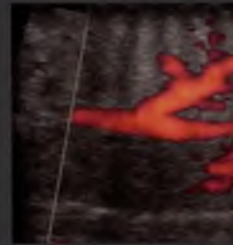


Get Full Access and More at

ExpertConsult.com

# CalLEN'S ULTRASONOGRAPHY IN OBSTETRICS AND GYNECOLOGY

SIXTH EDITION



MARY E.  
NORTON

LESLIE M.  
SCOUTT

VICKIE A.  
FELDSTEIN

ELSEVIER

CALLLEN'S  
ULTRASONOGRAPHY  
IN OBSTETRICS  
AND GYNECOLOGY

akushheringru



# CalLEN'S ULTRASONOGRAPHY IN OBSTETRICS AND GYNECOLOGY SIXTH EDITION

MARY E.

**NORTON, MD**

Professor  
Obstetrics, Gynecology, and Reproductive  
Sciences  
University of California San Francisco  
School of Medicine  
San Francisco, California

LESLIE M.

**SCOUTT, MD**

Professor of Radiology and Vascular Surgery  
Yale University  
School of Medicine  
New Haven, Connecticut

VICKIE A.

**FELDSTEIN, MD**

Professor  
Radiology and Biomedical Imaging  
Obstetrics, Gynecology, and  
Reproductive Sciences  
University of California San Francisco  
School of Medicine  
San Francisco, California

ELSEVIER

1600 John F. Kennedy Blvd.  
Ste 1800  
Philadelphia, PA 19103-2899

CALLAN'S ULTRASONOGRAPHY IN OBSTETRICS AND  
GYNECOLOGY, SIXTH EDITION

ISBN: 978-0-323-32834-0

Copyright © 2017 by Elsevier, Inc. All rights reserved.

No part of this publication may be reproduced or transmitted in any form or by any means, electronic or mechanical, including photocopying, recording, or any information storage and retrieval system, without permission in writing from the Publisher. Details on how to seek permission, further information about the Publisher's permissions policies and our arrangements with organizations such as the Copyright Clearance Center and the Copyright Licensing Agency, can be found at our website: [www.elsevier.com/permissions](http://www.elsevier.com/permissions).

This book and the individual contributions contained in it are protected under copyright by the Publisher (other than as may be noted herein).

#### Notices

Knowledge and best practice in this field are constantly changing. As new research and experience broaden our understanding, changes in research methods, professional practices, or medical treatment may become necessary.

Practitioners and researchers must always rely on their own experience and knowledge in evaluating and using any information, methods, compounds, or experiments described herein. In using such information or methods they should be mindful of their own safety and the safety of others, including parties for whom they have a professional responsibility.

With respect to any drug or pharmaceutical products identified, readers are advised to check the most current information provided (i) on procedures featured or (ii) by the manufacturer of each product to be administered, to verify the recommended dose or formula, the method and duration of administration, and contraindications. It is the responsibility of practitioners, relying on their own experience and knowledge of their patients, to make diagnoses, to determine dosages and the best treatment for each individual patient, and to take all appropriate safety precautions.

To the fullest extent of the law, neither the Publisher nor the authors, contributors, or editors, assume any liability for any injury and/or damage to persons or property as a matter of products liability, negligence or otherwise, or from any use or operation of any methods, products, instructions, or ideas contained in the material herein.

Previous editions copyrighted 2008, 2000, 1994, 1988, 1983.

#### Library of Congress Cataloging-in-Publication Data

Names: Callan, Peter W. | Norton, Mary E. (Professor in maternal health) | Scoutt, Leslie M. | Feldstein, Vickie A.

Title: Callan's ultrasonography in obstetrics and gynecology / [edited by] Mary E. Norton, MD, professor, Obstetrics, Gynecology, and Reproductive Sciences, University of California, San Francisco, San Francisco, California, Leslie Scoutt, MD, FACR, professor of radiology, Yale University School of Medicine, chief, Ultrasound Section, associate program director, Diagnostic Radiology, medical director, Non Invasive Vascular Laboratory, Yale New Haven Hospital, New Haven, Connecticut, Vickie A. Feldstein, MD, professor of radiology, University of California San Francisco School of Medicine, San Francisco, California.

Other titles: Ultrasonography in obstetrics and gynecology

Description: Sixth edition. | Philadelphia, PA : Elsevier, [2017] | Includes bibliographical references.

Identifiers: LCCN 2015048562 | ISBN 9780323328340 (hardcover : alk. paper)

Subjects: LCSH: Ultrasonics in obstetrics. | Generative organs, Female—Ultrasonic imaging.

Classification: LCC RG527.5.U48 U47 2017 | DDC 618.2/07543—dc23 LC record available at

<http://lcn.loc.gov/2015048562>

*Executive Content Strategist:* Robin Carter  
*Senior Content Development Manager:* Taylor Ball  
*Publishing Services Manager:* Patricia Tannian  
*Senior Project Manager:* Sharon Corell  
*Book Designer:* Brian Salisbury

Printed in China.

Last digit is the print number: 9 8 7 6 5 4 3 2 1



Working together  
to grow libraries in  
developing countries

[www.elsevier.com](http://www.elsevier.com) • [www.bookaid.org](http://www.bookaid.org)

To our families for their unwavering support and encouragement, to our residents and fellows who inspire us to be better teachers, to all the contributing authors for their hard work and excellent chapters, to our sonographers for their dedication to patient care, and to our colleagues who constantly stimulate us through their passion for the field of ultrasound.

M.E.N., L.M.S., V.A.F.

akusher-lib.ru



**Alfred Z. Abuhamad, MD**

Mason C. Andrews Professor and Chairman  
of Obstetrics and Gynecology  
Vice Dean for Clinical Affairs  
Eastern Virginia Medical School  
Norfolk, Virginia

**Nancy A. Ayres, MD**

Director of Fetal Cardiology  
Texas Children's Hospital Heart Center and  
Texas Children's Fetal Center  
Director of Non-Invasive Imaging  
Texas Children's Hospital Heart Center  
Department of Pediatrics  
Section of Cardiology  
Baylor College of Medicine  
Houston, Texas

**Robert H. Ball, MD**

Medical Director  
Obstetrix of the Mountain States  
Salt Lake City, Utah

**Oksana H. Baltarowich, MD**

Professor of Radiology  
Department of Radiology  
Thomas Jefferson University  
Philadelphia, Pennsylvania

**Beryl Benacerraf, MD**

Departments of Radiology and Obstetrics  
and Gynecology  
Brigham and Women's Hospital  
Department of Obstetrics and Gynecology  
Massachusetts General Hospital  
Harvard Medical School  
Boston, Massachusetts

**Genevieve L. Bennett, MD**

Assistant Professor of Radiology  
Department of Radiology  
Assistant Professor of Obstetrics and  
Gynecology  
Department of Obstetrics and Gynecology  
NYU Langone Medical Center  
New York, New York

**Carol B. Benson, MD**

Professor of Radiology  
Harvard Medical School  
Director of Ultrasound  
Co-Director of High-Risk Obstetrical  
Ultrasound  
Radiology Director of the Noninvasive  
Vascular Laboratory  
Brigham and Women's Hospital  
Boston, Massachusetts

**Vincenzo Berghella, MD**

Director  
Maternal-Fetal Medicine  
Professor  
Obstetrics and Gynecology  
Sidney Kimmel Medical College of Thomas  
Jefferson University  
Philadelphia, Pennsylvania

**Deborah Rose Berman, MD**

Associate Professor  
Department of Obstetrics and Gynecology  
University of Michigan Health System  
Ann Arbor, Michigan

**Priya Bhosale, MD**

Associate Professor of Radiology  
Department of Diagnostic Radiology  
MD Anderson Cancer Center  
Houston, Texas

**Douglas L. Brown, MD**

Professor of Radiology  
Mayo Clinic College of Medicine  
Rochester, Minnesota

**Peter W. Callen, MD**

Professor of Radiology, Obstetrics,  
Gynecology, and Reproductive Sciences  
Department of Radiology  
University of California San Francisco  
School of Medicine  
San Francisco, California

**Suneet P. Chauhan, MD**

Professor  
Department of Obstetrics and Gynecology  
McGovern Medical School at  
The University of Texas Health Science  
Center at Houston (UT Health)  
Houston, Texas

**Ramen H. Chmait, MD**

Associate Professor  
Obstetrics and Gynecology  
University of Southern California  
Director  
Los Angeles Fetal Surgery  
Los Angeles, California

**Jodi S. Dashe, MD**

Professor  
Department of Obstetrics and Gynecology  
University of Texas Southwestern Medical  
Center at Dallas  
Medical Director of Prenatal Diagnosis and  
Genetics  
Parkland Health and Hospital System  
Dallas, Texas

**Catherine Devine, MD**

Associate Professor of Radiology  
Department of Diagnostic Radiology  
MD Anderson Cancer Center  
Houston, Texas

**Jeffrey M. Dicke, MD**

Professor  
Department of Obstetrics and Gynecology  
Washington University School of Medicine  
St. Louis, Missouri

**Peter M. Doubilet, MD, PhD**

Professor of Radiology  
Harvard Medical School  
Senior Vice Chair  
Department of Radiology  
Brigham and Women's Hospital  
Boston, Massachusetts

**Sarah Ellestad, MD**

Assistant Professor  
Department of Obstetrics and Gynecology  
Division of Maternal-Fetal Medicine  
Medical Director  
Duke Perinatal  
Duke University Medical Center  
Durham, North Carolina

**Jimmy Espinoza, MD, MSc, FACOG**

Associate Professor  
Department of Obstetrics and Gynecology  
Division of Maternal and Fetal Medicine  
Texas Children's Hospital-Pavilion for  
Women  
Baylor College of Medicine  
Houston, Texas

**Vickie A. Feldstein, MD**

Professor  
Radiology and Biomedical Imaging  
Obstetrics, Gynecology, and Reproductive  
Sciences  
University of California San Francisco  
San Francisco, California

**Roy A. Filly, MD**

Professor Emeritus  
Radiology and Biomedical Imaging,  
Surgery, Obstetrics, Gynecology, and  
Reproductive Sciences  
University of California San Francisco  
School of Medicine  
San Francisco, California

**Mary C. Frates, MD**

Associate Professor of Radiology  
Harvard Medical School  
Assistant Director of Ultrasound  
Brigham and Women's Hospital  
Boston, Massachusetts

**Maynor Garcia, MD**

Department of Obstetrics and Gynecology  
Division of Maternal-Fetal Medicine  
Wayne State University  
School of Medicine  
Detroit, Michigan  
Perinatology Research Branch, NICHD/  
NIH/DHHS  
Bethesda, Maryland, and Detroit, Michigan

**Carly S. Gardner, MD**

Assistant Professor of Radiology  
Department of Radiology  
Baylor College of Medicine  
Houston, Texas

**Katherine R. Goetzinger, MD, MSCI**

Assistant Professor  
Division of Maternal Fetal Medicine  
Department of Obstetrics, Gynecology, and  
Reproductive Sciences  
University of Maryland  
School of Medicine  
Baltimore, Maryland

**Luis F. Gonçaves, MD**

Department of Radiology and Department  
of Obstetrics and Gynecology  
Beaumont Health System  
Divisions of Radiology and Fetal Imaging  
Royal Oak, Michigan  
Department of Radiology and Department  
of Obstetrics and Gynecology  
Oakland University William Beaumont  
Hospital  
School of Medicine  
Rochester, Michigan

**Edgar Hernandez-Andrade, MD, PhD**

Associate Professor  
Division of Maternal-Fetal Medicine  
Department of Obstetrics and Gynecology  
Wayne State University  
School of Medicine  
Detroit, Michigan  
Perinatology Research Branch NICHD/  
NIH/DHHS  
Bethesda, Maryland, and Detroit, Michigan

**Barbara L. Hoffman, MD**

Professor  
Department of Obstetrics and Gynecology  
University of Texas Southwestern Medical  
Center at Dallas  
Parkland Health and Hospital System  
Dallas, Texas

**Mindy M. Horrow, MD, FACR, FSRU,  
FAIUM**

Vice Chair  
Department of Radiology  
Einstein Medical Center  
Professor of Radiology  
Sidney Kimmel Medical College  
Thomas Jefferson University  
Philadelphia, Pennsylvania

**Kathryn Johnson Gray, MD, PhD**

Combined Maternal-Fetal Medicine/  
Genetics Fellow  
Maternal-Fetal Medicine  
Brigham and Women's Hospital  
Division of Genetics  
Boston Children's Hospital  
Boston, Massachusetts

**Adeeb Khalifeh, MD**

Fellow  
Obstetrics and Gynecology  
Jefferson Medical College of Thomas  
Jefferson University  
Philadelphia, Pennsylvania

**Jeffrey A. Kuller, MD**

Professor of Obstetrics and Gynecology  
Division of Maternal-Fetal Medicine  
Duke University Medical Center  
Durham, North Carolina

**Sherelle Laifer-Narin, MD**

Associate Professor of Radiology  
Department of Radiology  
Division of Body Imaging  
Chief  
Ultrasound and Fetal MRI  
Columbia University Medical Center  
New York, New York

**Jill E. Langer, MD**

Professor of Radiology  
Chief  
Ultrasound Section  
Department of Radiology  
The Perelman School of Medicine at the  
University of Pennsylvania  
Philadelphia, Pennsylvania

**Wesley Lee, MD**

Co-Director  
Texas Children's Fetal Center  
Section Chief  
Women's and Fetal Imaging  
Professor  
Department of Obstetrics and Gynecology  
Baylor College of Medicine  
Houston, Texas

**Mark E. Lockhart, MD, MPH**

Professor of Diagnostic Radiology  
Chief  
Abdominal Imaging Section  
Chief  
Genitourinary Imaging  
University of Alabama at Birmingham  
Birmingham, Alabama

**Suchaya Luewan, MD**

Maternal-Fetal Medicine Unit  
Department of Obstetrics and Gynecology  
Faculty of Medicine  
Chiang Mai University  
Chiang Mai, Thailand

**Everett F. Magann, MD**

Professor of Obstetrics and Gynecology  
Obstetrics and Gynecology  
University of Arkansas for the Medical  
Sciences  
Little Rock, Arkansas

**Shiraz A. Maskatia, MD**

Assistant Professor  
Department of Pediatrics  
Section of Cardiology  
Baylor College of Medicine  
Texas Children's Hospital Heart Center and  
Texas Children's Fetal Center  
Houston, Texas

**Hector Mendez-Figueroa, MD**

Assistant Professor  
Department of Obstetrics, Gynecology, and  
Reproductive Sciences  
Division of Maternal Fetal Medicine  
The University of Texas Health Science  
Center Houston  
Houston, Texas



**Malgorzata Mlynarczyk, MD, PhD**

Maternal Fetal Medicine Fellow  
Department of Obstetrics and Gynecology  
Eastern Virginia Medical School  
Norfolk, Virginia

**Tara A. Morgan, MD**

Clinical Instructor  
Radiology and Biomedical Imaging  
University of California San Francisco  
School of Medicine  
San Francisco, California

**Shaine A. Morris, MD, MPH**

Assistant Professor  
Pediatrics  
Division of Pediatric Cardiology  
Texas Children's Hospital Division of  
Pediatric Cardiology  
Houston, Texas

**Allan Nadel, MD**

Director of Prenatal Diagnosis  
Department of Obstetrics and Gynecology  
Massachusetts General Hospital  
Boston, Massachusetts

**Paulo Nassar de Carvalho, MD, MSc, PhD**

Perinatologist  
Department of Obstetrics  
Instituto Fernandes Figueira/FIOCRUZ  
Coordinator  
Department of Obstetrics  
Clinica Perinatal  
Rio de Janeiro, Brazil

**Mary E. Norton, MD**

Vice Chair of Clinical and Translational  
Genetics and Genomics; and  
David E. Thorburn, MD, and Kate  
McKee Thorburn Endowed Chair in  
Perinatal Medicine and Genetics  
Professor  
Obstetrics, Gynecology, and Reproductive  
Sciences  
University of California San Francisco  
San Francisco, California

**Anthony O. Odibo, MD, MSCE**

Professor of Obstetrics and Gynecology  
Director of Obstetric Ultrasound and Fetal  
Therapy  
USF Health—Morsani College of Medicine  
Department of Obstetrics and Gynecology  
Division of Maternal Fetal Medicine  
South Tampa Center for Advanced  
Healthcare  
Tampa, Florida

**Harriet J. Paltiel, MDCM**

Associate Professor of Radiology  
Harvard Medical School  
Radiologist  
Boston Children's Hospital  
Boston, Massachusetts

**Kate E. Pettit, MD**

Assistant Professor  
Department of Obstetrics and Gynecology  
Division of Maternal-Fetal Medicine  
University of Virginia  
Charlottesville, Virginia

**Andrew Phelps, MD**

Assistant Professor of Pediatric Radiology  
Radiology and Biomedical Imaging  
UCSF Benioff Children's Hospital  
San Francisco, California

**Gianluigi Pilu, MD**

Department of Obstetrics and Gynecology  
University of Bologna  
Bologna, Italy

**Liina Pöder, MD**

Associate Professor of Clinical Radiology  
Department of Radiology and Biomedical  
Imaging  
University of California San Francisco  
School of Medicine  
San Francisco, California

**Dolores H. Pretorius, MD**

Professor of Radiology  
Director of Imaging at UC San Diego  
Maternal-Fetal Care and Genetics  
Department of Radiology  
University of California San Diego  
San Diego, California

**Aliya Qayyum, MBBS, MRCP, FRCR**

Professor of Radiology  
Department of Diagnostic Radiology  
MD Anderson Cancer Center  
Houston, Texas

**Maryam Rezvani, MD**

Associate Professor of Radiology  
University of Utah School of Medicine  
Salt Lake City, Utah

**Britton D. Rink, MD, MS**

Director  
Perinatal Genetics  
Division of Maternal Fetal Medicine  
Mount Carmel Health System  
Columbus, Ohio

**Letty Romary, MD**

Professor  
Center for Molecular Medicine and Genetics  
Wayne State University  
Detroit, Michigan  
Maternal Fetal Medicine Fellow  
Department of Obstetrics and Gynecology  
Eastern Virginia Medical School  
Norfolk, Virginia

**Roberto Romero, MD, Med Sci**

Chief  
Program for Perinatal Research and  
Obstetrics  
Division of Intramural Research  
Eunice Kennedy Shriver National Institute  
of Child Health and Human  
Development  
National Institutes of Health  
Perinatology Research Branch, NICHD/  
NIH/DHHS  
Bethesda, Maryland, and Detroit, Michigan  
Professor  
Department of Obstetrics and Gynecology  
University of Michigan  
Ann Arbor, Michigan  
Professor  
Department of Epidemiology and  
Biostatistics  
Michigan State University  
East Lansing, Michigan

**Adam T. Sandlin, MD**

Assistant Professor  
Division of Maternal-Fetal Medicine  
Obstetrics and Gynecology  
University of Arkansas for Medical Sciences  
Little Rock, Arkansas

**Leslie M. Scoult, MD, FACR**

Professor of Radiology and Vascular Surgery  
Vice Chair  
Chief  
Ultrasound Section  
Medical Director  
Non-Invasive Vascular Laboratory  
Department of Radiology and Biomedical  
Imaging  
Yale University  
School of Medicine  
New Haven, Connecticut

**Howard T. Sharp, MD**

Professor of Obstetrics and Gynecology  
Chief  
Division of General Obstetrics and  
Gynecology  
Department of Obstetrics/Gynecology  
University of Utah Health Care  
Salt Lake City, Utah

**Lynn L. Simpson, MD**

Professor of Obstetrics and Gynecology  
Department of Obstetrics and Gynecology  
Columbia University Medical Center  
New York, New York

**Nga V. Tran, RDMS**

Sonographer  
Maternal Fetal Care and Genetics  
University of California San Diego  
San Diego, California

**Marjorie C. Treadwell, MD**

Professor  
Department of Obstetrics and Gynecology  
University of Michigan Health System  
Ann Arbor, Michigan

**Amanda S. Trudell, DO**

Clinical Fellow Maternal Fetal Medicine  
Department of Obstetrics and Gynecology  
Washington University School of Medicine  
St. Louis, Missouri

**Diane M. Twickler, MD**

Professor  
Departments of Radiology and Obstetrics  
and Gynecology  
University of Texas Southwestern  
Dallas, Texas

**Darci J. Wall, MD**

Assistant Professor of Radiology  
Mayo Clinic College of Medicine  
Rochester, Minnesota

**Milena M. Weinstein, MD**

Assistant Professor  
Division of Female Pelvic Medicine and  
Reconstructive Surgery  
Department of Obstetrics, Gynecology, and  
Reproductive Biology  
Harvard Medical School  
Massachusetts General Hospital  
Boston, Massachusetts

**Sarah Wheeler, MD**

Fellow  
Obstetrics and Gynecology  
Division of Maternal-Fetal Medicine  
Duke University Medical Center  
Durham, North Carolina

**Louise Wilkins-Haug, MD, PhD**

Professor  
Department of Obstetrics and Gynecology  
Brigham and Women's Hospital  
Boston, Massachusetts

**Thomas C. Winter, MD**

Professor of Radiology  
Adjunct Professor of Obstetrics/Gynecology  
Chief  
Adominal Imaging Section  
University of Utah School of Medicine  
Salt Lake City, Utah

**Lami Yeo, MD, FACOG, FAIUM**

Professor  
Division of Maternal-Fetal Medicine  
Department of Obstetrics and Gynecology  
Wayne State University School of Medicine  
Detroit, Michigan  
Director of Fetal Cardiology  
Perinatology Research Branch, NICHD,  
NIH, DHHS  
Bethesda, Maryland, and Detroit, Michigan



The first edition of this textbook was published well over 30 years ago, when Peter Callen was a young faculty member, we were in medical school, and obstetric sonography was an emerging subspecialty. Whereas the book has grown and evolved through the subsequent editions, it has remained one of the most highly regarded texts in obstetric and gynecologic ultrasound. The three of us grew up reading and learning from Callen's *Ultrasonography in Obstetrics and Gynecology*. Therefore, when we were invited to edit the sixth edition, it was an opportunity that we were eager to embrace, daunting though it was to follow in Peter's footsteps.

Over the years, many aspects of obstetric and gynecologic ultrasound have changed. Ultrasound technology and equipment continue to improve. The anatomic detail that can be visualized and the physiologic parameters that can be assessed have expanded the utility, as well as the complexity, of ultrasound imaging. As in other areas of medicine, care of the obstetric and gynecologic patient in today's practice has advanced to involve much more collaboration across disciplines. This sixth edition reflects this change and was truly a multidisciplinary effort reflecting contributions from experts in obstetrics and gynecology, maternal-fetal medicine, and diagnostic radiology and biomedical imaging. Mary recruited authors from the fields of obstetrics and maternal-fetal medicine and edited chapters on obstetric and fetal sonography. Leslie served as the gynecology editor, managing the recruitment of authors and editing of chapters focused on gynecologic imaging. Vickie helped ensure that the ultrasound images, diagrams, and medical illustrations were of the highest quality. The three of us have been fortunate to have been trained by, and subsequently worked alongside, some renowned leaders in the field of

obstetric and gynecologic imaging. Many of these colleagues and friends, names well known to those in this arena, have contributed to this textbook. The updated information highlights the clinical context and impact of imaging findings. We believe this approach has added to the richness, breadth, and depth of the content of this new edition.

The prior editions of this textbook were edited by Peter with meticulous care and attention. He was always mindful of including authors who are respected experts in their fields and whose writing is authoritative and clear. He ensured that each edition was a substantial update from the previous version and that each chapter was well and liberally illustrated with high-quality sonographic images, drawings, and diagrams to help clarify concepts and illustrate ideas. We aimed to follow his lead and have greatly benefited from his experience, advice, and help throughout this process.

In addition to Peter, who taught us so much and had faith that we could successfully carry on this tradition, there are many others to whom thanks is due. First and foremost, we want to acknowledge and thank all the authors who contributed such outstanding chapters, representing many hours of dedication and effort. The staff at Elsevier, including Taylor Ball in particular, was very helpful and patient as we moved through the production process. Many sonographers and sonologist colleagues helped us collect high-quality images. Finally and importantly, we must thank our families who tolerated so many late nights, early mornings, and weekends spent writing, editing, and tending to this text.

**Mary E. Norton, MD, Leslie M. Scutt, MD,  
and Vickie A. Feldstein, MD**

## SECTION I Obstetrics

- 1 Obstetric Ultrasound Examination, 2**  
*Peter W. Callen, Mary E. Norton*
- 2 Genetics and Prenatal Genetic Testing, 24**  
*Mary E. Norton, Britton D. Rink*
- 3 Ultrasound Evaluation of Fetal Aneuploidy in the First and Second Trimesters, 57**  
*Katherine R. Goetzinger, Anthony O. Odibo*
- 4 Ultrasound of the Early First Trimester, 82**  
*Peter M. Doubilet, Carol B. Benson*
- 5 Evaluation of Fetal Anatomy in the First Trimester, 98**  
*Amanda S. Trudell, Anthony O. Odibo*
- 6 Fetal Biometry and Growth, 118**  
*Carol B. Benson, Peter M. Doubilet*
- 7 Ultrasound Evaluation in Multiple Gestations, 132**  
*Lynn L. Simpson*
- 8 Ultrasound Evaluation of Normal Fetal Anatomy, 157**  
*Tara A. Morgan, Vickie A. Feldstein, Roy A. Filly*
- 9 Ultrasound Evaluation of the Fetal Central Nervous System, 220**  
*Gianluigi Pilu*
- 10 Ultrasound Evaluation of the Fetal Face and Neck, 243**  
*Kate E. Pettit, Nga V. Tran, Dolores H. Pretorius*
- 11 Fetal Musculoskeletal System, 272**  
*Edgar Hernandez-Andrade, Lami Yeo, Luís F. Gonçalves, Suchaya Luewan, Maynor Garcia, Roberto Romero*
- 12 Ultrasound Evaluation of the Fetal Thorax, 346**  
*Deborah Rose Berman, Marjorie C. Treadwell*
- 13 Sonographic Evaluation of the Fetal Heart, 371**  
*Shaine A. Morris, Nancy A. Ayres, Jimmy Espinoza, Shiraz A. Maskatia, Wesley Lee*
- 14 Ultrasound Evaluation of the Fetal Gastrointestinal Tract and Abdominal Wall, 460**  
*Allan Nadel*
- 15 Fetal Genitourinary Tract, 503**  
*Anthony O. Odibo, Jeffrey M. Dicke*
- 16 Ultrasound Features of Fetal Syndromes, 539**  
*Kathryn Johnson Gray, Louise Wilkins-Haug*
- 17 Evaluation of Hydrops Fetalis, 633**  
*Hector Mendez-Figueroa, Suneet P. Chauhan*
- 18 Ultrasound Evaluation of the Gravid Cervix, 653**  
*Vincenzo Berghella, Adeeb Khalifeh*
- 19 Ultrasound Evaluation of the Placenta, Membranes, and Umbilical Cord, 674**  
*Jodi S. Dashe, Barbara L. Hoffman*
- 20 Amniotic Fluid Volume in Fetal Health and Disease, 704**  
*Everett F. Magann, Adam T. Sandlin*
- 21 Antepartum Fetal Surveillance and the Role of Ultrasound, 720**  
*Sarah Ellestad, Sarah Wheeler, Jeffrey A. Kuller*
- 22 Role of Doppler Sonography in Obstetrics, 733**  
*Malgorzata Mlynarczyk, Letty Romary, Alfred Z. Abuhamad*
- 23 Role of Magnetic Resonance Imaging in Obstetrics, 749**  
*Sherelle Laifer-Narin, Diane M. Twickler*
- 24 Role of Sonography in Fetal Procedures, 775**  
*Ramen H. Chmait, Paulo Nassar de Carvalho, Robert H. Ball*

- 25 Obstetric Ultrasound Imaging and the Obese Patient, 799**  
*Beryl Benacerraf*

## SECTION II Gynecology

- 26 Normal Anatomy of the Female Pelvis and Transvaginal Sonography, 805**  
*Jill E. Langer*
- 27 Abnormal Uterine Bleeding: The Role of Ultrasound, 835**  
*Maryam Rezvani, Thomas C. Winter*
- 28 Ultrasound Evaluation of the Uterus, 846**  
*Liina Pöder*
- 29 Evaluation of Pelvic Pain in the Reproductive Age Patient, 883**  
*Genevieve L. Bennett*
- 30 Ultrasound Evaluation of the Ovaries, 919**  
*Douglas L. Brown, Darci J. Wall*
- 31 Ultrasound Evaluation of the Fallopian Tube, 934**  
*Mindy M. Horrow*
- 32 Sonographic Imaging in Infertility and Assisted Reproduction, 953**  
*Mary C. Frates*
- 33 Ectopic Pregnancy, 966**  
*Oksana H. Baltarowich, Leslie M. Scouff*
- 34 Gynecologic Sonography in the Pediatric and Adolescent Patient, 1001**  
*Harriet J. Paltiel, Andrew Phelps*
- 35 Ultrasound and Magnetic Resonance Imaging in Urogynecology, 1025**  
*Milena M. Weinstein, Mark E. Lockhart*
- 36 Role of Magnetic Resonance Imaging in the Evaluation of Gynecologic Disorders, 1045**  
*Priya Bhosale, Catherine Devine, Carly S. Gardner, Aliya Qayyum*
- 37 Role of Sonography in Gynecologic Interventions, 1076**  
*Howard T. Sharp, Thomas C. Winter*

## SECTION III Technical Considerations and Aberrations

- 38 Artifacts, Pitfalls, and Normal Variants, 1093**  
*Peter W. Callen*
- |                   |  |
|-------------------|--|
| <b>Appendix A</b> | <b>Measurements Frequently Used to Estimate Gestational Age and Fetal Biometry, 1155</b> |
| <b>Appendix B</b> | <b>Measurements Used in Assessing Fetal Weight, Growth, and Body Proportions, 1174</b>   |
| <b>Appendix C</b> | <b>Measurements for Amniotic Fluid Assessment, 1200</b>                                  |
| <b>Appendix D</b> | <b>Fetal Doppler Assessment (Noncardiac), 1204</b>                                       |
| <b>Appendix E</b> | <b>Doppler of the Middle Cerebral Artery to Assess Fetal Anemia, 1209</b>                |
| <b>Appendix F</b> | <b>Fetal Cardiac Measurements and Doppler Assessment, 1210</b>                           |
| <b>Appendix G</b> | <b>Sonographic Detection of Chromosomal Abnormalities, 1220</b>                          |





## ULTRASOUND OF THE EARLY FIRST TRIMESTER

### Sonography Showing Heartbeat

Chapter 4, Video 1—Peter M. Doubilet, Carol B. Benson

### Movement When Transducer Pressure Applied

Chapter 4, Video 2—Peter M. Doubilet, Carol B. Benson

### Failed Intrauterine Pregnancy

Chapter 4, Video 3—Peter M. Doubilet, Carol B. Benson

### Suspected Pregnancy Failure

Chapter 4, Video 4—Peter M. Doubilet, Carol B. Benson

### Suspected Pregnancy Failure Based on Expanded Amnion Sign

Chapter 4, Video 5—Peter M. Doubilet, Carol B. Benson

## SONOGRAPHIC EVALUATION OF THE FETAL HEART

### Four-Chamber View (4CV)

Chapter 13, Video 1—Shaine A. Morris, Nancy A. Ayres,

Jimmy Espinoza, Shiraz A. Maskatia, Wesley Lee

### Left-Ventricular Outflow Tract View (LVOT)

Chapter 13, Video 2—Shaine A. Morris, Nancy A. Ayres,

Jimmy Espinoza, Shiraz A. Maskatia, Wesley Lee

### Ebstein Anomaly and Other Tricuspid Valve Disorders

Chapter 13, Video 3—Shaine A. Morris, Nancy A. Ayres,

Jimmy Espinoza, Shiraz A. Maskatia, Wesley Lee

### Assessment of Atrioventricular Valves

Chapter 13, Video 4—Shaine A. Morris, Nancy A. Ayres,

Jimmy Espinoza, Shiraz A. Maskatia, Wesley Lee

### Bicausal View

Chapter 13, Video 5—Shaine A. Morris, Nancy A. Ayres,

Jimmy Espinoza, Shiraz A. Maskatia, Wesley Lee

### Long Axis of the Aortic Arch

Chapter 13, Video 6—Shaine A. Morris, Nancy A. Ayres,

Jimmy Espinoza, Shiraz A. Maskatia, Wesley Lee

### High Short Axis View of the Great Arteries

Chapter 13, Video 7—Shaine A. Morris, Nancy A. Ayres,

Jimmy Espinoza, Shiraz A. Maskatia, Wesley Lee

### Low Short Axis View of the Ventricles

Chapter 13, Video 8—Shaine A. Morris, Nancy A. Ayres,

Jimmy Espinoza, Shiraz A. Maskatia, Wesley Lee

### Muscular Ventricular Septal Defects

Chapter 13, Video 9—Shaine A. Morris, Nancy A. Ayres,

Jimmy Espinoza, Shiraz A. Maskatia, Wesley Lee

### Atrioventricular Canal Defects

Chapter 13, Video 10—Shaine A. Morris, Nancy A. Ayres,

Jimmy Espinoza, Shiraz A. Maskatia, Wesley Lee

### Incomplete or Partial Form of AVC

Chapter 13, Video 11—Shaine A. Morris, Nancy A. Ayres,

Jimmy Espinoza, Shiraz A. Maskatia, Wesley Lee

### Unbalanced AVC

Chapter 13, Video 12—Shaine A. Morris, Nancy A. Ayres,

Jimmy Espinoza, Shiraz A. Maskatia, Wesley Lee

### Tetralogy of Fallot

Chapter 13, Video 13—Shaine A. Morris, Nancy A. Ayres,

Jimmy Espinoza, Shiraz A. Maskatia, Wesley Lee

### Tetralogy of Fallot

Chapter 13, Video 14—Shaine A. Morris, Nancy A. Ayres,

Jimmy Espinoza, Shiraz A. Maskatia, Wesley Lee

### Pulmonary Blood Flow Fed by a Ductus Arteriosus

Chapter 13, Video 15—Shaine A. Morris, Nancy A. Ayres,

Jimmy Espinoza, Shiraz A. Maskatia, Wesley Lee

### Truncus Arteriosus

Chapter 13, Video 16—Shaine A. Morris, Nancy A. Ayres,

Jimmy Espinoza, Shiraz A. Maskatia, Wesley Lee

### Truncus Arteriosus

Chapter 13, Video 17—Shaine A. Morris, Nancy A. Ayres,

Jimmy Espinoza, Shiraz A. Maskatia, Wesley Lee

### Double Outlet Right Ventricle

Chapter 13, Video 18—Shaine A. Morris, Nancy A. Ayres,

Jimmy Espinoza, Shiraz A. Maskatia, Wesley Lee

### Hypoplastic Left Heart Syndrome

Chapter 13, Video 19—Shaine A. Morris, Nancy A. Ayres,

Jimmy Espinoza, Shiraz A. Maskatia, Wesley Lee

### Hypoplastic Left Heart Complex

Chapter 13, Video 20—Shaine A. Morris, Nancy A. Ayres,

Jimmy Espinoza, Shiraz A. Maskatia, Wesley Lee

### Fetal Aortic Stenosis in Hypoplastic Left Heart Syndrome

Chapter 13, Video 21—Shaine A. Morris, Nancy A. Ayres,

Jimmy Espinoza, Shiraz A. Maskatia, Wesley Lee

### Endocardial Fibroelastosis in Hypoplastic Left Heart Syndrome

Chapter 13, Video 22—Shaine A. Morris, Nancy A. Ayres,

Jimmy Espinoza, Shiraz A. Maskatia, Wesley Lee

### Endocardial Fibroelastosis in Hypoplastic Left Heart Syndrome

Chapter 13, Video 23—Shaine A. Morris, Nancy A. Ayres,

Jimmy Espinoza, Shiraz A. Maskatia, Wesley Lee

### Rhabdomyoma

Chapter 13, Video 24—Shaine A. Morris, Nancy A. Ayres,

Jimmy Espinoza, Shiraz A. Maskatia, Wesley Lee

### Intrapericardial Teratoma

Chapter 13, Video 25—Shaine A. Morris, Nancy A. Ayres,

Jimmy Espinoza, Shiraz A. Maskatia, Wesley Lee

### Ectopia Cordis/Pentalogy of Cantrell

Chapter 13, Video 26—Shaine A. Morris, Nancy A. Ayres,

Jimmy Espinoza, Shiraz A. Maskatia, Wesley Lee

## ANTEPARTUM FETAL SURVEILLANCE AND THE ROLE OF ULTRASOUND

### Tone Cine

Chapter 21, Video 1—Jeffrey A. Kuller, Sarahn Wheeler,

Sarah Ellestad

### Breathing Cine

Chapter 21, Video 2—Jeffrey A. Kuller, Sarahn Wheeler,

Sarah Ellestad

## ULTRASOUND AND FETAL PROCEDURES

### Aortic Valvuloplasty

Chapter 24, Video 1—Ramen H. Chmait, Paulo Nassar de Carvalho,

Robert H. Ball

## ULTRASOUND EVALUATION OF THE FALLOPIAN TUBE

### Normal Tube With Paratubal Cysts

Chapter 31, Video 1—Mindy M. Horrow

- Hydrosalpinx Medial to Right Ovary**  
Chapter 31, Video 2—Mindy M. Horrow
- Hematosalpinx**  
Chapter 31, Video 3—Mindy M. Horrow
- Tubal Torsion**  
Chapter 31, Video 4—Mindy M. Horrow

## **GYNECOLOGIC ULTRASOUND IN THE PEDIATRIC AND ADOLESCENT PATIENT**

- Unicornuate Left Uterus With Obstructed, Rudimentary Right Hemiuterus**  
Chapter 34, Video 1—Harriet J. Paltiel, Andrew Phelp

- Unicornuate Left Uterus With Obstructed, Rudimentary Right Hemiuterus**  
Chapter 34, Video 2—Harriet J. Paltiel, Andrew Phelps
- Cloacal Malformation**  
Chapter 34, Video 3—Harriet J. Paltiel, Andrew Phelps
- Polycystic Ovary Syndrome**  
Chapter 34, Video 4—Harriet J. Paltiel, Andrew Phelps
- Pyosalpinx**  
Chapter 34, Video 5—Harriet J. Paltiel, Andrew Phelps
- Incarcerated Inguinal Hernia**  
Chapter 34, Video 6—Harriet J. Paltiel, Andrew Phelps
- Right Ovarian Dysgerminoma**  
Chapter 34, Video 7—Harriet J. Paltiel, Andrew Phelps

SECTION I

Obstetrics

**CalLEN'S**  
ULTRASONOGRAPHY  
**IN** OBSTETRICS  
**AND** GYNECOLOGY

akusherstvo.ru

Obstetrics

akusher-lib.ru



# Obstetric Ultrasound Examination

Peter W. Callen, Mary E. Norton

## SUMMARY OF KEY POINTS

- Recent years have seen dramatic advances in ultrasound technology, including improved spatial and contrast resolution, routine use of three-dimensional (3D) and four-dimensional (4D) imaging, volumetric scanning, expanded indications for color and spectral Doppler, new and improved ultrasound scanning probes, and improved digital review workstations.
- With improved imaging comes the complicating corollary as to what minor findings should be reported to the patient and which merely lead to unnecessary anxiety.
- Although there is high-quality evidence that ultrasound is safe for the fetus when used appropriately, consensus statements conclude that Doppler examination of fetal vessels in early pregnancy should not be performed without a clinical indication.
- The nonmedical use of ultrasound for psychosocial or entertainment purposes is strongly discouraged by professional organizations such as the American Institute of Ultrasound in Medicine (AIUM).
- Only those with adequate training in a conventional training program should be performing and interpreting ultrasound examinations.
- Consensus guidelines and criteria for transvaginal sonographic diagnosis of pregnancy failure in a woman with an intrauterine pregnancy of uncertain viability have been established and should be followed.
- Although early detection of a morphologic abnormality is useful, the confident unequivocal detection of an abnormality is even more important. Unless one is extremely confident of the existence of an abnormality in the first trimester, a follow-up examination should be performed.
- Measurements made early in pregnancy, for the most part, are more accurate than those made near term.
- Although a diagnosis of oligohydramnios and polyhydramnios can be made subjectively, the extremes of amniotic fluid volume should also be assessed objectively using either the deepest vertical pocket (DVP) or amniotic fluid index (AFI).
- It is preferable to report the distance from the inferior edge of the placenta to the internal cervical os rather than relying on terms that may have differing meanings (e.g., marginal placenta).
- If a single obstetric ultrasound or a targeted examination is performed, it should be done at a gestational age of 18 to 20 weeks.
- Obstetric ultrasound examinations represented the majority of medical malpractice cases involving ultrasound.
- Ultrasound examination is a noninvasive, safe procedure that has a high degree of patient acceptance and can yield a wealth of information.

## OUTLINE

### Safety of Ultrasound Examination, 3

### Indications for Obstetric Ultrasound Examination, 4

Who Should Perform the Ultrasound Examination and How

Should It Be Performed?, 5

Nonmedical Use of Ultrasonography, 5

Terminology, 5

Ultrasound Lexicon, 6

### The American Institute of Ultrasound in Medicine Guidelines, 6

### Ultrasound Equipment and Documentation, 6

### The First Trimester Ultrasound Examination, 6

Identification of an Intrauterine Pregnancy, 6

Embryonic/Fetal Number, 12

Estimating Gestational Age, 12

Morphologic Abnormalities, 12

Placenta, 12

Uterus and Adnexa, 13

### The Second and Third Trimester Ultrasound Examinations, 13

Fetal Number and Fetal Life, 13

Fetal Position, 13

Assigning Gestational Age and Weight, 13

Amniotic Fluid Volume, 15

Amniotic Fluid Volume in Multiple Gestations, 16

Placenta, 16

Fetal Malformations, 17

Uterus and Adnexa, 17

### Verbiage Used in the AIUM/ACR/ACOG Guidelines, 17

### Interpretation of the Ultrasound Examination, 18

Reporting of Ultrasound Results, 18

Discussing the Examination With the Patient, 19

Evaluating the Obstetric-Gynecologic Ultrasound

Literature, 20

Malpractice and the Obstetric Ultrasound Examination, 20

### Conclusion, 21



It has now been over 4 decades since sonography was first used to evaluate the obstetric patient. At first, the questions this modality sought to answer were very basic: Is there a pregnancy? Is the fetus alive? Is there a singleton or a twin gestation? What is the location of the placenta? What is the gestational age? Probably, few envisioned the day when ultrasonography would be used to identify subtle anatomic defects such as cleft lip or palate, to predict obstetric complications such as placenta accreta, or to accurately detect the presence of fetal anemia. It is hard to believe that, at its inception, it was difficult to convince clinicians as to the usefulness of this new diagnostic modality in obstetric management. Now, it is routine for a patient to have at least one, and often several, ultrasound examinations during her pregnancy. The technologic advances in ultrasound imaging, including 3D/4D and volumetric measurements, the use of high-frequency transvaginal probes, and the utility for chromosomal screening in early pregnancy (e.g., nuchal translucency) have only expanded the indications for sonographic imaging in the obstetric patient.

Since the last edition of this textbook, there have been dramatic advances in ultrasound technology, including improved spatial and contrast resolution, routine use of 3D and 4D imaging, volumetric scanning, expanded indications for color and spectral Doppler, new and improved ultrasound scanning probes, and improved digital review workstations, to name a few. Likewise, our knowledge of normal fetal anatomy and pathology, and the pathophysiology of disease in general, has increased substantially. The Internet has made communication among and between researchers and clinicians easier. In addition, there have been many collaborative studies and refinements of the guidelines for the performance of the obstetric ultrasound examination. However, there are still differences in the approach to the obstetric ultrasound examination from one group to the next. Although guidelines have improved consistency in the conduct and reporting of obstetric examinations, several issues are often hotly debated: for example, what constitutes a basic ultrasound examination, what structures should be evaluated, what is the ideal timing of the examination, what is the appropriate role of the first trimester anatomic survey, who should perform and interpret the examination, how safe is ultrasound, how should it be recorded and documented, how should it be reported, and last, how should the patient be told the results of the examination? With improved images comes the complicating corollary as to what minor findings should be reported to the patient and which merely lead to unnecessary anxiety. These issues are addressed later in the text and some of them are discussed here.

## SAFETY OF ULTRASOUND EXAMINATION

It was not long after the inception of ultrasound imaging that questions were raised as to the safety of this new modality. Despite numerous claims for the safety of ultrasound to the mother and fetus, a number of studies have noted possible adverse effects of diagnostic ultrasound to the developing fetus. These studies have focused primarily on thermal and cavitation mechanisms leading to possible injuries to the developing fetus.<sup>1-5</sup>

Absorption of the ultrasound wave's energy by soft tissue and bone, and its conversion to heat, are measured by the thermal index (TI). A TI of 1 means an increase of 1° C. Several studies have suggested a general threshold of temperature elevation of 1.5° to 2° C above maternal core temperature before any evidence of a developmental effect occurs. With modern ultrasound machines, there is only a negligible rise in temperature, usually less than 1° C. The World Federation for Ultrasound in Medicine and Biology has stated that "a diagnostic exposure that produces a maximum in situ temperature rise of not more than 1.5° C above normal physiological levels may be used

without reservation on thermal grounds."<sup>6</sup> However, this organization further stated that "a diagnostic exposure that elevates embryonic and fetal in situ temperature above 41° C for 5 minutes should be considered potentially hazardous."<sup>6</sup> The conclusion overall is that it is unlikely that there is a deleterious effect of ultrasound in the first trimester during embryogenesis with routine gray-scale ultrasound.

However, when Doppler ultrasound is used during the first trimester, it is likely that temperature increases of over 1.5° C may occur. Studies of the effect of Doppler on soft tissues adjacent to bone and nerve conductance demonstrated a significant rise in temperature when the ultrasound Doppler beam was held for more than 30 seconds.<sup>17</sup> The European Federation for Societies in Medicine and Biology in 1998 concluded that "until further scientific information is available, investigations using pulsed or color Doppler should be carried out with careful control for output levels."<sup>18</sup> It is recommended that when performing Doppler imaging in early pregnancy, the displayed TI should be 1.0 or less and exposure time should be kept as short as possible, usually no longer than 5 to 10 minutes and not exceeding 60 minutes.<sup>9</sup> A thermal index for soft tissue (TIs) should be used at earlier than 10 weeks' gestation, and a thermal index for bone (TIb) should be used at 10 weeks' gestation or later when bone ossification is evident. In keeping with the ALARA (As Low As Reasonably Achievable) principle of prudent scanning, M-mode imaging should be used instead of spectral Doppler imaging to document embryonic/fetal heart rate.<sup>10</sup> Transvaginal ultrasound is not more harmful than transabdominal scanning; again, the risk is dependent on the TI.

Although the potential for embryonic effects from Doppler imaging exists, there is little evidence that ultrasound is teratogenic. As shown in one editorial on the subject, "Many of the studies to date have shown the embryo to be remarkably resilient to ultrasound exposure. Logic would suggest that Doppler techniques should not affect the embryo if the pulses are applied at a low level."<sup>11</sup> In one study, Zhu and associates<sup>12</sup> insonated pregnant rats with diagnostic levels of color Doppler ultrasound energy and studied the cell cycles of newborn rats by flow cytometry and factorial analysis. They found that the deoxyribonucleic acid content was not affected in any phase of the cell cycle in newborn rats by any of the different insonation times and frequencies. In another animal study, Pellicer and colleagues examined cellular damage in rats following exposure to low-intensity ultrasound for as long as 10 minutes. These investigators found that the longer the exposure time, the greater the liver cell damage that was observed.<sup>13</sup> Other animal studies have likewise demonstrated a relationship between the length of exposure to Doppler ultrasound and potential effects on the developing brain.<sup>14,15</sup> Although such studies support caution and minimizing unnecessary exposure, it is unclear whether such animal models can be extrapolated to humans and if such findings are important. However, at the present time, consensus statements conclude that Doppler examination of fetal vessels in early pregnancy should not be performed without a clinical indication.<sup>16</sup>

Cavitation involves the occurrence of gaseous bubble formation in an air-water interface.<sup>1</sup> One concern is that stress from the fluid adjacent to the gaseous body during the process of cavitation may disrupt cell membranes.<sup>1,17</sup> Cavitation has been difficult to document in mammalian fetuses, because, for the most part, there is not an air-water interface, which is needed for the cavitation mechanism.<sup>1</sup> The mechanical index (MI) is an onscreen indicator that provides a rough guide to the likelihood that ultrasound will induce an adverse biologic effect by a nonthermal mechanism, including cavitation. For all practical purposes, this index is probably not relevant for obstetric scanning owing to the relative absence of gas bubbles (air) in the fetus.<sup>18</sup>



A number of studies have evaluated the effect of prenatal ultrasound on neonatal and infant outcome in animal models. Although some studies have documented lower birth weights, shorter heights, and lowered white blood cell counts in neonates who were scanned in utero compared with control subjects, the size differences disappeared when studied after 3 months. In addition, hematologic parameters normalized by this time.<sup>19</sup> Neurodevelopmental studies revealed no significant differences in motor or cognitive tasks, or in learning skills.<sup>1,19</sup> Studies evaluating the human fetus and neonate have reached similar conclusions. Studies have found either no difference in birth weights between exposed and nonexposed fetuses, or a difference that, although present at birth, was not present at 6 to 7 years of age.<sup>20,21</sup>

The information on an association between ultrasound and congenital malformations is limited. Studies evaluating chromosomal aberration and ultrasound exposure have demonstrated little or no change.<sup>1,12,22</sup>

The major difficulties with the studies investigating a possible deleterious effect of diagnostic ultrasound evaluation are threefold: (1) experimental ultrasound exposure levels or time of exposure often far exceeded those that are normally used diagnostically; (2) the systems used to show ultrasound effect (plants, cell culture, laboratory animals) may not be applicable to humans; and (3) many studies that have demonstrated adverse effects in vitro have not been reproducible.<sup>23</sup>

One study evaluating the effect of diagnostic ultrasound on neuronal migration in mice raised much attention in the media.<sup>15</sup> Although this is an interesting study in mice, for the reasons stated earlier, it has little to no applicability in humans. There are two major criticisms of this study. Although the study did use commercially available equipment in which only slightly greater ultrasound frequency than normal was used (6.7 MHz vs. 3.5–5.0 MHz), the fixed duration of exposure far exceeded what would normally be used in humans. The study did not demonstrate statistically significant abnormal results until 30 minutes of exposure. More than 10 years ago, when a sonologist wished to determine whether an embryo was nonviable, the recommended evaluation of the embryo was 3 minutes of observation, demonstrating no evidence of embryonic or cardiac activity. Two minutes of evaluation, let alone 3 minutes, seemed like an eternity, and most examiners, in our experience, stopped after 1 minute. In the slightly older embryo and early fetus, greater than 5 to 10 minutes of sustained evaluation of the fetal brain would be excessive. In most cases, the transducer would be moving around the brain rather than being in a fixed position during the examination.

The second criticism relates to the timing of embryology and the relative sizes of the mouse and human brains. As stated by the authors of this study: “The duration of neuronal production and the migratory phase of cortical neurons in the human fetus lasts approximately 18 times longer than in mice (between 6 and 24 weeks of gestation in humans, with the peak occurring between 11 and 15 weeks, compared with the duration of only approximately 1 week (between E11 and E18) in a mouse).<sup>15,24,25</sup> Thus an exposure of 30 minutes represents a much smaller time dedicated to the development of the cerebral cortex in the human than in the mouse, and thus could have a lesser overall effect, making human corticogenesis less vulnerable to ultrasound waves.”

The AIUM statement on the clinical safety of diagnostic ultrasound reiterates previous findings that no confirmed bioeffects caused by exposure at intensities typical of present diagnostic instruments have ever been reported in patients or instrument operators.<sup>26</sup> This statement acknowledges the possibility that bioeffects may be identified in the future but emphasizes the current data indicating that the benefits of the prudent use of diagnostic sonography outweigh the risks, if any.<sup>26,27</sup> At a recent consensus conference on fetal imaging, it was

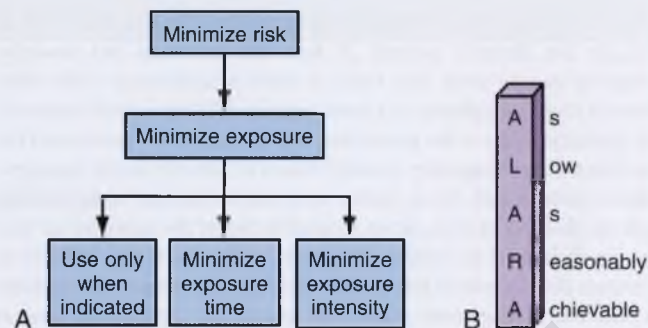


**FIG 1-1** Minimizing risk by minimizing exposure (A) is the cornerstone of the ALARA principle (B). (From Kremkau FW [ed]: *Diagnostic Ultrasound: Principles and Instruments*, 7th ed. Philadelphia, WB Saunders, 2006.)

concluded that there is high-quality evidence that ultrasound is safe for the fetus when used appropriately.<sup>28</sup> However, as stated by Kremkau,<sup>29</sup> “even if this risk is so minimal that it is difficult to identify, prudent practice dictates that routine measures be implemented to minimize the risk while obtaining the necessary information to achieve the diagnostic benefit. This is the ALARA (as low as reasonably achievable) principle of prudent scanning” (Fig. 1-1).

The sonographer’s knowledge of ultrasound and its safety is crucial to the safe implementation of this modality. Merritt, in an editorial, summarized it best: “In view of the rapid growth of sonography and its proliferation into the hands of minimally trained clinicians, it is likely that more patients are harmed each day by misdiagnosis resulting from improper indications, poor examination technique, and errors in interpretation than from all bioeffects.”<sup>27</sup>

## INDICATIONS FOR OBSTETRIC ULTRASOUND EXAMINATION

National guidelines from many organizations in the United States and elsewhere, including the American College of Obstetricians and Gynecologists (ACOG), the Royal College of Obstetricians and Gynaecologists, and the Society of Obstetricians and Gynaecologists of Canada, highlight the benefits of obstetric ultrasound examination, including accurate determination of gestational age, fetal number, cardiac activity, placental localization, and diagnosis of major fetal anomalies. Because of these benefits, and because most congenital anomalies occur in patients with no known risk factors, these organizations agree that second trimester ultrasonography should be offered routinely to all pregnant women and should follow specific guidelines.<sup>30–32</sup> In addition, ACOG recommends that all pregnant women should be offered first trimester screening for aneuploidy, which may include nuchal translucency sonography.<sup>33</sup>

The benefit of routine sonography in the detection of fetal anomalies has been debated. Large studies and systematic reviews report detection rates of 16% to 44% of anomalies prior to 24 weeks of gestation.<sup>31,34,35</sup> Higher detection rates of major and lethal anomalies, as high as 84%, have been reported.<sup>31</sup> The sensitivity of anomaly detection has been noted to vary with respect to the type of abnormality, patient factors, gestational age, and expertise of the imager.<sup>28</sup> Possible explanations for the variance in the detection rate of anomalous fetuses may include (1) differences in neonatal assessment, (2) differences in the definition of a major anomaly, (3) a differing risk status of the population, (4) differences in what is considered a routine or standard sonogram, and (5) the expertise of the examiner.<sup>36</sup>



## Who Should Perform the Ultrasound Examination and How Should It Be Performed?

Theoretically, the answer to who should perform the ultrasound examination should be extremely easy. In fact, it is one of the most controversial issues relating to the ultrasound examination. The answer should be that only those persons who have had adequate training (including didactic as well as supervised “hands-on” experience) should perform and interpret an ultrasound examination.

More than 30 years ago, the Joint Task Group on Training for Diagnosis in Obstetrical and Gynecologic Ultrasound developed guidelines for the post-resident physician who had completed residency programs in either radiology or obstetrics and gynecology that did not provide formal training in obstetric and gynecologic ultrasound evaluation.<sup>37</sup> These guidelines have been continuously updated, most recently in 2014, and include a recommendation of a minimum experience in obstetric and gynecologic ultrasound evaluation as well as training that includes basic physics, technique, performance, and interpretation. In addition, the physician should obtain practical and supervised experience (at least 300 examinations) before offering services as a physician competent in diagnostic ultrasound examination. Ongoing experience with at least 170 examinations per year is also recommended.<sup>38</sup>

The “turf” battles between radiologists and obstetricians as to who should perform the examination are unfortunate. As long as the examining physician is adequately trained and performs the minimum standard obstetric ultrasound examination, as per the guidelines of the American College of Radiology (ACR), AIUM, and ACOG, the specialty of the examiner does not matter.<sup>39,40</sup> However, we do not believe in the practice of self-referral. Self-referral examinations tend to be performed more and more frequently<sup>41</sup> and are often less “complete” and of a lower quality than when they are performed by a dedicated ultrasound practitioner. Except in localities where there are no diagnostic ultrasound specialists, patients should be referred to practitioners whose major practice is ultrasonography.

Guidelines for the performance of obstetric ultrasound examinations have been published by ACR, ACOG, and AIUM, and components of the standard fetal examination at 18 to 20 weeks of gestation were published in a consensus report by National Institute of Child Health and Human Development (NICHD), Society for Maternal-Fetal Medicine (SMFM), ACOG, ACR, AIUM, Society of Pediatric Radiology (SPR), and Society of Radiologists in Ultrasound (SRU) in 2014.<sup>28</sup> AIUM has likewise published guidelines for performance of a detailed fetal anatomic survey, referred to by the billing code 76811.<sup>42</sup> Although there may be sonologists who exceed these guidelines, the guidelines serve as a minimum standard for practitioners of basic and detailed obstetric ultrasonography.

## Nonmedical Use of Ultrasonography

The AIUM has published a “prudent use” statement, which was also endorsed by ACOG. The AIUM advocates the responsible use of diagnostic ultrasonography and strongly discourages its nonmedical use for psychosocial or entertainment purposes. The use of either 2D or 3D ultrasound imaging only to view the fetus, obtain a picture of the fetus, or determine the fetal sex without a medical indication is inappropriate and contrary to responsible medical practice. Although there are no confirmed biologic effects on patients caused by exposures from present diagnostic ultrasound instruments, the possibility exists that such biologic effects may be identified in the future. Thus, ultrasound imaging should be used in a prudent manner to provide medical benefit to the patient.<sup>43</sup> This position has been ethically defended.<sup>44</sup>

## Terminology

The latest classification<sup>45</sup> of fetal sonographic examinations by the AIUM, ACR, and ACOG groups the examinations into four major categories: (A) the first trimester ultrasound examination, (B) the standard second or third trimester examination, (C) the limited examination, and (D) specialized examinations. The standard second and third trimester obstetric examination is often referred to as a routine examination, basic examination, Level 1 examination, or complete ultrasound examination. Specialized examinations might include a detailed anatomic examination, as well as fetal Doppler ultrasound, a biophysical profile, a fetal echocardiogram, and additional biometric measurements. A detailed anatomic examination is generally performed when a patient is at high risk for a fetal anomaly, or when an anomaly is suspected on the basis of the history, biochemical abnormalities or abnormal results on other screening tests, or the results of either the limited or standard scan.

It is important to note that although those individuals performing detailed anatomic examinations must be proficient in evaluating patients for congenital anomalies, it is not acceptable for the Level 1 examiner to be unskilled. In an excellent editorial on the subject, Filly<sup>46</sup> notes that unfortunately some examiners have chosen to use the term “Level 1” as a shield for incompetency. As he states, the Level 1 sonogram is not defined by the technical capability of the examiner, nor by the cost of the sonographic instrumentation employed. In fact, the Level 1 examination “requires a high degree of competency” and should follow the standard second or third trimester obstetric sonographic examination as described in the AIUM/ACR/ACOG guidelines.<sup>10</sup>

The specialized examination (CPT 76811) has been referred to as the Level 2 examination, survey examination, or targeted examination. As the AIUM/ACR/ACOG guidelines state, this is a detailed anatomic examination that is performed when an anomaly is suspected on the basis of history, abnormalities detected on prenatal screening tests, or the results of either a limited or standard examination previously performed.<sup>45</sup>

The individuals performing the sonographic examination are referred to as either sonographers or sonologists. Traditionally, the technical component and initial production of images has been the responsibility of the sonographer (nonphysician), and the professional component and interpretation of images has been the responsibility of the sonologist (physician). The degree of collaboration between the two and their degree of involvement in the ultrasound examination vary from locality to locality. In many parts of the world, examinations are performed predominantly by physicians. Although the contribution of sonographers to the ultrasound examination is invaluable, it should be remembered, as stated by the AIUM, that “Ultrasound studies shall be supervised and interpreted by a physician with training and experience in the specific area of sonography. Findings must be recorded and results communicated in a timely fashion to the health care provider responsible for care. Although a sonographer may play a critical role in extracting the information essential to deriving a diagnosis, the rendering of the final diagnosis of ultrasound studies represents the practice of medicine, and, therefore, is the responsibility of the supervising physician.”<sup>47</sup>

Perhaps the least controversial aspect of this discussion should be who should interpret the ultrasound examination. This, we believe, is straightforward. Only those with adequate training in a conventional training programs (e.g., residency) in which there are didactic lectures, hands-on scanning, and physician supervision in the performance and interpretation of cases should be performing and interpreting ultrasound findings. Training by manufacturer’s training specialists or 1- to 2-week mini-courses do not constitute adequate training in ultrasound.



## Ultrasound Lexicon

Undoubtedly, hundreds of terms are used in obstetrics and ultrasonography that are either incorrect or confusing. Many of these terms are addressed later in this chapter and in other chapters in this text. Two areas in which terminology is often either misused or misunderstood in obstetric ultrasonography are fetal life and age. The term *viability* is defined as the ability to survive in the extrauterine environment. Even in cases of very late third trimester examinations, this statement cannot be used with complete certainty. We prefer to state that the embryo or fetus is living, if that is the case, and use the term *nonviable* for those embryos or fetuses that either are dead or are not capable of living in the extrauterine environment. Early pregnancy failure is another, perhaps even better, way of communicating this information.

The second often-confused term is gestational age. Taken as it sounds, this term would seem to imply the actual age of the fetus from conception to the present. In fact, this term, which is widely used by obstetricians and sonologists, is most often meant to be synonymous with menstrual age. Menstrual age refers to the length of time calculated from the first day of the last normal menstrual period to the point at which the pregnancy is being assessed. The true age of the embryo or fetus, *fetal age*, is rarely known accurately unless the patient has had assisted fertilization or has extremely regular menstrual periods and the day of conception is known. In general, the fetal age is 2 weeks less than the menstrual age.

In this text, the terms gestational age and menstrual age are used interchangeably. The important point for any examiner to remember is not which term is necessarily preferable but rather that the person interpreting the examination and the physician who ordered the examination both use the same terminology.

Another often-misused term is *fetal pole*. This term should be abandoned. It is most often used to describe the presence of the embryo in the early first trimester sonogram. The embryonic period lasts until the end of the 10th menstrual week; during this time the developing conceptus should be referred to as the embryo. Thereafter, the conceptus should be referred to as a fetus.

## THE AMERICAN INSTITUTE OF ULTRASOUND IN MEDICINE GUIDELINES

In 2013 the Practice Guideline for the Performance of an Antepartum Obstetric Ultrasound Examination was updated by the AIUM in collaboration with the ACR, the SRU, and ACOG.<sup>45</sup> It is a modification of previously developed guidelines that were first published in 1986. The actual ACR/AIUM/ACOG guidelines are presented in Table 1-1. What follows is our own bias as to what constitutes an appropriate ultrasound examination. In some respects, this discussion is an expansion of the guidelines previously mentioned. Because this multiauthor text is essentially a detailed review of the obstetric ultrasound examination, we recognize that our viewpoint in this chapter and those of the authors of the subsequent chapters may differ.

## ULTRASOUND EQUIPMENT AND DOCUMENTATION

It seems that there will always be differences of opinion as to which ultrasound machines produce the best images. With the present state of ultrasound technology, these differences are often subjective, particularly when discussing state-of-the-art machines. Most ultrasound machines use phased-array real-time technology and include 3D/4D ultrasound technology and color and pulsed Doppler flow capabilities and cine recording.

An often-debated issue is which transducer should be used for the ultrasound examination. The answer is as many transducers as are necessary should be used to answer the question for which the patient is referred. There is a misconception that the newest transducer introduced by a manufacturer may be the only one that is needed. When sector and, ultimately, transvaginal probes were first introduced, many practitioners believed that these transducers alone could be used for the entire examination. Many learned that using only a single transducer restricts the field of view or visualization of detail, making diagnosis more difficult.

The most common transducers, which are the workhorses of the ultrasound laboratory, are a convex linear array, a sector transducer (3 to 5 MHz), and a transvaginal probe (5 to 10 MHz). The higher frequency transducers are most useful in achieving high-resolution scans, particularly in the near-field, and the lower frequency transducers are useful in those circumstances in which increased penetration of the sound beam is necessary. Variations of transducer technology include convex linear transducers and multifrequency probes as well as probes allowing harmonic and 3D imaging and Doppler flow imaging.<sup>48</sup>

Whatever technology is used, images from the examination should be documented and stored. The purpose of documentation is twofold. First, the identification of normal structures is important so they can be viewed retrospectively and compared with later images if pathologic processes are ultimately demonstrated. Second, if a pathologic problem is identified, it can be shown to referring examiners, who will be doing further examinations.

Most imaging centers utilize picture archiving and communication systems (PACS). These systems allow for the storage of digital ultrasound images on computers and transmission of complete studies to computer workstations for viewing and interpretation. The quality of the images is excellent with these systems. Digital images can be also transmitted to remote locations (telemedicine) for review and consultation.<sup>49</sup>

In addition to digitally stored images, a written report of the ultrasound examination should be included in the patient's medical record. When significant pathologic processes are present, the referring physician should be notified immediately. This immediate communication should occur not only in cases of fetal malformations but also in cases of serious obstetric complications, such as oligohydramnios, diminished fetal movement, macrosomia, and fetal growth restriction. Physician notification should be documented.

## THE FIRST TRIMESTER ULTRASOUND EXAMINATION

### Identification of an Intrauterine Pregnancy

Patients referred for first trimester ultrasound evaluation often have vaginal bleeding, which raises the question of an ectopic pregnancy or a threatened abortion. The primary goal of ultrasound evaluation in the first trimester is to determine whether the pregnancy is intrauterine and whether the embryo is living. With present-day equipment, particularly transvaginal transducers, both of these tasks should be readily accomplished at very early stages of gestation. The same care taken in concluding that a pregnancy in the second or third trimester has a lethal malformation should be applied in deciding that an early pregnancy is nonviable. If there is reasonable doubt about embryonic life, a repeat examination in as few as 7 to 10 days will invariably make the conclusion unequivocal. In 2012 a consensus conference from the SRU established guidelines and criteria for transvaginal ultrasonographic

*Text continued on p. 12*



**TABLE 1-1 Guidelines for Performance of the Antepartum Obstetric Ultrasound Examination****I. Introduction**

The clinical aspects contained in specific sections of this guideline (Introduction, Classification of Fetal Sonographic Examinations, Specifications of the Examination, Equipment Specifications, and Fetal Safety) were revised collaboratively by the American Institute of Ultrasound in Medicine (AIUM), the American College of Radiology (ACR), the American College of Obstetricians and Gynecologists (ACOG), and the Society of Radiologists in Ultrasound (SRU).

Recommendations for personnel qualifications, written request for the examination, procedure documentation, and quality control vary among the organizations and are addressed by each separately.

This guideline has been developed for use by practitioners performing obstetric sonographic studies. Fetal ultrasound should be performed only when there is a valid medical reason, and the lowest possible ultrasonic exposure settings should be used to gain the necessary diagnostic information. A limited examination may be performed in clinical emergencies or for a limited purpose such as evaluation of fetal or embryonic cardiac activity, fetal position, or amniotic fluid volume. A limited follow-up examination may be appropriate for reevaluation of fetal size or interval growth or to reevaluate abnormalities previously noted if a complete prior examination is on record.

While this guideline describes the key elements of standard sonographic examinations in the first trimester and second and third trimesters, a more detailed anatomic examination of the fetus may be necessary in some cases, such as when an abnormality is found or suspected on the standard examination or in pregnancies at high risk for fetal anomalies. In some cases, other specialized examinations may be necessary as well.

While it is not possible to detect all structural congenital anomalies with diagnostic ultrasound, adherence to the following guidelines will maximize the possibility of detecting many fetal abnormalities.

**II. Classification of Fetal Sonographic Examinations****A. First-Trimester Examination**

A standard obstetric sonogram in the first trimester includes evaluation of the presence, size, location, and number of gestational sac(s). The gestational sac is examined for the presence of a yolk sac and embryo/fetus. When an embryo/fetus is detected, it should be measured and cardiac activity recorded by a 2-dimensional video clip or M-mode imaging. Use of spectral Doppler imaging is discouraged. The uterus, cervix, adnexa, and cul-de-sac region should be examined.

**B. Standard Second- or Third-Trimester Examination**

A standard obstetric sonogram in the second or third trimester includes an evaluation of fetal presentation, amniotic fluid volume, cardiac activity, placental position, fetal biometry, and fetal number, plus an anatomic survey. The maternal cervix and adnexa should be examined as clinically appropriate when technically feasible.

**C. Limited Examination**

A limited examination is performed when a specific question requires investigation. For example, in most routine nonemergency cases, a limited examination could be performed to confirm fetal heart activity in a bleeding patient or to verify fetal presentation in a laboring patient. In most cases, limited sonographic examinations are appropriate only when a prior complete examination is on record.

**D. Specialized Examinations**

A detailed anatomic examination is performed when an anomaly is suspected on the basis of the history, biochemical abnormalities, or the results of either the limited or standard scan. Other specialized examinations might include fetal Doppler ultrasound, a biophysical profile, a fetal echocardiogram, and additional biometric measurements.

**III. Qualifications and Responsibilities of Personnel**

See the AIUM Official Statement *Training Guidelines for Physicians Who Evaluate and Interpret Diagnostic Abdominal, Obstetric, and/or Gynecologic Ultrasound Examinations* and the *AIUM Standards and Guidelines for the Accreditation of Ultrasound Practices*.

**IV. Written Request for the Examination**

The written or electronic request for an ultrasound examination should provide sufficient information to allow for the appropriate performance and interpretation of the examination. The request for the examination must be originated by a physician or other appropriately licensed health care provider or under the provider's direction. The accompanying clinical information should be provided by a physician or other appropriate health care provider familiar with the patient's clinical situation and should be consistent with relevant legal and local health care facility requirements.

**V. Specifications of the Examination****A. First-Trimester Ultrasound Examination****1. Indications**

Indications for first-trimester sonography include but are not limited to:

- a. Confirmation of the presence of an intrauterine pregnancy;
- b. Evaluation of a suspected ectopic pregnancy;
- c. Defining the cause of vaginal bleeding;
- d. Evaluation of pelvic pain;
- e. Estimation of gestational (menstrual) age;
- f. Diagnosis or evaluation of multiple gestations;
- g. Confirmation of cardiac activity;
- h. Imaging as an adjunct to chorionic villus sampling, embryo transfer, and localization and removal of an intrauterine device;
- i. Assessing for certain fetal anomalies, such as anencephaly, in high-risk patients;
- j. Evaluation of maternal pelvic masses and/or uterine abnormalities;
- k. Measuring the nuchal translucency (NT) when part of a screening program for fetal aneuploidy; and
- l. Evaluation of a suspected hydatidiform mole.

**Comment**

A limited examination may be performed to evaluate interval growth, estimate amniotic fluid volume, evaluate the cervix, and assess the presence of cardiac activity.



**TABLE 1-1 Guidelines for Performance of the Antepartum Obstetric Ultrasound Examination—cont'd**

**2. Imaging Parameters**

**Comment**

Scanning in the first trimester may be performed either transabdominally or transvaginally. If a transabdominal examination is not definitive, a transvaginal scan or transperineal scan should be performed whenever possible.

- a. The uterus (including the cervix) and adnexa should be evaluated for the presence of a gestational sac. If a gestational sac is seen, its location should be documented. The gestational sac should be evaluated for the presence or absence of a yolk sac or embryo, and the crown-rump length should be recorded when possible.

**Comment**

A definitive diagnosis of intrauterine pregnancy can be made when an intrauterine gestational sac containing a yolk sac or embryo/fetus with cardiac activity is visualized. A small, eccentric intrauterine fluid collection with an echogenic rim can be seen before the yolk sac and embryo are detectable in a very early intrauterine pregnancy. In the absence of sonographic signs of ectopic pregnancy, the fluid collection is highly likely to represent an intrauterine gestational sac. In this circumstance, the intradecidual sign may be helpful. Follow-up sonography and/or serial determination of maternal serum human chorionic gonadotropin levels are/is appropriate in pregnancies of undetermined location to avoid inappropriate intervention in a potentially viable early pregnancy. The crown-rump length is a more accurate indicator of gestational (menstrual) age than is the mean gestational sac diameter. However, the mean gestational sac diameter may be recorded when an embryo is not identified.

Caution should be used in making the presumptive diagnosis of a gestational sac in the absence of a definitive embryo or yolk sac. Without these findings, an intrauterine fluid collection could represent a pseudo-gestational sac associated with an ectopic pregnancy.

- b. The presence or absence of cardiac activity should be documented with a 2-dimensional video clip or M-mode imaging.

**Comment**

With transvaginal scans, while cardiac motion is usually observed when the embryo is 2 mm or greater in length, if an embryo less than 7 mm in length is seen without cardiac activity, a subsequent scan in 1 week is recommended to ensure that the pregnancy is nonviable.

- c. Fetal number should be documented.

**Comment**

Amnionicity and chorionicity should be documented for all multiple gestations when possible.

- d. Embryonic/fetal anatomy appropriate for the first trimester should be assessed.

- e. The nuchal region should be imaged, and abnormalities such as cystic hygroma should be documented.

**Comment**

For those patients desiring to assess their individual risk of fetal aneuploidy, a very specific measurement of the NT during a specific age interval is necessary (as determined by the laboratory used). See the guidelines for this measurement below.

NT measurements should be used (in conjunction with serum biochemistry) to determine the risk of having a fetus with aneuploidy or other anatomic abnormalities such as heart defects. In this setting, it is important that the practitioner measure the NT according to established guidelines for measurement. A quality assessment program is recommended to ensure that false-positive and false-negative results are kept to a minimum.

Guidelines for NT Measurement:

- i. The margins of the NT edges must be clear enough for proper placement of the calipers.
- ii. The fetus must be in the midsagittal plane.
- iii. The image must be magnified so that it is filled by the fetal head, neck, and upper thorax.
- iv. The fetal neck must be in a neutral position, not flexed and not hyperextended.
- v. The amnion must be seen as separate from the NT line.
- vi. The + calipers on the ultrasound must be used to perform the NT measurement.
- vii. Electronic calipers must be placed on the inner borders of the nuchal line space with none of the horizontal crossbar itself protruding into the space.
- viii. The calipers must be placed perpendicular to the long axis of the fetus.
- ix. The measurement must be obtained at the widest space of the NT.

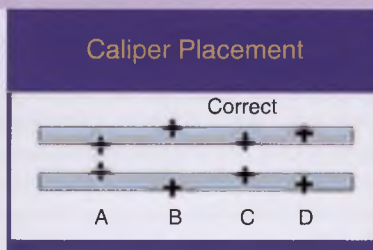


**TABLE 1-1 Guidelines for Performance of the Antepartum Obstetric Ultrasound Examination—cont'd**

- f. The uterus including the cervix, adnexal structures, and cul-de-sac should be evaluated. Abnormalities should be imaged and documented.

**Comment**

The presence, location, appearance, and size of adnexal masses should be documented. The presence and number of leiomyomata should be documented. The measurements of the largest or any potentially clinically significant leiomyomata should be documented. The cul-de-sac should be evaluated for the presence or absence of fluid. Uterine anomalies should be documented.

**B. Second- and Third-Trimester Ultrasound Examination**

**1. Indications**

Indications for second- and third-trimester sonography include but are not limited to:

- a. Screening for fetal anomalies;
- b. Evaluation of fetal anatomy;
- c. Estimation of gestational (menstrual) age;
- d. Evaluation of fetal growth;
- e. Evaluation of vaginal bleeding;
- f. Evaluation of abdominal or pelvic pain;
- g. Evaluation of cervical insufficiency;
- h. Determination of fetal presentation;
- i. Evaluation of suspected multiple gestation;
- j. Adjunct to amniocentesis or other procedure;
- k. Evaluation of a significant discrepancy between uterine size and clinical dates;
- l. Evaluation of a pelvic mass;
- m. Evaluation of a suspected hydatidiform mole;
- n. Adjunct to cervical cerclage placement;
- o. Suspected ectopic pregnancy;
- p. Suspected fetal death;
- q. Suspected uterine abnormalities;
- r. Evaluation of fetal well-being;
- s. Suspected amniotic fluid abnormalities;
- t. Suspected placental abruption;
- u. Adjunct to external cephalic version;
- v. Evaluation of premature rupture of membranes and/or premature labor;
- w. Evaluation of abnormal biochemical markers;
- x. Follow-up evaluation of a fetal anomaly;
- y. Follow-up evaluation of placental location for suspected placenta previa;
- z. History of previous congenital anomaly;
  - aa. Evaluation of the fetal condition in late registrants for prenatal care; and
  - bb. Assessment for findings that may increase the risk for aneuploidy.

**Comment**

In certain clinical circumstances, a more detailed examination of fetal anatomy may be indicated.

**2. Imaging Parameters for a Standard Fetal Examination**

- a. Fetal cardiac activity, fetal number, and presentation should be documented.

**Comment**

An abnormal heart rate and/or rhythm should be documented. Multiple gestations require the documentation of additional information: chorionicity, amnionicity, comparison of fetal sizes, estimation of amniotic fluid volume (increased, decreased, or normal) in each gestational sac, and fetal genitalia (when visualized).

- b. A qualitative or semiquantitative estimate of amniotic fluid volume should be documented.

**Comment**

Although it is acceptable for experienced examiners to qualitatively estimate amniotic fluid volume, semiquantitative methods have also been described for this purpose (eg, amniotic fluid index, single deepest pocket, and 2-diameter pocket).

- c. The placental location, appearance, and relationship to the internal cervical os should be documented. The umbilical cord should be imaged and the number of vessels in the cord documented. The placental cord insertion site should be documented when technically possible.

**Comment**

It is recognized that the apparent placental position early in pregnancy may not correlate well with its location at the time of delivery. Transabdominal, transperineal, or transvaginal views may be helpful in visualizing the internal cervical os and its relationship to the placenta. Transvaginal or transperineal ultrasound may be considered if the cervix appears shortened or cannot be adequately visualized during the transabdominal sonogram.

A velamentous (also called membranous) placental cord insertion that crosses the internal os of the cervix is vasa previa, a condition that has a high risk of fetal mortality if not diagnosed before labor.



**TABLE 1-1 Guidelines for Performance of the Antepartum Obstetric Ultrasound Examination—cont'd**

d. Gestational (menstrual) age assessment.

First-trimester crown-rump measurement is the most accurate means for sonographic dating of pregnancy. Beyond this period, a variety of sonographic parameters such as biparietal diameter, abdominal circumference, and femoral diaphysis length can be used to estimate gestational (menstrual) age. The variability of gestational (menstrual) age estimation, however, increases with advancing pregnancy. Significant discrepancies between gestational (menstrual) age and fetal measurements may suggest the possibility of a fetal growth abnormality, intrauterine growth restriction, or macrosomia.

Comment

The pregnancy should not be redated after an accurate earlier scan has been performed and is available for comparison.

- i. The biparietal diameter is measured at the level of the thalami and cavum septi pellucidi or columns of the fornix. The cerebellar hemispheres should not be visible in this scanning plane. The measurement is taken from the outer edge of the proximal skull to the inner edge of the distal skull.

Comment

The head shape may be flattened (dolichocephaly) or rounded (brachycephaly) as a normal variant. Under these circumstances, certain variants of normal fetal head development may make measurement of the head circumference more reliable than biparietal diameter for estimating gestational (menstrual) age.

- ii. The head circumference is measured at the same level as the biparietal diameter, around the outer perimeter of the calvarium. This measurement is not affected by head shape.
- iii. The femoral diaphysis length can be reliably used after 14 weeks' gestational (menstrual) age. The long axis of the femoral shaft is most accurately measured with the beam of insonation being perpendicular to the shaft, excluding the distal femoral epiphysis.
- iv. The abdominal circumference or average abdominal diameter should be determined at the skin line on a true transverse view at the level of the junction of the umbilical vein, portal sinus, and fetal stomach when visible.

Comment

The abdominal circumference or average abdominal diameter measurement is used with other biometric parameters to estimate fetal weight and may allow detection of intrauterine growth restriction or macrosomia.

e. Fetal weight estimation.

Fetal weight can be estimated by obtaining measurements such as the biparietal diameter, head circumference, abdominal circumference or average abdominal diameter, and femoral diaphysis length. Results from various prediction models can be compared to fetal weight percentiles from published nomograms.

Comment

If previous studies have been performed, appropriateness of growth should also be documented. Scans for growth evaluation can typically be performed at least 2 to 4 weeks apart. A shorter scan interval may result in confusion as to whether measurement changes are truly due to growth as opposed to variations in the technique itself.

Currently, even the best fetal weight prediction methods can yield errors as high as  $\pm 15\%$ . This variability can be influenced by factors such as the nature of the patient population, the number and types of anatomic parameters being measured, technical factors that affect the resolution of ultrasound images, and the weight range being studied.

f. Maternal anatomy.

Evaluation of the uterus, adnexal structures, and cervix should be performed when appropriate. If the cervix cannot be visualized, a transperineal or transvaginal scan may be considered when evaluation of the cervix is needed.

Comment

This will allow recognition of incidental findings of potential clinical significance. The presence, location, and size of adnexal masses and the presence of at least the largest and potentially clinically significant leiomyomata should be documented. It is not always possible to image the normal maternal ovaries during the second and third trimesters.

g. Fetal anatomic survey.

Fetal anatomy, as described in this document, may be adequately assessed by ultrasound after approximately 18 weeks' gestational (menstrual) age. It may be possible to document normal structures before this time, although some structures can be difficult to visualize due to fetal size, position, movement, abdominal scars, and increased maternal abdominal wall thickness. A second- or third-trimester scan may pose technical limitations for an anatomic evaluation due to imaging artifacts from acoustic shadowing. When this occurs, the report of the sonographic examination should document the nature of this technical limitation. A follow-up examination may be helpful. The following areas of assessment represent the minimal elements of a standard examination of fetal anatomy. A more detailed fetal anatomic examination may be necessary if an abnormality or suspected abnormality is found on the standard examination.

i. Head, face, and neck:

Lateral cerebral ventricles;

Choroid plexus;

Midline falx;

Cavum septi pellucidi;

Cerebellum;

Cistern magna; and

Upper lip.

Comment

A measurement of the nuchal fold may be helpful during a specific age interval to assess the risk of aneuploidy.

**TABLE 1-1 Guidelines for Performance of the Antepartum Obstetric Ultrasound Examination—cont'd**

- ii. Chest:
  - Heart:
    - Four-chamber view;
    - Left ventricular outflow tract; and
    - Right ventricular outflow tract.
- iii. Abdomen:
  - Stomach (presence, size, and situs);
  - Kidneys;
  - Urinary bladder;
  - Umbilical cord insertion site into the fetal abdomen; and
  - Umbilical cord vessel number.
- iv. Spine:
  - Cervical, thoracic, lumbar, and sacral spine.
- v. Extremities:
  - Legs and arms.
- vi. Sex:
  - In multiple gestations and when medically indicated.

**VI. Documentation**

Adequate documentation is essential for high-quality patient care. There should be a permanent record of the ultrasound examination and its interpretation.

Images of all appropriate areas, both normal and abnormal, should be recorded. Variations from normal size should be accompanied by measurements. Images should be labeled with the patient identification, facility identification, examination date, and side (right or left) of the anatomic site imaged. An official interpretation (final report) of the ultrasound findings should be included in the patient's medical record. Retention of the ultrasound examination should be consistent both with clinical needs and with relevant legal and local health care facility requirements.

Reporting should be in accordance with the *AIUM Practice Guideline for Documentation of an Ultrasound Examination*.

**VII. Equipment Specifications**

These studies should be conducted with real-time scanners, using a transabdominal and/or transvaginal approach. A transducer of appropriate frequency should be used. Real-time sonography is necessary to confirm the presence of fetal life through observation of cardiac activity and active movement.

The choice of transducer frequency is a trade-off between beam penetration and resolution. With modern equipment, 3- to 5-MHz abdominal transducers allow sufficient penetration in most patients while providing adequate resolution. A lower-frequency transducer may be needed to provide adequate penetration for abdominal imaging in an obese patient. During early pregnancy, a 5-MHz abdominal transducer or a 5- to 10-MHz or greater vaginal transducer may provide superior resolution while still allowing adequate penetration.

**VIII. Fetal Safety**

Diagnostic ultrasound studies of the fetus are generally considered safe during pregnancy. This diagnostic procedure should be performed only when there is a valid medical indication, and the lowest possible ultrasonic exposure setting should be used to gain the necessary diagnostic information under the ALARA (as low as reasonably achievable) principle.

A thermal index for soft tissue (Tis) should be used at earlier than 10 weeks' gestation, and a thermal index for bone (Tib) should be used at 10 weeks' gestation or later when bone ossification is evident. In keeping with the ALARA principle, M-mode imaging should be used instead of spectral Doppler imaging to document embryonic/fetal heart rate.

The promotion, selling, or leasing of ultrasound equipment for making "keepsake fetal videos" is considered by the US Food and Drug Administration to be an unapproved use of a medical device. Use of a diagnostic ultrasound system for these purposes, without a physician's order, may be in violation of state laws or regulations.

**IX. Quality Control and Improvement, Safety, Infection Control, and Patient Education**

Policies and procedures related to quality control, patient education, infection control, and safety should be developed and implemented in accordance with the *AIUM Standards and Guidelines for the Accreditation of Ultrasound Practices*.

Equipment performance monitoring should be in accordance with the *AIUM Standards and Guidelines for the Accreditation of Ultrasound Practices*.

**X. ALARA Principle**

The potential benefits and risks of each examination should be considered. The ALARA principle should be observed when adjusting controls that affect the acoustic output and by considering transducer dwell times. Further details on ALARA may be found in the AIUM publication *Medical Ultrasound Safety*, Second Edition.

Modified from American Institute of Ultrasound in Medicine: AIUM practice guideline for the performance of obstetric ultrasound examinations. *J Ultrasound Med* 32(6):1083-1101, 2013.



**TABLE 1-2 Guidelines for Transvaginal Ultrasonographic Diagnosis of Pregnancy Failure in a Woman With an Intrauterine Pregnancy of Uncertain Viability\***

Findings Diagnostic of Pregnancy Failure	Findings Suspicious for, But Not Diagnostic of, Pregnancy Failure <sup>†</sup>
Crown-rump length of $\geq 7$ mm and no heartbeat	Crown-rump length of $< 7$ mm and no heartbeat
Mean sac diameter of $\geq 25$ mm and no embryo	Mean sac diameter of 16-24 mm and no embryo
Absence of embryo with heartbeat $\geq 2$ wk after a scan that showed a gestational sac without a yolk sac	Absence of embryo with heartbeat 7-13 days after a scan that showed a gestational sac without a yolk sac
Absence of embryo with heartbeat $\geq 11$ days after a scan that showed a gestational sac with a yolk sac	Absence of embryo with heartbeat 7-10 days after a scan that showed a gestational sac with a yolk sac
	Absence of embryo $\geq 6$ wk after last menstrual period
	Empty amnion (amnion seen adjacent to yolk sac, with no visible embryo)
	Enlarged yolk sac ( $> 7$ mm)
	Small gestational sac in relation to the size of the embryo ( $< 5$ mm difference between mean sac diameter and crown-rump length)

\*Criteria are from the Society of Radiologists in Ultrasound Multispecialty Consensus Conference on Early First Trimester Diagnosis of Miscarriage and Exclusion of a Viable Intrauterine Pregnancy, October 2012.

<sup>†</sup>When there are findings suspicious for pregnancy failure, follow-up ultrasonography at 7 to 10 days to assess the pregnancy for viability is generally appropriate.

diagnosis of pregnancy failure in a woman with an intrauterine pregnancy of uncertain viability (see Table 1-2 and Chapter 4).

### Embryonic/Fetal Number

With a careful examination, the true number of embryos can be accurately determined even early in the first trimester. The literature has emphasized that it is important not to overestimate the number of developing gestations by misinterpreting findings such as a double sac sign, fluid in the uterine cavity, the yolk sac, or the presence of the amnion as evidence of multiple sacs or embryos and thus multiple gestations. However, the examiner may be just as likely to underestimate the number of developing gestations and embryos if a thorough evaluation of the gestational sac is not made for all embryos.<sup>50</sup> It is our experience that when multiple gestations are missed using ultrasound assessment, it is usually from a less than optimal first trimester examination. The head (crown) of one embryo may be added to the body (rump) of an adjacent embryo and measured as a singleton. This misdiagnosis, of course, occurs only in monochorionic gestations. For these reasons some investigators prefer that if one ultrasound examination is to be done concentrating on fetal number, it should be done in the early to middle second trimester of pregnancy.

### Estimating Gestational Age

The subject of estimating gestational age is covered in detail in Chapter 6. An estimate of gestational age should be made when an ultrasound examination is performed in the first trimester, as this is the most accurate time to determine gestational age. The two most common methods of gestational age estimation are mean gestational sac diameter and crown-rump length. For many years, the crown-rump length has been acclaimed as the most reliable method of estimating gestational age in utero. The crown-rump length is a highly accurate method of estimating gestational age using ultrasound evaluation (accuracy within 3 to 7 days). Other measurements, such as the head circumference or femur length, performed in the second trimester, are nearly as accurate and have the added benefit of allowing one to assess fetal morphologic features to a better advantage in a larger fetus. We believe that the first trimester ultrasound examination should not be done for the sole purpose of obtaining more accurate measurements if there is not a clinical reason why it cannot be done in the second trimester, and this approach was also affirmed in the NICHD Fetal Imaging Workshop consensus.<sup>28</sup>

### Morphologic Abnormalities

Recent years have seen continuous improvement in the resolution of ultrasound and many reports documenting morphologic abnormalities detected in the first trimester. Abnormalities involving virtually every organ system have been reported. In light of these reports, we are frequently asked when is the earliest time that a particular abnormality can be detected. Our reply is often that although early detection of a morphologic abnormality is useful, the confident unequivocal detection of an abnormality is even more important. Unless one is extremely confident of the existence of an abnormality in the first trimester, a follow-up examination should be performed.

One should be aware of four potential pitfalls in diagnosis in the first trimester: (1) the normal extra-abdominal position of the embryonic intestine simulating an abdominal wall defect, (2) the prominence of the developing cerebral vesicles (rhombencephalon), (3) the potential false negative diagnosis of anencephaly, and (4) the false positive diagnosis of cerebellar vermian and callosal abnormalities because of these structures not being fully developed at an early gestational age.<sup>51-53</sup>

### Placenta

In early pregnancies, it may be difficult to ascertain the site of the developing placenta. If, however, the examiner can confidently identify the site of placentation, either anterior or posterior, this information should be documented. It should be noted that the placenta either overlies the cervix or just reaches the cervix in up to 2% of pregnancies imaged transvaginally in the early second trimester.<sup>54,55</sup> Placental "migration," or resolution of placenta previa as pregnancy progresses, occurs in most cases, probably as a result of the faster growth of the placenta-free uterine wall relative to the uterine wall covered by the placenta.<sup>54</sup> Factors such as prior cesarean delivery and the degree to which the placenta overlies the cervix affect whether placenta previa in the second trimester will resolve prior to delivery. In general, the placenta commonly extends to the cervix before 16 weeks, and a placenta previa should not be reported. At 16 weeks and beyond, if the placental edge is within 2 cm of the internal os, a diagnosis of "low-lying placenta" is made and follow-up at 32 weeks of gestation is recommended.<sup>28</sup> If one is uncertain as to the location of the inferior edge of the placenta, a transvaginal scan will help clear up any confusion and prevent a patient being labeled as having a placenta previa.



## Uterus and Adnexa

The maternal uterus should be examined carefully for evidence of uterine abnormalities, particularly in high-risk patients. Late in pregnancy, these anomalies may be more difficult to detect. If uterine myomas are detected, their size, site, and relationship to the cervix should be recorded. It should be remembered that transient myometrial contractions may simulate myomas.

The adnexa should be carefully searched for the presence of cysts as well as ovarian neoplasms, both benign and malignant. Again, later in pregnancy, as the adnexal areas are displaced superiorly, they may be more difficult to evaluate adequately.

## THE SECOND AND THIRD TRIMESTER ULTRASOUND EXAMINATIONS

### Fetal Number and Fetal Life

Evaluating the number of fetuses should be extremely easy and accurate in the second and third trimesters. The increased perinatal morbidity and mortality risks of multiple gestations make it mandatory that a “surprise twin” at delivery be a rare event in any patient who has had a second or third trimester ultrasound examination. The major potential error in determining the number of fetuses is one of underestimation. This mistake, when made, is likely due to either not evaluating the fundal region or not making sure that the fetal head is associated with its body rather than that of a twin. When a multiple gestation is identified, it is important to determine the number of placentas and the number of amniotic sacs (the chorionicity and amnionicity).

In the ultrasound report, a statement should be made that the fetus was living, if this was the case, by virtue of cardiac motion being identified. If there is any doubt about fetal life, a confirmatory examination by another examiner should take place. The lack of fetal movement should not be interpreted as representing fetal death. Slow fetal heart rates often portend a poor prognosis; however, this observation alone should not be considered evidence of a nonviable pregnancy. Many cases of fetal heart rates less than 80 beats per minute result in normal outcomes.

### Fetal Position

Once fetal life and number have been identified, then the fetal lie and presenting part should be determined in patients beyond 20 weeks of gestation. Fetal lie refers to the relationship of the long axis of the fetus to the long axis of the uterus. Presentation defines the presenting fetal part closest to the cervix. The most common fetal lie is longitudinal, and the most common presenting part is the fetal head. Fetal lie or presentations other than these are referred to as malpresentations. Their significance lies in increased perinatal morbidity during delivery.

The advent of real-time ultrasound evaluation has placed an additional demand on the sonographer. If the sonologist interpreting the scans has not performed the examination, he or she must be able to deduce the lie and presentation from the sonographer's images. This may be done only by understanding the normal fetal anatomy and applying it to the scanning position (Figs. 1-2 and 1-3). Likewise, some congenital anomalies (e.g., dextrocardia, abnormal right-sided abdominal cystic mass) are recognized only fortuitously if a structure is identified as abnormal by virtue of its abnormal position related to the lie and presentation of the fetus.

As mentioned previously, the most common presenting part is the fetal head (cephalic presentation). (We prefer the term *cephalic* rather

than *vertex* because the latter term may also be used to describe a location on the fetal head.) When the head is adjacent to the lower uterine segment, it is likely that the fetus is in cephalic presentation; however, one must see all images before coming to that conclusion. The fetal body may also be low in the uterus with the fetal head, and, thus, the fetus would be in a transverse lie rather than in a cephalic presentation.

Fetal malpresentation requires that the sonographer extend the examination to answer two additional questions important to the referring obstetrician. First, what specifically is the presenting part (i.e., foot, buttocks in the case of a breech presentation, or shoulder in the case of a fetus in transverse lie) (Figs. 1-4 and 1-5)? Second, if a malpresentation persists into the latter third trimester, is there an associated fetal malformation or placental abnormality that may be causally related to the abnormal lie?<sup>56</sup>

### Assigning Gestational Age and Weight

The assignment of gestational age and weight is covered in detail in Chapter 6. It is important to remember several concepts when assigning gestational age using ultrasonography. First, measurements made early in pregnancy, for the most part, are more accurate than those made near term. In most cases, the measurements of the fetal head, body, and femur will be concordant with one another, within a week in the early to mid-second trimester. This is often not true in the late third trimester, when the femur may lag behind the other measurements and more variation is common and normal. In the early to mid-second trimester, if the femur or the head measurements are greater than 1 week less than the other measurements, this should raise a red flag and alert one to the possibility of either short-limbed bone dysplasia, trisomy 21, or microcephaly. Follow-up in these cases may be indicated. Second, pathologic states should be taken into consideration when deciding which body parts to use in assigning gestational age or weight. Most ultrasound machines allow the user to eliminate from the gestational age calculation those body parts that are abnormal. The abdominal circumference measurement is likely to be inaccurate in the presence of fetal ascites, and the femur length measurement is unreliable in fetuses with short-limbed dwarfism. Third, every obstetric ultrasound report should relate the calculated sonographic age to the patient's menstrual age or clinical gestational age. Because menstrual histories are frequently inaccurate, there is often a tendency to not believe a woman's menstrual history in deference to the calculated sonographic age. In doing so, however, one runs the risk of assigning an earlier gestational age to a fetus that is in fact older but growth restricted. Likewise, there is the possibility of assigning an earlier gestational age to a pregnancy that is post term, placing the fetus at risk for fetal postmaturity syndrome or in utero death. Fourth, the calculated fetal weight should be stated not only in grams but also as a percentile based on the patient's clinical gestational age or best obstetric estimate. Again, if the patient's menstrual dates are inaccurate, the obstetrician can make the decision not to become alarmed at a reported low-weight percentile. This is far better than misinterpreting a growth-restricted fetus as normal by relating the estimated weight only to the ultrasound-determined age. (Remember that although the formulas are different for the calculations of fetal age and weight, they are based upon the same biometric measurements and when compared to one another will often be near the 50% percentile.) Fifth, if there has been a previous ultrasound examination, there should be some statement in the report as to whether interval fetal growth has been normal or abnormal. Finally, sonograms attempting to assess normal or abnormal interval growth should have an interval of no less than 2 weeks. It may be difficult to determine whether there has been a growth abnormality versus a measurement error if scans are done with a shorter interval.





**FIG 1-2 A**, Illustration of a transverse plane of section of the gravid uterus. The fetus is in cephalic presentation, so this scan transects the fetal abdomen transversely. **B**, Longitudinal plane of section of the same fetus. These images are viewed with the maternal head to the left of the recorded image. F, foot; H, head; L, left; R, right.

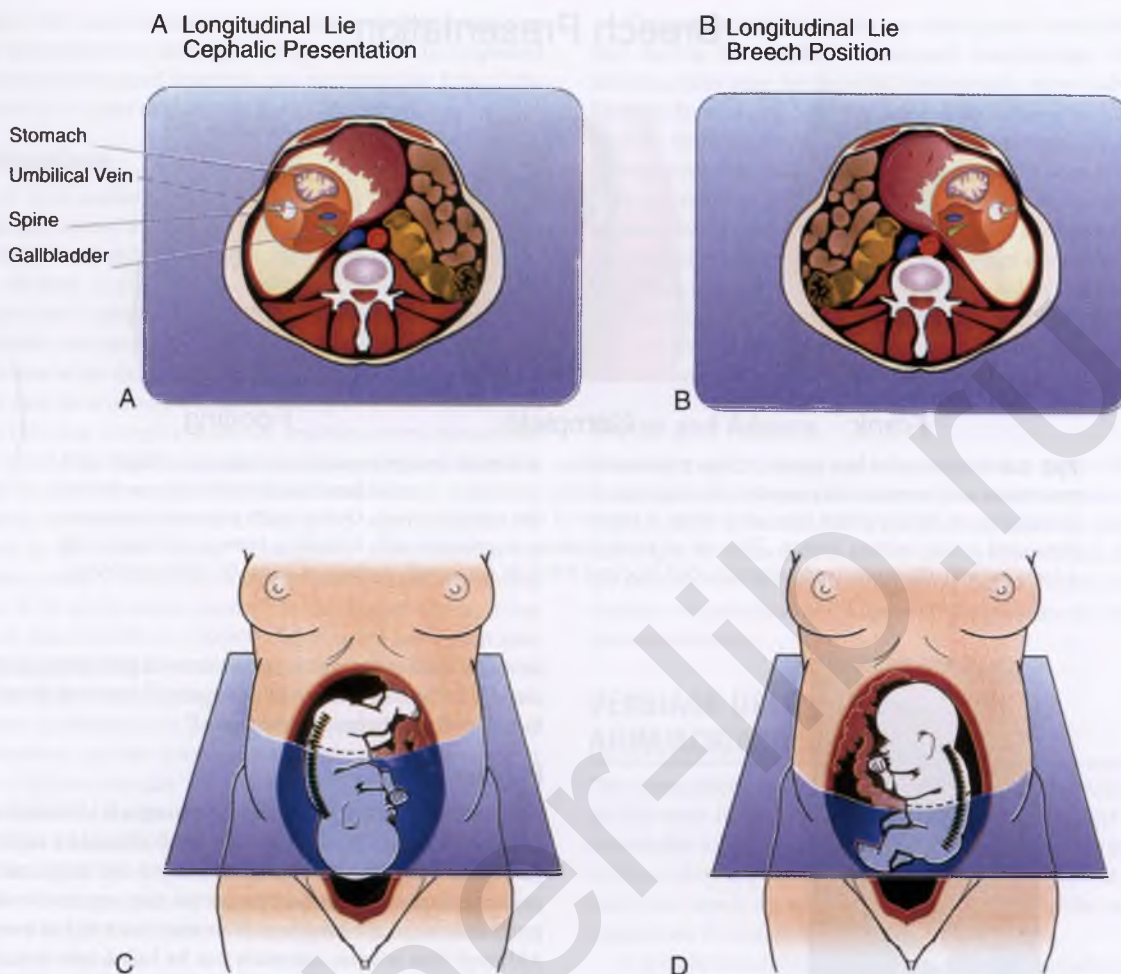


**FIG 1-3** Knowledge of the plane of section across the maternal abdomen (longitudinal or transverse) as well as the position of the fetal spine and left-sided (stomach) and right-sided (gallbladder) structures can be used to determine the fetal lie and presenting part. **A**, This transverse scan of the gravid uterus demonstrates the fetal spine on the maternal right with the fetus lying with its right side down (stomach anterior, gallbladder posterior). Because these images are viewed looking up from the patient's feet, the fetus must be in a longitudinal lie and cephalic presentation. **B**, When the gravid uterus is scanned transversely and the fetal spine is on the maternal left, with the right side down, the fetus is in a longitudinal lie and breech presentation. **C**, When a longitudinal plane of section demonstrates the fetal body to be transected transversely and the fetal spine is nearest the lower uterine segment with the fetal right side down, the fetus is in a transverse lie with the fetal head on the maternal left. **D**, When a longitudinal plane of section demonstrates the fetal body to be transected transversely and the fetal spine is nearest the uterine fundus with the fetal right side down, the fetus is in a transverse lie with the fetal head on the maternal right. Although real-time scanning of the gravid uterus quickly allows the observer to determine fetal lie and presentation, this maneuver of identifying specific right- and left-sided structures within the fetal body forces one to determine fetal position accurately and identify normal and pathologic fetal anatomy.

### Amniotic Fluid Volume

Amniotic fluid is an important consideration in assessing fetal development and well-being. Although there is relatively good agreement on the significance of extremes of amniotic fluid volume, there remains some controversy over the methodology used to make the diagnosis of either too much or too little amniotic fluid. Amniotic fluid volume should be assessed subjectively at all ultrasound examinations. Although a diagnosis of oligohydramnios and polyhydramnios can be made subjectively, the extremes of amniotic fluid volume should also be assessed objectively using either the DVP or AFI. The ability to assess amniotic fluid volume subjectively at different stages of gestation is readily learned and should not be difficult for most examiners. Two

points should be remembered when assessing amniotic fluid volume. First, amniotic fluid volume is large compared with fetal volume at early stages of gestation and should not be misinterpreted as polyhydramnios. Conversely, in term patients, the normal volume of amniotic fluid is quite small so that only small pockets may be seen. Second, patients who are obese often appear to have less than normal volumes of amniotic fluid. This may be due in part to scattering of sound with resultant artifactual echoes within the amniotic fluid.

In making the diagnosis of oligohydramnios, one should remember two points. First, because in many cases, it will imply the likelihood of a fetal renal malformation or severe growth restriction in the absence of ruptured membranes, this diagnosis should be made only when there is almost no amniotic fluid. An exception to this is when there is



## Breech Presentation



**FIG 1-4** Illustration of the types of breech presentation. In a frank breech presentation (the most common), the thighs are flexed at the hips with the legs and knees extended. In complete breech (the least common), the thighs are flexed at the hips, and there is flexion of the knees as well. One or both hips and knees are extended in the footling breech. The risk of cord prolapse is greatest with a footling breech and least with a frank breech. (Illustration copyright © 2006 Nucleus Medical Art, www.nucleusinc.com. All rights reserved.)



**FIG 1-5** Longitudinal scan of a footling breech presentation. In this scan, the leg (arrow) and foot extend into the lower uterine segment and cervix.

a small amount of fluid in an early or mid-second trimester examination (when normally large amounts of amniotic fluid would be anticipated). Second, because of the association of severe diminution of amniotic fluid in a compromised fetus with ultimate fetal demise, the obstetrician should be alerted immediately if this diagnosis is made, before the patient leaves the ultrasound evaluation area.

The diagnosis of polyhydramnios, although seeming to be less serious, in many cases may in fact be associated with significant complications to the mother and fetus. In the mother, preterm labor and ruptured membranes may occur as a result of polyhydramnios, and in the fetus, fetal anomalies may be present. Although many cases of polyhydramnios ultimately result in a normal fetus, the high number of anomalous fetuses with this condition reported in the literature should alert the sonographer to perform a thorough evaluation when this diagnosis is suggested.<sup>56-58</sup>

### Amniotic Fluid Volume in Multiple Gestations

If one looks at a list of causes of polyhydramnios in many obstetric texts, multiple gestations will most likely appear. Although increased

amniotic fluid volume may appear in twin gestations, in most cases the cause is some abnormality of pregnancy.<sup>59</sup> Many of these cases are due to twin-twin transfusion syndrome.<sup>60</sup>

### Placenta

As mentioned earlier, whenever the placenta is identified in pregnancy, its position and relationship to the cervix should be noted in the interpretation. The literature has emphasized the large number of false positive diagnoses of placenta previa that are made either early in pregnancy or in the presence of an overdistended urinary bladder.<sup>61,62</sup> Although this is true, one must not be lulled into a sense of security in thinking that all low-lying placentas will “go away” and be clinically unimportant. If the placenta is low lying during a second trimester examination, every effort should be made to answer the question as to whether there is or is not a placenta previa; this may require a transvaginal examination. However, if after a variety of maneuvers and transducers (Trendelenburg position, emptying the bladder, translabial or transvaginal scanning) one is still unsure about the relationship of the edge of the placenta to the cervical os, the placenta should be interpreted as low lying, and a placenta previa cannot be excluded. Therefore, these patients should have follow-up examination at 32 weeks of gestation. We prefer to report the distance from the inferior edge of the placenta to the internal cervical os rather than relying on terms that may have differing meanings (e.g., marginal placenta). In patients with a prior cesarean delivery and a placenta previa, the placenta should further be assessed for evidence of placenta accreta, as described in Chapter 19.

Abruptio placentae is a diagnosis that is often difficult to make using ultrasonography. One should remember that the myometrium and its vessels, as well as a transient myometrial contraction, may simulate a hematoma and that these potential false positive diagnoses should be avoided. Because most clinicians are aware that abruptio placentae is a difficult diagnosis, they often refer patients for ultrasound evaluation to exclude a placenta previa rather than to specifically view the abruptio. Patients with a true placental abruptio may not ever be seen in the ultrasound laboratory and go straight to labor and delivery.

Vasa previa, which is a variation of umbilical cord anatomy rather than a placental abnormality, is a serious and often overlooked condition. It occurs when fetal vessels cross the internal cervical os in an



attempt to reach the main substance of the placenta. Vasa previa can result in fetal exsanguination during delivery and should be suspected in cases of a velamentous cord insertion or a succenturiate lobe of the placenta, as well as in cases of “resolved” placenta previa.

### Fetal Malformations

The subject of fetal malformations is among the most emotionally charged issues that either the parents or a diagnostician may have to face. Over time, ultrasound evaluation has undergone a transformation that has allowed us to answer not only the basic question as to whether the patient is pregnant but also whether a fetal anomaly is present. As smaller and smaller abnormalities are identified, the question now becomes what degree of assurance should a patient expect from a report that no anomaly was seen during a routine ultrasound examination. This is a complex issue. To examine every patient for all anomalies would be highly impractical. Fortunately, most major anomalies can be detected as part of a routine evaluation.

Major genetic or structural birth defects affect approximately 3% of infants born in the United States.<sup>63</sup> Congenital malformations are the single leading cause of infant death in the United States, accounting for more than 21% of all infant deaths.<sup>64</sup> In the United States, it has been estimated that 100,000 to 150,000 children are born each year with major congenital malformations, and approximately 8000 of these babies die before completing their first year of life.<sup>64</sup> Children with congenital malformations account for approximately 30% of pediatric admissions, and the total cost of health care is estimated at more than \$1.4 billion annually.<sup>64-66</sup>

As was mentioned in the discussion of the first trimester ultrasound examination, fetal anomalies have been described in virtually every organ system at almost every gestational age. There is much controversy as to when a comprehensive scan of a pregnancy should occur. There has been a desire from many to accomplish this task at a time just before an amniocentesis (14 to 16 weeks) or even earlier, at the time of nuchal translucency measurement.<sup>67</sup> In particular, three advantages to earlier anatomic evaluation have been cited: (1) transient abnormalities such as an increased nuchal translucency and echogenic bowel (which may serve as markers for chromosomal and structural abnormalities) may disappear if scanning first occurs after 16 weeks<sup>68</sup>; (2) structures such as the fetal hands may be more readily seen, particularly with fingers extended, earlier than later in pregnancy<sup>68</sup>; and (3) if necessary, termination may be easier to accomplish and safer earlier than later in gestation.<sup>68</sup> Although it is true that many morphologic abnormalities will be detected particularly when using a transvaginal probe, certain abnormalities of the face, heart, and skeleton will not be detected at early gestational ages. Likewise, certain embryologic developmental stages, such as the development of the cerebellar vermis and corpus callosum, are not complete until the mid to late second trimester. If one has the economic luxury of performing several sonographic examinations during pregnancy, a scan at 11 to 14 weeks' gestation followed by a scan at 22 to 24 weeks' gestation might be ideal. It is certainly not unreasonable to exclude gross and potentially lethal abnormalities during the time of the nuchal translucency scan. This would obviously affect the timing of the next scan. However, it is our recommendation, and that of professional organizations (Reddy and coworkers<sup>28</sup>), that if a single ultrasound or a targeted (Level 2) examination is performed, it should be done at a gestational age of 18 to 20 weeks. The reason for this is that the fetus will be of a sufficient size to exclude most abnormalities and still allow time for a follow-up examination, if necessary. The slight loss of accuracy in assigning gestational age at this time is typically of limited clinical significance and is well worth the gain in visibility of fetal anatomy and pathologic malformation.

The patient and the referring obstetrician should be made aware that during the standard ultrasound examination, although many abnormalities may be detected fortuitously, more subtle lesions are likely to be detected only when the fetus is known to be at risk for a specific malformation. Anatomic malformations are likely to grow during pregnancy just as the fetus does; a defect seen at birth may have been too small to be detected earlier in pregnancy. Some lesions, such as duodenal atresia and achondroplasia, may not manifest until late in the second trimester. Finally, it is important for sonologists to know the limits of their expertise. If a malformation is suspected and the examiner has had little experience with the abnormality in question, the case should be referred to a more experienced examiner. Only in this way will patients be served best.

### Uterus and Adnexa

Evaluation of the uterus and adnexa becomes more difficult the later in gestation the examination occurs. The most common abnormalities that are likely to be detected are uterine myomas. As stated earlier, it is important to measure the size of the myoma, record the location of the myoma, and define the relationship of the myoma to the cervix. If ovarian abnormalities are suspected, patients should have a postpartum examination.

### VERBIAGE USED IN THE AIUM/ACR/ACOG GUIDELINES

The committees and individual members of the AIUM, ACR, and ACOG who helped develop the guidelines described earlier did a remarkable job. It is not easy producing a document such as this that will be widely applicable to ultrasound practitioners. In a few areas in which the words chosen were not clear we would like to give our own suggestions for interpretation.

It is understandable that the guidelines attempted to give the practitioner latitude in requirements for the obstetric ultrasound examination. They attempted to take into account the differences in maternal and fetal anatomy from one patient to the next as well as technical limitations at times. There are a number of instances in which the guidelines state that a structure or structures should be imaged. Unfortunately, additional wording is added that states “when possible” or “can also be attempted” or “when technically feasible.” As stated in the editorial mentioned earlier, “One could reasonably state that any of the views defined in the guidelines can only be obtained ‘if technically feasible.’” Indeed, the introduction to “Fetal Anatomic Survey” states that one may anticipate technical limitations: “some structures can be difficult to visualize due to fetal size, position, movement, abdominal scars, and increased maternal wall thickness.”<sup>28</sup> Adding these additional words, mentioned earlier, gives the examiner a “way out” to not examine important fetal or maternal anatomy. This issue occurs in discussion of the first trimester, when these modifying statements are made with respect to the cervix and amnionity and chorionity in multiple gestations. We do not know of a reason why the cervix cannot be assessed in the first trimester in any patient using a variety of methods available. Chorionity and amnionity can best be assessed in the first trimester of pregnancy; although the differentiation of monoamniotic from diamniotic twins may be difficult later in gestation, there is no reason chorionity cannot be determined at this time. In the extremities section, the legs and arms are mentioned. Medically, this would mean only the tibia/fibula and the humerus. We believe the intent was for the femur, humerus, tibia, fibula, radius, and ulna to be evaluated.

The fetal sex was stated as, “Medically indicated in low-risk pregnancies only for evaluation of multiple gestations.” Although we



appreciate the intent, we suggest that it should be noted that fetal sex should also be demonstrated in singleton gestations when medically indicated for diagnosis and counseling. Examples of this type of indication would include hemophilia or distal urinary obstruction, attempting to differentiate posterior urethra valves (predominantly male disorder) from a cloacal abnormality (predominantly female disorder). As for multiple gestations, there are many who would take issue with saying that any multiple pregnancy is low risk. It perhaps would have been better stated that “when chorionicity is difficult to determine in multiple gestation pregnancies, fetal sex determination, when different between the twins, will be helpful in excluding monozygosity.”

For weight determination, a statement is made that “Currently, even the best fetal weight prediction methods can yield errors as high as  $\pm 15\%$ .” Although we agree with this in concept, we would not have put what appears to be an upper limit on errors in weight estimation. This seems to imply that errors greater than this would be below the standard of care. Particularly in macrosomic fetuses, errors as high as 25% to 30% can be seen from what seemed to be reasonable biometry.

A statement regarding technical difficulties reads: “A second- or third-trimester scan may pose technical limitations for an anatomic evaluation due to imaging artifacts from acoustic shadowing. When this occurs, the report of the sonographic examination should document the nature of this technical limitation. A follow-up examination may be helpful.” Although we fully understand this limitation, which all of us have encountered, the recommendation is problematic. There are certain anatomic structures or situations in which the anatomy has to be imaged or an abnormality reported. The statement “follow-up examination may be helpful” is too vague. In far too many cases, failure to visualize normal anatomy was judged to be due to fetal position, when in fact the structure was abnormal. If the brain, heart, or kidneys and bladder (in the presence of oligohydramnios) are not seen, a short-interval follow-up examination should be performed. If failure to adequately visualize the anatomy is a result of maternal body habitus, follow-up in 2 to 4 weeks may be useful. If the structure is still not seen, the referring obstetrician should be notified and the conversation documented. Further follow-up should be recommended as clinically indicated.

## INTERPRETATION OF THE ULTRASOUND EXAMINATION

This is, of course, the focus of the remainder of this book; however, we would like to make several comments. Although the subspecialty of obstetric ultrasound seems to attract new biometric applications daily, we have never been much of advocates of the sole use of measurements to achieve a diagnosis. It seems that every day, someone has developed and published a new chart for the measurement of a fetal anatomic structure. We fully recognize that there are many measurements that are necessary for accurate ultrasound interpretation, fetal biometry for size and weight, cervical length, and fetal ventricular size, to name a few. For many of the abnormalities that can be recognized sonographically, we would prefer that the sonologist give more credence to his or her subjective eye than to a measurement when images or individual structures “just don’t seem right.” Although a measurement may appear to be within normal limits, with experience, there are times when subjectivity, in our opinion, wins out. It is acceptable to say that despite an AFI of 6, there is oligohydramnios or that the fetal bowel appears dilated without an objective measurement of the bowel lumen.

Another pitfall is making a measurement of an anatomic structure and not interpreting the significance of the measurement. For example,

some ultrasound laboratories believe that adding numerous measurements, for example, transcerebellar, renal, or intraorbital measurements, in addition to standard biometry (biparietal diameter [BPD], head circumference [HC], abdominal circumference [AC], femur length [FL]), will make the examination more complete. Although we will not argue the necessity of doing these additional measurements in some select cases, what is puzzling is that often the interpreter of the examination will not check these measurements against standard tables or nomograms to determine if they are normal or abnormal. In our opinion, this is a serious mistake.

Without launching into a discussion of statistics, suffice it to say that no measurement will likely be 100% accurate without false positive or false negative results. There are some situations in which false positive results may be acceptable (e.g., screening examinations for a serious abnormality). Every practitioner abhors the notion of being labeled an “over-reader” of examinations. The sonologist needs to consider whether the goal is to not miss any patients with a condition (thus, resulting in more potential false positive results), which may mean additional testing or intervention, or whether they wish fewer false positive results and thus risk missing the detection of an abnormality in some patients. With this in mind, one can set the threshold level for the test, either lower or higher. If the sonologist is calling a referring clinician or scheduling follow-up examinations four to six times a week with a suspected abnormality (pelviectasis, echogenic bowel, and so on), one should perhaps reevaluate the criteria for defining something as abnormal. However, if one calls a referring physician once every 2 to 4 weeks when one is “bothered” by a finding and wishes to call attention to it, one should not feel as if he or she is “over-calling” an abnormality. Likewise, one should not be embarrassed about calling the referring physician about a concern that something might be abnormal even if it ultimately proves to be normal. Only in this way will patients be best served.

## Reporting of Ultrasound Results

One would anticipate that this might be the least contentious topic when discussing the obstetric ultrasound examination. However, it is controversial. In concert with recommendations by various organizations (e.g., AIUM, ACR, ACOG) a written report should be produced at the completion of the ultrasound examination and should be placed in the patient’s medical records. With widespread implementation of electronic medical records, this report typically uses one of a number of available reporting packages. Such reporting packages have been developed to make reporting easier: they include but are not limited to obstetric worksheets or checklists, computer templates or canned reports, computer voice recognition, digital transcription systems accessed by telephone or computer, and traditional voice dictation that is typed by transcriptionists (on site or remotely). All of these methods have the potential for producing an accurate and readable report. However, in our experience, the easier the reporting method, the more likely that observations made during the examination will not be conveyed accurately. Too often, sonographers and sonologists finish an examination and quickly enter checks into boxes on a worksheet indicating that a particular structure was observed or was normal. It is inconceivable, watching the speed with which the worksheet is completed, that they ever asked themselves the question, Did I really see those structures? Although it is becoming antiquated, conventional dictation systems that require the examiner to pick up the recording device and say “the following structures were seen ...” or some similar device or mechanism probably had a better chance of succeeding in conveying accurate information.

There are mixed benefits to templates that contain standard paragraphs such as the following structures were seen: lateral ventricles,



cerebellum, and so on. Although this information may be necessary for reimbursement purposes, it is likely that sonologists or referring physicians rarely read these paragraphs. They also have the potential to be confusing when abnormalities are detected, particularly if the paragraph ends with “and these structures were normal.” If one does not alter the paragraph, the referring physician will read in this standard paragraph a sentence that says: “the fetal kidneys were normal” and in the next paragraph a sentence that reads “bilateral fetal hydro-nephrosis was seen.”

It is our practice and recommendation that when fetal abnormalities are detected, the referring physician should be contacted in person or by telephone and the discussion should be documented in the report.

A question often raised concerns what to do when a structure normally seen on routine (basic) sonograms (and listed in the guidelines) is not seen. Or what to do when one identifies a structure that has an unusual appearance but that one suspects is probably normal. Often, it is assumed that failure to see a structure or structures are secondary to technical limitations, such as shadowing or poor fetal position or fetal physiology (the fetus just urinated or fluid in the stomach passed into the duodenum). If the examination is performed in the early second trimester, the patient should return within 2 to 4 weeks for another evaluation. As was mentioned earlier, if a structure in question relates to the heart or brain or kidneys and bladder (when oligohydramnios is present), the study should be considered incomplete. If a follow-up examination is warranted, the referring physician should be contacted and the conversation documented. The rationale for these recommendations is the concern that adequate follow-up and evaluation will not occur, or if they do occur, they will not be performed in a timely fashion. Statements indicating “clinical correlation recommended” are appropriate when the abnormality seen needs to be correlated with patient’s medical condition, laboratory tests, family history, and the patient’s age, but not when an isolated abnormality is seen (dilated bowel loop).

### Discussing the Examination With the Patient

This topic is also controversial. The patient obviously wants to know that the fetus is healthy and to know the results at the time of the examination. As a general rule, the referring obstetrician knows the patient best and also often has important information about the patient’s menstrual history, family history, laboratory values, and emotional state. However, the performing sonologist may be more knowledgeable about the significance of a given finding and may be better able to explain the results to the patient and to counsel her effectively. In cases of suspected morphologic or genetic abnormalities, the advice of a reproductive geneticist may prove invaluable. As is discussed later, often the first words that are said to the patient are the things that she remembers. Despite what is said later, it may be difficult to undo what was said initially. It is appropriate to say that the diagnosing physician needs to evaluate all of the images together and possibly compare them with previous studies. At that time, the final report will be generated.

Counseling is often straightforward if the case is normal or when the diagnosis is unequivocally lethal (anencephaly). It becomes more complex in cases in which the outcome is less than 100% certain (e.g., mild isolated ventriculomegaly). It is important not to insert our own bias and values about raising children with disabilities. One cannot assume that if a serious malformation is detected that a patient will desire an abortion rather than to deliver a baby with disabilities. In some cases, the person informing the patient of the results is uncertain of the significance of the findings,<sup>69-71</sup> and the first information the patient hears may be unclear or misleading. This confusion may color

how patients perceive later information and may result in dissatisfaction with the bearer of the news.<sup>69,71</sup>

It is often assumed that women weigh equally the risk of delivering a baby with a congenital abnormality versus a procedure-related pregnancy loss (amniocentesis). In fact, studies have demonstrated that most women see the long-term consequences of raising a disabled child as worse than a miscarriage, although women vary widely in this regard.<sup>70</sup> It is important to remember that we do not know better than our patients what is best for them. Our challenge is to help them reach a decision that is best for them given their particular background, experience, and values.

Even when precise and correct information is transmitted in a counseling session, it may not be interpreted with the same intended meaning by the patient. Certain words tend to have more serious and worse connotations to the patient than alternative words.<sup>71</sup> The words “rare abnormality” are often interpreted as serious (even if it is a mild abnormality). The word “abnormality” is often interpreted as worse than a variation of normal. Likewise, technical genetic words often have a worse connotation. “Trisomy” sounds worse to most patients than “an extra chromosome.”<sup>71</sup> Choroid plexus cysts (CPCs) and echogenic intracardiac foci (EIF) are discussed in Chapter 3. One should be aware that even if the sonologist firmly believes that the finding of an isolated CPC or an EIF is likely a normal variant and of no consequence, for a patient, the fact that these structures are in the brain and heart is no small matter. The fact that there may not be a significant increased risk in that individual patient based on other findings or that the abnormality is of small size may not alleviate the patient’s anxiety once she is told of these findings.

There has been much debate regarding whether physicians should disclose that an isolated sonographic “soft marker” for a chromosomal abnormality has been detected in a fetus in the absence of other risk factors for aneuploidy.<sup>72-74</sup> A 2007 study by Lee and associates<sup>75</sup> found that the detection and communication of isolated aneuploidy markers (CPCs, EIF, renal pyelectasis, echogenic bowel) is associated with increased maternal anxiety and perhaps unnecessary amniocenteses. Their conclusion: “given the amount of maternal anxiety generated with detection of aneuploidy markers, serious consideration should be given to offering pre- and post-ultrasound genetic counseling or otherwise, nothing should be mentioned about ultrasound markers that may be normal variants in patients who have no other risk factors for aneuploidy.”<sup>75</sup>

The likelihood of having a normal child when an abnormality is suspected or a patient found to be at increased risk based on screening is almost always received more favorably by the family than being told of the small percentage of having an abnormal child. That is, a 99% chance of normal sounds less worrying than 1% chance of abnormal. When risk is given as a proportion, it often sounds worse than when it is given as a rate; in other words, 1/X sounds worse than X%.<sup>71</sup> One should be aware that a large portion of the public lacks functional knowledge of fractions, large numbers, or percentages.<sup>76,77</sup> In one study,<sup>78</sup> a third of adult women with less than a college education did not recognize that 1/1000 is less than 1%. It is interesting that although in most medical specialties, risk or prognosis is given as a percentage, for example, 10% chance of a cure or bad outcome, in prenatal genetic counseling, risk is often given as a proportion, which most patients do not fully understand. In a study by Grimes and Snively,<sup>76</sup> women of varying ages, education levels, and languages were asked to identify which proportion of bladder infection was higher: 1 in 384 or 1 in 112 persons. The same women were then asked to identify which rate of infection was higher: 2.6 per 1000 women or 8.9 per 1000 women. Overall, 73% correctly identified the higher risk in rate format (X/1000), in contrast with 56% who correctly answered the same



question framed as proportions (1/X).<sup>76</sup> Clearly, women understood rates better than proportions.

Perhaps the most important point of this discussion is what to do when a slight variation of normal or an unusual finding is seen. The first answer would be to consult your colleagues. If that does not answer the question, then one should discuss the case further with more experienced experts or refer the patient to a university or specialty center. In some cases, one will simply need to report that there is a finding and that you are uncertain of the significance. When the physician feels pressure to always give a black and white, or normal versus abnormal, answer without honest indecisiveness, this approach does a disservice to the patient.

## Evaluating the Obstetric-Gynecologic Ultrasound Literature

Whereas this text serves as a reference to many, as an aid to ongoing clinical problems, new and useful clinical information is reported constantly in the medical literature. It is appropriate that the reader keep current with new advances. It is also important to be vigilant for poorly constructed studies and conclusions. Although virtually every report will have some mention of the sensitivity and specificity of a new test, this is only a small part of an adequate analysis of the utility of a new technique. There are a number of areas that should be considered when evaluating a new report in the literature; these areas are outlined in Table 1-3.<sup>79</sup> Perhaps the most common error is that authors do not state the prevalence of "disease or abnormality" in their population or that readers do not take this into account when applying the report to

their own practice. This also holds true for both equipment and techniques used for analysis.

When the authors discuss a new technique or potentially helpful finding, it is invariably depicted in their first figure (i.e., Fig. 1-1). If after looking at Figure 1-1 in the new publication, as well as its legend and text description, the reader does not understand what is being demonstrated, the publication is likely to be of little value in clinical practice.

## Malpractice and the Obstetric Ultrasound Examination

It is likely that each person reading this text has been touched in some way by the ongoing malpractice crisis. For most of us, this crisis has resulted in increased costs of goods and services, and for some, it has meant being the defendant in a malpractice suit.

Medical malpractice actions typically arise from a patient's allegation of negligent diagnosis or treatment. In order to prevail, the patient must show that the physician fell below the applicable standard of care. Standard of care is established most commonly by the testimony of an expert witness. Although guidelines promulgated by various organizations (AIUM, ACR, ACOG) alone do not establish the standard of care introduced at trial, they do describe the general practice of obstetric ultrasound in many communities and are often referred to by medical experts.<sup>80</sup> The definition of standard of care varies slightly from state to state. California's instruction to juries regarding standard of care in medical malpractice cases is listed here:

### CALIFORNIA CIVIL JURY INSTRUCTIONS (CACI)

#### 501. Standard of Care for Health Care Professionals

[A/An] *[insert type of medical practitioner]* is negligent if [he/she] fails to use the level of skill, knowledge, and care in diagnosis and treatment that other reasonably careful *[insert type of medical practitioners]* would use in the same or similar circumstances. This level of skill, knowledge, and care is sometimes referred to as "the standard of care."

[You must determine the level of skill, knowledge, and care that other reasonably careful *[insert type of medical practitioners]* would use in the same or similar circumstances, based only on the testimony of the expert witnesses *[including [name of defendant]]* who have testified in this case.]

Data on the number of claims of malpractice and their settlements are difficult to obtain. In one report, Sanders<sup>78</sup> reported malpractice claims in diagnostic ultrasonography in 228 cases. Obstetric ultrasound examinations represented the majority (78%) of the cases.

Some of the more common reasons for the initiation of malpractice suits (whether legitimate or not) include the following:

- Unreasonable expectations of the ultrasound examination on the part of the patient and the referring physician
- Physician performing the examination having inadequate training or equipment
- Failure to seek consultation in difficult cases
- Inadequate or incomplete study
- Misinterpretation of the ultrasound examination (resulting in the inability to terminate before the legal state limit, a wrongful termination, or preterm or postterm delivery)
- Poor communication with referring clinicians (improper wording, lack of timely communication)
- Failure to maintain ultrasound equipment
- Failure to supervise personnel adequately

It is our desire that this text, through the education process of the sonographer and sonologist, will help alleviate errors in diagnosis

TABLE 1-3 Evaluating the Literature

#### Abstract

What are the objectives, findings, and conclusions of the study?

#### Introduction

What is the purpose of the diagnostic test?

#### Materials and Methods

How are the patients selected?

Are they representative of those who are ordinarily tested?

How is the test(s) performed and interpreted?

Are the interpretation criteria well defined and reproducible?

What is the gold standard for diagnosis? Is it appropriate?

Are the sonologists blinded from the final diagnosis and is the final diagnostician (pathologist) blinded from sonographic interpretation?

Is the gold standard applied uniformly?

In a comparison study, are the tests evaluated fairly?

#### Results

How is the accuracy reported?

Are the spectrum of disease and important covariates, such as comorbidity, age, sex, and body habitus, accounted for in tabular presentation of data?

Is the statistical analysis clearly described and appropriate?

#### Discussion

Are the deficiencies in the methodology of accuracy assessment acknowledged and discussed?

Are other relevant factors, such as disease prevalence, therapeutic effectiveness, and cost, adequately accounted for in the clinical recommendations?



and thus reduce the number of these cases. Unfortunately, despite the best medical care, some malpractice suits are brought against physicians.

## CONCLUSION

The appeal of the ultrasound examination is that it is a noninvasive, safe procedure that has a high degree of patient acceptance and can yield a wealth of information. It is always a delight to examine the obstetric patient and reassure her about her pregnancy, when appropriate.

When a pathologic process is first identified, the role of the sonologist is that of a detective who attempts to piece together all of the

information to arrive at the correct diagnosis (Fig. 1-6). Although discovering a pathologic process is always disconcerting, the sonologist can be a counselor to the patient and the clinician and can help guide them to appropriate management decisions. However, there are times when an abnormality is strongly suspected but it may be equivocal or may not fit into a specific category. Under these circumstances, the best pathway for the sonologist to follow may be to do a follow-up examination and seek consultation. If time does not allow a follow-up examination, then the sonologist should communicate to the referring physician and the patient that a definitive answer is not possible and that decisions will have to be made with less-than-perfect information.

We are hopeful that this text will serve two purposes: to educate and to excite. If those reading this text maintain the same enthusiasm

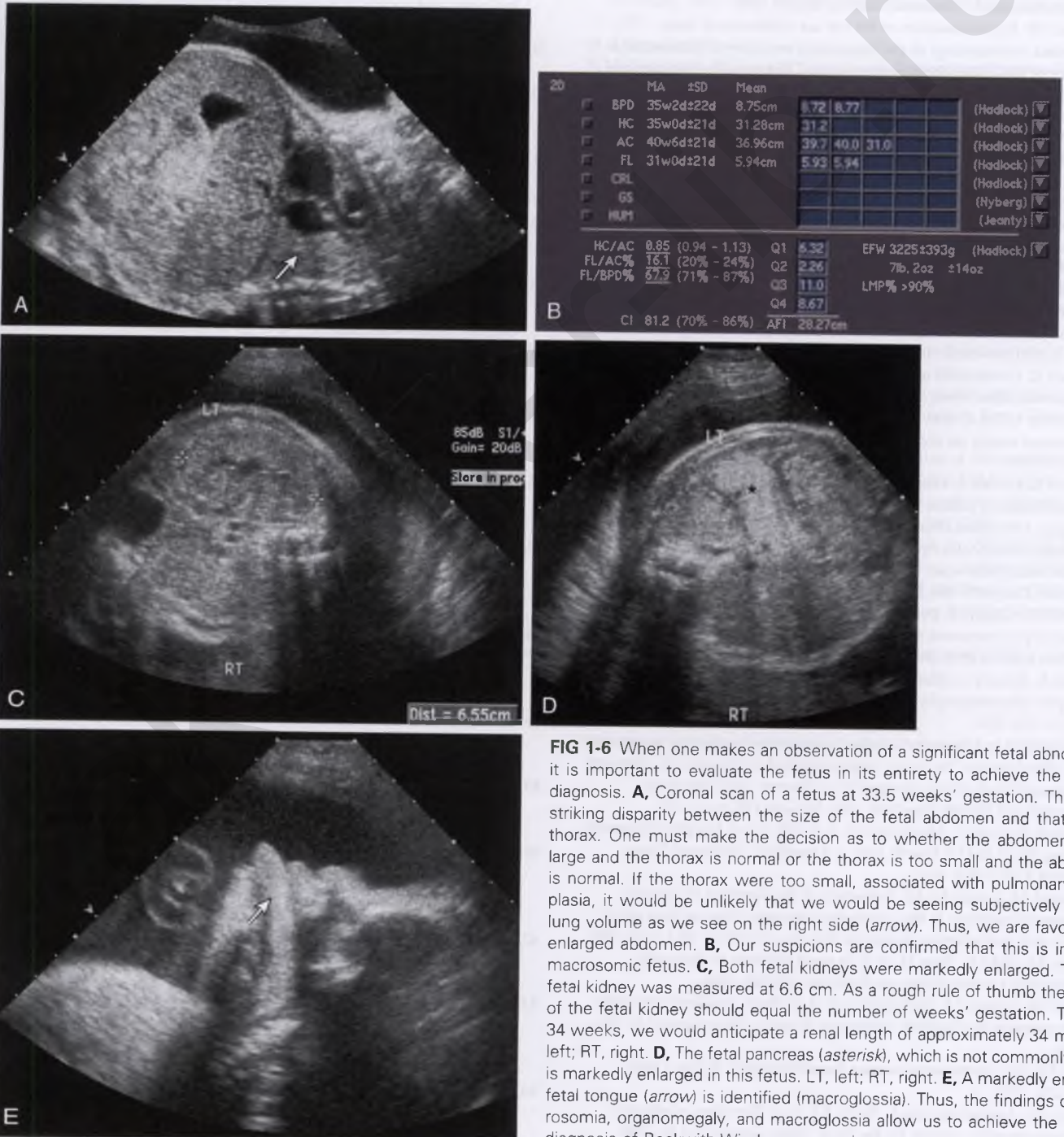


**FIG 1-6** When one makes an observation of a significant fetal abnormality it is important to evaluate the fetus in its entirety to achieve the correct diagnosis. **A**, Coronal scan of a fetus at 33.5 weeks' gestation. There is a striking disparity between the size of the fetal abdomen and that of the thorax. One must make the decision as to whether the abdomen is too large and the thorax is normal or the thorax is too small and the abdomen is normal. If the thorax were too small, associated with pulmonary hypoplasia, it would be unlikely that we would be seeing subjectively normal lung volume as we see on the right side (*arrow*). Thus, we are favoring an enlarged abdomen. **B**, Our suspicions are confirmed that this is in fact a macrosomic fetus. **C**, Both fetal kidneys were markedly enlarged. The left fetal kidney was measured at 6.6 cm. As a rough rule of thumb the length of the fetal kidney should equal the number of weeks' gestation. Thus, at 34 weeks, we would anticipate a renal length of approximately 34 mm. LT, left; RT, right. **D**, The fetal pancreas (*asterisk*), which is not commonly seen, is markedly enlarged in this fetus. LT, left; RT, right. **E**, A markedly enlarged fetal tongue (*arrow*) is identified (macroglossia). Thus, the findings of macrosomia, organomegaly, and macroglossia allow us to achieve the correct diagnosis of Beckwith-Wiedemann syndrome.



for obstetric and gynecologic sonography that we have, we will have fulfilled our goal.

## REFERENCES

- Hershkovitz R, Sheiner E, Mazor M: Ultrasound in obstetrics: a review of safety. *Eur J Obstet Gynecol Reprod Biol* 101:15, 2002.
- Cavicchi TJ, O'Brien WD, Jr: Heat generated by ultrasound in an absorbing medium. *J Acoust Soc Am* 76(4):1244, 1984.
- Nyborg WL, Steele RB: Temperature elevation in a beam of ultrasound. *Ultrasound Med Biol* 9:611, 1983.
- Flynn HG: Physics of acoustic cavitation in liquids. In Mason WP, editor: *Physical Acoustics* (vol 1B). New York, 1964, Academic Press.
- Child SZ, Hartman CL, Schery LA, et al: Lung damage from exposure to pulsed ultrasound. *Ultrasound Med Biol* 16:817, 1990.
- Barnett SB: *Recommendation on the safe use of ultrasound*. Paper presented at Proceedings of the Symposium on Safety of Ultrasound in Medicine, WFUMB (World Federation for Ultrasound in Medicine and Biology), 1998.
- Barnett SB, Rott HD, ter Haar GR, et al: The sensitivity of biological tissue to ultrasound. *Ultrasound Med Biol* 23(6):805, 1997.
- Rott HD: *Clinical Safety Statement for Diagnostic Ultrasound*. Tours, France, European Federation for Societies for Ultrasound in Medicine and Biology, 1998.
- Salvesen K, Lees C, Abramowicz J, et al: Board of International Society of Ultrasound in Obstetrics and Gynecology: ISUOG statement on the safe use of Doppler in the 11 to 13 + 6-week fetal ultrasound examination. *Ultrasound Obstet Gynecol* 37(6):628, 2011.
- American Institute of Ultrasound in Medicine: AIUM practice guideline for the performance of obstetric ultrasound examinations. *J Ultrasound Med* 32(6):1083–1101, 2013.
- Kossoff G: Contentious issues in safety of diagnostic ultrasound. *Ultrasound Obstet Gynecol* 10:151, 1997.
- Zhu J, Lin J, Zhu Z, et al: Effects of diagnostic levels of color Doppler ultrasound energy on the cell cycle of newborn rats. *J Ultrasound Med* 18:257, 1999.
- Pellicer B, Herraiz S, Taboas E, et al: Ultrasound bioeffects in rats: quantification of cellular damage in the fetal liver after pulsed Doppler imaging. *Ultrasound Obstet Gynecol* 37:643–648, 2011.
- Schneider-Kolsky ME, Ayobi Z, Lombardo P, et al: Ultrasound exposure of the foetal chick brain: effects on learning and memory. *Int J Dev Neurosci* 27(7):677–683, 2009.
- Ang ES, Jr, Gluncic V, Duque A, et al: Prenatal exposure to ultrasound waves impacts neuronal migration in mice. *Proc Natl Acad Sci U S A* 103(34):12903–12910, 2006.
- Bhide A, Acharya G, Bilardo CM, et al: ISUOG practice guidelines: use of Doppler ultrasonography in obstetrics. *Ultrasound Obstet Gynecol* 41:233–239, 2013.
- O'Brien WD, Jr: Ultrasound bioeffect issues related to obstetric sonography and related issues of the output display standard. In Fleischer AC, Manning FA, Jeanty P, et al, editors: *Sonography in Obstetrics and Gynecology, Principles and Practice*, New York, 1996, McGraw Hill, pp 17–33.
- Salvesen KA, Lees C, Abramowicz J, et al: Safe use of Doppler ultrasound during the 11 to 13 + 6-week scan: is it possible? *Ultrasound Obstet Gynecol* 37:625–628, 2011.
- Tarantal AF, Hendrickx AG: Evaluation of the bioeffects of prenatal ultrasound exposure in the cynomolgus macaque (*Macaca fascicularis*): II. Growth and behavior during the first year. *Teratology* 39(2):149, 1989.
- Lyons EA, Dyke C, Toms M, et al: In utero exposure to diagnostic ultrasound: a 6-year follow-up. *Radiology* 166:687, 1988.
- Stark CR, Orleans M, Haverkamp AD, et al: Short- and long-term risks after exposure to diagnostic ultrasound in utero. *Obstet Gynecol* 63:194, 1984.
- Lele PP: No chromosomal damage from ultrasound. *N Engl J Med* 287:254, 1972.
- Reece EA, Assimakopoulos E, Zheng XZ, et al: The safety of obstetric ultrasonography: concern for the fetus. *Obstet Gynecol* 76:139, 1990.
- Sidman RL, Rakic P: Neuronal migration, with special reference to developing human brain: a review. *Brain Res* 62:1, 1973.
- Letinic K, Zoncu R, Rakic P: Origin of GABAergic neurons in the human neocortex. *Nature* 417:645, 2002.
- American Institute of Ultrasound in Medicine, Bioeffects Committee: Bioeffects considerations for the safety of diagnostic ultrasound. *J Ultrasound Med* 7(9 Suppl):S1–S38, 1988.
- Merritt CR: Ultrasound safety: what are the issues? *Radiology* 173:304, 1989.
- Reddy UM, Abuhamad AZ, Levine D, Saade GR, Fetal Imaging Workshop Invited Participants: Fetal imaging: executive summary of a joint Eunice Kennedy Shriver National Institute of Child Health and Human Development, Society for Maternal-Fetal Medicine, American Institute of Ultrasound in Medicine, American College of Obstetricians and Gynecologists, American College of Radiology, Society for Pediatric Radiology, and Society of Radiologists in Ultrasound Fetal Imaging Workshop. *Obstet Gynecol* 123(5):1070–1082, 2014.
- Kremkau FW: *Diagnostic Ultrasound: Principles and Practice*, ed 7, Philadelphia, 2006, WB Saunders.
- American College of Obstetricians and Gynecologists: ACOG Practice Bulletin No. 101: ultrasonography in pregnancy. *Obstet Gynecol* 113:451–461, 2009.
- National Collaborating Centre for Women's and Children's Health: *Antenatal Care: Routine Care for the Healthy Pregnant Woman*, London, 2008, RCOG Press.
- Cargill Y, Morin L, Bly S, et al: Content of a complete routine second trimester obstetrical ultrasound examination and report. *J Obstet Gynaecol Can* 31(3):272–280, 2009.
- American College of Obstetricians and Gynecologists: ACOG Practice Bulletin No. 77: screening for fetal chromosomal abnormalities. *Obstet Gynecol* 109:217–227, 2007.
- Whitworth M, Bricker L, Neilson JP, Dowswell T: Ultrasound for fetal assessment in early pregnancy. *Cochrane Database Syst Rev* (4):CD007058, 2010.
- Grandjean H, Larroque D, Levi S: The performance of routine ultrasonographic screening of pregnancies in the Eurofetus Study. *Am J Obstet Gynecol* 181:446–454, 1999.
- VanDorsten JP, Hulsey TC, Newman RB, et al: Fetal anomaly detection by second-trimester ultrasonography in a tertiary center. *Am J Obstet Gynecol* 178:742, 1998.
- American Institute of Ultrasound in Medicine: Joint Task Group on Training for Diagnosis in Obstetrical and Gynecologic Ultrasound. AIUM Guidelines for minimum postresidency training in obstetrical and gynecological ultrasound. *J Ultrasound Med* 1:R40, 1982.
- American Institute of Ultrasound in Medicine: *Training Guidelines for Physicians Who Evaluate and Interpret Diagnostic Obstetric Ultrasound Examinations*. 10/31/2015. Available at <<http://www.aium.org/resources/viewStatement.aspx?id=59>>.
- American Institute of Ultrasound in Medicine: Guidelines for the performance of the antepartum obstetrical ultrasound examination. *J Ultrasound Med* 15:185, 1996.
- American College of Obstetricians and Gynecologists: ACOG Technical Bulletin No. 187, December 1993. Ultrasonography in pregnancy. *Int J Gynaecol Obstet* 44:173, 1994.
- Hillman BJ, Joseph CA, Mabry MR, et al: Frequency and costs of diagnostic imaging in office practice—a comparison of self-referring and radiologist-referring physicians. *N Engl J Med* 323:1604, 1990.
- Wax J, Minkoff H, Johnson A, et al: Consensus report on the detailed fetal anatomic ultrasound examination indications, components, and qualifications. *J Ultrasound Med* 33(2):189–195, 2014.
- American College of Obstetricians and Gynecologists ACOG Committee on Ethics: ACOG Committee Opinion No. 297, August 2004. Non-medical use of obstetric ultrasonography. *Obstet Gynecol* 104(2):423–424, 2004.
- Chervenak FA, McCullough LB: An ethical critique of boutique fetal imaging: a case for the medicalization of fetal imaging. *Am J Obstet Gynecol* 192(1):31–33, 2005.

45. American Institute of Ultrasound in Medicine: AIUM Practice Guideline for the performance of an antepartum obstetric ultrasound examination. *J Ultrasound Med* 22(10):1116, 2003.
46. Filly RA: Level 1, level 2, level 3 obstetric sonography: I'll see your level and raise you one. *Radiology* 172:312, 1989.
47. American Institute of Ultrasound in Medicine: *AIUM Official Statement—Interpretation of Ultrasound Examinations*. Approved March 26, 1997; revised June 22, 2005.
48. Szabo TL, Lewin PA: Ultrasound transducer selection in clinical imaging practice. *J Ultrasound Med* 32(4):573–582, 2013.
49. Malone FD, Nores JA, Athanassiou A, et al: Validation of fetal telemedicine as a new obstetric imaging technique. *Am J Obstet Gynecol* 177:626, 1997.
50. Doubilet PM, Benson CB: "Appearing twin": undercounting of multiple gestations on early first trimester sonograms. *J Ultrasound Med* 17:199, quiz 205, 1998.
51. Goldstein RB, Filly RA, Callen PW: Sonography of anencephaly: pitfalls in early diagnosis. *J Clin Ultrasound* 17:397, 1989.
52. Hertzberg BS, Bowie JD, Carroll BS, et al: Normal sonographic appearance of the fetal neck late in the first trimester: the pseudomembrane. *Radiology* 171:427, 1989.
53. Schmidt W, Yarkoni S, Crelin ES, et al: Sonographic visualization of physiologic anterior abdominal wall hernia in the first trimester. *Obstet Gynecol* 69:911, 1987.
54. Becker RH, Vonk R, Mende BC, et al: The relevance of placental location at 20–23 gestational weeks for prediction of placenta previa at delivery: evaluation of 8650 cases. *Ultrasound Obstet Gynecol* 17(6):496–501, 2001.
55. Lauria MR, Smith RS, Treadwell MC, et al: The use of second-trimester transvaginal sonography to predict placenta previa. *Ultrasound Obstet Gynecol* 8:337–340, 1996.
56. Neilson DR: Management of the large breech infant. A survey of 203 cases from Emanuel Hospital. *Am J Obstet Gynecol* 107:345, 1970.
57. Barkin SZ, Pretorius DH, Beckett MK, et al: Severe polyhydramnios: incidence of anomalies. *AJR Am J Roentgenol* 148:155, 1987.
58. Sivit CJ, Hill MC, Larsen JW, Lande IM: Second-trimester polyhydramnios: evaluation with US. *Radiology* 165(2):467, 1987.
59. Hashimoto B, Callen PW, Filly RA, et al: Ultrasound evaluation of polyhydramnios and twin pregnancy. *Am J Obstet Gynecol* 154:1069, 1986.
60. Mahony BS, Filly RA, Callen PW: Amnionicity and chorionicity in twin pregnancies: prediction using ultrasound. *Radiology* 155:205, 1985.
61. Laing FC: Placenta previa: avoiding false-negative diagnoses. *J Clin Ultrasound* 9:109, 1981.
62. Zemlyn S: The effect of the urinary bladder in obstetrical sonography. *Radiology* 128:169, 1978.
63. Centers for Disease Control and Prevention: *Update on Overall Prevalence of Major Birth Defects—Atlanta, Georgia, 1978–2005*. January 11, 2008. Available at <<http://www.cdc.gov/mmwr/preview/mmwrhtml/mm5701a2.htm>>.
64. Queisser-Luft A, Stopfkuchen H, Stolz G, et al: Prenatal diagnosis of major malformations: quality control of routine ultrasound examinations based on a five-year study of 20,248 newborn fetuses and infants. *Prenat Diagn* 18:567, 1998.
65. Sever L, Lynberg MC, Edmonds LD: The impact of congenital malformations on public health. *Teratology* 48:547, 1993.
66. Lynberg MC, Edmonds LD: Surveillance of birth defects. In Halperin W, Baker EL, Monson RR, editors: *Public Health Surveillance of Birth Defects*, New York, 1992, Van Nostrand Reinhold, pp 155–177.
67. Van Mieghem T, Hindryckx A, Van Calsteren K: Early fetal anatomy screening: who, what, when and why? *Curr Opin Obstet Gynecol* 27(2):143–150, 2015.
68. Bronshtein M, Zimmer EZ: Prenatal ultrasound examinations: for whom, by whom, what, when and how many? *Ultrasound Obstet Gynecol* 10:1, 1997.
69. Deleted in review.
70. Kuppermann M, Feeny D, Gates E, et al: Preferences of women facing a prenatal diagnostic choice: long-term outcomes matter most. *Prenat Diagn* 19:711, 1999.
71. Abramsky L, Fletcher O: Interpreting information: what is said, what is heard—a questionnaire study of health professionals and members of the public. *Prenat Diagn* 22:1188, 2002.
72. Filly RA, Benacerraf BR, Nyberg DA, et al: Choroid plexus cyst and echogenic intracardiac focus in women at low risk for chromosomal anomalies. *J Ultrasound Med* 23:447, 2004.
73. Doubilet PM, Copel JA, Benson CB, et al: Choroid plexus cyst and echogenic intracardiac focus in women at low risk for chromosomal anomalies: the obligation to inform the mother. *J Ultrasound Med* 23:883, 2004.
74. Filly RA: Echogenic intracardiac foci and choroid plexus cysts. *J Ultrasound Med* 23:1135, author reply 1138, 2004.
75. Lee MJ, Roman AS, Lusskin S, et al: Maternal anxiety and ultrasound markers for aneuploidy in a multiethnic population. *Prenat Diagn* 27:40, 2007.
76. Grimes DA, Snively GR: Patients' understanding of medical risks: implications for genetic counseling. *Obstet Gynecol* 93:910, 1999.
77. Shaw NJ, Dear PR: How do parents of babies interpret qualitative expressions of probability? *Arch Dis Child* 65:520, 1990.
78. Sanders RC: The effect of the malpractice crisis on obstetrical and gynecological ultrasound. In Chervenak F, editor: *Textbook of Obstetrical and Gynecological Ultrasound*, Boston, 1993, Little Brown, pp 263–276.
79. Black WC: How to evaluate radiology literature. *AJR Am J Roentgenol* 154:17, 1990.
80. Chervenak FA, Chervenak JL: Medical legal issues in obstetric ultrasound. *Clin Perinatol* 34:299–308, 2007.



# Genetics and Prenatal Genetic Testing

Mary E. Norton, Britton D. Rink

## SUMMARY OF KEY POINTS

- In the population, 2% to 3% of newborns have a congenital malformation or genetic disease identified at birth.
- Despite advances in genetics, the cause of more than half of human congenital abnormalities remains unknown.
- Chromosomal abnormalities are present in about 0.9% of newborns and include abnormalities of chromosome number as well as abnormalities of chromosome structure.
- The embryo is most sensitive to teratogenic effects between 3 and 8 weeks of development.
- Current available tools for fetal aneuploidy screening include cell-free DNA screening, various forms of multiple marker screening with first and second trimester maternal serum analytes, and ultrasound measurements, including nuchal translucency.
- The prevalence of many single gene disorders varies with race and ethnicity, and testing is often recommended based on an individual patient's background.
- Expanded carrier screening, including panels to simultaneously test for a large number of genetic conditions, is increasingly utilized for prenatal genetic screening.
- Chorionic villus sampling (CVS) and amniocentesis are both routinely used for prenatal diagnostic testing and can provide tissue for such tests as fluorescence in situ hybridization (FISH), karyotyping, chromosomal microarray analysis (CMA), and DNA-based tests.
- The loss rate attributable to CVS and amniocentesis is estimated to be between 1/500 and 1/1000 and decreases with provider experience.
- Many structural fetal abnormalities are associated with an increased risk of aneuploidy as well as copy number variants detectable with chromosomal microarray.

## OUTLINE

- Genetics and Birth Defects, 25
- Developmental Disorders: Causes, Mechanisms, and Patterns, 25
- Chromosomal Defects, 27**
  - Abnormalities of Chromosome Number, 27
    - Trisomy 21*, 27
    - Trisomy 18*, 28
    - Trisomy 13*, 28
    - Turner Syndrome*, 28
    - Klinefelter Syndrome*, 28
    - Triploidy*, 29
  - Abnormalities of Chromosome Structure, 29
  - Other Types of Chromosomal Rearrangements, 29
- Single Gene Disorders, 29**
  - Autosomal-Dominant Inheritance, 31
    - Penetrance and Expression*, 31
  - Autosomal-Recessive Disorders, 32
  - X-Linked Inheritance, 32
  - Other Novel Genetic Mechanisms, 32
  - Multifactorial Inheritance, 33
- Teratology, 34**
  - Recognized Teratogenic Agents, 35
  - Maternal Infections, 35
  - Medications, 35
  - Radiation, 35
  - Maternal Factors, 35
  - Mechanical Factors, 37
- Genetic Counseling, 37**
- Genetic Screening in Pregnancy, 37**
  - Carrier (Heterozygote) Screening for Single Gene Disorders, 38
    - Tay-Sachs Disease*, 38
    - Cystic Fibrosis*, 38
  - Screening for Structural Birth Defects, 40
    - Alpha-Fetoprotein and Open Neural Tube Defects*, 40
    - Elevated MSAFP*, 41
    - Other Abnormalities and Elevated AFP*, 41
    - Fetal Chromosomal Aneuploidy*, 41
- First Trimester Risk Assessment, 41**
- Second Trimester Risk Assessment, 42**
  - Sonographic "Soft Markers" for Aneuploidy, 43
- Combined First and Second Trimester Risk Assessment, 43**
  - Cell Free DNA Screening, 43
- Prenatal Screening in Multiple Gestations, 45**
- Third-Trimester Pregnancy Complications After Abnormal Serum Screening, 45**
- Genetic Diagnosis in Pregnancy, 45**
  - Genetic Counseling Before Prenatal Diagnostic Procedures, 46
  - Techniques for Prenatal Diagnosis, 46
    - Amniocentesis*, 46
    - Chorionic Villus Sampling*, 46

Multiple Gestations, 47
<i>Postprocedural Loss Rates in Multiple Gestations, 48</i>
<i>Selective Termination of Multifetal Pregnancies, 48</i>
Fetal Blood Sampling and Other Fetal Tissue Biopsy, 48
Preimplantation Genetic Diagnosis, 49

### Prenatal Testing for Congenital Malformations, 49

Techniques of Genetic Analysis, 50
Chromosome Identification, 50
Fluorescence in Situ Hybridization, 51
Molecular Techniques for DNA Analysis, 51
Chromosomal Microarray, 51

Genetic diseases are often perceived to be so rare that the average practitioner will seldom encounter them. However, increasing knowledge and technologic advances in genetic testing have demonstrated that this is far from the case. The availability of prenatal diagnosis for a wide range of disorders continues to increase with advances in genetics. In addition, progress has been made in population screening tests to identify couples who carry a genetic disorder. New techniques, such as cell-free DNA screening, have also changed the field of prenatal diagnosis significantly. These improvements in prenatal screening and diagnosis mean that many more at-risk couples are able to have unaffected children. In addition to reproductive choice, carrier screening and fetal diagnostic testing afford the important opportunity for preparation of the family and the delivery site for the birth of a fetus with a known genetic disorder.

Ultrasound plays a central role in the provision of prenatal screening and diagnosis. Not only is ultrasound key to guiding prenatal diagnostic procedures, but also integration of a genetics-based prenatal diagnosis program has been shown to increase the accuracy of diagnosis when compared to ultrasound alone.<sup>1</sup> This chapter includes a discussion of genetics, with an emphasis on recent advances relevant to prenatal diagnosis and a description of current strategies for genetic testing with a focus on how genetic screening and sonography together contribute to the provision of accurate and precise prenatal diagnosis.

### Genetics and Birth Defects

According to most studies, 2% to 3% of living newborns have a congenital malformation.<sup>2</sup> When considering birth defects noted in the first years of life, this incidence is nearly doubled. With the decline in infant mortality in the United States from infection and malnutrition, congenital malformations are now a leading cause of infant death (>20%) and are responsible for greater than 30% of intensive care nursery admissions.<sup>3</sup> Congenital defects range from enzyme deficiencies caused by single gene mutations to complex associations of structural defects. The continuum between purely biochemical abnormalities and structural birth defects includes disorders of structure, function, metabolism, and behavior.

Birth defects result from the interaction between the genetic makeup of the embryo and the environment in which it develops. The basic developmental information is encoded in genes, but the genotype is subjected to environmental influences that can impact the observed phenotype. In some cases, the genetic information is expressed regardless of environment, whereas in others, environmental causes interfere with normal development despite a normal genotype. Although some processes are primarily environmental and others mainly genetic, the distinctions between the two are not perfect.

Despite considerable advances and research over past several decades, the cause of more than half of human congenital abnormalities remains unknown. Of those with a recognized cause, approximately 15% to 20% are autosomal genetic diseases and 20% are cytogenetic in origin. Fewer than 1% of anomalies are thought to result from teratogenic medications. Some of the remaining defects are associated with other environmental exposures during pregnancy,

including infectious agents (3%), maternal disease states (4%), mechanical problems (1% to 2%), irradiation, and unknown environmental causes. The remainder are of unknown or complex causes (multifactorial, polygenic, spontaneous errors of development, and synergistic interactions of teratogens) (Fig. 2-1).<sup>3,4</sup>

### Developmental Disorders: Causes, Mechanisms, and Patterns

Errors in morphogenesis are often classified by dysmorphologists according to the underlying pathogenesis (Fig. 2-2). *Malformations* are defects in the structure of an organ resulting from a specific primary abnormality of development, such as a congenital heart or neural tube defect (NTD). *Deformations* are abnormalities of form, shape, or position caused by mechanical forces such as intrauterine molding or constraint. Factors leading to deformations may be extrinsic (e.g., oligohydramnios owing to ruptured membranes) or intrinsic (e.g., oligohydramnios owing to renal agenesis). Deformations may also occur postnatally; for example, an infant may develop a flat head from sleeping in one position. A *disruption* is a morphologic defect that results from breakdown of previously normal tissue. Disruptions can be due to extrinsic forces, internal interferences with a developmental process, or vascular insults. Examples of disruptions include amputations owing to amniotic bands, and gastroschisis and porencephaly, both thought to result from in utero vascular insults.

A *sequence* is a pattern of multiple abnormalities resulting from a single primary anomaly or mechanical factor; it may be a malformation, deformation, or disruption. An example is Potter sequence, in which oligohydramnios from any cause leads to similar features of fetal compression: characteristic facial features and abnormal positioning of the hands and feet. A *syndrome* is a pattern of multiple abnormalities known to have a common, specific cause. An example is Down

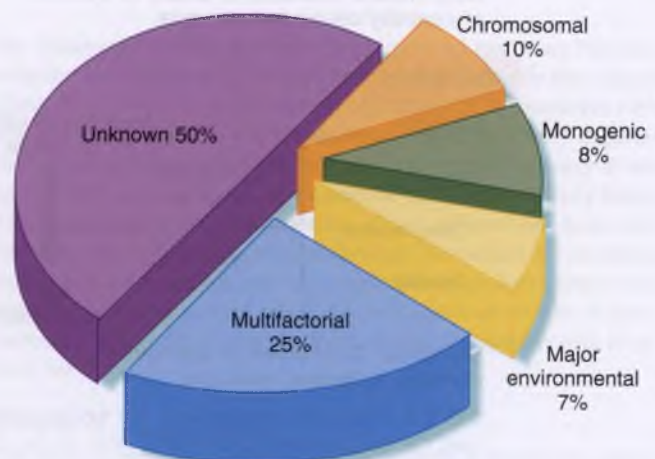
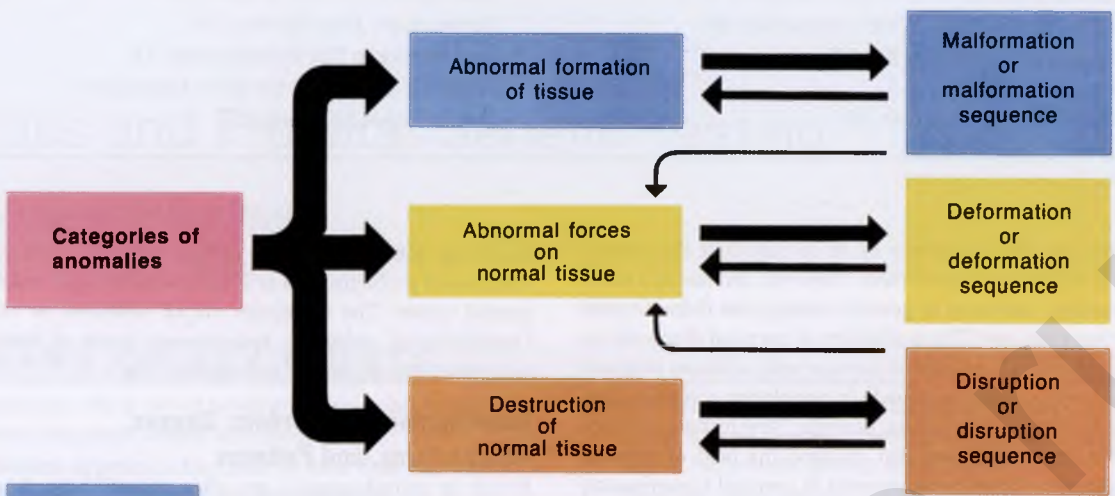


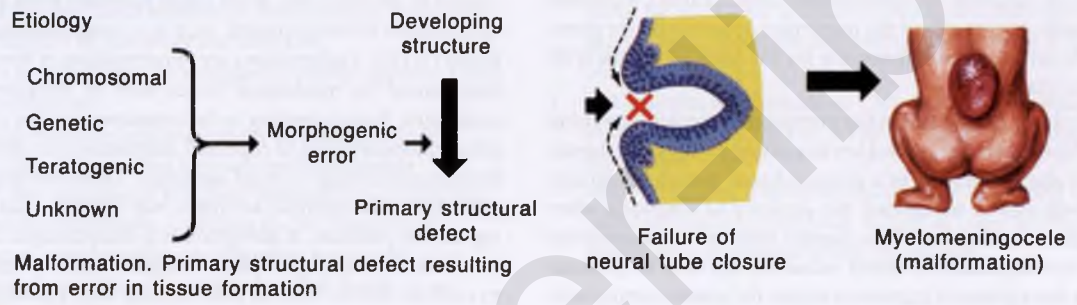
**FIG 2-1** Prevalence of genetic diseases in the population. (From Carlson BM: Human Embryology and Developmental Biology, 3rd ed. Philadelphia, Mosby/Elsevier, 2004, used with permission.)



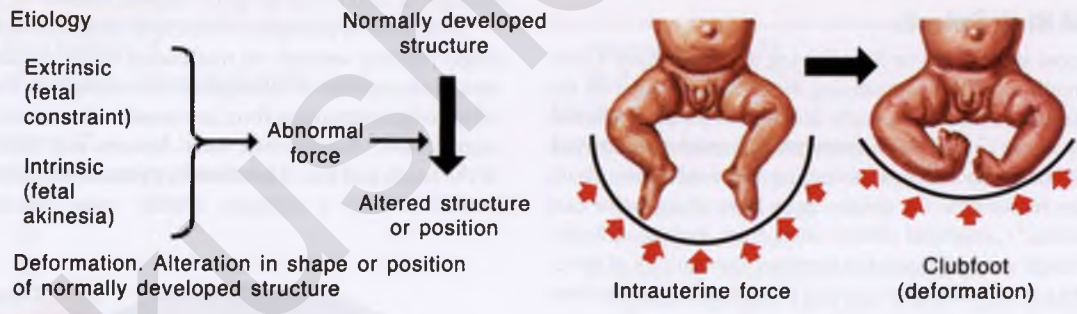
### Errors of Morphogenesis



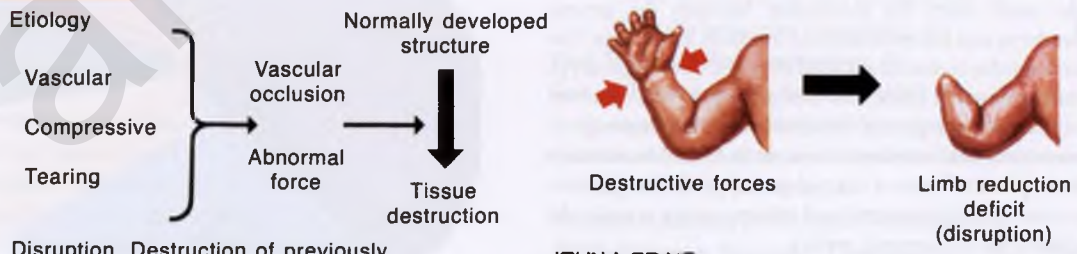
#### Malformation



#### Deformation



#### Disruption



JOHN A. CRAIG MD  
© CIBA-GEIGY

FIG 2-2 Errors of morphogenesis. For further explanation, see text. (From Nyhan WL: Structural Abnormalities: Clinical Symposia. CIBA-GEIGY, Vol. 42, No. 2, 1990, Plate 1, used with permission.)

syndrome (DS), which is caused by the presence of an extra copy of chromosome 21. Finally, the term *association* is used when two or more features occur together more commonly than expected by chance alone but for which no cause has been demonstrated. A common example is VACTERL association (Vertebral defects, Anal atresia, Cardiac defects, Tracheoesophageal fistula with Esophageal atresia, Renal anomalies, and Limb anomalies). This term does not imply a specific underlying cause but rather prompts the search for specific other defects when one component of the association is identified.

## CHROMOSOMAL DEFECTS

Chromosomal abnormalities occur in approximately 0.9% of newborns, and it is estimated that at least 10% to 15% of conceptions are chromosomally abnormal. Chromosome abnormalities are the leading cause of pregnancy loss, and at least 95% of chromosomally abnormal conceptions are lost before term. Abnormalities seen in abortuses differ from those seen in liveborn infants because the most severe chromosome abnormalities result in early arrest of development, whereas less severe abnormalities yield milder phenotypes that allow survival until later in pregnancy or even live birth. The most common abnormalities seen in first trimester spontaneous abortions are 45,X and 47,+16 (trisomy 16). Full or complete trisomy 16 is never seen in live births, whereas fewer than 1% of conceptions with 45,X survive until term.

Chromosome abnormalities can be either numeric or structural. They can involve one or more autosomes (chromosomes numbered 1-22), sex chromosomes, or both simultaneously. *Aneuploidy* refers to the presence of an abnormal number of chromosomes and is almost always associated with abnormalities of physical and cognitive development. *Translocations*, the exchange of segments between nonhomologous chromosomes, are relatively common and can be balanced, in which the appropriate amount of chromosomal material is present but rearranged, or unbalanced, in which some chromosomal material is gained or lost. Individuals with a balanced translocation are most often phenotypically normal unless the break for the rearrangement occurs in a critical gene and disrupts its function. Those with an unbalanced rearrangement most often have some phenotypic consequence including intellectual disability and structural birth defects as a result of being trisomic for one segment and monosomic for another. Many autosome translocations are unique, with some variation in expression of the additional or missing genetic material. A *Robertsonian translocation* is a rearrangement that involves any of the five acrocentric chromosomes, namely, 13, 14, 15, 21, and 22. The incidence of balanced Robertsonian translocations in the general population is 1/1000 and confers a higher risk for the relevant trisomies (most commonly trisomy 21 and 13) in offspring of balanced carriers. Balanced carriers are phenotypically normal and often only become aware of the rearrangement when they experience pregnancy with an abnormal karyotype, recurrent miscarriages, or male infertility.<sup>5</sup>

### Abnormalities of Chromosome Number

Aneuploidy is the most common clinically significant type of human chromosomal abnormality and occurs in 3% to 4% of recognized pregnancies. Nondisjunction in mitosis or meiosis is the cause of most aneuploidies. Maternal meiotic nondisjunction is known to increase with maternal age, and therefore the risk for aneuploid offspring also increases with advancing maternal age (Table 2-1). Both trisomy, the presence of three copies of an individual chromosome, and monosomy, the presence of a single copy of a chromosome, typically have significant phenotypic consequences. Monosomy is seen less frequently than trisomy because this situation is generally not compatible with

TABLE 2-1 Risk of Chromosomal Abnormalities in Liveborn Infants

Maternal Age (Years)	Risk for Down Syndrome	Total Risk for Chromosomal Abnormalities*
20	1/1667	1/526
21	1/1667	1/526
22	1/1429	1/500
23	1/1429	1/500
24	1/1250	1/476
25	1/1250	1/476
26	1/1176	1/476
27	1/1111	1/455
28	1/1053	1/435
29	1/1000	1/417
30	1/952	1/384
31	1/909	1/384
32	1/769	1/323
33	1/625	1/286
34	1/500	1/238
35	1/385	1/192
36	1/294	1/156
37	1/227	1/127
38	1/175	1/102
39	1/137	1/83
40	1/106	1/66
41	1/82	1/53
42	1/64	1/42
43	1/50	1/33
44	1/38	1/26
45	1/30	1/21
46	1/23	1/16
47	1/18	1/13
48	1/14	1/10
49	1/11	1/8

\*47,XXX excluded for ages 20 to 32 (data not available). Modified from the following sources: Hook EB, Cross PK, Schreinemachers DM: Chromosomal abnormality rates at amniocentesis and in live-born infants. *JAMA* 249:2034, 1983 (ages 33-49); Hook EB: Rates of chromosomal abnormalities at different maternal ages. *Obstet Gynecol* 58:282, 1981.

life. Trisomy or monosomy for any chromosome can occur theoretically, but in practice, some are seen much more frequently than others (Table 2-2). This is because most aneuploidies are incompatible with life, and aneuploid embryos spontaneously abort very early in gestation. Some chromosome abnormalities, for example, trisomy 8, are seen at birth only in mosaic form, and the full trisomy is likely lethal. *Mosaicism* is defined as the presence of two different cell lines with different genotypes in the same individual. Mosaicism is not always deleterious but can result in an abnormal phenotype depending on the degree and type of affected tissue. An entire extra set or sets of chromosomes, polyploidy, is also possible but is not compatible with long-term survival.

### Trisomy 21

The most common aneuploidy detected at birth is trisomy 21, which occurs in approximately 1/700 live births (Fig. 2-3). Trisomy 21 occurs as a result of maternal nondisjunction during meiosis in 95% of cases of DS; the remainder of cases is due to translocations involving



**TABLE 2-2 Population Frequency of Specific Chromosomal Disorders**

Disorder	Frequency per 1000 Live Births*
Trisomy 21	1.5
Trisomy 18	0.12
Trisomy 13	0.07
47,XXY (Klinefelter syndrome)	1.5
45,X (Turner syndrome)	0.4
XXX syndrome	1.5
XXX syndrome	0.65

\*Births of appropriate sex only for sex chromosomal abnormalities. From Harper PS: Practical Genetic Counseling, 6th ed. London, Arnold Publishers, 2004, p 66.

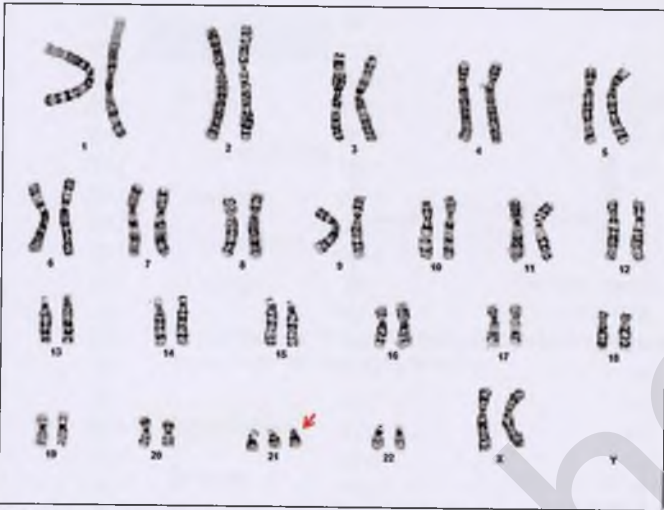


**FIG 2-3** Trisomy 21 karyotype. G-banded karyotype of a female with trisomy 21 (Down syndrome; 47,XX,+21). (Courtesy of Dr. Jingwei Yu, University of California, San Francisco, CA.)

chromosome 21. Karyotype analysis from the affected individual can differentiate between nondisjunction and translocation causes. Individuals with DS from either cause have a characteristic phenotype that includes distinctive facial features including midface hypoplasia and upslanting palpebral fissures, short stature, brachycephaly, a short neck with redundant skin on the nape, short broad hands with a single transverse palmar crease, and hypotonia. Other findings include intellectual disability, an increased risk for acute myeloid leukemia in the first 3 years of life, and thyroid dysfunction. Congenital heart defects (CHDs) are reported in 44% to 58% of affected newborns and are important contributors to morbidity and fatality.<sup>6,7</sup> Other structural birth defects associated with this diagnosis include hydronephrosis and duodenal atresia.

The recurrence risk of trisomy 21 (or other autosomal trisomies) is approximately 1% after one such child with nondisjunction-related aneuploidy is born to a couple. Although often requested, there is no indication for parental chromosomal evaluation after the birth of a child with trisomy 21 unless it is due to a translocation. A history of DS elsewhere in the family does not increase the risk of having a child with a chromosome abnormality, provided there is no familial translocation.

### Trisomy 18

Trisomy 18 occurs in about 1/8000 live births but is much more common at conception, with about 95% of such cases resulting in spontaneous abortion or stillbirth. Postnatal survival is poor, and the majority of liveborn neonates dies in early infancy. Characteristic findings include cardiac malformations, severe intellectual disability, growth restriction, a prominent occiput, dolicocephaly, small mandible, short sternum, clenched hands with overlapping digits, and rocker-bottom feet. Choroid plexus cysts are identified more frequently in this population, although most fetuses that demonstrate choroid plexus cysts are not aneuploid.

### Trisomy 13

Trisomy 13 occurs in about 1/20,000 live births. There is a high stillbirth rate among pregnancies with this diagnosis, and those who are liveborn typically die in early infancy. The phenotype includes midline defects including severe central nervous system (CNS) malformations such as holoprosencephaly, severe intellectual disability, growth restriction, cleft lip and palate, microphthalmia, omphalocele, polydactyly, clenched hands with overlapping digits, CHDs, and renal abnormalities such as polycystic kidneys.

### Turner Syndrome (45,X)

Although monosomy for an entire chromosome is almost always lethal, an important exception is monosomy X (45,X), which results in Turner syndrome. Turner syndrome is estimated to occur in 1% to 2% of all conceptions, but most end in miscarriage, resulting in a frequency of 1/2000 to 1/3000 live births. Females with Turner syndrome have a characteristic phenotype, which includes short stature, webbed neck, peripheral lymphedema at birth, CHDs, and renal abnormalities. Other features include ovarian dysgenesis with failure to develop secondary sexual characteristics and associated infertility. Prenatally, fetuses with Turner syndrome often have an increased nuchal translucency or cystic hygroma, lymphangiectasia, structural renal abnormalities, and CHDs, particularly left-sided obstructive lesions such as coarctation of the aorta. Females with Turner syndrome usually have normal intelligence, although they may have specific learning disabilities.

The chromosomal abnormalities that cause Turner syndrome vary. Only about 50% of patients have a nonmosaic 45,X karyotype. Approximately 30% to 40% of cases involve mosaicism, most commonly 45,X/46,XX or 45,X/46,XY. Patients with a Y chromosome may have ambiguous genitalia and are at risk for development of gonadoblastoma in their dysgenetic gonads. Structural abnormalities of the X chromosome are seen in 10% to 20% of cases and often involve mosaicism. The fact that these patients have more than one cell line can account for the variability in phenotype of individuals affected with Turner syndrome. Unlike the other diagnoses discussed, the nondisjunction that most often results in Turner syndrome is paternal in origin and is not associated with the age of either parent. There is no increased risk in subsequent pregnancies for another fetus with a chromosome abnormality.

### Klinefelter Syndrome (47,XXY)

Klinefelter syndrome (47,XXY) occurs in about 1/1000 male births and is a common cause of primary hypogonadism. Men with Klinefelter syndrome tend to be tall, with long arms and legs. They have small testes and are sterile owing to atrophy of the seminiferous tubules. Gynecomastia occurs in about 30%. There is an increased risk for learning disabilities, with intelligence quotient (IQ) about 10 to 15 points below that of unaffected siblings, although men with Klinefelter syndrome do not usually have significant intellectual disability. Because



the disorder is often subtle, men are often first diagnosed in infertility clinics. This condition is typically not identified by prenatal ultrasound findings because it is not associated with structural birth defects. In the prenatal setting, Klinefelter syndrome is most commonly incidentally identified by diagnostic testing done during pregnancy for another indication.

### Triploidy

Triploidy is a type of polyploidy and is defined as an entire extra set of chromosomes (69 chromosomes per cell). Triploidy is generally a lethal condition and is rarely reported in live births. Of those fetuses with triploidy who are liveborn, the longest reported survivors have lived to less than 1 year of age.<sup>8</sup> Congenital abnormalities seen in triploidy include micrognathia, prominent forehead, relative macrocephaly, low-set malformed ears, microphthalmia, hypertelorism, cleft lip and palate, omphalocele, syndactyly, and asymmetric development.

The extra chromosome set in triploid pregnancies can be of either maternal or paternal origin. Maternally derived triploidy results from fertilization of a diploid ovum by a haploid sperm and can involve either an XXX or XXY karyotype. Paternally derived triploidy can result from fertilization of a haploid ovum by either a diploid sperm or by two haploid sperm and can have either an XXX, XXY, or XYY karyotype.

The phenotype of triploid pregnancies depends on the parental source of the extra chromosome set. Triploids with an extra set of paternal chromosomes have a well-formed fetus with an abnormal placenta and may result in partial hydatidiform moles. By definition, all partial molar pregnancies are triploid but not all triploid fetuses have a molar placenta. Those with an extra set of maternal chromosomes usually have a small, growth-restricted fetus and a small, non-cystic placenta.<sup>9-11</sup>

### Abnormalities of Chromosome Structure

There are many types of abnormalities of chromosome structure, but all generally result from chromosome breakage, followed by recombination in an abnormal configuration. Overall, structural chromosome abnormalities occur in about 1/375 newborns. Reciprocal translocations involve an exchange of segments between nonhomologous chromosomes. These rearrangements are relatively common and can be balanced (that is, the appropriate amount of chromosomal material is present), typically resulting in a normal outcome, or unbalanced, in which some chromosomal material is gained or lost, therefore resulting in an abnormal outcome. There is an increased risk of unbalanced rearrangements in the offspring of people who carry balanced translocations, thereby leading to decreased fertility and an increased risk of offspring with structural malformations or intellectual disability.

A robertsonian translocation occurs when the long arms of two acrocentric chromosomes (chromosomes 13, 14, 15, 21, and 22) are fused and the corresponding two short arms are lost. Because the short arms of these chromosomes do not contain essential genetic material (they are made up of multiple copies of ribosomal RNA genes), the loss of this material does not result in an abnormal phenotype in a balanced robertsonian translocation carrier. The phenotype of an unbalanced robertsonian translocation is either miscarriage or a child with a trisomic condition such as trisomy 21 or trisomy 13 from the additional material. The most common robertsonian translocation involves chromosomes 14 and 21 and is responsible for about 5% of cases of DS. The recurrence of translocation DS depends on whether the translocation was inherited from a carrier parent. In 75% of cases, the translocation is de novo, and the recurrence risk is very low (<1%). If the translocation was inherited from a parent who carries a 14;21 balanced translocation, there is a 10% chance of

**TABLE 2-3 Common Microdeletion Syndromes**

Syndrome	Location	Frequency
Prader-Willi	15q11-13	1/10,000-1/30,000
Angelman	15q11-13	1/12,000-1/20,000
Velocardiofacial, DiGeorge	22q11.2	1/4000
Smith-Magenis	17p11.2	1/15,000-1/25,000
Williams	7q11.23	1/7500
Alagille	20p12	1/30,000-1/50,000
Rubinstein-Taybi	16p13.3	1/100,000
WAGR*	11p13	1/40,000
Miller-Dieker	17p13.3	1/85,000
Wolf-Hirschhorn	4p16.3	1/50,000
Cri-du-chat	5p15.2	1/20,000-1/50,000
Retinoblastoma	13q14.2	1/15,000-1/20,000

\*Wilms tumor, aniridia, genitourinary anomalies, retardation.

recurrence if the mother is the carrier and about a 2% chance if the father is the carrier.

When a balanced translocation or other rearrangement is identified in a fetus at the time of prenatal diagnosis, testing of the parents is recommended. If the translocation was inherited from a phenotypically normal parent, the fetus would be predicted to be normal. If a reciprocal translocation occurs as a de novo event, there is approximately a doubling of the background risk of phenotypic abnormality. This is thought to be due to subtle, undetected chromosomal imbalance or disruption of genes at the breakpoint(s).

### Other Types of Chromosomal Rearrangements

In addition to translocations, there are several other types of unbalanced chromosomal rearrangements. These types include *deletions*, which occur with the loss of a chromosome segment, resulting in partial monosomy. Such deletions can involve one or many genes and are responsible for a number of clinically distinct microdeletion syndromes (Table 2-3). One of the most common is the 22q deletion syndrome, which occurs in about 1/4000 live births. The 22q deletion is a relatively common cause of CHDs, particularly conotruncal abnormalities, such as truncus arteriosus and tetralogy of Fallot. Other features include cleft palate, velopharyngeal incompetence, renal malformations, characteristic facial features, immune deficiency, hypocalcemia, and learning difficulties. The majority of individuals (93%) has a de novo deletion identified by microarray or FISH. When an individual is diagnosed with this condition, parental testing is recommended because of the variable expressivity within a family and the small chance that one of the parents is a more mildly affected carrier.

*Duplications* of a chromosome segment also occur, resulting in partial trisomy. The size and region of the duplication confer risk for abnormal phenotype ranging from normal to significant structural defects and intellectual disability.

### SINGLE GENE DISORDERS

Many important genetic diseases occur as the result of a mutation at a single gene. Gregor Mendel first described the principles of segregation and independent assortment of genes in his well-known experiments with garden peas. This work led to the classic descriptions of autosomal-dominant (AD) and autosomal-recessive (AR) inheritance. X-linked inheritance occurs with conditions encoded on the X chromosome, and it may be either recessive or dominant. Figure 2-4 shows



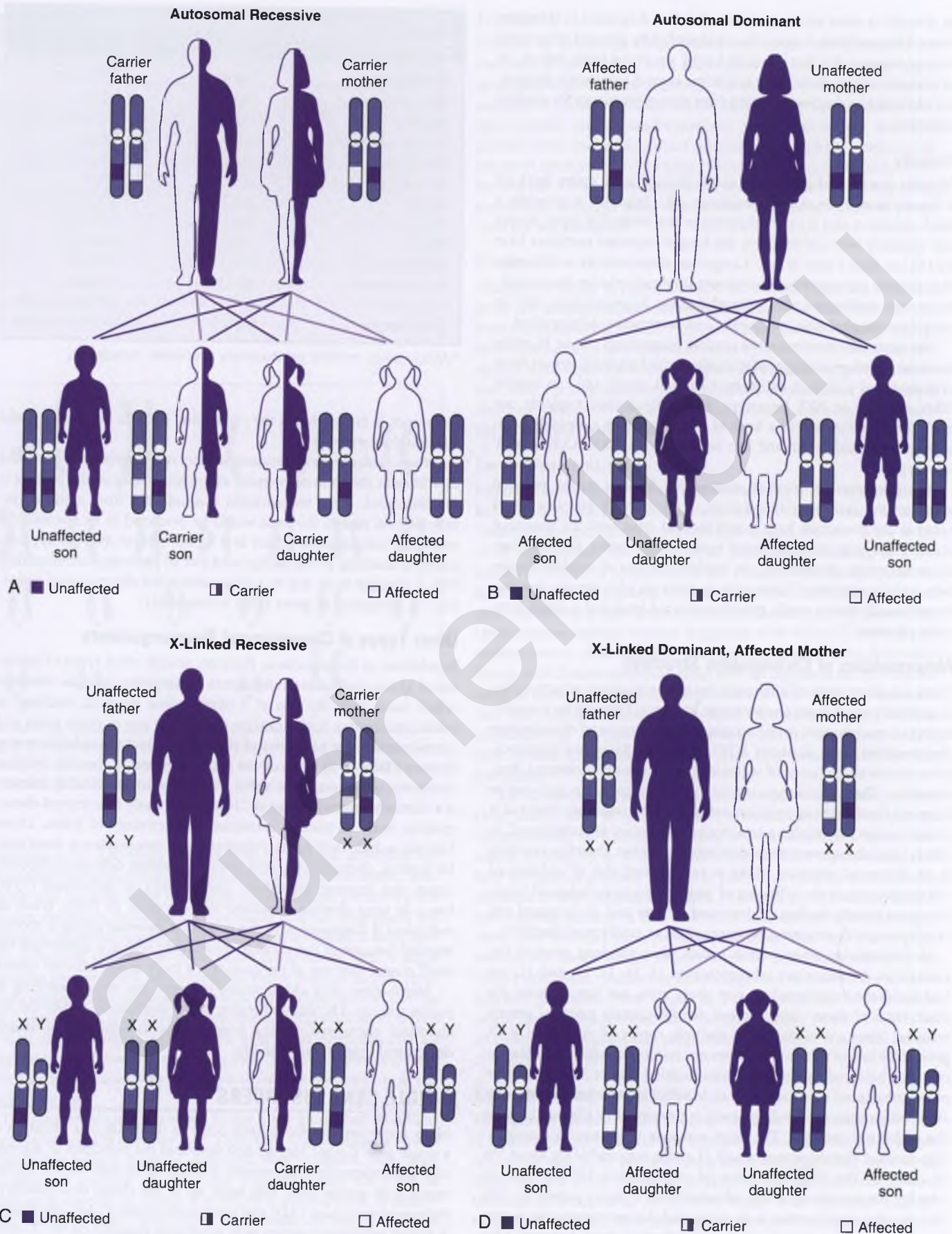
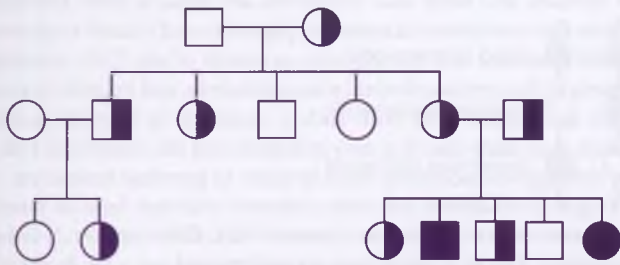


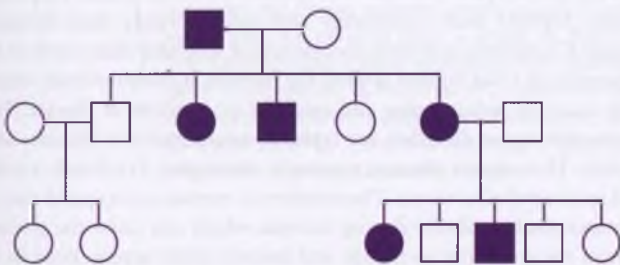
**FIG 2-4** Modes of inheritance: **A**, autosomal-recessive; **B**, autosomal-dominant; **C**, X-linked recessive; and **D**, X-linked dominant inheritance patterns. See text for explanation.



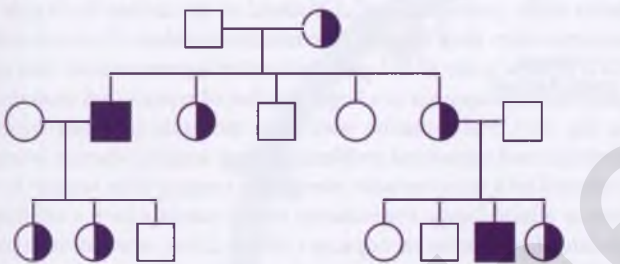
## A Autosomal-Recessive Inheritance



## B Autosomal-Dominant Inheritance



## C X-Linked Recessive Inheritance



■ Affected individuals      ● Unaffected carrier      ○ Unaffected individuals

**FIG 2-5** Pedigrees diagramming modes of inheritance. **A**, Autosomal-recessive inheritance. **B**, Autosomal-dominant inheritance. **C**, X-linked recessive inheritance. See text for further detail.

modes of inheritance; Figure 2-5 shows pedigrees demonstrating modes of inheritance.

The completion of the human genome project in 2003 was an epic chapter in laying the foundation for the study of human genes and the diagnosis and treatment of genetic disease. Although the human genome has now been sequenced, we still do not know how most genes work in either health or disease. We have gained an increased appreciation, however, for the complexity of human genetics. Relevant to clinical genetics, we have greatly increased our understanding of genetic heterogeneity, and the less than clear-cut association of one gene with one disorder. We now understand that mutations at more than one gene locus can lead to the same phenotype and that multiple different phenotypes also result from the interaction of genotype with the environment (including other genes), and there are numerous phenomena that advances in genetic technology have uncovered that make genetics far more fascinating, if far more complex.

### Autosomal-Dominant Inheritance

In AD inheritance, affected individuals are heterozygous for an abnormal allele that they transmit to 50% of their offspring, independent of

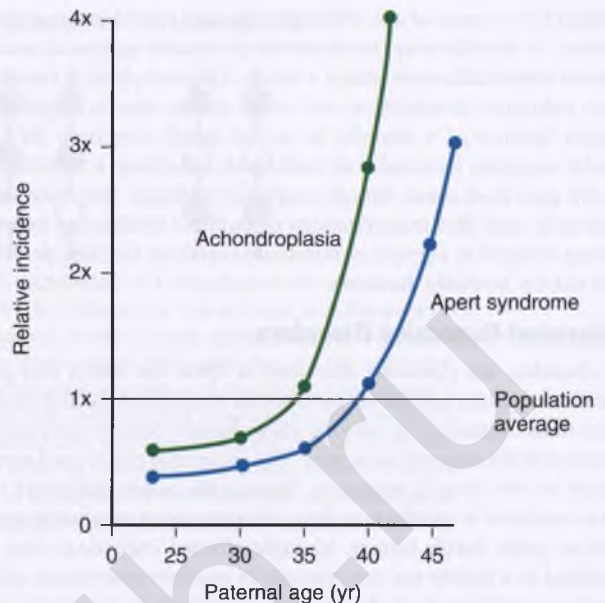


**FIG 2-6** Paternal age and risk of autosomal-dominant disorders. (Modified from Carlson BM: Human Embryology and Developmental Biology, 3rd ed. Philadelphia, Mosby/Elsevier, 2004.)

gender. Overall, approximately 1/200 individuals is affected with an AD condition, although individual conditions are generally rare.

In theory, AD inheritance is straightforward, but in actuality, there are numerous factors affecting gene expression that can make evaluation of such cases extremely complex. Counseling of families regarding AD disorders requires consideration of mechanisms such as the rate of new mutation, mosaicism, conditions with late or variable age of onset, incomplete penetrance, and variation in expressivity. AD disorders may be inherited from an affected parent or may result from a new mutation, with the risk varying with each specific condition. Paternal age has a demonstrable effect on the rate of such new mutations (Fig. 2-6) and is associated with an increased risk for AD disorders, including achondroplasia and neurofibromatosis (NF). No current screening or diagnostic testing is recommended for men who are aged 45 years or more, but genetic counseling, routine ultrasound, and discussion of this phenomena are indicated.

If a disorder occurs as a result of a new mutation, the risk of recurrence in a sibling is generally low. However, an individual may be mosaic for an AD mutation, meaning that there are cells of more than one genetic constitution present. If germline mosaicism is present, an apparently unaffected individual will have an increased risk of having affected offspring. Germline mosaicism is thought to occur in approximately 16% of cases of the perinatal lethal disorder osteogenesis imperfecta type II and can also occur in X-linked disorders such as Duchenne muscular dystrophy and hemophilia A. This means that the rate of recurrence is increased and is about 1.3% to 4% with osteogenesis imperfecta.<sup>12</sup>

### Penetrance and Expression

Further complicating recurrence risk counseling and clinical evaluation of AD disorders are the phenomena of penetrance and variable expression. A given individual may have a disease genotype but may not express the phenotype if a disorder is not 100% penetrant, as is the case with retinoblastoma, which affects only about 90% of individuals who inherit the causative mutation. Age is also an important consideration because a disorder such as polycystic kidney disease is about 80% to 90% penetrant by 20 years of age and nearly 100%



penetrant by 30 years of age, although only with careful imaging of the kidneys.<sup>13</sup> A disorder may also demonstrate variable expression among affected individuals, even within a family. Targeted physical examinations, radiologic investigation, and other studies may be required to identify features of a disorder in at-risk family members; NF is a notable example. Essentially all individuals inheriting a mutation in the NF gene have some clinical symptoms, although they may range from only mild skin manifestations to multiple debilitating neurofibromas. Referral to a geneticist is indicated for those families identified with risk for heritable disorders.

### Autosomal-Recessive Disorders

AR disorders are classically described as those for which two gene mutations must be present for the disorder to manifest. Such disorders occur most commonly in persons whose healthy parents each carry a mutation in the same recessive gene. The recurrence risk to such carrier parents is 25% in each pregnancy. Because the carrier frequency of a given condition is usually low, these disorders most commonly occur with no prior family history. Multiple affected individuals may be identified in a sibship but not typically in multiple generations unless there is consanguinity or the disorder is particularly common. Consanguinity increases the risk of having offspring with AR disorders because of the shared genetic material within a family. The increased risk to parents who are first cousins to have a child with a major genetic or congenital abnormality is about 6%, or twice the background rate.

Again, with advances in genetics, the exceptions to the traditional rules of AR inheritance are increasingly evident. It is now appreciated that carriers of many of these conditions may have subtle symptoms. Examples of this are cystic fibrosis (CF), in which male carriers have increased susceptibility to chronic pancreatitis and congenital bilateral absence of the vas deferens.<sup>14,15</sup> Similarly, sickle cell carriers may suffer splenic infarct at high altitudes and are at increased risk for urinary tract infection in pregnancy.

AR disorders demonstrate much less variation in expression, and lack of penetrance is rarely encountered, so counseling is more straightforward with these conditions. Genetic heterogeneity due to more than one causative locus, or multiple alleles at a single locus, is the major cause of variation in severity of a single disorder.

### X-Linked Inheritance

X-linked disorders can be dominant or recessive. Most X-linked conditions are recessive and are traditionally thought of as affecting only men, who have unaffected carrier mothers. Because women carry two X chromosomes whereas men carry only one, one X chromosome is randomly inactivated early in embryonic development, thereby allowing women to produce X-linked gene products in the same quantities as men (Lyon hypothesis). As X inactivation is random, some female heterozygote carriers of X-linked disorders will inactivate primarily their X chromosomes carrying the normal allele and therefore be symptomatic due to skewed X inactivation. This occurs in hemophilia A, in which some carriers can have a mild bleeding disorder because of reduced levels of factor VIII. Such affected women have symptoms that are usually, but not always, milder than their male counterparts. With isolated X-linked recessive disorders, it is helpful when possible to determine if an isolated case represents a new mutation or if the mother is a carrier. When molecular diagnosis or other methods of carrier detection are available, the situation can be clarified. However, such tests are not available for all conditions, and risks must often be empirically determined based on pedigree analysis and consideration of other factors such as the number of unaffected men in the pedigree. Increasingly, genomic sequencing is available to identify genetic mutations in individuals in whom a genetic disorder is suspected.

X-linked dominant disorders are less common than X-linked recessive diseases, and some such conditions are lethal in men. Examples include Rett syndrome, incontinenti pigmenti, and Aicardi syndrome. Aicardi syndrome is a rare disorder primarily of the CNS, including agenesis of the corpus callosum, microphthalmia, and infantile spasms. When an affected child with such a condition is born to healthy parents, it is likely due to a new mutation and the recurrence risk is low, although consideration must be given to germline mosaicism.

Fragile X syndrome, the most common inherited form of mental retardation, is an important disorder that demonstrates X-linked inheritance. Fragile X syndrome is characterized not only by mental retardation but also by behavioral difficulties including autism, and specific dysmorphic features. The condition affects males (approximately 1/4000) more commonly and more severely than females. Fragile X syndrome is a trinucleotide repeat disorder, characterized by expansion of DNA triplets beyond the normal, stable threshold, which may occur in certain genes and result in a condition or disease. Trinucleotide repeat disorders are typically neuromuscular diseases and include Huntington disease, myotonic dystrophy, Friedreich ataxia, and spinocerebellar ataxia. The number of repeats can expand due to chromosomal instability during meiosis, which can cause the phenotype of the condition to change and become more severe. Because of this, trinucleotide repeat disorders generally show genetic anticipation, in which the severity increases with each successive generation that inherits them. Individuals are considered to be carriers for fragile X syndrome when they have an intermediate number of trinucleotide (CGG) repeats in the *FMRI* gene (also called a premutation) that can expand during oogenesis to a larger number of repeats (full mutation) (see Fig. 2-5). Full-mutation men have moderate to severe mental retardation and behavioral problems such as autism, whereas women are affected by a more variable phenotype, ranging from normal to as severe as affected men. Premutation female carriers have a relatively high rate of premature menopause (15% to 25%), whereas male premutation carriers can have a tremor ataxia condition with an onset later in life.<sup>16,17</sup> For any patient with a family history of mental retardation, early menopause, or autism without an attributable diagnosis, or adults with parkinsonian features, carrier testing for fragile X syndrome is indicated.<sup>18</sup>

### Other Novel Genetic Mechanisms

Some genetic mutations have been noted to have a very different effect depending on the parent of origin, a phenomenon known as *genetic imprinting*. Imprinting is an epigenetic phenomenon by which certain genes are expressed or not expressed depending on the parent of origin (Fig. 2-7). As depicted in Figure 2-8, the imprinting cycle takes place in primordial germ cells early in development. A number of genetic disorders, including Prader-Willi syndrome (PWS) and Beckwith-Wiedemann syndrome (BWS), occur because of abnormalities of imprinted genes. Prader-Willi syndrome is characterized by neonatal and infantile hypotonia, hypogonadism, typical facial features, and feeding problems; these are followed in early childhood by excessive caloric intake resulting in morbid obesity and intellectual disability. The disorder occurs when there is no functional paternal copy of the *SNRPN* gene on chromosome 15. This can happen when both copies of chromosome 15 are maternally inherited, and no paternal copy is present, or when there is a deletion on the paternally inherited copy of chromosome 15. Several recent reports have indicated an association between imprinting disorders and in vitro fertilization (IVF) with intracytoplasmic sperm injection.<sup>19</sup>

Mitochondria, which produce adenosine triphosphate (ATP), have their own unique DNA in addition to nuclear DNA. Mitochondria are all maternally inherited and have a high mutation rate. Many



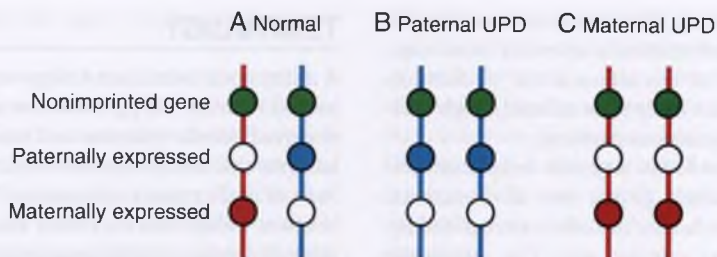


**FIG 2-7** Genomic imprinting and uniparental disomy (UPD). Schematic of a hypothetical chromosome pair representing genomic imprinting. The maternal chromosome is indicated by the red line, and the paternal copy by the blue line. Genes are represented by circles: colored circles indicate genes that are expressed, and the white circles represent genes that are inactive. The green circles are genes that are not imprinted, whereas red circles indicate genes in which only the maternal copy is active and the blue circles genes in which only the paternal copy is active. **A**, Normal state, with one chromosome inherited from each parent. The nonimprinted gene is expressed from both parents, whereas only one copy of the red or blue (imprinted) gene is expressed. **B**, Paternal UPD. With two copies of the paternal chromosome present, there is a double dose of the paternally expressed (blue) gene, and absence of expression of the maternally expressed gene. **C**, Maternal UPD. There is an absence of paternally expressed gene product (blue) and a double dose of the maternally expressed products (red).

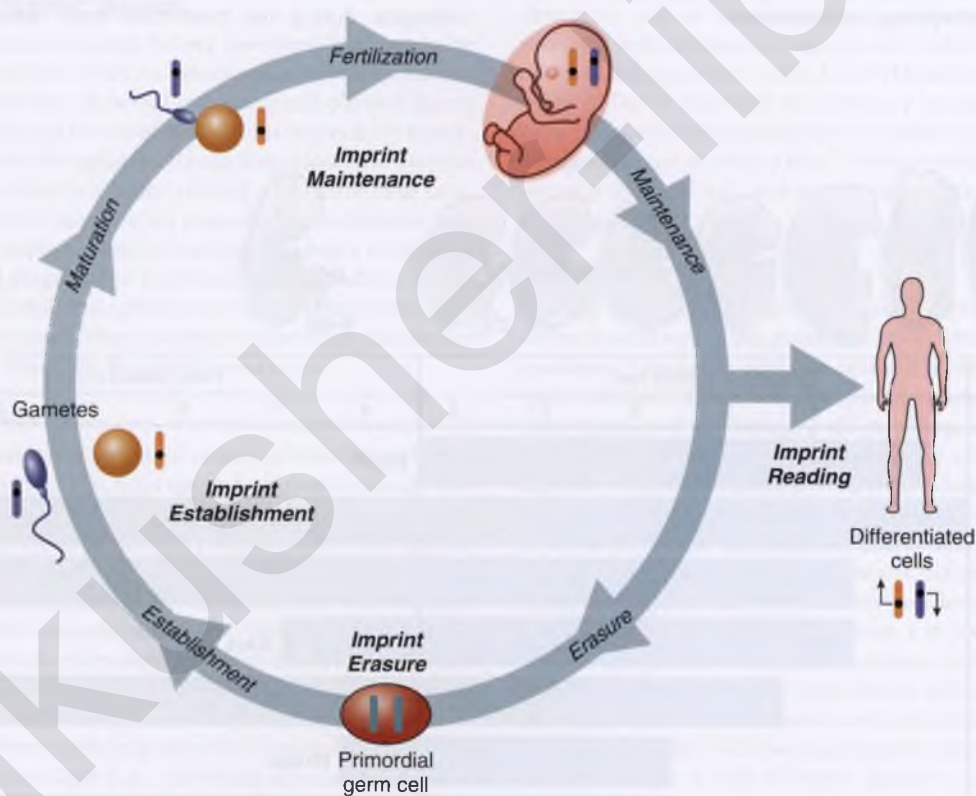


**FIG 2-8** Imprinting cycle. Imprinting occurs in primordial germ cells, early in development.

mitochondrial diseases have now been identified, and they are most commonly maternally inherited such that affected women pass the condition to all of their offspring and affected men do not pass the condition to any of their offspring. Mitochondrial disorders demonstrate variable expressivity within a family. Typical symptoms include neuromuscular abnormalities (such as loss of motor control, muscle weakness, and pain), gastrointestinal disorders and swallowing difficulties, poor growth, cardiac disease, liver disease, diabetes, respiratory complications, seizures, visual/hearing problems, lactic acidosis, developmental delays, and susceptibility to infection.

### Multifactorial Inheritance

Many common congenital malformations, including NTDs, cleft lip and palate, and CHDs, have an increased risk of recurrence in families above the baseline population risk. A small percentage of such defects have a specific cause, such as single gene disorders, chromosomal abnormalities, or teratogens. Most, however, are isolated defects that result from complex interactions among a number of factors, including genotype at one or more loci, and a variety of environmental exposures that trigger, accelerate, or exacerbate the disorder. Therefore, occurrence does not match simple mendelian inheritance but is complex and



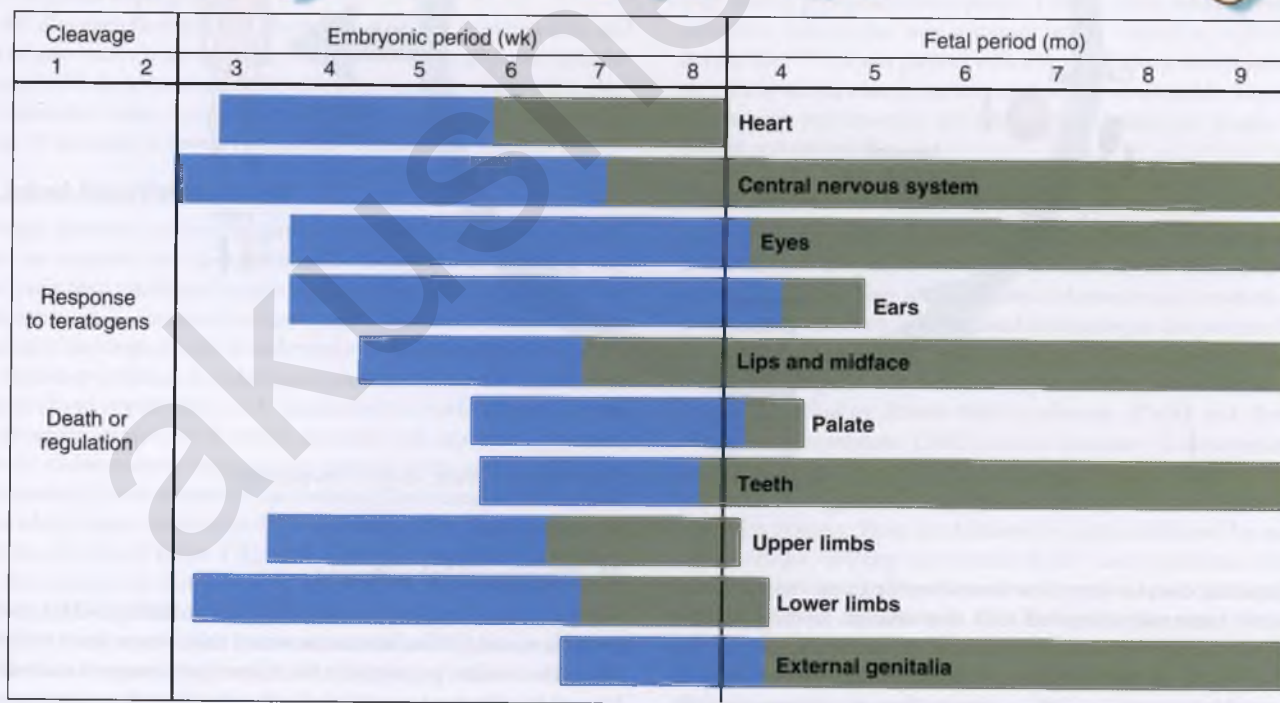
multifactorial. Recurrence risk of such disorders is increased by the presence of more than one affected relative, a severe or early-onset form of disease, an affected person of less common sex (in disorders in which persons of one sex are more likely to be affected), high heritability of the disorder, and consanguineous parentage.

NTDs have long been thought to follow a typical complex inheritance pattern determined by multiple genetic and environmental factors. Known environmental risk factors include maternal obesity, diabetes, and medications such as valproic acid. The association between lower socioeconomic status and NTD led investigators to consider nutritional deficiencies as risk factors. Therefore, it was a remarkable discovery that folate supplementation reduced the risk for NTD by approximately 80%, although most women with a fetal NTD diagnosed during pregnancy have normal range folate levels.<sup>20</sup> Public health initiatives to educate reproductive age women about the importance of folate and fortification of the food supply (cereals and breads) with folic acid have been instituted in the United States for the purpose of decreasing the incidence of NTDs. The mechanism for the protective action of folic acid in prevention of NTDs is not well understood.<sup>21</sup> Recent data suggest folate deficiency is not problematic unless present in combination with a mutated gene or genes; together these risk factors result in the embryologic malformation.<sup>22</sup>

## TERATOLOGY

A milestone in human teratology occurred in 1941, when an Australian named Norman Gregg noted the association between first trimester maternal rubella infection and serious birth defects.<sup>23</sup> Twenty years later, the thalidomide disaster sensitized the medical community to the risks of medications in pregnancy. Thalidomide, a very effective sedative, was widely used for several years in West Germany, Australia, and other countries until the association of prenatal exposure with phocomelia and amelia was recognized. Following the recognition of the potent teratogenicity of this drug, intense investigations into the safety of various medications in pregnancy heralded the modern age of teratology.

Embryos are more susceptible to teratogenic agents at specific critical periods of development (Fig. 2-9). The preorganogenetic phase, from conception until somite formation, is known as the all-or-none period, when insults to the embryo are likely to result in either death of the conceptus and miscarriage or in intact survival without sequelae.<sup>24</sup> At this stage, the embryo is undifferentiated, and repair and recovery are possible through multiplication of the still totipotential cells to replace those that have been lost. Exposure of embryos to teratogens during the presomitic stage usually does not cause



■ Highly sensitive period  
(major structural anomalies)

■ Less sensitive period  
(functional and/or minor  
structural anomalies)

**FIG 2-9** Periods and degrees of susceptibility of embryonic organs to teratogens. (From Carlson BM: Human Embryology and Developmental Biology, 3rd ed. Philadelphia, Mosby/Elsevier, 2004, used with permission.)



congenital malformations<sup>25</sup> unless the agent persists in the body beyond this period.

The embryonic period, between weeks 3 and 8 after conception, is when the basic steps of organogenesis occur. This is the period of maximum sensitivity to teratogenicity because tissues are differentiating rapidly and damage to them becomes irreparable. Exposure to teratogenic agents during this period has the greatest likelihood of causing a structural anomaly. Because teratogens are capable of affecting many organ systems, the pattern of anomalies produced depends upon which systems are differentiating at the time of teratogenic exposure. In general, organs that form first tend to be sensitive earlier, and very complex organs tend to have prolonged periods of high susceptibility to disruption.

The fetal phase, from the end of the embryonic stage to term, is the period when growth and functional maturation of organs and formed systems occur. Exposure to teratogens in this period will mainly affect fetal growth or the size or function of a specific organ. The brain in particular may be functionally affected almost throughout the entire pregnancy. Teratogens rarely cause gross structural anomalies during this time.<sup>26</sup>

### Recognized Teratogenic Agents

A large number of environmental factors have been reported to be associated with birth defects. They include chemical teratogens such as medications and hormones, maternal infections, and physical agents such as radiation. Although the list of medications suspected of teratogenicity is long, relatively few agents have been demonstrated to unquestionably cause birth defects in humans (Table 2-4). In some cases these medications must still be used during pregnancy, as the benefit outweighs the risk they impose. Patients must be made aware of the risks and benefits of use in pregnancy to treat the maternal condition versus the potential for harmful fetal effects and maternal morbidity and mortality risks if untreated. Often, maternal uncontrolled diseases are more harmful to the fetus than the administered drug.

### Maternal Infections

The incidence of intrauterine infections ranges between 3% and 15%. Rubella was one of the first infectious agents recognized to cause birth defects in humans and previously was one of the most common. Today, because of effective immunization programs against rubella, the number of affected fetuses has significantly decreased. Currently, the most common intrauterine infection with deleterious fetal effects is cytomegalovirus (CMV). Approximately 1 in 750 children born in the United States is born with or develops permanent problems as a result of this intrauterine infection.<sup>27</sup> Features include hearing and vision loss, seizures, intellectual disability, and rarely death.

Intrauterine infections with long-term fetal sequelae may be viral, parasitic, or bacterial (see Table 2-4). The timing of maternal infection can influence both the severity and likelihood of fetal infection. For example, rubella causes a high percentage of malformations in the first trimester, whereas toxoplasmosis causes fetal infection more commonly in the third trimester but with more severe consequences if contracted earlier. Infection of the fetus may occur owing to hematogenous spread through the placental barrier or via ascending infection through the fetal membranes with direct contamination of the amniotic fluid.

Fetal CMV infection may be suspected by ultrasound features identified during routine surveillance or in the course of evaluation for a known maternal exposure. Ultrasound findings may include fetal ascites or nonimmune hydrops, ventricular dilation and periventricular calcifications, echogenic bowel (EB), calcifications within the fetal liver, fetal growth restriction (FGR), and placental thickening.<sup>28</sup> Cases

of suspected intrauterine CMV infections can be evaluated by measuring serum levels of maternal specific antibodies, but the significance of antibody levels is often uncertain. Moreover, a rise in levels of maternal antibodies is diagnostic for maternal, but not necessarily for fetal, infection. To diagnose fetal infection, the infective agent should be identified in the amniotic fluid by culture or polymerase chain reaction (PCR) or by specific immunoglobulin M (IgM) in fetal blood. At birth, viral culture of the neonatal urine or saliva is the gold standard.

### Medications

Although many medications have been suspected of being human teratogens, there are a relatively small number for which there is convincing evidence linking the substance directly to congenital malformations in humans. Testing drugs to determine teratogenicity is difficult because agents may cause a high incidence of severe defects in animals but may not cause malformations in other species or in humans (e.g., cortisone causes cleft palate in mice but not humans). Conversely, thalidomide is a tragic example of an agent that is highly teratogenic in humans but not in animals. Antiepileptic drugs (AEDs) are classic examples of medications associated with structural birth defects as well as neurocognitive impairment. Risk for NTDs is increased with exposure to valproic acid (1-5% of exposed offspring) and carbamazepine (0.5-1.0%), but NTDs have not been reported with other AEDs.<sup>29,30</sup> Valproate monotherapy in utero exposure has also been associated with significantly lower IQ scores at the age of 3 when compared to use of other AEDs.<sup>30</sup> Therapy with more than one agent seems to compound the risk for not only structural changes but intellectual disability as well.

### Radiation

Ionizing radiation is a potent teratogen, with the response dependent on the dose as well as the gestational age at which the embryo/fetus is irradiated. Experience with the Japanese atomic bomb survivors as well as women treated with therapeutic radiation in pregnancy provides evidence of the damaging effects of large doses of ionizing radiation in humans. In contrast, there is no evidence that radiation exposure at typical diagnostic levels (e.g., a chest radiograph with two views and fetal exposure of 0.02-0.07 mrad) poses a significant threat to the embryo, and noncancerous health effects are not evident for fetal doses of less than 5 rads. Estimates indicate a slight increase in leukemia (approximately 1.5-2 times over baseline risk) with exposures of 1 to 2 rads (risk increases from 1 in 3000 background to 1 in 2000 with exposure to 1-2 rads).<sup>31</sup> Ionizing radiation at high doses (>5 rads) can cause a variety of anomalies in various organ systems. The most prominent radiation-associated abnormalities are defects in the CNS, ranging from NTD to neurocognitive impairment.<sup>22</sup> For fetuses exposed between 8 and 15 weeks' gestation, atomic bomb survivor data indicate that the decline in IQ score is approximately 25 to 31 points per 100 rads, at doses above 10 rads. At 16 to 25 weeks' gestation, the average IQ loss is approximately 13 to 21 points per 100 rads, at doses above 70 rads. After 26 weeks, at doses above 100 rads, the risks for stillbirth and neonatal death increase.<sup>32,33</sup> When evaluating the need for imaging or therapeutic radiation in pregnancy, the indication and both maternal and fetal health consequences should be discussed with the woman.

### Maternal Illnesses

A number of maternal illnesses and metabolic disorders have been implicated in the genesis of congenital malformations. Maternal diabetes is strongly associated with congenital malformations, with the



TABLE 2-4 Proven Teratogenic Agents in Humans

Agent	Effects
ACE inhibitors	CNS defects, congenital heart defects (first trimester exposure) Renal failure, skull hypoplasia (second trimester exposure)
Alcohol	Fetal alcohol syndrome: intrauterine growth retardation, microcephaly, developmental delay, characteristic facies, CHD, cleft palate
Carbamazepine	Neural tube defects, similar features to fetal hydantoin syndrome
Chemotherapeutic agents	Miscarriage, various malformations
Cocaine	Abruptio placentae, prematurity, fetal loss, decreased birth weight, microcephaly, limb defects, urinary tract anomalies, and poor neurodevelopmental performance
Coumarin anticoagulants	Fetal warfarin syndrome: hypoplasia and calcific stippling of the epiphyses, intrauterine growth retardation, developmental delay, CNS damage, eye defects, hearing loss
Diethylstilbestrol	Clear cell adenocarcinoma, benign adenosis of the vagina, female genital structural changes (cervix/uterus)
Folic acid antagonists	Fetal aminopterin syndrome: CNS defects (hydrocephalus, meningomyelocele), facial anomalies (cleft palate, high-arched palate, micrognathia, ocular hypertelorism, external ear anomalies), abnormal cranial ossification, abnormalities of first branchial arch derivatives, intrauterine growth retardation, mental retardation
Hydantoin	Fetal hydantoin syndrome: craniofacial dysmorphism (wide anterior fontanel, ocular hypertelorism, metopic ridge, broad depressed nasal bridge, short anteverted nose, bowed upper lip, cleft lip, cleft palate), hypoplasia of the distal phalanges, nail hypoplasia, growth retardation, mental deficiency, cardiac defects
Isotretinoin	Retinoic acid embryopathy: craniofacial anomalies (microtia or anotia, accessory parietal sutures, narrow sloping forehead, micrognathia, flat nasal bridge, cleft lip and palate, and ocular hypertelorism), cardiac defects (primarily conotruncal malformations), abnormalities in thymic development, and alterations in CNS development
Lithium	Cardiac defects, especially Ebstein anomaly
Misoprostol	Limb defects, Moebius sequence
Organic mercury	Mental retardation, cerebral atrophy, spasticity, blindness
Sodium iodide (I-131)	Ablation of fetal thyroid gland
Thalidomide	Limb defects, including phocomelia, polydactyly, syndactyly, and oligodactyly; defects of the external ears; facial capillary hemangiomas; palsies of cranial nerve VI or VII; cardiovascular defects; agenesis of kidneys, spleen, gallbladder, and appendix; atresia or stenosis of esophagus, duodenum, and anus
Trimethadione	Fetal trimethadione syndrome: characteristic craniofacial anomalies, growth retardation, delayed psychomotor development, clefting, and congenital heart defects
Valproate	Neural tube defects, fetal valproate syndrome: narrow bifrontal diameter, high forehead, epicanthal folds, infraorbital creases, telecanthus, low nasal bridge, short nose with anteverted nares, midfacial hypoplasia, long philtrum, thin vermilion border, small mouth, cardiovascular defects, long fingers and toes, hyperconvex fingernails, and cleft lip

#### INTRAUTERINE INFECTIONS

Cytomegalovirus	Cytomegalic inclusion disease: intrauterine growth retardation, microcephaly, chorioretinitis, seizures, blindness, optic atrophy Neonatal hepatosplenomegaly, jaundice, and thrombocytopenia
Rubella virus	Spontaneous abortion, congenital rubella syndrome: heart disease, deafness, cataracts, intrauterine growth retardation, encephalitis, abnormal long bones Neonatal hepatosplenomegaly, obstructive jaundice, thrombocytopenic purpura, mental retardation, neurologic deficits, and behavioral abnormalities
<i>Treponema pallidum</i> (causing syphilis)	Congenital malformations, prematurity, stillbirth, hepatosplenomegaly, osteochondritis or periostitis, jaundice, petechiae or purpuric skin lesions, lymphadenopathy, hydrops, edema, ascites, rhinitis, pneumonia, myocarditis, nephrosis, and bulbar pseudoparalysis
<i>Toxoplasma</i> (causing toxoplasmosis)	Encephalitis, hydrocephalus, intracranial calcifications, chorioretinitis, erythroblastosis, anemia, jaundice, hepatosplenomegaly, glomerulitis, myocarditis, myositis, CNS damage, seizures, mental retardation, cerebral palsy, deafness, and blindness
Varicella-zoster virus	Skin lesions, fetal growth retardation, limb hypoplasia, brain and eye defects, cerebral and cerebellar atrophy, seizures, developmental delay, and nerve palsies

CHD, congestive heart disease; CNS, central nervous system.

This table represents selected medications and their possible associations with fetal structural abnormalities. Many of the listed associations are based on isolated case reports that have appeared in the medical literature for which the association is unproved or on animal studies in which the dosage of medication far exceeded the normal clinical amount normally used. It is likely that in many cases the reported association was coincidental to, rather than resultant from, the medication. This table is not intended for patient counseling regarding the likelihood of fetal malformations or abnormalities. This table should be used by the sonologist/sonographer as a guide to evaluate specific organ systems in addition to a thorough sonographic examination. In all cases of suspected teratogenic effects a reproductive geneticist or teratologist and the drug manufacturer should be consulted.

From Diav-Citrin O, Ornoy A: Adverse environment and prevention of early pregnancy disorders. *Early Pregnancy* 4:5, 2000, used with permission. Modified from Brigs GG, Freeman RK, Yaffe SJ: *Drugs in Pregnancy and Lactation*, 5th ed. Philadelphia, Lippincott Williams & Wilkins, 1998.



risk to the embryo directly related to the degree of maternal glucose control.<sup>34,35</sup> The most common abnormalities include CHDs and NTDs, whereas caudal regression is rare but of greatly increased frequency in infants of diabetic mothers. The phenotype of the infants of diabetic mothers also includes macrosomia, polyhydramnios, and stillbirth, with hypoglycemia and erythroblastosis (increased fetal nucleated red blood cells) common neonatal complications. Maternal prepregnancy obesity is independently associated with fetal malformations including cleft palate, CHDs, NTDs, and congenital diaphragmatic hernias.<sup>36</sup> Untreated maternal phenylketonuria is also a potent teratogen and results in microcephaly, mental retardation, CHDs, and low birth weight. Risks to the fetus are related to the level of maternal phenylalanine and almost entirely eliminated with maternal dietary management and avoidance of phenylalanine in the diet of affected women during pregnancy.<sup>37</sup>

### Mechanical Factors

Mechanical disruption can result in a number of recognizable and characteristic sequence disorders. Mechanical forces may include multiple gestations, uterine myomas that distort the uterine cavity, or amniotic bands. Often, the underlying cause is less important than the common disruption pathway. Potter sequence, for example, results from early, longstanding oligohydramnios of any cause and consists of pulmonary hypoplasia, clubfeet, congenital hip dislocation, low-set ears, micrognathia, and flattened faces. This same phenotype can result from different causes of absent amniotic fluid, including bilateral renal agenesis and early rupture of the amniotic membrane.

## GENETIC COUNSELING

Clinical genetics is the discipline that is concerned with the diagnosis and management of the medical, social, and psychological aspects of hereditary disease. Often, people seeking genetic counseling are parents of a child with a potential or known genetic condition. Others who seek genetic counseling include adults with an abnormality or a family history of a condition such as cancer or neurodegenerative diseases. Genetic counseling is an integral part of genetic testing and screening programs, including prenatal testing.

The process of genetic evaluation involves several components: validation of the diagnosis, obtaining the family history, estimation of the risk of recurrence, helping the family to reach decisions and take appropriate action (i.e., genetic testing), and follow-up. An important part of genetic counseling involves understanding the family history. Health care providers in any field of medicine should include a three-generation pedigree as part of the patient history. Couples referred for prenatal testing for one specific indication will frequently have other risk factors identified when the family history is reviewed. Genetic counseling is based on the concept of nondirective counseling. Patients are not told what decisions to make with regard to testing and management options but, instead, are provided information and support.

A family may be referred to a medical genetics physician for evaluation and discussion of the diagnosis in question. The purpose could be to evaluate features in a parent or sibling suggestive of an underlying disorder or features of a fetus identified through ultrasound or testing that indicate a condition. The precise diagnosis must be certain in order to provide accurate prenatal diagnostic testing. The inheritance pattern must be known to provide correct risk assessment, as some disorders may have different patterns of inheritance in different families.

Making a precise diagnosis may have enormous implications for counseling a family. For example, if a prior male fetus was diagnosed

with hydrocephalus and the pregnancy terminated, a recurrence risk of 5% in future pregnancies would generally be quoted. Ultrasound would be offered for prenatal diagnosis, although in some cases of recurrence, ventriculomegaly may not manifest until late in pregnancy. On the other hand, more thorough evaluation of the prior fetus may have resulted in a diagnosis of X-linked aqueductal stenosis with identification of a mutation in the *LICAM* (cell-adhesion molecule) gene. In such cases, testing of the mother is indicated to determine if she is a carrier. The chance that a woman who has one affected son (and no family history) is a carrier of the mutated *LICAM* gene (or any X-linked male lethal condition) is approximately 2:3, or 67%, which is why genetic counseling and testing are important to consider. If she is a carrier, the recurrence risk is 50% for male offspring and very small for female offspring (although 50% of her daughters would also be carriers). Carrier females may manifest minor features such as adducted thumbs and intellectual disability. Rarely do females manifest the complete LI syndrome phenotype. CVS at 10 weeks would be possible for prenatal diagnosis if a molecular mutation has been identified. The spectrum of the disorder includes boys with mental retardation but without hydrocephalus, so ultrasound would not be adequate for ruling out a recurrence of this condition.

Patients who undergo genetic testing are also educated on the options of screening and diagnostic testing in pregnancy. The concept of screening as risk assessment for specific conditions in pregnancy must be clearly distinguished from the definitive nature of diagnostic procedures. It is currently recommended that both screening and diagnostic testing options should be offered to all women in pregnancy regardless of maternal age or perceived risk. Important counseling points to convey include the optional nature of all prenatal testing and the fact that a low-risk screening test result does not guarantee a healthy child and a high-risk screening test result does not mean the fetus has the disorder. Educational and counseling components must be provided both before and after all prenatal genetic tests. Issues of privacy and confidentiality of test results must be addressed.

## GENETIC SCREENING IN PREGNANCY

Screening is currently available and should be offered in pregnancy for a number of genetic (single gene or mendelian) disorders, chromosomal aneuploidy, and structural birth defects in the fetus regardless of maternal age or family history. A variety of tests provide risk assessment for genetic conditions and may be performed in the preconception period or in pregnancy. Screening for single gene defects such as CF or Tay-Sachs disease (TSD) has historically been targeted to the specific ethnic background of the patient, although this approach is changing and universal carrier screening for many disorders simultaneously is now available.<sup>38,39</sup> Screening for chromosomal abnormalities, traditionally associated with maternal age, is now recommended for all patients, with an overwhelming array of sonographic and maternal serum-based options available for carrying out risk assessment. Screening for structural birth defects, such as NTD, may involve maternal biochemical screening as well as ultrasound. Additionally, ultrasound should be considered a screening tool for genetic disorders and chromosomal aneuploidy, as many diagnoses have associated structural birth defects that are ascertained during a routine anatomic survey. As with any screening test, the patient should be made aware that a negative test result does not guarantee a healthy baby and a positive test result does not mean the fetus has the condition. In this scenario, the woman should undergo genetic counseling to understand the results, limitations of the test, and options for additional screening and diagnostic tests.



## Carrier (Heterozygote) Screening for Single Gene Disorders

The main purpose of carrier screening in pregnancy is to identify individuals who are themselves healthy but are at risk of having children with a genetic disorder. The majority of disorders in this category are AR diseases, in which both parents must be carriers of the gene but typically are unaffected. In the majority of cases, there is no family history of the disorder. Should a family history of a particular disorder be identified, that patient should undergo genetic counseling and be offered targeted genetic testing if indicated.

It has historically been agreed that the following criteria should be met for heterozygote screening programs to be effective: (1) disorder of sufficient severity to warrant screening, (2) high frequency of carriers in the screened population, (3) availability of an inexpensive and dependable test with low false negative and false positive results, (4) access to genetic counseling for couples identified as heterozygotes, (5) availability of prenatal diagnosis, and (6) acceptance and voluntary participation by the population targeted for screening. Testing directed at specific ethnic groups is increasingly criticized as our society becomes more multiethnic and it is recognized that genetic conditions do not occur uniquely in specific populations, as ethnicity-based screening limits accessibility of genetic information for individuals based on their reported ancestry. In addition, as genetic and genomic testing evolves, broad-based testing is available for many disorders, some very rare, simultaneously. This is rapidly changing the paradigm of genetic testing.

Because DNA-based screening tests generally look only at a set of the most common genetic mutations, not all carriers will be detected by a given screening test. Individuals with other mutations not included in the screening panel will not be detected. In some disorders, screening is more effective in a particular ethnic group in which a limited number of disease-causing gene mutations are seen. For example, DNA screening for CF is sensitive in the Ashkenazi Jewish population, in which greater than 95% of carriers can be detected because the majority of disease-causing mutations in this population is known. However, in Asian or African populations, fewer disease-causing mutations are known; therefore, fewer carriers of Asian or African descent will be identified by the current CF DNA test. It is important to remember that although a negative carrier test lowers the chance that an individual is a carrier, it does not rule it out (Table 2-5).

Table 2-6 lists the inherited disorders for which carrier screening is currently recommended. There are many other disorders for which screening is available and frequently performed. These disorders include fragile X syndrome, as well as extensive panels of diseases more common in the Ashkenazi Jewish population, and spinal muscular atrophy (SMA).<sup>18,40-42</sup> As genetic testing becomes more efficient and less expensive, clinicians and professional societies that establish practice

guidelines and policies are faced with the challenge of deciding which tests should be offered for general screening. Expanded, or universal, carrier screening is increasingly being offered as high-throughput genotyping and gene sequencing are able to rapidly provide information on many conditions, beyond those traditionally recommended in screening guidelines.<sup>39</sup> Many of the conditions have a variable phenotype and variable age of onset with a clinical course that is not well defined given the rarity of some of the included disorders. Pretest and posttest counseling is strongly recommended for patients undergoing expanded carrier screening to discuss the potential for unanticipated information and an inability to calculate a residual risk given the rare nature of many disorders included on panels.

### Tay-Sachs Disease

Carrier screening for TSD in the Ashkenazi Jewish population has been done on a large scale since 1969. Screening, followed by prenatal diagnosis when indicated, has resulted in a dramatic decrease in the incidence of TSD in the Jewish population.<sup>37</sup> A number of practical, social, and ethical complexities have also been identified in this prototypic population-based effort.<sup>43</sup> More than 100 mutations in the hexosaminidase A gene have been identified to date. Some are associated with later onset or more chronic forms of neuronal storage disease. In part because of this history of success with TSD screening, and in part because of cultural isolation, an increased number of tests for genetic disorders have been proposed for testing of the Ashkenazi Jewish population. Some of these tests have become routine, whereas others are provided through commercial laboratories that offer an extensive Ashkenazi Jewish panel.

### Cystic Fibrosis

CF is the most common severe AR disease to affect individuals with European ancestry, with an incidence of 1/2500 to 1/5000 corresponding to a carrier frequency of 1/25 to 1/35. The disease is characterized by chronic pulmonary obstruction and infection and by digestive disorders such as pancreatic insufficiency. It is caused by mutations in the gene that encodes the CF transmembrane receptor protein, or *CFTR*, on chromosome 7. Since the gene was cloned in 1989, more than 1800 mutations have been identified. The mutations have ethnic and geographic variation, as well as a wide range of phenotypic variation, from those causing classical, severe CF (such as the common delta F508 mutation) to those that may have subtle or no clinical manifestations.

Since 2001, the AGOC and the ACMG have recommended that screening for CF should be offered to women in pregnancy; the most recent guidelines recommend that testing be offered regardless of ancestry.<sup>38</sup> Implementing this recommendation is complex and therefore somewhat controversial. The complexity arises in part because the incidence of CF varies in people of different ethnic groups. It is most common in Ashkenazi Jewish and Northern European populations, in which 1/25 is a carrier, but is far less common in Hispanic, Black, and Asian-American persons. Furthermore, as mentioned earlier, the detection rate varies greatly among ethnic groups because not all alleles are known for each population. Most laboratories test for the most common mutations present in the population; in the United States this typically involves screening for the 23 to 32 mutations most common in the European population. Genetic counseling is particularly important in order to explain the limitations of testing (that is, not all carriers will be detected), especially for couples in which one or both partners is a carrier or has a positive family history or is of nonwhite ancestry. It is also imperative that individuals are made aware of the residual risk to be a carrier or have an affected child depending on the number of mutations analyzed and partner status.

**TABLE 2-5 Cystic Fibrosis Carrier Frequency and Detection Rates by Ethnic Group**

Group	Incidence	Carrier Risk	Detection Rate
Ashkenazi Jews	1/3300	1/24	94%
Europeans	1/3300	1/25	88%
Hispanics	1/8464	1/58	72%
African Americans	1/17,000	1/61	64%
Asian Americans	1/32,400	1/94	49%

TABLE 2-6 Genetic Screening Tests Currently Recommended by Ethnic Group

Condition	ACOG	ACMG	NSGC	Comment
Hemoglobinopathies <sup>a</sup>	African ancestry: hemoglobin electrophoresis  Mediterranean or Southeast Asian ancestry: If anemia and MCV less than 80 fL, evaluate for iron deficiency; if iron study results are normal, perform hemoglobin electrophoresis; if hemoglobin electrophoresis result is normal, molecular testing for $\alpha$ -thalassemia is indicated	No current guideline	No current guideline	Sickledex and other solubility tests do not identify variant hemoglobins other than hemoglobin S
Conditions prevalent among Ashkenazi Jewish population <sup>b,c</sup>	Offer screening for Tay-Sachs disease, cystic fibrosis (CF), Canavan disease, and familial dysautonomia to those with Ashkenazi Jewish ancestry; provide education materials and genetic counseling as requested for additional conditions	Offer screening for Tay-Sachs disease, CF, Canavan disease, and familial dysautonomia; also offer screening for Niemann-Pick disease (type A), Bloom syndrome, Fanconi anemia group C, mucopolipidosis IV, and Gaucher disease	No current guideline	Biomedical screening of hexosaminidase; this enzyme is the most sensitive screening test for Tay-Sachs disease in all populations
Cystic fibrosis <sup>d,e,f</sup>	Offer CF carrier screening to all women of reproductive age; complete sequencing of the CF gene is not appropriate for carrier screening	Offer population screening using a panel of 23 pathogenic variants in the <i>CFTR</i> gene associated with classic CF and present in at least 0.1% of patients with CF	Carrier testing for CF should be offered to all women of reproductive age, regardless of ancestry, preferably before pregnancy	
Spinal muscular atrophy <sup>g,h</sup>	Testing recommended only when a family history of spinal muscular atrophy is present	Offer screening regardless of ancestry or family history	No current guideline	
Fragile X syndrome <sup>h,i,j</sup>	Screening should be limited to individuals with family history of intellectual disability suggestive of fragile X syndrome, unexplained intellectual disability, or developmental delay, autism, or primary ovarian insufficiency	Screening should be limited to individuals with family history of intellectual disability suggestive of fragile X syndrome	Screening should be limited to individuals with family history of intellectual disability suggestive of fragile X syndrome	ACOG, ACMG, and NSGC do not recommend population carrier screening

<sup>a</sup>American College of Obstetricians and Gynecologists: ACOG Practice Bulletin No. 78: hemoglobinopathies in pregnancy. *Obstet Gynecol* 109:229-237, 2007.

<sup>b</sup>Gross SJ, Pletcher BA, Monaghan KG; Professional Practice and Guidelines Committee: Carrier screening in individuals of Ashkenazi Jewish descent. *Genet Med* 10:54-56, 2008.

<sup>c</sup>American College of Obstetricians and Gynecologists: ACOG Committee Opinion No. 442: preconception and prenatal carrier screening for genetic diseases in individuals of Eastern European Jewish descent. *Obstet Gynecol* 114:950-953, 2009.

<sup>d</sup>Watson MS, Cutting GR, Desnick RJ, et al: Cystic fibrosis population carrier screening: 2004 revision of American College of Medical Genetics mutation panel. *Genet Med* 6:387-391, 2004.

<sup>e</sup>American College of Obstetricians and Gynecologists: ACOG Committee Opinion No. 486: update on carrier screening for cystic fibrosis. *Obstet Gynecol* 117:1028-1031, 2011.

<sup>f</sup>Langfelder-Schwind E, Karczeki B, Strecker MN, et al: Molecular testing for cystic fibrosis carrier status practice guidelines: recommendations of the National Society of Genetic Counselors. *J Genet Couns* 23:5-15, 2014.

<sup>g</sup>Prior TW; Professional Practice and Guidelines Committee: Carrier screening for spinal muscular atrophy. *Genet Med* 10:840-842, 2008.

<sup>h</sup>American College of Obstetricians and Gynecologists: ACOG Committee Opinion No. 432: spinal muscular atrophy. *Obstet Gynecol* 113:1194-1196, 2009.

<sup>i</sup>American College of Obstetricians and Gynecologists: ACOG Committee Opinion No. 469: carrier screening for fragile X syndrome. *Obstet Gynecol* 116:1008-1010, 2010.

<sup>j</sup>Finucane B, Abrams L, Cronister A, et al: Genetic counseling and testing for FMR1 gene mutations: practice guidelines of the National Society of Genetic Counselors. *J Genet Couns* 21:752-760, 2012.

ACMG, American College of Medical Genetics; ACOG, American College of Obstetricians and Gynecologists; MCV, mean corpuscular volume; NSGC, American College of Medical Genetics.





**FIG 2-10** Hyperechogenic bowel (arrow) in a fetus with cystic fibrosis.

CF may be suspected in a fetus by the specific ultrasound finding of EB. Fetal EB, defined as bowel with sonographic density equal to or greater than that of surrounding bone, is diagnosed in 0.2% to 1.8% of fetuses during routine ultrasound examination in the second trimester of pregnancy. This increased echogenicity has been associated with chromosomal abnormalities, congenital infections, intestinal obstruction, and CF (Fig. 2-10).<sup>44</sup> In the case of CF, it is hypothesized that the malfunctioning CFTR protein leads to dehydration of mucous secretions, which become viscous and obstruct the bowel lumen, leading to meconium ileus. The risk for CF with EB has been extensively studied and reported to have a wide range, from 0% to 33%.<sup>45</sup> This range could result from differences in ascertainment, CF prevalence, and mutation detection rates.

## Screening for Structural Birth Defects

### Alpha-Fetoprotein and Open Neural Tube Defects

Population-based prenatal screening began in the late 1970s with the use of maternal serum alpha-fetoprotein (AFP) measurements to identify women at increased risk of carrying a fetus with an open NTD. AFP is the major serum protein early in fetal life.<sup>46</sup> This oncofetal protein is produced initially by the yolk sac and, after involution of this structure in early pregnancy, by the fetal liver. Relatively few data have been published on the biologic activities of AFP during fetal development. AFP is present in amniotic fluid initially through diffusion across immature skin, and later through the kidneys and fetal urination. The fetus recirculates swallowed amniotic fluid AFP (AFAFP), with eventual degradation by the fetal liver. Minute amounts of AFP are present in maternal serum through diffusion across the placenta and amnion. Nonpregnant, healthy women have levels of AFP that are barely detectable (1  $\mu\text{g/L}$ ), whereas normal median levels at 16 to 18 weeks of gestation range from 18 to 40  $\mu\text{g/L}$ . When the fetal serum level is 2 million  $\mu\text{g/L}$ , the corresponding AFAFP is 20,000  $\mu\text{g/L}$ , and the maternal serum level is 20  $\mu\text{g/L}$ .<sup>3</sup> Fetal plasma and amniotic fluid levels of AFP peak in the midtrimester of pregnancy, whereas maternal serum AFP (MSAFP) continues to increase until 28 to 32 weeks of gestation (Fig. 2-11). The discrepancy between amniotic fluid and maternal serum levels of AFP is not completely understood but may be due to the rapidly expanding placental and amniotic interfaces.

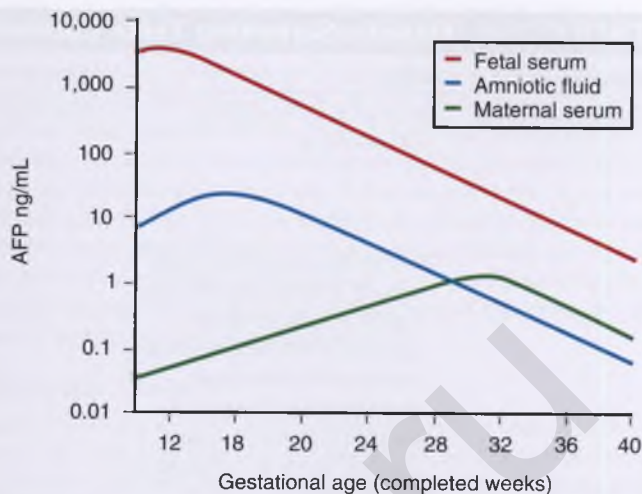


**FIG 2-11** Mean concentrations of alpha-fetoprotein (AFP) in maternal serum, amniotic fluid, and fetal serum. (Redrawn from Haddow JE: Prenatal screening for open neural tube defects, Down's syndrome, and other major fetal disorders. *Semin Perinatol* 14:488, 1990.)

In the fetus with a defect such as anencephaly or spina bifida, AFP enters the amniotic fluid in increased amounts, leading to higher levels in the maternal serum as well. Levels of AFP are elevated in amniotic fluid and maternal serum only when such lesions are open, that is, when the neural tissue is exposed or covered by only a thin membrane. When NTDs are skin covered, AFP does not escape from the fetal circulation, and such defects are generally not detected by MSAFP. Whereas essentially 100% of anencephaly lesions are open, approximately 20% of spina bifida cases are skin covered, as are 82% of encephaloceles.<sup>47</sup> Discussions of the sensitivity and specificity of AFP testing are generally restricted to open lesions, because it is assumed that closed lesions will not be detected. Elevated MSAFP is not uniquely associated with open NTDs. It may also be elevated in fetuses with abdominal wall defects, oligohydramnios, or renal abnormalities as well as in cases of placental dysfunction leading to later obstetric complications such as preterm birth, preeclampsia, and fetal growth restriction.<sup>48,49</sup>

Because more than 80% of infants with NTD are born into families with no prior history of the disorder, MSAFP screening is an important public health program. In laboratories providing AFP screening, results are expressed as multiples of the median (MoM). This provides less interlaboratory variation, which can be considerable, as well as a way to report results across a range of gestational ages. Encephaloceles are a less frequent cause of an elevated MSAFP, owing to both a lower incidence and a higher frequency of closed lesions. Given the extent of overlap between affected and unaffected pregnancies, it is not possible to detect all cases of open spina bifida with MSAFP screening, and likewise, most cases reported to be in need of further evaluation will ultimately be determined to be normal.

As discussed previously, AFP levels vary with gestational age. The optimal time for serum NTD screening is 16 to 18 weeks of gestation. Before 16 weeks, there is more overlap between affected and unaffected pregnancies. Whereas last menstrual period (LMP) dating is sufficiently accurate for NTD screening, sonographic dating is more accurate and its use improves sensitivity and specificity of screening. In addition, because second trimester biparietal diameter (BPD) measurements are usually smaller in fetuses with spina bifida, the MSAFP will appear higher, and this artifact improves the detection rate for this lesion. Other sonographic measurements (e.g., crown-rump length or composite biometry) can reliably date the pregnancy but do not have



this unique advantage of BPD dating. Therefore, in the second trimester, ultrasound dating based on BPD alone is recommended for pregnancies at 14 weeks of gestation or later for the purposes of AFP screening. Most laboratories have separate sets of distribution parameters for ultrasound versus LMP-dated pregnancies.

Several factors other than gestational age affect MSAFP levels, including maternal weight,<sup>50</sup> race,<sup>51,52</sup> insulin-dependent diabetes mellitus (IDDM),<sup>53,54</sup> and the number of fetuses. Studies have also suggested that second trimester MSAFP is consistently elevated after first trimester transabdominal multifetal pregnancy reduction (MFPR) and should not be performed in this setting.<sup>55</sup> Because larger maternal size results in greater dilution of AFP derived from the fetus, obese women have lower levels of MSAFP. Black and Asian women have levels that are 10% to 15% higher than nonblack women, and insulin-dependent diabetic women have levels that are lower than the general population. The physiologic basis for this lower value is unclear. Each of these factors is usually taken into account in the calculation of risk. Although other factors, such as maternal smoking<sup>56,57</sup> and IVF,<sup>58,59</sup> have a small impact on levels of MSAFP and other biochemical markers, these differences are not generally of sufficient magnitude to warrant correction.

### Elevated Maternal Serum Alpha-Fetoprotein

When the MSAFP level is above the cutoff (either 2.0 or 2.5 MoM), the accuracy of dating should be assessed. If dating based on LMP was used for the original calculation, an ultrasound is indicated to confirm dating and rule out multiple gestations and fetal demise, both of which can cause an elevated MSAFP. An anatomic survey should be performed as well to assess any identifiable structural birth defect to explain the elevation.

If the screening ultrasound does not identify a cause for the increased MSAFP, further assessment with more sophisticated sonography and potentially amniocentesis is indicated. The sensitivity of ultrasound for the detection of NTD and other significant structural abnormalities associated with increased MSAFP has been reported to be as high as 94% to 100%.<sup>60</sup> Ultrasound alone is reported to be more sensitive than MSAFP for the initial detection of NTD, although this varies with the experience and expertise of the ultrasound examiner.<sup>61</sup> Ultrasound is less expensive than amniocentesis and does not carry the risk of pregnancy loss.

Amniocentesis allows for measurement of both AFP and acetylcholinesterase (AChE) in the amniotic fluid. Measurement of AFAP and AChE has a 97% detection rate for NTDs, with a false positive rate of 0.5%.<sup>62</sup> Although many disorders can result in an elevated AFAP, AChE is more specific to neural tissue. Detection of AChE in the amniotic fluid generally indicates that an open NTD is present, although a positive AChE has also been reported with omphalocele, gastroschisis, cystic hygroma, fetal skin lesions, and fetal hydrops.<sup>63,64</sup>

A major cause of borderline AFAP elevations and false positive AChE results is contamination of the sample with fetal blood. Fetal blood AFP levels are more than 100 times higher than AFAP levels. False positive AChE results occur in about 2% of visibly bloodstained samples and 0.2% of samples that are not visibly bloodstained. Testing for the presence of fetal hemoglobin is indicated for samples with elevated AFAP, visible red blood cell contamination, and certain other indications (e.g., unexplained elevated MSAFP, reddish AFAP).

Several investigators have reported an association between elevated MSAFP and an increased risk of fetal aneuploidy, an additional argument for amniocentesis. These studies have estimated the prevalence of clinically significant aneuploidy in this setting at 1%, with approximately 55% of these being autosomal aneuploidies and 45% sex chromosomal abnormalities.<sup>65,66</sup>

### Other Abnormalities and Elevated Alpha-Fetoprotein

An elevated MSAFP can be associated with fetal defects other than NTDs (Fig. 2-12, Table 2-7), including omphalocele and gastroschisis. In addition, some fetal skin disorders allow increased diffusion of AFP into the amniotic fluid, resulting in an elevated MSAFP. Congenital nephrosis can cause extremely high levels of AFP owing to fetal proteinuria and is suspected with a normal ultrasound and markedly elevated MSAFP (often >10 MoM). This AR disorder results in renal failure early in life, and children often die in infancy or early childhood. It is relatively rare except in Finland, where the reported incidence of 1/2600 live births makes the disease a primary focus of an AFP screening program. DNA testing for Finnish nephrosis is now available, although it is of low yield in families not of Finnish descent.<sup>47,67,68</sup> Rarely, the source of an unexplained MSAFP can be maternal in nature and not reflective of the pregnancy. This includes maternal hepatic tumors or ovarian tumors that secrete AFP and confound the screening results. An unexplained MSAFP and AFAP have been associated with adverse obstetric outcomes including preeclampsia and preterm delivery.<sup>69</sup>

### Fetal Chromosomal Aneuploidy

Maternal age has historically been the most frequent method for identifying women at increased risk for fetal chromosome abnormalities and determining who should be offered prenatal diagnostic testing. As maternal age increases, the chance of delivering a child with DS increases from about 1/1000 at 30 years of age, to almost 1/400 at 35 years of age, and 1/100 at 40 years of age (see Table 2-1).<sup>70</sup> Paternal age does not affect aneuploidy risk. This clinical observation is consistent with studies demonstrating that greater than 90% of trisomy 21 results from nondisjunction in the oocyte, most commonly during meiosis I.<sup>71</sup> The mechanism of the nondisjunction event related to maternal age is not known. Because of the association of advancing maternal age with nondisjunction predisposing to aneuploidy, prenatal diagnosis has been offered to women 35 years of age or older for many years. At 35 years of age, the chance of identifying a fetus with DS approximates the chance of miscarriage due to the amniocentesis procedure. It is in part for this reason that testing has traditionally been offered at this point. For many women, however, the decision to undergo amniocentesis is difficult, because not all women weigh the risks equally. For some, the possibility of miscarriage is far more of a concern than the possibility of having a child with DS. For others, concerns over caring for a child with disabilities may be more serious.<sup>72</sup> All patients considering prenatal diagnosis should undergo genetic counseling to discuss the options available and the risks, benefits, and limitations of each testing choice.

### FIRST TRIMESTER RISK ASSESSMENT

First trimester risk assessment typically occurs between 9 and 14 weeks' gestation, depending on which markers are used, and provides risk assessment for trisomy 21 and 18 primarily, as well as for trisomy 13 in some laboratories. First trimester screening generally includes ultrasound measurement of the nuchal translucency, done at a crown-rump length of approximately 38 to 84 mm, and biochemical measurements of free  $\beta$ - or total human chorionic gonadotropin (hCG) and pregnancy-associated plasma protein A (PAPP-A). These markers are combined with maternal age and the number of fetuses to provide a patient-specific risk with a sensitivity of 85% for DS with a 5% false positive rate.<sup>73-78</sup> hCG level is typically elevated in pregnancies affected with fetal DS, whereas PAPP-A is lower. The nuchal translucency is often increased in fetuses with DS as well as a variety of other genetic conditions, including trisomy 13, trisomy 18, Turner syndrome, triploidy, and structural birth defects, particularly CHDs.<sup>77</sup> The nuchal



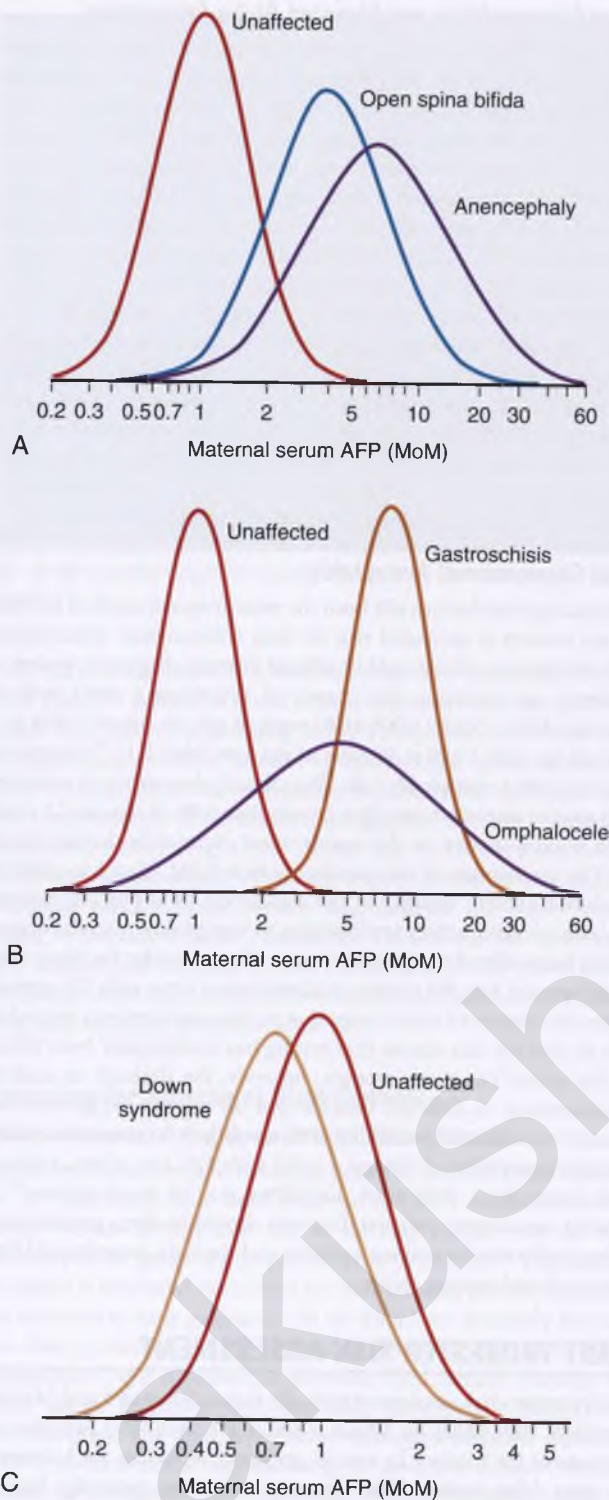


**FIG 2-12 A**, Distribution of second trimester maternal serum alpha-fetoprotein levels (MSAFP) in unaffected pregnancies and those affected by open spina bifida and anencephaly. The median for open spina bifida is 3.8 multiples of the median (MoM) and for anencephaly is 6.5 MoM. **B**, Distribution of second trimester MSAFP levels in unaffected pregnancies and those affected by gastroschisis and omphalocele. The median for gastroschisis pregnancies is 7.0 MoM and for omphalocele is 4.1 MoM. **C**, Distribution of second trimester MSAFP levels in unaffected pregnancies and those affected by Down syndrome. The median alpha-fetoprotein value is 0.75 MoM, and extensive overlap occurs between the affected and unaffected populations. (Redrawn from Haddow JE: Prenatal screening for open neural tube defects, Down's syndrome, and other major fetal disorders. *Semin Perinatol* 14:488, 1990.)

**TABLE 2-7 Causes of an Elevated Maternal Serum Alpha-Fetoprotein**

Multiple gestation
Fetal demise
Fetal-maternal hemorrhage
Placental abnormalities
Uterine abnormalities
Maternal ovarian or hepatic tumors
Fetal congenital defects
Neural tube defects
Spina bifida
Anencephaly
Encephalocele
Open ventral wall defects
Omphalocele
Gastroschisis
Congenital nephrosis
Triploidy
Bilateral renal agenesis
Congenital skin disorders
Epidermolysis bullosa
Aplasia cutis
Autosomal-recessive polycystic kidney disease
Sacrococcygeal teratoma
Cystic adenomatoid malformation of the lung

MSAFP, maternal serum alpha-fetoprotein.

measurement must be very precise and can be challenging to obtain accurately. It is also known to be dependent on the sonographer's experience and the quality of equipment, and therefore, proper training and quality management are important components of screening programs that include this ultrasound measurement in chromosomal aneuploidy risk assessment. The risk for aneuploidy increases as the nuchal translucency thickness increases (see Chapter 3). Cystic hygroma is a single or septated fluid-filled cavity usually involving the nuchal region that is the result of a lymphatic malformation and subsequent lymph accumulation. Approximately 50% of cystic hygromas identified in the first trimester are associated with chromosomal aneuploidy, and the majority of these are fetuses affected with DS.<sup>79</sup>

Women with a positive screening test in the first trimester should be counseled regarding the results and options for further testing including CVS as the most immediate diagnostic test available in the late first and early second trimester. Options for further screening include contingent and stepwise sequential screening as well as cell-free DNA testing. The benefit of identifying aneuploidy in the first trimester is that it affords patients information earlier in pregnancy so that decisions regarding pregnancy termination may be made at a time when services are more readily available and represent less maternal risk. The risk with early screening for chromosomal aneuploidy is the inherent loss rate in this population and the identification of a pregnancy that would go on to be spontaneously miscarried. Screening for NTDs by MSAFP or detailed ultrasound in the second trimester is recommended for those women who have first trimester genetic risk assessment.

## SECOND TRIMESTER RISK ASSESSMENT

Shortly after the introduction of MSAFP screening for NTD, it was recognized that fetuses with DS had a lower mean MSAFP in the second trimester.<sup>80,81</sup> Subsequent investigations have reported that maternal serum, amniotic fluid,<sup>81</sup> and fetal cord serum<sup>82</sup> levels of AFP



**TABLE 2-8 Pattern of Results Seen with Expanded AFP Screening in Fetal Disorders**

	AFP	uE <sub>3</sub>	hCG	Inhibin A
Open NTDs	↑	No change	No change	No change
Down syndrome	↓	↓	↑	↑
Trisomy 18	↑	↓	↓	No change

AFP, alpha-fetoprotein; hCG, human chorionic gonadotropin; NTDs, neural tube disorders; uE<sub>3</sub>, unconjugated estriol.

are all lower in pregnancies in which the fetus has DS. A number of other biochemical markers have also been studied for use in aneuploidy screening. Unconjugated estriol (uE<sub>3</sub>),<sup>83</sup> hCG,<sup>84</sup> and dimeric inhibin A<sup>76,77,85</sup> all add sensitivity and specificity to second trimester biochemical screening for DS and are included in a test routinely referred to as the *quad screen*.<sup>77,86</sup> Like AFP, uE<sub>3</sub> is 25% to 30% lower in DS pregnancy, whereas hCG and inhibin A are both increased with a median value about twice that of normal control subjects (Table 2-8).<sup>72</sup> With the use of quad screening, the detection rate for DS is 80% with a false positive rate of 5%.<sup>87</sup> In pregnancies in which the fetus is affected with trisomy 18, the levels of AFP, uE<sub>3</sub>, and hCG are all decreased, with median values of 0.6, 0.5, and 0.3 MoM, respectively. Inhibin A does not contribute to the detection of trisomy 18 and is not included in the screening algorithm. Use of a protocol evaluating this characteristic pattern is associated with an 80% detection rate for trisomy 18, but it identifies only 0.5% of women as high risk.<sup>88</sup> The second trimester maternal serum quad screen reports risk results for DS, trisomy 18, and NTDs. The quad screen does not reliably report risk assessment for trisomy 13 and is therefore not reported by most laboratories.

### Sonographic “Soft Markers” for Aneuploidy

A fetal anatomic survey in the second trimester has also been used as a screening tool for chromosomal aneuploidy (see Chapter 3). Approximately one third of fetuses with DS have an identifiable sonographic finding of either a major or minor structural variation. This includes CHDs (most commonly ventricular septal defects or endocardial cushion defects), ventriculomegaly, duodenal atresia, or a variety of “soft markers.” Soft markers include thickened nuchal skin fold, EB, renal pyelectasis, shortened femur and humerus, and hypoplastic or absent nasal bone. There are contrasting opinions on the utility of ultrasound to modify risk for DS. Most providers use the information to adjust prior risk from maternal age or standard screening results by applying likelihood ratios. In one large study of 7800 women to determine the effectiveness of ultrasound in genetic risk assessment, when performed by experienced providers, a genetic ultrasound alone had a detection rate for DS of 69% with a 5% false positive rate and enhanced the sensitivity of all other screening modalities.<sup>89</sup> A meta-analysis pooling data from 48 studies of low- and high-risk women indicate hypoplastic or absent nasal bone to be associated with the greatest risk for DS<sup>90</sup> (see Chapter 3).

### COMBINED FIRST AND SECOND TRIMESTER RISK ASSESSMENT

There are several ways to combine ultrasound and serum testing in the first trimester with second trimester serum analytes. Integrated testing has the highest DS detection rate (90%) with the lowest false positive rate (2%) compared to other blood and ultrasound test strategies in the first or second trimester.<sup>91</sup> This test includes blood and nuchal translucency ultrasound in the first trimester in addition to blood in

the second trimester to produce a single risk calculation for DS. The advantage of this test is the superior sensitivity and low false positive rate, whereas a disadvantage is that the information is not available until the second trimester. Stepwise sequential screening utilizes the same combination of nuchal translucency and first and second trimester serum analytes, but preliminary results are provided in the first trimester. For patients at high risk for aneuploidy, diagnostic testing is offered. Those whose risk is not increased can then have serum done in the second trimester and integrated with the first trimester results for a final risk calculation. The serum-integrated test (blood only) includes biochemical analytes from the first and second trimesters and is offered in locations where expertise in nuchal translucency ultrasound is limited or not available.<sup>92</sup>

### Cell Free DNA Screening

The quest to identify fetal genetic material in maternal blood began decades ago and was first described in 1969.<sup>93</sup> Efforts to isolate and purify intact fetal cells for prenatal testing ultimately proved to be unsuccessful, in part because of the scarcity of tissue and persistence of cells from antecedent pregnancies. The concept of cell-free DNA as a source of fetal genetic material was reported by Lo and colleagues in 1997.<sup>93</sup> Both maternal and fetal DNA are found circulating in plasma, and measurement of relative chromosomal content can be used to identify fetal trisomy<sup>94</sup> (Fig. 2-13). Fetal cell-free DNA is identifiable in maternal blood as early as 5 to 7 weeks' gestation, is found in relatively larger quantities than intact fetal cells, and is cleared from maternal circulation within hours of delivery, making this a better source of genetic material than intact cells. Approximately 10% of circulating DNA found in maternal plasma during pregnancy is fetal in origin, and this fetal fraction is almost entirely made up of trophoblast-derived DNA. This is important to understand, as there is potential for placental mosaicism, in which the placental and fetal genotypes differ, presenting the possibility of false positive or false negative results.

Cell-free fetal DNA testing was reported for the determination of fetal rhesus D genotype and early fetal sex identification for those at risk for X-linked male lethal disorders several years prior to the application for chromosomal aneuploidy risk assessment.<sup>95,96</sup> In October 2011, the first commercial laboratory began offering cell-free DNA (cfDNA) screening, also referred to as noninvasive prenatal testing or NIPT, for common aneuploidy conditions. Since that time, the utilization of this technique has markedly increased owing to the very high reported detection rate and low false positive rate, particularly for DS screening. Although highly accurate, cell-free DNA is considered a screening test and initial recommendations were that this test be reserved for high-risk women.<sup>97</sup> Most commercial laboratories report risk results for chromosomes 21, 13, 18, X, and Y. Laboratories that offer the technology use either massively parallel shotgun sequencing, which sequences DNA fragments from the whole genome, or targeted sequencing that looks only at regions of interest. In either scenario, high-throughput DNA sequencing undergoes extensive data analysis to detect abnormal amounts of genetic material specific to a chromosome or region of interest from the fetus. The sensitivity and specificity of cell-free DNA screening for the detection of DS has been reported to be between 96% and 100%, although this figure does not account for the subset of patients in which the testing is unsuccessful because of the low fraction of fetal DNA or high sequencing variance leading to difficulty in interpreting the results.<sup>98</sup> It is recommended that patients undergo pretest counseling to understand the screening nature of the test, that the test only detects common aneuploidies, the potential for unanticipated results or failure to obtain test results, and the options for diagnostic testing. Patients with a low-risk test should be aware that this does not guarantee an unaffected pregnancy. Because aneuploidy is relatively



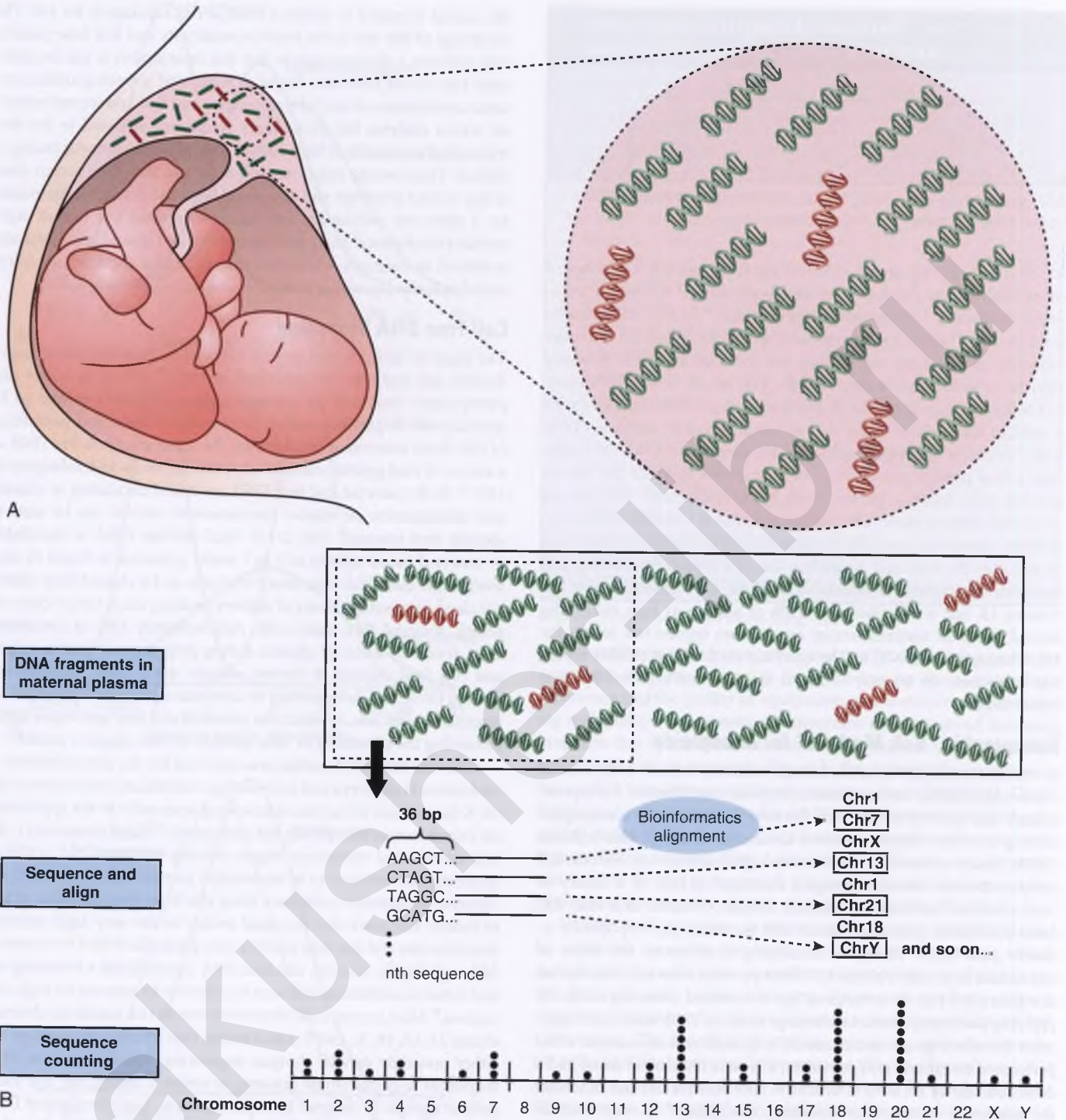


**FIG 2-13** **A**, Cell-free DNA from the placenta contributes approximately 10% to 12% of the total cell-free DNA in the maternal circulation. **B**, The approach to detecting trisomy through measurement of relative chromosomal contribution to the cell-free DNA in the maternal plasma. Alignment of each chromosomal fragment to the chromosome of origin, followed by a bioinformatics calculation of the relative contribution, can be used to calculate the likelihood of fetal trisomy. (With permission from *Circulating Cell-Free DNA in Women's Medicine* by Dr. Xiao Yan Zhong and Dr. Wolfgang Holgreve. *The Global Library of Women's Medicine*.)

uncommon, the positive predictive value or chance of an affected fetus given a positive result by cell-free DNA screening is likely 50% or less, depending on other risk factors and the particular aneuploidy.<sup>99</sup> Therefore, a patient with a high-risk test result should be referred for genetic counseling to discuss options for further testing.

In this evolving field of perinatal medicine, the technology is rapidly expanding to offer more and more clinical data. For example, some companies offer screening for 4 to 5 microdeletion conditions, such as 22q deletion and 1p36 deletion. Although most are individually rare, the 22q microdeletion is reported to occur in about 1/3000



newborns. These conditions are not associated with advanced maternal age, and some may lack structural birth defects on ultrasound evaluation.<sup>100</sup> The importance of pretest counseling and discussing possible results and implications for prenatally ascertained information should be reviewed.

Although cell-free DNA screening has changed the landscape of prenatal screening, further research to reduce cost and improve efficiency of the testing is ongoing. The concept of “precision medicine for the fetus” is evolving with work on the fetal transcriptome, metabolome, and proteome using epigenetic information, RNA, and microRNA. The entire fetal genome has been sequenced from DNA in maternal blood with important implications for future prenatal testing.<sup>101</sup> Many ethical issues have been raised regarding prenatal testing, including fetal autonomy in genetic testing, identification of adult-onset disorders in the prenatal setting, unanticipated or uncertain results, lack of appropriate resources and trained providers for counseling and interpretation of complex genetic information, and the role of industry in promoting research.

## PRENATAL SCREENING IN MULTIPLE GESTATIONS

A number of complexities arise in the screening of twin pregnancies. First, the incidence of DS appears to be lower than expected in twin pregnancies, making risk calculation more challenging.<sup>102</sup> Second, serum markers are approximately, but not exactly, twice those found in singleton pregnancies. Third, a single maternal serum value is used to provide information about multiple fetuses. In discordant cases, the normal co-twin will mask the abnormal marker production associated with the affected twin. Finally, with monozygotic twins, both are most commonly either affected or unaffected, whereas with dizygous twins, the risk of DS is independent. Although ultrasound determination of monochorionicity is diagnostic of monozygosity, with same-gender dichorionic pregnancies, zygosity is uncertain. Although rare, monozygous twins can have discordant karyotypes that most frequently involve sex chromosomes. Because nuchal translucency screening in the first trimester is able to evaluate each fetus individually, it may be the most useful screen for multiple pregnancies. In high-order multiple gestations, biochemical screening is generally not possible, and again, nuchal translucency is the most useful and often the only option in such cases. Large studies are needed to determine the optimal screening method in multiple pregnancies.

## THIRD-TRIMESTER PREGNANCY COMPLICATIONS AFTER ABNORMAL SERUM SCREENING

Extreme marker levels, both low and high, have been associated with third trimester pregnancy complications such as hypertensive disorders, FGR, and preterm birth. Most cases, however, are not due to fetal or maternal disease and ultimately result in a normal outcome. Numerous studies have demonstrated that women with elevated levels of MSAFP have an increased risk of complications, such as spontaneous abortion, small-for-gestational-age infants, pregnancy-associated hypertensive disorders, and preterm delivery. The magnitude of risk for any adverse outcome increases with increasing maternal serum levels, from a risk of 19% with levels of 2.5 to 2.9 MoM, to 67% with an MSAFP of greater than 6.0 MoM.<sup>103</sup> In cases of unexplained increased MSAFP, increased transplacental transfer is responsible for the elevated value. Such increased transfer occurs with various placental abnormalities, and these same placental abnormalities later result in perinatal complications. Abnormalities such as placenta accreta, increta, and percreta have also been reported with an elevated AFP,<sup>104,105</sup> and uterine anomalies have been reported to be 22 times more common in these patients as

well.<sup>106</sup> Because of the very large concentration gradient between fetal and maternal serum levels of AFP, even a slight compromise in uteroplacental integrity will allow detectably increased transport of AFP across the placenta.

Other biochemical markers and combinations of markers have also been studied with respect to adverse outcome in late pregnancy. Elevated hCG has been associated with an increased risk of FGR, hypertension/preeclampsia, fetal malformations, chromosomal abnormalities, and adverse perinatal outcome.<sup>48</sup> As with MSAFP, the highest levels of hCG are associated with the highest risk of poor outcome.<sup>107</sup> The risk of having an adverse outcome is most significantly increased if a patient has two or more abnormal markers.<sup>108</sup> Both singleton and twin pregnancies with elevated hCG and AFP have been associated with adverse obstetric outcomes.<sup>109-111</sup>

Women with low estriol (<0.75 MoM) have also been found to have an increased risk of adverse outcome, including FGR, oligohydramnios, and delivery of small-for-gestational-age infants, a risk that seems independent of elevated hCG or AFP.<sup>112</sup> About 0.27% of women will have a very low uE<sub>3</sub> (<0.15 MoM), a finding that has been associated with a number of metabolic and genetic disorders including Smith-Lemli-Opitz syndrome, steroid sulfatase deficiency, Kallmann syndrome, congenital adrenal hyperplasia, and other disorders associated with adrenal dysfunction. Smith-Lemli-Opitz syndrome is an AR disorder that results in multiple malformations, including CHDs, mental retardation, and ambiguous genitalia. Because the primary abnormality involves cholesterol biosynthesis, a lack of cholesterol precursors from the fetus renders the placenta unable to produce uE<sub>3</sub>.<sup>113</sup> Prenatal diagnosis is possible through detection of elevated levels of 7-OH-dehydrocholesterol in amniotic fluid or maternal urine.<sup>114</sup> The other, more common cause of very low estriol is the presence of X-linked steroid sulfatase in the fetus. Lack of this enzyme in the placenta also results in the inability to produce uE<sub>3</sub>. This disorder is an X-linked condition leading to ichthyosis as the primary symptom in offspring, and a careful family history will often reveal symptoms in a previously undiagnosed male relative (grandfather or brother). The diagnosis can be confirmed through molecular testing for the causative microdeletion on amniotic fluid. Although the disorder is relatively mild, prenatal diagnosis can reassure the family and physician that another, more serious condition is not present.<sup>115-117</sup>

Optimal management of pregnancies with unexplained abnormal biochemical screening, however, remains controversial.<sup>49</sup> Although many of the associations between adverse obstetric outcomes and abnormal serum markers are statistically significant, the low sensitivity and low predictive value of these tests precludes their use as a screening tool for complications. Various strategies of antenatal surveillance have been proposed using ultrasound for growth, Doppler studies, and other forms of fetal testing. For example, uterine artery Doppler may indicate pregnancies at risk for uteroplacental insufficiency in those with abnormal serum analytes, and some recommend that it be performed in the second trimester.<sup>49</sup> Ideally, further research will better define a model of care for patients with abnormal serum analytes in the absence of fetal aneuploidy and structural birth defects.

## GENETIC DIAGNOSIS IN PREGNANCY

For many families seeking genetic counseling, a major goal is learning the risk for heritable disease in their children and the options that are available for avoiding having an affected child. The principal goal of prenatal diagnosis is to provide at-risk families with definitive information so they can make informed choices during pregnancy. The potential benefits of prenatal diagnosis include (1) providing reassurance to at-risk families when the results are normal, (2) providing risk



information to couples who would not have a child without such reassurance, (3) allowing couples to prepare for the birth of an affected child, (4) allowing medical providers to plan for the delivery and postnatal care of an affected infant, and (5) providing risk information to couples for whom termination of an affected pregnancy is an option. Other considerations include the potential impact of the information for other family members and the possibility of unanticipated information or information of uncertain significance. As genetic testing has advanced, these latter considerations are increasingly important and relevant.

Prenatal diagnosis is typically performed early in pregnancy, at a time when termination of an affected fetus can be performed safely. Although prenatal diagnosis with termination of affected fetuses is one option for preventing the recurrence of a genetic disorder in a family, it is by no means a universal solution. There are still disorders for which prenatal diagnosis is not possible, and for many parents termination is not an acceptable option, even if prenatal diagnosis is available. Other measures for avoiding recurrence of a genetic disorder include avoiding childbirth through contraception or sterilization; adoption; sperm or ovum donation; or preimplantation genetic diagnosis (PGD) on embryos obtained through IVF (see later). For many families, even if termination of pregnancy is not an acceptable option, prenatal diagnosis can help them prepare mentally, emotionally, and financially and to seek support systems and arrange for appropriate neonatal care before the baby is born.

### Genetic Counseling Before Prenatal Diagnostic Procedures

Parents considering prenatal diagnosis need information that will allow them to understand their personal and clinical circumstances and to give (or withhold) consent for the prenatal diagnostic procedures. Genetic counseling before such procedures usually addresses the following: (1) the chance that the fetus will be affected, (2) the nature and consequences of the testable disorder(s), (3) the risks and limitations of the procedures being performed, (4) the time required before a report of the test results can be issued, and (5) the possibility of complications of the procedures such as a failed attempt to obtain a sufficient, testable sample, or inconclusive results. Options for dealing with abnormal results are usually discussed, and it is emphasized that undertaking prenatal diagnosis in no way obligates the parents to terminate a pregnancy if an abnormality is discovered.

### Techniques for Prenatal Diagnosis

#### Amniocentesis

In amniocentesis, a sample of amniotic fluid (20–30 mL) is removed by inserting a 20- or 22-G spinal needle through the maternal abdomen and uterine wall into the amniotic cavity under ultrasound guidance (Fig. 2-14). Amniotic fluid contains desquamated fetal cells that can be cultured and karyotyped or used for metabolic assays or DNA extraction if a specific indication is present. AFAFP levels are also usually routinely measured.

Amniocentesis is typically performed at 15 to 20 weeks' gestation. The volume of amniotic fluid at 15 menstrual weeks is 125 mL, and it increases 50 mL/week for the next 13 weeks.<sup>118</sup> In an attempt to provide earlier results, the feasibility and safety of amniocentesis as early as 11 weeks' gestation have been investigated. Results of a large, multicenter randomized trial of early (11 to 13½ weeks) versus midtrimester (15 to 16½ weeks) amniocentesis revealed a significantly increased loss rate in the early amniocentesis group (7.6% vs. 5.9%). In addition, there was a significantly increased incidence of talipes equinovarus in the early amniocentesis group (1.3% vs. 0.1%). Thus, it appears that early

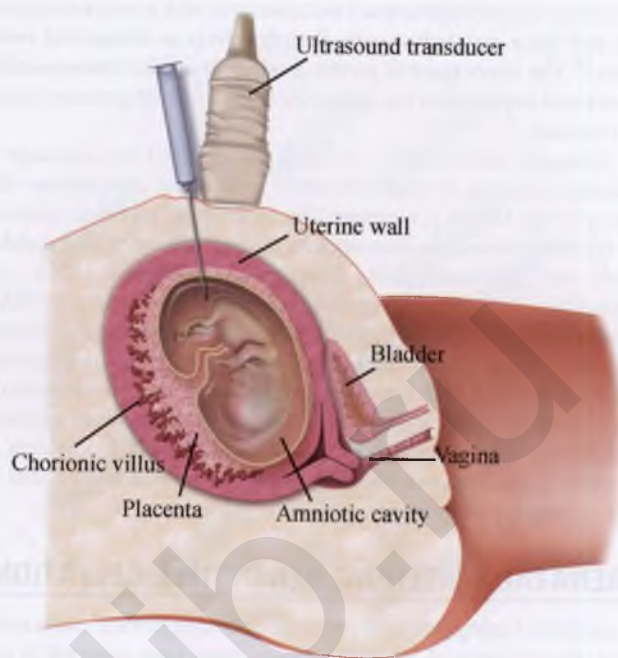


**FIG 2-14** Amniocentesis needle is positioned in the amniotic cavity under ultrasound guidance. (Illustration by James A. Cooper, MD, San Diego, CA.)

amniocentesis does carry an increased risk compared with midtrimester amniocentesis, and for this reason this procedure is not recommended prior to 15 weeks' gestation.<sup>119</sup>

The major complication of amniocentesis is the risk of miscarriage (above the 2% to 3% risk for any pregnancy at this gestational age unrelated to the procedure). The miscarriage risk of midtrimester amniocentesis at 15 to 20 weeks' gestation is typically quoted at 0.2% to 0.3% (1/300 to 1/500),<sup>120</sup> although risks as low as 1/1600 have been reported in some studies.<sup>121,122</sup> The only randomized trial that has been performed in low-risk patients was in the United Kingdom in 1986; this study demonstrated a 1% procedure-related loss rate.<sup>123</sup> Leakage of amniotic fluid following amniocentesis is not uncommon but typically resolves without long-term sequelae. Needle-associated injury to the fetus is rare, as is the incidence of maternal infection or intrauterine infection.

#### Chorionic Villus Sampling

In CVS, a biopsy of the developing placenta is performed at 10 to 13 weeks' gestation (Fig. 2-15). The primary advantage of CVS is that it can be performed earlier in gestation, which allows a decreased period of anxiety for patients at risk. Early results also permit first trimester termination, a safer and more readily available procedure than abortion in the second trimester. Indications for CVS are generally the same as those for amniocentesis, although AFP levels cannot be assessed on chorionic villi. Therefore, women who undergo CVS should be offered NTD screening with either MSAFP measurement or ultrasound later in pregnancy.

The two commonly used approaches to CVS are transcervical and transabdominal. Both are performed under ultrasound guidance, which is used to document fetal viability, gestational age, fetal number, localization of the placenta, and determination of the best approach and sampling path. With transcervical CVS, the patient is placed in the dorsal lithotomy position, a speculum inserted, and the vagina and cervix prepared with iodine antiseptic. A 16-G polyethylene catheter



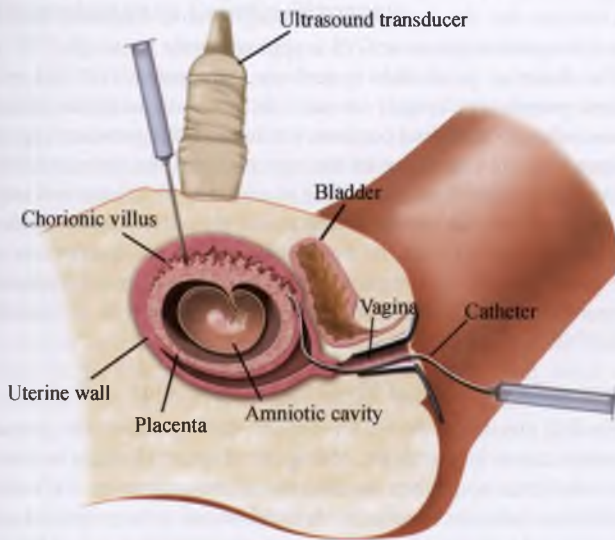


**FIG 2-15** Chorionic villus sampling. Either chorionic villus catheter or sampling needle is placed into the developing placenta under continuous ultrasound guidance. (Illustration by James A. Cooper, MD, San Diego, CA.)

with a flexible, stainless steel obturator is inserted through the cervix and into the developing placenta. With a transabdominal approach, a 20-G needle is inserted into the placenta in a fashion similar to that used for amniocentesis. In either approach, a 20-mL syringe is used to apply negative pressure and obtain a sample.

The risks of CVS were compared with those of amniocentesis in several trials performed shortly after introduction of the technique in the 1980s. A U.S. collaborative study demonstrated a loss rate 0.8% higher than that of midtrimester amniocentesis, a difference that was not statistically significant.<sup>124</sup> A Canadian trial also demonstrated a nonsignificant increase in losses of 0.6% above amniocentesis.<sup>125</sup> CVS does have a long learning curve, and the risks are very provider dependent; therefore, this equivalent loss rate may not be generalizable to all centers and providers.<sup>126</sup>

One important characteristic of CVS, different from amniocentesis, is the risk of confined placental mosaicism (CPM), which occurs in 1% to 2% of cases. CPM represents a discrepancy between the chromosomal makeup of the placenta and the fetus and is diagnosed when a mixture of aneuploid and normal cells are detected by CVS, whereas only normal cells are found on a subsequent amniocentesis or in the infant at birth. Most commonly, CPM represents a trisomic cell line present only in the placenta with a normal diploid chromosome complement in the fetus.<sup>127</sup> However, the fetus is truly mosaic in about 10% of cases,<sup>128</sup> although the risk is somewhat dependent on the specific trisomy identified.<sup>129</sup> Although some cases of CPM are associated with poor placental function and perinatal complications such as FGR and maternal hypertension, most commonly the outcome is normal. Such discordance between fetus and placenta can also confound results of cell-free DNA screening, which is based on placental trophoblast cells.

CPM can be associated with so-called trisomy rescue of an originally trisomic conception (Fig. 2-16). When this occurs, the fetus may be disomic but have uniparental disomy (UPD), a condition in which both chromosomes were inherited from the same parent. For example, if an embryo has trisomy 15 due to maternal nondisjunction, one or more cells in the inner cell mass, destined to become the fetus, may be “rescued” by loss of one chromosome 15. The mechanism is not well

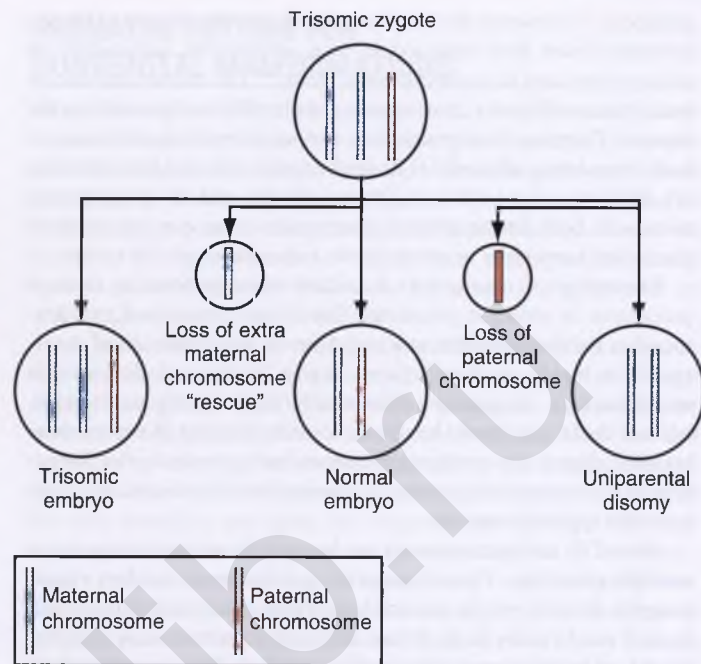


**FIG 2-16** Trisomy rescue and uniparental disomy. Diploid ovum is fertilized by a normal, haploid sperm, resulting in a trisomic zygote. The cells multiply and divide, and one cell reverts to a diploid state owing to anaphase lag. This may happen owing to loss of either of the maternal chromosomes, or of the paternal chromosome. If one of the maternal chromosomes is lost, the resulting cell or cells will be normal. If the paternal chromosome is lost, the cells will be diploid but uniparental disomy will result.

understood and the chromosome lost is thought to be random. If by chance the paternal copy is lost, there will be a normal chromosome number in the fetus, but maternal UPD 15. Trisomy rescue and UPD can potentially involve any chromosome, but if imprinted genes are present on the particular chromosome involved, this may have consequences for the fetus. Maternal UPD 15 is a cause of Prader-Willi syndrome (see earlier). In this scenario, there is no paternal contribution of chromosome 15. Therefore, testing for UPD is indicated as a follow-up to CPM detected by CVS when a chromosome containing known imprinted genes is involved (e.g., chromosomes 6, 7, 11, 14, and 15). If the chromosome involved in the original trisomy does not contain imprinted genes, no phenotypic consequences for the fetus would be predicted.

In the early 1990s, there were a number of reports of fetal limb reduction defects following CVS.<sup>130,131</sup> The procedures in the affected infants were largely performed between 55 and 66 days of gestation, and subsequent studies indicated that early gestational age (<10 completed weeks) at sampling increased the risk for this complication. After much investigation, including a large study of more than 140,000 cases of CVS submitted to the World Health Organization registry, it was concluded that there is no increased risk of limb reduction defects following CVS performed at greater than 10 weeks' gestation.<sup>132</sup> With both CVS and amniocentesis, the miscarriage rates are correlated with experience of the clinician and ongoing procedure volume.<sup>133,134</sup>

### Multiple Gestations

If a twin gestation is present, the risk of a chromosome abnormality has been thought to be increased as compared with a singleton pregnancy, and mathematically derived formulas have been used to estimate age-related risks of chromosomal abnormalities in twin



gestations.<sup>135</sup> However, the incidence of DS actually appears to be significantly lower than expected in twin pregnancies, particularly in older women and in monochorionic twins.<sup>102</sup> The chance that one or both fetuses will have a chromosome abnormality is dependent on the zygosity. There are three possibilities that would result in either one or both twins being affected: (1) dizygotic twins with one fetus affected, (2) dizygotic twins with both fetuses affected, and (3) monozygotic twins with both fetuses affected. Postzygotic errors can also result in discordant karyotypes in monozygotic twins, although this is rare.

Knowledge of chorionicity is critical when performing invasive procedures in multiple gestations. This is best determined by ultrasound in the first trimester, at which time the determination of chorionicity is highly accurate<sup>136</sup> (see Chapter 7). Prenatal diagnosis in monochorionic pregnancies theoretically requires only one sample, because the fetuses should be chromosomally identical. However, there is a small chance of postzygotic mutations leading to discordant karyotype or of incorrect assignment of chorionicity. For this reason, both twins are typically sampled.

Both CVS and amniocentesis can be used for prenatal diagnosis in multiple gestations. The technique for amniocentesis involves visualizing the dividing membrane and identifying an amniotic fluid pocket in each sac. In order to be certain that each amniotic sac is sampled, 0.5 mL of indigo carmine dye is often instilled after removal of fluid from the first sac. Aspiration of clear fluid from the second sac ensures proper placement. Indigo carmine has not been associated with risks to the fetus, whereas methylene blue dye should not be used owing to reports of fetal hemolysis, bowel atresia, and fetal demise when injected intra-amniotically.<sup>137-139</sup> A single-needle insertion technique for amniocentesis has also been reported, with puncture of the dividing membrane to access the second sac.<sup>140</sup> This raises the potential for admixture of samples with mosaic results, as well as disruption of the intertwin membrane. Reports of fetal abnormalities in twin gestations following rupture of the membrane,<sup>141</sup> and the possibility of creating an iatrogenic monoamniotic twin pregnancy with potential for umbilical cord entanglement, are also concerns.

With CVS, the procedure requires careful sonographic determination of placentation, because dye studies to mark the sample are not possible. Placing the tip of the aspiration device (catheter or needle) near the cord insertion can minimize the possibility of sampling the same fetus twice. A risk of less than 2% of sampling error has been reported with CVS in multiple gestations.<sup>142</sup> With either CVS or amniocentesis, detailed description of the relative locations of the fetuses and placentas is important, particularly if discordant karyotypes are present and selective termination is to be considered. Noting any structural abnormalities or other findings that can differentiate the fetuses is also helpful.

### Postprocedural Loss Rates in Multiple Gestations

Although genetic amniocentesis is frequently performed in multiple gestations, smaller numbers limit the availability of data regarding postprocedural losses in multiple gestations following either amniocentesis or CVS. A number of studies have been performed to assess fetal loss rate following amniocentesis in twins. The quoted rate of loss ranges from 2.7% to 8.1%, with a recent systematic review reporting an overall pregnancy loss rate of 3.07%.<sup>142-144</sup> Whereas some studies do suggest a higher postprocedural loss rate in twin pregnancies when compared with singletons, not all account for the higher background loss rate of twins.

With CVS, even more limited data are available to determine the safety and accuracy of this procedure in multiple gestations. Reported pregnancy loss rates in the largest recent trials reported in the literature range from 0.6% to 4.0%, again comparing favorably with the 6%

background loss rate reported for twin pregnancies.<sup>136,142-147</sup> Current data indicate that the excess risk following invasive diagnostic testing with either amniocentesis or CVS is approximately 1% to 2%.<sup>144,147</sup>

The choice as to whether to perform amniocentesis or CVS in a multiple pregnancy depends on many factors, such as the likelihood of proceeding to multifetal pregnancy reduction, the gestational age at presentation, the experience of the operator, and the technical difficulties of the specific case, including maternal body habitus and relative positions of the gestational sacs and placentas. Several studies have shown that CVS, in the hands of experienced operators, is at least as safe as second trimester amniocentesis for prenatal diagnosis in multiple pregnancies, with loss rates comparable to control twins.<sup>136,142-147</sup>

### Selective Termination of Multifetal Pregnancies

The finding of a single affected fetus in a multiple gestation can present a complex counseling situation. Management options include termination of the entire pregnancy, continuation of the pregnancy, or selective termination. Selective termination in a dichorionic twin pregnancy can be performed with fetal intracardiac injection of potassium chloride. Such an approach is effective, but it carries a loss rate of 4% to 12% for the remaining fetus or fetuses, depending on the gestational age of the pregnancy, starting number of fetuses, and location of the affected fetus.<sup>148,149</sup> If the pregnancy is monochorionic, but discordant for a chromosomal or structural abnormality, the ubiquitous presence of intertwin anastomoses makes intracardiac injection unsafe for the normal twin. If selective termination is desired in this situation, umbilical cord occlusion using laser, ligation, or bipolar coagulation is the only option. Few data exist as to risks to the pregnancy and the remaining twin if this approach is chosen, although there is an increased risk of pregnancy loss and preterm delivery of 15% to 25%.<sup>150,151</sup>

### Fetal Blood Sampling and Other Fetal Tissue Biopsy

Although there are theoretically many indications for accessing the fetal circulation directly, advances in molecular genetic technology have greatly decreased the need for percutaneous umbilical blood sampling (PUBS) as well as for performing biopsy of tissues such as fetal muscle, skin, or liver. PUBS has frequently been used to obtain fetal blood for rapid karyotyping, but again, the availability of FISH to detect the most common trisomies has decreased the need for this technique. Disorders such as hemophilia, hemoglobinopathies, immunodeficiencies, and diseases expressed in muscle, skin, and liver that have, in the past, required direct biochemical evaluation of fetal tissue can now commonly be detected through DNA analysis on amniocytes or chorionic villi. At present, PUBS is most commonly used in the evaluation and treatment of fetal alloimmunization when a need for in utero transfusion is suspected. When this procedure is performed, it is done under continuous ultrasound guidance. The umbilical cord insertion into the placenta is identified; this site is commonly used for sampling because the cord is fixed at this location. The cord insertion into the fetus or a free loop of cord can also be accessed; however, this may be more difficult owing to movement of the cord and fetus. The mother may be given parenteral sedation both for her comfort and to decrease fetal movement. Intramuscular or intravascular injection of a short-acting paralytic medication is also occasionally used to eliminate fetal movement, although the long-term effects of fetal paralysis are unknown.<sup>152,153</sup> Once the optimal site for accessing the cord has been identified, the maternal abdomen is prepped and draped, and the insertion site is infiltrated with a local anesthetic. Under ultrasound guidance, a 20- or 22-G spinal needle is advanced into the umbilical vein. Samples of fetal blood are aspirated into heparinized syringes.<sup>154</sup>



### Preimplantation Genetic Diagnosis

PGD is a prenatal testing technique in which early embryos, conceived through IVF, undergo genetic testing while being cultured in vitro, before reimplantation in the uterus (Fig. 2-17). *Preimplantation genetic screening* (PGS) is a term used to specifically describe cases in which aneuploidy testing is performed to screen for chromosomal abnormalities in the embryo. In either case, only those embryos with normal results are transferred. PGD can be used to test for most genetic disorders in which a mutation has been identified and can be helpful for couples at high risk of having a fetus affected by a genetic disease for whom pregnancy termination after CVS or amniocentesis is not an option. Because the genetic testing done in cases of PGD must be performed using just one or two cells from these early embryos, with a very rapid turnaround time (generally less than 24 hours), the technique is complex and errors can occur. The rate of error is generally quoted as less than 5%,<sup>155</sup> and it is recommended that CVS or amniocentesis be used to confirm results from PGD. Again, large studies to determine the accuracy and efficacy of PGD are clearly needed.<sup>156</sup> PGD is also used to select euploid embryos in couples who are carriers of balanced translocations. Although the use of IVF with PGS and selection of only euploid embryos is appealing for couples with unexplained recurrent pregnancy loss, the prognosis for live birth in a subsequent pregnancy without any intervention is approximately 75%.<sup>157</sup> Whether the outcome of IVF with PGS for common aneuploidies in women of advanced reproductive age is of benefit remains controversial.<sup>158-160</sup>

### PRENATAL TESTING FOR CONGENITAL MALFORMATIONS

Anomalies such as NTD, cleft lip and palate, and CHDs usually occur as multifactorial traits, caused by an interaction of multiple genes with environmental factors. Because these disorders have an elevated risk of recurrence in families, prenatal testing is often requested. Owing to their complex genetic causes, congenital malformations cannot be identified by amniocentesis or CVS. In most cases, prenatal testing consists of detailed ultrasound evaluation aimed at the detection or elucidation of specific fetal birth defects.

As in all other areas of medicine, providing appropriate information and treatment relies on a correct diagnosis. In the prenatal diagnosis of congenital disorders, providing prognostic information or evaluating a possible recurrence in a future pregnancy relies first and foremost on ensuring the correct diagnosis of the original affected child (or other relative). Increasingly, prenatal intervention is offered for such disorders, and again, the prognosis and outcome with such intervention also are dependent on accurate diagnosis of the abnormality and associated findings. Whereas many congenital malformations are isolated traits, they can also occur as part of a syndrome in which a pattern of malformations and features results from a single cause. The cause of a syndrome can involve an entire chromosome (that is, trisomy), deletion of a small chromosome region, or a single gene mutation. Often the other features of the syndrome cannot be detected by ultrasound, and therefore, careful counseling of the family, as well as consideration of other testing, is important.

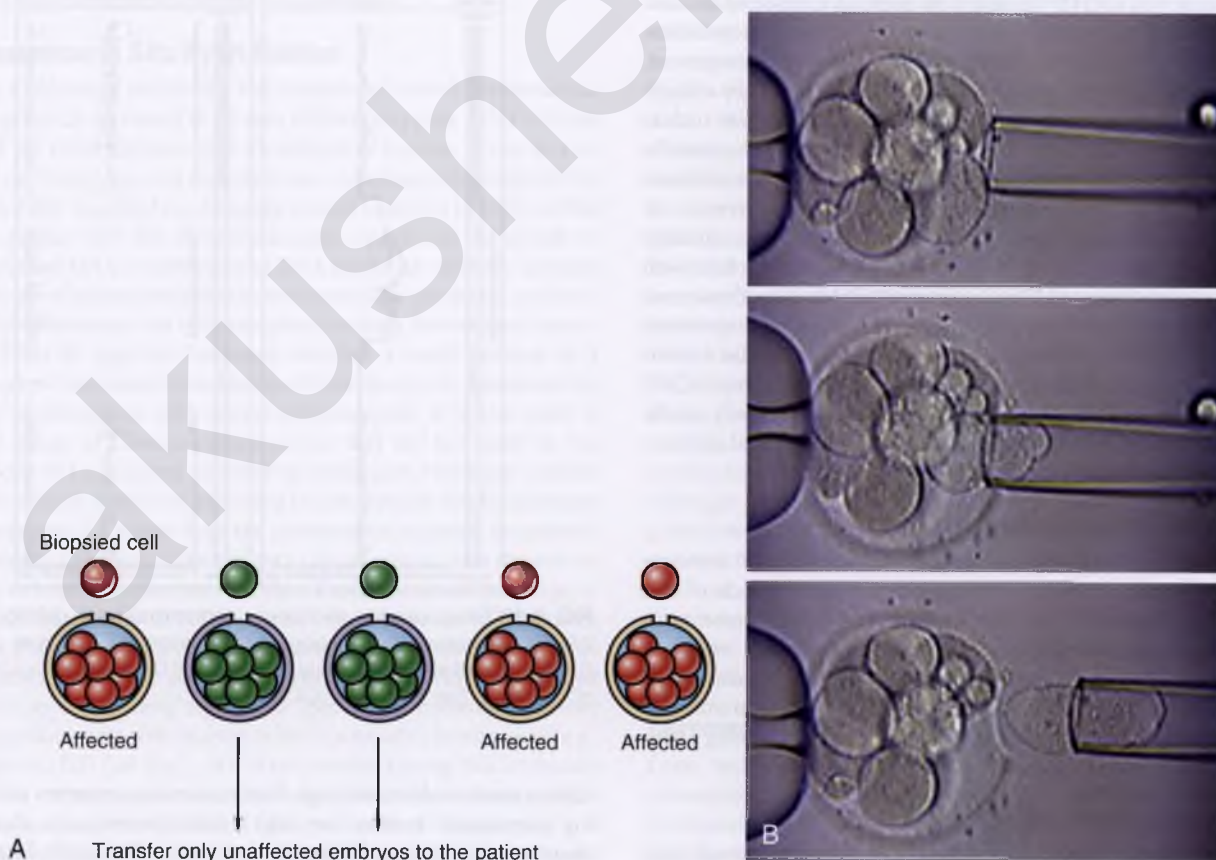


**FIG 2-17** **A** and **B**, Technique of preimplantation genetic diagnosis. In vitro fertilization is used to create embryos. One or two cells are removed for genetic analysis, and unaffected embryos are transferred to the uterus.



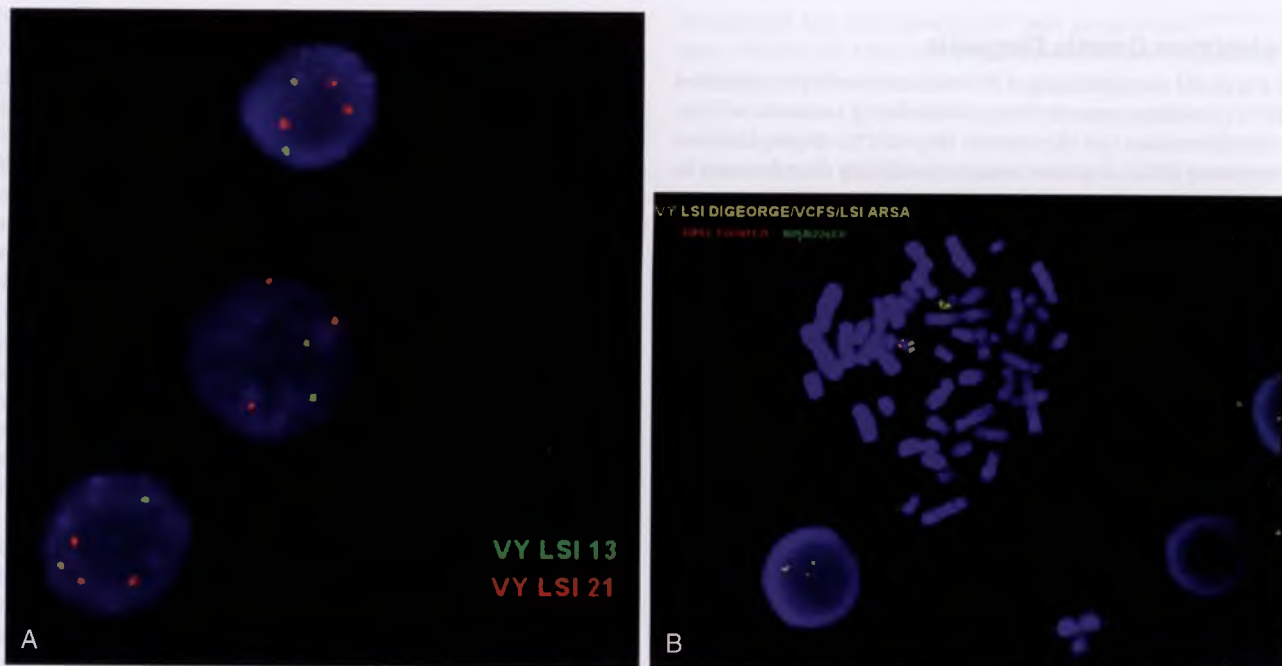


**FIG 2-18** **A**, Fluorescence in situ hybridization in interphase cells. Probes to chromosome 21 (test) are red and to chromosome 13 (control) are green. Presence of three red signals indicates the presence of trisomy 21. **B**, Fluorescence in situ hybridization in metaphase cell. Probes to chromosome 22q11 (test) are red, and to 22q13 (control) are green. Presence of a single red signal indicates a 22q11.2 deletion and the presence of 22q11.2 deletion syndrome.

As an example, a CHD identified on prenatal ultrasound is commonly an isolated finding. However, it may occur as part of a syndrome in which other abnormalities, such as mental retardation, are present. CHDs are heterogeneous in etiology, caused in some cases by a single gene or chromosomal mechanism, and in others by teratogens such as rubella infection or poorly controlled maternal diabetes. The cause in most cases is unknown, and the majority is believed to be multifactorial in origin. First-degree relatives have an increased recurrence risk of 2% to 4%. Prenatal ultrasound (echocardiography) is typically offered to couples with a strong family history or a previous fetus with CHD. In cases in which a CHD is unexpectedly detected by ultrasound, amniocentesis is offered to test for chromosome abnormalities, which underlie 10% to 15% of fetal CHD. Amniocentesis can also test for genetic abnormalities that increase the risk of CHD. For example, CHD is often associated with chromosomal microdeletions, which can be detected through the use of FISH (Fig. 2-18) or chromosomal microarray on fetal tissue obtained by amniocentesis (Fig. 2-19).

### Techniques of Genetic Analysis

Over the past 2 decades, advances in genetics have included increases in our understanding of novel genetic mechanisms. Much of this increased understanding has come about from improvements in genetic technology, allowing more detailed investigation of genes, mechanisms of mutation, and genetic variation in the population. As these techniques are used and investigated, an increasing number of clinically available tests are offered, with more and more being applicable to and useful for evaluation of the fetus.

### Chromosome Identification

Standard prenatal diagnosis involves evaluation of the individual chromosomes making up the fetal karyotype. Giemsa staining, which produces a specific banding pattern called G banding, is the technique that has been most widely used in clinical cytogenetics laboratories for

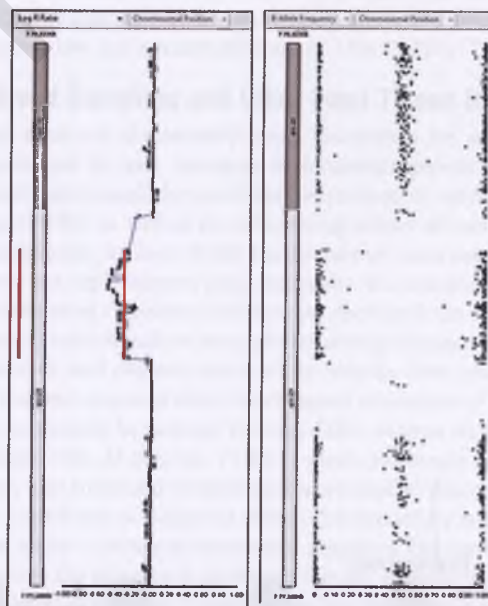


**FIG 2-19** Chromosomal microarray demonstrating a deletion in the William syndrome critical region on chromosome 7 (red line). *Left*, log R ratio; *right*, B-allele frequency. (Courtesy of Dr. Jingwei Yu, University of California, San Francisco, CA.)

chromosome analysis, although chromosomal microarrays are becoming increasingly routine (see later). Each chromosome stains in a characteristic pattern of light and dark bands (Fig. 2-20). In an internationally accepted system of chromosome classification, the dark and light bands on each chromosome are numbered. This numbering system allows the location of any particular band and its involvement



FIG 2-20 G-banded male karyotype.

in any chromosome abnormality to be described unambiguously and precisely.

### Fluorescence in Situ Hybridization

FISH is a technique that allows visualization of a small chromosomal region, generally too small to be seen with karyotyping. FISH can also be used for rapid chromosome identification because it can be performed on interphase cells and, therefore, culturing is not required for analysis. FISH is carried out by using a small fragment of DNA (called a DNA probe) with the same nucleotide sequence as the stretch of chromosomal DNA of interest. The DNA probe is covalently attached to a fluorescent label; hybridized with metaphase, prophase, or interphase chromosomes; and then visualized under a fluorescence microscope. FISH is used to determine whether a small portion of a chromosome (too small to be seen on the karyotype) is deleted and to identify translocations and marker chromosomes. It is also used to identify pieces of chromosomal material that are too small or too ambiguous to be localized by banding techniques. Normally, a probe will hybridize in two places, reflecting the presence of two homologous chromosomes. If a probe from the chromosome segment in question hybridizes to only one of the patient's chromosomes, then the patient is likely to have a deletion on the other. Excess chromosomal material can also be detected with FISH, in which case the probe will hybridize in more than two places. As a rapid assessment for trisomy (or other aneuploidy), interphase cells can be analyzed with FISH probes that hybridize to centromeric regions of specific chromosomes, thereby allowing a fast count of the copy number of a specific chromosome (e.g., 21 to rule out DS) (see Fig. 2-18). In the prenatal setting, this is typically targeted to chromosomes 13, 18, 21, X, and Y with results from analysis of interphase nuclei available in 24 to 48 hours. The sensitivity and specificity for the detection of aneuploidy are greater than 99.6% and greater than 99.9%, respectively. Because only specific chromosomes are queried, the technique is not comprehensive. It cannot detect balanced rearrangements, inversions, or Robertsonian translocations.

### Molecular Techniques for DNA Analysis

It is surprisingly easy to isolate pure DNA, which is generally very stable when compared with enzymes and other molecules. DNA can be extracted from any cell type that has a nucleus, including white blood cells, buccal cells, amniocytes, chorionic villi, and skin fibroblasts. PCR can be used to amplify very small quantities of DNA, allowing small samples to be used for the detection of specific mutations.

Genetic mutations generally occur as a result of point mutations, deletions, or duplications. PCR and Southern blotting are commonly used techniques for the identification of genetic mutations in DNA samples. Automated techniques of DNA sequencing are also available; such sequencing was used to complete the human genome project in 2003. Use of sequencing in clinical practice is increasingly common but is complicated by the potential for identification of previously undescribed mutations of uncertain clinical significance.

When a molecular cause of a disorder is identified, this allows a specific test to be applied to at-risk relatives or for prenatal diagnosis. Although gene sequencing is a powerful tool for the identification of genetic mutation, it is critical that firm proof of the diagnosis exists and that the gene mutation identified is known to be causative. In addition, detection of a mutation in a person (or fetus) at risk does not make a diagnosis of a clinical disorder and all the previously described caveats are critical to accurate diagnosis and management of genetic disorders, particularly in the prenatal setting.

### Chromosomal Microarray

Other techniques for molecular evaluation of the genome, such as chromosomal microarray analysis (CMA), have been relatively recently developed and introduced into clinical use. CMA is increasingly used for prenatal evaluation of chromosomes and chromosome abnormalities in the fetus. Currently, CMA is recommended by the ACMG as a first-tier test in the evaluation of children with intellectual disabilities, autism spectrum disorders, and birth defects of undetermined origin,



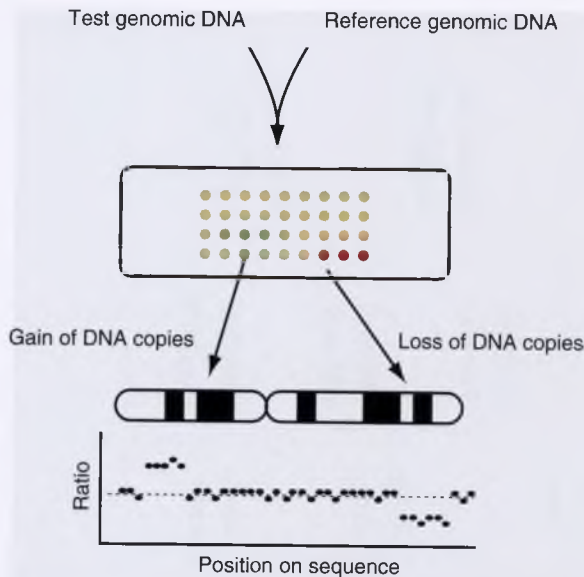


**FIG 2-21** Array comparative genomic hybridization (CGH) technique. DNA to be tested is labeled green, and control reference DNA is red. Labeled DNA is hybridized to a microarray containing hundreds to thousands of DNA clones, and copy number is analyzed for each clone. The ratio of test to reference DNA at each clone is indicated on the graph. Increase in ratio of test DNA indicates duplication or trisomy, and decrease in ratio indicates deletion or monosomy for each clone.

and this technique is now also recommended by the ACOG for the evaluation of fetuses with structural abnormalities.<sup>161</sup> CMA can be performed by two techniques: comparative genomic hybridization (CGH) and single nucleotide polymorphism (SNP) array. CGH is a technique whereby DNA from a test subject is hybridized together with control DNA. Differential labeling of the test versus control DNA allows comparative analysis of copy number, thus screening for decrease or increase in copy number across the genome. This method of testing cannot identify triploidy. Deletions or duplications in a particular region are identified by computer analysis of signal intensity. CMA by single nucleotide polymorphism array is a technique whereby only the fetal DNA is affixed to the slide where labeled control DNA has been applied. This modality of testing can identify regions of homozygosity, suggesting consanguinity or UPD (see earlier) as well as triploidy. Originally developed primarily for use in cancer, CMA has great utility in pediatric and prenatal cases, in which features suggest a chromosomal abnormality but are not specific enough to indicate a single FISH analysis (Figs. 2-20 and 2-21).<sup>162</sup>

The benefit of CMA in the prenatal setting is the ability to perform the test from nearly any tissue including archived tissue or tissue that cannot be cultured. The test may be customized to focus on known disease-causing regions in the genome commonly identified in prenatal testing and has a higher yield than standard karyotype analysis. In 2012, a multicenter trial was published comparing prenatal CMA with standard karyotype analysis. CMA identified all of the clinically significant aneuploidies identified by conventional karyotype. In addition, the array CGH technique identified additional clinically significant abnormalities in approximately 6% of pregnancies in which there were structural abnormalities identified by ultrasound that were not detected by karyotype. CMA also detected an abnormality in 1.7% of structurally normal fetuses that had a normal karyotype.<sup>100</sup>

Limitations of CMA include an inability to identify a balanced rearrangement (although this is not typically disease causing unless there is disruption of a critical gene by the chromosome break) and an

inability to detect low levels of mosaicism. The time to results is not as rapid as FISH, which is often important in the prenatal setting. Although CMA can detect whole chromosomal aneuploidy, when common aneuploidy is suspected (trisomy 21, trisomy 18, or sex chromosome), conventional karyotype analysis may be more appropriate because of cost. The interpretation of microarray results can be challenging with variations of unknown significance or alterations in regions of unknown clinical significance. In the prenatal setting, clinically uncertain variants, variants associated with adult-onset disorders, and complex results may cause significant parental anxiety. Therefore, pretest and posttest genetic counseling is recommended.<sup>161</sup>

## REFERENCES

1. Evans MI, Hume RF, Jr, Johnson MP, et al: Integration of genetics and ultrasonography in prenatal diagnosis: just looking is not enough. *Am J Obstet Gynecol* 174:1925, 1996.
2. Heinonen OP, Sloane D, Shapiro S: *Birth Defects and Drugs in Pregnancy*, Littleton, MA, 1977, Publishing Sciences Group.
3. Carlson BM, editor: *Human Embryology and Developmental Biology*, ed 3, St. Louis, 2004, Mosby.
4. Schardein JL: *Chemically Induced Birth Defects*, ed 2, New York, 1993, Marcel-Dekker, p 2.
5. Therman E, Susman B, Denniston C: The nonrandom participation of human acrocentric chromosomes in Robertsonian translocations. *Ann Hum Genet* 53:49–65, 1989.
6. Freeman SB, Bean LH, Allen EG, et al: Ethnicity, sex, and the incidence of congenital heart defects: a report from the National Down Syndrome Project. *Genet Med* 10:173–180, 2008.
7. De Rubens FJ, del Pozzo MB, Hach JLP, et al: Heart malformations in children with Down syndrome. *Rev Esp Cardiol* 56:894–899, 2003.
8. Lakovscek IC, Streubel B, Ulm B: Natural outcome of trisomy 13, trisomy 18, and triploidy after prenatal diagnosis. *Am J Med Genet A* 155A(11):2626–2633, 2011.
9. Zaragoza MV, Surti U, Redline RW, et al: Parental origin and phenotype of triploidy in spontaneous abortions: predominance of diandry and association with the partial hydatidiform mole. *Am J Hum Genet* 66:1807, 2000.
10. Redline RW, Hassold T, Zaragoza MV: Prevalence of the partial molar phenotype in triploidy of maternal and paternal origin. *Hum Pathol* 29:505, 1998.
11. McFadden DE, Kalousek DK: Two different phenotypes of fetuses with chromosomal triploidy: correlation with parental origin of the extra haploid set. *Am J Med Genet* 38:535, 1991.
12. Pyott SM, Pepin MG, Schwarze U, et al: Recurrence of perinatal lethal osteogenesis imperfecta in sibships: parsing the risk between parental mosaicism for dominant mutations and autosomal recessive inheritance. *Genet Med* 13(2):125–130, 2011.
13. Ravine D, Gibson RN, Walker RG, et al: Evaluation of ultrasonographic diagnostic criteria for autosomal dominant polycystic kidney disease. *Lancet* 343:824, 1994.
14. Yu J, Chen Z, Ni Y, Li Z: CFTR mutations in men with congenital bilateral absence of the vas deferens (CBAVD): a systemic review and meta-analysis. *Hum Reprod* 27(1):25–35, 2012.
15. Steiner B, Rosendahl J, Witt H, et al: Common CFTR haplotypes and susceptibility to chronic pancreatitis and congenital bilateral absence of the vas deferens. *Hum Mutat* 32(8):912–920, 2011.
16. Allingham-Hawkins DJ, Babul-Hirji R, Chitayat D, et al: Fragile X premutation is a significant risk factor for premature ovarian failure: the International Collaborative POF in fragile X study. Preliminary data. *Am J Med Genet* 83:322, 1999.
17. Schwartz CE, Dean J, Howard-Peebles PN, et al: Obstetrical and gynecological complications in fragile X carriers: a multicenter study. *Am J Med Genet* 51:400, 1994.
18. American College of Obstetricians and Gynecologists Committee on Genetics: ACOG Committee Opinion No. 469: carrier screening for fragile X syndrome. *Obstet Gynecol* 116(4):1108–1110, 2010.



19. Lazaraviciute G, Kausar M, Bhattacharya S, et al: A systematic review and meta-analysis of DNA methylation levels and imprinting disorders in children conceived by IVF/ICSI compared with children conceived spontaneously. *Hum Reprod Update* 20(6):840–852, 2014.
20. Bradley LA, Palomaki GE, McDowell GA, ONTD Working Group; ACMG Laboratory Quality Assurance Committee: Technical standards and guidelines: prenatal screening for open neural tube defects. *Genet Med* 7(5):355, 2005.
21. Copp AJ, Stanier P, Greene ND: Neural tube defects: recent advances, unresolved questions, and controversies. *Lancet Neurol* 12(8):799–810, 2013.
22. Burren KA, Savery D, Massa V, et al: Gene-environment interactions in the causation of neural tube defects: folate deficiency increases susceptibility conferred by loss of Pax3 function. *Hum Mol Genet* 17:3675–3685, 2008.
23. Gregg NM: Congenital cataract following German measles in the mother. *Aust N Z J Ophthalmol* 19(267):1991, 1941.
24. Fabro S, Scialli AR: *Drug and Chemical Action in Pregnancy*, New York, 1986, Marcel-Dekker, p 239.
25. Moore KL, Persaud TVN: *The Developing Human: Clinically Oriented Embryology*, ed 6, Philadelphia, 1998, WB Saunders.
26. Diav-Citrin O, Ornoy A: *Adverse Environment and Prevention of Early Pregnancy Disorders. Early Pregnancy: Biology and Medicine*, vol 4, Cherry Hill, NJ, 2000, Siep Publications, p 5.
27. Centers for Disease Control and Prevention: *Congenital CMV Infection Trends and Statistics*. June 5, 2013. Available at <<http://www.cdc.gov/CMV/trends-stats.html>>.
28. Puder KS, Treadwell MC, Gonik B: Ultrasound characteristics of in utero infection. *Infect Dis Obstet Gynecol* 5(3):262–270, 1997.
29. Perucca E: Birth defects after prenatal exposure to antiepileptic drugs. *Lancet Neurol* 4(11):781–786, 2005.
30. Meador KJ, Baker GA, Browning N, et al: Cognitive function at 3 years of age after fetal exposure to antiepileptic drugs. *N Engl J Med* 360(16):1597–1605, 2009.
31. American College of Obstetricians and Gynecologists Committee on Obstetric Practice: ACOG Committee Opinion No. 299, September 2004 (replaces No. 158, September 1995). Guidelines for diagnostic imaging during pregnancy. *Obstet Gynecol* 104:647–651, 2004.
32. Centers for Disease Control and Prevention: *Prenatal Radiation Exposure: A Fact Sheet for Physicians*. Available at <<http://www.bt.cdc.gov/radiation/prenatalphysician.asp>>.
33. Schull WJ: *Effects of Atomic Radiation, a Half-Century of Studies from Hiroshima and Nagasaki*, New York, 1995, Wiley-Liss & Sons.
34. Wender-Ozegowska E, Wroblewska K, Zawiejaska A, et al: Threshold values of maternal blood glucose in early diabetic pregnancy—prediction of fetal malformations. *Acta Obstet Gynecol Scand* 84(1):17, 2005.
35. Temple R, Aldridge V, Greenwood R, et al: Association between outcome of pregnancy and glycaemic control in early pregnancy in type 1 diabetes: population based study. *BMJ* 325:1275, 2002.
36. Block SR, Watkins SM, Salemi JL, et al: Maternal pre-pregnancy body mass index and risk of selected birth defects: evidence of a dose-response relationship. *Paediatr Perinat Epidemiol* 27(6):521–531, 2013.
37. Levy HL: Historical background for the maternal PKU syndrome. *Pediatrics* 112:1516, 2003.
38. American College of Obstetricians and Gynecologists Committee on Genetics: ACOG Committee Opinion No. 486: update on carrier screening for cystic fibrosis. *Obstet Gynecol* 117(4):1028–1031, 2011.
39. Edwards JG, Feldman G, Goldberg J, et al: Expanded carrier screening in reproductive medicine—points to consider: a joint statement of the American College of Medical Genetics and Genomics, American College of Obstetricians and Gynecologists, National Society of Genetic Counselors, Perinatal Quality Foundation, and Society for Maternal-Fetal Medicine. *Obstet Gynecol* 125(3):653–662, 2015.
40. American College of Obstetricians and Gynecologists Committee on Genetics: ACOG Committee Opinion No. 442: preconception and prenatal carrier screening for genetic diseases in individuals of Eastern European Jewish descent. *Obstet Gynecol* 114:950–953, 2009.
41. American College of Obstetricians and Gynecologists Committee on Genetics: ACOG Committee Opinion No. 432: spinal muscular atrophy. *Obstet Gynecol* 113:1194–1196, 2009.
42. Prior TW, Professional Practice and Guidelines Committee: Carrier screening for spinal muscular atrophy. *Genet Med* 10(11):840–842, 2008.
43. Kaback M: Population-based genetic screening for reproductive counseling: the Tay-Sachs disease model. *Eur J Pediatr* 159:S192, 2000.
44. Berlin BM, Norton ME, Sugarman EA, et al: Cystic fibrosis and chromosome abnormalities associated with echogenic fetal bowel. *Obstet Gynecol* 94:135, 1999.
45. Scotet V, De Braekeleer M, Audrezet MP, et al: Prenatal detection of cystic fibrosis by ultrasonography: a retrospective study of more than 346,000 pregnancies. *J Med Genet* 39:443, 2002.
46. Bergstrand CG, Czar B: Demonstration of a new protein fraction in serum from the human fetus. *Scand J Clin Lab* 8:174, 1956.
47. Haddow JE: Prenatal screening for open neural tube defects, Down's syndrome, and other major fetal disorders. *Semin Perinatol* 14:488, 1990.
48. Baer RJ, Currier RJ, Norton ME, et al: Obstetric, perinatal, and fetal outcomes in pregnancies with false-positive integrated screening results. *Obstet Gynecol* 123(3):603–609, 2014.
49. Dugoff L: First and second-trimester maternal serum markers for aneuploidy and adverse obstetric outcomes. *Obstet Gynecol* 115(5):1052–1061, 2010.
50. Haddow JE, Knight GJ, Kloza EM: Relation between maternal weight and serum alpha-fetoprotein concentration during the second trimester. *Clin Chem* 27:133, 1981.
51. Johnson AM: Racial differences in MSAFP screening. In Jizejewski GH, Porter IH, editors: *Alpha-Fetoprotein and Congenital Disorders*, New York, 1985, Academic Press.
52. O'Brien JE, Drugan A, Chervenak F: Maternal serum alpha-fetoprotein screening: the need to use race/ethnic specific medians in Asians. *Fetal Diagn Ther* 8:367, 1993.
53. Wald NJ, Cuckle HS, Boreham J, et al: Maternal serum alpha-fetoprotein and diabetes mellitus. *Br J Obstet Gynaecol* 86:101, 1979.
54. Huttly W, Rudnicka A, Wald NJ: Second trimester prenatal screening markers for Down syndrome in women with insulin-dependent diabetes mellitus. *Prenat Diagn* 24:804, 2004.
55. Lynch L, Berkowitz RL: Maternal serum alpha-fetoprotein and coagulation profiles after multifetal pregnancy reduction. *Am J Obstet Gynecol* 169:987, 1993.
56. Palomaki GE, Knight GJ, Haddow JE, et al: Cigarette-smoking and levels of maternal serum alpha-fetoprotein, unconjugated estriol, and hCG: impact on Down syndrome screening. *Obstet Gynecol* 81:675, 1993.
57. Rudnicka AR, Wald NJ, Huttly W, Hackshaw AK: Influence of maternal smoking on the birth prevalence of Down syndrome and on second trimester screening performance. *Prenat Diagn* 22:893, 2002.
58. Muller F, Dreux S, Lemeur A, et al: Medically assisted reproduction and second-trimester maternal serum marker screening for Down syndrome. *Prenat Diagn* 23:1073, 2003.
59. Lambert-Messerlian G, Dugoff L, Vidaver J, et al: First- and second-trimester Down syndrome screening markers in pregnancies achieved through assisted reproductive technologies (ART): a FASTER trial study. *Prenat Diagn* 26:672, 2006.
60. Nadel AS, Green JK, Holmes LB, et al: Absence of need for amniocentesis in patients with elevated levels of maternal serum alpha-fetoprotein and normal ultrasonographic examinations. *N Engl J Med* 323:557, 1990.
61. Norem CT, Schoen EJ, Walton DL, et al: Routine ultrasonography compared with maternal serum alpha-fetoprotein for neural tube defect screening. *Obstet Gynecol* 106:747, 2005.
62. Milunsky A, Saperstein VS: Prenatal diagnosis of open neural tube defects using the amniotic fluid acetylcholinesterase assay. *Obstet Gynecol* 59:1, 1982.
63. Mirlesse V, Duguy N, Cynober E, et al: Alphafoetoprotein and acetylcholinesterase in amniotic fluid as a factor suggesting fetal skin and nerve lesions in a case of congenital varicella syndrome. *Prenat Diagn* 24:498, 2004.



64. Kelly JC, Petrocik E, Wassman ER: Amniotic fluid acetylcholinesterase ratios in prenatal diagnosis of fetal abnormalities. *Am J Obstet Gynecol* 161:703, 1989.
65. Feuchtbaum LB, Cunningham G, Waller DK, et al: Fetal karyotyping for chromosome abnormalities after unexplained maternal serum alpha-fetoprotein screening. *Obstet Gynecol* 86:248, 1995.
66. Megerian G, Godmilow L, Donnenfeld A: Ultrasound-adjusted risk and spectrum of fetal chromosomal abnormality in women with elevated maternal serum alpha-fetoprotein. *Obstet Gynecol* 85:952, 1995.
67. Crandall BF, Matsumoto M: Risks associated with an elevated amniotic fluid alpha-fetoprotein level. *Am J Med Genet* 39:64, 1991.
68. Ryyanen M, Seppala M, Kuusela P, et al: Antenatal screening for congenital nephrosis in Finland by maternal serum alpha-fetoprotein. *Br J Obstet Gynaecol* 90:437, 1983.
69. Wenstrom KD, Owen J, Davis RO, et al: Prognostic significance of unexplained elevated amniotic fluid alpha-fetoprotein. *Obstet Gynecol* 87:213, 1996.
70. Savva GM, Morris JK, Mutton DE, Alberman E: Maternal age-specific fetal loss rates in Down syndrome pregnancies. *Prenat Diagn* 26:499, 2006.
71. Antonarakis SE: Parental origin of the extra chromosome in trisomy 21 as indicated by analysis of DNA polymorphisms. Down Syndrome Collaborative Group. *N Engl J Med* 324:872, 1991.
72. Wald NJ, Cuckle HS, Densem JW, et al: Maternal serum screening for Down syndrome in early pregnancy. *Br Med J* 297(6653):883–887, 1988.
73. Wald NJ, Hackshaw AK: Combining ultrasound and biochemistry in first-trimester screening for Down syndrome. *Prenat Diagn* 17(9):821, 1997.
74. Canick JA, Lambert-Messerlian GM, Palomaki GE, et al: Comparison of serum markers in first-trimester Down syndrome screening. *Obstet Gynecol* 108(5):1192, 2006.
75. Nicolaides KH: Nuchal translucency and other first-trimester sonographic markers of chromosomal abnormalities. *Am J Obstet Gynecol* 191(1):45, 2004.
76. Lambert-Messerlian GM, Canick JA, Palomaki GE, et al: Second trimester levels of maternal serum inhibin A, total inhibin, alpha inhibin precursor, and activin in Down syndrome pregnancy. *J Med Screen* 3(2):58, 1996.
77. Malone FD, Canick JA, Ball RH, et al: First- and second-trimester evaluation of risk (FASTER) research consortium. First-trimester or second-trimester screening, or both, for Down's syndrome. *N Engl J Med* 353:2001, 2005.
78. Wapner R, Thom E, Simpson JL, et al: First-trimester screening for trisomies 21 and 18. *N Engl J Med* 349(15):1405–1413, 2003.
79. Malone FD, Ball RH, Nyberg DA, et al: First-trimester septated cystic hygroma: prevalence, natural history and pediatric outcome. *Obstet Gynecol* 106(2):288, 2005.
80. Wald NJ, Cuckle HS: Biochemical screening. In Brock DJH, Rodeck CH, Ferguson-Smith MA, editors: *Prenatal Diagnosis and Screening*, Edinburgh, 1992, Churchill Livingstone, p 556.
81. Merkatz IR, Nitowsky HM, Macri JN, et al: An association between low maternal serum alpha-fetoprotein and fetal chromosome abnormalities. *Am J Obstet Gynecol* 148:886, 1984.
82. Cuckle HS, Wald NJ, Lindenbaum RH: Cord serum alpha-fetoprotein and Down syndrome. *Br J Obstet Gynaecol* 93:407, 1986.
83. Jorgensen PI, Trolle D: Low urinary oestriol excretion during pregnancy in women giving birth to infants with Down syndrome. *Lancet* 2:782, 1972.
84. Bogart MH, Pandian MR, Jones OW: Abnormal maternal serum chorionic gonadotropin levels in pregnancies with fetal chromosome abnormalities. *Prenat Diagn* 7:623, 1987.
85. Wallace EM, Swanston IA, McNeilly AS, et al: Second trimester screening for Down syndrome using maternal serum dimeric inhibin A. *Clin Endocrinol* 44:17, 1996.
86. Canick JA, MacRae AR: Second trimester serum markers. *Semin Perinatol* 29:203, 2005.
87. Wald NJ, Kennard A, Hackshaw A, McGuire A: Antenatal screening for Down's syndrome. *J Med Screen* 4(4):181, 1997.
88. Palomaki GE, Knight GJ, Haddow JE, et al: Prospective trial of a screening protocol to identify trisomy 18 using maternal serum alpha-fetoprotein, unconjugated estriol, and human chorionic gonadotropin. *Prenat Diagn* 49(Suppl):227, 1991.
89. Aagaard-Tillery KM, Malone FD, Nyberg DA, et al: Role of second-trimester genetic sonography after Down syndrome screening. *Obstet Gynecol* 114(6):1189, 2009.
90. Agathokleous M, Chaveeva P, Poon LCY, et al: Meta-analysis of second trimester markers for trisomy 21. *Ultrasound Obstet Gynecol* 41:247, 2013.
91. Wald NJ, Rodeck C, Hackshaw AK, et al: First and second trimester antenatal screening for Down's syndrome: the results of the Serum, Urine and Ultrasound Screening Study (SURUSS). *Health Technol Assess* 7(11):1, 2003.
92. Platt LD, Greene N, Johnson A, et al: Sequential pathways of testing after first-trimester screening for trisomy 21. *Obstet Gynecol* 104(4):661–666, 2004.
93. Lo YM, Corbetta N, Chamberlain PF, et al: Presence of fetal DNA in maternal plasma and serum. *Lancet* 350:485–487, 1997.
94. Norton ME, Brar H, Weiss J, et al: Non-Invasive Chromosomal Evaluation (NICE) Study: results of a multi-center prospective cohort study for detection of fetal trisomy 21 and trisomy 18. *Am J Obstet Gynecol* 207(2):137.e1–137.e8, 2012.
95. Zimmermann B, El-Sheikhah A, Nicolaides K, et al: Optimized real-time quantitative PCR measurement of male fetal DNA in maternal plasma. *Clin Chem* 51(9):2005, 1598–1604.
96. Kolialexi A, Tounta G, Mavrou A: Noninvasive fetal RhD genotyping from maternal blood. *Exp Rev Mol Diagn* 10(3):285–296, 2010.
97. American College of Obstetricians and Gynecologists Committee on Genetics: ACOG Committee Opinion No. 545: noninvasive prenatal testing for fetal aneuploidy. *Obstet Gynecol* 120:1532–1534, 2012.
98. Mersy E, Smits LJ, Van Winden LA, et al: Noninvasive detection of fetal trisomy 21: systematic review and report of quality and outcomes of diagnostic accuracy studies performed between 1997 and 2012. *Hum Reprod Update* 19(4):318, 2013.
99. Bianchi DW, Parker RL, Wentworth J, et al: DNA sequencing versus standard prenatal aneuploidy screening. *N Engl J Med* 370:799–808, 2014.
100. Wapner RJ, Martin CL, Levy B, et al: Chromosomal microarray versus karyotyping for prenatal diagnosis. *N Engl J Med* 367(23):2175–2184, 2012.
101. Fan HC, Gu W, Wang J, et al: Non-invasive prenatal measurement of the fetal genome. *Nature* 487(7407):320–324, 2012.
102. Boyle B, Morris JK, McConkey R, et al: Prevalence and risk of Down syndrome in monozygotic and dizygotic multiple pregnancies in Europe: implications for prenatal screening. *Br J Obstet Gynaecol* 121:809–820, 2014.
103. Robinson L, Grau P, Crandall BF: Pregnancy outcomes after increasing levels of maternal serum alpha-fetoprotein. *Obstet Gynecol* 74:17, 1989.
104. Zelop C, Nadel AS, Frigoletto F, et al: Placenta accreta, percreta and increta: a cause of increased maternal serum alpha-fetoprotein. *Obstet Gynecol* 80:693, 1992.
105. Hung TH, Shau WY, Hsieh CC, et al: Risk factors for placenta accreta. *Obstet Gynecol* 93:545–550, 1999.
106. Heinonen S, Ryyanen M, Kirkinen P, et al: Uterine malformation: a cause of elevated maternal serum alpha-fetoprotein concentrations. *Prenat Diagn* 16:635, 1996.
107. Palacio M, Jauniaux E, Kingdom J, et al: Perinatal outcome in pregnancies with a positive serum screening for Down's syndrome due to elevated levels of free beta-human chorionic gonadotropin. *Ultrasound Obstet Gynecol* 13:58, 1999.
108. Dugoff L, Hobbins JC, Malone FD, et al, FASTER Trial Research Consortium: Quad screen as a predictor of adverse pregnancy outcome. *Obstet Gynecol* 106(2):260, 2005.
109. Lepage N, Chitayat D, Kingdom J, Huang T: Association between second-trimester isolated high maternal serum maternal serum human chorionic gonadotropin levels and obstetric complications in singleton and twin pregnancies. *Am J Obstet Gynecol* 188:1354, 2003.



110. Onderoglu LS, Kabukcu A: Elevated second trimester human chorionic gonadotropin level associated with adverse pregnancy outcome. *Int J Gynaecol Obstet* 56:245, 1997.
111. Duric K, Skrabljin S, Lesin J, et al: Second trimester total human chorionic gonadotropin, alpha-fetoprotein and unconjugated estriol in predicting pregnancy complications other than fetal aneuploidy. *Eur J Obstet Gynecol Reprod Biol* 110:12, 2003.
112. Kowalczyk TD, Cabaniss ML, Cusmano L: Association of low unconjugated estriol in the second trimester and adverse pregnancy outcome. *Obstet Gynecol* 91:396, 1998.
113. Kelley RI: Inborn errors of cholesterol biosynthesis. *Adv Pediatr* 47:1, 2000.
114. Kratz LE, Kelley RI: Prenatal diagnosis of the RSH/Smith-Lemli-Opitz syndrome. *Am J Med Genet* 82:376, 1999.
115. Schoen E, Norem C, O'Keefe J, et al: Maternal serum unconjugated estriol as a predictor for Smith-Lemli-Opitz syndrome and other fetal conditions. *Obstet Gynecol* 102:167, 2003.
116. Kashork CD, Sutton VR, Fonda Allen JS, et al: Low or absent unconjugated estriol in pregnancy: an indicator for steroid sulfatase deficiency detectable by fluorescence in situ hybridization and biochemical analysis. *Prenat Diagn* 22:1028, 2002.
117. Bradley LA, Canick JA, Palomaki GE, Haddow JE: Undetectable maternal serum unconjugated estriol levels in the second trimester: risk of perinatal complications associated with placental sulfatase deficiency. *Am J Obstet Gynecol* 176:531, 1997.
118. Fuchs F: Volume of amniotic fluid at various stages of pregnancy. *Clin Obstet Gynecol* 9:449, 1966.
119. The Canadian Early and Mid-trimester Amniocentesis Trial (CEMAT) Group: Randomised trial to assess safety and fetal outcome of early and midtrimester amniocentesis. *Lancet* 351(9098):242, 1998.
120. American College of Obstetricians and Gynecologists Committee on Obstetric Practice and Committee on Genetics: ACOG Practice Bulletin No. 88: invasive prenatal testing for aneuploidy. *Obstet Gynecol* 110(6):1459–1467, 2007.
121. Odibo AO, Gray DL, Dicke JM, et al: Revisiting the fetal loss rate after second-trimester genetic amniocentesis: a single center's 16-year experience. *Obstet Gynecol* 111(3):589–595, 2008.
122. Akolekar R, Beta J, Picciarelli G, et al: Procedure-related risk of miscarriage following amniocentesis and chorionic villus sampling: a systematic review and meta-analysis. *Ultrasound Obstet Gynecol* 45(1):16–26, 2015.
123. Tabor A, Philip J, Madsen M, et al: Randomised controlled trial of genetic amniocentesis in 4606 low-risk women. *Lancet* 1:1287, 1986.
124. Rhoads GG, Jackson LG, Schlesselman SE, et al: The safety and efficacy of chorionic villus sampling for early prenatal diagnosis of cytogenetic abnormalities. *N Engl J Med* 320:609, 1989.
125. Canadian Collaborative CVS-Amniocentesis Clinical Trial Group: Multicentre randomised clinical trial of chorion villus sampling and amniocentesis. First report. *Lancet* 1(8628):1–6, 1989.
126. Wijnberger LD, van der Schouw YT, Christiaens GC: Learning in medicine: chorionic villus sampling. *Prenat Diagn* 20:241, 2000.
127. Robinson WP, Barrett IJ, Bernard L, et al: Meiotic origin of trisomy in confined placental mosaicism is correlated with presence of fetal uniparental disomy, high levels of trisomy in trophoblast, and increased risk of fetal intrauterine growth restriction. *Am J Hum Genet* 60:917, 1997.
128. Phillips OP, Tharapel AT, Lerner JL, et al: Risk of fetal mosaicism when placental mosaicism is diagnosed by chorionic villus sampling. *Am J Obstet Gynecol* 174:850, 1996.
129. Goldberg JD, Wohlferd MM: Incidence and outcome of chromosomal mosaicism found at the time of chorionic villus sampling. *Am J Obstet Gynecol* 176:1349, 1997.
130. Firth HV, Boyd PA, Chamberlain P, et al: Severe limb abnormalities after chorion villus sampling at 56–66 days' gestation. *Lancet* 1:762, 1991.
131. Hsieh FJ, Shyu MK, Sheu BC, et al: Limb defects after chorionic villus sampling. *Obstet Gynecol* 85:84, 1995.
132. Froster UG, Jackson L: Limb defects and chorionic villus sampling: results from an international registry, 1992–94. *Lancet* 347:489, 1996.
133. Tabor A, Vestergaard CH, Lidegaard Ø: Fetal loss rate after chorionic villus sampling and amniocentesis: an 11-year national registry study. *Ultrasound Obstet Gynecol* 34(1):19–24, 2009.
134. Caughey AB, Hopkins LM, Norton ME: Chorionic villus sampling compared with amniocentesis and the difference in the rate of pregnancy loss. *Obstet Gynecol* 108(3 Pt 1):612–616, 2006.
135. Rodis JF, Egan JGX, Craffey A, et al: Calculated risk of chromosomal abnormalities in twin gestations. *Obstet Gynecol* 76:1037, 1990.
136. Brambati B, Tului L, Guerclena S, Alberti E: Ultrasound outcome of first-trimester chorionic villus sampling for genetic investigation in multiple pregnancy. *Obstet Gynecol* 17:209, 2001.
137. McEnerney JK, McEnerney LN: Unfavorable neonatal outcome after intraamniotic injection of methylene blue. *Obstet Gynecol* 35:61, 1983.
138. Van der Pol JG, Wolf H, Boer K, et al: Jejunal atresia related to the use of methylene blue in genetic amniocentesis in twins. *Br J Obstet Gynaecol* 99:141, 1992.
139. Kidd SA, Lancaster PA, Anderson JC, et al: Fetal death after exposure to methylene blue dye during mid-trimester amniocentesis in twin pregnancy. *Prenat Diagn* 16:39, 1996.
140. Bahado-Singh R, Schmitt R, Hobbins JC: New technique for genetic amniocentesis in twins. *Obstet Gynecol* 79:304, 1992.
141. Gilbert WM, Davis SE, Kaplan C, et al: Morbidity associated with prenatal disruption of the dividing membrane in twin gestations. *Obstet Gynecol* 78:623, 1991.
142. Rochon M, Stone J: Invasive procedures in multiple gestations. *Curr Opin Obstet Gynecol* 15:167, 2003.
143. Yaron Y, Bryant-Greenwood PK, Dave N, et al: Multifetal pregnancy reductions of triplets to twins: comparison with nonreduced triplets and twins. *Am J Obstet Gynecol* 180:1268, 1999.
144. Agarwal K, Alfirevic Z: Pregnancy loss after chorionic villus sampling and genetic amniocentesis in twin pregnancies: a systematic review. *Ultrasound Obstet Gynecol* 40:128–134, 2012.
145. De Catte L, Liebaers I, Foulon W: Outcome of twin gestations after first-trimester chorionic villus sampling. *Obstet Gynecol* 96:714, 2000.
146. Antsaklis A, Souka AP, Daskalakis G, et al: Second-trimester amniocentesis vs. chorionic villus sampling for prenatal diagnosis in multiple gestations. *Ultrasound Obstet Gynecol* 20:476, 2002.
147. Cahill AG, Macones GA, Stamilio DM, et al: Pregnancy loss rate after mid-trimester amniocentesis in twin pregnancies. *Am J Obstet Gynecol* 200(3):257.e1–257.e6, 2009.
148. Evans MI, Goldberg JD, Horenstein J, et al: Selective termination for structural, chromosomal and Mendelian anomalies: international experience. *Am J Obstet Gynecol* 181:893, 1999.
149. Eddleman KD, Stone JL, Lynch L, Berkowitz RL: Selective termination of anomalous fetuses in multifetal pregnancies: two hundred cases at a single center. *Am J Obstet Gynecol* 187:1168, 2002.
150. Kumar S, Paramasivam G, Zhang E, et al: Perinatal- and procedure-related outcomes following radiofrequency ablation in monochorionic pregnancy. *Am J Obstet Gynecol* 210(5):454.e1–454.e6, 2014.
151. Moise KJ, Jr, Johnson A, Moise KY, Nickleit V: Radiofrequency ablation for selective reduction in the complicated monochorionic gestation. *Am J Obstet Gynecol* 198(2):198.e1–198.e5, 2008.
152. De Crespigny LC, Robinson HP, Quinn M, et al: Ultrasound-guided fetal blood transfusion for severe rhesus isoimmunization. *Obstet Gynecol* 66:529, 1985.
153. Seeds JW, Bowes WA: Ultrasound-guided fetal intravascular transfusion in severe rhesus isoimmunization. *Am J Obstet Gynecol* 154:1105, 1986.
154. Berry SM, Stone J, Norton ME, et al: Society for Maternal-Fetal Medicine (SMFM): Fetal blood sampling. *Am J Obstet Gynecol* 209(3):170–180, 2013.
155. Ray PF, Ao A, Taylor DM, et al: Assessment of the reliability of single blastomere analysis for preimplantation diagnosis of the delta F508 deletion causing cystic fibrosis in clinical practice. *Prenat Diagn* 18:1402, 1998.
156. Baruch S, Adamson GD, Cohen J, et al: Genetic testing of embryos: a critical need for data. *Reprod Biomed Online* 11:667, 2005.



157. Clifford K, Rai R, Regan L: Future pregnancy outcome in unexplained recurrent first trimester miscarriage. *Hum Reprod* 12(2):387–389, 1997.
158. Mastenbroek S, Repping S: Preimplantation genetic screening: back to the future. *Hum Reprod* 29(9):1846–1850, 2014.
159. Hardarson T, Hanson C, Lundin K, et al: Preimplantation genetic screening in women of advanced maternal age caused a decrease in clinical pregnancy rate: a randomized controlled trial. *Hum Reprod* 23:2806–2812, 2008.
160. Mastenbroek S, Twisk M, van Echten-Arends J, et al: In vitro fertilization with preimplantation genetic screening. *N Engl J Med* 357:9–17, 2007.
161. American College of Obstetricians and Gynecologists Committee on Genetics: ACOG Committee Opinion No. 581: the use of chromosomal microarray analysis in prenatal diagnosis. *Obstet Gynecol* 122:1374–1377, 2013.
162. Rickman L, Fiegler H, Carter NP, Bobrow M: Prenatal diagnosis by array-CGH. *Eur J Med Genet* 48:232, 2005.

akusherlib.ru

# Ultrasound Evaluation of Fetal Aneuploidy in the First and Second Trimesters

Katherine R. Goetzinger, Anthony O. Odibo

## SUMMARY OF KEY POINTS

- Major fetal malformations are highly associated with fetal chromosomal abnormalities, particularly central nervous system anomalies, facial abnormalities, cystic hygroma, diaphragmatic hernia, cardiac defects, gastrointestinal abnormalities, genitourinary anomalies, nonimmune hydrops fetalis (NIHF), and abnormalities involving the extremities.
- The combination of nuchal translucency (NT) measurement and maternal serum analytes, pregnancy-associated plasma protein-A (PAPP-A) and free  $\beta$ -hCG (human chorionic gonadotropin), is the most common aneuploidy screening paradigm in the first trimester of pregnancy.
- Incorporation of first trimester nasal bone documentation into NT and serum screening can increase the detection rate of trisomy 21 without significantly altering the false positive rate.
- The genetic sonogram is a targeted second trimester ultrasound examination that is performed at the time of the anatomic survey and assesses for major fetal malformations as well as minor markers of aneuploidy. The presence or absence of these markers, either alone or in combination, can adjust a patient's aneuploidy risk, specifically for trisomy 21.
- Likelihood ratios (LRs) have been established for each individual sonographic marker of aneuploidy; they can be multiplied by the patient's *a priori* risk to determine the patient's posttest odds for aneuploidy.
- Thickened nuchal skinfold and absent/hypoplastic nasal bone are the sonographic markers most specifically associated with trisomy 21 in the second trimester.
- In a low-risk population, pyelectasis, echogenic intracardiac foci, and choroid plexus cysts are not associated with an increased risk for aneuploidy when observed in isolation.
- The finding of one sonographic marker of aneuploidy should prompt a more targeted ultrasound examination to evaluate for additional signs of aneuploidy.

## OUTLINE

### Structural Abnormalities, 58

#### First Trimester Markers of Aneuploidy, 63

- Nuchal Translucency, 63
- Cystic Hygroma, 67
- Absent Nasal Bone, 67
- Ductus Venosus Doppler Studies, 68
- Tricuspid Regurgitation, 69
- Frontomaxillary Facial Angle, 69

#### The Second Trimester Genetic Sonogram, 69

- Thickened Nuchal Fold, 70
- Absent/Hypoplastic Nasal Bone, 70

Hyperechoic Bowel, 72

Femoral/Humeral Shortening, 72

Pyelectasis, 73

Echogenic Intracardiac Focus, 73

Other Minor Markers for Down Syndrome, 74

#### Second Trimester Sonographic Markers for Other Aneuploidies, 75

Choroid Plexus Cysts, 75

Single Umbilical Artery, 75

Abnormalities of the Extremities, 76

#### Conclusions, 77

In addition to biochemical screening, sonography is a noninvasive method used to perform risk assessment for fetal aneuploidy. In addition to the major congenital anomalies discussed later and listed in Table 3-1, multiple other first and second trimester ultrasound findings are associated with aneuploidy. Such findings, commonly referred to as *minor markers* or *soft markers*, typically are not structural anomalies per se and usually have no clinical significance to the fetus except for their association with aneuploidy. The presence or absence of these minor markers can be used to adjust a patient's *a priori* risk for aneuploidy based on biochemical screening results or maternal age. This

becomes particularly important in screening for trisomy 21, as approximately 75% of fetuses affected by trisomy 21 will not have ultrasound-detectable major congenital anomalies at the time of the second trimester anatomic survey.<sup>1</sup> This is in contrast to fetuses affected by trisomies 18 and 13, of which greater than 90% will have major structural malformations detectable by sonography in the second trimester of pregnancy.<sup>2-4</sup>

This chapter will review the most common first and second trimester ultrasound findings associated with fetal aneuploidy. We will discuss major malformations, as well as soft markers and their



**TABLE 3-1 Major Congenital Anomalies Associated With Fetal Aneuploidy**

Trisomy 21	Trisomy 13	Trisomy 18
AV canal defect	Cardiac defects	Cardiac defects
Duodenal atresia	CNS abnormalities	Spina bifida
Ventriculomegaly	Cleft lip/palate	Micrognathia
Other cardiac defects	Omphalocele	Omphalocele
Cystic hygroma	Midline facial anomalies	Clenched hands/wrists
Nonimmune hydrops	Echogenic kidneys	Radial aplasia
	Urogenital anomalies	Clubfeet
	Polydactyly	Cerebellar dysgenesis
	Rocker bottom feet	Cystic hygroma
	Cystic hygroma	Nonimmune hydrops
	Nonimmune hydrops	
	Congenital diaphragmatic hernia	Congenital diaphragmatic hernia

AV, atrioventricular; CNS, central nervous system.

Modified from Nyberg DA, Souter VL: Sonographic markers of fetal trisomies. *J Ultrasound Med* 20:655-674, 2001.

screening efficiency as well as their current role in aneuploidy risk calculation in the era of first trimester biochemical screening and prenatal screening using cell-free DNA (cfDNA).

## STRUCTURAL ABNORMALITIES

Structural abnormalities are more common in aneuploid fetuses, particularly central nervous system anomalies, facial abnormalities, cystic hygroma, diaphragmatic hernia, cardiac defects, gastrointestinal abnormalities, genitourinary anomalies, NIHF, and abnormalities involving the extremities. The large majority of fetuses with trisomies 13 and 18 have multiple major structural anomalies. Fetuses with Down syndrome, in contrast, are less likely to have structural abnormalities identified by second trimester sonography; it is reported that just 25% of second trimester fetuses with Down syndrome have sonographically detectable major congenital anomalies.<sup>5</sup> In two prenatal series before 20 weeks, structural anomalies were detected by sonography in only 16% to 17% of trisomy 21 fetuses.<sup>6,7</sup>

Identification of *cardiac malformations* on prenatal sonography substantially increases the risk for chromosomal abnormalities, with a frequency of aneuploidy reported to be as high as 22% to 32%.<sup>8,9</sup> The frequency of aneuploidy varies with the type of cardiac defect present and is higher with hypoplastic heart (Fig. 3-1), atrioventricular canal defects, tetralogy of Fallot, and double-outlet right ventricle as compared with isolated ventricular septal defects or valvular stenosis.<sup>10</sup> Atrioventricular canal defects have a very high risk of aneuploidy, particularly Down syndrome. In one series of 38 atrioventricular septal defects, aneuploidy was present in 22 (58%), with Down syndrome ( $n = 19$ ), trisomy 18 ( $n = 1$ ), trisomy 13 ( $n = 1$ ), and mosaicism ( $n = 1$ ) all identified.<sup>11</sup>

Approximately 50% of infants with Down syndrome have cardiac defects. However, most of these are ventricular septal defects (Fig. 3-2) and common atrioventricular canal defects (Fig. 3-3), and their detection by prenatal sonography is quite variable. One study reported that heart defects were detected in just over one half of fetuses with Down syndrome.<sup>12</sup> DeVore reported that nonspecific cardiac findings (such as tricuspid regurgitation, pericardial effusion, and right-left disproportion) were present in 76% of fetuses with Down syndrome, whereas just 9% had a characteristic atrioventricular septal defect.<sup>13</sup> In contrast,



**FIG 3-1** Apical four-chamber view in a second trimester fetus demonstrating hypoplastic left-sided heart syndrome.



**FIG 3-2** Apical four-chamber view of the fetal heart showing an inlet ventricular septal defect.

cardiac malformations are present in more than 90% of fetuses with trisomy 18 and 13. Studies have reported that major congenital heart defects can be identified sonographically in over 80% of fetuses with trisomy 18.<sup>4,14</sup>

*Duodenal atresia* (Fig. 3-4) is rarely recognized until after 20 to 24 weeks of pregnancy, when the characteristic double bubble sign (dilated fluid-filled stomach and proximal duodenum) and polyhydramnios become apparent. Duodenal atresia is the leading cause of intestinal obstruction among newborns and is highly associated with Down syndrome. Among cases of duodenal atresia detected prenatally, trisomy 21 is present in approximately one third of cases.<sup>10</sup>

The differential diagnosis of NIHF is extensive (Fig. 3-5); this disorder can result from a variety of both maternal and fetal causes. NIHF is recognized sonographically by ascites, pericardial effusions, pleural effusions, polyhydramnios, thickened placenta, and skin edema (see





**FIG 3-3** Transverse axial view of the fetal chest, showing a complete atrioventricular canal defect of the heart in a Down syndrome fetus. Note the primum atrial septal defect and inlet ventricular septal defect at the crux of the heart, along with a single atrioventricular valve.



Chapter 17). Aneuploidy is a common cause of NIHF, accounting for up to 16% of cases.<sup>15,16</sup> The most common karyotype abnormalities associated with hydrops include Turner syndrome (45,X); trisomies 21, 18, and 13; and triploidy. NIHF is most highly associated with aneuploidy when diagnosed earlier in pregnancy; a higher incidence of aneuploidy is identified in the second trimester as compared with the latter half of pregnancy.<sup>17</sup> The combination of generalized hydrops and cystic hygroma is often referred to as lymphangiectasia, which has a very poor prognosis. Lymphangiectasia is associated with aneuploidy, especially Turner syndrome, in approximately two thirds of cases (Fig. 3-6).

*Hydrothorax* (pleural effusion, chylothorax) has been linked to aneuploidy, especially Turner syndrome, Down syndrome, and trisomy 13. Among 82 cases of isolated fetal pleural effusion (Fig. 3-7) reported in the literature, Down syndrome was present in 4.9%.<sup>18</sup> Ascites (see Fig. 3-5) may also occur in isolation without other signs of hydrops. This finding has also been associated with aneuploidy; in one report of 18 fetuses with ascites, 5.6% ( $n = 1$ ) had Down syndrome.<sup>19</sup>

*Diaphragmatic hernia* (Fig. 3-8) results from a congenital defect in the fetal diaphragm, with herniation of abdominal viscera into the fetal chest (see Chapter 12). This abnormality carries an increased risk for aneuploidy, particularly trisomy 18 (most common), trisomy 13,

**FIG 3-4** Duodenal atresia in a fetus with Down syndrome. **A**, A transverse axial scan of the abdomen in the third trimester demonstrates the classic "double bubble" sign. **B**, Polyhydramnios was also present, as was echogenic bowel **(C)** (arrow).





**FIG 3-5** Transverse axial view of the fetal abdomen, demonstrating ascites (arrow) associated with nonimmune hydrops.



**FIG 3-6** Gross image of a stillborn fetus with a massive cystic hygroma surrounding the neck.

Down syndrome, Turner syndrome, and other chromosomal abnormalities. The frequency of aneuploidy is reported to be as high as 34%, although it generally ranges from 10% to 20% in reported series.<sup>20-22</sup>

An *omphalocele* (Figs. 3-9 and 3-10) occurs when there is a central abdominal wall defect that results in herniation of intra-abdominal structures into the base of the umbilical cord, which is covered by a membrane. Omphaloceles are associated with other fetal anomalies and aneuploidy, which complicates more than half of prenatally diagnosed cases. Associated aneuploidies include trisomies 18 and 13 (which are most frequent), Down syndrome, Turner syndrome, and

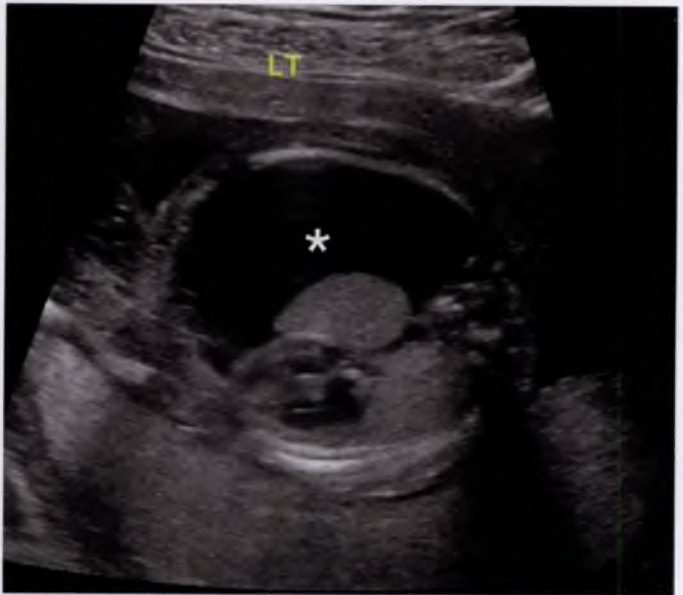


**FIG 3-7** Transverse axial view of the fetal chest, demonstrating a large, unilateral pleural effusion (asterisk) pushing the heart to the right side of the chest. LT, left thorax.



**FIG 3-8** Transverse axial view of the fetal chest, demonstrating a left-sided congenital diaphragmatic hernia (asterisk). The stomach (S) is herniated into the chest, and the heart (H) is displaced to the right. LT, left thorax; RT, right thorax.

triploidy. Similarly to other fetal malformations, there appears to be a higher frequency of aneuploidy in prenatal (30-40%) as compared with neonatal studies (which have a combined rate of 12%) owing to in utero lethality.<sup>10</sup> In one study of 35 cases of prenatally diagnosed omphalocele, 54% had aneuploidy: trisomy 18 ( $n = 17$ ), triploidy ( $n = 1$ ), and Klinefelter syndrome ( $n = 1$ ).<sup>23</sup> Small omphaloceles containing only bowel (see Fig. 3-10) have a higher aneuploidy risk than those containing liver, with one series reporting an aneuploidy rate of





**FIG 3-9** Sagittal view of a fetus with an omphalocele (arrow) at 13 weeks' gestation. Fetus also has an enlarged nuchal translucency (double arrows).

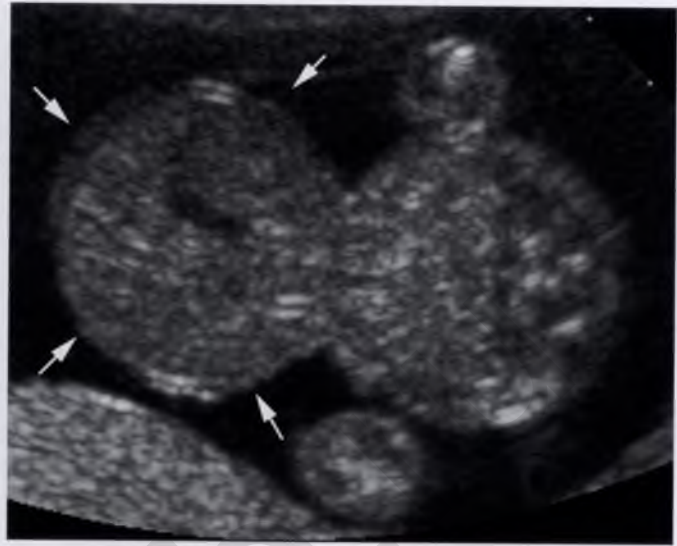


**FIG 3-11** Large liver containing omphalocele (arrows) in a second trimester patient. The omphalocele is larger than the native fetal abdomen.

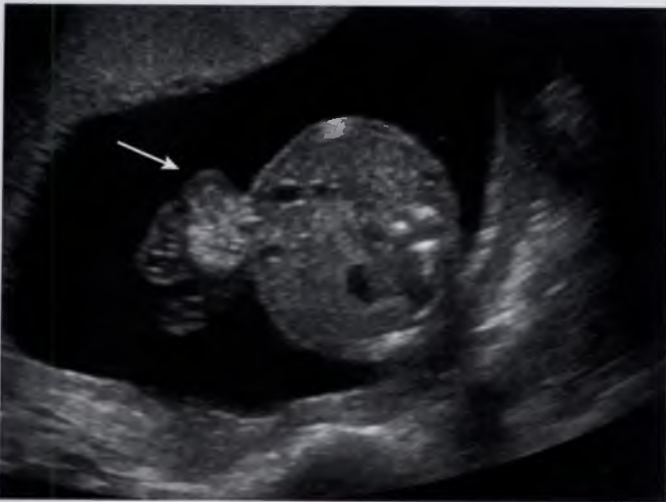


**FIG 3-10** Transverse scan of abdomen in a second trimester fetus demonstrating a small omphalocele (arrow) containing only small bowel.

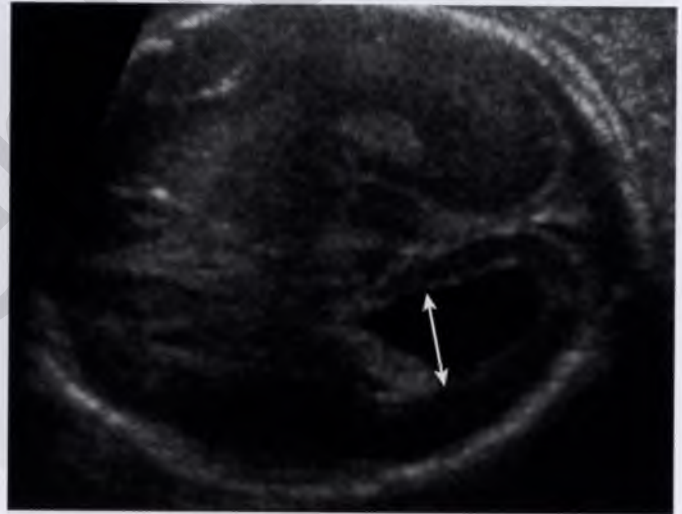


**FIG 3-12** Transverse axial scan at midgestation demonstrates mild ventriculomegaly associated with trisomy 21 (arrow).

87% in bowel only omphaloceles versus 9% in those containing liver (Fig. 3-11).<sup>24</sup>

Many central nervous system abnormalities carry an increased risk for fetal aneuploidy. Cerebral *ventriculomegaly* (Fig. 3-12), which is diagnosed when the atrial diameter of the cranial lateral ventricle reaches 10 mm or more, is relatively common finding on prenatal sonography. Ventriculomegaly (even mild) is associated with an increased risk for aneuploidy, particularly Down syndrome. However, mild ventriculomegaly may also be seen as a normal variant in the second trimester (after 20 weeks' gestation) and in male fetuses.<sup>10</sup> In one study of 31 fetuses with isolated borderline ventriculomegaly (10-15 mm), 9.7% ( $n = 3$ ) were found to have aneuploidy (Down syndrome [ $n = 2$ ] and trisomy 13 [ $n = 1$ ]).<sup>25</sup> In large series, 3.8% of fetuses with mild ventriculomegaly are karyotypically abnormal, with Down syndrome the most common aneuploidy.<sup>6</sup> In chromosomally normal, aneuploid, and Down syndrome fetuses, mild ventriculomegaly is observed in 0.5%, 6.8%, and 5.5%, respectively.<sup>6</sup>

*Hydrocephalus* (Fig. 3-13) and *spina bifida* (Fig. 3-14) are both associated with chromosomal abnormalities, primarily trisomy 18, trisomy 13, and triploidy.<sup>26</sup> In a review of 107 fetuses with central

nervous system abnormalities, aneuploidy was found in 3%, 8%, and 33% of fetuses with hydrocephalus, hydrocephalus and spina bifida, and spina bifida alone, respectively.<sup>26</sup> In one study of 38 fetuses with trisomy 18, 19% had neural tube defects and 8% had ventriculomegaly or hydrocephalus.<sup>4</sup>

Cerebellar abnormalities, such as Dandy-Walker malformation (DWM) or cerebellar hypoplasia, are associated with an increased risk for aneuploidy<sup>27</sup> (Figs. 3-15 to 3-17). Trisomy 18 is the most common aneuploidy seen with these anomalies, but other chromosomal abnormalities may also be observed. *Agnesis of the corpus callosum* (Fig. 3-18) can be complete or partial. The diagnosis is made by showing absence of the complex formed by the corpus callosum and cavum septum pellucidum, along with various other sonographic findings such as colpocephaly (disproportionate enlargement of the occipital horns) (Fig. 3-19). Aneuploidy is reported in approximately 20% of prenatally diagnosed cases, primarily trisomies 18, 8, and 13,<sup>28</sup> although a variety of other chromosomal abnormalities are also reported. A study reported in 2009 examined cases of agnesis of the corpus callosum diagnosed prenatally and postnatally.<sup>29</sup> Among the prenatally



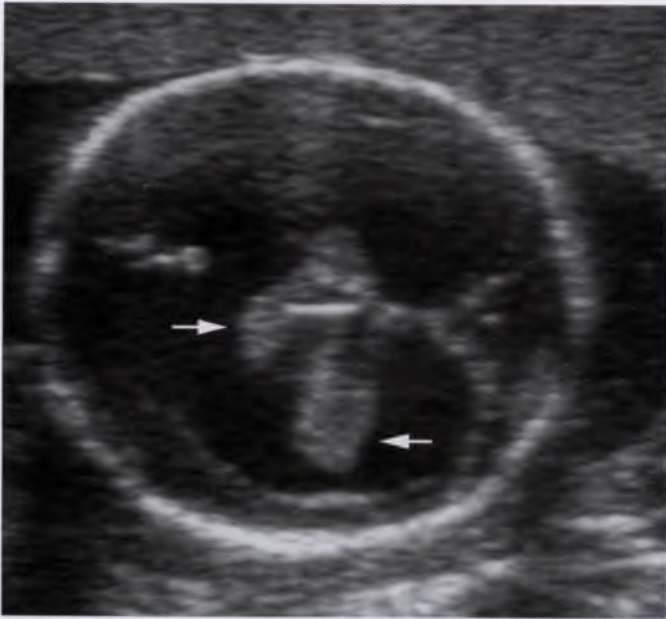


**FIG 3-13** Marked dilation of both lateral ventricles with dangling choroid plexuses (arrows) in a fetus with hydrocephalus.

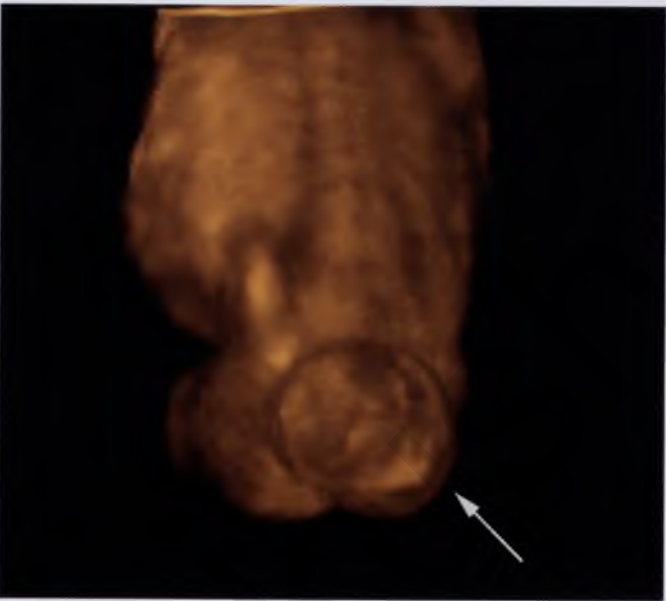


**FIG 3-14** Three-dimensional sonogram showing the fetal back affected by a neural tube defect (arrow) in the lumbosacral area.

diagnosed cases, aneuploidy was present in 8%, as compared with 4% in postnatal cases.

**Holoprosencephaly** (Figs. 3-20 and 3-21) is a midline abnormality of the brain, resulting from absent or incomplete division of the prosencephalon (embryonic forebrain) and formation of the midline structures. It is embryologically related to development of the midface, hence the common association with median facial anomalies (Fig. 3-22). There are three major types of holoprosencephalies, depending on the degree of anatomic abnormality: alobar, semilobar, and lobar. Aneuploidy is present in 50% to 60% of fetuses with alobar or semilobar holoprosencephaly. Of the various types of chromosomal abnormalities, trisomy 13 or a variant of trisomy 13 is the most common (found in 50-75% of those with abnormal karyotype). However, a wide variety of other aneuploidies has been reported. In fetuses with trisomy



**FIG 3-15** Dandy-Walker malformation in a trisomy 13 fetus. In a transverse axial plane, an enlarged fourth ventricle (arrow) is seen along with a defect in the cerebellar vermis. Note that the cerebellar hemispheres are splayed (asterisk).

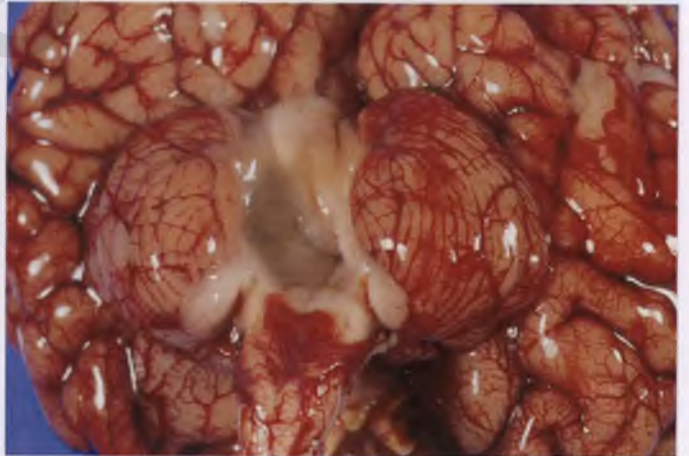


**FIG 3-16** Pathologic specimen of brain shows cerebellar hemispheres bilaterally, but with complete absence of the vermis, consistent with Dandy-Walker malformation.

13, holoprosencephaly was reported in 39%.<sup>30</sup> When other abnormalities are present, in addition to holoprosencephaly, the risk for aneuploidy is increased.

Abnormalities of the facial profile are common in fetuses or neonates with chromosomal abnormalities. Some chromosomally abnormal fetuses or neonates demonstrate *micrognathia* (Figs. 3-23 and 3-24), a sloping forehead (see Fig. 3-24), flattened profile (Fig. 3-25), or *retrognathia*. In one study examining the sonographic features of 38 fetuses with trisomy 18, approximately one half (53%) had facial anomalies identified.<sup>4</sup> Twenty-nine percent had an abnormal profile

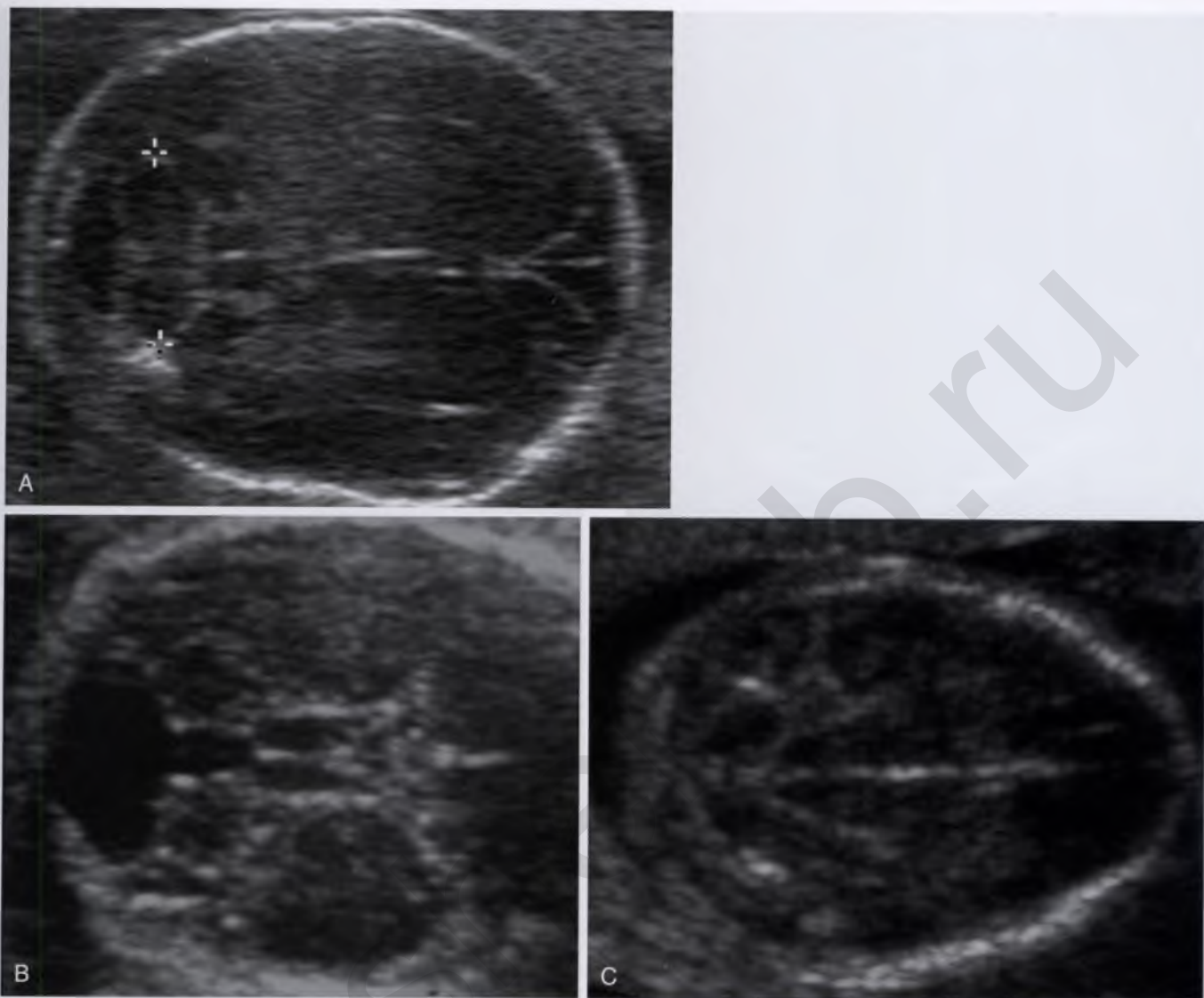


**FIG 3-17** **A**, Normal posterior fossa. **B**, Vermian agenesis. **C**, Chiari II malformation.

(excluding micrognathia), 21% had micrognathia, and 18% had hypotelorism.

The presence of *cleft lip/palate* (Figs. 3-26 and 3-27) is associated with aneuploidy such as trisomies 13 and 18, especially when other anomalies are also present. One study of fetuses with cleft lip and palate reported aneuploidy in 0%, 32%, 59%, and 82% in unilateral cleft lip, unilateral cleft lip and palate, bilateral cleft lip and palate, and median cleft lip and palate, respectively.<sup>10</sup>

Ocular anomalies, such as *hypotelorism* (Fig. 3-28), *hypertelorism*, *microphthalmia*, *anophthalmia*, and *cyclopia* (see Fig. 3-22), can be associated with fetal chromosomal abnormalities. Most importantly, when they are seen along with other malformations (especially holoprosencephaly), the risk of aneuploidy is particularly increased.

Genitourinary abnormalities can be associated with fetal chromosomal abnormalities. The highest frequency of aneuploidy has been reported in those fetuses with *urethrovesical obstruction* (bladder outlet obstruction), most commonly trisomy 18 or 13.<sup>10</sup> In one cohort of 39 fetuses with obstruction at or distal to the urethrovesical junction, chromosomal abnormalities were reported in 23%.<sup>31</sup> With urinary tract abnormalities that are more proximal, aneuploidy is reported with less frequency. In unilateral renal abnormalities such as

ureteropelvic junction obstruction and multicystic dysplastic kidneys, the risk of aneuploidy is low.<sup>32</sup>

Although the presence of most congenital malformations significantly increases the risk for fetal aneuploidy, there are some notable exceptions. They generally involve disorders that are thought to result from tissue or vascular disruption, such as *gastroschisis*, *tumors*, *limb-body wall complex*, *hydranencephaly*, and *amniotic band syndrome*.

## FIRST TRIMESTER MARKERS OF ANEUPLOIDY

### Nuchal Translucency

The term *nuchal translucency* (NT) was first coined by Nicolaides and colleagues in 1992 to describe the finding of an increased translucent region behind the neck of fetuses who were diagnosed with aneuploidy at the time of chorionic villus sampling.<sup>33</sup> This group published the first large cohort study on the association between NT and aneuploidy in 1995.<sup>34</sup> This sonographic marker for aneuploidy was subsequently validated by several investigators and is now an integral component of most first trimester screening tests for chromosomal disorders.<sup>35-45</sup> Despite widespread use of the NT measurement, the pathologic basis for enlargement of the NT in fetuses with aneuploidy is not known.



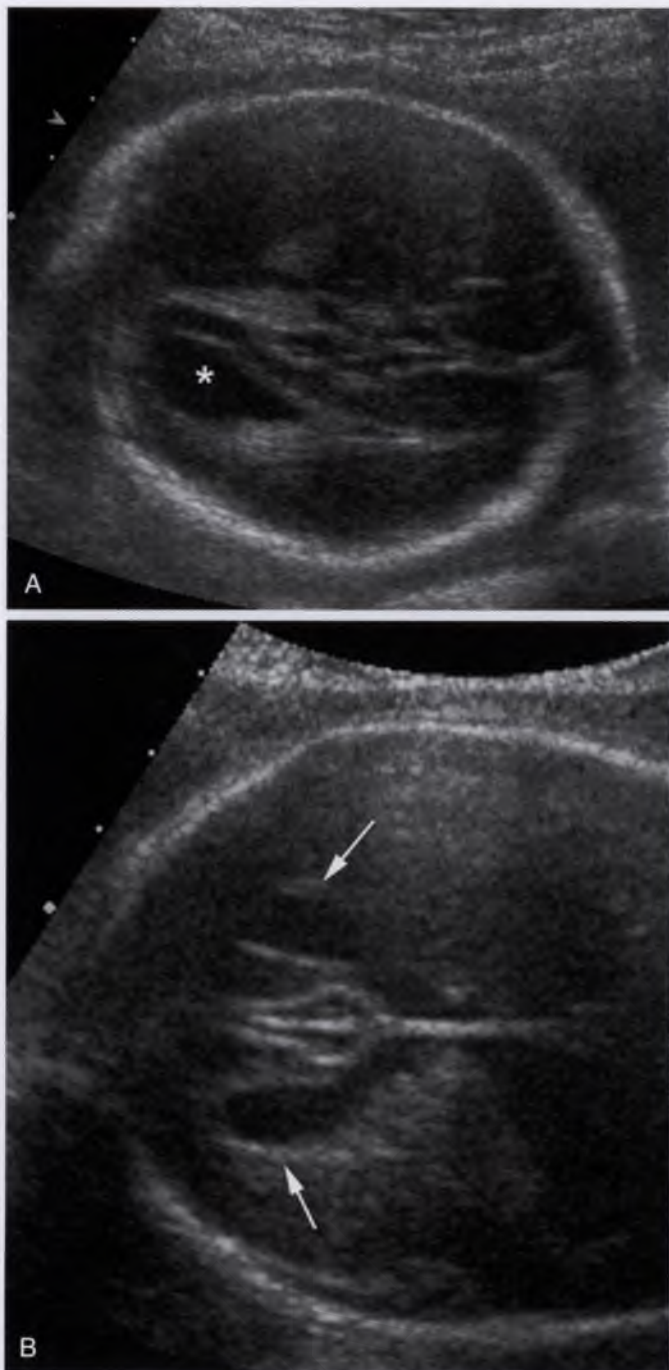


**FIG 3-18** Fetus with agenesis of corpus callosum. **A**, Transverse axial scan through the lateral ventricle shows the characteristic teardrop shape of lateral ventricles or disproportionate enlargement of the occipital horns (colpocephaly) (*asterisk*), which is indicative of agenesis of corpus callosum. **B**, Widely separated frontal horns (*arrows*) are seen with absence of the cavum septum pellucidum.

Suggested mechanisms include a decrease in cardiac function and impaired circulation, increased collagen and hyaluronan content within fetal skin, dysfunction within the jugular-lymphatic drainage system, and increased intrathoracic pressure.<sup>46-50</sup>

The most common first trimester screening paradigm combines the measurement of the NT with serum markers including PAPP-A and hCG to modify a woman's a priori risk for aneuploidy based on her age. The reported sensitivity for trisomy 21 detection using the

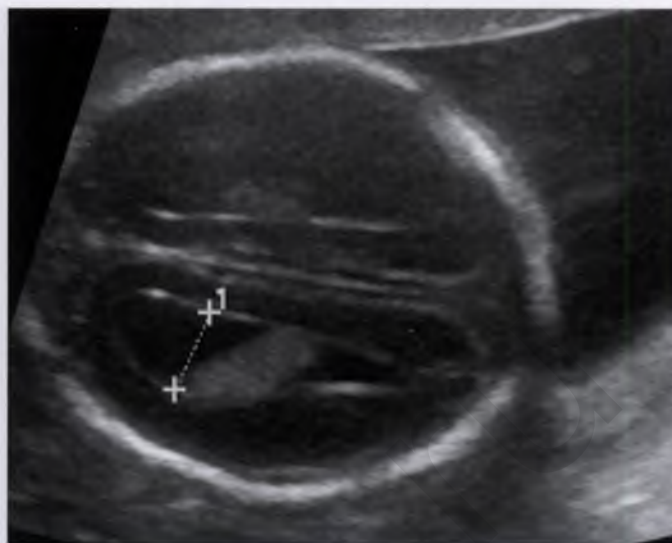


**FIG 3-19** Agenesis of the corpus callosum. Transverse scan of the fetal head demonstrates mild ventriculomegaly, a characteristic teardrop shape of the lateral ventricle, and absence of the cavum septum pellucidum.

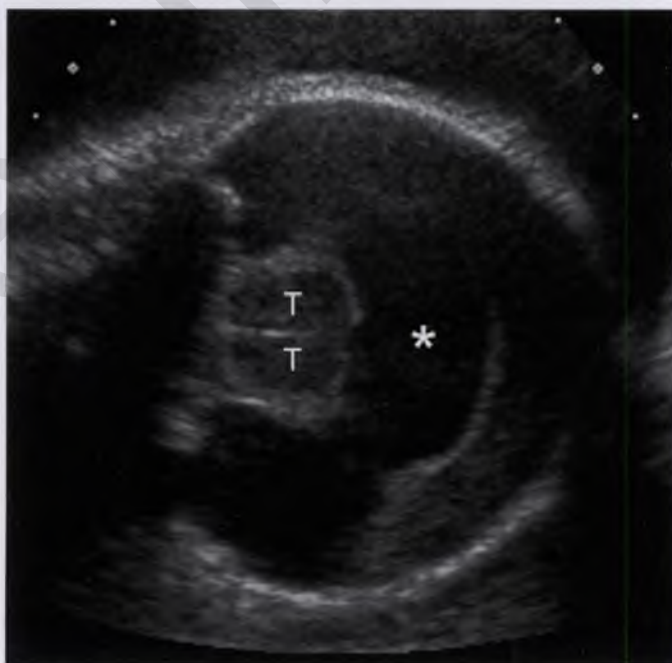


**FIG 3-20** Transaxial view through the head of a trisomy 13 fetus, showing alobar holoprosencephaly. Note the fused thalami (T) surrounded by a single monoventricle (*asterisk*).

combined first trimester approach alone ranges from 80% to 91%, with a specificity of 91% to 96%.<sup>33,35,38,43-45</sup> When the first trimester approach is combined with second trimester serum markers including unconjugated estriol, alpha-fetoprotein, and inhibin A in a modified sequential or integrated protocol, the sensitivity approaches 95% with specificity ranging from 95% to 98%.<sup>36,45,51</sup>

Detection rates for aneuploidies other than trisomy 21 are lower, but the NT is similarly enlarged, with many different chromosomal abnormalities. The combined first trimester screening test or the presence of cystic hygroma detected 78% of all non-Down syndrome aneuploidies with a 6% false positive rate in the FASTER (First and

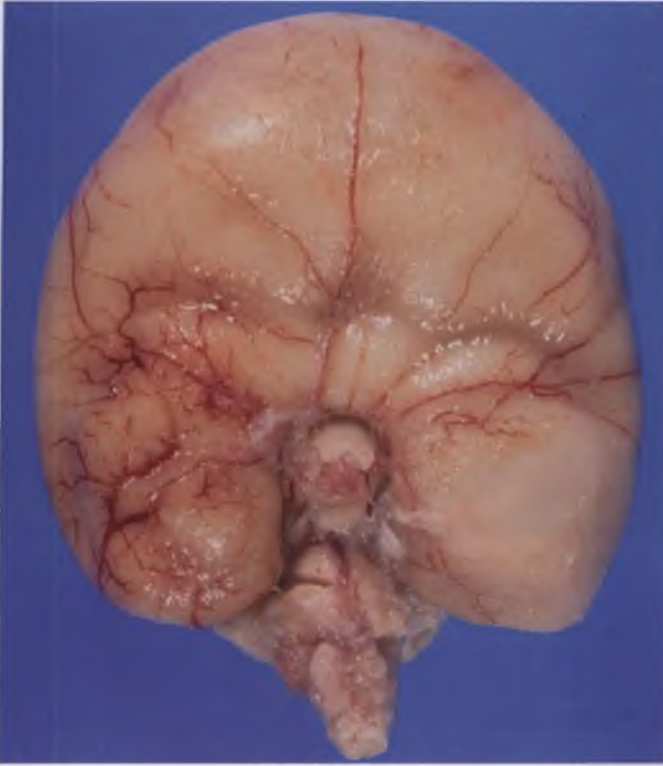


**FIG 3-21** Surgical pathologic specimen of alobar holoprosencephaly in neonate affected with trisomy 13.



**FIG 3-22** Gross pathologic features seen in the face of a neonate with alobar holoprosencephaly. A single eye globe (cyclopia) and a proboscis located above the median eye are present. Also note the clenched hands bilaterally.

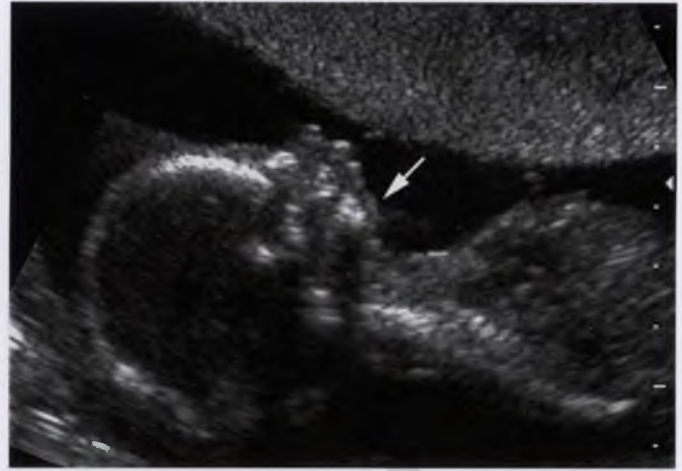


**FIG 3-23** Abnormal facial profile, showing severe micrognathia (arrow).



**FIG 3-24** Gross pathologic features seen in the face of a neonate with trisomy 9. Note the sloping forehead, flat profile, small nose, and micrognathia (arrow).



**FIG 3-25** Facial profile of fetus with trisomy 18. The profile is flattened and there is a hypoplastic nasal bone.



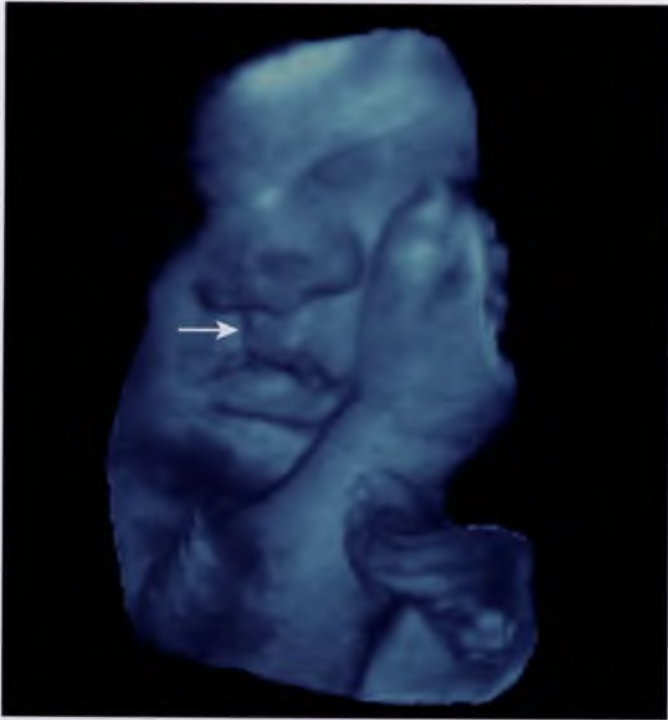


**FIG 3-26** Three-dimensional image of the fetal face showing unilateral cleft lip (arrow).



**FIG 3-27** Three-dimensional image of the fetal face showing bilateral cleft lip.

Second Trimester Evaluation of Risk) trial, a large multicenter trial of aneuploidy screening in over 30,000 pregnant women.<sup>51</sup>

It is important to emphasize the need for meticulous technique in evaluating the NT, which must be measured accurately to achieve the previously described screening efficiency. An important observation since the introduction of NT-based aneuploidy screening is the importance of maintaining good quality measurements to achieve optimal screening effectiveness. Unlike biochemical markers that display low interrater variability, NT measurement can be subject to large interobserver variation if not performed under a strict protocol.



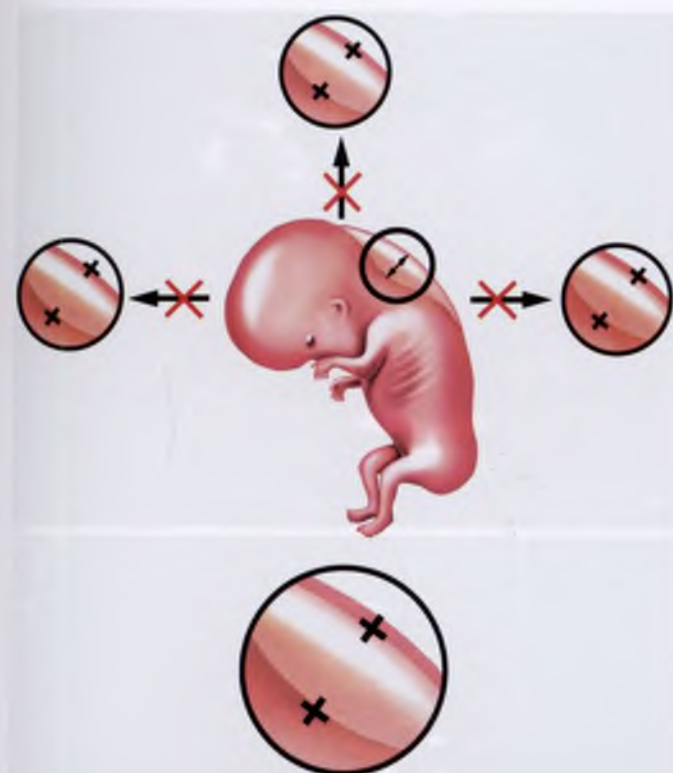
**FIG 3-28** Marked hypotelorism in a fetus with trisomy 13.

Measurements should be performed when the crown-rump length measurement is between 36 and 84 mm, depending on the laboratory used. In addition, some important criteria must be fulfilled for a good quality measurement (Fig. 3-29):

- The image should be magnified to occupy 75% of the screen and should show only the fetal head, neck, and upper thorax.
- The fetus must be in the midsagittal plane.
- The fetal neck must be in a neutral position—not hyperextended or hyperflexed.
- Three echogenic lines indicating the inner and outer borders of the fetal skin and the amnion must be displayed.
- The ultrasound calipers must be placed with the horizontal cross on the inner borders of the echolucent space and perpendicular to the fetal axis.
- The measurement of the NT must be taken at the widest space.

The impact of poor quality measurements of the NT on aneuploidy detection can be twofold. Undermeasurement can result in lower detection rates, whereas exaggerated measurement can increase the false positive rate. A modeling study by Cuckle suggested that a 10% undermeasurement may result in a 6% reduction in the trisomy 21 detection rate.<sup>53</sup> In a multicenter study published shortly after the introduction of NT-based screening, the importance of adequate training and monitoring of sonographers was highlighted by a reported low detection rate for Down syndrome of 31%.<sup>54</sup> The Nuchal Translucency Quality Review (NTQR) program and the Fetal Medicine Foundation are two organizations that provide NT training, certification, and oversight and have helped ensure maintenance of high-quality programs offering first trimester screening. Despite the institution of these quality assurance steps, a 2015 review of approximately 1.5 million ultrasound images performed for NT measurement still revealed wide variability among providers, with the more experienced providers demonstrating measurements closer to the expected norms.<sup>55</sup>

When NT-based screening was first introduced, absolute or categorical NT cutoffs were suggested to define an abnormal screening result. It was soon realized that the NT increases with gestational age even in the short-term window between the 10th and 14th weeks when these tests are performed.<sup>56,57</sup> Therefore, NT measurements must be adjusted for gestational age. The approach to adjusting involves converting the NT to multiples of the median (MoM) for gestational age and using either the 95th percentile for the MoM or the delta value of the observed NT from that expected for the gestational age or crown-rump length.



### A Conventional Measurement



**FIG 3-29** Technique for obtaining accurate first trimester nuchal translucency (NT) measurement. **A**, Demonstration of appropriate caliper placement. **B**, Demonstration of appropriate magnification, fetal neck position, and visualization of the amnion. Illustration by James A. Cooper, MD, San Diego, CA.

Sophisticated software is used to perform such calculations, and these measurements are now considered the gold standard. However, it is also important to note that an enlarged NT (greater than 3.0 mm) may be considered an indication for diagnostic testing, regardless of gestational age correction, given that the risk for aneuploidy exceeds 1 in 6 at this threshold. Further adjustment using first trimester serum analytes will not significantly alter the risk for aneuploidy in most cases.<sup>58</sup>

### Cystic Hygroma

Cystic hygromas represent an abnormality of the fetal lymphatic system and occur in approximately 1 in 285 first trimester pregnancies.<sup>59</sup> This diagnosis is made when the nuchal space is enlarged with

large posterior or posterolateral fluid-filled cavities noted within the fetal neck, with or without the presence of septations. This edema can extend caudally along the upper back of the fetus (Fig. 3-30). The presence of a cystic hygroma in the first trimester confers a 50% risk for fetal aneuploidy, with the most common chromosomal abnormalities being Turner syndrome (45,X), trisomy 21, and trisomy 18. In euploid fetuses with cystic hygromas, 50% to 60% will be diagnosed with major fetal structural abnormalities later in pregnancy.<sup>59</sup> Debate continues as to whether cystic hygromas represent a continuum of thickened NT and if the presence or absence of septations alters the aneuploidy risk. Based on the available data, it would appear that in the presence of either a thickened NT or cystic hygroma with or without septations, the aneuploidy risk remains comparably very high, and this distinction is clinically relatively unimportant. In either case, invasive diagnostic testing should be offered.<sup>60</sup>

### Absent Nasal Bone

The appearance of a small nose with a low nasal bridge in children and adults with Down syndrome initially led to the investigation of the fetal nasal bone as a marker for this condition. In 2002, Sonek and Nicolaiades reported on three unselected first trimester fetuses with Down syndrome. Two of those fetuses had sonographically undetectable nasal bones, and the third had a nasal bone that was below the 2.5th percentile in length for gestational age.<sup>61</sup> A 2003 study performed NT screening on 5532 fetuses from 5425 pregnancies and found that the nasal bone was absent in 70% of fetuses with Down syndrome versus in 0.2% of euploid fetuses. Not only did the authors show an association of absent nasal bone with Down syndrome, but they also demonstrated that appropriate imaging of the nasal bone was attainable in a large percentage of the study population, with a 99.8% visualization rate.<sup>62</sup>

Additional studies have confirmed the association of absent nasal bone and Down syndrome. One study demonstrated that a successful view of the fetal profile could be obtained in 1752 of 1906 consecutive fetuses undergoing NT scanning (91.9%).<sup>63</sup> In this study, the nasal bone was absent or hypoplastic in 12 of 19 fetuses with chromosomal abnormalities and in 8 of 10 with trisomy 21. Absence of the nasal bone was recorded in only 24 of 1733 chromosomally normal fetuses (1.4%). In an additional study, investigators successfully assessed the nasal bone in 1027 of 1089 (94.3%) fetuses and found that the nasal bone was absent in 10 of 1000 (1.0%) unaffected cases and in 10 of 15 (66.7%) Down syndrome cases.<sup>64</sup>

To assess the nasal bone sonographically, the fetal profile is first viewed in the midsagittal plane. The transducer can then be rocked sideways to maintain the angle of insonation at 45 or 135 degrees.<sup>65</sup> The nasal bone is visualized as an echogenic line below and parallel to the overlying skin. When present, the nasal bone and skin appear similar to an equal sign<sup>66</sup> (Fig. 3-31). Although obtaining sonographic images of the fetal nasal bone is straightforward, there is a learning curve associated with developing proficiency. In 2003, Cicero and colleagues determined that it took sonographers with NT imaging expertise an average of 80 nasal bone images, with a range of 40 to 120, to become competent in examining the fetal nasal bone.<sup>67</sup>

Recent research has attempted to incorporate nasal bone evaluation into current first trimester screening protocols in order to improve the accuracy of aneuploidy diagnosis. In 2005, a prospective cohort study assessing the utility of incorporating nasal bone assessment into screening with standard first trimester markers (NT, free  $\beta$ -hCG, PAPP-A) was performed. Incorporating nasal bone measurement improved the detection rate of Down syndrome to 90% and reduced the false positive rate to 2.5%.<sup>68</sup> Cicero and colleagues observed similar results with the incorporation of fetal nasal bone into first trimester screening.<sup>69</sup>





**FIG 3-30** **A**, Coronal view of a septated cystic hygroma in the first trimester of pregnancy in a fetus ultimately diagnosed with trisomy 18. **B**, Transverse view of the fetal head and neck in the same fetus demonstrating a midline septation. **C**, Sagittal view of another fetus with a cystic hygroma (*arrow*) with subcutaneous edema (*double arrows*).



**FIG 3-31** **A**, First trimester ultrasound examination at 13 weeks' gestation demonstrating the presence of a nasal bone (*arrow*) below and parallel to the overlying skin. **B**, Absent nasal bone (*arrow*) in a fetus with trisomy 21. The nuchal translucency is also enlarged in this fetus.

It has been noted that race and ethnicity are associated with an absent nasal bone. In a study reported in 2003, in 3358 karyotypically normal fetuses, absent nasal bone was identified in 2.8% of Caucasians, 10.4% of African Caribbeans, and 6.8% of Asians.<sup>70</sup> The finding of racial variation and absent nasal bone was reinforced by another large series of patients. In that study, the fetal profile was successfully examined in 5851 cases (98.9%), and absent nasal bone in chromosomally normal fetuses was seen in 2.2% of Caucasians, 9.0% of African Caribbeans, and 5.0% of Asians.<sup>71</sup> These findings have led investigators to question whether the simple presence or absence of the nasal bone is applicable when evaluating the nasal bone in the first trimester, given that race and ethnicity may not be known or easily incorporated into risk adjustment.

### Ductus Venosus Doppler Studies

The ductus venosus is a unique fetal blood vessel that shunts highly oxygenated blood from the umbilical vein to the right atrium, after



which it is shunted through the foramen ovale to provide oxygenated blood to the fetal circulation. Doppler study of the ductus venosus normally will show triphasic, pulsatile forward flow. However, an absent or reversed a wave during atrial systole has been observed in cases of fetal cardiac malformations and aneuploidy. In 1998, Matias and colleagues demonstrated the feasibility of first trimester ductus venosus Doppler sonography to screen for aneuploidy, showing that 57 of 63 (90.5%) chromosomally abnormal fetuses had either an absent or reversed a wave.<sup>72</sup> A subsequent study by Prefumo and colleagues demonstrated a positive LR of 7.05 for Down syndrome in the setting of abnormal ductus venosus flow in a high-risk population undergoing chorionic villus sampling.<sup>73</sup> Using ductus venosus Doppler studies as an adjunct to NT screening appears to be more discriminatory than using either test alone.<sup>74,75</sup>

In chromosomally normal fetuses with a normal NT, abnormal ductus venosus blood flow in the first trimester has been associated with adverse fetal outcome such as congenital heart disease and fetal growth restriction.<sup>76,77</sup> Despite these reports, the technical feasibility of successfully interrogating such a small fetal vessel (~2 mm) with Doppler sonography in the first trimester of pregnancy may preclude its practical use in screening for fetal abnormalities.

### Tricuspid Regurgitation

Tricuspid regurgitation has also been proposed as an adjunct to first trimester aneuploidy screening. This measurement is obtained by using pulse-wave Doppler imaging of the tricuspid valve in the apical four-chamber view with insonation parallel to the ventricular septum. A regurgitant jet must be present over at least half of systole with a velocity over 60 to 80 cm/second for a diagnosis of tricuspid regurgitation.<sup>78</sup> Falcon and colleagues demonstrated significant tricuspid regurgitation in 74% of Down syndrome fetuses compared to 6.9% of normal fetuses.<sup>78</sup> The addition of tricuspid regurgitation to first trimester serum screening and NT measurement has been shown to increase the detection rate of Down syndrome from 91% to 96% at a 3% fixed false positive rate.<sup>79</sup> Similar to first trimester ductus venosus Doppler screening, the technical difficulties and need for experienced sonographers with training in fetal echocardiography limit the utility of this measurement for screening in the general population.

### Frontomaxillary Facial Angle

In 2007, Sonek and colleagues proposed the use of first trimester fetal frontomaxillary facial (FMF) angle as a sonographic screening tool for aneuploidy based on the characteristic flat facial profile observed in children and adults with Down syndrome.<sup>80</sup> This measurement is taken by first obtaining a midsagittal view of the fetal profile. The FMF angle is defined as the angle between a line along the upper surface of the upper palate and a line that traverses the upper corner of the anterior aspect of the maxilla and extends to the external surface of the frontal bone at the point of its greatest anterior excursion.<sup>80</sup> This angle measurement has been demonstrated to be significantly larger in Down syndrome fetuses compared to euploid fetuses.<sup>80,81</sup> Incorporation of this measurement into first trimester screening increases the Down syndrome detection rate from 90% to 94% at a 5% false positive rate.<sup>82</sup>

## THE SECOND TRIMESTER GENETIC SONOGRAM

The sonographic detection of a major structural abnormality significantly increases the risk that a fetal chromosome abnormality is present. Some structural abnormalities are particularly associated with a specific aneuploidy (see Table 3-1). However, many aneuploid fetuses, particularly those with Down syndrome, do not have major structural abnormalities that are readily detected in the first or second trimester.

Because Down syndrome is the most common clinically significant chromosome abnormality, identification of minor features of Down syndrome, or so-called sonographic soft signs, is often employed as a screening tool.

Prior to the introduction of the genetic sonogram, the only additional option available for patients with elevated aneuploidy risks obtained by second trimester serum screening was to undergo amniocentesis. As the association between ultrasound markers and Down syndrome became more apparent, the genetic sonogram was introduced as an alternative noninvasive method to further refine aneuploidy risk, most specifically for Down syndrome.

The genetic sonogram is a targeted second trimester ultrasound study performed at the time of the anatomic survey, which assesses for major fetal malformations as well as minor markers of aneuploidy, including increased nuchal skinfold, shortened long bones, pyelectasis, absent/hypoplastic nasal bone, hyperechoic bowel, and echogenic intracardiac focus (EIF) as well as a number of other, less common markers. The presence or absence of these markers, either alone or in combination, can adjust a patient's aneuploidy risk obtained by second trimester screening results, potentially aiding in the decision as to whether or not to pursue invasive testing with amniocentesis. The components of the genetic sonogram have been revised over the years with markers such as widened pelvic angle and sandal gap toe deformity falling out of favor and newer sonographic findings such as aberrant right subclavian artery (ARSA), prenatal thickness, and FMF angle gaining more popularity.<sup>83,84</sup>

In isolation, each sonographic marker typically carries low to moderate sensitivity and specificity for the detection of Down syndrome. However, the presence of multiple markers can substantially improve the detection rate while also lowering the false positive rate. Studies have demonstrated Down syndrome detection rates ranging from 50% to 93% in the presence of one or more minor aneuploidy markers on genetic sonogram.<sup>85-88</sup> In addition, LRs have been established for each individual marker; these ratios can be multiplied by the patient's a priori risk for aneuploidy calculated by serum screening results or age alone to provide an age-adjusted ultrasound risk assessment [AAURA] of the patient's posttest odds for aneuploidy. These LRs weight the influence of each individual marker by their strength of association with Down syndrome. Bromley and colleagues demonstrated an exponential increase in the chance of Down syndrome based on the number of markers observed on ultrasound imaging, ranging from 1.9 in the presence of one marker to 80 in the presence of three or more markers.<sup>89</sup> Table 3-2 presents individual LRs as reported in several studies.<sup>89-92</sup> The differences between studies likely stem from the heterogeneity of the populations studied, thereby making interpretation difficult. In the setting of multiple markers, it has been proposed that it is appropriate to multiply the LR of each individual marker by the patient's a priori aneuploidy risk. However, caution must be taken with this approach, as the independence of the various markers has not been proved.

In addition to the utility of these calculated positive LRs, the absence of any of these markers on second trimester sonography can decrease a patient's aneuploidy risk. It has been demonstrated that a normal genetic sonogram can decrease the risk of Down syndrome by 60% to 80%, correlating to a negative LR of 0.2 to 0.4.<sup>89,90</sup> This result may provide additional reassurance to patients with a positive second trimester serum screen, although it is important that patients understand the nature and limitations of this screening test and that these findings cannot diagnose or rule out Down syndrome with certainty.

The genetic sonogram originally was targeted toward a high-risk population (i.e., advanced maternal age, positive second trimester serum screening) and was found to significantly decrease the rate of invasive testing with amniocentesis.<sup>93,94</sup> The application of the genetic



TABLE 3-2 Likelihood Ratios for Minor Markers of Aneuploidy

Marker	Bromley, 2002 <sup>89</sup>	Nyberg, 2001 <sup>90</sup>	Smith-Bindman, 2001 <sup>91</sup>	Agathokleous, 2013 <sup>92</sup>
None	0.22	0.4	NA	0.37
Nuchal fold	Infinite	11	17	23.27
Absent/hypoplastic nasal bone	NA	NA	NA	23.30
Hyperechoic bowel	NA	6.7	6.1	11.44
Short humerus	5.8	5.1	7.5	4.81
Short femur	1.2	1.5	2.7	3.72
Echogenic intracardiac focus	1.4	2.0	2.8	5.83
Pyelectasis	1.5	1.5	1.9	7.63

Superscript numbers indicate references at the end of the chapter. NA, not applicable.

sonogram to low-risk populations has been more controversial. Given the low prevalence of aneuploidy in this population, positive findings on a genetic sonogram carry low predictive values and high false positive rates, resulting in increased patient anxiety. The presence of isolated minor markers such as echogenic intracardiac foci, pyelectasis, and femoral/humeral shortening confers only a small effect on the pretest odds for Down syndrome in this population.<sup>91,92</sup> However, the finding of one minor marker of aneuploidy should prompt a more thorough search for other associated markers or structural abnormalities as well as a review of the patient's aneuploidy risk based on age or other screening tests.

In the current era of first trimester biochemical and cfDNA screening, the utility of the second trimester genetic sonogram has been questioned. The FASTER trial attempted to answer this question in a subset of patients and found a modest increase in the Down syndrome detection rate with application of the genetic sonogram after normal screening. When the genetic sonogram was added to the quadruple screen in an integrated, stepwise, or contingent manner, the detection rate of Down syndrome increased from 93%, 97%, and 95% to 98%, 98%, and 97%, respectively. However, substituting the genetic sonogram for second trimester serum screening did not appear to be useful, yielding only a 90% Down syndrome detection rate.<sup>95</sup> Kranz and colleagues performed a simulation study to determine the effectiveness of the genetic sonogram following negative first trimester combined screening results. Using individual marker LRs, the genetic sonogram identified an additional 6.1% of Down syndrome cases, resulting in a total detection rate of 94.6% with a false positive rate of 5.4%.<sup>96</sup>

Given the recent introduction of cfDNA screening into clinical practice, studies specifically addressing the performance of the genetic sonogram following cfDNA screening are not yet available. With the increased ability to diagnose aneuploidy early in pregnancy, the prevalence of Down syndrome at the time of the second genetic sonogram has decreased, therefore decreasing the positive predictive value of these sonographic markers. Despite this fact, the genetic sonogram likely still can play a role in aneuploidy screening in populations with limited access to cfDNA, in twins and higher-order multiple gestations, and in patients with borderline or failed cfDNA results.<sup>97</sup>

### Thickened Nuchal Fold

The association between a thickened nuchal skinfold (NF) and Down syndrome was first described by Benacerraf and colleagues in 1985 and remains one of the most specific second trimester markers for Down syndrome.<sup>98</sup> This sonographic finding phenotypically correlates to the redundant soft tissue in the posterior neck that is characteristic of newborns affected by Down syndrome.<sup>99</sup> Although it initially was thought, and seems logical, that a second trimester thickened NF

measurement results from a first trimester thickened NT, these markers do not appear to be correlated and, therefore, can be used independently to assess aneuploidy risk.<sup>100,101</sup>

The NF is typically measured between 15 and 21 weeks by obtaining a transverse plane of the fetal head at the level of the biparietal diameter. The transducer is then angled caudally to include the cerebellum and occipital bone. The NF is measured by placing calipers on the outer skull and outer skin edge<sup>98</sup> (Fig. 3-32). Significant fetal neck extension or excessive abdominal pressure with the ultrasound probe may falsely increase this measurement.<sup>102</sup> Thresholds of 5 mm or greater and 6 mm or more have been proposed; however, 6 mm or greater seems to be the most accepted standard value to define abnormal.<sup>98,103,104</sup> Using this threshold, positive LRs as high as 94.7 have been reported; however, more recent meta-analyses indicate a more modest association, with LRs ranging between 11 and 17.<sup>89,91,92</sup> Importantly, the false positive rate for this sonographic marker is exceedingly low (0.1–1.3%), making this one of the most specific second trimester sonographic markers for Down syndrome.<sup>3,98,103</sup> Nuchal skinfold thickness has been found to increase with advancing gestational age, leading many investigators to evaluate gestational age-specific nomograms to extend the utility of this measurement up to 24 weeks' gestation.<sup>105,106</sup> Alternatively, some fetuses with Down syndrome may experience complete resolution of nuchal thickness as gestation advances, suggesting that following serial sonograms for resolution is unwarranted and may even provide false reassurance.<sup>107</sup>

### Absent/Hypoplastic Nasal Bone

As discussed earlier in this chapter, studies utilizing the absence of the nasal bone in the first trimester have clearly shown an association with Down syndrome. However, concerns exist regarding maternal ethnic variability as well as the potential for late ossification of the nasal bone in select populations. To minimize false positive results and to offer screening options to the patient who presents for later prenatal care, attention shifted to nasal bone screening in the second trimester. The addition of absent nasal bone to the second trimester genetic sonogram as a marker of Down syndrome has been shown to significantly increase the sensitivity of the examination (Fig. 3-33).

When evaluating the facial profile for the nasal bone, the correct technique and angle of insonation should be used. The profile should be viewed in the midsagittal plane, with care taken to keep the angle of insonation close to 45 degrees or 135 degrees. With angles less than 45 degrees or greater than 135 degrees, the nasal bone may artificially appear to be absent. On the other hand, as the angle approaches 90 degrees, edges of the bone may become difficult to delineate precisely because of echo scatter, and the measurement may be artificially large. The nasal bone should be visualized as a linear echogenic structure if the correct technique is used (Figs. 3-34 and 3-35).



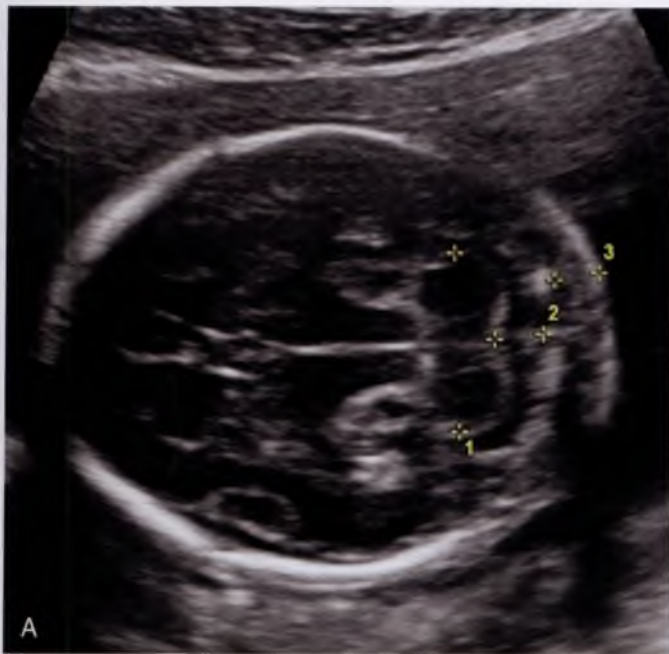


**FIG 3-32** **A**, Transverse view through the posterior fossa with placement of electronic calipers demonstrating a normal cerebellum (1), cisterna magna (2), and nuchal skinfold (3) measurement at 20 weeks' gestation. **B**, Transverse view through the posterior fossa demonstrating a thickened nuchal skinfold, measuring 9.6 mm.

The definition of nasal bone hypoplasia is important because its inclusion into screening strategies that utilize other sonographic markers can significantly improve Down syndrome detection rates while minimizing false positive rates—much in the same manner as first trimester screening strategies. In 2006, Odibo and colleagues evaluated second trimester nasal bone hypoplasia as a marker for fetal aneuploidy and demonstrated that its incorporation into risk assessment with other markers of fetal aneuploidy significantly improved the sensitivity and specificity for karyotype abnormalities. When used



**FIG 3-33** Second trimester midsagittal fetal facial profile view demonstrating absence of the nasal bone.



**FIG 3-34** Normal facial profile showing presence of the fetal nasal bone (arrow).



**FIG 3-35** Hypoplastic nasal bone. Facial profile of another fetus showing a small nasal bone (arrow).



alone, nasal bone hypoplasia had a sensitivity of 23% to 64% and a specificity of 57% to 99% for detecting Down syndrome. The ranges depended on the definition of nasal bone hypoplasia that was used. When combined with other markers (nuchal fold, femur and humeral lengths, choroid plexus cysts, echogenic bowel), the sensitivity increased from 59% to 82%, and the specificity improved from 74% to 87%.<sup>108</sup> Interestingly, a recent study comparing nasal bone with NF thickness found absent nasal bone to be a more efficient marker for Down syndrome. This study also evaluated a cohort that had not been well studied—the low-risk patient population. The authors found that nasal bone and NF thickness were equally efficient Down syndrome markers in both high- and low-risk populations.<sup>109</sup> Finally, a recent meta-analysis demonstrated a positive LR of 23.27 for absent or hypoplastic nasal bone; this LR is high enough that it would categorize essentially all patients with this finding as “screening positive” regardless of maternal age.<sup>92</sup>

Although absent nasal bone as a dichotomous marker for Down syndrome has been shown to have superior screening efficiency, other measures to assess nasal bone hypoplasia have been proposed. One such measure is the use of fetal biometry ratios. A commonly reported ratio is the fetal biparietal diameter/nasal bone length (BPD/NBL). By utilizing a ratio, the influence of gestational age is potentially offset. In 2002, Bromley and colleagues used a BPD/NBL ratio and compared Down syndrome and euploid infants. They reported 100% sensitivity for the detection of affected fetuses using a BPD/NBL ratio of 9 or greater. However, this high sensitivity was associated with a false positive rate of 22%.<sup>110</sup> Subsequent studies have tried to balance the rate of detection with a more acceptable false positive rate. In 2004, Odibo and colleagues reported that a ratio of BPD/NBL greater than 11 identified 50% of Down syndrome fetuses and had a false positive rate of 7%.<sup>111</sup> More recent studies have shown that using MoM values of the nasal bone could improve specificity for detecting Down syndrome. Results from a prospective cohort study reported that nasal bone MoM less than 0.75 was the best definition of NB hypoplasia, with a sensitivity of 49% and a specificity of 92%, as compared to a sensitivity of 61% and a specificity of 84% for BPD/NBL ratio greater than 11.<sup>65</sup> Although the optimal threshold to define nasal bone hypoplasia is uncertain, this marker is one of the best sonographic predictors of Down syndrome in both the first and second trimesters.

### Hyperechoic Bowel

Hyperechoic bowel, also referred to as echogenic bowel or bright bowel, is a nonspecific finding that is observed in 0.2% to 1.8% of routine second trimester ultrasound examinations. This sonographic finding is somewhat subjective and is diagnosed when the fetal bowel appears as bright as surrounding bone, typically as compared to the iliac wing (see Fig. 3-36). The echogenicity of fetal bowel can be affected by the frequency of the transducer used; therefore, the diagnosis of hyperechoic bowel should always be confirmed with a low-frequency transducer, less than 5 Mz, and without utilizing harmonics. Although grading systems to classify the degree of bowel echogenicity have been proposed, they have not been routinely accepted into clinical practice.<sup>112</sup>

After thickened NF and absent nasal bone, hyperechoic bowel is the next most sensitive sonographic marker for the detection of Down syndrome. The association between hyperechoic bowel and aneuploidy was first reported by Nyberg in 1990, when he observed a 7% prevalence of hyperechoic bowel in 94 fetuses with Down syndrome.<sup>7</sup> This finding has been duplicated in subsequent studies, with LRs ranging from 6 to 14.<sup>90-92,112-114</sup> Decreased bowel motility and increased water absorption leading to subsequent dehydration of meconium is the proposed mechanism that results in this finding in aneuploid fetuses.<sup>115</sup>

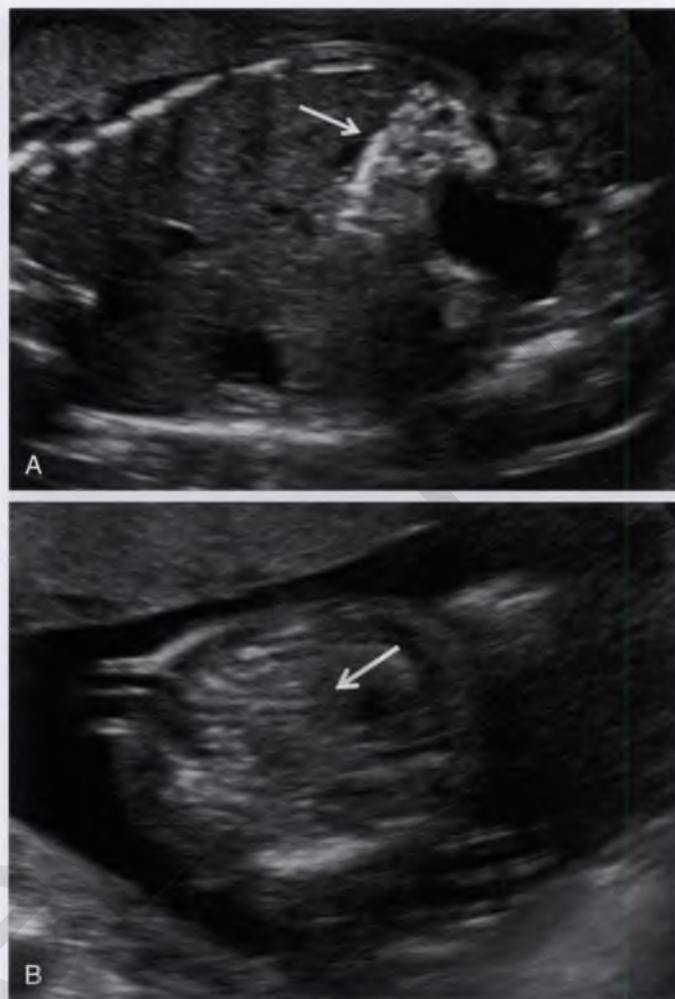


**FIG 3-36 A**, Coronal view of the fetal abdomen demonstrating an echogenic area of bowel (arrow) adjacent to the fetal bladder. **B**, Transverse view of the fetal abdomen at the level of the abdominal cord insertion site, demonstrating areas of speckled echogenicity (arrow) throughout the fetal bowel.

Although Down syndrome is the most common chromosome abnormality associated with hyperechoic bowel, it has also been reported with trisomy 18, trisomy 13, triploidy, and monosomy X.<sup>112</sup> As with other sonographic markers, the predictive value of hyperechoic bowel for aneuploidy is greatly increased in the presence of other sonographic findings.

Once aneuploidy is excluded, the differential diagnosis for hyperechoic bowel includes fetal swallowing of intra-amniotic blood, cystic fibrosis, congenital infection, and primary gastrointestinal disease.<sup>116-119</sup> In addition, isolated hyperechoic bowel has been associated with adverse pregnancy outcomes such as fetal growth restriction and intrauterine fetal demise.<sup>114,120</sup>

### Femoral/Humeral Shortening

Given that the majority of individuals with Down syndrome are short in stature, it was theorized that affected fetuses may also demonstrate shortening of their long bones. Multiple definitions to classify a shortened femur and humerus in the second trimester have been proposed, including biparietal diameter/femur length (BPD/FL) and BPD/humerus length (HL) greater than 1.5 MoM for gestational age; observed to expected (O/E) ratios of FL and HL measuring 0.91 or less



and 0.89 or less, respectively; and FL and HL measurements below the 5th percentile for gestational age.<sup>121-124</sup> Regardless of which definition is used, it is imperative that femur and humerus diaphysis lengths be measured with the long bone positioned horizontally in the image, in order not to falsely truncate the measurement.

Benacerraf and colleagues first reported that 68% of fetuses with Down syndrome had a shortened FL as measured by O/E ratio.<sup>123</sup> Using BPD/FL ratios, Lockwood and colleagues demonstrated a 50% sensitivity for the detection of Down syndrome at a 7% false positive rate.<sup>125</sup> However, as an isolated marker, short femur lacks discriminatory effectiveness, with positive LRs of only 1.2 to 1.5.<sup>89,90</sup> Shortened humeral length appears to be a superior marker, with reported Down syndrome detection rates of approximately 50%.<sup>124,126</sup> In 2009, Gray and colleagues revisited the optimal definition of short humeral length and demonstrated that an HL below the 5th percentile for gestational age was the most discriminatory definition, with a positive LR as high as 25.<sup>122</sup> Combining short femur and short humeral length yields an 11-fold increase in Down syndrome risk and has a lower false positive rate compared to using either marker alone.<sup>127</sup> Given the probable ethnic and gender variation in long bone measurements, race- and gender-specific nomograms have been proposed. However, such nomograms have not been found to substantially improve Down syndrome detection rates.<sup>128-130</sup>

### Pyelectasis

Pyelectasis (also referred to as pelviectasis) is observed in 1% to 3% of normal fetuses during second trimester anatomic survey.<sup>131</sup> This diagnosis is made when the anteroposterior dimension of the fluid-filled renal pelvis exceeds 4 mm prior to 32 weeks' gestation. Measurements of the renal pelvis should be taken with the fetal spine at either the 12 o'clock or 6 o'clock position to ensure greatest accuracy (see Fig. 3-37). Pyelectasis is often seen as a normal variant or may be an early sign of genitourinary obstruction (see Chapter 15). In 1990, Benacerraf and colleagues demonstrated an association between fetal pyelectasis and Down syndrome, with 25% of Down syndrome fetuses in their cohort having pyelectasis, as compared to only 2.8% of euploid control subjects.<sup>132</sup> Subsequent studies confirmed this association, although the sensitivities remain low, ranging from 17% to 25%, with false positive rates of 2% to 3%.<sup>131,132</sup> Although this finding is more common in male fetuses, gender does not appear to alter the risk of aneuploidy.<sup>133</sup>



**FIG 3-37** Transverse view of the fetal kidneys at the midtrimester; ultrasound image demonstrates mild bilateral pyelectasis. The anteroposterior diameters of the renal pelvises measure 0.67 and 0.80 cm on the right (RT) and left (LT), respectively.

When combined with other sonographic markers, the finding of pyelectasis in the detection of Down syndrome can make a modest contribution, with LRs ranging from 5.5 to 8.8.<sup>89,90,92</sup> In a 2007 retrospective review of a large amniocentesis database, Bornstein and colleagues demonstrated an eightfold increased risk of major fetal trisomy when pyelectasis was identified with another single sonographic marker and a 62-fold increase when pyelectasis was identified in combination with multiple other markers.<sup>134</sup> Conversely, the performance of pyelectasis as an isolated marker remains more controversial. Prior studies reported very low LRs (1.5-1.9) in the setting of isolated fetal pyelectasis, suggesting that this isolated finding would not significantly alter the a priori risk of aneuploidy in low-risk women with normal serum screening results.<sup>89,90</sup> More recent studies have attempted to further refine these risk estimates. In 2010, Carbone and colleagues demonstrated a greater than twofold increased risk for Down syndrome with isolated pyelectasis. This increased risk remained significant when stratified by maternal age.<sup>135</sup> A recent meta-analysis evaluating the risk of Down syndrome in the setting of isolated pyelectasis revealed similar results, calculating a pooled positive LR of 2.78. Interestingly, this study also calculated a negative LR of 0.99, suggesting that the absence of this sonographic finding does not decrease the likelihood of Down syndrome.<sup>136</sup> Although these results suggest that the presence of isolated pyelectasis may impact the risk of Down syndrome in a high-risk population (advanced maternal age, abnormal serum screening results), it remains a dilemma how to handle this finding in a low-risk population. However, based on the preceding data, it seems unlikely that isolated pyelectasis substantially impacts aneuploidy risk in an otherwise low-risk population and should not be a sole indication for invasive diagnostic testing.

### Echogenic Intracardiac Focus

An EIF is the most common sonographic soft marker observed at the time of second trimester anatomic survey, occurring in 3% to 5% of normal fetuses.<sup>137</sup> This finding is thought to represent microcalcification and fibrosis of the papillary muscle and chordae tendineae and is diagnosed when an echogenic area, as bright as bone, is visualized in the fetal heart, most commonly within the left ventricle. An EIF is best appreciated in the apical four-chamber view but must be identified in two distinct cardiac planes to make the diagnosis (Fig. 3-38). An isolated EIF is not associated with structural cardiac abnormalities or myocardial dysfunction based on pathologic correlation and long-term childhood follow-up studies.<sup>138,139</sup>

The association between microcalcifications of the fetal papillary muscle and chromosome abnormalities was first made in the early 1990s when Roberts and Genest noted that this finding was present on pathologic examination in 16% of Down syndrome fetuses as compared to only 2% of normal fetuses.<sup>140</sup> Subsequent ultrasound studies were able to identify this finding sonographically and demonstrated a greater than fourfold increased risk for Down syndrome in the presence of an EIF.<sup>141,142</sup> Similar to pyelectasis, EIF tends to perform best for the detection of Down syndrome in the presence of other sonographic markers, with positive LRs ranging from 2.8 to 8.0.<sup>89-92</sup> Performance of EIF as an isolated marker remains more controversial. In 2009, Shanks and colleagues demonstrated that an EIF was not significantly associated with an increased risk for Down syndrome in patients not otherwise at an increased risk for aneuploidy.<sup>143</sup> Other studies have drawn similar conclusions, stating that EIF should not be considered a marker for aneuploidy in patients without an elevated a priori risk, specifically in those under the age of 35 with negative first or second trimester screening results.<sup>144-147</sup> In contrast, a 2003 meta-analysis reported a relatively high pooled LR estimate of 5.4 for fetal Down syndrome in the presence of an isolated EIF. However, heterogeneity



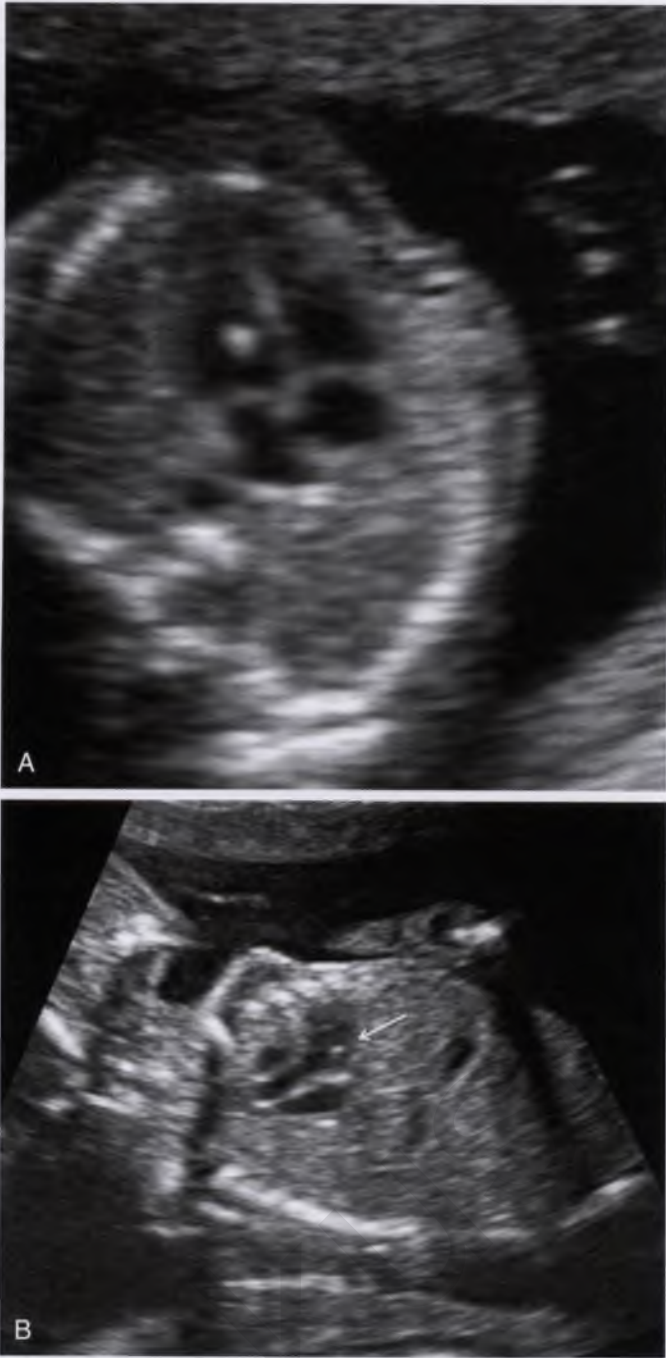


**FIG 3-38** **A**, Apical four-chamber cardiac view demonstrating the presence of an echogenic intracardiac focus in the right ventricle. **B**, View of the left ventricular cardiac outflow tract demonstrating the presence of an echogenic intracardiac focus (arrow) in the left ventricle.

of the included studies must be taken into consideration and limited the strength of the conclusions to some degree.<sup>148</sup>

Given these conflicting results, obstetricians have struggled with the dilemma of whether or not to disclose the finding of an isolated EIF and offer diagnostic genetic testing to low-risk patients, especially given how commonly this finding is identified on routine sonography. Supporters of full disclosure cite an ethical responsibility of physicians to fully inform and counsel patients. Others have argued that disclosure of this finding, which is common and only weakly associated with

Down syndrome, creates unnecessary parental anxiety and leads to an increased rate of invasive diagnostic testing with the potential for fetal loss without significantly improving detection of aneuploidy.<sup>149,150</sup> Caughey and colleagues published a decision analysis evaluating the impact of offering routine amniocentesis to all patients younger than 35 years old with an isolated EIF on second trimester sonogram. This study estimated that more than 100,000 additional amniocenteses would be performed per year to identify 244 additional cases of Down syndrome. This would correlate to 2.4 procedure-related losses per Down syndrome fetus identified.<sup>151</sup> More recently, Chasen and Razavi reported that rates of amniocentesis were significantly higher in low-risk patients following disclosure of an isolated EIF compared to patients without an EIF at a similar level of risk.<sup>152</sup> The issue of disclosure remains an ethical dilemma for obstetric providers. With improvements in prenatal aneuploidy screening, including introduction of cfDNA, this option may allow follow-up testing and alleviation of patient anxiety without concern over unnecessary fetal loss from amniocentesis.

### Other Minor Markers for Down Syndrome

Based on the phenotypic features of children with Down syndrome, investigators have suggested that ultrasound findings such as widened iliac wing angle, shortened ear length, clinodactyly, and sandal gap toe deformity be included as part of the second trimester genetic sonogram. However, over the years, these findings have fallen out of favor given their lack of specificity and reproducibility. Instead, other novel markers have been introduced, some of which have demonstrated promise.

An aberrant right subclavian artery (ARSA) has been reported to occur in up to 35% of individuals with Down syndrome.<sup>153</sup> Typically, the right subclavian artery arises as the first branch of the brachiocephalic artery as it originates as the first vessel from the aortic arch. With ARSA, the right subclavian artery arises anomalously as a fourth branch of the aortic arch. This is best visualized in the trachea and three-vessel view of the fetal heart, in which color Doppler demonstrates a fourth vessel coursing from the aorta to the right side of the fetus. In 2005, Chaoui and colleagues noted that an ARSA could be identified in 35.7% of fetuses with Down syndrome.<sup>154</sup> This finding has been confirmed in subsequent studies, with positive LRs as high as 23.27 to 45 in the setting of other sonographic markers.<sup>83,155,156</sup> A recent 2013 meta-analysis demonstrated a positive LR of 3.94 when ARSA was evaluated as an isolated marker. However, few studies were available for the analysis, given that this is a relatively recently reported finding.<sup>92</sup>

In 2005, Maymon and colleagues proposed measurement of prenasal thickness as a second trimester marker of Down syndrome, extrapolating from the physical finding of poor skin elasticity in children with this disorder.<sup>157</sup> To acquire this measurement, the fetal facial profile view is obtained, and a measurement between the frontonasal angle and outer skin edge is taken. In the original study, the prenasal thickness was significantly increased in Down syndrome compared to euploid fetuses. Using both nasal bone and prenasal thickness, the detection rate for Down syndrome was 70%, compared to 43% using nasal bone alone.<sup>157</sup> A subsequent study evaluated prenasal thickness/nasal bone length ratio and demonstrated that a ratio above the 95th percentile resulted in a 100% detection rate for Down syndrome, with a 5% false positive rate and a positive LR of 21.2.<sup>158</sup> Using receiver operator curve analysis, another study found that a prenasal thickness/nasal bone length ratio of 0.76 or greater resulted in an 80% detection rate for Down syndrome at a 5% false positive rate.<sup>159</sup> The optimal threshold for use of prenasal thickness in clinical practice remains to be determined.



As with first trimester imaging, the FMF angle measurement has also been proposed as a second trimester marker for Down syndrome.<sup>160,161</sup> Sonek and colleagues demonstrated an 85% detection rate of Down syndrome when the FMF angle measured above the 95th percentile.<sup>160</sup> Odibo and colleagues demonstrated less promising results, with the FMF angle identifying only 9.5% of Down syndrome fetuses. When used together with nasal bone, the FMF angle identified only one additional case of Down syndrome.<sup>162</sup> It remains unclear whether this angle measurement is dependent on gestational age and ethnicity. Future large prospective studies are needed to determine the true association between this finding and Down syndrome and to standardize measurement technique and optimal threshold values.

## SECOND TRIMESTER SONOGRAPHIC MARKERS FOR OTHER ANEUPLOIDIES

### Choroid Plexus Cysts

Choroid plexus cysts occur in 1% to 2% of normal fetuses.<sup>163,164</sup> The normal choroid plexus fills the atrium of the lateral cerebral ventricles prior to 16 weeks and can be best visualized in the transventricular view just superior to the plane of the biparietal diameter. Choroid plexus cysts are typically identified between 16 and 23 weeks and are seen as round hypoechoic structures within the choroid plexus (Fig. 3-39). They can vary greatly in size and can be unilateral or bilateral, single or multiple. These cysts tend to be transient, typically resolving by 26 weeks, and have no effect on structure or neurodevelopment of the fetus.<sup>165</sup>

The incidence of choroid plexus cysts in fetuses with Down syndrome appears to approximate the incidence in the general population; therefore, this finding is not thought to be a sonographic marker for that condition.<sup>166,167</sup> Several studies have demonstrated positive LRs that approximate 1.0 for the association between choroid plexus cysts and Down syndrome, indicating no increased risk over the background risk.<sup>91,168</sup>

In contrast, choroid plexus cysts have been associated with a significantly increased risk for trisomy 18. Snijders and colleagues demonstrated that choroid plexus cysts are found in approximately 50% of fetuses with trisomy 18 in the midtrimester. As isolated findings, these cysts only marginally increase the risk of aneuploidy. However, when

identified in combination with other markers of aneuploidy, the risk for trisomy 18 may be increased by 20-fold.<sup>169</sup> Gupta and colleagues reported a risk for trisomy 18 of 1 in 3 when choroid plexus cysts were identified in conjunction with other anatomic abnormalities. That study also found that the risk for aneuploidy was not related to cyst size, laterality, or regression over the course of gestation.<sup>170</sup>

Debate in the literature remains regarding the significance of choroid plexus cysts as isolated sonographic findings. In a meta-analysis by Ghidini and colleagues, the finding of an isolated choroid plexus cyst increased the risk of trisomy 18 by a factor of 7.<sup>171</sup> More recent data suggest that the presence of an isolated choroid plexus cyst in an otherwise low-risk patient does not increase the risk of trisomy 18.<sup>172-174</sup> These studies support the role of targeted sonography to evaluate for other features of trisomy 18 when a choroid plexus cyst is identified (Figs. 3-40 through 3-42). Similar to EIF, disclosure of this isolated finding remains controversial.<sup>149,150</sup>

### Single Umbilical Artery

The normal umbilical cord contains three vessels, one vein and two arteries, surrounded by Wharton jelly. The finding of a single umbilical artery (SUA) is common, occurring in approximately 1% of all live singleton births.<sup>175</sup> Primary agenesis or thrombotic atrophy of one of the umbilical arteries versus persistence of a single allantoic artery are potential explanations for this finding.<sup>176</sup> On prenatal ultrasound imaging, the umbilical arteries are best viewed as they course around either side of the fetal bladder in a transverse view of the fetal pelvis. Using color or power Doppler, demonstration of an absent intra-abdominal segment of one umbilical artery can make the diagnosis of SUA (Fig. 3-43A). Alternatively, a cross-sectional view of a free-floating loop of cord demonstrating only two vessels can also aid in diagnosis (Fig. 3-43B). Some investigators have noted that SUA can be diagnosed as early as 11 to 14 weeks' gestation; however, this finding more typically is diagnosed at the time of the midtrimester anatomic survey.<sup>177</sup>

The association between SUA and major aneuploidies is well established, with trisomy 18 being the most common aneuploidy in affected fetuses. Trisomy 13, monosomy X, and triploidy have also been observed in the setting of SUA.<sup>177-181</sup> Although there have been reports of trisomy 21 in the setting of SUA, there appears to be no significant association or increased risk.<sup>179</sup> Granese and colleagues demonstrated

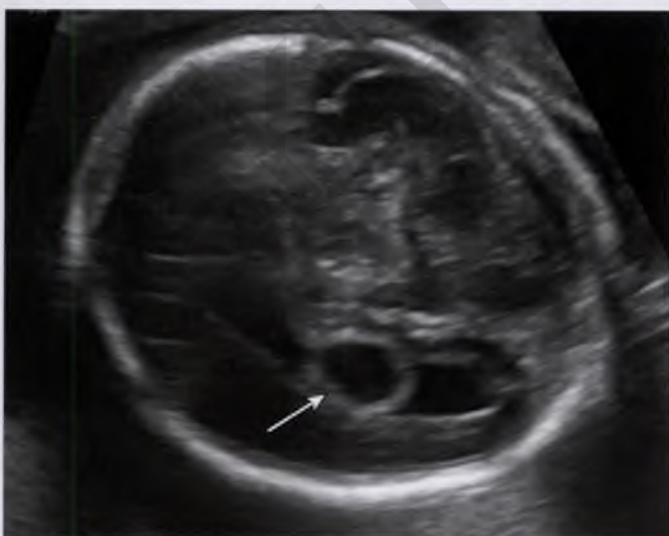


**FIG 3-39** Transverse view of the fetal head at the level of the choroid plexus demonstrating the presence of a single choroid plexus cyst (arrow).



**FIG 3-40** Sonogram of fetus with trisomy 18 shows bilateral clenched hands, which persisted throughout the sonographic examination.





**FIG 3-41** Three-dimensional image of fetus with trisomy 18 shows persistently bilateral clenched hands in front of the face. These hand findings are characteristic of this aneuploidy.

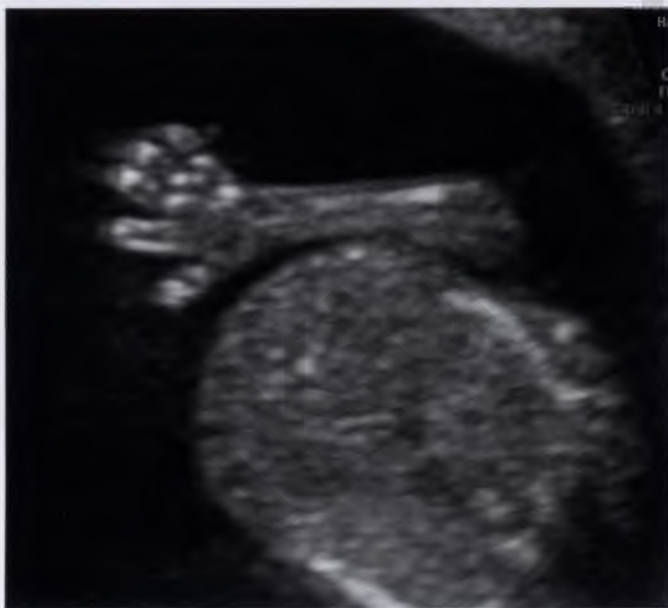


**FIG 3-42** Normal open fetal hand. The absence of the characteristic clenched hands seen in trisomy 18 is an important component of a fetal evaluation when choroid plexus cysts are identified.

a 41.6% incidence of chromosomal malformations in fetuses with SUA and a concomitant major anomaly compared to a 2.56% incidence when SUA was an isolated finding.<sup>179</sup> In a 2010 population-based retrospective cohort study of greater than 200,000 fetuses and neonates, SUA conferred a 15.35 times greater risk of chromosomal



**FIG 3-43 A**, Transverse power Doppler ultrasound image of the fetal pelvis demonstrating the presence of a single umbilical artery coursing adjacent to the bladder. **B**, Cross section of a free loop of umbilical cord showing the larger umbilical vein and the adjacent small single umbilical artery (SUA).

abnormalities overall.<sup>182</sup> Another recent study demonstrated no cases of aneuploidy in the setting of isolated SUA, a 3.7% risk in fetuses with one additional defect, and a 50.7% risk in fetuses with multiple defects.<sup>181</sup> Finally, a recent meta-analysis demonstrated no increased risk for aneuploidy in fetuses with isolated SUA.<sup>183</sup> Based on these data, it would appear that the association between SUA and aneuploidy is strongest in the setting of other major anomalies, and there is little evidence to support an increased risk of aneuploidy in the setting of an isolated SUA. However, this sonographic finding should prompt more detailed targeted examination to evaluate for other markers of aneuploidy. In the absence of aneuploidy, SUA has also been associated with other major anomalies, specifically cardiac and renal abnormalities, as well as fetal growth restriction<sup>182,184</sup> (see Chapter 19).

### Abnormalities of the Extremities

Malformations of the fetal extremities are commonly observed in fetuses with autosomal trisomies. Abnormal positioning of the fetal hands, including clenched fists and overlapping digits, is one of the most common findings seen in fetuses with trisomy 18. These findings may be subtle sonographically and are best observed during real-time imaging. Shields and colleagues found that 89% of fetuses with trisomy 18 demonstrated persistent abnormal positioning of the fetal fingers during ultrasound examinations between 14 and 22 weeks.<sup>185</sup> These





**FIG 3-44** Left-sided clubfoot identified at 20 weeks' gestation. LT, left.

investigators suggested that sonographic documentation of an open hand should significantly decrease trisomy 18 risk (see Fig. 3-42). Similarly, Watson and colleagues demonstrated that abnormalities of the position of the fetal hands were the second most common sonographic finding in trisomy 18 (43%), following cardiac defects (62%).<sup>186</sup> These fetal hand abnormalities may be one of the earliest sonographic findings in trisomy 18 fetuses, identifiable as early as 12 to 13 weeks' gestation.<sup>187,188</sup>

“Rocker-bottom feet” are pathognomonic for trisomy 18, with the fetal feet having the sonographic appearance of a rocking chair bottom instead of the typical inward arch of the plantar surface of the foot. This finding has been reported in 10% to 52% of fetuses with trisomy 18.<sup>3,189,190</sup> Other reported extremity malformations in trisomy 18 include hypoplastic/absent thumb, syndactyly of the fingers and toes, and radial/ulnar deviation of the hands.<sup>190</sup>

Talipes equinovarus (clubfoot) has also been associated with trisomy 18, trisomy 13, and sex chromosome abnormalities.<sup>191</sup> This abnormality is diagnosed when the foot is rotated inward and fixed in a plantar-flexed position (Fig. 3-44). Clubfeet are identified in approximately 20% to 40% of all fetuses with trisomy 18. However, as reported previously, the vast majority of these fetuses will also have additional associated abnormalities.<sup>3,189</sup> As an isolated finding, the incidence of aneuploidy associated with clubfoot ranges from 1.7% to 3.6% and is generally not thought to be an indication for invasive genetic testing in a low-risk patient.<sup>192,193</sup>

Polydactyly is diagnosed when more than five digits are located on either the hand or foot. Postaxial polydactyly is diagnosed when the digit is located on the ulnar or fibular side of the hand or foot and has been associated with trisomy 13.<sup>4,194,195</sup> Recent studies demonstrate a 7% to 10% incidence of postaxial polydactyly in trisomy 13 fetuses.<sup>194,195</sup> Because this extra digit is often a simple skintag without the presence of ossified bone, it can be difficult to detect sonographically.

## CONCLUSIONS

A large number of major and minor sonographic findings have been associated with fetal aneuploidy in the first and second trimesters of

pregnancy. Although structural anomalies are strongly associated with chromosome abnormalities, a search for major malformations will identify relatively few cases of Down syndrome. For this reason, so-called soft markers are often used to identify fetuses at risk. The presence of an isolated soft marker usually does not represent a markedly elevated risk for Down syndrome, the exception being an absent nasal bone or a thickened nuchal fold. The identification of one soft marker should result in a careful assessment for other markers and structural abnormalities, as well as a determination of the patient's baseline aneuploidy risk.

## REFERENCES

- Vintzileos AM, Egan JF: Adjusting the risk for trisomy 21 on the basis of second-trimester ultrasonography. *Am J Obstet Gynecol* 172(3):837–844, 1995.
- Nyberg DA, Kramer D, Resta RG, et al: Prenatal sonographic findings of trisomy 18: review of 47 cases. *J Ultrasound Med* 12(2):103–113, 1993.
- Yeo L, Guzman ET, Day-Salvatore D, et al: Prenatal detection of fetal trisomy 18 through abnormal sonographic features. *J Ultrasound Med* 22(6):581–590, 2003.
- Lehman CD, Nyberg DA, Winter TC, et al: Trisomy 13 syndrome: prenatal ultrasound findings in a review of 33 cases. *Radiology* 194(1): 217–222, 1995.
- Vintzileos AM, Egan JF: Adjusting the risk for trisomy 21 on the basis of second-trimester ultrasonography. *Am J Obstet Gynecol* 172:837, 1995.
- Sohl BD, Scioscia AL, Budorick NE, Moore TR: Utility of minor ultrasonographic markers in the prediction of abnormal fetal karyotype at a prenatal diagnostic center. *Am J Obstet Gynecol* 181:898, 1999.
- Nyberg DA, Resta R, Luthy DA, et al: Prenatal sonographic findings of Down syndrome: review of 94 cases. *Obstet Gynecol* 76:370, 1990.
- Crawford DC, Chita SK, Allan LD: Prenatal detection of congenital heart disease: factors affecting obstetric management and survival. *Am J Obstet Gynecol* 159:352, 1988.
- Copel JA, Pilu G, Kleinman CS: Congenital heart disease and extracardiac anomalies: associations and indications for fetal echocardiography. *Am J Obstet Gynecol* 154:1121, 1986.
- Nyberg DA, Souter VL: Chromosomal abnormalities. In Nyberg DA, McGahan JP, Pretorius DH, Pilu G, editors: *Diagnostic Imaging of Fetal Anomalies*, Philadelphia, 2003, Lippincott Williams & Wilkins, pp 86–906.
- Delisle MF, Sandor GG, Tessier F, Farquharson DF: Outcome of fetuses diagnosed with atrioventricular septal defect. *Obstet Gynecol* 94:763, 1999.
- Paladini D, Tartaglioine A, Agangi A, et al: The association between congenital heart disease and Down syndrome in prenatal life. *Ultrasound Obstet Gynecol* 15:104, 2000.
- DeVore GR: Trisomy 21: 91% detection rate using second-trimester ultrasound markers. *Ultrasound Obstet Gynecol* 16:133, 2000.
- DeVore GR: Second trimester ultrasonography may identify 77 to 97% of fetuses with trisomy 18. *J Ultrasound Med* 19:565, 2000.
- Anandakumar C, Biswas A, Wong YC, et al: Management of non-immune hydrops: 8 years' experience. *Ultrasound Obstet Gynecol* 8:196, 1996.
- Society for Maternal-Fetal Medicine (SMFM), Norton ME, Chauhan SP, Dashe JS: Society for maternal-fetal medicine (SMFM) clinical guideline #7: nonimmune hydrops fetalis. *Am J Obstet Gynecol* 212(2):127–139, 2015.
- Iskaros J, Jauniaux E, Rodeck C: Outcome of nonimmune hydrops fetalis diagnosed during the first half of pregnancy. *Obstet Gynecol* 90:321, 1997.
- Hagay Z, Reece A, Roberts A, et al: Isolated fetal pleural effusion: A prenatal management dilemma. *Obstet Gynecol* 81:147, 1993.
- Zelop C, Benacerraf BR: The causes and natural history of fetal ascites. *Prenat Diagn* 14:941, 1994.
- Dillon E, Renwick M, Wright C: Congenital diaphragmatic herniation: Antenatal detection and outcome. *Br J Radiol* 73:360, 2000.



21. Bollmann R, Kalache K, Mau H, et al: Associated malformations and chromosomal defects in congenital diaphragmatic hernia. *Fetal Diagn Ther* 10:52, 1995.
22. Howe DT, Kilby MD, Sirry H, et al: Structural chromosome anomalies in congenital diaphragmatic hernia. *Prenat Diagn* 16:1003, 1996.
23. Gilbert WM, Nicolaides KH: Fetal omphalocele: Associated malformations and chromosomal defects. *Obstet Gynecol* 70:633, 1987.
24. Getachew MM, Goldstein RB, Edge V, et al: Correlation between omphalocele contents and karyotypic abnormalities: Sonographic study in 37 cases. *AJR Am J Roentgenol* 158:133, 1992.
25. Pilu G, Falco P, Gabrielli S, et al: The clinical significance of fetal isolated cerebral borderline ventriculomegaly: Report of 31 cases and review of the literature. *Ultrasound Obstet Gynecol* 14:320, 1999.
26. Kolble N, Wisser J, Kurmanavicius J, et al: Dandy-Walker malformation: Prenatal diagnosis and outcome. *Prenat Diagn* 20:318, 2000.
27. Serur D, Jeret JS, Wisniewski K: Agenesis of the corpus callosum. Clinical, neuroradiological and cytogenetic studies. *Neuropediatr* 19:87, 1986.
28. Serur D, Jeret JS, Wisniewski K: Agenesis of the corpus callosum. Clinical, neuroradiological and cytogenetic studies. *Neuropediatr* 19:87, 1986.
29. Lehman CD, Nyberg DA, Winter TC, et al: Trisomy 13 syndrome: Prenatal ultrasound findings in a review of 33 cases. *Radiology* 194:217, 1995.
30. Bogart MH, Pandian MR, Jones OW: Abnormal maternal serum chorionic gonadotropin levels in pregnancies with fetal chromosome abnormalities. *Prenat Diagn* 7:623, 1987.
31. Nicolaides KH, Snijders RJ, Gosden CM, et al: Ultrasonographically detectable markers of fetal chromosomal abnormalities. *Lancet* 340:704, 1992.
32. Rizzo N, Gabrielli S, Pilu G, et al: Prenatal diagnosis and obstetrical management of multicystic dysplastic kidney disease. *Prenat Diagn* 7:109, 1987.
33. Nicolaides KH, Azar G, Byrne D, et al: Fetal nuchal translucency: ultrasound screening for chromosomal defects in first trimester of pregnancy. *BMJ* 304(6831):867-869, 1992.
34. Pandya PP, Kondylios A, Hilbert L, et al: Chromosomal defects and outcome in 1015 fetuses with increased nuchal translucency. *Ultrasound Obstet Gynecol* 5(1):15-19, 1995.
35. Spencer K, Souter V, Tul N, et al: A screening program for trisomy 21 at 10-14 weeks using fetal nuchal translucency, maternal serum free  $\beta$ -human chorionic gonadotropin and pregnancy associated plasma protein-A. *Ultrasound Obstet Gynecol* 13(4):231-237, 1999.
36. Wald N, Watt H, Hackshaw A: Integrated screening for Down syndrome based on tests performed in the first and second trimesters. *N Engl J Med* 341(7):461-467, 1999.
37. Kornman LH, Morssink LP, Beekhuis JR, et al: Nuchal translucency cannot be used as a screening test for chromosomal abnormalities in the first trimester of pregnancy in a routine ultrasound practice. *Prenat Diagn* 16(9):797-805, 1996.
38. Economides DL, Whitlow BJ, Kadir R, et al: First trimester sonographic detection of chromosomal abnormalities in an unselected population. *Br J Obstet Gynaecol* 105(1):58-62, 1998.
39. Snijders RJ, Noble P, Sebire N, et al: UK multicenter project on assessment of risk of trisomy 21 by maternal age and fetal nuchal-translucency thickness at 10-14 weeks of gestation. *Lancet* 352(9125):343-346, 1998.
40. Krantz DA, Hallahan TW, Orlandi F, et al: First-trimester Down syndrome screening using dried blood biochemistry and nuchal translucency. *Obstet Gynecol* 96(2):207-213, 2000.
41. Brizot ML, Carvalho MH, Liao AW, et al: First-trimester screening for chromosomal abnormalities by fetal nuchal translucency in a Brazilian population. *Ultrasound Obstet Gynecol* 18(6):652-655, 2001.
42. Malone FD, Dalton ME, Society for Maternal-Fetal Medicine: First-trimester sonographic screening for Down syndrome. *Obstet Gynecol* 102(5 Pt1):1066-1079, 2003.
43. Crossley JA, Aitken DA, Cameron AD, et al: Combined ultrasound and biochemical screening for Down's syndrome in the first trimester: a Scottish multicenter study. *Br J Obstet Gynaecol* 109(6):667-676, 2002.
44. Wapner R, Thom E, Simpson JL, et al: First trimester Maternal Serum Biochemistry and Fetal Nuchal Translucency Screening (BUN) Study Group: First trimester screening for trisomies 21 and 18. *N Engl J Med* 349(15):1405-1413, 2003.
45. Wald NJ, Rodeck C, Hackshaw AK, et al: First and second trimester antenatal screening for Down's syndrome: the results of the Serum, Urine and Ultrasound Screening Study (SURUSS). *J Med Screen* 10(2):56-104, 2003.
46. Bohlandt S, von Kaisenberg CS, Wewetzer K, et al: Hyaluronan in the nuchal skin of chromosomally abnormal fetuses. *Hum Reprod* 15(5):1155-1158, 2000.
47. Sebire NJ, Snijders RJ, Davenport M, et al: Fetal nuchal translucency thickness at 10-14 weeks' gestation and congenital diaphragmatic hernia. *Obstet Gynecol* 90(6):943-946, 1997.
48. Hyett J, Perdu M, Sharland G, et al: Using nuchal translucency to screen for major cardiac defects at 10-14 weeks of gestation: population based cohort study. *BMJ* 318(7176):81-85, 1999.
49. Mol BWJ: Down's syndrome, cardiac anomalies and nuchal translucency. *BMJ* 318(7176):70-71, 1999.
50. von Kaisenberg CS, Krenn V, Ludwig M, et al: Morphological classification of nuchal skin in human fetuses with trisomy 21, 18, and 13 at 12-18 weeks and in a trisomy 16 mouse. *Anat Embryol (Berl)* 197(2):105-124, 1998.
51. Malone FD, Canick JA, Ball RH, et al: First- and Second-Trimester Evaluation of Risk (FASTER) Research Consortium: First-trimester or second-trimester screening, or both, for Down's syndrome. *N Engl J Med* 353(19):2001-2011, 2005.
52. Breathnach FM, Malone FD, Lambert-Messerlian G, et al: First and Second Trimester Evaluation of Risk (FASTER) Research Consortium: First- and second-trimester screening: detection of aneuploidies other than Down syndrome. *Obstet Gynecol* 110(3):651-657, 2007.
53. Cuckle H: Monitoring quality control of nuchal translucency. *Clin Lab Med* 30(3):593-604, 2010.
54. Haddow JE, Palomaki GE, Knight GJ, et al: Screening of maternal serum for fetal Down's syndrome in the first trimester. *N Engl J Med* 338(14):955-961, 1998.
55. Nuchal Translucency Quality Review Program of the Perinatal Quality Foundation, Cuckle H, Platt LD, et al: Nuchal Translucency Quality Review (NTQR) program: first one and half million results. *Ultrasound Obstet Gynecol* 45(2):199-204, 2015.
56. Scott F, Boogert A, Sinosich M, Anderson J: Establishment and application of a normal range for nuchal translucency across the first trimester. *Prenat Diagn* 16(7):629-634, 1996.
57. Schuchter K, Wald N, Hackshaw AK, et al: The distribution of nuchal translucency at 10-13 weeks of pregnancy. *Prenat Diagn* 18(3):281-286, 1998.
58. Comstock CH, Malone FD, Ball RH, et al: Is there a nuchal translucency millimeter measurement above which there is no added benefit from first-trimester serum screening? *Am J Obstet Gynecol* 195(3):843-847, 2006.
59. Malone FD, Ball RH, Nyberg DA, et al: FASTER Trial Research Consortium: First-trimester septated cystic hygroma: prevalence, natural history, and pediatric outcome. *Obstet Gynecol* 106(2):288-294, 2005.
60. Molina FS, Avgidou K, Kagan KO, et al: Cystic hygromas, nuchal edema, and nuchal translucency at 11-14 weeks of gestation. *Obstet Gynecol* 107(3):678-683, 2006.
61. Sonek JD, Nicolaides KH: Prenatal ultrasonographic diagnosis of nasal bone abnormalities in three fetuses with Down syndrome. *Am J Obstet Gynecol* 186(1):139-141, 2002.
62. Zoppi MA, Ibba RM, Axiana C, et al: Absence of fetal nasal bone and aneuploidies at first-trimester nuchal translucency screening in unselected pregnancies. *Prenat Diagn* 23(6):496-500, 2003.
63. Viora E, Masturzo B, Errante G, et al: Ultrasound evaluation of fetal nasal bone at 11 to 14 weeks in a consecutive series of 1906 fetuses. *Prenat Diagn* 23(10):784-787, 2003.



64. Orlandi F, Bilardo CM, Campogrande M, et al: Measurement of nasal bone length at 11–14 weeks of pregnancy and its potential role in Down syndrome risk assessment. *Ultrasound Obstet Gynecol* 22(1):36–39, 2003.
65. Odibo AO, Sehdev HM, Stamilio DM, et al: Defining nasal bone hypoplasia in second-trimester Down syndrome screening: does the use of multiples of the median improve screening efficacy? *Am J Obstet Gynecol* 197(4):361.e1–361.e4, 2007.
66. Rosen T, D'Alton ME, Platt LD, Wapner R: First-trimester ultrasound assessment of the nasal bone to screen for aneuploidy. *Obstet Gynecol* 110(2 Pt 1):399–404, 2007.
67. Cicero S, Dezergega V, Andrade E, et al: Learning curve for sonographic examination of the fetal nasal bone at 11–14 weeks. *Ultrasound Obstet Gynecol* 22(2):135–137, 2003.
68. Orlandi F, Rossi C, Orlandi E, et al: First-trimester screening for trisomy-21 using a simplified method to assess the presence or absence of the fetal nasal bone. *Am J Obstet Gynecol* 192(4):1107–1111, 2005.
69. Cicero S, Avgidou K, Rembouskos G, et al: Nasal bone in first-trimester screening for trisomy 21. *Am J Obstet Gynecol* 195(1):109–114, 2006.
70. Cicero S, Longo D, Rembouskos G, et al: Absent nasal bone at 11–14 weeks of gestation and chromosomal defects. *Ultrasound Obstet Gynecol* 22(1):31–35, 2003.
71. Cicero S, Rembouskos G, Vandecruys H, et al: Likelihood ratio for trisomy 21 in fetuses with absent nasal bone at the 11–14-week scan. *Ultrasound Obstet Gynecol* 23(3):218–223, 2004.
72. Matias A, Gomes C, Flack N, et al: Screening for chromosomal abnormalities at 10–14 weeks: the role of ductus venosus blood flow. *Ultrasound Obstet Gynecol* 12(6):380–384, 1998.
73. Prefumo F, Sethna F, Sairam S, et al: First-trimester ductus venosus, nasal bones, and Down syndrome in a high-risk population. *Obstet Gynecol* 105(6):1348–1354, 2005.
74. Zoppi MA, Putzolu M, Ibba RM, et al: First-trimester ductus venosus velocimetry in relation to nuchal translucency thickness and fetal karyotype. *Fetal Diagn Ther* 17(1):52–57, 2002.
75. Mavrides E, Sairam S, Hollis B, Thilaganathan B: Screening for aneuploidy in the first trimester by assessment of blood flow in the ductus venosus. *Br J Obstet Gynaecol* 109(9):1015–1019, 2002.
76. Oh C, Harman C, Baschat AA: Abnormal first-trimester ductus venosus blood flow: a risk factor for adverse outcome in fetuses with normal nuchal translucency. *Ultrasound Obstet Gynecol* 30(2):192–196, 2007.
77. Martinez JM, Comas M, Borrell A, et al: Abnormal first-trimester ductus venosus blood flow: a marker of cardiac defects in fetuses with normal karyotype and nuchal translucency. *Ultrasound Obstet Gynecol* 35(3):267–272, 2010.
78. Falcon O, Auer M, Gerovassili A, et al: Screening for trisomy 21 by fetal tricuspid regurgitation, nuchal translucency and maternal serum free  $\beta$ -hCG and PAPP-A at 11 + 0 to 13 + 6 weeks. *Ultrasound Obstet Gynecol* 27(2):151–155, 2006.
79. Kagan KO, Valencia C, Livanos P, et al: Tricuspid regurgitation in screening for trisomies 21, 18 and 13 and Turner syndrome at 11+0 to 13+6 weeks of gestation. *Ultrasound Obstet Gynecol* 33(1):18–22, 2009.
80. Sonek J, Borenstein M, Dagleis T, et al: Frontomaxillary facial angle in fetuses in trisomy 21 at 11–13(6) weeks. *Am J Obstet Gynecol* 196(3):271, 2007.
81. Alphonse J, Cox J, Clarke JL, et al: Frontomaxillary facial angle measurement in trisomy 21 and euploid fetuses: two- and three-dimensional assessment during routine first trimester screening. *Fetal Diagn Ther* 36(3):183–189, 2014.
82. Borenstein M, Persico N, Kagan KO, et al: Frontomaxillary facial angle in screening for trisomy 21 at 11+0 to 13+6 weeks. *Ultrasound Obstet Gynecol* 32(1):5–11, 2008.
83. Zalel Y, Achiron R, Yagel S, Kivilevich Z: Fetal aberrant right subclavian artery in normal and Down syndrome fetuses. *Ultrasound Obstet Gynecol* 31(1):25–29, 2008.
84. Vos FI, De Jong-Pleij EA, Ribbert LS, et al: Three-dimensional ultrasound imaging and measurement of nasal bone length, prenasal thickness and frontomaxillary facial angle in normal second- and third-trimester fetuses. *Ultrasound Obstet Gynecol* 39(6):636–641, 2012.
85. Benacerraf BR, Neuberger D, Bromley B, Frigoletto FD, Jr: Sonographic scoring index for prenatal detection of chromosomal abnormalities. *J Ultrasound Med* 11(9):449–458, 1992.
86. Nyberg DA, Luthy DA, Cheng EY, et al: Role of prenatal ultrasonography in women with positive screen for Down syndrome on the basis of maternal serum markers. *Am J Obstet Gynecol* 173(4):1030–1035, 1995.
87. Vintzileos AM, Campbell WA, Rodis JF, et al: The use of second-trimester genetic sonogram in guiding clinical management of patients at increased risk for trisomy 21. *Obstet Gynecol* 87(6):948–952, 1996.
88. Devore GR, Romero R: Combined use of genetic sonography and maternal serum triple-marker screening: an effective method for increasing the detection of trisomy 21 in women younger than 35 years. *J Ultrasound Med* 20(6):645–654, 2001.
89. Bromley B, Lieberman E, Shipp TD, Benacerraf BR: The genetic sonogram: a method of risk assessment for Down syndrome in the second trimester. *J Ultrasound Med* 21(10):1087–1096, 2002.
90. Nyberg DA, Souter VL, El-Bastwissi A, et al: Isolated sonographic markers for detection of fetal Down syndrome in the second trimester of pregnancy. *J Ultrasound Med* 20(10):1053–1063, 2001.
91. Smith-Bindman R, Hosmer W, Feldstein VA, et al: Second-trimester ultrasound to detect fetuses with Down syndrome: a meta-analysis. *JAMA* 285(8):1044–1055, 2001.
92. Agathokleous M, Chaveeva P, Poon LCY, et al: Meta-analysis of second-trimester markers for trisomy 21. *Ultrasound Obstet Gynecol* 41(3):247–261, 2013.
93. Vintzileos AM, Guzman ER, Smulian JC, et al: Choice of second-trimester genetic sonogram for detection of trisomy 21. *Obstet Gynecol* 90(2):187–190, 1997.
94. Pinette MG, Garrett J, Salvo A, et al: Normal midtrimester (17–20 weeks) genetic sonogram decreases amniocentesis rate in a high-risk population. *J Ultrasound Med* 20(6):639–644, 2001.
95. Aagard-Tillery KM, Malone FD, Nyberg DA, et al: Role of second-trimester genetic sonography after Down syndrome screening. *Obstet Gynecol* 114(6):1189–1196, 2009.
96. Krantz DA, Hallahan TW, Macri VJ, Macri JN: Genetic sonography after first-trimester Down syndrome screening. *Ultrasound Obstet Gynecol* 29(6):666–670, 2007.
97. Odibo AO, Ghidini A: Role of the second trimester “genetic sonogram” for Down syndrome screen in the era of first-trimester screening and noninvasive prenatal testing. *Prenat Diagn* 34(6):511–517, 2014.
98. Benacerraf BR, Gelman R, Frigoletto FD: A sonographic sign for the detection in the second trimester of the fetus with Down's syndrome. *Am J Obstet Gynecol* 151(8):1078–1079, 1985.
99. Down JL: Observations on an ethnic classification of idiots. 1866. *Ment Retard* 33(1):54–56, 1985.
100. Maymon R, Zimmerman AL, Weintraub Z, et al: Correlation between nuchal translucency and nuchal skin-fold measurements in Down syndrome and unaffected fetuses. *Ultrasound Obstet Gynecol* 32(4):501–505, 2008.
101. Salomon LJ, Bernard JP, Taupin P, et al: Relationship between nuchal translucency at 11–14 weeks and nuchal fold at 20–24 weeks of gestation. *Ultrasound Obstet Gynecol* 18(6):636–637, 2001.
102. Olson G, Saade GR, Zlatnik M, et al: The effect of fetal neck position on nuchal fold thickness. *Am J Obstet Gynecol* 183(4):995–997, 2000.
103. Gray DL, Crane JP: Sonographically measured nuchal skinfold thickness as a screening tool for Down syndrome: results of a prospective clinical trial. *Obstet Gynecol* 77(4):533–536, 1991.
104. Watson WJ, Miller RC, Menard MK: Ultrasonographic measurements of fetal nuchal skin to screen for chromosomal abnormalities. *Am J Obstet Gynecol* 170(2):583–586, 1994.
105. Gray DL, Crane JP: Optimal nuchal skin-fold thresholds based on gestational age for prenatal detection of Down syndrome. *Am J Obstet Gynecol* 171(5):1282–1286, 1994.
106. Singh C, Biswas A: Impact of gestational age on nuchal fold thickness in the second trimester. *J Ultrasound Med* 33(4):687–690, 2014.
107. Bromley B, Benacerraf BR: The resolving nuchal fold in second trimester fetuses: not necessarily a reassuring finding. *J Ultrasound Med* 14(3):253–255, 1995.



108. Odibo AO, Sehdev HM, Sproat L, et al: Evaluating the efficiency of using second-trimester nasal bone hypoplasia as a single or a combined marker for fetal aneuploidy. *J Ultrasound Med* 25(4):437–441, 2006.
109. Odibo AO, Sehdev HM, Gerkowicz S, et al: Comparing the efficiency of second-trimester nasal bone hypoplasia and increased nuchal fold in Down syndrome screening. *Am J Obstet Gynecol* 199(3):281, 2008.
110. Bromley B, Lieberman E, Shipp TD, Benacerraf BR: Fetal nose bone length: a marker for Down syndrome in the second trimester. *J Ultrasound Med* 21(12):1387–1394, 2002.
111. Odibo AO, Sehdev HM, Dunn L, et al: The association between fetal nasal bone hypoplasia and aneuploidy. *Obstet Gynecol* 104(6):1229–1233, 2004.
112. Nyberg DA, Dubinsky T, Resta RG, et al: Echogenic fetal bowel during the second trimester: clinical importance. *Radiology* 188(2):527–531, 1993.
113. Ghose I, Mason GC, Martinez D, et al: Hyperechogenic fetal bowel: a prospective analysis of sixty consecutive cases. *Br J Obstet Gynaecol* 107(3):426–429, 2000.
114. Al-Kouatly HB, Chasen ST, Streltsoff J, Chervenak FA: The clinical significance of fetal echogenic bowel. *Am J Obstet Gynecol* 185(5):1035–1038, 2001.
115. Brock DJH: A comparative study of microvillar enzyme activities in the prenatal diagnosis of cystic fibrosis. *Prenat Diagn* 5(2):129–134, 1985.
116. Caspi B, Elchalal U, Lancet M, Chemke J: Prenatal diagnosis of cystic fibrosis. Ultrasonographic appearance of meconium ileus in the fetus. *Prenat Diagn* 8(5):379–382, 1998.
117. Forouzan I: Fetal abdominal echogenic mass: an early sign of intrauterine cytomegalovirus infection. *Obstet Gynecol* 80(3 Pt 2):535–537, 1992.
118. Strocker AM, Snijders RJ, Carlson DE, et al: Fetal echogenic bowel: parameters to be considered in the differential diagnosis. *Ultrasound Obstet Gynecol* 16(6):519–523, 2000.
119. Sepulveda W, Reid R, Nicolaidis P, et al: Second-trimester echogenic bowel and intraamniotic bleeding: association between fetal bowel echogenicity and amniotic fluid spectrophotometry at 410 nm. *Am J Obstet Gynecol* 174(3):839–842, 1996.
120. Goetzinger KR, Cahill AG, Macones GA, Odibo AO: Echogenic bowel on second-trimester ultrasonography: evaluating the risk of adverse pregnancy outcome. *Obstet Gynecol* 117(6):1341–1348, 2011.
121. Dicke JM, Gray DL, Songster GS, Crane JP: Fetal biometry as a screening tool for the detection of chromosomally abnormal pregnancies. *Obstet Gynecol* 74(5):726–729, 1989.
122. Gray DL, Dicke JM, Dickerson R, et al: Reevaluating humeral length for the detection of fetal trisomy 21. *J Ultrasound Med* 28(10):1325–1330, 2009.
123. Benacerraf BR, Gelman R, Frigoletto FD: Sonographic identification of second-trimester fetuses with Down's syndrome. *N Engl J Med* 317(22):1371–1376, 1987.
124. Benacerraf BR, Neuberger D, Frigoletto FD: Humeral shortening in second-trimester fetuses with Down syndrome. *Obstet Gynecol* 77(2):223–227, 1991.
125. Lockwood C, Benacerraf B, Krinsky A, et al: A sonographic screening method for Down syndrome. *Am J Obstet Gynecol* 157(4 Pt 1):803–808, 1987.
126. Fitzsimmons J, Droste S, Shepard TH, et al: Long-bone growth in fetuses with Down syndrome. *Am J Obstet Gynecol* 161(5):1174–1177, 1989.
127. Nyberg DA, Resta RG, Luthy DA, et al: Humerus and femur length shortening in the detection of Down's syndrome. *Am J Obstet Gynecol* 168(2):534–538, 1993.
128. Borgida AF, Zelop C, Deroche M, et al: Down syndrome screening using race-specific femur length. *Am J Obstet Gynecol* 189(4):977–979, 2003.
129. Harper LM, Gray DL, Dicke JM, et al: Do race-specific definitions of short long bones improve the detection of Down syndrome on second-trimester genetic sonograms? *J Ultrasound Med* 29(2):231–235, 2010.
130. Goetzinger KR, Dicke JM, Gray DL, et al: The effect of fetal gender in predicting Down syndrome using long bone ultrasonographic measurements. *Prenat Diagn* 30(10):950–955, 2010.
131. Corteville JE, Dicke JM, Crane JP: Fetal pyelectasis and Down syndrome: is genetic amniocentesis warranted? *Obstet Gynecol* 79(5 Pt 1):770–772, 1992.
132. Benacerraf BR, Mandel J, Estroff JA, et al: Fetal pyelectasis: a possible association with Down syndrome. *Obstet Gynecol* 76(1):58–60, 1990.
133. Bornstein E, Barnhard Y, Donnenfeld AE, et al: Fetal pyelectasis: does gender modify the risk of major trisomies? *Obstet Gynecol* 107(4):877–879, 2006.
134. Bornstein E, Barnhard Y, Donnenfeld AE, et al: The risk of a major trisomy in fetuses with pyelectasis: the impact of an abnormal maternal serum screen or additional sonographic markers. *Am J Obstet Gynecol* 196(5):e24–e26, 2007.
135. Carbone JF, Tuuli MG, Dicke JM, et al: Revisiting the risk for aneuploidy in fetuses with isolated pyelectasis. *Prenat Diagn* 31(6):566–570, 2011.
136. Orzechowski KM, Berghella V: Isolated fetal pyelectasis and the risk of Down syndrome: a meta-analysis. *Ultrasound Obstet Gynecol* 42(6):615–621, 2013.
137. Levy DW, Mintz MC: The left ventricular echogenic focus: a normal finding. *AJR Am J Roentgenol* 150(1):85–86, 1988.
138. Wax JR, Donnelly J, Carpenter M, et al: Childhood cardiac function after prenatal diagnosis of intracardiac echogenic foci. *J Ultrasound Med* 22(8):783–787, 2003.
139. Tennstedt C, Chaoui R, Vogel M, et al: Pathologic correlation of sonographic echogenic foci in the fetal heart. *Prenat Diagn* 20(4):287–292, 2000.
140. Roberts DJ, Genest D: Cardiac histologic pathology characteristics of trisomies 13 and 21. *Hum Pathol* 23(10):1130–1140, 1992.
141. Winter TC, Anderson AM, Cheng EY, et al: Echogenic intracardiac focus in 2nd trimester fetuses with trisomy 21: usefulness as a US marker. *Radiology* 216(2):450–456, 2000.
142. Bromley B, Lieberman E, Laboda L, Benacerraf BR: Echogenic intracardiac focus: a sonographic sign for fetal Down syndrome. *Obstet Gynecol* 86(6):998–1001, 1995.
143. Shanks AL, Odibo AO, Gray DL: Echogenic intracardiac foci: associated with increased risk for trisomy 21 or not? *J Ultrasound Med* 28(12):1639–1643, 2009.
144. Coco C, Jeanty P, Jeanty C: An isolated echogenic heart focus is not an indication for amniocentesis in 12,672 unselected patients. *J Ultrasound Med* 23(4):489–496, 2004.
145. Prefumo F, Presti F, Mavrides E, et al: Isolated echogenic foci in the fetal heart: do they increase risk of trisomy 21 in a population previously screened by nuchal translucency? *Ultrasound Obstet Gynecol* 18(2):126–130, 2001.
146. Anderson N, Jyoti R: Relationship of isolated fetal intracardiac echogenic focus to trisomy 21 at the mid-trimester sonogram in women younger than 35. *Ultrasound Obstet Gynecol* 21(4):354–358, 2003.
147. Lamont RF, Havutcu E, Salgia S, et al: The association between isolated fetal echogenic cardiac foci on second-trimester ultrasound scan and trisomy 21 in low-risk unselected women. *Ultrasound Obstet Gynecol* 23(4):346–351, 2004.
148. Sotiriadis A, Makrydimas G, Ioannidis JPA: Diagnostic performance of intracardiac echogenic foci for Down syndrome: a meta-analysis. *Obstet Gynecol* 101(5 Pt 1):1009–1016, 2003.
149. Doubilet PM, Copel JA, Benson CB, et al: Choroid plexus cyst and echogenic intracardiac focus in women at low risk for chromosomal anomalies. *J Ultrasound Med* 23(7):883–885, 2004.
150. Filly RA, Benacerraf BR, Nyberg DA, Hobbins JC: Choroid plexus cyst and echogenic intracardiac focus in women at low risk for chromosomal anomalies. *J Ultrasound Med* 23(4):447–449, 2004.
151. Caughey AB, Lyell DJ, Filly RA, et al: The impact of the use of the isolated echogenic intracardiac focus as a screen for Down syndrome in women under the age of 35 years. *Am J Obstet Gynecol* 185(5):1021–1027, 2001.



152. Chasen ST, Razavi AS: Echogenic intracardiac foci: disclosure and the rate of amniocentesis in low-risk patients. *Am J Obstet Gynecol* 209(4):377, 2013.
153. Goldenstein WB: Aberrant right subclavian artery in mongolism. *Am J Roentgenol Radium Ther Nucl Med* 95:131–134, 1965.
154. Chaoui R, Heling K, Sarioglu N, et al: Aberrant right subclavian artery as a new cardiac sign in second- and third-trimester fetuses with Down syndrome. *Am J Obstet Gynecol* 192(1):257–263, 2005.
155. Borenstein M, Minekawa R, Zidere V, et al: Aberrant right subclavian artery at 16 to 23+6 weeks of gestation: a marker for chromosomal abnormality. *Ultrasound Obstet Gynecol* 36(5):548–552, 2010.
156. Yazicioglu HF, Sevket O, Akin H, et al: Aberrant right subclavian artery in Down syndrome fetuses. *Prenat Diagn* 33(3):209–213, 2013.
157. Maymon R, Levinsohn-Tavor O, Cuckle H, et al: Second trimester ultrasound prenatal thickness combined with nasal bone length: a new method of Down syndrome screening. *Prenat Diagn* 25(10):906–911, 2005.
158. De Jong-Pleij EAP, Vos FI, Ribbert SM, et al: Prenasal thickness-to-nasal bone length ratio: a strong and simple second- and third-trimester marker for trisomy 21. *Ultrasound Obstet Gynecol* 39(2):185–190, 2012.
159. Ozcan T, Ozlu T, Allen J, et al: Predictive role of prenasal thickness and nasal bone for Down syndrome in the second trimester. *Eur J Obstet Gynecol Reprod Biol* 171(2):220–224, 2013.
160. Sonek J, Borenstein M, Downing C, et al: Frontomaxillary facial angles in screening for trisomy 21 at 14–23 weeks' gestation. *Am J Obstet Gynecol* 197(2):160, 2007.
161. Molina F, Persic N, Borenstein M, et al: Frontomaxillary facial angle in trisomy 21 fetuses at 16–24 weeks of gestation. *Ultrasound Obstet Gynecol* 31(4):384–387, 2008.
162. Odibo AO, Schoenborn JA, Haas K, Macones GM: Does the combination of fronto-maxillary facial angle and nasal bone evaluation improve the detection of Down syndrome in the second trimester? *Prenat Diagn* 29(10):947–951, 2009.
163. Naeini RM, Yoo JH, Hunter JV: Spectrum of choroid plexus lesions in children. *AJR Am J Roentgenol* 192(1):32–40, 2009.
164. Chinn DH, Miller EI, Worthy LM, Towers CV: Sonographically detected fetal choroid plexus cysts. Frequency and association with aneuploidy. *J Ultrasound Med* 10(5):255–258, 1991.
165. Twining P, Zuccollo J, Clewes J, Swallow J: Fetal choroid plexus cysts: a prospective study and review of the literature. *Br J Radiol* 64(758):98–102, 1991.
166. Bromley B, Lieberman R, Benacerraf BR: Choroid plexus cysts: not associated with Down syndrome. *Ultrasound Obstet Gynecol* 8(4):232–235, 1996.
167. Yoder PR, Sabbagha RE, Gross SJ, Zelop CM: The second-trimester fetus with isolated choroid plexus cysts: a meta-analysis of risk of trisomies 18 and 21. *Obstet Gynecol* 93(5 Pt 2):869–872, 1999.
168. Goetzinger KR, Stamilio DM, Dicke JM, et al: Evaluating the incidence and likelihood ratios of chromosomal abnormalities in fetuses with common central nervous system malformations. *Am J Obstet Gynecol* 199(3):285, 2008.
169. Snijders RJ, Shawa L, Nicolaidis KH: Fetal choroid plexus cysts and trisomy 18: assessment of risk based on ultrasound findings and maternal age. *Prenat Diagn* 14(12):1119–1127, 1994.
170. Gupta JK, Cave M, Lilford RJ, et al: Clinical significance of fetal choroid plexus cysts. *Lancet* 346(8977):724–729, 1995.
171. Ghidini A, Strobelt N, Locatelli A, et al: Isolated fetal choroid plexus cysts: role of ultrasonography in establishment of the risk of trisomy 18. *Am J Obstet Gynecol* 182(4):972–977, 2000.
172. Demasio K, Canterino J, Ananth C, et al: Isolated choroid plexus cyst in low-risk women less than 35 years old. *Am J Obstet Gynecol* 187(5):1246–1249, 2002.
173. Bronsteen R, Lee W, Vettraino IM, et al: Second-trimester sonography and trisomy 18. *J Ultrasound Med* 23(2):241–245, 2004.
174. Beke A, Barakonyi E, Belics Z, et al: Risk of chromosome abnormalities in the presence of bilateral or unilateral choroid plexus cysts. *Fetal Diagn Ther* 23(3):185–191, 2008.
175. Heifetz SA: Single umbilical artery. A statistical analysis of 237 autopsy cases and review of the literature. *Perspect Pediatr Pathol* 8(4):345–378, 1984.
176. Gornall AS, Kurinczuk JJ, Konje JC: Antenatal detection of a single umbilical artery: does it matter? *Prenat Diagn* 23(2):117–123, 2003.
177. Rembouskos G, Cicero S, Longo D, et al: Single umbilical artery at 11–14 weeks' gestation: relation to chromosomal defects. *Ultrasound Obstet Gynecol* 22(6):567–570, 2003.
178. Saller DN, Keene CL, Sun CC, Schwartz S: The association of single umbilical artery with cytogenetically abnormal pregnancies. *Am J Obstet Gynecol* 163(3):922–925, 1990.
179. Granese R, Coco C, Jeanty P: The value of single umbilical artery in the prediction of fetal aneuploidy: findings in 12,672 pregnant women. *Ultrasound Q* 23(2):117–121, 2007.
180. Geipel A, Germer U, Welp T, et al: Prenatal diagnosis of single umbilical artery: determination of the absent side, associated anomalies, Doppler findings and perinatal outcome. *Ultrasound Obstet Gynecol* 15(2):114–117, 2000.
181. Dagklis T, Defigueiredo D, Staboulidou I, et al: Isolated single umbilical artery and fetal karyotype. *Ultrasound Obstet Gynecol* 36(3):291–295, 2010.
182. Murphy-Kaulbeck L, Dodds L, Joseph KS, Van den Hof M: Single umbilical artery risk factors and pregnancy outcomes. *Obstet Gynecol* 116(4):843–850, 2010.
183. Voskamp BJ, Fleurke-Rozema H, Oude-Rengerink K, et al: Relationship of isolated single umbilical artery to fetal growth, aneuploidy and perinatal mortality: systematic review and meta-analysis. *Ultrasound Obstet Gynecol* 42(6):622–628, 2013.
184. Hua M, Odibo AO, Macones GA, et al: Single umbilical artery and its associated findings. *Obstet Gynecol* 115(5):930–934, 2010.
185. Shields LE, Carpenter LA, Smith KM, Nghiem HV: Ultrasonographic diagnosis of trisomy 18: is it practical in the early second trimester? *J Ultrasound Med* 17(5):327–331, 1998.
186. Watson WJ, Miller RC, Wax JR, et al: Sonographic findings of trisomy 18 in the second trimester of pregnancy. *J Ultrasound Med* 27(7):1033–1038, 2008.
187. Quintero RA, Johnson MP, Mendoza G, Evans MI: Ontogeny of clenched-hand development in trisomy 18 fetuses: a serial transabdominal fetoscopic observation. *Fetal Diagn Ther* 14(2):68–70, 1999.
188. Lam YH, Tang MH: Sonographic features of fetal trisomy 18 at 13 and 14 weeks: four case reports. *Ultrasound Obstet Gynecol* 13(5):366–369, 1999.
189. Isaksen CV, Eik-Nes SH, Blaas HG, et al: A correlative study of prenatal ultrasound and post-mortem findings in fetuses and infants with an abnormal karyotype. *Ultrasound Obstet Gynecol* 16(1):37–45, 2000.
190. Hsiao CC, Tsao LY, Chen HN, et al: Changing clinical presentations and survival pattern in trisomy 18. *Pediatr Neonat* 50(4):147–151, 2009.
191. Benacerraf BR: Antenatal sonographic diagnosis of congenital clubfoot: a possible indication for amniocentesis. *J Clin Ultrasound* 14(9):703–706, 1986.
192. Malone FD, Marino T, Biachi DW, et al: Isolated club foot diagnosed prenatally: is karyotyping indicated? *Obstet Gynecol* 95(3):437–440, 2000.
193. Lauson S, Alvarez C, Patel MS, Langlois S: Outcome of prenatally diagnosed isolated clubfoot. *Ultrasound Obstet Gynecol* 35(6):708–714, 2010.
194. Papp C, Beke A, Ban Z, et al: Prenatal diagnosis of trisomy 13: analysis of 28 cases. *J Ultrasound Med* 25(4):429–435, 2006.
195. Watson WJ, Miller RC, Wax JR, et al: Sonographic detection of trisomy 13 in the first and second trimesters of pregnancy. *J Ultrasound Med* 26(9):1209–1214, 2007.



# Ultrasound of the Early First Trimester

Peter M. Doubilet, Carol B. Benson

## SUMMARY OF KEY POINTS

- The progression of transvaginal sonographic findings in normal early first trimester pregnancies follows a highly predictable pattern, with a gestational age variability of approximately  $\pm 0.5$  week: gestational sac at 5.0 weeks, yolk sac at 5.5 weeks, embryo with heartbeat at 6.0 weeks, and amnion at 7.0 weeks.
- In a woman with a positive pregnancy test and no evidence of an intrauterine or ectopic pregnancy on ultrasound (pregnancy of unknown location [PUL]), a single hCG measurement does not reliably distinguish a normal intrauterine pregnancy from a failed intrauterine pregnancy or an ectopic pregnancy.
- In a woman with a positive pregnancy test, any round or oval intrauterine fluid collection should be interpreted as highly likely to be a gestational sac, not a pseudogestational sac or decidual cyst, and treatments that could damage an intrauterine pregnancy should be avoided.
- An extraovarian mass can be distinguished from an intraovarian lesion, such as a corpus luteum, by observing its motion relative to the ovary when pressure is applied by the transvaginal transducer.
- Sonographic findings definitive for failed intrauterine pregnancy include crown-rump length (CRL) of at least 7 mm without cardiac activity, mean sac diameter (MSD) of at least 25 mm without an embryo, and no embryo with a heartbeat on a follow-up scan at specific time intervals after the initial scan.
- Sonographic findings suspicious, but not definitive, for failed intrauterine pregnancy include CRL of less than 7 mm without cardiac activity, MSD of 16 to 24 mm without an embryo, no embryo with a heartbeat 6 weeks or more after the first day of the last menstrual period (LMP), empty amnion sign, expanded amnion sign, and a large yolk sac.
- Risk factors for pregnancy failure when embryonic heartbeat is seen include slow heart rate, large subchorionic hematoma, and small gestational sac size.
- Pregnancy number (singleton, twin, triplet, and higher order multiples) assessed prior to 6 weeks of gestation may subsequently decrease owing to the vanishing twin phenomenon or may increase by one or more additional embryos that appear on a follow-up scan.

## OUTLINE

### Normal Transvaginal Sonographic Findings in the Early First Trimester, 83

### Confirmation or Exclusion of Intrauterine Pregnancy When No Yolk Sac or Embryo Is Seen, 84

Ultrasound Demonstrates No Intrauterine Fluid Collection and No Adnexal Abnormality (No Extraovarian Adnexal Mass or Significant Free Fluid), 84

Ultrasound Demonstrates an Intrauterine Fluid Collection and No Adnexal Abnormality, 85

Ultrasound Demonstrates a Complex or Solid Adnexal Mass, 87

### Assignment of Gestational Age by Early First Trimester Ultrasound, 87

### Diagnosis of Failed Intrauterine Pregnancy (Miscarriage), 88

Sonographic Findings Definitive for Failed Intrauterine Pregnancy, 88

*Crown-Rump Length With No Embryonic Heartbeat, 88*

*Mean Sac Diameter With No Embryo, 88*

*Time-Based Criteria for Pregnancy Failure, 89*

Sonographic Findings Suspicious (but Not Definitive) for Failed Intrauterine Pregnancy, 90

*Crown-Rump Length With No Embryonic Heartbeat, 90*

*Mean Sac Diameter With No Embryo, 90*

*Time-Based Criteria Suspicious for Pregnancy Failure, 90*

*Empty Amnion Sign, 90*

*Expanded Amnion Sign, 90*

*Large Yolk Sac, 91*

### Risk Factors for Impending Pregnancy Failure When Embryonic Heartbeat Is Seen, 91

Slow Embryonic Heart Rate, 92

Subchorionic Hematoma, 93

Small Gestational Sac Size in Relation to the Embryo, 93

### Assessment of Pregnancy Number, 93

Vanishing Twin, 94

Appearing Twin, 94

A developing pregnancy generally becomes visible on transvaginal ultrasound at 5 weeks' gestational age, which corresponds to 3 weeks after conception and 5 weeks after the first day of the LMP in a woman with regular 28-day cycles. This chapter will address sonographic evaluation of pregnancies during the gestational age range of 5.0 to 8.0 weeks. Since the 1970s, this age range has been a major focus of ultrasound research.<sup>1</sup> Improvements in ultrasound technology over the past 3 decades, especially the introduction and dissemination of transvaginal sonography, have made ultrasound an increasingly valuable tool.

During the early part of the first trimester, very careful sonographic technique and interpretation are critical because of the small size of the pregnancy-related structures in the uterus and adnexa, including the intrauterine or ectopic gestational sac and corpus luteum. If done well, ultrasound can confirm the presence and location of pregnancy and accurately determine the gestational age. If done poorly, an intrauterine pregnancy can be mistaken for an ectopic pregnancy,<sup>2,3</sup> or a normal pregnancy in the uterus can be mistaken for a failed pregnancy (also termed *miscarriage*), mistakes that can have serious consequences.

### NORMAL TRANSVAGINAL SONOGRAPHIC FINDINGS IN THE EARLY FIRST TRIMESTER

Approximately 1 week after fertilization, the pregnancy implants in the decidua on one side of the uterine cavity<sup>4</sup> (Fig. 4-1), but it is not yet visible on ultrasound for about 2 more weeks. The progression of findings on transvaginal sonography in normal early first trimester pregnancies follows a highly predictable pattern,<sup>5-8</sup> with a gestational age variability of approximately  $\pm 0.5$  week. The gestational sac is first seen on transvaginal sonography at 5.0 weeks of gestation as a fluid collection 2 to 3 mm in diameter normally located in the central echogenic region of the uterus, which corresponds to the decidua (Figs. 4-2 and 4-3). It grows at the rate of 1 mm/day over the course of the next week.<sup>8</sup>

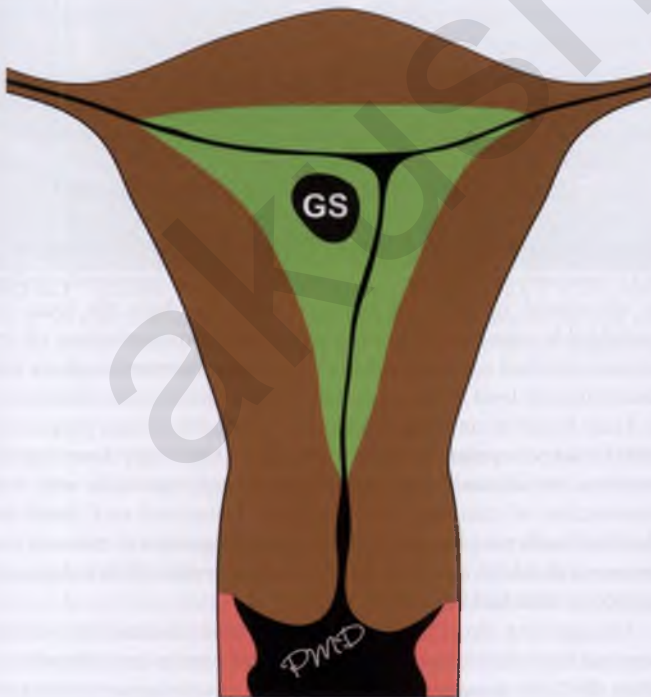


**FIG 4-1** Diagram of the early gestational sac (GS) at approximately 5.0 weeks of gestation. The sac is implanted within the decidua (depicted in green). The uterine cavity (thin black lines) is collapsed.

The first structure that is identifiable within the gestational sac is the yolk sac, which appears as a circular structure up to 6 mm in diameter (Fig. 4-4). It can be seen beginning at 5.5 weeks and remains visible for most of the first trimester. The embryo is first visible at 6.0 weeks, initially appearing as a 1- to 4-mm echogenic structure adjacent to the yolk sac with a flickering motion inside it, representing the beating heart (Fig. 4-5, Video 4-1, Table 4-1).

By 7.0 weeks, the embryo is approximately 1 cm in length<sup>9,11</sup> and is still fairly featureless. At that point, the amnion first becomes visible around the embryo, as the amniotic cavity enlarges with fluid between the embryo and the amnion (Figs. 4-6 and 4-7).<sup>12</sup> By 8.0 weeks' gestation, the embryo is 16 mm in length, and individual body parts can be identified on ultrasound. The embryonic head can be distinguished from the trunk, and limb buds are visible (Fig. 4-8).

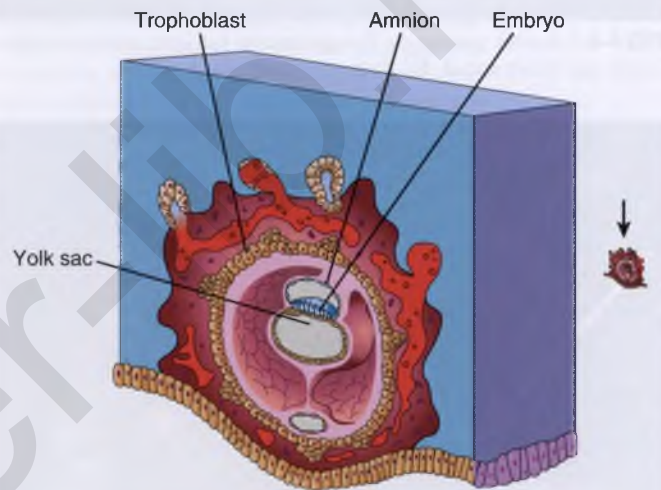


**FIG 4-2** Diagram of the blastocyst at the end of the conceptus stage of development. The gestational sac, which is now visible by sonography, measures approximately 5 mm in diameter and contains the secondary yolk sac lying opposite the amniotic cavity. A developing embryo is interposed between these two fluid-filled cavities. Sonography variably identifies the secondary yolk sac, although the embryo cannot yet be seen. (From Moore KL, Persaud TVN: *The Developing Human: Clinically Oriented Embryology*, 7th ed. Philadelphia, WB Saunders, 2003.)

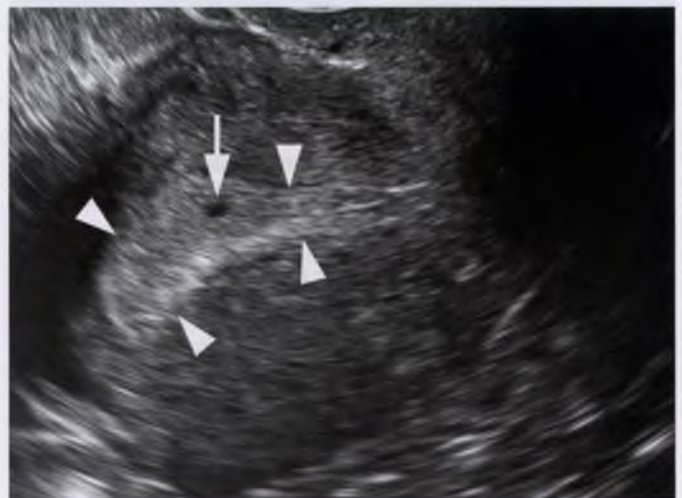


**FIG 4-3** 5.0-week pregnancy. The gestational sac (arrow), with no identifiable internal structures, lies within the decidua (arrowheads).



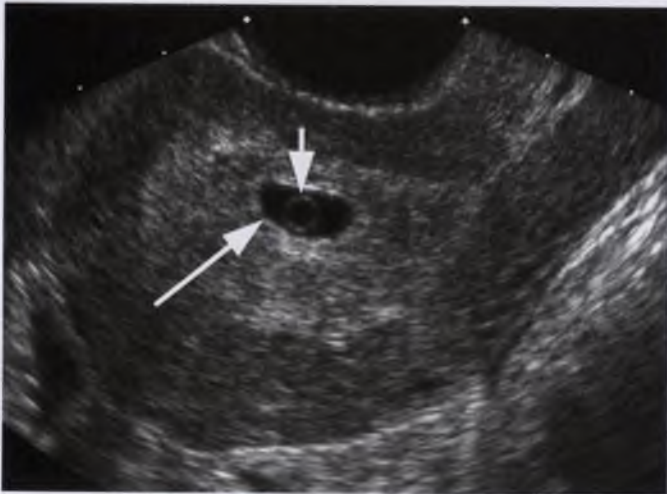


**FIG 4-4** 5.5-week pregnancy. The gestational sac (*long arrow*) contains a yolk sac (*short arrow*). No embryo is seen.

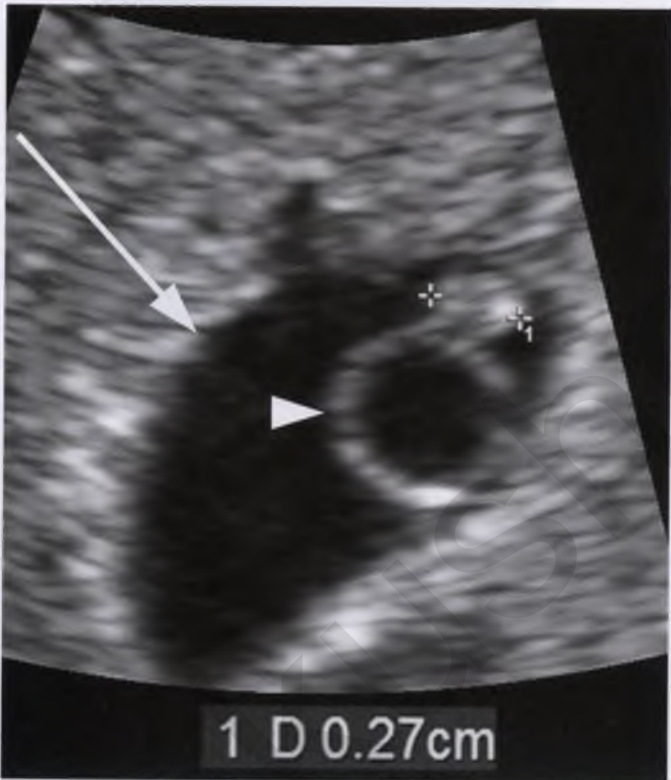


**FIG 4-5** 6.0-week pregnancy. The gestational sac (*arrow*) contains an embryo (*calipers*) lying beside the yolk sac (*arrowhead*). The embryo is 2.7 mm in length, and a heartbeat was perceived within it on real-time sonography. (See Video 4-1, which shows the heartbeat.)

### CONFIRMATION OR EXCLUSION OF INTRAUTERINE PREGNANCY WHEN NO YOLK SAC OR EMBRYO IS SEEN

When a sonogram is performed on a woman with a positive pregnancy test, a fundamental question concerns where the pregnancy is located: intrauterine or ectopic. The question is answered based on the sonographic findings in the uterus and adnexa. The sonographic finding that is definitive for a gestational sac in either location is a fluid collection containing a yolk sac or an embryo with cardiac activity. In the

**TABLE 4-1 Normal Transvaginal Sonographic Findings in the Early First Trimester**

Gestational Age (Weeks)	Structure First Appears on Ultrasound*	Mean Sac Diameter (mm) <sup>8</sup>	Crown-Rump Length (mm) <sup>10</sup>
5.0	Gestational sac	2	—
5.5	Yolk sac	6	—
6.0	Embryo with heartbeat	10	3
6.5		14	6
7.0	Amnion	18	10
7.5		22	13
8.0		26	16

\*±0.5-week age range for first visibility of each structure.

Superscript numbers in table indicate references at the end of the chapter.

absence of such a fluid collection, the diagnosis is less straightforward. We will consider a number of scenarios involving various potential sonographic appearances of the uterus and adnexa.

### Ultrasound Demonstrates No Intrauterine Fluid Collection and No Adnexal Abnormality (No Extraovarian Adnexal Mass or Significant Free Fluid)

When the human chorionic gonadotropin (hCG) test is positive but ultrasound demonstrates neither an intrauterine nor ectopic pregnancy, the woman is said to have a pregnancy of unknown location (PUL). The diagnostic possibilities in this setting are a normal intrauterine pregnancy that is too early to be visualized, a failed intrauterine pregnancy (miscarriage), and an ectopic pregnancy. The quantitative hCG is of some value in distinguishing among these possibilities, but care must be taken not to rely on a single hCG level.<sup>13</sup>

The concept of the hCG *discriminatory zone* was introduced by a study published in 1981.<sup>14</sup> That study demonstrated that, in women with normal intrauterine pregnancies, a gestational sac was not generally identifiable on transabdominal ultrasound (the ultrasound technique in general use at that time) when the hCG was below 6000 mIU/mL, and a gestational sac was consistently seen when the hCG was above 6500 mIU/mL. Since that time, the latter of these values—the hCG measurement above which a gestational sac is consistently visible on ultrasound, or the discriminatory level—has been the focus of considerable attention. The rationale is that nonvisualization of an intrauterine fluid collection when the hCG measurement is above the discriminatory level largely excludes a normal intrauterine pregnancy, so it may be safe to undertake treatment for possible ectopic pregnancy without fear of causing harm to a pregnancy that might have a good outcome. As ultrasound technology improved, especially with the introduction of transvaginal sonography, gestational sacs could be identified earlier in pregnancy. This led to a progressive decrease in the recommended hCG discriminatory level. By the mid-1980s it dropped to 1000 to 2000 mIU/mL.<sup>5,15-17</sup>

Management algorithms based on the hCG discriminatory level were put forth for women with bleeding and pain in early pregnancy, when the hCG measurement is above the discriminatory level and no intrauterine or ectopic pregnancy is identified on ultrasound. One algorithm advocates administering systemic methotrexate for suspected ectopic pregnancy in this setting.<sup>18</sup> Another algorithm



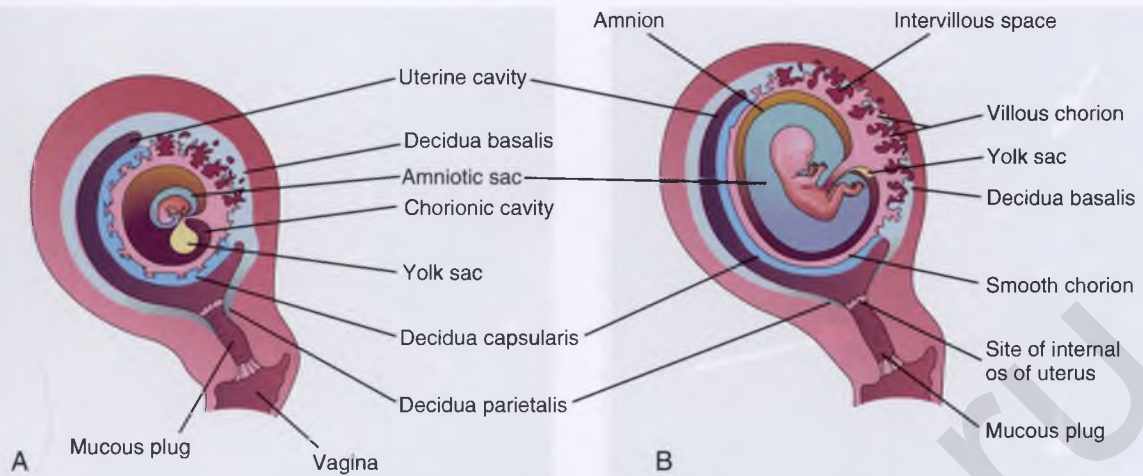


**FIG 4-6 A**, At 7 weeks' gestational age, chorionic villi completely surround the gestational sac and are relatively thick where they contact underlying endometrial tissue (decidua basalis). As the sac enlarges, the chorion and overlying decidual tissue (decidua capsularis) protrude into the compressed uterine cavity and come into contact with the decidua parietalis. This anatomic configuration gives rise to the double decidual sac sign. **B**, The compressed and avascular chorionic tissue becomes smooth and is defined by sonologists as the chorionic "membrane." Because of its fixed anatomic relationship to the developing placenta, in the event of placental bleeding, blood can dissect between the chorionic membrane and overlying decidual tissue, giving rise to a subchorionic hematoma. (From Moore KL, Persaud TVN: *The Developing Human: Clinically Oriented Embryology*, 7th ed. Philadelphia, WB Saunders, 2003.)

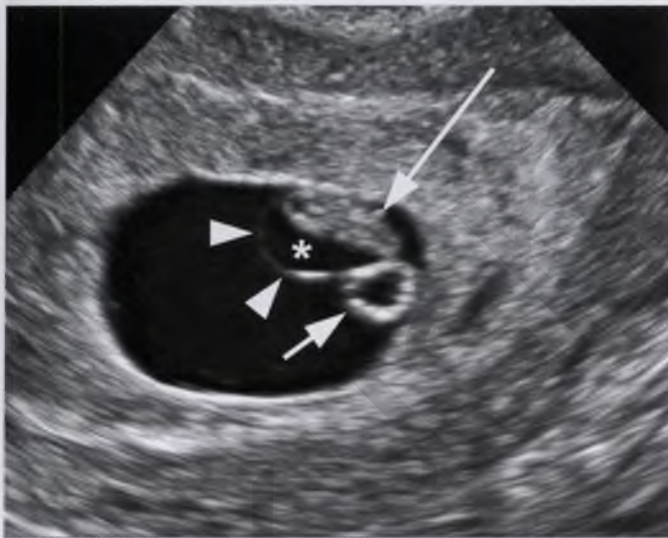


**FIG 4-7** 7.0-week pregnancy. The embryo (*long arrow*) is surrounded by a thin membrane, the amnion (*arrowheads*), adjacent to the yolk sac (*short arrow*). Fluid (\*) is present within the amniotic cavity, separating the amnion from the embryo.

recommends performing a dilatation and curettage procedure (D&C) and then administering systemic methotrexate if no chorionic villi are retrieved.<sup>19</sup>

Over the past several years, however, it has become clear that these management algorithms are overly simplistic and can result in serious errors. As our knowledge of PUL has increased, a number of important points have been learned:

- The discriminatory level does not reliably exclude a normal intrauterine pregnancy. In particular, an hCG value above 2000 mIU/mL, or even above 3000 mIU/mL, in conjunction with a sonogram demonstrating no intrauterine saclike structure, does not fully exclude a normal intrauterine pregnancy.<sup>20</sup>

- A single hCG measurement in a woman with PUL does not reliably distinguish a normal intrauterine pregnancy from a failed intrauterine pregnancy or an ectopic pregnancy.<sup>21</sup>
- Delaying treatment by a few days in a woman with ectopic pregnancy and no adnexal mass on ultrasound carries little risk if she is hemodynamically stable.<sup>22</sup>

Thus, treatment of a woman with a PUL based on a single hCG measurement runs the risk of inadvertently harming a normal intrauterine pregnancy or unnecessarily administering methotrexate to a woman with a failed intrauterine pregnancy. Instead, proper management entails sequential testing with hCG or sonography over a period of 2 or more days.<sup>13</sup> The hCG ratio—ratio of hCG value at 48 hours to initial hCG value—provides more diagnostic information than does a single hCG measurement.<sup>23</sup> A number of management algorithms based on sequential testing have been put forth.<sup>24-26</sup> Regardless of which management approach a facility chooses to follow, the key message is as follows: if ultrasound shows no evidence of intrauterine or ectopic pregnancy and the woman is hemodynamically stable, one should not intervene based on a single hCG measurement but instead do follow-up testing with at least one additional sonogram and hCG measurement.<sup>13</sup>

### Ultrasound Demonstrates an Intrauterine Fluid Collection and No Adnexal Abnormality

In a woman with a positive pregnancy test, an intrauterine fluid collection without a yolk sac or embryo can represent a gestational sac, fluid (blood or secretions) in the uterine cavity, or a cyst in the decidua. Around 1980, ultrasound practitioners observed that some women with an ectopic pregnancy have fluid in the uterine cavity.<sup>27,28</sup> Despite the fact that the location of this fluid is different from that of a gestational sac—the former is situated in the uterine cavity and the latter within the decidua—the limited resolution of ultrasound equipment at that time often made it difficult to distinguish between them. As a result, intrauterine fluid in women with ectopic pregnancy was termed a *pseudogestational sac*.<sup>28</sup> Subsequently, it was noted that decidual cysts can also be seen in some women with ectopic pregnancy.<sup>29</sup>



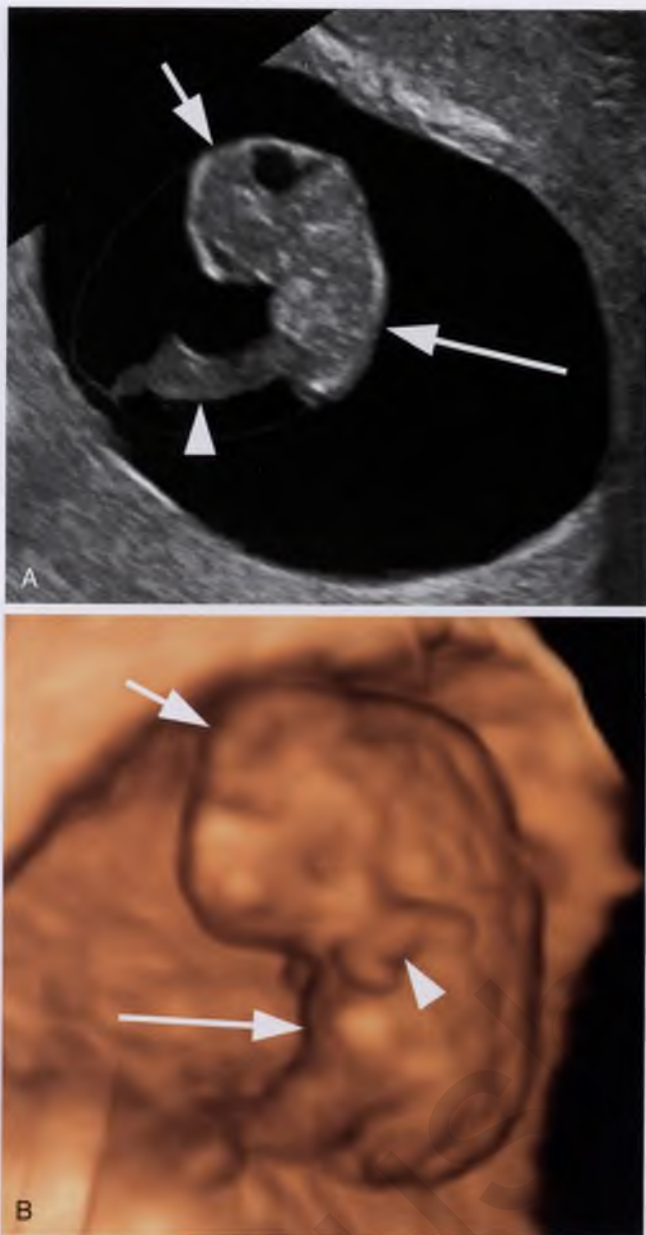


**FIG 4-8** 8.0-week pregnancies. **A**, The head (*short arrow*) and trunk (*long arrow*) are identifiable. The umbilical cord (*arrowhead*) connects to the anterior abdominal wall. **B**, On a three-dimensional sonogram of another embryo, the head (*short arrow*), trunk (*long arrow*), and an upper extremity (*arrowhead*) are identifiable.

Because of the importance of diagnosing intrauterine pregnancies and distinguishing them from ectopic pregnancies, early practitioners sought criteria that would permit them to conclude that a fluid collection in the uterus was a gestational sac. Two signs of intrauterine pregnancy were put forth: the *double sac sign*<sup>30</sup> and the *intradecidual sign*<sup>31</sup> (Fig. 4-9). The double sac sign refers to the presence of two concentric echogenic rings surrounding at least part of the fluid collection, hypothesized to represent the decidua capsularis and parietalis. The intradecidual sign refers to an intrauterine fluid collection eccentrically located in the decidua, anterior or posterior to a thin white line representing the collapsed uterine cavity.

The development and wide dissemination of transvaginal ultrasound in the mid- to late 1980s revolutionized early pregnancy

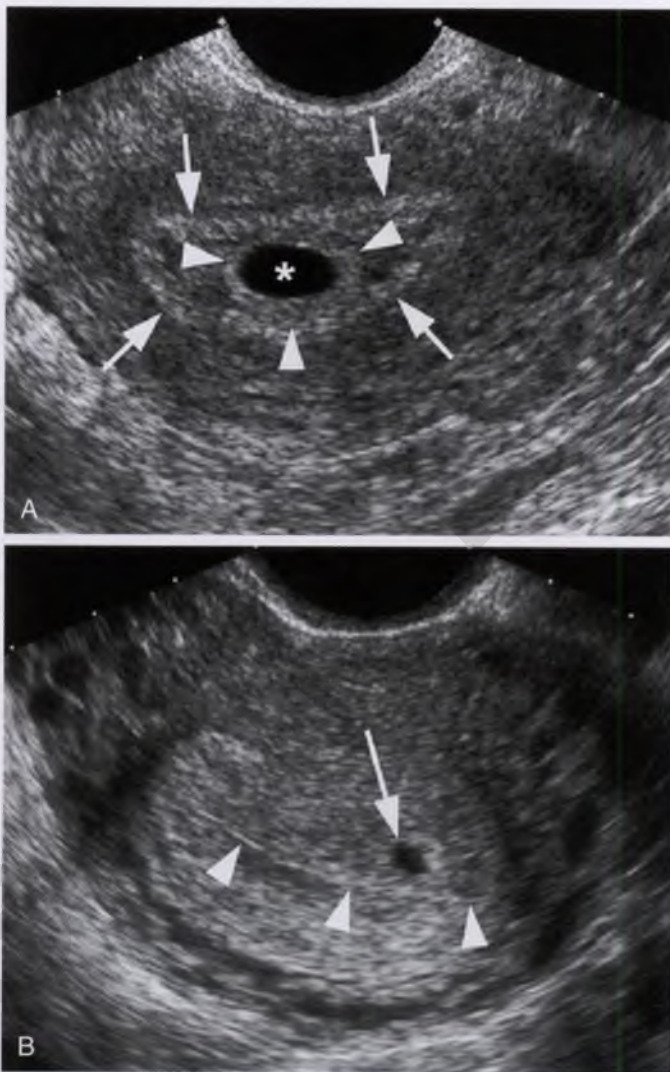


**FIG 4-9** Double sac and intradecidual signs. **A**, The gestational sac (\*) is surrounded by an inner echogenic ring (*arrowheads*) and an outer echogenic ring (*arrows*). The presence of two surrounding rings constitutes the double sac sign of early intrauterine pregnancy. **B**, The gestational sac (*arrow*) is eccentrically located in the echogenic decidua, anterior to a thin white line (*arrowheads*) representing the collapsed uterine cavity. This appearance constitutes the intradecidual sign of early intrauterine pregnancy.

sonography. With this technique, gestational sacs can be seen earlier in pregnancy and with different sonographic characteristics than via transabdominal sonography. In particular, normal early gestational sacs frequently display neither the double sac sign nor the intradecidual sign on transvaginal sonography<sup>32</sup> (Fig. 4-3). Furthermore, intrauterine fluid in women with ectopic pregnancy can often be distinguished from gestational sacs when scanning transvaginally, in that the fluid with ectopic pregnancy often conforms to the shape and location of the uterine cavity, has an irregular shape, and is filled with debris<sup>33</sup> (Fig. 4-10).

Despite the far greater resolution of transvaginal sonography, some practitioners continue to rely on the concepts of pseudogestational sac, double sac sign, and intradecidual sign that were defined using transabdominal sonography, even when interpreting transvaginal scans in early pregnancy. Furthermore, a misconception about these signs appears to be fairly common: “the presence of a double sac sign or



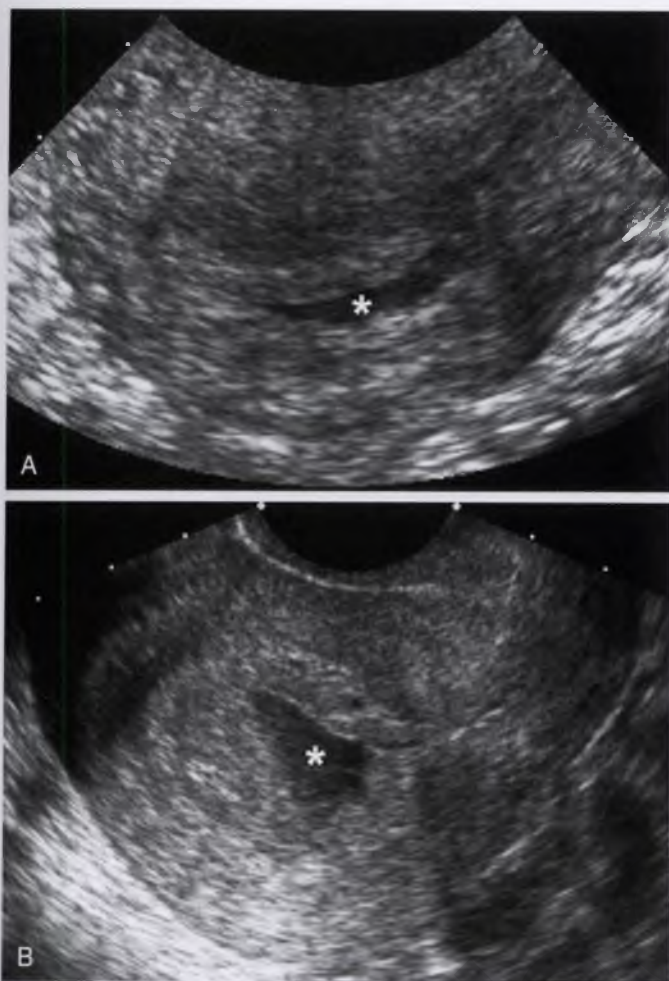


**FIG 4-10** Intrauterine fluid in women with ectopic pregnancy. **A**, There is a fluid collection (\*), with internal debris, conforming to the shape and location of the uterine cavity. **B**, In another woman with ectopic pregnancy, an irregularly shaped fluid collection (\*) with internal debris is seen within the uterine cavity.

intradecidual sign indicates intrauterine pregnancy” (correct interpretation) is sometimes assumed to mean “the absence of a double sac sign or intradecidual sign excludes intrauterine pregnancy” (incorrect interpretation). Such misinterpretation may lead to management errors in early pregnancy: small intrauterine fluid collections in early pregnancy, representing gestational sacs, are incorrectly diagnosed as pseudogestational sacs associated with ectopic pregnancy, leading to treatments (systemic methotrexate or D&C) that damage the intrauterine pregnancy. Reports of malpractice lawsuits for this error<sup>3</sup> and the existence of online support groups for women mismanaged in this way<sup>34</sup> are evidence that this is not a rare occurrence.

A straightforward calculation based on recent data is informative. Approximately half (range: 35-70%) of early intrauterine gestational sacs have a nonspecific saclike appearance: they are oval or round with no double sac sign or intradecidual sign.<sup>32</sup> About 3% of women with ectopic pregnancies have an intrauterine fluid collection with a similar cystic appearance.<sup>33</sup> Two percent of all pregnancies in the United States are ectopic, and 98% are intrauterine.<sup>35</sup> Combining these values, it follows that, when an intrauterine saclike fluid collection without a double sac sign or intradecidual sign is seen on ultrasound in the absence of an adnexal mass or significant free pelvic fluid, the

likelihood is at least 99% that it is a gestational sac and at most 1% that the diagnosis is ectopic pregnancy.<sup>32,33</sup>

The takeaway message is that any round or oval intrauterine fluid collection in early pregnancy should be interpreted as highly likely to be a gestational sac and that treatments that would damage a desired intrauterine pregnancy should be avoided unless a potentially normal intrauterine pregnancy is subsequently ruled out.

### Ultrasound Demonstrates a Complex or Solid Adnexal Mass

When an adnexal mass is seen in a woman with a positive hCG test, the crucial distinction is whether it is intraovarian or extraovarian. An intraovarian mass is almost certainly a corpus luteum (unless the flicker of a heartbeat is seen within it), whereas an extraovarian mass is highly likely to represent an ectopic pregnancy. An extraovarian mass with a “tubal ring” appearance—anechoic center surrounded by an echogenic ring—has the highest probability of representing an ectopic pregnancy, but even in the absence of such characteristics, a complex or solid adnexal mass outside the ovary in a woman with a positive pregnancy and no intrauterine pregnancy has a high probability of indicating ectopic pregnancy.<sup>36</sup>

In most cases, the sonographic distinction between intraovarian and extraovarian mass is straightforward. In some cases, however, it is uncertain whether a mass is abutting the ovary or is within the ovary. A number of sonographic features of the mass have been suggested for making this important distinction, including its grayscale appearance, its Doppler characteristics, and its movement when pressure is applied by a transvaginal transducer.

One study found that a tubal ring of ectopic pregnancy is usually more echogenic than the ovarian parenchyma, whereas the echogenicity of a corpus luteum is generally less than or equal to that of the ovarian parenchyma.<sup>37</sup> However, the comparison of these echogenicities is not definitive for distinguishing a tubal ring from a corpus luteum: in this series, 6 of 39 (15%) tubal rings were equal or lower in echogenicity than the ovary, whereas 3 of 45 (7%) corpora lutea were more echogenic than the ovary.

When assessed by Doppler, an adnexal mass of ectopic pregnancy typically has prominent flow on color Doppler and a low impedance pattern on spectral Doppler.<sup>38,39</sup> When there is an adnexal mass indeterminate for being within, as opposed to abutting, the ovary, however, the presence of these Doppler characteristics in the mass does not reliably establish the diagnosis of ectopic pregnancy because a corpus luteum can have similar Doppler findings.<sup>38</sup>

The most definite way to demonstrate that a mass abutting the ovary is extraovarian is to observe its motion relative to the ovary when pressure is applied by the transvaginal transducer.<sup>40</sup> If the mass slides along the ovary, then it is extraovarian and the probable diagnosis is ectopic pregnancy (see Fig. 4-11, Video 4-2). If the mass and ovary move together, the mass is likely to be a corpus luteum within the ovary, and the probable diagnosis is intrauterine pregnancy. In an ultrasound facility that has the capability of storing video clips, it is good practice to store a clip of the adnexa while transducer pressure is applied.

### ASSIGNMENT OF GESTATIONAL AGE BY EARLY FIRST TRIMESTER ULTRASOUND

Prior to visualization of an embryo, gestational age can be assigned based either on the contents or the size of the gestational sac. The former approach assigns a gestational age of 5.0 weeks if the sonogram demonstrates a gestational sac with no visible internal structures and 5.5 weeks if a yolk sac is seen. Alternatively, the gestational age can be assigned based on the MSD (average of the anteroposterior, transverse,



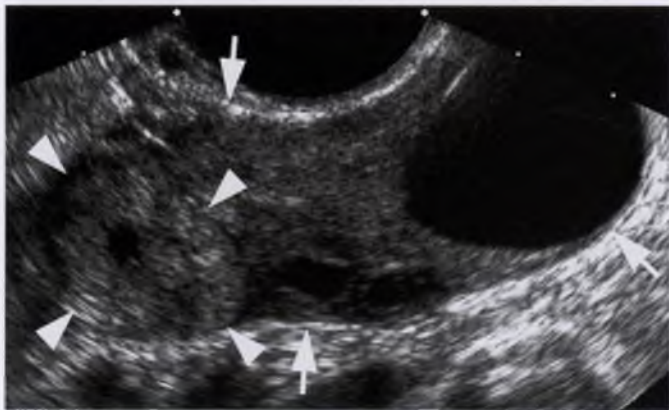


**FIG 4-11** Movement with transducer pressure distinguishing ectopic pregnancy from corpus luteum. Note the structure with an echogenic rim and anechoic center (*arrowheads*) lying in or adjacent to the ovary (*arrows*). When pressure was applied with the transvaginal ultrasound transducer, the structure was seen to move separately from the ovary, confirming it as being extraovarian and thus representing an ectopic pregnancy. (Video 4-2 shows the movement when transducer pressure is applied.)

and sagittal measurements of the gestational sac) via a table that correlates MSD and age (see Table 4-1).<sup>8</sup>

Once the embryo is visible, the most accurate way to assign gestational age is via the CRL. A number of formulas and tables have been devised for this purpose.<sup>9,10</sup> Using the gold standard of gestational age in pregnancies achieved via in vitro fertilization, a variety of published CRL formulas and tables have been shown to have minimal bias in estimating gestational age.<sup>11,41</sup>

All of these approaches, whether based on sac contents, MSD, or CRL, provide a highly accurate age estimate in normal early pregnancies. Each has a 95% confidence range of approximately  $\pm 0.5$  week.<sup>41</sup>

## DIAGNOSIS OF FAILED INTRAUTERINE PREGNANCY (MISCARRIAGE)

A previous section presented the normal progression of sonographic findings in early pregnancy. Failure to meet one or more of the expected early milestones raises concern for pregnancy failure, but it is important to distinguish between those that are definitive for pregnancy failure and those that are merely suspicious for that diagnosis. A suspicious finding should prompt a follow-up sonogram, generally 7 to 10 days later. If, on the other hand, there is a finding that is definitive for pregnancy failure, there is no need for a follow-up scan and it would be safe to undertake an intervention such as uterine evacuation.

Because erroneous diagnosis of early pregnancy failure can have serious consequences, such as uterine evacuation in a woman with a normal, desired pregnancy, criteria for definite pregnancy failure should be strict. That is, these criteria should virtually eliminate false positive diagnoses, which means that they should have specificities of very close to 100%. Furthermore, they should apply to a broad range of ultrasound facilities that meet at least minimum quality criteria, not solely to experts in early obstetric ultrasound.

Criteria for definite pregnancy failure fall into three categories<sup>13</sup>: (1) embryo above a certain size (measured by the CRL) with no visible heartbeat, (2) gestational sac above a certain size (measured by the MSD) with no visible embryo, and (3) no embryo with heartbeat visible after a certain time interval since an initial scan. Less stringent variants of these criteria, as well as a number of other sonographic findings, are suspicious for pregnancy failure.

**TABLE 4-2 Sonographic Findings Definitive for Failed Intrauterine Pregnancy**

Category	Criterion for Definite Pregnancy Failure
Embryo with no cardiac activity	CRL $\geq 7$ mm
Gestational sac containing no embryo with heartbeat	MSD $\geq 25$ mm
Time-based findings	No embryo with heartbeat on a follow-up scan at least 2 weeks after an initial scan that showed a gestational sac without a yolk sac No embryo with heartbeat on a follow-up scan at least 11 days after an initial scan that showed a gestational sac with a yolk sac

CRL, crown-rump length; MSD, mean sac diameter.

## Sonographic Findings Definitive for Failed Intrauterine Pregnancy

### Crown-Rump Length With No Embryonic Heartbeat

In a normal intrauterine pregnancy, the flickering motion of cardiac activity is generally seen once the embryo is identifiable, regardless of embryonic size. A number of researchers over the past 3 decades have sought to answer the following question: at what CRL is cardiac activity always (not merely generally) seen in a normal intrauterine pregnancy? Studies reported in the 1990s concluded that cardiac activity is consistently visible by a CRL of 4 mm<sup>42,43</sup> or 5 mm.<sup>44,45</sup> Based on that research, the transvaginal sonographic finding of an embryo with CRL of at least 5 mm and no cardiac activity became widely accepted as a criterion for definite pregnancy failure (Table 4-2).<sup>46-50</sup>

In recent years, serious doubts have arisen regarding the 5-mm CRL cutoff, for a number of reasons. First, despite the importance of avoiding false positive diagnoses of pregnancy failure, the studies on which the 5-mm CRL had been based had small study populations. A meta-analysis concluded that, because of the small study sizes, the 5-mm criterion may have a specificity as low as 90%,<sup>51</sup> undercutting its value for definitively diagnosing pregnancy failure. Second, there were reported cases of embryos measuring 5 to 6 mm without cardiac activity on an initial scan, in which a heartbeat was apparent on a follow-up scan.<sup>52,53</sup> Third, a study found an interobserver variability of  $\pm 15\%$  (95% confidence range) in CRL measurements at 6 to 9 weeks of gestation,<sup>54</sup> so that an embryo measuring 6 mm by one observer may be measured as high as 6.9 mm by a second observer. On the basis of these factors, 7 mm has become the generally accepted CRL cutoff for diagnosing pregnancy failure in the absence of cardiac activity<sup>13,55</sup> (Fig. 4-12, Video 4-3).

### Mean Sac Diameter With No Embryo

The criterion for diagnosing pregnancy failure based on nonvisualization of an embryo by a certain gestational sac size has followed a progression of events similar to that described previously for CRL with no heartbeat. Around 1990, a number of studies found that an embryo with a heartbeat is consistently visible on ultrasound when the MSD is 16 mm<sup>56</sup> or 17 mm.<sup>57</sup> Based on these studies, nonvisualization of an embryo with a heartbeat with an MSD of at least 16 mm became a generally accepted criterion as definitive for pregnancy failure.<sup>48,49</sup>

In more recent years, a number of doubts about the reliability of this criterion arose, similar to those discussed earlier for the CRL with





**FIG 4-12** Failed intrauterine pregnancy. An embryo (*calipers*) 9 mm in length is seen within the uterus. No heartbeat was detected within it. (Video 4-3 shows the absence of cardiac activity.)

no visible heartbeat. First, the initial studies that led to the MSD criterion of 16 mm with no embryo involved small patient populations, so that subsequent reanalysis demonstrated that the specificity had a wide 95% confidence range of 0.88 to 1.00.<sup>51</sup> Second, there were a number of reported cases in which the MSD was 17 to 20 mm and no embryo was seen, and then a subsequent scan demonstrated an embryo with cardiac activity.<sup>52,58</sup> Third, the measurement of the MSD has an interobserver confidence range of  $\pm 19\%$  (95% confidence interval),<sup>54</sup> so that a measurement of 20 mm may be 19% higher, or 24 mm, when measured by another examiner.

Thus, the generally accepted criterion for early pregnancy failure based on an MSD with no visible embryo has become more stringent: one should diagnose failed pregnancy only if the MSD is at least 25 mm and no embryo is seen on transvaginal sonography<sup>13,55</sup> (Fig. 4-13).

### Time-Based Criteria for Pregnancy Failure

The CRL and MSD criteria described earlier permit pregnancy failure to be diagnosed on a single scan in early pregnancy. The diagnosis can also be established when there is abnormal progression of findings on sequential scans. These time-based criteria for pregnancy failure are needed because, in many cases of early pregnancy failure, the CRL and MSD never reach a size of 7 mm and 25 mm, respectively.

As noted previously, the gestational sac, yolk sac, and embryo are first visible at 5, 5.5, and 6 weeks, respectively, with a variability of  $\pm 0.5$  week. Based on these values, pregnancy failure can be diagnosed with certainty in either of the following situations: (1) an initial scan shows a gestational sac without yolk sac or embryo, followed by a scan at least 2 weeks later in which no embryo with a heartbeat is seen, or (2) an initial scan demonstrates a gestational sac with a yolk sac but no embryo, followed by a scan at least 11 days later in which no embryo with a heartbeat is seen.<sup>13</sup>

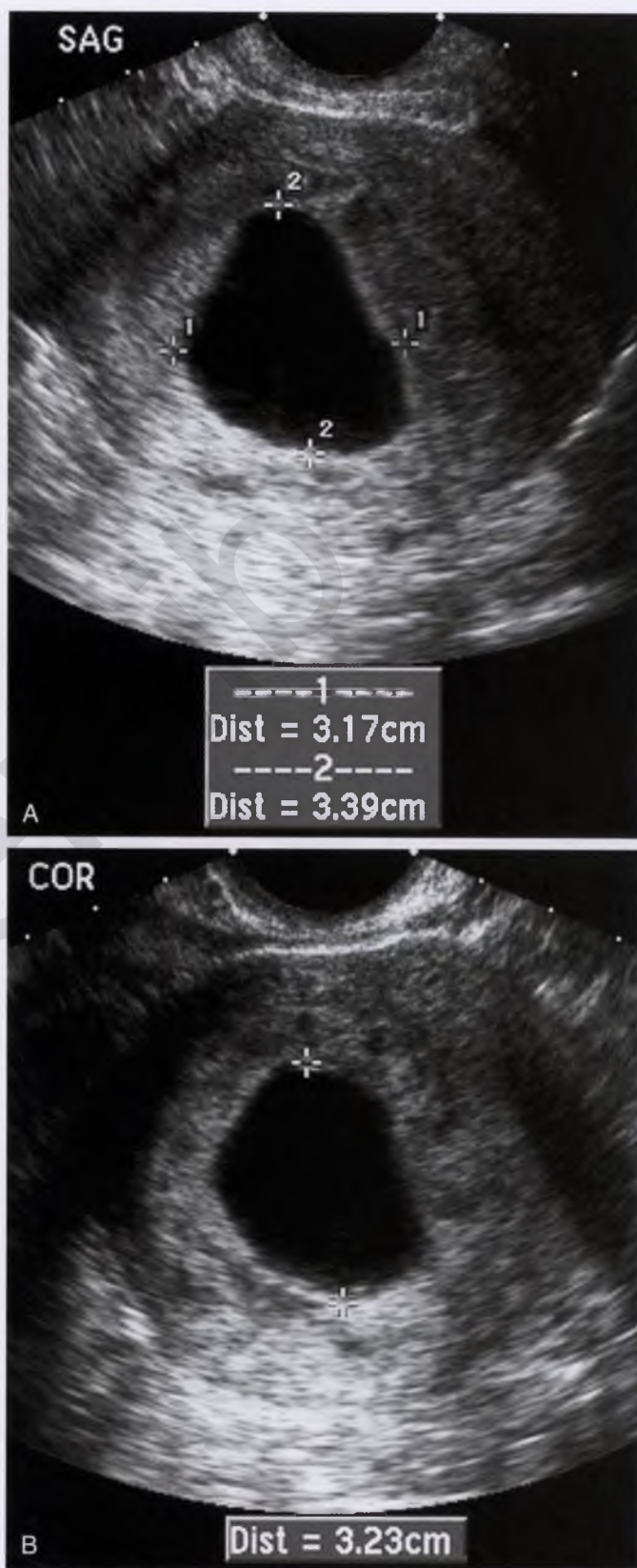


**FIG 4-13** Failed intrauterine pregnancy. **A** and **B**, The mean sac diameter is 32.6 mm, the average of the anteroposterior, transverse, and sagittal measurements of the gestational sac on sagittal (SAG) and coronal (COR) images of the gestational sac. No embryo is seen.



## Sonographic Findings Suspicious (but Not Definitive) for Failed Intrauterine Pregnancy

### Crown-Rump Length With No Embryonic Heartbeat

Because cardiac activity is usually identifiable in any embryo seen on transvaginal ultrasound, the presence of an embryo without a heartbeat is always a worrisome (if not definitively abnormal) finding. Although not definitive, absence of cardiac activity when the CRL is below the cutoff of 7 mm is suspicious for pregnancy failure (Fig. 4-14, Video 4-4, Table 4-3).

### Mean Sac Diameter With No Embryo

Pregnancy outcome may, in rare cases, be normal when no embryo is seen in a gestational sac whose MSD is at least 16 mm (the previously accepted cutoff for definite pregnancy failure) but less than 24 mm (the currently accepted cutoff). The fact that this happens infrequently means that the finding of an MSD of 16 to 24 mm without identifiable embryo is suspicious for pregnancy failure (Fig. 4-15).

### Time-Based Criteria Suspicious for Pregnancy Failure

When an initial scan shows a gestational sac and a follow-up scan shows no embryo with a heartbeat, this is worrisome if the time interval between scans is only slightly less than that required for diagnosis of definite pregnancy failure. In particular, the following sequences are suspicious for pregnancy failure: (1) an initial scan shows a gestational sac without yolk sac or embryo, and there is no visible embryo with a heartbeat on a subsequent scan 7 to 13 days later, and (2) an initial scan shows a gestational sac with yolk sac but no embryo, and there is still no visible embryo with a heartbeat on a subsequent scan 7 to 10 days later.<sup>13</sup>



**FIG 4-14** Suspected pregnancy failure. An embryo (*calipers*) 3.09 mm in length is seen within the uterus. No heartbeat was seen within it. (Video 4-4 shows the absence of cardiac activity.)

Another time-based finding that is suspicious for pregnancy failure is nonvisualization of an embryo with a heartbeat 6 weeks or more after the first day of the LMP. In view of variable cycle lengths<sup>59</sup> and often unreliable recollection of LMP,<sup>60,61</sup> failure to identify an embryo with a heartbeat at any point after the LMP reported by the mother should not be taken as definitive proof of pregnancy failure.

### Empty Amnion Sign

The normal order of visibility of structures within the early gestational sac is yolk sac, then embryo, then amnion. Thus, it can be normal to see an embryo and no amnion<sup>62</sup> but not to see an amnion and no embryo. The latter combination has been termed the *empty amnion sign*.<sup>62,63</sup> This sign is present when the gestational sac contains two adjacent circular structures, representing the yolk sac and amnion, but no embryo (Fig. 4-16).

The empty amnion sign carries a poor prognosis. In two studies that included 15 patients<sup>62</sup> and 68 patients<sup>63</sup> with this sign, pregnancy failure was confirmed in all 83 cases. Because both of these studies were done at the same institution, and because two yolk sacs in a case of early monochorionic diamniotic twins could potentially be mistaken for the empty amnion sign, this sign should be considered a suspicious, but not definitive, indicator of pregnancy failure.

### Expanded Amnion Sign

Embryonic cardiac activity is normally seen before the amnion is first identifiable around the embryo.<sup>64,65</sup> The term *expanded amnion sign* has been coined to describe the following combination of findings on an early pregnancy sonogram: visualization of an embryo that is surrounded by an amnion and has no cardiac activity (Fig. 4-17, Video 4-5). Among 108 patients with this finding who had a CRL at or below

**TABLE 4-3 Sonographic Findings Suspicious (but Not Definitive) for Failed Intrauterine Pregnancy**

Category	Finding Suspicious for Pregnancy Failure*
Embryo with no cardiac activity	CRL < 7 mm
Gestational sac containing no embryo with heartbeat	MSD 16-24 mm
Time-based findings	No embryo with heartbeat on a follow-up scan 7-13 days after an initial scan that showed a gestational sac without a yolk sac No embryo with heartbeat on a follow-up scan 7-10 days after an initial scan that showed a gestational sac with a yolk sac No embryo with heartbeat at least 6 weeks after LMP
Empty amnion	Amnion seen adjacent to yolk sac, with no visible embryo
Expanded amnion	Embryo with no cardiac activity, with amnion visible around it
Enlarged yolk sac	>7 mm

\*When findings are suspicious for pregnancy failure, follow-up ultrasound in 7 to 10 days is generally appropriate. CRL, crown-rump length; LMP, last menstrual period; MSD, mean sac diameter.





**FIG 4-15** Suspected pregnancy failure. **A** and **B**, The mean sac diameter is 21.8 mm, the average of the anteroposterior, transverse, and sagittal measurements of the gestational sac on sagittal (SAG) and coronal (COR) images of the gestational sac. No embryo is seen.

5.4 mm and known outcome, pregnancy failure was confirmed in all 108.<sup>65</sup>

### Large Yolk Sac

The upper limit of normal yolk sac diameter in the early first trimester is approximately 4.5 mm when measured inner-to-inner<sup>66</sup> and 6 mm when measured outer-to-outer.<sup>67</sup> A large yolk sac is an indicator of poor prognosis. Although the causal relationship between a large yolk sac and pregnancy prognosis is unclear, a number of studies have documented a high rate of pregnancy failure when the diameter of the yolk sac is more than 7 mm<sup>66,68</sup> (Fig. 4-18).



**FIG 4-16** Suspected pregnancy failure based on empty amnion sign. Two circular structures (*arrowheads*) are within the gestational sac, representing the yolk sac and amnion. No embryo is visible.

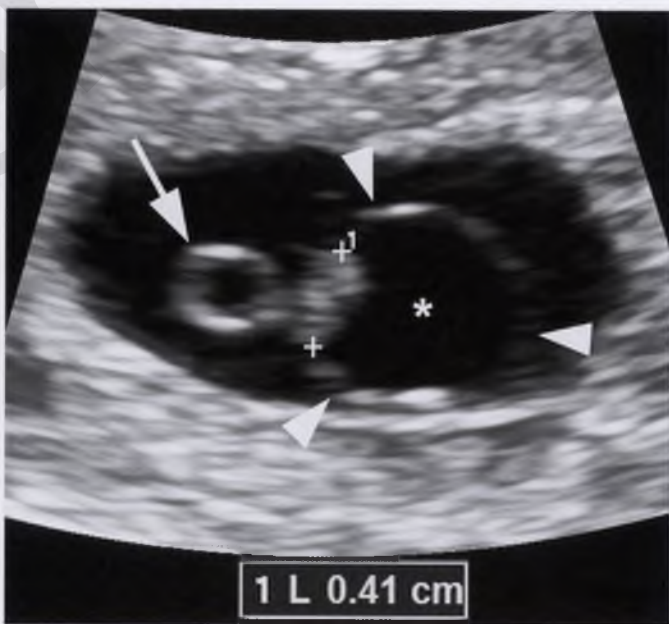


**FIG 4-17** Suspected pregnancy failure based on expanded amnion sign. There is an embryo (*calipers*), 4.1 mm in length, surrounded by the amnion (*arrowheads*), lying adjacent to the yolk sac (*arrow*). No heartbeat was detected within the embryo. (Video 4-5 shows the absence of cardiac activity.)

### RISK FACTORS FOR IMPENDING PREGNANCY FAILURE WHEN EMBRYONIC HEARTBEAT IS SEEN

Visualization of an embryonic heartbeat is a reassuring finding on an early first trimester sonogram, but it does not guarantee a good pregnancy outcome. Subsequent pregnancy failure is always a potential occurrence, but the chance of this untoward event is higher if the heart



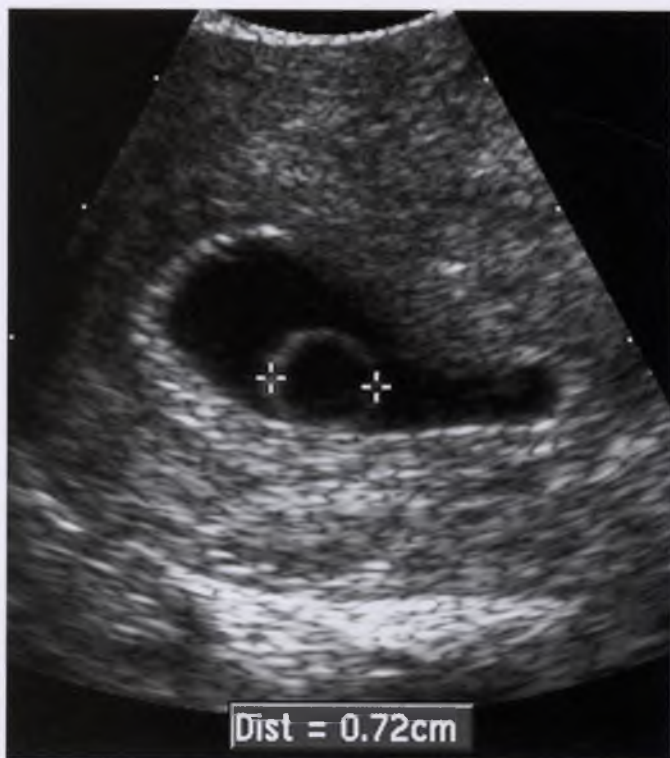


**FIG 4-18** Suspected pregnancy failure based on enlarged yolk sac. The yolk sac (*calipers*) measures 7.2 mm in diameter.

**TABLE 4-4 Risk Factors for Impending Pregnancy Failure When Embryonic Heartbeat Is Seen**

Category	Finding Suspicious for Impending Pregnancy Failure
Slow embryonic heart rate	GA 6.0-6.2 weeks or CRL 1-4 mm: <ul style="list-style-type: none"> <li>• Slow: &lt;90 bpm</li> <li>• Borderline: 90-99 bpm</li> </ul> GA 6.3-7 weeks or CRL 5-9 mm: <ul style="list-style-type: none"> <li>• Slow: &lt;110 bpm</li> <li>• Borderline: 110-119 bpm</li> </ul>
Large subchorionic hematoma	Variably diagnosed as large by the following: <ul style="list-style-type: none"> <li>• Subjective assessment</li> <li>• Hematoma surrounds at least two thirds of the gestational sac</li> <li>• Volume of hematoma <math>\geq</math> 60 mL</li> </ul>
Small gestational sac size in relation to the embryo	MSD – CRL < 5 mm (or subjective assessment)

bpm, beats per minute; CRL, crown-rump length; GA, gestational age; LMP, last menstrual period; MSD, mean sac diameter.

rate is slow, a large subchorionic hematoma is present, or the gestational sac is abnormally small (Table 4-4).

### Slow Embryonic Heart Rate

The mean embryonic heart rate increases from 100 to 110 beats per minute (bpm) at 6 weeks to approximately 150 bpm at 8 to 9 weeks, and then plateaus for the rest of pregnancy.<sup>69-71</sup> A slow heart rate in the

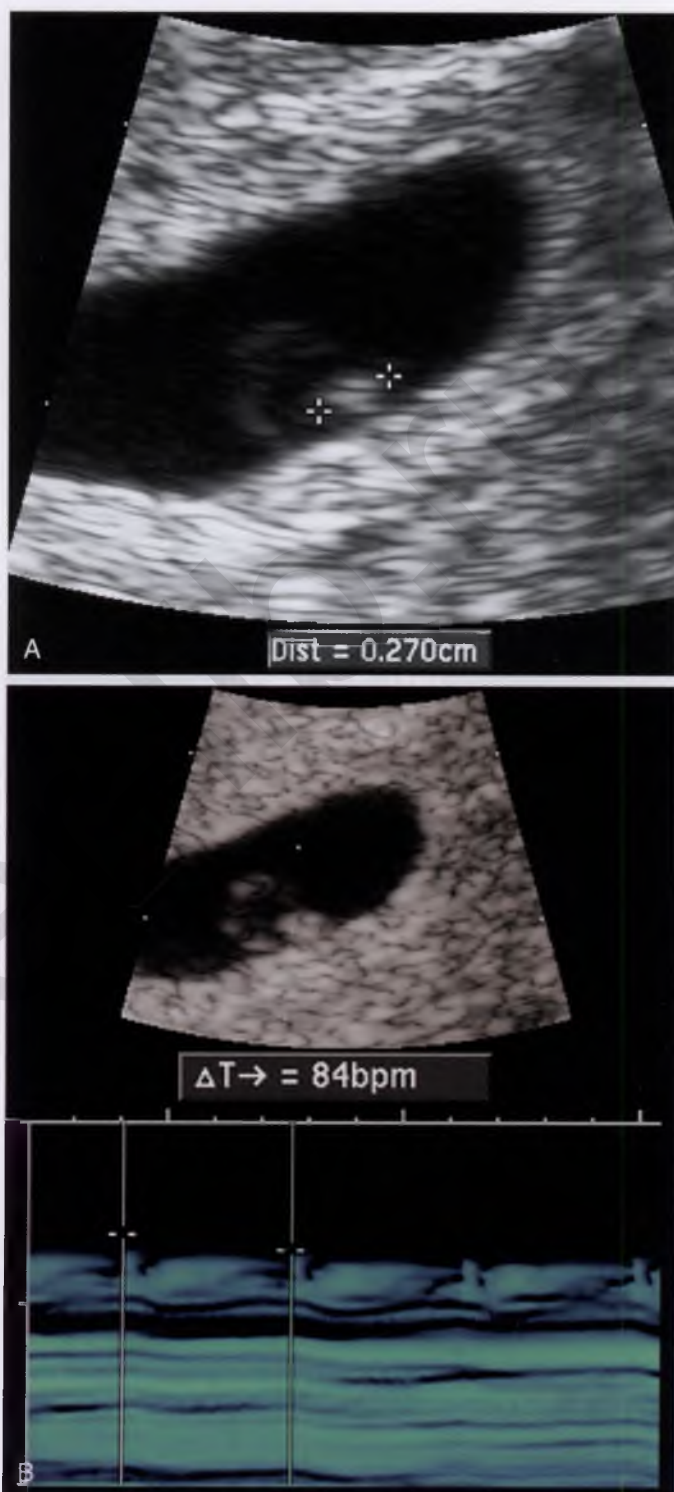


**FIG 4-19** Slow embryonic heartbeat. **A**, There is a 2.7-mm embryo in the uterus. **B**, The heart rate, measured via M-mode, is 84 beats per minute. There was no cardiac activity on a follow-up scan 2 weeks later.

early first trimester carries a high risk that the pregnancy will fail by the end of the first trimester.<sup>69-73</sup> The slower the rate, the worse the prognosis. At 6.0 to 6.2 weeks, when the CRL is up to 4 mm, almost all pregnancies will subsequently miscarry if the heart rate is less than 80 bpm and a majority will fail if the rate is 80 to 89 bpm, so any rate below 90 bpm should be considered abnormal (Fig. 4-19). The prognosis is better for heart rates of 90 to 99 bpm and plateaus for heart



rates of 100 bpm or above, so a rate of 90 to 99 bpm should be considered borderline and one of 100 bpm or above is normal. At 6.3 to 7.0 weeks, corresponding to a CRL of 5 to 9 mm, the corresponding heart rates are 20 bpm higher: a heart rate of less than 110 bpm is abnormal, a rate of 110 to 119 bpm is borderline, and one of 120 bpm and above is normal.<sup>73</sup>

It is appropriate to perform a follow-up sonogram in 1 to 2 weeks when a scan at 6.0 to 6.2 weeks reveals a heart rate less than 90 bpm or a 6.3- to 7.0-week scan demonstrates a heart rate less than 110 bpm. In most cases, the cardiac activity will have ceased by the time of the follow-up scan. In a minority of cases, cardiac activity will still be present, occasionally with a normal heart rate. When this occurs, the prognosis is better but still not normal, as 25% will go on to miscarry by the end of the first trimester.<sup>74</sup> If the fetus is still alive at the end of the first trimester, the likelihood of pregnancy loss then reverts to normal, but the risk of fetal anomalies may be somewhat elevated.<sup>73</sup>

### Subchorionic Hematoma

A subchorionic hematoma appears on ultrasound as an irregular hypoechoic space, sometimes crescent-shaped, around part of the gestational sac. The hematoma usually has internal echoes and is separated from the fluid inside the gestational sac by a thick band of tissue (Fig. 4-20). It must be differentiated from separation of the amnion from the chorion, a normal finding in the first trimester, in which the very thin, smooth amnion lies between the inner amniotic fluid and the outer chorionic fluid.

Several studies have assessed the prognostic significance of subchorionic hematomas in pregnancies with a live embryo. These studies have differed considerably in design, both with respect to the gestational age range of the study population and the way that the size of the hematoma is determined. Studies variously classify the hematoma as small, moderate, or large based on subjective assessment<sup>75</sup> or on the fraction of the gestational sac surrounded by the hematoma.<sup>76</sup> Still others use a quantitative estimate of the hematoma's volume, despite the fact that determining the volume of an irregular space is prone to error. Even among these latter studies there is considerable variability, with one study comparing outcomes with hematoma volume greater versus less than 60 mL<sup>77</sup> and another comparing those greater or less than 15 mL.<sup>78</sup>

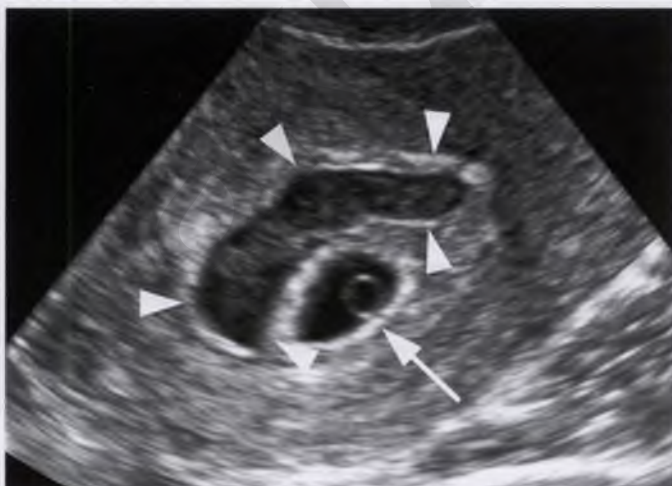


**FIG 4-20** Subchorionic hematoma. An irregular, somewhat crescent-shaped, fluid collection with internal debris (*arrowheads*) lies adjacent to the gestational sac (*arrow*). A thick band of tissue separates the hematoma from the fluid in the gestational sac.

Despite these differences, there is general consensus that a small subchorionic hematoma carries little or no risk.<sup>75-79</sup> Most studies,<sup>75-78</sup> though not all,<sup>80</sup> have found that a large subchorionic hematoma carries an elevated risk of subsequent pregnancy loss. In one study that provides separate data for early first trimester cases up to 8 weeks of gestation, 5 of 22 cases (22.7%) with a large hematoma went on to pregnancy loss, compared to 12 of 88 (13.6%) with a moderate and 14 of 116 (12.1%) with a small hematoma.<sup>76</sup>

### Small Gestational Sac Size in Relation to the Embryo

The gestational sac is normally considerably larger than the embryo. One group of authors has proposed using the metric of MSD minus CRL to distinguish gestational sacs that are abnormally small in relation to the embryo from those that are normal. In particular, they diagnose the sac as being abnormally small if MSD – CRL is less than 5 mm and normal if 5 mm or greater.<sup>81</sup> In their case series of 16 early first trimester pregnancies with normal embryonic heart rates and small sac size, 15 (94%) ended in pregnancy loss. Although most practitioners do not use objective criteria to assess the size of the gestational sac in relation to the embryo, relying instead on subjective assessment, the results of this study confirm that small size of the gestational sac in relation to the embryo is an indicator of poor prognosis (Fig. 4-21).

### ASSESSMENT OF PREGNANCY NUMBER

One of the basic elements of obstetric ultrasound is to assess pregnancy number: singleton, twin, triplet, or higher order multiples. It is important to recognize that the number determined on an early first trimester scan may subsequently increase or decrease, owing to the “vanishing” and “appearing” twin phenomena.



**FIG 4-21** Small gestational sac size in relation to the embryo. Very little fluid is seen around the embryo (*calipers*).



### Vanishing Twin

It was reported as early as the 1970s that a woman diagnosed as having twins on a first trimester scan may go on to have a singleton on subsequent scans or at delivery.<sup>82-84</sup> Because the ultrasound scanners in use at that time had low resolution and did not display images in real time, their cases likely fell into two categories: (1) pregnancies that began as twins, with one of the gestations failing to progress beyond an early stage, or (2) singleton pregnancies with a second fluid collection (e.g., subchorionic hematoma) misinterpreted as a second gestational sac.

After real-time sonography was introduced, a published report documented a series of twin pregnancies with two heartbeats on an initial scan followed by a single live fetus on subsequent scans.<sup>85</sup> In this series, the incidence of first trimester twinning was 3.3%, and 21% of early twins had loss of one. When there is loss of one twin in the early first trimester, the remaining singleton has a good prognosis, and in most cases, the second sac is no longer seen later in pregnancy or at birth, leading to the term *vanishing twin* (Fig. 4-22).

Loss of one twin can occur at any time during pregnancy but is most common during the early first trimester. Among early first trimester twins with two heartbeats, 70% to 80% result in live twins, and most of the remaining 20% to 30% deliver a live singleton.<sup>86-88</sup> The likelihood of loss of one twin is greatest if the twins are monochorionic<sup>86,87</sup> or the woman has symptoms of vaginal bleeding at the time of the initial scan.<sup>88</sup>

### Appearing Twin

From 6 weeks onward, pregnancy number is determined by counting embryos or fetuses with heartbeats. Prior to 6 weeks, when the embryo may not be visible, the assessment of number is less straightforward and more prone to error. At that stage, it is done by counting gestational sacs and yolk sacs. Undercounting of twins or higher order multiples can occur in a number of ways. When more than one gestation implants in the uterus, one or more of them might not be visible at the time of the initial scan because of its small size or location. This is especially true when image quality is suboptimal due to patient body habitus, uterine myomas, or uterine orientation. Monochorionic twins scanned prior to visualization of yolk sacs (i.e., before about 5.5 weeks) will always be mistaken for a singleton gestation, as will monochorionic monoamniotic twins scanned prior to visualization of embryos (i.e., before about 6.0 weeks), because monoamniotic twin gestations typically have only a single yolk sac.

One case series assessed the frequency of undercounting. Using a database of ultrasound reports, all reports with findings of at least two heartbeats were retrieved, and then the subset of these cases that had been scanned prior to 6 weeks' gestation was identified. Of the 325 cases in this subset, 47 cases (14%) had undercounted pregnancy number on the ultrasound performed before 6 weeks' gestation (Figs. 4-23 and 4-24). Undercounting occurred more frequently at 5 to 5.4 weeks than at 5.5 to 5.9 weeks (19% vs. 9%), in higher order multiples than in twin gestations (16% vs. 14%), and in monochorionic twin gestations than in dichorionic twins (86% vs. 11%). There was no difference in pregnancy outcome in undercounted cases as compared to correctly counted cases.<sup>89</sup>

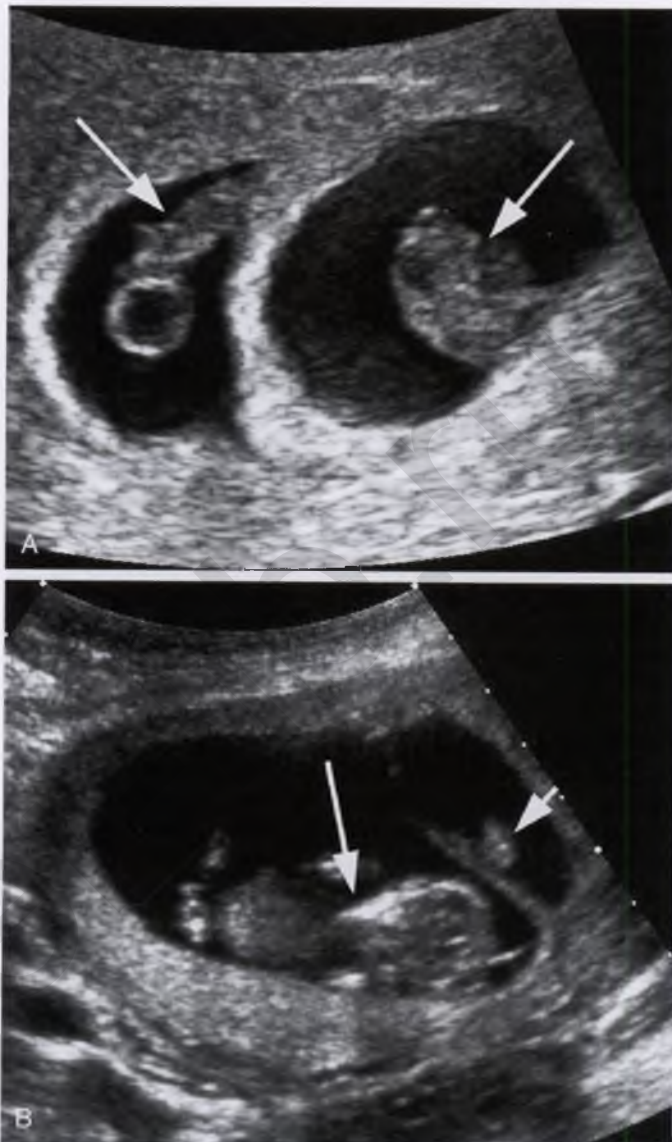


**FIG 4-22** “Vanishing” twin. **A**, Sonogram at 7.9 weeks' gestation demonstrates two gestational sacs, each containing an embryo with heartbeat (*arrows*). **B**, Follow-up scan 4 weeks later demonstrates a normal fetus that had cardiac activity (*long arrow*) and a second, much smaller, fetus (*short arrow*) that had no cardiac activity. Subsequent second and third trimester scans showed no evidence of the demised twin or its gestational sac.

Thus, although pregnancy number should be assessed on any obstetric ultrasound, it should be understood that, for ultrasound scans performed in early pregnancy, the count is preliminary. The number may subsequently decrease because of the vanishing twin phenomenon, and the number may increase by one or more embryos that appear on a follow-up scan.



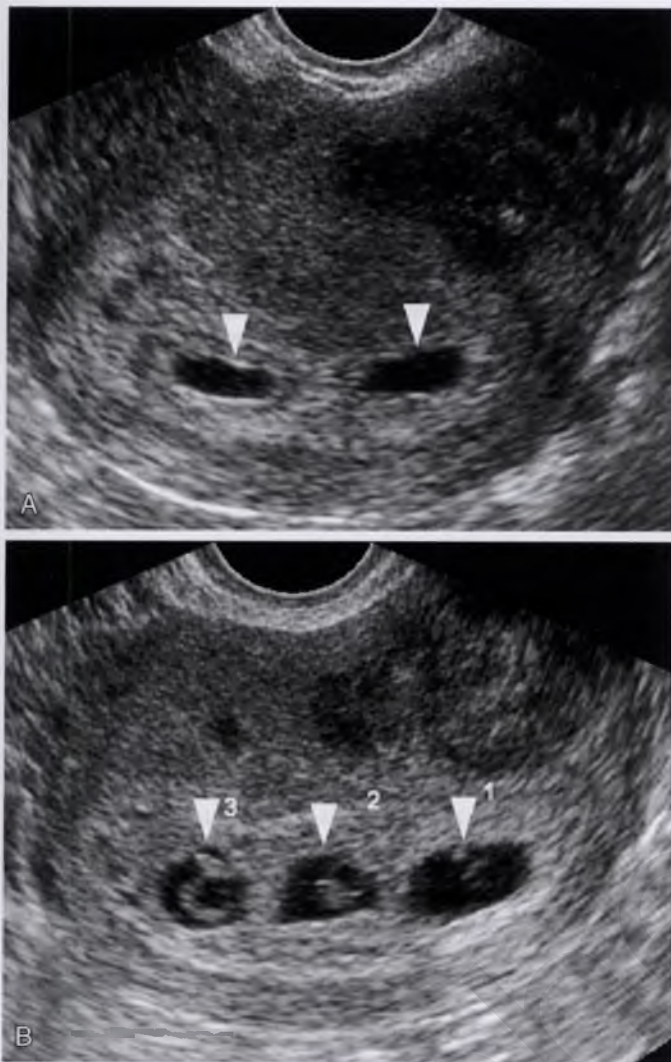


**FIG 4-23** “Appearing” triplet. **A**, Sonogram at 5.3 weeks’ gestation demonstrates two gestational sacs (arrowheads). **B**, Follow-up scan 1 week later demonstrates three gestational sacs (arrowheads), each of which contains an embryo with cardiac activity.

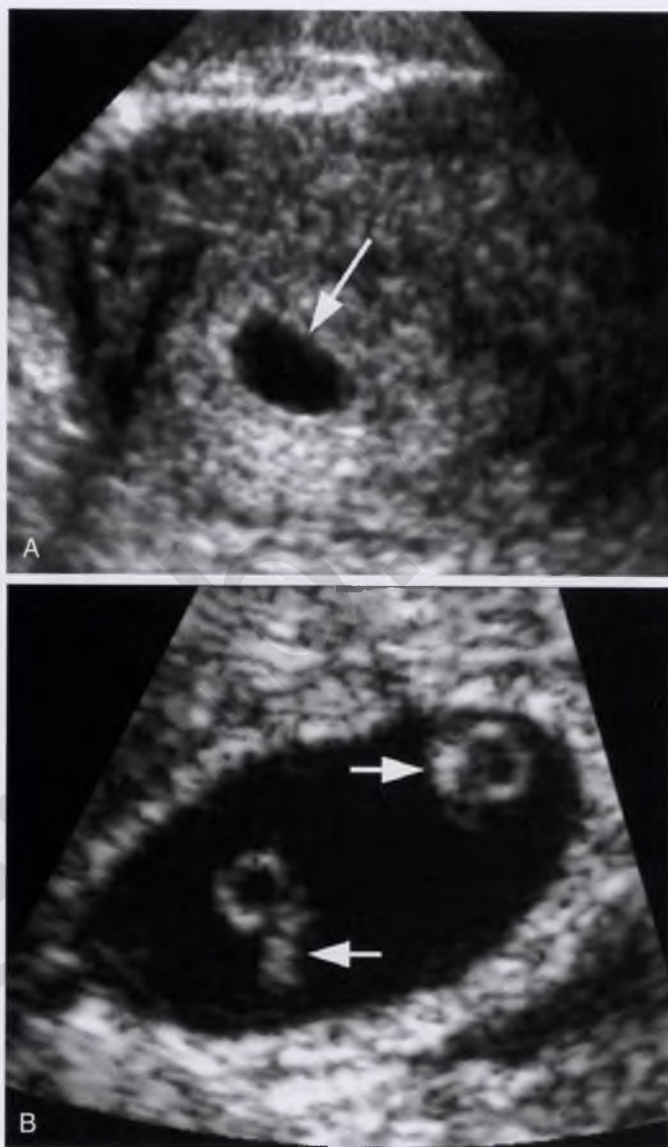


**FIG 4-24** “Appearing” twin. **A**, Sonogram at 5.0 weeks’ gestation demonstrates a gestational sac (arrow). **B**, Follow-up scan 1 week later demonstrates two embryos (arrows) with heartbeats. They are located within a single gestational sac, indicating that they are monozygotic twins.

## REFERENCES

- Benson CB, Doubilet PM: The history of imaging in obstetrics. RSNA centennial radiology select. *Radiology* 273:S92–S110, 2014.
- Doubilet PM, Benson CB: First, do no harm ... to early pregnancies. *J Ultrasound Med* 29(5):685–689, 2010.
- Shwyder JM: Waiting for the tide to change: reducing risk in the turbulent sea of liability. *Obstet Gynecol* 116:8–15, 2010.
- Moore KL, Persaud TVN, Torchia MG: *The Developing Human: Clinically Oriented Embryology*, ed 9, Philadelphia, 2013, WB Saunders.
- Bree RL, Edwards M, Bohm-Velez M, et al: Transvaginal sonography in the evaluation of early pregnancy: correlation with hCG level. *Am J Roentgenol* 153:75–79, 1989.
- Goldstein I, Zimmer EA, Tamir A, et al: Evaluation of normal gestational sac growth: appearance of embryonic heartbeat and embryo body movements using the transvaginal technique. *Obstet Gynecol* 77:885–888, 1991.
- Fossum GT, Davajan V, Kletzky OA: Early detection of pregnancy with transvaginal ultrasound. *Fertil Steril* 49:788–791, 1988.
- Daya S, Woods S, Ward S, et al: Early pregnancy assessment with transvaginal ultrasound scanning. *Can Med Assoc J* 144:441–446, 1991.
- Robinson HP, Fleming JEE: A critical evaluation of sonar “crown-rump length” measurements. *Br J Obstet Gynaecol* 82(9):702–710, 1975.
- Hadlock FP, Shah YP, Kanon DJ, Lindsey JV: Fetal crown-rump length: reevaluation of relation to menstrual age (5–18 weeks) with high-resolution real-time US. *Radiology* 182(2):501–505, 1992.
- Sladkevicius P, Saltvedt S, Almstrom H, et al: Ultrasound dating at 12–14 weeks of gestation: a prospective cross-validation of established dating formulae in in-vitro fertilized pregnancies. *Ultrasound Obstet Gynecol* 26:504–511, 2005.
- Ikegawa A: First-trimester detection of amniotic sac in relation to miscarriage. *J Obstet Gynaecol Res* 23(3):283–288, 1997.
- Doubilet PM, Benson CB, Bourne T, et al: Early first trimester diagnostic criteria for nonviable pregnancy. *N Engl J Med* 369:1443–1451, 2013.
- Kadar N, DeVore G, Romero R: Discriminatory hCG zone: its use in the sonographic evaluation for ectopic pregnancy. *Obstet Gynecol* 58:156–161, 1981.



15. Bateman BG, Nunley WC, Kolp LA, et al: Vaginal sonography findings and hCG dynamics of early intrauterine and tubal pregnancies. *Obstet Gynecol* 75:421–427, 1990.
16. Bernashek G, Rudelstorfer R, Csaicsich P: Vaginal sonography versus serum human chorionic gonadotropin in early detection of pregnancy. *Am J Obstet Gynecol* 158:608–612, 1988.
17. Cacciatore B, Stenman UH, Ylostalo P: Diagnosis of ectopic pregnancy by vaginal ultrasonography in combination with a discriminatory serum hCG level of 1000 IU/L (IRP). *Br J Obstet Gynecol* 97:904–908, 1990.
18. Stovall TG: Medical management of ectopic pregnancy. *Curr Opin Obstet Gynecol* 6:510–515, 1994.
19. Seeber BE, Barnhart KT: Suspected ectopic pregnancy. *Obstet Gynecol* 107:399–413, 2006.
20. Doubilet PM, Benson CB: Further evidence against the reliability of the hCG discriminatory level. *J Ultrasound Med* 30:1637–1642, 2011.
21. Condous G, Kirk E, Lu C, et al: Diagnostic accuracy of varying discriminatory zones for the prediction of ectopic pregnancy in women with a pregnancy of unknown location. *Ultrasound Obstet Gynecol* 26:770–775, 2005.
22. Morse CB, Sammel MD, Shaunik A, et al: Performance of human chorionic gonadotropin curves in women at risk for ectopic pregnancy: exceptions to the rules. *Fertil Steril* 97:101–106, 2012.
23. Bignardi T, Condous G, Alhamsan D, et al: The hCG ratio can predict the ultimate viability of the intrauterine pregnancies of uncertain viability in the pregnancy of unknown location population. *Hum Reprod* 23:1964–1967, 2008.
24. Condous G, Van Calster B, Kirk E, et al: Prediction of ectopic pregnancy in women with a pregnancy of unknown location. *Ultrasound Obstet Gynecol* 29:680–687, 2007.
25. Kirk E, Condous G, Van Calster B, et al: Rationalizing the follow-up of pregnancies of unknown location. *Hum Reprod* 22:1744–1750, 2007.
26. Van Calster B, Abdallah Y, Guha S, et al: Rationalizing the management of pregnancies of unknown location: temporal and external validation of a risk model on 1962 pregnancies. *Hum Reprod* 28:609–616, 2013.
27. Marks WM, Filly RA, Callen PW, Laing FC: The decidual cast of ectopic pregnancy: a confusing ultrasonographic appearance. *Radiology* 133:451–454, 1979.
28. Nyberg DA, Laing FA, Filly RA, et al: Ultrasonographic differentiation of the gestational sac of early intrauterine pregnancy from pseudogestational sac of ectopic pregnancy. *Radiology* 146:755–759, 1983.
29. Ackerman TE, Levi CS, Lyons EA, et al: Decidual cyst: transvaginal sonographic sign of ectopic pregnancy. *Radiology* 189:727–731, 1993.
30. Bradley WG, Fiske CE, Filly RA: The double sac sign of early pregnancy: use in exclusion of ectopic pregnancy. *Radiology* 143:223–226, 1982.
31. Yeh H, Goodman JD, Carr L, Rabinowitz JG: Intradecidual sign: a US criterion of early intrauterine pregnancy. *Radiology* 161:463–467, 1986.
32. Doubilet PM, Benson CB: Double sac sign and intradecidual sign in early pregnancy: interobserver reliability and frequency of occurrence. *J Ultrasound Med* 32:1207–1214, 2013.
33. Benson CB, Doubilet PM, Peters HE, Frates MC: Intrauterine fluid with ectopic pregnancy: a reappraisal. *J Ultrasound Med* 32:389–393, 2013.
34. Misdiagnosed Ectopic, Given Methotrexate: Facebook website. Available at <<http://www.facebook.com/groups/misduagnosedectopic/>>.
35. Current trends in ectopic pregnancy—United States 1990–1992: *MMWR Morb Mortal Wkly Rev* 44:46–48, 1995.
36. Brown DL, Doubilet PM: Transvaginal sonography for diagnosing ectopic pregnancy: positivity criteria and performance characteristics. *J Ultrasound Med* 13:259–266, 1994.
37. Frates MC, Visweswaran A, Laing FC: Comparison of tubal ring and corpus luteum echogenicities: a useful differentiating characteristic. *J Ultrasound Med* 20:27–31, 2001.
38. Pellerito JS, Taylor KJW, Quedens-Case C, et al: Ectopic pregnancy: evaluation with transvaginal color flow imaging. *Radiology* 183:407–411, 1992.
39. Emerson DS, Cartier MS, Altieri LA, et al: Diagnostic efficacy of transvaginal color Doppler flow imaging in an ectopic pregnancy screening program. *Radiology* 183:413–420, 1992.
40. Blaivas M, Lyon M: Reliability of adnexal mass mobility in distinguishing possible ectopic pregnancy from corpus luteum cysts. *J Ultrasound Med* 24:599–603, 2005.
41. Doubilet PM: Should a first trimester dating scan be routine for all pregnancies? *Semin Perinatol* 37:307–309, 2013.
42. Levi CS, Lyons EA, Zheng XH, et al: Transvaginal ultrasound: demonstration of cardiac activity in embryos of less than 5.0 mm in crown-rump length. *Radiology* 176:71–74, 1990.
43. Goldstein SR: Significance of cardiac activity on transvaginal ultrasound in very early embryos. *Obstet Gynecol* 80:670–672, 1992.
44. Brown DL, Emerson DS, Felker RE, et al: Diagnosis of embryonic demise by transvaginal sonography. *J Ultrasound Med* 9:631–636, 1990.
45. Pennell RG, Needleman L, Pajak T, et al: Prospective comparison of vaginal and abdominal sonography in normal early pregnancy. *J Ultrasound Med* 10:63–67, 1991.
46. American Institute of Ultrasound in Medicine: AIUM practice guideline for the performance of pelvic ultrasound examinations. *J Ultrasound Med* 29(1):166–172, 2010.
47. American College of Obstetricians and Gynecologists: ACOG Practice Bulletin: ultrasonography in pregnancy. *Obstet Gynecol* 113(2 Pt 1):451–461, 2009.
48. American College of Radiology: *ACR Appropriateness Criteria: First Trimester Bleeding*. Reston, VA, Department of Quality & Safety, American College of Radiology, 2012 (date of origin 1996).
49. Moore C, Promes SB: Ultrasound in pregnancy. *Emerg Clin North Am* 22:697–722, 2004.
50. Deutchman M, Tubay AT, Turok DK: First trimester bleeding. *Am Fam Physician* 79:985–992, 2009.
51. Jevc Y, Rana R, Bhide A, Thangaratinam S: Accuracy of first trimester ultrasound in the diagnosis of early embryonic demise: a systematic review. *Ultrasound Obstet Gynecol* 38:489–496, 2011.
52. Abdallah Y, Daemen A, Kirk E, et al: Limitations of current definitions of miscarriage using mean gestational sac diameter and crown-rump length measurements: a multicenter observational study. *Ultrasound Obstet Gynecol* 38:497–502, 2011.
53. Hamilton J, Hamilton J: The 6 mm crown-rump length threshold for detecting fetal heart movements—what is the evidence? *Ultrasound Obstet Gynecol* 38(S1):7, 2011.
54. Pexsters A, Luts J, van Schoubroeck D, et al: Clinical implications of intra- and interobserver reproducibility of transvaginal sonographic measurements of gestational sac and crown-rump length at 6–9 weeks' gestation. *Ultrasound Obstet Gynecol* 38(5):510–515, 2011.
55. Lane BF, Wong-You-Cheong JJ, Javitt MC, et al: ACR appropriateness criteria for first trimester bleeding. *Ultrasound Q* 29(2):91–96, 2013.
56. Levi CS, Lyons EA, Lindsay DJ: Early diagnosis of nonviable pregnancy with transvaginal US. *Radiology* 167:383–385, 1988.
57. Tongsong T, Wanapirak C, Sirsomboon J, et al: Transvaginal ultrasound in threatened abortions with empty gestational sacs. *Int J Gynecol Obstet* 46:297–301, 1994.
58. Rowling SE, Coleman BG, Langer JE, et al: First-trimester US parameters of failed pregnancy. *Radiology* 203:211–217, 1997.
59. Wilcox AJ, Baird DD, Weinberg CR: Time of implantation of the conceptus and loss of pregnancy. *N Engl J Med* 340:1796–1799, 1999.
60. Wegienka G, Baird DD: A comparison of recalled date of last menstrual period with a menstrual diary. *J Women's Health* 14:248–252, 2005.
61. Savitz DA, Terry JW, Dole N, et al: Comparison of pregnancy dating by last menstrual period, ultrasound scanning, and their combination. *Am J Obstet Gynecol* 187:1660–1666, 2002.
62. McKenna KM, Feldstein VA, Goldstein RB, Filly RA: The empty amnion: a sign of early pregnancy failure. *J Ultrasound Med* 14:117–121, 1995.
63. Yegul NT, Filly RA: Further observations on the “empty amnion sign.” *J Clin Ultrasound* 38(3):113–117, 2010.
64. Horrow MM: Enlarged amniotic cavity: a new sonographic sign of early embryonic death. *AJR Am J Roentgenol* 158:359–362, 1992.
65. Yegul NT, Filly RA: The expanded amnion sign: evidence of early embryonic death. *J Ultrasound Med* 28:1331–1335, 2009.

66. Lindsay DJ, Lovett IS, Lyons EA, et al: Yolk sac diameter and shape at transvaginal US: predictors of pregnancy outcome in the first trimester. *Radiology* 183:115–118, 1992.
67. Cepni I, Bese T, Ocal P, et al: Significance of yolk sac measurements with the vaginal sonography in the first trimester in the prediction of pregnancy outcome. *Acta Obstet Gynecol Scand* 76:969–972, 1997.
68. Stampone C, Nicotra M, Muttinelli C, Cosmi EV: Transvaginal sonography of the yolk sac in normal and abnormal pregnancy. *J Clin Ultrasound* 24:3–9, 1996.
69. Laboda LA, Estroff JA, Benacerraf BR: First trimester bradycardia. A sign of impending fetal loss. *J Ultrasound Med* 8(10):561–563, 1989.
70. Hertzberg BS, Mahoney BS, Bowie JD: First trimester fetal cardiac activity. Sonographic documentation of a progressive early rise in heart rate. *J Ultrasound Med* 7:573–575, 1988.
71. Achiron R, Tadmor O, Mashiach S: Heart rate as a predictor of first-trimester spontaneous abortion after ultrasound-proven viability. *Obstet Gynecol* 78:330–334, 1991.
72. Benson CB, Doubilet PM: Slow embryonic heart rate in early first trimester: indicator of poor pregnancy outcome. *Radiology* 192:343–344, 1994.
73. Doubilet PM, Benson CB: Embryonic heart rate in the early first trimester: what rate is normal? *J Ultrasound Med* 14:431–434, 1995.
74. Doubilet PM, Benson CB: First trimester outcome of pregnancies in which the embryo has a slow heart rate at 6–7 weeks gestation and a normal heart rate on a follow-up scan by 8 weeks. *Radiology* 236:643–646, 2005.
75. Benson CB, Doubilet PM, Cooney MJ, et al: Early singleton pregnancy outcome: effects of maternal age and mode of conception. *Radiology* 203:399–403, 1997.
76. Bennett GL, Bromley B, Lieberman E, Benacerraf BR: Subchorionic hemorrhage in first-trimester pregnancies: prediction of pregnancy outcome with sonography. *Radiology* 200:803–806, 1996.
77. Sauerbrei EE, Pham DH: Placental abruption and subchorionic hemorrhage in the first half of pregnancy: US appearance and clinical outcome. *Radiology* 160:109–112, 1983.
78. Mandruzzato GP, D'Ottavio G, Rustico A, et al: The intrauterine hematoma: diagnostic and clinical aspects. *J Clin Ultrasound* 17:503–510, 1989.
79. Stabile I, Campbell S, Grudzinskas JG: Threatened miscarriage and intrauterine hematomas. Sonographic and biochemical studies. *J Ultrasound Med* 8(6):289–292, 1989.
80. Joupilla P: Clinical consequences after ultrasonic diagnosis of intrauterine hematoma in threatened abortion. *J Clin Ultrasound* 13:107–111, 1985.
81. Bromley B, Harlow B, Laboda L, Benacerraf BR: Small sac size in the first trimester: a predictor of poor fetal outcome. *Radiology* 178:375–377, 1991.
82. Levi S: Ultrasonic assessment of the high rate of human multiple pregnancy in the first trimester. *J Clin Ultrasound* 4:3–5, 1976.
83. Robinson HP, Caines JS: Sonar evidence of early pregnancy failure in patients with twin conceptions. *Br J Obstet Gynaecol* 84(1):22–25, 1977.
84. Finberg HJ, Birnholz JC: Ultrasound observations in multiple gestation with first trimester bleeding: the blighted twin. *Radiology* 132:137–142, 1979.
85. Landy HL, Weiner S, Corson SL, et al: The “vanishing twin”: ultrasonographic assessment of fetal disappearance in the first trimester. *Am J Obstet Gynecol* 155:14–19, 1986.
86. Benson CB, Doubilet PM, Laks MP: Outcome of twin gestations following sonographic demonstration of two heart beats in the first trimester. *Ultrasound Obstet Gynecol* 3:343–345, 1993.
87. Benson CB, Doubilet PM, David V: Prognosis of first trimester twin pregnancies: polychotomous logistic regression analysis. *Radiology* 192:765–768, 1994.
88. Sampson A, de Crespigny LC: Vanishing twins: the frequency of spontaneous fetal reduction of a twin pregnancy. *Ultrasound Obstet Gynecol* 2:107–109, 1992.
89. Doubilet PM, Benson CB: The “appearing twin”: undercounting of multiple gestations on early first trimester sonograms. *J Ultrasound Med* 17:199–203, 1998.



# Evaluation of Fetal Anatomy in the First Trimester

Amanda S. Trudell, Anthony O. Odibo

## SUMMARY OF KEY POINTS

- Evaluation of fetal anatomy, including a detailed fetal cardiac examination, is possible in the late first trimester.
- Many anatomic abnormalities can be detected in the first trimester, giving families time to make important decisions regarding pregnancy management and the opportunity for early termination of pregnancy to reduce maternal morbidity risks.
- Doppler techniques and four-dimensional spatiotemporal image correlation (4D STIC) are modalities used to help examine the fetal heart in detail during the first trimester, although detection rates using STIC technology are reported to be slightly lower than with two-dimensional (2D) sonography.
- In experienced centers, or when educational programs are instituted, the reliability and detection rates of first trimester anatomic evaluation have been demonstrated to parallel those of second trimester anatomic evaluation.
- The cost effectiveness of first trimester anatomic screening in the general population remains unknown at this time.
- It is important to keep the ALARA (as low as reasonably achievable) principle in mind when performing detailed anatomic evaluation in the first trimester. This point becomes particularly important when using modalities that employ higher frequencies, such as power Doppler sonography.
- The thermal index for soft tissue (TIS) and thermal index for bone (TIB) should be kept below 1.0.

## OUTLINE

### Fetal Development in the First Trimester, 98

Embryonic Period (Weeks 4-9 Post Conception), 99

Fetal Period (Weeks 9-14), 101

### Normal Ultrasound Findings in the First Trimester, 101

Head and Neck, 101

Chest, 102

Abdomen, 106

Extremities, 107

### Abnormal Ultrasound Findings in the First Trimester, 108

Head and Neck, 108

Chest, 110

Abdomen, 111

Extremities, 113

### Limitations of First Trimester Fetal Anatomic Survey, 113

Detection Rates, 114

Cost Effectiveness, 114

Safety, 114

Conclusions, 115

First trimester fetal anatomy evaluation has developed over the past several decades. As a result of advances in technology, the resolution of sonography has improved, and subsequently, our ability to image the fetus with increasing detail. Initially, first trimester sonography was limited to use as a means of measuring crown-rump length for pregnancy dating. As the utilization of high-frequency transvaginal sonography evolved through the 1980s, sonographic investigation of the anatomic development of the embryo and early fetus became possible.<sup>1</sup> With the boom in first trimester aneuploidy screening in the 1990s came the discovery of increased nuchal translucency as a marker of aneuploidy, propelling further investigation into the potential for first trimester anatomy evaluation.<sup>2</sup> As reports of normal and abnormal first trimester fetal anatomy continued to surface in the literature and detection rates and technical aspects began to be published, our ability to image the fetus in the first trimester became

more refined. Today, the possibility of performing a detailed anatomic assessment, including fetal echocardiography, between 12 and 14 weeks is a reality.

## FETAL DEVELOPMENT IN THE FIRST TRIMESTER

The first trimester marks a period of rapid fetal growth and development (Fig. 5-1, Table 5-1). Prior to embarking on a detailed description of the use of sonography to assess fetal anatomy in the first trimester, it is important to understand the structure and development of the embryo and fetus, as this directly impacts the potential of ultrasound to detect abnormal structures. Note that embryonic development is typically described by weeks post conception, whereas sonographic findings are described using clinical menstrual age dating. Menstrual age dating is typically 2 weeks greater than conceptional age (see Chapter 6).



**FIG 5-1** Development of the early embryo/fetus from 5 through 13 weeks of gestation (menstrual weeks). See text for details.

### Embryonic Period (Weeks 4-9 Post Conception)<sup>3</sup>

**Week 4:** The 4th week marks significant development of the embryonic body, with formation of the primordium of the brain from the previously formed neural tube, the oropharyngeal membrane, and the foregut (primordium of the pharynx, esophagus, and lower respiratory tract). Primitive erythroblasts enter the embryo proper at 4 weeks' gestation, and the primordial heart begins to develop and contract. During the 4th week, hematopoietic cells begin to colonize the newly forming liver, which serves as the major site of hematopoiesis.<sup>4</sup> As the embryo folds in both the cephalocaudal and lateral directions, the intraembryonic coelom is divided by the septum transversum (future diaphragm), located just caudal to the heart. The septum transversum divides the primordial body cavities into the cranial pericardial cavity and the caudal peritoneal cavity. The maxilla and mandible begin to take form. The prominence of the forebrain results in the classic

C-shaped curve of the embryo. Caudal folding results in the caudal eminence, a tail-like structure, with lower limb buds visible by the end of the 4th week.

**Week 5:** The 5th week is marked by accelerated growth, with head growth outpacing the other embryonic structures. The face begins to take form, and the mesonephric ridges develop to mark the site of the future kidneys. The embryonic heart develops into a four-chambered structure.

**Week 6:** By the 6th week, the limb buds begin to differentiate into upper and lower limbs with large hand plates, which develop primordial digits. The lower extremities lag behind the upper limbs by approximately 4 to 5 days. The primordial ear develops and the eyes become obvious as the retina becomes pigmented. The fetal liver occupies the majority of the abdominal cavity at the 6th week. As the rapid growth of the intestines exceeds the growth of the abdominal cavity



**TABLE 5-1 Appearance of Embryonic Structures on Ultrasound Imaging Through the First Trimester**

Structure	GESTATIONAL WEEK									
	5	6	7	8	9	10	11	12	13	14
Gestational sac	■									
Yolk sac		■	■	■	■	■	■	■	■	■
Fetal pole		■	■	■	■	■	■	■	■	■
Single ventricle			■	■	■	■	■	■	■	■
Falx				■	■	■	■	■	■	→
Spine			■	■	■	■	■	■	■	→
Choroid plexus				■	■	■	■	■	■	→
Forebrain				■	■	■	■	■	■	→
Hindbrain					■	■	■	■	■	→
Face					■	■	■	■	■	→
Nuchal translucency										
Heartbeat		■	■	■	■	■	■	■	■	→
Four-chamber view							■	■	■	■
Midgut herniation				■	■	■	■	■	■	■
Kidneys						■	■	■	■	→
Lower limbs						■	■	■	■	→
Upper limbs						■	■	■	■	→
Limb movement						■	■	■	■	→
Fingers							■	■	■	→
Toes								■	■	→

Modified from Timor-Tritsch IE, Farine D, Rosen MG: A close look at early embryonic development with the high-frequency transvaginal transducer. Am J Obstet Gynecol 159(3):676-681, 1988; and Timor-Tritsch IE, Bashiri A, Monteagudo A, Arslan AA: Qualified and trained sonographers in the US can perform early fetal anatomy scans between 11 and 14 weeks. Am J Obstet Gynecol 191(4):1247-1252, 2004.

the physiologic herniation of the intestines into the umbilical cord occurs. Spontaneous twitching movements and reflex responses to touch begin to take place.

**Week 7:** The most notable change in structure at 7 weeks is limb development as the digits become distinct and ossification begins. The plantar surfaces of the feet face each other. The developing central nervous system (CNS) is divided into the prosencephalon (forebrain), mesencephalon (midbrain), and rhombencephalon (hindbrain); however, the midline falx cerebri has not formed, and what will become the lateral ventricles is a single ventricle at this point.

**Week 8:** The 8th week marks the final week of the embryonic period. By then, the heart has developed all of its adult components, pulmonary veins, tricuspid and mitral valves, coronary arteries, inferior and superior vena cava, interventricular septum, and aortic and pulmonary valves. Near the end of the 8th week, the choroid plexus begins to fold inward and the falx cerebri develops, thus dividing the single ventricle into two lateral ventricles.<sup>5</sup> The face takes form over the course of weeks 5 through 8. By the end of the 8th week, the mandibular, maxillary, and nasal processes have merged in the midline, and the primary and secondary palates have fully fused to produce the two palatal shelves of the definitive palate.<sup>6</sup>

### Fetal Period (Weeks 9-14)

**Weeks 9 to 12:** At 9 weeks, 50% of the fetus is composed of the head, and the 9th through 12th weeks are marked by acceleration in body growth. At 10 weeks, the knees begin to rotate ventrally and the soles of the feet become reoriented with the plantar surface on the ventral aspect.<sup>7</sup> In the 10th week, the hindbrain develops and the cerebellum takes form. It is not until 12 weeks that the corpus callosum begins the first stages of development that will continue through the second trimester.<sup>5,8,9</sup> From 10 to 12 weeks, the male and female genitalia differentiate. The intestines begin to return to the abdominal cavity in the 10th week with full return by the end of the 11th week. Between weeks 10 through 12, the two shelves of the definitive palate fuse in the midline. Primary ossification centers appear by 12 weeks; the lower limbs have reached their final relative length, and the upper limbs are nearly at their relative length. Between 9 and 12 weeks the fetal kidneys begin urine production and excretion into the amniotic fluid.

**Weeks 13 to 14:** Weeks 13 through 14 are marked by more fetal growth. Limb movements become coordinated by 14 weeks. The eyes begin to rotate from anterolateral to anterior.

## NORMAL ULTRASOUND FINDINGS IN THE FIRST TRIMESTER

### Head and Neck

#### Central Nervous System

In the embryonic period, the brain is hypoechoic and characterized in the sagittal plane by the presence of three echogenic structures: prosencephalon (forebrain), mesencephalon (midbrain), and rhombencephalon (hindbrain). The rhombencephalon can be visualized as early as 7 weeks and is the most prominent cavity owing to its relatively larger size compared to the other two cavities.<sup>10</sup> These fluid-filled cavities are positioned in a triangular fashion, laid out as to predict their future site of structure and function. The base of the triangle is formed by the forebrain in the anterior position and the hindbrain in the posterior position with the midbrain forming the apex of the triangle in between<sup>10</sup> (Fig. 5-2).

**Forebrain and Midbrain.** The cerebral hemispheres are only tiny buds at 7 weeks, but by 9 weeks Blaas and associates demonstrated the appearance of measurable hemispheres in 79% of embryos with



**FIG 5-2** Ultrasound image of a normal fetal central nervous system in the midsagittal plane at 12 weeks' gestation. The thalamus (T), midbrain (M), brainstem (B), medulla oblongata (MO), and choroid plexus (CP) of the fourth ventricle are noted. The normal intracranial translucency (IT) of the fourth ventricle is present.



**FIG 5-3** Coronal view demonstrating normal choroid plexus (CP), falx cerebri (F), and lateral ventricles (LV) at 12 weeks.

visualization in all fetuses by 10 weeks. As the hemispheres grow, they conceal the diencephalon and meet in the midline at 11 to 12 weeks. At 12 weeks the mean measurements of the cerebral hemisphere in the sagittal view are length 16.4 mm (12.4-20.9 mm); width 6.1 mm (4.2-8.4 mm); and height 2.0 mm (1.4-2.5 mm).<sup>11</sup> As the first trimester progresses from the 8th week onward, the mesencephalon gradually moves toward a more central location, and the third and fourth ventricles become more organized with a distinct isthmus visible between the cavities of the prosencephalon and mesencephalon by the 9th week.

**Lateral Ventricles.** At 7 weeks, a single ventricle is visible, as the midline falx cerebri has not yet developed. Timor-Tritsch and colleagues demonstrated variability in the development of the falx. Although the falx was visible in the majority (75%) of embryos by 9 weeks, in a small proportion the division of the ventricles was not visible until the 10th week, when the falx was clearly visualized dividing the two lateral ventricles in all embryos.<sup>7</sup> The choroid plexus can be visualized routinely within each of the lateral ventricles by the middle of the 9th week, and by the 12th week it fills most of the space of the lateral ventricles<sup>11</sup> (Fig. 5-3).



At 12 weeks, the corpus callosum is not visible, but the trunk from which it will continue to develop may be seen. The cavum septi pellucidum (CSP), an important marker of normal CNS development, can be seen in 40% of pregnancies at 15 weeks and in 82% at 16 to 17 weeks.<sup>12</sup>

**Cerebellum and Posterior Fossa.** The rhombencephalon is the most obvious structure of the early embryonic CNS. As the cerebellar hemispheres grow, they become measurable by the middle of the 10th week and appear to meet in the midline by 11 to 12 weeks.<sup>10</sup> The choroid plexuses of the fourth ventricle are visible by the middle of the 10th week as echogenic areas that traverse the roof of the fourth ventricle.<sup>5,10</sup>

**Spine.** The spine will be detectable as two parallel lines as early as the 8th week in a majority of embryos.<sup>7</sup> The cervical, thoracic, and lumbar spine can be visualized in 80%, 81%, and 72% of fetuses between 11 and 12 weeks and 89%, 87%, and 72% of fetuses between 13 and 14 weeks.<sup>13</sup> The sacral spine is more difficult to visualize in the first trimester, with visualization rates of 35% between 11 and 12 weeks and 48% between 13 and 14 weeks<sup>13</sup> (Fig. 5-4A and B).

### Skeletal Structures/Face

**Skull.** The bony cranium begins to ossify at 9 weeks and can be precisely measured after 9 weeks using high-frequency transvaginal sonography.<sup>1</sup> Using a combination of transvaginal and transabdominal sonography, Souka and colleagues were able to visualize the fetal head, including the complete cranium and the presence of the falx in all cases between 11 and 14 weeks' gestation<sup>14</sup> (Fig. 5-5A).

**Face.** The structure of the face changes dramatically throughout the first trimester and therefore is not reliably imaged until the 11th

or 12th week.<sup>7</sup> Souka and colleagues were able to visualize the fetal face, including the orbits, lenses, and profile 99.7% of the time using a combination of transabdominal and transvaginal sonography from 11 to 14 weeks.<sup>14</sup> In addition, there does not seem to be a significant difference in the ability to detect the structures of the face, including the lenses, profile, nose, and lips between 11 and 12 weeks compared to 13 and 14 weeks.<sup>13</sup> In the embryonic and early fetal periods, the forehead is the dominant feature of the developing human face. After 11 weeks, the fetal profile takes on the expected contour with balance between the mandible, the maxilla, and the forehead. At 12 weeks a coronal section of the face can reliably be obtained and allows assessment for symmetry through imaging of the orbits, mandible, and maxilla<sup>7</sup> (Fig. 5-6). In the coronal section of the face, the fetal lenses can be visualized as an echogenic ring with a sonolucent center in 91% of fetuses at 11 to 12 weeks' gestation.<sup>7</sup>

By 11 weeks, imaging of the palate and lips can be reliably performed<sup>7</sup> (Fig. 5-7). The nose also becomes fully formed by 11 weeks, and the presence or absence of the nasal bone can be evaluated at this time. The frontomaxillary facial angle measured using three-dimensional (3D) volumes of the fetal face has been investigated as a screening tool for trisomy 21, which is associated with significant flattening of the face. The frontomaxillary angle decreases with increasing crown-rump length. Nomograms for chromosomally normal fetuses have been reported.<sup>15</sup>

The international 3D focus group has published recommendations regarding imaging of the fetal face in the first trimester. These recommendations include imaging specifications that are unique to the developing first trimester face and are particularly useful for correct visualization of the nasal bone and excluding face malformations.<sup>16</sup>

### Neck

Evaluation of the nuchal anatomy in the first trimester has been a stepping stone that has led to the development of fetal anatomic assessment in the first trimester. The measurement of the nuchal translucency (NT) is now a widely accepted tool used for first trimester aneuploidy screening.<sup>2,17</sup> The nuchal translucency is gestational age dependent and can be reliably measured from 11 to 14 weeks' gestation<sup>18,19</sup> (Fig. 5-8).

### Chest

The fetal chest, imaged between 11 and 14 weeks' gestation, demonstrates improved visualization of the pulmonary and cardiac structures occurring over the course of time. Using a combination of transvaginal and transabdominal sonography, Timor-Tritsch and colleagues demonstrated a significant difference in the ability to visualize the fetal lungs between 13 and 14 weeks compared with 11 to 12 weeks (77% vs. 64%,  $P = 0.02$ ). The fetal diaphragm was visualized by the same group in 87% of fetuses from 11 to 12 weeks<sup>7</sup> (Fig. 5-9).

### Cardiac Features

Using high-frequency transvaginal sonography, the fetal heart motion is first visualized from 5 weeks and 4 days to 5 weeks and 6 days, with an average rate at 6 weeks of 104 bpm.<sup>1,7,20</sup> In a longitudinal study of cardiac development in the first trimester, Blaas and colleagues demonstrated that the fetal heart rate follows an inverted-U curve from 7 weeks to 12 weeks. The fetal heart rate was noted to be at 138 bpm at 7 weeks, peaks at 175 bpm at 9 weeks, and then decreases to 166 bpm at 12 weeks.<sup>21</sup>

Although it has been demonstrated that the major structures of the heart can be visualized as early as 10 weeks, the success rate of visualizing these structures has been shown by several authors to improve with each advancing week.<sup>21-24</sup> In addition, Gembruch and colleagues

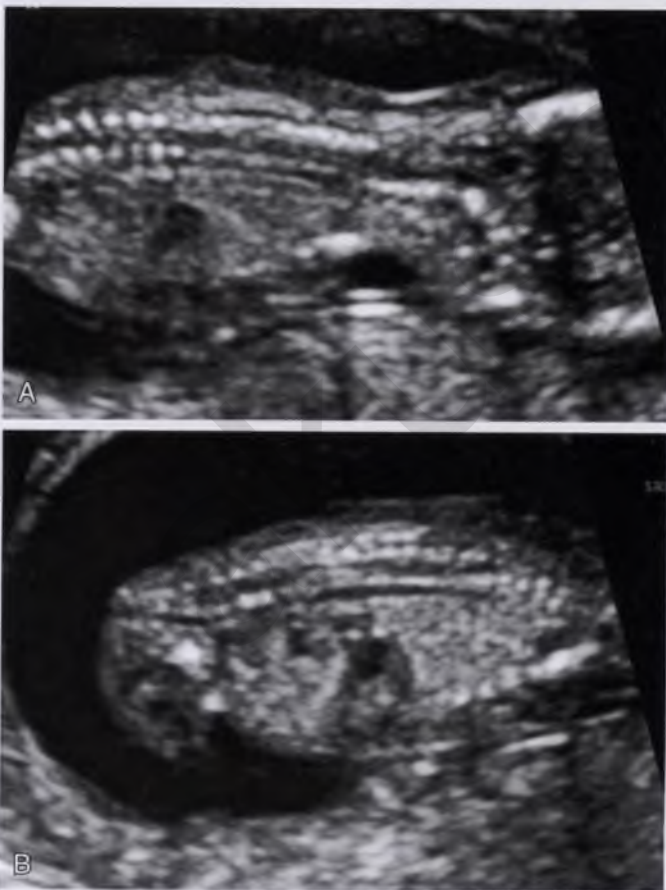


**FIG 5-4** Normal fetal spine at 12 weeks' gestation. **A.** Cervical and thoracic spine. **B.** Thoracic and lumbar spine.



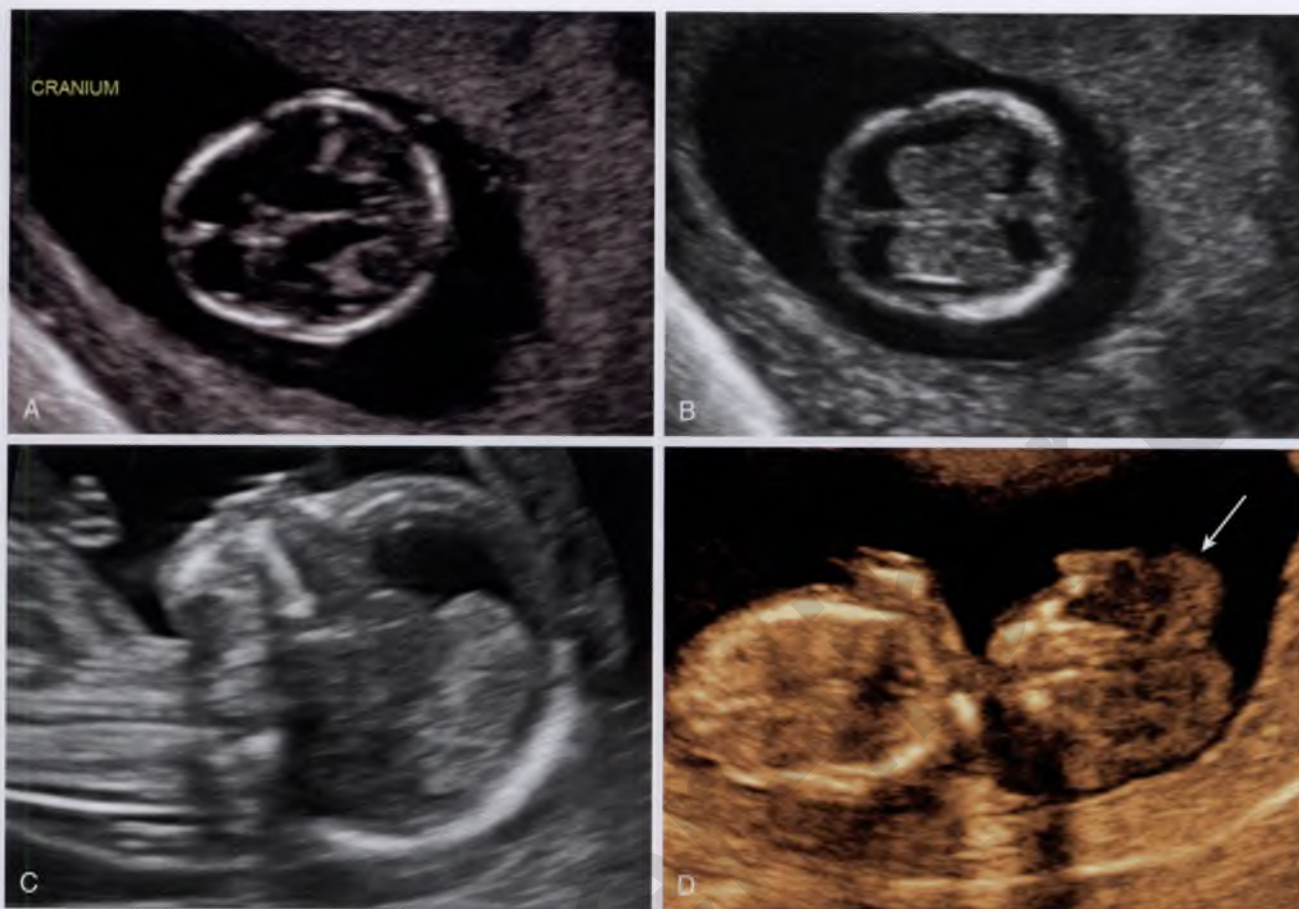


**FIG 5-5** Fetal head at 12 weeks' gestation demonstrating a normal cranial vault (**A**) and normal choroid plexus (**B**). The midline falx is also demonstrated. **C**, The large echolucent area anterior to the choroid plexus is normal at this gestational age. **D**, This 13-week fetus has acrania or exencephaly, with absence of the cranial vault and irregular brain tissue floating in the amniotic fluid (*arrow*). (Courtesy of Barbora Mrazek-Pugh.)



**FIG 5-6** Coronal view of the normal fetal face at 12 weeks demonstrating the symmetry of the orbits, mandible, and maxilla.



**FIG 5-7** Normal fetal palate (*arrow*) at 12 weeks.





**FIG 5-8** Nuchal translucency (NT). **A**, Normal NT in a normal fetus. **B**, Enlarged NT and absent nasal bone (arrow) in a fetus with trisomy 21.



**FIG 5-9** Image of the fetal chest and abdomen at 12 weeks demonstrating stomach (S) below the intact diaphragm (arrows).



**FIG 5-10** Four-chamber view of the heart at 12 weeks demonstrating normal cardiac axis of approximately 45 degrees. LT, left thorax.

have demonstrated better visualization using transvaginal sonography compared to transabdominal sonography from 10 to 13 weeks, equivalent visualization of the two approaches at 14 weeks, and after 14 weeks superiority of the abdominal approach.<sup>24</sup>

Situs can be confirmed by documenting appropriate orientation with the aorta to the right of the spine, inferior vena cava anterior and right of the spine, and the heart lying on the left side of the chest with the appropriate axis.<sup>25</sup> Compared to the  $45 \pm 10$  degree cardiac axis in the mid-second and third trimesters, the cardiac axis in the first trimester begins much more midline and gradually rotates to the 45-degree position by about the 12th week.<sup>26</sup> From the 8th through the 9th weeks the heart sits at approximately  $25 \pm 12$  degrees, from the 10th through the 11th week the axis rotates to  $40 \pm 9$  degrees, and between the 12th and 15th weeks it reaches the final cardiac axis at  $49 \pm 7$  degrees<sup>26</sup> (Fig. 5-10).

At 12 weeks the four-chamber view can be obtained reliably in 90% of fetuses using transvaginal sonography.<sup>23</sup> Two equally sized ventricles and atria with an intact ventricular septum up to the cardiac crux are

seen in the normal four-chamber view<sup>23</sup> (Fig. 5-11A and C). The atrial appendages are more pronounced in the first trimester fetal heart compared to later in gestation, and the ventricles are in a spiral arrangement; however, the resolution of 2D sonography limits our ability to appreciate these differences, which have been demonstrated using 4D high-resolution transvaginal sonography (4D HREVS).<sup>27</sup> The right and left ventricles can be difficult to distinguish because of their spiral orientation, but they can be distinguished by identification of the offset of the atrioventricular valves with the tricuspid valve on the right side positioned slightly lower than the mitral valve on the left. The atrioventricular septum grows relatively late in the first trimester, and as such, the offset of the mitral and tricuspid valves may not be apparent until after 12 weeks.<sup>25</sup> Doppler sonography can be used to help identify the morphologic features of the right and left ventricles. Lombardi and colleagues described the “banana-shaped” right ventricle and

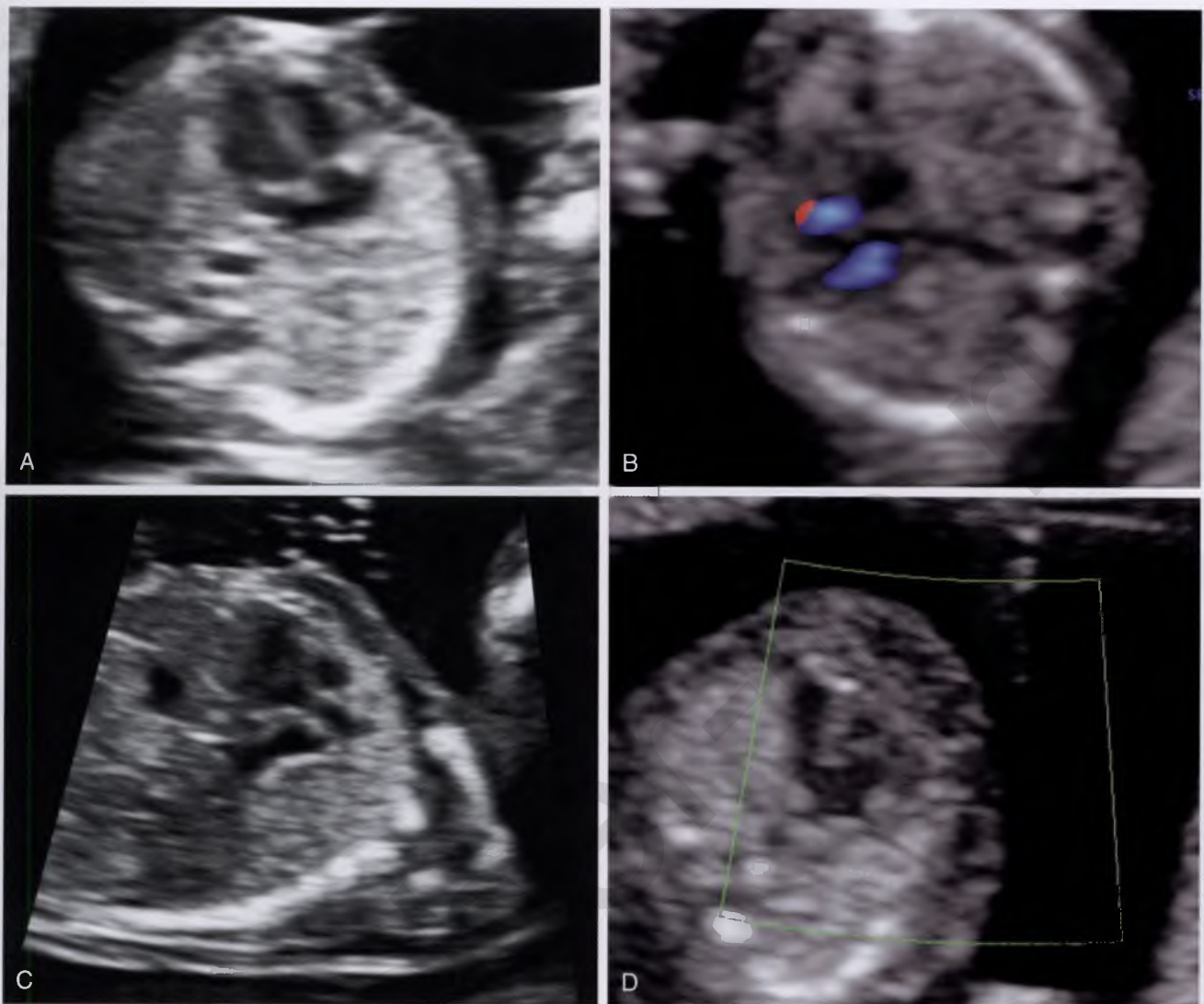


**FIG 5-11** Fetal heart in the late first trimester. **A**, Four-chamber view of the heart at 14 weeks' gestation. **B**, Four-chamber view visualized with color Doppler. **C**, Left ventricular outflow tract. **D**, Atrioventricular canal defect at 12 weeks' gestation.

“ballerina shoe-shaped” left ventricle with its less severe curvature.<sup>25</sup> In addition, a combination of color Doppler and power Doppler is also recommended to help define the septal aortic continuity, evaluate normal valvular flow, and show pulmonary vein flow into the left atrium. The short axis view of the great vessels, which demonstrates the wrapping of the pulmonary artery from the right ventricle continuous with the branching of the ductus arteriosus, also demonstrates the tricuspid and pulmonary valves and is therefore useful for measuring flow across these valves.<sup>25,28</sup> It should be noted that in the first trimester it is particularly important to apply the ALARA principle and keep the thermal index below 1, which can become an issue when Doppler is used.<sup>29</sup>

Demonstration of the outflow tracts can be achieved in many fetuses by the 12th week, with improved visualization in the 13th week.<sup>25</sup> The long-axis view of the aorta with the aorta arising from the left ventricle adequately demonstrates the left ventricular outflow tract (LVOT) in 68% of fetuses in the 12th week, increasing to 92% in the 13th week<sup>22</sup> (Fig. 5-11B). In the long-axis view of the aorta, the continuity of the ventricular septum with the anterior wall of the aorta and

the anterior mitral leaflet with the posterior wall of the aorta can be visualized. By angling the transducer toward the fetal right side, if the aorta and pulmonary artery are oriented in their normal crossover configuration, the long-axis view of the pulmonary artery can be obtained, which demonstrates the right ventricular outflow tract as the pulmonary artery branches off the right ventricle cephalad toward the fetal left side.

The aorta is seen arising centrally from the left ventricle and the pulmonary trunk from the anterior right ventricle with the pulmonary trunk crossing over the ascending aorta to the left side of the fetus (Fig. 5-12). The ductal arch is anterior to the transverse section of the aortic arch and heads almost directly posterior toward the spine where it converges with the descending aorta to the left of the spine (Fig. 5-13). The three-vessel view with the pulmonary trunk originating from the right ventricle, the aorta, and the superior vena cava is useful for identifying and comparing the sizes of the great vessels. The use of color Doppler can confirm forward flow through the outflow tracts. Using power Doppler, the normal orientation of the great vessels can be demonstrated using the X sign, which identifies the normal crossover





**FIG 5-12** Normal aortic arch at 12 weeks.



**FIG 5-13** Normal ductal arch at 12 weeks.

of the pulmonary trunk over the aorta, and the b sign, which demonstrates a transverse plane at the level of the sweeping arch of the aorta and near linear path of the pulmonary artery.<sup>25</sup>

Nomograms for cardiac biometry between the 10 and 15 weeks have been published by Smrcek and coworkers.<sup>28</sup>

### Abdomen

Examination of the abdomen in the first trimester begins with evaluation of the ventral wall (Fig. 5-14). The physiologic herniation of the midgut can be seen as early as 7 weeks and becomes most identifiable from 9 to 10 weeks with retraction back into the abdominal cavity from the middle of the 10th week through the 11th week<sup>21</sup> (Fig. 5-15). By 12 weeks the thickening of the umbilical cord associated with midgut herniation has resolved, and the umbilical cord insertion into the abdominal cavity is able to be evaluated.<sup>1,7,30</sup>



**FIG 5-14** Axial view through the fetal abdomen at 13 weeks of gestation, demonstrating an intact abdominal wall and normal fetal cord insertion.

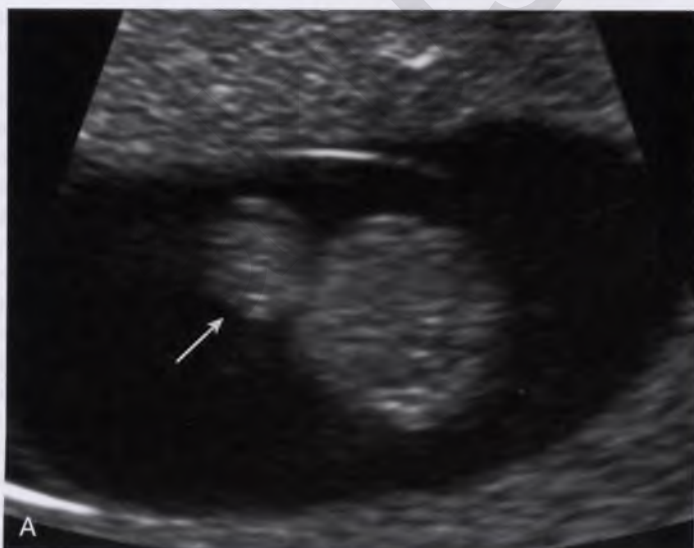


**FIG 5-15** Physiologic bowel herniation. **A**, At 11 weeks' gestation, bowel can be seen in the base of the umbilical cord (*arrow*). **B**, At 18 weeks' gestation, the ventral wall and umbilical cord insertion site are now normal.

### Gastrointestinal Tract

**Stomach.** As early as 8 weeks, the stomach can be visualized as a left-sided hypoechoic cavity in the upper abdomen.<sup>21,30</sup> By 11 to 14 weeks the stomach is visible in 99% of fetuses<sup>14</sup> (Fig. 5-16).

**Bowel.** After 12 weeks the entire bowel is intra-abdominal, with visualization more successful between 13 and 14 weeks compared to 11 to 12 weeks (88% vs. 77%,  $P = 0.02$ )<sup>13</sup> (Fig. 5-17).

### Genitourinary Tract

**Kidneys.** The fetal kidneys appear as hyperechoic structures with hypoechoic centers lateral to the spine. Using a combination of transvaginal and transabdominal sonography between 11 and 14 weeks, the visualization rate for the kidneys in the first trimester ranges from 80% to 95%.<sup>13,14</sup> Timor-Tritsch and associates demonstrated improved visualization rates for the kidneys later in the first trimester with 80%

visualization between 11 and 12 weeks compared to 91% visualization between 13 and 14 weeks ( $P = .02$ )<sup>13</sup> (Fig. 5-18).

**Bladder.** The normal first trimester fetal bladder is identified as a hypoechoic structure in the fetal pelvis visualized in 93% to 100% of fetuses between 11 and 14 weeks.<sup>13,14,31,32</sup> Using color Doppler, the umbilical arteries can be seen coursing from the umbilical cord insertion around the bladder in 84% of fetuses from 11 to 12 weeks<sup>13</sup> (Fig. 5-19). Normal measurements of the fetal kidney from 12 to 14 weeks have been published by Bronshtein and coworkers.<sup>32</sup>

**Genitalia.** Early accurate determination of fetal gender has been reported as early 11 weeks with an accuracy rate ranging from 46% to 70%.<sup>33,34</sup> The male and female genitalia are best distinguished in the first trimester by the direction of the genital tubercle (future phallus or clitoris) seen in the sagittal plane. The male genital tubercle points in the cephalad direction, whereas the female genital tubercle is directed caudally or on the horizontal. Subjective assessment of the first trimester gender has been described and quantified for accuracy using a combination of the sagittal view and the transverse view. In the transverse view identification of a round structure at the base of the genital tubercle representing the scrotal swelling, or a midline echo at the base of the genital tubercle, representing the median penile raphe, aid in identifying the male fetus. Two, or four, parallel lines, representing the labia minora and majora, help to identify the female fetus. When the subjective two-view assessment is used 67% of male fetuses are correctly identified at 11 weeks with improvement in identification of male fetuses at 12 weeks to 89% without further significant improvement beyond 12 weeks. This is in contrast to the female fetus in which correct gender identification occurs 83% of the time but does not improve until 14 weeks when it is correct 95% of the time.<sup>33</sup> Using an objective cutoff of 30 degrees from the horizontal for the direction of the genital tubercle in the sagittal view appears to have improved accuracy over the subjective two-view method, although there is no study directly comparing the two methods. Using a cutoff of 30 degrees, the gender is accurately determined in 70% of fetuses at 11 weeks, 99% at 12 weeks, and 100% at 13 weeks. Male fetuses are incorrectly assigned as female 56% of the time at 11 weeks, but only 3% of the time at 12 weeks, and 0% at 13 weeks. In contrast, female fetuses will be incorrectly assigned only 5% of the time at 11 weeks and 0% at 12 and 13 weeks.<sup>34</sup>



**FIG 5-16** Transverse image through fetal abdomen demonstrating normal fetal stomach (arrow) at 12 weeks' gestation and documentation of situs. LT, left thorax.



**FIG 5-17** Transverse view at the level of the umbilical cord insertion (U) demonstrating intact abdominal wall and intra-abdominal location of the bowel.

### Extremities

Using high-frequency transvaginal sonography, the upper and lower limb buds can be imaged from 7 weeks onward. At this early gestational



**FIG 5-18** Normal fetal kidneys at 13 weeks' gestation (arrows).



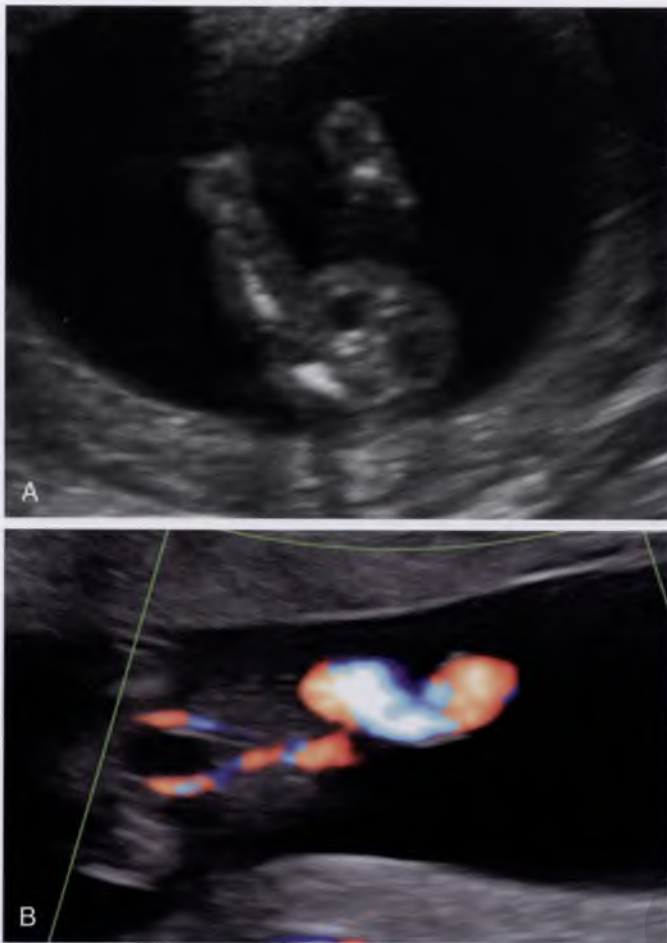


**FIG 5-19** Fetal bladder. **A**, Bladder is easily demonstrated with gray-scale imaging in this 12-week fetus. **B**, Color Doppler demonstrates umbilical arteries bifurcating around the fetal bladder.

age, the tail of the embryo is longer than the lower limb buds and will be prominent. By the 10th week, the full length of the limbs are able to be fully imaged.<sup>7</sup> Using a combination of high-frequency transvaginal and transabdominal sonography, full examination of the extremities including biometry of the short and long bones, the fingers, toes, and the movement and posture of the joints is possible in 100% of fetuses by 11 weeks<sup>14</sup> (Fig. 5-20).

## ABNORMAL ULTRASOUND FINDINGS IN THE FIRST TRIMESTER

### Head and Neck

#### Central Nervous System

CNS anomalies account for approximately 11% of abnormalities detected in the first trimester.<sup>35</sup>

**Neural Tube Defects.** Closure of the neural tube occurs early in embryogenesis, from 4 to 6 weeks' conceptional age. When there is disruption in this closure, the result is a neural tube defect (NTD). Open spina bifida (myelomeningocele) is a specific type of NTD that occurs when the caudal portion of the neural tube fails to close at 4 weeks. Myelomeningocele is distinct from anencephaly, which results when the cranial portion of the neural tube fails to close. Exencephaly is the finding that precedes anencephaly when the floating brain tissue is still present (Fig. 5-5D).



**FIG 5-20** Normal fetal hand demonstrating five normal digits.

**Anencephaly (Exencephaly).** Imaging of the cranial vault is reliable at 11 weeks, making the diagnosis of anencephaly possible at this early gestational age. In the first trimester, the cerebral hemispheres have not yet eroded away, but with absence of the cranium, in the sagittal view the “Mickey Mouse sign” has been shown to be 100% sensitive and specific for lethal anomalies associated with a missing cranium including anencephaly and acrania.<sup>36</sup>

**Myelomeningocele.** The diagnosis and management of myelomeningocele have evolved dramatically over the past century.<sup>37</sup> Lesion level has been closely correlated to short- and long-term outcomes, and advances in open fetal surgery available in select cases at specialty centers has made early diagnosis and characterization of the defect important for patient counseling.<sup>38-40</sup>

In addition to the visualization of an obvious myelomeningocele, which may be present as early as 9 weeks, there are several signs unique to the first trimester that have been described in association with open NTDs. Small biparietal diameter (BPD) in the first trimester has been associated with myelomeningocele, with nearly 50% of cases having a BPD below the 5th percentile between 11 and 14 weeks.<sup>41-43</sup> Bernard and associates demonstrated that the combination of first trimester BPD below the 5th percentile with maternal serum markers, maternal serum alpha-fetoprotein, and free  $\beta$ -hCG (human chorionic gonadotropin), improves the first trimester detection rate for myelomeningocele to 70% with a fixed false positive rate of 10%.<sup>42</sup>

Imaging of the posterior fossa can be helpful for ruling out and diagnosing NTDs in the first trimester. Intracranial translucency, which was first noted during nuchal translucency screening, is the normal fluid-filled area of the fourth ventricle seen in the midsagittal view (see Fig. 5-2). Chaoui and coworkers retrospectively evaluated 191 fetuses and found that myelomeningocele was successfully ruled out in 100% of fetuses with a normal intracranial translucency.<sup>44</sup> Larger prospective studies are still needed before widespread search for this sign can be proposed. In addition, using 3D sonography, cisterna magna width and measurements of the brainstem in comparison to the brainstem-occipital bone distance have been identified as potential first trimester screening signs for open spina bifida.<sup>45</sup>

Beyond the posterior fossa, an overall reduction in cerebrospinal fluid with corresponding reduction in the area of the cerebral ventricular system has also been associated with myelomeningocele.<sup>46</sup>



**Encephalocele.** Encephalocele is a herniation of neural tissue through a cranial defect, which can be located either in the occipital or, less commonly, frontal locations. Occipital encephaloceles are considered on the spectrum of NTDs. Several autosomal recessive conditions are associated with encephalocele, the most common of which is Meckel-Gruber syndrome. When high-frequency transvaginal sonography was used to screen women with a previous pregnancy complicated by Meckel-Gruber syndrome, encephalocele was able to be diagnosed as early as 11 weeks and as early as 12 weeks in low-risk populations undergoing first trimester anatomic screening.<sup>47-49</sup>

**Holoprosencephaly.** Incomplete cleavage of the forebrain results in holoprosencephaly, which can range from complete fusion (alobar), partial fusion with separation of the posterior cerebral hemispheres (semilobar), and partial fusion with separation of both the anterior and posterior cerebral hemispheres (lobar). Chervenak and coworkers described the diagnostic findings of holoprosencephaly to include absence of a midline echo with hypotelorism; however, the authors acknowledge that hypotelorism may be absent in cases with normal facial structure. Ventriculomegaly with either microcephaly or macrocephaly is also often present in cases of holoprosencephaly.<sup>50</sup> Beyond the CNS findings, there is a range of midface abnormalities that can result from incomplete facial development including cyclopia, proboscis, bilateral or unilateral cleft lip, single nostril or blind ended nose, flat nose, iris coloboma, single maxillary incisor, or simply absent philtrum.<sup>51</sup> Transverse views of the normal fetal head in the first trimester reveal the symmetric shape of a butterfly including clear demarcation of the midline. Systematic imaging of the choroid plexus from 11 to 14 weeks by Sepulveda and colleagues demonstrated absence of the butterfly sign in cases of holoprosencephaly.<sup>52</sup>

### Skeletal/Face

**Clefts.** Oral clefts are one of the most prevalent fetal anomalies, occurring at a rate of 1.05/1000 live births and fetal deaths with cleft lip alone occurring at a lower rate, 0.66/1000 in live births and fetal deaths combined. In the majority (73.8%) of cases of cleft lip with or without cleft palate the anomaly is isolated; however, when the palate is involved it is less likely to be an isolated anomaly (48.3%).<sup>53</sup> Using 2D sonography in the second trimester, the RADIUS (Routine Antenatal Diagnostic Imaging with Ultrasound) trial demonstrated relatively low detection rates for oral clefts (30%).<sup>54</sup> However, with the ability to systematically manipulate multiplanar images using 3D sonography, detection rates of 90% have been reported.<sup>55</sup> In the first trimester, using 2D sonography, Sepulveda and colleagues described the systematic examination of the natural triangle formed between the frontal processes of the maxilla and the palate, termed *retronasal triangle*, as a screening tool for oral clefting. The authors used 2D sonography to identify abnormalities of the alveolar ridge and nasal bone using the view of the retronasal triangle; these abnormalities were then further evaluated using manipulation of 3D datasets, which demonstrated accurate detection in 100% of primary palate clefts and 86% of secondary palate clefts, with a false positive rate of less than 1%.<sup>56,57</sup>

**Micrognathia.** Micrognathia is associated with many chromosomal and genetic syndromes. During their investigation of the retronasal angle, Sepulveda and colleagues recognized normal fetuses to have a gap between the mandibular bodies and have since published the finding of an absent mandibular gap as found in 100% of fetuses with micrognathia (77.8%) or severe retrognathia (22.2%).<sup>58</sup>

**Absent Nasal Bone.** The sagittal view allows imaging of the fetal nasal bone and the frontomaxillary angle, abnormalities of which have been associated with trisomy 21 (Fig. 5-8B). The likelihood ratio for trisomy 21 when the nasal bone is absent was reported to be 146 (95% confidence interval [CI] 50-434) by Cicero and colleagues. This group

also demonstrated a trisomy 21 detection rate of 90% with a false positive rate of 5% when first trimester examination of the nasal bone was incorporated into a screening strategy that included nuchal translucency, serum free  $\beta$ -hCG, and pregnancy-associated plasma protein A (PAPP-A).<sup>59,60</sup>

**Increased Frontomaxillary Angle.** The frontomaxillary angle can be measured in the sagittal view and when combined with maternal age, nuchal translucency, and serum free  $\beta$ -hCG and PAPP-A gives a detection rate for trisomy 21 of 94.3% with a false positive rate of 5%, which was increased over the detection rate of 89.5% when the frontomaxillary angle was not included.<sup>61</sup>

### Neck

Increased nuchal translucency has been well established as a risk factor for aneuploidy (see Chapter 3). Nuchal translucency screening alone identifies 75% to 80% of trisomy 21 fetuses with a false positive rate of 5%<sup>62</sup> and when combined with measurement of serum levels of free  $\beta$ -hCG and PAPP-A identifies 82% to 87% of trisomy 21 fetuses (fixed false positive rate of 5%) and 78% of non-trisomy 21 aneuploid fetuses (false positive rate of 6%).<sup>63,64</sup> One third of fetuses with a nuchal translucency greater than the 95th percentile will be aneuploid and the remaining two thirds will be euploid.<sup>65</sup> Among euploid fetuses with increased nuchal translucency, there is an increased risk of structural malformations, syndromes, and perinatal death<sup>65-67</sup> (Fig. 5-21B). Nicolaides and associates first described a nuchal translucency cutoff of 3.0 mm as a useful screening tool for aneuploidy screening.<sup>2</sup> Since that time, several cutoffs have been studied including 2.5 mm, 3.0 mm, 3.5 mm, 95th and 99th percentiles, and multiples of the median (MoM) of 2 or delta value 1.5.<sup>68,69</sup> In a large trial of 96,127 women across 22 centers in the United Kingdom, 95th percentile for nuchal translucency measurement was noted to change significantly with crown-rump length, but the 99th percentile remained relatively constant at 3.5 mm.<sup>19,67</sup> Although 92% of euploid fetuses with a nuchal translucency of less than 3.5 mm will result in a healthy infant, this number decreases to 20% for a nuchal translucency greater than 6.5 mm.<sup>65</sup> The prevalence of cardiac anomalies has been shown to increase exponentially with increasing nuchal translucency thickness (Table 5-2).<sup>67,70</sup> The American Institute of Ultrasound in Medicine recommends fetal echocardiogram when there is a first-degree relative with a congenital heart defect.<sup>71</sup> The baseline prevalence of congenital heart disease in the general population is approximately 8/1000 (0.8%),<sup>72</sup> and the risk of congenital heart disease among siblings increases from this baseline to

**TABLE 5-2 Prevalence of Major Cardiac Defects by Nuchal Translucency Thickness**

Nuchal Translucency Thickness	Prevalence of Major Cardiac Defect
<95th percentile	1.6/10,000*
95th percentile to 3.4 mm	10/1000†
3.5-4.4 mm	27/1000†
4.5-5.4 mm	43/1000†
5.5-6.4 mm	63/1000†
≥6.5 mm	169/1000†

\*From Souka AP, Von Kaisenberg CS, Hyett JA, et al: Increased nuchal translucency with normal karyotype. *Am J Obstet Gynecol* 192(4):1005-1021, 2005.

†From Souka AP, Snijders RJ, Novakov A, et al: Defects and syndromes in chromosomally normal fetuses with increased nuchal translucency thickness at 10-14 weeks of gestation. *Ultrasound Obstet Gynecol* 11(6):391-400, 1998.





**FIG 5-21** Omphalocele at 13 weeks' gestation on axial (A) and sagittal (B) views. This fetus also has an enlarged nuchal translucency.

approximately 30/1000 (3%).<sup>73</sup> Therefore, it is reasonable to use a nuchal translucency of greater than or equal to 3.5 mm, associated with a prevalence of 2.7% (see Table 5-1), as the cutoff for referral to specialized fetal echocardiogram.<sup>70,74,75</sup>

**Cystic Hygroma.** Cystic hygroma is a malformation of the lymphatic system that causes collection of edema at the fetal neck and may encompass the entire fetus (Fig. 5-22). Early cystic hygromas are associated with congenital syndromes and other malformations and should be distinguished from cystic hygromas developing later in pregnancy that are generally isolated lymphangiomas. Using data from the FASTER trial,<sup>63</sup> Malone and colleagues reported on the short- and long-term outcomes of a total of 134 septated cystic hygromas compared to the general population of 38,033 fetuses. The authors defined cystic hygroma as a septated hypoechoic area behind the fetal neck extending along the fetal back to make the distinction from simple increased nuchal translucency thickness. Chromosomal abnormalities were diagnosed in 51% (67/132) of cases (Table 5-3). Among the chromosomally normal cases, 33.8% were complicated by a major structural anomaly, with cardiac malformations being the most common (72.7%) followed by skeletal abnormalities (27.3%). The



**FIG 5-22** Cystic hygroma, with subcutaneous edema extending down the fetal back and surrounding the abdominal wall.

**TABLE 5-3 Chromosomal and Structural Abnormalities of 132 Cases of Septated Cystic Hygroma**

Outcome	N (%)
<b>Chromosomal Abnormality</b>	67/132
Trisomy 21	25/67 (37.3)
Monosomy X	19/67 (28.3)
Trisomy 18	13/67 (19.4)
Trisomy 13	6/67 (9.0)
Triploidy	3/67 (4.5)
Mosaic deletion of chromosome 9	1/67 (1.5)
<b>Structural Malformation</b>	22/65
Cardiac	16/22
Skeletal	6/22

Modified from Malone FD, Ball RH, Nyberg DA, et al: First-trimester septated cystic hygroma: prevalence, natural history, and pediatric outcome. *Obstet Gynecol* 106(2):288-294, 2005.

most common cardiac defect was a single ventricle, that is, hypoplastic left-sided or right-sided heart syndrome (25%). Termination of pregnancy was chosen by 60% of patients, and stillbirth occurred in an additional 15% (25% chromosomally normal). In all, there were 23 structurally and chromosomally normal liveborn infants followed for a mean of 25 months, 22 of whom remained developmentally normal and one who developed spastic diplegia for which no cause of cerebral palsy could be identified. In addition, the authors demonstrated a significant increase in the odds for aneuploidy (odds ratio [OR] 5.2, 95% CI 2.9-9.6), cardiac malformation (OR 12.4, 95% CI 3.2-56.3), and fetal or neonatal death (6.0, 95% CI 1.4-26.2) among cases of septated cystic hygroma compared to simple increased nuchal translucency thickness ( $\geq 3.0$  MoM).<sup>76</sup>

### Chest

Most of the literature regarding identification of chest abnormalities in the first trimester focuses on congenital heart disease; however, a general overview of the chest in the first trimester can identify other malformations.



### Extracardiac Masses/Congenital Diaphragmatic Hernia

First trimester detection of pulmonary sequestration, cystic adenomatoid malformation, and congenital diaphragmatic hernia has been reported.<sup>67,77,78</sup> Although these malformations may be detected in the first trimester, visualization will depend on size, and continued growth may aid detection in the second trimester. In a randomized trial of routine 12-week anatomic survey versus routine 18-week anatomic survey, Saltvedt and colleagues detected 0% of the three diaphragmatic hernias in the 12-week group but 50% of four diaphragmatic hernias in the 18-week group, but this difference was not statistically significant because of the overall low prevalence of congenital diaphragmatic hernia in the cohort (7/36,108).<sup>78</sup>

### Cardiac Disease

Congenital heart disease is one of the most common severe congenital abnormalities, with a prevalence of 8/1000 live births.<sup>22,72,79,80</sup> Over the past 2 decades, imaging of the fetal heart in the first trimester has evolved considerably to include full echocardiographic studies, with several authors reporting diagnosis of congenital heart disease in the first trimester<sup>22,30,79-81</sup> (Fig. 5-23). In a retrospective study of 2165 singleton pregnancies that underwent fetal echocardiogram from 1997 to 2003 Smrcek and colleagues reported the frequency of congenital heart malformations diagnosed between 11 and 13 weeks, with atrioventricular septal defects being the most frequent by about 4.5-fold (18/29), followed by ventricular septal defect (4/29), and tetralogy of Fallot (3/29).<sup>28</sup> Additionally, ectopia cordis, hypoplastic left-sided and right-sided heart syndrome, double outlet right ventricle, transposition of the great arteries, absence of the pulmonary valves, aortic stenosis, aortic coarctation, left and right atrial isomerism, pulmonary stenosis, truncus arteriosus, tricuspid atresia, and total anomalous pulmonary venous return have all been reported as either isolated findings or in combination as complex congenital heart disease.<sup>22,28,81-83</sup> The majority of studies evaluating first trimester fetal cardiac evaluation have included a selected population referred for specialized fetal echocardiogram in which the indication most commonly was increased nuchal translucency but may also include risk factors such as cardiac findings on a nonspecialized routine first trimester sonogram, multiple gestation, or family history. Detection rates for cardiac malformations in a high-risk population have been reported to range from 70% to 84.2%.<sup>81,83</sup> Orlandi and colleagues prospectively evaluated a systematic



**FIG 5-23** Atrioventricular canal defect detected at 10 weeks' gestation in a fetus with a cystic hygroma. Cell-free fetal DNA test is positive for trisomy 13. Patient opted for termination of pregnancy.

approach at first trimester fetal cardiac imaging, which did not include a full fetal echocardiogram but evaluated the four-chamber view and outflow tracts. The overall detection rate for cardiac abnormalities was 66%, 80% for major defects and 42% for minor defects with no false positive major congenital heart defects.<sup>84</sup>

Advances in technology have led to developments in 4D sonography with STIC, which allows the offline manipulation and evaluation of images.<sup>85</sup> First trimester use of 4D STIC for the detection of cardiac malformations has demonstrated detection rates in the range of 90% to 95% in high-risk populations attending specialty centers.<sup>86,87</sup> The benefit of 4D STIC over traditional 2D sonography for the detection of cardiac anomalies has not been demonstrated, as Bennasar and colleagues identified 2D modalities to be slightly better than STIC, with a detection rate of 98% with no false positive results.<sup>86</sup> Even so, the value in 4D STIC may go beyond detection rates and likely lies in the ability to manipulate and evaluate images offline, which could aid in efficiency by enabling cardiac evaluation via a small number of specialists trained in this modality.<sup>85</sup> However, the acquisition of high-quality images is technically difficult, which limits the application of this technology.<sup>87</sup> Therefore, the role of 4D STIC at this time continues to be in the investigational arena.

### Abdomen

Abnormalities of the fetal abdomen that are detectable by ultrasound can be divided into gastrointestinal malformations, which primarily include abdominal wall defects, and the genitourinary system abnormalities of the kidneys and bladder.

### Gastrointestinal Malformations

First trimester diagnosis of esophageal atresia and duodenal atresia have been described, but abdominal wall defects are more frequent and as such have received the most attention in the literature on first trimester anatomic evaluation.<sup>77,88-90</sup>

**Abdominal Wall Defects.** Omphalocele has been reported to affect 1.4 to 2.5/10,000 live births.<sup>91-94</sup> Compared to omphalocele, the prevalence of gastroschisis is greater at 4.4/10,000 live births and has increased in prevalence over time. There has been significant epidemiologic variation in the prevalence of gastroschisis over time. In a large U.S. study of over 14,000 cases of gastroschisis occurring across 15 states, the prevalence of gastroschisis rose from 2.32/10,000 in 1995 to 4.42/10,000 in 2005, with the majority of the increased prevalence occurring among mothers younger than 20 years of age (11.45/10,000).<sup>95</sup>

The midgut herniation resolves by 12 weeks' gestation; therefore, unless it is equal to or greater than the size of the abdomen, any midgut herniation should be considered physiologic prior to this time<sup>96</sup> (see Figs. 5-15 and 5-21). In theory, gastroschisis should be able to be distinguished from the physiologic herniation and omphalocele in the first trimester by its location lateral to the umbilicus (typically right-sided) (Fig. 5-24); however, image resolution or fetal position and movement may limit the ability to adequately characterize any bowel herniation prior to 12 weeks and requires confirmation after 12 weeks.

When gastroschisis or omphalocele is detected in the first trimester, the next step is ruling out additional anomalies. Although gastroschisis is typically an isolated anomaly, it can be associated with abnormalities of the brain (4.5%), heart (2.5%), limbs (2.2%), and kidneys (1.9%) and with chromosomal syndromes (1.2%) and non-chromosomal syndromes (0.7%).<sup>97</sup> In contrast to gastroschisis, omphaloceles are much more commonly associated with other major structural anomalies or chromosomal syndromes. In a study of 98 fetuses diagnosed with omphalocele prior to 14 weeks' gestation, 45.9% of fetuses had an additional major structural malformation and





**FIG 5-24** Fetal gastroschisis (arrows) at 12 weeks' gestation in sagittal (A), axial (B), and three-dimensional (3D) (C) images. The 3D image clearly demonstrates the typical defect with extruded bowel to the right of the umbilical cord insertion. (Courtesy of Barbora Mrazek-Pugh.)

53.8% of 80 fetuses karyotyped were affected by a chromosomal abnormality, most frequently trisomy 18 (72.1%). In addition, the authors reported on 33 fetuses with an apparently isolated omphalocele seen prior to 14 weeks that underwent an additional anatomic survey at 16 weeks, and 6 of these cases (18.2%) were found to have an additional malformation and 21 (63.6%) had an intact abdominal wall, stressing the importance of follow-up ultrasound assessment when omphalocele is suspected in the first trimester. Outcomes for fetuses with omphalocele are largely dependent on whether the abdominal wall defect is isolated or complicated by additional anomalies or aneuploidy. Tassin and colleagues reported the outcomes of isolated omphalocele diagnosed prior to 14 weeks.<sup>90</sup> Of 79 cases there

were 15 (19%) medically indicated terminations, 4 (5%) elective terminations, 6 (8%) stillbirths, and 54 (68%) live births. The authors investigated the omphalocele/transabdominal diameter ratio and suggest a ratio of greater than or equal to 0.8 for a threshold to discriminate increased neonatal morbidity. Although the sensitivity of this threshold in the study was shown to be 86.7%, the specificity remained low at 50% ( $P = .017$ ), and neither this measure nor this threshold has been externally validated to date.<sup>90</sup>

#### Genitourinary Abnormalities

The most commonly detected genitourinary abnormality seen on ultrasound images in the first trimester is megacystis; however,



hydronephrosis and cystic kidneys have also been reported. The detection of renal agenesis in the first trimester is technically difficult because of confusion with the adrenal glands.<sup>98</sup>

**Megacystis.** Megacystis is a sign of lower urinary tract obstruction (LUTO), which may have several causes. When megacystis is diagnosed in the first trimester, because the fetus is young and the obstructive cause may resolve or progress throughout the pregnancy, a spectrum of outcomes are possible, ranging from complete resolution without sequelae to dysplastic nonfunctioning kidneys with resulting anhydramnios, accompanying pulmonary disease, and death. In a retrospective investigation of pregnancies in the United Kingdom enrolled in a protocol to evaluate screening nuchal translucency in the general population from 10 to 14 weeks, megacystis was found in 0.06% of 24,492 fetuses screened.<sup>99,100</sup> Among the cases of megacystis the authors found the minimum longitudinal bladder diameter to be 8 mm with a minimum bladder/crown-rump length ratio of 13%. When a control group of 3000 normal fetuses were selected for comparison, the maximum bladder diameter was 6 mm and the median bladder/crown-rump length ratio was 5.4% (0-10.4%). Chromosomal abnormalities were found in 20% of the cases of megacystis, trisomy 21, trisomy 13, and a balanced translocation of chromosomes 14 and 20, and nuchal translucency was found to be greater than the 95th percentile in 40% of cases, the two trisomy cases, and four additional euploid cases. Spontaneous abortion occurred in one chromosomally normal fetus. Megacystis was found to resolve spontaneously by 20 weeks' gestation in 7 of the 11 chromosomally normal surviving cases (63%), of which 4 cases were found to have pyelectasis at 20 weeks persisting to the postnatal period in only 1 case. Of the remaining four chromosomally normal pregnancies repeat ultrasound examinations demonstrated progression, with two of the parents opting for termination, one after vesicocentesis indicated elevated urine calcium. Of the remaining two progressive cases, vesicoamniotic shunt was performed followed by spontaneous abortion within 1 week of the procedure in both cases.<sup>99</sup>

There has been some evidence showing that the cause of megacystis diagnosed in the first half of pregnancy may be more likely to be due to a functional obstruction from banding of the wolffian ducts as opposed to posterior urethral valves (the most common cause of LUTO diagnosed in the second half of pregnancy).<sup>101</sup> It has been hypothesized that sudden decompression with vesicocentesis may successfully relieve a functional obstruction of the urethra in these cases and should be the first line of therapy in progressing megacystis diagnosed in the first trimester; however, the evidence to support this theory is limited, and therefore, serial vesicocentesis for the resolution of megacystis remains investigative at this time. Additionally, urine biochemistry has been used to prognosticate which fetuses may benefit from vesicoamniotic shunting. However, current evidence suggests first trimester urine biochemistry does not correlate with prognosis which may, in part, be due to physiologic differences in first trimester fetal renal function and preclude the use of currently published urine biochemistry cutoff values in fetuses younger than 16 weeks. Further, vesicoamniotic shunts have been shown to be associated with a high rate of fetal loss when performed in the first trimester, and the benefit is questionable at this time.<sup>99,102-104</sup> The Prenatal Treatment of Lower Urinary Tract Obstruction (PLUTO) trial of LUTO, which was stopped early because of poor recruitment, did not show a significant benefit of vesicoamniotic shunting, but the trial was not focused on first trimester cases of LUTO.<sup>105</sup>

### Extremities

Skeletal anomalies detected in the first trimester can vary greatly, ranging from osteochondrodysplasias to minor abnormalities such as



**FIG 5-25** Right focal femoral (RT FEM) deficiency detected at 13 weeks' gestation. LT FEM, left femoral.

polydactyly. Grande and colleagues found that the most common skeletal abnormalities detected in the first trimester among low-risk women were osteochondrodysplasias followed by limb-reduction defects and arthrogryposis, with detection rates of 86%, 57%, and 50%, respectively (Fig. 5-25). The authors also reported detection of minor skeletal abnormalities such as clubfoot, syndactyly, and polydactyly but with a much lower overall detection rate of 9%.<sup>98</sup>

### LIMITATIONS OF FIRST TRIMESTER FETAL ANATOMIC SURVEY

Despite great progress in the ability to perform a comprehensive fetal anatomic survey in the first trimester, several limitations must be mentioned. First, at the present time, most sonographers and physicians have only limited experience with complete anatomic evaluation in the first trimester. Second, even in experienced hands, several abnormalities develop and change throughout pregnancy and may not be appreciated in the first trimester. Major examples include congenital diaphragmatic hernia, skeletal dysplasias, and congenital heart defects such as cardiomyopathy and abnormalities of single ventricle physiology (i.e., hypoplastic left-sided heart syndrome), which may evolve from stenotic valves that can be difficult to appreciate in the first trimester.<sup>106</sup>

Also, several limitations are specific to first trimester fetal echocardiography. High termination rates have been reported in pregnancies with cardiac abnormalities identified in the first trimester; therefore, follow-up and confirmation rates remain low, at 20%, which makes true detection rates difficult to determine.<sup>107</sup> Even with recent advances in technology, the resolution of 4D STIC imaging remains in the range of 50 to 100  $\mu\text{m}$ , and therefore, subtle differences that may be visible later in pregnancy, such as offset of the atrioventricular valves, may not be perceived in the first trimester. Additionally, Votino and colleagues demonstrated that 4D sonography is no better than 2D sonography for the detection of cardiac malformations in the first trimester.<sup>87</sup> The normal fetal heart is a developing organ that has demonstrable physiologic differences in the first trimester that could be falsely interpreted as normal or abnormal if we assume that baseline parameters for fetal cardiac structure and function developed in the second and third trimesters apply in the first trimester. For example, tricuspid regurgitation was present in the first trimester in 27% of fetuses that were later confirmed to have a normal heart.<sup>82</sup> Concerns regarding resource



utilization secondary to the time-intensive and technically challenging nature of fetal echocardiography have also been raised.<sup>108</sup> To counter this argument, Lombardi and colleagues demonstrated that with an initial investment of a 1-week intensive course, sonographers were able to reliably perform first trimester fetal echocardiogram in 10 minutes on average. However, the cost effectiveness of this strategy remains to be determined.<sup>25</sup>

## DETECTION RATES

The overall detection rate of first trimester fetal anatomic survey for structural abnormalities reported in the literature varies greatly, from 17% to 90%.<sup>109</sup> Aside from the technical limitations including education and skill development, much of this heterogeneity exists because of study selection criteria.

There is no doubt that sonography is a valuable tool to assess first trimester fetal anatomy, but with the preceding limitations in mind, the controversial question to address is whether first trimester anatomic survey should be applied as a screening tool offered to all pregnancies or reserved for a selected group of high-risk patients. To answer this question, the Swedish Nuchal Translucency (NUPP) trial randomized patients to one routine ultrasound examination either at 12 to 14 weeks or at 18 weeks. The authors found no statistically significant difference in overall detection rates for fetal anomalies among pregnancies with normal chromosomes in the first trimester compared to the second trimester (20% vs. 25%,  $P = 0.11$ ). These detection rates were noted to be low in contrast to the U.S. RADIUS trial (35%).<sup>54</sup> RADIUS randomized women to receive two ultrasound screening examinations at 18 to 20 weeks and at 31 to 33 weeks, which may account for the improved detection rates. The NUPP trial did demonstrate that detection rates for lethal or severe anomalies improved, but again, they did not differ between the first versus the second trimester groups (38% vs. 47%,  $P = 0.06$ ). Of note, lethal anomalies were detected at the initial 12- to 14-week ultrasound examination in 69% of fetuses in the early ultrasound examination group.<sup>78</sup> This study was not powered to find significant differences in detection rates of specific anomalies, but the group published an additional analysis of the NUPP trial to examine detection rates of major congenital heart malformations.<sup>80</sup> Overall, detection rates for cardiac abnormalities were low and did not differ between the 12- to 14-week group and the 18-week group (11% vs. 15%,  $P = 0.60$ ). Only a limited cardiac examination was performed in which the four-chamber view was the only obligatory view and evaluation of the outflow tracts was not required, which may account for the low detection rates compared to cardiac evaluation that includes the outflow tracts.<sup>84</sup> Referral for echocardiogram was made if the four-chamber view was difficult to interpret or abnormal, if the nuchal translucency was 3.5 mm or greater, or first trimester trisomy 21 risk was 1:250 or greater and the chromosomes were normal or karyotype was declined.

To date, two systematic reviews with diagnostic meta-analyses have been published which report similar pooled detection rates for first trimester ultrasound examination to detect anatomic abnormalities of about 50% (45.2% and 51%).<sup>109,110</sup> Rossi and Prefumo demonstrated varying detection rates depending on the location of the anomaly<sup>110</sup> (Table 5-4). The detection of cardiac abnormalities was higher in fetuses that underwent focused fetal echocardiogram compared to those that underwent anatomic survey alone (53% vs. 43%,  $P = 0.040$ ). In addition, the authors found that the use of Doppler did not seem to improve detection rates (52% vs. 44%,  $P = 0.11$ ). Heterogeneity due to population differences was also explored, and as expected, detection in a high-risk population was significantly better than detection in a low-risk population (65% vs. 50%,  $P < 0.001$ ).

**TABLE 5-4 First Trimester Detection Rate by Location of Fetal Anomaly**

Location of Anomaly	Detection Rate*
Neck	92%
Abdomen	88%
Brain and spine	51%
Heart	48%
Limbs	34%
Genitourinary system	34%
Face	34%

\*Modified from Rossi AC, Prefumo F: Accuracy of ultrasonography at 11-14 weeks of gestation for detection of fetal structural anomalies: a systematic review. *Obstet Gynecol* 122(6):1160-1167, 2013.

## COST EFFECTIVENESS

Overall, there is limited quality evidence on the cost effectiveness of ultrasound surveillance for the detection of fetal anomalies.<sup>111</sup> It should be kept in mind that a majority of studies evaluating first trimester fetal anatomy go on to offer additional ultrasound screening in the second trimester. In a prospective cross-sectional study of unselected women undergoing first trimester sonographic screening of fetal anatomy, Roberts and associates<sup>111</sup> estimated the cost of such screening in their unit in 1999 was £7470 (USD \$9268.22) per case for detecting fetal aneuploidy and £6258 (USD \$7764.46) per case for detecting structural abnormalities. In our experience these estimates are low; the cost of first trimester sonography in our perinatal laboratory in the midwestern United States in 2014 is \$170 compared to £33 (USD \$40.94) used by the authors to generate their cost estimates (based on 2014 exchange rates).

At this time, the current evidence does not support routine anatomic screening with ultrasound in the first trimester, and first trimester fetal anatomic evaluation should be reserved for a selected population of high-risk patients, such as those with a significant family or genetic history or prior child with a structural anomaly, poorly controlled diabetes, teratogen exposure, or increased nuchal translucency thickness. Additionally, there is evidence that second trimester anatomic evaluation is difficult in women with a body mass index higher than 40 kg/m<sup>2</sup>.<sup>112-114</sup> First trimester anatomic evaluation may be improved while the uterus remains low in the pelvis, which facilitates abdominal imaging below the pannus and may be additionally aided with the use of transvaginal imaging.

## SAFETY

Ultrasound is generally considered to be safe in pregnancy, but as a source of energy, it does have the potential for biological harm.<sup>115</sup> Unfortunately, human data on the safety of ultrasound are limited. In a World Health Organization (WHO) systematic review on the safety of ultrasound, the authors reviewed clinical trials, case control studies, and cohort studies reporting any long-term or short-term effects of ultrasound exposure.<sup>116</sup> Of over 6000 citations identified, 61 studies were reviewed, and not a single study included evaluation of ultrasound safety as a specific objective.<sup>116</sup> In general, the thermal index should be kept below 1, and the ALARA principle should be respected, reserving ultrasound use to clinically indicated situations, for the shortest duration with the lowest amount of acoustic energy to achieve an accurate diagnosis.<sup>29</sup> The thermal index is the amount of energy required to raise tissue temperature by 1° C, and the American Institute of Ultrasound in Medicine recommends the use of a thermal index for



soft tissue (TIS) prior to 8 weeks and a thermal index for bone (TIB) at 8 weeks or greater when bone ossification is identified.<sup>117</sup> The first trimester fetus is particularly vulnerable to teratogenicity, and the use of color Doppler ultrasound increases the acoustic energy exposure such that safe levels can easily be exceeded if one is not cautious. Therefore, when fetal anatomic survey is performed in the first trimester it is particularly important to be mindful of ultrasound safety and respect the ALARA principle.

## CONCLUSIONS

As ultrasound technology has continued to advance, our ability to reliably assess the fetal anatomy in the first trimester has come to parallel that of the second trimester in experienced hands. Complete, detailed, fetal anatomic assessment including fetal echocardiography is possible in the first trimester, but at the current time, controversy exists surrounding the application of this tool. Although routine first trimester anatomic screening has not been shown to improve detection rates compared to second trimester anatomic screening, the cost effectiveness of such a screening strategy also remains unproved.<sup>78</sup>

## REFERENCES

- Timor-Tritsch IE, Farine D, Rosen MG: A close look at early embryonic development with the high-frequency transvaginal transducer. *Am J Obstet Gynecol* 159(3):676–681, 1988.
- Nicolaides KH, Azar G, Byrne D, et al: Fetal nuchal translucency: ultrasound screening for chromosomal defects in first trimester of pregnancy. *BMJ* 304(6831):867–869, 1992.
- Moore KL, Persaud TVN, Torchia MG: *The Developing Human: Clinically Oriented Embryology*, ed 9, Philadelphia, 2013, Saunders/Elsevier.
- Palis J, Segel GB: Developmental biology of erythropoiesis. *Blood Rev* 12(2):106–114, 1998.
- Blaas HG, Eik-Nes SH: Sonoembryology and early prenatal diagnosis of neural anomalies. *Prenat Diagn* 29(4):312–325, 2009.
- Larsen WJ: *Human Embryology*, ed 3, New York, 2002, Churchill Livingstone.
- Timor-Tritsch IE, Peisner DB, Raju S: Sonoembryology: an organ-oriented approach using a high-frequency vaginal probe. *J Clin Ultrasound* 18(4):286–298, 1990.
- Crelin ES: Development of the nervous system. A logical approach to neuroanatomy. *Clin Symp* 26(2):1–32, 1974.
- Lachmann R, Sodre D, Barmpas M, et al: Midbrain and falx in fetuses with absent corpus callosum at 11–13 weeks. *Fetal Diagn Ther* 33(1):41–46, 2013.
- Blaas HG, Eik-Nes SH, Kiserud T, Hellevik LR: Early development of the hindbrain: a longitudinal ultrasound study from 7 to 12 weeks of gestation. *Ultrasound Obstet Gynecol* 5(3):151–160, 1995.
- Blaas HG, Eik-Nes SH, Kiserud T, Hellevik LR: Early development of the forebrain and midbrain: a longitudinal ultrasound study from 7 to 12 weeks of gestation. *Ultrasound Obstet Gynecol* 4(3):183–192, 1994.
- Falco P, Gabrielli S, Visentin A, et al: Transabdominal sonography of the cavum septum pellucidum in normal fetuses in the second and third trimesters of pregnancy. *Ultrasound Obstet Gynecol* 16(6):549–553, 2000.
- Timor-Tritsch IE, Bashiri A, Monteagudo A, Arslan AA: Qualified and trained sonographers in the US can perform early fetal anatomy scans between 11 and 14 weeks. *Am J Obstet Gynecol* 191(4):1247–1252, 2004.
- Souka AP, Pilalis A, Kavalakis Y, et al: Assessment of fetal anatomy at the 11–14-week ultrasound examination. *Ultrasound Obstet Gynecol* 24(7):730–734, 2004.
- Borenstein M, Persico N, Kaihura C, et al: Frontomaxillary facial angle in chromosomally normal fetuses at 11 + 0 to 13 + 6 weeks. *Ultrasound Obstet Gynecol* 30(5):737–741, 2007.
- Merz E, Abramovic J, Baba K, et al: 3D imaging of the fetal face—recommendations from the International 3D Focus Group. *Ultraschall Med* 33(2):175–182, 2012.
- Taipale P, Hiilesmaa V, Salonen R, Ylostalo P: Increased nuchal translucency as a marker for fetal chromosomal defects. *N Engl J Med* 337(23):1654–1658, 1997.
- Braithwaite JM, Morris RW, Economides DL: Nuchal translucency measurements: frequency distribution and changes with gestation in a general population. *Br J Obstet Gynaecol* 103(12):1201–1204, 1996.
- Snijders RJ, Noble P, Sebire N, et al: UK multicentre project on assessment of risk of trisomy 21 by maternal age and fetal nuchal-translucency thickness at 10–14 weeks of gestation. Fetal Medicine Foundation First Trimester Screening Group. *Lancet* 352(9125):343–346, 1998.
- Leiva MC, Tolosa JE, Binotto CN, et al: Fetal cardiac development and hemodynamics in the first trimester. *Ultrasound Obstet Gynecol* 14(3):169–174, 1999.
- Blaas HG, Eik-Nes SH, Kiserud T, Hellevik LR: Early development of the abdominal wall, stomach and heart from 7 to 12 weeks of gestation: a longitudinal ultrasound study. *Ultrasound Obstet Gynecol* 6(4):240–249, 1995.
- Haak MC, Twisk JW, Van Vugt JM: How successful is fetal echocardiographic examination in the first trimester of pregnancy? *Ultrasound Obstet Gynecol* 20(1):9–13, 2002.
- Dolkart LA, Reimers FT: Transvaginal fetal echocardiography in early pregnancy: normative data. *Am J Obstet Gynecol* 165(3):688–691, 1991.
- Gembruch U, Shi C, Smrcek JM: Biometry of the fetal heart between 10 and 17 weeks of gestation. *Fetal Diagn Ther* 15(1):20–31, 2000.
- Lombardi CM, Bellotti M, Fesslova V, Cappellini A: Fetal echocardiography at the time of the nuchal translucency scan. *Ultrasound Obstet Gynecol* 29(3):249–257, 2007.
- McBrien A, Howley L, Yamamoto Y, et al: Changes in fetal cardiac axis between 8 and 15 weeks' gestation. *Ultrasound Obstet Gynecol* 42(6):653–658, 2013.
- Gindes L, Matsui H, Achiron R, et al: Comparison of ex-vivo high-resolution episcopic microscopy with in-vivo four-dimensional high-resolution transvaginal sonography of the first-trimester fetal heart. *Ultrasound Obstet Gynecol* 39(2):196–202, 2012.
- Smrcek JM, Berg C, Geipel A, et al: Early fetal echocardiography: heart biometry and visualization of cardiac structures between 10 and 15 weeks' gestation. *J Ultrasound Med* 25(2):173–182, quiz 183–175, 2006.
- Reddy UM, Abuhamad AZ, Levine D, Saade GR: Fetal imaging: executive summary of a joint Eunice Kennedy Shriver National Institute of Child Health and Human Development, Society for Maternal-Fetal Medicine, American Institute of Ultrasound in Medicine, American College of Obstetricians and Gynecologists, American College of Radiology, Society for Pediatric Radiology, and Society of Radiologists in Ultrasound Fetal Imaging Workshop. *Obstet Gynecol* 123(5):1070–1082, 2014.
- Bronshtein M, Yoffe N, Zimmer EZ: Transvaginal sonography at 5 to 14 weeks' gestation: fetal stomach, abnormal cord insertion, and yolk sac. *Am J Perinatol* 9(5–6):344–347, 1992.
- Bronshtein M, Rottem S, Yoffe N, et al: Early determination of fetal sex using transvaginal sonography: technique and pitfalls. *J Clin Ultrasound* 18(4):302–306, 1990.
- Bronshtein M, Kushnir O, Ben-Rafael Z, et al: Transvaginal sonographic measurement of fetal kidneys in the first trimester of pregnancy. *J Clin Ultrasound* 18(4):299–301, 1990.
- Whitlow BJ, Lazanakis MS, Economides DL: The sonographic identification of fetal gender from 11 to 14 weeks of gestation. *Ultrasound Obstet Gynecol* 13(5):301–304, 1999.
- Efrat Z, Akinfenwa OO, Nicolaides KH: First-trimester determination of fetal gender by ultrasound. *Ultrasound Obstet Gynecol* 13(5):305–307, 1999.
- Chen M, Lee CP, Lam YH, et al: Comparison of nuchal and detailed morphology ultrasound examinations in early pregnancy for fetal structural abnormality screening: a randomized controlled trial. *Ultrasound Obstet Gynecol* 31(2):136–146, discussion 146, 2008.
- Chatzipapas IK, Whitlow BJ, Economides DL: The “Mickey Mouse” sign and the diagnosis of anencephaly in early pregnancy. *Ultrasound Obstet Gynecol* 13(3):196–199, 1999.



37. Trudell AS, Odibo AO: Diagnosis of spina bifida on ultrasound: always termination? *Best Pract Res Clin Obstet Gynaecol* 28(3):367–377, 2014.
38. Cochrane DD, Wilson RD, Steinbok P, et al: Prenatal spinal evaluation and functional outcome of patients born with myelomeningocele: information for improved prenatal counselling and outcome prediction. *Fetal Diagn Ther* 11(3):159–168, 1996.
39. Adzick NS, Thom EA, Spong CY, et al: A randomized trial of prenatal versus postnatal repair of myelomeningocele. *N Engl J Med* 364(11):993–1004, 2011.
40. American College of Obstetricians and Gynecologists: ACOG Committee Opinion No. 550: maternal-fetal surgery for myelomeningocele. *Obstet Gynecol* 121(1):218–219, 2013.
41. Karl K, Benoit B, Entezami M, et al: Small biparietal diameter in fetuses with spina bifida on 11-13-week and mid-gestation ultrasound. *Ultrasound Obstet Gynecol* 40(2):140–144, 2012.
42. Bernard JP, Cuckle HS, Stirnemann JJ, et al: Screening for fetal spina bifida by ultrasound examination in the first trimester of pregnancy using fetal biparietal diameter. *Am J Obstet Gynecol* 207(4):306.e1–306.e5, 2012.
43. Khalil A, Coates A, Papageorghiou A, et al: Biparietal diameter at 11-13 weeks' gestation in fetuses with open spina bifida. *Ultrasound Obstet Gynecol* 42(4):409–415, 2013.
44. Chaoui R, Benoit B, Mitkowska-Wozniak H, et al: Assessment of intracranial translucency (IT) in the detection of spina bifida at the 11-13-week scan. *Ultrasound Obstet Gynecol* 34(3):249–252, 2009.
45. Scheier M, Lachmann R, Petros M, Nicolaidis KH: Three-dimensional sonography of the posterior fossa in fetuses with open spina bifida at 11-13 weeks' gestation. *Ultrasound Obstet Gynecol* 38(6):625–629, 2011.
46. Loureiro T, Ushakov F, Montenegro N, et al: Cerebral ventricular system in fetuses with open spina bifida at 11-13 weeks' gestation. *Ultrasound Obstet Gynecol* 39(6):620–624, 2012.
47. Sepulveda W, Sebire NJ, Souka A, et al: Diagnosis of the Meckel-Gruber syndrome at eleven to fourteen weeks' gestation. *Am J Obstet Gynecol* 176(2):316–319, 1997.
48. Eckmann-Scholz C, Jonat W, Zerres K, Ortiz-Bruchle N: Earliest ultrasound findings and description of splicing mutations in Meckel-Gruber syndrome. *Arch Gynecol Obstet* 286(4):917–921, 2012.
49. Jones D, Fiozzo F, Waters B, et al: First trimester diagnosis of Meckel-Gruber syndrome by fetal ultrasound, with molecular identification of CC2D2A mutations by next-generation sequencing. *Ultrasound Obstet Gynecol* 44(6):719–721, 2014.
50. Chervenak FA, Isaacson G, Hobbins JC, et al: Diagnosis and management of fetal holoprosencephaly. *Obstet Gynecol* 66(3):322–326, 1985.
51. Peebles DM: Holoprosencephaly. *Prenat Diagn* 18(5):477–480, 1998.
52. Sepulveda W, Dezerega V, Be C: First-trimester sonographic diagnosis of holoprosencephaly: value of the "butterfly" sign. *J Ultrasound Med* 23(6):761–765, quiz 766–767, 2004.
53. Croen LA, Shaw GM, Wasserman CR, Tolarova MM: Racial and ethnic variations in the prevalence of orofacial clefts in California, 1983-1992. *Am J Med Genet* 79(1):42–47, 1998.
54. Crane JP, LeFevre ML, Winborn RC, et al: A randomized trial of prenatal ultrasonographic screening: impact on the detection, management, and outcome of anomalous fetuses. The RADIUS Study Group. *Am J Obstet Gynecol* 171(2):392–399, 1994.
55. Chmait R, Pretorius D, Jones M, et al: Prenatal evaluation of facial clefts with two-dimensional and adjunctive three-dimensional ultrasonography: a prospective trial. *Am J Obstet Gynecol* 187(4):946–949, 2002.
56. Sepulveda W, Wong AE, Martinez-Ten P, Perez-Pedregosa J: Retronasal triangle: a sonographic landmark for the screening of cleft palate in the first trimester. *Ultrasound Obstet Gynecol* 35(1):7–13, 2010.
57. Martinez-Ten P, Adiego B, Illescas T, et al: First-trimester diagnosis of cleft lip and palate using three-dimensional ultrasound. *Ultrasound Obstet Gynecol* 40(1):40–46, 2012.
58. Sepulveda W, Wong AE, Vinals F, et al: Absent mandibular gap in the retronasal triangle view: a clue to the diagnosis of micrognathia in the first trimester. *Ultrasound Obstet Gynecol* 39(2):152–156, 2012.
59. Cicero S, Curcio P, Papageorghiou A, et al: Absence of nasal bone in fetuses with trisomy 21 at 11-14 weeks of gestation: an observational study. *Lancet* 358(9294):1665–1667, 2001.
60. Cicero S, Avgidou K, Rembouskos G, et al: Nasal bone in first-trimester screening for trisomy 21. *Am J Obstet Gynecol* 195(1):109–114, 2006.
61. Borenstein M, Persico N, Kagan KO, et al: Frontomaxillary facial angle in screening for trisomy 21 at 11 + 0 to 13 + 6 weeks. *Ultrasound Obstet Gynecol* 32(1):5–11, 2008.
62. Nicolaidis KH: Nuchal translucency and other first-trimester sonographic markers of chromosomal abnormalities. *Am J Obstet Gynecol* 191(1):45–67, 2004.
63. Malone FD, Canick JA, Ball RH, et al: First-trimester or second-trimester screening, or both, for Down's syndrome. *N Engl J Med* 353(19):2001–2011, 2005.
64. Breathnach FM, Malone FD, Lambert-Messerlian G, et al: First- and second-trimester screening: detection of aneuploidies other than Down syndrome. *Obstet Gynecol* 110(3):651–657, 2007.
65. Bilardo CM, Muller MA, Pajkrt E, et al: Increased nuchal translucency thickness and normal karyotype: time for parental reassurance. *Ultrasound Obstet Gynecol* 30(1):11–18, 2007.
66. Souka AP, Snijders RJ, Novakov A, et al: Defects and syndromes in chromosomally normal fetuses with increased nuchal translucency thickness at 10-14 weeks of gestation. *Ultrasound Obstet Gynecol* 11(6):391–400, 1998.
67. Souka AP, Krampfl E, Bakalis S, et al: Outcome of pregnancy in chromosomally normal fetuses with increased nuchal translucency in the first trimester. *Ultrasound Obstet Gynecol* 18(1):9–17, 2001.
68. Makrydimas G, Sotiriadis A, Ioannidis JP: Screening performance of first-trimester nuchal translucency for major cardiac defects: a meta-analysis. *Am J Obstet Gynecol* 189(5):1330–1335, 2003.
69. Maymon R, Tercanli S, Dreazen E, et al: Comparison of pregnancy outcome of euploid fetuses with increased nuchal translucency (NT) expressed in NT MoM or delta-NT. *Ultrasound Obstet Gynecol* 23(5):477–481, 2004.
70. Souka AP, Von Kaisenberg CS, Hyett JA, et al: Increased nuchal translucency with normal karyotype. *Am J Obstet Gynecol* 192(4):1005–1021, 2005.
71. American Institute of Ultrasound in Medicine: *AIUM Practice Guideline for the Performance of Fetal Echocardiography*. Laurel, MD, 2013, American Institute of Ultrasound in Medicine. Available at: <<http://www.aium.org/resources/guidelines/fetalecho.pdf>>.
72. Reller MD, Strickland MJ, Riehle-Colarusso T, et al: Prevalence of congenital heart defects in metropolitan Atlanta, 1998-2005. *J Pediatr* 153(6):807–813, 2008.
73. Oyen N, Poulsen G, Boyd HA, et al: Recurrence of congenital heart defects in families. *Circulation* 120(4):295–301, 2009.
74. Alfirevic Z: DISQ 8: management of patients with an increased first-trimester Down syndrome screening risk and normal fetal karyotype. *Ultrasound Obstet Gynecol* 31(2):232, 2008.
75. Bilardo CM, Timmerman E, Pajkrt E, van Maarle M: Increased nuchal translucency in euploid fetuses—what should we be telling the parents? *Prenat Diagn* 30(2):93–102, 2010.
76. Malone FD, Ball RH, Nyberg DA, et al: First-trimester septated cystic hygroma: prevalence, natural history, and pediatric outcome. *Obstet Gynecol* 106(2):288–294, 2005.
77. Syngelaki A, Chelemen T, Dagklis T, et al: Challenges in the diagnosis of fetal non-chromosomal abnormalities at 11-13 weeks. *Prenat Diagn* 31(1):90–102, 2011.
78. Saltvedt S, Almstrom H, Kublickas M, et al: Detection of malformations in chromosomally normal fetuses by routine ultrasound at 12 or 18 weeks of gestation: a randomised controlled trial in 39,572 pregnancies. *Br J Obstet Gynaecol* 113(6):664–674, 2006.
79. Hyett J, Moscoso G, Papapanagiotou G, et al: Abnormalities of the heart and great arteries in chromosomally normal fetuses with increased nuchal translucency thickness at 11-13 weeks of gestation. *Ultrasound Obstet Gynecol* 7(4):245–250, 1996.
80. Westin M, Saltvedt S, Bergman G, et al: Routine ultrasound examination at 12 or 18 gestational weeks for prenatal detection of major congenital



- heart malformations? A randomised controlled trial comprising 36,299 fetuses. *Br J Obstet Gynaecol* 113(6):675–682, 2006.
81. McAuliffe FM, Trines J, Nield LE, et al: Early fetal echocardiography—a reliable prenatal diagnosis tool. *Am J Obstet Gynecol* 193(3 Pt 2):1253–1259, 2005.
  82. Huggon IC, Ghi T, Cook AC, et al: Fetal cardiac abnormalities identified prior to 14 weeks' gestation. *Ultrasound Obstet Gynecol* 20(1):22–29, 2002.
  83. Becker R, Wegner RD: Detailed screening for fetal anomalies and cardiac defects at the 11-13-week scan. *Ultrasound Obstet Gynecol* 27(6):613–618, 2006.
  84. Orlandi E, Rossi C, Perino A, et al: Simplified first-trimester fetal cardiac screening (four chamber view and ventricular outflow tracts) in a low-risk population. *Prenat Diagn* 34(6):558–563, 2014.
  85. Vinals F, Poblete P, Giuliano A: Spatio-temporal image correlation (STIC): a new tool for the prenatal screening of congenital heart defects. *Ultrasound Obstet Gynecol* 22(4):388–394, 2003.
  86. Bennasar M, Martinez JM, Olivella A, et al: Feasibility and accuracy of fetal echocardiography using four-dimensional spatiotemporal image correlation technology before 16 weeks' gestation. *Ultrasound Obstet Gynecol* 33(6):645–651, 2009.
  87. Votino C, Cos T, Abu-Rustum R, et al: Use of spatiotemporal image correlation at 11-14 weeks' gestation. *Ultrasound Obstet Gynecol* 42(6):669–678, 2013.
  88. Ebrashy A, El Kateb A, Momtaz M, et al: 13-14-week fetal anatomy scan: a 5-year prospective study. *Ultrasound Obstet Gynecol* 35(3):292–296, 2010.
  89. Souka AP, Pilalis A, Kavalakis I, et al: Screening for major structural abnormalities at the 11- to 14-week ultrasound scan. *Am J Obstet Gynecol* 194(2):393–396, 2006.
  90. Tassin M, Descriaud C, Elie C, et al: Omphalocele in the first trimester: prediction of perinatal outcome. *Prenat Diagn* 33(5):497–501, 2013.
  91. Baird PA, MacDonald EC: An epidemiologic study of congenital malformations of the anterior abdominal wall in more than half a million consecutive live births. *Am J Hum Genet* 33(3):470–478, 1981.
  92. Lindham S: Omphalocele and gastroschisis in Sweden 1965-1976. *Acta Paediatr Scand* 70(1):55–60, 1981.
  93. Rankin J, Dillon E, Wright C: Congenital anterior abdominal wall defects in the north of England, 1986-1996: occurrence and outcome. *Prenat Diagn* 19(7):662–668, 1999.
  94. Stoll C, Alembik Y, Dott B, Roth MP: Risk factors in congenital abdominal wall defects (omphalocele and gastroschisis): a study in a series of 265,858 consecutive births. *Ann Genet* 44(4):201–208, 2001.
  95. Kirby RS, Marshall J, Tanner JP, et al: Prevalence and correlates of gastroschisis in 15 states, 1995 to 2005. *Obstet Gynecol* 122(2 Pt 1): 275–281, 2013.
  96. van Zalen-Sprock RM, Vugt JM, van Geijn HP: First-trimester sonography of physiological midgut herniation and early diagnosis of omphalocele. *Prenat Diagn* 17(6):511–518, 1997.
  97. Mastroiacovo P, Lisi A, Castilla EE, et al: Gastroschisis and associated defects: an international study. *Am J Med Genet A* 143(7):660–671, 2007.
  98. Grande M, Arigita M, Borobio V, et al: First-trimester detection of structural abnormalities and the role of aneuploidy markers. *Ultrasound Obstet Gynecol* 39(2):157–163, 2012.
  99. Sebire NJ, Von Kaisenberg C, Rubio C, et al: Fetal megacystis at 10-14 weeks of gestation. *Ultrasound Obstet Gynecol* 8(6):387–390, 1996.
  100. Pandya PP, Snijders RJ, Johnson SP, et al: Screening for fetal trisomies by maternal age and fetal nuchal translucency thickness at 10 to 14 weeks of gestation. *Br J Obstet Gynaecol* 102(12):957–962, 1995.
  101. Jouannic JM, Hyett JA, Pandya PP, et al: Perinatal outcome in fetuses with megacystis in the first half of pregnancy. *Prenat Diagn* 23(4):340–344, 2003.
  102. Wisser J, Kurmanavicius J, Lauper U, et al: Successful treatment of fetal megavesica in the first half of pregnancy. *Am J Obstet Gynecol* 177(3): 685–689, 1997.
  103. Evans MI, Sacks AJ, Johnson MP, et al: Sequential invasive assessment of fetal renal function and the intrauterine treatment of fetal obstructive uropathies. *Obstet Gynecol* 77(4):545–550, 1991.
  104. Carroll SG, Soothill PW, Tizard J, Kyle PM: Vesicocentesis at 10-14 weeks of gestation for treatment of fetal megacystis. *Ultrasound Obstet Gynecol* 18(4):366–370, 2001.
  105. Morris RK, Malin GL, Quinlan-Jones E, et al: Percutaneous vesicoamniotic shunting versus conservative management for fetal lower urinary tract obstruction (PLUTO): a randomised trial. *Lancet* 382(9903):1496–1506, 2013.
  106. Timor-Tritsch IE, Fuchs KM, Monteagudo A, D'Alton ME: Performing a fetal anatomy scan at the time of first-trimester screening. *Obstet Gynecol* 113(2 Pt 1):402–407, 2009.
  107. Persico N, Moratalla J, Lombardi CM, et al: Fetal echocardiography at 11-13 weeks by transabdominal high-frequency ultrasound. *Ultrasound Obstet Gynecol* 37(3):296–301, 2011.
  108. Rustico MA, Benettoni A, D'Ottavio G, et al: Early screening for fetal cardiac anomalies by transvaginal echocardiography in an unselected population: the role of operator experience. *Ultrasound Obstet Gynecol* 16(7):614–619, 2000.
  109. Farraposo S, Montenegro N, Matias A: Evaluation of the role of first-trimester obstetric ultrasound in the detection of major anomalies: a systematic review. *J Perinat Med* 42(2):141–149, 2014.
  110. Rossi AC, Prefumo F: Accuracy of ultrasonography at 11-14 weeks of gestation for detection of fetal structural anomalies: a systematic review. *Obstet Gynecol* 122(6):1160–1167, 2013.
  111. Roberts T, Henderson J, Mugford M, et al: Antenatal ultrasound screening for fetal abnormalities: a systematic review of studies of cost and cost effectiveness. *Br J Obstet Gynaecol* 109(1):44–56, 2002.
  112. Aagaard-Tillery KM, Flint Porter T, Malone FD, et al: Influence of maternal BMI on genetic sonography in the FaSTER trial. *Prenat Diagn* 30(1):14–22, 2010.
  113. Hendler I, Blackwell SC, Bujold E, et al: The impact of maternal obesity on midtrimester sonographic visualization of fetal cardiac and craniospinal structures. *Int J Obes Relat Metab Disord* 28(12):1607–1611, 2004.
  114. Dashe JS, McIntire DD, Twickler DM: Maternal obesity limits the ultrasound evaluation of fetal anatomy. *J Ultrasound Med* 28(8):1025–1030, 2009.
  115. American College of Obstetricians and Gynecologists: ACOG Practice Bulletin No. 101: ultrasonography in pregnancy. *Obstet Gynecol* 113(2 Pt 1):451–461, 2009.
  116. Torloni MR, Vedmedovska N, Merialdi M, et al: Safety of ultrasonography in pregnancy: WHO systematic review of the literature and meta-analysis. *Ultrasound Obstet Gynecol* 33(5):599–608, 2009.
  117. American Institute of Ultrasound in Medicine: AIUM practice guideline for the performance of obstetric ultrasound examinations. *J Ultrasound Med* 32(6):1083–1101, 2013.



# Fetal Biometry and Growth

Carol B. Benson, Peter M. Doubilet

## SUMMARY OF KEY POINTS

- In the first trimester, gestational age should be assigned to the pregnancy based on sonographic findings or mean sac diameter prior to the visualization of the embryo and by embryonic or fetal crown-rump length (CRL) thereafter.
- In the second trimester, gestational age should be assigned based on head measurements that take into account head shape—namely, the corrected biparietal diameter or head circumference (HC)—or a composite age formula.
- By the latter part of the third trimester, neither dating by ultrasound nor dating by last menstrual period (LMP) is very accurate.
- Once gestational age has been assigned by an accurate method, such as sonography, the pregnancy should not be redated nor should the estimated due date be changed, because the earlier the gestational age is determined, the more accurate the dating of the pregnancy.
- Estimating fetal growth is best performed through estimating fetal weight and weight percentile, starting in the latter part of the second trimester and during the third trimester.
- The diagnosis of fetal growth restriction (FGR) should be suspected if the estimated weight falls below the 10th percentile for gestational age.
- The diagnosis of fetal macrosomia is suspected when the estimated fetal weight (EFW) is greater than 4000 g in a diabetic patient and above 4500 g in a nondiabetic patient.
- The diagnosis of a large for gestational age fetus is suspected when the EFW is above the 90th percentile for gestational age.
- In addition to its role in assessing gestational age and monitoring growth, fetal biometry is also important for identifying fetal abnormalities that are characterized by abnormal size of specific body parts, such as long bones with skeletal dysplasias.

## OUTLINE

Assignment of Gestational Age, 119

First Trimester Dating, 119

Second and Third Trimester Dating, 119

Measurements, 119

Assigning Gestational Age in the Second and Third Trimesters, 121

Fetal Weight Estimation and Weight Percentiles, 123

Abnormal Fetal Growth, 126

Fetal Growth Restriction and Small for Gestational Age Fetuses, 126

Macrosomic and Large for Gestational Age Fetuses, 127

Fetal Anomalies Associated With Abnormal Biometry, 127

Conclusion, 128

Sonographic measurements of fetal structures provide an accurate means of determining the age of a pregnancy, estimating fetal weight, and assessing the normality of a number of fetal body parts. This chapter will discuss various fetal measurements and how they are used to date pregnancy, monitor fetal growth, diagnose fetal growth disturbances, and diagnose fetal abnormalities that are characterized by abnormal size of specific fetal structures.

*Gestational age* is the term most commonly used for specifying the age of a pregnancy. Prior to the advent of sonography, gestational age referred to the time elapsed since the first day of the woman's last menstrual period (LMP). This is also termed *menstrual age*. With the development of means of dating pregnancies that are often more accurate than LMP, the term *gestational age* is no longer tied to the LMP. Instead, it refers to the time since the estimated conception date plus 2 weeks. Because women typically conceive at or close to 2 weeks after their LMP, gestational age and menstrual age are generally the same, but gestational age is a more accurate measure of the age of the

pregnancy than is menstrual age in a woman with irregular cycle length. Full term is 40 weeks' gestational age. The *estimated due date* (EDD) or *estimated date of confinement* (EDC) is calculated as the date at which the gestational age of a pregnancy will reach 40 weeks.

Another term sometimes used to date pregnancy is *conceptional age*, defined as the time since the date of conception. In some situations, such as in patients conceiving through *assisted reproductive techniques* (ART), conceptional age can be determined very accurately. In these cases, gestational age is equally accurate, because it is equal to the precisely known conceptional age plus 2 weeks. To avoid using different terms for dating pregnancies in ART patients, the term *gestational age* is the preferred term for dating all pregnancies, regardless of the mode of conception.<sup>1</sup>

Accurate dating of pregnancy is extremely important for managing the obstetric patient, as many clinical decisions during pregnancy are dependent on gestational age. In the first trimester, the timing of prenatal testing for fetal chromosomal abnormalities is gestational age

dependent. For assessment of some fetal structures, gestational age must be taken into account when distinguishing some normal from abnormal findings. For example, protrusion of intra-abdominal contents into the base of the umbilical cord can be a normal finding prior to 12 weeks' gestation (physiologic bowel herniation) but is abnormal in the second trimester, when it represents an omphalocele.<sup>2</sup> In the second trimester, selecting the best time to perform the sonographic fetal survey to assess for anomalies requires knowledge of the gestational age.<sup>3</sup> Accurate dating is also important to determine if a fetal structure is abnormal in size. For example, if the femur is small for gestational age, concern for Down syndrome or a skeletal dysplasia should be raised.<sup>4,5</sup> In the third trimester, accurate dating is needed to diagnose and manage preterm labor and to diagnose postterm pregnancies and determine when intervention is required.

Accurate assignment of gestational age is also essential for assessing fetal growth, because a key method for assessing growth is determining whether the EFW is within the normal range for gestational age or abnormally low or abnormally high. Abnormally small fetuses may require increased prenatal surveillance<sup>6,7</sup> and possibly early delivery. Cesarean delivery may be appropriate for fetuses measuring abnormally large for gestational age.<sup>8,9</sup>

## ASSIGNMENT OF GESTATIONAL AGE

The gestational age of a pregnancy can be assigned based on either clinical factors or sonographic findings. In general, clinical factors, such as LMP or uterine size estimation, are less accurate than ultrasound for dating pregnancies. Dating based on LMP is fraught with inaccuracies, including incorrect recall, irregular menstrual cycles, menstrual cycles longer or shorter than 28 days,<sup>10-12</sup> and variable timing of ovulation during the cycle.<sup>13</sup> Dating based on physical examination assessment of uterine size is even less accurate than LMP, because the assessment of uterine size is affected by body habitus as well as myomas and other uterine abnormalities.

Dating by ultrasound, particularly before the third trimester, is generally more accurate than clinical dating by LMP or physical examination.<sup>10,11,14,15</sup> One exception in which clinical information is more accurate than ultrasound for dating is in pregnancies conceived by ART. Such pregnancies can be dated very accurately because the exact date of conception is known. Based on that date of conception, gestational age is assigned as the number of weeks since known conception plus 2 weeks.<sup>1</sup>

Once gestational age has been assigned by sonography or by clinical information in an ART patient, the pregnancy should not be redated nor should the EDD be changed. This is because the earlier in pregnancy the gestational age is determined, the more accurate the dating of the pregnancy.<sup>11,16,17</sup> Selecting the appropriate sonographic method for dating pregnancy depends on how far along the pregnancy is, and therefore, dating for each trimester will be discussed separately.

## FIRST TRIMESTER DATING

Early in the first trimester, before the embryo is visible, gestational age can be assigned based on transvaginal sonographic findings. The earliest sonographic finding of pregnancy is a small rounded intrauterine fluid collection in the central portion of the uterus.<sup>18-23</sup> The fluid collection may or may not demonstrate the intradecidual sign<sup>18,19</sup> or the double sac sign.<sup>24</sup> When ultrasound demonstrates an intrauterine fluid collection with no visible yolk sac or embryo, the pregnancy can be accurately assigned a gestational age of 5.0 weeks. When the fluid collection contains a yolk sac but no embryo, the pregnancy can be accurately assigned a gestational age of 5.5 weeks. The presence of a small

embryo, less than 2 mm in size, with the embryonic heartbeat visible adjacent to the yolk sac, can be accurately dated as 6.0 weeks' gestation (Fig. 6-1). The accuracy of these early sonographic milestones for dating pregnancy is  $\pm 0.5$  week.<sup>22-24</sup>

An alternate method for dating early pregnancy is to measure the mean sac diameter of the gestational sac. This is done by averaging the sagittal, coronal, and anteroposterior measurements of the fluid component of the gestational sac (Fig. 6-2) and assigning gestational age based on published tables (Table 6-1) or formulas.<sup>25-27</sup> Dating by mean sac diameter very early in pregnancy has similar accuracy to dating by sonographic milestones.<sup>21,23,25,26,28</sup> However, once the embryo is large enough to measure, dating based on the size of the embryo is more accurate than using the mean sac diameter.<sup>11,29</sup>

From the time the embryo is visible until the end of the first trimester, dating is based on the length of the embryo or fetus, measured from the top of the head to the bottom of the rump, the CRL. Gestational age is assigned based on CRL by using published formulas or tables (Table 6-2).<sup>27,29-32</sup> Dating by CRL is more accurate in the early first trimester, when accuracy is  $\pm 0.5$  week, than toward the end of the first trimester, when accuracy approaches  $\pm 1.0$  week.<sup>27-33</sup> Care must be taken to measure the CRL correctly, particularly toward the end of the first trimester. The fetus should be in neutral position, neither hyperextended nor hyperflexed with the chin tucked against the chest. The calipers should be placed at the top of the fetal head and the bottom of the rump, making sure not to include the yolk sac or lower extremities in the measurement (Fig. 6-3).<sup>28-32</sup>

When dating a pregnancy during the first trimester, sonography is more accurate than LMP.<sup>14,15</sup> However, it is acceptable to use the LMP to date a pregnancy if the LMP is certain and the difference between gestational age by LMP and gestational age by first trimester sonography is less than 7 days.<sup>11</sup>

## SECOND AND THIRD TRIMESTER DATING

### Measurements

During the second and third trimesters of pregnancy, measurements of specified fetal parts can be used individually or in combination to estimate gestational age of the pregnancy. The most commonly used measurements for gestational age assignment are the biparietal diameter (BPD), occipitofrontal diameter (OFD), head circumference (HC), abdominal diameter (AD), abdominal circumference (AC), and femur length (FL).

The BPD, OFD, and HC are measured on an axial image of the fetal head at the level of the paired thalami, third ventricle, and cavum septum pellucidum (Figs. 6-4 and 6-5).<sup>34,35</sup> With a true axial view, the calvarium and intracranial contents appear symmetric on either side of the falx and paired thalami. The BPD is measured by placing the caliper closer to the transducer (i.e., at the top of the image) at the outer edge of the bony calvarium, while the caliper farther from the transducer should be placed on the inner edge of the bony calvarium. That is, the BPD is measured from leading edge to leading edge of the calvarium.<sup>34,36</sup> Improper measurements, either from using an image at an incorrect plane of section through the fetal head or from misplacement of the sonographic calipers, will lead to errors in estimating gestational age and fetal weight.

The OFD and HC can be measured on the same view of the fetal head as the BPD, provided the image is a true axial view that includes the entire head from the frontal bone to the occipital bone. For the OFD measurement, one caliper is placed in the anterior midline in the middle of the echogenic line of the frontal bone, and the second is placed posteriorly in the middle of the echogenic line of the occipital bone.<sup>34,36</sup> The HC is measured by using elliptical calipers to outline the



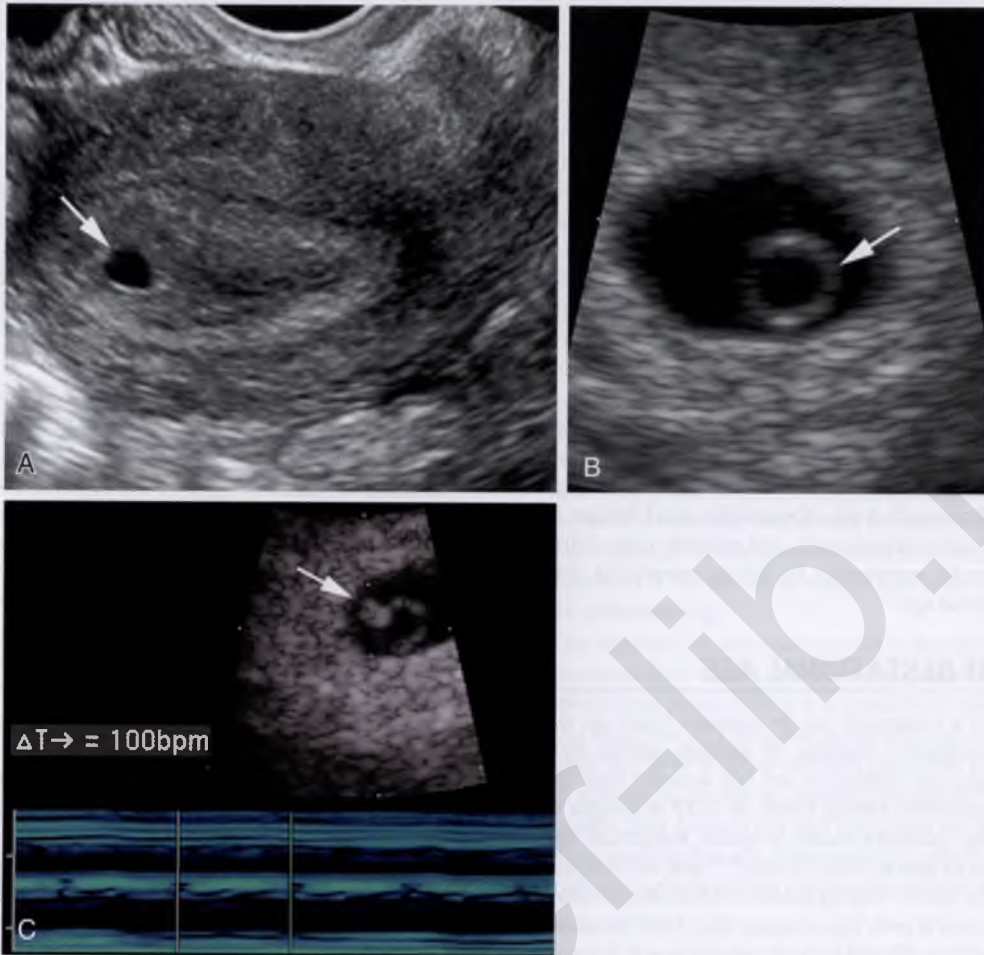


**FIG 6-1** Early first trimester dating with sonographic milestones. **A**, Sagittal image showing a small rounded intrauterine fluid collection (*arrow*) in the central portion of the uterus, consistent with 5.0 weeks' gestation. **B**, Intrauterine gestational sac containing a yolk sac (*arrow*), consistent with 5.5 weeks' gestation. **C**, Intrauterine gestational sac containing a small embryo with heartbeat (*arrow*) adjacent to the yolk sac. M-mode tracing through the embryo documents a heart rate of 100 beats per minute. These findings are consistent with gestational age of 6.0 weeks.

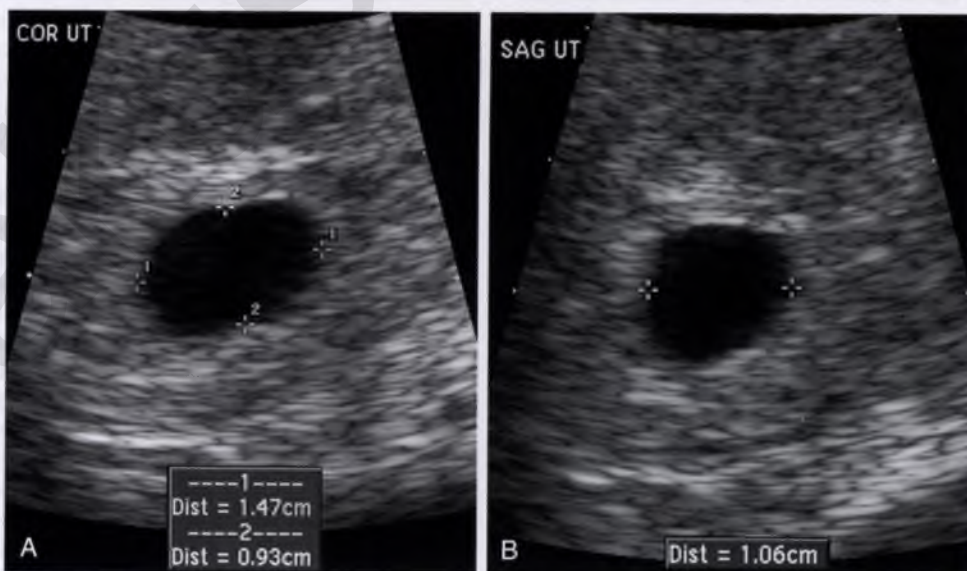


**FIG 6-2** Mean sac diameter in early pregnancy. **A**, Coronal image of intrauterine gestational sac measuring approximately 15 mm in transverse diameter and 9 mm in anteroposterior diameter (*calipers*). **B**, Longitudinal view of gestational sac with sagittal measurement of approximately 11 mm. The mean sac diameter of this pregnancy is 12 mm.

**TABLE 6-1 Gestational Dating by Mean Sac Diameter in the Early First Trimester**

Mean Sac Diameter (mm)	Gestational Age (Weeks)*
2	5.0
3	5.1
4	5.2
5	5.4
6	5.5
7	5.6
8	5.7
9	5.9
10	6.0

95% confidence interval =  $\pm 0.5$  week.

\*Values from Daya S, Woods S, Ward S, et al: Early pregnancy assessment of transvaginal ultrasound scanning. *Can Med Assoc J* 144(4):441-446, 1991.

outer edge of the skull (see Figs. 6-4 and 6-5A). The HC can also be calculated from the BPD and OFD:

$$HC = 1.62 \times (BPD + OFD)$$

This formula is based on the circumference of an ellipse with diameters BPD and OFD with a correction factor because these diameters are not outer-to-outer.<sup>36-38</sup>

The OFD is also used in conjunction with the BPD to take into account the shape of the fetal head. A standard-shaped fetal head has an OFD:BPD ratio of 1.265. When the OFD:BPD ratio is higher or lower than 1.265, a corrected BPD can be calculated with the formula:

$$\text{Corrected BPD} = \text{square root of } [(BPD \times OFD) / 1.265]$$

The corrected BPD represents the BPD of a standard-shaped fetal head with the same cross-sectional area.<sup>38</sup>

The AD and AC are measured on an axial image of the fetal abdomen at the level of the stomach and intrahepatic portion of the umbilical vein.<sup>36,39,40</sup> The abdomen should be as round as possible, and the outer skin surface should be visible all the way around. For the AD, two perpendicular measurements are taken with the calipers placed on the outer surface of the skin. The anteroposterior AD is measured from the anterior midline to the posterior midline, the latter behind the spine. The transverse AD is measured perpendicular to the anteroposterior AD, with calipers placed on the skin surface on both sides of the fetal abdomen (Fig. 6-6). The AC is measured via elliptical calipers outlining the outer surface of the skin around the abdomen (Figs. 6-6 and 6-7). The AC can also be calculated from the two orthogonal AD measurements as:

$$AC = 1.57 \times (\text{anteroposterior AD} + \text{transverse AD})$$

When measuring the fetal abdomen, care must be taken to make sure the image is at the correct level, the entire abdomen is included on the image, the outer skin surface is visible, and the calipers are placed appropriately. Images showing part of a kidney are too low in the abdomen and will yield inaccurate estimations of fetal age and weight. Misplacement of the calipers inside the fetal skin layer or the abdomen will lead to underestimation of the gestational age and weight.<sup>41,42</sup>

The measurement of the fetal femur is actually a measurement of the femoral diaphysis, because, for most of pregnancy, only the diaphysis of the bone is ossified. For most accurate femur measurements, an attempt should be made to image the femur as perpendicular to the ultrasound beam as possible. On the image, the femur is measured by

**TABLE 6-2 Gestational Age Estimation by Crown-Rump Length (CRL)**

CRL (mm)	Gestational Age (Weeks)*	CRL (mm)	Gestational Age (Weeks)*
5	6.0	45	11.1
6	6.2	46	11.2
7	6.4	47	11.3
8	6.6	48	11.4
9	6.8	49	11.4
10	7.0	50	11.5
11	7.2	51	11.6
12	7.4	52	11.7
13	7.5	53	11.8
14	7.7	54	11.8
15	7.8	55	11.9
16	8.0	56	12.0
17	8.1	57	12.1
18	8.3	58	12.2
19	8.4	59	12.2
20	8.5	60	12.3
21	8.7	61	12.4
22	8.8	62	12.4
23	8.9	63	12.5
24	9.0	64	12.6
25	9.1	65	12.7
26	9.3	66	12.7
27	9.4	67	12.8
28	9.5	68	12.9
29	9.6	69	12.9
30	9.7	70	13.0
31	9.8	71	13.1
32	9.9	72	13.2
33	10.0	73	13.2
34	10.1	74	13.3
35	10.2	75	13.4
36	10.3	76	13.4
37	10.4	77	13.5
38	10.5	78	13.5
39	10.6	79	13.6
40	10.7	80	13.7
41	10.8		
42	10.8		
43	10.9		
44	11.0		

\*Values derived from Robinson HP, Fleming JEE: A critical evaluation of sonar "crown-rump length" measurements. *Br J Obstet Gynecol* 82:702-710, 1975.

placing the calipers at either end of the ossified diaphysis (Figs. 6-8 and 6-9). It is important not to include any of the femoral epiphysis, which can appear as a linear projection from the proximal or distal end of the diaphysis.<sup>36,43</sup>

### Assigning Gestational Age in the Second and Third Trimesters

In the second and third trimesters, gestational age can be assigned based on a single measurement, such as the BPD, corrected BPD, HC, or FL (Tables 6-3 through 6-5), or on a combination of measurements, such as with composite age formulas. Head measurements that take into account the shape of the fetal head—namely, the corrected BPD





**FIG 6-3** Crown-rump length measurement. Sonogram of fetus in gestation sac with crown-rump length measured (*calipers*). The yolk sac (*arrow*) is visible adjacent to the fetus, not included in the crown-rump length measurement

and the HC—are more accurate than the BPD alone or FL alone in the second trimester. Accuracy of the corrected BPD and the HC before 20 weeks is approximately  $\pm 1.2$  weeks.<sup>44-46</sup> As pregnancy progresses, the accuracy of all measurements decreases, such that, by the end of the third trimester, the accuracy of gestational age estimation by head measurements is about  $\pm 3.5$  weeks (Table 6-6).<sup>44-46</sup> Although head measurements are more accurate than FL in the second trimester, by the third trimester, the accuracy of the FL is similar to that of head measurements. The AC is a poor predictor of gestational age, particularly later in pregnancy, and should not be used on its own to assign gestational age.

Composite age formulas estimate gestational age via two or more fetal measurements,<sup>47-49</sup> such as the BPD, HC, FL, and AC. The accuracy of gestational age estimation using these composite age formulas is similar to the accuracy of the corrected BPD and HC and is more accurate than age estimation using the FL.<sup>44,46,50</sup> One drawback of using the composite gestational age formulas is the potential to miss an abnormal measurement or anomaly. For example, if the fetal head is abnormally small and the FL and AC are normal for gestational age, the composite age formula that incorporates measurements of the BPD, HC, FL, and AC will be an underestimation of the true age. In such cases, the interpreter of the sonogram might not recognize that the head is abnormally small, because its size might be within the normal range for the calculated gestational age, an underestimate.

Therefore, when the first ultrasound examination during pregnancy is in the second trimester, the best approach to assigning gestational age at that time is either to use a head measurement that takes into account head shape—namely, the corrected BPD or HC—or to use a composite age formula. Both have similar accuracy during the second trimester of about  $\pm 1.2$  weeks early in this trimester and approximately  $\pm 2.0$  weeks by the end of the trimester.<sup>44-46</sup> When the first ultrasound examination is not until the third trimester, any of the

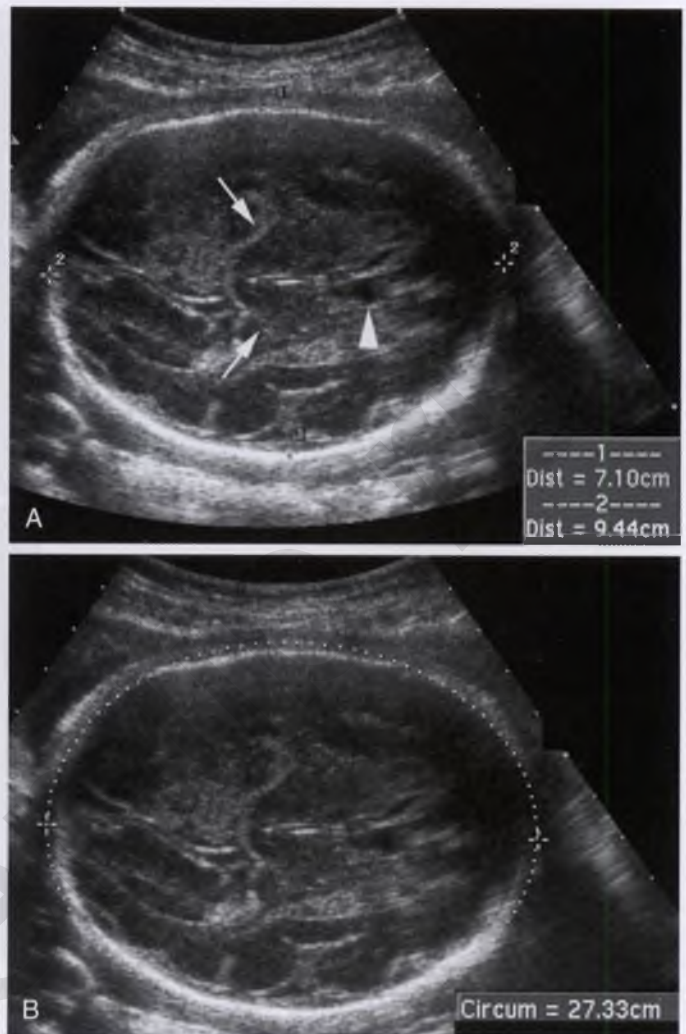


**FIG 6-4** Head measurements. **A**, Axial image of fetal head at the level of the paired thalami (*arrows*), third ventricle, and cavum septum pellucidum (*arrowhead*), with biparietal diameter (*calipers 1*) and occipitofrontal diameter (*calipers 2*) measured. **B**, Head circumference measured with elliptical caliper tracing (*dotted line*) on the same image used to measure the biparietal and occipitofrontal diameters.

corrected BPD, HC, or FL can be used to assign gestational age, or a composite age formula can be used. However, caution must be used when assigning gestational age this late in pregnancy because of the broad error range of more than  $\pm 3.0$  weeks.<sup>11,44-46</sup>

An acceptable alternative to sonographic dating in the second trimester is to use the LMP to date the pregnancy when the difference in gestational age by LMP and gestational age by ultrasound is less than 10 days. Similarly, for dating in the early third trimester, up until 28 weeks' gestation, it is acceptable to date by the LMP if the age difference between dating by LMP and dating by ultrasound is less than 14 days.<sup>11</sup> By the latter part of the third trimester, neither dating by ultrasound nor dating by LMP is very accurate.<sup>11</sup>

As mentioned previously, once the gestational age has been assigned based on sonographic findings or measurements, the dating should not be changed based on measurements of the fetus on subsequent examinations. Rather, measurements on subsequent sonograms should be assessed to ensure that the fetus is growing appropriately and that all measurements are within normal limits for gestational age.



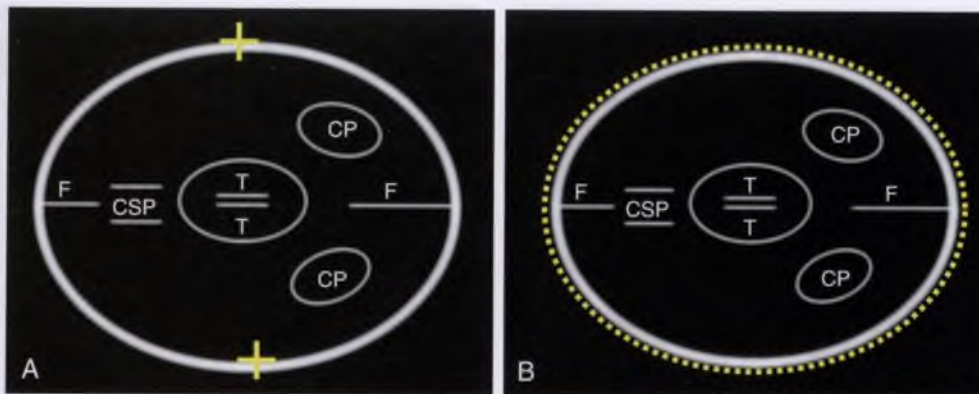


**FIG 6-5** Diagram demonstrating anatomy at the level of appropriate measurement of the fetal biparietal diameter (**A**) and head circumference (**B**). CP, choroid plexus; CSP, cavum septum pellucidum; F, falx; T, thalami.

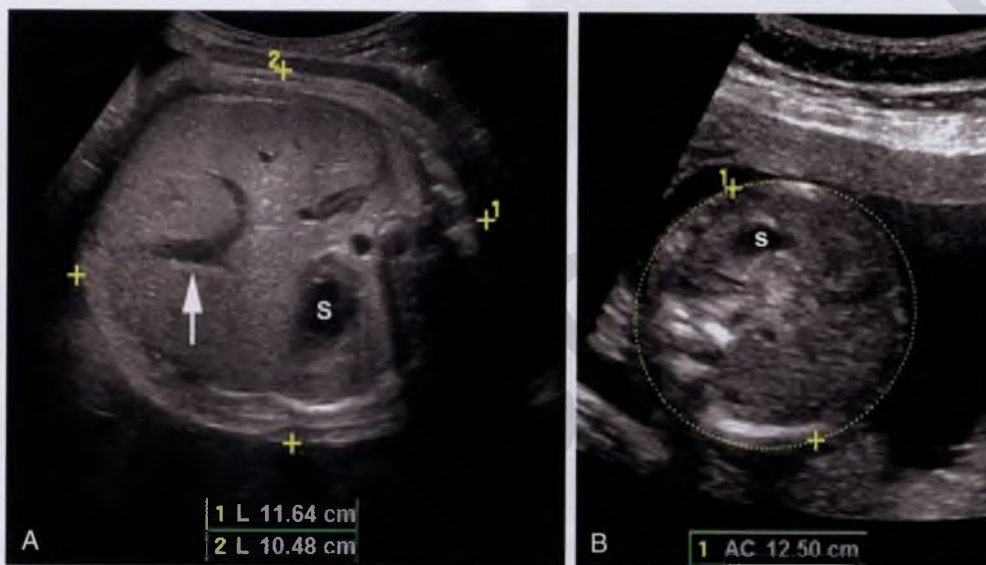


**FIG 6-6** Abdominal diameter and circumference measurements. **A**, Axial image of the fetal abdomen at the level of the stomach (S) and intrahepatic portion of the umbilical vein (arrow) where it joins the left portal vein with the anteroposterior diameter (calipers 1) and transverse diameter (calipers 2) measured. **B**, Axial image of another fetal abdomen with the abdominal circumference measured with elliptical caliper tracing (dotted line). S, stomach.

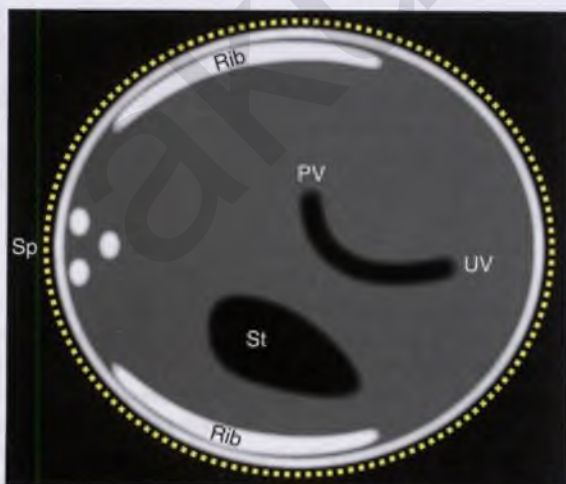


**FIG 6-7** Diagram demonstrating anatomy at the level of appropriate measurement of the fetal abdominal circumference. PV, right portal vein; Sp, spine; St, stomach; UV, umbilical vein.

## FETAL WEIGHT ESTIMATION AND WEIGHT PERCENTILES

Fetal weight is estimated using a formula based on fetal measurements. Each formula was developed using a population of fetuses scanned close to the time of delivery by assessing the sonographic measurements in relation to birth weight. Numerous weight estimation formulas have been developed<sup>51-57</sup> and tested.<sup>58-61</sup> From these studies testing various formulas, several conclusions can be drawn.

- Formulas that use measurements of the fetal head, abdomen, and femur have a mean error of 15% ( $\pm 2$  standard deviations [SDs]).<sup>62</sup> Formulas that use fewer than three measurements of fetal body parts perform less well (i.e., have larger standard deviations).
- Adding other measurements to the head, abdomen, and femur, such as the thigh circumference or thickness of thigh soft tissue<sup>63,64</sup> or three-dimensional volume calculations,<sup>61,65-67</sup> does not improve accuracy of weight estimation.
- Despite considerable improvements in sonographic equipment, the accuracy of estimating fetal weight has not changed since the development of formulas 3 decades ago.<sup>58-61,68,69</sup>



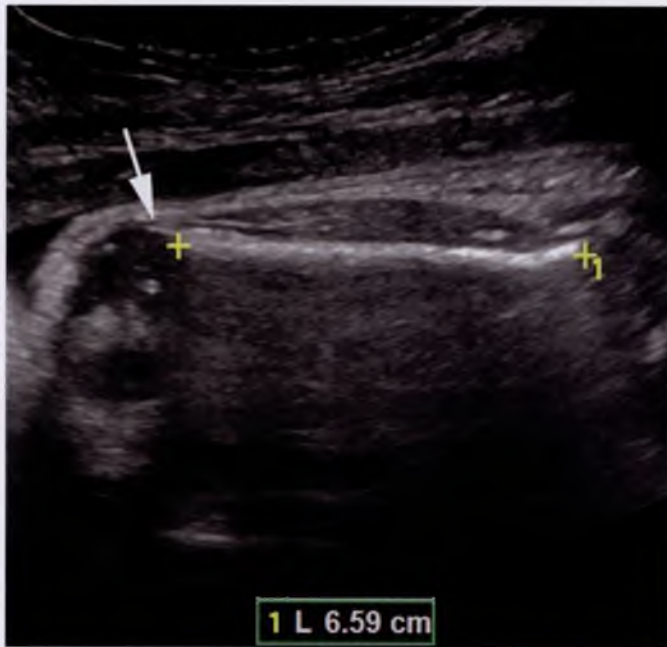


**FIG 6-8** Femur length measurement. Sonogram of femur with ossified diaphysis measured (*calipers*). The linear projection from the diaphysis of the femoral epiphysis (*arrow*) is not included in the measurement.

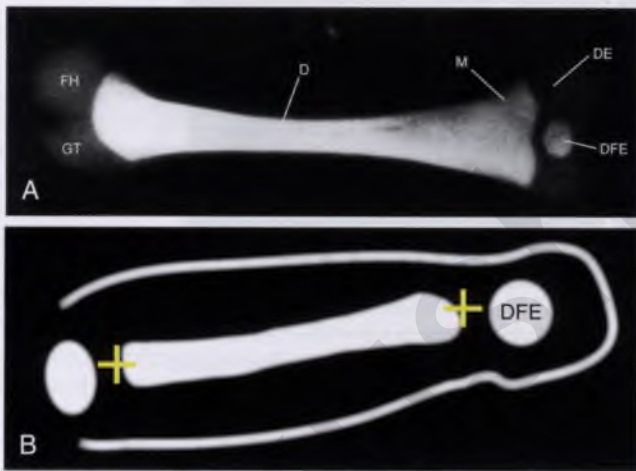


**FIG 6-9** Radiograph (A) from a term neonatal autopsy specimen and illustration (B) of the femur. Sonographic measurements of the "femur" include only the ossified portion of the diaphysis (D) and metaphysis (M). The cartilaginous femoral head (FH), greater trochanter (GT), and distal epiphysis (DE) are not included in the measurement. When it ossifies, the distal femoral epiphyseal (DFE) secondary ossification center is also not included in the measurement.

- Formulas designed for singletons can also be used for estimating weight in twin gestations, because formulas developed specifically for twins are no more accurate than those developed for singletons.<sup>61,70</sup>
- The accuracy of fetal weight estimates is not affected by maternal body mass index or fetal sex,<sup>61</sup> nor is it affected by oligohydramnios or polyhydramnios.<sup>41,53,71,72</sup>
- Fetal weight estimation is less accurate in diabetic mothers than in nondiabetic mothers<sup>73</sup> and less accurate in very small fetuses (i.e., those weighing less than 1000 g).<sup>41</sup>

**TABLE 6-3 Gestational Age Estimation by Biparietal Diameter**

BPD or BPDc (mm)	Gestational Age (Weeks)	BPD or BPDc (mm)	Gestational Age (Weeks)
20	13.2	60	24.2
21	13.4	61	24.5
22	13.6	62	24.9
23	13.8	63	25.3
24	14.0	64	25.7
25	14.3	65	26.1
26	14.5	66	26.5
27	14.7	67	26.9
28	14.9	68	27.3
29	15.1	69	27.7
30	15.4	70	28.1
31	15.6	71	28.5
32	15.8	72	29.0
33	16.1	73	29.4
34	16.3	74	29.9
35	16.6	75	30.3
36	16.8	76	30.8
37	17.1	77	31.2
38	17.3	78	31.7
39	17.6	79	32.2
40	17.9	80	32.7
41	18.1	81	33.2
42	18.4	82	33.7
43	18.7	83	34.2
44	19.0	84	34.7
45	19.3	85	35.2
46	19.6	86	35.8
47	19.9	87	36.3
48	20.2	88	36.9
49	20.5	89	37.4
50	20.8	90	38.0
51	21.1	91	38.6
52	21.4	92	39.2
53	21.7	93	39.8
54	22.1	94	40.4
55	22.4	95	41.0
56	22.8	96	41.6
57	23.1	≥97	42.0
58	23.5		
59	23.8		

BPD, biparietal diameter; BPDc, corrected BPD.

From Doubilet PM, Benson CB: Improved prediction of gestational age in the late third trimester. *J Ultrasound Med* 12:647-653, 1993.

- The intraobserver and interobserver variability is high for fetal weight estimation. Higher quality scans result in more accurate weight estimation.<sup>41,42</sup> Thus, attempts should be made to minimize this variability by averaging several measurements of each body part, using careful measurement techniques and optimizing image quality such that anatomic landmarks are clearly visible.<sup>61</sup> Among the most widely used formulas for estimating fetal weight are those published in 1985 by Hadlock and colleagues (Table 6-7).<sup>56</sup> These formulas have been tested by multiple authors. Although attempts have been made to improve fetal weight prediction with other

TABLE 6-4 Gestational Age Estimation by Head Circumference (HC)

HC (mm)	Gestational Age (Weeks)	HC (mm)	Gestational Age (Weeks)
80	13.4	225	24.5
85	13.7	230	25.0
90	14.0	235	25.5
95	14.3	240	26.1
100	14.7	245	26.6
105	15.0	250	27.1
110	15.3	255	27.7
115	15.6	260	28.3
120	16.0	265	28.9
125	16.3	270	29.4
130	16.6	275	30.0
135	17.0	280	30.7
140	17.3	285	31.3
145	17.7	290	31.9
150	18.1	295	32.6
155	18.4	300	33.3
160	18.8	305	33.9
165	19.2	310	34.6
170	19.6	315	35.3
175	20.0	320	36.1
180	20.4	325	36.8
185	20.8	330	37.6
190	21.3	335	38.3
195	21.7	340	39.1
200	22.2	345	39.9
205	22.6	350	40.7
210	23.1	355	41.6
215	23.6	360	42.4
220	24.0		

Values derived from Law RG, MacRae KD: Head circumference as an index of fetal age. *J Ultrasound Med* 1:281-288, 1982.

formulas, none has been developed that outperforms the Hadlock formulas consistently and across all types of patient populations.<sup>58-62,68-73</sup>

Fetal size in proportion to that expected for age is assessed by comparing the EFW to norms for gestational age. The metric used for this purpose is the weight percentile. Determining the weight percentile, once the gestational age has been established and the fetal weight estimated, is accomplished using published formulas or tables (Table 6-8).<sup>74-77</sup> Selecting the most appropriate table is important for making sure the weight percentiles apply to the population being scanned. Because babies are born larger than they were several decades ago, newer tables, such as that published by Alexander and associates in 1991,<sup>75</sup> are likely better than older ones.<sup>76,77</sup> Those based on more accurate sonographic dating are likely to be even better<sup>74,78</sup> than those in which dating may be less precise. However, even weight tables based on known birth weights and gestational age have an important drawback. Prior to term, the weight percentiles do not reflect those of normal fetuses but rather reflect those of preterm neonates. Because neonates born premature are smaller than fetuses of the same gestational age who will remain in utero until term, the weight tables based on neonatal birth weights contain lower weights at each percentile than what is likely the norm.<sup>79-81</sup>

Estimating fetal size for gestational age via weight percentile is best performed in the latter part of the second trimester and during the

TABLE 6-5 Gestational Age Estimation by Femur Length (FL)

FL (mm)	Gestational Age (Weeks)	FL (mm)	Gestational Age (Weeks)
10	13.7	45	24.5
11	13.9	46	24.9
12	14.2	47	25.3
13	14.4	48	25.7
14	14.6	49	26.2
15	14.9	50	26.6
16	15.1	51	27.0
17	15.4	52	27.5
18	15.6	53	28.0
19	15.9	54	28.4
20	16.2	55	28.9
21	16.4	56	29.4
22	16.7	57	29.9
23	17.0	58	30.4
24	17.3	59	30.9
25	17.6	60	31.4
26	17.9	61	31.9
27	18.2	62	32.5
28	18.5	63	33.0
29	18.8	64	33.6
30	19.1	65	34.1
31	19.4	66	34.7
32	19.7	67	35.3
33	20.1	68	35.9
34	20.4	69	36.5
35	20.7	70	37.1
36	21.1	71	37.7
37	21.4	72	38.3
38	21.8	73	39.0
39	22.2	74	39.6
40	22.5	75	40.3
41	22.9	76	40.9
42	23.3	77	41.6
43	23.7	≥78	42.0
44	24.1		

From Doubilet PM, Benson CB: Improved prediction of gestational age in the late third trimester. *J Ultrasound Med* 12:647-653, 1993.

third trimester. Prior to this time, weight estimation is less accurate.<sup>41,61-68</sup> The fetal weight percentile is used to assess whether or not the fetus is growing appropriately. Appropriate weight percentiles are those between the 10th and 90th percentiles for gestational age. An EFW below the 10th percentile is concerning for an abnormally small fetus, which may be due to FGR. An infant with a birth weight below the 10th percentile is termed *small for gestational age* (SGA), and one above the 90th percentile is termed *large for gestational age* (LGA).<sup>82</sup>

Fetal interval growth from one ultrasound scan to the next can be estimated to make sure the fetus is gaining weight at an appropriate rate. Because of the wide 95% confidence interval of fetal weight estimation of  $\pm 15\%$  (2 SDs), assessment of fetal growth between two sonograms should be performed after an interval of at least 7 days. Normal fetuses grow fairly steadily from 30 to 40 weeks' gestation at a rate of approximately 220 g per week. After 40 weeks, the growth rate declines.<sup>74,76</sup> The fetal growth rate from one examination to the



**TABLE 6-6 Gestational Age Assignment by Initial Ultrasound Scan**

Stage of Pregnancy	Basis for GA	Table	Accuracy (Weeks)*
<b>First Trimester</b>			
Early (5-6 weeks)	Sonographic milestones or MSD	1	±0.5
Mid to late (6-13 weeks)	CRL	2	±0.5-1.0
<b>Second Trimester</b>			
If OFD measurable	BPDc or HC	3 and 4	±1.2 (14-20)
If OFD not measurable	BPD or FL	3 and 5	±1.9 (20-26)
			±1.4 (14-20)
			±2.1-2.5 (20-26)
<b>Third Trimester</b>			
If OFD measurable	BPDc, HC, or FL	3, 4, and 5	±3.1-3.4 (26-32)
If OFD not measurable	FL	5	±3.5-3.8 (32-42)
			±3.1 (26-32)
			±3.5 (36-42)

\*Two standard deviations, or 95% confidence interval.

BPD, biparietal diameter; BPDc, corrected BPD; CRL, crown-rump length; FL, femur length; GA, gestational age; HC, head circumference; MSD, mean sac diameter; OFD, occipitofrontal diameter.

**TABLE 6-7 Approach to Fetal Weight Estimation**

Body Parts Imaged	Formula Used for Weight Estimate*
Head, abdomen, and femur	
OFD measurable	Formula 1, using corrected BPD in place of BPD
OFD not measurable	Formula 1
Head and abdomen	
OFD measurable	Formula 2, using corrected BPD in place of BPD
OFD not measurable	Formula 2
Abdomen and femur	Formula 3

Formula 1

$$\text{Log}_{10}(\text{EFW}) = 1.4787 - 0.003343 \text{ AC} \times \text{FL} + 0.001837 \text{ BPD}^2 + 0.0458 \text{ AC} + 0.158 \text{ FL}$$

Formula 2

$$\text{Log}_{10}(\text{EFW}) = 1.1134 + 0.05845 \text{ AC} - 0.000604 \text{ AC}^2 - 0.007365 \text{ BPD}^2 + 0.00595 \text{ BPD} \times \text{AC} + 0.1694 \text{ BPD}$$

Formula 3

$$\text{Log}_{10}(\text{EFW}) = 1.3598 + 0.051 \text{ AC} + 0.1844 \text{ FL} - 0.0037 \text{ AC} \times \text{FL}$$

AC, abdominal circumference, in cm; BPD, biparietal diameter, in cm; EFW, estimated fetal weight, in g; FL, femur length, in cm; OFD, occipitofrontal diameter, in cm.

\*Data from Hadlock FP, Harrist RB, Carpenter RJ, et al: Sonographic estimation of fetal weight: the value of femur length in addition to head and abdomen measurements. *Radiology* 150:535-540, 1984.

**TABLE 6-8 Fetal Weight Percentiles in the Third Trimester\***

Gestational Age (Weeks)	WEIGHT PERCENTILES (g)		
	10th	50th	90th
26	570	860	1320
27	660	990	1470
28	770	1150	1660
29	890	1310	1890
30	1030	1460	2100
31	1180	1630	2290
32	1310	1810	2500
33	1480	2010	2690
34	1670	2220	2880
35	1870	2430	3090
36	2190	2650	3290
37	2310	2870	3470
38	2510	3030	3610
39	2680	3170	3750
40	2750	3280	3870
41	2800	3360	3980
42	2830	3410	4060
43	2840	3420	4100
44	2790	3390	4110

\*From Doubilet PM, Benson CB, Nadel AS, Ringer SA: Improved birth weight table for neonate developed from gestations dated by early ultrasonography. *J Ultrasound Med* 16:241-249, 1997.

next can be calculated by taking the difference between the two estimated weights and dividing by the number of weeks that have elapsed.

Another way to assess fetal interval growth is to compare the weight percentiles from one sonogram to the next. If the weight percentiles for gestational age are similar from one examination to the next, the fetal growth is likely to be normal. If, however, the weight percentile falls considerably between two examinations, concern should be raised that the fetus is not growing appropriately.

## ABNORMAL FETAL GROWTH

### Fetal Growth Restriction and Small for Gestational Age Fetuses

The term *fetal growth restriction* is used to describe a fetus that is abnormally small for gestational age, often due to complications of placental insufficiency. The term *small for gestational age* (SGA) is used to describe a neonate whose weight falls below the 10th percentile for gestational age. FGR fetuses are at increased risk of perinatal morbidity and mortality, including in utero demise,<sup>83,84</sup> brain injury, fetal distress,<sup>85</sup> neonatal hypothermia, hypoglycemia, hyperbilirubinemia, and decreased immune function.<sup>86-93</sup> When FGR is diagnosed prenatally and close fetal monitoring is instituted, including nonstress tests, biophysical profiles, and umbilical artery Doppler, the neonatal outcome is better than that of neonates born with FGR that were not diagnosed prenatally.<sup>6,7,83,94-96</sup>

The terms FGR and SGA are often used interchangeably because the most common definition of FGR is a neonate with birth weight below the 10th percentile for gestational age, the same as the definition of SGA.<sup>6,84,94,95</sup> In utero, SGA and FGR are diagnosed when the EFW is below the 10th percentile for gestational age. Although some have tried to differentiate SGA fetuses who are constitutionally small but are achieving their expected growth potential from FGR fetuses whose



growth is compromised, in practice it is often difficult to make this distinction.<sup>97</sup> It has been shown that the smaller the fetal size for gestational age, the greater the likelihood that fetal growth is compromised.<sup>83</sup> SGA neonates have significantly higher postnatal mortality rates in the first week of life, the first month of life, and the first year as compared to neonates who are appropriate or LGA.<sup>98</sup> Thus, identification of a small fetus (i.e., one whose weight is below the 10th percentile for gestational age) will identify fetuses at risk of being FGR neonates and prompt close surveillance in an attempt to improve outcome.<sup>6,85,96-98</sup>

Although the diagnosis of FGR in utero is most often made based on an EFW below the 10th percentile,<sup>94,95,97,98</sup> not all such fetuses truly have FGR. Because of this, a number of other sonographic criteria have been proposed to improve the accuracy of diagnosing FGR prenatally. However, none of these criteria, including the EFW percentile, has both a high sensitivity and high positive predictive value. The EFW, for example, has a fairly high sensitivity of 89% for FGR, but its positive predictive value is only 45%.<sup>99</sup> Using multiple parameters can improve the sensitivity and positive predictive value of sonographic diagnosis of FGR.<sup>100-102</sup> One method for predicting FGR using multiple parameters is the FGR score, which incorporates EFW, amniotic fluid volume, and maternal blood pressure status (normal vs. hypertensive) to diagnosis or exclude FGR with high sensitivity and positive predictive value.<sup>100,101</sup> For each week of data on gestation, amniotic fluid volume classification, and maternal blood pressure status, the table presents an EFW range. For a particular fetus, if the EFW is below the lower end of the EFW range, then the fetus can be confidently diagnosed with FGR. If the EFW is above the upper end of the range, FGR can be excluded with confidence. If the EFW falls within the range, the likelihood of FGR is elevated but indeterminate, because FGR cannot be diagnosed or excluded with confidence. These combined criteria perform even better if the pregnancy has accurate early dating with first trimester ultrasound than if dating was assigned later in pregnancy. In those pregnancies with first trimester dating, only the lower value in the EFW range is used, with a diagnosis of FGR made with confidence if the EFW is below the lower EFW number and excluded with confidence if the EFW is above the lower EFW number.<sup>100,101</sup>

Doppler criteria, including umbilical and uterine artery Doppler measurements, have previously been suggested for diagnosing FGR. However, all proposed Doppler criteria have low sensitivities and positive predictive values and, therefore, are not reliable for diagnosing FGR.<sup>6,97,103,104</sup> In a fetus already suspected of being growth restricted, however, umbilical artery Doppler is useful for fetal monitoring and for guiding management decisions<sup>6,83,94,95,97</sup> (see Chapter 22).

When a fetus is diagnosed with FGR, attempts should be made to determine the cause. Maternal factors should be considered, including genetic and nutritional factors, as well as medical diseases, such as hypertension, vasculitis, and renal disease.<sup>97,105</sup> Fetal abnormalities should be investigated, including fetal anomalies and aneuploidy.<sup>107</sup> Lastly, placental abnormalities, such as circumvallate placenta or velamentous cord insertion, or an abnormally invasive placenta with accreta, can be the cause of FGR.<sup>105</sup>

### Macrosomic and Large for Gestational Age Fetuses

The term *macrosomia* is defined as a large neonate with a birth weight above a defined value such as 4000 g or 4500 g, independent of gestational age. The term *large for gestational age* is used to describe a neonate with birth weight above the 90th percentile for gestational age.<sup>74,106-111</sup> Macrosomic fetuses are at increased risk of shoulder dystocia, birth injury, and neonatal hypoglycemia and have a lifelong increased risk of obesity.<sup>82,109,110</sup> Accompanying the fetal and neonatal

risks are maternal risks, including anal sphincter tears and postpartum hemorrhage.<sup>109</sup> The higher the birth weight, the greater the risks. Identifying a fetus as macrosomic prior to delivery can direct management decisions regarding delivery, often prompting cesarean delivery when appropriate.<sup>80,109,111-115</sup>

Infants of diabetic mothers have different body proportions than those of nondiabetic mothers, such that their shoulders and trunk tend to be bigger compared to their head size, because of overgrowth of internal organs and increased subcutaneous fat. Thus, fetuses of diabetic mothers have a higher rate of perinatal complications, including shoulder dystocia, for the same birth weight.<sup>112,116-118</sup> As a result, some advocate defining macrosomia in diabetic mothers as greater than 4000 g, whereas they may define macrosomia in nondiabetic mothers as greater than 4500 g.<sup>109,112-114</sup> LGA fetuses are at increased risk of the same fetal and maternal complications as macrosomic fetuses, particularly when they are carried to term.<sup>106,112,116,119</sup>

The prenatal diagnosis of macrosomia relies on the EFW. A weight above 4500 g in a nondiabetic mother or a weight above 4000 g in a diabetic mother suggests macrosomia.<sup>82,109,112-114</sup> The prenatal diagnosis of LGA, like macrosomia, relies on the EFW as well as reliable dating. An EFW above the 90th percentile for gestational age suggests an LGA fetus.

Although sonographically EFWs are somewhat imprecise, using the EFW is still the best way to predict macrosomia and LGA, and better than physical examination or maternal estimates of fetal size.<sup>82,109,110</sup> This holds true despite the fact that EFWs are less precise in diabetic mothers than nondiabetic mothers and less accurate in large fetuses than in those who are average size.<sup>73,82,120-123</sup>

In addition to EFW and fetal weight percentile, a number of other criteria have been proposed to predict LGA and macrosomia. However, none of these proposed criteria has both a higher sensitivity and higher positive predictive value than the EFW.<sup>106,120,121,124-129</sup>

### FETAL ANOMALIES ASSOCIATED WITH ABNORMAL BIOMETRY

In addition to its role in determining gestational age and evaluating fetal size and growth, fetal biometry is important for identifying a number of abnormalities that are characterized by abnormal size of individual fetal structures. Examples include skeletal dysplasias, many of which are associated with abnormally small bones, and microcephaly, in which the head size is small. Furthermore, fetal biometry can assist in the diagnosis of trisomy 21 and other forms of aneuploidy.

When interpreting an obstetric ultrasound image, it is important to assess the normality of all individual body parts that are measured. In addition, a number of measurement ratios, including the HC:AC ratio,<sup>130,131</sup> the FL:AC ratio,<sup>132-134</sup> the BPD:FL ratio,<sup>4,135</sup> and the BPD:HL ratio,<sup>136-138</sup> can be helpful for detecting fetal abnormalities. Once calculated, these ratios can be compared to the norm for gestational age to help identify abnormal measurements within the fetal biometry.

If fetal head measurements are small, such that the HC falls more than 2 SDs below the mean for gestational age, concern for microcephaly should be raised. The smaller the head is for gestational age, the more likely it is that the neonate will be microcephalic at birth and have associated neurologic deficits.<sup>139-141</sup>

Each time the FL is measured, its size should be compared to norms for gestational age. In the second trimester, an FL below the 10th percentile for gestational age has been associated with Down syndrome<sup>136,142</sup> and should prompt further investigation into the likelihood of Down syndrome in the fetus. A very short femur, one falling more than 2 SDs below the mean for gestational age, raises concern for a skeletal dysplasia or FGR, with the latter much more often the



cause than the former.<sup>143,144</sup> An extremely short femur, one falling more than 4 SDs below the mean for gestational age, is usually the result of a skeletal dysplasia.<sup>145-147</sup> In such cases, the other long bones should be assessed for size by comparing their measurements to norms for gestational age,<sup>148,149</sup> and all long bones should be examined for fractures or bowing.<sup>145-147</sup>

The humeral length can also be used as a marker for Down syndrome. In particular, a humeral length that is small compared to the BPD is associated with an increased risk of Down syndrome.<sup>136-138</sup> The fetus should be examined for other markers, such as an absent or small nasal bone.<sup>150,151</sup>

Abnormalities of a single long bone or several bones in one limb can be diagnosed with ultrasound. Such abnormalities may be isolated or may represent one characteristic of a broader syndrome. For example, a very short or hypoplastic radius is associated with a variety of syndromes, including Holt-Oram, Nager, and vertebral defects, anal atresia, cardiac defects, tracheo-esophageal fistula, renal anomalies, and limb abnormalities (VACTERL).<sup>152,153</sup>

Tables and formulas listing normal measurements for gestational age of a variety of other fetal structures beyond the head, abdomen, and femur have been developed, including other long bones in the extremities,<sup>148,149</sup> the clavicle,<sup>154,155</sup> the foot,<sup>156,157</sup> and binocular distance,<sup>158,159</sup> as well as nonbony structures, such as the cerebellum,<sup>160,161</sup> and others.<sup>162,163</sup> (see Appendices). These tables and formulas can be used when evaluating a fetus for anomalies. For example, a binocular distance abnormally small for gestational age is called *hypotelorism*, an anomaly often associated with holoprosencephaly.

## CONCLUSION

In summary, pregnancy dating is important for optimal obstetric care, and sonography is the most accurate method for assigning gestational age. The earlier in pregnancy that gestational age is assigned with ultrasound, the more accurate is the dating of the pregnancy. Once assigned, the pregnancy should not be redated and the EDD should not be changed. Beginning in the late second trimester and thereafter, fetal biometry should be used to estimate fetal weight and calculate the fetal weight percentile. An EFW between the 10th and 90th percentiles for gestational age is normal. EFW below the 10th percentile should raise concern for FGR, whereas EFW above the 90th percentile should raise concern for an LGA fetus. An EFW above 4500 g in a nondiabetic mother suggests fetal macrosomia, as does an EFW above 4000 g in a diabetic mother. Fetal measurements are also used to diagnose fetal abnormalities involving abnormal size of one or more fetal structures.<sup>164</sup> For all of the reasons mentioned here and others discussed in this chapter, fetal measurements are an important component of obstetric ultrasound evaluation throughout gestation.

## REFERENCES

- Delpachitra P, Palmer K, Onwude J, et al: Ultrasound reference chart based on IVF dates to estimate gestational age at 6-9 weeks' gestation. *ISRN Obstet Gynecol* 2012:938583, 2012.
- Bowerman RA: Sonography of fetal midgut herniation: normal size criteria and correlation with crown-rump length. *J Ultrasound Med* 12:251-254, 1993.
- Reddy UM, Abuhamad ZA, Levine D, Saade GR, for the Fetal Imaging Workshop Invited Participants: Executive Summary of a Joint Eunice Kennedy Shriver National Institute of Child Health and Human Development, Society for Maternal-Fetal Medicine, American Institute of Ultrasound in Medicine, American College of Obstetricians and Gynecologists, American College of Radiology, Society for Pediatric Radiology, and Society of Radiologists in Ultrasound Fetal Imaging Workshop. *Obstet Gynecol* 123:1070-1082, 2014. *Am J Obstet Gynecol* 210:387-397, 2014; and *J Ultrasound Med* 33:745-757, 2014.
- Benacerraf BR, Gelman R, Frigoletto FD: Sonographic identification of second-trimester fetuses with Down's syndrome. *N Engl J Med* 317:1371-1376, 1987.
- Filly RA, Golbus MS, Carey JC, Hall JG: Short-limbed dwarfism: ultrasonographic diagnosis by mensuration of fetal femoral length. *Radiology* 138:653-656, 1981.
- Society for Maternal-Fetal Medicine Publications Committee, Berkley E, Chauhan SP, Abuhamad A: Doppler assessment of the fetus with intrauterine growth restriction. *Am J Obstet Gynecol* 206:300-308, 2012.
- Visentin S, Londero AP, Grumolato F, et al: Timing of delivery and neonatal outcomes for small-for-gestational-age fetuses. *J Ultrasound Med* 33:1721-1728, 2014.
- O'Leary JA, Leonetti HB: Shoulder dystocia: prevention and treatment. *Am J Obstet Gynecol* 162:5-9, 1990.
- Benedetti TJ, Gabbe SG: Shoulder dystocia: a complication of fetal macrosomia and prolonged second stage of labor with midpelvic delivery. *Obstet Gynecol* 52:526-529, 1978.
- Savitz DA, Terry JW, Jr, Dole N, et al: Comparison of pregnancy dating by last menstrual period, ultrasound scanning, and their combination. *Am J Obstet Gynecol* 187:1660-1666, 2002.
- Committee Opinion No. 611: Method for estimating due date. *Obstet Gynecol* 124(4):863-866, 2014.
- Wegienka G, Baird DD: A comparison of recalled date of last menstrual period with prospectively recorded dates. *J Womens Health* 14:248-252, 2005.
- Matsumoto S, Nogami Y, Ohkuri S: Statistical studies on menstruation: a criticism on the definition of normal menstruation. *J Med Sci* 11:294-318, 1962.
- Verburg BO, Steegers EA, De Ridder M, et al: New charts for ultrasound dating of pregnancy and assessment of fetal growth: a population-based cohort study. *Ultrasound Obstet Gynecol* 31:388-396, 2008.
- Bennett KA, Crane JMG, O'Shea P, et al: First trimester ultrasound screening is effective in reducing postterm labor induction rates: a randomized controlled trial. *Am J Obstet Gynecol* 190:1077-1081, 2004.
- Caughey AB, Nicholson JM, Washington AE: First- vs second-trimester ultrasound: the effect on pregnancy dating and perinatal outcomes. *Am J Obstet Gynecol* 198:703-706, 2008.
- Kalish RB, Thaler HT, Chasen ST, et al: First- and second-trimester ultrasound assessment of gestational age. *Am J Obstet Gynecol* 191:975-978, 2004.
- Doubilet PM, Benson CB: First, do no harm ... to early pregnancies. *J Ultrasound Med* 29:285-289, 2010.
- Doubilet PM, Benson CB: Double sac sign and intradecidual sign in early pregnancy: interobserver reliability and frequency of occurrence. *J Ultrasound Med* 32:1207-1214, 2013.
- Doubilet PM, Benson CB, Bourne T, et al: Diagnostic criteria for nonviable pregnancy early in the first trimester. *N Engl J Med* 369:1443-1451, 2013.
- De Crespigny LC, Cooper D, McKenna M: Early detection of intrauterine pregnancy with ultrasound. *J Ultrasound Med* 7:7-10, 1988.
- Fossum GT, Davajan V, Kletzky OA: Early detection of pregnancy with transvaginal ultrasound. *Fertil Steril* 49:788-791, 1988.
- Bree RL, Edwards M, Bohm-Velez M, et al: Transvaginal sonography in the evaluation of normal early pregnancy: correlation with HCG level. *AJR Am J Roentgenol* 153(1):75-79, 1989.
- Bradley WF, Fiske CE, Filly RA: The double sac sign in early intrauterine pregnancy: use in exclusion of ectopic pregnancy. *Radiology* 148:223-226, 1982.
- Daya S, Woods S, Ward S, et al: Early pregnancy assessment of transvaginal ultrasound scanning. *Can Med Assoc J* 144(4):441-446, 1991.
- Daya S, Woods S, Ward S, et al: Transvaginal ultrasound scanning in early pregnancy and correlation with human chorionic gonadotropin levels. *J Clin Ultrasound* 19:139-142, 1991.



27. Papaioannou GI, Syngelaki A, Poon LCY, et al: Normal ranges of embryonic length, embryonic heart rate, gestational sac diameter and yolk sac diameter at 6-10 weeks. *Fetal Diagn Ther* 28:207-219, 2010.
28. Nyberg DA, Filly RA, Mahony BS, et al: Early gestation: correlation of HCG levels and sonographic identification. *AJR Am J Roentgenol* 144:951-954, 1985.
29. Robinson HP, Fleming JEE: A critical evaluation of sonar "crown-rump length" measurements. *Br J Obstet Gynecol* 82:702-710, 1975.
30. Daya S: Accuracy of gestational age estimation using fetal crown-rump measurements. *Am J Obstet Gynecol* 168:903-908, 1993.
31. Hadlock FP, Shah YP, Kanon DJ, Lindsey JV: Fetal crown-rump length: reevaluation of relation to menstrual age (5-18 weeks) with high resolution real-time US. *Radiology* 182:501-505, 1992.
32. Drumm JE, Clinch J, MacKenzie G: The ultrasonic measurement of fetal crown-rump length as a method of assessing gestational age. *Br Obstet Gynaecol* 83:417-421, 1976.
33. MacGregor SN, Tamura RK, Sabbagha RE, et al: Underestimation of gestational age by conventional crown-rump length dating curves. *Obstet Gynecol* 70:344-348, 1987.
34. Hadlock FP, Deter RL, Harrist RB, Park SK: Fetal biparietal diameter: a critical re-evaluation of the relation to menstrual age by means of real-time ultrasound. *J Ultrasound Med* 1:97-104, 1982.
35. Shepard M, Filly RA: A standardized plane for biparietal diameter measurement. *J Ultrasound Med* 1:145-150, 1982.
36. Salomon LJ, Alfirevic Z, Berghella V, et al: Practice guidelines for performance of the routine mid-trimester fetal ultrasound scan. *Ultrasound Obstet Gynecol* 37:116-126, 2010.
37. Hadlock FP, Deter RL, Harrist RB, Park SK: Fetal head circumference: relation to menstrual age. *AJR Am J Roentgenol* 138:649-653, 1982.
38. Doubilet PM, Greenes RA: Improved prediction of gestational age from fetal head measurements. *AJR Am J Roentgenol* 142:797-800, 1984.
39. Hadlock FP, Kent WR, Loyd JL, et al: An evaluation of two methods for measuring fetal head and body circumferences. *J Ultrasound Med* 1:359-360, 1982.
40. Smulian JC, Ranzini AC, Ananth CV, et al: Comparison of three sonographic circumference measurement techniques to predict birth weight. *Obstet Gynecol* 93:692-696, 1999.
41. Townsend RR, Filly RA, Callen PW, Laros RK: Factors affecting prenatal sonographic estimation of weight in extremely low birth weight infants. *J Ultrasound Med* 7:183-187, 1988.
42. Pineau JC, Grange G, Kapitaniak B, et al: Estimation of fetal weight: accuracy of regression models versus accuracy of ultrasound data. *Fetal Diagn Ther* 24:140-145, 2008.
43. Goldstein RB, Filly RA, Simpson G: Pitfalls in femur length measurements. *J Ultrasound Med* 6:203-207, 1987.
44. Doubilet PM, Benson CB: Improved prediction of gestational age in the late third trimester. *J Ultrasound Med* 12:647-653, 1993.
45. Guihard-Costa AM, Droulle P, Thiebaugeorges O, Hascoet JM: A longitudinal study of fetal growth variability. *Biol Neonate* 78:8-12, 2000.
46. Benson CB, Doubilet PM: Fetal measurements for predicting gestational age in the second and third trimesters: a reappraisal with a more reliable gold standard. *Radiology* 169(P):210, 1988.
47. Hadlock FP, Deter RL, Harrist RB, Park SK: Estimating fetal age: computer-assisted analysis of multiple fetal growth parameters. *Radiology* 152:497-501, 1984.
48. Hadlock FP, Harrist RB, Shah YP, et al: Estimating fetal age using multiple parameters: a prospective evaluation in a racially mixed population. *Am J Obstet Gynecol* 156:955-957, 1987.
49. Mongelli M, Chew S, Yuxin NG, Biswas A: Third-trimester ultrasound dating algorithms derived from pregnancies conceived with artificial reproductive techniques. *Ultrasound Obstet Gynecol* 26:129-131, 2005.
50. Johnsen SL, Rasmussen S, Sollien R, Kiserud T: Fetal age assessment based on femur length at 10-25 weeks of gestation, and reference ranges for femur length to head circumference ratios. *Acta Obstet Gynecol Scand* 84:725-733, 2005.
51. Warsof SL, Gohari P, Berkowitz RL, Hobbins JC: The estimation of fetal weight by computer assisted analysis. *Am J Obstet Gynecol* 128:881-892, 1977.
52. Shepard MJ, Richards VA, Berkowitz RL, et al: An evaluation of two equations for predicting fetal weight by ultrasound. *Am J Obstet Gynecol* 142:47-54, 1982.
53. Thurnau GR, Tamura RK, Sabbagha R, et al: A simple estimated fetal weight equation based on real time ultrasound measurements of fetuses less than thirty four weeks' gestation. *Am J Obstet Gynecol* 145:557-561, 1983.
54. Jordaan HVF: Estimation of fetal weight by ultrasound. *J Clin Ultrasound* 11:59-66, 1983.
55. Hadlock FP, Harrist RB, Carpenter RJ, et al: Sonographic estimation of fetal weight: the value of femur length in addition to head and abdomen measurements. *Radiology* 150:535-540, 1984.
56. Hadlock FP, Harrist RB, Sharman RS, et al: Estimation of fetal weight with the use of head, body, and femur measurements: a prospective study. *Am J Obstet Gynecol* 151:333-337, 1985.
57. Birnholz JC: An algorithmic approach to accurate ultrasonic fetal weight estimation. *Invest Radiol* 21:571-576, 1986.
58. Siemer J, Egger N, Hart N, et al: Fetal weight estimation by ultrasound: comparison of 11 different formulae and examiners with differing skill levels. *Ultraschall Med* 29(2):159-164, 2008.
59. Hoopmann M, Abele H, Wagner N, et al: Performance of 36 different weight estimation formulae in fetuses with macrosomia. *Fetal Diagn Ther* 27:204-213, 2010.
60. Scott F, Beeby P, Abbott J, et al: New formula for estimating fetal weight below 1000 g: comparison with existing formulas. *J Ultrasound Med* 15:669-672, 1996.
61. Dudley NJ: A systematic review of the ultrasound estimation of fetal weight. *Ultrasound Obstet Gynecol* 25:80-89, 2005.
62. Barel O, Vaknin Z, Tovbin J, et al: Assessment of the accuracy of multiple sonographic fetal weight estimation formulas, a 10-year experience from a single center. *J Ultrasound Med* 32(5):815-823, 2013.
63. Scioscia M, Scioscia F, Vimercati A, et al: Estimation of fetal weight by measurement of fetal thigh soft-tissue thickness in the late third trimester. *Ultrasound Obstet Gynecol* 31:314-320, 2008.
64. Vintzileos AM, Campbell WA, Rodis JF, et al: Fetal weight estimation formulas with head, abdominal, femur, and thigh circumference measurements. *Am J Obstet Gynecol* 157:410-414, 1987.
65. Lee W, Deter RL, Ebersole JD, et al: Birth weight prediction by three-dimensional ultrasonography. *J Ultrasound Med* 20:1283-1292, 2001.
66. Song TB, Moore TR, Lee JY, et al: Fetal weight prediction by thigh volume measurement with three-dimensional ultrasonography. *Obstet Gynecol* 96:157-161, 2000.
67. Schild RL, Fimmers R, Hansmann M: Fetal weight estimation by three-dimensional ultrasound. *Ultrasound Obstet Gynecol* 16:445-452, 2000.
68. Anderson NG, Jolley IJ, Wells JE: Sonographic estimation of fetal weight: comparison bias, precision and consistency using 12 different formulae. *Ultrasound Obstet Gynecol* 30(2):173-179, 2007.
69. Kehl S, Schmidt U, Spaich S, et al: What are the limits of accuracy in fetal weight estimation with conventional biometry in two dimensional ultrasound? A novel postpartum study. *Ultrasound Obstet Gynecol* 39:543-548, 2012.
70. Khalil A, D'Antonia F, Dias T, et al: Ultrasound estimation of birth weight in twin pregnancy: comparison of biometry algorithms in the STORK multiple pregnancy cohort. *Ultrasound Obstet Gynecol* 44:2210-2220, 2014.
71. Ashwal E, Hiersch L, Melamed N, et al: Does the level of amniotic fluid have an effect on the accuracy of sonographic estimated fetal weight at term? *J Matern Fetal Neonatal Med* 28(6):638-642, 2015.
72. Chauhan SP, Scardo JA, Hendrix NW, et al: Accuracy of sonographically estimated fetal weight with and without oligohydramnios. *J Reprod Med* 44:969-973, 1999.
73. Benson CB, Doubilet PM, Saltzman DH: Sonographic determination of fetal weights in diabetic pregnancies. *Am J Obstet Gynecol* 156:441-444, 1987.
74. Doubilet PM, Benson CB, Nadel AS, Ringer SA: Improved birth weight table for neonate developed from gestations dated by early ultrasonography. *J Ultrasound Med* 16:241-249, 1997.



75. Alexander GR, Himes JH, Kaufmann RB, et al: A United States national reference for fetal growth. *Obstet Gynecol* 87:163–168, 1996.
76. Brenner WE, Edelman DA, Hendricks CH: A standard of fetal growth for the United States of America. *Am J Obstet Gynecol* 126:555–564, 1976.
77. Lubchenco LO, Hansman C, Dressler M, Boyd E: Intrauterine growth as estimated from liveborn birth weight data at 24 to 42 weeks of gestation. *Pediatrics* 32:793–800, 1963.
78. Hadlock FP, Harrist RB, Martinez-Poyer J: In utero analysis of fetal growth: a sonographic weight standard. *Radiology* 181(1):129–133, 1991.
79. Doubilet PM, Benson CB, Wilkins-Haug L, Ringer S: Fetuses subsequently born premature are smaller than gestational-age-matched fetuses not born premature. *J Ultrasound Med* 22:359–363, 2003.
80. Lysikiewicz A, Bracero LA, Tejani N: Sonographically estimated fetal weight percentile as a predictor of preterm delivery. *J Matern Fetal Med* 10(1):44–47, 2001.
81. Mercer BM, Merlino AA, Milluzzi CJ, Moore JJ: Small fetal size before 20 weeks' gestation: associations with maternal tobacco use, early preterm birth, and low birthweight. *Am J Obstet Gynecol* 198:673–678, 2008.
82. Abramowicz JS, Ahn JT: Fetal macrosomia. *UpToDate* 2014. Available at <<http://www.uptodate.com/contents/fetal-macrosomia>>.
83. Pilliod RA, Chen YW, Snowden JM, et al: The risk of intrauterine fetal death in the small-for-gestational-age fetus. *Am J Obstet Gynecol* 207:318.e1–318.e6, 2012.
84. Chauhan SP, Ananth DV: Induction of labor in the United States: a critical appraisal of appropriateness and reducibility. *Semin Perinatol* 36:336–343, 2012.
85. Lindqvist PG, Molin J: Does antenatal identification of small-for-gestational age fetuses significantly improve their outcome? *Ultrasound Obstet Gynecol* 25:258–264, 2005.
86. Doctor BA, O'Riordan MA, Kirchner HL, et al: Perinatal correlates and neonatal outcomes of small for gestational age infants born at term gestation. *Am J Obstet Gynecol* 185:652–659, 2001.
87. Kramer MS, Olivier M, McLean FH, et al: Impact of intrauterine growth retardation and body proportionality on fetal and neonatal outcome. *Pediatrics* 86:707–713, 1990.
88. Hakanson DO, Oh W: Hyperviscosity in the small-for-gestational age infant. *Biol Neonate* 37:109–112, 1980.
89. Ferguson AC: Prolonged impairment of cellular immunity in children with intrauterine growth retardation. *J Pediatr* 93:52–56, 1978.
90. Williams RL, Creasy RK, Cunningham GC, et al: Fetal growth and perinatal viability in California. *Obstet Gynecol* 59:624–632, 1982.
91. Wennergren M, Wennergren G, Vilbergsson G: Obstetric characteristics and neonatal performance in a four-year small for gestational age population. *Obstet Gynecol* 72:615–620, 1988.
92. Piper JM, Xenakis EM, McFarland M: Do growth-retarded premature infants have different rates of perinatal morbidity and mortality than appropriately grown premature infants? *Obstet Gynecol* 87:169–174, 1996.
93. Kok JH, den Ouden AL, Verloove-Vanhorick SP, Brand R: Outcome of very preterm small for gestational age infants: the first nine years of life. *Br J Obstet Gynaecol* 105:162–168, 1998.
94. Divon MY: Fetal growth restriction: diagnosis. *UpToDate* 2014. Available at <[http://www.uptodate.com/contents/fetal-growth-restriction-diagnosis?source=search\\_result&search=growth+restriction&selectedTitle=2~150](http://www.uptodate.com/contents/fetal-growth-restriction-diagnosis?source=search_result&search=growth+restriction&selectedTitle=2~150)>.
95. American College of Obstetricians and Gynecologists: ACOG Practice Bulletin No. 134: fetal growth restriction. *Obstet Gynecol* 121(5):1122–1133, 2013.
96. Baschat AA: Doppler application in the delivery timing of the preterm growth-restricted fetus: another step in the right direction. *Ultrasound Obstet Gynecol* 23:111–118, 2004.
97. Mayer C, Joseph KS: Fetal growth: a review of terms, concepts and issues relevant to obstetrics. *Ultrasound Obstet Gynecol* 41:136–145, 2013.
98. Chen HY, Chauhan SP, Ward TC, et al: Aberrant fetal growth and early, late, and postneonatal mortality: an analysis of Milwaukee births, 1996–2007. *Am J Obstet Gynecol* 204(3):261.e1–261.e10, 2011.
99. Benson CB, Doubilet PM, Saltzman DH: Intrauterine growth retardation: predictive value of ultrasound criteria for antenatal diagnosis. *Radiology* 160:415–417, 1986.
100. Benson CB, Boswell SB, Brown DL, et al: Improved prediction of intrauterine growth retardation with use of multiple parameters. *Radiology* 168:7–12, 1988.
101. Benson CB, Belville JS, Lentini JF, et al: Diagnosis of intrauterine growth retardation using multiple parameters: a prospective study. *Radiology* 177:499–502, 1990.
102. Stirnemann JJ, Benoist G, Salomon LJ, et al: Optimal risk assessment of small-for-gestational-age fetuses using 31–34-week biometry in a low-risk population. *Ultrasound Obstet Gynecol* 43:311–316, 2014.
103. Benson CB, Doubilet PM: Doppler criteria for intrauterine growth retardation: predictive values. *J Ultrasound Med* 7:655–659, 1988.
104. Morris RK, Malin G, Robson SC, et al: Fetal umbilical artery Doppler to predict compromise of fetal/neonatal wellbeing in a high-risk population: systematic review and bivariate meta-analysis. *Ultrasound Obstet Gynecol* 37:135–142, 2011.
105. Lin CC, Santolaya-Forgas J: Current concepts of fetal growth restriction: part I. Causes, classification, and pathophysiology. *Obstet Gynecol* 92(6):1044–1055, 1998.
106. Ott WJ: The diagnosis of altered fetal growth. *Obstet Gynecol Clin North Am* 15:237–263, 1988.
107. Mintz MC, Landon MB: Sonographic diagnosis of fetal growth disorders. *Clin Obstet Gynecol* 31:44–52, 1988.
108. Landon MB, Mintz MC, Gabbe SG: Sonographic evaluation of fetal abdominal growth: predictor of the large for gestational age infant in pregnancies complicated by diabetes mellitus. *Am J Obstet Gynecol* 160:115–121, 1989.
109. Chauhan SP, Grobman WA, Gherman RA, et al: Suspicion and treatment of the macrosomic fetus: a review. *Am J Obstet Gynecol* 193(2):332–346, 2005.
110. Campbell S: Fetal macrosomia: a problem in need of a policy. *Ultrasound Obstet Gynecol* 43:3–10, 2014.
111. Pagani G, Palai N, Zatti S, et al: Fetal weight estimation in gestational diabetic pregnancies: comparison between conventional and three-dimensional fractional thigh volume methods using gestation-adjusted projection. *Ultrasound Obstet Gynecol* 43:72–76, 2014.
112. Acker DB, Sachs BP, Friedman EA: Risk factors for shoulder dystocia. *Obstet Gynecol* 66:762–768, 1985.
113. Langer O, Berkus MK, Huff RW, Sumueloff A: Shoulder dystocia: should the fetus weighing R4000 grams be delivered by cesarean section? *Am J Obstet Gynecol* 165:831–837, 1991.
114. Lipscomb KR, Gregory K, Shaw K: The outcome of macrosomic infants weighing at least 4500 grams: Los Angeles county plus University of Southern California experience. *Obstet Gynecol* 85:558–564, 1995.
115. Deter RL, Hadlock FP: Use of ultrasound in the detection of macrosomia: a review. *J Clin Ultrasound* 13:519–524, 1985.
116. Gross SJ, Shime J, Farine D: Shoulder dystocia: predictors and outcome. A five-year review. *Am J Obstet Gynecol* 156(2):334–336, 1987.
117. Bochner CJ, Medearis AL, Williams J, 3rd, et al: Early third-trimester ultrasound screening in gestational diabetes to determine the risk of macrosomia and labor dystocia at term. *Am J Obstet Gynecol* 157(3):703–708, 1987.
118. Sandmire HF, O'Halloin TJ: Shoulder dystocia: its incidence and associated risk factors. *Int J Gynaecol Obstet* 26:65–73, 1988.
119. Golditch IM, Kirkman K: The large fetus: management and outcome. *Obstet Gynecol* 52:26–30, 1978.
120. Benacerraf BR, Gelman R, Frigoletto FD: Sonographically estimated fetal weights: accuracy and limitation. *Am J Obstet Gynecol* 159:1118–1121, 1988.
121. Miller JM, Korndorffer FA, Gabert HA: Fetal weight estimates in late pregnancy with emphasis on macrosomia. *J Clin Ultrasound* 14:437–442, 1986.
122. Sabbagha RE, Minogue J, Tamura RK, Hungerford SA: Estimation of birth weight by use of ultrasonographic formulas targeted to large, appropriate, and small for gestational age fetus. *Am J Obstet Gynecol* 160:854–860, 1989.



123. Miller JM, Kissling GA, Brown HL, Gabert HA: Estimated fetal weight: applicability to small and large for gestational age fetus. *J Clin Ultrasound* 16:95–97, 1988.
124. Doubilet PM, Benson CB: Fetal growth disturbances. *Semin Roentgenol* 25:309–316, 1990.
125. Miller JM, Korndorffer FA, Kissling GE, et al: Recognition of the overgrown fetus: in utero ponderal indices. *Am J Perinatol* 4:86–89, 1987.
126. Chamberlain PF, Manning FA, Morrison I: Ultrasound evaluation of amniotic fluid volume. II. The relationship of increased amniotic fluid volume to perinatal outcome. *Am J Obstet Gynecol* 150:250–254, 1984.
127. Benson CB, Doubilet PM: Amniotic fluid volume in the large for gestational age fetus. *Radiology* 173(P):248, 1989.
128. Miller JM, Brown HL, Khawli OF, et al: Ultrasonographic identification of the macrosomic fetus. *Am J Obstet Gynecol* 159:1110–1114, 1988.
129. Chauhan SP, West DJ, Scardo JA, et al: Antepartum detection of macrosomic fetus: clinical versus sonographic, including soft-tissue measurements. *Obstet Gynecol* 95:639–642, 2000.
130. Campbell S, Thomas A: Ultrasound measurement of the fetal head to abdominal circumference in the assessment of growth retardation. *Br J Obstet Gynaecol* 84:165–174, 1977.
131. Tongsong T, Wanapirak C, Takapijitra A: Ultrasonic measurement of the fetal head to abdominal circumference ratio in normal pregnancy. *J Med Assoc Thai* 76(3):153–158, 1993.
132. Hadlock FP, Harrist RB, Fearneyhough TC, et al: Use of femur length/abdominal circumference ratio in detecting the macrosomic fetus. *Radiology* 154:503–505, 1985.
133. Hadlock FP, Deter RL, Harrist RB, et al: A date-independent predictor of intrauterine growth retardation: femur length/abdominal circumference ratio. *AJR Am J Roentgenol* 141(5):979–984, 1983.
134. Benson CB, Doubilet PM, Saltzman DH, Jones TB: FL/AC ratio: poor predictor of intrauterine growth retardation. *Invest Radiol* 20:727–730, 1985.
135. Hadlock FP, Harrist RB, Martinez-Poyer J: Fetal body ratios in second trimester: a useful tool for identifying chromosomal abnormalities? *J Ultrasound Med* 11(2):81–85, 1992.
136. Nyberg DA, Resta RG, Luthy DA, et al: Humerus and femur length shortening in the detection of Down's syndrome. *Am J Obstet Gynecol* 168:534–538, 1993.
137. Benacerraf BR, Neuberger D, Frigoletto FD: Humeral shortening in second-trimester fetuses with Down syndrome. *Obstet Gynecol* 77:223–227, 1991.
138. Agathokleous M, Chaveeva P, Poon LC, et al: Meta-analysis of second-trimester markers for trisomy 21. *Ultrasound Obstet Gynecol* 41:247–261, 2013.
139. Pilu G, Falco P, Milano V, et al: Prenatal diagnosis of microcephaly assisted by vaginal sonography and power Doppler. *Ultrasound Obstet Gynecol* 11:357–360, 1998.
140. Bromley B, Benacerraf BR: Difficulties in the prenatal diagnosis of microcephaly. *J Ultrasound Med* 14:303–306, 1995.
141. Lorenz JM, Whitaker AH, Feldman JF, et al: Indices of body and brain size at birth and at the age of 2 years: relations to cognitive outcome at the age of 16 years in low birth weight infants. *J Dev Behav Pediatr* 30(6):535–543, 2009.
142. Gale CR, O'Callaghan FJ, Bredow M, et al: The influence of head growth in fetal life, infancy, and childhood on intelligence at the ages of 4 and 8 years. *Pediatrics* 118(4):1486–1492, 2006.
143. Vermeer N, Bekker MN: Association of isolated short fetal femur with intrauterine growth restriction. *Prenat Diagn* 33:365–370, 2013.
144. de Carvalho AA, Carvalho JA, Figueiredo I Jr, et al: Association of midtrimester short femur and short humerus with fetal growth restriction. *Prenat Diagn* 33:130–133, 2013.
145. Doray B, Favre R, Viville B, et al: Prenatal sonographic diagnosis of skeletal dysplasias. A report of 47 cases. *Ann Genet* 43:163–169, 2000.
146. Parilla BV, Leeth EA, Kambich MP, et al: Antenatal detection of skeletal dysplasias. *J Ultrasound Med* 22:255–258, 2003.
147. Krakow D, Alanay Y, Rimoin LP, et al: Evaluation of prenatal onset osteochondrodysplasias by ultrasonography: a retrospective and prospective analysis. *Am J Med Genet A* 146A(15):1917–1924, 2008.
148. Jeanty PJ, Rodesch F, Delbeke D, Dumont JE: Estimation of gestational age from measurements of fetal long bones. *J Ultrasound Med* 3:75–79, 1984.
149. Jeanty P, Dramaix-Wilmet M, van Kerkem J, et al: Ultrasonic evaluation of fetal limb growth: part II. *Radiology* 143:751–754, 1982.
150. Malone FD, Ball RH, Nyberg DA, et al: FASTER Research Consortium: First-trimester nasal bone evaluation for aneuploidy in the general population. *Obstet Gynecol* 104(6):1222–1228, 2004.
151. Sepulveda W, Wong AE, Dezerega V: First-trimester ultrasonographic screening for trisomy 21 using fetal nuchal translucency and nasal bone. *Obstet Gynecol* 109:1040–1045, 2007.
152. Bromley B, Benacerraf B: Abnormalities of the hands and feet in the fetus: sonographic findings. *AJR Am J Roentgenol* 165:1239–1243, 1995.
153. Pajkrt E, Cicero S, Griffin DR, et al: Fetal forearm anomalies: prenatal diagnosis, associations and management strategy. *Prenat Diagn* 32:1084–1093, 2012.
154. Yarkoni S, Schmidt W, Jeanty P, et al: Clavicular measurement: a new biometric parameter for fetal evaluation. *J Ultrasound Med* 4:467–470, 1985.
155. Sherer DM, Sokolowski M, Dalloul M, et al: Fetal clavicle length throughout gestation: a nomogram. *Ultrasound Obstet Gynecol* 27:306–310, 2006.
156. Mercer BM, Sklar S, Shariatmadar A, et al: Fetal foot length as a predictor of gestational age. *Am J Obstet Gynecol* 156:350–355, 1987.
157. Hern WM: Correlation of fetal age and measurements between 10 and 26 weeks of gestation. *Obstet Gynecol* 63:26–32, 1984.
158. Mayden KL, Tortora M, Berkowitz RL, et al: Orbital diameters. A new parameter for prenatal diagnosis and dating. *Am J Obstet Gynecol* 144:289–297, 1982.
159. Jeanty P, Cantraine F, Coussaert E, et al: The binocular distance. A new way to estimate fetal age. *J Ultrasound Med* 3:241–243, 1984.
160. Goldstein I, Reece EA, Pilu G, et al: Cerebellar measurements with ultrasonography in the evaluation of fetal growth and development. *Am J Obstet Gynecol* 156:1065–1069, 1987.
161. Hata K, Hata T, Senoh D, et al: Ultrasonographic measurement of the fetal transverse cerebellum in utero. *Gynecol Obstet Invest* 28:111–112, 1989.
162. Konje JC, Abrams KR, Bell SC, Taylor DJ: Determination of gestational age after the 24th week of gestation from fetal kidney length measurements. *Ultrasound Obstet Gynecol* 19:592–597, 2002.
163. Sherer DM, Sokolowski M, Santoso PG, et al: Nomograms of sonographic measurements throughout gestation of the fetal hard palate width, length and area. *Ultrasound Obstet Gynecol* 24:35–41, 2004.
164. Law RG, MacRae KD: Head circumference as an index of fetal age. *J Ultrasound Med* 1:281–288, 1982.



# Ultrasound Evaluation in Multiple Gestations

Lynn L. Simpson

## SUMMARY OF KEY POINTS

- Early diagnosis and determination of chorionicity in the first trimester are critical for the optimal management of multiple gestations.
- Dichorionic twins may be either monozygotic or dizygotic, whereas essentially all monochorionic twins are monozygotic.
- In addition to risks for aneuploidy and malformations, increased nuchal translucency (NT) in monochorionic twins reflects the potential for complications related to inter-twin anastomoses within a shared placenta.
- Pregnancy risk for fetal structural anomalies is increased in multiple gestations, being highest in those with monochorionic placentation.
- Even with monozygotic twins, most structural anomalies are discordant and uncommonly affect both fetuses.
- Transvaginal sonography may be useful to assess for placenta previa, vasa previa, and cervical shortening, which are all increased in multiple pregnancies.
- Because of limitations of the physical examination and risks associated with abnormal fetal growth and amniotic fluid volume, monthly ultrasound examinations are recommended in multiple gestations.
- Multiples with monochorionic placentation require increased scrutiny and serial surveillance for a variety of unique complications such as twin-twin transfusion syndrome (TTTS), unequal placental sharing with discordant twin growth or selective fetal growth restriction (FGR), and twin anemia-polycythemia sequence (TAPS).

## OUTLINE

Embryology of Twins, 132  
 Pregnancy Dating, 133  
 Chorionicity, 135  
 Nuchal Translucency, 137  
 Anatomic Survey, 138  
 Placental Evaluation, 139  
 Cervical Length, 140  
 Fetal Growth Studies, 140  
 Serial Surveillance, 143

Monoamniotic Twins, 143  
 Conjoined Twins, 144  
 Twin Reversed Arterial Perfusion Syndrome, 144  
 Twin-Twin Transfusion Syndrome, 145  
 Twin Anemia-Polycythemia Sequence, 147  
 Unequal Placental Sharing With Discordant Twin Growth or Selective Fetal Growth Restriction, 148  
 Single Twin Demise, 148  
 Conclusion, 150

Ultrasound technology plays a critical role in the management of multiple gestations, which now compose over 3% of all live births in the United States<sup>1</sup> (Figs. 7-1 and 7-2). Advances in reproductive technologies have contributed to this increase, and, fortunately, these cases are detected early owing to the routine use of sonography in practices that provide these services. In contrast, half of all of twin pregnancies were undiagnosed until delivery in the years before sonography was integrated into obstetric practice.<sup>2</sup> Today, with wide availability of sonography, most multiple gestations are identified in the first trimester, providing the opportunity to individualize and optimize the care of these complicated pregnancies.

Multiple gestations pose special considerations as well as unique conditions that may necessitate additional imaging studies. Standard indications for sonography in multiple gestations include pregnancy dating, determination of chorionicity, nuchal translucency (NT) assessment, anatomic survey, placental evaluation, cervical length

assessment, routine fetal growth studies, and serial surveillance of pregnancies complicated by anomalies, fetal growth disturbances, and amniotic fluid abnormalities. Multiples with monochorionic placentation require increased scrutiny for monoamnicity, conjoined twins, twin reversed arterial perfusion (TRAP) syndrome, twin-twin transfusion syndrome (TTTS), unequal placental sharing with discordant twin growth or selective fetal growth restriction (FGR), twin anemia-polycythemia sequence (TAPS), and single fetal demise. Undoubtedly, ultrasound evaluation is essential for the supervision of multiple gestations in modern obstetrics.

## EMBRYOLOGY OF TWINS

The embryology of twin gestations includes the added complexity of the development of two embryos and either one or two placentas. Twins may be monozygotic or dizygotic, depending on the number of

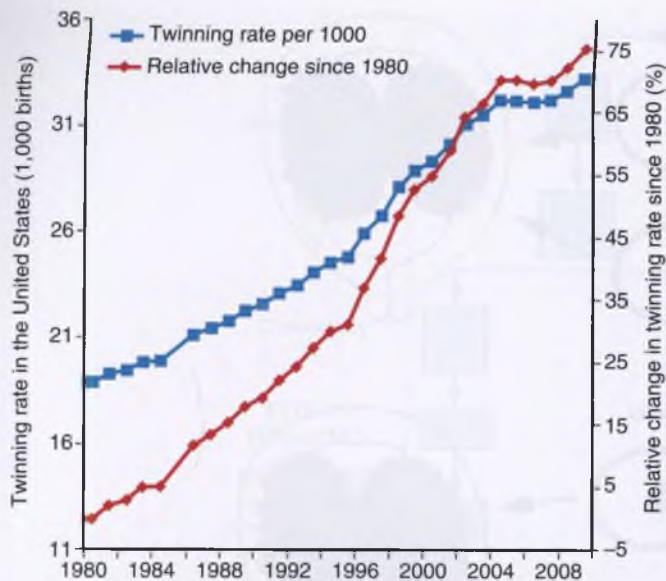


**FIG 7-1** Temporal trends in the rate of twinning (per 1,000 births), and the change in twinning rates in the United States, 1980 to 2009. (From Ananth CV, Chauhan SP: Epidemiology of twinning in developed countries. *Semin Perinatol* 36(3):156-161, 2012.)

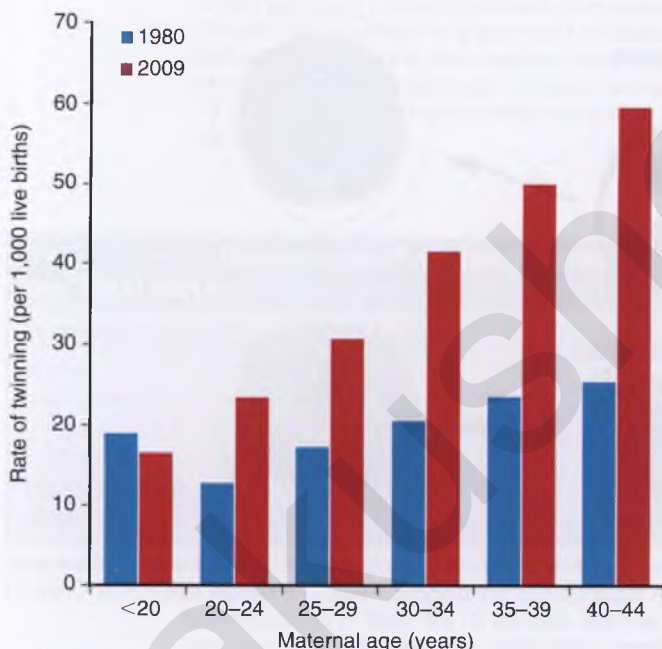


**FIG 7-2** Changes in the rate of twinning (per 1,000 births) in relation to maternal age in the United States, 1980 and 2009. (From Ananth CV, Chauhan SP: Epidemiology of twinning in developed countries. *Semin Perinatol* 36(3):156-161, 2012.)

ova that are fertilized at conception (Fig. 7-3). Monozygotic twins result from fertilization of one ovum by one sperm with subsequent division into two embryos. Because they have the same genome, they are often referred to as “identical” twins, although influences on development after conception mean that monozygotic twins are not truly identical. Dizygotic twins result from fertilization of two ova by two sperm (Figs. 7-3 and 7-4). These fetuses are no more closely related than other siblings and are therefore sometimes referred to as “fraternal twins.”

Unlike dizygotic twinning, the rate of monozygotic twinning is constant worldwide and occurs in approximately 1/250 pregnancies (Table 7-1). The timing of cleavage in monozygotic twins determines the type of placentation and the likelihood of additional complications. This effect is depicted in Figure 7-5 and Table 7-2, which demonstrate the timing and types of placentation. Dichorionic placentation is present in approximately 1/3 of monozygotic twins and results from cleavage very early, in the first 3 days after conception. Monochorionic placentation occurs in 2/3 of monozygotic twins and results from cleavage between days 4 and 8 after conception. Monoamniotic pregnancies are much less common, reported in fewer than 1% of monozygotic gestations, and result from splitting on days 9 to 12. Finally, conjoined twins result from very late attempts at cleavage on day 13 or later. With very rare exceptions, dizygotic twins always have dichorionic-diamniotic placentation.

Although the rate of monozygotic twinning is relatively constant in spontaneous twin gestations, it is increased by assisted reproductive technologies (ARTs), particularly those that involve embryo manipulation or later embryo transfer.<sup>3,4</sup> The rate of monozygotic twinning with ART is increased approximately 2- to 12-fold. The frequency of dizygotic twinning, in contrast, varies and is associated with maternal age, race, geography, and use of fertility treatment.<sup>5,6</sup> Prior to the widespread use of assisted reproduction, the highest rates of dizygotic twinning were in Nigeria, where 49/1,000 live births were twin pregnancies, and lowest in Japan at 1.3/1,000 live births (see Table 7-1). It is thought that the high rate in Nigerian women results from higher baseline levels of follicle-stimulating hormone.<sup>5</sup> The peak maternal age for spontaneous multiple gestations is 37 years old.<sup>6</sup>

With greater use of fertility treatments, including ovulation induction as well as ARTs, the geographic differences in rates of twinning have changed over time. In one survey in the United Kingdom in 2003, it was reported that 1.4% of deliveries were twins and 0.01% were triplets. ARTs were used in 1.9% of all pregnancies, with 13.5% of ART pregnancies associated with multiple gestations versus 1.2% in spontaneous conceptions.<sup>7</sup> Recognition of the higher perinatal morbidity and mortality risks in multifetal pregnancies has resulted in efforts to decrease the rate of this complication by judicious use of ovulation induction as well as an emphasis on single embryo transfer in ART pregnancies.<sup>8</sup>

## PREGNANCY DATING

Accurate pregnancy dating is important for the timing of screening and diagnostic testing as well as the correct interpretation of fetal growth in multiple gestations. Experts now recommend that uncomplicated dichorionic twins be delivered at 38 weeks, monochorionic twins at 36 weeks, and monoamniotic twins at 34 weeks.<sup>9</sup> Early confirmation of gestational age, with establishment of a fixed due date, is necessary for delivery planning in multiple pregnancies.

As in singletons, determining gestational age is best accomplished in the first trimester using the crown-rump length (CRL)<sup>10</sup> (Fig. 7-6). Accuracy of the CRL, obtained prior to 14 weeks, to predict the due date is  $\pm 5$  to 7 days.<sup>11</sup> After the first trimester, multiple biometric measurements should be used to date the pregnancy but this approach is less precise. For multiples conceived by in vitro fertilization (IVF), dating by embryo transfer is comparable to dating by CRL in the first trimester. In both spontaneous and IVF conceived multiple gestations, dating can be uncertain if there is a significant discrepancy in size between the fetuses. In these cases, dating based on the size of the larger fetus decreases the risk of overlooking early FGR, although the smaller CRL has been shown to be more accurate in the estimation of gestational age.<sup>12,13</sup>



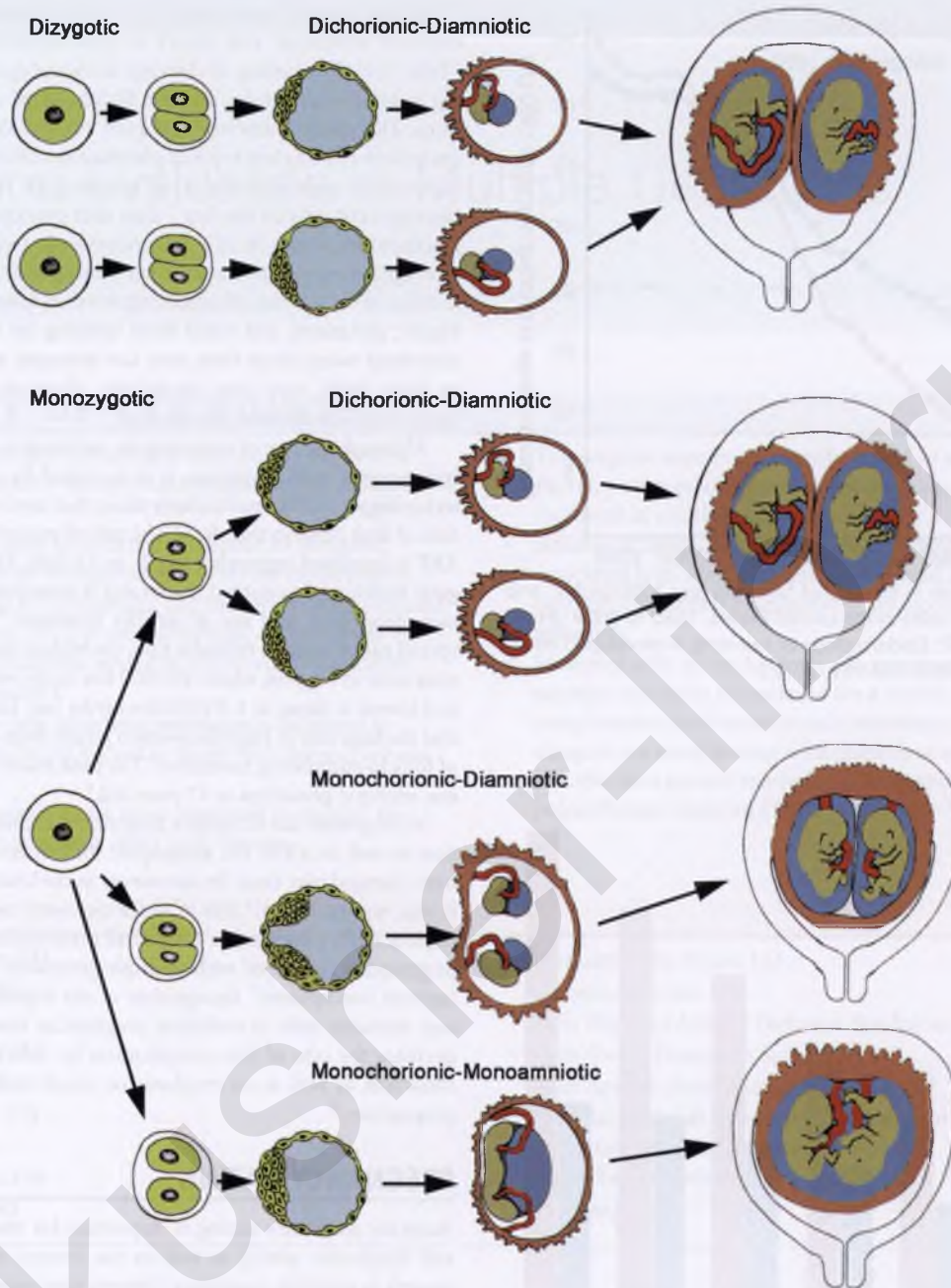
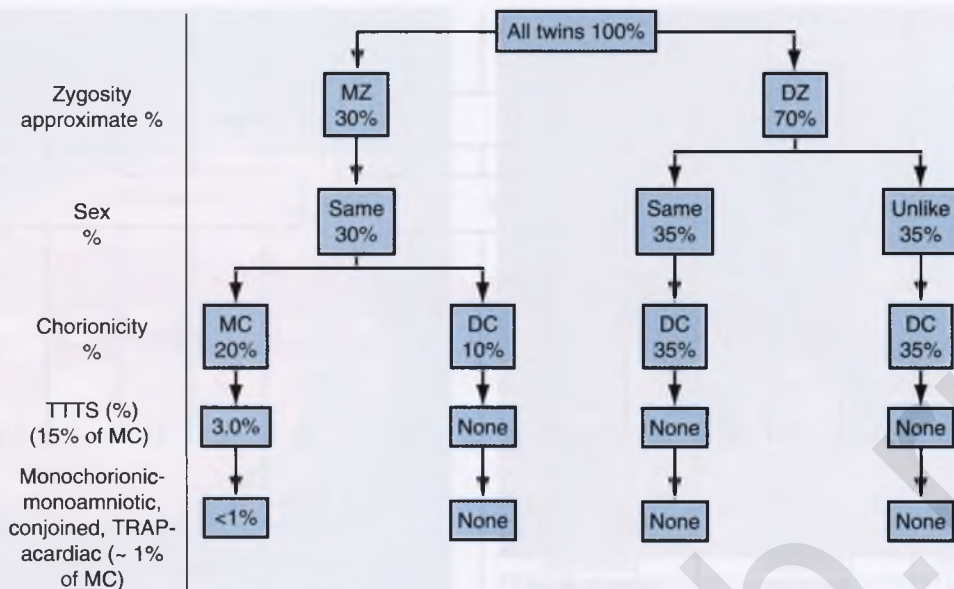


**FIG 7-3** Diagram of the development and placentation of dizygotic and monozygotic twins. The degree to which monozygotic twins share placentas, chorions, and amnions depends on the stage of development at which splitting occurs. (Modified from Larsen WJ: Human Embryology, 2nd ed. New York, Churchill Livingstone, 1997.)



MZ monozygous, DZ dizygous, MC monochorionic, DC dichorionic, TTTS twin to twin transfusion syndrome, TRAP twin reversed arterial perfusion.

**FIG 7-4** Approximate distribution of monozygous (MZ) and dizygous (DZ) twinning with chorionicity and complications of monozygous twins as a percentage of all twins. This represents the approximate distribution of twin gestations in the United States by zygoty and chorionicity. Both monochorionic (MC) and dichorionic (DC) twin gestations are at greater risk for maternal and fetal/neonatal complications (such as preeclampsia, diabetes, structural fetal abnormalities, aneuploidy, growth restriction) when compared with singleton gestations. Complications found only in monochorionic twin gestations include twin-twin transfusion syndrome (TTTS), monochorionic-monoamniotic twins, twin reversed arterial perfusion (TRAP) acardiac twins, conjoined twins, and fetus in fetu.

**TABLE 7-1 Geographic Twinning Rates per 1000 Births**

Geographic Area	Monozygotic	Dizygotic
Nigeria	5.0	49.0
United States		
Black	4.7	11.1
White	4.2	7.1
England and Wales	3.5	8.8
Japan	3.0	1.3

Adapted from MacGillivray I: Epidemiology of twin pregnancy. *Semin Perinatol* 10:4, 1986.

**CHORIONICITY**

Chorionicity impacts obstetric management as well as the risk of possible complications and adverse perinatal outcomes in multiple pregnancies. Selective reduction of an abnormal fetus or multifetal reduction in higher-order multiple pregnancies relies on accurate determination of chorionicity to inform procedural decisions. Correct assignment of chorionicity using sonography is nearly 100% when done in the first trimester compared to an approximate 10% likelihood of error in the second trimester.<sup>14,15</sup> A 2014 study found that before 20 weeks, sonography incorrectly assigned chorionicity in 6.4% of twins overall, with 4% of dichorionic twins and 19% of monochorionic twins misclassified.<sup>16</sup> Although dizygous twins are always dichorionic, placentation in monozygous twins varies, depending on the timing of embryo division after fertilization, and is more difficult to assess with

advancing gestational age<sup>17</sup> (Table 7-3). Therefore, chorionicity should be established at the time of the initial sonogram, optimally in the first trimester.

The approach to assigning chorionicity depends on gestational age. Early in the first trimester, the number of gestational sacs equals the number of chorions (Fig. 7-7 and Table 7-4). Late in the first trimester, the visualization of two separate placentas can be used to diagnose dichorionicity (Fig. 7-8). In cases with a single placenta or adjacent apparently “fused” placentas, evaluation of the intervening membrane can help distinguish between monochorionic and dichorionic placentation. Membrane thickness, number of membrane layers, and presence of either the lambda sign or T-sign at the base on the intervening membrane can be evaluated using ultrasound imaging. In dichorionic twins, the separating membrane tends to be thicker, as it is composed of two layers of amnion and two layers of chorion, compared to only two layers of amnion in monochorionic twins. Although a membrane thickness of 2 mm has been used as a threshold to distinguish between dichorionic and monochorionic twins, it does not perform reliably as a diagnostic test.<sup>18</sup> The lambda sign, consisting of a small triangular wedge of echogenic chorionic tissue observed between layers of the intervening membrane at its base, where it meets the fetal surface of the placenta, is diagnostic of dichorionicity<sup>19</sup> (Figs. 7-9 and 7-10). The lambda sign is best visualized in the late first and early second trimesters of pregnancy. It is important to remember that this sign does not necessarily persist on follow-up scans later in pregnancy, but when seen, it helps confirm dichorionicity. The T-sign, which appears as a thin linear structure, composed of two opposing layers of amnion, forming a perpendicular angle where it intersects the fetal surface of the shared placenta, is characteristic of monochorionic placentation



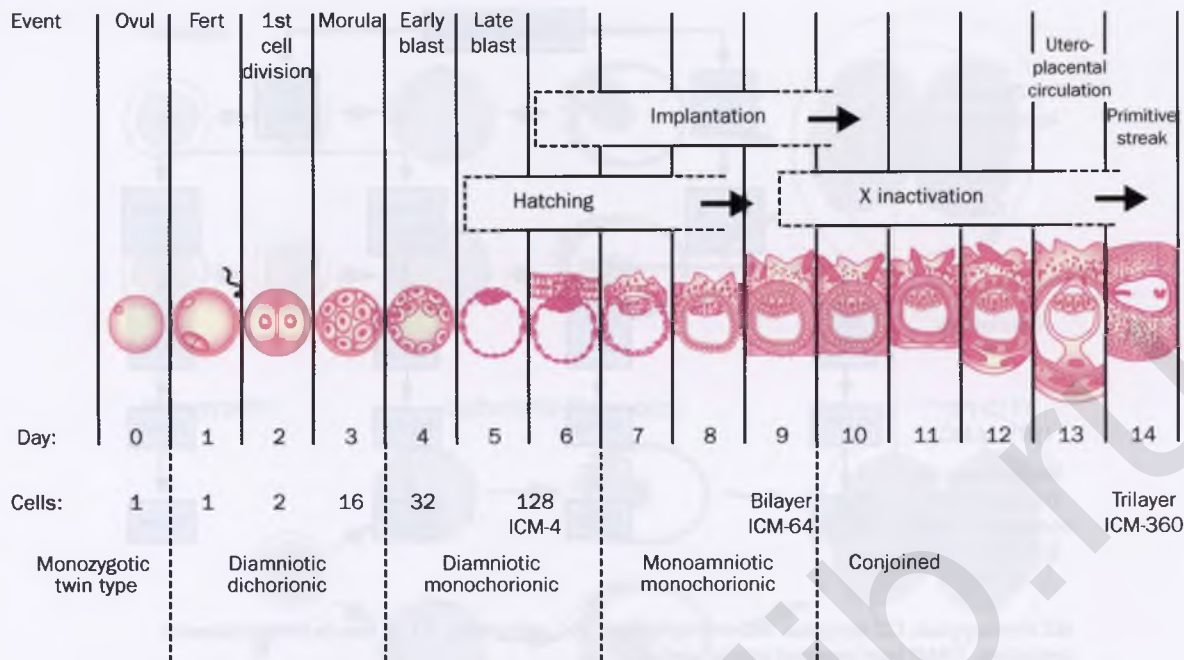


**FIG 7-5** The timing of monozygotic twinning demonstrating the impact of the day cleavage occurs on placentation and complications, that is, monochorionic monoamniotic placenta or conjoined twins. Fert, fertilization; ICM, inner cell mass; Ovul, ovulation. (Modified from JG Hall: Twins and twinning. In Rimoin DL, Connor JM, Pyeritz RE (eds): Emery and Rimoin's Principles and Practice of Medical Genetics, 4th ed. New York, Churchill Livingstone, 2001, vol. 1, pp 501-513.)

**TABLE 7-2** Types of Monozygotic Twins Related to Time of Division After Ovum Fertilization

Chorion	Amnion	Time to Division (Days)	Frequency
Dichorionic	Diamniotic	0-3	25%
Monochorionic	Diamniotic	4-8	75%
Monochorionic	Monoamniotic	9-12	~1%
Monochorionic	Monoamniotic (conjoined twins)	13-15	Rare

**TABLE 7-3** Types of Monozygotic Twins

Embryo Division After Fertilization	Chorion	Amnion	Frequency
0-3 days	Dichorionic	Diamniotic	25%
4-8 days	Monochorionic	Diamniotic	75%
9-12 days	Monochorionic	Monoamniotic	1%
13-15 days	Monochorionic	Monoamniotic (conjoined twins)	Rare

Modified from Egan JFX, Borgida AF: Ultrasound evaluation of multiple pregnancies. In Callen PW (ed): Ultrasonography in Obstetrics and Gynecology, 5th ed. Philadelphia, Saunders Elsevier, 2008.



**FIG 7-6** First trimester crown-rump length (CRL) optimal for pregnancy dating. GA, gestational age.

(Figs. 7-10 and 7-11). Toward the end of the first trimester and beyond, fetal sex can also be assessed to aid in determination of chorionicity. Although this finding is not useful if both twins appear to be the same sex, different phenotypic findings (one with male and one with female external genitalia) imply dichorionicity except in very rare cases. These principles also apply when evaluating higher-order multiple gestations.

Establishing amnionicity is also important in the evaluation of multiples with monochorionic placentation because fetuses that share a single amniotic sac face increased risks and are managed differently. This is particularly true when caring for higher-order multiple

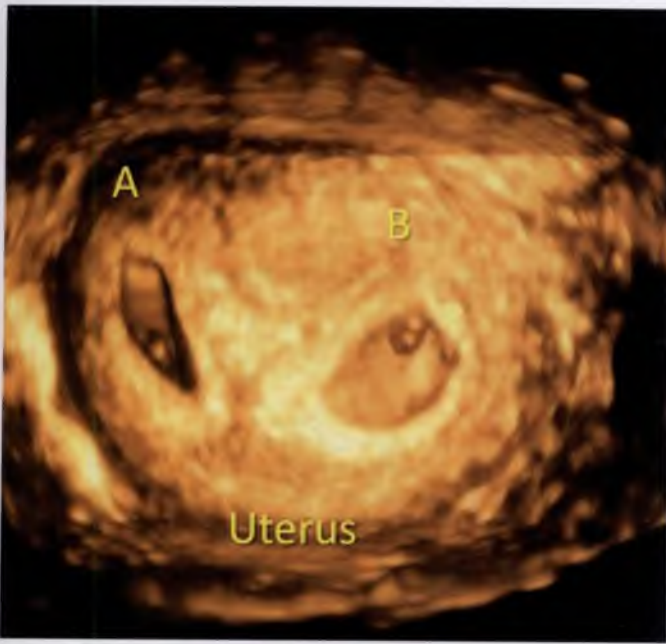


**FIG 7-7** Three-dimensional image of two distinct gestational sacs (A and B) indicating a dichorionic twin pregnancy.

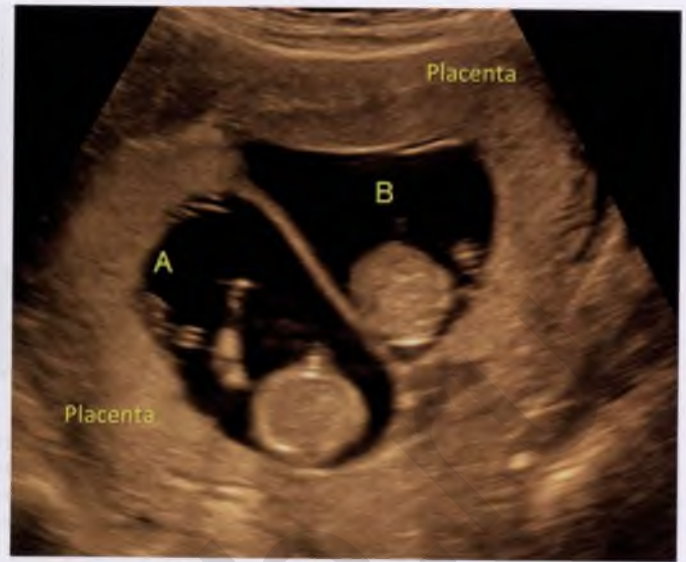


**FIG 7-8** Visualization of two separate placentas confirms dichorionicity.

**TABLE 7-4 Sonographic Determination of Chorionicity and Amnionicity in First Trimester Twin Gestations**

Placentation	Gestational Sacs	Yolk Sacs	Embryos/ Sac	Amniotic Cavities
DC, DA	2	2	1	2
MC, DA	1*	2	2*	2
MC, MA	1*	1 or partially divided*	2*	1

\*Amnionicity cannot be determined by this finding.

DA, diamniotic; DC, dichorionic; MA, monoamniotic; MC, monochorionic.

gestations that include a monochorionic twin pair. Although the number of yolk sacs seen early in gestation tends to equal the number of amnions, this is not a reliable diagnostic criterion. A transvaginal sonogram early in gestation can often demonstrate the two amnions of a monochorionic twin pregnancy (Fig. 7-12). Visualization of a separating inter-twin membrane ensures the presence of two amnions in both dichorionic and monochorionic gestations. In monochorionic twins, the intervening membrane can be very thin and difficult to identify, possibly leading to an incorrect diagnosis of monoamnioticity (Fig. 7-13). A transvaginal sonogram and repeat imaging in the first trimester may be required to distinguish between monochorionic diamniotic and monochorionic monoamniotic twin gestations (Fig. 7-14).

## NUCHAL TRANSLUCENCY

In both singleton and multiple gestations, NT measurements have been used in the evaluation of risk for aneuploidy and fetal anomalies. Overall, the sensitivity of NT combined with maternal age for detection of trisomy 21 in twins is comparable to that in singletons at over

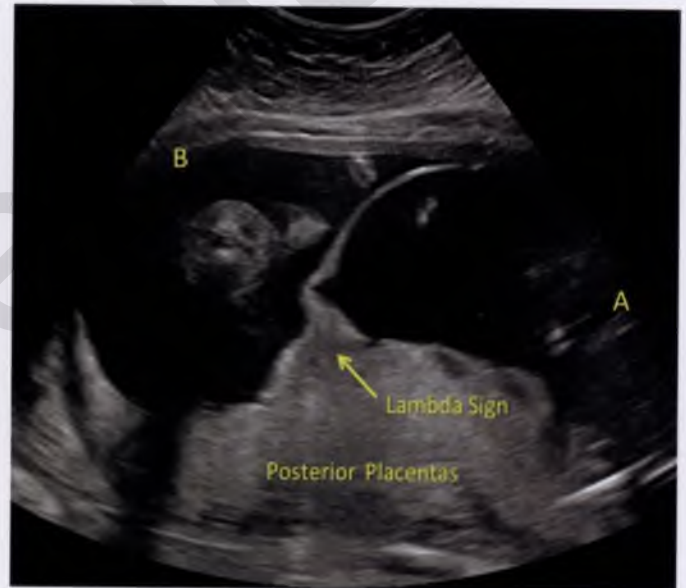


**FIG 7-9** The lambda sign (arrow) represents chorionic tissue wedged between layers of the intervening membrane (separating the gestational sacs of twins A and B) where it meets the fetal surface of the abutting placentas. This finding is not always present, but when seen, it is a useful indicator of dichorionicity.

70%, but the screen positive rate is higher, particularly in monochorionic twins.<sup>20</sup> Monochorionic twins have been observed to have increased NT measurements compared to dichorionic twins<sup>21</sup> (Fig. 7-15). This difference may reflect the higher likelihood of structural malformations in monozygotic twins as well as the potential for complications related to inter-twin vascular anastomoses within a shared placenta. The detection rate for Down syndrome in twin pregnancies can be increased by combining maternal age and NT with maternal serum analytes, although it is important that chorionicity be taken into consideration.<sup>22</sup> Because maternal serum screening has not been adequately studied in higher-order multiples and there are likewise limited data regarding the utility of cell-free DNA screening in multiple pregnancies, NT screening is still worthwhile for identifying



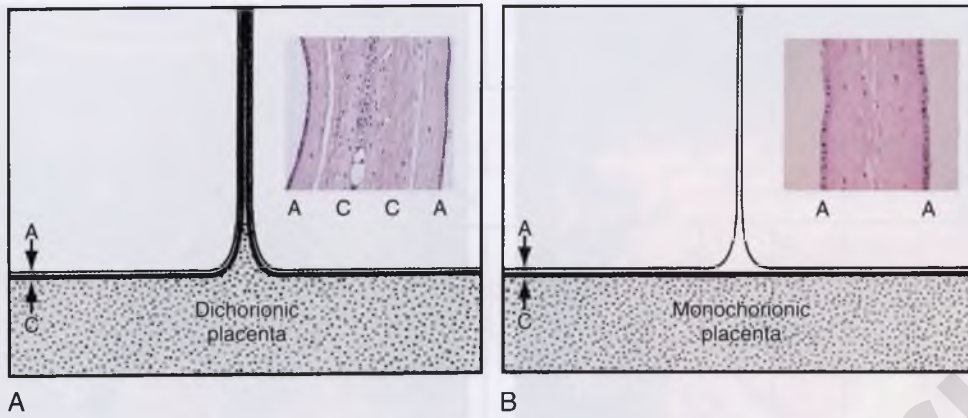


**FIG 7-10** Twin peak sign with placental pathologic images of fetal membranes. **A**, Diagram of the twin peak sign in dichorionic twin gestations. The chorion (C) and amnion (A) of each twin reflect away from the fused placenta to form the inter-twin membrane. A potential space exists between the membranes, which are filled with the amniotic and chorionic mesoderm as seen in the pathologic images of dichorionic membranes (see *inset*). **B**, In monochorionic-diamniotic twins the inter-twin membrane is composed of only two amnions. A single chorion does not allow the chorionic mesoderm to access the potential space between the diamniotic membranes as seen in the pathologic sample of monochorionic fetal membranes (see *inset*). (From Finberg HJ: The “twin peak” sign: reliable evidence of dichorionic twinning. *J Ultrasound Med* 11:571, 1992; pathologic images courtesy Melinda Sanders, MD, and Erika Walz, PA, University of Connecticut Health Center, Farmington, CT.)



**FIG 7-11** The T-sign (*arrow*) formed by the thin inter-twin membrane (composed of two layers of amnion, separating the sacs of A and B) where it meets perpendicular to the fetal surface of the single shared placenta—indicating a monochorionic diamniotic twin pregnancy.

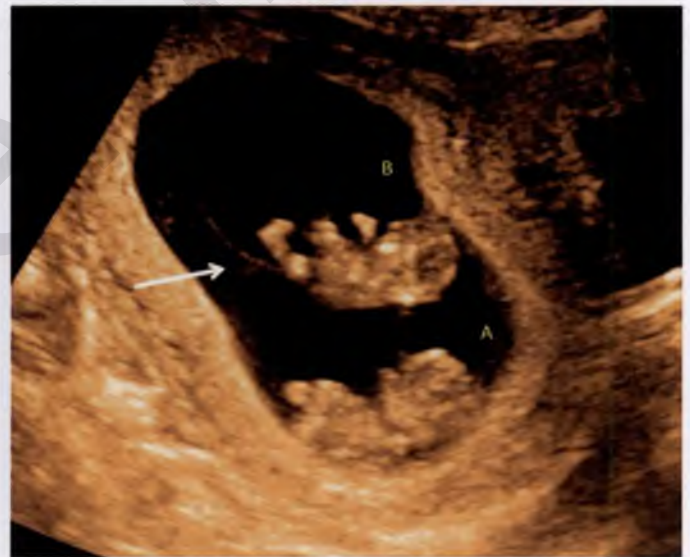


**FIG 7-12** Two amniotic sacs, each containing one twin (A and B), can be seen on this transvaginal ultrasound image. The thin separating membrane of this monochorionic diamniotic pregnancy will be formed by the two opposing layers of amnion (*arrow*).

a potentially abnormal fetus in a multiple gestation warranting further investigation.<sup>23</sup>

Cystic hygroma or hydrops identified at the time of NT assessment may reflect chromosomal or structural abnormalities in both singletons and multiples (Fig. 7-16). Although many different malformations have been associated with enlarged NT and first trimester cystic hygroma, both are recognized risk factors for major cardiac anomalies.<sup>24,25</sup> Furthermore, both structural and functional types of heart disease are more common in monochorionic twins, and an increased NT may identify those cases most at risk. An added benefit of assessing NT in monochorionic twins is that a 20% inter-twin difference in NT measurement is associated with a greater than 30% risk of fetal death or subsequent development of severe TTTS, thereby identifying those cases that warrant increased scrutiny during follow-up sonographic

surveillance.<sup>26</sup> Observation of enlarged NT, cystic hygroma, or early hydrops in a monochorionic pair of a higher-order multiple gestation may also influence recommendations and clinical decisions.

## ANATOMIC SURVEY

The main objective of the anatomic sonographic survey in multiples is the same as that in singletons: to provide reassurance that the fetuses are developing normally with no evidence of structural abnormalities. Overall, twin and triplet pregnancies have a higher background risk of major malformations, greater than the 2% reported in singletons.<sup>27</sup> Although the rate per fetus remains roughly the same in dizygotic





**FIG 7-13** Dichorionic triplet gestation with a monozygotic pair (B and C) in which amnionicity could not be firmly established early in the pregnancy. A membrane (arrow) was seen separating triplet A from B and C.



**FIG 7-14** Lack of an intervening membrane and visualization of a single amnion (arrow) confirms monozygotic monoamniotic twin pregnancy.

twins or trizygotic triplets, this amounts to an overall rate of 4% and 6% for such pregnancies, respectively (Fig. 7-17). The prevalence of birth defects in monozygotic twins is even higher, nearly twice that observed in dichorionic twins.<sup>28</sup> Interestingly, when both twins are found to have a structural malformation, only 10% of dichorionic and 20% of monozygotic twin pairs have the same defect.<sup>27</sup> Of twin pregnancies with congenital anomalies, only one twin is affected in about 90% of cases.<sup>27</sup> Heightened awareness with careful inspection for malformations is warranted whenever scanning twins and higher-order multiples.



**FIG 7-15** Monozygotic diamniotic twin pregnancy in which twin A was noted to have an enlarged nuchal translucency (NT) measuring 0.59 cm.

Approximately one third to one half of all birth defects are identified prenatally in singleton pregnancies, and the detection rate in twins and triplets is expected to be even lower.<sup>29</sup> Certain anomalies, such as those involving the central nervous system, are often recognized prenatally, whereas major cardiac abnormalities are frequently missed in twins<sup>29</sup> (Fig. 7-18). This difference is of clinical importance because congenital heart disease is more common in monozygotic twins, in which the prevalence is reported to be about 7.5%.<sup>30</sup> Although controversial, there are some data to suggest that fetuses conceived by IVF are also at increased risk for cardiac defects.<sup>31,32</sup> The standard cardiac screening examination, consisting of the four-chamber view of the heart and views of the great vessels and outflow tracts, identifies about one third of major heart defects prenatally.<sup>33,34</sup> Today, IVF, monozygosity, and increased NT are all accepted indications for fetal echocardiography, which when done in experienced centers can detect close to 100% of major cardiac anomalies.<sup>35</sup> Given the challenge of imaging multiple fetuses in variable positions at midgestation, repeat ultrasound examinations may be necessary to complete the anatomic sonographic surveys in these pregnancies. The management of discordant anomalies in multiples depends upon the gestational age at diagnosis, placentation, type of defect, and potential for associated pregnancy complications. Prenatal diagnosis in twin pregnancies is discussed in Chapter 2.

## PLACENTAL EVALUATION

The ultrasound evaluation of each placenta is essential in the assessment of multiple pregnancies. Placenta previa is 40% more common in twin and triplet gestations than in singletons, related in part to the greater placental mass and larger implantation site.<sup>36</sup> Vasa previa is also more common, secondary to the higher proportion of velamentous placental cord insertions (PCIs) noted in multiples, particularly those with monozygotic placentation.<sup>37</sup> Color flow Doppler ultrasound imaging during transvaginal sonography can help identify the presence of placental tissue or a fetal vessel overlying the cervix (Fig. 7-19).

Color flow Doppler sonography can also be used to identify and evaluate the PCI of each fetus, an important component of the ultrasound examination (Fig. 7-20). Both sonographic and pathologic studies have reported that marginal and velamentous cord insertions are more frequent in monozygotic diamniotic twins and that



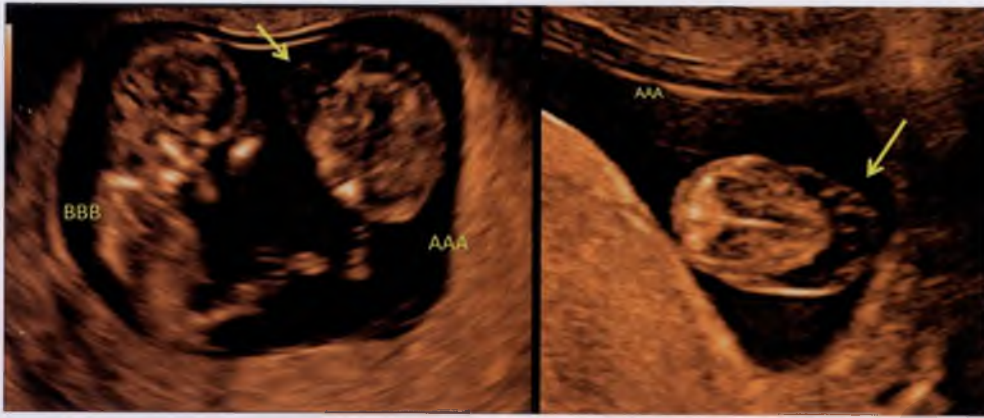


**FIG 7-16** Monozygotic monoamniotic twin pregnancy with cystic hygroma (arrows) shown affecting the twin labeled AAA. The twin labeled BBB appeared normal.



**FIG 7-17** Three-dimensional ultrasound image of triamniotic triplet pregnancy (labeled A, B, and C), each with a 2% risk of structural anomalies amounting to a total pregnancy risk of 6%.

velamentous cord insertion, in particular, is associated with an increased likelihood of TTTS, unequal placental sharing with discordant twin growth, and selective FGR<sup>38,39</sup> (Fig. 7-21). With velamentous insertion, fetal vessels are devoid of protective Wharton jelly as they traverse the membranes; this lack may contribute to the threefold increase in perinatal mortality rate observed in pregnancies with monozygotic placentation and velamentous PCI<sup>38</sup> (Fig. 7-22). PCI determination early in gestation can help identify those monozygotic diamniotic twins or higher-order multiples with a monozygotic twin pair that merit increased sonographic surveillance for TTTS and disturbances in twin growth.<sup>40</sup> Early detection of these complications should trigger adjustments in clinical management that may help decrease the risk of perinatal morbidity and mortality.

## CERVICAL LENGTH

Although universal screening of cervical length is controversial, its assessment can be useful in the management of patients with



**FIG 7-18** Absence of the calvarium (arrow) suggesting acrania in twin A of a monozygotic diamniotic pregnancy.

preexisting risk factors for preterm delivery. Over half of all twins deliver prior to term, as do almost all higher-order multiples, and thus, an awareness of cervical length can influence patient counseling and management of multiple gestations<sup>41</sup> (Fig. 7-23). Transvaginal sonography is optimal for visualization of the cervix and measurement of its length and its response to the Valsalva maneuver or fundal pressure. In the second trimester, a cervical length of 20 to 25 mm or less is observed in 5% to 10% of twins and increases the likelihood of preterm delivery threefold to fivefold.<sup>42</sup> The negative predictive value of a midtrimester cervical length measuring greater than 35 mm is over 90%, which provides reassurance to patients carrying twins.<sup>43</sup> Although the optimal cervical length threshold and the appropriate frequency of follow-up evaluation are uncertain, a baseline measurement in the midtrimester with serial assessment at the time of subsequent growth studies in the second and early third trimesters can identify those at highest risk for spontaneous preterm delivery. Despite a lack of data, this is a reasonable approach when caring for higher-order multiple pregnancies as well.

## FETAL GROWTH STUDIES

Ongoing sonographic assessment of fetal growth is necessary when managing multiple gestations. Abnormal growth may be evident as



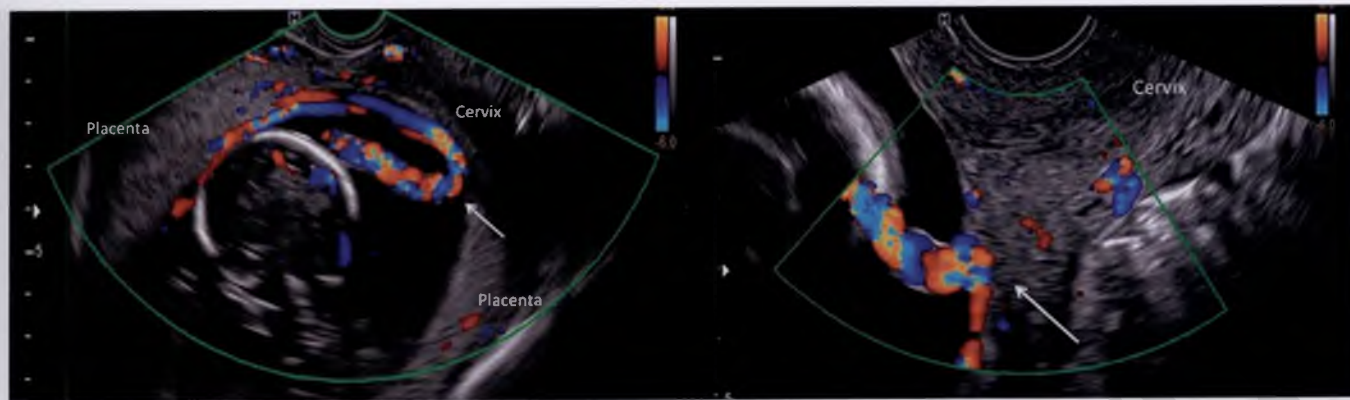


**FIG 7-19** Transvaginal sonography with color Doppler flow imaging demonstrates vasa previa, with fetal vessels crossing the cervix. The cord insertion is velamentous (*arrow*), in close proximity to the internal cervical os.



**FIG 7-20** Color flow Doppler ultrasound imaging is used to identify each placental cord insertion (PCI) of the monozygotic diamniotic twin pair (A and B). The thin inter-twin membrane is in close proximity to twin B (*arrow*).

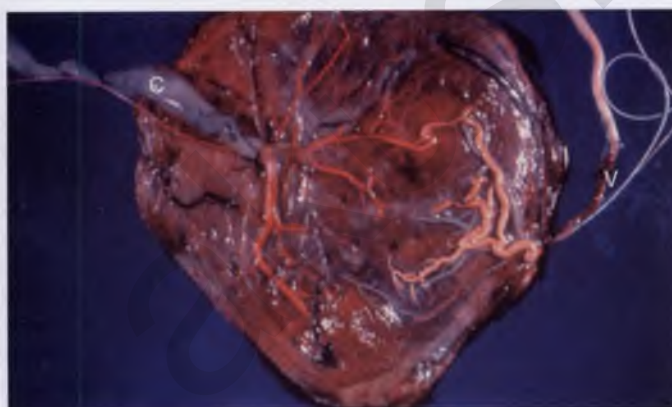


**FIG 7-21** Photograph of a monozygotic placenta. The cord insertion sites are shown to be central (C) for one twin and velamentous (V) for the other. (Courtesy Geoffrey A. Machin, MD, PhD.)



**FIG 7-22** Two-dimensional ultrasound image demonstrates a velamentous cord insertion (*arrow*) of twin B, directly into the separating inter-twin membrane.

can identify those cases that might benefit from increased antenatal surveillance.

Healthy singletons and twins tend to follow similar growth patterns until the third trimester, at which time twin growth begins to lag behind that of singletons.<sup>45</sup> FGR, defined as estimated fetal weight corresponding to less than the 10th percentile for gestational age, can be determined using singleton growth curves. Following twin or triplet growth using singleton curves assures that cases of suboptimal growth are not overlooked, as physiologic growth potential is best estimated with singleton growth curves. The downside of this approach is that many healthy fetuses of higher-order multiple pregnancies will be labeled as having FGR. The most commonly used definition of growth discordance between fetuses in a multiple gestation is variance of 20% or more, which is calculated as the difference between the estimated fetal weights of two fetuses, divided by the estimated fetal weight of the larger fetus. An early sonographic clue of impending discordant growth is disparate abdominal circumferences (Fig. 7-25). An inter-twin abdominal circumference difference of 20 mm or greater and a ratio of less than 0.93 are predictive of discordant birth weights.<sup>46</sup> Both

early as the first trimester (Fig. 7-24). Physical examination with abdominal palpation and symphysis-fundal height measurements are unreliable in predicting fetal sizes in multiple pregnancies, so sonographic estimation of twin or triplet growth is justified.<sup>44</sup> Serial sonographic estimations of fetal weight can detect early growth restriction or discordance that might otherwise be missed and



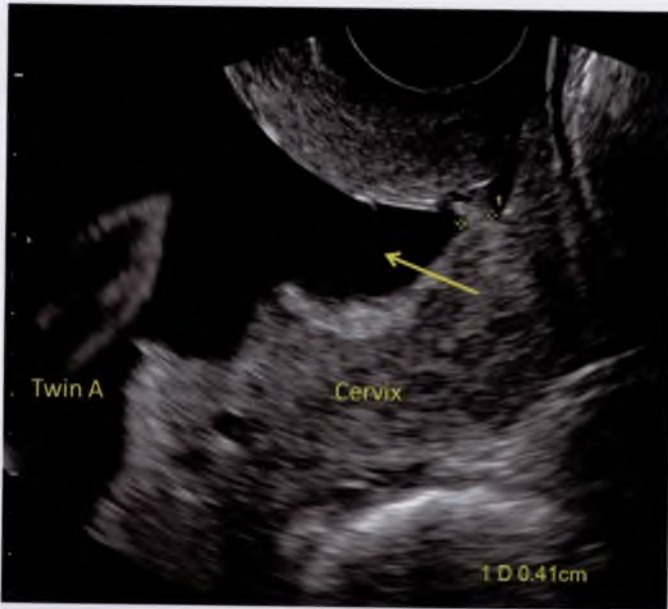


**FIG 7-23** Transvaginal ultrasound image showing a funneled short cervix, measuring 0.41 cm in length, in a monochorionic diamniotic twin gestation with oligohydramnios-polyhydramnios sequence. A portion of the amniotic membrane of the presenting twin A (arrow) is seen within the dilated cervical canal.



**FIG 7-24** Early discrepancy in crown-rump lengths (CRL) shown between a monochorionic diamniotic twin pair, labeled A and B. GA, gestational age.

FGR and twin discordance are associated with higher likelihood of fetal and perinatal death compared to normally grown and concordant twins.<sup>47,48</sup> The use of sonography to assess fetal size and growth every 4 weeks in multiple gestations is recommended for the early detection of growth abnormalities and timely initiation of antenatal fetal testing.

Amniotic fluid abnormalities may also be identified during routine sonographic examinations in multiple gestations, forewarning of potential complications (Fig. 7-26). Folding of the intervening membrane upon itself can sometimes be seen and may suggest early discrepancies in amniotic fluid volume between the two sacs (Fig. 7-27). Different methods to assess amniotic fluid volume in multiple gestations may be used, but a common approach is to measure the maximal vertical pocket (MVP) in each sac (Fig. 7-28). Using this method,



**FIG 7-25** Significant discordance in abdominal circumferences noted in this monochorionic diamniotic pregnancy, with lagging growth of twin B compared to twin A.



**FIG 7-26** Monochorionic diamniotic pregnancy with less amniotic fluid in the sac of twin A compared to the sac of twin B.



**FIG 7-27** Slight redundancy and focal fold of the thin separating membrane (arrow) of this monochorionic diamniotic twin pregnancy. Although this may be a normal observation, it can be seen in cases of evolving oligohydramnios-polyhydramnios sequence.



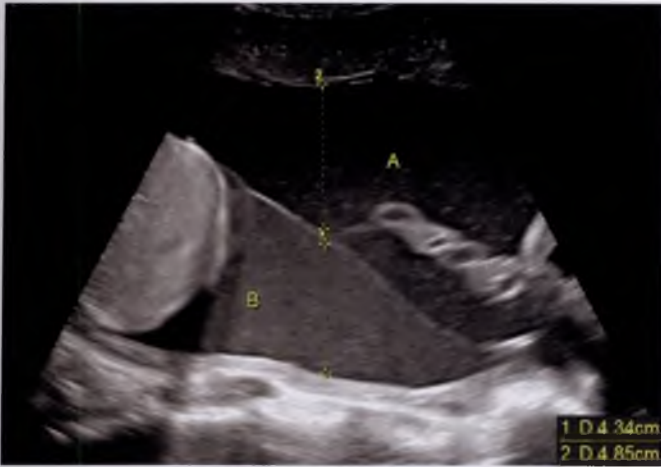


**FIG 7-28** Normal pocket of amniotic fluid shown and measured for each twin (A and B) in a monochorionic diamniotic pair.



**FIG 7-29** Twin-twin transfusion syndrome with polyhydramnios in the sac of twin A and oligohydramnios in the sac of twin B.

oligohydramnios is defined as an MVP smaller than 2 cm and polyhydramnios as an MVP larger than 8 cm.<sup>19,40</sup> As with singletons, pregnancies with oligohydramnios or polyhydramnios require additional investigation to determine the underlying cause, as well as serial antenatal testing to ensure fetal well-being. TTTS should be considered and addressed when both oligohydramnios and polyhydramnios are detected in pregnancies with monochorionic diamniotic placentation<sup>40</sup> (Fig. 7-29). In the third trimester, the position and presentation of the fetuses should be determined by sonography and reported, to aid in delivery planning. Sonography plays a key role in assessing potential candidates for vaginal delivery of a nonpresenting nonvertex twin. As experience and skills with breech delivery decline, planned cesarean delivery is increasing for all twin pregnancies to avoid combined vaginal-cesarean births. Although higher-order multiples are routinely delivered by cesarean, presentation as well as placental location of each fetus may inform intraoperative decision making.

## SERIAL SURVEILLANCE

Although serial surveillance by sonography is indicated in multiple pregnancies diagnosed with anomalies, fetal growth disturbances, and

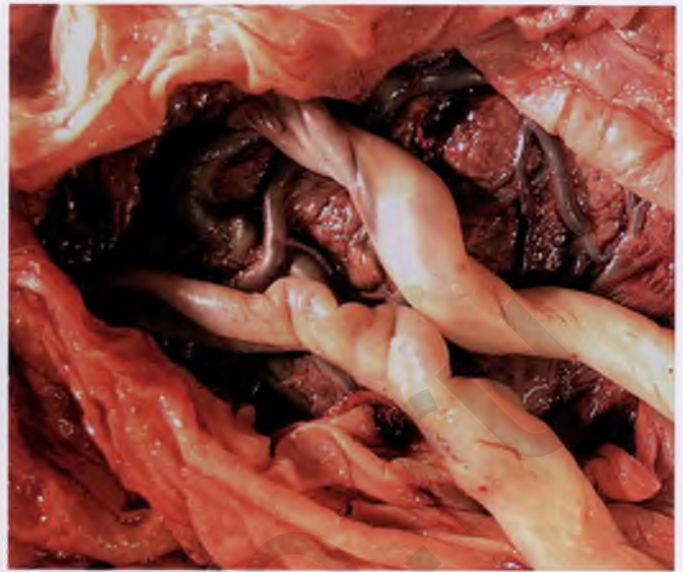


**FIG 7-30** Placenta showing both umbilical cords close to one another with no intervening membranes. (Pathologic image courtesy Melinda Sanders, MD, and Erika Walz, PA, University of Connecticut Health Center, Farmington, CT.)

amniotic fluid abnormalities, seemingly uncomplicated monochorionic twins require extra scrutiny as they are at risk for developing a number of unique conditions. These disorders are overrepresented in IVF-conceived pregnancies, as IVF appears to increase the risk of embryo splitting.<sup>49</sup> Nevertheless, all twin or higher-order multiple gestations with a monochorionic pair should be carefully evaluated for the following possible complications.

### Monoamniotic Twins

Overall, about 1% of monozygotic twins are monoamniotic, which should be suspected when a separating membrane cannot be visualized on serial sonograms.<sup>50</sup> The number of yolk sacs does not reliably reflect the number of amnions and therefore should not be used to determine amnionicity.<sup>51</sup> The thin intervening membrane associated with monochorionic diamniotic placentation can be difficult to visualize and is frequently missed in early pregnancy, leading to an incorrect diagnosis of monoamnicity. Monoamniotic gestation can also be incorrectly diagnosed later in pregnancy when the separating membrane encasing a “stuck” twin is closely apposed to the fetus with oligohydramnios and therefore is thought to be absent. This error can be avoided by repositioning the patient during the sonogram and reassessing fetal location, looking for monoamniotic twin fetuses to move freely within the shared amniotic sac. Possible errors in diagnosis must be taken into consideration when counseling patients with suspected monoamniotic twins in the first trimester. Twins sharing a single placenta within a single sac confirmed on repeat ultrasound imaging establishes the diagnosis of monoamnicity (Fig. 7-30). Entanglement of the umbilical cords also confirms that the twins share a common amniotic sac (Figs. 7-31 and 7-32). Color flow imaging has demonstrated entwined cords in virtually all monochorionic monoamniotic twins.<sup>52</sup>

The confirmation of monoamnicity affects patient counseling and alters pregnancy management. In women carrying higher-order multiple pregnancies, selective termination of a monoamniotic twin pair may be considered in order to decrease difficult management decisions and optimize healthy outcome of the remaining fetus(es). Congenital structural anomalies are found in up to 10% and cardiac defects in 4% of monoamniotic twins, with additional risks related to





**FIG 7-31** Color Doppler ultrasound image demonstrating entangled umbilical cords of monochorionic monoamniotic twins. PCI, placental cord insertion of twins A and B.

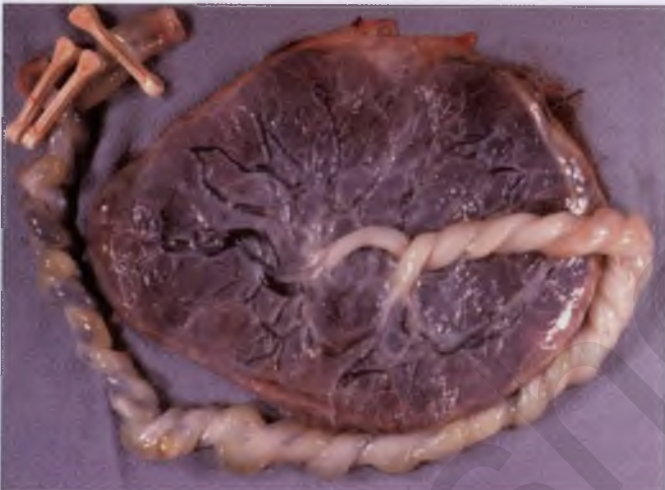


**FIG 7-32** The placenta of a monochorionic monoamniotic twin pregnancy with entanglement and twisting of the umbilical cords. (Courtesy Geoffrey A. Machin, MD, PhD.)

the single shared placenta.<sup>53</sup> Single or dual intrauterine fetal demise may result from cord entanglement, so increased antenatal testing of these high-risk twins is appropriate.<sup>53</sup> After careful detailed patient counseling, daily fetal monitoring and serial growth scans for monoamniotic pregnancies are initiated at approximately the age of fetal viability; management usually involves hospitalization for close surveillance at 24 to 28 weeks' gestation. This careful rigorous approach has resulted in decreased perinatal mortality rate from 30% to 50% to 10% to 20% in recent series.<sup>53,54</sup>

### Conjoined Twins

Conjoined twins are rare, affecting less than 1% of monozygotic twin pairs.<sup>55</sup> The diagnosis should be suspected when monozygotic fetuses are shown to consistently hold the same fixed position relative to each other. The location and extent of fusion between the twins determine the potential for surgical separation and postnatal survival. Conjoined twins are classified based upon the location of attachment, with thoracopagus twins representing over 40% of reported cases<sup>55</sup> (Table 7-5 and Figs. 7-33 and 7-34). All types of conjoined twins are at risk for

**TABLE 7-5 Common Types of Conjoined Twins (N = 383 cases)**

Type	Description	Frequency
Thoracopagus	Ventrally joined; thorax to upper abdomen, involves heart	42%
Parapagus dicephalus	Laterally joined; one trunk, two heads	11.6%
Cephalopagus	Laterally joined; top of head to umbilicus, two faces	5.5%
Omphalopagus	Ventrally joined; abdomen to lower thorax, never the heart	5.5%
Parasitic	Asymmetric, fetus in fetus	3.9%
Craniopagus	Skulls joined; shared meninges, not face or trunk	3.4%
Parapagus diprosopus	Laterally joined; one trunk, one head, two faces	2.9%
Ischiopagus	Lower abdomen and pelvic bones joined	1.8%
Rachipagus	Dorsally fused; dorsolumbar vertebrae area	1.0%
Pygopagus	Dorsally fused; perineal and sacrococcygeal area	1.0%
Unspecified	Rare types	21.4%

Data from Mutchinick OM, Luna-Munoz L, Amar E, et al: Conjoined twins: a worldwide collaborative epidemiological study of the International Clearinghouse for Birth Defects Surveillance and Research. *Am J Med Genet* 157:274-287, 2011.

associated structural malformations, which impact prognosis (Fig. 7-35). Although shared organs can be visualized on gray-scale sonography, color flow mapping with Doppler can delineate vascular communications between the circulations. If significant, these vascular connections can lead to cardiovascular compromise and twin death.

Early diagnosis of conjoined twins is important, as many patients will opt for termination because of the grave prognosis. When this condition is identified in higher-order multiple gestations, selective reduction of the conjoined pair is usually recommended to optimize outcome for the remaining fetus(es). Beyond the first trimester, termination of conjoined twins can be technically very difficult and in the third trimester, cesarean delivery is often necessary for patient safety. Overall, intrauterine fetal demise complicates over 10% of affected pregnancies and fewer than half of liveborn conjoined twins survive.<sup>56</sup> Sonographic surveillance in ongoing pregnancies should be individualized based on the condition of the conjoined twins, recommendations from the multidisciplinary team of providers, and input from the patient.

### Twin Reversed Arterial Perfusion Syndrome

TRAP syndrome complicates approximately 1% of monochorionic twins, with 75% occurring in diamniotic and 25% in monoamniotic twin pairs.<sup>57</sup> TRAP is characterized by a pump twin perfusing a dysmorphic acardiac fetus through aberrant arterioarterial anastomoses within the shared single placenta (Figs. 7-36 and 7-37). The sonographic diagnosis requires monochorionic placentation, a normal-appearing pump twin, an abnormal-appearing co-twin without discernible cardiac activity, and reversed arterial flow directed toward, rather than away from, the anomalous acardiac fetus (Fig. 7-38).<sup>57</sup> The use of color and spectral duplex Doppler interrogation, which indicate direction and character of flow, is particularly helpful in this setting, to confirm the diagnosis of TRAP (see Fig. 7-38). It is theorized that



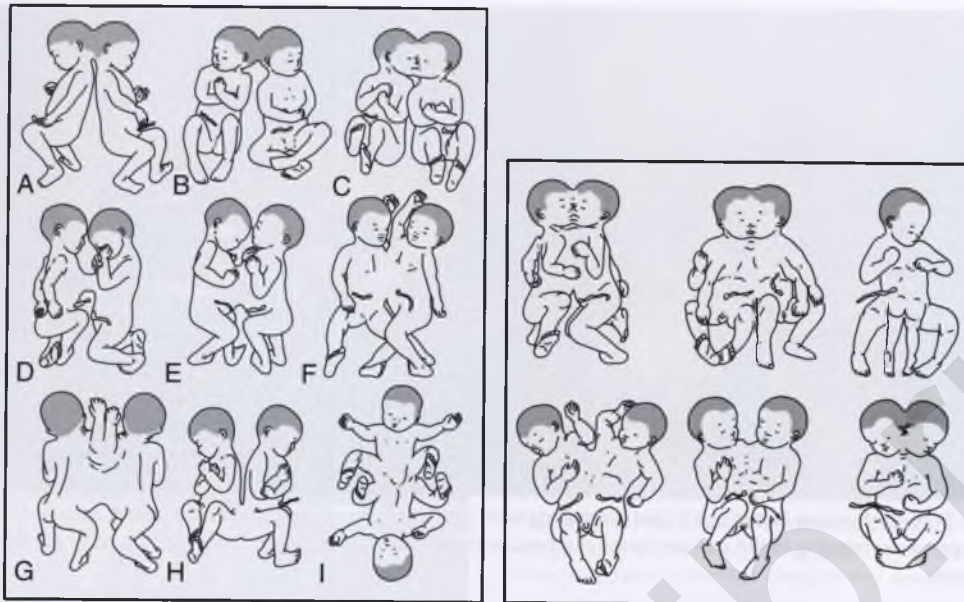


**FIG 7-33** Different types of conjoined twins. *Left*, Examples of limited fusions in which heads and limbs are separate and retain their identity: **A to C**, craniopagus; **D to G**, thoracopagus; **H and I**, pyopagus. *Right*, Examples of more extensive fusion. (From Patten BM: Human Embryology, 4th ed. New York, McGraw Hill, 1976, Figs. VIII-5, VIII-6, pp 128-129.)



**FIG 7-34** Newborn conjoined thoraco-omphalopagus twins.

the relatively deoxygenated arterial blood flowing away from the pump twin perfusing its co-twin contributes to the abnormal development of the acardiac fetus. The acardiac twin often lacks a recognizable head, trunk, and upper extremities but has lower extremity development and demonstrable internal flow on Doppler ultrasound imaging (Fig. 7-39). Up to 10% of cases have karyotype abnormalities, and 5% to 10% of pump twins have structural malformations, including cardiac anomalies, so genetic counseling and comprehensive evaluation of the pump twin are recommended in ongoing pregnancies.<sup>58</sup> In addition to evaluating for possible structural defects, fetal echocardiography is indicated to assess the cardiac function of the pump twin owing to the risk of hemodynamic compromise from the additional burden and high-output state related to perfusion of the acardiac co-twin.

The risk of developing cardiac failure in the pump twin influences the possible need for in utero intervention; this threat is greatest

when the estimated size of the acardiac twin measures 50% or larger than the pump twin.<sup>59,60</sup> Various methods are used to estimate the size of the acardiac twin. One approach is to estimate its weight using the equation for volume of a prolate ellipsoid by multiplying length  $\times$  width  $\times$  height (in centimeters)  $\times$  0.52 (this factor is used to generate a volume in cubic centimeters and convert this figure into estimated weight, in grams), or to simply compare the abdominal circumferences of the twins.<sup>59,60</sup> In ongoing pregnancies with TRAP, serial sonographic surveillance and fetal echocardiography are warranted to monitor cardiac function of the pump twin and assess for hydrops, as deterioration may be an indication for intervention such as cord occlusion of the acardiac twin, in utero medical therapy, or early delivery depending on gestational age. High-output cardiac failure in the pump twin may also be accompanied by polyhydramnios, placing the patient at increased risk for cervical shortening, premature rupture of membranes, or preterm labor and delivery. Historically, the perinatal mortality rate in TRAP pregnancies was over 50%, but recent series have reported 85% to 90% survival rate of the pump twin with judicious use of umbilical cord occlusion techniques, such as radiofrequency ablation of flow to the acardiac twin.<sup>59-62</sup>

### Twin-Twin Transfusion Syndrome

TTTS affects approximately 10% of monochorionic twins, occurring almost exclusively in monochorionic diamniotic twin pairs.<sup>40</sup> Although the exact pathophysiologic mechanism of TTTS is not completely understood, placental anastomoses linking the circulations of the twins are critical for its development. Inter-twin vascular anastomoses are present in virtually all monochorionic placentas, and net flow between the twins is "balanced" in the majority of cases. However, in pregnancies affected by TTTS, blood flow becomes unbalanced with one twin, the donor, transferring a net volume (with unidirectional flow through arteriovenous connections) to its co-twin, the recipient (Figs. 7-40 and 7-41). Differences between twins in CRL, NT, abdominal circumference, and amniotic fluid volume identify a subset of monochorionic diamniotic pairs more likely to be diagnosed with TTTS.<sup>40</sup> The risk of



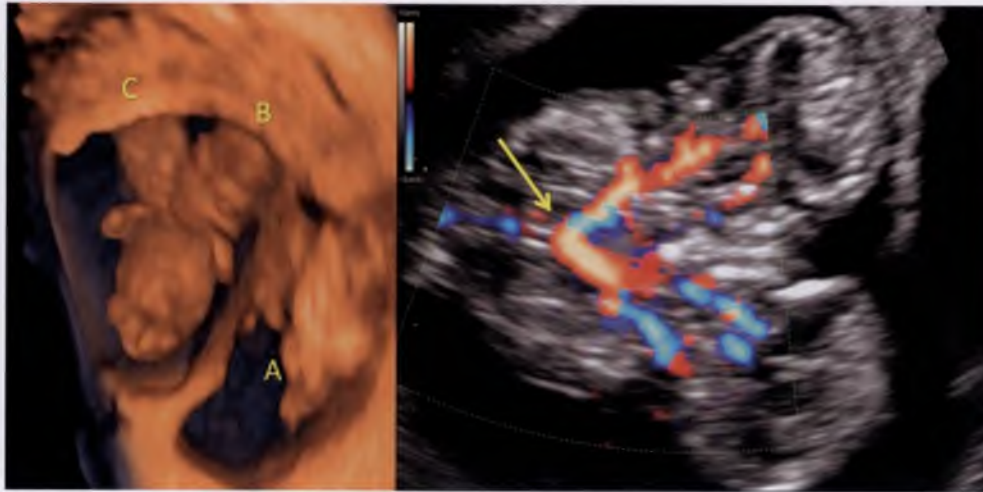


**FIG 7-35** Dichorionic diamniotic triplet pregnancy with parapagus dicephalus conjoined pair (B and C). Color Doppler flow imaging (*right*) demonstrates the head and neck vessels of B and C arising from a single heart (*arrow*).



**FIG 7-36** Longitudinal ultrasound image shows abnormal upper body development of the anomalous acardiac twin, which lacked demonstrable cardiac activity despite continued growth. The image includes an axial view through the brain of the morphologically normal pump twin.



**FIG 7-37** Acardiac twin demonstrating the amorphous, vestigial structures cephalad and caudad as the distance from the umbilical cord arterial circulation increases. (Pathologic image courtesy Melinda Sanders, MD, and Erika Walz, PA, University of Connecticut Health Center, Farmington, CT.)

TTTS also appears to be increased when velamentous cord insertions, for one or both fetuses, into the shared placenta are seen.<sup>63</sup>

Sonography is used to categorize TTTS into stages, with less favorable outcomes observed with advanced stages of the disorder<sup>64</sup> (Table 7-6). Serial sonographic surveillance of monochorionic twins is recommended, aiming to detect TTTS in its earliest stages. The finding of monochorionic twins with concomitant oligohydramnios (low fluid in one amniotic sac) and polyhydramnios (high fluid in the other) is essential for the diagnosis of TTTS<sup>40</sup> (see Fig. 7-29). The “donor” twin with oligohydramnios may appear “stuck” in its sac, plastered against the placenta or uterine wall with membrane closely draped over its body (Figs. 7-42 and 7-43). With advanced stages of TTTS, the bladder of the donor twin is not visualized (stage II) and abnormal arterial or venous Doppler waveforms may be seen in the donor or recipient (stage III) (Fig. 7-44). Doppler velocimetry of the middle cerebral artery (MCA) may demonstrate elevated peak systolic velocity in the donor twin, suggesting fetal anemia and reduced peak systolic velocity in the recipient twin implying polycythemia—consistent with coexisting TAPS (see later).<sup>65</sup> Fetal echocardiography and fetal magnetic resonance imaging (MRI), targeting the developing brains, are ancillary

studies that may provide additional information about the impact of TTTS and the status of the twins. The imbalance of blood flow from the donor to the recipient twin increases preload, resulting in adaptive responses within the recipient’s cardiovascular system (Fig. 7-45). Cardiac dysfunction, biventricular hypertrophy, and functional or structural right ventricular outflow obstruction may develop in the recipient twin over time<sup>40</sup> (Fig. 7-46). Central nervous system abnormalities such as hemorrhagic and ischemic white matter changes, which carry a poor prognosis, have been detected in both donors and recipients in cases with TTTS.<sup>66</sup>

Given the risk of developing TTTS, ultrasound evaluation of monochorionic twin pregnancies is recommended every 2 weeks beginning in the second trimester.<sup>40</sup> Management options for TTTS vary depending on gestational age and stage at time of diagnosis. These options may include pregnancy termination, selective reduction of an anomalous growth-restricted or hydropic co-twin, fetoscopic laser photocoagulation of inter-twin placental vascular anastomoses,



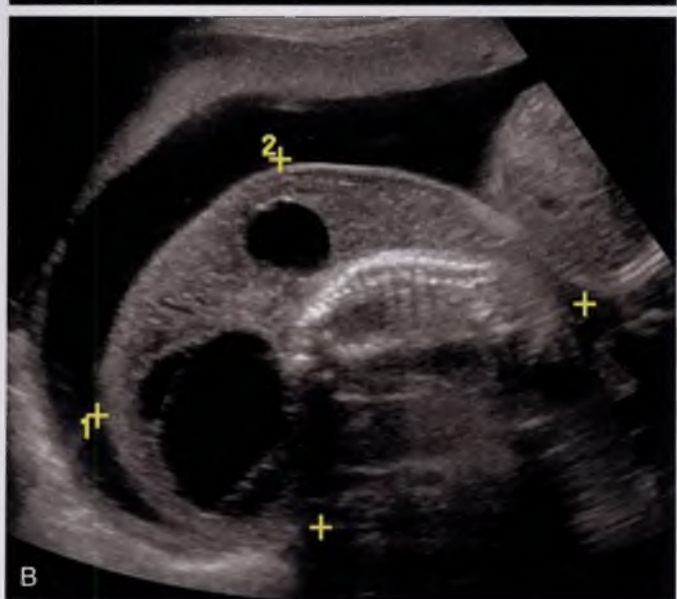
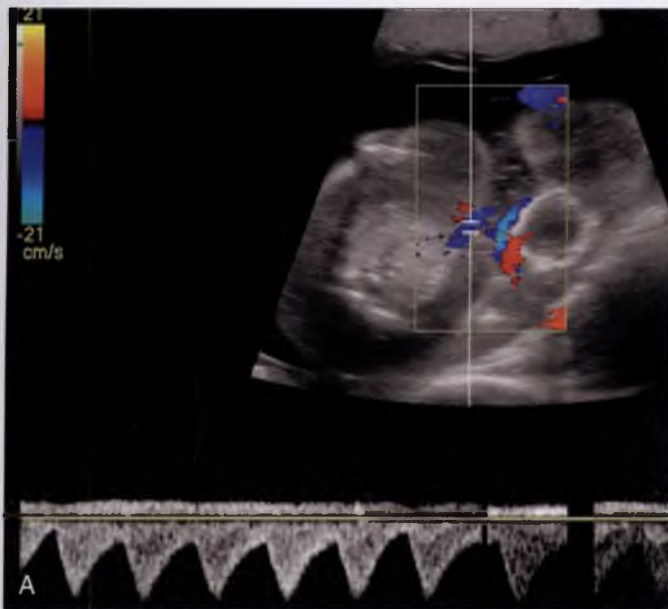


**FIG 7-38** Twin reversed arterial perfusion (TRAP). **A**, Color and spectral duplex Doppler interrogation demonstrates reversed arterial flow directed into the acardiac fetus at the level of the umbilical cord insertion at the anterior abdominal wall. **B**, Electronic calipers placed to measure a large anencephalic acardiac parabolic twin. Diffuse integumentary edema and large cystic hygromas are noted.

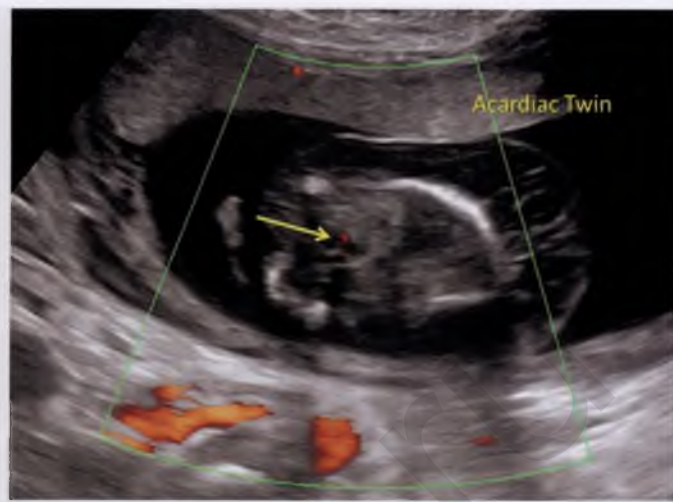


**FIG 7-39** Power Doppler ultrasound image demonstrating signal, indicating flow, at the level of the umbilical cord insertion (arrow), but no flow was seen within the chest of this acardiac twin.

most remain stable, resolve spontaneously, or do not recur after a single amnioreduction.<sup>67,68</sup>

Following fetoscopic laser photocoagulation for advanced TTTS, serial sonographic surveillance is recommended to assess the twins' response to treatment. In the majority of cases, TTTS resolves with normalization of amniotic fluid volume in each sac, visualization of the donor twin's bladder, and improvement in the recipient twin's cardiac function.<sup>69</sup> Umbilical artery Doppler ultrasound findings may remain abnormal in the presence of coexistent unequal placental sharing with discordant twin growth and in these cases, antenatal fetal testing should be incorporated into third trimester management. Serial assessment by sonography is also used to evaluate for recurrent TTTS, reversed TTTS, TAPS, and unequal placental sharing until delivery.<sup>40</sup>

The outcome of pregnancies with TTTS is dependent on the gestational age at diagnosis, clinical stage, and progression of disease. Mild, early stage TTTS that presents after 26 weeks and does not progress tends to have a favorable outcome for both twins. However, most cases of severe advanced TTTS present in the second trimester. Without treatment, perinatal mortality rate in cases with advanced stages of TTTS is 70% to 100%.<sup>40,70</sup> Following intervention with laser to treat TTTS, perinatal survival rate is reported to be 50% to 70%.<sup>40</sup> In general, two twins survive in 50% of cases, a single twin survives in 30% of cases, and there are no survivors in 20% of cases treated with fetoscopic laser photocoagulation.<sup>40</sup> Procedure-related twin loss is a recognized complication of fetoscopic intervention. In addition, survival with neurologic impairment is a potential serious long-term sequela of TTTS, with or without treatment. Intracranial abnormalities, including intraventricular hemorrhage and cystic periventricular leukomalacia, and subsequent diagnosis of neurodevelopmental delay and cerebral palsy remain risks for survivors of TTTS. Long-term neurologic sequelae are observed in 5% to 20% of survivors of TTTS treated with fetoscopic laser.<sup>40</sup> Additional risks related to preterm delivery and prematurity of these complicated monochorionic diamniotic pregnancies likely impact the long-term outcomes of surviving twins.

### Twin Anemia-Polycythemia Sequence

Spontaneous TAPS complicates 5% of monochorionic diamniotic twins and is usually diagnosed after birth when one twin is pale and the other plethoric and the twins are found to have discordant

amnioreduction, expectant observation, or delivery. The options are similar for complicated triplet pregnancies, but with early detection, some patients may opt for selective reduction of the TTTS pair. Most cases of TTTS are diagnosed in the second trimester and in ongoing pregnancies with advanced stages of TTTS (stage II-IV), fetoscopic laser photocoagulation of vascular anastomoses within the shared placenta is currently considered the best therapeutic intervention to improve perinatal survival<sup>40</sup> (see Chapter 24). This procedure is typically performed between 16 and 26 weeks' gestation and is done in conjunction with post-laser amnioreduction, with aspiration of excess amniotic fluid from the recipient's sac. The management of stage I TTTS is controversial, as only 10% to 30% of cases progress, whereas



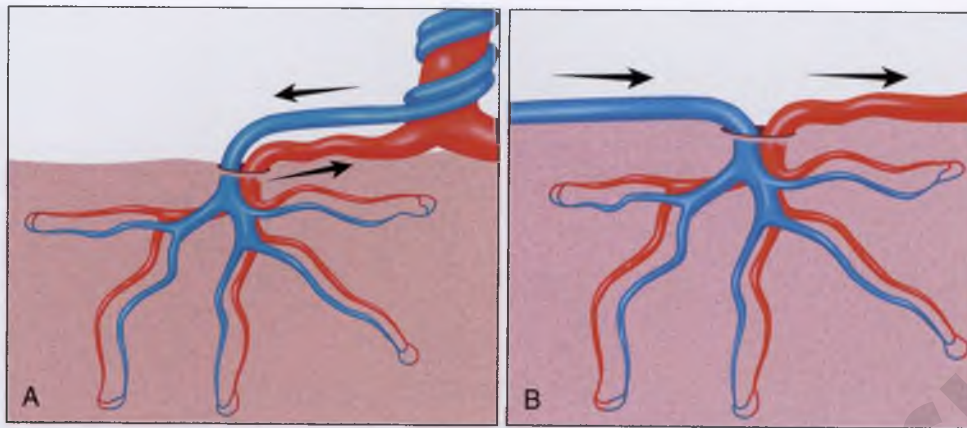


**FIG 7-40** Illustrations of normal-paired branch vessels from the umbilical cord (A) and arteriovenous anastomosis in monochorionic twin placenta (B). **A**, Normal paired branches of the umbilical artery (*blue*) and umbilical vein (*red*) are seen coursing together on the fetal surface of the placenta. Blood flows from the umbilical cord toward the placenta by way of the umbilical artery and returns by way of the umbilical vein. **B**, Unpaired vessels course on the fetal surface of the placenta. A branch of the donor umbilical artery (*blue*) meets a branch of the recipient umbilical vein (*red*) where they enter and exit the placental cotyledon by way of a common foramen. Note that the arteriovenous communication occurs deep within the placenta. (Courtesy Vickie Feldstein, MD, University of California, San Francisco, School of Medicine, San Francisco, CA.)

hemoglobin values (Fig. 7-47).<sup>65</sup> As in cases of TTTS, it is theorized that inter-twin vascular anastomoses in the single shared placenta result in a chronic imbalance of blood flow from donor to recipient. However, in TAPS the flow is presumably low volume and slow, such that significant amniotic fluid abnormalities do not develop. Iatrogenic TAPS, observed in up to 10% of TTTS cases treated with fetoscopic laser photocoagulation, is more likely to be recognized in utero because of increased sonographic surveillance following laser treatment.<sup>65</sup> It has been reported that incomplete photocoagulation of inter-twin vascular anastomoses, particularly small unidirectional connections, contributes to the development of postprocedure TAPS.<sup>71</sup>

Serial sonographic surveillance for iatrogenic TAPS is often recommended after laser photocoagulation. The diagnosis is confirmed when peak systolic velocity in the MCA is more than 1.5 multiples of median (MoM) in one twin and less than 0.8 MoM in the co-twin<sup>65</sup> (Fig. 7-48). Screening for spontaneous TAPS in otherwise uncomplicated monochorionic twins is not routine but is performed in some centers when minor variance in amniotic fluid volumes is detected. MCA Doppler velocimetry may be the only sonographic marker of TAPS complicating a monochorionic diamniotic twin pregnancy. Although TAPS and TTTS can occur concomitantly, the observation of both oligohydramnios in one twin and polyhydramnios in the other is not seen in cases of pure “isolated” TAPS. The management of TAPS is controversial, but options include termination, observation, repeat laser intervention, intrauterine fetal transfusion, or delivery, depending on gestational age. The perinatal outcome of TAPS is also variable, ranging from double twin demise to liveborn twins with no obvious long-term sequelae.<sup>65</sup>

### Unequal Placental Sharing With Discordant Twin Growth or Selective Fetal Growth Restriction

Although discordant growth and FGR may complicate any multiple gestation, the cause and implications are more wide-ranging with monochorionic placentation. Overall, significant discordance in growth occurs in 15% to 25% of monochorionic twins.<sup>72,73</sup> When compared to monochorionic twins concordant in size, velamentous PCIs and unequally shared placentas are more common in cases with

growth disturbance.<sup>74,75</sup> Selective FGR of one twin in a monochorionic pair has been classified into three groups based upon findings on Doppler interrogation of the umbilical artery: type I has normal Doppler waveforms with diastolic flow; type II has persistent absent or reversed end-diastolic flow; and type III has intermittent absent or reversed end-diastolic flow<sup>73</sup> (Fig. 7-49).

As in all multiple pregnancies, growth disorders in twins that share a common placenta may present at any time in gestation. Early disturbances in twin growth, particularly when associated with abnormal diastolic flow in the umbilical artery, have the poorest prognosis with reported 15% to 20% risk of intrauterine fetal demise.<sup>73</sup> TTTS often occurs in conjunction with unequal placental sharing, thereby complicating the diagnosis and management of the pregnancy. For instance, abnormal umbilical artery Doppler waveforms in monochorionic twins may represent uteroplacental insufficiency but may also be related to inter-twin anastomoses and changes in vascular reactivity. Close sonographic surveillance is recommended for all multiple gestations complicated by discordant growth but is of increased importance in monochorionic pregnancies as death of one monochorionic twin increases the likelihood of death or neurologic injury in the co-twin. In general, the latency between development of abnormal diastolic flow in the umbilical artery and fetal deterioration necessitating delivery tends to be longer in monochorionic twins compared to singletons with FGR, but frequent surveillance is still warranted once fetal viability is reached.<sup>76</sup>

### Single Twin Demise

Similar to singleton pregnancies, spontaneous loss in the first trimester occurs in 15% to 20% of dichorionic twin gestations and may be recognized as an empty sac or absent cardiac activity in one embryo.<sup>77</sup> Overall, it is expected that only 50% of spontaneous twin pregnancies identified in the first trimester will result in two liveborn infants.<sup>77</sup> Fortunately, the finding of a “vanishing twin” early in gestation is associated with a favorable prognosis for the surviving twin, similar to that of a singleton pregnancy. However, cases with neurologic injury following in utero demise of a monochorionic co-twin have been reported as early as 14 weeks’ gestation.<sup>78</sup>

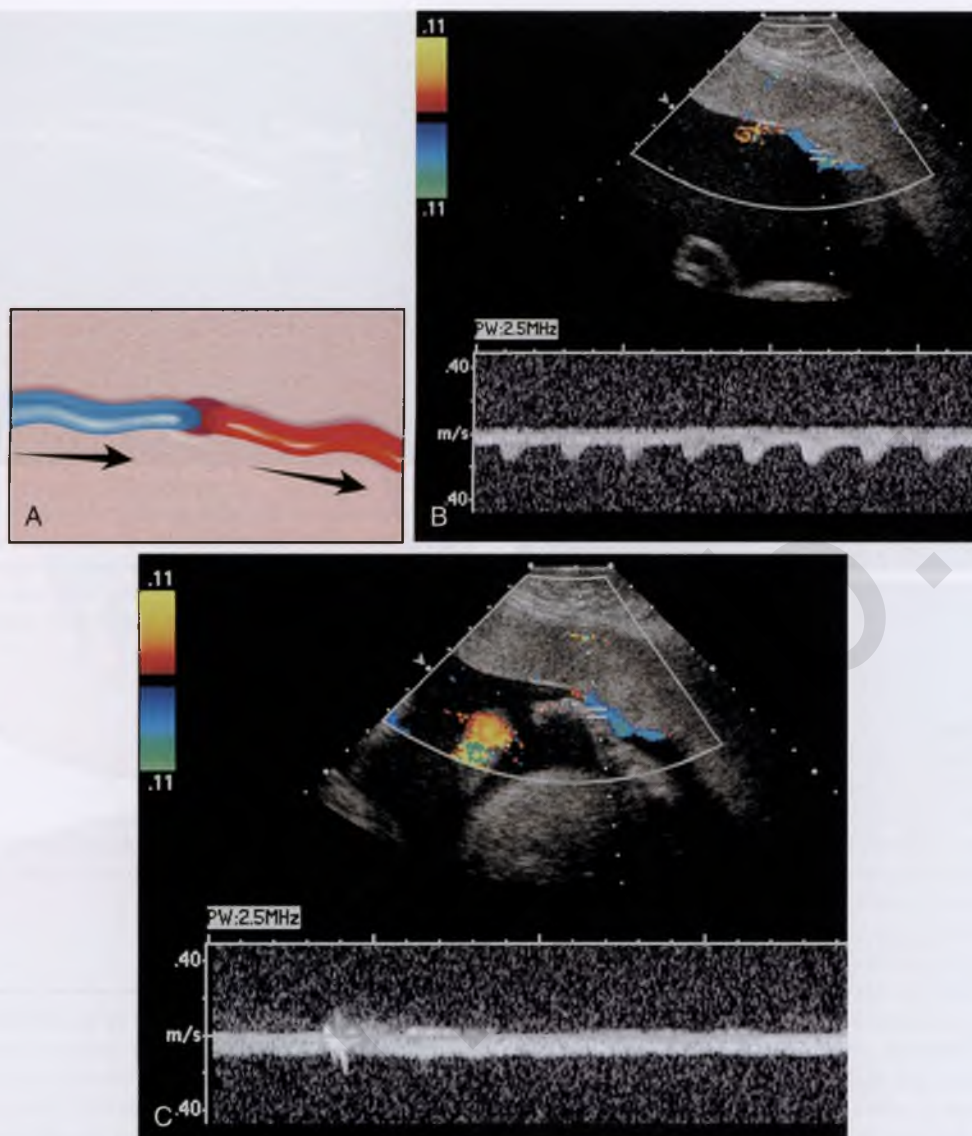


**FIG 7-41** Color and pulsed Doppler of the surface-communicating vessels in monozygotic twins. **A**, Arteriovenous anastomosis in a monozygotic placenta. Overview from the fetal surface of the placenta shows feeding branch of umbilical artery from donor (*blue*) and draining branch of umbilical vein of recipient (*red*) entering the placenta via a common foramen. **B** and **C**, Color Doppler ultrasound study demonstrates an unpaired vascular structure on the placental surface. Spectral Doppler waveforms reveal a feeding arterial branch (in **B**) and draining venous branch (in **C**), with flow directed from the donor toward the recipient. **D**, Placental pathologic injection study showing an arteriovenous anastomosis (*arrow*) with donor-feeding arterial branch blue and recipient-draining venous branch red. **E**, Pulsed-wave color Doppler insonation of placental surface vessel showing the characteristic periodic bidirectional interference pattern of an arterio-arterial anastomosis. (A through C courtesy Vickie Feldstein, MD, University of California, San Francisco, School of Medicine, San Francisco, CA; D courtesy Geoffrey Machin, MD, Permanente Medical Group, Oakland, CA.)



**TABLE 7-6 Quintero Staging of Twin-Twin Transfusion Syndrome**

TTTS	
Stage	Ultrasound Features
I	MVP fluid <2 cm in the donor sac and >8 cm in the recipient sac
II	Nonvisualization of the fetal bladder in donor twin for >60 minutes
III	Absent or reversed umbilical artery diastolic flow, reversed ductus venosus a wave flow, or pulsatile umbilical vein flow
IV	Fetal hydrops in one or both twins
V	Fetal demise of one or both twins

MVP, maximal vertical pocket; TTTS, twin-twin transfusion syndrome. Data from Quintero RA, Morales WJ, Allen MH, et al: Staging of twin-twin transfusion syndrome. *J Perinatol* 19:550-555, 1999.

The majority of cases with subsequent in utero demise of a twin will be diagnosed at the time of routine sonographic surveillance for fetal growth and well-being. Beyond the first trimester, intrauterine demise of one fetus occurs in about 5% of twin gestations.<sup>79</sup> Twins with structural malformations are more likely to die in utero than their morphologically normal co-twins. The smaller twin of a discordant pair or a twin with early-onset FGR is also at greater risk of in utero demise.<sup>73</sup> As with singletons, the cause of fetal death in a multiple gestation is often unknown, although there is a threefold to fourfold increase in the rate of intrauterine death in monochorionic compared to dichorionic twins.<sup>80</sup> Complications unique to monochorionic twin pregnancies that contribute to a higher likelihood of single twin demise include cord entanglement in monoamniotic twins, conjoined twins, TRAP, TTTS, unequal placental sharing, and TAPS. Unlike the loss of one twin in a dichorionic gestation, intrauterine demise of one twin in a monochorionic pair increases the risk of specific adverse events, including 10% risk of dual fetal demise and 10% to 30% risk of neurologic injury in the surviving co-twin.<sup>80</sup> Immediate delivery of a monochorionic twin following demise of its co-twin does not eliminate the risk of neurologic compromise. The intracranial insult that a fetus may sustain following demise of a monochorionic co-twin is best assessed by means of in utero MRI, as it is more sensitive than sonography for the detection of hypoxic-ischemic brain injury. Clinical management of these pregnancies depends on gestational age and evidence of fetal or maternal complications. Figure 7-50 shows an ultrasound image of a 21-week twin gestation with in utero demise of one fetus. The head circumference and abdominal circumference of the deceased twin are much smaller than those of the surviving fetus. Figure 7-51

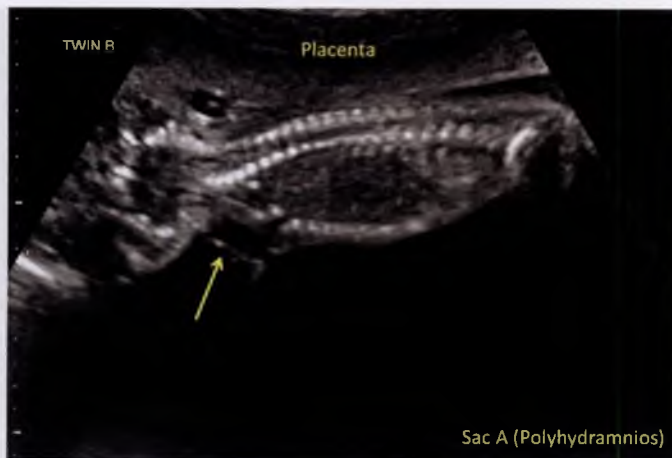


**FIG 7-42** Monochorionic diamniotic pregnancy complicated by twin-twin transfusion syndrome with oligohydramnios and polyhydramnios. Twin B, the donor, appears plastered against the anterior placenta with marked oligohydramnios. Polyhydramnios is noted in the sac of the recipient twin A. The thin separating inter-twin membrane is barely visible (arrow) as it is adjacent and closely apposed to the “stuck” twin B.

is a photograph of a fetus papyraceus, mummified remains of the lost twin found in the folds of the membranes of the placenta after delivery of the surviving twin at 38 weeks.

## CONCLUSION

Despite the expanding literature on twins and higher-order multiples, recommendations about the use of obstetric sonography in multiple gestations are based primarily on level II and III evidence with few randomized controlled trials<sup>81</sup> (Table 7-7). Many of the indications for sonography in multiple pregnancies parallel those for sonographic evaluation in singletons. Pregnancy dating, NT assessment, structural anatomic survey, and placental evaluation should be standard practice. Multiple pregnancies warrant careful sonographic determination of chorionicity early in gestation. Cervical length assessment and sonograms with biometry to evaluate fetal growth are recommended in multiple gestations, but the optimal timing and frequency of these measurements remain uncertain. However, it is evident that multiple gestations with a monochorionic pair require careful serial sonographic surveillance searching for a multitude of potential complications unique to twins that share a single placenta.

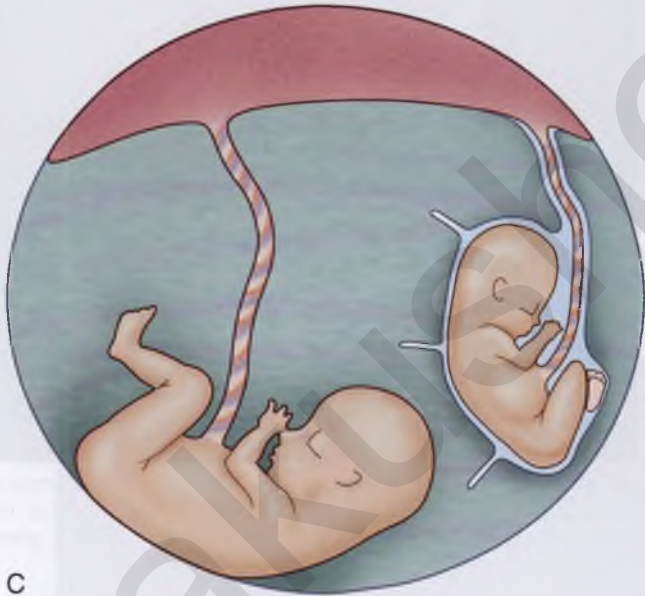
*Text continued on p. 155*



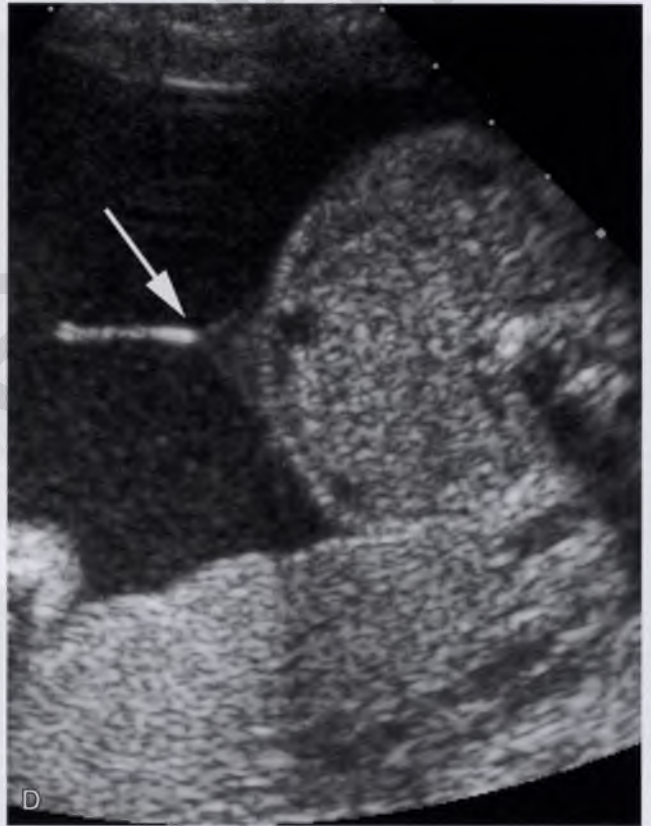
A



B



C



D

**FIG 7-43** Twin-twin transfusion syndrome (TTTS) with a "sling" around the "stuck" twin. When there is little to no amniotic fluid in the amniotic sac of the donor "stuck" twin, the membrane appears as a sling around the fetus. In the absence of amniotic fluid in this sac, the fluid surrounding this twin may wrongly be assumed to be in its sac, when in fact it is the fluid in the adjacent recipient twin's sac with polyhydramnios. **A**, A pregnancy with TTTS in which the fetus on the right is enshrouded by its membrane in an oligohydramniotic sac. **B**, In this case of TTTS, the donor twin is in an anhydramniotic sac. The apposed membranes appear as a single membrane (*arrow*). The surrounding amniotic fluid (*asterisks*) is in the other twin's amniotic sac. **C**, A pregnancy with TTTS in which the fetus on the right is enshrouded by its membrane in an oligohydramniotic sac. Redundant amnion is seen projecting from the fetus and at times presents a confusing appearance. **D**, Scan of a donor fetus with severe oligohydramnios and redundant amnion (*arrow*) seen projecting into the amniotic fluid of the other fetus. (A and C courtesy Vickie A. Feldstein, MD, University of California School of Medicine, San Francisco, CA.)



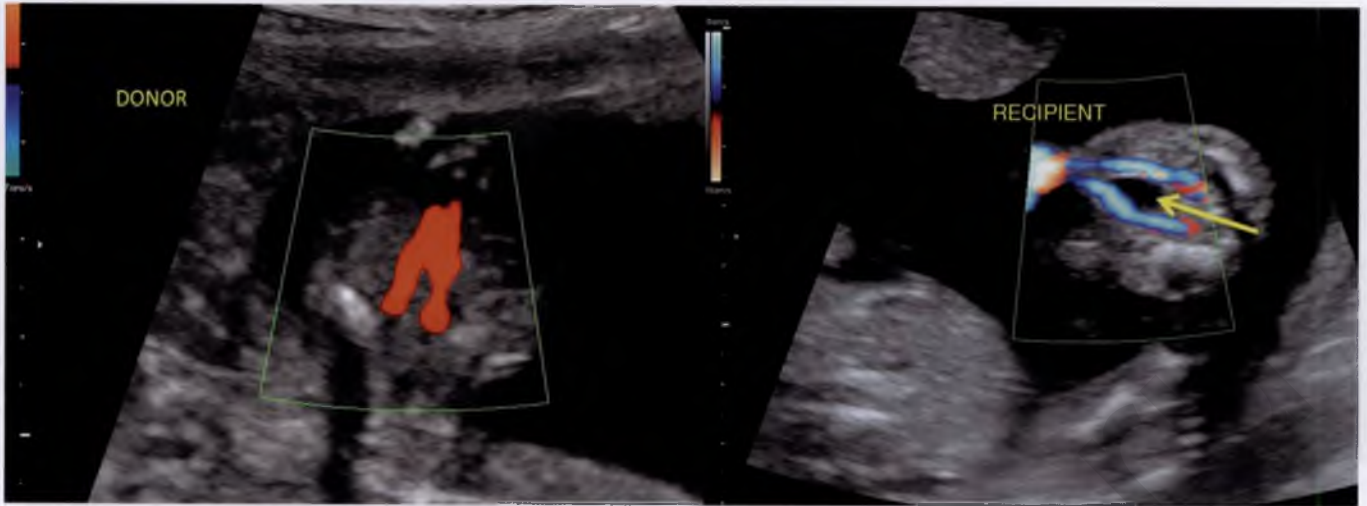


**FIG 7-44** Twin-twin transfusion syndrome, stage II. Monozygotic diamniotic twin pregnancy with oligohydramnios and polyhydramnios (not shown). Nonvisualization of the empty bladder in the donor. Fluid shown within the normal-appearing bladder (*arrow*) of the recipient. Color Doppler demonstrates flow within the umbilical arteries, which flank the bladder, of each twin.

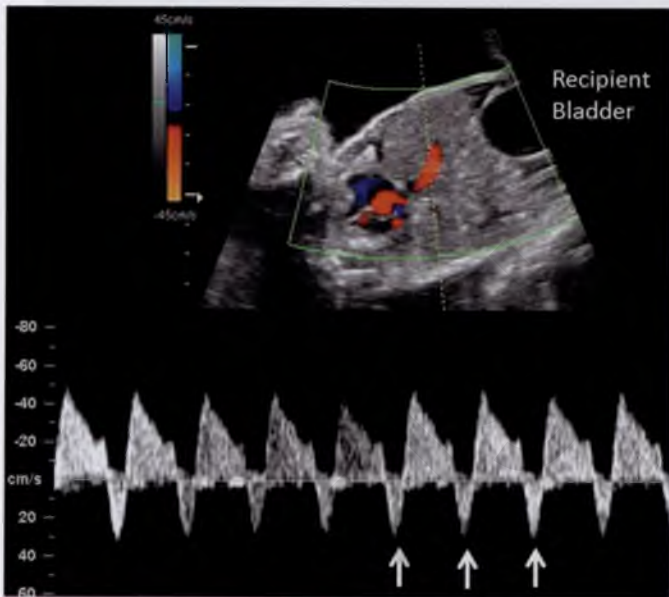


**FIG 7-45** Twin-twin transfusion syndrome. Recipient twin with distended urinary bladder. Spectral Doppler waveform of the ductus venosus demonstrates reversed a-wave flow (*arrows*), indicative of cardiac diastolic dysfunction associated with overload.



**FIG 7-46** Twin-twin transfusion syndrome. Biventricular hypertrophy in the recipient twin is noted early in the second trimester. The thick-walled right cardiac ventricle (*arrow*) was noted to be more affected than the left.



**FIG 7-47** Placenta in a case of twin-twin transfusion syndrome. The donor's placental disc is paler, suggesting fetal anemia, whereas the recipient's placental disc is darker, suggesting polycythemia. The donor's hematocrit was 22% and the recipient's was 54%. (Courtesy Melinda Sanders, MD, and Erika Walz, PA, University of Connecticut Health Center, Farmington, CT.)

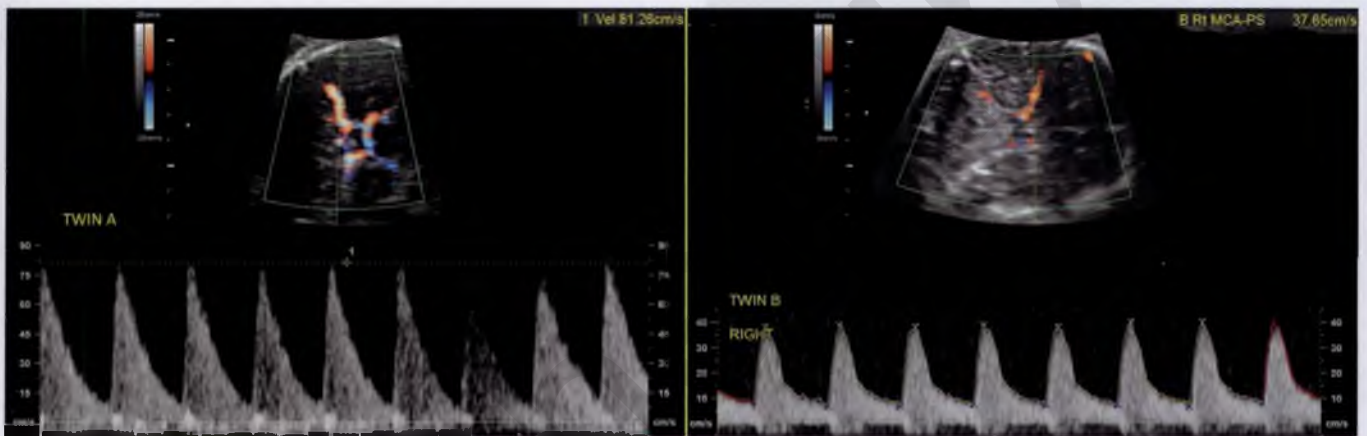


**FIG 7-48** Twin anemia-polycythemia sequence (TAPS). Elevated peak systolic (PS) velocity in the middle cerebral artery (MCA) in twin A (measuring 81.26 cm/second) and decreased in twin B (measuring 37.65 cm/second) characteristic of TAPS.

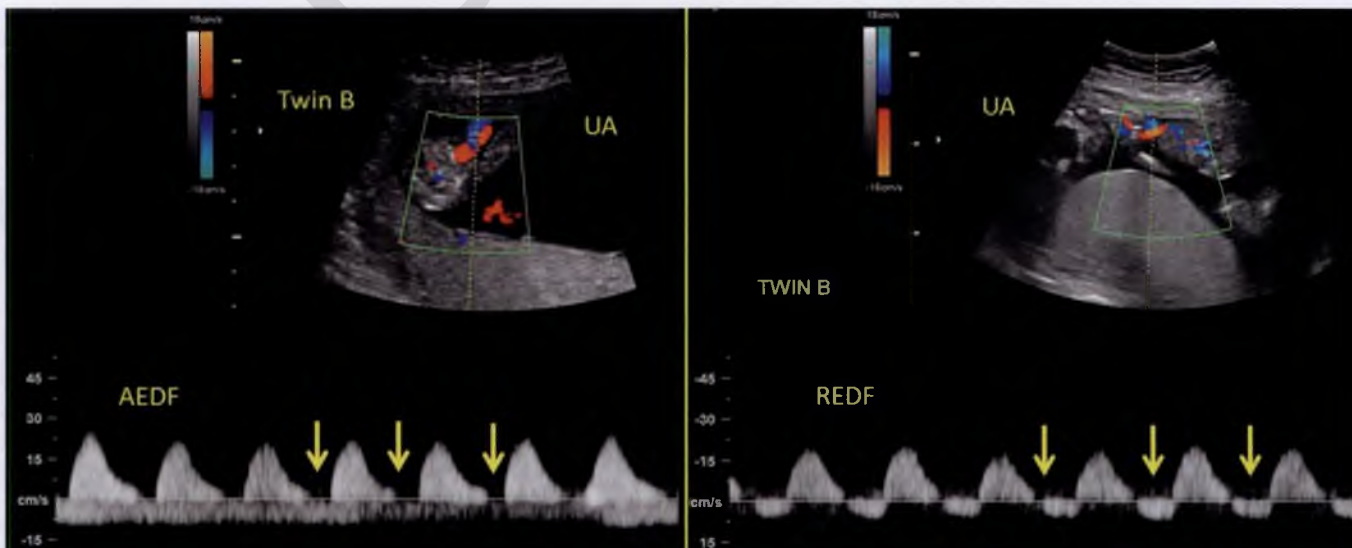


**FIG 7-49** Abnormal umbilical artery (UA) Doppler waveforms in growth-restricted twin B of a monozygotic diamniotic pair. At left, initially, absent end-diastolic flow (AEDF) was observed (arrows). On right, follow-up sonogram revealed progression (arrows) with reversed end-diastolic flow (REDF) in this case with suspected unequal placental sharing.





**FIG 7-50** Fetal demise of one twin with a surviving co-twin at 21 weeks' gestation. **A**, The collapsed cranium of the twin with the fetal demise compared with the surviving twin's cranium. **B**, The abdominal circumference of the fetal demise is compared with that of the surviving twin.



**FIG 7-51** Fetus papyraceus resulting from a midtrimester fetal demise of a co-twin. This fetus was noted on inspection of the placenta and membranes following a term delivery of the surviving twin. (Pathologic image courtesy Melinda Sanders, MD, and Erika Walz, PA, University of Connecticut Health Center, Farmington, CT.)

**TABLE 7-7** Ultrasound Evaluation in Multiple Gestations

Reason for Evaluation	Timing	Points
Pregnancy dating	1st trimester	Optimal at 7-10 weeks using CRL
Determination of chorionicity	1st trimester	Close to 100% accuracy if done prior to 2nd trimester
Nuchal translucency assessment	10-13 weeks	Increased with aneuploidy, malformations, TTTS
Anatomic survey	2nd trimester	Optimal at 18-22 weeks; consider fetal echocardiography for IVF and presence of monochorionic twin pair
Placental evaluation	2nd trimester	Transvaginal imaging to exclude placenta previa and vasa previa; color imaging for PCI localization
Cervical length	2nd trimester	Transvaginal imaging optimal
Interval fetal growth	2nd and 3rd trimesters	Every 4 weeks for uncomplicated multiple gestations
Serial surveillance	2nd and 3rd trimesters	Every 2 weeks for uncomplicated monochorionic twins; daily testing for viability for monoamniotic twins; frequency and type of testing of twins and higher-order multiples depends on chorionicity, risk, and complications

CRL, crown-rump length; IVF, in vitro fertilization; PCI, placental cord insertion; TTTS, twin-twin transfusion syndrome.

Modified from Simpson LL: Ultrasound in twins: dichorionic and monochorionic. *Semin Perinatol* 37:348-358, 2013.

## REFERENCES

1. Martin JA, Hamilton BE, Osterman MJ: Three decades of twin births in the United States, 1980-2009. *NCHS Data Brief* 80:1-8, 2012.
2. Kurtz GR, Keating WJ, Loftus JB: Twin pregnancy and delivery: analysis of 500 twin pregnancies. *Obstet Gynecol* 6:370-378, 1995.
3. Wenstrom KD, Syrop CH, Hammitt DG, et al: Increased risk of monozygotic twinning associated with assisted reproduction. *Fertil Steril* 60:510, 1993.
4. Blickstein I: Monozygosity in perspective. *Ultrasound Obstet Gynecol* 27:235, 2006.
5. Nylander PP: The factors that influence twinning rates. *Acta Genet Med Gemellol (Roma)* 30(3):189, 1981.
6. Campbell DM, Campbell AJ, MacGillivray I: Maternal characteristics of women having twin pregnancies. *J Biosoc Sci* 6(4):463, 1974.
7. Bardis N, Maruthini D, Balen AH: Modes of conception and multiple pregnancy: a national survey of babies born during one week in 2003 in the United Kingdom. *Fertil Steril* 84:1727, 2005.
8. Practice Committee of American Society for Reproductive Medicine; Practice Committee of Society for Assisted Reproductive Technology: Criteria for number of embryos to transfer: a committee opinion. *Fertil Steril* 99(1):44-46, 2013.
9. Lee YM: Delivery of twins. *Semin Perinatol* 36:195-200, 2012.
10. Morin L, Lim K: Ultrasound in twin pregnancies. *J Obstet Gynaecol Can* 33(6):643-656, 2011.
11. American College of Obstetricians and Gynecologists: ACOG Committee Opinion No. 611: method for estimating due date. *Obstet Gynecol* 124:863-866, 2014.
12. Chaudhuri K, Su LL, Wong PC, et al: Determination of gestational age in twin pregnancy: which fetal crown-rump length should be used? *J Obstet Gynaecol Res* 39:761-765, 2013.
13. Salomon LJ, Cavicchioli O, Bernard JP, et al: Growth discrepancy in twins in the first trimester of pregnancy. *Ultrasound Obstet Gynecol* 26:512-516, 2005.
14. Carroll SG, Soothill PW, Abdel-Fattah SA, et al: Prediction of chorionicity in twin pregnancies at 10-14 weeks gestation. *Br J Obstet Gynaecol* 109:182-186, 2002.
15. Lee YM, Cleary-Goldman J, Thanker HM, et al: Antenatal sonographic prediction of twin chorionicity. *Am J Obstet Gynecol* 195:863-867, 2006.
16. Blumenfeld YJ, Momirova V, Rouse DJ, et al: Accuracy of sonographic chorionicity classification in twin gestations. *J Ultrasound Med* 33:2187-2192, 2014.
17. Egan JFX, Borgida AF: Ultrasound evaluation of multiple pregnancies. In Callen PW, editor: *Ultrasonography in Obstetrics and Gynecology*, ed 5, Philadelphia, 2008, Saunders Elsevier.
18. Bracero LA, Byrne DW: Ultrasound determination of chorionicity and perinatal outcome in twin pregnancies using dividing membrane thickness. *Gynecol Obstet Invest* 55:50-57, 2003.
19. DeJesus Allison SO, Javitt MC, Glanc P, et al, American College of Radiology: ACR Appropriateness Criteria® Multiple gestations. *Ultrasound Q* 28(2):149-155, 2012.
20. Sebire NJ, Snijders RJ, Hughes K, et al: Screening for trisomy 21 in twin pregnancies by maternal age and fetal translucency at 10-14 weeks of gestation. *Br J Obstet Gynaecol* 103:999-1003, 1996.
21. Cheng PJ, Huang SY, Shaw SW, et al: Difference in nuchal translucency between monozygotic and dizygotic spontaneously conceived twins. *Prenat Diagn* 30:247-250, 2010.
22. Madsen HN, Ball S, Wright D, et al: A reassessment of biochemical marker distributions in trisomy 21-affected and unaffected twin pregnancies in the first trimester. *Ultrasound Obstet Gynecol* 37:38-47, 2011.
23. American College of Obstetricians and Gynecologists: ACOG Committee Opinion No. 545: noninvasive prenatal testing for fetal aneuploidy. *Obstet Gynecol* 120:1532-1534, 2012.
24. Simpson LL, Malone FD, Bianchi DW, et al: Nuchal translucency and the risk of congenital heart disease. *Obstet Gynecol* 109:376-383, 2007.
25. Malone FD, Ball RH, Nyberg DA, et al: First-trimester septated cystic hygroma: prevalence, natural history, and pediatric outcome. *Obstet Gynecol* 106:288-294, 2005.
26. Kagan KO, Gazzoni A, Sepulveda-Gonzalez G, et al: Discordance in nuchal translucency thickness in the prediction of severe twin-to-twin transfusion syndrome. *Ultrasound Obstet Gynecol* 29:527-532, 2007.
27. Boyle B, McConkey R, Garne E, et al: Trends in the prevalence, risk and pregnancy outcome of multiple births with congenital anomaly: a registry-based study in 14 European countries 1984-2007. *Br J Obstet Gynaecol* 120:707-716, 2013.
28. Glinianaia SV, Rankin J, Wright C: Congenital anomalies in twins: a register-based study. *Hum Reprod* 23:1306-1311, 2008.
29. Zhang XH, Qiu LQ, Huang JP: Risk of birth defects increased in multiple births. *Birth Defects Res* 91:34-38, 2011.
30. Pettit KE, Merchant M, Machin GA, et al: Congenital heart defects in a large, unselected cohort of monozygotic twins. *J Perinatol* 33:457-461, 2013.
31. Reefhuis J, Honein MA, Schieve LA, et al: Assisted reproductive technology and major structural birth defects in the United States. *Hum Reprod* 24:360-366, 2009.
32. Bahtiyar MO, Campbell K, Dulay AT, et al: Is the rate of congenital heart defects detected by fetal echocardiography among pregnancies conceived by in vitro fertilization really increased? A case-historical control study. *J Ultrasound Med* 29:917-922, 2010.
33. Acherman RJ, Evans WN, Luna CF, et al: Prenatal detection of congenital heart disease in southern Nevada: the need for universal fetal cardiac evaluation. *J Ultrasound Med* 26:1715-1719, 2007.
34. Friedberg MK, Silverman NH, Moon-Grady AJ, et al: Prenatal detection of congenital heart disease. *J Pediatr* 155:26-31, 2009.
35. Fetal Echocardiography Task Force; American Institute of Ultrasound in Medicine Clinical Standards Committee; American College of Obstetricians and Gynecologists; Society for Maternal-Fetal Medicine: AIUM practice guideline for the performance of fetal echocardiography. *J Ultrasound Med* 30(1):127-136, 2011.
36. Ananth CV, Demissie K, Smulian JC, et al: Placenta previa in singleton and twin births in the United States, 1989 through 1998: a comparison of risk factor profiles and associated conditions. *Am J Obstet Gynecol* 188:275-281, 2003.
37. Gandhi M, Cleary-Goldman J, Ferrara L, et al: The association between vasa previa, multiple gestations, and assisted reproductive technology. *Am J Perinatol* 25:587-589, 2008.
38. Hack KE, Nikkels PG, Koopman-Esseboom C, et al: Placental characteristics of monozygotic diamniotic twin pregnancies in relation to perinatal outcome. *Placenta* 29(11):976-981, 2008.
39. De Paepe ME, Shapiro S, Young L, et al: Placental characteristics of selective birth weight discordance in diamniotic-monozygotic twin gestations. *Placenta* 31(5):380-386, 2010.
40. Society for Maternal-Fetal Medicine, Simpson LL: Twin-twin transfusion syndrome. *Am J Obstet Gynecol* 208(1):3-18, 2013.
41. To MS, Fonseca EB, Molina FS, et al: Maternal characteristics and cervical length in the prediction of spontaneous early preterm delivery in twins. *Am J Obstet Gynecol* 194:1360-1365, 2006.
42. Conde-Agudelo A, Romero R, Hassan SS, et al: Transvaginal sonographic cervical length for the prediction of spontaneous preterm birth in twin pregnancies: a systematic review and meta-analysis. *Am J Obstet Gynecol* 203:128.e1-128.e12, 2010.
43. Schwartz R, Prieto J: Shortened cervical length as a predictor of preterm delivery in twin gestations. *J Reprod Med* 55:147-150, 2010.
44. Reddy UM, Abuhamad AZ, Levine D, et al: Fetal imaging: executive summary of a Joint Eunice Kennedy Shriver National Institute of Child Health and Human Development, Society for Maternal-Fetal Medicine, American Institute of Ultrasound in Medicine, American College of Obstetricians and Gynecologists, American College of Radiology, Society for Pediatric Radiology, and Society of Radiologists in Ultrasound Fetal Imaging Workshop. *Am J Obstet Gynecol* 210(5):387-397, 2014.
45. Papageorghiou AT, Bakoulas V, Sebire NJ, et al: Intrauterine growth in multiple pregnancies in relation to fetal number, chorionicity and gestational age. *Ultrasound Obstet Gynecol* 32:890-893, 2008.
46. Klam SL, Rinfret R, Leduc L: Prediction of growth discordance in twins with the use of abdominal circumference ratios. *Am J Obstet Gynecol* 192:247-251, 2005.



47. Odibo AO, McDonald RE, Stamilio DM, et al: Perinatal outcomes in growth-restricted twins compared with age-matched growth-restricted singletons. *Am J Perinatol* 22:269–273, 2005.
48. Wen SW, Fung KF, Huang L, et al: Fetal and neonatal mortality among twin gestations in a Canadian population: the effect of in utero birthweight discordance. *Am J Perinatol* 22:279–286, 2005.
49. Knopman JM, Krey LC, Oh C, et al: What makes them split? Identifying risk factors that lead to monozygotic twins after in vitro fertilization. *Fertil Steril* 102:82–89, 2014.
50. Rossi AC, Prefumo F: Impact of cord entanglement on perinatal outcome of monoamniotic twins: a systematic review of the literature. *Ultrasound Obstet Gynecol* 41:131–135, 2013.
51. Murakoski T, Ishii K, Matsushita M, et al: Monochorionic monoamniotic twin pregnancies with two yolk sacs may not be a rare finding: a report of two cases. *Ultrasound Obstet Gynecol* 36:384–386, 2010.
52. Dias T, Mahsud-Doman S, Bhide A, et al: Cord entanglement and perinatal outcome in monoamniotic twin pregnancies. *Ultrasound Obstet Gynecol* 35:201–204, 2010.
53. Morikawa M, Yamada T, Yamada T, et al: Prospective risk of intrauterine fetal death in monoamniotic twin pregnancies. *Twin Res Hum Genet* 15(4):522–526, 2012.
54. Hack KE, Derks JB, Schaap AH, et al: Perinatal outcome of monoamniotic twin pregnancies. *Obstet Gynecol* 113:353–360, 2009.
55. Mutchinick OM, Luna-Munoz L, Amar E, et al: Conjoined twins: a worldwide collaborative epidemiological study of the International Clearinghouse for Birth Defects Surveillance and Research. *Am J Med Genet* 157:274–287, 2011.
56. Chen CB, Hsu CY, Su JW, et al: Conjoined twins detected in the first trimester: a review. *Taiwan J Obstet Gynecol* 50:424–431, 2011.
57. Chalouhi GE, Stirnemann JJ, Salomon LJ, et al: Specific complications of monochorionic twin pregnancies: twin-twin transfusion syndrome and twin reversed arterial perfusion sequence. *Semin Fetal Neonatal Med* 15:349–356, 2010.
58. Hanafy A, Peterson CM: Twin-reversed arterial perfusion (TRAP) sequence: case reports and review of literature. *Aust N Z J Obstet Gynaecol* 37:187–191, 1997.
59. Jelin E, Hirose S, Rand L, et al: Perinatal outcome of conservative management versus fetal intervention for twin reversed arterial perfusion sequence with a small acardiac twin. *Fetal Diagn Ther* 27:138–141, 2010.
60. Cabassa P, Fichera A, Prefumo F, et al: The use of radiofrequency in the treatment of reversed arterial perfusion sequence: a case series and review of the literature. *Eur J Obstet Gynecol Reprod Biol* 166:127–132, 2013.
61. Moore TR, Gale S, Benirschke K: Perinatal outcome of forty-nine pregnancies complicated by acardiac twinning. *Am J Obstet Gynecol* 163:907–912, 1990.
62. Lee H, Wagner AJ, Sy E, et al: Efficacy of radiofrequency ablation for twin-reversed arterial perfusion sequence. *Am J Obstet Gynecol* 196(5):459.e1–459.e4, 2007.
63. De Paepe ME, Shapiro S, Greco D, et al: Placental markers of twin-to-twin transfusion syndrome in diamniotic-monochorionic twins: a morphometric analysis of deep artery-to-vein anastomoses. *Placenta* 31:269–276, 2010.
64. Quintero RA, Morales WJ, Allen MH, et al: Staging of twin-twin transfusion syndrome. *J Perinatol* 19:550–555, 1999.
65. Slaghekke F, Kist WJ, Oepkes D, et al: Twin anemia-polycythemia sequence: diagnostic criteria, classification, perinatal management and outcome. *Fetal Diagn Ther* 27:181–190, 2010.
66. Quarello E, Molho M, Ville Y: Incidence, mechanisms, and patterns of fetal cerebral lesions in twin-to-twin transfusion syndrome. *J Matern Fetal Neonatal Med* 20:589–597, 2007.
67. Bebbington MW, Tiblad E, Huesler-Charles M, et al: Outcomes in a cohort of patients with stage I twin-to-twin transfusion syndrome. *Ultrasound Obstet Gynecol* 36:48–51, 2010.
68. Rossi C, D'Addario V: Survival outcomes of twin-twin transfusion syndrome in stage I: a systemic review of the literature. *Am J Perinatol* 30:5–10, 2013.
69. Van Mieghem T, Klaritsch P, Done E, et al: Assessment of fetal cardiac function before and after therapy for twin-to-twin transfusion syndrome. *Am J Obstet Gynecol* 200:400.e1–400.e7, 2009.
70. Berghella V, Kaufmann M: Natural history of twin-twin transfusion syndrome. *J Reprod Med* 46:480–484, 2001.
71. Chmait RH, Assaf SA, Benirschke K: Residual vascular communications in twin-twin transfusion syndrome treated with sequential laser surgery: frequency and clinical implications. *Placenta* 31:611–614, 2010.
72. Gratacos E, Ortiz JU, Martinez JM: A systemic approach to the differential diagnosis and management of the complications of monochorionic twin pregnancies. *Fetal Diagn Ther* 32:145–155, 2012.
73. Gratacos E, Lewi L, Munoz B, et al: A classification system for selective intrauterine growth restriction in monochorionic pregnancies according to umbilical artery Doppler flow in the smaller twin. *Ultrasound Obstet Gynecol* 30:28–34, 2007.
74. Lopriore E, Pasman SA, Klumper FJ, et al: Placental characteristics in growth-discordant monochorionic twins: a matched case-control study. *Placenta* 33:171–174, 2012.
75. Fick AL, Feldstein VA, Norton ME, et al: Unequal placental sharing and birth weight discordance in monochorionic diamniotic twins. *Am J Obstet Gynecol* 195(1):178–183, 2006.
76. Vanderheyden TM, Fichera A, Pasquini L, et al: Increased latency of absent end-diastolic flow in the umbilical artery of monochorionic twin fetuses. *Ultrasound Obstet Gynecol* 26:44–49, 2005.
77. Samuels P: Ultrasound in the management of the twin gestation. *Clin Obstet Gynecol* 31:110–122, 1988.
78. Weiss JL, Cleary-Goldman J, Tanji K, et al: Multicystic encephalomalacia after first-trimester intrauterine fetal death in monochorionic twins. *Am J Obstet Gynecol* 190:563–565, 2004.
79. Kilby MD, Govind A, O'Brien PM: Outcome of twin pregnancies complicated by a single intrauterine death: a comparison with viable twin pregnancies. *Obstet Gynecol* 84:107–109, 1994.
80. Ong SS, Zamora J, Khan KS, Kilby MD: Prognosis for the co-twin following single-twin death: a systematic review. *Br J Obstet Gynaecol* 113:992–998, 2006.
81. Simpson LL: Ultrasound in twins: dichorionic and monochorionic. *Semin Perinatol* 37:348–358, 2013.

# Ultrasound Evaluation of Normal Fetal Anatomy

*Tara A. Morgan, Vickie A. Feldstein, Roy A. Filly*

## SUMMARY OF KEY POINTS

- Continued advancement of ultrasound technology including increase in frequency and choice of focal position have improved visualization of fetal anatomy and therefore have also increased the required anatomic knowledge of these structures for those performing and interpreting fetal sonograms.
- Superficial anatomy of the fetus can be delineated with either two-dimensional or three-dimensional sonography and can be useful in confirming normal formation of facial structures and genitalia.
- Fetal skeletal structures are the earliest recognizable fetal features, and their sonographic evaluation is highly dependent on the position of the fetus.
- Identification of a normal three-vessel umbilical cord and normal portal venous anatomy is useful in determining whether cardiovascular development is normal.
- The liver is the largest gastrointestinal organ and is the largest contributor to the size of the abdominal circumference.
- The lungs become more echogenic later in pregnancy; however, the change is not related to lung maturity.
- Kidneys grow throughout pregnancy, with a ratio of kidney circumference to abdominal circumference of 0.27 to 0.30.
- The calvaria can obscure the portion of the brain nearest the transducer. Bone-free windows through the fontanelles can be used to increase visualization, and when one hemisphere is not well seen, symmetry is assumed unless images prove otherwise.

## OUTLINE

**Superficial Anatomy of the Fetus, 161**  
**Musculoskeletal System, 161**  
**Cardiovascular System, 183**  
**Gastrointestinal System, 191**

**Respiratory System, 197**  
**Genitourinary System, 199**  
**Central Nervous System, 200**

Our understanding of normal fetal anatomy as seen on sonograms continues to evolve. Instrumentation has improved steadily, yielding both improved and more consistent image quality. Among the most significant advances in fetal imaging has been the ability to choose the depth of the zone of best focus of the ultrasonic beam and to select frequency without changing transducers. With these capabilities, the area of anatomy being observed can be consistently inspected with the focused portion of the beam at an optimal frequency, both highly significant advantages. Recent technologic advances allow imaging at higher frequencies than a mere decade ago.

In addition to these technologic advances, sonologists have gradually improved their understanding of the anatomy portrayed on in utero sonograms. Unquestionably, clearer images have led the way to our improved understanding, but other factors have been involved; not the least of these has been the surge in ultrasonic imaging of premature neonates.<sup>1,2</sup> These tiny neonates are the equivalent of second trimester fetuses as early, at times, as 24 weeks' gestation. Visualization of their brains<sup>1,2</sup> (Fig. 8-1) and abdominal (Fig. 8-2) anatomy in the ex utero environment, which permits the use of higher frequency transducers, a greater selection of planes of section, and comparison with other imaging modalities, has done much to improve our understanding of fetal anatomy. This information can be, to a large extent, extrapolated

to younger fetuses. As well, as magnetic resonance imaging (MRI) continues to be a growth area in fetal imaging, our ability to compare sonographic anatomy of the fetus with that portrayed on MR imaging further enhances our understanding of fetal sonographic anatomy<sup>3-7</sup> (Fig. 8-3).

The ability of sonography to detect intrafetal structures is a balance between spatial resolution and contrast.<sup>8</sup> This balance, however, strongly favors contrast as the more important aspect of perception. For example, a large white dot on a white wall is difficult or impossible to see because no contrast differential exists even though the eye can spatially resolve easily a tiny black dot (high contrast) on the same wall. Structures possessing high levels of subject contrast can be consistently detected at a smaller size (often equating to an earlier age) than those displaying poor contrast. Although sonographic contrast agents are available for imaging in adults and children, current agents do not cross the placenta in sufficient concentration to affect fetal organs.<sup>9</sup> Therefore, sonologists possess no agents to alter contrast of fetal organs and thus are totally dependent on subject contrast (inherent contrast) for visualization of internal fetal morphologic details. Clearly, spatial resolution is also a critical feature in defining morphologic structure but has not been the limiting factor in demonstrating fetal anatomy. Fortunately, sophisticated modern sonographic imaging systems have



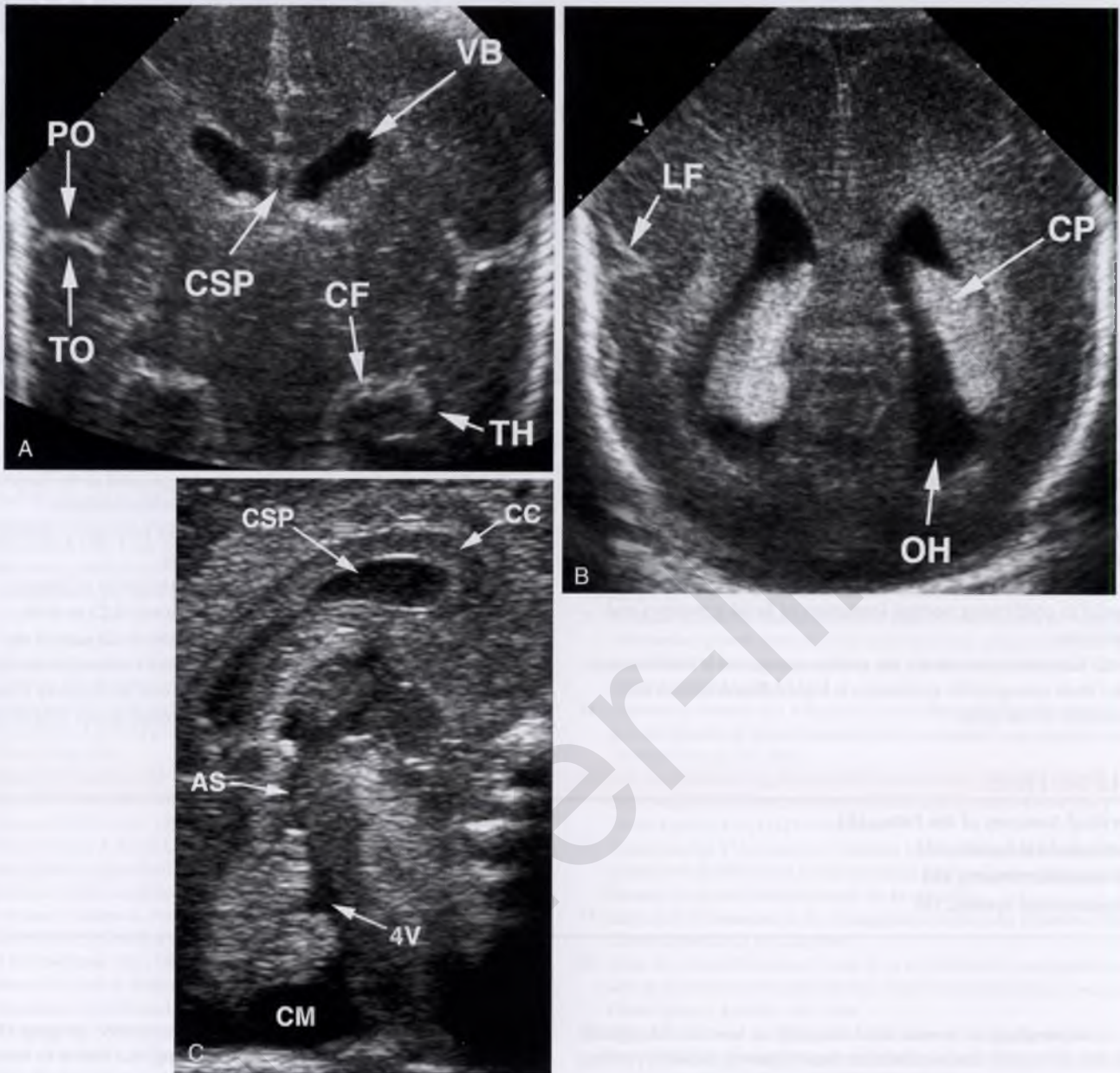


**FIG 8-1** Neonatal head sonograms. Coronal (**A**), axial (**B**), and midsagittal (**C**) images enable correlation with fetal examinations. AS, sylvian aqueduct; CC, corpus callosum; CF, choroidal fissure; CM, cisterna magna; CP, choroid plexus; CSP, cavum septi pellucidum; LF, lateral fissure; OH, occipital horn; PO, parietal operculum; TH, temporal horn; TO, temporal operculum; VB, lateral ventricular body; 4V, fourth ventricle.

the ability to choose varying contrast settings, which enhance inherent tissue differences. An important aspect of the technical advancements allowing ever higher frequency imaging is that at higher frequencies, contrast differences between organs change, which can have diagnostic impact.

Another technology that has improved fetal imaging, particularly for earlier gestations, is the intracavitary (transvaginal) transducer.<sup>10-12</sup> Certain aspects of fetal and even embryonic anatomy can be seen with amazing detail (Fig. 8-4). Although this methodology is crucial to modern imaging, we intend to concentrate our discussion on anatomy visualized by transabdominal transducers in fetuses beyond the 14th week. When examining later pregnancies, in the context of fetal anatomic imaging, we use transvaginal transducers predominantly to visualize the presenting part when transabdominal transducers fail to

adequately image this region of the fetal anatomy (e.g., distal sacrum in a breech fetus).

Other parameters, important in fetal imaging, also cannot be controlled. Sonography is a tomographic technique. Appropriate positioning for obtaining the best tomographic plane is always desirable. However, we are unable to control fetal position to attain this end. We also cannot control maternal body habitus or the amount of amniotic fluid, both of which may dramatically alter our ability to discern fetal anatomy. Despite these problems, a large number of fetal structures are consistently visible sonographically.

High-resolution, real-time scanners with their flexible approach to imaging are mandatory for modern fetal sonography.<sup>13-15</sup> In the following sections, various aspects of fetal anatomy are detailed as seen on such instrumentation. An estimate is made of the ability of



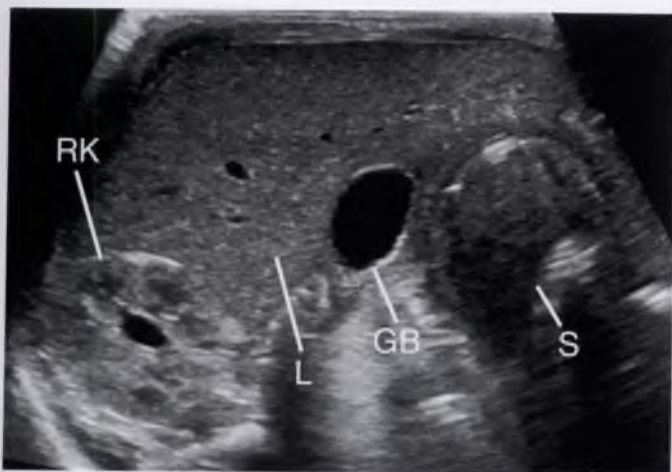


**FIG 8-2** Neonatal abdominal sonogram. Transverse axial image in a 1-month-old infant born premature at 24 weeks' gestation demonstrates the right kidney (RK), liver (L), gallbladder (GB), and stomach (S).



**FIG 8-3** T2-weighted fetal magnetic resonance imaging in a 21-week fetus demonstrates normal anatomy of the liver (L), cerebral lateral ventricle (LV), stomach (S), heart (H), right lung (RL), small bowel (SB), and bladder (B).



**FIG 8-4** Transvaginal sonogram of a 17-mm embryo. This midsagittal view demonstrates the large early fourth ventricle formed by the folding of the rhombencephalon (R). A, amnion.

ultrasound instrumentation to consistently demonstrate the anatomic part under consideration as well as an attempt to estimate when the fetus has attained sufficient size such that the anatomic structure is large enough to be detected. It is important to recall that size and visualization may be relative at any given stage of development. For example, in a small fetus with a well-distended urinary bladder, identification of the bladder is relatively easy. Alternatively, identification of the bladder will be difficult in a term fetus that has recently voided. The urine, in this instance, provides the “contrast” that ordinarily makes the urinary bladder an easy structure to perceive. If this contrast agent drains away, the size of the fetus (and thus its bladder) will not rescue one from the loss of contrast. Also important is the concept that the human eye sees best in the “relative” rather than the “absolute” sense of size. Thus, in a young fetus, the cerebral ventricle is much more readily seen than in an older fetus because the relative size of the ventricle compared with overall brain size is larger early (even though the absolute size is larger later).

If the sonographer begins with a specific intent to image a particular fetal part, it is frequently possible to succeed.<sup>8,16</sup> To accomplish this end, the sonographer must (1) assess the precise fetal position; (2) consider whether the anatomic part of interest is best visualized in planes perpendicular to the fetal long axis or parallel to the fetal long axis; and (3) adjust acoustic imaging parameters, particularly time-gain compensation, and transducer angulation to visualize the area to best advantage. Obviously, such rules are the same throughout all of sonography. The challenge of imaging intrafetal structures is to apply these rules when fetal position is changing such that the current scanning plane is no longer applicable for the part one wishes to visualize.

The flexibility offered by real-time sonographic systems enables one to survey the fetus quickly to determine precise position. Second, the sonographic tomograms, which are rapidly generated (virtually “real-time” imaging), enable one to view a large volume of the fetus with closely spaced sections. Such a rapid look at many contiguous tomograms eliminates one of the basic flaws of tomographic imaging of a moving target. Finally, fetal movements are viewed directly, which enables one to quickly reorient the transducer to the optimal plane of section to image the structure of interest. As digital image storage and viewing continues to expand, cine clip technology has greatly improved the capture and viewing of many fetal parts, especially those that are



in motion, like the heart. Surprisingly, many imaging groups fail to take advantage of cine technology when recording fetal examinations. This immensely powerful technology should not be left on the sidelines by imaging specialists.

Currently, three-dimensional imaging systems have reached a clinically relevant stage of development.<sup>17-19</sup> These instruments depend on *volume imaging*. That is, a volume of tissue within the fetus is insonated and the data are gathered in the processing computer. From this volume, three-dimensional images are generated. Of perhaps greater importance in the future, individual planes of section in virtually any orientation can be computed. When and if it becomes possible to generate equivalent planar images to those obtained with a hand-held transducer, the current method of "fluoroscopic" sonography, the entire nature of sonography will change. The technical challenges of sonography will be greatly reduced (Fig. 8-5).

Fetal parts of interest to the sonologist fall into three major categories of subject contrast that subsequently determine the relative ease with which the structure is sonographically visible: (1) structures that generate high-amplitude reflections (e.g., ossified bones, submucosa of fetal bowel, leptomeninges); (2) structures that generate no internal

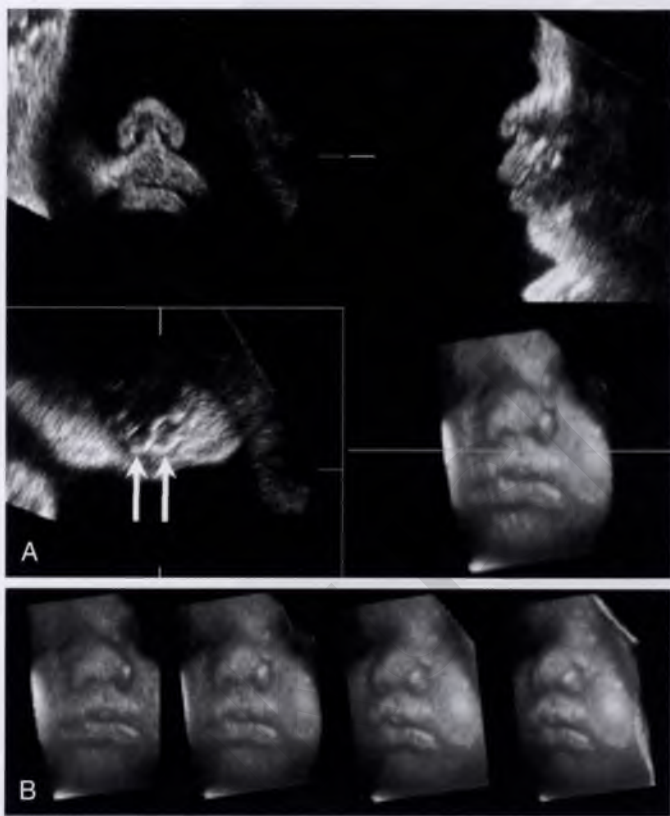


**FIG 8-5** Normal fetal face at 35 menstrual weeks. **A**, Multiplanar and volume-rendered images of the fetal face are displayed. *Upper left*, a coronal view through the nose and lips is seen. *Upper right*, a sagittal or profile view of the face is seen. *Lower left*, an axial plane through the anterior alveolar ridge of the primary palate is shown. *Lower right*, a volume-rendered image of the face using surface and light techniques is shown. A line is visible crossing the upper lip of the fetus, which identifies the level of the axial plane in the lower left box. Note two tooth buds in the anterior alveolar ridge (*arrows*). **B**, Images from multiple rotations of the fetal face are shown. Generally, a volume is rotated with a knob on the work panel to provide the impression of three-dimensionality. (From Pretorius DH, Nelson TR: Three-dimensional ultrasound in gynecology and obstetrics. *Ultrasound Q* 14:218-233, 1998.)

echoes (e.g., fluid-containing viscera); and (3) structures that generate midrange gray echoes (e.g., the parenchymal organs such as the lungs, brain, spleen, liver, kidneys, and muscles). The categories are listed from most visible to least visible. Within the last category, one may anticipate seeing a spectrum of gray shades that will enable distinction between parenchymal organs and intraorgan components. For example, the medullary portions of the fetal renal parenchyma generate lower amplitude internal echoes than do the surrounding cortical tissues and Bertin septa, thus enabling recognition of this separate component of renal tissue (Fig. 8-6).<sup>20</sup> Modern imaging systems enable distinctions previously not possible. An example from a relatively common pathologic circumstance is the apposition of the herniated spleen against the lung in left congenital diaphragmatic hernia. Previously these organs "blended" together, but currently they are readily discriminated, resulting in better estimations of residual lung volume in affected fetuses (Fig. 8-7).

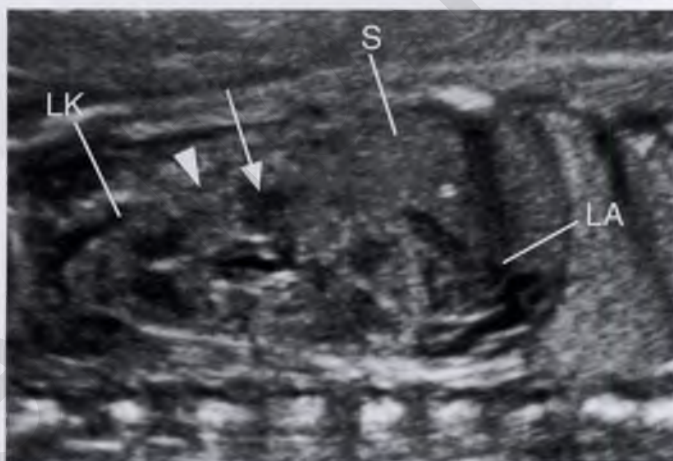


**FIG 8-6** Sonogram of a fetal left kidney (LK) in longitudinal axis. The medullary pyramids (*arrow*) are darker, triangular areas distinguishable from the surrounding cortical tissues and septa of Bertin (*arrowhead*). LA, left adrenal gland; S, spleen.

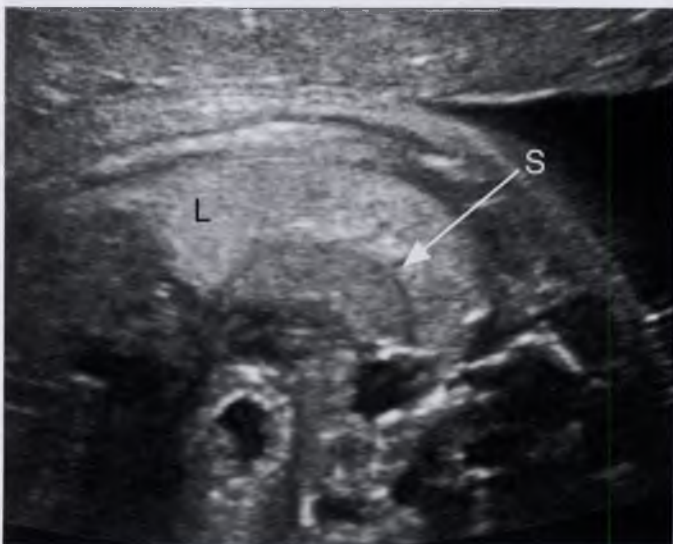


**FIG 8-7** Transverse sonogram of the left fetal hemithorax with congenital diaphragmatic hernia demonstrates that the spleen (S) within the chest is well differentiated from and less echogenic than the adjacent fetal lung (L).



A feature of critical importance for organ imaging is the fetal position. A prone fetus is in an optimal position for imaging the kidneys, ordinarily difficult to perceive, but in a poor position to demonstrate the urinary bladder, which is usually easy to image. Determination of fetal position should be accomplished in all obstetric sonographic examinations from the second trimester onward. The fetal position should be determined as precisely as possible before an interpretation of fetal anatomy is begun, because the position of a structure will often influence our interpretation. The general fetal orientation is first assessed (e.g., cephalic, breech, oblique, or transverse). Once this is determined, the location of the fetal spine is noted. If, for example, the fetal spine is on the maternal left side and the fetus is in a cephalic presentation, one can judge that the fetus is lying on its left side (Fig. 8-8). Conversely, if the fetus is breech, then it must be lying on its right side. The reverse is the case for breech and cephalic fetuses when the fetal spine lies on the maternal right side. In the transverse or oblique fetal positions the same rules apply but with a different orientation.

Such an analysis of fetal position is vital for proper interpretation of abdominal and thoracic situs (now a requirement of the AIUM/ACR/ACOG [American Institute of Ultrasound in Medicine/American College of Radiology/American College of Obstetricians and Gynecologists] practice guidelines for second and third trimester obstetric sonograms) and for identification of abnormal fetal structures. For instance, a rounded, fluid-filled structure in the left posterior portion of the upper fetal abdomen may be assumed to represent the fundus of the fetal stomach. However, a structure of identical appearance but located on the right side of the upper fetal abdomen must be interpreted as a pathologic lesion or an abnormality of situs.

It is important to recall that pathologic structures are frequently more visible than their normal counterparts (e.g., dilated small bowel loops are easier to detect than normal small bowel loops). However, it is even more important to keep in mind that the most difficult pathologic observation is to recognize the absence of a structure that ordinarily could be visualized (i.e., a missing portion of an extremity or the inability to see the stomach when esophageal atresia without tracheoesophageal fistula is present).

## SUPERFICIAL ANATOMY OF THE FETUS

Routine sonography for obstetric indications in many cases does not require a survey of superficial fetal structures. However, when an anomaly is suspected, a careful look at superficial features of the fetus becomes important or even mandatory. Superficial anatomy considered in this section includes the face, ears, hair, and external genitalia. Importantly, technologic advancements in three-dimensional renderings of fetal sonograms have had a dramatic impact on visualization of superficial fetal anatomy.<sup>21-23</sup>

The fetal face can be viewed with considerable clarity with two-dimensional sonography. Expectant mothers are often surprised to see their fetus so clearly (Figs. 8-9 to 8-11). The brow, cheeks, eyelids (and occasionally even eyelashes), nose, lips, and chin can be seen with consistency. The nose and lips are the more important to image in detail (to exclude clefting). The alae, columella, and nares can be clearly depicted (Figs. 8-12 and 8-13). The upper lip is more important diagnostically than the lower lip and fortunately easier to see. Visualization is usually good enough to identify the philtrum. The cheeks are prominent, as expected, and the subcutaneous tissues of the cheek, because of the presence of a large fat pad, are brightly echogenic (Fig. 8-14). The profile is also readily demonstrated (see Fig. 8-11) and provides useful information about the brow (e.g., frontal bossing), chin (e.g., hypognathia), and nose (e.g., midface hypoplasia and Down syndrome).

The ears can be visualized quite well and their progressive maturation noted.<sup>24</sup> The external auditory canal, helix (and antihelix in older fetuses), lobule, and tragus can be depicted (Fig. 8-15), but the relative position of the ear (e.g., as in low-set ears) is difficult to judge—a task more readily accomplished with three-dimensional imaging. The ear may be protuberant and can be mistaken for an abnormality, especially an encephalocele.<sup>25</sup>

When present, scalp hair is readily perceived in late fetuses. The bright linear echoes protruding from or paralleling the scalp and neck are quite conspicuous. The only benefit of recognizing hair is not to be misled into mistaking long hair for a pathologic process—namely, an encephalocele or cystic hygroma—because longer hair, wet and matted by the amniotic fluid, may trap some of the fluid between it and the skin of the occiput or neck, creating the false impression of a cystic mass in this location (Fig. 8-16).

The external genitalia can be appreciated from early second trimester onward. Fetal sex can be quite accurately assigned.<sup>26-28</sup> Ordinarily, this is not of clinical consequence. However, in certain circumstances, fetal sex should always be determined. These situations include all living twins in which a single placental site is seen or when monozygotic twinning, other than for reasons of placentation, would be considered detrimental to pregnancy outcome.<sup>29</sup> All fetuses with suspected lower urinary tract obstruction should have fetal sex determined because the differential diagnosis is different in males and females. Certain other circumstances would require determination of sex if karyotyping were refused or impractical to perform and cell-free DNA screening were not possible or inconclusive. These indications include, but are not limited to, risk for X-linked disorders or when Turner syndrome is suspected because of a dysmorphic feature (e.g., cystic hygroma).

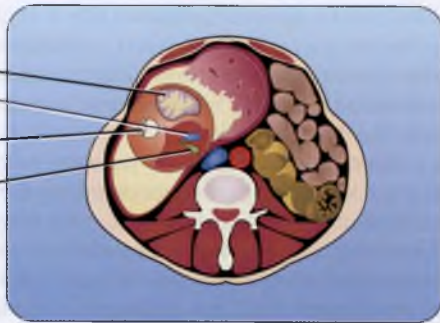
Female sex should be assigned only by identification of the major and minor labia (Fig. 8-17). Assigning female sex based solely on an inability to see a penis will result in many diagnostic errors. Male genitalia are readily seen (Fig. 8-18). The penis and scrotum are most obvious. Testes may be seen in the scrotal sac, sometimes as early as the beginning of the third trimester (the testes are intra-abdominal during most of gestation but are only visualized in the presence of ascites). Care should be taken to image the entirety of the phallus to avoid false foreshortening. Details of the penis, including the glans, urethra, and corpora cavernosa, may be appreciated (Fig. 8-19). Even the foreskin is visible in some cases.

## MUSCULOSKELETAL SYSTEM

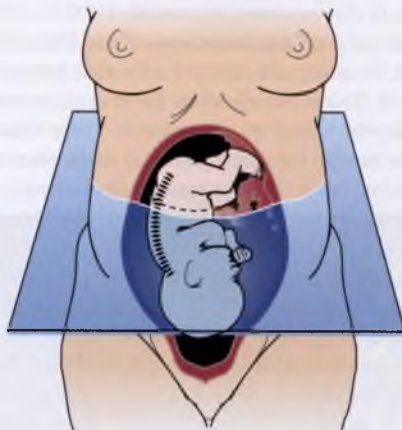
Real-time ultrasonography provides the most appropriate format for imaging fetal bones. The resolution and flexibility offered by such systems enable one to survey the fetal skeleton rapidly. Of all structures within the fetus, the ossified portions of the skeleton possess the highest level of subject contrast and thus are seen earlier and more consistently than any other organ system.<sup>13,30-33</sup> Sonography surpasses all other imaging modalities in fetal skeletal imaging. Although radiographs of abortuses demonstrate bony morphologic appearance more advantageously than would a sonogram,<sup>34,35</sup> the reverse is true of fetuses in the womb, where overlying maternal soft tissues and bones, fetal movement, and inappropriate fetal position degrade radiographic images of the early fetal skeleton. With volumetric imaging (three-dimensional sonography), special processing can give a more global view of fetal skeletal structures than can be achieved with two-dimensional sonography.<sup>36-38</sup> This enhances the image and diagnostic process for assessment of both normal and pathologic findings (Fig. 8-20).

Fetal position dramatically affects visualization of the bony structures. The posterior elements of the fetal spine may be clearly imaged



Longitudinal lie  
cephalic presentationLongitudinal lie  
breech position

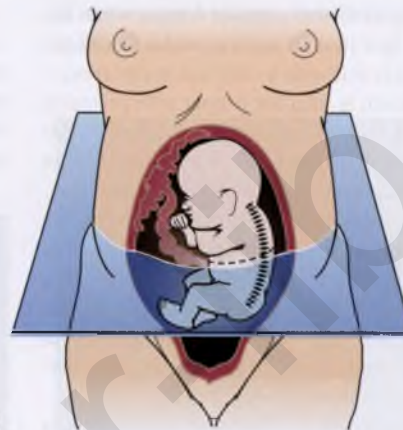
Stomach  
Umbilical vein  
Spine  
Gallbladder



A

Transverse lie  
head, maternal left

C



B

Transverse lie  
head, maternal right

D

**FIG 8-8** Knowledge of the plane of section across the maternal abdomen (longitudinal or transverse) as well as the position of the fetal spine and left-sided (stomach) and right-sided (gallbladder) structures can be used to determine fetal lie and presenting part. **A**, This transverse scan of the gravid uterus demonstrates the fetal spine on the maternal right with the fetus lying with its right side down (stomach anterior, gallbladder posterior). Because these images are viewed looking up from the patient's feet, the fetus must be in a longitudinal lie and in cephalic presentation. **B**, When the gravid uterus is scanned transversely and the fetal spine is on the maternal left, with the right side down, the fetus is in a longitudinal lie and in breech presentation. **C**, When a longitudinal plane of section demonstrates the fetal body to be transected transversely and the fetal spine is nearest the lower uterine segment, with the fetal right side down, the fetus is in a transverse lie with the fetal head on the maternal left. **D**, When a longitudinal plane of section demonstrates the fetal body to be transected transversely and the fetal spine is nearest the uterine fundus with the fetal right side down, the fetus is in a transverse lie with the fetal head on the maternal right. Although real-time scanning of the gravid uterus quickly allows the observer to determine fetal lie and presentation, this maneuver of identifying specific right- and left-sided structures within the fetal body forces one to determine fetal position accurately and identify normal and pathologic fetal anatomy.





**FIG 8-9** Coronal section of the fetal face that demonstrates the palpebral fissures (PF) particularly well. NB, nasal bone.

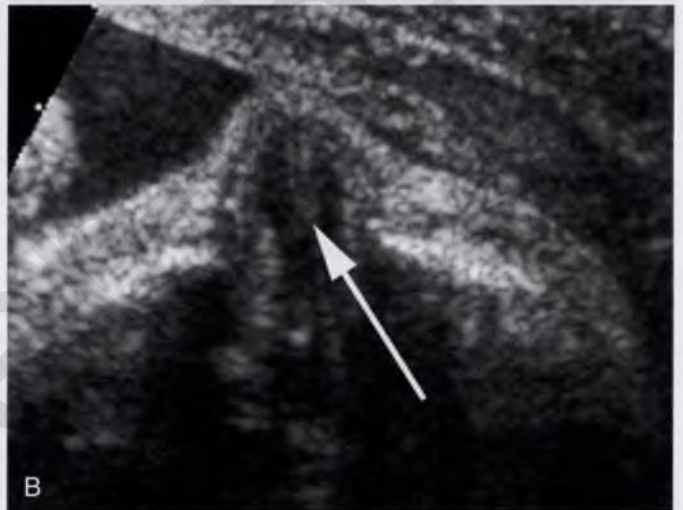
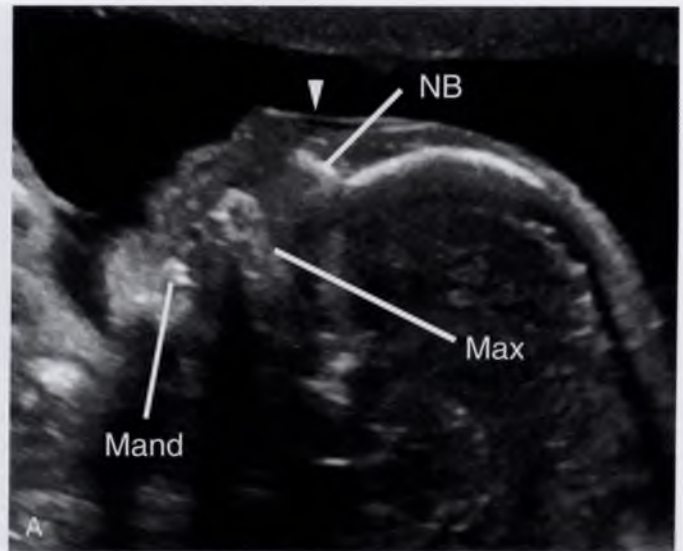


**FIG 8-11 A**, Midsagittal view of the fetal face (profile view). **B**, Axial sonogram through the nose. Note that the cartilaginous nasal septum (arrow) is well seen. Mand, mandible; Max, maxilla; amniotic membrane (arrowhead); NB, nasal bone.

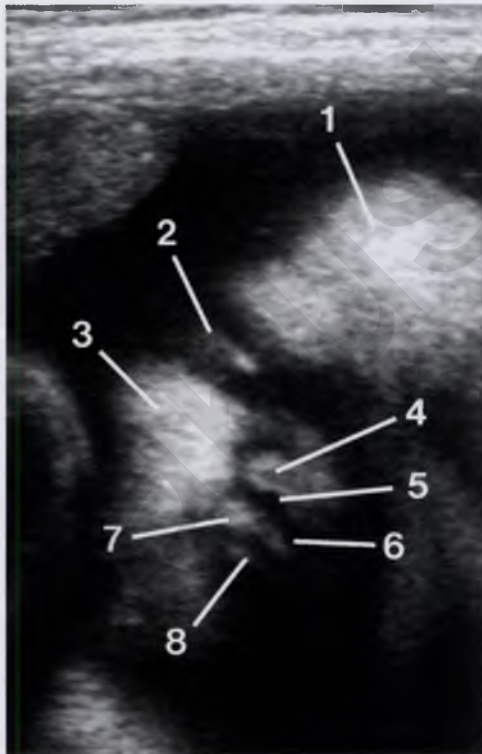


**FIG 8-10** Sonogram of the fetal face. Even though this image is a tomogram with relatively little depth, facial features are seen well. Amniotic fluid surrounding the face provides the "contrast" for visualization. 1, brow; 2, eyelid; 3, cheek; 4, ala of nose; 5, nostril; 6, philtrum; 7, upper lip; 8, lower lip.



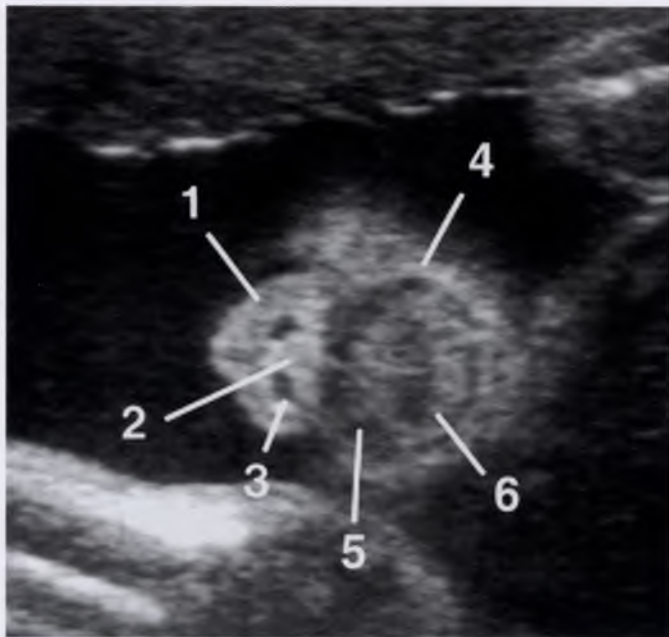


**FIG 8-12** "Coronal" sonogram of the nose and mouth. Nasal structure is particularly well seen: 1, ala; 2, column; 3, nostril. The mouth displays less detail, although consistent and characteristic layering of echoes is seen. These layers are (presumably) the subcutaneous fat (4) and muscular tissue (5), the orbicularis oris muscle, and (6) the mucosal tissue.

with the fetus in a prone or decubitus position but are difficult to image when the fetus is supine.<sup>39</sup> Similarly, the extremities are imaged to excellent advantage when floating freely in the amniotic fluid, yet when tucked under the fetus an extremity will be quite difficult to adequately assess.

Despite these potential problems, fetal skeletal structures remain the earliest and most readily recognized fetal anatomic structures. The earliest structures seen with consistency are the ossification centers of the maxilla, mandible, and clavicle, the first bones of the human body to ossify.<sup>13</sup> The calvaria can be imaged from the late first trimester onward. The same is true of the long bones of the upper and lower extremities (Fig. 8-21). Visibility of bony detail rapidly increases, and by 15 to 16 menstrual weeks (sometimes earlier) even phalanges can be visualized. Bones as small as 2 to 3 mm can be consistently imaged by sonography, provided that no unusual impediments to the scanning procedure exist (Fig. 8-22). Many specific bony structures can be depicted. Bones in both the appendicular and axial skeleton are well imaged.

Sonography has the capacity to visualize not only the ossified portions of the fetal skeleton but also the cartilaginous portions.<sup>13</sup> Bones entirely in cartilage can be seen sonographically (Fig. 8-23). Cartilaginous ends of the long bones may be seen by the early second trimester. It is also important to recognize that the full thickness of the ossified diaphysis of long bones is not seen sonographically.<sup>40</sup> This is due to acoustic shadowing. The cartilaginous ends of long bones help us to recognize this aberration. By matching up the width of the epiphysis, the full thickness of which can be seen, with the apparent width of the bony diaphysis, it is clear that they are unequal (Figs. 8-24 and 8-25). This observation helps to eliminate perceptual errors that can lead to erroneous diagnoses. For example, the inability to see the full thickness of the femoral diaphysis creates the impression that the fetal femur farther from the transducer is bowed (Fig. 8-26).<sup>40</sup> This error is caused by visualization of only the medial cortex of the femoral diaphysis

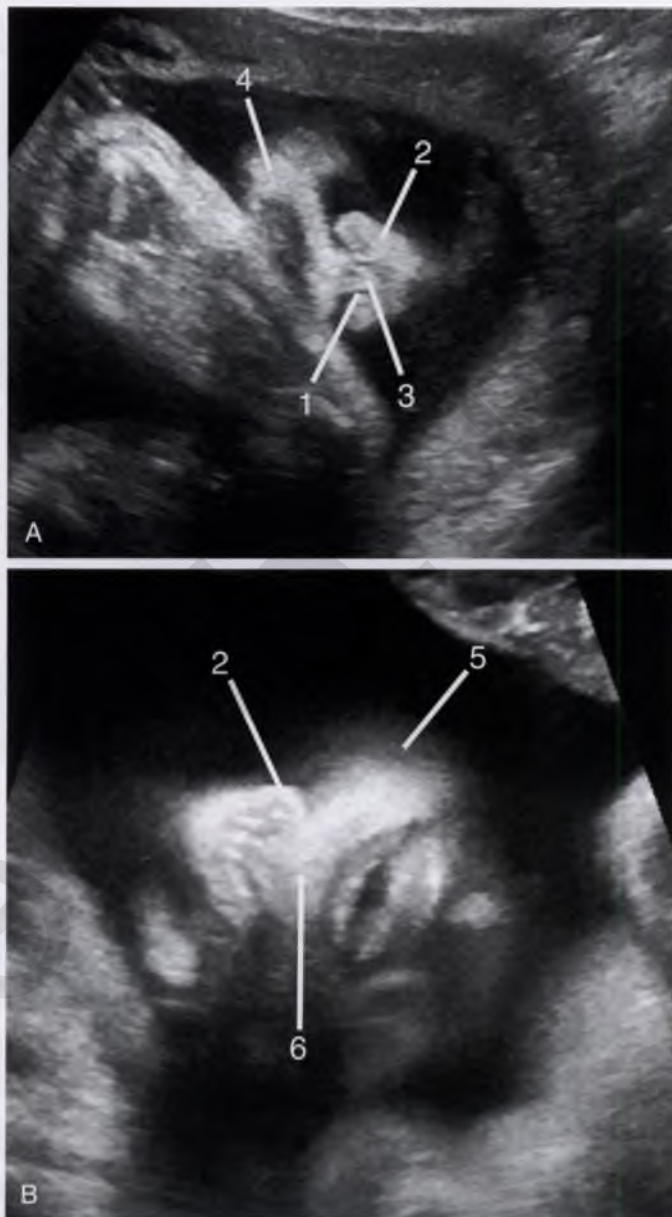


**FIG 8-13 A**, True coronal image of the nose and upper lip. **B**, Inclined coronal image demonstrates a slightly different perspective. 1, nostril; 2, ala; 3, column; 4, upper lip; 5, cheek; 6, philtrum.

(which is normally curved) (Fig. 8-27). However, the inability to visually correct this normal curvature by simultaneous observation of the straight lateral cortex may cause a perceptual error.

The majority of the bones of the appendicular skeleton can be seen in the early to mid-second trimester, although phalanges may be difficult to perceive in some instances. It is a general rule of appendicular skeletal imaging that the more proximal a bone, the more readily it is identified. This rule in one sense is untrue of the hands and feet, where the metacarpals and metatarsals are seen more readily and earlier than either the carpal or tarsal bones (Figs. 8-22 and 8-28). This is because the metacarpals and metatarsals are well ossified at 4 months, whereas the carpals and tarsals (except for the tarsal calcaneus and talus) remain cartilaginous throughout pregnancy. The tarsal calcaneus and talus ossify between the 5th and 6th months, whereas the remaining tarsals and carpals do not ossify until after birth (Figs. 8-29 and 8-30).



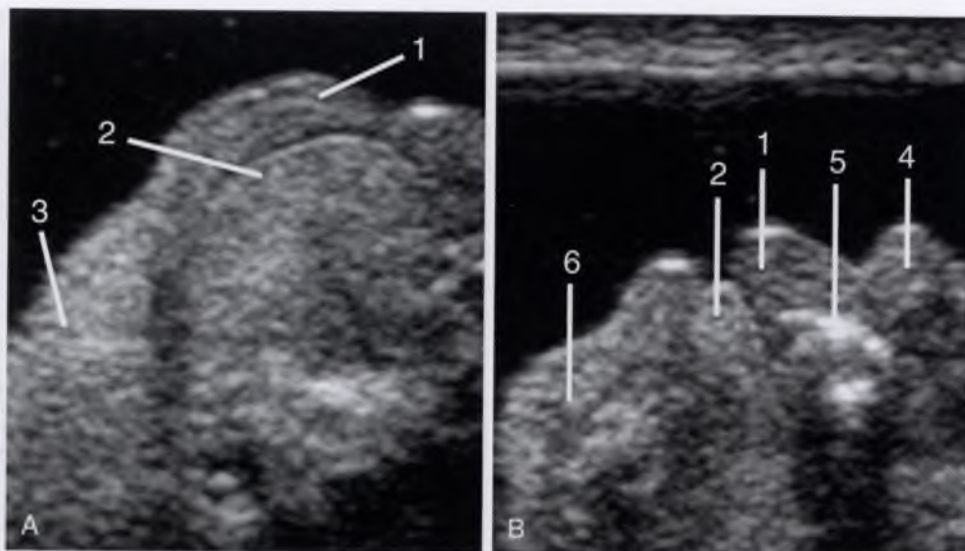


**FIG 8-14** **A**, Axial section of the fetal face demonstrating the tongue. **B**, Midsagittal section of the fetal face demonstrating the tongue. 1, lip; 2, tongue; 3, fat pad of cheek; 4, nose; 5, maxilla; 6, chin.

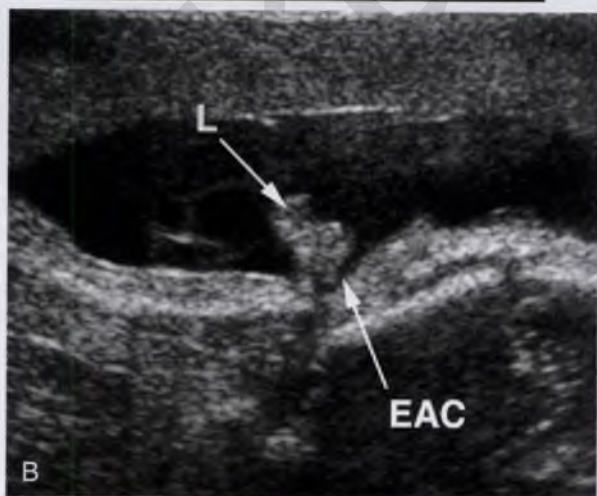
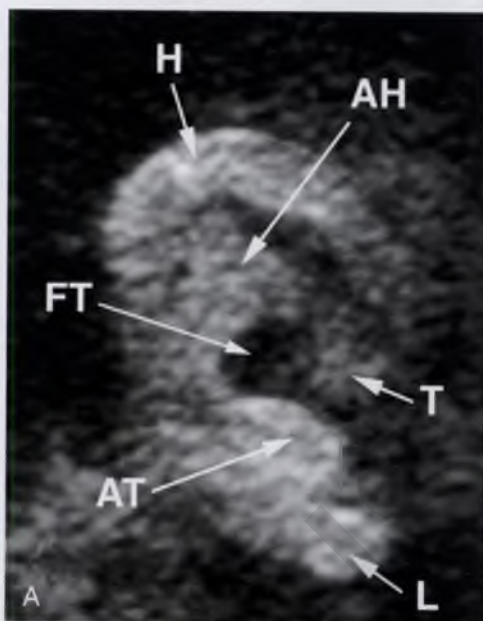


**FIG 8-15** Parasagittal (**A**) and coronal (**B**) sonograms of the fetal ear. AH, antihelix; AT, antitragus; EAC, external auditory canal; FT, fossa triangularis; H, helix; L, lobule; T, tragus.

The scapula (Figs. 8-31 and 8-32), clavicle (Fig. 8-33), humerus (Figs. 8-31 and 8-34), radius (Fig. 8-35), ulna (see Figs. 8-34 and 8-35), metacarpals (see Figs. 8-22 and 8-35), and phalanges (Fig. 8-36) can be imaged in most cases. Interestingly, the clavicle may be difficult to see, presumably because of the flexed position of the fetal neck, which draws the calvaria into an obscuring position. Nonetheless, if one desires to see the clavicle, this can nearly always be accomplished. Measurements exist for normal clavicular length at various gestational ages.<sup>41</sup> Similarly, the femur (Figs. 8-37 to 8-40), tibia (Figs. 8-41 and 8-42), fibula (see Fig. 8-41), metatarsals (see Figs. 8-28 and 8-29), and phalanges (see Fig. 8-28) of the lower extremity can be appreciated well sonographically. The figures demonstrating the hip joint, femur, and knee (see Figs. 8-37 to 8-41) demonstrate the remarkably detailed anatomy that can be achieved with high-resolution sonography.

The simplest way to identify the types of long bones of the extremity viewed on the sonogram is to obtain planes of section that traverse the short axis of the limb. Sonograms obtained in such a plane through the forearm and lower leg will demonstrate two bones. In the lower leg, the more lateral bone is the fibula, and the medial bone is the tibia (see Fig. 8-41). This method works as well in the forearm but is less precise because pronation may cause the radius and ulna to “cross.” In the normal fetus, the tibia and fibula and radius and ulna end at the same level distally (see Fig. 8-35). Proximally, the ulna is longer than the radius (see Fig. 8-34) and the tibia is longer than the fibula. This allows both ready differentiation of the tibia and fibula in the lower extremity and of the radius from the ulna in the upper extremity. Knowledge that both paired long bones of the upper and lower extremity end at the same level distally is important in assessing possible limb reduction abnormalities.

The hand can be assessed more critically than the foot.<sup>42-44</sup> With patience one can usually discern all four fingers and the thumb. The hand is frequently clenched in a fist-like fashion, which can complicate the counting of fingers. However, even under this circumstance, one can frequently make the necessary observations. The toes, although smaller than the fingers, can be seen relatively well with modern equipment (see Figs. 8-28 and 8-30). If difficulty arises, it is usually the functionally less important fourth and fifth toes that are not seen.

It is possible in the late third trimester fetus to identify the distal femoral (Figs. 8-25 and 8-43) and proximal tibial (see Fig. 8-43)

*Text continued on p. 176*



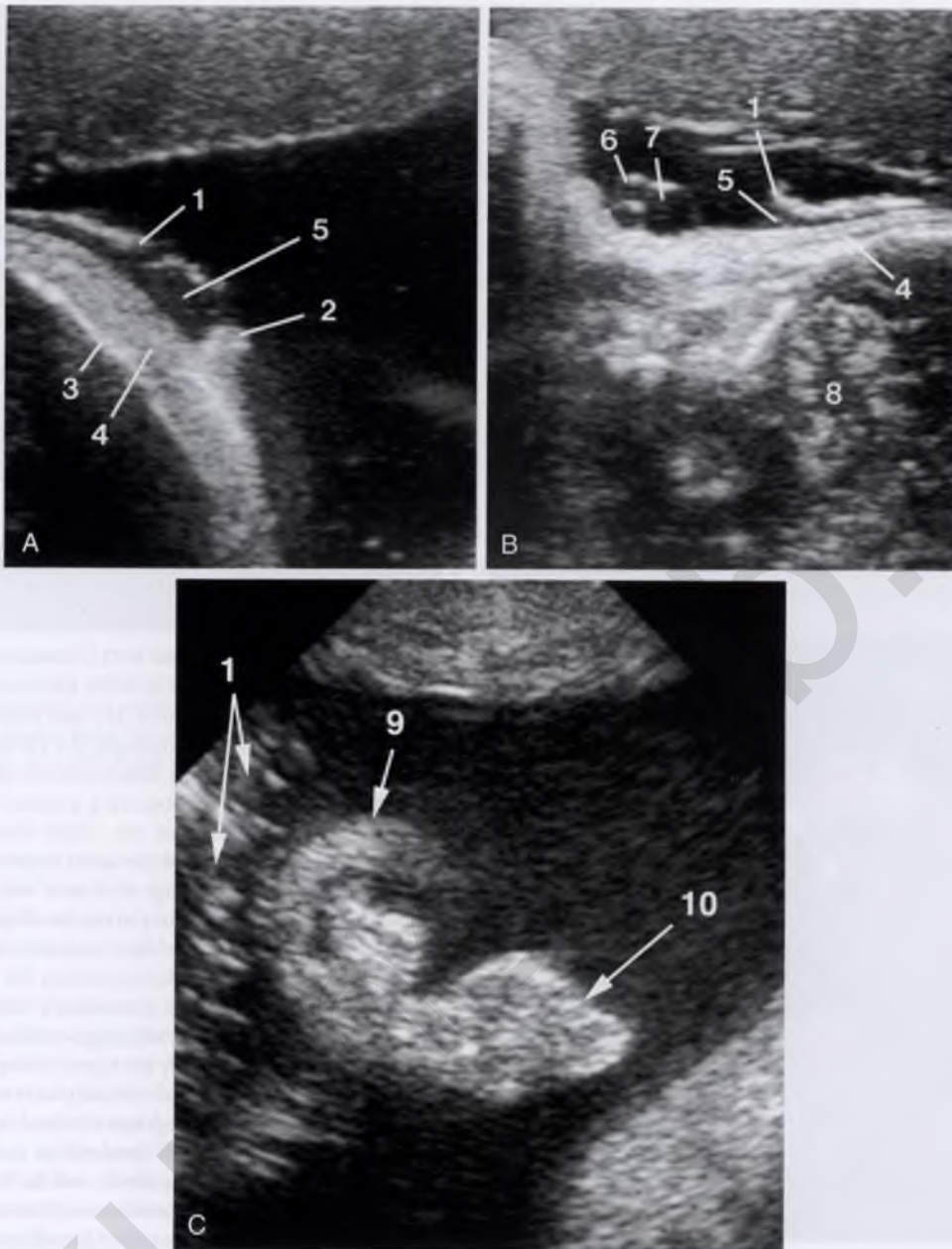


**FIG 8-16** **A**, Hair may be mistaken for the outer membrane of a cystic mass in an older fetus. **B**, Scan at 90 degrees to **A**. This image clarifies that the fetus is normal. **C**, Parasagittal plane through a different fetus demonstrates hair above the ear. 1, hair; 2, portion of ear; 3, occipital bone; 4, subcutaneous tissues and muscles in the occipital region; 5, "trapped" amniotic fluid; 6, umbilical artery; 7, umbilical vein; 8, cerebellum; 9, helix; 10, lobule.

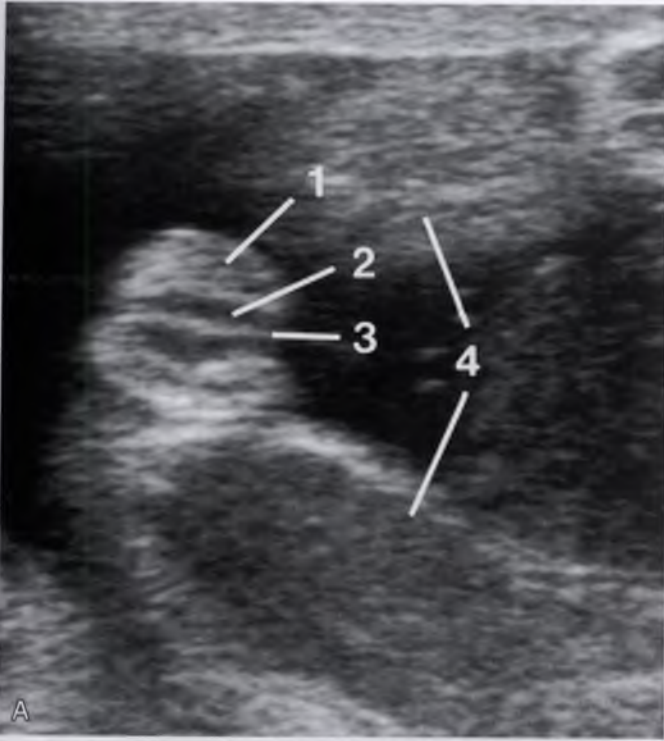


**FIG 8-17** Coronal (A) and axial (B) views. External (and “internal”) female genitalia. Of interest, the uterus (Ut) can be seen to asymmetrically indent the bladder of female fetuses (Ants Toi, MD, personal communication). 1, major labium; 2, minor labium; 3, vaginal cleft; 4, thighs.

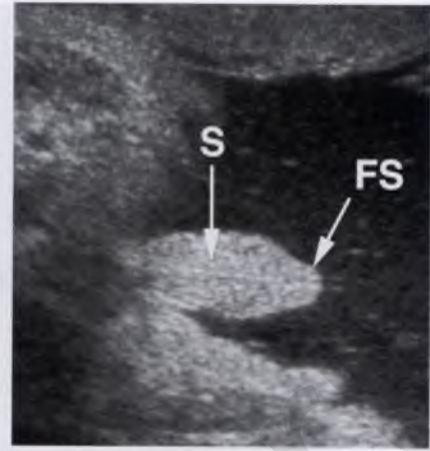


**FIG 8-18** Nonerect fetal penis seen sonographically. FS, foreskin; S, shaft.



**FIG 8-19** Details in an erect fetal penis. 1, urethra; 2, corpus cavernosum; 3, shaft; 4, glans; 5, foreskin.

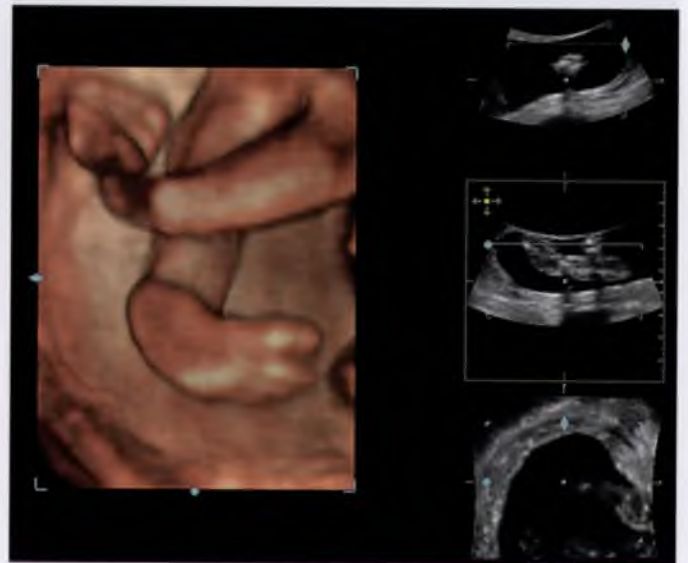


**FIG 8-20** Three-dimensional image (left) reconstructed from the multiplanar two-dimensional images (right) demonstrates bilateral clubbed feet in a 20-week fetus.





**FIG 8-21** Sonogram of a 10.5-week embryo demonstrates the tiny (approximately 1 mm) primary ossification center of the femur (*arrow*). (From Mahony BS, Filly RA: High-resolution sonographic assessment of the fetal extremities. *J Ultrasound Med* 3:489, 1984.)

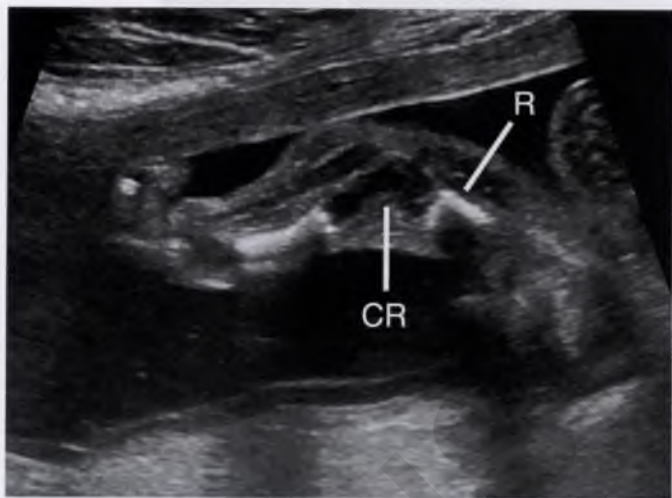


**FIG 8-22** Sonogram of a 25-week fetal wrist. CR, cartilaginous carpal bones; R, radial diaphysis (distal radial epiphysis is also cartilaginous).

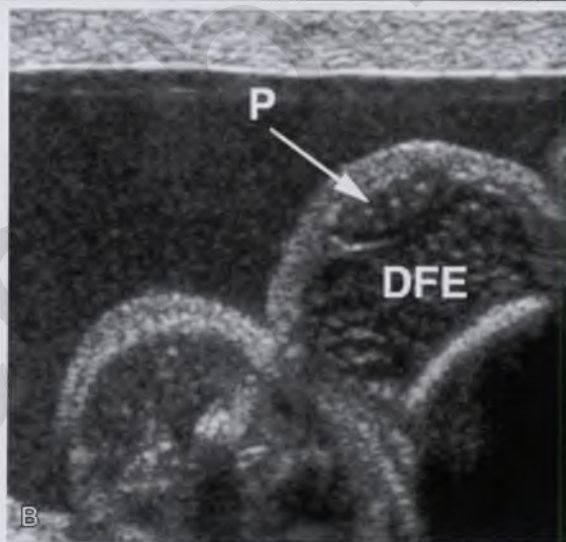
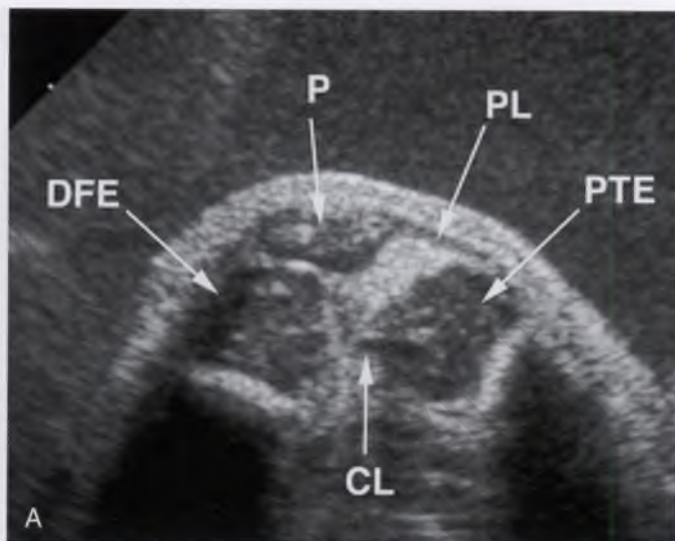


**FIG 8-23 A**, Midsagittal sonogram of the fetal knee. **B**, Axial sonogram (similar to the knee radiograph called the *sunrise view*). Note the echogenic synovium located between the patella, patellar ligament, and epiphyses. P, patella (a bone that is entirely cartilaginous); DFE, distal femoral epiphysis; CL, posterior cruciate ligament; PL, patellar ligament; PTE, proximal tibial epiphysis.

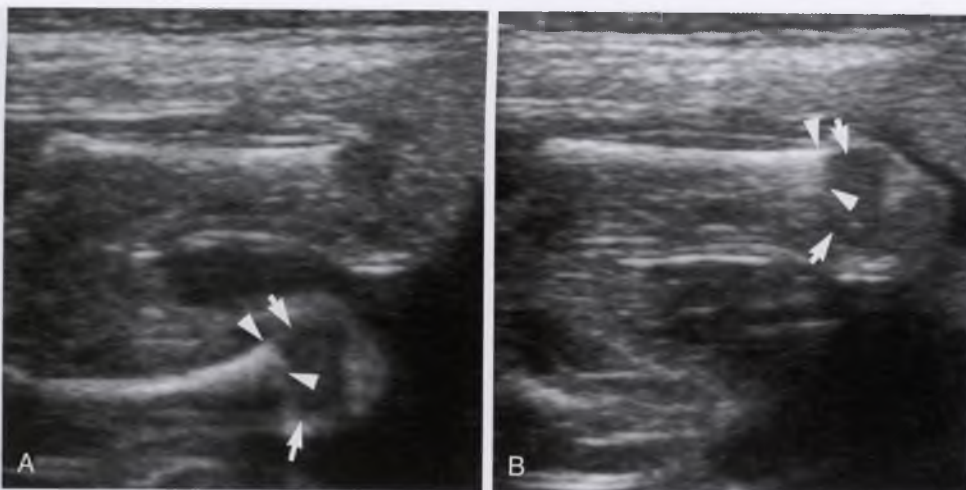


**FIG 8-24** **A**, Sonogram best demonstrating the femur farther from the transducer. Arrows mark the edges of the distal epiphysis. Arrowheads mark the apparent "edges" of the distal femoral diaphysis. The more medial edge of the diaphysis matches the edge of the medial condyle, but the lateral edges of "diaphysis" and lateral condyle are widely disparate. **B**, The same exercise can be performed on the nearer femur. Again, arrows mark the edges of the distal epiphysis, and arrowheads mark the "edges" of the femoral diaphysis. Shadowing by the bone but not the cartilage causes this deceptive appearance.

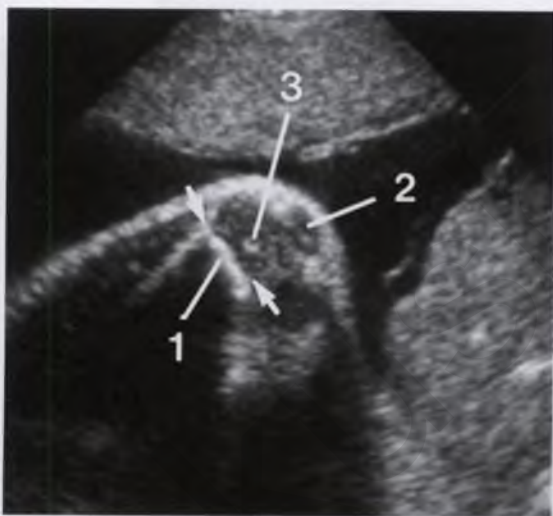


**FIG 8-25** Sector sonogram of the distal femur taken such that the lines of sight from the transducer intersect the inferior end of the femoral metaphysis at the epiphyseal plate (1). By this maneuver, the full thickness of the distal ossified femur is seen sonographically (compare with Fig. 8-24). Now, the thickness of the epiphysis (arrows) and ossified femoral shaft match perfectly. 2, patella; 3, secondary ossification center of the distal femoral epiphysis.

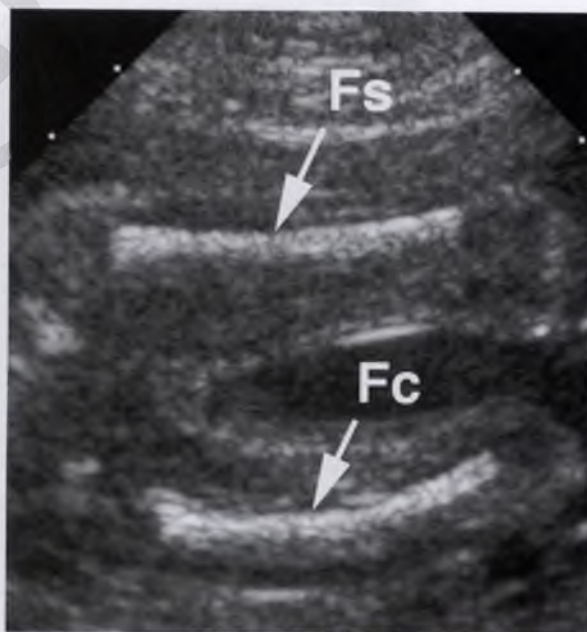


**FIG 8-26** In this sonogram the diaphysis of the femur nearer to the transducer appears straight (Fs). The full thickness of the diaphysis is not seen. The diaphysis of the femur farther from the transducer appears curved (Fc). Compare with Figure 8-27. This is a normal shape of the medial aspect of the bone. However, the straight lateral cortex seen in the radiograph but not the sonogram visually compensates the curvature because the full thickness of bone is not perceived.



**FIG 8-27** Radiograph of a midtrimester fetal femur. Note that our eye compensates for the curvature of the medial diaphyseal cortex (*curved arrows*) by noting the straight lateral diaphyseal cortex (*straight arrows*). Compare with Figure 8-26.

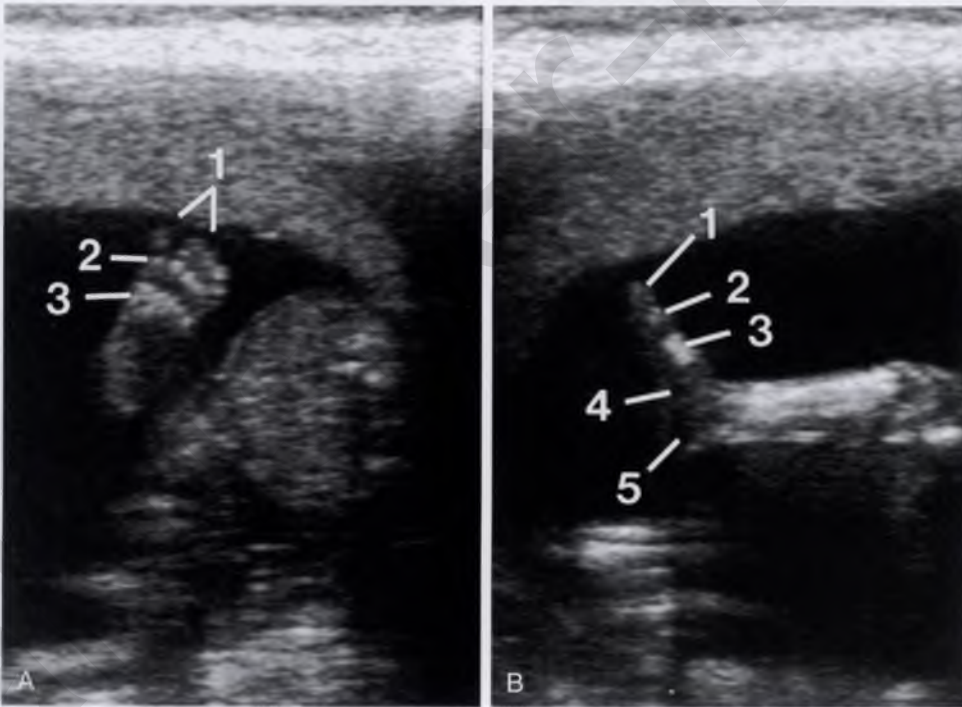


**FIG 8-28** Fetal foot at 16 weeks' gestation in transverse axial (**A**) and parasagittal (**B**) planes. 1, toes; 2, proximal phalangeal ossification centers; 3, metatarsal ossification centers; 4, tarsal cuboid in cartilage; 5, tarsal calcaneus in cartilage.

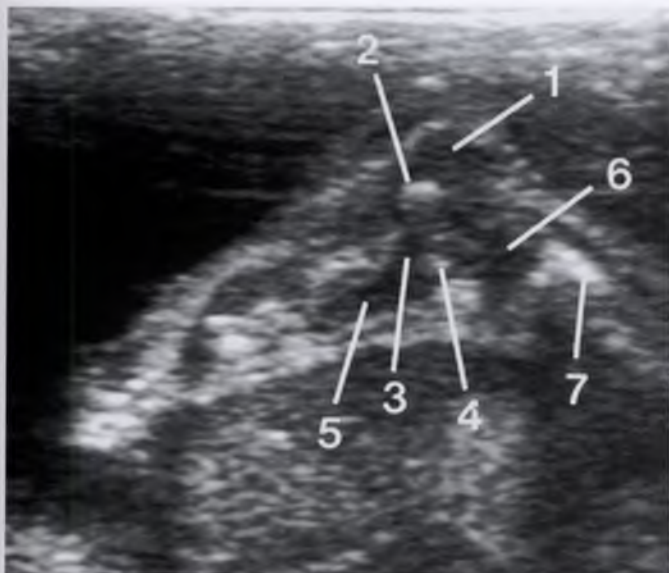


**FIG 8-29** Midsagittal sonogram of the fetal foot in late second trimester. 1, cartilaginous calcaneus; 2, primary ossification center of calcaneus; 3, cartilaginous talus; 4, primary ossification center of talus; 5, tarsal navicular in cartilage; 6, distal tibial epiphysis; 7, distal tibial diaphysis.

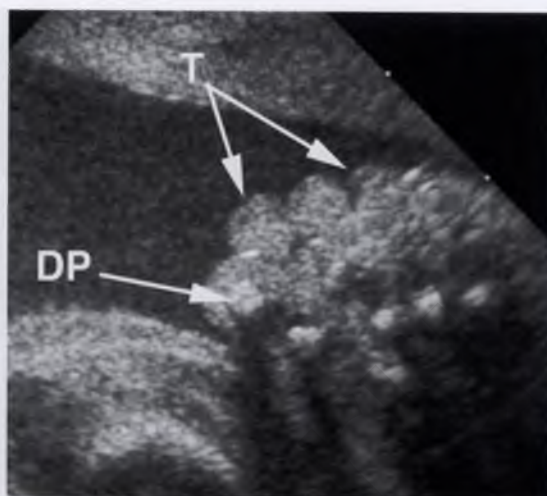


**FIG 8-30** Axial sonogram of the fetal toes (T) demonstrating the soft tissues. Little bony structure is seen, although the distal phalanx (DP) of the great toe is visible.

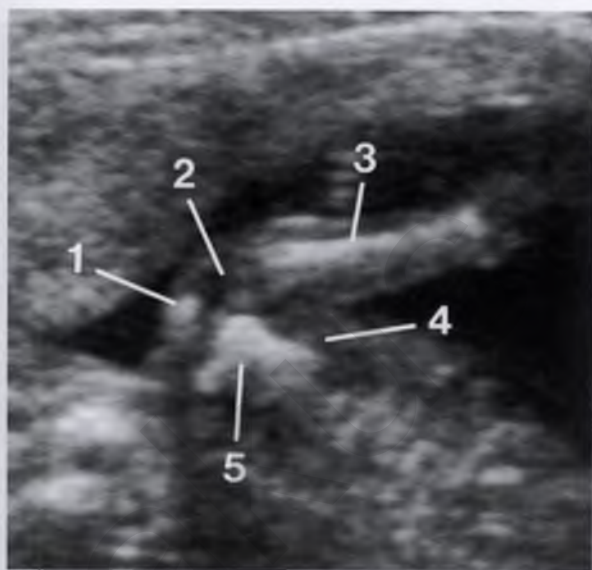


**FIG 8-31** Coronal sonogram of the shoulder and upper arm. 1, distal clavicle; 2, cartilaginous humeral head; 3, ossified humeral diaphysis; 4, latissimus dorsi muscle; 5, scapula.

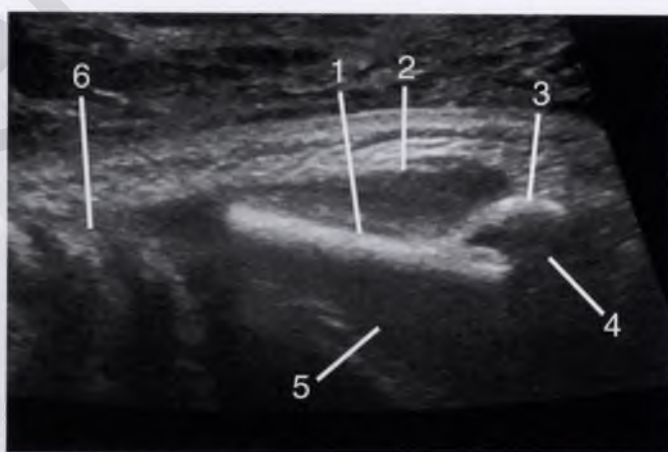


**FIG 8-32** Parasagittal sonogram of the scapula. 1, infraspinous fossa; 2, infraspinatus muscle; 3, scapular spine; 4, supraspinatus muscle; 5, subscapularis muscle; 6, ribs in short axis.



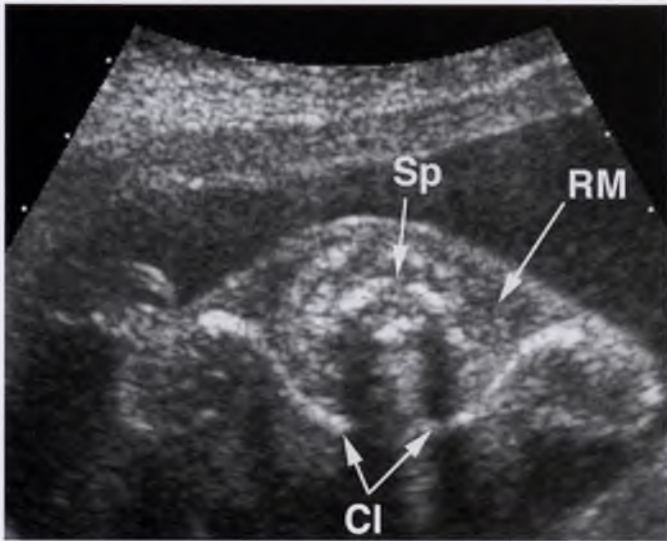


**FIG 8-33** Axial sonogram of the clavicles (CI). RM, rhomboid muscle; Sp, spine.

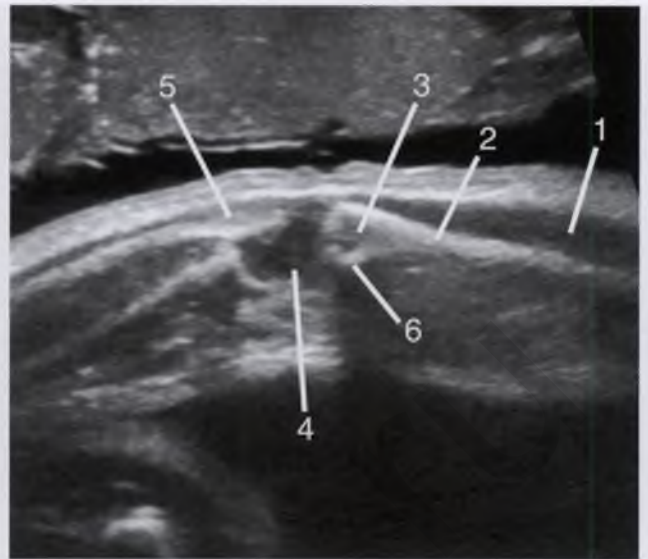


**FIG 8-34** Fetal elbow, hand pronated, coronal sonogram. 1, triceps muscle; 2, ossified humeral diaphysis; 3, cartilaginous olecranon fossa; 4, conglomerate cartilages about the elbow joint; 5, proximal ulnar diaphysis; 6, medial humeral epicondyle.

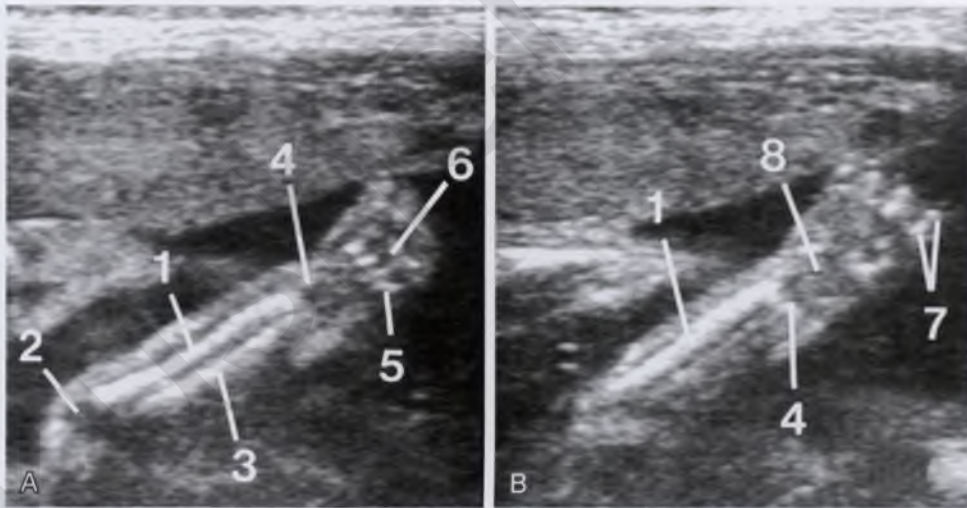


**FIG 8-35 A and B**, Coronal sonograms of the forearm and wrist. 1, ulnar diaphysis; 2, olecranon in cartilage; 3, radial diaphysis; 4, distal ulnar epiphysis; 5, metacarpal diaphysis; 6, distal metacarpal epiphysis; 7, phalangeal ossification centers; 8, carpal arch seen as a conglomerate cartilage.

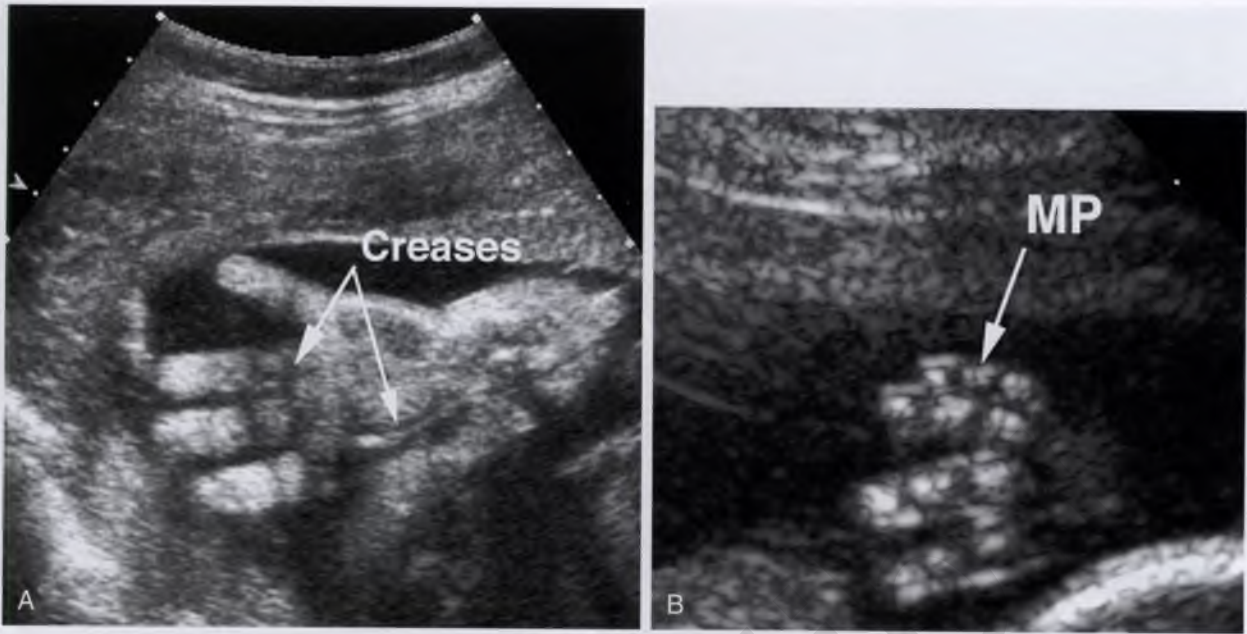


**FIG 8-36** **A**, Coronal sonogram of the fetal hand demonstrating the soft tissues of the fingers and palm. Creases at the interphalangeal joints and palmar creases are seen. **B**, Coronal sonogram of the hand demonstrating some of the bony detail of the developing phalanges. MP, middle phalanx.

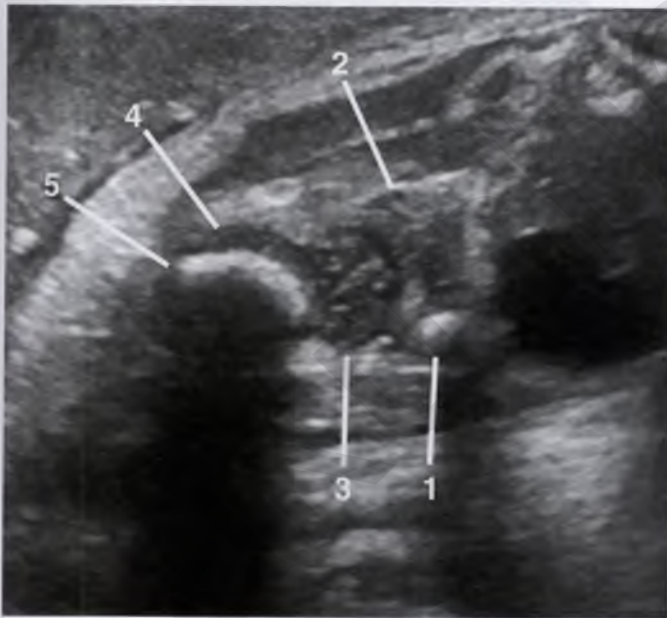


**FIG 8-37** Coronal oblique image of the fetal hip. 1, ischial ossification center; 2, cartilaginous acetabulum; 3, femoral head in cartilage; 4, greater trochanter in cartilage; 5, femoral metaphysis.



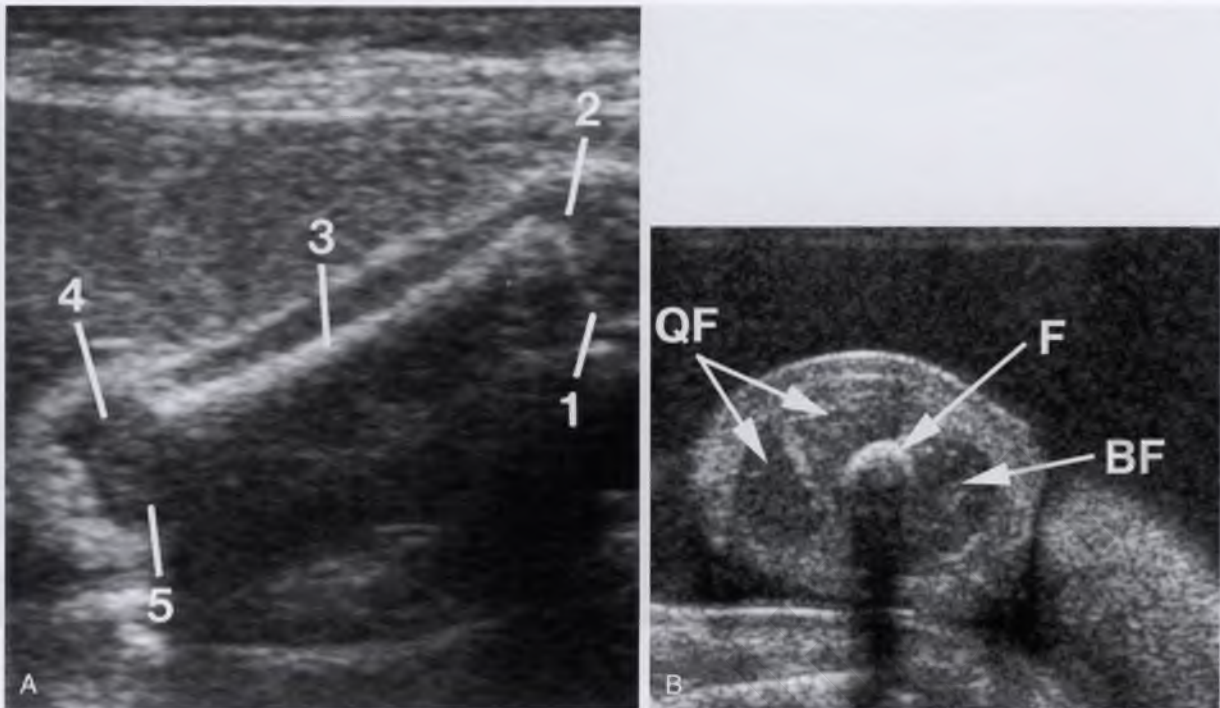


**FIG 8-38** Longitudinal (**A**) and transverse axial (**B**) sonograms of the fetal thigh. 1, posterior hip joint capsule; 2, greater trochanter; 3, femoral diaphysis; 4, lateral condyle; 5, medial condyle; BF, biceps femoris muscle; F, femoral diaphysis; QF, quadriceps femoris muscle.

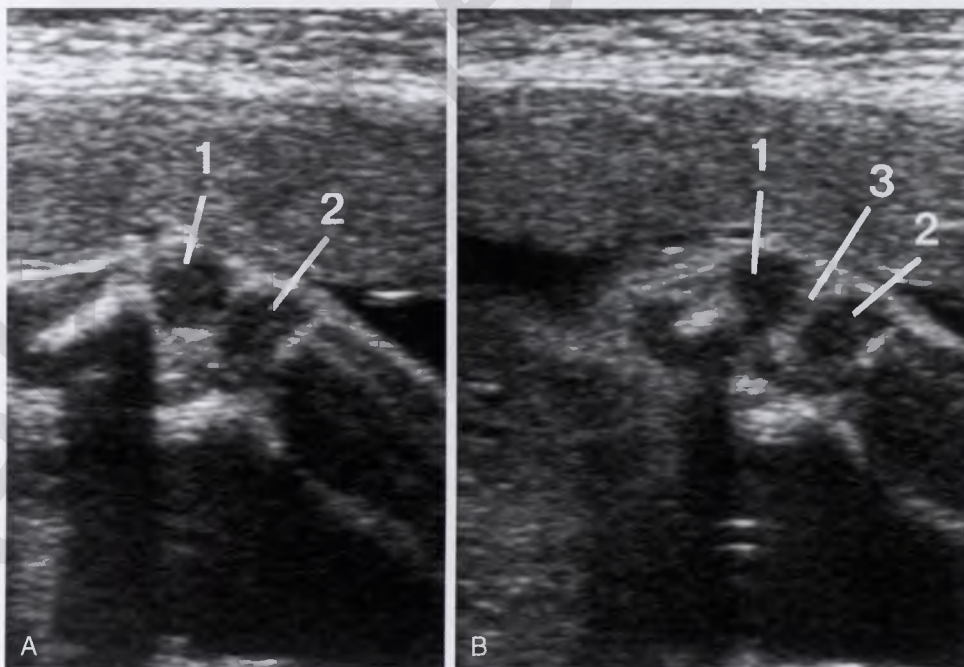


**FIG 8-39 A**, Parasagittal sonogram of the fetal knee. The femoral condyle (1) articulates with the tibial plateau (proximal tibial epiphysis). **B**, Midsagittal sonogram of the fetal knee. The gap (3) between the distal femoral epiphysis (1) and the proximal tibial epiphysis (2) is due to the intercondylar notch (see Fig. 8-40).

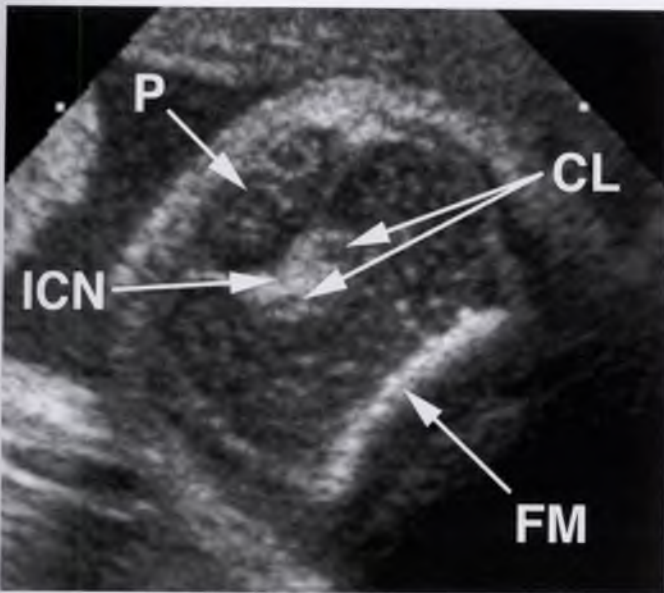


**FIG 8-40** Axial sonogram of the knee in flexion. CL, cruciate ligaments; FM, femoral metaphysis; ICN, intercondylar notch (note the brightly echogenic synovium within the joint); P, patella.

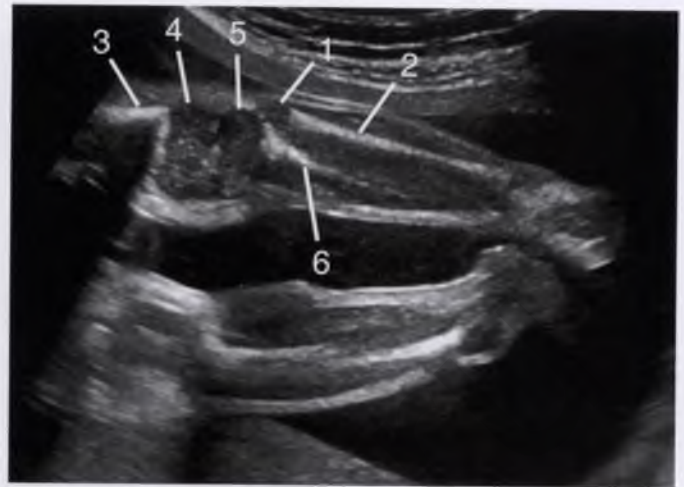


**FIG 8-41** Coronal sonograms of the knee. 1, proximal fibular epiphysis; 2, fibular diaphysis; 3, femoral metaphysis; 4, lateral femoral condyle; 5, proximal tibial epiphysis; 6, tibial diaphysis.

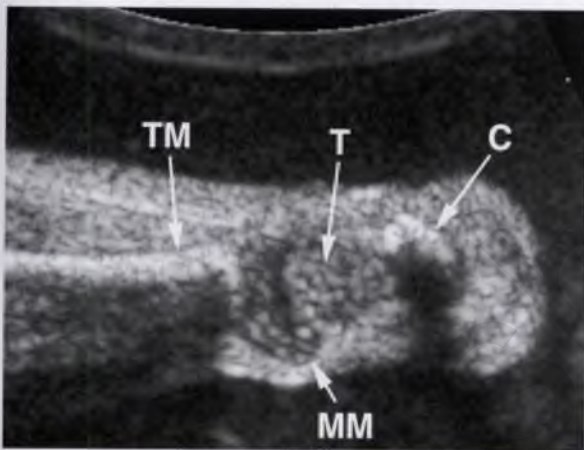


**FIG 8-42** Axial sonogram of the distal tibia and a portion of the ankle joint. C, calcaneus; MM, medial malleolus; T, talus (a bone that is entirely cartilaginous); TM, tibial metaphysis.

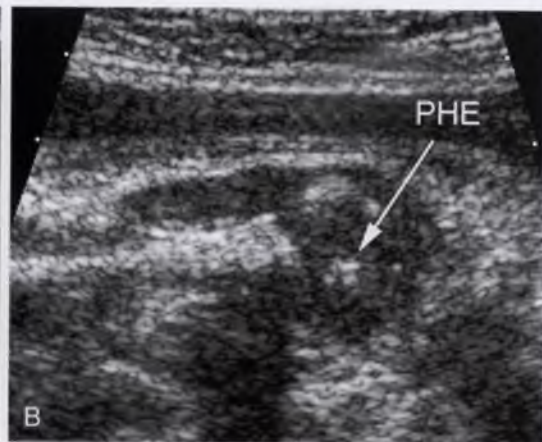
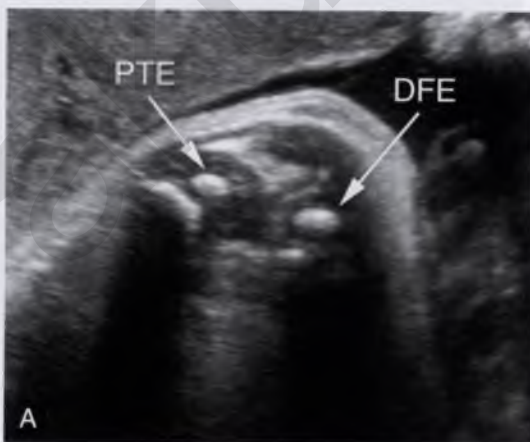


**FIG 8-43** **A**, Coronal sonogram of the distal thigh in a term fetus. Note the large and similar sizes of the ossification centers, a virtually certain sign of a near-term fetus. **B**, Coronal sonogram through the proximal humerus shows an early secondary ossification center in the humeral head, another finding indicating a later gestation. DFE, ossification center of distal femoral epiphysis; PHE, ossification center of proximal humeral epiphysis; PTE, ossification center of proximal tibial epiphysis.



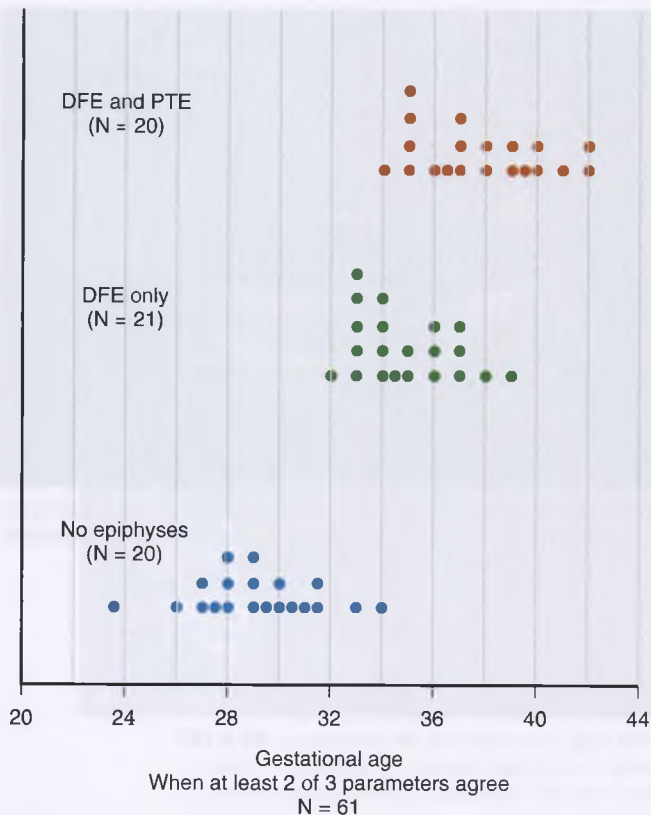


**FIG 8-44** Appearance time of the distal femoral epiphysis (DFE) and proximal tibial epiphysis (PTE) in a mixed group of 61 fetuses when two of the following three dating parameters agreed: last menstrual period, early sonogram, and Dubowitz scores. (From Chinn DH, Bolding DB, Callen PW, et al: Ultrasonographic identification of fetal lower extremity epiphyseal ossification centers. *Radiology* 147:815-818, 1983.)

epiphyseal ossification centers.<sup>45,46</sup> Ossification of these epiphyses, as seen on radiographs, is known to be an indicator of fetal maturity. Identification of the epiphyseal ossification centers about the knee provides a different type of parameter that sonologists can use in the assessment of gestational age in the third trimester of pregnancy. In general, visualization of a distal femoral epiphyseal ossification center indicates a gestational age of at least 33 weeks (Figs. 8-44 to 8-46). Similarly, the same data suggest that demonstration of the proximal tibial epiphysis indicates a gestational age of at least 35 weeks. These ossification centers appear earlier, on average, in female fetuses (see Fig. 8-45).<sup>46</sup> The size of the distal femoral ossification center correlates with late gestational age (see Fig. 8-46).<sup>46</sup> The proximal humeral epiphyseal ossification center is usually the last of the secondary ossification centers to ossify and generally can be seen at a gestational age of 38 weeks or later.

As stated earlier, many bones of the fetal appendicular skeleton are entirely cartilaginous. Some of these still can be imaged sonographically. For example, the patella, which does not begin to ossify until after birth, can be seen rather commonly (see Figs. 8-23 and 8-25). All of the carpal and most of the tarsal bones are entirely cartilaginous (see Figs. 8-22, 8-28, 8-29, and 8-35). The carpal bones cannot be seen discretely. Rather, they are perceived as a conglomerate hypoechoic band spanning the gap from the distal radius and ulna to the proximal metacarpal ossification centers (see Fig. 8-35). This gap includes the cartilaginous epiphyses of the long bones as well. Conversely, some of the tarsal bones can be discretely identified from time to time (see Figs.

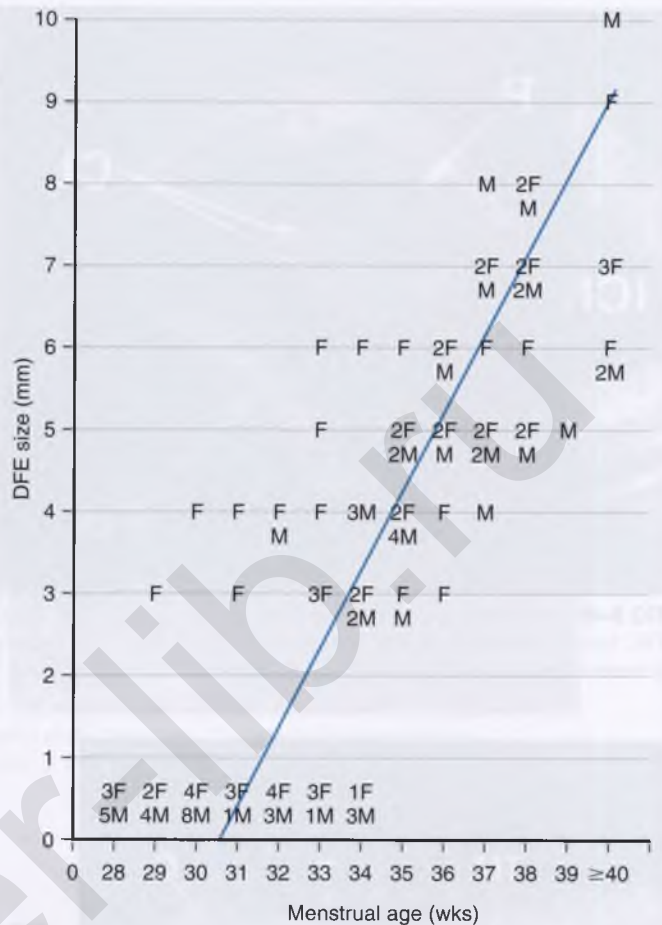


**FIG 8-45** Variation in the distal femoral epiphysis (DFE) appearance time and size in male (M) and female (F) fetuses. (From Mahony SB, Callen PW, Filly RA: The distal femoral epiphyseal ossification center in the assessment of third trimester menstrual age: sonographic identification and measurement. *Radiology* 155:201-204, 1985.)

8-28 and 8-29). These include, most notably, the early calcaneus and talus (before 24 weeks) and the tarsal navicular and cuboid throughout gestation.

Visualization of the cartilaginous ends of the long bones assists in their measurement in two ways. The measurement of fetal long bones is confined to the ossified portion. A potential error is to foreshorten the bone by failing to obtain the plane of section through the true long axis of the bone. To avoid underestimating length, this shortcoming is often compensated for by assuming the "longest" measurement obtained in several attempts to be the most accurate, an assumption that can lead to serious overestimates, as is discussed shortly. However, if both cartilaginous ends of the desired bone to be measured are seen, this guarantees that the plane of section has passed through the longest axis of the bone (Fig. 8-47). The only remaining task to minimize error is to accurately position measurement cursors at the ends of the bone.

Another common misconception in measurement of the femur is that no other tissue in proximity to the bony termination will yield an echo of equal brightness to the bone. Thus, one should always place measurement cursors from the edge of the distal brightest reflection to the edge of the proximal brightest reflection. This longstanding belief is unfortunately untrue, especially in older fetuses, although younger fetuses are not exempt from this potentially significant error in femur length estimation.<sup>47</sup> Figure 8-48 demonstrates that a

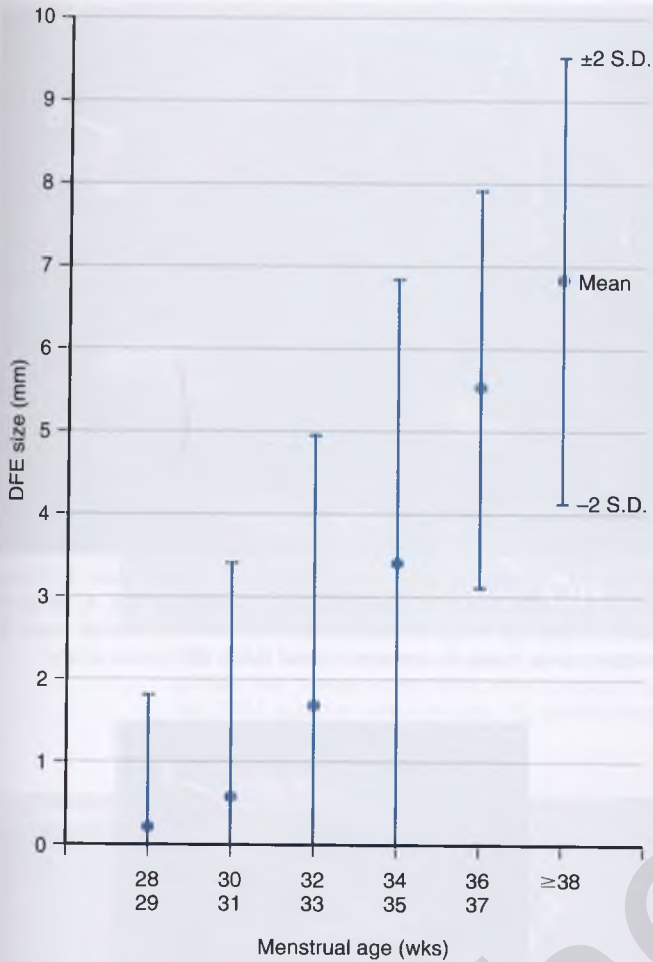


**FIG 8-46** Mean diameter of the distal femoral epiphysis (DFE) with increasing age. S.D., standard deviation. (From Mahony SB, Callen PW, Filly RA: The distal femoral epiphyseal ossification center in the assessment of third trimester menstrual age: sonographic identification and measurement. *Radiology* 155:201-204, 1985.)

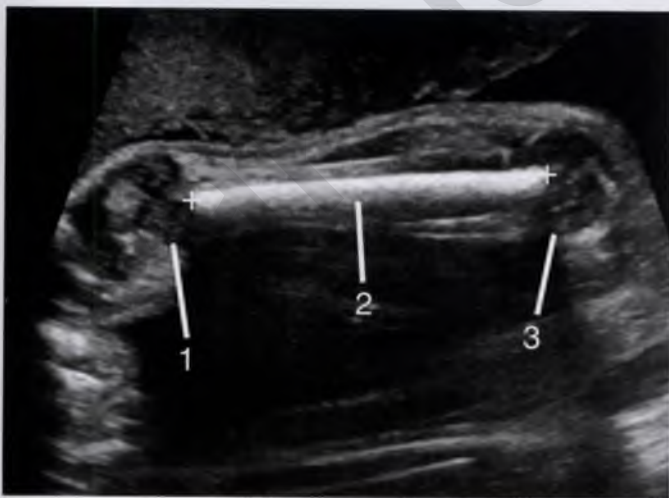


**FIG 8-47** Longitudinal view of femur for measurement. Visualization of the proximal (3) and distal (1) cartilaginous bone ensures that the plane of section is through the long axis of the diaphysis (2). Only proper positioning of the cursors (+) remains to ensure an accurate measurement.

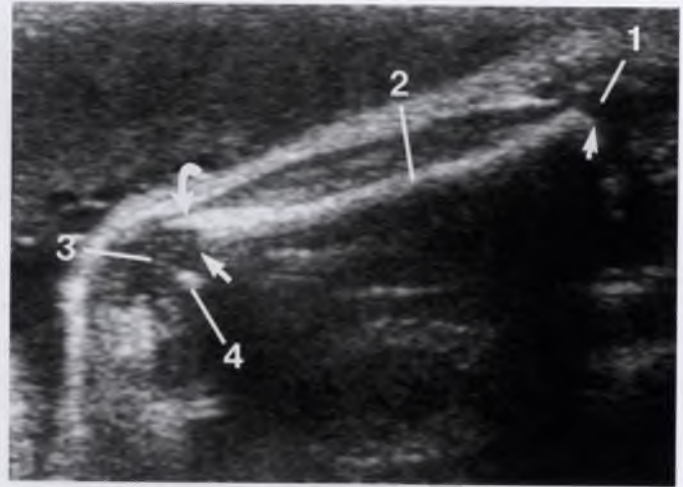


**FIG 8-48** View of the fetal femur, third trimester. A bright reflector (curved arrow) is seen in continuity with the lateral femoral metaphysis. This structure is not part of the ossified femur. End points of femur measurement are marked by straight arrows. 1, greater trochanter; 2, femoral diaphysis; 3, lateral condyle; 4, ossification center of the distal epiphysis.

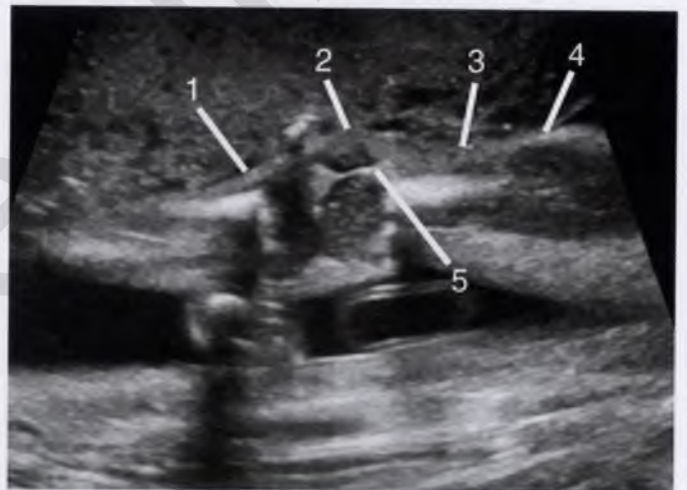


**FIG 8-49** Midsagittal sonogram of the extended knee. In addition to structures pointed out in earlier figures, note the patellar ligament (1), patella (2), quadriceps tendon (3), quadriceps muscle (4), and synovium (5) contained by the knee joint.

nonosseous, but nonetheless equally bright, reflection is returned from tissues distal to the epiphyseal plate but in immediate contiguity with the distal femoral metaphysis. This is called the distal femoral point for lack of a more precise anatomic term.<sup>47</sup> That this “point” is not part of the ossified femur can be determined by noting its relationship to the cartilaginous lateral condyle. The femoral metaphysis ends at the beginning of the distal femoral epiphysis and does not overlap the edge of the epiphysis. Compare the radiograph of the fetal femur in Figure 8-27 with the sonogram of the fetal femur in Figure 8-48. No such ossified femoral point exists.

Sonography, from time to time, demonstrates rather extraordinarily detailed anatomy of the musculoskeletal system of the extremities such as individual tendons and ligaments. At present, no known diagnostic usefulness for this information has been established, nor is it possible to demonstrate such structures with the consistency necessary to use their visualization in diagnostic pursuits. However, several of these remarkable features are demonstrated in Figures 8-49 to 8-51.



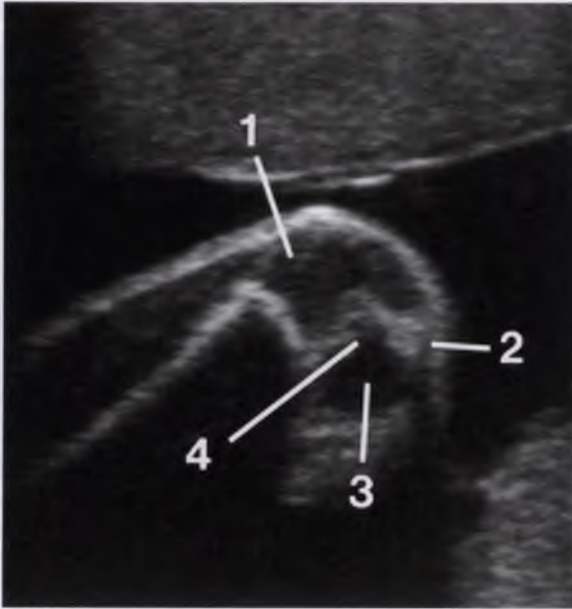


**FIG 8-50** Midsagittal sonogram of the fetal knee in flexion shows the distal femoral epiphysis (1), patellar ligament (2), and proximal tibial epiphysis (3). These three structures marginate the knee joint. Within the knee joint is a large quantity of highly echogenic tissue, presumably synovium. Clearly outlined by the bright "synovium" is the cruciate ligament (4).

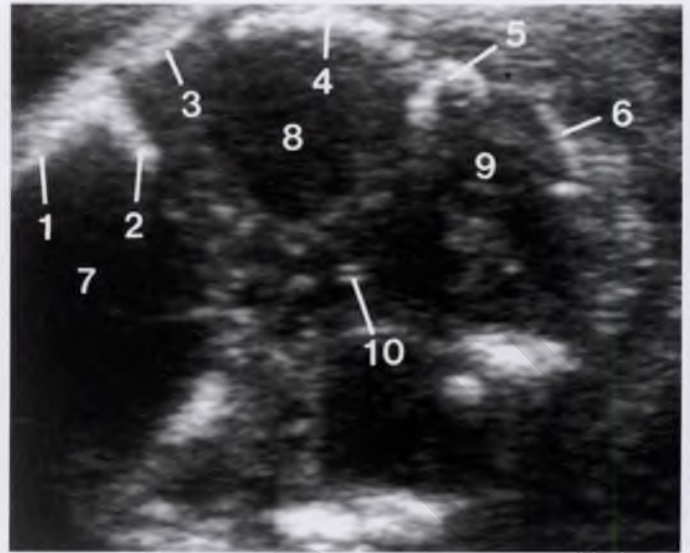


**FIG 8-52** Transverse axial sonogram near the skull base. 1, frontal bone; 2, greater wing of sphenoid bone; 3, parietal bone; 4, temporal bone; 5, petrous ridge; 6, occipital bone; 7, anterior cranial fossa; 8, middle cranial fossa; 9, posterior cranial fossa; 10, basilar artery.

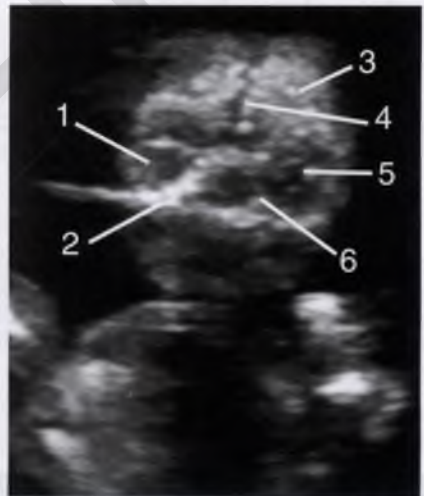


**FIG 8-53** Fetal orbits, early second trimester. 1, orbit; 2, maxilla; 3, frontal bone; 4, metopic suture; 5, lens; 6, nasal bone.



**FIG 8-51** Coronal sonogram through the dorsal soft tissues of the forearm and hand. 1, extensor muscle group; 2, extensor tendons.

Many bones or components of bones of the axial skeleton are also routinely visualized. In the skull region, one can perceive a number of bones individually or as a conglomerate. The greater wings of the sphenoid and petrous ridge are easily identified and define the anterior, middle, and posterior cranial fossae (Fig. 8-52). Both orbits can be visualized without difficulty unless the more anteriorly positioned orbit severely shadows the more posteriorly positioned orbit (Fig. 8-53). Standards have been established for fetal interorbital distances to evaluate hypotelorism and hypertelorism.<sup>48</sup> In older fetuses, surprising detail of the intraorbital contents can be appreciated, including the wall of the globe, lens, retrobulbar fat, optic nerve, and rectus muscles (Fig. 8-54). Portions of the maxilla and nearly the entire mandible can be identified, as can the bony nasal ridge (see Fig. 8-53). Similarly, the frontal, parietal, and squama of the temporal and occipital bones, the bones making up the calvaria, can be seen clearly. The cartilaginous zones of articulation of these bones, the coronal, sagittal, and lambdoid sutures, are commonly visible (Fig. 8-55). The fontanelles may be seen



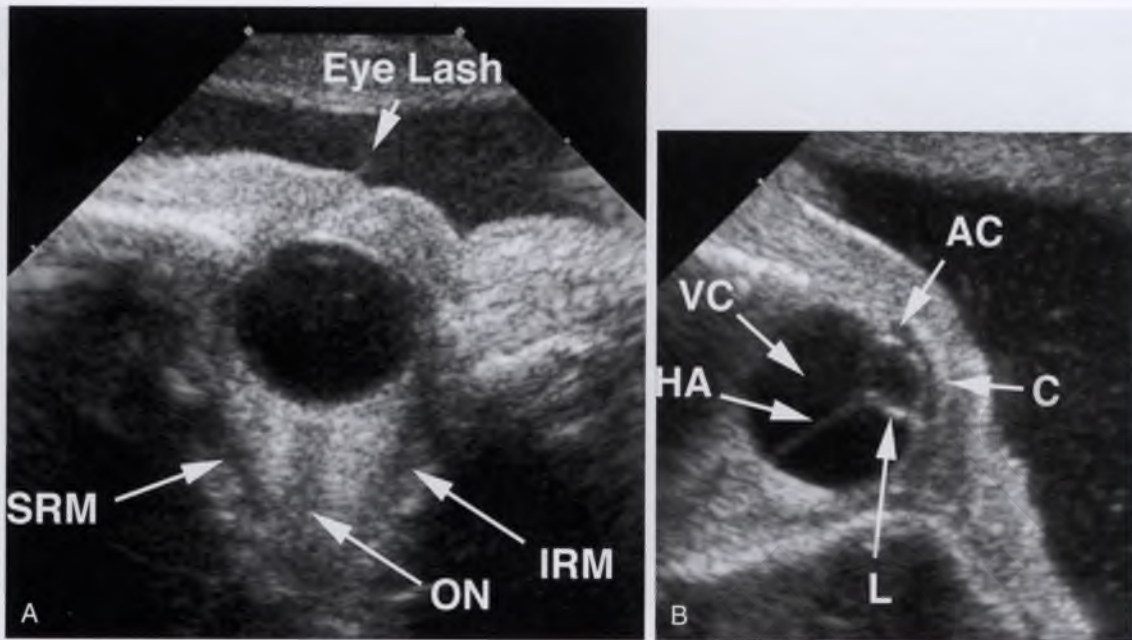


**FIG 8-54** Fetal orbits and contents seen on parasagittal sonograms (**A** and **B**). AC, anterior chamber; C, cornea; HA, hyaloid artery; IRM, inferior rectus muscle; L, lens; ON, optic nerve (traversing the retrobulbar fat); SRM, superior rectus muscle; VC, primary vitreous. Note the eyelash extending from the closed eyelids (also visible in B).

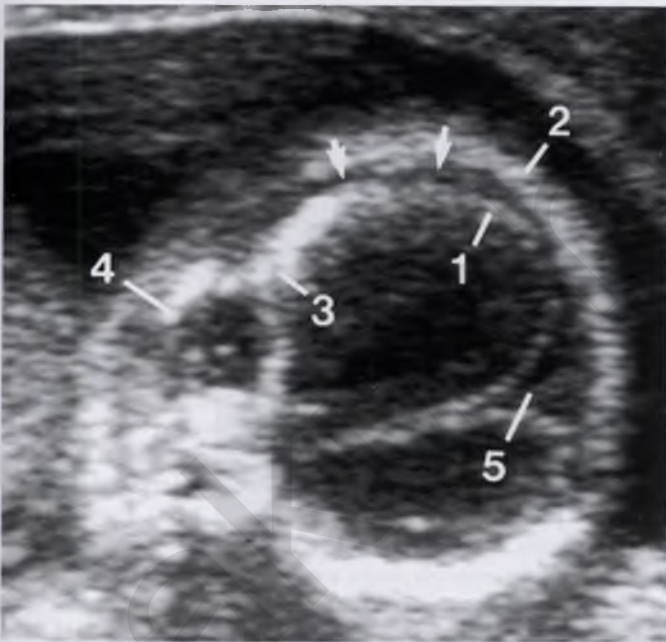


**FIG 8-55** Oblique view demonstrating the coronal suture (arrows). 1, frontal bone; 2, parietal bone; 3, greater wing of sphenoid bone; 4, maxilla; 5, interhemispheric fissure with brain edges showing brightly reflective covering of pia-arachnoid.

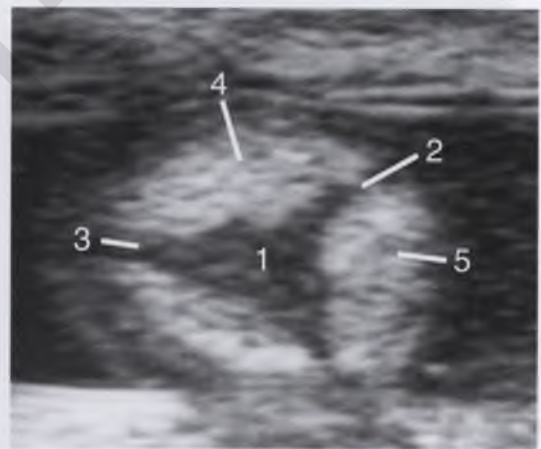


**FIG 8-56** Transverse axial sonogram of the posterior fontanelle (1). 2, lambdoid suture; 3, sagittal suture; 4, parietal bone; 5, occipital bone.

as well (Fig. 8-56). These anatomic features are particularly well seen in three-dimensional reconstructions of the calvaria, as demonstrated in Chapter 11. Sutures and fontanelles function as windows for brain imaging (Fig. 8-57). Although many individuals who perform sonography do not realize that they are employing sutures and fontanelles to image the fetal brain, they visually ascertain that, as they move the transducer, “fuzzy” brain images suddenly become clearer. The reason, of course, is that as they move the transducer the beam inevitably

passes through a suture or fontanelle, enabling even the unsophisticated imager to take advantage of these gaps between the calvarial plates.

The ribs, spine, and pelvis are easily imaged and serve as excellent anatomic landmarks. In the pelvis, the iliac ossification centers are easily observed from the early second trimester onward (ossified at 2.5 to 3 fetal months). Ischial ossification (see Fig. 8-37) is present at 4 months, whereas pubic ossification is not present until 6 months.

The spine is an extremely important structure in fetal diagnosis.<sup>39,49-51</sup> With the advent of maternal serum  $\alpha$ -fetoprotein screening, as well as the concurrent development of sophisticated high-resolution ultrasound imaging technology, the potential exists to diagnose nearly all lesions of spina bifida before the 20th week of pregnancy.<sup>52</sup> These changes in obstetric care mandate that the morphologic appearance of the fetal spine be well understood by sonologists. The sequence of development of ossification centers in the fetal vertebral column has



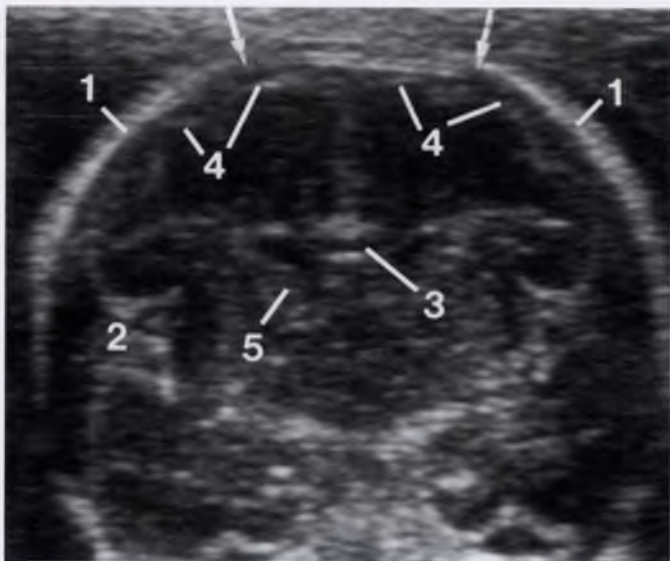


**FIG 8-57** The sonographic beam was directed through the anterior fontanelle (arrows) in a midtrimester fetus, enabling recognition of striking detail in the fetal brain because of the "bone-free window." 1, parietal bone; 2, lateral fissure; 3, corpus callosum; 4, brain edges over the most cephalic portions of the parietal lobes; 5, head of caudate nucleus.



**FIG 8-58** Early ossification centers in the sacral spine. Anteriorly is the centrum, and posteriorly (POC) the ossifications of the posterior arch appear near the base of the transverse processes. IW, iliac wings. (From Filly RA, Simpson GF, Linkowski G: Fetal spine morphology and maturation during the second trimester: sonographic evaluation. *J Ultrasound Med* 6:631, 1987.)

been extensively studied in the past with radiologic and histologic methods.<sup>34,35</sup> Each vertebra usually has three primary ossification centers, one for the body (centrum) and one on each side of the posterior neural arch. The centra are ossified first in the lower thoracic and upper lumbar regions followed by progressive ossification in both the cephalic and caudal directions. By contrast, and in general, the ossification centers for the posterior neural arch appear in a more standard cephalocaudal direction. The posterior neural arch first begins to ossify (sonographically recognizable high-amplitude reflections) at the base of the transverse process (Fig. 8-58). Ossification proceeds from this center to progressively include the laminae and pedicles. The progression of ossification of the laminae is more important for the diagnosis of neural tube defects because spina bifida is the most consistently demonstrable dysmorphic lesion in open spinal

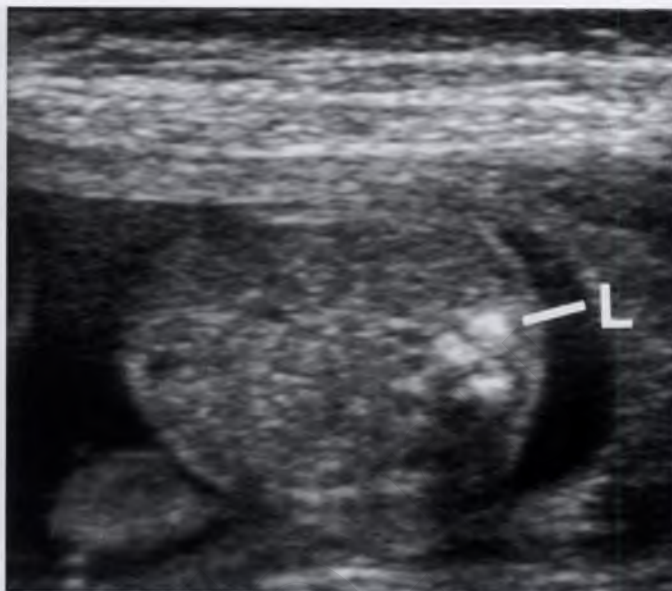


**FIG 8-59** Lumbar vertebra, transverse axial sonogram. The laminae (L) demonstrate early ossification, causing the appearance of "inward angulation" of the posterior arch. (From Filly RA, Simpson GF, Linkowski G: Fetal spine morphology and maturation during the second trimester: sonographic evaluation. *J Ultrasound Med* 6:631, 1987.)

defects. This abnormality is recognized sonographically by an abnormal outward flaring of the posterior neural arch ossification centers.

Varying degrees of maturation of spinal ossification are present at differing levels of the spine when we are most frequently called on to assess normality of the fetal spine.<sup>39</sup> Although there are some exceptions as noted previously, ossification in the neural arch first appears at the base of the transverse process. Early posterior neural arch ossification then progresses anteriorly into the pedicles, also contributing a portion of the vertebral body, and posteriorly into the laminae. Additionally, craniocaudal extension into the articular processes and lateral extension into the transverse processes occur. Because the critical observation in the diagnosis of open spinal neural tube defects is the demonstration of spina bifida (seen as an outward flaring of the posterior arch ossification centers), the ideal situation to confirm normality is to observe the antithesis of this pathologic state (i.e., inward angulation of the laminae). This is readily achieved when visible ossification is present in the normal laminae (Fig. 8-59). Unfortunately, there is insufficient ossification of the laminae to perceive inward angulation of the posterior neural arch ossification centers in the lower spine to confirm normality of the fetal spine during the crucial stage of gestation when this sonographic diagnosis must be made (18 to 22 menstrual weeks) (see Fig. 8-58).<sup>49,52</sup> This is particularly important when considering the most common location of such lesions (i.e., lumbar and sacral regions).<sup>49</sup> Easily identifiable ossification of the laminae is visible in the cervical region in all fetuses by 18 to 19 menstrual weeks, whereas thoracic ossification of the laminae is only partially visible during 18 to 19 menstrual weeks.<sup>39</sup> There is no ossification of the laminae in the lumbar or sacral regions of fetuses examined before 19 menstrual weeks (see Fig. 8-58). The thoracic vertebrae consistently demonstrate partial ossification of the laminae in the range of 20 to 22 weeks; the lumbar region does not demonstrate a similar degree of ossification until 22 to 24 weeks (Fig. 8-60). The sacral spine reveals no evidence of ossification in the laminae before 22 weeks. Only after 25 weeks is there consistently recognizable ossification of the arch





**FIG 8-60** Lumbar spine, transverse axial sonogram, 23 weeks, showing well-defined ossification of the laminae (L) and neurocentral synchondroses (arrows). C, centrum.



**FIG 8-61** Sacral spine, transverse axial sonogram, 26 weeks. L, laminae; IW, iliac wing.



**FIG 8-62** Transverse axial sonograms, sacral spine, in prone (A) and decubitus (B) positions. The posterior arch (POC) anatomy is seen well in either position. (From Filly RA, Simpson GF, Linkowski G: Fetal spine morphology and maturation during the second trimester: sonographic evaluation. *J Ultrasound Med* 6:631, 1987.)

in the sacral region (Fig. 8-61). Fetal position (either prone or decubitus) does not appear to affect appreciably the ability to discern the degree of neural arch ossification, although the prone position usually results in the clearest images (Fig. 8-62). If the fetus is supine, a critical examination of the posterior neural arch cannot be accomplished (Fig. 8-63).<sup>39</sup>

The spine may be seen in both longitudinal and transverse axial planes. Although both planes are important, the transverse axial plane demonstrates the anatomy to best advantage. On longitudinal planes of section the posterior elements are seen as “parallel” bands of echoes. In fact, they are not precisely parallel because they flare in the upper cervical region and converge in the sacrum. In addition, careful scanning usually discloses a slight widening of the lumbar area. It is

important not to mistake this slight lumbar widening as a pathologic event. Because the fetal spine is normally kyphotic, usually one cannot visualize the entire spine in a single longitudinal coronal plane. For this reason, transverse axial planes of section are necessary to be certain that the entire spine has been imaged on a segment-by-segment basis. Caution must be exercised as well to ensure that the spine has been examined in its entirety on transverse planes. At the cephalic end, no problem arises because one encounters the calvaria. However, the caudal end is more difficult. The ischial ossification centers can be successfully used as landmarks to ensure that the caudal end of the spine has been reached (Fig. 8-64). In older fetuses, both vertebral and spinal canal anatomy can often be quite dramatically depicted (Figs. 8-65 and 8-66).



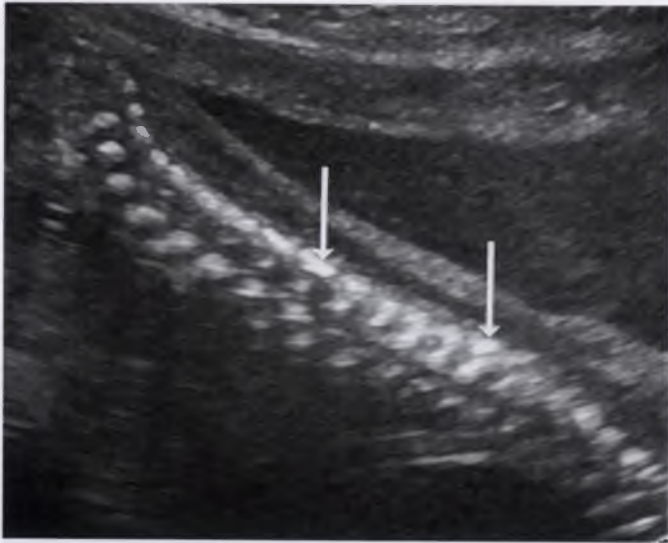


**FIG 8-63** Supine fetus, second trimester. The vertebral bodies, lying between the arrows, are clearly seen, but the posterior arch cannot be well appreciated. Note that the vertebral body ossification centers smoothly align along their anterior surfaces.

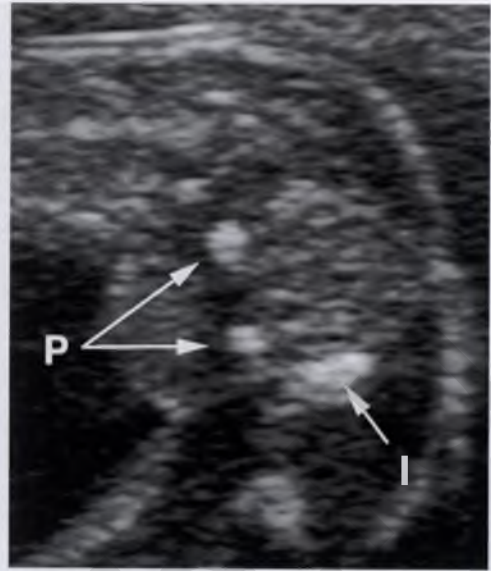


**FIG 8-64** Axial sonogram of the pelvis demonstrating the early ossification centers of the pubis (P). Also seen is an ischial ossification (I).

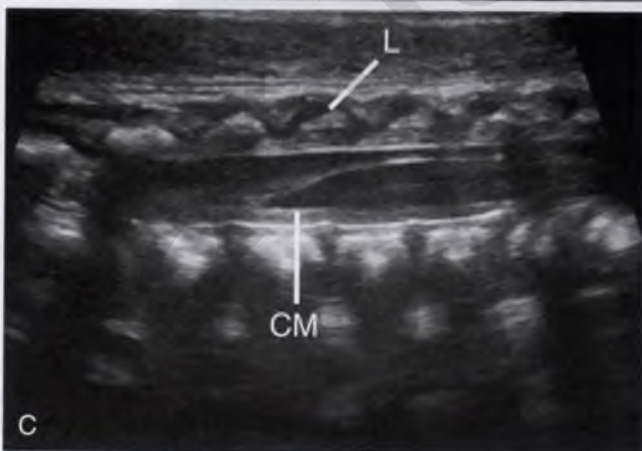
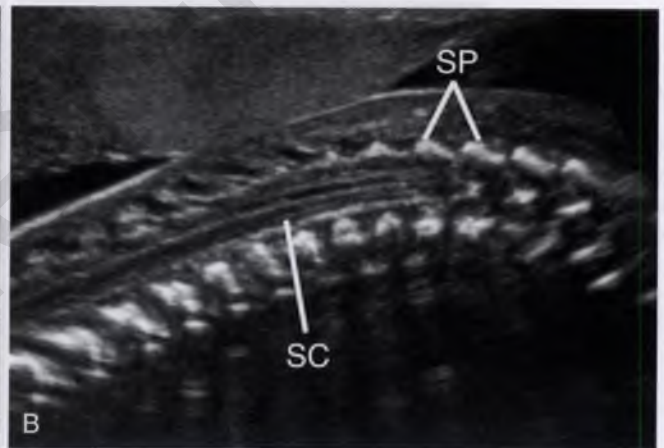
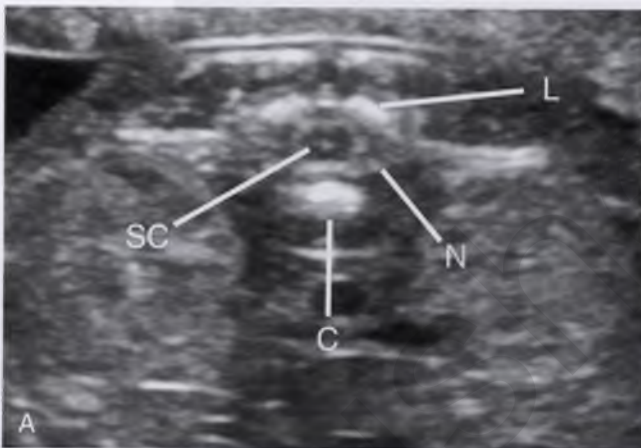


**FIG 8-65** **A**, Lumbar spine of 20-week fetus, axial section. Longitudinal scans of the thoracolumbar (**B**) and lumbosacral (**C**) spine. C, centrum; CM, conus medullaris; L, laminae; N, neurocentral synchondrosis; SC, spinal cord (note bright linear echo from central canal); SP, spinous process (in cartilage).



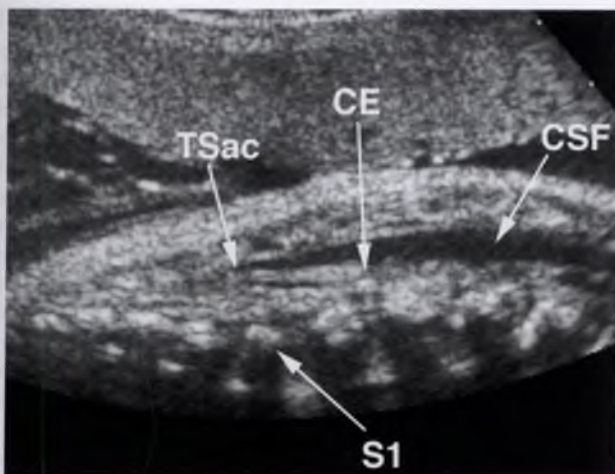


**FIG 8-66** Midsagittal sonogram of the fetal spine demonstrating the termination of the thecal sac (TSac). The S1 vertebral body is marked. Overlying the echogenic cauda equina (CE) (echogenic owing to the leptomeninges that cover the nerve roots) is lucent cerebrospinal fluid (CSF).

Cartilaginous structures in the axial skeleton are less conspicuous than in the appendicular skeleton but nonetheless are visible in virtually all fetuses. The sutures of the calvarial vault already have been noted. The cartilaginous neurocentral synchondrosis of the spine (the junction of the centrum and the posterior ossification centers) is visible in all fetuses from the end of the first trimester onward (see Figs. 8-58 to 8-62).<sup>39</sup> Similarly, the gaps between the vertebral body ossification centers are a composite of the nonossified margin of the adjoining vertebral bodies plus the intervertebral disk (see Fig. 8-63). The margin of cartilage in the vertebral body is best appreciated posteriorly, lying between the ossification center and the dura of the spinal canal (Fig. 8-65A and C). The spinous processes of the posterior neural arch are also occasionally seen and again are composed entirely of cartilage in fetal life (Fig. 8-65B).

A feature of the fetal musculoskeletal system that is poorly judged sonographically is the degree of bony ossification. Increased ossification, as in osteopetrosis, is completely unrecognized on sonograms. Similarly, diminished ossification is difficult to recognize. Only in the most extremely osteopenic bone can one appreciate diminished ossification on sonograms. Examples are the nearly nonossified calvaria in fetuses with osteogenesis imperfecta lethalis or recessive hypophosphatasia<sup>53-55</sup> or the spine in fetuses with achondrogenesis.<sup>56</sup>

Little attention is typically devoted to the fetal muscular system, even though many muscles and muscle groups can be very well visualized (see Fig. 8-32). In general, normal muscles are quite hypoechoic, at times so much so that they simulate fluid collections. This is most notable of the abdominal wall musculature, which may simulate ascites (pseudoascites) (Fig. 8-67).<sup>57</sup> Currently, high-resolution sonographic equipment decreases the propensity to “overcall” ascites caused by this artifactual situation because the layers of the abdominal wall can be individually discerned.<sup>58</sup>

The abdominal wall muscles, the internal and external oblique and the transversus abdominis, at times, are so clearly visible that the individual layers can be detected. More commonly seen as a single layer of muscles, this tissue is easily recognized as lying within the abdominal wall by noting its position between the subcutaneous and peritoneal fat (Fig. 8-67B). The latter is traced from the paranephric fat as it curves along the lateroconal fascia. Furthermore, the abdominal wall

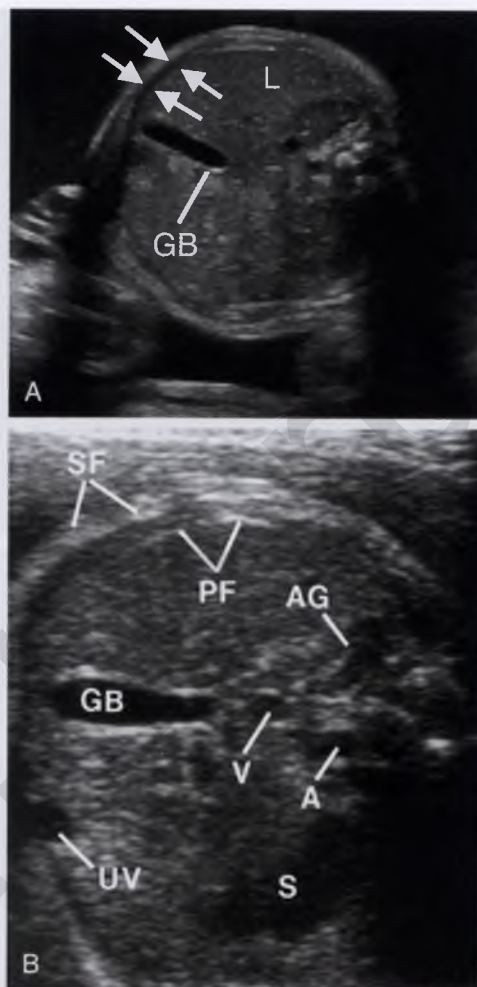


**FIG 8-67** Transverse axial sonograms, fetal abdomen. **A**, Lucent abdominal wall musculature (arrows) may erroneously give the impression that ascites is present. **B**, Abdominal wall musculature lies between the subcutaneous fat (SF) and the properitoneal fat (PF). Individual layers can be appreciated. A, aorta; AG, adrenal gland; GB, gallbladder; L, liver; S, stomach; UV, umbilical vein; V, inferior vena cava.

muscles “meet” the ends of the lower thoracic ribs, whereas ascites would pass “between” the ribs and the abdominal viscera.<sup>58</sup>

## CARDIOVASCULAR SYSTEM

The anatomy of the heart and great vessels is discussed in detail in Chapter 13. Here, the focus is on those fetal vessels visible within the uterus and fetal corpus that are not covered elsewhere. A surprisingly large number of individual fetal blood vessels can be seen. Color Doppler sonography has greatly added to our ability to consistently demonstrate fetal vessels.

The fetal circulation begins in the placenta. In virtually all second and third trimester fetuses, surface (fetal) vessels of the placenta can be detected, and with color Doppler sonography these vessels are seen penetrating the placental substance. The surface vessels coalesce at the cord “insertion.” The identification of the cord insertion is important in the performance of percutaneous umbilical (fetal) blood sampling (PUBS) and intrauterine fetal transfusion for diagnosis and management of a number of fetal disorders (Chapter 24).<sup>59</sup> As well, velamentous and peripheral cord insertions can have obstetric implications.



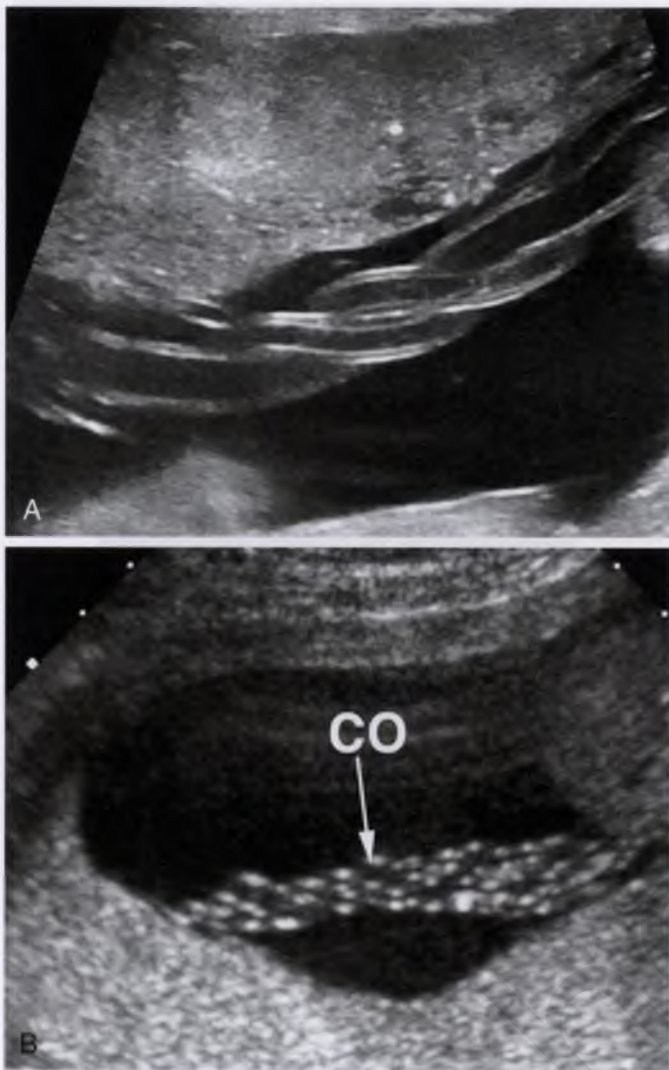


**FIG 8-68** **A**, Longitudinal sonogram of a three-vessel umbilical cord with a typical amount of coiling. **B**, Longitudinal sonogram of a three-vessel umbilical cord (CO) with a greater than usual amount of coiling (there is an issue as to whether this is a variant or an abnormal circumstance).

The cord “insertion” is often easily seen, but if not, it is worthwhile to search for large placental surface vessels using color Doppler and trace these vessels to where they collabesce with the cord.

The normal umbilical cord is composed of two arteries and a vein (Fig. 8-70). The cord is virtually always coiled and sometimes extremely so, or “hypercoiled.” This arrangement leads to a variety of appearances of the cord when viewed with tomographic sections as generated by sonography (Fig. 8-69). The seemingly “simple” task of counting cord vessels can be made quite frustrating by numerous coils. To obtain the correct count of cord vessels consistently, one must rely on a true transverse axial section. Longitudinal or oblique views can be misleading and result in error.

Umbilical vessels enter the fetus, by definition, at the umbilicus and there immediately diverge.<sup>60</sup> The umbilical vein proceeds cephalically (Fig. 8-70); the umbilical arteries egress from a caudal direction. The umbilical arteries proceed along the margin of the urinary bladder from their origin at the iliac arteries in their course toward the umbilicus (Fig. 8-71). As they course along the bladder margin, they should not be mistaken for dilated ureters, a distinction easily made by

interrogating them with color Doppler sonography. Regardless of the degree of bladder distention, normal umbilical arteries *always* flank the bladder wall. Thus, this relationship can be employed both to detect the umbilical arteries or the urinary bladder, particularly when some defect or disease has altered the expected appearance of the bladder. Although not representing certain evidence of a three-vessel cord, the identification of two umbilical arteries flanking the bladder lumen represents excellent evidence for a three-vessel cord and, employing color Doppler sonography, constitutes the easiest method of “confirming” a three-vessel cord. If using the technique of color Doppler identification of umbilical arteries flanking the bladder to determine “cord vessel number”—a common practice—caution should be exercised to avoid mistaking an iliac artery for an umbilical artery. The iliac artery will also “light up” on color Doppler and is sufficiently close to the umbilical artery to create confusion from time to time.

The umbilical vein joins the fetal portal circulation, which is seen with a high degree of consistency on sonograms. Obviously, the larger the fetus, the more readily one will see the smaller elements of this system. Many of the illustrations in the literature incorrectly interpret the fetal umbilical and portal venous anatomy. Confusion has led not only to improper nomenclature but also to use of inappropriate landmarks for obtaining important fetal measurements. With a clear understanding of fetal portal vein anatomy, these pitfalls can be avoided and similarity of the fetal and adult segmental hepatic anatomy better appreciated.

The dynamics of fetal circulation determine the details of fetal hepatic portal venous and segmental anatomy.<sup>61</sup> Because there are no blood-diverting branches of the umbilical vein, the volume of placental blood entering the left portal venous system equals that in the umbilical vein. Thus, the umbilical vein and the portion (umbilical segment) of the left portal vein that it joins have the same diameter (see Fig. 8-70). Therefore, the left portal vein of the fetus is larger than the right, the reverse of the situation seen in the child and adult. From this point, blood may reach the right atrium through several pathways. A common misconception of the fetal circulation is that the bulk of umbilical venous blood bypasses the liver capillary bed through a large patent ductus venosus. In utero, the ductus venosus averages only one seventh the diameter of the umbilical vein<sup>62</sup> and even may be closed (see Fig. 8-70).<sup>63</sup> It should be remembered, however, that the peripheral resistance of the hepatic vascular bed is not present in the ductus venosus, enabling this smaller caliber vessel to carry a larger quantity of blood than might be expected. A significant portion of umbilical venous blood, which carries the highest concentration of nutrients and oxygen in the fetus, circulates through the left lobe of the fetal liver through branches supplying the medial and lateral segments before entering the systemic venous system through the left and middle hepatic veins (Fig. 8-72). Although the right lobe of the liver receives a small amount of umbilical venous blood from the left portal vein, the bulk of blood entering the right portal vein is derived from the main portal vein, which, in the fetus, contains low concentrations of both nutrients and oxygen.<sup>63</sup> The unequal distribution of nutrients to the fetal liver partially accounts for the relatively large size of the left lobe of the fetal liver. After closure of the umbilical vein at birth, the nutrient supply to the entire liver equalizes and the relative size of the left lobe decreases.

In the fetus, the umbilical vein courses cephalically in the free margin of the falciform ligament (see Fig. 8-70). As noted earlier, it joins the umbilical portion of the left portal vein near the caudal margin of the left intersegmental fissure of the liver.<sup>64</sup> After birth, the umbilical vein thromboses, collapses, and ultimately becomes the ligamentum teres hepatis, a classical marker of the left intersegmental fissure (for a very long time this structure was considered the line of division of the left and right hepatic lobes). The precise line of division



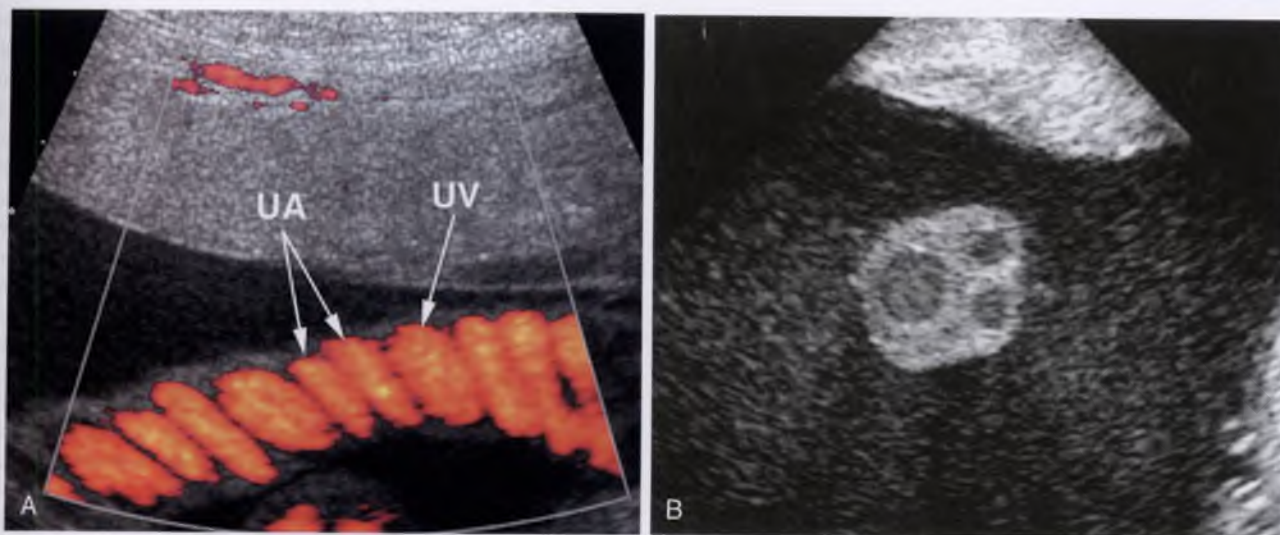


**FIG 8-69** **A**, Longitudinal nondirectional color Doppler sonogram of the umbilical cord. The umbilical vein (UV) is interlaced by the two umbilical arteries (UA). **B**, Transverse axial sonogram of the umbilical cord.

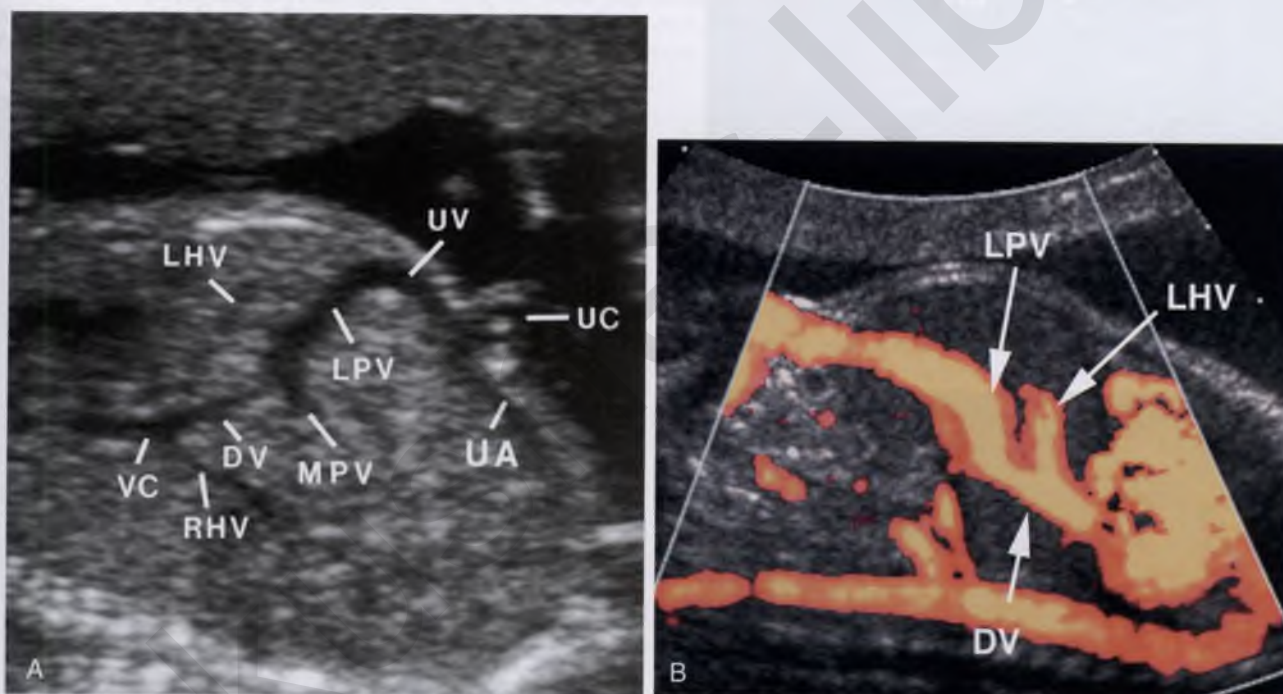


**FIG 8-70** Midsagittal sonograms of the umbilical circulation in gray scale (**A**) and nondirectional color Doppler (**B**). DV, ductus venosus; LHV, left hepatic vein; LPV, umbilical segment of left portal vein; MPV, main portal vein; RHV, right hepatic vein; UA, umbilical artery; UC, umbilical cord; UV, umbilical vein; VC, inferior vena cava.

between the umbilical vein and the umbilical segment of the left portal vein is the point at which the most anterior of the medial and lateral segmental branches to the left hepatic lobe egress the left portal vein (the branches to segments 3 and 4). Remember, the umbilical vein has no blood diverting branches. Therefore, these two hepatic intraparenchymal vessels had to originate from the umbilical segment of the left portal vein.

The umbilical portion of the left portal vein has a predominantly posterior course but also courses superiorly in the left intersegmental fissure (see Fig. 8-70). As noted, its branches supply the medial and lateral segments of the left lobe of the liver.<sup>65</sup> The left portal vein then courses abruptly to the right, exits the left intersegmental fissure, and

forms the transverse portion (pars transversa) of the left portal vein (Figs. 8-72 and 8-73). The pars transversa joins imperceptibly with the right portal vein at the main lobar fissure. The ductus venosus originates from the pars transversa (but occasionally more rightward).<sup>66</sup> The ductus continues posteriorly but assumes a more cephalad course than the umbilical portion of the left portal vein (see Fig. 8-73). It continues as an unbranched structure to join the left or, less commonly, the middle hepatic vein (this distinction is somewhat artificial as the left hepatic vein, the middle hepatic vein, and the ductus venosus most commonly form a confluence before entering the inferior vena cava). In this position the ductus venosus lies in the superior extension of the gastrohepatic ligament, which separates the developing caudate lobe



posteriorly from the lateral segment of the left hepatic lobe anteriorly (the gastrohepatic ligament, the dominant ligament of the lesser omentum, also separates the greater and lesser peritoneal cavities). After birth, the ductus venosus closes and becomes the fibrous ligamentum venosum.<sup>64</sup>

Sonograms of the upper portion of the fetal abdomen clearly demonstrate the anatomy described previously (see Figs. 8-70 to 8-73).

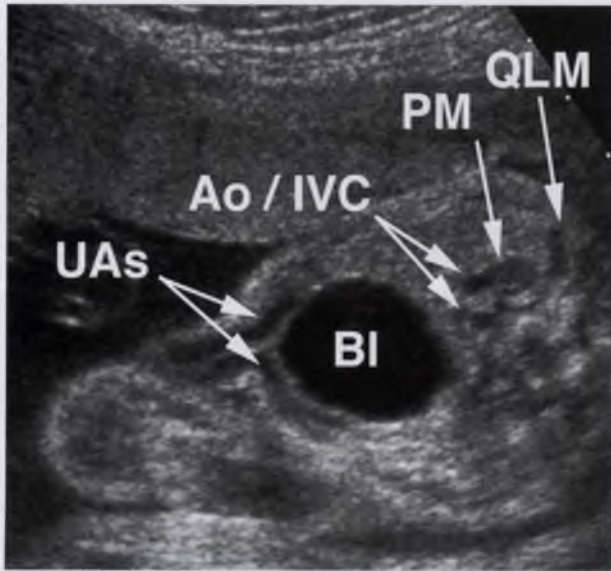


**FIG 8-71** Umbilical cord insertion into the fetus. The umbilical arteries (UAs) egress from a caudal direction, coursing along the margin of the urinary bladder (BI). Ao/IVC, aorta and inferior vena cava; PM, psoas muscle; QLM, quadratus lumborum muscle.

Because the umbilical vein courses cephalically, transversely oriented planes of section intersect this vessel's short axis (see Fig. 8-67). Slight cephalad movement of the transducer demonstrates a position at which this venous structure abruptly courses posteriorly (see Figs. 8-72 and 8-73). This posteriorly coursing vein represents the umbilical portion of the left portal vein rather than the cephalic portion of the umbilical vein, as it is commonly mislabeled in the literature. Confirmation that this vessel is the left portal vein is easily made by observation of branches arising from this vein to the medial and lateral segments of the left hepatic lobe (see Figs. 8-72 and 8-73). When the umbilical portion of the left portal vein is seen throughout its entire course, one can be certain that some angulation has been introduced into the scan plane because this venous structure courses not only posterior but slightly cephalad (see Fig. 8-70). A variety of branches of the umbilical segment of the left portal vein are occasionally imaged; they include the medial, superolateral, and inferolateral branches (see Fig. 8-72).

The right portal vein divides into anterior and posterior segmental branches, the same as in the adult (see Fig. 8-73). Each supplies a respective segment of the right hepatic lobe. The hepatic veins can be recognized by their relationship to portal veins<sup>64</sup> and can be seen to radiate toward the inferior vena cava, coalescing with this venous channel immediately before it enters the right atrium (Fig. 8-74). These veins divide the liver into lobes and segments. The hepatic veins are most easily sought near the level of the diaphragm where their caliber is the largest.<sup>67</sup> Nonetheless, the middle and right hepatic veins are commonly seen in more inferior planes of section by noting their relative position compared with the right portal vein divisions (see Fig. 8-73). The right hepatic vein passes between as well as bisecting the distance between the anterior and posterior divisions of the right portal vein, whereas the middle hepatic vein always crosses anterior to the right portal vein (in the main lobar fissure) and bisects the distance

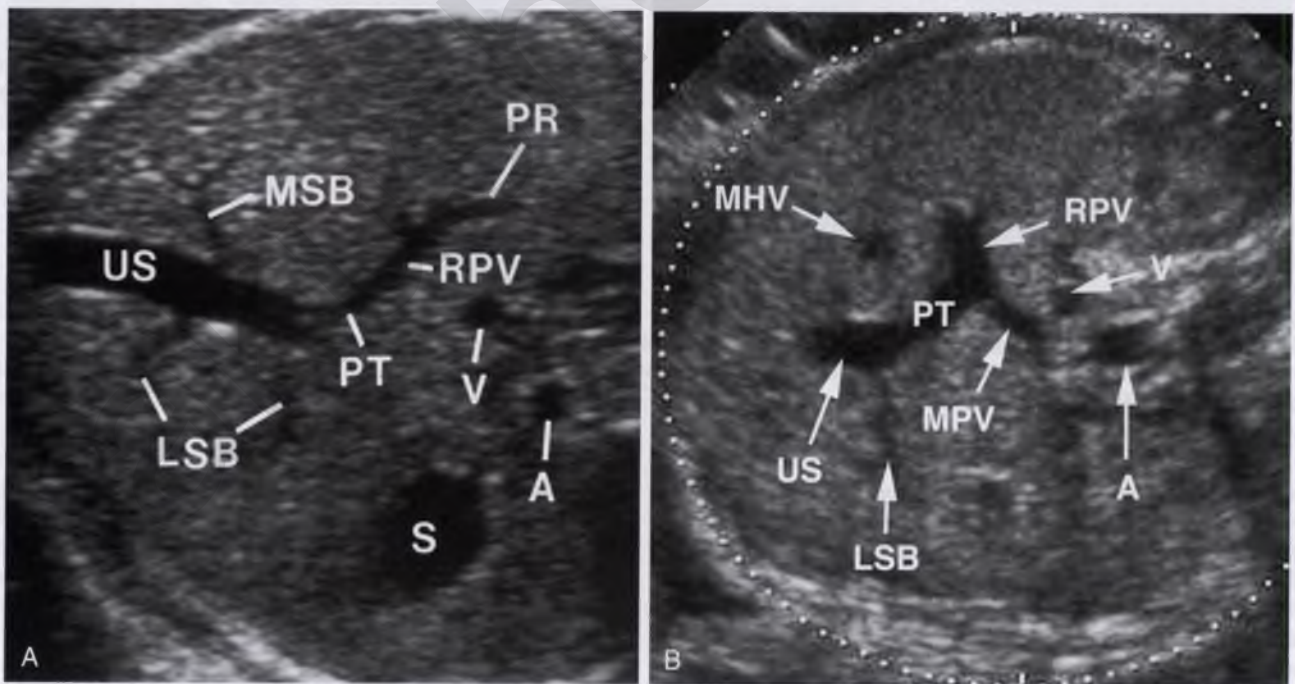


**FIG 8-72 A**, Fetal portal circulation. Umbilical segment (US) of the left portal vein begins at the point where the medial (MSB) and the distal lateral (LSB) segmental branches originate (proximal to that point the vessel is the umbilical vein). **B**, Note that the main portal vein (MPV) is the appropriate line of division between the right portal vein (RPV) and the first portion of the left portal vein, the pars transversa (PT). A, aorta; MHV, middle hepatic vein; PR, posterior division of right portal vein; S, stomach; V, vena cava.



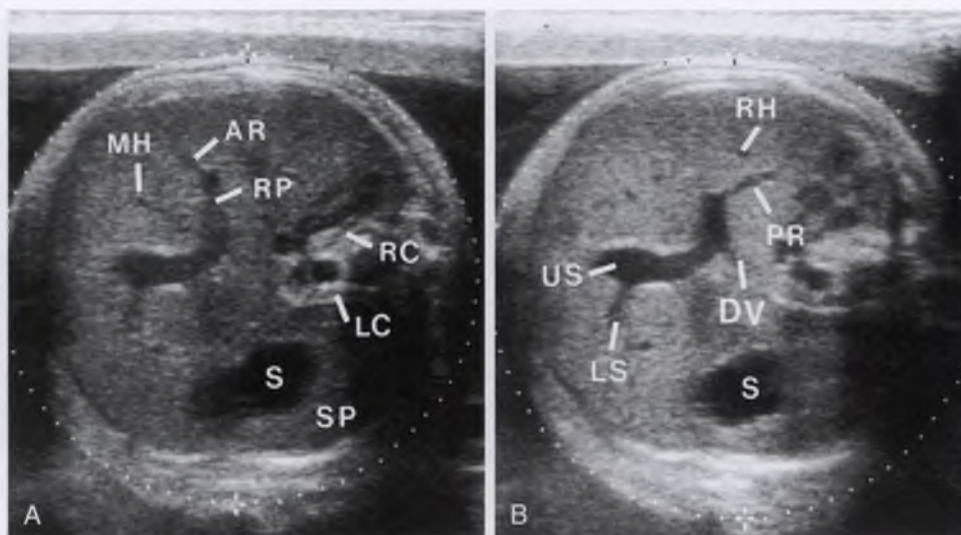


**FIG 8-73** **A** and **B**, Transverse axial sonograms of fetal liver. AR, anterior division of right portal vein; DV, ductus venosus (alternatively, this may represent a partial section through the main portal vein—see Fig. 8-72B); LC, left diaphragmatic crura; LS, lateral segmental branch; MH, middle hepatic vein; PR, posterior division of right portal vein; RC, right diaphragmatic crura; RH, right hepatic vein; RP, right portal vein; S, stomach; SP, spleen; US, umbilical segment of left portal vein.

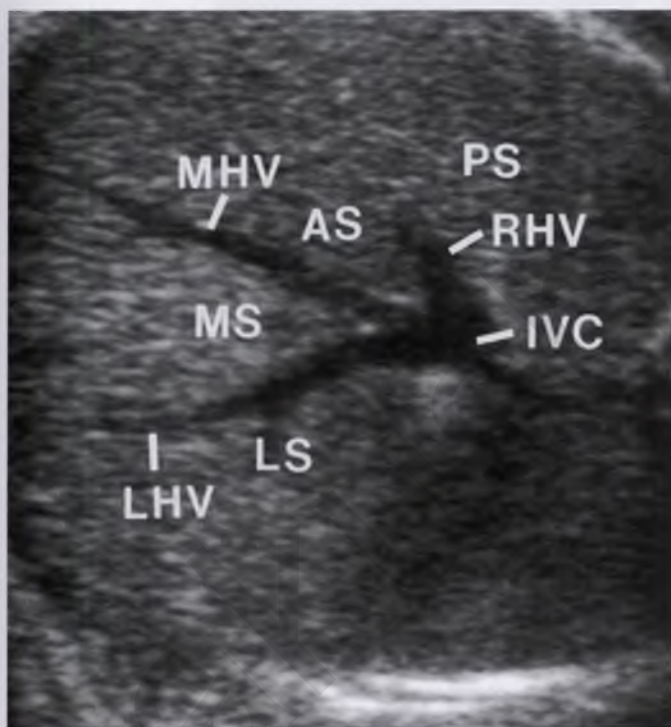


**FIG 8-74** Sonogram through the long axis of the proximal fetal hepatic veins: IVC, inferior vena cava; LHV, left hepatic vein; MHV, middle hepatic vein; RHV, right hepatic vein. These veins divide the liver into lobes and segments: AS and PS, anterior and posterior segments of the right hepatic lobe; MS and LS, medial and lateral segments of the left hepatic lobe.

between the anterior branch of the right portal vein and the umbilical segment of the left portal vein. The aorta and inferior vena cava have a similar course in the lower abdomen but diverge in the upper abdomen, where the aorta penetrates the diaphragm posteriorly (in contact with the spine), whereas the inferior vena cava turns anteriorly to join the right atrium (Fig. 8-75).

The great vessels and heart are described in detail in Chapter 13. Briefly, a second or third trimester sonogram of all pregnancies should include a four-chamber heart view (Fig. 8-76). Outflow tract views of the left and right cardiac ventricles also are required in the most recent guidelines.<sup>68</sup> Useful information about the position and size of the great vessels can be quickly gleaned from a transverse axial view of the upper mediastinum by simply moving the transducer cephalically from the four-chamber heart view. This section traverses the superior vena cava, the ascending and descending thoracic aorta, and the pulmonary artery. As well, one or more branches of the pulmonary artery will be seen. These may be one or the other or both the right or left pulmonary arteries or the ductus arteriosus (coursing from the pulmonary artery to the descending thoracic aorta) (Fig. 8-77).

The vessels arising from the transverse aorta are frequently visible and normally comprise the brachiocephalic, left common carotid, and left subclavian arteries (Fig. 8-78A). The common carotid arteries and jugular veins are also commonly seen in the neck of an older fetus. The brachial artery and vein are less frequently seen adjacent to the humerus but again can be found using color Doppler sonography.

Intracranial arterial structures are easily perceived using color Doppler sonography (Fig. 8-79). These include the vessels of the circle of Willis located in the basal cistern and surrounding the inferior portion of the third ventricle. The middle cerebral artery can be identified coursing in the sylvian cistern, the posterior cerebral artery in the ambient cistern, and the anterior cerebral arteries in the interhemispheric cistern (near the genu of the corpus callosum). The basilar artery lies ventral to the pons in the prepontine space and upon reaching the interpeduncular cistern it bifurcates. The basilar artery is most often seen on sonograms depicting the interpeduncular cistern where it is part of the circle of Willis. Also commonly seen after the formation of the corpus callosum commences is the pericollousal artery coursing along its body.

The abdominal aorta and inferior vena cava are easily identified, as are the common iliac arteries and veins (Fig. 8-78B and C). Other branches of the abdominal aorta can be consistently visualized using color Doppler sonography. They include the celiac axis, the superior mesenteric artery, and the renal arteries. Similarly, the renal veins can be consistently seen.



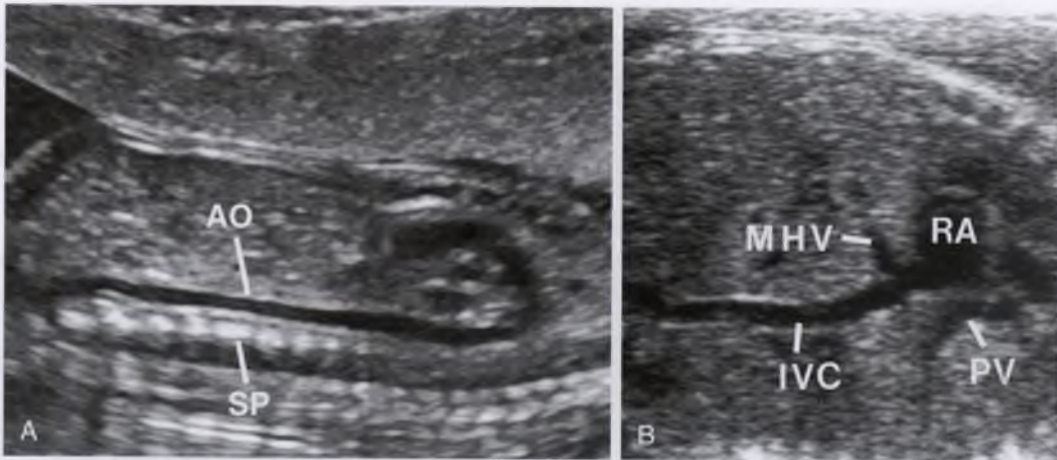


**FIG 8-75** **A**, Longitudinal view of the aorta (AO). **B**, Longitudinal view of the inferior vena cava (IVC). MHV, middle hepatic vein; PV, pulmonary vein; RA, right atrium; SP, spine.

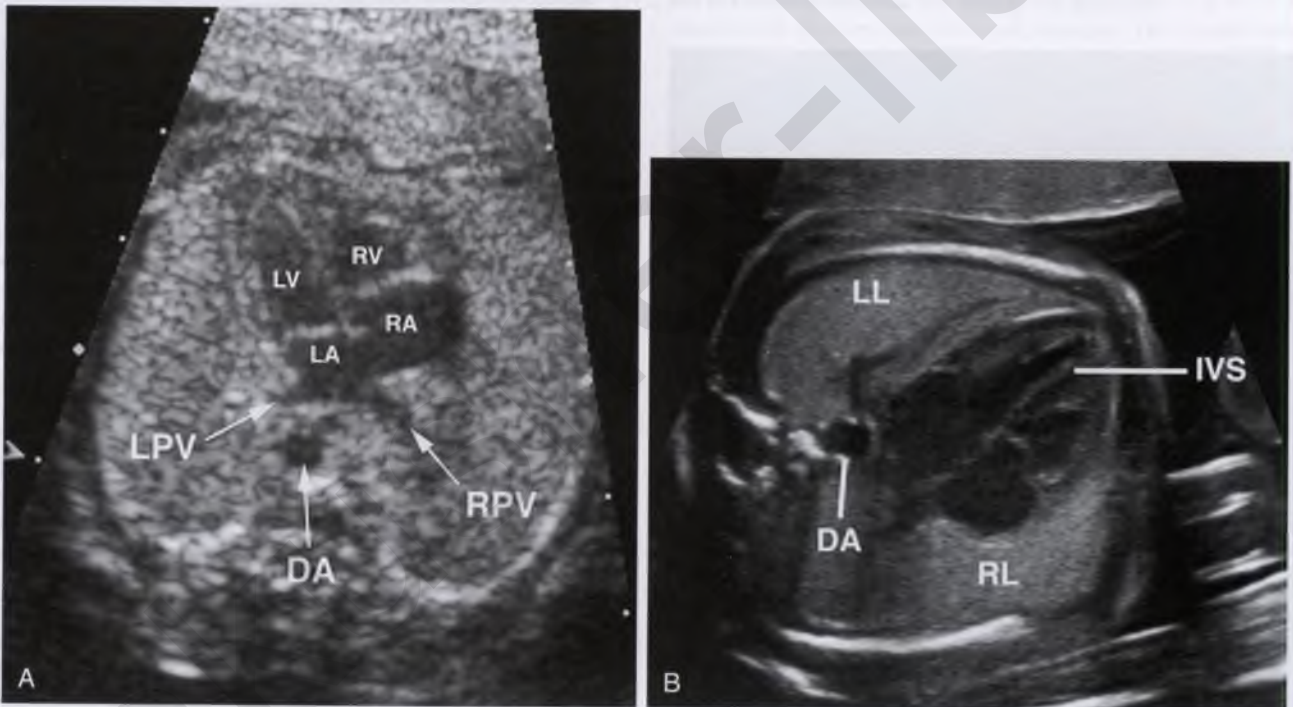


**FIG 8-76** Transverse axial sonograms through the fetal thorax, the "four-chamber view." In **A**, the fetus is supine. In **B**, the fetus is in right decubitus position. DA, descending thoracic aorta; IVS, interventricular septum; LA, left atrium; LL, left lung; LPV, left pulmonary vein; LV, left ventricle; RA, right atrium; RL, right lung; RPV, right pulmonary vein; RV, right ventricle.

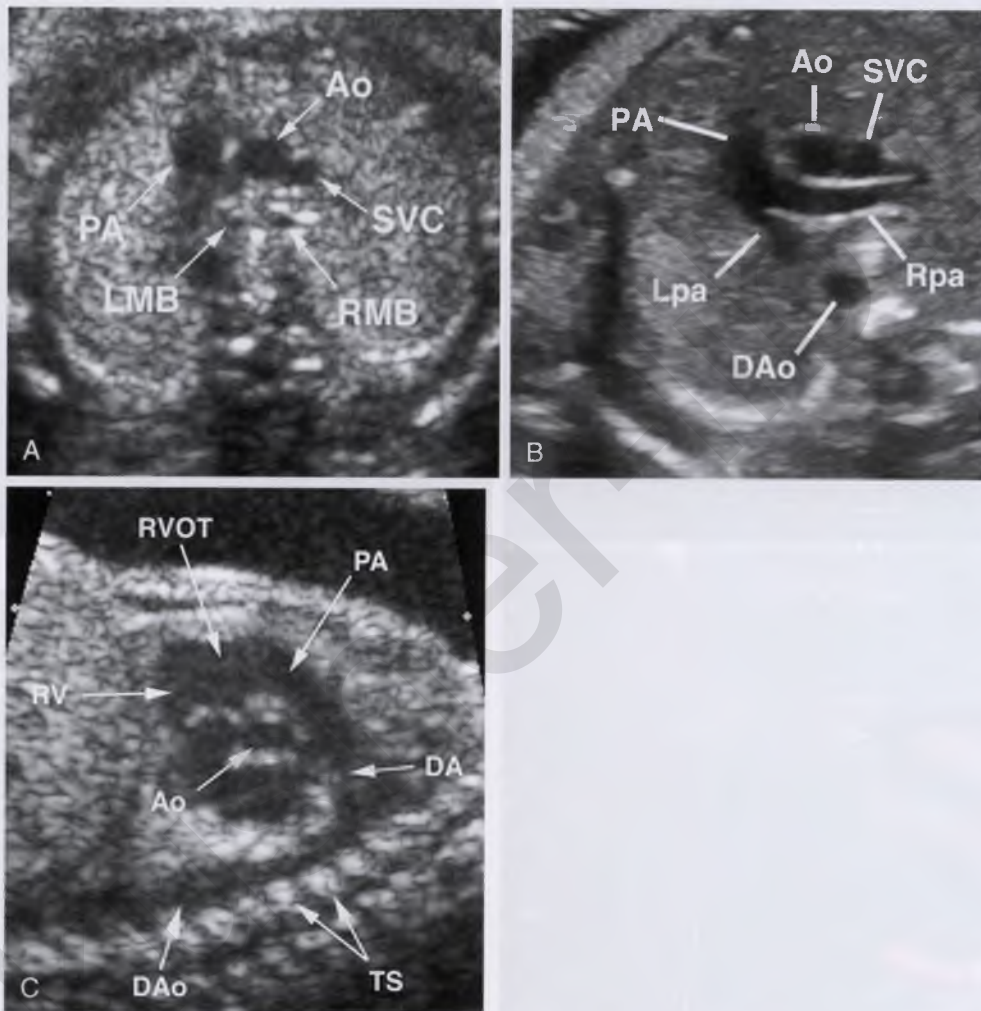


**FIG 8-77** **A** and **B**, Transverse axial sonograms through the fetal chest. **C**, Midsagittal sonogram of the fetal chest. In transaxial sonograms (**A** and **B**) the great vessels lie sequentially from right to left and posterior to anterior as follows: superior vena cava (SVC), aorta (Ao), and pulmonary artery (PA). The descending aorta (DAo) lies immediately anterior to the thoracic spine (TS). The right pulmonary artery (Rpa) passes directly posterior to the aorta and superior vena cava. The right (RMB) and left (LMB) mainstem bronchi lie posterior to the great vessels. DA, ductus arteriosus; Lpa, left pulmonary artery; RV, right ventricle; RVOT, right ventricular outflow tract.

## GASTROINTESTINAL SYSTEM

The gastrointestinal system is the most complex of the fetal systems. It is the only system that is not fully developed at birth. The system is composed of the esophagus, stomach, small intestine, large intestine, and rectum. The system is responsible for the digestion and absorption of nutrients from the mother's milk or formula. The system is also responsible for the elimination of waste from the body.

The gastrointestinal system is the most complex of the fetal systems. It is the only system that is not fully developed at birth. The system is composed of the esophagus, stomach, small intestine, large intestine, and rectum. The system is responsible for the digestion and absorption of nutrients from the mother's milk or formula. The system is also responsible for the elimination of waste from the body.



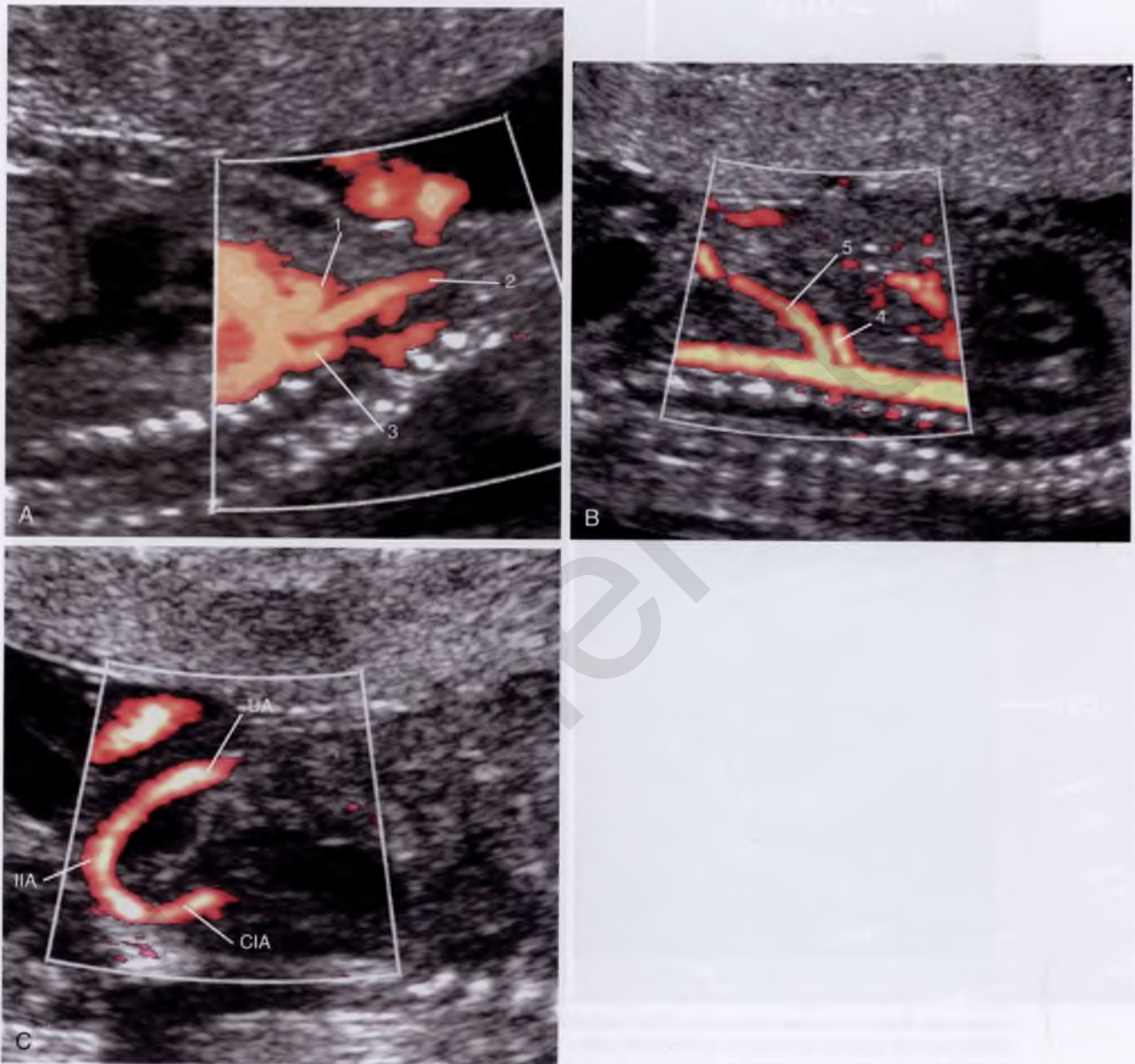


**FIG 8-78** Series of nondirectional color Doppler sonograms of the fetal torso. **A**, The aortic arch is seen to good advantage. 1, brachiocephalic artery; 2, left common carotid artery; 3, left subclavian artery. **B**, Midsagittal sonogram of the abdominal aorta. 4, celiac axis; 5, superior mesenteric artery. **C**, Oblique sonogram through the fetal pelvis demonstrating the umbilical artery (UA) joining the internal iliac artery (IIA) and continuing into the common iliac artery (CIA).



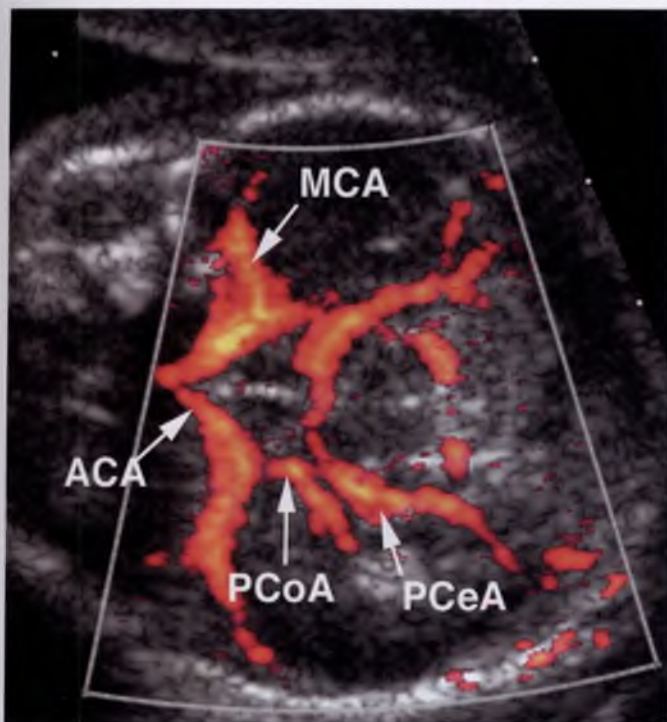


**FIG 8-79** The circle of Willis is well seen on this nondirectional color Doppler image. ACA, anterior cerebral artery; MCA, middle cerebral artery; PCeA, posterior cerebral artery; PCoA, posterior communicating artery.

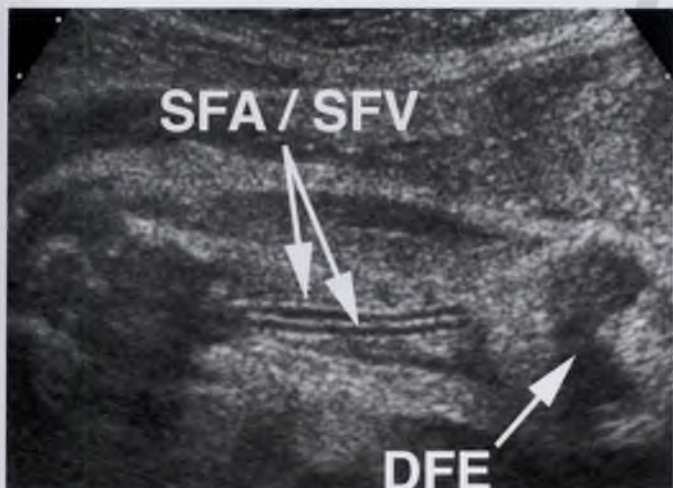


**FIG 8-80** Superficial femoral artery and vein (SFA/SFV) seen side by side in the mid- and distal thigh. DFE, distal femoral epiphysis.

In the leg, the superficial femoral artery and vein (Fig. 8-80) may be visualized in older fetuses. When the knee is extended, it is not difficult to trace these vessels to the level of the popliteal artery and vein, a virtually impossible task when the knee is flexed.

## GASTROINTESTINAL SYSTEM

Many components of the gastrointestinal system can be seen sonographically, some as early as the end of the first trimester.<sup>69</sup> The liver, the largest parenchymal organ of the system and of the torso, is seen consistently from the second trimester onward, although its margins

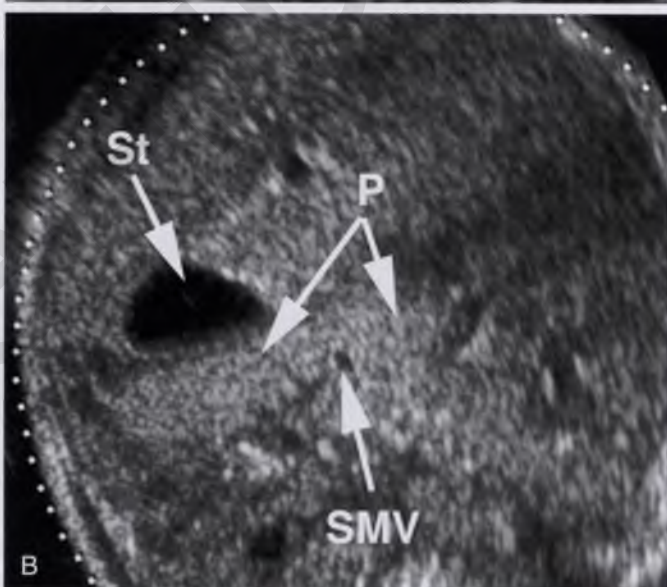
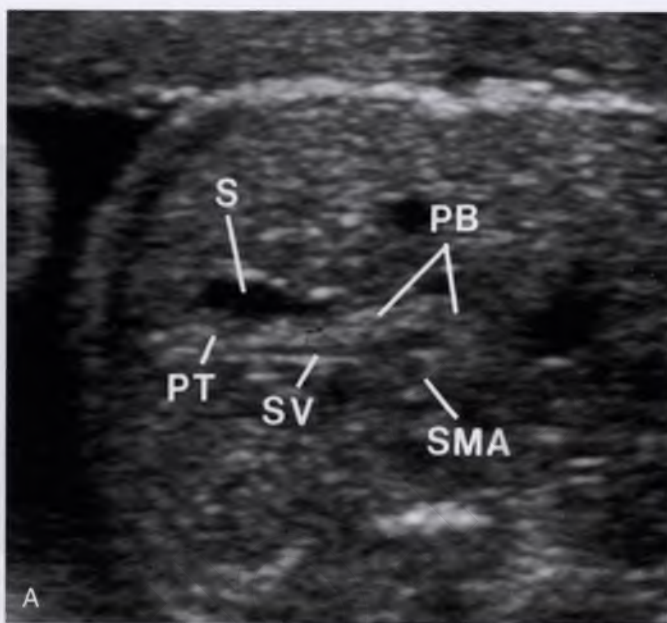


**FIG 8-81 A and B**, The fetal pancreas is not commonly seen discretely but is well depicted in these sonograms. When sought, it can often be detected. Those who perform abdominal sonograms in adults and children will recognize the familiar landmarks. In **B** the pancreas (P) is enlarged (Beckwith-Wiedemann syndrome). The pancreas lies between the splenic vein (SV) and the posterior stomach wall (St). PB, pancreatic body; PT, pancreatic tail; S, stomach; SMA, superior mesenteric artery; SMV, superior mesenteric vein.

are often indistinct in earlier gestations. With the latest equipment the liver is usually easily discriminated from surrounding structures. Conversely, the other major parenchymal organ of the gastrointestinal system, the pancreas, is much less commonly seen, even in third trimester fetuses (Fig. 8-81). The spleen, more appropriately a part of the reticuloendothelial system and not the gastrointestinal system although considered here, is also visible consistently in the second trimester, but similar to the liver in early pregnancy, its margins are frequently indistinct (Figs. 8-73 and 8-82). Conversely, those portions of the fetal gastrointestinal system that consistently contain fluid, the stomach (see Figs. 8-67, 8-72, and 8-73) and gallbladder



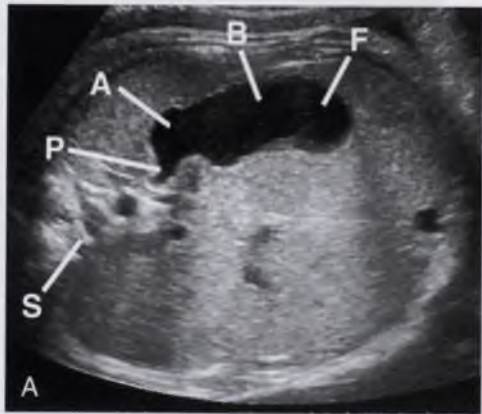


**FIG 8-82** **A**, Coronal image of the stomach demonstrating all portions of the stomach including the fundus (F), body (B), antrum (A), and pylorus (P). S, spine. **B**, Axial sonogram of the fetal stomach showing the fundus (F) and body (B). A portion of the left lung (L) and spleen (Sp) are included. D, diaphragm.

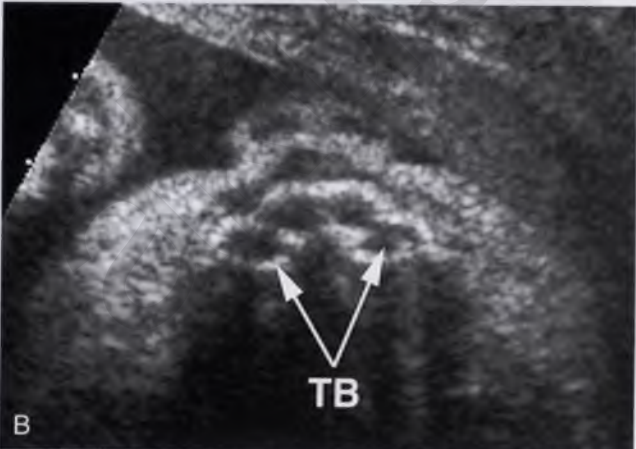
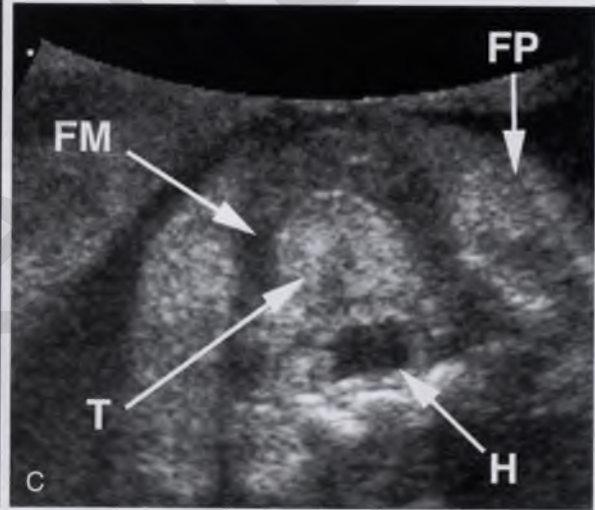
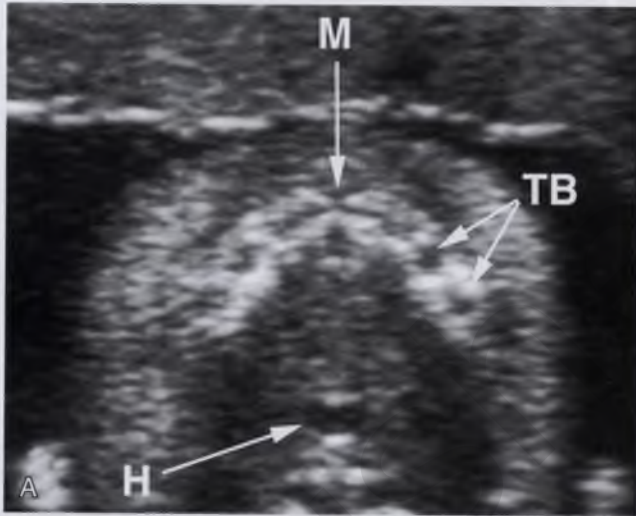


**FIG 8-83** Transverse axial sonograms of the mandible (**A**), maxilla (**B**), and tongue (**C**). FM, facial musculature; FP, cheek fat pads (Bichat); H, hypopharynx; M, mandibular mentum; T, tongue; TB, tooth buds.

(see Fig. 8-67), are among the earliest and most consistently seen of fetal structures.

The components within and about the oral cavity are seen relatively well sonographically.<sup>70</sup> The lips and cheeks have been described in the section on superficial anatomy (see Figs. 8-12 and 8-13). The tongue

(Fig. 8-83) is also consistently seen and to best advantage during swallowing movements. The gingival ridge with tooth buds is seen commonly in fetuses of 20 weeks or more (Fig. 8-83A). The hard palate is difficult to define consistently but with practice can be detected. For this reason, cleft palate is more difficult to detect than cleft lip. Cleaving



of the soft palate is difficult to diagnosis sonographically because the soft palate cannot be discretely recognized. The oropharynx and laryngeal pharynx frequently contain fluid and thus are seen relatively often when sought (Figs. 8-83 and 8-84). Transverse axial scans through the upper neck are quite successful for visualization of the pharynx, but longitudinal coronal images, although more difficult to obtain, display the anatomy to greater advantage. In longitudinal coronal planes, the continuity of the pharyngeal zones can be appreciated as well as the larynx protruding into the pharynx (see Fig. 8-84). The piriform sinuses, valliculae, and glottis may also be appreciated.

The mid- and distal esophagus may be seen surprisingly often when sought (Fig. 8-85).<sup>70</sup> The proximal esophagus is extraordinarily difficult, if not impossible, to visualize in the normal fetus. The mid- and distal esophagus may be seen, although inconsistently, in both longitudinal coronal and transverse axial images. The key to identification of this structure is its relationship to the descending thoracic aorta, a structure easily seen. The mid- and distal portions of the esophagus lie immediately anterior to the descending thoracic aorta. The aorta is first visualized in a longitudinal coronal plane. The transducer is then slowly moved anteriorly. As the aorta disappears from view, the esophagus comes into view but is much more difficult to recognize. It is seen

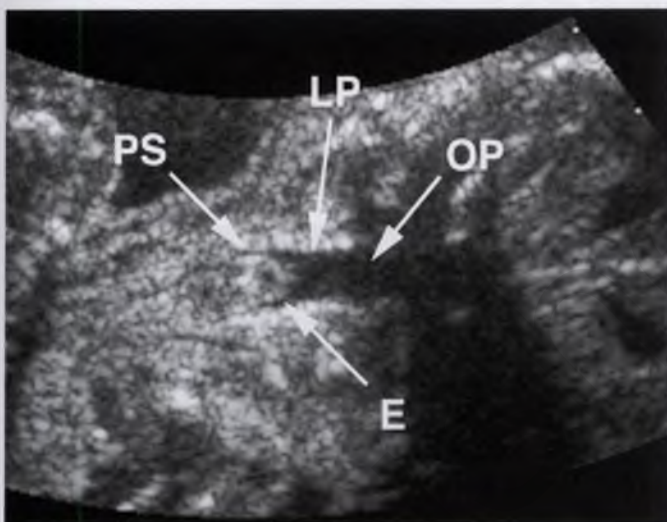


**FIG 8-84** Coronal sonogram of the fetal hypopharynx. The fluid-filled oropharynx (OP) and laryngopharynx (LP) are well seen. Fluid slightly distends the piriform sinuses (PS). E, epiglottis.

as five parallel linear echoes. The hyperechoic serosa, submucosa, and lumen and the hypoechoic muscular wall (Fig. 8-86) create these. Conceptually, one could apply a similar strategy to visualization of the upper third of the esophagus. In this instance, one would image the trachea (see following section) in a longitudinal coronal plane and then slowly move the transducer posteriorly. As the trachea disappears, the esophagus should again come into view. Unfortunately, this concept, although anatomically correct, is practically less successful.

The stomach and gallbladder are the only portions of the subdiaphragmatic fetal gastrointestinal system that consistently contain fluid (Figs. 8-67, 8-72, and 8-73).<sup>69,71,72</sup> Thus, any fluid-containing small bowel should be viewed with suspicion, although in late fetuses one not infrequently sees very small amounts of normal succus entericus in the small bowel lumen, usually made more obvious by accompanying peristalsis. In particular, fluid in the duodenum should be viewed with suspicion. However, the normal duodenum can be seen and can contain very small amounts of succus entericus. If one wishes to interrogate the duodenum, it is most easily found by its anatomic relationship to the gallbladder. These two organs always touch in the absence of an intervening pathologic structure (Fig. 8-87). Fluid contained within the normal fetal stomach is almost entirely imbibed. The fetus begins to swallow amniotic fluid at approximately 16 weeks.<sup>71,72</sup> The volume that the fetus swallows increases dramatically throughout pregnancy and reaches 400 to 500 mL by term. There is a relative proportionality between the volume of urine produced and the amount of amniotic fluid imbibed by the fetus. This proportionality (production versus absorption) maintains the equilibrium of the amniotic fluid volume. In the absence of a patent esophagus, the stomach will be empty (invisible) except in two circumstances. First, and most common, is the concomitant presence of a tracheoesophageal fistula, enabling the lung fluid that is produced by the fetus to enter the esophagus via the fistula and thence to the stomach.<sup>73</sup> This malformation is commonly associated with polyhydramnios in late pregnancy but not always before 24 weeks. Second, the association of esophageal atresia without tracheoesophageal fistula but with a second proximal gastrointestinal tract atresia or obstruction will allow secretions from the stomach to accumulate within the gastric lumen.

The stomach varies considerably in size depending, presumably, on how much amniotic fluid has been recently imbibed by the fetus.<sup>71,72</sup> A prominent stomach never should be taken as sole evidence of obstruction. When the stomach is well distended, its various parts (i.e., the fundus, body, and antrum) can be identified (see Fig. 8-82). The fundus is most posterior, whereas the antrum is most anterior. The incisura angularis can be noted when the stomach is well distended.

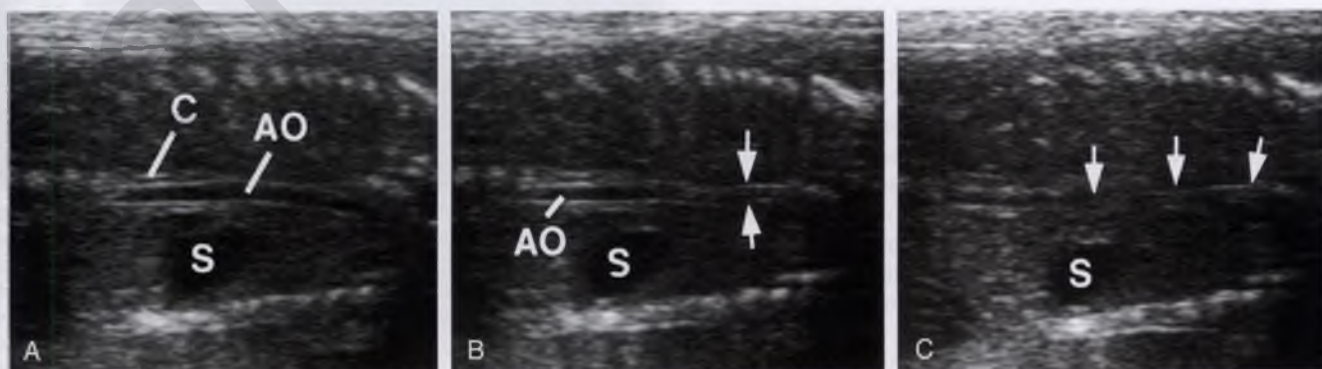


**FIG 8-85** Coronal sonograms depicting the mid- and distal esophagus. First (**A**), the descending aorta (AO) is localized. **B** and **C**, As the transducer is moved anteriorly, the esophagus (arrows) comes into view. C, diaphragmatic crura; S, stomach.



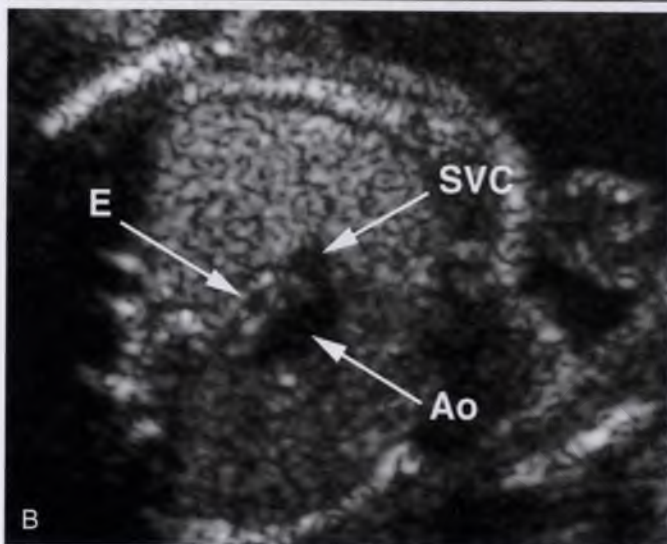
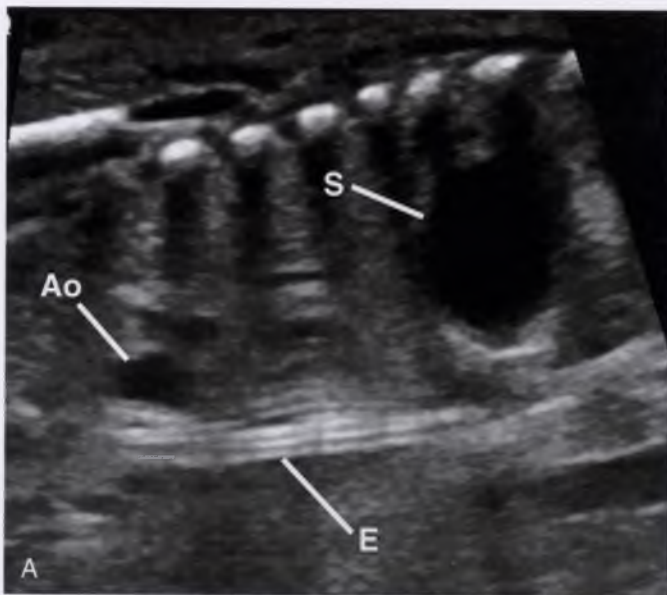


**FIG 8-86** Coronal (A) and transverse axial (B) sonograms demonstrating the esophagus (E). The serosa and lumen appear hyperechoic, and the muscular wall is hypoechoic. Distally, the esophagus lies anterior to the descending aorta (compare Fig. 8-83). Proximally, it lies posterior to the transverse aorta (in B) and medial to the ascending aorta (in A). Ao, aorta; S, stomach; SVC, superior vena cava.

The incisura angularis is a notch of variable depth that is usually found along the lesser curvature between the body and antrum of the stomach. If the incisura angularis is deep enough it is possible to generate a sonographic plane of section, which simulates a “double bubble.”<sup>74</sup>

Small bowel becomes progressively more visible through the second and third trimesters. This is particularly true of the echogenically bright submucosa of the small bowel. This may impart the appearance of a “conglomerate” zone of increased echogenicity in the mid- and lower abdomen of the fetus. This should not be mistaken either for an abnormal mass (pseudomass of bowel)<sup>75-77</sup> or for a bowel abnormality (so-called echogenic bowel). With passage of time, and somewhat dependent on ease of imaging, discrete small bowel loops become visible (Fig. 8-88). With modern equipment, the bowel wall is seen to good advantage. The submucosa and serosa display greater

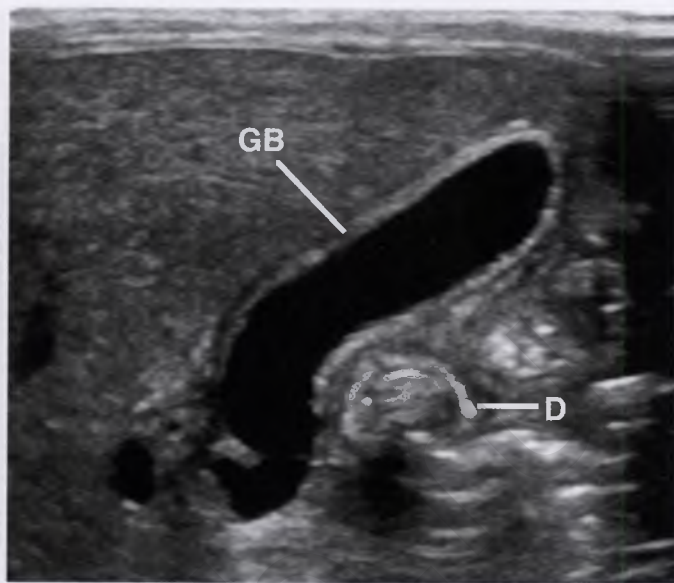


**FIG 8-87** Longitudinal image through the gallbladder in a 1-month-old infant born premature at 24 weeks' gestation demonstrates the normal relationship of the gallbladder (GB) with the duodenum (D), closely opposed without any intervening structure.



**FIG 8-88** Discrete small bowel (SB) loops are clearly visible on images through the fetal abdomen. The morphology of the bowel wall is well shown. The dominant feature of the small bowel wall is the submucosa (SM), which demonstrates bright echoes (not to be mistaken for “echogenic bowel”). The muscularis mucosa (MM) lies “inside” the submucosa and is hypoechoic. Note that the anterior abdominal wall musculature (AWM), like all musculature, demonstrates darker gray echoes. If one looks closely, one can appreciate the more echogenic small bowel mucosa “sandwiched” between the layers of muscularis mucosa.



echogenicity than the muscular layers, the thinner muscularis mucosa and thicker muscularis propria. Later in pregnancy, deposition of fat in the mesentery probably accentuates the separation of individual bowel loops and increases echogenicity in the region of the abdomen where the small bowel resides.

Importantly, “increased echogenicity” of the bowel has been implicated as a harbinger of several serious abnormalities of the fetus.<sup>78,79</sup> It is therefore important to discriminate increased echogenicity of the bowel content (potentially indicating a problem) from echogenicity caused by normal bowel structure, but perceived in conglomerate to represent “increased bowel echogenicity” (unlikely to indicate a problem). Examining to see if the echogenicity is due to well-visualized submucosa or mesenteric fat will avoid these issues. Generally, high-frequency transducers demonstrate the submucosa of the small bowel to much greater advantage, thus giving the examiner the impression that the bowel is “echogenic.”<sup>80</sup> When transducers with frequencies greater than 5 MHz are being employed, the probability that fetal bowel wall structure has resulted in an impression of “increased echogenicity” is great. Confirmation with lower frequent transducers should be performed. By late pregnancy, almost regardless of equipment quality, discrete small bowel containing small amounts of fluid (succus entericus) can be visualized in nearly all fetuses.<sup>81</sup>

The colon tends to become visible near the beginning of the third trimester and, again, is seen progressively better with increasing gestational age.<sup>81,82</sup> The colon tends to be relatively hypoechoic (Figs. 8-89 and 8-90). As such, colon should not be mistaken for dilated small bowel. It is the characteristic course of the colon that most readily permits distinction from pathologically dilated small bowel. The

ascending colon courses along the right flank (see Fig. 8-86A) in relation to the right kidney. As it approaches the liver, it bends leftward, in the hepatic flexure (see Fig. 8-89A). The transverse colon courses along the free edge of the liver (see Fig. 8-89B) and passes inferior to the stomach. At the splenic flexure, the colon turns posteriorly and again comes into intimate relationship with the kidney; of course, in this instance it is the left kidney. Frequently, when imaging the kidneys, the colon is detected. If one kidney is absent, the colon occupies the renal fossa and should not be misinterpreted as a normal or abnormal kidney. Finally, the sigmoid colon arcs over the urinary bladder to join the rectum (see Figs. 8-89C and 8-90B). Occasionally, haustral markings can be noted in the colon wall. A redundant sigmoid colon should not be mistaken for dilated small bowel. The anus can be visualized at the base of the gluteal cleft (see Fig. 8-90C). A normal appearance of the anus is helpful to exclude anal atresia when dilated colon is suspected.

The liver, as noted earlier, is proportionately larger in the fetus than in the child or adult.<sup>83</sup> Similarly, in the early second trimester, the liver constitutes 10% of the total fetal weight but only 5% of the total weight at term. The fetal liver, in addition, has a substantially larger left lobe. Blood with a high degree of nutrients and oxygen enters the umbilical segment of the left portal vein. Thus, the left hepatic lobe is nourished with the highest levels of nutrients. Conversely, the blood going to the right hepatic lobe comes almost exclusively from the main portal vein, which has the lowest levels of nutrients (it has already passed through a capillary network). The fetal liver spans the entire width of the abdomen throughout pregnancy, the left lobe always contacting the left abdominal wall. This would be unusual but possible in an adult. The

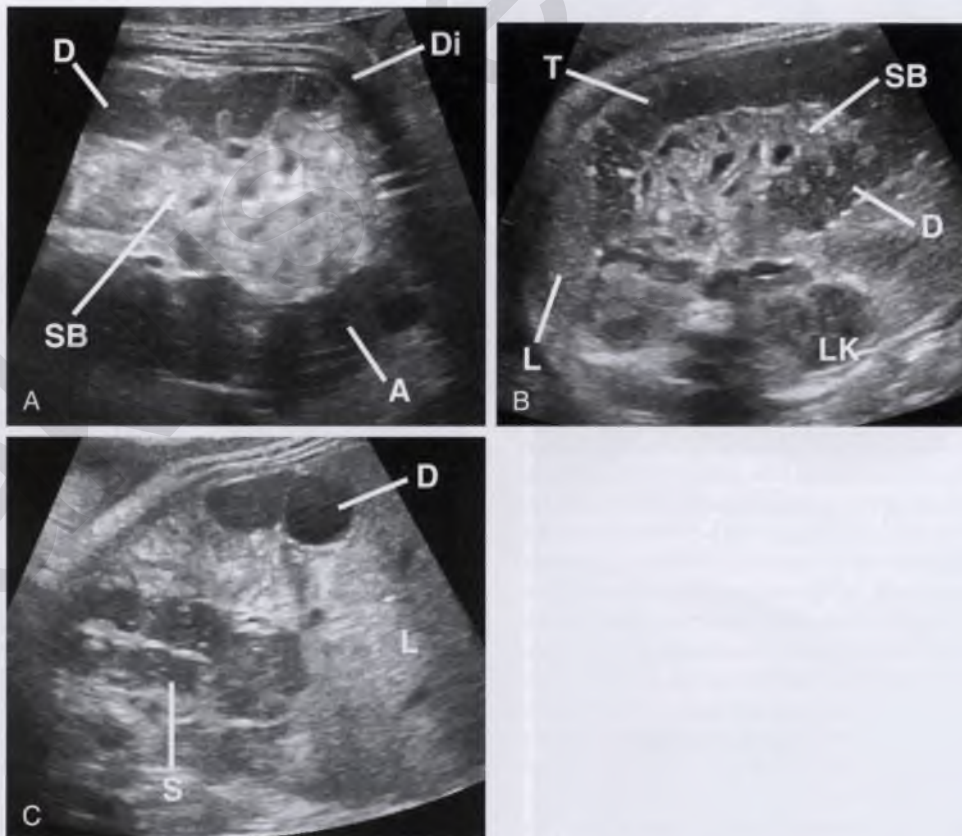


**FIG 8-89** Coronal (A and C) and transverse (B) sonograms of the fetal abdomen demonstrating, by position, the ascending (A), transverse (T), descending (D), and sigmoid (S) colon. Di, diaphragm; L, liver; LK, left kidney; SB, small bowel.



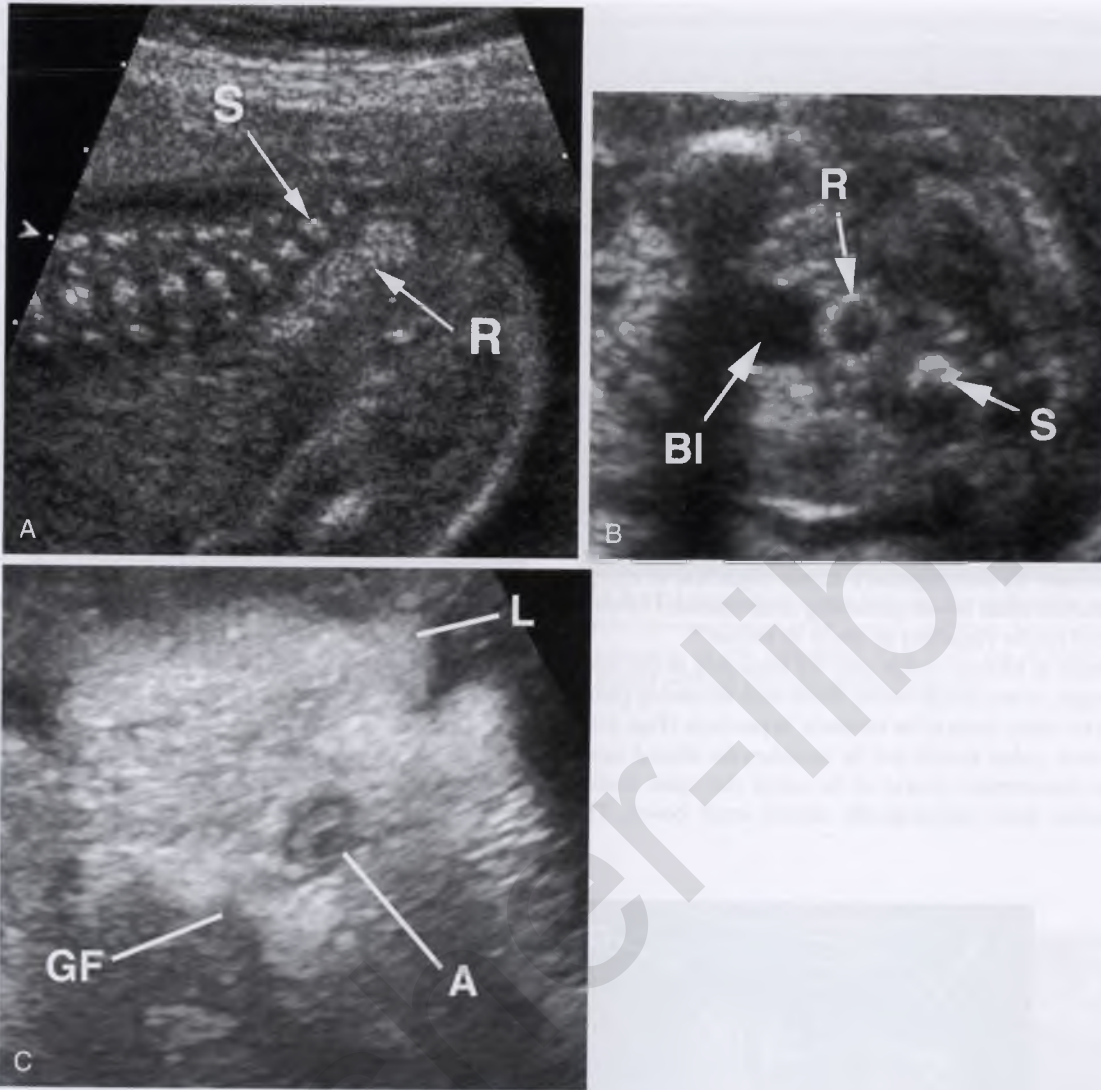


**FIG 8-90** **A**, Midsagittal sonogram demonstrates the rectum (R) anterior to the sacrum (S). **B**, A transverse axial sonogram demonstrates the rectum (R) lying between the bladder (Bl) and sacrum (S). **C**, Transverse axial sonogram demonstrates the anus (A). GF, gluteal fold, L, labia majora.

two major segments of each hepatic lobe can be seen in older fetuses (see Fig. 8-74) and to some extent even in early second trimester fetuses.<sup>61,64</sup> The lateral segment of the left lobe extends to the left of the umbilical segment of the left portal vein (see Figs. 8-72 and 8-73). The medial segment of the left lobe is the tissue lying between the gallbladder (or middle hepatic vein more superiorly) and the umbilical segment of the left portal vein or the intersegmental fissure more caudally (Fig. 8-91). The right lobe is all of the hepatic tissue lying to the right of the gallbladder, middle hepatic vein, and inferior vena cava (see Figs. 8-67 and 8-73). These latter three structures all reside in the main lobar fissure. The left portal vein and left hepatic vein mark the left intersegmental fissure. Finally, the right intersegmental fissure is marked by the right hepatic vein cephalically and its anterior branch inferiorly.

As equipment has improved, the pancreas is more readily perceived from the midtrimester onward. The pancreatic tissue lies posterior to the stomach, an area that can be visualized consistently in the fetus. The pancreatic tissue is more echogenic than the liver or the left kidney,

making its visualization somewhat easier. One should not presume that acoustic enhancement from fluid in the stomach is the cause of the greater intensity echoes from the pancreas (although acoustic enhancement increases the brightness of all echoes in its path). Definitive recognition of the pancreas requires demonstration of the splenic vein and origin of the superior mesenteric artery in a transverse axial plane of section (see Fig. 8-81). The pancreas then is the band of tissue between these vessels and the posterior gastric wall.

The spleen is not truly a gastrointestinal organ (see Figs. 8-73 and 8-82B). It is part of the reticuloendothelial system. However, as an upper abdominal organ it fits most appropriately in this section. The spleen is bounded by the diaphragm superiorly, the lower ribs laterally, the stomach medially, and the diaphragm and kidney posteriorly. It is only the inferior margin that is difficult to delimit. In the fetus, spleen echogenicity is similar to that of the liver. In the adult, the liver is slightly less echogenic than the spleen.<sup>84-87</sup> The spleen grows progressively through fetal life, and nomograms of splenic size are available in the literature.<sup>84</sup>



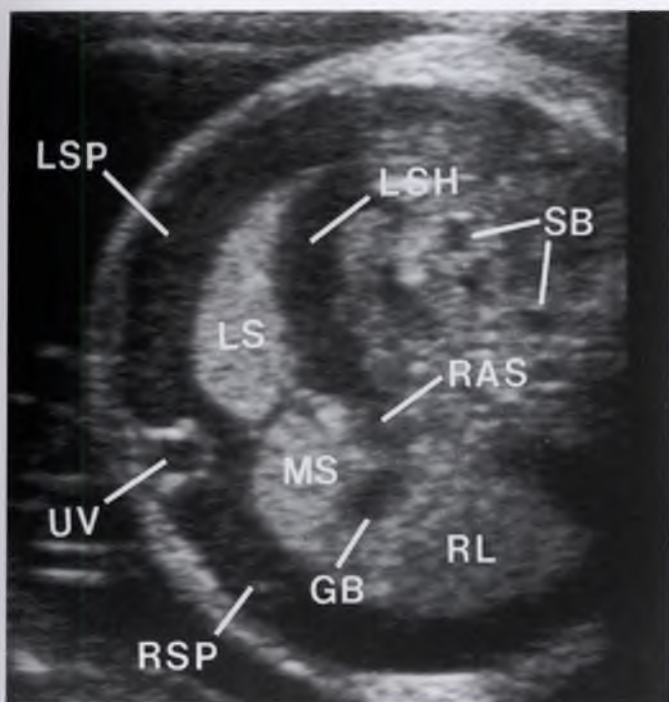


**FIG 8-91** Transverse axial sonogram of the fetal abdomen after an intraperitoneal transfusion for Rh isoimmunization enables recognition of many peritoneal spaces, including the right (RSP) and left (LSP) subphrenic spaces and the right anterior (RAS) and left subhepatic (LSH) spaces. Segmental anatomy of the fetal liver is also well seen, including the medial (MS) and lateral (LS) segments of the left hepatic lobe. GB, gallbladder; RL, right hepatic lobe; SB, small bowel; UV, umbilical vein.

## RESPIRATORY SYSTEM

The upper respiratory tract system is seen partially. The nose has been previously illustrated (see Figs. 8-12 and 8-13). The nasal cavity, septum, and palate can be detected with practice. As noted earlier, portions of the pharynx and hypopharynx are commonly visible because of the presence of fluid.<sup>70</sup> The piriform sinuses are seen when fluid filled (see Fig. 8-84). When relatively large amounts of fluid are present in the pharynx of an older fetus, the epiglottis may be seen protruding into the fluid (Fig. 8-92). The epiglottis is particularly visible during swallowing.

The larynx is virtually always visible when the hypopharynx is fluid filled (see Figs. 8-84 and 8-92). Details of laryngeal anatomy are not particularly evident, but the larynx itself is easily recognized as a superior constriction of the tracheal fluid column protruding into the hypopharynx and flanked by the piriform sinuses. If the head is markedly flexed, the overlying mandible frequently defeats efforts to visualize the larynx and hypopharynx. The larger thyroid cartilage of the larynx is hypoechoic as are virtually all cartilaginous structures in the fetus. Thus, it is commonly seen as two thin hypoechoic bands paralleling the upper tracheal fluid column of the fetus on longitudinal sections of the trachea (Fig. 8-93).

As noted earlier, the trachea is a relatively easy structure to visualize (Figs. 8-92 to 8-95).<sup>70</sup> Again, this is predominantly because it is consistently fluid filled. Not only do the lungs produce fluid that is expelled into the trachea, but additionally, the trachea, along much of its length, is flanked by the conspicuous pulsations of the common carotid arteries. The trachea can usually be traced to its distal end, coursing posterior to the aortic arch (Fig. 8-94A), but the carina and bronchi are quite difficult to perceive. Because mainstem bronchi are usually invisible, smaller ramifications of the bronchi are, for all intents and purposes, universally invisible at this time in the development of fetal sonography.

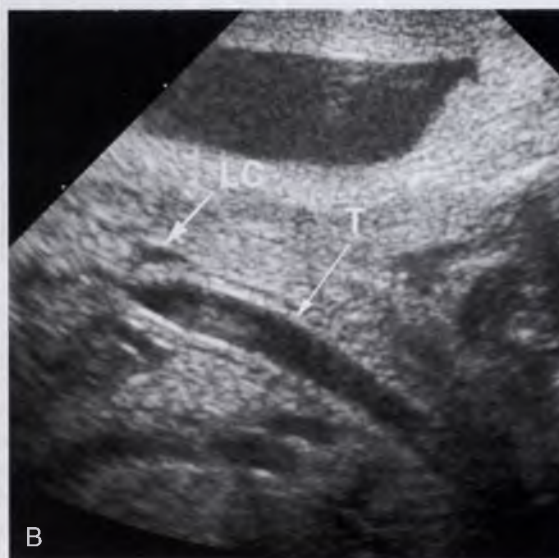
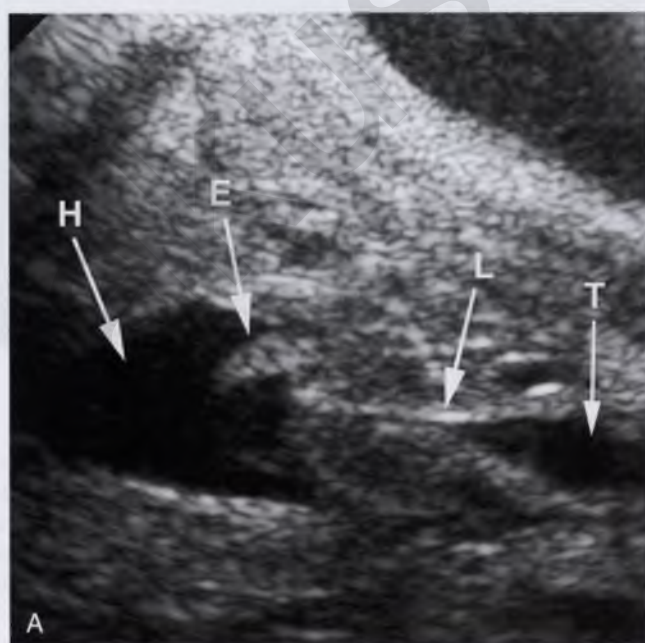


**FIG 8-92 A and B**, Coronal sections through the hypopharynx (H), larynx (L), and trachea (T). E, epiglottis; LC, laryngeal cartilage.



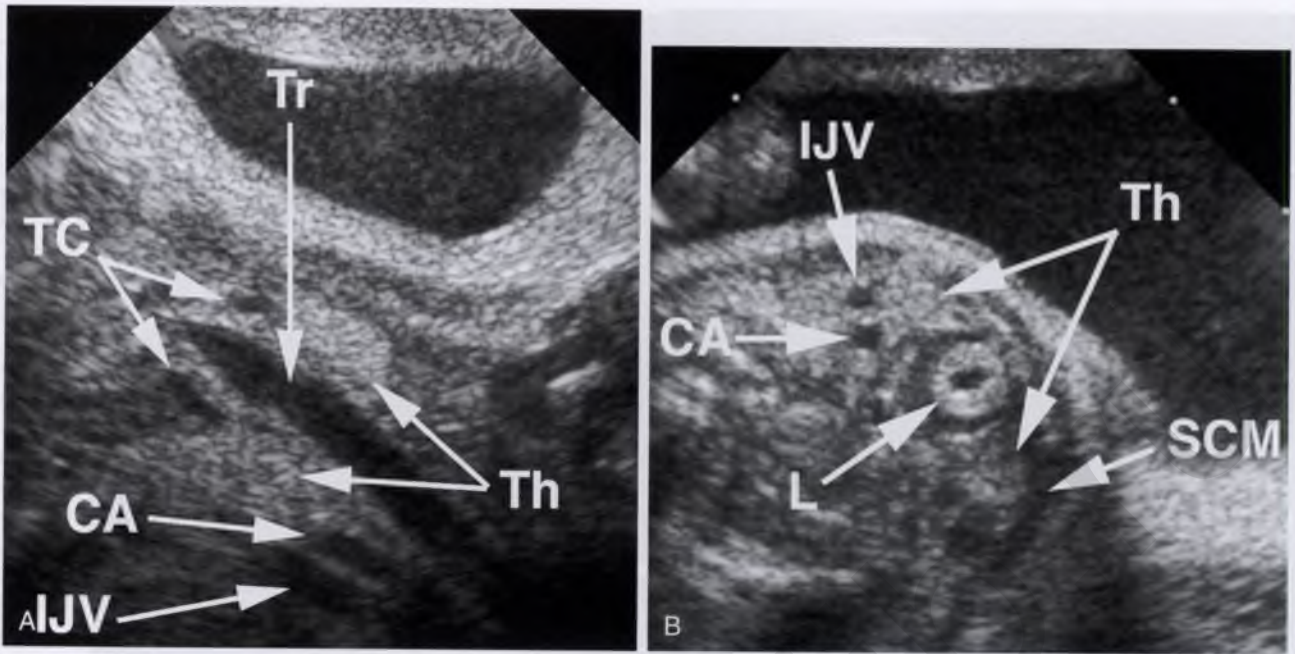


**FIG 8-93** Longitudinal (A) and axial (B) sonograms of the fetal neck. CA, carotid artery; IJV, internal jugular veins; L, larynx; SCM, sternocleidomastoid muscle; TC, thyroid cartilages; Th, thyroid lobes; Tr, trachea.

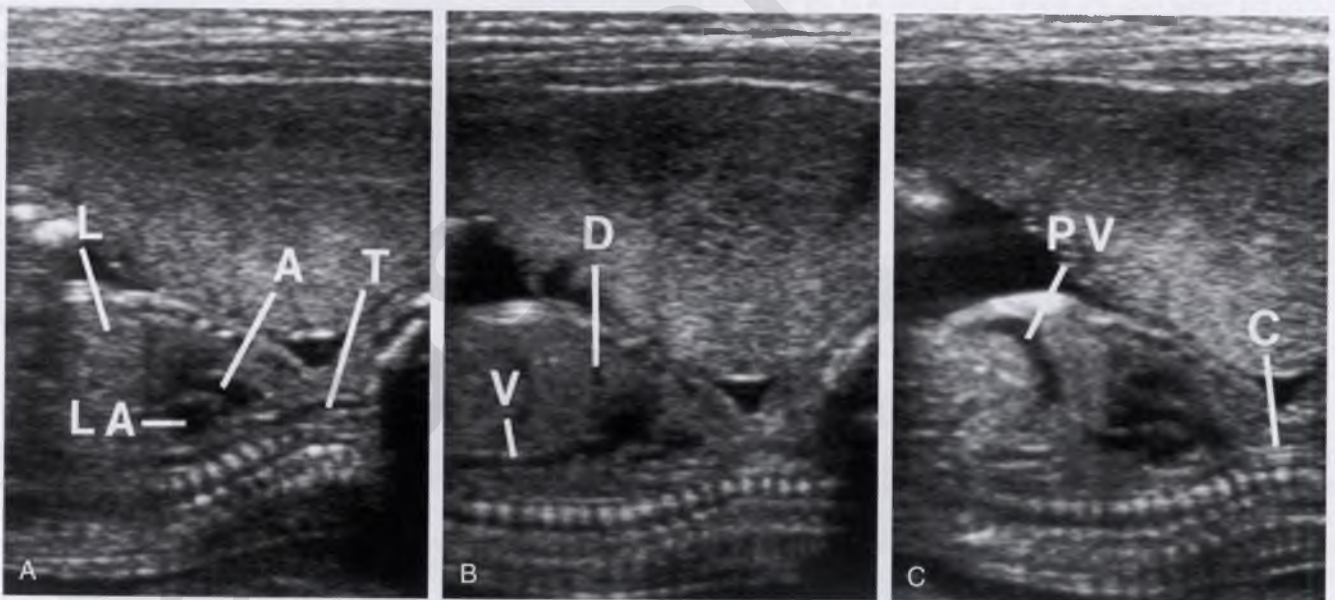


**FIG 8-94** Relationships of mediastinal and neck structures. Midsagittal (A) and parasagittal (B and C) sonograms demonstrate the trachea (T) down to the level of the aortic arch (A). The cervical esophagus (C) lies posterior to the trachea in the neck (note again the muscular and mucosal layering). D, diaphragm; L, liver; LA, left atrium; PV, left portal vein; V, inferior vena cava.



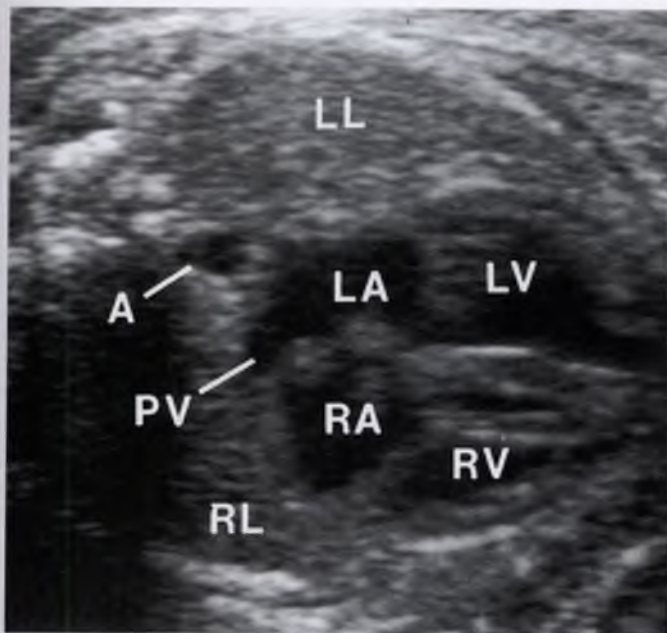


**FIG 8-95** Transverse axial sonogram of the fetal thorax. A, descending aorta; LA, left atrium; LL, left lung; LV, left ventricle; PV, pulmonary vein; RA, right atrium; RL, right lung; RV, right ventricle.



**FIG 8-96** Axial section through the fetal thorax. (Arrows), pulmonary veins; LL, left lung; RL, right lung.

The right and left pulmonary arteries and pulmonary veins (Figs. 8-95 and 8-96) are visible in a large percentage of second and third trimester fetuses. However, one generally pursues visualization of these major vessels during examination of the heart rather than of the lungs. Details of the pulmonary arterial and venous anatomy are found in Chapter 13.

The lung (at least lung tissue) can be seen from late first trimester onward. Early in pregnancy, definition of the lung is drawn more from the structures that surround it. These include, predominantly, the ribs

superolaterally and the heart (and to a lesser extent other mediastinal structures) medially. Inferiorly, the early lung blends imperceptibly with the liver. These two organs are equal in echogenicity throughout some of the second trimester. As pregnancy progresses, the lung becomes more echogenic than the liver (Fig. 8-97). The reason for this is unknown. It was speculated that this difference may signal pulmonary maturity, a notion that is certainly erroneous because a lung of greater echogenicity than the liver can be seen earlier in pregnancy than lung maturity can possibly develop.<sup>88,89</sup> Furthermore, the muscular portion of the diaphragm becomes progressively more visible with fetal growth and the hypertrophy of the diaphragmatic muscle that occurs as the fetus “breathes” against atelectatic, fluid-filled lungs (Fig. 8-98). These markers of the inferior extent of the lung improve pulmonary tissue visibility with advancing gestational age. Discrete pulmonary lobes are not visible in the normal fetus, but when a pleural effusion is present, insinuation of fluid into the major fissures (and the minor fissure on the right) marks lobar boundaries.

## GENITOURINARY SYSTEM

Although the extreme variability of fetal positioning and the lack of subject contrast between kidney and the surrounding tissues do not permit consistent identification of both fetal kidneys, normal fetal kidneys are commonly identified in their paraspinous location after the early second trimester. In longitudinal section, fetal kidneys appear as bilateral elliptical structures, and in transverse section they have an ovoid to circular appearance adjacent to the lumbar spinal ossification centers bilaterally (Fig. 8-99). Later in pregnancy, echogenic retroperitoneal fat, which surrounds the kidneys, assists in their sonographic visualization (Fig. 8-100). The fetal renal pyramids can be discriminated from the surrounding cortex and columns of Bertin in most fetuses and are arranged in an anterior and posterior row (see Fig. 8-99A) in a configuration corresponding to the calices that contact the apices of the pyramids (the papillae).<sup>20</sup> The echogenicity of the normal fetal renal cortex, which usually approximates or may even be slightly greater than that of the surrounding tissues, highlights the relatively hypoechoic pyramids. The characteristic position of the pyramids avoids any potential confusion with renal parenchymal cysts. Confusion with dilated calices is avoided by noting the interspaced columns of Bertin and the lack of communication with dilated infundibula and pelvis. Within the renal sinus of fetuses, there is a paucity, or more commonly a frank absence, of fat. Intrarenal collecting structures, the pelvis and infundibula, are commonly seen in fetuses because they frequently contain fluid,<sup>91,92</sup> a topic that is addressed in Chapter 15. The normal fetal ureter is, for all intents and purposes, not identifiable in fetuses. Visualization of a fetal ureter should always suggest pathologic dilatation.

The fetal kidneys grow throughout gestation. Standards for renal length, width, thickness, volume, and circumference have been established as a function of menstrual age and correspond with measurements of renal size obtained on stillborn fetuses postnatally.<sup>93-95</sup> Throughout pregnancy, the ratio of kidney circumference to abdominal circumference remains relatively constant at 0.27 to 0.30. Such measurements are more efficient for detecting enlarged kidneys than small kidneys. Diminution in renal size is more difficult to detect because the exact renal border, especially of small kidneys, may be partially obscured, because the plane of section may not be through the longest renal axis, and because of the wide standard deviation in renal size.<sup>93-95</sup>

As early as 15 menstrual weeks the normal fetal urinary bladder can be identified (see Fig. 8-71). Less than a milliliter of bladder urine is needed to allow ready visualization in a young fetus. Because the fetus



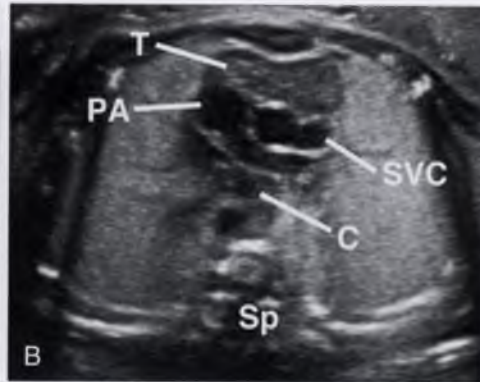
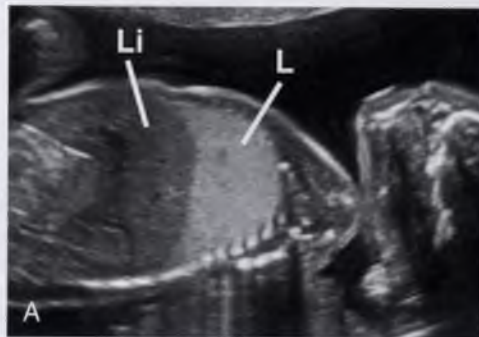


**FIG 8-97** **A**, Sagittal sonogram through the fetal chest. Echogenicity differences between lung (L) and liver (Li) are easily seen in this older fetus. **B**, Axial sonogram through the fetal chest. Again, the echogenicity differences between the lung and thymus (T) are easily seen. C, carina; PA, pulmonary artery; Sp, spine; SVC, superior vena cava.

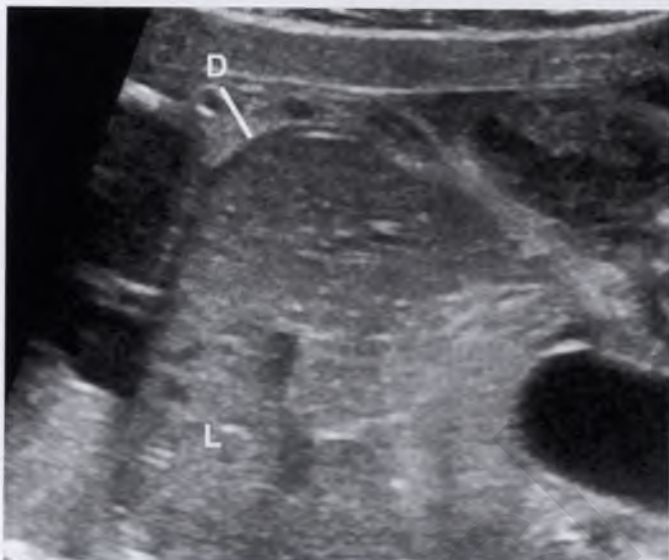


**FIG 8-98** The muscular diaphragm (D) is relatively hypoechoic. L, liver.

normally fills and empties the urinary bladder every 30 to 45 minutes, the bladder will frequently be seen to increase in size and to empty during the course of a sonographic examination.<sup>96-98</sup> Similarly, fetuses in whom the urinary bladder is not visualized can be examined at intervals for bladder filling. If the bladder cannot be seen in the presence of oligohydramnios, sequential imaging to test for bladder filling is mandatory.

At 32 weeks of gestation, the maximum fetal bladder volume measures 10 mL. By term, the normal fetal bladder volume quadruples. Similarly, fetal urine production, as calculated by determination of change in bladder volume with time, increases from 9.6 mL/hour at 30 weeks to 27.3 mL/hour at 40 weeks menstrual age.<sup>96,97</sup> Of course, term fetuses void; thus, the bladder may be empty.<sup>98</sup> Filling and emptying of the fetal urinary bladder confirm that the fetus produces urine but does not indicate the “quality” of urine produced. The normal fetal urinary bladder, the wall of which is very thin and virtually invisible when the bladder is well distended, occupies a midline position within the fetal pelvis (Fig. 8-101). Changes in volume of the urinary bladder with time differentiate it from cystic pathologic pelvic structures. Recall that the umbilical arteries, regardless of the degree of bladder

distention, always flank the urinary bladder. This anatomic relationship is extremely useful for identification of a persistently empty urinary bladder or the confirmation of a massively overdistended bladder.

The normal fetal urethra may be identified, from time to time, as an echogenic line extending the length of an erect penis (see Fig. 8-19). In females and in males examined when the penis is flaccid, the normal urethra is difficult or impossible to identify. The uterus and ovaries cannot be visualized in normal female fetuses. The testes can be visualized in male fetuses only after they have descended into the scrotum under normal circumstances. The prostate cannot be visualized. The external genitalia were discussed previously in the section entitled “Superficial Anatomy of the Fetus.”

The fetal adrenal gland, although not part of the genitourinary system, is seen quite routinely when searching for the kidneys (Figs. 8-100 and 8-102).<sup>99,110</sup> Even in the presence of agenesis of one or both kidneys, the adrenal glands can be appreciated in their expected paraspinous locations. The fetal adrenal glands may often be imaged after 20 menstrual weeks. The adrenal glands have a specific size, shape, and echogenicity. The echo pattern is so characteristic that the cortex and medulla can be appreciated separately (see Figs. 8-6, 8-67, and 8-102). In the fetus, both adrenal glands cap the upper renal poles (in the adult the left adrenal gland most often lies anterior to the upper pole).<sup>100</sup> The right adrenal is seen more consistently. Its upper portion lies immediately posterior to the proximal inferior vena cava (see Fig. 8-102).

## CENTRAL NERVOUS SYSTEM

The fetal brain was one of the first areas of investigational interest in the diagnosis of fetal anomalies.<sup>101</sup> This was a result of two factors: (1) the fetal head was imaged routinely to obtain a biparietal diameter for the determination of gestational age, and (2) central nervous system anomalies are among the most common birth defects. At first, only gross morphologic aberrations such as anencephaly or advanced hydrocephalus were discovered prenatally. As instrumentation has improved to the present day, many more malformations of the brain can be diagnosed with accuracy.<sup>102-107</sup>

The path to the diagnosis of anomalous development, as always, begins with a firm grasp of normal developmental anatomy. Initially, many errors were made when interpreting normal fetal intracranial anatomy as seen by sonography.<sup>108-110</sup> This was due to the unusual circumstance that “fluid” and “solid” areas of the brain did not behave in an anticipated manner. It was initially expected that the sonographic



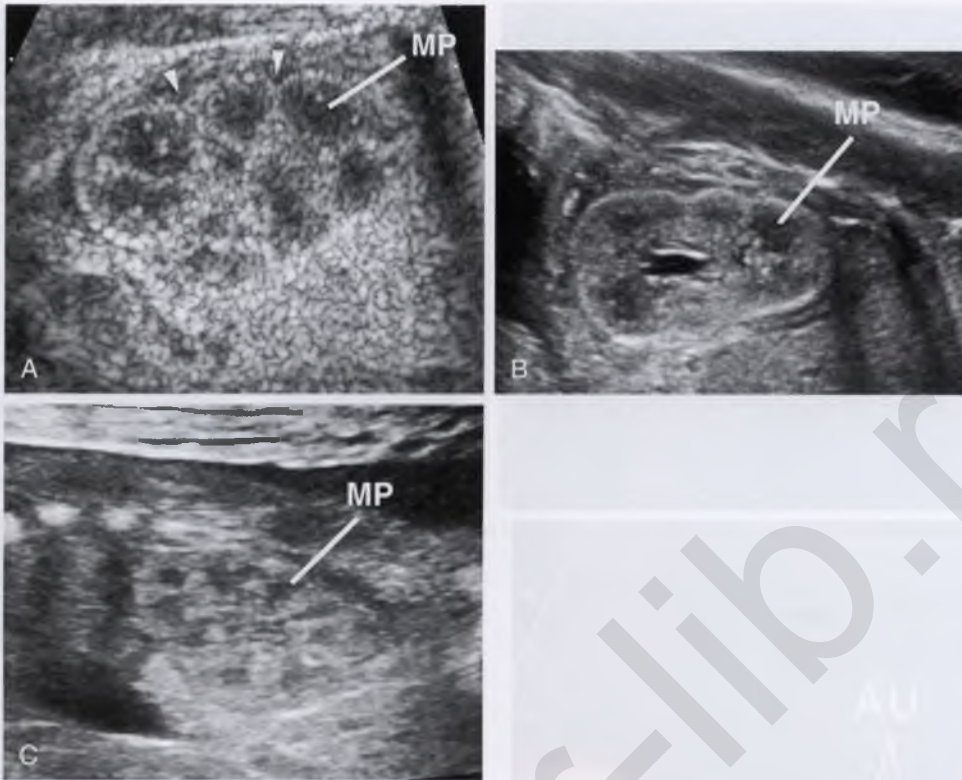


**FIG 8-99** **A**, Longitudinal sonogram through the early second trimester fetal kidney (*arrowheads*). **B**, Longitudinal sonogram through a late second trimester fetal kidney. Note that the medullae (MP) appear more prominent earlier. This is because cortical growth is greater than that of medullary growth, and thus the relative size of the medullae decreases. **C**, Longitudinal sonogram through a third trimester fetal kidney. Among the normal variations of fetal renal appearances, note that the renal echogenicity can be relatively increased because the cortical tissue is echogenic, thus better outlining the more echolucent medullary pyramids (MP).



**FIG 8-100** Transverse axial sonogram of a fetal kidney margined by perirenal fat (*arrows*). The brightly echogenic perirenal fat helps to sonographically outline the less echogenic renal parenchyma.

appearance of the lateral ventricles would be dominated by cerebrospinal fluid, which would render them echolucent. Instead, their appearance was dominated by highly echogenic choroid plexus (Figs. 8-103 to 8-106).<sup>111,112</sup> Conversely, the bulk of neural tissue, the telencephalon, diencephalon, and mesencephalon, is quite hypoechoic compared with other solid tissues in the human body (see Fig. 8-103).<sup>111,113</sup> The more recent entrant into the area of diagnostic sonography can well imagine the potential for misinterpretation among early researchers when the largest fluid-containing areas of the brain yielded the greatest amplitude echoes whereas the solid tissue yielded the lowest. To further complicate matters, dramatic changes occur as brain development progresses, resulting in ever-changing positions of certain “landmarks.” These changes had never been observed *in vivo*, and postmortem examination of the brain can be at variance with its appearance during life.

A series of key observations led to the clear delineation of normal developmental neuroanatomy as viewed sonographically. These observations included recognition of the fetal third ventricle, the brightly echogenic choroid plexus,<sup>111</sup> and pulsating vasculature in several cisterns.<sup>113</sup> The first two identified the supratentorial ventricular system. The last enabled identification of the sylvian cistern (middle cerebral artery pulsation), interpeduncular cisterns (basilar artery pulsation), and ambient cisterns (posterior cerebral artery pulsations) (see Fig. 8-79). The landmarks established by these observations provided a



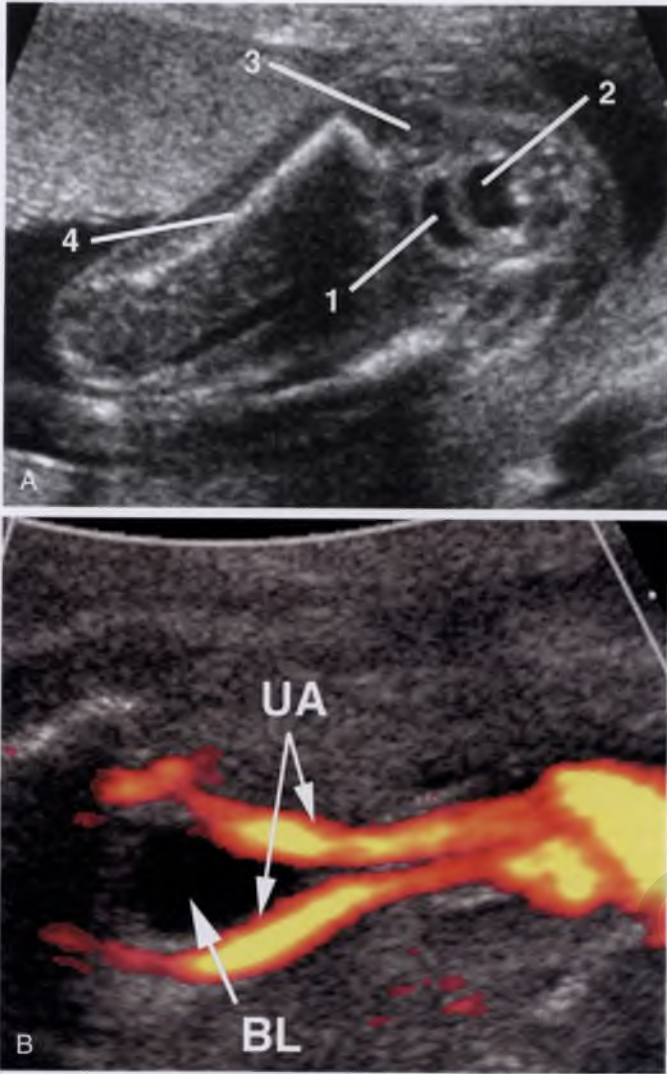


**FIG 8-101 A**, Transverse axial sonogram through the fetal pelvis. 1, urinary bladder; 2, rectum; 3, femoral head; 4, femoral diaphysis. **B**, Oblique axial sonogram through the fetal pelvis with nondirectional color Doppler. The umbilical arteries (UA) mark the lateral margins of the bladder (BL).

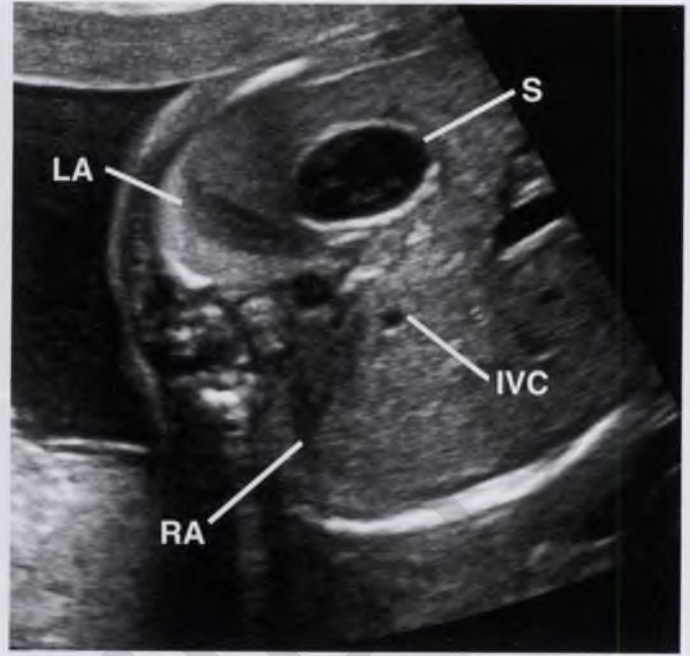


**FIG 8-102** Transverse axial sonogram of the adrenal glands; much anatomy can be seen on this image of the upper fetal abdomen. Note both limbs of the right adrenal gland (RA) immediately posterior to the inferior vena cava (IVC), and the left adrenal gland (LA) is to the left of the aorta and posterior to the stomach (S). See also Figure 8-6 for the typical triangular appearance of the adrenal gland in the coronal plane superior to the kidney.

symmetric appearance of the brain as these structures narrow the developing third ventricle into a midline specular reflector.<sup>119-122</sup>

By the end of the first trimester, the thalamus, third ventricle, mid-brain, brainstem, and cerebellar hemispheres have achieved an appearance that will remain largely unchanged, other than progressive enlargement, throughout the remaining period of sonographic observation of the fetus (see Fig. 8-103). Therefore, the vast majority of the changes that are observed—and they are substantial—relate to the growth and development of the telencephalon. As mentioned, by the end of the first and beginning of the second trimesters, the lateral ventricles (see Figs. 8-103 and 8-104) dominate the sonographic appearance of the telencephalon. The brightly echogenic choroid plexus dominates these in turn. By 12 to 13 weeks, the lateral ventricles can be clearly seen, appear ovoid, and are largely filled with choroid plexus. Only the frontal horns are devoid of choroid plexus, as they are throughout life (see Figs. 8-103B, 8-104, and 8-105). At this stage of development, only the rudiment of a temporal horn (see Fig. 8-104B) is seen, and an occipital horn has yet to develop. The frontal horn, body of the ventricle, and atrium of the ventricle are large and easily detected. The choroid is the easiest structure to recognize because of its size and high-amplitude echogenicity. Conversely, the mantle of developing cerebral cortex surrounding the lateral ventricle is more difficult to delineate because of its low-amplitude echogenicity (see Fig. 8-103A), but a demarcation between the lateral ventricle and the cerebral mantle can be appreciated from specular reflections arising from the walls of the lateral ventricle (see Figs. 8-103B and 8-104B). These are seen where the acoustic beam intersects the ventricular wall perpendicularly. By 16 to 18 weeks the mantle of developing cortical tissue has thickened appreciably (compare Figs. 8-104 and 8-106). As the occipital lobe has increased in volume, an occipital horn of the lateral ventricle has gradually appeared (see Figs. 8-104 through 8-106).

framework for subsequent identification of other specific neural structures.<sup>114-118</sup>

Later in the course of the development of sonography, the neonatal brain came under study (Figs. 8-1 and 8-107).<sup>1,2,112</sup> Interestingly, this resulted in much greater understanding of the appearance of the fetal brain because examination of “newborn children” now begins commonly at 24 to 25 weeks of development (essentially a second trimester fetus) (see Fig. 8-1). Investigators then began to apply neuroanatomy as learned from the neonatal brain, which was imaged with great clarity through the anterior fontanelle, to the developing fetal brain. The following analysis of fetal intracranial anatomy is presented on the basis of these observations.

The fetal head can be clearly discriminated from the fetal torso when an embryo reaches a crown-rump length of 10 to 15 mm. By the 10th to 11th week after the last normal menstrual period (see Fig. 8-4), one can already begin to appreciate anatomy inside the developing fetal head. At this point, the intracranial tissue components consist almost entirely of the thalamus and corpus striatum, which yield the



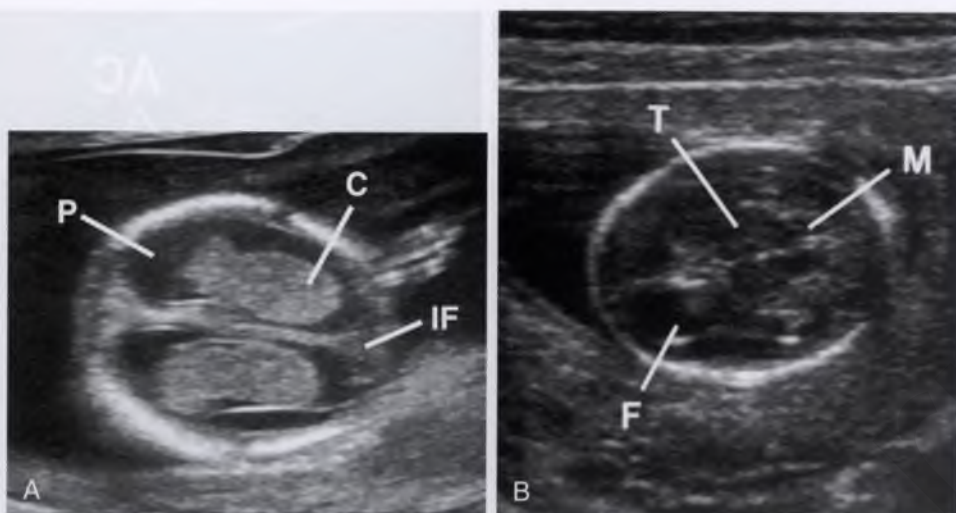


**FIG 8-103** **A**, Transverse axial scan at the level of the lateral ventricular atria in a 14-week fetus. The brain parenchyma (P) is very lucent. C, choroid plexus; IF, interhemispheric fissure. **B**, Slightly caudal scan demonstrates well-developed thalami (T) and midbrain (M). The frontal horns (F) are large and filled with cerebrospinal fluid.

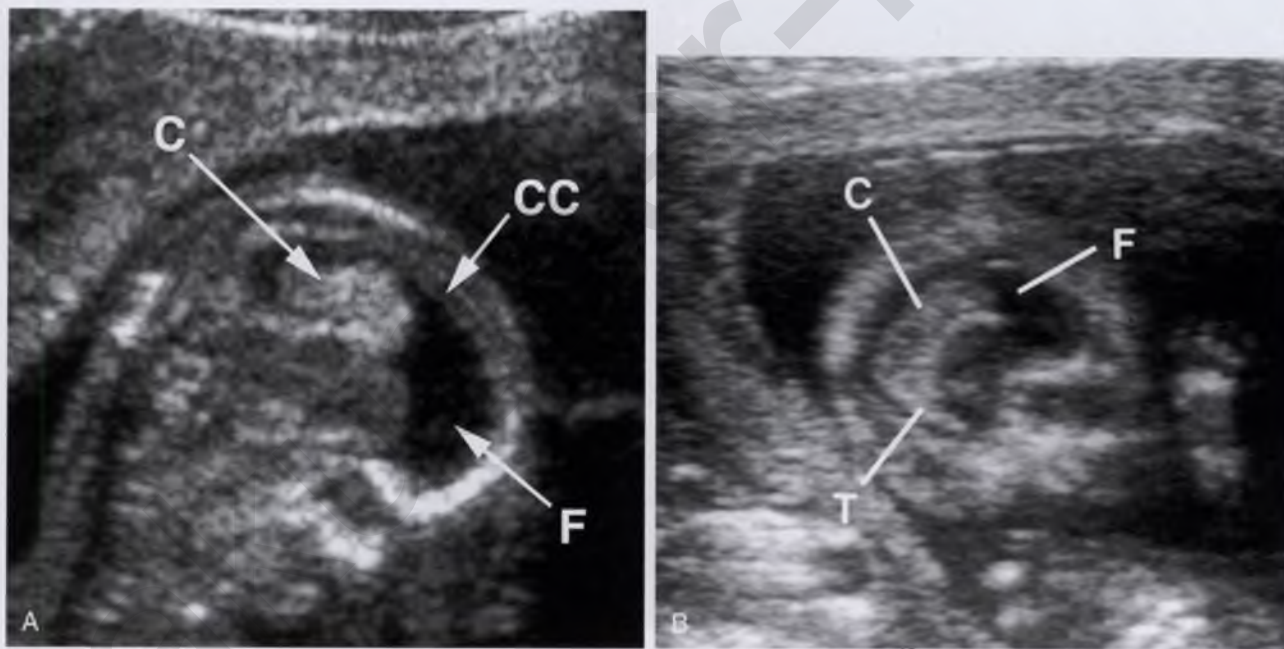


**FIG 8-104** **A** and **B**, Parasagittal sonograms in late first trimester demonstrate that, even this early in development, choroid plexus (C) fills the posterior and inferior portions of the ventricle. Specular reflectors demarcate the frontal horn (F), which is devoid of choroid plexus and thus seen as a "fluid-containing" portion of the ventricular system. The early temporal horn is seen (T). Note absence of an occipital horn. Choroid plexus fills the body, atrium, and early temporal horn. Note as well how remarkably thin the cerebral cortical (CC) tissue is.



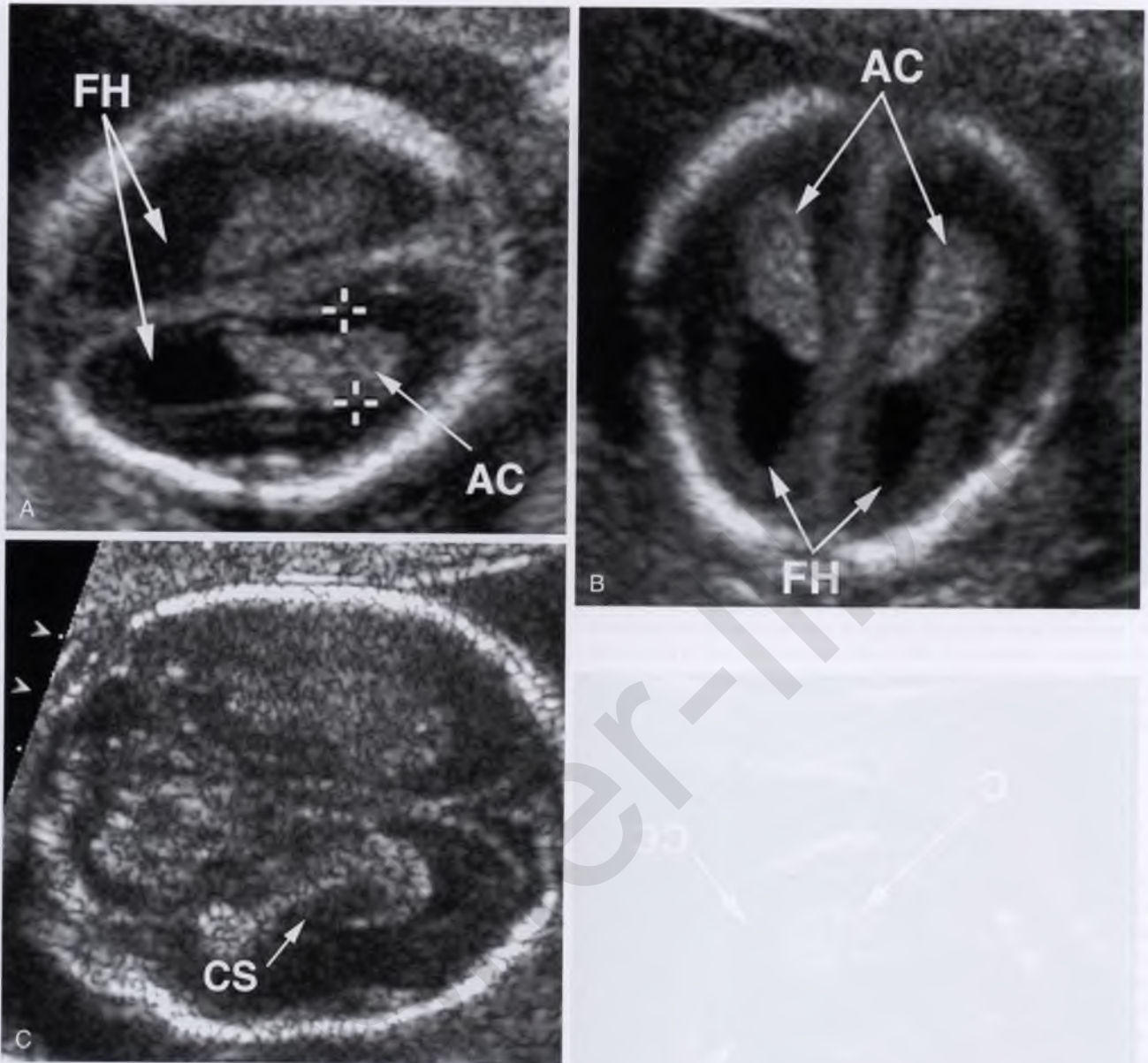


**FIG 8-105** Three axial sonograms through the lateral ventricles of early second trimester fetuses. **A**, Axial sonogram demonstrates degradation of visualization of the near ventricle due to calvarial reverberation artifact. Note the difference in clarity of the frontal horns (FH). AC, atrial choroid. **B**, By imaging through the posterior fontanelle, calvarial reverberation is nearly eliminated, and the frontal horns are now seen with equal clarity. **C**, At this early stage of development the corpus striatum (CS) is prominent and indents the ventricular choroid. This should not be mistaken for an abnormality (sometimes, when more lucent, it masquerades as a choroid plexus cyst).

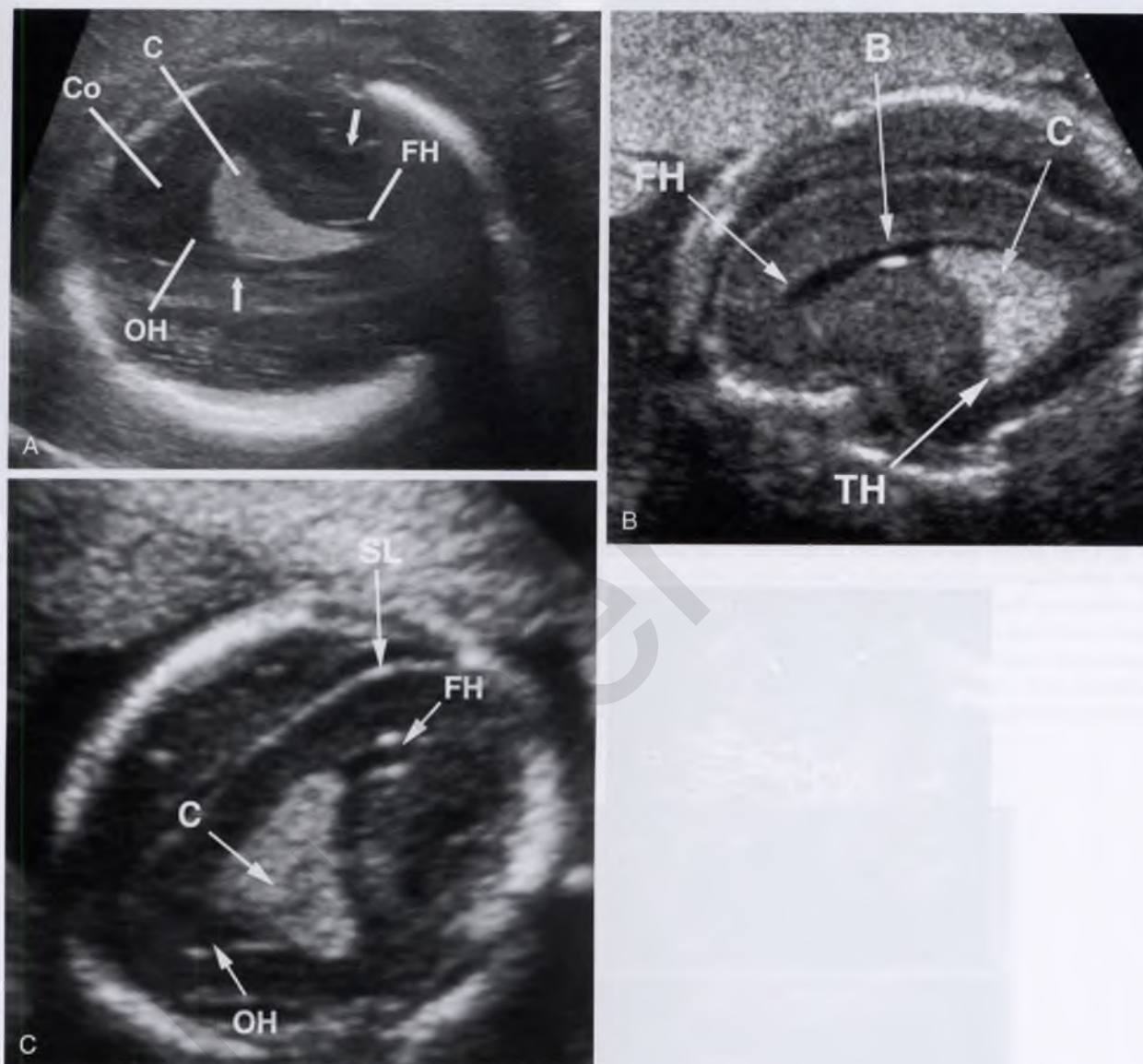


**FIG 8-106** **A** through **C**, Parasagittal sonograms through the ventricle of 16- to 18-week fetuses. The choroid (**C**) defines the ventricular size and the position of the ventricular atrium. Note the substantial increase in cortical brain (**Co**) thickness compared with fetuses only a few weeks younger (see Fig. 8-104). Bright echoes marginate the edge of the telencephalon (*straight arrows*). The bright reflector represents surface leptomeninges (**SL**). Note the beginnings of an occipital horn (**OH**) in **A**, and compare with the more developed occipital horn in **C**. Note, as well, that the frontal horn (**FH**) is much narrower in craniocaudal diameter because growth of the head of the caudate nucleus has reshaped this portion of the ventricle. **B**, ventricular body; **TH**, developing temporal horn.



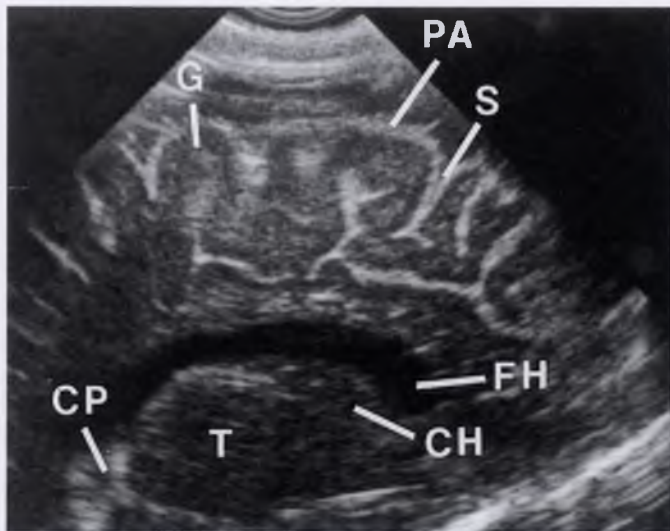


**FIG 8-107** Parasagittal sonogram of the brain of a 6-month-old child. Gyri (G) are well developed. Pia-arachnoid (PA) tissues cover the surface of the brain and make the sulci (S) highly conspicuous. Careful inspection of gyri shows that cortical "gray matter" is less echogenic than the "white matter" (this is almost certainly not a difference due to gray and white matter distinction but to the vessels coursing through the central gyrus). CH, caudate head; CP, choroid plexus; FH, frontal horn; T, thalamus.

The relative echogenicity of structures, which will be viewed throughout the remainder of gestation, is largely established at this time. Two types of tissues are brightly echogenic and, therefore, most easily seen during the examination of the fetal brain. These tissues are the choroid plexus, as noted earlier, and the brain coverings: the dura (pachymeninx) and pia-arachnoid (leptomeninges). Interestingly, the choroid develops from the vascular pia. The leptomeninges demarcate the edges of the brain with a brightly reflective margin of echoes (Figs. 8-106 through 8-108). Peripheral to this echogenic margin are the subarachnoid spaces that contain cerebrospinal fluid (Figs. 8-107 through 8-109). A characteristic feature is the relative lack of change in echogenicity between the peripheral (i.e., cortical brain) tissue and the cerebrospinal fluid space as seen across the brightly reflecting marginal echo from the pia-arachnoid (the cerebrospinal fluid-containing space may be more echogenic) (see Figs. 8-108 and 8-109). This perceptual problem originates from the anticipation that the subarachnoid spaces should be anechoic whereas the brain parenchyma should be echogenic. This reasonable assumption is untrue in many instances. These spaces have both cerebrospinal fluid and pia-arachnoid tissue within them, and it is the relative amount of these two components that determines the sonographic appearance of the subarachnoid spaces. Small subarachnoid cisterns (such as the basal and perimesencephalic cisterns) have an appearance dominated by pia-arachnoid and thus are seen as brightly echogenic spaces (Fig. 8-110). This is not to say that these cisterns are devoid of cerebrospinal fluid, but the fluid does not significantly influence their sonographic appearance.

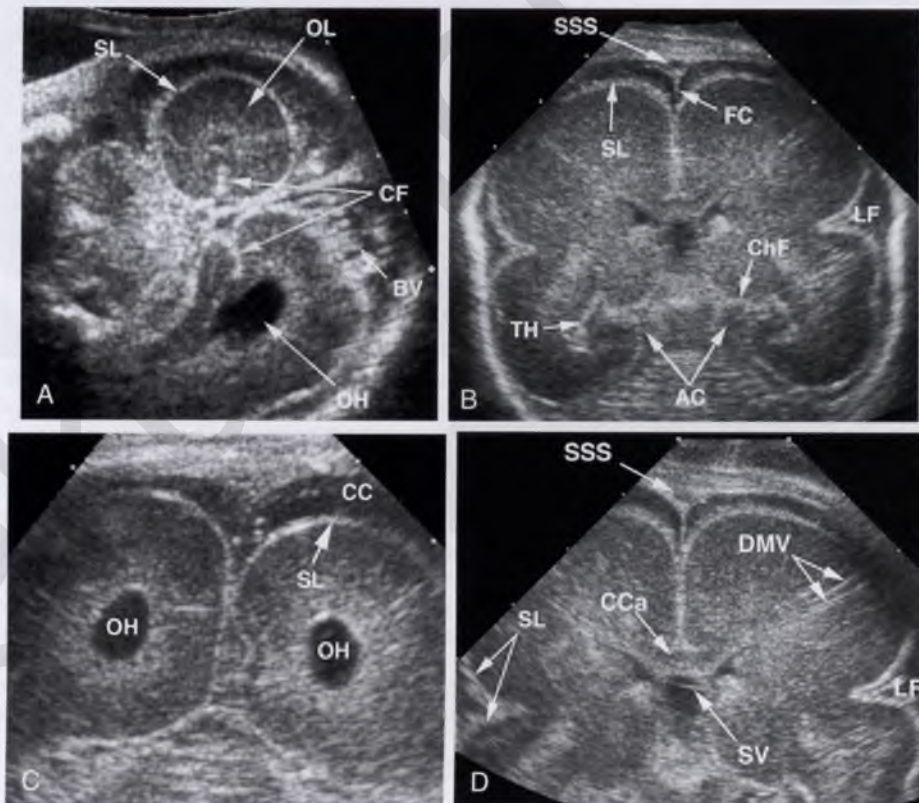


**FIG 8-108 A through D**, Sequence of sonograms obtained through fontanelles and sutures. This technique enables one to see symmetric brain anatomy. The surface leptomeninges (SL) are crucial to discriminating the edge of the brain tissue and the adjacent cisterns. AC, ambient cistern; BV, bridging veins; CC, convexity cistern; CCa, corpus callosum; CF, calcarine fissure; ChF, choroidal fissure; DMV, deep medullary veins; FC, falx cerebri; LF, lateral fissure; OH, occipital horn; OL, occipital lobe; SSS, superior sagittal sinus; SV, septal vein; TH, temporal horn.



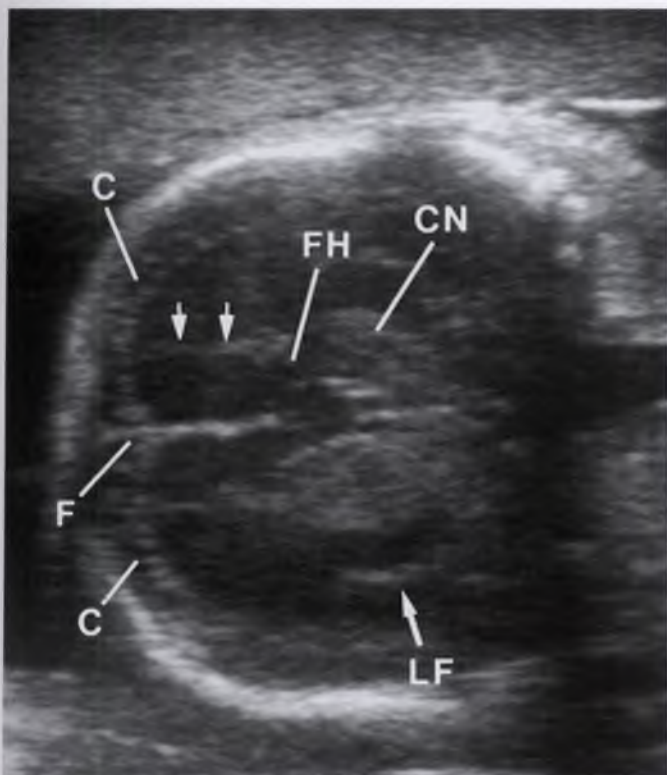


**FIG 8-109** Coronal section through the heads of the caudate nuclei (CN). The frontal horn (FH), which is not well seen, drapes over the caudate. Extending between the ventricular margin and the edge of the brain are linear echogenic structures previously mistaken for ventricles (arrows). Also seen are bridging strands of pia-arachnoid through the cistern (C) over the convexities (probably bridging veins covered with pia-arachnoid). F, falx; LF, lateral fissure.

Conversely, larger subarachnoid spaces, such as those over the convexities of the hemispheres (see Fig. 8-107 and 8-108) and the cisterna magna (Fig. 8-111), have an appearance dominated by cerebrospinal fluid. Thus, they behave, in the sonographic sense, as one would anticipate for a fluid-containing cavity. Intermediate-sized subarachnoid spaces will have both anechoic zones from visible cerebrospinal fluid and brightly echogenic zones from visible pia-arachnoid tissues (see Figs. 8-108 through 8-110). The bright margination provided by the leptomeninges enables one to visualize, for example, the midbrain quite elegantly (see Fig. 8-110). Without these margin echoes our perception of the midbrain would be greatly hindered.

As noted earlier, brightly reflecting structures dominate the sonographic appearance of the fetal brain. The choroid plexus and brain coverings (pia-arachnoid and dura) are the two major components within the developing calvaria that produce bright reflections. The important dural structures from the perspective of sonographic fetal brain anatomy are the falx cerebri and the tentorium (Figs. 8-108 through 8-112). Some neural structures generate high-amplitude reflections. This is particularly true of the basal ganglia, especially the lenticular nuclei (see Fig. 8-111). The cerebellar vermis and the surface tissues of the cerebellar hemispheres also appear very bright (Figs. 8-113 and 8-114), but this appearance is again secondary to leptomeninges. The cerebellar folia “drag” meninges below the “surface” of the hemisphere, making the surface tissues appear bright (see Fig. 8-113B). The cerebellar vermis has the greatest number of folia and intertwined meninges. Thus, it often appears strikingly echogenic (see Fig. 8-114B).

Also important as high-amplitude echoing structures are specular reflections from the walls of the ventricular system (see Figs. 8-103B, 8-104B, 8-105A, and 8-106C). Such reflections occur when the ultrasonic beam strikes the smooth ventricular wall perpendicularly or nearly so. Thus, one would assume that points and lines of brightness so produced might vary from moment to moment depending on the direction in which the transducer was pointed. This, however, is not the case for two reasons. First, fetal brain images are predominantly

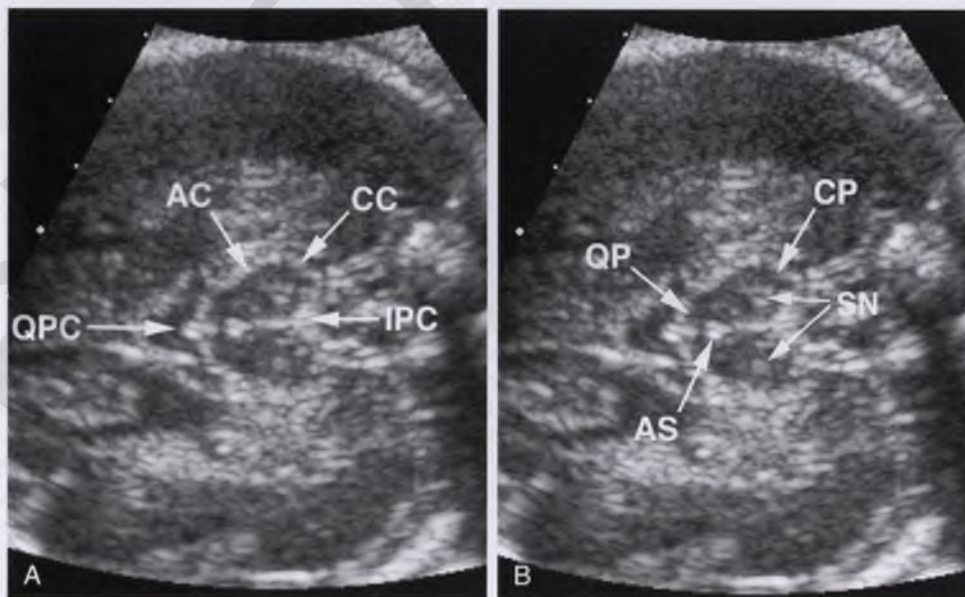


**FIG 8-110 A and B**, Sonograms demonstrating the midbrain. The midbrain is seen well because of the sharp outline provided by the brightly echogenic perimesencephalic cisterns (the leptomeninges provide the bright line of demarcation). These cisterns marginate the cerebral peduncles (CP) and the quadrigeminal plate (QP). AC, ambient cistern; AS, aqueduct of Sylvius; CC, crural cistern; IPC, interpeduncular cistern; QPC, quadrigeminal plate cistern. SN, substantia nigra.



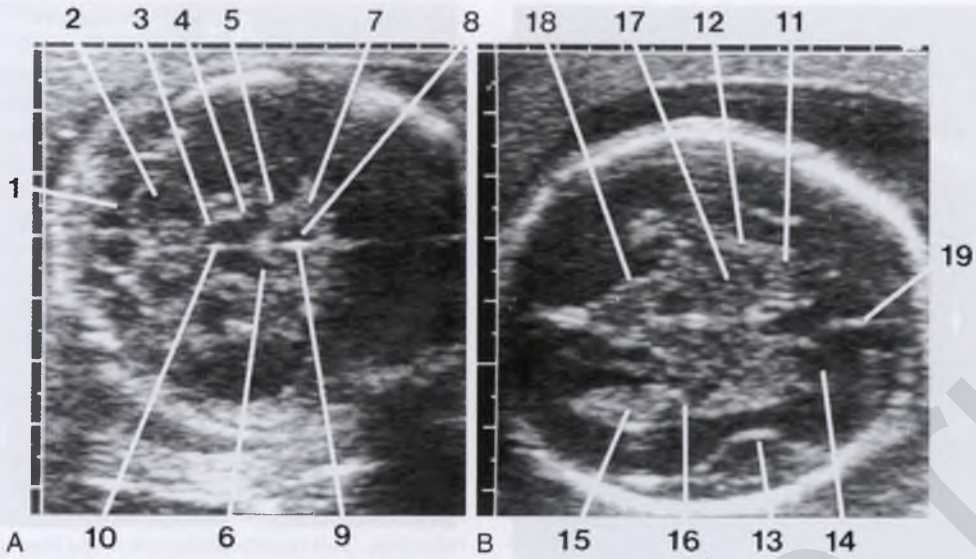


**FIG 8-111 A and B,** Transverse axial sonograms demonstrating many discrete neural structures. Note the varying echogenicities of the cisterns. Large cisterns (1, cisterna magna) have an appearance dominated by cerebrospinal fluid. Small cisterns (7, basal cisterns) are dominated by pia-arachnoid. 2, cerebellar hemisphere; 3, quadrigeminal cistern; 4, ambient cistern; 5, crural cistern; 6, interpeduncular cistern (note walls of basilar artery centrally in this cistern); 8, hypothalamus; 9, inferior recess of third ventricle; 10, sylvian aqueduct; 11, head of caudate; 12, lentiform nuclei; 13, lateral fissure; 14, frontal horn; 15, atrial choroid; 16, posterior limb of internal capsule; 17, thalamus; 18, tentorial hiatus; 19, falx cerebri.

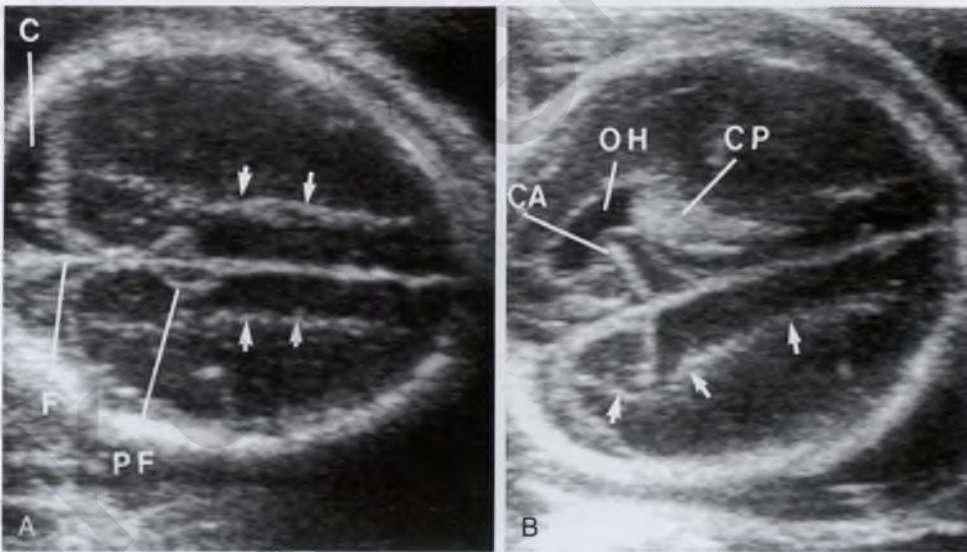


**FIG 8-112 A,** Transverse axial sonogram near the vertex. Bright linear echoes (*arrows*) often mistaken for lateral ventricles are clearly seen. Note that these echoes extend to the brain edge. C, convexity cistern with cerebrospinal fluid and hair-like bridging veins covered by brightly echogenic pia-arachnoid; F, falx; PF, parieto-occipital fissure. **B,** Off-axis scan through both the lateral ventricle and the linear echo (*arrows*) seen in **A**. The occipital horn (OH) is now well seen. Note again that the linear echo extends to the brain edge, whereas the occipital horn is entirely margined by brain tissue. CA, calcar avis; CP, choroid.



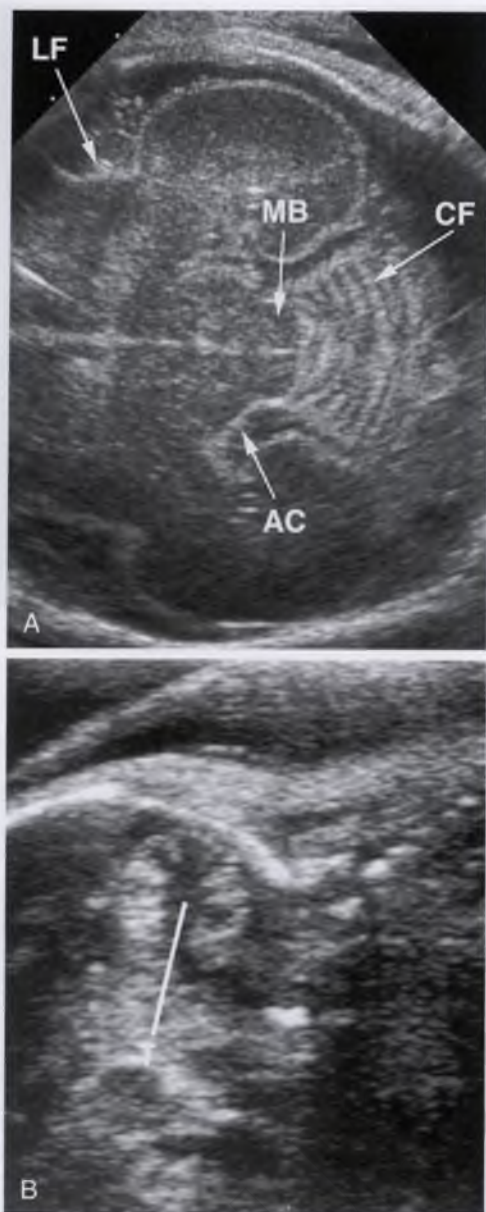


**FIG 8-113 A**, Posterior fossa view (transverse axial) demonstrating cerebellar folia (CF). AC, ambient cistern; LF, lateral fissure; MB, midbrain. **B**, Parasagittal sonogram of the posterior fossa. Cerebellar white matter tracts (T) are well seen. The bright margin of the cerebellum is “artificial” in that it is due to reflections from leptomeninges drawn into the cerebellum by folia formation (gray matter is hypoechoic).

produced in transverse axial planes (appropriate for both biparietal diameter and head circumference measurements) (see Fig. 8-103B) and less commonly coronal or parasagittal (see Fig. 8-106C) planes. In these planes, the beam tends to intersect the ventricular system perpendicularly at the same interfaces. Second, the curvature of the bony calvaria limits the number of axial, coronal, and parasagittal planes that can be achieved as a result of significant beam divergence when the beam intersects curved portions of calvaria. Thus, the specular reflections from the ventricular walls tend to be seen in stable locations and can be used as important and reproducible anatomic landmarks.

Additionally, within the substance of the brain, most notably in the region of the cerebral white matter tracks, other bright reflections are

noted (Figs. 8-108 to 8-110 and 8-115). Although these reflectors might be mistaken for the lateral ventricular walls, with which they are contiguous (see Figs. 8-109 and 8-112),<sup>110,113,119</sup> origins of these reflections are blood vessels draining the deeper white matter regions (see Figs. 8-108D, 8-109, 8-112, and 8-115).<sup>120</sup> Interestingly, pia accompanies these vessels as they course through the brain substance. Therefore, again it is the leptomeninges that account for bright echoes in the fetal brain. Thus, the brightly echoing structures of the fetal brain, including the surface echoes, cisterns, draining veins of the deep white matter, and choroid plexus, are all tied to the pia mater. As Dr. James Bowie observed regarding the grand unifying theory of bright echoes in the brain, “it’s all pia” (personal communication, 1991).

The sonographic “skeleton” of the developing fetal brain originates from the brightly reflective structures just considered. Using these structures as the framework, numerous discrete neural tissue areas are discernible sonographically (Figs. 8-110, 8-111, and 8-116).<sup>12</sup> As the brain develops, multiple areas of the telencephalon, diencephalon, midbrain, pons, and cerebellum become anatomically identifiable. They are recognized by variations in the echogenicity of specific nuclei and tracts that pass through these zones (see Figs. 8-109, 8-111, 8-113B, 8-114, 8-115A, and 8-116). Several brain nuclei, as well as some other areas of neural tissue, demonstrate a moderate increase in echo amplitude compared with surrounding brain elements (Figs. 8-109, 8-111, 8-116, and 8-117A). These nuclei demonstrate lower amplitude signals than choroid or leptomeninges. Among these structures are the caudate and lenticular nuclei, separated by the internal capsule. Less commonly, the claustrum, marginated by the extreme and external capsules, is visible. Similarly, the substantia nigra (see Fig. 8-110B) in the midbrain and dentate nuclei of the cerebellum (Fig. 8-111A, not labeled) are discernible. Also the pars ventralis (belly) of the pons is seen as a zone of moderate echogenicity as opposed to the pars dorsalis (tegmentum), which returns low-amplitude echoes (Fig. 8-118A).<sup>1</sup>

The appearance of the lateral ventricles undergoes characteristic changes throughout growth and development of the fetal brain. By 18 weeks, easily recognizable occipital horns and temporal horns are visible (see Fig. 8-106). The lateral ventricles have achieved their adult components. From this point onward, the lateral ventricles change in shape and proportion as influenced by neural tissues growing adjacent to their walls. For example, the growth of the caudate nucleus markedly reshapes the frontal horn of the lateral ventricles (see Fig. 8-106).<sup>121</sup> However, throughout the period of observation of fetal lateral ventricles (from 13 to 40 weeks), the size of the atria remains largely unchanged. The transverse diameter of the ventricular atrium at the level of the glomus of the choroid plexus shows an average dimension of approximately 7 mm and an upper limit of 10 mm throughout the second and third trimesters.<sup>122</sup> This is the most convenient area to recognize fetal ventricular enlargement, as is discussed in detail in the section on ventriculomegaly in Chapter 9.<sup>111,112,122</sup> The developing fetus is the most dynamic structure an imager will ever confront. Within this dynamic organism, there is only one structure that remains stable in size throughout the second and third trimesters. That structure is the ventricular atrium, and this stability is nature’s gift to the prenatal diagnostician.

It is important to note that the frontal (anterior) and occipital (posterior) horns of the lateral ventricles do not possess choroid plexus (see Figs. 8-104 through 8-106). Between 24 weeks and term, the telencephalon undergoes little structural change other than increased cortical growth and the consequent increase in convolutions (and thus sulcal markings), which can be recognized adjacent to the convexities (Fig. 8-119A and 8-120B).<sup>123</sup> The increase in brain volume causes the lateral ventricles, which are growing more slowly, to become progressively less conspicuous.



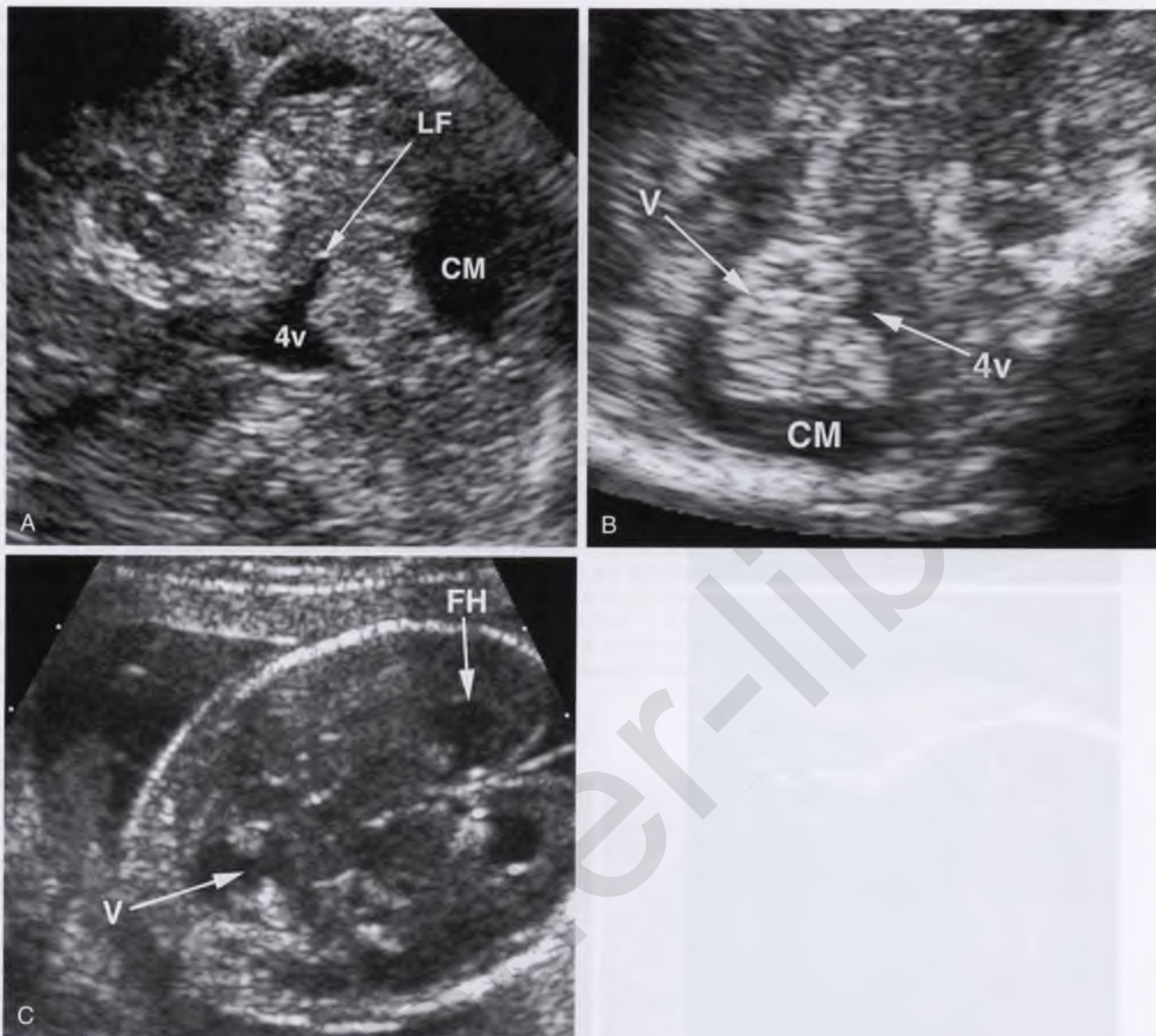


**FIG 8-114** Three images of the posterior fossa at different stages of cerebellar development. **A** and **B** are images of later fetuses whereas **C** is obtained in the early second trimester. **A**, Transverse axial sonogram of the posterior fossa demonstrating the fourth ventricle (4v) and the Luschka foramen (LF). Lying between the fourth ventricle and the cisterna magna (CM) is the fully developed inferior vermis. **B**, Parasagittal sonogram of the posterior fossa. The fully developed vermis (V) is seen. The fourth ventricle is outlined by the superior peduncle and ala lobula centralis superiorly and the nodule and tonsil inferiorly. The inferior vermis is well depicted between the fourth ventricle and cisterna magna (CM). Note that the vermis appears very brightly echogenic because of the large number of folia and, most importantly, the intervening leptomeninges covering the surfaces of the folia. **C**, Transverse axial sonogram of the posterior fossa demonstrating the fourth ventricle communicating freely with the cisterna magna across an incompletely formed inferior vermis (V). This is a normal finding at this early stage of pregnancy. FH, frontal horn.



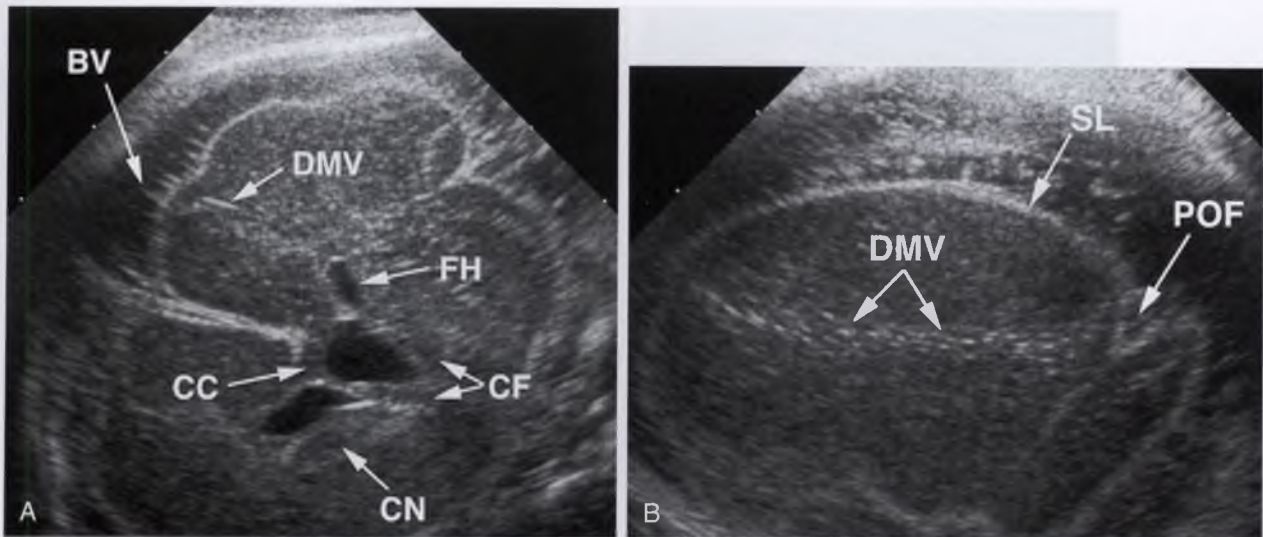


**FIG 8-115** **A**, Coronal plane. **B**, Parasagittal plane. The deep medullary veins (DMV) and the bridging veins (BV) are invested with pia mater and thus are brightly reflective. Brightly reflective surface leptomeninges (SL) demarcate the brain surface and help to delineate fissures and sulci such as the parieto-occipital fissure (POF). CC, corpus callosum; CF, columns of the fornix; CN, caudate nucleus; FH, frontal horn.

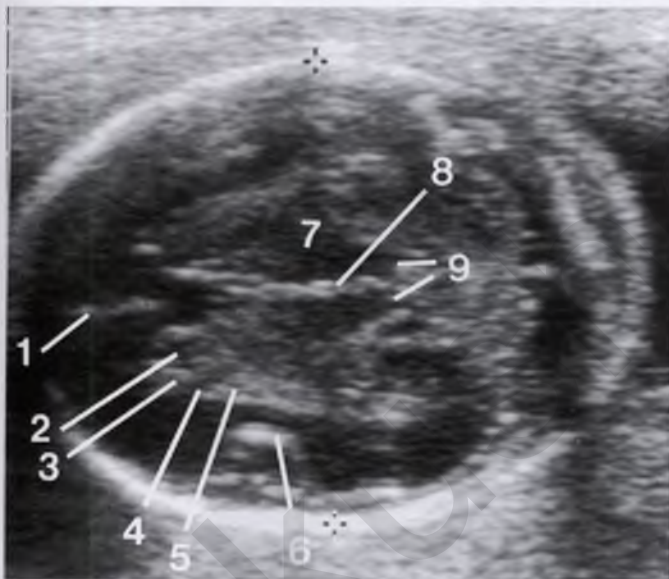


**FIG 8-116** Transverse axial sonogram. 1, falx; 2, frontal horn; 3, caudate head; 4, anterior limb of internal capsule; 5, lentiform nuclei; 6, lateral sulcus; 7, thalamus; 8, third ventricle; 9, quadrigeminal bodies.

As opposed to sulci, which are narrow and develop later as gyri form, fissures are broader, present earlier in development, and can be seen before 20 weeks.<sup>116</sup> Of the two that are commonly seen, the parieto-occipital fissure, an indentation medially adjacent to the interhemispheric cistern, is smaller (see Figs. 8-112A, 8-115B, and 8-119A). The lateral fissure (insula and sylvian fossa/fissure) is a deep groove in the lateral margin of the developing telencephalon.<sup>122,124,125</sup> The groove is seen as a smooth depression as early as 14 weeks (see Fig. 8-105C).<sup>116</sup> Subsequently, its appearance gradually changes as the frontoparietal and temporal opercula develop (see Figs. 8-109, 8-111, 8-113, 8-116, and 8-120).<sup>116</sup> This important fissure results in frequent confusion because it causes a portion of the brain surface to be invaginated deeply into the hemisphere (see Figs. 8-109, 8-111, 8-113, and 8-116). The

pia-arachnoid on the surface of the insula, the tissue at the base of the lateral fissure, generates a curvilinear reflection that appears to lie within the brain substance rather than at its “edge.” This echo is often mistaken for a specular reflection from the lateral wall of the lateral ventricle, an error leading to misdiagnoses of hydrocephalus. With progressive growth of the temporal and parietal lobes, this fissure progressively closes, burying the previously exposed insular cortex behind the developing temporal and parietal opercula (Figs. 8-120 and 8-121). By term (38 to 42 weeks), the lateral fissure closes and ultimately becomes the sylvian cistern complex.

Other fissures and sulci become visible at predictable times during fetal brain development. This developmental sequence, or the failure thereof, enables one to diagnose or exclude certain brain malformations associated with migrational abnormalities. Among these are either the absence of formation of fissures and sulci (lissencephalic anomalies) or the appearance of fissures and sulci in aberrant locations (dysplastic brain).<sup>116,126</sup> The calcarine fissure (sulcus) (see Fig. 8-108A) is associated with the parieto-occipital fissure. The calcarine fissure angles caudally from the midportion of the parieto-occipital fissure, creating a prominent fold in the medial occipital lobe (the two fissures form a “Y” lying on its side). The calcarine fissure’s greatest importance is that, as it grows, it indents the medial aspect of the occipital horn, thereby actually changing the shape of the ventricle at the junction of the atrium and occipital horn (the other piece of developing brain that greatly reshapes ventricular configuration is the caudate nucleus). The folded tissue is called the *calcar avis* (translated, the “bird’s heel” which it somewhat resembles [at least to the anatomist who described it—I would have called it the “bird’s beak”]) (see Figs. 8-112B and 8-120B). The calcarine fissure is easily seen on coronal sections of the posterior brain (see Fig. 8-108A). In the coronal plane one would think that it is the parieto-occipital fissure except that the coronal plan favors visualization of the calcarine fissure whereas the axial plane favors visualization of the parieto-occipital fissure (see Fig. 8-119B). The calcarine fissure (sulcus) becomes visible by the 24th week.<sup>116</sup> The cingulate sulcus, the sulcus that parallels the superior surface of the corpus callosum (see Fig. 8-118), also becomes visible at approximately the same time as the calcarine sulcus.<sup>116</sup> The cingulate sulcus is important in that



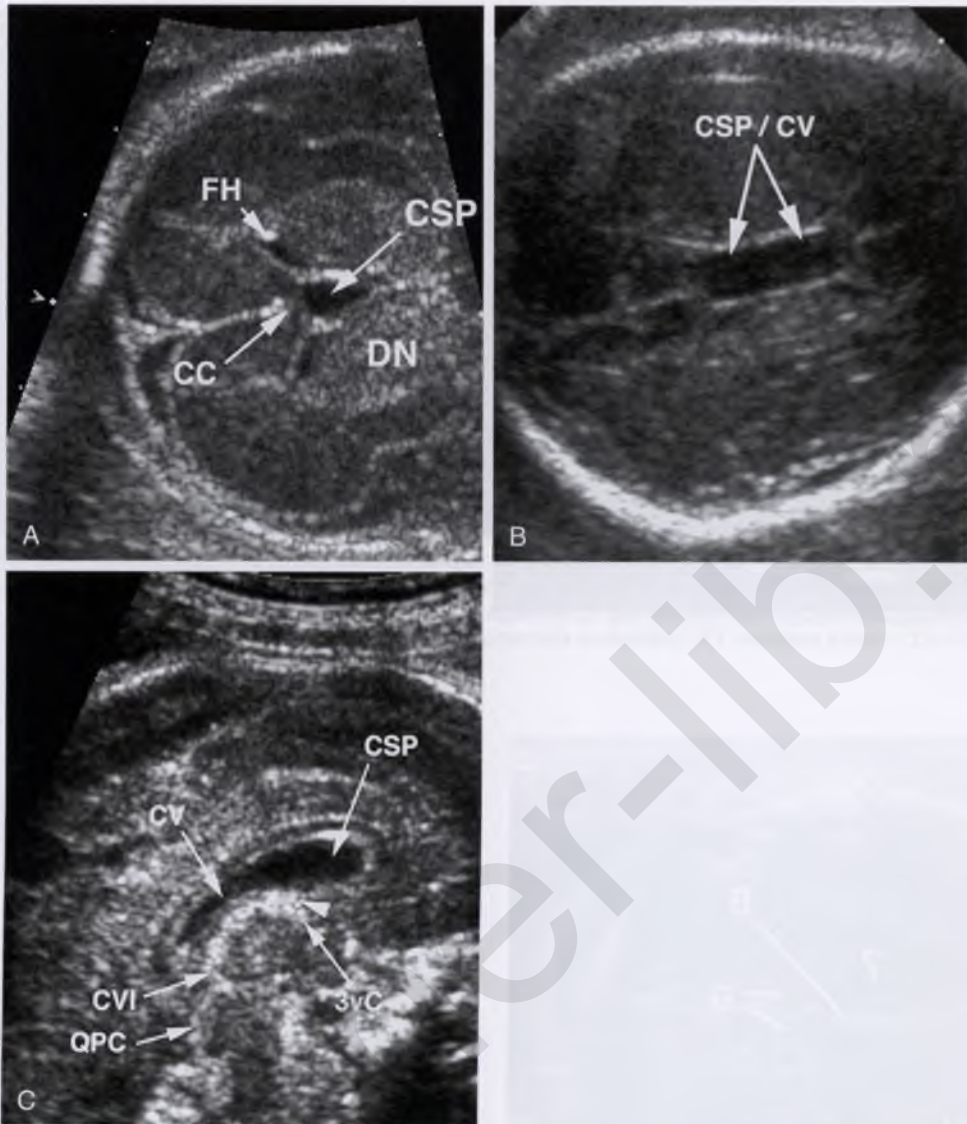


**FIG 8-117** Coronal (**A**), transverse axial (**B**), and midsagittal (**C**) sonograms of the cavum septi pellucidi/cavum vergae complex. **A**, In the coronal plane the cavum septi pellucidi (CSP) lies between the frontal horns of the lateral ventricle (FH). The genu of the corpus callosum (CC) marks its roof. DN, deep gray matter nuclei. **B**, An axial sonogram demonstrates a relatively large cavum septi pellucidi complex (CSP/CV). A line of division between these entities cannot be adequately drawn in this plane of section. **C**, In the midsagittal plane the line of division between the cavum septi pellucidi and cavum vergae is more readily determined. First, the cavae lie between the brightly echogenic choroid in the roof of the third ventricle (3vC) and the corpus callosum (not labeled). The cavum septi pellucidi (CSP) "ends" where the third ventricular choroid begins (*arrowhead*). Posterior to that point it is most appropriately called the *cavum vergae* (CV). The third ventricular choroid blends imperceptibly with the brightly echogenic leptomeninges in the cistern of the velum interpositum (CVI) and the quadrigeminal plate cistern (QPC). Occasionally there is also a "cavum of the velum interpositum" that can produce a cyst-like small mass inferior to the splenium of the corpus callosum. This is a normal variant.

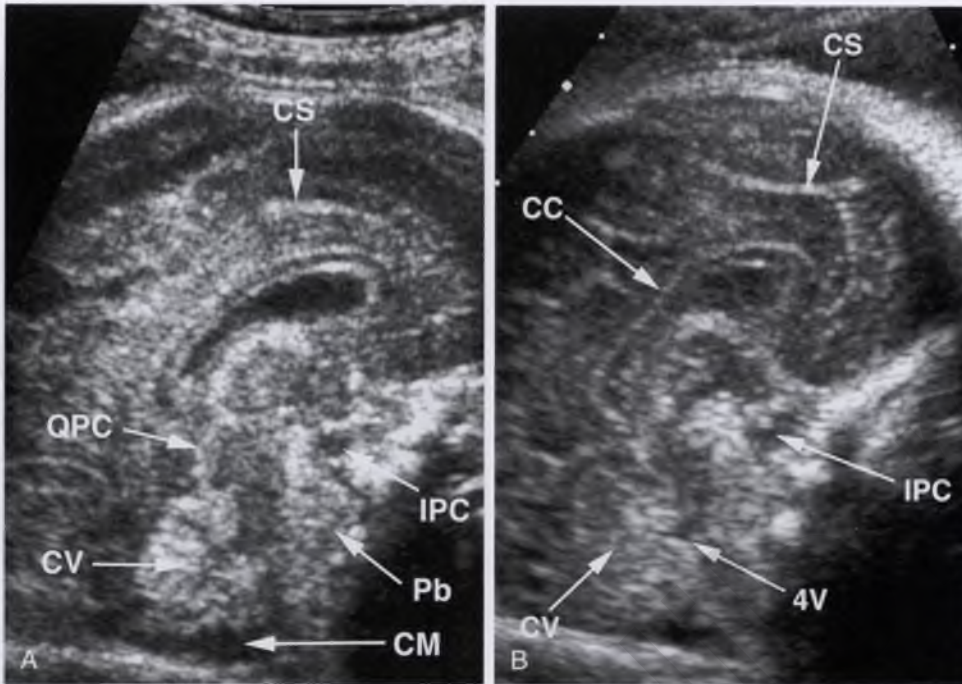


**FIG 8-118** Midsagittal sonograms of a younger (**A**) and older (**B**) fetus. The cingulate sulcus (CS) is readily seen. The cingulate gyrus (not labeled) lies between the cingulate sulcus and the corpus callosum (CC). In the older fetus more visible sulci along the medial frontal and parietal lobes are visible. CM cisterna magna; CV, cerebellar vermis; IPC, interpeduncular cistern; Pb, belly of pons; QPC, quadrigeminal plate cistern; 4V, fourth ventricle.

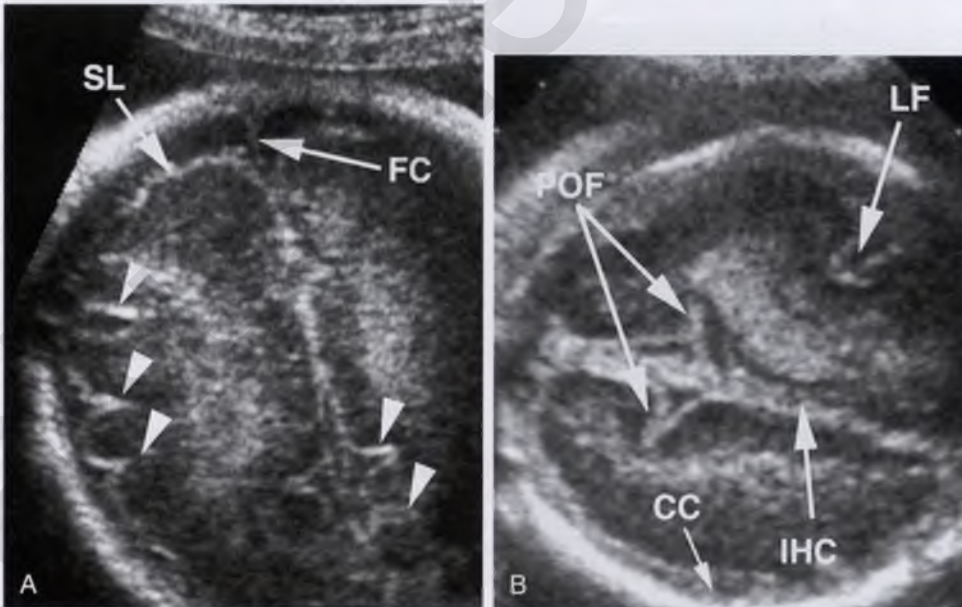


**FIG 8-119** **A**, Older fetus. **B**, Younger fetus. Sonograms concentrating on the brain surface. In the younger fetus the brain surface is relatively smooth, although some of the major developing fissures are visible. In the older fetus, numerous sulci and gyri are visible (*arrowheads*). CC, convexity cistern; FC, falx cerebri; IHC, interhemispheric cistern; LF, lateral fissure; POF, parieto-occipital fissure; SL, surface leptomeninges.



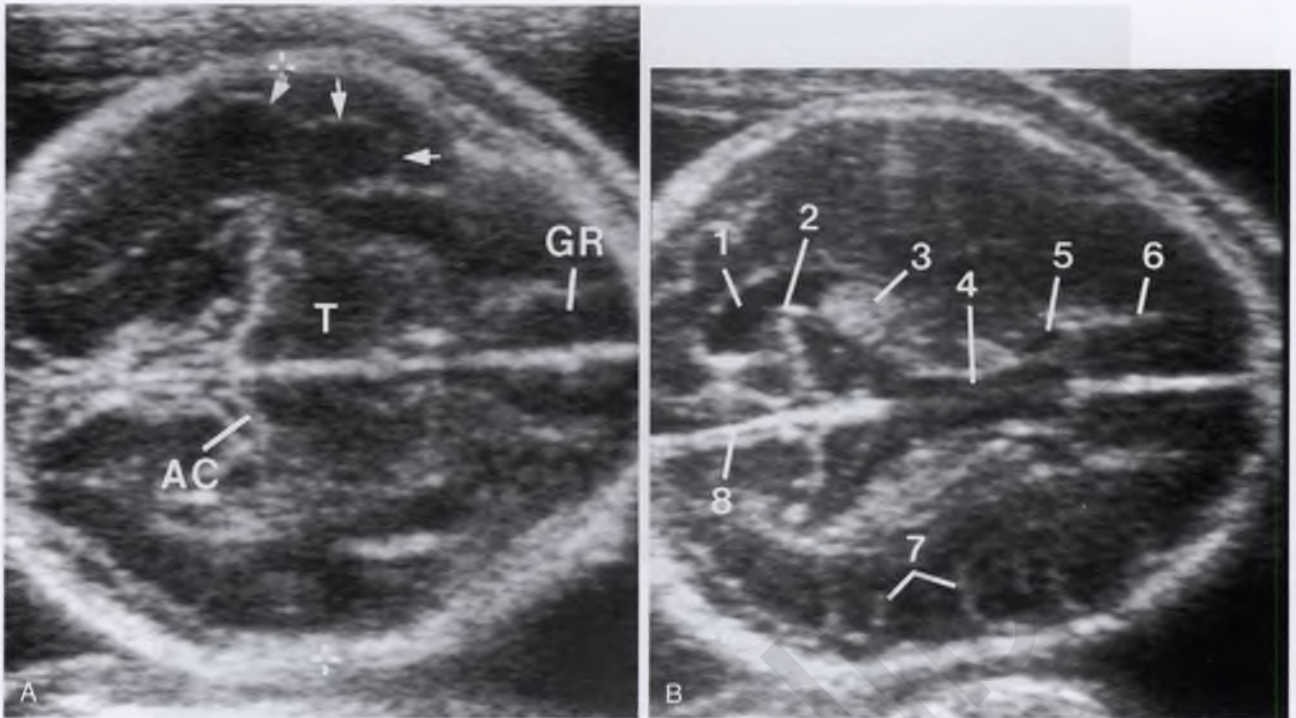


**FIG 8-120** Transverse axial sonograms of a fetus with little calcification of the calvaria (recessive osteogenesis imperfecta). **A**, Note the lack of near calvarial reverberation artifact enabling visualization of the near temporal lobe (*short arrows*) with greater clarity than the far temporal lobe. AC, ambient cistern; GR, gyrus rectus; T, thalamus. **B**, Note the clarity which with the near ventricle is visualized. 1, occipital horn; 2, calcar avis; 3, atrial choroid; 4, corpus callosum (it is very unusual to see so much of the corpus callosum in an axial plane); 5, frontal horn; 6, deep medullary veins; 7, sulci; 8, falx cerebri.

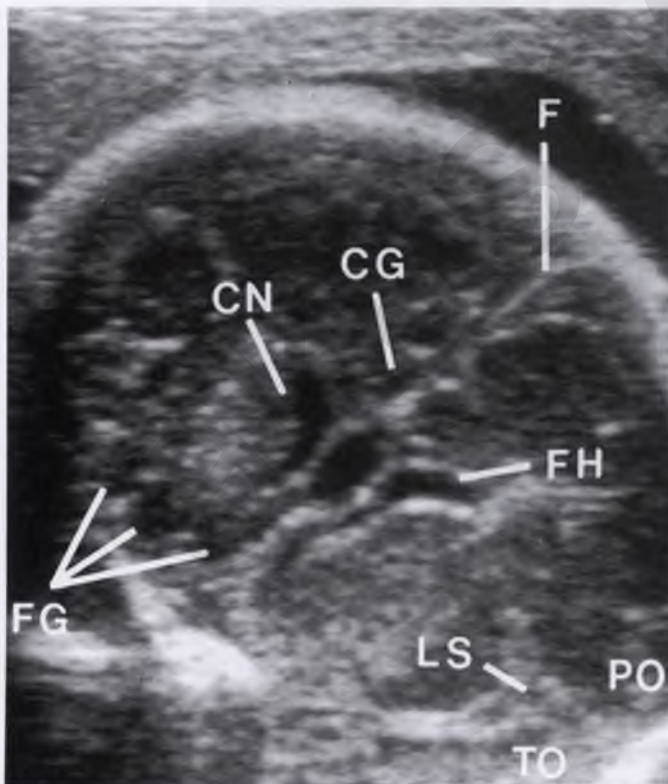


**FIG 8-121** Coronal sonogram, anterior. CG, cingulate gyrus; CN, caudate nucleus; F, falx; FG, frontal gyri; FH, frontal horn; LS, lateral sulcus; PO, parietal operculum; TO, temporal operculum.

it does not form when there is complete agenesis of the corpus callosum. Thus, the formation of the corpus callosum is the “causative” element determining sulcation of the medial frontoparietal cortex. As the cingulate sulcus is the first of the medial sulci to develop, its presence is helpful in excluding complete agenesis. Finally, the sulci over the convexities gradually become increasingly visible from the beginning of the third trimester onward.<sup>116</sup> Other recognizable sulci include those on the inferior frontal lobe that help define the gyrus rectus (see Figs. 8-120 and 8-121).

A structure of great importance in fetal neuroanatomy is the corpus callosum (Fig. 8-122). The corpus callosum begins its development between the 10th and 11th weeks of gestation. It has achieved its adult configuration by the end of the 17th week. The development starts at the genu and proceeds posteriorly to the splenium. However, the rostrum (the most anterior part of the corpus callosum) forms last. The rostrum is not usually seen on prenatal sonograms. Sonographic imaging of the corpus callosum for the detection of abnormal formation should not be attempted in earnest until after 17 weeks (see Fig. 8-122D). The best views of the corpus callosum are obtained in the midsagittal plane (see Figs. 8-118B and 8-122B). However, information about the corpus callosum can be obtained in other planes of section. The body and genu can be seen in coronal and axial planes (see Figs. 8-115A, 8-117A, and 8-122A). Unfortunately, when partial agenesis (dysgenesis) of the corpus callosum is present, typically the splenium and distal body are missing. Importantly, the splenium can be imaged in axial planes of section, although with some difficulty, because the plane of section must approach from the occipital region (see Fig. 8-122C). Occipital ossification and the smaller posterior fontanelle make this approach difficult at times.



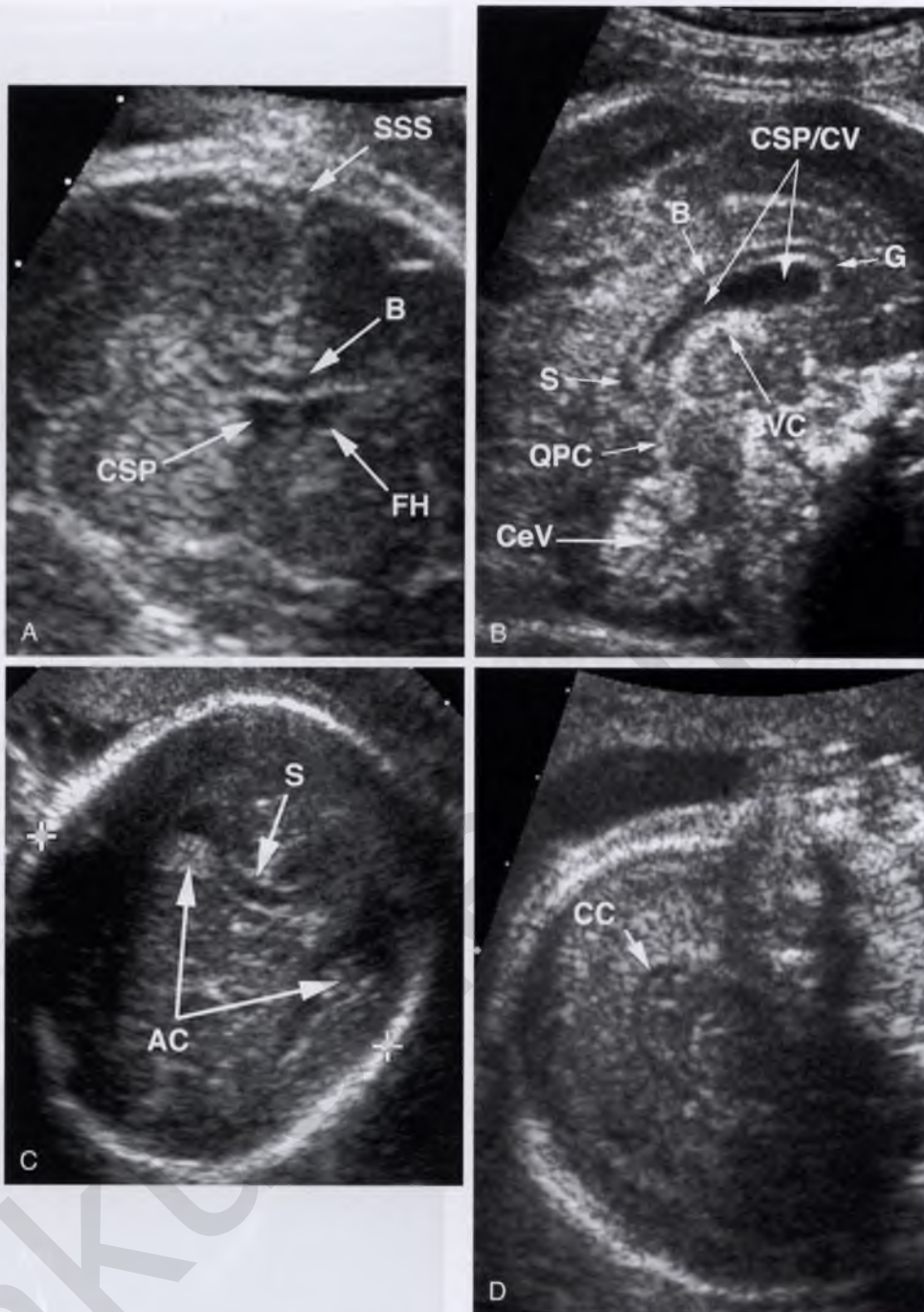


**FIG 8-122** **A**, Coronal section through the body (B) of the corpus callosum. **B**, Midsagittal sonogram shows the corpus callosum to best advantage. **C**, Axial view "aimed" at the occiput demonstrates the splenium (S), the most crucial portion of the corpus callosum to visualize. In an "occiput up" fetus, a midsagittal sonogram of the corpus callosum would be nearly impossible to obtain. **D**, A 19-week fetus with corpus callosum well demonstrated. AC, atrial choroid; B, body; CC, corpus callosum; CeV, vermis of the cerebellum; CSP, cavum septi pellucidi; CV, cavum vergae; FH, frontal horn; G, genu; QPC, quadrigeminal plate cistern; S, splenium; SSS, superior sagittal sinus; 3VC, choroid plexus in the roof of the third ventricle.



An extremely helpful structure, both in terms of visualization of the corpus callosum and for excluding complete agenesis of the corpus callosum, is the cavum septi pellucidi/cavum vergae complex (see Fig. 8-117). The cavum septi pellucidi is the median cleft between the two laminae of the septum pellucidum. Sometimes called the fifth ventricle, it is not. It is not lined by ependyma. The cavum vergae (described by the Italian anatomist, Andrea Verga) is the posterior extension of the cavum septi pellucidi (see Fig. 8-117C). The actual line of division is the fornix, but as the fornix is not visible in a midsagittal plane, the Monroe foramen can be used to demarcate the end of one cavum and the beginning of the other (see Fig. 8-117C). The corpus callosum is the roof of the cava, and the roof of the third ventricle is the floor of the cava. Fortunately, we have an excellent marker of the roof of the third ventricle. This is because the third ventricular choroid recurves along the roof (see Figs. 8-117C and 8-122B). The most anterior extent of the third ventricular choroid (see Fig. 8-117C) marks the position of the Monroe foramen and thus is a very reasonable dividing line between the cavum septi pellucidi and the cavum vergae. In axial planes of section, a reasonable line of division cannot be drawn (see Fig. 8-117B). A final aspect of callosal development is that formation of the cingulate gyrus (and thus the cingulate sulcus) is dependent on the formation of the corpus callosum (see Fig. 8-118).

The cerebellar vermis, like the corpus callosum, is also a late structure to develop (see Fig. 8-114). Of the major parts of the fetal brain to develop, the cerebellar vermis is last in line. The cerebellum is well imaged throughout the second and third trimesters (except near term when occipital ossification is sufficiently great to thwart passage of the acoustic beam) (see Figs. 8-113, 8-114, 8-118, and 8-122B). Like the corpus callosum, the cerebellar vermis develops from “front to back.” Thus, the inferior portion of the vermis does not complete its formation until relatively late (in the range of the 18th gestational week). Sonographically, one detects the inferior vermis lying between the fourth ventricle and the cisterna magna, or Blake pouch (see Figs. 8-114A, 8-114B, and 8-118A). In midsagittal planes the fourth ventricle is outlined by the superior peduncle and ala lobula centralis superiorly and the nodule and tonsil inferiorly. The inferior vermis is well depicted between the fourth ventricle and cisterna magna. Note that the vermis appears very brightly echogenic because of its large number of folia (see Fig. 8-114B) and, most importantly, the intervening leptomeninges covering the surfaces of the folia. By contrast, in a fetus 16 to 17 weeks old, a transverse axial sonogram of the posterior fossa typically demonstrates the fourth ventricle communicating freely with the cisterna magna across an incompletely formed inferior vermis (see Fig. 8-114C). This is a normal finding at this early stage of pregnancy. The cerebellar hemispheres are outlined by the fluid in the cisterna magna (see Fig. 8-114). The fourth ventricle can be depicted throughout the second and third trimesters unless technical imaging problems confound its visualization (the “fourth ventricle” is even seen in the first trimester [see Fig. 8-4]).

Blake pouch is clearly seen in the majority of fetuses during the second trimester. One sees two septa extending posteriorly from the midcerebellum and crossing the cisterna magna. At one point, these septa were thought to represent separated dural leaves. However, when dural leaves separate they do so to house a venous sinus. This is not the origin of these septa. Robinson and Goldstein showed these septa to represent Blake pouch.<sup>127</sup> Blake pouch is an early embryologic structure that persists. It is a posteriorly positioned membranous structure protruding from the region of the developing fourth ventricle. Details of the formation of this structure are discussed in the original article. Other landmarks in the posterior fossa (like the torcular herophili) become important when addressing the differential diagnosis of posterior fossa cysts. These landmarks are seen to better advantage with

MRI. All posterior fossa cysts should be imaged with MRI before a diagnosis is offered, in the opinion of these authors.

One of the difficulties in mastering the sonographic anatomy of intracranial structures is the usual inability to see both hemispheres of the brain symmetrically.<sup>128</sup> The hemisphere nearest to the transducer is virtually always “clouded” over by reverberation artifacts generated as the acoustic beam passes through the near calvarial wall. Calvarial ossification appears to be at the root of this artifact because the artifact is markedly reduced in fetuses with the most severe form of osteogenesis imperfecta or other bone dysplasias wherein calvarial ossification is nearly absent (see Fig. 8-120). Unfortunately, essentially all other fetuses possess calvarial ossification. The following rule should always be applied: the sonologist must assume that the intracranial anatomy of the fetus is asymmetric, whether normal or abnormal, unless images document an asymmetry. Visualization of the near hemisphere requires that we use bone-free windows in the near calvaria. The “windows” are the anterolateral and posterolateral fontanelles in axial approach or the anterior and posterior fontanelles in coronal imaging. Because the anterolateral and posterolateral fontanelles are nearer to the base of the brain than to the vertex, using the anterolateral and posterolateral fontanelles results in images of the near hemisphere that are off axis to the axial plane (at least in most images). Therefore, caution must be exercised in the interpretation of the off-axis planes, particularly when judging the size of the near ventricular atrium.

As noted earlier, the fetal spine is seen well from 15 to 16 weeks onward. However, we often delay evaluation for suspected myelomeningocele until 18 to 20 weeks of gestation because of the significant and favorable maturational changes in the spine that occur during this period. The posterior ossification centers begin at the base of the transverse processes (see Figs. 8-58 to 8-63). As ossification progresses, the laminae become visible (see Figs. 8-59 to 8-61 and 8-65). The inward angulation of the normal laminae is the opposite of the outward splaying of the laminae seen in spina bifida, an optimal situation for detecting this anomaly. Spina bifida is the bony anomaly seen in all myelomeningoceles. The spinal cord neural tissue, like that of most brain tissue, is echogenic (see Fig. 8-65). The conus medullaris (see Fig. 8-65C) and the craniocervical junction (Fig. 8-123) can be seen,

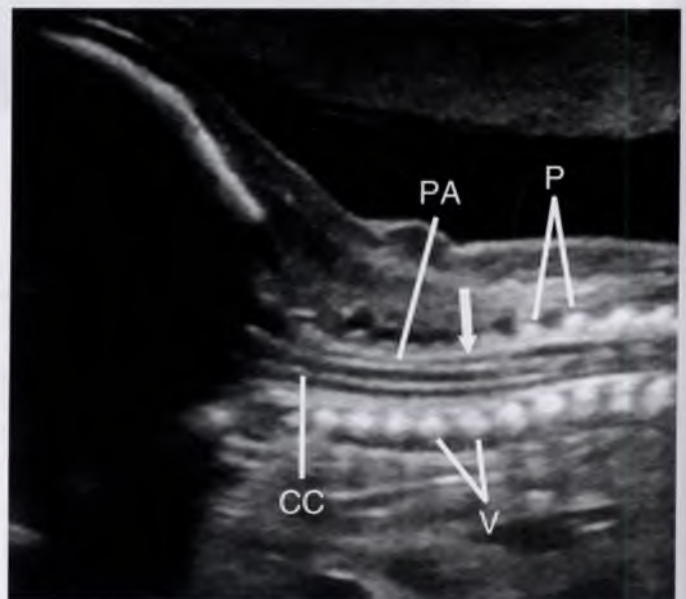


**FIG 8-123** Longitudinal sonogram at the craniocervical junction demonstrating the cervical cord (CC). (Arrow), dura; P, posterior arch ossification centers; PA, pia-arachnoid; V, vertebral body ossification centers.



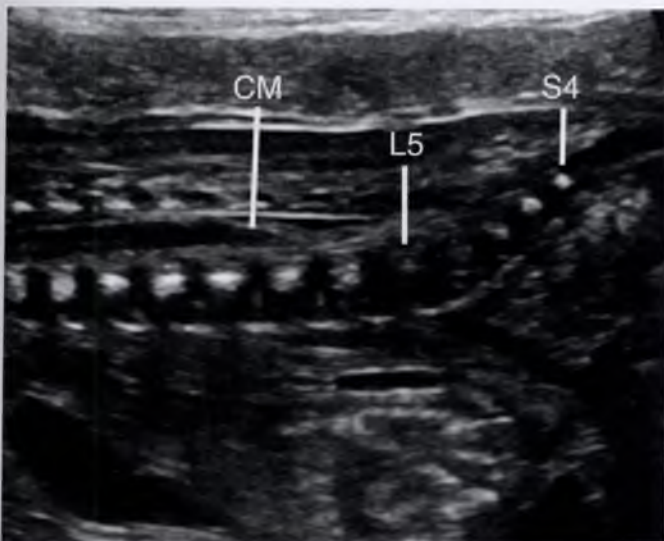


**FIG 8-124** Sagittal plane of section of the spine in a 20 weeks' gestation fetus. The spinal level can be determined by counting up from the last ossified vertebral segment (assumed to be S4 in the second trimester and S5 in the third trimester). In this case the S4 ossification center is the most distal segment present and is used to count cephalad to identify L5. Note the conus medullaris (CM) at the L2-L3 level.

albeit inconsistently, in nearly all fetuses by 18 to 20 menstrual weeks. The tissues surrounding the cord (leptomeninges) are brightly echogenic, as are those that surround the brain, and the dura is usually also seen discretely as a linear bright reflector (see Fig. 8-65 and 8-66). In fetuses with myelomeningoceles, determination of the most cephalic spinal level of the lesion is an important factor in prognosis. This level can be determined by counting up from the last ossified vertebral segment (assumed to be S4 in the second trimester and S5 in the third trimester) (Fig. 8-124).

## REFERENCES

1. Yousefzadeh DK, Naidich TP: US anatomy of the posterior fossa in children: correlation with brain sections. *Radiology* 156(2):353–361, 1985.
2. Naidich TP, Gusnard DA, Yousefzadeh DK: Sonography of the internal capsule and basal ganglia in infants: 1. Coronal sections. *AJNR Am J Neuroradiol* 6(6):909–917, 1985.
3. Amin RS, Nikolaidis P, Kawashima A, et al: Normal anatomy of the fetus at MR imaging. *Radiographics* 19(Spec No):S201–S214, 1999.
4. Coakley FV, Glenn OA, Qayyum A, et al: Fetal MRI: a developing technique for the developing patient. *AJR Am J Roentgenol* 182(1):243–252, 2004.
5. Glenn OA: Fetal central nervous system MR imaging. *Neuroimaging Clin North Am* 16(1):1–17, vii, 2006.
6. Levine D, Smith AS, McKenzie C: Tips and tricks of fetal MR imaging. *Radiol Clin North Am* 41(4):729–745, 2003.
7. Trop I, Levine D: Normal fetal anatomy as visualized with fast magnetic resonance imaging. *Top Magn Reson Imaging* 12(1):3–17, 2001.
8. Filly RA, Callen PW: Ultrasonographic evaluation of normal fetal anatomy. In Sanders RC, James AE, editors: *The Principles and Practice of Ultrasonography in Obstetrics and Gynecology*, ed 2, New York, 1980, Appleton Century Crofts.
9. Simpson DH, Burns PN, Averkiou MA: Techniques for perfusion imaging with microbubble contrast agents. *IEEE Trans Ultrason Ferroelectr Freq Control* 48(6):1483–1494, 2001.
10. Monteagudo A, Timor-Tritsch IE: First trimester anatomy scan: pushing the limits. What can we see now? *Curr Opin Obstet Gynecol* 15(2):131–141, 2003.

11. Souka AP, Nicolaides KH: Diagnosis of fetal abnormalities at the 10-14-week scan. *Ultrasound Obstet Gynecol* 10(6):429–442, 1997.
12. Timor-Tritsch IE: Transvaginal sonographic evaluation of fetal anatomy at 14 to 16 weeks. Why is this technique not attractive in the United States? *J Ultrasound Med* 20(7):705–709, 2001.
13. Mahony BS, Filly RA: High-resolution sonographic assessment of the fetal extremities. *J Ultrasound Med* 3(11):489–498, 1984.
14. Cooperberg PL, Chow T, Kite V, Austin S: Biparietal diameter: a comparison of real time and conventional B scan techniques. *J Clin Ultrasound* 4(6):421–423, 1976.
15. Docker MF, Settattree RS: Comparison between linear array real time ultrasonic scanning and conventional compound scanning in the measurement of the fetal biparietal diameter. *Br J Obstet Gynaecol* 84(12):924–929, 1977.
16. Filly RA: Sonographic anatomy of the normal fetus. In Harrison MR, Golbus MS, Filly RA, editors: *The Unborn Patient: Prenatal Diagnosis and Treatment*, ed 2, Philadelphia, 1991, WB Saunders.
17. Benacerraf BR, Shipp TD, Bromley B: Three-dimensional US of the fetus: volume imaging. *Radiology* 238(3):988–996, 2006.
18. Dyson RL, Pretorius DH, Budorick NE, et al: Three-dimensional ultrasound in the evaluation of fetal anomalies. *Ultrasound Obstet Gynecol* 16(4):321–328, 2000.
19. Goncalves LF, Lee W, Espinoza J, Romero R: Three- and 4-dimensional ultrasound in obstetric practice: does it help? *J Ultrasound Med* 24(12):1599–1624, 2005.
20. Bowie JD, Rosenberg ER, Andreotti RF, Fields SI: The changing sonographic appearance of fetal kidneys during pregnancy. *J Ultrasound Med* 2(11):505–507, 1983.
21. Hata T, Yonehara T, Aoki S, et al: Three-dimensional sonographic visualization of the fetal face. *AJR Am J Roentgenol* 170(2):481–483, 1998.
22. Rotten D, Levallant JM: Two- and three-dimensional sonographic assessment of the fetal face. 2. Analysis of cleft lip, alveolus and palate. *Ultrasound Obstet Gynecol* 24(4):402–411, 2004.
23. Rotten D, Levallant JM: Two- and three-dimensional sonographic assessment of the fetal face. 1. A systematic analysis of the normal face. *Ultrasound Obstet Gynecol* 23(3):224–231, 2004.
24. Birnholz JC: The fetal external ear. *Radiology* 147(3):819–821, 1983.
25. Fink IJ, Chinn DH, Callen PW: A potential pitfall in the ultrasonographic diagnosis of fetal encephalocele. *J Ultrasound Med* 2(7):313–314, 1983.
26. Elejalde BR, de Elejalde MM, Heitman T: Visualization of the fetal genitalia by ultrasonography: a review of the literature and analysis of its accuracy and ethical implications. *J Ultrasound Med* 4(12):633–639, 1985.
27. Birnholz JC: Determination of fetal sex. *N Engl J Med* 309(16):942–944, 1983.
28. Natsuyama E: Sonographic determination of fetal sex from twelve weeks of gestation. *Am J Obstet Gynecol* 149(7):748–757, 1984.
29. Mahony BS, Filly RA, Callen PW: Amnionicity and chorionicity in twin pregnancies: prediction using ultrasound. *Radiology* 155(1):205–209, 1985.
30. Filly RA, Golbus MS: Ultrasonography of the normal and pathologic fetal skeleton. *Radiol Clin North Am* 20(2):311–323, 1982.
31. Filly RA, Golbus MS, Carey JC, Hall JG: Short-limbed dwarfism: ultrasonographic diagnosis by mensuration of fetal femoral length. *Radiology* 138(3):653–656, 1981.
32. O'Brien GD, Queenan JT, Campbell S: Assessment of gestational age in the second trimester by real-time ultrasound measurement of the femur length. *Am J Obstet Gynecol* 139(5):540–545, 1981.
33. Jeanty P, Kirkpatrick C, Dramaix-Wilmet M, Struyven J: Ultrasonic evaluation of fetal limb growth. *Radiology* 140(1):165–168, 1981.
34. Meyer DB, O'Rahilly R: Roentgenographic investigation of the human skeleton during early fetal life. *Am J Roentgenol Radium Ther Nucl Med* 76(3):455–468, 1956.
35. Bagnall KM, Harris PF, Jones PR: A radiographic study of the human fetal spine. 2. The sequence of development of ossification centres in the vertebral column. *J Anat* 124(Pt 3):791–802, 1977.



36. Garjian KV, Pretorius DH, Budorick NE, et al: Fetal skeletal dysplasia: three-dimensional US—initial experience. *Radiology* 214(3):717–723, 2000.
37. Riccabona M, Johnson D, Pretorius DH, Nelson TR: Three dimensional ultrasound: display modalities in the fetal spine and thorax. *Eur J Radiol* 22(2):141–145, 1996.
38. Yanagihara T, Hata T: Three-dimensional sonographic visualization of fetal skeleton in the second trimester of pregnancy. *Gynecol Obstet Invest* 49(1):12–16, 2000.
39. Filly RA, Simpson GE, Linkowski G: Fetal spine morphology and maturation during the second trimester. Sonographic evaluation. *J Ultrasound Med* 6(11):631–636, 1987.
40. Abrams SL, Filly RA: Curvature of the fetal femur: a normal sonographic finding. *Radiology* 156(2):490, 1985.
41. Yarkoni S, Schmidt W, Jeanty P, et al: Clavicular measurement: a new biometric parameter for fetal evaluation. *J Ultrasound Med* 4(9):467–470, 1985.
42. Jeanty P, Romero R, d'Alton M, et al: In utero sonographic detection of hand and foot deformities. *J Ultrasound Med* 4(11):595–601, 1985.
43. Benacerraf BR, Frigoletto FD: Prenatal ultrasound diagnosis of clubfoot. *Radiology* 155(1):211–213, 1985.
44. Hashimoto BE, Filly RA, Callen PW: Sonographic diagnosis of clubfoot in utero. *J Ultrasound Med* 5(2):81–83, 1986.
45. Chinn DH, Bolding DB, Callen PW, et al: Ultrasonographic identification of fetal lower extremity epiphyseal ossification centers. *Radiology* 147(3):815–818, 1983.
46. Mahony BS, Callen PW, Filly RA: The distal femoral epiphyseal ossification center in the assessment of third-trimester menstrual age: sonographic identification and measurement. *Radiology* 155(1):201–204, 1985.
47. Goldstein RB, Filly RA, Simpson G: Pitfalls in femur length measurements. *J Ultrasound Med* 6(4):203–207, 1987.
48. Jeanty P, Cantraine F, Cousaert E, et al: The binocular distance: a new way to estimate fetal age. *J Ultrasound Med* 3(6):241–243, 1984.
49. Dennis MA, Drose JA, Pretorius DH, Manco-Johnson ML: Normal fetal sacrum simulating spina bifida: "pseudodysraphism." *Radiology* 155(3):751–754, 1985.
50. Abrams SL, Filly RA: Congenital vertebral malformations: prenatal diagnosis using ultrasonography. *Radiology* 155(3):762, 1985.
51. Birnholz JC: Fetal lumbar spine: measuring axial growth with US. *Radiology* 158(3):805–807, 1986.
52. Hashimoto BE, Mahony BS, Filly RA, et al: Sonography, a complementary examination to alpha-fetoprotein testing for fetal neural tube defects. *J Ultrasound Med* 4(6):307–310, 1985.
53. Brown BS: The prenatal ultrasonographic diagnosis of osteogenesis imperfecta lethalis. *J Can Assoc Radiol* 35(1):63–66, 1984.
54. Kousseff BG, Mulivor RA: Prenatal diagnosis of hypophosphatasia. *Obstet Gynecol* 57(6 Suppl):9S–12S, 1981.
55. Merz E, Goldhofer W: Sonographic diagnosis of lethal osteogenesis imperfecta in the second trimester: case report and review. *J Clin Ultrasound* 14(5):380–383, 1986.
56. Mahony BS, Filly RA, Cooperberg PL: Antenatal sonographic diagnosis of achondrogenesis. *J Ultrasound Med* 3(7):333–335, 1984.
57. Rosenthal SJ, Filly RA, Callen PW, Sommer FG: Fetal pseudoascites. *Radiology* 131(1):195–197, 1979.
58. Hashimoto BE, Filly RA, Callen PW: Fetal pseudoascites: further anatomic observations. *J Ultrasound Med* 5(3):151–152, 1986.
59. Daffos F: Fetal blood sampling under ultrasound guidance. In Harrison MR, Golbus MS, Filly RA, editors: *The Unborn Patient: Prenatal Diagnosis and Treatment*, ed 2, Philadelphia, 1991, WB Saunders.
60. Moore KL: The placenta and fetal membranes. In Moore KL, editor: *The Developing Human: Clinically Oriented Embryology*, ed 4, Philadelphia, 1988, WB Saunders.
61. Chinn DH, Filly RA, Callen PW: Ultrasonic evaluation of fetal umbilical and hepatic vascular anatomy. *Radiology* 144(1):153–157, 1982.
62. Barron DH: The changes in the fetal circulation at birth. *Physiol Rev* 24:277–295, 1944.
63. Emery JL: Functional asymmetry of the liver. *Ann N Y Acad Sci* 111:37–44, 1963.
64. Marks WM, Filly RA, Callen PW: Ultrasonic anatomy of the liver: a review with new applications. *J Clin Ultrasound* 7(2):137–146, 1979.
65. Gupta SC, Gupta CD, Arora AK: Intrahepatic branching patterns of portal vein. A study by corrosion cast. *Gastroenterology* 72(4 Pt 1):621–624, 1977.
66. Rosen MS, Reich SB: Umbilical venous catheterization in the newborn: identification of correct positioning. *Radiology* 95(2):335–340, 1970.
67. Hattan RA, Rees GK, Johnson ML: Normal fetal anatomy. *Radiol Clin North Am* 20(2):271–284, 1982.
68. American Institute of Ultrasound in Medicine: AIUM practice guideline for the performance of obstetric ultrasound examination. *J Ultrasound Med* 32(6):1083–1101, 2013.
69. Goldstein RB, Callen PW: Ultrasound evaluation of the fetal thorax and abdomen. In Callen PW, editor: *Ultrasonography in Obstetrics and Gynecology*, ed 2, Philadelphia, 1988, WB Saunders.
70. Cooper C, Mahony BS, Bowie JD, et al: Ultrasound evaluation of the normal fetal upper airway and esophagus. *J Ultrasound Med* 4(7):343–346, 1985.
71. Pritchard JA: Fetal swallowing and amniotic fluid volume. *Obstet Gynecol* 28(5):606–610, 1966.
72. Abramovich DR: Fetal factors influencing the volume and composition of liquor amnii. *J Obstet Gynaecol Br Commonw* 77(10):865–877, 1970.
73. Pretorius DH, Meier PR, Johnson ML: Diagnosis of esophageal atresia in utero. *J Ultrasound Med* 2(10):475–476, 1983.
74. Gross BH, Filly RA: Potential for a normal fetal stomach to simulate the sonographic "double bubble" sign. *J Can Assoc Radiol* 33(1):39–40, 1982.
75. Grand RJ, Watkins JB, Torti FM: Development of the human gastrointestinal tract. A review. *Gastroenterology* 70(5 Pt 1):790–810, 1976.
76. Manco LG, Nunan FA, Jr, Sohnen H, Jacobs EJ: Fetal small bowel simulating an abdominal mass at sonography. *J Clin Ultrasound* 14(5):404–407, 1986.
77. Fakhry J, Reiser M, Shapiro LR, et al: Increased echogenicity in the lower fetal abdomen: a common normal variant in the second trimester. *J Ultrasound Med* 5(9):489–492, 1986.
78. Al-Kouatly HB, Chasen ST, Streltsoff J, Chervenak FA: The clinical significance of fetal echogenic bowel. *Am J Obstet Gynecol* 185(5):1035–1038, 2001.
79. Kesrouani AK, Guibourdenche J, Muller F, et al: Etiology and outcome of fetal echogenic bowel. Ten years of experience. *Fetal Diagn Ther* 18(4):240–246, 2003.
80. Vincoff NS, Callen PW, Smith-Bindman R, Goldstein RB: Effect of ultrasound transducer frequency on the appearance of the fetal bowel. *J Ultrasound Med* 18(12):799–803, quiz 805–806, 1999.
81. Ziliani M, Fernandez S: Correlation of ultrasonic images of fetal intestine with gestational age and fetal maturity. *Obstet Gynecol* 62(5):569–573, 1983.
82. Nyberg DA, Mack LA, Patten RM, Cyr DR: Fetal bowel. Normal sonographic findings. *J Ultrasound Med* 6(1):3–6, 1987.
83. Crelin ES: *Functional Anatomy of the Newborn*, New Haven, CT, 1973, Yale University Press.
84. Schmidt W, Yarkoni S, Jeanty P, et al: Sonographic measurements of the fetal spleen: clinical implications. *J Ultrasound Med* 4(12):667–672, 1985.
85. Potter EL: *Pathology of the Fetus and Infant*, Chicago, 1961, Year Book Medical.
86. Gruenwald P, Hoang Ngoc M: Evaluation of body and organ weights in perinatal pathology. I. Normal standards derived from autopsies. *Am J Clin Pathol* 34:247–253, 1960.
87. Mittlestaedt CA: Ultrasound of the spleen. *Semin Ultrasound* 2:233, 1981.
88. Fried AM, Loh FK, Umer MA, et al: Echogenicity of fetal lung: relation to fetal age and maturity. *AJR Am J Roentgenol* 145(3):591–594, 1985.
89. Cayea PD, Grant DC, Doubilet PM, Jones TB: Prediction of fetal lung maturity: inaccuracy of study using conventional ultrasound instruments. *Radiology* 155(2):473–475, 1985.
90. Lawson TL, Foley WD, Berland LL, Clark KE: Ultrasonic evaluation of fetal kidneys. *Radiology* 138(1):153–156, 1981.
91. Hoddick WK, Filly RA, Mahony BS, Callen PW: Minimal fetal renal pyelectasis. *J Ultrasound Med* 4(2):85–89, 1985.



92. Arger PH, Coleman BG, Mintz MC, et al: Routine fetal genitourinary tract screening. *Radiology* 156(2):485–489, 1985.
93. Grannum P, Bracken M, Silverman R, Hobbins JC: Assessment of fetal kidney size in normal gestation by comparison of ratio of kidney circumference to abdominal circumference. *Am J Obstet Gynecol* 136(2):249–254, 1980.
94. Jeanty P, Dramaix-Wilmet M, Elkhazen N, et al: Measurements of fetal kidney growth on ultrasound. *Radiology* 144(1):159–162, 1982.
95. Bertagnoli L, Lalatta F, Gallicchio R, et al: Quantitative characterization of the growth of the fetal kidney. *J Clin Ultrasound* 11(7):349–356, 1983.
96. Wladimiroff JW, Campbell S: Fetal urine-production rates in normal and complicated pregnancy. *Lancet* 1(7849):151–154, 1974.
97. Campbell S, Wladimiroff JW, Dewhurst CJ: The antenatal measurement of fetal urine production. *J Obstet Gynaecol Br Commonw* 80(8):680–686, 1973.
98. Chamberlain PF, Manning FA, Morrison I, Lange IR: Circadian rhythm in bladder volumes in the term human fetus. *Obstet Gynecol* 64(5):657–660, 1984.
99. Rosenberg ER, Bowie JD, Andreotti RF, Fields SI: Sonographic evaluation of fetal adrenal glands. *AJR Am J Roentgenol* 139(6):1145–1147, 1982.
100. Co CS, Filly RA: Normal fetal adrenal gland location. *J Ultrasound Med* 5(2):117–118, 1986.
101. Goldberg BB, Isard HJ, Gershon-Cohen J, Ostrum BJ: Ultrasonic fetal cephalometry. *Radiology* 87(2):328–332, 1966.
102. Hidalgo H, Bowie J, Rosenberg ER, et al: Review. In utero sonographic diagnosis of fetal cerebral anomalies. *AJR Am J Roentgenol* 139(1):143–148, 1982.
103. Fiske CE, Filly RA: Ultrasound evaluation of the normal and abnormal fetal neural axis. *Radiol Clin North Am* 20(2):285–296, 1982.
104. Pasto ME, Kurtz AB: The prenatal examination of the fetal cranium, spine, and central nervous system. *Semin Ultrasound CT MR* 5:170, 1984.
105. Filly RA: Ultrasonography. In Harrison MR, Golbus MS, Filly RA, editors: *The Unborn Patient: Prenatal Diagnosis and Treatment*, Orlando, FL, 1984, Grune & Stratton, pp 33–123.
106. Carrasco CR, Stierman ED, Harnsberger HR, Lee TG: An algorithm for prenatal ultrasound diagnosis of congenital CNS abnormalities. *J Ultrasound Med* 4(4):163–168, 1985.
107. Edwards MSD, Filly RA: Diagnosis and management of fetal disorders of the central nervous system. In Hoffman HJ, Epstein F, editors: *Disorders of the Developing Nervous System: Diagnosis and Treatment*, Boston, 1986, Blackwell Scientific Publications, pp 55–73.
108. Young GB: The “arrow” pattern. A new “anatomical” fetal biparietal diameter. *Radiology* 137(2):445–449, 1980.
109. Jeanty P, Chervenak FA, Romero R, et al: The sylvian fissure: a commonly mislabeled cranial landmark. *J Ultrasound Med* 3(1):15–18, 1984.
110. Denkhau H, Winsberg F: Ultrasonic measurement of the fetal ventricular system. *Radiology* 131(3):781–787, 1979.
111. Chinn DH, Callen PW, Filly RA: The lateral cerebral ventricle in early second trimester. *Radiology* 148(2):529–531, 1983.
112. Fiske CE, Filly RA, Callen PW: The normal choroid plexus: ultrasonographic appearance of the neonatal head. *Radiology* 141(2):467–471, 1981.
113. Johnson ML, Dunne MG, Mack LA, Rashbaum CL: Evaluation of fetal intracranial anatomy by static and real-time ultrasound. *J Clin Ultrasound* 8(4):311–318, 1980.
114. Pugash D, Hendson G, Dunham CP, et al: Sonographic assessment of normal and abnormal patterns of fetal cerebral lamination. *Ultrasound Obstet Gynecol* 40(6):642–651, 2012.
115. Kline-Fath BM, Calvo-Garcia MA: Prenatal imaging of congenital malformations of the brain. *Semin Ultrasound CT MR* 32(3):167–188, 2011.
116. Toi A, Lister WS, Fong KW: How early are fetal cerebral sulci visible at prenatal ultrasound and what is the normal pattern of early fetal sulcal development? *Ultrasound Obstet Gynecol* 24(7):706–715, 2004.
117. Monteagudo A, Timor-Tritsch IE: Fetal neurosonography of congenital brain anomalies. In Timor-Tritsch IE, Monteagudo A, Cohen HL, editors: *Ultrasonography of the Prenatal and Neonatal Brain*, New York, 2001, McGraw-Hill, pp 151–258.
118. Patriquin H, Fontaine S, Michaud J, et al: Development of the fetal brain in the second trimester: an anatomic and ultrasonographic demonstration. *Can Assoc Radiol J* 43:131–137, 1992.
119. Jeanty P, Dramaix-Wilmet M, Delbeke D, et al: Ultrasonic evaluation of fetal ventricular growth. *Neuroradiology* 21(3):127–131, 1981.
120. Hertzberg BS, Burger PC, Bowie JD, et al: Sonographic characteristics of small cerebral blood vessels. An in vivo and postmortem study. *J Ultrasound Med* 9(12):697–703, 1990.
121. Day WR: Casts of foetal lateral ventricles. *Brain* 82(1):109–115, 1959.
122. Siedler DE, Filly RA: Relative growth of the higher fetal brain structures. *J Ultrasound Med* 6(10):573–576, 1987.
123. Worthen NJ, Gilbertson V, Lau C: Cortical sulcal development seen on sonography: relationship to gestational parameters. *J Ultrasound Med* 5(3):153–156, 1986.
124. Pilu G, De Palma L, Romero R, et al: The fetal subarachnoid cisterns: an ultrasound study with report of a case of congenital communicating hydrocephalus. *J Ultrasound Med* 5(7):365–372, 1986.
125. Laing FC, Stamler CE, Jeffrey RB: Ultrasonography of the fetal subarachnoid space. *J Ultrasound Med* 2:29, 1983.
126. Fong KW, Ghai S, Toi A, et al: Prenatal ultrasound findings of lissencephaly associated with Miller-Dieker syndrome and comparison with pre- and postnatal magnetic resonance imaging. *Ultrasound Obstet Gynecol* 24(7):716–723, 2004.
127. Robinson AJ, Goldstein R: The cisterna magna septa. Vestigial remnants of Blake’s pouch and a potential new marker for normal development of the rhombencephalon. *J Ultrasound Med* 26:83–95, 2007.
128. Reuter KL, D’Orsi CJ, Raptopoulos VD, et al: Sonographic pseudoasymmetry of the prenatal cerebral hemispheres. *J Ultrasound Med* 1(3):91–95, 1982.



# Ultrasound Evaluation of the Fetal Central Nervous System

Gianluigi Pilu

## SUMMARY OF KEY POINTS

- Central nervous system (CNS) anomalies are among the most frequent malformations encountered by antenatal sonography.
- Ultrasound allows detection of a large proportion of all CNS malformations in early gestation. However, in some cases the findings may be subtle, whereas in others the anomaly may be progressive and manifest only in late gestation or after birth. Ultrasound will also frequently demonstrate normal anatomic variations difficult to differentiate from true malformations.
- Magnetic resonance imaging (MRI) is often useful with CNS anomalies to improve diagnostic accuracy.
- One of the most common antenatal diagnoses, enlargement of the lateral cerebral ventricles or ventriculomegaly, may be associated with other CNS malformations and requires a detailed workup.
- Neural tube defects, such as anencephaly and open spina bifida, are often recognized in early gestation. Demonstration of the spinal defect in spina bifida may be difficult, but the diagnosis is facilitated by frequently associated abnormalities of intracranial anatomy.
- Alobar and semilobar holoprosencephaly may be recognized in early gestation; more subtle varieties, such as the lobar type, are more difficult to identify.
- Complete agenesis of the corpus callosum (ACC) can be recognized by midgestation. Counseling regarding prognosis is difficult because the prognosis is variable and studies suggest that many infants diagnosed in utero may have normal intelligence. Partial agenesis is much more difficult to identify by prenatal sonography.
- Cystic and cyst-like anomalies of the posterior fossa are often difficult to diagnose with certainty. Although the increased fluid is easily recognized, a specific diagnosis is often difficult because many different entities exist and there is much overlap with normal variants.

## OUTLINE

### Embryology, 221

- Ventriculomegaly, 222
- Neural Tube Defects, 222
- Midline Anomalies, 225
- Cystic and Cyst-like Abnormalities of the Posterior Fossa, 229
- Intrauterine Cerebral Injuries, 231
- Microcephaly, 231

### Intracranial Cysts and Tumors, 232

- Vascular Abnormalities, 237
- Cortical Malformations and Anomalies of Neuronal Migration, 237
- Conclusions, 240

CNS malformations are among the most common congenital abnormalities encountered at birth. The true incidence of these anomalies, however, is probably underestimated; most epidemiologic surveys are based upon clinical examinations performed in the neonatal period, and many cerebral malformations will only be discovered later in life. Long-term follow-up studies suggest that the true incidence may be as high as 1 in 100.<sup>1</sup>

Detection of CNS anomalies was one of the early goals of sonography in pregnancy. Although there has been much debate regarding the value of ultrasound screening, it is now clear that open neural tube defects, including anencephaly, open spina bifida, and large cephaloceles, as well as other severe malformations such as holoprosencephaly, are easily identified in early gestation. Improvements in image quality have led to increased detection of relatively minor malformations, such that the challenge sonologists now face is not sensitivity, but rather

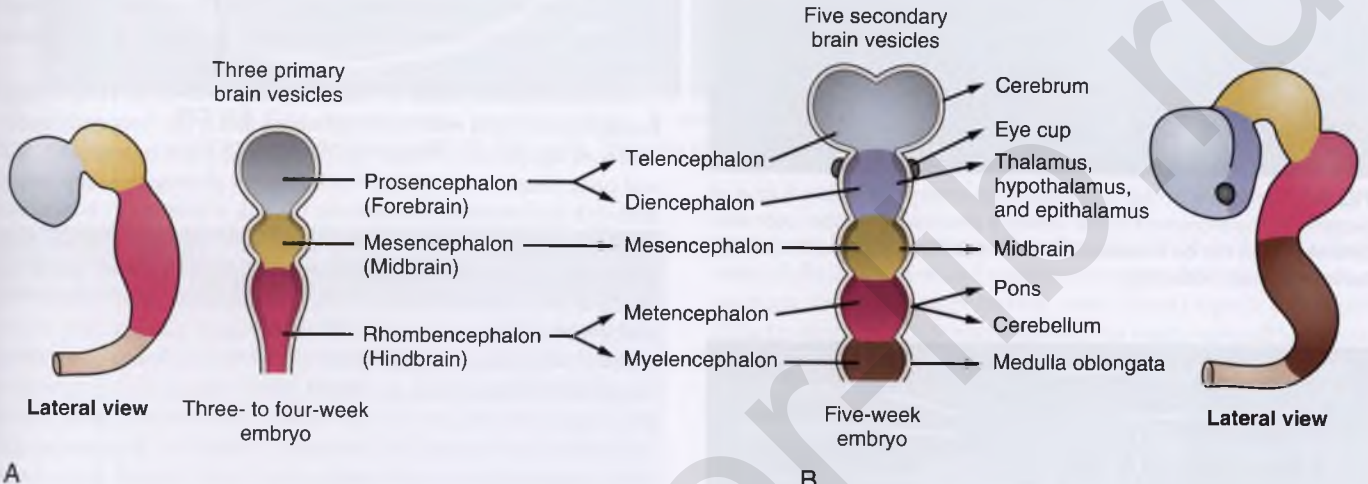
specificity. Many CNS anomalies that are poorly understood (ACC and posterior fossa cysts are representative examples) are now detected antenatally and for many such abnormalities, the postnatal consequences are difficult to predict. Furthermore, there is often significant overlap between normal variation and pathologic changes, as with enlargement of the ventricular system and small dimensions of the fetal head. Fetal sonography can precisely diagnose some lethal or severe malformations. But in a significant proportion of patients (e.g., enlargement of the lateral ventricles alone has an in utero prevalence of 1%), CNS findings carry uncertain prognostic significance that can provoke much anxiety in expectant couples, require difficult decisions, and may eventually result in the loss of normal fetuses. It has been suggested that MRI may add important diagnostic and prognostic information, although the precise impact of this technique continues to be debated.

**EMBRYOLOGY**

The nervous system develops from the neural plate, a thickened area of embryonic ectoderm. It is the notochord and paraxial mesoderm that induce the overlying ectoderm to differentiate into the neural plate. The neural plate folds along its central axis to form a neural groove lined on each side by a neural fold. The two neural folds fuse together and pinch off to become the neural tube. Fusion of the neural folds begins in the middle of the embryo and moves cranially and caudally. The cranial open end of the tube is the anterior (rostral) neuropore, and the caudal open end of the tube is the posterior

(caudal) neuropore (Figs. 9-1 and 9-2). The rostral neuropore closes on or before day 26 and the caudal neuropore closes 2 days later. The walls of the neural tube thicken to form the brain and spinal cord. The neural canal of the neural tube is converted into the ventricular system of the brain and the central canal of the spinal cord.

At about 8 to 10 weeks' gestation, a focal dilatation of the neural tube is seen in the dorsal aspect of the developing hindbrain; it is the rhombencephalic vesicle, the predecessor to the fourth ventricle. This structure may appear quite prominent and should not be misinterpreted as representing ventriculomegaly or another CNS anomaly (Figs. 9-3 and 9-4).



A

B

**FIG 9-1** The embryonic brain develops complexity through enlargements of the neural tube called vesicles. **A**, The primary vesicle stage has three regions. **B**, The secondary vesicle stage has five regions. (From OpenStax College: Anatomy & Physiology, CNX Web site, June 19, 2013. Available at <http://cnx.org/content/col11496/1.6/>.)

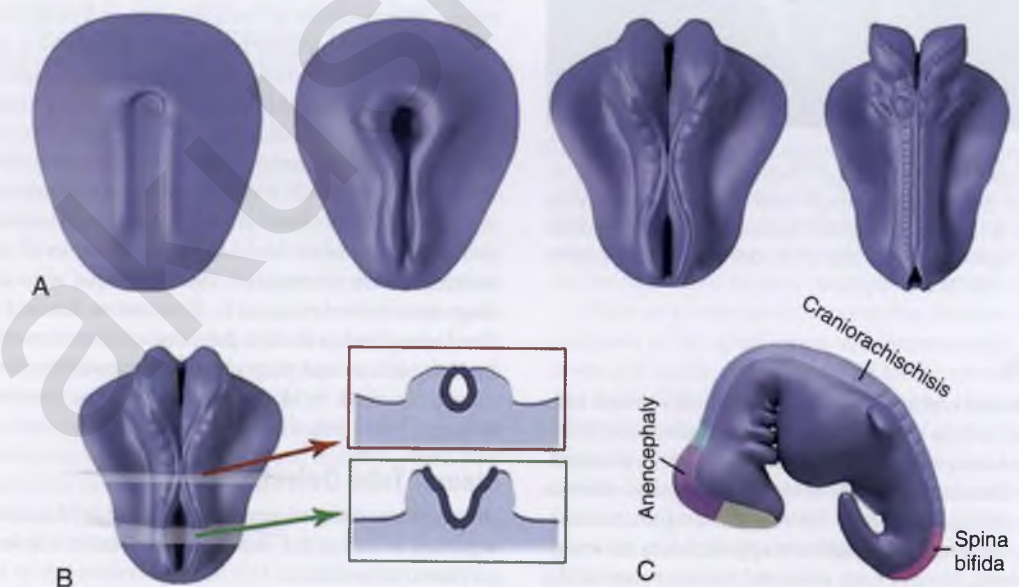


**FIG 9-2 A**, Successive images showing the time course of neural tube closure in a stylized vertebrate embryo (rostral = up). Initially, the central nervous system is a flat sheet; paired neural folds elevate along the rostrocaudal axis and move medially, eventually fusing to enclose the neural tube. **B**, Cross sections illustrate closed (red arrow) and open (green arrow) regions of the neural tube. **C**, Region-specific neural tube defects. (From Wallingford JB, Niswander LA, Shaw GM, Finnell RH: The continuing challenge of understanding, preventing, and treating neural tube defects. *Science* 339(6123):1222002, 2013.)





**FIG 9-3** Sonogram of the fetal brain in an embryo (8 weeks 5 days of gestation). The prominent fourth ventricle precursor (rhombencephalon) (arrow) should not be mistaken for ventriculomegaly or another central nervous system anomaly.

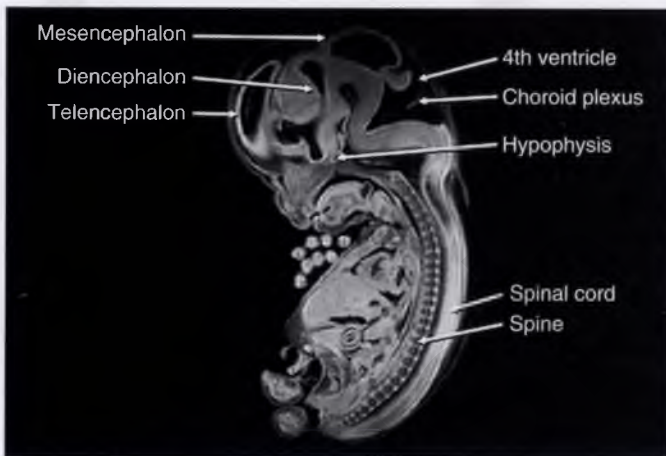


**FIG 9-4** Sectional magnetic resonance image of Carnegie stage 23 (10 weeks' gestational age) human embryo. (From Pooh RK, Shiota K, Kurjak A: Imaging of the human embryo with magnetic resonance imaging microscopy and high-resolution transvaginal 3-dimensional sonography: human embryology in the 21st century. *Am J Obstet Gynecol* 204(1):77.e1-16, 2011.)

## Ventriculomegaly

Enlargement of the lateral cerebral ventricles, commonly referred to as *ventriculomegaly* (Fig. 9-5), is a nonspecific marker of abnormal brain development. The presence of normal fetal lateral ventricles on ultrasound examination decreases the risk of a CNS anomaly, whereas detection of ventriculomegaly increases the risk that a significant malformation is present. Although many different approaches to the evaluation of the lateral ventricles have been proposed, measurement of the width of the atrium (or posterior horn) of the lateral ventricle is currently favored. In a normal fetus, the measurement of the lateral ventricle should be less than 10 mm between 15 and 40 weeks' gestation. In most fetuses with significant ventricular enlargement, the ventricles are symmetrically affected whereas cases with milder degrees of ventriculomegaly are more commonly unilateral. Male fetuses have a

slightly larger atrial size than female fetuses. A study by Patel and associates<sup>2</sup> demonstrated that atrial size demonstrated a near-normal distribution, with mean size for all subjects  $6.1 \text{ mm} \pm 1.3$  (standard deviation [SD]). When separated by sex, the mean atrial diameter of 122 female fetuses was  $5.8 \text{ mm} \pm 1.3$ , and the mean atrial diameter of 97 male fetuses was  $6.4 \text{ mm} \pm 1.3$ . The difference in mean size was statistically significant ( $P < 0.005$ ).<sup>2</sup> Thus, a ventricular atrial measurement of 10 to 11 mm will have more significance in a female fetus than in a male fetus.

A ventricular atrial width of more than 15 mm indicates *severe ventriculomegaly*. This is almost always associated with an intracranial malformation, although the outcome is variable and depends largely upon the underlying cause. The available studies suggest that fetuses with isolated severe ventriculomegaly have an increased risk of perinatal death and a probability of severe long-term neurologic sequelae in at least 50% of survivors.<sup>2</sup>

An intermediate value of the atrial width, 10 to 15 mm, is commonly referred to as *mild ventriculomegaly* and is less frequently associated with significant CNS anomalies, although it can be seen with ACC and open neural tube defects.<sup>3,4</sup> Mild ventriculomegaly is also associated with chromosomal aberrations: the risk of trisomy 21 is increased 3.8 times when ventricular enlargement is an isolated finding.<sup>5</sup> Fetal infections, such as cytomegalovirus (CMV), may result in ventricular enlargement, although usually other sonographic abnormalities are also present (areas of focal cerebral increased echogenicity, microcephaly, and porencephaly). When mild ventriculomegaly is isolated, and associated anomalies are absent, most infants are asymptomatic after birth. However, several reports have indicated that some fetuses are found to have severe CNS anomalies in advanced gestation or after birth (hydrocephalus, white matter injury, and cortical plate abnormalities), and some studies have reported an increased risk of neurologic compromise. Studies reporting on the prognosis of mild ventriculomegaly have been limited by the lack of standardized follow-up protocols and difficulty in defining "normal" neurologic outcome. However, most fetuses with mild ventriculomegaly will have a normal outcome, whereas about 10% demonstrate neurodevelopmental abnormalities of variable types and magnitude.<sup>4</sup>

When mild ventriculomegaly is encountered, it is important to rule out associated anomalies. A targeted sonographic survey of fetal anatomy should be performed, with particular attention to details of the CNS. Fetal diagnostic testing for aneuploidy should be offered, and chromosomal microarray should be considered. Detailed ultrasound assessment of the CNS may be enhanced by transvaginal scanning, particularly if the fetus is in cephalic presentation. There is some debate as to whether fetal MRI is indicated in all cases of apparently isolated ventriculomegaly.<sup>4</sup> This technique may provide significant diagnostic information, as it allows more detailed assessment of the developing fetal brain and detection of disorders of sulcation, cortical malformations, and migrational abnormalities. In continuing pregnancies in which mild ventriculomegaly has been identified, standard obstetric management is recommended.

## Neural Tube Defects

The incidence, cause, and recurrence risk of neural tube defects are reported in Tables 9-1 through 9-3. There are several different forms of neural tube defects.

*Anencephaly* is characterized by the absence of the cranial vault and telencephalon. The diagnosis is made by ultrasound in the second and third trimesters and relies upon demonstration of the absence of the cranial vault. In addition, most cases can be confidently identified by 11 to 13 weeks' gestation. At this time, the fetal head can be recognized as overtly abnormal owing to lack of an ossified calvarium (Fig. 9-6).<sup>6</sup>



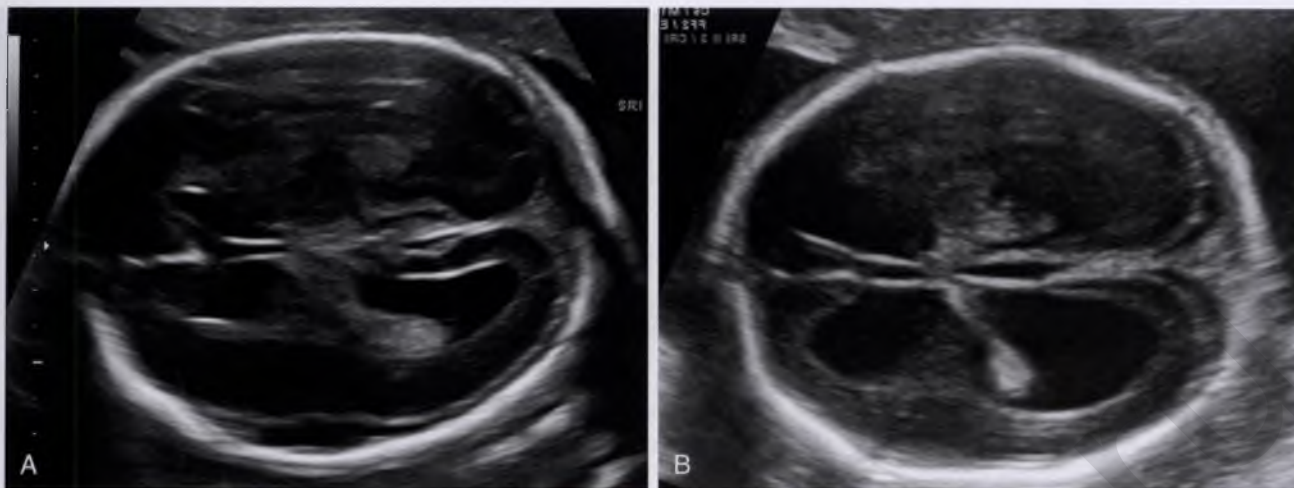


**FIG 9-5** Fetal lateral cerebral ventriculomegaly. **A**, Mild ventriculomegaly (atrial width 11 mm); **B**, severe ventriculomegaly (atrial width 16 mm) with “dangling choroid.”

**TABLE 9-1** Incidence of Neural Tube Defects

Geographic Area	Spina Bifida Incidence per 1000 Births	Anencephaly Incidence per 1000 Births
South Wales	4.1	3.5
Southampton	3.2	1.9
Birmingham, UK	2.8	2.0
Charleston		
White	1.5	1.2
Black	0.6	0.2
Alexandria	0	3.6
Japan	0.3	0.6

Modified from Brocklehurst G: Spina bifida. In Vinken PJ, Bruyn GW (eds): Handbook of Clinical Neurology. Amsterdam, Elsevier/North Holland Biomedical Press, 1978, vol. 32, pp 519–578.

The terms *acrania* and *exencephaly* have also been used to describe this appearance; these represent early stages in the development of anencephaly. The outcome of anencephaly is uniformly fatal.

*Spina bifida* can occur in open as well as closed forms. Open spina bifida is characterized by a full-thickness defect of the skin, underlying soft tissues, and vertebral arches, with exposure of the neural canal. These defects may vary considerably in size, with the lumbar and sacral areas most frequently affected. Leakage of cerebrospinal fluid through the defect results in an increased concentration of alpha-fetoprotein (AFP) and acetylcholinesterase in the amniotic fluid and maternal serum, and measurement of maternal serum and amniotic fluid AFP can be used to screen for neural tube defects.

Open spina bifida can be identified sonographically by demonstrating the opening of the neural tube and the defect in the vertebrae (splaying outward of the posterior elements) as well as the overlying soft tissues (Fig. 9-7). A cyst formed by the fusion of the malformed cord and meninges (myelomeningocele) is usually found. In a minority of cases, there is no covering membrane (myelocoele). The diagnosis of a neural tube defect may be difficult and requires meticulous scanning. Examination of the fetal head is of great utility, as open spina bifida is consistently associated with characteristic and readily recognizable

intracranial lesions. Leakage of cerebrospinal fluid leads to displacement of the cerebellum and medulla oblongata through the foramen magnum inside the upper cervical canal (Chiari type II or Arnold-Chiari malformation). Sonographically, this results in small head measurements in the midtrimester, as well as obliteration of the cisterna magna; small size and abnormal shape of the cerebellum (banana sign), which is located deep in the posterior fossa; scalloping of the frontal bones (lemon sign); and ventriculomegaly. Another characteristic abnormality is a “pointed” appearance of the occipital horns of the lateral ventricle. The occipital point is a common supratentorial feature of the Chiari II malformation. It is seen more commonly in fetuses younger than 24 weeks and in those with normal-sized ventricles. Interestingly, it is seen as commonly among fetuses with mild posterior fossa deformations as in those with more severe distortions<sup>7</sup> (see Fig. 9-7). Overall, the detection rate of open spina bifida at the midtrimester obstetric sonogram has been reported to be at least 90%.<sup>8-10</sup> Abnormalities of the posterior fossa and lateral ventricles have also been described at 11 to 13 weeks’ gestation, but the diagnostic accuracy of these findings to screen for spina bifida is still being assessed.

Several other neural axis abnormalities are frequently associated with myelomeningocele and Chiari II malformation, both intracranial and extracranial. These abnormalities are known to exist in the presence of myelomeningocele, and thus, when observed, the fetus should not be considered to have “multiple anomalies” (Table 9-4).

There is a correlation between the location (vertebral level) and extension of the spinal lesion and the neurologic outcome. In general, lower and smaller defects result in less severe neurologic compromise. The level of the bony spinal lesion can be determined by counting the affected vertebrae either from the most distal vertebra (in the second trimester fetus, the lowest ossified vertebra is S4) or from the rib cage (which ends at T12). Antenatal ultrasound assessment correlates reasonably well with postnatal assessment (75%), and MRI has been found to add little to determination of the bony level of the defect. However, it is not possible to precisely predict motor function, morbidity, or developmental milestones.<sup>11</sup> Of note, the degree of ventricular enlargement does correlate with the need for postnatal shunting.<sup>12</sup>

Antenatal counseling after detection of fetal spina bifida is complex and should involve a multidisciplinary team. Postnatal hydrocephalus requiring shunting, causing incontinence, and resulting in motor



**TABLE 9-2 Recognized Causes of Neural Tube Defects****Multifactorial Inheritance**

Anencephaly, myelomeningocele, meningocele, and encephalocele

**Mendelian Syndromes**

Pallister-Hall syndrome

Meckel-Gruber syndrome, autosomal recessive (phenotype includes occipital encephalocele and rarely anencephaly)

Median-cleft face syndrome, possibly autosomal dominant (phenotype includes anterior encephalocele)

Robert syndrome, autosomal recessive (phenotype includes anterior encephalocele)

Syndrome of anterior sacral meningomyelocele and anal stenosis (dominant, either autosomal or X-linked)

Jarcho-Levin syndrome, autosomal recessive (phenotype includes meningomyelocele)

HARD(E) syndrome (hydrocephalus, agyria, retinal dysplasia,  $\pm$  encephalocele), autosomal recessive (phenotype includes encephalocele)

**Chromosome Abnormalities**

Trisomy 13

Trisomy 18

Triploidy

Other abnormalities, such as unbalanced translocations and ring chromosome

**Probably Hereditary but Mode of Transmission Not Established**

Syndrome of occipital encephalocele, myopia, and retinal dysplasia  
Anterior encephalocele among Bantus and Thais

**Teratogens**

Valproic acid (spina bifida)

Phenytoin

Carbamazepine

Aminopterin/amethopterin (anencephaly and encephalocele)

Exposure to high heat caused by fever

Monozygotic twinning

**Maternal Predisposing Factors**

Diabetes mellitus (anencephaly more frequently than spina bifida)

Obesity

Methyltetrahydrofolate reductase (*MTHFR*) gene carrier

**Specific Phenotypes, Without Known Cause**

Syndrome of craniofacial and limb defects secondary to amniotic bands (phenotype includes multiple encephaloceles)

Cloacal exstrophy (phenotype includes myelocystocele)

Sacroccygeal teratoma (phenotype includes myelomeningocele)

Modified from Main DM, Mennuti MT: Neural tube defects: issues in prenatal diagnosis and counselling. *Obstet Gynecol* 67(1):1-16, 1986.

weakness requiring wheelchair use is common. Options for management of an affected pregnancy include termination, expectant management with postnatal repair, and in utero surgical repair<sup>13-15</sup> (see Chapter 24). The benefit of cesarean delivery to improve neurologic outcome of infants with open spina bifida is uncertain.<sup>16,17</sup>

Closed spina bifida is characterized by a vertebral defect (schisis) covered by skin. Most defects are small, involving only a few vertebral segments, and the classic intracranial signs (lemon-shaped calvarium,

**TABLE 9-3 Estimated Incidence of Neural Tube Defects (NTDs) Based on Specific Risk Factors in the United States**

Population	Incidence per 1000 Live Births
<b>Mother as Reference</b>	
General incidence	1.4-1.6
Women undergoing amniocentesis for advanced maternal age	1.3-3.0
Women with diabetes mellitus	20
Women on valproic acid in first trimester	10-20
<b>Fetus as Reference</b>	
One sibling with NTD	15-30
Two siblings with NTD*	57
Parent with NTD	11
Half sibling with NTD	8
First cousin (mother's sister's child)	10
Other first cousins	3
Sibling with severe scoliosis secondary to multiple vertebral defects	15-30
Sibling with occult spinal dysraphism	15-30
Sibling with sacroccygeal teratoma or hemartoma	~15-30

\*Risk is higher in British studies. Risk increases further for three or more siblings or combinations of other close relatives.

Modified from Main DM, Mennuti MT: Neural tube defects: issues in prenatal diagnosis and counselling. *Obstet Gynecol* 67(1):1-16, 1986.

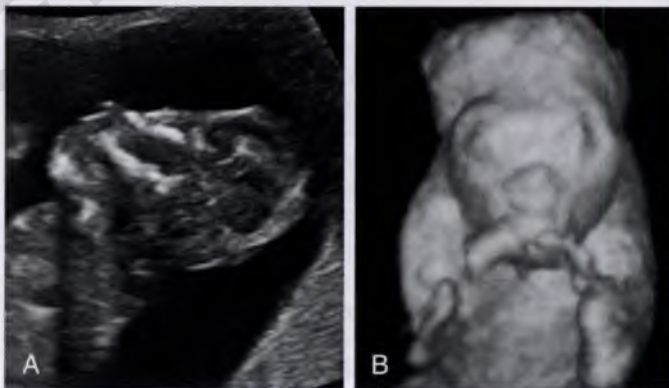


**FIG 9-6** Anencephaly at 13 weeks' gestation. **A**, Two-dimensional midline sagittal sonographic image; **B**, three-dimensional sonogram.

banana-shaped cerebellum, ventriculomegaly) are absent (Fig. 9-8). As a consequence, the sonographic diagnosis of closed spina bifida is difficult and in practice is only possible in those cases that are associated with a subcutaneous mass, such as a meningocele or lipoma overlying the bony defect.<sup>8</sup> The outcome of closed spina bifida is difficult to predict. These infants do not develop Arnold-Chiari malformation or hydrocephalus. However, those with subcutaneous masses may suffer from neurologic sequelae, including weakness or paralysis of the lower extremities and incontinence, usually as a consequence of tethering or compression of the spinal cord.

The term *cephalocele* is used to describe a protrusion of intracranial contents through a bony defect of the skull.<sup>18-20</sup> Most commonly, these lesions arise from the midline, in the occipital area; they arise less commonly from the parietal or frontal bones. *Encephaloceles* are



**FIG 9-7** Open spina bifida (myelomeningocele). **A**, Typical associated intracranial findings including scalloping of the bilateral frontal bones and small posterior fossa with obliteration of the cisterna magna. **B**, Large vertebral defect with overlying septated cyst. **C**, Axial sonographic image of a fetus with Chiari II malformation and normal-size ventricle showing pointed configuration (*arrow*) of the occipital horn. (C from Callen AL, Filly RA: Supratentorial abnormalities in the Chiari II malformation, I: the ventricular point J. *Ultrasound Med* 27:33–38, 2008.)

**TABLE 9-4** Frequency of Brain and Spine Anomalies in Patients With Chiari II Malformations

Anomaly	Frequency
Myelomeningocele	Always
Hydrocephalus	Almost always
Dysplastic tentorium	Almost always
Small posterior fossa	Almost always
Luckenschädel	Almost always
Caudal displacement of brainstem	Usually
Cervicomedullary kink	Usually
Upward cerebellar herniation	Usually
Large massa intermedia	Usually
Elongated cranial nerves	Usually
Tectal beak	Usually
Callosal hypogenesis	Usually
Syringohydromyelia	~50%
Malformations of cortical development	Occasionally
Aqueductal stenosis	Occasionally

From Barkovich AJ, Raybaud C (eds): *Pediatric Neuroimaging*, 5th ed. Philadelphia, Lippincott Williams & Wilkins, 2012.

characterized by the presence of brain tissue in the lesion. When only meninges protrude, the term *cranial meningocele* is used. Cephaloceles often cause impaired cerebrospinal fluid circulation and hydrocephalus, and massive encephaloceles may be associated with microcephaly. Associated anomalies are frequent (Table 9-5). Fetal cephaloceles are suspected when a paracranial mass is seen on sonography (Fig. 9-9). The diagnosis of encephalocele is typically straightforward, as the presence of brain tissue inside the sac is striking on ultrasound images, although distinguishing a cranial meningocele from soft tissue edema or a cystic hygroma of the neck may be difficult. The diagnosis of cephalocele is favored when it is possible to demonstrate a bony defect in the cranial vault or associated cerebral abnormalities, such as ventriculomegaly. The pediatric literature suggests that the outcome of cephaloceles is primarily related to the presence or absence of brain tissue inside the lesion. The largest available antenatal series reports a dismal prognosis for both varieties,<sup>21</sup> with the possible exception of small lesions associated with normal intracranial anatomy.

### Midline Anomalies

Midline cerebral anomalies include a group of brain defects that encompass a wide spectrum of severity and are often associated with craniofacial malformations.

The *holoprosencephalies* are complex abnormalities of the forebrain characterized by incomplete separation of the cerebral hemispheres and formation of diencephalic structures. They are rarely seen at birth owing to a high intrauterine mortality rate, although these disorders are relatively common in series of antenatally detected CNS anomalies. The cause of holoprosencephaly is heterogeneous, and in most cases, the anomaly is isolated and sporadic. However, holoprosencephaly may also be associated with chromosomal abnormalities (trisomy 13 and polyploidy), a number of single gene disorders, and other anatomic abnormalities.

The most widely accepted classification of these disorders recognizes three major varieties: the alobar, semilobar, and lobar types. In addition, a middle interhemispheric variant is described (Fig. 9-10).

The alobar, semilobar, and middle interhemispheric variant types have a similar appearance on antenatal ultrasound imaging: there is no midline echo anteriorly (absent septum pellucidum), and a single ventricular cavity is present (Fig. 9-11). In the *alobar* form, which is the most severe, the interhemispheric fissure, falx cerebri, and corpus callosum are absent; there is a single primitive ventricle; the thalami are fused in the midline; and there is absence of the third ventricle, neurohypophysis, and the olfactory bulbs and tracts. In *semilobar* holoprosencephaly, the two cerebral hemispheres are partially separated posteriorly but there is still a single ventricular cavity. The splenium of the corpus callosum is present without the genu or body of the corpus callosum.<sup>18,22,23</sup> In both alobar and semilobar holoprosencephaly, the roof of the ventricular cavity, the *tela choroidea* (which is normally enfolded within the brain), may balloon out between the cerebral convexity and the skull to form a cyst of variable size called the *dorsal sac*. Both of these forms are often associated with microcephaly, though they can sometimes be associated with macrocephaly because of a dorsal cyst or obstructive hydrocephalus.

In *lobar holoprosencephaly*, the interhemispheric fissure is well developed posteriorly and anteriorly, but there is a variable degree of fusion of the cingulate gyrus and the lateral ventricles, and the septum pellucidum is absent. In the *middle hemispheric* variant, fusion occurs primarily at the level of the bodies of the lateral ventricles, whereas the frontal horns and posterior horns are relatively well developed.<sup>24</sup>



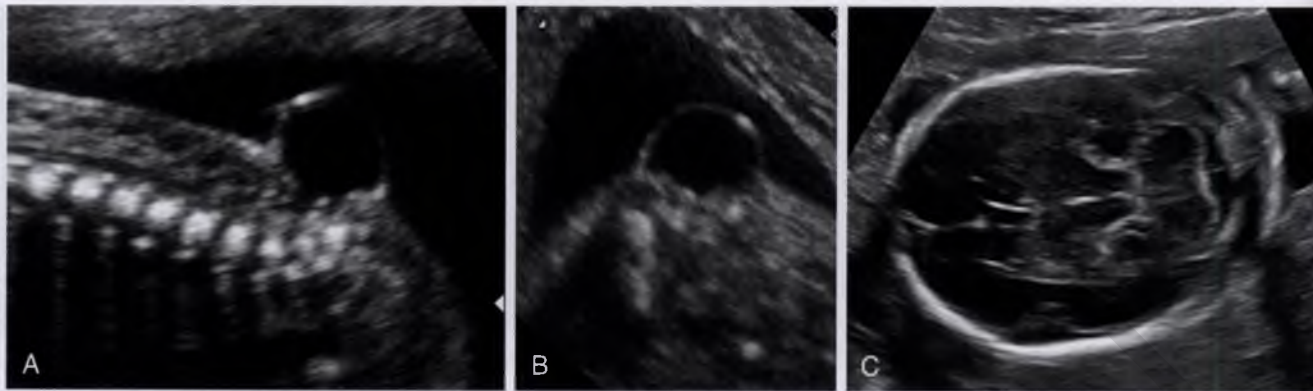


**FIG 9-8** Closed, or skin-covered, cystic spina bifida (meningocele). **A** and **B**, Small vertebral defect with an overlying nonseptated cyst; **C**, normal intracranial anatomy.

### TABLE 9-5 Conditions Associated With Cephaloceles

Amniotic band syndrome (sporadic)
Multiple cephaloceles, predominantly anterior
Amputations of digits or limbs
Bizarre oral clefts
Chemke syndrome (AR)
Hydrocephaly
Agyria
Cerebellar dysgenesis
Cryptophthalmos syndrome (AR)
Forehead skin covers one or both eyes
Ear abnormalities
Soft tissue syndactyly
Dyssegmental dysplasia (AR)
Short limb skeletal dysplasia
Metaphyseal widening
Small thorax
Micrognathia
Frontonasal dysplasia (sporadic, some cases are familial)
Frontal cephalocele
Ocular hypertelorism
Meckel-Gruber syndrome (AR)
Polycystic kidneys
Polydactyly
Microphthalmia
Orofacial clefting
Ambiguous genitalia
von Voss-Cherstvoy syndrome
Agenesis of the corpus callosum
Phocomelia
Urogenital anomalies
Thrombocytopenia
Warfarin syndrome
Nasal hypoplasia
Bone stippling
Limb shortening
Hydrocephaly

Modified from Cohen MM Jr, Lemire RJ: Syndromes with cephaloceles. *Teratology* 25(2):161-172, 1982.

Gross facial abnormalities (cyclopia, hypotelorism, and absence of the nose) are frequently associated with alobar and semilobar holoprosencephaly (Fig. 9-12). Facial malformations include cyclopia and severe hypotelorism with median cleft lip/palate. The nose may be absent, replaced by a proboscis, or flattened.<sup>25</sup> Facial anomalies are rarely associated with lobar holoprosencephaly or the middle inter-hemispheric variant.

Prenatal diagnosis of alobar or semilobar holoprosencephaly depends on the demonstration of a single rudimentary cerebral ventricle, which may protrude posteriorly through the incompletely enfolded cortex to form a dorsal sac. Additional findings of typical facial anomalies can assist in confirming the diagnosis. In most cases, the diagnosis is possible at 11 to 13 weeks' gestation. The lobar variety is associated with more subtle findings (absence of the septum pellucidum with central fusion of the frontal horns), and this diagnosis is rarely made prior to 20 weeks' gestation (Fig. 9-13).<sup>25</sup>

Infants affected by alobar and semilobar holoprosencephaly have an invariably poor prognosis. Antenatally diagnosed lobar holoprosencephaly is also associated with poor postnatal neurodevelopmental outcomes.<sup>26</sup>

ACC is an anomaly of uncertain prevalence and variable clinical significance. The best estimates suggest a prevalence of approximately 1.4 per 10,000 live births in the general population and 2% to 3% in the developmentally disabled.<sup>27,28</sup> The cause of ACC is heterogeneous. Genetic causes are common, and the anomaly is associated with a number of different genetic syndromes. The high frequency of associated malformations and chromosomal aberrations suggests that ACC is often part of a widespread developmental disturbance. ACC may be either complete or partial. In the latter case, also referred to as dysgenesis or partial agenesis, the caudad or posterior portion is missing to varying degrees. *Hypoplasia* refers to a corpus callosum of normal length but with much decreased thickness; this is rarely identified by prenatal sonography.

The diagnosis of ACC is possible from midgestation onward<sup>29</sup> but can be challenging even for expert sonologists.<sup>30</sup> The anatomic elements useful for reaching this diagnosis are summarized in Figure 9-14.

Characteristic changes of the ventricular system and cerebral hemispheres were first described by Davidoff and Dyke in 1934 based upon observations made by pneumoencephalography.<sup>31</sup> They noticed:

- Lateral separation of the frontal horns and bodies of the lateral ventricles
- Angled lateral peaks of the frontal horns and bodies of the lateral ventricles





**FIG 9-9** Cephalocele. **A**, Small occipital cephalocele; **B**, small occipital cephalocele with severe ventriculomegaly; **C**, large occipital cephalocele with large cranial defect and marked extracranial displacement of the brain.



**FIG 9-10** Categorization of holoprosencephaly.

- Elevation and variable dilatation of the third ventricle
- Dilatation of the occipital horns
- Concave medial wall of the lateral ventricles related to the bundles of Probst
- Abnormal radial orientation of medial cerebral gyri extending from the roof of the third ventricle

In a series of fetuses with ACC, Bertino and colleagues<sup>32</sup> reported that a minority demonstrated a characteristic midline cyst. They described three findings that might lead one to suspect ACC on routine transverse views of the fetal brain:

1. Disproportionate enlargement of the occipital horn (colpocephaly)
2. Demonstration of both medial and lateral ventricular walls at a level where the single periventricular line is normally demonstrated
3. A more parallel course of both ventricular walls than normal

Complete ACC is usually suspected on midgestation obstetric sonograms based on absence of the cavum septi pellucidi (CSP) and characteristic configuration of the lateral ventricles with increased separation of the frontal horns and mild enlargement of the posterior horns with “teardrop” shape, frequently associated with mild ventriculomegaly. The two hemispheres tend to appear more separated than usual in the central portion of the brain. In coronal section, the frontal horns appear more widely spaced than usual and have a comma-like shape. In the transverse axial plane, the lateral ventricles have a teardrop shape with posterior enlargement of the atria and occipital horns, referred to as *colpocephaly*.

Once suspected, definitive diagnosis of ACC may be made by demonstrating absence of the corpus callosum in the coronal and sagittal

planes (Fig. 9-15).<sup>20</sup> Diagnosis of partial agenesis is also possible, although the sonographic findings are subtler than those seen in complete ACC. With partial agenesis, the CSP is usually present and the axial images may be unremarkable. The diagnosis requires a midline sagittal view demonstrating that the corpus callosum is shorter than normal and does not form a complete arch over the third ventricle (Fig. 9-16). Visualization of the pericallosal artery with color Doppler sonography may be useful if complete or partial ACC is suspected (Fig. 9-17). Charts listing normal size of the corpus callosum are available for reference but should be used with caution as partial agenesis is relatively rare, and a clear threshold defining pathologic appearance has not been established. Most cases diagnosed antenatally have had a reduction in size of 50% or more. We have detected many cases with measurements of the corpus callosum below the 5th centile, and most have resulted in the birth of normal children.

Complete or partial ACC is frequently associated with a genetic syndrome (Table 9-6) or other malformations. One syndrome that may be associated with ACC is Aicardi syndrome, an X-linked dominant syndrome that consists of infantile spasms, callosal agenesis or hypogenesis, chorioretinopathy, severe global developmental delay, and medical refractory epilepsy.<sup>33,34</sup> Imaging findings include ACC, heterotopias, cortical dysplasia, posterior fossa cysts, cerebellar hypoplasia, choroid plexus papillomas, and microphthalmia. Assessment of fetal sex can be helpful if this disorder is suspected, as it is seen at birth only in female infants.

A recent systematic review of 16 studies assessed neurodevelopmental outcome in 132 fetuses with isolated ACC.<sup>35</sup> With complete ACC, the outcome was normal in 74.3%, borderline or with moderate disability in 14.3%, and associated with severe disability in 11.4%. The outcome was slightly less favorable, although not significantly different, with partial ACC (65.5%, 6.9%, and 27.6%, respectively). When considering only those studies using MRI confirmation and standardized tools of neurodevelopmental assessment, in cases with complete ACC, the rates were 83.7%, 8.2%, and 8.2% for normal, borderline/moderate, and severe disability, respectively. The corresponding rates for partial ACC were not reported because of the small number of cases. The authors of the review highlighted many limitations in existing studies, including limited and inconsistent data that prevented subgroup analyses. Providing a precise estimate of the risk of neurodevelopmental delay is difficult, and one important limitation of the available studies is the length of time of follow-up. In most cases, assessment was made in the preschool period. This may represent an important shortcoming, as in one series a progressive decline of



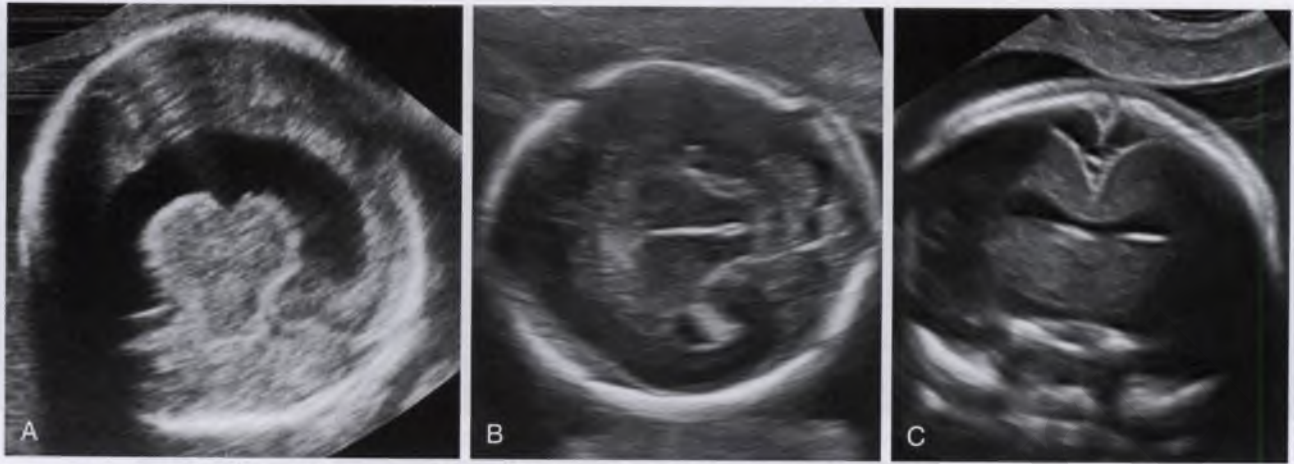


**FIG 9-11** Holoprosencephaly. **A**, Alobar holoprosencephaly with a large single ventricular cavity (monovertricle) and fused thalami; **B**, milder case with subtle findings—the anterior midline structures are absent. The single ventricular cavity and absent septum were best demonstrated by means of transvaginal sonographic image in the coronal plane (**C**).

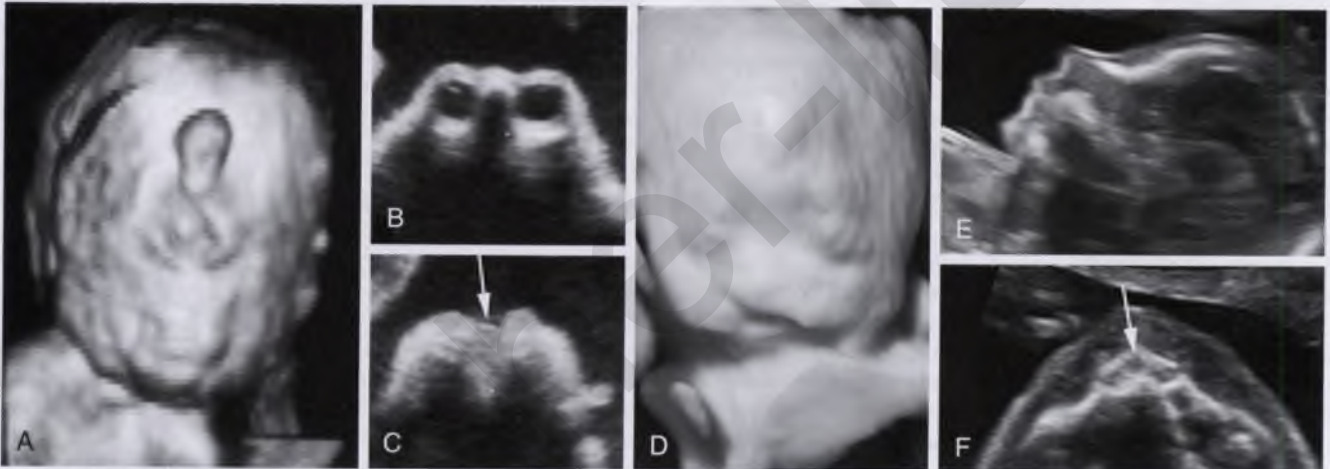


**FIG 9-12** Facial anomalies associated with holoprosencephaly. **A**, Three-dimensional ultrasound image of cyclopia, with proboscis protruding above the single orbit; **B** through **D**, marked hypotelorism and median cleft lip (*arrow*); **E** and **F**, subtle facial features of holoprosencephaly—although the midline sagittal profile view appears normal, meticulous scanning reveals a single median incisor tooth (*arrow*).

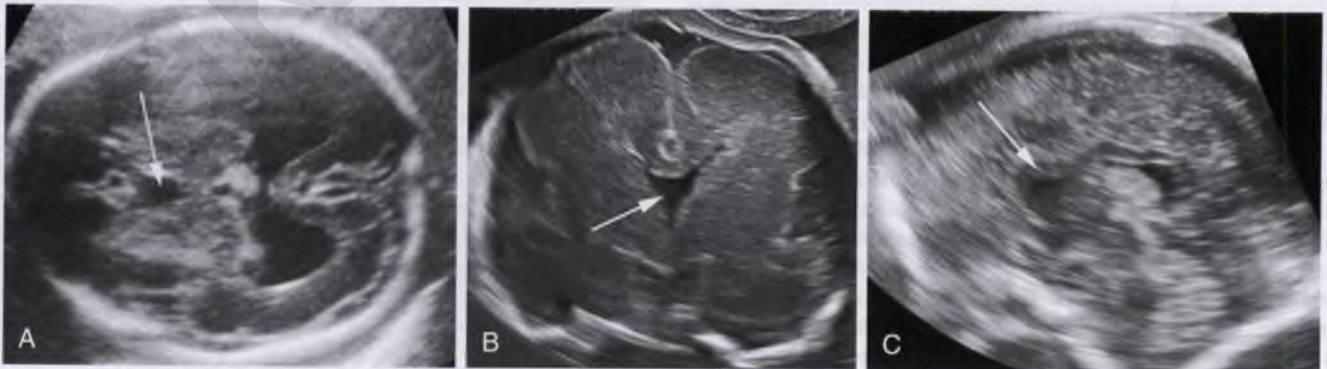


**FIG 9-13** Lobar holoprosencephaly. **A** and **B**, The predominant finding on axial and coronal ultrasound images is the absence of the septum pellucidum (*arrows*) and the diminutive frontal horns. **C**, The typical configuration of the corpus callosum is absent and has been replaced by irregular fibers connecting the two hemispheres in the midline (*arrow*).



intellect was noted, with a considerable number of children demonstrating learning difficulties in school.

The *septum pellucidum*, with the inferior fornix, forms the medial border of the lateral ventricles. It contains two leaves that in fetal life are separated by a fluid-filled cavity, the CSP. The leaves fuse in late gestation or immediately after birth, and the cavity is seen only in a minority of adults. Absence of the *septum pellucidum* in fetuses can be associated with a number of CNS anomalies including ACC, holoprosencephaly, destruction secondary to raised intraventricular pressure, schizencephaly, and septo-optic dysplasia (de Morsier syndrome). Isolated absence of the septal leaves with central fusion of the frontal horns is possible and is usually of no consequence (Fig. 9-18). The greatest challenge is to differentiate isolated absence of the CSP from septo-optic dysplasia. Visualization of the optic chiasma by either MRI or three-dimensional ultrasound is useful but does not always provide a definitive diagnosis. Although data are limited, two thirds of fetuses

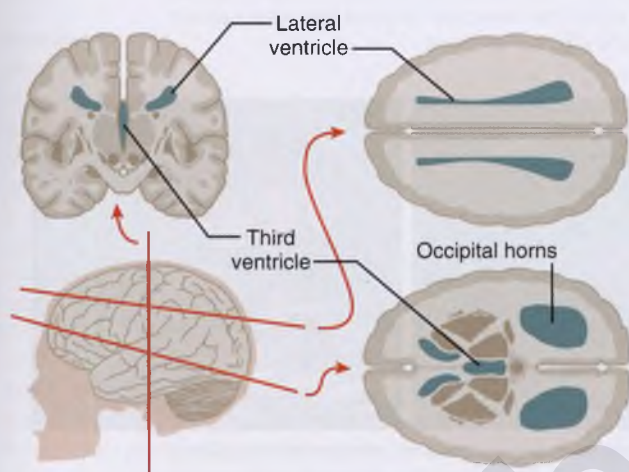


**FIG 9-14** Schematic diagram of agenesis of the corpus callosum without interhemispheric cyst. On a coronal view (*top left*), the widely spaced lateral ventricles are shown pointing cephalad. On an axial view superiorly (*top right*), both medial and lateral walls of the lateral ventricles are identified. A more inferior axial view (*bottom right*) reveals dilatation of the occipital horns (colpocephaly) and separation of the frontal horns. The third ventricle may or may not be dilated.

with absent CSP have been reported to be normal at birth. If a normal optic chiasma can be demonstrated, the probability of a normal outcome increases to 90%.<sup>36</sup>

### Cystic and Cyst-like Abnormalities of the Posterior Fossa

Fluid collections in the fetal posterior fossa encompass a wide spectrum of entities, ranging from normal variants to severe anomalies (Table 9-7).

In the late first trimester, the fourth ventricle is large and the cerebellum is relatively small. In the following weeks, the cerebellum grows to completely enfold the fourth ventricle. However, a small finger-like appendage of the fourth ventricle, the Blake pouch, is frequently seen protruding into the cisterna magna, caudal to the cerebellum. It has been suggested that there is a continuum of anatomic anomalies involving the fourth ventricle–Blake pouch complex (Fig. 9-19).<sup>37-40</sup> The mildest of these anomalies is the *Blake pouch cyst*, an isolated persistence of the Blake pouch. This term was originally introduced in the pediatric neuroradiology literature to indicate a compressive cyst of the posterior fossa that displaced the cerebellar vermis superiorly and caused obstructive hydrocephalus. Recently, the same term has been used more frequently in fetal imaging to describe cases in which a posterior fossa cyst was seen to superiorly displace an intact cerebellar vermis, typically in association with a normal ventricular system and normal size of the posterior fossa. The entities described in the original neonatal literature and later described in fetal reports are likely different, as the latter typically has a normal outcome and is rarely associated with ventriculomegaly. *Mega-cisterna magna* may be a variation of the Blake pouch cyst that does not result in superior displacement of the vermis.

In the largest available series, Blake pouch cyst and mega-cisterna magna were the two most common entities described antenatally, representing about 50% of all cystic anomalies of the fetal posterior fossa.<sup>39</sup> These two conditions share many clinical similarities. Although they may be associated with other anomalies, when isolated, they undergo spontaneous resolution during gestation in one third of cases, and regardless of resolution, they result in normal postnatal neurodevelopment in about 90% of cases.<sup>39</sup>

*Dandy-Walker malformation* (DWM) is relatively rare, with an estimated prevalence of approximately 1 in 30,000 births, and is associated

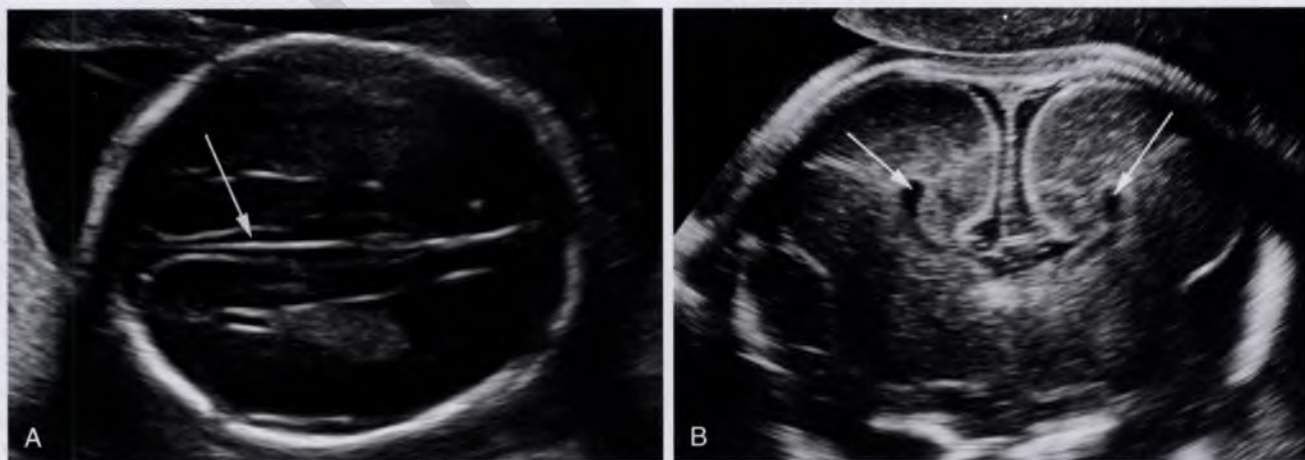


**FIG 9-15** Complete agenesis of the corpus callosum. **A**, The axial plane reveals mild enlargement of the lateral ventricles, which have a typical teardrop shape, absence of the cavum septi pellucidum and distention of the interhemispheric fissure, which is centrally partitioned by the falx cerebri (*arrow*). **B**, The coronal plane demonstrates the large interhemispheric fissure, the absence of any bridging structure connecting the two hemispheres, and the lateral separation of the frontal horns that appear medially concave (*arrows*).



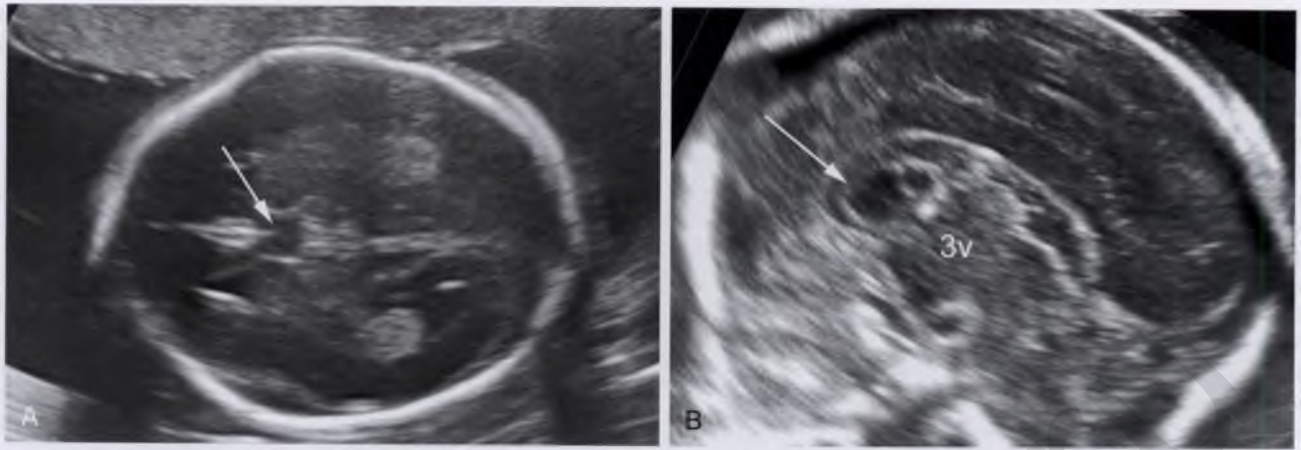


**FIG 9-16** Partial agenesis of the corpus callosum. **A**, This axial image shows a relatively normal appearance of the cavum septi pellucidi (arrow). **B**, The midline sagittal view demonstrates a corpus callosum (arrow) that is short (the arch does not completely cover the area of the third ventricle [3v] and the measurement is about 50% the expected length at this gestational age) and irregular in shape.



**FIG 9-17** Pericallosal artery. **A**, In a normal fetus, color Doppler sonography demonstrates the pericallosal artery, which courses adjacent to and highlights the corpus callosum. **B**, In complete agenesis of the corpus callosum, the loop of the pericallosal artery is lost. The anterior cerebral artery ascends vertically and branches with a tree-like configuration. **C**, In partial agenesis of the corpus callosum, the pericallosal artery forms an unusually short loop.

with 4% to 12% of infantile hydrocephalus. The main features of DWM are enlargement of the cisterna magna and superior displacement of the cerebellar vermis, which may be intact or incompletely formed. Historically, hydrocephalus was considered an essential diagnostic element of DWM, but more recent evidence suggests that it is not present at birth in most patients, though it may develop later in life. DWM is frequently associated with other CNS (ACC, holoprosencephaly, or encephalocele) and non-CNS anomalies (polycystic kidneys, cardiovascular defects, and facial clefts) and genetic conditions (Table 9-8). When isolated, the outcome is variable. In antenatal studies, approximately 50% of surviving infants are reported to have normal intelligence, and 50% have variable degrees of neurodevelopmental disability.<sup>39</sup>

*Vermian agenesis/hypoplasia* is characterized by an absent or small cerebellar vermis with a normal cisterna magna. This condition was originally labeled *Dandy-Walker variant*, a term that has fallen out of favor. Follow-up studies of children with antenatally diagnosed vermian agenesis or hypoplasia have reported widely variable outcomes, ranging from largely normal in some series, to a high prevalence of neurologic compromise in others.<sup>39,41</sup>

*Joubert syndrome* and related disorders are a group of conditions characterized by hypoplasia of the cerebellar vermis with a characteristic neuroradiologic finding described as the *molar tooth sign*, which refers to elongation of the superior cerebellar peduncles that gives an

appearance reminiscent of a molar or wisdom tooth (Fig. 9-20). These CNS findings can be associated with a variety of non-CNS anomalies and therefore may constitute different syndromes, although all generally share an unfavorable neurologic outcome.<sup>42</sup>

*Arachnoid cysts* of the posterior fossa are rare and most frequently result in a mass effect on the cerebellar structures. They may be difficult to differentiate from mega-cisterna magna or DWM and should be considered in the differential diagnosis of cystic lesions of the posterior fossa (see later section for further discussion).

With the exception of mega-cisterna magna, in which the diagnostic criteria are clear-cut (the widely accepted definition is a cisterna magna with anteroposterior diameter measuring >10 mm with normal-appearing cerebellum and cerebellar vermis), the other cystic anomalies of the fetal posterior fossa can appear quite similar to each other and thus the differential diagnosis is often difficult. Blake pouch cyst, DWM, vermian hypoplasia/agenesis, and Joubert syndrome share a similar finding: the impression, on an axial image, of communication between the fourth ventricle and the cisterna magna (open fourth ventricle sign). This communication is created by the presence of a cystic structure extending from the roof of the fourth ventricle into the cisterna magna beneath the cerebellar vermis. This observation is frequent in early gestation and becomes significant only when it is demonstrated after 20 weeks' gestation. After this time, the most valuable diagnostic information is obtained from a midsagittal view of the



**TABLE 9-6 Syndromes Featuring Agenesis of the Corpus Callosum****Frequent in:**

Acrocallosal syndrome (AR)  
 Aicardi syndrome (X-linked dominant)  
 Andermann syndrome (AR)  
 Cerebro-oculo-facio-skeletal (COFS) syndrome (AR)  
 Fryns syndrome (AR)  
 Marden-Walker syndrome (AR)  
 Meckel-Gruber syndrome (AR)  
 Microphthalmia-linear skin defects syndrome (X-linked dominant)  
 Miller-Dieker syndrome (lissencephaly syndrome)  
 Neu-Laxova syndrome (AR)  
 Septo-optic dysplasia sequence  
 Walker-Warburg syndrome (X-linked dominant)  
 Zellweger syndrome (AR)

**Occasional in:**

Apert syndrome (AR)  
 Baller-Gerold syndrome (AR)  
 Calloso-genital dysplasia syndrome (AR)  
 Coffin-Siris syndrome (?AR)  
 Congenital microgastria-limb reduction complex (unknown)  
 Crouzon syndrome (AD)  
 Duplication 4p syndrome  
 Fetal alcohol syndrome  
 Fetal warfarin syndrome  
 FG syndrome (X-linked recessive)  
 Frontonasal dysplasia sequence (sporadic/AD)  
 Gorlin syndrome (AD)  
 Greig cephalopolysyndactyly syndrome (AD)  
 Hydrolethrus syndrome (AR, X-linked dominant)  
 Lens dysplasia (X-linked recessive)  
 Marshall-Smith syndrome (unknown)  
 Oculo-auriculo-vertebral spectrum (unknown)  
 Oculo-cerebro-cutaneous syndrome (Delleman syndrome) (unknown)  
 Opitz syndrome (AD, X-linked recessive)  
 Oral-facial-digital syndrome type 1 (X-linked dominant)  
 Peters-plus syndrome (AR)  
 Radial aplasia-thrombocytopenia syndrome (AR)  
 Rubinstein-Taybi syndrome (sporadic)  
 Shapiro syndrome (X-linked recessive)  
 Simpson-Golabi-Behmel syndrome (X-linked recessive)  
 Trisomy 8 syndrome  
 Trisomy 13 syndrome  
 Trisomy 18 syndrome  
 X-linked hydrocephalus spectrum (X-linked recessive)  
 Turner syndrome (45,X)  
 49,XXXXY syndrome (hypoplastic)  
 Yunis-Varon syndrome  
 Metabolic disorders

AD, autosomal dominant; AR, autosomal recessive.

Modified from Blum A, André M, Droullé P, et al: Prenatal echographic diagnosis of corpus callosum agenesis. The Nancy experience 1982-1989.

brain. Antenatal studies combining the use of sonography and MRI report diagnoses consistent with postnatal confirmation in approximately 90% of cases. Differentiating a Blake pouch cyst from a DWM and diagnosing vermian hypoplasia in early gestation remain diagnostic challenges.<sup>38,39,41</sup>

**Intrauterine Cerebral Injuries**

Many congenital anomalies of the brain are not the consequence of an embryogenetic malformative process but are due to destructive injury. The pathophysiology is frequently unclear and most of these conditions are idiopathic. An association with obstetric complications may be found in some cases.

*Intracranial hemorrhage* (ICH) is a frequent complication in premature infants. Rarely, it may occur antenatally, as a consequence of fetal thrombocytopenia or other coagulopathies, trauma, or other unrecognized factors. The sonographic appearance is extremely variable depending upon the type (Table 9-9), location, severity, and chronicity of the bleed (Fig. 9-21). Blood initially appears as a hyperechoic collection; with time, the blood clot retracts and demonstrates hypoechoic components. Antenatal ICH is frequently associated with ventricular dilatation. Large intraventricular hemorrhages may be complicated by infarction and destruction of the surrounding white matter.

As with neonates, there is a correlation between the grade of the in utero fetal hemorrhage and the neurologic outcome. The prognosis is typically favorable with grade 1 and 2 hemorrhage (involving the germinal matrix only, or extending into the ventricle but without ventriculomegaly), which may resolve in utero. More significant degrees of ICH, including grade 3 and 4 lesions (intraventricular hemorrhage with ventriculomegaly, or intraparenchymal involvement), are associated with a higher likelihood of abnormal neurologic development. Most cases identified prenatally are grade 3 or 4; in one review of the literature, 50% of these fetuses died in the perinatal period and 50% of survivors were neurologically impaired.<sup>43</sup> If ICH is suspected, the possibility of fetal alloimmune thrombocytopenia should be addressed. Fetal MRI is particularly helpful in confirming ICH, assessing extent of associated injury, and distinguishing hemorrhage from other intracranial injuries.

*Fetal stroke* has been documented antenatally.<sup>44</sup> The cause is heterogeneous, but most reported cases have been identified in monozygotic twin gestations, usually as a consequence of in utero co-twin demise or severe hemodynamic compromise associated with twin-to-twin transfusion syndrome. The appearance is variable (Fig. 9-22). Following the initial insult, focal areas of increased cerebral echogenicity may be seen. With evolution, microcephaly, cystic intraparenchymal cavities (porencephaly, schizencephaly, periventricular leukomalacia), and cortical malformations may develop. The outcome is determined by the size and location of the lesion. Microcephaly and extensive porencephaly have a guarded prognosis.

*Intrauterine infection* is an important cause of congenital brain lesions. Fetuses with CMV infection affecting the brain may present with a wide range of intracranial abnormalities, including periventricular and intraparenchymal echogenic foci, ventriculomegaly, cerebellar hypoplasia, microcephaly, and cortical abnormalities. The most characteristic findings include hyperechoic periventricular halo and septations within the occipital horns of the lateral ventricles (Fig. 9-23). Patients with recent CMV infection and characteristic cerebral findings have symptomatic infection at birth in virtually all cases. The negative predictive value of ultrasound in the setting of maternal CMV infection is more limited, as sonography does not reliably detect intracranial fetal findings in all cases. Recent series suggest that a normal obstetric ultrasound image in the setting of fetal CMV infection is more common in the second trimester than in the third.<sup>45</sup>

**Microcephaly**

Microcephaly refers to the association of abnormal neurologic development and a small head. The association between both brain mass and total cell number in *microcephalic infants* is well established. The



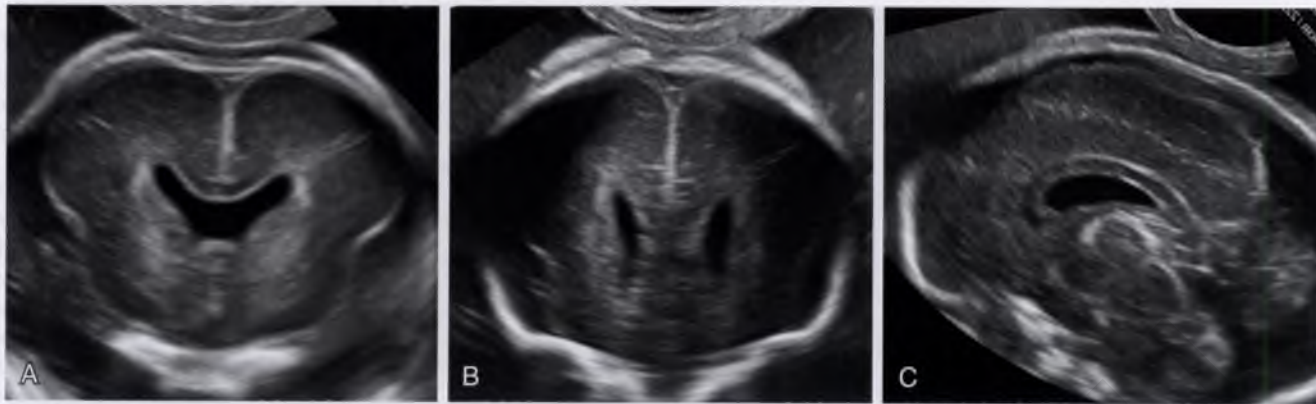


**FIG 9-18** Absence of the septum pellucidum. **A**, The frontal horns of the lateral ventricles communicate centrally, and no intervening leaves of the septum pellucidum are seen. **B** and **C**, The anterior coronal and sagittal views appear within normal limits.

**TABLE 9-7 Sonographic Findings of Posterior Fossa Cyst and Cyst-like Anomalies**

Anomaly	Findings
Mega-cisterna magna	Intact cerebellum; cisterna magna >10 mm
Blake pouch cyst	Cerebellum of normal size, intact vermis with mild rotation (usually <30 degrees)
Dandy-Walker malformation	Cerebellum of normal or diminished size, normal to small vermis with significant rotation (usually >45 degrees), large cisterna magna
Vermian hypoplasia	Cerebellum of normal or diminished size, small dysmorphic vermis with or without moderate rotation (usually <45 degrees), normal cisterna magna
Joubert syndrome	Cerebellum and cisterna magna of normal size, extremely small or absent vermis, typical configuration of fourth ventricle and cerebellar peduncles
Posterior fossa arachnoid cyst and other extra-axial cysts	Cystic asymmetric enlargement of the cisterna magna with a mass effect on the cerebellum

smaller the head dimensions, the greater the probability of microcephaly, although there is not an absolute quantitative cutoff point. The prevalence of microcephaly is estimated to be 1.6 per 1000 live births, but a minority of microcephalic infants diagnosed in the first year of life are detected at birth.

Microcephaly is not a single clinical entity but rather can result from primary cerebral malformations or exposure to teratogens or as part of a variety of syndromes. Microcephaly can also be transmitted with mendelian inheritance, usually as an autosomal recessive trait (Table 9-10). Association with abnormal intracranial anatomy is common, including abnormal convolitional patterns, such as macrogyria, microgyria, and agyria. The ventricles may be enlarged. Microcephaly is frequently found in cases of porencephaly, lissencephaly, and holoprosencephaly.

Microcephaly is a progressive condition, and therefore, definitive prenatal diagnosis is not possible in most cases. The natural history of fetal microcephaly is largely unknown. About 80% of infants affected with microcephaly have a normal head circumference at birth, and

about 90% of those diagnosed at birth had normal cranial measurements in the second trimester. Cases diagnosed in utero represent the exception and typically include fetuses with extreme reduction of head dimensions, usually with multiple anomalies.

Traditionally, microcephaly is suspected if the head circumference is 2 SDs or more below the mean for gestational age. However, only when the measurement is 5 SD or more below the mean is the diagnosis certain.<sup>46</sup> In those cases in which the head measurements are small and of concern, a detailed neurosonographic examination or MRI scan may be useful, as two thirds of microcephalic infants have abnormal CNS anatomy, including holoprosencephaly, anomalies of the corpus callosum, or cortical malformations. The forehead is often sloping, and demonstration of this feature should increase the index of suspicion.

The outcome of microcephaly varies, in part depending on the presence of associated anomalies. For infants without associated malformations, the prognosis is related to head size. The pediatric literature suggests that the risk of intellectual disability with head circumference between 2 and 3 SDs below the mean is in the range of 10% and 30%, rising to 50% to 60% for measurements of 3 SDs below the mean. Prenatal data, however, are more limited. In the largest available series, of the 20 infants found in utero to have head circumference between -2 and -3 SD below the mean, none had intellectual disability or neurocognitive abnormalities on long-term follow-up.<sup>47</sup>

*Megalencephaly*, or an abnormally large brain, usually results in normal neurologic outcome, although it can be associated with intellectual impairment.<sup>48</sup> Megalencephaly is part of some congenital syndromes, including Beckwith-Wiedemann syndrome, achondroplasia, neurofibromatosis, and tuberous sclerosis. Obstetric and pediatric sonologists are often challenged by the problem of possible megalencephaly, a condition that should be suspected with abnormally large head measurements but normal intracranial anatomy. In such cases, examination of the parents can be helpful, as a large head size can be familial.

## INTRACRANIAL CYSTS AND TUMORS

Intracranial *arachnoid cysts* are accumulations of clear cerebrospinal-like fluid between the dura and the brain substance. The histologic diagnosis is not always available, and the term is frequently used to indicate any intracranial cyst located in the subarachnoid space.

Arachnoid cysts may occur anywhere in the CNS, including the spinal canal. Most cases diagnosed antenatally involve supratentorial



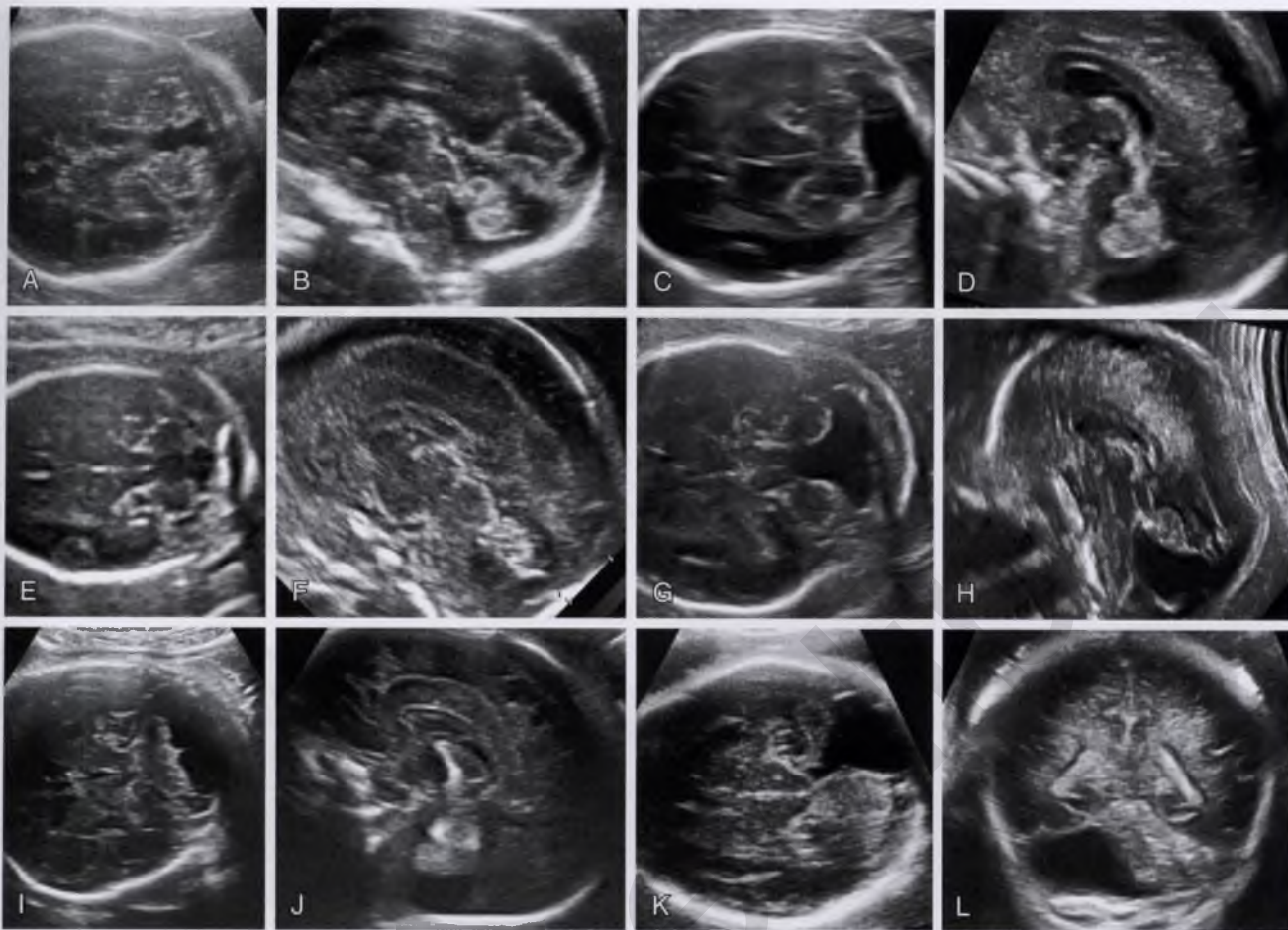


**FIG 9-19** Posterior fossa fluid collections (see Table 9-7). **A** and **B**, Blake pouch cyst; **C** and **D**, megacisterna magna; **E** and **F**, vermian hypoplasia; **G** and **H**, Dandy-Walker malformation; **I** and **J**, cerebellar hypoplasia; **K** and **L**, arachnoid cyst of the posterior fossa. (From Gandolfi Colleoni G, Contro E, Carletti A, et al: Prenatal diagnosis and outcome of fetal posterior fossa fluid collections. *Ultrasound Obstet Gynecol* 39(6):625–631, 2012, used with permission.)

cysts in the midline, or between the skull and the hemispheres. They appear as well-defined anechoic lesions, occasionally associated with ventriculomegaly, that usually develop in late gestation (Fig. 9-24). Arachnoid cysts should be differentiated from other cystic lesions with different prognostic implications; the most important feature is that they are external to the hemispheres and do not involve the brain parenchyma. Porencephalic cysts occur within the brain substance and frequently communicate with the ventricular system (see Fig. 9-22). Arachnoid cysts may be asymptomatic, although in some cases they may be associated with seizures, mild motor or sensory abnormalities, or hydrocephalus. Neurosurgical series generally suggest a good prognosis with absence of symptoms in more than 70% of cases.

**Choroid plexus cysts (CPCs)** appear as round sonolucent structures within the choroid plexus of the lateral ventricles and are found in 1% to 3% of midtrimester fetuses (Fig. 9-25). They may be unilateral or bilateral and are sometimes multiple. They are typically found in the atria of the lateral ventricles. CPCs are benign findings, although they have been associated with an increased likelihood of trisomy 18. The available data do not indicate an association with other chromosomal aberrations, including trisomy 21. As fetuses with trisomy 18 typically have severe malformations readily detectable with in utero ultrasound, there is general consensus that isolated CPCs do not present a significantly increased risk for trisomy 18 in the absence of other risk factors

or findings. The identification of isolated CPCs should not modify standard obstetric management, and as no deleterious effects on the fetus have been reported, there is no need for follow-up sonography. A handful of cases of very large cysts of the choroid plexus leading to increased intracranial pressure have been described in the neurosurgical literature, but these cysts likely represent a separate clinical entity.

Fetal **intracranial tumors** are rare, present in about 3 to 4 cases per 1 million live births. Teratomas account for most cases. The remaining minority include neuroepithelial tumors, lipomas, and craniopharyngiomas (Table 9-11). Ultrasound will rarely allow a specific diagnosis, as teratomas, astrocytomas, and craniopharyngiomas have a similar appearance, all presenting as a complex mass distorting the brain architecture, possibly associated with macrocephaly, ventriculomegaly, and intracranial calcifications (Fig. 9-26).<sup>49</sup> Only intracranial lipomas and choroid plexus papillomas have distinct sonographic appearances. Lipomas appear as well-defined echogenic areas, usually located in the midline, in the position normally occupied by the corpus callosum, and within the bodies of the lateral ventricles. Choroid plexus papillomas appear as large choroid plexuses, most frequently in association with ventriculomegaly and subarachnoid space enlargement. Cerebral tumors typically develop rapidly in late gestation, and many cases have been reported in which the midtrimester sonogram was unremarkable. The differential diagnosis of intracranial tumors includes other



space-occupying intracranial lesions, and it may be challenging in some cases to distinguish between a tumor and an acute intraparenchymal hemorrhage.

The prognosis of congenital CNS tumors is generally poor, with overall mortality rates in the range of 75%.<sup>40</sup> No clear data are available with regard to degree of neurologic impairment in survivors, but this is likely to be high as well. Large complex masses distorting intracranial anatomy (usually teratomas, astrocytomas, or craniopharyngiomas) have particularly dismal prognoses, with an overall survival rate of only

14%.<sup>49</sup> Intracranial lipomas represent an exception in that the reported survival rate is 100% and developmental handicap is rare.

Tuberous sclerosis is a syndrome characterized by multiorgan involvement, including the CNS, heart, and kidneys. Although transmitted as an autosomal dominant trait, the syndrome frequently arises from a spontaneous new mutation. Intellectual disability is present in 50% to 80% of cases and appears to be more frequent when the diagnosis is made antenatally or in early infancy. The most typical brain lesions are tubers, which are nodules of variable size composed of poorly differentiated neurons and glial cells disseminated in the neural plate or periventricular area. The CNS lesions are difficult to identify by antenatal sonography, although they can be seen more readily by MRI. The condition is usually suspected antenatally when cardiac tumors are identified (see Chapters 13 and 16). About 90% of such tumors are rhabdomyomas, and about 75% of fetuses with sonographic rhabdomyomas will be affected by tuberous sclerosis.<sup>50</sup> The risk appears to be higher when multiple cardiac tumors are present. Therefore, whenever cardiac tumors are identified, a search for cerebral lesions is warranted. Sonographic diagnosis is possible, although MRI is generally considered to be more sensitive.

**TABLE 9-8 Abnormalities Associated With Dandy-Walker Malformation**

Malformations	Chromosomal Abnormalities	Environmental Causes
<ul style="list-style-type: none"> <li>Holoprosencephaly</li> <li>Agenesis of the corpus callosum</li> <li>Neural tube defects</li> <li>Cleft lip</li> <li>Congenital heart disease</li> <li>Cornelia de Lange syndrome</li> <li>Goldenhar syndrome</li> <li>Kidney abnormalities</li> <li>Facial hemangiomas</li> <li>Klippel-Feil syndrome</li> <li>Polysyndactyly</li> </ul>	<ul style="list-style-type: none"> <li>6p-</li> <li>Dup 5p</li> <li>Dup 8p</li> <li>Dup 8q</li> <li>Trisomy 9</li> <li>Triploidy</li> <li>Dup 17q</li> </ul>	<ul style="list-style-type: none"> <li>Rubella</li> <li>Coumadin</li> <li>Alcohol</li> <li>Cytomegalovirus</li> <li>Diabetes</li> <li>Isotretinoin</li> </ul>
Mendelian Syndromes		
<ul style="list-style-type: none"> <li>Walker-Warburg syndrome (AR)</li> <li>Aase-Smith syndrome (AD)</li> <li>Ruvalcaba syndrome (AD/X-linked)</li> <li>Coffin-Siris syndrome (AR)</li> <li>Oral-facial-digital syndrome, type II (AR)</li> <li>Meckel-Gruber syndrome (AR)</li> <li>Aicardi syndrome (X-linked dominant)</li> <li>Ellis-van Creveld syndrome (AR)</li> <li>Fraser cryptophthalmos syndrome (AR)</li> </ul>		

AD, autosomal dominant; AR, autosomal recessive.  
Modified from Murray JC, Johnson JA, Bird TD: Dandy-Walker malformation: etiologic heterogeneity and empiric recurrence risk. Clin Genet 28:272, 1985.

**TABLE 9-9 Categorization and Grading of Fetal Intracranial Hemorrhage**

Type of Hemorrhage	Findings
Intracranial hemorrhage, grade I	Hemorrhage limited to the germinal matrix, subependymal
Intracranial hemorrhage, grade II	Intraventricular extension with ventricles <15 mm, intact brain parenchyma
Intracranial hemorrhage, grade III	Intraventricular extension with ventricles >15 mm, intact brain parenchyma
Intracranial hemorrhage, grade IV	Intraventricular hemorrhage and periventricular lesions/parenchymal involvement
Cerebellar hemorrhage	Hemorrhage within the cerebellar parenchyma
Subarachnoid hemorrhage and subdural hematoma	Accumulation of blood external to the hemispheres (extra-axial); the two entities are difficult to discriminate by antenatal ultrasound

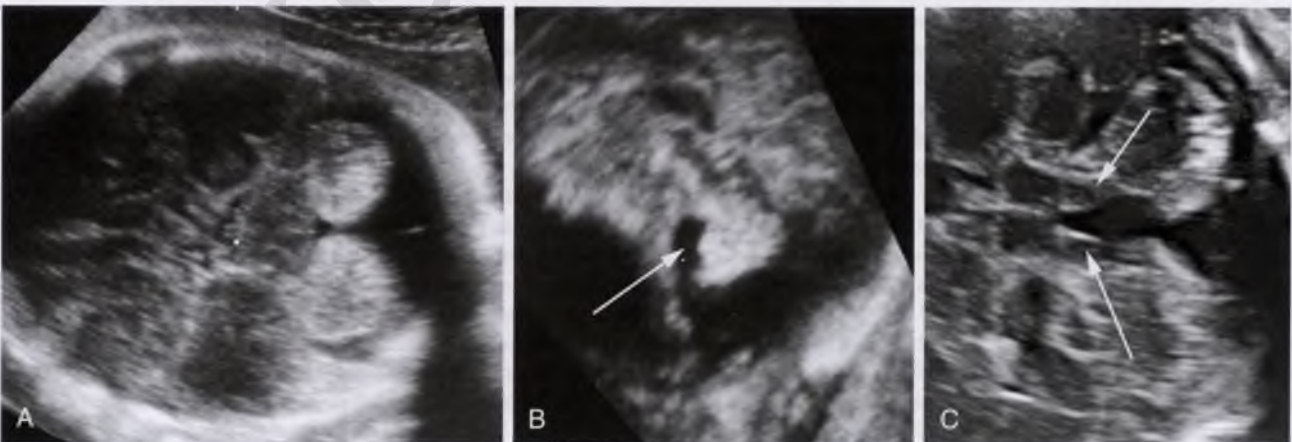


**FIG 9-20** Joubert syndrome. **A**, Posterior opening of the fourth ventricle is seen in the axial plane. **B**, A midline sagittal view reveals an irregular shape of the fourth ventricle (arrow) and absence of the normal configuration of the cerebellar vermis. **C**, Pathognomonic posterior separation of the cerebellar peduncles (arrows) seen in the axial plane (molar tooth sign).



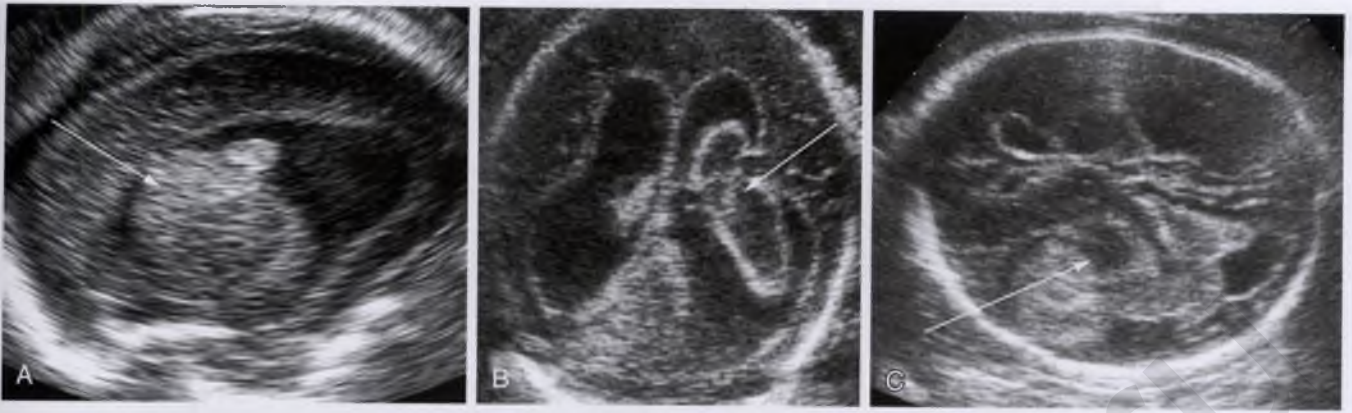


**FIG 9-21** Intracranial hemorrhage. **A**, Shortly after acute hemorrhage, the blood is markedly echogenic (*arrow*) in this grade II bleed, with intraventricular extension. **B**, In this older, subacute grade III hemorrhage, the coronal scan demonstrates moderately echogenic intraventricular blood clot (*arrow*) and ventricular enlargement. **C**, Grade IV hemorrhage with extension and associated parenchymal injury of the adjacent periventricular white matter (*arrow*).

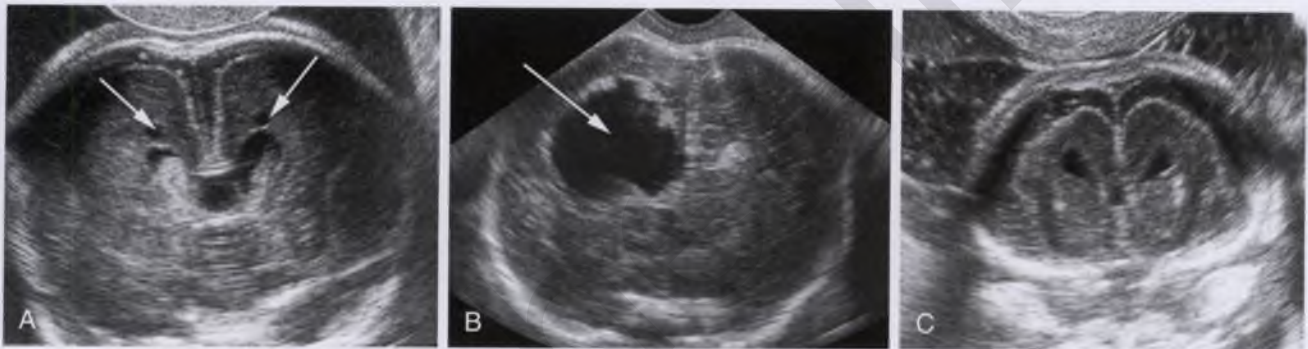


**FIG 9-22** Variable appearance of fetal stroke following severe hypoxic-ischemic events. **A**, Small fluid-filled cavities (*arrows*) adjacent to the frontal horns of bilateral lateral ventricles suggest periventricular leukomalacia. **B**, Large porencephalic cyst (*arrow*) communicating with the ipsilateral ventricle. **C**, Microcephaly. Small echogenic foci noted in the bilateral basal ganglia.

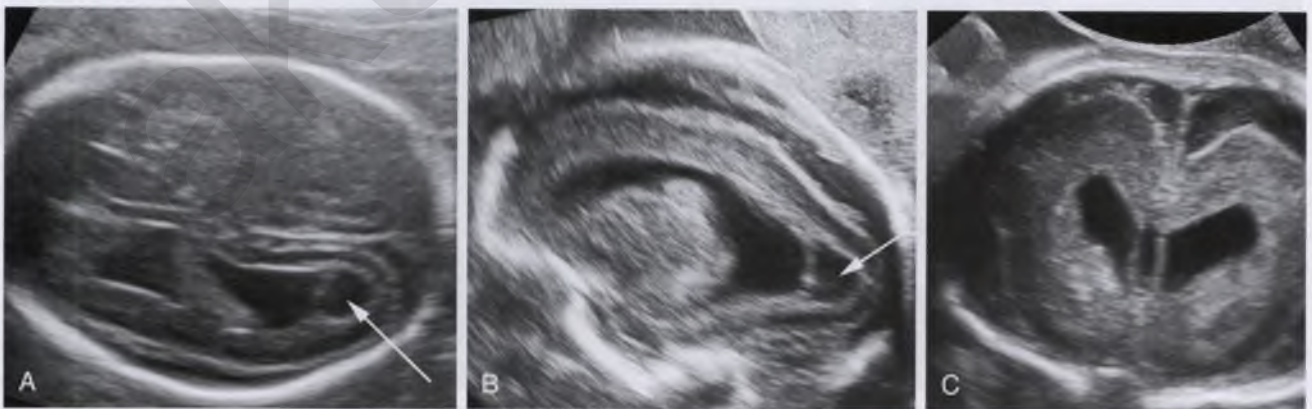


**FIG 9-23** Cerebral sequelae of in utero cytomegalovirus infection. **A** and **B**, An apparent septation is suggested within the posterior aspect of the lateral ventricle (*arrow*). This appearance is the result of parenchymal injury with cystic degeneration of periventricular white matter in the occipital lobe (*arrow*). **C**, In the coronal view, the ventricles and extra-axial subarachnoid spaces appear slightly enlarged, and the cerebral parenchyma appears irregularly echogenic.



TABLE 9-10 Etiologic Classification of Microcephaly

**I. Microcephaly With Associated Malformations****A. Genetic causes**

## 1. Chromosomal aberrations

Down syndrome (trisomy 21)

Trisomy 13

Trisomy 18

Trisomy 22

4p-

Cri-du-chat syndrome (5p-)

18p-

18q-

Langer-Giedion syndrome (8q24.1 deletion)

Williams syndrome (7q11.23 deletion)

## 2. Mendelian syndromes

Bloom syndrome (AR)

Borjeson-Forsman-Lehmann syndrome (XLR)

Cockayne syndrome (AR)

De Sanctis-Cacchione syndrome (AR)

Dubowitz syndrome (AR)

Fanconi pancytopenia (AR)

Focal dermal hypoplasia (XLD)

Incontinentia pigmenti (XLD)

Lissencephaly syndrome (AR)

Meckel-Gruber syndrome (AR)

Menkes syndrome (XLR)

Roberts syndrome (AR)

Rubenstein-Taybi syndrome

Seckel syndrome (AR)

Smith-Lemli-Opitz syndrome (AR)

**B. Environmental causes**

## 1. Prenatal infections

Rubella syndrome

Cytomegalovirus disease

Herpesvirus hominis infection

Toxoplasmosis

## 2. Prenatal exposure to drugs or chemicals

Fetal alcohol syndrome

Fetal hydantoin syndrome

Aminopterin syndrome

## 3. Maternal phenylketonuria

**C. Unknown causes**

## 1. Recognized syndromes

Coffin-Siris syndrome

DeLange syndrome

Johanson-Blizzard syndrome

## 2. Undefined combinations

**II. Microcephaly Without Associated Malformations****A. Genetic causes**

## 1. Primary microcephaly (AR)

## 2. Paine syndrome (XLR)

## 3. Alpers disease (AR)

## 4. Inborn errors of metabolism

Disorders of folic acid metabolism (AR)

Hyperlysinemia (AR)

Methylmalonic acidemia (AR)

Maternal phenylketonuria (AR)

**B. Environmental causes**

## 1. Prenatal exposure to radiation

## 2. Fetal malnutrition

## 3. Perinatal trauma or hypoxia

## 4. Postnatal infections

**C. Other causes**

## 1. Angelman syndrome

AR, autosomal recessive; XLD, X-linked dominant; XLR, X-linked recessive.

Modified from Ross JJ, Frias JL: Microcephaly. In Vinken PJ, Bruyn GW (eds): *Congenital Malformations of the Brain and Skull*. Handbook of Clinical Neurology, vol. 30. Amsterdam, Elsevier North Holland Biomedical Press, 1977, pp 507-524.**FIG 9-24** Midline arachnoid cyst. Large irregular anechoic fluid-filled structures shown by ultrasound in the axial (A), sagittal (B), and coronal (C) imaging planes.

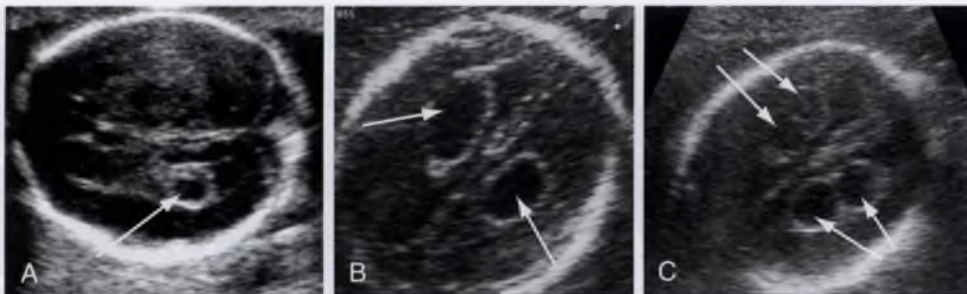


**FIG 9-25** Choroid plexus cysts (arrows). **A**, Single and small cyst; **B**, large bilateral cyst; and **C**, multiple cysts.

### TABLE 9-11 Classification of Congenital Intracranial Tumors

Embryonic tumors
Teratoma
Epidermoid
Dermoid
Germinal tumors
Germinoma
Embryonal carcinoma
Choriocarcinoma
Endodermal sinus tumor
Teratoma
Neuroblastic tumors
Medulloblastoma
Neuroblastoma
Retinoblastoma
Tumors related to embryonal remnant tissues
Craniopharyngioma
Chordoma
Tumors of ependymal origin
Ependymoma
Subependymal mixed glioma
Choroid plexus papilloma
Glioblastoma multiforme
Malignant astrocytoma
Tumors associated with genetic diseases
Tuberous sclerosis
Neurofibromatosis
Systemic angiomatosis of the central nervous system and eye (Von Hippel-Lindau syndrome)
Colloid cyst of the third ventricle
Heterotopia and hamartoma
Lipoma
Vascular tumors: hemangioblastoma

Modified from Mori K: *Neuroradiology and Neurosurgery*. New York, Thieme-Stratton, 1985; Wilson et al: *Classification of intracranial tumors*. In Newton TH, Potts DG (eds): *Radiology of the Skull and Brain*. Anatomy and Pathology. St. Louis, CV Mosby, 1977.

### Vascular Abnormalities

Vascular abnormalities of the fetal brain are relatively rare, and only a limited number of cases have been described. The majority of reports refer to vein of Galen vascular malformations.

The term *aneurysm of the vein of Galen* refers to a spectrum of arteriovenous malformations, ranging from a single large aneurysmal dilatation of the vein of Galen to multiple communications between

the vein and the carotid and vertebrobasilar systems. The typical finding is an elongated anechoic area at the level of the cistern of the vein of Galen, with color and spectral Doppler evidence of turbulent venous or arterial intraluminal blood flow (Fig. 9-27). The cerebral architecture may be intact or may be distorted owing to associated ventriculomegaly, porencephaly, and cerebral edema suggested by increased echogenicity of the cortex. A large arteriovenous shunt may lead to increased cardiac work and result in high-output heart failure and hydrops. The available experience with prenatal diagnosis suggests a mortality rate of about 50%, and normal neurodevelopment in about 50% of survivors.<sup>51</sup> The outcome is strongly dependent on antenatal evidence of other intracranial abnormalities (hydrocephalus, brain edema, porencephaly) and hydrops. When any of these is identified, the prognosis is poor. In general, cases with normal postnatal development had isolated vascular lesions, without cerebral or cardiovascular compromise in utero, and were treated after birth with angiographic embolization.

It may be difficult to distinguish an aneurysm of the vein of Galen from a pial arteriovenous malformation.<sup>52</sup> The latter is a vascular malformation within the brain parenchyma that results in enlargement of the cerebral venous system in general and the vein of Galen in particular. The outcome is similar to that of vein of Galen aneurysm, and the prognosis is poor when there are associated abnormal cerebral findings or evidence of cardiac overload.

Several cases of in utero *thrombosis of the dural sinuses* have been described. The sonographic findings include identification of a posterior, fluid-filled structure displacing the fetal brain anteriorly and usually containing an echogenic core likely representing thrombus (Fig. 9-28). The cause of antenatal cases is uncertain. Thrombophilias may be found, but usually the condition is idiopathic. Although the intrauterine appearance may be quite dramatic, complete remission occurs frequently,<sup>53</sup> and if there are no signs of cerebral compromise, the outcome is good in most cases.

### Cortical Malformations and Anomalies of Neuronal Migration

The neuronal cells that form the gray matter of the CNS originate from the surface of the lateral ventricles and later migrate along radially aligned glial cells to reach the outer surface of the brain. The migration occurs in different waves that last for several weeks. Most of the process takes place between 8 and 16 weeks' gestation, but this migration continues until 25 weeks. Once the neuronal cells have reached their destination on the surface of the brain, they undergo a process of maturation and differentiation, grow axons and dendrites, and develop synapses with other neurons, giving rise to a well-ordered, six-layer cortex. Cortical malformations are characterized by the incomplete formation of the cortical layers, with abnormal locations of neurons that have failed to reach their intended final destination. The migrational process may be arrested by environmental factors (ischemia,



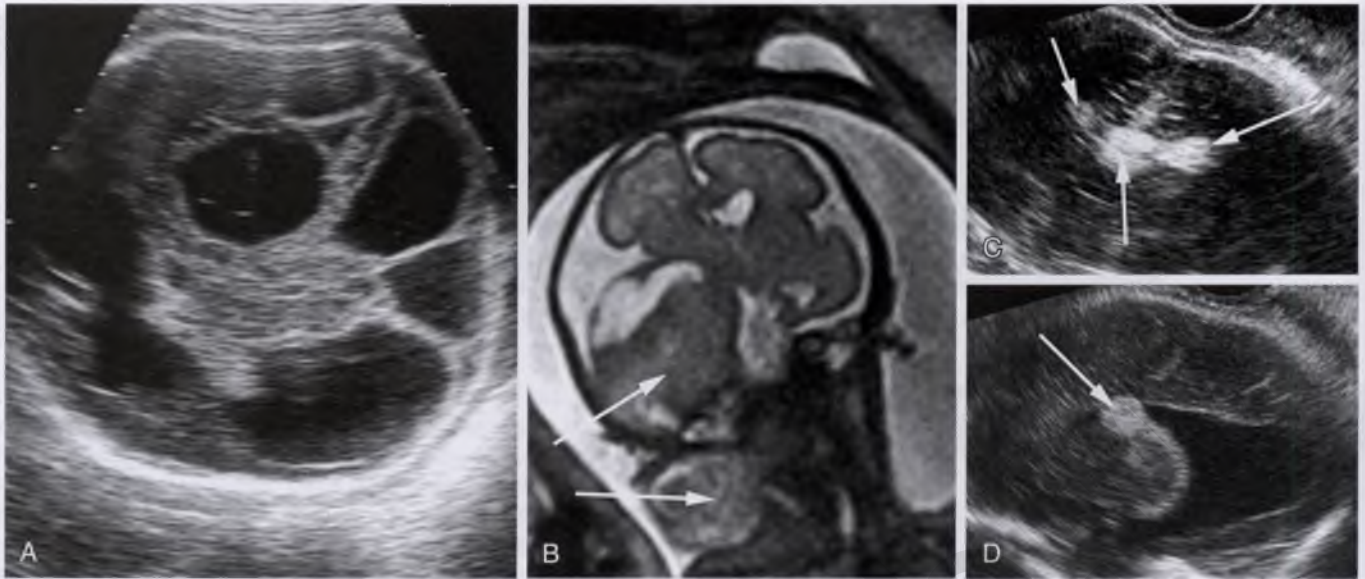


**FIG 9-26** Fetal intracranial tumors: intracranial teratoma as visualized by ultrasound (**A**) and magnetic resonance imaging (**B**) (arrows). Multiple lipomas appear as echogenic round masses (arrows) in a fetus with associated agenesis of the corpus callosum (**C** and **D**).

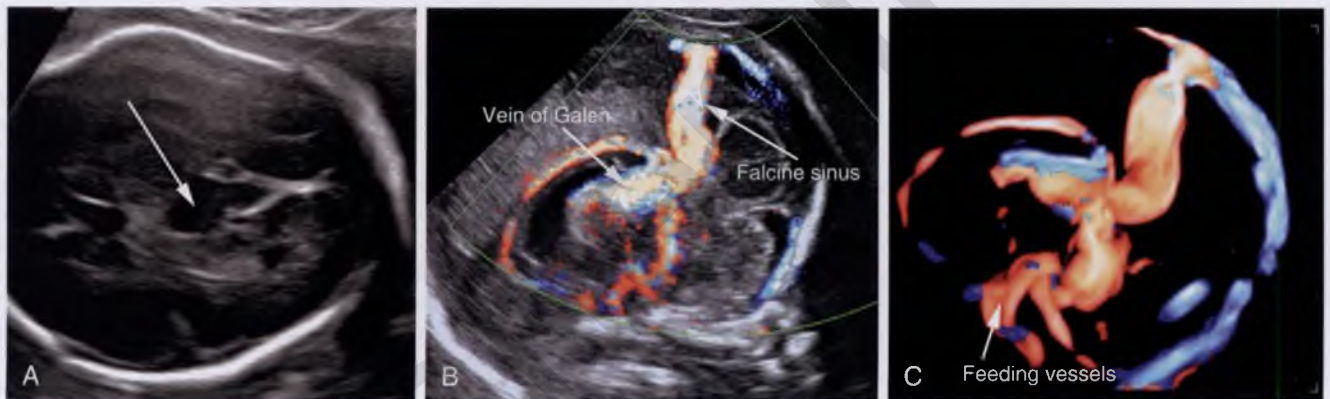


**FIG 9-27** Aneurysm of the vein of Galen: **A**, The aneurysm appears as a hypoechoic tubular midline structure; **B**, with prominent turbulent intraluminal flow on color Doppler sonography, draining into a large falcine sinus; and **C**, 3D color Doppler sonogram delineating the vascular anatomy with abnormal arterial feeding vessels supplying the large vein of Galen.

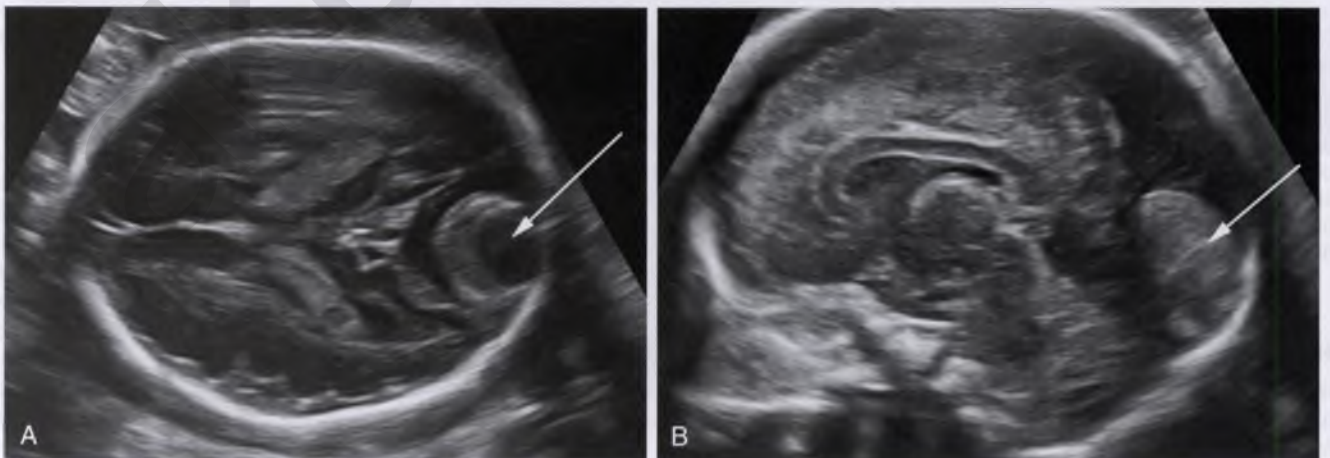


**FIG 9-28** Thrombosis of the sinus confluence: a large hypoechoic collection containing an echogenic core suggestive of thrombus is seen in the occipital region, posterior to the brain on axial (**A**) and midline sagittal (**B**) images (arrows).



teratogens) but for some anomalies, a genetic predisposition is present. Although the anatomy may be variable, with many cortical malformations the cortex is abnormally thickened by a large, disorganized layer of neurons, whereas the underlying white matter is thin. Macroscopically, the primary finding is an alteration in the convolitional pattern of the brain, which may be associated with modifications in brain mass and ventricle size.

Cortical malformations should be considered in the differential diagnosis of ventriculomegaly, microcephaly, and macrocephaly and are suspected when an anomalous pattern of cerebral convolutions is present.<sup>54</sup> These disorders include a broad spectrum of anomalies, including *lissencephaly*, in which there is absence or reduction of convolutions; *polymicrogyria*, an increased number of small convolutions; *unilateral megalencephaly*; *schizencephaly*; and *gray matter heterotopias*.

The entities most frequently described in antenatal studies are summarized in Table 9-12 and Figure 9-29. The optimal imaging technique for the diagnosis and evaluation of these anomalies postnatally is MRI, as this allows clear discrimination between white and gray matter. Antenatally, faster sequences are used because of fetal movement, and these have more limited resolution. In addition, the neural plate is incompletely formed antenatally, and this also limits diagnosis of many CNS anomalies. In utero MRI can, however, provide a panoramic view of the fetus and improved visualization of the cerebral surface and is therefore an important complementary imaging modality (see Chapter 23). With improvements in imaging quality and resolution, detection of typical macroscopic abnormalities of the brain, such as cortical clefts and gyral anomalies, is sometimes possible prenatally, although usually only in late gestation (Figs. 9-30 and 9-31). Studies have documented the

**TABLE 9-12 Sonographic Findings Associated With Cortical Malformations**

Anomaly	Sonographic Findings
Lissencephaly	Smooth brain contour without recognizable convolutions/gyri; ventriculomegaly and microcephaly may be present
Unilateral megalencephaly	Macrocephaly; shift of the midline with overgrowth of one hemisphere; abnormal thick gyri and ventriculomegaly frequently present in the larger hemisphere
Schizencephaly	Cleft of the brain resulting in connection between the subarachnoid space and the ventricular ependyma; may be unilateral or bilateral
Periventricular nodular heterotopia	Irregular margin of the lateral ventricle due to small subependymal nodules of heterotopic gray matter; may be focal or diffuse
Polymicrogyria	Excessive number of small gyri; may be generalized or focal
Pachygyria	Large thick convolutions/gyri of the cerebral cortex

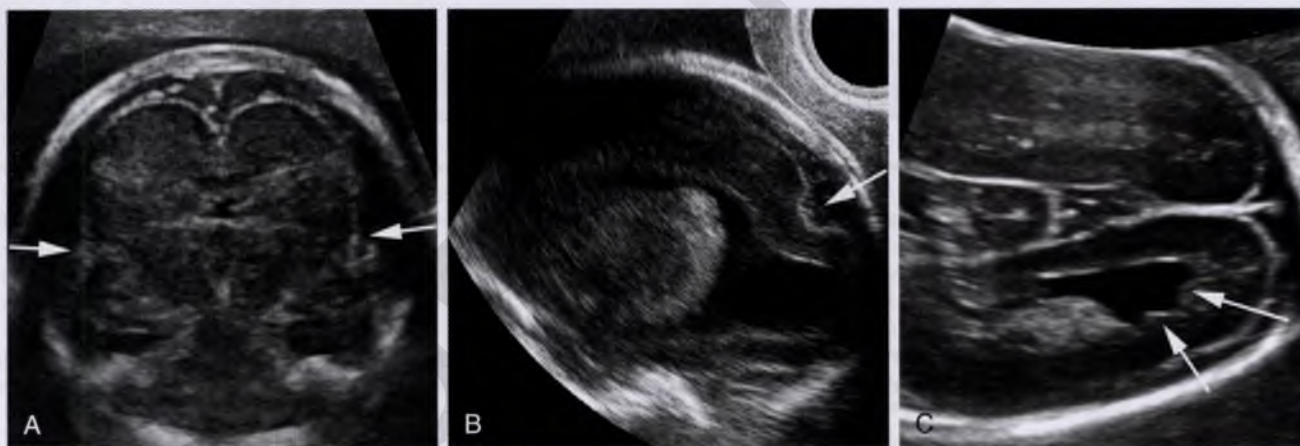


**FIG 9-29** Cortical malformations (see Table 9-12). **A**, Lissencephaly; in this third trimester fetus, the brain contour appears abnormally smooth on this coronal ultrasound image, without evidence of convolutions or development of the sylvian fissures (arrows). **B**, An irregular sulcus/infolding (arrow) is noted in this fetus, diagnosed after birth with polymicrogyria. **C**, Irregular contour of the posterior aspect of the dependent lateral ventricle (arrows) suggests periventricular nodular heterotopia.

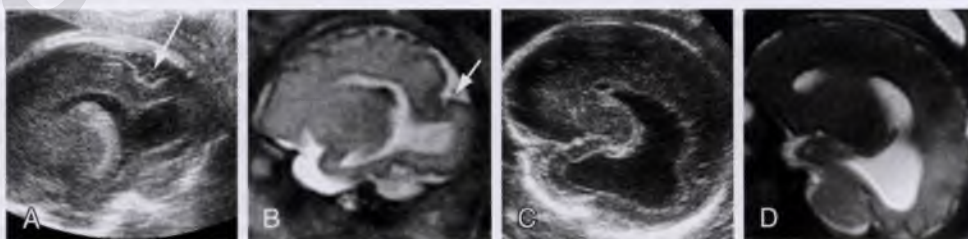


**FIG 9-30** Fetal cortical abnormalities demonstrated by sonography and magnetic resonance imaging. **A** and **B**, Abnormal convolution associated with unusual shape of the cortex (arrows) and underlying lateral ventricle. **C** and **D**, This fetus at 34 weeks' gestation has a very smooth brain and an unusual echogenicity of the cortex.



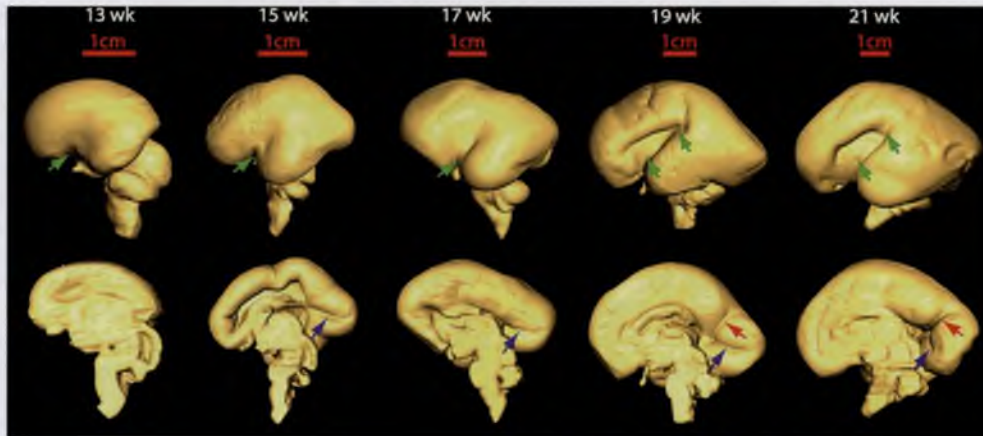


**FIG 9-31** Three-dimensional reconstruction of the lateral (*top row*) and medial (*bottom row*) surface of 13- to 21-week fetal brains to reveal the development of the sylvian fissure (*green arrows*), the calcarine fissure (*blue arrows*), and the parieto-occipital sulcus (*red arrows*). (From Huang H, Xue R, Zhang J, et al: Anatomical characterization of human fetal brain development with diffusion tensor magnetic resonance imaging. *J Neurosci* 29(13):4263–4273, 2009.)

**TABLE 9-13 Gestational Age\* When Primary Fissures and Sulci Become Visible at Anatomic, Sonographic, and Magnetic Resonance Imaging Examinations**

Visible Feature	Anatomic Examination	SONOGRAPHIC EXAMINATION†		MAGNETIC RESONANCE IMAGING‡	
		First Seen	Always Seen	First Seen	Always Seen
Parieto-occipital fissure	16	18.5	20.5	18-19	22-23
Calcarine fissures	16	18.5	21.9	18-19	22-23
Cingulate sulcus	18	23.2	24.3	24-25	28-29
Central sulcus	20			26-27	26-27
Convexity sulci	20-25	23.2	27.9	26-27	28-29

\*In weeks.

†Data from Toi A, Lister WS, Fong KW: How early are fetal cerebral sulci visible at prenatal ultrasound and what is the normal pattern of early fetal sulcal development? *Ultrasound Obstet Gynecol* 24:706–715, 2004.

‡Data from Levine D, Barnes P: Cortical maturation in normal and abnormal fetuses as assessed with prenatal MR imaging. *Radiology* 210:751–758, 1999.

From Ghai S, Fong KD, Toi A: Prenatal US and MR imaging findings of lissencephaly: review of fetal cerebral sulcal development. *Radiographics* 26:389–405, 2006.

sonographic appearance of developing brain structures such as the parieto-occipital fissure, calcarine fissure, cingulate sulcus, and other convexity sulci. In a study by Toi and coworkers,<sup>55</sup> the authors reported the youngest age at which a specific sulcus was first visible in a fetus and the age after which the sulcus was visible in all fetuses (Table 9-13). Sulci could be seen by transabdominal sonography as early as 18.5 weeks. The medial hemispheric sulcus and the insula were visible earlier and more confidently than convexity sulci. The earliest gestational ages at which specific sulci could be seen in any fetus were as follows: parieto-occipital fissure, 18.5 weeks; calcarine fissure, 18.5 weeks; cingulate sulcus, 23.2 weeks; and convexity sulci, 23.2 weeks. In this series, the gestational ages at which these sulci were always visible were the parieto-occipital fissure, after 20.5 weeks; calcarine fissure, after 21.9 weeks; cingulate sulcus, after 24.3 weeks; and convexity sulci, after 27.9 weeks.<sup>55</sup> Failure of identification of sulcation beyond these gestational ages would prompt one to suspect lissencephaly.

## CONCLUSIONS

Modern ultrasound equipment affords unique potential for the visualization and evaluation of normal and abnormal fetal CNS development. A large number of congenital anomalies can be consistently

recognized. Transvaginal sonography can extend antenatal diagnosis to very early gestation, and MRI can be used to improve the accuracy of the diagnosis in many cases.

Nevertheless, there are many limitations to the prenatal diagnosis of CNS anomalies. Some studies of low-risk patients undergoing basic sonographic examinations have reported sensitivities in excess of 80%.<sup>56,57</sup> However, these results probably overestimate the diagnostic performance of the technique. These surveys typically had very short postnatal follow-up, and almost all included cases of open neural tube defects, with recognition of these lesions facilitated by systematic screening with maternal serum AFP. Pitfalls of prenatal sonography are well documented. One of the most important limitations is related to the continuation of brain development in the second half of gestation and into early childhood, limiting the detection of some anomalies such as microcephaly and cortical malformations. Furthermore, some cerebral lesions do not result from abnormal embryologic development but represent the consequence of acquired prenatal, perinatal, and postnatal insults. Even in expert hands, some fetal CNS anomalies may be difficult or impossible to diagnose in utero.<sup>58</sup>

When abnormal intracranial anatomy is identified, accurate and compassionate counseling of the parents is critically important but frequently difficult. Some cerebral anomalies have outcomes that are

relatively predictable, as with catastrophic lesions such as anencephaly and severe holoprosencephaly. Others are more variable, although a relatively predictable range of outcomes can be provided such as with spina bifida. There are, however, a large number of conditions that can be correctly identified in utero and yet have uncertain progression and prognosis. Representative examples of such conditions include mild ventriculomegaly, ACC, intracranial cysts, and posterior fossa anomalies. When the sonographic findings are uncertain, MRI can often be helpful. However, the available literature reports some conflicting results, and the precise role of this technique is yet to be defined.

## REFERENCES

- Myriantopoulos NC: Epidemiology of central nervous system malformations. In Vinken PJ, Bruyn GW, editors: *Handbook of Clinical Neurology*, Amsterdam, 1977, Elsevier, pp 139–171.
- Patel MD, Goldstein RB, Tung S, Filly RA: Fetal ventricular atrium: difference in size according to sex. *Radiology* 194:713–715, 1995.
- Gupta JK, Bryce FC, Lilford RJ: Management of apparently isolated fetal ventriculomegaly. *Obstet Gynecol Surv* 49(10):716–721, 1994.
- Melchiorre K, Bhida A, Gika AD, et al: Counseling in isolated mild fetal ventriculomegaly. *Ultrasound Obstet Gynecol* 34(2):212–224, 2009.
- Agathokleous M, Chaveeva P, Poon LC, et al: Meta-analysis of second-trimester markers for trisomy 21. *Ultrasound Obstet Gynecol* 41(3):247–261, 2013.
- Johnson SP, Sebire NJ, Snijders RJ, et al: Ultrasound screening for anencephaly at 10–14 weeks of gestation. *Ultrasound Obstet Gynecol* 9(1):14–16, 1997.
- Callen AL, Filly RA: Supratentorial abnormalities in the Chiari II malformation. I: the ventricular point. *J Ultrasound Med* 27:33–38, 2008.
- Ghi T, Pilu G, Falco P, et al: Prenatal diagnosis of open and closed spina bifida. *Ultrasound Obstet Gynecol* 28(7):899–903, 2006.
- Van den Hof MC, Nicolaides KH, Campbell J, Campbell S: Evaluation of the lemon and banana signs in one hundred thirty fetuses with open spina bifida. *Am J Obstet Gynecol* 162(2):322–327, 1990.
- Roman AS, Gupta S, Fox NS, et al: Is MSAFP still a useful test for detecting open neural tube defects and ventral wall defects in the era of first-trimester and early second-trimester fetal anatomical ultrasounds? *Fetal Diagn Ther* 37(3):206–210, 2015.
- Appasamy M, Roberts D, Pilling D, Buxton N: Antenatal ultrasound and magnetic resonance imaging in localizing the level of lesion in spina bifida and correlation with postnatal outcome. *Ultrasound Obstet Gynecol* 27(5):530–536, 2006.
- Khalil A, Caric V, Papageorgiou A, et al: Prenatal prediction of need for ventriculoperitoneal shunt in open spina bifida. *Ultrasound Obstet Gynecol* 43(2):159–164, 2014.
- Bruner JP, Tulipan N: Tell the truth about spina bifida. *Ultrasound Obstet Gynecol* 24:595, 2004.
- Shurtluff DB, Luthy DA, Nyberg DA, et al: Meningomyelocele: management in utero and post natum. *Ciba Found Symp* 181:270, discussion 280, 1994.
- Shurtluff DB, Luthy DA, Nyberg DA, et al: The outcome of fetal myelomeningocele brought to term. *Eur J Pediatr Surg* 4(Suppl 1):25, 1994.
- Luthy DA, Wardinsky T, Shurtluff DB, et al: Cesarean section before the onset of labor and subsequent motor function in infants with meningomyelocele diagnosed antenatally. *N Engl J Med* 324:662, 1991.
- Hill AE, Beattie F: Does caesarean section delivery improve neurological outcome in open spina bifida? *Eur J Pediatr Surg* 4(Suppl 1):32–34, 1994.
- Barkovich JA: Congenital malformations of the brain and skull. In Barkovich JA, editor: *Pediatric Neuroimaging*, ed 4, Philadelphia, 2005, Lippincott Williams & Wilkins.
- Diebler C, Dulac O: Cephaloceles: clinical and neuroradiological appearance. Associated cerebral malformations. *Neuroradiology* 25:199, 1983.
- Santo S, D'Antonio F, Homfray T, et al: Counseling in fetal medicine: agenesis of the corpus callosum. *Ultrasound Obstet Gynecol* 40(5):513–521, 2012.
- Goldstein RB, LaPidus AS, Filly RA: Fetal cephaloceles: diagnosis with US. *Radiology* 180(3):803–808, 1991.
- Barkovich JA: Apparent atypical callosal dysgenesis: analysis of MR findings in six cases and their relationship to holoprosencephaly. *Am J Neuroradiol* 11:333, 1990.
- Barkovich JA, Norman D: Anomalies of the corpus callosum: correlation with further anomalies of the brain. *Am J Roentgenol* 151:171, 1988.
- Malinger G, Lev D, Kidron D, et al: Differential diagnosis in fetuses with absent septum pellucidum. *Ultrasound Obstet Gynecol* 25:42, 2005.
- Blaas HG, Eriksson AG, Salvesen KA, et al: Brains and faces in holoprosencephaly: pre- and postnatal description of 30 cases. *Ultrasound Obstet Gynecol* 19(1):24–38, 2002.
- Pilu G, Sandri F, Perolo A, et al: Prenatal diagnosis of lobar holoprosencephaly. *Ultrasound Obstet Gynecol* 2:88, 1992.
- Han JS, Benson JE, Kaufman B, et al: MR imaging of pediatric cerebral abnormalities. *J Comput Assist Tomogr* 9:103, 1985.
- Jeret JS, Serur D, Wisniewski K, et al: Frequency of agenesis of the corpus callosum in the developmentally disabled population as determined by computerized tomography. *Pediatr Neurosci* 12:101, 1985.
- Pilu G, Sandri F, Perolo A, et al: Sonography of fetal agenesis of the corpus callosum: a survey of 35 cases. *Ultrasound Obstet Gynecol* 3:318, 1993.
- Bennett GL, Bromley B, Benacerraf BR: Agenesis of the corpus callosum: prenatal detection usually is not possible before 22 weeks of gestation. *Radiology* 199:447, 1996.
- Gowan LR, Masten MG: Agenesis of the corpus callosum: diagnosis of a case by encephalography. *Am J Dis Child* 60(6):1381–1385, 1940.
- Bertino RE, Nyberg DA, Cyr DR, Mack LA: Prenatal diagnosis of agenesis of the corpus callosum. *J Ultrasound Med* 7(5):251–260, 1988.
- Aicardi G, Lefebvre J, Lericque-Koechlin A: A new syndrome: spasm in flexion, callosal agenesis, ocular abnormalities. *Electroencephalogr Clin Neurophysiol* 19:609, 1965.
- Rosser TL, Acosta MT, Packer RJ: Aicardi syndrome: spectrum of disease and long-term prognosis in 77 females. *Pediatr Neurol* 27:343, 2002.
- Sotiriadis A, Makrydimas G: Neurodevelopment after prenatal diagnosis of isolated agenesis of the corpus callosum: an integrative review. *Am J Obstet Gynecol* 206(4):337.e1–337.e5, 2012.
- Bault JP, Salomon LJ, Guibaud L, Achiron R: Role of three-dimensional ultrasound measurement of the optic tract in fetuses with agenesis of the septum pellucidum. *Ultrasound Obstet Gynecol* 37(5):570–575, 2011.
- Tortori-Donati P, Fondelli MP, Rossi A, et al: Cystic malformations of the posterior cranial fossa originating from a defect of the posterior membranous area. Mega cisterna magna and persisting Blake's pouch: two separate entities. *Childs Nerv Syst* 12:303, 1996.
- Robinson AJ: Inferior vermian hypoplasia—preconception, misconception. *Ultrasound Obstet Gynecol* 43(2):123–136, 2014.
- Gandolfi Colleoni G, Contro E, Carletti A, et al: Cystic diagnosis and outcome of fetal posterior fossa fluid collections. *Ultrasound Obstet Gynecol* 39(6):625–631, 2012.
- Nelson MD, Jr, Maher K, Gilles FH: A different approach to cysts of the posterior fossa. *Pediatr Radiol* 34:720, 2004.
- Limperopoulos C, Robertson RL, Estroff JA, et al: Diagnosis of inferior vermian hypoplasia by fetal magnetic resonance imaging: potential pitfalls and neurodevelopmental outcome. *Am J Obstet Gynecol* 194(4):1070–1076, 2006.
- Quarello E, Molho M, Garel C, et al: Prenatal abnormal features of the fourth ventricle in Joubert syndrome and related disorders. *Ultrasound Obstet Gynecol* 43(2):227–232, 2014.
- Ghi T, Simonazzi G, Perolo A, et al: Outcome of antenatally diagnosed intracranial hemorrhage: case series and review of the literature. *Ultrasound Obstet Gynecol* 22(2):121–130, 2003.
- Govaert P: Prenatal stroke. *Semin Fetal Neonatal Med* 14(5):250–266, 2009.
- Picone O, Teissier N, Cordier AG, et al: Detailed in utero ultrasound description of 30 cases of congenital cytomegalovirus infection. *Prenat Diagn* 34(6):518–524, 2014.
- Chervenak FA, Rosenberg J, Brightman RC, et al: A prospective study of the accuracy of ultrasound in predicting fetal microcephaly. *Obstet Gynecol* 69(6):908–910, 1987.



47. Stoler-Poria S, Lev D, Schweiger A, et al: Developmental outcome of isolated fetal microcephaly. *Ultrasound Obstet Gynecol* 36(2):154–158, 2010.
48. DeMyer W: Megalencephaly: types, clinical syndromes, and management. *Pediatr Neurol* 2:321, 1986.
49. Schlembach D, Bornemann A, Rupprecht T, Beinder E: Fetal intracranial tumors detected by ultrasound: a report of two cases and review of the literature. *Ultrasound Obstet Gynecol* 14(6):407–418, 1999.
50. Tworetzky W, McElhinney DB, Margossian R, et al: Association between cardiac tumors and tuberous sclerosis in the fetus and neonate. *Am J Cardiol* 92(4):487–489, 2003.
51. Sepulveda W, Platt CC, Fisk NM: Prenatal diagnosis of cerebral arteriovenous malformation using color Doppler ultrasonography: case report and review of the literature. *Ultrasound Obstet Gynecol* 6(4):282–286, 1995.
52. Garel C, Azarian M, Lasjaunias P, Luton D: Pial arteriovenous fistulas: dilemmas in prenatal diagnosis, counseling and postnatal treatment. Report of three cases. *Ultrasound Obstet Gynecol* 26(3):293–296, 2005.
53. Laurichesse Delmas H, Winer N, Gallot D, et al: Prenatal diagnosis of thrombosis of the dural sinuses: report of six cases, review of the literature and suggested management. *Ultrasound Obstet Gynecol* 32(2):188–198, 2008.
54. Malinger G, Kidron D, Schreiber L, et al: Prenatal diagnosis of malformations of cortical development by dedicated neurosonography. *Ultrasound Obstet Gynecol* 29(2):178–191, 2007.
55. Toi A, Lister WS, Fong KW: How early are fetal cerebral sulci visible at prenatal ultrasound and what is the normal pattern of early fetal sulcal development? *Ultrasound Obstet Gynecol* 24:706–715, 2004.
56. Ewigman BG, Crane JP, Frigoletto FD, et al: Effect of prenatal ultrasound screening on perinatal outcome. RADIUS Study Group. *N Engl J Med* 329:821, 1993.
57. Crane JP, LeFevre ML, Winborn RC, et al: A randomized trial of prenatal ultrasonographic screening: impact on the detection, management, and outcome of anomalous fetuses. The RADIUS Study Group. *Am J Obstet Gynecol* 171:392, 1994.
58. Malinger G, Lerman-Sagie T, Waternberg N, et al: A normal second-trimester ultrasound does not exclude intracranial structural pathology. *Ultrasound Obstet Gynecol* 20:51, 2002.

# Ultrasound Evaluation of the Fetal Face and Neck

Kate E. Pettit, Nga V. Tran, Dolores H. Pretorius

## SUMMARY OF KEY POINTS

- The diagnosis of a typical orofacial cleft involving the palate can be suspected as early as the first trimester by the presence of an anechoic space or discontinuity in the retranasal triangle (RNT) view.
- Using two-dimensional (2D) ultrasound, identifying typical clefts in the second trimester is best done by utilizing the coronal view of the nose and lips and the axial view of the fetal palate.
- Three-dimensional (3D) ultrasound, particularly the rendering function, can be helpful in the diagnosis of clefts of the hard and soft palate as well as in showing the surface rendered images to the family.
- Hypertelorism and hypotelorism, which can be defined by standard tables, are associated with a range of genetic syndromes.
- Micro- and retrognathia are identified in the sagittal profile view, and the diagnosis can be made subjectively or objectively with the use of facial angles.
- Craniosynostosis, the premature closure of cranial sutures, should be suspected in the presence of significant dolichocephaly or brachycephaly and may be associated with other anomalies or syndromes.
- Nuchal cystic hygromas are often associated with aneuploidy, with a higher frequency of trisomy 21 in the first trimester and Turner syndrome in the second trimester.
- Facial tumors and neck masses can compromise the fetal airway at birth and may require the use of an ex utero intrapartum treatment (EXIT) procedure at the time of delivery.

## OUTLINE

### Normal Sonographic Anatomy of the Fetal Face, 243

#### Craniofacial Anomalies, 245

Typical Facial Clefts, 245

Atypical Facial Clefts, 250

Orbital and Ocular Defects, 252

Micrognathia and Retrognathia, 255

Macroglossia, 257

Tumors of the Face, 257

Ears, 262

#### Craniosynostosis, 262

#### Anomalies of the Neck, 265

Nuchal Cystic Hygroma, 265

Other Neck Masses, 266

#### Conclusions, 268

## NORMAL SONOGRAPHIC ANATOMY OF THE FETAL FACE

The fetal face can be evaluated in three different planes using 2D ultrasound—sagittal, axial or transverse, and coronal (Fig. 10-1). Each plane has a unique contribution to the evaluation of fetal craniofacial anatomy. The sagittal plane allows for assessment of the fetal profile and can illustrate any dysmorphism of the forehead or nose and the presence of the nasal bone as well as the positioning of the fetal chin to evaluate for micrognathia or retrognathia (Table 10-1). The axial or transverse plane is integral at two different levels (Table 10-2). The first key image is that of the orbits and eyes, which can be obtained caudad to the image displaying the biparietal diameter. Romero and associates have published nomograms for the various ocular parameters including binocular distance, interocular distance, and ocular diameter (Table 10-3).<sup>1</sup> Moving the transducer further caudad on the fetal head, one arrives at the level of the superior lip and palate followed by the fetal mandible.

3D ultrasound has an integral role in the evaluation and diagnosis of craniofacial anomalies. Though not yet validated for routine use in low-risk pregnancies, its use in the context of a detected or suspected craniofacial anomaly is quite apparent. A single midsagittal volume obtained with 3D ultrasound can allow for the evaluation of the sagittal, axial, and coronal views using multiplanar reconstruction. The rendering mode can create a realistic image of the exterior facial features as well as a 3D image of the fetal palate. In order to obtain a volume, a pocket of amniotic fluid needs to be present in front of the fetal face. These techniques can be applied to the routine anatomic survey in the midtrimester as well as the late first trimester. In addition to being used as a diagnostic modality, 3D ultrasound can also help to illustrate the appearance of a particular anomaly and to display the location and severity of the anomaly to consulting surgical specialists as well as families.

As discussed previously, there are multiple displays of 3D ultrasound that can be used to explore a craniofacial anomaly. The multiplanar display allows the simultaneous display of three perpendicular





**FIG 10-1** Normal images of fetal face. **A**, Sagittal image showing profile. **B**, Axial image through orbits. **C**, Axial image through palate showing toothbuds. **D**, Coronal image showing lips and nostrils.

**TABLE 10-1** Normal Appearance of Fetal Facial Features on Ultrasound Image in the Midsagittal Section Plane

Structure	Normal Appearance
Forehead	Almost linear immediately above the articulation between the nasal bones and the frontal bone, followed by a smooth backward bend. This view allows measurement of the thickness of the frontal skin (at the level of the middle of the frontal bend).
Nasal bones	Oblique along a frontocaudal direction. This view allows measurement of the length of the nasal bones and of the superior facial angle (angle between the vertical section of the frontal bone and the nasal bones).
Nasal soft tissues	The columella is oblique or horizontal but should not be vertical.
Upper lip	The philtrum is linear and should present no bulging. This view allows measurement of the length of the philtrum.
Secondary palate	Thick echoic line, beginning at the alveolar level, and extending horizontally backward. Its middle is marked by a notch, present on both the superior and inferior edges, and corresponds to the transverse palatal suture. The notch is mostly visible on the superior edge.
Oral cavity	The tongue is slightly oblique upward (10-15 degrees). Its tip lies immediately behind the alveolar ridge.
Inferior lip	Rests edge to edge with the upper lip. Both lips are arranged along the same axis; there should be no anteroposterior shift between them.
Chin	At the level of the vertical line traced on the prefrontal skin (esthetic vertical line of the face).

From Rotten D, Levailant JM: Two- and three-dimensional sonographic assessment of the fetal face. 1. A systematic analysis of the normal face. *Ultrasound Obstet Gynecol* 23:224, 2004.

planes—namely, sagittal, axial, and coronal—of the fetal head and face (Fig. 10-2). These planes can be manipulated by the sonographer to highlight the region of interest. The surface rendering mode can be used to create a model of a frontal view of the fetal face (Fig. 10-3). The maximum and transparent modes can be mixed to evaluate the hyperechoic bony structures including the fetal sutures, which can be useful in the diagnosis of craniosynostosis (Fig. 10-4). The same volume may be viewed with both surface rendering and skeletal displays.

Abnormalities of the fetal hard palate, particularly the secondary palate, can be challenging to evaluate with 2D ultrasonography.

**TABLE 10-2** Normal Appearance of Fetal Facial Features on Ultrasound Image in the Axial Section Planes

Structure	Normal Appearance
Orbits	The interorbital axis is perpendicular to the strict sagittal axis. This view allows measurement of the inner and outer interorbital lengths.
Nasal septum, molar	The nasal septum is perpendicular to the axial plane. The two malar arches are symmetric with regard to arches to the nasal septum.
Upper lip, maxilla	There is no lack of continuity of the upper lip. The maxilla appears as a regular, U-shaped echoic bend. The alveolus and tooth buds appear as hypoechoic spots regularly distributed along the alveolar ridge. There is no shift between adjacent alveoli. The hard palate appears as an echoic structure, with a complex shape. The anterior part is semicircular and lies immediately posterior to the alveolar ridge. The posterior part presents as a rectangular figure, with a notch on its distal side. This view allows measurement of the size of the maxilla.
Oral cavity	The tongue occupies the totality of the oral cavity and is glued to the alveolar ridge. Posteriorly, the tongue ends at the oropharynx level. This view allows measurement of the width and length of the tongue.
Mandible	Appears as a regular V-shaped echoic image. Both hemimandibles are almost rectilinear. The symphysis menti is clearly visible. The alveoli appear as regularly distributed hypoechoic spots. This view allows measurement of the size of the mandible (e.g., mandible width and computation of mandible width/maxilla width ratio).

From Rotten D, Levailant JM: Two- and three-dimensional sonographic assessment of the fetal face. 1. A systematic analysis of the normal face. *Ultrasound Obstet Gynecol* 23:224, 2004.

Acquiring a volume in the axial plane and then rendering the hard palate from a viewing plane inferior to the palate in an axial plane can be helpful (Fig. 10-5); this approach is a modification of the “flipped face” reported by Platt and colleagues and by Faure and coworkers.<sup>2-4</sup> Other techniques that have been used include the “reverse face” view using a coronal plane through the hard palate and oblique face views (Fig. 10-6).<sup>5,6</sup> Parallel slice imaging can use a single 3D volume to create

TABLE 10-3 Nomograms for Growth of the Ocular Parameters, by Percentile

Age (Weeks)	BINOCULAR DISTANCE (mm)			INTEROCULAR DISTANCE (mm)			OCULAR DIAMETER (mm)		
	5th	50th	95th	5th	50th	95th	5th	50th	95th
11	5	13	20	—	—	—	—	—	—
12	8	15	23	4	9	13	1	3	6
13	10	18	25	5	9	14	2	4	7
14	13	20	28	5	10	14	3	5	8
15	15	22	30	6	10	14	4	6	9
16	17	25	32	6	10	15	5	7	9
17	19	27	34	6	11	15	5	8	10
18	22	29	37	7	11	16	6	9	11
19	24	31	39	7	12	16	7	9	12
20	26	33	41	8	12	17	8	10	13
21	28	35	43	8	13	17	8	11	13
22	30	37	44	9	13	18	9	12	14
23	31	39	46	9	14	18	10	12	15
24	33	41	48	10	14	19	10	13	15
25	35	42	50	10	15	19	11	13	16
26	36	44	51	11	15	20	12	14	16
27	38	45	53	11	16	20	12	14	17
28	39	47	54	12	16	21	13	15	17
29	41	48	56	12	17	21	13	15	18
30	42	50	57	13	17	22	14	16	18
31	43	51	58	13	18	22	14	16	19
32	45	52	60	14	18	23	14	16	19
33	46	53	61	14	19	23	15	17	19
34	47	54	62	15	19	24	15	17	20
35	48	55	63	15	20	24	15	18	20
36	49	56	64	16	20	25	16	18	20
37	50	57	65	16	21	25	16	18	21
38	50	58	65	17	21	26	16	18	21
39	51	59	66	17	22	26	16	19	21
40	52	59	67	18	22	26	16	19	21

From Romero R, Pilu G, Jeanty P, et al: Prenatal Diagnosis of Congenital Anomalies. Norwalk, CT, Appleton & Lange, 1988, p 83.

multiple parallel slices, similar to a computed tomography (CT) scan, which can be useful in diagnosing abnormalities of the fetal hard palate (Fig. 10-7). Magnetic resonance imaging (MRI) can be helpful in selected cases to better elucidate fetal craniofacial clefts, particularly when there is a concern for associated neurologic abnormalities.<sup>7</sup>

## CRANIOFACIAL ANOMALIES

Craniofacial anomalies are relatively common findings, both in prenatal diagnosis as well as in liveborn infants. The basic ultrasonographic survey of the fetal face should include the upper lip, and a more detailed examination could potentially include the profile, nose, orbits and lenses, palate, maxilla, mandible, tongue, and ear position and size.<sup>8</sup> The prenatal sonographic diagnosis of a craniofacial anomaly should indicate the need for a more detailed full anatomic examination to evaluate for concomitant anomalies. In addition, patients should be offered prenatal diagnostic testing to evaluate for associated genetic syndromes.

The accuracy of ultrasonographic diagnoses of craniofacial anomalies varies by the patient population as well as the expertise and experience of the institution and examiner. A systematic review of 21 studies cited a large range in the prenatal detection rates for orofacial clefts, from 0% to 73%, in low-risk women with 2D ultrasound.<sup>9</sup> In a more

contemporary study of a population of more than 30,000 women, both low and high risk, the sensitivity for cleft lip with or without cleft palate reached 88%.<sup>10</sup> In high-risk women, in whom 3D ultrasound was used as an adjunct to 2D imaging, the detection rate in specialized centers has been quoted as high as 100%.<sup>9</sup> 3D ultrasound has much to offer in the elucidation of the detailed anatomy and extent of craniofacial anomalies.

## Typical Facial Clefts

Orofacial clefts are relatively common and occur in 1 in 700 live births.<sup>11</sup> The rate varies by ethnicity, with higher rates seen in Asian and Native American populations and significantly lower rates in African populations.<sup>12</sup> Typical facial clefts can occur as isolated cleft lip (CL), isolated cleft palate (CP), or as a combination of both cleft lip and cleft palate (CL+CP). They are often further subdivided into the categories of CL±CP and isolated CP. Clefts most often run from one or both of the nostrils to the central part of the posterior palate. An in-depth anatomic classification system was proposed by Tessier in 1976.<sup>13</sup>

Of all orofacial clefts, CL with CP represents 50% of cases, isolated CL 25% of cases, and isolated CP 25% of cases.<sup>14,15</sup> Clefts involving the lip are more common in males, with a ratio of 2:1, and isolated CP clefts are more common in females, also with a ratio of 2:1.<sup>12</sup> A large



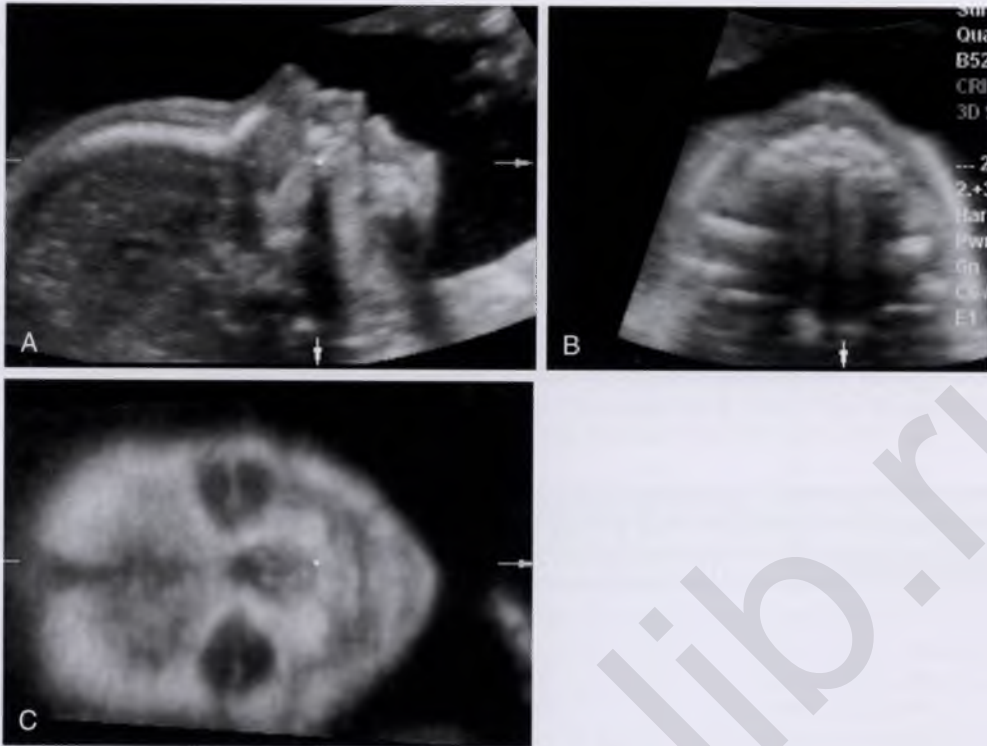


**FIG 10-2** Three-dimensional ultrasound images of normal fetal face. Multiplanar display demonstrating simultaneously sagittal (A), axial (B), and coronal views (C) of the fetal face.



**FIG 10-3** Three-dimensional ultrasound images of fetal face. Surface rendering of the fetal face at 11 weeks (A), 19 weeks (B), and 37 weeks (C).

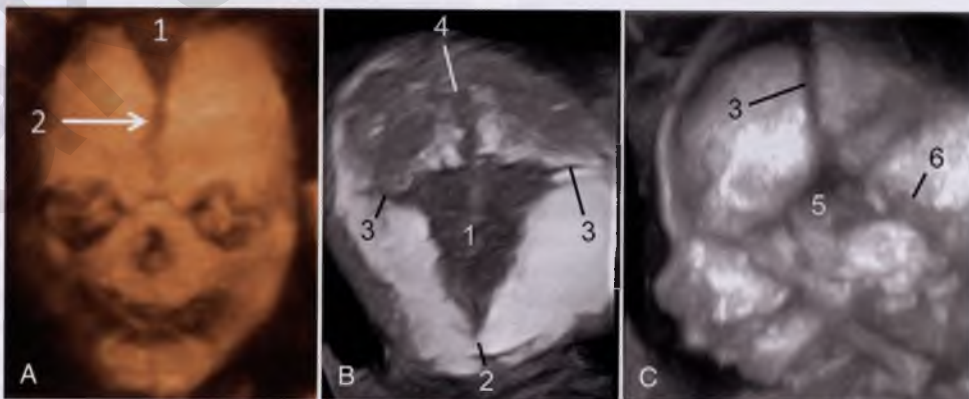


**FIG 10-4** Three-dimensional ultrasound image showing skeleton of the face and skull using maximum/transparent mode. The different sutures and fontanelles are depicted in the coronal (A), superior (B), and lateral (C) views of the skull: 1, bregmatic fontanelle; 2, frontal or metopic suture; 3, coronal suture; 4, parietal suture; 5, sphenoid fontanelle; 6, mastoid suture.



**FIG 10-5** Normal palate at 24 weeks: **A**, Axial two-dimensional ultrasound image of normal palate showing toothbuds in the anterior alveolar ridge (*solid arrow*), posterior aspect of hard palate (*dashed arrow*), and pharynx (P). **B**, Axial three-dimensional ultrasound image of normal palate.

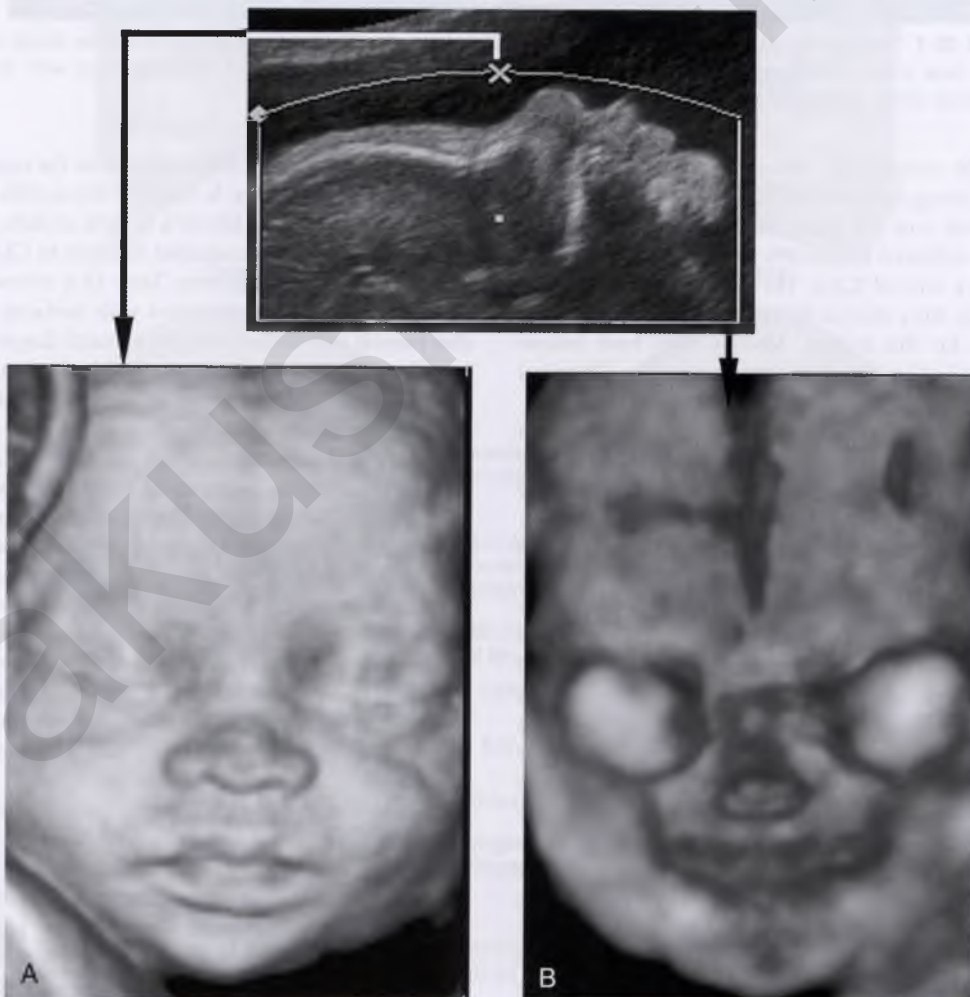


**FIG 10-6** Three-dimensional ultrasound images showing anterior surface rendering (**A**) and reverse view skeletal rendering (**B**) of the fetal face. The same ultrasound volume is used, and the rendering displays are changed. The reverse view provides an image of the anterior palate and nasal fossa.



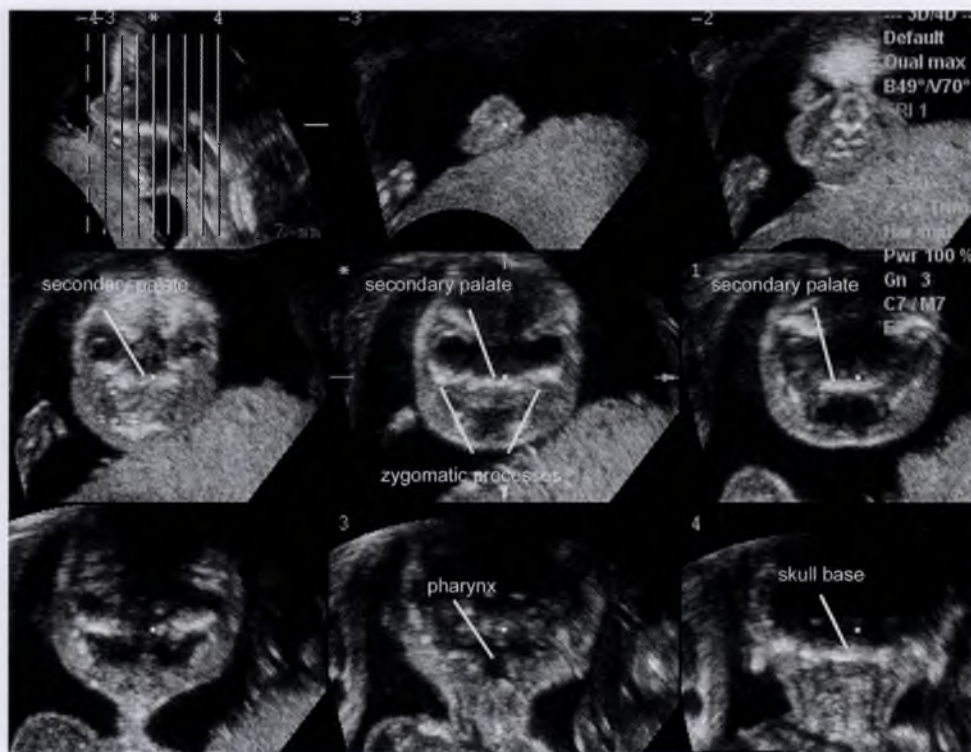


**FIG 10-7** Three-dimensional ultrasound imaging: Tomographic ultrasound imaging (TUI) (multiple slices) of the fetal palate visualized with an angled approach. Comparing the reference midsagittal view with the coronal slices, the entire secondary palate is clearly demonstrated.

study of almost 50,000 deliveries in Norway with 77 fetuses with CL±CP revealed that among cases of CL±CP, 64% were unilateral and 34% were bilateral, with only 3% being midline.<sup>15</sup> The same study demonstrated that in unilateral clefts, 69% were left-sided and 31% were right-sided, with a ratio of 2.3:1. The left-sided predominance has also been shown in other studies; however, there is no definitive anatomic explanation for this finding. Median clefts have unique causes and associations and are detailed in the next section (“Atypical Facial Clefts”).

An appreciation for the embryologic development of the face can help in the understanding of the development of orofacial clefts. The face arises from five prominences that surround the mouth—the central frontonasal prominence and the paired maxillary and mandibular prominences. These prominences are composed of neural crest cells and are present by the fourth week of embryogenesis (Fig. 10-8). By the fifth week, the nasal placodes have formed, separating each side of the inferior portion of the frontonasal prominence into lateral and medial nasal processes. The upper lip and primary palate are formed by the end of the sixth week, when the medial nasal processes fuse with each other and the paired maxillary processes. This sixth week is a sensitive time for development, and teratogenic exposures at this time can result in orofacial clefts. The purpose of the secondary palate is to separate the oral and nasal cavities. The development of the secondary palate begins in the sixth week and is completed by the tenth week. The secondary palate is formed from paired palatal shelves that are outgrowths of the maxillary processes. These shelves fuse during the seventh week and differentiate into the hard and soft palate. By the tenth week, the primary palate and nasal septum have fused with the secondary palate (Fig. 10-9).<sup>16-18</sup> Clefting can occur during multiple stages of the embryogenesis process and results in different anatomic variations depending on the timing and which prominences are affected (Fig. 10-10).

Orofacial clefts are often divided into the categories of syndromic and nonsyndromic clefts. In CL±CP, 70% to 90% of clefts are nonsyndromic, and in isolated CP, 60% to 80% of clefts are nonsyndromic.<sup>19</sup> Isolated CL should be counseled similarly to CL+CP because it has a similar developmental pattern. Table 10-4 reviews some of the more common syndromic associations with orofacial clefts. It is essential that parents with fetuses with the prenatal diagnosis of orofacial clefts be offered further genetic workup with chorionic villus sampling or amniocentesis and evaluation of chromosomal abnormalities with karyotyping and chromosomal microarray.

All types of orofacial clefts can potentially be associated with other structural anomalies. In one study, 43% of those with CL±CP and 58% of those with isolated CP had associated structural anomalies.<sup>15</sup> Rates of associated anomalies vary, with another study reporting 35% of patients with CL±CP as having an associated anomaly or suspected genetic syndrome.<sup>20</sup> A third study suggested a lower level of association with anomalies, reporting that those with unilateral CL±CP had a rate of associated structural anomalies of 9.8%, whereas bilateral CL+CP had associated anomalies in 25%.<sup>21</sup> Most of these studies are biased by tertiary care subselection; in our practice, we counsel a risk of associated anomalies of approximately 10% when an isolated CL±CP is identified on prenatal ultrasound images.

In addition to genetic causes, orofacial clefts have been linked to several environmental factors and medications. Organic solvent and agricultural chemical exposure may contribute to the risk for cleft anomalies.<sup>22,23</sup> Antiepileptic medications, including the older generation drugs such as diazepam, phenytoin, and phenobarbital as well as some of the newer generation drugs such as topiramate and lamotrigine have been associated with an increased risk of orofacial clefts in some studies.<sup>17,24-26</sup> Early exposure to retinoid medications and corticosteroids has also been linked to fetal craniofacial anomalies.<sup>27,28</sup> Maternal smoking has been consistently associated with CL±CP with

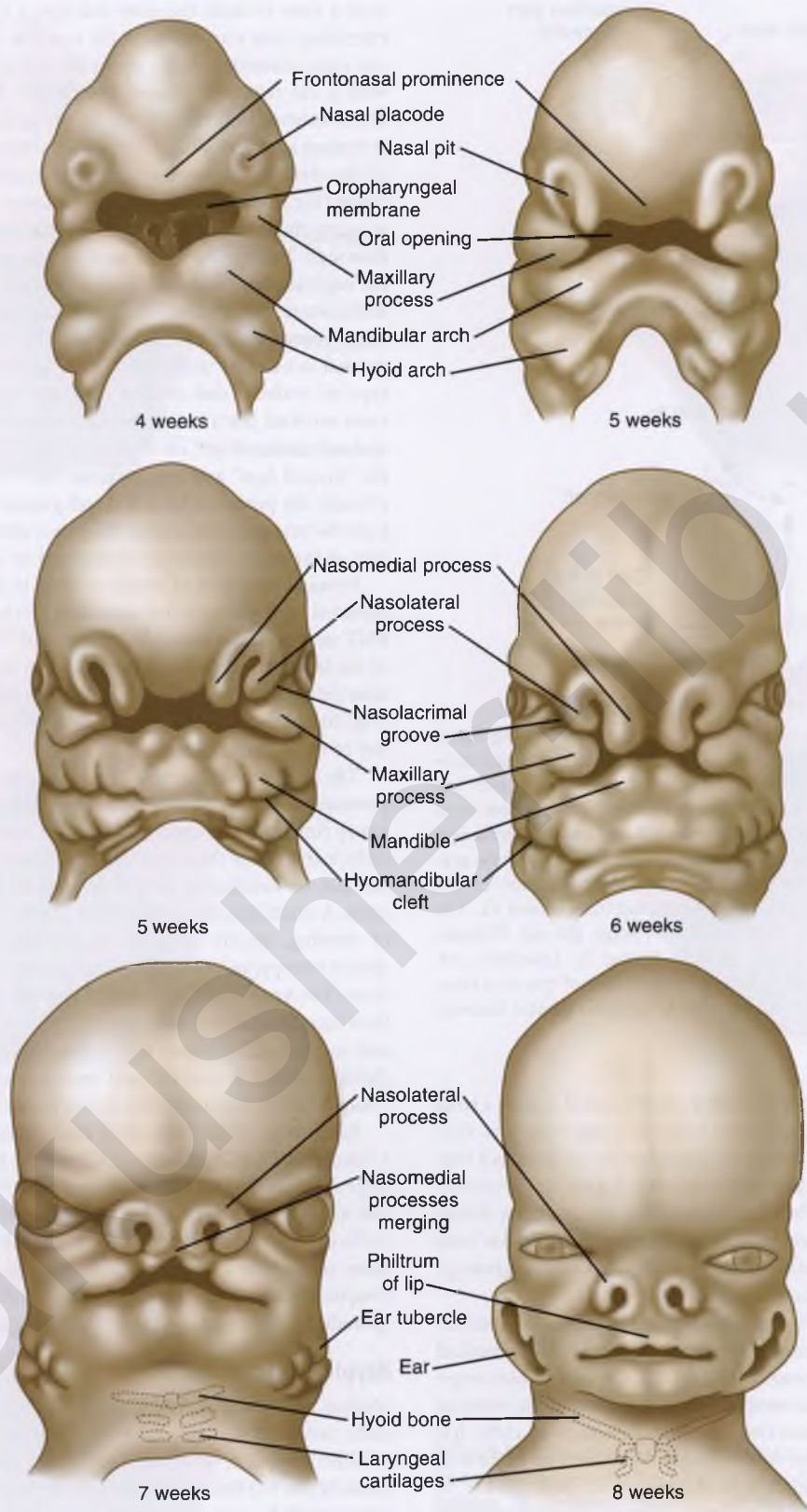


**FIG 10-8** Frontal views of the heads of human embryos from 4 to 8 weeks of age. (From Carlson BM [ed]: Human Embryology and Developmental Biology, 3rd ed. Philadelphia, Mosby/Elsevier, 2004, p 322.)



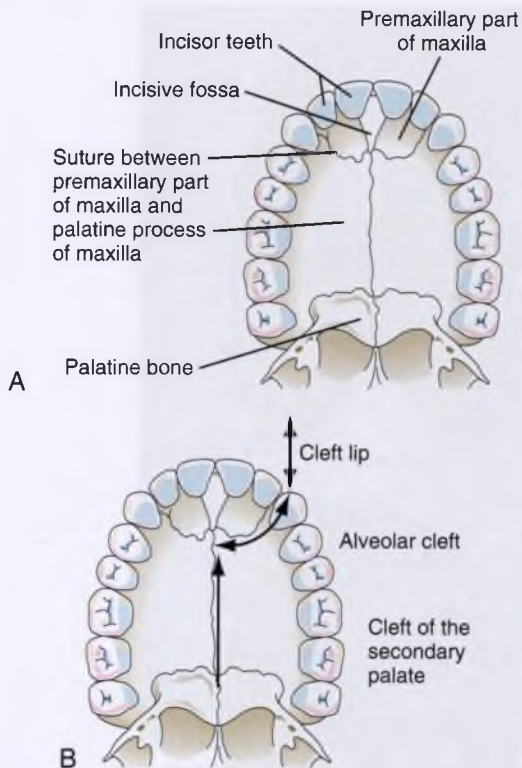


**FIG 10-9 A**, Drawing of the human palate in the axial plane highlights the anatomy of the premaxillary part of the maxilla and the lateral palatine processes of the secondary palate. Their points of fusion are indicated by the black lines between them. The four incisor teeth arise from the premaxillary portion of the primary palate, and the remaining teeth, from the canines posteriorly, arise from the lateral palatine processes of the secondary palate. **B**, Schematic representation of the various cleft constituents of the palate. (A adapted from Moore KL: *The Developing Human: Clinically Oriented Embryology*, 6th ed. Philadelphia, WB Saunders, 1998, p 245; B from Rotten D, Levailant JM: Two- and three-dimensional sonographic assessment of the fetal face. 2. Analysis of cleft lip, alveolus and palate. *Ultrasound Obstet Gynecol* 24:402, 2004.)

a relative risk of 1.34 and CP alone with a relative risk of 1.22 in a large meta-analysis.<sup>29</sup> There is inconsistent evidence suggesting that folic acid deficiency may yield an increased risk for orofacial clefts and thus that supplementation could potentially decrease the risk of recurrence in a subsequent pregnancy, but this relationship has not been definitively established.<sup>30,31</sup> The early prenatal use of multivitamins has been associated with a 25% reduction in the risk for CL±CP and a nonsignificant 12% reduction in the risk for CP.<sup>30</sup>

Prenatal diagnosis of clefts can allow parents to choose options for further genetic testing and can also prepare them for the child's medical course if they continue the pregnancy. In 1981, Christ and Meinger reported the first prenatal ultrasonographic diagnosis of an orofacial cleft.<sup>32</sup> Research has demonstrated that the detection of clefts has improved over time, with one study citing a detection rate of 34% in the period of 1987-1995 and 58% in the period of 1996-2004.<sup>9,15</sup> A systematic review of 21 studies reported a broad range in prenatal detection rates for low-risk women, from 9% to 100% for CL±CP and 0% to 22% for CP only. Detection of isolated CP in particular continues to be poor, with some large contemporary studies showing a detection rate of 0%.<sup>15,21</sup>

In the second trimester, CL±CP and CP can be best visualized by utilizing both coronal and axial planes. In the anterior coronal plane,

with a view of both the nose and lips, a CL is identified as a defect extending from one nostril to the oral rim (Table 10-5). These defects can cause distortion of the upper lip and nose, which can be seen well with a 3D rendered image (Fig. 10-11). To determine whether the defect extends into the alveolus or the primary palate, the axial plane is the best approach (Table 10-6). This view can demonstrate the extent of the cleft and determine if it also involves the secondary or hard palate (Fig. 10-12, Table 10-7). As discussed, identifying an isolated CP is quite challenging, and these defects are often missed, even with thorough 2D or 3D ultrasonography. In the case of bilateral CL+CP, the sagittal plane with the fetal profile can be helpful. This view can demonstrate the protrusion of the central palate and lip, often termed the *premaxillary mass* (Fig. 10-13). The sagittal plane will likely be normal in cases of unilateral CL+CP or with bilateral CL. When any type of orofacial cleft is suspected, 3D ultrasound can often offer a more accurate portrayal of the facial anatomy and specifically the hard and soft palate (Figs. 10-14 and 10-15).<sup>3,33,34</sup> As previously reviewed, the "flipped face" and the "reversed face" view allow the examiner to evaluate the posterior hard and soft palates.<sup>2,3,34</sup> MRI may better illustrate the extent of orofacial clefting, as it allows for improved visualization of the palate, particularly the hard or secondary palate.<sup>7</sup>

Prenatal diagnosis of orofacial clefts in the first trimester has been reported by Sepulveda and associates.<sup>35</sup> It has been proposed that the RNT view may be a useful diagnostic tool. This view is a coronal image of the fetal face posterior to the nose that includes the three echogenic lines formed by the two frontal processes of the maxilla and the palate (Fig. 10-16).<sup>35</sup> A hypoechoic defect in the palate region can be indicative of an orofacial cleft.

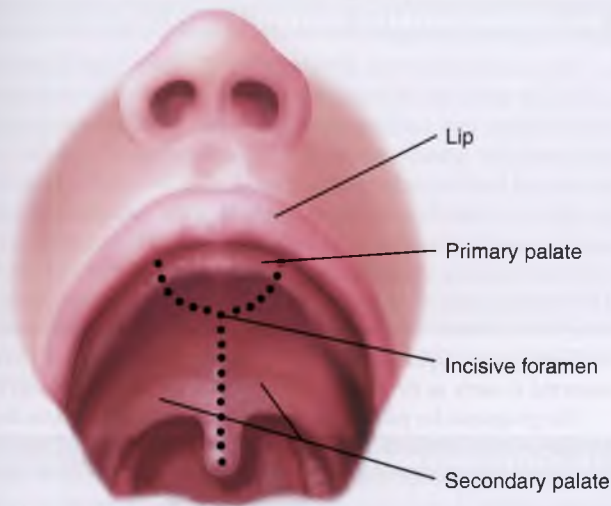
The prognosis of orofacial clefts depends first and foremost on the presence of associated anomalies or genetic syndromes. Feeding, respiratory function, and speech attainment may be compromised with all clefts, particularly those involving the palate. The cosmetic appearance can also be debilitating to a child's psychological and social development. A multidisciplinary approach is a necessity with the involvement of nursing, plastic surgery, maxillofacial surgery, otolaryngology, speech therapy, audiology, counseling, genetics, orthodontics, and dentistry. The American Cleft Palate–Craniofacial Association 2009 guidelines recommend surgical repair of a CL in the first 12 months of life and surgical palate repair by 18 months, or earlier if possible.<sup>36</sup> Most children with CL and CP will undergo approximately 10 surgeries (related to the cleft and tubes for ears) by the age of 10 years.

Recurrence of orofacial clefts tends to be type-specific, with either a history of CL±CP or isolated CP within the same familial line. In a large study of over 54,000 relatives from 1952 to 2005, the recurrence risk in those with first-degree relatives with orofacial clefts was 3.5% (95% confidence interval 3.1-4.0%).<sup>19</sup> Table 10-8 details the approximate recurrence risks for various degrees of familial relationships. Despite the hereditary risk factors, the majority of orofacial clefts are sporadic.

### Atypical Facial Clefts

Median and lateral facial clefts are far less common than the typical clefts reviewed earlier. Only about 3% of clefts are located at the midline.<sup>15</sup> Median or midline clefts are associated with two distinct phenotypes: (1) the median cleft, which is often associated with holoprosencephaly, and (2) frontonasal dysplasia or median cleft face syndrome.

The processes of midline and facial defects and brain development are closely linked. Inadequate development of the frontonasal prominence can result in a midline facial defect. This is often correlated with holoprosencephaly, a process in which the embryonic forebrain has incomplete cleavage.<sup>37</sup> In 1964, DeMyer and coworkers described the



A



B



C



D



E

**FIG 10-10** Drawings of common forms of cleft lip/palate: **A**, Normal lip and palate showing the fusion lines of the primary and secondary palates. **B**, Unilateral isolated cleft lip. **C**, Unilateral cleft lip and palate. (Note that the cleft palate can extend for variable distance: it may be confined to the anterior palate and end at the incisive foramen or may extend all the way to the uvula or for any distance in between.) **D**, Bilateral isolated cleft lip. **E**, Bilateral cleft lip and palate with characteristic premaxillary protrusion. (Illustration by James A. Cooper, MD, San Diego, CA.)



**TABLE 10-4 Most Frequent Syndromes Associated With Facial Clefts**

**Chromosomal Aberrations**

Deletion 4p (Wolf-Hirschhorn syndrome)  
Trisomy 10  
Trisomy 13  
Trisomy 18  
Trisomy 22  
Trisomy 9

**Malformations and Sequences**

Amniotic bands  
Arthrogryposis  
Camptomelic dysplasia  
Caudal regression syndrome/syrenomelia  
CHARGE association  
Diastrophic dysplasia  
Ectrodactyly, ectodermal dysplasia, clefting  
Holoprosencephaly  
Hydrolethalus  
Majewski (short rib polydactyly) syndrome, type 2  
Median cleft face (frontonasal dysplasia)  
Pierre Robin sequence

**Syndromes**

Crouzon  
Femoral hypoplasia, unusual facies  
Fryns  
Goldenhar  
Gorlin  
Klippel-Feil  
Larsen  
Marfan  
Meckel-Gruber  
Multiple pterygium  
MURCS association  
Nager  
Neu-Laxova  
Oral-facial-digital (Mohr)  
Pena Shokeir  
Roberts  
Shprintzen  
Smith-Lemli-Opitz  
Treacher Collins  
Van der Woude  
Walker-Warburg

CHARGE, coloboma of the eye, heart anomaly, choanal atresia, retardation, and genital and ear anomalies; MURCS, müllerian duct aplasia, renal agenesis, and cervicothoracic somite dysplasia.

spectrum of facial phenotypes that can accompany holoprosencephaly, which can range from a median quadrangular CL±CP with orbital hypotelorism and a flattened nose to cyclopia with arhinia and a proboscis (Figs. 10-17 through 10-19).<sup>38</sup> The degree of facial dysmorphism is often reflective of the degree of holoprosencephaly.

The prognosis of median clefts associated with holoprosencephaly is universally poor. The majority of the time, the condition will be lethal and the few survivors are affected by significant neurodevelopmental disability.<sup>39</sup> Holoprosencephaly occurs in 1 in 8000 live births,<sup>40</sup>

with chromosomal abnormalities, most commonly trisomy 13, present in 37% to 67% of cases.<sup>37,39</sup>

The second phenotype associated with median facial clefts is frontonasal dysplasia or the median cleft face syndrome. In contrast to the hypotelorism and midline clefts associated with holoprosencephaly, this condition instead presents with hypertelorism and the unique features of median clefting affecting the nose or both the nose and lip or palate, broadening of the nasal root, with unilateral or bilateral colobomas of the nasal alae, lack of formation of the nasal tip, anterior cranium bifidum occultum, and a widow's peak hair distribution.<sup>41</sup> The identification of hypertelorism on ultrasound image in the axial scan differentiates this condition from the median cleft associated with holoprosencephaly. Prenatal ultrasonographic diagnosis has been reported as early as the first trimester, utilizing 3D ultrasonography.<sup>42</sup>

The prognosis for patients with median cleft face syndrome depends on the severity of the defects and also on the presence of any central nervous system malformations. Patients with median cleft face syndrome usually do not typically present with developmental disability, though one small series of 21 patients cited a prevalence of neurodevelopmental abnormalities in approximately 50% of cases, associated with a high frequency of agenesis of the corpus callosum.<sup>43</sup> The surgical correction of these multiple facial malformations, including the midline defect as well as the hypertelorism, can be a significant undertaking.

Lateral facial clefts are another form of atypical facial cleft. They often begin at the corners of the mouth and extend outward, with the most severe forms reaching the ear. These anomalies occur in 1 in 50,000 to 1 in 175,000 live births.<sup>44</sup> Such clefts, like the typical clefts, may develop as errors of early embryogenesis, although they may also be due to the disruptive effects of amniotic band syndrome and occur later in development.<sup>45,46</sup>

The clinical finding when a lateral cleft is present is termed *macrostomia*, or widening of the oral commissure. These clefts can be associated with skeletal malformations of the lateral face and external ear including the maxilla, zygomatic bone, and ascending branch of the mandible.<sup>47</sup> This type of cleft is challenging to diagnose on prenatal ultrasound examination, particularly with 2D ultrasound. The widening of the mouth and facial asymmetry are best seen in the coronal view (Fig. 10-20).<sup>44</sup> If such a cleft is suspected, 3D ultrasound in surface mode may be helpful to further elucidate the location and extent of the cleft. Given the frequent involvement of nearby skeletal structures, surgical repair of these types of clefts is a difficult and multistep process.

**Orbital and Ocular Defects**

Approximately 22 days after conception, the development of the eye begins, and formation of the globe structure is complete by 42 days. Differentiation of the lens and eye structures occurs following these initial steps.<sup>48</sup> The orbit itself is complex and made up of seven different bones—the frontal, zygomatic, sphenoid, ethmoidal, maxillary, lacrimal, and palatine.<sup>49</sup> The eyes grow in size and move medially with advancing gestation, with the eventual goal to allow stereoscopic vision. The angle between the optic nerves is initially 180 degrees and at birth is only 70 degrees.<sup>49</sup> Sonographically, the vitreous and lens of the eye are normally hypoechoic, whereas the lens outline and orbit are hyperechoic.

Hypotelorism is defined prenatally as an interocular distance below the 5th percentile (see Table 10-3).<sup>1,50</sup> Burns and associates have published tables of normal values of orbital distances based on gestational age.<sup>50</sup> In our experience, hypotelorism should be suspected if the space between the orbits is not equivalent to at least the size of one orbit. Hypotelorism is associated with holoprosencephaly and is also found

**TABLE 10-5 Sonographic Characteristics of Unilateral or Bilateral Cleft Lip**

Section Plane	Unilateral Cleft	Bilateral Cleft
Sagittal and parasagittal	The midsagittal view is usually normal. The parasagittal views show the cleft of the upper lip as a defect between two thickened zones, with visible asymmetry between both sides of the defect. The narinal bridge is always complete, but there is a flattened narinal bend.	The normal image of the lip is replaced by the protruding premaxillary prolabium. The prolabium is stuck to the nose and consequently flattened. The columella cannot be analyzed.
Axial premaxillary	The loss of continuity of the labial arc is clearly apparent. The nostrils are asymmetric and distorted, but the nasal aisles are always present, constituting a bridge over the cleft.	On each side, the protruding prolabium is separated from the remaining upper lip extremities by the clefts. Both nostrils are flattened but complete.
Coronal	The loss of lip continuity is clearly apparent.	The defects in lip continuity are clearly apparent.

From Rotten D, Levailant JM: Two- and three-dimensional sonographic assessment of the fetal face. 2. Analysis of cleft lip, alveolus and palate. *Ultrasound Obstet Gynecol* 24:402, 2004.

**TABLE 10-6 Sonographic Characteristics of Unilateral or Bilateral Cleft Alveolus**

Section Plane	Unilateral Cleft	Bilateral Cleft
Axial	The alveolar defect ranges from a simple slant to a cleft involving the alveolus and premaxilla. Clefts involving the alveolus present as a defect in alveolar continuity. A simple irregularity in the alveolar lining signals an alveolar slant. A defect in alveolar regularity with anteroposterior shift between the two hemimaxillas signals a cleft involving the alveolus and premaxilla.	The premaxilla is protruded together with the prolabium. The premaxillary mass is analyzed (size, soft tissue, and bone content). The external parts of both alveoli are symmetric.
Coronal	There is a defect in alveolar continuity, with missing buds.	There is a median defect in alveolar continuity. This defect contrasts with an intact hard palate.

From Rotten D, Levailant JM: Two- and three-dimensional sonographic assessment of the fetal face. 2. Analysis of cleft lip, alveolus and palate. *Ultrasound Obstet Gynecol* 24:402, 2004.

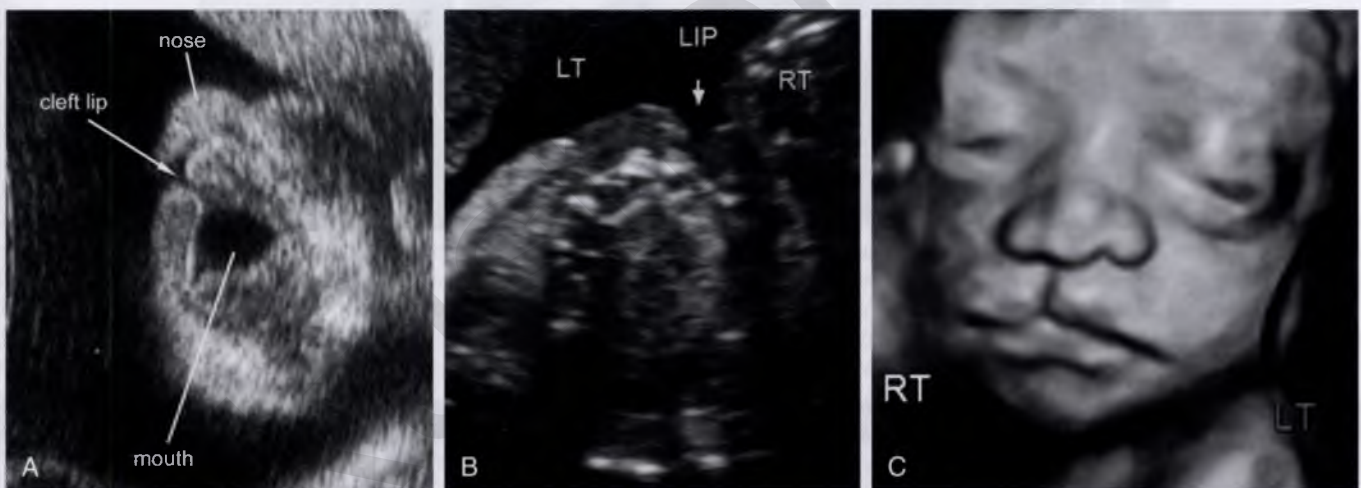


**FIG 10-11** Unilateral right cleft lip in fetus at 27 weeks: **A**, Frontal two-dimensional ultrasound image of lip and nose showing cleft lip (arrow). **B**, Axial two-dimensional image of palate showing intact primary and secondary palate with unilateral right cleft lip (arrow). **C**, Frontal three-dimensional surface rendered image of right unilateral cleft lip.

in OMIM (Online Mendelian Inheritance in Man) to be associated with over 80 syndromes. The same mechanisms that result in the excessive central migration of the orbits also contribute to the formation of the forebrain.<sup>50</sup> The prognosis of hypertelorism depends largely on the associated anomalies and the presence or absence of holoprosencephaly.<sup>51</sup>

Hypertelorism is defined prenatally as an interocular distance above the 95th percentile (see Table 10-3)<sup>1,50</sup> and is found in OMIM to be associated with over 500 syndromes. It can be associated with the median cleft face syndrome or frontonasal dysplasia, as previously discussed under "Atypical Facial Clefts."<sup>52</sup> Hypertelorism can be seen

with typical CL and CP as well. Isolated mild hypertelorism can also be seen as a normal variant. As with hypotelorism, the prognosis depends on whether the fetus is affected with other anomalies or a genetic syndrome. Surgical procedures that have been proposed for correction of hypertelorism include canthoplasty, orbitoplasty, surgical positioning of the eyebrows, and rhinoplasty.<sup>53</sup>

Microphthalmia is defined as decreased size of the eye as reflected by a decreased ocular diameter, and anophthalmia is the absence of the eye structures on pathologic examination (Table 10-3, Figs. 10-21 and 10-22). Prenatal sonographic diagnosis of microphthalmia was first reported by Feldman and coworkers in 1985.<sup>54</sup> This finding can be



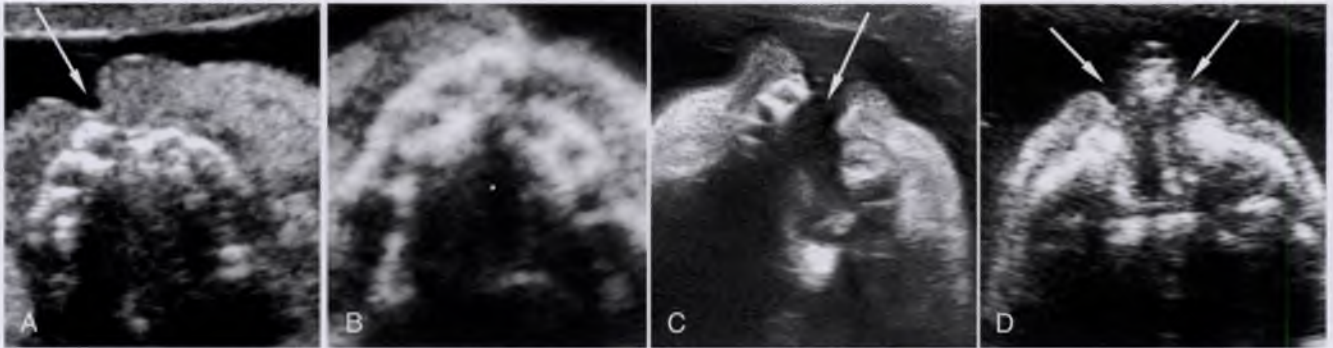


**FIG 10-12** Axial planes of the maxilla in fetuses with facial clefts: **A**, Isolated cleft lip (*arrow*): the alveolar ridge is intact albeit irregular in shape as frequently happens in these cases. **B**, Unilateral cleft lip and palate: the defect extends only to the alveolar ridge; note that one toothbud is missing but that the secondary palate does look intact; this defect is frequently referred to as *cleft alveolus*. **C**, Unilateral cleft lip and palate; the defect is seen extending to the secondary palate (*arrow*). **D**, Bilateral cleft lip and palate (*arrows*); the anterior protrusion of the central portion of the maxilla (or premaxilla) indicates that the defect extends posteriorly to the secondary palate.

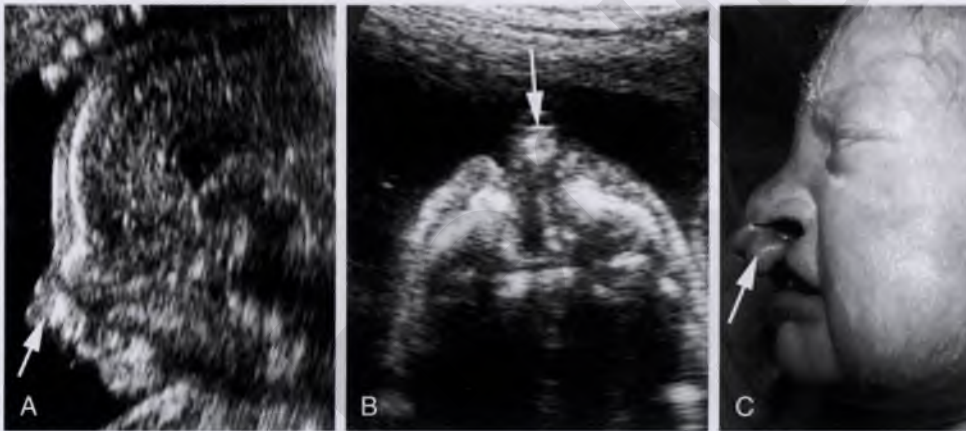


**FIG 10-13** Protrusion of the premaxilla (*arrows*) in a fetus with bilateral cleft lip and palate: **A**, Sagittal view; **B**, axial view; **C**, postnatal image for comparison.

**TABLE 10-7 Sonographic Characteristics of Unilateral or Bilateral Secondary Palate Cleft**

Section Plane	Secondary Palate Cleft With a Unilateral CLA	Secondary Palate Cleft With a Bilateral CLA
Midsagittal and parasagittal	The successive views show a defect in hard palate continuity. This defect is asymmetric. It is not strictly median but lateralized, usually toward the same side as the CLA.	A hyperechoic midline image is present in the midsagittal view. Care must be taken: although a median line is present, it is not the palate but the vomer bone. On each side of the sagittal view, the parasagittal views show the hard palate defects.
Axial	When looking for the palate caudally to the alveolus (remember that the alveoli are separated by a defect and a shift), one does not find it. The only apparent image is that of an oblique vomer bone.	The anteroposterior hyperechoic line corresponding to the vomer bone is present. Anteriorly, it extends onto the premaxillary prolabium. On each side of this median structure, the cleft is readily apparent.
Coronal	Medially, the palatal arch is interrupted by a defect. Actually, this defect is not symmetric but lateralized on the same side as the CLA. Thus, the two half arches are not symmetric. The wider half is on the nonpathologic side. The vomer bone is deflected toward the half arch situated on the pathologic side and rests on it.	The hard palate cannot be imaged. The vomer appears as a suspended midline line, with no supportive structure to rest on. The palatal arch is reduced to two small lateral structures.

CLA, cleft lip and alveolus.

From Rotten D, Levailant JM: Two- and three-dimensional sonographic assessment of the fetal face. 2. Analysis of cleft lip, alveolus and palate. *Ultrasound Obstet Gynecol* 24:402, 2004.

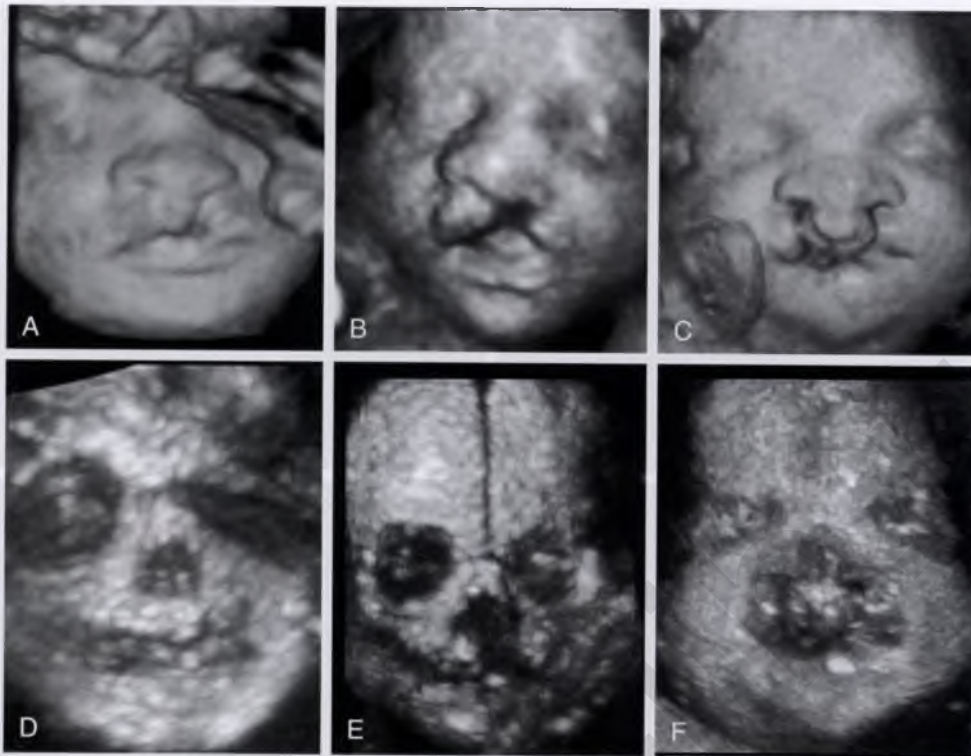


**FIG 10-14** Three-dimensional ultrasound imaging of cleft lip in surface mode (A through C) and maximum mode (D through F). A and D, Unilateral cleft lip. B and E, Unilateral cleft lip and palate. C and F, Bilateral cleft lip and palate.

unilateral or bilateral and may be associated with many genetic syndromes including Goldenhar syndrome, a condition of hemifacial microsomia thought to occur secondary to a vascular event involving the first and second branchial arches.<sup>55</sup> It can also be a result of infection or exposure to a teratogen.<sup>56</sup> It is possible to detect microphthalmia in the early second trimester fetal survey; however, it can also develop over time, as there are cases of microphthalmia in the third trimester with normal ocular diameters documented in the second trimester.<sup>56</sup> Infants and children with microphthalmia are often affected by vision impairment and blindness; 3.2% to 11.2% of all blind children have microphthalmia.<sup>57</sup>

Congenital cataracts are rare, occurring in 1 to 6 per 10,000 live births.<sup>58</sup> They can be detected on prenatal ultrasound image, as the lens will be very echogenic (see Fig. 10-21).<sup>59</sup> The cause of congenital cataracts can be genetic (either autosomal dominant, recessive, or X-linked) or related to aneuploidy or other syndromes, infections, and metabolic conditions.<sup>59,60</sup> Unilateral cataracts are genetic in 30% of cases, and bilateral cataracts are genetic in 50% of cases.<sup>59</sup> Surgery via lens removal for infants is recommended prior to 6 weeks for unilateral cataracts, and prior to 10 weeks for bilateral cataracts, in order to optimize visual outcome.<sup>60</sup>

Dacrocystoceles can present prenatally as anechoic masses medial and inferior to the eye and can be imaged well with tomographic ultrasound imaging (TUI) (Fig. 10-23). They are caused by obstruction of the lacrimal drainage system that then results in dilation of the nasolacrimal sac.<sup>61</sup> The differential diagnosis for this finding includes an encephalocele, hemangioma, and dermoid cyst. Some dacrocystoceles will resolve in utero, and the majority will resolve postnatally without intervention.<sup>61,62</sup> For those that do not resolve spontaneously, initial therapy can include warm compresses, massage, and antibiotics,

with surgery for unresolved cases in the form of nasolacrimal duct probing or marsupialization.<sup>63</sup>

### Micrognathia and Retrognathia

In the 4th week of gestation, neural crest cells travel to the head and neck area and stimulate pharyngeal arch formation. The mandibular and maxillary prominences form from the first pharyngeal arch. The mandible or jaw is derived from the mandibular prominence.<sup>64</sup> It is likely that defects in mandibular development begin at this early stage.

Micrognathia refers to a small chin secondary to an underdeveloped mandible, whereas retrognathia refers to the posterior displacement of the chin. These two findings can be difficult to differentiate sonographically and may also occur simultaneously; the terms are often used interchangeably. It is possible to mimic micrognathia if a suboptimal image of the fetal profile is taken obliquely, rather than in a true midsagittal plane. With true micrognathia, a normal fetal profile image cannot be obtained.

Micrognathia is often associated with syndromes and other abnormalities. In one series of 58 cases identified prenatally, Luedders and colleagues found that 43% had musculoskeletal disorders, 15% had nonskeletal anomalies, and only 7% were isolated; only 15% were alive postnatally.<sup>65</sup> Micrognathia is commonly associated with the Pierre Robin sequence, a condition that includes a U-shaped palatal cleft and glossoptosis.<sup>66</sup> Pierre Robin sequence can be isolated or may be associated with other anomalies, aneuploidy, or other syndromes, such as Treacher Collins, Stickler syndrome, and the 22q11.2 deletion syndrome. It occurs in 1 in 8500 to 1 in 14,000 live births and is isolated in approximately 40% of cases.<sup>67</sup> The original triad as published by Robin in 1923 did not include the palatal cleft but rather included respiratory compromise with airway complications.<sup>68</sup> However, 90%



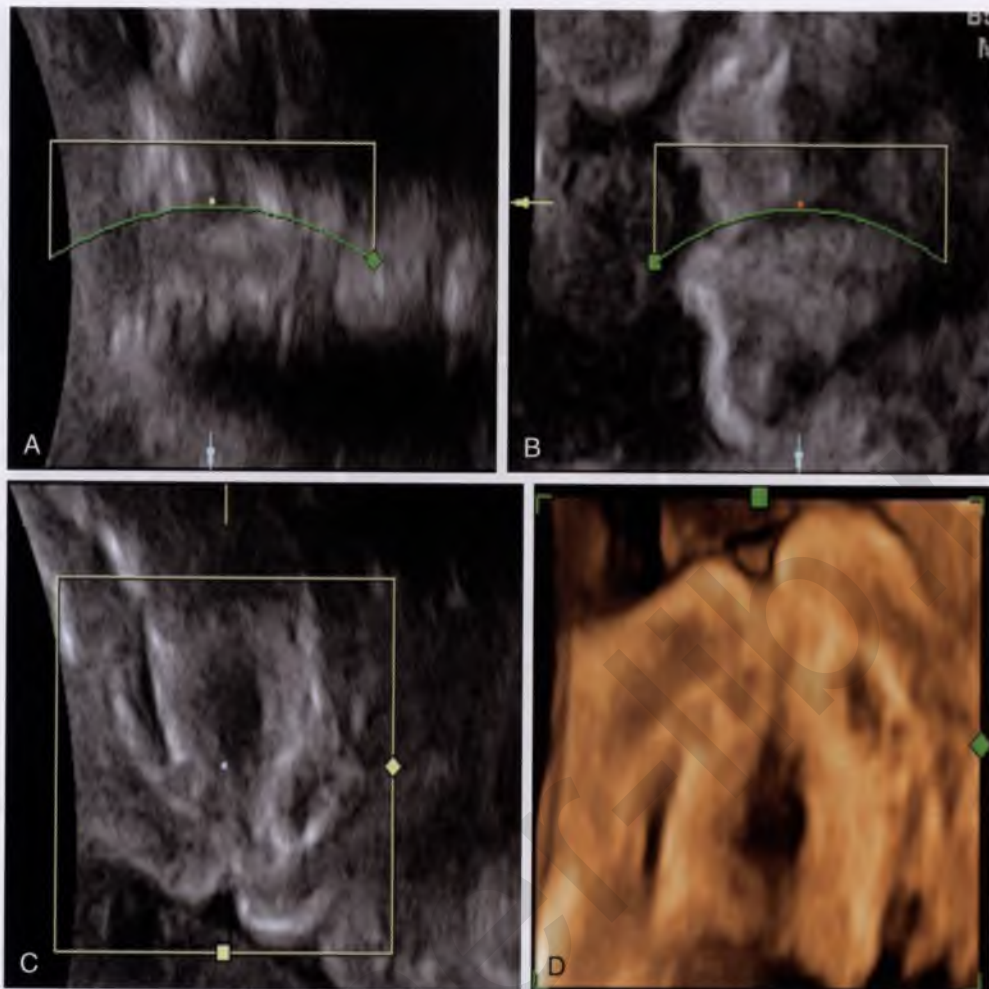


**FIG 10-15** Multiplanar display of cleft lip and palate: **A**, Frontal view of palate. **B**, Sagittal view of palate. **C**, Axial view of palate. **D**, Rendered image of cleft palate including alveolar ridge and hard palate. Notice that the green rendering line is curved and viewed from the inferior direction of the palate/maxilla in images A and B.

of children with Pierre Robin sequence have an accompanying CP.<sup>69</sup> The initial mandibular malformation likely causes the upward and posterior displacement of the tongue, which prevents palatal closure, leading to the cleft.

The first approach to sonographic assessment of mandibular size and position is the sagittal profile view. This view allows determination as to whether the midportion of the mandible is aligned with the maxilla. Subjective estimation of the presence of micrognathia or retrognathia is generally done on the sagittal image; however, quantitative methods have also been explored. Multiple quantitative methods have been proposed for the diagnosis of micrognathia with both 2D and 3D ultrasound imaging.<sup>70-73</sup> For the diagnosis of retrognathia, measurement of the inferior facial angle (IFA) has been suggested. This angle is represented by the angle between a line orthogonal to the vertical part of the forehead at the level of the synostosis of the nasal bones (reference line) and a line joining the tip of the mentum and the anterior border of the more protrusive lip (profile line) (Fig. 10-24). In a study by Rotten and coworkers, an IFA less than 50 degrees at 18 to 28 weeks was consistent with retrognathia.<sup>73</sup> Despite advances in the manipulation of sonographic images, the prenatal diagnosis of micrognathia and retrognathia remains challenging. This is particularly true of retrognathia, which can be a normal variant early in the second

trimester, with mandibular growth occurring after 20 weeks' gestation and postnatally.<sup>69</sup> 3D rendered images can be created to better demonstrate the realistic appearance of retrognathia (see Fig. 10-24).

First trimester identification of micrognathia or retrognathia has also been reported. Sepulveda and colleagues proposed the use of the RNT view to identify mandibular abnormalities. The RNT view, also used for the identification of clefts, is an image in the coronal plane of the face in which the primary palate and the frontal processes of the maxilla are simultaneously visualized.<sup>74</sup> In their study, the presence of a gap in the mandible was seen in 204 normal fetuses, and an absence of a mandibular gap was seen in nine fetuses with micrognathia (see Fig. 10-16).

The essential issues for neonates with these mandibular abnormalities, particularly Pierre Robin sequence, are airway obstruction and feeding difficulties.<sup>66,69</sup> At birth, the neonatal team should be prepared for difficult airway management and possible intubation. In addition, 38% to 62% of neonates with Pierre Robin sequence will have challenges with feeding. This can be addressed with nasogastric tube feeding.

Depending on the severity of the micrognathia or retrognathia, multiple treatment modalities are available after birth. Nonsurgical approaches include prone positioning and the use of a nasopharyngeal

airway.<sup>69</sup> In a study by Meyer and associates, 68% of infants with isolated Pierre Robin sequence responded to one of these interventions.<sup>75</sup> Surgical procedures include tongue-lip adhesion, mandibular distraction osteogenesis, and tracheotomy.<sup>69</sup> Many infants with Pierre Robin sequence have accompanying anomalies or concomitant genetic syndromes, and their postnatal prognosis is based on these factors as well as their response to treatment for the mandibular abnormality.<sup>66</sup>

### Macroglossia

Macroglossia is subjectively defined as a protruding tongue that extends beyond the teeth and lips. This finding is characteristic of Beckwith-Wiedemann syndrome, an overgrowth syndrome that has been detected successfully on antenatal ultrasound image (Fig. 10-25).<sup>76</sup> Trisomy 21, an absent thyroid, triploidy, metabolic storage disorders, and multiple other genetic syndromes may also present with macroglossia either prenatally or, more often, after birth. Protrusion of the

tongue is best seen on the sagittal profile view but is often not detected until the late second or third trimester.

### Tumors of the Face

The differential diagnosis of congenital tumors of the oropharyngeal region includes teratoma, hemangioma, lymphangioma, neurofibroma, and granular cell tumor.<sup>77</sup> Hemangiomas may appear as cystic or solid lesions and arise from subcutaneous tissues. Lymphangiomas are largely cystic masses that typically originate from the nuchal region, although sublingual lymphangiomas have been reported.<sup>78</sup> Epignathus is a rare benign oral cavity tumor that occurs in 1 in 35,000 to 1 in 200,000 live births.<sup>79</sup> These tumors occur more often in females than males, with a ratio of 3:1.<sup>80</sup> The tumor is a teratoma with derivatives of foreign tissue from any or all of the three germinal layers.<sup>81</sup> Patients often present with elevated maternal serum alpha-fetoprotein. The tumor most commonly grows from the hard palate or the mandible but can also arise from other oral cavity tissues and structures<sup>80</sup> and will appear as a large solid or cystic mass protruding from the mouth (Figs. 10-26 and 10-27). Tumors may develop through gestation, as cases have been documented with normal sonograms in the second trimester and with the epignathus identified only later in the pregnancy.<sup>80</sup> The tumors can be unidirectional, growing only outward through the mouth, or bidirectional and extend intracranially.<sup>81</sup> The latter portends a poor prognosis with no reported surviving infants.<sup>80,81</sup> For cases with unidirectional spread, delivery and survival may be

*Text continued on p. 262*

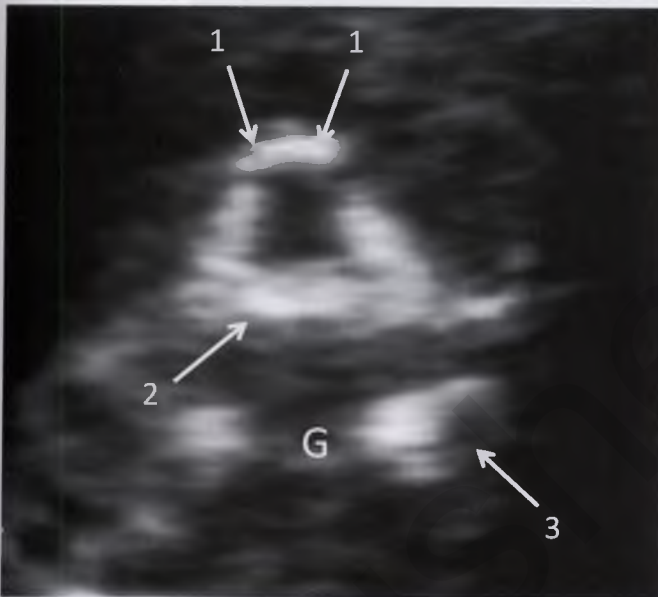


**FIG 10-16** Normal two-dimensional first trimester retronasal triangle image at 12 weeks. The normal gap (G) in the mandible signifies the lack of retrognathia. 1, nasal bones; 2, primary palate (maxilla); 3, mandible.

**TABLE 10-8 Risk of Recurrent Cleft Lip/Cleft Palate in Subsequent Offspring**

Variable	Cleft Lip/Palate (%)
<b>Unaffected Parent</b>	
No affected offspring	0.1
No affected offspring but one affected first cousin	0.4
One affected offspring	4.0
Two affected offspring	9.0
One affected offspring plus one affected relative	4.0
<b>Affected Parents</b>	
One parent but no affected offspring	4.0
One parent plus one affected offspring	10-17
Two parents plus one affected offspring	60.0

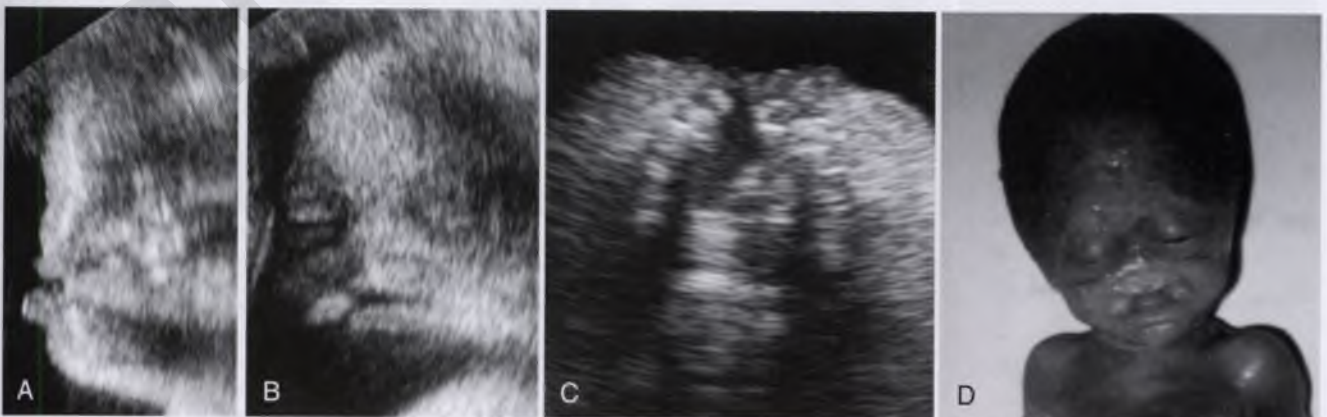


**FIG 10-17** Median cleft lip and flattened nose in a fetus with alobar holoprosencephaly seen in sagittal (A), coronal (B), and axial (C) planes of section and postnatally (D).





A



B



C



D



E

**FIG 10-18** Facial abnormalities associated with holoprosencephaly compared with the normal face. **A**, Normal face. **B**, Cyclopia with proboscis. **C**, Ethmocephaly with proboscis. **D**, Cebocephaly with single nostril. **E**, Midline cleft. (Modified from Coates TL, McGahan JP: The fetal face. In McGahan JP, Porto A [eds]: *Diagnostic Obstetrical Ultrasound*. Philadelphia, Lippincott, 1994, p 212. Illustration by James A. Cooper, MD, San Diego, CA.)

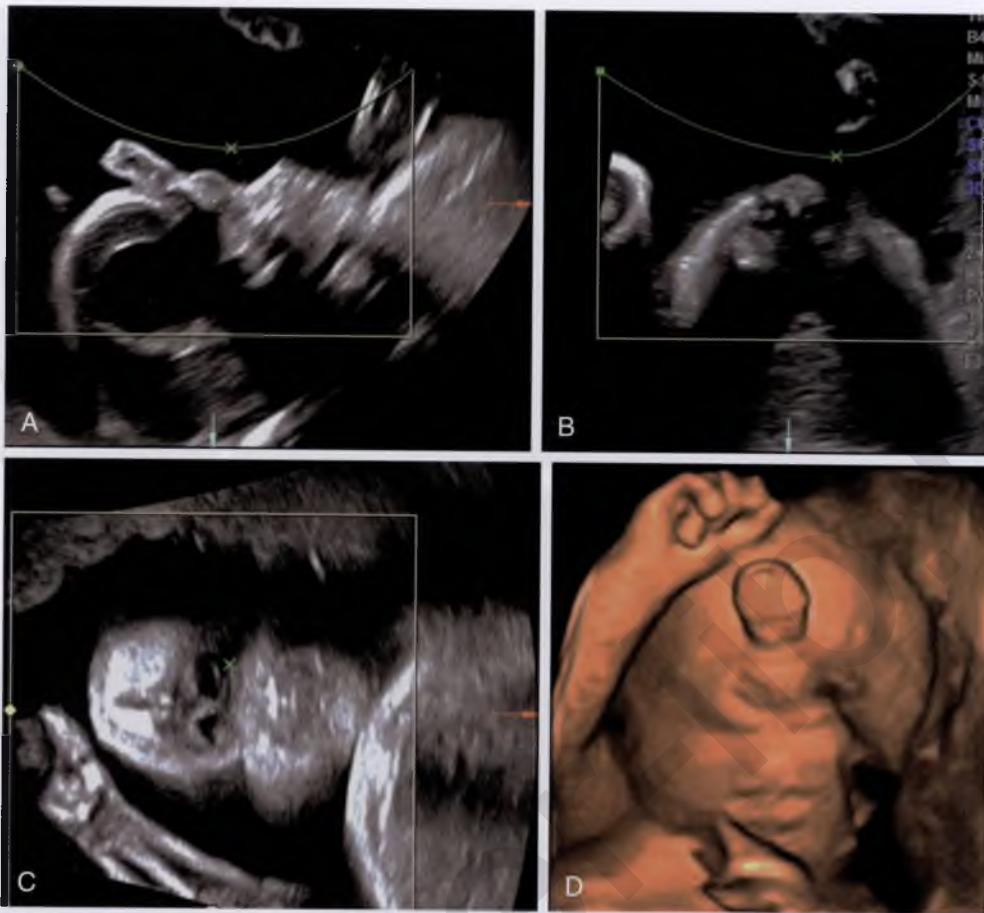


**FIG 10-19** Fetus with proboscis and hypotelorism at 26 weeks: **A**, Sagittal image showing proboscis. **B**, Axial image of orbits showing hypotelorism. **C**, Coronal image of face showing hypotelorism. **D**, Three-dimensional rendered image of face showing proboscis and hypotelorism.

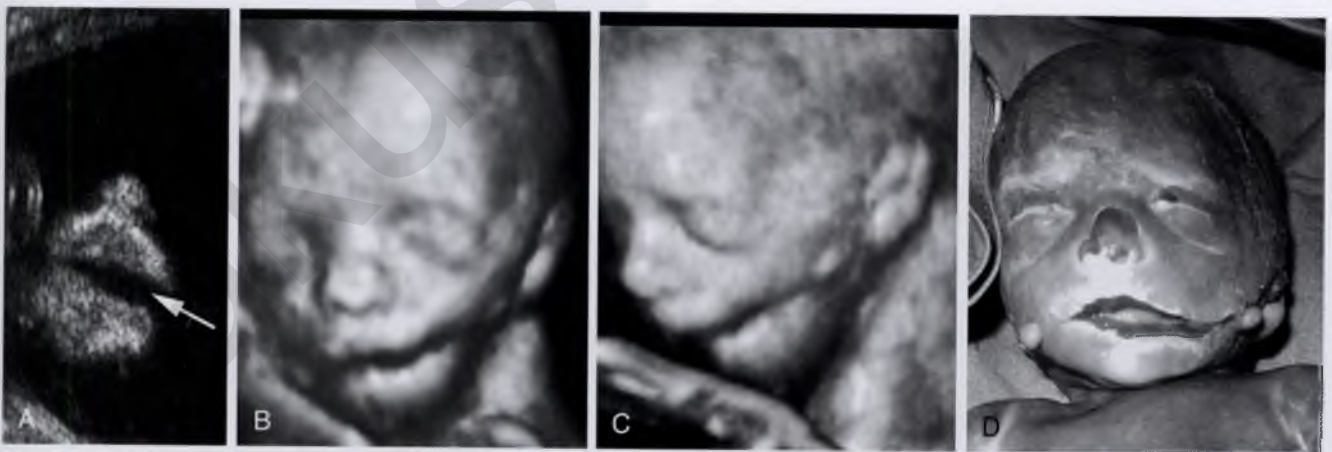


**FIG 10-20** Lateral cleft of the fetal face: **A**, Anterior coronal scan demonstrating the lips and nose; asymmetry in the shape of the mouth is noted (*arrow*). **B** and **C**, Three-dimensional ultrasound surface mode demonstrates a lateral cleft associated with a typically sunken cheek and a skin tag. **D**, Postnatal image.



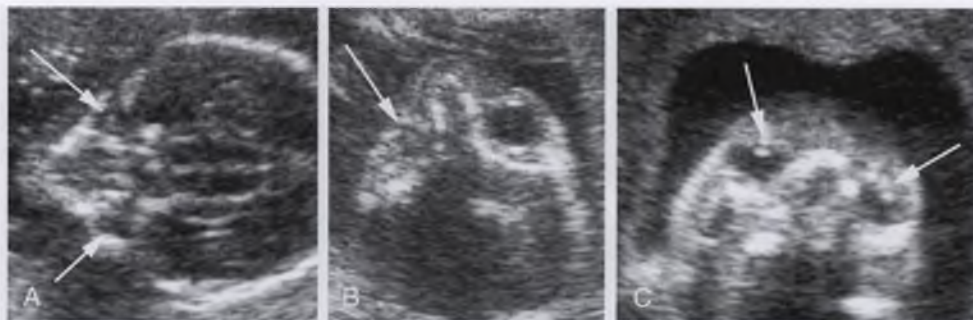


**FIG 10-21** Ocular anomalies: **A** and **B**, Bilateral and unilateral microphthalmia (arrows); **C**, cataract (arrows).

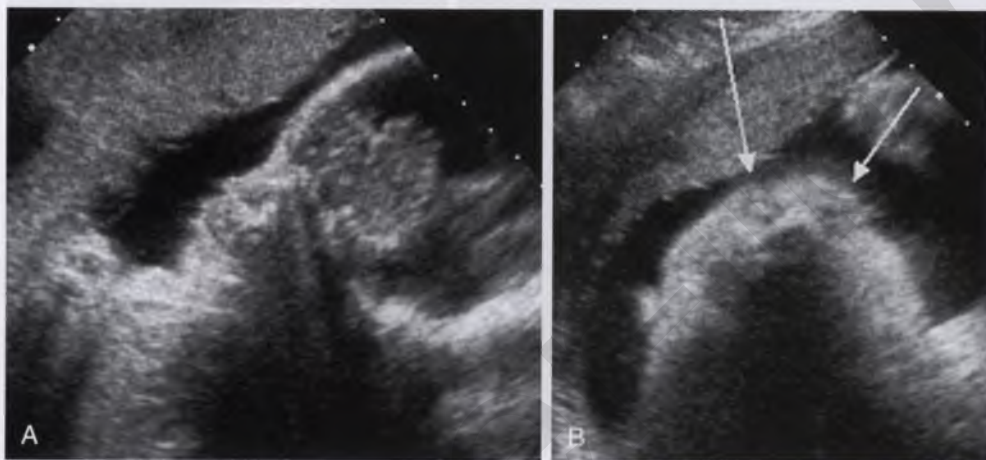


**FIG 10-22** **A** and **B**, Anophthalmia. Abnormal profile on midline sagittal image (**A**) with absent globes (arrows) on axial view (**B**).

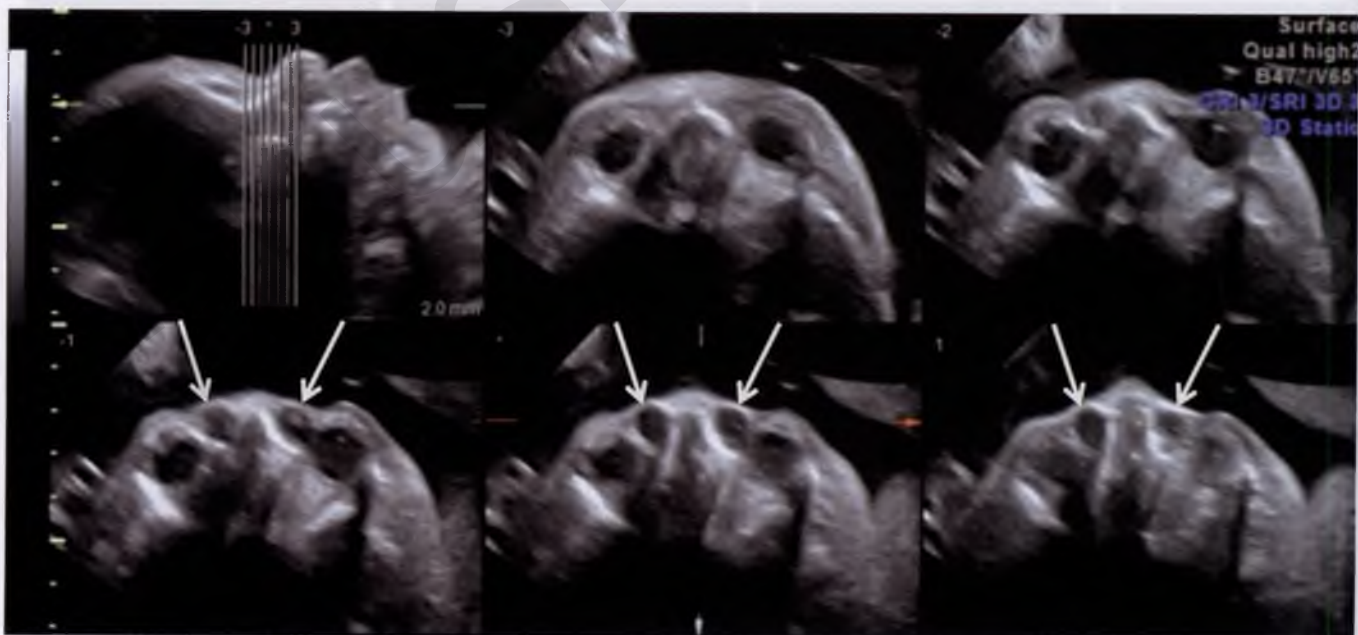


**FIG 10-23** Bilateral dacryocystoceles: Tomographic ultrasound imaging (multiple parallel slices) through fetal face demonstrating orbits and dacryocystoceles (arrows).

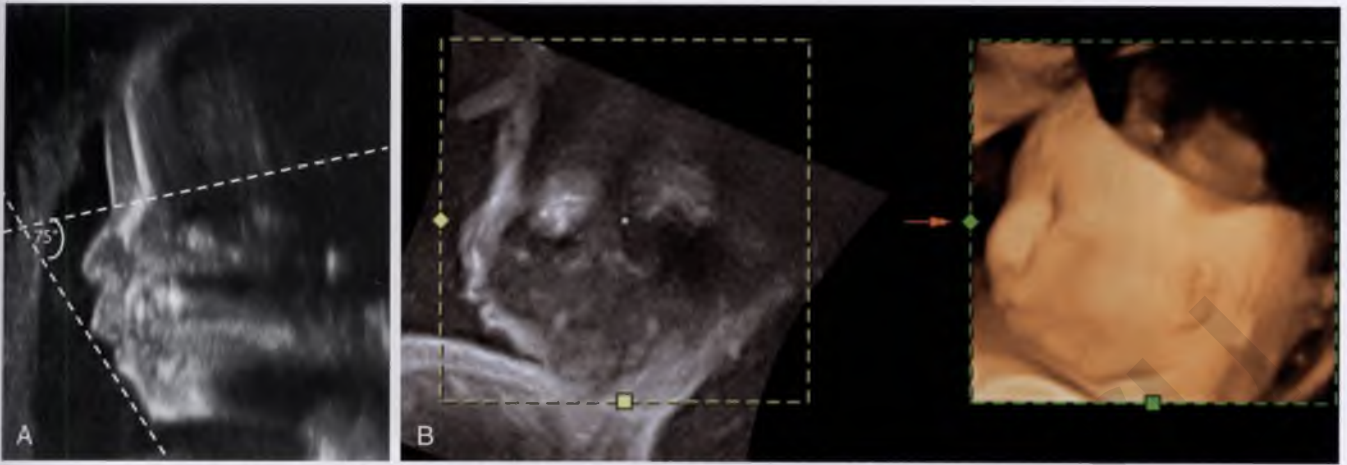


**FIG 10-24** Profile of normal and abnormal fetuses: **A**, Normal 24-week fetus showing normal facial angle of 75 degrees. **B**, Fetus with micrognathia with two-dimensional image on left and three-dimensional rendered image on right.



**FIG 10-25** Beckwith-Wiedemann syndrome in a second trimester fetus. A protruding tongue is seen (arrow) in the profile view.

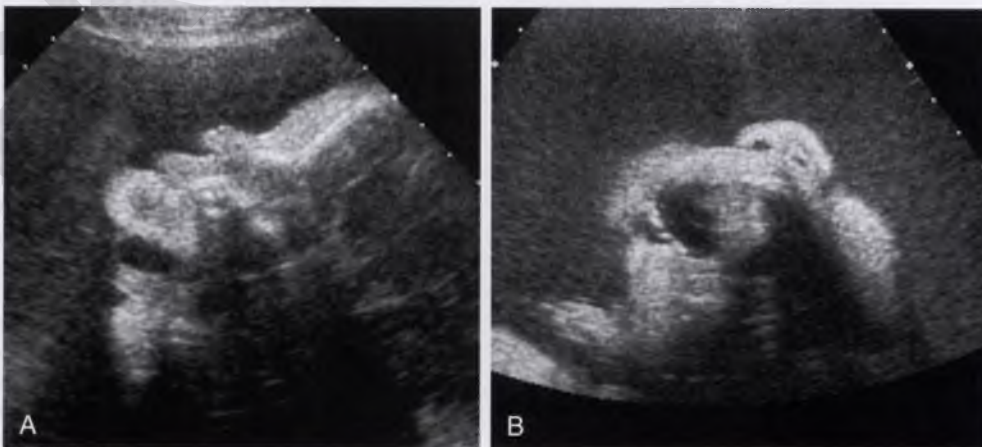


**FIG 10-26** Epignathus. Small solid and cystic mass protruding from fetal mouth in sagittal (**A**) and axial (**B**) views.



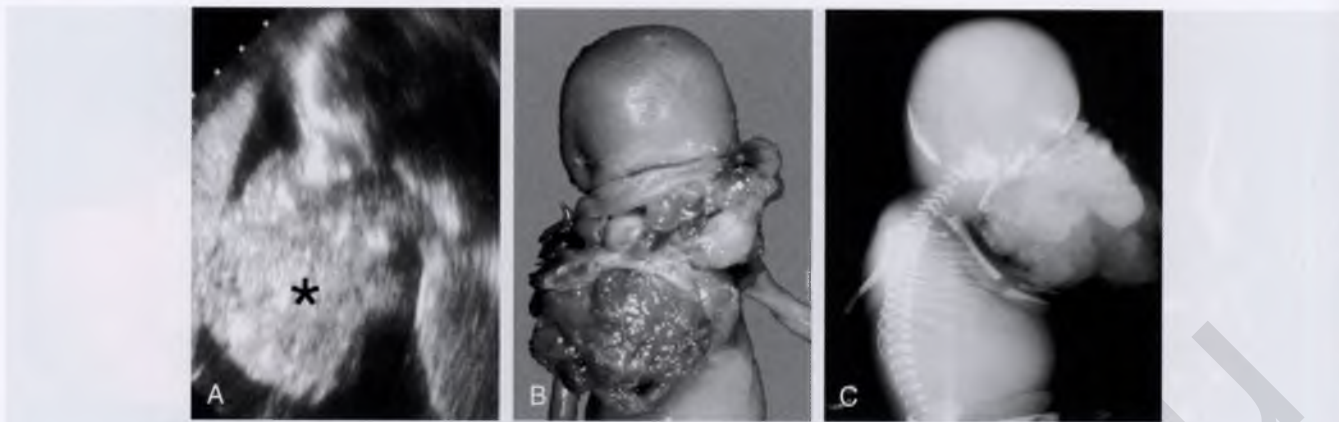


**FIG 10-27** Epignathus: **A**, Antenatal sonogram demonstrating a large mass (*asterisk*). **B** and **C**, Postnatal images in a similar case. (B and C courtesy of Frank Chervenak, MD, New York, NY, and [www.TheFetus.net](http://www.TheFetus.net)).



**FIG 10-28** Orbital teratoma. Large cystic and solid mass (*arrow*) projecting beyond the orbit.

possible with an EXIT procedure, in which a cesarean delivery is performed and the placenta is left in the uterus and attached to the fetus via the umbilical cord, allowing continued oxygen supply while the fetal airway is addressed via intubation or tracheotomy. These procedures are performed only in specialized centers with appropriate multidisciplinary support. The size and location of the lesion are features predictive of postnatal prognosis. Intracranial tumors such as teratomas can also present as facial tumors if they are extensive (Fig. 10-28).

## Ears

Embryologically, the ears are derived from the first and second branchial arches. Development of the ears begins as early as week 3 after conception and is usually fully completed by week 20.<sup>82</sup> Beyond 20 weeks, only progressive growth of the inner, middle, and external ear structures occurs. At the time of birth, the inner and middle ear structures have reached adult size, whereas the external ear continues to

grow throughout childhood (Fig. 10-29). Ear abnormalities can include anotia (absent ear), microtia (small ear), large ears, and abnormal shape and position.

Conditions associated with ear abnormalities include the trisomies (13, 18, and 21), Turner syndrome, first and second pharyngeal arch syndromes, holoprosencephaly, anencephaly, Crouzon syndrome, Treacher Collins syndrome, the CHARGE association (coloboma of the eye, heart anomaly, choanal atresia, retardation, and genital and ear anomalies), and VACTERL syndrome (abnormalities of vertebrae, anus, cardiovascular tree, trachea, esophagus, renal system, and limb buds).<sup>83</sup> In 1955, it was first suggested that small ear size or microtia may be associated with aneuploidy, particularly Down syndrome or trisomy 21.<sup>84</sup> Hall noted that 60% of newborns with Down syndrome had abnormal ears.<sup>85</sup>

Prenatal diagnosis of ear abnormalities is possible, particularly with 3D ultrasound (Fig. 10-30). Shih and colleagues obtained adequate images of the fetal ears in 84% of cases utilizing 3D ultrasound.<sup>85</sup> Chang and coworkers determined that 3D ultrasound was superior to 2D ultrasound given that 3D ultrasound allowed for the evaluation of ear shape in 93% of cases versus only 40% with 2D ultrasound.<sup>86</sup> Ear length, width, and area have been shown to correlate with increasing gestational age,<sup>86</sup> and various nomograms have been established. In one study, the sensitivity and specificity for aneuploidy in fetuses with structural malformations if fetal ear length was below the 5th percentile were 80% and 84%, respectively.<sup>87</sup> The authors suggested that fetal ear length may be as useful for aneuploidy risk assessment as other commonly used soft signs, such as a thickened nuchal fold. Dysmorphic ear shape can also be a sign of an underlying syndrome, and attention should be paid to assessing for associated anomalies if abnormal ears are identified (see Fig. 10-30).

Beyond ultrasound technology, fetal MRI, when obtained to evaluate cranial or brain abnormalities, may also be useful in the diagnosis of ear abnormalities, particularly when obtained after 25 weeks' gestation. This can apply to external as well as internal ear abnormalities.<sup>88</sup>

## CRANIOSYNOSTOSIS

Craniosynostosis is defined as premature closure of single or multiple cranial sutures.<sup>89</sup> The overall prevalence of craniosynostosis is approximately 4.3 per 10,000 births.<sup>90</sup> Isolated craniosynostosis represents approximately 85% of cases, whereas craniosynostosis associated with syndromes or other anomalies accounts for the remainder (Fig. 10-31).<sup>91</sup>



**FIG 10-29** Three-dimensional ultrasound imaging of normal ear. **A**, Rendered profile with normal ear at 19 weeks. **B**, Rendered profile with normal ear at 31 weeks.

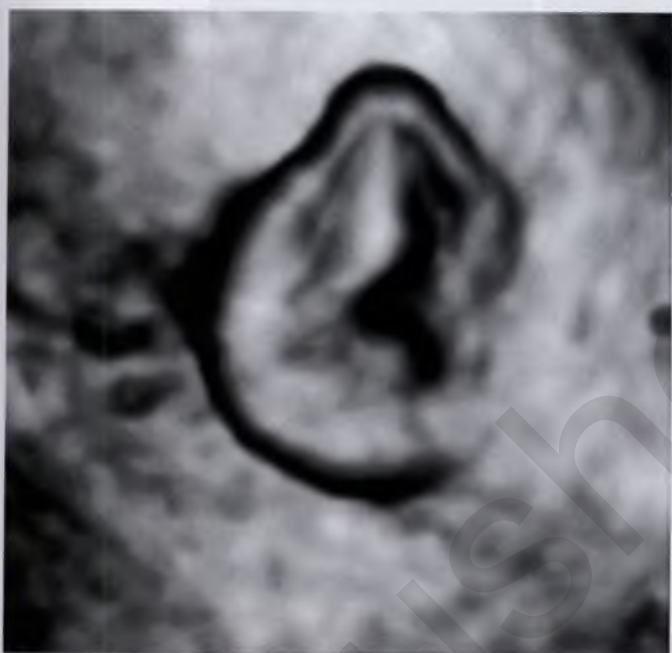


**FIG 10-30** Three-dimensional ultrasound image of abnormal ear. Unfurled ear at 33 weeks; fetus had tetralogy of Fallot and mother had coarctation of aorta. Both mother and neonate had unilateral abnormal ears.

In single suture synostosis, the most commonly affected suture is the sagittal suture, followed by the coronal, metopic, and lambdoid sutures.<sup>92</sup> Skull shape is dependent on the sutures involved: sagittal suture synostosis results in scaphocephaly (also called dolichocephaly), and coronal synostosis results in brachycephaly.<sup>91</sup> A rarer form of craniosynostosis, Kleeblattschädel, which usually involves fusion of the majority of the sutures, results in a cloverleaf-shaped skull (Fig. 10-32).<sup>93</sup>

Isolated and syndromic craniosynostosis have multiple causes. In one study of a prospective cohort of craniosynostosis cases over 10 years, 21% of the cases were given a genetic diagnosis.<sup>92</sup> Of these, 86% were single gene disorders and 15% were chromosome abnormalities (one patient had both findings). In addition, Kleeblattschädel synostosis specifically is associated with thanatophoric dysplasia type 2 and Pfeiffer syndrome type 2.<sup>93,94</sup>

Syndromic craniosynostosis is often more severe and tends to be associated with other anomalies. Some syndromes involving craniosynostosis include Crouzon, Apert, Pfeiffer, Saethre-Chotzen, Jackson-Weiss, Antley-Bixler, and Carpenter syndromes.<sup>91</sup> These conditions differ both in the types of sutures involved (Fig. 10-33) and the accompanying anomalies.

Apert syndrome was originally described in 1906 by Eugène Apert in a sentinel report describing nine patients with similar characteristics.<sup>95</sup> It usually involves the fusion of the coronal, sagittal, and lambdoid sutures (Fig. 10-34).<sup>91</sup> Rare, the incidence is approximately 6 to 15 per 1 million live births.<sup>96-98</sup> This is an autosomal dominant condition, and it is recognized that advanced paternal age is a risk factor for the development of de novo autosomal dominant mutations.<sup>99</sup> Unique clinical features include maxillary hypoplasia, proptosis, and syndactyly of the hands and feet (Figs. 10-31 and 10-35).<sup>100</sup> The hands are often called mitten hands, as there is fusion of all of the fingers aside from the thumb. Up to 75% of patients can have CP or a bifid uvula.<sup>101</sup> Intelligence levels range from significant developmental disability to normal intelligence.<sup>102</sup>

Crouzon syndrome is slightly more common than Apert syndrome, with an estimated incidence of 16 per 1 million live births.<sup>97</sup> It is also an autosomal dominant condition. In this syndrome, the coronal and sagittal sutures are both fused.<sup>91</sup> However, the facial and cranial features tend to be less severe than those in Apert syndrome. In addition, there is no evidence of syndactyly with Crouzon syndrome, and the children usually have normal intelligence.

Pfeiffer syndrome is less common than either Apert or Crouzon syndrome, and the condition is also autosomal dominant.<sup>103</sup> Pfeiffer syndrome is divided into three types, with type 2 and 3 having more severe features and poorer prognoses given that multiple sutures are frequently involved (see Fig. 10-31).<sup>94</sup> A variable extent of syndactyly is seen in this syndrome, which is not usually as significant as that seen in Apert syndrome.

Another unique craniosynostosis condition is trigonocephaly, which results from the closure of an isolated suture, the metopic suture, and is not usually syndromic. Closure of the metopic suture creates the appearance of a triangular forehead (see Fig. 10-31).

Prenatal detection of craniosynostosis can be challenging, and often only the severe cases are identified by prenatal ultrasound examination.<sup>94,104</sup> The hyperechogenic bones of the skull have been visualized as early as 9 weeks of gestation.<sup>94</sup> The hypoechoic sutures become thinner as gestation advances. Abnormal fetal head shape or growth parameters (biparietal and occipitofrontal diameters) or the inability



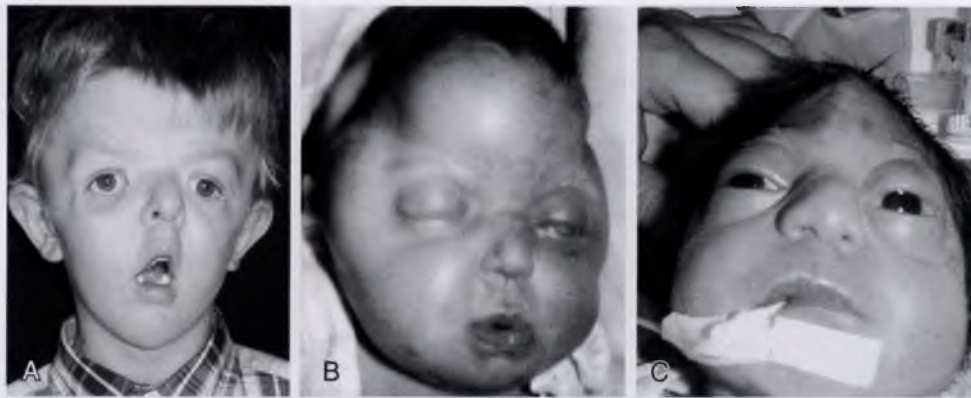


**FIG 10-31** Craniosynostosis syndromes: **A**, Apert syndrome. **B**, Pfeiffer syndrome, lethal variety (cloverleaf skull). **C**, Trigonocephaly.

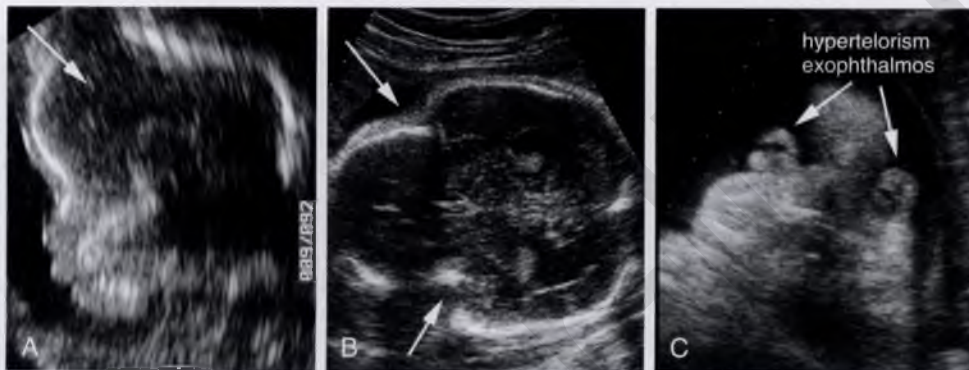


**FIG 10-32** Antenatal sonogram from the case demonstrated in Figure 10-27B: **A** and **B**, Sagittal and axial sonograms demonstrating the cloverleaf skull (arrows). **C**, Exophthalmos and hypertelorism.

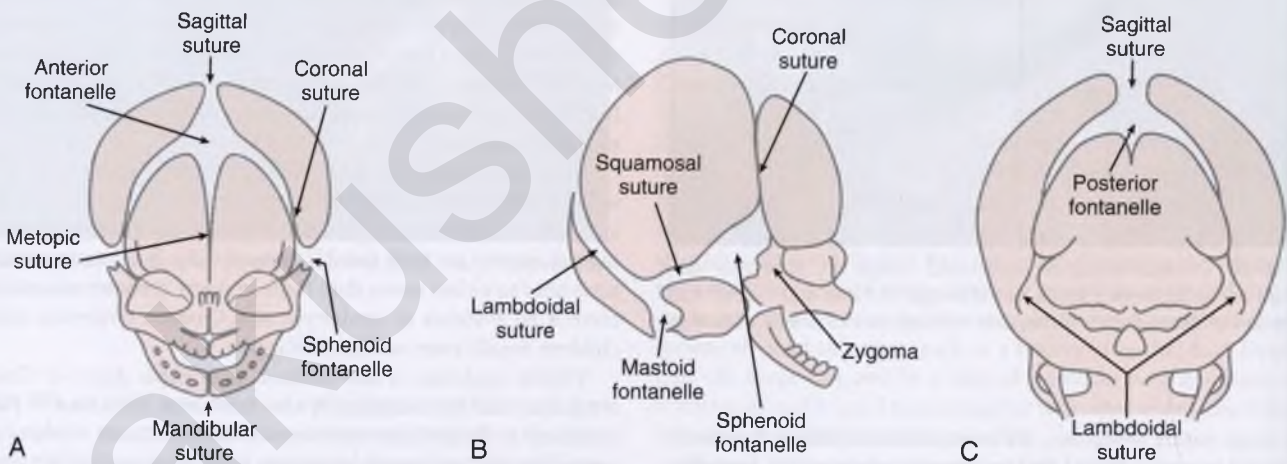


**FIG 10-33** Diagram of fetal sutures and fontanelles: **A**, Anterior view. **B**, Lateral view. **C**, Posterior view. (From Pretorius DH, Nelson TR: Prenatal visualization of cranial sutures and fontanelles with three-dimensional ultrasonography. *J Ultrasound Med* 13(11):872, 1994.)

to visualize the intervening sutures should raise concern for craniosynostosis. However, the abnormal skull shape may appear later, 4 to 16 weeks prior to the full closure of the sutures.<sup>91</sup> Widening of the nonfused sutures can also be noted and is best visualized with 3D ultrasound. The volumes need to be acquired by targeting each specific suture; otherwise, refractive shadows may simulate sutures. For example, the coronal suture should be acquired from an axial scan of the head, whereas the metopic suture should be acquired from a frontal view of the face, whether axial or sagittal. It is important to place the

region of interest rendering boundaries along one suture at a time so that there is no overlapping of bones (see Fig. 10-34). Fetal MRI has been reported to be an excellent adjunct to ultrasound technology for the detection of craniosynostosis and the associated anomalies in small series.<sup>99,105</sup>

Treatment for craniosynostosis is surgical and involves several stages in those with multiple suture synostosis. The goals of care are to correct skull deformities and reduce the risk of raised intracranial pressure and subsequent neurologic damage.<sup>92</sup> The procedures can

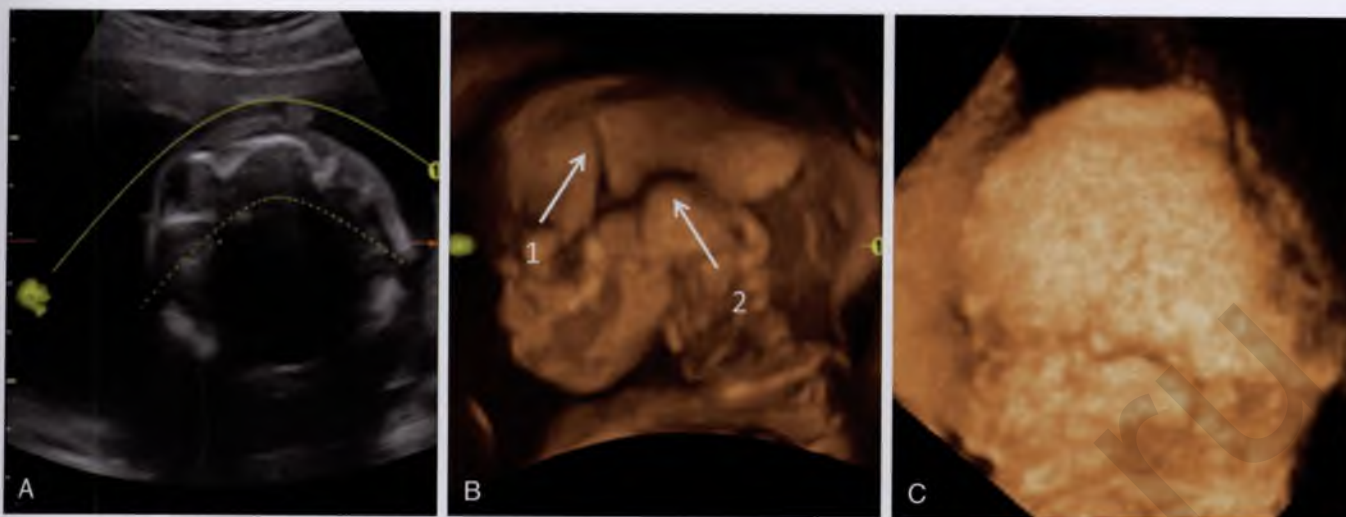


**FIG 10-34** Normal and abnormal cranial sutures. **A**, Normal four-dimensional OmniView reference image of sutures at 26 weeks showing curved line over skull. **B**, Rendered image of normal sutures obtained using OmniView. 1, coronal suture; 2, squamosal suture. **C**, Craniosynostosis of coronal suture in Apert syndrome at 21 weeks.

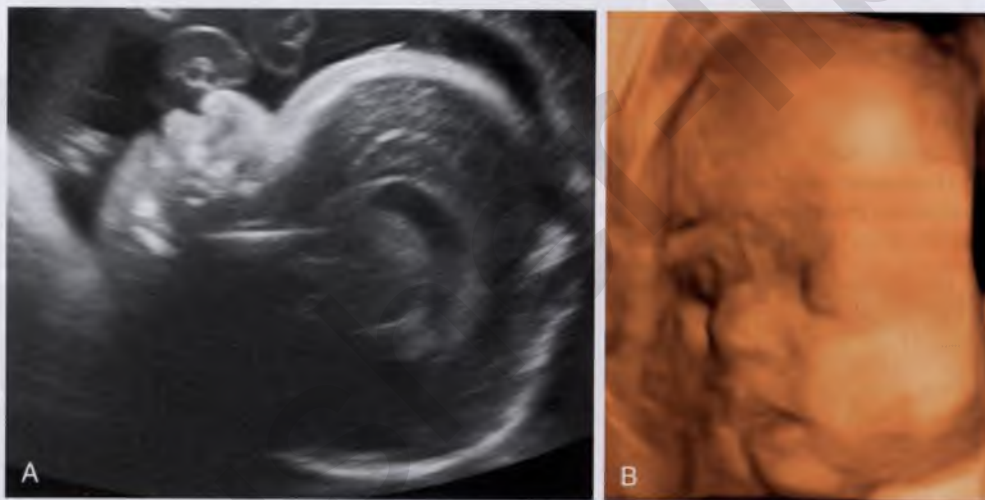


**FIG 10-35** Apert syndrome. Craniosynostosis with altered facies as seen on midline sagittal image (**A**) and surface rendering (**B**).

include craniosynostosis release with fronto-orbital advancement at age 6 to 8 months followed by midface advancement later in childhood and possibly again in adolescence.<sup>106,107</sup> Airway management during these procedures can be difficult.<sup>108</sup>

The recurrence risks for craniosynostosis are likely less than 5% in those with nonsyndromic sagittal, metopic, or unicoronal synostosis but up to 30% to 50% in bicoronal and multisuture synostosis.<sup>92</sup> The autosomal dominant conditions can recur if there is germline mosaicism.

## ANOMALIES OF THE NECK

Using a combination of 2D and 3D ultrasound imaging, a detailed assessment of the fetal neck can be made. In a study by Liberty and coworkers of 582 fetuses undergoing routine screening ultrasonography, the fetal neck structures were adequately visualized in 23% of fetuses at 10 to 13 weeks, 29% at 14 to 16 weeks, 35% at 17 to 19 weeks, and 88% at 20 to 24 weeks.<sup>109</sup> The success of imaging was therefore gestational age dependent. Structures that can be appreciated included

multiple components of the fetal pharynx and larynx as well as the esophagus. Assessment of five standardized planes was proposed to evaluate the larynx and pharynx, including a posterior coronal plane, anterior coronal plane, and three axial planes (high, mid, low) (Fig. 10-36).<sup>109</sup> Standardized tables were established for the larynx and pharynx based on the study by Liberty and coworkers. These images are best accomplished by 3D multiplanar reconstruction; however, 2D real-time ultrasound is useful in detecting flow of amniotic fluid by color Doppler via both the pharynx and larynx into the fetal lungs and via the esophagus to the fetal stomach. The fetal esophagus, when decompressed, appears as two echogenic lines representing the serosa and mucosa with surrounding hypoechoic muscular walls. Potential anomalies that can be detected via imaging of these basic structures of the fetal neck include laryngeal or esophageal atresia or a tracheo-esophageal fistula (see Chapter 14).

### Nuchal Cystic Hygroma

A cystic hygroma is a cystic lymphatic structure, usually occurring predominantly in the occipitocervical region, though it can extend



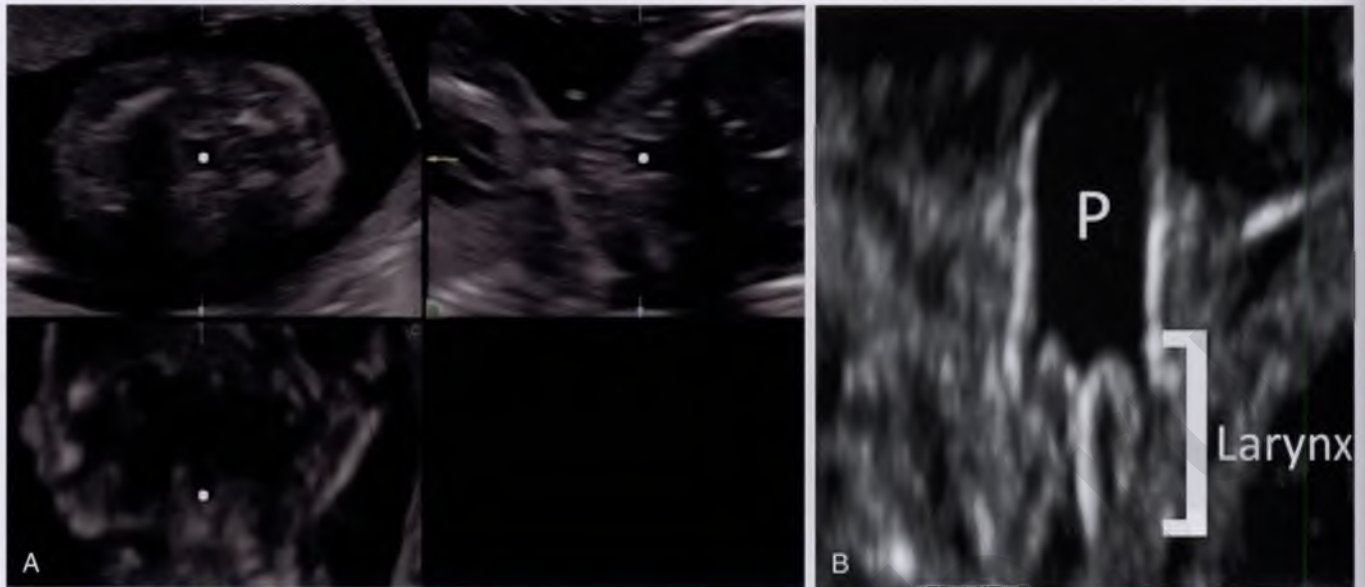


**FIG 10-36** Normal ultrasound images of the fetal neck: **A**, Three-dimensional multiplanar display of the fetal neck acquired in the axial plane. The white cursor dot is centered in the pharynx in all three planes; upper left is axial, upper right is coronal, and lower left is sagittal. **B**, Coronal image of the fetal neck showing the pharynx (P) and larynx.

along the entire length of the fetus.<sup>110,111</sup> The proposed physiology of the formation of cystic hygromas was termed the *jugular lymphatic-obstruction sequence* by Smith and Graham.<sup>112</sup> In theory, the lymph fluid in a fetus first flows into the jugular lymphatic sacs, and the jugular sacs then develop connections to the venous system. They ultimately become the terminal portions of the right lymphatic duct and thoracic duct.<sup>112,113</sup> Distention of the jugular sacs and cystic hygromas occurs when this sequence is unsuccessful and the venous connections are not made. This can eventually result in global lymphedema and fetal hydrops (often called *congenital lymphangiectasia*) and fetal death (Fig. 10-37). Cystic hygromas may resolve in some cases as gestation progresses, with the theory that in these fetuses, recanalization of the lymph vessels occurs and collaterals develop.<sup>110</sup> For continuing pregnancies, isolated cystic hygromas identified in the first trimester, in otherwise normal fetuses, have been shown to resolve 78% of the time.<sup>111</sup>

In a large contemporary study of almost 40,000 patients screened in the first trimester, the frequency of cystic hygromas was found to be 1 in 285, whereas other studies report a frequency of 1.7%.<sup>110,111</sup> Some consider cystic hygroma to be the extreme of an enlarged nuchal translucency.

On ultrasound imaging, cystic hygromas and bilateral distention of the jugular sacs appear as hypoechoic structures in the fetal nuchal space. They may be septated or nonseptated. Multiple fibrous septa can give the hygroma a honeycomb appearance (Fig. 10-38). The hygromas vary in size and may be associated with sonographic findings of hydrops, including skin edema, pleural and pericardial effusions, and ascites.<sup>53</sup>

Cystic hygromas are concerning sonographic findings, as they are associated with aneuploidy, fetal anomalies, and fetal death. In a study of 134 cases, 51% were associated with confirmed aneuploidy whereas 34% of the remaining cases were affected with a major structural malformation.<sup>111</sup> Hygromas in the first trimester have been shown to be associated more often with trisomy 21 and in the second trimester with 45,X (Turner syndrome), although they can be seen with other aneuploidies as well.<sup>111,113</sup> Septa and larger cystic hygromas have been shown to be particularly concerning in terms of the association with aneuploidy and anomalies.<sup>110,111</sup> A cystic hygroma in a euploid fetus



**FIG 10-37** Nuchal cystic hygroma with lymphatic obstruction sequence.

can also result in pterygium colli (webbed neck) after birth. Anterior hygromas or lymphangiomas, rather than posterior, do not have the same association with aneuploidy.

The finding of a cystic hygroma warrants a thorough evaluation, including consideration of an invasive diagnostic procedure (chorionic villous sampling or amniocentesis) for genetic diagnosis and a detailed anatomic survey and fetal echocardiogram for those with continuing pregnancies. Only 17% of fetuses with the finding of a cystic hygroma in the first trimester will have normal pediatric outcomes.<sup>111</sup>

### Other Neck Masses

The differential diagnosis for a fetal neck mass includes cystic hygroma, lymphangioma, hemangioma, cervical teratoma, goiter, branchial cleft cyst, and thyroglossal duct cyst.<sup>114</sup> All of these neck masses can be associated with polyhydramnios secondary to fetal esophageal compression and can potentially result in compromise of the neonatal airway at birth. Evaluating these masses to assess for potential involvement of vital neck structures such as the trachea and esophagus with





**FIG 10-38** Nuchal cystic hygroma: **A**, Small hygroma in a second trimester fetus: two separate fluid accumulations (jugular sacs) are seen on each side of the neck (arrows). **B**, Large cystic hygroma (arrow) with septations in a fetus at 14 weeks' gestation. **C**, Three-dimensional ultrasound in surface mode in a fetus with a cystic hygroma (arrow).

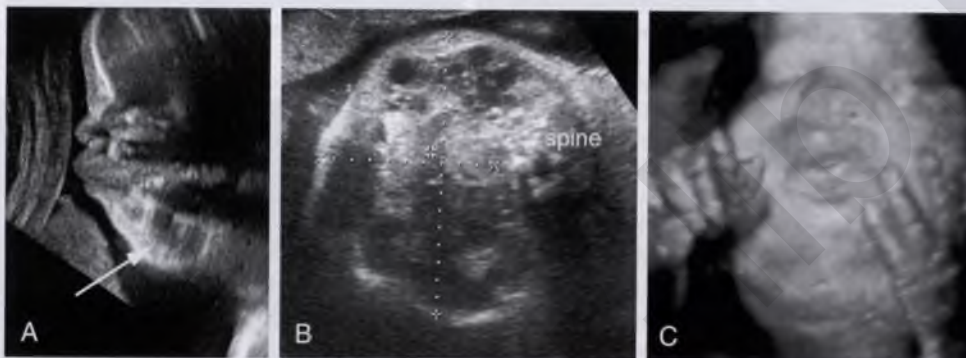


**FIG 10-39** Although the antenatal diagnosis was cervical teratoma, this fetus was found at birth to have a cavernous lymphangioma infiltrating the neck tissues. **A** and **B**, Two-dimensional sonograms demonstrating the large neck mass. **C**, Surface rendered 3D sonogram demonstrating the mass.

the use of 3D and 4D ultrasound, as well as MRI, can be helpful.<sup>115-117</sup> If tracheal occlusion is suspected with any of these masses, an EXIT procedure may be required.<sup>118</sup>

Lymphangiomas are lymphatic malformations similar to cystic hygromas that infiltrate the subcutaneous space and muscular septa.<sup>115</sup> They can be seen by prenatal ultrasound as fetal neck masses of varied sizes with cystic components infiltrating the surrounding tissues (Fig. 10-39). They can require immediate surgical treatment either at the time of birth in the event of airway compromise or surgery in early neonatal life. Spontaneous resolution is less likely.

Hemangiomas are benign vascular malformations that can be located in the area of the fetal head and neck and have an appearance similar to lymphangiomas on prenatal ultrasound images. They are found in the dermis and subcutaneous tissues. There are three types—capillary, cavernous, and nevus flammeus.<sup>119</sup> Cavernous hemangiomas are found in 2% of infants and can be detected on prenatal ultrasound images as echogenic soft tissue masses.<sup>119</sup> The borders of these benign tumors are often hard to differentiate from surrounding tissues.<sup>120</sup> Color power Doppler examination has been used to demonstrate significant vascularity of the lesions, which is a distinctive finding differentiating them from lymphangiomas.<sup>119</sup> High-output cardiac failure can occur with cavernous hemangiomas, which can lead to fetal hydrops, and they therefore require close monitoring, particularly if they are large. Depending on the location and size of the hemangioma, some can be managed expectantly postnatally, whereas others will require surgical intervention.

Teratomas are rare tumors, occurring in 1 in 20,000 to 1 in 40,000 live births, and about 5% of them are located in the cervical region.<sup>121-123</sup> They are most often benign, though malignant transformation has been reported.<sup>124</sup> Like epignathus tumors of the mouth,



**FIG 10-40** Parasagittal sonographic image showing large exophytic solid and cystic cervical teratoma.

these tumors can be derived from all three germ cell layers. On ultrasound imaging, the tumors appear as pharyngeal masses usually crossing the midline with solid and cystic components (Figs. 10-40 and 10-41). Approximately 50% of teratomas display calcifications.<sup>121</sup> Thirty percent of these tumors are associated with polyhydramnios.<sup>114,121</sup> Treatment is via surgical excision, and fetuses with airway



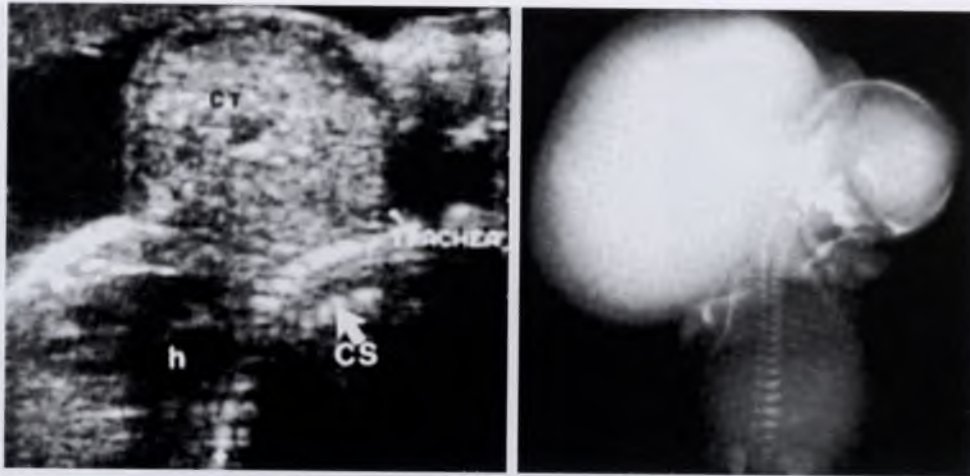


**FIG 10-41** Large cervical teratoma (CT). CS, cervical spine; h, heart.

compression may require delivery by means of the EXIT procedure, like several of the other neck masses, depending on the size and the structures involved.

Fetal goiter can also manifest as an anterior neck mass that may lead to tracheal compression and neonatal airway concerns at birth. On ultrasound imaging, it is a homogeneous, uniform well-demarcated central neck mass that may result in hyperextension/retroflexion of the fetal neck (Fig. 10-42).<sup>125</sup> Iodine deficiency, overtreatment of maternal Graves disease or other causes of hyperthyroidism, excessive thyroid replacement, and congenital hypothyroidism can lead to the development of a fetal goiter.<sup>125,126</sup> If the cause is a maternal medical issue, it can be addressed appropriately; however, if there is concern for congenital hypothyroidism, percutaneous umbilical blood sampling may be necessary to assess the fetal thyroid status and determine if treatment is warranted. If significant fetal hypothyroidism is identified, it has been successfully treated with intra-amniotic levothyroxine; this treatment can result in reduction of the size of the goiter and decrease the risk of tracheal compression at birth.<sup>126,127</sup> If tracheal patency is highly suspected on prenatal sonography and MRI, and the mass is not expected to pose an airway problem at the time of birth, fetal goiter has also been managed conservatively with treatment of the congenital hypothyroidism initiated after birth.<sup>125</sup>

Establishing a definitive diagnosis of a fetal neck mass on prenatal imaging can be challenging, even with the use of advanced ultrasound technology and MRI.<sup>114,120</sup> Attention must be paid to the presence of solid or calcified components, which are more common in teratomas, whereas hemangiomas and lymphangiomas are more often fluid-filled structures.<sup>114,121</sup> One of the essential goals of prenatal imaging is to identify whether the trachea appears patent as this finding can alter delivery planning and the need for an EXIT procedure.<sup>118</sup> It is highly recommended that infants with large neck masses be delivered in a tertiary care center to allow for involvement of a multispecialty team and avoid any delay in necessary immediate treatment.

## CONCLUSIONS

Orofacial clefts are among the most common fetal and neonatal anomalies. With improved access to and expertise in both 2D and 3D sonography, the frequency and accuracy of prenatal diagnosis are improving. Particularly with clefts that involve the palate only, 3D ultrasound imaging can be essential. Other abnormalities of the fetal face and head amenable to potential prenatal detection include ocular defects, micrognathia and retrognathia, and craniosynostosis. Identifying a facial



**FIG 10-42** Fetal goiter (arrow) that was found to be associated with hypothyroidism as a consequence of excessive maternal propylthiouracil intake.

anomaly should always signal the need for a complete detailed fetal anatomic survey, particularly the brain, to evaluate for any associated anomalies that could represent a known chromosomal abnormality or syndrome. The same is true of the finding of fetal neck abnormalities, particularly the cystic hygroma. The prognosis for fetal facial anomalies depends on the severity of the finding, the presence of an underlying syndrome, and any associated neurologic abnormalities. The outcome for fetal facial tumors and neck masses relies on the ability to treat and resect such lesions. Advances in prenatal ultrasound imaging of the fetal face and neck assist in preparing the patient and the surgical teams for the optimal care of the neonate.



## REFERENCES

- Romero R, Pilu G, Jeanty P, et al: *Prenatal Diagnosis of Congenital Anomalies: The Face*, Norwalk, CT, 1988, Appleton & Lange.
- Platt LD, DeVore GR, Pretorius DH: Improving cleft palate/cleft lip antenatal diagnosis by 3-dimensional sonography the “flipped face” view. *J Ultrasound Med* 25(11):1423–1430, 2006.
- Faure J, Captier G, Baumler M, Boulot P: Sonographic assessment of normal fetal palate using three-dimensional imaging: a new technique. *Ultrasound Obstet Gynecol* 29:159–165, 2007.
- Ramos GA, Romine LE, Gindes L, et al: Evaluation of the fetal secondary palate by 3-dimensional ultrasonography. *J Ultrasound Med* 29:357–364, 2010.
- Campbell S, Lees C, Moscoso G, Hall P: Ultrasound antenatal diagnosis of cleft palate by a new technique: the 3D “reverse face” view. *Ultrasound Obstet Gynecol* 25(1):12–18, 2005.
- Martínez Ten P, Pérez Pedregosa J, Santacruz B, et al: Three-dimensional ultrasound diagnosis of cleft palate: “reverse face,” “flipped face” or “oblique face”—which method is best? *Ultrasound Obstet Gynecol* 33:399–406, 2009.
- Mailáth-Pokorny M, Worda C, Krampl-Bettelheim E, et al: What does magnetic resonance imaging add to the prenatal ultrasound diagnosis of facial clefts? *Ultrasound Obstet Gynecol* 36:445–451, 2010.
- Wax J, Minkoff H, Johnson A, et al: Consensus report on the detailed fetal anatomic ultrasound examination: indications, components, and qualifications. *J Ultrasound Med* 33:189–195, 2014.
- Maarse W, Berge SJ, Pistorius L, et al: Diagnostic accuracy of transabdominal ultrasound in detecting prenatal cleft lip and palate: a systematic review. *Ultrasound Obstet Gynecol* 35:495–502, 2010.
- Maarse W, Pistorius L, Van Eeten W, et al: Prenatal ultrasound screening for orofacial clefts. *Ultrasound Obstet Gynecol* 38:434–439, 2011.
- Mossey P, Castilla E: *Global Registry and Database on Craniofacial Anomalies*, Geneva, 2003, World Health Organization, pp 85–89.
- Dixon MJ, Marazita ML, Beaty TH, et al: Cleft lip and palate: understanding genetic and environmental influences. *Nat Rev Genet* 12:167–178, 2011.
- Tessier P: Anatomical classification of facial, cranio-facial and latero-facial clefts. *J Maxillofac Surg* 4:69–92, 1976.
- Gorlin R, Cervenká J, Pruzansky S: Facial clefting and its syndromes. *Birth Defects Orig Artic Ser* 7(7):3–49, 1971.
- Offerdal K, Jebens N, Syvertsen T, et al: Prenatal ultrasound detection of facial clefts: a prospective study of 49,314 deliveries in a non-selected population in Norway. *Ultrasound Obstet Gynecol* 31(6):639–646, 2008.
- Sperber GH: Formation of the primary and secondary palate. In Wyszynski DF, editor: *Cleft Lip and Palate: From Origin to Treatment*, New York, 2002, Oxford University Press, pp 5–24.
- Mossey PA, Little J, Munger RG, et al: Cleft lip and palate. *Lancet* 374:1773–1785, 2009.
- Moxham B: The development of the palate—a brief review. *Eur J Anat* 7:53–74, 2003.
- Grosen D, Chevrier C, Skytthe A, et al: A cohort study of recurrence patterns among more than 54,000 relatives of oral cleft cases in Denmark: support for the multifactorial threshold model of inheritance. *J Med Genet* 47:162–168, 2010.
- Chmait R, Pretorius D, Moore T, et al: Prenatal detection of associated anomalies in fetuses diagnosed with cleft lip with or without cleft palate in utero. *Ultrasound Obstet Gynecol* 27:173–176, 2006.
- Gillham J, Anand S, Bullen P: Antenatal detection of cleft lip with or without cleft palate: incidence of associated chromosomal and structural anomalies. *Ultrasound Obstet Gynecol* 34:410–415, 2009.
- Shaw GM, Nelson V, Iovannisci DM, et al: Maternal occupational chemical exposures and biotransformation genotypes as risk factors for selected congenital anomalies. *Am J Epidemiol* 157:475–484, 2003.
- Gordon JE, Shy CM: Agricultural chemical use and congenital cleft lip and/or palate. *Arch Environ Health* 36:213–221, 1981.
- Holmes LB, Hernandez-Diaz S: Newer anticonvulsants: lamotrigine, topiramate and gabapentin. *Birth Defects Res A Clin Mol Teratol* 94(8):599–606, 2012.
- Margulis AV, Mitchell AA, Gilboa SM, et al: Use of topiramate in pregnancy and risk of oral clefts. *Am J Obstet Gynecol* 207:405.e1–405.e7, 2012.
- Tomson T, Battino D: Teratogenic effects of antiepileptic drugs. *Lancet Neurol* 11:803–813, 2012.
- Lammer EJ, Chen DT, Hoar RM, et al: Retinoic acid embryopathy. *N Engl J Med* 313:837–841, 1985.
- Park-Wyllie L, Mazzotta P, Pastuszak A, et al: Birth defects after maternal exposure to corticosteroids: prospective cohort study and meta-analysis of epidemiological studies. *Teratology* 62(6):385–392, 2000.
- Little J, Cardy A, Munger RG: Tobacco smoking and oral clefts: a meta-analysis. *Bull World Health Organ* 82(3):213–218, 2004.
- Johnson CY, Little J: Folate intake, markers of folate status and oral clefts: is the evidence converging? *Int J Epidemiol* 37:1041–1058, 2008.
- Wehby GL, Murray JC: Folic acid and orofacial clefts: a review of the evidence. *Oral Dis* 16:11–19, 2010.
- Christ JE, Meininger MG: Ultrasound diagnosis of cleft lip and cleft palate before birth. *Plast Reconstr Surg* 68:854–859, 1981.
- Johnson DD, Pretorius DH, Budorick NE, et al: Fetal lip and primary palate: three-dimensional versus two-dimensional US. *Radiology* 217:236–239, 2000.
- Pilu G, Segata M: A novel technique for visualization of the normal and cleft fetal secondary palate: angled insonation and three-dimensional ultrasound. *Ultrasound Obstet Gynecol* 29:166–169, 2007.
- Sepulveda W, Wong AE, Martínez-Ten P, et al: Retronasal triangle: a sonographic landmark for the screening of cleft palate in the first trimester. *Ultrasound Obstet Gynecol* 35:7–13, 2010.
- American Cleft Palate-Craniofacial Association: Parameters for evaluation and treatment of patients with cleft lip/palate or other craniofacial anomalies. *Cleft Palate Craniofac J* 30(Suppl):S1–S16, 1993.
- Blaas HG, Eriksson A, Salvesen K, et al: Brains and faces in holoprosencephaly: pre- and postnatal description of 30 cases. *Ultrasound Obstet Gynecol* 19:24–38, 2002.
- DeMyer W, Zeman W, Palmer CG: The face predicts the brain: diagnostic significance of median facial anomalies for holoprosencephaly (arhinencephaly). *Pediatrics* 34:256–263, 1964.
- Petracchi F, Crespo L, Michia C, et al: Holoprosencephaly at prenatal diagnosis: analysis of 28 cases regarding etiopathogenic diagnoses. *Prenat Diagn* 31:887–891, 2011.
- Leoncini E, Baranello G, Orioli IM, et al: Frequency of holoprosencephaly in the International Clearinghouse Birth Defects Surveillance Systems: searching for population variations. *Birth Defects Res A Clin Mol Teratol* 82:585–591, 2008.
- Fox JW, Golden GT, Edgerton MT: Frontonasal dysplasia with alar clefts in two sisters: genetic considerations and surgical correction. *Plast Reconstr Surg* 57:553–561, 1976.
- Sleus E, Goncalves L, Johnson A, et al: First-trimester three-dimensional ultrasonographic findings in a fetus with frontonasal malformation. *J Matern Fetal Neonatal Med* 16:187–197, 2004.
- Guion-Almeida ML, Richieri-Costa A, Saavedra D, et al: Frontonasal dysplasia: analysis of 21 cases and literature review. *Int J Oral Maxillofac Surg* 25:91–97, 1996.
- Presti F, Celentano C, Marcuzzo L, et al: Ultrasound prenatal diagnosis of a lateral facial cleft (Tessier number 7). *Ultrasound Obstet Gynecol* 23:606–608, 2004.
- Muraskas JK, McDonnell JE, Chudik RJ, et al: Amniotic band syndrome with significant orofacial clefts and disruptions and distortions of craniofacial structures. *J Pediatr Surg* 38:635–638, 2003.
- Stelnicki EJ, Hoffman WY, Vanderwall K, et al: A new in utero model for lateral facial clefts. *J Craniofac Surg* 8:460–465, 1997.
- Pilu G, Visentin A, Ambrosini G, et al: Three-dimensional sonography of unilateral Tessier number 7 cleft in a mid-trimester fetus. *Ultrasound Obstet Gynecol* 26:98–99, 2005.
- Paquette L, Randolph L, Incerpi M, et al: Fetal microphthalmia diagnosed by magnetic resonance imaging. *Fetal Diagn Ther* 24:182–185, 2008.



49. Dollfus H, Verloes A: Dysmorphology and the orbital region: a practical clinical approach. *Surv Ophthalmol* 49:547–561, 2004.
50. Burns NS, Iyer RS, Robinson AJ, et al: Diagnostic imaging of fetal and pediatric orbital abnormalities. *AJR Am J Roentgenol* 201:W797–W808, 2013.
51. Pineda-Alvarez DE, Solomon BD, Roessler E, et al: A broad range of ophthalmologic anomalies is part of the holoprosencephaly spectrum. *Am J Med Genet A* 155A(11):2713–2720, 2011.
52. Sedano HO, Gorlin RJ: Frontonasal malformation as a field defect and in syndromic associations. *Oral Surg Oral Med Oral Pathol* 65(6):704–710, 1988.
53. Callen P: Ultrasonography in obstetrics and gynecology. In Pilu G, et al, editors: *Ultrasound Evaluation of the Fetal Face and Neck*, ed 5, Philadelphia, 2008, WB Saunders, pp 392–418.
54. Feldman E, Shalev E, Weiner E, et al: Microphthalmia—prenatal ultrasonic diagnosis: a case report. *Prenat Diagn* 5:205–207, 1985.
55. Feingold M, Baum J: Goldenhar's syndrome. *Am J Dis Child* 132:136–138, 1978.
56. Blazer S, Zimmer EZ, Mezer E, et al: Early and late onset fetal microphthalmia. *Am J Obstet Gynecol* 194:1354–1359, 2006.
57. Verma AS, FitzPatrick DR: Anophthalmia and microphthalmia. *Orphanet J Rare Dis* 2:47, 2007.
58. Francis P, Berry V, Bhattacharya S, et al: The genetics of childhood cataract. *J Med Genet* 37:481–488, 2000.
59. Léonard A, Bernard P, Hiel AL, et al: Prenatal diagnosis of fetal cataract: case report and review of the literature. *Fetal Diagn Ther* 26(2):61–67, 2009.
60. Chan WH, Biswas S, Ashworth JL, et al: Educational paper. *Eur J Pediatr* 171:625–630, 2012.
61. Sepulveda W, Wojakowski AB, Elias D, et al: Congenital dacryocystocele prenatal 2- and 3-dimensional sonographic findings. *J Ultrasound Med* 24:225–230, 2005.
62. Goldberg H, Sebire N, Holwell D, et al: Prenatal diagnosis of bilateral dacryocystoceles. *Ultrasound Obstet Gynecol* 15:448–449, 2000.
63. Shekunov J, Griepentrog GJ, Diehl NN, et al: Prevalence and clinical characteristics of congenital dacryocystocele. *J AAPOS* 14(5):417–420, 2010.
64. Singh DJ, Bartlett SP: Congenital mandibular hypoplasia: analysis and classification. *J Craniofac Surg* 16:291–300, 2005.
65. Luedders DW, Bohlmann MK, Germer U, et al: Fetal micrognathia: objective assessment and associated anomalies on prenatal sonogram. *Prenat Diagn* 31:146–151, 2011.
66. Van den Elzen AP, Semmekrot BA, Bongers EM, et al: Diagnosis and treatment of the Pierre Robin sequence: results of a retrospective clinical study and review of the literature. *Eur J Pediatr* 160:47–53, 2001.
67. Izumi K, Konczal LL, Mitchell AL, et al: Underlying genetic diagnosis of Pierre Robin sequence: retrospective chart review at two children's hospitals and a systematic literature review. *J Pediatr* 160:645–650.e2, 2012.
68. Robin P: A fall of the base of the tongue considered as a new cause of nasopharyngeal respiratory impairment: Pierre Robin sequence, a translation. 1923. *Plast Reconstr Surg* 93(6):1301–1303, 1994.
69. Evans KN, Sie KC, Hopper RA, et al: Robin sequence: from diagnosis to development of an effective management plan. *Pediatrics* 127:936–948, 2011.
70. Otto C, Platt L: The fetal mandible measurement: an objective determination of fetal jaw size. *Ultrasound Obstet Gynecol* 1:12–17, 1991.
71. Chitty LS, Campbell S, Altman DG: Measurement of the fetal mandible—feasibility and construction of a centile chart. *Prenat Diagn* 13:749–756, 1993.
72. Paladini D, Morra T, Teodoro A, et al: Objective diagnosis of micrognathia in the fetus: the jaw index. *Obstet Gynecol* 93:382–386, 1999.
73. Rotten D, Levaillant J, Martinez H, et al: The fetal mandible: a 2D and 3D sonographic approach to the diagnosis of retrognathia and micrognathia. *Ultrasound Obstet Gynecol* 19:122–130, 2002.
74. Sepulveda W, Wong AE, Vinals F, et al: Absent mandibular gap in the retroronasal triangle view: a clue to the diagnosis of micrognathia in the first trimester. *Ultrasound Obstet Gynecol* 39:152–156, 2012.
75. Meyer AC, Lidsky ME, Sampson DE, et al: Airway interventions in children with Pierre Robin sequence. *Otolaryngol Head Neck Surg* 138:782–787, 2008.
76. Williams DH, Gauthier DW, Maizels M: Prenatal diagnosis of Beckwith-Wiedemann syndrome. *Prenat Diagn* 25(10):879–884, 2005.
77. Meizner I, Shalev J, Mashiach R, et al: Prenatal ultrasonographic diagnosis of congenital oral granular cell myoblastoma. *J Ultrasound Med* 19:337–339, 2000.
78. Paladini D, Morra T, Guida F, et al: Perinatal diagnosis and perinatal management of a lingual lymphangioma. *Ultrasound Obstet Gynecol* 11(2):141, 1998.
79. Ruano R, Benachi A, Aubry MC, et al: The impact of 3-dimensional ultrasonography on perinatal management of a large epignathus teratoma without ex utero intrapartum treatment. *J Pediatr Surg* 40(11):e31–e34, 2005.
80. Clement K, Chamberlain P, Boyd P, et al: Prenatal diagnosis of an epignathus: a case report and review of the literature. *Ultrasound Obstet Gynecol* 18:178–181, 2001.
81. Takeuchi K, Masuda Y, Narita F, et al: Prenatal evaluation of bidirectional epignathus: comparison of ultrasonography and magnetic resonance imaging. *Fetal Diagn Ther* 18:26–28, 2003.
82. Tracy JC, Lee AS, Scott AR, et al: *Embryology and Anomalies of the External Ear. Advanced Cosmetic Otoplasty*, New York, 2013, Springer, pp 3–13.
83. Shih JC, Shyu MK, Lee CN, et al: Antenatal depiction of the fetal ear with three-dimensional ultrasonography. *Obstet Gynecol* 91:500–505, 1998.
84. Allen G, Baroff G: Mongoloid twins and their siblings. *Hum Hered* 5:294–326, 1954.
85. Hall B: Mongolism in newborn infants. An examination of the criteria for recognition and some speculations on the pathogenic activity of the chromosomal abnormality. *Clin Pediatr (Phila)* 5:4–12, 1966.
86. Chang CH, Chang FM, Yu CH, et al: Fetal ear assessment and prenatal detection of aneuploidy by the quantitative three-dimensional ultrasonography. *Ultrasound Med Biol* 26(5):743–749, 2000.
87. Shimizu T, Salvador L, Dawson L, et al: The role of reduced ear size in the prenatal detection of chromosomal abnormalities. *Prenat Diagn* 17:545–549, 1997.
88. Moreira NC, Teixeira J, Raininko R, et al: The ear in fetal MRI: what can we really see? *Neuroradiology* 53:1001–1008, 2011.
89. Marchac D, Renier D: Craniosynostosis. *World J Surg* 13:358–365, 1989.
90. Boulet SL, Rasmussen SA, Honein MA: A population based study of craniosynostosis in metropolitan Atlanta, 1989–2003. *Am J Med Genet A* 146A(8):984–991, 2008.
91. Delahaye S, Bernard J, Renier D, et al: Prenatal ultrasound diagnosis of fetal craniosynostosis. *Ultrasound Obstet Gynecol* 21:347–353, 2003.
92. Wilkie AO, Byren JC, Hurst JA, et al: Prevalence and complications of single-gene and chromosomal disorders in craniosynostosis. *Pediatrics* 126:e391–e400, 2010.
93. Cohen MM, Jr: Cloverleaf skulls: etiologic heterogeneity and pathogenetic variability. *J Craniofac Surg* 20:652–656, 2009.
94. Muenke M, Kress W, Collmann H, et al: *Craniosynostoses: Molecular Genetics, Principles of Diagnosis and Treatment*, Basel, 2011, Karger Medical and Scientific Publishers.
95. Apert M: De l'acrocephalosyndactylie. *Bull Soc Med Hop (Paris)* 23:1310–1330, 1906.
96. Blank C: Apert's syndrome (a type of acrocephalosyndactyly)—observations on a British series of thirty-nine cases. *Ann Hum Genet* 24:151–164, 1959.
97. Cohen MM, Kreiborg S, Lammer EJ, et al: Birth prevalence study of the Apert syndrome. *Am J Med Genet* 42:655–659, 1992.
98. Tolarova MM, Harris JA, Ordway DE, et al: Birth prevalence, mutation rate, sex ratio, parents' age, and ethnicity in Apert syndrome. *Am J Med Genet* 72:394–398, 1997.

99. Giacotti A, D'Ambrosio V, De Filippis A, et al: Comparison of ultrasound and magnetic resonance imaging in the prenatal diagnosis of Apert syndrome: report of a case. *Childs Nerv Syst* 30(8):1445–1448, 2014.
100. Cohen MM, Jr, Kreiborg S: A clinical study of the craniofacial features in Apert syndrome. *Int J Oral Maxillofac Surg* 25(1):45–53, 1996.
101. Kreiborg S, Cohen MM, Jr: The oral manifestations of Apert syndrome. *J Craniofac Genet Dev Biol* 12(1):41–48, 1992.
102. Cohen MM, Jr, Kreiborg S: An updated pediatric perspective on the Apert syndrome. *Am J Dis Child* 147:989–993, 1993.
103. Rutland P, Pulleyn LJ, Reardon W, et al: Identical mutations in the FGFR2 gene cause both Pfeiffer and Crouzon syndrome phenotypes. *Nat Genet* 9:173–176, 1995.
104. Miller C, Losken HW, Towbin R, et al: Ultrasound diagnosis of craniosynostosis. *Cleft Palate Craniofac J* 39(1):73–80, 2002.
105. Fjörtöft MI, Sevely A, Boetto S, et al: Prenatal diagnosis of craniosynostosis: value of MR imaging. *Neuroradiology* 49:515–521, 2007.
106. Cedars MG, Linck DL, Chin M, et al: Advancement of the midface using distraction techniques. *Plast Reconstr Surg* 103:429–441, 1999.
107. Wong GB, Kakulis EG, Mulliken JB: Analysis of fronto-orbital advancement for Apert, Crouzon, Pfeiffer, and Saethre-Chotzen syndromes. *Plast Reconstr Surg* 105:2314–2323, 2000.
108. Abouleish AE: Neonatal craniosynostosis. *Anesthesiology* 115:1103, 2011.
109. Liberty G, Boldes R, Shen O, et al: The fetal larynx and pharynx: structure and development on two- and three-dimensional ultrasound. *Ultrasound Obstet Gynecol* 42:140–148, 2013.
110. Rosati P, Guariglia L: Prognostic value of ultrasound findings of fetal cystic hygroma detected in early pregnancy by transvaginal sonography. *Ultrasound Obstet Gynecol* 16:245–250, 2000.
111. Malone FD, Ball RH, Nyberg DA, et al: First-trimester septated cystic hygroma: prevalence, natural history, and pediatric outcome. *Obstet Gynecol* 106:288–294, 2005.
112. Smith D, Graham J: *Jugular Lymphatic Obstruction Sequence. Recognizable Patterns of Human Malformation*, ed 3, Philadelphia, 1982, WB Saunders, pp 472–473.
113. Chervenak FA, Isaacson G, Blakemore KJ, et al: Fetal cystic hygroma: cause and natural history. *N Engl J Med* 309:822–825, 1983.
114. Rempen A, Feige A: Differential diagnosis of sonographically detected tumours in the fetal cervical region. *Eur J Obstet Gynecol Reprod Biol* 20:89–105, 1985.
115. Paladini D, Vassallo M, Sglavo G, et al: Cavernous lymphangioma of the face and neck: prenatal diagnosis by three-dimensional ultrasound. *Ultrasound Obstet Gynecol* 26:300–302, 2005.
116. Kathary N, Bulas DI, Newman KD, et al: MRI imaging of fetal neck masses with airway compromise: utility in delivery planning. *Pediatr Radiol* 31:727–731, 2001.
117. Ogura T, Hamada H, Obata-Yasuoka M, et al: Antepartum assessment of fetal cystic lymphangioma by magnetic resonance imaging. *Gynecol Obstet Invest* 53:237–239, 2002.
118. Marwan A, Crombleholme TM: The EXIT procedure: principles, pitfalls, and progress. *Semin Pediatr Surg* 15(2):107–115, 2006.
119. Viora E, Grassi Pirrone P, Comoglio F, et al: Ultrasonographic detection of fetal cranio-facial hemangioma: case report and review of the literature. *Ultrasound Obstet Gynecol* 15:431–434, 2000.
120. Yoshida S, Kikuchi A, Naito S, et al: Giant hemangioma of the fetal neck, mimicking a teratoma. *J Obstet Gynaecol Res* 32:47–54, 2006.
121. Kerner B, Flaum E, Mathews H, et al: Cervical teratoma: prenatal diagnosis and long-term follow-up. *Prenat Diagn* 18:51–59, 1998.
122. Bergé SJ, Von Lindern J, Appel T, et al: Diagnosis and management of cervical teratomas. *Br J Oral Maxillofac Surg* 42:41–45, 2004.
123. Shine NP, Sader C, Gollow I, Lannigan FJ: Congenital cervical teratomas: diagnostic, management and postoperative variability. *Auris Nasus Larynx* 33(1):107–111, 2006.
124. Muscatello L, Giudice M, Feltri M: Malignant cervical teratoma: report of a case in a newborn. *Eur Arch Otorhinolaryngol* 262:899–904, 2005.
125. Blumenfeld YJ, Davis A, Milan K, et al: Conservatively managed fetal goiter: an alternative to in utero therapy. *Fetal Diagn Ther* 34:184–187, 2013.
126. Bliddal S, Rasmussen ÅK, Sundberg K, et al: Graves' disease in two pregnancies complicated by fetal goitrous hypothyroidism: successful in utero treatment with levothyroxine. *Thyroid* 21:75–81, 2011.
127. Davidson KM, Richards DS, Schatz DA, et al: Successful in utero treatment of fetal goiter and hypothyroidism. *N Engl J Med* 324:543–546, 1991.



# Fetal Musculoskeletal System

*Edgar Hernandez-Andrade, Lami Yeo, Luís F. Gonçalves, Suchaya Luewan,  
Maynor Garcia, Roberto Romero*

## SUMMARY OF KEY POINTS

- The prevalence of skeletal dysplasias is about 2.4/10,000 births, and 9.1/1000 among perinatal deaths; the most common anomalies are thanatophoric dysplasia, achondroplasia, osteogenesis imperfecta, and achondrogenesis.
- The new edition of Nosology and Classification of Genetic Skeletal Disorders includes 436 clinical conditions classified into 42 groups involving 364 affected genes; therefore, molecular diagnosis is possible in about 75% of skeletal disorders.
- Molecular diagnosis can be offered to couples with a family history of skeletal dysplasia to estimate the risk in a future pregnancy, or to pregnant women with ultrasound signs suggestive of fetal skeletal dysplasia.
- Two-dimensional (2D) and three-dimensional (3D) sonography and 3D helical computed tomography (3D-HCT) are the main imaging modalities used to evaluate a fetus with suspected skeletal dysplasia.
- Thanatophoric dysplasia and achondrogenesis account for 60% of all lethal skeletal dysplasias and are characterized by extremely reduced thoracic dimensions and very short long bones.
- A complete fetal ultrasound evaluation, including assessment of fetal movements, should be performed if a skeletal disorder is suspected.
- Ultrasound signs suggestive of a skeletal dysplasia include bones with reduced length, abnormal shape, reduced mineralization, and fractures; abnormal fetal facial profile; polyhydramnios; and abnormal pattern of fetal movements.
- The diagnosis of a possible skeletal dysplasia during pregnancy should be corroborated by molecular diagnosis and neonatal or pathologic evaluation.

## OUTLINE

### Development of the Fetal Skeleton, 273

Skeletogenesis (Genetics and Embryology), 273

Endochondral Ossification, 273

Intramembranous Ossification, 275

### Skeletal Dysplasias, 275

Birth Prevalence and Contribution to Perinatal Mortality, 275

Classification of Skeletal Dysplasias, 275

Terminology Frequently Used to Describe Bone Dysplasias, 277

Clinical Presentation, 288

Diagnostic Imaging and Prenatal Diagnosis of Skeletal Dysplasias, 288

Approach to the Diagnosis of Skeletal Dysplasias, 291

Increased Nuchal Translucency and Skeletal Dysplasias, 303

### Osteochondrodysplasias, 303

Achondroplasia, Thanatophoric Dysplasia, and Hypochondroplasia, 303

Fibrochondrogenesis and Atelosteogenesis, 306

Achondrogenesis, 307

Osteogenesis Imperfecta and Hypophosphatasia, 309

Diastrophic Dysplasia, 310

Kniest-like Disorders, 311

Dyssegmental Dysplasia, 312

Campomelic Dysplasia, 312

Skeletal Dysplasias Characterized by a Hypoplastic Thorax, 313

Skeletal Dysplasias With Predominant Membranous Bone Involvement, 316

Limb Deficiency or Congenital Amputations, 317

Syndromes With Absent Limbs and Facial Anomalies, 318

Limb Reduction Defects Associated With Other Anomalies, 319

### Split Hand and Foot Deformities, 320

Ectrodactyly Ectodermal Dysplasia–Cleft Lip/Palate Syndrome, 320

### Clubhand Deformities, 321

Radial Clubhand, 321

Radial Clubhand and Hematologic Disorders, 321

Radial Clubhand and Scoliosis, 322

Other Conditions Associated With Radial Clubhand, 323

Polydactyly, 323

Arthrogyposis, 323

### Clubfoot, 325

## DEVELOPMENT OF THE FETAL SKELETON

The skeleton is formed by 206 skeletal elements constituted by two tissues (bone and cartilage) and three cell types (osteoblasts, osteoclasts, and chondrocytes).<sup>1,2</sup> Skeletal tissues derive from three embryonic cell lineages: (1) cranial neural crest cells, from which the craniofacial skeleton originates; (2) paraxial mesoderm cells or somites, which are the embryologic precursors of the axial skeleton; and (3) the lateral plate mesoderm, which is responsible for limb formation.<sup>1,3-6</sup> Limb buds begin to develop during the 4th week of embryonic life (6th menstrual week) as clusters of mesenchymal cells covered by a layer of ectoderm.<sup>1-3</sup> Mesenchymal models of bone (anlagen: templates for future bones) form around the 5th week of embryonic life (7th menstrual week) (Fig. 11-1).<sup>3</sup> Development of the upper limbs precedes the lower limbs in bud appearance, differentiation, and final relative limb size. Limbs develop in a proximodistal sequence, with the anlagen of the humerus and femur forming first, followed by the radius and ulna, the tibia and fibula, the metacarpal and metatarsal bones, and phalanges.<sup>1,2,7</sup>

### Skeletogenesis (Genetics and Embryology)

Skeletogenesis involves four steps: patterning, organogenesis, growth, and homeostasis.<sup>4</sup> Patterning is the process by which the final size, shape, number, and arrangement of bones are determined.<sup>2,4</sup> This process takes place long before skeletogenesis, and three signaling regions have been identified: (1) an apical ectodermal ridge; (2) an area consisting of ectoderm covering the sides of the bud; and (3) a zone of polarizing activity.<sup>5</sup> The apical ectodermal ridge consists of densely packed ectodermal cells located at the tip of the limb bud, which express several fibroblast growth factors (FGFs) that initiate and control limb outgrowth.<sup>5,8,9</sup> The ectoderm covering the sides of the bud regulates dorsoventral patterning.<sup>5</sup> The zone of polarizing activity is

located on the posterior limb bud margin. It is responsible for antero-posterior patterning and, thus, the formation of digits.<sup>9,10</sup> Besides FGFs, other genes are involved in the control of limb patterning, including Sonic hedgehog (Shh), GLI-Kruppel family member GLI3 (Gli3), sal-like 1 (Sall1), Hoxd13, Hoxa13, bone morphogenetic/cartilage-derived morphogenetic protein (CDMP), growth differentiation factors (GDFs), Noggin (Nog), Wn7-a, engrailed (en), and LIM homeobox transcription factor 1 beta (Lmx1b).<sup>1,11-16</sup>

Bone and cartilage are formed during the organogenesis period, which consists of three phases: condensation, cell differentiation, and histogenesis. Condensation is of great importance in skeletal development, because the templates for future bones are defined at this stage.<sup>6</sup> Condensation initiation, boundary set, proliferation, adhesion, and growth are regulated by complex interactions between extracellular matrix molecules, cell surface receptors, cell adhesion molecules (e.g., fibronectin, tenascin, Noggin, syndecan, and neural cell adhesion molecule [N-CAM]), homeobox genes (e.g., Hoxa-2, Hoxa-13, Hoxd-11, and Hoxd-11-13), transcription factors (e.g., runt-related transcription factor 2 [RUNX2], winged-helix transcription factor [CFKH-1], mesenchyme forkhead 1 [MFH-1], paired box transcription factors 1 and 9 [PAX-1, PAX-9], periaxin 1 and 2 [PRX-1 and PRX-2], scleraxis, and mammalian SRY box 9 [SOX-9]), and growth factors (e.g., bone morphogenetic proteins, fibroblast growth factor 2 [FGF-2], transforming growth factor beta [TGF- $\beta$ ]).<sup>17,18</sup> Osteogenesis initiates during the 7th week of embryonic development (9th menstrual week), with bones developing by either endochondral or membranous ossification.<sup>4</sup>

### Endochondral Ossification

The axial and appendicular skeletons are formed by endochondral ossification (Fig. 11-2). The axial skeleton (e.g., vertebrae and the dorsal part of the ribs) originates from the somites. Cartilaginous

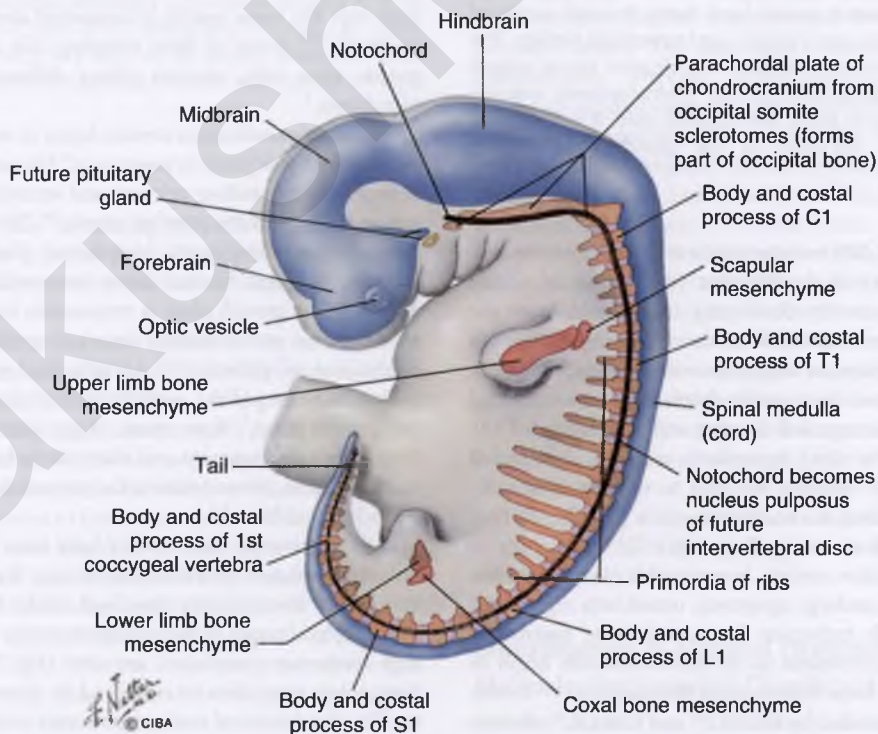


**FIG 11-1** Diagram of the mesenchymal precartilaginous primordia of the axial and appendicular skeletons at 5 weeks' embryonic age (7 weeks' menstrual age). These primordia develop further and eventually ossify to form skeletal structures. (Illustration by Netter FH; from Crelin ES: *Development of the musculoskeletal system*. CIBA Clin Symp 33:6, 1981. Used with permission from CIBA-GEIGY Corporation, Summit, NJ.)



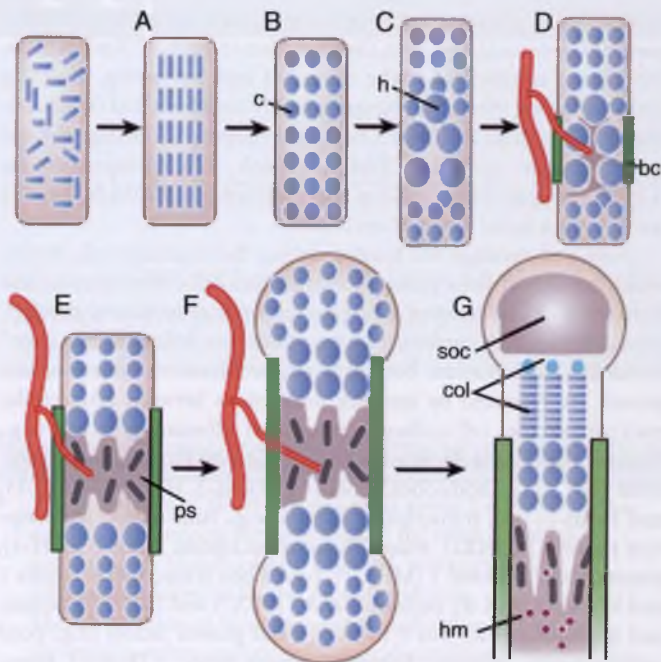


**FIG 11-2** Endochondral bone formation. **A**, Mesenchymal cells condense. **B**, Cells of condensations become chondrocytes (c). **C**, Chondrocytes at the center of condensation stop proliferating and become hypertrophic (h). **D**, Perichondrial cells adjacent to hypertrophic chondrocytes direct the formation of mineralized matrix, attract blood vessels, and undergo apoptosis. **E**, Osteoblasts of primary spongiosa accompany vascular invasion forming the primary spongiosa (ps). **F**, Chondrocytes continue to proliferate, lengthening the bone. Osteoblasts of primary spongiosa are precursors of eventual trabecular bone; osteoblasts of bone collar become cortical bone. **G**, At the edge of the bone, the secondary ossification center (soc) forms through cycles of chondrocyte hypertrophy, vascular invasion, and osteoblast activity. The growth plate below the secondary center of ossification forms orderly columns of proliferating chondrocytes (col). Hematopoietic marrow (hm) expands in marrow space along with stromal cells. (From Kronenberg HM: Developmental regulation of the growth plate. *Nature* 423:332-336, 2003.)

models of the future bones differentiate within mesenchymal condensations during the 6th week of development (8th menstrual week), with primary ossification centers developing in the middle of the anlagen between the 7th and 12th weeks of development (9th to 14th menstrual weeks).<sup>3</sup> *SOX9* plays an important role in chondrogenesis. Mutations in this gene cause campomelic dysplasia, a severe skeletal disorder characterized by congenital bowing and angulation of the long bones (especially of the tibia), hypoplastic scapulae, sex reversal in male fetuses, and a high lethality rate due to respiratory insufficiency.<sup>9</sup> Another gene involved in chondrogenesis is procollagen type II alpha 1 (*COL2A1*), which encodes collagen type II.<sup>1,19</sup>

Within primary ossification centers, hypertrophic cartilage matrix is degraded, chondrocytes undergo apoptosis, osteoblasts replace the disappearing cartilage with trabecular bone, and bone marrow is formed.<sup>1</sup> Simultaneously, osteoblasts in the perichondrium begin to deposit a collar of compact bone matrix along the diaphysis.<sup>1,19</sup> Osteoblast differentiation is controlled by *RUNX2*<sup>20</sup> and *Osterix*,<sup>21</sup> whereas proliferation is controlled by the low-density lipoprotein receptor-related protein 5 (*LPR5*) signaling pathway.<sup>2</sup> Eventually, cartilage in the center of the anlagen degrades, mineralizes, and is removed by osteoclasts.<sup>3,6</sup> Vascular ingrowth is stimulated by vascular endothelial growth

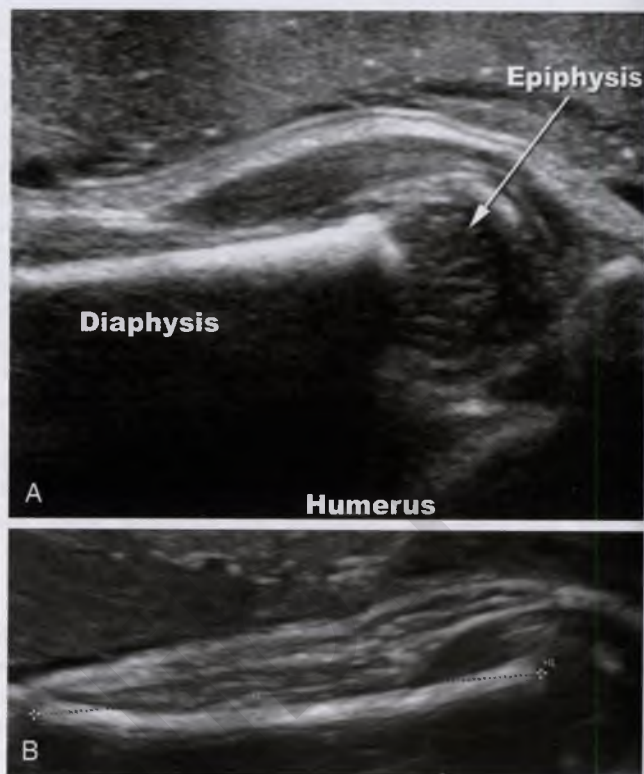


**FIG 11-3 A**, Proximal humeral epiphysis imaged with a high-frequency linear transducer (10 MHz) in a fetus at 29 weeks' gestation. **B**, Measurement of the femur in a third trimester. The femur should be measured along the ossified bone (between the electronic calipers).

factor, with the influx of osteoprogenitor cells occurring at the same time that the bone matrix is deposited along the periosteum of the midshaft.<sup>3,6,22</sup> Some of these invading cells differentiate into hematopoietic stem cells, whereas others differentiate into osteoclasts or osteoblasts.<sup>4</sup>

Secondary ossification centers begin to appear at the extremities of bones (epiphyses) later in pregnancy.<sup>3</sup> The portion of cartilage trapped between the expanding primary and secondary ossification centers is known as the growth plate or physis.<sup>3,9</sup> This structure is formed by a cartilaginous component (epiphyseal plate), a bony component (metaphysis), and fibrous tissue surrounding the periphery of the plate.<sup>23,24</sup> The growth plate is responsible for the longitudinal growth of long bones until definitive fusion of epiphyses and diaphyses occurs at the end of puberty.<sup>3,6,19</sup> Longitudinal growth is coordinated by Indian hedgehog (*Ihh*), a stimulator of chondrocyte proliferation at the growth plate.<sup>1</sup> Bone mass, shape, and strength are maintained throughout development and adult life by balancing bone destruction and formation. Homeostasis is the process that controls the continuing remodeling of bones.<sup>4</sup>

It is noteworthy that when a long bone is imaged by ultrasound, only the diaphyses are measured, because the epiphyses are hypoechoic and are not always clearly visualized. Under favorable conditions, good sonographic images of the epiphysis can be obtained, especially when high-frequency transducers are used (Fig. 11-3). Secondary ossification centers may often be visualized by ultrasound in the third trimester. The distal femoral ossification center may be seen at approximately 32 to 33 weeks of gestation, the proximal tibial epiphyseal center at 34 to 35 weeks, and the proximal humeral epiphyseal ossification center at 37 to 38 weeks of gestation (Fig. 11-4). When all three centers are identified, it is likely that the fetus is at least 37 weeks' gestational age.



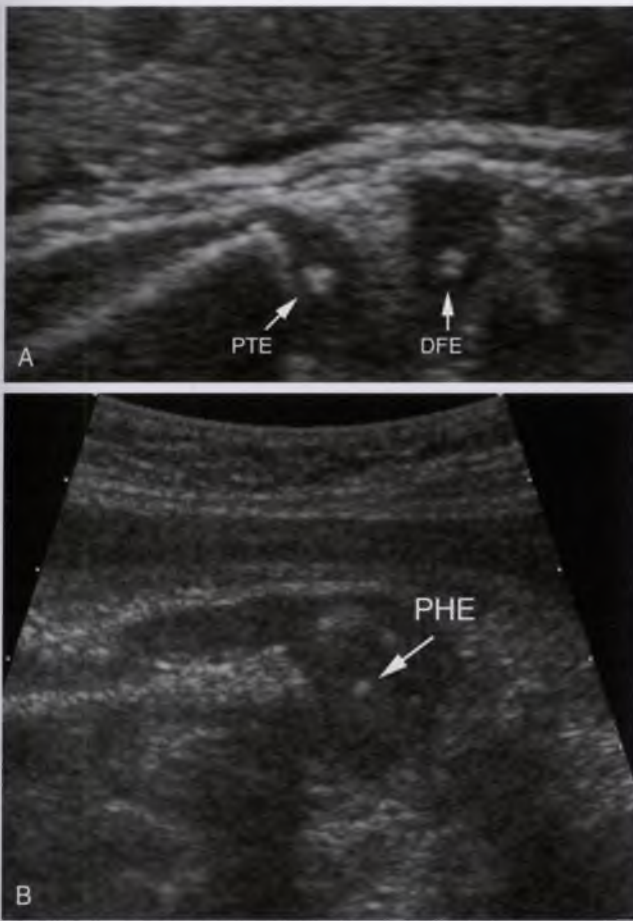


**FIG 11-4** **A**, Sonogram of the knee in a fetus at 35 weeks' gestation. Increased echogenicity from the secondary ossification centers of distal femoral (DFE) and proximal tibial (PTE) epiphyses are seen. **B**, Sonogram of the proximal humerus in a fetus at 38 weeks' gestation. Ossification of the proximal humeral epiphysal ossification center (PHE) is noted.

These ossification centers may be seen slightly earlier in female fetuses than in male fetuses. The timeline for radiographic and histologic appearance of primary and secondary ossification centers is illustrated in Figure 11-5.

Formation and detachment of new somites in the axial skeleton from the paraxial mesoderm occur in craniocaudal direction following a molecular clock produced by oscillations of cycling genes (e.g., *c-hairy-1*, *lunatic fringe [l-fng]*, and *naked cuticle 1 [nkd1]*) that stimulate Notch receptor signaling waves that sweep through the paraxial mesoderm.<sup>25-28</sup> Spatial coordination is provided by a decreasing gradient of FGF8 from the posterior to the anterior pole of the embryo.<sup>5,28,29</sup> Differential expression of delta-like (Dll) proteins determines the size and polarity of the somites,<sup>5</sup> which mature as they move rostrally and differentiate into dermatomyotomes and sclerotomes.<sup>5,28</sup> Dermatomyotomes give rise to the appendicular and axial musculatures, as well as the dorsal epithelium. The sclerotome is the precursor of the axial skeleton, and its formation is initiated and controlled by the Sonic hedgehog gene (*SHH*).<sup>5,30,31</sup>

### Intramembranous Ossification

The craniofacial skeleton and clavicles develop by intramembranous ossification.<sup>1</sup> This process differs from endochondral ossification by

the direct differentiation of mesenchymal cells into osteoblasts, which produce a bone matrix rich in type I collagen.<sup>1-3,19,22</sup> Bone remodeling is accomplished by continuous and concerted action of osteoblasts (cells that produce bone matrix) and osteoclasts (cells that remove bone).

## SKELETAL DYSPLASIAS

Abnormal development, growth, or maintenance of cartilage and bone tissues results in skeletal dysplasias. Skeletal dysplasias are a heterogeneous group of disorders affecting the development of chondroosseous tissues leading to abnormalities in the size, mineralization, and shape of various segments of the skeleton. Despite recent advances in imaging and molecular genetics,<sup>32-34</sup> accurate prenatal diagnosis of skeletal dysplasias remains a clinical challenge.<sup>35</sup> In the most recent revision of the International Nosology and Classification of Constitutional Disorders of Bone<sup>36</sup> it is mentioned that in approximately 25% of all bone disorders the mutated gene has not been yet identified. It is important to acknowledge the contribution of the International Skeletal Dysplasia Registry<sup>37</sup> in the identification and study of skeletal anomalies, assisting providers and patients in the diagnosis and clinical management of skeletal disorders.

In subsequent sections of this chapter, we will review the birth prevalence, classification, and molecular genetics of skeletal dysplasias that are identifiable at birth.

### Birth Prevalence and Contribution to Perinatal Mortality

In a large multicenter study conducted by Camera and Mastroiacovo<sup>38</sup> the birth prevalence of skeletal dysplasias (excluding limb amputations) was estimated as 2.4/10,000 births. Twenty-three percent of the affected infants were stillborn, whereas 32% died during the first week of life. The overall frequency of skeletal dysplasias among perinatal deaths was 9.1/1000. This study also reported on the birth prevalence of the different skeletal dysplasias and their relative frequency among perinatal deaths. The four most common skeletal dysplasias were thanatophoric dysplasia, achondroplasia, osteogenesis imperfecta (OI), and achondrogenesis. Thanatophoric dysplasia and achondrogenesis accounted for 62% of all lethal skeletal dysplasias, and the most common nonlethal skeletal dysplasia was achondroplasia.<sup>38</sup> In another large series from western Scotland, the prevalence of skeletal dysplasias at birth was 1.1/10,000 births. The most frequent conditions were thanatophoric dysplasia (1/42,000), OI (1/56,000), chondrodysplasia punctata (1/84,000), campomelic syndrome (1/112,000), and achondrogenesis (1/112,000).<sup>39</sup> Rasmussen and associates<sup>40</sup> reported a prevalence of 2.1/10,000 deliveries in a longitudinal study, which included elective pregnancy termination, stillborn infants at more than 20 weeks of gestation, and liveborn infants diagnosed by the 5th day of life. The rate of lethal cases in this study was 0.95/10,000 deliveries.<sup>40</sup> Of interest, the study reporting the highest prevalence of skeletal dysplasias at birth (9.5/10,000 births) was conducted in a population with a high rate of consanguineous unions.<sup>41</sup> An overview of the prevalence of skeletal dysplasias in different populations is presented in Table 11-1.

### Classification of Skeletal Dysplasias

#### Molecular-Pathogenetic Classification of Skeletal Dysplasias

The first classification of skeletal anomalies was proposed more than 40 years ago and was mainly based on clinical and radiographic findings.<sup>50</sup> Since that time, the classification has continuously evolved owing to the contribution of imaging and molecular biology techniques.<sup>33,34,51-55</sup> This classification is currently known as Nosology and



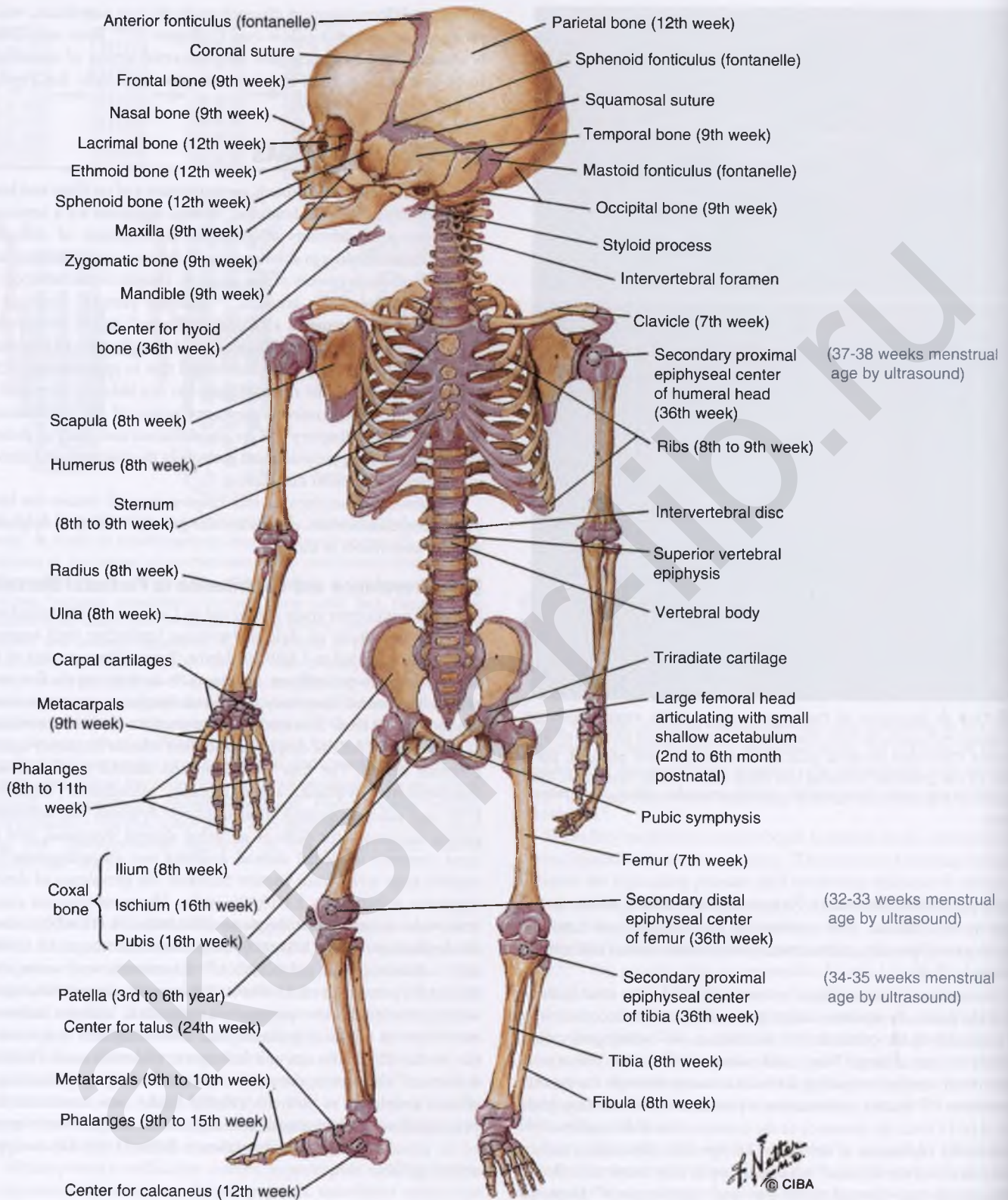


**FIG 11-5** Diagram of the skeleton of a full-term newborn. The times that the ossification centers appear are designated in embryologic weeks (add 2 weeks for menstrual age). These times are somewhat different from those using ultrasound because ultrasound is more sensitive for detection of ossification than radiographic methods. All refer to the primary ossification centers unless otherwise designated. Only at birth do the lower extremities have the same length as the upper extremities; subsequently, the lower extremities become longer than the upper extremities. (Illustration by Netter FH; from Crelin ES: Development of the musculoskeletal system. CIBA Clin Symp 33:13, 1981. Used with permission from CIBA-GEIGY Corporation, Summit, NJ.)



**TABLE 11-1 Prevalence of Skeletal Dysplasias**

Study*	Prevalence	Comment
Gustavson and Jorulf <sup>42</sup>	1/2117	Newborns
Camera and Mastroiacovo <sup>38</sup>	1/4600	Neonates
Connor et al <sup>39</sup>	1/8900	Neonates
Weldner et al <sup>35</sup>	1/1333	Achondroplasia
Orioli et al <sup>43</sup>	1/4347	First 3 days of life
Stoll et al <sup>44</sup>	1/3125	First 8 days of life
Andersen <sup>45</sup>	1/6667	At birth
Kallen et al <sup>46</sup>	1/6250	Multicenter study
Rasmussen et al <sup>40</sup>	1/4166	First 5 days of life
Barbosa-Buck et al <sup>47</sup>	1/21,276	Thanatophoric dysplasia
Donnelly et al <sup>48</sup>	1/8000	Thanatophoric dysplasia
Stevenson et al <sup>49</sup>	1/7900	Osteogenesis imperfecta

\*Studies are listed in the references at the end of the chapter.

Classification of Genetic Skeletal Disorders.<sup>36</sup> Most skeletal anomalies are a phenotypic manifestation of a mutation in a gene and altered protein expression; therefore, they can be grouped according to the affected genes as they share similar clinical characteristics. The International Skeletal Dysplasia Society (ISDS) periodically reviews this classification, and the last version corresponding to the 9th edition was published in 2015.<sup>36</sup> In this document, the authors acknowledge the contribution of next-generation sequencing technologies and the increasing availability of whole exome sequencing, allowing the discovery of more gene-related skeletal anomalies. For this review, 436 clinical conditions were classified into 42 groups involving 364 affected genes (Table 11-2). The classification provides (1) the group/name of the skeletal disorder; (2) type of inheritance; (3) MIM (Mendelian Inheritance in Man) number; (4) locus of the mutation in the gene; (5) affected protein; and (6) associations/difference with other skeletal anomalies. Skeletal dysplasias, metabolic bone disorders, dysostosis, skeletal malformations, and reduction syndromes are included in this classification. However, the authors also clarify that in approximately 25% of skeletal disorders, the mutated gene has not yet been identified. The genetic basis for classification of very rare diseases was done by family pedigree, or was based on homogeneity or phenotype in unrelated families. The classification aims to provide more complete information for prenatal counseling and clinical management. The full document can be consulted at the ISDS website.<sup>56</sup>

### Skeletal Dysplasias Seen at Birth

The molecular pathogenic classification of genetic disorders of the skeleton is very extensive and includes many conditions that may not be apparent at birth and therefore are not amenable to prenatal diagnosis by imaging methods.<sup>33</sup> A more clinically relevant list of skeletal dysplasias that may be recognizable during pregnancy along with their mode of inheritance and causative genes has been published by Krakow<sup>57</sup> (Table 11-3). The authors acknowledge that for a full classification of skeletal anomalies the Nosology and Classification of Genetic Skeletal Disorders should be consulted.<sup>36</sup>

### Clinically Oriented Classification

A skeletal anomaly is suspected prenatally either by family history or by ultrasound findings, while after birth, the diagnosis is suspected based on family history and on clinical and radiographic findings. When a previous family member is affected, a gene panel can be offered to the mother (and if necessary to the father) to evaluate the risk to

the fetus. Direct testing can also be performed and genetic panels evaluated on amniotic fluid or chorionic villus samples when sonographic findings suggestive of a skeletal anomaly are identified. Krakow and colleagues<sup>58</sup> compiled a practical list of abnormal ultrasonographic findings seen in skeletal dysplasias along with a list of differential diagnoses for each finding (Table 11-4). Once the differential diagnoses have been narrowed down to the most likely disorder(s), definitive genetic testing can be offered. Limitations of genetic panels include study cost, time to obtain the results, and that the genetic basis of all skeletal anomalies are not known. A benefit of molecular testing is that identification of the gene mutation can provide information on the severity of the disease.

### Terminology Frequently Used to Describe Bone Dysplasias

Shortening of the extremities can involve the entire limb (micromelia), the proximal segment (rhizomelia), the intermediate segment (mesomelia), or the distal segment (acromelia) (Fig. 11-6). The diagnosis of rhizomelia or mesomelia requires comparing the bony dimensions of the lower legs and forearms with those of the thighs and arms. Figures 11-7 and 11-8 display the relationships between the humerus and ulna, as well as the femur and tibia, which can be used for the objective assessment of rhizomelia and mesomelia. Table 11-5 presents a list of skeletal dysplasias characterized by rhizomelia, mesomelia, and micromelia.

Several skeletal dysplasias feature alterations of the hands and feet. The term *polydactyly* refers to the presence of more than five digits. It is classified as postaxial if the extra digits are on the ulnar or fibular side, and preaxial if they are located on the radial or tibial side. *Syn-dactyly* refers to soft tissue or bony fusion of adjacent digits. *Clinodactyly* consists of deviation of a finger or fingers.

The most common spinal abnormality seen in skeletal dysplasias is platyspondyly, which consists of flattening of the vertebrae (Fig. 11-9).<sup>59-65</sup> Xyphosis, scoliosis<sup>66-70</sup> (Figs. 11-10 and 11-11), hemivertebra (Fig. 11-12),<sup>66,71,72</sup> and coronal clefing of vertebral bodies have been also reported.<sup>68</sup>

Long bone biometry has been used extensively for the prediction of gestational age. Nomograms for this purpose display the distribution of bone lengths in relation to gestational weeks. For the proper use of these nomograms, the clinician must know the accurate gestational age of the fetus. Therefore, patients at risk for skeletal dysplasias are advised to seek prenatal care at an early gestational age in order to assess all clinical estimators of gestational age. Tables 11-6 and 11-7 present nomograms of the measurement of limb biometry for the upper and lower extremities, respectively. Comparisons between the limb dimensions and head circumference can be used for patients presenting with uncertain gestational age (Figs. 11-13 and 11-14).

The nomograms and figures in this chapter provide the mean, 3rd, and the 97th percentiles of limb biometric parameters. The reader should be aware that approximately 6% of the general population will fall outside these boundaries. Ideally, a more stringent criterion, such as the 1st percentile of limb growth for gestational age, should be used for diagnosis. Unfortunately, none of the currently available nomograms has been based on a sufficient number of patients to provide an accurate discrimination between the 3rd and the 1st percentiles. However, most skeletal dysplasias diagnosed in utero or at birth are associated with dramatic long bone shortening, and under these circumstances, the precise boundary used (i.e., 1st or 3rd percentile) is not critical. An exception to this is achondroplasia, in which limb biometry is only mildly affected until the third trimester, when abnormal growth can be detected by examining the slope of growth of the

*Text continued on p. 288*



TABLE 11-2 Nosology and Classification of Genetic Skeletal Disorders

GROUPS/NAME OF DISORDER	GROUPS/NAME OF DISORDER
1. FGFR3 chondrodysplasia group <ul style="list-style-type: none"> <li>a. Thanatophoric dysplasia type 1 (TD1), type 2 (TD2)</li> <li>b. Severe achondroplasia with developmental delay and acanthosis nigricans (SADDAN)</li> <li>c. Achondroplasia</li> <li>d. Hypochondroplasia</li> <li>e. Camptodactyly, tall stature, and hearing loss syndrome (CATSHL)</li> <li>f. Hypochondroplasia-like dysplasia(s)</li> </ul>	8. TRPV4 group <ul style="list-style-type: none"> <li>a. Metatropic dysplasia</li> <li>b. Spondyloepimetaphyseal dysplasia, Maroteaux type (pseudo-Morquio syndrome type 2)</li> <li>c. Spondylometaphyseal dysplasia, Kozlowski type</li> <li>d. Brachyolmia, autosomal dominant type</li> <li>e. Familial digital arthropathy with brachydactyly</li> </ul>
2. Type 2 collagen group <ul style="list-style-type: none"> <li>a. Achondrogenesis type 2 (ACG2; Langer-Saldino)</li> <li>b. Platspondylic dysplasia, Torrance type</li> <li>c. Hypochondrogenesis</li> <li>d. Spondyloepiphyseal dysplasia congenita (SEDC)</li> <li>e. Spondyloepimetaphyseal dysplasia (SEMD), Strudwick type</li> <li>f. Kniest dysplasia</li> <li>g. Spondyloperipheral dysplasia</li> <li>h. Mild SED with premature onset arthrosis</li> <li>i. SED with metatarsal shortening (formerly Czech dysplasia)</li> <li>j. Stickler syndrome type 1</li> </ul>	9. Ciliopathies with major skeletal involvement <ul style="list-style-type: none"> <li>a. Chondroectodermal dysplasia (Ellis-van Creveld)</li> <li>b. Short rib-polydactyly syndrome (SRPS) type 1/3 (Saldino-Noonan/Verma-Naumoff)</li> <li>c. Asphyxiating thoracic dysplasia (ATD; Jeune)</li> <li>d. SRPS type 2 (Majewski)</li> <li>e. SRPS type 4 (Beemer)</li> <li>f. SRPS type 5</li> <li>g. Oral-facial-digital syndrome type 4 (Mohr-Majewski)</li> <li>h. Cranioectodermal dysplasia (Levin-Sensenbrenner) types 1, 2</li> <li>i. Thoracolumbar pelvic dysplasia (Barnes)</li> </ul>
3. Type 11 collagen group <ul style="list-style-type: none"> <li>a. Stickler syndrome type 2</li> <li>b. Marshall syndrome</li> <li>c. Stickler syndrome type 3 (nonocular)</li> <li>d. Fibrochondrogenesis</li> <li>e. Oto-spondylo-mega-epiphyseal dysplasia (OSMED), recessive type</li> <li>f. Oto-spondylo-mega-epiphyseal dysplasia (OSMED), dominant type (Weissenbacher-Zweymüller syndrome, Stickler syndrome type 3)</li> </ul>	10. Multiple epiphyseal dysplasia and pseudoachondroplasia group <ul style="list-style-type: none"> <li>a. Pseudoachondroplasia (PSACH)</li> <li>b. Multiple epiphyseal dysplasia (MED) type 1 (EDM1)</li> <li>c. Multiple epiphyseal dysplasia (MED) type 2 (EDM2)</li> <li>d. Multiple epiphyseal dysplasia (MED) type 3 (EDM3)</li> <li>e. Multiple epiphyseal dysplasia (MED) type 5 (EDM5)</li> <li>f. Multiple epiphyseal dysplasia (MED) type 6 (EDM6)</li> <li>g. Multiple epiphyseal dysplasia (MED), other types</li> <li>h. Stickler syndrome, recessive type</li> <li>i. Familial hip dysplasia (Beukes)</li> <li>j. Multiple epiphyseal dysplasia with microcephaly and nystagmus (Lowry-Wood)</li> </ul>
4. Sulfation disorders group <ul style="list-style-type: none"> <li>a. Achondrogenesis type 1B (ACG1B)</li> <li>b. Atelosteogenesis type 2 (AO2)</li> <li>c. Diastrophic dysplasia (DTD)</li> <li>d. MED, autosomal recessive type (rMED; EDM4)</li> <li>e. SEMD, PAPSS2 type</li> <li>f. Brachyolmia, recessive type</li> <li>g. Chondrodysplasia gPAPP type (includes Catel-Manzke-like syndrome)</li> <li>h. Chondrodysplasia with congenital joint dislocations, CHST3 type (recessive Larsen syndrome)</li> <li>i. Ehlers-Danlos syndrome, CHST14 type ("musculoskeletal variant")</li> </ul>	11. Metaphyseal dysplasias <ul style="list-style-type: none"> <li>a. Metaphyseal dysplasia, Schmid type (MCS)</li> <li>b. Cartilage-hair hypoplasia (CHH; metaphyseal dysplasia, McKusick type)</li> <li>c. Metaphyseal dysplasia, CHH-like, POP1 type</li> <li>d. Metaphyseal dysplasia, Jansen type</li> <li>e. Eiken dysplasia</li> <li>f. Metaphyseal dysplasia with pancreatic insufficiency and cyclic neutropenia (Shwachman-Bodian-Diamond syndrome, SBDS)</li> <li>g. Metaphyseal anadysplasia types 1, 2</li> <li>h. Metaphyseal dysplasia, Spahr type</li> <li>i. Metaphyseal dysplasia with maxillary hypoplasia</li> </ul>
5. Perlecan group <ul style="list-style-type: none"> <li>a. Dyssegmental dysplasia, Silverman-Handmaker type</li> <li>b. Dyssegmental dysplasia, Rolland-Desbuquois type</li> <li>c. Schwartz-Jampel syndrome (myotonic chondrodystrophy)</li> </ul>	12. Spondylometaphyseal dysplasias (SMD) <ul style="list-style-type: none"> <li>a. Spondyloenchondrodysplasia (SPENCD)</li> <li>b. Odontochondrodysplasia (ODCD)</li> <li>c. SMD, Sutcliffe type or corner fractures type</li> <li>d. SMD with cone-rod dystrophy</li> <li>e. SMD with retinal degeneration, axial type</li> </ul>
6. Aggrecan group <ul style="list-style-type: none"> <li>a. SED, Kimberley type</li> <li>b. SEMD, Aggrecan type</li> <li>c. Familial osteochondritis dissecans</li> </ul>	13. Spondylo-epi-(meta-)physeal dysplasias (SE(M)D) <ul style="list-style-type: none"> <li>a. Dyggve-Melchior-Clausen dysplasia (DMC)</li> <li>b. Immuno-osseous dysplasia (Schimke)</li> <li>c. SED, Wolcott-Rallison type</li> <li>d. SEMD, Matrilin type</li> <li>e. SEMD, short limb-abnormal calcification type</li> <li>f. SED tarda, X-linked (SED-XL)</li> <li>g. Spondylodysplastic Ehlers-Danlos syndrome</li> <li>h. SPONASTRIME dysplasia</li> <li>i. Platspondylic (brachyolmia) with amelogenesis imperfecta</li> <li>j. CODAS syndrome</li> </ul>
7. Filamin group and related disorders <ul style="list-style-type: none"> <li>a. Frontometaphyseal dysplasia</li> <li>b. Osteodysplasty Melnick-Needles</li> <li>c. Otopalatodigital syndrome type 1 (OPD1)</li> <li>d. Otopalatodigital syndrome type 2 (OPD2)</li> <li>e. Terminal osseous dysplasia with pigmentary defects (TODPD)</li> <li>f. Atelosteogenesis type 1 (AO1)</li> <li>g. Atelosteogenesis type 3 (AO3)</li> <li>h. Larsen syndrome (dominant)</li> <li>i. Spondylo-carpal-tarsal dysplasia</li> <li>j. Frank-ter Haar syndrome</li> </ul>	

TABLE 11-2 Nosology and Classification of Genetic Skeletal Disorders—cont'd

GROUPS/NAME OF DISORDER	GROUPS/NAME OF DISORDER
14. Severe spondylodysplastic dysplasias <ul style="list-style-type: none"> <li>a. Achondrogenesis type 1A (ACG1A)</li> <li>b. Schneckenbecken dysplasia</li> <li>c. Spondylometaphyseal dysplasia, Sedaghatian type</li> <li>d. Severe spondylometaphyseal dysplasia (SMD Sedaghatian-like)</li> <li>e. Opsismodysplasia</li> <li>f. Mitochondria-associated granulocyte macrophage colony stimulating factor-signaling gene (MAGMAS) related skeletal dysplasia</li> </ul>	20. Dysplasias with multiple joint dislocations <ul style="list-style-type: none"> <li>a. Desbuquois dysplasia (with accessory ossification center in digit 2)</li> <li>b. Desbuquois dysplasia with short metacarpals and elongated phalanges (Kim type)</li> <li>c. Desbuquois dysplasia type 2</li> <li>d. Pseudodiastrophic dysplasia</li> <li>e. SEMD with joint laxity (SEMD-JL) leptodactylic or Hall type</li> <li>f. SEMD with joint laxity (SEMD-JL) Beighton type</li> </ul>
15. Acromelic dysplasias <ul style="list-style-type: none"> <li>a. Tricho-rhino-phalangeal dysplasia types 1/3</li> <li>b. Tricho-rhino-phalangeal dysplasia type 2 (Langer-Giedion)</li> <li>c. Acrocapitofemoral dysplasia</li> <li>d. Geleophysic dysplasia</li> <li>e. Acromicric dysplasia</li> <li>f. Weill-Marchesani</li> <li>g. Myhre dysplasia</li> <li>h. Acrodysostosis               <ul style="list-style-type: none"> <li>i. Angel-shaped phalango-epiphyseal dysplasia (ASPED)</li> <li>j. Albright hereditary osteodystrophy</li> </ul> </li> </ul>	21. Chondrodysplasia punctata (CDP) group <ul style="list-style-type: none"> <li>a. CDP, X-linked dominant, Conradi-Hünermann type (CDPX2)</li> <li>b. CDP, X-linked recessive, brachytelephalangi type (CDPX1)</li> <li>c. CHILD (congenital hemidysplasia, ichthyosis, limb defects)</li> <li>d. Keutel syndrome</li> <li>e. Greenberg dysplasia</li> <li>f. Rhizomelic CDP types 1, 2, 3</li> <li>g. CDP tibial-metacarpal type</li> <li>h. Astley-Kendall dysplasia</li> </ul>
16. Acromesomelic dysplasias <ul style="list-style-type: none"> <li>a. Acromesomelic dysplasia type Maroteaux (AMDM)</li> <li>b. Grebe dysplasia</li> <li>c. Fibular hypoplasia and complex brachydactyly (Du Pan)</li> <li>d. Acromesomelic dysplasia with genital anomalies</li> <li>e. Acromesomelic dysplasia, Osebold-Remondini type</li> </ul>	22. Neonatal osteosclerotic dysplasias <ul style="list-style-type: none"> <li>a. Blomstrand dysplasia</li> <li>b. Desmosterolosis</li> <li>c. Caffey disease (including prenatal, infantile, and attenuated)</li> <li>d. Caffey dysplasia (severe variants with prenatal onset)</li> <li>e. Raine dysplasia (lethal and nonlethal forms)</li> </ul>
17. Mesomelic and rhizomesomelic dysplasias <ul style="list-style-type: none"> <li>a. Dyschondrosteosis (Leri-Weill)</li> <li>b. Langer type (homozygous dyschondrosteosis)</li> <li>c. Omodysplasia</li> <li>d. Omodysplasia, dominant</li> <li>e. Robinow syndrome, recessive type and dominant type</li> <li>f. Mesomelic dysplasia, Kantaputra type</li> <li>g. Mesomelic dysplasia, Nievergelt type</li> <li>h. Mesomelic dysplasia, Kozlowski-Reardon type</li> <li>i. Mesomelic dysplasia with acral synostoses (Verloes-David-Pfeiffer type)</li> <li>j. Mesomelic dysplasia, Savarirayan type (triangular tibia-fibular aplasia)</li> </ul>	23. Osteopetrosis and related disorders <ul style="list-style-type: none"> <li>a. Osteopetrosis, severe neonatal or infantile forms (OPTB1)</li> <li>b. Osteopetrosis, severe neonatal or infantile forms (OPTB4)</li> <li>c. Osteopetrosis, severe neonatal or infantile forms (OPTB8)</li> <li>d. Osteopetrosis, infantile form, with nervous system involvement (OPTB5)</li> <li>e. Osteopetrosis, intermediate form, osteoclast-poor (OPTB2)</li> <li>f. Osteopetrosis, infantile form, osteoclast-poor with immunoglobulin deficiency (OPTB7)</li> <li>g. Osteopetrosis, intermediate form (OPTB6)</li> <li>h. Osteopetrosis, intermediate form (OPTA2)</li> <li>i. Osteopetrosis with renal tubular acidosis (OPTB3)</li> <li>j. Osteopetrosis, late-onset form type 1 (OPTA1)</li> <li>k. Osteopetrosis, late-onset form type 2 (OPTA2)</li> <li>l. Osteopetrosis with ectodermal dysplasia and immune defect (OLEDAID)</li> </ul>
18. Campomelic dysplasia and related disorders <ul style="list-style-type: none"> <li>a. Campomelic dysplasia (CD)</li> <li>b. Stuve-Wiedemann dysplasia</li> <li>c. Kyphomelic dysplasia, several forms</li> </ul>	<ul style="list-style-type: none"> <li>m. Osteopetrosis, moderate form with defective leukocyte adhesion (LAD3)</li> <li>n. Osteopetrosis, moderate form with defective leukocyte adhesion</li> <li>o. Pyknodysostosis</li> <li>p. Osteopoikilosis</li> <li>q. Melorheostosis with osteopoikilosis</li> <li>r. Osteopathia striata with cranial sclerosis (OSCS)</li> <li>s. Melorheostosis</li> <li>t. Dysosteosclerosis</li> </ul>
19. Slender bone dysplasia group <ul style="list-style-type: none"> <li>a. 33-M syndrome</li> <li>b. Kenny-Caffey dysplasia</li> <li>c. Osteocraniostenosis</li> <li>d. Microcephalic osteodysplastic primordial dwarfism types 1/3 (MOPD1)</li> <li>e. Microcephalic osteodysplastic primordial dwarfism type 2 (MOPD2, Majewski type)</li> <li>f. IMAGE syndrome (intrauterine growth retardation, metaphyseal dysplasia, adrenal hypoplasia, and genital anomalies)</li> <li>g. Hallermann-Streiff syndrome</li> </ul>	

Continued



TABLE 11-2 Nosology and Classification of Genetic Skeletal Disorders—cont'd

GROUPS/NAME OF DISORDER	GROUPS/NAME OF DISORDER
<p>24. Other sclerosing bone disorders</p> <ul style="list-style-type: none"> <li>a. Craniometaphyseal dysplasia, autosomal dominant type</li> <li>b. Diaphyseal dysplasia Camurati-Engelmann</li> <li>c. Hematodiaphyseal dysplasia Ghosal</li> <li>d. Hypertrophic osteoarthropathy</li> <li>e. Pachydermoperiostosis (hypertrophic osteoarthropathy, primary, autosomal dominant)</li> <li>f. Oculo-dento-osseous dysplasia (ODOD) mild type</li> <li>g. Oculo-dento-osseous dysplasia (ODOD) severe type</li> <li>h. Osteoectasia with hyperphosphatasia (juvenile Paget disease)</li> <li>i. Scleroosteosis</li> <li>j. Endosteal hyperostosis, van Buchem type</li> <li>k. Trichodento-osseous dysplasia</li> <li>l. Craniometaphyseal dysplasia,</li> </ul> <p>m. Diaphyseal medullary stenosis with malignant fibrous histiocytoma</p> <ul style="list-style-type: none"> <li>n. Craniodiaphyseal dysplasia</li> <li>o. Craniometadiaphyseal dysplasia, Wormian bone type</li> <li>p. Endosteal sclerosis with cerebellar hypoplasia</li> <li>q. Lenz-Majewski hyperostotic dysplasia</li> <li>r. Metaphyseal dysplasia, Braun-Tinschert type</li> <li>s. Pyle disease</li> </ul>	<p>27. Lysosomal storage diseases with skeletal involvement (dysostosis multiplex group)</p> <ul style="list-style-type: none"> <li>a. Mucopolysaccharidosis type 1H/1S (Hurler, Hurler-Scheie, Scheie)</li> <li>b. Mucopolysaccharidosis type 2 (Hunter)</li> <li>c. Mucopolysaccharidosis type 3A (Sanfilippo A)</li> <li>d. Mucopolysaccharidosis type 3B (Sanfilippo B)</li> <li>e. Mucopolysaccharidosis type 3C (Sanfilippo C)</li> <li>f. Mucopolysaccharidosis type 3D (Sanfilippo D)</li> <li>g. Mucopolysaccharidosis type 4A (Morquio A)</li> <li>h. Mucopolysaccharidosis type 4B (Morquio B)</li> <li>i. Mucopolysaccharidosis type 6 (Maroteaux-Lamy)</li> <li>j. Mucopolysaccharidosis type 7 (Sly)</li> <li>k. Fucosidosis</li> <li>l. Alpha-mannosidosis</li> <li>m. Beta-mannosidosis</li> <li>n. Aspartylglucosaminuria</li> <li>o. GM1 gangliosidosis, several forms</li> <li>p. Sialidosis, several forms</li> <li>q. Sialic acid storage disease (SIASD)</li> <li>r. Galactosialidosis, several forms</li> <li>s. Multiple sulfatase deficiency</li> <li>t. Mucopolipidosis II (I-cell disease), alpha/beta type</li> <li>u. Mucopolipidosis III (pseudo-Hurler polydystrophy), alpha/beta type</li> <li>v. Mucopolipidosis III (pseudo-Hurler polydystrophy), gamma type</li> </ul>
<p>25. Osteogenesis imperfecta and decreased bone density group</p> <ul style="list-style-type: none"> <li>a. Osteogenesis imperfecta, nondeforming form (OI type 1)</li> <li>b. Osteogenesis imperfecta, perinatal lethal form (OI type 2)</li> <li>c. Osteogenesis imperfecta, progressively deforming type (OI type 3)</li> <li>d. Osteogenesis imperfecta, moderate form (OI type 4)</li> <li>e. Osteogenesis imperfecta with calcification of the interosseous membranes and/or hypertrophic callus (OI type 5)</li> <li>f. X-linked osteoporosis</li> <li>g. Bruck syndrome type 1 (BS1)</li> <li>h. Bruck syndrome type 2 (BS2)</li> <li>i. Osteoporosis-pseudoglioma syndrome</li> <li>j. LRP5 primary osteoporosis</li> <li>k. Calvarial doughnut lesions with bone fragility</li> <li>l. Idiopathic juvenile osteoporosis</li> </ul> <p>m. Cole-Carpenter dysplasia (bone fragility with craniosynostosis)</p> <ul style="list-style-type: none"> <li>n. Spondylo-ocular dysplasia</li> <li>o. Osteopenia with radiolucent lesions of the mandible</li> <li>p. Ehlers-Danlos syndrome, progeroid form</li> <li>q. Geroderma osteodysplasticum</li> <li>r. Cutis laxa, autosomal recessive form, type 2B (ARCL2B)</li> <li>s. Cutis laxa, autosomal recessive form, type 2A (ARCL2A) (Wrinkly skin syndrome)</li> <li>t. Singleton-Merten dysplasia</li> </ul>	<p>28. Osteolysis group</p> <ul style="list-style-type: none"> <li>a. Familial expansile osteolysis</li> <li>b. Mandibuloacral dysplasia type A, B</li> <li>c. Progeria, Hutchinson-Gilford type</li> <li>d. Torg-Winchester syndrome</li> <li>e. Hajdu-Cheney syndrome</li> <li>f. Multicentric carpal-tarsal osteolysis with and without nephropathy</li> </ul>
<p>26. Abnormal mineralization group</p> <ul style="list-style-type: none"> <li>a. Hypophosphatasia, perinatal lethal, infantile and juvenile forms</li> <li>b. Hypophosphatasia, juvenile and adult forms</li> <li>c. Hypophosphatemic rickets, X-linked dominant</li> <li>d. Hypophosphatemic rickets, autosomal dominant</li> <li>e. Hypophosphatemic rickets, autosomal recessive, type 1 (ARHR1)</li> <li>f. Hypophosphatemic rickets, autosomal recessive, type 2 (ARHR2)</li> <li>g. Hypophosphatemic rickets with hypercalciuria, X-linked recessive</li> <li>h. Hypophosphatemic rickets with hypercalciuria, autosomal recessive (HHRH)</li> <li>i. Neonatal hyperparathyroidism, severe form</li> <li>j. Familial hypocalciuric hypercalcemia with transient neonatal hyperparathyroidism</li> <li>k. Calcium pyrophosphate deposition disease (familial chondrocalcinosis) type 2</li> </ul>	<p>29. Disorganized development of skeletal components group</p> <ul style="list-style-type: none"> <li>a. Multiple cartilaginous exostoses 1, 2, 3</li> <li>b. Cherubism</li> <li>c. Fibrous dysplasia, polyostotic form (McCune-Albright)</li> <li>d. Progressive osseous heteroplasia</li> <li>e. Gnathodiaphyseal dysplasia</li> <li>f. Metachondromatosis</li> <li>g. Osteoglophonic dysplasia</li> <li>h. Fibrodysplasia ossificans progressiva (FOP)</li> <li>i. Neurofibromatosis type 1 (NF1)</li> <li>j. Carpotarsal osteochondromatosis</li> <li>k. Cherubism with gingival fibromatosis (Ramon syndrome)</li> <li>l. Dysplasia epiphysealis hemimelica (Trevor)</li> <li>m. Lipomembranous osteodystrophy with leukoencephalopathy (presenile dementia with bone cysts; Nasu-Hakola)</li> <li>n. Enchondromatosis (Ollier) and enchondromatosis with hemangiomata (Maffucci)</li> <li>o. Metaphyseal chondromatosis with D-2-hydroxyglutaric aciduria</li> <li>p. Genochondromatosis</li> <li>q. Gorham-Stout</li> </ul>

TABLE 11-2 Nosology and Classification of Genetic Skeletal Disorders—cont'd

GROUPS/NAME OF DISORDER	GROUPS/NAME OF DISORDER
30. Overgrowth (tall stature) syndromes with skeletal involvement <ol style="list-style-type: none"> <li>Weaver syndrome</li> <li>Sotos syndrome</li> <li>Sotos-like syndrome</li> <li>Marshall-Smith syndrome</li> <li>Proteus syndrome</li> <li>CLOVES</li> <li>Marfan syndrome</li> <li>Congenital contractural arachnodactyly</li> <li>Loeys-Dietz syndrome types 1A,1B, 2A, 2B, 3, 4</li> <li>Overgrowth syndrome with 2q37 translocations</li> <li>Overgrowth with macrodactyly and NPR2 gain of function</li> <li>Overgrowth syndrome with skeletal dysplasia (Nishimura-Schmidt, endochondral gigantism)</li> </ol>	35. Dysostoses with predominant vertebral with and without costal involvement <ol style="list-style-type: none"> <li>Currarino triad</li> <li>Spondylocostal dysostosis type 1 (SCDO1), type 2 (SCDO2), type 3(SCDO3), type 4 (SCDO4), type 5 (SCDO5)</li> <li>Spondylothoracic dysostosis (STD)</li> <li>Vertebral segmentation defect (congenital scoliosis) with variable penetrance</li> <li>Klippel-Feil anomaly with laryngeal malformation</li> <li>Cerebro-costo-mandibular syndrome (rib gap syndrome)</li> <li>Cerebro-costo-mandibular-like syndrome with vertebral defects</li> <li>Diaphanospondylydysostosis</li> <li>Spondylo-megaepiphyseal-metaphyseal dysplasia (SMMD)</li> </ol>
31. Genetic inflammatory/rheumatoid-like osteoarthropathies <ol style="list-style-type: none"> <li>Progressive pseudorheumatoid dysplasia (PPRD; SED with progressive arthropathy)</li> <li>Chronic infantile neurologic cutaneous articular syndrome (CINCA)/ neonatal onset multisystem inflammatory disease (NOMID)</li> <li>Sterile multifocal osteomyelitis, periostitis, and pustulosis (CINCA/NOMID-like)</li> <li>Chronic recurrent multifocal osteomyelitis with congenital dyserythropoietic anemia (CRMO with CDA; Majeed syndrome)</li> <li>Hyperostosis/hyperphosphatemia syndrome</li> <li>Hyaline fibromatosis syndrome</li> </ol>	36. Patellar dysostoses <ol style="list-style-type: none"> <li>Ischiopatellar dysplasia (small patella syndrome)</li> <li>Nail-patella syndrome</li> <li>Genitopatellar syndrome</li> <li>Ear-patella-short stature syndrome (Meier-Gorlin)</li> </ol>
32. Cleidocranial dysplasia and related disorders <ol style="list-style-type: none"> <li>Cleidocranial dysplasia</li> <li>CDAGS syndrome (craniosynostosis, delayed fontanelle closure, parietal foramina, imperforate anus, genital anomalies, skin eruption)</li> <li>Yunis-Varon dysplasia</li> <li>Parietal foramina (isolated)</li> </ol>	37. Brachydactyly (without extraskeletal manifestations) <ol style="list-style-type: none"> <li>Brachydactyly types A1, A2, B, B2, C, D, E</li> <li>Brachydactyly with anonychia (Cooks syndrome)</li> </ol>
33. Craniosynostosis syndromes <ol style="list-style-type: none"> <li>Pfeiffer syndrome (FGFR1-related)</li> <li>Apert syndrome</li> <li>Craniosynostosis with cutis gyrata (Beare-Stevenson)</li> <li>Crouzon syndrome</li> <li>Bent bone dysplasia</li> <li>Crouzon-like craniosynostosis with acanthosis nigricans (Crouzodermoskeletal syndrome)</li> <li>Craniosynostosis, Muenke type</li> <li>Antley-Bixler syndrome</li> <li>Craniosynostosis Boston type</li> <li>Saethre-Chatzen syndrome</li> <li>Shprintzen-Goldberg syndrome</li> <li>Baller-Gerold syndrome</li> <li>Carpenter syndrome</li> <li>Coronal craniosynostosis</li> <li>Complex craniosynostosis</li> </ol>	38. Brachydactyly (with extraskeletal manifestations) <ol style="list-style-type: none"> <li>Brachydactyly-mental retardation syndrome</li> <li>Hyperphosphatasia with mental retardation, brachytelephalangy, and distinct face</li> <li>Brachydactyly-hypertension syndrome (Bilginturan)</li> <li>Microcephaly-oculo-digito-esophageal-duodenal syndrome (Feingold syndrome)</li> <li>Hand-foot-genital syndrome</li> <li>Rubinstein-Taybi syndrome</li> <li>Brachydactyly, Temtamy type</li> <li>Christian type brachydactyly</li> <li>Coffin-Siris syndrome1</li> <li>Adams-Oliver</li> <li>Catel-Manzke syndrome</li> </ol>
34. Dysostoses with predominant craniofacial involvement <ol style="list-style-type: none"> <li>Mandibulofacial dysostosis (Treacher-Collins, Franceschetti-Klein)</li> <li>Oral-facial-digital syndrome type I (OFD1)</li> <li>Weyers acrofacial (acrofacial) dysostosis</li> <li>Endocrine-cerebro-osteodysplasia (ECO)</li> <li>Craniofrontonasal syndrome</li> <li>Frontonasal dysplasia, types 1, 2, 3</li> <li>Hemifacial microsomia</li> <li>Miller syndrome (postaxial acrofacial dysostosis)</li> <li>Acrofacial dysostosis, Nager type</li> <li>Acrofacial dysostosis, Rodriguez type</li> <li>Mandibulofacial dysostosis with microcephaly</li> </ol>	39. Limb hypoplasia—reduction defects group <ol style="list-style-type: none"> <li>Ulnar-mammary syndrome</li> <li>de Lange syndrome</li> <li>Fanconi anemia</li> <li>Thrombocytopenia—absent radius (TAR)</li> <li>Thrombocythemia with distal limb defects</li> <li>Holt-Oram syndrome</li> <li>Okhiro syndrome (Duane—radial ray anomaly)</li> <li>Cousin syndrome</li> <li>Roberts syndrome</li> <li>Split-hand-foot malformation with long bone deficiency (SHFLD3)</li> <li>Tibial hemimelia</li> <li>Tibial hemimelia-polysyndactyly-triphalangeal thumb</li> </ol>
	m. Acheiropodia n. Tetra-amelia o. Terminal transverse defect p. Al-Awadi Raas-Rothschild limb-pelvis hypoplasia-aplasia q. Fuhrmann syndrome r. RAPADILINO syndrome s. Femoral hypoplasia-unusual face syndrome (FHUFS) t. Femur-fibula-ulna syndrome (FFU) u. Hanhart syndrome (hypoglossia-hypodactyly) v. Gollop-Wolfgang w. Scapulo-iliac dysplasia (Kosenow)



TABLE 11-2 Nosology and Classification of Genetic Skeletal Disorders—cont'd

GROUPS/NAME OF DISORDER	GROUPS/NAME OF DISORDER
40. Ectrodactyly with and without other manifestations	o. Acrocallosal syndrome
a. Ectrodactyly with and without other manifestations	p. Acro-pectoral syndrome
b. Ankyloblepharon-ectodermal dysplasia-cleft lip/palate (AEC)	q. Acro-pectoro-vertebral dysplasia (F-syndrome)
c. Ectrodactyly-ectodermal dysplasia cleft-palate syndrome type 3 (EEC3)	r. Mirror-image polydactyly of hands and feet (Laurin-Sandrow syndrome)
d. Ectrodactyly-ectodermal dysplasia cleft-palate syndrome type 1 (EEC1)	s. Cenani-Lenz syndactyly
e. Ectrodactyly-ectodermal dysplasia-macular dystrophy syndrome (EEM)	t. Cenani-Lenz-like syndactyly
f. Limb-mammary syndrome (including ADULT syndrome)	u. Syndactyly, Malik-Percin type
g. Split hand-foot malformation, isolated form, type 4 (SHFM4)	v. STAR syndrome (syndactyly of toes, telecanthus, ano- and renal malformations)
h. Split hand-foot malformation, isolated form, type 1 (SHFM1)	w. Syndactyly type Lueken
i. Split hand-foot malformation, isolated form, type 3 (SHFM3)	x. Oculodentodigital dysplasia, syndactyly type 3 (IV-V)
j. Split hand-foot malformation, isolated form, type 5 (SHFM5)	y. Syndactyly Haas type
k. Hartsfield syndrome	z. Syndactyly with metacarpal and metatarsal fusion
41. Polydactyly-syndactyly-triphalangism group	aa. Metacarpal 4-5 fusion syndrome
a. Preaxial polydactyly type 1 (PPD1)	bb. Syndactyly with craniosynostosis (Philadelphia type)
b. Postaxial polydactyly type A	cc. Syndactyly with microcephaly and mental retardation (Filippi syndrome)
c. Postaxial polydactyly type B	dd. Meckel syndrome types 1, 2, 3, 4, 5, 6
d. Triphalangeal thumb (TPT)-polydactyly syndrome	42. Defects in joint formation and synostoses
e. Preaxial polydactyly type 3 (PPD3)	a. Multiple synostoses syndrome type 3
f. Preaxial polydactyly type 4 (PPD4)	b. Proximal symphalangism type 1
g. Greig cephalopolysyndactyly syndrome	c. Proximal symphalangism type 2
h. Pallister-Hall syndrome	d. Radioulnar synostosis with amegakaryocytic thrombocytopenia
i. Synpolydactyly (complex, fibulin 1-associated)	e. Liebenberg syndrome
j. Synpolydactyly	f. Congenital clubfoot
k. Townes-Brocks syndrome (renal-ear-anal-radial syndrome)	
l. Lacrimo-auriculo-dento-digital syndrome (LADD Gene FGFR2)	
m. Lacrimo-auriculo-dento-digital syndrome (LADD Gene FGFR3)	
n. Lacrimo-auriculo-dento-digital syndrome (LADD Gene FGF10)	

Adapted from Bonafe L, Cormier-Daire V, Hall C, et al: Nosology and classification of genetic skeletal disorders: 2015 revision. *Am J Med Genet A* 167(12):2869-2892, 2015.

TABLE 11-3 Well-Defined Skeletal Disorders Seen During the Neonatal Period

Group or Name of the Disorder	Mode of Inheritance	Gene Symbol	Group or Name of the Disorder	Mode of Inheritance	Gene Symbol
<b>Fibroblast Growth Factor Receptor 3 (FGFR3) Disorders</b>			<b>Sulfation Disorders</b>		
Thanatophoric dysplasia	AD	<i>FGFR3</i>	Achondrogenesis IB	AR	<i>SLC26A2</i>
Achondroplasia	AD	<i>FGFR3</i>	Atelosteogenesis II	AR	<i>SLC26A2</i>
Hypochondroplasia	AD	<i>FGFR3</i>	Diastrophic dysplasia	AR	<i>SLC26A2</i>
Severe achondroplasia with developmental delay and acanthosis nigricans (SADDAN)	AD	<i>FGFR3</i>	Chondrodysplasia with congenital joint dislocations	AR	<i>CHST3</i>
<b>Type II Collagen Disorders</b>			<b>Perlecan Disorders</b>		
Achondrogenesis II	AD	<i>COL2A1</i>	Dyssegmental dysplasia	AR	<i>PLC</i>
Hypochondrogenesis	AD	<i>COL2A1</i>	Dyssegmental dysplasia, Silverman-Handmaker type	AR	<i>PLC</i>
Spondyloepiphyseal dysplasia congenita (SEDC)	AD	<i>COL2A1</i>	Dyssegmental dysplasia, Rolland-Desbuquois type	AR	<i>PLC</i>
Kniest dysplasia	AD	<i>COL2A1</i>			
<b>Type XI Collagen Disorders</b>			<b>Filamin Disorders and Similar Disorders</b>		
Fibrochondrogenesis	AR	<i>COL11A1</i>	Otopalatodigital syndrome I and II	XLD	<i>FLNA</i>
Fibrochondrogenesis	AD	<i>COL11A1</i> , <i>COL11A2</i>	Osteodysplasty, Melnick-Needles	XLD	<i>FLNA</i>
Otospondylomegaepiphyseal dysplasia (OSMED)	AR	<i>COL11A2</i>	Atelosteogenesis types I and III	AD	<i>FLNB</i>
			Larsen syndrome	AD	<i>FLNB</i>
			Spondylo-carpal-tarsal dysplasia	AR	<i>FLNB</i>
			Serpentine fibula-polycystic kidney syndrome	AD	<i>NOTCH2</i>

TABLE 11-3 Well-Defined Skeletal Disorders Seen During the Neonatal Period—cont'd

Group or Name of the Disorder	Mode of Inheritance	Gene Symbol	Group or Name of the Disorder	Mode of Inheritance	Gene Symbol
<b>TRPV4 Disorders</b>			<b>Chondrodysplasia Punctata Group (CDP)</b>		
Metatropic dysplasia	AD	<i>TRPV4</i>	CDP, X-linked dominant	XLD	<i>EBP</i>
<b>Short Rib Dysplasias (With and Without Polydactyly)</b>			Conradi-Hunermann type (CDPX2)	XLR	<i>ARSE</i>
Chondroectodermal dysplasia (Ellis-van Creveld)	AR	<i>DYNC2H1</i>	Brachytelephalangic type (CDPX1)	XLD	<i>NSDHL</i>
Short rib-polydactyly syndrome I, II, III, and IV including asphyxiating thoracic dystrophy	AR	<i>IFT80 NEK</i> <i>WDR35</i>	Congenital hemidysplasia with ichthyosiform erythroderma and limb defects (CHILD) syndrome	XLD	<i>EBP</i>
Thoracolaryngeal dysplasia	AD	Unknown	Greenberg dysplasia	AR	<i>LBR</i>
<b>Metaphyseal Dysplasias</b>			Rhizomelic CDP type 1	AR	<i>PEX7</i>
Cartilage-hair hypoplasia	AR	<i>RMRP</i>	Rhizomelic CDP type 2	AR	<i>DHPAT</i>
Metaphyseal dysplasia, Jansen type	AD	<i>PTHR1</i>	Rhizomelic CDP type 3	AR	<i>AGPS</i>
<b>Spondylo-Epi-(Meta)-Physeal Dysplasia (SEMD)</b>			<b>Neonatal Osteosclerotic Dysplasias</b>		
SEMD, short limb abnormal calcification type	AR	<i>DDR2</i>	Bloomstrand dysplasia	AR	<i>PTHR1</i>
<b>Severe Spondylodysplastic Dysplasias</b>			Desmosterolosis	AR	<i>DHCR24</i>
Achondrogenesis 1A	AR	<i>GMAP210</i>	Caffey disease (infantile)	AD	<i>COL1A1</i>
Schneckenbecken dysplasia	AR	<i>SLC35D1</i>	Raine dysplasia	AR	<i>FAM20C</i>
Opsismodysplasia	AR	<i>INPPL1</i>	<b>Increased Bone Density Group</b>		
<b>Acromesomelic Disorders</b>			Osteopetrosis (severe neonatal or infantile forms)	AR	<i>TCIRG1</i>
Acromesomelic dysplasia, type Maroteaux	AR	<i>NPR2</i>	Osteopetrosis (severe neonatal or infantile forms)	AR	<i>CLCN7</i>
<b>Mesomelic and Rhizomesomelic Dysplasias</b>			Dysosteosclerosis	AR	<i>SLC29A3</i>
Langer type (homozygous dyschondrosteosis)	Pseudo-AR/XLD	<i>SHOX</i>	Lenz-Majewski hyperostotic dysplasia	SP	<i>PTDSS1</i>
Omodysplasia	AR	<i>GPC6</i>	<b>Osteogenesis Imperfecta and Decreased Bone Density Group</b>		
Robinow syndrome, recessive	AR	<i>ROR2</i>	Osteogenesis imperfecta (OI), moderate, severe, and perinatal lethal	AD	<i>COL1A1</i> , <i>COL1A2</i> , <i>IFITM5</i> ,
Robinow syndrome, dominant	AD	<i>WNT5</i>	OI, moderate, severe, and perinatal lethal	AR	<i>CRTAP</i> , <i>P3H1</i> , <i>PPBI</i> , <i>FKBP10</i> , <i>HSP47</i> , <i>SP7</i> , <i>WNT1</i> , <i>TMEM33B</i> ,
<b>Bent Bone Dysplasias</b>			Bruck syndrome		<i>PLOD2</i> , <i>FKBP10</i> , <i>LRP5</i>
Campomelic dysplasia	AD	<i>SOX9</i>	Osteoporosis-pseudoglioma syndrome	AR	
Stuve-Wiedemann dysplasia	AR	<i>LIFR</i>	Cole-Carpenter dysplasia	SP	<i>LRP5</i> , <i>SEC24D</i> , <i>P4HB</i> , <i>CRTAP</i>
Bent bone dysplasia FGFR2 type	AD	<i>FGFR2</i>	<b>Abnormal Mineralization Group</b>		
<b>Slender Bone Dysplasias</b>			Hypophosphatasia, perinatal and infantile forms	AR	<i>ALPL</i>
Microcephalic osteodysplastic primordial dwarfism (MOPD1)	AR	<i>RNU4ATAC</i>			
Microcephalic osteodysplastic primordial dwarfism (MOPD2)	AR	<i>PCNT</i>			
<b>Dysplasias With Multiple Joint Dislocations</b>					
Desbuquois dysplasia	AR	<i>CANT1</i> , <i>XYLT1</i>			
Pseudodiathrophic dysplasia	AR	Unknown			

From Krakow D: Skeletal dysplasias. Clin Perinatol 42:301-319, 2015.



**TABLE 11-4 Common Abnormal Ultrasound Findings and Differential Diagnosis of Skeletal Disorders**

Disorders	MIM No.	Gene Defect	Disorders	MIM No.	Gene Defect
<b>Poor Mineralization of the Calvarium</b>			<b>Poor Mineralization of the Vertebrae</b>		
Achondrogenesis IA	200600	Unknown	Achondrogenesis IA	200600	Unknown
Cleidocranial dysplasia	119600	<i>RUNX2</i>	Achondrogenesis IB	600972	<i>SLC26A2</i>
Hypophosphatasia	241500	<i>ALPL</i>	Achondrogenesis II	200610	<i>COL2A1</i>
Osteogenesis imperfecta type II	166210	<i>COL1A1</i>	Atelosteogenesis I	108720	<i>FLNB</i>
	166210	<i>COL1A2</i>	Atelosteogenesis II	256050	<i>SLC26A2</i>
	610854	<i>CRTAP</i>	Atelosteogenesis III	108721	<i>FLNB</i>
<b>Fractures of Long Bones (Particular Femora)</b>			Opsismodysplasia	258480	Unknown
Hypophosphatasia	241500	<i>ALPL</i>	SMD—sedaghatian type	250220	Unknown
Neurofibromatosis	162200	<i>NF1</i>	Thanatophoric dysplasia types I and II	187600	<i>FGFR3</i>
Osteogenesis imperfecta types II and III	166210	<i>COL1A1</i>	187601	<i>FGFR3</i>	
	166210	<i>COL1A2</i>			
	610854	<i>CRTAP</i>			
	259440	<i>P3H1</i>			
<b>Bent/Bowed Bones by Ultrasound</b>			<b>Absent/Hypoplastic Scapula</b>		
Achondrogenesis IA	200600	Unknown	Campomelic dysplasia	114290	<i>SOX9</i>
Achondrogenesis IB	600972	<i>SLC26A2</i>	<b>Equinovarus</b>		
Antley-Bixler syndrome	207410	<i>FGFR2</i>	Achondrogenesis IA	200600	Unknown
Atelosteogenesis I	108720	<i>FLNB</i>	Achondrogenesis IB	600972	<i>SLC26A2</i>
Atelosteogenesis II	256050	<i>SLC26A2</i>	Achondrogenesis II	200610	<i>COL2A1</i>
Atelosteogenesis III	108721	<i>FLNB</i>	Atelosteogenesis I	108720	<i>FLNB</i>
Campomelic dysplasia	114290	<i>SOX9</i>	Atelosteogenesis II	256050	<i>SLC26A2</i>
Diastrophic dysplasia	222600	<i>SLC26A2</i>	Atelosteogenesis III	108721	<i>FLNB</i>
Hypophosphatasia	241500	<i>ALPL</i>	Campomelic dysplasia	114290	<i>SOX9</i>
Osteogenesis types II and III	166210	<i>COL1A1</i>	Desbuquois dysplasia	251450	Unknown
	166210	<i>COL1A2</i>	Diastrophic dysplasia	222600	<i>SLC26A2</i>
	610854	<i>CRTAP</i>	Ehler-Danlos syndrome types VIIA and B	130060	<i>COL1A1, COL1A2</i>
	259440	<i>P3H1</i>	Hypophosphatasia	241500	<i>ALPL</i>
Short-rib polydactyly syndromes (types I-IV)	263530	Unknown	Larsen syndrome	150250	<i>FLNB</i>
	263520	Unknown	Osteogenesis imperfecta types II and III	166210	<i>COL1A1</i>
	263510	Unknown	166210	<i>COL1A2</i>	
	269860	Unknown	610854	<i>CRTAP</i>	
	601559	<i>LIFR</i>	259440	<i>P3H1</i>	
Thanatophoric dysplasia types I and II	187600	<i>FGFR3</i>	Pseudodiastrophic dysplasia	264180	Unknown
	187601	<i>FGFR3</i>	Short-rib polydactyly syndromes (types I-IV)	263530	Unknown
			263520	Unknown	
			263510	Unknown	
			269860	Unknown	
			187600	<i>FGFR3</i>	
			187601	<i>FGFR3</i>	

MIM, Mendelian Inheritance in Man; SMD, spondylometaphyseal dysplasia.

From Krakow D, Lachman RS, Rimoin DL: Guidelines for the prenatal diagnosis of fetal skeletal dysplasias. *Genet Med* 11:127-133, 2009.

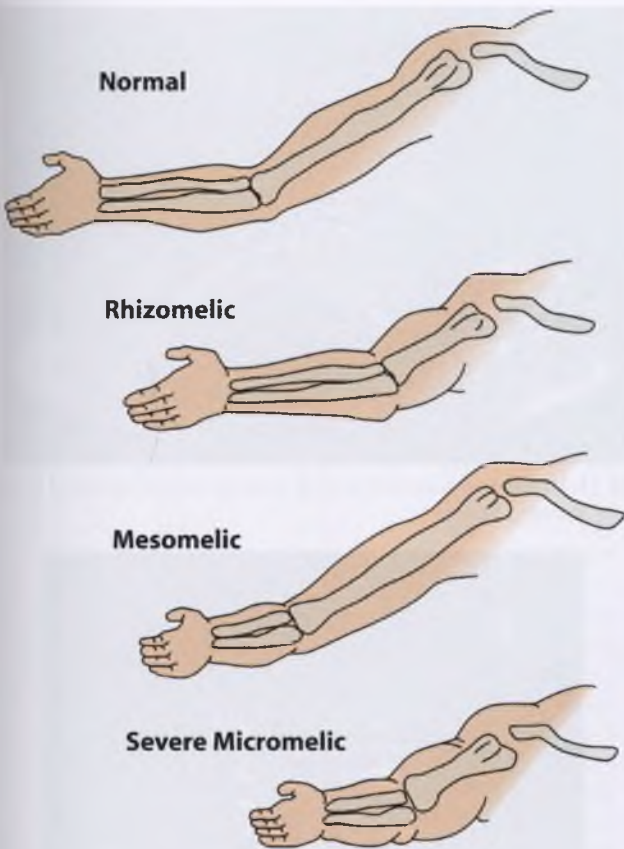


FIG 11-6 Varieties of short limb dysplasia according to the involved segment.

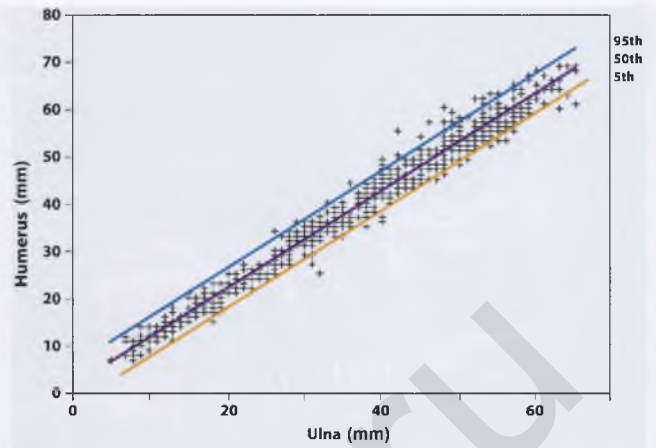


FIG 11-7 Relationship between the lengths of the ulna (mm) and the humerus (mm).

**TABLE 11-5 Skeletal Dysplasias Characterized by Rhizomelia, Mesomelia, and Micromelia**

Rhizomelia	
	Thanatophoric dysplasia
	Atelosteogenesis
	Chondrodysplasia punctata (rhizomelic type)
	Congenital short femur
	Achondroplasia
	Hypochondroplasia
Mesomelia	
	Mesomelic dysplasia (Langer, Reinhardt, and Robinow types)
	Ellis-van Creveld syndrome (chondroectodermal dysplasia)
Acromesomelia	
	Ellis-van Creveld syndrome (chondroectodermal dysplasia)
Micromelia	
	Achondrogenesis
	Atelosteogenesis
	Short rib-polydactyly syndrome
	Diastrophic dysplasia
	Fibrochondrogenesis
	Osteogenesis imperfecta (type II)
	Kniest dysplasia
	Dyssegmental dysplasia
	Roberts syndrome

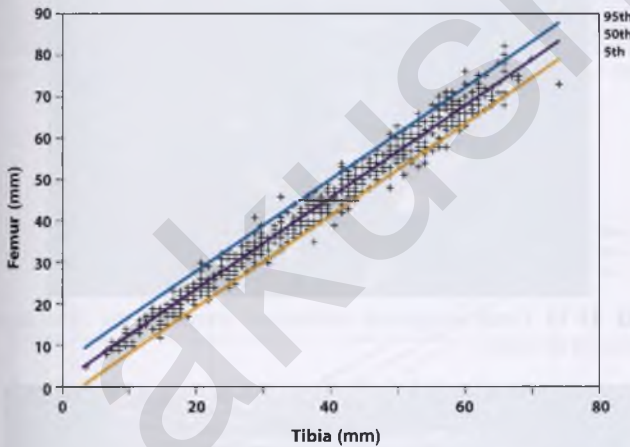


FIG 11-8 Relationship between the lengths of the tibia (mm) and femur (mm).





A



B

**FIG 11-9 A**, Longitudinal scan of the spine in a fetus with thanatophoric dysplasia and platyspondyly. The intervertebral disks (*white arrows*) are greater in height than the vertebrae (*black arrows*), which are flat. **B**, Lateral spine radiograph from a fetus with platyspondyly and thanatophoric dysplasia. Note the markedly flattened vertebrae.



**FIG 11-10** Coronal scan of the fetal spine by two-dimensional sonography showing scoliosis.

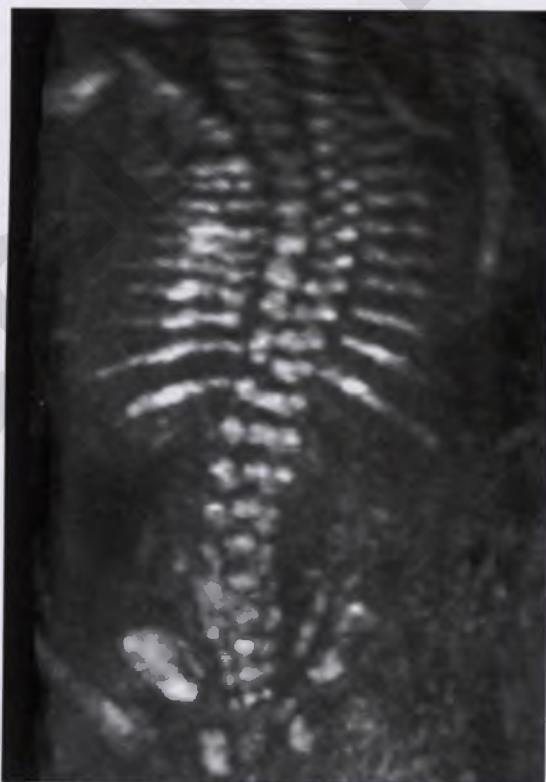


**FIG 11-11** Three-dimensional ultrasound image of the fetal spine showing scoliosis.

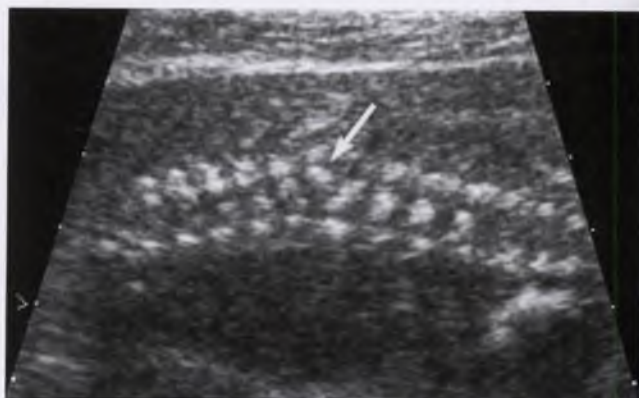


**FIG 11-12** Coronal scan of the fetal spine showing lateral hemivertebra (*arrow*) in the thoracic segment.

**TABLE 11-6 Normal Values (3rd, 50th, 97th Percentiles) of the Lower Limb Bones (Millimeters)**

Week	FEMUR			TIBIA			FIBULA		
	3rd	50th	97th	3rd	50th	97th	3rd	50th	97th
12	4.4	7.7	11.1	4.4	7.6	10.8	3.6	6.8	10.0
13	7.5	10.9	14.4	5.8	9.2	12.5	5.2	8.5	11.8
14	10.6	14.1	17.6	8.0	11.4	14.8	7.4	10.8	14.2
15	13.6	17.2	20.8	10.6	14.1	17.6	10.0	13.5	17.0
16	16.5	20.3	24.0	13.3	16.9	20.5	12.8	16.4	20.0
17	19.4	23.3	27.2	16.2	19.9	23.5	15.6	19.3	23.0
18	22.3	26.3	30.2	19.0	22.8	26.6	18.4	22.2	26.0
19	25.1	29.2	33.3	21.8	25.7	29.6	21.2	25.1	29.0
20	27.9	32.1	36.3	24.5	28.5	32.5	23.9	27.9	31.8
21	30.6	34.9	39.2	27.2	31.2	35.3	26.4	30.5	34.6
22	33.2	37.6	42.0	29.7	33.8	38.0	28.9	33.1	37.3
23	35.8	40.3	44.8	32.1	36.4	40.6	31.2	35.5	39.8
24	38.3	42.9	47.6	34.4	38.8	43.1	33.5	37.9	42.3
25	40.8	45.5	50.2	36.6	41.0	45.5	35.6	40.1	44.6
26	43.1	48.0	52.8	38.7	43.2	47.8	37.6	42.2	46.8
27	45.4	50.4	55.3	40.7	45.3	49.9	39.6	44.3	49.0
28	47.6	52.7	57.8	42.6	47.3	52.0	41.4	46.2	51.0
29	49.8	55	60.1	44.4	49.2	54.0	43.1	48.0	52.9
30	51.8	57.1	62.4	46.1	51.0	55.9	44.8	49.8	54.8
31	53.8	59.2	64.6	47.7	52.7	57.7	46.4	51.5	56.6
32	55.7	61.2	66.7	49.3	54.4	59.5	47.9	53.1	58.3
33	57.5	63.1	68.7	50.8	55.9	61.1	49.3	54.6	59.9
34	59.2	64.9	70.6	52.2	57.5	62.7	50.7	56.1	61.5
35	60.8	66.6	72.4	53.5	58.9	64.3	52.0	57.5	63.0
36	62.3	68.2	74.1	54.8	60.3	65.7	53.2	58.8	64.4
37	63.7	69.7	75.8	56	61.6	67.2	54.4	60.1	65.8
38	64.9	71.1	77.3	57.2	62.9	68.5	55.5	61.3	67.1
39	66.1	72.4	78.7	58.3	64.1	69.8	56.6	62.5	68.4
40	67.2	73.6	79.9	59.4	65.2	71.1	57.6	63.6	69.6
41	68.1	74.6	81.1	60.4	66.4	72.3	58.6	64.7	70.8
42	69.0	75.6	82.2	61.4	67.4	73.5	59.5	65.8	72.0

From Chitty LS, Altman DG: Charts of fetal size: limb bones. Br J Obstet Gynaecol 109:919-929, 2002.

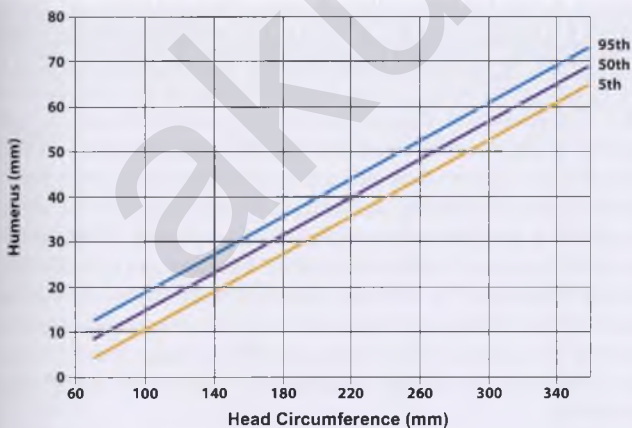


**FIG 11-13** Relationship between the head circumference (mm) and the length of the humerus (mm).

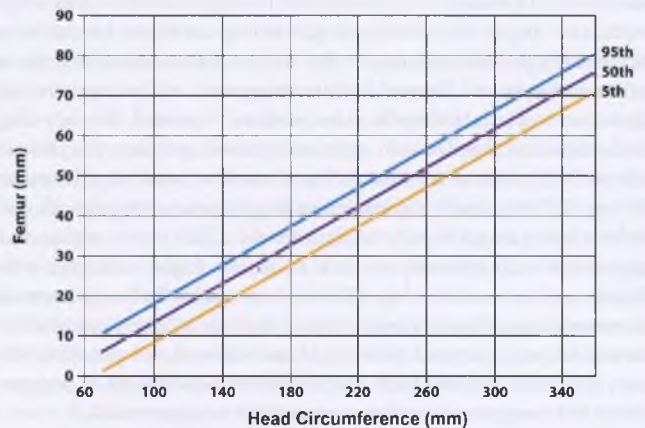


**FIG 11-14** Relationship between the head circumference (mm) and the length of the femur (mm).



**TABLE 11-7 Normal Values (3rd, 50th, 97th Percentiles) for the Upper Limb Bones (Millimeters)**

Week	HUMERUS			ULNA			RADIUS		
	3rd	50th	97th	3rd	50th	97th	3rd	50th	97th
12	3.7	7.1	10.6	3.9	7.3	10.7	2.2	5.5	8.8
13	7.2	10.7	14.2	6.2	9.6	13.1	4.8	8.2	11.6
14	10.5	14.1	17.7	8.8	12.4	15.9	7.6	11.0	14.5
15	13.7	17.3	21.0	11.6	15.3	18.9	10.3	13.9	17.4
16	16.7	20.4	24.2	14.5	18.2	22.0	13.0	16.7	20.3
17	19.6	23.4	27.2	17.3	21.2	25.0	15.6	19.3	23.1
18	22.3	26.2	30.1	20.1	24.0	28.0	18.1	21.9	25.7
19	24.9	28.9	32.9	22.8	26.8	30.8	20.4	24.4	28.3
20	27.4	31.5	35.5	25.3	29.4	33.5	22.7	26.7	30.7
21	29.8	34.0	38.1	27.8	32.0	36.2	24.8	28.9	32.9
22	32.1	36.3	40.5	30.1	34.4	38.7	26.8	30.9	35.1
23	34.3	38.6	42.9	32.3	36.6	41.0	28.6	32.9	37.1
24	36.4	40.7	45.1	34.3	38.8	43.3	30.4	34.7	39.1
25	38.4	42.8	47.2	36.3	40.9	45.5	32.0	36.5	40.9
26	40.3	44.8	49.3	38.2	42.8	47.5	33.6	38.1	42.6
27	42.1	46.7	51.3	39.9	44.7	49.5	35.1	39.7	44.3
28	43.9	48.5	53.2	41.6	46.5	51.3	36.5	41.2	45.8
29	45.5	50.2	55.0	43.2	48.2	53.1	37.8	42.6	47.3
30	47.1	51.9	56.7	44.7	49.8	54.8	39.0	43.9	48.7
31	48.6	53.5	58.4	46.2	51.3	56.4	40.2	45.1	50.1
32	50.0	55.0	59.9	47.5	52.7	58.0	41.3	46.4	51.4
33	51.4	56.4	61.5	48.8	54.1	59.4	42.4	47.5	52.6
34	52.7	57.8	62.9	50.0	55.4	60.8	43.4	48.6	53.8
35	53.9	59.1	64.3	51.2	56.7	62.2	44.3	49.6	54.9
36	55.1	60.3	65.6	52.3	57.9	63.5	45.2	50.6	56.0
37	56.2	61.5	66.8	53.4	59.1	64.7	46.1	51.6	57.0
38	57.2	62.6	68.0	54.4	60.2	65.9	46.9	52.5	58.0
39	58.2	63.7	69.2	55.4	61.2	67.1	47.7	53.3	59.0
40	59.1	64.7	70.3	56.3	62.2	68.2	48.4	54.2	59.9
41	60.0	65.6	71.3	57.2	63.2	69.3	49.1	55.0	60.8
42	60.8	66.5	72.2	58.0	64.1	70.3	49.8	55.7	61.6

From Chitty LS, Altman DG: Charts of fetal size: limb bones. *Br J Obstet Gynaecol* 109:919-929, 2002.

femur length.<sup>73</sup> In a study including 127 cases of 17 skeletal dysplasias, Gonçalves and Jeanty<sup>74</sup> concluded, with the use of discriminant analysis, that the degree of femur length shortening can be used as the initial step in distinguishing among the five most common disorders: thanatophoric dysplasia, OI type II, achondrogenesis, achondroplasia, and hypochondroplasia. Gabrielli and coworkers<sup>75</sup> reported the early diagnosis of skeletal dysplasias in eight women with previous pregnancies affected with skeletal dysplasias. Five recurrent cases were identified during the first trimester by the femur length/crown rump length ratio and the femur length/biparietal diameter ratio. The results of this study suggest that early evaluation of fetal structures might be helpful in the diagnosis of severe skeletal dysplasias. Nomograms for long bone measurements according to crown rump length in a large population of normal fetuses examined between 11 and 14 weeks of gestation have been published, but still their role in the early assessment of pregnancies at risk for skeletal dysplasias remains to be determined.<sup>76</sup>

### Clinical Presentation

In general, the challenges of the prenatal diagnosis of skeletal dysplasias presents in one of two ways: (1) a patient who has delivered an infant with a skeletal dysplasia and desires antenatal assessment in a subsequent pregnancy or (2) the incidental finding of a shortened, bowed,

or anomalous extremity during a routine sonographic examination. In patients at risk, the examination is easier when the particular phenotype of the skeletal dysplasia is known. The inability to obtain reliable information about skeletal mineralization and the effect of depth on sonography is a limiting factor in establishing an accurate diagnosis after identification of an incidental finding. Another limitation is the paucity of information about the in utero natural history of these disorders. Yet, despite these difficulties and limitations, good medical reasons justify attempting an accurate prenatal diagnosis of skeletal dysplasias. A number of these disorders are uniformly lethal, whereas others are associated with severe physical handicap and neurodevelopmental disabilities.<sup>77</sup> In addition, there is a group of disorders associated with thrombocytopenia for which vaginal delivery may expose the infant to an increased risk of intracranial hemorrhage. Therefore, accurate diagnosis of skeletal dysplasias is important for prenatal counseling.

### Diagnostic Imaging and Prenatal Diagnosis of Skeletal Dysplasias

Despite increasing availability of molecular testing, in about one third of skeletal dysplasias their molecular basis has not been defined.<sup>34</sup> The role of diagnostic imaging in the prenatal investigation of skeletal

dysplasias is (1) to narrow the differential diagnosis of skeletal dysplasias, so that appropriate confirmatory molecular tests can be done; (2) to predict lethality; and (3) to identify the fetus with a skeletal dysplasia early enough in gestation so that the diagnostic workup can be completed before the limit of fetal viability.<sup>78-82</sup>

Sonography is the primary imaging modality used for detection of an affected fetus.<sup>59,73,83-94</sup> The prevalence of skeletal dysplasias identified by ultrasound examination during the second and third trimesters of pregnancy is about 7.5/10,000 pregnancies.<sup>95</sup> In early pregnancy (11-14 weeks) the most frequently diagnosed skeletal dysplasias are thanatophoric dysplasia and achondrogenesis. However, despite ultrasound findings highly suggestive of skeletal dysplasia, the definitive diagnosis should only be determined by molecular testing and confirmation of the ultrasound findings later in pregnancy.<sup>96</sup> Table 11-8 summarizes the sensitivity of 2D sonography for the prenatal diagnosis of skeletal dysplasias.<sup>35,93,99-102</sup> Schramm and associates<sup>103</sup> reported a 67.9% (110/162) correct diagnosis and a 30.9% (50/162) partially correct diagnosis of skeletal dysplasia by evaluating the following sonographic parameters: (1) measurements of all segments of the long bones; (2) examination of the hands, spine, and head; (3) assessment of mineralization and shape of the bones; and (4) a full anatomic survey. For lethal skeletal dysplasias, the accuracy of sonographic findings was 99% (113/114). The authors reported that an accurate diagnosis of skeletal dysplasias before 24 weeks of gestation was possible in 62% of cases, although achondroplasia was the only skeletal dysplasia that could not be diagnosed before 24 weeks of gestation. When there is a family history of skeletal dysplasias, the following should be carefully evaluated on ultrasound imaging: complete biometry including the biparietal diameter, head and abdominal circumferences, lengths of all long bones, femur-foot ratio, and measurements of the mandible, clavicle, scapula, skull, chest, and spine. Other ultrasound parameters that might also be helpful in differentiating skeletal dysplasias include the fetal facial profile (e.g., flattened nasal bridge), presence and shape of vertebral bodies, appearance of the hands and feet (e.g., extra, missing, or malformed digits), and fetal thorax to assess the risk for lethality.<sup>58</sup> More recently, Nelson and colleagues<sup>104</sup> reported an overall prevalence of skeletal dysplasias of 2/10,000 pregnancies. In their series, 60% of skeletal dysplasias survived to hospital discharge, although 20% died in the neonatal period, 4% were stillbirths, and 16% were terminated. The authors reported that a femur/abdominal circumference

ratio less than 0.16 was the main discriminator among fetuses with lethal skeletal dysplasias, and that this measurement had better performance than femur shortening, thoracic circumference, and thoracic circumference/abdominal circumference ratio.

Several investigators have also proposed that 3D ultrasonography may improve the prenatal diagnostic accuracy for skeletal dysplasias and arthrogyposis.<sup>105-119</sup> It allows observation of phenotypic features that can be difficult to detect by 2D sonography such as detailed evaluation of the face, scapular anomalies, and abnormal calcification patterns.<sup>108,116</sup> As an example, Moeglin and Benoit<sup>112</sup> applied the multiplanar view to demonstrate the pointed appearance of the upper femoral diaphysis in achondroplasia. 3D reconstruction of the fetal bones is best performed using the maximum intensity projection or skeletal mode, a rendering algorithm that prioritizes the display of the brightest voxels contained within a region of interest selected by the operator<sup>108,112</sup> (Fig. 11-15). It is noteworthy that if a fetus is examined early enough in pregnancy, the entire skeleton can be included within the region of interest, and therefore, panoramic imaging can be obtained.<sup>108</sup> However, in some skeletal dysplasias the abnormal features may not be detectable until later in fetal development. Case reports and small series of skeletal dysplasias have described phenotypic characteristics or skeletal features for which 3D sonography may provide additional information (Table 11-9).<sup>106,108-112,114-116,118,120</sup>

3D-HCT has been proposed as an adjunctive imaging modality for improving the prenatal diagnosis and clinical management of skeletal dysplasias (Fig. 11-16).<sup>121-129</sup> 3D-HCT overcomes the main limitation of 2D and 3D ultrasonography for assessment of bones (i.e., acoustic shadowing), allowing easy and exquisite 3D rendering of mineralized bones at the expense of a mild radiation exposure to the fetus.<sup>130,131</sup> Long bone measurements in fetuses with suspected skeletal dysplasias obtained using ultrasound show a good correlation with measurements obtained by postmortem 3D-HCT within 24 hours of delivery.<sup>132</sup> Measurements obtained from 3D-HCT are not distance dependent and therefore are more accurate.<sup>128</sup> Excellent panoramic images of the fetal skeleton can be obtained without superimposition of the maternal skeleton (which occurs with radiography).<sup>123</sup> Yet, because of the low radiation dose currently used in pregnancy, 3D-HCT provides limited visualization of bone density, of fetal metaphyseal deformities, and of the feet and hands at early gestational ages.<sup>133,134</sup>

The contribution of 3D-HCT, 3D sonography, and 2D sonography in the evaluation of skeletal dysplasias was analyzed by Ruano and coworkers,<sup>121</sup> who compared the phenotypic characteristics of fetuses with skeletal dysplasias (achondroplasia [ $n = 3$ ], OI [ $n = 2$ ], and chondrodysplasia punctata [ $n = 1$ ]) using these three imaging modalities. Deformation of the fetal pelvis and an increase in the intervertebral space of the lumbar vertebrae were diagnosed more often using 3D-HCT. In contrast, some phenotypic characteristics of fetuses with skeletal dysplasias were demonstrated only by ultrasound such as phalangeal hypoplasia, point-calcified epiphysis (by both 2D and 3D sonography), and facial dysmorphism (by 3D sonography only). Although the overall count of correct phenotypic characteristics detected prenatally favored 3D-HCT over 3D sonography (94.3% [33/35] vs. 77.1% [27/35];  $P = 0.03$ ), the diagnostic performance of 3D-HCT was not superior to that of 3D sonography, as the correct prenatal diagnosis was established by both modalities in all cases. However, 3D sonography has two important advantages over 3D-HCT, namely the lack of radiation exposure and wider availability in the clinical setting. It is also noteworthy that the overall experience with 3D sonography for the diagnosis of skeletal dysplasias is still limited.<sup>105-108,111-118,120,135-141</sup> Nevertheless, even in the study of Ruano and coworkers<sup>121</sup> 3D sonography performed better than 2D sonography in the identification of phenotypic characteristics (77.1% [27/35]

**TABLE 11-8 Sensitivity of Ultrasound in the Prenatal Diagnosis of Skeletal Dysplasias**

Author	Year	Number of Cases	Sensitivity (%) (n)
Gordienko et al <sup>99</sup>	1996	26	73 (9)
Gaffney et al <sup>93</sup>	1998	35	31 (11)
Tretter et al <sup>100</sup>	1998	27	48 (13)
Hersh et al <sup>101</sup>	1998	23	48 (11)
Doray et al <sup>102</sup>	2000	47	60 (28)
Parilla et al <sup>95</sup>	2003	31	65 (20)
Witters et al <sup>97</sup>	2008	38	66 (25)
Schramm et al <sup>103</sup>	2009	162	68 (110)
Yeh et al <sup>98</sup>	2011	40	70 (28)
Khalil et al <sup>96</sup>	2011	15	40 (6)

Superscript numbers indicate references listed at the end of the chapter.

Modified from Hall CM, Offiah AC, Forzano F, et al: Fetal and Skeletal Dysplasias; an Atlas of Multimodality Imaging. London, Radcliffe Publishing, 2012, p 11.



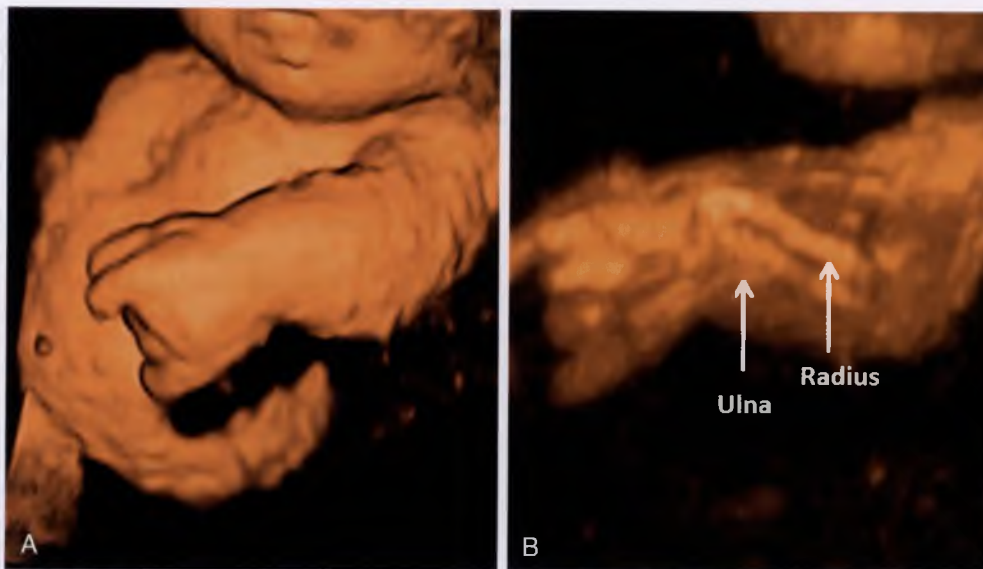


**FIG 11-15** Comparison between the surface rendering mode (A) and the maximum intensity projection mode (B) for visualization of the fetal arm in a fetus with mesomelic shortening of the long bones. Using the maximum intensity projection mode, only voxels with the highest intensity are displayed, thus allowing a clear representation of the mesomelic shortening of the radius and ulna.

**TABLE 11-9 Additional Phenotypic Findings and Improved Visualization in Skeletal Dysplasias Imaged by Prenatal Three-Dimensional Ultrasound (3DUS) as Compared to Two-Dimensional Ultrasound (2DUS)**

Skeletal Dysplasia	Phenotypic Characteristics Identified Better by 3DUS than 2DUS
Platyspondylic lethal chondrodysplasia <sup>106</sup>	Enhanced visualization of femoral and tibial bowing;
Campomelic dysplasia <sup>118,141</sup>	Better characterization of the facial soft tissues with surface rendering
Thanatophoric dysplasia <sup>109,110</sup>	Micrognathia, flat face, hypoplastic scapulae, bifid foot, fan-like position of the toes
Achondroplasia <sup>116</sup>	Improved characterization of frontal bossing and depressed nasal bridge;
	Demonstration of redundant skinfolds;
	Low-set dysmorphic ears
	Improved characterization of frontal bossing and depressed nasal bridge;
	Superior evaluation of the epiphyses and metaphyses of the long bones, with demonstration of a vertical metaphyseal slope;
	Caudal narrowing of the interpedicular distance;
	Clear visualization of trident hand;
	Better visualization of disproportion between limb segments
Chondrodysplasia punctata, rhizomelic form <sup>116</sup>	Improved characterization of the Binder facies (depressed nasal bridge, midface hypoplasia, small nose with upturned alae);
Achondrogenesis <sup>116</sup>	Identification of laryngeal stippling
Jarcho-Levin syndrome <sup>115</sup>	Panoramic demonstration of short neck and severe shortening of all segments of the limbs
Spondylocostal dysostosis <sup>138</sup>	Vertebral defects with absence of ribs and transverse process
Larsen syndrome <sup>120</sup>	Fan-like rib cage with rib fusion
Cleidocranial dysplasia <sup>140</sup>	Genu recurvatum, midface hypoplasia, low-set ears
Apert syndrome <sup>137</sup>	Widened cranial sutures, poor mineralization of the occipital bones, pseudoarthrosis of the clavicle
	Coronal craniosynostosis

Phenotypic characteristics of osteogenesis imperfecta,<sup>108</sup> and short rib–polydactyly (SRP) syndrome,<sup>114</sup> have also been described using 3DUS, although no additional findings to 2DUS were observed.

Superscript numbers indicate references listed at the end of the chapter.

vs. 51.4% [18/35];  $P = 0.004$ ) and in establishing an accurate diagnosis.

Fetal magnetic resonance imaging (MRI) is useful when the ultrasound examination is inconclusive because of oligohydramnios, maternal obesity, late gestational age, or fetal position. Both skeleton and muscle can be assessed by MRI using echoplanar imaging,<sup>142</sup> with thick slab T2-weighted and dynamic sequences.<sup>143-149</sup> Echoplanar

imaging can demonstrate epimetaphyseal characteristics used in measurement of fetal long bones,<sup>150</sup> increasing the accuracy of diagnosing short long bones.<sup>148,151</sup> MRI can also be useful in differentiating between normal bone development and bone dysplasia caused by a disruption of endochondral ossification.<sup>152</sup> Moreover, MRI can be applied to measure fetal thoracic and lung volumes, which are used to predict lethality in skeletal dysplasias.<sup>153</sup>

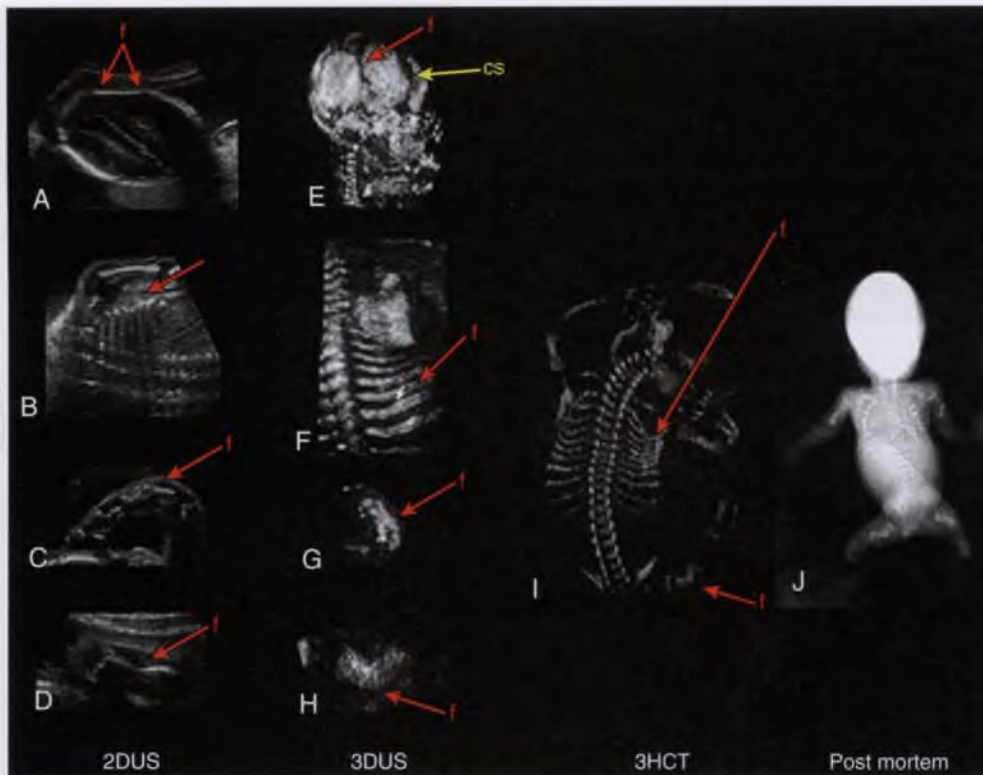


**FIG 11-16** Comparison of phenotypic features of osteogenesis imperfecta by three-dimensional helical computed tomography (3HCT), three-dimensional ultrasound (3DUS) images, two-dimensional ultrasound (2DUS) images, and postmortem radiographs. **A**, 2DUS: transverse section of fetal head with a skull fracture (f) deformed by the transducer pressure. **B**, 2DUS: coronal section of fetal thorax showing irregular ribs (arrow). **C**, 2DUS: sagittal section of the right superior limb showing a short and bowed arm. **D**, 2DUS: sagittal section of fetal femur with a fracture (f). **E**, 3DUS image showing lateral view of fetal skull with a fracture (f) that could be differentiated from a normal coronal suture (CS) by the location and the abnormal shape depending on the transducer pressure; this was confirmed by postmortem examination. **F**, 3DUS-rendered bone mode demonstrating posterior view of fetal thorax showing fractured and irregular ribs (f). **G**, 3DUS-rendered bone mode image showing short and bowed radius and ulna. **H**, 3DUS-rendered bone mode image showing a fractured femur (f). **I**, 3HCT: posterior view of entire fetus confirming fractures (f) of ribs and femur as well as decreased mineralization of the skull. **J**, Postmortem radiologic examination, confirming shortening, bowing, and fracture of long bones. (From Ruano R, Molho M, Roume J, et al: Prenatal diagnosis of fetal skeletal dysplasias by combining two-dimensional and three-dimensional ultrasound and intrauterine three-dimensional helical computer tomography. *Ultrasound Obstet Gynecol* 24:134, 2004.)

## Approach to the Diagnosis of Skeletal Dysplasias

A proposed systematic approach to the prenatal diagnosis of skeletal dysplasias is summarized in Table 11-10 and described in greater detail in the following section.

### Evaluation of the Long Bones

**Measurements.** All long bones must be measured in all extremities. Comparisons with other segments should be performed to establish whether the limb shortening is predominantly rhizomelic, mesomelic, or acromelic, or whether it involves all segments (see Figs. 11-6 to 11-8). A detailed examination of each bone is necessary to exclude absence or hypoplasia of individual bones (fibula, tibia, ulna, radius, clavicles, and scapulae).<sup>90,154-157</sup> From a group of fetuses less than 24 weeks of gestation with a short femur length, Papageorghiou and associates<sup>158</sup> reported that 35% presented with skeletal dysplasias; all affected fetuses had associated anomalies. The authors suggested that in the presence of a short femur, a complete fetal anatomic evaluation is necessary. The most frequently associated skeletal dysplasias were

asphyxiating thoracic dystrophy, osteogenesis imperfecta, thanatophoric dysplasia, and campomelic dysplasia.

**Degree of Mineralization.** An attempt should be made to characterize the degree of mineralization, which can be assessed by examining the acoustic shadow behind the bone as well as the echogenicity of the bone itself. Signs of demineralization include visualization of an unusually prominent falx in the fetal brain and the absence of or decreased echogenicity of the spine. It should be emphasized that there are limitations to the sonographic evaluation of long bone mineralization and that other structures, such as the fetal skull, may be better suited for such assessment (Fig. 11-17).

**Degree of Long Bone Curvature.** At present, there is no objective means to assess long bone curvature, and experience is necessary to assist the operator in discerning the boundary between normality and abnormality. Bowed or angulated femora (campomelia) (Fig. 11-18) is characteristic of campomelic dysplasia, thanatophoric dysplasia, osteogenesis imperfecta, short rib dysplasia, and hypophosphatasia.<sup>159</sup>

**Metaphyseal Flaring.** Metaphyseal flaring denotes widening at the level of the metaphyseal growth plate. It can be observed in many



conditions, including achondroplasia, hypochondroplasia, hypochondrogenesis, asphyxiating thoracic dysplasia, chondrodysplasia punctata, diastrophic dysplasia, hypophosphatasia, Kniest dysplasia, kyphomelic dysplasia, metatropic dysplasia, and OI.<sup>18</sup>

**Femoral Angle.** Khalil and colleagues<sup>160</sup> reported an increased diaphysis-metaphysis femoral angle measured at 20 weeks to 23 weeks

### TABLE 11-10 Checklist for Ultrasound Evaluation of a Fetus With Suspected Skeletal Dysplasia

1. Long bones
  - Presence/absence
  - Length/shape
  - Mineralization/fractures
2. Hands and feet
  - Presence/absence
  - Position/movements
  - Fingers and toes: number/position/movements
3. Spine
  - Shape/curvatures
  - Mineralization
  - Clefts
  - Size and number of vertebral bodies
4. Skull
  - Shape/mineralization/size
5. Face
  - Profile
  - Hypertelorism/hypotelorism
  - Clefts
6. Thorax
  - Shape
  - Lung and thoracic areas/volumes
  - Ribs: shape/fractures/number
  - Scapula/clavicle
7. Fetal movements
8. Complete anatomic evaluation
9. Echocardiography
10. Amniotic fluid

and 6 days of gestation in fetuses later diagnosed with achondroplasia. The femoral angle in affected fetuses was 125 degrees as compared to 95 degrees in normal fetuses. The authors conclude that estimation of the femoral angle might improve the early detection of fetuses with achondroplasia.

**Fractures.** Fractures can be found in certain skeletal dysplasias such as OI and hypophosphatasia (Fig. 11-19). The fractures may be extremely subtle or may lead to angulation and separation of segments of the affected bone (Fig. 11-20).

### Prediction of Pulmonary Hypoplasia

Skeletal dysplasias associated with a hypoplastic thorax frequently have lung hypoplasia, which is the most frequent cause of death for these conditions. When a severe skeletal dysplasia is diagnosed, the presence



**FIG 11-17** Demineralization of the skull in a case of osteogenesis imperfecta. The lateral ventricle and choroid plexus in the near field are well visualized because of lack of normal mineralization of the calvarium. In normal fetuses, reverberation artifact from the calvarium would obscure the ultrasound image of these structures.



**FIG 11-18** Bowing of long bones of the limbs (arrows) in fetuses with campomelic dysplasia (A) and with thanatophoric dysplasia (B).

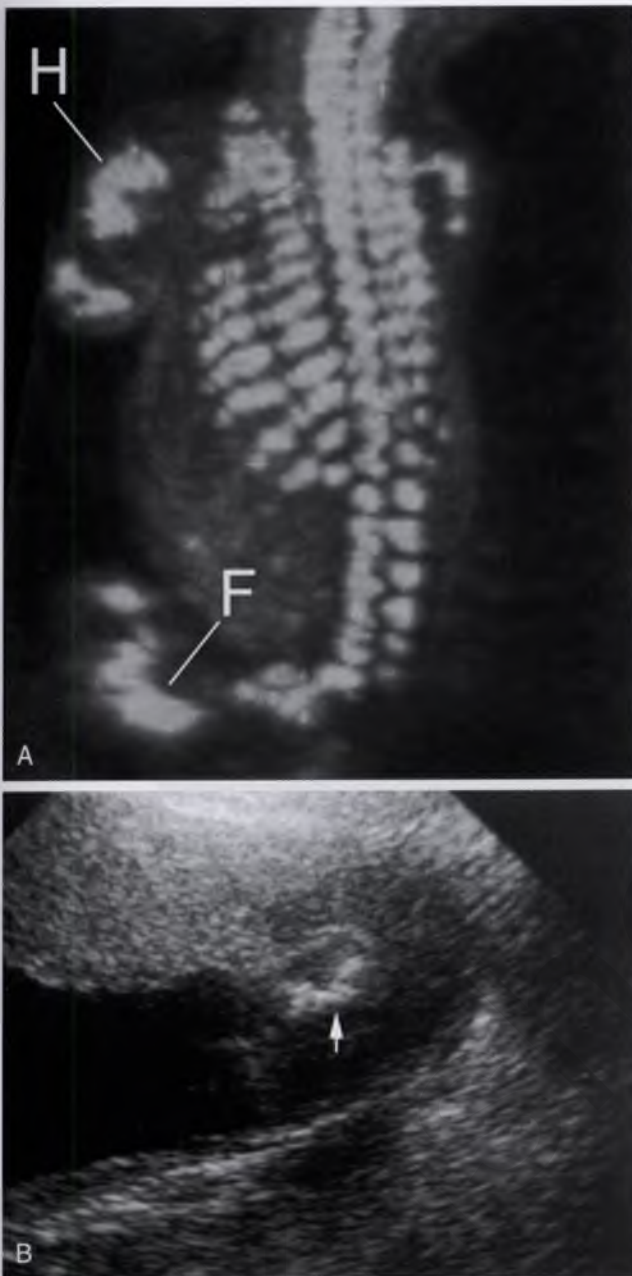


**FIG 11-19 A**, Three-dimensional sonogram in a fetus with osteogenesis imperfecta type II. The volume dataset was rendered using the maximum intensity mode. Multiple fractures in the ribs are present. Note the severe bowing and shortening of the femur (F) and humerus (H). **B**, Sonogram of a fetus with osteogenesis imperfecta type II. The femur is markedly shortened (arrow) with multiple fractures.

of marked thoracic involvement and pulmonary hypoplasia will allow the clinician to counsel the parents regarding prognosis, even though the specific type of skeletal dysplasia may be unknown. A number of sonographic parameters have been investigated for the prediction of pulmonary hypoplasia. They include measurements of the thorax and lungs, ratios between thoracic measurements and other biometric parameters, Doppler velocimetry of the pulmonary arteries, Doppler evaluation of tracheal fluid flow, and more recently, three-dimensional volumetric measurements of the fetal lungs by either sonography or MRI.

A detailed evaluation of the thorax in order to answer the following questions can assist in the diagnosis of the particular skeletal dysplasia<sup>161</sup>:

- Is the thorax extremely small? (thanatophoric dysplasia)
- Is the thorax long and narrow? (Jeune syndrome)
- Are the ribs extremely short? (short rib–polydactyly syndromes)
- Are there rib fractures? (osteogenesis imperfecta type II)
- Are there gaps within the ribs? (cerebra-costo-mandibular syndrome)
- Are there fused ribs? (spondylocostal dysplasia)
- Is there clavicular aplasia, hypoplasia, or pseudoarthrosis? (cleidocranial dysplasia)
- Are the scapulae abnormal? (hypoplasia or absence in campomelic dysplasia)

**Evaluation of Thoracic and Lung Dimensions by Two-Dimensional Ultrasound.** Thoracic and lung biometry has been extensively studied to identify fetuses at high risk for pulmonary hypoplasia.<sup>162-173</sup> Table 11-11 lists the skeletal dysplasias associated with altered thoracic dimensions, and Figures 11-21 and 11-22 illustrate features associated with a hypoplastic thorax. Methods used to measure the thorax, lungs, and heart by 2D sonography are illustrated in Figure 11-23. Thoracic areas and volumes in fetuses with a known gestational age can be evaluated using the nomograms reproduced in Tables 11-12 and 11-13. When gestational age is uncertain, age-independent ratios, such as the thoracic/abdominal circumference ratio (normal value: 0.77 to 1.01) and the thoracic/head circumference ratio (normal value: 0.56 to 1.04) can be used.<sup>164</sup>

A summary of the diagnostic accuracy of biometric parameters for the diagnosis of pulmonary hypoplasia is presented in Table 11-14.<sup>153,163,165-170,173-182</sup> Of particular interest are measurements of the right lung diameter, or the ratio between right lung diameter and the bony thoracic circumference proposed by Merz and associates,<sup>171</sup> who reported that fetuses with pulmonary hypoplasia all had a right lung diameter below the 5th percentile for gestational age, regardless of the primary disorder (skeletal dysplasias [ $n = 7$ ], renal agenesis [ $n = 11$ ], diaphragmatic hernia [ $n = 7$ ], and hydrothorax [ $n = 2$ ]).<sup>177</sup> In another study of 19 fetuses with congenital diaphragmatic hernia, Bahlmann and colleagues<sup>178</sup> demonstrated that the ratio of right lung diameter/bony thoracic circumference detected all fetuses with pulmonary hypoplasia with 100% sensitivity and 100% specificity.

**Short Femur Length and Prediction of Lethality in Skeletal Dysplasias.** Rahemtullah and coworkers<sup>183</sup> studied 18 fetuses with skeletal dysplasias in which all lethal cases were associated with a femur length/abdominal circumference ratio of 0.16. Although the test detected lethal cases with 100% sensitivity, two cases of achondroplasia were erroneously identified as lethal using this method. A different approach has been proposed by Hersh and associates,<sup>101</sup> who predicted lethality in 23 out of 25 cases of skeletal dysplasias with a femur length below the 1st percentile for gestational age and presence of bell-shaped thorax or decreased bone echogenicity.

**Lung Volumetry by Three-Dimensional Sonography.** Fetal lung volumetry by 3D sonography has been performed using two techniques: multiplanar<sup>184-190</sup> (Fig. 11-24) and VOCAL (Virtual Organ Computer-Aided Analysis, GE Medical Systems, Milwaukee, WI) (Fig. 11-25).<sup>191-198</sup> Nomograms for lung volumetry using 3D sonography are available in the literature (see Table 11-12).<sup>198</sup> Kalache and colleagues<sup>191</sup> demonstrated that both the 3D multiplanar and 3D VOCAL modes can be used to measure fetal lung volumes, an observation that was subsequently confirmed by Moeglin and associates.<sup>196</sup> A potential advantage of the VOCAL technique is the possibility of obtaining fine contours of the lungs, which may be particularly valuable when

*Text continued on p. 298*



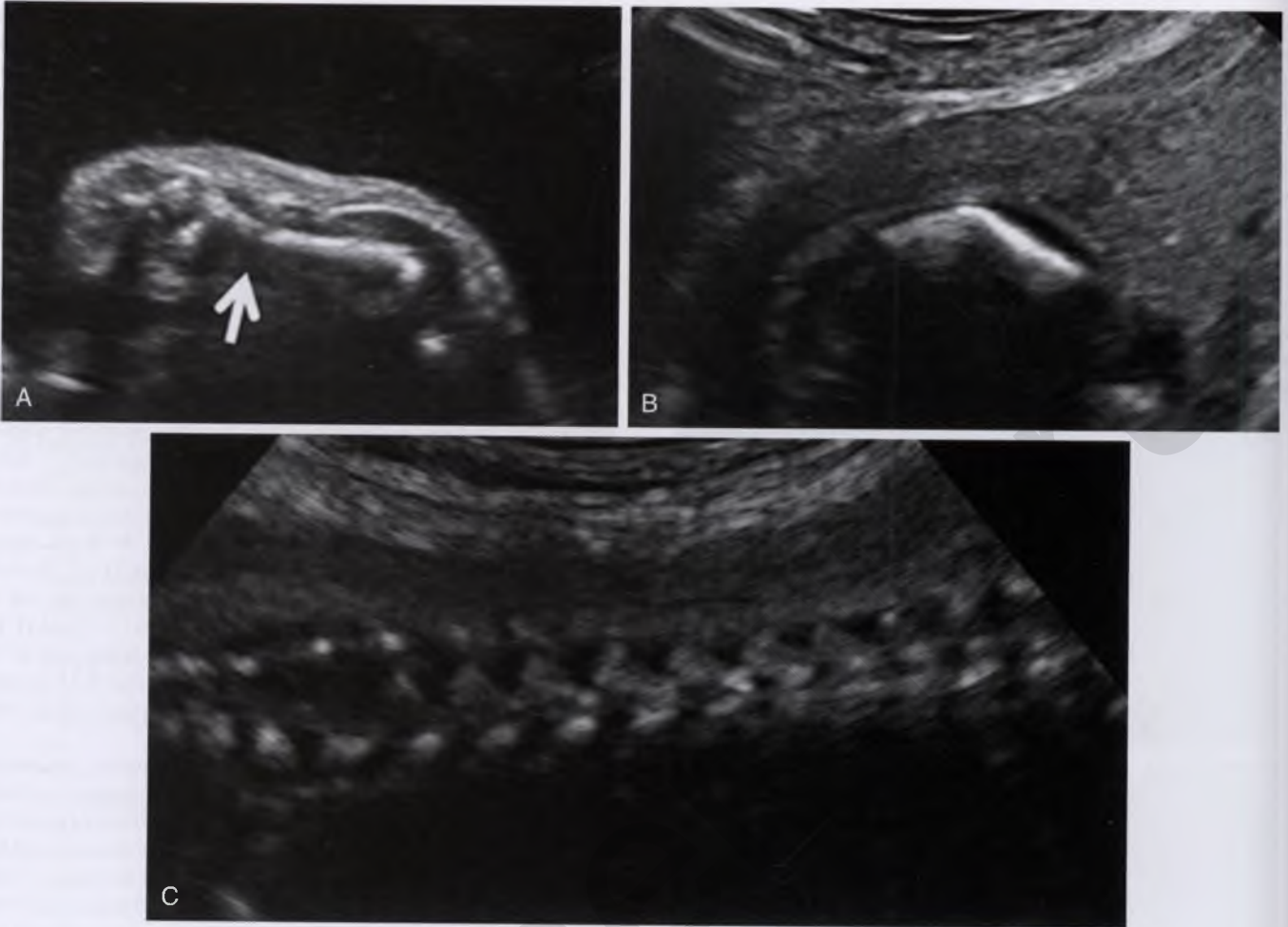


**FIG 11-20** In utero fracture (A) and bowing (B) of the long bones in a fetus with osteogenesis imperfecta. The arrow indicates the hypoechoic fracture line. Hypomineralization of the spine is shown in the longitudinal view (C).



**FIG 11-21** Longitudinal section of a fetus with thanatophoric dysplasia. Note the significant disproportion between the chest and abdomen.



**FIG 11-22** Extremely short ribs in a fetus with short rib-polydactyly syndrome.

**TABLE 11-11 Skeletal Dysplasias Associated With Altered Thoracic Dimensions****Long, Narrow Thorax**

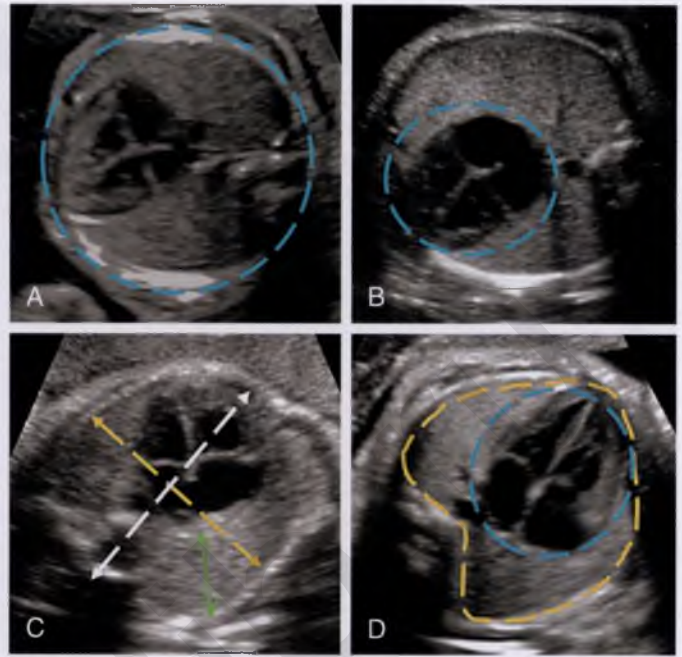
Asphyxiating thoracic dysplasia (Jeune)  
 Chondroectodermal dysplasia (Ellis-van Creveld)  
 Metatropic dysplasia  
 Fibrochondrogenesis  
 Atelosteogenesis  
 Camptomelic dysplasia  
 Jarcho-Levin syndrome  
 Achondrogenesis  
 Osteogenesis imperfecta type II  
 Hypophosphatasia  
 Dyssegmental dysplasia  
 Cleidocranial dysplasia

**Short Thorax**

Osteogenesis imperfecta (type II)  
 Kniest dysplasia (metatropic dysplasia type II)  
 Pena-Shokeir syndrome

**Hypoplastic Thorax**

Short rib-polydactyly syndrome (type I, type II)  
 Thanatophoric dysplasia  
 Cerebrocostomandibular syndrome  
 Cleidocranial dysplasia syndrome  
 Homozygous achondroplasia  
 Melnick-Needles syndrome (osteodysplasty)  
 Fibrochondrogenesis  
 Otopalatodigital syndrome type II

**FIG 11-23** Illustration of the various methods to measure thoracic, lung, and heart dimensions. **A**, Thoracic circumference. **B**, Cardiac circumference. **C**, Lung diameter/thoracic area ratio. **D**, Cardiac area/lung area ratio.**TABLE 11-12 Lung Area (Manual Tracing [2.5th, 50th, 97.5th Percentiles]) and Lung Volume From 12 to 32 Gestational Weeks**<sup>174,198</sup>

Weeks	LEFT LUNG AREA			RIGHT LUNG AREA			LEFT LUNG VOLUME			RIGHT LUNG VOLUME			TOTAL LUNG VOLUME		
	2.5th	50th	97.5th	2.5th	50th	97.5th	2.5th	50th	97.5th	2.5th	50th	97.5th	2.5th	50th	97.5th
12	20	36	51	44	58	71	0.63	0.64	0.65	0.59	0.6	0.62	1.37	1.56	1.75
13	26	47	68	42	69	96	0.37	0.57	0.77	0.5	0.75	1	0.85	1.4	1.94
14	36	62	89	48	88	129	0.26	0.69	1.11	0.54	1.06	1.58	0.7	1.65	2.61
15	49	82	114	61	115	169	0.31	0.97	1.64	0.7	1.53	2.36	0.9	2.32	3.74
16	65	104	144	80	148	215	0.49	1.42	2.35	1	2.16	3.33	1.42	3.36	5.31
17	83	130	177	105	186	267	0.79	2.02	3.24	1.42	2.96	4.51	2.25	4.77	7.29
18	103	158	213	134	229	323	1.22	2.76	4.3	1.97	3.92	5.87	3.36	6.52	9.67
19	125	188	252	168	275	383	1.75	3.63	5.51	2.64	5.04	7.44	4.72	8.57	12.4
20	148	220	293	204	325	447	2.38	4.62	6.85	3.43	6.31	9.19	6.31	10.9	15.5
21	172	254	335	243	378	512	3.09	5.71	8.33	4.33	7.73	11.1	8.1	13.5	18.9
22	196	288	380	283	432	580	3.87	6.9	9.92	5.34	9.28	13.2	10.1	16.3	22.6
23	220	323	425	325	486	648	4.71	8.16	11.6	6.45	11	15.5	12.2	19.3	26.5
24	244	358	471	366	541	716	5.58	9.49	13.4	7.64	12.8	17.9	14.4	22.5	30.7
25	268	392	517	406	595	783	6.49	10.9	15.3	8.9	14.7	20.5	16.6	25.8	35
26	290	426	563	445	647	849	7.4	12.3	17.2	10.2	16.7	23.2	18.9	29.2	39.5
27	310	459	609	482	697	913	8.31	13.7	19.1	11.6	18.8	26	21.2	32.7	44.1
28	328	491	653	515	744	973	9.19	15.1	21.1	13	21	29	23.5	36.1	48.7
29	344	521	697	545	787	1029	10	16.6	23.1	14.4	23.2	32	25.7	39.6	53.4
30	358	548	738	569	825	1081	10.8	17.9	25	15.9	25.5	35.1	27.7	42.9	58.1
31	368	573	777	589	858	1127	11.5	19.3	27	17.2	27.7	38.2	29.6	46.2	62.7
32	374	594	814	602	885	1167	12.1	20.5	28.9	18.6	30	41.3	31.3	49.3	67.3

From Peralta CF, Cavoretto P, Csapo B, et al: Assessment of lung area in normal fetuses at 12-32 weeks. *Ultrasound Obstet Gynecol* 26:718-724, 2005; Peralta CF, Cavoretto P, Csapo B, et al: Lung and heart volumes by three-dimensional ultrasound in normal fetuses at 12-32 weeks' gestation. *Ultrasound Obstet Gynecol* 27:128-133, 2006.



**TABLE 11-13 Thoracic Diameters (10th, 50th, 90th Percentiles) From 12 to 41 Weeks of Gestation**

Weeks	THORACIC ANTEROPOSTERIOR DIAMETER			THORACIC TRANSVERSE DIAMETER			THORACIC CIRCUMFERENCE		
	10th	50th	90th	10th	50th	90th	10th	50th	90th
12	11.7	14.2	16.5	11.7	14.2	16.5	11.7	14.2	16.5
13	14.3	17.2	19.8	14.3	17.2	19.8	14.3	17.2	19.8
14	17.1	20.3	23.3	17.1	20.3	23.3	17.1	20.3	23.3
15	19.9	23.4	26.7	19.9	23.4	26.7	19.9	23.4	26.7
16	22.8	26.5	30.2	22.8	26.5	30.2	22.8	26.5	30.2
17	25.8	29.6	33.6	25.8	29.6	33.6	25.8	29.6	33.6
18	28.7	32.6	37.0	28.7	32.6	37.0	28.7	32.6	37.0
19	31.6	35.6	40.5	31.6	35.6	40.5	31.6	35.6	40.5
20	34.2	38.5	43.9	34.2	38.5	43.9	34.2	38.5	43.9
21	36.8	41.4	47.2	36.8	41.4	47.2	36.8	41.4	47.2
22	39.2	44.3	50.4	39.2	44.3	50.4	39.2	44.3	50.4
23	41.5	47.2	53.6	41.5	47.2	53.6	41.5	47.2	53.6
24	43.9	50.0	56.6	43.9	50.0	56.6	43.9	50.0	56.6
25	46.5	52.8	59.5	46.5	52.8	59.5	46.5	52.8	59.5
26	49.1	55.5	62.3	49.1	55.5	62.3	49.1	55.5	62.3
27	51.7	58.2	64.9	51.7	58.2	64.9	51.7	58.2	64.9
28	54.2	60.8	67.4	54.2	60.8	67.4	54.2	60.8	67.4
29	56.6	63.4	69.8	56.6	63.4	69.8	56.6	63.4	69.8
30	58.9	65.9	72.3	58.9	65.9	72.3	58.9	65.9	72.3
31	61.1	68.4	74.9	61.1	68.4	74.9	61.1	68.4	74.9
32	63.2	70.9	77.7	63.2	70.9	77.7	63.2	70.9	77.7
33	65.1	73.2	80.6	65.1	73.2	80.6	65.1	73.2	80.6
34	67.0	75.4	83.4	67.0	75.4	83.4	67.0	75.4	83.4
35	68.8	77.3	85.8	68.8	77.3	85.8	68.8	77.3	85.8
36	70.6	79.0	88.0	70.6	79.0	88.0	70.6	79.0	88.0
37	72.5	80.5	90.0	72.5	80.5	90.0	72.5	80.5	90.0
38	74.3	81.9	91.8	74.3	81.9	91.8	74.3	81.9	91.8
39	75.9	83.1	93.5	75.9	83.1	93.5	75.9	83.1	93.5
40	77.5	84.1	94.9	77.5	84.1	94.9	77.5	84.1	94.9
41	78.8	84.9	95.8	78.8	84.9	95.8	78.8	84.9	95.8

From Lessoway VA, Schulzer M, Wittmann BK, et al: Ultrasound fetal biometry charts for a North American Caucasian population. J Clin Ultrasound 26(9):433-453, 1998.

TABLE 11-14 Biometric Parameters Proposed for the Evaluation of Lung Hypoplasia

Author	Parameter	Fetuses at Risk	Prevalence (%)	Sensitivity (%)	Specificity (%)	Accuracy (%)	Population
Nimrod et al <sup>163</sup>	TC	45	38	88	96	93	PROM; oligohydramnios; pleural effusion; other conditions affecting lung growth
Heling et al <sup>179</sup>	TTD	29	55	44	50	46	Bilateral renal agenesis; bilateral multicystic kidneys; chronic PROM < 25 weeks of gestational age; hydrothorax
	APTD			57	42	52	
	LL			29	66	42	
Laudy et al <sup>180,185,208</sup>	TC	40	43	94	38	61	Prolonged oligohydramnios due to PROM or congenital renal disease
	CC/TC			76	50	61	
	TC/AC			69	71	70	
	LD			71	93	82	
	TC/AC			86	85	85	
	FL/AC			86	85	85	
Gerards et al <sup>181</sup>	TC	33	48.5	71	89	83	2DUS and 3DUS in 33 fetuses at risk of pulmonary hypoplasia
	3D LV			62	100	81	
	TC vs FL			25	100	64	
	TC/AC			81	59	70	
Vergani et al <sup>182</sup>	TA/HA	32	41	94	47	70	35 fetuses at risk of pulmonary hypoplasia including skeletal malformations, rupture of membranes, hydrothorax and bilateral renal dysplasia
	3D LV			85	95	93	
	TC			23	89	62	
	TC/AC			46	74	63	
Weaver et al <sup>153</sup>	TA/HA	23	52	23	95	65	23 fetuses with confirmed skeletal dysplasia
	FL/AC < 0.124			75	91	83	
	FL/AC < 0.16			83.3	41	63	
	O/E TLV < 47.9	75	81	78			

2D, two-dimensional; 3D, three-dimensional; AC, abdominal circumference; APTD, anteroposterior thoracic diameter; CC, cardiac circumference; FL, femur length; HA, heart area; LD, lung diameter; LL, lung length; LV, lung volume; O/E TLV, observed-to-expected total lung volume; PROM, premature rupture of membranes; TA, thoracic area; TC, thoracic circumference; TTD, transverse thoracic diameter; US, ultrasonography.

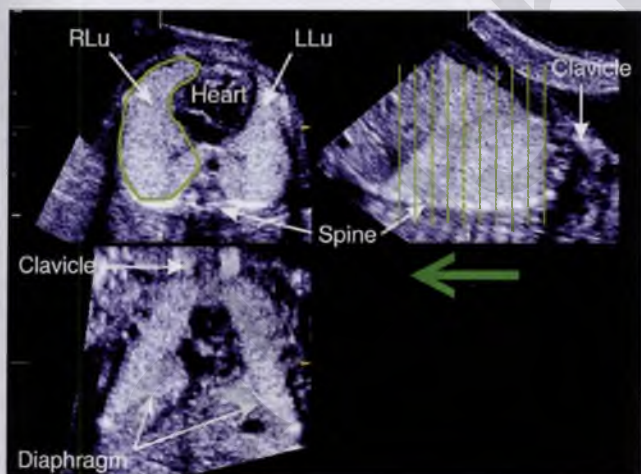


**FIG 11-24** Three-dimensional ultrasound fetal lung measurements using the multiplanar technique. Note the image sequences (green vertical lines) used to obtain transverse views of the lung. The right lung (RLu) is outlined. Fetal lung volume is obtained by scrolling through the transverse plane (green arrow). LLu, left lung. (From Kalache KD, Espinoza J, Chaiworapongsa T, et al: Three-dimensional ultrasound fetal lung volume measurement: a systematic study comparing the multiplanar method with the rotational (VOCAL) technique. *Ultrasound Obstet Gynecol* 21;111, 2003.)

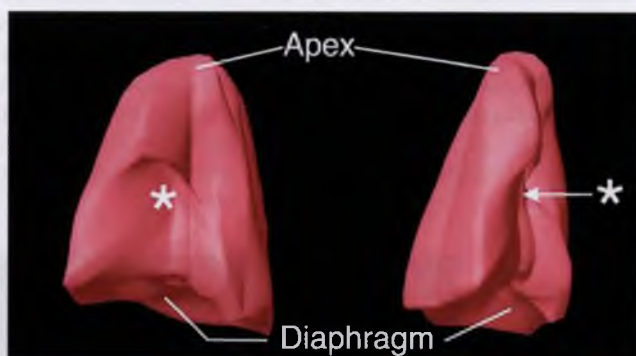


**FIG 11-25** Three-dimensional ultrasound model of the right lung volume obtained using VOCAL. Note the indentation of the fetal heart (asterisk). The frontal view is shown on the left and the lateral view on the right. (From Kalache KD, Espinoza J, Chaiworapongsa T, et al: Three-dimensional ultrasound fetal lung volume measurement: a systematic study comparing the multiplanar method with the rotational (VOCAL) technique. *Ultrasound Obstet Gynecol* 21;111, 2003.)



the outline of the organ is irregular, such as in cases of congenital diaphragmatic hernia. In contrast, obtaining lung volume measurements using the 3D multiplanar technique is faster, taking usually less than 5 minutes to perform.<sup>196</sup> Volumes are best estimated when datasets are acquired using a transverse view of the fetal thorax.<sup>186,198</sup> Ruano and coworkers<sup>197</sup> compared volumetric measurements of the fetal lungs obtained using the VOCAL method with lung volumes calculated at the time of autopsy in 8 cases of congenital diaphragmatic hernia and in 25 control fetuses without pulmonary malformations. The mean relative error of 3D sonography to estimate the actual lung volume was  $-7.19\%$  (range:  $-42.70\%$  to  $+18.11\%$ ) in cases of congenital diaphragmatic hernia and  $-0.72\%$  (range:  $-30.25\%$  to  $+19.22\%$ ) in normal fetuses. Barros and colleagues<sup>190</sup> studied 24 fetuses with skeletal dysplasia and measured the total lung volume using VOCAL. An abnormally reduced lung volume was defined as below the 5th percentile for gestational age. From 18 fetuses diagnosed at birth with lethal pulmonary hypoplasia, 83% had a total lung volume below the 5th percentile for gestational age. Lung volume more accurately predicted pulmonary hypoplasia than thoracic circumference, thoracic circumference/abdominal circumference ratio, and thoracic area/cardiac area ratio.

**Estimation of Pulmonary Hypoplasia by Magnetic Resonance Imaging.** Parameters proposed to evaluate lung volume by MRI include the relative lung volume (observed/expected lung volume ratio), lung volume/estimated fetal weight (LV/EFW) ratio, and the lung/spinal fluid signal intensity (L/SF) ratio.<sup>199-206</sup> Fetal lung volume shows a linear increase across gestational age with the right lung volume accounting for 56% of the total fetal lung volume.<sup>200</sup> Lung volume evaluated by MRI is significantly reduced in fetuses at risk of pulmonary hypoplasia,<sup>203</sup> and MRI might perform better than sonography.<sup>204</sup> In addition, reduced signal intensity and altered L/SF ratio on T2-weighted imaging have been reported in fetuses with pulmonary hypoplasia.<sup>202,205,206</sup>

**Doppler Assessment of Tracheal Fluid Flow.** Kalache and coworkers<sup>207</sup> proposed that the volume of lung fluid displaced in the trachea could be useful for the analysis of fetal lung function. The investigators tested this hypothesis in a case-control study that included six cases of congenital diaphragmatic hernia and in a control group of five healthy fetuses matched for gestational age. Parameters that were analyzed included the (1) length of the inspiratory phase; (2) length of the

expiratory phase; (3) peak velocities during inspiration and expiration; and (4) volume estimation of the displaced fluid in the trachea during breathing, calculated as

$$\text{Volume} = \text{VTI} \times \pi \times (d \times 0.5)^2$$

where VTI = velocity time interval and  $d$  = distance. The estimated breathing-related tracheal volume flow in uncomplicated pregnancies increased with gestational age (from  $0.21 \pm 0.10$  mL/breath at 26 weeks, to  $1.37 \pm 0.48$  mL/breath at 36 weeks of gestation) and was significantly lower in fetuses with diaphragmatic hernia who died of pulmonary hypoplasia. Tracheal volume flow in survivors was comparable to that in control subjects.

**Doppler Velocimetry of the Pulmonary Arteries.** Underdevelopment and structural changes of the pulmonary vascular bed in cases of pulmonary hypoplasia may result in increased pulmonary vascular resistance and reduced pulmonary arterial compliance.<sup>208</sup> Therefore, several investigators have attempted to use Doppler measurements of the pulmonary arteries and its branches in an attempt to identify fetuses at risk for pulmonary hypoplasia.<sup>180,209-213</sup> However the observed increment in the resistance or pulsatility indices in fetuses at risk of pulmonary hypoplasia<sup>209,211</sup> has not been consistently documented,<sup>210</sup> and when present it has not been found superior to thoracic measurements.<sup>180</sup> Other Doppler parameters, such as acceleration time, have been also proposed for identification of fetuses at risk of pulmonary hypoplasia.<sup>214</sup>

### Evaluation of Hands and Feet

The fetal hands and feet should be examined to exclude polydactyly (Fig. 11-26), brachydactyly, and extreme postural deformities, such as those seen in diastrophic dysplasia. Table 11-15 shows a nomogram of fetal foot size throughout gestation. Table 11-16 displays disorders associated with hand and foot deformities. Disproportion between the hands and feet and other parts of the extremity may also be a sign of skeletal dysplasias. Figure 11-27 illustrates the relationship between femur length and foot length. The femur length/foot length ratio is nearly constant from 14 to 40 weeks of gestation, with a mean value of 0.99 (standard deviation  $\pm 0.06$ ). A ratio below 0.87 is considered abnormal.<sup>215</sup> Although fetuses with skeletal dysplasias have been reported to have abnormally low ratios, more experience is required to establish the diagnostic value of this method.<sup>216</sup> It is expected that

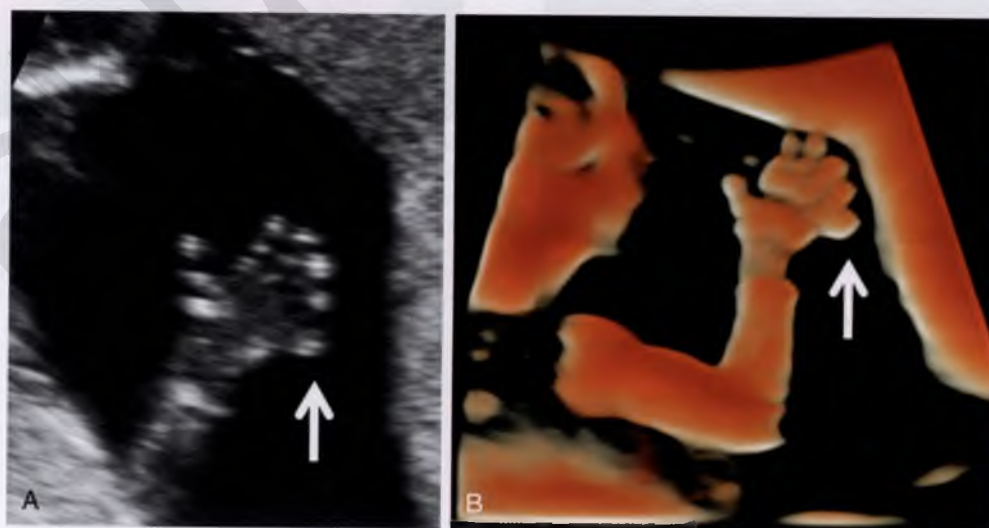


**FIG 11-26** Two-dimensional (A) and three-dimensional (B) ultrasound-rendered volume using HDlive mode showing postaxial polydactyly (arrow).

**TABLE 11-15 Nomogram of Fetal Foot Length (3rd, 50th, and 97th Percentiles) Throughout Gestation (Centimeters)**

Weeks	FOOT LENGTH		
	3rd	50th	97th
12	5.9	8.9	11.8
13	8.5	11.7	14.9
14	11.3	14.6	18.0
15	14.0	17.6	21.2
16	16.8	20.6	24.4
17	19.6	23.6	27.6
18	22.4	26.6	30.8
19	25.2	29.6	34.0
20	28.0	32.6	37.2
21	30.8	35.6	40.4
22	33.5	38.6	43.6
23	36.2	41.5	46.7
24	38.9	44.4	49.8
25	41.5	47.2	52.8
26	44.1	50.0	55.8
27	46.6	52.7	58.7
28	49.1	55.3	61.6
29	51.4	57.9	64.3
30	53.7	60.4	67.0
31	55.9	62.8	69.6
32	58.0	65.1	72.1
33	60.0	67.3	74.5
34	61.9	69.4	76.8
35	63.7	71.4	79.0
36	65.4	73.3	81.1
37	66.9	75.0	83.1
38	68.4	76.7	85.0
39	69.7	78.2	86.7
40	70.9	79.6	88.3
41	71.9	80.8	89.7
42	72.8	81.9	91.0

From Chitty LS, Altman DG: Charts of fetal size: limb bones. *Br J Obstet Gynaecol* 109:919-929, 2002.

a small proportion of normal fetuses may have an abnormal ratio. As in the case of other limb biometric parameters, large deviations from the lower limit of normal are likely to be significant.

### Evaluation of the Fetal Cranium

Several skeletal dysplasias are associated with defects of membranous ossification, and, therefore, skull bones are affected. Examination of the skull bones may reveal poor ossification (see Fig. 11-17), frontal bossing (Fig. 11-28), or cloverleaf deformity (Fig. 11-29). Table 11-17 presents abnormalities of the skull and face in various skeletal dysplasias.

### Evaluation of the Fetal Face

Sonographic examination of the fetal face is of major importance in the assessment and diagnosis of skeletal dysplasias, because many of these disorders are associated with characteristic abnormalities.<sup>217</sup> Sonographic evaluation of the fetal face is easily performed in a high percentage of patients from 16 to 20 weeks of gestation onward. The single most reliable view in detecting facial abnormalities is the sagittal plane. This view permits determination of midface hypoplasia, which

**TABLE 11-16 Skeletal Dysplasias Associated With Polydactyly and Syndactyly**

#### Postaxial Polydactyly

Chondroectodermal dysplasia  
Short rib–polydactyly syndrome (type I, type II)  
Asphyxiating thoracic dysplasia  
Otopalatodigital syndrome  
Mesomelic dysplasia, Werner type (associated with absence of thumbs)

#### Preaxial Polydactyly

Chondroectodermal dysplasia  
Short rib–polydactyly syndrome type II  
Carpenter syndrome

#### Syndactyly

Poland syndrome  
Acrocephalosyndactyly (Carpenter syndrome, Apert syndrome)  
Otopalatodigital syndrome type II  
Mesomelic dysplasia, Werner type  
Thrombocytopenia with absent radius (TAR) syndrome

#### Brachydactyly

Mesomelic dysplasia, Robinow type  
Otopalatodigital syndrome

#### Hitchhiker Thumbs

Diastrophic dysplasia

#### Clubfoot Deformity

Diastrophic dysplasia  
Osteogenesis imperfecta  
Kniest dysplasia  
Spondyloepiphyseal dysplasia

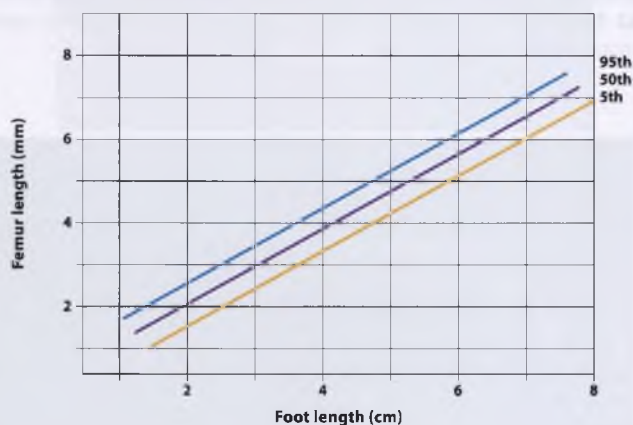


**FIG 11-27** Relationship between femur length (mm) and foot length (cm).

occurs in several skeletal dysplasias, such as thanatophoric dysplasia, achondroplasia, campomelic dysplasia, osteogenesis imperfecta, and spondyloepiphyseal dysplasia congenita.<sup>86,217</sup>

In cases of median cleft lip, the central portion of the upper lip is absent, and on the midline sagittal view, no upper lip will be demonstrated. In bilateral cleft lip, the midline view will have a variable appearance, depending upon the amount of residual premaxillary tissue present in the midline. In unilateral cleft lip, the midline sagittal scan may be relatively normal but the parasagittal view will reveal



the cleft. Clefts should be confirmed by imaging the lips in the coronal plane.

Cleft palate occurs in 66% of patients with cleft lip. Isolated cleft palate is more difficult to diagnose with ultrasound due to the shadowing from the facial bones. 3D sonography has been shown to be superior to 2D sonography for prenatal diagnosis of cleft lip and palate.<sup>135,218,219</sup> Potential advantages of 3D sonography over 2D sonography include the following: (1) a true coronal view of the lips can be displayed, even when the original scanning plane was obtained from a different orientation; (2) 3D standardized multiplanar imaging makes it easier to successfully demonstrate the maxillary tooth-bearing alveolar ridge in suspected cases; and (3) the maxillary tooth-bearing alveolar ridge can be more accurately localized by the multiplanar technique because this region can easily be mistaken for the mandibular ridge.<sup>220,221</sup> Rendered views of the cleft lip/palate have also been particularly useful for patient counseling.<sup>220,222,223</sup> A novel technique for visualization of the fetal palate, called the 3D reverse face view, has been proposed for



**FIG 11-28** Frontal bossing (arrow) in a sagittal plane of a fetus with achondroplasia.

the antenatal characterization of facial clefting; specifically, clefting of the hard palate.<sup>224</sup> This technique consists of rotating the volume dataset 180 degrees around the vertical axis in order to examine the secondary palate. Campbell and associates<sup>225</sup> reported that a cleft in the soft palate was missed in only one of eight cases of suspected orofacial clefting with the use of this rendering technique. Recent studies recommend the use of MRI in the evaluation of fetal cleft lip and palate identified by sonography. MRI appears to provide a better assessment of the degree of involvement of the secondary palate and of cleft extent since shadowing artifacts from adjacent osseous structures do not affect fetal MR images.<sup>226-230</sup>

Micrognathia is frequently observed in cases of skeletal dysplasia (Table 11-18).<sup>231-233</sup> In an attempt to provide an objective tool to diagnose micrognathia prenatally, Paladini and colleagues<sup>234</sup> proposed the jaw index, which is computed as the ratio between the anteroposterior mandibular diameter and the biparietal diameter. In a population of 198 fetuses with congenital anomalies (11 of which had micrognathia at necropsy or at birth), a jaw index below 23 correctly identified all cases of micrognathia with a false positive rate of 2%. Rotten and coworkers<sup>235</sup> proposed two parameters to differentiate between retrognathia and micrognathia: the inferior facial angle (Fig. 11-30) and the mandible width/maxilla width (MD/MX) ratio (Fig. 11-31). The inferior facial angle is defined as the angle between two lines traced on a sagittal profile view of the fetal face: (1) a reference line, orthogonal to the vertical part of the forehead, at the level of the synostosis of the nasal bones, and (2) the profile line, joining the tip of the mentum to the anterior border of the more protruding lip. In a population of fetuses at high risk for facial anomalies, an inferior facial angle less than 50 degrees identified retrognathia with a sensitivity of 100% and specificity of 98.9%. The MD/MX ratio was computed using transverse sections of the mandible and maxilla, with the actual measurements performed 10 mm posteriorly to the anterior osseous border; an MD/MX ratio less than 0.8 (between 18 and 28 weeks of gestation) correctly identified micrognathia in three cases of Treacher Collins syndrome.

Intraorbital and interorbital diameters should also be measured, because hypertelorism may occur in cases of skeletal dysplasia (Table 11-19).

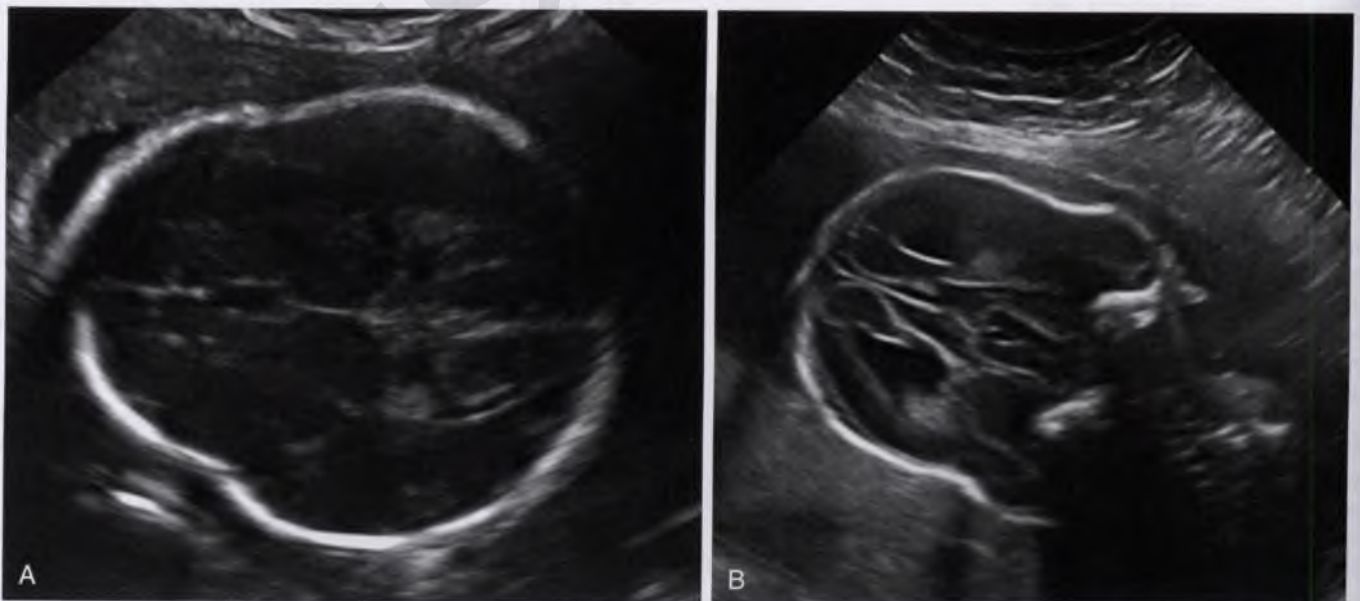


**FIG 11-29** Mild cloverleaf skull in a patient with thanatophoric dysplasia. **A**, Cross-sectional plane. **B**, Coronal plane.

**TABLE 11-17 Skeletal Dysplasias Associated With Skull and Face Deformities****Large Head**

Achondroplasia  
 Achondrogenesis  
 Thanatophoric dysplasia  
 Osteogenesis imperfecta  
 Cleidocranial dysplasia  
 Hypophosphatasia  
 Campomelic dysplasia  
 Short rib–polydactyly syndrome, type III  
 Robinow mesomelic dysplasia  
 Otopalatodigital syndrome

**Cloverleaf Skull**

Thanatophoric dysplasia  
 Campomelic dysplasia

**Other Craniostenosis**

Apert syndrome  
 Carpenter syndrome

**Congenital Cataracts**

Condrosyplasia punctata

**Cleft Palate**

Asphyxiating thoracic dysplasia  
 Kniest dysplasia  
 Diastrophic dysplasia  
 Spondyloepiphyseal dysplasia  
 Campomelic dysplasia  
 Jarcho-Levin syndrome  
 Ellis–van Creveld syndrome  
 Short rib–polydactyly syndrome, type II  
 Metatropic dysplasia  
 Otopalatodigital syndrome, type II  
 Dyssegmental dysplasia  
 Robert syndrome

**Short Upper Lip**

Chondroectodermal dysplasia

**Micrognathia**

Campomelic dysplasia  
 Diastrophic dysplasia  
 Weissenbacher-Zweymüller syndrome  
 Otopalatodigital syndrome  
 Pena-Shokeir syndrome  
 Thrombocytopenia–absent radius (TAR) syndrome  
 Langer syndrome

**TABLE 11-18 Skeletal Dysplasias Associated With Micrognathia**

Campomelic dysplasia	Treacher Collins syndrome
Diastrophic dysplasia	Nager acrofacial dysostosis
Otopalatodigital syndrome	Oromandibular limb hypogenesis
Achondrogenesis	Goldenhar syndrome
Mesomelic dysplasia	Atelosteogenesis
Pena-Shokeir syndrome	Hydroletharus syndrome

**Evaluation of the Fetal Spine**

Sonographic assessment of the fetal spine must be performed in all fetuses with suspected skeletal dysplasias. The following parameters should be assessed:

**Vertebral Bodies.** Fetal vertebral bodies are composed of three ossification centers representing the vertebral body and two laminae.<sup>236-239</sup> Abnormalities of the ossification centers of the fetal vertebral bodies may result in hemivertebra (see Fig. 11-12), butterfly vertebrae, spinal dysgenesis (Fig. 11-32), or block vertebrae causing congenital scoliosis (see Figs. 11-10 and 11-11). A study of the associated anomalies in 27 cases of prenatally detected hemivertebra noted that 16 (59%) have additional associated anomalies, including gastrointestinal, renal, facial, limb, and cranial anomalies; only five of the fetuses with additional anomalies survived.<sup>236</sup> Usually these anomalies are not a risk factor for aneuploidy. Rib defects are often associated with thoracic vertebral body anomalies.

Platyspondyly can be diagnosed using high-resolution sonography (see Fig. 11-9).<sup>240</sup> An objective evaluation of platyspondyly is obtained

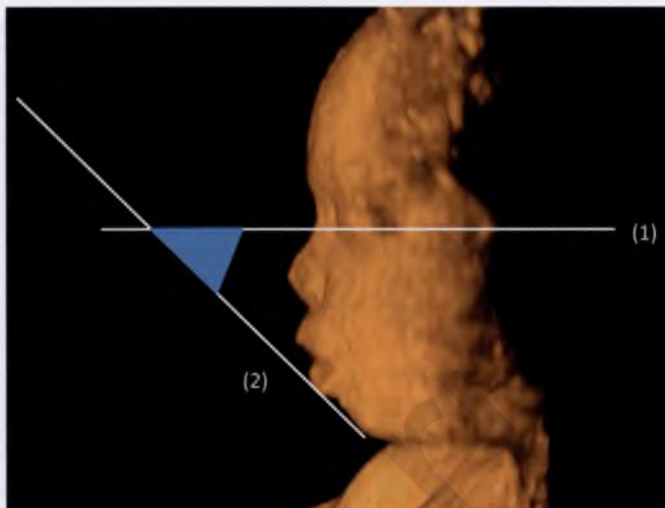


**FIG 11-30** Inferior facial angle obtained from a sagittal view of the fetal face. The angle is formed by a reference line (1), orthogonal to the vertical part of the forehead at the level of the synostosis of the nasal bones, and the profile line (2), joining the tip of the mentum to the anterior border of the more protruding lip. (From Mittermayer C, Blaicher W, Brugger PC, et al: Foetal facial clefts: prenatal evaluation of lip and primary palate by 2D and 3D ultrasound. *Ultraschall Med* 25:120-125, 2004.)

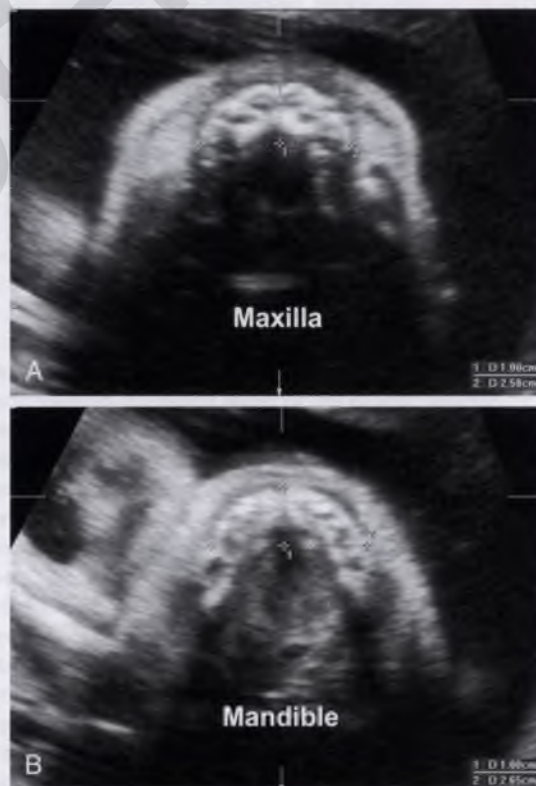


**FIG 11-31** The mandible/maxilla (MD/MX) ratio is calculated using transverse sections of the mandible (B) and maxilla (A), with measurements performed 10 mm posterior to the anterior osseous border.

by estimating the ratio between measurements of the vertebral interspace and of vertebral body height.<sup>59</sup>

Clefting of the vertebrae may be longitudinal or transverse and complete or incomplete.<sup>68</sup> Coronal vertebral clefts are a result of missed fusion between the anterior and posterior primary ossification centers



**TABLE 11-19 Skeletal Dysplasias Associated With Hypertelorism**

Otopalatodigital syndrome	Coffin syndrome
Arthrogryposis multiplex congenita	Klippel-Feil syndrome
Larsen syndrome	Apert syndrome
Roberts syndrome	Sprengel deformity
Cleidocranial dysplasia	Mesomelic dysplasia
Achondroplasia	Holt-Oram syndrome
Campomelic dysplasia	

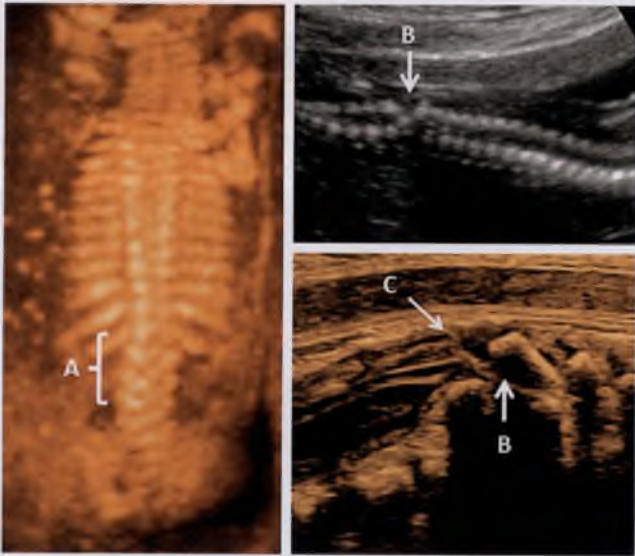


**FIG 11-32** Spinal dysgenesis showing complex vertebral segmentation between the thoracic and lumbar segments (A), obliteration of the spinal canal (B), and tethered spinal cord (C).

beyond 16 weeks of gestation and can be observed by prenatal sonography.<sup>241,242</sup> Sagittal clefts in the vertebral bodies are believed to represent localized splitting of the notochord due to adhesions between ectoderm and endoderm during the embryonic period. The role of vertebral clefting in the diagnosis of skeletal dysplasias was assessed by Westvik and Lachman<sup>242</sup> based on the International Skeletal Dysplasia Registry. The authors reported coronal and sagittal clefts in 40 different skeletal anomalies. Coronal clefts were more common than sagittal clefts and were mainly located in the thoracolumbar region. Clefts were most frequently observed in atelosteogenesis (88%), followed by chondrodysplasia punctata (79%), dyssegmental dysplasia (73%), Kniest dysplasia (63%), and short rib–polydactyly syndrome (SRPS) (53%).<sup>242</sup> The authors concluded that vertebral clefts are of major diagnostic value in these groups of skeletal dysplasias.

**Spinal Curvature.** The most common osseous anomaly causing scoliosis is unilateral unsegmented bar with contralateral hemivertebra.<sup>236,243-246</sup> Spinal dysraphism may also occur with congenital scoliosis. An apparent etiologic relationship exists between neural tube defects and other vertebral anomalies. Siblings of infants with congenital scoliosis have a 4% risk of neural tube defects.<sup>247</sup> This increased risk is present in siblings of children with a single hemivertebra, as well as multiple vertebral anomalies (with or without neural arch defects). The differential diagnosis of fetal scoliosis includes neural tube defects, large abdominal wall defects, amniotic band syndrome, caudal

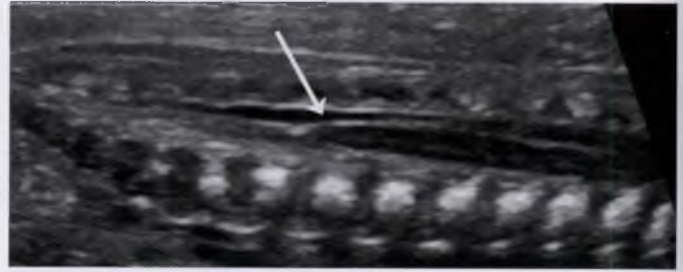


**FIG 11-33** Conus medullaris (arrow) in a fetus at 21 weeks of gestation.

regression, and hemivertebra. Nonossification of the lumbar vertebral bodies has been detected in achondrogenesis and other diseases.<sup>248-250</sup>

**Conus Medullaris.** Hoopmann and associates<sup>251</sup> performed detailed sonographic evaluation of the fetal spine and reported that the distance from the tip of the conus medullaris to the sacrum was useful in identifying fetuses with skeletal dysplasias with a shortened trunk (Fig. 11-33). In their study, all fetuses with a shortened trunk at birth had a considerably shorter distance from the tip of the conus medullaris to the sacrum as compared with normal fetuses. The authors suggest that evaluation of the conus medullaris might be useful in the evaluation of skeletal dysplasias.

### Evaluation of the Internal Organs

A detailed examination of the cardiovascular, genitourinary, gastrointestinal, and central nervous system (CNS) organs should be performed for differential diagnosis among syndromes presenting with fetal skeletal anomalies. For example, congenital heart disease is a prominent feature of Ellis–van Creveld and Holt-Oram syndromes.<sup>252,253</sup>

### Fetal Movements

The normal pattern of fetal movements can be identified as early as 11 weeks of gestation through a detailed anatomic evaluation.<sup>254-257</sup> Abnormal fetal movements can be observed in skeletal disorders involving joint contractures, neural muscular connective tissue disorders, amyoplasia (lack of muscle growth), vascular compromise, and anomalies of the spinal cord. The most frequent conditions associated with abnormal or absent fetal movements are fetal akinesia deformation sequence (FADS) or Pena-Shokeir syndrome, and arthrogryposis.<sup>258</sup> In FADS there is a significant reduction in the amplitude, velocity, and complexity of fetal movements.<sup>259,260</sup> In arthrogryposis, there is fixed position of the distal parts of the limbs and reduced amplitude in limb movements. Abdulkadir and colleagues<sup>261</sup> reported a characteristic pattern of movements in a fetus with thanatophoric dysplasia at 32 weeks of gestation including rigid abduction of the limbs, flexed elbows and knees, lack of synchronous movements, hyperextended neck, and rhythmic segmentation of trunk movements.

### Newborn Evaluation

Even when all efforts have been made to establish an accurate prenatal diagnosis, a careful study of the newborn is always required.<sup>92</sup> The evaluation should include radiographs of the skeleton and a detailed physical examination performed by a geneticist or by a professional with experience in the field of skeletal dysplasias. The radiographs should include anteroposterior (AP), lateral, and Towne views of the skull, as well as AP views of the spine, extremities, and scapula,<sup>262</sup> with separate films of the hands and feet. Veeramani and coworkers<sup>263</sup> reported that a full skeletal x-ray survey helped to establish the correct



diagnosis in 69% of all skeletal dysplasias. In lethal skeletal dysplasias, histologic examination of the chondro-osseous tissue should be performed as this information may help the physician reach a specific diagnosis. Chromosomal studies should also be included, as there is a specific group of constitutional bone disorders associated with cytogenetic abnormalities. Biochemical studies are helpful in some cases (e.g., hypophosphatasia). Enzymatic activity assays may be considered if the phenotype suggests a metabolic disorder (e.g., mucopolysaccharidosis). Molecular diagnosis can be performed for disorders in which a specific genetic mutation has been identified or if a specific diagnosis is suspected, and it is recommended that DNA should be saved in all cases.<sup>33,34,264</sup> Increasingly, whole exome sequencing is helpful in the diagnosis of suspected genetic disorders.

### Increased Nuchal Translucency and Skeletal Dysplasias

In chromosomally normal pregnancies, increased nuchal translucency (NT) thickness is associated with a higher risk of major anomalies,<sup>265-268</sup> including skeletal dysplasias.<sup>115,268-272</sup> In one multicenter screening project for trisomy 21 performed in 100,000 pregnancies by the combination of maternal age and NT, a significant association between increased NT and a wide range of skeletal dysplasias was found.<sup>265</sup> In addition, several case reports and small series have confirmed that in chromosomally normal fetuses, an association may exist between increased NT thickness and skeletal anomalies. The skeletal dysplasias associated with increased thickness of NT are listed in Table 11-20.

**TABLE 11-20 Skeletal Dysplasias Associated With Increased Nuchal Translucency Thickness**

Skeletal Dysplasia	Author, Year
Achondrogenesis	Hewitt, 1993 <sup>273</sup> ; Soothill, 1997 <sup>274</sup> ; Fisk, 1991 <sup>452</sup>
Achondroplasia	Fukada, 1997 <sup>275</sup> ; Hernadi, 1997 <sup>276</sup>
Asphyxiating thoracic dysplasia	Ben Ami, 1997 <sup>672</sup> ; Hsieh, 1999 <sup>591</sup>
Blomstrand osteochondrodysplasia	den Hollander, 1997 <sup>277</sup>
Campomelic acampomelic dysplasia	Michel-Calemard, 2004 <sup>271</sup>
Campomelic dysplasia	Hafner, 1998 <sup>278</sup>
Cleidocranial dysplasia	Hjippala, 2001 <sup>279</sup>
Chondroectodermal dysplasia (Ellis-van Creveld)	Venkat-Raman, 2005 <sup>280</sup>
Diastrophic dysplasia	Ngo, 2007 <sup>281</sup>
Ectrodactyly ectodermal dysplasia	Leung, 1995 <sup>282</sup>
Fanconi anemia	Tercanli, 2001 <sup>283</sup>
Fetal akinesia deformation sequence	Souka, 1998 <sup>288</sup> ; Hyett, 1997 <sup>284</sup> ; Madazli, 2002 <sup>285</sup>
Hypophosphatasia	Souka et al, 2002 <sup>270</sup>
Jarcho-Levin syndrome	Eliyahu, 1997 <sup>286</sup> ; Souka, 1998 <sup>288</sup>
Osteogenesis imperfecta II	Makridymas, 2001 <sup>289</sup>
Osteogenesis imperfecta III	Vimecarti, 2013 <sup>287</sup>
Short rib–polydactyly syndrome	Hill, 1998 <sup>288</sup>
Sirenomelia	Hewitt, 1993 <sup>273</sup>
Thanatophoric dysplasia	Ferreira et al, 2004 <sup>289</sup>
Thrombocytopenia–radial aplasia	Witters et al, 2005 <sup>272</sup>
VACTERL association	Souka, 1998 <sup>288</sup>

VACTERL, vertebral, anal atresia, cardiac defects, tracheoesophageal fistula, renal anomalies, limb defects.

Superscript numbers indicate references listed at the end of the chapter.

## OSTEOCHONDRODYSPLASIAS

A growing number of skeletal dysplasias have been recognized in utero, and a complete account of each disorder is beyond the scope of this chapter. For detailed information on classification and molecular diagnosis of skeletal disorders, the interested reader should consult the International Nosology and Classification of Constitutional Disorders of Bone.<sup>36</sup> For detailed information on prenatal and postnatal imaging methods applied to evaluate skeletal dysplasias, we highly recommend the book *Fetal and Perinatal Skeletal Dysplasias; An Atlas of Multimodality Imaging* by Christine Hall, Amaka Offiah, Francesca Forzano, Mario Lituania, Michelle Fink, and Deborah Krakow.<sup>161</sup> The following discussion presents a few of the most common disorders relevant to prenatal diagnosis.

### Achondroplasia, Thanatophoric Dysplasia, and Hypochondroplasia

Achondroplasia, thanatophoric dysplasia, and hypochondroplasia are discussed in the same section because these disorders are caused by different mutations in the fibroblast growth factor receptor-3 gene (*FGFR3*).<sup>290-297</sup> Mutations in *FGFR3* are gain-of-function mutations that produce a constitutively active protein capable of initiating intracellular signal pathways in the absence of ligand binding.<sup>298,299</sup> This activation leads to premature maturation of the bone.<sup>299</sup> The critical clinical difference between thanatophoric dysplasia and achondroplasia/hypochondroplasia is severe shortening of the ribs in thanatophoric dysplasia, resulting in restricted lung volumes, respiratory insufficiency, and death within hours or days after birth.<sup>300</sup>

### Achondroplasia

The most common nonlethal skeletal dysplasia is achondroplasia, an autosomal dominant condition with complete penetrance and an estimated prevalence ranging from 1:10,000 to 1:50,000 births.<sup>301-303</sup> It is clinically characterized by rhizomelic shortening of the limbs and mild limb bowing, exaggerated lumbar lordosis, and an enlarged head.<sup>304</sup> The bones of the hands and feet are short (brachydactyly). The head is large (macrocephaly), with frontal bossing, midface hypoplasia, a flattened nasal bridge, and a broad mandible. Achondroplasia is frequently misdiagnosed during pregnancy.<sup>305</sup> Modaff and associates<sup>306</sup> retrospectively collected data from 37 consecutive referrals of infants with achondroplasia in whom prenatal sonography was performed. Nine of the 37 (24%) infants had a positive family history of achondroplasia; all 9 were correctly diagnosed prenatally. Of the 28 infants with no family history of achondroplasia, 16 (57%) were recognized to have abnormalities on ultrasound imaging, although none was diagnosed with certainty. Five received an appropriate diagnosis of “most likely” achondroplasia, and four others were given a nonspecific (but appropriate) diagnosis of some skeletal dysplasia, not otherwise specified. In seven instances (25%), an incorrect diagnosis of a lethal or very severe disorder was provided.

The major difficulty in the prenatal diagnosis of this condition is that abnormal long bone growth is not recognized in most cases until the third trimester of pregnancy.<sup>74,304</sup> However, prenatal diagnosis of achondroplasia is possible and has been reported.<sup>307-310</sup> For example, the “trident hand” (an increased interspace between the third and fourth digit) is a specific finding for achondroplasia<sup>311,312</sup> (Fig. 11-34). A distinct difference in the femoral length growth curves of homozygous, heterozygous, and unaffected children of achondroplastic parents was described by Patel and Filly.<sup>313</sup> Fetuses with homozygous achondroplasia demonstrated early shortening of the femora less than the 3rd percentile at 14.0 to 16.5 weeks of gestation (mean 15.6 weeks), but fetuses with heterozygous achondroplasia showed femoral





**FIG 11-34** **A**, Drawing demonstrating separation between the third and fourth digit. **B**, Photograph of a child with achondroplasia and trident hand. **C**, In utero sonogram of a fetus with achondroplasia and trident hand with separation between the third and fourth digits (arrow).

shortening less than the 3rd percentile at 18.2 to 26.2 weeks of gestation (mean 21.5 weeks).<sup>313</sup> Recently, Tonni and colleagues<sup>303</sup> reported the association of first trimester increased NT in a fetus with achondroplasia, and Karadimas and associates<sup>314</sup> reported a fetus with achondroplasia and multiple craniosynostoses. Khalil and colleagues suggested that widening of the proximal femoral angle at 20 to 23 weeks of gestation can identify fetuses with achondroplasia.<sup>160</sup>

More than 99% of individuals with achondroplasia have one of two mutations in the *FGFR3* gene, which is located on the short arm of chromosome 4.<sup>315-317</sup> The most common mutation is a guanine-to-adenine (G-to-A) transition, at nucleotide 1138 in the amino acid 380,

and about 1% of affected individuals have a guanine-to-cytosine (G-to-C) transversion at the same nucleotide.<sup>290,317</sup> A transversion occurs when a pyrimidine replaces a purine or vice versa, and a point mutation occurs when a pyrimidine replaces a pyrimidine or a purine replaces a purine.<sup>264</sup> The G380R mutation has been shown to result in constitutive activation of the *FGFR3* gene, which inhibits chondrocyte proliferation and differentiation and is responsible for the shortness of long bones. It is noteworthy that all new mutations occur on the paternal allele, suggesting an increased mutability of *FGFR3* during spermatogenesis is associated with increased paternal age.<sup>318</sup> Molecular diagnosis is possible in pregnancies in which one or both parents have



achondroplasia, either in placental tissue obtained by chorionic villus sampling (CVS) or in fetal cells obtained by amniocentesis.<sup>308,319,320</sup>

Molecular analysis can also identify mutations in fetuses suspected to have achondroplasia based on ultrasound findings.

Heterozygous achondroplasia is compatible with normal life and intellectual development. However, cervicomedullary junction abnormalities, which may lead to spinal cord compression, put the infant with achondroplasia at risk for lethal sequelae.<sup>321</sup> Cervicomedullary decompressive surgery can be lifesaving by decreasing neurologic complications associated with damage of the spinal cord and may eliminate the risk of central apnea that can cause sudden death.<sup>322</sup> In the homozygous state (which occurs in 25% of the offspring of two parents with achondroplasia), the disease is usually lethal during the first 2 years of life.<sup>301</sup> However, a case of survival until 37 months has been reported.<sup>323</sup> The radiologic characteristics of homozygous achondroplasia lie between those of thanatophoric dysplasia and those of heterozygous achondroplasia.

Administration of growth hormone (GH) has been proposed for the treatment of achondroplasia.<sup>324</sup> Children treated with GH for 2 years showed an increment in annual height ( $6.5 \pm 1.8$  cm in the first year, and  $4.6 \pm 1.6$  cm in the second year) significantly greater than before treatment ( $3.9 \pm 1.0$  cm).<sup>325</sup> However, individual variability in response to GH treatment has been reported.<sup>326</sup> Other innovative therapeutic approaches include downregulation of the tyrosine kinase activity of the *FGFR3* by selective chemical inhibitors,<sup>302</sup> blocking antibodies to interfere with the binding of FGF ligands to *FGFR3*,<sup>302</sup> and targeted overexpression of C-type natriuretic peptide.<sup>327</sup>

**Severe Achondroplasia With Developmental Delay and Acanthosis Nigricans.** Tavormina and associates<sup>328</sup> identified a *FGFR3* missense mutation in four unrelated individuals with skeletal dysplasias approaching the severity observed in thanatophoric dysplasia type I. Three of the four individuals developed extensive areas of acanthosis nigricans beginning in early childhood, suffered from severe neurologic impairments, and survived past infancy without prolonged life support measures. The *FGFR3* mutation associated with this phenotype (A1949T:Lys650Met) occurs at the nucleotide adjacent to the thanatophoric dysplasia type II mutation (A1948G:Lys650Glu) and results in a different amino acid substitution. The authors of the study referred to the phenotype caused by the Lys650Met mutation as "severe achondroplasia with developmental delay and acanthosis nigricans" (SADDAN) because it differs significantly from the phenotypes of other known *FGFR3* mutations. SADDAN is also associated with unusual bone deformities, such as femoral bowing with reverse (i.e., posterior apex) tibial and fibular bowing, and so-called ram's horn bowing of the clavicle. This condition has not been associated with cloverleaf skull or craniosynostosis.<sup>329</sup>

### Thanatophoric Dysplasia

Thanatophoric dysplasia is the most common lethal skeletal dysplasia,<sup>38</sup> and it is characterized by severe rhizomelia, normal trunk length with a narrow thorax, and a large head with prominent forehead. It occurs in 0.24 to 0.69 of 10,000 births.<sup>39,40,293,330</sup> Two subtypes (I and II) have been identified, which are phenotypically differentiated by the skull shape and femur morphology. Type I typically presents with bowed "telephone receiver" femora<sup>331</sup> (Fig. 11-35) and no or mild cloverleaf skull, whereas the type II phenotype is characterized by a severe cloverleaf skull (see Fig. 11-29) and short but straight long bones.<sup>331-335</sup> Cloverleaf skull results from premature closure of the coronal and lambdoid sutures, defective development of the cranial base with secondary synostosis, or a primary developmental disorder of the brain with secondary deformation of the skull. The differential diagnosis between the two types depends on the radiographic findings

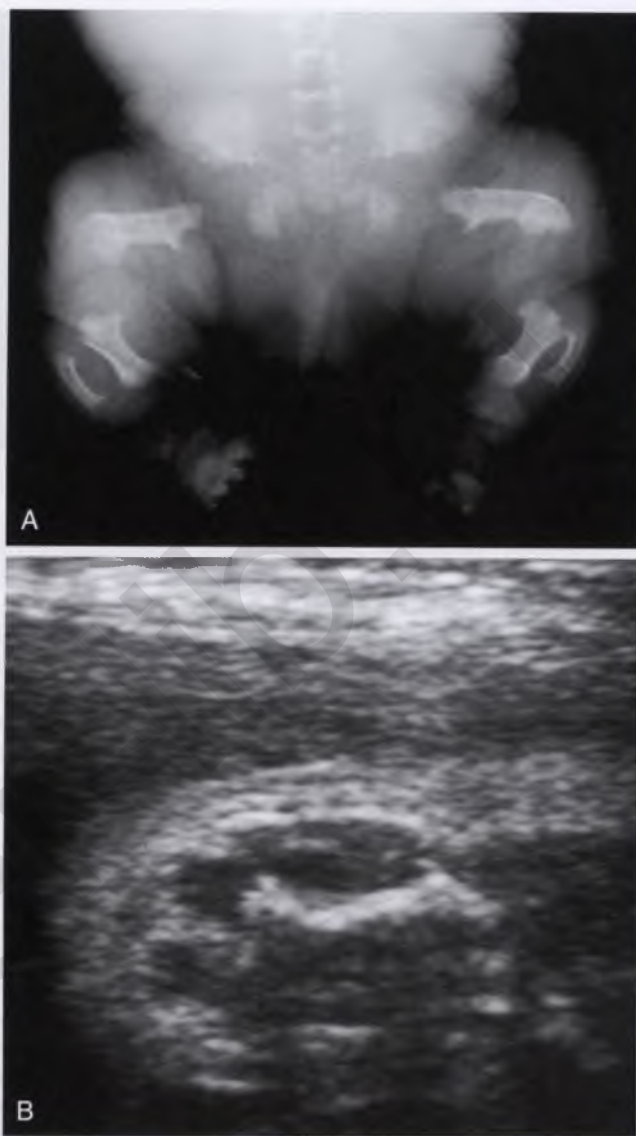


**FIG 11-35** **A**, Radiograph of a patient with thanatophoric dysplasia. Marked limb shortening and characteristic bowed "telephone receiver" femora. **B**, Sonogram of a fetus with thanatophoric dysplasia with marked femoral shortening and bowing.

and histologic characteristics. Both types of thanatophoric dysplasia are inherited in an autosomal dominant manner. The majority of cases of thanatophoric dysplasia (all type I and most cases of type II) are sporadic. Some familial cases of type II have been reported.<sup>336-339</sup> Distinct mutations in the *FGFR3* gene cause each one of the two types of thanatophoric dysplasia.<sup>301,336,338,340</sup> Three common mutations (R248C, Y373C, and S249C) are found in approximately 90% of the patients with thanatophoric dysplasia type I.<sup>298,341,342</sup> Importantly, up to 99% of the mutations causing type I and more than 99% of mutations causing type II thanatophoric dysplasia can be identified through molecular genetic testing of *FGFR3*. The *FGFR3* mutation p.Lys650Glu has been identified in all individuals with type II thanatophoric dysplasia,<sup>343</sup> and one mutation (K650E) is found in almost all cases of type II thanatophoric dysplasia.<sup>343-345</sup> Camera and colleagues<sup>346</sup> described an individual with the common thanatophoric dysplasia type I mutation and the clinical phenotype of achondroplasia. Although mosaicism was considered as a possible explanation for the milder phenotype, no trace of mosaicism was found in buccal mucosal cells or blood.





**FIG 11-36** Platyspondyly in a fetus with thanatophoric dysplasia. (Courtesy of Theera Tongsong, MD, and Suchaya Luewan, MD.)

The prenatal sonographic findings depend on the specific type of thanatophoric dysplasia.<sup>241</sup> The association of cloverleaf skull with micromelia is specific to thanatophoric dysplasia type II. Although campomelic syndrome may also be associated with cloverleaf skull, micromelia is not a feature of that condition. Ventriculomegaly, macrocranium, and polyhydramnios are frequently seen in thanatophoric dysplasia. Cerebellar hypoplasia is observed in approximately 37% of cases in postnatal series.<sup>300</sup> There is a relatively large calvarium with a prominent forehead, a saddle nose, and hypertelorism. Additional findings include short ribs, platyspondyly (see Fig. 11-9 and Fig. 11-36), and short and broad tubular bones in the hands and feet.

Thanatophoric dysplasia is associated with a specific pattern of brain malformations, characterized by megalencephaly (100%), hippocampal dysplasia (100%), rudimentary dentate gyrus (100%), polymicrogyria (97%), enlarged temporal lobes (93%), abnormal deep transverse sulci across the inferomedial temporal lobe (88%), subependymal neuronal heterotopia (81%), and subarachnoid neuroglial heterotopia (79%).<sup>300</sup> This pattern of brain anomalies has been extensively described in the neuropathology literature and has been observed with similar frequency in the two types of thanatophoric dysplasia.<sup>300</sup> Research conducted in mouse models for thanatophoric dysplasia suggests that the cortical malformations result from compound disturbances in cortical patterning, proliferation, and apoptosis. The result is gyral pattern abnormalities, regional dysplasia, and altered surface area (especially temporal lobe hyperplasia and premature sulcation).<sup>300,347</sup> Macroscopic gyral abnormalities and enlargement of the temporal lobes are specific for the disease, and are already present at midgestation by the time ultrasonography is performed.<sup>300,348</sup>

The differential diagnoses for thanatophoric dysplasia include SRPS, homozygous achondroplasia (in which both parents are typically affected), and asphyxiating thoracic dysplasia (differentiated by slight shortening of the long bones and normal vertebrae). On a review of radiologic findings of several cases of thanatophoric dysplasia, Horton and colleagues<sup>349</sup> were able to discern a group of distinct entities characterized by severe platyspondyly. These disorders include Torrance, San Diego, Lutton, and Shiraz types of platyspondylic lethal osteochondrodysplasias. The differential diagnosis among these entities is based on histologic and radiologic characteristics. Individuals with platyspondylic lethal skeletal dysplasia-San Diego type, have *FGFR3* mutations that have been previously reported in association with thanatophoric dysplasia type I.<sup>350</sup>

Thanatophoric dysplasia is a uniformly lethal disorder, although survival for several months has been reported.<sup>339,349,351-354</sup> Diagnosis by prenatal sonography has been documented,<sup>111,249,355-372</sup> including a case in a triplet pregnancy.<sup>237</sup> Prenatal diagnosis by CVS or amniocentesis is available.<sup>135,373-375</sup>

### Hypochondroplasia

Hypochondroplasia is an autosomal dominant disorder that resembles achondroplasia,<sup>376</sup> although the clinical symptoms and radiologic features in hypochondroplasia are generally milder than those seen in achondroplasia. Hypochondroplasia can result from a mutation in the *FGFR3* gene,<sup>377,378</sup> even though genetic heterogeneity has been suspected.<sup>379,380</sup> The incidence and prevalence of this disorder have not been determined, in part because of lack of agreement on a definitive set of diagnostic criteria, which makes it difficult to review data from many studies reported in the literature. Most cases occur sporadically as a result of a new mutation.<sup>381</sup>

Two *FGFR3* mutations (C1620A and C1620G) result in a lysine for asparagine substitution at codon 540 (N540K) and have been shown to cause hypochondroplasia.<sup>291,382</sup> Several other *FGFR3* mutations have been proposed to cause a small number of cases of hypochondroplasia. In addition, the *IGF1* gene has been proposed to be associated with hypochondroplasia although no pathogenetic mutations have been identified.<sup>379</sup>

The differential diagnosis between this condition and achondroplasia is based on sparing of the head and lack of tibial bowing in hypochondroplasia.<sup>376,383-387</sup> However, it is noteworthy that medial temporal lobe dysgenesis, similar to that observed in patients with thanatophoric dysplasia, has been described in three patients with a C1620A mutation in the *FGFR3* gene.<sup>388,389</sup> Thus, brain abnormalities that are commonly seen in hypochondroplasia and thanatophoric dysplasia can be used to distinguish them from achondroplasia.<sup>388-390</sup> In contrast to achondroplasia, the skull, pelvis, and hands are essentially normal.

Although hypochondroplasia is generally first detected during childhood, prenatal diagnosis has been reported in fetuses at risk.<sup>309,384</sup> A reduced femur length and a normal growth of the skull have been suggested as a potential sonographic marker for the prenatal diagnosis of hypochondroplasia.<sup>391</sup> DNA-based diagnosis through CVS or amniocentesis may be possible. It has been recommended that molecular analysis should include both achondroplasia and hypochondroplasia mutations.<sup>392</sup> Wang and coworkers<sup>393</sup> reported the molecular diagnosis in a Chinese family with a history of hypochondroplasia, using microarray-based next-generation sequencing (NGS) to evaluate disease-related genes *FGFR3* and cartilage oligomeric matrix protein (COMP). Similarly, Chen and associates<sup>394</sup> reported a mutation in *FGFR3* in a fetus presenting with very short limbs. The initial diagnosis was achondroplasia; however, study of *FGFR3* showed a de novo mutation for hypochondroplasia. The most common mutations are N540K in the tyrosine kinase 1 domain, G342C, and Y278C.<sup>394,395</sup> Hypochondroplasia has also been reported in Léri-Weill dyschondrosteosis<sup>396</sup> and shares similar clinical characteristics with Turner syndrome.<sup>397</sup>

### Fibrochondrogenesis and Atelosteogenesis

These two conditions have a clinical presentation similar to that of thanatophoric dysplasia. The differential diagnosis between these disorders in utero is difficult. Fibrochondrogenesis and atelosteogenesis are extremely rare, and only a few cases of each have been reported.<sup>68,398-405</sup>

### Fibrochondrogenesis

This skeletal disorder is a very rare lethal chondrodysplasia.<sup>406</sup> The first case was described in 1978 by Lazzaroni-Fossati and colleagues.<sup>407</sup> This disorder is inherited in an autosomal recessive fashion and is



characterized by micromelia with significant metaphyseal flaring, normal head size, flat face, flattened nasal bridge with anteverted nostrils, prominent eyes, undermineralized skull, platyspondyly, clefting of the vertebral bodies, and a narrow and bell-shaped thorax.<sup>404,408-411</sup> Metaphyseal flaring is not a feature of thanatophoric dysplasia.<sup>399,407,412,413</sup> This condition has been described in four consanguineous families.<sup>400,407,410,414</sup> Other conditions to be considered in the differential diagnosis include metatropic dysplasia and Kniest dysplasia. Histologic examination is characterized by chondrocytes with fibroblastic appearance and poor endochondral ossification.<sup>404,410</sup> The prenatal diagnosis of fibrochondrogenesis by ultrasound has been reported as early as 17 weeks of gestation.<sup>399,400,404</sup> The recurrence risk for fibrochondrogenesis is 25%, which emphasizes the importance of genetic counseling.<sup>404</sup> At present, the molecular defect involved in fibrochondrogenesis is not known.<sup>415</sup> However, Bekdache and coworkers<sup>416</sup> studied 20 cases in which fibrochondrogenesis was identified prenatally. Among them, 6 pregnancies were terminated, 13 were delivered, and 11 died within 3 months after birth. In the two surviving children, a mutation in the gene *COL11A1* was observed. The authors suggested that molecular diagnosis might be possible for fibrochondrogenesis.

### Atelosteogenesis

This condition includes a heterogeneous group of disorders with overlapping phenotypic features. It is a lethal chondrodysplasia characterized by severe micromelia (with hypoplasia of the distal segments of the humerus and femur), bowing of long bones, flat nasal bridge, cleft palate, micrognathia, narrow thorax with short ribs, coronal and sagittal vertebral clefts,<sup>68</sup> and dislocation at the level of the elbow and knee. Clubfoot deformities may also be present.<sup>417</sup> Three subtypes of atelosteogenesis (I, II, and III) have been described based on radiologic and pathologic findings.<sup>418-421</sup> Sillence and associates<sup>421</sup> retrospectively collected data from 17 referrals of fetuses and newborns with atelosteogenesis during a 20-year period. Clinically, all cases had marked limb shortening, and micrognathia, flattened nasal bridge, cleft palate, and pulmonary hypoplasia were more common in atelosteogenesis type II. Talipes was present in 80% of the cases of atelosteogenesis type I. Radiographic findings of atelosteogenesis type I (5 cases) showed distal hypoplasia of the femur; the humerus was absent or segment shaped; the radius, ulna, and tibia were bowed; there was absence of the fibula; and all cases had coronal clefts in the lumbar vertebrae. In atelosteogenesis type II (11 cases), the femora were shortened with expanded club-like ends and not distally tapered, and the humeri presented with distal hypoplasia and pointing. The forearm was shorter due to distal hypoplasia of the ulnae and proximal hypoplasia of the radii. In the lower limbs, the tibiae were short and bowed, and the fibulae had proximal or distal hypoplasia and pointing. The sacrum was horizontal. All cases had an S-shaped cervical spine. Only one case of atelosteogenesis type III was reported, with distal tapering of the femur and humerus, absence of ossification of the fibula, and an S-shaped cervical spine.<sup>421</sup>

Atelosteogenesis types I and III are sporadic and caused by missense mutations in the gene encoding filamin B, a protein that has a role in vertebral segmentation, joint formation, and endochondral ossification.<sup>422</sup> Atelosteogenesis type I shows giant cells in the growth plate cartilage and a mutation in the filamin B gene (*BLNB*).<sup>423</sup> Atelosteogenesis type II is inherited in an autosomal recessive pattern and is caused by a mutation in the diastrophic dysplasia sulfate transporter (*DTDST*) gene (*SLC26A2*).<sup>375-378</sup> It overlaps phenotypically and genetically with diastrophic dysplasia and achondrogenesis type IB.<sup>421,424,425</sup>

Differential diagnoses include diastrophic dysplasia and de la Chapelle dysplasia.<sup>426,427</sup> Three cases of a lethal dysplasia termed

boomerang dysplasia (so-called boomerang-like tibia) may actually represent the same disorder as atelosteogenesis type I.<sup>428</sup>

### Achondrogenesis

This skeletal dysplasia, also known as anosteogenesis, is a lethal chondrodystrophy characterized by extreme micromelia, a short trunk, and macrocrania. Prevalence at birth varies from 0.09 to 0.23 in 10,000 births.<sup>39,40,89,93,100</sup> Traditionally, this disorder has been classified into two types: the more severe form or type I achondrogenesis (Parenti-Fraccaro) and the less severe form or type II achondrogenesis (Langer-Saldino). In 1998, type I was subdivided into two types: type IA (Houston-Harris) and type IB (Fraccaro).<sup>429,430</sup> Although hypochondrogenesis had been considered a separate disorder from achondrogenesis, evidence now suggests that hypochondrogenesis and achondrogenesis type II are phenotypic variants of the same disorder.<sup>330,431,432</sup> Indeed, clinically and radiologically, achondrogenesis type II, hypochondrogenesis, and neonatal spondyloepiphyseal dysplasia congenita form a continuous spectrum of disease.<sup>433</sup> The fundamental biochemical disorder seems to be allelic mutations of the gene coding for type II procollagen.<sup>434</sup>

Type IA achondrogenesis (Houston-Harris) is characterized by micromelia, lack of ossification of vertebral bodies (but ossification of the pedicles in the cervical and upper thoracic region), and short ribs with multiple fractures. The calvarium is demineralized. Type IB (Fraccaro), which is a recessively inherited chondrodysplasia, is caused by a mutation in the *DTDS* gene<sup>435-437</sup> and is similar to type IA achondrogenesis. The calvarium, however, is ossified, and fractured ribs cannot be seen; the pedicles of the vertebral bodies show some degree of ossification. Type II achondrogenesis is characterized by micromelia; lack of mineralization of all or many of the vertebral bodies, sacrum, and ischium; an enlarged calvarium with normal ossification; variable shortening of the ribs; and absence of fractures (Fig. 11-37).<sup>438</sup> Table 11-21 illustrates the characteristics of the different types of achondrogenesis.<sup>439,440</sup>

Prenatal diagnosis should be suspected on the basis of micromelia, lack of vertebral ossification, and a large head with various degrees of ossification of the calvarium.<sup>248,438-451</sup> Polyhydramnios and hydrops have been associated with achondrogenesis. An association between cystic hygromas and achondrogenesis has been reported in a fetus with normal karyotype.<sup>438,441,452</sup>

Achondrogenesis types IA and IB are inherited in an autosomal recessive pattern, whereas most cases of achondrogenesis type II and hypochondrogenesis have been sporadic (new autosomal dominant mutations). Some severe cases of type II achondrogenesis follow an autosomal recessive pattern.<sup>453</sup> The distinction between achondrogenesis type IB (which has a recurrence risk of 25%), and the more frequent autosomal dominant achondrogenesis type II, which has a lower recurrence risk, is important for genetic counseling. A couple at risk of having a child with achondrogenesis type IB may take advantage of the possibility of molecular prenatal diagnosis by CVS or amniocentesis, or preimplantation genetic diagnosis.<sup>324,454,455</sup>

Achondrogenesis type IA is caused by a homozygous or compound heterozygous mutation in the thyroid receptor-interacting protein 11 gene (*TRIP11*) on chromosome 14q32. *TRIP11* encodes the Golgi microtubule-associated protein (GMAP) 210, which is associated with development of the skeletal system.<sup>456</sup> Achondrogenesis type IB is caused by a homozygous or compound heterozygous mutation in the diastrophic dysplasia sulfate transporter (*DTDST*) gene (*SLC26A2*) located in chromosome 5q32.<sup>455,457</sup> This gene is required for synthesis of sulfated proteoglycans in cartilage. It is also affected in atelosteogenesis type II (AO2), diastrophic dysplasia (DTD), diastrophic dysplasia variant (DTDv), and recessively inherited multiple epiphyseal



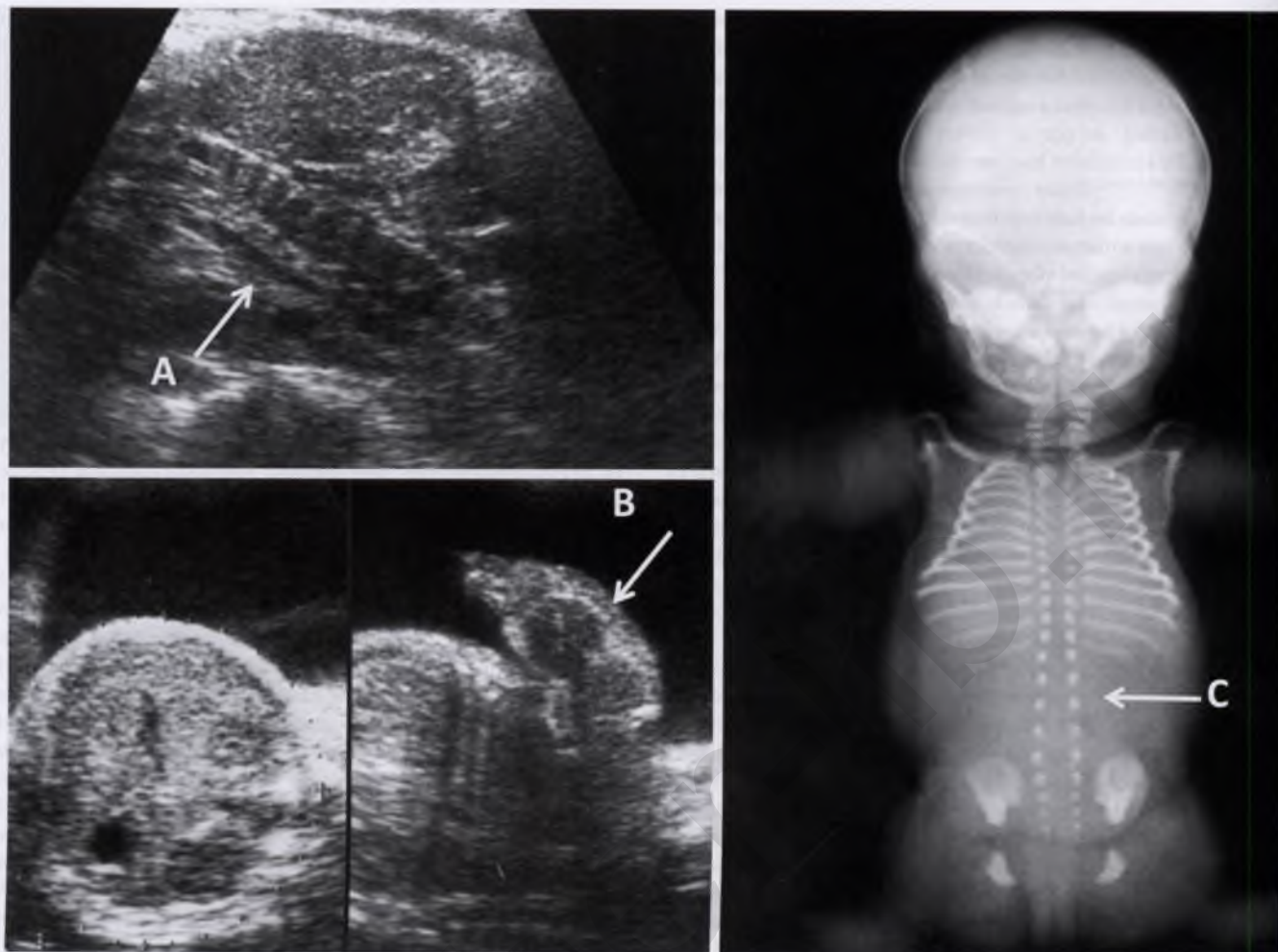


**FIG 11-37** Frontal and lateral views of a fetus with achondrogenesis type II. Hypomineralization of the spine ischial bones and vertebral bodies (A). The long bones are extremely short with metaphyseal flaring and cupping (B). The thorax is bell-shaped, with short and straight ribs and no fractures (C). (Courtesy of Theera Tongsong, MD, and Suchaya Luewan, MD.)

**TABLE 11-21 Radiologic Differences Between Achondrogenesis Type I (A-B), Type II, and Hypochondrogenesis**

	<b>Type IA (Houston-Harris)</b>	<b>Type IB (Fraccaro)</b>	<b>Type II (Langer-Saldino)</b>	<b>Hypochondrogenesis</b>
Skull	Membranous calvarium	All parts of ossified skull well seen	Normal ossification	Normal ossification
Long bones	Extremely shortened with metaphyseal cupping and spurs Rectangular bones	Arms and legs shorter than with type IA with minimal ossification; abundant metaphyseal spiking or spurring on lower leg bones Square or stellate bones	Short and bowed with metaphyseal flaring and cupping Mushroom stem bones	Less bowed and shortened with irregular or smooth metaphyses
Thorax	Short and barrel-shaped Short ribs with cupped metaphyses and multiple fractures	Same as in type IA with unfractured ribs	Short and barrel- or bell-shaped with short unfractured ribs	Near normal but shallow cage with short unfractured ribs
Spine	Vertebral bodies unossified, with partly ossified pedicles	Vertebral bodies minimally or not ossified, pedicles ossified	Variable pattern of ossified or unossified vertebral bodies and pedicles	Thoracic and upper lumbar vertebral bodies ossified but still platyspondylic Cervical and lower lumbar bodies unossified
Pelvis	Poorly formed and ossified, with iliac bones and ischial bones poorly ossified, pubic bones unossified	Iliac bones same aspect as in type IA Ischial and pubic bones unossified	Halberd-like iliac bones with unossified ischial and pubic bones	Near normally developed iliac bones with partial ossification of ischial bones and unossified pubic bones

From Spranger J: Pattern recognition in bone dysplasias. In Papadatos CJ, Bartsocas CS (eds): Endocrine Genetics and Genetics of Growth. New York, Alan R. Liss, 1985, p 315.

dysplasia (rMED).<sup>436,454,455,458</sup> Achondrogenesis type II is caused by a heterozygous mutation in the collagen, type II, alpha 1 gene (*COL2A1*) located in chromosome 12q13.<sup>459,460</sup> Prenatal diagnosis by molecular analysis of the *COL2A1* gene is available.

### Osteogenesis Imperfecta and Hypophosphatasia

Osteogenesis imperfecta (OI) and hypophosphatasia are discussed together because they are characterized by skeletal demineralization.

#### Osteogenesis Imperfecta

The term OI was introduced over a century ago to describe a newborn with extremely brittle bones (see Figs. 11-17, 11-19, and 11-20). At present, the term refers to a heterogeneous group of disorders caused (in most cases) by mutations in one or two structural genes for type I procollagen.<sup>461-467</sup> Extraskelatal malformations are variably associated with the disorder and include blue sclerae, dentinogenesis imperfecta, hyperlaxity of ligaments and skin, hearing impairment, and presence of wormian bones on skull radiographs.<sup>467</sup> Advanced paternal age is considered a risk factor for OI.<sup>468</sup> The prevalence of OI is 0.18 per 10,000 births.<sup>39,40</sup>

The most popular classification is that proposed by Silience and colleagues.<sup>469</sup> Further modifications of this classification included four additional types (V, VI, VII, and VIII)<sup>467,470</sup> [Table 11-22]. Clinically, the most relevant characteristic of OI is bone fragility, with severity increasing in the following order: (1) type I (less severe); (2) types IV, V, VI, and VII; (3) type VIII; (4) type III, and (5) type II (more severe).<sup>467</sup>

In OI type I (autosomal dominant), there are no prenatal deformities. After birth, patients are affected by bone fragility, blue sclerae (all ages), and hearing loss. Other findings include osteoporosis, a normal calvarium, and no dentinogenesis imperfecta. Fractures may range from none to multiple, especially vertebral fractures that can lead to mild scoliosis.<sup>467</sup> Mutations resulting in OI type I cause premature termination codons that lead to decreased production of type I procollagen.<sup>464</sup>

OI type II is an autosomal dominant condition.<sup>471</sup> It is also known as the perinatal variety and is uniformly lethal. Other features include almost no ossification of the skull; beaded ribs; shortened, crumpled long bones; and multiple fractures in utero (see Fig. 11-19). The thorax

is short, but not narrow. Type II is subclassified into three subtypes (IIA, IIB, and IIC) according to radiologic criteria: (1) subtype A has short, broad, crumpled long bones, angulation of tibiae, and continuously beaded ribs; (2) subtype B has short, broad, crumpled femora, angulation of tibiae, but normal ribs, or ribs with incomplete beading; and (3) subtype C has long, thin, inadequately modeled long bones with multiple fractures and thin beaded ribs.<sup>472</sup>

OI type III (autosomal recessive/rare) is a nonlethal variety characterized by blue sclerae and multiple fractures present at birth. The sclerae become white with time. The membranous skull is severely deossified, and the long bones are mildly shortened but with marked angulation. Type IIB and type III OI are difficult to distinguish and may represent different degrees of severity of the same disorder.<sup>473</sup>

In OI type IV (autosomal dominant), the long bones and sclerae are normal. There is mild to moderate osseous fragility, and 25% of the newborns have fractures. There is significant heterogeneity in disease expression, even within the same family.<sup>474</sup> From this heterogeneous group, Rauch and Glorieux<sup>467</sup> have identified three separate clinical entities based on distinct clinical and bone histologic features. These disorders have been classified as OI types V, VI, and VII.<sup>467,474-476</sup>

OI types V and VI have in common primary defects in endochondral bone ossification or mineralization. Type V is associated with a heterozygous mutation in *IFITM5* (interferon-induced transmembrane protein 5).<sup>477</sup> It is characterized by moderate to severe bone fragility, calcification of the interosseous membrane at the forearm that severely limits movements of the hand, radial head dislocation, and predisposition for developing hyperplastic calluses during fracture healing. The color of the sclerae is variable, and no teeth anomalies are seen.<sup>478</sup> The characterization of OI type VI is based on bone histologic findings showing an increased amount of osteoid and an abnormal pattern of lamellation. Individuals with type VI have mutations of the gene *SERPINF1*.<sup>479</sup> Type VI has also been associated with a defect in the gene encoding for pigment epithelium-derived factor (PEDF).<sup>475,480</sup> These patients are usually asymptomatic during the first year of life; however, afterward, they develop deformed bones, fractures, vertebral compression, and reduced bone mineral density.

OI type VII is a recessive disorder with bone fragility, rhizomelia, and coxa vara. This type has been described in a community of Native Americans in northern Quebec.<sup>467</sup>

TABLE 11-22 Expanded Classification of Osteogenesis Imperfecta

Type	Clinical Severity	Typical Features	Typically Associated Mutations
I	Mild nondeforming	Normal height or mild short stature; blue sclera; no dentinogenesis imperfecta	Premature stop codon in <i>COL1A1</i>
II	Perinatal lethal	Multiple rib and long bone fractures at birth; pronounced deformities; broad long bones; low density of skull bones on radiographs; dark sclerae	Glycine substitutions in <i>COL1A1</i> or <i>COL1A2</i>
III	Severely deforming	Very short stature; triangular face; severe scoliosis; grayish sclerae; dentinogenesis imperfecta	Glycine substitutions in <i>COL1A1</i> or <i>COL1A2</i>
IV	Moderately deforming	Moderately short stature; mild to moderate scoliosis; grayish or white sclerae; dentinogenesis imperfecta	Glycine substitutions in <i>COL1A1</i> or <i>COL1A2</i>
V	Moderately deforming	Mild to moderate short stature; dislocation of radial head; mineralized interosseous membrane; hyperplastic callus; white sclerae; no dentinogenesis imperfecta	<i>IFITM5</i>
VI	Moderately to severely deforming	Moderately short stature; scoliosis; accumulation of osteoid in bone tissue, fish-scale pattern of bone lamellation; white sclerae; no dentinogenesis imperfecta	<i>IFITM5</i> , <i>SERPINF1</i>
VII	Moderately deforming	Mild short stature; short humeri and femora; coxa vara; white sclerae; no dentinogenesis imperfecta	<i>CRTAP</i>
VIII	Moderately to severely deforming	Growth deficiency and extreme undermineralization of the skeleton, white sclerae	<i>LEPRE1</i>



OI type VIII is similar to OI types II and III in appearance and symptoms, except for white sclerae, and is characterized by severe growth deficiency and extreme undermineralization of the skeleton. It is caused by absence or severe deficiency of prolyl 3-hydroxylase activity due to mutations in the *LEPRE1* gene.<sup>481</sup>

Types I to IV and VII are caused by a collagen defect. OI type I is caused by a premature stop codon in *COL1A1*.<sup>463</sup> Types II, III, and IV typically result from mutations that lead to substitutions for glycine within the triple helical domain of the pro- $\alpha$  chain, disrupting the normal folding of the molecule and initiating the production of abnormal collagen.<sup>482,483</sup> Approximately 90% of patients with a clinical diagnosis of OI have a mutation in either the *COL1A1* or *COL1A2* gene, resulting in an abnormal molecular constitution of procollagen type I.<sup>467,483-485</sup>

The natural history of OI in utero is variable. Prenatal diagnosis of OI type II has been reported numerous times,<sup>108,486-507</sup> in some cases as early as 12 weeks of gestation by either 2D or 3D sonography.<sup>508-511</sup> It is noteworthy, however, that fractures and limb shortening may not be observed until the second or even the third trimester.<sup>512-514</sup> A typical sonographic finding associated with OI type II is the improved visualization of intracranial structures. Prenatal diagnosis of OI types I, III, and IV has also been reported using ultrasound, biochemistry, or molecular techniques.<sup>515-519</sup> The differential diagnosis should include other skeletal disorders such as hypophosphatasia, achondrogenesis, and campomelic dysplasia.

### Hypophosphatasia

This rare autosomal recessive disorder has an estimated incidence of 1 in 100,000 births.<sup>520</sup> It is characterized by demineralization of bones and low alkaline phosphatase (ALP) in serum and other tissues.<sup>521,522</sup> The severity of the disease is inversely related to serum levels of ALP activity.<sup>523</sup> ALP acts on pyrophosphate and other phosphate esters, leading to the accumulation of inorganic phosphates, altering the formation of bone crystals, and increasing bone fragility.<sup>524</sup>

Hypophosphatasia has been subdivided into six clinical types according to the age of onset: (1) perinatal (lethal); (2) infantile; (3) childhood; (4) adult; (5) odontohypophosphatasia; and (6) pseudohypophosphatasia.<sup>525</sup> The perinatal form is associated with stillbirth or early neonatal death due to intracranial hemorrhage or respiratory insufficiency secondary to poorly developed ribs and reduced thoracic volume.<sup>526,527</sup> The infantile variant may cause craniosynostosis and nephrocalcinosis from hypercalcemia and hypercalciuria during the first year of life and is often lethal. Premature loss of deciduous teeth and rickets are the cardinal clinical features of hypophosphatasia during childhood. In the adult form, recurrent metatarsal stress fractures and pseudofractures in long bones can be the hallmark. Odontohypophosphatasia refers to especially mildly affected individuals who have dental, but no skeletal, manifestations. The teeth are predisposed to cavities and may be lost prematurely. Pseudohypophosphatasia is an extremely rare variant characterized by typical clinical, radiologic, and biochemical findings of infantile hypophosphatasia with the exception that the total serum ALP concentrations are normal or increased.<sup>525</sup> The perinatal and infantile varieties have an autosomal recessive pattern of inheritance, and the childhood, adult, and odontohypophosphatasia forms can be transmitted as either an autosomal dominant or autosomal recessive trait.<sup>528</sup>

Fetuses with congenital hypophosphatasia have generalized demineralization of the skeleton with shortening and bowing of tubular bones with multiple fractures.<sup>529</sup> The generalized and marked demineralization of the cranial vault results in deformation of the skull after external compression. This sonographic sign is also present in OI type II and achondrogenesis type IA. Prenatal diagnosis of

this condition has been reported using ultrasound as early as 18 weeks of gestation.<sup>451,530-539</sup> Other sonographic findings include short and beaded ribs, markedly reduced mineralization of the spine (mainly in the thoracic region), and a small chest.<sup>529,540</sup> Identification of bone spurs projecting perpendicular from the limbs can be considered pathognomonic for lethal hypophosphatasia.<sup>540,541</sup> Bone spurs have been identified using 3D sonography as early as 18 weeks of gestation.<sup>541</sup>

ALP can be measured from tissue obtained by CVS<sup>521,542,543</sup> or amniotic fluid culture. However, ALP measurement in amniotic fluid is not a reliable method to make the diagnosis of hypophosphatasia because most of the ALP in amniotic fluid is of intestinal origin.<sup>544,545</sup> Involved isoenzymes in hypophosphatasia are bone and liver ALPs, and these isoenzymes contribute only 16% of the total amniotic fluid enzymatic activity.<sup>546</sup> Therefore, although prenatal diagnosis by DNA analysis is possible,<sup>547</sup> it requires sequencing the entire gene, which increases the complexity of the process.

Hypophosphatasia has been shown to be caused by mutations in the ALP liver gene (*ALPL*), also called the tissue nonspecific alkaline phosphatase gene (*TNSALP*), located on chromosome 1p36.1-p34.<sup>548-551</sup> A large spectrum of mutations is observed in the Caucasian population.<sup>549,552,553</sup> All reported gene mutations are continuously updated,<sup>554</sup> and about 80% of all mutations are missense.<sup>523</sup> Missense mutations in the gene lead to variable residual enzymatic activity and the extremely high phenotypic heterogeneity observed in hypophosphatasia.<sup>292,555</sup>

### Diastrophic Dysplasia

Diastrophic dysplasia is an autosomal recessive disease with low frequency in most populations, but highly prevalent in Finland, with a carrier frequency of 1% to 2% of a mutation in the dystrophy sulfate transporter (*DTDST*) gene or *SLC26A2*.<sup>457,556</sup> The condition is characterized by micromelia, clubfoot, hand deformities, multiple joint flexion contractures, and scoliosis.<sup>557</sup> The diagnosis may be difficult at birth because of phenotypic variability, and milder cases are often diagnosed at a later age.<sup>558</sup> The clinical features include rhizomelic-type micromelia, joint contractures, hand deformities with an abducted position of the thumbs (so-called "hitchhiker thumb" [Figs. 11-38 and 11-39]), spine disorders (e.g., scoliosis, kyphosis, spina bifida occulta, spinal stenosis, lumbar lordosis), and severe talipes equinovarus. The head is normal, but micrognathia and cleft palate may be seen.<sup>559</sup> Diastrophic dysplasia is a generalized disorder of cartilage leading to destruction of the cartilage matrix, formation of fibrous scar tissue and subsequent ossification. The latter process is responsible for the contractures. The mutations in the *DTDST* gene (*SLC26A2*), located on chromosome 5q32-q33.1,<sup>560,561</sup> are associated with reduced sulfate transport in chondrocytes, resulting in undersulfation of proteoglycans, leading to abnormal cartilage formation.<sup>454,561-563</sup> Five common *SLC26A2* mutations (R279W, IVS1 + 2T>C, delV340, R178X, and C653S) account for approximately 65% of disease alleles.<sup>561</sup> Sequence analysis of the coding region can detect mutations in greater than 90% of alleles in individuals with typical clinical, radiologic, and histologic features.<sup>561</sup>

The prenatal diagnosis of diastrophic dysplasia has been made in patients at risk based on severe shortening and bowing of all long bones.<sup>67,70,558,564-567</sup> Sepulveda and coworkers<sup>568</sup> suggested that 3D sonography can improve the visualization of limbs and face deformities. Prenatal diagnosis in at-risk pregnancies in which the familial mutations have been identified can be accomplished by DNA analysis of fetal cells obtained by CVS or amniocentesis.<sup>569</sup> Biochemical studies of fibroblasts and chondrocytes are available and may be useful for cases in which molecular genetic tests fail to identify *SLC26A2*



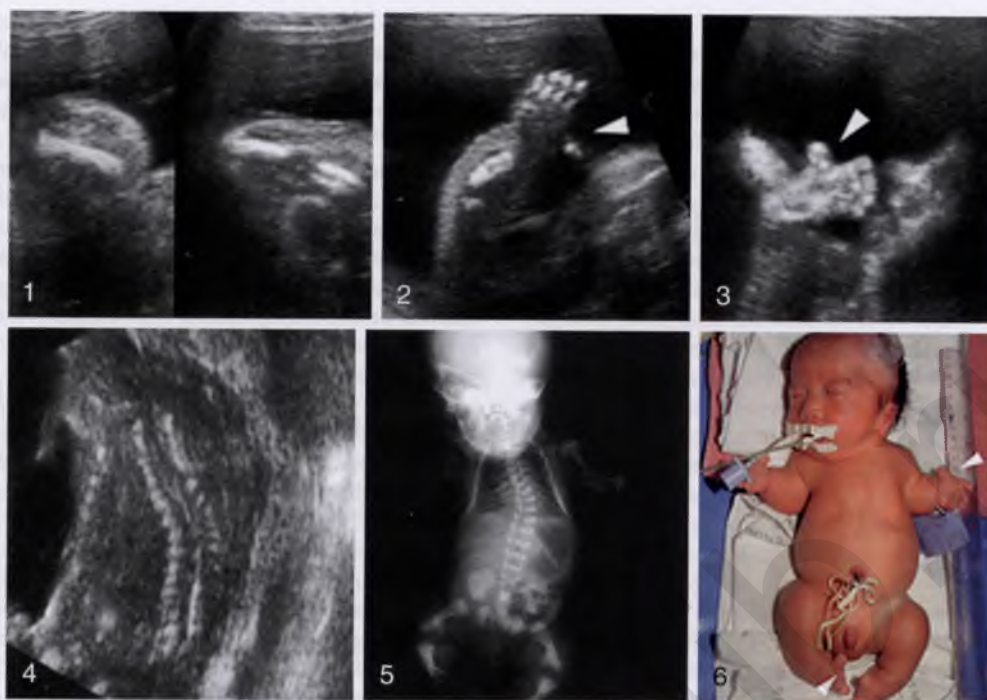


**FIG 11-38** Sonograms of a fetus with diastrophic dysplasia showing short long bones (1), hitchhiker thumb (2), separation of the great toe (3), and kyphoscoliosis (4). Kyphoscoliosis was corroborated after birth (5). Appearance of newborn (6). (Courtesy of Theera Tongsong, MD, and Suchaya Luewan, MD.)



**FIG 11-39** Hitchhiker thumb in diastrophic dysplasia.

mutations. This disorder has a wide spectrum, and some cases may not be diagnosable in utero.

Diastrophic dysplasia is not universally lethal. Intelligence and sexual development are unaffected. However, joint contractures and painful osteoarthroses are associated with severe physical handicaps

that require corrective orthopedic surgery.<sup>457</sup> An increased mortality rate in the neonatal period and infancy is due to upper airway obstruction secondary to tracheobronchomalacia and medullary compression caused by severe cervical kyphosis.<sup>457,570</sup>

The differential diagnoses include arthrogyposis multiplex congenita, atelosteogenesis type II, and pseudodiastrophic dysplasia. Pseudodiastrophic dysplasia has a similar presentation as diastrophic dysplasia<sup>571</sup> and is inherited in an autosomal recessive pattern.<sup>40</sup> Histologic examination is required for differential diagnosis, because the distinctive morphologic abnormalities of the growth plate noted in diastrophic dysplasia have not been observed in pseudodiastrophic dysplasia. Cetta and associates<sup>572</sup> demonstrated that a patient with pseudodiastrophic dysplasia had no defect in the DTDST gene and that both sulfate uptake by skin fibroblasts as well as sulfation of proteoglycans were normal.

### Kniest-like Disorders

The term Kniest-like disorders is used in reference to a group of conditions that share histologic and radiologic characteristics with Kniest syndrome but differ in terms of clinical presentation and inheritance.

### Kniest Syndrome

In 1952, Dr. Wilhelm Kniest<sup>573</sup> published the case of a 3.5-year-old girl with “skeletal changes showing a certain relationship to classical chondrodystrophy but differing in many of its manifestations.” His publication clarified the phenotypic differences between this condition and other forms of chondrodystrophies. Kniest syndrome is one of the type II collagenopathies, which are disorders that not only impair fetal growth but are also characterized by ocular and otolaryngologic abnormalities.<sup>574-577</sup> The pattern of inheritance is autosomal dominant,<sup>337</sup> and these diseases are usually caused by de novo mutations in the *COL2A1* gene.<sup>575,577,578</sup> Other type II collagenopathies include spondyloepiphyseal dysplasia and Stickler dysplasia type I.<sup>579</sup>



Phenotypic features of Kniest syndrome include rhizomelic shortening of the long bones with widened metaphyses and prominent joints. Spinal involvement is common and characterized by platyspondyly and coronal clefts. The thorax is broad and short. Other manifestations, which may be detected during prenatal life, include micrognathia and cleft palate. However, Kniest syndrome may be difficult to recognize at midgestation because long bone biometry does not become remarkably abnormal until the third trimester of pregnancy.<sup>580</sup> Prenatal diagnosis has been reported using 3D helical computed tomography showing abnormal shape in the femora, platyspondyly, and clefts in the lumbar vertebral body,<sup>580</sup> and by MRI demonstrating enlarged hyaline cartilage structures, abnormal T2 signal intensity, delayed ossification of the pubic and ischiatic bones, and platyspondyly.<sup>581</sup> The prognosis varies widely, ranging from long-term survival with short stature, kyphoscoliosis, and craniofacial anomalies to lethality in the neonatal period secondary to tracheomalacia and respiratory insufficiency.<sup>582</sup> Other long-term disabilities include feeding difficulties, hearing impairment, and blindness.

### Dyssegmental Dysplasia

Dyssegmental dysplasia is a disorder characterized by anarchic ossification of the vertebral bodies (anisospondyly), metaphyseal flaring, and severe bowing of the long bones.<sup>583,584</sup> Two distinct types have been recognized: the mild Rolland-Desbuquois, and the lethal

Silverman-Handmaker.<sup>583,585-587</sup> Encephaloceles are frequently present in the Silverman-Handmaker type,<sup>588</sup> and prenatal diagnosis has been established in patients at risk.<sup>585,589-591</sup> The Silverman-Handmaker type is caused by a functional null mutation in the gene encoding perlecan (*HSPG2*).<sup>592-594</sup> The Rolland-Desbuquois type has milder radiographic features resembling Kniest dysplasia. Although long-term survival is possible, a substantial proportion of affected individuals die during the first year of life.<sup>336,582</sup> Decreased levels of matrix metalloproteinase-2 and the tissue inhibitor of metalloproteinase-1 have been reported in cases of the Rolland-Desbuquois type of dyssegmental dysplasia.<sup>595</sup> The inheritance of both conditions is autosomal recessive.<sup>584</sup> Other disorders associated with vertebral disorganization include Jarcho-Levin syndrome and mesomelic dysplasia.

### Campomelic Dysplasia

First described by Maroteaux in 1971, campomelic dysplasia (CMD) is a rare lethal disorder.<sup>596</sup> The prevalence varies between 0.05 and 1.6/10,000.<sup>596,597</sup> The disorder is characterized by bowing of the long bones of the lower extremities, an enlarged and elongated skull with a peculiarly small face, hypoplastic scapulae, and several associated anomalies such as micrognathia, cleft palate, talipes equinovarus, congenital dislocation of the hip, macrocephaly, hydrocephalus, hydronephrosis, and congenital heart defects.<sup>596,597</sup> (Fig. 11-40). The most important and significant features are bowing of the femur and tibia;



**FIG 11-40** Fetus with campomelic dysplasia showing hypoplasia of the scapula (A) and bowing of the tibia and clubfoot with normal ossification (B). C, Postnatal appearance. (Courtesy of Theera Tongsong, MD, and Suchaya Luewan, MD.)

other tubular bones are normal in length (see Fig. 11-18A). The thorax is narrow, can be bell-shaped, and 11 pairs of ribs are usually present. Cervical vertebrae are hypoplastic and poorly ossified.<sup>598</sup> Campomelic dysplasia is considered a sporadic autosomal dominant condition.<sup>596</sup>

There are two short-bone varieties of campomelic dysplasia, representing distinct syndromes: (1) the normocephalic form, known as kyphomelic dysplasia, and (2) the craniostenotic type, which appears to be identical to Antley-Bixler syndrome. The antenatal diagnosis of campomelic dysplasia has been reported several times and the differential diagnosis includes OI, thanatophoric dysplasia, and hypophosphatasia.<sup>100,141,241,599-602</sup>

A unique aspect of campomelic dysplasia is that 75% of affected infants with a male karyotype present with sex reversal syndrome and have female or ambiguous genitalia.<sup>353,596,603</sup> The histologic features of the gonads vary, from gonads with testicular differentiation to dysgenetic gonads with primary follicles. Indeed, mutations in the *SOX9* gene, which is also a fundamental testis-differentiation gene common to all vertebrates,<sup>604</sup> have been reported in several patients with this disorder.<sup>353,603,605-608</sup> These mutations interfere with DNA binding by *SOX9* or truncate the carboxy-terminal transactivation domain, thereby impeding the ability of *SOX9* to activate target genes during organ development.<sup>607</sup> Molecular genetic testing of *SOX9* detects mutations or chromosome rearrangements in approximately 95% of affected individuals.<sup>596</sup> In approximately 5% of cases with campomelic dysplasia, routine karyotype analysis may identify de novo reciprocal translocations and a de novo interstitial deletion of 17q.<sup>609-614</sup> In rare cases, the translocation may be familial; thus, parental karyotypes should be analyzed when an abnormality is identified in the proband. Campomelic dysplasia is an autosomal dominant condition; however,

most cases are de novo mutations in *SOX9*; thus, parents are not typically affected. Recurrence in siblings has occurred, and somatic and germline mosaicism have been also reported. Campomelic dysplasia is frequently lethal in infancy, although some cases of survivors have been reported.<sup>599,615-619</sup> The cause of death is respiratory insufficiency due to tracheomalacia.

### Skeletal Dysplasias Characterized by a Hypoplastic Thorax

A dysplastic process involving the ribs and other bones of the thorax occurs in many skeletal dysplasias. A reduction in thoracic dimensions leads to restriction of lung growth and, consequently, pulmonary hypoplasia, which is the main cause of death in lethal skeletal dysplasias. Dysplasias in which thoracic hypoplasia is a cardinal feature include: asphyxiating thoracic dysplasia, Ellis-van Creveld syndrome, SRPS, and campomelic dysplasia. Table 11-23 illustrates criteria for the differential diagnoses of some of these conditions. Other disorders presenting with altered thoracic dimensions include thanatophoric dysplasia, atelosteogenesis, fibrochondrogenesis, achondrogenesis, and Jarcho-Levin syndrome (Fig. 11-41).<sup>620</sup>

### Asphyxiating Thoracic Dysplasia (Jeune Syndrome)

Jeune syndrome is a rare autosomal recessive condition, with an estimated prevalence of 0.14/10,000 births.<sup>621-624</sup> Asphyxiating thoracic dysplasia is characterized by a combination of a small thorax, varying degrees of brachymelia, polydactyly, pelvic abnormalities, and renal involvement.<sup>625,626</sup> Phenotypic expression is wide and includes lethal,<sup>627</sup> mild,<sup>624,628</sup> and latent<sup>622</sup> forms. In severe cases, thoracic narrowing is responsible for pulmonary hypoplasia, respiratory failure, and death in early infancy.<sup>629</sup> In the milder forms, the presence and degree of renal

TABLE 11-23 Skeletal Disorders With Thoracic Dysplasia and Polydactyly

	Asphyxiating Thoracic Dysplasia (Jeune)	Chondroectodermal Dysplasia (Ellis-van Creveld)	Polydactyly Syndrome Type I (Saldino-Noonan)	Polydactyly Syndrome Type II (Majewski)	Short-Rib Syndrome Type III (Naumoff)	Short-Rib Syndrome Type IV (Beemer-Langer)
<b>Relative Prevalence</b>	Common	Uncommon	Common	Extremely rare	Rare	Rare
<b>Clinical Features</b>						
Thoracic constriction	++	+	+++	+++	+++	+++
Polydactyly	+	++	++	++	++	++
Limb shortening	+	+	+++	+	++	++
Congenital heart disease	-	++	++	++	-	-
Other abnormalities	Renal disease	Ectodermal dysplasia	Genitourinary and gastrointestinal anomalies	Cleft lip and palate	Renal abnormality	Cleft lip and palate and genitourinary and gastrointestinal anomalies
<b>Radiographic Features</b>						
Tubular bone shortening	+	+	+++	++	+++	++
Distinctive features in femora	-	-	Pointed ends	-	Marginal spurs	-
Short, horizontal ribs	++	++	+++	+++	+++	+++
Vertical shortening of ilia and flat acetabula	++	++	++	-	++	-
Defective ossification of vertebral bodies	-	-	++	-	+	++
Shortening of skull base	-	-	-	-	+	-

+, not common; ++, common; +++, most common; -, absent

From Cremim BJ: Bone Dysplasias of Infancy. A Radiological Atlas. Berlin, Springer-Verlag, 1978, reproduced with permission.



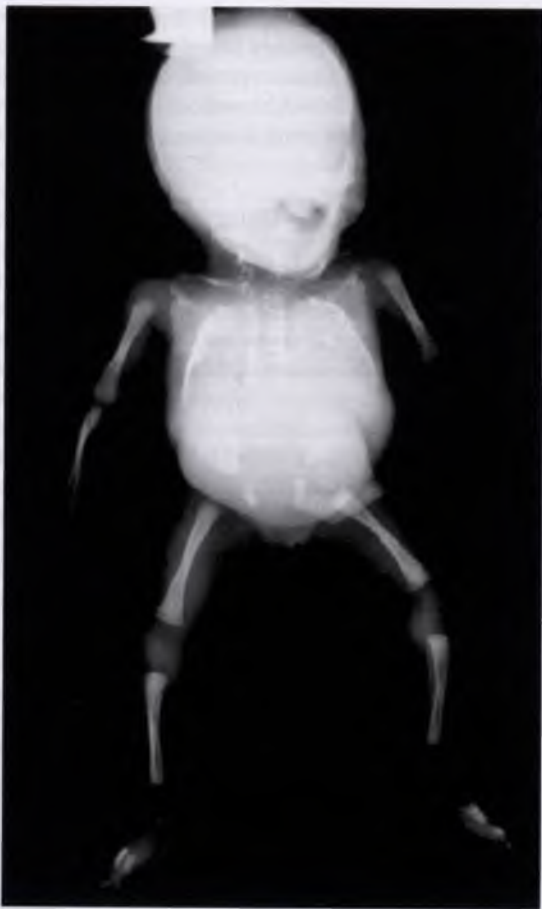


**FIG 11-41** Jarcho-Levin syndrome. There is dramatic spinal shortening with disorganization of the vertebral bodies, a characteristic chest deformity (crab-like appearance with posterior fusion and anterior flaring of the ribs), and unaffected long bones.

involvement<sup>630-641</sup> constitute the main prognostic factor.<sup>628,632,642</sup> Individuals surviving childhood are likely to have a clinical course complicated by respiratory insufficiency, recurrent pulmonary infections,<sup>641</sup> hepatic involvement,<sup>630,638,642-649</sup> and pancreatic involvement.<sup>650,651</sup> Ocular/retinal manifestations have been sporadically described in association with Jeune syndrome.<sup>638,652-654</sup>

**Skeletal Findings.** The thorax is described as narrow and bell-shaped, and the ribs are short, broad, and horizontally oriented.<sup>640,655</sup> Brachymelia (if present) is predominantly of the rhizomelic type.<sup>654,656,657</sup> Long bones may be bowed<sup>655,657</sup> and have visible proximal ossification centers at birth in two thirds of cases.<sup>657</sup> Postaxial polydactyly can be present, with both the upper and lower limbs variably affected.<sup>642,655,656,658,659</sup> Pelvic findings include small-squared iliac wings, a trident pelvis (shortened ilia with a downward hook of the greater sciatic notches), and horizontal acetabular roofs with spur-shaped projections.<sup>656,658</sup> A handlebar-like conformation of clavicles has been reported.<sup>657</sup> Cleft lip and palate can also occur.

**Renal Findings.** The degree of renal involvement is the main prognostic factor for individuals surviving the neonatal period.<sup>628,634,638,640,642</sup> Renal failure can occur during childhood<sup>632,635,638,640</sup> and may require renal transplantation.<sup>637,639,641</sup> Cystic or scleroatrophic changes, partly indistinguishable from those associated with juvenile nephronophthisis, are the two characteristic histologic patterns of renal involvement.<sup>634,640,660</sup> Cystinuria has also been described in patients with Jeune syndrome.<sup>636,661</sup>

**Hepatic Findings.** Liver involvement ranges from subclinical to biliary cirrhosis and progressive portal hypertension,<sup>647,649,662</sup> requiring transplantation during childhood.<sup>649</sup> Intralobular bile ducts loss, portal tract periphery bile duct proliferation, and fibrosis are the most frequent histologic findings.<sup>630,638,649</sup> Because liver involvement at early stages can be subclinical and manifest as early as in the neonatal period,<sup>644,646</sup> early diagnostic workup and close follow-up of hepatic function has been proposed.<sup>647</sup>

**Other Findings.** Ophthalmologic evaluation of long-term survivors has revealed a wide spectrum of retinal anomalies such as pigmentation, dystrophy, degeneration, and aplasia.<sup>652,653,663</sup> Visual loss and night blindness have been sporadically reported as the initial manifestation of mild forms of Jeune syndrome.<sup>652</sup> Other associated anomalies include Dandy-Walker malformation,<sup>646,664</sup> agenesis of the corpus callosum,<sup>665</sup> situs inversus,<sup>666</sup> neuroectodermal tumor in the soft tissue of the chest wall,<sup>637</sup> Hirschsprung disease,<sup>667</sup> and asplenia.<sup>666</sup>

**Prenatal Diagnosis.** The prenatal sonographic diagnosis of Jeune syndrome has been reported in the literature.<sup>625,642,655-657,659,668-674</sup> A positive family history contributes to second trimester recognition of recurrent forms,<sup>359,656,657,669</sup> while diagnosis in low-risk pregnancies is more challenging and has been reported in the third trimester of pregnancy.<sup>625</sup>

Although the locus for asphyxiating thoracic dystrophy maps to chromosome 15q13, mutation analysis of two candidate genes (*GREMLIN* and *FORMIN*) did not reveal pathogenic mutations.<sup>675</sup> In 2013 Baujau and colleagues<sup>676</sup> studied 39 families in which one of the members presented with asphyxiating thoracic dysplasia and reported in 23 families (59% of cases) with mutations in the *DYNC2H1* gene (dynein cytoplasmic 2 heavy chain 1). The authors concluded that *DYNC2H1* is a major gene responsible for asphyxiating thoracic dysplasia.

**Surgical Management for Respiratory Insufficiency.** Lateral thoracic expansion, a surgical procedure that attempts to enlarge the thoracic cage by separating ribs from their periosteum and plating them together with titanium struts, has been performed in a handful of patients with asphyxiating thoracic dysplasia, resulting in improvement in respiratory function or eliminating the need for external ventilators.

### Short Rib–Polydactyly Syndromes

SRPSs are a heterogeneous group of disorders inherited as autosomal recessive conditions.<sup>677</sup> Traditionally, four major types of short rib–polydactyly syndromes have been described: type I (Saldino–Noonan),<sup>678</sup> type II (Majewski),<sup>679,680</sup> type III (Verma–Naumoff),<sup>681</sup> and type IV (Beemer–Langer).<sup>682</sup> These conditions are classified within the family *short rib dysplasia with or without polydactyly*, which also includes asphyxiating thoracic dysplasia (Jeune syndrome) and chondroectodermal dysplasia (Ellis–van Creveld dysplasia). Because SRPSs I to IV are lethal in the newborn period (due to severe pulmonary hypoplasia and associated anomalies) and, conversely, Ellis–van Creveld and Jeune syndromes are not uniformly lethal, accurate prenatal diagnosis is important in order to provide adequate counseling.

SRPSs I to IV are characterized by short limbs/micromelic dwarfism, constricted thorax, usually polydactyly, and multiple anomalies of major organs (Fig. 11-42).<sup>683,684</sup> Scarano and coworkers<sup>685</sup> indicated that the absence of polydactyly does not exclude the diagnosis of this condition. In fact, although polydactyly is a constant feature in SRPS type II (Majewski) and is commonly found in types I and III (Saldino–Noonan and Verma–Naumoff),<sup>686</sup> patients with SRPS type IV (Beemer) seldom have polydactyly. Type IV is also characterized by ambiguous genitalia, anophthalmia, cleft lip and palate, pulmonary hypoplasia, renal dysplasia, and occasionally hydrops.<sup>687</sup>





**FIG 11-42** Short rib–polydactyly syndrome. There is severe shortening of all long bones, very short and horizontal ribs, and postaxial polydactyly in all four extremities. Note the angulation of the bones in the forearm.

**Differential Diagnosis.** SRPSs have been identified prenatally by 2D and 3D sonography.<sup>688-690</sup> Table 11-23 illustrates the differential diagnosis and features of the disorders characterized by polydactyly and a narrow thorax. The differential diagnosis is often challenging, especially before birth, because a high degree of overlap exists in clinical and radiologic features. Indeed, there is debate as to whether the various forms of SRPSs are related to different genes, to different mutations on the same gene, or to variability of expression of the same mutant gene.<sup>633,691</sup> Chen and associates<sup>692,693</sup> reported a mutation in the *NEK1* gene, which encodes NIMA (never in mitosis gene A-related kinase 1), in fetuses with type II and type III SRPS.

**Molecular Diagnosis.** Mutations have been identified in several intraflagellar transport (IFT) genes responsible for SRPS III, including *DYNC2H1*, *IFT80*, *WDR34*, *WDR35*, and *WDR60*.<sup>694-697</sup> IFT proteins are involved in chondrocyte maturation through bone morphogenetic protein signaling. Recently, Mei and colleagues<sup>698</sup> reported the identification of novel compound heterozygous mutations of *DYNC2H1* in a fetus with SRPS III, using targeted next-generation sequencing.

### Chondroectodermal Dysplasia (Ellis–van Creveld Syndrome)

Ellis–van Creveld syndrome is a rare autosomal recessive condition with an estimated birth prevalence of 1/60,000 in the general population and 5/1000 among the Amish community.<sup>699</sup> Ellis–van Creveld syndrome is defined by the tetrad of chondrodysplasia, ectodermal dysplasia, polydactyly, and congenital heart disease.<sup>700</sup> The combination and severity of each of these features are extremely variable, and,

as a consequence, the clinical course and prognosis range from death in the neonatal period due to cardiopulmonary complications to long-term survival.<sup>701,702</sup>

**Skeletal Findings.** In Ellis–van Creveld syndrome, the long bones most commonly present as mesomelic<sup>703</sup> or acromesomelic shortening.<sup>700</sup> The presence and severity of rib cage dysplasia are important factors in determining prognosis. A narrow thorax with short and horizontal ribs is frequently associated with pulmonary hypoplasia, early respiratory failure, and recurrent pulmonary infections.<sup>702,704</sup>

Postaxial polydactyly (Fig. 11-43) can involve the hands and feet in several combinations: only hands bilaterally,<sup>705</sup> both hands and both feet,<sup>706</sup> or both hands and one foot.<sup>707</sup> Clinodactyly<sup>701</sup> and syndactyly<sup>708</sup> have also been reported. Bowing of the long bones, genu valgum, and pelvic radiologic anomalies (including broad, squared, and vertically short ilia; trident configuration of the acetabula; spur-like projections at the acetabular roof) are additional phenotypic features.<sup>700,703</sup> The vertebrae and skull have a normal appearance.<sup>673</sup>

**Cardiac Defects.** Congenital heart disease occurs in up to 60% of affected individuals, and its presence and severity are strongly correlated to mortality rate.<sup>703,709</sup> The most common cardiac anomalies are those characterized by defects of endocardial cushion closure, such as atrial septal defects, ventricular septal defects, atrioventricular canal, and single atrium<sup>710-712</sup>; however, complex cardiac malformations have also been reported.<sup>713</sup>

**Ectodermal Dysplasia.** Clinical manifestations of ectodermal dysplasia are present in 70% of cases.<sup>714</sup> The most frequent are dystrophic changes of the fingernails, thin and sparse hair, and oral and dental abnormalities.<sup>715</sup> A short upper lip, multiple and hyperplastic frenula, and fusion of the upper lip to the gingival margin are common.<sup>716</sup> Dental anomalies include dysmorphic cone-shaped and microdontic teeth, taurodontism, delay in eruption or anodontia,<sup>717</sup> and natal and neonatal teeth.<sup>716</sup> Sporadic cases of micrognathia and mandibular malocclusion have also been reported.<sup>718</sup> This variety of oral manifestations requires multidisciplinary dental treatment, with special attention to the high incidence of cardiac defects in these patients.<sup>716</sup>

**Other Manifestations.** Central nervous system anomalies can occasionally occur in association with Ellis–van Creveld syndrome, including ventriculomegaly<sup>719</sup> and Dandy–Walker anomaly.<sup>720</sup> The kidneys are rarely involved, although there are sporadic reports of renal agenesis, congenital megaureter,<sup>721</sup> renal medullary dysplasia,<sup>722</sup> and nephronophthisis.<sup>723</sup> An association between Ellis–van Creveld syndrome and bile duct dysplasia requiring liver transplantation has been reported.<sup>722</sup> Thymic hypoplasia,<sup>724</sup> Hodgkin disease, nodular sclerosing at young age,<sup>725</sup> and retinal dystrophy<sup>726</sup> are other less common associations. Prenatal diagnosis by ultrasound has been reported during the second<sup>727,728</sup> and third trimesters,<sup>729</sup> as well as in the first trimester.<sup>730</sup>

**Differential Diagnosis.** Differentiating between Ellis–van Creveld and Jeune syndrome can be challenging because there is a great degree of overlap in the phenotypic features of these two conditions. McKusick–Kaufman syndrome shares with Ellis–van Creveld postaxial polydactyly and heart defects,<sup>731</sup> but differentiating characteristics include absence of chondrodysplasia and ectodermodydysplasia as well as hydrometrocolpos.<sup>732</sup> Weyers acrofacial dysostosis, an autosomal dominant condition, shares with Ellis–van Creveld syndrome the mild short stature and postaxial polydactyly, as well as dental and nail dystrophy, but thoracic dysplasia and congenital heart disease are not typical features in Weyers acrofacial dysostosis. Linkage and haplotype analysis have raised the possibility that Weyers acrofacial dysostosis is the heterozygous expression of a mutation that, in the homozygous form, causes Ellis–van Creveld syndrome.<sup>733</sup>





**FIG 11-43** **A**, Postaxial polydactyly in a fetus with Ellis-van Creveld syndrome. **B**, Sonographic image of the hand shown in **A**. Note the abnormal angulation of the extra digit on the ulnar side of the forearm (*arrow*).

**Genetics and Molecular Diagnosis.** Mutations on the two nonhomologous genes *EVC1* and *EVC2* located in the short arm of chromosome 4 (4p16) have been related to Ellis-van Creveld syndrome<sup>734,735</sup>; however, not all affected subjects present with these mutations.<sup>736</sup> Typing of microsatellite markers flanking the *EVC* locus has been reported for the first trimester diagnosis of Ellis-van Creveld syndrome in a family with a previously affected child.<sup>737</sup> There is debate about the possibility of partial manifestations in heterozygous carriers.<sup>738</sup>

### Skeletal Dysplasias With Predominant Membranous Bone Involvement

This group of skeletal dysplasias is characterized by disruption in the process of intramembranous bone ossification. They include cleidocranial dysplasia, Yunis-Varon syndrome, and isolated parietal foramina. Among these disorders, cleidocranial dysplasia is the one more often diagnosed prenatally.

#### Cleidocranial Dysplasia

Cleidocranial dysplasia is an autosomal dominant condition characterized by clavicular aplasia or hypoplasia, brachycephaly, midface hypoplasia, patent or delayed closure of fontanelles (Fig. 11-44), delayed eruption of permanent teeth, and relatively short stature with an estimated incidence of 0.5/100,000 live births.<sup>739</sup> Cleidocranial dysplasia is caused by mutations in the human osteoblast-specific transcription factor gene (*RUNX2*) located in chromosome 6p21.<sup>740,741</sup> The *RUNX2* gene is essential for osteoblast differentiation and affects membranous and endochondral bone formation. *RUNX2* induces and regulates the expression of genes involved in bone matrix formation and remodeling by modification of chromatin or interaction with co-regulatory proteins.<sup>742,743</sup>

The sonographic prenatal diagnosis of cleidocranial dysplasia has been reported as early as 13 weeks of gestation.<sup>744,745</sup> The most common finding is unilateral and bilateral hypoplastic and hypomineralized clavicles, although pseudoarthrosis (fracture) of the clavicle (Fig. 11-45) has also been reported.<sup>140</sup> Other features include hypomineralization/poor ossification of the spine, cranial bones, and pelvis; large fontanelles with wide sutures; obvious corpus callosum; brachycephaly; frontoparieto-occipital bossing; low nasal bridge; and long bones below the 5th percentile.<sup>744,746,747</sup> Molecular prenatal diagnosis for *RUNX2* mutations can be accomplished by CVS or amniocentesis, or through analysis of fetal tissue.<sup>748</sup>

The differential diagnosis includes disorders characterized by poor mineralization of the calvarium (such as hypophosphatasia) as well as disorders that have fracture/pseudoarthrosis of the clavicle (e.g., congenital pseudoarthrosis of the clavicle and Yunis-Varon syndrome). Congenital pseudoarthrosis defines a spontaneous fracture that progresses to nonunion, and it is associated with abnormal movement at the site. The mechanisms proposed for this clavicular defect include an abnormal elevation of the first rib and right subclavian artery, or a failure of fusion of the two ossification centers (congenital pseudoarthrosis).<sup>749</sup>

#### Yunis-Varon Syndrome

This severe autosomal recessive disorder is characterized by skeletal defects and severe neurologic involvement. It shares characteristics with cleidocranial dysplasia but additionally includes micrognathia, bilateral absence of the thumbs and of the distal phalanges of the fingers, as well as hypoplasia of the great toes.<sup>750</sup> The skeletal defects include wide fontanelles with calvarial dysostosis, and aplasia or hypoplasia of the clavicles. Pelvic bone dysplasia, absent sternal ossification

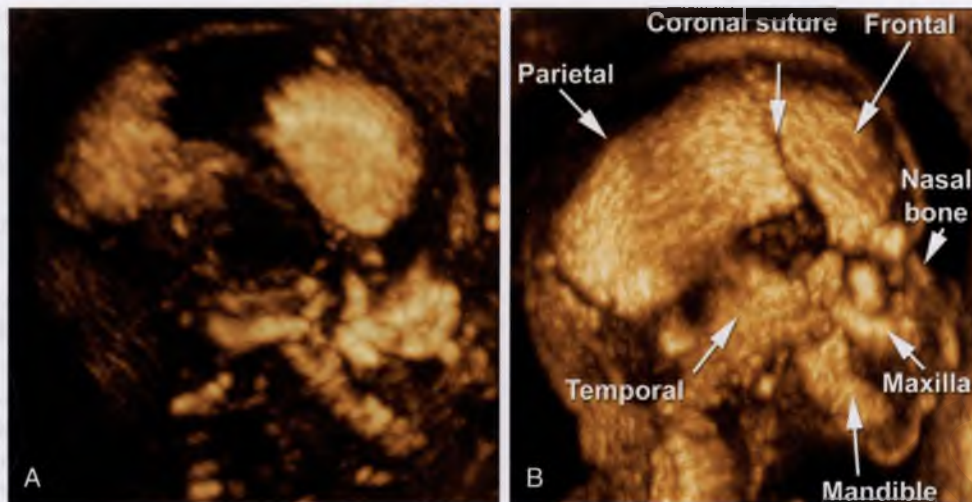


**FIG 11-44** **A**, Three-dimensional ultrasound image of the fetal skull at 18 $\frac{3}{4}$  weeks of gestation using the maximum intensity projection mode demonstrates widening of the coronal suture, absence of the squamous portion of the temporal bone, and absence of the nasal bones in a fetus with cleidocranial dysplasia. **B**, Labeled three-dimensional ultrasound image of a normal fetal skull at 18 $\frac{3}{4}$  weeks (control). (From Soto E, Richani K, Goncalves LF, et al: Three-dimensional ultrasound in the prenatal diagnosis of cleidocranial dysplasia associated with B-cell immunodeficiency. *Ultrasound Obstet Gynecol* 27:574, 2006.)

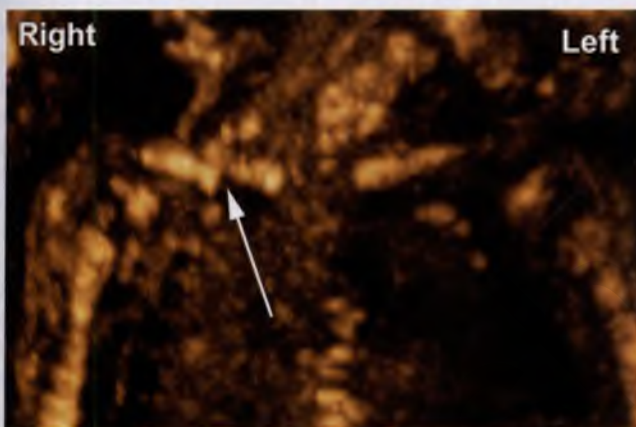


**FIG 11-45** Three-dimensional ultrasound-rendered image of the fetal shoulders using the maximum intensity projection mode in a fetus with cleidocranial dysplasia. The arrow points to a site of pseudoarthrosis (fracture) of the clavicle (From Soto E, Richani K, Goncalves LF, et al: Three-dimensional ultrasound in the prenatal diagnosis of cleidocranial dysplasia associated with B-cell immunodeficiency. *Ultrasound Obstet Gynecol* 27:574, 2006.)

centers, and bony fractures are also frequent. Neurologic findings include diffuse atrophy of the cerebellar vermis, corpus callosum, basal ganglia, and frontal lobes.<sup>751</sup> Prenatal ultrasound imaging can demonstrate limb abnormalities, polyhydramnios, and hydrops fetalis.<sup>752</sup> Recently, mutations of the *FIG4* gene on chromosome 6q21 (also known as *SAC3*), a 5'-phosphoinositide phosphatase which is essential for endosome/lysosome function, have been identified as a cause of Yunis-Varon syndrome.<sup>753,754</sup>

### Limb Deficiency or Congenital Amputations

Occasionally, the only identifiable anomaly is the absence of an extremity (limb deficiency) or a segment of an extremity (congenital amputation) (Table 11-24). These disorders differ from osteochondrodysplasias,

**TABLE 11-24** Congenital Amputations

Absent limbs only
Single absent limb
Multiple absent limbs
Absent limbs with rings
Congenital ring constriction syndrome
Absent limbs and face anomaly
Aglossia-adactylia syndromes
Moebius syndrome
Absent limbs with other anomalies
Ichthyosiform skin (CHILD syndrome)
Fibula agenesis-complex brachydactyly (Du Pan syndrome)
Splenogonadal fusion
Skull and scalp defects (Adams-Oliver syndrome)
Phocomelia
Thalidomide syndrome
Thrombocytopenia with absent radius (TAR) syndrome
Roberts pseudothalidomide-SC syndrome
Grebe syndrome
Proximal femoral focal deficiency
Femoral hypoplasia-unusual facies syndrome
Femur-fibula-ulna complex
Femur-tibia-radius complex
Split hand/split foot (SH/SF) syndromes
Only SH/SF
SH/SF and absent long bones
Ectrodactyly, ectodermal dysplasia, cleft lip and palate syndrome
Others
SF and triphalangeal thumb, autosomal dominant
SF, or SH and central polydactyly (see central polydactyly)
SH/SF and congenital nystagmus (Karsch-Neugebauer syndrome)
SH/SF and renal malformations (Acrorenal syndrome)
SF and mandibulofacial dysostosis (Fontaine syndrome), autosomal dominant

From Goldberg MD: *The Dysmorphic Child: An Orthopedic Perspective*. New York, Raven Press, 1987, reproduced with permission.



and the terms used to refer to limb reduction abnormalities include the following<sup>755</sup>:

- Amelia: absence of a limb or limbs
- Hemimelia: absence of a longitudinal segment of a limb (e.g., radial aplasia, radial hypoplasia)
- Phocomelia: hypoplasia of the limbs, with hands and feet attached to the shoulder and hips
- Acheira: absence of the hands
- Apodia: absence of a foot or feet
- Acheiropodia: absence of hands and feet

The overall incidence of congenital limb reduction deformities ranges from 0.49 to 3.5 per 10,000 births.<sup>756</sup> It has been estimated that approximately 50% of these limb reduction defects are simple transverse reduction deficiencies of one forearm or hand without associated anomalies.<sup>757</sup> The remainder consist of multiple reduction deficiencies, with an approximate 23% incidence of additional anomalies of the internal organs or craniofacial structures.<sup>758</sup>

Limb deficiencies can present alone or as part of a specific syndrome. An isolated limb deficiency of the upper extremity (e.g., distal segment of an arm) is generally an isolated anomaly. The hand often deviates in the direction of the absent bone (Fig. 11-46). In contrast, congenital amputation of the leg generally occurs within the context of a syndrome, as do bilateral amputations or reduction of all limbs.<sup>759</sup>

Isolated amputation of an extremity can be due to amniotic band syndrome, to a vascular accident, or to exposure to a teratogen. In most cases, the anomaly is sporadic, and the risk of recurrence is negligible. Sonographic findings related to these conditions have been reviewed in depth by Bromley and Benacerraf.<sup>760</sup>

In a large European study including 709,030 births from 20 malformation registries in 12 European countries, the overall prenatal detection rate for limb reduction defects was 35.6% (89/250), with a higher detection rate observed among cases with associated malformations (49.1% [55/112]).<sup>756</sup> The frequency of chromosomal anomalies in the presence of associated malformations was 14.3% (16/112), with eight cases of trisomy 18, two cases of trisomy 21, and one case each of triple X, Klinefelter syndrome, deletion 7q, isochromosome 12p, deletion 3q, and an unbalanced translocation: t(5;14)(p13;q13). Among fetuses with a normal karyotype and associated anomalies, 33.9% (38/112) have been related with the following syndromes: Poland, Hanhart B, Brachmann-De Lange, thrombocytopenia-radial aplasia (TAR), ulnar

mammary, Holt-Oram, Roberts, femur-fibula-ulna, Aarskog, Adams-Oliver, Otofaciodigital type 2, Robinow, and Carey-Fineman-Ziter; and with the following sequences or associations: amniotic bands, VATER/VACTER (vertebral, anal atresia, cardiac defects, tracheoesophageal fistula, renal anomalies) limb body wall complex, caudal regression, Fanconi anemia, and twin-reversed arterial perfusion sequence.

The following section reviews syndromes in which a limb amputation or deficiency is associated with other anomalies. We follow the classification proposed by Goldberg (see Table 11-24).<sup>758</sup>

## Syndromes With Absent Limbs and Facial Anomalies

### Aglossia-Adactylia Syndrome

This syndrome consists of transverse amputations of the limbs and malformations of the mouth, including micrognathia, vestigial tongue (hypoglossia), dental abnormalities, and ankylosis of the tongue to the hard palate, the floor of the mouth, or the lips (glossopalatine ankylosis). The spectrum of limb anomalies is variable, ranging from absent digits to severe deficiencies of all four extremities. Intelligence is generally normal; however, associations between aglossia-adactylia syndrome and mental retardation have been reported.<sup>761</sup> As the defects are usually asymmetric and distal, this condition has been attributed to a vascular accident or to an interruption of the blood supply to different regions of the embryo.<sup>762</sup> It includes the Moebius sequence, Hanhart syndrome, glossopalatine ankylosis syndrome, and limb deficiency-splenogonadal fusion syndrome.<sup>763-765</sup> There is confusion in the classification of these patients because of the associated anomalies and the frequency of overlapping features. Although some authors have considered Hanhart syndrome and glossopalatine ankylosis syndrome as distinct entities, the differential diagnosis is extremely difficult.

### Moebius Sequence

This condition consists of a number of facial anomalies attributed to paralysis of the sixth and seventh cranial nerves.<sup>766</sup> Limited jaw mobility and micrognathia are present, and ptosis is a common feature.<sup>767</sup> The Moebius sequence is generally sporadic, but autosomal dominant, autosomal recessive, and X-linked recessive forms have been described.<sup>768</sup> An association between prenatal exposure to misoprostol and Moebius sequence has been reported by several authors.<sup>769-771</sup> The associated limb reduction anomalies (25% of cases) are generally

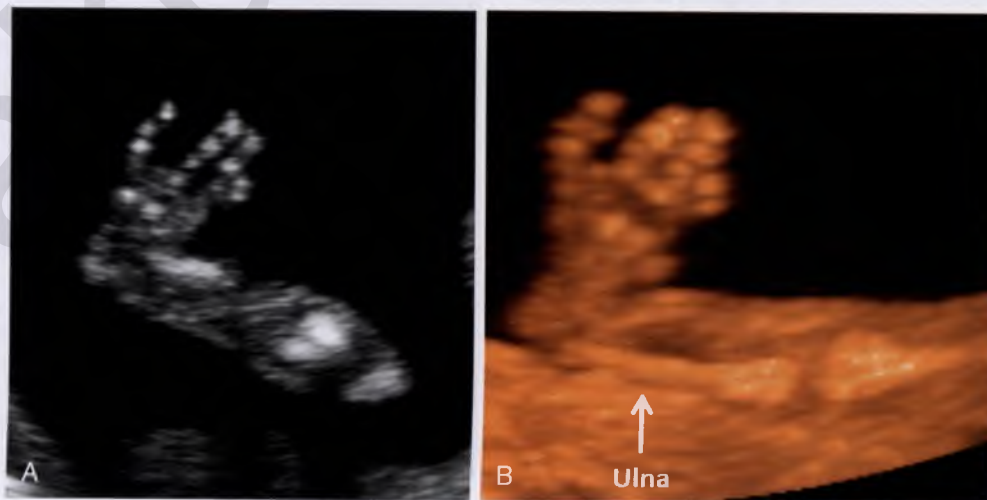


**FIG 11-46** Sonogram of a fetus with radial aplasia using two-dimensional ultrasound (**A**) and three-dimensional maximum intensity projection mode (**B**). The hand deviates toward the side of the absent bone (radius).



present in the upper extremities and range from transverse deficiencies to absent digits. The Moebius, Poland, and Klippel-Feil syndromes have been considered as subclavian artery supply disruption sequences, and it is hypothesized that interruption of the early embryonic blood supply to the subclavian and vertebral arteries and their branches may lead to these conditions.<sup>772,773</sup>

### Limb Reduction Defects Associated With Other Anomalies

#### Congenital Hemidysplasia With Ichthyosiform Erythroderma and Limb Defects Syndrome

Congenital hemidysplasia with ichthyosiform erythroderma and limb defects (CHILD) syndrome is characterized by strict demarcation of the lesions to one side of the midline.<sup>774,775</sup> The presence of unilateral defects of long bones is an important feature of the syndrome.<sup>776</sup> Limb deficiencies vary from hypoplasia of phalanges or metacarpals to complete absence of an extremity. The calvarium, scapulae, or ribs may also be involved. Zellweger syndrome, chondrodysplasia punctata, and warfarin embryopathy may present with similar findings. Visceral anomalies include congenital heart disease, unilateral hydronephrosis, hydroureter, and unilateral absence of the kidney, fallopian tube, ovaries, adrenal gland, and thyroid.<sup>776,777</sup> CHILD syndrome predominantly affects females (by a ratio of 19:1)<sup>774,778</sup> and is caused by mutations in the *NSDHL* gene (NAD[P]H steroid dehydrogenase-like protein), located at Xq28 and encoding a beta-hydroxysteroid dehydrogenase involved in the cholesterol biosynthetic pathway.<sup>778-781</sup> The detection of 4-carboxylsterols in affected skin flakes may be a marker for diagnosis.<sup>782-784</sup> Genetic testing from CVS is available. Raychaudhury and coworkers<sup>785</sup> reported an unusual phenotype of CHILD syndrome, most likely resulting from a novel X-chromosomal microdeletion encompassing the promoter region and exon 1 of the nicotinamide adenine dinucleotide phosphate steroid dehydrogenase-like protein gene, the neighboring gene *CETN2*, and more than 10 kb of noncoding DNA.<sup>785</sup> The prognosis is highly variable and mainly based upon skeletal or cardiac anomalies. Cases of minimal involvement can carry a risk of severe disease in the offspring.

#### Fibula Aplasia Complex Brachydactyly (Du Pan Syndrome)

Du Pan syndrome is an extremely rare condition characterized by bilateral agenesis of the fibula with abnormalities of the metacarpals and proximal phalanges. Limb reduction defects can involve the lower extremities.<sup>786,787</sup> An autosomal recessive pattern of inheritance has been suggested.<sup>786</sup> Faiyaz-Ul-Haque and associates<sup>788</sup> have examined genomic DNA from a family with Du Pan syndrome for mutations in the *CDMP1* gene. Affected individuals were homozygous for a missense mutation, T1322C, in the coding region of the *CDMP1* gene. Homozygous *CDMP1* mutations also cause Hunter-Thompson and Grebe syndromes.<sup>789</sup> Douzgou and colleagues<sup>790</sup> identified compound heterozygosity for two mutations (P436T and R378Q) in the growth differentiation factor 5 (*GDF5*) gene in mild forms of Du Pan type chondrodysplasia.

#### Splenogonadal Fusion Syndrome

Splenogonadal fusion (SGF) syndrome is characterized by limb reduction defects and splenogonadal fusion.<sup>791</sup> When associated with terminal limb defects, it is called splenogonadal fusion limb defect syndrome (SGLDS).<sup>792</sup> Mandibular hypoplasia, micrognathia, spina bifida, cleft palate, and complex cardiac malformations have been reported in cases of SGLDS. Most reported cases of SGF have occurred in boys.<sup>793</sup> Typically, there is a mass in the scrotum and an ectopic spleen can be identified during surgery. There is a variant in which the normally

located spleen is connected to the gonad by bands or cords of splenic tissue.<sup>794</sup> A review of 14 reported cases indicates that there is some overlap between this syndrome and the aglossia-adactylia syndrome or Hanhart syndrome.<sup>795</sup>

#### Adams-Oliver Syndrome

This group of disorders is characterized by the association of limb reduction defects and scalp anomalies (aplasia cutis and deficiency of bony calvarium).<sup>796-798</sup> Other organ systems may be involved, and there are reports of associated cardiovascular, brain, pulmonary, hepatic, and renal anomalies.<sup>799-801</sup> Congenital heart defects include ventricular septal defects, anomalies of the great arteries and their valves, and tetralogy of Fallot.<sup>802</sup>

Becker and coworkers<sup>803</sup> reported the sonographic prenatal diagnosis of two cases of Adams-Oliver syndrome in the same family, the first at 13 weeks, and the second at 23 weeks of gestation. Both cases showed limb reduction defects, and in the second case, the scalp defect was diagnosed as an echo-free space between the scalp and bone. Papadopolou and associates<sup>804</sup> reported bilateral dilatation of lateral ventricles and periventricular cysts at 26 weeks of gestation by MRI in a fetus that was diagnosed after birth with Adams-Oliver syndrome. At 14 months of age the child presented with aplasia cutis congenita, distal limb traverse defects, growth retardation, a wide atrial septal defect, periventricular leukomalacia, and enlarged ventricles.

Eye anomalies have been also described in an autosomal recessive variant of Adams-Oliver syndrome,<sup>805-807</sup> and retinal hypervascularization is a recurrent finding.<sup>802</sup> Facial features include hypertelorism, epicanthal folds, blue sclerae, and micrognathia.<sup>808,809</sup> Vandersteen and colleagues<sup>810</sup> described an autosomal dominant form of Adams-Oliver syndrome involving characteristic scalp defects and terminal limb defects, but without congenital heart defects or immune defects. An association between mutations in *DOCK6* and the autosomal recessive form of Adams-Oliver syndrome has been reported.<sup>811</sup>

#### Phocomelia

In phocomelia, the hands and feet are present, but the intervening arms and legs are absent. Hands and feet may be normal or abnormal.<sup>812</sup> Three syndromes should be considered in the differential diagnosis of phocomelia: Roberts syndrome, some varieties of the TAR syndrome, and Grebe syndrome. Phocomelia also can be caused by exposure to thalidomide.<sup>813</sup> Prenatal diagnosis of phocomelia has been reported using 3D sonography.<sup>814</sup>

#### Roberts Syndrome

This autosomal recessive disorder is characterized by the association of tetraphocomelia and craniofacial dysmorphism, including macrocephaly, hypertelorism, shallow orbits, facial clefting defects, and hypoplastic nasal alae. The upper extremities are generally more severely affected than the lower extremities. Polyhydramnios has been noted, and other anomalies associated with the syndrome include horseshoe kidney, ventriculomegaly, cephalocele, and spina bifida.<sup>815</sup> 3D sonography might provide clearer visualization of the short bones, contracted legs, and additional anomalies.<sup>816</sup> Roberts syndrome is caused by mutations in the *ESCO2* gene (establishment of cohesion 1 homolog 2) similar to SC phocomelia syndrome<sup>817</sup> (named after the first descriptions in two families with surnames beginning with S and C, respectively).<sup>818</sup> SC phocomelia is considered a mild variant of Roberts syndrome and is characterized by (1) nearly symmetric reductive malformations of the limbs, resembling phocomelia; (2) flexion contractures of various joints; (3) minor anomalies, including capillary hemangioma of the face, forehead, and ears, hypoplastic cartilages of the ears and nose, micrognathia, scanty silvery blond hair, and cloudy



corneas; (4) growth restriction; and (5) mental retardation. Mental retardation may be mild, and survival into adulthood is common.<sup>819</sup>

### Grebe Syndrome (Grebe-Quelce-Salgado Chondrodystrophy)

This autosomal recessive nonlethal acromesomelic skeletal disorder was first described in two girls by Grebe,<sup>820</sup> and subsequently in 47 Brazilian individuals by Quelce-Salgado.<sup>821</sup> Affected individuals have a normal head, neck, and trunk skeleton, relatively normal humeri and femora, short and deformed radii, ulnae, tibiae, and fibulae, and severe abnormalities of hands and feet. Polydactyly is frequent. Digits are very small and have been variously described as bulbous,<sup>822</sup> bud-like,<sup>823</sup> mere knobs, globular appendages,<sup>824</sup> or stubby toe-like fingers. The proximal and middle phalanges of the fingers and toes are invariably absent, and the distal phalanges are present. Radiographic and computed tomography imaging provide information on subtle clinical characteristics for obligate heterozygotes such as polydactyly, brachydactyly, hallux valgus, and metatarsus adductus.<sup>825-827</sup> The disease is caused by a missense mutation in the gene encoding cartilage-derived morphogenetic protein-1 (*CDMP1*).<sup>828,829</sup> Survivors have normal intelligence and develop normal secondary sexual characteristics. Prenatal diagnosis of Grebe syndrome has been made based on the phenotypic features of the disease (acromesomelic dysplasia and dysmorphic distal appendages with normal craniofacial and axial skeletal development)<sup>822,830,831</sup> and by the identification of mutations in the *CDMP1* gene.<sup>831</sup>

### Congenital Short Femur (Proximal Femoral Focal Deficiency)

Congenital short femur refers to a group of disorders encompassing a wide range of congenital developmental anomalies of the femur. The disorder has been classified into five groups, types I through V: (I) simple hypoplasia of the femur; (II) short femur with angulated shaft; (III) short femur with coxa vara (most common); (IV) absent or defective proximal femur;<sup>832,833</sup> and (V), absent or rudimentary femur (Fig. 11-47). One or both femora can be affected, although the right femur is more frequently involved. Anomalies of the upper limbs can also be present and do not exclude the diagnosis.<sup>39</sup> Proximal femoral focal deficiency syndrome may be associated with umbilical or inguinal hernias. If both femora are affected, it is important to examine the face carefully, because the disorder may be *bilateral femoral hypoplasia and unusual facies syndrome*,<sup>834,835</sup> which consists of bilateral femoral hypoplasia and facial anomalies, including short nose with broad tip, long philtrum, micrognathia, and cleft palate. Long bone abnormalities can

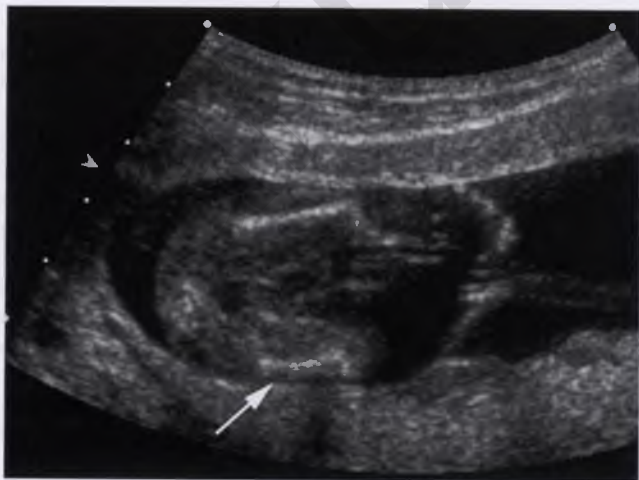


**FIG 11-47** Second trimester sonogram in a fetus with proximal femoral focal deficiency. The right femur (arrow) is significantly shorter than the left femur.

extend to other segments of the lower extremities (absent fibula) and to the upper extremities. Femoral focal deficiency syndrome is considered a sporadic condition, but a familial form has been described. Except in bilateral proximal focal deficiency, the diagnosis is usually suspected when there is unilateral short femur, in the absence of other anomalies.<sup>835-841</sup> If the defect is unilateral, it may correspond to the femur-fibula-ulnar or femur-tibia-radius complex. These two syndromes have different implications for genetic counseling: the former is nonfamilial, whereas the second has a strong genetic component.<sup>840</sup>

### Thrombocytopenia With Absent Radius Syndrome

TAR syndrome is discussed in detail later in the section titled "Radial Clubhand and Hematologic Disorders."

## SPLIT HAND AND FOOT DEFORMITIES

The term split-hand-and-foot syndrome is used to refer to a group of disorders characterized by splitting of the hand and foot into two parts. Other terms include lobster-claw deformity, ectrodactyly, and aborted fingers.<sup>841</sup> The conditions are classified into typical and atypical varieties.<sup>842</sup> The typical form consists of absence of both the finger and the metacarpal bone, resulting in a deep V-shaped central defect that clearly divides the hand into an ulnar and radial part. It occurs in 1 per 90,000 live births and has a familial tendency (usually inherited in an autosomal dominant fashion).<sup>843</sup> The atypical variety is characterized by a much wider cleft formed by a defect of the metacarpals and the middle fingers. As a consequence, the cleft is U-shaped and wide, with only thumb and small finger remaining. The atypical variety occurs in 1 per 150,000 live births.<sup>844</sup>

Although a complex system for the classification of these disorders (based on the distribution of remaining fingers) has been proposed,<sup>845</sup> it is not helpful in differential diagnosis and syndrome classification. Split-hand-and-foot deformities can occur as isolated anomalies or as part of a more complex syndrome. The syndromic types are more frequently encountered.

The split-hand-and-foot and absent-long-bones syndromes include two conditions in which there is split hand and aplasia of the tibia, or split foot with aplasia of the ulna. However, skeletal anomalies are not limited to these bones; the clavicle, femur, and fibula can also be affected. The pattern of inheritance of these disorders has not been clearly determined. Autosomal dominant, recessive, and X-linked recessive patterns have been proposed.<sup>846</sup>

## ECTRODACTYLY ECTODERMAL DYSPLASIA–CLEFT LIP/PALATE SYNDROME

Ectrodactyly ectodermal dysplasia–cleft lip/palate syndrome is an autosomal dominant condition characterized by the triad of ectrodactyly, ectodermal dysplasia, and facial clefting.<sup>847</sup> Ectrodactyly generally involves the four extremities, with more severe deformities of the hands.<sup>848,849</sup> The spectrum of ectodermal defects is wide and includes hypopigmentation, dry skin, sparse hair, and dental defects.<sup>850-852</sup> Tear duct anomalies and decreased lacrimal secretions lead to chronic keratoconjunctivitis and severe loss of visual acuity.<sup>853,854</sup> Cleft lip is generally bilateral, obstructive uropathy often occurs in this condition,<sup>855</sup> and intelligence is generally normal.<sup>856</sup> There is a marked phenotypic variability even within members of the same family showing isolated or combined limb defects as split hand/foot and mesoaxial polydactyly, cleft lip/palate, and ectodermal manifestations such as blond sparse hair with slow growth, thin nails, periorbital hyperpigmentation, dental caries, hypodontia, edentulism, and micturition and defecation



difficulties.<sup>857</sup> Mutations in the P63 gene account for most cases of ectodermal dysplasia–cleft lip/palate syndrome,<sup>858</sup> and some individuals are mosaic for the mutation.<sup>859</sup> Differential diagnosis includes a group of syndromes with associations of the split-hand-and-foot deformity with other anomalies such as Karsch-Neugebauer syndrome (split hand and foot with congenital nystagmus) and mandibulofacial dysostosis (Fontaine syndrome).<sup>856</sup>

## CLUBHAND DEFORMITIES

Clubhand deformities are classified into two main categories: radial and ulnar. Radial clubhand includes a wide spectrum of disorders that encompass absent thumb, thumb hypoplasia, thin first metacarpal, and absent radius (Table 11-25). Ulnar clubhand is much less frequent than radial clubhand and ranges from mild deviations of the hand on the ulnar side of the forearm to complete absence of the ulna. Although radial clubhand is frequently syndromic, ulnar clubhand is usually an isolated anomaly.<sup>860,861</sup> Table 11-26 displays conditions that present with ulnar ray defects.

Whenever a clubhand is identified, it is important to conduct a thorough examination of the fetus and newborn to delineate associated anomalies that may suggest a syndrome. Fetal blood sampling can be helpful, and fetal echocardiography is recommended. A complete blood cell count, including platelets, is important for the diagnosis of Fanconi pancytopenia, TAR syndrome, and Diamond-Blackfan anemia. A fetal karyotype is indicated because several chromosomal abnormalities (e.g., trisomy 18 and trisomy 21) have been reported in association with clubhand deformities. Congenital heart disease is an important feature of the Holt-Oram syndrome, the Lewis upper limb–cardiovascular syndrome, and in some cases of TAR syndrome.

### Radial Clubhand

An isolated radial clubhand is usually a sporadic nonsyndromic disorder<sup>861-863</sup>; however, other structural anomalies may be present (e.g., scoliosis and congenital heart disease). A detailed list of conditions associated with radial clubhands is presented in Table 11-25.

### Radial Clubhand and Hematologic Disorders

Radial clubhand may be part of the three syndromes characterized by hematologic abnormalities: Fanconi pancytopenia, TAR syndrome, and Diamond-Blackfan anemia.

### Fanconi Anemia

Fanconi anemia (pancytopenia) is an autosomal recessive disease characterized by the association of bone marrow failure (anemia, leukopenia, and thrombocytopenia) and skeletal anomalies, including radial clubhand with absent thumbs, radial hypoplasia, and a high frequency of chromosomal instability (demonstrated in amniotic fluid cells or fetal lymphocytes as a high rate of chromosomal breakage after incubation with diepoxybutane).<sup>864-866</sup> Approximately 25% of affected individuals do not have limb reduction anomalies. Other associated findings include microcephaly, congenital dislocation of the hips, scoliosis, cardiac, pulmonary, and gastrointestinal anomalies, and fetal growth restriction.<sup>867</sup>

It is assumed that the basic defect is related to the inability to repair DNA damage, in particular that of so-called DNA cross-links. At least 11 complementation groups (A, B, C, D1/BRCA2, D2, E, F, G, I, J, and L)<sup>868</sup> and 8 associated genes have been identified: *FANCA*, *FANCC*, *FANCD2*, *FANCE*, *FANCF*, *FANCG/XRCC9*, *FANCL*, and *FANCD1 (BRCA2)*.<sup>869-871</sup> About 200 mutations have been described, and among these, mutations in the gene for complementation group FA-A (*FANCA*) account for approximately 65% of the cases.<sup>868</sup> Prenatal

**TABLE 11-25 Radial Ray Defects: A Differential Diagnosis of Congenital Deficiency of the Radius and Radial Ray**

- I. Isolated: nonsyndromic
- II. Syndromes with blood dyscrasias
  - A. Fanconi anemia
  - B. Thrombocytopenia with absent radii syndrome
  - C. Diamond-Blackfan syndrome: congenital anemia, non-opposable triphalangeal thumb, scaphoid and distal radius hypoplasia, radioulnar synostosis, short stature with narrow shoulders, autosomal recessive
- III. Syndromes with congenital heart disease
  - A. Holt-Oram syndrome
  - B. Lewis upper limb–cardiovascular syndrome: more extensive arm malformations and more complex heart anomalies than with Holt-Oram but probably not a separate syndrome, autosomal dominant
- IV. Syndromes with craniofacial abnormalities
  - A. Nager acrofacial dysostosis
  - B. Radial clubhand and cleft lip and/or cleft palate: sporadic
  - C. Juberg-Hayward syndrome: cleft lip and palate, hypoplastic thumbs, short radius, radial head subluxation, autosomal recessive
  - D. Baller-Gerold syndrome: craniosynostosis, bilateral radial clubhand, absent/hypoplastic thumb, autosomal recessive
  - E. Rothmund-Thomson syndrome: prematurely aged skin changes, juvenile cataract, sparse gray hair, absent thumbs, radial clubhands, occasional knee dysplasia (see progeria syndromes)
  - F. Duane-radial dysplasia syndrome: abnormal ocular movements: inability to abduct and eyeball retraction with adduction, radius and radial ray hypoplasia, vertebral anomalies, renal malformation, autosomal dominant (see Klippel-Feil variants)
  - G. The IVIC syndrome (Instituto Venezolano de Investigaciones Científicas): radial ray deficiency, hypoplastic or absent thumbs and radial clubhands, impaired hearing, abnormal movements of extraocular muscles with strabismus, autosomal dominant
  - H. LARD syndrome (lacrimo-auriculo-radial-dental; Levy-Hollister): absent lacrimal structures, protuberant ears, thumb and radial hypoplasia, abnormal teeth, autosomal dominant
  - I. Radial defects with ear anomalies and cranial nerve dysfunction
  - J. Radial hypoplasia, triphalangeal thumb, hypospadias, diastema or maxillary central incisors, autosomal dominant
- V. Syndromes with congenital scoliosis
  - A. VATER/VACTER association
  - B. Goldenhar syndrome (oculo-auriculo-vertebral dysplasia)
  - C. Klippel-Feil syndrome
- VI. Radial aplasia and chromosome aberrations
- VII. Syndromes with mental retardation
  - A. Seckel's syndrome (bird-headed dwarfism): microcephaly, beaklike protrusion of nose, mental retardation, absent/hypoplastic thumbs, bilateral dislocated hips
- VIII. Thalidomide embryopathy (of historical interest, but some 60% had radial clubhand)

VACTER, vertebral, anal atresia, cardiac defects, tracheoesophageal fistula, renal anomalies.

From Goldberg MD: The Dysmorphic Child: An Orthopedic Perspective. New York, Raven Press, 1987, reproduced with permission.



**TABLE 11-26 Ulnar Ray Defects: A Differential Diagnosis of Congenital Deficiency of the Ulna and Ulnar Ray**

- I. Isolated: nonsyndromic absent ulna
- II. Ulna hypoplasia and skeletal deficiency elsewhere
  - A. Ulna aplasia with lobster claw deformity of hand and/or foot, autosomal dominant
  - B. Femur-fibula-ulna complex
- III. Syndromes with ulna deficiency
  - A. Cornelia de Lange syndrome
  - B. Miller syndrome (postaxial acrofacial dysostosis): absent ulna and ulnar rays and absent fourth and fifth toes; Treacher Collins mandibulofacial hypoplasia, autosomal recessive; distinguish from Nagai preaxial acrofacial dysostosis
  - C. Pallister ulnar-mammary syndrome (autosomal dominant): hypoplasia of ulna and ulnar rays; hypoplasia of the breast and absence of apocrine sweat glands
  - D. Pillay syndrome (ophthalmomandibulomelic dysplasia; autosomal dominant): absent distal third of ulna, absent olecranon, hypoplastic trochlea and proximal radius, fusion of interphalangeal joints in ulnar fingers, knee dysplasia; corneal opacities, fusion of temporomandibular joint
  - E. Weyers oligodactyly syndrome (sporadic): deficiency of ulna and ulnar rays, antecubital webbing, short sternum, malformed kidney and spleen, cleft lip and palate
  - F. Schnitzel syndrome (autosomal dominant): absent/hypoplastic fourth, fifth metacarpals and phalanges, hypogenitalism, anal atresia
  - G. Mesomelic dwarfism, Reinhardt-Pfeiffer type (ulno-fibula dysplasia; autosomal dominant): a generalized bone dysplasia but with a disproportionate hypoplasia of the ulna and fibula
  - H. Mesomelic dwarfism, Langer type: a generalized bone dysplasia, but with aplasia of the distal ulna and proximal fibula and hypoplasia of the mandible

From Goldberg MD: *The Dysmorphic Child: An Orthopedic Perspective*. New York, Raven Press, 1987, reproduced with permission.

diagnosis is possible with DNA testing for the most common mutations.<sup>872,873</sup> For those cases in which the affected gene and parental mutations are not known (e.g., in case of radial ray abnormalities identified by sonography but negative family history), chromosome breakage studies after exposure to DNA cross-linking agents,<sup>874</sup> single-cell parameter flow cytometry of amniotic fluid cell cultures, or bivariate flow cytometry of umbilical cord cell cultures have been used for prenatal diagnosis. The rationale for using flow cytometry to test for Fanconi anemia is the hypersensitivity of Fanconi anemia cells to alkylating agents leading to elevated G2-phase cell fractions in positive cases.<sup>875</sup>

### Thrombocytopenia With Absent Radius Syndrome

TAR syndrome is an autosomal recessive disorder characterized by thrombocytopenia (platelet count of less than 100,000/mm<sup>3</sup>) and bilateral absence of the radius.<sup>876,877</sup> Thumbs and metacarpals are always present. The ulna and humerus may be absent, and clubfoot deformities may occur. Congenital heart disease is present in 33% of cases (e.g., tetralogy of Fallot and septal defects). Delivery by cesarean section is recommended, because these fetuses are at risk for intracranial hemorrhage.<sup>878</sup> TAR has been successfully diagnosed in utero.<sup>879,880</sup> Houeijeh

and coworkers<sup>881</sup> reported that the presence of 1q21.1 deletion can be associated with TAR syndrome.

### Diamond-Blackfan Syndrome/Aase Syndrome

Diamond-Blackfan syndrome is an autosomal recessive condition characterized by congenital hypoplastic anemia and a radial clubhand with bilateral triphalangeal thumb and a hypoplastic distal radius.<sup>882,883</sup> Triphalangeal thumbs are a feature of several bone dysostoses and malformation syndromes. They may also occur in random association with other defects and as isolated, often familial, anomalies.<sup>884</sup> The differential diagnosis of this condition includes Holt-Oram syndrome, chromosomal abnormalities, and fetal hydantoin syndrome.<sup>885</sup> Diamond-Blackfan syndrome has been associated with mutations and deletions of different ribosomal protein (RP) genes.<sup>886-889</sup>

### Holt-Oram Syndrome

Holt-Oram syndrome is an autosomal dominant disorder characterized by congenital heart disease (mainly atrial and ventricular septal defects and interrupted aortic arch), aplasia or hypoplasia of the radius, and triphalangeal or absent thumbs.<sup>890-892</sup> Limb defects are often asymmetric, with the left side being more affected than the right side. There is no correlation between the severity of the limb defects and cardiac anomalies.<sup>893</sup> Indeed, some individuals have only a skeletal anomaly. Other findings include hypertelorism and chest wall and vertebral anomalies. This condition has been diagnosed prenatally by 2D and 3D sonography.<sup>891,894</sup> Holt-Oram syndrome is caused by mutations in the *TBX5* gene,<sup>895,896</sup> and preimplantation diagnosis of this condition has been reported.<sup>897</sup>

### Radial Clubhand and Scoliosis

Radial clubhand may also be associated with congenital scoliosis. Three conditions should be considered in the differential diagnosis: VATER/VACTER association, some cases of the Goldenhar syndrome, and Klippel-Feil syndrome.

### VATER/VACTER Association

VATER/VACTER association is the result of a defective mesodermal development during embryogenesis before the 35th day of gestation.<sup>898</sup> The typical findings are vertebral segmentation defects, anal atresia, tracheoesophageal fistula, cardiac defects, esophageal atresia, single umbilical artery, and radial and renal defects.<sup>899-901</sup> VATER/VACTER association occurs sporadically, although recurrence within a sibship may occur.<sup>902</sup> The features of VATER/VACTER can be detected by prenatal sonography.<sup>903,904</sup>

### Goldenhar Syndrome

Goldenhar syndrome is characterized by hemifacial microsomia, vertebral anomalies, and radial defects.<sup>905</sup> Alterations in the morphogenesis of the first and second brachial arches result in hypoplasia of the malar, maxillary, or mandibular region; microtia; and ocular and oropharyngeal anomalies.<sup>906,907</sup> Prenatal diagnosis based on ultrasound findings has been reported.<sup>907-909</sup>

### Klippel-Feil Syndrome

Klippel-Feil syndrome is characterized by fusion of two cervical vertebrae, resulting in short neck, low posterior hairline, and restricted mobility of the upper spine. Several associated anomalies may be present, including spina bifida, encephalocele, cleft palate, rib abnormalities, lung disorders, congenital heart disease, and limb anomalies.<sup>910,911</sup> Herman and associates<sup>911</sup> reported a large occipital encephalocele, abnormal kidney, and marked dilatation of the duodenum on fetal MRI at 31 weeks of gestation. Postnatally, segmentation



anomalies of the cervical spine and cervical vertebral body fusion are consistent findings in Klippel-Feil syndrome.

### Other Conditions Associated With Radial Clubhand

Radial clubhand has also been reported in association with chromosomal anomalies, including trisomy 18, and deletion of the long arm of chromosome 13.<sup>912,913</sup>

Some disorders present with craniofacial abnormalities and radial clubhand deformities. These conditions are sporadic and have common features that make a prenatal differential diagnosis difficult. The most common craniofacial anomaly is cleft lip and palate.<sup>914</sup>

### Ulnar Clubhand

Ulnar clubhand usually occurs as an isolated, nonsyndromic anomaly. Syndromes that may have ulnar clubhand as part of their phenotype (e.g., Poland syndrome) are described in Table 11-26.<sup>915</sup>

### Polydactyly

Polydactyly is the presence of an additional digit, and it is the most common hereditary limb deformation.<sup>916</sup> The extra digit may range from a fleshy nubbin to a complete digit with controlled flexion and extension (see Figs. 11-42 and 11-43). Polydactyly can be classified as postaxial (the most common form), preaxial, and central (see Table 11-16). Postaxial polydactyly occurs on the ulnar side of the hand and on the fibular side of the foot. Preaxial polydactyly is present on the radial side of the hand and on the tibial side of the foot (Fig. 11-48).<sup>917</sup> Central polydactyly consists of an extra digit that is usually hidden between the long and the ring finger.<sup>918</sup>

Evidence from mouse models suggests that several types of polydactyly involve the hedgehog pathway, either directly or indirectly.<sup>919,920</sup> Specifically, mutations in the downstream effector of Shh, *GLI3*, give rise to different polydactyly phenotypes, the mildest of which are postaxial polydactyly type I and preaxial polydactyly type IV (or Greig cephalopolysyndactyly).<sup>921</sup> Postaxial polydactyly type I is about 10 times more frequent in blacks than in whites and is characterized by a well-developed extra digit that articulates with the fifth digit. Greig cephalopolysyndactyly is characterized by pre- or postaxial polysyndactyly of variable degrees, frontal bossing, and hypertelorism.<sup>921</sup> The most severe malformations are found in Pallister-Hall syndrome, which is characterized by hypothalamic hamartomas, craniofacial anomalies, polysyndactyly, and anal defects.<sup>922</sup>

Although the majority of cases of polydactyly are isolated and inherited as an autosomal dominant trait, polydactyly is a phenotypic trait in 119 disorders (97 syndromic and 22 nonsyndromic), 39 of which are caused by mutations in known genes and 16 are mapped to a locus in the genome.<sup>923</sup> Central polydactyly is often bilateral and may be associated with other hand and foot malformations. Preaxial polydactyly, however, especially when a triphalangeal thumb is present, is more likely to be part of a syndrome.

### Arthrogryposis

The term arthrogryposis multiplex congenita (AMC) refers to multiple joint contractures present at birth with an intact skeleton.<sup>924</sup> The prevalence of AMC has been estimated as 8.5/100,000 births in a population-based study including 8.9 million births from 1980 to 2006.<sup>925</sup> The inheritance pattern of AMC was analyzed in 320 cases and reported as follows: 46% were part of syndromes with no recurrence risk; 23% were inherited with a mendelian pattern (autosomal dominant, autosomal recessive, or X-linked); and 3% were associated with chromosomal anomalies. In 28% of AMC cases no direct cause or associations were observed.<sup>926</sup> Table 11-27 shows a list of motor disorders that can lead to AMC.



**FIG 11-48** Femoral hypoplasia–unusual facies syndrome. Note the absence of the left femur and only a tiny portion of ossified bone on the right side. There is partial fusion of the tibia and fibula. Of interest is the presence of preaxial polydactyly (arrows) in both feet.

Normal fetal movement between 7 and 8 weeks of gestation onward is important for development of the joints; limitation of fetal joint motion leads to development of contractures and AMC.<sup>927</sup> This has been confirmed in experimental rats exposed to a viral myopathy induced by coxsackie A viruses.<sup>928,929</sup> AMC is therefore a syndrome, not a specific disorder, associated to neurologic, muscular, connective, and skeletal abnormalities and, with reduced intrauterine space, that can lead to impaired fetal motion and development of AMC.<sup>930-932</sup> In most cases of AMC, deformities are symmetric and involve the four limbs (Figs. 11-49 and 11-50). Anomalies of the lower extremities only, or bimelic involvement, can also occur. The severity of deformities increases distally with the hands and feet typically being the most affected.<sup>933</sup>

Cardinal findings on prenatal ultrasonography include absence of fetal movement on real-time examination and severe flexion deformities.<sup>924,934</sup> Zelop and Benacerraf<sup>935</sup> evaluated the clinical significance and outcome of postural deformities and contractures of the upper extremities detected prenatally. Among 52 fetuses with sonographically detected abnormalities of the upper extremities, 59% ( $n = 26$ ) had aneuploidies, mostly trisomy 18 (88% [23/26]). Fetuses with a normal karyotype presented with a variety of syndromic conditions, including three cases of AMC and one case each of Pierre-Robin sequence, Freeman-Sheldon syndrome, and Whistler syndrome, and bilateral syndactyly requiring multiple corrective surgical procedures. The



**TABLE 11-27 Disorders of the Developing Motor System Leading to Immobilization**

Disorders of the developing neuromuscular system
Loss of anterior horn cells
Radicular disease with collagen proliferation
Peripheral neuropathy with neurofibromatosis
Congenital myasthenia
Neonatal myasthenia (maternal myasthenia gravis)
Amyoplasia congenita
Congenital muscular dystrophy
Central core disease
Congenital myotonic dystrophy
Glycogen accumulation myopathy
Disorders of developing connective tissue or connective tissue disease
Muscular and articular connective tissue dystrophy
Articular defects by mesenchymal dysplasia
Increased collagen synthesis
Disorders of developing medulla or medullar disease
Congenital spinal epidural hemorrhage
Congenital duplication of the spinal canal
Disorders of brain development (e.g., porencephaly or brain disease)
Congenital encephalopathy



**FIG 11-49** Arthrogyposis multiplex congenita; note flexion of the upper limbs with hyperextension of the lower limbs.

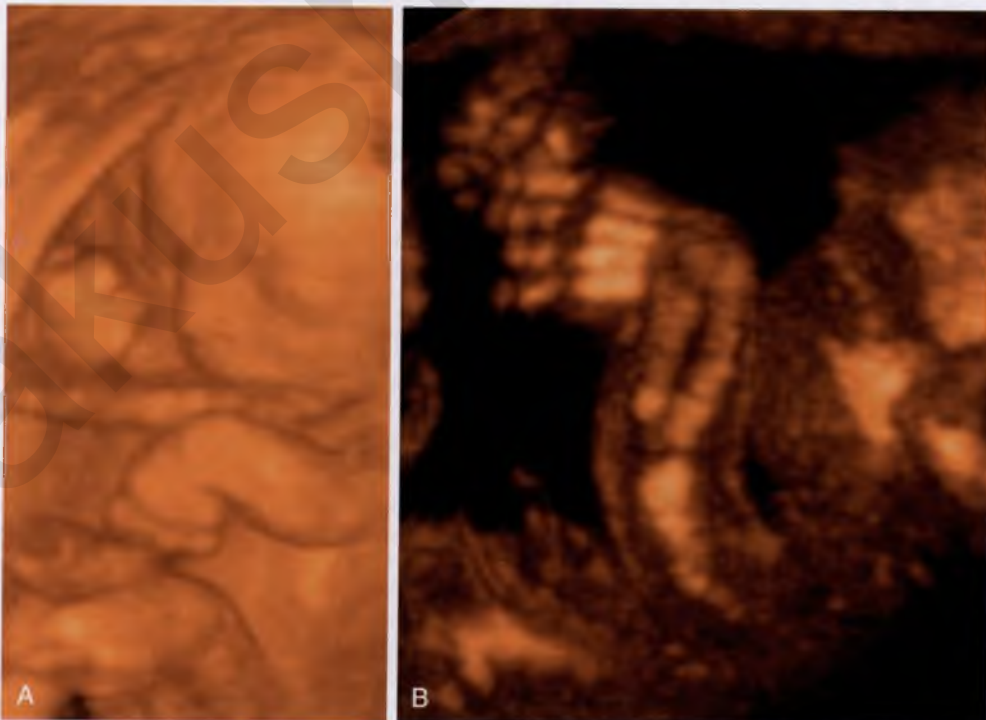


**FIG 11-50** Bilateral hyperflexed wrists in a fetus at 23 weeks of gestation with arthrogyposis multiplex congenita. Three-dimensional ultrasound rendered images using surface mode (A) and maximum intensity projection mode (B). (Courtesy of Maynor Garcia, MD.)

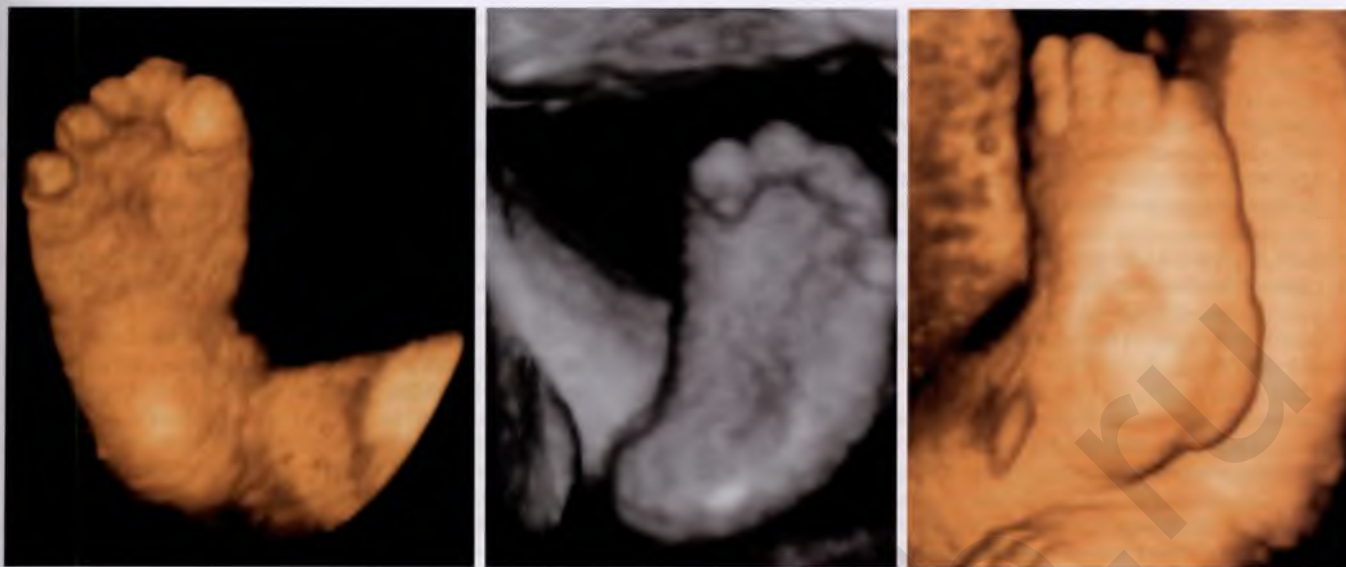


**FIG 11-51** Two-dimensional ultrasound images using surface mode in a fetus with unilateral clubfoot showing internal rotation and hyperflexed toes.

survival rate was 5% (8/52), and only one of the survivors was phenotypically normal after birth. Dicke and colleagues<sup>936</sup> reported that ultrasound can detect up to 81% of cases of AMC before 22 weeks of gestation.

The prognosis of AMC depends on the specific cause. Although some cases are uniformly lethal, others are associated with mild to moderate handicap. Polyhydramnios is considered a poor prognostic sign.<sup>937</sup>

## CLUBFOOT

Clubfoot (talipes equinovarus) is a congenital malformation of the bones of the ankle and foot, resulting in adduction of the forefoot, inversion of the heel, and plantar flexion of the forefoot and ankle.<sup>938</sup> There is subluxation of the talocalcaneonavicular joint. As a result of this malformation, the dorsal aspect of the foot is often rotated medially, which assumes a clublike appearance. The sonographic diagnosis is made when the metatarsals and phalanges of the foot are seen in the same plane as the tibia and fibula<sup>939,940</sup> (Fig. 11-51).

The severity of the clubfoot deformity varies from (1) a postural deformity often requiring no treatment; (2) an isolated clubfoot deformity needing casting and possible surgery, often with a favorable outcome; or (3) a complex clubfoot abnormality associated with other chromosomal, neuromuscular, or structural abnormalities. Clubfoot may also result from restriction of movement in utero, as in severe oligohydramnios.<sup>941</sup> The prevalence is often reported as 1 per 1000 live births with a 2:1 male-to-female predisposition.<sup>942</sup> Several series reported that an initially diagnosed isolated clubfoot is usually associated with other abnormalities, appearing either later in pregnancy or in the neonatal period.<sup>943</sup> The association of an isolated clubfoot with aneuploidy is controversial. Shipp and Benacerraf found that 5.9% of 87 fetuses with isolated clubfoot had an abnormal karyotype and concluded that amniocentesis is indicated after such diagnosis.<sup>944</sup> Other investigators do not suggest invasive testing for chromosomal anomalies in fetuses with isolated unilateral clubfoot.<sup>945</sup>

## ACKNOWLEDGMENTS

This work was supported by the Perinatology Research Branch, Division of Intramural Research, Eunice Kennedy Shriver National Institute of Child Health and Human Development, National Institutes of Health, and Department of Health and Human Services (NICHD/NIH/DHHS).

This chapter is an update of the chapter appearing in the previous edition: Gonçalves LF, Kusanovic JP, Gotsch F, et al: The fetal musculoskeletal system. In Callen PW (ed): *Ultrasonography in Obstetrics and Gynecology*, 5th ed. Philadelphia, Saunders Elsevier, 2008.

## REFERENCES

- Olsen BR, Reginato AM, Wang W: Bone development. *Annu Rev Cell Dev Biol* 16:191–220, 2000.
- Karsenty G: The complexities of skeletal biology. *Nature* 423:316–318, 2003.
- Moore KL, Persaud TVN: *The Developing Human: Clinically Oriented Embryology*, Philadelphia, 1998, Saunders.
- Mundlos S: Skeletal morphogenesis. *Methods Mol Biol* 136:61–70, 2000.
- Kornak U, Mundlos S: Genetic disorders of the skeleton: a developmental approach. *Am J Hum Genet* 73:447–474, 2003.
- Savarirayan R, Rimoin DL: Skeletal dysplasias. *Adv Pediatr* 51:209–229, 2004.
- Summerbell D, Lewis JH, Wolpert L: Positional information in chick limb morphogenesis. *Nature* 244:492–496, 1973.
- Brand-Saberi B, Krenn V, Christ B: The control of directed myogenic cell migration in the avian limb bud. *Anat Embryol (Berl)* 180(6):555–566, 1989.
- Koussoulakos S: Vertebrate limb development: from Harrison's limb disk transplantations to targeted disruption of Hox genes. *Anat Embryol (Berl)* 209:93–105, 2004.
- MacCabe JA, MacCabe AB, Abbott UK, McCarrey JR: Limb development in diplopodia: a polydactylous mutation in the chicken. *J Exp Zool* 191:383–394, 1975.



11. Li J, Kim KS, Park JS, et al: BMP-2 and CDMP-2: stimulation of chondrocyte production of proteoglycan. *J Orthop Sci* 8:829–835, 2003.
12. Knosp WM, Scott V, Bachinger HP, Stadler HS: HOXA13 regulates the expression of bone morphogenetic proteins 2 and 7 to control distal limb morphogenesis. *Development* 131:4581–4592, 2004.
13. Li Y, Qiu Q, Watson SS, et al: Uncoupling skeletal and connective tissue patterning: conditional deletion in cartilage progenitors reveals cell-autonomous requirements for *Lmx1b* in dorsal-ventral limb patterning. *Development* 137:1181–1188, 2010.
14. Gerhart J, Scheinfeld VL, Milito T, et al: Myo/Nog cell regulation of bone morphogenetic protein signaling in the blastocyst is essential for normal morphogenesis and striated muscle lineage specification. *Dev Biol* 359(1):12–25, 2011.
15. Clendenning DE, Mortlock DP: The BMP ligand *Gdf6* prevents differentiation of coronal suture mesenchyme in early cranial development. *PLoS ONE* 7:e36789, 2012.
16. Deckelbaum RA, Holmes G, Zhao Z, et al: Regulation of cranial morphogenesis and cell fate at the neural crest-mesoderm boundary by engrailed 1. *Development* 139:1346–1358, 2012.
17. Shukunami C, Ohta Y, Sakuda M, Hiraki Y: Sequential progression of the differentiation program by bone morphogenetic protein-2 in chondrogenic cell line ATDC5. *Exp Cell Res* 241(1):1–11, 1998.
18. Hall BK, Miyake T: All for one and one for all: condensations and the initiation of skeletal development. *Bioessays* 22(2):138–147, 2000.
19. Kronenberg HM: Developmental regulation of the growth plate. *Nature* 423:332–336, 2003.
20. Ducy P: *Cbfa1*: a molecular switch in osteoblast biology. *Dev Dyn* 219:461–471, 2000.
21. Nakashima K, Zhou X, Kunkel G, et al: The novel zinc finger-containing transcription factor *osterix* is required for osteoblast differentiation and bone formation. *Cell* 108:17–29, 2002.
22. Zelzer E, Olsen BR: The genetic basis for skeletal diseases. *Nature* 423:343–348, 2003.
23. Brighton CT: Morphology and biochemistry of the growth plate. *Rheum Dis Clin North Am* 13:75–100, 1987.
24. von Pfeil DJ, DeCamp CE: The epiphyseal plate: physiology, anatomy, and trauma. *Compend Contin Educ Vet* 31:E1–E12, 2009.
25. Conlon RA, Reaume AG, Rossant J: *Notch1* is required for the coordinate segmentation of somites. *Development* 121:1533–1545, 1995.
26. Palmeirim I, Henrique D, Ish-Horowicz D, Pourquie O: Avian hairy gene expression identifies a molecular clock linked to vertebrate segmentation and somitogenesis. *Cell* 91(5):639–648, 1997.
27. Ishikawa A, Kitajima S, Takahashi Y, et al: Mouse *Nkd1*, a Wnt antagonist, exhibits oscillatory gene expression in the PSM under the control of Notch signaling. *Mech Dev* 121:1443–1453, 2004.
28. Baker RE, Schnell S, Maini PK: A clock and wavefront mechanism for somite formation. *Dev Biol* 293:116–126, 2006.
29. Dubrulle J, McGrew MJ, Pourquie O: FGF signaling controls somite boundary position and regulates segmentation clock control of spatiotemporal Hox gene activation. *Cell* 106:219–232, 2001.
30. Fan CM, Tessier-Lavigne M: Patterning of mammalian somites by surface ectoderm and notochord: evidence for sclerotome induction by a hedgehog homolog. *Cell* 79(7):1175–1186, 1994.
31. Johnson RL, Laufer E, Riddle RD, Tabin C: Ectopic expression of Sonic hedgehog alters dorsal-ventral patterning of somites. *Cell* 79(7):1165–1173, 1994.
32. Maymon R, Ogle RF, Chitty LS: Smith-Lemli-Opitz syndrome presenting with persisting nuchal oedema and non-immune hydrops. *Prenat Diagn* 19:105–107, 1999.
33. Superti-Furga A, Bonafe L, Rimoin DL: Molecular-pathogenetic classification of genetic disorders of the skeleton. *Am J Med Genet* 106:282–293, 2001.
34. Superti-Furga A: Growing bone knowledge. *Clin Genet* 66:399–401, 2004.
35. Parilla BV, Leeth EA, Kambich MP, et al: Antenatal detection of skeletal dysplasias. *J Ultrasound Med* 22:255–261, 2003.
36. Bonafe L, Cormier-Daire V, Hall C, et al: Nosology and classification of genetic skeletal disorders: 2015 revision. *Am J Med Genet A* 167(12):2869–2892, 2015.
37. *International Skeletal Dysplasia Registry (ISDR)*: Available at <<http://ortho.ucla.edu>>.
38. Camera G, Mastroiacovo P: Birth prevalence of skeletal dysplasias in the Italian Multicentric Monitoring System for Birth Defects. *Prog Clin Biol Res* 104:441–449, 1982.
39. Connor JM, Connor RA, Sweet EM, et al: Lethal neonatal chondrodysplasias in the West of Scotland 1970–1983 with a description of a thanatophoric, dysplasia-like, autosomal recessive disorder, Glasgow variant. *Am J Med Genet* 22:243–253, 1985.
40. Rasmussen SA, Bieber FR, Benacerraf BR, et al: Epidemiology of osteochondrodysplasias: changing trends due to advances in prenatal diagnosis. *Am J Med Genet* 61:49–58, 1996.
41. Al-Gazali LI, Bakir M, Hamid Z, et al: Birth prevalence and pattern of osteochondrodysplasias in an inbred high risk population. *Birth Defects Res A Clin Mol Teratol* 67:125–132, 2003.
42. Gustavson KH, Jorulf H: Different types of osteochondrodysplasia in a consecutive series of newborns. *Helv Paediatr Acta* 30:307–314, 1975.
43. Orioli IM, Castilla EE, Barbosa-Neto JG: The birth prevalence rates for the skeletal dysplasias. *J Med Genet* 23:328–332, 1986.
44. Stoll C, Dott B, Roth MP, Alembik Y: Birth prevalence rates of skeletal dysplasias. *Clin Genet* 35:88–92, 1989.
45. Andersen PE, Jr: Prevalence of lethal osteochondrodysplasias in Denmark. *Am J Med Genet* 32:484–489, 1989.
46. Kallen B, Knudsen LB, Mutchinick O, et al: Monitoring dominant germ cell mutations using skeletal dysplasias registered in malformation registries: an international feasibility study. *Int J Epidemiol* 22:107–115, 1993.
47. Barbosa-Buck CO, Orioli IM, da Graca Dutra M, et al: Clinical epidemiology of skeletal dysplasias in South America. *Am J Med Genet A* 158A:1038–1045, 2012.
48. Donnelly DE, McConnell V, Paterson A, Morrison PJ: The prevalence of thanatophoric dysplasia and lethal osteogenesis imperfecta type II in Northern Ireland—a complete population study. *Ulster Med J* 79(3):114–118, 2010.
49. Stevenson DA, Carey JC, Byrne JL, et al: Analysis of skeletal dysplasias in the Utah population. *Am J Med Genet A* 158A:1046–1054, 2012.
50. McKusick VA, Scott CI: A nomenclature for constitutional disorders of bone. *J Bone Joint Surg Am* 53:978–986, 1971.
51. Erlebacher A, Filvaroff EH, Gitelman SE, Derynck R: Toward a molecular understanding of skeletal development. *Cell* 80:371–378, 1995.
52. Gilbert-Barnes E, Opitz JM: Abnormal bone development: histopathology of skeletal dysplasias. *Birth Defects Orig Artic Ser* 30(1):103–156, 1996.
53. Horton WA: Progress in human chondrodysplasias: molecular genetics. *Ann N Y Acad Sci* 785:150–159, 1996.
54. Horton WA: Molecular genetic basis of the human chondrodysplasias. *Endocrinol Metab Clin North Am* 25:683–697, 1996.
55. Reardon W: Skeletal dysplasias detectable by DNA analysis. *Prenat Diagn* 16:1221–1236, 1996.
56. *International Skeletal Dysplasia Society*: Available at <<http://www.isds.ch/>>.
57. Krakow D: Skeletal dysplasias. *Clin Perinatol* 42:301–319, 2015.
58. Krakow D, Lachman RS, Rimoin DL: Guidelines for the prenatal diagnosis of fetal skeletal dysplasias. *Genet Med* 11:127–133, 2009.
59. Rouse GA, Filly RA, Toomey F, Grube GL: Short-limb skeletal dysplasias: evaluation of the fetal spine with sonography and radiography. *Radiology* 174:177–180, 1990.
60. Chitayat D, Gruber H, Mullen BJ, et al: Hydrops-ectopic calcification-moth-eaten skeletal dysplasia (Greenberg dysplasia): prenatal diagnosis and further delineation of a rare genetic disorder. *Am J Med Genet* 47:272–277, 1993.
61. Seller MJ, Berry AC, Maxwell D, et al: A new lethal chondrodysplasia with platyspondyly, long bone angulation and mixed bone density. *Clin Dysmorphol* 5:213–215, 1996.



62. Brodie SG, Lachman RS, Jewell AF, et al: Lethal osteosclerotic osteochondrodysplasia with platyspondyly, metaphyseal widening, and intracellular inclusions in sibs. *Am J Med Genet* 80:423–428, 1998.
63. Wilcox WR, Lucas BC, Loebel B, et al: Pacman dysplasia: report of two affected sibs. *Am J Med Genet* 77:272–276, 1998.
64. Chen CP, Chern SR, Shih SL, et al: Kyphomelic dysplasia in two sib fetuses. *J Med Genet* 35:65–69, 1998.
65. Trajkovski Z, Vrcakovski M, Saveski J, Gucev ZS: Greenberg dysplasia (hydrops-ectopic calcification-moth-eaten skeletal dysplasia): prenatal ultrasound diagnosis and review of literature. *Am J Med Genet* 111:415–419, 2002.
66. Benacerraf BR, Greene MF, Barss VA: Prenatal sonographic diagnosis of congenital hemivertebra. *J Ultrasound Med* 5:257–259, 1986.
67. Gembruch U, Niesen M, Kehrberg H, Hansmann M: Diastrophic dysplasia: a specific prenatal diagnosis by ultrasound. *Prenat Diagn* 8:539–545, 1988.
68. Nores JA, Rotmensch S, Romero R, et al: Atelosteogenesis type II: sonographic and radiological correlation. *Prenat Diagn* 12:741–753, 1992.
69. Song TB, Kim YH, Oh ST, et al: Prenatal ultrasonographic diagnosis of congenital kyphosis due to anterior segmentation failure. *Asia Oceania J Obstet Gynaecol* 20(1):31–33, 1994.
70. Tongsong T, Wanapirak C, Sirichotiyakul S, Chanprapaph P: Prenatal sonographic diagnosis of diastrophic dwarfism. *J Clin Ultrasound* 30:103–105, 2002.
71. Ryu JK, Cho JY, Choi JS: Prenatal sonographic diagnosis of focal musculoskeletal anomalies. *Korean J Radiol* 4:243–251, 2003.
72. Weisz B, Achiron R, Schindler A, et al: Prenatal sonographic diagnosis of hemivertebra. *J Ultrasound Med* 23:853–857, 2004.
73. Kurtz AB, Wapner RJ: Ultrasonographic diagnosis of second-trimester skeletal dysplasias: a prospective analysis in a high-risk population. *J Ultrasound Med* 2:99–106, 1983.
74. Goncalves L, Jeanty P: Fetal biometry of skeletal dysplasias: a multicentric study. *J Ultrasound Med* 13:977–985, 1994.
75. Gabrielli S, Falco P, Pilu G, et al: Can transvaginal fetal biometry be considered a useful tool for early detection of skeletal dysplasias in high-risk patients? *Ultrasound Obstet Gynecol* 13:107–111, 1999.
76. De Biasio P, Prefumo F, Lantieri PB, Venturini PL: Reference values for fetal limb biometry at 10–14 weeks of gestation. *Ultrasound Obstet Gynecol* 19:588–591, 2002.
77. Coffin GS, Siris E, Wegienka LC: Mental retardation with osteocartilaginous anomalies. *Am J Dis Child* 112:205–213, 1966.
78. Baker ER, Goldberg MJ: Diagnosis and management of skeletal dysplasias. *Semin Perinatol* 18:283–291, 1994.
79. Azouz EM, Teebi AS, Eydoux P, et al: Bone dysplasias: an introduction. *Can Assoc Radiol J* 49:105–109, 1998.
80. Vanhoenacker FM, Van Hul W, Gielen J, De Schepper AM: Congenital skeletal abnormalities: an introduction to the radiological semiology. *Eur J Radiol* 40:168–183, 2001.
81. Unger S: A genetic approach to the diagnosis of skeletal dysplasia. *Clin Orthop Relat Res* 401:32–38, 2002.
82. Goncalves LF, Espinoza J, Mazor M, Romero R: Newer imaging modalities in the prenatal diagnosis of skeletal dysplasias. *Ultrasound Obstet Gynecol* 24:115–120, 2004.
83. Pretorius DH, Rumack CM, Manco-Johnson ML, et al: Specific skeletal dysplasias in utero: sonographic diagnosis. *Radiology* 159:237–242, 1986.
84. Donnenfeld AE, Mennuti MT: Second trimester diagnosis of fetal skeletal dysplasias. *Obstet Gynecol Surv* 42:199–217, 1987.
85. McGuire J, Manning F, Lange I, et al: Antenatal diagnosis of skeletal dysplasia using ultrasound. *Birth Defects Orig Artic Ser* 23:367–384, 1987.
86. Escobar LF, Bixler D, Weaver DD, et al: Bone dysplasias: the prenatal diagnostic challenge. *Am J Med Genet* 36:488–494, 1990.
87. Kurtz AB, Needleman L, Wapner RJ, et al: Usefulness of a short femur in the in utero detection of skeletal dysplasias. *Radiology* 177:197–200, 1990.
88. Spirt BA, Oliphant M, Gottlieb RH, Gordon LP: Prenatal sonographic evaluation of short-limbed dwarfism: an algorithmic approach. *Radiographics* 10:217–236, 1990.
89. Sharony R, Browne C, Lachman RS, Rimoin DL: Prenatal diagnosis of the skeletal dysplasias. *Am J Obstet Gynecol* 169:668–675, 1993.
90. Bowerman RA: Anomalies of the fetal skeleton: sonographic findings. *AJR Am J Roentgenol* 164:973–979, 1993.
91. MacDonald MR, Welsh MP: Perinatal approach to skeletal dysplasia. *Nebr Med J* 80(11):334–335, 1995.
92. Carvalho L, Soares M, Feijoo MJ, et al: A collaborative approach to the diagnosis of a lethal short limb skeletal dysplasia. *Genet Couns* 8:139–143, 1997.
93. Gaffney G, Manning N, Boyd PA, et al: Prenatal sonographic diagnosis of skeletal dysplasias—a report of the diagnostic and prognostic accuracy in 35 cases. *Prenat Diagn* 18:357–362, 1998.
94. Ermito S, Dinatale A, Carrara S, et al: Prenatal diagnosis of limb abnormalities: role of fetal ultrasonography. *J Prenat Med* 3:18–22, 2009.
95. Weldner BM, Persson PH, Ivarsson SA: Prenatal diagnosis of dwarfism by ultrasound screening. *Arch Dis Child* 60:1070–1072, 1985.
96. Khalil A, Pakr E, Chitty LS: Early prenatal diagnosis of skeletal anomalies. *Prenat Diagn* 31:115–124, 2011.
97. Witters I, Moerman P, Fryns JP: Skeletal dysplasias: 38 prenatal cases. *Genet Couns* 19:267–275, 2008.
98. Yeh P, Saeed F, Paramasivam G, et al: Accuracy of prenatal diagnosis and prediction of lethality for fetal skeletal dysplasias. *Prenat Diagn* 31:515–518, 2011.
99. Gordienko I, Grechanina E, Sopko NI, et al: Prenatal diagnosis of osteochondrodysplasias in high risk pregnancy. *Am J Med Genet* 63:90–97, 1996.
100. Tretter AE, Saunders RC, Meyers CM, et al: Antenatal diagnosis of lethal skeletal dysplasias. *Am J Med Genet* 75:518–522, 1998.
101. Hersh JH, Angle B, Pietrantonio M, et al: Predictive value of fetal ultrasonography in the diagnosis of a lethal skeletal dysplasia. *South Med J* 91:1137–1142, 1998.
102. Doray B, Favre R, Viville B, et al: Prenatal sonographic diagnosis of skeletal dysplasias. A report of 47 cases. *Ann Genet* 43:163–169, 2000.
103. Schramm T, Gloning KP, Minderer S, et al: Prenatal sonographic diagnosis of skeletal dysplasias. *Ultrasound Obstet Gynecol* 34:160–170, 2009.
104. Nelson DB, Dashe JS, McIntire DD, Twickler DM: Fetal skeletal dysplasias: sonographic indices associated with adverse outcomes. *J Ultrasound Med* 33:1085–1090, 2014.
105. Merz E, Bahlmann F, Weber G, Macchiella D: Three-dimensional ultrasonography in prenatal diagnosis. *J Perinat Med* 23:213–222, 1995.
106. Steiner H, Spitzer D, Weiss-Wichert PH, et al: Three-dimensional ultrasound in prenatal diagnosis of skeletal dysplasia. *Prenat Diagn* 15:373–377, 1995.
107. Ploekinger-Ulm B, Ulm MR, Lee A, et al: Antenatal depiction of fetal digits with three-dimensional ultrasonography. *Am J Obstet Gynecol* 175:571–574, 1996.
108. Garjian KV, Pretorius DH, Budorick NE, et al: Fetal skeletal dysplasia: three-dimensional US—initial experience. *Radiology* 214:717–723, 2000.
109. Achiron R, Gindes L, Zalel Y, et al: Three- and four-dimensional ultrasound: new methods for evaluating fetal thoracic anomalies. *Ultrasound Obstet Gynecol* 32:36–43, 2008.
110. Chen CP, Chern SR, Shih JC, et al: Prenatal diagnosis and genetic analysis of type I and type II thanatophoric dysplasia. *Prenat Diagn* 21:89–95, 2001.
111. Machado LE, Bonilla-Musoles F, Raga F, et al: Thanatophoric dysplasia: ultrasound diagnosis. *Ultrasound Q* 17:235–243, 2001.
112. Moeglin D, Benoit B: Three-dimensional sonographic aspects in the antenatal diagnosis of achondroplasia. *Ultrasound Obstet Gynecol* 18:81–83, 2001.
113. Kos M, Hafner T, Funduk-Kurjak B, et al: Limb deformities and three-dimensional ultrasound. *J Perinat Med* 30:40–47, 2002.
114. Viora E, Sciarone A, Bastonero S, et al: Three-dimensional ultrasound evaluation of short-rib polydactyly syndrome type II in the second trimester: a case report. *Ultrasound Obstet Gynecol* 19:88–91, 2002.
115. Clementschitsch G, Hasenohrl G, Steiner H, Staudach A: Early diagnosis of a fetal skeletal dysplasia associated with increased nuchal



- translucency with 2D and 3D ultrasound. *Ultraschall Med* 24(5):349–352, 2003.
116. Krakow D, Williams J, 3rd, Poehl M, et al: Use of three-dimensional ultrasound imaging in the diagnosis of prenatal-onset skeletal dysplasias. *Ultrasound Obstet Gynecol* 21:467–472, 2003.
  117. Benoit B: The value of three-dimensional ultrasonography in the screening of the fetal skeleton. *Childs Nerv Syst* 19:403–409, 2003.
  118. Seow KM, Huang LW, Lin YH, et al: Prenatal three-dimensional ultrasound diagnosis of a camptomelic dysplasia. *Arch Gynecol Obstet* 269:142–144, 2004.
  119. Lin IW, Chueh HY, Chang SD, Cheng PJ: The application of three-dimensional ultrasonography in the prenatal diagnosis of arthrogyposis. *Taiwan J Obstet Gynecol* 47:75–78, 2008.
  120. Shih JC, Peng SS, Hsiao SM, et al: Three-dimensional ultrasound diagnosis of Larsen syndrome with further characterization of neurological sequelae. *Ultrasound Obstet Gynecol* 24:89–93, 2004.
  121. Ruano R, Molho M, Roume J, Ville Y: Prenatal diagnosis of fetal skeletal dysplasias by combining two-dimensional and three-dimensional ultrasound and intrauterine three-dimensional helical computer tomography. *Ultrasound Obstet Gynecol* 24:134–140, 2004.
  122. Bonnefoy O, Delbosc JM, Maugey-Laulom B, et al: Prenatal diagnosis of hypochondroplasia: three-dimensional multislice computed tomography findings and molecular analysis. *Fetal Diagn Ther* 21:18–21, 2006.
  123. Cassart M, Massez A, Cos T, et al: Contribution of three-dimensional computed tomography in the assessment of fetal skeletal dysplasia. *Ultrasound Obstet Gynecol* 29:537–543, 2007.
  124. Miyazaki O, Nishimura G, Sago H, et al: Prenatal diagnosis of chondrodysplasia punctata tibia-metacarpal type using multidetector CT and three-dimensional reconstruction. *Pediatr Radiol* 37:1151–1154, 2007.
  125. Tsutsumi S, Sawai H, Nishimura G, et al: Prenatal diagnosis of thanatophoric dysplasia by 3-D helical computed tomography and genetic analysis. *Fetal Diagn Ther* 24:420–424, 2008.
  126. Ulla M, Aiello H, Cobos MP, et al: Prenatal diagnosis of skeletal dysplasias: contribution of three-dimensional computed tomography. *Fetal Diagn Ther* 29:238–247, 2011.
  127. Yamada T, Nishimura G, Nishida K, et al: Prenatal diagnosis of short-rib polydactyly syndrome type 3 (Verma-Naumoff type) by three-dimensional helical computed tomography. *J Obstet Gynaecol Res* 37:151–155, 2011.
  128. Adler-Levy Y, Yagel S, Nadjari M, et al: Use of low dose computed tomography with 3D reconstructions for the prenatal evaluation of suspected skeletal dysplasia. *Isr Med Assoc J* 17(1):42–46, 2015.
  129. Akizawa Y, Nishimura G, Hasegawa T, et al: Prenatal diagnosis of osteogenesis imperfecta type II by three-dimensional computed tomography: the current state of fetal computed tomography. *Congenit Anom (Kyoto)* 52(4):203–206, 2012.
  130. Brink JA: Technical aspects of helical (spiral) CT. *Radiol Clin North Am* 33:825–841, 1995.
  131. Wilting JE: Technical aspects of spiral-CT. *Medica Mundi* 43:34–43, 1989.
  132. Braillon PM, Buenerd A, Lapillonne A, Bouvier R: Skeletal and total body volumes of human fetuses: assessment of reference data by spiral CT. *Pediatr Radiol* 32:354–359, 2002.
  133. Victoria T, Epelman M, Coleman BG, et al: Low-dose fetal CT in the prenatal evaluation of skeletal dysplasias and other severe skeletal abnormalities. *AJR Am J Roentgenol* 200:989–1000, 2013.
  134. Cassart M: Suspected fetal skeletal malformations or bone diseases: how to explore. *Pediatr Radiol* 40:1046–1051, 2010.
  135. Chen ML, Chang CH, Yu CH, et al: Prenatal diagnosis of cleft palate by three-dimensional ultrasound. *Ultrasound Med Biol* 27:1017–1023, 2001.
  136. Blaumeiser B, Loquet P, Wuyts W, Nothen MM: Prenatal diagnosis of Pfeiffer syndrome type II. *Prenat Diagn* 24:644–646, 2004.
  137. Esser T, Rogalla P, Bamberg C, Kalache KD: Application of the three-dimensional maximum mode in prenatal diagnosis of Apert syndrome. *Am J Obstet Gynecol* 193:1743–1745, 2005.
  138. Wong GY, Wong SE, Chan WP, Ng WF: Three-dimensional ultrasound findings of spondylocostal dysostosis in the second trimester of pregnancy. *Ultrasound Obstet Gynecol* 27:580–582, 2006.
  139. Faro C, Chaoui R, Wegrzyn P, et al: Metopic suture in fetuses with Apert syndrome at 22–27 weeks of gestation. *Ultrasound Obstet Gynecol* 27:28–33, 2006.
  140. Soto E, Richani K, Goncalves LF, et al: Three-dimensional ultrasound in the prenatal diagnosis of cleidocranial dysplasia associated with B-cell immunodeficiency. *Ultrasound Obstet Gynecol* 27:574–579, 2006.
  141. Promsonthi P, Wattanasirichaigoon D: Prenatal diagnosis of campomelic dysplasia with three-dimensional ultrasound. *Ultrasound Obstet Gynecol* 27:583–585, 2006.
  142. Nemeč U, Nemeč SF, Krakow D, et al: The skeleton and musculature on foetal MRI. *Insights Imaging* 2(3):309–318, 2011.
  143. Teng SW, Guo WY, Sheu MH, Wang PH: Initial experience using magnetic resonance imaging in prenatal diagnosis of osteogenesis imperfecta type II: a case report. *Clin Imaging* 27:55–58, 2003.
  144. Miller E, Blaser S, Miller S, et al: Fetal MR imaging of atelosteogenesis type II (AO-II). *Pediatr Radiol* 38:1345–1349, 2008.
  145. Nemeč SF, Kasprian G, Brugger PC, et al: Abnormalities of the upper extremities on fetal magnetic resonance imaging. *Ultrasound Obstet Gynecol* 38:559–567, 2011.
  146. Nemeč SF, Nemeč U, Brugger PC, et al: MR imaging of the fetal musculoskeletal system. *Prenat Diagn* 32:205–213, 2012.
  147. Pugash D, Brugger PC, Bettelheim D, Prayer D: Prenatal ultrasound and fetal MRI: the comparative value of each modality in prenatal diagnosis. *Eur J Radiol* 68:214–226, 2008.
  148. Nemeč SF, Nemeč U, Brugger PC, et al: Skeletal development on fetal magnetic resonance imaging. *Top Magn Reson Imaging* 22:101–106, 2011.
  149. Giancotti A, D'Ambrosio V, De Filippis A, et al: Comparison of ultrasound and magnetic resonance imaging in the prenatal diagnosis of Apert syndrome: report of a case. *Childs Nerv Syst* 30:1445–1448, 2014.
  150. Nemeč U, Nemeč SF, Weber M, et al: Human long bone development in vivo: analysis of the distal femoral epimetaphysis on MR images of fetuses. *Radiology* 267:570–580, 2013.
  151. Donne HD, Jr, Faundes A, Tristao EG, et al: Sonographic identification and measurement of the epiphyseal ossification centers as markers of fetal gestational age. *J Clin Ultrasound* 33:394–400, 2005.
  152. Doger E, Kopuk SY, Cakiroglu Y, et al: Unilateral isolated proximal femoral focal deficiency. *Case Rep Obstet Gynecol* 2013:637904, 2013.
  153. Weaver KN, Johnson J, Kline-Fath B, et al: Predictive value of fetal lung volume in prenatally diagnosed skeletal dysplasia. *Prenat Diagn* 34:1326–1331, 2014.
  154. Pashayan H, Fraser FC, McIntyre JM, Dunbar JS: Bilateral aplasia of the tibia, polydactyly and absent thumb in father and daughter. *J Bone Joint Surg Br* 53:495–499, 1971.
  155. Luthy DA, Hall JG, Graham CB: Prenatal diagnosis of thrombocytopenia with absent radii. *Clin Genet* 15:495–499, 1979.
  156. Filkins K, Russo J, Bilinki I, et al: Prenatal diagnosis of thrombocytopenia absent radius syndrome using ultrasound and fetoscopy. *Prenat Diagn* 4:139–142, 1984.
  157. Graham M: Congenital short femur: prenatal sonographic diagnosis. *J Ultrasound Med* 4:361–363, 1985.
  158. Papageorghiou AT, Fratelli N, Leslie K, et al: Outcome of fetuses with antenatally diagnosed short femur. *Ultrasound Obstet Gynecol* 31:507–511, 2008.
  159. Alanay Y, Krakow D, Rimoin DL, Lachman RS: Angulated femurs and the skeletal dysplasias: experience of the International Skeletal Dysplasia Registry (1988–2006). *Am J Med Genet A* 143A:1159–1168, 2007.
  160. Khalil A, Morales-Rosello J, Morlando M, et al: Widening of the femoral proximal diaphysis—metaphysis angle in fetuses with achondroplasia. *Ultrasound Obstet Gynecol* 44:69–75, 2014.
  161. Hall C, Offiah AC, Forzano F, et al: *Fetal and Perinatal Skeletal Dysplasias: an Atlas of Multimodality Imaging*, London, UK, 2010, Radcliffe.
  162. DeVore GR, Horenstein J, Platt LD: Fetal echocardiography. VI. Assessment of cardiothoracic disproportion—a new technique for the diagnosis of thoracic hypoplasia. *Am J Obstet Gynecol* 155:1066–1071, 1986.
  163. Nimrod C, Davies D, Iwanicki S, et al: Ultrasound prediction of pulmonary hypoplasia. *Obstet Gynecol* 68:495–498, 1986.



164. Chitkara U, Rosenberg J, Chervenak FA, et al: Prenatal sonographic assessment of the fetal thorax: normal values. *Am J Obstet Gynecol* 156:1069–1074, 1987.
165. Johnson A, Callan NA, Bhutani VK, et al: Ultrasonic ratio of fetal thoracic to abdominal circumference: an association with fetal pulmonary hypoplasia. *Am J Obstet Gynecol* 157:764–769, 1987.
166. Fong K, Ohlsson A, Zalev A: Fetal thoracic circumference: a prospective cross-sectional study with real-time ultrasound. *Am J Obstet Gynecol* 158:1154–1160, 1988.
167. Songster GS, Gray DL, Crane JP: Prenatal prediction of lethal pulmonary hypoplasia using ultrasonic fetal chest circumference. *Obstet Gynecol* 73:261–266, 1989.
168. Vintzileos AM, Campbell WA, Rodis JF, et al: Comparison of six different ultrasonographic methods for predicting lethal fetal pulmonary hypoplasia. *Am J Obstet Gynecol* 161:606–612, 1989.
169. D'Alton M, Mercer B, Riddick E, Dudley D: Serial thoracic versus abdominal circumference ratios for the prediction of pulmonary hypoplasia in premature rupture of the membranes remote from term. *Am J Obstet Gynecol* 166:658–663, 1992.
170. Maeda H, Nagata H, Tsukimori K, et al: Prenatal evaluation and obstinatal management of fetuses at risk of developing lung hypoplasia. *J Perinat Med* 21:355–361, 1993.
171. Merz E, Wellek S, Bahlmann F, Weber G: Normal ultrasound curves of the fetal osseous thorax and fetal lung. *Geburtshilfe Frauenheilkd* 55(2):77–82, 1995.
172. Abuhamad AZ, Sedule-Murphy SJ, Kolm P, et al: Prenatal ultrasonographic fetal rib length measurement: correlation with gestational age. *Ultrasound Obstet Gynecol* 7:193–196, 1996.
173. Yoshimura S, Masuzaki H, Gotoh H, et al: Ultrasonographic prediction of lethal pulmonary hypoplasia: comparison of eight different ultrasonographic parameters. *Am J Obstet Gynecol* 175:477–483, 1996.
174. Peralta CF, Cavoretto P, Csapo B, et al: Assessment of lung area in normal fetuses at 12–32 weeks. *Ultrasound Obstet Gynecol* 26:718–724, 2005.
175. Roberts AB, Mitchell JM: Direct ultrasonographic measurement of fetal lung length in normal pregnancies and pregnancies complicated by prolonged rupture of membranes. *Am J Obstet Gynecol* 163:1560–1566, 1990.
176. Ohlsson A, Fong K, Rose T, et al: Prenatal ultrasonic prediction of autopsy-proven pulmonary hypoplasia. *Am J Perinatol* 9:334–337, 1992.
177. Merz E, Miric-Tesanic D, Bahlmann F, et al: Prenatal sonographic chest and lung measurements for predicting severe pulmonary hypoplasia. *Prenat Diagn* 19:614–619, 1999.
178. Bahlmann F, Merz E, Hallermann C, et al: Congenital diaphragmatic hernia: ultrasonic measurement of fetal lungs to predict pulmonary hypoplasia. *Ultrasound Obstet Gynecol* 14:162–168, 1999.
179. Heling KS, Tennstedt C, Chaoui R, et al: Reliability of prenatal sonographic lung biometry in the diagnosis of pulmonary hypoplasia. *Prenat Diagn* 21:649–657, 2001.
180. Laudy JA, Tibboel D, Robben SG, et al: Prenatal prediction of pulmonary hypoplasia: clinical, biometric, and Doppler velocity correlates. *Pediatrics* 109:250–258, 2002.
181. Gerards FA, Twisk JW, Fetter WP, et al: Predicting pulmonary hypoplasia with 2- or 3-dimensional ultrasonography in complicated pregnancies. *Am J Obstet Gynecol* 198:140.e1–140.e6, 2008.
182. Vergani P, Andreani M, Greco M, et al: Two- or three-dimensional ultrasonography: which is the best predictor of pulmonary hypoplasia? *Prenat Diagn* 30:834–838, 2010.
183. Rahemtullah A, McGillivray B, Wilson RD: Suspected skeletal dysplasias: femur length to abdominal circumference ratio can be used in ultrasonographic prediction of fetal outcome. *Am J Obstet Gynecol* 177:864–869, 1997.
184. Lee A, Kratochwil A, Stumpflen I, et al: Fetal lung volume determination by three-dimensional ultrasonography. *Am J Obstet Gynecol* 175:588–592, 1996.
185. Laudy JA, Janssen MM, Struyk PC, et al: Three-dimensional ultrasonography of normal fetal lung volume: a preliminary study. *Ultrasound Obstet Gynecol* 11:13–16, 1998.
186. Pohls UG, Rempen A: Fetal lung volumetry by three-dimensional ultrasound. *Ultrasound Obstet Gynecol* 11:6–12, 1998.
187. Bahmaie A, Hughes SW, Clark T, et al: Serial fetal lung volume measurement using three-dimensional ultrasound. *Ultrasound Obstet Gynecol* 16:154–158, 2000.
188. Osada H, Iitsuka Y, Masuda K, et al: Application of lung volume measurement by three-dimensional ultrasonography for clinical assessment of fetal lung development. *J Ultrasound Med* 21:841–847, 2002.
189. Gerards FA, Engels MA, Twisk JW, van Vugt JM: Normal fetal lung volume measured with three-dimensional ultrasound. *Ultrasound Obstet Gynecol* 27:134–144, 2006.
190. Barros CA, Rezende GC, Araujo Junior E, et al: Prediction of lethal pulmonary hypoplasia by means fetal lung volume in skeletal dysplasias: a three-dimensional ultrasound assessment. *J Matern Fetal Neonatal Med* 29(11):1725–1730, 2016.
191. Kalache KD, Espinoza J, Chaiworapongsa T, et al: Three-dimensional ultrasound fetal lung volume measurement: a systematic study comparing the multiplanar method with the rotational (VOCAL) technique. *Ultrasound Obstet Gynecol* 21:111–118, 2003.
192. Kalache KD, Espinoza J, Chaiworapongsa T, et al: Three-dimensional reconstructed fetal lung using VOCAL. *Ultrasound Obstet Gynecol* 21:205, 2003.
193. Ruano R, Benachi A, Joubin L, et al: Three-dimensional ultrasonographic assessment of fetal lung volume as prognostic factor in isolated congenital diaphragmatic hernia. *Br J Obstet Gynaecol* 111:423–429, 2004.
194. Ruano R, Joubin L, Sonigo P, et al: Fetal lung volume estimated by 3-dimensional ultrasonography and magnetic resonance imaging in cases with isolated congenital diaphragmatic hernia. *J Ultrasound Med* 23:353–358, 2004.
195. Ruano R, Benachi A, Martinovic J, et al: Can three-dimensional ultrasound be used for the assessment of the fetal lung volume in cases of congenital diaphragmatic hernia? *Fetal Diagn Ther* 19:87–91, 2004.
196. Moeglin D, Talmant C, Duyme M, Lopez AC: Fetal lung volumetry using two- and three-dimensional ultrasound. *Ultrasound Obstet Gynecol* 25:119–127, 2005.
197. Ruano R, Martinovic J, Dommergues M, et al: Accuracy of fetal lung volume assessed by three-dimensional sonography. *Ultrasound Obstet Gynecol* 26:725–730, 2005.
198. Peralta CF, Cavoretto P, Csapo B, et al: Lung and heart volumes by three-dimensional ultrasound in normal fetuses at 12–32 weeks' gestation. *Ultrasound Obstet Gynecol* 27:128–133, 2006.
199. Coakley FV, Lopoo JB, Lu Y, et al: Normal and hypoplastic fetal lungs: volumetric assessment with prenatal single-shot rapid acquisition with relaxation enhancement MR imaging. *Radiology* 216:107–111, 2000.
200. Rypens F, Metens T, Rocourt N, et al: Fetal lung volume: estimation at MR imaging—initial results. *Radiology* 219:236–241, 2001.
201. Paek BW, Coakley FV, Lu Y, et al: Congenital diaphragmatic hernia: prenatal evaluation with MR lung volumetry—preliminary experience. *Radiology* 220:63–67, 2001.
202. Kuwashima S, Nishimura G, Iimura F, et al: Low-intensity fetal lungs on MRI may suggest the diagnosis of pulmonary hypoplasia. *Pediatr Radiol* 31:669–672, 2001.
203. Williams G, Coakley FV, Qayyum A, et al: Fetal relative lung volume: quantification by using prenatal MR imaging lung volumetry. *Radiology* 233:457–462, 2004.
204. Tanigaki S, Miyakoshi K, Tanaka M, et al: Pulmonary hypoplasia: prediction with use of ratio of MR imaging-measured fetal lung volume to US-estimated fetal body weight. *Radiology* 232:767–772, 2004.
205. Osada H, Kaku K, Masuda K, et al: Quantitative and qualitative evaluations of fetal lung with MR imaging. *Radiology* 231:887–892, 2004.
206. Keller TM, Rake A, Michel SC, et al: MR assessment of fetal lung development using lung volumes and signal intensities. *Eur Radiol* 14:984–989, 2004.
207. Kalache KD, Chaoui R, Hartung J, et al: Doppler assessment of tracheal fluid flow during fetal breathing movements in cases of congenital diaphragmatic hernia. *Ultrasound Obstet Gynecol* 12:27–32, 1998.



208. Laudy JA, Wladimiroff JW: The fetal lung. 2: pulmonary hypoplasia. *Ultrasound Obstet Gynecol* 16:482–494, 2000.
209. Mitchell JM, Roberts AB, Lee A: Doppler waveforms from the pulmonary arterial system in normal fetuses and those with pulmonary hypoplasia. *Ultrasound Obstet Gynecol* 11:167–172, 1998.
210. Achiron R, Heggesh J, Mashiach S, et al: Peripheral right pulmonary artery blood flow velocimetry: Doppler sonographic study of normal and abnormal fetuses. *J Ultrasound Med* 17:687–692, 1998.
211. Chaoui R, Kalache K, Tennstedt C, et al: Pulmonary arterial Doppler velocimetry in fetuses with lung hypoplasia. *Eur J Obstet Gynecol Reprod Biol* 84:179–185, 1999.
212. Yoshimura S, Masuzaki H, Miura K, et al: Diagnosis of fetal pulmonary hypoplasia by measurement of blood flow velocity waveforms of pulmonary arteries with Doppler ultrasonography. *Am J Obstet Gynecol* 180:441–446, 1999.
213. Rizzo G, Capponi A, Angelini E, et al: Blood flow velocity waveforms from fetal peripheral pulmonary arteries in pregnancies with preterm premature rupture of the membranes: relationship with pulmonary hypoplasia. *Ultrasound Obstet Gynecol* 15:98–103, 2000.
214. Fuke S, Kanzaki T, Mu J, et al: Antenatal prediction of pulmonary hypoplasia by acceleration time/ejection time ratio of fetal pulmonary arteries by Doppler blood flow velocimetry. *Am J Obstet Gynecol* 188:228–233, 2003.
215. Campbell J, Henderson A, Campbell S: The fetal femur/foot length ratio: a new parameter to assess dysplastic limb reduction. *Obstet Gynecol* 72:181–184, 1988.
216. Hershey DW: The fetal femur/foot length ratio: a new parameter to assess dysplastic limb reduction. *Obstet Gynecol* 73:682, 1989.
217. Turner GM, Twining P: The facial profile in the diagnosis of fetal abnormalities. *Clin Radiol* 47:389–395, 1993.
218. Chmait R, Pretorius D, Jones M, et al: Prenatal evaluation of facial clefts with two-dimensional and adjunctive three-dimensional ultrasonography: a prospective trial. *Am J Obstet Gynecol* 187:946–949, 2002.
219. Mittermayer C, Blaicher W, Brugger PC, et al: Foetal facial clefts: prenatal evaluation of lip and primary palate by 2D and 3D ultrasound. *Ultraschall Med* 25:120–125, 2004.
220. Johnson DD, Pretorius DH, Budorick NE, et al: Fetal lip and primary palate: three-dimensional versus two-dimensional US. *Radiology* 217:236–239, 2000.
221. Lee W, Kirk JS, Shaheen KW, et al: Fetal cleft lip and palate detection by three-dimensional ultrasonography. *Ultrasound Obstet Gynecol* 16:314–320, 2000.
222. Pretorius DH, Nelson TR: Fetal face visualization using three-dimensional ultrasonography. *J Ultrasound Med* 14:349–356, 1995.
223. Mittermayer C, Lee A: Three-dimensional ultrasonographic imaging of cleft lip: the winners are the parents. *Ultrasound Obstet Gynecol* 21:628–629, 2003.
224. Campbell S, Lees CC: The three-dimensional reverse face (3D RF) view for the diagnosis of cleft palate. *Ultrasound Obstet Gynecol* 22:552–554, 2003.
225. Campbell S, Lees C, Moscoso G, Hall P: Ultrasound antenatal diagnosis of cleft palate by a new technique: the 3D “reverse face” view. *Ultrasound Obstet Gynecol* 25:12–18, 2005.
226. Ghi T, Tani G, Savelli L, et al: Prenatal imaging of facial clefts by magnetic resonance imaging with emphasis on the posterior palate. *Prenat Diagn* 23:970–975, 2003.
227. Mailath-Pokorny M, Worda C, Krampl-Bettelheim E, et al: What does magnetic resonance imaging add to the prenatal ultrasound diagnosis of facial clefts? *Ultrasound Obstet Gynecol* 36:445–451, 2010.
228. Wang G, Shan R, Zhao L, et al: Fetal cleft lip with and without cleft palate: comparison between MR imaging and US for prenatal diagnosis. *Eur J Radiol* 79:437–442, 2011.
229. Manganaro L, Tomei A, Fierro F, et al: Fetal MRI as a complement to US in the evaluation of cleft lip and palate. *Radiol Med* 116:1134–1148, 2011.
230. Arangio P, Manganaro L, Pacifici A, et al: Importance of fetal MRI in evaluation of craniofacial deformities. *J Craniofac Surg* 24:773–776, 2013.
231. Pilu G, Reece EA, Romero R, et al: Prenatal diagnosis of craniofacial malformations with ultrasonography. *Am J Obstet Gynecol* 155:45–50, 1986.
232. Bromley B, Benacerraf BR: Fetal micrognathia: associated anomalies and outcome. *J Ultrasound Med* 13:529–533, 1994.
233. Prows CA, Bender PL: Beyond Pierre Robin sequence. *Neonatal Netw* 18:13–19, 1999.
234. Paladini D, Morra T, Teodoro A, et al: Objective diagnosis of micrognathia in the fetus: the jaw index. *Obstet Gynecol* 93:382–386, 1999.
235. Rotten D, Levallant JM, Martinez H, et al: The fetal mandible: a 2D and 3D sonographic approach to the diagnosis of retrognathia and micrognathia. *Ultrasound Obstet Gynecol* 19:122–130, 2002.
236. Abrams SL, Filly RA: Congenital vertebral malformations: prenatal diagnosis using ultrasonography. *Radiology* 155:762, 1985.
237. Zelop CM, Pretorius DH, Benacerraf BR: Fetal hemivertebrae: associated anomalies, significance, and outcome. *Obstet Gynecol* 81:412–416, 1993.
238. Achiron R, Lipitz S, Grisaru D, et al: Second-trimester ultrasonographic diagnosis of segmental vertebral abnormalities associated with neurological deficit: a possible new variant of occult spinal dysraphism. *Prenat Diagn* 16:760–763, 1996.
239. Kozlowski K, Bieganski T, Gardner J, Beighton P: Osteochondrodysplasias with marked platyspondyly and distinctive peripheral anomalies. *Pediatr Radiol* 29:1–5, 1999.
240. Wells TR, Landing BH, Bostwick FH: Studies of vertebral coronal cleft in rhizomelic chondrodysplasia punctata. *Pediatr Pathol* 12:593–600, 1992.
241. Lachman RS: Fetal imaging in the skeletal dysplasias: overview and experience. *Pediatr Radiol* 24:413–417, 1994.
242. Westvik J, Lachman RS: Coronal and sagittal clefts in skeletal dysplasias. *Pediatr Radiol* 28:764–770, 1998.
243. McMaster MJ: Occult intraspinal anomalies and congenital scoliosis. *J Bone Joint Surg Am* 66:588–601, 1984.
244. McMaster MJ, David CV: Hemivertebra as a cause of scoliosis. A study of 104 patients. *J Bone Joint Surg Br* 68:588–595, 1984.
245. McMaster MJ: Congenital scoliosis caused by a unilateral failure of vertebral segmentation with contralateral hemivertebrae. *Spine* 23(9):998–1005, 1998.
246. McMaster MJ, Singh H: Natural history of congenital kyphosis and kyphoscoliosis. A study of one hundred and twelve patients. *J Bone Joint Surg Am* 81:1367–1383, 1999.
247. Connor JM, Conner AN, Connor RA, et al: Genetic aspects of early childhood scoliosis. *Am J Med Genet* 27:419–424, 1987.
248. Johnson VP, Yiu-Chiu VS, Wierda DR, Holzwarth DR: Midtrimester prenatal diagnosis of achondrogenesis. *J Ultrasound Med* 3:223–226, 1984.
249. Mahony BS, Filly RA, Callen PW, Golbus MS: Thanatophoric dwarfism with the cloverleaf skull: a specific antenatal sonographic diagnosis. *J Ultrasound Med* 4:151–154, 1985.
250. Serge G, Ruggieri M, Lachman RS: Spondyloperipheral dysplasia. *Am J Med Genet* 59:139–142, 1995.
251. Hoopmann M, Sonek J, Schramm T, et al: Position of the conus medullaris in fetuses with skeletal dysplasia. *Prenat Diagn* 32:1313–1317, 2012.
252. Katsouras CS, Thomadakis C, Michalis LK: Cardiac Ellis-van Creveld syndrome. *Int J Cardiol* 87:315–316, 2003.
253. Bossert T, Walther T, Gummert J, et al: Cardiac malformations associated with the Holt-Oram syndrome—report on a family and review of the literature. *Thorac Cardiovasc Surg* 50:312–314, 2002.
254. de Vries JI, Fong BF: Normal fetal motility: an overview. *Ultrasound Obstet Gynecol* 27:701–711, 2006.
255. Filges I, Hall JG: We are failing to identify disorders of fetal movement—why? *Prenat Diagn* 32(10):919–920, 2012.
256. Filges I, Hall JG: Failure to identify antenatal multiple congenital contractures and fetal akinesia—proposal of guidelines to improve diagnosis. *Prenat Diagn* 33:61–74, 2013.
257. Nowlan NC: Biomechanics of foetal movement. *Eur Cell Mater* 29:1–21, 2015.
258. de Vries JI, Fong BF: Changes in fetal motility as a result of congenital disorders: an overview. *Ultrasound Obstet Gynecol* 29:590–599, 2007.



259. Donker ME, Eijkelhof BH, Tan GM, de Vries JI: Serial postural and motor assessment of Fetal Akinesia Deformation Sequence (FADS). *Early Hum Dev* 85:785–790, 2009.
260. Hoellen F, Schroer A, Kelling K, et al: Arthrogryposis multiplex congenita and Pena-Shokeir phenotype: challenge of prenatal diagnosis—report of 21 cases, antenatal findings and review. *Fetal Diagn Ther* 30:289–298, 2011.
261. Abdulkadir AY, Isyaku K, Dare A, et al: Prenatal third trimester sonographic behavior of a thanatophoric dwarfs. *J Prenat Med* 2:42–46, 2008.
262. Mortier GR, Rimoin DL, Lachman RS: The scapula as a window to the diagnosis of skeletal dysplasias. *Pediatr Radiol* 27:447–451, 1997.
263. Veeramani AK, Higgins P, Butler S, et al: Diagnostic use of skeletal survey in suspected skeletal dysplasia. *J Clin Res Pediatr Endocrinol* 1:270–274, 2009.
264. Francomano CA: The genetic basis of dwarfism. *N Engl J Med* 332:58–59, 1995.
265. Nicolaides KH, Azar G, Byrne D, et al: Fetal nuchal translucency: ultrasound screening for chromosomal defects in first trimester of pregnancy. *BMJ* 304:867–869, 1992.
266. Pandya PP, Kondyliou A, Hilbert L, et al: Chromosomal defects and outcome in 1015 fetuses with increased nuchal translucency. *Ultrasound Obstet Gynecol* 5:15–19, 1995.
267. Brady AF, Pandya PP, Yuksel B, et al: Outcome of chromosomally normal livebirths with increased fetal nuchal translucency at 10–14 weeks' gestation. *J Med Genet* 35:222–224, 1998.
268. Souka AP, Snijders RJ, Novakov A, et al: Defects and syndromes in chromosomally normal fetuses with increased nuchal translucency thickness at 10–14 weeks of gestation. *Ultrasound Obstet Gynecol* 11:391–400, 1998.
269. Makrydimas G, Souka A, Skentou H, et al: Osteogenesis imperfecta and other skeletal dysplasias presenting with increased nuchal translucency in the first trimester. *Am J Med Genet* 98:117–120, 2001.
270. Souka AP, Raymond FL, Mornet E, et al: Hypophosphatasia associated with increased nuchal translucency: a report of two affected pregnancies. *Ultrasound Obstet Gynecol* 20:294–295, 2002.
271. Michel-Calemard L, Lesca G, Morel Y, et al: Campomelic acampomelic dysplasia presenting with increased nuchal translucency in the first trimester. *Prenat Diagn* 24:519–523, 2004.
272. Witters I, Claerhout P, Fryns JP: Increased nuchal translucency thickness in thrombocytopenia-absent-radius syndrome. *Ultrasound Obstet Gynecol* 26:581–582, 2005.
273. Hewitt B: Nuchal translucency in the first trimester. *Aust N Z J Obstet Gynaecol* 33:389–391, 1993.
274. Soothill P, Kyle P: Fetal nuchal translucency test for Down's syndrome. *Lancet* 350(9091):1629–1632, 1997.
275. Fukada Y, Yasumizu T, Takizawa M, et al: The prognosis of fetuses with transient nuchal translucency in the first and early second trimester. *Acta Obstet Gynecol Scand* 76:913–916, 1997.
276. Hernadi L, Torocsik M: Screening for fetal anomalies in the 12th week of pregnancy by transvaginal sonography in an unselected population. *Prenat Diagn* 17:753–759, 1997.
277. den Hollander NS, van der Harten HJ, Vermeij-Keers C, et al: First-trimester diagnosis of Blomstrand lethal osteochondrodysplasia. *Am J Med Genet* 73:345–350, 1997.
278. Hafner E, Schuchter K, Liebhart E, Philipp K: Results of routine fetal nuchal translucency measurement at weeks 10–13 in 4233 unselected pregnant women. *Prenat Diagn* 18:29–34, 1998.
279. Hiippala A, Eronen M, Taipale P, et al: Fetal nuchal translucency and normal chromosomes: a long-term follow-up study. *Ultrasound Obstet Gynecol* 18:18–22, 2001.
280. Venkat-Raman N, Sebire NJ, Murphy KW, et al: Increased first-trimester fetal nuchal translucency thickness in association with chondroectodermal dysplasia (Ellis-Van Creveld syndrome). *Ultrasound Obstet Gynecol* 25:412–414, 2005.
281. Ngo C, Viot G, Aubry MC, et al: First-trimester ultrasound diagnosis of skeletal dysplasia associated with increased nuchal translucency thickness. *Ultrasound Obstet Gynecol* 30:221–226, 2007.
282. Leung KY, MacLachlan NA, Sepulveda W: Prenatal diagnosis of ectrodactyly: the “lobster claw” anomaly. *Ultrasound Obstet Gynecol* 6:443–446, 1995.
283. Tercanli S, Miny P, Siebert MS, et al: Fanconi anemia associated with increased nuchal translucency detected by first-trimester ultrasound. *Ultrasound Obstet Gynecol* 17:160–162, 2001.
284. Hyett J, Noble P, Sebire NJ, et al: Lethal congenital arthrogryposis presents with increased nuchal translucency at 10–14 weeks of gestation. *Ultrasound Obstet Gynecol* 9:310–313, 1997.
285. Madazli R, Tuysuz B, Aksoy F, et al: Prenatal diagnosis of arthrogryposis multiplex congenita with increased nuchal translucency but without any underlying fetal neurogenic or myogenic pathology. *Fetal Diagn Ther* 17:29–33, 2002.
286. Eliyahu S, Weiner E, Lahav D, Shalev E: Early sonographic diagnosis of Jarcho-Levin syndrome: a prospective screening program in one family. *Ultrasound Obstet Gynecol* 9:314–318, 1997.
287. Vimercati A, Panzarino M, Totaro I, et al: Increased nuchal translucency and short femur length as possible early signs of osteogenesis imperfecta type III. *J Prenat Med* 7:5–8, 2013.
288. Hill LM, Leary J: Transvaginal sonographic diagnosis of short-rib polydactyly dysplasia at 13 weeks' gestation. *Prenat Diagn* 18:1198–1201, 1998.
289. Ferreira A, Matias A, Brandao O, Montenegro N: Nuchal translucency and ductus venosus blood flow as early sonographic markers of thanatophoric dysplasia. A case report. *Fetal Diagn Ther* 19:241–245, 2004.
290. Shiang R, Thompson LM, Zhu YZ, et al: Mutations in the transmembrane domain of FGFR3 cause the most common genetic form of dwarfism, achondroplasia. *Cell* 78:335–342, 1994.
291. Bellus GA, McIntosh I, Smith EA, et al: A recurrent mutation in the tyrosine kinase domain of fibroblast growth factor receptor 3 causes hypochondroplasia. *Nat Genet* 10:357–359, 1995.
292. Ozono K: Recent advances in molecular analysis of skeletal dysplasia. *Acta Paediatr Jpn* 39(4):491–498, 1997.
293. Wilcox WR, Tavormina PL, Krakow D, et al: Molecular, radiologic, and histopathologic correlations in thanatophoric dysplasia. *Am J Med Genet* 78:274–281, 1998.
294. Climent C, Lorda-Sanchez I, Urioste M, et al: Achondroplasia: molecular study of 28 patients. *Med Clin (Barc)* 110:492–494, 1998.
295. Cohen MM, Jr: Achondroplasia, hypochondroplasia and thanatophoric dysplasia: clinically related skeletal dysplasias that are also related at the molecular level. *Int J Oral Maxillofac Surg* 27:451–455, 1998.
296. Wilkin DJ, Szabo JK, Cameron R, et al: Mutations in fibroblast growth-factor receptor 3 in sporadic cases of achondroplasia occur exclusively on the paternally derived chromosome. *Am J Hum Genet* 63:711–716, 1998.
297. Lemyre E, Azouz EM, Teebi AS, et al: Bone dysplasia series. Achondroplasia, hypochondroplasia and thanatophoric dysplasia: review and update. *Can Assoc Radiol J* 50:185–197, 1999.
298. Rousseau F, el Ghouzzi V, Delezoide AL, et al: Missense FGFR3 mutations create cysteine residues in thanatophoric dwarfism type I (TD1). *Hum Mol Genet* 5:509–512, 1996.
299. Cohen MM, Jr: Some chondrodysplasias with short limbs: molecular perspectives. *Am J Med Genet* 112:304–313, 2002.
300. Hevner RF: The cerebral cortex malformation in thanatophoric dysplasia: neuropathology and pathogenesis. *Acta Neuropathol* 110:208–221, 2005.
301. Vajo Z, Francomano CA, Wilkin DJ: The molecular and genetic basis of fibroblast growth factor receptor 3 disorders: the achondroplasia family of skeletal dysplasias, Muenke craniostylosis, and Crouzon syndrome with acanthosis nigricans. *Endocr Rev* 21:23–39, 2000.
302. Aviezer D, Golemb M, Yayon A: Fibroblast growth factor receptor-3 as a therapeutic target for achondroplasia—genetic short limbed dwarfism. *Curr Drug Targets* 4:353–365, 2003.
303. Tonni G, Ventura A, De Felice C: First trimester increased nuchal translucency associated with fetal achondroplasia. *Am J Perinatol* 22:145–148, 2005.
304. Ramaswami U, Rumsby G, Hindmarsh PC, Brook CG: Genotype and phenotype in hypochondroplasia. *J Pediatr* 133:99–102, 1998.



305. Kurtz AB, Filly RA, Wapner RJ, et al: In utero analysis of heterozygous achondroplasia: variable time of onset as detected by femur length measurements. *J Ultrasound Med* 5:137-140, 1986.
306. Modaff P, Horton VK, Pauli RM: Errors in the prenatal diagnosis of children with achondroplasia. *Prenat Diagn* 16:525-530, 1996.
307. Elejalde BR, de Elejalde MM, Hamilton PR, Lombardi JM: Prenatal diagnosis in two pregnancies of an achondroplastic woman. *Am J Med Genet* 15:437-439, 1983.
308. Mesoraca A, Pilu G, Perolo A, et al: Ultrasound and molecular mid-trimester prenatal diagnosis of de novo achondroplasia. *Prenat Diagn* 16:764-768, 1996.
309. Huggins MJ, Mernagh JR, Steele L, et al: Prenatal sonographic diagnosis of hypochondroplasia in a high-risk fetus. *Am J Med Genet* 87:226-229, 1999.
310. Chitayat D, Fernandez B, Gardner A, et al: Compound heterozygosity for the achondroplasia-hypochondroplasia FGFR3 mutations: prenatal diagnosis and postnatal outcome. *Am J Med Genet* 84:401-405, 1999.
311. Cordone M, Lituania M, Bocchino G, et al: Ultrasonographic features in a case of heterozygous achondroplasia at 25 weeks' gestation. *Prenat Diagn* 13:395-401, 1993.
312. Guzman ER, Day-Salvatore D, Westover T, et al: Prenatal ultrasonographic demonstration of the trident hand in heterozygous achondroplasia. *J Ultrasound Med* 13:63-66, 1994.
313. Patel MD, Filly RA: Homozygous achondroplasia: US distinction between homozygous, heterozygous, and unaffected fetuses in the second trimester. *Radiology* 196:541-545, 1995.
314. Karadimas C, Trouvas D, Haritatos G, et al: Prenatal diagnosis of achondroplasia presenting with multiple-suture synostosis: a novel association. *Prenat Diagn* 26:258-261, 2006.
315. Francomano CA, Ortiz de Luna RI, Hefferon TW, et al: Localization of the achondroplasia gene to the distal 2.5 Mb of human chromosome 4p. *Hum Mol Genet* 3:787-792, 1994.
316. Velinov M, Slangenaupt SA, Stoilov I, et al: The gene for achondroplasia maps to the telomeric region of chromosome 4p. *Nat Genet* 6:314-317, 1994.
317. Rousseau F, Bonaventure J, Legeai-Mallet L, et al: Mutations in the gene encoding fibroblast growth factor receptor-3 in achondroplasia. *Nature* 371:252-254, 1994.
318. Dakouane Giudicelli M, Serazin V, Le Sciellour CR, et al: Increased achondroplasia mutation frequency with advanced age and evidence for G1138A mosaicism in human testis biopsies. *Fertil Steril* 89:1651-1656, 2008.
319. James PA, Shaw J, du Sart D, et al: Molecular diagnosis in a pregnancy at risk for both spondyloepiphyseal dysplasia congenita and achondroplasia. *Prenat Diagn* 23:861-863, 2003.
320. Schrijver I, Lay MJ, Zehnder JL: Rapid combined genotyping assay for four achondroplasia and hypochondroplasia mutations by real-time PCR with multiple detection probes. *Genet Test* 8(2):185-189, 2004.
321. Lachman RS: Neurologic abnormalities in the skeletal dysplasias: a clinical and radiological perspective. *Am J Med Genet* 69:33-43, 1997.
322. Ho NC, Guarnieri M, Brant LJ, et al: Living with achondroplasia: quality of life evaluation following cervico-medullary decompression. *Am J Med Genet A* 131:163-167, 2004.
323. Pauli RM, Conroy MM, Langer LO, Jr, et al: Homozygous achondroplasia with survival beyond infancy. *Am J Med Genet* 16:459-473, 1983.
324. Seino Y, Moriwake T, Tanaka H, et al: Molecular defects in achondroplasia and the effects of growth hormone treatment. *Acta Paediatr Suppl* 88(428):118-120, 1999.
325. Tanaka H, Kubo T, Yamate T, et al: Effect of growth hormone therapy in children with achondroplasia: growth pattern, hypothalamic-pituitary function, and genotype. *Eur J Endocrinol* 138:275-280, 1998.
326. Weber G, Prinster C, Meneghel M, et al: Human growth hormone treatment in prepubertal children with achondroplasia. *Am J Med Genet* 61:396-400, 1996.
327. Yasoda A, Komatsu Y, Chusho H, et al: Overexpression of CNP in chondrocytes rescues achondroplasia through a MAPK-dependent pathway. *Nat Med* 10:80-86, 2004.
328. Tavormina PL, Bellus GA, Webster MK, et al: A novel skeletal dysplasia with developmental delay and acanthosis nigricans is caused by a Lys650Met mutation in the fibroblast growth factor receptor 3 gene. *Am J Hum Genet* 64:722-731, 1999.
329. Bellus GA, Bamshad MJ, Przylepa KA, et al: Severe achondroplasia with developmental delay and acanthosis nigricans (SADDAN): phenotypic analysis of a new skeletal dysplasia caused by a Lys650Met mutation in fibroblast growth factor receptor 3. *Am J Med Genet* 85:53-65, 1999.
330. Spranger J: International nomenclature of constitutional bone diseases (the Paris nomenclature). *Fortschr Geb Rontgenstr Nuklearmed* 115:283-287, 1971.
331. Brodie SG, Kitho H, Lipson M, et al: Thanatophoric dysplasia type I with syndactyly. *Am J Med Genet* 80:260-262, 1998.
332. Spranger J: International classification of osteochondrodysplasias. The International Working Group on Constitutional Diseases of Bone. *Eur J Pediatr* 151:407-415, 1992.
333. Weber M, Johannisson R, Carstens C, et al: Thanatophoric dysplasia type II: new entity? *J Pediatr Orthop B* 7:10-22, 1998.
334. Iannaccone G, Gerlini G: The so-called "cloverleaf skull syndrome." A report of three cases with a discussion of its relationships with thanatophoric dwarfism and the craniostenoses. *Pediatr Radiol* 2:175-184, 1974.
335. Jasnosz KM, MacPherson TA: Perinatal pathology casebook. Thanatophoric dysplasia with cloverleaf skull. *J Perinatol* 13:162-164, 1993.
336. Yang SS, Heidelberger KP, Brough AJ, et al: Lethal short-limbed chondrodysplasia in early infancy. *Perspect Pediatr Pathol* 3:1-40, 1976.
337. McKusick VA, Francomano CA, Antonarakis SE: *Mendelian Inheritance in Man: Catalogs of Autosomal Dominant, Autosomal Recessive, and X-Linked Phenotypes*, Baltimore, 1990, Johns Hopkins University Press.
338. Tavormina PL, Shiang R, Thompson LM, et al: Thanatophoric dysplasia (types I and II) caused by distinct mutations in fibroblast growth factor receptor 3. *Nat Genet* 9:321-328, 1995.
339. Schild RL, Hunt GH, Moore J, et al: Antenatal sonographic diagnosis of thanatophoric dysplasia: a report of three cases and a review of the literature with special emphasis on the differential diagnosis. *Ultrasound Obstet Gynecol* 8:62-67, 1996.
340. d'Avis PY, Robertson SC, Meyer AN, et al: Constitutive activation of fibroblast growth factor receptor 3 by mutations responsible for the lethal skeletal dysplasia thanatophoric dysplasia type I. *Cell Growth Differ* 9(1):71-78, 1998.
341. Passos-Bueno MR, Wilcox WR, Jabs EW, et al: Clinical spectrum of fibroblast growth factor receptor mutations. *Hum Mutat* 14:115-125, 1999.
342. Li D, Liao C, Ma X: Prenatal diagnosis and molecular analysis of type I thanatophoric dysplasia. *Int J Gynaecol Obstet* 91:268-270, 2005.
343. Bellus GA, Spector EB, Speiser PW, et al: Distinct missense mutations of the FGFR3 lys650 codon modulate receptor kinase activation and the severity of the skeletal dysplasia phenotype. *Am J Hum Genet* 67:1411-1421, 2000.
344. Rousseau F, Saugier P, Le Merrer M, et al: Stop codon FGFR3 mutations in thanatophoric dwarfism type I. *Nat Genet* 10:11-12, 1995.
345. Gorlin RJ: Fibroblast growth factors, their receptors and receptor disorders. *J Craniomaxillofac Surg* 25:69-79, 1997.
346. Camera G, Baldi M, Strisciuglio G, et al: Occurrence of thanatophoric dysplasia type I (R248C) and hypochondroplasia (N540K) mutations in two patients with achondroplasia phenotype. *Am J Med Genet* 104:277-281, 2001.
347. Inglis-Broadgate SL, Thomson RE, Pellicano F, et al: FGFR3 regulates brain size by controlling progenitor cell proliferation and apoptosis during embryonic development. *Dev Biol* 279:73-85, 2005.
348. Knisely AS, Ambler MW: Temporal-lobe abnormalities in thanatophoric dysplasia. *Pediatr Neurosci* 14:169-176, 1988.
349. Horton WA, Rimoin DL, Hollister DW, Lachman RS: Further heterogeneity within lethal neonatal short-limbed dwarfism: the platyspondylic types. *J Pediatr* 94:736-742, 1979.



350. Brodie SG, Kitoh H, Lachman RS, et al: Platyospondylic lethal skeletal dysplasia, San Diego type, is caused by FGFR3 mutations. *Am J Med Genet* 84:476–480, 1999.
351. Moir DH, Kozlowski K: Long survival in thanatophoric dwarfism. *Pediatr Radiol* 5:123–125, 1976.
352. Stensvold K, Ek J, Hovland AR: An infant with thanatophoric dwarfism surviving 169 days. *Clin Genet* 29:157–159, 1986.
353. Foster JW, Dominguez-Steglich MA, Guioli S, et al: Campomelic dysplasia and autosomal sex reversal caused by mutations in an SRY-related gene. *Nature* 372:525–530, 1994.
354. Baker KM, Olson DS, Harding CO, Pauli RM: Long-term survival in typical thanatophoric dysplasia type 1. *Am J Med Genet* 70:427–436, 1997.
355. Fink IJ, Filly RA, Callen PW, Fiske CC: Sonographic diagnosis of thanatophoric dwarfism in utero. *J Ultrasound Med* 1:337–339, 1982.
356. Chervenak FA, Blakemore KJ, Isaacson G, et al: Antenatal sonographic findings of thanatophoric dysplasia with cloverleaf skull. *Am J Obstet Gynecol* 146:984–985, 1983.
357. Beetham FG, Reeves JS: Early ultrasound diagnosis of thanatophoric dwarfism. *J Clin Ultrasound* 12:43–44, 1984.
358. Burrows PE, Stannard MW, Pearrow J, et al: Early antenatal sonographic recognition of thanatophoric dysplasia with cloverleaf skull deformity. *AJR Am J Roentgenol* 143:841–843, 1984.
359. Elejalde BR, de Elejalde MM: Thanatophoric dysplasia: fetal manifestations and prenatal diagnosis. *Am J Med Genet* 22:669–683, 1985.
360. Weiner CP, Williamson RA, Bonsib SM: Sonographic diagnosis of cloverleaf skull and thanatophoric dysplasia in the second trimester. *J Clin Ultrasound* 14:463–465, 1986.
361. Meizner I, Levy A, Carmi R, Simhon T: Early prenatal ultrasonic diagnosis of thanatophoric dwarfism. *Isr J Med Sci* 26:287–289, 1990.
362. Kassanos D, Botsis D, Katassos T, et al: Prenatal sonographic diagnosis of thanatophoric dwarfism. *Int J Gynaecol Obstet* 34:373–376, 1991.
363. Corsello G, Maresi E, Rossi C, et al: Thanatophoric dysplasia in monozygotic twins discordant for cloverleaf skull: prenatal diagnosis, clinical and pathological findings. *Am J Med Genet* 42:122–126, 1992.
364. Gerihauser H, Schuster C, Immervoll H, Sochor G: Prenatal diagnosis of thanatophoric dwarfism. *Ultraschall Med* 13(1):41–45, 1992.
365. Camera G, Doderio D, Camandona F, Camera A: Prenatal diagnosis of thanatophoric dysplasia at 21st week of pregnancy. *Pathologica* 85(1096):215–219, 1993.
366. Marin-Ruiz R, Alarcon Hernandez C, Montiel Ramirez W, Gonzalez Moreno JM: Thanatophoric dysplasia. Its prenatal ultrasonic diagnosis. A case report. *Ginecol Obstet Mex* 61:344–347, 1993.
367. van der Harten HJ, Brons JT, Dijkstra PF, et al: Some variants of lethal neonatal short-limbed platyspondylic dysplasia: a radiological ultrasonographic, neuropathological and histopathological study of 22 cases. *Clin Dysmorphol* 2:1–19, 1993.
368. Szatmary FP, Szabo L, Toth T, Kristof A: Prenatal diagnosis of thanatophoric dysplasia. *Orv Hetil* 136(2):75–78, 1995.
369. Todros T, Sciarone A, Voglino G, et al: Prenatal diagnosis of thanatophoric dysplasia at the 20th week of pregnancy using ultrasonography. *Pathologica* 87(6):723–725, 1995.
370. Yuca MA, Yardim T, Kurtul M, et al: Prenatal diagnosis of thanatophoric dwarfism in second trimester. A case report. *Clin Exp Obstet Gynecol* 25:149–150, 1998.
371. Sun CC, Grumbach K, DeCosta DT, et al: Correlation of prenatal ultrasound diagnosis and pathologic findings in fetal anomalies. *Pediatr Dev Pathol* 2:131–142, 1999.
372. Sahinoglu Z, Uludogan M, Gurbuz A, Karateke A: Prenatal diagnosis of thanatophoric dysplasia in the second trimester: ultrasonography and other diagnostic modalities. *Arch Gynecol Obstet* 269:57–61, 2003.
373. Sawai H, Komori S, Ida A, et al: Prenatal diagnosis of thanatophoric dysplasia by mutational analysis of the fibroblast growth factor receptor 3 gene and a proposed correction of previously published PCR results. *Prenat Diagn* 19:21–24, 1999.
374. De Biasio P, Prefumo F, Baffico M, et al: Sonographic and molecular diagnosis of thanatophoric dysplasia type I at 18 weeks of gestation. *Prenat Diagn* 20:835–837, 2000.
375. Chen CP, Chern SR, Chang TY, et al: Second trimester molecular diagnosis of a stop codon FGFR3 mutation in a type I thanatophoric dysplasia fetus following abnormal ultrasound findings. *Prenat Diagn* 22:736–737, 2002.
376. Hall BD, Spranger J: Hypochondroplasia: clinical and radiological aspects in 39 cases. *Radiology* 133:95–100, 1979.
377. Cohn DH: Mutations affecting multiple functional domains of FGFR3 cause different skeletal dysplasias: a personal retrospective in honor of John Wasmuth. *Ann N Y Acad Sci* 785:160–163, 1996.
378. Matsui Y, Yasui N, Kimura T, et al: Genotype phenotype correlation in achondroplasia and hypochondroplasia. *J Bone Joint Surg Br* 80:1052–1056, 1998.
379. Mullis PE, Patel MS, Brickell PM, et al: Growth characteristics and response to growth hormone therapy in patients with hypochondroplasia: genetic linkage of the insulin-like growth factor I gene to chromosome 12q23 to the disease in a subgroup of these patients. *Clin Endocrinol (Oxf)* 34:265–274, 1991.
380. Song SH, Balce GC, Agashe MV, et al: New proposed clinico-radiologic and molecular criteria in hypochondroplasia: FGFR 3 gene mutations are not the only cause of hypochondroplasia. *Am J Med Genet A* 158A(10):2456–2462, 2012.
381. Bailey AJ, Sims TJ, Stanescu V, et al: Abnormal collagen cross-linking in the cartilage of a diastrophic dysplasia patient. *Br J Rheumatol* 34:512–515, 1995.
382. Prinso P, Costa T, Sommer A, et al: A common FGFR3 gene mutation in hypochondroplasia. *Hum Mol Genet* 4:2097–2101, 1995.
383. Scott CI, Jr: Achondroplastic and hypochondroplastic dwarfism. *Clin Orthop Relat Res* 114:18–30, 1976.
384. Stoll C, Manini P, Bloch J, Roth MP: Prenatal diagnosis of hypochondroplasia. *Prenat Diagn* 5:423–426, 1985.
385. Stoilov I, Kilpatrick MW, Tsiouras P, Costa T: Possible genetic heterogeneity in hypochondroplasia. *J Med Genet* 32:492–493, 1995.
386. Angle B, Hersh JH, Christensen KM: Molecularly proven hypochondroplasia with cloverleaf skull deformity: a novel association. *Clin Genet* 54:417–420, 1998.
387. Prinster C, Carrera P, Del Maschio M, et al: Comparison of clinical-radiological and molecular findings in hypochondroplasia. *Am J Med Genet* 75:109–112, 1998.
388. Grosso S, Farnetani MA, Berardi R, et al: Medial temporal lobe dysgenesis in Muenke syndrome and hypochondroplasia. *Am J Med Genet A* 120A:88–91, 2003.
389. Kannu P, Hayes IM, Mandelstam S, et al: Medial temporal lobe dysgenesis in hypochondroplasia. *Am J Med Genet A* 138:389–391, 2005.
390. Cesaretti C, Spaccini I, Rustico M, et al: Prenatal magnetic resonance imaging detection of temporal lobes and hippocampal anomalies in hypochondroplasia. *Prenat Diagn* 34:1015–1017, 2014.
391. Kataoka S, Sawai H, Yamada H, et al: Radiographic and genetic diagnosis of sporadic hypochondroplasia early in the neonatal period. *Prenat Diagn* 24:45–49, 2004.
392. Karadimas C, Sifakis S, Valsamopoulos P, et al: Prenatal diagnosis of hypochondroplasia: report of two cases. *Am J Med Genet A* 140:998–1003, 2006.
393. Wang H, Sun Y, Wu W, et al: A novel missense mutation of FGFR3 in a Chinese female and her fetus with hypochondroplasia by next-generation sequencing. *Clin Chim Acta* 423:62–65, 2013.
394. Chen CP, Su YN, Lin TH, et al: Detection of a de novo Y278C mutation in FGFR3 in a pregnancy with severe fetal hypochondroplasia: prenatal diagnosis and literature review. *Taiwan J Obstet Gynecol* 52:580–585, 2013.
395. Heuertz S, Le Merrer M, Zabel B, et al: Novel FGFR3 mutations creating cysteine residues in the extracellular domain of the receptor cause achondroplasia or severe forms of hypochondroplasia. *Eur J Hum Genet* 14:1240–1247, 2006.
396. Ross JL, Bellus G, Scott CI, Jr, et al: Mesomelic and rhizomelic short stature: the phenotype of combined Leri-Weill dyschondrosteosis and achondroplasia or hypochondroplasia. *Am J Med Genet A* 116A:61–65, 2003.



397. Laurencikas E, Savendahl L, Jorulf H: Metacarpophalangeal pattern profile analysis: useful diagnostic tool for differentiating between dyschondrosteosis, Turner syndrome, and hypochondroplasia. *Acta Radiol* 47:518–524, 2006.
398. Chervenak FA, Isaacson G, Rosenberg JC, Kardon NB: Antenatal diagnosis of frontal cephalocele in a fetus with atelosteogenesis. *J Ultrasound Med* 5:111–113, 1986.
399. Hunt NC, Vujanic GM: Fibrochondrogenesis in a 17-week fetus: a case expanding the phenotype. *Am J Med Genet* 75:326–329, 1998.
400. Megarbane A, Haddad S, Berjaoui L: Prenatal ultrasonography: clinical and radiological findings in a boy with fibrochondrogenesis. *Am J Perinatol* 15:403–407, 1998.
401. Bejjani BA, Oberg KC, Wilkins I, et al: Prenatal ultrasonographic description and postnatal pathological findings in atelosteogenesis type 1. *Am J Med Genet* 79:392–395, 1998.
402. Schultz C, Langer LO, Laxova R, Pauli RM: Atelosteogenesis type III: long term survival, prenatal diagnosis, and evidence for dominant transmission. *Am J Med Genet* 83:28–42, 1999.
403. Ueno K, Tanaka M, Miyakoshi K, et al: Prenatal diagnosis of atelosteogenesis type I at 21 weeks' gestation. *Prenat Diagn* 22:1071–1075, 2002.
404. Randrianaivo H, Haddad G, Roman H, et al: Fetal fibrochondrogenesis at 26 weeks' gestation. *Prenat Diagn* 22:806–810, 2002.
405. Wessels MW, Den Hollander NS, De Krijger RR, et al: Prenatal diagnosis of boomerang dysplasia. *Am J Med Genet A* 122A:148–154, 2003.
406. Kulkarni ML, Matadh PS, Praveen Prabhu SP, Kulkarni PM: Fibrochondrogenesis. *Indian J Pediatr* 72:355–357, 2005.
407. Lazzaroni-Fossati F, Stanescu V, Stanescu R, et al: Fibrochondrogenesis. *Arch Fr Pediatr* 35:1096–1104, 1978.
408. Eteson DJ, Adomian GE, Ornoy A, et al: Fibrochondrogenesis: radiologic and histologic studies. *Am J Med Genet* 19:277–290, 1984.
409. Al-Gazali LI, Bakalinova D, Bakir M, Dawodu A: Fibrochondrogenesis: clinical and radiological features. *Clin Dysmorphol* 6:157–163, 1997.
410. Leeners B, Funk A, Cotarello CL, Sauer I: Two sibs with fibrochondrogenesis. *Am J Med Genet A* 127A:318–320, 2004.
411. Kunderangi NG, Taori K, Jathar C, Disawal A: Fibrochondrogenesis, an antenatal and postnatal correlation. *J Clin Imaging Sci* 2:5, 2012.
412. Whitley CB, Langer LO, Jr, Ophoven J, et al: Fibrochondrogenesis: lethal, autosomal recessive chondrodysplasia with distinctive cartilage histopathology. *Am J Med Genet* 19:265–275, 1984.
413. Martinez-Frias ML, Garcia A, Cuevas J, et al: A new case of fibrochondrogenesis from Spain. *J Med Genet* 33:429–431, 1996.
414. Al-Gazali LI, Bakir M, Dawodu A, Haas D: Recurrence of fibrochondrogenesis in a consanguineous family. *Clin Dysmorphol* 8:59–61, 1999.
415. Hall CM, Elcioglu NH: Metatropic dysplasia lethal variants. *Pediatr Radiol* 34:66–74, 2004.
416. Bekdache GN, Begam MA, Chedid F, et al: Fibrochondrogenesis: prenatal diagnosis and outcome. *J Obstet Gynaecol* 33:663–668, 2013.
417. Maroteaux P, Spranger J, Stanescu V, et al: Atelosteogenesis. *Am J Med Genet* 13:15–25, 1982.
418. Sillence DO, Lachman RS, Jenkins T, et al: Spondylohumerothoracic hypoplasia (giant cell chondrodysplasia): a neonatally lethal short-limbed skeletal dysplasia. *Am J Med Genet* 13:7–14, 1982.
419. Yang SS, Roskamp J, Liu CT, et al: Two lethal chondrodysplasias with giant chondrocytes. *Am J Med Genet* 15:615–625, 1983.
420. McAlister WH, Crane JR, Bucy RP, Craig RB: A new neonatal short limbed dwarfism. *Skeletal Radiol* 13:271–275, 1985.
421. Sillence D, Worthington S, Dixon J, et al: Atelosteogenesis syndromes: a review, with comments on their pathogenesis. *Pediatr Radiol* 27:388–396, 1997.
422. Krakow D, Robertson SP, King LM, et al: Mutations in the gene encoding filamin B disrupt vertebral segmentation, joint formation and skeletogenesis. *Nat Genet* 36:405–410, 2004.
423. Wessels A, Wainwright HC, Beighton P: Atelosteogenesis type I: autopsy findings. *Pediatr Dev Pathol* 14:496–500, 2011.
424. Rossi A, van der Harten HJ, Beemer FA, et al: Phenotypic and genotypic overlap between atelosteogenesis type 2 and diastrophic dysplasia. *Hum Genet* 98:657–661, 1996.
425. Newbury-Ecob R: Atelosteogenesis type 2. *J Med Genet* 35(1):49–53, 1998.
426. De la Chapelle A, Maroteaux P, Havu N, Granroth G: A rare lethal bone dysplasia with recessive autosomic transmission. *Arch Fr Pediatr* 29:759–770, 1972.
427. Whitley CB, Burke BA, Granroth G, Gorlin RJ: de la Chapelle dysplasia. *Am J Med Genet* 25(1):29–39, 1986.
428. Kozlowski K, Sillence D, Cortis-Jones R, Osborn R: Boomerang dysplasia. *Br J Radiol* 58:369–371, 1985.
429. Borochowitz Z, Ornoy A, Lachman R, Rimoin DL: Achondrogenesis II-hypochondrogenesis: variability versus heterogeneity. *Am J Med Genet* 24:273–288, 1986.
430. Borochowitz Z, Lachman R, Adomian GE, et al: Achondrogenesis type I: delineation of further heterogeneity and identification of two distinct subgroups. *J Pediatr* 112:23–31, 1988.
431. Godfrey M, Keene DR, Blank E, et al: Type II achondrogenesis-hypochondrogenesis: morphologic and immunohistopathologic studies. *Am J Hum Genet* 43:894–903, 1988.
432. van der Harten HJ, Brons JT, Dijkstra PF, et al: Achondrogenesis-hypochondrogenesis: the spectrum of chondrogenesis imperfecta. A radiological, ultrasonographic, and histopathologic study of 23 cases. *Pediatr Pathol* 8:571–597, 1988.
433. Murray LW, Bautista J, James PL, Rimoin DL: Type II collagen defects in the chondrodysplasias. I. Spondyloepiphyseal dysplasias. *Am J Hum Genet* 45:5–15, 1989.
434. Whitley CB, Gorlin RJ: Achondrogenesis: new nosology with evidence of genetic heterogeneity. *Radiology* 148:693–698, 1983.
435. Wenstrom KD, Williamson RA, Hoover WW, Grant SS: Achondrogenesis type II (Langer-Saldino) in association with jugular lymphatic obstruction sequence. *Prenat Diagn* 9:527–532, 1989.
436. Superti-Furga A, Hastbacka J, Wilcox WR, et al: Achondrogenesis type IB is caused by mutations in the diastrophic dysplasia sulphate transporter gene. *Nat Genet* 12:100–102, 1996.
437. Cai G, Nakayama M, Hiraki Y, Ozono K: Mutational analysis of the DTDST gene in a fetus with achondrogenesis type 1B. *Am J Med Genet* 78:58–60, 1998.
438. Won HS, Yoo HK, Lee PR, et al: A case of achondrogenesis type II associated with huge cystic hygroma: prenatal diagnosis by ultrasonography. *Ultrasound Obstet Gynecol* 14:288–290, 1999.
439. Golbus MS, Hall BD, Filly RA, Poskanzer LB: Prenatal diagnosis of achondrogenesis. *J Pediatr* 91:464–466, 1977.
440. Ozeren S, Yuksel A, Tukul T: Prenatal sonographic diagnosis of type I achondrogenesis with a large cystic hygroma. *Ultrasound Obstet Gynecol* 13:75–76, 1999.
441. Anteby SO, Aviad I, Weinstein D: Prenatal diagnosis of achondrogenesis. *Radiol Clin (Basel)* 46:109–114, 1977.
442. Smith WL, Breitweiser TD, Dinno N: In utero diagnosis of achondrogenesis, type I. *Clin Genet* 19:51–54, 1981.
443. Mahony BS, Filly RA, Cooperberg PL: Antenatal sonographic diagnosis of achondrogenesis. *J Ultrasound Med* 3:333–335, 1984.
444. Benacerraf B, Osathanondh R, Bieber FR: Achondrogenesis type I: ultrasound diagnosis in utero. *J Clin Ultrasound* 12:357–359, 1984.
445. Glenn LW, Teng SS: In utero sonographic diagnosis of achondrogenesis. *J Clin Ultrasound* 13:195–198, 1985.
446. Schramm T, Nerlich A: Sonographic diagnosis of a case of type I achondrogenesis in the 2d trimester. *Geburtshilfe Frauenheilkd* 49:917–919, 1989.
447. Balakumar K: Antenatal diagnosis of Parenti-Fraccaro type achondrogenesis. *Indian Pediatr* 27:496–499, 1990.
448. Jeesson UC, Prabhu S, Nambiar D: Prenatal diagnosis of achondrogenesis. *Indian Pediatr* 27:190–193, 1990.
449. Mandjee D, Clement F, Belin M, et al: Achondrogenesis. Ultrasonic diagnosis and clinical and anatomopathologic comparison. *Rev Fr Gynecol Obstet* 86:391–396, 399–400, 1991.



450. Boudier E, Zurlinden B, Cour A, et al: Antenatal diagnosis of achondrogenesis. Two successive cases in the same family. *J Gynecol Obstet Biol Reprod (Paris)* 20:623–626, 1991.
451. Tongsong T, Sirichotiyakul S, Siriangkul S: Prenatal diagnosis of congenital hypophosphatasia. *J Clin Ultrasound* 23:52–55, 1995.
452. Fisk NM, Vaughan J, Smidt M, Wigglesworth J: Transvaginal ultrasound recognition of nuchal edema in the first-trimester diagnosis of achondrogenesis. *J Clin Ultrasound* 19:586–590, 1991.
453. Luthy DA, Mack L, Hirsch J, Cheng E: Prenatal ultrasound diagnosis of thrombocytopenia with absent radii. *Am J Obstet Gynecol* 141:350–351, 1981.
454. Hastbacka J, Superti-Furga A, Wilcox WR, et al: Atelosteogenesis type II is caused by mutations in the diastrophic dysplasia sulfate-transporter gene (DTDST): evidence for a phenotypic series involving three chondrodysplasias. *Am J Hum Genet* 58:255–262, 1996.
455. Superti-Furga A: Achondrogenesis type IB. *J Med Genet* 33:957–961, 1996.
456. Smits P, Bolton AD, Funari V, et al: Lethal skeletal dysplasia in mice and humans lacking the golgin GMAP-210. *N Engl J Med* 362:206–216, 2010.
457. Hastbacka J, de la Chapelle A, Mahtani MM, et al: The diastrophic dysplasia gene encodes a novel sulfate transporter: positional cloning by fine-structure linkage disequilibrium mapping. *Cell* 78:1073–1087, 1994.
458. Dwyer E, Hyland J, Modaff P, Pauli RM: Genotype-phenotype correlation in DTDST dysplasias: atelosteogenesis type II and diastrophic dysplasia variant in one family. *Am J Med Genet A* 152A:3043–3050, 2010.
459. Vissing H, D'Alessio M, Lee B, et al: Glycine to serine substitution in the triple helical domain of pro- $\alpha$ 1 (II) collagen results in a lethal perinatal form of short-limbed dwarfism. *J Biol Chem* 264:18265–18267, 1989.
460. Comstock JM, Putnam AR, Sangle N, et al: Recurrence of achondrogenesis type 2 in sibs: additional evidence for germline mosaicism. *Am J Med Genet A* 152A:1822–1824, 2010.
461. Kuivaniemi H, Tromp G, Prockop DJ: Mutations in collagen genes: causes of rare and some common diseases in humans. *FASEB J* 5:2052–2060, 1991.
462. Byers PH, Steiner RD: Osteogenesis imperfecta. *Annu Rev Med* 43:269–282, 1992.
463. Willing MC, Pruchno CJ, Atkinson M, Byers PH: Osteogenesis imperfecta type I is commonly due to a COL1A1 null allele of type I collagen. *Am J Hum Genet* 51:508–515, 1992.
464. Wang Q, Orrison BM, Marini JC: Two additional cases of osteogenesis imperfecta with substitutions for glycine in the  $\alpha$ 2(I) collagen chain. A regional model relating mutation location with phenotype. *J Biol Chem* 268:25162–25167, 1993.
465. Willing MC, Deschenes SP, Slayton RL, Roberts EJ: Premature chain termination is a unifying mechanism for COL1A1 null alleles in osteogenesis imperfecta type I cell strains. *Am J Hum Genet* 59:799–809, 1996.
466. Dyne KM, Valli M, Forlino A, et al: Deficient expression of the small proteoglycan decorin in a case of severe/lethal osteogenesis imperfecta. *Am J Med Genet* 63:161–166, 1996.
467. Rauch F, Glorieux FH: Osteogenesis imperfecta. *Lancet* 363:1377–1385, 2004.
468. Orioli IM, Castilla EE, Scarano G, Mastroiacovo P: Effect of paternal age in achondroplasia, thanatophoric dysplasia, and osteogenesis imperfecta. *Am J Med Genet* 59:209–217, 1995.
469. Silience DO, Senn A, Danks DM: Genetic heterogeneity in osteogenesis imperfecta. *J Med Genet* 16:101–116, 1979.
470. Van Dijk FS, Pals G, Van Rijn RR, et al: Classification of osteogenesis imperfecta revisited. *Eur J Med Genet* 53:1–5, 2010.
471. Young ID, Thompson EM, Hall CM, Pembrey ME: Osteogenesis imperfecta type IIA: evidence for dominant inheritance. *J Med Genet* 24:386–389, 1987.
472. Silience DO, Barlow KK, Garber AP, et al: Osteogenesis imperfecta type II delineation of the phenotype with reference to genetic heterogeneity. *Am J Med Genet* 17:407–423, 1984.
473. Silience DO, Barlow KK, Cole WG, et al: Osteogenesis imperfecta type III. Delineation of the phenotype with reference to genetic heterogeneity. *Am J Med Genet* 23:821–832, 1986.
474. Andersen PE, Jr, Hauge M: Osteogenesis imperfecta: a genetic, radiological, and epidemiological study. *Clin Genet* 36:250–255, 1989.
475. Glorieux FH, Ward LM, Rauch F, et al: Osteogenesis imperfecta type VI: a form of brittle bone disease with a mineralization defect. *J Bone Miner Res* 17:30–38, 2002.
476. Ward LM, Rauch F, Travers R, et al: Osteogenesis imperfecta type VII: an autosomal recessive form of brittle bone disease. *Bone* 31:12–18, 2002.
477. Farber CR, Reich A, Barnes AM, et al: A novel IFITM5 mutation in severe atypical osteogenesis imperfecta type VI impairs osteoblast production of pigment epithelium-derived factor. *J Bone Miner Res* 29:1402–1411, 2014.
478. Forlino A, Marini JC: Osteogenesis imperfecta. *Lancet* Epub 2015 Nov 2.
479. Minillo RM, Sobreira N, de Faria Soares Mde F, et al: Novel deletion of SERPINF1 causes autosomal recessive osteogenesis imperfecta type vi in two Brazilian families. *Mol Syndromol* 5:268–275, 2014.
480. Glorieux FH, Rauch F, Plotkin H, et al: Type V osteogenesis imperfecta: a new form of brittle bone disease. *J Bone Miner Res* 15:1650–1658, 2000.
481. Marini JC, Cabral WA, Barnes AM: Null mutations in LEPRE1 and CRTAP cause severe recessive osteogenesis imperfecta. *Cell Tissue Res* 339:59–70, 2010.
482. Byers PH, Starman BJ, Cohn DH, Horwitz AL: A novel mutation causes a perinatal lethal form of osteogenesis imperfecta. An insertion in one  $\alpha$ 1 (I) collagen allele (COL1A1). *J Biol Chem* 263:7855–7861, 1988.
483. Wenstrup RJ, Cohn DH, Cohen T, Byers PH: Arginine for glycine substitution in the triple-helical domain of the products of one  $\alpha$ 2(I) collagen allele (COL1A2) produces the osteogenesis imperfecta type IV phenotype. *J Biol Chem* 263:7734–7740, 1988.
484. Barsh GS, Byers PH: Reduced secretion of structurally abnormal type I procollagen in a form of osteogenesis imperfecta. *Proc Natl Acad Sci U S A* 78:5142–5146, 1981.
485. Chu ML, Gargiulo V, Williams CJ, Ramirez F: Multiexon deletion in an osteogenesis imperfecta variant with increased type III collagen mRNA. *J Biol Chem* 260:691–694, 1985.
486. Chervenak FA, Romero R, Berkowitz RL, et al: Antenatal sonographic findings of osteogenesis imperfecta. *Am J Obstet Gynecol* 143:228–230, 1982.
487. Milsom I, Mattsson LA, Dahlen-Nilsson I: Antenatal diagnosis of osteogenesis imperfecta by real time ultrasound: two case reports. *Br J Radiol* 55:310–312, 1982.
488. Elejalde BR, de Elejalde MM: Prenatal diagnosis of perinatally lethal osteogenesis imperfecta. *Am J Med Genet* 14:353–359, 1983.
489. Griffin ER, 3rd, Webster JC, Almarino VP: Ultrasonic and radiological features of osteogenesis imperfecta congenita: case report. *Mil Med* 148(2):157–158, 1983.
490. Patel ZM, Shah HL, Madon PF, Ambani LM: Prenatal diagnosis of lethal osteogenesis imperfecta (OI) by ultrasonography. *Prenat Diagn* 3:261–263, 1983.
491. Stephens JD, Filly RA, Callen PW, Golbus MS: Prenatal diagnosis of osteogenesis imperfecta type II by real-time ultrasound. *Hum Genet* 64:191–193, 1983.
492. Woo JS, Ghosh A, Liang ST, Wong VC: Ultrasonic evaluation of osteogenesis imperfecta congenita in utero. *J Clin Ultrasound* 11:42–44, 1983.
493. Aylsworth AS, Seeds JW, Guilford WB, et al: Prenatal diagnosis of a severe deforming type of osteogenesis imperfecta. *Am J Med Genet* 19:707–714, 1984.
494. Brown BS: The prenatal ultrasonographic diagnosis of osteogenesis imperfecta lethalis. *J Can Assoc Radiol* 35:63–66, 1984.
495. Ghosh A, Woo JS, Wan CW, Wong VC: Simple ultrasonic diagnosis of osteogenesis imperfecta type II in early second trimester. *Prenat Diagn* 4:235–240, 1984.
496. Bradley FJ, Essex T: Osteogenesis imperfecta: report of 2 cases. *J Am Osteopath Assoc* 85:462–466, 1985.



497. Carpenter MW, Abuelo D, Neave C: Midtrimester diagnosis of severe deforming osteogenesis imperfecta with autosomal dominant inheritance. *Am J Perinatol* 3:80–83, 1986.
498. Merz E, Goldhofer W: Sonographic diagnosis of lethal osteogenesis imperfecta in the second trimester: case report and review. *J Clin Ultrasound* 14:380–383, 1986.
499. Brons JT, van der Harten HJ, Wladimiroff JW, et al: Prenatal ultrasonographic diagnosis of osteogenesis imperfecta. *Am J Obstet Gynecol* 159:176–181, 1988.
500. Munoz C, Filly RA, Golbus MS: Osteogenesis imperfecta type II: prenatal sonographic diagnosis. *Radiology* 174:181–185, 1990.
501. Pfutzenreuter N, Panzer F, Bastert G: Prenatal diagnosis of osteogenesis imperfecta congenita; a case report. *Eur J Obstet Gynecol Reprod Biol* 34:189–194, 1990.
502. Constantine G, McCormack J, McHugo J, Fowlie A: Prenatal diagnosis of severe osteogenesis imperfecta. *Prenat Diagn* 11:103–110, 1991.
503. Morin LR, Herlicovitz M, Loisel JC, et al: Prenatal diagnosis of lethal osteogenesis imperfecta in twin pregnancy. *Clin Genet* 39:467–470, 1991.
504. D'Ottavio G, Tamaro LF, Mandruzzato G: Early prenatal ultrasonographic diagnosis of osteogenesis imperfecta: a case report. *Am J Obstet Gynecol* 169:384–385, 1993.
505. Berge LN, Marton V, Tranebjaerg L, et al: Prenatal diagnosis of osteogenesis imperfecta. *Acta Obstet Gynecol Scand* 74:321–323, 1995.
506. Chen FP, Chang LC: Prenatal diagnosis of osteogenesis imperfecta congenita by ultrasonography. *J Formos Med Assoc* 95:386–389, 1996.
507. Tongsong T, Wanapirak C, Siringkul S: Prenatal diagnosis of osteogenesis imperfecta type II. *Int J Gynaecol Obstet* 61:33–38, 1998.
508. DiMaio MS, Barth R, Koprivnikar KE, et al: First-trimester prenatal diagnosis of osteogenesis imperfecta type II by DNA analysis and sonography. *Prenat Diagn* 13:589–596, 1993.
509. Buisson O, Senat MV, Laurenceau N, Ville Y: Update on prenatal diagnosis of osteogenesis imperfecta type II: an index case report diagnosed by ultrasonography in the first trimester. *J Gynecol Obstet Biol Reprod (Paris)* 31:672–676, 2002.
510. McEwing RL, Alton K, Johnson J, et al: First-trimester diagnosis of osteogenesis imperfecta type II by three-dimensional sonography. *J Ultrasound Med* 22:311–314, 2003.
511. Ruano R, Picone O, Benachi A, et al: First-trimester diagnosis of osteogenesis imperfecta associated with encephalocele by conventional and three-dimensional ultrasound. *Prenat Diagn* 23:539–542, 2003.
512. Bulas DI, Stern HJ, Rosenbaum KN, et al: Variable prenatal appearance of osteogenesis imperfecta. *J Ultrasound Med* 13:419–427, 1994.
513. Bishop NJ: Osteogenesis imperfecta calls for caution. *Nat Med* 5:466–467, 1999.
514. Bischoff H, Freitag P, Jundt G, et al: Type I osteogenesis imperfecta: diagnostic difficulties. *Clin Rheumatol* 18:48–51, 1999.
515. Robinson LP, Worthen NJ, Lachman RS, et al: Prenatal diagnosis of osteogenesis imperfecta type III. *Prenat Diagn* 7:7–15, 1987.
516. Thompson EM: Non-invasive prenatal diagnosis of osteogenesis imperfecta. *Am J Med Genet* 45:201–206, 1993.
517. Pepin M, Atkinson M, Starman BJ, Byers PH: Strategies and outcomes of prenatal diagnosis for osteogenesis imperfecta: a review of biochemical and molecular studies completed in 129 pregnancies. *Prenat Diagn* 17:559–570, 1997.
518. Nuytinck L, Sayli BS, Karen W, De Paep A: Prenatal diagnosis of osteogenesis imperfecta type I by COL1A1 null-allele testing. *Prenat Diagn* 19:873–875, 1999.
519. Ries L, Frydman M, Barkai G, et al: Prenatal diagnosis of a novel COL1A1 mutation in osteogenesis imperfecta type I carried through full term pregnancy. *Prenat Diagn* 20:876–880, 2000.
520. Mornet E, Simon-Bouy B: Genetics of hypophosphatasia. *Arch Pediatr* 11:444–448, 2004.
521. Mornet E, Muller F, Ngo S, et al: Correlation of alkaline phosphatase (ALP) determination and analysis of the tissue non-specific ALP gene in prenatal diagnosis of severe hypophosphatasia. *Prenat Diagn* 19:755–757, 1999.
522. Mornet E, Nunes ME: Hypophosphatasia. In Pagon RA, Adam MP, Ardinger HH, et al, editors: *GeneReviews*, Seattle, 1993–2016, University of Washington.
523. Komaru K, Ishida Y, Amaya Y, et al: Novel aggregate formation of a frame-shift mutant protein of tissue-nonspecific alkaline phosphatase is ascribed to three cysteine residues in the C-terminal extension. Retarded secretion and proteasomal degradation. *FEBS J* 272(7):1704–1717, 2005.
524. Vandevijver N, De Die-Smulders CE, Offermans JP, et al: Lethal hypophosphatasia, spur type: case report and fetopathological study. *Genet Couns* 9:205–209, 1998.
525. Whyte MP: Hypophosphatasia and the role of alkaline phosphatase in skeletal mineralization. *Endocr Rev* 15:439–461, 1994.
526. Terada S, Suzuki N, Ueno H, et al: A congenital lethal form of hypophosphatasia: histologic and ultrastructural study. *Acta Obstet Gynecol Scand* 75:502–505, 1996.
527. Sergi C, Mornet E, Troeger J, Voigtlaender T: Perinatal hypophosphatasia: radiology, pathology and molecular biology studies in a family harboring a splicing mutation (648+1A) and a novel missense mutation (N400S) in the tissue-nonspecific alkaline phosphatase (TNSALP) gene. *Am J Med Genet* 103:235–240, 2001.
528. Sawai H, Kanazawa N, Tsukahara Y, et al: Severe perinatal hypophosphatasia due to homozygous deletion of T at nucleotide 1559 in the tissue nonspecific alkaline phosphatase gene. *Prenat Diagn* 23:743–746, 2003.
529. Guguloth A, Aswani Y, Anandpara KM: Prenatal diagnosis of hypophosphatasia congenita using ultrasonography. *Ultrasonography* 35(1):83–86, 2016.
530. Wladimiroff JW, Niermeijer MF, Van der Harten JJ, et al: Early prenatal diagnosis of congenital hypophosphatasia: case report. *Prenat Diagn* 5:47–52, 1985.
531. Warren RC, McKenzie CF, Rodeck CH, et al: First trimester diagnosis of hypophosphatasia with a monoclonal antibody to the liver/bone/kidney isoenzyme of alkaline phosphatase. *Lancet* 2:856–858, 1985.
532. Yagel S, Milwidsky A, Ornoy A, et al: Imaging case of the month. Hypophosphatasia. *Am J Perinatol* 2:261–262, 1985.
533. DeLange M, Rouse GA: Prenatal diagnosis of hypophosphatasia. *J Ultrasound Med* 9:115–117, 1990.
534. Hall C: Pre-natal diagnosis of lethal dwarfism using ultrasound. *Radiogr Today* 57(654):22–23, 1991.
535. Kleinman G, Uri M, Hull S, Keene C: Perinatal ultrasound casebook. Antenatal findings in congenital hypophosphatasia. *J Perinatol* 11:282–284, 1991.
536. Moore CA, Curry CJ, Henthorn PS, et al: Mild autosomal dominant hypophosphatasia: in utero presentation in two families. *Am J Med Genet* 86:410–415, 1999.
537. Pauli RM, Modaff P, Sipes SL, Whyte MP: Mild hypophosphatasia mimicking severe osteogenesis imperfecta in utero: bent but not broken. *Am J Med Genet* 86:434–438, 1999.
538. Gortzak-Uzan L, Sheiner E, Gohar J: Prenatal diagnosis of congenital hypophosphatasia in a consanguineous Bedouin couple. A case report. *J Reprod Med* 45:588–590, 2000.
539. Tongsong T, Pongsatha S: Early prenatal sonographic diagnosis of congenital hypophosphatasia. *Ultrasound Obstet Gynecol* 15:252–255, 2000.
540. Zankl A, Mornet E, Wong S: Specific ultrasonographic features of perinatal lethal hypophosphatasia. *Am J Med Genet A* 146A(9):1200–1204, 2008.
541. Sinico M, Levaillant JM, Vergnaud A, et al: Specific osseous spurs in a lethal form of hypophosphatasia correlated with 3D prenatal ultrasonographic images. *Prenat Diagn* 27:222–227, 2007.
542. Brock DJ, Barron L: First-trimester prenatal diagnosis of hypophosphatasia: experience with 16 cases. *Prenat Diagn* 11:387–391, 1991.
543. Sato S, Matsuo N: Genetic analysis of hypophosphatasia. *Acta Paediatr Jpn* 39:528–532, 1997.
544. Rudd NL, Miskin M, Hoar DJ, et al: Prenatal diagnosis of hypophosphatasia. *N Engl J Med* 295:146–148, 1976.



545. Rattenbury JM, Blau K, Sandler M, et al: Letter: Prenatal diagnosis of hypophosphatasia. *Lancet* 1(7954):306, 1976.
546. Orimo H, Nakajima E, Hayashi Z, et al: First-trimester prenatal molecular diagnosis of infantile hypophosphatasia in a Japanese family. *Prenat Diagn* 16:559–563, 1996.
547. Henthorn PS, Whyte MP: Infantile hypophosphatasia: successful prenatal assessment by testing for tissue-non-specific alkaline phosphatase isoenzyme gene mutations. *Prenat Diagn* 15:1001–1006, 1995.
548. Weiss MJ, Cole DE, Ray K, et al: A missense mutation in the human liver/bone/kidney alkaline phosphatase gene causing a lethal form of hypophosphatasia. *Proc Natl Acad Sci U S A* 85:7666–7669, 1988.
549. Smith M, Weiss MJ, Griffin CA, et al: Regional assignment of the gene for human liver/bone/kidney alkaline phosphatase to chromosome 1p36.1-p34. *Genomics* 2:139–143, 1988.
550. Watanabe A, Yamamasu S, Shinagawa T, et al: Prenatal genetic diagnosis of severe perinatal (lethal) hypophosphatasia. *J Nippon Med Sch* 74:65–69, 2007.
551. Watanabe A, Satoh S, Fujita A, et al: Perinatal hypophosphatasia caused by uniparental isodisomy. *Bone* 60:93–97, 2014.
552. Mornet E, Taillandier A, Peyramaure S, et al: Identification of fifteen novel mutations in the tissue-nonspecific alkaline phosphatase (TNSALP) gene in European patients with severe hypophosphatasia. *Eur J Hum Genet* 6:308–314, 1998.
553. Suzumori N, Mornet E, Mizutani E, et al: Prenatal diagnosis of familial lethal hypophosphatasia using imaging, blood enzyme levels, chorionic villus sampling and archived fetal tissue. *J Obstet Gynaecol Res* 37:1470–1473, 2011.
554. Simon-Bouy B, Taillandier A, Fauvert D, et al: Hypophosphatasia: molecular testing of 19 prenatal cases and discussion about genetic counseling. *Prenat Diagn* 28:993–998, 2008.
555. Zurutuza L, Muller F, Gibrat JF, et al: Correlations of genotype and phenotype in hypophosphatasia. *Hum Mol Genet* 8:1039–1046, 1999.
556. Honorio JC, Bruns RF, Grundtner LF, et al: Diastrophic dysplasia: prenatal diagnosis and review of the literature. *Sao Paulo Med J* 131:127–132, 2013.
557. Horton WA, Rimoin DL, Lachman RS, et al: The phenotypic variability of diastrophic dysplasia. *J Pediatr* 93:609–613, 1978.
558. Kaitila I, Ammala P, Karjalainen O, et al: Early prenatal detection of diastrophic dysplasia. *Prenat Diagn* 3:237–244, 1983.
559. Canto MJ, Buixeda M, Palau J, Ojeda F: Early ultrasonographic diagnosis of diastrophic dysplasia at 12 weeks of gestation in a fetus without previous family history. *Prenat Diagn* 27:976–978, 2007.
560. Hastbacka J, Kaitila I, Sistonen P, de la Chapelle A: Diastrophic dysplasia gene maps to the distal long arm of chromosome 5. *Proc Natl Acad Sci U S A* 87:8056–8059, 1990.
561. Rossi A, Superti-Furga A: Mutations in the diastrophic dysplasia sulfate transporter (DTDST) gene (SLC26A2): 22 novel mutations, mutation review, associated skeletal phenotypes, and diagnostic relevance. *Hum Mutat* 17:159–171, 2001.
562. Karniski LP: Mutations in the diastrophic dysplasia sulfate transporter (DTDST) gene: correlation between sulfate transport activity and chondrodysplasia phenotype. *Hum Mol Genet* 10:1485–1490, 2001.
563. Megarbane A, Farkh I, Haddad-Zebouni S: How many phenotypes in the DTDST family chondrodysplasias? *Clin Genet* 62:189–190, 2002.
564. Gollop TR, Eigier A: Prenatal ultrasound diagnosis of diastrophic dysplasia at 16 weeks. *Am J Med Genet* 27:321–324, 1987.
565. Jung C, Sohn C, Sergi C: Case report: prenatal diagnosis of diastrophic dysplasia by ultrasound at 21 weeks of gestation in a mother with massive obesity. *Prenat Diagn* 18:378–383, 1998.
566. Severi FM, Bocchi C, Sanseverino F, Petraglia F: Prenatal ultrasonographic diagnosis of diastrophic dysplasia at 13 weeks of gestation. *J Matern Fetal Neonatal Med* 13:282–284, 2003.
567. Wax JR, Carpenter M, Smith W, et al: Second-trimester sonographic diagnosis of diastrophic dysplasia: report of 2 index cases. *J Ultrasound Med* 22:805–808, 2003.
568. Sepulveda W, Sepulveda-Swatson E, Sanchez J: Diastrophic dysplasia: prenatal three-dimensional ultrasound findings. *Ultrasound Obstet Gynecol* 23:312–314, 2004.
569. Hastbacka J, Salonen R, Laurila P, et al: Prenatal diagnosis of diastrophic dysplasia with polymorphic DNA markers. *J Med Genet* 30:265–268, 1993.
570. Remes V, Helenius I, Peltonen J, et al: Lung function in diastrophic dysplasia. *Pediatr Pulmonol* 33:277–282, 2002.
571. Eteson DJ, Beluffi G, Burgio GR, et al: Pseudodiastrophic dysplasia: a distinct newborn skeletal dysplasia. *J Pediatr* 109:635–641, 1986.
572. Cetta G, Rossi A, Burgio GR, Beluffi G: Diastrophic dysplasia sulfate transporter (DTDST) gene is not involved in pseudodiastrophic dysplasia. *Am J Med Genet* 73:493–494, 1997.
573. Kniest W: Differential diagnosis between dysostosis enchondralis and chondrodystrophy. *Z Kinderheilkd* 70:633–640, 1952.
574. Siggers CD, Rimoin DL, Dorst JP, et al: The Kniest syndrome. *Birth Defects Orig Artic Ser* 10:193–208, 1974.
575. Winterpacht A, Hilbert M, Schwarze U, et al: Kniest and Stickler dysplasia phenotypes caused by collagen type II gene (COL2A1) defect. *Nat Genet* 3:323–326, 1993.
576. Fernandes RJ, Wilkin DJ, Weis MA, et al: Incorporation of structurally defective type II collagen into cartilage matrix in kniest chondrodysplasia. *Arch Biochem Biophys* 355:282–290, 1998.
577. Weis MA, Wilkin DJ, Kim HJ, et al: Structurally abnormal type II collagen in a severe form of Kniest dysplasia caused by an exon 24 skipping mutation. *J Biol Chem* 273:4761–4768, 1998.
578. Wilkin DJ, Bogaert R, Lachman RS, et al: A single amino acid substitution (G103D) in the type II collagen triple helix produces Kniest dysplasia. *Hum Mol Genet* 3:1999–2003, 1994.
579. Nishimura G, Haga N, Kitoh H, et al: The phenotypic spectrum of COL2A1 mutations. *Hum Mutat* 26:36–43, 2005.
580. Wada R, Sawai H, Nishimura G, et al: Prenatal diagnosis of Kniest dysplasia with three-dimensional helical computed tomography. *J Matern Fetal Neonatal Med* 24:1181–1184, 2011.
581. Yazici Z, Kline-Fath BM, Laor T, et al: Fetal MR imaging of Kniest dysplasia. *Pediatr Radiol* 40:348–352, 2010.
582. Chen H, Yang SS, Gonzalez E: Kniest dysplasia: neonatal death with necropsy. *Am J Med Genet* 6:171–178, 1980.
583. Handmaker SD, Campbell JA, Robinson LD, et al: Dyssegmental dwarfism: a new syndrome of lethal dwarfism. *Birth Defects Orig Artic Ser* 13:79–90, 1977.
584. Aleck KA, Grix A, Clericuzio C, et al: Dyssegmental dysplasias: clinical, radiographic, and morphologic evidence of heterogeneity. *Am J Med Genet* 27:295–312, 1987.
585. Andersen PE, Jr, Hauge M, Bang J: Dyssegmental dysplasia in siblings: prenatal ultrasonic diagnosis. *Skeletal Radiol* 17:29–31, 1988.
586. Prabhu VG, Kozma C, Leftridge CA, et al: Dyssegmental dysplasia Silverman-Handmaker type in a consanguineous Druze Lebanese family: long term survival and documentation of the natural history. *Am J Med Genet* 75:164–170, 1998.
587. Stoll C, Alembik Y, Repetto M: Congenital bilateral fibular deficiency with facial dysmorphism, brachydactyly and mental retardation in a girl. *Genet Couns* 9:147–152, 1998.
588. Fasanelli S, Kozlowski K, Reiter S, Sillence D: Dyssegmental dysplasia (report of two cases with a review of the literature). *Skeletal Radiol* 14:173–177, 1985.
589. Kim HJ, Costales F, Bouzouki M, Wallach RC: Prenatal diagnosis of dyssegmental dwarfism. *Prenat Diagn* 6:143–150, 1986.
590. Izquierdo LA, Kushnir O, Aase J, et al: Antenatal ultrasonic diagnosis of dyssegmental dysplasia: a case report. *Prenat Diagn* 10:587–592, 1990.
591. Hsieh YY, Chang CC, Tsai HD, et al: Prenatal diagnosis of dyssegmental dysplasia. A case report. *J Reprod Med* 44:303–305, 1999.
592. Arikawa-Hirasawa E, Wilcox WR, Le AH, et al: Dyssegmental dysplasia, Silverman-Handmaker type, is caused by functional null mutations of the perlecan gene. *Nat Genet* 27:431–434, 2001.
593. Rieubland C, Jacquemont S, Mittaz L, et al: Phenotypic and molecular characterization of a novel case of dyssegmental dysplasia, Silverman-Handmaker type. *Eur J Med Genet* 53:294–298, 2010.
594. Ladhani NN, Chitayat D, Nezarati MM, et al: Dyssegmental dysplasia, Silverman-Handmaker type: prenatal ultrasound findings and molecular analysis. *Prenat Diagn* 33:1039–1043, 2013.



595. Uchide K, Ueno H, Takizawa N, Okada Y: Reduced levels of MMP-2 and TIMP-1 in dyssegmental dysplasia. *J Bone Miner Res* 18:381–382, 2003.
596. Mansour S, Hall CM, Pembrey ME, Young ID: A clinical and genetic study of campomelic dysplasia. *J Med Genet* 32:415–420, 1995.
597. Normann EK, Pedersen JC, Stüris G, van der Hagen CB: Campomelic dysplasia—an underdiagnosed condition? *Eur J Pediatr* 152:331–333, 1993.
598. Houston CS, Opitz JM, Spranger JW, et al: The campomelic syndrome: review, report of 17 cases, and follow-up on the currently 17-year-old boy first reported by Maroteaux et al in 1971. *Am J Med Genet* 15:3–28, 1983.
599. Fryns JP, van den Berghe K, van Assche A, van den Berghe H: Prenatal diagnosis of campomelic dwarfism. *Clin Genet* 19:199–201, 1981.
600. Cordone M, Lituania M, Zampatti C, et al: In utero ultrasonographic features of campomelic dysplasia. *Prenat Diagn* 9:745–750, 1989.
601. Sanders RC, Greyson-Fleg RT, Hogge WA, et al: Osteogenesis imperfecta and campomelic dysplasia: difficulties in prenatal diagnosis. *J Ultrasound Med* 13:691–700, 1994.
602. Tongsong T, Wanapirak C, Pongsatha S: Prenatal diagnosis of campomelic dysplasia. *Ultrasound Obstet Gynecol* 15:428–430, 2000.
603. Wunderle VM, Critcher R, Hastie N, et al: Deletion of long-range regulatory elements upstream of SOX9 causes campomelic dysplasia. *Proc Natl Acad Sci U S A* 95:10649–10654, 1998.
604. Kanai Y, Hiramatsu R, Matoba S, Kidokoro T: From SRY to SOX9: mammalian testis differentiation. *J Biochem* 138:13–19, 2005.
605. Goji K, Nishijima E, Tsugawa C, et al: Novel missense mutation in the HMG box of SOX9 gene in a Japanese XY male resulted in campomelic dysplasia and severe defect in masculinization. *Hum Mutat Suppl* 1:S114–S116, 1998.
606. Hageman RM, Cameron FJ, Sinclair AH: Mutation analysis of the SOX9 gene in a patient with campomelic dysplasia. *Hum Mutat Suppl* 1:S112–S113, 1998.
607. McDowall S, Argentaro A, Ranganathan S, et al: Functional and structural studies of wild type SOX9 and mutations causing campomelic dysplasia. *J Biol Chem* 274:24023–24030, 1999.
608. Pop R, Zaragoza MV, Gaudette M, et al: A homozygous nonsense mutation in SOX9 in the dominant disorder campomelic dysplasia: a case of mitotic gene conversion. *Hum Genet* 117:43–53, 2005.
609. Maraia R, Saal HM, Wangsa D: A chromosome 17q de novo paracentric inversion in a patient with campomelic dysplasia: case report and etiologic hypothesis. *Clin Genet* 39:401–408, 1991.
610. Young ID, Zuccollo JM, Maltby EL, Broderick NJ: Campomelic dysplasia associated with a de novo 2q;17q reciprocal translocation. *J Med Genet* 29:251–252, 1992.
611. Tommerup N, Schempp W, Meinecke P, et al: Assignment of an autosomal sex reversal locus (SRA1) and campomelic dysplasia (CMPD1) to 17q24.3-q25.1. *Nat Genet* 4:170–174, 1993.
612. Ninomiya S, Narahara K, Tsuji K, et al: Acampomelic campomelic syndrome and sex reversal associated with de novo t(12;17) translocation. *Am J Med Genet* 56:31–34, 1995.
613. Savarirayan R, Bankier A: Acampomelic campomelic dysplasia with de novo 5q;17q reciprocal translocation and severe phenotype. *J Med Genet* 35:597–599, 1998.
614. Pfeifer D, Kist R, Dewar K, et al: Campomelic dysplasia translocation breakpoints are scattered over 1 Mb proximal to SOX9: evidence for an extended control region. *Am J Hum Genet* 65:111–124, 1999.
615. Beluffi G, Fraccaro M: Genetical and clinical aspects of campomelic dysplasia. *Prog Clin Biol Res* 104:53–68, 1982.
616. Ray S, Bowen JR: Orthopaedic problems associated with survival in campomelic dysplasia. *Clin Orthop Relat Res* 185:77–82, 1984.
617. Cooke CT, Mulcahy MT, Cullity GJ, et al: Campomelic dysplasia with sex reversal: morphological and cytogenetic studies of a case. *Pathology* 17:526–529, 1985.
618. Offiah AC, Mansour S, McDowall S, et al: Surviving campomelic dysplasia has the radiological features of the previously reported ischio-pubic-patella syndrome. *J Med Genet* 39(9):e50, 2002.
619. Mansour S, Offiah AC, McDowall S, et al: The phenotype of survivors of campomelic dysplasia. *J Med Genet* 39:597–602, 2002.
620. Romero R, Ghidini A, Eswara MS, et al: Prenatal findings in a case of spondylocostal dysplasia type I (Jarcho-Levin syndrome). *Obstet Gynecol* 71:988–991, 1988.
621. Jeune M, Beraud C, Carron R: Asphyxiating thoracic dystrophy with familial characteristics. *Arch Fr Pediatr* 12:886–891, 1955.
622. Kozlowski K, Masel J: Asphyxiating thoracic dystrophy without respiratory disease: report of two cases of the latent form. *Pediatr Radiol* 5:30–33, 1976.
623. Maarup LP, Host A: The Jeune syndrome, asphyxiating thoracic dysplasia. A review and description of 2 sibs. *Ugeskr Laeger* 147(21):1676–1678, 1985.
624. Capilupi B, Olappi G, Cornaglia AM, Novati GP: Asphyxiating thoracic dysplasia or Jeune's syndrome. Description of 2 mild familial cases. *Pediatr Med Chir* 18:529–532, 1996.
625. Chen CP, Lin SP, Liu FF, et al: Prenatal diagnosis of asphyxiating thoracic dysplasia (Jeune syndrome). *Am J Perinatol* 13(8):495–498, 1996.
626. Tuysuz B, Baris S, Aksoy F, et al: Clinical variability of asphyxiating thoracic dystrophy (Jeune) syndrome: evaluation and classification of 13 patients. *Am J Med Genet A* 149A:1727–1733, 2009.
627. Poggiani C, Gasparoni MC, Mangili G, Colombo A: Asphyxiating thoracic dysplasia in a lethal form: radiological and sonographic findings. *Minerva Pediatr* 52:63–67, 2000.
628. Giorgi PL, Gabrielli O, Bonifazi V, et al: Mild form of Jeune syndrome in two sisters. *Am J Med Genet* 35:280–282, 1990.
629. Reiterer F, Muller WD, Wendler H: Variance in the clinical picture and course of asphyxiating thoracic dysplasia (Jeune syndrome). *Klin Padiatr* 198:340–343, 1986.
630. Edelson PJ, Spackman TJ, Belliveau RE, Mahoney MJ: A renal lesion in asphyxiating thoracic dysplasia. *Birth Defects Orig Artic Ser* 10:51–56, 1974.
631. Caraballo A, Lopez Barrios A, Martin Govantes J, et al: Thoracic asphyxiating dystrophy and renal disease (author's transl). *An Esp Pediatr* 10(1):88–95, 1977.
632. Shah KJ: Renal lesion in Jeune's syndrome. *Br J Radiol* 53:432–436, 1980.
633. Bernstein R, Isdale J, Pinto M, et al: Short rib-polydactyly syndrome: a single or heterogeneous entity? A re-evaluation prompted by four new cases. *J Med Genet* 22:46–53, 1985.
634. Donaldson MD, Warner AA, Trompeter RS, et al: Familial juvenile nephronophthisis, Jeune's syndrome, and associated disorders. *Arch Dis Child* 60:426–434, 1985.
635. Ring E, Zobel G, Ratschek M, et al: Retrospective diagnosis of Jeune's syndrome in two patients with chronic renal failure. *Child Nephrol Urol* 10:88–91, 1990.
636. Clayton-Smith J: Jeune syndrome and cystinuria. *Am J Med Genet* 41:531–532, 1991.
637. Redmond J, 3rd, Richter MP, Stein HD, et al: Primitive neuroectodermal tumor of the chest wall in a patient with Jeune's syndrome and renal transplant. *Am J Kidney Dis* 21:449–451, 1993.
638. Novakovic I, Kostic M, Popovic-Rolovic M, et al: Jeune's syndrome (3 case reports). *Srp Arh Celok Lek* 124(Suppl 1):244–246, 1996.
639. Amirou M, Bourdat-Michel G, Pinel N, et al: Successful renal transplantation in Jeune syndrome type 2. *Pediatr Nephrol* 12:293–294, 1998.
640. Ozcay F, Derbent M, Demirhan B, et al: A family with Jeune syndrome. *Pediatr Nephrol* 16:623–626, 2001.
641. Banerjee D, Desai A, Burke GW, Roth D: Retransplantation in a patient with type 2 Jeune's syndrome. *Am J Kidney Dis* 39:E9, 2002.
642. Tongsong T, Chanprapaph P, Thongpadungroj T: Prenatal sonographic findings associated with asphyxiating thoracic dystrophy (Jeune syndrome). *J Ultrasound Med* 18:573–576, 1999.
643. Herdman RC, Langer LO: The thoracic asphyxiating dystrophy and renal disease. *Am J Dis Child* 116:192–201, 1968.
644. Whitley CB, Schwarzenberg SJ, Burke BA, et al: Direct hyperbilirubinemia and hepatic fibrosis: a new presentation of Jeune syndrome (asphyxiating thoracic dystrophy). *Am J Med Genet Suppl* 3:211–220, 1987.



645. Landing BH, Wells TR, Lipsey AI, Oyemade OA: Morphometric studies of cystic and tubulointerstitial kidney diseases with hepatic fibrosis in children. *Pediatr Pathol* 10:959–972, 1990.
646. Trabelsi M, Hammou-Jeddi A, Kammoun A, et al: Asphyxiating thoracic dysplasia associated with hepatic ductal hypoplasia, agenesis of the corpus callosum and Dandy-Walker syndrome. *Pediatrie* 45(1):35–38, 1990.
647. Labrune P, Fabre M, Trioche P, et al: Jeune syndrome and liver disease: report of three cases treated with ursodeoxycholic acid. *Am J Med Genet* 87:324–328, 1999.
648. Esmer C, Alvarez-Mendoza A, Lieberman E, et al: Liver fibrocystic disease and polydactyly: proposal of a new syndrome. *Am J Med Genet* 101:12–16, 2001.
649. Yerian LM, Brady L, Hart J: Hepatic manifestations of Jeune syndrome (asphyxiating thoracic dystrophy). *Semin Liver Dis* 23:195–200, 2003.
650. Hopper MS, Boulton JE, Watson AR: Polyhydramnios associated with congenital pancreatic cysts and asphyxiating thoracic dysplasia. A case report. *S Afr Med J* 56(1):32–33, 1979.
651. Georgiou-Theodoropoulos M, Agapitos M, Theodoropoulos P, Koutselinis A: Jeune syndrome associated with pancreatic fibrosis. *Pediatr Pathol* 8:541–544, 1988.
652. Phillips CI, Stokoe NL, Bartholomew RS: Asphyxiating thoracic dystrophy (Jeune's disease) with retinal aplasia: a sibship of two. *J Pediatr Ophthalmol Strabismus* 16(5):279–283, 1979.
653. Wilson DJ, Weleber RG, Beals RK: Retinal dystrophy in Jeune's syndrome. *Arch Ophthalmol* 105:651–657, 1987.
654. Casteels I, Demandt E, Legius E: Visual loss as the presenting sign of Jeune syndrome. *Eur J Paediatr Neurol* 4:243–247, 2000.
655. Elejalde BR, de Elejalde MM, Pansch D: Prenatal diagnosis of Jeune syndrome. *Am J Med Genet* 21:433–438, 1985.
656. Schinzel A, Savoldelli G, Briner J, Schubiger G: Prenatal sonographic diagnosis of Jeune syndrome. *Radiology* 154:777–778, 1985.
657. den Hollander NS, Robben SG, Hoogeboom AJ, et al: Early prenatal sonographic diagnosis and follow-up of Jeune syndrome. *Ultrasound Obstet Gynecol* 18:378–383, 2001.
658. Tahernia AC, Stamps P: "Jeune syndrome" (asphyxiating thoracic dystrophy). Report of a case, a review of the literature, and an editor's commentary. *Clin Pediatr (Phila)* 16:903–908, 1977.
659. Lipson M, Waskey J, Rice J, et al: Prenatal diagnosis of asphyxiating thoracic dysplasia. *Am J Med Genet* 18:273–277, 1984.
660. Bernstein J: Glomerulocystic kidney disease—nosological considerations. *Pediatr Nephrol* 7:464–470, 1993.
661. Rinaldi S, Dionisi-Vici C, Goffredo B, et al: Jeune syndrome associated with cystinuria: report of two sisters. *Am J Med Genet* 37:301–303, 1990.
662. Hudgins L, Rosengren S, Treem W, Hyams J: Early cirrhosis in survivors with Jeune thoracic dystrophy. *J Pediatr* 120:754–756, 1992.
663. Bard LA, Bard PA, Owens GW, Hall BD: Retinal involvement in thoracic-pelvic-phalangeal dystrophy. *Arch Ophthalmol* 96:278–281, 1978.
664. Silengo M, Gianino P, Longo P, et al: Dandy-Walker complex in a child with Jeune's asphyxiating thoracic dystrophy. *Pediatr Radiol* 30(6):430, 2000.
665. Dugoff L, Thieme G, Hobbins JC: First trimester prenatal diagnosis of chondroectodermal dysplasia (Ellis-van Creveld syndrome) with ultrasound. *Ultrasound Obstet Gynecol* 17:86–88, 2001.
666. Majewski E, Ozturk B, Gillessen-Kaesbach G: Jeune syndrome with tongue lobulation and preaxial polydactyly, and Jeune syndrome with situs inversus and asplenia: compound heterozygosity Jeune-Mohr and Jeune-Ivemark? *Am J Med Genet* 63:74–79, 1996.
667. Aurora P, Wallis CE: Jeune syndrome (asphyxiating thoracic dystrophy) associated with Hirschsprung disease. *Clin Dysmorphol* 8:259–263, 1999.
668. Skiptunas SM, Weiner S: Early prenatal diagnosis of asphyxiating thoracic dysplasia (Jeune's syndrome). Value of fetal thoracic measurement. *J Ultrasound Med* 6:41–43, 1987.
669. Panero Lopez AL, Puyol Buil PJ, Belaustegui Cueto A, Sotelo MT: Asphyxiating thoracic dysplasia in 2 dizygotic twins. *An Esp Pediatr* 26(6):453–456, 1987.
670. Kapoor R, Saha MM, Gupta NC: Antenatal diagnosis of asphyxiating thoracic dysplasia. *Indian Pediatr* 26:495–497, 1989.
671. Ardura Fernandez J, Alvarez Gonzalez C, Rodriguez Fernandez M, Andres de Llano J: Asphyxiating thoracic dysplasia associated with proximal myopathy and arachnoid cyst. *An Esp Pediatr* 33:592–596, 1990.
672. Ben Ami M, Perlitz Y, Haddad S, Matilsky M: Increased nuchal translucency is associated with asphyxiating thoracic dysplasia. *Ultrasound Obstet Gynecol* 10:297–298, 1997.
673. Das BB, Nagaraj A, Fayemi A, et al: Fetal thoracic measurements in prenatal diagnosis of Jeune syndrome. *Indian J Pediatr* 69:101–103, 2002.
674. Chen CP, Shih JC, Chang JH, et al: Prenatal diagnosis of right pulmonary agenesis associated with VACTERL sequence. *Prenat Diagn* 23:515–518, 2003.
675. Morgan NV, Bacchelli C, Gissen P, et al: A locus for asphyxiating thoracic dystrophy, ATD, maps to chromosome 15q13. *J Med Genet* 40:431–435, 2003.
676. Baujat G, Huber C, El Hokayem J, et al: Asphyxiating thoracic dysplasia: clinical and molecular review of 39 families. *J Med Genet* 50:91–98, 2013.
677. Davis JT, Long FR, Adler BH, et al: Lateral thoracic expansion for Jeune syndrome: evidence of rib healing and new bone formation. *Ann Thorac Surg* 77:445–448, 2004.
678. Saldino RM, Noonan CD: Severe thoracic dystrophy with striking micromelia, abnormal osseous development, including the spine, and multiple visceral anomalies. *Am J Roentgenol Radium Ther Nucl Med* 114:257–263, 1972.
679. Majewski E, Pfeiffer RA, Lenz W, et al: Polysyndactyly, short limbs, and genital malformations—a new syndrome? *Z Kinderheilkd* 111:118–138, 1971.
680. Basgul Yigiter A, Guducu N, Kavak ZN, et al: A short rib polydactyly syndrome overlapping both lethal and nonlethal types. *Genet Couns* 23:231–237, 2012.
681. Naumoff P, Young LW, Mazer J, Amortegui AJ: Short rib-polydactyly syndrome type 3. *Radiology* 122:443–447, 1977.
682. Beemer FA, Langer LO, Jr, Klep-de Pater JM, et al: A new short rib syndrome: report of two cases. *Am J Med Genet* 14:115–123, 1983.
683. Sarafoglou K, Funai EF, Fefferman N, et al: Short rib-polydactyly syndrome: more evidence of a continuous spectrum. *Clin Genet* 56:145–148, 1999.
684. Elcioglu NH, Hall CM: Diagnostic dilemmas in the short rib-polydactyly syndrome group. *Am J Med Genet* 111:392–400, 2002.
685. Scarano G, Della Monica M, Capece G, et al: A case of short-rib syndrome without polydactyly in a stillborn: a new type? *Birth Defects Orig Artic Ser* 30:95–101, 1996.
686. Yang SS, Roth JA, Langer LO, Jr: Short rib syndrome Beemer-Langer type with polydactyly: a multiple congenital anomalies syndrome. *Am J Med Genet* 39:243–246, 1991.
687. Taori KB, Sharbidre KG, Krishnan V, et al: Diagnosis of short rib polydactyly syndrome type IV (Beemer-Langer syndrome) with cystic hygroma: a case report. *J Clin Ultrasound* 37:406–409, 2009.
688. Sirichotiyakul S, Tongsong T, Wanapirak C, Chanprapaph P: Prenatal sonographic diagnosis of Majewski syndrome. *J Clin Ultrasound* 30:303–307, 2002.
689. Naki MM, Gur D, Zemheri E, et al: Short rib-polydactyly syndrome. *Arch Gynecol Obstet* 272:173–175, 2005.
690. Chen CP, Shih JC, Tzen CY, et al: Recurrent short-rib polydactyly syndrome: prenatal three-dimensional ultrasound findings and associations with congenital high airway obstruction and pyelectasia. *Prenat Diagn* 25:417–418, 2005.
691. Ho NC, Francomano CA, van Allen M: Jeune asphyxiating thoracic dystrophy and short-rib polydactyly type III (Verma-Naumoff) are variants of the same disorder. *Am J Med Genet* 90:310–314, 2000.
692. Chen CP, Chern SR, Chang TY, et al: Prenatal diagnosis and molecular genetic analysis of short rib-polydactyly syndrome type III (Verma-Naumoff) in a second-trimester fetus with a homozygous splice site



- mutation in intron 4 in the NEK1 gene. *Taiwan J Obstet Gynecol* 51:266–270, 2012.
693. Chen CP, Chang TY, Chen CY, et al: Short rib-polydactyly syndrome type II (Majewski): prenatal diagnosis, perinatal imaging findings and molecular analysis of the NEK1 gene. *Taiwan J Obstet Gynecol* 51:100–105, 2012.
694. Beales PL, Bland E, Tobin JL, et al: IFT80, which encodes a conserved intraflagellar transport protein, is mutated in Jeune asphyxiating thoracic dystrophy. *Nat Genet* 39:727–729, 2007.
695. Dagonneau N, Goulet M, Genevieve D, et al: DYNC2H1 mutations cause asphyxiating thoracic dystrophy and short rib-polydactyly syndrome, type III. *Am J Hum Genet* 84:706–711, 2009.
696. Huber C, Wu S, Kim AS, et al: WDR34 mutations that cause short-rib polydactyly syndrome type III/severe asphyxiating thoracic dysplasia reveal a role for the NF-kappaB pathway in cilia. *Am J Hum Genet* 93:926–931, 2013.
697. McInerney-Leo AM, Schmidts M, Cortes CR, et al: Short-rib polydactyly and Jeune syndromes are caused by mutations in WDR60. *Am J Hum Genet* 93:515–523, 2013.
698. Mei L, Huang Y, Pan Q, et al: Targeted next-generation sequencing identifies novel compound heterozygous mutations of DYNC2H1 in a fetus with short rib-polydactyly syndrome, type III. *Clin Chim Acta* 447:47–51, 2015.
699. McKusick VA, Egeland JA, Eldridge R, Krusen DE: Dwarfism in the Amish I. The Ellis-van Crevelde syndrome. *Bull Johns Hopkins Hosp* 115:306–336, 1964.
700. Arya L, Mendiratta V, Sharma RC, Solanki RS: Ellis-van Crevelde syndrome: a report of two cases. *Pediatr Dermatol* 18:485–489, 2001.
701. da Silva EO, Janovitz D, de Albuquerque SC: Ellis-van Crevelde syndrome: report of 15 cases in an inbred kindred. *J Med Genet* 17:349–356, 1980.
702. Tongsong T, Chanprapaph P: Prenatal sonographic diagnosis of Ellis-van Crevelde syndrome. *J Clin Ultrasound* 28:38–41, 2000.
703. Al-Khenaizan S, Al-Sanna N, Teebi AS: What syndrome is this? Chondroectodermal dysplasia—the Ellis-van Crevelde syndrome. *Pediatr Dermatol* 18:68–70, 2001.
704. Sergi C, Voigtlander T, Zoubaa S, et al: Ellis-van Crevelde syndrome: a generalized dysplasia of enchondral ossification. *Pediatr Radiol* 31:289–293, 2001.
705. Spranger S, Tariverdian G: Symptomatic heterozygosity in the Ellis-van Crevelde syndrome? *Clin Genet* 47:217–220, 1995.
706. Qureshi F, Jacques SM, Evans MI, et al: Skeletal histopathology in fetuses with chondroectodermal dysplasia (Ellis-van Crevelde syndrome). *Am J Med Genet* 45:471–476, 1993.
707. Goldblatt J, Minutillo C, Pemberton PJ, Hurst J: Ellis-van Crevelde syndrome in a Western Australian aboriginal community. Postaxial polydactyly as a heterozygous manifestation? *Med J Aust* 157:271–272, 1992.
708. Lal H, Manchanda SS, Thaman OP: Chondroectodermal dysplasia (Ellis-van Crevelde syndrome) (a case report). *Indian J Pediatr* 32:10–13, 1965.
709. Santos JM, Pipa J, Antunes L, et al: The Ellis-van Crevelde syndrome. Apropos 2 clinical cases. *Rev Port Cardiol* 13:45–50, 1994.
710. Lynch JJ, Perry LW, Takakuwa T, Scott LP, 3rd: Congenital heart disease and chondroectodermal dysplasia. Report of two cases, one in a negro. *Am J Dis Child* 115:80–87, 1968.
711. Donlan MA, Murphy JJ, Brakel CA: Ellis-van Crevelde syndrome associated with complete situs inversus. *Clin Pediatr (Phila)* 8:366–368, 1969.
712. Sajeev CG, Roy TN, Venugopal K: Images in cardiology: common atrium in a child with Ellis-Van Crevelde syndrome. *Heart* 88:142, 2002.
713. Giknis FL: Single atrium and the Ellis-van Crevelde syndrome. *J Pediatr* 62:558–564, 1963.
714. Goor D, Rotem Y, Friedman A, Neufeld HN: Ellis-van Crevelde syndrome in identical twins. *Br Heart J* 27:797–804, 1965.
715. Hattab FN, Yassin OM, Sasa IS: Oral manifestations of Ellis-van Crevelde syndrome: report of two siblings with unusual dental anomalies. *J Clin Pediatr Dent* 22:159–165, 1998.
716. Cahuana A, Palma C, Gonzales W, Gean E: Oral manifestations in Ellis-van Crevelde syndrome: report of five cases. *Pediatr Dent* 26:277–282, 2004.
717. Feingold M: Ellis-van Crevelde syndrome. *Clin Pediatr (Phila)* 5:431–436, 1966.
718. Pratesi C, Carattoli MT: The Ellis-Van Crevelde syndrome. (Description of a case with associated micrognathia). *Riv Clin Pediatr* 77(2):57–68, 1966.
719. Blackburn MG, Belliveau RE: Ellis-van Crevelde syndrome. A report of previously undescribed anomalies in two siblings. *Am J Dis Child* 122:267–270, 1971.
720. Zangwill KM, Boal DK, Ladda RL: Dandy-Walker malformation in Ellis-van Crevelde syndrome. *Am J Med Genet* 31:123–129, 1988.
721. Rosemberg S, Carneiro PC, Zerbini MC, Gonzalez CH: Brief clinical report: chondroectodermal dysplasia (Ellis-van Crevelde) with anomalies of CNS and urinary tract. *Am J Med Genet* 15:291–295, 1983.
722. Bohm N, Fukuda M, Staudt R, Helwig H: Chondroectodermal dysplasia (Ellis-van Crevelde syndrome) with dysplasia of renal medulla and bile ducts. *Histopathology* 2:267–281, 1978.
723. Moudgil A, Bagga A, Kamil ES, et al: Nephronophthisis associated with Ellis-van Crevelde syndrome. *Pediatr Nephrol* 12:20–22, 1998.
724. Akar H, Konuralp C, Baysal K, Kolbakir F: Ellis-van Crevelde syndrome associated with thymic hypoplasia. *Asian Cardiovasc Thorac Ann* 10:336–338, 2002.
725. Datta V, Chaturvedi P: Ellis-van Crevelde syndrome associated with nodular sclerosing Hodgkin's disease and nephrotic syndrome. *Indian J Pediatr* 67:929–930, 2000.
726. Calver D, Keast-Butler J, Taylor D: The extra digit. A pointer to the eye? *Trans Ophthalmol Soc U K* 101:35–38, 1981.
727. Frikiche A, Verloes A, Stassen M, et al: Ellis-Van Crevelde syndrome. Apropos of a case diagnosed in utero. *Rev Med Liege* 44:68–72, 1989.
728. Rahmani R, Sterling CL, Bedford HM: Prenatal diagnosis of Jeune-like syndromes with two-dimensional and three-dimensional sonography. *J Clin Ultrasound* 40:222–226, 2012.
729. Kunderagi NG, Taori K, Kumawat R, et al: Ellis van Crevelde syndrome with synpolydactyly, an antenatal diagnosis with postnatal correlation. *J Clin Imaging Sci* 1:59, 2011.
730. Chen CP, Chen CY, Chern SR, et al: First-trimester prenatal diagnosis of Ellis-van Crevelde syndrome. *Taiwan J Obstet Gynecol* 51:643–648, 2012.
731. Digilio MC, Marino B, Giannotti A, Dallapiccola B: Atrioventricular canal defect and postaxial polydactyly indicating phenotypic overlap of Ellis-van Crevelde and Kaufman-McKusick syndromes. *Pediatr Cardiol* 18:74–75, 1997.
732. Castel Y, Toudic L, Alix D, et al: Postaxial polydactyly in a female neonate associated with hydrocolpos due to vaginal atresia and with a congenital cardiopathy: the McKusick-Kaufman syndrome. *J Genet Hum* 30:329–337, 1982.
733. Ruiz-Perez VL, Ide SE, Strom TM, et al: Mutations in a new gene in Ellis-van Crevelde syndrome and Weyers acrodistal dysostosis. *Nat Genet* 24:283–286, 2000.
734. Chen CP, Su YN, Hsu CY, et al: Ellis-van Crevelde syndrome: prenatal diagnosis, molecular analysis and genetic counseling. *Taiwan J Obstet Gynecol* 49:481–486, 2010.
735. Peraita-Ezcurra M, Martinez-Garcia M, Ruiz-Perez VL, et al: Ellis-van Crevelde syndrome in a fetus with rhizomelia and polydactyly. Report of a case diagnosed by genetic analysis, and correlation with pathological and radiologic findings. *Gene* 499:223–225, 2012.
736. Takamine Y, Krejci P, Mekikian PB, Wilcox WR: Mutations in the EVC1 gene are not a common finding in the Ellis-van Crevelde and short rib-polydactyly type III syndromes. *Am J Med Genet A* 130A:96–97, 2004.
737. Torrente I, Mangino M, De Luca A, et al: First-trimester prenatal diagnosis of Ellis-van Crevelde syndrome using linked microsatellite markers. *Prenat Diagn* 18:504–506, 1998.
738. Shen W, Han D, Zhang J, et al: Two novel heterozygous mutations of EVC2 cause a mild phenotype of Ellis-van Crevelde syndrome in a Chinese family. *Am J Med Genet A* 155A:2131–2136, 2011.



739. Mendoza-Londono R, Lee B: Cleidocranial dysplasia. In Pagon RA, Adam MP, Ardinger HH, et al, editors: *GeneReviews*, Seattle, 1993-2016, University of Washington.
740. Cohen MM, Jr: RUNX genes, neoplasia, and cleidocranial dysplasia. *Am J Med Genet* 104:185-188, 2001.
741. Otto F, Kanegane H, Mundlos S: Mutations in the RUNX2 gene in patients with cleidocranial dysplasia. *Hum Mutat* 19:209-216, 2002.
742. Ziros PG, Basdra EK, Papavassiliou AG: Runx2: of bone and stretch. *Int J Biochem Cell Biol* 40:1659-1663, 2008.
743. Cohen MM, Jr: Perspectives on RUNX genes: an update. *Am J Med Genet A* 149A:2629-2646, 2009.
744. Hove HD, Hermann NV, Jorgensen C, et al: An echo-poor spine at 13 weeks: an early sign of cleidocranial dysplasia. *Fetal Diagn Ther* 24:103-105, 2008.
745. Hermann NV, Hove HD, Jorgensen C, et al: Prenatal 3D ultrasound diagnostics in cleidocranial dysplasia. *Fetal Diagn Ther* 25:36-39, 2009.
746. Hassan J, Sepulveda W, Teixeira J, et al: Prenatal sonographic diagnosis of cleidocranial dysostosis. *Prenat Diagn* 17:770-772, 1997.
747. Paladini D, Lamberti A, Agangi A, Martinelli P: Cleidocranial dysostosis. Prenatal ultrasound diagnosis of a late onset form. *Ultrasound Obstet Gynecol* 16:100-101, 2000.
748. Cavalli P, Santorelli FM, Bontardelli M, et al: Prenatal exclusion of cleidocranial dysplasia. *Prenat Diagn* 23:945-946, 2003.
749. Lloyd-Roberts GC, Apley AG, Owen R: Reflections upon the aetiology of congenital pseudarthrosis of the clavicle. With a note on cranio-cleido dysostosis. *J Bone Joint Surg Br* 57:24-29, 1975.
750. Yunis E, Varon H: Cleidocranial dysostosis, severe micrognathism, bilateral absence of thumbs and first metatarsal bone, and distal aphyalangia: a new genetic syndrome. *Am J Dis Child* 134:649-653, 1980.
751. Reutter H, Bagci S, Muller A, et al: Primary pulmonary hypertension, congenital heart defect, central nervous system malformations, hypo- and aplastic toes: another case of Yunis-Varon syndrome or report of a new entity. *Eur J Med Genet* 55:27-31, 2012.
752. Basel-Vanagaite L, Kornreich L, Schiller O, et al: Yunis-Varon syndrome: further delineation of the phenotype. *Am J Med Genet A* 146A(4):532-537, 2008.
753. Nakajima J, Okamoto N, Shiraishi J, et al: Novel FIG4 mutations in Yunis-Varon syndrome. *J Hum Genet* 58:822-824, 2013.
754. Campeau PM, Lenk GM, Lu JT, et al: Yunis-Varon syndrome is caused by mutations in FIG4, encoding a phosphoinositide phosphatase. *Am J Hum Genet* 92:781-791, 2013.
755. Romero R, Pilu G, Jeanty P, et al: Skeletal dysplasias. In Romero R, Pilu G, Jeanty P, editors: *Prenatal Diagnosis of Congenital Anomalies*, Norwalk, CT, 1987, Appleton & Lange, pp 311-402.
756. Stoll C, Wiesel A, Queisser-Luft A, et al: Evaluation of the prenatal diagnosis of limb reduction deficiencies. EUROSCAN Study Group. *Prenat Diagn* 20:811-818, 2000.
757. Bod M, Czeizel A, Lenz W: Incidence at birth of different types of limb reduction abnormalities in Hungary 1975-1977. *Hum Genet* 65:27-33, 1983.
758. Goldberg MJ: *The Dysmorphic Child: An Orthopedic Perspective*, New York, 1987, Raven Press.
759. Zhu J, Miao L, Xu C, et al: Analysis of 822 infants with limb reduction defect in China. *Hua Xi Yi Ke Da Xue Xue Bao* 27:400-403, 1996.
760. Bromley B, Benacerraf B: Abnormalities of the hands and feet in the fetus: sonographic findings. *AJR Am J Roentgenol* 165:1239-1243, 1995.
761. Seven M, Yosunkaya E, Guven G, Yuksel A: The very rare aglossia adactylia syndrome with a novel finding of mental retardation. *Genet Couns* 23:81-85, 2012.
762. Lecannellier J, Vischer D: The aglossia-adactylia syndrome. *Helv Paediatr Acta* 31:77-84, 1976.
763. Robinow M, Marsh JL, Edgerton MT, et al: Discordance in monozygotic twins for aglossia-adactylia, and possible clues to the pathogenesis of the syndrome. *Birth Defects Orig Artic Ser* 14:223-230, 1978.
764. Canete Estrada R, Gil Rivas R, Alvarez Marcos R, et al: Hanhart syndrome (aglossia-adactylia syndrome). Report of 2 cases. *An Esp Pediatr* 33:465-468, 1990.
765. Marti-Herrero M, Cabrera-Lopez JC, Toledo L, et al: Moebius syndrome. Three different forms of presentation. *Rev Neurol* 27:975-978, 1998.
766. Abramson DL, Cohen MM, Jr, Mulliken JB: Mobius syndrome: classification and grading system. *Plast Reconstr Surg* 102:961-967, 1998.
767. Chorazy M, Lesniewicz R, Posmyk R, et al: The natural history of Mobius syndrome in a 32-year-old man. *Neurol Neurochir Pol* 45:74-79, 2011.
768. Journal H, Roussey M, Le Marec B: MCA/MR syndrome with oligodactyly and Mobius anomaly in first cousins: new syndrome or familial facial-limb disruption sequence? *Am J Med Genet* 34:506-510, 1989.
769. da Silva Dal Pizzol T, Knop FP, Mengue SS: Prenatal exposure to misoprostol and congenital anomalies: systematic review and meta-analysis. *Reprod Toxicol* 22:666-671, 2006.
770. Bos-Thompson MA, Hillaire-Buys D, Roux C, et al: Mobius syndrome in a neonate after mifepristone and misoprostol elective abortion failure. *Ann Pharmacother* 42:888-892, 2008.
771. Pirmez R, Freitas ME, Gasparetto EL, Araujo AP: Moebius syndrome and holoprosencephaly following exposure to misoprostol. *Pediatr Neurol* 43:371-373, 2010.
772. Matsui A, Nakagawa M, Okuno M: Association of atrial septal defect with Poland-Moebius syndrome: vascular disruption can be a common etiologic factor. A case report. *Angiology* 48:269-271, 1997.
773. Issaivanan M, Viridi VS, Parmar VR: Subclavian artery supply disruption sequence-Klippel-Feil and Mobius anomalies. *Indian J Pediatr* 69:441-442, 2002.
774. Happle R, Koch H, Lenz W: The CHILD syndrome. Congenital hemidysplasia with ichthyosiform erythroderma and limb defects. *Eur J Pediatr* 134:27-33, 1980.
775. Hebert AA, Esterly NB, Holbrook KA, Hall JC: The CHILD syndrome. Histologic and ultrastructural studies. *Arch Dermatol* 123:503-509, 1987.
776. Hoeger PH, Adwani SS, Whitehead BF, et al: Ichthyosiform erythroderma and cardiomyopathy: report of two cases and review of the literature. *Br J Dermatol* 139:1055-1059, 1998.
777. Happle R, Effendy I, Megahed M, et al: CHILD syndrome in a boy. *Am J Med Genet* 62:192-194, 1996.
778. Konig A, Happle R, Bornholdt D, et al: Mutations in the NSDHL gene, encoding a 3beta-hydroxysteroid dehydrogenase, cause CHILD syndrome. *Am J Med Genet* 90:339-346, 2000.
779. Hummel M, Cunningham D, Mullett CJ, et al: Left-sided CHILD syndrome caused by a nonsense mutation in the NSDHL gene. *Am J Med Genet A* 122A:246-251, 2003.
780. Seeger MA, Paller AS: The role of abnormalities in the distal pathway of cholesterol synthesis in the Congenital Hemidysplasia with Ichthyosiform erythroderma and Limb Defects (CHILD) syndrome. *Biochim Biophys Acta* 1841:345-352, 2014.
781. Morimoto M, Souich C, Trinh J, et al: Expression profile of NSDHL in human peripheral tissues. *J Mol Histol* 43(1):95-106, 2012.
782. Porter FD, Herman GE: Malformation syndromes caused by disorders of cholesterol synthesis. *J Lipid Res* 52:6-34, 2011.
783. Kanungo S, Soares N, He M, Steiner RD: Sterol metabolism disorders and neurodevelopment-an update. *Dev Disabil Res Rev* 17:197-210, 2013.
784. Heda GD, Valivade V, Sanghavi P, et al: CHILD syndrome. *Indian J Dermatol Venereol Leprol* 80:483, 2014.
785. Raychaudhury T, George R, Mandal K, et al: A novel X-chromosomal microdeletion encompassing congenital hemidysplasia with ichthyosiform erythroderma and limb defects. *Pediatr Dermatol* 30:250-252, 2013.
786. Ahmad M, Abbas H, Wahab A, Haque S: Fibular hypoplasia and complex brachydactyly (Du Pan syndrome) in an inbred Pakistani kindred. *Am J Med Genet* 36:292-296, 1990.
787. Uyguner ZO, Kocaoglu M, Toksoy G, et al: Novel indel mutation in the GDF5 gene is associated with brachydactyly type C in a four-generation Turkish family. *Mol Syndromol* 5:81-86, 2014.
788. Faiyaz-Ul-Haque M, Ahmad W, Zaidi SH, et al: Mutation in the cartilage-derived morphogenetic protein-1 (CDMP1) gene in a kindred affected with fibular hypoplasia and complex brachydactyly (DuPan syndrome). *Clin Genet* 61:454-458, 2002.



789. Savarirayan R, White SM, Goodman FR, et al: Broad phenotypic spectrum caused by an identical heterozygous CDMP-1 mutation in three unrelated families. *Am J Med Genet A* 117A:136–142, 2003.
790. Douzgou S, Lehmann K, Mingarelli R, et al: Compound heterozygosity for GDF5 in Du Pan type chondrodysplasia. *Am J Med Genet A* 146A:2116–2121, 2008.
791. McPherson F, Frias JL, Spicer D, et al: Splenogonadal fusion-limb defect “syndrome” and associated malformations. *Am J Med Genet A* 120A:518–522, 2003.
792. Basbug M, Akgun H, Ozgun MT, et al: Prenatal sonographic findings in a fetus with splenogonadal fusion limb defect syndrome. *J Clin Ultrasound* 37:298–301, 2009.
793. Speare R, Roberts J, Cohen M, Wales J: Splenogonadal fusion and sex reversal. *J Pediatr Endocrinol Metab* 25:541–542, 2012.
794. Bonneau D, Roume J, Gonzalez M, et al: Splenogonadal fusion limb defect syndrome: report of five new cases and review. *Am J Med Genet* 86:347–358, 1999.
795. Bonafede RP, Beighton P: Autosomal dominant inheritance of scalp defects with ectrodactyly. *Am J Med Genet* 3:35–41, 1979.
796. Fryns JP, Legius E, Demaerel P, van den Berghe H: Congenital scalp defect, distal limb reduction anomalies, right spastic hemiplegia and hypoplasia of the left arteria cerebri media. Further evidence that interruption of early embryonic blood supply may result in Adams-Oliver (plus) syndrome. *Clin Genet* 50:505–509, 1996.
797. Snape KM, Ruddy D, Zenker M, et al: The spectra of clinical phenotypes in aplasia cutis congenita and terminal transverse limb defects. *Am J Med Genet A* 149A:1860–1881, 2009.
798. Meester JA, Southgate L, Stittrich AB, et al: Heterozygous loss-of-function mutations in DLL4 cause Adams-Oliver syndrome. *Am J Hum Genet* 97:475–482, 2015.
799. Bamforth JS, Kaurah P, Byrne J, Ferreira P: Adams Oliver syndrome: a family with extreme variability in clinical expression. *Am J Med Genet* 49:393–396, 1994.
800. Brancati E, Garaci FG, Mingarelli R, Dallapiccola B: Abnormal neuronal migration defect in the severe variant subtype of Adams-Oliver syndrome. *Am J Med Genet A* 146A:1622–1623, 2008.
801. Silva G, Braga A, Leitao B, et al: Adams-Oliver syndrome and portal hypertension: fortuitous association or common mechanism? *Am J Med Genet A* 158A:648–651, 2012.
802. Stittrich AB, Lehman A, Bodian DL, et al: Mutations in NOTCH1 cause Adams-Oliver syndrome. *Am J Hum Genet* 95:275–284, 2014.
803. Becker R, Kunze J, Horn D, et al: Autosomal recessive type of Adams-Oliver syndrome: prenatal diagnosis. *Ultrasound Obstet Gynecol* 20:506–510, 2002.
804. Papadopoulou E, Sifakis S, Raissaki M, et al: Antenatal and postnatal evidence of periventricular leukomalacia as a further indication of vascular disruption in Adams-Oliver syndrome. *Am J Med Genet A* 146A:2545–2550, 2008.
805. Temtamy SA, Aglan MS, Ashour AM, Zaki MS: Adams-Oliver syndrome: further evidence of an autosomal recessive variant. *Clin Dysmorphol* 16:141–149, 2007.
806. Prothero J, Nicholl R, Wilson J, Wakeling EL: Aplasia cutis congenita, terminal limb defects and falciform retinal folds: confirmation of a distinct syndrome of vascular disruption. *Clin Dysmorphol* 16:39–41, 2007.
807. Shaheen R, Faqeih E, Sunker A, et al: Recessive mutations in DOCK6, encoding the guanidine nucleotide exchange factor DOCK6, lead to abnormal actin cytoskeleton organization and Adams-Oliver syndrome. *Am J Hum Genet* 89:328–333, 2011.
808. McGoey RR, Lacassie Y: Adams-Oliver syndrome in siblings with central nervous system findings, epilepsy, and developmental delay: refining the features of a severe autosomal recessive variant. *Am J Med Genet A* 146A:488–491, 2008.
809. Hassed SJ, Wiley GB, Wang S, et al: RBPJ mutations identified in two families affected by Adams-Oliver syndrome. *Am J Hum Genet* 91:391–395, 2012.
810. Vandersteen AM, Dixon JW: Adams-Oliver syndrome, a family with dominant inheritance and a severe phenotype. *Clin Dysmorphol* 20:210–213, 2011.
811. Shaheen R, Aglan M, Keppler-Noreuil K, et al: Mutations in EOGT confirm the genetic heterogeneity of autosomal-recessive Adams-Oliver syndrome. *Am J Hum Genet* 92:598–604, 2013.
812. Shukla AK, Sanjay SC, Krishna L, Krishnappa N: Tetra-phocomelia: a rarest of rare case. *J Clin Diagn Res* 9(3):TD3–TD4, 2015.
813. Newman CG: The thalidomide syndrome: risks of exposure and spectrum of malformations. *Clin Perinatol* 13:555–573, 1986.
814. Lee A, Kratochwil A, Deutinger J, Bernaschek G: Three-dimensional ultrasound in diagnosing phocomelia. *Ultrasound Obstet Gynecol* 5:238–240, 1995.
815. Gordillo M, Vega H, Jabs EW: Roberts syndrome. In Pagon RA, Adam MP, Ardinger HH, et al, editors: *GeneReviews*, Seattle, 1993–2016, University of Washington.
816. Dulnuan DJ, Matsuoka M, Uketa E, et al: Antenatal three-dimensional sonographic features of Roberts syndrome. *Arch Gynecol Obstet* 284:241–244, 2011.
817. Morita A, Nakahira K, Hasegawa T, et al: Establishment and characterization of Roberts syndrome and SC phocomelia model medaka (*Oryzias latipes*). *Dev Growth Differ* 54(5):588–604, 2012.
818. Herrmann J, Feingold M, Tuffli GA, Opitz JM: A familial dysmorphogenetic syndrome of limb deformities, characteristic facial appearance and associated anomalies: the “pseudothalidomide” or “SC-syndrome.” *Birth Defects Orig Artic Ser* 3:81–89, 1969.
819. Schule B, Oviedo A, Johnston K, et al: Inactivating mutations in ESCO2 cause SC phocomelia and Roberts syndrome: no phenotype-genotype correlation. *Am J Hum Genet* 77:1117–1128, 2005.
820. Grebe H: Die Achondrogenesis: ein einfach rezessives Erbmerkmal. *Folia Hered Path* 2:23–28, 1952.
821. Quelce-Salgado A: A new type of dwarfism with various bone aplasias and hypoplasias of the extremities. *Acta Genet Stat Med* 14:63–66, 1964.
822. Kulkarni ML, Kulkarni BM, Nasser PU: Antenatal diagnosis of Grebe syndrome in a twin pregnancy by ultrasound. *Indian Pediatr* 32:1007–1011, 1995.
823. Rittler M, Higa S: Grebe syndrome: a second case with extremely severe manifestations. *J Med Genet* 34:1038, 1997.
824. Costa T, Ramsby G, Cassia F, et al: Grebe syndrome: clinical and radiographic findings in affected individuals and heterozygous carriers. *Am J Med Genet* 75:523–529, 1998.
825. Kumar D, Curtis D, Blank CE: Grebe chondrodysplasia and brachydactyly in a family. *Clin Genet* 25:68–72, 1984.
826. Beighton P: Heterozygous manifestations in the heritable disorders of the skeleton. *Pediatr Radiol* 27:397–401, 1997.
827. Al Kaissi A, Chehida FB, Ganger R, Grill F: Neonatal death dwarfism in a girl with distinctive bone dysplasia compatible with grebe chondrodysplasia: analysis by CT scan-based phenotype. *J Clin Imaging Sci* 4:53, 2014.
828. Thomas JT, Kilpatrick MW, Lin K, et al: Disruption of human limb morphogenesis by a dominant negative mutation in CDMPL. *Nat Genet* 17:58–64, 1997.
829. Martinez-Garcia M, Garcia-Canto E, Fenollar-Cortes M, et al: Characterization of an acromesomelic dysplasia, Grebe type case: novel mutation affecting the recognition motif at the processing site of GDF5. *J Bone Miner Metab Epub* 2015 Aug 15.
830. Munoz Rojas MV, Goncalves LF: Grebe-Quelce-Salgado chondrodysplasia: prenatal diagnosis of two new cases in unrelated families in Southern Brazil. *Am J Med Genet* 113:193–199, 2002.
831. Cordero DR, Goldberg Y, Basel D, et al: Prenatal sonographic diagnosis of Grebe syndrome. *J Ultrasound Med* 25:115–121, 2006.
832. Daentl DL, Smith DW, Scott CI, et al: Femoral hypoplasia—unusual facies syndrome. *J Pediatr* 86:107–111, 1975.
833. Hamanishi C: Congenital short femur. Clinical, genetic and epidemiological comparison of the naturally occurring condition with that caused by thalidomide. *J Bone Joint Surg Br* 62:307–320, 1980.
834. Sanpera I, Jr, Fixsen JA, Sparks LT, Hill RA: Knee in congenital short femur. *J Pediatr Orthop B* 4:159–163, 1995.
835. Makino Y, Inoue T, Shirota K, et al: A case of congenital familial short femur diagnosed prenatally. *Fetal Diagn Ther* 13:206–208, 1998.



836. Hadi HA, Wade A: Prenatal diagnosis of unilateral proximal femoral focal deficiency in diabetic pregnancy: a case report. *Am J Perinatol* 10:285–287, 1993.
837. Goncalves LF, De Luca GR, Vitorello DA, et al: Prenatal diagnosis of bilateral proximal femoral hypoplasia. *Ultrasound Obstet Gynecol* 8:127–130, 1996.
838. Kalaycioglu A, Aynaci O: Proximal focal femoral deficiency, contralateral hip dysplasia in association with contralateral ulnar hypoplasia and cleft hand: a case report and review of literatures of PFFD and/or FFU. *Okajimas Folia Anat Jpn* 78:83–89, 2001.
839. Filly AL, Robnett-Filly B, Filly RA: Syndromes with focal femoral deficiency: strengths and weaknesses of prenatal sonography. *J Ultrasound Med* 23(11):1511–1516, 2004.
840. Sen Gupta DK, Gupta SK: Familial bilateral proximal femoral focal deficiency. Report of a kindred. *J Bone Joint Surg Am* 66:1470–1472, 1984.
841. Frey M, Williams J: What is your diagnosis? Radiographic diagnosis—ectrodactyly. *J Am Vet Med Assoc* 206:619–620, 1995.
842. Miura T, Suzuki M: Clinical differences between typical and atypical cleft hand. *J Hand Surg [Br]* 9:311–315, 1984.
843. Glicenstein J, Guero S, Haddad R: Median clefts of the hand. Classification and therapeutic indications apropos of 29 cases. *Ann Chir Main Memb Super* 14:253, 1995.
844. Tada K, Yonenobu K, Swanson AB: Congenital central ray deficiency in the hand—a survey of 59 cases and subclassification. *J Hand Surg Am* 6(5):434–441, 1981.
845. van den Berghe H, Dequeker J, Fryns JP, David G: Familial occurrence of severe ulnar aplasia and lobster claw feet: a new syndrome. *Hum Genet* 42:109–113, 1978.
846. Verma IC, Joseph R, Bhargava S, Mehta S: Split-hand and split-foot deformity inherited as an autosomal recessive trait. *Clin Genet* 9:8–14, 1976.
847. Brunner HG, Hamel BC, Van Bokhoven H: The p63 gene in EEC and other syndromes. *J Med Genet* 39:377–381, 2002.
848. Rudiger RA, Haase W, Passarge E: Association of ectrodactyly, ectodermal dysplasia, and cleft lip–palate. *Am J Dis Child* 120:160–163, 1970.
849. Roelfsema NM, Cobben JM: The EEC syndrome: a literature study. *Clin Dysmorphol* 5:115–127, 1996.
850. Miller CI, Hashimoto K, Shwayder T, et al: What syndrome is this? Ectrodactyly, ectodermal dysplasia, and cleft palate (EEC) syndrome. *Pediatr Dermatol* 14:239–240, 1997.
851. Kasman B, Ruprecht KW: Ocular manifestations in a father and son with EEC syndrome. *Graefes Arch Clin Exp Ophthalmol* 235:512–516, 1997.
852. Kronic AL, Vesic SA, Goldner B, et al: Ectrodactyly, soft-tissue syndactyly, and nodulocystic acne: coincidence or association? *Pediatr Dermatol* 14:31–35, 1997.
853. Maas SM, de Jong TP, Buss P, Hennekam RC: EEC syndrome and genitourinary anomalies: an update. *Am J Med Genet* 63:472–478, 1996.
854. Gershoni-Baruch R, Goldscher D, Hochberg Z: Ectrodactyly-ectodermal dysplasia-clefting syndrome and hypothalamo-pituitary insufficiency. *Am J Med Genet* 68:168–172, 1997.
855. Leiter E, Lipson J: Genitourinary tract anomalies in lobster claw syndrome. *J Urol* 115:339–341, 1976.
856. Halal F, Homsy M, Perreault G: Acro-renal-ocular syndrome: autosomal dominant thumb hypoplasia, renal ectopia, and eye defect. *Am J Med Genet* 17:753–762, 1984.
857. Sripathomsawat W, Tanpaiboon P, Heering J, et al: Phenotypic analysis of Arg227 mutations of TP63 with emphasis on dental phenotype and micturition difficulties in EEC syndrome. *Am J Med Genet A* 155A:228–232, 2011.
858. Celli J, Duijff P, Hamel BC, et al: Heterozygous germline mutations in the p53 homolog p63 are the cause of EEC syndrome. *Cell* 99:143–153, 1999.
859. Kosaki R, Ohashi H, Yoshihashi H, et al: A de novo mutation (R279C) in the P63 gene in a patient with EEC syndrome. *Clin Genet* 60:314–315, 2001.
860. Bujdoso G, Lenz W: Monodactylous splithand-splitfoot. A malformation occurring in three distinct genetic types. *Eur J Pediatr* 133:207–215, 1980.
861. Wood VE: Congenital thumb deformities. *Clin Orthop Relat Res* 195:7–25, 1985.
862. Chan KM, Lamb DW: Triphalangeal thumb and five-fingered hand. *Hand* 15:329–334, 1983.
863. Goldberg MJ, Meyn M: The radial clubhand. *Orthop Clin North Am* 7:341–359, 1976.
864. Lanneaux J, Poidvin A, Soole F, et al: Fanconi anemia in 2012: diagnosis, pediatric follow-up and treatment. *Arch Pediatr* 19:1100–1109, 2012.
865. Vundint BR: Chromosomal instability and molecular mutations in multi spectrum disease of Fanconi anemia. *Mol Cytogenet* 7:147, 2012.
866. Bogliolo M, Surralles J: Fanconi anemia: a model disease for studies on human genetics and advanced therapeutics. *Curr Opin Genet Dev* 33:32–40, 2015.
867. Umana LA, Magoulas P, Bi W, Bacino CA: A male newborn with VACTERL association and Fanconi anemia with a FANCB deletion detected by array comparative genomic hybridization (aCGH). *Am J Med Genet A* 155A:3071–3074, 2011.
868. Levran O, Diotti R, Pujara K, et al: Spectrum of sequence variations in the FANCA gene: an International Fanconi Anemia Registry (IFAR) study. *Hum Mutat* 25:142–149, 2005.
869. Strathdee CA, Duncan AM, Buchwald M: Evidence for at least four Fanconi anaemia genes including FACC on chromosome 9. *Nat Genet* 1(3):196–198, 1992.
870. Lo Ten Foe JR, Rooimans MA, Bosnoyan-Collins L, et al: Expression cloning of a cDNA for the major Fanconi anaemia gene, FAA. *Nat Genet* 14:320–323, 1996.
871. Ianzano L, D'Apolito M, Centra M, et al: The genomic organization of the Fanconi anemia group A (FAA) gene. *Genomics* 41:309–314, 1997.
872. Lee HJ, Park S, Kang HJ, et al: A case report of Fanconi anemia diagnosed by genetic testing followed by prenatal diagnosis. *Ann Lab Med* 32:380–384, 2012.
873. Smogorzewska A, Desetty R, Saito TT, et al: A genetic screen identifies FAN1, a Fanconi anemia-associated nuclease necessary for DNA interstrand crosslink repair. *Mol Cell* 39:36–47, 2010.
874. Fargo JH, Rochowski A, Giri N, et al: Comparison of chromosome breakage in non-mosaic and mosaic patients with Fanconi anemia, relatives, and patients with other inherited bone marrow failure syndromes. *Cytogenet Genome Res* 144:15–27, 2014.
875. Bechtold A, Friedl R, Kalb R, et al: Prenatal exclusion/confirmation of Fanconi anemia via flow cytometry: a pilot study. *Fetal Diagn Ther* 21:118–124, 2006.
876. Sekine I, Hagiwara T, Miyazaki H, et al: Thrombocytopenia with absent radii syndrome: studies on serum thrombopoietin levels and megakaryopoiesis in vitro. *J Pediatr Hematol Oncol* 20:74–78, 1998.
877. Toriello HV: Thrombocytopenia-absent radius syndrome. *Semin Thromb Hemost* 37(6):707–712, 2011.
878. de Vries LS, Connell J, Bydder GM, et al: Recurrent intracranial haemorrhages in utero in an infant with alloimmune thrombocytopenia. Case report. *Br J Obstet Gynaecol* 95:299–302, 1988.
879. Donnenfeld AE, Wiseman B, Lavi E, Weiner S: Prenatal diagnosis of thrombocytopenia absent radius syndrome by ultrasound and cordocentesis. *Prenat Diagn* 10:29–35, 1990.
880. Bellver J, Lara C, Perez-Aytes A, et al: First-trimester diagnosis of thrombocytopenia-absent radius (TAR) syndrome in a triplet pregnancy. *Prenat Diagn* 25:332–334, 2005.
881. Houeijeh A, Andrieux J, Saugier-Verber P, et al: Thrombocytopenia-absent radius (TAR) syndrome: a clinical genetic series of 14 further cases. Impact of the associated 1q21.1 deletion on the genetic counselling. *Eur J Med Genet* 54:e471–e477, 2011.
882. Muis N, Beemer FA, van Dijken P, et al: The Aase syndrome. Case report and review of the literature. *Eur J Pediatr* 145:153–157, 1986.
883. Hing AV, Downton SB: Aase syndrome: novel radiographic features. *Am J Med Genet* 45:413–415, 1993.
884. Dror Y, Durie P, Marcon P, Freedman MH: Duplication of distal thumb phalanx in Shwachman-Diamond syndrome. *Am J Med Genet* 78:67–69, 1998.



885. Vlachos A, Blanc L, Lipton JM: Diamond Blackfan anemia: a model for the translational approach to understanding human disease. *Expert Rev Hematol* 7:359–372, 2014.
886. Boria I, Garelli E, Gazda HT, et al: The ribosomal basis of Diamond-Blackfan anemia: mutation and database update. *Hum Mutat* 31:1269–1279, 2010.
887. Gazda HT, Preti M, Sheen MR, et al: Frameshift mutation in p53 regulator RPL26 is associated with multiple physical abnormalities and a specific pre-ribosomal RNA processing defect in Diamond-Blackfan anemia. *Hum Mutat* 33:1037–1044, 2012.
888. Landowski M, O'Donohue MF, Buros C, et al: Novel deletion of RPL15 identified by array-comparative genomic hybridization in Diamond-Blackfan anemia. *Hum Genet* 132:1265–1274, 2013.
889. Gerrard G, Valganon M, Foong HE, et al: Target enrichment and high-throughput sequencing of 80 ribosomal protein genes to identify mutations associated with Diamond-Blackfan anaemia. *Br J Haematol* 162:530–536, 2013.
890. Bennhagen RG, Menaheem S: Holt-Oram syndrome and multiple ventricular septal defects: an association suggesting a possible genetic marker? *Cardiol Young* 8:128–130, 1998.
891. Law KM, Tse KT: Prenatal sonographic diagnosis of familial Holt-Oram syndrome associated with type B interrupted aortic arch. *Hong Kong Med J* 14:317–320, 2008.
892. Barisic I, Boban L, Greenlees R, et al: Holt Oram syndrome: a registry-based study in Europe. *Orphanet J Rare Dis* 9:156, 2014.
893. Sletten LJ, Pierpont ME: Variation in severity of cardiac disease in Holt-Oram syndrome. *Am J Med Genet* 65:128–132, 1996.
894. Sunagawa S, Kikuchi A, Sano Y, et al: Prenatal diagnosis of Holt-Oram syndrome: role of 3-D ultrasonography. *Congenit Anom (Kyoto)* 49:38–41, 2009.
895. Porto MP, Vergani N, Carvalho AC, et al: Novel mutations in the TBX5 gene in patients with Holt-Oram syndrome. *Genet Mol Biol* 33:232–236, 2010.
896. Jhang WK, Lee BH, Kim GH, et al: Clinical and molecular characterisation of Holt-Oram syndrome focusing on cardiac manifestations. *Cardiol Young* 25:1093–1098, 2015.
897. He J, McDermott DA, Song Y, et al: Preimplantation genetic diagnosis of human congenital heart malformation and Holt-Oram syndrome. *Am J Med Genet A* 126A:93–98, 2004.
898. Temtamy SA, Miller JD: Extending the scope of the VATER association: definition of the VATER syndrome. *J Pediatr* 85:345–349, 1974.
899. Solomon BD: VACTERL/VATER Association. *Orphanet J Rare Dis* 6:56, 2011.
900. Bartels E, Schulz AC, Mora NW, et al: VATER/VACTERL association: identification of seven new twin pairs, a systematic review of the literature, and a classical twin analysis. *Clin Dysmorphol* 21:191–195, 2012.
901. Khalid S, Faizan M, Alam MM, et al: Congenital longitudinal radial deficiency in infants: spectrum of isolated cases to VACTERL syndrome. *J Clin Neonatol* 2:193–195, 2013.
902. Auchterlonie IA, White MP: Recurrence of the VATER association within a sibship. *Clin Genet* 21:122–124, 1982.
903. Tongsong T, Chanprapaph P, Khunamornpong S: Prenatal diagnosis of VACTERL association: a case report. *J Med Assoc Thai* 84:143–148, 2001.
904. Mori M, Matsubara K, Abe E, et al: Prenatal diagnosis of persistent cloaca associated with VATER (vertebral defects, anal atresia, tracheoesophageal fistula, and renal dysplasia). *Tohoku J Exp Med* 213(4):291–295, 2007.
905. Lal P, Agrawal P, Krishna A: Goldenhar syndrome. *Indian Pediatr* 34:837–838, 1997.
906. Araneta MR, Moore CA, Olney RS, et al: Goldenhar syndrome among infants born in military hospitals to Gulf War veterans. *Teratology* 56:244–251, 1997.
907. Herwig MC, Gembruch U, Born M, et al: Preterm diagnosis of choristoma and choroidal coloboma in Goldenhar's syndrome. *Pediatr Dev Pathol* 14:322–326, 2011.
908. Ghi T, Contro E, Carletti A, et al: Prenatal sonographic imaging of Goldenhar syndrome associated with cystic eye. *Prenat Diagn* 28:362–363, 2008.
909. Guzelmansur I, Ceylaner G, Ceylaner S, et al: Prenatal diagnosis of Goldenhar syndrome with unusual features by 3D ultrasonography. *Genet Couns* 24:319–325, 2013.
910. Tracy MR, Dormans JP, Kusumi K: Klippel-Feil syndrome: clinical features and current understanding of etiology. *Clin Orthop Relat Res* 424:183–190, 2004.
911. Herman TE, Siegel MJ, Vachharajani A: Klippel Feil syndrome with occipital encephalocele, duodenal web, left pelvic kidney, ASD, anorectal malformation fetal and postnatal imaging. *J Perinatol* 33:245–247, 2013.
912. Chemke J, Fishel E, Zalish M, Sagiv M: Multiple skeletal anomalies in the "13q" syndrome. *Eur J Pediatr* 128:27–31, 1978.
913. Sepulveda W, Treadwell MC, Fisk NM: Prenatal detection of preaxial upper limb reduction in trisomy 18. *Obstet Gynecol* 85:847–850, 1995.
914. Uuspaa V: Upper extremity deformities associated with the orofacial clefts. *Scand J Plast Reconstr Surg* 12:157–162, 1978.
915. Cogulu O, Ozkinay F, Yalman O: Poland anomaly and ulna shortage in two cousins. *Indian J Pediatr* 67:471–472, 2000.
916. Malik S: Polydactyly: phenotypes, genetics and classification. *Clin Genet* 85:203–212, 2014.
917. Kleanthous JK, Kleanthous EM, Hahn PJ, Jr: Polydactyly of the foot. Overview with case presentations. *J Am Podiatr Med Assoc* 88:493–499, 1998.
918. Guo B, Lee SK, Paksima N: Polydactyly: a review. *Bull Hosp Jt Dis (2013)* 71(1):17–23, 2013.
919. Gildea DE, Luettkeimer ES, Bao X, et al: The pleiotropic mouse phenotype extra-toes spotting is caused by translation initiation factor Eif3c mutations and is associated with disrupted sonic hedgehog signaling. *FASEB J* 25:1596–1605, 2011.
920. Rix S, Calmont A, Scambler PJ, Beales PL: An Ift80 mouse model of short rib polydactyly syndromes shows defects in hedgehog signalling without loss or malformation of cilia. *Hum Mol Genet* 20(7):1306–1314, 2011.
921. Raposo L, Fachada H, Santos Paulo A, et al: Prenatal diagnosis of Greig cephalopolysyndactyly syndrome: a case report. *Prenat Diagn* 35:203–205, 2015.
922. Kang S, Graham JM, Jr, Olney AH, Biesecker LG: GLI3 frameshift mutations cause autosomal dominant Pallister-Hall syndrome. *Nat Genet* 15:266–268, 1997.
923. Biesecker LG: Polydactyly: how many disorders and how many genes? *Am J Med Genet* 112:279–283, 2002.
924. Sucuoglu H, Ornek NI, Caglar C: Arthrogyriposis multiplex congenita: multiple congenital joint contractures. *Case Rep Med* 2015:379730, 2015.
925. Hoff JM, Loane M, Gilhus NE, et al: Arthrogyriposis multiplexa congenita: an epidemiologic study of nearly 9 million births in 24 EUROCAT registers. *Eur J Obstet Gynecol Reprod Biol* 159:347–350, 2011.
926. Hall JG: An approach to research on congenital contractures. *Birth Defects Orig Artic Ser* 20:8–30, 1984.
927. Hall JG: Arthrogyriposis multiplex congenita: etiology, genetics, classification, diagnostic approach, and general aspects. *J Pediatr Orthop B* 6:159–166, 1997.
928. Jacobson L, Polizzi A, Vincent A: An animal model of maternal antibody-mediated arthrogyriposis multiplex congenita (AMC). *Ann NY Acad Sci* 841:565–567, 1998.
929. Drachman DB, Weiner LP, Price DL, Chase J: Experimental arthrogyriposis caused by viral myopathy. *Arch Neurol* 33:362–367, 1976.
930. Banker BQ: Neuropathologic aspects of arthrogyriposis multiplex congenita. *Clin Orthop Relat Res* 194:30–43, 1985.
931. Swinyard CA: Concepts of multiple congenital contractures (arthrogyriposis) in man and animals. *Teratology* 25:247–258, 1982.
932. Quinn CM, Wigglesworth JS, Heckmatt J: Lethal arthrogyriposis multiplex congenita: a pathological study of 21 cases. *Histopathology* 19:155–162, 1991.
933. Dane B, Dane C, Aksoy F, et al: Arthrogyriposis multiplex congenita: analysis of twelve cases. *Clin Exp Obstet Gynecol* 36:259–262, 2009.
934. Dimitrakaki M, Tsikouras P, Bouchlariotou S, et al: Prenatal assessment of arthrogyriposis. A review of the literature. *J Matern Fetal Neonatal Med* 24:32–36, 2011.

935. Zelop C, Benacerraf B: Sonographic diagnosis of fetal upper extremity dysmorphology: significance and outcome. *Ultrasound Obstet Gynecol* 8:391–396, 1996.
936. Dicke JM, Piper SL, Goldfarb CA: The utility of ultrasound for the detection of fetal limb abnormalities—a 20-year single-center experience. *Prenat Diagn* 35:348–353, 2015.
937. Fahy MJ, Hall JG: A retrospective study of pregnancy complications among 828 cases of arthrogyposis. *Genet Couns* 1(1):3–11, 1990.
938. Bacino CA, Hecht JT: Etiopathogenesis of equinovarus foot malformations. *Eur J Med Genet* 57:473–479, 2014.
939. Mammen L, Benson CB: Outcome of fetuses with clubfeet diagnosed by prenatal sonography. *J Ultrasound Med* 23:497–500, 2004.
940. Bar-On E, Mashiach R, Inbar O, et al: Prenatal ultrasound diagnosis of club foot: outcome and recommendations for counselling and follow-up. *J Bone Joint Surg Br* 87:990–993, 2005.
941. Christianson C, Huff D, McPherson E: Limb deformations in oligohydramnios sequence: effects of gestational age and duration of oligohydramnios. *Am J Med Genet* 86:430–433, 1999.
942. Yamamoto H: A clinical, genetic and epidemiologic study of congenital club foot. *Jinrui Idengaku Zasshi* 24:37–44, 1979.
943. Nemeč U, Nemeč SF, Kasprian G, et al: Clubfeet and associated abnormalities on fetal magnetic resonance imaging. *Prenat Diagn* 32(9):822–828, 2012.
944. Shipp TD, Benacerraf BR: The significance of prenatally identified isolated clubfoot: is amniocentesis indicated? *Am J Obstet Gynecol* 178:600–602, 1998.
945. Malone FD, Marino T, Bianchi DW, et al: Isolated clubfoot diagnosed prenatally: is karyotyping indicated? *Obstet Gynecol* 95:437–440, 2000.

akusherlib.ru



# Ultrasound Evaluation of the Fetal Thorax

*Deborah Rose Berman, Marjorie C. Treadwell*

## SUMMARY OF KEY POINTS

- The most common chest masses are congenital pulmonary airway malformations (CPAMs) and congenital diaphragmatic hernias (CDHs). For both, the displacement of the heart from its normal position is the most commonly recognized ultrasound finding.
- CPAMs are unilateral 98% of the time and appear as echogenic areas of the lung, with or without identified cysts. The CPAM volume ratio (CVR) can be used to subdivide these malformations into high- and low-risk categories for development of fetal hydrops.
- Fluid-filled dilated airways should raise suspicion for bronchial or laryngeal atresia. Bilateral hyperechogenic lungs with fluid-filled airways are characteristic of congenital high airway obstruction syndrome (CHAOS), whereas a unilateral hyperechogenic lung with fluid-filled airways suggests bronchial atresia or congenital lobar emphysema (CLE).
- Hydrothorax may be primary or secondary. Primary hydrothorax is usually chylous in origin and may progress to hydrops, usually associated with significant skin edema. A large unilateral hydrothorax, even if associated with significant hydrops, may respond to prenatal drainage and shunting.
- CDHs are left-sided and posterior in 85% of cases. They are associated with other anomalies (structural and chromosomal) in 40% to 50% of cases.
- Prognosis for CDHs depends on the presence of associated abnormalities, the gestational age at delivery, and the degree of pulmonary hypoplasia.
- Estimation of lung volume by two-dimensional ultrasound lung-head ratios or volumes obtained through magnetic resonance imaging (MRI) or three-dimensional ultrasound may help guide counseling.

## OUTLINE

### Embryology, 346

Embryonic Phase, 349

Pseudoglandular Phase, 349

Canalicular Phase, 349

Saccular Phase, 349

Alveolar Phase, 349

### Key Features for Assessment, 349

### Pulmonary Hypoplasia, 350

### Congenital Pulmonary Airway Malformation, 351

### Bronchogenic Cyst, 354

### Bronchial Atresia, 355

### Congenital Lobar Emphysema, 357

### Congenital High Airway Obstruction Syndrome, 357

### Congenital Hydrothorax, 359

### Congenital Diaphragmatic Hernia, 362

The neonatal identification of chest lesions frequently relies on decompensation of the newborn. Prenatal identification allows for appropriate triaging for site of delivery as well as early and appropriate treatment. Better definition and prenatal identification of chest lesions along with enhanced understanding of the natural history of these lesions has resulted in improvements in counseling. In addition, prenatal therapies are now available for many different types of chest abnormalities. The appropriate use of these therapies depends on accurate identification and assessment of the lesion and the associated pathologic changes. Identifying prognostic factors facilitates continued improvement in the understanding of the natural course of the disease.

This chapter will explore the range of chest lesions that can be identified prenatally and will discuss factors associated with a thorough sonographic diagnosis to facilitate complete and accurate counseling for patients.

## EMBRYOLOGY

Although an intact pulmonary system is not required for intrauterine viability, the prenatal development of the respiratory system is integral to ex utero life and survival. To allow successful transition to neonatal life, fetal lungs must proceed through both structural and functional maturation processes, which occur from the early embryonic period and continue after birth. During structural development, there is branching of the airways and development of alveolar spaces, allowing gas exchange to occur once the first breath is taken at delivery. Functional development results in the creation of a surfactant system. This system is composed of phospholipids that decrease alveolar surface tension, inhibiting alveolar collapse during exhalation. The surfactant system develops in the third trimester and is typically mature at 36 weeks' gestation. Birth prior to the development of the surfactant

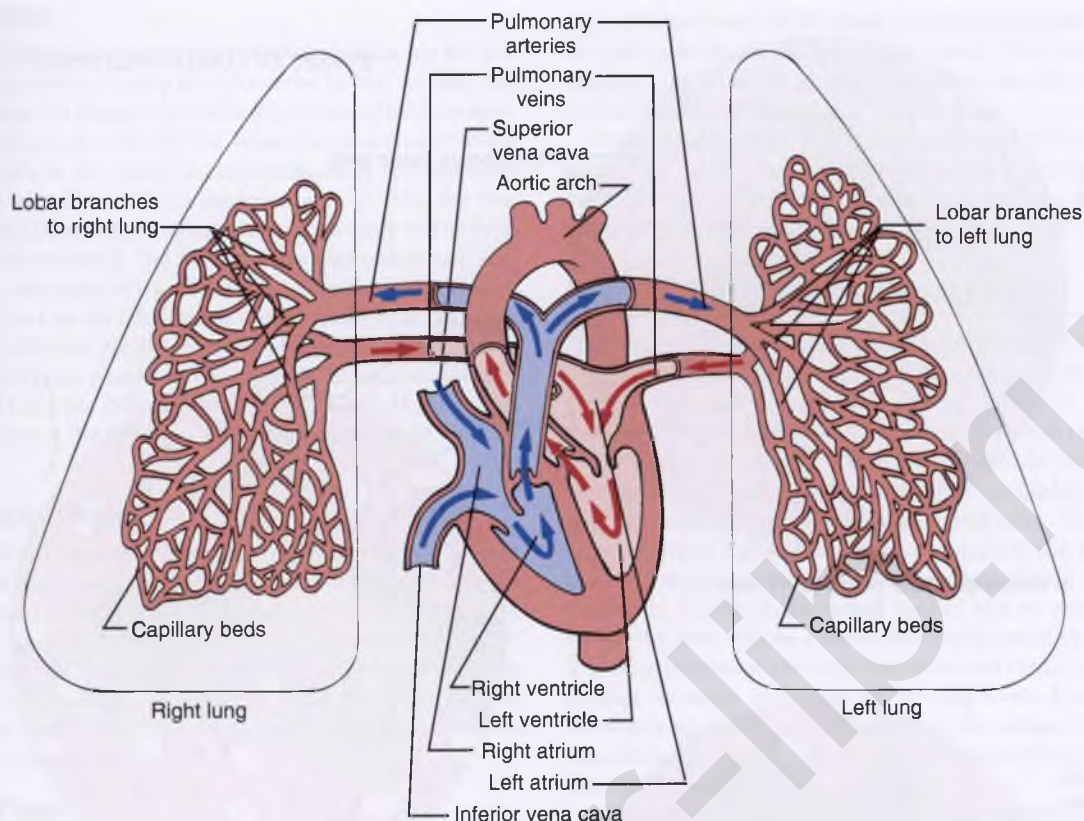


**FIG 12-1** The pulmonary circulation. The right and left pulmonary veins and arteries and the branching capillaries are illustrated. (From Brashers VL: Structure and function of the pulmonary system. In McCance KL, Huether SE (eds): Pathophysiology: The Biologic Basis for Disease in Adults and Children. St. Louis, Elsevier, Mosby, 2006.)

system or completed pulmonary development results in neonatal respiratory compromise.

The respiratory diverticulum (lung bud) appears as an outgrowth of the ventral wall of the foregut. The epithelium of the internal lining of the larynx, trachea, bronchi, and lungs is entirely of endodermal origin. The cartilaginous, smooth muscle, and connective tissues of the trachea and lungs are derived from splanchnic mesoderm that surrounds the tubular framework. The lung bud is in open communication with the foregut. The diverticulum develops in a craniocaudal direction, leading to development of the upper respiratory structures (nose and pharynx) prior to the lower structures. Two tracheoesophageal ridges separate the diverticulum from the foregut. The dorsal portion of the foregut divides into the esophagus and the ventral portion into the trachea and lung buds.<sup>1</sup>

The pulmonary circulation is a highly specialized vascular network, connecting the interdependent heart and lungs (Fig. 12-1). The vascular bed parallels the airways and links the arterial and venous poles of the heart. The pulmonary vasculature has been described as appearing de novo within the mesoderm ventral and lateral to the foregut endoderm, suggesting that this mesoderm pool gives rise to the future pulmonary vasculature as lung develops from the foregut.<sup>2</sup> The lungs have two sets of lymphatic vessels, a superficial set located beneath the pleura and a deep set which follows the blood vessels and extends along the bronchi. Both sets end within the bronchial glands. Efferent lymphatic vessels travel up the trachea, ending at the left-sided thoracic duct or the right-sided lymphatic duct. The fetal lungs play a key role in amniotic fluid volume maintenance: 15 mL/kg of body weight in fluid is produced by the lungs and flows out via the trachea and mouth, circulating and contributing to the amniotic fluid that is swallowed.<sup>3</sup>

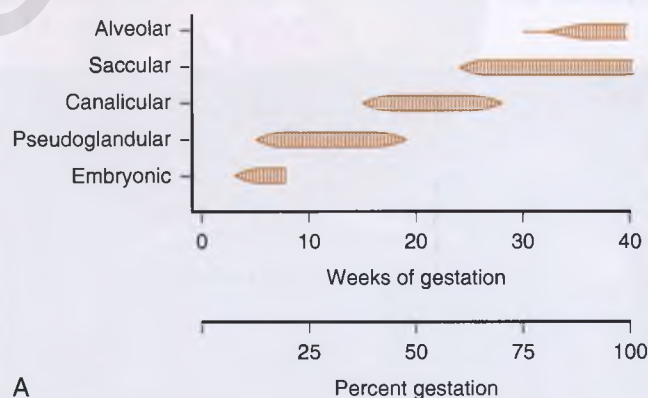


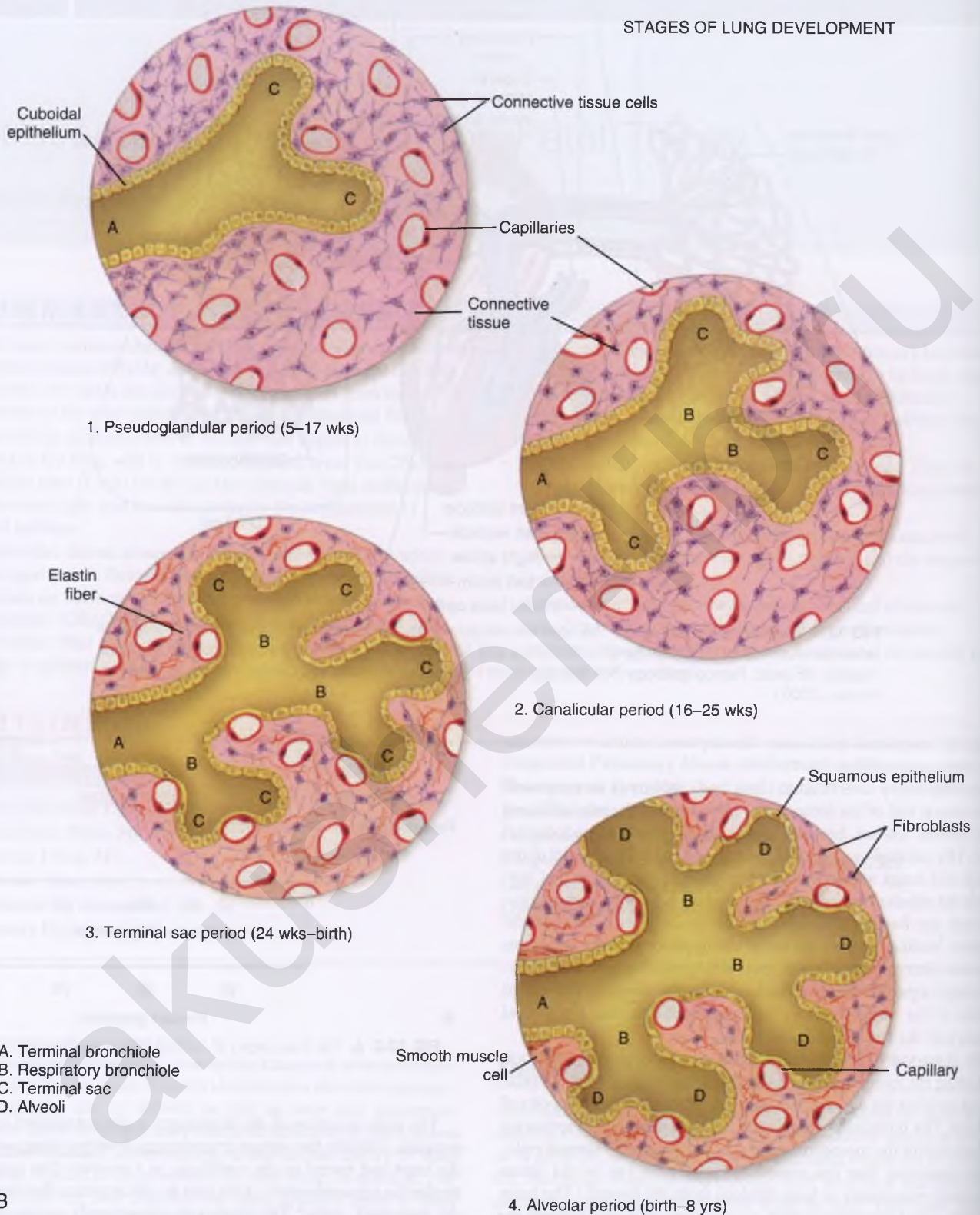
**FIG 12-2 A**, The five stages of normal fetal lung development.

The basic structure of the diaphragm is also established early in gestation. Initially, the septum transversum develops, lying caudal to the heart and rostral to the umbilicus, in a position that eventually divides the intraembryonic cavity into the pleuropericardial cavity and the peritoneal cavity.<sup>4</sup> The diaphragm subsequently undergoes programmed muscularization; this represents the final stage in the formation of the basic foundation of the diaphragm and is completed by 14 weeks' gestation.

Fetal lung development occurs in five stages: embryonic, pseudoglandular, canalicular, saccular, and alveolar (Fig. 12-2). The timing of these phases is approximate. Transitions between stages are gradual, with overlap from one stage to the next.



## STAGES OF LUNG DEVELOPMENT



B

## 4. Alveolar period (birth–8 yrs)

**FIG 12-2, cont'd B,** Histologic sections illustrating progressive stages of lung development. 1. Pseudoglandular period (about 8 weeks). 2. Late canalicular period (about 24 weeks). 3. Early terminal sac period (about 26 weeks). 4. Early alveolar period (newborn infant). Note that the alveolocapillary membrane is thin and that some of the capillaries have begun to bulge into the primordial alveoli. (A from Pringle KC: Human fetal lung development and related animal models. *Clin Obstet Gynecol* 3:502, 1986; B from Moore KL, Persaud TVN, Shiota K [eds]: *Color Atlas of Clinical Embryology*, 2nd ed. Philadelphia, WB Saunders, 2000.)



### Embryonic Phase

The embryonic phase of lung development takes place during the first 4 to 5 weeks of gestation. During this phase, the larynx, trachea, and lung bud form from the foregut. The embryonic phase of lung development begins at about day 28 with the formation of a groove in the ventral lower pharynx, the sulcus laryngotrachealis. A few days later, at about day 30, a bud forms from the lower part, creating the true lung primordium.<sup>5</sup> Development progresses in the 8-week-old embryo as the lobar buds subdivide and form the bronchopulmonary segments. Early on, the asymmetry of the main bronchi is established, with the smaller bud on the left directed more laterally than the larger one on the right, which is parallel to the esophagus and directed more caudally. The embryonic phase proceeds with the unequal dividing of the endodermal branches followed by further division. At the end of the embryonic period, the five lobes of the lungs (three right and two left) are present.

### Pseudoglandular Phase

The pseudoglandular stage takes place between the 7th and 16th weeks of embryonic development. Conducting airways are formed by progressive branching of the original lung buds into smaller and more numerous areas. Each bud eventually becomes an independent respiratory unit, served by a bronchiole surrounded by capillary vessels that will bring blood to the lungs for oxygen. During this stage, the first differentiation of lung epithelium occurs. By 13 weeks' gestation, cilia appear in the proximal airways.

### Canalicular Phase

Lasting until approximately 25 weeks' gestational age, the canalicular phase is crucial for the development of the gas-exchanging portion of the lung. By 20 weeks, there is differentiation into type I pneumocytes, the primary structural cell of the alveolus. Capillaries grow in close proximity to the distal surface of the alveolar cells. Lamellar bodies develop in type II alveolar cells and are the site of surfactant storage prior to release into the alveoli. A sufficient differentiation of the type II pneumocytes into the type I pneumocytes and the proliferation of the capillaries into the mesenchyme marks an important step toward the fetus being able to survive outside the uterus. By the end of this stage, structural development has progressed sufficiently such that gas exchange is possible and neonatal survival can occur. Amniotic fluid is required for the canalicular stage to occur. Fetal lung growth is stimulated in part by the distending force of lung fluid in the airways, which occurs during fetal breathing and is inhibited by anhydramnios.<sup>6</sup>

### Saccular Phase

The saccular phase encompasses the period from 26 weeks until term, when the last generation of airspaces of the bronchial tree evolve. During this stage, there is a decrease in interstitial tissue, and a thinning of the airspace, resulting in a smaller population of collagen and elastic fibers. Surfactant production begins in the lungs. At the end of each respiratory tract passage, smooth-walled sacculi form, coated with type I and type II pneumocytes. Lamellar bodies of the type II cells store surfactant, which is rich in phosphatidylinositol, a necessary component for alveolar stability. Neonatal lung stability correlates with the number of lamellar bodies present. In the absence of surfactant, the lung alveoli are prone to collapse.

### Alveolar Phase

The last phase of lung development spans the period from approximately 32 weeks' gestation into early childhood. In addition to further surfactant production, lung development during this period is characterized by growth of more bronchioles and alveoli. This allows the

gas-exchange tissues of the lungs to expand and makes them capable of moving more air as the neonate grows. This final stage of lung development primarily occurs during postnatal life, building on the several million alveoli already present.<sup>5</sup>

Understanding these processes provides important insight into the aberrations in development associated with pulmonary lesions. The failure of normal physical development of the lung at any phase can result in pathologic lesions and potential respiratory compromise.

### KEY FEATURES FOR ASSESSMENT

Complete assessment of the thoracic structures includes evaluation of lung structure and appearance. The lung fields should appear homogeneous with no fluid collections present (Fig. 12-3). The size of the thorax relative to the fetal abdomen and the overall chest size relative to the size of the heart structures are nonspecific but are important components of evaluation. The cardiac circumference should be approximately 50% of the thoracic circumference. When the heart is large relative to thoracic size, further evaluation will determine if the chest is too small (potential pulmonary hypoplasia) or whether cardiomegaly is present. Abnormal cardiac axis or abnormal position within the chest may be a marker for displacement by a chest mass or a missing portion of the lung. Any abnormal cardiac position should prompt thorough evaluation of the lung fields. In addition to the homogeneous appearance of lung fields, the echogenicity of the lungs should also be assessed, with normal echogenicity being slightly greater than that of the fetal liver.

Adequate evaluation of the diaphragm requires sweeping side to side to assess continuity of the structure. The diaphragm will appear echolucent on ultrasound images (Fig. 12-4). Shadowing from the ribs may present a challenge to visualization of the entire diaphragm. Particular care should be taken to examine the posterolateral portions, where most defects will occur. It is important that diaphragm



**FIG 12-3** Normal transaxial image of the fetal chest with four-chamber view of the heart. Normal cardiac position and axis. The bilateral lung tissue appears homogeneous.



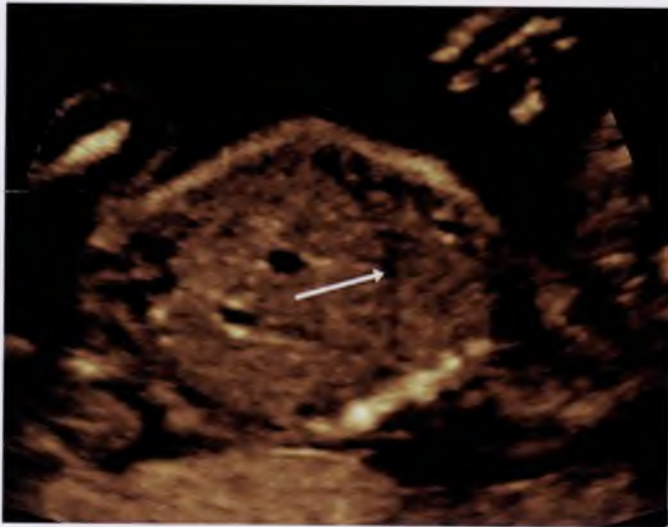


**FIG 12-4** Sagittal section through the fetal chest showing the echolucent diaphragm (arrow). Note the convex shape of the diaphragm.

continuity is confirmed and not just assumed based on other organs that are not appreciated in the chest. The contour of the diaphragm should also be assessed, as some abnormalities may be associated with eversion of the diaphragm downward.

## PULMONARY HYPOPLASIA

Pulmonary hypoplasia occurs as a spectrum characterized by incomplete development of unilateral or bilateral lung tissue. Clinically, it presents as respiratory compromise, with the severity reflecting the degree of reduction in lung size or in the number of lung cells, alveoli, or degree of bronchial branching.<sup>7</sup> The severity is related to the timing of the insult in relation to the stage of embryologic development.<sup>8,9</sup> Normal lung development requires adequate thoracic space as well as sufficient distention of the lungs through fluid exchange. Hypoplasia may therefore be caused by restriction or compression of developing fetal lung as well as by lack of amniotic fluid. Space-occupying lesions within the hemithorax, such as CDH, CPAM, massive cardiomegaly, and pleural effusion, can all cause pulmonary hypoplasia through mass effect, inhibiting normal formation of the pulmonary airways and alveoli. Thoracic musculoskeletal abnormalities, such as skeletal dysplasias and neuromuscular disorders, prohibit full expansion of the thoracic cage, with the restriction of chest size leading to hypoplasia.<sup>10</sup> Additionally, oligohydramnios associated with renal or urinary tract abnormalities or preterm premature rupture of membranes during crucial embryologic stages reduces the development of normal pulmonary components. The mechanism by which lack of amniotic fluid inhibits lung growth is unknown. However, inhibition of fetal breathing movements or increased loss of fetal lung fluid into the amniotic space have been suggested as two possible mechanisms for pulmonary hypoplasia in the setting of oligohydramnios. The incidence of neonatal pulmonary hypoplasia with premature rupture of membranes between 18 and 26 weeks' gestation ranges from 9% to 28%.<sup>11,12</sup>

Although it is relatively uncommon, the high mortality rate associated with pulmonary hypoplasia makes prenatal prediction critical for appropriate counseling. Subjective ultrasound assessment of relative chest size is helpful only in extreme cases (Fig. 12-5). Two-dimensional ultrasound measurements of fetal thoracic circumference, thoracic length, and the thoracic circumference to abdominal circumference (TC/AC) ratio have all been established (Table 12-1) but also have



**FIG 12-5** Axial view through the chest in a fetus with pulmonary hypoplasia. Note the heart occupying nearly the entire thorax.

limited predictive value except at the extremes. The use of the lung-to-head ratio (LHR) and lung volume measurements has been described more frequently with CDH<sup>10</sup> (see later discussion under "Congenital Diaphragmatic Hernia"). Other methods, such as the quantitative lung index (QLI), have been employed in attempts to mathematically quantify lung volumes.<sup>13,14</sup> This index, which is obtained by calculating lung area/(head circumference/10)<sup>2</sup>, has been described as a calculation that is fetal age independent. It has been reported to have minimal variation throughout pregnancy, with near constant parameters. Recent studies have provided reference ranges for normal 20- to 36-week fetal lung areas and LHRs (using the longest diameter and area tracing methods).<sup>15</sup> Unfortunately, these indirect measurements of lung volumes do not reliably and uniformly predict pulmonary hypoplasia, lung function, or likelihood of survival. The use of three-dimensional ultrasound to obtain volume measurements either directly or through the VOCAL technique (Virtual Organ Computer-Aided Analysis, General Electric Medical Systems) would seem more promising but have not been shown to be superior. MRI has also been used to calculate lung volumes (Fig. 12-6). The risk for pulmonary hypoplasia is assessed by comparing lung volumes measured by MRI with normal reference values based on the gestational age.<sup>16</sup> MRI has the advantage of more clearly delineating lung tissue from mediastinal structures and is not compromised by some of the limitations of ultrasound in the presence of oligohydramnios or high maternal body mass index (BMI). However, the ability of MRI to predict prognosis and survival has also been inconsistent, and the superiority of MRI in this regard remains controversial.<sup>13,17</sup>

Pulmonary hypoplasia is associated with a need for prolonged respiratory support and can even result in infant death despite aggressive postnatal management. It is important to understand that neither sonography nor MRI uniformly predicts hypoplasia except in extreme cases. Despite the limitations, measurements obtained from both

TABLE 12-1 Fetal Thoracic Circumference Measurements\*

Gestational Age (Week)	No.	PREDICTIVE PERCENTILES								
		2.5	5	10	25	50	75	90	95	97.5
16	6	5.9	6.4	7.0	8.0	9.1	10.3	11.3	11.9	12.4
17	22	6.8	7.3	7.9	8.9	10.0	11.2	12.2	12.8	13.3
18	31	7.7	8.2	8.8	9.8	11.0	12.1	13.1	13.7	14.2
19	21	8.6	9.1	9.7	10.7	11.9	13.0	14.0	14.6	15.1
20	20	9.5	10.0	10.6	11.7	12.8	13.9	15.0	15.5	16.0
21	30	10.4	11.0	11.6	12.6	13.7	14.8	15.8	16.4	16.9
22	18	11.3	11.9	12.5	13.5	14.6	15.7	16.7	17.3	17.8
23	21	12.2	12.8	13.4	14.4	15.5	16.6	17.6	18.2	18.8
24	27	13.2	13.7	14.3	15.3	16.4	17.5	18.5	19.1	19.7
25	20	14.1	14.6	15.2	16.2	17.3	18.4	19.4	20.0	20.6
26	25	15.0	15.5	16.1	17.1	18.2	19.3	20.3	21.0	21.5
27	24	15.9	16.4	17.0	18.0	19.1	20.2	21.3	21.9	22.4
28	24	16.8	17.3	17.9	18.9	20.0	21.2	22.2	22.8	23.3
29	24	17.7	18.2	18.8	19.8	21.0	22.1	23.1	23.7	24.2
30	27	18.6	19.1	19.7	20.7	21.9	23.0	24.0	24.6	25.1
31	24	19.5	20.0	20.6	21.6	22.8	23.9	24.9	25.5	26.0
32	28	20.4	20.9	21.5	22.6	23.7	24.8	25.8	26.4	26.9
33	27	21.3	21.8	22.5	23.5	24.6	25.7	26.7	27.3	27.8
34	25	22.2	22.8	23.4	24.4	25.5	26.6	27.6	28.2	28.7
35	20	23.1	23.7	24.3	25.3	26.4	27.5	28.5	29.1	29.6
36	23	24.0	24.6	25.2	26.2	27.3	28.4	29.4	30.0	30.6
37	22	24.9	25.5	26.1	27.1	28.2	29.3	30.3	30.9	31.5
38	21	25.9	26.4	27.0	28.0	29.1	30.2	31.2	31.9	32.4
39	7	26.8	27.3	27.9	28.9	30.0	31.1	32.2	32.8	33.3
40	6	27.7	28.2	28.8	29.8	30.9	32.1	33.1	33.7	34.2

\*Measurements in centimeters.

From Chitkara U, Rosenberg J, Chervenak FA, et al: Prenatal sonographic assessment of the fetal thorax: normal values. *Am J Obstet Gynecol* 156:1069, 1987.

modalities may assist with predicted range of disease severity, allowing for appropriate counseling of families while sharing the limitations.

## CONGENITAL PULMONARY AIRWAY MALFORMATION

Fetal chest masses include CPAM (formerly referred to as *congenital cystic adenomatoid malformation* [CCAM]) and bronchopulmonary sequestration (BPS). CPAMs are the most common lung lesions identified by fetal ultrasound imaging. On occasion, hybrid lesions are found, with imaging and pathologic features of both CPAM and BPS. Historically, CPAMs were thought to be infrequent, with reported incidence between 1 in 25,000 and 1 in 35,000 live births. With ongoing improvements in ultrasound resolution, smaller CPAMs are now being diagnosed with increasing frequency, and the incidence of CPAM is now reported to be as high as 1 in 12,000 live births,<sup>18,19</sup> accounting for 30% to 47% of fetal thoracic lung lesions.<sup>20</sup> These lesions are most often unilateral (95%) and are rarely bilateral. The right and left lungs are involved with equal frequency, with the lower lobes more commonly affected.<sup>21,22</sup> Current theories of pathogenesis suggest maturational arrest in bronchopulmonary development, resulting in dysplastic tissue distal to this segment.<sup>23,24</sup>

CPAMs have best been described as hamartomatous malformations of the lung characterized by abnormal branching of immature bronchioles. They communicate with the normal tracheobronchial tree and derive their blood supply from normal pulmonary circulation. These lesions develop during the pseudoglandular period, at 7 to 16 weeks.<sup>25</sup>

Stocker and associates initially classified the most common types of CPAMs into three categories.<sup>25</sup> Type 1 is described as a lesion with a dominant cyst (3-10 cm in diameter); type 2 comprises multiple small cysts (0.5-2.0 cm diameter) that are distributed evenly and blend in with adjacent normal tissue; and type 3 is the small microcyst or what appears to be solid type of cyst on sonographic images (Fig. 12-7). Recently, Stocker added two subtypes: type 0 (acinar dysplasia) and type 4 (large peripheral cyst of the distal acinus lined with alveolar cells), expanding the classification of CPAMs into five subtypes.<sup>26</sup> However, this categorization was intended to be applied to resected lung specimens, rather than sonographic diagnoses. As the various types of CPAMs have little clinical significance, and the size and presence of larger cysts have more prognostic importance, the most common current practice is to describe the CPAM lesion as microcystic or macrocystic and to report its size.<sup>27</sup>

BPS describes a mass of nonfunctioning lung tissue that does not communicate with the bronchial tree. These lesions have aberrant systemic arterial blood supply (which is how they can be differentiated from CPAM), commonly arising from the descending thoracic aorta<sup>28,29</sup> (Fig. 12-8). BPS may be intralobar, with the same pleural covering as normal lung tissue, or extralobar, with a distinct and separate pleural covering. Almost all prenatally diagnosed cases of BPS are extralobar, above the diaphragm, and most frequently in the lower left side of the chest.<sup>30</sup> Extralobar lesions may occur within the abdomen, appearing as echogenic masses below the diaphragm<sup>31,32</sup> (Fig. 12-9).

The identification of CPAM is often aided by shift in the location or axis of the fetal heart. The affected lung tissue will appear to have



increased echogenicity with possible presence of discrete cysts (see Fig. 12-7). Sometimes the increased echogenicity is confined to a single lobe of the lung, most often a lower lung field (Fig. 12-10). Polyhydramnios may be seen in the later stages of pregnancy and might be a consequence of decreased swallowing of amniotic fluid owing to mass

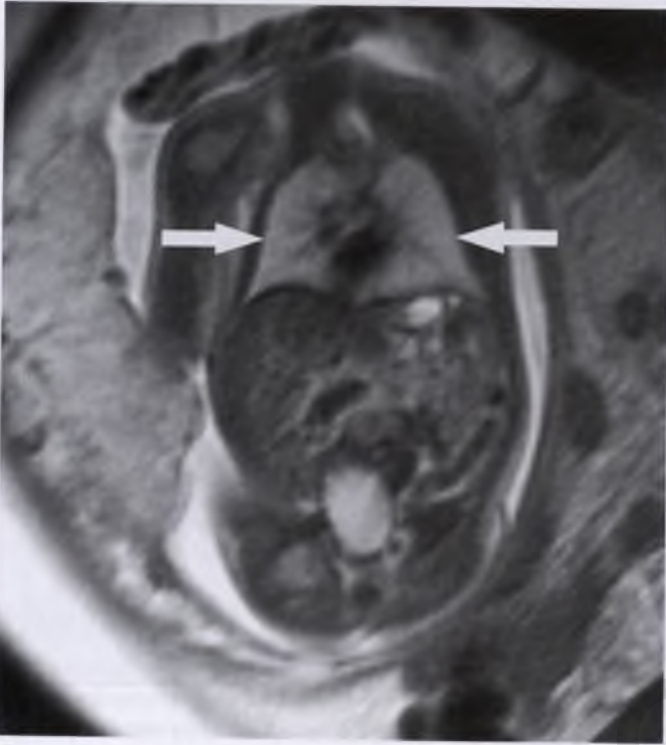


**FIG 12-6** Magnetic resonance imaging (MRI) obtained in a 29-year-old pregnant woman at 30 weeks' gestation in whom detailed prenatal ultrasound depicted a normal fetal chest and fetal abdomen; MRI was performed because placenta accreta was suspected. Coronal single-shot rapid acquisition with relaxation enhancement (T2-weighted MR image 8/90, 4-mm section) of the fetal chest and fetal abdomen shows lungs (arrows) with high signal intensity. Use of this sequence facilitated easy identification of the lungs and planimetry. (From Williams G, Coakley FV, Qayyum A, et al: Fetal relative lung volume: quantification by using prenatal MR imaging lung volumetry. *Radiology* 233:457, 2004.)

effect by the lesion resulting in esophageal compression or increased fluid production by the abnormal lung (Fig. 12-11).<sup>33</sup> With larger masses, there is a risk of fetal hydrops.

The overall prognosis for CPAM lesions has improved considerably, in part owing to the diagnosis of smaller lesions but also because of prenatal therapy for larger masses. For the individual patient, the natural history and prognosis depend primarily on the size of the lesion, the presence of mediastinal shift, and fetal hemodynamic alterations.<sup>34</sup> The presence of hydrops without therapy is associated with a poor outcome and is generally an indication for fetal intervention.

Because the outcome of CPAM is most closely related to the size of the mass, attempts have been made to quantify lesion size to provide prognosis. The CVR is one approach used for risk assessment and patient counseling.<sup>35</sup> The volume of the chest mass is calculated by multiplying the maximal length, width, and depth dimensions (in cm) of the lesion: craniocaudal  $\times$  anteroposterior  $\times$  mediolateral dimensions). This product (in  $\text{cm}^3$ ) is then multiplied by a correction factor of 0.52, resulting in a calculated lesion volume (formula for determining volume of a prolate ellipsoid). Then, to control for gestational age, this estimated volume is divided by the fetal head circumference (in cm) (Fig. 12-12):

$$\text{CVR} = (\text{length} \times \text{width} \times \text{depth} \times 0.52) / \text{head circumference}$$

In calculating CVR, it is important to include the margins of the lesion and to measure its maximal dimensions (Fig. 12-13).

CPAMs tend to stabilize in size in the late second/early third trimester, at a mean gestational age of 26 weeks. However, in some cases these lesions may continue to grow late into the third trimester. The size of the lesions, the variable growth behavior, the presence of a dominant cyst, and possible systemic venous obstruction all play a role in prognosis and in potential development of hydrops.

For an individual patient, the volume of the lesion relative to the size of the fetus, as measured by the CVR, is the best predictor of both prenatal development of hydrops and the presence of respiratory symptoms at birth. A CVR greater than 1.6 is associated with risk for fetal hydrops. A maximum CVR greater than 1.0 at any point in gestation is associated with respiratory symptoms at birth and an increased risk of requiring neonatal surgical intervention (positive predictive value 75%; negative predictive value 98%).<sup>36</sup> Hydrops is associated with close to 100% mortality rate and is considered an indication for prenatal therapy.<sup>37</sup> Open fetal surgery has been offered to patients with



**FIG 12-7** **A**, Macrocystic congenital pulmonary airway malformation, type 1, with several sizable cysts in the left-sided chest mass. **B**, Echogenic congenital pulmonary airway malformation, type 2, within the chest, displacing the heart. Small peripheral cysts are seen. **C**, Displacement of the fetal heart toward the right facilitates identification of homogeneous left-sided mass. The solid-appearing mass is consistent with congenital pulmonary airway malformation, type 3. No discrete cysts are seen. Small amount of normal-appearing lung is present on the right. LT, left thorax; RT, right thorax.



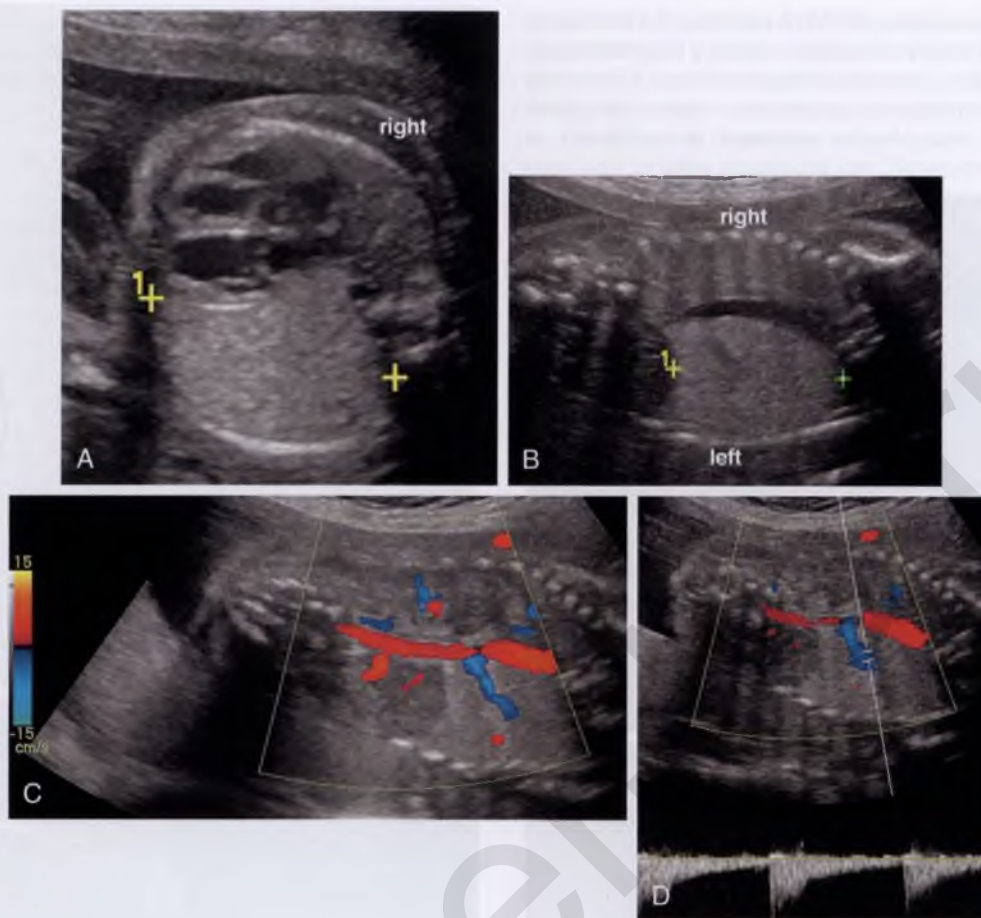


**FIG 12-8** Axial (A) and coronal (B) views through the fetal chest with homogeneous left-sided mass consistent with bronchopulmonary sequestration (BPS). Note rightward cardiomeastinal shift. Color (C) and spectral (D) Doppler sonographic images of left-sided BPS demonstrating anomalous arterial supply to the lesion arising from the descending aorta.

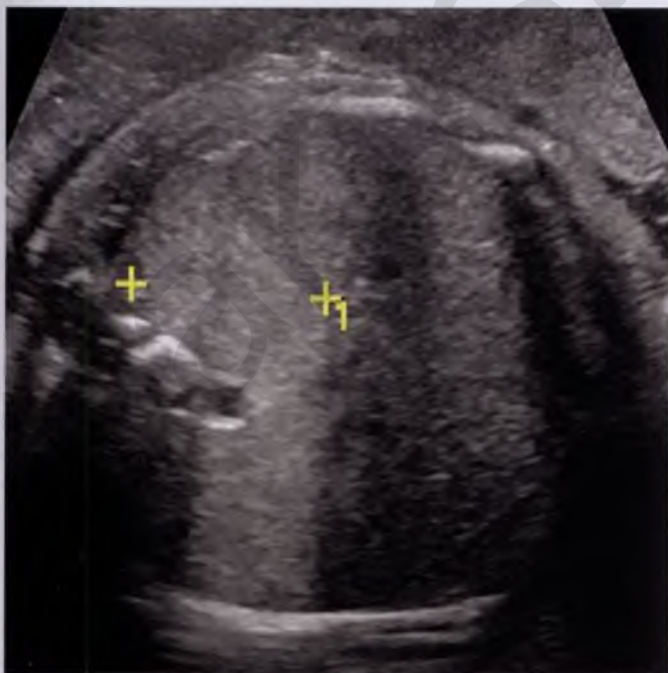


**FIG 12-9** Axial sonographic image through the fetal upper abdomen demonstrating a subdiaphragmatic sequestration.

large microcystic CPAM lesions in the setting of hydrops or early decompensation of the fetus.<sup>38</sup> Survival rates of 52% have been reported, with mean gestational age at delivery of 31.3 weeks.<sup>39</sup> The associated risks including preterm labor, preterm rupture of membranes, fetal demise, and potential maternal complications have to be balanced against high risk of mortality for the fetus. Less invasive approaches including cyst aspiration have been performed as temporizing measures to slow disease progression and to determine if thoracoamniotic shunting will be effective. Placement of thoracoamniotic shunts in hydropic fetuses results in an overall survival rate approaching 60%.<sup>39</sup>

Prenatal administration of corticosteroids has been shown to be an effective alternative to the more invasive surgical approach.<sup>40,41</sup> When administered in the setting of CPAM and fetal hydrops, reversal of hydrops is reported in 78% of cases, with 83% survival rate to neonatal discharge.<sup>41-43</sup> Additionally, when corticosteroids were administered in the setting of CPAM with CVR greater than 1.6, hydrops did not develop.<sup>43</sup> Ongoing research is focused on ideal timing, dosing, and selection of candidates for steroid therapy.

Management of CPAM includes observation for signs of lesion growth or development of hydrops with serial scans every 2 weeks (Fig. 12-14). For patients at highest risk of hydrops (i.e., CVR > 1.6), weekly assessment may be appropriate. Frequent observation is recommended until there is evidence of a plateau in growth and stabilization in size of the lesion based on CVR measurements. Corticosteroid



administration may be considered if CVR is more than 1.6 and should be offered if signs of hydrops are present, without a single dominant cyst. If a single dominant cyst is noted within the lesion, in the setting of hydrops or decompensation, percutaneous ultrasound-guided drainage of the cystic lesion can be considered. In the absence of

contraindications, term delivery is recommended. If the maximum CVR measures more than 1.0 at any point during the pregnancy, delivery at a tertiary care center should be considered because of the possible need for neonatal respiratory support.<sup>36</sup>

## BRONCHOGENIC CYST

Bronchogenic cysts result from abnormal budding of the primitive esophagus and tracheobronchial tree during embryogenesis. Because they form between 4 and 8 weeks' gestation, prior to the development of distal airways, they rarely connect to a normal bronchus. Lesions arising before or during the separation of the embryonic foregut are located in the mediastinum (30%). The more common location is within the lung parenchyma, where the lesion arises after separation of the airway and the esophagus (70%).<sup>44</sup> The cyst wall is lined with ciliated epithelium and contains structural elements of the airway, including cartilage, smooth muscle, mucous glands, and respiratory epithelium.<sup>45</sup>

Bronchogenic cysts usually appear as a single anechoic unilocular cyst located in the central area of the lung parenchyma<sup>45</sup> (Fig. 12-15); they may also present as multiple cysts. Most are right-sided, near the midline, and in close proximity to the tracheobronchial tree. On rare

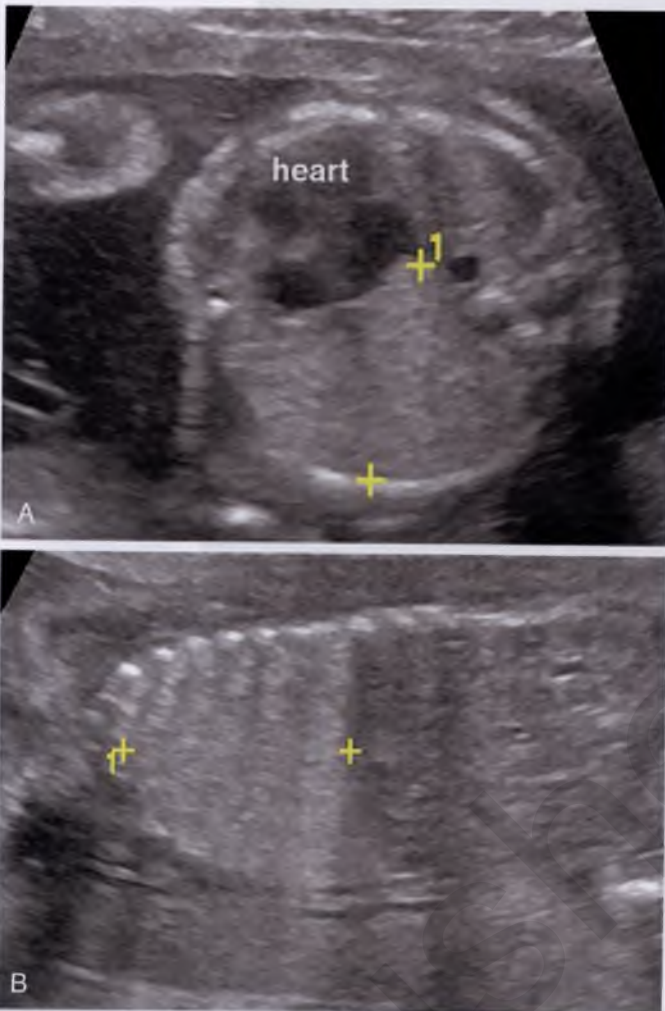
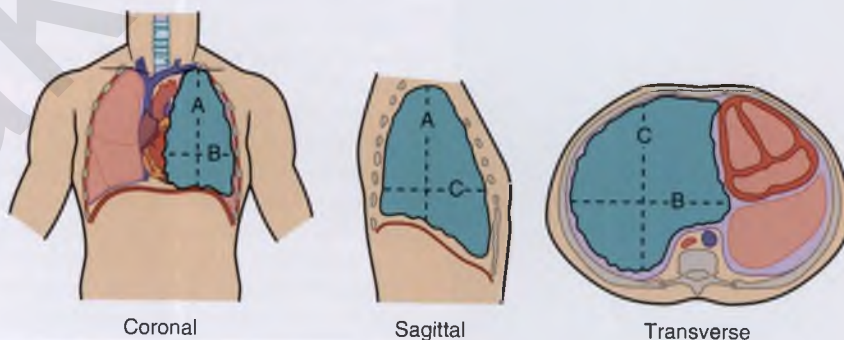


**FIG 12-10** Homogeneous, echogenic chest mass shown in axial (A) and sagittal (B) views, consistent with type 3 congenital pulmonary airway malformation.



**FIG 12-11** Fetus with homogeneous echogenic lung mass and polyhydramnios.



$$\text{CVR} = \frac{[A \times B \times C \text{ (all in cm)}] \times 0.52}{\text{Head circumference (in cm)}}$$

**FIG 12-12** Diagram illustrating technique for calculating CPAM volume ratio (CVR). A, craniocaudal; B, mediolateral; C, anteroposterior; CPAM, congenital pulmonary airway malformation.



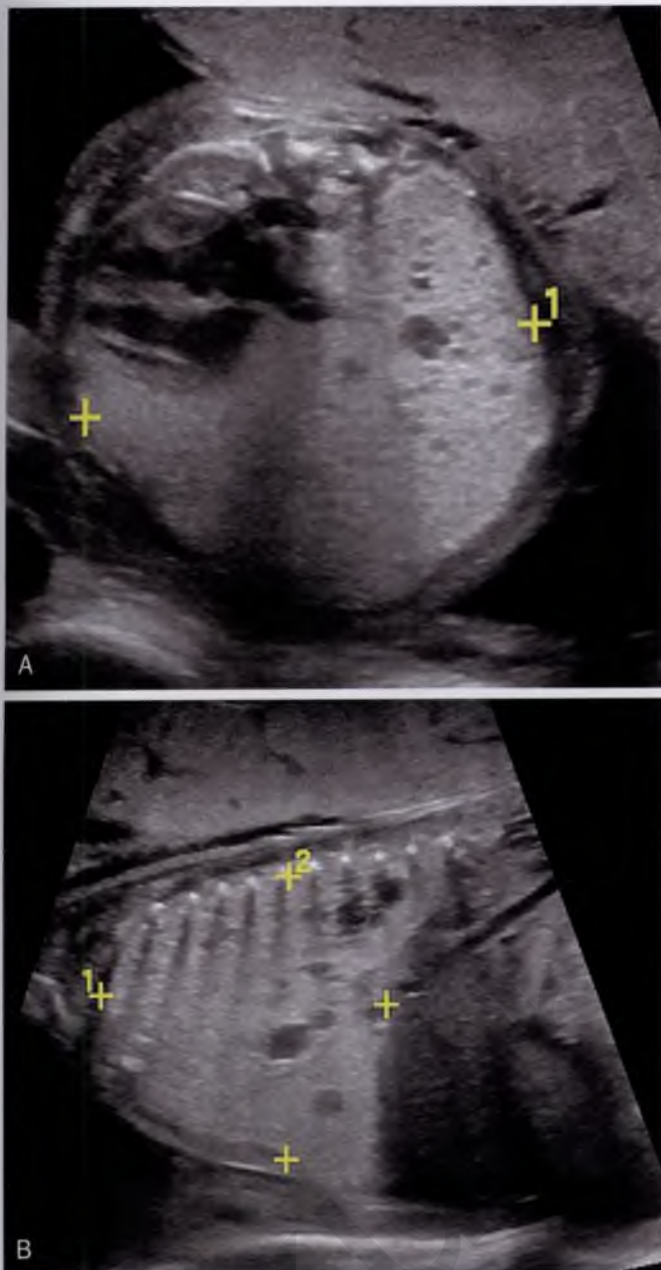


**FIG 12-13** Large solid and cystic congenital pulmonary airway malformation (CPAM) on axial (**A**) and sagittal (**B**) views. Electronic calipers are placed to measure the three dimensions of the lesion—used to calculate CVR (CPAM volume ratio). See Figure 12-12.

occasions, they migrate to the perihilar area or even subdiaphragmatic regions.<sup>46</sup> Cyst size is variable, ranging from 2 to 10 cm in diameter.<sup>47</sup> Bronchogenic cysts may be difficult to distinguish from macrocystic CPAM with a single dominant cyst, but the location and the absence of surrounding echogenic lung tissue characteristic of CPAM will aid in reaching the correct diagnosis.

Bronchogenic cysts can enlarge with advancing gestation and cause compression of surrounding normal lung parenchyma. The compression of the mediastinum and the surrounding lung tissue may be associated with hydrops as well as pulmonary hypoplasia.<sup>48</sup> In utero aspiration of the cyst can be performed if there is evidence of hydrops or compromise of cardiac function; thoracoamniotic shunting will decompress enlarging cysts and may reverse the mediastinal

compression and hydrops. Most often these lesions are closely followed and managed in the neonatal period with thoracotomy and cyst excision. Wedge resection, segmental resection, and lobectomy have been described to improve neonatal respiratory status.<sup>49</sup>

The differential diagnosis of a sizeable cystic lesion within the fetal chest also includes neurenteric cyst. Neurenteric cysts are posterior enteric remnants that result from incomplete separation of the notochord from the foregut in the 3rd to 4th weeks of embryogenesis.<sup>50-53</sup> Approximately 90% of neurenteric cysts occur in the right posterior mediastinum, superior to the carina, and about 50% are associated with vertebral abnormalities such as scoliosis, segmentation abnormalities with hemivertebrae, and butterfly vertebrae. The cysts may be unilocular, though often they have an internal septation. Neurenteric cysts can be distinguished from the other cystic lesions discussed based on their association with vertebral anomalies.

## BRONCHIAL ATRESIA

Bronchial atresia is on the spectrum of developmental disorders related to the variable timing of airway obstruction. Congenital bronchial atresia is a relatively rare lesion characterized by localized atresia or stenosis of a segmental bronchus. It results from focal obliteration of a proximal segmental or subsegmental bronchus, with normal development of the distal structures. Bronchial atresia can involve lobar, segmental, or mainstem bronchi, more often affecting segmental or subsegmental bronchi. Prenatally diagnosed CLE can be caused by lobar bronchial atresia.<sup>44</sup> The short atretic segment leads to mucous accumulation within the distal bronchi, resulting in a bronchocele.<sup>45</sup>

Prenatal ultrasound findings of bronchial atresia demonstrate an extremely large, massively overexpanded unilateral lung or lung segment. The mass will typically result in mediastinal shift from mass effect, with compression of chest structures and often with eversion of the ipsilateral hemidiaphragm<sup>54</sup> (Fig. 12-16). Contralateral lung volumes may appear small. Branching fluid-filled structures may be seen within the enlarged echogenic lung, representing dilated airways peripheral to the central obstructed bronchus.<sup>45,46</sup> Serial sonograms should be performed to delineate anatomy, assess for enlargement of the lesion and development of hydrops, and search for possible concomitant anomalies. MRI may be helpful to identify the atretic airway and to distinguish this lesion from a large CPAM (Fig. 12-17). When these lesions are suspected, MRI acts as an adjunctive imaging tool, assisting with tissue characterization, determining level and location of atresia, and delineating complex anatomy. As lesions enlarge and change, they may affect the development of surrounding lung, obstruct venous return, and result in lung hypoplasia.<sup>49</sup>

Ultrasound differentiation between bronchial atresia and CPAM may be challenging, as the large echogenic lung appears very similar to microcystic (type 3) CPAM. The central versus peripheral location of cystic components and the involvement of multiple lobes of the lung should raise suspicion for bronchial atresia and may prompt further imaging. Serial sonograms are recommended, as these lesions typically enlarge during pregnancy. In this way, they differ from CPAMs, which typically plateau in size during gestation. The risk of hydrops is increased with larger lesions, but the ability to prognosticate based on lesion size at the time of initial diagnosis or based on CVR measurements is not very reliable with bronchial atresia.<sup>48</sup>

Bronchial atresia more commonly affects segmental or subsegmental bronchi, and therefore, it is often asymptomatic or may not present until adolescence.<sup>55,56</sup> Prenatally diagnosed segmental CLE caused by bronchial atresia has been reported and is managed surgically in the newborn period.<sup>57</sup> Although segmental and lobar bronchial atresias may be compatible with ex utero survival, the outcome for mainstem





**FIG 12-14** Large solid and cystic type 2 congenital pulmonary airway malformation shown on axial (**A**) and coronal (**B** and **C**) views. Note the small amount of ascites present at the upper abdomen. There is marked leftward displacement of the heart (H). S, stomach.

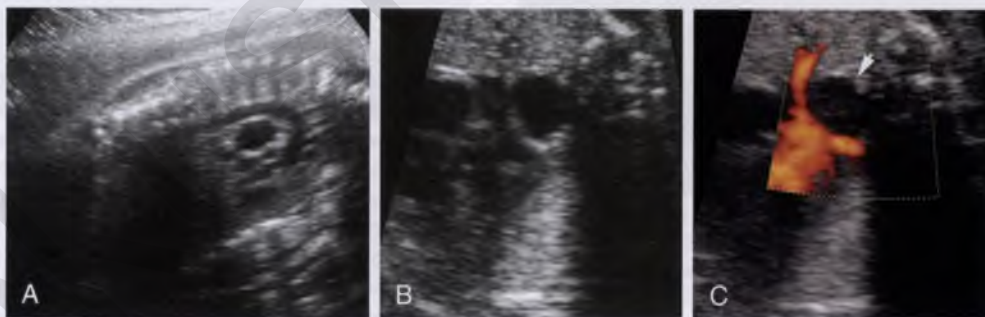


**FIG 12-15** Bronchogenic cyst (*arrow*) in fetus at 28 weeks' gestation, shown in longitudinal (**A**) and transverse (**B**) planes and transverse image with power Doppler sonographic evaluation (**C**).

bronchial atresia is grim.<sup>47</sup> Optimal management for a fetus with main-stem bronchial atresia remains uncertain. It is possible that fetal surgical resection may provide the best opportunity for survival, although benefits have not been clearly documented. Prenatal intervention to remove the enlarged lung segment has been attempted; reported outcomes have been poor to date, with prematurity remaining a significant complication.<sup>58</sup> In one reported case, maternal betamethasone administration was thought to explain the lack of fetal hydrops. However, the lung lesion was smaller (CVR 2.6) and may have represented only partial bronchial obstruction.<sup>48</sup>

It is recommended that a fetus with bronchial atresia be delivered in a tertiary care center because of possible pulmonary hypoplasia and potential for air trapping in the alveoli supplied by the affected bronchi. There is a wide spectrum of involvement and severity with this lesion. When a larger lesion is noted, ex utero intrapartum treatment (EXIT) and a primed extracorporeal membrane oxygenation (ECMO) circuit may be considered for delivery.<sup>59</sup> Overall prognosis remains poor for the larger lesions identified by massive unilateral hyperplasia, marked distention of the obstructed bronchi, bronchiectasis, as well as fluid-filled airspaces seen at the time of postnatal surgery.



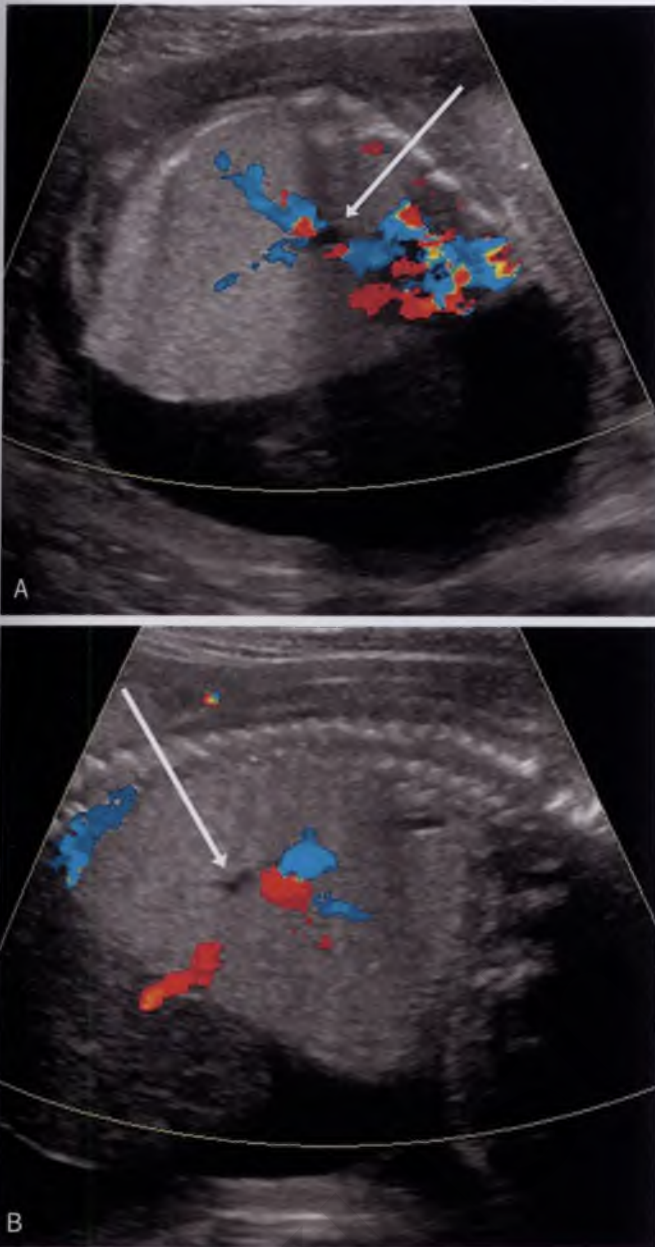


**FIG 12-16** Color Doppler images through fetal chest. Axial (**A**) and sagittal (**B**) images demonstrate markedly enlarged echogenic lung, with eversion of the hemidiaphragm, consistent with bronchial atresia. Note fluid-filled airway (arrow).

## CONGENITAL LOBAR EMPHYSEMA

CLE is a developmental abnormality of the lower respiratory tract that is characterized by entrapment of fluid in the lungs, resulting in hyperinflation of one or more of the pulmonary lobes. Bronchial atresia, with an atretic portion of the bronchus, is one of many causes of CLE. The prevalence prenatally is not certain, but it is reported to affect approximately 1 in 20,000 to 1 in 30,000 newborns.<sup>60</sup> It has been postulated that CLE may result from intrinsic obstruction caused by defects in the bronchial wall, such as deficient or dysplastic bronchial cartilage leading to obstruction of the lower airway. Extrinsic compression causing obstruction may also result from aberrant cardiopulmonary vasculature or other intrathoracic lesions, including anomalous

pulmonary venous return, duplication cysts, teratomas, or bronchogenic cysts.<sup>61,62</sup> This results in altered distal development and diffuse bronchial abnormalities. Approximately 25% of the time, CLE is caused by an intrinsic obstruction.<sup>63</sup> Whether the bronchi are underdeveloped or obstructed, collapsed distal lung prohibits normal lung fluid homeostasis. This, in turn, leads to progressive lobar hyperinflation. Postnatally, airway obstruction leads to a “ball-valve” mechanism in which a greater volume of air enters the affected lobe during inspiration than leaves during expiration. This air trapping in distal areas of the lung results in emphysema.<sup>64</sup>

Sonographic appearance of the fetal thorax with CLE demonstrates a homogeneous echogenic lung mass, usually without cystic components. This mass appears as a unilateral lesion because of the inflated lung distal to the obstruction. The mass often crosses the midline and results in displacement and compression of the heart.<sup>65</sup> Mediastinal shift, polyhydramnios, and fetal hydrops can also be seen and are predictors of severe respiratory distress and increased risk of death. Ninety-five percent of lesions occur in the upper and middle lobes and are unilateral.<sup>66</sup> The lower pulmonary tissue is typically normal in appearance. Mass effect may result in downward displacement of the diaphragm. Blood supply is derived from the normal pulmonary artery and vein. CLE is most often diagnosed in the neonatal period secondary to respiratory symptoms.

The differential diagnosis of an echogenic lung mass is diverse and includes CPAM, BPS, and unilateral bronchial atresia. BPS may be recognized if anomalous arterial supply arising from the aorta is observed. Dilated fluid-filled airways will not be seen in CPAM and when they are noted, the differential diagnosis is limited to CLE or bronchial atresia. Because CLE occurs secondary to obstruction, it may resolve during the course of the pregnancy. CPAM typically demonstrates a plateau or gradual decrease in lesion size after 26 weeks’ gestation. CLE should be considered if a striking reduction in size of a chest mass is observed over a short interval, as relief of the obstruction may result in resolution of hyperinflated echogenic lung. Unfortunately, resolution of in utero findings with CLE does not always confer normalization of lung function after birth. As with bronchial atresia, fetal MRI may help confirm and delineate the underlying pathologic process.

The appropriate treatment of CLE in neonates with respiratory distress is surgical resection of the affected lobe.<sup>67</sup> Historically, open thoracotomy was performed. Recent advances in minimally invasive thoracoscopic surgery have resulted in decreased morbidity associated with neonatal resection.<sup>68</sup>

## CONGENITAL HIGH AIRWAY OBSTRUCTION SYNDROME

Congenital high airway obstruction syndrome (CHAOS) results from obstruction of the fetal upper airway. This obstruction, whether partial or complete, is most often secondary to atresia or stenosis of the larynx or trachea. Laryngeal agenesis, subglottic stenosis or atresia, and laryngeal webs or cysts are also reported causes of this condition.<sup>69</sup> When complete atresia is seen, tracheoesophageal fistula is often present.<sup>70</sup> Although rare, with an uncertain incidence,<sup>71,72</sup> it is understood that tracheal atresia occurs secondary to deficient recanalization of the upper airway at about the 10th week of gestation.<sup>71</sup> The prenatal diagnosis of CHAOS was first described in the late 1980s.<sup>73</sup> The increasing frequency of CHAOS diagnosis and reporting has allowed for a better understanding of the pathophysiologic mechanisms (Fig. 12-18).

Although some fluid secreted by the fetal lung is absorbed through the tracheobronchial tree, the bulk of secreted fluid is released into the amniotic sac. When an obstruction is present in the tracheobronchial



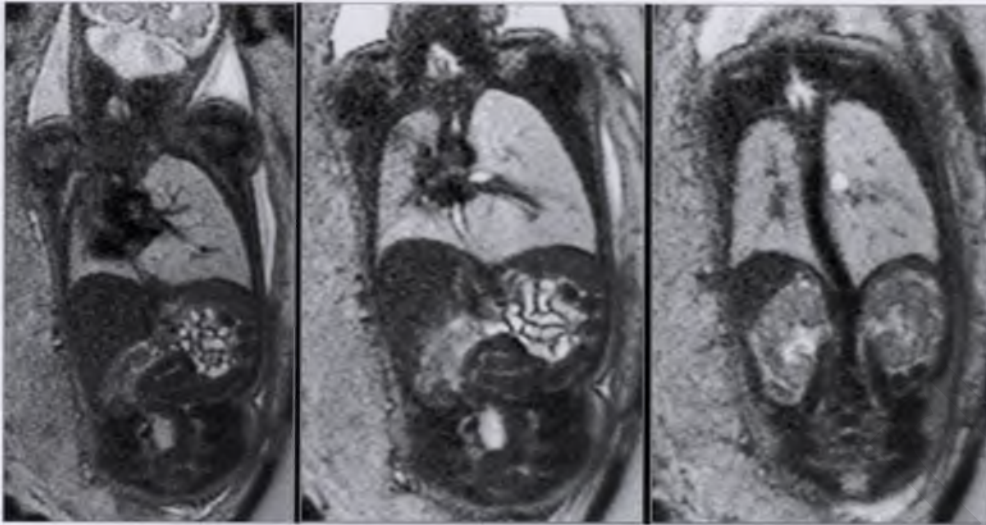


**FIG 12-17** Coronal fetal magnetic resonance images showing unilateral hyperexpanded left lung. Note the left perihilar T2-weighted hyperintense structure consistent with a dilated, fluid-filled airway.

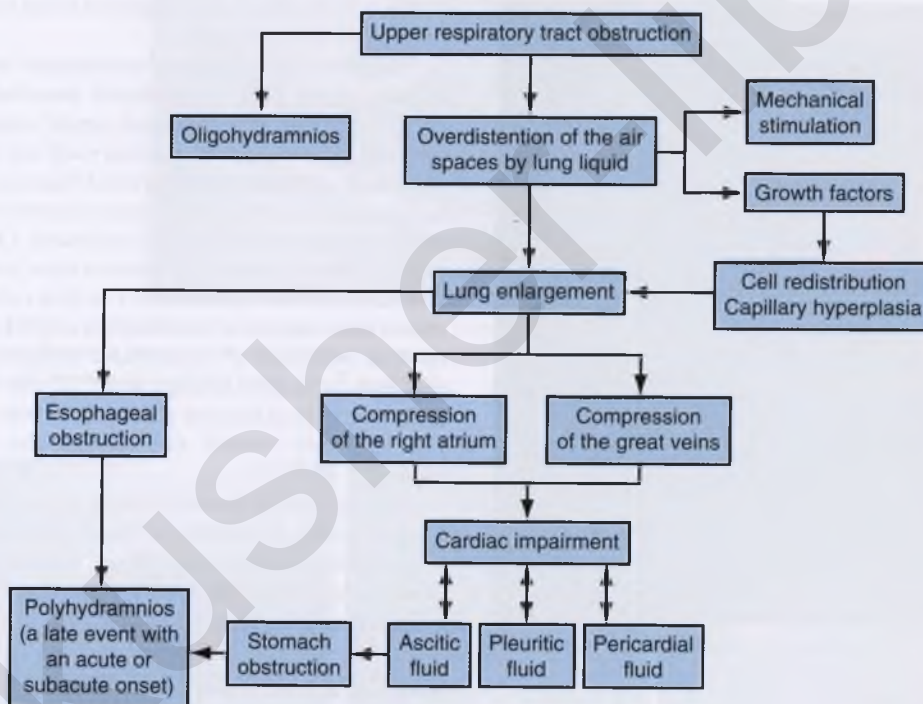


**FIG 12-18** The pathophysiologic mechanisms and sonographic findings of upper respiratory atresia sequence in congenital high airway obstruction syndrome. (From Kassanos D, Christodoulou CN, Agapitos E, et al: Prenatal ultrasonographic detection of the tracheal atresia sequence. *Ultrasound Obstet Gynecol* 10:133, 1997.)

tree and prevents fluid egress into the amniotic sac, the accumulated fetal lung fluid causes increased intratracheal pressure and distention of the lungs. The enlarged fetal lungs compress the heart, resulting in central deviation of the cardiac structures (Fig. 12-19). The classic sonographic findings of high upper airway obstruction, which may be more readily appreciated on coronal or sagittal views, include bilateral symmetric enlarged hyperechoic fetal lungs, flattened or everted hemidiaphragms, and dilated, fluid-filled trachea.

Increased intrathoracic pressure, decreased venous return to the heart, and impaired cardiac contractility can lead to the development of ascites, placentomegaly, and nonimmune hydrops with effusions

and polyhydramnios.<sup>74</sup> Compression of the esophagus by dilated lungs may result in impaired swallowing, a potential additional contributing factor to the later development of polyhydramnios seen in some, but not all, cases of CHAOS.<sup>75</sup>

Spontaneous resolution of the ultrasound findings of CHAOS has been reported.<sup>70,76</sup> This may result from spontaneous perforation of an obstructing web with decompression of the lungs as the fluid is released into the amniotic cavity. Recurrent obstruction is possible and patients should be followed with serial sonograms even after apparent resolution. Unfortunately, resolution of the ultrasound findings is not always associated with improvement in lung function, and there may be



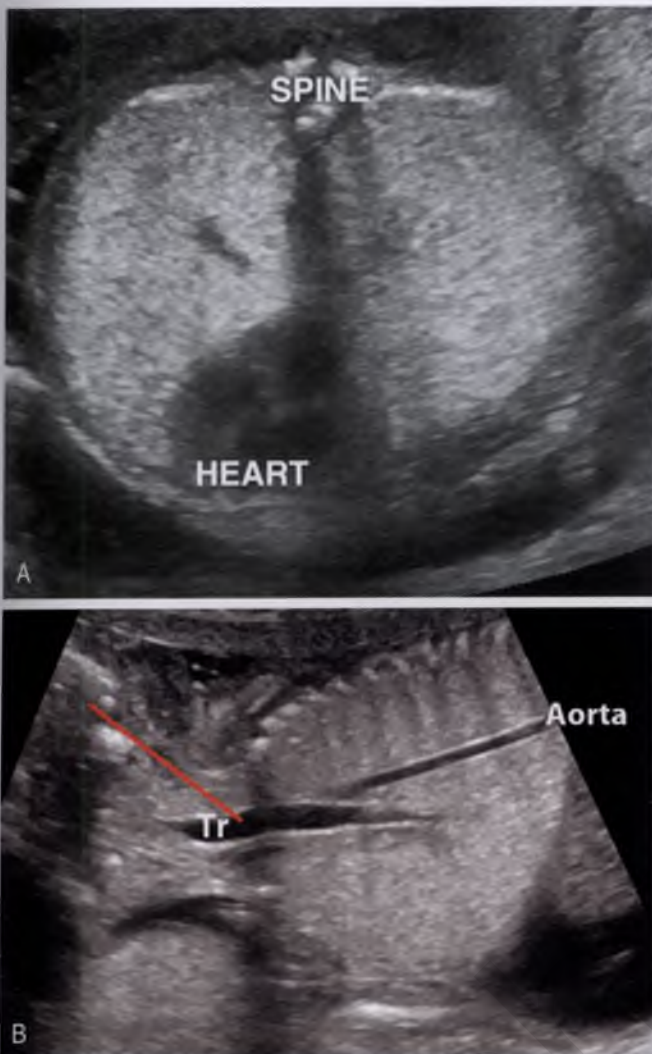


**FIG 12-19** Congenital high airway obstruction syndrome (CHAOS). Two views, axial (**A**) and coronal (**B**), showing markedly enlarged hyper-echoic bilateral fetal lungs. The heart is in the midline, displaced anteriorly, and the fluid-filled trachea (Tr) is visualized (red line).

significant pulmonary compromise at birth even after apparent prenatal resolution.

Because of the lack of a patent airway, CHAOS is frequently lethal. There are also high reported rates of intrauterine fetal demise.<sup>74</sup> Prenatal sonographic diagnosis allows improved neonatal survival, and antenatal recognition of CHAOS allows for a multidisciplinary delivery management plan. MRI may allow for improved visualization of dilated airways with detection of the level and structure of the obstruction,<sup>77</sup> and these findings may assist with counseling and delivery planning<sup>69,78</sup> (Fig. 12-20). EXIT may be offered if the location of the obstruction is compatible with establishment of an airway and CHAOS is an isolated finding.<sup>70,79</sup> By improving identification of the level of obstruction, sonography and MRI have allowed appropriate delivery planning. Postnatally, diaphragmatic dysfunction is commonly due to diaphragmatic stretching, and survivors may require extended ventilator support.<sup>74</sup>

Although CHAOS is most often an isolated finding, it may be seen with syndromes or isolated unilateral lung agenesis (Figs. 12-21 and 12-22). Fraser syndrome, an autosomal recessive genetic disorder,

includes microphthalmia, cryptophthalmos, polydactyly, and syndactyly in association with upper airway obstruction.<sup>80</sup> Other syndromes that have been reported in association with CHAOS are cri du chat syndrome, short-rib polydactyly syndrome, and 22q11.2 deletion syndrome.<sup>81</sup> A thorough anatomic survey identifying additional findings allows for optimal counseling regarding anticipated prognosis and inheritance implications for future pregnancies.<sup>74</sup>

The differential diagnosis of CHAOS includes bilateral CLE, bronchial atresia, or bilateral CPAM. CHAOS must be distinguished from extrinsic causes of tracheolaryngeal obstruction such as lymphatic malformation, cervical teratoma, and vascular rings, as accurate distinction is crucial for management planning.<sup>70</sup>

## CONGENITAL HYDROTHORAX

Congenital fetal hydrothorax, also known as primary pleural effusion, is the abnormal accumulation of fluid in the pleural space. The estimated incidence of hydrothorax has been reported as 1:10,000 to 1:15,000 pregnancies<sup>82</sup> and may initially be either unilateral or bilateral. As the fluid increases, mass effect may result in compression of adjacent thoracic structures, compromising heart function as well as lung development. It is worth remembering that fetal pleural effusions can be associated with nonimmune hydrops—either as a primary cause or as a consequence. Unilateral hydrothorax in particular can lead to nonimmune hydrops if the effusion is large and asymmetric, as these effusions can cause a mass effect with cardiomeastinal shift and eversion of the ipsilateral hemidiaphragm. Primary hydrothorax as a cause of nonimmune hydrops should be suspected with a very large, unilateral effusion or markedly asymmetric bilateral effusions; this cause of nonimmune hydrops is important to recognize, as it can be effectively treated with in utero percutaneous aspiration or thoracoamniotic shunting. Such treatment may be lifesaving for an otherwise normal fetus.

Isolated pleural effusions present as echolucent fluid collections between the lungs and chest wall. They are differentiated from pericardial effusions by the extension of fluid around the lung structures (Fig. 12-23). Sonographic findings range from small amounts of fluid adjacent to the normal-appearing lung (typically more prominent in the anterior chest) to larger effusions causing mediastinal shift and downward displacement of the diaphragm (Fig. 12-24). Polyhydramnios is often seen with larger pleural effusions.

The natural history of hydrothoraces varies from spontaneous prenatal resolution (22%) to generalized hydrops fetalis or even death. The mortality rate for isolated effusions has been reported to be between 15% and 36%.<sup>83,84</sup> A worse prognosis is associated with bilateral effusions, the presence of hydrops, persistence of effusions, or premature delivery.<sup>85</sup> When generalized hydrops fetalis is present, mortality rate may approach 95% without treatment (Fig. 12-25).<sup>86,87</sup> Prenatal therapy including drainage and shunting of the pleural effusion is reported to improve the survival rate to over 70%.<sup>88-91</sup> The presence of polyhydramnios tends to be associated with a poorer prognosis,<sup>85</sup> in part because of the association with larger effusions and presence of hydrops.

The most common cause of isolated pleural effusion is chylothorax. Prenatal confirmation is made by ultrasound-guided thoracentesis and identification of high lymphocyte count (>80%) in the aspirated fluid.<sup>92</sup> Aspiration of the fluid and drainage of the chest allows for diagnosis, in addition to potential therapeutic benefits.<sup>89</sup> Drainage also allows for pulmonary reexpansion and evaluation of lung tissue to ensure that no underlying abnormalities are present. It also may facilitate evaluation of the heart and mediastinal structures to assess for possible associated structural abnormalities. Impaired venous return





**FIG 12-20** Coronal T2-weighted fetal MR images showing enlarged bilateral lungs with eversion of the diaphragm and fluid-filled trachea (*arrow*) consistent with congenital high airway obstruction syndrome, owing to laryngeal atresia. Associated hydrops with moderate volume of fetal ascites is evident.

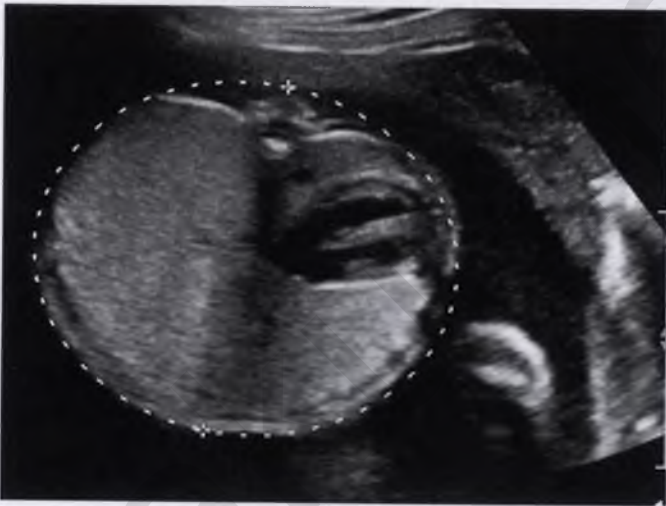


**FIG 12-21** Transverse ultrasound image shows marked deviation of the fetal heart toward the left. The right lung appears enlarged and echogenic, suggesting unilateral bronchial atresia.

secondary to compression and tamponade-like effects on the heart may result in the development of hydrops. When pleural effusions are first seen in a fetus with hydrops, it can be challenging to identify the underlying cause. Hydrops secondary to primary pleural effusion is usually associated with significant skin edema and with volume of pleural fluid significantly larger than the volume of ascites. In addition, hydrops most commonly results from unilateral effusion with associated mass effect, and less commonly it is the consequence of bilateral effusions. In the setting of fetal hydrops with bilateral effusions, attention should be paid to the relative size of the effusions and the presence



**FIG 12-22** Coronal T2-weighted fetal magnetic resonance image of unilateral bronchial atresia with markedly enlarged right lung. Distended fluid-filled airway seen centrally (*arrow*). Associated hydrops with marked fetal ascites. The contralateral left lung was not visualized.





**FIG 12-23** Axial image showing unilateral right-sided hydrothorax with associated mediastinal shift.



**FIG 12-24** Large unilateral right pleural effusion causing significant mass effect with leftward cardiomeastinal shift.

or absence of mass effect. Large primary hydrothorax can result in hydrops with development of contralateral pleural fluid, though typically there is significant discrepancy in volume and marked cardiomeastinal shift.

Fetuses whose effusions rapidly reaccumulate after aspiration may benefit from ultrasound-guided percutaneous placement of a thoracoamniotic shunt<sup>93</sup> (Fig. 12-26). Thoracoamniotic shunt placement allows for lung reexpansion, permitting normal development of compressed pulmonary tissue and resolution of mediastinal shift with improved cardiovascular function.<sup>87</sup> Resolution of significant hydrops occurs gradually after successful shunt placement. Preterm delivery prior to 32 weeks is more likely to result in neonatal demise of the fetus with significant pleural effusions; pulmonary hypoplasia remains a major complication for some neonates despite prenatal shunting. The



**FIG 12-25** Significant integumentary edema associated with large pleural effusion at 24 weeks' gestation. Patient underwent ultrasound-guided thoracoamniotic shunt placement and subsequently delivered a healthy infant at 38 weeks' gestation.



**FIG 12-26** Thoracoamniotic shunt adjacent to and within the fetal chest (arrows). Though ascites is still present, there is no residual pleural fluid in the chest.

most common complication of prenatal shunting is the need for shunt replacement because of obstruction or dislodgment (37%).<sup>94</sup>

Neonates with pleural effusions may be symptomatic with respiratory distress at birth from compression of otherwise normal lung by the fluid or from residual pulmonary hypoplasia.<sup>95</sup> Delivery in a tertiary care center is recommended owing to uncertainty regarding pulmonary function and need for resuscitation. For a newborn with a catheter in place at delivery, it is important to occlude the bidirectional shunt at the time of birth to prevent pneumothorax. Long term, there is increased risk of childhood asthma when prenatal pleural effusions were identified.<sup>96</sup>

Causes for congenital pleural effusions, in addition to primary chylothorax, include infection, congenital heart disease, genetic or chromosomal abnormalities, pulmonary lesions including CPAM, or other lesions such as CDH or tracheoesophageal fistula.<sup>92</sup> The two most commonly associated abnormalities are CDH and trisomy 21.<sup>97,98</sup> Alternatively, the fluid collection may be one of several findings seen in hydrops fetalis due to other causes.



Cystic or fluid-filled structures within the thorax such as CDH, cystic CPAM, bronchogenic cyst, and pericardial fluid may simulate pleural fluid collections or may be associated with pleural effusions. It is important to clearly delineate the anatomy to allow for appropriate diagnosis and therapy.

### CONGENITAL DIAPHRAGMATIC HERNIA

CDH results from absence or deficiency of a portion of the diaphragm owing to incomplete formation of the structure, with subsequent herniation of abdominal contents into the fetal chest (Fig. 12-27). The incidence of CDH in the United States is estimated at 1088 cases per year, or 1 in 3836 live births.<sup>99</sup> The reported incidence may be lower than the actual incidence because of a higher rate of intrauterine demise and early (undiagnosed) neonatal death in infants with CDH.

CDH is most often a sporadic condition, and 85% of the defects are posterolateral and on the fetal left side (Fig. 12-28). Right-sided defects are seen in approximately 10% to 15% of cases, and 2% of defects occur bilaterally or centrally<sup>102</sup> (Fig. 12-29). Females and males are equally affected. The normal primitive diaphragm is formed by the end of the 8th week of gestation with development of the muscular diaphragm completed by the 14th week. Although the failure of fusion of the pleuroperitoneal canal occurs early in gestation, the herniation of intra-abdominal contents may not occur until later in fetal life, making small defects difficult to identify early in pregnancy. Most CDHs are detected at the time of the 18- to 20-week fetal anatomy sonogram, with a median gestational age at diagnosis of 19 weeks. An eventration of the diaphragm may appear as herniation of intra-abdominal contents into the fetal chest and can be mistaken for CDH. Eventration results from failure of muscularization of the otherwise intact primitive diaphragm and has a better prognosis.

It is frequently the abnormal position of the fetal heart that provides the first clue to the presence of a diaphragmatic defect. On a transaxial image through the thorax, a shift of the mediastinum and heart toward the right will be seen in most left-sided lesions. With a right-sided lesion, it is possible for the heart to appear in the usual



**FIG 12-27** Pathologic specimen of intrauterine fetal demise associated with left-sided congenital diaphragmatic hernia. Failure of closure of the diaphragm allowed herniation of the bowel and stomach into the fetal chest. (Image courtesy of Mason Barr, MD.)

location. Therefore, in every examination, care must be taken to assess the echogenicity and morphologic appearance of the intrathoracic contents, to assure that herniated bowel or liver is not misinterpreted as lung tissue. The presence of the fluid-filled stomach in the chest is easily recognized. A bowel-containing CDH with normal-appearing, normally located stomach at the left upper quadrant of the abdomen, which may occur with small left-sided lesions, is more challenging to detect. Review of real-time images may demonstrate peristalsis, allowing for recognition of herniated bowel, but it is often the echotexture of the intrathoracic tissue that raises suspicion (Fig. 12-30). The inability to visualize the fluid-filled fetal stomach is often associated with esophageal atresia but may also occur in some cases of CDH, and this

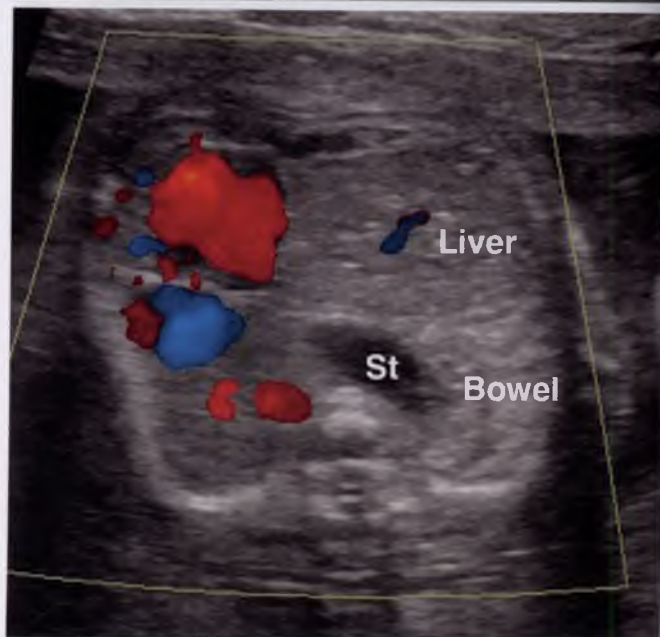


**FIG 12-28** Two axial sonographic views through the chest in a fetus with a left congenital diaphragmatic hernia. Stomach (St), bowel, and portion of liver are herniated into the left hemithorax. Rightward shift of the heart (H) is also evident.



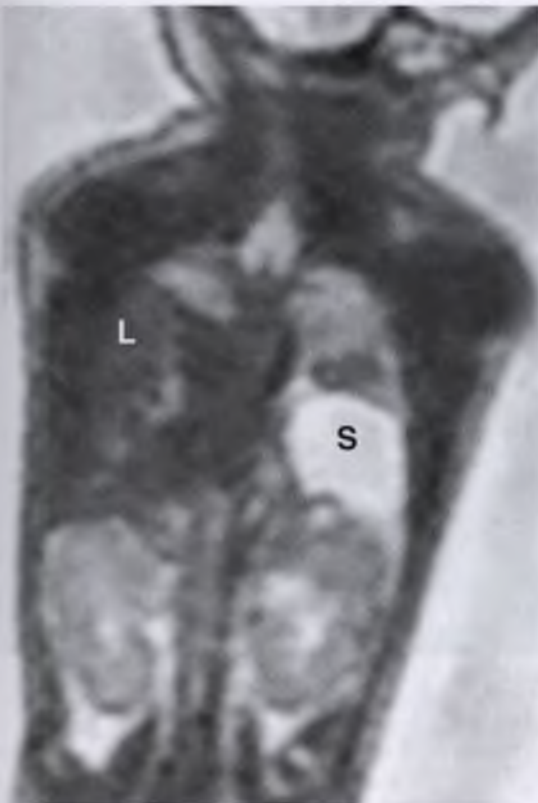


**FIG 12-29** Coronal fetal magnetic resonance imaging showing bilateral congenital diaphragmatic hernia with liver (L) and stomach (S) herniated into the right and left hemithorax, respectively.



**FIG 12-31** Parasagittal sonographic image with discontinuity and defect at the posterior aspect of the left hemidiaphragm. Herniation of the fluid-filled stomach and bowel into the left hemithorax.



**FIG 12-32** Transverse plane through the fetal chest with left-sided congenital diaphragmatic hernia and associated rightward cardiome-diastinal shift.



**FIG 12-30** Transverse image through the fetal chest demonstrates mild rightward shift of the heart. The fluid-filled stomach (not shown on this view) was identified in the expected location at the left upper quadrant, within the abdomen. Heterogeneous echogenic material within the left hemithorax represents herniated, nondilated small bowel segments. It, left thorax; rt, right thorax.

possibility should be considered in the differential diagnosis when no stomach is identified. A fluid-filled stomach noted at the expected level of the diaphragm (Fig. 12-31) or within the fetal chest facilitates the diagnosis of CDH (Fig. 12-32). The location of the stomach is also helpful in assessing the severity and the presence of other herniated abdominal contents, in particular the left lobe of the liver. With left CDH, liver herniation is more likely if the stomach is located in the mid- or posterior left chest. Polyhydramnios frequently accompanies CDH but is usually a late finding, seen most often in the third trimester.

Paradoxical motion of the hemidiaphragm with fetal breathing movements is diagnostic of a diaphragmatic abnormality. This observation is manifest by descent of one hemidiaphragm with ascent of the other, observed on coronal imaging during fetal inspiration.<sup>100</sup> This sign can be useful, particularly in patients in whom heart deviation is noted, but suboptimal sonographic resolution makes the diagnosis difficult.



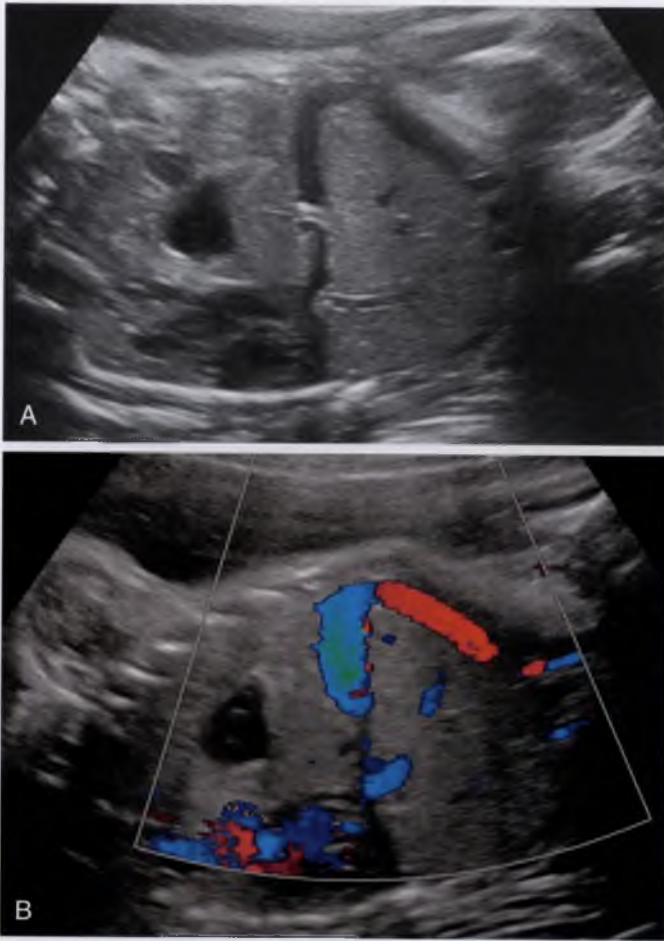


**FIG 12-33** Left congenital diaphragmatic hernia (CDH). Coronal sonographic image (A) with liver herniation confirmed by color Doppler (B) showing flow in deviated umbilical/left portal vein.

In cases of left CDH, assessment of the location of the fetal liver is necessary for providing prognosis and patient counseling. Liver herniation is consistently associated with higher rate of postnatal mortality as well as morbidity, and increased liver herniation appears to predict outcome.<sup>101</sup> As mentioned, a portion of the left hepatic lobe is likely herniated into the thorax (liver “up”) if the fetal stomach is located posteriorly within the chest. This can also be suggested by deviation/distortion of the midhepatic portion of the umbilical vein toward the left<sup>102</sup> (Fig. 12-33). This altered hepatic venous anatomy can be differentiated from an intrahepatic persistent right umbilical vein by assessing the location of the gallbladder. Color Doppler sonography to identify hepatic vessels and demonstrate crossing at the expected level of the diaphragm can be used to recognize liver herniation. The observation of a horizontal stomach in the abdomen has been described as early as 13 weeks’ gestation as a marker for liver herniation with right-sided CDH.<sup>103</sup>

Pleural effusions are not uncommon with CDH and are seen much more often with right-sided (29.2%) than with left-sided hernias (5.2%)<sup>104</sup> (Fig. 12-34). Interestingly, if pleural effusions are noted in a fetus with suspected left-sided CDH, the possibility of diaphragmatic eventration should be raised, as over half of fetuses with eventration will have pleural and pericardial effusions.<sup>105</sup> Diaphragmatic hernia and eventration may be difficult to distinguish on ultrasound images, and in these cases additional evaluation by MRI may be helpful.



**FIG 12-34** Right congenital diaphragmatic hernia with liver and fluid shown in the right hemithorax. Note associated leftward shift of the heart. LT, left thorax; RT, right thorax.

The presence of effusions with CDH does not confer the same poor prognosis as generalized hydrops or effusions caused by other conditions. The cause of pleural fluid with CDH is not certain but may be secondary to liver congestion related to hepatic venous kinking, especially with right-sided lesions. It is possible that pleural fluid is associated with bowel irritation. Pleural effusions communicate with the peritoneal cavity through the diaphragmatic defect, and in half of the cases of CDH with pleural effusion, peritoneal fluid is also seen. In addition, there is a high incidence of chylothorax following postnatal CDH repair. It is not known whether this is due to surgical insult or thoracic duct dysfunction. In general, the observation of ascites and pleural effusions in association with “isolated” CDH does not significantly alter the prognosis.<sup>104</sup>

The differential diagnosis of CDH includes any intrathoracic lesion that displaces the fetal heart or lungs, including masses in the spectrum of CPAMs. Bronchogenic cysts, cystic teratomas in the anterior mediastinum, and neurogenic tumors in the posterior mediastinum may also be considered. Dextrocardia and unilateral lung hypoplasia or agenesis can be manifest as abnormal position of the heart and should be considered if no specific chest mass or abnormal intrathoracic tissue is identified.

The prognosis of CDH depends on the presence of associated anomalies and the degree of pulmonary hypoplasia. The severity of pulmonary hypoplasia is related to gestational age at diagnosis (as earlier detection is associated with larger lesions and more herniated contents) and to the presence and degree of liver herniation. Survival is influenced by gestational age at delivery.

Risk factors for CDH include maternal pregestational diabetes and alcohol use.<sup>106</sup> Previous studies have also suggested an association with low maternal BMI.<sup>107</sup> The presence of associated anomalies greatly influences survival in neonates with CDH. From 40% to 50% of fetuses will have associated anomalies including chromosomal abnormalities, single gene disorders and genetic syndromes, and other structural



lesions. The incidence of karyotype abnormality is 34%, the majority being deletions, translocations, marker chromosomes, and other unusual chromosomal abnormalities.<sup>108</sup> Multiple syndromes have been described in association with CDHs including Fryns, Cornelia de Lange, Perlman, Beckwith-Wiedemann, and others. Identification and differentiation of various syndromes are not always possible, but suspicion should be raised, particularly if growth abnormalities are noted. In addition, identification of subtle dysmorphic features, including hand and ear anomalies, may facilitate reaching a complete, correct diagnosis.

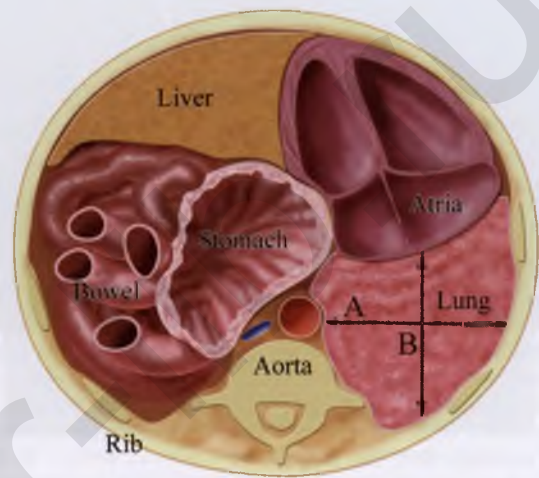
Fetuses affected with both major cardiac anomalies and CDH face much worse prognosis. Overall survival rate appears more closely related to the severity of the cardiovascular malformation than the CDH.<sup>109</sup> It is important to recognize that mild heart defects are common with left-sided CDH. In a series of 125 left-sided CDH patients, 111 had small left-sided cardiac structures based on aortic valve and mitral valve diameters, with the left ventricle contributing only 33% of prenatal cardiac output as compared to the expected 40% to 50%. Z-scores of left-sided cardiac structures increased to normal in postnatal life. The small size is likely secondary to reduced flow and to mass effect with increased external pressure on the heart.<sup>110</sup> The presence of concomitant major congenital heart disease, intrathoracic herniation of a portion of the liver, and premature birth all significantly impact survival of infants with CDH. However, minor left side of the heart dimension and reduced left-sided heart flow on prenatal echo are not associated with postnatal outcome independent of other cardiac findings.

In the absence of associated anomalies, the degree of lung hypoplasia determines the ultimate outcome for a fetus with CDH. The degree of pulmonary hypoplasia correlates with gestational age at herniation and with herniated structures present in the fetal chest. Liver herniation is associated with a greater degree of pulmonary hypoplasia. In general, right-sided hernias (which typically contain liver) are associated with worse prognosis than left-sided lesions. For left-sided CDH, the presence and degree of liver herniation impact outcome.<sup>111</sup> Although the presence of a hernia sac has been associated with less pulmonary hypoplasia, this is often difficult to discern on prenatal ultrasound.<sup>112</sup>

Multiple attempts have been made to prenatally identify those fetuses at highest risk of demise or other poor outcome, including requirement for ECMO due to respiratory compromise. This prognostic information is helpful for counseling families, for selecting the most appropriate location for delivery, and for identifying those who might benefit from referral to specialized centers offering fetal intervention. The use of the LHR was first described in 1996 in a retrospective cohort.<sup>113</sup> The authors found that in fetuses with left-sided CDH, the LHR measurement correlated with survival and inversely with the need for ECMO. Since that time, additional retrospective and prospective studies have shown the value of LHR in predicting outcome for fetuses with left-sided CDH, and it has been widely incorporated into this assessment.<sup>114</sup> A higher LHR is associated with improved neonatal outcomes and with lower risk of pulmonary hypertension.<sup>115</sup>

Three main methods of determining LHR in the setting of left-sided CDH have been described. LHR is calculated by measuring the size of the right lung, as seen on a transaxial image of the fetal chest at the level of the four-chamber view of the heart, and dividing that by the head circumference—to control for gestational age and fetal size (Fig. 12-35). In a fetus with a small left-sided hernia and minimal cardio-mediastinal shift, there is more right lung visible, greater right lung size to measure, larger numerator in the formula, and higher calculated LHR. The three main approaches to calculating the numerator (right

lung size) include the anteroposterior diameter method, the longest diameter method, and the tracing method. The measurement is best done on a technically optimized, transaxial sonographic image at the appropriate level. Avoiding acoustic shadowing by the ribs and enlarging the image so the chest fills the screen allow for more accurate assessment<sup>116</sup> (Figs. 12-36 and 12-37). The tracing method has been shown to be the most reliable and the longest diameter method the least.<sup>116</sup> There is a learning curve associated with reliability and



$$\text{LHR} = \frac{A \times B \text{ (mm)}}{\text{HC (mm)}}$$



### A Head Circumference

**FIG 12-35 A**, Diagrammatic illustration of the method for measuring the lung-to-head ratio (LHR) in a fetus with congenital diaphragmatic hernia. The measurement of the right lung (in the typical left congenital diaphragmatic hernia) uses a transverse axial plane of section of the fetal thorax at the level of the four-chamber view of the fetal heart. The plane of section should be symmetric so that a single rib is seen on each side. A measurement in millimeters (mm) is made from the thoracic aorta to the lateral inner chest wall (A). Another measurement, also in mm, is made in a plane perpendicular to the first measurement from the outer wall of the atrium to the inner aspect of the posterior chest wall (B). These two measurements are multiplied and their product is divided by the measurement of the head circumference (HC), also in mm.



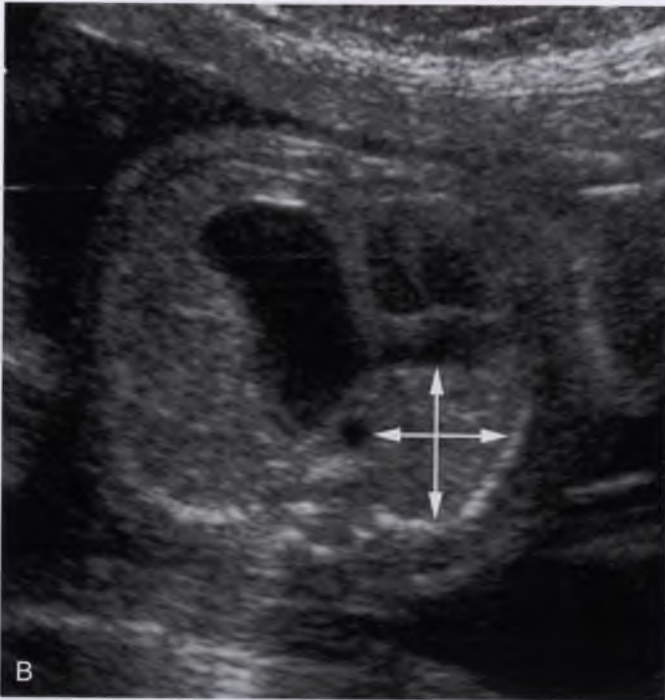


**FIG 12-35, cont'd B**, Transverse axial sonogram of a fetus with a left congenital diaphragmatic hernia. The two diameters (arrows) used in measuring the remaining area of the right lung are shown. (In A, sonogram courtesy of Roy A. Filly, MD, San Francisco, CA. Illustration by James A Cooper, MD, San Diego, CA.)

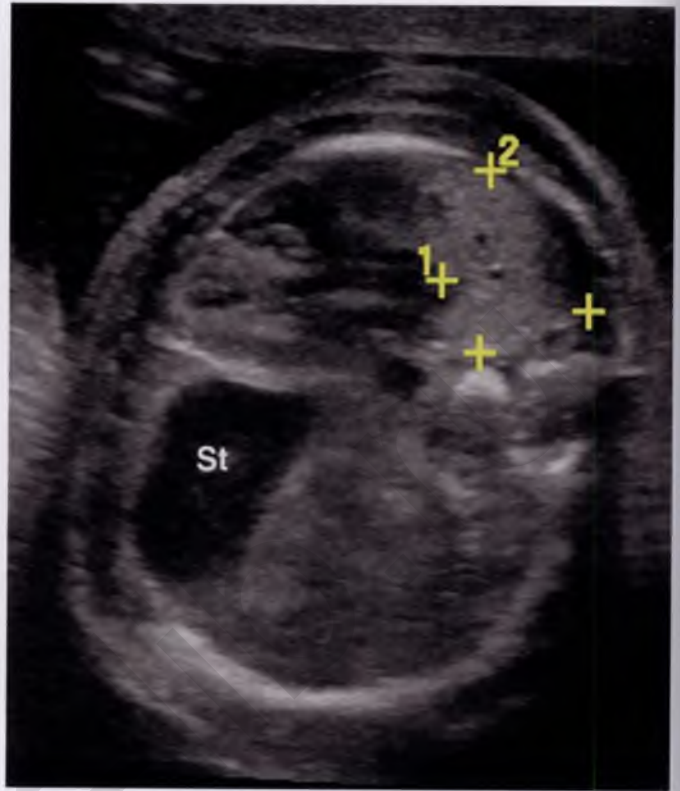
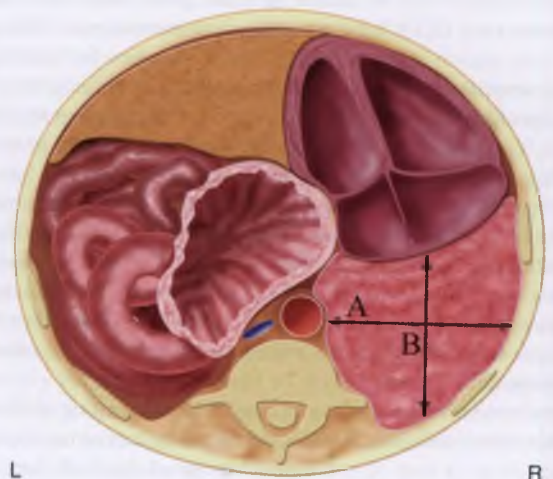


**FIG 12-36** Axial view of fetus with left congenital diaphragmatic hernia (CDH). Herniated fluid-filled stomach (St) is shown in the left side of the chest. Electronic calipers are measuring dimensions of the right lung (used to calculate the numerator in LHR [lung-to-head ratio]).

reproducibility of LHR measurements. The technique can be practiced on images of normal fetuses, with approximately 70 to 80 measurements needed to reach consistency among examiners.<sup>117</sup>

Variable cutoffs for LHR have been reported in the literature for prediction of poor postnatal outcome in fetuses with CDH. Some of this variation results from difference in gestational age at time of measurement, alternate techniques in caliper placement, range in operator experience, and application in fetuses with and without liver herniation. There is an 18-fold increase in lung area between 12 and 32 weeks' gestation with a fourfold increase in head circumference during that same time period.<sup>118</sup> Utilizing observed-to-expected LHRs rather than LHR alone may thus result in improved outcome prediction across gestational ages.<sup>113,119</sup> Still, the reported positive predictive value for survival is only 46% with a false positive rate of 10%.<sup>119</sup> The possibility of in utero intervention with tracheal occlusion in the treatment of severe CDH relies on accurate diagnosis and prognosis. The most severe lesions—those with herniated liver, significant mass effect, low LHR measurements, and predicted poor outcome—are considered for in utero intervention as they are most likely to benefit.

Fetal endoscopic tracheal occlusion has been used prenatally in the treatment of CDH. In utero, the fetal lungs secrete fluid into the airways that is eventually drained into the amniotic fluid through fetal breathing movements. With in utero intervention, occlusion of the trachea prevents this drainage of secretions, resulting in growth and stretching of the fetal lung parenchyma. This technique has been shown to stimulate fetal lung growth in a variety of animal models.<sup>120</sup> In this procedure, usually done between 22 and 26 weeks' gestation, an



$$\text{LHR} = \frac{A \times B \text{ (in mm)}}{\text{Head circumference (in mm)}}$$

**FIG 12-37** Diagram illustrating caliper placement for measurement of numerator in lung-to-head ratio.



endoscope is passed through the fetal mouth, and a balloon is deployed just above the carina (Fig. 12-38). Following balloon placement, ultrasound surveillance ensures the balloon's structural integrity and measures the fetal pulmonary response. At approximately 34 weeks' gestation, the balloon is deflated and removed. Ultimately, the goal of fetal endoscopic tracheal occlusion is to minimize pulmonary hypoplasia and pulmonary arterial hypertension. Following delivery, neonates still require diaphragm repair. Although results of one randomized trial of tracheal occlusion did not show improved outcomes over standard postnatal repair, better selection of the most severe cases and prenatal removal of the balloon are advances that appear to result in better outcomes. However, the ultimate utility of this intervention remains uncertain.<sup>121,122</sup>

Although measurement of the LHR is helpful in predicting outcome and selecting cases most likely to benefit from in utero therapy, it does not successfully identify fetuses at highest risk for pulmonary hypertension, another major cause of postnatal morbidity. Measurement of the pulmonary artery Doppler waveform has been studied, but further research is needed to identify prenatal factors that predict pulmonary hypertension in the neonate. Other areas of investigation to better evaluate and predict outcome in fetuses with CDH include prenatal MRI and three-dimensional ultrasound measurement of lung volumes<sup>123,124</sup> (Fig. 12-39). As with other conditions, the extremes may have higher predictive value than lung volumes in the middle of the spectrum. The best way to assess and predict outcome in these cases is continuing to evolve.

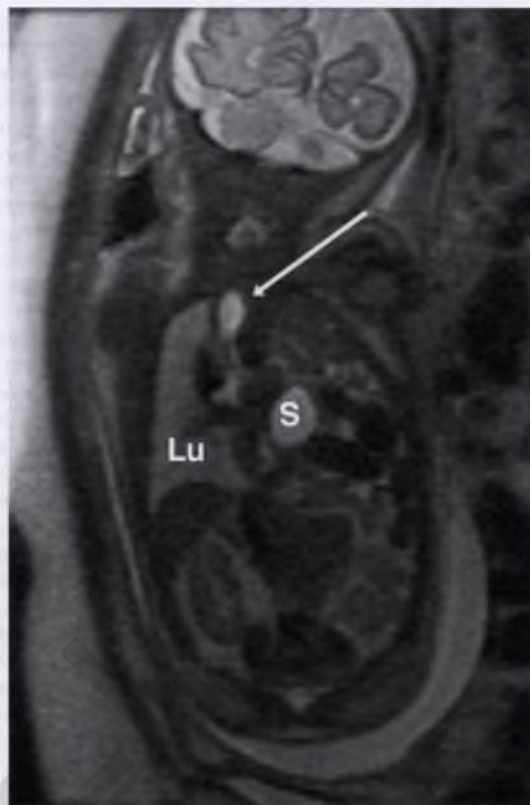


**FIG 12-38** Coronal T2-weighted magnetic resonance imaging of fetus with large left congenital diaphragmatic hernia. Stomach (S) and bowel are shown within the left hemithorax. Fetoscopic intervention had been performed with placement of fluid-filled balloon (arrow) within the fetal trachea. Lu, right lung.

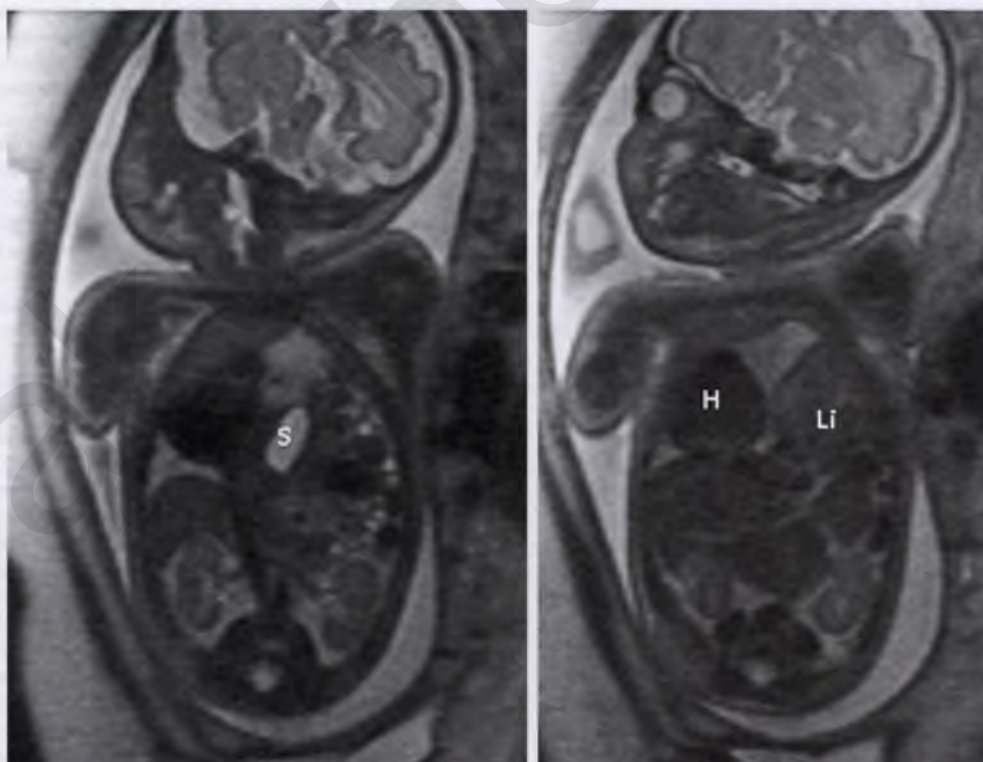


**FIG 12-39** Fetal left congenital diaphragmatic hernia shown on coronal T2-weighted images. Fluid-filled stomach (S) is noted within the left hemithorax with rightward shift of the heart (H). High signal intensity lung tissue can be visualized and distinguished from herniated contents including portion of left lobe of the liver (Li).



## REFERENCES

- Sadler T: *Langman's Medical Embryology*, ed 10, Philadelphia, 2006, Lippincott Williams & Wilkins, p 37.
- Parera MC, van Dooren M, van Kempen M, et al: Distal angiogenesis: a new concept for lung vascular morphogenesis. *Am J Physiol Lung Cell Mol Physiol* 288:L141–L149, 2005.
- Hooper SB, Harding R: Fetal lung liquid: a major determinant of the growth and functional development of the fetal lung. *Clin Exp Pharmacol Physiol* 22(4):235–247, 1995.
- Clugston RD, Greer JJ: Diaphragm development and congenital diaphragmatic hernia. *Semin Pediatr Surg* 16:94–100, 2007.
- Zeltner TB, Burri PH: The postnatal development and growth of the human lung. II. Morphology. *Respir Physiol* 67(3):269–282, 1987.
- McMillan JA: Chronic diffuse interstitial lung disease in childhood. In McMillan JA, editor: *Oski's Pediatrics*, ed 4, Philadelphia, 2006, Lippincott Williams & Wilkins.
- Wigglesworth JS, Desai R, Guerrini P: Fetal lung hypoplasia: biochemical and structural variations and their possible significance. *Arch Dis Child* 56:606–615, 1981.
- Thibeault DW, Haney B: Lung volume, pulmonary vasculature, and factors affecting survival in congenital diaphragmatic hernia. *Pediatrics* 101(2):289–295, 1998.
- Thurlbeck WM: Prematurity and the developing lung. *Clin Perinatol* 19(3):497–519, 1992.
- Laudy JA, Wladimiroff JW: The fetal lung, 2: pulmonary hypoplasia. *Ultrasound Obstet Gynecol* 16:482–494, 2000.
- Thibeault DW, Beatty EC, Jr, Hall RT, et al: Neonatal pulmonary hypoplasia with premature rupture of fetal membranes and oligohydramnios. *J Pediatr* 107:273–277, 1985.
- Winn HM, Chen M, Amon E, et al: Neonatal pulmonary hypoplasia and perinatal mortality in patients with midtrimester rupture of amniotic membranes—a critical analysis. *Am J Obstet Gynecol* 182:1638–1644, 2000.
- Mahieu-Caputo D, Sonigo P, Dommergues M, et al: Fetal lung volume measurement by magnetic resonance imaging in congenital diaphragmatic hernia. *Br J Obstet Gynaecol* 108:863–868, 2001.
- Peralta CF, Jani JC, Van Schoubroeck D, et al: Fetal lung volume after endoscopic tracheal occlusion in the prediction of postnatal outcome. *Am J Obstet Gynecol* 198:60, 2008.
- Britto IS, Araujo Júnior E, Sangi-Haghpeykar H, et al: Reference ranges for 2-dimensional sonographic lung measurements in healthy fetuses: a longitudinal study. *J Ultrasound Med* 33(11):1917–1923, 2014.
- Deshmukh S, Rubesova E, Barth R: MR assessment of normal fetal lung volumes: a literature review. *AJR Am J Roentgenol* 194(2):W212–W217, 2010.
- Rypens F, Metens T, Rocourt N, et al: Fetal lung volume: estimation at MR imaging—initial results. *Radiology* 219:236–241, 2001.
- Tsai AY, Liechty KW, Hedrick HL, et al: Outcomes after postnatal resection of prenatally diagnosed asymptomatic cystic lung lesions. *J Pediatr Surg* 43:513–517, 2008.
- Laberge JM, Flageole H, Pugash D, et al: Outcome of the prenatally diagnosed congenital cystic adenomatoid lung malformation: a Canadian experience. *Fetal Diagn Ther* 16:178–186, 2001.
- Shanti CM, Klein MD: Cystic lung disease. *Semin Pediatr Surg* 17:2–8, 2008.
- De Santis M, Masini L, Noia G, et al: Congenital cystic malformation of the lung: antenatal ultrasound findings and fetal-neonatal outcome. Fifteen years of experience. *Fetal Diagn Ther* 15:246–248, 2001.
- Rempen A, Feige A, Wunsch P: Prenatal diagnosis of bilateral cystic adenomatoid malformation of the lung. *J Clin Ultrasound* 15:3–8, 1987.
- Marshall KW, Blane CE, Teitelbaum DH, VanLeeuwen K: Congenital cystic adenomatoid malformation: impact of prenatal diagnosis and changing strategies in the treatment of the asymptomatic patient. *AJR Am J Roentgenol* 175:1551–1554, 2000.
- Cangiarella J, Greco MA, Askin F, et al: Congenital cystic adenomatoid malformation of the lung: insights into the pathogenesis utilizing quantitative analysis of vascular marker CD34 (QBEND-10) and cell proliferation maker MIB-1. *Med Pathol* 8:913–918, 1995.
- Stocker JT, Madewell JER, Drake RM: Congenital cystic adenomatoid malformation of the lung: classification and morphologic spectrum. *Hum Pathol* 8:155–171, 1977.
- Stocker JT: Congenital pulmonary airway malformation: a new name and an extended classification of congenital cystic adenomatoid malformation of the lung. *Histopathology* 41:424–431, 2002.
- Adzick NS: Management of fetal lung lesions. *Clin Perinatol* 36:363–376, 2009.
- Alamo L, Gudinchet F, Reinberg O, et al: Prenatal diagnosis of congenital lung malformations. *Pediatr Radiol* 42:273–283, 2012.
- Achiron R, Hagesh J, Yagel S: Fetal lung lesions: a spectrum of disease. New classification based on pathogenesis, two-dimensional and color Doppler ultrasound. *Ultrasound Obstet Gynecol* 24:107–114, 2004.
- Biyyam DR, Chapman T, Ferguson MR, et al: Congenital lung abnormalities: embryologic correlation. *Radiographics* 30:1721–1738, 2010.
- Kalenahalli KV, Garg N, Goolahally LN, et al: Infradiaphragmatic extralobar pulmonary sequestration: masquerading as suprarenal mass. *J Clin Neonatol* 2(3):146–148, 2013.
- Yang HJ, Lee SW, Lee HJ, et al: Extralobar pulmonary sequestration mimicking an adrenal tumor. *J Soc Laparosc Surg* 16(4):671–674, 2012.
- Lima JS, Camargos PA, Aguiar RA, et al: Pre and perinatal aspects of congenital cystic adenomatoid malformation of the lung. *J Matern Fetal Neonatal Med* 27:228–232, 2014.
- Ruchonnet-Metrailler I, Leroy-Terquem E, Stirnemann J, et al: Neonatal outcomes of prenatally diagnosed congenital pulmonary malformations. *Pediatrics* 133(5):e1285–e1291, 2014.
- Crombleholme TM, Coleman B, Hedrick H, et al: Cystic adenomatoid malformation volume ratio predicts outcome in prenatally diagnosed cystic adenomatoid malformation of the lung. *J Pediatr Surg* 37:331–338, 2002.
- Ehrenberg-Buchner S, Stapf AM, Berman DR, et al: Fetal lung lesions: can we start to breathe easier? *Am J Obstet Gynecol* 208:151, 2013.
- Adzick NS, Harrison MR, Glick PL, et al: Fetal cystic adenomatoid malformation: prenatal diagnosis and natural history. *J Pediatr Surg* 20:483–488, 1985.
- Grethel EJ, Wagner AJ, Clifton MS, et al: Fetal intervention for mass lesions and hydrops improves outcome: a 15-year experience. *J Pediatr Surg* 42:117–123, 2007.
- Wilson RD: In utero therapy for fetal thoracic abnormalities. *Prenat Diagn* 28:619–625, 2008.
- Curran PF, Jelin EB, Rand L, et al: Prenatal steroids for microcystic congenital cystic adenomatoid malformations. *J Pediatr Surg* 45:145–150, 2010.
- Morris LM, Lim FY, Livingston JC, et al: High risk fetal congenital pulmonary airway malformations have a variable response to steroids. *J Pediatr Surg* 44:60–65, 2009.
- Tsao K, Hawgood S, Vu L, et al: Resolution of hydrops fetalis in congenital cystic adenomatoid malformation after prenatal steroid therapy. *J Pediatr Surg* 38:508–510, 2003.
- Peranteau WH, Wilson RD, Liechty KW, et al: Effect of maternal betamethasone administration on prenatal congenital cystic adenomatoid malformation growth and fetal survival. *Fetal Diagn Ther* 22:365–371, 2007.
- Parikh D, Samuel M: Congenital cystic lung lesions: is surgical resection essential? *Pediatr Pulmonol* 40(6):533–537, 2005.
- Albright EB, Crane JP, Shackelford GD: Prenatal diagnosis of a bronchogenic cyst. *J Ultrasound Med* 7:90–95, 1988.
- El Youssef R, Fleseriu M, Sheppard BC: Adrenal and pancreatic presentation of subdiaphragmatic retroperitoneal bronchogenic cysts. *Arch Surg* 145:302–304, 2010.
- Ronson RS, Duarte I, Miller JJ: Embryology and surgical anatomy of the mediastinum with clinical implications. *Surg Clin North Am* 80:157–169, 2000.
- Kumar N: Perinatal management of common neonatal thoracic lesions. *Indian J Pediatr* 75:931–937, 2008.
- Fievet L, D'Journo XB, Guys JM, et al: Bronchogenic cyst: best time for surgery? *Ann Thorac Surg* 94:1695–1699, 2012.



50. Uludag S, Madazli R, Erdogan E, et al: A case of prenatally diagnosed fetal neuroenteric cyst. *Ultrasound Obstet Gynecol* 18:277, 2001.
51. Reed JG, Sobonya RE: Morphologic analysis of foregut cysts in the thorax. *Am J Roentgenol Radium Ther Nucl Med* 120:851, 1974.
52. Strollo DC, Rosado-de-Christenson ML, Jett JR: Primary mediastinal tumors: part II. Tumors of the middle and posterior mediastinum. *Chest* 112:1344, 1997.
53. Ryckman FC, Rosenkrantz JG: Thoracic surgical problems in infancy and childhood. *Surg Clin North Am* 65:1423, 1985.
54. Keswani SG, Crombleholme TM, Pawel BR, et al: Prenatal diagnosis and management of mainstem bronchial atresia. *Fetal Diagn Ther* 20:74–78, 2005.
55. Seo T, Ando H, Kaneko K, et al: A Two cases of prenatally diagnosed congenital lobar emphysema caused by lobar bronchial atresia. *J Pediatr Surg* 41:e17–e20, 2006.
56. Kamata S, Sawai T, Usui N, et al: Case of congenital bronchial atresia detected by fetal ultrasound. *Pediatr Pulmonol* 35:227–229, 2003.
57. Cass DL, Olutoye OO, Cassady CI, et al: Prenatal diagnosis and outcome of fetal lung masses. *J Pediatr Surg* 46:292–298, 2011.
58. Zamora IJ, Sheikh F, Olutoye OO, et al: Mainstem bronchial atresia: a lethal anomaly amenable to fetal surgical treatment. *J Pediatr Surg* 49:706–711, 2014.
59. Mychaliska GB, Bealer JF, Graf JL, et al: Operating on placental support: the ex utero intrapartum treatment procedure. *J Pediatr Surg* 32(2):227–230, discussion 230–231, 1997.
60. Olutoye OO, Coleman BG, Hubbard AM, Adzick NS: Prenatal diagnosis and management of congenital lobar emphysema. *J Pediatr Surg* 35:792–795, 2000.
61. Stigers KB, Woodring JH, Kanga JF: The clinical and imaging spectrum of findings in patients with congenital lobar emphysema. *Pediatr Pulmonol* 14:160–170, 1992.
62. Cochran ST, Gyepes MT, Smith LE: Obstruction of the airways by the heart and pulmonary vessels in infants. *Pediatr Radiol* 6:81–87, 1977.
63. Kravitz RM: Congenital malformations of the lung. *Pediatr Clin North Am* 41:453, 1994.
64. Özçelik U, Göçmen A, Kiper N, et al: Congenital lobar emphysema: evaluation and long-term follow-up of thirty cases at a single center. *Pediatr Pulmonol* 35:384, 2003.
65. Babu R, Lyle P, Spicer RD: Prenatal sonographic features of congenital lobar emphysema. *Fetal Diagn Ther* 16:200–202, 2001.
66. Pariente G, Aviram M, Landau D, Hershkovitz R: Prenatal diagnosis of congenital lobar emphysema: case report and review of the literature. *J Ultrasound Med* 28:1081–1084, 2009.
67. Dogan R, Dogan OF, Yilmaz M, et al: Surgical management of infants with congenital lobar emphysema and concomitant congenital heart disease. *Heart Surg Forum* 7:E644–E649, 2004.
68. Lau CT, Leung L, Chan IH, et al: Thoracoscopic resection of congenital cystic lung lesions is associated with better post-operative outcomes. *Pediatr Surg Int* 29:341–345, 2013.
69. Courtier J, Poder L, Wang ZJ, et al: Fetal tracheolaryngeal airway obstruction: prenatal evaluation by sonography and MRI. *Pediatr Radiol* 40:1800–1805, 2010.
70. Guimaraes CV, Linam LE, Kline-Fath BM, et al: Prenatal MRI findings of fetuses with congenital high airway obstruction sequence. *Korean J Radiol* 10:129–134, 2009.
71. Roybal JL, Liechty KW, Hedrick HL, et al: Predicting the severity of congenital high airway obstruction syndrome. *J Pediatr Surg* 45:1633–1639, 2010.
72. Vanhaesebrouck P, De Coen K, Defoort P, et al: Evidence for autosomal dominant inheritance in prenatally diagnosed CHAOS. *Eur J Pediatr* 165:706–708, 2006.
73. Kassaros D, Christodoulou CN, Agapitos E, et al: Prenatal ultrasonographic detection of the tracheal atresia sequence. *Ultrasound Obstet Gynecol* 10:133, 1997.
74. Lim FY, Crombleholme TM, Hedrick HL, et al: Congenital high airway obstruction syndrome: natural history and management. *J Pediatr Surg* 38:940–945, 2003.
75. Artunc Ulkumen B, Pala HG, Nese N, et al: Prenatal diagnosis of congenital high airway obstruction syndrome: report of two cases and brief review of the literature. *Case Rep Obstet Gynecol* 2013:728974.
76. Kuwashima S, Kitajima K, Kaji Y, et al: MR imaging appearance of laryngeal atresia (congenital high airway obstruction syndrome): unique course in a fetus. *Pediatr Radiol* 38:344–347, 2008.
77. Mong A, Johnson AM, Kramer SS, et al: Congenital high airway obstruction syndrome: MR/US findings, effect on management, and outcome. *Pediatr Radiol* 38:1171–1179, 2008.
78. Coakley FV, Hricak H, Filly RA, et al: Complex fetal disorders: effect of MR imaging on management: preliminary clinical experience. *Radiology* 213:691–696, 1999.
79. Oepkes D, Teunissen AK, Van De Velde M, et al: Congenital high airway obstruction syndrome successfully managed with ex-utero intrapartum treatment. *Ultrasound Obstet Gynecol* 22:437–439, 2003.
80. Mesens T, Witters I, Van Robaeyns J, et al: Congenital high airway obstruction syndrome (CHAOS) as part of Fraser syndrome: ultrasound and autopsy findings. *Genet Couns* 24(4):367–371, 2013.
81. Joshi P, Satija L, George RA, et al: Congenital high airway obstruction syndrome-antenatal diagnosis of a rare case of airway obstruction using multimodality imaging. *Med J Armed Forces India* 68(1):78–80, 2012.
82. Longaker MT, Laberge JM, Dansereau J, et al: Primary fetal hydrothorax: natural history and management. *J Pediatr Surg* 24:573–576, 1989.
83. Petersen S, Kaur R, Thomas JT, et al: The outcome of isolated primary fetal hydrothorax: a 10-year review from a tertiary center. *Fetal Diagn Ther* 34:69–76, 2013.
84. Estoff JA, Parad RB, Frigoletto FD, Benacerraf BR: The natural history of isolated fetal hydrothorax. *Ultrasound Obstet Gynecol* 2:162–165, 1992.
85. Aubard Y, Derouineau I, Aubard V, et al: Primary fetal hydrothorax: a literature review and proposed antenatal clinical strategy. *Fetal Diagn Ther* 13:325–333, 1998.
86. Randenberg AL: Nonimmune hydrops fetalis part II: does etiology influence mortality? *Neonatal Netw* 29(6):367–380, 2010.
87. Bebbington M, Rosner M, Wilson RD, et al: Perinatal outcomes with fetal chest shunts. *Am J Obstet Gynecol* 192:S138, 2008.
88. Kuo YL, Chan TF: Treatment of unilateral fetal pleural effusion by intrauterine thoracocentesis. *Taiwan J Obstet Gynecol* 51:303–304, 2012.
89. Mann S, Johnson MP, Wilson D: Fetal thoracic and bladder shunts. *Semin Fetal Neonatal Med* 15:28–33, 2010.
90. Murabayashi N, Sugiyama T, Kusaka H, et al: Thoracoamniotic shunting with double-basket catheters for fetal chylothorax in the second trimester. *Fetal Diagn Ther* 22:425–427, 2007.
91. Bianchi S, Lista G, Castoldi F, et al: Congenital primary hydrothorax: effect of thoracoamniotic shunting on neonatal clinical outcome. *J Matern Fetal Neonatal Med* 23:1225–1229, 2010.
92. Yinon Y, Kelly E, Ryan G: Fetal pleural effusions. *Best Pract Res Clin Obstet Gynaecol* 22:77–96, 2008.
93. Derderian CS, Trivedi S, Farrell J, et al: Outcomes of fetal intervention for primary hydrothorax. *J Pediatr Surg* 49:900–903, 2014.
94. Chernicka V, Reed MH: Pneumothorax and chylothorax in the neonatal period. *J Pediatr* 76:624–632, 1970.
95. Caserio S, Gallego C, Martin P, et al: Congenital chylothorax: from foetal life to adolescence. *Acta Paediatr* 99(10):1571–1577, 2010.
96. Achiron R, Weissman A, Lipitz S, et al: Fetal pleural effusion: the risk of fetal trisomy. *Gynecol Obstet Invest* 39:153–156, 1995.
97. Waller K, Chaithongwongwatthana S, Yamasmit W, et al: Chromosomal abnormalities among 246 fetuses with pleural effusions detected on prenatal ultrasound examination: factors associated with an increased risk of aneuploidy. *Genet Med* 7:417–421, 2005.
98. Colvin J, Bower C, Dickinson JE, Sokol J: Outcomes of congenital diaphragmatic hernia: a population-based study in Western Australia. *Pediatrics* 116:e356–e363, 2005.
99. Centers for Disease Control and Prevention: *Birth Defects: Data & Statistics*. Available at: <[www.cdc.gov/ncbddd/birthdefects/data](http://www.cdc.gov/ncbddd/birthdefects/data)>, 2015.



100. Comstock C, Bronsteen RA, Whitten A, Lee W: Paradoxical motion: a useful tool in the prenatal diagnosis of congenital diaphragmatic hernias and eventrations. *J Ultrasound Med* 28:1365–1367, 2009.
101. Lusk LA, Wai KC, Mood-Grady AJ, et al: Fetal ultrasound markers of severity predict resolution of pulmonary hypertension in congenital diaphragmatic hernia. *Am J Obstet Gynecol* 213(2):216.e1–216.e8, 2015.
102. Richards DS, Kays DM: Fetal umbilical vein deviation in congenital diaphragmatic hernia. *J Ultrasound Med* 32:263–268, 2013.
103. Conturso R, Giorgetta F, Bellussi F, et al: Horizontal stomach: a new sonographic clue to the antenatal diagnosis of right-sided congenital diaphragmatic hernia. *Ultrasound Obstet Gynecol* 41:340–341, 2013.
104. Van Mieghem T, Cruz-Martinez R, Allegaert K, et al: Outcome of fetuses with congenital diaphragmatic hernia and associated intrafetal fluid effusions managed in the era of fetal surgery. *Ultrasound Obstet Gynecol* 39:50–55, 2012.
105. Jeanty C, Nien JK, Espinoza J, et al: Pleural and pericardial effusion: a potential ultrasonographic marker for the prenatal differential diagnosis between congenital diaphragmatic eventration and congenital diaphragmatic hernia. *Ultrasound Obstet Gynecol* 29:378–387, 2007.
106. McAteer JP, Hecht A, De Roos AJ, Goldin AB: Maternal medical and behavioral risk factors for congenital diaphragmatic hernia. *J Pediatr Surg* 49:34–38, 2014.
107. Waller DK, Tita AT, Werler MM, Mitchell AA: Association between prepregnancy maternal body mass index and the risk of having an infant with a congenital diaphragmatic hernia. *Birth Defects Res A Clin Mol Teratol* 67(1):73–76, 2003.
108. Howe DT, Kilby MD, Sirry H, et al: Structural chromosome anomalies in congenital diaphragmatic hernia. *Prenat Diagn* 16:1003–1009, 1996.
109. Takahashi S, Sago H, Kanamori Y, et al: Prognostic factors of congenital diaphragmatic hernia accompanied by cardiovascular malformation. *Pediatr Int* 55:492–497, 2013.
110. Vogel M, McElhinney DB, Marcus E, et al: Significance and outcome of left heart hypoplasia in fetal congenital diaphragmatic hernia. *Ultrasound Obstet Gynecol* 35:310–317, 2010.
111. Lazar DA, Ruano R, Cass DL, et al: Defining “liver-up”: does the volume of liver herniation predict outcome for fetuses with isolated left-sided congenital diaphragmatic hernia? *J Pediatr Surg* 47:1058–1062, 2012.
112. Spaggiari E, Stirnemann J, Bernard JP, et al: Prognostic value of a hernia sac in congenital diaphragmatic hernia. *Ultrasound Obstet Gynecol* 41:286–290, 2013.
113. Metkus AP, Filly RA, Stinger MD, et al: Sonographic predictors of survival in fetal diaphragmatic hernia. *J Pediatr Surg* 31:148–152, 1996.
114. Lipshutz GS, Albanese CT, Feldstein VA, et al: Prospective analysis of lung-to-head ratio predicts survival for patients with prenatally diagnosed congenital diaphragmatic hernia. *J Pediatr Surg* 32(11):1634–1636, 1997.
115. Spaggiari E, Stirnemann JJ, Sonigo P, et al: Prenatal prediction of pulmonary arterial hypertension in congenital diaphragmatic hernia. *Ultrasound Obstet Gynecol* 45(5):572–577, 2015.
116. Jani JC, Peralta CF, Nicolaides KH: Lung-to-head ratio: a need to unify the technique. *Ultrasound Obstet Gynecol* 39:2–6, 2012.
117. Cruz-Martinez R, Figueras F, Moreno-Alvarez O, et al: Learning curve for lung area to head circumference ratio: measurement in fetuses with congenital diaphragmatic hernia. *Ultrasound Obstet Gynecol* 36:32–36, 2010.
118. Peralta CFA, Cavoretto P, Csapo B, et al: Assessment of lung area in normal fetuses at 12–32 weeks. *Ultrasound Obstet Gynecol* 26(7):718–724, 2005.
119. Kehl S, Siemer J, Brunnemer S, et al: Prediction of postnatal outcomes in fetuses with isolated congenital diaphragmatic hernias using different lung-to-head ratio measurements. *J Ultrasound Med* 33(5):759–767, 2014.
120. Nardo L, Hooper SB, Harding R: Lung hypoplasia can be reversed by short-term obstruction of the trachea in fetal sheep. *Pediatr Res* 38:690–696, 1995.
121. Harrison MR, Keller RL, Hawgood SB, et al: A randomized trial of fetal endoscopic tracheal occlusion for severe fetal congenital diaphragmatic hernia. *N Engl J Med* 349(20):1916–1924, 2003.
122. Ruano R, Yoshisaki CT, da Silva MM, et al: A randomized controlled trial of fetal endoscopic tracheal occlusion versus postnatal management of severe isolated congenital diaphragmatic hernia. *Ultrasound Obstet Gynecol* 39:20–27, 2012.
123. Bebbington M, Victoria T, Danzer E, et al: Comparison of ultrasound and magnetic resonance imaging parameters in predicting survival in isolated left-sided congenital diaphragmatic hernia. *Ultrasound Obstet Gynecol* 43:670–674, 2014.
124. Ruano R, Lazar DA, Cass DL, et al: Fetal lung volume and quantification of liver herniation by magnetic resonance imaging in isolated congenital diaphragmatic hernia. *Ultrasound Obstet Gynecol* 43:662–669, 2014.

# Sonographic Evaluation of the Fetal Heart

Shaine A. Morris, Nancy A. Ayres, Jimmy Espinoza,  
Shiraz A. Maskatia, Wesley Lee

## SUMMARY OF KEY POINTS

- Prenatal diagnosis of congenital heart disease (CHD) can reduce morbidity and mortality rates by means of delivery and intervention planning.
- With the proper technology and skill, some forms of fetal cardiac disease can be detected using first trimester and early second trimester sonography.
- The addition of outflow tracts to the four-chamber view in the standard midtrimester screening examination greatly improves the detection of fetal cardiac disease and is recommended.
- Use of standard scan planes and systematic assessment of the fetal cardiovascular system is useful in evaluating for cardiac disease.
- Ventricular septal defects (VSDs) are the most common CHD, and their size and location determine the clinical course and management.
- Conotruncal defects may be difficult to differentiate and are associated with widely variable outcomes, so accurate diagnosis is important. For these lesions, the key to diagnosis is determining the source of pulmonary blood flow.
- There are varying patterns of left-sided heart hypoplasia. In evolving hypoplastic left heart syndrome (HLHS) due to aortic stenosis, the four-chamber view may initially appear normal in early gestation; the key to early detection is to assess for left-sided heart growth as pregnancy advances and for the development of left ventricular dysfunction and endocardial fibroelastosis.
- Fetal heart failure is a common pathway for both primary and secondary cardiovascular disorders. Careful assessment of signs of cardiac failure can help determine prognosis and possible need for intervention.

## OUTLINE

Fetal Cardiovascular Physiology, 372

Ultrasound Equipment, 372

First and Early Second Trimester Fetal Cardiac Evaluation, 372

Cardiac Examination, 372

Effectiveness of Early Gestation Cardiovascular Evaluation, 376

Second Trimester Fetal Cardiac Evaluation, 378

Rationale and Effectiveness, 378

Cardiac Screening, 378

Fetal Echocardiography, 391

3D and 4D Fetal Cardiac Evaluation, 396

Acquisition of Volume Datasets With 4D Sonography and STIC, 396

Display Modalities in 4D Sonography and STIC, 397

Rendering Techniques in 4D Sonography and STIC, 400

Accuracy and Reproducibility of 4D Sonography in the Prenatal Diagnosis of Congenital Heart Disease, 400

First and Early Second Trimester 4D Fetal Echocardiography, 401

Fetal Cardiovascular Disease, 401

Overview, 401

Congenital Heart Lesions, 402

Cardiac Masses and Tumors, 437

Fetal Cardiac Arrhythmias, 440

Pericardial Effusions, 444

Fetal Heart Failure/Impaired Cardiovascular Performance, 444

Extracardiac Masses, 445

A major purpose of fetal sonographic evaluation is detection of cardiovascular disease to optimize counseling and care of the fetus. This noninvasive approach has been used to evaluate the fetal heart since the 1970s,<sup>1</sup> and in the current era, with advances in imaging technology, up to 95% of major CHD can be prenatally detected by detailed fetal echocardiography.<sup>2-4</sup> However, in population studies, the rate of prenatal diagnosis of major congenital heart lesions by screening methodology is much lower and highly variable by practice and region.<sup>5-10</sup> This lower rate is likely due to a combination of factors, including limitations in access to prenatal care, equipment, and

experience of the sonographer or medical care provider; time constraints; and certain patient factors, such as poor acoustic windows.

A large portion of fetal cardiovascular disease is composed of CHD. CHD is associated with significant morbidity and mortality risks; in fact, CHD is the primary contributor to birth defect-related infant fatality, accounting for nearly one quarter of infant deaths from birth defects.<sup>11,12</sup> Approximately 18 per 10,000 live births have critical congenital heart defects, defined as defects requiring surgery or catheter intervention in the first year of life.<sup>13,14</sup> Outcomes are highly variable by lesion and coexisting conditions. For example, isolated VSD has



nearly 100% infant survival rate, HLHS has 70% to 80% infant survival rate, but HLHS with Turner syndrome has less than 10% survival rate.<sup>15-20</sup> Fetal cardiovascular disease also consists of fetal arrhythmia, cardiac dysfunction and high output heart failure, pericardial effusions, and cardiac and extracardiac thoracic masses.

Prenatal diagnosis of CHD or arrhythmia allows for many potential benefits for the family and fetus. These benefits include emotional preparation for the parents, fetal therapy when indicated, and parental choice of the hospital that will provide postnatal care and intervention. Parents can plan delivery at an institution with considerable expertise and experience to provide the best postnatal care for the infant. Prenatal diagnosis, by conferring these benefits to families, is associated with improved presurgical status of the infant with CHD, as well as lower morbidity and mortality rates in infants with complex CHD.<sup>21-24</sup> Prenatal detection of CHD also allows time for families to accept and understand the diagnosis prior to the birth of the infant. Although prenatal diagnosis has been shown to increase stress during pregnancy, families overwhelmingly state they would prefer to have this knowledge sooner than to learn of CHD after birth.<sup>25-27</sup>

In this chapter, we review normal fetal cardiovascular anatomy and physiology, recommended approaches for prenatal cardiac screening and detailed evaluation, ultrasound findings associated with common types of CHD, and specific imaging tools for common fetal heart diseases.

## FETAL CARDIOVASCULAR PHYSIOLOGY

Our fundamental understanding of the human fetal circulation and changes attributable to CHD was originally extrapolated from early work with fetal lambs.<sup>28-30</sup> The introduction of fetal ultrasound imaging and more recently the use of fetal cardiac magnetic resonance imaging (MRI) have refined our understanding of fetal cardiac physiology.<sup>31,32</sup> Unlike the postnatal heart, in which blood flow is in series, the right and left fetal ventricular outputs are parallel circuits (Fig. 13-1A). Starting from the placenta, maternal oxygenated blood courses through the umbilical vein and enters the inferior vena cava via the ductus venosus (DV). This oxygenated blood accounts for approximately 50% of blood returning to the right atrium (RA) (Fig. 13-2). Oxygenated blood enters the RA, but instead of predominantly then flowing to the right ventricle (RV), oxygen-rich blood is directed across the fetal foramen ovale to the left atrium (LA) by the eustachian valve. Most fetal left-sided blood flow is provided in this manner (~63% per MRI estimates<sup>32</sup>). Blood then courses from the LA across the mitral valve to the left ventricle (LV) and is ejected across the aortic valve into the ascending aorta. Blood flow is then directed to the brain and upper extremities (73% of aortic outflow) while the rest is ejected to the inferior portion of the fetal body (28% of aortic output, 11% of combined cardiac output [CCO]) and joins blood from the ductus arteriosus (72% of pulmonary output, 41% of CCO) in the descending aorta.

Some of the blood that was delivered to the head, arms, and lower extremity organs and muscles eventually returns deoxygenated to the heart via the superior vena cava and inferior vena cava (52% of CCO), while some is returned to the placenta via the umbilical artery (approximately 29% of CCO). Deoxygenated blood with lower glucose levels returning through the fetal systemic veins courses through the RA, RV, and across the pulmonary valve into the pulmonary artery, and primarily traverses the ductus arteriosus into the descending aorta. A small proportion of blood in fetal life is directed into the branch pulmonary arteries into the lungs (approximately 28% of pulmonary flow, 16% of CCO) and returns to the LA via the pulmonary veins. Three percent of cardiac output supplies the coronary artery system. This normal fetal circulation essentially allows the most oxygen-rich,

glucose-rich blood to reach the fetal brain, and may be significantly altered when CHD is present.

At the time of birth, when placental blood flow ceases, oxygen-rich umbilical venous blood is no longer directed into the fetal heart (see Fig. 13-1B). However, at the same time, the newborn infant has started to breathe, and much of the blood flow from the pulmonary artery that was directed across the ductus arteriosus in fetal life is now redirected to the pulmonary arteries to perfuse the newly expanded lungs. This blood becomes oxygenated and returns to the LA via the pulmonary veins. During this transition, the ductus arteriosus closes<sup>33</sup> and in most infants the foramen ovale also closes. Blood flow to the left side of the heart transitions from being supplied via the foramen ovale to being supplied by the pulmonary veins. Failure of the foramen ovale or the ductus arteriosus to close results in patency of these structures; these defects are considered CHD (patent foramen ovale [PFO] and patent ductus arteriosus [PDA]).

## ULTRASOUND EQUIPMENT

Contemporary two-dimensional (2D) ultrasound systems for fetal cardiac screening provide gray-scale and Doppler ultrasound capabilities. Broadband ultrasound transducers are designed to minimize ergonomic stress with a small scanning footprint that can be angled or maneuvered between fetal ribs for satisfactory views of the heart. Higher frequency transducers provide greater resolution, but at the expense of decreased penetration. Harmonic imaging, speckle reduction, and write priority for balancing color Doppler with gray-scale ultrasound images are commonly available. Optimal cardiac studies will be achieved while using high frame rates because temporal resolution should adequately capture movement of anatomic structures throughout the cardiac cycle. Digital video clips are recommended to document fetal cardiac findings.<sup>34</sup>

## FIRST AND EARLY SECOND TRIMESTER FETAL CARDIAC EVALUATION

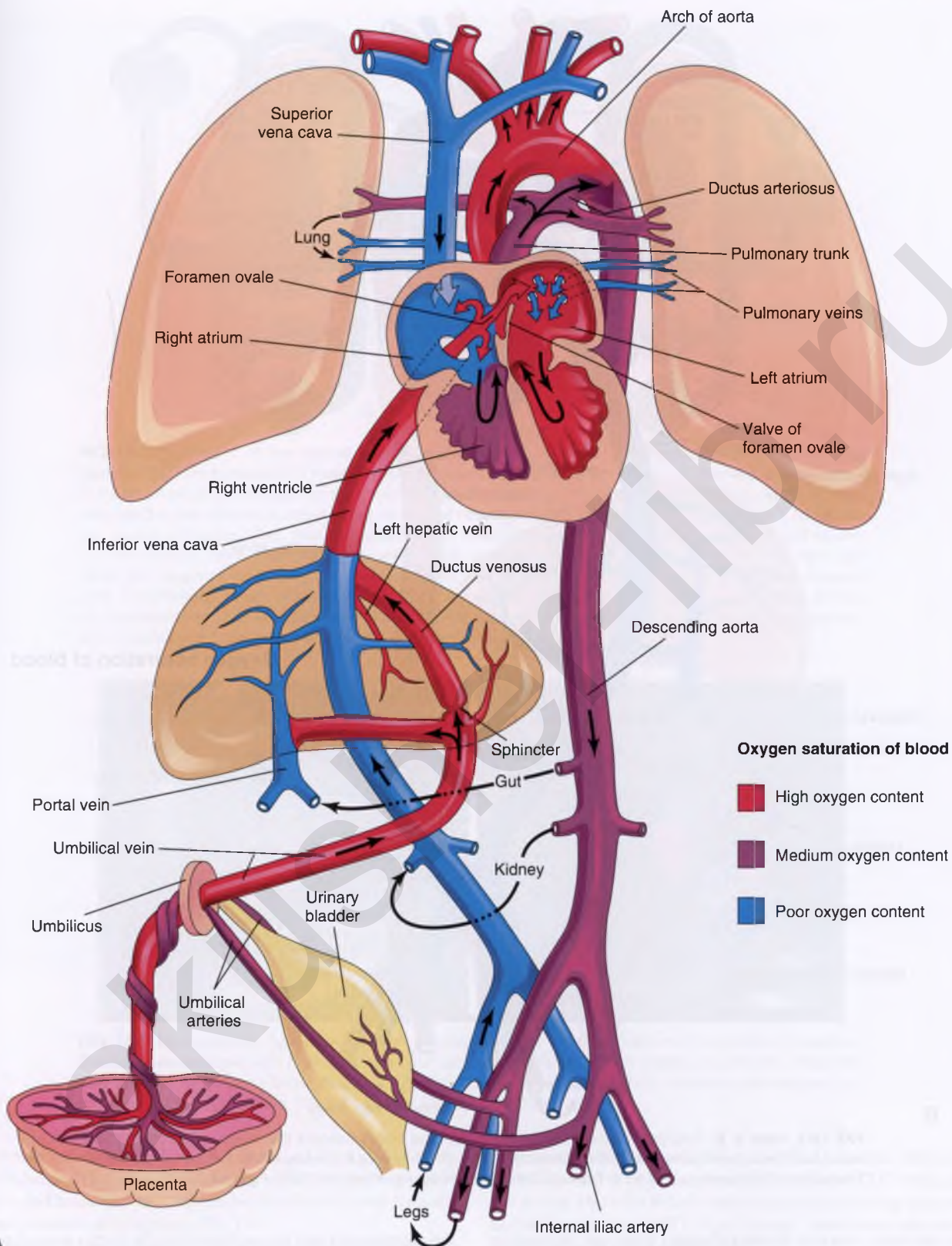
Our ability to identify heart defects in the prenatal period is limited by the following factors: (1) early or late gestational age; (2) structural complexity of the fetal heart, particularly in the abnormal heart; (3) the extensive training required to become proficient in, and maintain expertise in, fetal cardiac sonography; (4) frequent fetal and maternal motion; (5) maternal obesity; (6) limited or excessive amniotic fluid volume; (7) fetal position; and (8) maternal abdominal scar tissue. Limitations are especially present in early pregnancy, when small fetal structures are most difficult to image.

### Cardiac Examination

The American Institute of Ultrasound in Medicine (AIUM) recommends routine documentation for the presence or absence of cardiac activity with a 2D video clip or M-mode imaging when a standard viability first trimester ultrasound examination is performed.<sup>35</sup> However, additional cardiac evaluation may be performed when indicated, as discussed later.

High-frequency, high-resolution transvaginal and transabdominal probes, with improvements in magnification imaging and signal processing, have increased the visualization of the fetal heart during the first and early second trimesters of pregnancy. The standard fetal cardiac screening 2D views (details in next section) typically performed in second and third trimester cardiac screening can also be performed in the first trimester and early second trimester, usually no earlier than 11 weeks' gestation. Visualization of these sonographic planes can be facilitated by using color Doppler imaging.<sup>36-52</sup>





A

FIG 13-1 Cardiovascular circulation before and after birth. A, Prenatal cardiovascular circulation.

Continued



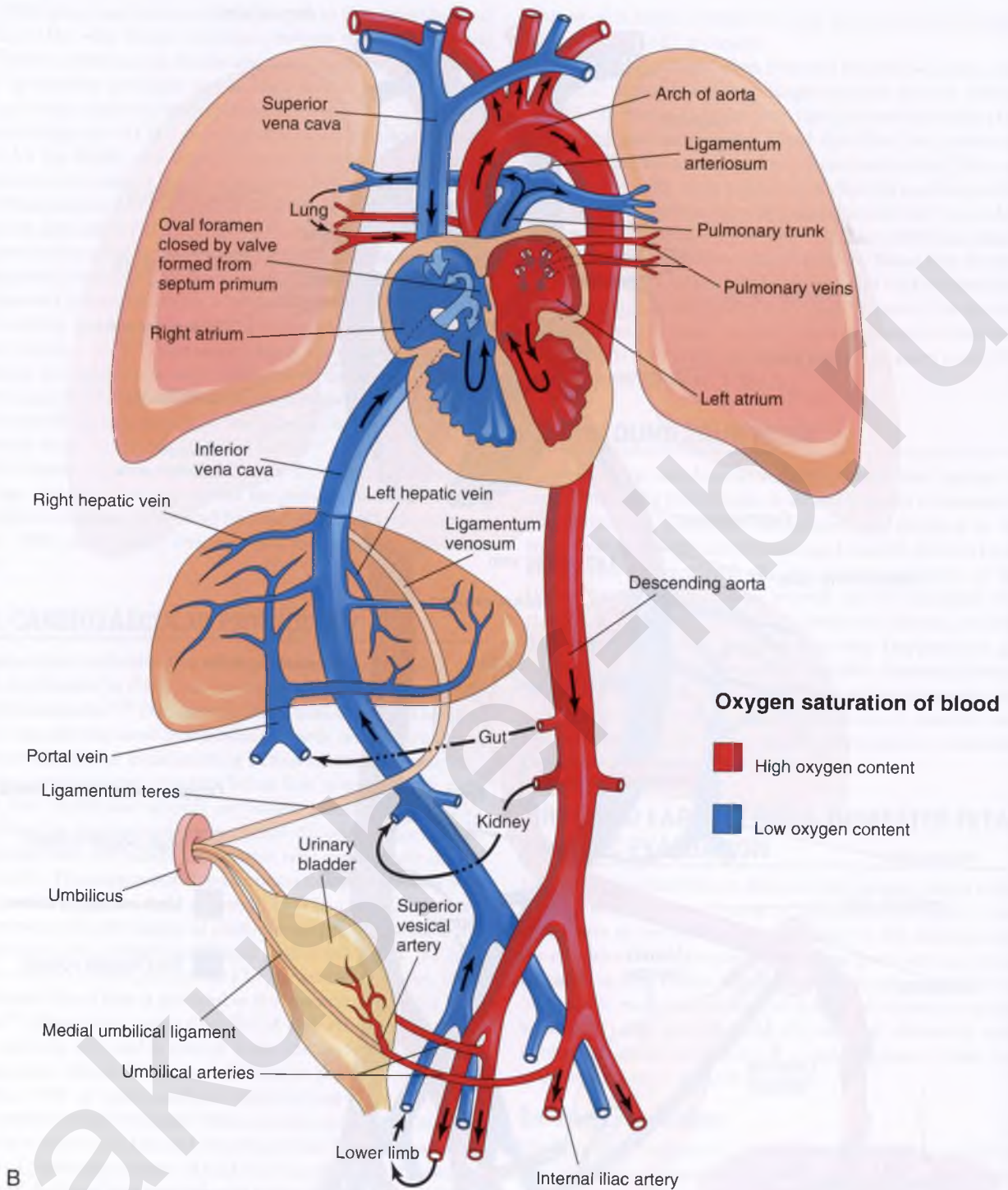


**FIG 13-1, cont'd B**, Postnatal cardiovascular circulation. The colors indicate the oxygen saturation of the blood, and the arrows demonstrate the direction of flow. (From Moore K, Persaud TVN: *Before We Are Born: Essentials of Embryology and Birth Defects*, 9th ed. Philadelphia, Elsevier, 2015, Figs. 14-32, 14-33.)

Early gestation views in the four-chamber plane are depicted in Figure 13-3A. Color flow mapping helps in the evaluation of the four-chamber view to delineate the flow into both ventricles and gives an approximate estimation of the ventricular size (Fig. 13-3B).

Early gestation imaging in the left ventricular outflow tract (LVOT) view can be performed and may be better visualized with color Doppler early in pregnancy (Fig. 13-4). In the three-vessel and trachea (3VT) view (Fig. 13-5A), color flow mapping is useful in delineating

the great arteries and the confluence of the ductus arteriosus and the aortic arch (V sign) (Fig. 13-5B). Color and spectral Doppler evaluation can also help in the identification of valvar regurgitation. For the spectral Doppler evaluation of tricuspid regurgitation, a sample gate of 2 mm to 3 mm is recommended, which should be positioned above the tricuspid valve in an apical four-chamber view with an angle of insonation of less than 20 degrees. The diagnosis of tricuspid regurgitation can be made with the demonstration of a spectral Doppler

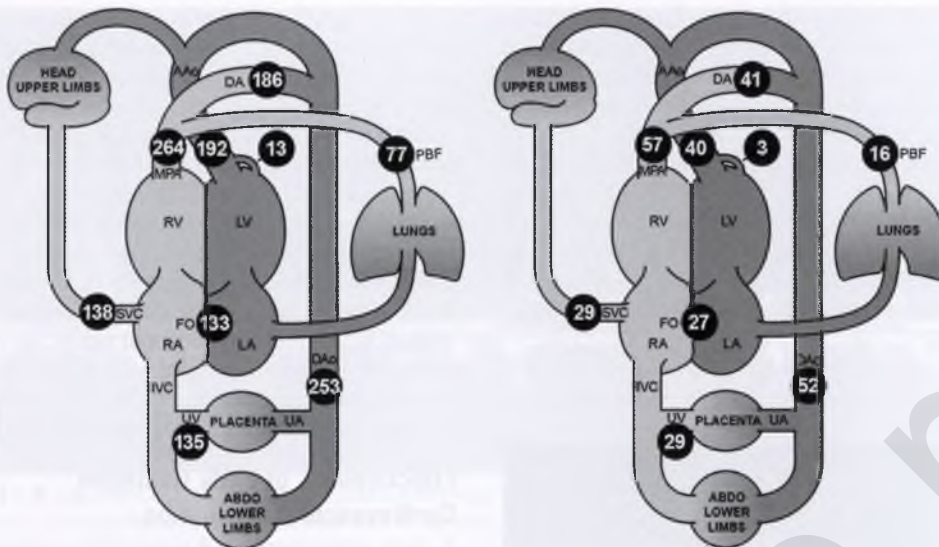


**FIG 13-2** Distribution of the normal human fetal circulation measured by phase-contrast MRI in 40 late-gestation fetuses expressed as mean flows (mL/minute per kg) (numbers in black circles, *left*) and converted to modeled mean percentages of the combined ventricular output (numbers in black circles, *right*). FO flow calculated as the difference between left ventricular output and PBF. AAo, ascending aorta; ABDO, abdomen; DA, ductus arteriosus; Dao, descending aorta; FO, foramen ovale; IVC, inferior vena cava; LA, left atrium; LV, left ventricle; MPA, main pulmonary artery; PBF, pulmonary blood flow; RA, right atrium; RV, right ventricle; SVC, superior vena cava; UA, umbilical artery; UV, umbilical vein. (From Prsa M, Sun L, van Amerom J, et al: Reference ranges of blood flow in the major vessels of the normal human fetal circulation at term by phase-contrast magnetic resonance imaging. *Circ Cardiovasc Imaging* 7:663-670, 2014, used with permission. Courtesy of Luke Itani, The Hospital for Sick Children, Toronto, Canada.)

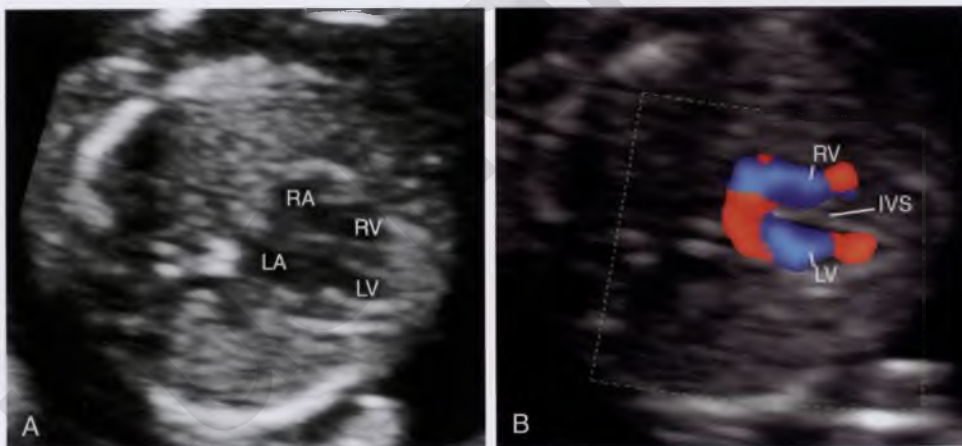


**FIG 13-3** Early gestation four-chamber view. **A**, Four-chamber view in a fetus at 13½ weeks of gestation. **B**, Four-chamber view with high definition color Doppler in a fetus at 13½ weeks of gestation. Note that color Doppler allows for a better delineation of the interventricular septum. IVS, interventricular septum; LA, left atrium; LV, left ventricle; RA, right atrium; RV, right ventricle.

waveform that involves at least half of systole and a velocity of more than 80 cm/second (Fig. 13-6).<sup>53</sup> In cases of severe tricuspid regurgitation such as in Ebstein anomaly this can be visualized by color Doppler in the first trimester of pregnancy (Fig. 13-7).

If normality of situs and cardiac connections, atrioventricular (AV) connections, right- and left-sided symmetry, and ventriculoarterial connections can confidently be demonstrated, most major structural malformations can be excluded.<sup>15</sup> However, septal defects and developmental lesions may be overlooked; thus, there is a need for follow-up in the second trimester of pregnancy. The additional use of color flow mapping to assess intracardiac flow velocities will enhance detection of valvar lesions, such as aortic and pulmonary stenosis, which may

progress to critical stenosis during the third trimester. Methods have been described to optimize prenatal detection of CHD using adjunctive evaluation of the fetus in early pregnancy, including assessment of nuchal translucency (NT), fetal Doppler waveforms, aberrant right subclavian artery, and cardiac axis.<sup>54-61</sup>

Mounting evidence supports the association of increased NT between 11 and 14 weeks of gestation and an increased risk for CHDs in both high-risk<sup>54-57</sup> and low-risk populations.<sup>62</sup> Among fetuses with increased NT measurements, the higher the NT measurement, the higher the prevalence of CHDs.<sup>54,57</sup> However, increased NT measurement is only modestly predictive of CHD. In a large meta-analysis involving more than 58,000 fetuses, the detection rate of an increased



NT measurement was only 31%, for a false positive rate of 1%.<sup>63</sup> Thus, other approaches had been used to evaluate the risk for CDH in the first trimester of pregnancy, including a combination of increased NT measurement, tricuspid regurgitation, and abnormal spectral flow waveforms in the DV (Fig. 13-8).<sup>58,59</sup>

Abnormal DV waveforms, including negative/reversed a wave and increased pulsatility index for the veins (PIV), have been associated with structural cardiac abnormalities in euploid first trimester fetuses.<sup>59</sup> The sensitivity and specificity of abnormal DV waveforms in the identification of CHDs are 80% and 83% in fetuses with increased NT, whereas the respective values in fetuses regardless of their NT measurement are 50% and 93%.<sup>64</sup>

Other findings during the first trimester scan associated with CHD include abnormal cardiac axis (Fig. 13-9)<sup>65</sup> and aberrant subclavian

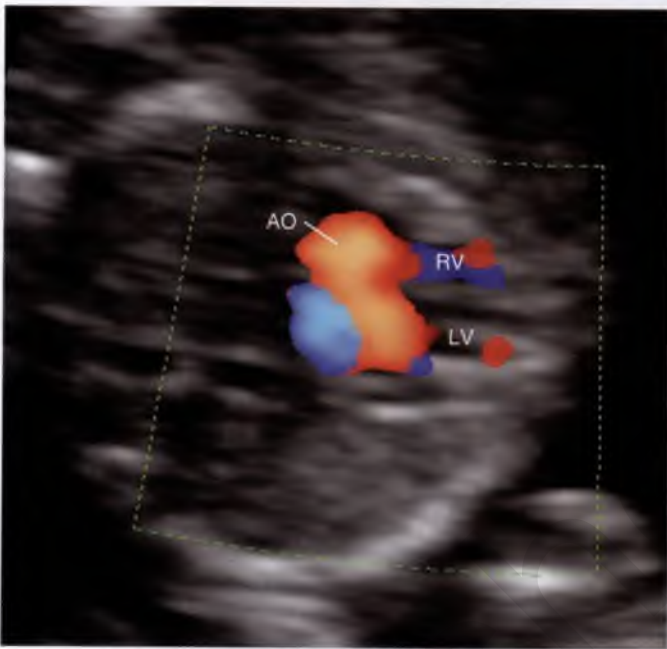


**FIG 13-4** Color Doppler imaging demonstrates a five-chamber view in the first trimester of pregnancy; the aortic root is visualized arising from the left ventricle. AO, aorta; LV, left ventricle; RV, right ventricle.

artery.<sup>60,61</sup> Sinkovskaya and associates<sup>65</sup> measured the cardiac axis on the four-chamber view in a prospective study between 11 and 14 weeks' gestation. The authors reported that the mean value for the cardiac axis in fetuses without cardiac anomalies was 47 degrees with limits of normality between 35 degrees and 60 degrees. An abnormal axis was seen in four of the six cases with CHD (of which three showed a structurally abnormal four-chamber view): one with HLHS, two with atrioventricular septal defects (AVSDs, one unbalanced, one associated with isomerism), and one with tetralogy of Fallot (TOF). The authors concluded that this approach may help to identify pregnancies at risk of CHD.<sup>65</sup> Of note, women with a body mass index (BMI) of 30 or higher were excluded from the study, and nearly one in five cases required a combined transabdominal and transvaginal approach. Thus, for CHD screening purposes, this strategy may be applicable only in facilities with availability and expertise in transvaginal sonography.

### Effectiveness of Early Gestation Cardiovascular Evaluation

A study using transvaginal sonography reported that the success rate of visualization of the four-chamber view, LVOT view, pulmonary trunk with three-vessel view (3VV) and crossover of the great arteries increased with gestational age, from 20% in week 11 to 92% in week 13.<sup>41</sup> In a study among women undergoing chorionic villus sampling between 11 and 13 weeks of gestation, the authors reported a 93.1% accuracy in the identification of CHDs using a high-frequency linear transducer.<sup>52</sup> In another study in high-risk women, using a combination of transabdominal and transvaginal sonography, the authors reported a 70% sensitivity and a 98% specificity in the identification of CHDs before 16 weeks' gestation.<sup>47</sup> In a large low-risk population, the authors reported that in 29 of the 39 cases of CHDs the heart defect was suspected in the first trimester.<sup>66</sup> Of note, in the latter study all examinations were performed using transabdominal sonography; however, in 7.3% of the cases a transvaginal scan was also required.

In a more recent study, Zidere and coworkers<sup>67</sup> performed a comparison of fetal echocardiography findings at less than 15 weeks of gestation in 1200 patients and a follow-up scan at least 6 weeks later.<sup>67</sup> The authors reported a high degree of accuracy in the identification of CHD by early fetal echocardiography (sensitivity 84.8%, 95% confidence interval [CI] 75.0-91.9; specificity 95.3%, 95% CI 93.9-96.4). Discordance between the two scans was found in 85 patients. In 50 of

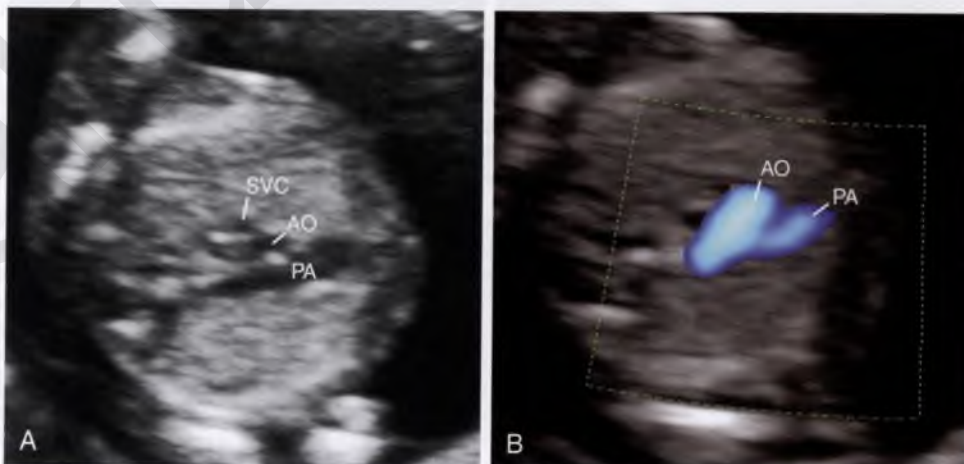


**FIG 13-5** The three-vessel and trachea view demonstrates the main pulmonary artery in communication with the ductus arteriosus (A). Color flow mapping is useful in the delineating the great arteries and the confluence of the ductus arteriosus and the aortic arch (V sign) (B). AO, aorta; PA, pulmonary artery; SVC, superior vena cava.

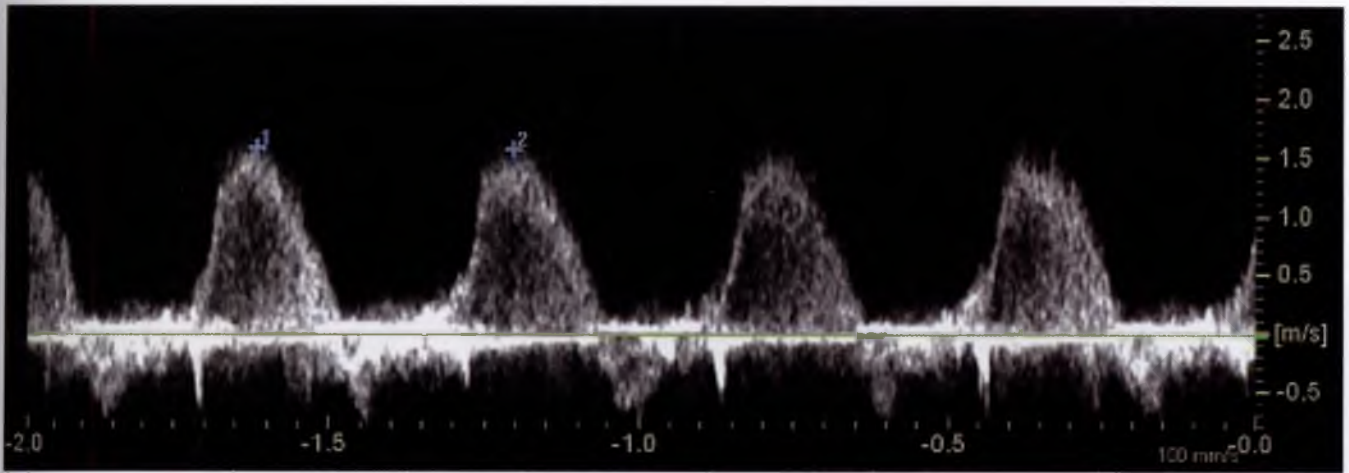


**FIG 13-6** Spectral Doppler in a first trimester fetus with severe tricuspid valve regurgitation. Note that the duration of regurgitation extends for over half of systole.



**FIG 13-7** Color Doppler imaging demonstrates severe tricuspid regurgitation in a fetus with Ebstein anomaly at 13½ weeks of gestation. DAO, descending aorta; LV, left ventricle; RV, right ventricle; TR, tricuspid regurgitation.

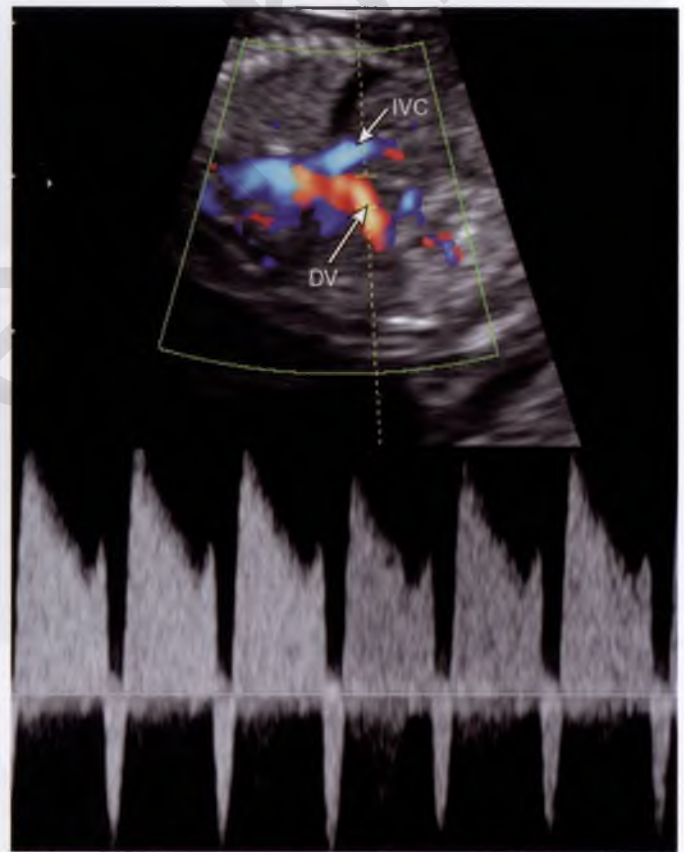


**FIG 13-8** Reversed a wave in the ductus venosus in a fetus with trisomy 18 and tricuspid atresia. DV, ductus venosus; IVC, inferior vena cava.

them, there was mild tricuspid regurgitation ( $n = 44$ ), mild mitral regurgitation ( $n = 3$ ), or both ( $n = 3$ ) at the early scan and no abnormal findings at the second scan. In three cases, CHD was suspected at the first scan but was not confirmed at the second scan (false positive diagnoses), and in four cases, less complex CHD than originally suspected at the first scan was found at the second scan. In 29 fetuses, an abnormality was found at the second scan that had not been detected at, or that had changed in severity since, the early study. The discordance was considered significant in 15 of the 29 cases. The authors suggested that in 10 cases of the latter group the significant differences between the early and later scans represented true progression of findings between the early and later scans, rather than missed or incorrect diagnoses. The authors concluded that early fetal echocardiography between 12 and 14 completed weeks' gestation is highly specific for the

detection of CHD. However, the identification of every case of TOF and mild AV canal variants presents particular diagnostic challenges in early fetal echocardiography. Changes in severity appear to occur particularly in obstructive lesions at the aortic and pulmonary valves and in the aortic arch, and there are limitations on accuracy with more subtle malformations. In an accompanying editorial the author cautioned that in the study of Zidere and coworkers,<sup>67</sup> if fetuses with resolving mild functional abnormality are removed from the denominator, 7/81 (9%) had a false positive diagnosis of CHD. A further 15/81



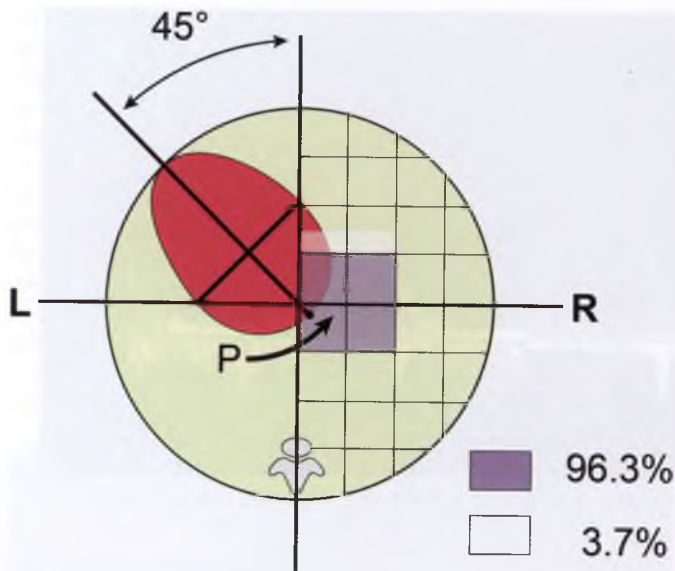


**FIG 13-9** Fetal cardiac axis and position. The mean cardiac axis is 45 degrees (2 SD = 20 degrees, range 22-75 degrees). A line through the intervententricular axis is extended to the posterior border of the heart to produce point P, the location of which can be used to define cardiac position. The percentages represent the proportion of time point "P" is in the indicated location. L, left; R, right; SD, standard deviation. (Modified from Comstock CH: Normal fetal heart axis and position. *Obstet Gynecol* 70:255-259, 1987.)

(18.5%) had important discordant findings at the second trimester scan, with 10/15 thought to be due to progression of disease that led to an alteration in counseling. Thus, even in expert hands, over 27% of important fetal structural CHD were missed or the parents were counseled inappropriately for the eventual outcome. The author proposed that concerns about the quality of information that can be obtained from the early human heart in euploid fetuses should make us pause to reconsider echocardiography in the first trimester and perhaps defer it until later in pregnancy.

## SECOND TRIMESTER FETAL CARDIAC EVALUATION

### Rationale and Effectiveness

Given that CHD is the most common birth defect, one of the major goals of the standard second trimester ultrasound examination is to evaluate for cardiac disease. Of highest priority is the identification of fetuses at risk for ductal dependency and hypoxemia after birth (Table 13-1). The examination is typically performed at 18 to 22 weeks' gestation. Of note, a prospective randomized study of second trimester fetal cardiac screening suggests that unselected pregnant women are less likely to require an additional scan at 20 to 22 weeks' gestation than at 18 weeks' gestation.<sup>68</sup>

Earlier practice guidelines for fetal cardiac screening encouraged visualization of the four-chamber view or "basic scan" with inclusion of the cardiac outflow tracts as part of an "extended basic scan" only if technically feasible.<sup>34,69</sup> However, additional assessment of both ventricular outflow tracts can improve the cardiac anomaly detection rate to approximately 80%.<sup>70-72</sup> A large retrospective review of over 18,000 midtrimester screening examinations with normal four-chamber views were examined at a single institution to determine how often outflow tracts could be obtained during a routine scan.<sup>73</sup> In 7.0% of 1308 scans, the main pulmonary artery, aortic outflow tract, or both were poorly visualized. In 778 scans (4.2%), poor visualization of the aorta only was noted. In 297 scans (1.6%), poor visualization of the

**TABLE 13-1 Critical Congenital Heart Disease Lesions and Associated Clinical Characteristics**

Lesion	Prevalence*	Hypoxemia	Ductus Arteriosus Dependent
<b>Outflow Tract Defects</b>			
Tetralogy of Fallot	6.1	Most	Uncommon
D-transposition of the great arteries	4.0	All	Uncommon
Double-outlet right ventricle	1.7	Some	Some
Truncus arteriosus	1.0	All	None
TAPVC	1.2	All	None
Ebstein anomaly	0.6	Some	Some
<b>Right Obstructive Defects</b>			
Tricuspid atresia	0.5	All	Some
Pulmonary atresia, intact septum	0.8	All	All
Pulmonary stenosis, atresia	6.3	Some	Some
<b>Left Obstructive Defects</b>			
Hypoplastic left heart	3.3	All	All
Coarctation of the aorta	4.7	Some	Some
Aortic arch atresia or hypoplasia	1.0	Some	All
Aortic valve stenosis (critical)	1.6	Uncommon	Some
Other major heart defects	12.4	Some	Some

\*Per 10,000 livebirths. Data are derived from the Metropolitan Atlanta Congenital Defects Program.

TAPVC, total anomalous pulmonary venous connection.

From Mahle WT, Newburger JW, Matherne P, et al: Role of pulse oximetry in examining newborns for congenital heart disease: a scientific statement from the American Heart Association and American Academy of Pediatrics. *Circulation* 120:447-458, 2009, used with permission.

pulmonary artery only was noted. In 233 scans (1.3%), neither ventricular outflow tract could be visualized. Given the significantly improved detection of CHD, and the low rate of poor visualization of the outflow tracts, recent guidelines now consider visualization of both arterial outflow tracts to be an integral part of the midtrimester fetal cardiac screening examination.<sup>34,74</sup>

The effectiveness of routine midtrimester fetal cardiac evaluation was reported in a large screening study of over 30,000 pregnancies in a nonselected Norwegian population.<sup>75</sup> This study was performed at a single institution where 98% of pregnancies received routine midtrimester screening scans at approximately 18 weeks' gestation that included a four-chamber view with visualization of the great arteries. Over one half (57%) of the 97 CHD cases with major cardiac defects were detected prenatally. Their findings underscored the importance of examiner experience for the effective detection of major CHD.<sup>75</sup>

### Cardiac Screening

The cardiac screening examination is optimally performed between 18 and 22 weeks' gestation, typically as part of a routine fetal anatomic survey.<sup>34</sup> Standardized transverse scanning planes are used to screen

fetuses for CHD using basic principles that have been based on a sequential segmental approach to describing sonographic findings.<sup>34,76,77</sup> Cardiac ultrasound images are typically optimized by adjusting image display depth, modifying acoustic focus for the heart, and maintaining low frame persistence. A relatively narrow scan angle will permit satisfactory temporal resolution.

**Standardized Scan Planes.** Because the relatively enlarged fetal liver displaces the fetal heart into a more horizontal position, the

examiner can use standardized transverse planes to systematically evaluate fetal cardiac anatomy (Figs. 13-10 through 13-12).

The four-chamber view permits assessment of major anatomic landmarks with particular emphasis on the AV junctions. Further examination of the size and relationship of the aortic and pulmonary outflow tracts, 3VV, and 3VT view (Figs. 13-13 and 13-14) provides a means to evaluate the size, number, alignment, and appearance of the great arteries in relation to their ventriculoarterial junctions and surrounding anatomy. The same views used in cardiac screening are used

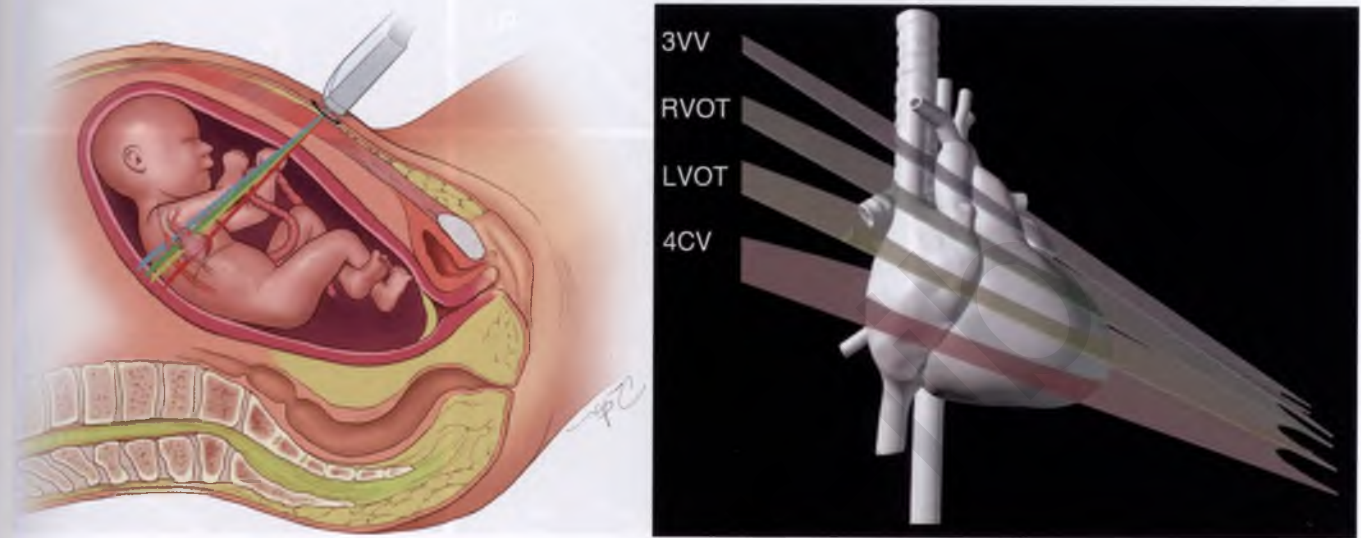


**FIG 13-10** Basic sonographic approach for the midtrimester fetal cardiac screening examination. Cephalad sweep of an ultrasound transducer toward the fetal head is used to visualize a four-chamber view (4CV), left ventricular outflow tract (LVOT), right ventricular outflow tract (RVOT), and three-vessel view (3VV), respectively.

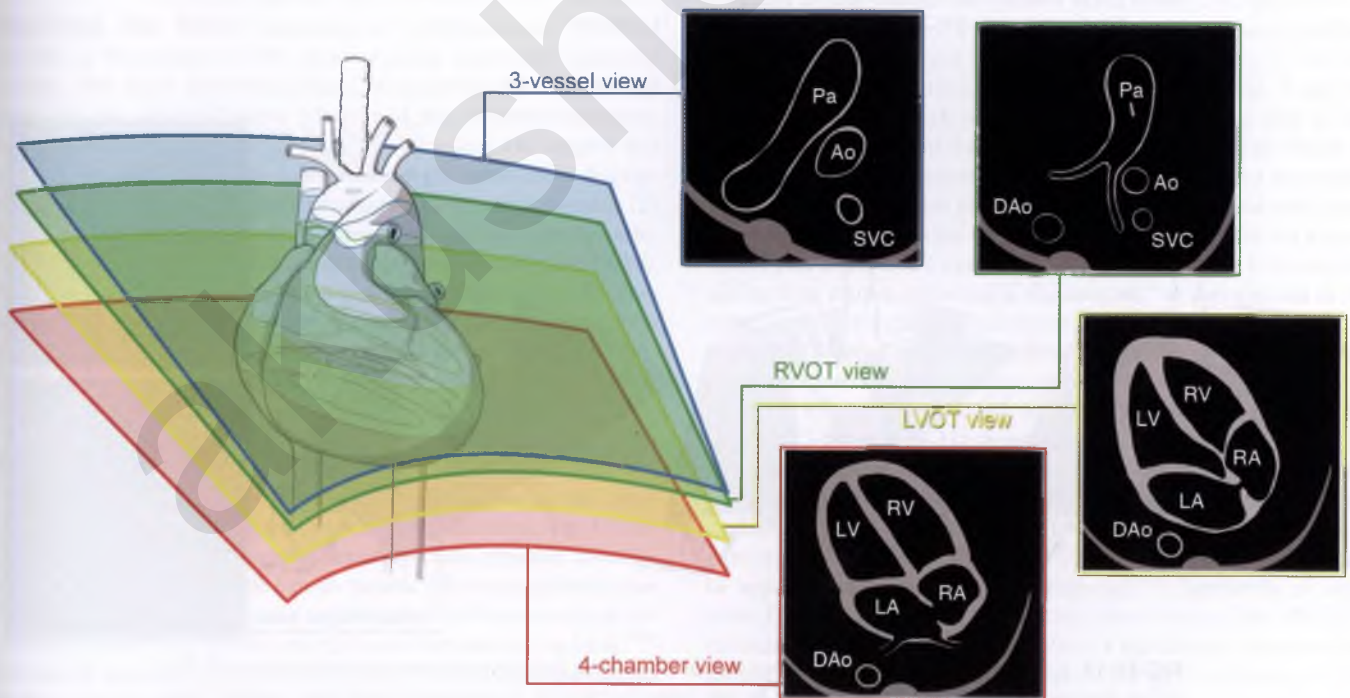


**FIG 13-11** Sonographic scanning planes for fetal cardiac screening. The most inferior transverse plane is used to confirm that the stomach and heart are both on the left side of the fetus (not shown). A cephalad sweep of an ultrasound transducer toward the fetal head is used to visualize (1) four-chamber view; (2) left ventricular outflow tract (LVOT); (3) right ventricular outflow tract (RVOT); (4) and three-vessel view. Ao, ascending aorta; DAo, descending aorta; LA, left atrium; LV, left ventricle; Pa, pulmonary artery; RA, right atrium; RV, right ventricle; SVC, superior vena cava.



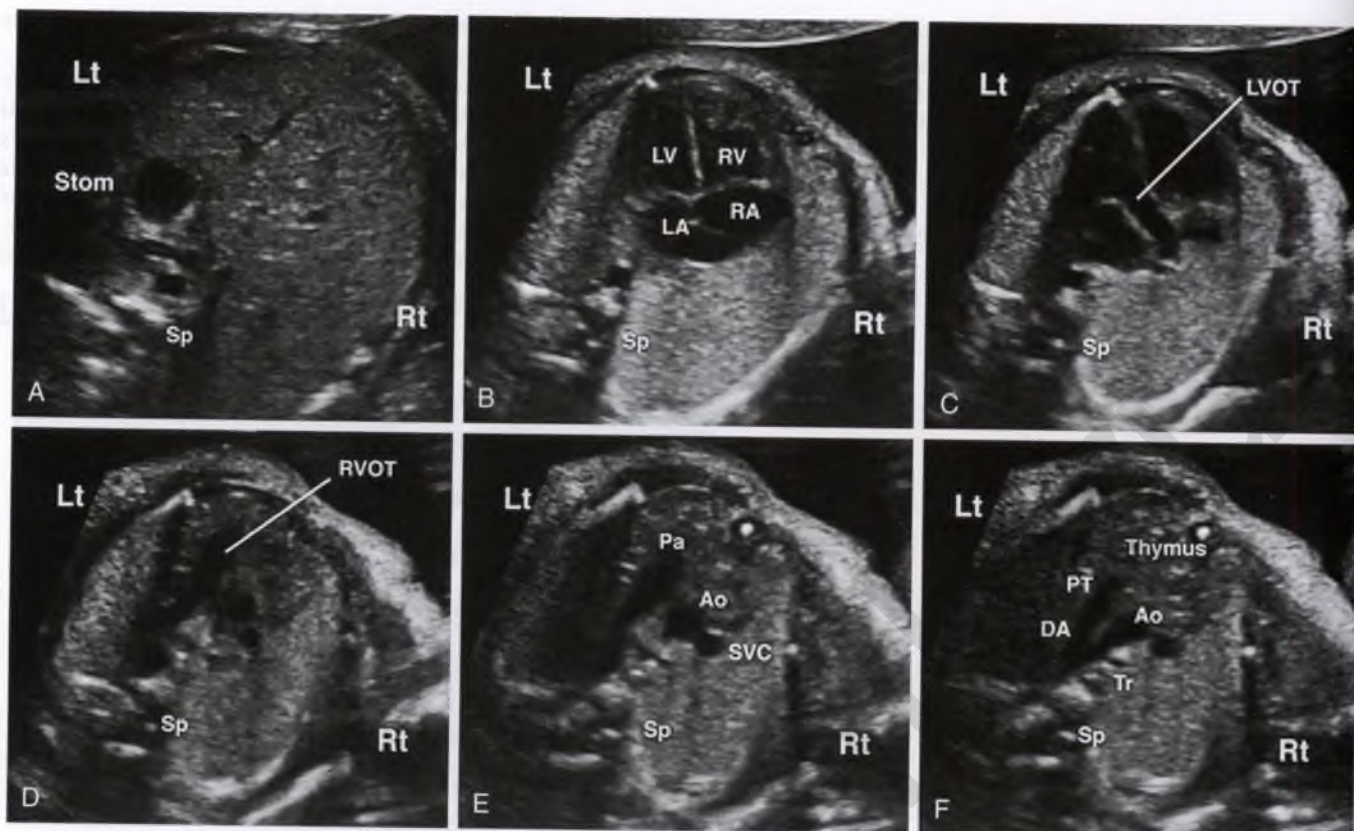


**FIG 13-12** Standard ultrasound scanning planes are used to evaluate the fetal heart by evaluating the following: **A**, abdominal situs; **B**, four-chamber view; **C**, left ventricular outflow tract; **D**, right ventricular outflow tract; **E**, three-vessel view; and **F**, three-vessel and trachea view. Ao, ascending aorta; DA, ductus arteriosus; LA, left atrium; Lt, left; LV, left ventricle; LVOT, left ventricular outflow tract; Pa, pulmonary artery; PT, pulmonary artery trunk; RA, right atrium; Rt, right; RV, right ventricle; RVOT, right ventricular outflow tract; Sp, spine; Stom, stomach; SVC, right superior vena cava; Tr, trachea.

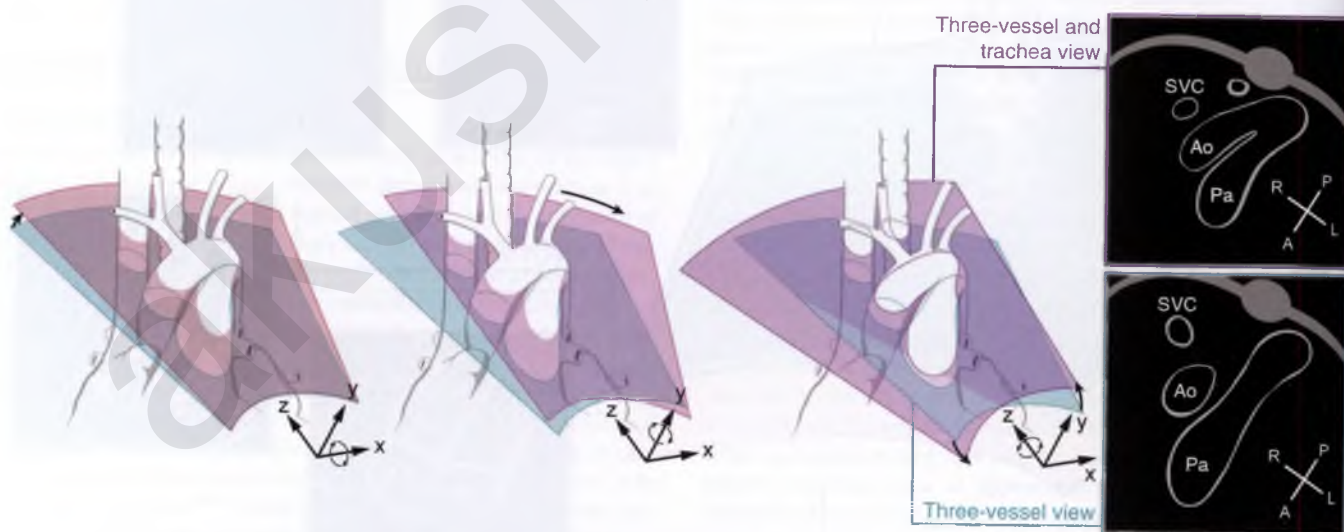


**FIG 13-13** Subtle transition between a three-vessel view (3VV) and three-vessel and trachea view (3VTV). A final transverse scan plane (purple plane, far left figure) completes the cephalad transducer sweep. Next, this plane is slightly rotated clockwise (purple plane with *curved arrow*, middle figure) and followed by a counterclockwise roll that allows the plane to intersect the ductus arteriosus as part of a “V-connection” between the aorta (Ao) and pulmonary artery (Pa) (purple plane, far right figure). Some investigators place more emphasis on the 3VTV because it captures similar diagnostic information as the 3VV and permits identification of anomalies such as a right aortic arch or vascular ring. A, anterior; L, left; P, posterior; R, right; SVC, right superior vena cava.



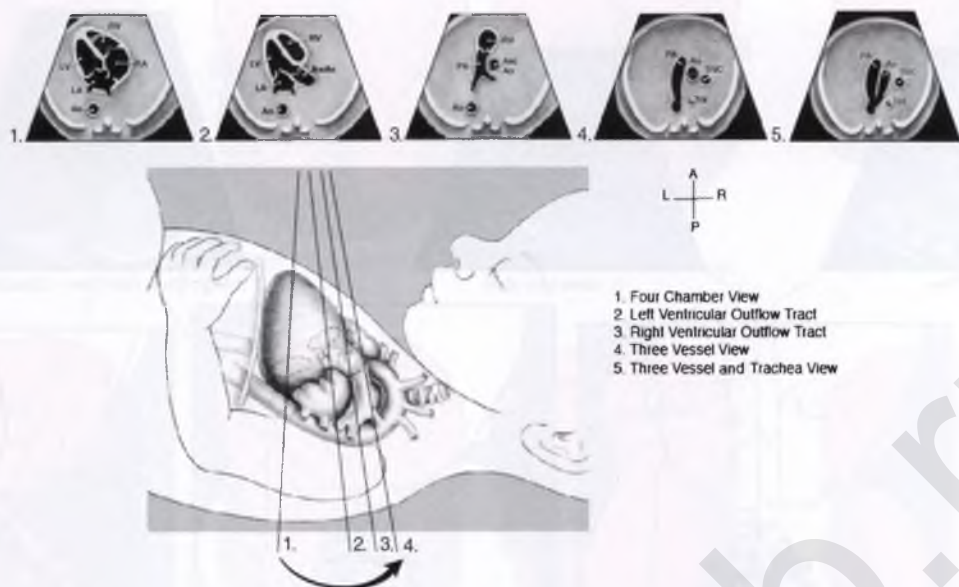


**FIG 13-14** Standardized transverse scanning planes for fetal echocardiography include an evaluation of the four-chamber view (1), arterial outflow tracts (2 and 3), and the three-vessel and three-vessel and trachea views (4 and 5). A, anterior; Ao, descending aorta; Asc Ao, ascending aorta; L, left; LA, left atrium; LV, left ventricle; P, posterior; PA, pulmonary artery; R, right; RA, right atrium; RV, right ventricle; and Tra, trachea. (From American Institute of Ultrasound in Medicine: AIUM practice guideline for the performance of fetal echocardiography. *J Ultrasound Med* 32:1067-1082, 2013, used with permission.)

in formal fetal echocardiography, in addition to a series of other views obtained in different planes (Figs. 13-14 and 13-15). The additional views are discussed further later in this section (“Standard Views”).

**Describing the Heart.** Evaluation of cardiovascular structures includes a description of the anatomy using sequential segmental analysis. Two main historical schools of nomenclature are typically used: the Van Praagh/Boston school and the Anderson/European school, as well as consensus-based nomenclature for CHD surgery that is typically used for databases.<sup>78</sup> Regardless of the names used, description of the heart typically includes evaluation of (1) atrial anatomy, (2) AV connections, (3) ventricular looping/topology, (4) ventriculoarterial connections, and (5) description of the great arteries (Fig. 13-16). Abnormalities of these normal relationships are present in many types of heart disease, as detailed in the following sections. Some examples of abnormal atrial anatomy, AV connections, ventricular looping, ventriculoarterial connections, and great artery arrangement are illustrated in Figure 13-17.

### Standard Views

**Plane 1: Transabdominal View.** A transverse view of the upper fetal abdomen is first evaluated to confirm normal situs (Fig. 13-18). The most caudal transabdominal scanning plane typically reveals a left-sided fetal stomach with a main hepatic lobe and gallbladder on the right side. This view is useful in heterotaxy syndromes such as left atrial isomerism (polysplenia) and right atrial isomerism (asplenia)<sup>79,80</sup> that may be associated with complex cyanotic heart disease and cardiac rhythm disturbances.

**Plane 2: Four-Chamber View.** After one verifies the stomach on the left side and liver on the right, the transducer is swept cephalad across the fetal thorax toward the head to obtain a four-chamber view and to assess cardiac position and direction of the apex (Figs. 13-11, 13-12B, 13-14, and 13-19, Video 13-1). The four-chamber view is defined by a

specific set of diagnostic imaging criteria that have been well summarized by the International Society of Ultrasound in Obstetrics and Gynecology<sup>34</sup> (Table 13-2).

**Plane 3: Left Ventricular Outflow Tract View.** Continuation of a transducer sweep toward the fetal head will reveal an aortic outflow tract that originates from the LV (Figs. 13-11, 13-12C, 13-14, and 13-20, Video 13-2). Although not required for screening, it may be possible to visualize neck vessels of the transverse aortic arch as one follows the distal end of the LVOT. The medial aortic wall should be continuous with the ventricular septum. Membranous or conoseptal VSDs will be seen in this plane and will not be visualized on a four-chamber view. Use of color or spectral Doppler imaging is not a mandatory part of the LVOT evaluation, although familiarity in its use and adding it to routine screening is encouraged,<sup>34</sup> as they can aid in the identification of aortic stenosis or aortic regurgitation.

**Plane 4: Right Ventricular Outflow Tract View.** The next scanning plane demonstrates a pulmonary artery that originates from a morphologic RV that is identified by a moderator band (Figs. 13-11, 13-12D, 13-14, and 13-21). A pulmonary artery bifurcation may be visualized (Fig. 13-21C), although this finding is not a required element for a technically satisfactory cardiac screening examination. An example of a right ventricular outflow tract (RVOT) abnormality is narrowing of part of the RVOT in TOF, although narrowing may not be apparent until later stages of pregnancy.<sup>81,82</sup> Familiarity of using color Doppler sonography for routine assessment of the RVOT is encouraged, although it is not considered a mandatory component for cardiac screening.<sup>34</sup> Color and spectral Doppler evaluation of the RVOT can aid in the identification of pulmonary stenosis or pulmonary regurgitation.

**Plane 5: Three-Vessel View.** A 3VV provides a transverse view of the upper fetal mediastinum. In this plane, the main pulmonary artery, ascending aorta, and superior vena cava are arranged in a straight line that extends from the left anterior to right posterior aspect of the



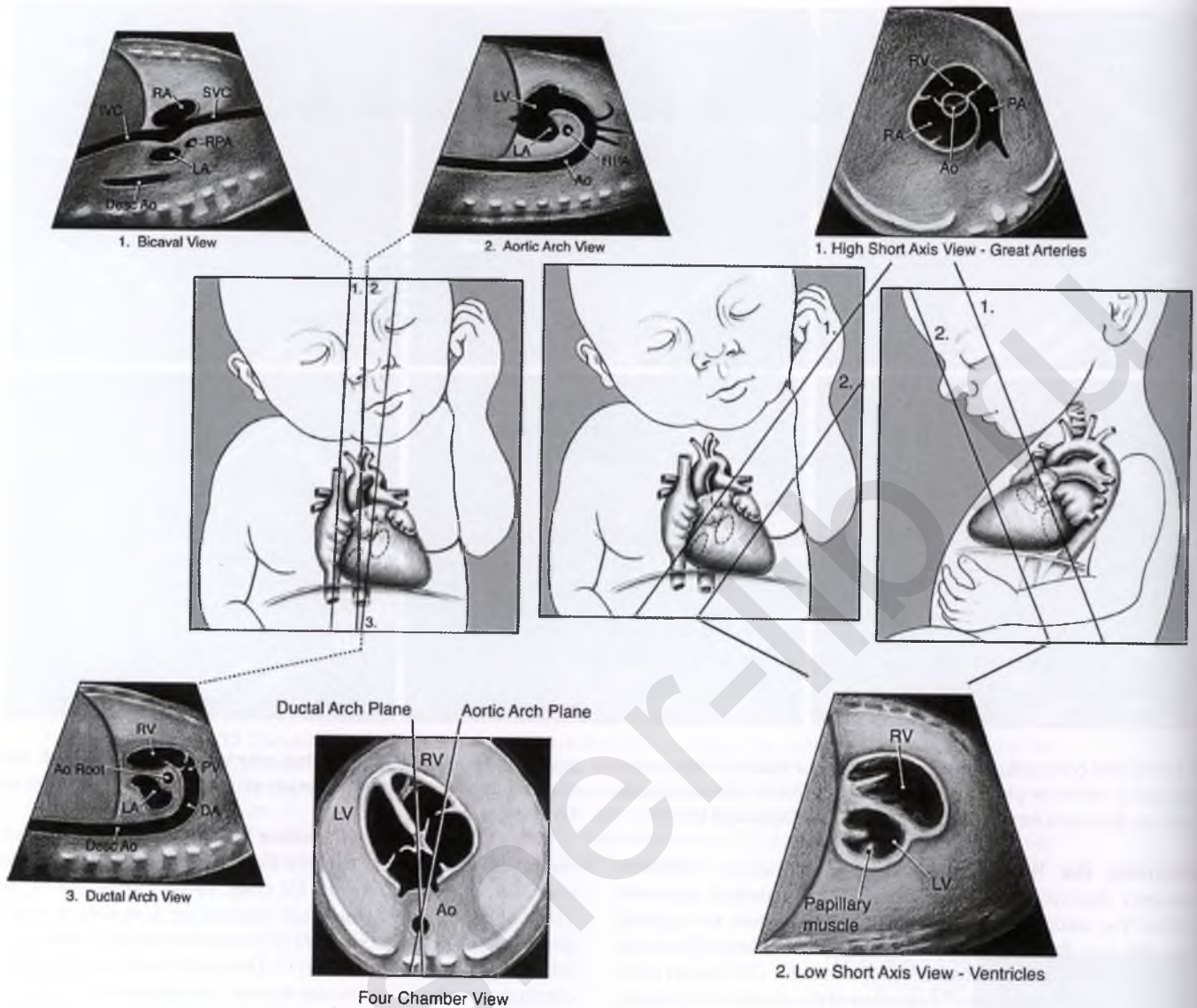


**FIG 13-15** Sagittal views of the superior and inferior venae cavae, aortic arch, and ductal arch, as well as low and high short-axis views of the fetal heart. Ao, aorta; Ao Root, aortic root; DA, ductus arteriosus; Desc Ao, descending aorta; IVC, inferior vena cava; LA, left atrium; LV, left ventricle; PA, main pulmonary artery; PV, pulmonary valve; RA, right atrium; RPA, right pulmonary artery; RV, right ventricle; SVC, superior vena cava. (From American Institute of Ultrasound in Medicine: AIUM practice guideline for the performance of fetal echocardiography. *J Ultrasound Med* 32:1067-1082, 2013, used with permission.)

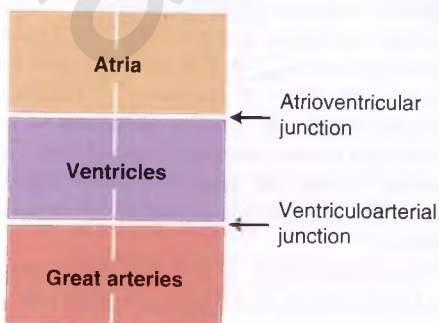
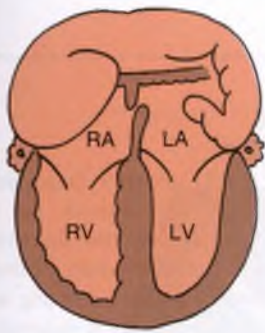


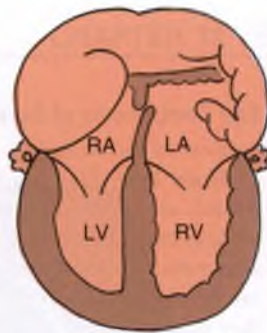
**FIG 13-16** Basic cardiac segments and junctions.

mediastinum with decreasing magnitude of their vessel diameters<sup>83</sup> (Figs. 13-11, 13-12E, 13-13, 13-14, and 13-22). If technically feasible, the 3VV should be attempted as a routine part of a midtrimester screening examination.<sup>34</sup> Color Doppler sonography is not a mandatory part of the 3VV, although familiarity in its use and adding it to routine screening is encouraged.<sup>34</sup>

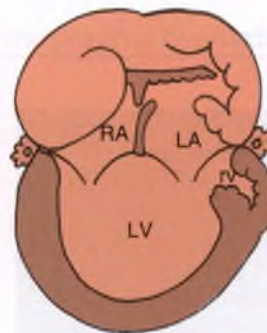
Normal and abnormal examples for using color Doppler sonography with the 3VV have also been reported.<sup>84</sup> Abnormalities in vessel number, size, alignment, and arrangements may provide clues for anomalies of the great vessel such as right aortic arch or a persistent left superior vena cava. Paladini<sup>85</sup> has also described how the internal mammary arteries can be used to outline the fetal thymus from a 3VT view for fetuses at risk for chromosome 22q11.2 microdeletion.



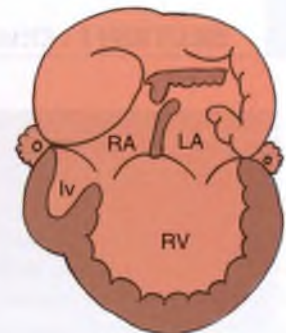
Concordant connection



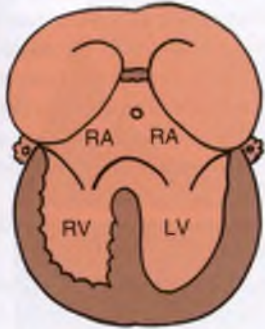
Discordant connection



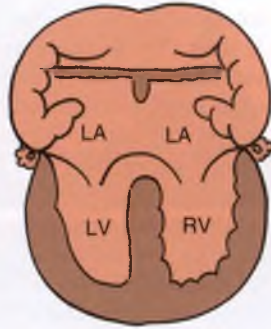
Double inlet left ventricle



Double inlet right ventricle



Right isomeric atria connected to D-loop ventricles



Left isomeric atria connected to L-loop ventricles



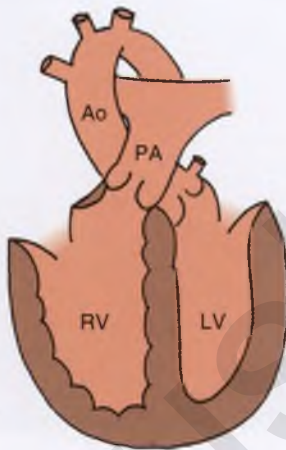
Absent right atrioventricular connection



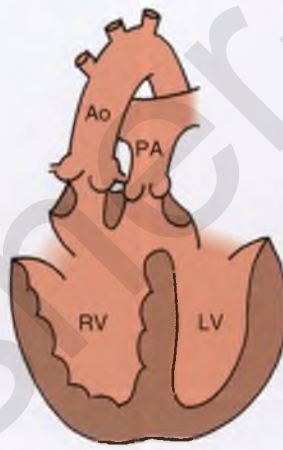
Absent left atrioventricular connection

A

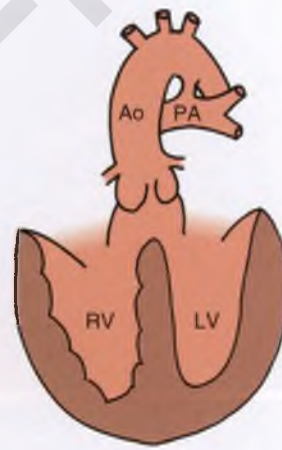
B



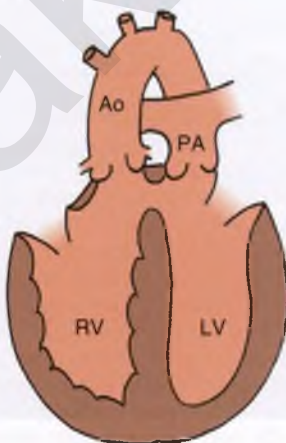
Concordant connection



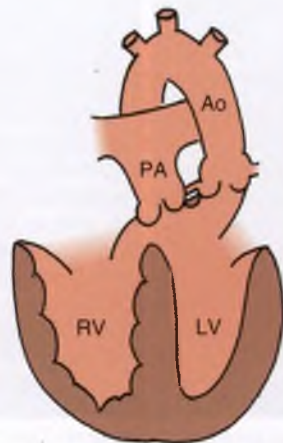
Double-outlet right ventricle



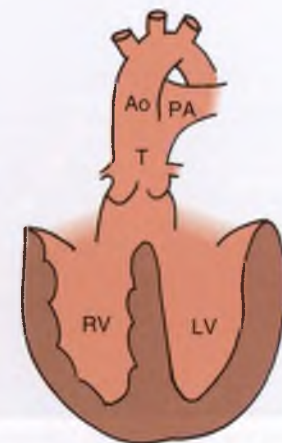
Single arterial trunk



Discordant connection



Double-outlet left ventricle



Common arterial trunk

**FIG 13-17** Biventricular atrioventricular connections (A), univentricular atrioventricular connections (B), and types of ventriculoarterial connections (C). Ao, ascending aorta; LA, left atrium; LV (lv), left ventricle; PA, main pulmonary artery; RA, right atrium; RV (rv), right ventricle; T, truncus.



**Plane 6: Three-Vessel and Trachea View.** Finally, a 3VT view is obtained just a few millimeters above the 3VV after slight counterclockwise angulation toward the left from an axial plane<sup>86</sup> (Figs. 13-12F, 13-13, 13-14, 13-22, and 13-23). This plane is used to evaluate major vessels in the fetal mediastinum. The transverse aortic arch and isthmus merge into the descending aorta, as does the pulmonary trunk and ductus arteriosus, creating a V-shaped configuration. Note the presence of an anterior fetal thymus gland in this view as well and how the V-shaped landmark lies just to the left of the trachea.

A 3VT view is very similar to the 3VV except that the aortic and ductal arches are both visualized just superior to the carina (see Fig. 13-13). Both arches are normally visualized to the left of the spine and trachea. Much like the 3VV, the 3VT view can be used to assess the number, size, and alignment of the main pulmonary artery, aorta, and right superior vena cava. However, the 3VT view will likely allow the detection of life-threatening ductus-dependent cardiac malformations.<sup>87</sup> In this regard, color Doppler sonography can be very useful for identifying ductus-dependent lesions in this scanning plane. The 3VT view has also been used for the detection of aortic arch anomalies and aberrant right subclavian artery (ARSA).<sup>88,89</sup> In a study of 106 second trimester Down syndrome fetuses, the incidence of aberrant right subclavian artery was 25%.<sup>90</sup>

## Key Components of Screening

### General Assessment

**Heart Rate.** Fetal heart rate (FHR) reference ranges during the second and third trimesters typically fall between 120 and 160 beats/minute (bpm) with occasional and limited decelerations or accelerations beyond these limits.<sup>91</sup> Benign episodes of fetal bradycardia can occur during a second trimester screening scan, but they quickly recover to normal values, especially if maternal abdominal pressure of the ultrasound transducer is reduced. Although fetal bradycardia has been broadly accepted as a heart rate less than 100 bpm, the American College of Obstetricians and Gynecologists (ACOG) has defined bradycardia as a heart rate less than 110 bpm.<sup>92,93</sup> Sustained bradycardia below this threshold may be caused by heart block. Mild tachycardia (>160 bpm) can transiently occur in normal fetuses, although persistent tachycardia ( $\geq 180$  bpm) should be further investigated for problems such as supraventricular tachycardia (SVT), chorioamnionitis, fetal distress, or hyperthyroidism.

**Heart Size.** Cardiac circumference measurements provide quantitative verification when cardiomegaly is suspected.<sup>94,95</sup> Enlarged hearts can be associated with cardiac dysfunction, especially in the presence of pericardial effusion. Cardiomegaly is generally defined as

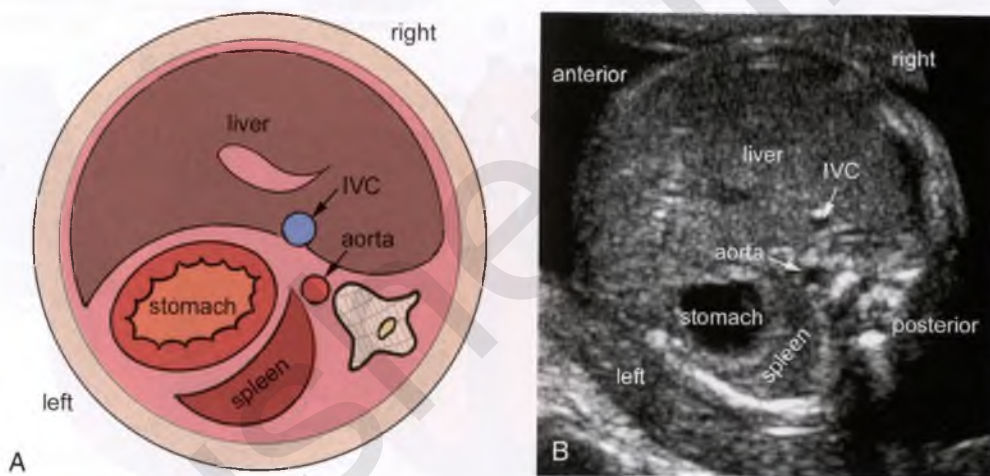


**FIG 13-18** Transverse view of the upper abdomen, diagram (A) and sonographic image (B). The larger lobe of the liver is on the right, and the stomach on the left. The descending aorta is at the left anterior aspect of the spine. The inferior vena cava (IVC) is on the right side of the midline. Note that the IVC is located anteriorly at some distance from the spine as it courses forward to connect to the right atrium above this level.

**FIG 13-19** Diagram (A) and sonographic images (B through F) in the four-chamber view. The right- and left-sided chambers are symmetric in size. The atrioventricular valves have offset attachments (dots in B-D) to the septum, with the tricuspid valve having more apical attachment than the mitral valve. The apex of the right ventricle (RV) is obliterated in B and C by the moderator band (asterisk). The moderator band can also be seen as a distinct muscle bundle as shown in D. Right and left lower pulmonary veins (RLPV and LLPV) course obliquely forward as they connect to the left atrium (LA). The central part of the atrial septum is the septum primum (arrows in C). It is thin and mobile and bulges into the LA. The descending aorta (ao) is seen at the left anterior corner of the spine. E shows a slice just inferior to the four-chamber view. The coronary sinus (CS) is seen as a tubular structure between the left ventricle (LV) and the inferior vena cava (IVC) orifice. Note that the proximal part of the coronary sinus can be seen as a small circle at the left atrioventricular junction in a regular four-chamber view. The color Doppler image (F) shows both lower pulmonary veins and the right upper pulmonary vein (RUPV). Both lower pulmonary veins course obliquely forward, whereas the RUPV courses obliquely backward as it connects to the LA. RA, right atrium. (A from American Institute of Ultrasound in Medicine: AIUM practice guideline for the performance of fetal echocardiography. J Ultrasound Med 32:1067-1082, 2013.)



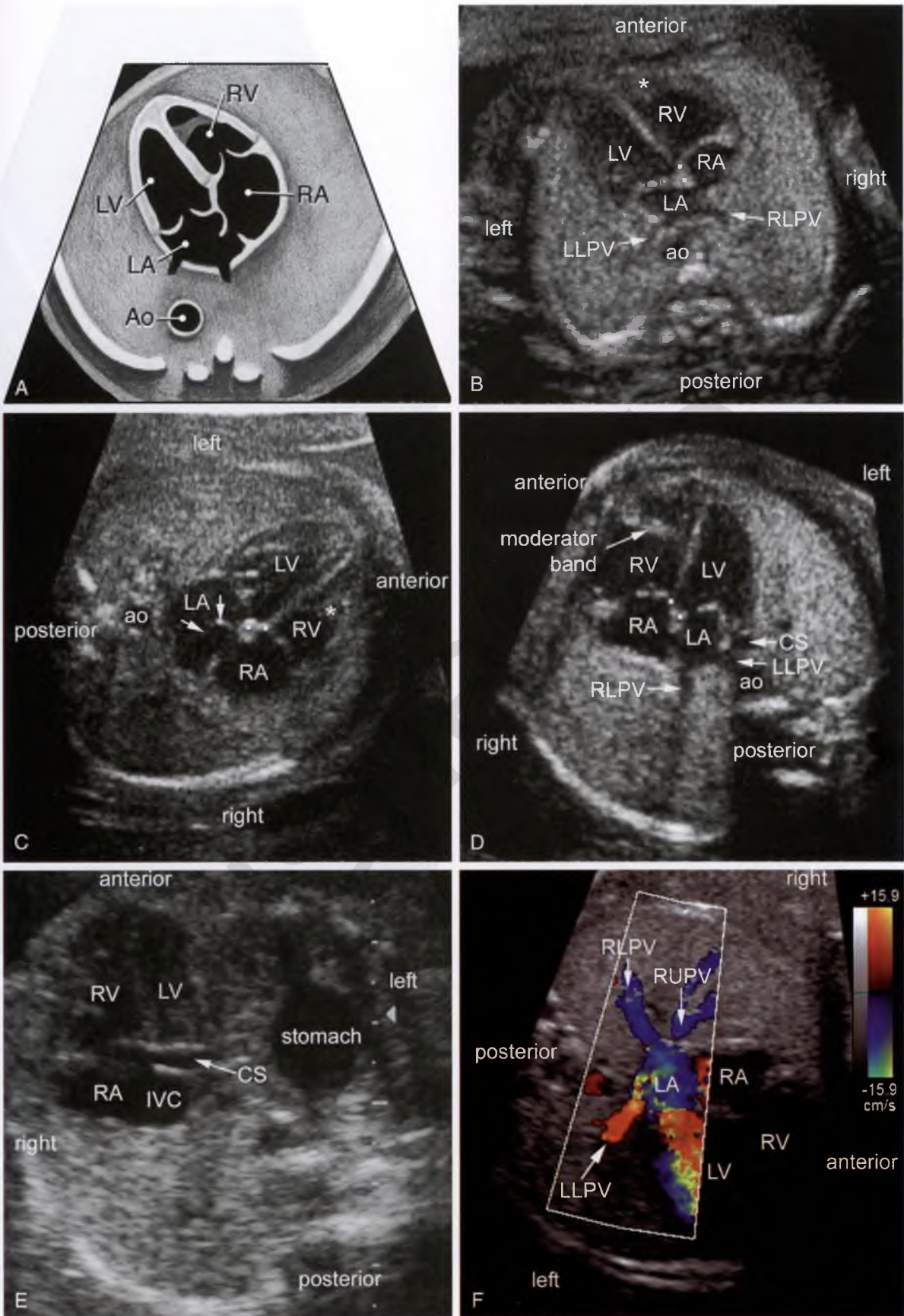




**TABLE 13-2 Fetal Situs/Laterality and Four-Chamber View of the Fetal Heart**

**General Assessment**

1. Fetal laterality (identify right and left sides of fetus)
2. Stomach and heart on left
3. Normal cardiac rate and rhythm
4. Heart occupies no more than a third of thoracic area
5. Majority of heart in left side of chest
6. Normal cardiac axis and position
7. Four cardiac chambers present
8. No pericardial effusion or hypertrophy

**Atrial Chambers**

1. Two atria, approximately equal in size
2. Foramen ovale flap in left atrium
3. Atrium septum primum present (near to crux)
4. Pulmonary vein enters left atrium

**Ventricular Chambers**

1. Two ventricles, approximately equal in size
2. No ventricular wall hypertrophy
3. Moderator band at right ventricular apex
4. Ventricular septum intact (apex to crux)

**Atrioventricular Junction and Valves**

1. Intact cardiac crux
2. Two atrioventricular valves open and move freely
3. Differential offsetting: tricuspid valve leaflet inserts on ventricular septum closer to cardiac apex than does mitral valve

Adapted from International Society of Ultrasound in Obstetrics and Gynecology; Carvalho JS, Allan LD, Chaoui R, et al: ISUOG Practice Guidelines (updated): sonographic screening examination of the fetal heart. *Ultrasound Obstet Gynecol* 41(3):348-359, 2013.

a cardiothoracic circumference ratio greater than 0.50 or a cardiothoracic area ratio greater than 0.25.<sup>96,97</sup>

**Cardiac Axis and Position.** Cardiac axis is determined from a line that is drawn from the spine to the anterior chest wall.<sup>98</sup> This line divides the fetal chest into equal halves with an angle that the interventricular septum makes with this line as the cardiac axis. The fetal heart is located in the left hemithorax with a cardiac axis of  $45 \pm 20$  degrees (see Fig. 13-9). The heart can point toward the midline (mesocardia) or be deviated toward the right side of the chest (dextrocardia) as a normal variant. The same line can be extended to the most posterior cardiac border where it intersects the posterior wall as a "P point." Point P is located within a specific area of the thorax in 96.3% of fetuses.

Both cardiac axis and position are constant throughout pregnancy. Although left cardiac axis deviation ( $>75$  degrees to left) can occur as a normal variant, most cases will be associated with structural malformations, particularly conotruncal anomalies and coarctation, which may not otherwise be detectable from a four-chamber view.<sup>99</sup> Right cardiac deviation (heart axis from 25 degrees to the left of midline to anywhere in the midline or right side of the chest) has been associated with polysplenia/asplenia, situs inversus, AVSD, double-outlet right ventricle (DORV), or common atria.<sup>100</sup> Abnormal cardiac position deviated into the right chest (dextroposition) warrants a further search for either a left-sided congenital diaphragmatic hernia or space-occupying mass such as a cystic adenomatoid malformation.

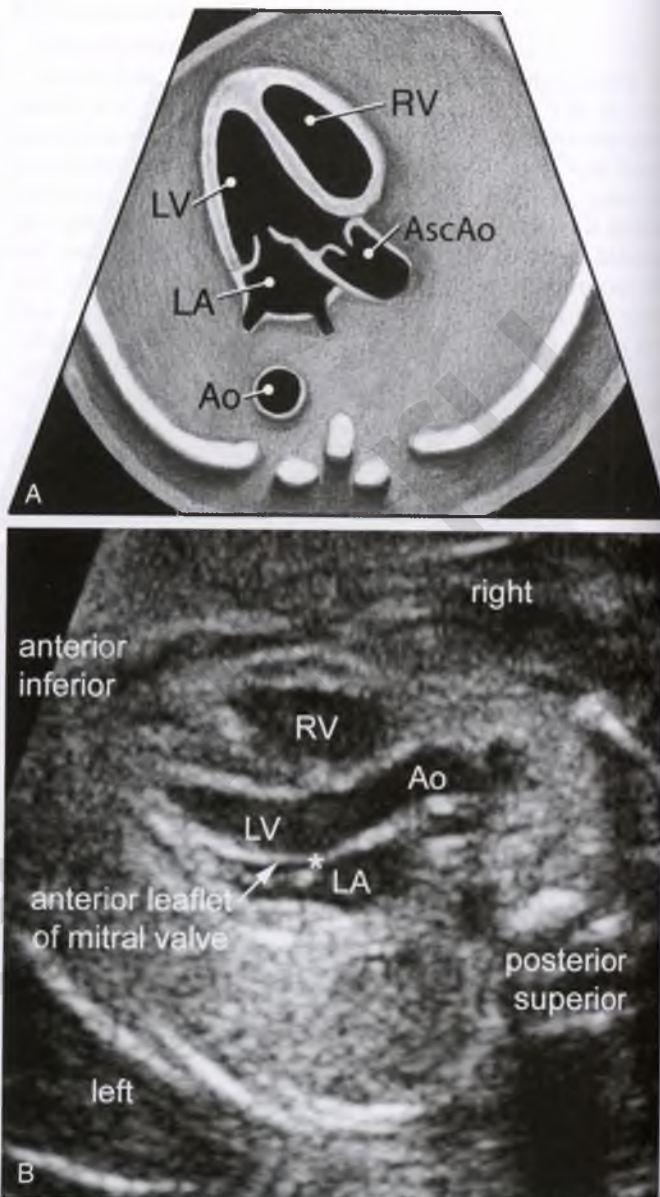


**FIG 13-20** Diagram (A) and sonographic image (B) in the left ventricular outflow tract view. Ao, aorta; AscAo, ascending aorta; LA, left atrium; LV, left ventricle; RV, right ventricle. (A from American Institute of Ultrasound in Medicine: AIUM practice guideline for the performance of fetal echocardiography. *J Ultrasound Med* 32:1067-1082, 2013.)

**Four Cardiac Chambers Present.** The presence of four cardiac chambers is an essential component of a normal four-chamber view. However, a simple count of four chambers alone should not be mistaken as being sufficient to fulfill diagnostic criteria for a technically acceptable four-chamber view. In a normal four-chamber view the two atria and the two ventricles will be symmetric in size (see Fig. 13-19A through D).

**No Pericardial Effusion or Hypertrophy.** Pericardial effusions are occasionally identified at the time of a routine cardiac screening examination (Fig. 13-24). A pericardial fluid collection of more than 2 mm in thickness is considered abnormal.<sup>101,102</sup> Isolated effusions can spontaneously resolve with good postnatal outcomes, although this finding can also be associated with a genetic syndrome such as trisomy 21.





Age-specific reference values for left and right ventricular wall thickness have been reported in fetuses.<sup>103</sup>

**Atrial Chambers.** A normal fetal cardiac screening examination identifies two atrial chambers of approximately the same size with a normal-appearing foramen ovale flap in the LA (see Fig. 13-19A through D). The primum atrial septum is intact and pulmonary veins enter the left atrial chamber. The coronary sinus can be visualized in the left AV groove when sweeping inferiorly (see Fig. 13-19E).

One of the primary reasons for investigating atrial morphologic appearance is to rule out heterotaxy (also known as isomerism), in which the heart has inappropriate symmetry. Berg and colleagues reviewed 30 prenatally diagnosed cases of heterotaxy and have described two types of atrial morphologic features<sup>104</sup>: (1) sickle shape with tip pointing laterally and apically and (2) blunt shape resembling the usual atrial appearance in the four-chamber view (see Fig. 13-17A). Their results suggest that prenatally diagnosed heterotaxy most often presents with an isomeric morphologic appearance in the four-chamber view, and that differentiation between bilateral left (sickle-shaped) and bilateral right (blunt and pyramidal) isomerism can be determined. This differentiation is particularly significant because the greatest attrition in left atrial isomerism occurs during fetal life, whereas neonates with right atrial isomerism are more likely to experience postnatal problems associated with complex CHD. However, caution should be exercised when applying these findings to a screening population. More information regarding evaluating heterotaxy in the fetal echocardiogram is given in the discussion of congenital heart lesions (“Situs Abnormalities”).

Atrial septal aneurysm may also be visualized from the four-chamber view. A retrospective study of 1302 fetal echocardiograms found a 7.6% incidence of atrial septal aneurysm that was defined as redundant tissue extending at least halfway across the LA. They observed that 36% of fetuses with atrial septal aneurysm had premature atrial beats that appeared to be related to the degree of septal bulging. Their results suggest that such aneurysms almost always resolve after birth and are not typically associated with major cardiac dysrhythmias.<sup>105</sup> Severe atrial septal aneurysms that extend over the mitral valve apparatus have been reported with left-right asymmetry on fetal evaluation, and occasionally with coarctation of the aorta.<sup>106</sup>

Routine screening should also include assessment of the pulmonary veins. A normal four-chamber screening examination usually demonstrates at least two of the four pulmonary veins entering the LA (see Fig. 13-19B through D and F). Total anomalous pulmonary venous return (TAPVC) should be suspected when the connection between the pulmonary veins and the LA is not evident. The diagnosis of TAPVC should always be considered in cases of heterotaxy, especially in fetuses suspected to have right isomerism.<sup>107</sup> Ganesan and colleagues described sonographic findings for 26 fetuses with a prenatal diagnosis of TAPVC.<sup>108</sup> They concluded that the diagnosis of TAPVC can be suspected on standard axial views during the cardiac screening examination and confirmed on fetal echocardiography based on pulsed-Doppler studies. More detailed information on anomalies of pulmonary

**FIG 13-21** Diagram (A) and sonographic images (B and C) in the right ventricular outflow tract view and extended view including the branch pulmonary arteries. Ao, aorta; Asc Ao, ascending aorta; L, left pulmonary artery; LV, left ventricle; PA, main pulmonary artery; R, right pulmonary artery; RV, right ventricle; SVC, superior vena cava. (A from American Institute of Ultrasound in Medicine: AIUM practice guideline for the performance of fetal echocardiography. *J Ultrasound Med* 32:1067-1082, 2013.)



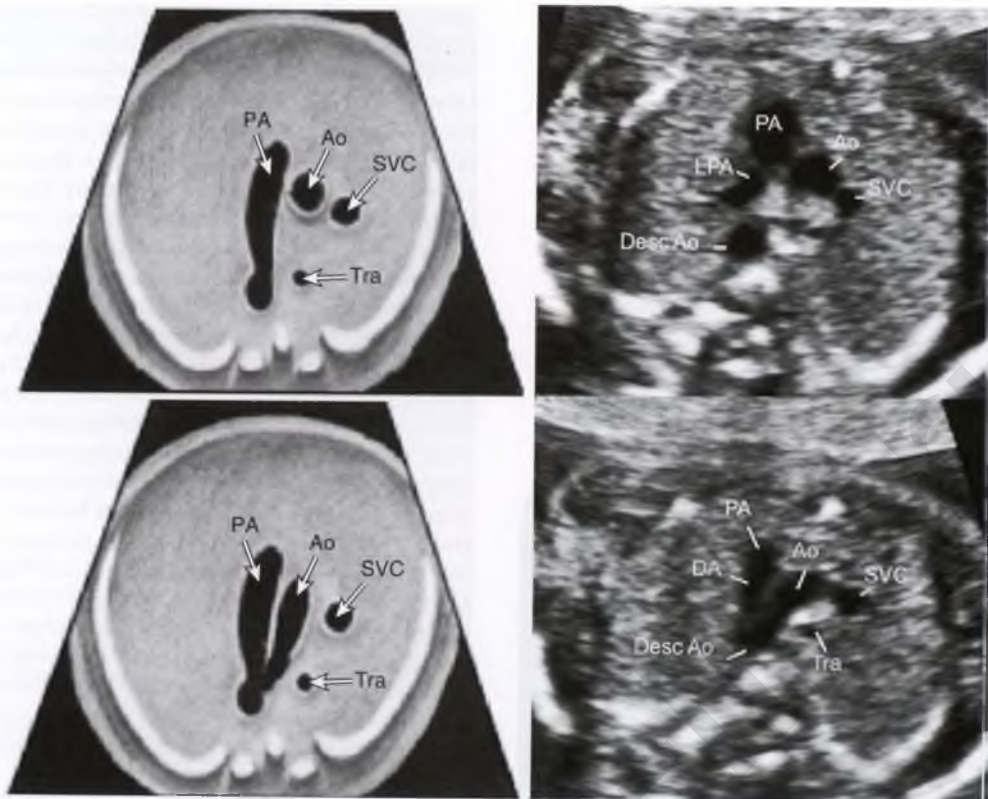


**FIG 13-22** Diagrams (*left*) and sonographic images (*right*) in the three-vessel view (3VV) and three-vessel and trachea view (3VTV). The 3VTV plane is situated only a few millimeters more cephalad from the 3VV plane. The V-shaped connection between the aorta and ductus arteriosus is obtained by a slight counterclockwise rotation of the ultrasound transducer. Ao, ascending aorta; DA, ductal arch; Desc Ao, descending aorta; LPA, left pulmonary artery; PA, main pulmonary artery; SVC, superior vena cava; Tra, trachea. (Diagrams adapted from American Institute of Ultrasound in Medicine: AIUM practice guideline for the performance of fetal echocardiography. *J Ultrasound Med* 32:1067-1082, 2013.)

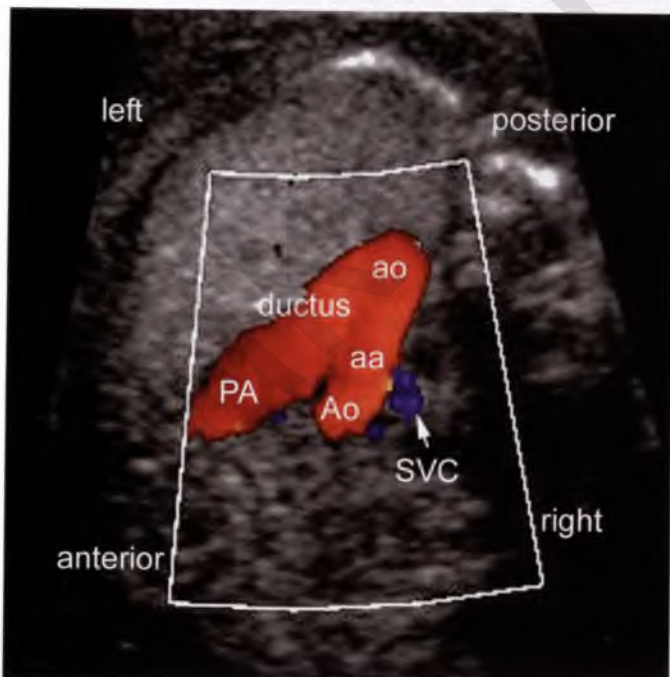


**FIG 13-23** Three-vessel and trachea view using color Doppler imaging. aa, aortic arch; Ao, ascending aorta; ao, descending aorta; DA, ductal arch; PA, pulmonary artery; SVC, superior vena cava.



**FIG 13-24** Circumferential pericardial effusion in the fetus. Desc ao, descending aorta; LA, left atrium; LV, left ventricle; RA, right atrium; RV, right ventricle.



venous return is provided later in this chapter under “Anomalous Pulmonary Venous Connection.”

**Ventricular Chambers.** A normal four-chamber view requires confirmation of two cardiac ventricles that are approximately the same size, although the RV is usually slightly larger, particularly in late gestation. The normal RV/LV size ratio increases with progressing gestational age (90% CIs ranging from 0.79 to 1.24).<sup>109</sup> Ventricular size discrepancy may be an initial clue for cardiac anomalies during the screening examination despite the presence of normal ventricular diameter measurements.

**Left Ventricle.** A cone-shaped LV lies posterior to and leftward of the RV (see Fig. 13-19A through E). The LV has two distinct papillary muscles, the anterolateral and posteromedial. Both papillary muscles have chordae tendineae, which connect to the mitral valve. The LV septal surface is smooth with fine apical trabeculations and no septal connection to the mitral valve.

**Right Ventricle.** The morphologic anterior right ventricular chamber has a moderator band near the cardiac apex (see Fig. 13-19A through D). Chordae tendineae extend from the septal tricuspid valve leaflet and insert into papillary muscles that arise from the right ventricular septal surface. Unlike the LV, the inlet and apical portions of the RV are heavily trabeculated.

#### Atrioventricular Junction and Valves

**Mitral and Tricuspid Valves.** The AV valves prevent ventricular blood from backing up into the atrial chambers. On the screening examination, valve leaflets do not appear thickened and should move freely throughout the cardiac cycle. Although not required, color Doppler imaging of the AV valves is the most useful way to assess for AV valve regurgitation, which is commonly seen in fetal heart disease, especially in atrioventricular canal defects (AVCDs), Ebstein anomaly and other tricuspid valve disorders (Video 13-3), and fetal primary or secondary cardiac dysfunction (Fig. 13-25). AV valves should also be assessed for appropriate connections to the ventricles, as conditions such as tricuspid atresia and mitral atresia can have absent connections to the ventricles, and double-inlet LV can have both AV valves entering the LV (Fig. 13-26 and Video 13-4).

**Offset Atrioventricular Valves.** In the normal heart, the tricuspid valve annulus is slightly offset from the center crux of the heart and more apically positioned than the mitral valve annulus (see Fig. 13-18).

Absence of this normal offsetting suggests an abnormality. For example, in Ebstein anomaly, there is excessive apical displacement of the septal tricuspid valve leaflet (Fig. 13-27).<sup>110</sup> In AVCDs and variants, the normal valve offsetting is not present as there is either a common AV valve or separate AV valves at the same level.<sup>111</sup> The normal valve offsetting may not be apparent in fetuses with a dilated coronary sinus,<sup>112</sup> or may be challenging to recognize due to technical factors.

Offset AV valves can usually be visually confirmed in fetuses, although occasionally it may be helpful to measure the distance between insertions of the medial leaflets of the mitral and tricuspid valves (MTD). Calipers are placed parallel to the ventricular septum

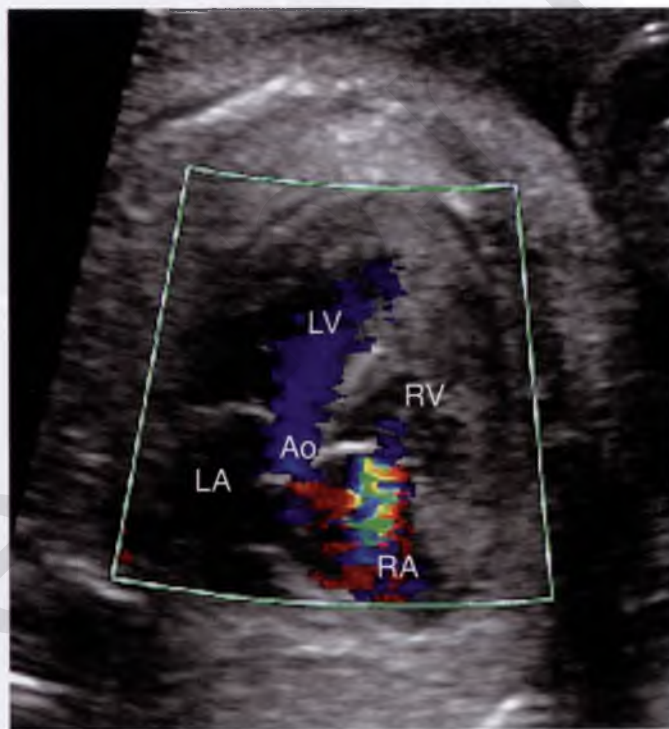


**FIG 13-25** Moderate to severe tricuspid valve regurgitation. Ao, aorta; LA, left atrium; LV, left ventricle; RA, right atrium; RV, right ventricle.

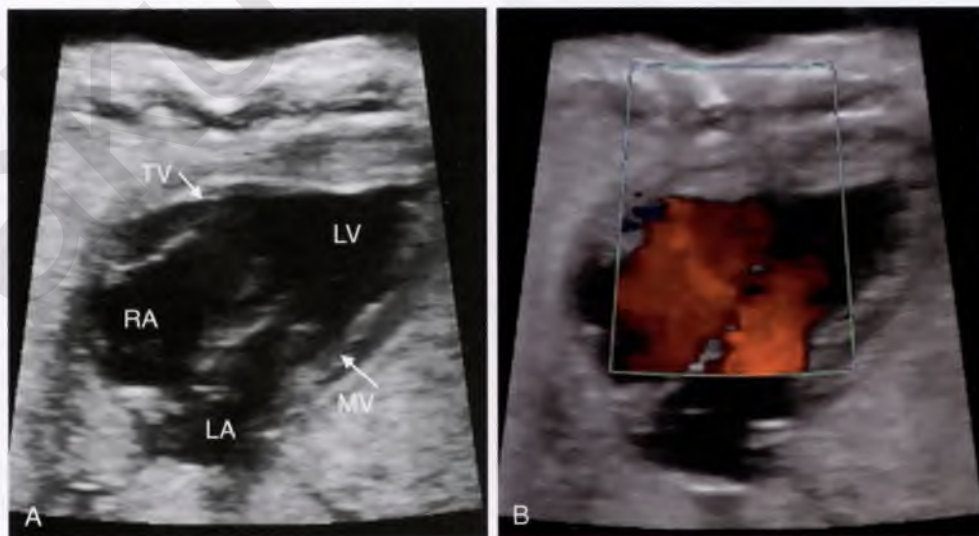


**FIG 13-26** Double-inlet left ventricle (LV) by two-dimensional imaging (A) and color Doppler imaging (B). Both the tricuspid valve (TV) and the mitral valve (MV) open into the LV. The right ventricle is severely hypoplastic and not visible from this view. LA, left atrium; RA, right atrium.



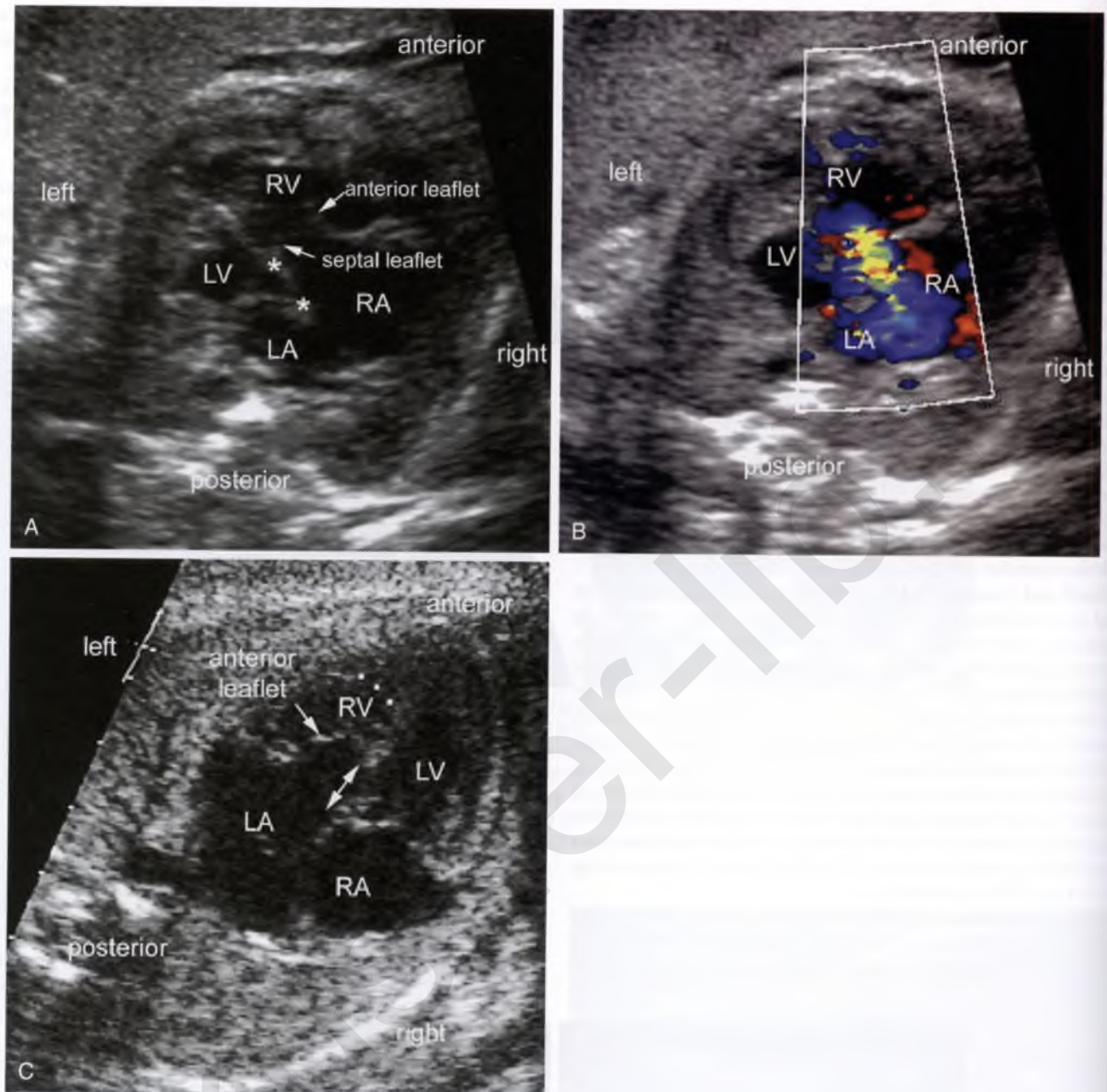


**FIG 13-27** Ebstein malformation of the tricuspid valve. **A**, Four-chamber view shows a big heart with dilatation of the right atrium (RA) and right ventricle (RV). Note the displaced attachment of the septal leaflet of the tricuspid valve (*upper asterisk*). The anterior leaflet of the mitral valve has a normal insertion to the septum (*lower asterisk*). The anterior leaflet of the tricuspid valve is large, whereas the septal leaflet is small. **B**, Color Doppler image in the same view as **A** shows moderate tricuspid regurgitation. **C**, Ebstein malformation in a patient with congenitally corrected transposition of the great arteries (atrioventricular discordance with ventriculoarterial discordance). LA, left atrium; LV, left ventricle. (From Yoo SJ, Jaeggi ET: Ultrasound evaluation of the fetal heart. In Callen PW [ed]: *Ultrasonography in Obstetrics and Gynecology*. London, Elsevier Health Sciences, 2011, pp 511-586, used with permission.)

using a standard four-chamber view. The first caliper is placed at the junction of the insertion point of the atrial surface of the tricuspid valve and ventricular septum, and the second caliper is placed at the level of insertion of the atrial surface of the mitral valve and the ventricular septum. In the second trimester, the mean MTD is  $2.8 \pm 0.9$  mm, and in the third trimester the mean MTD is  $4.6 \pm 1.1$  mm.<sup>113</sup>

#### **Ventriculoarterial Junction and Valves**

**Aortic and Pulmonary Valves.** The aortic and pulmonary valves prevent blood from backing up into the ventricular chambers during diastole. On the screening examination, normal valve leaflets appear thin and mobile throughout the cardiac cycle.

**Arterial Outflow Tracts.** The aorta normally arises from the LV and the pulmonary artery arises from the RV. Conotruncal

abnormalities involve a spectrum of anatomic defects such as DORV, TOF, transposition of the great arteries (TGA), and truncus arteriosus that are not usually evident in a four-chamber view. Identification of conotruncal anomalies remains a challenging task for those who routinely screen fetuses for CHD.

The great vessels should appear approximately equal in size and cross over each other at approximately 80 degrees from their respective ventricular chambers.<sup>114</sup> The addition of color and spectral Doppler to outflow tracts is not mandatory, but may facilitate making the diagnosis of valvar regurgitation or stenosis.

## Fetal Echocardiography

**Guidelines.** Fetuses at risk for CHD should be further examined using a detailed echocardiogram. A practice guideline consensus was recently developed on behalf of several organizations that included the AIUM, ACOG, Society for Maternal-Fetal Medicine (SMFM), American Society of Echocardiography (ASE), and American College of Radiology (ACR).<sup>74</sup> In brief, this collaborative document outlined common maternal and fetal indications for fetal echocardiography but emphasized that most referrals are not associated with known risk factors. Further details on the rationale for fetal cardiac diagnosis and treatment, including a more detailed list of indications for prenatal echocardiography, can be found in a multidisciplinary Scientific Statement from the American Heart Association<sup>115</sup> (Table 13-3).

**Timing of Fetal Echocardiogram.** The timing of the first fetal echocardiogram depends on the study indication. For most practitioners

and programs, fetal echocardiography is easily performed after 18 weeks' gestation. There are many reports, however, of fetal echocardiography performed at 13 to 18 weeks with accurate results, although this option is not offered in all programs.<sup>4,47,67</sup> When there is a structural anomaly suspected on screening ultrasound images, fetal echocardiography should be performed shortly after to provide early counseling. When fetal echocardiography is indicated because of increased risk secondary to another condition (e.g., family history, maternal diabetes mellitus), recommendations are generally for fetal echocardiography to be performed at 18 to 22 weeks.<sup>115</sup> It still should be kept in mind that some lesions progress over the course of the pregnancy, and the abnormality may be more evident later in gestation.

**Fetal Echocardiography Views.** Specific components of the fetal echocardiogram as recommended by the American Heart Association 2014 guidelines are listed in Table 13-4. Evaluation in standard planes can be useful, including those listed earlier for cardiac screening (see Fig. 13-14), along with the following additional views (see Fig. 13-15): (1) the bicaval view, (2) long-axis view of the aortic arch, (3) long-axis view of the ductal arch, (4) high short-axis view—great arteries, and (5) low short-axis view—ventricles. Details of these views are listed next. In addition to gray-scale imaging in all views, color and spectral Doppler are performed. Sweeps of the heart allow anatomic definition of the fetal heart. Measuring cardiac structures is optional, although this step should be considered for suspected structural or functional anomalies. Reference values have been published for most fetal cardiac structures, and free gestational age-based or size-based Z-score

**TABLE 13-3 Common Indications for Referral for Fetal Echocardiogram**

Indications With Higher Risk Profile (estimated >2% absolute risk)	Indications With Lower Risk Profile (estimated >1% but <2% absolute risk)	Not Indicated (≤1% risk)
Maternal pregestational diabetes mellitus	Maternal medications	Maternal gestational diabetes mellitus with HbA <sub>1c</sub> <6%
Diabetes mellitus diagnosed in the first trimester	Anticonvulsants	Maternal medications
Maternal phenylketonuria (uncontrolled)	Lithium	SSRIs (other than paroxetine)
Maternal autoantibodies (SSA/SSB*)	Vitamin A	Vitamin K agonists (Coumadin), although fetal survey is recommended
Maternal medications	SSRIs (only paroxetine)	Maternal infection other than rubella with seroconversion only
ACE inhibitors	NSAIDs in 1st/2nd trimester	Isolated CHD in other than first- or second-degree relative
Retinoic acid	CHD in second-degree relative of fetus	
NSAIDs in third trimester	Fetal abnormality of the umbilical cord or placenta	
Maternal first trimester rubella infection	Fetal intra-abdominal venous anomaly	
Maternal infection with suspicion of fetal myocarditis		
Assisted reproductive technology		
CHD in first-degree relative of fetus (maternal, paternal, or sibling with CHD)		
First- or second-degree relative with disorder with mendelian inheritance with CHD association		
Fetal cardiac abnormality suspected on obstetric ultrasound		
Fetal extracardiac abnormality suspected on obstetric ultrasound		
Fetal karyotype abnormality		
Fetal tachycardia or bradycardia, or frequent or persistent irregular heart rhythm		
Fetal increased NT >95% (≥3 mm)		
Monochorionic twinning		
Fetal hydrops or effusions		

ACE, angiotensin-converting enzyme; CHD, congenital heart disease; HbA<sub>1c</sub>, hemoglobin A<sub>1c</sub>; NSAIDs, nonsteroidal anti-inflammatory drugs; NT, nuchal translucency; SSRI, selective serotonin reuptake inhibitor.

From Donofrio MT, Moon-Grady AJ, Hornberger LK, et al: Diagnosis and treatment of fetal cardiac disease: a scientific statement from the American Heart Association. *Circulation* 129(21):2183-2242, 2014.



TABLE 13-4 Components of the Fetal Echocardiogram

Two-Dimensional Imaging	Rhythm Assessment	Color Flow Map Imaging	Pulsed Doppler Interrogation	Continuous Wave Doppler	Ventricular Function
Cardiac size (qualitative)	Heart rate	Tricuspid and mitral valves/ventricular inflows	Tricuspid and mitral inflows	<i>Valvar insufficiency (if present)</i>	Exclusion of hydrops
Cardiac axis	AV relationship/rhythm	Pulmonary and aortic inflows	Pulmonary and aortic outflows	<i>Ventricular outflows (if pulse Doppler abnormal)</i>	Exclusion of cardiomegaly
Cardiac position	<i>Mechanical PR (AV interval)†</i>	Pulmonary and aortic outflows/ventricular outflows	Ductus venosus	<i>Ductus arteriosus (if pulse Doppler abnormal)</i>	Qualitative assessment of ventricular contractility
Visceral and atrial situs	<i>Description of AV relation including arrhythmia onset/offset, duration‡</i>	Aortic/ductal arches	<i>Umbilical vein</i>		<i>Systemic venous Doppler examination*</i>
Systemic venous anatomy		Ventricular and atrial septal flow	<i>Umbilical artery</i>		<i>Pulmonary venous Doppler examination*</i>
Pulmonary venous anatomy		Superior and inferior venae cavae	<i>Aortic and ductal arches</i>		<i>Ventricular Doppler inflow examination*</i>
Qualitative atrial size		Pulmonary veins	<i>Superior/inferior venae cavae</i>		<i>Right and left ventricular cardiac output*</i>
Atrial septal morphology/localization of defect if present		Ductus venosus	<i>Branch pulmonary arteries†</i>		<i>Ventricular shortening fraction*</i>
AV connections		Proximal branch pulmonary arteries	<i>Middle cerebral artery Doppler†</i>		<i>Isovolumetric contraction and relaxation time*</i>
Tricuspid/mitral valve morphology and size		Umbilical vein			<i>Myocardial performance index*</i>
Ventricular morphology, looping, size		Umbilical artery			<i>Cardiovascular profile score*</i>
Ventricular septal morphology with description of defect if present					
Ventricular-arterial connections					
Pulmonary/aortic valve morphology and size					
Great artery relationship/size					
Aortic/ductal arch morphology					
Aortic/ductal relationship relative to the trachea					
Proximal right and left branch pulmonary arteries					
Pericardial or pleural effusions					
<i>Tricuspid/mitral annulus diameters</i>					
<i>Atrial dimensions</i>					
<i>Ventricular length and width</i>					
<i>Pulmonary and aortic valve annulus diameters</i>					
<i>Main pulmonary artery and ascending aorta diameters</i>					
<i>Ductus arteriosus diameter</i>					
<i>Aortic transverse arch diameter</i>					
<i>Cardiothoracic ratio measurement*</i>					
<i>Branch pulmonary artery diameters†</i>					

Required (class I) elements for fetal echocardiography are in plain text; elements that are reasonable to include (class IIa) are indicated in italics. Note: In specific clinical situations, italicized elements may be recommended and therefore mandatory to perform.

AV, atrioventricular.

\*Elements that can be used for assessment of a known/suspected cardiac function abnormality.

†Additional elements for which usefulness is not well established but which may be considered (class IIb).

‡Required elements (class I) for a known/suspected rhythm abnormality or if indication for examination relates to potential for rhythm abnormality.

From Donofrio MT, Moon-Grady AJ, Hornberger LK, et al: Diagnosis and treatment of fetal cardiac disease: a scientific statement from the American Heart Association. *Circulation* 129(21):2183-2242, 2014.

calculators are available<sup>116,117</sup> using published reference values.<sup>97,118-121</sup> This detailed assessment may include an advanced assessment of cardiac function such as ventricular strain and myocardial performance index (MPI) measurements.

**Plane 7: Bicaval View.** The bicaval view is obtained by sagittal imaging of the fetal chest, just to the left of midline (Fig. 13-28 and Video 13-5). This view confirms that the suprahepatic portion of the inferior vena cava is intact (may be interrupted in heterotaxy) and that a right superior vena cava is present. This view is also the best view to visualize the foramen ovale. Color Doppler should be used to assess the direction of flow across the foramen ovale, which is normally from the RA to the LA, but may be left to right in cases of HLHS.

**Plane 8: Long-Axis View of the Aortic Arch.** The long-axis view of the aortic arch, or “candy-cane” view, is obtained by sagittal imaging of the fetal thorax and angling slightly leftward (Fig. 13-29 and Video 13-6). It can also be obtained by aligning the transverse arch with the ultrasound beam in the 3VT view and turning the probe 90 degrees. The arch should be assessed for hypoplasia or coarctation, and measurements can be performed and compared with the normal range for age.<sup>122</sup> Flow should be toward the descending aorta. Reversal of flow in the arch indicates that the ductus arteriosus is supplying some of the flow to the head and upper extremities circulation and may be seen when there are hypoplastic left-sided structures or an atrial septal aneurysm obstructing mitral valve inflow.<sup>106</sup>



**FIG 13-28** Diagram (A) and sonographic image (B) in the bicaval view. The atrial septum and foramen ovale are best seen from this view as well between the left atrium (LA) and right atrium (RA). Ao, descending aorta; IVC, inferior vena cava; RPA, right pulmonary artery; RV, right ventricle; SVC, superior vena cava. (A from American Institute of Ultrasound in Medicine: AIUM practice guideline for the performance of fetal echocardiography. *J Ultrasound Med* 32:1067-1082, 2013.)

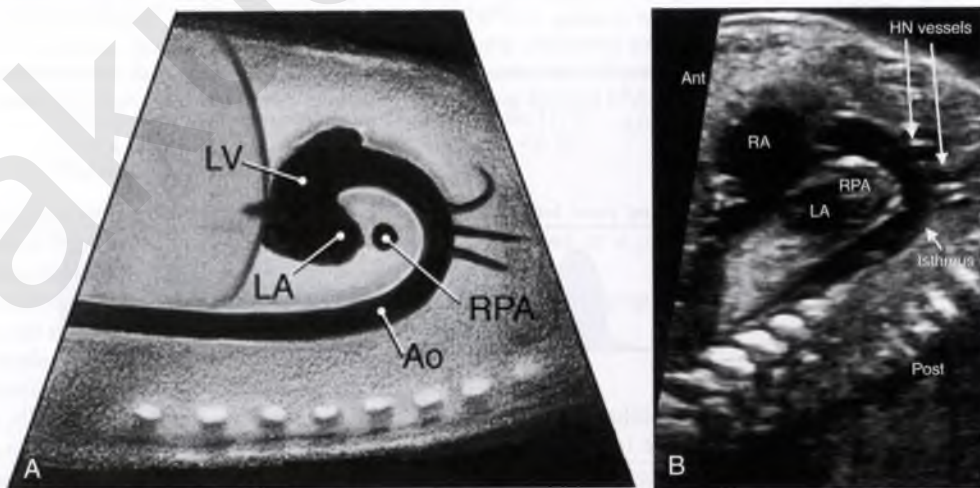


**FIG 13-29** Diagram (A) and sonographic image (B) in the long axis of the aortic arch. In addition to the arch and the head and neck (HN) vessels, the right atrium (RA), left atrium (LA), and atrial septum can often be seen in this view. Ant, anterior; Ao, aorta; LV, left ventricle; Post, posterior; RPA, right pulmonary artery. (A from American Institute of Ultrasound in Medicine: AIUM practice guideline for the performance of fetal echocardiography. *J Ultrasound Med* 32:1067-1082, 2013.)

**Plane 9: Long-Axis View of the Ductal Arch.** The long-axis view of the ductal arch, or “hockey stick” view, is usually accomplished by obtaining a direct sagittal view of the fetal thorax, just left of center (Fig. 13-30). The ductus should be assessed for restriction and direction of flow. By spectral Doppler, a restrictive ductus arteriosus typically has a peak velocity greater than 2.0 m/second and an abnormal flow pattern with continuous flow. Continuous high-velocity flow is also usually evident by color Doppler imaging. Flow reversal in the ductus arteriosus is present with severe right-sided obstructive lesions, such as severe pulmonary stenosis or pulmonary atresia.

**Plane 10: High Short-Axis View—Great Arteries.** Imaging in cross section of the heart can be very useful in assessing the outflow tracts, the ventricular septum, function, and AV valve anatomy. The first short-axis view is the high short-axis view, which demonstrates the aortic valve en face, surrounded by the pulmonary artery wrapping around the aorta (Fig. 13-31 and Video 13-7). The proximal branch pulmonary arteries can also be seen bifurcating, and the tricuspid valve is well seen in this view. The high short-axis view is best for demonstrating RVOT obstruction and for differentiating types of VSDs that involve the outlet portion of the ventricular septum. Tricuspid regurgitation can also be assessed from this view.

**Plane 11: Low Short-Axis View—Ventricles.** The low short-axis view is the best view to assess ventricular function and to evaluate for muscular VSDs (Fig. 13-32 and Video 13-8). As muscular VSDs are often very small, the use of color Doppler to show flow across the septum is usually necessary to detect or confirm these defects. The AV valve morphologic appearance can be assessed as well, including detection of a common AV valve or mitral valve cleft.

**Assessment of Cardiovascular Function.** Detailed functional assessment should be performed if cardiac function appears impaired. The assessment of cardiac function in the fetus can be complex. In an effort to standardize the assessment of cardiovascular function, Huhta and colleagues developed the Cardiovascular Profile Score (CPS), a scoring system that incorporates cardiac and extracardiac aspects of fetal cardiovascular function.<sup>123</sup> Figure 13-33 details the five categories of the CPS (hydrops, umbilical venous Doppler, heart size, abnormal myocardial function, and arterial Doppler), each worth 2 points, for a total score of 10. A lower value signifies worsened cardiovascular



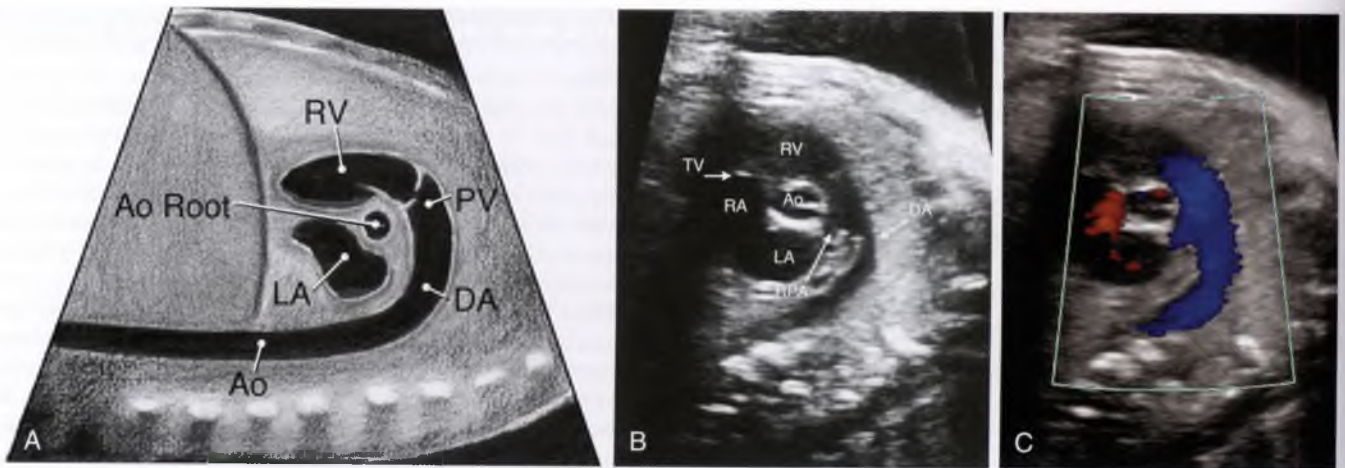


**FIG 13-30** Diagram (A) and sonographic images (B and C) in the long axis of the ductal arch by two-dimensional and color Doppler imaging. Ao, aorta; Ao Root, aortic root; DA, ductal arch; LA, left atrium; PV, pulmonary valve; RA, right atrium; RPA, right pulmonary artery; RV, right ventricle; TV, tricuspid valve. (A from American Institute of Ultrasound in Medicine: AIUM practice guideline for the performance of fetal echocardiography. *J Ultrasound Med* 32:1067-1082, 2013.)

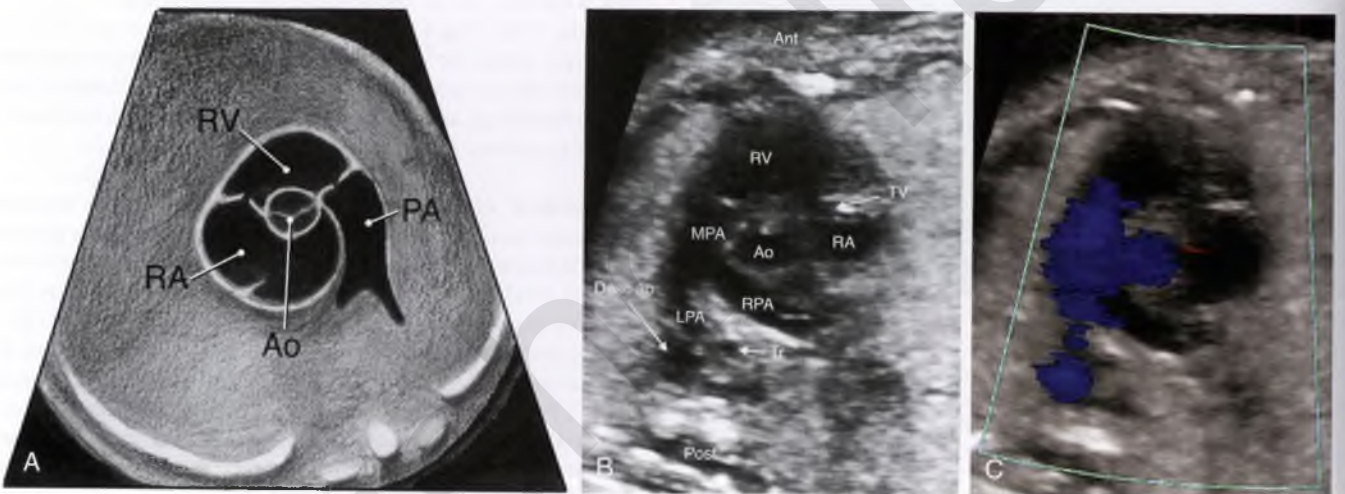


**FIG 13-31** Diagram (A) and sonographic images (B and C) in the high short-axis view of the great arteries by two-dimensional and color Doppler imaging. Ant, anterior; Ao, aortic root; Desc aorta, descending aorta; LPA, left pulmonary artery; MPA, main pulmonary artery; PA, main pulmonary artery; Post, posterior; RA, right atrium; RPA, right pulmonary artery; RV, right ventricle; Tr, trachea; TV, tricuspid valve. (A from American Institute of Ultrasound in Medicine: AIUM practice guideline for the performance of fetal echocardiography. *J Ultrasound Med* 32:1067-1082, 2013.)

function, although a discrete cutoff point for predicting poor fetal outcome has varied between studies, from lower than 6 to lower than 10.<sup>124-132</sup>

Cardiac output (CO) can be estimated by echocardiography using the following formula:

$$CO = VTI \times \pi \times (D/4) \times HR$$

where VTI = velocity time integral of flow across that semilunar valve, D = diameter of the semilunar valve, and HR = heart rate. In the fetus, because of the parallel circulation physiology, aortic cardiac output can be added to pulmonary cardiac output to arrive at an estimated combined cardiac output (CCO).<sup>133,134</sup> Fetal estimates of CCO have correlated with cardiovascular profile score in high cardiac output lesions such as sacrococcygeal teratoma<sup>126</sup> and with worse outcomes in twin-twin transfusion syndrome.<sup>135</sup>

The MPI, or Tei index, is a commonly used and extensively studied measure of fetal cardiac function. The MPI is obtained by measuring the AV valve closure to opening time (systole) and the semilunar valve ejection time. The ejection time is then subtracted from the AV valve closure to opening time in order to arrive at the sum of isovolumetric contraction and isovolumetric relaxation times. This sum is then divided by the ejection time (Fig. 13-34). Normal values of the MPI change slightly throughout gestation. Generally, values less than 0.43 to 0.45 are considered to be normal.<sup>136</sup> Elevations of MPI values reflect alternations in both systolic and diastolic function.

Myocardial deformation imaging is a relatively new technique, which has begun to be applied to fetal echocardiography. Deformation refers to the degree to which myocardial tissue fibers shorten over the cardiac cycle. Discrete layers of ventricular muscle fibers oriented in longitudinal, circumferential, and radial dimensions play specific roles

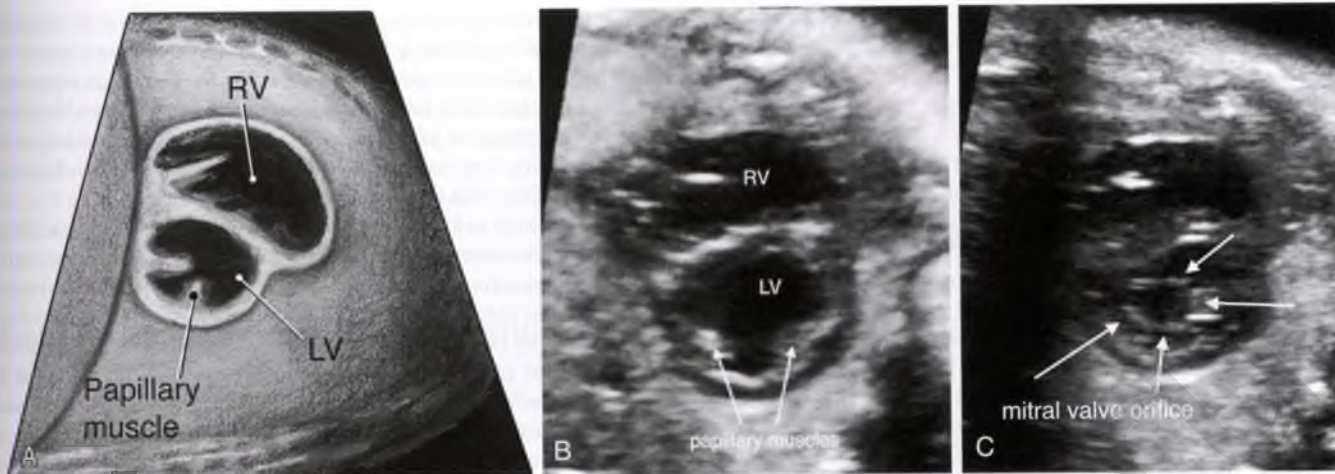


**FIG 13-32** Diagram (A) and sonographic images (B and C) in the low short-axis view of the ventricles. At the midventricular level two papillary muscles are seen in the left ventricle. Just basal to this (closer to the atria), the mitral valve can be visualized en face to ensure there is not a cleft and that there is not a common atrioventricular valve. LV, left ventricle; RV, right ventricle. (A from American Institute of Ultrasound in Medicine: AIUM practice guideline for the performance of fetal echocardiography. *J Ultrasound Med* 32:1067-1082, 2013.)

	Normal	-1 point	-2 points
Hydrops	None	Ascites or pleural effusion or pericardial effusion	Skin edema
Venous Doppler (umbilical vein) (ductus venosus)			
UV			
DV			
Heart size (Heart area/chest area)	>0.20 and ≤0.35	0.35–0.50	>0.50 or <0.20
Cardiac function	Normal TV and MV RV/LV SF >0.28 Biphasic diastolic filling	Holosystolic TR or RV/LV SF <0.28	Holosystolic MR or TR dP/dt <400 or monophasic filling
Arterial Doppler (umbilical artery)	UA 	UA (AEDV) 	UA (REDV) 

**FIG 13-33** Components of the Cardiovascular Profile Score. The score is 10 if there are no abnormal signs and reflects 2 points for each of 5 categories: hydrops, venous Doppler, heart size, cardiac function, and arterial Doppler. AEDV, absent end-diastolic velocity; dP/dt, change in pressure over time of TR jet; DV, ductus venosus; LV, left ventricle; MR, mitral valve regurgitation; MV, mitral valve; REDV, reversed end-diastolic velocity; RV, right ventricle; SF, ventricular shortening fraction; TR, tricuspid valve regurgitation; TV, tricuspid valve; UA, umbilical artery; UV, umbilical vein. (From Falkensammer CB, Paul J, Huhta JC: Fetal congestive heart failure: correlation of Tei-index and Cardiovascular-score. *J Perinat Med* 29:390-398, 2001, used with permission.)



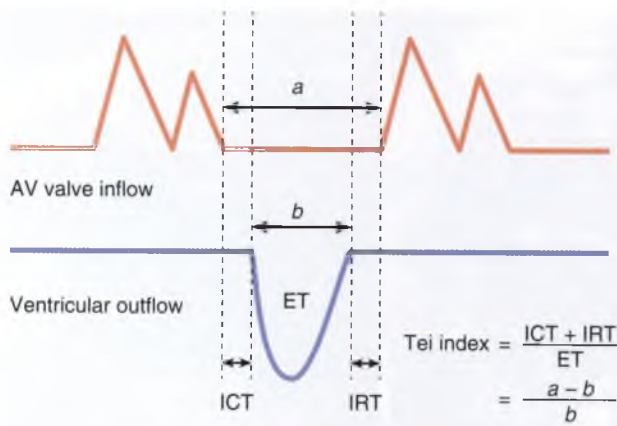


**FIG 13-34** Calculation of the myocardial performance index (MPI, or Tei index). AV, atrioventricular; ET, ejection time; ICT, isovolumetric contraction time; IRT, isovolumetric relaxation time. (From Sugiura T, Suzuki S, Hussein MH, et al: Usefulness of a new Doppler index for assessing both ventricular functions and pulmonary circulation in newborn piglet with hypoxic pulmonary hypertension. *Pediatr Res* 53:927-932, 2003, used with permission.)

in the cardiac cycle. The most commonly reported measures of deformation are strain and strain rate. Strain ( $\epsilon$ ) represents the fractional change in length ( $L$ ) of a myocardial segment caused by an applied force.<sup>137</sup>

$$\epsilon = \frac{L - L_0}{L_0} = \frac{\Delta L}{L_0}$$

Strain rate represents the rate of myocardial deformation (strain per unit time). Speckle tracking echocardiography is an imaging technique that involves tracking the motion of natural acoustic markers throughout the cardiac cycle in order to calculate strain and strain rate.<sup>138,139</sup> Deviations of the angle of interrogation are overcome by this method, which makes it very attractive for fetal cardiac imaging. Furthermore, standard measures of systolic dysfunction are ominous, late findings in fetal cardiovascular disease, thus making a more sensitive measure of diminished contractility appealing. However, the small fetal heart mass and fast heart rate pose significant challenges to applying existing myocardial deformation technology. In order to reduce undersampling throughout the cardiac cycle, optimal temporal resolution (high frame rate) and optimal spatial resolution are required.<sup>140,141</sup> Despite these concerns, multiple studies have reported successfully tracking the fetal heart and have reported normal strain and strain rate values at various gestational ages.<sup>142-148</sup>

Within the past few years, there have been studies of differences in myocardial deformation values between normal fetuses and those with CHD,<sup>149-153</sup> those exposed to maternal diabetes,<sup>154,155</sup> those with growth restriction,<sup>156</sup> and those with twin-twin transfusion syndrome.<sup>157</sup> Although concerns for reproducibility and uncertainty about the actual added clinical benefit of myocardial deformation imaging currently limit its clinical use, it is a promising technique for the assessment of fetal cardiac function.

### 3D AND 4D FETAL CARDIAC EVALUATION

3D sonography can be used evaluate the anatomy of the heart, but does not incorporate time. 4D technology has been developed that allows 3D evaluation of the fetal heart plus the aspect of time as the fourth dimension. Spatiotemporal image correlation (STIC) is a feature of 4D sonography that allows the acquisition of volume datasets akin to

blocks of pathologic specimens, in which all the anatomic information is contained in the block and the information displayed depends on the level at which the block is cut. STIC has the additional advantages that these planes can be assessed in a virtual beating heart, that fetal electrocardiographic triggering is not needed, and that rendering techniques can be used to gain additional insight into the structure and function of the fetal heart.<sup>40,50,158,159</sup>

With the use of STIC, volume datasets from fetal heart are acquired with a single automated sweep of the transducer, and spatial and temporal information is combined to display images that can be extracted from volume datasets. Thus, standardized planes for fetal echocardiography can be obtained from the volume datasets at the time of the sonographic examination or afterward; moreover, novel planes to examine the fetal heart can also be obtained including coronal views. In addition to this anatomic information, functional information of the fetal heart can be obtained including the direction of blood flow if the volume dataset was obtained with color Doppler or high definition (HD) power Doppler.

Several studies suggest that 4D sonography facilitates examination of the fetal heart.<sup>158-169</sup> Thus, 4D fetal echocardiography has the potential to reduce the operator dependency of 2D sonography. Prenatal diagnosis of CHDs is challenging because of the complexity of the fetal heart and the expertise required in performing fetal echocardiography. In addition, fetal and maternal motion, maternal body mass index, gestational age, adequacy of the amniotic fluid volume, and fetal position are important factors that can affect image quality. This section of the chapter reviews some technical aspects of 4D sonography including volume acquisition and rendering, displays modalities in 4D sonography, and summarizes the evidence evaluating the accuracy and reproducibility of 4D sonography in the prenatal diagnosis of CHDs.

#### Acquisition of Volume Datasets With 4D Sonography and STIC

**Volume Acquisition With Mechanical Transducers.** Volume acquisition is performed with an automated sweep of the transducer, acquiring sequential frames at a rapid rate. Acquisition time ranges from 5 to 15 seconds; the longer the acquisition time, the better the spatial resolution. During acquisition, on the basis of changes in the cardiac motion, the STIC algorithm detects the FHR and synchronizes 2D images. Frames acquired during the same phase in the cardiac cycle are merged into one volume dataset representing approximately 40 volumes. After analysis and rearrangement the dynamic images are displayed on the screen in three planes that are orthogonal to each other.<sup>158</sup>

The image quality contained in a STIC cardiac volume dataset can be improved by optimizing the settings before acquisition by adjusting the 2D gray-scale and color Doppler parameters. Our preference is to use low persistence, high contrast, and high frame rate settings. Typical acquisition time ranges from 5 to 15 seconds. Shorter acquisition times can be used to minimize motion artifacts but this reduces the image spatial resolution.

**Volume Acquisition With Matrix Array Technology.** Matrix array transducers utilize several thousand elements and have eliminated the need for internal moving parts. Each element fires an ultrasound beam that is used to create a pyramidal group of ultrasound voxels, with an opening angle between 6 and 100 degrees. This allows real-time 4D imaging that does not require mechanical translation of the ultrasound transducer. Additionally, the large aperture in the elevation plane provides for superior resolution. Volume dataset acquisition with mechanical transducers relies on approximately 40 volume datasets to reconstruct a virtual volume. In contrast, the 4D volume dataset

obtained with matrix transducers divides the volume into four sub-volumes. Acquisition of a spatially and temporally correlated volume takes approximately 25% of the time that is required using a mechanical transducer. Typically, STIC acquisitions take about 5 to 15 seconds, during which time the fetus may move and affect the quality of volume acquired. With matrix array technology, the volume acquisition takes about 3 seconds with less motion artifact in addition to increased spatial and temporal resolution. Hence, the real-time data acquisition is less prone to artifact from fetal movement and maternal respiratory motion.

### Display Modalities in 4D Sonography and STIC

2D sonography relies on standard anatomic views of the fetal heart, as described previously.<sup>71,170-172</sup> Acquisition of these views can be facilitated using different display modalities of 4D sonography.<sup>168,173-183</sup>

**Dynamic Multiplanar Display.** This modality in 3D and 4D sonography allows for the simultaneous display of three anatomic planes that are orthogonal to each other: the transverse, sagittal, and coronal planes. Moreover, an imaging tool referred to as the reference dot allows for the identification of anatomic structures in these three orthogonal planes (Fig. 13-35). This display modality can also be used to scroll through the volume dataset to visualize the transverse view of the upper abdomen, four-chamber view, five-chamber view, and the 3VV. For example, in cardiac rhabdomyomas, the transverse plane allows visualization of the cardiac tumor in the four-chamber-view, whereas the sagittal and coronal planes reveal additional smaller tumors that are not seen in the axial plane (Fig. 13-36). One approach is to display the standard transverse view used in fetal cardiac evaluation in panel A, to place the dot in the abnormal vascular structure, and to identify the structure in the sagittal and coronal planes in panels B and C (Fig. 13-37).

Novel algorithms using the multiplanar display have been proposed for simultaneous display of both outflow tracts,<sup>158</sup> to visualize the aortic and ductal arches,<sup>184</sup> and to determine the nature of vascular connections to the fetal heart using the spin technique.<sup>185</sup> The latter technique involves positioning the reference dot in the center of the structure and “spinning” the volume dataset around the y-axis to determine its spatial relationship with the heart and other vascular structures.

The sagittal view of the ductal arch can be easily obtained using 4D volume datasets of the fetal heart acquired with STIC (Fig. 13-38).<sup>186</sup> A retrospective study using this approach<sup>186</sup> reported that the visualization rate of the sagittal view of the ductal arch was significantly lower in fetuses with conotruncal anomalies than among normal fetuses and those with other CHDs. The authors concluded that the inability to visualize the ductal arch using the proposed algorithm should raise the possibility of conotruncal anomalies.

**Automated Display of Multiple Slices.** This modality allows for the simultaneous display of up to eight parallel planes whose distance can be adjusted for better visualization of anatomic planes. Tomographic ultrasound imaging (TUI) (GE Healthcare, Milwaukee, WI) allows the visualization of multiple sections of a beating heart at the same time.<sup>187-190</sup> An overview image, which is shown on the upper left corner, shows a plane orthogonal to the slices, and parallel lines demarcate the position of the slices within the volume dataset (Fig. 13-39). However, the simple use of planes parallel to the four-chamber view of the heart does not allow for the visualization of the long-axis view of the left outflow tract and the short-axis view of the aorta, which are considered part of an integral examination of the fetal heart.<sup>71,171,172,191</sup>

An algorithm using TUI with STIC was developed that allows for the simultaneous visualization of the standard planes for fetal cardiac screening including the four-chamber view, 3VV, long-axis view of the

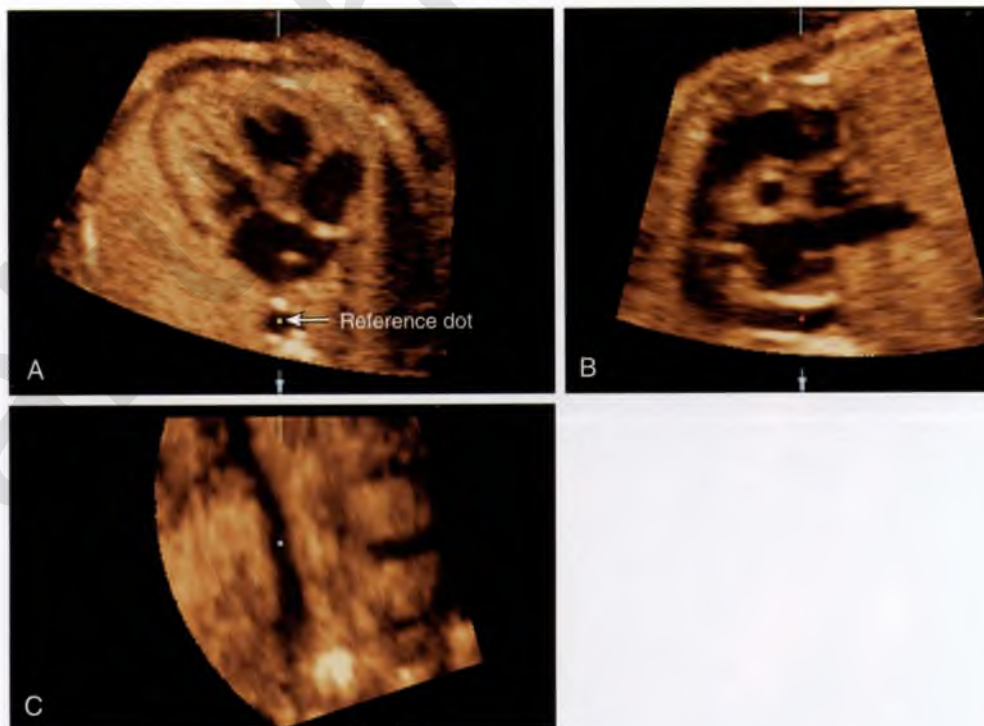


**FIG 13-35** Multiplanar display in three- and four-dimensional sonography allows for the simultaneous display of three anatomic planes that are orthogonal to each other: the transverse (A), sagittal (B), and coronal (C) planes. An imaging tool referred to as the reference dot allows for the identification of anatomic structures in these three orthogonal planes.



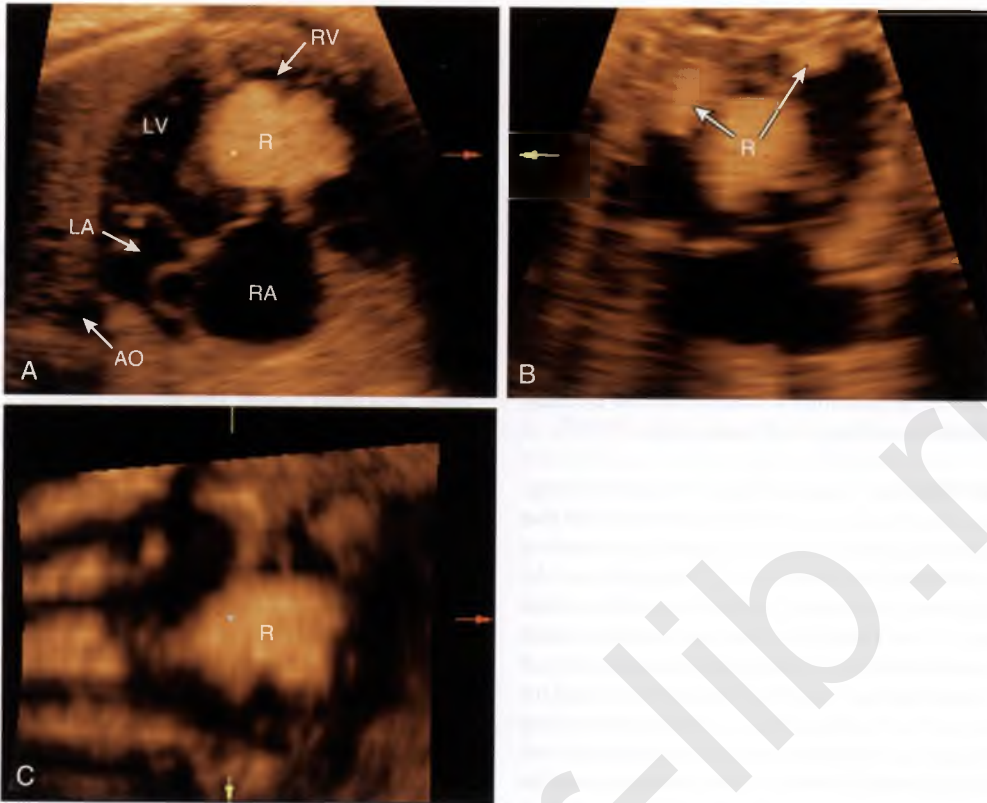


**FIG 13-36** Multiplanar display of a fetus with cardiac rhabdomyomas allowing the simultaneous visualization of a large cardiac tumor in the four-chamber view (**A**) filling most of the right ventricle (RV), whereas the sagittal (**B**) and coronal (**C**) planes reveal additional smaller tumors that are not seen in the axial plane. AO, aorta; LA, left atrium; LV, left ventricle; R, rhabdomyoma; RA, right atrium.

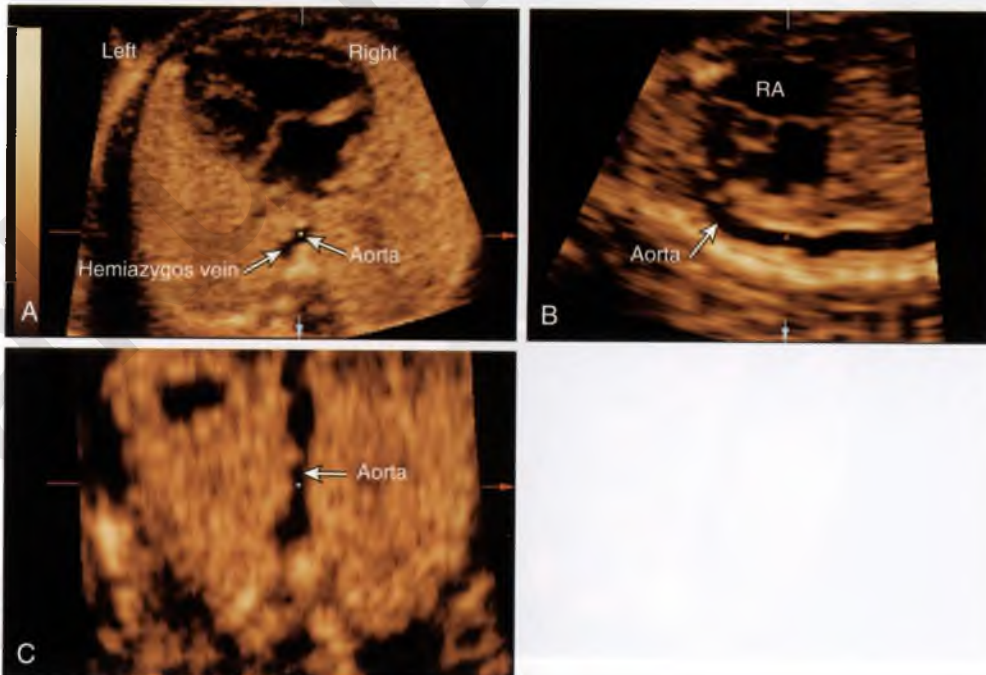


**FIG 13-37** Multiplanar display of a dilated hemiazygos vein in a fetus with interrupted inferior vena cava. The reference dot was placed on the aorta in the four-chamber view (**A**). The corresponding orthogonal images are displayed in the sagittal (**B**) and coronal (**C**) views. RA, right atrium.

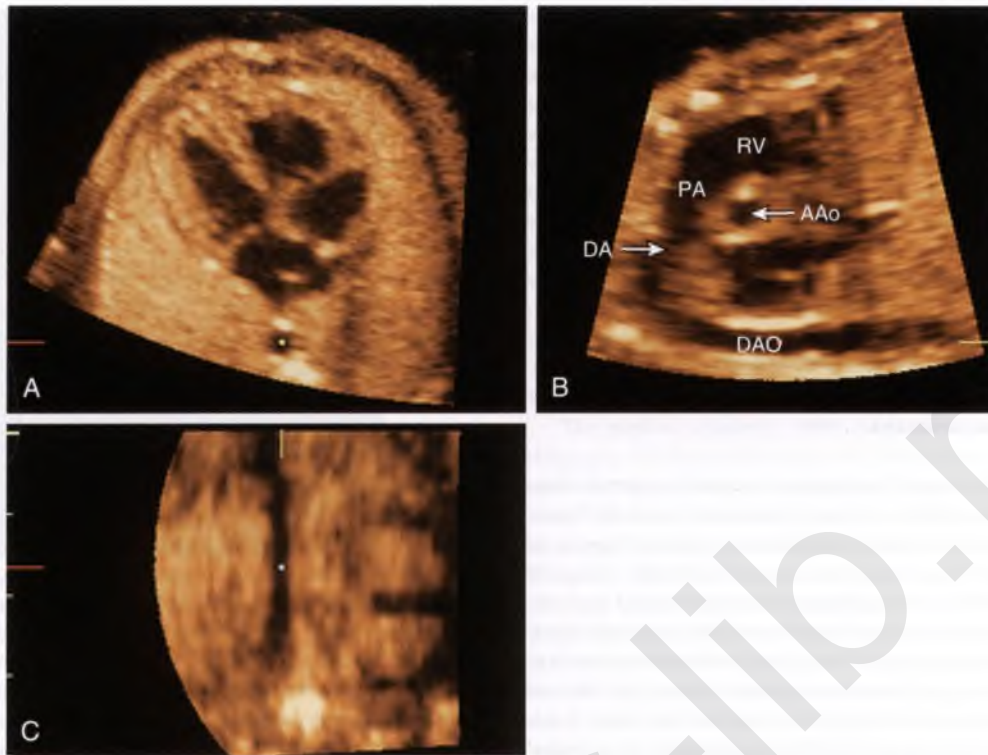


**FIG 13-38** Multiplanar display of a normal fetal heart in the second trimester of pregnancy. **A**, The four-chamber view. **B**, The components of the sagittal view of the ductal arch including the right ventricular (RV) outlet, main pulmonary artery (PA), ductus arteriosus (DA), descending aorta (DAO), and a cross section of the ascending aorta (AAo). **C**, The coronal view of the DAO.

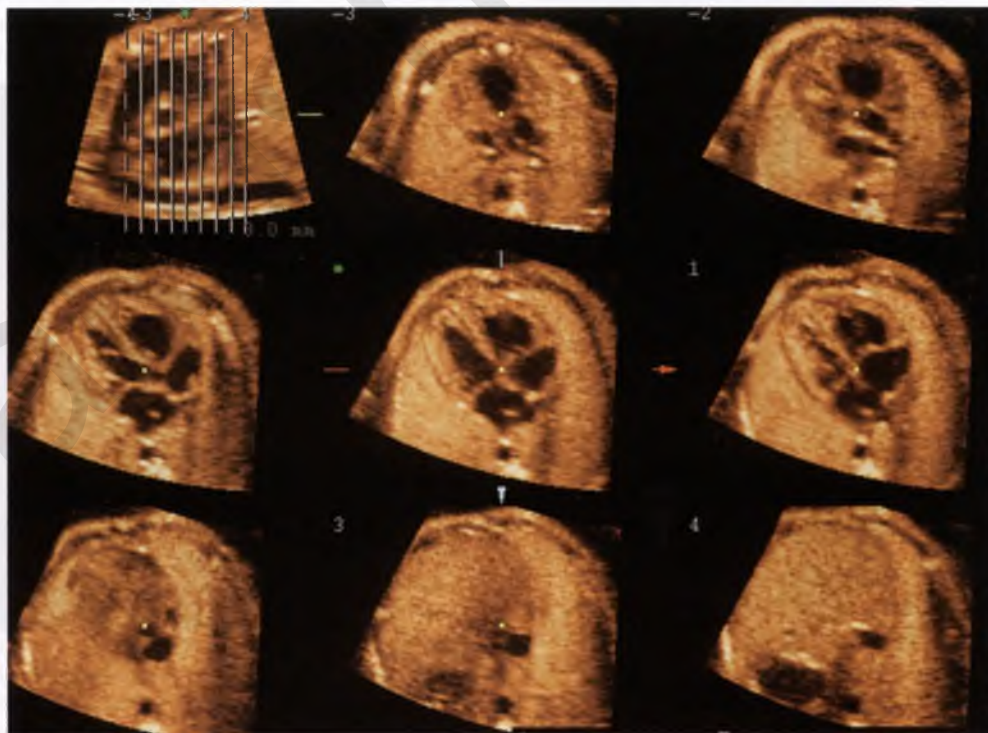


**FIG 13-39** Tomographic ultrasound imaging: an overview image is shown in the upper left corner; the parallel lines in the overview image demarcate the position of the slices within the volume dataset.



left outflow tract, and short-axis view (right outflow tract) in most fetuses without CHDs.<sup>192</sup> With the use of this algorithm a normal four-chamber view, five-chamber view, longitudinal view of the ductal arch, 3VT view, view of the left outflow tract, and short-axis view were visualized in 99%, 96.9%, 98.5%, 88.2%, 93.3%, and 87.2% of the volume datasets, respectively. Similar results were recently reported by Rizzo and associates<sup>193</sup> using STIC and a simplified method referred to as the “three-step technique.” Other algorithms designed to evaluate the fetal heart using multiplanar display includes the Four-chamber view And Swing Technique (FAST) echo<sup>194</sup> and Fetal Intelligent Navigation Echocardiography (FINE)<sup>195</sup> techniques.

### Rendering Techniques in 4D Sonography and STIC

Several rendering algorithms have been described for visualization of the fetal cardiovascular structures.

**Inversion Mode.** This mode transforms echolucent structures into solid structures. Thus, anechoic structures such as the heart chambers, lumen of the great vessels, stomach, and bladder appear echogenic on the rendered image, whereas structures that are normally echogenic become anechoic. Postprocessing adjustments are performed as necessary, including adjustments of the gamma curve, threshold, and transparency to improve image quality. The technique allows examiners to obtain 4D rendered images of cardiovascular structures from volume datasets acquired with gray-scale only. For example, the value of this display modality can be observed in the visualization of a dilated azygous vein in a case of interrupted IVC in heterotaxy complex (Fig. 13-40).

**Transparency Modes.** The minimum projection mode (MPM) is another volume-rendering tool that allows preferential display of minimum gray-scale values within a volume dataset. This algorithm can be useful for displaying vascular structures and fluid-filled organs.<sup>196,197</sup> The MPM can provide important insight into the spatial relationships of abnormal vascular connections to the fetal heart in the upper mediastinum and could potentially be useful in the determination of atrial morphologic features in cases of left and right isomerism.<sup>168</sup>

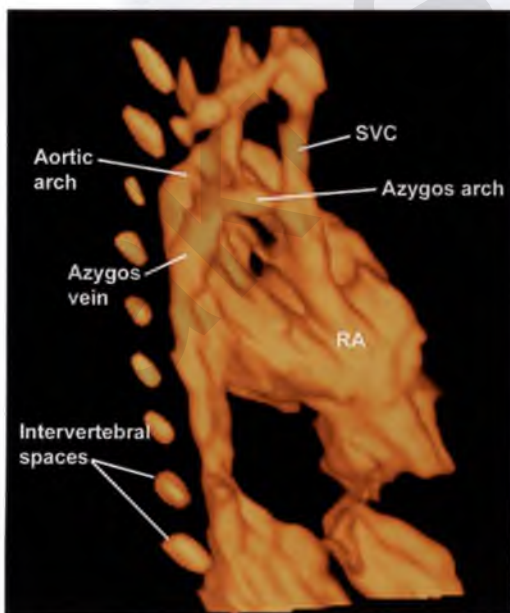


**FIG 13-40** Three-dimensional reconstruction of a fetal heart rendered with the inversion mode in a case of interrupted inferior vena cava with azygous vein continuation. RA, right atrium; SVC, superior vena cava.

**B-Flow Rendering.** This 4D display modality enhances signals from weak blood reflectors from vessels and, at the same time, suppresses strong signals from surrounding tissues.<sup>198-200</sup> Because this technology does not rely on Doppler methods to display blood flow, it is angle-independent and does not interfere with the frame rate. This modality is potentially advantageous over color or power Doppler imaging when used in conjunction with STIC for the evaluation of the fetal vasculature. In B-flow imaging, the echoes from the tissue and the blood flow can be displayed with high resolution and without the overlay that characterizes color Doppler imaging. Moreover, B-flow may have less signal dropout when the ultrasound beam is perpendicular to the vessel. B-flow imaging can provide important insight into abnormal vascular connections to the fetal heart including TAPVC<sup>201</sup> (Fig. 13-41) and tortuous aorta in cases of coarctation<sup>202</sup> (Fig. 13-42).

### Accuracy and Reproducibility of 4D Sonography in the Prenatal Diagnosis of Congenital Heart Disease

The accuracy and reproducibility of 4D sonography with STIC in the diagnosis of CHDs were recently evaluated in two multicenter studies in the second trimester of pregnancy.<sup>203,204</sup> One cross-sectional study included seven international centers with expertise in 4D sonography where fetuses with and without confirmed heart defects were scanned between 18 to 26 weeks' gestation and their volume datasets were uploaded onto a centralized FTP (file transfer protocol) server.<sup>204</sup> The authors reported that the median (range) sensitivity, specificity, and positive and negative predictive values as well as false positive and false negative results for the identification of fetuses with CHDs were as follows: 93% (77%-100%), 96% (84%-100%), 96% (83%-100%), 93% (79%-100%), 4.8% (2.7%-25%), and 6.8% (5%-22%), respectively. Moreover, there was excellent intercenter agreement (kappa statistic = 0.97) in the identification of CHDs. The authors concluded that 4D volume datasets can be remotely acquired and accurately interpreted by different centers and that among centers with technical expertise 4D sonography is an accurate and reliable method for fetal echocardiography. However, 10% of volume datasets have limited clinical value because the image quality was not adequate, the volume dataset

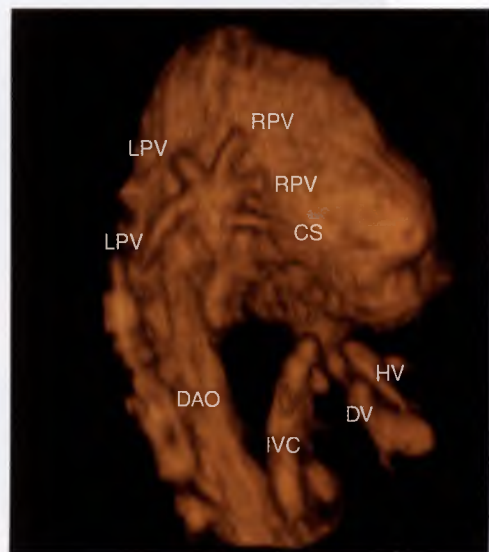


**FIG 13-41** B-flow imaging of a fetus with total anomalous pulmonary venous return. The confluence of pulmonary vein, behind the right atrium and above the coronary sinus, resembles a starfish; CS, coronary sinus; DAO, descending aorta; DV, ductus venosus; HV, hepatic vein; IVC, inferior vena cava; LPV, left pulmonary vein; RPV, right pulmonary vein.



**FIG 13-42** B-flow imaging of a narrow and tortuous aortic arch (Ao Arch) and its relationship with the heart and other vascular structures: DAo, descending aorta; IVC, inferior vena cava; UV, umbilical vein.

did not include sufficient anatomic information, or image artifacts limited the visualization of the anatomic structures. Of note, the median time required to upload or download each volume dataset into the centralized FTP server was 2 minutes (range: 1-3 minutes), and the median time required to analyze each volume dataset was 6 minutes (range: 2-15 minutes). Similarly, in another study involving 167 normal fetuses and 175 fetuses with CHDs the authors reported that the sensitivity, specificity, and positive and negative predictive values of 4D sonography with STIC in the identification of CHDs were 91.6%, 94.9%, 88.1%, 89.7%, and 94.0%, respectively. Two different sonographers with expertise in 4D sonography read the volume datasets in a blinded fashion and agreed in the final diagnosis in 74% of the cases.<sup>203</sup> However, in a different report the same authors reported good or excellent intraobserver and interobserver agreement in the identification of fetal cardiac structures using 4D sonography and STIC in all trimesters of pregnancy.<sup>205</sup>

One study evaluated if 3D and 4D sonography can improve the ability of 2D sonography in the identification of CHDs. The authors compared 2D cine loops and 4D volume datasets from 181 fetuses with CHDs. The authors reported that with different 4D rendering modalities 12 CHDs were identified by 3D/4D sonography but not by 2D cine loops. These cases included one case of right aortic arch with anomalous branching, one case of TGA with pulmonary atresia, one case of segmental interrupted aortic arch, one case of RV aneurysm, two cases of total anomalous pulmonary venous connections (TAPVCs), and four cases of VSDs.<sup>206</sup>

### First and Early Second Trimester 4D Fetal Echocardiography

A 2014 study evaluated the role of 4D sonography in the identification of CHDs between 11 and 15 weeks of gestation.<sup>207</sup> The study included 48 volume datasets from fetuses with normal ( $n = 17$ ) and abnormal ( $n = 16$ ) hearts. Overall, the median (range) accuracy, sensitivity, and specificity, as well as the positive and negative likelihood ratios, for the identification of fetuses with CHDs were 79% (77-83%), 90% (70-96%), 59% (58-93%), 2.35% (2.05-9.8%), and 0.18% (0.08-0.32%), respectively. Of note, there was only a moderate intercenter agreement ( $\kappa = 0.6$ ); and between 15% and 23% of volume datasets were considered to have limited clinical value because the image quality was

not adequate, the volume dataset did not include sufficient anatomic information, or image artifacts limited the visualization of the anatomic structures. Moreover, participating centers with lower diagnostic indices reviewed a higher proportion of suboptimal volume datasets than those with higher diagnostic indices. The authors concluded that 4D sonography can be performed in the first trimester and early second trimester of pregnancy and that 4D volume datasets obtained from fetuses between 11 and 15 weeks can be remotely acquired and accurately interpreted by different centers. These results are in keeping with a 2008 report indicating that standardized planes for fetal echocardiography can be obtained from 4D volume datasets obtained in the first trimester of pregnancy in a reproducible manner<sup>50</sup> and with a 2009 report indicating that 4D fetal echocardiography in the first trimester can identify CHDs with 95.3% accuracy.<sup>208</sup>

The median sensitivity (90%) of 4D first trimester fetal echocardiography for the identification of CHDs reported in the multicenter study is comparable with the results of a study done at a single institution.<sup>208</sup> However, the median specificity (59%) is lower than previously reported. This may be a reflection of moderate intercenter agreement. The observation that in almost one fifth of the cases 4D volume datasets had limited clinical value appears to be a reflection of the challenges of 4D first trimester fetal echocardiography due to frequent fetal motion, the size of the cardiac structures, and the frequent need to rely on color Doppler imaging to evaluate these structures. However, in many instances the anatomic information contained in these volume datasets was sufficient to differentiate normal from abnormal cases and to diagnose the specific CHD.

The evidence reviewed in this section indicates that 4D fetal echocardiography with STIC can facilitate the examination of the fetal heart with the use of multiple display and rendering modalities. Moreover, 4D sonography appears to be an accurate and reproducible technique for the identification of CHDs in the second trimester of pregnancy. The initial reports on the value of 4D sonography in the first trimester and early second trimester of pregnancy are promising. However, larger studies are required to confirm these results. Another important area for research is the evaluation of 4D sonography in the screening of CHDs as well as the use of automated or semiautomated algorithms using 4D sonography and STIC in the screening and diagnosis of CHDs. The practical application of STIC for fetal cardiac screening, versus a role better suited to a specialized echocardiographic procedure, requires further investigation in the context of emerging technologies.

## FETAL CARDIOVASCULAR DISEASE

### Overview

**Epidemiology.** Fetal cardiovascular disease most commonly consists of structural heart disease, fetal arrhythmias, or secondary heart disease, but also includes fetal myocarditis and cardiomyopathy, pericardial effusions, and cardiac tumors. The prevalence of fetal cardiovascular disease is unknown and difficult to ascertain. Given that some fetuses with CHD do not survive to term, it is suspected that the prevalence of CHD in the fetus is significantly higher than the liveborn estimate of 6 to 10/1000, although this topic has not been extensively studied.<sup>209,210</sup>

**Etiology.** The cause of CHD is unknown in most cases, but is clearly multifactorial. Maternal exposures that have been associated with CHD include environmental (dioxins, polychlorinated biphenyls, pesticides),<sup>211,212</sup> ingested (alcohol, isotretinoin, thalidomide),<sup>213</sup> and infectious (rubella).<sup>214</sup> Maternal fever alone, regardless of the cause, has also been implicated in CHD,<sup>215,216</sup> as has the increasingly prevalent health conditions of obesity and diabetes.<sup>217-219</sup>



There are genetic influences on development of CHD, both inherited and sporadic. A large number of syndromic disorders are associated with CHD, and genetic disorders have also been shown to be associated with isolated CHD (Table 13-5).<sup>212</sup> Genetic disease with CHD may be due to aneuploidies, such as Down syndrome or Turner

syndrome; may result from chromosomal deletions, such as chromosome 22q11.2 deletion; or may be secondary to a single DNA base mutation that causes abnormal protein transcription, such as Alagille syndrome due to a *JAG1* mutation. Given the frequent associations between CHD and genetic disorders, many advocate that genetic evaluation should be performed in any fetus or child with CHD.

Of note, however, at this time only a minority of CHDs can be attributed to a recognized genetic condition. The majority of infants born with CHD are born to parents with no identifiable risk factors. Therefore, despite discovered risk factors, the most important tool for detection of prenatal CHD is a high-quality second trimester ultrasound examination.

**TABLE 13-5 Commonly Diagnosed Genetic Disorders in the Fetus and Cardiovascular Associations**

Condition	Cardiovascular Findings
Turner syndrome (monosomy X)	Left-sided disease: hypoplastic left heart syndrome, bicuspid aortic valves, coarctation of the aorta Systemic venous anomalies: absence of the ductus venosus, left superior vena cava Pulmonary venous anomalies: partial anomalous pulmonary venous return
Down syndrome (trisomy 21)	Atrioventricular canal defect Atrioventricular canal defect with tetralogy of Fallot Isolated ventricular septal defect
22q11.2 deletion	Tetralogy of Fallot Truncus arteriosus Double-outlet right ventricle Pulmonary atresia with ventricular septal defect Right aortic arch Aberrant right or left subclavian artery Double aortic arch
Edwards syndrome (trisomy 18)	Atrial septal defect Ventricular septal defect Polyvalvar disease
Patau syndrome (trisomy 13)	Atrial septal defect Ventricular septal defect Polyvalvar disease
Williams syndrome ( <i>ELN</i> mutation)	Supravalvar aortic stenosis, branch pulmonary artery stenosis, mitral valve and aortic valve disorders
Alagille syndrome ( <i>JAG1</i> mutation)	Tetralogy of Fallot Branch pulmonary artery stenosis
CHARGE syndrome	Atrial septal defect Ventricular septal defect Tetralogy of Fallot

CHARGE, coloboma, heart defects, choanal atresia, retarded growth and development, genital abnormalities, and ear anomalies.

From Fahed AC, Gelb BD, Seidman JG, Seidman CE: Genetics of congenital heart disease: the glass half empty. *Circ Res* 112(4): 707-720, 2013.

**Neurodevelopmental Outcomes.** Over the last 30 years, there have been significant advances in understanding neurodevelopment sequelae in children with CHD. Although the vast majority of nonsyndromic children with CHD do not have severe neurodevelopmental impairments, children who have undergone cardiac surgery are more likely to have neurodevelopmental abnormalities than children without cardiac disease.<sup>220</sup> A 23% incidence of structural brain abnormalities has been identified by fetal MRI in children with complex forms of CHD as compared to normal control subjects (<2%).<sup>221</sup> Owen and colleagues<sup>222</sup> have also reported impaired brain volume growth before cardiac surgery in infants with CHD. Given that prenatal diagnosis has been shown to improve the preoperative status of newborns with critical CHD, prenatal coordinated multidisciplinary care and possibly early interventions may result in improved neurodevelopmental outcomes.<sup>223</sup>

### Congenital Heart Lesions

This section highlights the anatomy and imaging pearls of the most common CHDs. Detection of these lesions can most easily be accomplished by use of sweeps through the heart that are centered on the key views listed earlier.

#### Ventricular Septal Defect

**Definition.** A VSD is a communication between the RVs and LVs. There are several types of VSDs and multiple names for the same lesion, depending on nomenclature used (Table 13-6).<sup>224-226</sup> The Congenital Heart Surgery Nomenclature and Database Project addressed this topic, simply classifying VSD types as types 1 through 4.<sup>227</sup> For the purposes of this chapter, the Van Praagh classification will be used.

**Epidemiology.** When excluding the residual fetal structures PFO and PDA, VSDs represent the most common type of CHD. The birth prevalence of VSD has been increasing over the last several decades,

**TABLE 13-6 Ventricular Septal Defect Nomenclature**

Congenital Heart Surgery Nomenclature and Database Project	Van Praagh	Anderson	Other
Type I	Conalseptal	Doubly committed juxtarterial or Muscular—outlet or infundibular	Supracristal Infundibular Juxtarterial Conal Right ventricular outlet Subarterial
Type II	Conoventricular—membranous type or Conoventricular—malalignment type	Perimembranous—outlet	
Type III	Atrioventricular canal type	Perimembranous—inlet*	Inlet
Type IV	Muscular	Muscular—trabecular or Muscular—inlet	

\*Unless defect is associated with an endocardial cushion defect, in which case it would not be included in VSD classifications.

and in recent series it is approximately 300/100,000.<sup>9,228</sup> The increase over time appears to be primarily due to nonsurgical perimembranous and muscular defects.<sup>14</sup> Given this, there has been speculation that the increase in VSDs is at least in part due to improved cardiovascular imaging.<sup>229,230</sup>

**Anatomy.** The various potential locations of VSDs as seen from the right ventricular side of the ventricular septum are displayed in Figure 13-43. Membranous types of conoventricular VSDs (more commonly referred to simply as membranous VSDs, Fig. 13-44) are bordered by the aortic valve and the tricuspid valve and are one of the most common types of VSD. Malalignment type of conoventricular VSDs (commonly referred to as conoventricular VSDs) are also bordered by the tricuspid and aortic valves, but the conal septum is either anteriorly or posteriorly deviated, resulting in overriding of the aorta or of the pulmonary artery, respectively (Fig. 13-45). Anteriorly malalignment defects are the type most commonly seen in TOF, and posterior malalignment defects are most commonly seen with interrupted aortic arch.

Defects that are in the trabecular septum are termed muscular VSDs (Fig. 13-46 and Video 13-9), which may be further described as apical, midmuscular, posterior, and anterior. Muscular VSDs are the most common type of VSD. Defects in the inlet septum that borders both AV valves are called AV canal type VSDs (perimembranous inlet type by Anderson terminology, Fig. 13-47).

Conalseptal defects (Fig. 13-48) are the least common and are present when the septum between the RVOT and the LV is incomplete. These defects often are bordered by both the pulmonary valve annulus and the aortic annulus, hence the name given in the Anderson nomenclature is *doubly committed juxtarterial*. If a defect is in this region, but completely surrounded by muscular tissue (instead or bordered by a valve), it would be classified using Anderson terminology as muscular outlet VSD.

**Genetic Considerations.** Genetic disorders must be considered when a VSD is noted. One study reported that among fetuses noted to have a VSD, 46% had a genetic abnormality.<sup>231</sup> Of note, however, all patients except one with genetic abnormalities had an abnormal NT, were high risk for aneuploidy, or had known extracardiac defects. When broken down into those with and without risk factors, 2.5% of those with none of the previous factors had a genetic abnormality, whereas 58% of those with risk factors had a genetic disorder. Another

paper showed similar findings, with only 1.2% of patients with a VSD but no extracardiac anomalies having a genetic disorder.<sup>229</sup>

Particular VSD types significantly increase the risk of a genetic disorder. For example, if an AV canal type VSD is seen, one must be sure this is not a complete AVCD, which would confer an almost 50% risk of Down syndrome. If a malalignment type VSD is associated with pulmonary stenosis or a right aortic arch, the risk of 22q11.2 deletion syndrome increases substantially to as high as 25%. If poly-valvar disease is present with a VSD, the risk of trisomy 13 or 18 is very high.

**Interventions and Prognosis.** A VSD typically has one of three fates. It can close spontaneously, can be closed with surgery, or can be left alone without intervention if it is not hemodynamically significant. Both muscular and membranous VSDs may close spontaneously, and this may occur in utero.<sup>229,231-233</sup> Studies suggest that muscular defects close in fetal life 2% to 31% of the time, with another 19% to 75% closing in the next 12 months.<sup>229,232-234</sup> An estimated 0% to 15% of muscular defects discovered in utero will require surgery.<sup>229,233</sup> For membranous defects, studies suggest 4% to 35% of them close in fetal life, and another 1% to 23% in first 12 months, with an estimated 42% needing surgery.<sup>229,231,234</sup> AV canal type VSDs, malalignment VSDs, and conalseptal defects rarely close spontaneously and will require surgical repair.

For VSDs that require intervention, in the absence of other congenital heart lesions, the procedure can usually be deferred to several months of age, although diuretic therapy may be used in the interim to improve symptoms. At present, surgical repair for pediatric VSD is the preferred therapy in most centers, although catheter-based techniques are demonstrating an improved safety profile compared to prior decades.<sup>235-238</sup> Pulmonary artery banding is largely reserved for critically ill infants with multiple VSDs or for those with associated anomalies.

In isolation, prognosis of children with VSDs is excellent. Even if surgical repair is necessary, most pediatric cardiac surgical programs have mortality rates for VSD closure below 1%.<sup>236</sup> There are potential complications of postoperative arrhythmia (~4%, usually temporary) and postoperative AV block (~1%). Patients with conalseptal defects and membranous or malalignment defects may develop aortic regurgitation or aortic dilation far beyond the surgery, so lifetime follow-up is recommended.

**Diagnostic Imaging Features.** VSDs are some of the most commonly missed CHD lesions by prenatal imaging, likely because of wide variation in size and equal ventricular pressures in the fetus precluding easy observation of shunting.<sup>239</sup> Medium to large VSDs can be detected in the fetus with careful imaging. Smaller defects are able to be visualized, but it can be challenging to distinguish them from artifact. In some cases, the “T-sign” may be helpful in distinguishing a true VSD from artifact, although it is not completely reliable. The T-sign refers to an area of dropout bordered by an echobright, sharp structure that represents the blunted end of the intact portion of the septum (Fig. 13-50C).<sup>239a</sup> In both early and later gestation, a combination of 2D sonography and Doppler color imaging can help identify VSDs, to optimize detection and minimize false positive diagnoses.<sup>232</sup> Although large defects may be easily seen by 2D imaging, VSDs should always be confirmed by color Doppler imaging, which usually demonstrates bidirectional flow across the large defects.

#### Diagnostic Imaging Tips

##### Membranous Ventricular Septal Defect (See Fig. 13-44)

- Defects are seen from many views.
- Aortic valve or tricuspid valve will always be in the picture as a border of the defect.
- If one starts from a four-chamber view, and sweeps superiorly, the defect will be seen just as the aortic valve comes into view.

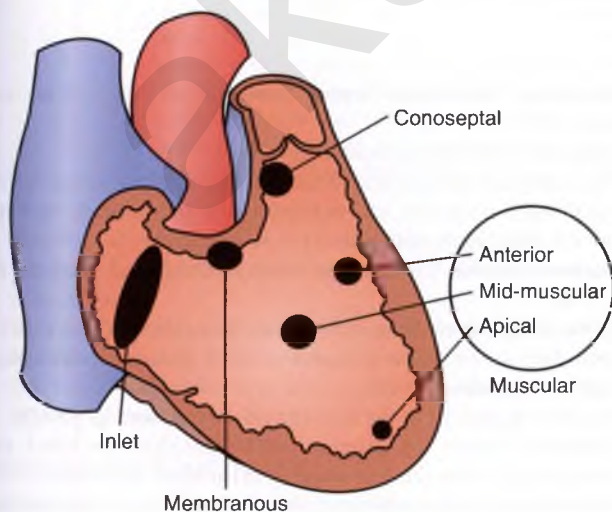


**FIG 13-43** Diagram of location of ventricular septal defects from the view of the right ventricular septum.



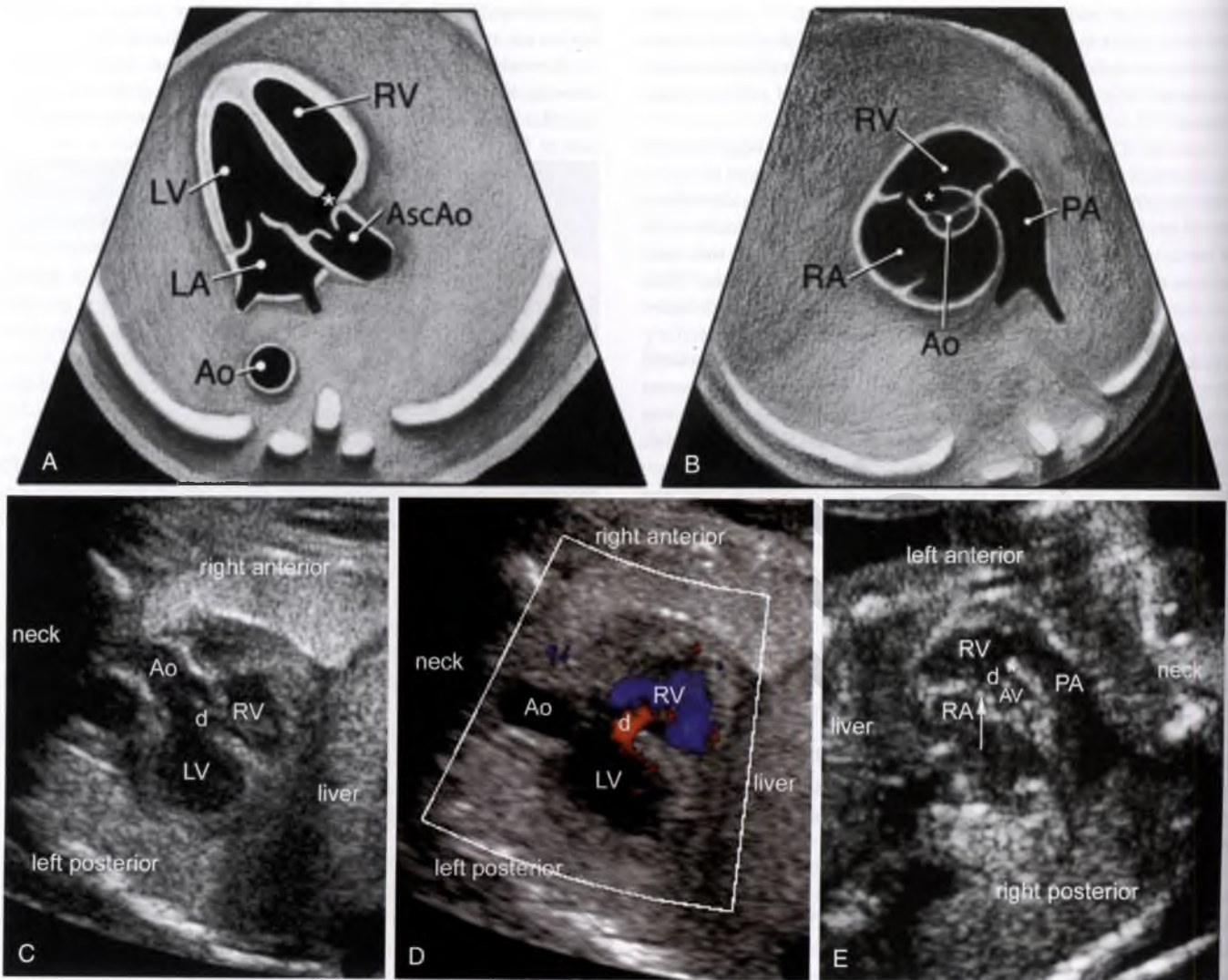


**FIG 13-44** Diagrams and sonograms of membranous (also known as perimembranous) ventricular septal defects by two-dimensional and color Doppler imaging. A membranous defect is typically bordered by the tricuspid valve and the aortic valve and is best seen in a left ventricular outflow tract view or a high short-axis view, as shown by the asterisks in **A** and **B**, and the letter "d" in **C** through **E**. There is remnant outlet septum seen in **E** (asterisk) anterosuperior to the defect. By color Doppler (**D**), shunting across the defect is typically bidirectional; in this image there is left-to-right shunting in a systole frame. Ao, aorta; AscAo, ascending aorta; AV, aortic valve; d, ventricular septal defect; LA, left atrium; LV, left ventricle; PA, main pulmonary artery; RA, right atrium; RV, right ventricle.

- False positive findings are common, as the membranous septum is the thinnest part of the septum and can appear to be missing even when present. Findings should always be confirmed by color Doppler.

#### Conoventricular Ventricular Septal Defect (See Fig. 13-45)

- Defects can exist in isolation, but are most frequently associated with other defects, specifically TOF (anterior malalignment) and interrupted aortic arch (posterior malalignment).
- Conoventricular VSDs frequently are associated with outflow tract obstruction and therefore warrant close evaluation of great artery size discrepancy and obstruction.
- There is a higher association with right aortic arch.
- Classically, the aorta appears to be overriding (anterior malalignment). The pulmonary artery can also appear to be overriding (posterior malalignment), which is usually associated with aortic arch hypoplasia or interrupted aortic arch.

#### Muscular Ventricular Septal Defects (See Fig. 13-46 and Video 13-9)

- Muscular VSDs do not border any valves.
- They may appear fenestrated on imaging, as some defects have a single opening on the left ventricular side and multiple openings on the right ventricular side.

#### Atrioventricular Canal Type Ventricular Septal Defect (See Fig. 13-47)

- If the aortic valve is seen at the same time as the VSD, the defect is probably not an AV canal type VSD, or it occurs in combination with a membranous VSD.
- It is best diagnosed in the four-chamber view (see Fig. 13-47B).
- Carefully inspect for primum ASD (four-chamber view) and common AV valve (en face imaging in the short-axis view).
- Defect must be seen when the AV valves are in view because they serve as borders of this defect.



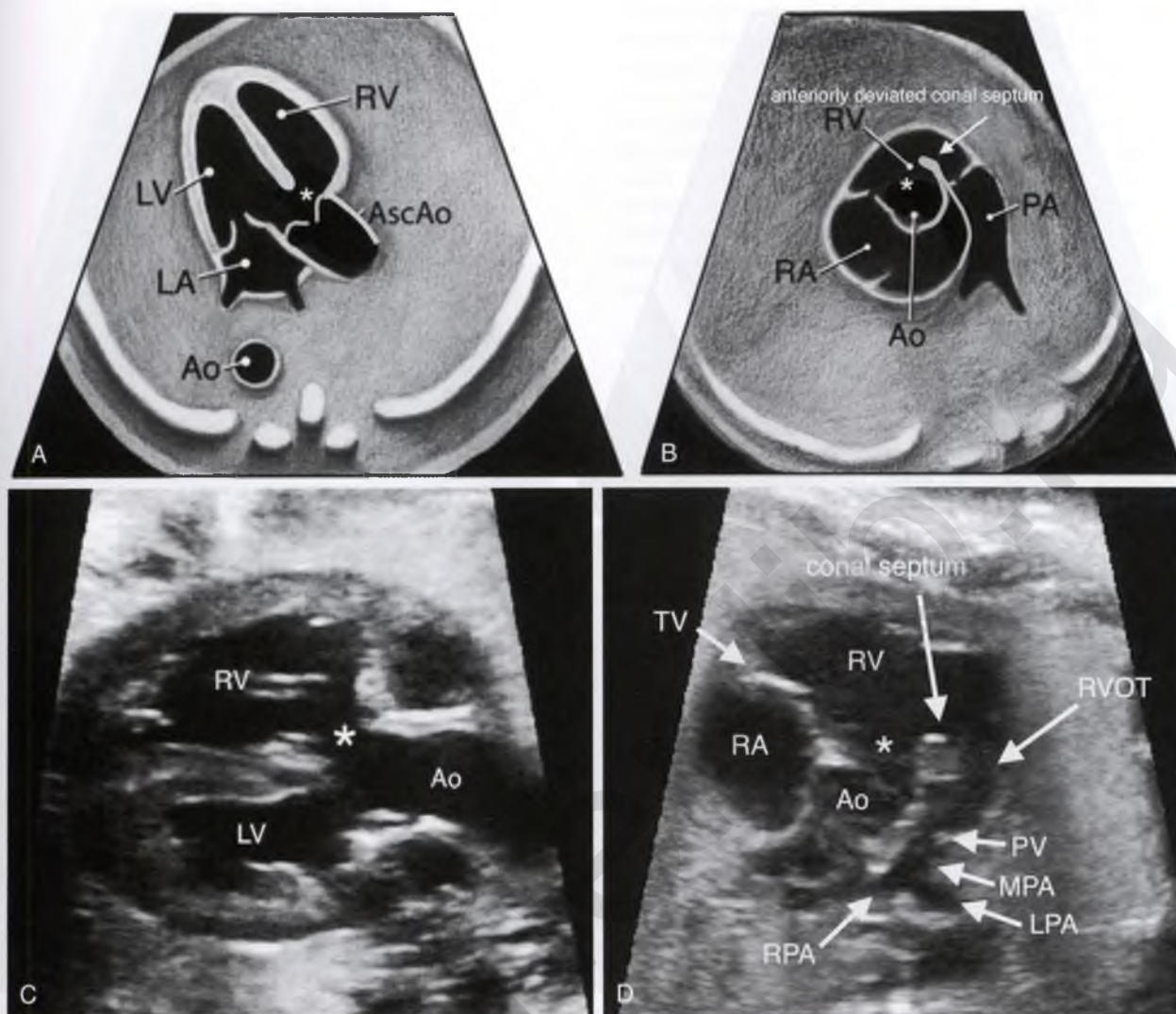


**FIG 13-45** Diagrams and sonographic images of conoventricular (also known as anterior malalignment or perimembranous outlet) ventricular septal defects in tetralogy of Fallot. Conoventricular septal defects are most often associated with anterior deviation of the conal septum, as is seen in tetralogy of Fallot. The defect is indicated by an asterisk in the images. The defect typically borders the tricuspid valve (TV) and the aortic valve, but is differentiated from a nonmalalignment membranous ventricular septal defect (VSD) by the abnormal conal septum. **A** and **C**, Left ventricular outflow tract view shows a large conoventricular septal defect and overriding aorta. **B** and **D**, The high short-axis view shows narrowing of the right ventricular outflow tract (RVOT) due to deviation of the conal septum. The VSD (*asterisk*) is seen bordering the TV and aorta. The pulmonary valve annulus is also mildly hypoplastic. Ao, aorta; AscAo, ascending aorta; LA, left atrium; LPA, left pulmonary artery; LV, left ventricle; MPA, main pulmonary artery; PA, main pulmonary artery; PV, pulmonary valve; RA, right atrium; RPA, right pulmonary artery; RV, right ventricle. (**D** from Morris SA, Maskatia SA, Altman CA, Ayres NA: *Fetal and perinatal cardiology*. In Allen HD, Shaddy RE, Penny DJ et al [eds]: *Moss and Adams' Heart Disease in Infants, Children, and Adolescents Including the Fetus and Young Adult*, 9th ed. Philadelphia, Wolters Kluwer, 2016, used with permission.)

#### Conalseptal Ventricular Septal Defect (See Fig. 13-48)

- This least common VSD may be confused with a membranous VSD in some views.
- With this diagnosis, VSD cannot be bordered by the tricuspid valve.
- The defect lies close to the pulmonary valve.
- Short-axis imaging is best to distinguish membranous defects from conalseptal defects.

#### Atrioventricular Canal Defects

**Definition.** An atrioventricular canal defect (AVCD) is also known as an atrioventricular septal defect (AVSD) or an endocardial cushion

defect. For this section, AVCD terminology will be used. This cardiac malformation has a septum primum atrial septal defect (ASD), an AV canal type VSD, and an abnormal common AV valve, usually composed of five leaflets (Fig. 13-49 and Video 13-10). The defect is an anomaly of the crux of the heart resulting in an ASD in the atrial septum near the AV valves and a VSD in the inlet ventricular septum. There is failure of the common AV valve to be septated by the endocardial cushions. The common AV valve has a single annulus that connects both atria and ventricles. The common AV valve crosses both ventricles at the same level at the crux of the heart resulting in the absence of the normal AV valve offsetting.



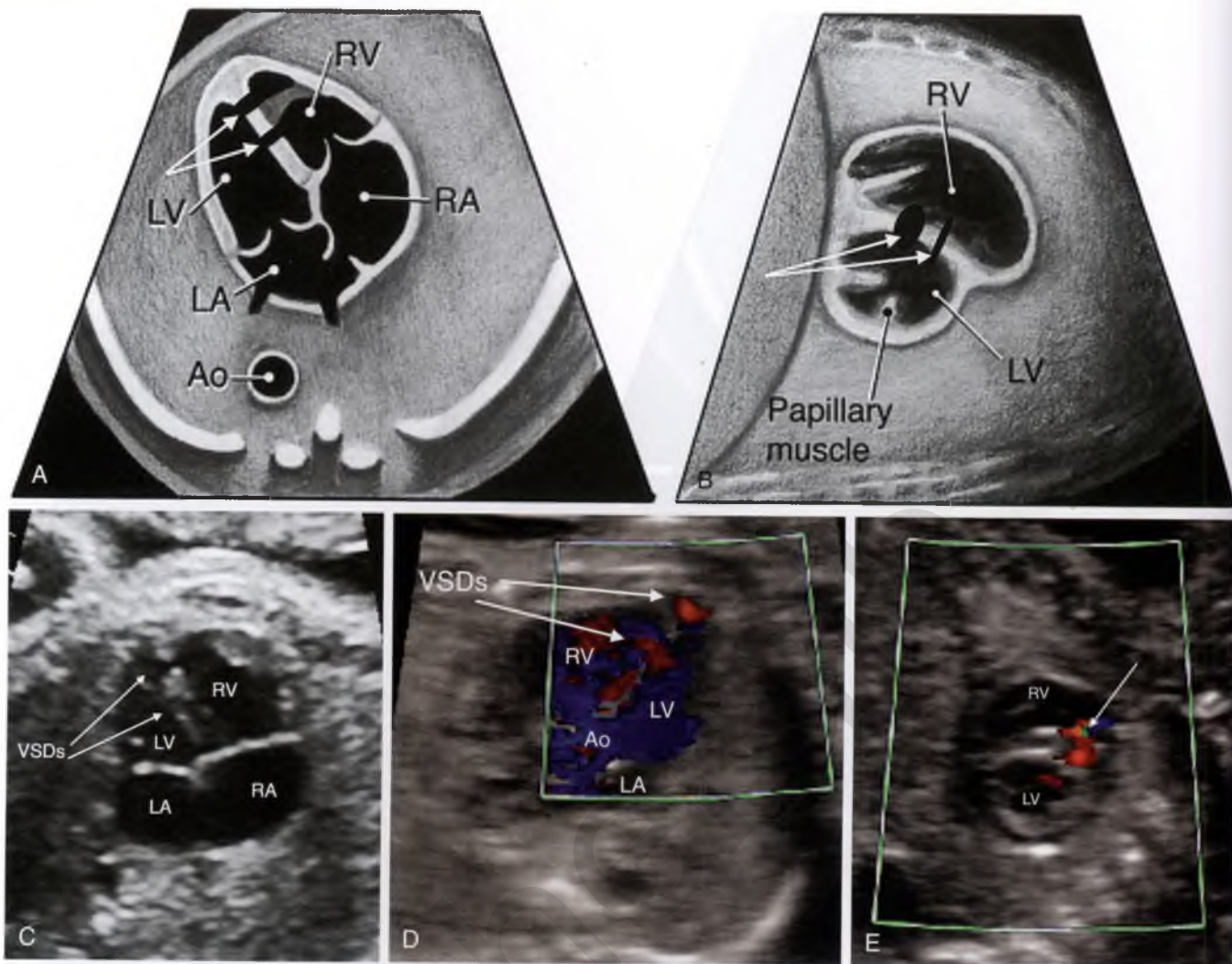


**FIG 13-46** Diagrams and sonographic images of muscular ventricular septal defects (VSDs). The VSDs are indicated by the arrows. The first diagram (A) and the images in C and D show a midmuscular and apical muscular VSD. The second diagram (B) shows two midmuscular defects, and E shows an anterior muscular defect. Ao, aorta; LA, left atrium; LV, left ventricle; RA, right atrium; RV, right ventricle. (A, Adapted with permission from American Institute of Ultrasound in Medicine: AIUM practice guideline for the performance of fetal echocardiography. *J Ultrasound Med* 32:1067-1082, 2013.)

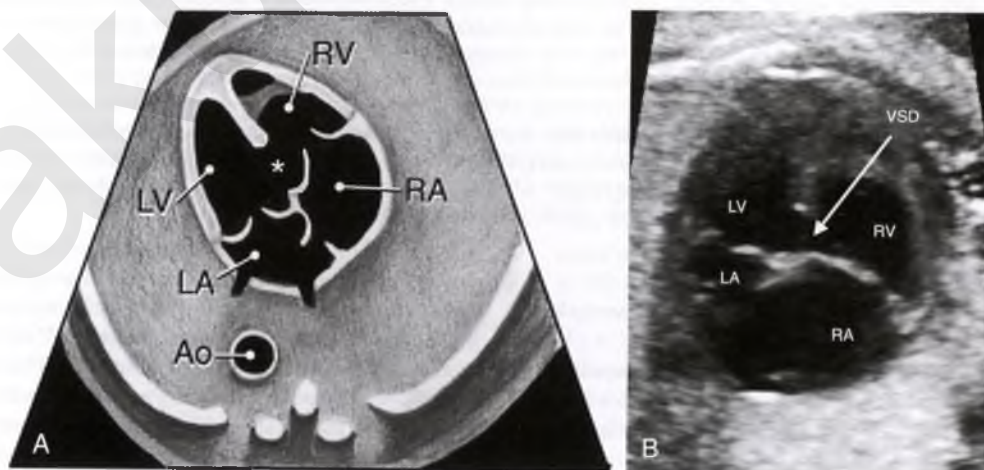


**FIG 13-47** Diagram (A) and sonographic image (B) of atrioventricular canal type (also known as perimembranous inlet) ventricular septal defects (VSDs). VSDs are indicated by an asterisk in A, and the arrow in B. Note that there are two atrioventricular valves, and there is no primum atrial septal defect in this defect. Ao, aorta; LA, left atrium; LV, left ventricle; RA, right atrium; RV, right ventricle. (A, Adapted with permission from American Institute of Ultrasound in Medicine: AIUM practice guideline for the performance of fetal echocardiography. *J Ultrasound Med* 32:1067-1082, 2013.)



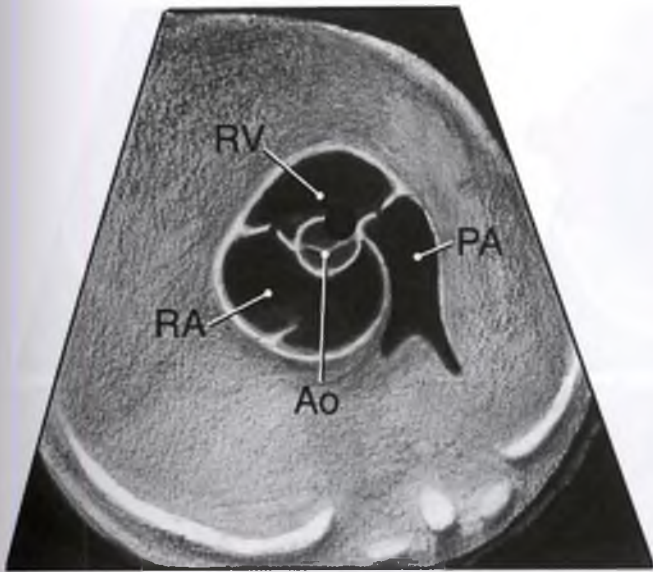


**FIG 13-48** Diagram of a conoseptal type ventricular septal defect. Ao, aorta; PA, main pulmonary artery; RA, right atrium; RV, right ventricle. (Adapted with permission from American Institute of Ultrasound in Medicine: AIUM practice guideline for the performance of fetal echocardiography. *J Ultrasound Med* 32:1067-1082, 2013.)

**Epidemiology.** AVCD accounts for 4% to 5% of infants with CHD and occurs in 0.19 to 0.35 per 1000 live births.<sup>209,240,241</sup> In a large prospective study of fetal CHD, AVCD was the most common cardiac diagnosis and was found in 18% of abnormal fetal hearts.<sup>242</sup> In AVCD, the four-chamber view is diagnostic given that the ASD, VSD, and common AV valve are evident (Fig. 13-50).

Because the dextrodorsal conus cushion contributes to the right AV valve development and the outflow tracts, AVCD may be associated with conotruncal anomalies such as TOF and DORV. Complete AVCD and variations of AVCDs with TOF can be seen in trisomy 21 patients. Unbalanced AVCD occurs when the AV valve connection is shifted primarily toward one ventricle and the contralateral ventricle has hypoplasia. AVCD also occurs in heterotaxy syndrome and is more common in asplenia (bilateral right atrial isomerism) than in polysplenia (bilateral left atrial isomerism).

**Anatomy.** AVCD defines a group of cardiac defects resulting from an abnormal development of the endocardial cushions during cardiogenesis. Failure of the endocardial superior and inferior cushions to fuse results in a defect in the inferior atrial septum and the inlet ventricular septum. There is a common AV valve with the left and right components of the common AV valve attaching at the same septal insertion level. The inferior displacement of the left component of the common valve results in the absence of the normal offsetting of the AV valves. The distance from the crux of the heart to the apex is foreshortened and the distance from the apex to the aorta is increased and results in an elongated LVOT with the aorta anteriorly displaced. The aorta is “sprung” and is not normally wedged between the two AV valves. The elongated, narrowed LVOT has the appearance of a “goose neck.” The narrowed LVOT and abnormal attachment of the anterior bridging leaflet to the ventricular septum can result in subaortic stenosis and LVOT obstruction after surgical repair.

A complete AVCD is characterized by a large primum ASD and AV canal type VSD, with the common AV valve positioned between both defects. The ostium primum ASD is located anterior and inferior to the fossa ovalis and adjacent to the AV valves. An AVCD is classified by the morphologic features of the anterior (sometimes called superior) bridging leaflet as described by Giancarlo Rastelli. In type A, which is

the most common, the anterior bridging leaflet inserts entirely on the anterosuperior rim of the ventricular septum. Type B is the least common, and the anterior bridging leaflet is larger and straddles the ventricular septum with chordal attachments along the right ventricular septum or moderator band. Type C has an anterior bridging leaflet that is not attached to the ventricular septum and has chordal attachments to the right anterior papillary muscle. The type C anterior bridging leaflet is described as a “free-floating” leaflet with no septal chordal attachments and it “floats” over the VSD.<sup>243</sup> The papillary muscles in AVCD are rotated counterclockwise. The papillary muscles may be closely positioned or fused as a single papillary muscle.

An incomplete or partial form of AVCD occurs when both the anterior and posterior (sometimes called inferior) bridging leaflets have dense septal attachments to the crest of the ventricular septum, which results in no VSD. There is a large primum ASD but no VSD (Fig. 13-49B and C, Fig. 13-51, and Video 13-11). The AV valves are at the same level with a common, single AV valve annulus, but there are two separate orifices due to a tongue of AV valve tissue centrally connecting the superior and inferior bridging leaflets. The left AV valve component has a cleft in the anterior leaflet, which is directed toward the middle portion of the ventricular septum. A “transitional” AVCD is similar to the incomplete AVCD but the chordae are less dense and there is a restrictive VSD or multiple small VSDs.

When the AV valve is equally connected to both ventricles, the AVCD is balanced. An unbalanced AVCD occurs when the AV inlet is primarily committed to one ventricle (Video 13-12). Unbalanced AVCDs account for about 10% of all AVCDs. Approximately two thirds of unbalanced AVSDs are RV dominant with more than half of the common AV valve committed to the RV. In RV-dominant AVCD, the LV is hypoplastic, and there are frequently LVOT obstruction, aortic valve hypoplasia, and aortic arch anomalies such as coarctation of the aorta. In LV-dominant AVCD, the RV is hypoplastic, and there are associated RVOT obstruction and pulmonary stenosis or atresia. In trisomy 21 patients with an unbalanced AVCD, the LV-dominant type is common.<sup>244</sup>

**Genetic Considerations.** Approximately 40% to 45% of children with trisomy 21 have congenital cardiac anomalies. Of children with trisomy 21 and heart disease, about 45% have an AVCD. Of the patients with AVCD, more than 75% have trisomy 21.<sup>245</sup> Thus, in the prenatal diagnosis of AVCD, trisomy 21 should be high in the differential diagnosis. A common atrium with an absent atrial septum and common AV valve and no VSD is associated with Ellis-van Creveld syndrome, an inherited condition with an autosomal recessive pattern of inheritance.<sup>246</sup>

**Interventions and Prognosis.** Incomplete or partial AVCD has the physiology of a large ASD and because there is no ventricular component, these patients undergo surgical repair in the first 2 years of life to patch the ASD and repair the cleft in the left anterior AV valve leaflet. The morbidity and mortality rates are very low in this lesion. Left residual AV valve regurgitation may be a chronic problem and is more commonly seen in children repaired after 4 years of age.<sup>247,248</sup>

Over the last several decades AVCD has become one of the most successfully repaired congenital heart anomalies. The Pediatric Heart Network recently reported an overall 1-month mortality rate of 2.5% and a 6-month mortality rate of 4%. In complete AVCD, a residual ASD or VSD was common at 1 month but at 6 months only 1% had a residual VSD of significance.<sup>247,249</sup> Late operations occurred in approximately 20% of complete AVCD patients and include repair of residual AV valve regurgitation (most often the left AV valve), AV valve stenosis, LVOT obstruction, and residual VSD. The most common reason for a subsequent surgery is moderate to severe residual left AV valve regurgitation, which may be repaired but in some cases requires replacement.<sup>244,249-253</sup>



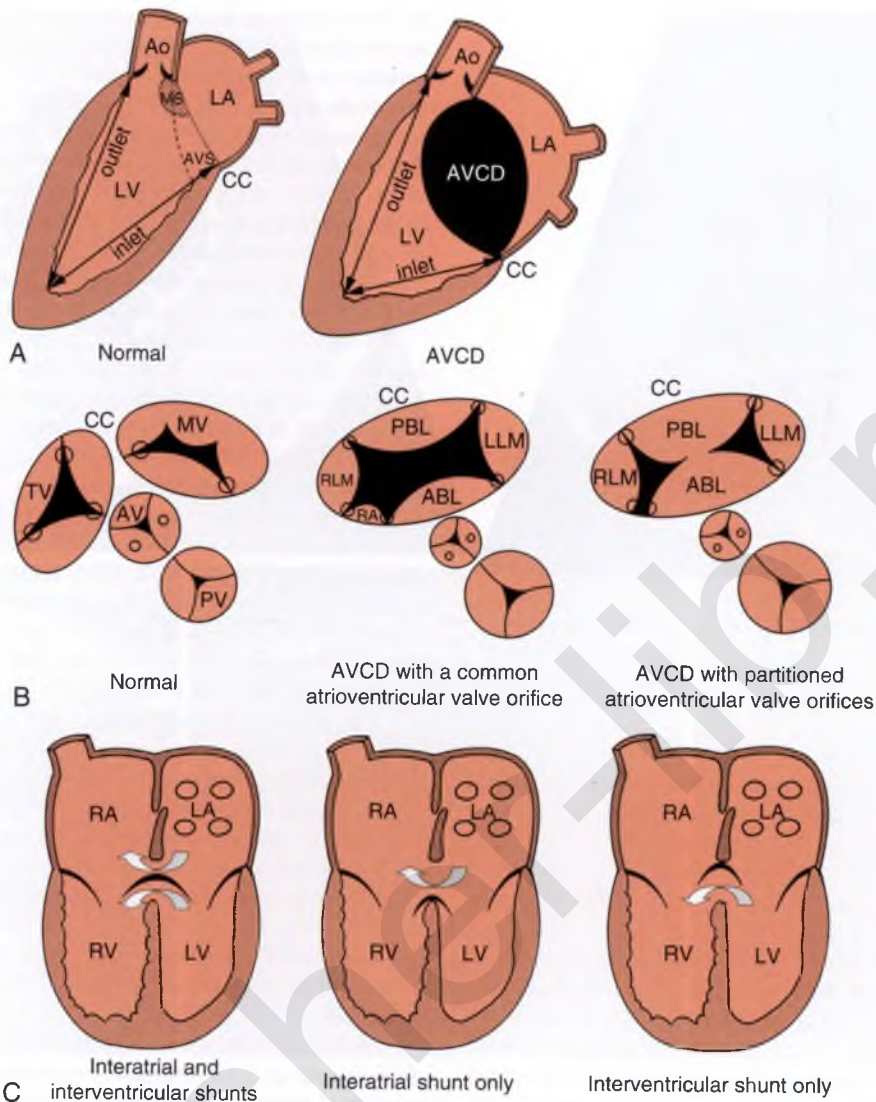


**FIG 13-49** Diagrams showing characteristic features of atrioventricular septal defect (AVSD). **A**, Left ventricle (LV) seen from the left side showing inlet-outlet disproportion and increased distance between the aorta (Ao) and crux cordis (CC) in AVSD. **B**, Atrioventricular valves seen from above. Note the wedged position of the aortic valve (AV) between the tricuspid (TV) and mitral (MV) valves in the normal heart. The aortic valve has an unwedged position in AVSD with an increased distance between the AV and CC because of a common atrioventricular annulus. The five leaflets of AVSD are the anterior and posterior bridging leaflets (ABL and PBL), the left and right lateral mural leaflets (LLM and RLM), and the right anterior leaflet (RA). **C**, Level of shunts. The level of shunt across the AVSD is determined by the relationship of the bridging leaflets to the septal margins of the defect. LA, left atrium; MS, membranous septum; PV, pulmonary valve; RA, right atrium; RV, right ventricle.

**Diagnostic Imaging Features.** All types of AVSD (see Figs. 13-50 and 13-51 and Video 13-10) have the following features:

- AV valve leaflets insert at the same level at the cardiac crux.
- Cleft in the left AV valve component is directed toward the ventricular septum.
- Aorta is unwedged and anteriorly displaced.
- LVOT is elongated.
- Primum ASD is located anteroinferior to the margin of the fossa ovalis.
- LV papillary muscles are rotated counterclockwise.

Complete AVCDs (see Fig. 13-50 and Video 13-10) have all the previous findings as well as the following:

- Large AV canal type VSD.
- Common AV valve crossing between the large ASD and large VSD.
- Unbalanced AVC when the common AV is committed primarily to one ventricle. Given this possibility, examination should include evaluation of the contralateral hypoplastic ventricle for outflow tract and distal semilunar valve obstruction. In RV-dominant AVC, evaluation for aortic arch obstruction is required.

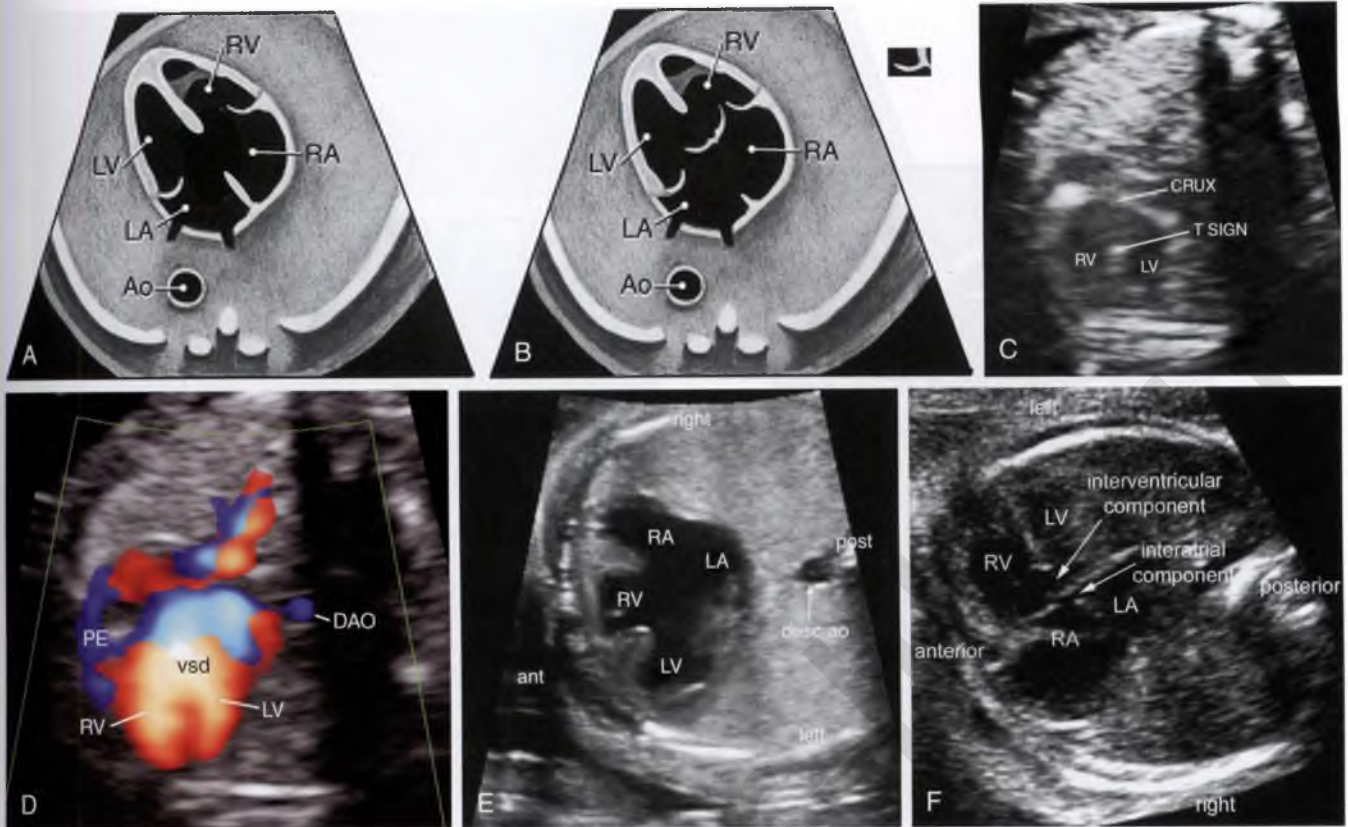


**FIG 13-50** Diagrams (**A** and **B**) and sonographic images (**C** through **F**) of a complete atrioventricular canal defect (atrioventricular septal defect). Depending on the angle of the transducer and point in the cardiac cycle, more or less of the common atrioventricular valve may be seen. The four-chamber view in a fetus with trisomy 13 and a complete atrioventricular canal at 13<sup>5</sup>/<sub>7</sub> weeks of gestation is shown by two-dimensional (**C**) and color Doppler (**D**) imaging. ant, anterior; Ao, aorta; DAO, descending aorta; desc ao, descending aorta; LA, left atrium; LV, left ventricle; PE, pericardial effusion; post, posterior; RA, right atrium; RV, right ventricle; vsd, ventricular septal defect. (**A** and **B**, Adapted with permission from American Institute of Ultrasound in Medicine: AIUM practice guideline for the performance of fetal echocardiography. *J Ultrasound Med* 32:1067-1082, 2013.)

Features of an incomplete or partial AVC (see Fig. 13-51):

- No VSD.
- Common AV valve with a connecting tongue of AV valve tissue creates two separate orifices in the single AV valve annulus.
- The left AV valve component has a cleft in the anterior leaflet, which is directed toward the middle portion of the ventricular septum (Fig. 13-51C).

Features of the transitional AVC:

- Small, restrictive VSD.
- Common AV valve with a connecting tongue of AV valve tissue creates two separate orifices in the single AV valve annulus.

### Tetralogy of Fallot and Pulmonary Atresia With Ventricular Septal Defect

**Definition.** In 1671, Niels Stensen initially described a constellation of findings now known to represent TOF.<sup>254,255</sup> Over 200 years later, Etienne Fallot described a “blue malady” linked to four distinct structural anomalies of the heart: a large VSD, aortic override, right ventricular hypertrophy, and stenosis of the pulmonary artery (Figs. 13-45 and 13-52, Videos 13-13 and 13-14).<sup>256</sup> It is now well understood that TOF is the result of four unrelated structural cardiac lesions. In fact, underdevelopment and anterosuperior deviation of the infundibular septum is the pathognomonic feature.<sup>257</sup> This deviation of the infundibular septum is crucial to the echocardiographic diagnosis of TOF (Fig. 13-45B and D). Pulmonary atresia with a ventricular septal defect

(PA-VSD) represents the most severe form of TOF, with complete obliteration of the RVOT (see Fig. 13-46).

**Epidemiology.** TOF is the most common cyanotic heart defect, with a prevalence of approximately 0.5 per 1000 live births.<sup>209,258</sup> In the absence of a genetic syndrome, a mother who has had a child with TOF has a 3% to 4% risk of having a second child with CHD.<sup>259-261</sup>

**Anatomy.** Although the presence of a conotruncal defect may be readily identified, distinguishing between conotruncal diagnoses can be challenging.<sup>262,263</sup> In the long-axis view of the LV, the appearance of a VSD and an overriding semilunar valve can signal the presence of any of a variety of lesions, including TOF, PA-VSD, truncus arteriosus, some forms of DORV, or aortic atresia with large VSD (Figs. 13-45A and C and 13-53A through C). Distinguishing these lesions and searching for known associated abnormalities is of the utmost importance.

TOF represents a wide spectrum of disease. In contrast to infants with very little obstruction to pulmonary blood flow and VSD physiology (“pink tet”), infants with severe outflow tract obstruction require prostaglandin administration at delivery to assure sufficient pulmonary blood flow (“blue tet”). Evaluation of the RVOT is crucial. Color and spectral Doppler interrogation at the pulmonary valve and of the ductus arteriosus, as well as 2D measurements of the pulmonary valve and main pulmonary artery, can aid in predicting the need for prostaglandin infusion after delivery, for early intervention, and for a transannular patch during the initial repair.<sup>264-267</sup> Specifically, severe pulmonary valve annular hypoplasia, significantly elevated flow



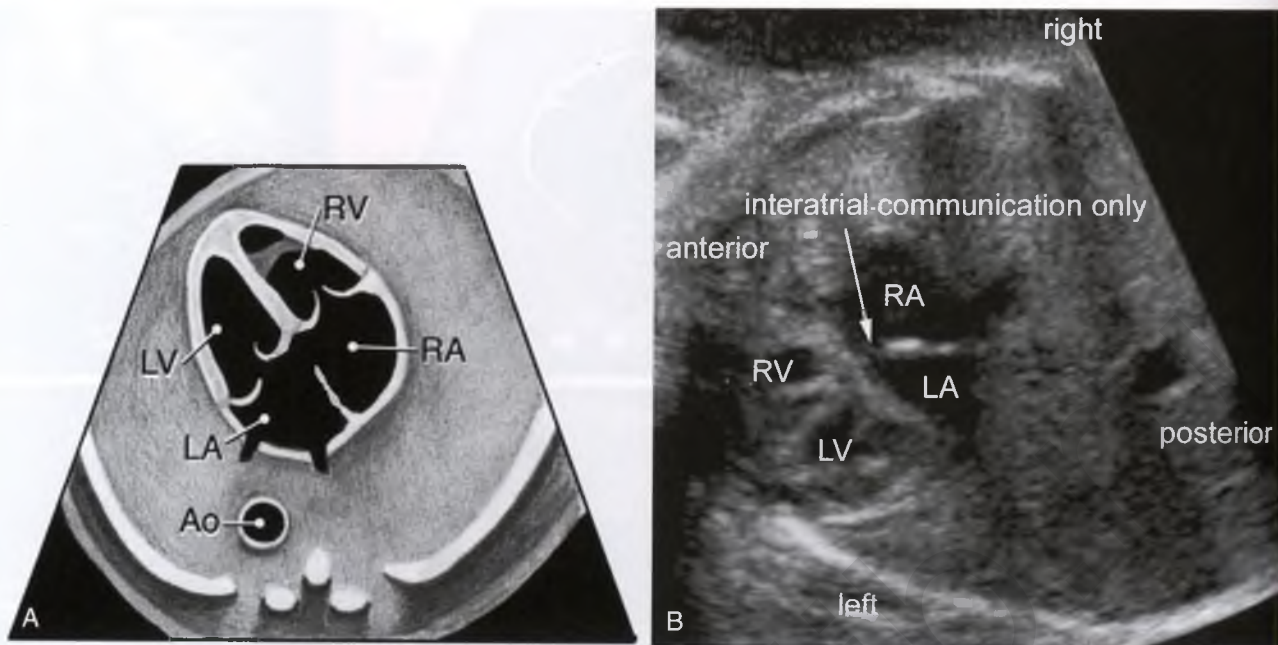


**FIG 13-51** **A** and **B**, Diagram and sonographic images of a partial atrioventricular canal (atrioventricular septal) defect, with a primum atrial septal defect and cleft left atrioventricular valve. **A** shows the low short-axis view, with en face imaging of the left atrioventricular valve showing abnormal attachment to the ventricular septum and a cleft in the anterior leaflet. No ventricular septal component of the defect is seen. AL, anterior leaflet of the mitral valve; LA, left atrium; LV, left ventricle; PL, posterior leaflet of the mitral valve; RA, right atrium; RV, right ventricle. (**A**, Adapted with permission from American Institute of Ultrasound in Medicine: AIUM practice guideline for the performance of fetal echocardiography. *J Ultrasound Med* 32:1067-1082, 2013.)

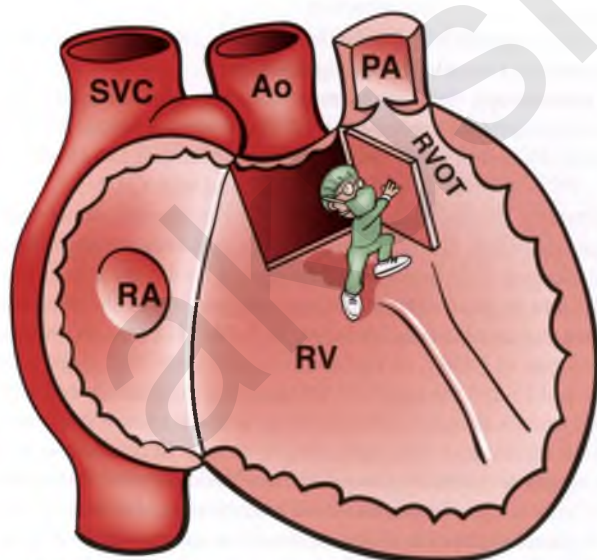


**FIG 13-52** Cartoon showing pathogenic mechanism of tetralogy of Fallot. The essential feature of tetralogy is leftward, anterior, and superior deviation of the outlet septum, causing right ventricular outflow tract (RVOT) narrowing and malalignment type of ventricular septal defect. Ao, aorta; PA, pulmonary artery; RA, right atrium; RV, right ventricle; SVC, superior vena cava. (From Yoo SJ, Jaeggi ET, used with permission.)

velocity at the level of the pulmonary valve, and flow reversal in the ductus arteriosus are all signs of more severe obstruction, requiring prostaglandin administration at delivery. Additionally, the presence of associated cardiac anomalies, such as additional VSDs, a right-sided aortic arch (Fig. 13-53D), and branch pulmonary artery hypoplasia should be investigated.

Determining the source of pulmonary blood flow in pulmonary atresia is crucial. In the case of pulmonary blood flow fed by a ductus arteriosus (see Fig. 13-53A through D), prostaglandin initiation would be necessary at birth, as would neonatal surgery to establish a stable source of pulmonary blood flow. When the pulmonary blood flow is supplied by multiple aortopulmonary collateral arteries (MAPCAs) (Fig. 13-53E and F), pulmonary blood flow is stable at birth. In the case of pulmonary blood flow supplied by a ductus arteriosus, the ductus is tortuous and elongated (Fig. 13-53A and B and Video 13-15).

**Genetic Considerations.** The common features among conotruncal defects are further highlighted by their association with 22q11.2 deletion syndrome (i.e., DiGeorge syndrome, but this describes only a subset of findings in 22q11.2 deletion syndrome). CHD of some form is present in approximately 80% of liveborn patients with 22q11.2 deletion syndrome. Cardiac anomalies most closely linked to 22q11.2 deletion include absent pulmonary valve syndrome, pulmonary atresia and MAPCAs, truncus arteriosus, and type B interrupted aortic arch (Table 13-7). In addition, the presence of a right aortic arch, anomalous subclavian artery, and crossing pulmonary arteries further increase the risk of 22q11.2 in these populations.<sup>268</sup> A fetal study published in



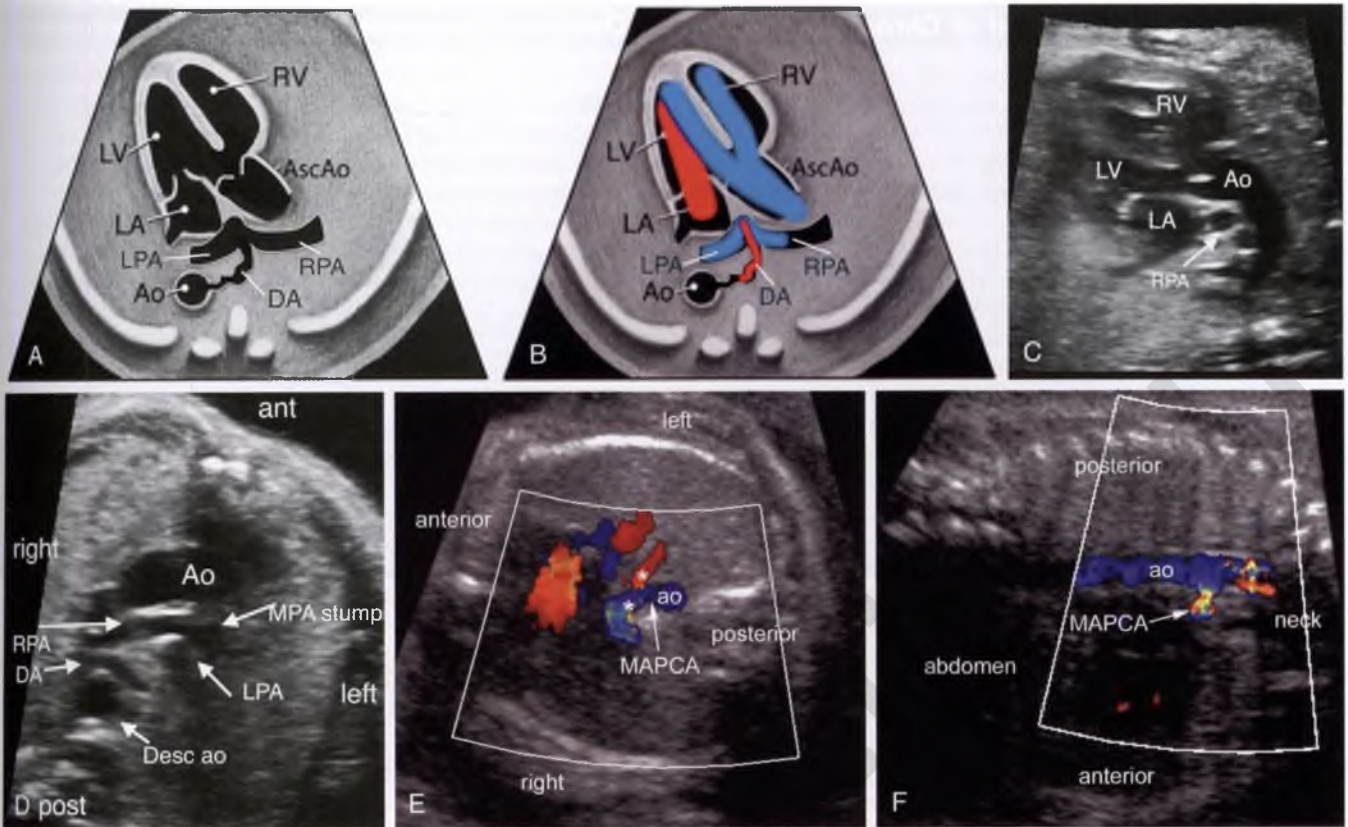


**FIG 13-53** Diagrams (**A** and **B**) and sonographic images (**C** through **F**) of pulmonary atresia with ventricular septal defect (PA-VSD). PA-VSD with confluent branch pulmonary arteries are shown in **A** through **D**, and PA-VSD with multiple aortopulmonary collateral arteries (MAPCAs) are shown in **E** and **F**. In **A** and **B** the schematic shows how outflows look with subtle superior sweeping with and without color Doppler. From the left ventricular outflow tract view (**A** through **C**), a large conoventricular VSD is seen with an overriding aorta. From this view, it is difficult to distinguish tetralogy of Fallot (TOF) with pulmonary stenosis, pulmonary atresia with VSD, truncus arteriosus, and TOF-type double-outlet right ventricle from looking at intracardiac anatomy alone. To distinguish these, pulmonary blood flow must be determined. With anterosuperior sweeps, no right ventricular outflow tract is seen; a main pulmonary artery (MPA) stump is seen in **D**. In **A** and **B**, the tortuous ductus arteriosus (DA) arises in the typical fashion from the descending aorta in a left-sided arch. In **D**, the aortic arch is right-sided, and the ductus arises from the origin of the left innominate artery; the ductus is only partially seen in the image. In **E**, a MAPCA (*asterisks*) is seen arising from the anterior wall of the descending aorta (desc ao). **F**, Axial view shows a MAPCA bifurcating into branches to both lungs. Ant, anterior; Ao, aorta; AscAo, ascending aorta; DA, ductus arteriosus; Desc ao, descending aorta; LA, left atrium; LPA, left pulmonary artery; LV, left ventricle; MPA, main pulmonary artery; post, posterior; RPA, right pulmonary artery; RV, right ventricle. (**A**, Adapted with permission from American Institute of Ultrasound in Medicine: AIUM practice guideline for the performance of fetal echocardiography. *J Ultrasound Med* 32:1067-1082, 2013.)

2001 demonstrated a 45% prevalence of 22q11.2 deletion in patients with an interrupted aortic arch compared to 38% in absent pulmonary valve syndrome, 31% in truncus arteriosus, 18% in PA-VSD, 14% in TOF, and 12% in complex TGA.<sup>269</sup> Interestingly, the association between TGA and 22q11.2 is not consistently observed postnatally, indicating that this transposition with 22q11.2 deletion may represent a group at risk for fetal demise.<sup>268</sup>

**Interventions and Prognosis.** TOF requires surgical repair to eliminate shunting across the VSD and to prevent cyanosis. For most children, the initial repair is performed within the first 6 months of life (but not as a neonate) and involves closing the VSD and establishing unobstructed pulmonary blood flow. For neonates with pulmonary atresia or severe pulmonary obstruction, complete repair may be performed in the neonatal period, or a systemic to pulmonary artery shunt may be placed to provide pulmonary blood flow until a few

months of age, when the complete repair is performed. After repair, patients typically have some degree of pulmonary insufficiency. If severe, patients may require repeat pulmonary valve replacement later in life. Those with pulmonary atresia will require serial replacement of a prosthetic conduit from the RV to the pulmonary artery, necessitating repeat surgery over a lifetime.

Fetal demise in TOF is rare.<sup>269</sup> The long-term outcomes of patients with TOF with or without pulmonary atresia hinge upon the health of the RV.<sup>270-272</sup> Overall, survival is excellent, with survival rate in those undergoing surgery since 2000 over 98%.<sup>272</sup> Children and adults with TOF and PA-VSD do need to be followed throughout their lifetime for complications of the heart conditions and repairs, including arrhythmias, exercise intolerance, and impairment of the right side of the heart.

**Diagnostic Imaging Features.** Features of TOF (see Fig. 13-45 and Videos 13-13 and 13-14):



TABLE 13-7 Likelihood of Chromosome 22q11.2 Deletion Syndrome With Different Lesions

Lesion	% With 22q11.2 Deletion	Lesion	% With 22q11.2 Deletion
Isolated right aortic arch	6-30%	D-transposition of the great arteries	0-0.4%
Right aortic arch, mirror image branching	0-22%	L-transposition of the great arteries	0%
Right aortic arch, aberrant left subclavian artery	12-32%	Double-outlet right ventricle	0-5%
Isolated double aortic arch	14%	VSD with coarctation	26%
Tetralogy of Fallot, all	9-21%	Posterior malalignment type VSD with coarctation	33-67%
TOF with left arch, normal branching	6-11%	Truncus arteriosus	30-41%
TOF with any arch anomaly	21%	Type A1	25-42%
TOF with left arch, aberrant left subclavian artery	0-31%	Type A2	17-33%
TOF with right arch, mirror image branching	10-24%	Type A3	63-100%
TOF with right arch, aberrant right subclavian artery	0-40%	Type A4	25-50%
Pulmonary atresia with VSD	21-47%	Absent pulmonary valve syndrome	14-40%
PA-VSD and RAA	70%	Interrupted aortic arch with VSD	45-89%
PA-VSD with PDA	0-22%	Type A	0%
PA-VSD with MAPCAs	43-77%	Type B	56-57%
PA-VSD with MAPCAs and RAA	100%		

MAPCAs, multiple aortopulmonary collateral arteries; PA-VSD, pulmonary atresia with a ventricular septal defect; PDA, patent ductus arteriosus; RAA, right aortic arch; TOF, tetralogy of Fallot; VSD, ventricular septal defect.

Data obtained from the following published sources:

Momma K: Cardiovascular anomalies associated with chromosome 22q11.2 deletion syndrome. *Am J Cardiol* 105(11):1617-1624, 2010.

Boudjemline Y, Fermont L, Le Bidois J, et al: Prevalence of 22q11 deletion in fetuses with conotruncal cardiac defects: a 6-year prospective study. *J Pediatr* 138(4):520-524, 2001.

Song MS, Hu A, Dyamenahalli U, et al: Extracardiac lesions and chromosomal abnormalities associated with major fetal heart defects: comparison of intrauterine, postnatal and postmortem diagnoses. *Ultrasound Obstet Gynecol* 33(5):552-559, 2009.

Goldmuntz E, Crenshaw ML, Lin AE: Genetic aspects of congenital heart defects. In Allen HD, Driscoll DJ, Shaddy RE, Feltes TF (eds): *Moss & Adams' Heart Disease in Infants, Children, and Adolescents*, 8th ed. Philadelphia, Lippincott Williams & Wilkins, 2013, pp 617-643.

Iserin L, de Lonlay P, Viot G, et al: Prevalence of the microdeletion 22q11 in newborn infants with congenital conotruncal cardiac anomalies. *Eur J Pediatr* 157(11):881-884, 1998.

Momma K, Matsuoka R, Takao A: Aortic arch anomalies associated with chromosome 22q11 deletion (CATCH 22). *Pediatr Cardiol* 20(2):97-102, 1999.

Momma K, Kondo C, Matsuoka R: Tetralogy of Fallot with pulmonary atresia associated with chromosome 22q11 deletion. *J Am Coll Cardiol* 27(1):198-202, 1996.

Hofbeck M, Leipold G, Rauch A, et al: Clinical relevance of monosomy 22q11.2 in children with pulmonary atresia and ventricular septal defect. *Eur J Pediatr* 158(4):302-307, 1999.

Frohn-Mulder IM, Wesby Swaay E, Bouwhuis C, et al: Chromosome 22q11 deletions in patients with selected outflow tract malformations. *Genet Couns* 10(1):35-41, 1999.

Maeda J, Yamagishi H, Matsuoka R, et al: Frequent association of 22q11.2 deletion with tetralogy of Fallot. *Am J Med Genet* 92(4):269-272, 2000.

Peyvandi S, Lupo PJ, Garbarini J, et al: 22q11.2 Deletions in patients with conotruncal defects: data from 1,610 consecutive cases. *Pediatr Cardiol* 34(7):1687-1694, 2013.

McElhinney DB, Clark BJ 3rd, Weinberg PM, et al: Association of chromosome 22q11 deletion with isolated anomalies of aortic arch laterality and branching. *J Am Coll Cardiol* 37(8):2114-2119, 2001.

- The four-chamber view may appear normal. The lesion is commonly detected by a sweep from the four chambers to the outflow tracts, which demonstrates the VSD and aortic override (Fig. 13-45A and C). TOF may be confused with truncus arteriosus, DORV, and aortic atresia with VSD. Look carefully at the outflow tracts and arch morphologic features to distinguish them from each other.
- The distinction between TOF and PA-VSD is that in TOF, there is still forward flow across the pulmonary valve, which is best seen by color Doppler imaging.
- The VSD is typically of the conoventricular type (see earlier). Rarely it is of the conoseptal type.
- Zooming in on the RVOT and branch pulmonary arteries can help determine the location of the obstruction by 2D imaging. Any of the following may be present: subvalvar stenosis, pulmonary

annular hypoplasia, valvar stenosis, supra-valvar stenosis, branch pulmonary artery stenosis.

- In the fetus, the velocity is rarely elevated across the RVOT by spectral Doppler, even in cases of moderate to severe obstruction. 2D imaging and Z-scores are better able to determine the degree of hypoplasia.

Features of PA-VSD (see Fig. 13-53 and Video 13-15):

- In PA-VSD, all pulmonary blood flow is from another source, either retrograde from the ductus arteriosus or via MAPCAs, which usually arise from the descending aorta.
- MAPCAs are best seen by putting a color Doppler box at a low Nyquist limit over the descending aorta and looking for small vessels with anteriorly directed continuous flow.
- Fetuses may have a combination of hypoplastic branch pulmonary arteries and MAPCAs.

## Truncus Arteriosus

**Definition.** Truncus arteriosus is a complex lesion that is defined as a congenital cardiovascular malformation in which a single great artery arises from the base of the heart and gives origin to the coronary, pulmonary, and systemic arteries.<sup>273</sup> It may easily be confused with PA-VSD or aortic atresia with VSD on fetal cardiac evaluation, because one of the great arteries in those conditions is severely hypoplastic.

**Epidemiology.** Truncus arteriosus has an estimated birth incidence of approximately 7 to 21 per 100,000 live births.<sup>274-276</sup> There is some suggestion that the prevalence of truncus arteriosus in both the United States and Europe is decreasing, perhaps associated with improved prenatal diagnosis and subsequent termination.<sup>228,274</sup>

**Anatomy.** There are various subtypes of truncus arteriosus (Figs. 13-54 and 13-55), typically categorized by one of two classifications: The Van Praagh Classification<sup>273</sup>:

- Type A1: The branch pulmonary arteries arise from a common pulmonary trunk (most common type) (Video 13-16).
- Type A2: The branch pulmonary arteries arise separately from the truncal artery (second most common). Of note, types A1 and A2 may be difficult to distinguish, even in the initial case series, in which 9% were unclear.<sup>273</sup>
- Type A3: Either the right or left pulmonary artery branch is absent. Collateral arteries supply the lung that does not receive a pulmonary artery branch from the truncus arteriosus (rare).
- Type A4: Underdevelopment of the aortic arch results in preductal hypoplasia, coarctation, atresia, or aortic arch interruption (Video 13-17).

The Collet-Edwards Classification<sup>277</sup>:

- Type I: same as Van Praagh type A1.
- Type II: same as Van Praagh type A2.

- Type III: similar to type II, but pulmonary arteries arise separately from the lateral walls of the truncus (as opposed to posterior truncus); this type is included in Van Praagh type A2.
- Type IV: Previously called truncus arteriosus, this type is now more correctly labeled pulmonary atresia with aortopulmonary collaterals (discussed earlier).

**Genetic Considerations.** Approximately 50% of newborns with truncus arteriosus are found to have a genetic disorder,<sup>275</sup> most commonly the chromosome 22q11.2 deletion syndrome.<sup>278</sup> However, truncus arteriosus has also been described in trisomy 18,<sup>279</sup> trisomy 21,<sup>280</sup> 14q deletion,<sup>281</sup> *GATA6* mutations,<sup>282</sup> and chromosome 3q22.3 deletions.<sup>283</sup>

**Interventions and Prognosis.** Truncus arteriosus is typically repaired in the newborn period by creating a baffle that closes the VSD and connects the LV to the aorta and by placing an RV to pulmonary artery conduit. The conduit does not grow with the child and therefore usually needs replacing, often multiple times over the course of a lifetime. Other possible complications include the development of carotid obstruction, conduit regurgitation, branch pulmonary artery obstruction, and aortic dilation/regurgitation. Many of these complications can be treated with catheter-based techniques. If they do need to be surgically addressed, the procedure may be performed at the time of a conduit replacement.

In the current era, outcomes of truncus repair surgery are quite good, with operative mortality rate less than 10% in most centers.<sup>284-286</sup> Despite this, overall mortality rate in truncus arteriosus is still relatively high, estimated at 10% to 20% in infancy, primarily because of additional cardiac lesions, such as interrupted aortic arch, as well as non-cardiac problems including necrotizing enterocolitis, extracardiac birth defects, and immunodeficiency associated with DiGeorge syndrome.<sup>278,284,286</sup>

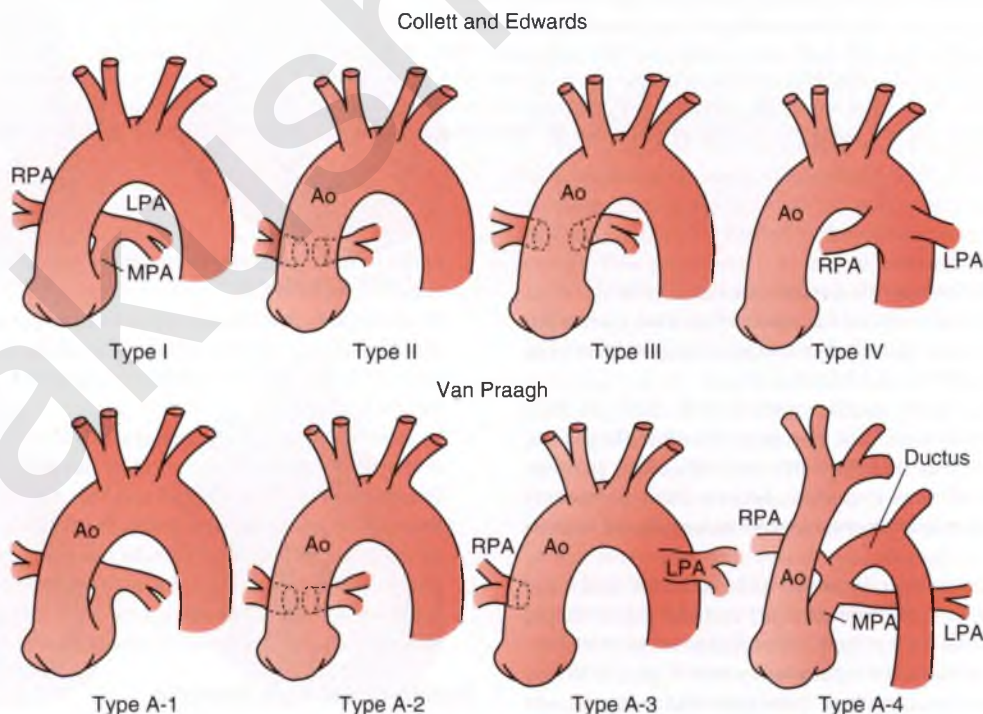


**FIG 13-54** Classifications of truncus arteriosus. Ao, ascending aorta; LPA, left pulmonary artery; MPA, main pulmonary artery; RPA, right pulmonary artery. (Adapted from St Louis JD: Persistent truncus arteriosus. In Nichols DG, Ungerleider RM, Spevak PJ, et al [eds]: *Critical Heart Disease in Infants and Children*. Philadelphia, Mosby, 2006, p 690.)



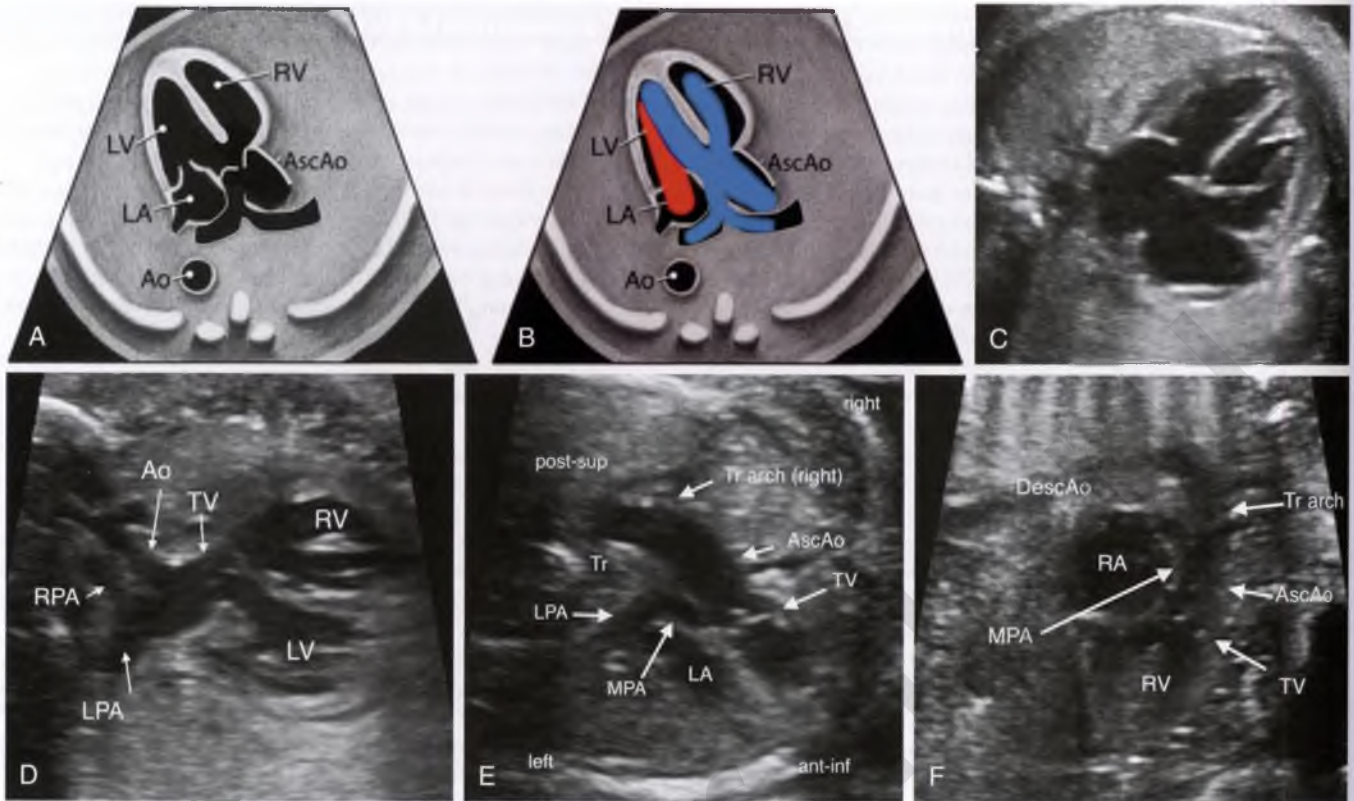


**FIG 13-55** Diagrams and sonographic images of truncus arteriosus. **A** and **B**, These schematics show how outflows look with subtle superior sweeping with and without color Doppler. **C**, The deceptively normal four-chamber view. **D**, The left ventricular outflow tract view shows a large VSD and overriding aorta. In **D** and **E**, evaluation of the great arteries shows a main pulmonary artery arising from the aorta (Van Praagh type A1, Collet-Edwards type I). **D** shows a hypoplastic ascending aorta and interrupted aortic arch (arch anatomy not visible in image). **E** shows a right-sided aortic arch. In **F**, the main pulmonary artery and ascending aorta arise from the same truncal valve in this patient with a right aortic arch. No ductus arteriosus is present. ant-inf, anterior-inferior; Ao, aorta; AscAo, ascending aorta; DescAo, descending aorta; LA, left atrium; LPA, left pulmonary artery; LV, left ventricle; MPA, main pulmonary artery; post-sup, posterior-superior; RA, right atrium; RPA, right pulmonary artery; RV, right ventricle; Tr, trachea; Tr arch, transverse arch; TV, truncal valve. (**A**, Adapted with permission from American Institute of Ultrasound in Medicine: AIUM practice guideline for the performance of fetal echocardiography. *J Ultrasound Med* 32:1067-1082, 2013.)

### Diagnostic Imaging Features

- The four-chamber view appears normal (see Fig. 13-55C).
- This malformation can be detected on the outflow tract views when only one arterial trunk is identified overriding a large VSD (see Fig. 13-55A, B, and D and Videos 13-16 and 13-17).
- Truncus arteriosus can be easily confused with TOF, PA-VSD, DORV, or aortic atresia with VSD, as in these situations the pulmonary artery or aorta may be hypoplastic and difficult to visualize. Making this distinction is important because both pulmonary atresia and aortic atresia are ductus-dependent lesions and truncus arteriosus is not.
- The ductus arteriosus is typically absent (see Fig. 13-55E and F and Video 13-16). Therefore, only one great artery and *one* arch should be evident. If two arches are present, other diagnoses must be considered, including aortic atresia, pulmonary atresia, and DORV.
- To distinguish truncus arteriosus from pulmonary atresia, one should identify the blood source of the branch pulmonary arteries. In truncus arteriosus, the branch arteries arise from the single great artery, but in pulmonary atresia either the branch pulmonary arteries arise from the ductus arteriosus, which will have retrograde flow,

or the branch pulmonary arteries are hypoplastic and the lungs are supplied via MAPCAs.

- To distinguish truncus arteriosus from aortic atresia with VSD, one should evaluate the arch anatomy. In aortic atresia, there will be a severely hypoplastic ascending aorta and arch, and flow in the arch will be retrograde.
- In approximately 1% of cases, truncus arteriosus is associated with severe coarctation of the aorta or interrupted aortic arch (Van Praagh type A4) (Fig. 13-55D and Video 13-17). In these cases, the ductus arteriosus is present and is the primary source of blood flow to the lower half of the body. In cases of coarctation, two arches may be present, with the aortic arch being hypoplastic. Much more common is interrupted aortic arch with truncus arteriosus, and in this situation the ductus arteriosus is usually the only arch present.

### Double-Outlet Right Ventricle

**Definition.** DORV comprises a group of complex lesions, and various definitions of DORV are used. Some define DORV as greater than 50% override of the posterior great artery over the VSD, others define the condition as a lack of continuity between the mitral and



aortic valves, and still others diagnose DORV only when both great vessels completely arise from the RV.<sup>287</sup> The Congenital Heart Surgery Nomenclature and Database Project considered DORV in 2000, and their consensus definition of DORV was made deliberately broad by stating, "DORV is a type of ventriculoarterial connection in which both great vessels arise either entirely or predominantly from the right ventricle."<sup>287</sup>

**Epidemiology.** DORV is thought to occur in approximately 6 to 15 infants per 100,000 live births.<sup>288,289</sup> There appears to be a larger proportion of males with DORV than females, with estimates of approximately 1.6 males to every female.<sup>289</sup>

**Anatomy.** Nearly all patients with DORV also have a VSD. Rare exceptions include mitral valve atresia and DORV in which no VSD is apparent. VSDs in DORV are traditionally classified as subpulmonary, subaortic, doubly committed, and remote (Fig. 13-56). Subpulmonary and subaortic VSDs are most similar to the membranous (perimembranous outlet) VSD described earlier and are bordered by an AV valve and the posterior semilunar valve (or semilunar valve closest to the ventricular septum if the great arteries are side by side). Therefore, if the aorta is the posterior/leftward vessel, this defect would be subaortic (Fig. 13-57A through C). If the pulmonary artery is posterior and leftward, the defect is called subpulmonary (Fig. 13-57D). The great artery closest to the ventricular septum may appear to override the VSD (see Fig. 13-57D). The doubly committed VSD is most closely related to conalseptal hypoplasia (doubly committed subarterial), described previously. A doubly committed VSD is bordered by both the aortic and pulmonary valves and occurs when the conal

septum is hypoplastic or absent. Remote VSDs include other VSDs that are not bordered by a semilunar valve, and often include AV canal type VSDs.

Because many variations of DORV are possible, the cardiac hemodynamics will ultimately determine the child's prognosis and required interventions. Apart from DORV associated with single ventricle lesions (such as mitral atresia with DORV), there are three major physiologic types: TOF type, TGA type, and VSD type. In TOF type DORV, the pulmonary artery is usually anterior, there is a subaortic VSD, and a degree of pulmonary stenosis is present.<sup>290</sup> The infant has decreased pulmonary blood flow in accordance with the relative degree of pulmonary stenosis. In TGA type DORV, the aorta is typically anterior and the VSD is subpulmonary (see Fig. 13-57D). The physiology will mimic that of TGA, with systemic desaturation at birth. This type is also referred to as Taussig-Bing anomaly. The third type, VSD type DORV, typically is associated with a large subaortic VSD, an anterior pulmonary artery, and no outflow tract obstruction. This type of DORV presents with VSD physiology and pulmonary overcirculation with normal or near-normal oxygen systemic saturation. In a recent study, VSD type DORV was the most common subtype among the prenatal group (64%), with TOF type making up 26%, and TGA type DORV composing 10%.<sup>290</sup> The postnatal group consisted of 52% with VSD type DORV, 35% with TGA type, and only 13% with TOF type (see Fig. 13-2 and Table 13-2).<sup>290</sup>

**Genetic Considerations.** All mothers carrying a fetus with DORV should be offered genetic counseling and testing, given that up to 43% of patients with DORV have a genetic disorder.<sup>291</sup> The most commonly associated chromosomal abnormalities are trisomy 13 and trisomy 18. DORV has also been associated with 22q11.2 microdeletion, trisomy 21, and Klinefelter syndrome.<sup>278,292</sup>

**Interventions and Prognosis.** Surgery for DORV usually depends on the physiologic nature of the lesion and can vary greatly. For TOF type DORV with severe pulmonary stenosis, an aortopulmonary shunt may be required in the neonatal period to augment pulmonary blood flow, followed by complete repair later in infancy, although some institutions will perform a complete neonatal repair.<sup>290,293,294</sup> A complete repair would include VSD closure, eliminating of obstruction of the RVOT, and shunt takedown.

For TGA type VSD, an arterial switch and VSD closure can often be performed. However, if associated with significant subpulmonary or pulmonary stenosis, an RV to pulmonary artery conduit may be placed with the VSD baffled to the anterior aorta instead of an arterial switch. This procedure is known as a Rastelli repair.<sup>295</sup> In VSD type DORV, VSD closure including a baffle to direct left ventricular flow to the aorta is typically performed. Occasionally in this lesion the pulmonary overcirculation becomes significant at a very young age, and a pulmonary artery band may be placed prior to other surgeries to limit pulmonary blood flow temporarily. In any type of DORV, when there is a remote VSD or significant straddling of the AV valves, a single ventricle palliation may be the only option.<sup>296</sup>

Many coexisting lesions can occur with DORV, and they may also need to be addressed with intervention, including ASDs, coarctation of the aorta, and pulmonary vein anomalies. Sometimes DORV is associated with mitral or tricuspid atresia, and these patients will require single ventricle palliation.<sup>290,293-296</sup>

DORV is associated with a high risk of early demise and complex postnatal care.<sup>290</sup> Factors associated with fetal demise include hydrops, chromosomal abnormalities, and tricuspid regurgitation,<sup>290</sup> which occur in approximately 8% of DORV.<sup>290</sup> The primary factor associated with infant death prior to surgery is the presence of extracardiac malformations. Heterotaxy complex and single ventricle physiology are associated with worse surgical outcomes. For children able to undergo

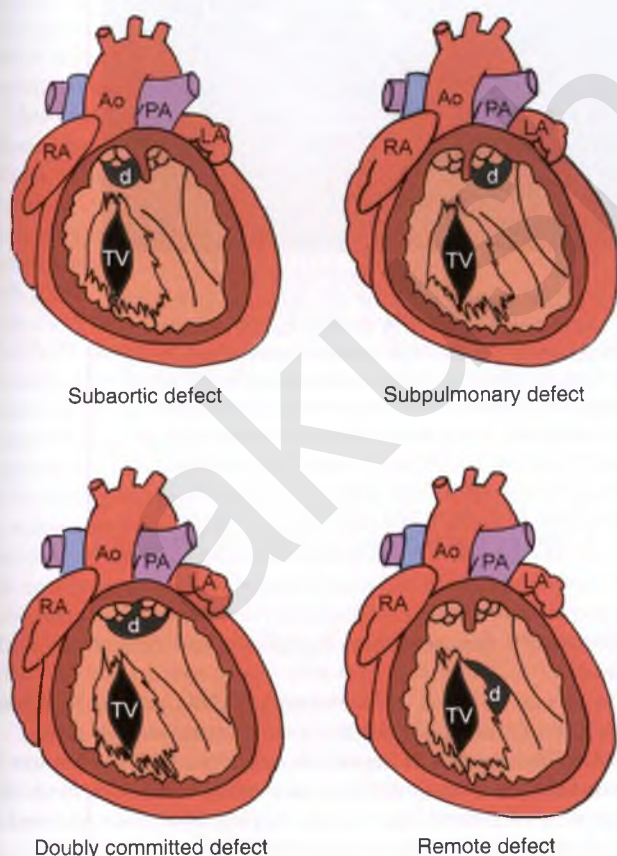


**FIG 13-56** Types of ventricular septal defects in double-outlet right ventricle. Ao, ascending aorta; d, ventricular septal defect; LA, left atrium; PA, main pulmonary artery; RA, right atrium; TV, tricuspid valve.



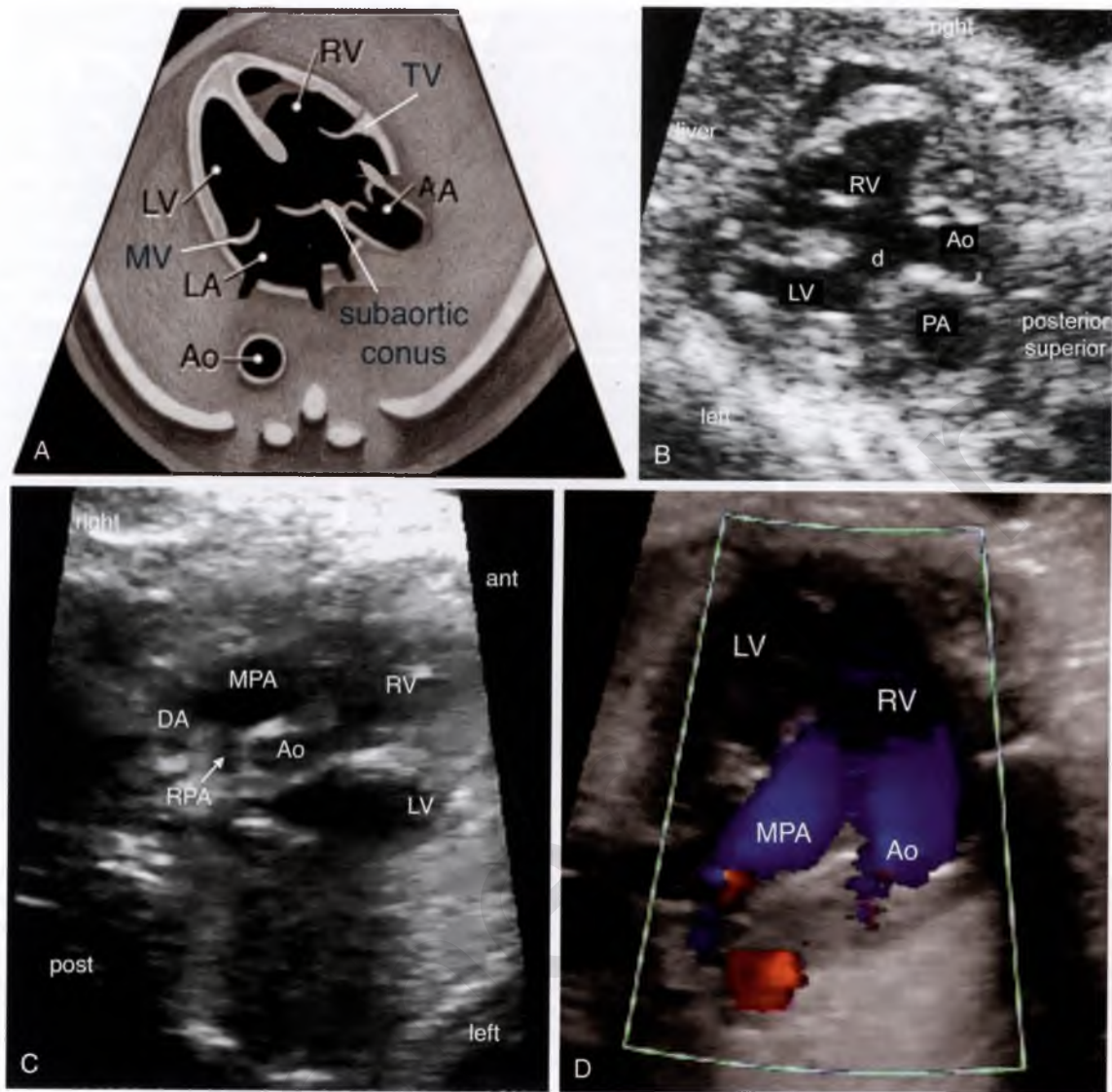


**FIG 13-57** Diagram and sonographic images of double-outlet right ventricle (DORV). The diagram (**A**) shows that the great artery closest to the ventricular septum (which typically arises from the left ventricle) arises from the right ventricle in DORV, as does the anterior great artery (not shown). In **A** through **C**, the aorta is closest to the ventricular septal defect (VSD), and there is a subaortic conus. In **D** the pulmonary artery is closest to the VSD. For all, the ventricular septal defect (d in **B**) is below the aortic valve and is the only outlet of the left ventricle. **B** shows subaortic narrowing. In **D** both outflow tracts are unobstructed and the great vessels are malposed, with the aorta rightward and anterior. AA, ascending aorta; ant, anterior; Ao, aorta; d, ventricular septal defect; DA, ductus arteriosus; LA, left atrium; LV, left ventricle; MPA, main pulmonary artery; MV, mitral valve; PA, main pulmonary artery; post, posterior; RPA, right pulmonary artery; RV, right ventricle; TV, tricuspid valve. (**A**, Adapted with permission from American Institute of Ultrasound in Medicine: AIUM practice guideline for the performance of fetal echocardiography. *J Ultrasound Med* 32:1067-1082, 2013.)

biventricular repair, chance of survival is much better, with survival rate to discharge 93% to 95%<sup>293</sup> and approximately 85% to 91% survival rate at 5 years. Reinterventions among those with biventricular repair are common but are associated with low morbidity and mortality rates.<sup>297</sup>

**Diagnostic Imaging Features.** General features (Fig. 13-57 and Video 13-18):

- DORV is associated with other cardiac anomalies. Common associations include venous anomalies such as TAPVC, partial anomalous pulmonary venous return (PAPVC), and left superior vena cava; endocardial cushion defects including complete AVCDs;

pulmonary stenosis; aortic hypoplasia; and coarctation of the aorta.

- Secundum ASDs are also common in DORV but may be difficult to assess in the fetus, given the widely patent foramen ovale.
- DORV is common in heterotaxy conditions. If DORV is seen in combination with an AVCD or any venous anomalies, heterotaxy must be considered, and careful imaging should be performed of all cardiovascular, thoracic, and abdominal structures.
- A sweep toward the fetal head starting in a four-chamber view is often helpful to delineate which great artery is more inferior and posterior and to delineate left-right relationships.



Features of TOF physiology DORV:

- Aorta is closest to the VSD (therefore VSD is subaortic) and may appear to override the VSD, but to a greater degree than that in TOF.
- Subpulmonary or pulmonary valve stenosis is present.

Features of TGA physiology DORV (see Fig. 13-57D):

- Pulmonary artery is closest to the VSD (thus subpulmonary VSD) and may appear to override the VSD.
- The great arteries are malpositioned with the aorta, usually either anterior and rightward or adjacent but rightward of the pulmonary artery.
- Pulmonary stenosis or aortic and arch hypoplasia may be present.
- Coarctation and aortic arch hypoplasia are more common in TGA type DORV.

Features of VSD physiology DORV:

- Neither great artery is obstructed.
- The pulmonary artery is usually anterior.

### Transposition of the Great Arteries

**Definition.** D-transposition of the great arteries (DTGA), also known as complete transposition of the great arteries, is a congenital heart defect in which there is atrial situs solitus (usual atrial arrangement) and AV concordance but ventricular arterial discordance, with the RV connection to the aorta, and the LV connection to the pulmonary artery (Fig. 13-58). The aorta is rightward and anterior to the pulmonary artery, which is leftward and posterior. The great artery relationship is designated as D-transposed in which “D” indicates *dexter*, the Latin word meaning “right.”

**Epidemiology.** DTGA is a relatively common congenital cardiac anomaly, occurring in 5% to 7% of all congenital cardiac defects, with an incidence of 0.33 cases per 1000 live births and a 2:1 male-female predominance.<sup>298,299</sup> Extracardiac anomalies are extremely rare in patients with DTGA when no other cardiac lesions are present.

**Anatomy.** DTGA is seen in isolation with no additional cardiac anomalies other than a persistent PFO or PDA in approximately 50% of cases. The most commonly associated cardiac anomaly is a VSD, occurring in about 40% to 45% of DTGA patients; one third of the VSDs are small and of no hemodynamic significance. LVOT obstruction occurs in 20% to 30% of DTGA. LVOT obstruction is associated with a VSD in approximately 30% of DTGA. However, the combination of a VSD with significant LVOT obstruction occurs in nearly 10%. The LVOT obstruction can be a dynamic obstruction related to septal deviation into the LVOT, which is most common with an intact interventricular septum (IVS) because the right ventricular systolic pressure exceeds that in the LV. Fixed LVOT obstruction can be secondary to a subpulmonary fibromuscular membrane and tunnel-like fibromuscular narrowing. Subpulmonary obstruction can also be noted secondary to redundant mitral valve tissue or abnormal anterior mitral valve chordae in the LVOT. Redundant tricuspid valve tissue or aneurysm of the membranous septum bulging across the VSD during systole can also cause LVOT obstruction. Pulmonary valve stenosis and hypoplasia of the pulmonary valve annulus are rarely seen with DTGA with an intact IVS but are seen in approximately 30% of DTGA/VSD, which often have complex LVOT obstruction.<sup>300,301</sup>

Taussig-Bing anatomy is a term used for DORV with malposition of the great arteries, and the physiology closely resembles that of DTGA. In this anatomy, there is a large subpulmonary VSD. As the pulmonary artery may override the aorta, sometimes this is referred to as Taussig-Bing type of TGA instead of DORV. In Taussig-Bing anatomy, there is a subaortic conus or infundibulum, which may be malaligned anteriorly and often results in subaortic obstruction. This is associated with aortic valve hypoplasia, aortic arch hypoplasia, and

coarctation of the aorta. The pulmonary valve annulus overrides the VSD and the pulmonary artery is significantly larger than the aorta.<sup>300</sup>

**Genetic Considerations.** There is a low incidence of extracardiac or chromosomal anomalies with isolated DTGA. DTGA may occur in association with heterotaxy (most commonly asplenia syndrome/right atrial isomerism), most commonly when DORV or complete AVCDs are also present. In some patients with DTGA and heterotaxy (and rare cases of isolated DTGA), mutations of *ZIC3*, *CFC1*, and *NODAL* genes (laterality genes) have been observed.

DTGA occurs in pregnant mice treated with retinoic acid or with retinoic acid inhibitors. In humans, some families have recurrence of DTGA or congenitally corrected transposition of the great arteries (CCTGA) cases in first-degree relatives.<sup>302,303</sup> These data suggest that monogenic inheritance with a variable phenotypic expression could explain the familial aggregation of DTGA and CCTGA. The prevalence of DTGA is also higher in infants of diabetic mothers, following maternal infection (i.e., flu with fever) during critical cardiogenesis, with intake of ibuprofen, and in cases of in vitro fertilization.<sup>302-306</sup>

**Interventions and Prognosis.** DTGA is well tolerated in utero. Following delivery, there are parallel systemic and pulmonary cardiac circuits. The deoxygenated systemic venous return is to the RA-RV-aorta, and the oxygenated pulmonary venous return is to the LA-LV-PA. To survive, the newborn requires either intracardiac mixing at either the atrial (ASD) or ventricular (VSD) level or at the level of the great arteries via a PDA. A newborn with DTGA with an intact ventricular septum and a restrictive atrial septum or PDA may present with profound hypoxemia and acidosis after delivery. Some studies suggest that prenatal diagnosis can lower the mortality rate in infants with DTGA, given the ability to rapidly diagnose and intervene at birth.<sup>21,22</sup>

Surgical repair in DTGA involves an arterial switch operation. The native pulmonary valve becomes the neo-aorta and the coronary arteries are reimplanted into the sinuses of the neo-aorta. The native aortic valve and root become the neopulmonary valve. If there is a VSD or ASD, the septal defects are closed. If there is complex LVOT obstruction or significant pulmonary valve stenosis, an arterial switch is not an option for repair. DTGA and VSD with significant LVOT obstruction are best palliated by baffling the VSD patch to the anteriorly positioned aorta. This requires placing a valved conduit from the RV to the branch pulmonary arteries (Rastelli operation). DTGA and DTGA with a VSD have excellent results in major congenital cardiovascular surgical centers.<sup>307</sup> In the current era, the mortality rate for an arterial switch ranges from 0% to 2.8% in experienced congenital cardiovascular centers. Patients with complex DTGA with LVOT obstruction have increased risk of recurrence of LVOT obstruction and higher morbidity and mortality rates.<sup>308-311</sup>

**Diagnostic Imaging Features.** Isolated DTGA with an intact ventricular septum, which is seen in up to 50% of patients, will have a normal-appearing four-chamber view (see Fig. 13-58C). Thus, DTGA is commonly missed on a prenatal anatomic scan; a large national series gathering data over 21 years of fetal cardiac screening noted a detection rate of DTGA of only about 26%.<sup>298</sup> Improved detection of DTGA is expected with the inclusion of a detailed evaluation of the outflow tracks in addition to the four-chamber view.<sup>70</sup>

Two very important structures to define in the DTGA fetus are the PFO and the PDA, which, if restrictive, suggest the newborn is at risk of developing severe hypoxemia at birth.<sup>312-314</sup> Fetuses with DTGA who are at risk for severe neonatal hypoxemia have abnormal flow in the fetal PDA, in which there is retrograde diastolic flow in the PDA and low-velocity systolic prograde PDA flow. In the fetus with DTGA and no atrial septal restriction, the atrial septum bows into the LA with continuous right-to-left flow. A fetus with DTGA and either a restrictive foramen ovale or a hypermobile, redundant atrial septum



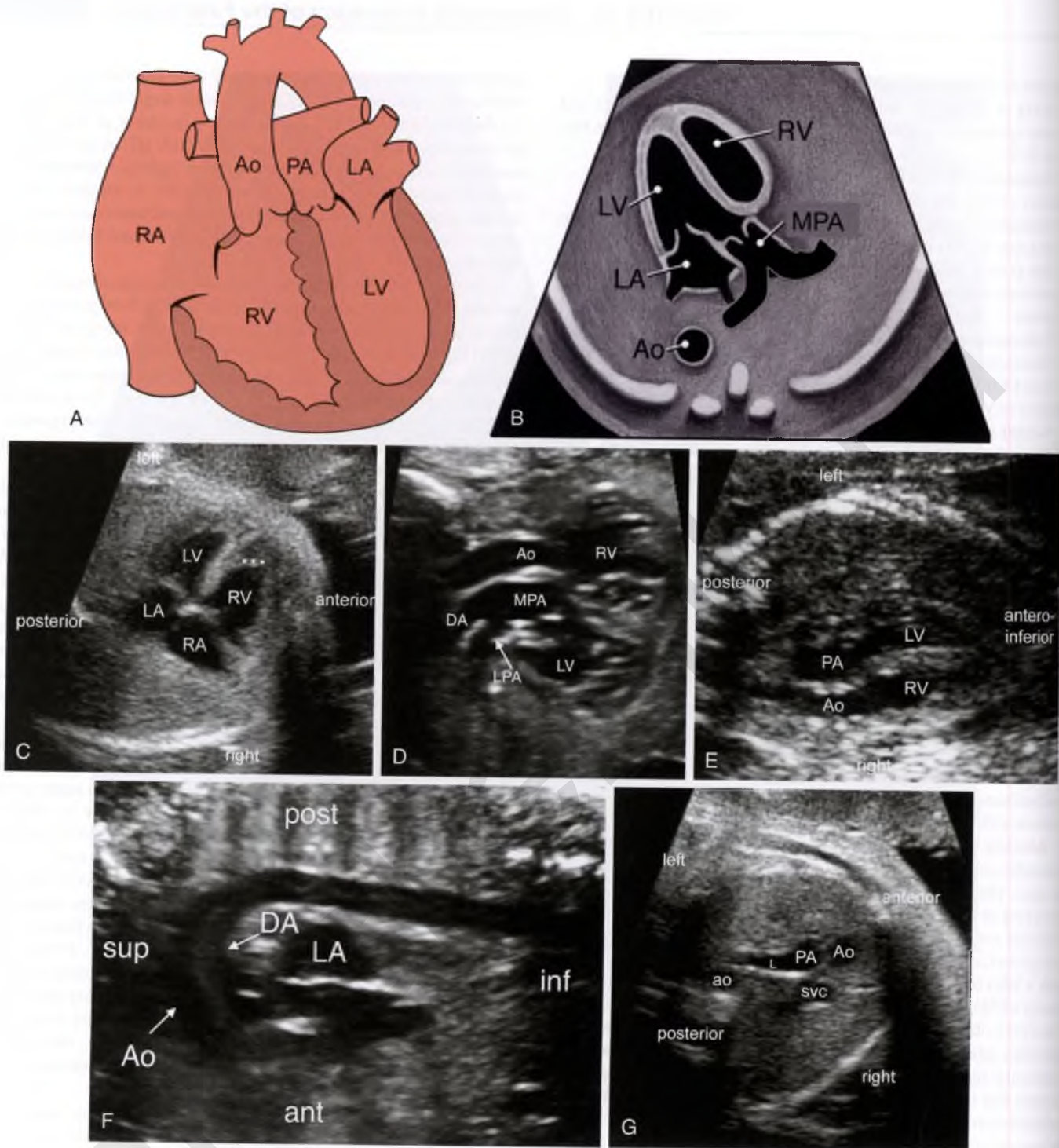


**FIG 13-58** Diagrams and sonographic images of D-transposition of the great arteries (DTGA, also known as complete transposition of the great arteries). **A**, Anatomy of DTGA. **B**, Fetal echocardiographic diagram of the left ventricular outflow tract view; small sweeps show the bifurcation of the branch pulmonary arteries. **C**, The four-chamber view shows normal cardiac anatomy. The apex of the right ventricle (RV) is obliterated by the moderator band (*asterisks*). **D**, A view obtained between the short-axis views and the arch views. The parallel great arteries are easily visualized, and the left pulmonary artery and ductus arteriosus can be seen arising from the posterior great artery, that helps identify it as the pulmonary artery. **E**, Ventricular outflow tract view shows discordant ventriculoarterial connections with parallel courses. **F**, View of the arches shows that the aortic arch has a more anterior origin and is more "hockey-stick-shaped" in DTGA, and the ductal arch originates more posteriorly and is more "candy-cane-shaped." **G**, Three-vessel view shows triangular arrangement of the three vessels. The aorta (Ao) is located right and anterior to the main pulmonary artery (PA). ant, anterior; ao, aorta; DA, ductus arteriosus; inf, inferior; L, left pulmonary artery; LA, left atrium; LV, left ventricle; post, posterior; RA, right atrium; sup, superior; svc, superior vena cava. (**B**, Adapted with permission from American Institute of Ultrasound in Medicine: AIUM practice guideline for the performance of fetal echocardiography. *J Ultrasound Med* 32:1067-1082, 2013. **D** and **E** from Morris SA, Maskatia SA, Altman CA, Ayres NA: *Fetal and perinatal cardiology*. In Allen HD, Shaddy RE, Penny DJ, et al [eds]: *Moss and Adams' Heart Disease in Infants, Children, and Adolescents Including the Fetus and Young Adult*, 9th ed. Philadelphia: Lippincott Wolters Kluwer, 2016, used with permission.)



that undulated between the left and right atria is at risk for neonatal hypoxemia.<sup>312-315</sup>

#### Imaging Tips

- The outflow tracts will be parallel (Fig. 13-58D through F).
- The main pulmonary artery is typically short, arises posteriorly from the LV, and bifurcates (Fig. 13-58B and D).
- 3VV will demonstrate the aorta as the anterior great artery, and the pulmonary artery as posterior (Fig. 13-58G). At times, the vessels cannot be seen in the same view, as the aorta ascends more superiorly than the pulmonary artery (Fig. 13-58F).
- The aorta is superior or cephalad to the pulmonary artery and this elongates the transverse arch and has a more “hockey stick” appearance (Fig. 13-58F). Note the head and neck vessels arising from the superior and anterior aorta. Color Doppler can assist in the differentiation of the two great arteries.
- If TGA is suspected, inspect the PDA for retrograde flow. Note ductal pulsatility index (PI) because a PI of 1.8 or less is associated with ductal restriction and may be a harbinger of neonatal hypoxemia.
- Inspect the atrial septal status for any restriction or bidirectional shunting at the atrial level. Determine if the atrial septum is hypermobile or excessively redundant because this too may indicate a high risk of neonatal hypoxemia and need for urgent intervention.
- Inspect the ventricular septum for a VSD.
- Evaluate the mitral valve and tricuspid valve for any abnormalities or evidence of LVOT obstruction.
- Evaluate the LVOT and pulmonary valve for obstruction, which is more frequently noted with VSD; more severe and complex LVOT obstruction has increased the morbidity rate due to the complex surgical repair.
- Compare the size of the aorta and pulmonary artery. If the pulmonary artery is abnormally large, evaluate the subaortic region for obstruction due to a malaligned conus. This defect is associated with arch hypoplasia and obstruction as seen in Taussig-Bing type of DTGA.

### Congenitally Corrected Transposition of the Great Arteries

**Definition.** CCTGA occurs when there is both AV and ventriculoarterial discordance. In other words, the great arteries are transposed, as are the morphologic LVs and RVs (Fig. 13-59A).

**Epidemiology.** CCTGA is relatively rare and occurs in approximately 0.03 per 1000 live births and accounts for 0.05% of CHD.<sup>316</sup>

**Anatomy.** In CCTGA (see Fig. 13-59), systemic venous return is to the RA, which is connected to the morphologic LV via the mitral valve. The LV gives rise to the pulmonary artery that is positioned rightward and posterior to the aorta. Pulmonary venous return is to the morphologic LA, which connects to the morphologic RV via the tricuspid valve. The RV gives rise to the aorta, which is anterior and to the left of the pulmonary artery. In this defect, the unoxygenated systemic venous return is to the lungs via the morphologic LV and pulmonary artery, and the oxygenated pulmonary venous return is directed to the aorta via the morphologic RV. Thus, there is physiologic correction in terms of blood oxygen saturation due to the discordance of both the AV and ventriculoarterial connections. In CCTGA, abnormal leftward looping/topology of the ventricles results in the ventricular septum being in a more sagittal or horizontal plane.

Only 1% to 2% of CCTGA patients have no additional cardiac anomaly.<sup>317</sup> VSD is the most commonly associated defect with CCTGA and is present in approximately 80% of CCTGA cases (Fig. 13-59D). Other coexisting anomalies are subpulmonary valve stenosis, pulmonary valve stenosis, tricuspid valve anomalies, ASD, and congenital complete heart block. Approximately 5% of patients with CCTGA have an abnormality of atrial situs.<sup>317,318</sup>

The most common type of VSD is a membranous defect, and they are often large and have anterior extension. The location of the perimembranous VSD is in close proximity to the tricuspid valve septal leaflet and the posterior mitral valve leaflet. Less frequently seen are conoseptal and muscular VSDs.

The right AV valve is a morphologic mitral valve with two papillary muscles. In majority of CCTGA, the mitral valve has chordal attachments only to the morphologic left ventricular free wall. However, mitral valve abnormalities occur in up to 10% of CCTGA patients and may account for subpulmonary obstruction due to abnormal or accessory chordae attached to the crest of the ventricular septum or redundant or accessory mitral valve tissue in the LVOT.<sup>319,320</sup> The pulmonary vein is wedged between the two AV valves, and with the absence of the subpulmonary infundibulum or conus, the mitral valve is in close proximity to the pulmonary vein. This creates a substrate for LVOT obstruction.

The left AV valve is the morphologic tricuspid valve connected to the morphologic RV that is left in position. The tricuspid valve has an approximately 90% incidence of valve abnormalities of varying degrees, with Ebstein anomaly the most common (Fig. 13-27C).<sup>317,321</sup> A subaortic infundibulum or conus positions the aorta superiorly and anteriorly. Thus, the aorta is to the left of the pulmonary artery. The subaortic conus causes the lack of fibrous continuity between the tricuspid valve and the aortic valve. The subaortic conus elevates the aortic valve more superior than the left AV valve, and thus the tricuspid valve, which is the left AV valve, is not seen in the same plane as the aortic valve.<sup>316</sup> Both AV valves can contribute to LVOT obstruction secondary to the anatomic proximity to the LVOT, resulting in straddling of either AV valve into the VSD.<sup>317</sup>

**Rhythm Abnormalities.** Congenital complete heart block is associated with CCTGA. In utero, the fetus with complete AV block has a better prognosis when associated with normal cardiac chamber dimensions.<sup>322</sup> CCTGA has also been associated with atrial ectopy, reentry tachycardia, accessory bypass track, and ventricular tachycardia.<sup>322</sup>

**Genetic Considerations.** Familial recurrence of CCTGA is uncommon; however, in a large clinical case series from four Italian centers the authors noted a 5.2% risk for a sibling to have a cardiac anomaly. The most common congenital cardiac defect seen in siblings of CCTGA patients was DTGA. Recurrence risk of DTGA for relatives of CCTGA patients was 2.6%. Five families with nonaffected parents had two children each with one child with CCTGA and the other child with DTGA. Vertical transmission was seen in one mother with CCTGA, who had a son with DTGA.<sup>303</sup> The recurrence risks were significantly higher than prior published epidemiologic studies, which have reported a recurrence risk of 1% to 3% for parents with a child with CHD.<sup>323</sup> The study suggests single gene involvement in some cases, and possibly autosomal recessive inheritance. Environmental factors have also been shown to be associated with CCTGA.<sup>303,324,325</sup>

Another study reported six twin sets in which one twin had CCTGA and the other twin had no cardiac anomalies. This study and others have documented an increased incidence of CHD in twin pregnancies, suggesting that the twinning process itself increases the risk of one twin having a cardiac defect due to epigenetic or environmental effects on monozygotic twins with identical genetic makeup.<sup>326,327</sup>

In all vertebrates, the linear heart tube undergoes rightward looping, which is essential for proper orientation of the pulmonary (right) and systemic (left) ventricles, and for alignment of the heart chambers with the vasculature. The molecular mechanisms governing cardiac looping remain unknown, but identification of genes differentially expressed along the outer and inner curvatures of the looped heart tube suggests that intrinsic properties of the two surfaces may underlie this critical morphogenetic event. The direction of cardiac looping is determined



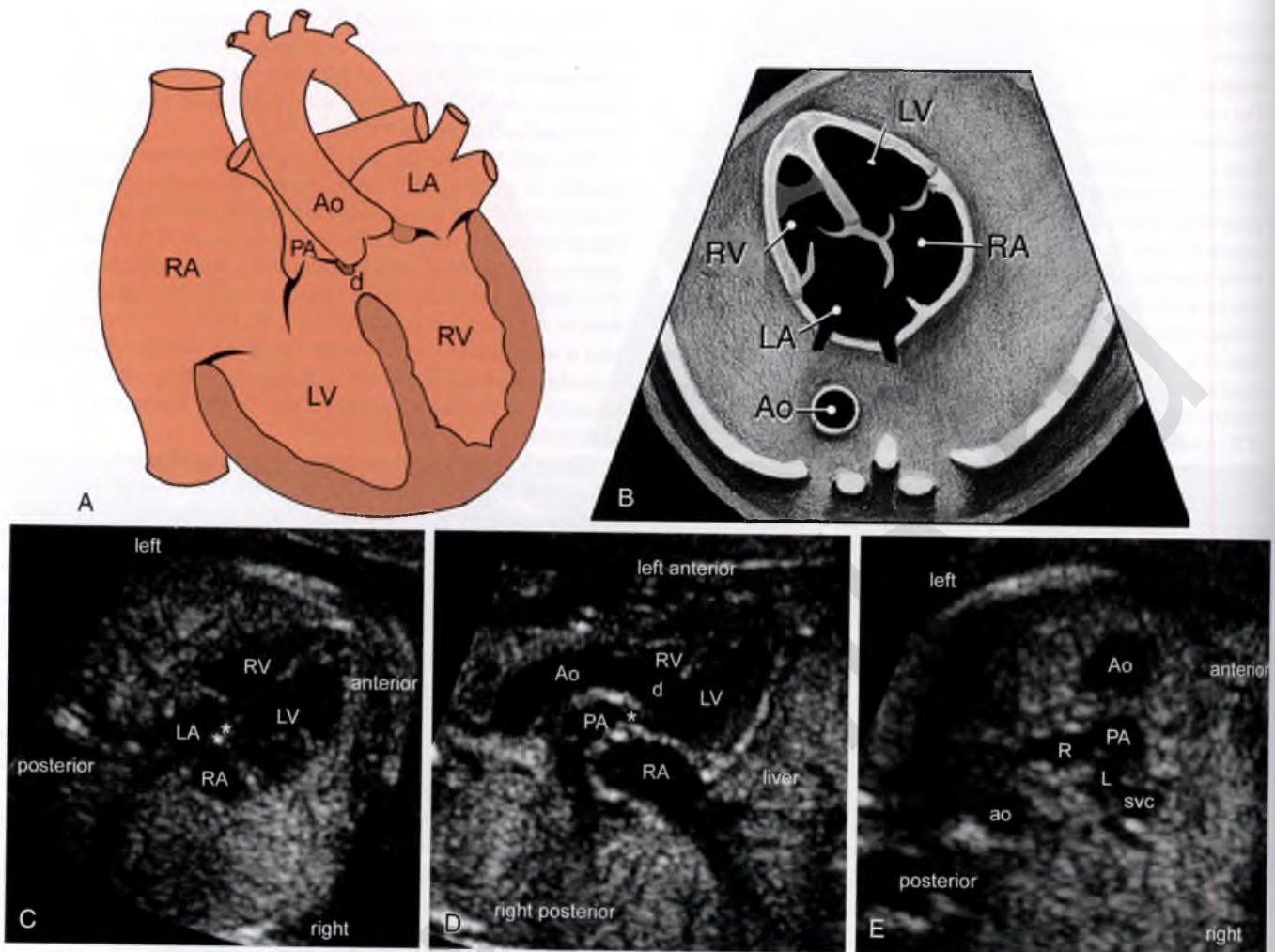


**FIG 13-59** Diagrams and sonographic images of congenitally corrected transposition of the great arteries (CCTGA, also known as discordant atrioventricular and ventriculoarterial connections). **A**, Anatomy of CCTGA. **B** and **C**, Diagram and sonographic image in the four-chamber view, with left ventricular looping (left-handed topology), with the morphologically right ventricle (RV) on the left and the morphologically left ventricle (LV) on the right, and discordant atrioventricular connections. Note the more apical attachment of the left-sided atrioventricular valve to the septum (*asterisks*). **D**, Right anterior oblique view shows a superoinferior relationship of the parts of the ventricles and discordant ventriculoarterial connection. The subpulmonary outflow tract (*asterisk*) shows narrowing. **E**, The three-vessel view shows a grossly abnormal great artery relationship with the ascending aorta (Ao) on the left anterior aspect of the main pulmonary artery (PA). This position is most commonly seen in and is highly suggestive of corrected transposition of the great arteries in situs solitus. Ao, aorta; d, ventricular septal defect; L, left pulmonary artery; LA, left atrium; R, right pulmonary artery; RA, right atrium; SVC, superior vena cava. (**B**, Adapted with permission from American Institute of Ultrasound in Medicine: AIUM practice guideline for the performance of fetal echocardiography. *J Ultrasound Med* 32:1067-1082, 2013.)

by an asymmetric axial signaling system that also affects the location of the lungs, liver, spleen, and gut. Before organ formation begins, this signaling cascade directs the asymmetric expression of sonic hedgehog and Nodal, members of the transforming growth factor (TGF) family, in the lateral mesoderm. Interpretation of left-right signals is mediated in part by the transcription factor Ptx2, which is expressed along the left side of developing organs, including the early heart tube. Mouse models of left-right defects demonstrate absent, bilaterally symmetric, or reversed Nodal and Ptx2 expression. In humans, mirror-image reversal of left-right asymmetry is often associated with normal organogenesis. But a discordance of cardiac, pulmonary, and visceral asymmetry (heterotaxy syndrome) reflects a lack of coordinated left-right signaling and is universally associated with defects in organogenesis.

The common association of human cardiac alignment defects with abnormalities in left-right asymmetry points to intersecting pathways that regulate the direction and process of cardiac looping, and highlights the clinical significance of this area of study.<sup>305,328</sup> Pregnant mice receiving retinoic acid and retinoic acid inhibitors have fetuses with CCTGA.<sup>304</sup> Thus, the cause of CCTGA is heterogeneous and multifactorial.

**Interventions and Prognosis.** A classic or physiologic complete repair of CCTGA is VSD closure and addressing any LVOT obstruction or pulmonary valve stenosis. The classic repair leaves the morphologic RV as the systemic ventricle and the tricuspid valve is the systemic AV valve. The morphologic RV supports systemic circulation, which leads to progressive RV dilation and subsequently increasing tricuspid valve



insufficiency and chronic heart failure. Long-term outcomes include increased morbidity and mortality risks due to significant tricuspid valve insufficiency, AV block and secondary heart failure due to RV dysfunction. The systemic RV has single coronary supply, which can also contribute to RV dysfunction. The classic repair does not address the ventricular arterial discordance.<sup>329</sup> Survival rate at 1 year is approximately 84% with a decline to 60% at 15 years.<sup>330-332</sup>

More recently, CCTGA has been repaired via double switch. The systemic venous return is baffled to the tricuspid valve via a Mustard or Senning atrial switch. The great arteries are switched and coronary arteries reimplanted into the neo-aorta. The LV must be “prepared” and have systemic or near systemic pressures prior to the double switch. In the presence of significant pulmonary valve or subvalvular stenosis, the LV is accustomed to high systolic pressures. A pulmonary artery band is placed when there is no significant pulmonary or subpulmonary valve stenosis. In CCTGA cases with a large VSD, the VSD closure baffles the LV to the anterior aorta and there is an RV to pulmonary artery conduit placed (Rastelli procedure) in addition to the atrial switch for an anatomic repair. The anatomic repair commits the morphologic LV and mitral valve to systemic pressures. An anatomic repair is preferred when there is significant tricuspid valve regurgitation. The double switch has about 7% early death risk, but at 10-year follow-up in one study, the patients were heart failure free and had a 10-year survival rate of 77% to 84%.<sup>333-336</sup> Late LV dysfunction has been noted in CCTGA patients with an anatomic repair and complete heart block.<sup>337,338</sup> Overall, an anatomic repair to commit the LV to the systemic ventricle has a better long-term outcome than the classic repair.

#### Diagnostic Imaging Features

- Left AV valve is inferiorly displaced and lower in position than the right AV valve (Fig. 13-59C).
- Left AV valve has chordal attachments to the ventricular septum.
- The ventricle on the right has two papillary muscles and the right AV valve most frequently has no septal attachments.
- A moderator band is noted in the posterior leftward positioned morphologic RV (Fig. 13-59B).
- Aorta is anterior and leftward and is often just posterior to the sternum (Fig. 13-59E).
- VSDs are present in 80% of CCTGA so careful inspection of the ventricular septum is important.
- Pulmonary valve and subpulmonary valve are coexisting anomalies.
- CCTGA can present with complete heart block, bradycardia, or atrial tachycardia, so evaluation of the rhythm is critical.
- In the 3VV, the aorta is to the left of the pulmonary artery and more superior and anteriorly positioned (see Fig. 13-59E).
- The pulmonary artery is wedged between the two AV valves.

### Hypoplastic Left Heart Syndrome

**Definition.** HLHS is one of the most severe heart conditions and is a spectrum of cardiac malformations, characterized by a severe underdevelopment of the left heart-aorta complex, consisting of aortic or mitral valve atresia, stenosis, or hypoplasia with marked hypoplasia or absence of the LV, and hypoplasia of the ascending aorta and of the aortic arch (Fig. 13-60 and Video 13-19).<sup>339</sup>

As discussed later, hypoplasia of the left-sided cardiac structures, including the mitral valve, the LV, aorta, and aortic arch, can occur without meeting criteria for HLHS.

**Birth Prevalence/Epidemiology.** HLHS occurs in approximately 1 in 5000 to 6000 live births.<sup>24,230</sup> Without surgery, this condition is lethal, and comfort care previously was the only option. However, major

changes over the last 30 years in diagnosis, surgical intervention, and medical management of HLHS have now allowed survival into adulthood for the majority of patients.<sup>15</sup>

**Anatomy.** Although HLHS is used collectively to describe the collection of features described previously, there are likely several mechanisms of developing left-sided hypoplasia,<sup>15</sup> and HLHS defines the most severe form. Understanding of this process has been improved with modern fetal imaging.<sup>340</sup> Most mechanisms appear to be related to the “no flow, no grow” phenomenon: when blood flow is impaired, growth of the affected fetal heart structures halts.

Classic HLHS is severe mitral stenosis or atresia with severe aortic stenosis or atresia and a severely hypoplastic slit-like LV cavity and severely hypoplastic aortic arch (see Fig. 13-60 and Video 13-19). Although sometimes the LV is severely hypoplastic on the first fetal evaluation and a diagnosis of HLHS is clear, it is not uncommon to see moderate left ventricular hypoplasia in the fetus that progresses to HLHS later in pregnancy.

There are two general patterns to left ventricular hypoplasia when classic HLHS is not already present—a long thin LV or a short fat LV. When the left-sided structures are not clearly small enough to meet criteria for HLHS, it may be referred to as a “borderline LV.”<sup>296</sup> The pattern of a long, thin hypoplastic LV is most commonly seen when arch hypoplasia is present and is often first recognized as left-right ventricular asymmetry (Fig. 13-61).<sup>341</sup> The presence of left-right asymmetry (with left side smaller) on fetal echocardiography should trigger concern for developing coarctation of the aorta (Fig. 13-61A). When there is asymmetry in addition to moderate to severe hypoplasia of multiple small left-sided structures, this pattern is also often referred to as Shone complex, although Shone and colleagues described a very specific set of anatomic features that are not always present in this pattern of findings.<sup>296,342</sup> Others have referred to this as “hypoplastic left heart complex.”<sup>339,343</sup> In this pattern of hypoplasia, the mitral valve and aortic valve are often hypoplastic and subaortic obstruction may be present (Fig. 13-62 and Video 13-20). Endocardial fibroelastosis is typically not present. For many of these patients, the LV may actually expand with improved filling after birth, and single ventricle palliation may not be necessary. Many children with the long thin LV pattern will require aortic arch repair, and possible mitral valve surgery and subaortic or aortic surgery, and sometimes in severe cases may require single ventricle palliation.<sup>341</sup>

For those with a long thin LV, a main cause is postulated to be obstruction of inflow into the LV, as this pattern of hypoplasia has been described with various associations, including abnormal or small PFO,<sup>344</sup> left superior vena cava to coronary sinus (Fig. 13-63),<sup>345,346</sup> aneurysmal atrial septum obstructing mitral valve flow,<sup>106</sup> and leftward malattachment of the atrial septum.<sup>344,347</sup>

The second pattern of left ventricular hypoplasia when frank HLHS is not present is a short LV, which is almost universally associated with severe fetal aortic stenosis (Fig. 13-64).<sup>348,349</sup> In fetal aortic stenosis, the LV first becomes dilated and severely dysfunctional (Video 13-21). Endocardial fibroelastosis develops, and the pressure generated by the LV decreases. Left ventricular growth halts, and right-sided structures grow around the left side of the heart, resulting in HLHS (Videos 13-22 and 13-23).<sup>348,350,351</sup> Endocardial fibroelastosis and ventricular dysfunction are nearly universal in late fetal aortic stenosis. Mitral valve abnormalities and arch obstruction are also common. Fetal aortic stenosis is particularly easy to miss on cardiac screening, as the LV may appear normal on the four-chamber view (see Video 13-21) and only later develop dilation and ongoing left ventricular growth arrest and left ventricular dysfunction.<sup>352</sup> Clues for development of HLHS in the fetus in the absence of a severely small LV are severe left ventricular dysfunction, endocardial fibrosis (Fig. 13-64A and B), monophasic mitral



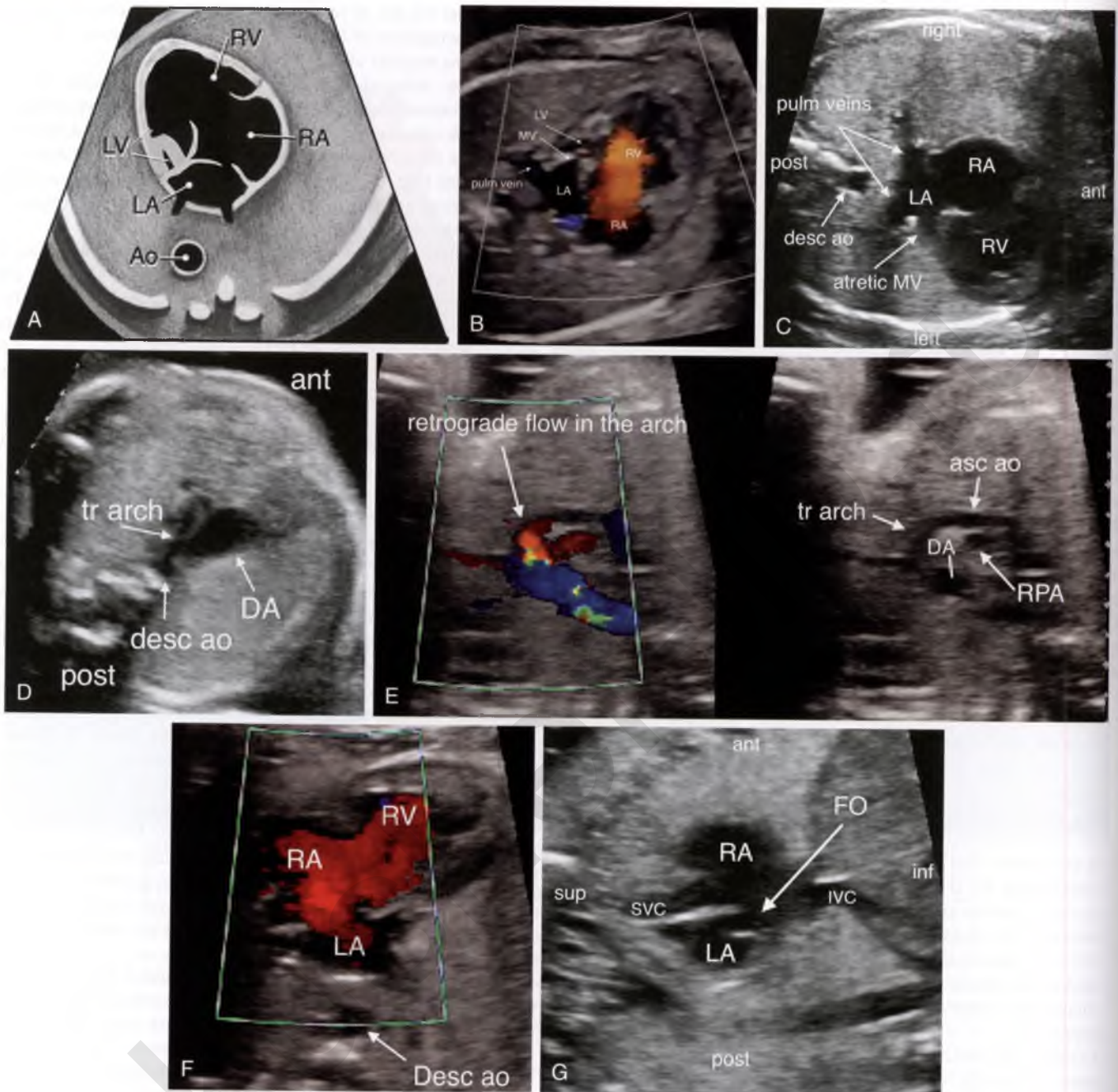


**FIG 13-60** Diagram and sonographic images of hypoplastic left heart syndrome (HLHS). **A** through **C**, Diagram and color Doppler images of HLHS in the four-chamber view. **B** shows HLHS with severe mitral stenosis and aortic atresia (not in image), with a severely hypoplastic left ventricle. In **C**, the fetus has mitral and aortic atresia, and there is no discernible left ventricle. **D**, Three-vessel and trachea view shows a severely hypoplastic transverse aortic arch. **E**, A long-axis view of the aortic with two-dimensional and color Doppler imaging shows a severely hypoplastic ascending aorta and transverse arch. **F**, Unrestrictive atrial septum with left-to-right flow across the foramen ovale. **G**, The bicaval view is often the best way to evaluate the atrial septum in HLHS. ant, anterior; Ao, aorta; asc ao, ascending aorta; DA, ductal arch; desc ao, descending aorta; FO, foramen ovale; inf, inferior; IVC, inferior vena cava; LA, left atrium; LV, left ventricle; MV, mitral valve; post, posterior; pulm vein(s), pulmonary vein; RA, right atrium; RPA, right pulmonary artery; RV, right ventricle; sup, superior; SVC, superior vena cava; tr arch, transverse arch. (**A**, Adapted with permission from American Institute of Ultrasound in Medicine: AIUM practice guideline for the performance of fetal echocardiography. *J Ultrasound Med* 32:1067-1082, 2013.)



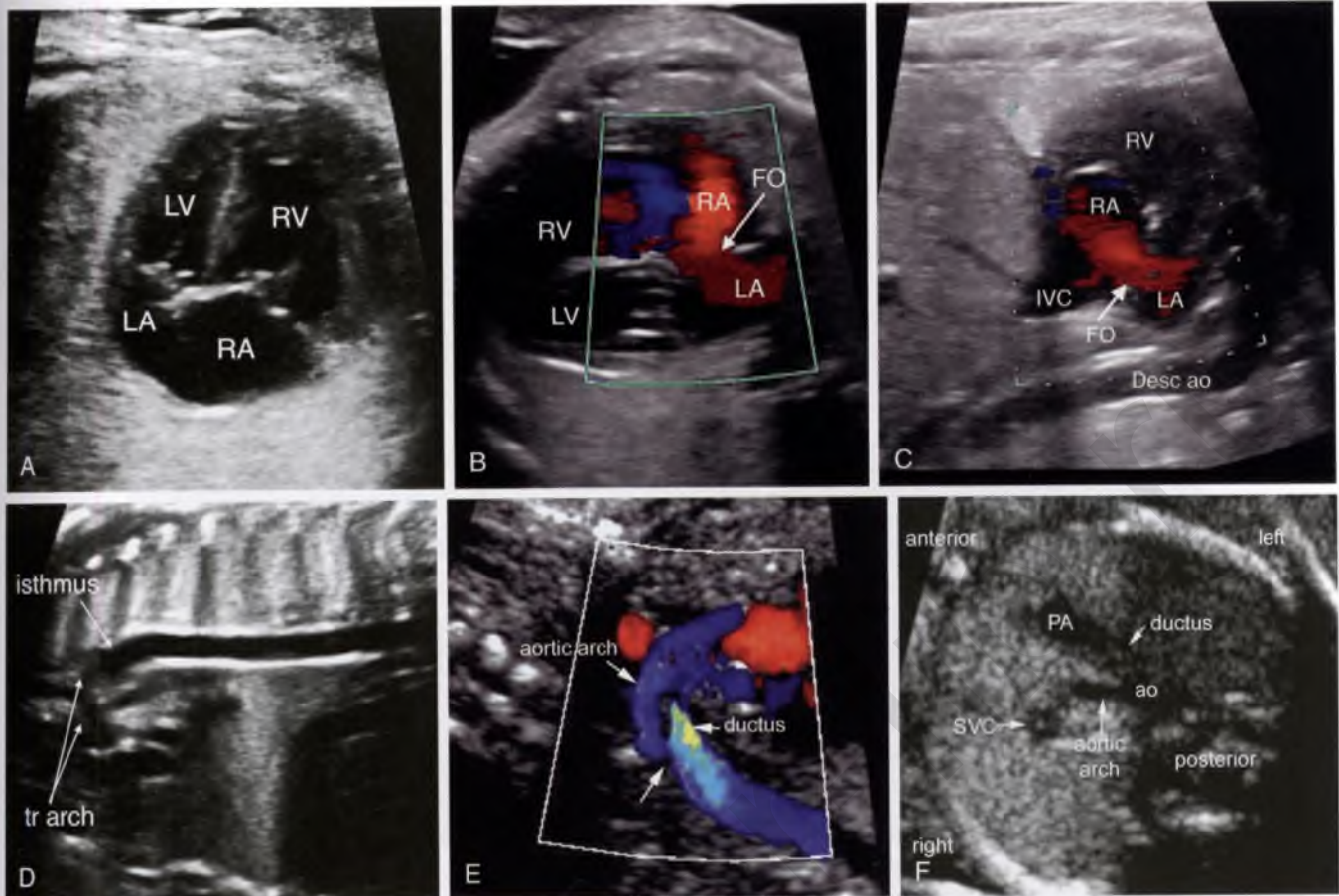


**FIG 13-61** Coarctation of the aorta. **A**, In the four-chamber view, there is left-right ventricular size discrepancy, with the left ventricle smaller, but forming an apex. **B** and **C**, Atrial level shunting is typically bidirectional or left to right. **D** and **E**, The arch may appear hypoplastic. In this arch, all flow is forward. **F**, From the three-vessel and trachea view, the transverse arch is much smaller than the ductal arch. Ao and Desc ao, descending aorta; FO, foramen ovale; IVC, inferior vena cava; LA, left atrium; LV, left ventricle; PA, main pulmonary artery; RA, right atrium; RV, right ventricle; SVC, superior vena cava; tr arch, transverse arch.

inflow (Fig. 13-64D), retrograde flow in the aortic arch (Fig. 13-64E), and left-to-right flow across the atrial septum.

A portion of patients with HLHS will develop severe restriction at the atrial septum or closure of the foramen ovale, which confers a much worse prognosis because there is no exit of pulmonary blood flow.<sup>340,353,354</sup> For this reason, fetal intervention or emergent postnatal intervention are often offered.<sup>353,355-357</sup> Interrogation of the pulmonary venous Doppler pattern may help determine the severity of atrial level restriction (Fig. 13-65).

**Genetic Considerations.** From 10% to 19% of patients with HLHS are ultimately found to have either extracardiac birth defects or a genetic abnormality.<sup>24,291,340,358,359</sup> The most common of these is Turner syndrome, occurring in approximately 6% of liveborn females with HLHS.<sup>20</sup> Given that survival is poor in patients with Turner syndrome and HLHS,<sup>360,361</sup> counseling regarding the prognostic utility of diagnostic testing is particularly important in female fetuses with HLHS. Other genetic disorders that have been associated with HLHS include trisomy 13, trisomy 18, Noonan syndrome, chromosome 7 deletions, Holt-Oram syndrome, Smith-Lemli-Opitz syndrome, partial trisomy 9, Jacobsen syndrome, and others.<sup>39,291,349,358,362</sup> Extracardiac anomalies associated with HLHS include agenesis of the corpus callosum,

diaphragmatic hernia, duodenal atresia, tracheoesophageal fistula, and omphalocele, among others (see Video 13-21).<sup>361,363</sup> The large majority of fetuses with HLHS and genetic disorders also have extracardiac birth defects.<sup>39</sup>

**Interventions and Prognosis.** Two fetal interventions are available for fetuses with evolving complete HLHS, depending on the anatomy. In cases of fetal aortic stenosis where the LV is not yet hypoplastic, in utero aortic valvuloplasty has been offered to promote forward flow.<sup>364,365</sup> Early results suggest that fetal aortic valvuloplasty may be associated with an increased chance of a biventricular repair, but this intervention is associated with fetal fatality and the effects on overall mortality rate and outcomes are unclear.<sup>365-368</sup>

For fetuses with a highly restrictive or intact atrial septum, atrial septal perforation and stenting have been performed.<sup>354,356</sup> The purpose of this procedure is to open the atrial septum early in order to allow the pulmonary vasculature to improve over the rest of the pregnancy and to perform the intervention under “maternal bypass,” as opposed to after birth, when the infant will be in extremis because of the profound hypoxemia and subsequent acidosis. After birth, the highly restrictive or intact atrial septum results in the oxygenated blood returning from the newborn’s lungs being trapped in the LA, and





**FIG 13-62** Left-sided heart hypoplasia/hypoplastic left heart complex/Shone complex. This form of left ventricular hypoplasia is almost universally associated with arch hypoplasia/coarctation of the aorta, mitral annular hypoplasia, aortic annular hypoplasia, and an apex-forming, but narrow left ventricle (LV). **A**, Four-chamber view of a long, thin LV with a hypoplastic mitral valve annulus. **B**, Left ventricular outflow tract view shows a hypoplastic aortic valve annulus. **C**, Low short-axis view shows that the LV is much narrower than the right ventricle (RV). **D** and **E**, Hypoplastic aortic arch that has retrograde flow by color Doppler, secondary to inadequate prograde flow across the left side of the heart. **F**, Atrial level shunting is typically bidirectional or left to right. Asc ao, ascending aorta; AV, aortic valve; FO, foramen ovale; IVC, inferior vena cava; LA, left atrium; pulm vein, pulmonary vein; RA, right atrium; SVC, superior vena cava; tr arch, transverse arch.

therefore this condition requires an emergent atrial intervention. Although technical success of in utero intervention has been reported, complications are common.<sup>354,369</sup>

For infants born with HLHS, surgery can be anticipated within the first week of life, and a minimum of three palliative surgeries are typically required in the first 5 years of life. For those with an intact or highly restrictive atrial septum, emergent postnatal intervention is necessary for survival, although this may not be sufficient.<sup>354,361</sup> The

Norwood operation includes aortic arch reconstruction, atrial septectomy, and anastomosis of the main pulmonary artery to the aorta, creating a neo-aorta. Pulmonary blood flow is supplied by either an aortopulmonary (Blalock-Taussig) shunt or Sano conduit (RV to pulmonary artery conduit).<sup>15</sup> Less commonly a hybrid operation is offered as the first stage, which includes an atrial septostomy, PDA stent, and bilateral pulmonary artery banding. Although this strategy may be an option for the most critically ill newborns, in most centers

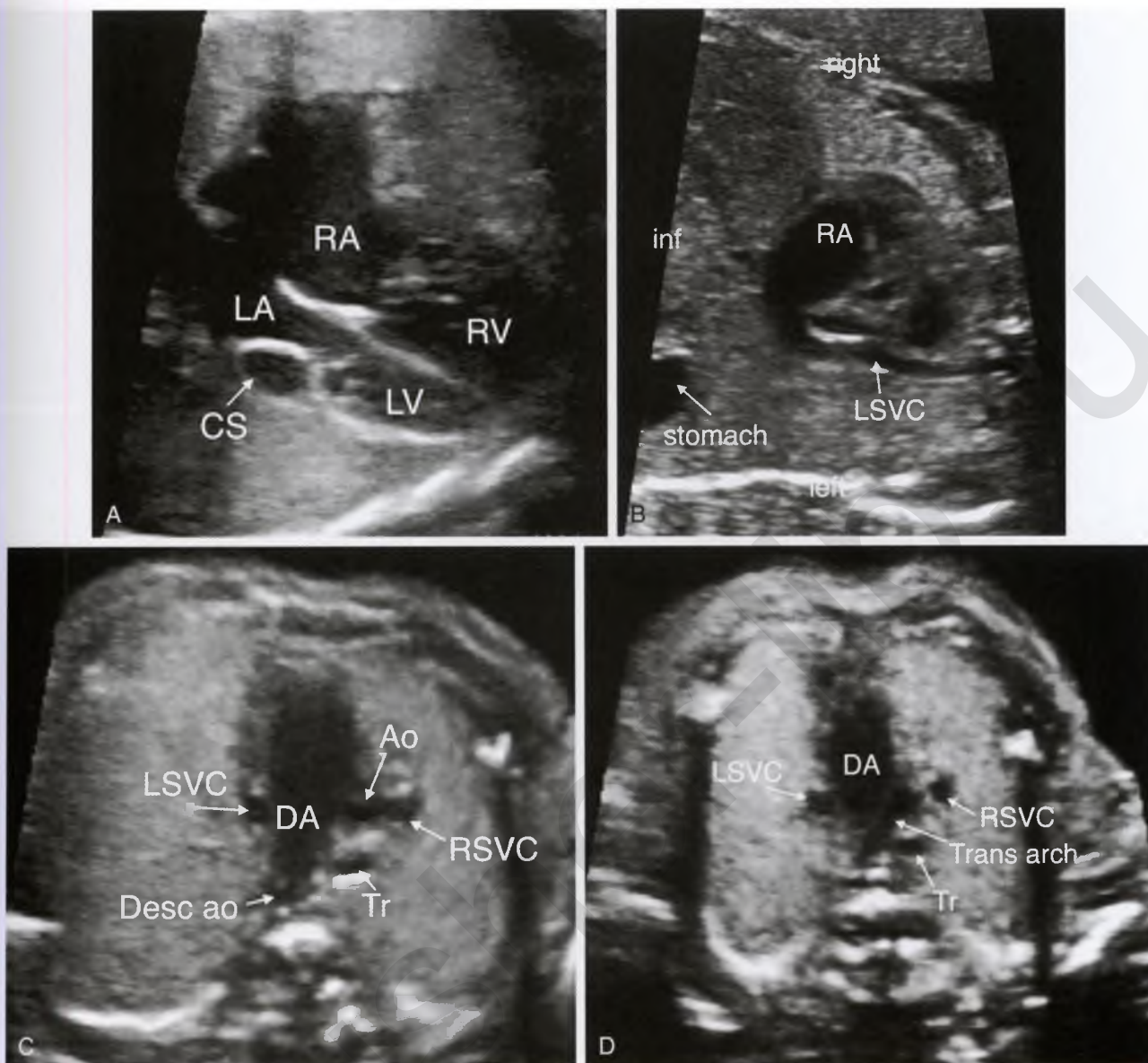


**FIG 13-63** Left superior vena cava (LSVC) to coronary sinus and left-sided heart hypoplasia. **A**, Four-chamber view shows a long, thin left ventricle, a dilated coronary sinus (CS), and hypoplastic mitral valve annulus. **B**, A coronal view of the fetal chest shows the LSVC draining to a CS and emptying into the right atrium (RA). **C**, A three-vessel view shows an extra vessel on the left that is the LSVC. **D**, The three-vessel and trachea view shows the LSVC on the left mirroring the right superior vena cava (RSVC). The transverse arch also appears hypoplastic and the ductal arch is larger than usual. Ao, ascending aorta; DA, ductal arch; inf, inferior; LA, left atrium; LV, left ventricle; RV, right ventricle; Tr, trachea; trans arch, transverse arch.

it is not the standard surgery offered for HLHS.<sup>355,370</sup> The Glenn procedure (anastomosis of the superior vena cava to the pulmonary artery) is typically performed at approximately 3 to 6 months of age. The Fontan procedure to create a conduit from the inferior vena cava to the pulmonary arteries is then typically performed between 2 and 4 years of age. In most cases, after the Fontan procedure, the patient is no longer cyanotic, as all of the systemic blood flow is passively directed to the lung.<sup>15</sup>

Termination rates for HLHS vary widely throughout the world and have been reported to range from 16% to 79% in countries that allow termination.<sup>340,358,359,371</sup> Although fetal demise may occur in HLHS, it is rare unless there is severe AV valve regurgitation or intact atrial

septum.<sup>15,339</sup> Fatality in the neonatal period, however, is common and occurs both before and after surgery. Presurgical mortality rate is estimated to be as high as 10% in epidemiologic studies, although it is only about 3% in patients born in or surviving transfer to a cardiac surgical center.<sup>24,371</sup> Presurgical fatality is associated with delivery far from a surgical center, major extracardiac congenital anomalies, and obstructed pulmonary venous return. Mortality rate following the Norwood operation is high compared to that for other CHDs, but has significantly improved since the introduction of this procedure. Recent estimates suggest that hospital mortality rate in patients undergoing a Norwood procedure is 7% to 26%.<sup>372-375</sup> Mortality rate of 2% to 16% may occur between the first and second stages,<sup>23,376-379</sup> and death may



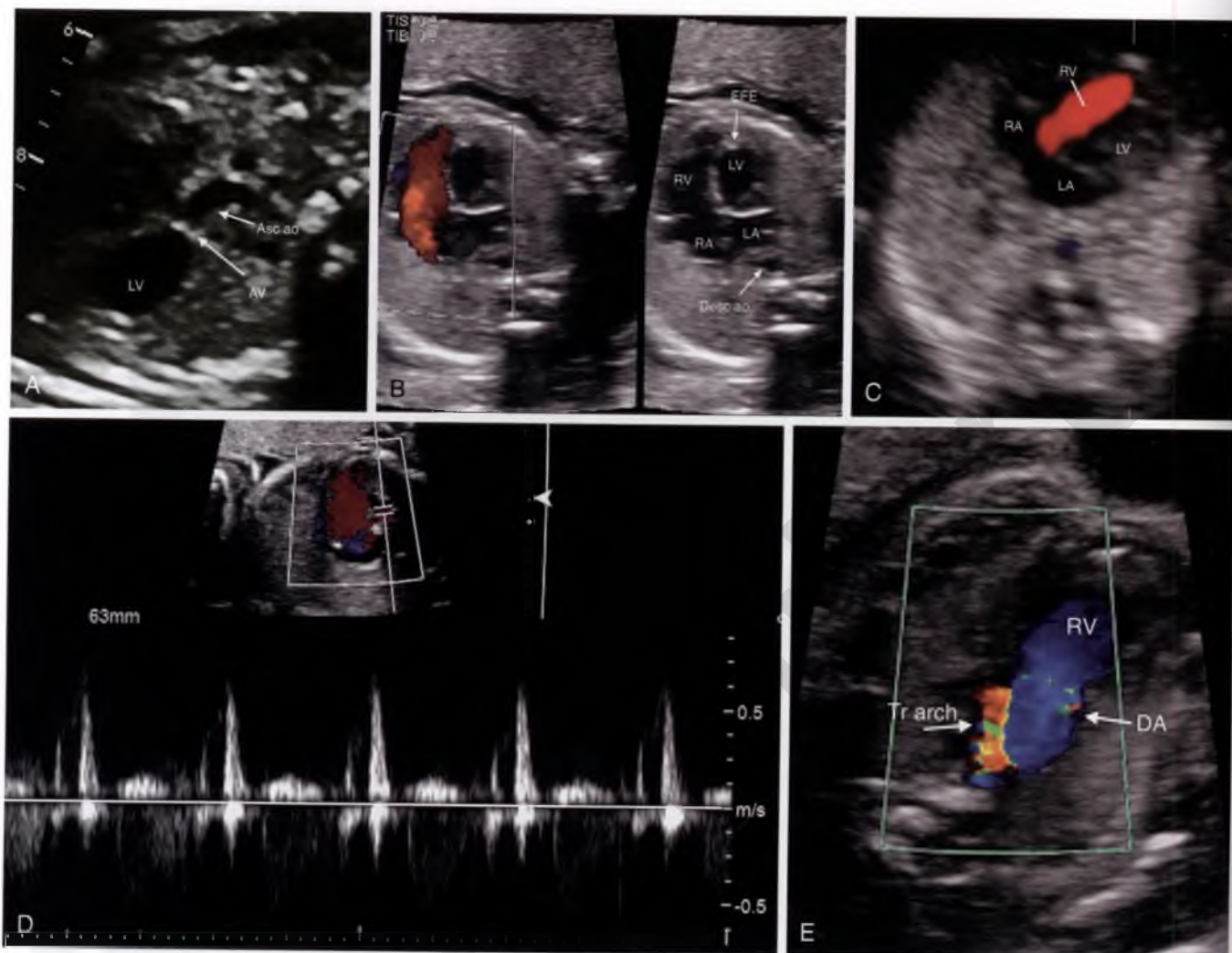


**FIG 13-64** Severe aortic stenosis (AS). **A**, Left ventricular outflow tract view shows a hypoplastic aortic valve and ascending aorta. The aortic valve leaflets are echobright. The left ventricle (LV) is globular. Echobright lining of the endocardium is consistent with endocardial fibroelastosis (EFE). **B**, Two-dimensional (2D) and color Doppler imaging in the four-chamber view. By 2D imaging, the LV appears globular and is lined with EFE. Although color Doppler imaging shows inflow into the right ventricle, no inflow is seen into the LV due to severe mitral stenosis. **C**, Four-chamber view in a fetus with aortic stenosis evolving into hypoplastic left heart syndrome (HLHS) at 12 $\frac{1}{2}$  weeks of gestation; note a thickened myocardium, a small LV, and no flow into the LV. **D**, Spectral Doppler pattern of inflow across the mitral valve shows monophasic inflow, suggesting progression to HLHS. **E**, Retrograde flow in the aortic arch in a three-vessel and trachea view. Asc ao, ascending aorta; AV, aortic valve; DA, ductal arch; Desc ao, descending aorta; EFE, endocardial fibroelastosis; LA, left atrium; LV, left ventricle; RA, right atrium; RV, right ventricle; Tr arch, transverse arch. (A and D from Morris SA, Maskatia SA, Altman CA, Ayres NA: Fetal and perinatal cardiology. In Allen HD, Shaddy RE, Penny DJ, et al [eds]: Moss and Adams' Heart Disease in Infants, Children, and Adolescents Including the Fetus and Young Adult, 9th ed. Philadelphia, Lippincott Wolters Kluwer, 2016, used with permission.)

occur with later procedures as well. In the current era, 50% to 70% of newborns will survive the three surgeries to age 5, and the survival rate continues to improve over time.<sup>374,380,381</sup>

Aside from fatality, long-term complications associated with HLHS include learning disabilities, attention-deficit/hyperactivity disorder, arrhythmias, and heart failure, among others. Many patients with a Fontan circulation develop hepatic impairment with age, and the ultimate therapeutic option is heart transplant for the adult population with HLHS, although much work is being done to develop alternative solutions.<sup>15</sup>

**Diagnostic Imaging Features.** Features of HLHS (see Fig. 13-60):

- The LV is severely hypoplastic.
- The mitral valve annulus is severely hypoplastic (atresia) with minimal or no flow.
- The aortic valve annulus is severely hypoplastic (atresia) with minimal or no flow.
- Aortic arch flow is completely retrograde.
- Foramen ovale flow is completely left to right. In some cases the foramen ovale may be severely restrictive or the atrial septum may be intact. In these cases, the pulmonary veins often appear dilated,

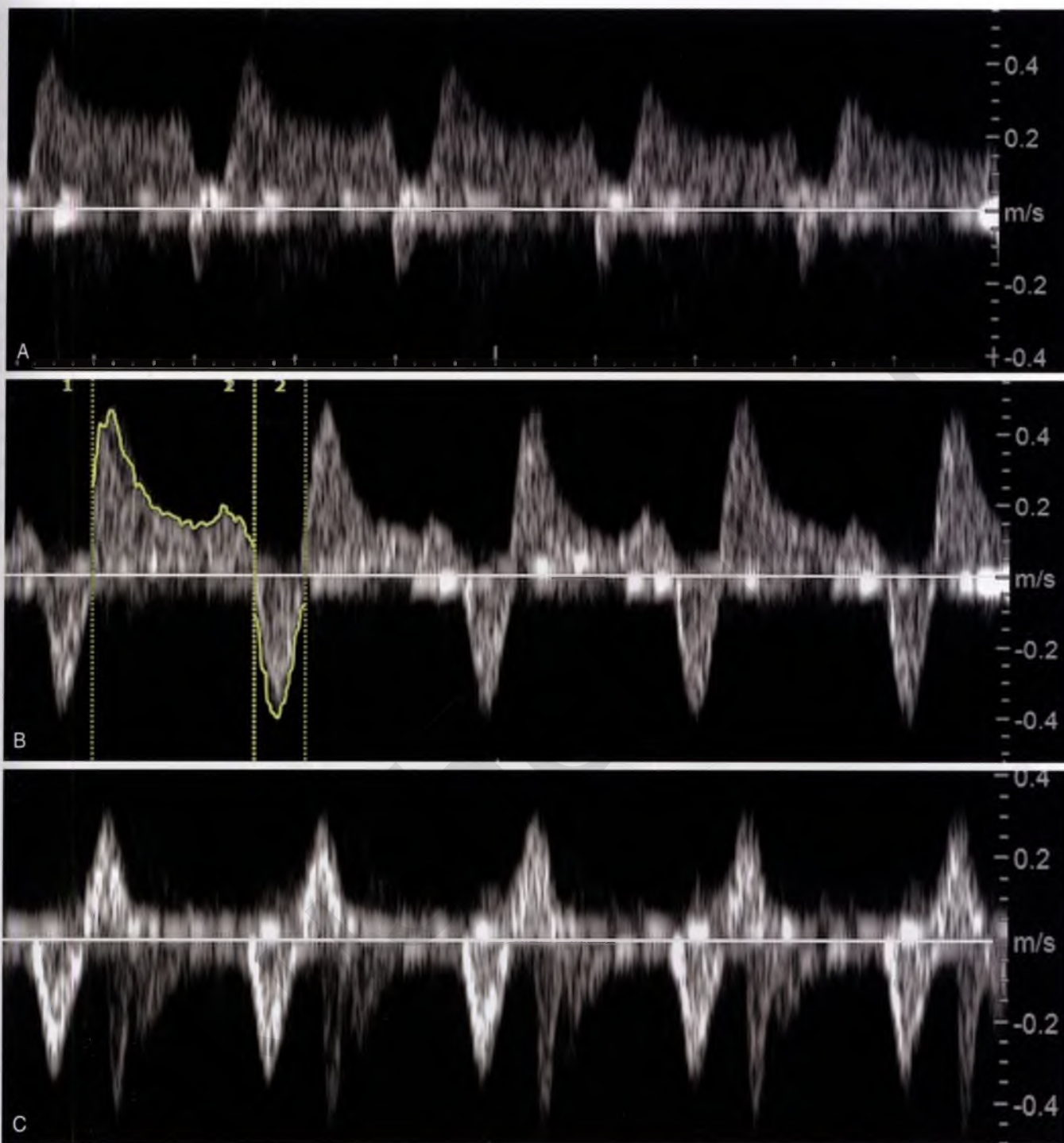


**FIG 13-65** Pulmonary venous Doppler patterns with increasing degrees of atrial level restriction. **A**, Pulmonary venous Doppler pattern seen with no atrial septal restriction, with a very short period of a-wave reversal. **B**, Pulmonary venous Doppler pattern seen with mild to moderate obstruction at the atrial septal level. Both a systolic wave and a diastolic wave are seen, but there is more prolonged a-wave reversal. Measurement of the ratio of prograde-retrograde velocity time integral (VTI) is greater than 3 and suggests there will likely not be decompensation at birth. **C**, Pattern of pulmonary venous flow seen with severe atrial level restriction in HLHS. The VTI of the antegrade flow (below line) is just slightly larger than the VTI of retrograde flow (above line) and suggests acute decompensation postnatally. (From Morris SA, Maskatia SA, Altman CA, Ayres NA: Fetal and perinatal cardiology. In Allen HD, Shaddy RE, Penny DJ, et al [eds]: Moss and Adams' Heart Disease in Infants, Children, and Adolescents Including the Fetus and Young Adult, 9th ed. Philadelphia, Lippincott Wolters Kluwer, 2016, used with permission. Information from Divanović A, Hor K, Cnota J, et al: Prediction and perinatal management of severely restrictive atrial septum in fetuses with critical left heart obstruction: clinical experience using pulmonary venous Doppler analysis. *J Thorac Cardiovasc Surg* 141(4):988-994, 2011.)



and pulmonary venous flow is both prograde and retrograde (see Fig. 13-65). Fetuses with severe restriction have a much worse prognosis at birth, and fetuses with this physiology may therefore be candidates for fetal cardiac intervention.

Features of the coarctation complex/Shone complex with a long thin LV (Figs. 13-61 and 13-62):

- The LV is usually long and narrow and forms an apex.
- Endocardial fibrosis is usually not present.
- The mitral valve and aortic valve annuli are usually hypoplastic.
- The mitral valve apparatus is often abnormal with short chordae, closely spaced papillary muscles, or a single papillary muscle.
- Mitral valve inflow is typically biphasic.
- Subaortic narrowing may be present.
- Aortic arch hypoplasia is typically present.
- Flow reversal and arch may be present.
- It may be associated with atrial septal aneurysm or left superior vena cava (Fig. 13-63).

Features of severe aortic stenosis (Fig. 13-64):

- The LV appears globular (more round than long) and may be dilated and dysfunctional.
- Endocardial fibroelastosis is often present; this condition appears as an echobright lining of the LV.

- Spectral Doppler across the mitral valve demonstrates monophasic inflow.
- Flow across the atrial septum is usually left to right.
- Aortic arch flow is often bidirectional or completely retrograde.
- Flow across the aortic valve may be high velocity, but in severe cases with near atresia, a small amount of low-velocity flow may be visible and the velocity of the mitral regurgitation jet may be helpful in determining whether the fetus is a good candidate for in utero aortic valvuloplasty, as higher velocities portend better response to fetal intervention.

### Tricuspid Valve Atresia

**Definition.** Tricuspid valve atresia (TVA) is complete absence of the tricuspid valve with no direct communication of the RA to the RV (Fig. 13-66). The lack of right ventricular inflow results in hypoplasia of the RV, which is variable in severity due to the frequent association of a VSD with this condition.

**Birth Prevalence/Epidemiology.** TVA is an uncommon congenital cardiac anomaly and accounts for 1% to 3% of congenital cardiac lesions. One study reported a prevalence of TVA of 0.056/1000 live births.<sup>239</sup>

**Anatomy.** TVA results in an obligatory right-to-left atrial level shunt. The four morphologic types of TVA are muscular (62%),

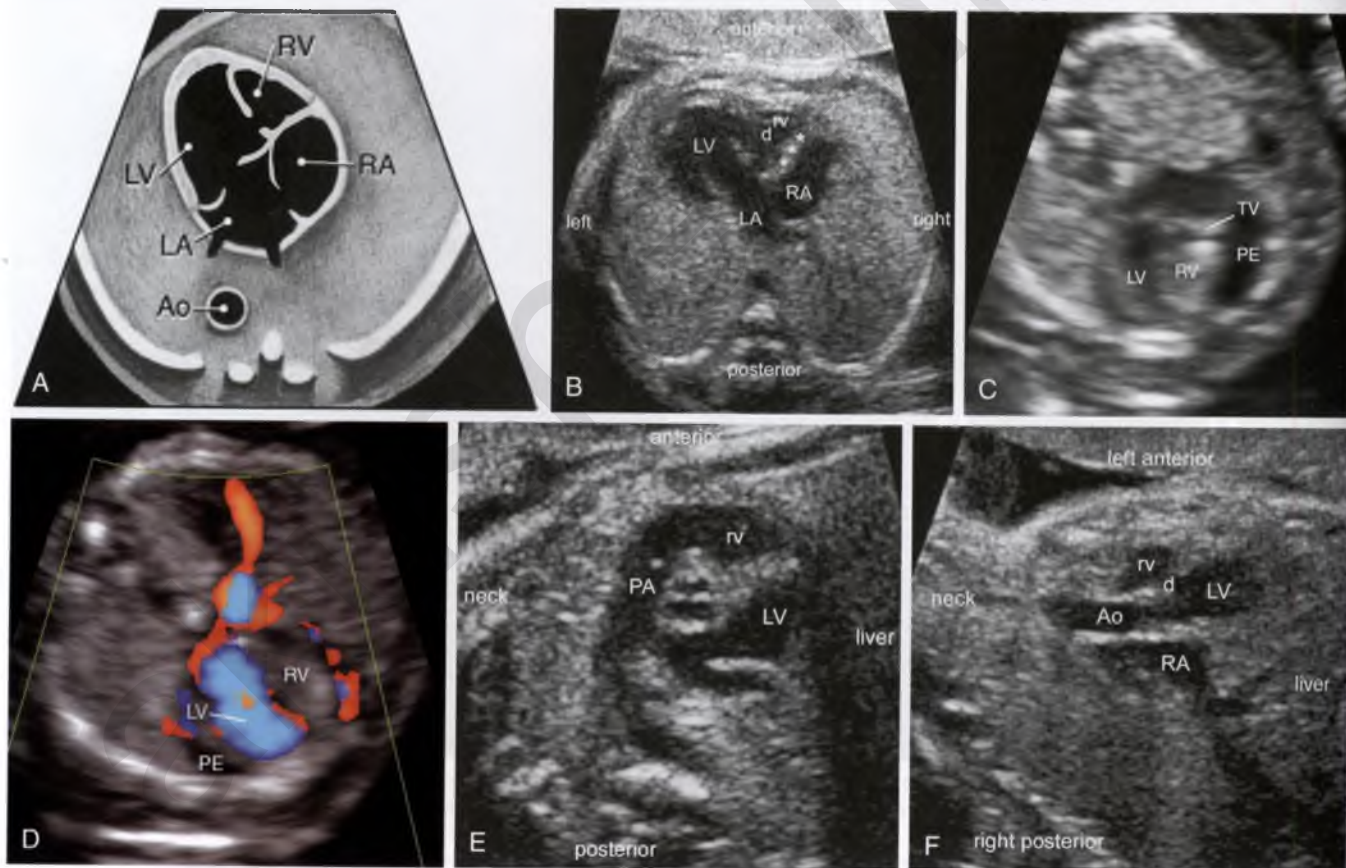


**FIG 13-66** Tricuspid atresia with normally related great arteries. **A** and **B**, Fetal echocardiographic diagram and sonographic image of tricuspid atresia in the four-chamber view. This view shows that the muscular floor (*asterisks*) separates the right atrium (RA) from the underlying small right ventricle (rv). There is an unrestrictive ventricular septal defect (d) between the large left ventricle (LV) and the small right ventricle. **C** and **D**, Four-chamber view in a fetus with tricuspid atresia at 13½ weeks of gestation; note the lack of blood flow to the right ventricle (RV) by both 2D sonography (**C**) and color Doppler imaging (**D**). **E**, Oblique sagittal view through the right ventricle shows the pulmonary artery (PA) arising from the right ventricle. **F**, Oblique sagittal view through the left ventricular outflow tract shows the aorta (Ao) arising from the left ventricle. ao, descending aorta; LA, left atrium; PE, pericardial effusion; TV, tricuspid valve. (**A**, Adapted with permission from American Institute of Ultrasound in Medicine: AIUM practice guideline for the performance of fetal echocardiography. *J Ultrasound Med* 32:1067-1082, 2013.)



membranous (29%), Ebstein-like (6%), and valvar (3%). Muscular TVA has a muscular floor to the RA and no valve tissue. With membranous TVA, the floor of the RA is the membranous AV septum. The Ebstein-like TVA is seen with the imperforate tricuspid valve leaflets plastered to the inferiorly displaced tricuspid valve tissue, resulting in sealed off "atrialized" RV resulting in no connection of the RA to the RV. In valvar TVA tricuspid valve tissue and chordae are visualized but the valve is completely imperforate. In all forms, the inlet RV is absent. Thus, the RV is composed of only the trabecular and infundibular segments of the RV.<sup>382</sup> The overall size of the RV is directly related to the presence and size of an accompanying VSD. If there is no VSD, the RV is diminutive or absent, whereas a larger VSD is typically associated with a larger RV. The sizes of the VSD and RV are also directly related to the sizes of the RVOT and pulmonary valve annulus. When the VSD is restrictive, there is often pulmonary valve stenosis and hypoplasia.

TVA has been classified according to the relationship of the great arteries. Type I TVA is the most common, accounting for approximately 70% to 80% of the patients. Type I TVA has normally related great arteries and, using the Van Praagh segment notation, is designated as {S, D, S}, which describes normal atrial situs (S), normally D-looped ventricles (D), and normally related great arteries (S). Type I TVA with no VSD has pulmonary valve atresia and is a ductus-dependent lesion with the pulmonary arteries being supplied by the ductus arteriosus. Type I TVA with a VSD is more frequently found. In type I TVA with a VSD, the size of the VSD determines the amount of pulmonary blood flow. A recent study of 150 type I TVA infants noted absent antegrade pulmonary blood flow in 19%, restricted pulmonary blood flow in 54%, and unrestricted blood flow in 28%.<sup>383</sup>

Type II comprises approximately 12% to 25% of TVA cases and is associated with TGA. The segmental Van Praagh definition is {S, D, D}, indicating that the RV gives rise to the aorta secondary to transposed great arteries. Thus, the systemic blood flow is dependent upon the sizes of the VSD and RV. Type II TVA has an increased incidence of RV and aortic hypoplasia, aortic valve stenosis, aortic arch hypoplasia, and coarctation of the aorta. Only about 8% of type II TVA have an associated coarctation of the aorta. Type III TVA is uncommon and accounts for approximately 3% to 6% of TVA patients. Type III comprises a complex form of TVA associated with L-transposition of the great arteries. The Van Praagh segments are {S, L, L} with L-looped ventricles or ventricular inversion and an atretic, leftward-positioned tricuspid valve, which is connected to the systemic RV. In addition, the morphologic RV is connected to the L-transposed anteriorly positioned aorta. The systemic AV valve is an atretic tricuspid valve and flow to the aorta is via a VSD into the morphologic RV that is leftward in orientation.

In TVA, the PFO is usually large and unrestrictive, which is critical in this defect because all the systemic venous return and hence the right cardiac output must cross right to left through the PFO. The PFO in the type III TVA may become restrictive, as the pulmonary venous return is limited in the fetus and with the atretic left tricuspid valve, the only egress from the LA is left to right across the atrial septum.

TVA is generally an isolated defect. A small percentage (<20%) of associated defects are seen in TVA patients. Associated cardiac anomalies include left juxtaposed atrial appendages, left superior vena cava, and a right aortic arch.

**Genetic Considerations.** To date, the genetic mechanism responsible for the development of TVA remains obscure.<sup>384,385</sup> There are isolated case reports of chromosome 22q11.2 deletion with TVA but they appear sporadic.<sup>386,387</sup>

**Interventions and Prognosis.** TVA is an obligatory single ventricle repair, and all TVA patients are ultimately managed as a single ventricle

palliation with a Glenn shunt in the first year of life and a Fontan operation as a toddler. Management of type I TVA with normally related great arteries is dependent upon the degree of pulmonary blood flow. If the neonate has inadequate pulmonary blood flow, then an arterial to pulmonary shunt is placed. Later, TVA is managed via a single ventricular pathway. When an infant with an aortopulmonary shunt develops desaturation in the first year, the pulmonary blood flow is augmented with a Glenn shunt (superior vena cava [SVC] to right pulmonary artery shunt) and takedown of the arterial shunt. Later a Fontan baffle is performed to baffle the systemic venous return (inferior vena cava [IVC]) to the pulmonary artery.

In type I TVA with a large VSD and unrestricted pulmonary blood flow, a pulmonary artery band is placed to prevent pulmonary overcirculation and pulmonary hypertension. The later management is the Glenn shunt followed by a Fontan procedure.

In type II TVA with TGA, the size of the VSD impacts the size of the RV and the degree of aortic valve and arch hypoplasia. If there is type II TVA with aortic arch obstruction or coarctation of the aorta, the aortic arch obstruction is repaired. In cases of aortic arch obstruction and RV hypoplasia, an arterial switch operation results in the LV being the systemic ventricle and resolving the RV outflow tract obstruction. The neopulmonary artery is connected to the hypoplastic RV, which subsequently restricts the pulmonary arterial blood flow. In TVA, the long-term goal is a Glenn shunt and Fontan baffle, which connects the systemic venous return directly to the pulmonary arteries. A Damus-Kaye-Stansel procedure (anastomosis of the pulmonary valve and main pulmonary artery to the proximal aorta) with an aortic arch repair or a type I Norwood procedure has also been a surgical repair used in type II TVA with significant aortic valve and arch obstruction as the first palliative procedure.

Outcomes of TVA reflect the severity of these lesions. A large multicenter series of prenatally diagnosed TVA reported four in utero demises. Survival rate of the liveborn neonates was 91% at 1 month, 87% at 6 months, and 83% at 1 year with no subsequent deaths for 13 years.<sup>388</sup> A more recent series of 54 prenatally diagnosed TVA cases reported two in utero demises. Fifty-two percent ( $n = 28$ ) had normally related great arteries and 14 of those 28 had pulmonary outflow obstruction. Forty-six percent ( $n = 25$ ) had transposed great arteries of which 14 of the 25 had aortic outflow obstruction. The overall survival rate of the continued pregnancies was 89% at 2 years with the greatest loss occurring in the first year of life.<sup>389</sup> A study of 150 type I TVA neonates reported an 86% 5-year survival rate and improved outcomes when a smaller aortopulmonary shunt was placed in neonates with confounding mitral regurgitation.<sup>383</sup>

Overall long-term Fontan survival rate in TVA patients ranges from 79% to 82% in 25-year and 10-year follow-up respective series.<sup>390,391</sup> The more complicated type II TVA-TGA with systemic outflow tract obstruction has a survival rate of 68% at 6 years.<sup>392</sup> The independent risk factors for fatality are low birth weight, premature birth, aortic arch obstruction, and RV hypoplasia.<sup>391</sup>

#### Diagnostic Imaging Features

- Both 2D sonography and Doppler color imaging in the four-chamber view can aid in recognition of the ventricular disproportion that is seen in TVA (Figs. 13-66A to D and 13-67).
- When TVA is suspected, the following steps are important in evaluation:
  - Assess the great artery relationship. With normally related great arteries, assess for degrees of pulmonary blood flow obstruction.
  - When the great arteries are normally related, the size of the VSD determines the amount of pulmonary blood flow. Assess the direction of flow in the ductus arteriosus. Normal forward antegrade flow in the ductus arteriosus implies adequate blood flow



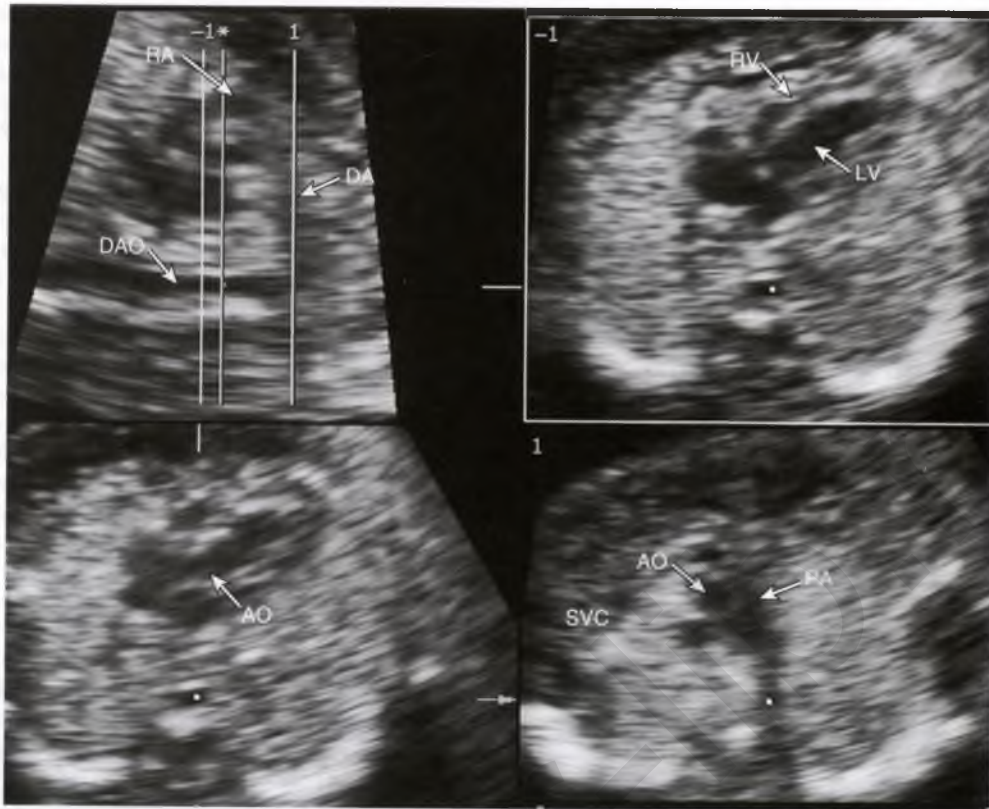


**FIG 13-67** Early gestation imaging of tricuspid atresia. Tomographic ultrasound imaging in a fetus with tricuspid atresia and normally related great arteries at 12 $\frac{5}{7}$  weeks of gestation. The image on the upper left corner corresponds to the ductal arch plane. The four-chamber view is displayed on upper right corner, which demonstrates a small right ventricle (RV); the five-chamber view is displayed in lower left corner. A very small pulmonary artery (PA) is seen on the three-vessel view. AO, aorta; DA, ductus arteriosus; DAO, descending aorta; LV, left ventricle; RA, right atrium; SVC, superior vena cava.

after delivery. Retrograde ductus arteriosus implies significant RVOT obstruction or pulmonary obstruction and a ductus-dependent pulmonary blood flow.

- In type II TVA with transposed great arteries, assess for aortic outflow tract and aortic arch obstruction. Note if retrograde flow in the proximal or transverse arch indicates significant systemic outflow track obstruction and ductus-dependent postnatal systemic circulation.
- Most type I and type II TVA fetuses have a wide PFO, but the atretic tricuspid valve will cause a reduction in the DV flow with atrial contraction. Venous pulsations in the umbilical vein suggest atrial septal restriction.
- Type III TVA with ventricular inversion and an atretic left AV connection between the LA and RV presents a risk of atrial level restriction and requires thorough evaluation of the atrial septum. Most fetuses tolerate mild to moderate atrial level restriction, but after birth with increased cardiac output any significant atrial level restriction may require an urgent neonatal balloon atrial septostomy.
- Although both TVA and severe pulmonary stenosis or pulmonary atresia with an intact ventricular septum (PA-IVS) may have a hypoplastic RV and flow reversal in the ductus arteriosus (Fig. 13-68), three features help to distinguish the two: (1) At least a small amount of tricuspid inflow and regurgitation will usually be present in PA-IVS. (2) A VSD is typically associated with TVA, but not with PA-IVS. (3) RV-coronary fistulas are commonly present in PA-IVS, but not in TVA.

### Anomalous Pulmonary Venous Connection

**Definition.** Normally there are two pulmonary veins from the right lung and two pulmonary veins from the left lung with all the veins connected to the LA. When anomalous pulmonary venous connection is present, the pulmonary veins connect directly with a systemic vein or drain directly into the RA. With TAPVC, there is no connection of the pulmonary veins to the LA (Fig. 13-69). In PAPVC at least one pulmonary vein returns normally to the LA, and at least one returns anomalously.

**Birth Prevalence/Epidemiology.** TAPVC occurs in approximately 0.9/10,000 live births and accounts for approximately 2% of CHD.<sup>324</sup> One of the most common coexisting conditions is heterotaxy syndrome; TAPVC is common in right atrial isomerism/asplenia, whereas PAPVC is more common in left atrial isomerism/polysplenia. Disruption of the left-right asymmetry pathways has been shown in mice to affect alignment of cardiac and visceral structures and to be associated with anomalous pulmonary venous return and heterotaxy syndrome.<sup>305</sup>

**Anatomy.** The classification of pulmonary venous anomalies is based upon embryologic origins of the pulmonary veins. Thus, a brief review of the embryologic development of the pulmonary veins follows. The primordia of the lungs, larynx, and tracheobronchial tree are derived from divisions of the human embryo foregut. The lungs are enmeshed by the splanchnic vascular plexus of the foregut. During pulmonary differentiation, part of the splanchnic plexus forms the pulmonary vascular bed. Early in development, there is no direct connection with the fetal heart. At this stage, the pulmonary vascular bed

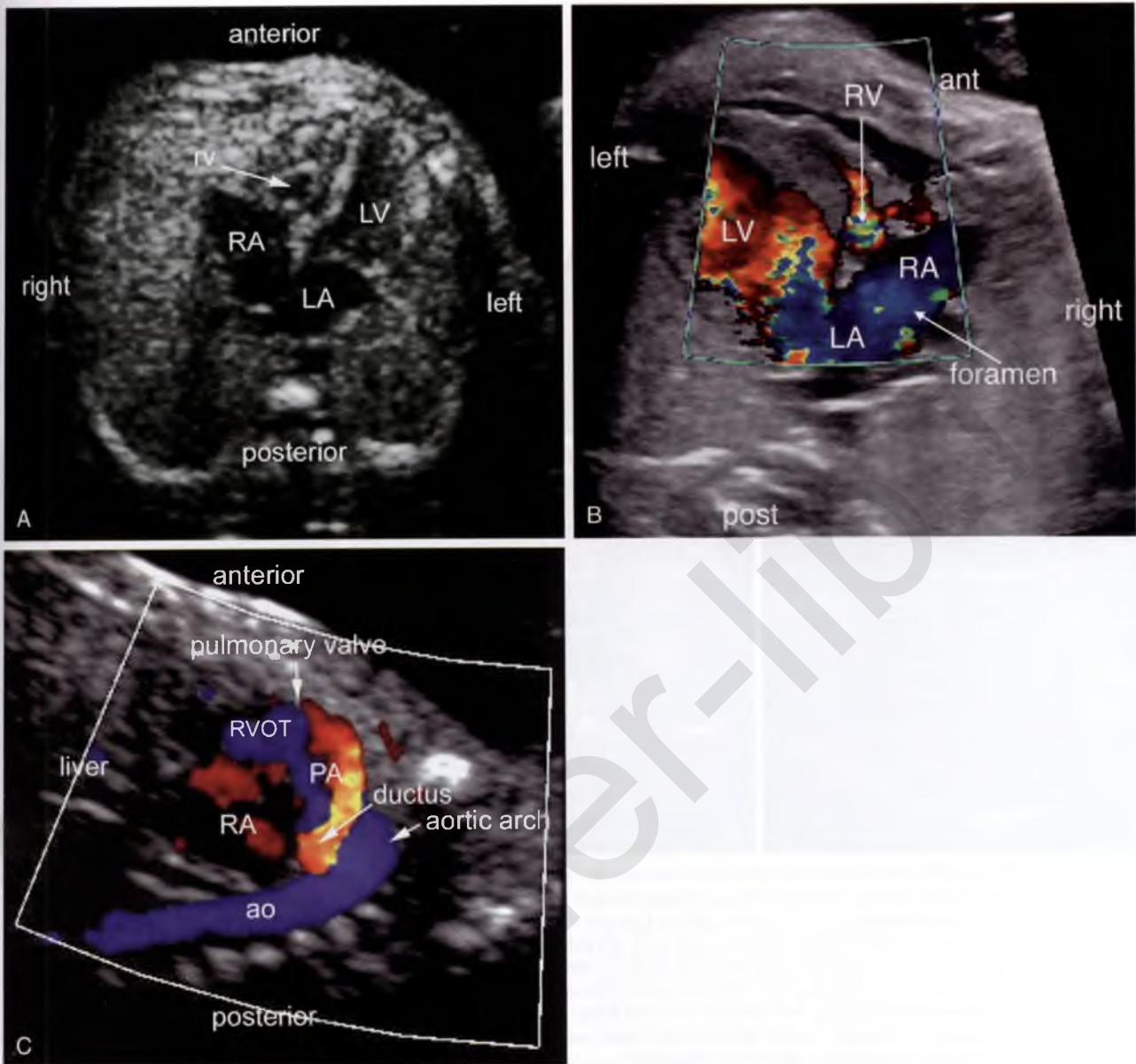


**FIG 13-68** Pulmonary atresia with intact ventricular septum. **A**, Four-chamber view shows severe hypoplasia of the right ventricular cavity (rv) and markedly thickened right ventricular free wall. **B**, A four-chamber view using color Doppler shows minimal inflow into the right ventricle (RV). **C**, Ductal arch view with color Doppler shows left-to-right shunt across the ductus. The blood flow from the right ventricle (*blue* signal in right ventricular outflow tract [RVOT]) and the retrograde flow in the main pulmonary artery (*red* signal) collide at the atretic pulmonary valve. ant, anterior; ao, aorta; LA, left atrium; LV, left ventricle; PA, main pulmonary artery; post, posterior; RA, right atrium.

has drainage via the veins of the umbilicovitelline and cardinal systems from the splanchnic plexus. By the end of the first month of gestation, the intraparenchymal pulmonary veins become connected with a common pulmonary vein that evaginates into the LA. The common pulmonary evagination is positioned cephalad to the right and left horns of the sinus venosus and to the left of the developing septum primum.<sup>393</sup> Failure of the normal development of the common pulmonary vein to develop or failure of evagination of the common pulmonary into the LA results in TAPVC of drainage. The abnormal pulmonary venous connections or drainage is via the veins of the primitive umbilicovitelline and cardinal systems from the splanchnic plexus. Thus, abnormal pulmonary venous connections can be total,

with all the pulmonary veins draining anomalously, or partial, in which one, two, or three veins have failed to connect to the common pulmonary vein and thus the LA, with the anomalous vein(s) connecting back to the heart via a residual connection to one of the primitive umbilicovitelline and cardinal veins from the splanchnic plexus.

**Supracardiac TAPVC.** There are several types of TAPVC with the supracardiac being the most common. The pulmonary veins form a confluence posterior to the LA, and a venous channel originates from the confluence and ascends anterior to the left pulmonary artery and bronchus. The vertical venous channel is a derivative of the left cardinal venous system. This vertical venous channel often ascends anterior to the aorta and into the superior mediastinum where the vertical vein



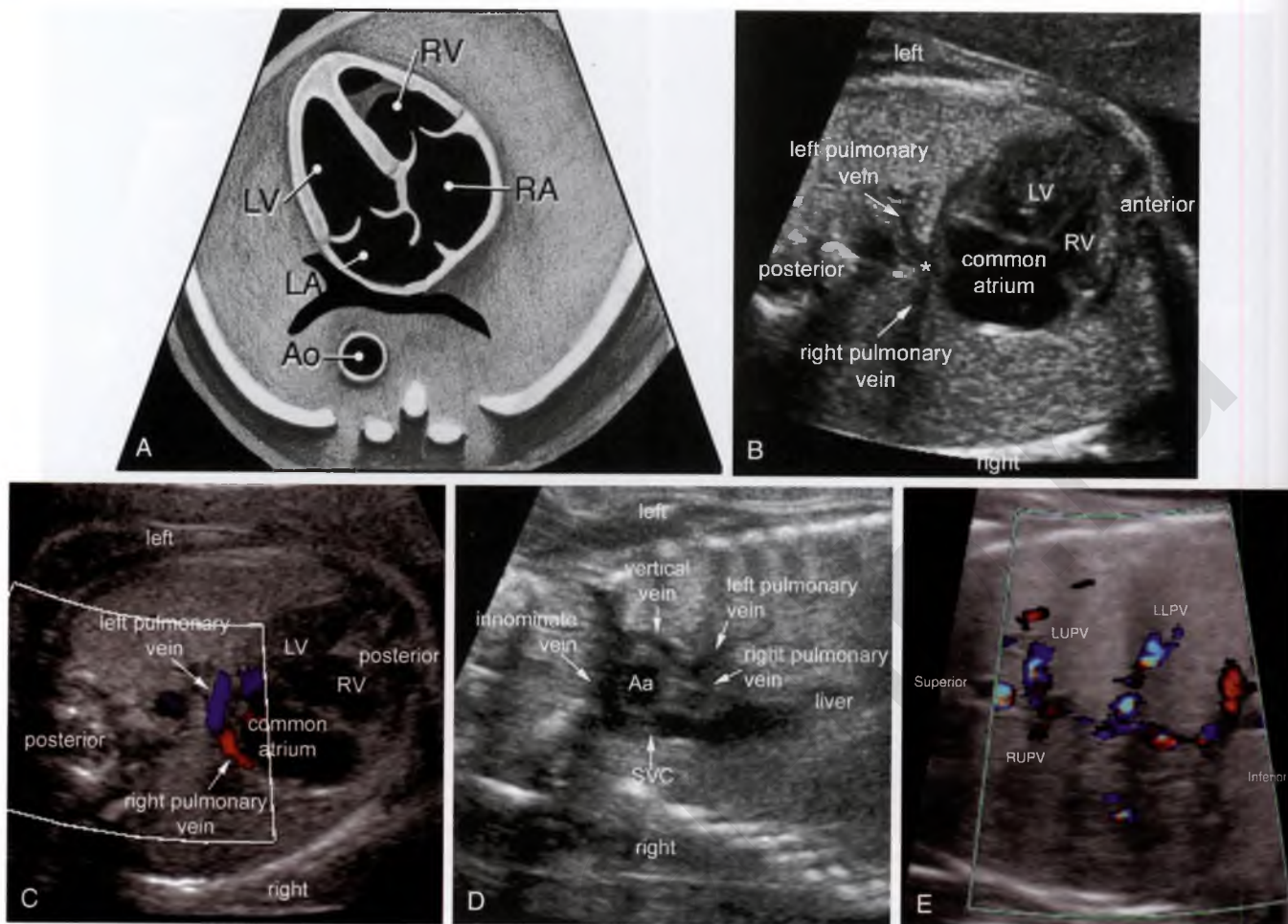


**FIG 13-69** Total anomalous pulmonary venous return (TAPVC). **A** through **C**, Diagram and images in the four-chamber view show that the pulmonary venous confluence (*asterisk* in **B**) is in close proximity to but does not connect to the left atrium. **B** and **C** show a fetus with right atrial isomerism. **D**, Coronal view in supracardiac TAPVC shows that the right and left pulmonary veins make a confluence to the vertical vein that connects to the innominate vein. The superior vena cava (SVC) is dilated. **E**, Coronal view in infracardiac TAPVC shows two left and one right pulmonary veins returning to a long descending vein. Aa, aortic arch; Ao, descending aorta; LA, left atrium; LLPV, left lower pulmonary vein; LUPV, left upper pulmonary vein; LV, left ventricle; RA, right atrium; RUPV, right upper pulmonary vein; RV, right ventricle. (**E** from Morris SA, Maskatia SA, Altman CA, Ayres NA: Fetal and perinatal cardiology. In Moss and Adams' Heart Disease in Infants, Children, and Adolescents Including the Fetus and Young Adult, 9th ed. Allen HD, Shaddy RE, Penny DJ, et al [eds]: Philadelphia, Lippincott Wolters Kluwer, 2016, used with permission.)

joins the left innominate vein proximal the insertions of the left subclavian and left jugular veins. When the left vertical vein passes between the left pulmonary artery and left bronchus, the extrinsic compression of the bronchus frequently causes pulmonary venous obstruction. The pulmonary venous return traverses to the left innominate vein and proceeds into the SVC, joining the RA. The embryologic splanchnic venous plexus is a midline structure and this explains why pulmonary venous return may cross the midline with left veins draining to the right cardinal venous system and right veins crossing to the left cardinal venous system. TAPVC to the left innominate vein is seen in approximately 36% of all TAPVC cases, whereas TAPVC to the right SVC is seen less frequently, in about 10% of cases.

**TAPVC to the Heart.** TAPVC to the coronary sinus occurs in approximately 16% of cases of TAPVC. The posterior venous confluence connects to the coronary sinus in the region of the left AV groove. The coronary sinus follows the normal course entering the RA. TAPVC

to the coronary sinus is unobstructed because the course of the anomalous drainage is all within the pericardium.

**Infracardiac TAPVC.** In this form of TAPVC, the umbilicovitelline venous system allows anomalous pulmonary venous drainage to return below the diaphragm. This form occurs in approximately 13% of cases of TAPVC. The venous confluence is posterior to the LA, and a common vessel descends from the confluence anterior to the esophagus and passes through the esophageal hiatus into the abdomen. Most often the descending vein connects with the portal system via the confluence of the splenic and superior mesenteric veins. When the descending vein connects with the umbilicovitelline venous system, pulmonary venous obstruction is seen in the fetus, which is exacerbated after delivery with increased pulmonary venous return. The descending vein can also connect with the IVC, hepatic vein, or via the DV.<sup>394</sup>

**TAPVC to the Right Atrium.** In cases of heterotaxy syndrome with an absent septum secundum (often with polysplenia), the septum



primum is displaced superiorly and leftward, which results in the pulmonary veins being incorporated into the RA. The pulmonary veins are connected normally to the posterior atrial wall between the right and left SVCs but drain abnormally into the RA as a result of the abnormal atrial septal displacement.<sup>395</sup>

**Mixed TAPVC.** Mixed type of TAPVC occurs in approximately 7% and occurs when the pulmonary veins connect to different venous structures and not all connect or drain via the same systemic vein.<sup>394</sup>

**Partial Anomalous Pulmonary Venous Connection.** Partial anomalous pulmonary venous connection or drainage (PAPVC) occurs when one or more, but not all, of the pulmonary veins are connected to a systemic vein. PAPVC exhibits a wide spectrum of variable venous connections. Left pulmonary veins frequently connect anomalously with the derivatives of the left cardinal system—either the left innominate vein or the coronary sinus, whereas the right pulmonary veins connect to the derivatives of the right cardinal system—the SVC or IVC. In the most common type of PAPVC the left pulmonary veins connect to the left innominate vein. In the second most common type, the right pulmonary veins connect to the IVC.

Scimitar syndrome is seen in the fetus with anomalous right pulmonary venous drainage to the junction of the IVC with the RA. There is also hypoplasia of the right lung and the right pulmonary artery along with anomalous arterial pulmonary blood flow from the aorta. This results in pulmonary sequestration. The right lung hypoplasia results in subsequent shift of the heart into the right side of the chest.<sup>396,397</sup>

PAPVC to the right SVC or into the RA occurs in association with a sinus venosus ASD, which is a superiorly positioned ASD at the junction of the SVC with the superior atrial septum. This defect has not been reported to be detected in utero.

**Genetic Considerations.** Isolated case reports of siblings with recurrence of TAPVC has suggested a possible autosomal-recessive cause.<sup>398-401</sup> There are also case reports of TAPVC and heterotaxy syndrome in patients with a frameshift in *NKX2.5* gene.<sup>402</sup> Cat eye syndrome, a duplication of chromosome 22q11.2, has been associated with TAPVC.<sup>403</sup> PAPVC is also seen in Turner and Noonan syndromes.

**Interventions and Prognosis.** Infants with infradiaphragmatic TAPVC almost always have obstruction and present in the first 12 hours of life with cyanosis, acidosis, and pulmonary venous congestion. Obstructed TAPVC below the diaphragm commonly requires emergent surgical repair. About 50% or more of supracardiac TAPVC infants also have obstruction and have similar symptoms as the subdiaphragmatic TAPVC and require early surgical repair. The systemic cardiac output is dependent upon the size of the ASD or PFO. Any restriction of the atrial septum will contribute to symptoms and can result in decreased systemic cardiac output if the atrial septum is restrictive.

Surgical repair connects the pulmonary venous confluence to the posterior LA wall and patch-closes the ASD or PFO. The vertical ascending or descending vein is ligated. If there is an additional defect such as a VSD or PDA, the additional defect is closed at the time of surgery. Unobstructed pulmonary veins present with the physiology of a large ASD with right-sided heart volume loading and enlargement due to pulmonary overcirculation and are electively repaired.

TAPVC to the coronary sinus has the physiology of a large ASD. Repair is to excise the common wall of the coronary sinus and LA and close the ASD.

An international, multicenter study of 422 TAPVC patients noted a 3-year mortality rate of 15%. Independent risk factors for death were hypoplastic or stenotic pulmonary veins, earlier age at surgery, associated complex cardiac defects, postoperative pulmonary hypertension, and postoperative pulmonary venous obstruction. Following TAPVC repair, 60 neonates (15%) developed pulmonary venous obstruction and had a 3-year mortality rate of 41%.<sup>404</sup>

A 2014 report of surgical outcomes after TAPVC repair compared patients with isolated TAPVC to those with additional congenital heart disease lesions.<sup>405</sup> Supracardiac TAPVC comprised 48%, intracardiac 20%, infracardiac 20%, and mixed 12% of all TAPVC patients. Obstructed pulmonary venous connection was seen in 33% of all TAPVC, with infradiaphragmatic type demonstrating the most frequent type with obstruction at the level of the diaphragm or in the liver. Overall operative mortality rate in isolated TAPVC was 6.9%, whereas it was 41.2% in TAPVC with more complex heart disease. The risk factors for higher operative fatality were weight less than 3 kg, single ventricle physiology, and aortic cross-clamp time of longer than 1 hour. The late mortality rate combined with the surgical mortality rate was 17% in isolated TAPVC and was 77% in complex TAPVC.<sup>405</sup>

Surgical series note that intrinsic pulmonary venous obstruction and pulmonary vein stenosis have increased morbidity and mortality rates. A 2015 study evaluated 46 isolated TAPVC cases. Those presenting hours after delivery in shock with hypoxemia, hypotension, and severe pulmonary venous congestion were deemed to have intrinsic pulmonary vein obstruction. This group had a 10-year survival rate of 69%. These neonates required prolonged nitric oxide and ventilation along with higher reoperation risk than the other TAPVC neonates without immediate symptoms after birth. Neonates who developed obstruction during the first day of life owing to obstruction of a vertical vein and descending vein because of increasing pulmonary blood flow had a 10-year survival rate of 88%. Neonates presenting with unobstructed TAPVC and pulmonary overcirculation had a 96% 10-year survival rate. Intrinsic pulmonary venous obstruction has a worse prognosis than the nonobstructed TAPVC infants.<sup>406</sup>

Repair of scimitar syndrome involves redirecting the anomalous right pulmonary veins to the LA. Because 70% of scimitar patients have an ASD, the anomalously draining right pulmonary veins are often baffled through the ASD to the LA. Reimplantation of the anomalous right pulmonary vein is also a technique used to reimplant the anomalous veins to the LA. The anomalous aortopulmonary vessels from the descending aorta are either occluded with coils in a preoperative cardiac catheterization or occluded at the time of surgery. The highest risk patients are those with pulmonary hypertension and symptomatic infants requiring surgery prior to 1 year of age. The most successful repairs are performed in older children, of whom many are asymptomatic over a long term.<sup>407,408</sup>

**Diagnostic Imaging Features.** Series have described TAPVC detected in fetal life, although it is one of the hardest lesions to detect prenatally when isolated.<sup>108</sup> Ganesan and colleagues described sonographic findings for 26 fetuses with a prenatal diagnosis of TAPVC.<sup>108</sup> Lack of visible pulmonary venous connections back to the atrium (100%) and the presence of a visible venous confluence on axial four-chamber views (96%) were the most consistent findings (see Fig. 13-69). The presence of additional vertical venous channels on 3VV or axial abdominal views were also sometimes noted.

There may be a size discrepancy with the RA and RV appearing larger than the LA and LV, although in the Ganesan study, cardiac asymmetry was observed but not consistently in the fetus. When asymmetry is present, it is usually present later in pregnancy as the pulmonary blood flow in the fetus increases. During the last 10 weeks of pregnancy, the pulmonary venous return increases from 20% to 25% of the combined cardiac output. When the pulmonary venous return is abnormal and diverted away from the left side of the heart, a relative left-sided heart hypoplasia can develop. The location of the abnormal pulmonary connection impacts the degree of left-sided heart hypoplasia. Supracardiac TAPVC and TAPVC to the RA and coronary sinus increase the RA and RV volume and thus the right-sided heart enlargement is often more evident, whereas infradiaphragmatic TAPVC



returns via the umbilicovitelline venous system and the IVC, and the blood is directed across the atrial septum. In some infradiaphragmatic TAPVC cases, the left side of the heart can be normal in size and is less likely to have significant hypoplasia.<sup>401</sup>

More rarely, TAPVC is associated with intrinsic pulmonary vein stenosis and hypoplasia, which may also result in decreased pulmonary flow and some degree of left-sided heart hypoplasia due to intrinsic pulmonary venous obstruction. Severe intrinsic pulmonary venous hypoplasia and stenosis are associated with severe hypoxemia, acidosis, and shock in the first several hours of life. Thus, if pulmonary veins are not seen or abnormal flow within the pulmonary veins is noted, the fetus may have the most critical type of TAPVC.

Normal pulmonary venous flow velocity and volume increases during the third trimester.<sup>409</sup> Abnormal spectral Doppler with turbulence by color Doppler may be seen at the site of obstruction in a vertical or descending vein. At the site of obstruction, there is an abnormally high velocity (0.6-1.4 m/second in late gestation) for a pulmonary vein and continuous flow. This is a similar spectral Doppler pattern seen after delivery. Proximal to the pulmonary venous obstruction, the flow in the pulmonary venous channel is low velocity and monophasic. In TAPVC, there is no direct connection of a pulmonary vein to the LA. There is also a separation between the posterior LA wall and the descending aorta, as well as a posterior venous confluence that may be star-shaped or oval between the posterior LA wall and the descending aorta. The aorta is the only normal vessel in the retrocardiac space, and any additional structure or vessel requires interrogation for possible TAPVC and a vertical or descending venous channel.<sup>108,397</sup> A disproportional size in the SVC and IVC is seen when either the IVC or SVC is connected to the anomalous pulmonary venous connection. The systemic vein draining the TAPVC will be larger than the systemic vein with normal venous return.

#### **Imaging Tips for TAPVC**

- Size discrepancy may be present, with the right heart chambers and pulmonary artery being larger than the left heart chambers and aorta.
- The LA may appear small, with no venous connections.
- Posterior pulmonary venous confluence is posterior to the LA and anterior to the descending aorta. The posterior confluence may be twig-like star-shaped or ellipsoid.
- An additional vertical structure in the thorax may be seen, with low-velocity venous monophasic flow directed either superiorly or inferiorly. Turbulence is seen in the vertical structure with obstructed flow pattern of increased velocity of 0.6 to 1.4 m/second, and monophasic flow is seen with pulmonary venous obstruction.
- A dilated IVC or SVC should be interrogated for possible TAPVC connection.
- A markedly dilated SVC and innominate vein along with a vertical vein with venous flow superiorly directed into the innominate vein is seen with supracardiac TAPVC. The size of the SVC is dilated in the 3VV and along with the pulmonary artery appears larger than the aorta.
- Abnormal, additional venous structure crossing from the thorax inferiorly through the diaphragm entering the IVC, portal veins, DV, or hepatic veins with increased turbulent flow in the liver is seen with infradiaphragmatic TAPVC.
- Small LA with moderate or greater enlargement of the coronary sinus and lack of pulmonary veins to the LA may be seen with TAPVC to the coronary sinus.
- Small right pulmonary artery, dextroposition of the heart, relative hypoplasia of the right lung, and increased venous return to the IVC are seen with scimitar syndrome and anomalous right pulmonary venous drainage to the IVC.

- Pulmonary veins require spectral and color Doppler analysis and attention to anatomic connection with the LA. In TAPVC the four pulmonary veins may enter a confluence just posterior to the LA, but there will be a horizontal membrane (the posterior LA wall) separating the pulmonary venous confluence from the LA.
- PAPVC in the absence of scimitar syndrome is a more difficult diagnosis in the fetus and may not be detected.

### **Situs Abnormalities**

**Definition.** Abnormalities of situs are complex and will be discussed only briefly. These conditions refer to abnormalities of laterality in the thorax and abdomen and are discussed because they frequently involve cardiac anomalies. Laterality defects are typically divided into two major forms: situs inversus totalis and heterotaxy (also known as heterotaxy syndrome or isomerism, Fig. 13-70).

**Birth Prevalence/Epidemiology.** The estimated birth prevalence of nonsyndromic laterality defects is approximately 0.9 to 1.4 per 10,000 live births, with 73% representing heterotaxy and 27% representing situs inversus totalis.<sup>14,240,324,410-412</sup>

Situs defects have been shown to be more prevalent among non-white mothers under 20 years of age.<sup>410</sup> Approximately 17% of patients with heterotaxy are born small for gestational age, which is approximately twice the prevalence in the normal population. Although situs inversus totalis has an associated CHD presence of approximately 40%, about a third of these are simple defects. In contrast, heterotaxy is associated with CHD in over 90% of cases, with over 83% of cases having complex heart disease.<sup>410</sup>

**Anatomy.** In situs inversus totalis, the position of all thoracic and abdominal organs is entirely reversed, which includes dextrocardia, a rightward stomach, a leftward liver, and inverted cardiac anatomy (see Fig. 13-70). This form includes pulmonary venous return to a right-sided atrium and systemic venous return to a left-sided atrium, left-handed cardiac ventricular looping, and leftward malposed arteries (aorta anterior and leftward). Situs inversus totalis is not typically associated with major cardiac defects, but it is commonly associated with minor cardiac defects.<sup>410,413</sup>

Heterotaxy is much more complicated and typically involves abnormal thoracic status, abdominal visceral situs, and cardiovascular anatomy (Figs. 13-70 and 13-71). Traditionally two overall forms of heterotaxy are described, although many variations can occur.<sup>414</sup> The two historical forms of heterotaxy are (1) polysplenia complex (Van Praagh nomenclature), also known as left atrial isomerism (Anderson nomenclature), and (2) asplenia complex (Van Praagh nomenclature), also known as right atrial isomerism (Anderson nomenclature). As the Anderson nomenclature is more descriptive of this lesion, that terminology will be used for this section. Left atrial isomerism is associated with "duplication" or mirror image of the left-sided structures with the classic involvement of absence of the IVC with azygous continuation, ipsilateral pulmonary venous return with right pulmonary veins to the RA and left pulmonary veins to the LA, and frequent absence of the sinoatrial node with associated sinus node dysfunction. Right atrial isomerism is associated with an intact IVC, TAPVC, right or bilateral SVC, and secondary sinoatrial nodes. Both conditions are associated with AVCDs, although they are more common in right atrial isomerism; they are present in approximately 55% of cases of right atrial isomerism compared to 26% of left atrial isomerism cases. Bilateral SVC, broad-based midline liver, DORV, and pulmonary stenosis are seen in similar frequency in right and left forms.<sup>410</sup>

**Genetic Considerations.** Over 100 genes have been identified as important in left-right asymmetry in animal models,<sup>413</sup> and disruption of these pathways is implicated in human laterality defects. Primary

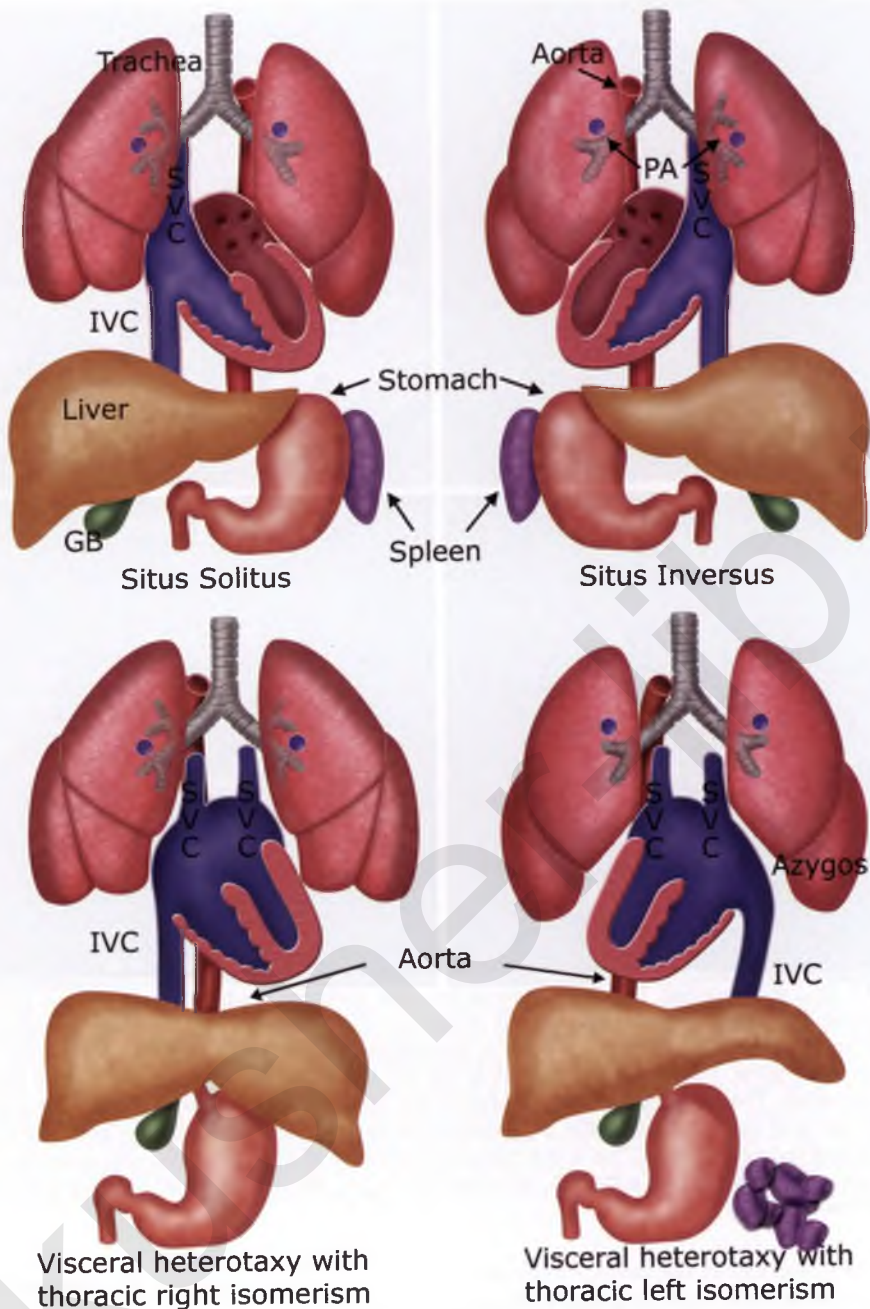


**FIG 13-70** Types of visceral situs. GB, gallbladder; IVC, inferior vena cava; PA, branch pulmonary artery; SVC, superior vena cava. (Illustration by Shi-Joon Yoo, MD.)

ciliary dyskinesia (PCD), previously known as immotile cilia syndrome, is one of the most widely recognized ciliopathies and is associated with situs inversus approximately 20% of the time.<sup>413</sup> PCD may be caused by a variety of gene defects, but is almost always an autosomal recessive condition.<sup>413</sup> Studies indicate that heterotaxy can also be caused by single gene mutations, although it is most often sporadic, and there is probably extensive locus heterogeneity.<sup>415</sup> Autosomal dominant, autosomal recessive, and X-linked inheritance have all been shown. Some of the genes implicated in heterotaxy include *NODAL*, *ZIC3*, *CFC1*, *CRELD1*, *SHROOM3*, and *ACVR2B*.<sup>413,415,416</sup> As these mutations will not typically be detected on karyotype or chromosomal microarray, a heterotaxy gene panel or whole exome sequencing may be considered for patients with laterality defects.<sup>416</sup>

**Interventions and Prognosis.** Surgical therapies are widely varied for heterotaxy complex and are based on the lesions that are present. These procedures are broad and can include repair of anomalous pulmonary veins, AVCD repairs, VSD repairs, and single ventricle palliations when a biventricular repair cannot be achieved. It is not uncommon for pacemaker placement to be indicated for either sinus node dysfunction or AV block. Ablation may also be needed for SVT secondary to dual AV node physiology.

Fetal demise and stillbirth may occur in the presence of heterotaxy syndrome with reports ranging from 7% to 31%.<sup>79,80</sup> When fetal demise occurs it is most often in association with significant AV valve regurgitation or bradyarrhythmia, at median ages in studies ranging from 24 to 26 weeks' gestation.<sup>80,417</sup> Termination rates are relatively high in



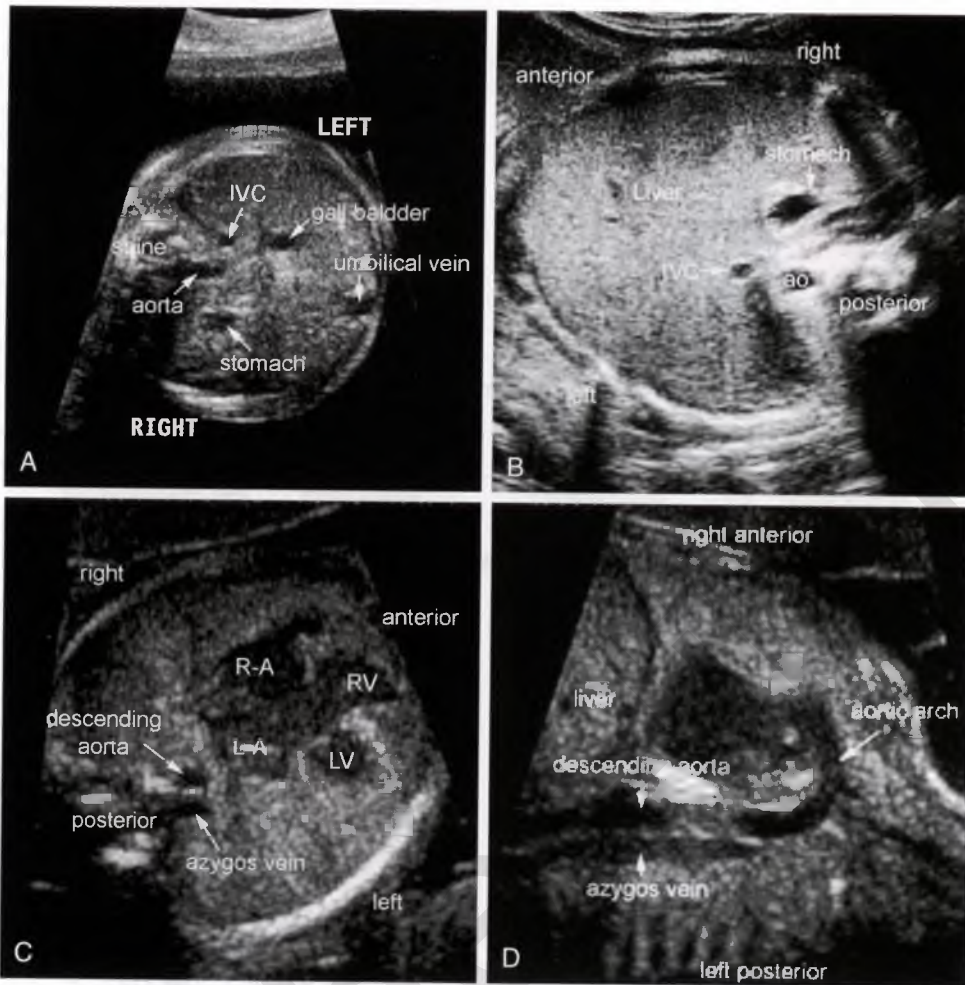


**FIG 13-71** Situs abnormalities. Transverse view of the upper abdomen in situs inversus (A), and heterotaxy with asplenia/right atrial isomerism (B). **A**, Situs inversus is characterized by mirror-image arrangement of the abdominal organs. **B**, The abdominal aorta is piggybacked behind the inferior vena cava (IVC) on the same side of the spine. This juxtaposed position of the IVC and abdominal aorta is seen in more than 90% of right isomerism. The liver extends from one side of the abdomen to the other. **C** and **D**, Left isomerism with interruption of the IVC. Two parallel large vessels are seen in front of the spine in both four-chamber (A) and oblique coronal (B) views. This is the characteristic feature of interrupted IVC with azygous or hemiazygous venous connection. ao, aorta; L-A, left-sided atrium; LV, left ventricle; R-A, right-sided atrium; RV, right ventricle.

published series, especially among those with single ventricle physiology, and have been reported to vary from 22% to 55%.<sup>79,80,417</sup>

Of those who are liveborn, the mortality rate is higher with right atrial isomerism, and death is often due to pulmonary vein stenosis and noncardiac anomalies.<sup>79,80,418</sup> Estimated 5-year survival rate in a recent report was 83% in left atrial isomerism and 55% in right atrial isomerism.<sup>80</sup>

#### Diagnostic Imaging Features

- Abdominal situs abnormalities may be the first sign of abnormal cardiac situs (Fig. 13-71A and B).
- The presence of an AVCD or dextrocardia should trigger a careful evaluation of systemic and pulmonary venous anatomy to evaluate for possible heterotaxy (Fig. 13-71C).
- Although both left and right ventricular hypoplasias are common in heterotaxy, they are rarely secondary to lesions such as HLHS or pulmonary atresia with intact ventricular septum. Rather, they are most frequently representative of an unbalanced AVCD.

- Look for the SVC anatomy using the 3VV or 3VT view; determine if there are bilateral SVCs or only a left SVC (Fig. 13-63C and D).
- To determine the location of IVC and hepatic venous drainage, a coronal view of the fetus is often helpful.
- Both 2D and color imaging to carefully evaluate systemic and pulmonary veins should be performed when heterotaxy is suspected (Fig. 13-71D).
- Pulmonary stenosis and atresia are commonly present in heterotaxy. In the case of severe pulmonary stenosis or pulmonary atresia there is usually a tortuous ductus arteriosus with retrograde flow.
- A right aortic arch is very common in heterotaxy and can be best diagnosed sweeping through the 3VT view to determine the relationship of the trachea and the arch. When the arch is right-sided, the duct often arises from the innominate artery and not the underside of the aortic arch.



**FIG 13-72** Cardiac tumors. **A**, Rhabdomyomas. Four-chamber view shows multiple tumors (asterisks) involving both ventricles, interventricular septum, and right atrium (RA). **B**, Hemangioma. Large pericardial teratoma in a four-chamber view. The tumor is heterogeneous and appears adherent to the RA, which is compressed. The heart is displaced leftward in the chest, and there is a large pericardial effusion taking up most of the chest. **C** and **D**, These four-chamber views show a hemangioma at 32 weeks and 35 weeks of gestation. In **C**, at 32 weeks, there is a round protruding mass (arrow) arising from the posterior wall of the RA. **D** shows growth of the mass and development of an echolucent cystic area. The removed mass showed histologic features of hemangioma with central hemorrhage. LA, left atrium; LV, left ventricle; RV, right ventricle.

## Cardiac Masses and Tumors

### General Features

**Definition.** A cardiac tumor is an abnormal mass or structure in the heart, myocardium, or pericardial space (Fig. 13-72). The mass may be single or multiple. Most pediatric primary cardiac tumors are benign. The natural history of a cardiac tumor is dependent upon the histologic composition and anatomic location. Fetal tumors that are large may result in hemodynamic obstruction of normal intracardiac flow patterns and hemodynamic compromise. Large tumors may present with myocardial dysfunction and hydrops fetalis. Fetal arrhythmias, such as atrial tachycardia, ventricular tachycardia, and bradycardia, may be the presenting findings of a fetal cardiac tumor. Fetal cardiac tumors have been noted in fetal demise cases.<sup>419</sup>

**Epidemiology.** An autopsy series in children reported an incidence of fetal cardiac tumors of 0.027% to 0.08%.<sup>420</sup> A large multicenter study evaluated 14,000 fetal echoes to document the frequency of fetal cardiac tumors, which were present in 19 pregnancies, or approximately 0.14%. Single tumors were found in 10 fetuses and multiple

tumors in 9. Tumor size ranged from 0.4 × 0.4 cm to 3.5 × 4 cm. There were 17 rhabdomyomas, 1 fibroma, and 1 atrial hemangioma. Tuberosus sclerosis complex (TSC) was diagnosed in 10 of the 17 (54%) fetuses with rhabdomyomas. Rhabdomyomas in 8 patients had partial or complete regression in size and in 5 fetuses there was no change. Three had cardiac hemodynamic obstruction and required tumor resection after birth.<sup>421</sup> The most common reason for a fetal echocardiogram was cardiac mass on routine obstetric ultrasound.

A study evaluating 224 patients (89 fetuses and 135 neonates) with cardiac tumors reported that rhabdomyoma was the most common, followed by teratoma, fibromas, and hemangiomas. In this study, rhabdomyoma accounted for 64% of the fetal tumors detected, teratoma accounted for 23%, fibroma approximately 6% to 7%, and vascular tumors such as hemangioma approximately 6% to 7%.<sup>419</sup> Toronto investigators reported on a series of 40 fetuses with cardiac tumors.<sup>422</sup> Hydrops fetalis was seen in 18%, ventricular obstruction in 30%, arrhythmias in 13%, and ventricular dysfunction in 5%. Rhabdomyomas were seen in 33 fetuses; 3 had elective termination. Four fetuses with rhabdomyomas died at birth. TSC was found in 88% of



the 26 fetuses with rhabdomyomas who survived. Three intrapericardial teratomas were found with pericardial effusions, and all had a fetal demise.<sup>422</sup>

A cardiac tumor may be the initial presentation of a genetic disorder such as tuberous sclerosis, neurofibromatosis, familial myxoma syndrome (cardiac myxoma, skin and mucous membrane lesions, and endocrine gland lesions in pituitary, adrenal gland, and testis), Gorlin syndrome (basal cell nevoid carcinoma syndrome), and rarely Beckwith-Wiedemann syndrome (macroglossia, macrosomia, and omphalocele).<sup>419</sup>

### Anatomy

**Rhabdomyoma.** Rhabdomyomas are the most frequently detected fetal cardiac tumor (Fig. 13-72 and Video 13-24). Rhabdomyomas are found within the ventricular wall and septum in the subepicardial region and within the atria. Rhabdomyomas are frequently multiple, well-circumscribed, nonencapsulated white or gray-white intramural or intracavitary nodules. On fetal echo, rhabdomyomas appear as rounded, homogeneous, and hyperechogenic masses. Less often, rhabdomyomas are single lesions.<sup>419</sup> When large, these intramural tumors may encroach on the intracavitary ventricular space or the outflow tract. The large tumors can also impinge upon the function of the AV and semilunar valves.

Rhabdomyomas have a biphasic growth pattern in the fetus. The tumor size typically increases between 20 and 32 weeks' gestation and subsequently either begins to regress or remains the same size in the fetus. During the first year of life, rhabdomyomas exhibit partial to complete regression in approximately 50% of cases.<sup>421</sup>

Multiple large rhabdomyomas may result in primary myocardial dysfunction. Depending on location, large tumors can also severely compromise blood flow in the outflow tracts and lead to hydrops fetalis. Fetal arrhythmias can be associated with rhabdomyomas and include atrial ectopy, SVT, bradycardia, and ventricular tachycardia, any of which can also precipitate hydrops fetalis and potentially in utero fetal demise. Tumor size 20 mm or larger and fetal arrhythmia are associated with poor fetal and neonatal outcomes.<sup>421-428</sup>

Rhabdomyomas are generally not associated with CHD, although there are sporadic case reports of rhabdomyomas seen with endocardial fibroelastosis, TOF, Ebstein anomaly, hypoplastic tricuspid valve, and HLHS.<sup>421,429,430</sup>

**Fibroma.** Fibromas are the second most common pediatric intracardiac tumor, but they are much less frequently seen in the fetus.<sup>421</sup> Fibromas are predominantly single, white, nonencapsulated intramural tumors located in the free wall, apex or IVS of the LV. Less frequently, fibromas can be in the right ventricular free wall, atrial septum, or atrial free wall. These lesions may demonstrate calcifications and cystic degeneration, which assist in differentiating them from a single rhabdomyoma, which is more homogeneous in character. Fibromas have been noted to increase in size prenatally and typically do not regress.<sup>431</sup> Again, this feature can help differentiate these lesions from rhabdomyomas.

**Intrapericardial Teratoma.** Intrapericardial teratomas are rare tumors that often present in the fetus with a large pericardial effusion (Fig. 13-72B and Video 13-25), and detection of a large pericardial effusion should lead to investigation for an intrapericardial teratoma. These lesions are single, encapsulated, bosselated tumors containing multiple cysts and attached at the base of the heart either by a broad-based stalk or pedicle to the aortic root and wedged between the SVC and the base of the aorta. The tumor most frequently is right-sided, arising from the aorta, and infrequently arises from the pulmonary artery. Intrapericardial teratomas can be three to four times the size of the fetal or newborn heart, and the solid tumor mass is contained within the restrictive fibrous pericardium. The large mass has a

propensity to obstruct and compress the heart. The development of a pericardial effusion may be related to obstructed or impaired lymphatics and SVC venous obstruction. These lesions are associated with fetal demise and a high mortality rate.

**Cardiac Hemangiomas.** Cardiac hemangiomas are single, highly vascular tumors, which may be epicardial, intramural, or intracavitary (Fig. 13-72C and D). They may be polypoid or sessile with central areas of necrosis and calcification.<sup>432</sup> Hemagioendotheliomas are commonly located in the RA with vascular flow from the coronary arteries.

**Myxoma.** Myxomas are rare fetal cardiac tumors and form exophytic intracavitary masses in the endocardium. A left atrial origin via a pedicle or a broad base off the fossa ovalis is seen in 75% of myxomas. Single right atrial tumors account for approximately 25% of myxomas. Rarely, myxomas originate in the ventricle, from valves or valve chordae. Calcification and cystic regions can develop. They are friable tumors with regions of thrombosis, which may result in peripheral emboli. Myxoma is the most common tumor in adults but is uncommon in the pediatric and prenatal populations.<sup>431</sup>

**Genetic Considerations.** Cardiac rhabdomyomas are associated with TSC. Fetal studies report that between 59% and 79% of fetuses with cardiac rhabdomyomas have TSC.<sup>421,433-435</sup> Mutations of the *TSC1* and *TSC2* genes cause TSC, and this disorder can be diagnosed in many cases by DNA analysis of *TSC1* (hamartin gene on chromosome 9q34) and *TSC2* (tuberin gene on chromosome 16p13.3). Both of these genes are tumor suppressor genes.<sup>436</sup> The clinical manifestations of TSC include mental retardation, seizures, and tumor-like malformations in the brain, kidney, retina, pancreas, and skin. TSC has an autosomal dominant mode of inheritance, although approximately 50% of TSC cases occur because of spontaneous mutations with no family history.<sup>432</sup>

Approximately 7% of myxomas are familial. Cardiac myxomas are seen in the pediatric age group as part of multiple lentiginos syndrome and may be associated with non-neoplastic endocrine disorders.<sup>432</sup>

**Outcomes.** Some large *rhabdomyomas* may obstruct tricuspid valve inflow or cause RVOT obstruction and present with cyanosis due to right-to-left shunting at the atrial level. LVOT obstruction can be severe and cause low cardiac output symptoms and right-to-left shunting at the PDA. Severe RVOT or LVOT obstruction may be ductus-dependent at birth and require surgical resection. Rhabdomyomas 20 mm or greater and fetal arrhythmias increase the risk for hydrops fetalis and in utero demise and are associated with poorer outcomes.

Depending on size, a *fibroma* may encroach upon the intracavitary space, obstruct the LVOT or RVOT, and present with symptoms of low cardiac output when obstructing the LVOT and cyanosis with significant RVOT obstruction. In severe outflow tract obstruction, surgical resection is necessary. Ventricular tachycardia is an arrhythmia associated with fibromas and may be the cause for sudden death in fibroma patients.<sup>427</sup> Prenatal diagnosis of an *intrapericardial teratoma* can allow for fetal intervention with pericardial fluid drainage or tumor resection. With prenatal pericardial fluid drainage, reaccumulation is typical. Delivery at a tertiary medical center with planned neonatal intrapericardial tumor resection allows for an excellent outcome because these tumors are seldom malignant or recurrent. Thus, surgical resection is considered curative with an excellent long-term outcome.<sup>437-441</sup> Large *hemangiomas* in the RA have been associated with hydrops fetalis and fetal demise.<sup>442,443</sup> *Myxoma* is rare, but prenatal diagnosis has been reported, and this condition has also been reported in a stillbirth.<sup>444</sup>

### Diagnostic Imaging Features

#### Rhabdomyoma

- Multiple rounded, homogeneous, hyperechoic lesions are seen in the ventricular, septal, and atrial myocardium; rarely is rhabdomyoma a single tumor.



- Associated arrhythmias include both tachycardia and bradycardia.

#### Fibroma

- This single, often large intramural tumor may be found in the free wall, apex, or septum of the LV.
- It is nonhomogeneous due to regions of calcification and cystic degeneration.
- Fibroma is associated with ventricular tachycardia.

#### Intrapericardial Teratoma

- This tumor is a large single, nonhomogeneous, lobular mass arising from the base of the heart.
- Echolucent cystic regions and calcifications are echogenic foci.
- Attachments to the base of the aorta or less frequently the pulmonary artery are seen.
- It is associated with large pericardial effusions.

#### Cardiac Hemangioma

- This nonhomogeneous hemangioma may include calcifications or regions of cystic necrosis.
- It is highly vascular, with vascular flow often from coronary arteries.
- The cardiac hemangioma is frequently found in the RA; large tumors in the RA can obstruct the tricuspid valve.

#### Myxoma

- Myomas are nonhomogeneous and friable.
- A single LA > RA tumor is attached to the fossa ovalis by a broad base or pedicle.
- It can be mobile and cross to and from either atrium.
- In diastole, it protrudes across the AV valve. In systole, it moves into the atria.

### Ectopia Cordis/Pentology of Cantrell

**Definition.** Ectopia cordis is a form of a pericardial defect and is marked by displacement of the heart outside the thorax (Fig. 13-73 and Video 13-26). There can be partial or complete displacement of the heart, and this condition is further classified by the location of the heart: cervical (3%), thoracic (60%), thoracoabdominal (7%), or abdominal (30%).<sup>410,445,446</sup> Pentology of Cantrell consists of an anterior diaphragmatic deficiency, midline abdominal wall defect, a diaphragmatic pericardial defect, and a lower sternal defect.<sup>447</sup>

**Epidemiology.** Ectopia cordis accounts for less than 0.1% of all congenital heart defects. The failure of the fetal embryonic sternum to fuse inferiorly results in a sternal cleft, which allows the heart to protrude outside the thorax. The incidence ranges from 5.5 to 7.9 per 1 million live births.<sup>448</sup> However, the true incidence may be higher, but unknown because of in utero demise. Ectopia cordis is a complex field defect, which involves a deficiency in the sternum, the diaphragm, and the anterior body wall. The development of the sternum begins during the 6th week of gestation when a pair of parallel mesenchymal bands of condensed mesenchyme migrate medially from two lateral plates on either side of the anterior chest wall. Fusion of the midline sternum occurs in a ventrolateral and craniocaudal fashion by the 10th week of gestation.<sup>445,449</sup>

**Anatomy.** Regardless of the subtype, coincident CHD is common in the setting of ectopia cordis, and outcomes are almost universally poor.<sup>448,450,451</sup> Although various cardiac structural defects have been reported, conotruncal abnormalities such as DORV and TOF predominate.<sup>448,451</sup> Coincident abdominal wall defects should prompt careful inspection of the position of the heart.

Most often, pentology of Cantrell presents in an incomplete form, with one or more of the previously mentioned diagnoses absent. Associated intracardiac defects are common, and various defects have been reported, including ASD, VSD, TOF, and Ebstein anomaly.<sup>452</sup> Demise is common in pentology of Cantrell, and the mortality rate is



**FIG 13-73** Ectopia cordis. This transverse view of the chest shows the heart protruding out of the thorax through a sternal cleft. The ribs are impinging on the atria, and the ventricles are outside the chest. Ant, anterior; Desc Ao, descending aorta; LA, left atrium; LV, left ventricle; Post, posterior; RA, right atrium; RV, right ventricle.

higher in complete forms and in cases with coincident extracardiac anomalies.<sup>453</sup>

Ectopia cordis is commonly associated with other anomalies, including a variety of intracardiac defects and midline body wall defects. Pentology of Cantrell was originally described as five associated anomalies, including a midline supraumbilical abdominal wall defect, a cleft in the inferior sternum, a deficiency of the anterior diaphragm, a pericardial diaphragmatic defect, and an intracardiac malformation. The hallmark of this syndrome is an omphalocele associated with ectopia cordis. Cantrell's series of ectopia cordis reported the following intracardiac defects: VSD (100%), ASD (53%), TOF (20%), and ventricular diverticulum (20%).<sup>447</sup> Other conotruncal anomalies such as DORV, pulmonary stenosis/atresia, aortic valve stenosis, TGA, and truncus arteriosus have been reported, as have many other cardiac defects. A small thorax can occur with ectopia cordis and be associated with lung hypoplasia and pulmonary artery hypoplasia, which has a very poor outcome. This disorder often presents as an incomplete form of pentology of Cantrell and exhibits a wide spectrum of other congenital anomalies, including omphalocele, diastasis recti, gastroschisis, craniofacial defects (such as cleft lip and palate), neural tube defects (such as encephalocele, hydrocephalus, and craniorachischisis), and skeletal anomalies.<sup>448,453-455</sup>

In thoracic ectopia cordis, the heart either partially or completely protrudes through the sternal cleft with the apex of the ventricles pointing cephalad. In thoracoabdominal ectopia cordis, there is a partial absence or a cleft in the inferior sternum, a midline anterior diaphragmatic defect, and a defect in the diaphragmatic pericardium, which allows the ventricular portion of the heart to enter the epigastrium. The heart may also protrude ventrally into an omphalocele or supraumbilical abdominal wall defect such as a gastroschisis. Often the heart appears to be sitting on top of the liver. Cervical ectopia cordis is very rare and is seen with either an intact sternum or partial cleft in the superior sternum. Abdominal ectopia cordis results from an anterior pericardial defect and diaphragmatic hernia, with the heart positioned in the abdomen.

**Genetic Considerations.** Familial cases have been reported, and some suggest a possible X-linked inheritance.<sup>456</sup> Trisomy 21, trisomy



18, trisomy 13, and Turner syndrome have also been reported with ectopia cordis, although the majority of ectopia cordis patients have a normal karyotype.<sup>457</sup> Ectopia cordis has been associated with maternal teratogens and viral infections and has been induced in animal models.<sup>458,459</sup>

**Outcomes.** In utero and postnatal demise is common in the setting of ectopia cordis, although survival following repair of the thoracic defect has been reported.<sup>448,451,460,461</sup>

**Interventions and Prognosis.** Treatment strategy for ectopia cordis consists of corrective or palliative cardiovascular surgery, correction of the ventral hernia diaphragmatic defects, and correction of associated anomalies. The overall outcome is dependent upon the size of the abdominal wall defect, the associated intracardiac abnormality, and the location of the ectopia cordis. A multistage repair is recommended, with the initial stage used to cover the heart with skin. Untreated, death occurs as a result of desiccation, trauma, or kinking of the heart and vessels, in addition to hypoxemia, sepsis, and arrhythmias. High morbidity and mortality rates are associated with attempted repair of pentology of Cantrell. Overall, surgical repair carries a survival rate of 40% to 50% and often is associated with prolonged ventilatory support and poor quality long-term outcomes.<sup>453,462</sup> Management is multidisciplinary, involving neonatology, congenital heart surgery, pediatric surgery, plastic surgery, obstetrics, and pediatric cardiology. If attempted repair is planned, delivery should be cesarean and neonatal resuscitation is required along with sterile coverage of the heart. Temporary coverage of the heart and abdominal defects is followed by repair of the diaphragmatic hernia and palliative or complete repair of the cardiac defect. The intracardiac repairs are based on the type of cardiac lesion. A multistaged approach has been the most successful. The best outcomes are related to ectopia cordis with no associated intracardiac defect. However, there are case reports of single ventricles undergoing successful repair and repair of ectopia cordis in staged surgeries.<sup>448,463-466</sup>

Cervical ectopia cordis has an extremely poor prognosis due to kinking of the great arteries and cardiac constriction, which occurs with attempts to reposition the heart. Abdominal ectopia cordis involves migration of the heart into the upper abdomen, and the outcomes are dependent upon the intracardiac anomalies, size of thorax, and degree of pulmonary hypoplasia.

#### Diagnostic Imaging Features

- Location of the heart must be carefully evaluated, as it may be partially or completely outside of the thorax (see Fig. 13-73).
- Cardiac anatomy should be carefully assessed, as VSDs and other associated anomalies are common.
- The degree of thoracic and pulmonary hypoplasia should be assessed.
- A careful evaluation for extracardiac anomalies is warranted, as they are common and significantly affect prognosis.

### Fetal Cardiac Arrhythmias

**General Features.** The cardiac conduction system consists of highly specialized tissue that rhythmically generates electrical signals from the sinoatrial node. This electrical signal is propagated through the atria to the AV node and into the His-Purkinje system in the ventricles. Synchronized depolarization and repolarization of the atrial and ventricular myocardial tissues corresponds to the rhythmic contraction and relaxation of the cardiac chambers, which allows synchronized filling and emptying. Derangements in the normal rhythm sequence of contraction or an abnormal rate result in abnormal filling and emptying. Therefore, persistent tachycardia or bradycardia result in myocardial dysfunction, low cardiac output, and congestive heart

failure. In the fetus, congestive heart failure typically manifests as hydrops fetalis.

Fetal arrhythmias are detected in 1% to 2% of pregnancies and are a common obstetric reason for a referral for fetal echocardiogram. The normal FHR ranges between 120 and 180 bpm with limited beat-to-beat variability. Fetal bradycardia is defined as FHR less than 100 bpm and fetal tachycardia as FHR greater than 180 bpm. An irregular rhythm is frequently due to atrial premature beats and infrequently due to ventricular extrasystoles. In the fetus, atrial ectopy is often encountered and ventricular ectopy is uncommon.

#### Echocardiographic Assessment of the Fetal Cardiac Rhythm.

Arrhythmias are traditionally diagnosed by electrocardiography, which measures the rate and morphologic and chronologic features of the atrial and ventricular electrical events. This assessment is challenging in the fetus because there is no conventional electrocardiography for the fetus. Current research tools use fetal magnetocardiography and fetal electrocardiography, but these tools are available at only a few centers.<sup>467-469</sup> Echocardiography is therefore used to measure the fetal chronology and temporal relationship of the atrial and ventricular myocardial sequence of contractions. For reference, normal Doppler signals of various cardiovascular structures are pictured in Figure 13-74. The fetal rhythm is determined by timing the atrial and ventricular mechanical contractions, which occur after depolarization. Both M-mode and Doppler imaging can be used to time the atrial and ventricular rates and the relationship of mechanical chamber contractions.

From the four-chamber view, positioning the M-mode beam through an atrial free wall and the opposite ventricular free wall near the AV groove, is preferred because these regions exhibit the greatest lateral excursion during the cardiac cycle (Fig. 13-75). An alternative view, placing the M-mode cursor across an atrial wall and the aortic valve in cross section, also allows timing of atrial systole and ventricular systolic ejection. By M-mode, the atrial contraction is the inward motion of the atrial wall, whereas the aortic valve opening represents the ventricular systolic ejection period. Mechanical events are not precisely recorded by M-mode measurements; rather, a more precise timing of cardiac events is defined using spectral Doppler sonography. The SVC and aorta are anatomically adjacent to each other, allowing a wide spectral Doppler sample volume to be positioned within both the aorta and the SVC. In the SVC, there is a larger S wave followed by a D wave directed toward the heart during ventricular systole (S) and in early diastole (D), and with atrial systole there is a brief retrograde a wave (A) that occurs following atrial depolarization and correlates with the P wave. The aortic ejection occurs after ventricular depolarization, which correlates with the QRS complex. The onset of the a wave to the onset of ventricular systole (onset of aortic flow) or AV interval correlates with the electrical PR interval and can be measured in the fetus. Doppler sonography can also be used to measure the timing of pulmonary vein and artery flow; with atrial systole there is a brief cessation of pulmonary venous flow, whereas pulmonary artery flow represents ventricular systole. These features again represent the AV duration and correlate to the PR interval.<sup>470</sup>

In normal sinus rhythm, the FHR most often ranges between 120 and 160 bpm and there is a 1:1 relationship between an atrial contraction followed by a ventricular contraction. The AV chronology and AV conduction ratio are also determined when evaluating the fetal cardiac rhythm. Analysis of the regularity of the atrial to atrial events and ventricular to ventricular events is important along with the relationship of the atrial and ventricular events.

**Irregular Fetal Rhythm.** The most common reason for an irregular fetal cardiac rhythm is premature atrial contractions (PACs), which



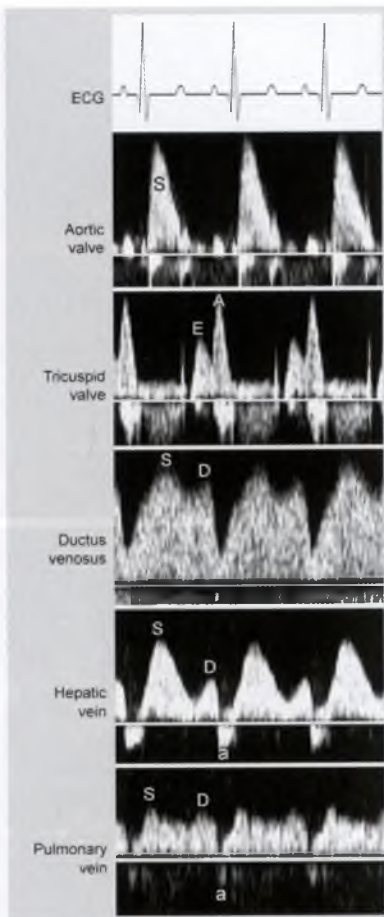


**FIG 13-74** Normal fetal cardiovascular Doppler tracings and correlation with an electrocardiogram (ECG). The aortic valve (and pulmonary valve) Doppler waveforms show a systolic ejection pattern, with no significant flow in diastole. The tricuspid valve (and mitral valve) waveforms are diastolic and biphasic: the shorter peak (E) occurs in early diastole, and the second peak (A) occurs with atrial contraction. For normal atrioventricular valves, there is no flow in systole. In the case of significant atrioventricular valve regurgitation, Doppler interrogation demonstrates a long, high-velocity systolic waveform (Fig. 13-6). The ductus venosus, hepatic veins, and pulmonary veins have a venous waveform, with systolic (S) and diastolic (D) waves. The normal hepatic vein and pulmonary vein Doppler waveforms may also have short a-wave reversal. A-wave reversal in the ductus venosus, however, is a sign of fetal heart failure.

occur in 1% to 3% of pregnancies. An atrial cell that electrically fires prior to the sinoatrial node results in a premature atrial beat or contraction. The PAC is either conducted to the ventricle or may be blocked, with no ventricular contraction (Fig. 13-76). With a blocked PAC, there is an increased V-V interval and a pause in the rhythm as the sinus node resets. Blocked atrial PAC followed by a sinus beat results in atrial bigeminy, with every other beat alternating between a sinoatrial beat and a blocked PAC, and two atrial events for each ventricular event. There is a short A-A interval between the sinus atrial beat and the blocked PAC, followed by a longer A-A interval between the blocked PAC and next sinoatrial beat. This short A-A interval followed by a longer A-A interval results in a consistent and repetitive pattern in persistent blocked atrial bigeminy and is characterized by a ventricular rate that ranges between 70 and 100 bpm but is never less than 65 bpm.<sup>471</sup> Approximately 10% to 14% of fetuses with blocked

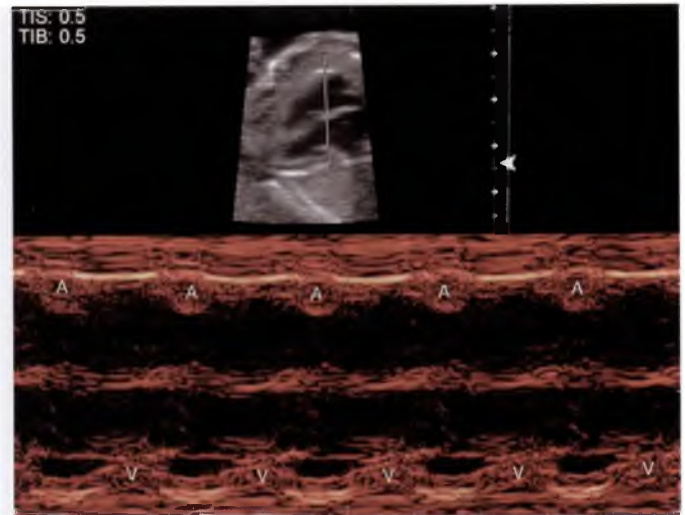


**FIG 13-75** Normal M-mode tracing for cardiac rhythm assessment using a four-chamber view. The M-mode beam is directed through the atrial and ventricular wall, and timing of contractions is observed. In normal sinus rhythm, every atrial contraction (A) is followed by one ventricular contraction (V).

atrial bigeminy develop SVT later in the pregnancy or after delivery, but most cases spontaneously resolve.

Frequent atrial couplets, two conducted PACs in a row, or frequent PACs present a risk for the development of SVT and should be monitored every 1 to 2 weeks. Atrial ectopy can be seen with intracardiac rhabdomyomas and with very redundant, aneurysmal atrial septum.

Premature ventricular beats or contractions are uncommon in the fetus and are most often benign. They can be seen in fetuses with rhabdomyomas and ventricular fibromas. Fetal premature ventricular contractions have also been associated with myocarditis in the fetal heart and with long QT syndrome.

**Fetal Bradycardia.** Fetal bradycardia is defined as an FHR of 110 bpm or less. FHRs in the 100 to 110 bpm range remain hemodynamically stable and there is no progressive cardiac dysfunction.

**Sinus or Low Atrial Bradycardia.** Left and right atrial isomerism can be associated with a low atrial rhythm ranging between 90 and 130 bpm, or dual sinoatrial nodes. Fetuses with heterotaxy syndrome frequently have associated intracardiac anomalies. The sinus node can also have acquired damage, as in fetuses born to women with Sjögren syndrome (SSA or SSB antibodies). The sinus node can be damaged by fetal myocarditis and present with a low atrial bradycardia.<sup>115</sup>

**Second-Degree Heart Block.** In second-degree heart block, the A-A interval is regular with very little variability, and there are two atrial events for every ventricular event (2:1 block). The ventricular rate ranges between 60 and 75 bpm, and this arrhythmia can be difficult to distinguish from complete heart block. If second-degree heart block is suspected at 16 to 26 weeks' gestation, maternal testing for SSA/SSB antibodies is indicated to determine if the fetal bradycardia may represent evolving fetal complete heart block. Channelopathies, such as Brugada syndrome and progressive cardiac conduction disease (*NKX2.5*, *hERG*, *SCN5A* mutations) and long QT syndromes (*LQT2*, *LQT3*, *LQT8*), can manifest as second- and third-degree heart block, and in some cases genetic testing is helpful.<sup>472</sup>



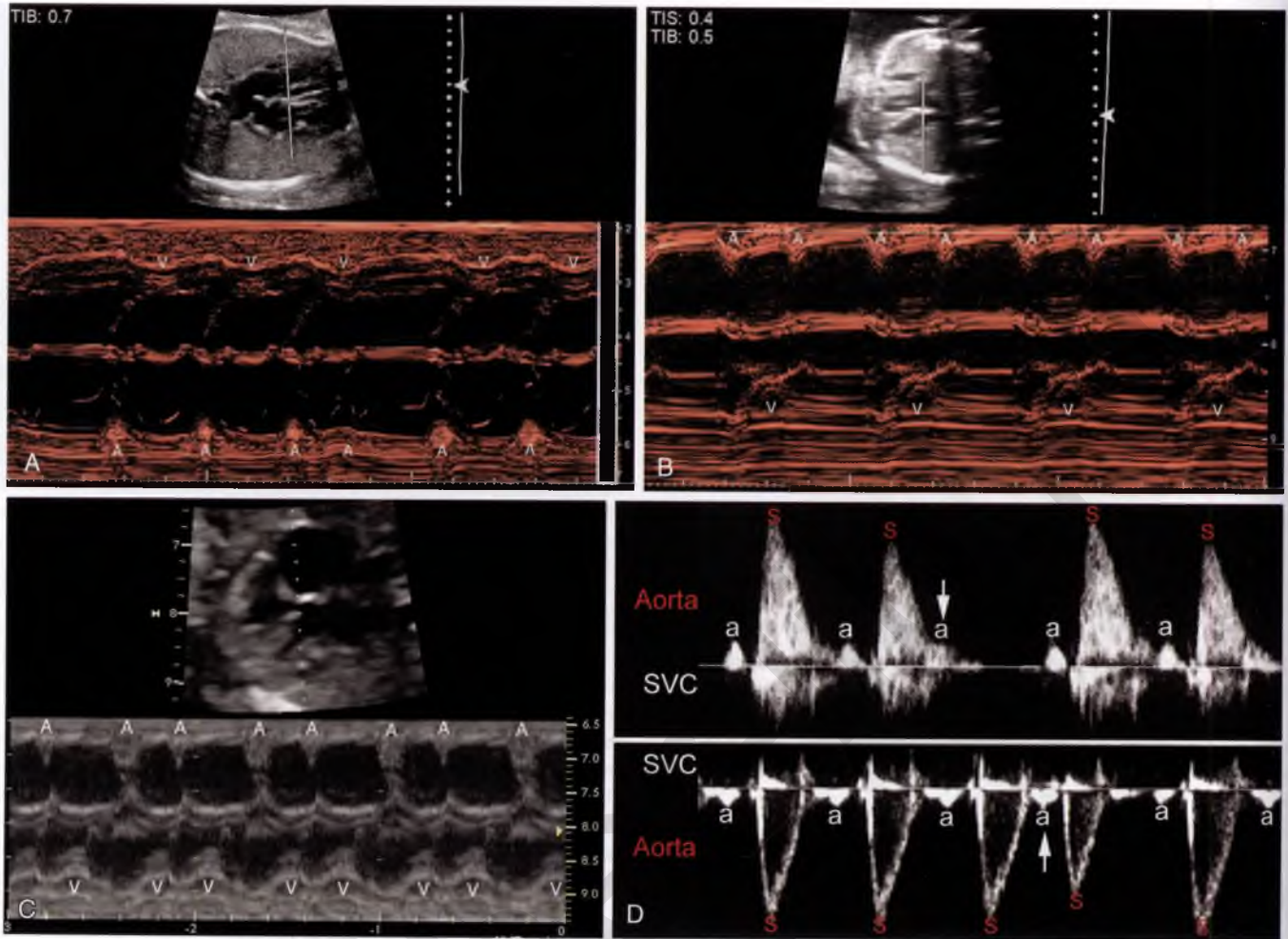


**FIG 13-76** Premature atrial contractions. **A**, M-mode through the ventricles (*above*) and atria (*below*) during a single premature atrial contraction that is not conducted (A, atrial contraction; V, ventricular contraction). The fourth atrial contraction is premature and is not followed by a ventricular contraction. **B**, Blocked atrial bigeminy. M-mode through the ventricles (*below*) and atria (*above*). Every other atrial contraction is early; the premature contractions are not followed by a ventricular contraction. **C**, Conducted atrial bigeminy. M-mode through the ventricles (*below*) and atria (*above*). Every other atrial contraction is early; the premature contractions are always followed by a ventricular contraction. **D**, Premature atrial contractions. Simultaneous Doppler tracing of the superior vena cava (SVC) and ascending aorta showing isolated blocked (*upper panel*) and conducted (*lower panel*) premature atrial contractions (*arrows*). a, atrial contraction; s, ventricular contraction.

### Third-Degree Heart Block: Congenital Complete Heart Block.

With third-degree or complete heart block (CHB) there is atrial and ventricular dissociation with the atrial rate in the normal range and the ventricular rate less than 60 bpm (Fig. 13-77).<sup>471</sup> CHD can be associated with complex cardiac defects and a malformed conduction system (50-55%) or with SSA/SSB antibodies, which represent approximately 40%. Heterotaxy syndrome, complex AVCDs, and congenitally corrected TGA may all present with CHB. A small number of CHB fetuses have no identified cause.<sup>115</sup>

When the FHR is less than 55 bpm, there is a risk of hydrops, and maternal  $\beta$ -sympathomimetics (terbutaline, salbutamol, isoprenaline) are sometimes suggested to augment the FHR. Maternal therapy is sometimes used in the setting of a faster FHR if there is an associated structural cardiac anomaly and signs of fetal cardiac compromise or evolving hydrops. Placement of a fetal pacemaker has not been successful and is considered experimental.<sup>115,472-475</sup>

With immune-mediated CHB, there have been reports of some limited benefit from maternal treatment with fluorinated steroids, IVIG (intravenous immunoglobulin) infusions, or a combination of both. If the fetus has first-degree heart block (defined as a fetal mechanical PR interval of  $>150$  ms<sup>476-478</sup>) or second-degree heart block and additional signs of inflammation, such as echogenicity of the fetal myocardium, valve regurgitation, cardiac dysfunction, or effusions, it has been hypothesized that treatment might prevent progression to CHB. A maternal trial of dexamethasone 4 to 8 mg/day has been proposed as a clinical treatment option.<sup>479</sup> The effect on the fetal heart is closely monitored along with assessment for fetal complications of maternal steroid treatment, which include growth restriction, oligohydramnios, and ductal constriction.<sup>115,477</sup> Once CHB is present, maternal steroids have not been found to be useful. One study reported better outcomes in fetuses treated with maternal steroids compared to untreated fetuses, with improvement in dilated cardiomyopathy,



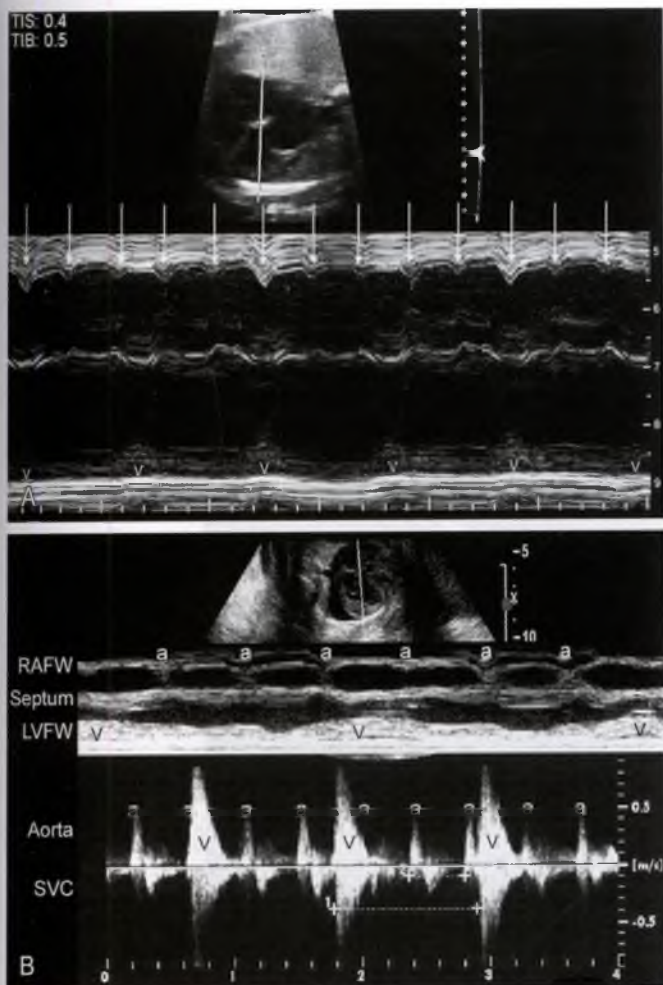


**FIG 13-77** Complete heart block. **A**, M-mode through the ventricular (below) and atrial (above) walls show that there are many more atrial contractions (arrows) than ventricular contractions (V). The ventricular rate is 52 beats per minute, whereas the atrial rate is 120 to 130 beats per minute. **B**, Doppler tracing of the superior vena cava (SVC) and ascending aorta (lower panel) showing complete atrioventricular dissociation related to complete atrioventricular block. The atrial rate (a-a) is 140 beats per minute, and the ventricular rate (V-V) is 54 beats per minute. LAFW, left atrial free wall; RAFW, right atrial free wall.

myocardial dysfunction, and hydrops. The maternal steroid therapy was speculated to be treating an immune-mediated fetal myocarditis.<sup>480</sup> However, a 2011 large European study of 175 CHB patients reported no overall difference in fetal or neonatal mortality rate in steroid-treated fetuses versus those with no therapy.<sup>481</sup> This study reported that the fetuses with the poorest outcomes were those presenting with CHB at less than 20 weeks' gestation, with FHR 50 bpm or less, ventricular dysfunction, and hydrops.<sup>473,474,481-483</sup>

### Fetal Tachycardia

**Sinus Tachycardia.** With sinus tachycardia, there is a 1:1 ratio of atrial:ventricular events (Fig. 13-78A), and a heart rate in the 160 to 180 bpm range. The rate has some variability and does not abruptly start or stop. Sinus tachycardia is often seen with fetal movement. Some disorders, such as anemia, hypoxemia, maternal infections, and maternal thyrotoxicosis, are also known to cause fetal sinus tachycardia. If there is an underlying maternal or fetal cause, it should be addressed and the FHR will typically return to normal for the gestational age.<sup>472</sup>

**Supraventricular Tachycardia.** SVT is caused by an AV node reentry accessory pathway, which is a rapidly conducting pathway from the ventricles to the atria. The ventriculoatrial (VA) time interval as measured by Doppler is short because of the fast conduction in the reentry pathway. In reentry SVT, the AV time interval is longer than the VA time interval, there is 1:1 A:V conduction, and the rate is in the 180 to 300 bpm range (Fig. 13-78B). The onset and cessation of SVT are both abrupt. When the fetus is in SVT more than 50% of the imaging time, maternal pharmacologic treatment is indicated as incessant SVT can lead to low cardiac output, myocardial dysfunction, AV valve regurgitation, hydrops fetalis, and fetal demise. The first line of choice is digoxin and if a second antiarrhythmic is needed, options include sotalol or flecainide. Amiodarone has also been used to treat fetal SVT, although it is used less frequently owing to potential maternal and fetal side effects.

Fetal SVT can also occur secondary to an ectopic atrial focus. The ectopic atrial tachycardia has a long VA time interval and measurement of this time interval can be used to differentiate the various causes of fetal SVT.<sup>484</sup> The rate is also 180 to 300 bpm and is managed similar to reentrant fetal SVT. For the fetus presenting late in gestation, an expedited delivery followed by a newborn cardioversion may be the best option.<sup>485-488</sup>

Fetal SVT that exhibits a long VA time interval, which is longer than the AV time interval, is due to atrial ectopic tachycardia (AET) or paroxysmal junctional reciprocating tachycardia (PJRT). This less common form of fetal SVT may be more recalcitrant to therapy. The time intervals are easily measured by spectral Doppler imaging.<sup>472,478</sup>

**Atrial Flutter.** Atrial flutter is an atrial macroreentry tachycardia that accounts for approximately 30% of fetal SVT and typically occurs in the third trimester. It has been speculated that the fetal atrium reaches a critical size for the appearance of the circuit at 27 to 30 weeks' gestation.<sup>489</sup> Fetal atrial flutter is defined as a rapid regular atrial rate of 300 to 600 bpm and is accompanied by a fixed or variable AV conduction block (Fig. 13-79). Thus, the ventricular rate is slower than the atrial rate, and there is typically a 2:1 A:V block. Atrial flutter is considered incessant if present for more than 50% of a 45-minute study and intermittent if the tachycardia is present less than 50% of the time. Digoxin is often the therapy of choice, as this prolongs the AV conduction and can increase the degree of block. Sotalol has also been effective in converting atrial flutter, especially with hydrops as it crosses the hydropic placenta more effectively.<sup>485-488</sup>

**Ventricular Tachycardia.** Ventricular tachycardia (VT) is extremely rare in the fetus, with the most important predisposing factor being long QT syndrome (LQTS). LQTS should be considered in the fetus presenting with baseline bradycardia and intermittent tachycardia, which may represent torsades de pointes type of VT. The hallmark of VT is AV dissociation, with the ventricular rate being higher than the atrial rate.

VT may also present in a fetus with myocarditis and ventricular tumors, such as rhabdomyoma and ventricular fibromas. Fetal VT has been treated with maternal IV lidocaine, magnesium, maternal oral mexiletine, sotalol, and amiodarone.<sup>472,490-492</sup>

### Diagnostic Imaging Features

- Simultaneous M-mode tracing of atrial and ventricular walls should be performed to determine the sequence and timing of mechanical contraction of the atria and ventricles.
- Simultaneous spectral Doppler of a vein and artery can measure the ratio of atrial to ventricular frequency.
- A:V ratio of 1:1 with a short VA < AV interval is AV node reentry tachycardia.
- A:V ratio of 1:1 with a long VA > AV interval is AET or PJRT.



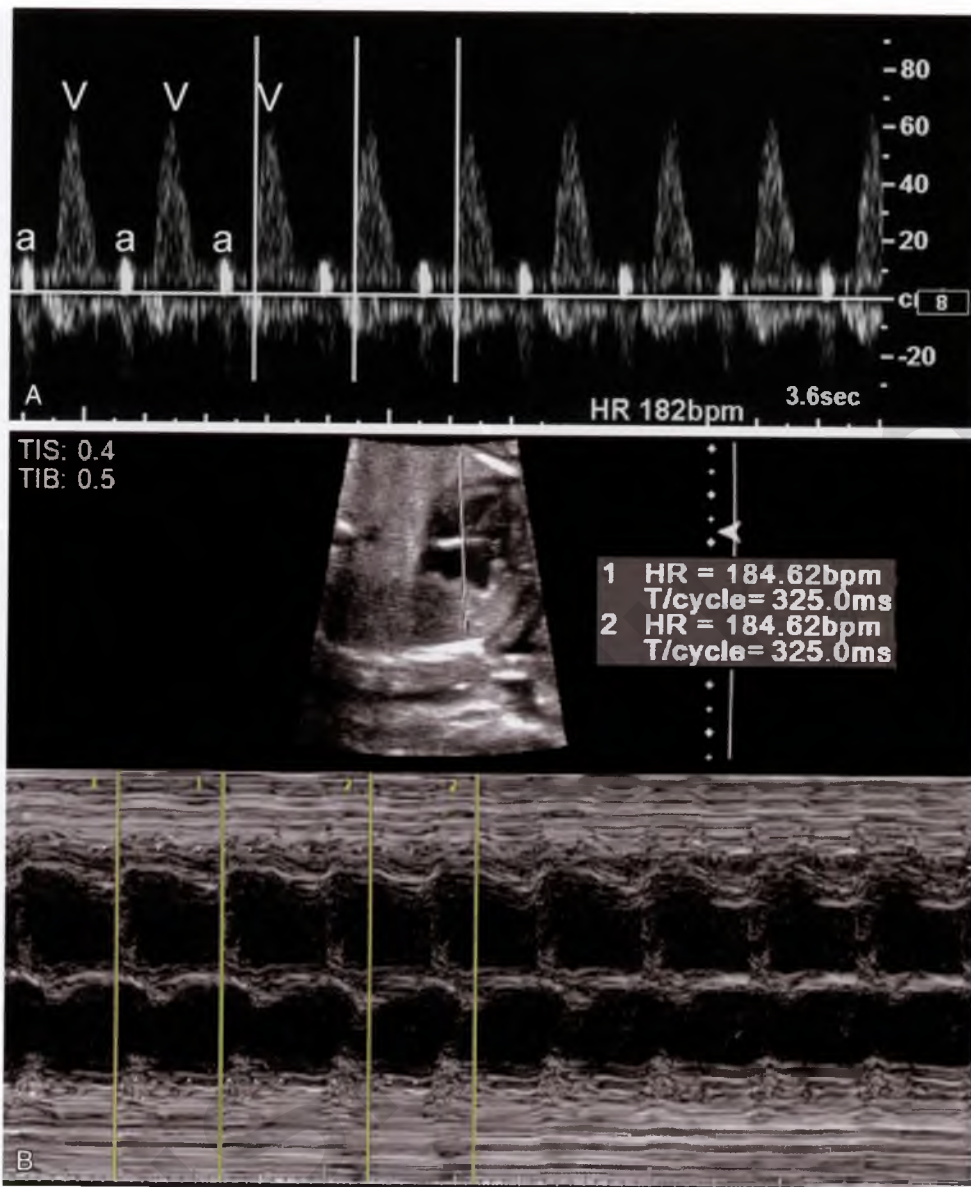


**FIG 13-78** Supraventricular tachycardia. **A**, Tachycardia with 1:1 atrioventricular relationship. Simultaneous Doppler tracing of the superior vena cava and ascending aorta show fetal tachycardia of 182 beats per minute with normal atrioventricular time intervals. This form of tachycardia may be caused by sinus tachycardia, permanent junctional reciprocating tachycardia (PJRT), and atrial ectopic tachycardia (AET). **B**, M-mode through the ventricles (*above*) and atria (*below*). Tachycardia at 184 beats per minute with 1:1 atrioventricular relationship. Although there is a ventricular contraction (V) for every atrial contraction (A), the ventricular contraction is closely followed by the atrial contraction, suggesting a reentrant mechanism to the tachycardia. HR, heart rate.

- A > V ratio represents either atrial flutter or, when consistently irregular, atrial fibrillation.
- A < V ratio is VT or junctional ectopic tachycardia.
- An atrial rate in the normal range and ventricular rate less than 60 bpm is complete heart block and AV dissociation.
- Atrial bigeminy with blocked PACs may have a ventricular rate of 70 to 100 bpm.

### Pericardial Effusions

Pericardial effusions are rarely seen in isolation and are typically associated with a primary abnormality (see Fig. 13-24), including structural heart disease, dysrhythmias, chromosomal abnormalities,

and extracardiac defects. Although the combination of a pericardial effusion and one of these defects often portends a poor outcome, outcomes of fetuses with isolated pericardial effusions are generally favorable.<sup>493</sup>

### Fetal Heart Failure/Impaired Cardiovascular Performance

Fetal cardiovascular performance can be affected by a wide variety of cardiac and noncardiac conditions. Cardiomyopathy, infection, alloimmune disease, anemia, arrhythmia, and exposure to toxins can all directly affect the fetal myocardium. Derangements in fetal preload or afterload due to structural heart disease, mass effect from other

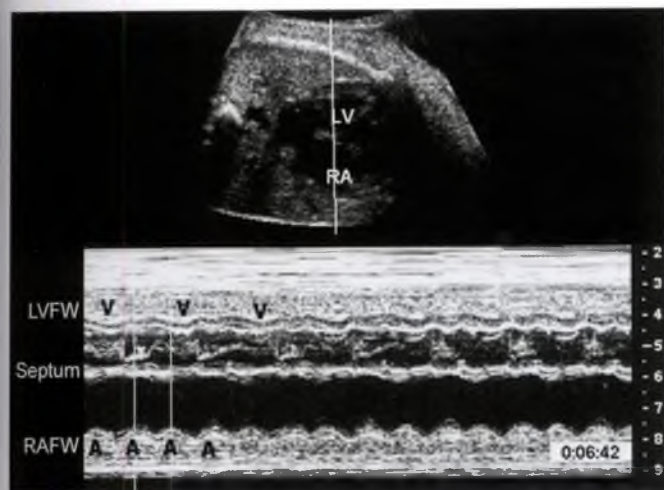


**FIG 13-79** Atrial flutter. M-mode tracing through the left ventricle (LV) and right atrium (RA) shows a fast atrial (A) rate (420 beats per minute) that is twice the ventricular (V) rate (210 beats per minute). The underlying arrhythmia is atrial flutter with 2:1 atrioventricular conduction. LVFW, left ventricular free wall; RAFW, right atrial free wall.

congenital anomalies, placental abnormalities, vascular tumors, malformations, and humoral factors can also affect cardiovascular performance (Fig. 13-80).<sup>494-498</sup>

**Assessment Parameters.** Stroke volume is determined by preload, afterload, and contractility of the ventricle. Cardiac output is a function of both stroke volume and heart rate. Fetal cardiac output stays relatively constant over a wide variety of heart rates, from approximately 50 to 200 bpm. Beyond this range, cardiac output will decrease owing to depletion of glucose and calcium stores. Higher extracellular water content, diminished calcium stores in the sarcoplasmic reticulum, lower albumin concentration, higher heart rate, and lower systemic arterial pressure result in markedly reduced compliance compared with the postnatal myocardium, and thus also respond poorly to increases in preload.<sup>499,500</sup> Fetal cardiac output is also sensitive to afterload. In cases of increased placental resistance, the afterload on the fetal RV increases, resulting in reduced output of that ventricle.<sup>501-503</sup>

The fetal RV and LV have different circulatory responsibilities in comparison to those of the child and adult. The fetal LV, instead of supporting the entire systemic circulation, provides circulation to the head and upper body. The fetal RV, on the other hand, provides circulation to the lower body and placenta (see Fig. 13-1). The fetal circulation, therefore, operates in parallel, and not in series, and the fetal RV is larger and has a larger cardiac output as compared to the left.<sup>32,121,133,341,504,505</sup>

Congestive heart failure is defined as inadequate oxygen delivery for normal end-organ function. Early signs of congestive heart failure include markers of diastolic dysfunction. They include AV valvar regurgitation, umbilical venous pulsations, flow reversal in the DV, and monophasic AV valve inflow. As heart failure progresses, fluid accumulates in a variety of potential spaces, leading to fetal hydrops.<sup>496,506,507</sup> As heart failure advances, systolic dysfunction develops. Although a variety of more sophisticated measures of systolic function exist, the most commonly used is shortening fraction. Shortening fraction of less than 28% is defined as abnormal, regardless of gestational age.

The most common manifestations of abnormal fetal hemodynamics include AV valve regurgitation, monophasic inflow into the ventricles, reduced ventricular stroke volume, and depressed ventricular

function with poor cardiac output, which results in the development of pericardial and pleural effusions, ascites, skin edema, and hydrops fetalis.

**Cardiomyopathy and Myocarditis.** Once a fetus with impaired cardiovascular performance is identified, a thorough evaluation for primary cause should be undertaken. This evaluation includes a thorough maternal history, assessment of fetal heart rhythm, evaluation for anemia, maternal serologic testing to assess for inflammatory and infectious disorders, and detailed structural ultrasound examination of the fetal heart, fetal extracardiac vasculature, and the placenta. If a fetal or maternal cause cannot be found, then myocarditis or cardiomyopathy should be considered.

Viral myocarditis presents as a cardiomyopathy in utero and can be due to a number of agents, including coxsackievirus, adenovirus, parvovirus B19, *Toxoplasma gondii*, herpes simplex virus, and human immunodeficiency virus.<sup>494,508-513</sup> Although large series do not exist, outcomes in fetuses diagnosed with myocarditis and cardiac dysfunction are thought to be quite poor. Prenatal treatment with steroid or immunoglobulins have been suggested, although neither has been studied in a meaningful way.<sup>509</sup>

Abnormally thick or trabeculated myocardium should signal the need for a detailed fetal structural cardiac evaluation. A recent review of fetuses diagnosed with left ventricular noncompaction demonstrated that the majority (92%) had coincident structural heart disease. Compared to other fetuses with structural heart disease, this group of patients represents a particularly high-risk cohort, as 81% of patients with known follow-up died or underwent heart transplantation.<sup>514</sup>

As knowledge of the genetics of myocardial disease advances, so may the accuracy of diagnosis of the cause of a fetal cardiomyopathy. Currently, primary fetal cardiomyopathy is most often a diagnosis of exclusion, and the rarity of this condition makes it difficult to study. The inclusion criteria for the small number of published studies differed, limiting their generalizability.<sup>132,494,513,515</sup> However, these series report generally poor outcomes, which are worse with hydrops and in cases with a cardiovascular profile score 6 or less (see Fig. 13-33). Additionally, a morphologic classification system including nonhypertrophic and hypertrophic cardiomyopathy has been proposed, as those fetuses with nonhypertrophic disease appeared to have better outcomes in one series.<sup>132</sup> Importantly, elevated myocardial performance index (see Fig. 13-34) appears to be a common finding in fetuses with cardiomyopathy but limited in its ability to predict outcome. Overall reported survival rates of fetal cardiomyopathy have improved dramatically over time, likely owing to improved rates of fetal diagnosis in the less severe cases. In contrast to earlier reports, in which the majority of fetuses had severe cardiomyopathy with accompanying hydrops, recent series have reported survival rate to infancy to be as high as 89%, and survival rate to 1 and 5 years to be as high as 85% and 75%, respectively.<sup>132,494,513,515</sup> Figure 13-81 depicts a fetus with cardiomyopathy who was successfully delivered but ultimately died in the neonatal period.

### Extracardiac Masses

Extracardiac masses can also affect cardiovascular status. High output vascular malformations such as sacrococcygeal teratoma, chorioangiomas, and arteriovenous malformations can dramatically increase the volume load on the fetal heart, and result in high output cardiac failure. Multiple series exist that describe vascular malformations in the fetus and predictors of poor outcome. Predictors of cardiovascular status or demise have included increased estimated combined cardiac output, cardiomegaly, worsened cardiovascular profile score, and hydrops.<sup>126,516-520</sup> When associated with fetal hydrops at a previable



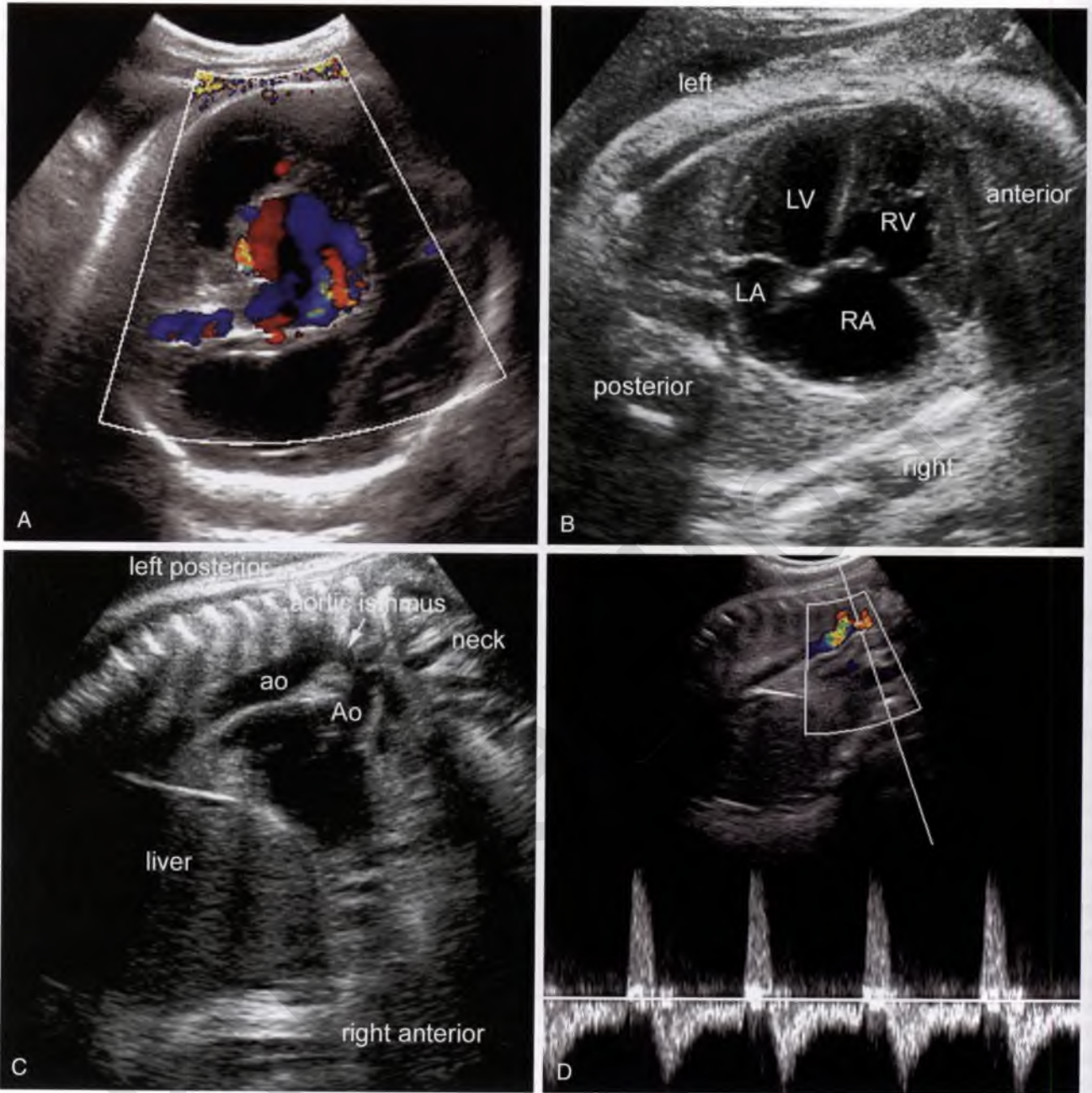


**FIG 13-80** Vein of Galen malformation with coarctation of aorta. **A**, Transverse view of the brain shows an aneurysmally dilated vein of Galen and hydrocephalus. **B**, Four-chamber view shows cardiomegaly with dilatation of the right atrium (RA) and right ventricle (RV). The right ventricle is also hypertrophied. **C**, Aortic arch view shows narrow aortic isthmus. **D**, Spectral Doppler tracing of the aortic isthmus shows systolic forward and diastolic retrograde flow. Ao, ascending aorta; ao, descending aorta; LA, left atrium; LV, left ventricle.

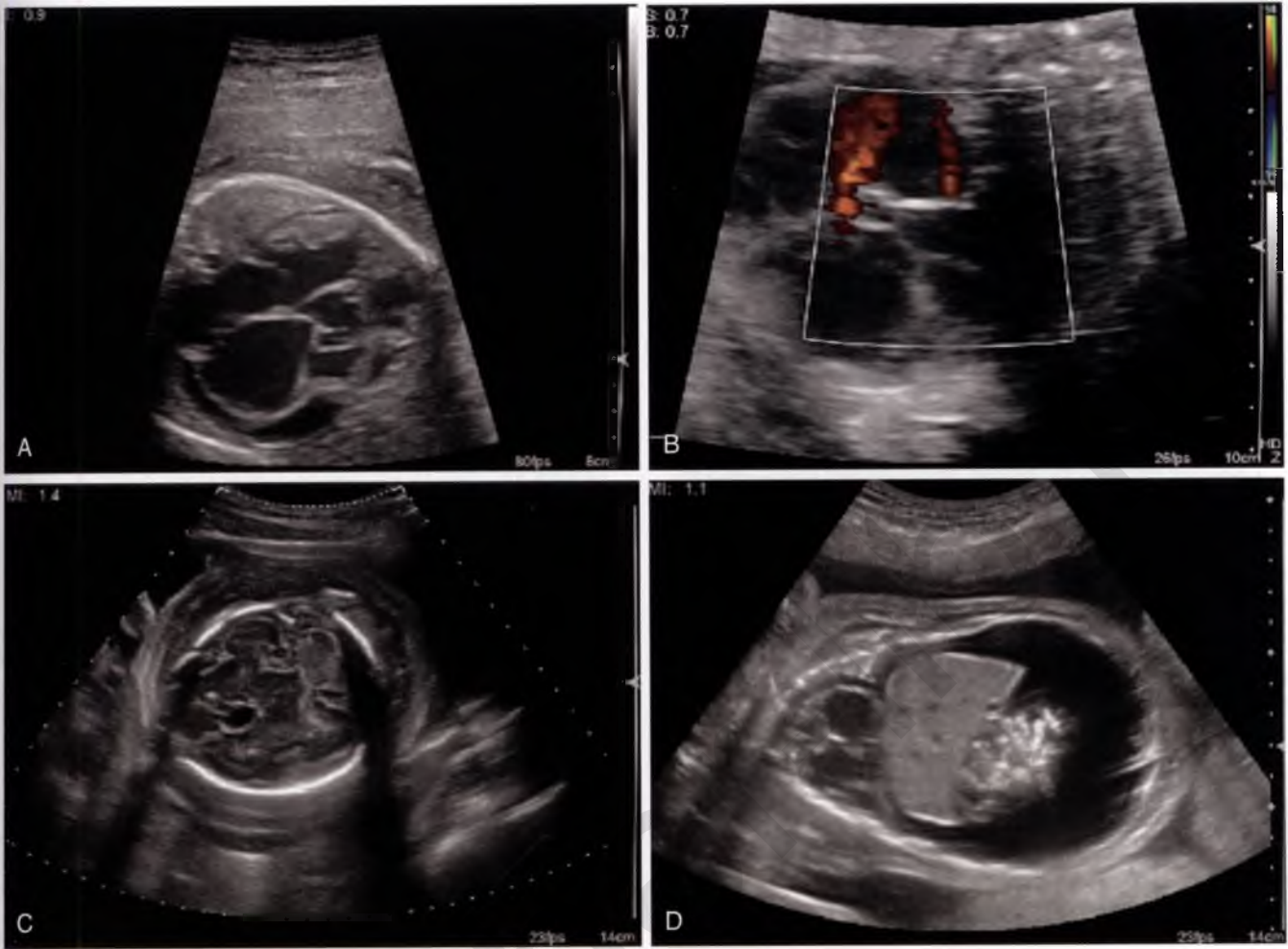


**FIG 13-81** Fetus with primary cardiomyopathy. **A**, The four-chamber view demonstrates marked hypertrabeculation of both ventricles with severe enlargement of the atria and a pericardial effusion. **B**, Color Doppler demonstrates moderate mitral and severe tricuspid regurgitation. **C** and **D**, There is fetal hydrops, as evidenced by scalp edema, body wall edema, and ascites.

gestational age, high output vascular malformations are almost universally fatal, although in utero intervention for some of these malformations may improve outcomes.<sup>517,521</sup>

## ACKNOWLEDGMENTS

Thank you to Maggie Nguyen, RDCS, and Lacey Schoppe, RDCS, for their constant pursuit of excellence in imaging and preparation of the fetal echocardiography video clips.

## REFERENCES

- Kleinman CS, Hobbins JC, Jaffe CC, et al: Echocardiographic studies of the human fetus: prenatal diagnosis of congenital heart disease and cardiac dysrhythmias. *Pediatrics* 65(6):1059–1067, 1980.
- Berghella V, Pagotto L, Kaufman M, et al: Accuracy of prenatal diagnosis of congenital heart defects. *Fetal Diagn Ther* 16(6):407–412, 2001.
- Jorgensen DE, Vejstrup N, Jorgensen C, et al: Prenatal detection of congenital heart disease in a low risk population undergoing first and second trimester screening. *Prenat Diagn* 35(4):325–330, 2015.
- Pike JJ, Krishnan A, Donofrio MT: Early fetal echocardiography: congenital heart disease detection and diagnostic accuracy in the hands of an experienced fetal cardiology program. *Prenat Diagn* 34(8):790–796, 2014.
- Oster ME, Kim CH, Kusano AS, et al: A population-based study of the association of prenatal diagnosis with survival rate for infants with congenital heart defects. *Am J Cardiol* 113(6):1036–1040, 2014.
- Levey A, Glickstein JS, Kleinman CS, et al: The impact of prenatal diagnosis of complex congenital heart disease on neonatal outcomes. *Pediatr Cardiol* 31(5):587–597, 2010.
- Baardman ME, du Marchie Sarvaas GJ, de Walle HE, et al: Impact of introduction of 20-week ultrasound scan on prevalence and fetal and neonatal outcomes in cases of selected severe congenital heart defects in The Netherlands. *Ultrasound Obstet Gynecol* 44(1):58–63, 2014.
- Brown DW, Cohen KE, O'Brien P, et al: Impact of prenatal diagnosis in survivors of initial palliation of single ventricle heart disease: analysis of the National Pediatric Cardiology Quality Improvement Collaborative database. *Pediatr Cardiol* 36(2):314–321, 2015.
- Wren C, Reinhardt Z, Khawaja K: Twenty-year trends in diagnosis of life-threatening neonatal cardiovascular malformations. *Arch Dis Child Fetal Neonatal Ed* 93(1):F33–F35, 2008.
- Quartermain MD, Pasquali S, Hill K, et al: National variation in prenatal diagnosis of congenital heart disease by state and lesion type: an analysis of thoracic surgeons congenital heart surgery (STS-CHS) database (Abstract). *J Am Coll Cardiol* 63(12):A497, 2014.
- Matthews TJ, Macdorman MF: Infant mortality statistics from the 2010 period linked birth/infant death data set. *Natl Vital Stat Rep* 62(8):1–26, 2013.



12. Broussard CS, Gilboa SM, Lee KA, et al: Racial/ethnic differences in infant mortality attributable to birth defects by gestational age. *Pediatrics* 130(3):e518–e527, 2012.
13. Mahle WT, Newburger JW, Matherne GP, et al: Role of pulse oximetry in examining newborns for congenital heart disease: a scientific statement from the American Heart Association and American Academy of Pediatrics. *Circulation* 120(5):447–458, 2009.
14. Reller MD, Strickland MJ, Riehle-Colarusso T, et al: Prevalence of congenital heart defects in metropolitan Atlanta, 1998–2005. *J Pediatr* 153(6):807–813, 2008.
15. Feinstein JA, Benson DW, Dubin AM, et al: Hypoplastic left heart syndrome: current considerations and expectations. *J Am Coll Cardiol* 59(1 Suppl):S1–S42, 2012.
16. Gabriel HM, Heger M, Innerhofer P, et al: Long-term outcome of patients with ventricular septal defect considered not to require surgical closure during childhood. *J Am Coll Cardiol* 39(6):1066–1071, 2002.
17. Jacobs JP, O'Brien SM, Pasquali SK, et al: Variation in outcomes for benchmark operations: an analysis of The Society of Thoracic Surgeons Congenital Heart Surgery Database. *Ann Thorac Surg* 92(6):2184–2192, 2011.
18. Cramer JW, Bartz PJ, Simpson PM, Zangwill SD: The spectrum of congenital heart disease and outcomes after surgical repair among children with Turner syndrome: a single-center review. *Pediatr Cardiol* 35(2):253–260, 2013.
19. Madriago E, Nguyen T, McFerson M, et al: Frequency and outcomes of cardiac operations and catheter interventions in Turner syndrome. *Am J Cardiol* 110(4):580–585, 2012.
20. Lara D, Ethen M, Canfield M, et al: Mortality in patients with Turner syndrome and hypoplastic left heart syndrome (Abstract). *J Am Coll Cardiol* 65(10):A545, 2015.
21. Bonnet D, Coltri A, Butera G, et al: Detection of transposition of the great arteries in fetuses reduces neonatal morbidity and mortality. *Circulation* 99(7):916–918, 1999.
22. van Velzen CL, Haak MC, Reijnders G, et al: Prenatal detection of transposition of the great arteries reduces mortality and morbidity. *Ultrasound Obstet Gynecol* 45(3):320–325, 2015.
23. Tworetzky W, McElhinney DB, Reddy VM, et al: Improved surgical outcome after fetal diagnosis of hypoplastic left heart syndrome. *Circulation* 103(9):1269–1273, 2001.
24. Morris SA, Ethen MK, Penny DJ, et al: Prenatal diagnosis, birth location, surgical center, and neonatal mortality in infants with hypoplastic left heart syndrome. *Circulation* 129(3):285–292, 2014.
25. Arya B, Glickstein JS, Levasseur SM, Williams IA: Parents of children with congenital heart disease prefer more information than cardiologists provide. *Congenit Heart Dis* 8(1):78–85, 2013.
26. Rosenberg KB, Monk C, Glickstein JS, et al: Referral for fetal echocardiography is associated with increased maternal anxiety. *J Psychosom Obstet Gynaecol* 31(2):60–69, 2010.
27. Rychik J, Donaghue DD, Levy S, et al: Maternal psychological stress after prenatal diagnosis of congenital heart disease. *J Pediatr* 162(2):302–307, 2013.
28. Rudolph AM, Heymann MA: The fetal circulation. *Annu Rev Med* 19(1):195–206, 1968.
29. Rudolph AM: The effects of postnatal circulatory adjustments in congenital heart disease. *Pediatrics* 36(5):763–772, 1965.
30. Rudolph AM: Congenital cardiovascular malformations and the fetal circulation. *Arch Dis Child Fetal Neonatal Ed* 95(2):F132–F136, 2010.
31. Clavero JA, Negueruela J, Ortiz L, et al: Blood flow in the intervillous space and fetal blood flow. I. Normal values in human pregnancies at term. *Am J Obstet Gynecol* 116(3):340–346, 1973.
32. Prsa M, Sun L, van Amerom J, et al: Reference ranges of blood flow in the major vessels of the normal human fetal circulation at term by phase-contrast magnetic resonance imaging. *Circ Cardiovasc Imaging* 7(4):663–670, 2014.
33. Eldridge FL, Hultgren HN: The physiologic closure of the ductus arteriosus in the newborn infant. *J Clin Invest* 34(7 Pt 1):987–996, 1955.
34. International Society of Ultrasound in Obstetrics and Gynecology, Carvalho JS, Allan LD, et al: ISUOG Practice Guidelines (updated): sonographic screening examination of the fetal heart. *Ultrasound Obstet Gynecol* 41(3):348–359, 2013.
35. American Institute of Ultrasound in Medicine: AIUM practice guideline for the performance of obstetric ultrasound examinations. *J Ultrasound Med* 32(6):1083–1101, 2013.
36. Carvalho JS, Moscoso G, Ville Y: First-trimester transabdominal fetal echocardiography. *Lancet* 351(9108):1023–1027, 1998.
37. Zosmer N, Souter VL, Chan CS, et al: Early diagnosis of major cardiac defects in chromosomally normal fetuses with increased nuchal translucency. *Br J Obstet Gynaecol* 106(8):829–833, 1999.
38. Huhta JC: The first trimester cardiologist: one standard of care for all children. *Curr Opin Pediatr* 13(5):453–455, 2001.
39. Galindo A, Comas C, Martínez JM, et al: Cardiac defects in chromosomally normal fetuses with increased nuchal translucency at 10–14 weeks of gestation. *J Matern Fetal Neonatal Med* 13(3):163–170, 2003.
40. DeVore GR: First-trimester fetal echocardiography: is the future now? *Ultrasound Obstet Gynecol* 20(1):6–8, 2002.
41. Haak MC, Twisk JR, Van Vugt JM: How successful is fetal echocardiographic examination in the first trimester of pregnancy? *Ultrasound Obstet Gynecol* 20(1):9–13, 2002.
42. Haak MC, Bartelings MM, Gittenberger-De Groot AC, Van Vugt JM: Cardiac malformations in first-trimester fetuses with increased nuchal translucency: ultrasound diagnosis and postmortem morphology. *Ultrasound Obstet Gynecol* 20(1):14–21, 2002.
43. Huggon IC, Ghi T, Cook AC, et al: Fetal cardiac abnormalities identified prior to 14 weeks' gestation. *Ultrasound Obstet Gynecol* 20(1):22–29, 2002.
44. Lopes LM, Brizot ML, Lopes MA, et al: Structural and functional cardiac abnormalities identified prior to 16 weeks' gestation in fetuses with increased nuchal translucency. *Ultrasound Obstet Gynecol* 22(5):470–478, 2003.
45. Smrcek JM, Gembruch U, Krokowski M, et al: The evaluation of cardiac biometry in major cardiac defects detected in early pregnancy. *Arch Gynecol Obstet* 268(2):94–101, 2003.
46. Carvalho JS: Clinical impact of first and early second trimester fetal echocardiography on high risk pregnancies. *Heart* 90(8):921–926, 2004.
47. McAuliffe FM, Trines J, Nield LE, et al: Early fetal echocardiography—a reliable prenatal diagnosis tool. *Am J Obstet Gynecol* 193(3):1253–1259, 2005.
48. Rasiyah SV, Publicover M, Ewer AK, et al: A systematic review of the accuracy of first-trimester ultrasound examination for detecting major congenital heart disease. *Ultrasound Obstet Gynecol* 28(1):110–116, 2006.
49. Yagel S, Cohen SM, Messing B: First and early second trimester fetal heart screening. *Curr Opin Obstet Gynecol* 19(2):183–190, 2007.
50. Viñals F, Ascenzo R, Naveas R, et al: Fetal echocardiography at 11 + 0 to 13 + 6 weeks using four-dimensional spatiotemporal image correlation telemedicine via an Internet link: a pilot study. *Ultrasound Obstet Gynecol* 31(6):633–638, 2008.
51. Martínez JM, Comas M, Borrell A, et al: Abnormal first-trimester ductus venosus blood flow: a marker of cardiac defects in fetuses with normal karyotype and nuchal translucency. *Ultrasound Obstet Gynecol* 35(3):267–272, 2010.
52. Persico N, Moratalla J, Lombardi CM, et al: Fetal echocardiography at 11–13 weeks by transabdominal high-frequency ultrasound. *Ultrasound Obstet Gynecol* 37(3):296–301, 2011.
53. Khalil A, Nicolaides KH: Fetal heart defects: potential and pitfalls of first-trimester detection. *Semin Fetal Neonatal Med* 18(5):251–260, 2013.
54. Ghi T, Huggon IC, Zosmer N, Nicolaides KH: Incidence of major structural cardiac defects associated with increased nuchal translucency but normal karyotype. *Ultrasound Obstet Gynecol* 18(6):610–614, 2001.
55. Hyett J, Moscoso G, Papapanagiotou G, et al: Abnormalities of the heart and great arteries in chromosomally normal fetuses with increased nuchal translucency thickness at 11–13 weeks of gestation. *Ultrasound Obstet Gynecol* 7(4):245–250, 1996.
56. Hyett J: Does nuchal translucency have a role in fetal cardiac screening? *Prenat Diagn* 24(13):1130–1135, 2004.

57. Hyett JA, Perdu M, Sharland GK, et al: Increased nuchal translucency at 10-14 weeks of gestation as a marker for major cardiac defects. *Ultrasound Obstet Gynecol* 10(4):242-246, 1997.
58. Pereira S, Ganapathy R, Syngelaki A, et al: Contribution of fetal tricuspid regurgitation in first-trimester screening for major cardiac defects. *Obstet Gynecol* 117(6):1384-1391, 2011.
59. Timmerman E, Clur SA, Pajkrt E, Bilardo CM: First-trimester measurement of the ductus venosus pulsatility index and the prediction of congenital heart defects. *Ultrasound Obstet Gynecol* 36(6):668-675, 2010.
60. Zapata H, Edwards JE, Titus JL: Aberrant right subclavian artery with left aortic arch: associated cardiac anomalies. *Pediatr Cardiol* 14(3):159-161, 1993.
61. Ramaswamy P, Lytrivi ID, Thanjan MT, et al: Frequency of aberrant subclavian artery, arch laterality, and associated intracardiac anomalies detected by echocardiography. *Am J Cardiol* 101(5):677-682, 2008.
62. Mavrides E, Cobian-Sanchez F, Tekay A, et al: Limitations of using first-trimester nuchal translucency measurement in routine screening for major congenital heart defects. *Ultrasound Obstet Gynecol* 17(2):106-110, 2001.
63. Makrydimas G, Sotiriadis A, Ioannidis JP: Screening performance of first-trimester nuchal translucency for major cardiac defects: a meta-analysis. *Am J Obstet Gynecol* 189(5):1330-1335, 2003.
64. Papatheodorou SI, Evangelou E, Makrydimas G, Ioannidis J: First-trimester ductus venosus screening for cardiac defects: a meta-analysis. *Br J Obstet Gynaecol* 118(12):1438-1445, 2011.
65. Sinkovskaya E, Horton S, Berkley EM, et al: Defining the fetal cardiac axis between 11 + 0 and 14 + 6 weeks of gestation: experience with 100 consecutive pregnancies. *Ultrasound Obstet Gynecol* 36(6):676-681, 2010.
66. Volpe P, Ubaldo P, Volpe N, et al: Fetal cardiac evaluation at 11-14 weeks by experienced obstetricians in a low-risk population. *Prenat Diagn* 31(11):1054-1061, 2011.
67. Zidere V, Bellsham-Revell H, Persico N, Allan LD: Comparison of echocardiographic findings in fetuses at less than 15 weeks' gestation with later cardiac evaluation. *Ultrasound Obstet Gynecol* 42(6):679-686, 2013.
68. Schwarzler P, Senat MV, Holden D, et al: Feasibility of the second-trimester fetal ultrasound examination in an unselected population at 18, 20 or 22 weeks of pregnancy: a randomized trial. *Ultrasound Obstet Gynecol* 14(2):92-97, 1999.
69. Lee W: Performance of the basic fetal cardiac ultrasound examination. *J Ultrasound Med* 17(9):601-607, 1998.
70. Simpson LL: Screening for congenital heart disease. *Obstet Gynecol Clin North Am* 31(1):51-59, 2004.
71. Bromley B, Estroff JA, Sanders SP, et al: Fetal echocardiography: accuracy and limitations in a population at high and low risk for heart defects. *Am J Obstet Gynecol* 166(5):1473-1481, 1992.
72. Kirk JS, Riggs TW, Comstock CH, et al: Prenatal screening for cardiac anomalies: the value of routine addition of the aortic root to the four-chamber view. *Obstet Gynecol* 84(3):427-431, 1994.
73. Vettriano IM, Lee W, Bronsteen RA, Comstock CH: Sonographic evaluation of the ventricular cardiac outflow tracts. *J Ultrasound Med* 24(4):566, 2005.
74. American Institute of Ultrasound in Medicine: AIUM practice guideline for the performance of fetal echocardiography. *J Ultrasound Med* 32(6):1067-1082, 2013.
75. Tegnander E, Williams W, Johansen OJ, et al: Prenatal detection of heart defects in a non-selected population of 30,149 fetuses—detection rates and outcome. *Ultrasound Obstet Gynecol* 27(3):252-265, 2006.
76. Yoo SJ, Lee YH, Cho KS, Kim DY: Sequential segmental approach to fetal congenital heart disease. *Cardiol Young* 9(4):430-444, 1999.
77. Yagel S, Cohen SM, Achiron R: Examination of the fetal heart by five short-axis views: a proposed screening method for comprehensive cardiac evaluation. *Ultrasound Obstet Gynecol* 17(5):367-369, 2001.
78. Jacobs JP, Jacobs ML, Mavroudis C, et al: Nomenclature and databases for the surgical treatment of congenital cardiac disease—an updated primer and an analysis of opportunities for improvement. *Cardiol Young* 18(Suppl 2):38-62, 2008.
79. Taketazu M, Loughheed J, Yoo SJ, et al: Spectrum of cardiovascular disease, accuracy of diagnosis, and outcome in fetal heterotaxy syndrome. *Am J Cardiol* 97(5):720-724, 2006.
80. Escobar-Diaz MC, Friedman K, Salem Y, et al: Perinatal and infant outcomes of prenatal diagnosis of heterotaxy syndrome (asplenia and polysplenia). *Am J Cardiol* 114(4):612-617, 2014.
81. Lee W, Smith RS, Comstock CH, et al: Tetralogy of Fallot: prenatal diagnosis and postnatal survival. *Obstet Gynecol* 86(4 Pt 1):583-588, 1995.
82. Hornberger LK, Need L, Benacerraf BR: Development of significant left and right ventricular hypoplasia in the second and third trimester fetus. *J Ultrasound Med* 15(9):655-659, 1996.
83. Yoo SJ, Lee YH, Kim ES, et al: Three-vessel view of the fetal upper mediastinum: an easy means of detecting abnormalities of the ventricular outflow tracts and great arteries during obstetric screening. *Ultrasound Obstet Gynecol* 9(3):173-182, 1997.
84. Chaoui R, McEwing R: Three cross-sectional planes for fetal color Doppler echocardiography. *Ultrasound Obstet Gynecol* 21(1):81-93, 2003.
85. Paladini D: How to identify the thymus in the fetus: the thy-box. *Ultrasound Obstet Gynecol* 37(4):488-492, 2011.
86. Yagel S, Arbel R, Anteby EY, et al: The three vessels and trachea view (3VT) in fetal cardiac scanning. *Ultrasound Obstet Gynecol* 20(4):340-345, 2002.
87. Gardiner H, Chaoui R: The fetal three-vessel and tracheal view revisited. *Semin Fetal Neonatal Med* 18(5):261-268, 2013.
88. Achiron R, Rotstein Z, Heggesh J, et al: Anomalies of the fetal aortic arch: a novel sonographic approach to in-utero diagnosis. *Ultrasound Obstet Gynecol* 20(6):553-557, 2002.
89. Chaoui R, Heling KS, Sarioglu N, et al: Aberrant right subclavian artery as a new cardiac sign in second- and third-trimester fetuses with Down syndrome. *Am J Obstet Gynecol* 192(1):257-263, 2005.
90. Paladini D, Sglavo G, Pastore G, et al: Aberrant right subclavian artery: incidence and correlation with other markers of Down syndrome in second-trimester fetuses. *Ultrasound Obstet Gynecol* 39(2):191-195, 2012.
91. Carvalho JS: Primary bradycardia: keys and pitfalls in diagnosis. *Ultrasound Obstet Gynecol* 44(2):125-130, 2014.
92. American College of Obstetricians and Gynecologists: ACOG Practice Bulletin No. 106: intrapartum fetal heart rate monitoring: nomenclature, interpretation, and general management principles. *Obstet Gynecol* 114(1):192-202, 2009.
93. Hankins GD, Miller DA: A review of the 2008 NICHD Research Planning Workshop: recommendations for fetal heart rate terminology and interpretation. *Clin Obstet Gynecol* 54(1):3-7, 2011.
94. Awadh AMA, Prefumo F, Bland JM, Carvalho JS: Assessment of the intraobserver variability in the measurement of fetal cardiothoracic ratio using ellipse and diameter methods. *Ultrasound Obstet Gynecol* 28(1):53-56, 2006.
95. Lee W, Riggs T, Amula V, et al: Fetal echocardiography: z-score reference ranges for a large patient population. *Ultrasound Obstet Gynecol* 35(1):28-34, 2010.
96. Tongsong T, Wanapirak C, Sirichotiyakul S, et al: Fetal sonographic cardiothoracic ratio at midpregnancy as a predictor of Hb Bart disease. *J Ultrasound Med* 18(12):807-811, 1999.
97. Hoffmann R, von Bardeleben S, ten Cate F, et al: Assessment of systolic left ventricular function: a multi-centre comparison of cineventriculography, cardiac magnetic resonance imaging, unenhanced and contrast-enhanced echocardiography. *Eur Heart J* 26(6):607-616, 2005.
98. Comstock CH: Normal fetal heart axis and position. *Obstet Gynecol* 70(2):255-259, 1987.
99. Smith RS, Comstock CH, Kirk JS, et al: Ultrasonographic left cardiac axis deviation: a marker for fetal anomalies. *Obstet Gynecol* 85:187, 1995.
100. Comstock CH, Smith R, Lee W, Kirk JS: Right fetal cardiac axis: clinical significance and associated findings. *Obstet Gynecol* 91(4):495-499, 1998.



101. Shenker L, Reed KL, Anderson CF, Kern W: Fetal pericardial effusion. *Am J Obstet Gynecol* 160(6):1505–1508, 1989.
102. Di Salvo DN, Brown DL, Doubilet PM, et al: Clinical significance of isolated fetal pericardial effusion. *J Ultrasound Med* 13(4):291–293, 1994.
103. Oyer CE, Sung CJ, Friedman R, et al: Reference values for valve circumferences and ventricular wall thicknesses of fetal and neonatal hearts. *Pediatr Dev Pathol* 7(5):499–505, 2004.
104. Berg C, Geipel A, Kohl T, et al: Fetal echocardiographic evaluation of atrial morphology and the prediction of laterality in cases of heterotaxy syndromes. *Ultrasound Obstet Gynecol* 26(5):538–545, 2005.
105. Papa M, Fragasso G, Camesasca C, et al: Prevalence and prognosis of atrial septal aneurysm in high risk fetuses without structural heart defects. *Ital Heart J* 3(5):318–321, 2002.
106. Channing A, Szwast A, Natarajan S, et al: Maternal hyperoxygenation improves left heart filling in the fetus with atrial septal aneurysm causing impediment to left ventricular inflow. *Ultrasound Obstet Gynecol* 45:664–669, 2014.
107. Patel CR, Steele MA, Stewart JW: Double-outlet right ventricle with partial anomalous pulmonary venous connection: prenatal diagnosis. *J Ultrasound Med* 24(6):861–864, 2005.
108. Ganesan S, Brook MM, Silverman NH, Moon-Grady AJ: Prenatal findings in total anomalous pulmonary venous return: a diagnostic road map starts with obstetric screening views. *J Ultrasound Med* 33(7):1193–1207, 2014.
109. Kirk JS, Comstock CH, Lee W, et al: Fetal cardiac asymmetry: a marker for congenital heart disease. *Obstet Gynecol* 93(2):189–192, 1999.
110. Gussenhoven EJ, Stewart PA, Becker AE, et al: “Offsetting” of the septal tricuspid leaflet in normal hearts and in hearts with Ebstein’s anomaly. *Am J Cardiol* 54(1):172–176, 1984.
111. Berg C, Kaiser C, Bender F, et al: Atrioventricular septal defect in the fetus—associated conditions and outcome in 246 cases. *Ultraschall Med* 30(1):25–32, 2009.
112. Park JK, Taylor DK, Skeels M, Towner DR: Dilated coronary sinus in the fetus: misinterpretation as an atrioventricular canal defect. *Ultrasound Obstet Gynecol* 10(2):126–129, 1997.
113. Vettriano IM, Huang R, Comstock CH: The normal offset of the tricuspid septal leaflet in the fetus. *J Ultrasound Med* 21(10):1099–1104, 2002.
114. Espinoza J, Romero R, Kusanovic JP, et al: OP12.09: The value of the sagittal view of the “ductal arch plane” in the prenatal diagnosis and counseling of conotruncal anomalies using 4D ultrasonography. *Ultrasound Obstet Gynecol* 30(4):495–496, 2007.
115. Donofrio MT, Moon-Grady AJ, Hornberger LK, et al: Diagnosis and treatment of fetal cardiac disease: a scientific statement from the American Heart Association. *Circulation* 129(21):2183–2242, 2014.
116. *Innovative Resources for Fractional Limb Volume, Fetal Echocardiography, and Individualized Growth Assessment*. Available at <obsono.org>.
117. *Z-scores for fetal echocardiography*. Available at <fetal.parameterz.com>.
118. Comas M, Crispi F, Gómez O, et al: Gestational age- and estimated fetal weight-adjusted reference ranges for myocardial tissue Doppler indices at 24–41 weeks’ gestation. *Ultrasound Obstet Gynecol* 37(1):57–64, 2011.
119. McElhinney DB, Marshall AC, Wilkins-Haug LE, et al: Predictors of technical success and postnatal biventricular outcome after in utero aortic valvuloplasty for aortic stenosis with evolving hypoplastic left heart syndrome. *Circulation* 120(15):1482–1490, 2009.
120. Pasquini L, Mellander M, Seale A, et al: Z-scores of the fetal aortic isthmus and duct: an aid to assessing arch hypoplasia. *Ultrasound Obstet Gynecol* 29(6):628–633, 2007.
121. Schneider C, McCrindle BW, Carvalho JS, et al: Development of z-scores for fetal cardiac dimensions from echocardiography. *Ultrasound Obstet Gynecol* 26(6):599–605, 2005.
122. Achiron R, Zimand S, Hegesh J, et al: Fetal aortic arch measurements between 14 and 38 weeks’ gestation: in-utero ultrasonographic study. *Ultrasound Obstet Gynecol* 15(3):226–230, 2000.
123. Falkensammer CB, Paul J, Huhta JC: Fetal congestive heart failure: correlation of Tei-index and Cardiovascular-score. *J Perinat Med* 29(5):390–398, 2001.
124. Wieczorek A, Hernandez-Robles J, Ewing L, et al: Prediction of outcome of fetal congenital heart disease using a cardiovascular profile score. *Ultrasound Obstet Gynecol* 31(3):284–288, 2008.
125. Li Y, Fang J, Zhou K, et al: Prediction of fetal outcome without intrauterine intervention using a cardiovascular profile score: a systematic review and meta-analysis. *J Matern Fetal Neonatal Med* 28(16):1965–1972, 2015.
126. Statile CJ, Cnota JF, Gomien S, et al: Estimated cardiac output and cardiovascular profile score in fetuses with high cardiac output lesions. *Ultrasound Obstet Gynecol* 41(1):54–58, 2013.
127. Shah AD, Border WL, Crombleholme TM, Michelfelder EC: Initial fetal cardiovascular profile score predicts recipient twin outcome in twin-twin transfusion syndrome. *J Am Soc Echocardiogr* 21(10):1105–1108, 2008.
128. Ezon DS, Khan MS, Adachi I, et al: Pediatric ventricular assist device use as a bridge to transplantation does not affect long-term quality of life. *J Thorac Cardiovasc Surg* 147(4):1334–1343, 2014.
129. Hofstaetter C, Hansmann M, Eik-Nes SH, et al: A cardiovascular profile score in the surveillance of fetal hydrops. *J Matern Fetal Neonatal Med* 19(7):407–413, 2006.
130. Iacovella C, Chandrasekaran N, Khalil A, et al: Fetal and placental vascular tumors: persistent fetal hyperdynamic status predisposes to poorer long-term neurodevelopmental outcome. *Ultrasound Obstet Gynecol* 43(6):658–661, 2014.
131. Patel D, Cuneo B, Viesca R, et al: Digoxin for the treatment of fetal congestive heart failure with sinus rhythm assessed by cardiovascular profile score. *J Matern Fetal Neonatal Med* 21(7):477–482, 2008.
132. Weber R, Kantor P, Chitayat D, et al: Spectrum and outcome of primary cardiomyopathies diagnosed during fetal life. *JACC Heart Fail* 2(4):403–411, 2014.
133. Mielke G, Benda N: Cardiac output and central distribution of blood flow in the human fetus. *Circulation* 103(12):1662–1668, 2001.
134. Stewart WJ, Jiang L, Mich R, et al: Variable effects of changes in flow rate through the aortic, pulmonary and mitral valves on valve area and flow velocity: impact on quantitative Doppler flow calculations. *J Am Coll Cardiol* 6(3):653–662, 1985.
135. Maskatia SA, Ruano R, Shamshirsaz AA, Javadian P: Increased estimated cardiac output and functional improvement in fetuses in response to laser therapy for twin-twin transfusion syndrome. *Circulation* 128(22 Supplement):A17384, 2013.
136. Tsutsumi T, Ishii M, Eto G, et al: Serial evaluation for myocardial performance in fetuses and neonates using a new Doppler index. *Pediatr Int* 41(6):722–727, 1999.
137. D’hooge J, Heimdal A, Jamal F, et al: Regional strain and strain rate measurements by cardiac ultrasound: principles, implementation and limitations. *Eur J Echocardiogr* 1(3):154–170, 2000.
138. Modesto KM, Cauduro S, Dispenzieri A, et al: Two-dimensional acoustic pattern derived strain parameters closely correlate with one-dimensional tissue Doppler derived strain measurements. *Eur J Echocardiogr* 7(4):315–321, 2006.
139. Serri K, Reant P, Lafitte M, et al: Global and regional myocardial function quantification by two-dimensional strain: application in hypertrophic cardiomyopathy. *J Am Coll Cardiol* 47(6):1175–1181, 2006.
140. Perk G, Tunick PA, Kronzon I: Non-Doppler two-dimensional strain imaging by echocardiography—from technical considerations to clinical applications. *J Am Soc Echocardiogr* 20(3):234–243, 2007.
141. Marwick TH: Measurement of strain and strain rate by echocardiography: ready for prime time? *J Am Coll Cardiol* 47(7):1313–1327, 2006.
142. Kapusta L, Mainzer G, Weiner Z, et al: Changes in fetal left and right ventricular strain mechanics during normal pregnancy. *J Am Soc Echocardiogr* 26(10):1193–1200, 2013.
143. Kim SH, Miyakoshi K, Kadohira I, et al: Comparison of the right and left ventricular performance during the fetal development using velocity vector imaging. *Early Hum Dev* 89(9):675–681, 2013.
144. Ishii T, McElhinney DB, Harrild DM, et al: Circumferential and longitudinal ventricular strain in the normal human fetus. *J Am Soc Echocardiogr* 25(1):105–111, 2012.

145. Kapusta L, Mainzer G, Weiner Z, et al: Second trimester ultrasound: reference values for two-dimensional speckle tracking-derived longitudinal strain, strain rate and time to peak deformation of the fetal heart. *J Am Soc Echocardiogr* 25(12):1333–1341, 2012.
146. Di Salvo G, Russo MG, Paladini D, et al: Two-dimensional strain to assess regional left and right ventricular longitudinal function in 100 normal fetuses. *Eur J Echocardiogr* 9(6):754–756, 2008.
147. Pu DR, Zhou QC, Zhang M, et al: Assessment of regional right ventricular longitudinal functions in fetus using velocity vector imaging technology. *Prenat Diagn* 30(11):1057–1063, 2010.
148. Crispi F, Sepulveda-Swatson E, Cruz-Lemini M, et al: Feasibility and reproducibility of a standard protocol for 2D speckle tracking and tissue Doppler-based strain and strain rate analysis of the fetal heart. *Fetal Diagn Ther* 32(1–2):96–108, 2012.
149. Brooks PA, Khoo NS, Hornberger LK: Systolic and diastolic function of the fetal single left ventricle. *J Am Soc Echocardiogr* 27(9):972–977, 2014.
150. Nemes A, Katona M, Kalapos A, et al: Three-dimensional speckle tracking echocardiographic analysis of a fetal heart with hypoplastic left heart syndrome—a case from the MAGYAR-Fetus Study. *Int J Cardiol* 176(3):e81–e82, 2014.
151. Ishii T, McElhinney DB, Harrild DM, et al: Ventricular strain in fetuses with aortic stenosis and evolving hypoplastic left heart syndrome before and after prenatal aortic valvuloplasty. *Fetal Diagn Ther* 35(1):18–26, 2014.
152. Truong UT, Sun HY, Tacy TA: Myocardial deformation in the fetal single ventricle. *J Am Soc Echocardiogr* 26(1):57–63, 2013.
153. Miller TA, Puchalski MD, Weng C, Menon SC: Regional and global myocardial deformation of the fetal right ventricle in hypoplastic left heart syndrome. *Prenat Diagn* 32(10):949–953, 2012.
154. Pauliks LB: The effect of pregestational diabetes on fetal heart function. *Expert Rev Cardiovasc Ther* 13(1):67–74, 2015.
155. Liu F, Liu S, Ma Z, et al: Assessment of left ventricular systolic function in fetuses without myocardial hypertrophy of gestational diabetes mellitus mothers using velocity vector imaging. *J Obstet Gynaecol* 32(3):252–256, 2012.
156. Crispi F, Bijmens B, Sepulveda-Swatson E, et al: Postsystolic shortening by myocardial deformation imaging as a sign of cardiac adaptation to pressure overload in fetal growth restriction. *Circ Cardiovasc Imaging* 7(5):781–787, 2014.
157. Taylor-Clarke MC, Matsui H, Roughton M, et al: Ventricular strain changes in monozygotic twins with and without twin-to-twin transfusion syndrome. *Am J Obstet Gynecol* 208(6):462.e1–462.e6, 2013.
158. Gonçalves LF, Lee W, Chaiworapongsa T, et al: Four-dimensional ultrasonography of the fetal heart with spatiotemporal image correlation. *Am J Obstet Gynecol* 189(6):1792–1802, 2003.
159. DeVore GR, Falkensammer P, Sklansky MS, Platt LD: Spatio-temporal image correlation (STIC): new technology for evaluation of the fetal heart. *Ultrasound Obstet Gynecol* 22(4):380–387, 2003.
160. Sklansky MS, Nelson TR, Pretorius DH: Usefulness of gated three-dimensional fetal echocardiography to reconstruct and display structures not visualized with two-dimensional imaging. *Am J Cardiol* 80(5):665–668, 1997.
161. Nelson TR: Three-dimensional fetal echocardiography. *Prog Biophys Mol Biol* 69(2–3):257–272, 1998.
162. Scharf A, Geka F, Steinborn A, et al: 3D real-time imaging of the fetal heart. *Fetal Diagn Ther* 15(5):267–274, 2000.
163. Bega G, Kuhlman K, Lev-Toaff A, et al: Application of three-dimensional ultrasonography in the evaluation of the fetal heart. *J Ultrasound Med* 20(4):307–313, quiz 315–316, 2001.
164. Deng J, Yates R, Birkett AG, et al: Online motion-gated dynamic three-dimensional echocardiography in the fetus—preliminary results. *Ultrasound Med Biol* 27(1):43–50, 2001.
165. Meyer-Wittkopf M, Cooper S, Vaughan J, Sholler G: Three-dimensional (3D) echocardiographic analysis of congenital heart disease in the fetus: comparison with cross-sectional (2D) fetal echocardiography. *Ultrasound Obstet Gynecol* 17(6):485–492, 2001.
166. Maulik D, Nanda NC, Singh V, et al: Live three-dimensional echocardiography of the human fetus. *Echocardiography* 20(8):715–721, 2003.
167. Chaoui R, Hoffmann J, Heling KS: Three-dimensional (3D) and 4D color Doppler fetal echocardiography using spatio-temporal image correlation (STIC). *Ultrasound Obstet Gynecol* 23(6):535–545, 2004.
168. Espinoza J, Gonçalves LF, Lee W, et al: The use of the minimum projection mode in four-dimensional examination of the fetal heart with spatiotemporal image correlation (STIC) (Abstract). *Ultrasound Obstet Gynecol* 24(3):277–278, 2004.
169. Yagel S, Valsky DV, Messing B: Detailed assessment of fetal ventricular septal defect with 4D color Doppler ultrasound using spatio-temporal image correlation technology. *Ultrasound Obstet Gynecol* 25(1):97–98, 2005.
170. Benacerraf BR: Sonographic detection of fetal anomalies of the aortic and pulmonary arteries: value of four-chamber view vs direct images. *AJR Am J Roentgenol* 163(6):1483–1489, 1994.
171. Chaoui R: The examination of the normal fetal heart using two-dimensional fetal echocardiography. In Yagel S, Silverman NH, Gembruch U, editors: *Fetal Cardiology*, London, 2002, CRC Press, pp 141–149.
172. Allan LD: Technique of fetal echocardiography. *Pediatr Cardiol* 25(3):223–233, 2004.
173. Kalache K, Romero R, Gonçalves LF, et al: Three-dimensional color power imaging of the fetal hepatic circulation. *Am J Obstet Gynecol* 189(5):1401–1406, 2003.
174. Ruano R, Benachi A, Aubry MC, et al: Perinatal three-dimensional angiosonographic presentation of aneurysm of the vein of Galen (Abstract). *Ultrasound Obstet Gynecol* 22(S1):1357–1362, 2003.
175. Lee W, Kalache KD, Chaiworapongsa T, et al: Three-dimensional power Doppler ultrasonography during pregnancy. *J Ultrasound Med* 22(1):91–97, 2003.
176. Chaoui R, Schneider MBE, Kalache KD: Right aortic arch with vascular ring and aberrant left subclavian artery: prenatal diagnosis assisted by three-dimensional power Doppler ultrasound. *Ultrasound Obstet Gynecol* 22(6):661–663, 2003.
177. Gonçalves LF, Romero R, Espinoza J, et al: Four-dimensional ultrasonography of the fetal heart using color Doppler spatiotemporal image correlation. *J Ultrasound Med* 23(4):473–481, 2004.
178. Gonçalves LF, Espinoza J, Lee W, et al: Three- and four-dimensional reconstruction of the aortic and ductal arches using inversion mode: a new rendering algorithm for visualization of fluid-filled anatomical structures. *Ultrasound Obstet Gynecol* 24(6):696–698, 2004.
179. Espinoza J, Gonçalves LF, Lee W, et al: A novel method to improve prenatal diagnosis of abnormal systemic venous connections using three- and four-dimensional ultrasonography and “inversion mode.” *Ultrasound Obstet Gynecol* 25(5):428–434, 2005.
180. Benacerraf BR: Inversion mode display of 3D sonography: applications in obstetric and gynecologic imaging. *AJR Am J Roentgenol* 187(4):965–971, 2006.
181. Deng J, Rodeck CH: New fetal cardiac imaging techniques. *Prenat Diagn* 24(13):1092–1103, 2004.
182. Gonçalves LF, Espinoza J, Lee W, et al: A new approach to fetal echocardiography: digital casts of the fetal cardiac chambers and great vessels for detection of congenital heart disease. *J Ultrasound Med* 24(4):415–424, 2005.
183. Volpe P, Campobasso G, Stanziano A, et al: Novel application of 4D sonography with B-flow imaging and spatio-temporal image correlation (STIC) in the assessment of the anatomy of pulmonary arteries in fetuses with pulmonary atresia and ventricular septal defect. *Ultrasound Obstet Gynecol* 28(1):40–46, 2006.
184. Bega G, Lev-Toaff A, Kuhlman K, et al: Three-dimensional ultrasonographic imaging in obstetrics: present and future applications. *J Ultrasound Med* 20(4):391–408, 2001.
185. DeVore GR, Polanco B, Sklansky MS, Platt LD: The “spin” technique: a new method for examination of the fetal outflow tracts using three-dimensional ultrasound. *Ultrasound Obstet Gynecol* 24(1):72–82, 2004.
186. Espinoza J, Romero R, Kusanovic JP, et al: The role of the sagittal view of the ductal arch in identification of fetuses with conotruncal anomalies using 4-dimensional ultrasonography. *J Ultrasound Med* 26(9):1181–1188, quiz 1189–1190, 2007.



187. DeVore GR, Polanko B: Tomographic ultrasound imaging of the fetal heart: a new technique for identifying normal and abnormal cardiac anatomy. *J Ultrasound Med* 24(12):1685–1696, 2005.
188. Gonçalves LF, Espinoza J, Romero R, et al: Four-dimensional ultrasonography of the fetal heart using a novel tomographic ultrasound imaging display. *J Perinatal Med* 34(1):39–55, 2006.
189. Rizzo G, Capponi A, Cavicchioni O, et al: Application of automated sonography on 4-dimensional volumes of fetuses with transposition of the great arteries. *J Ultrasound Med* 27(5):771–776, quiz 777, 2008.
190. Rizzo G, Capponi A, Vendola M, et al: Role of tomographic ultrasound imaging with spatiotemporal image correlation for identifying fetal ventricular septal defects. *J Ultrasound Med* 27(7):1071–1075, 2008.
191. Carvalho JS, Mavrides E, Shinebourne EA, et al: Improving the effectiveness of routine prenatal screening for major congenital heart defects. *Heart* 88(4):387–391, 2002.
192. Espinoza J, Kusanovic JP, Gonçalves LF, et al: A novel algorithm for comprehensive fetal echocardiography using 4-dimensional ultrasonography and tomographic imaging. *J Ultrasound Med* 25(8):947–956, 2006.
193. Rizzo G, Capponi A, Muscatello A, et al: Examination of the fetal heart by four-dimensional ultrasound with spatiotemporal image correlation during routine second-trimester examination: the “three-steps technique.” *Fetal Diagn Ther* 24(2):126–131, 2008.
194. Yeo L, Romero R, Jodick C, et al: Four-chamber view and “swing technique” (FAST) echo: a novel and simple algorithm to visualize standard fetal echocardiographic planes. *Ultrasound Obstet Gynecol* 37(4):423–431, 2011.
195. Yeo L, Romero R: Fetal Intelligent Navigation Echocardiography (FINE): a novel method for rapid, simple, and automatic examination of the fetal heart. *Ultrasound Obstet Gynecol* 42(3):268–284, 2013.
196. Baba K, Okai T, editors: *Three-Dimensional Ultrasound in Obstetrics and Gynecology*, New York, 1997, Taylor & Francis.
197. Kettl K, Gritzky A: Introduction to three-dimensional ultrasound technology and future aspects. In Kurjak A, editor: *Three-Dimensional Power Doppler in Obstetrics and Gynecology*, New York, 2000, Taylor & Francis, pp 1–7.
198. Pooh RK: New application of B-flow sono-angiography in perinatology. *Ultrasound Obstet Gynecol* 15(2):163, 2000.
199. Deane C: Extended field-of-view and B-flow ultrasound: fashion or future? *Ultrasound Obstet Gynecol* 15(2):96–97, 2000.
200. DeVore GR: Three-dimensional and four-dimensional fetal echocardiography: a new frontier. *Curr Opin Pediatr* 17(5):592–604, 2005.
201. Lee W, Espinoza J, Cutler N, et al: The “starfish” sign: a novel sonographic finding with B-flow imaging and spatiotemporal image correlation in a fetus with total anomalous pulmonary venous return. *Ultrasound Obstet Gynecol* 35(1):124–125, 2010.
202. Espinoza J, Romero R, Kusanovic JP, et al: Prenatal diagnosis of coarctation of the aorta with the multiplanar display and B-flow imaging using 4-dimensional sonography. *J Ultrasound Med* 28(10):1375–1378, 2009.
203. Bennasar M, Martínez JM, Gómez O, et al: Accuracy of four-dimensional spatiotemporal image correlation echocardiography in the prenatal diagnosis of congenital heart defects. *Ultrasound Obstet Gynecol* 36(4):458–464, 2010.
204. Espinoza J, Lee W, Romero R, et al: Collaborative study on four-dimensional echocardiography for the diagnosis of fetal heart defects: the COFEHD study. *Am J Obstet Gynecol* 201(6):S38, 2009.
205. Bennasar M, Martínez JM, Gómez O, et al: Intra- and interobserver repeatability of fetal cardiac examination using four-dimensional spatiotemporal image correlation in each trimester of pregnancy. *Ultrasound Obstet Gynecol* 35(3):318–323, 2010.
206. Yagel S, Cohen SM, Rosenak D, et al: Added value of three-/four-dimensional ultrasound in offline analysis and diagnosis of congenital heart disease. *Ultrasound Obstet Gynecol* 37(4):432–437, 2011.
207. Espinoza J, Lee W, Vinals F, et al: Collaborative study of 4-dimensional fetal echocardiography in the first trimester of pregnancy. *J Ultrasound Med* 33(6):1079–1084, 2014.
208. Bennasar M, Martínez JM, Olivella A, et al: Feasibility and accuracy of fetal echocardiography using four-dimensional spatiotemporal image correlation technology before 16 weeks’ gestation. *Ultrasound Obstet Gynecol* 33(6):645–651, 2009.
209. Hoffman JJ, Kaplan S: The incidence of congenital heart disease. *J Am Coll Cardiol* 39(12):1890–1900, 2002.
210. Hoffman JJ: Incidence of congenital heart disease: II. Prenatal incidence. *Pediatr Cardiol* 16(4):155–165, 1995.
211. Kopf PG, Walker MK: Overview of developmental heart defects by dioxins, PCBs, and pesticides. *J Environ Sci Health C Environ Carcinog Ecotoxicol Rev* 27(4):276–285, 2009.
212. Fahed AC, Gelb BD, Seidman JG, Seidman CE: Genetics of congenital heart disease: the glass half empty. *Circ Res* 112(4):707–720, 2013.
213. Zhu H, Kartiko S, Finnell RH: Importance of gene-environment interactions in the etiology of selected birth defects. *Clin Genet* 75(5):409–423, 2009.
214. Dewan P, Gupta P: Burden of congenital rubella syndrome (CRS) in India: a systematic review. *Indian Pediatr* 49(5):377–399, 2012.
215. Tikkanen J, Heinonen OP: Maternal hyperthermia during pregnancy and cardiovascular malformations in the offspring. *Eur J Epidemiol* 7(6):628–635, 1991.
216. Dreier JW, Andersen AMN, Berg-Beckhoff G: Systematic review and meta-analyses: fever in pregnancy and health impacts in the offspring. *Pediatrics* 133(3):e674–e688, 2014.
217. Madsen NL, Schwartz SM, Lewin MB, Mueller BA: Prepregnancy body mass index and congenital heart defects among offspring: a population-based study. *Congenit Heart Dis* 8(2):131–141, 2012.
218. Wren C: Cardiovascular malformations in infants of diabetic mothers. *Br Heart J* 89(10):1217–1220, 2003.
219. Cai GJ, Sun XX, Zhang L, Hong Q: Association between maternal body mass index and congenital heart defects in offspring: a systematic review. *Am J Obstet Gynecol* 211(2):91–117, 2014.
220. Donofrio MT, Duplessis AJ, Limperopoulos C: Impact of congenital heart disease on fetal brain development and injury. *Curr Opin Pediatr* 23(5):502–511, 2011.
221. Brossard-Racine M, Duplessis AJ, Vezina G, et al: Prevalence and spectrum of in utero structural brain abnormalities in fetuses with complex congenital heart disease. *Am J Neuroradiol* 35(8):1593–1599, 2014.
222. Owen M, Shevell M, Donofrio MT, et al: Brain volume and neurobehavior in newborns with complex congenital heart defects. *J Pediatr* 164(5):1121–1127.e1, 2014.
223. Donofrio MT, Levy RJ, Schuette JJ, et al: Specialized delivery room planning for fetuses with critical congenital heart disease. *Am J Cardiol* 111(5):737–747, 2013.
224. Van Praagh R, Geva T, Kreutzer J: Ventricular septal defects: how shall we describe, name and classify them? *J Am Coll Cardiol* 14(5):1298–1299, 1989.
225. Soto B, Becker AE, Moulart AJ, et al: Classification of ventricular septal defects. *Br Heart J* 43(3):332–343, 1980.
226. Anderson RH, Wilcox BR: The surgical anatomy of ventricular septal defect. *J Card Surg* 7(1):17–35, 1992.
227. Jacobs JP, Burke RP, Quintessenza JA, Mavroudis C: Congenital heart surgery nomenclature and database project: ventricular septal defect. *Ann Thorac Surg* 69(4 Suppl):S25–S35, 2000.
228. Bjornard K, Riehle-Colarusso T, Gilboa SM, Correa A: Patterns in the prevalence of congenital heart defects, metropolitan Atlanta, 1978 to 2005. *Birth Defects Res A Clin Mol Teratol* 97(2):87–94, 2013.
229. Gómez O, Martínez JM, Olivella A, et al: Isolated ventricular septal defects in the era of advanced fetal echocardiography: risk of chromosomal anomalies and spontaneous closure rate from diagnosis to age of 1 year. *Ultrasound Obstet Gynecol* 43(1):65–71, 2014.
230. van der Linde D, Konings EE, Slager MA, et al: Birth prevalence of congenital heart disease worldwide: a systematic review and meta-analysis. *J Am Coll Cardiol* 58(21):2241–2247, 2011.
231. Mosimann B, Zidere V, Simpson JM, Allan LD: Outcome and requirement for surgical repair following prenatal diagnosis of ventricular septal defect. *Ultrasound Obstet Gynecol* 44(1):76–81, 2014.

232. Axt-Fliedner R, Schwarze A, Smrcek J, et al: Isolated ventricular septal defects detected by color Doppler imaging: evolution during fetal and first year of postnatal life. *Ultrasound Obstet Gynecol* 27(3):266–273, 2006.
233. Erol O, Sevket O, Keskin S, et al: Natural history of prenatal isolated muscular ventricular septal defects. *J Turk Ger Gynecol Assoc* 15(2):96–99, 2014.
234. Jin Y, Wang A, Wang Y, et al: Natural history of prenatal ventricular septal defects and their association with foetal echocardiographic features. *Cardiol Young* 22(03):323–326, 2011.
235. Scully BB, Morales DLS, Zafar F, et al: Current expectations for surgical repair of isolated ventricular septal defects. *Ann Thorac Surg* 89(2):544–549, 2010.
236. O'Brien SM, Clarke DR, Jacobs JP, et al: An empirically based tool for analyzing mortality associated with congenital heart surgery. *J Thorac Cardiovasc Surg* 138(5):1139–1153, 2009.
237. Oses P, Hugues N, Dahdah N, et al: Treatment of isolated ventricular septal defects in children: Amplatzer versus surgical closure. *Ann Thorac Surg* 90(5):1593–1598, 2010.
238. Kanaan M, Ewert P, Berger F, et al: Follow-up of patients with interventional closure of ventricular septal defects with Amplatzer Duct Occluder II. *Pediatr Cardiol* 36(2):379–385, 2015.
239. Garne E, Stoll C, Clementi M: Euroscan Group: Evaluation of prenatal diagnosis of congenital heart diseases by ultrasound: experience from 20 European registries. *Ultrasound Obstet Gynecol* 17(5):386–391, 2001.
- 239a. Jaffe CC, Atkinson P, Taylor KJW: Physical parameters affecting the visibility of small ventricular septal defects using two-dimensional echocardiography. *Invest Radiol* 14(2):149–155, 1979.
240. Report of the New England Regional Infant Cardiac Program. *Pediatrics* 65(2 Pt 2):375–461, 1980.
241. Samánek M: Children with congenital heart disease: probability of natural survival. *Pediatr Cardiol* 13(3):152–158, 1992.
242. Allan LD, Sharland GK, Milburn A, et al: Prospective diagnosis of 1,006 consecutive cases of congenital heart disease in the fetus. *J Am Coll Cardiol* 23(6):1452–1458, 1994.
243. Konstantinov IE, Rosapepe F, Dearani JA, et al: A tribute to Giancarlo Rastelli. *Ann Thorac Surg* 79(5):1819–1823, 2005.
244. Cetta F, Minich LL, Maleszewski JJ, et al: Atrioventricular septal defects. In Allen HD, Driscoll DJ, Shaddy RE, Feltes TF, editors: *Moss & Adams' Heart Disease in Infants, Children, and Adolescents*, ed 8, Philadelphia, 2013, Lippincott Williams & Wilkins, pp 691–712.
245. Freeman SB, Taft LF, Dooley KJ, et al: Population-based study of congenital heart defects in Down syndrome. *Am J Med Genet* 80(3):213–217, 1998.
246. Hills CB, Kochilas LK, Schimmenti LA, Moller JH: Ellis-van Creveld syndrome and congenital heart defects: presentation of an additional 32 cases. *Pediatr Cardiol* 32(7):977–982, 2011.
247. Minich LL, Atz AM, Colan SD, et al: Partial and transitional atrioventricular septal defect outcomes. *Ann Thorac Surg* 89(2):530–536, 2010.
248. Stulak JM, Burkhart HM, Dearani JA, et al: Reoperations after repair of partial atrioventricular septal defect: a 45-year single-center experience. *Ann Thorac Surg* 89(5):1352–1359, 2010.
249. Atz AM, Hawkins JA, Lu M, et al: Surgical management of complete atrioventricular septal defect: associations with surgical technique, age, and trisomy 21. *J Thorac Cardiovasc Surg* 141(6):1371–1379, 2011.
250. Stulak JM, Burkhart HM, Dearani JA, et al: Reoperations after initial repair of complete atrioventricular septal defect. *Ann Thorac Surg* 87(6):1872–1877, 2009.
251. Myers PO, del Nido PJ, Marx GR, et al: Improving left ventricular outflow tract obstruction repair in common atrioventricular canal defects. *Ann Thorac Surg* 94(2):599–605, 2012.
252. Bakhtiyari F, Takacs J, Cho MY, et al: Long-term results after repair of complete atrioventricular septal defect with two-patch technique. *Ann Thorac Surg* 89(4):1239–1243, 2010.
253. Hoochenkerk GJF, Bruggemans EF, Koolbergen DR, et al: Long-term results of reoperation for left atrioventricular valve regurgitation after correction of atrioventricular septal defects. *Ann Thorac Surg* 93(3):849–855, 2012.
254. Stensen N: Embryo monstro affinis Parisiis dissectus. In Bartholin T, editor: *Acta Medica et Philosophica Hafniensia*, Hafnia, P., 1671–1672, Haubold, pp 202–203.
255. Acierno LJ: Etienne-Louis Fallot: is it his tetralogy? *Clin Cardiol* 22(4):321–322, 1999.
256. Fallot E-L: Contribution à l'anatomie pathologique de la maladie bleue (cyanose cardiaque). *Marseille Méd* 25:77–93, 1888.
257. Anderson RH, Weinberg PM: The clinical anatomy of tetralogy of Fallot. *Cardiol Young* 15(Suppl 1):38–47, 2005.
258. Marelli AJ, Mackie AS, Ionescu-Ittu R, et al: Congenital heart disease in the general population: changing prevalence and age distribution. *Circulation* 115(2):163–172, 2006.
259. Burn J, Brennan P, Little J, et al: Recurrence risks in offspring of adults with major heart defects: results from first cohort of British collaborative study. *Lancet* 351(9099):311–316, 1998.
260. Nora JJ, Nora AH: Recurrence risks in children having one parent with a congenital heart disease. *Circulation* 53(4):701–702, 1976.
261. Digilio MC, Marino B, Giannotti A, et al: Recurrence risk figures for isolated tetralogy of Fallot after screening for 22q11 microdeletion. *J Med Genet* 34(3):188–190, 1997.
262. Sivanandam S, Glickstein J, Printz B, et al: Prenatal diagnosis of conotruncal malformations: diagnostic accuracy, outcome, chromosomal abnormalities, and extracardiac anomalies. *Am J Perinatol* 23(4):241–246, 2006.
263. Tometzki AJR, Suda K, Kohl T, et al: Accuracy of prenatal echocardiographic diagnosis and prognosis of fetuses with conotruncal anomalies. *J Am Coll Cardiol* 33(6):1696–1701, 1999.
264. Escribano D, Herraiz I, Granados M, et al: Tetralogy of Fallot: prediction of outcome in the mid-second trimester of pregnancy. *Prenat Diagn* 31(12):1126–1133, 2011.
265. Kwon EN, Parness IA, Srivastava S, et al: Subpulmonary stenosis assessed in midtrimester fetuses with tetralogy of Fallot: a novel method for predicting postnatal clinical outcome. *Pediatr Cardiol* 34(6):1314–1320, 2013.
266. Hirji A, Bernasconi A, McCrindle BW, et al: Outcomes of prenatally diagnosed tetralogy of Fallot: implications for valve-sparing repair versus transannular patch. *Can J Cardiol* 26(1):e1–e6, 2010.
267. Arya B, Levasseur SM, Woldu K, et al: Fetal echocardiographic measurements and the need for neonatal surgical intervention in tetralogy of Fallot. *Pediatr Cardiol* 35(5):810–816, 2014.
268. Momma K: Cardiovascular anomalies associated with chromosome 22q11.2 deletion syndrome. *Am J Cardiol* 105(11):1617–1624, 2010.
269. Boudjemline Y, Fermont L, Le Bidois J, et al: Prevalence of 22q11 deletion in fetuses with conotruncal cardiac defects: a 6-year prospective study. *J Pediatr* 138(4):520–524, 2001.
270. Geva T, Sandweiss BM, Gauvreau K, et al: Factors associated with impaired clinical status in long-term survivors of tetralogy of Fallot repair evaluated by magnetic resonance imaging. *J Am Coll Cardiol* 43(6):1068–1074, 2004.
271. Gatzoulis MA, Balaji S, Webber SA, et al: Risk factors for arrhythmia and sudden cardiac death late after repair of tetralogy of Fallot: a multicentre study. *Lancet* 356(9234):975–981, 2000.
272. Ylitalo P, Nieminen H, Pitkanen OM, et al: Need of transannular patch in tetralogy of Fallot surgery carries a higher risk of reoperation but has no impact on late survival: results of Fallot repair in Finland. *Eur J Cardiothorac Surg* 48(1):91–97, 2015.
273. Calder L, Van Praagh R, Van Praagh S, et al: Truncus arteriosus communis. Clinical, angiographic, and pathologic findings in 100 patients. *Am Heart J* 92(1):23–38, 1976.
274. Egbe A, Uppu S, Lee S, et al: Changing prevalence of severe congenital heart disease: a population-based study. *Pediatr Cardiol* 35(7):1232–1238, 2014.
275. Long J, Ramadhani T, Mitchell LE: Epidemiology of nonsyndromic conotruncal heart defects in Texas, 1999–2004. *Birth Defects Res A Clin Mol Teratol* 88(11):971–979, 2010.
276. Canfield MA, Honein MA, Yuskiv N, et al: National estimates and race/ethnic-specific variation of selected birth defects in the United States, 1999–2001. *Birth Defects Res A Clin Mol Teratol* 76(11):747–756, 2006.



277. Collett RW, Edwards JE: Persistent truncus arteriosus; a classification according to anatomic types. *Surg Clin North Am* 29(4):1245–1270, 1949.
278. Goldmuntz E, Clark BJ, Mitchell LE, et al: Frequency of 22q11 deletions in patients with conotruncal defects. *J Am Coll Cardiol* 32(2):492–498, 1998.
279. Moore JW, Wight NE, Jones MC, Krous HF: Truncus arteriosus associated with trisomy 18. *Pediatr Cardiol* 15(3):154–156, 1994.
280. Francalanci P, Gallo P, Dallapiccola B, et al: A genetic assessment of trisomy 21 in a patient with persistent truncus arteriosus who died 38 years ago. *Am J Cardiol* 79(2):245–247, 1997.
281. Oehl-Jaschkowitz B, Vanakker OM, De Paep A, et al: Deletions in 14q24.1q24.3 are associated with congenital heart defects, brachydactyly, and mild intellectual disability. *Am J Med Genet* 164(3):620–626, 2013.
282. Gong M, Simaite D, Kuhnen P, et al: Two novel GATA6 mutations cause childhood-onset diabetes mellitus, pancreas malformation and congenital heart disease. *Horm Res Paediatr* 79(4):250–256, 2013.
283. Rea G, McCullough S, McNerlan S, et al: Delineation of a recognisable phenotype of interstitial deletion 3 (q22.3q25.1) in a case with previously unreported truncus arteriosus. *Eur J Med Genet* 53(3):162–167, 2010.
284. Swanson TM, Selamat Tierney ES, Tworetzky W, et al: Truncus arteriosus: diagnostic accuracy, outcomes, and impact of prenatal diagnosis. *Pediatr Cardiol* 30(3):256–261, 2009.
285. Volpe P, Paladini D, Marasini M, et al: Common arterial trunk in the fetus: characteristics, associations, and outcome in a multicentre series of 23 cases. *Heart* 89(12):1437–1441, 2003.
286. Russell HM, Pasquali SK, Jacobs JP, et al: Outcomes of repair of common arterial trunk with truncal valve surgery: a review of the Society of Thoracic Surgeons congenital heart surgery database. *Ann Thorac Surg* 93(1):164–169, 2012.
287. Walters HL, Mavroudis C, Tchervenkov CI, et al: Congenital Heart Surgery Nomenclature and Database Project: double outlet right ventricle. *Ann Thorac Surg* 69(4 Suppl):S249–S263, 2000.
288. Shuler CO, Black GB, Jerrell JM: Population-based treated prevalence of congenital heart disease in a pediatric cohort. *Pediatr Cardiol* 34(3):606–611, 2013.
289. Pradat P, Francannet C, Harris JA, Robert E: The epidemiology of cardiovascular defects, part I: a study based on data from three large registries of congenital malformations. *Pediatr Cardiol* 24(3):195–221, 2003.
290. Lagopoulos ME, Manlihot C, McCrindle BW, et al: Impact of prenatal diagnosis and anatomical subtype on outcome in double outlet right ventricle. *Am Heart J* 160(4):692–700, 2010.
291. Song MS, Hu A, Dyamenahalli U, et al: Extracardiac lesions and chromosomal abnormalities associated with major fetal heart defects: comparison of intrauterine, postnatal and postmortem diagnoses. *Ultrasound Obstet Gynecol* 33(5):552–559, 2009.
292. Obler D, Juraszek AL, Smoot LB, Natowicz MR: Double outlet right ventricle: aetiologies and associations. *J Med Genet* 45(8):481–497, 2008.
293. Li S, Ma K, Hu S, et al: Surgical outcomes of 380 patients with double outlet right ventricle who underwent biventricular repair. *J Thorac Cardiovasc Surg* 148(3):817–824, 2014.
294. Mahle WT, Martinez R, Silverman NH, et al: Anatomy, echocardiography, and surgical approach to double outlet right ventricle. *Cardiol Young* 18(Suppl 3):39–51, 2008.
295. Rastelli GC, Wallace RB, Ongley PA: Complete repair of transposition of the great arteries with pulmonary stenosis. A review and report of a case corrected by using a new surgical technique. *Circulation* 39(1):83–95, 1969.
296. Pitkanen OM, Hornberger LK, Miner SES, et al: Borderline left ventricles in prenatally diagnosed atrioventricular septal defect or double outlet right ventricle: echocardiographic predictors of biventricular repair. *Am Heart J* 152(1):163.e1–163.e7, 2006.
297. Hayes DA, Jones S, Quaegebeur JM, et al: Primary arterial switch operation as a strategy for total correction of Taussig-Bing anomaly: a 21-year experience. *Circulation* 128(11 Suppl 1):S194–S198, 2013.
298. Marek J, Tomtek V, Skovranek J, et al: Prenatal ultrasound screening of congenital heart disease in an unselected national population: a 21-year experience. *Heart* 97(2):124–130, 2011.
299. Johnson TR: Conotruncal cardiac defects: a clinical imaging perspective. *Pediatr Cardiol* 31(3):430–437, 2010.
300. Wernovsky G: Transposition of the great arteries. In Allen HD, Driscoll DJ, Shaddy RE, Feltes TF, editors: *Moss & Adams' Heart Disease in Infants, Children, and Adolescents*, ed 8, Philadelphia, 2013, Lippincott Williams & Wilkins, pp 1097–1146.
301. Kirklin JW, Barratt-Boyes BG: Complete transposition of the great arteries. In Kirklin JW, Barratt-Boyes BG, editors: *Cardiac Surgery*, ed 2, New York, 1993, Churchill Livingstone.
302. Thammineni K, Lohr J, Trefz M, Sivanandam S: Familial recurrence of congenital heart diseases. *J Perinatol* 31(11):742–743, 2011.
303. Piacentini G, Digilio MC, Capolino R, et al: Familial recurrence of heart defects in subjects with congenitally corrected transposition of the great arteries. *Am J Med Genet* 137(2):176–180, 2005.
304. Unolt M, Putotto C, Silvestri LM, et al: Transposition of great arteries: new insights into the pathogenesis. *Front Pediatr* 1:11, 2013.
305. Srivastava D: Genetic regulation of cardiogenesis and congenital heart disease. *Annu Rev Pathol* 1(1):199–213, 2006.
306. Digilio MC, Casey B, Toscano A, et al: Complete transposition of the great arteries: patterns of congenital heart disease in familial recurrence. *Circulation* 104(23):2809–2814, 2001.
307. Skinner J, Hornung T, Rumball E: Transposition of the great arteries: from fetus to adult. *Heart* 94(9):1227–1235, 2008.
308. Stoica S, Carpenter E, Campbell D, et al: Morbidity of the arterial switch operation. *Ann Thorac Surg* 93(6):1977–1983, 2012.
309. Fricke TA, d'Udekem Y, Richardson M, et al: Outcomes of the arterial switch operation for transposition of the great arteries: 25 years of experience. *Ann Thorac Surg* 94(1):139–145, 2012.
310. Villafane J, Lantin-Hermoso MR, Bhatt AB, et al: D-transposition of the great arteries: the current era of the arterial switch operation. *J Am Coll Cardiol* 64(5):498–511, 2014.
311. Khairy P, Clair M, Fernandes SM, et al: Cardiovascular outcomes after the arterial switch operation for D-transposition of the great arteries. *Circulation* 127(3):331–339, 2013.
312. Al-Naami GH, Al-Mesned AA: Transposition of great arteries with constrictive ductus arteriosus revisited. *Pediatr Cardiol* 29(4):827–829, 2008.
313. Maeno YV, Kamenir SA, Sinclair B, et al: Prenatal features of ductus arteriosus constriction and restrictive foramen ovale in D-transposition of the great arteries. *Circulation* 99(9):1209–1214, 1999.
314. Pun R, Silverman NH: Fetal predictors of urgent balloon atrial septostomy in neonates with complete transposition. *J Am Soc Echocardiogr* 24(4):425–430, 2011.
315. Donofrio MT: Images in cardiovascular medicine. Premature closure of the foramen ovale and ductus arteriosus in a fetus with transposition of the great arteries. *Circulation* 105(11):e65–e66, 2002.
316. Atallah J, Rutledge JM, Dyck JD: Congenitally corrected transposition of the great arteries (atrioventricular and ventriculoarterial discordance). In Allen HD, Driscoll DJ, Shaddy RE, Feltes TF, editors: *Moss & Adams' Heart Disease in Infants, Children, and Adolescents*, ed 8, Philadelphia, 2013, Lippincott Williams & Wilkins, pp 1147–1160.
317. Marino AL, Levy RJ, Berger JT, Donofrio MT: Pentalogy of Cantrell with a single-ventricle cardiac defect: collaborative management of a complex disease. *Pediatr Cardiol* 32(4):498–502, 2011.
318. Witham AC: Double outlet right ventricle; a partial transposition complex. *Am Heart J* 53(6):928–939, 1957.
319. Penny DJ, Somerville J, Redington AN: Echocardiographic demonstration of important abnormalities of the mitral valve in congenitally corrected transposition. *Br Heart J* 68(5):498–500, 1992.
320. Razzouk L, Applebaum RM, Okamura C, Saric M: The windsock syndrome: subpulmonic obstruction by membranous ventricular septal aneurysm in congenitally corrected transposition of great arteries. *Echocardiography* 30(8):E243–E248, 2013.

321. Van Praagh R, Papagiannis J, Grünenfelder J, et al: Pathologic anatomy of corrected transposition of the great arteries: medical and surgical implications. *Am Heart J* 135(5):772–785, 1998.
322. Jaeggi ET, Hamilton RM, Silverman ED, et al: Outcome of children with fetal, neonatal or childhood diagnosis of isolated congenital atrioventricular block. *J Am Coll Cardiol* 39(1):130–137, 2002.
323. Nora J, Berg K, Nora A: *Cardiovascular Disease: Genetics, Epidemiology and Prevention*, New York, 1991, Oxford University Press.
324. Ferencz C, Rubin JD, Loffredo CA, Magee CA: *Epidemiology of Congenital Heart Disease: the Baltimore-Washington Infant Study*, Mount Kisco, NY, 1993, Futura Publishing Company.
325. Kuehl KS, Loffredo CA: Population-based study of L-transposition of the great arteries: possible associations with environmental factors. *Birth Defects Res A Clin Mol Teratol* 67(3):162–167, 2003.
326. Al Rais F, Feldstein VA, Srivastava D, et al: Monochorionic twins discordant for congenital heart disease: a referral center's experience and possible pathophysiologic mechanisms. *Prenat Diagn* 31(10):978–984, 2011.
327. Bruneau BG, Srivastava D: Congenital heart disease: entering a new era of human genetics. *Circ Res* 114(4):598–599, 2014.
328. Srivastava D, Olson EN: A genetic blueprint for cardiac development. *Nature* 407(6801):221–226, 2000.
329. Alghamdi AA, McCrindle BW, Van Arsdell GS: Physiologic versus anatomic repair of congenitally corrected transposition of the great arteries: meta-analysis of individual patient data. *Ann Thorac Surg* 81(4):1529–1535, 2006.
330. Bogers AJ, Head SJ, de Jong PL, et al: Long term follow up after surgery in congenitally corrected transposition of the great arteries with a right ventricle in the systemic circulation. *J Cardiothorac Surg* 5(1):74, 2010.
331. Graham TP, Jr, Bernard YD, Mellen BG, et al: Long-term outcome in congenitally corrected transposition of the great arteries. *J Am Coll Cardiol* 36(1):255–261, 2000.
332. Hraska V, Duncan BW, Mayer JE, Jr, et al: Long-term outcome of surgically treated patients with corrected transposition of the great arteries. *J Thorac Cardiovasc Surg* 129(1):182–191, 2005.
333. Murtuza B, Barron DJ, Stumper O, et al: Anatomic repair for congenitally corrected transposition of the great arteries: a single-institution 19-year experience. *J Thorac Cardiovasc Surg* 142(6):1348–1357.e1, 2011.
334. Duncan B: Results of the double switch operation for congenitally corrected transposition of the great arteries. *Eur J Cardio Thorac Surg* 24(1):11–20, 2003.
335. Ma K, Gao H, Hua Z, et al: Palliative pulmonary artery banding versus anatomic correction for congenitally corrected transposition of the great arteries with regressed morphologic left ventricle: Long-term results from a single center. *J Thorac Cardiovasc Surg* 148(4):1566–1571, 2014.
336. Myers PO, del Nido PJ, Geva T, et al: Impact of age and duration of banding on left ventricular preparation before anatomic repair for congenitally corrected transposition of the great arteries. *Ann Thorac Surg* 96(2):603–610, 2013.
337. Bautista-Hernandez V, Marx GR, Gauvreau K, et al: Determinants of left ventricular dysfunction after anatomic repair of congenitally corrected transposition of the great arteries. *Ann Thorac Surg* 82(6):2059–2066, 2006.
338. Bautista-Hernandez V, Myers PO, Cecchin F, et al: Late left ventricular dysfunction after anatomic repair of congenitally corrected transposition of the great arteries. *J Thorac Cardiovasc Surg* 148(1):254–258, 2014.
339. Tchervenkov CI, Jacobs ML, Tahta SA: Congenital heart surgery nomenclature and database project: hypoplastic left heart syndrome. *Ann Thorac Surg* 69(4 Suppl):S170–S179, 2000.
340. Galindo A, Nieto O, Villagrà S, et al: Hypoplastic left heart syndrome diagnosed in fetal life: associated findings, pregnancy outcome and results of palliative surgery. *Ultrasound Obstet Gynecol* 33(5):560–566, 2009.
341. Quartermain MD, Cohen MS, Dominguez TE, et al: Left ventricle to right ventricle size discrepancy in the fetus: the presence of critical congenital heart disease can be reliably predicted. *J Am Soc Echocardiogr* 22(11):1296–1301, 2009.
342. Shone JD, Sellers RD, Anderson RC, et al: The developmental complex of “parachute mitral valve,” supraavalvular ring of left atrium, subaortic stenosis, and coarctation of aorta. *Am J Cardiol* 11:714–725, 1963.
343. Tchervenkov CI, Tahta SA, Jutras LC, Beland MJ: Biventricular repair in neonates with hypoplastic left heart complex. *Ann Thorac Surg* 66(4):1350–1357, 1998.
344. Feit LR, Copel JA, Kleinman CS: Foramen ovale size in the normal and abnormal human fetal heart: an indicator of transatrial flow physiology. *Ultrasound Obstet Gynecol* 1(5):313–319, 1991.
345. Blecher SR: Left heart hypoplasia with associated anomalies. *Heart* 24(6):801–804, 1962.
346. Pasquini L, Fichera A, Tan T, et al: Left superior caval vein: a powerful indicator of fetal coarctation. *Heart* 91(4):539–540, 2005.
347. Chin AJ, Weinberg PM, Barber G: Subcostal two-dimensional echocardiographic identification of anomalous attachment of septum primum in patients with left atrioventricular valve underdevelopment. *J Am Coll Cardiol* 15(3):678–681, 1990.
348. Makikallio K, McElhinney DB, Levine JC, et al: Fetal aortic valve stenosis and the evolution of hypoplastic left heart syndrome: patient selection for fetal intervention. *Circulation* 113(11):1401–1405, 2006.
349. Axt-Fliedner R, Kreiselmair P, Schwarze A, et al: Development of hypoplastic left heart syndrome after diagnosis of aortic stenosis in the first trimester by early echocardiography. *Ultrasound Obstet Gynecol* 28(1):106–109, 2006.
350. Allan LD, Sharland G, Tynan MJ: The natural history of the hypoplastic left heart syndrome. *Int J Cardiol* 25(3):341–343, 1989.
351. Danford DA, Cronican P: Hypoplastic left heart syndrome: progression of left ventricular dilation and dysfunction to left ventricular hypoplasia in utero. *Am Heart J* 123(6):1712–1713, 1992.
352. Freud LR, Moon-Grady AJ, Escobar-Diaz MC, et al: Low rate of prenatal diagnosis among neonates with critical aortic stenosis: insight into the natural history in utero. *Ultrasound Obstet Gynecol* 45(3):326–332, 2015.
353. Michelfelder E, Polzin W, Hirsch R: Hypoplastic left heart syndrome with intact atrial septum: utilization of a hybrid catheterization facility for cesarean section delivery and prompt neonatal intervention. *Catheter Cardiovasc Interv* 72(7):983–987, 2008.
354. Vida VL, Bacha EA, Larrazabal A, et al: Hypoplastic left heart syndrome with intact or highly restrictive atrial septum: surgical experience from a single center. *Ann Thorac Surg* 84(2):581–585, 2007.
355. Barker GM, Forbess JM, Guleserian KJ, Nugent AW: Optimization of preoperative status in hypoplastic left heart syndrome with intact atrial septum by left atrial decompression and bilateral pulmonary artery bands. *Pediatr Cardiol* 35(3):479–484, 2014.
356. Marshall AC, Levine J, Morash D, et al: Results of in utero atrial septoplasty in fetuses with hypoplastic left heart syndrome. *Prenat Diagn* 28(11):1023–1028, 2008.
357. Glatz JA, Tabbutt S, Gaynor JW, et al: Hypoplastic left heart syndrome with atrial level restriction in the era of prenatal diagnosis. *Ann Thorac Surg* 84(5):1633–1638, 2007.
358. Brackley KJ, Kilby MD, Wright JG, et al: Outcome after prenatal diagnosis of hypoplastic left-heart syndrome: a case series. *Lancet* 356(9236):1143–1147, 2000.
359. Axt-Fliedner R, Enzensberger C, Fass N, et al: Fetal diagnosis of hypoplastic left heart, associations and outcomes in the current era. *Ultraschall Med* 33(07):E51–E56, 2012.
360. Jacobs JP, O'Brien SM, Chai PJ, et al: Management of 239 patients with hypoplastic left heart syndrome and related malformations from 1993 to 2007. *Ann Thorac Surg* 85(5):1691–1697, 2008.
361. Rychik J, Szwast A, Natarajan S, et al: Perinatal and early surgical outcome for the fetus with hypoplastic left heart syndrome: a 5-year single institutional experience. *Ultrasound Obstet Gynecol* 36(4):465–470, 2010.
362. Patel A, Hickey E, Mavroudis C, et al: Impact of noncardiac congenital and genetic abnormalities on outcomes in hypoplastic left heart syndrome. *Ann Thorac Surg* 89(6):1805–1813, 2010.
363. Natowicz M, Chatten J, Clancy R, et al: Genetic disorders and major extracardiac anomalies associated with the hypoplastic left heart syndrome. *Pediatrics* 82(5):698–706, 1988.



364. Arzt W, Wertaschnigg D, Veit I, et al: Intrauterine aortic valvuloplasty in fetuses with critical aortic stenosis: experience and results of 24 procedures. *Ultrasound Obstet Gynecol* 37(6):689–695, 2011.
365. Freud LR, McElhinney DB, Marshall AC, et al: Fetal aortic valvuloplasty for evolving hypoplastic left heart syndrome: postnatal outcomes of the first 100 patients. *Circulation* 130(8):638–645, 2014.
366. Rychik J: Hypoplastic left heart syndrome: can we change the rules of the game? *Circulation* 130(8):629–631, 2014.
367. Moon-Grady AJ, Belfort M, Chmait R, et al: Outcomes after in-utero cardiac interventions: a preliminary report of the collaborative international fetal cardiac intervention registry (Abstract). *Circulation* 130(Suppl 2):A16469, 2014.
368. Kovacevic A, Mellander M, Tulzer G, et al: Does fetal aortic valvuloplasty alter the natural history of aortic stenosis? (Abstract). *Circulation* 130(Suppl 2):A13233, 2014.
369. Kalish BT, Tworetzky W, Benson CB, et al: Technical challenges of atrial septal stent placement in fetuses with hypoplastic left heart syndrome and intact atrial septum. *Catheter Cardiovasc Interv* 84(1):77–85, 2014.
370. Galantowicz M, Cheatham JP: Lessons learned from the development of a new hybrid strategy for the management of hypoplastic left heart syndrome. *Pediatr Cardiol* 26(2):190–199, 2005.
371. Atz AM, Trivison TG, Williams IA, et al: Prenatal diagnosis and risk factors for preoperative death in neonates with single right ventricle and systemic outflow obstruction: screening data from the Pediatric Heart Network Single Ventricle Reconstruction Trial. *J Thorac Cardiovasc Surg* 140(6):1245–1250, 2010.
372. Mahle WT, Clancy RR, McGaurn SP, et al: Impact of prenatal diagnosis on survival and early neurologic morbidity in neonates with the hypoplastic left heart syndrome. *Pediatrics* 107(6):1277–1282, 2001.
373. Stasik CN, Gelehrter S, Goldberg CS, et al: Current outcomes and risk factors for the Norwood procedure. *J Thorac Cardiovasc Surg* 131(2):412–417, 2006.
374. Tweddell JS, Hoffman GM, Mussatto KA, et al: Improved survival of patients undergoing palliation of hypoplastic left heart syndrome: lessons learned from 115 consecutive patients. *Circulation* 106(12 Suppl 1):182–189, 2002.
375. Gaynor JW, Mahle WT, Cohen MI, et al: Risk factors for mortality after the Norwood procedure. *Eur J Cardiothorac Surg* 22(1):82–89, 2002.
376. Srinivasan C, Sachdeva R, Morrow WR, et al: Standardized management improves outcomes after the Norwood procedure. *Congenit Heart Dis* 4(5):329–337, 2009.
377. Hehir DA, Dominguez TE, Ballweg JA, et al: Risk factors for interstage death after stage I reconstruction of hypoplastic left heart syndrome and variants. *J Thorac Cardiovasc Surg* 136(1):94–99.e1–3, 2008.
378. Furck AK, Uebing A, Hansen JH, et al: Outcome of the Norwood operation in patients with hypoplastic left heart syndrome: a 12-year single-center survey. *J Thorac Cardiovasc Surg* 139(2):359–365, 2010.
379. Tweddell JS, Hoffman GM, Fedderly RT, et al: Patients at risk for low systemic oxygen delivery after the Norwood procedure. *Ann Thorac Surg* 69(6):1893–1899, 2000.
380. Bove EL, Ohye RG, Devaney EJ: Hypoplastic left heart syndrome: conventional surgical management. *Semin Thorac Cardiovasc Surg Pediatr Card Surg Annu* 7:3–10, 2004.
381. McGuirk SP, Griselli M, Stumper OF, et al: Staged surgical management of hypoplastic left heart syndrome: a single institution 12 year experience. *Heart* 92(3):364–370, 2006.
382. Rychik J, Tian Z: *Fetal Cardiovascular Imaging*, Philadelphia, 2011, Saunders Elsevier.
383. Karamloul T, Ashburn DA, Caldarone CA, et al: Matching procedure to morphology improves outcomes in neonates with tricuspid atresia. *J Thorac Cardiovasc Surg* 130(6):1503–1510, 2005.
384. Sarkozy A, Conti E, D'Agostino R, et al: ZFPM2/FOG2 and HEY2 genes analysis in nonsyndromic tricuspid atresia. *Am J Med Genet* 133A(1):68–70, 2005.
385. Fischer A, Klamt B, Schumacher N, et al: Phenotypic variability in Hey2<sup>-/-</sup> mice and absence of HEY2 mutations in patients with congenital heart defects or Alagille syndrome. *Mamm Genome* 15(9):711–716, 2004.
386. Lee MY, Won HS, Baek JW, et al: Variety of prenatally diagnosed congenital heart disease in 22q11.2 deletion syndrome. *Obstet Gynecol Sci* 57(1):11–16, 2014.
387. Marino B, Digilio MC, Novelli G, et al: Tricuspid atresia and 22q11 deletion. *Am J Med Genet* 72(1):40–42, 1997.
388. Wald RM, Tham EB, McCrindle BW, et al: Outcome after prenatal diagnosis of tricuspid atresia: a multicenter experience. *Am Heart J* 153(5):772–778, 2007.
389. Berg C, Lachmann R, Kaiser C, et al: Prenatal diagnosis of tricuspid atresia: intrauterine course and outcome. *Ultrasound Obstet Gynecol* 35(2):183–190, 2010.
390. Mair DD, Puga FJ, Danielson GK: The Fontan procedure for tricuspid atresia: early and late results of a 25-year experience with 216 patients. *J Am Coll Cardiol* 37(3):933–939, 2001.
391. Sittiwangkul R, Azakie A, Van Arsdell GS, et al: Outcomes of tricuspid atresia in the Fontan era. *Ann Thorac Surg* 77(3):889–894, 2004.
392. Lan YT, Chang RK, Laks H: Outcome of patients with double-inlet left ventricle or tricuspid atresia with transposed great arteries. *J Am Coll Cardiol* 43(1):113–119, 2004.
393. Lucas RV, Anderson RC, Amplatz K, et al: Congenital causes of pulmonary venous obstruction. *Pediatr Clin North Am* 10:781–836, 1963.
394. Burroughs JT, Edwards JE: Total anomalous pulmonary venous connection. *Am Heart J* 59:913–931, 1960.
395. Edwards JE: Pathologic and developmental considerations in anomalous pulmonary venous connection. *Proc Staff Meet Mayo Clin* 28(17):441–452, 1953.
396. Bhide A, Murphy D, Thilaganathan B, Carvalho JS: Prenatal findings and differential diagnosis of scimitar syndrome and pulmonary sequestration. *Ultrasound Obstet Gynecol* 35(4):398–404, 2010.
397. Valsangiacomo ER, Hornberger LK, Barrea JF, et al: Partial and total anomalous pulmonary venous connection in the fetus: two-dimensional and Doppler echocardiographic findings. *Ultrasound Obstet Gynecol* 22(3):257–263, 2003.
398. Eronen M, Kajantie E, Boldt T, et al: Right atrial isomerism in four siblings. *Pediatr Cardiol* 25(2):141–144, 2004.
399. Cesko I, Hajdú J, Marton T, et al: Polysplenia and situs inversus in siblings. Case reports. *Fetal Diagn Ther* 16(1):1–3, 2001.
400. Seale AN, Carvalho JS, Gardiner HM, et al: Total anomalous pulmonary venous connection: impact of prenatal diagnosis. *Ultrasound Obstet Gynecol* 40(3):310–318, 2001.
401. Allan LD, Sharland GK: The echocardiographic diagnosis of totally anomalous pulmonary venous connection in the fetus. *Heart* 85(4):433–437, 2001.
402. Izumi K, Noon S, Wilkens A, Krantz ID: NKX2.5 mutation identification on exome sequencing in a patient with heterotaxy. *Eur J Med Genet* 57(10):558–561, 2014.
403. Chen CP, Ko TM, Chen YY, et al: Prenatal diagnosis and molecular cytogenetic characterization of mosaicism for a small supernumerary marker chromosome derived from chromosome 22 associated with cat eye syndrome. *Gene* 527(1):384–388, 2013.
404. Seale AN, Uemura H, Webber SA, et al: Total anomalous pulmonary venous connection: morphology and outcome from an international population-based study. *Circulation* 122(25):2718–2726, 2010.
405. Padalino MA, Cavalli G, De Franceschi M, et al: Surgical outcomes of total anomalous pulmonary venous connection repair: a 22-year experience. *J Card Surg* 29(5):678–685, 2014.
406. Hoashi T, Kagisaki K, Kurosaki K, et al: Intrinsic obstruction in pulmonary venous drainage pathway is associated with poor surgical outcomes in patients with total anomalous pulmonary venous connection. *Pediatr Cardiol* 36(2):432–437, 2015.
407. Brink J, Yong MS, d'Udekem Y, et al: Surgery for scimitar syndrome: the Melbourne experience. *Interac Cardiovasc Thorac Surg* 20(1):31–34, 2015.
408. Vida VL, Padalino MA, Boccuzzo G, et al: Scimitar syndrome: a European Congenital Heart Surgeons Association (ECHSA) multicentric study. *Circulation* 122(12):1159–1166, 2010.

409. Lenz F, Chaoui R: Reference ranges for Doppler-assessed pulmonary venous blood flow velocities and pulsatility indices in normal human fetuses. *Prenat Diagn* 22(9):786–791, 2002.
410. Lin AE, Krikov S, Riehle-Colarusso T, et al: Laterality defects in the national birth defects prevention study (1998–2007): birth prevalence and descriptive epidemiology. *Am J Med Genet* 164(10):2581–2591, 2014.
411. Bedard T, Lowry RB, Sibbald B, et al: Congenital heart defect case ascertainment by the Alberta Congenital Anomalies Surveillance System. *Birth Defects Res A Clin Mol Teratol* 94(6):449–458, 2012.
412. Khoshnood B, Loane M, Garne E, et al: Recent decrease in the prevalence of congenital heart defects in Europe. *J Pediatr* 162(1):108–113.e2, 2013.
413. Sutherland MJ, Ware SM: Disorders of left–right asymmetry: heterotaxy and situs inversus. *Am J Med Genet C Semin Med Genet* 151C(4):307–317, 2009.
414. Jacobs JP, Anderson RH, Weinberg PM, et al: The nomenclature, definition and classification of cardiac structures in the setting of heterotaxy. *Cardiol Young* 17(Suppl 2):1–28, 2007.
415. Belmont JW, Mohapatra B, Towbin JA, Ware SM: Molecular genetics of heterotaxy syndromes. *Curr Opin Cardiol* 19(3):216–220, 2004.
416. Tariq M, Belmont JW, Lalani S, et al: SHROOM3 is a novel candidate for heterotaxy identified by whole exome sequencing. *Genome Biol* 12(9):R91, 2011.
417. Berg C, Geipel A, Smrcek J, et al: Prenatal diagnosis of cardiopulmonary syndromes: a 10-year experience. *Ultrasound Obstet Gynecol* 22(5):451–459, 2003.
418. Anagnostopoulos PV, Pearl JM, Octave C, et al: Improved current era outcomes in patients with heterotaxy syndromes. *Eur J Cardiothorac Surg* 35(5):871–877, 2009.
419. Isaacs H: Fetal and neonatal cardiac tumors. *Pediatr Cardiol* 25(3):252–273, 2004.
420. Nadas AS, Ellison RC: Cardiac tumors in infancy. *Am J Cardiol* 21(3):363–366, 1968.
421. Holley DG, Martin GR, Brenner JJ, et al: Diagnosis and management of fetal cardiac tumors: a multicenter experience and review of published reports. *J Am Coll Cardiol* 26(2):516–520, 1995.
422. Yinon Y, Chitayat D, Blaser S, et al: Fetal cardiac tumors: a single-center experience of 40 cases. *Prenat Diagn* 30(10):941–949, 2010.
423. Groves AM, Fagg NL, Cook AC, Allan LD: Cardiac tumours in intrauterine life. *Arch Dis Child* 67(10 Spec No):1189–1192, 1992.
424. Chao AS, Chao A, Wang TH, et al: Outcome of antenatally diagnosed cardiac rhabdomyoma: case series and a meta-analysis. *Ultrasound Obstet Gynecol* 31(3):289–295, 2008.
425. Pruksanusak N, Suntharasaj T, Suwanrath C, et al: Fetal cardiac rhabdomyoma with hydrops fetalis. *J Ultrasound Med* 31(11):1821–1824, 2012.
426. Schlaegel F, Takacs Z, Solomayer EF, et al: Prenatal diagnosis of giant cardiac rhabdomyoma with fetal hydrops in tuberous sclerosis. *J Prenat Med* 7(3):39–41, 2013.
427. Miyake CY, Del Nido PJ, Alexander ME, et al: Cardiac tumors and associated arrhythmias in pediatric patients, with observations on surgical therapy for ventricular tachycardia. *J Am Coll Cardiol* 58(18):1903–1909, 2011.
428. Hirakubo Y, Ichihashi K, Shiraishi H, Momoi MY: Ventricular tachycardia in a neonate with prenatally diagnosed cardiac tumors: a case with tuberous sclerosis. *Pediatr Cardiol* 26(5):655–657, 2005.
429. Watanabe T, Hojo Y, Kozaki T, et al: Hypoplastic left heart syndrome with rhabdomyoma of the left ventricle. *Pediatr Cardiol* 12(2):121–122, 1991.
430. Russell GA, Dhasmana JP, Berry PJ, Gilbert-Barnes EF: Coexistent cardiac tumours and malformations of the heart. *Int J Cardiol* 22(1):89–98, 1989.
431. Freedom RM, Lee KJ, MacDonald C, Taylor G: Selected aspects of cardiac tumors in infancy and childhood. *Pediatr Cardiol* 21(4):299–316, 2000.
432. Marx GR, Moran AM: Cardiac tumors. In Allen HD, Driscoll DJ, Shaddy RE, Feltes TF, editors: *Moss & Adams' Heart Disease in Infants, Children, and Adolescents*, ed 8, Philadelphia, 2013, Lippincott Williams & Wilkins, pp 1549–1564.
433. Twaretzky W, McElhinney DB, Margossian R, et al: Association between cardiac tumors and tuberous sclerosis in the fetus and neonate. *Am J Cardiol* 92(4):487–489, 2003.
434. Bader RS, Chitayat D, Kelly E, et al: Fetal rhabdomyoma: prenatal diagnosis, clinical outcome, and incidence of associated tuberous sclerosis complex. *J Pediatr* 143(5):620–624, 2003.
435. Lacey SR, Donofrio MT: Fetal cardiac tumors: prenatal diagnosis and outcome. *Pediatr Cardiol* 28(1):61–67, 2007.
436. Milunsky A, Ito M, Maher TA, et al: Prenatal molecular diagnosis of tuberous sclerosis complex. *Am J Obstet Gynecol* 200(3):321.e1–321.e6, 2009.
437. Fagiana AM, Barnett S, Reddy VS, Milhoan KA: Management of a fetal intrapericardial teratoma: a case report and review of the literature. *Congenit Heart Dis* 5:51–55, 2010.
438. Gobbi D, Rubino M, Chiandetti L, et al: Neonatal intrapericardial teratoma: a challenge for the pediatric surgeon. *J Pediatr Surg* 42(1):E3–E6, 2007.
439. Soor GS, Chakrabarti MO, Luk A, et al: Prenatal intrapericardial teratomas: diagnosis and management. *Cardiovasc Pathol* 19(1):e1–e4, 2010.
440. Sydorak RM, Kelly T, Feldstein VA, et al: Prenatal resection of a fetal pericardial teratoma. *Fetal Diagn Ther* 17(5):281–285, 2002.
441. Laforgia N, Calderoni G, Di Mauro A, et al: A case of neonatal intrapericardial teratoma. Clinical and pathological findings. *Acta Paediatr* 100(8):e90–e92, 2011.
442. Hou CF, Chao A, Wang CJ, et al: Atrial hemangioma: a rare cause of hydrops fetalis and intrauterine fetal death. *Eur J Obstet Gynecol Reprod Biol* 130(2):271–272, 2007.
443. Mackie AS, Kozakewich HP, Geva T, et al: Vascular tumors of the heart in infants and children: case series and review of the literature. *Pediatr Cardiol* 26(4):344–349, 2004.
444. Paladini D, Tartaglione A, Vassallo M, Martinelli P: Prenatal ultrasonographic findings of a cardiac myxoma. *Obstet Gynecol* 102(5 Pt 2):1174–1176, 2003.
445. Engum SA: Embryology, sternal clefts, ectopia cordis, and Cantrell's pentalogy. *Semin Pediatr Surg* 17(3):154–160, 2008.
446. Kanagasuntheram R, Verzin JA: Ectopia cordis in man. *Thorax* 17:159–167, 1962.
447. Cantrell JR, Haller JA, Ravitch MM: A syndrome of congenital defects involving the abdominal wall, sternum, diaphragm, pericardium, and heart. *Surg Gynecol Obstet* 107(5):602–614, 1958.
448. Hornberger LK, Colan SD, Lock JE, et al: Outcome of patients with ectopia cordis and significant intracardiac defects. *Circulation* 94(9 Suppl):1132–1137, 1996.
449. Sadler TW, Feldkamp ML: The embryology of body wall closure: relevance to gastroschisis and other ventral body wall defects. *Am J Med Genet C Semin Med Genet* 148C(3):180–185, 2008.
450. Amato JJ, Douglas WI, Desai U, Burke S: Ectopia cordis. *Chest Surg Clin N Am* 10(2):297–316, 2000.
451. Lawrence EJ, Morris SA, Sexson-Tejtel K, et al: OP15.08: fetal echocardiography findings and outcomes in ectopia cordis; a case series. *Ultrasound Obstet Gynecol* 44(S1):110, 2014.
452. Morales JM, Patel SG, Duff JA, et al: Ectopia cordis and other midline defects. *Ann Thorac Surg* 70(1):111–114, 2000.
453. van Hoorn JH, Moonen RM, Huysentruyt CJ, et al: Pentalogy of Cantrell: two patients and a review to determine prognostic factors for optimal approach. *Eur J Pediatr* 167(1):29–35, 2008.
454. Repondek-Liberska M, Janiak K, Wloch A: Fetal echocardiography in ectopia cordis. *Pediatr Cardiol* 21(3):249–252, 2014.
455. Gabriel A, Donnelly J, Kuc A, et al: Ectopia cordis: a rare congenital anomaly. *Clin Anat* 27(8):1193–1199, 2014.
456. Martin RA, Cunniff C, Erickson L, Jones KL: Pentalogy of Cantrell and ectopia cordis, a familial developmental field complex. *Am J Med Genet* 42(6):839–841, 1992.
457. Fogel M, Copel JA, Cullen MT, et al: Congenital heart disease and fetal thoracoabdominal anomalies: associations in utero and the importance of cytogenetic analysis. *Am J Perinatol* 8(6):411–416, 1991.



458. Gavrilov S, Lacy E: Genetic dissection of ventral folding morphogenesis in mouse: embryonic visceral endoderm-supplied BMP2 positions head and heart. *Curr Opin Genet Dev* 23(4):461–469, 2013.
459. Ma X, Adelstein RS: A point mutation in myh10 causes major defect in heart development and body wall closure. *Circ Cardiovasc Genet* 7:257–265, 2014.
460. Scott GW: Ectopia cordis; report of a case successfully treated by operation. *Guys Hosp Rep* 104(1):55–66, 1955.
461. Dobell AR, Williams HB, Long RW: Staged repair of ectopia cordis. *J Pediatr Surg* 17(4):353–358, 1982.
462. O'Gorman CS, Tortoriello TA, McMahon CJ: Outcome of children with pentalogy of Cantrell following cardiac surgery. *Pediatr Cardiol* 30(4):426–430, 2009.
463. Mohan R, Peralta M, Perez R, et al: Chest wall reconstruction in a pediatric patient with ectopia cordis. *Ann Plast Surg* 65(2):211–213, 2010.
464. Sadlecki P, Krekora M, Krasomski G, et al: Prenatally evolving ectopia cordis with successful surgical treatment. *Fetal Diagn Ther* 30(1):70–72, 2011.
465. Sakasai Y, Thang BQ, Kanemoto S, et al: Staged repair of pentalogy of Cantrell with ectopia cordis and ventricular septal defect. *J Cardiol Surg* 27:390–392, 2012.
466. Marino AL, Levy RJ, Berger JT, Donofrio MT: Pentalogy of Cantrell with a single-ventricle cardiac defect: collaborative management of a complex disease. *Pediatr Cardiol* 32(4):498–502, 2011.
467. Wiggins DL, Strasburger JF, Gotteiner NL, et al: Magnetophysiologic and echocardiographic comparison of blocked atrial bigeminy and 2:1 atrioventricular block in the fetus. *Heart Rhythm* 10(8):1192–1198, 2013.
468. Strasburger JF, Cheulkar B, Wakai RT: Magnetocardiography for fetal arrhythmias. *Heart Rhythm* 5(7):1073–1076, 2008.
469. Das B, Cuneo BF, Ovadia M, et al: Magnetocardiography-guided management of an unusual case of isoimmune complete atrioventricular block complicated by ventricular tachycardia. *Fetal Diagn Ther* 24(3):282–285, 2008.
470. Maeno Y, Hirose A, Kanbe T, Hori D: Fetal arrhythmia: prenatal diagnosis and perinatal management. *J Obstet Gynaecol Res* 35(4):623–629, 2009.
471. Eliasson H, Wahren-Herlenius M, Sonesson SE: Mechanisms in fetal bradyarrhythmia: 65 cases in a single center analyzed by Doppler flow echocardiographic techniques. *Ultrasound Obstet Gynecol* 37(2):172–178, 2011.
472. Strasburger JF, Wakai RT: Fetal cardiac arrhythmia detection and in utero therapy. *Nat Rev Cardiol* 7(5):277–290, 2010.
473. Hutter D, Silverman ED, Jaeggi ET: The benefits of transplacental treatment of isolated congenital complete heart block associated with maternal anti-Ro/SSA antibodies: a review. *Scand J Immunol* 72(3):235–241, 2010.
474. Cuneo BF, Zhao H, Strasburger JF, et al: Atrial and ventricular rate response and patterns of heart rate acceleration during maternal–fetal terbutaline treatment of fetal complete heart block. *Am J Cardiol* 100(4):661–665, 2007.
475. Miyoshi T, Maeno Y, Sago H, et al: Evaluation of transplacental treatment for fetal congenital bradyarrhythmia: nationwide survey in Japan. *Circ J* 76(2):469–476, 2012.
476. Buyon JP, Clancy RM, Friedman DM: Autoimmune associated congenital heart block: integration of clinical and research clues in the management of the maternal/foetal dyad at risk. *J Intern Med* 265(6):653–662, 2009.
477. Buyon JP, Clancy RM, Friedman DM: Cardiac manifestations of neonatal lupus erythematosus: guidelines to management, integrating clues from the bench and bedside. *Nat Clin Pract Rheumatol* 5(3):139–148, 2009.
478. Srinivasan S, Strasburger J: Overview of fetal arrhythmias. *Curr Opin Pediatr* 20(5):522–531, 2008.
479. Llanos C, Friedman DM, Saxena A, et al: Anatomical and pathological findings in hearts from fetuses and infants with cardiac manifestations of neonatal lupus. *Rheumatology (Oxford)* 51(6):1086–1092, 2012.
480. Jaeggi ET: Transplacental fetal treatment improves the outcome of prenatally diagnosed complete atrioventricular block without structural heart disease. *Circulation* 110(12):1542–1548, 2004.
481. Eliasson H, Sonesson SE, Sharland G, et al: Isolated atrioventricular block in the fetus: a retrospective, multinational, multicenter study of 175 patients. *Circulation* 124(18):1919–1926, 2011.
482. Friedman DM, Llanos C, Izmirly PM, et al: Evaluation of fetuses in a study of intravenous immunoglobulin as preventive therapy for congenital heart block: results of a multicenter, prospective, open-label clinical trial. *Arthritis Rheum* 62(4):1138–1146, 2010.
483. Donofrio MT, Gullquist SD, Mehta ID, Moskowitz WB: Congenital complete heart block: fetal management protocol, review of the literature, and report of the smallest successful pacemaker implantation. *J Perinatol* 24(2):112–117, 2004.
484. Perles Z, Gavri S, Rein A: Tachyarrhythmias in the fetus: state of the art diagnosis and treatment. *Prog Pediatr Cardiol* 22(1):95–107, 2006.
485. Jaeggi ET, Carvalho JS, De Groot E, et al: Comparison of transplacental treatment of fetal supraventricular tachyarrhythmias with digoxin, flecainide, and sotalol: results of a nonrandomized multicenter study. *Circulation* 124(16):1747–1754, 2011.
486. van der Heijden LB, Oudijk MA, Manten GT, et al: Sotalol as first-line treatment for fetal tachycardia and neonatal follow-up. *Ultrasound Obstet Gynecol* 42(3):285–293, 2013.
487. Shah A, Moon-Grady A, Bhogal N, et al: Effectiveness of sotalol as first-line therapy for fetal supraventricular tachyarrhythmias. *Am J Cardiol* 109(11):1614–1618, 2012.
488. Vigneswaran TV, Callaghan N, Andrews RE, et al: Correlation of maternal flecainide concentrations and therapeutic effect in fetal supraventricular tachycardia. *Heart Rhythm* 11(11):2047–2053, 2014.
489. Wren C: Mechanisms of fetal tachycardia. *Heart* 79(6):536–537, 1998.
490. Simpson JM, Maxwell D, Rosenthal E, Gill H: Fetal ventricular tachycardia secondary to long QT syndrome treated with maternal intravenous magnesium: case report and review of the literature. *Ultrasound Obstet Gynecol* 34(4):475–480, 2009.
491. Rein AJ, Levine JC, Nir A: Use of high-frame rate imaging and doppler tissue echocardiography in the diagnosis of fetal ventricular tachycardia. *J Am Soc Echocardiogr* 14(2):149–151, 2001.
492. Schleich JM, Bernard Du Haut Cilly F, Laurent MC, Almange C: Early prenatal management of a fetal ventricular tachycardia treated in utero by amiodarone with long term follow-up. *Prenat Diagn* 20(6):449–452, 2000.
493. Slesnick TC, Ayres NA, Altman CA, et al: Characteristics and outcomes of fetuses with pericardial effusions. *Am J Cardiol* 96(4):599–601, 2005.
494. Pedra SR, Smallhorn JF, Ryan G, et al: Fetal cardiomyopathies: pathogenic mechanisms, hemodynamic findings, and clinical outcome. *Circulation* 106(5):585–591, 2002.
495. Gardiner HM, Pasquini L, Wolfenden J, et al: Increased periconceptual maternal glycated haemoglobin in diabetic mothers reduces fetal long axis cardiac function. *Heart* 92(8):1125–1130, 2006.
496. Hansmann M, Gembruch U, Bald R: New therapeutic aspects in nonimmune hydrops fetalis based on four hundred and two prenatally diagnosed cases. *Fetal Ther* 4(1):29–36, 1989.
497. Yinon Y, Yagel S, Hegesh J, et al: Fetal cardiomyopathy—in utero evaluation and clinical significance. *Prenat Diagn* 27(1):23–28, 2007.
498. Machin GA: Hydrops revisited: literature review of 1,414 cases published in the 1980s. *Am J Med Genet* 34(3):366–390, 1989.
499. Friedman WF: The intrinsic physiologic properties of the developing heart. *Prog Cardiovasc Dis* 15(1):87–111, 1972.
500. Thornburg KL, Morton MJ: Filling and arterial pressures as determinants of RV stroke volume in the sheep fetus. *Am J Physiol* 244(5):H656–H663, 1983.
501. Api O, Emeksziz MB, Api M, et al: Modified myocardial performance index for evaluation of fetal cardiac function in pre-eclampsia. *Ultrasound Obstet Gynecol* 33(1):51–57, 2009.
502. Crispi F, Comas M, Hernandez-Andrade E, et al: Does pre-eclampsia influence fetal cardiovascular function in early-onset intrauterine growth restriction? *Ultrasound Obstet Gynecol* 34(6):660–665, 2009.

503. Kiserud T, Ebbing C, Kessler J, Rasmussen S: Fetal cardiac output, distribution to the placenta and impact of placental compromise. *Ultrasound Obstet Gynecol* 28(2):126–136, 2006.
504. Rudolph AM, Heymann MA: The circulation of the fetus in utero methods for studying distribution of blood flow, cardiac output and organ blood flow. *Circ Res* 21(5):741–746, 1967.
505. Rasanen J, Wood DC, Weiner S, et al: Role of the pulmonary circulation in the distribution of human fetal cardiac output during the second half of pregnancy. *Circulation* 94(5):1068–1073, 1996.
506. Wafelman LS, Pollock BH, Kreutzer J, et al: Nonimmune hydrops fetalis: fetal and neonatal outcome during 1983–1992. *Biol Neonate* 75(2):73–81, 1999.
507. Iskaros J, Jauniaux E, Rodeck C: Outcome of nonimmune hydrops fetalis diagnosed during the first half of pregnancy. *Obstet Gynecol* 90(3):321–325, 1997.
508. Porter HJ, Khong TY, Evans MF, et al: Parvovirus as a cause of hydrops fetalis: detection by in situ DNA hybridisation. *J Clin Pathol* 41(4):381–383, 1988.
509. Bonnin A, Tassin M, Vauloup-Fellous C, et al: Case of a healthy infant born following antenatal enterovirus myocarditis and hydrops. *J Clin Virol* 61(3):459–462, 2014.
510. Ouellet A, Sherlock R, Toye B, Fung KF: Antenatal diagnosis of intrauterine infection with coxsackievirus B3 associated with live birth. *Infect Dis Obstet Gynecol* 12(1):23–26, 2004.
511. Barron SD, Pass RF: Infectious causes of hydrops fetalis. *Semin Perinatol* 19(6):493–501, 1995.
512. Ashshi AM, Cooper RJ, Klapper PE, et al: Detection of human herpes virus 6 DNA in fetal hydrops. *Lancet* 355(9214):1519–1520, 2000.
513. Sivasankaran S, Sharland GK, Simpson JM: Dilated cardiomyopathy presenting during fetal life. *Cardiol Young* 15(4):409–416, 2005.
514. Arunamata A, Punn R, Cuneo B, et al: Echocardiographic diagnosis and prognosis of fetal left ventricular noncompaction. *J Am Soc Echocardiogr* 25(1):112–120, 2012.
515. Ezon DS, Ayres NA, Altman CA, et al: In primary fetal cardiomyopathy, concurrent use of the tei index and the cardiovascular profile score may improve prognostic value. *J Am Soc Echocardiogr* 26(6):B128, 2013.
516. Russell RT, Carlin A, Ashworth M, Welch CR: Diffuse placental chorioangiomas and fetal hydrops. *Fetal Diagn Ther* 22(3):183–185, 2007.
517. Van Mieghem T, Al-Ibrahim A, Deprest J, et al: Minimally invasive therapy for fetal sacrococcygeal teratoma: case series and systematic review of the literature. *Ultrasound Obstet Gynecol* 43(6):611–619, 2014.
518. Wilson RD, Hedrick H, Flake AW, et al: Sacrococcygeal teratomas: prenatal surveillance, growth and pregnancy outcome. *Fetal Diagn Ther* 25(1):15–20, 2009.
519. Zanardini C, Papageorgiou A, Bhide A, Thilaganathan B: Giant placental chorioangioma: natural history and pregnancy outcome. *Ultrasound Obstet Gynecol* 35(3):332–336, 2010.
520. Henrich W, Fuchs I, Bührer C, et al: Isolated cardiomegaly in the second trimester as an early sign of fetal hydrops due to intracranial arteriovenous malformation. *J Clin Ultrasound* 31(8):445–449, 2003.
521. Ruano R, Duarte S, Zugaib M: Percutaneous laser ablation of sacrococcygeal teratoma in a hydropic fetus with severe heart failure—too late for a surgical procedure? *Fetal Diagn Ther* 25(1):26–30, 2009.



# Ultrasound Evaluation of the Fetal Gastrointestinal Tract and Abdominal Wall

Allan Nadel

## SUMMARY OF KEY POINTS

- Detection of gastrointestinal tract obstruction is often difficult. Duodenal and small intestinal obstructions are easily visualized, but usually not until the third trimester, whereas esophageal atresia and anal atresia may be difficult to detect at any gestational age.
- Echogenic small intestine is a nonspecific finding that is associated with an increased risk for Down syndrome, cystic fibrosis, congenital cytomegalovirus (CMV) infection, fetal growth restriction (FGR), and fetal demise. However, unless there is an increased a priori risk, most fetuses with isolated echogenic bowel have a normal outcome.
- Several sonographic findings in the fetal abdomen can be associated with cystic fibrosis, including echogenic bowel, meconium peritonitis, meconium ileus, and absent gallbladder. If detected, these findings should be correlated with genetic screening results for cystic fibrosis, which is routinely offered in pregnancy.
- Ventral wall defects can often be diagnosed between 11 and 14 weeks, but be aware that isolated small omphaloceles may spontaneously resolve and can perhaps best be thought of as delayed resolution of physiologic bowel herniation.
- Omphalocele can almost always be distinguished from gastroschisis because it involves the umbilicus, is covered by a membrane, and often contains liver. Gastroschisis involves free loops of externalized bowel that have herniated to the right of the umbilical cord insertion site.
- Omphalocele is more likely than gastroschisis to be associated with aneuploidy and other anomalies. Although gastroschisis is typically isolated, affected fetuses have an increased risk of FGR and fetal demise and may have a prolonged course in the neonatal nursery.
- The risk of aneuploidy in a fetus with an omphalocele is directly related to the presence of associated anomalies, and inversely related to the gestational age.

## OUTLINE

### Embryology, 460

### Esophagus and Stomach, 461

Esophageal Atresia, 461

### Small Intestine, 465

Duodenal Obstruction, 465

Echogenic Bowel, 465

Jejunioileal Obstruction, 469

Meconium Peritonitis, 470

### Rectum, 471

Anorectal Malformations, 471

### Liver, Spleen, and Gallbladder, 475

Liver, 475

Gallbladder, 476

Spleen, 478

Ascites, 478

### Cysts, 479

Differential Diagnosis, 479

Ovarian Cysts, 480

Enteric Duplication Cysts, 481

Rare Causes of Cysts, 481

### Ventral Wall Defects, 483

Omphalocele, 483

Gastroschisis, 493

Bladder and Cloacal Exstrophy/OEIS Complex, 496

Pentalogy of Cantrell, 497

Limb-Body Wall Complex/Amniotic Band Syndrome, 497

Urachal Cyst, 497

## EMBRYOLOGY

The gastrointestinal tract begins its development early in the 3rd and 4th weeks, as longitudinal and lateral folding of the embryo results in incorporation of the dorsal part of the yolk sac.<sup>1</sup> As this occurs, the endoderm germ cell layer is incorporated into the embryo and forms the primordial (primitive) gut tube (Fig. 14-1).<sup>1</sup> This primitive gut is

closed at the cranial end by the oropharyngeal membrane and at the caudal end by the cloacal membrane.<sup>2</sup> The endoderm of the primitive gut gives rise to most of the epithelium and glands of the digestive tract. The epithelium at the cranial and caudal ends of the tract is derived from the ectoderm of the stomodeum (primitive mouth) and proctodeum (anal pit), respectively. The muscular layer, connective tissue, and other layers of the wall of the digestive tract are derived

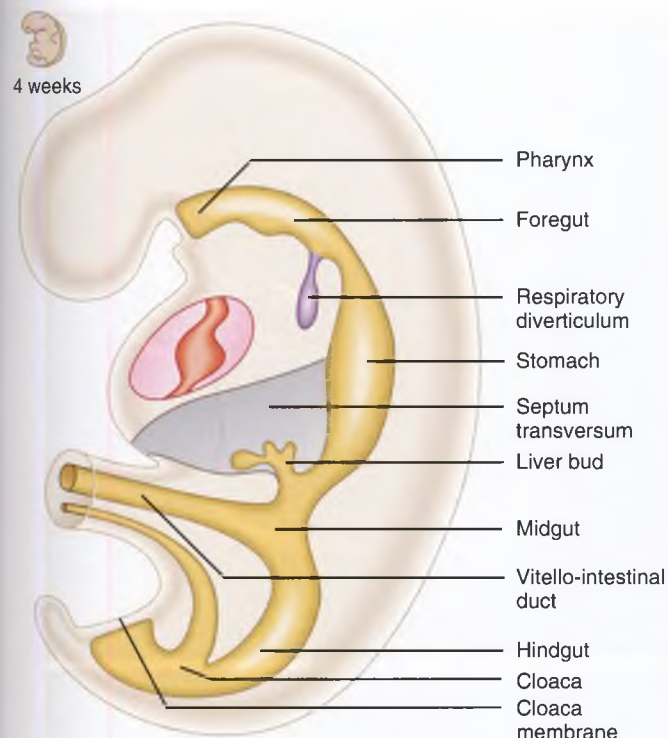


**FIG 14-1** The gut tube in a 4-week embryo. (From Mitchell B, Sharma R: *Embryology: An Illustrated Colour Text*. Edinburgh, Elsevier/Churchill Livingstone, 2005, p 39.)

from the splanchnic mesenchyme surrounding the primitive gut.<sup>2</sup> In the anterior portion of the embryo, incorporation of the endoderm into the head fold results in the formation of the foregut, whereas in the posterior portion of the embryo the hindgut forms.<sup>2</sup> The foregut is divided into a cranial and a caudal portion. The cranial portion develops in the head and neck as the pharynx. In the middle region, the midgut forms, and initially this is in direct continuity with the yolk sac. In addition to the primitive gut tube, the endodermal layer also gives rise to the parenchyma of the two large glandular organs associated with the gastrointestinal duct, the liver and pancreas.<sup>1</sup>

## ESOPHAGUS AND STOMACH

The normal esophagus is a collapsed structure that is not routinely imaged. Although it is possible to see the esophagus with a high-frequency transducer after 19 weeks in the majority of cases,<sup>3</sup> this is not part of routine sonography. The presence of a patent and normally functioning esophagus is usually inferred by noting fluid in the fetal stomach, the so-called “stomach bubble.” This normally appears as a sonolucent area in the left upper quadrant of the abdomen (Fig. 14-2A and C), which can be seen as early as the first trimester.<sup>4</sup> There may be echogenic material in the fetal stomach bubble, thought to be debris in the amniotic fluid that has been swallowed by the fetus and is of no clinical significance.<sup>5</sup>

The stomach is located on the right side of the abdomen in *situs inversus totalis*, which involves left-right reversal of otherwise normal gross anatomy such that the heart, stomach, and spleen are to the right and the liver is to the left. In about one fourth of cases *situs inversus totalis* is associated with *primary ciliary dyskinesia* (*Kartagener syndrome*), which can cause respiratory distress in newborns, chronic respiratory tract infections, and male infertility.<sup>6</sup>

The stomach can be on the left, in the middle, or on the right side of the abdomen in *heterotaxy syndromes*, a group of disorders of laterality that include polysplenia (bilateral left-sidedness) and asplenia (bilateral right-sidedness).<sup>7,8</sup> Most cases of heterotaxy syndrome are associated with congenital heart disease.

The stomach is frequently displaced by diaphragmatic hernia. It is usually in the thorax, but in milder cases can remain in the abdomen.

The amount of fluid in the stomach is highly variable among normal fetuses as, over time, in an individual fetus the stomach cyclically fills after fetal swallowing and empties through the pyloric valve into the duodenum.<sup>9</sup> A larger than average quantity of fluid in the stomach is common and is generally of no clinical significance as long as there is a normal amount of amniotic fluid and the stomach bubble does not cross the midline, which would suggest duodenal obstruction. *Pyloric atresia* is associated with a large stomach bubble, but is extremely rare and is usually accompanied by polyhydramnios<sup>10</sup> and possibly esophageal dilation.<sup>11</sup> Pyloric stenosis does not become symptomatic until after the child is born and generally cannot be detected in utero.

A small or absent stomach bubble in the absence of polyhydramnios is most often a transient finding seen in a normal fetus. Having the patient return in an hour or so, if at all possible, should cause the patient less anxiety and inconvenience than having her return for a follow-up scan in 1 or 2 weeks.<sup>12</sup> A persistently small or absent stomach bubble, particularly when accompanied by polyhydramnios, suggests an abnormality such as esophageal atresia.

## Esophageal Atresia

Esophageal atresia is an interruption of the esophagus such that the upper esophagus ends in a blind pouch, most often at or above the tracheal bifurcation<sup>13</sup> (Fig. 14-3). The prevalence of esophageal atresia is about 2.4 per 10,000.<sup>14</sup> In as many as 90% of cases, esophageal atresia is associated with a tracheoesophageal fistula, which is almost always from the trachea to the distal esophagus.

Associated abnormalities are common. In the EUROCAT (European Registry of Congenital Anomalies and Twins) series of 1222 cases over a 20-year period, esophageal atresia was isolated in less than half of cases<sup>14</sup> (Table 14-1). Associated abnormalities are even more common in prenatal compared to pediatric series of esophageal atresia and indeed may dominate the sonographic picture and result in a poorer prognosis. In an early series, 7 of 16 cases of correctly diagnosed esophageal atresia had trisomy 18, and only 4 survived the neonatal period.<sup>15</sup> Two more recent series found additional abnormalities in 76% of prenatally diagnosed cases.<sup>16,17</sup>

## Sonographic Diagnosis

Esophageal atresia is suspected when the amount of fluid in the stomach is less than normal, particularly in the presence of polyhydramnios. The stomach bubble may not be completely absent, because when there is a distal tracheoesophageal fistula (present in the majority of cases) tracheal fluid can flow across the fistula into the distal esophagus and stomach. Even in the setting of esophageal atresia without fistula, gastric secretions may produce a small amount of fluid in the stomach (see Fig. 14-2). Unfortunately, there are no good criteria that define the lower limit of normal size for the fetal stomach. Retrospective reviews describe a “small or absent stomach bubble”<sup>15-19</sup> or an “absent or collapsed fetal stomach”<sup>12</sup> without quantification.

Assessment of stomach size can be subjective and presents a tradeoff between sensitivity and specificity. Sonologists who consider very small stomach bubbles to be normal will occasionally miss an anomalous fetus. Conversely, sonologists who raise concern for these same small stomach bubbles will have many more false positive



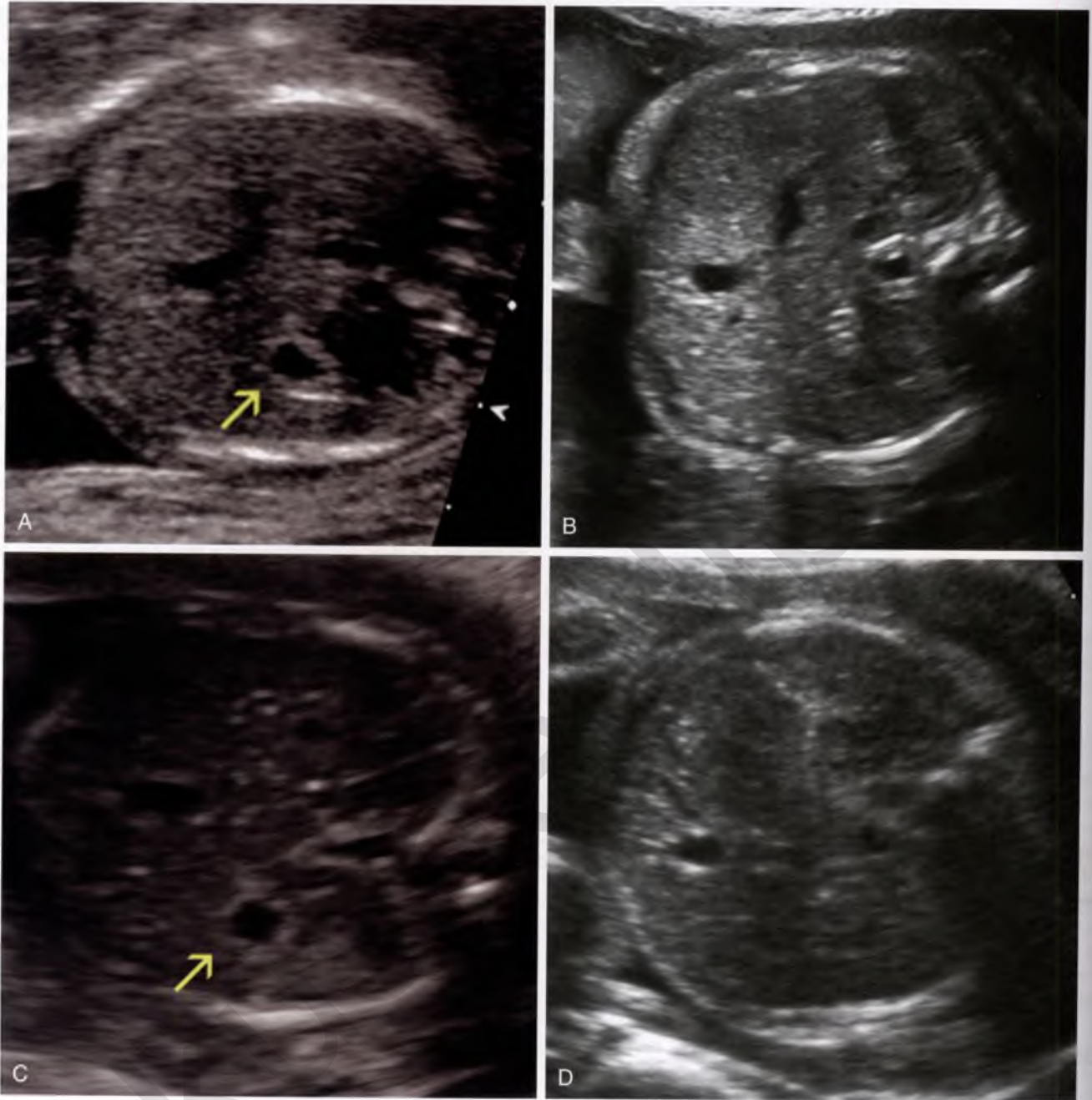


**FIG 14-2** Esophageal atresia. **A**, This fetus had multiple anomalies seen at 19 weeks. The stomach bubble (*arrow*) and the amniotic fluid volume were normal. **B**, The same fetus as in A at 30 weeks. At this time the stomach bubble was absent and there was mild polyhydramnios. The child had esophageal atresia with tracheoesophageal fistula and CHARGE syndrome (see Table 14-3). **C**, The patient was 41 years old and declined aneuploidy screening. At 19 weeks, the fetal stomach bubble (*arrow*) and the amniotic fluid volume were normal. **D**, The same fetus as in C at 28 weeks. At this time the stomach bubble was absent and there was mild polyhydramnios. The child had esophageal atresia (without tracheoesophageal fistula) and Down syndrome.

diagnoses, resulting in more anxious patients, an increased number of follow-up sonograms, and potentially unnecessary amniocenteses.

A completely absent stomach bubble is more likely than a small stomach bubble to represent esophageal atresia, particularly in the presence of polyhydramnios. For example, in one study esophageal atresia was present in all five fetuses with polyhydramnios and an absent stomach bubble but was found in only three of six fetuses with polyhydramnios and a small stomach bubble.<sup>20</sup> As expected, a small

stomach bubble with normal amniotic fluid volume was often a transient finding in a normal fetus.

Care must be taken to confirm that the stomach is not in an unusual location, as may be the case with situs inversus, heterotaxy syndrome, diaphragmatic hernia, or ventral wall defect. A persistently absent or very tiny stomach bubble suggests an inability of the fetus to swallow amniotic fluid and transport it to the stomach. There are several possible causes in addition to esophageal atresia (Table 14-2).

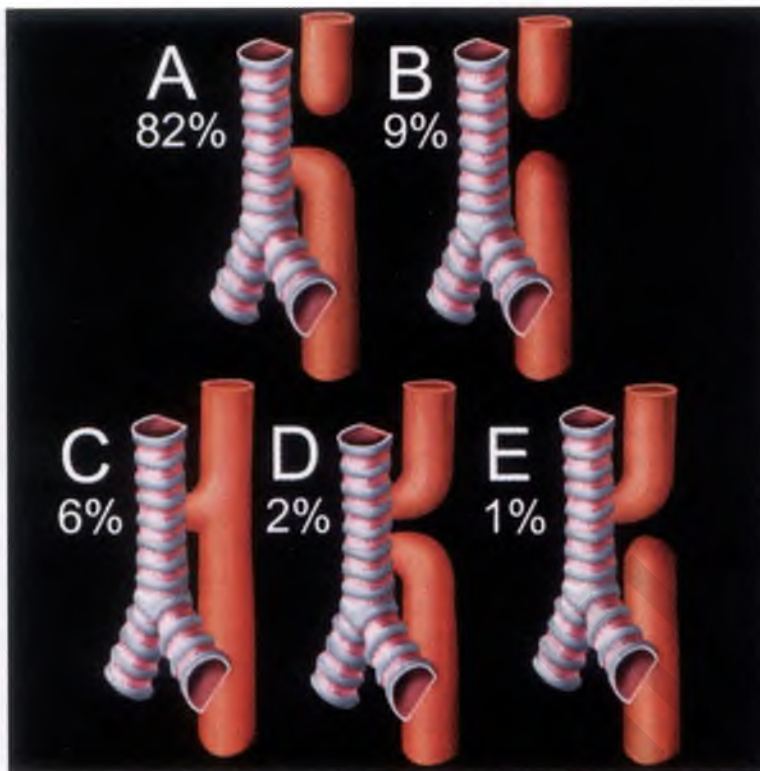


**FIG 14-3** Graphic illustration of the five main types of esophageal atresia with and without tracheoesophageal fistula. (From Donnelly LF, Jones BV, O'Hara SM, et al [eds]: *Diagnostic Imaging, Pediatrics*. Salt Lake City, Amirsys, 2005, p 44.)

**TABLE 14-1 Etiology of Esophageal Atresia**

Cause	Incidence
<b>Aneuploidy</b>	
Trisomy 18	6%
Down syndrome	2%
Other	1%
<b>Genetic Syndromes</b>	
CHARGE*	1%
Other	5%
VACTERL*	10%
Unclassified multiple malformations	31%
Isolated	45%

\*See Table 14-3.

Data from Pederson R, Calzolari E, Husby S, Game E; EUROCAT Working group: Oesophageal atresia: prevalence, prenatal diagnosis and associated anomalies in 23 European regions. *Arch Dis Child* 97(3):227-232, 2012.

Therefore, sonographic evaluation of the fetus with a small or absent stomach bubble should always involve meticulous inspection of the rest of the anatomy with particular attention to amniotic fluid volume, fetal activity, and the fetal face, neck, and chest. A 2010 series<sup>12</sup> reported a wide variety of conditions in association with persistent nonvisualization of the fetal stomach: esophageal atresia was found in only 8/48 cases (17%) after excluding those with oligohydramnios or aberrant location of the stomach. Seven fetuses were ultimately found to be normal. Fetal akinesia sequence was present in six cases.

**TABLE 14-2 Pathologic Causes for Persistently Small or Absent Stomach Bubble in the Fetus**

*Oligohydramnios* from any cause (e.g., preterm premature rupture of membranes, bilateral renal disease, urethral obstruction, donor twin in twin-twin transfusion syndrome) presumably because there is less fluid to swallow.

*Neuromuscular disorder* that impairs active swallowing: any condition that is associated with hypokinesia and/or arthrogyriposis.

*Abnormalities of the face or neck* that can interfere with active swallowing or cause a mechanical obstruction: micrognathia (often associated with hypokinesia syndromes), orofacial cleft, epignathus (teratoma originating from the mouth), neck mass (teratoma, large goiter).

*Esophageal atresia* with or without tracheoesophageal fistula.

The detection rate of esophageal atresia is poor. There were 152 cases of esophageal atresia with complete data in Northern England between 1985 and 1997; only 14 were prenatally diagnosed, for a detection rate of 9%.<sup>18</sup> The EUROCAT registry reported that the detection rate increased only slightly over time, from 26% during the years 1987 to 1996 to 36% in the following decade.<sup>14</sup> The best results were obtained in Norway: 46% of 46 cases were detected, although 32 of these cases were referred because of sonographic abnormalities.<sup>16</sup> A recent, more representative review of children treated for esophageal atresia in Texas between 2002 and 2014 showed that only 16% of 91 cases were prenatally diagnosed,<sup>21</sup> suggesting that the “real world” detection rate remains low.



In addition, prenatal diagnosis of esophageal atresia, when made, tends to occur late in gestation. Approximately one third are diagnosed prior to 28 to 30 weeks,<sup>15-17</sup> with median gestational age of in utero diagnosis of esophageal atresia of 31 to 32 weeks<sup>16,18</sup> (see Fig. 14-2).

As previously noted, the sonographic diagnosis of esophageal atresia is often incorrect.<sup>12</sup> Esophageal atresia was found in 17% of fetuses with a small or absent stomach bubble; this increased to 34% to 44% when there was also increased amniotic fluid volume.<sup>15,18</sup> In a more recent study, esophageal atresia was found in 8/18 euploid fetuses that had persistent nonvisualization of the stomach and polyhydramnios; 2 fetuses were normal, and the remaining 8 had a variety of other problems.<sup>12</sup> In a series of 22 fetuses with suspected esophageal atresia, the diagnosis was more likely to be correct if subsequent scans showed a persistently absent stomach bubble and development of polyhydramnios<sup>22</sup>; 11 fetuses in this study did not have esophageal atresia, and 5 were found to be normal.

In an effort to improve the accuracy of prenatal sonographic diagnosis of esophageal atresia, several authors have suggested use of the *pouch sign* representing the proximally dilated esophagus in the neck or thorax. This sign was present in 43% of fetuses with esophageal atresia,<sup>16</sup> and most authors feel that it is very specific, so when seen, the diagnosis is most frequently correct. However, an esophageal pouch should not be confused with a normal pharynx; false positive results have been reported.<sup>23</sup>

More recent studies have utilized magnetic resonance imaging (MRI); at a mean gestational age of 30 weeks an esophageal pouch was seen in 10/12 fetuses (83%) with and in 0/11 fetuses without postnatally confirmed esophageal atresia.<sup>24</sup> In another recent (2014) study at a mean gestational age of 32 weeks, an abnormal MRI was correct in all 8 cases, whereas a normal MRI was correct in only 5 of 7.<sup>25</sup> Note that both of these series evaluated fetuses in the third trimester.

### Antepartum Management

When esophageal atresia is suspected because of a persistently small or absent stomach bubble, a careful ultrasound examination should be performed, with special attention to the following:

1. Fetal activity to exclude the possibility of diminished fetal swallowing due to fetal hypokinesia
2. The face and neck to exclude the possibility of an anatomic obstruction
3. Findings associated with VACTERL (vertebral anomalies, anal atresia, cardiac defects, tracheoesophageal fistula and/or esophageal atresia, renal anomalies, and limb defects) (Table 14-3): including vertebral bodies, rectum and anus, heart, kidneys, extremities (especially radii and thumbs) and umbilical arteries
4. Findings associated with aneuploidy (especially Down syndrome and trisomy 18)

Because of the high prevalence of associated congenital heart disease, a fetal echocardiogram is recommended. An MRI can be considered, both to evaluate the esophagus and to search for additional anomalies not detected by ultrasound examination. The possibility of fetal aneuploidy should be addressed. If amniocentesis is performed, testing for the *CHD7* gene associated with CHARGE (see Table 14-3) syndrome can be considered.

Serial sonograms should be obtained to search for additional anomalies and evaluate fetal growth. The diagnosis of esophageal atresia typically becomes more evident over time, with a persistently absent stomach bubble and development of polyhydramnios (see Fig. 14-2). A pediatric surgery consult is advised, and delivery should be at a tertiary care center.

### TABLE 14-3 Characteristics of VACTERL Association and CHARGE Syndrome

VACTERL is an acronym that refers to an association of nonrandom co-occurring structural anomalies involving multiple body parts and organ systems.<sup>a</sup>

V: vertebral anomalies such as segmentation defects, e.g., hemivertebrae (60%-80%)

A: anorectal malformations, e.g., anal atresia (55%-90%)

C: cardiac abnormalities (40%-80%)

TE: esophageal atresia with or without tracheoesophageal fistula (50%-80%)

R: renal abnormalities (50%-80%)

L: limb malformations, such as radial ray defects (40%-50%)

By common agreement, at least three anomalies must be present to warrant this diagnosis/label, without evidence of overlapping genetic conditions, such as Fanconi anemia.

Additional anomalies are frequently associated with VACTERL. For example, single umbilical artery is seen in 20% of cases.<sup>b</sup>

The prevalence of VACTERL association is reported to be 1:10,000 to 1:40,000.<sup>c</sup> The underlying cause is not known, although changes in genes coding for transcription factors have been implicated.<sup>c</sup> Although most cases are sporadic, 9% of probands have a first-degree relative with at least one component of this association.<sup>d</sup>

CHARGE syndrome is caused by a mutation in *CHD7* gene.

Coloboma of the eye

Heart defects

Atresia choanae (also known as choanal atresia)

Retardation of growth and/or development

Genital and/or urinary abnormalities

Ear abnormalities

Although not part of the acronym, tracheoesophageal fistula is found in 20% of cases (see Fig. 14-2).<sup>e</sup>

<sup>a</sup>Solomon BD: VACTERL/VATER association. *Orphanet J Rare Dis* 6:56, 2011.

<sup>b</sup>de Jong EM, Felix JF, Deurloo JA, et al: Non-VACTERL-type anomalies are frequent in patients with esophageal atresia/tracheoesophageal fistula and full or partial VACTERL association. *Birth Defects Res A Clin Mol Teratol* 82(2):92-97, 2008.

<sup>c</sup>Shaw-Smith C: Genetic factors in esophageal atresia, tracheoesophageal fistula and the VACTERL association: roles for *FOXF1* and the 16q24.1 *FOX* transcription factor gene cluster, and review of the literature. *Eur J Med Genet* 53:6-13, 2010.

<sup>d</sup>Solomon BD, Pineda-Alvarez DE, Raam MS, Cummings DA: Evidence for inheritance in patients with VACTERL association. *Hum Genet* 127(6):731-733, 2010.

<sup>e</sup>Zentner GE, Layman WS, Martin DM, Scacheri PC: Molecular and phenotypic aspects of *CHD7* mutation in CHARGE syndrome. *Am J Med Genet A* 152A:674-686, 2010.

### Neonatal Management

Feeding should be withheld. Passage of a catheter into the stomach is attempted and a radiograph is obtained. In the presence of esophageal atresia, the tip of the catheter is kinked at about T2 to T4.<sup>13</sup>

Repair of the most common form of esophageal atresia, with a distal tracheoesophageal fistula, can be done via either thoracotomy or thoroscopic approach. If there is no distal fistula, repair can be more complicated and may require initial placement of a gastrostomy.

Survival rate for full-term infants without associated anomalies approaches 100%.<sup>26</sup> Complications can include anastomotic leaks, esophageal stricture, and recurrent tracheoesophageal fistula. Other

long-term problems include tracheomalacia, disordered esophageal peristalsis, gastroesophageal reflux, vocal cord dysfunction, and respiratory problems.

## SMALL INTESTINE

### Duodenal Obstruction

Duodenal obstruction can be intrinsic, most commonly because of atresia, or extrinsic, from constriction. An annular pancreas may occur in conjunction with an intrinsic defect rather than representing a true constricting lesion.<sup>27</sup> A duodenal web can cause partial obstruction. The prevalence of duodenal obstruction is about 1.8 per 10,000 births.<sup>28</sup>

### Ultrasound Diagnosis

The characteristic “double bubble sign” of duodenal obstruction, usually seen in conjunction with polyhydramnios, was one of the first fetal anomalies that could be detected by ultrasound. However, a more specific diagnosis requires demonstration of continuity of the dilated duodenum with fluid in the stomach, crossing the midline of the fetus<sup>29</sup> (Fig. 14-4). If such continuity cannot be established, other causes of an upper abdominal cyst (such as choledochal, mesenteric, hepatic, or enteric duplication cyst) should be considered. The differential diagnosis also includes duodenal duplication.<sup>30</sup>

Cases of transient duodenal dilation have been reported, presumably caused by transit of fluid across the pyloric valve, so assessment of suspected dilation should include documentation for a reasonable length of time.

Duodenal obstruction can rarely, if ever, be diagnosed in the first trimester.<sup>31,32</sup> At the routine 20-week obstetric sonogram, the detection rate may be as high as 50%,<sup>29,33</sup> but like other obstructions of the gastrointestinal tract, this diagnosis is more reliably made in the third trimester.

### Associated Anomalies

Up to one half of children with duodenal obstruction have Down syndrome.<sup>29,34</sup> This is not surprising considering that the relative risks of duodenal atresia and annular pancreas for Down syndrome are 264 and 430, respectively.<sup>35</sup> That is, the finding of duodenal obstruction increases the odds that a fetus has Down syndrome by a factor of at least 264.

In addition to Down syndrome, duodenal obstruction is associated with a wide variety of structural abnormalities, in particular congenital heart disease, additional intestinal problems such as malrotation and atresia, and all of the anomalies that are part of the VACTERL association (see Table 14-3).<sup>29,34</sup>

### Prognosis

As is true with many conditions, the prognosis for duodenal obstruction is highly dependent on the presence or absence of associated anomalies. In isolated duodenal obstruction, survival rate approaches 100%<sup>29</sup>; there is a wide variation in mortality rate in complicated cases, dependent on the nature of the associated anomalies.

### Antenatal Management

At the time of diagnosis, a detailed search for additional abnormalities should include a fetal echocardiogram. The risk of aneuploidy should be addressed. Duodenal obstruction is associated with a high rate of prematurity, possibly because of polyhydramnios, and an increased rate of unexpected fetal demise.<sup>36</sup> Antenatal surveillance is sometimes considered, although the benefit is unclear. A pediatric surgery consult is advised, and delivery should be at a tertiary care center.

### Neonatal Management

Fluid resuscitation and gastric decompression are followed by surgical repair, which can be either laparoscopic or by open duodeno-duodenostomy. Long-term survival is excellent for term infants without associated anomalies but complications such as gastroesophageal reflux and delayed gastric emptying can occur.<sup>37</sup>

### Echogenic Bowel

#### Definition

On second trimester ultrasound imaging, the fetal liver, lung, small intestine, and bone demonstrate increasing echogenicity in that order (Fig. 14-5A). In the 1990s it was noted that sometimes the echogenicity of small intestine is increased, such that it appears as bright as bone. This was referred to as “echogenic bowel,” a term often used interchangeably with echogenic small intestine. At that time, standard transducers used for obstetric ultrasound imaging had frequencies of 3.5 to 5 MHz and were without harmonic signal processing. Present-day transducer frequencies are typically 5 to 8 MHz and harmonics are routinely employed. These newer transducers offer improved resolution and thereby enhance prenatal diagnosis. They also make the disparity in echogenicity between small intestine and liver more conspicuous, thereby making the diagnosis of echogenic bowel more difficult<sup>38</sup> (Fig. 14-5B and C).

For these reasons, it is now recommended that when echogenic small intestine is suspected, a low-frequency transducer ( $\leq 5$  MHz) should be used. Some authors suggest that the gain be turned down to allow for comparison between the echogenicity of small intestine and bone. Despite these caveats, the detection of echogenic small intestine remains very subjective, more than most other sonographic observations<sup>39</sup> (Fig. 14-6A). There are no standardized criteria for the sonographic diagnosis of echogenic small intestine.<sup>40</sup>

A 2011 review states that the prevalence of echogenic small intestine in routine second trimester sonograms ranges from 0.2% to 1.8%.<sup>41</sup> This ninefold range in prevalence attests to the subjectivity of this finding.

#### Etiology

Echogenic small intestine is thought to be due to abnormal characteristics of intraluminal bowel contents or edema of the bowel wall.<sup>40</sup> Factors such as decreased amniotic fluid volume, presence of meconium, intestinal hypomotility because of ischemia, and swallowed blood after intra-amniotic bleeding have been associated with echogenic bowel.

#### Association With Adverse Outcomes (Table 14-4)

**Down Syndrome.** The odds that a fetus has Down syndrome is increased in the presence of echogenic small intestine. The amount that it is increased is defined by the *likelihood ratio* (LR). Owing in part to the subjective nature of echogenic bowel, LR values as disparate as

**TABLE 14-4 Adverse Outcomes Associated With Echogenic Bowel**

Aneuploidy, in particular Down syndrome
Cystic fibrosis
Growth restriction and fetal demise
Congenital infection, in particular cytomegalovirus (CMV)
Gastrointestinal obstruction



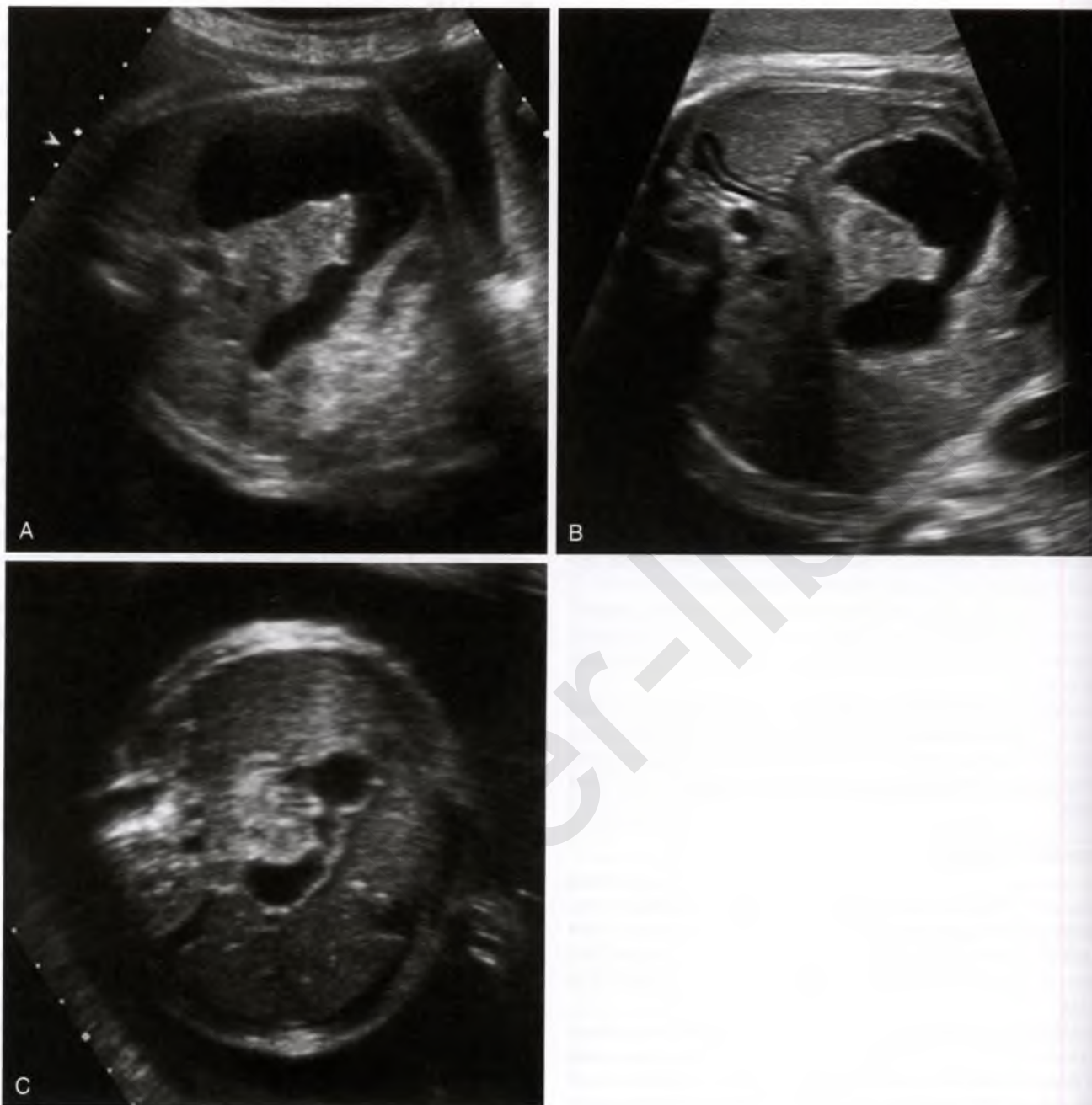


**FIG 14-4** Duodenal obstruction. In these three fetuses the diagnosis of duodenal obstruction was made in the third trimester. All three demonstrate similar, characteristic ultrasound findings with fluid shown in the stomach and proximal duodenum. **A**, This fetus was first seen at 34 weeks. On postnatal evaluation, he was found to have an annular pancreas and normal chromosomes. He is doing well except for gastroesophageal reflux. **B**, Duodenal atresia in a fetus with Down syndrome. **C**, This pregnancy was followed for mild fetal ascites (see Fig. 14-18). Evidence of duodenal obstruction and mild polyhydramnios was noted by ultrasound examination at 31 weeks. The child has Down syndrome and underwent an open duodeno-duodenostomy on day 9 of life.

1.7<sup>42</sup> and 5.5 to 6.7<sup>43</sup> have been cited in a meta-analysis and in the executive summary of a National Institutes of Health (NIH)-sponsored workshop, respectively. In addition, the positive LR of an *isolated* finding (such as echogenic bowel) depends on the product of the negative LRs of all of the other sonographic markers, referred to as “soft signs.” The earlier studies cited by the NIH workshop<sup>43</sup> did not include evaluation of the nasal bone, which has a negative LR of approximately 0.5. Conversely the meta-analysis<sup>42</sup> considered

evaluation for an aberrant subclavian artery, which is not frequently done. If evaluation of the nasal bone is added to the NIH workshop estimate, the LR for isolated echogenic bowel decreases to about 3, and if evaluation of the subclavian artery is removed from the meta-analysis, the LR for isolated echogenic bowel increases to 2.4. Thus the two estimates can be more closely reconciled.

**Cystic Fibrosis.** Cystic fibrosis has been detected in about 8% of fetuses with echogenic small intestine.<sup>44</sup> However, these patients were

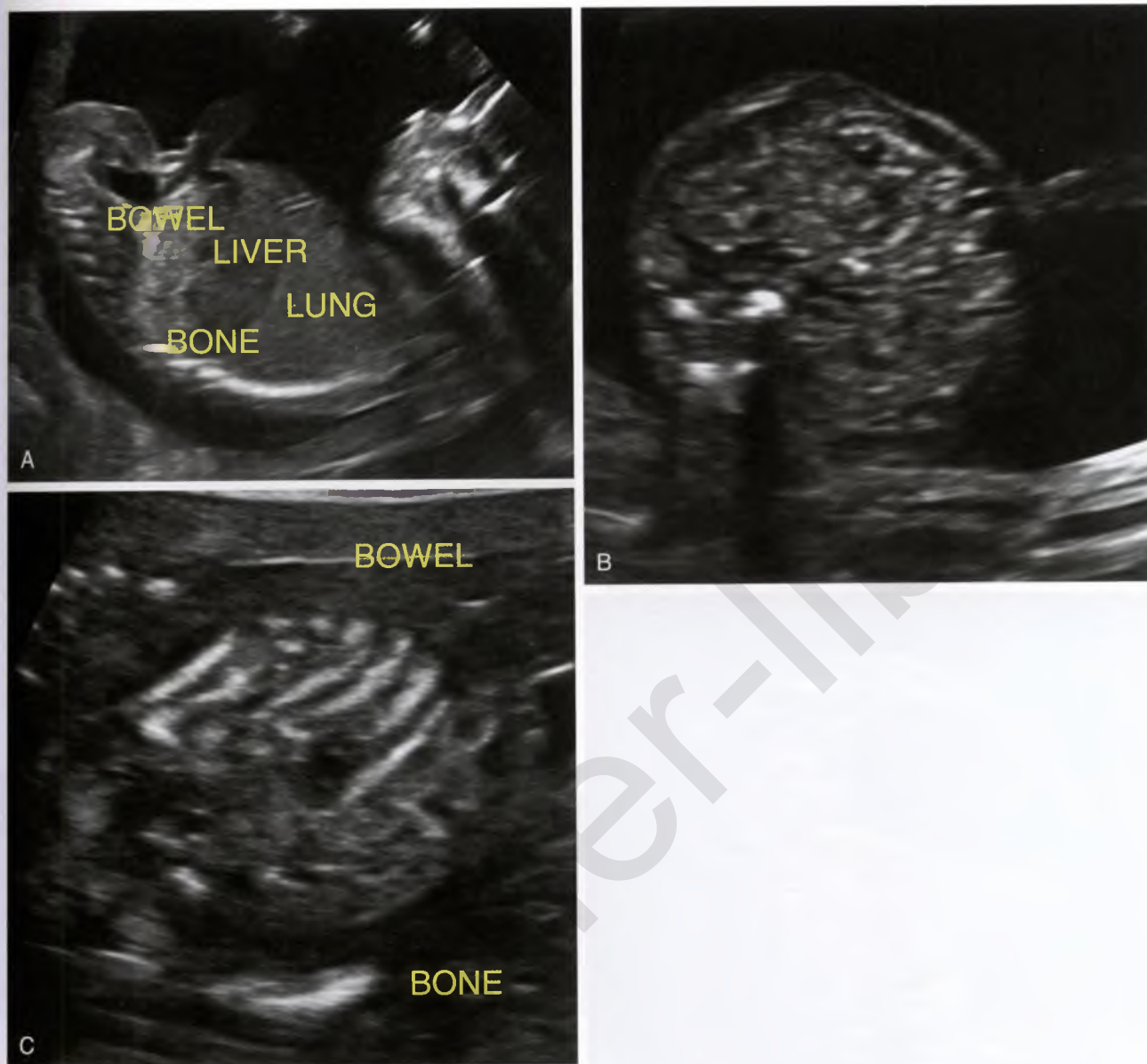


**FIG 14-5** Normal intestine in the second trimester. **A**, Midline sagittal view through the normal fetal abdomen. In order of increasing echogenicity: liver, lung, bowel, bone. **B**, Characteristic appearance of fetal intestine in the second trimester, shown on this transaxial view through the midabdomen. **C**, Using a 9-MHz transducer, the settings were deliberately manipulated to give the intestine an abnormal appearance such that, as a result of artifact, the echogenicity of bowel is as bright as iliac bone.

not previously screened for cystic fibrosis carrier status, which can detect approximately 90% of heterozygotes in the caucasian population; offering such screening is the standard of care in the United States. The frequency of cystic fibrosis in a *prescreened* population with echogenic bowel would clearly be much less. In some cases, sequencing of the cystic fibrosis transmembrane receptor gene may be helpful in patients with echogenic fetal bowel and normal cystic fibrosis screening results.

**Congenital Infection.** In one study, there were reported to be sonographic findings in 30 of 69 cases of congenital CMV infection, including 9 cases of echogenic small intestine.<sup>45</sup> Other sonographic findings associated with congenital CMV infection included growth restriction, head circumference below the 5th percentile, brain calcifications, and ventriculomegaly. An earlier study demonstrated similar results: 7 of 154 fetuses (5%) with documented congenital CMV infection had

echogenic bowel, whereas 131 fetuses (85%) had no sonographic findings.<sup>46</sup> Conversely, the likelihood of CMV infection in a fetus with echogenic small intestine is at most 3%<sup>46</sup> and the association with other infections is even less.<sup>40</sup>

**Fetal Growth Restriction and Stillbirth.** In recent years, increasing attention has been directed toward the association between echogenic small intestine and obstetric complications. The likelihood of fetal demise and of FGR was increased by a factor of 9.6 and 2.1, respectively, in fetuses with echogenic small intestine.<sup>47</sup> The median gestational age at fetal demise was 24 weeks, and in this study all spontaneous fetal losses that were observed in the setting of isolated echogenic small intestine occurred at or before 30 weeks. A subsequent study reported very similar findings, with an increase in the likelihood of growth restriction from 1.3% to 9.9% and an increase in the likelihood of fetal demise from 0.5% to 8.9% in fetuses with isolated echogenic



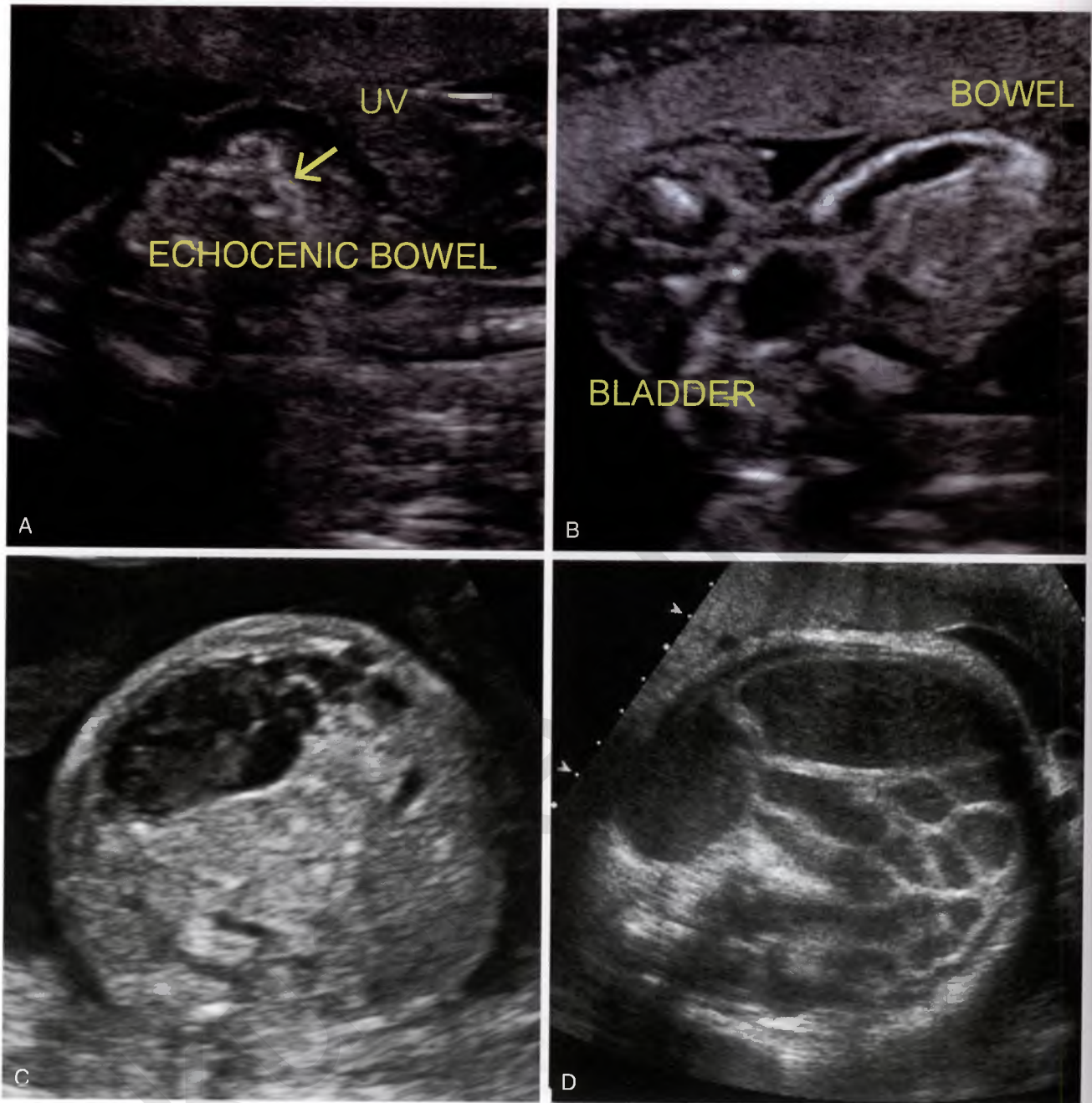


**FIG 14-6** Evolution of jejunoileal obstruction. **A**, Typical sonographic appearance of echogenic fetal bowel (*arrow*) at 19 weeks. UV, umbilical vein. **B**, Of note on this follow-up examination, a slightly dilated loop of small bowel with an echogenic rim is shown. **C**, At 23 weeks, a heterogeneous intra-abdominal cystic structure with echogenic margins was noted, indicating a meconium pseudocyst. **D**, Progressive dilatation of fluid-filled small bowel segments was observed on serial obstetric sonograms. This is the appearance at 37 weeks. Immediately after birth, the child underwent resection of 27 cm of small bowel, with anastomosis of 104 cm of proximal to 52 cm of distal small bowel. She is now doing well without nutritional deficiencies. (**D**, Courtesy of Mary Frates, MD.)

small intestine. Again, the median gestational age at fetal demise was 24 weeks and all spontaneous losses occurred prior to 30 weeks.<sup>48</sup> These data suggest that the advantage of antenatal surveillance starting at 32 weeks may be limited.

Additional factors that may further increase the likelihood of obstetric complications in fetuses with echogenic small intestine include elevated maternal serum alpha-fetoprotein<sup>49,50</sup> and abnormal uterine artery Doppler.<sup>51</sup>

Echogenic small intestine is rarely associated with other anomalies, such as  $\alpha$ -thalassemia<sup>40</sup> and intestinal obstruction (see Fig. 14-6).

#### Management of Isolated Echogenic Small Intestine

1. Targeted sonographic evaluation of fetal anatomy, including search for other markers of aneuploidy or evidence of congenital CMV infection, to ensure that the echogenic small intestine is indeed an isolated finding.

- Evaluation of a priori risk of aneuploidy based on maternal age and previously obtained screening results. If the patient desires, additional prenatal testing for aneuploidy can be offered. Given that the increased risk of aneuploidy is relatively modest and is mainly limited to trisomy 21, cell-free DNA testing is a useful option to consider in this setting.
- Evaluation of a priori risk of cystic fibrosis based on parental ethnicity and previously obtained carrier screening for *CFTR* mutations, which should be offered if not previously obtained. Even if the mother screened negative, there is a residual risk that she is a carrier, and that the fetus could be affected. If the prospective parents wish to address this concern, the next step would be to obtain blood from the father of the fetus for carrier screening, and if he tests positive, one or both parents could pursue gene sequencing, which can detect mutations not identified through genotyping panels.
- Evaluation for congenital infection with maternal serologic tests. Blood is routinely drawn to test for CMV antibodies, both IgG and IgM. To help assess if the infection is acute in the setting of positive IgM antibody, IgG avidity can be determined. Although it is possible to have fetal manifestations from recurrent or secondarily infected CMV, the likelihood is low. Unless there are specific concerns, serologic tests for other infections such as toxoplasmosis may not be warranted.<sup>41</sup> If the maternal serologic tests indicate evidence of acute infection, further evaluation such as amniocentesis for CMV RNA using polymerase chain reaction should be offered.

- Fetal surveillance in the second half of pregnancy. This typically entails serial ultrasound examinations, often every 4 weeks, to assess growth and amniotic fluid volume. Many institutions also institute weekly or biweekly nonstress tests or biophysical profiles after 32 weeks. Follow-up sonograms will detect most cases with bowel complications.

As a rule, providers taking care of the newborn should always be apprised of antenatal sonographic findings. If the child appears well, no further evaluation is necessary after an in utero finding of isolated echogenic small intestine: follow-up of 48 such infants demonstrated a normal outcome.<sup>52</sup>

### Jejunioileal Obstruction

When performing a second trimester obstetric sonogram using a high-frequency transducer, particularly in a thin patient, individual loops of fetal bowel can often be discerned (see Fig. 14-5B). During the third trimester, fluid can be seen within the bowel lumen; the maximal diameter of normal fetal small intestine is reported to be 7 mm.<sup>53</sup>

The hallmark of distal small bowel obstruction is dilated loops of bowel (Fig. 14-6D). This is rarely seen before the third trimester. Polyhydramnios, a dilated stomach, and echogenic bowel are nonspecific findings that are sometimes associated with or are precursors to identification of frank obstruction<sup>54</sup> (Table 14-5).

Obstructed fetal small bowel should not be confused with normal fetal colon, which becomes more prominent during gestation, typically appearing as hypoechoic bowel segments, of varying size, at the periphery of the abdomen (Fig. 14-7A). The small intestine tends to

**TABLE 14-5 Sonographic Comparison Between Jejunal and Ileal Atresia in the Second Half of Pregnancy**

Segment	Intestinal Loops	Stomach	Peritoneal Calcification	Ascites	Associated Anomalies	Polyhydramnios
Jejunum	Marked dilation of loops, most of them on the left abdominal side	Large	Frequent	Very rare	Frequent	Frequent
Ileum	Enlargement of duodenum is common Usually only minor dilation of a few loops	Normal	Frequent	Frequent	Rare	Rare

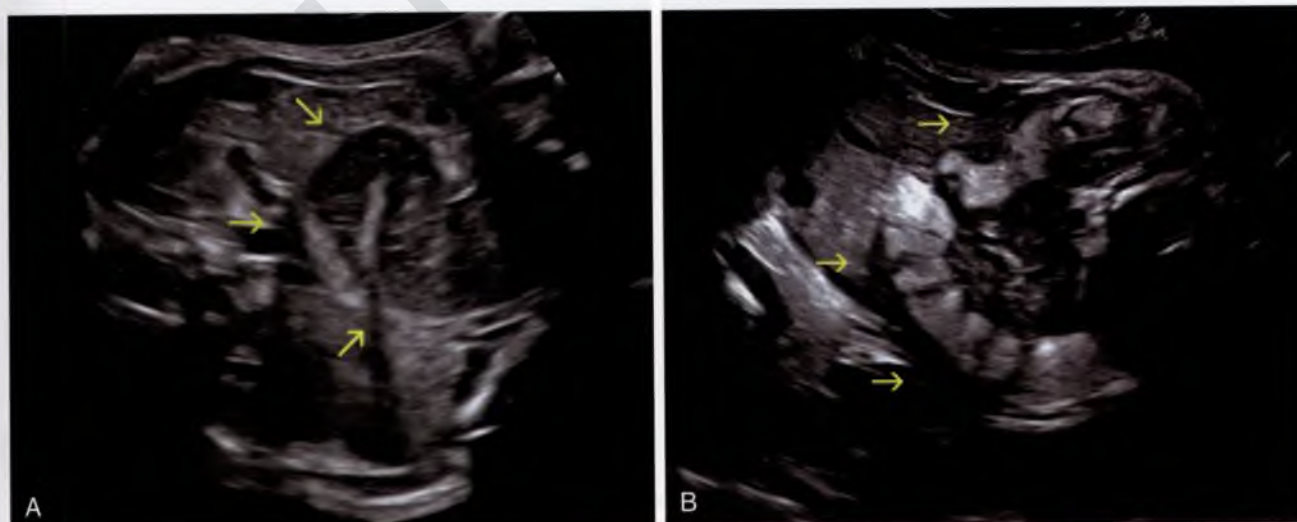


**FIG 14-7** Normal fetal colon. **A**, Normal fetal colon in the third trimester appears as hypoechoic loops of varying size at the periphery of the abdomen and in the pelvis (arrows). **B**, Echogenic colon (arrows) is a benign finding when seen after 36 weeks.



be more centrally located. Rarely, late in the third trimester, the large intestine can have a characteristic echogenic appearance (Fig. 14-7B). This is considered an innocuous finding unless it is detected prior to 36 weeks, when it has been associated with cystinuria.<sup>55</sup>

### Etiology

Atresia of a segment of jejunum or ileum is thought to most often be a consequence of vascular disruption leading to ischemic necrosis of a variable length of small bowel.<sup>56</sup> Evidence of swallowed amniotic fluid distal to the atresia suggests that the ischemic event occurred relatively late in gestation.<sup>27</sup> This finding is usually sporadic and the risk of extraintestinal anomalies varies, depending on level of obstruction. In one series of 38 children with jejunal atresia, there were 10 with cystic fibrosis, 4 with congenital heart disease, and 5 with a variety of other defects including one with Down syndrome. In contrast, only 1 of 45 children with ileal atresia had an associated anomaly.<sup>56</sup> Other abnormalities of the gastrointestinal tract, such as esophageal atresia, duodenal obstruction, and anorectal malformation, are sometimes seen in association with jejunoleal obstruction.

Some rare autosomal recessive syndromes are associated with jejunoleal atresia: "apple peel" atresia is associated with an extensive atretic segment and therefore has a guarded prognosis,<sup>57</sup> and another syndrome with multiple atretic segments has a poor prognosis.<sup>58</sup> Midgut volvulus, with<sup>59</sup> or without<sup>60</sup> the whirlpool sign, has also been reported prenatally. Meconium ileus, which is sometimes due to cystic fibrosis, is a common cause of fetal small bowel obstruction. This occurs from an accumulation of inspissated meconium in the distal ileum.

### Evaluation and Antenatal Management

The differential diagnosis includes congenital intestinal pseudo-obstruction, colonic atresia, Hirschsprung disease, and congenital chloride diarrhea.<sup>61</sup> Hydronephrosis should be reasonably easy to distinguish from dilated bowel by ultrasound imaging as it can be traced to

the bladder or kidney. In some studies, fetal MRI has been reported to be useful.<sup>62</sup>

Fetal small bowel obstruction has been associated with a high incidence of prematurity and growth restriction, possibly related to an inability to obtain oral nourishment from the amniotic fluid.<sup>63</sup>

### Neonatal Management

Treatment for jejunoleal atresia is surgical, and the prognosis is excellent unless there are multiple sites of atresia or extensive "apple peel" atresia. The treatment for volvulus is also surgical and prognosis depends on the length and condition of the affected bowel; "short gut" syndrome is the major cause of long-term morbidity.

Initial treatment for simple meconium ileus is one or more isotonic water-soluble contrast enemas, which is successful in the majority of cases.

### Meconium Peritonitis

Meconium peritonitis is thought to result from inflammation that occurs in response to intestinal rupture. The perforation can be due to intestinal atresia, volvulus, intussusception, internal hernia, or vascular compromise; often the cause is unknown.<sup>64</sup> In the past, pediatric series of symptomatic newborns reported high rates of morbidity and mortality<sup>65</sup> but the prognosis of sonographically detected prenatal cases is much better; in two recent papers, there were 5 deaths out of a total of 107 cases.<sup>64,66</sup>

Meconium peritonitis is suspected when extraluminal abdominal calcifications and ascites are seen. Extraluminal calcifications form along the visceral or parietal peritoneum, often on the surface of the liver or under the diaphragm, and appear as linear echogenic densities possibly with posterior acoustic shadowing (Fig. 14-8A). These changes may also extend through the patent processus vaginalis into the scrotum<sup>67</sup> (Fig. 14-8B). Ascites may be observed initially and then noted to resolve over time.

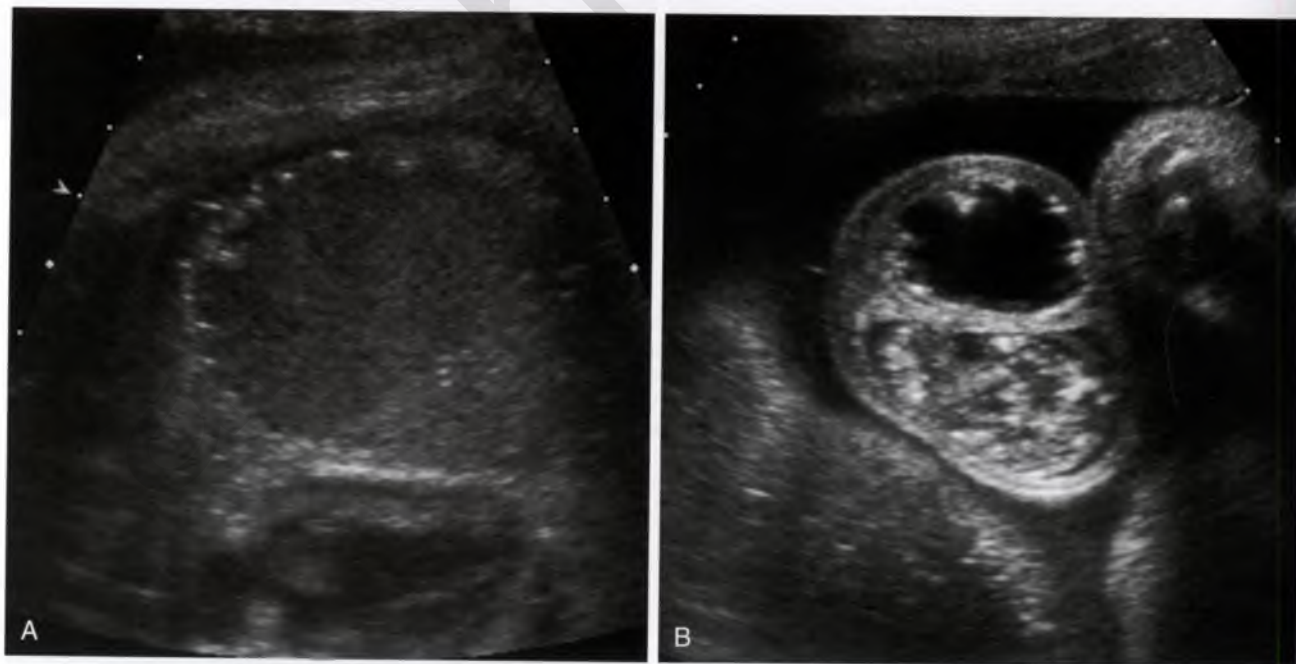


**FIG 14-8** Meconium peritonitis. **A**, Multiple tiny echogenic foci indicating peritoneal calcifications along the surface of the liver at 37 weeks. **B**, Because of patency of the processus vaginalis in the fetus, calcifications related to meconium peritonitis may also be seen within the scrotum. The child appeared healthy at birth and was discharged without any special testing, although he did undergo bilateral inguinal hernia repair at 5 weeks of age.

A *meconium pseudocyst* occurs when extravasated intestinal contents become walled off. It typically appears as a complex, round intra-abdominal cystic collection with an echogenic wall (Fig. 14-6C).

Several methods of grading the severity of meconium peritonitis have been suggested; all agree that the greater the severity, the greater the likelihood that the newborn will be symptomatic. Using one such classification system, when sonographic abnormalities included only intraperitoneal calcifications, 0/18 infants required surgical intervention; but when there were additional findings such as ascites, pseudocyst, bowel dilation, or polyhydramnios the likelihood of surgical intervention increased.<sup>64</sup> The authors suggest that it may be safe to deliver a fetus with only scattered intraperitoneal calcifications in a community hospital, but when other sonographic findings are noted, delivery in a tertiary care center is probably warranted.

Pediatric series have demonstrated a strong association between meconium peritonitis and cystic fibrosis.<sup>65</sup> Interestingly, cases

associated with cystic fibrosis are less likely to demonstrate intraperitoneal calcifications, perhaps because the intestinal contents are less inflammatory or remain more localized.<sup>66</sup> Genetic testing for cystic fibrosis is routinely offered early in pregnancy, and results of such testing should be evaluated if meconium peritonitis is identified. Other factors that have been reported in association with meconium peritonitis include parvovirus infection<sup>69</sup> and hepatitis A.<sup>70</sup>

## RECTUM

### Anorectal Malformations

Anorectal malformations result from abnormal partitioning of the cloaca by the urorectal septum into the urogenital sinus anteriorly and the rectum posteriorly (Fig. 14-9); these malformations are also referred to as *urogenital sinus malformations*. Earlier failure of development of the urorectal septum results in a higher, more severe

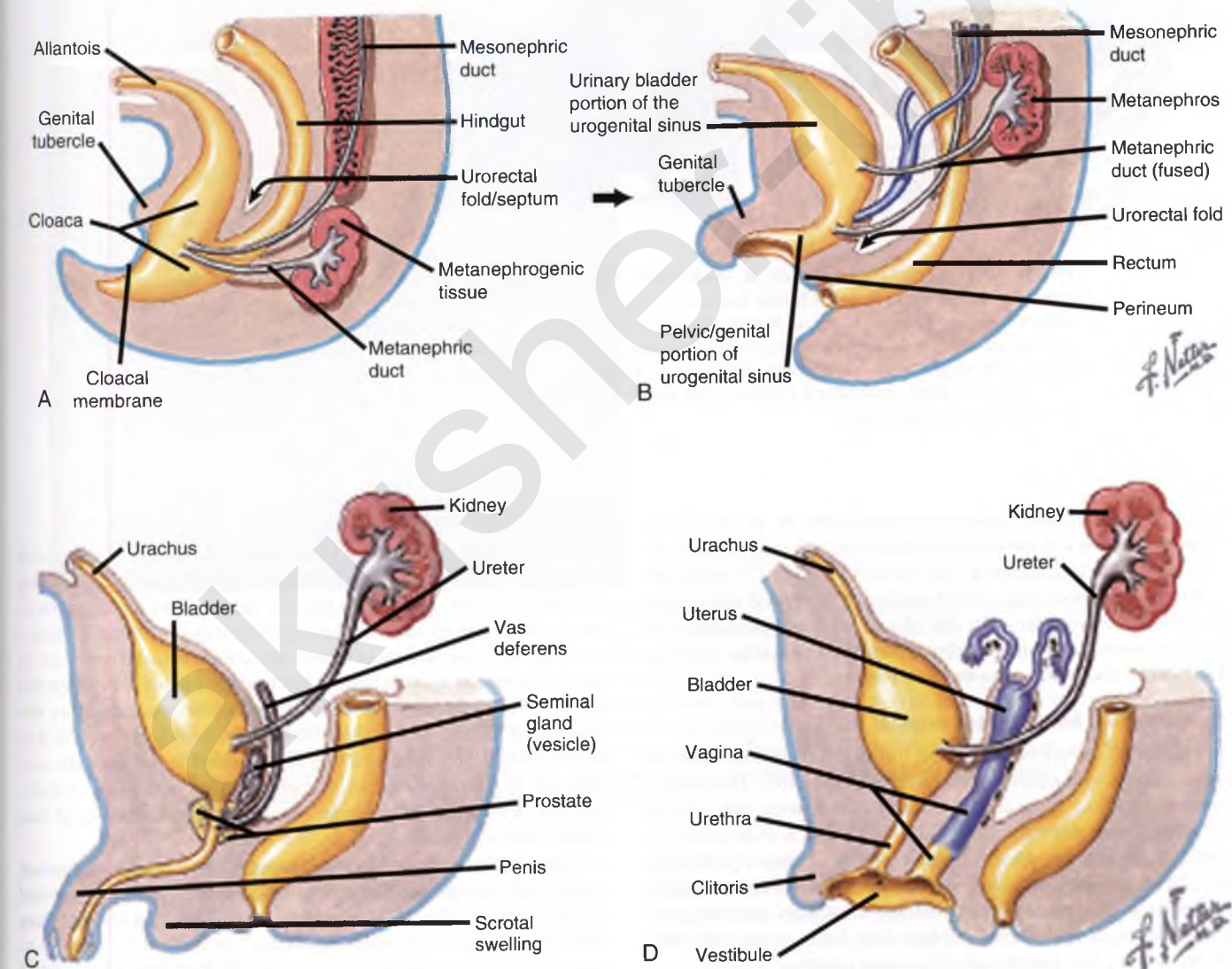


**FIG 14-9** Normal embryology: division of the cloaca. The urorectal septum grows in a caudal direction (A) until it reaches the cloacal membrane, where it becomes the perineum (B). The remaining cloacal membrane perforates posteriorly to form the anus, and anteriorly to form the urethra in males (C) and the urethra/vestibule/vagina in females (D). (Copyright Netterimages.com.)



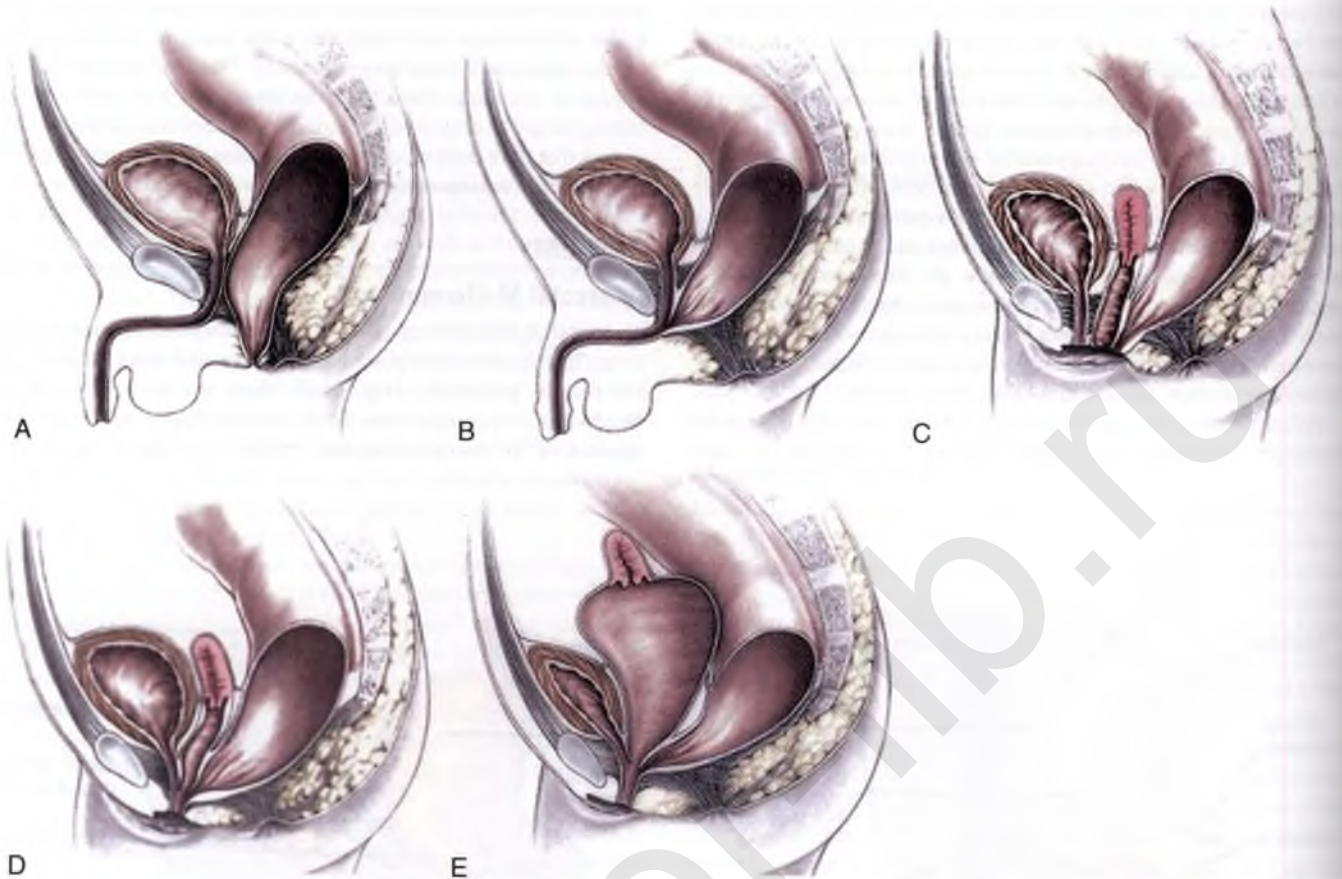


**FIG 14-10** Anorectal malformations. **A**, Imperforate anus with rectoperineal fistula opening anterior to the anal muscle complex. **B**, Imperforate anus with rectourethral fistula. This is the most common anorectal defect in males. **C**, Imperforate anus with rectovestibular fistula. This is the most common anorectal defect in females and has an excellent functional prognosis. **D**, Persistent cloaca. **E**, Persistent cloaca with hydrocolpos. The vagina often has a longitudinal septum, not shown in this drawing. (From Holcomb GW, Murphy JP, Ostlie DJ [eds]: *Ashcraft's Pediatric Surgery*. Philadelphia, Elsevier, 2014, Figs. 35-1, 35-3A, 35-7A, 35-8B, 35-10A, respectively.)

abnormality. The mildest defects are often referred to as *anal atresia* or *imperforate anus* and often involve a rectal fistula that opens anterior to the anal muscular complex (Fig. 14-10A through C). Anorectal malformation without fistula, which is strongly associated with Down syndrome,<sup>71</sup> accounts for only 4% of anorectal malformations. In females, the most severe abnormality is *persistent cloaca* (Fig. 14-10D), which will be discussed separately.

### Prevalence and Associated Anomalies

The EUROCAT survey of 4.6 million births identified 1846 cases of anal anomalies, with a prevalence of 4 per 10,000 births.<sup>72</sup> Fortunately lower lesions are far more common than higher lesions; only 10% of anal atresias were above the level of the levator ani. A wide variety of additional findings are present in the majority of cases and include VACTERL (see Table 14-3), chromosomal abnormalities, other known syndromes and sequences, and multiple anomalies involving the genital system, central nervous system, face, limbs, musculoskeletal system, and to a lesser extent, all other organ systems.<sup>73</sup>

Although most cases are sporadic, like some other abnormalities, there is often a genetic component, and anorectal malformations are associated with a variety of single gene syndromes.<sup>74</sup> There are also reports of familial nonsyndromic anorectal malformations.

### Sonographic Diagnosis

Cystic fluid collections in the first trimester have been associated with anal atresia<sup>75</sup> (Fig. 14-11A and B). In the second trimester, observation of a dilated rectum allowed for the prenatal sonographic diagnosis in only 11 of 69 (16%) cases of anal atresia and in only 3 cases when it was isolated.<sup>76</sup> Calcified intraluminal meconium is sometimes seen in cases of anorectal malformations, but it is not known how often this occurs.<sup>77</sup> These findings are likely related to the presence of an enterourinary fistula, which allows urine to distend the rectum and interact with meconium, resulting in a calcified appearance. In contrast, one might not see any sonographic findings in the case of rectoperineal or rectovestibular fistulas (see Fig. 14-10A and C) or of anal atresia without a fistula.

More recent studies address the possibility of direct visualization of the fetal anal sphincter as a circular hypoechoic area with a small echogenic center (Fig. 14-12B), which can be identified in more than 90% of fetuses after 23 weeks' gestation.<sup>78</sup> In one study, inability to image this structure allowed for the prenatal diagnosis of 17 cases of anal atresia.<sup>79</sup> Some groups utilize three-dimensional (3D) sonography for this purpose.<sup>80</sup> A combination of 2D and 3D techniques was used to evaluate 189 fetuses at increased risk for anorectal malformation based on the presence of one or more other congenital structural

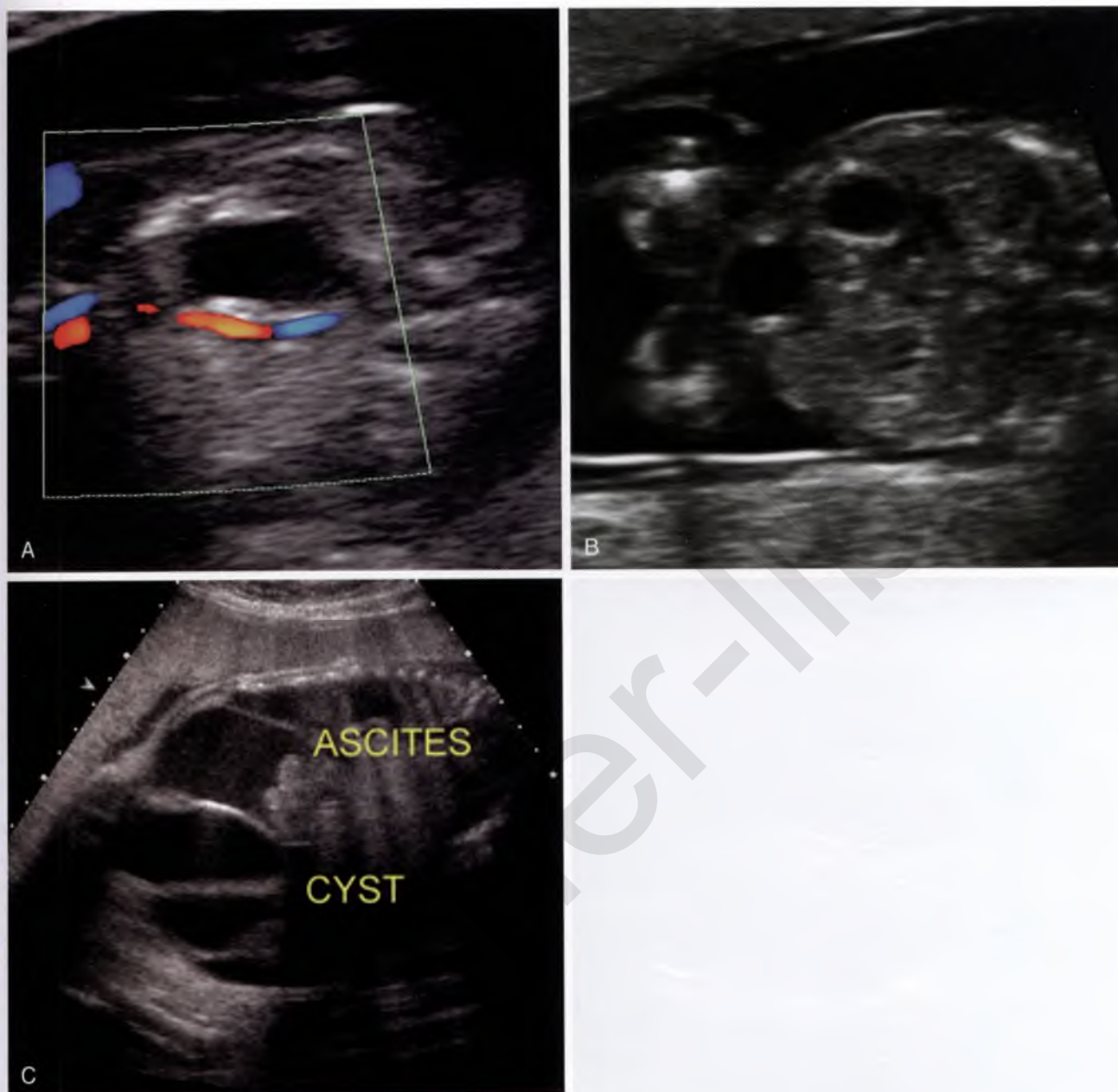


**FIG 14-11** Persistent cloaca. **A**, At 13 weeks, fluid-filled structure thought to be a large bladder with adjacent single umbilical artery, shown by color Doppler sonography. **B**, Also observed at 13 weeks was a small round abdominal cyst. The karyotype was normal. The fetal anatomic survey at 18 weeks demonstrated intra-abdominal calcifications, echogenic bowel wall, and umbilical cord cyst. **C**, In the third trimester, a septated cystic mass was shown posterior to a normal-appearing bladder. Also noted was marked ascites, with low level echoes present within the peritoneal fluid. The kidneys appeared normal. The diagnosis was urogenital sinus malformation with septated hydrocolpos (persistent cloaca). There was in utero fetal demise due to thrombosis of the single umbilical artery. The diagnosis was confirmed at autopsy. (**A** and **B**, Courtesy of Rosemary Reiss, MD; **C**, Courtesy of Mary Frates, MD.)

anomalies known to be associated with anorectal malformations. The investigators correctly excluded anorectal malformation in 175 fetuses and correctly detected an abnormality of the anus in the other 14.<sup>81</sup>

### Persistent Cloaca

This most severe form of anorectal malformation is found only in females. It is very uncommon, with a prevalence of only 0.2 per 10,000.<sup>72</sup> With persistent cloaca, the distal portion of the urinary tract, vagina, and rectum all lead to a single common channel that opens

onto the perineum (see Fig. 14-10D). In 30% of cases, hydrocolpos develops as a result of passage of urine and meconium into the vagina, which is more compliant than the bladder or rectum (Fig. 14-10E).<sup>82</sup> Development of hydrocolpos can result in several additional pathologic changes, some of which can be seen by ultrasound imaging in the third trimester (Figs. 14-11 and 14-13).

Hydrocolpos presents as a midline cystic mass in the pelvis, posterior to the bladder, extending to the perineum (Fig. 14-11C).<sup>83</sup> There is often a longitudinal vaginal septum, and there may be fluid/fluid



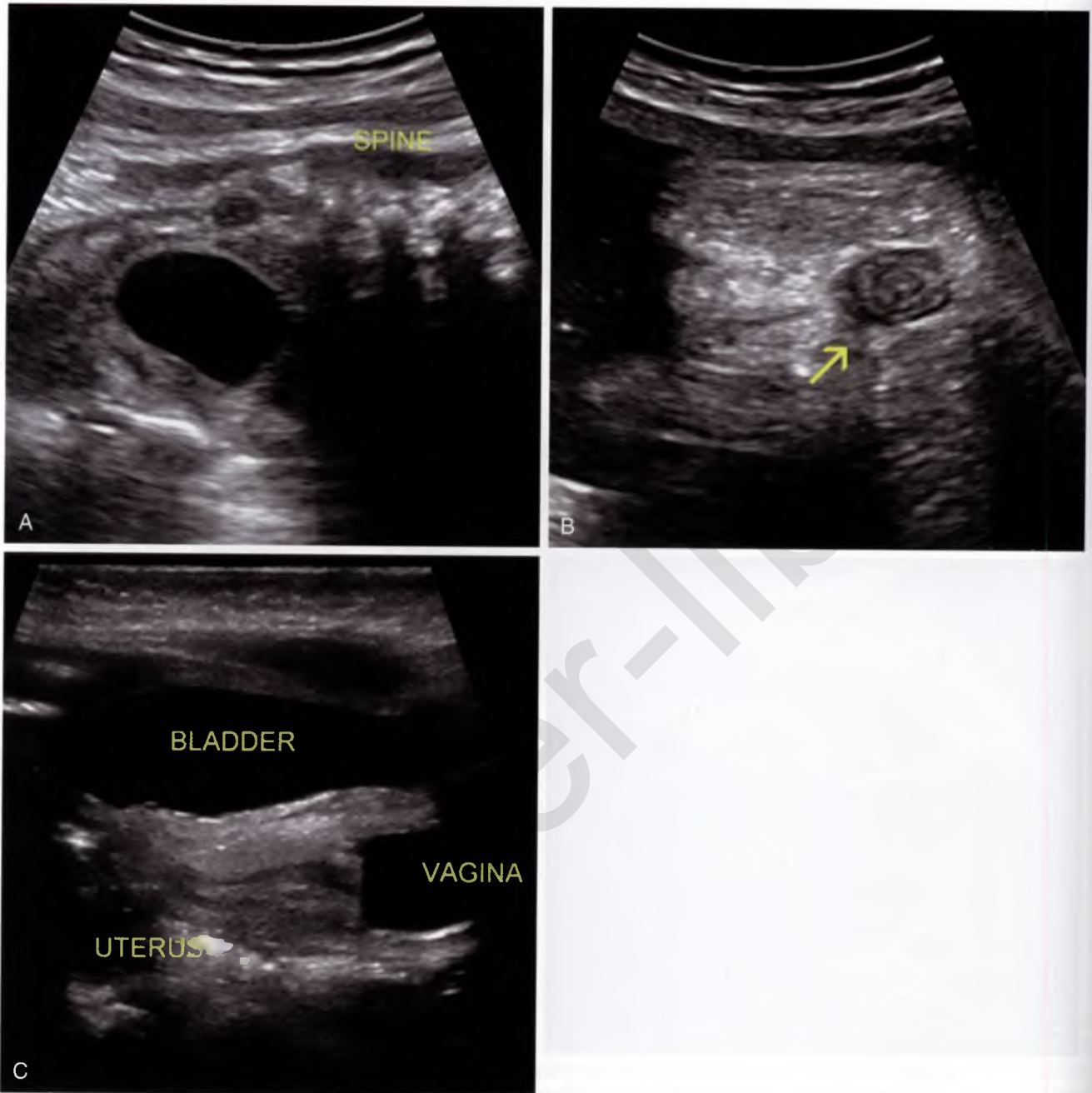


**FIG 14-12** Isolated hydrocolpos. **A**, A 2.5-cm anechoic cyst in the pelvis, anterior to the sacrum and posterior to the bladder. **B**, As part of the targeted sonographic evaluation, a normal anus, appearing as a circular structure (arrow) with echogenic center, was visualized. **C**, Postnatal transabdominal pelvic sonogram showing fluid in the distended vagina, posterior to the fluid-filled urinary bladder.

levels due to mixture of urine and meconium. The contents of the cystic mass will not be uniformly sonolucent as is the case in megacystis.

Hydrocolpos is frequently associated with urinary tract obstruction; hydronephrosis and oligohydramnios were the next most common abnormalities seen on prenatal ultrasound imaging.<sup>84</sup> If obstruction is at the level of the bladder outlet, there will be megacystis; if obstruction is at the level of the trigone, the bladder will appear normal or small.

Ascites is seen in a minority of cases. It is thought that this occurs as a result of retrograde passage of cloacal contents through the

fallopian tubes.<sup>83</sup> Because of the inflammatory response triggered by this material, abdominal calcifications characteristic of meconium peritonitis may be seen.<sup>85,86</sup> In some cases, dilated loops of bowel will demonstrate intraluminal calcifications due to mixing of meconium with urine.<sup>83,84,86</sup> Additional findings that may be seen in this setting include multicystic dysplastic kidney, ectopic/malpositioned kidney, single umbilical artery, and spinal abnormalities.<sup>83</sup>

The prenatal diagnosis of persistent cloaca is challenging, and in two recent series was made in only 6% of cases.<sup>84,86</sup> This is likely related to the rarity of this condition, the complex and variable nature of the ultrasound findings with hydrocolpos present in less than half. When

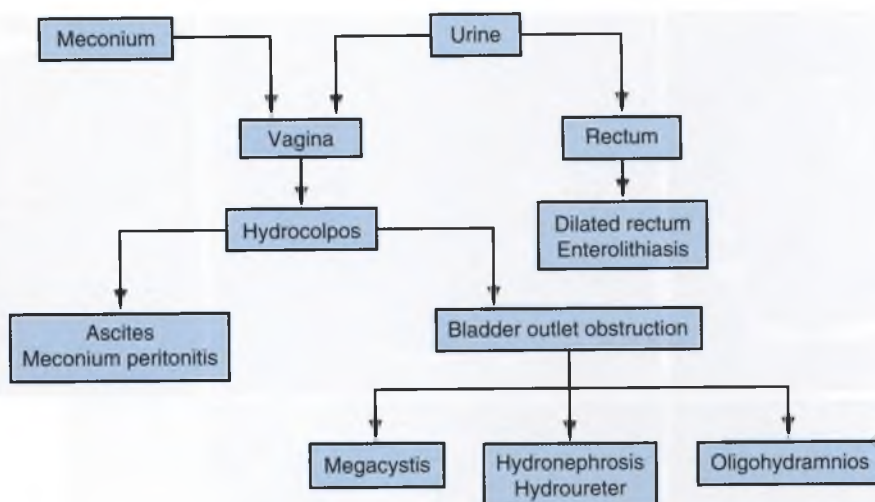


**FIG 14-13** Pathophysiology of persistent cloaca with hydrocolpos. In 30% of cases urine and meconium can pass into the most distensible organ, the vagina, causing hydrocolpos. This can be identified as a midline pelvic mass, often with a longitudinal vaginal septation. Some of this fluid can pass in retrograde fashion through the fallopian tubes resulting in free peritoneal fluid, sometimes with evidence of peritonitis and calcifications. Also, some urine can pass into the rectum, causing dilation and enterolithiasis from mixing with meconium. Hydrocolpos may be associated with obstruction of the urinary tract; if there is bladder outlet obstruction, megacystis, hydronephrosis, and hydroureter may be seen. Complete obstruction results in oligohydramnios.

this diagnosis is suspected, fetal MRI is often useful.<sup>85,87</sup> On a sagittal view of a normal third trimester fetus, the rectum should extend at least 10 mm below the bladder; in 5 of 6 fetuses with persistent cloaca, third trimester MRI demonstrated a high and dilated rectum.<sup>88</sup>

### Neonatal Management

Examination of the perineum of the neonate will often establish the diagnosis. In males, waiting 24 hours is suggested so that intraluminal pressure in the rectum can increase sufficiently to allow passage of meconium through a fistula, either on the perineum or in the urine. In females, inspection of the perineum can demonstrate a single orifice, signifying the presence of a cloaca, or reveal a fistula in the vestibule or on the perineum. Careful evaluation for associated anomalies by physical examination and imaging is also important.

Definitive surgical repair depends upon the level of the lesion. A low lesion with a fistula on the perineum can undergo primary repair, whereas a higher fistula often requires placement of a colostomy followed by a more complex surgical procedure.

## LIVER, SPLEEN, AND GALLBLADDER

### Liver

The umbilical vein enters the lower abdomen and travels in a cephalad and posterior direction to enter the liver. Within the liver, the largest branch curves toward the right, away from the stomach, where it connects with the ductus venosus and drains into the inferior vena cava just below the right atrium. In the transverse plane, at the level where abdominal circumference is measured, the vein is a prominent C-shaped structure within the liver, curving away from the stomach bubble (see Fig. 14-2A).

Occasionally the umbilical vein is noted to curve toward the left side of the fetal abdomen, toward the stomach (Fig. 14-14A). This represents *persistence of the right umbilical vein*, which may be associated with other anomalies but when isolated is considered a normal variant.<sup>89</sup>

*Choleliths* result from dilation of the biliary tract, most often fusiform dilation of the common bile duct (Fig. 14-15). They present as sonolucent cysts at the hepatic hilum. The differential diagnosis includes benign hepatic cyst (Fig. 14-14B). The diagnosis is confirmed after birth by ultrasound imaging and magnetic resonance cholangiopancreatography.<sup>90</sup> Treatment requires surgical excision and biliary-enteric anastomosis (hepatojejunostomy or hepatooduodenostomy) to prevent obstructive jaundice, cholangitis, pancreatitis, liver fibrosis, and malignancy; the timing of surgery is controversial.<sup>90</sup>

*Hepatic calcifications/echogenic foci* in the liver parenchyma (Fig. 14-14C) should be distinguished from calcifications along the surface of the liver from meconium peritonitis (see Fig. 14-8A) and from echogenic material within the gallbladder (Fig. 14-16B). Hepatic parenchymal calcifications are relatively common; the prevalence may be as high as 1:1000. In the largest reported series, 40 of 61 cases had additional sonographic abnormalities; of these, there were 10 cases with aneuploidy and 1 with congenital CMV infection.<sup>91</sup> Outcomes were better for the 21 cases with isolated hepatic calcifications: 1 fetus had parvovirus and 1 had trisomy 21, but the others fared well. In a review of the four largest series,<sup>92</sup> 93% of 63 cases with isolated intrahepatic echogenic foci had normal outcomes compared with 39% of 54 cases when there were other ultrasound findings.

Therefore, when an echogenic focus in the fetal liver is identified, a detailed study should be performed, searching for additional anomalies, particularly those associated with aneuploidy or congenital infection. Maternal blood should be obtained and tested for possible infection, particularly for CMV. Depending on the a priori risk of aneuploidy related to maternal age and screening test results, amniocentesis or cell-free DNA screening could be considered. If there is no evidence of infection and the risk of aneuploidy is low, the patient whose fetus has an isolated intrahepatic echogenic focus can be reassured.

Hepatic tumors found by prenatal sonography are rare and are the subject of case reports and literature reviews.<sup>93,94</sup> Survival statistics are based on small numbers.



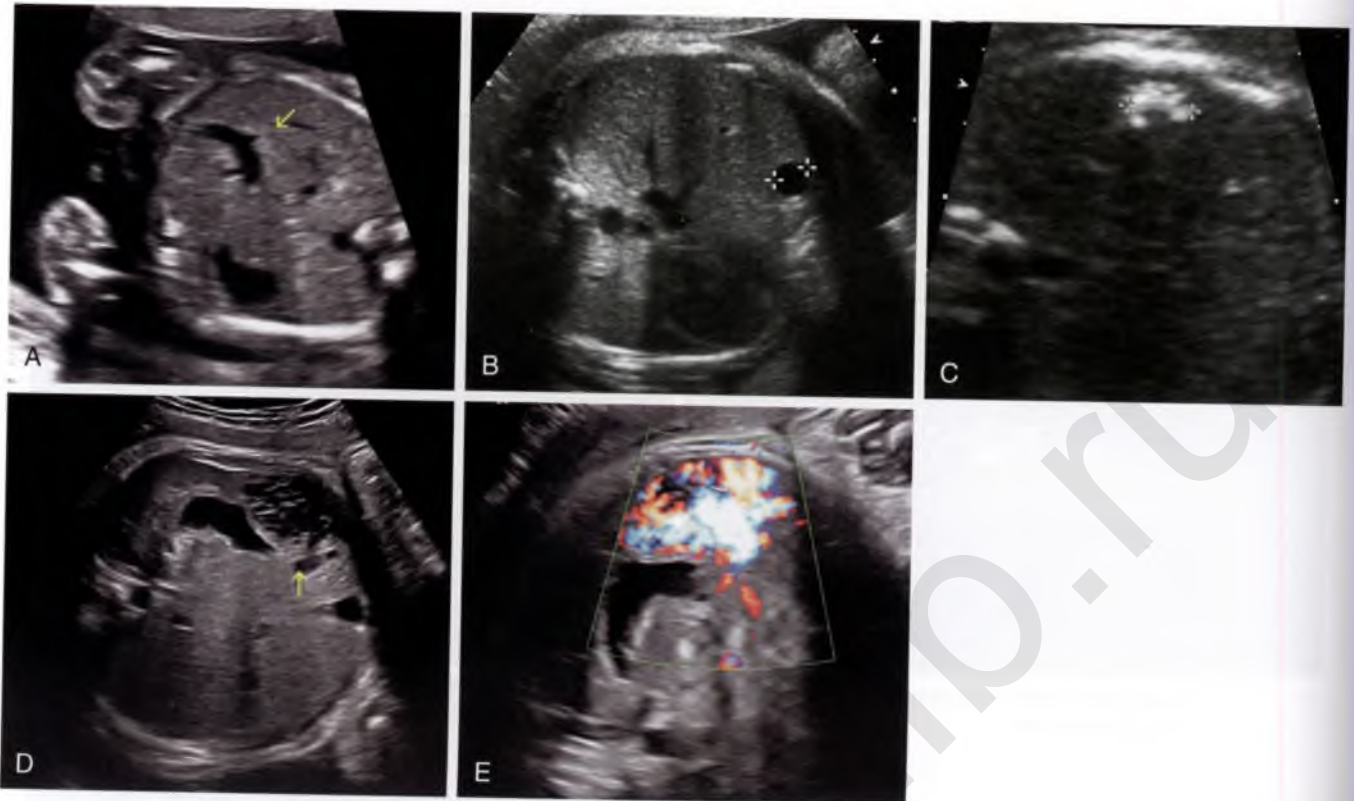


**FIG 14-14** Liver malformations. **A**, Persistent right umbilical vein (*arrow*), curving toward the left-sided stomach (compare to Fig. 14-2A). This fetus also had a horseshoe kidney, which was confirmed after birth. **B**, Small round anechoic hepatic cyst (*cursors*) seen on an oblique transaxial sonographic image of the upper abdomen. **C**, Hepatic calcification (*cursors*). Note the intraparenchymal dense echogenic foci at the periphery of the liver with slight posterior acoustic shadowing. This observation would prompt testing for possible infection, such as cytomegalovirus. **D**, Hepatic arteriovenous malformation (*arrow*). Heterogeneous hypoechoic mass within the left hepatic lobe, adjacent to the fluid-filled stomach. **E**, The same fetus as in D, with color Doppler sonography demonstrating marked vascularity. This lesion gradually involuted over the first 6 months of life.

1. *Hemangiomas and hemangioendotheliomas* can be focal, with reported survival rate of 73%, or multifocal. They can appear hypo- or hyperechoic or have mixed heterogeneous echogenicity. They are highly vascular and color Doppler interrogation can be helpful, although hepatic arteriovenous malformations may have a similar appearance (Fig. 14-14D and E). Anemia and coagulopathy can occur as a result of platelet sequestration (Kasabach-Merritt syndrome). These benign tumors tend to regress spontaneously in infancy, and regression may be hastened by administration of corticosteroids.
2. *Mesenchymal hamartomas* have a survival rate of 64%. They may be completely solid or solid with multiseptated cystic components.
3. *Hepatoblastomas* are reported to have a survival rate of only 22%. They can appear as large, echogenic solid masses; one reported case of a very large tumor had focal hemorrhage and necrosis and was highly vascular on Doppler interrogation.<sup>95</sup>
4. *Metastases from congenital neuroblastoma* may present as single or multiple hypoechoic nodules.

Rapid growth of hepatic tumors can lead to high-output cardiac failure and hydrops. If the tumor has a prominent cystic component, the differential diagnosis would include hepatic cyst (see Fig. 14-14B) and choledochal cyst. MRI may be useful in determining the cause of a hepatic mass. Because rupture can lead to massive hemorrhage, elective cesarean delivery is sometimes recommended.

## Gallbladder

The fetal gallbladder typically appears as a teardrop-shaped cystic structure in the right upper quadrant of the fetal abdomen angling obliquely toward the pelvis. It can be identified as early as the first trimester and is visualized in most fetuses in the second and third trimesters (Fig. 14-16A). Echogenic material in the fetal gallbladder is occasionally seen, mainly in the third trimester. This is relatively common and has a variable appearance<sup>96</sup> (see Fig. 14-16B). It is attributed to gallstones and is thought to be of no clinical significance because it usually resolves after birth.<sup>97,98</sup> Conservative management with sonographic surveillance of the child until resolution is suggested.

Nonvisualization of the fetal gallbladder is often a transient finding and should be reassessed on a subsequent scan. Persistent nonvisualization of the fetal gallbladder is of greater concern, particularly when associated with additional findings. In a series of 16 fetuses with isolated nonvisualization of the gallbladder, one fetus had cystic fibrosis and the remainder had normal outcomes.<sup>99</sup> In a larger series of 85 cases with persistent nonvisualization of the fetal gallbladder and no other anomalies at a mean gestational age of 23 weeks, the gallbladder was subsequently identified in 55 fetuses; of the remaining 30 fetuses, 22 had congenital agenesis of the gallbladder, which is clinically benign. However, there were three fetuses in this group with cystic fibrosis and five fetuses with congenital biliary atresia.<sup>100</sup>

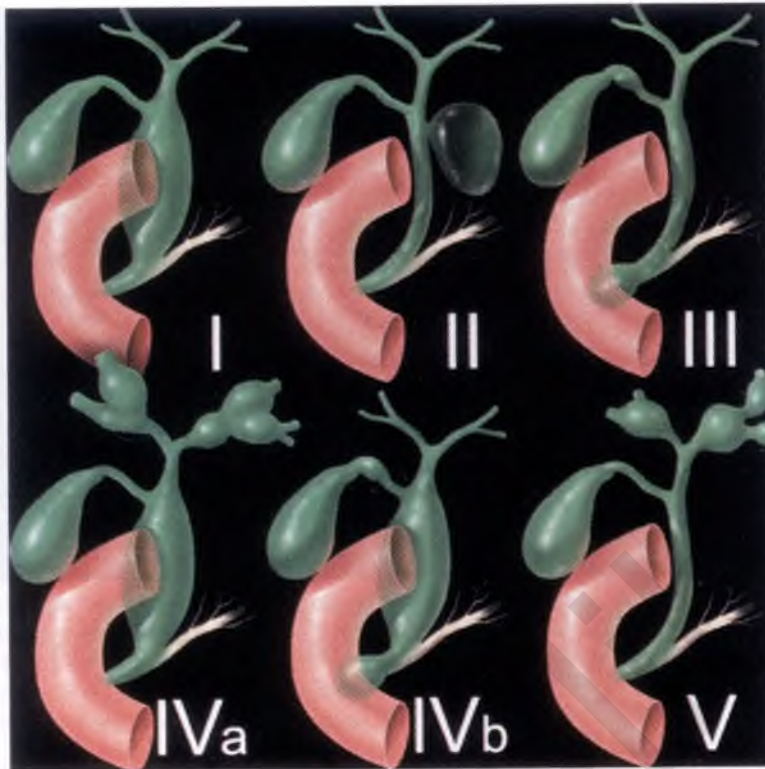


**FIG 14-15** Various types of choledochal malformation. Note the anomalous pancreaticobiliary junction; the pancreatic duct inserts into common bile duct proximal to the sphincter of Oddi. (From Donnelly LF, Jones BV, O'Hara SM, et al [eds]: *Diagnostic Imaging: Pediatrics*. Salt Lake City, Amirsys, 2005, p 96.)

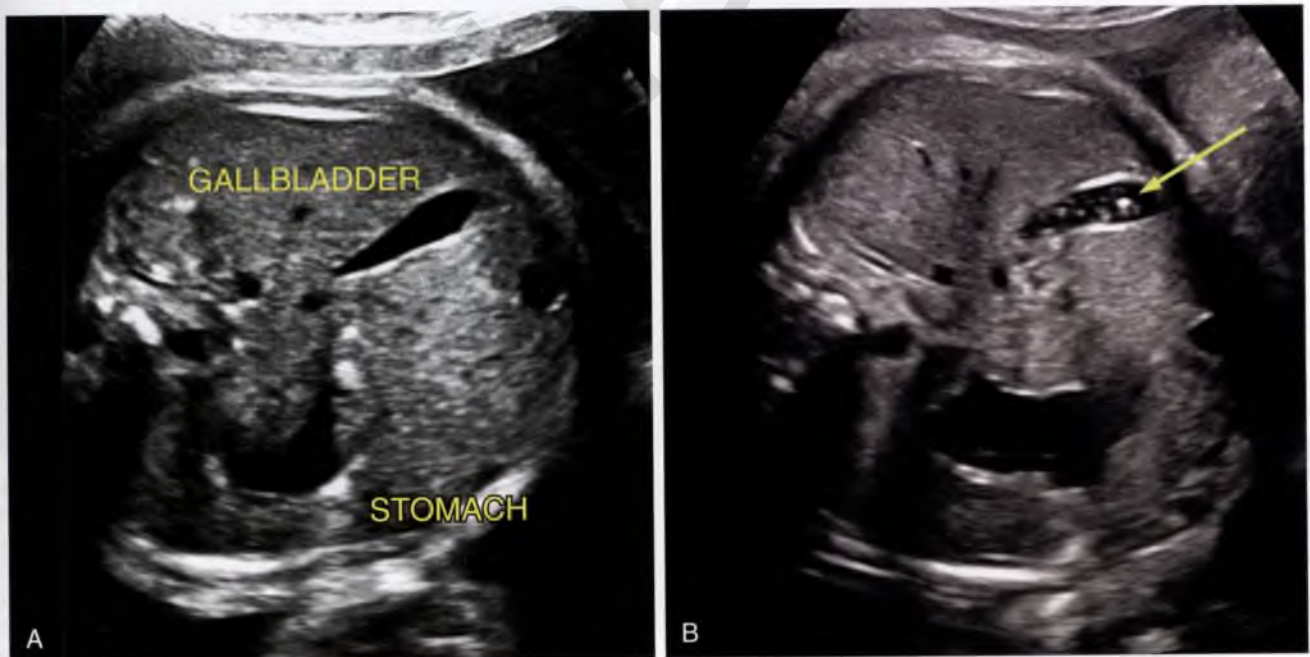


**FIG 14-16** Gallbladder. **A**, Normal fetal gallbladder in the third trimester. **B**, Similar transaxial sonographic view of the upper abdomen in a different fetus showing gallstones (*arrow*), which are relatively common and usually resolve spontaneously after birth.



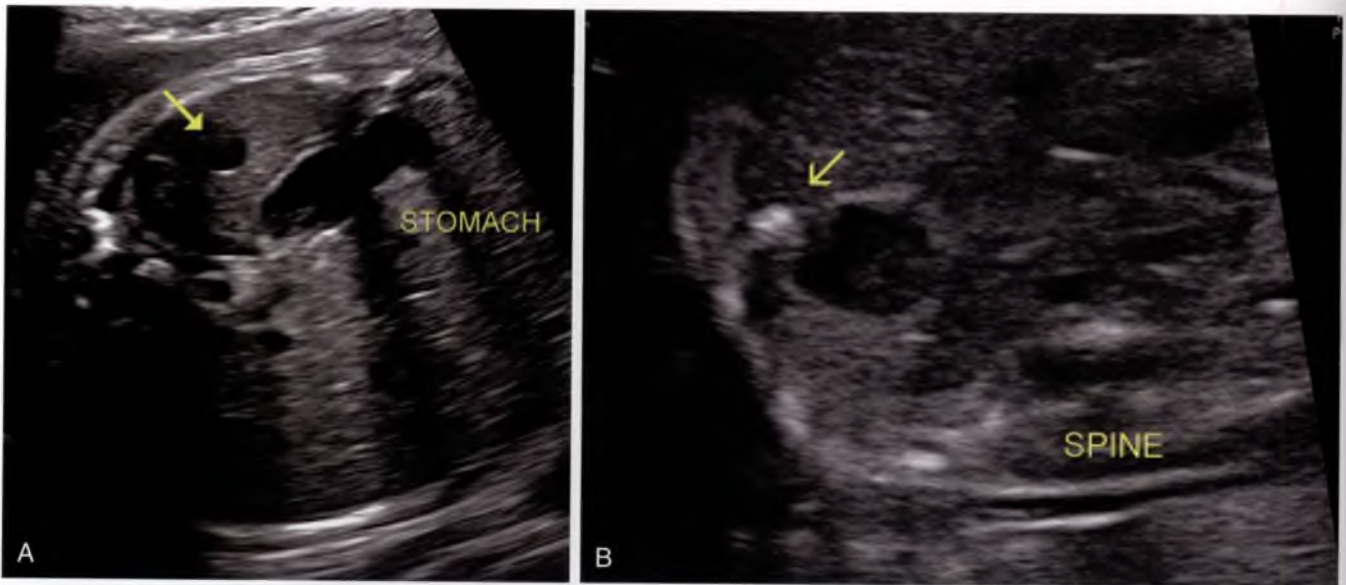


**FIG 14-17** Benign findings in the spleen. **A**, Small unilocular anechoic cyst within the spleen (*arrow*). The cyst remained small, stable in size over several weeks. **B**, Small echogenic focus (*arrow*) indicating calcification at the left upper quadrant, adjacent and lateral to the fluid-filled stomach. These are seen fairly often and are considered benign and inconsequential.

In the United States, patients are routinely offered genetic screening for cystic fibrosis early in pregnancy. Therefore, detection of biliary atresia would be the rationale for incorporating visualization of the gallbladder as part of the routine anatomic survey. Biliary atresia is a serious condition that requires postnatal surgical correction and may result in the need for liver transplantation. Fortunately it is rare, with a prevalence of 7 per 100,000 in the United States.<sup>101</sup> Amniocentesis with evaluation of digestive enzymes can provide additional information but cannot always differentiate biliary atresia from more benign conditions. Although some would advocate adding evaluation of the gallbladder to the routine second trimester sonographic survey to detect biliary atresia<sup>102</sup> others have expressed concern about false positive results.

### Spleen

Splenic cysts are usually simple serous epithelial cysts. If small and sonolucent, these are likely to regress spontaneously<sup>103</sup> (Fig. 14-17A). A small echogenic focus at the left upper quadrant of the fetal abdomen is not uncommonly visualized on mid-trimester ultrasound imaging; they are typically not clinically significant<sup>104</sup> (Fig. 14-17B).

### ASCITES

Ascites is an excess amount of free intraperitoneal fluid in the fetal abdomen. A trace amount of fluid between bowel loops can sometimes be seen in normal fetuses when using a high-frequency transducer. (See Fig. 14-5B.) Mild ascites, when present, can best be visualized adjacent to the cord insertion and bladder (Fig. 14-18). Moderate and severe ascites is readily apparent as fluid surrounds bowel loops and liver. Depending on the cause of the ascites, the amniotic fluid volume can be normal, increased, or decreased. Because there are many causes of fetal ascites and there is overlap with generalized hydrops, a careful evaluation is warranted, starting with maternal and family history and including a detailed sonographic evaluation of the fetus (Table 14-6).<sup>105,106</sup>

Many cases of ascites will have an obvious explanation on ultrasound imaging. Any space-occupying lesion in the chest, including



**FIG 14-18** Ascites. Mild ascites is most readily detectable near the cord insertion at the anterior abdominal wall.

congenital pulmonary airway malformation, pulmonary sequestration, or congenital high airway obstruction can result in ascites.

In addition, as mentioned earlier in this chapter, abnormalities of the fetal gastrointestinal tract may result in microperforation of bowel, with leakage of intraluminal contents and ascites.

*Urinary ascites* can be the cause of free fluid within the peritoneal cavity. This results from leakage or rupture of urine from an obstructed urinary collecting system, most commonly bladder outlet obstruction

**TABLE 14-6 Sonographically Detectable Causes of Fetal Ascites**

Space-occupying thoracic mass
Urinary tract obstruction (i.e., urinary ascites)
Ventral wall defect
Bowel obstruction
Meconium peritonitis
Persistent cloaca
Ovarian cyst
Generalized hydrops
Evidence of cytomegalovirus (CMV) infection
Evidence of aneuploidy

due to posterior urethral valves. Sonographic evaluation of the genitourinary system will be abnormal in fetuses with urinary ascites, with findings such as hydronephrosis, hydroureter, and enlarged or ruptured, thick-walled urinary bladder.

Note that ascites may be an early manifestation of generalized hydrops from a systemic cause such as cardiac dysfunction or anemia. Thus, targeted attention to the fetal heart anatomy and function and follow-up examinations are warranted. Very rarely, generalized hydrops might occur as a result of ascites, perhaps secondary to vena caval compression.

It is very important to routinely consider systemic causes of fetal ascites. Fetal echocardiography can be considered. Measurement of the peak systolic velocity in the fetal middle cerebral artery to assess for possible anemia should be performed. Even if the fetus does not appear to be anemic, maternal blood type and antibody screen, Kleihauer-Betke test, and parvovirus titers may be considered. Infectious causes that can lead to ascites include CMV infection, toxoplasmosis, hepatitis, syphilis, and infection from additional organisms.<sup>105</sup> Maternal serologic titers should be obtained, particularly if there are additional findings such as intracranial calcifications or echogenic bowel. The possibility of fetal aneuploidy should be addressed.

Genetic causes of hydrops and congenital ascites include metabolic syndromes such as lysosomal storage diseases. Congenital chylous ascites is due to lymphatic obstruction, similar to chylothorax, and could theoretically be detected by demonstration of elevated lymphocyte count in peritoneal fluid, but this would require fetal paracentesis. As many as 10% of cases of fetal ascites are idiopathic, and they tend to have a favorable prognosis.

The management and ultimate prognosis of fetal ascites depend upon the cause. If no cause is found on the initial evaluation, follow-up sonograms should be performed; occasionally an underlying cause will become apparent. Not surprisingly, severe ascites, early gestational age at diagnosis,<sup>106</sup> and development of hydrops are associated with worse prognosis. When ascites remained isolated and no cause was found, prognosis was favorable in some<sup>107,108</sup> but not all<sup>109</sup> series. Diagnostic or therapeutic paracentesis may be warranted in a minority of cases; because fluid often rapidly reaccumulates, shunt placement has been attempted.<sup>105</sup>

## CYSTS

### Differential Diagnosis

The differential diagnosis of a fetal abdominal cyst is lengthy and therefore a systematic approach to sonographic assessment is useful (Table 14-7). The first step is to identify normal anatomy: normal cystic structures in the fetal abdomen include the stomach, gallbladder,

**TABLE 14-7 Fetal Abdominal Cystic Structures**

Normal structures
Stomach
Gallbladder
Urinary bladder
Umbilical vein
Renal abnormalities
Hydronephrosis
Renal cyst
Perinephric urinoma
Hydroureter
Adrenal abnormalities
Neuroblastoma
Adrenal hemorrhage
Benign adrenal cyst
Umbilical vein varix
Intestinal obstruction
Duodenal
Jejunioileal
Cystic structures in the upper abdomen
Choledochal cyst
Hepatic cyst
Splenic cyst
Gallbladder duplication
Cystic structures in the lower abdomen
Ovarian cyst
Type IV sacrococcygeal teratoma
Anterior sacral meningocele
Hydrocolpos (isolated, in association with persistent cloaca)
Cystic structures in variable locations
Meconium pseudocyst
Enteric duplication cyst
Mesenteric/omental cyst

and urinary bladder. Each of these structures varies in size. When identifying the stomach and gallbladder at the upper abdomen, it is important to confirm normal situs because, although rare, situs inversus or heterotaxy syndrome can cause confusion. A cystic structure in the pelvis almost always represents the urinary bladder; it can be seen to fill and empty during the course of a typical ultrasound examination. Use of color Doppler sonography to identify the umbilical arteries flanking the bladder can be helpful, and many do this routinely to document two umbilical arteries.

The intrahepatic umbilical vein/portal vein has a typical C-shaped appearance, curving away from the left-sided stomach. If there is any doubt, color Doppler sonography may be helpful (see Fig. 14-2A). With an intrahepatic persistent right umbilical vein, the vessel curves in the opposite direction, toward the stomach (see Fig. 14-14A).

The next step is to evaluate the renal collecting system. A fluid-filled structure in or adjacent to one or both kidneys can be due to hydronephrosis, renal cyst(s), or perinephric urinoma. Typically, a normal nondilated ureter cannot be visualized, whereas hydroureter appears as a tortuous, tubular, fluid-filled structure situated between the kidney and bladder. The bladder itself can be dilated because of urethral obstruction. A ureterocele can sometimes be identified within the bladder. An umbilical vein varix adjacent to the bladder can be distinguished from a pelvic cyst by the use of color Doppler sonography.



Dilation of the gastrointestinal tract may demonstrate a cystic appearance by ultrasound imaging. A cystic collection at the right upper quadrant may represent duodenal obstruction if a connection to the stomach can be demonstrated (see Fig. 14-4). Jejunioileal obstruction typically presents as multiple fusiform fluid-filled components rather than a single cystic collection (see Fig. 14-6D).

Having addressed all of these structures, the next step is to consider the location of the cyst (see Table 14-7).

### Ovarian Cysts

Ovarian cyst is the most common lower abdominal or pelvic cyst in a female fetus during the second half of pregnancy.<sup>110</sup> These cysts can be thin-walled, anechoic, “simple” cysts (Fig. 14-19A and C), or they may have a heterogeneous appearance; these “complex” cysts can manifest fluid/debris levels, septations, and low level echoes<sup>111,112</sup> thought to be the result of hemorrhage or torsion (Fig. 14-19B). Rarely, ovarian cysts

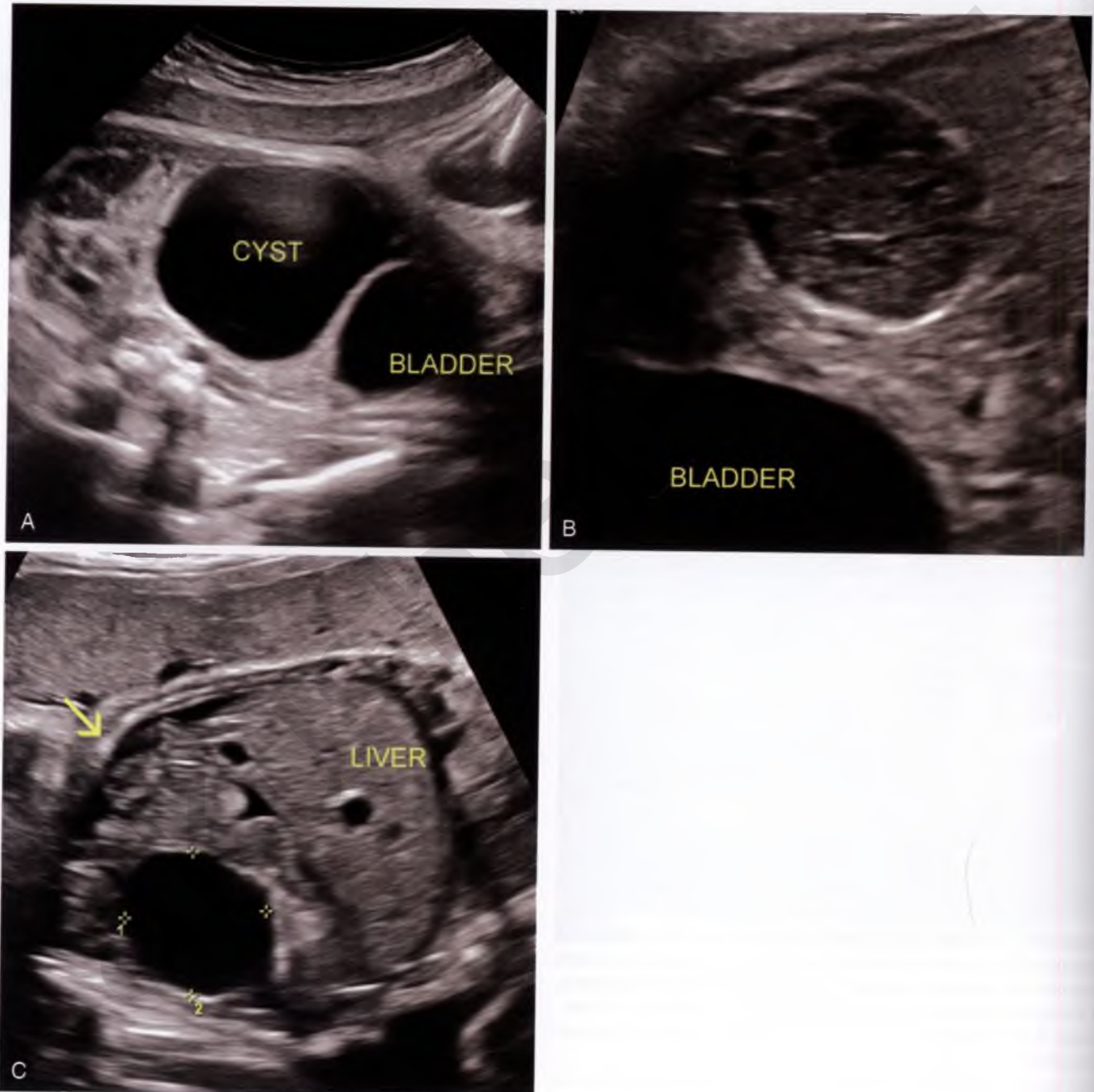


**FIG 14-19** Ovarian cyst. **A**, Large thin-walled anechoic cyst, first seen at 36 weeks, adjacent to the urinary bladder. Color Doppler sonography can be used to identify the bladder, flanked by the umbilical arteries. The child underwent percutaneous drainage of the cyst 1 week after birth, but the fluid reaccumulated. Surgical excision was performed at 11 weeks of age and ovarian torsion with necrosis was found. **B**, A 3-cm ovarian cyst, with internal echoes and strands suggesting hemorrhage, adjacent to the bladder. **C**, A 4-cm unilocular thin-walled anechoic ovarian cyst (*cursors*) seen at 36 weeks. Mild ascites (*arrow*) also present. The ascites rapidly resolved, and the cyst gradually involuted postnatally. The child did not require surgery.

can be associated with polyhydramnios, ascites<sup>111</sup> (see Fig. 14-19C), or fetal anemia due to hemorrhage.<sup>112</sup>

The differential diagnosis includes all of the other cysts found in the lower abdomen and pelvis described in this chapter. However, when such a cyst is identified in a female fetus in the third trimester without any additional findings, the likelihood is high that it represents an ovarian cyst. If there is doubt, MRI can be used to confirm the diagnosis.<sup>113</sup>

Fetal ovarian cysts are, with very rare exceptions, functional rather than neoplastic, related to stimulation by maternal hormones; there is generally no concern regarding possible malignancy.<sup>110,114</sup> Management is directed toward preserving ovarian tissue and avoiding unnecessary interventions. Simple cysts are generally managed conservatively. Some authors suggest in utero percutaneous aspiration of simple cysts once they reach a certain size in an effort to prevent torsion and hemorrhage<sup>115</sup>; others oppose this.<sup>110,111</sup> The postnatal management of hemorrhagic cysts is increasingly conservative, as many of these cysts spontaneously resolve. There is little evidence that early neonatal intervention in an asymptomatic child prevents functional loss of the ovary.

### Enteric Duplication Cysts

Enteric duplication cysts (Fig. 14-20) can arise at any level of the gastrointestinal tract, although 80% are intra-abdominal.<sup>116</sup> They can be round or tubular, single or multiple. Sonographic demonstration of a double wall sign and the presence of peristalsis support the diagnosis; if there is uncertainty, MRI may be helpful. Associated malformations are seen in one third of cases, so fetal echocardiogram is recommended. Obstetric management includes follow-up sonograms; there are case reports of prenatal ultrasound-guided drainage. The decision regarding delivery at a tertiary care center can be individualized. Because these cysts may cause pain, intussusception, intestinal obstruction,

ulceration with perforation, or hemorrhage, they are typically resected within the first 6 months of life, either by laparoscopic or open surgical procedure.

### Rare Causes of Cysts

Other relatively rare causes of lower abdominal or pelvic cysts include the following:

#### Sacrococcygeal Teratoma

Most sacrococcygeal teratomas are external and exophytic; only 10% are type IV, completely internal. Most sacrococcygeal teratomas have a solid or vascular component, although there is at least one case report of a cystic type IV sacrococcygeal teratoma.<sup>117</sup>

#### Anterior Sacral Meningocele

*Anterior sacral meningocele* may appear as an anechoic pelvic cyst, possibly mimicking hydrometrocolpos at 20 weeks.<sup>118</sup>

#### Hydrocolpos

*Hydrocolpos* is most often seen in association with persistent cloaca (discussed elsewhere in this chapter) but can rarely be isolated, related to vaginal atresia or imperforate hymen; in such cases, spontaneous resolution after birth can be expected.<sup>119</sup> Hydrocolpos should be considered when a hypoechoic structure is seen posterior to the bladder (see Fig. 14-12). MRI may be useful in establishing this diagnosis.<sup>119</sup>

#### Mesenteric/Omental Cyst

Mesenteric or omental cyst is often a presumptive diagnosis for a small, unilocular, thin-walled anechoic cyst in a variable intra-abdominal location that becomes increasingly inconspicuous with advancing gestation and with fetal growth.

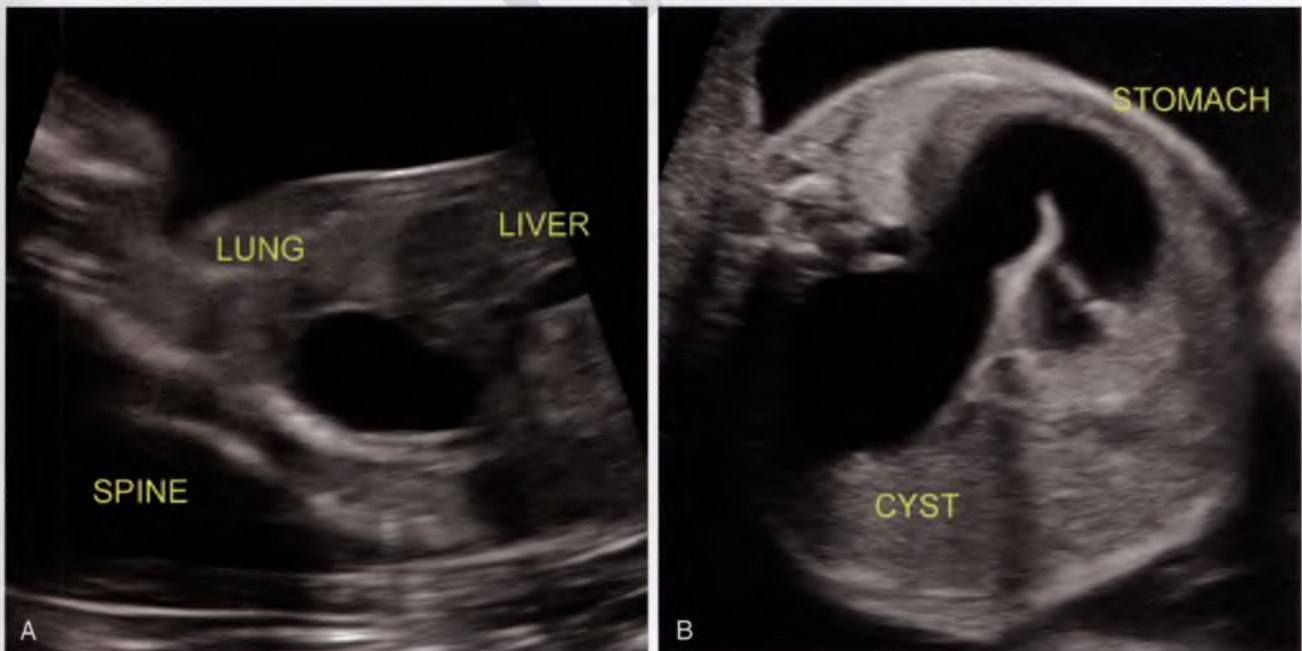


**FIG 14-20** Enteric duplication cyst. **A**, At 21 weeks, a unilocular anechoic cyst, shown on this parasagittal ultrasound image, extended above and below the level of the diaphragm. **B**, At 26 weeks, the cyst had enlarged and appeared contiguous with the fluid-filled stomach. The cyst was resected at 3 weeks of age and appeared to originate near the esophageal-gastric junction. Pathologic examination showed it was lined by primitive columnar epithelium with focal areas of gastric epithelium.



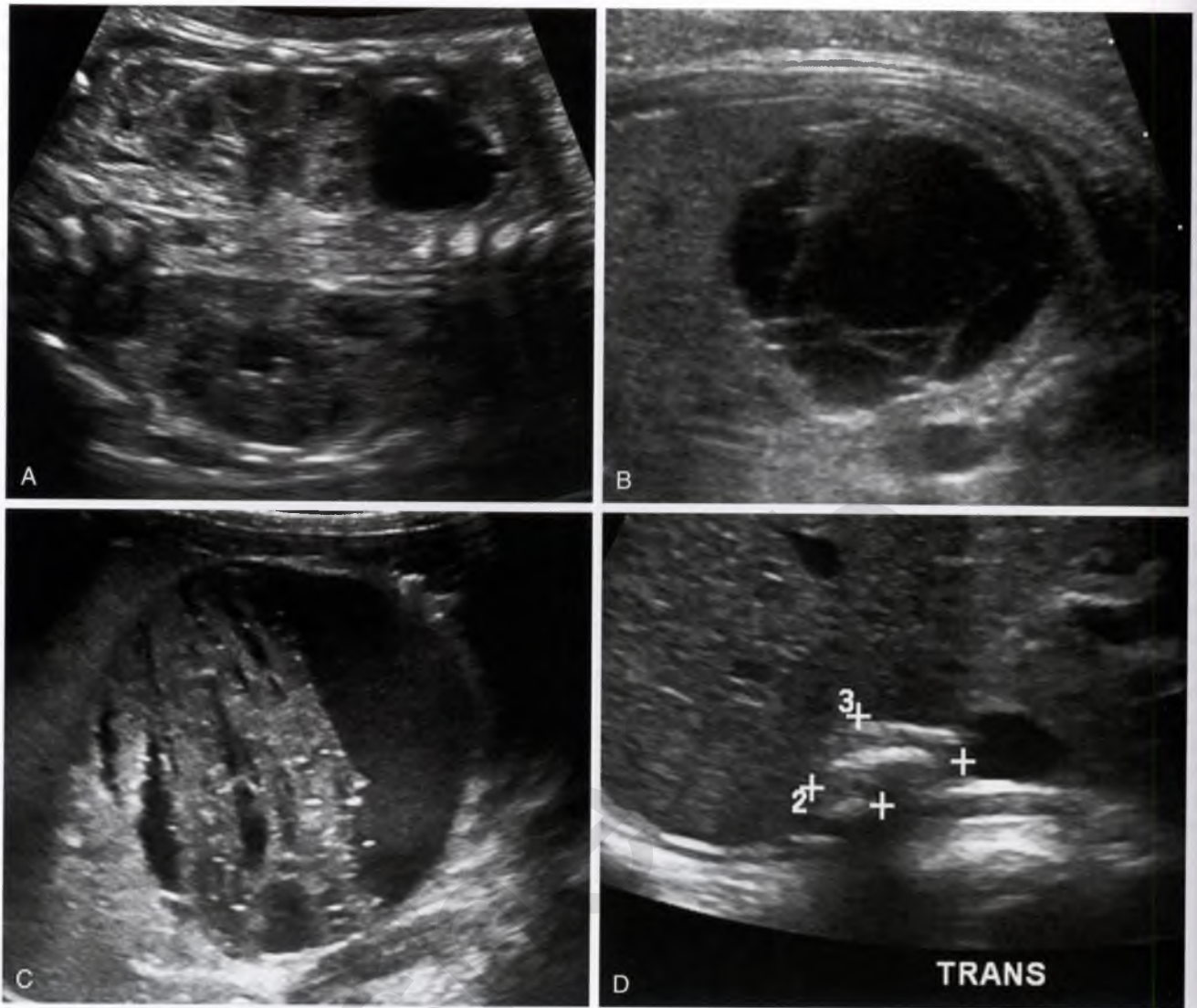


**FIG 14-21** Adrenal neuroblastoma, cystic. **A**, Coronal sonographic image obtained at 31 weeks shows a thin-walled anechoic cyst cephalad to the right kidney. The bilateral kidneys appear normal with expected corticomedullary differentiation. **B**, Two weeks later, the mass appears slightly larger with internal echoes and strands suggesting hemorrhage. **C**, Transabdominal sonogram of the hemorrhagic cystic adrenal mass obtained shortly after birth. **D**, The child was managed conservatively with follow-up imaging. At 4 years of age, involution of the adrenal lesion (*calipers*) with calcification is shown.

### Adrenal Cyst

*Adrenal cyst* can be detected in the third trimester in a characteristic location, cephalad to a kidney. The differential diagnosis includes subdiaphragmatic extralobar pulmonary sequestration, benign cyst, and adrenal hemorrhage. Some adrenal cysts detected in utero represent neuroblastomas<sup>120,121</sup> (Fig. 14-21). Hemorrhage is the most common cause of an apparent adrenal mass in a newborn but rarely occurs before birth.<sup>122</sup>

Most neuroblastomas diagnosed in utero are of adrenal origin, and they are often cystic. Fortunately, prenatally diagnosed neuroblastomas, particularly cystic lesions, usually represent localized stage I disease with an excellent prognosis; indeed, they may spontaneously

regress, and conservative management is an acceptable strategy<sup>121,123</sup> (Fig. 14-21D).

### First Trimester Abdominal Cyst (Fig. 14-22)

With improved ultrasound resolution and increased attention to fetal anatomy early in gestation, a number of cases of first trimester abdominal cysts have been reported.<sup>75</sup> The origin of these cysts is often not determined, in part because spontaneous resolution is common. In 20 cases of apparently isolated first trimester abdominal cysts, 13 resolved and these children did well. However, in this series, 4 fetuses with first trimester lower abdominal cysts were later found to have anorectal malformations. Outcomes were worse if the cysts persisted or if there

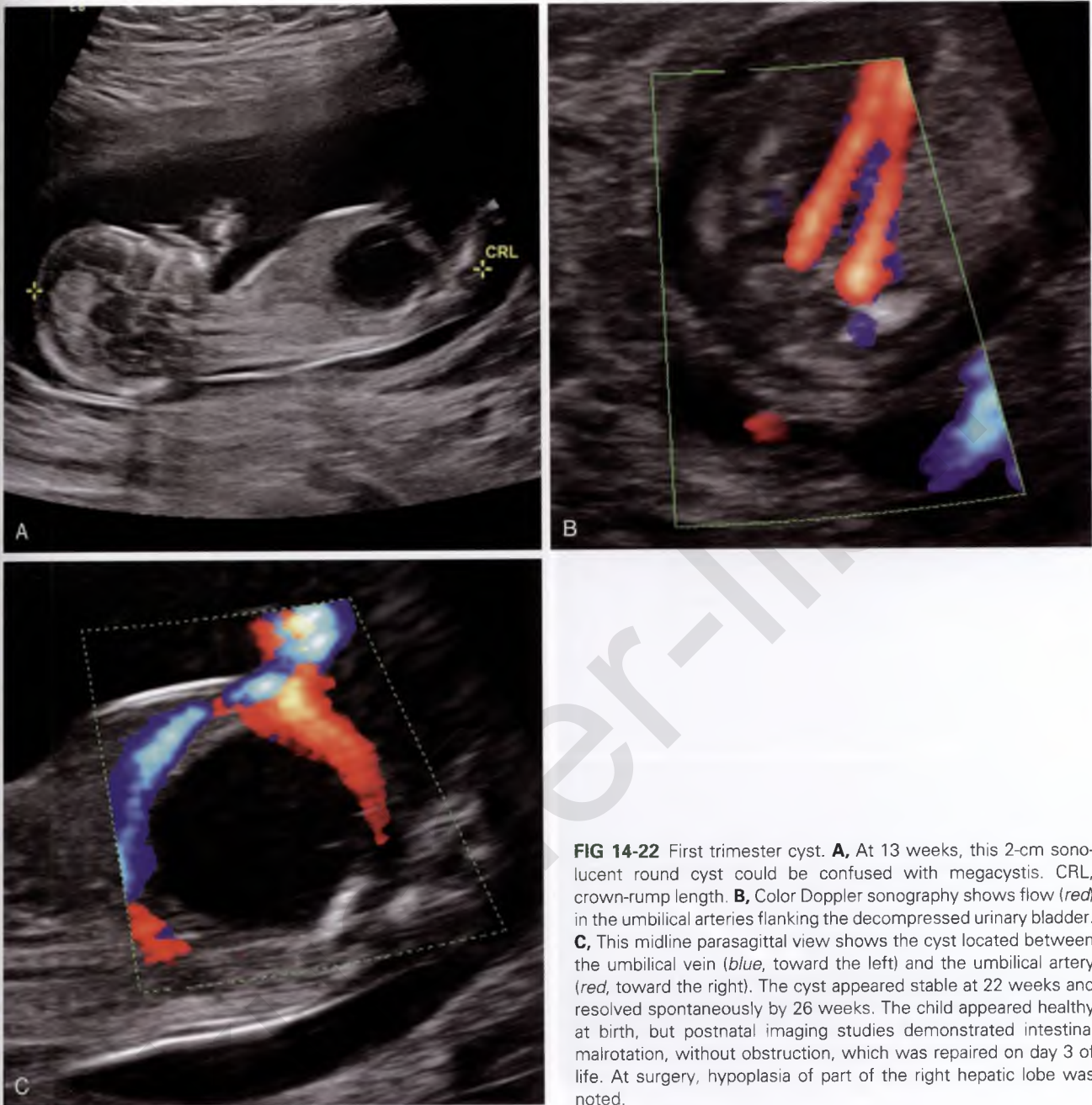


**FIG 14-22** First trimester cyst. **A**, At 13 weeks, this 2-cm sonolucent round cyst could be confused with megacystis. CRL, crown-rump length. **B**, Color Doppler sonography shows flow (*red*) in the umbilical arteries flanking the decompressed urinary bladder. **C**, This midline parasagittal view shows the cyst located between the umbilical vein (*blue*, toward the left) and the umbilical artery (*red*, toward the right). The cyst appeared stable at 22 weeks and resolved spontaneously by 26 weeks. The child appeared healthy at birth, but postnatal imaging studies demonstrated intestinal malrotation, without obstruction, which was repaired on day 3 of life. At surgery, hypoplasia of part of the right hepatic lobe was noted.

were additional abnormalities. After considering megacystis, the differential diagnosis consists primarily of cysts originating from the gastrointestinal tract.

## VENTRAL WALL DEFECTS

The differential diagnosis for a ventral abdominal wall defect includes several anomalies (Table 14-8), but the most common are omphalocele and gastroschisis. These two entities differ in several important ways (Table 14-9).

### Omphalocele

Omphalocele is also referred to by the term *exomphalos*. Omphalocele is often categorized based on whether the omphalocele sac contains

liver (extracorporeal liver) or bowel only (intracorporeal liver). The embryology of these two types probably differs, as the latter can be thought of as failure of resolution of physiologic bowel herniation seen in the first trimester. Given that in normal development the liver is never located outside the abdomen, the embryology of omphalocele with extracorporeal liver may be different. The cause of omphalocele is reported by some to be different when diagnosed in the first compared to the second trimester (Table 14-10).

### Prevalence

The prevalence of omphalocele among live births, stillbirths, and induced abortions is about 2.0 to 2.6 per 10,000<sup>124-127</sup> and has been reasonably stable since 1980, despite changes in prenatal diagnosis. Despite the strong association of omphalocele with aneuploidy, and of



TABLE 14-8 Ventral Wall Defects

Omphalocele
Gastroschisis
Bladder and cloacal exstrophy, OEIS complex (omphalocele, exstrophy, imperforate anus, spinal abnormalities)
Pentalogy of Cantrell
Limb-body wall complex/amniotic band syndrome
Urachal cyst*

\*Not a true ventral wall defect, but may have a similar sonographic appearance.

TABLE 14-9 Sonographic Features Distinguishing Omphalocele From Gastroschisis

Assessment Category	Omphalocele	Gastroschisis
Maternal age	U-shaped age distribution	Younger
Ultrasound findings	Membrane covers intestine	Free loops of externalized intestine
	Cord involvement	Located to right of cord insertion
	Liver out: common	Liver out: rare
	Dilated/thickened bowel: rare	Dilated/thickened bowel: common
Associated nonbowel abnormalities	Common	Uncommon
Aneuploidy	Common	Uncommon
Risk of FGR/IUFD	Uncommon	Common
Surgical complications	Uncommon	Common

FGR, fetal growth restriction; IUFD, in utero fetal demise.

TABLE 14-10 Omphalocele: First Versus Second Trimester Diagnosis

Liver Status	First Trimester Diagnosis	Second Trimester Diagnosis
Intracorporeal liver	May resolve	Will not resolve
	Risk of aneuploidy: high	Risk of aneuploidy: high
Extracorporeal liver	Will not resolve	Will not resolve
	Risk of aneuploidy: high	Risk of aneuploidy: low

TABLE 14-11 Omphalocele: Etiology and Associated Anomalies

Study	Years	N	Prenatal Diagnosis	Abnormal Karyotype	Syndromic	Multiple Malformations	Isolated
EUROCAT <sup>124</sup>	1980-1990	732		94 (13%)	≈ 30 (4%)	273 (37%)	335 (46%)
Euroscan Study Group <sup>125</sup>	1996-1998	137	103 (75%)	34 (25%)	14 (10%)	29 (21%)	60 (44%)
Brantberg <sup>130</sup>	1985-2004	90	90 (100%)	44 (49%)	0 (0%)	36 (40%)	10 (11%)
Stoll <sup>126</sup>	1979-2003	86	39 (45%)	25 (29%)	13 (15%)	26 (30%)	22 (26%)

EUROCAT, European Registry of Congenital Anomalies and Twins. Superscript numbers indicate references at the end of the chapter.

aneuploidy with advanced maternal age, the age distribution for omphalocele appears to be U-shaped, highest in the youngest and oldest mothers,<sup>128,129</sup> especially among chromosomally normal cases.<sup>124</sup>

Table 14-11 includes data from recent reported series of omphaloceles. More than half of fetuses with omphaloceles have additional malformations and chromosomal abnormalities, but there are large discrepancies among the reports, likely due to differences in the populations studied. As is the case for many anomalies, prenatally diagnosed cases differ markedly from pediatric series. The EUROCAT registry<sup>124</sup> surveyed birth certificates, maternity and pediatric records, hospital discharge summaries, and pathologic reports in 2.9 million births from 1980 to 1990. In this report, prenatally diagnosed cases were underrepresented, which likely explains the relatively low rates of aneuploidy and additional malformations, and the high rate of isolated omphalocele. In contrast, Brantberg and associates<sup>130</sup> reviewed prenatally diagnosed cases and reported high rates of aneuploidy and multiple malformations and a low rate of isolated omphalocele. The two additional included studies with intermediate prenatal diagnosis rates also had intermediate rates of isolated lesions.

### Associated Aneuploidies

Trisomy 18 is the most common aneuploidy associated with omphalocele, accounting for 62% to 75% of aneuploidy found in the four studies referenced. Trisomy 13 is also common, accounting for 11% to 24%. Together, these two trisomies account for 86% of aneuploidies found in cases of omphalocele. Down syndrome, triploidy, and sex chromosome abnormalities were seen less commonly.

The association of aneuploidy with omphalocele is inversely associated with gestational age at diagnosis and directly associated with the presence of additional structural abnormalities. Also, the presence of liver in the omphalocele sac is associated with decreased likelihood of chromosomal abnormality in the second trimester, but not the first.<sup>131</sup>

In addition to abnormalities seen on standard karyotype, microdeletions and microduplications detected as copy number variations by chromosomal microarray have been reported.<sup>132,133</sup>

### Associated Syndromes

In the EUROCAT study, Beckwith-Wiedemann syndrome (BWS) was associated with 4% of omphaloceles.<sup>124</sup> In a more recent report, BWS was found in 6 of 30 cases of "isolated" omphalocele without autosomal aneuploidy; 3 of these 6 were conceived using assisted reproductive technology.<sup>134</sup> Fetuses with BWS may demonstrate additional abnormalities such as macrosomia, macroglossia (with a protruding tongue), and polyhydramnios, but these findings are generally not seen until the third trimester. Very rarely, enlarged kidneys or a cystic pancreas may be seen. Because BWS can be caused by a variety of molecular mechanisms affecting the imprinted genes on chromosome 11p15.5,<sup>135</sup> specialized DNA testing is required for diagnosis.

Omphalocele is rarely associated with other genetic syndromes.<sup>130,136</sup> There are a total of 73 entries found under “omphalocele” in OMIM (Online Mendelian Inheritance in Man).<sup>137</sup>

### Nonchromosomal Anomalies

Even after excluding cases with aneuploidy, omphalocele is associated with a wide variety of anomalies encompassing almost every organ system.<sup>124,126</sup> Of particular importance are cardiac anomalies, which were present in a total of 36% of 97 cases in these two referenced articles.

### Sonographic Diagnosis

By ultrasound imaging, exteriorized abdominal viscera are shown, covered by a thin membrane derived from parietal peritoneum and amnion (Figs. 14-23 through 14-25). The umbilical cord inserts into the base of the omphalocele sac (Fig. 14-23B). Most often, segments of small intestine, with or without liver, protrude beyond the abdomen; sometimes other organs including the colon, stomach, spleen, and rarely kidneys can be exteriorized. Ascites or Wharton jelly is often noted within the omphalocele sac.



**FIG 14-23** Serial assessment of omphalocele. **A**, Moderate-size omphalocele, which appears to contain liver, shown on this midline sagittal ultrasound image at 13 weeks. CRL, crown-rump length. **B**, At 18 weeks, the omphalocele (*calipers*) measures approximately 1.5 cm in diameter. Note the cord insertion into the base of the omphalocele sac. **C**, Photograph of the newborn shows the omphalocele was quite small; it was easily repaired surgically. **D**, Midsagittal view of a different fetus with a similar appearance at 12 weeks. In this case, an abnormal karyotype was found.



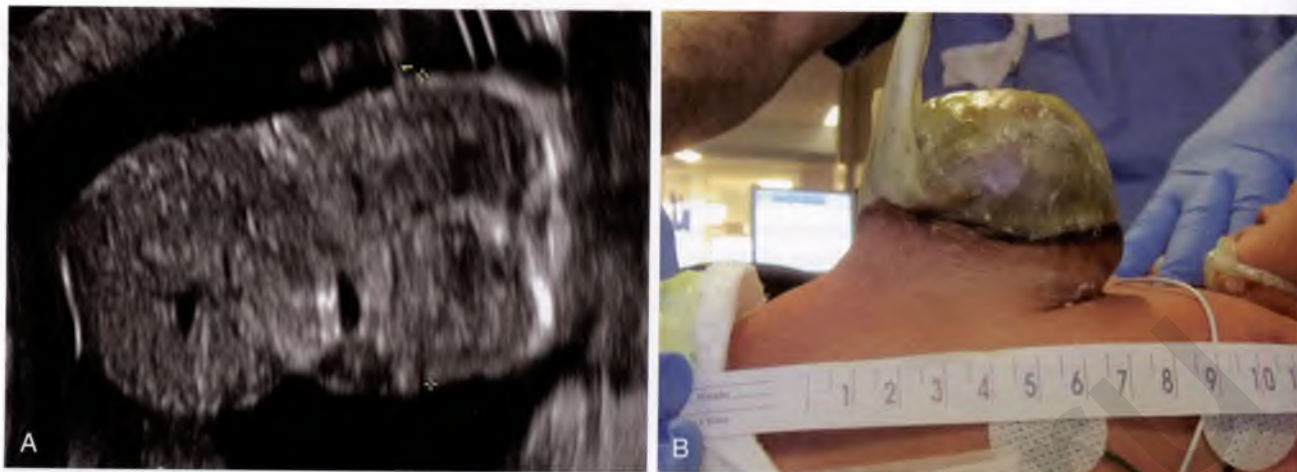


**FIG 14-24** Large omphalocele. **A**, Sonogram at 23 weeks. On this transverse view, the fetal abdomen is toward the right, between the cursors. The large liver-containing omphalocele is toward the left. **B**, Photograph obtained after birth showing the large omphalocele. A primary surgical closure was performed.

The differential diagnosis primarily includes other types of ventral wall defects (see Table 14-8 and Figs. 14-26 through 14-35). In gastroschisis, free loops of bowel (and rarely liver) are prolapsed to the right of the cord insertion at the abdominal wall. Pentalogy of Cantrell is a defect of the upper abdominal wall and diaphragm such that part of the heart is also exteriorized. Bladder and cloacal exstrophy are defects of the lower abdominal wall that involve the bladder; demonstration of a normal bladder is essential to exclude these entities. OEIS complex (omphalocele, exstrophy, imperforate anus, spinal defects) can be thought of as cloacal exstrophy with involvement of the spine. Limb-body wall complex is characterized by severe abnormalities of the spine, abdomen, and legs. A urachal cyst may communicate with the bladder and contains urine.

### Prognosis

Despite advances in neonatal care and surgical repair, the prognosis for prenatally diagnosed omphalocele is guarded. In a series of 90 cases in Norway from 1985 to 2004, there were 49 pregnancy terminations and 6 antepartum, 5 intrapartum and 9 postnatal deaths.<sup>130</sup> Of the 21 survivors, 13 had various additional anomalies or impairments. Only 8 children (9% of the original cohort) were considered healthy on follow-up evaluation at ages 1 to 17 years. Similar follow-up findings were reported in a series of 445 cases treated in London from 1991 to 2002.<sup>138</sup> Most aneuploid pregnancies were either terminated or died in the antepartum or neonatal period. Of 176 fetuses with normal or unknown karyotype, there were 96 terminations, 27 fetal demises, and 9 neonatal deaths. Only 44 children underwent surgery (10% of the original cohort), and all of them survived.

The poor outcomes for omphalocele are related to the high incidence of associated abnormalities, especially aneuploidy. The prognosis for isolated omphalocele is much better. After birth, these infants often have an easier postoperative course compared to those with gastroschisis, presumably because the omphalocele membrane protects the externalized intestine.

However, those with large liver-containing omphaloceles (see Fig. 14-24) may face additional complications, including respiratory insufficiency and complex extended surgical repair. *Giant omphalocele* is often defined as more than 75% of liver located exterior to the abdomen. As might be expected, prognosis for these fetuses is significantly worse than for those with smaller isolated omphaloceles. In a series of 10 such pregnancies, there were 2 antepartum and 2 infant

**TABLE 14-12 First Trimester Omphalocele**

Crown-Rump Length (mm)	Prevalence of Bowel-Only Omphalocele (per 10,000)
45-55	102
55-65	12.5
65-85	4.8

Data from Kagan KO, Staboulidou I, Syngelaki A, et al: The 11-13-week scan: diagnosis and outcome of holoprosencephaly, exomphalos and megacystis. *Ultrasound Obstet Gynecol* 36:10-14, 2010.

deaths. Of the 6 survivors, 4 had respiratory insufficiency and there were various long-term problems including developmental delay in 2.<sup>139</sup>

### Diagnosis at 11 to 14 Weeks

Ventral wall defects can be reliably diagnosed by ultrasound imaging performed between 11 and 14 weeks (see Fig. 14-23A and D and Fig. 14-25A-C). Indeed, detection rate may approach 100%; in one series, all 60 fetuses with omphalocele (50 with bowel only and 10 with extracorporeal liver) were detected, as were all 19 cases with gastroschisis.<sup>31</sup>

When a ventral wall defect is detected, evaluation of the cord insertion site with color Doppler sonography may be helpful to distinguish omphalocele and gastroschisis (Fig. 14-26B). At times this distinction is deferred until a subsequent ultrasound examination can be performed, typically at about 16 weeks.

The prevalence of omphalocele depends on the gestational age at which the fetus/infant is examined. In a database of 57,119 singleton pregnancies that underwent sonograms between 11 and 14 weeks, there were 150 fetuses with omphalocele (prevalence 26 per 10,000).<sup>140</sup> This is 10 times greater than the reported prevalence found at birth in the EUROCAT registry. Even between 11 and 14 weeks, the prevalence of omphalocele is inversely related to gestational age (Table 14-12).

There are two explanations for the reported high prevalence of omphalocele at early gestational ages. Many of these fetuses are aneuploid and undergo demise in utero. In addition, many of these presumed "omphaloceles" appear to resolve. In one series of 150 cases of omphalocele detected in the first trimester, apparent spontaneous

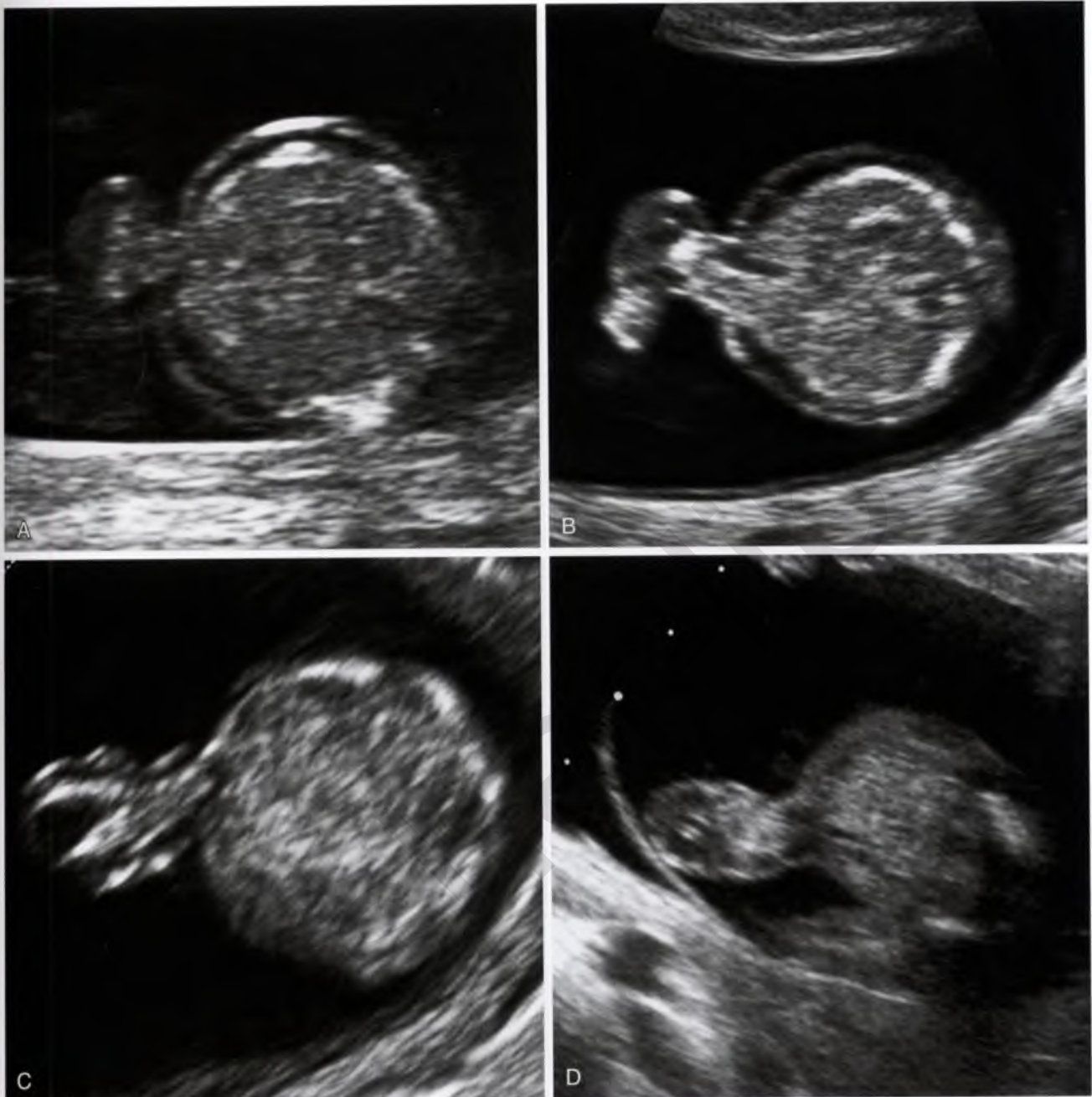


**FIG 14-25** Small first trimester omphalocele. **A**, Fetus at 11 weeks 2 days with nuchal translucency measuring 3.0 mm. The small omphalocele resolved and the child was normal at 4 years of age. **B**, Fetus at 11 weeks 4 days with nuchal translucency measuring 4.0 mm. Mild integumentary edema of the abdominal wall is shown. The omphalocele resolved but the fetus developed growth restriction and underwent a difficult delivery; the child now has dysmorphic features, hydrocephalus, and developmental delay. **C**, Small bowel-only omphalocele at 12 weeks 3 days was the only finding by ultrasound imaging. Amniocentesis at 15 weeks revealed a familial unbalanced translocation, despite a normal preimplantation microarray. **D**, Same fetus as in C at 17 weeks 4 days. At this time there were additional sonographic findings including an abdominal cyst and craniosynostosis.



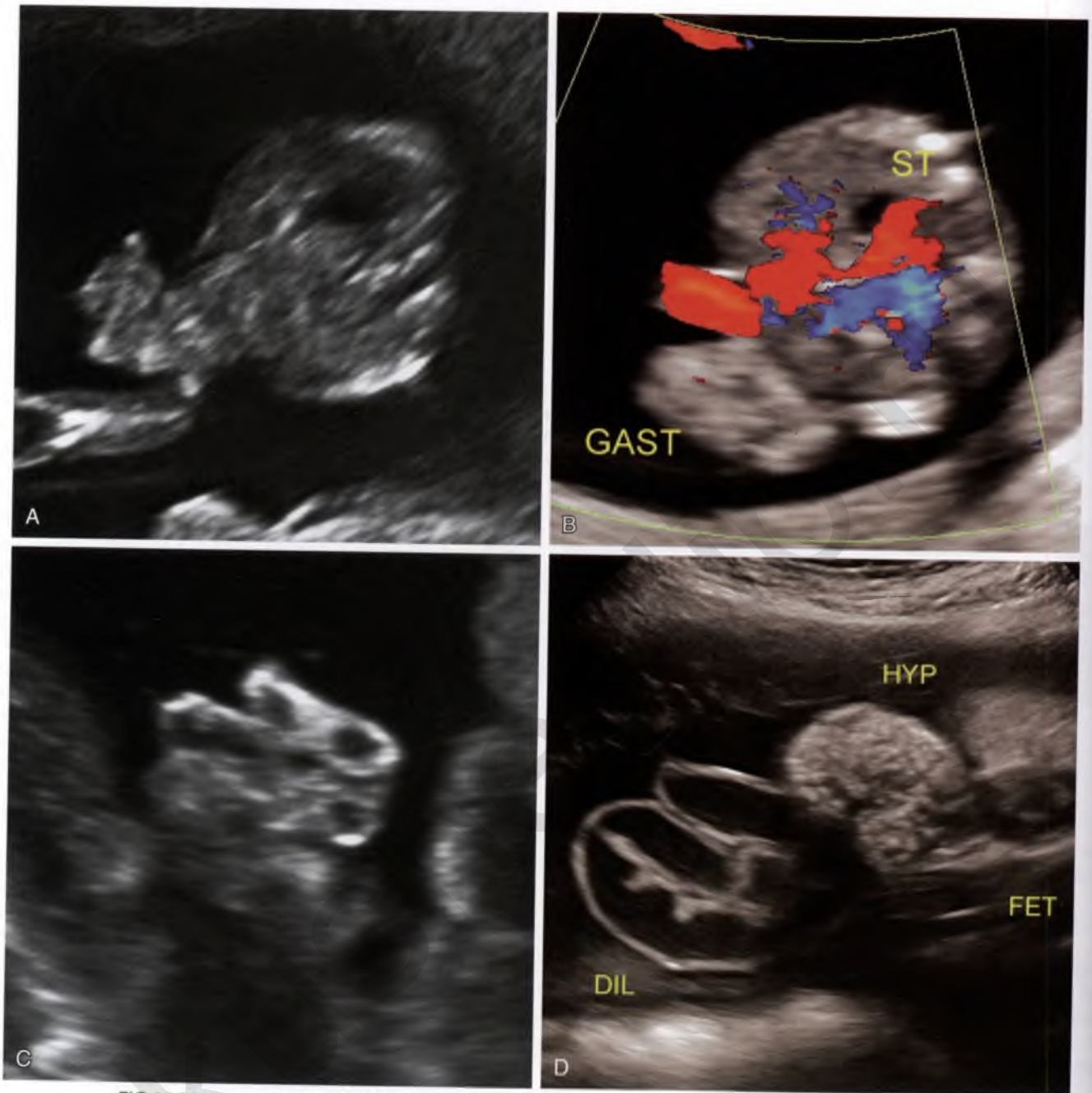


**FIG 14-26** Gastroschisis. **A**, At 13 weeks, externalized segments of free-floating bowel are seen, suggesting gastroschisis rather than omphalocele. **B**, Color Doppler sonography demonstrates flow within the umbilical cord. The abdominal wall defect is right paramedian, adjacent to the cord insertion, typical of gastroschisis. ST, stomach; GAST, gastroschisis. **C**, Free loops of externalized nondilated bowel, surrounded by amniotic fluid, are more easily demonstrated at 22 weeks. **D**, In the third trimester, this fetus (FET) developed dilated loops of extra-abdominal intestine (DIL) and a hyperechoic segment (HYP), presumably from inspissated meconium within colon. These findings did not alter obstetric management. The infant weighing 1.7 kg (<1st percentile) was delivered at 37 weeks. The gastroschisis was reduced using a silo, the fascial defect was closed on day 11, and the child was discharged on day of life 55.

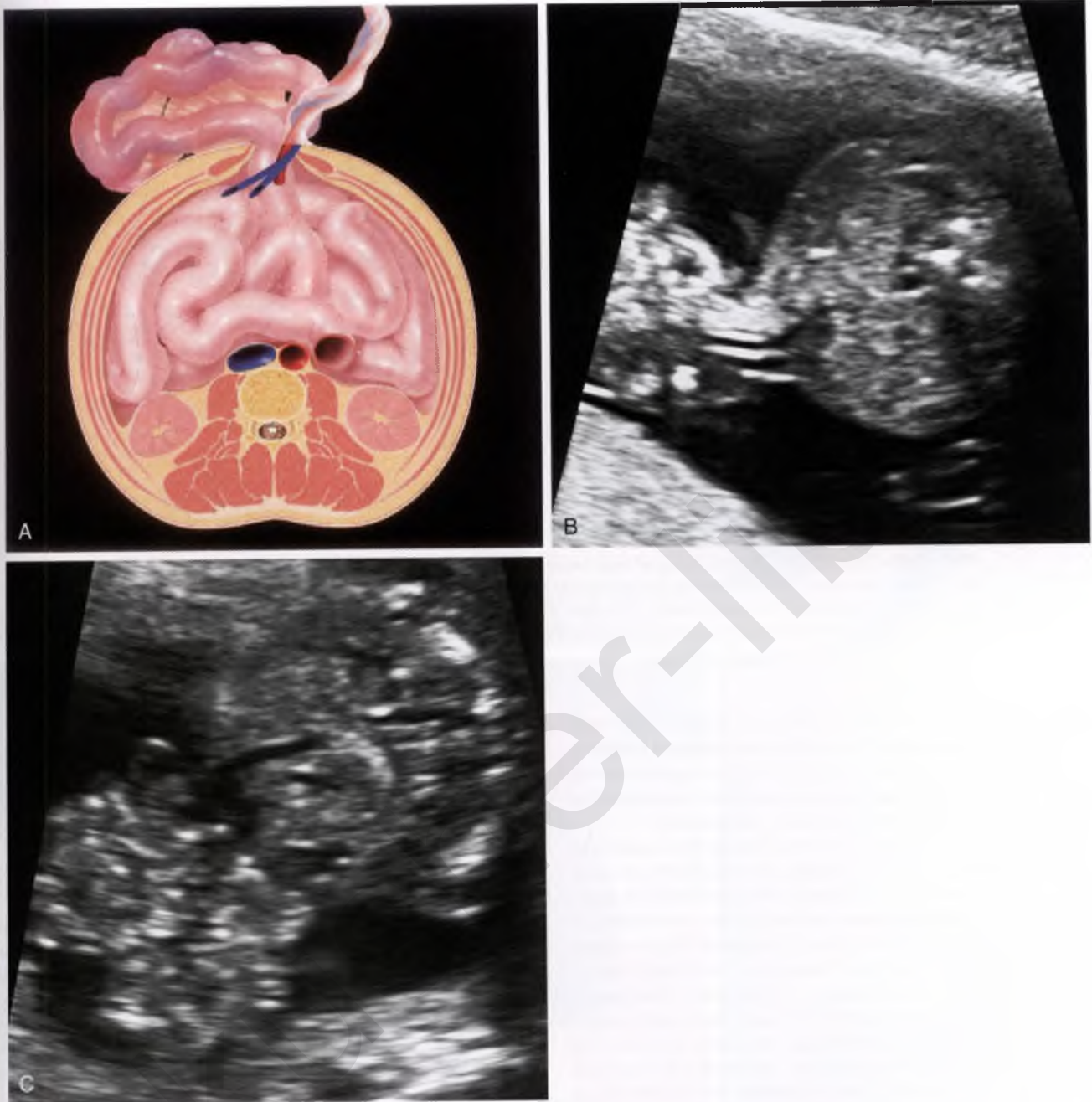


**FIG 14-27** Gastroschisis. **A**, Graphic presentation of an abdominal wall defect with herniation of small bowel. The defect is to the right and adjacent to the normally inserted umbilical cord. **B**, At 17 weeks, an anterior abdominal wall defect is shown adjacent to and to the right of the umbilical cord insertion. **C**, Free loops of nondilated externalized intestine are shown surrounded by amniotic fluid. This child had a primary postnatal repair and was discharged on day of life 19. (A from Donnelly LF, Jones BV, O'Hara SM, et al [eds]. *Diagnostic Imaging: Pediatrics*. Salt Lake City, Amirsys, 2005.)



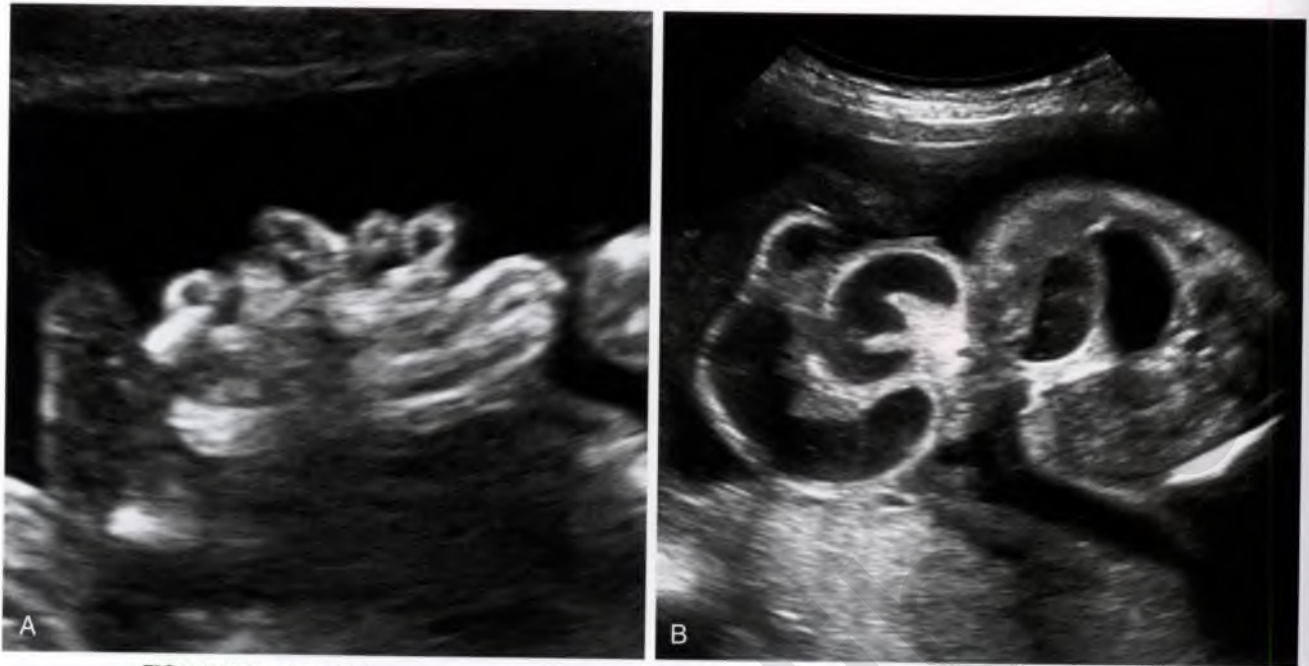


**FIG 14-28** Gastroschisis. **A**, Free loops of externalized nondilated, slightly thick-walled bowel at 17 weeks. **B**, Dilated intra- and extra-abdominal bowel segments shown at 32 weeks. These findings did not alter obstetric management. The patient went into labor at 35 weeks and the infant weighing 1.7 kg (<1st percentile) was delivered. The gastroschisis was reduced using a silo, the fascial defect was closed on day 12, and the child was discharged on day of life 79.

resolution occurred by 20 weeks in 83% of 59 euploid fetuses with bowel-only lesions, and in these cases, the infants appeared healthy at birth.<sup>140</sup> These findings raise the possibility that physiologic herniation of bowel into the base of the umbilical cord had been misconstrued as bowel-only omphalocele by early ultrasound examinations.

Although in most cases physiologic bowel herniation resolves by 11 weeks' gestation (crown-rump length 45 mm), there are occasional exceptions. Therefore, an isolated small omphalocele containing only bowel (no other anomalies, normal nuchal translucency) at 11 to 12 weeks may represent delayed resolution of physiologic bowel herniation. Like other manifestations of embryonic dysynchrony, such as delayed development of lymphatics resulting in nuchal edema, delayed ossification of the nasal bone, and delayed coordination of micturition resulting in megacystis, this can be a transient finding that is best regarded as a soft marker for increased risk of chromosomal or other genetic problem, rather than a true structural abnormality.

Another study investigated the outcome of 98 fetuses in whom omphalocele was detected between 11 and 14 weeks.<sup>141</sup> Of 45 fetuses with an additional abnormality on the 11- to 14-week scan, there were no survivors, and there were only 3 survivors among the 22 with increased nuchal translucency. However, the 31 fetuses with apparent isolated omphalocele fared better—in 18, resolution of the omphalocele occurred by 16 weeks and all of these fetuses were liveborn. Of the 11 cases in whom omphalocele persisted, 5 had other anomalies detected at 16 weeks, resulting in 1 surviving infant; 6 had isolated omphaloceles, resulting in 4 surviving infants.

Counseling a patient carrying a pregnancy with ventral wall defect suspected at the 11- to 14-week scan must therefore be done with great care. There is almost a bimodal distribution of prognosis: the majority do poorly, because of aneuploidy or additional structural malformations. Yet a significant fraction, perhaps 1 in 5, result in the birth of a healthy child who does not require surgery. This latter scenario occurs

in the majority of cases when the omphalocele is isolated and small, and the nuchal translucency is normal. Management options include noninvasive aneuploidy screening with cell-free DNA or pregnancy-associated plasma protein A (PAPP-A) and human chorionic gonadotropin (hCG), invasive testing by chorionic villus sampling (CVS) or amniocentesis, and follow-up sonograms at 16 and 20 weeks.

### Counseling and Obstetric Management

As mentioned previously, counseling patients carrying fetuses with isolated bowel-only omphalocele seen in the first trimester must be circumspect, as many of these fetuses will have normal outcomes. If there is liver in the omphalocele sac, increased nuchal translucency, or associated anomalies, or if the omphalocele persists beyond the first trimester, evaluation for aneuploidy should be offered. If CVS or amniocentesis is performed, consideration should be given to obtaining a microarray and testing for BWS in addition to standard karyotype. If the patient declines diagnostic testing, cell-free DNA screening should detect the majority of trisomies associated with omphalocele. This finding is important because a diagnosis of trisomy 13 or 18 may inform obstetric and neonatal management.

Because of the high risk of associated anomalies and our desire to provide early diagnosis, we offer a structural survey at 16 weeks and again at 20 weeks. A fetal echocardiogram should be performed, although if the heart appears normal on the obstetric sonogram, it may be delayed until 22 weeks. The role of MRI in the evaluation of these fetuses is not well established<sup>142</sup> but can be considered, particularly in unusual or difficult cases.

We routinely obtain follow-up sonograms every 4 to 6 weeks. Macrosomia, polyhydramnios, or macroglossia suggests BWS. We recommend that prospective parents meet with a pediatric surgeon at an appropriate time, usually after 20 weeks when the search for associated anomalies is complete, but earlier if the patient is anxious or is contemplating termination. Delivery should be in a tertiary care center.



**FIG 14-29** Gastroschisis repair using a spring-loaded prefabricated silo. The sequential photographs show gradual reduction of herniated bowel. In the final image, the infant is ready to undergo surgical closure of the fascia. (From Holcomb GW, Murphy JP, Ostlie DJ [eds]: *Ashcraft's Pediatric Surgery*. Philadelphia, Elsevier, 2014, Fig. 48-5.)



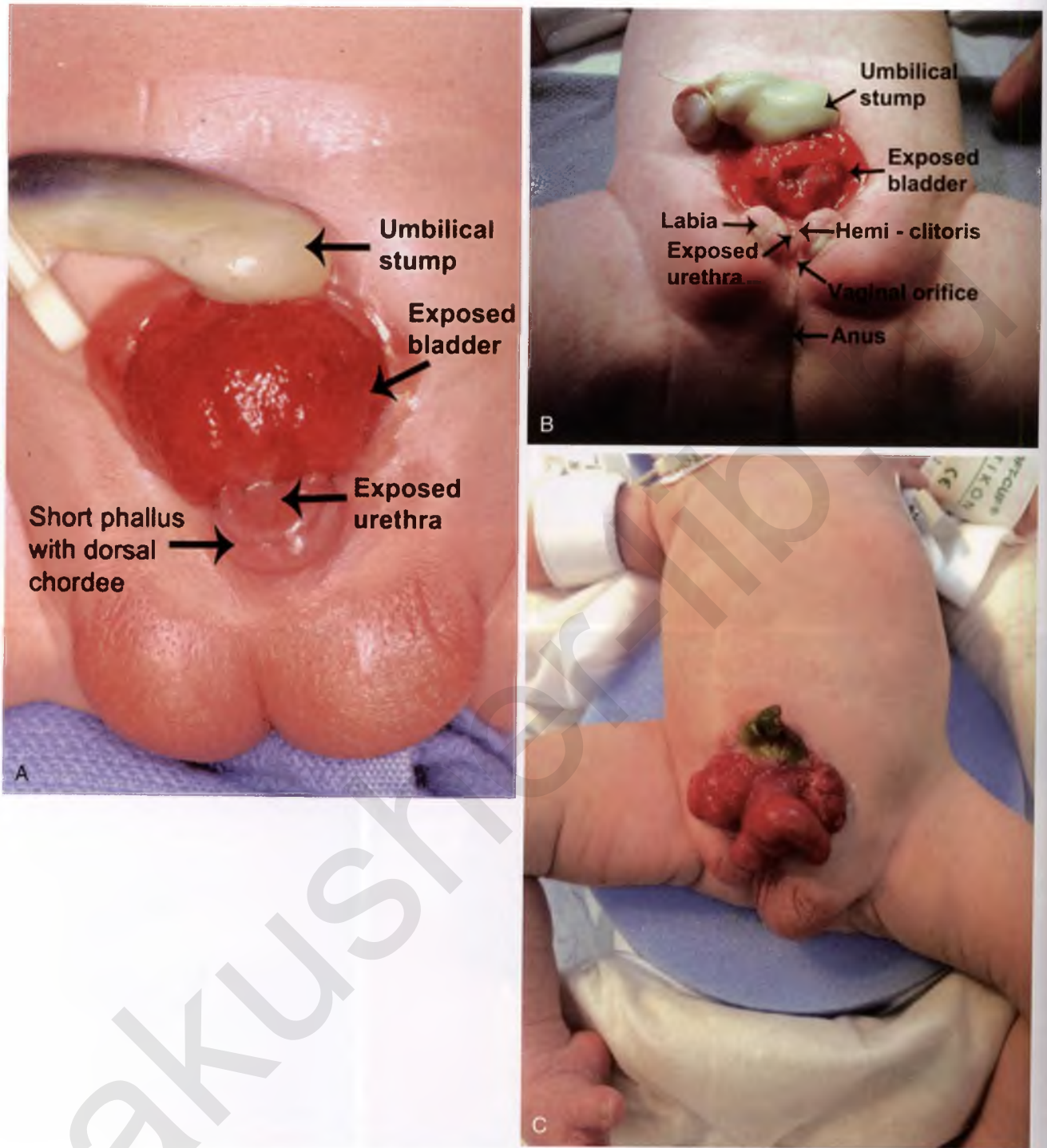


**FIG 14-30** Bladder and cloacal exstrophy. **A**, Bladder exstrophy in a newborn male. **B**, Bladder exstrophy in a newborn female. **C**, Cloacal exstrophy. The hindgut is herniated between two exposed hemibladders. (A and B from Pierre K, Borer J, Phelps A, Chow J: Bladder exstrophy: current management and postoperative imaging. *Pediatr Radiol* 44(7):768-786, 2014, Figs. 2 and 3; C from Clements MB, Chalmers DJ, Meyers ML, Vemulakonda VM: Prenatal diagnosis of cloacal exstrophy: a case report and review of the literature. *Urology* 83(5):1162-1164, 2014, Fig. 3.)

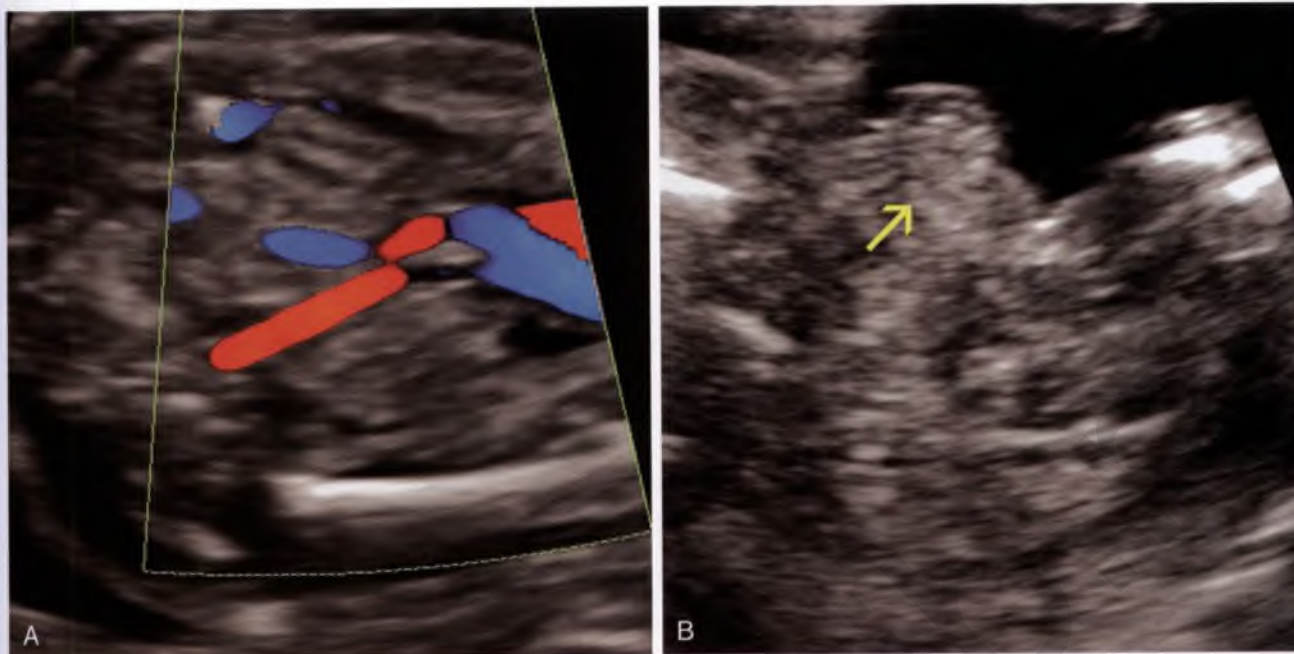


**FIG 14-31** Bladder exstrophy. **A**, Color Doppler ultrasound image at the level of the umbilical arteries. The urinary bladder was not visualized and could not be identified on repeated attempts during a prolonged examination. The bilateral fetal kidneys and amniotic fluid volume appeared normal. This constellation of findings suggests bladder exstrophy. **B**, Exposed redundant bladder tissue (*arrow*) is noted at the ventral aspect of the inferior abdominal wall. Compare to Figure 14-30A. This child underwent successful complete primary surgical repair.

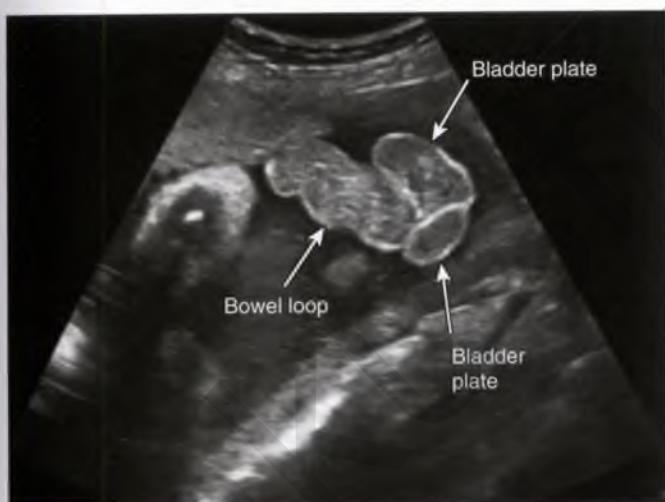


**FIG 14-32** Cloacal exstrophy. Bowel loops are herniated between two hemibladders. Compare to Figure 14-30C. (From Clements MB, Chalmers DJ, Meyers ML, Vemulakonda VM: Prenatal diagnosis of cloacal exstrophy: a case report and review of the literature. *Urology* 83(5):1162-1164, 2014, Fig. 2.)

Cesarean delivery has not been shown to improve outcome, although this option can be considered for giant omphalocele.

### Neonatal Management

The exteriorized organs are wrapped in warm saline-soaked gauze covered with plastic to prevent evaporative loss. Intravenous hydration and nasogastric decompression are begun promptly. Serial blood sugar determinations should be obtained because of the possibility of BWS, which can be associated with neonatal hypoglycemia.

The surgical approach depends largely on the size of the lesion. Small omphaloceles are amenable to primary closure. A variety of surgical techniques have been used to repair large omphaloceles. Although there can be issues with gastroesophageal reflux, respiratory problems, and feeding difficulty with failure to thrive, long-term outcomes are determined largely by the presence or absence of associated abnormalities.

### Gastroschisis

#### Definition

The International Clearinghouse for Birth Defects Research and Surveillance defines gastroschisis as “a congenital malformation characterized by visceral herniation through a right-sided abdominal wall defect adjacent to an intact umbilical cord and not covered by a membrane.”<sup>143</sup>

Note that almost all cases of gastroschisis are right-sided and consist of externalized bowel, without liver herniation (see Figs. 14-26 and 14-27). Thus left-sided gastroschisis or gastroschisis with liver involvement is rare and atypical. A report of three cases of left-sided gastroschisis noted extraintestinal anomalies in all three.<sup>144</sup> A recent series found liver herniation in 6% of 117 cases of gastroschisis.<sup>145</sup> Some of these atypical cases may represent confusion of gastroschisis with other abdominal wall defects such as omphalocele, limb-body wall complex/amniotic band syndrome/body stalk anomaly, or cloacal exstrophy. In a report of 296 cases with ventral wall defects, the diagnosis was changed in 6%.<sup>146</sup>

#### Prevalence and Risk Factors

Gastroschisis is nearly unique among congenital anomalies, as there has been a 10- to 20-fold increase in prevalence from the 1960s until the present.<sup>143</sup> The prevalence of gastroschisis is inversely associated



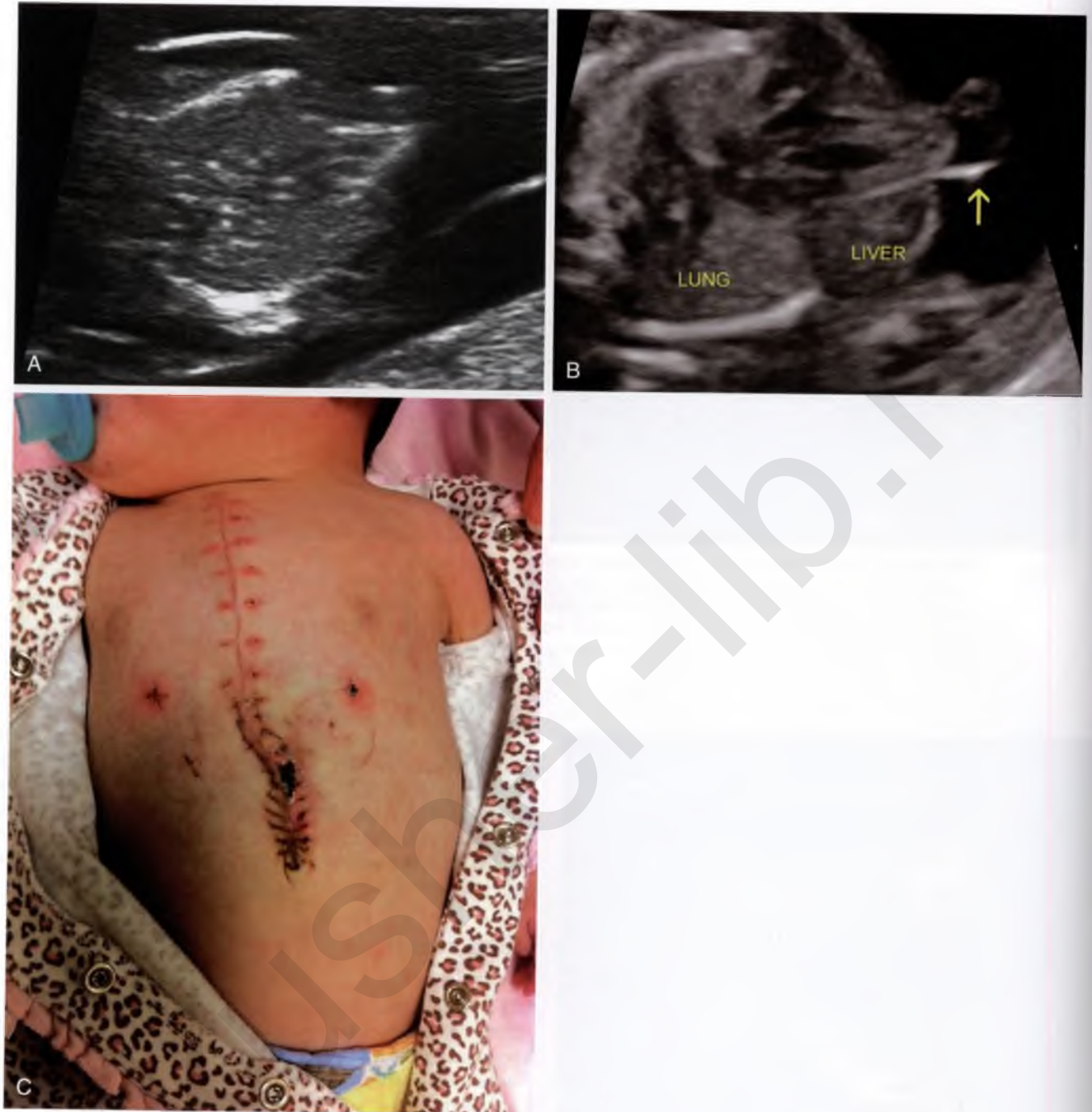


**FIG 14-33** Pentology of Cantrell. **A**, Fetus referred at 11 weeks 5 days with cystic hygroma. The apex of the heart protrudes through the ventral chest wall. This abnormality was more conspicuous on real-time imaging, with cardiac pulsation observed. **B**, Oblique transaxial sonographic view through the chest and upper abdomen demonstrates caudal angulation of the ectopic heart, herniating through the ventral defect, surrounded by a thin membrane (*arrow*). **C**, Photograph obtained following surgical correction of transposition of the great arteries with pulmonary stenosis and repair of the diaphragmatic defect and omphalocele. The infant was doing well at 6 months of age.



**FIG 14-34** Limb–body wall complex at 10 weeks. The cranial portion of the fetus is located in the amniotic cavity, but the caudal portion of the fetus is in the extra-amniotic chorionic space. (Three-dimensional rendering by Bryann Bromley, MD.)

with maternal age; this condition is more than 60 times more common in women younger than 20 years of age, compared to women older than 35.<sup>147</sup> In some studies, exposure to several substances including aspirin, pseudoephedrine and related drugs, and cigarettes and alcohol has been associated with a modest increased risk of gastroschisis.<sup>148,149</sup> The recurrence risk of gastroschisis is thought to be low, although one study calculated a risk of 2.4%.<sup>150</sup> Investigations suggest an environmental rather than genetic cause of this condition.

### Associated Anomalies

Abnormalities of the gastrointestinal tract such as atresia, stenosis, necrosis, perforation, malrotation, and volvulus are considered part of the primary defect rather than associated abnormalities. The reported incidence of these bowel complications varies from 4% to 21%,<sup>151-155</sup> with no obvious explanation for the discrepancy in rates.

It is often stated that extraintestinal anomalies are rarely associated with gastroschisis. However, they were found in 6% of 64 prenatally diagnosed fetuses<sup>151</sup> and 7% of 143 registered births.<sup>152</sup> Another study found additional nonbowel anomalies in 5% of 108 fetuses in the prenatal period and a total of 13% of 108 cases after birth.<sup>156</sup> The largest study, a review of 3322 cases of gastroschisis contributed by 24 registries,<sup>157</sup> found that 469 cases (14%) were not isolated: there were 41 cases of aneuploidy, mainly trisomy 13 and 18; 24 nonchromosomal syndromes; and a total of 615 additional defects in 404 fetuses that were grouped together as “multiple congenital anomalies.” These anomalies included 147 central nervous system anomalies with 42 cases of hydrocephalus; 83 cardiovascular anomalies; 46 oral clefts; 60 genital anomalies; 61 urinary tract anomalies; and 72 limb anomalies. These authors suggest that some of these cases may be attributed to misclassification. In particular, they propose that cases of trisomy 13 and 18 might have represented misdiagnosed omphaloceles. Still, the incidence of extraintestinal congenital anomalies associated with gastroschisis may be higher than previously reported.<sup>158</sup>

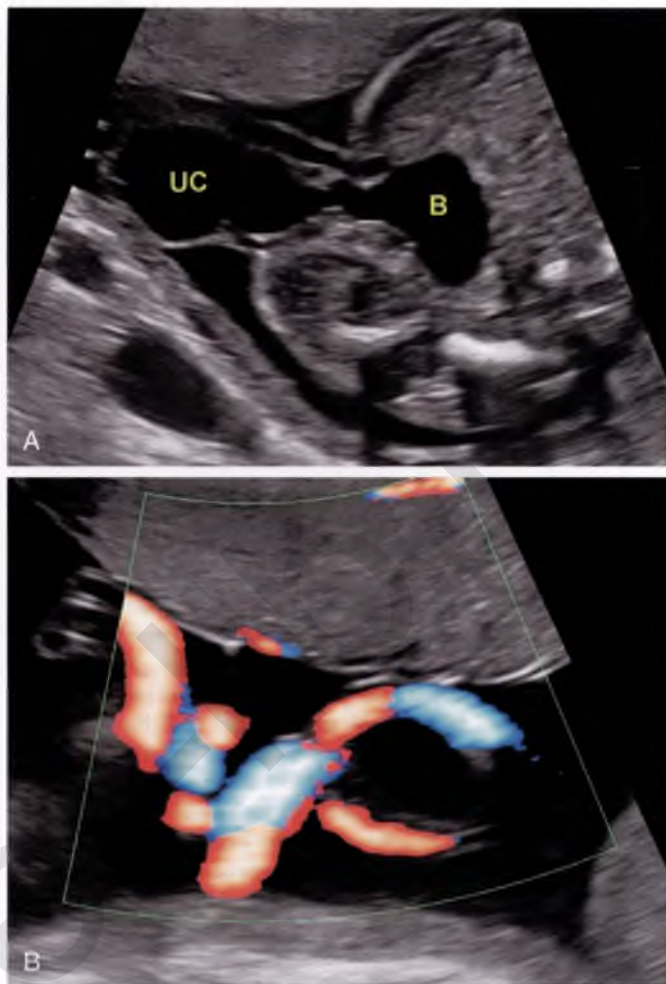


**FIG 14-35** Urachal cyst. **A**, Sonolucent urachal cyst (UC) at the ventral aspect of the fetus, near the cord insertion. Initially, this lesion may resemble an omphalocele without prolapsed organs or soft tissue. On closer examination, the cyst can be seen to communicate with the fluid-filled urinary bladder (B). **B**, Color Doppler ultrasound image shows characteristic spaying of the umbilical arteries on either side of the urachal cyst. The urachal remnant was easily repaired with surgery done shortly after birth.

### Pathophysiology

Gastroschisis is often thought to be due to a vascular event, perhaps disruption of the right vitelline artery or abnormal involution of the right umbilical vein. However, this does not easily explain the increased risk of associated anomalies. Several additional hypotheses have been suggested: (1) failure of mesoderm to form in the body wall, (2) rupture of the amnion around the umbilical ring, (3) abnormal folding of the body wall resulting in a ventral body wall defect through which the gut herniates,<sup>148</sup> and (4) failure to incorporate the yolk sac and related vitelline structures into the umbilical stalk.<sup>159</sup>

### Adverse Obstetric Outcomes

The incidence of growth restriction, fetal demise, and spontaneous preterm delivery is increased. Brantberg and associates<sup>151</sup> found 22% of 64 affected infants weighed less than 2 standard deviations below the mean for gestational age. Netta and colleagues<sup>160</sup> found that 61% of 36 infants were below the 10th percentile and 44% were below the 5th percentile.



In a recent meta-analysis of 3276 pregnancies with gastroschisis, there were 177 stillbirths (risk of fetal demise 4.5%, seven times that in the general population), despite antenatal surveillance and early elective delivery in many of the studies.<sup>161</sup> It is not clear to what extent fetal demise may be due to placental insufficiency as there is not a strong correlation between FGR and stillbirth. Other possible causes of stillbirth include cord compression, protein loss with hypovolemia, cytokine-mediated inflammation, and vascular compromise due to intestinal volvulus.<sup>161</sup>

There is a high rate of spontaneous preterm delivery. In one study, the rate of preterm birth was 28% and the mean gestational age at spontaneous delivery was 36.6 weeks.<sup>162</sup> In a more recent report, 24% of 98 pregnancies were complicated by preterm birth or premature rupture of membranes.<sup>155</sup>

### Sonographic Diagnosis and Obstetric Management

Ventral wall defects can reliably be diagnosed by ultrasound examinations as early as 11 to 14 weeks.<sup>31</sup> It is important to confirm the diagnosis of gastroschisis, as opposed to other ventral wall defects, based on the observation of free-floating loops of intestine without a covering membrane herniating to the right of an intact umbilical cord insertion. The use of color Doppler sonography is often helpful (see Figs. 14-26 through 14-28). If the patient fits the demographic profile and there are no additional anomalies in any other organ system, the diagnosis of gastroschisis would seem secure and the prospective parents can be counseled accordingly. A fetal echocardiogram can be offered, although the incidence of congenital heart disease of 2.5%<sup>157</sup> to 4%<sup>163</sup> is somewhat lower than that seen with many other anomalies. Additional testing for aneuploidy can be discussed, although the likelihood of chromosomal abnormality is low. Fetal MRI and amniocentesis add little to the diagnosis after a targeted sonogram performed by an experienced examiner. However, if there are any atypical features, then more extensive evaluation should be recommended.

The most important goal of subsequent obstetric care is to avoid stillbirth, which is not always related to growth restriction. Some form of fetal surveillance is warranted, most often including serial sonographic evaluation for growth, amniotic fluid volume, and appearance of the intestines. Many centers also perform antepartum fetal heart rate monitoring of fetuses with gastroschisis.<sup>164</sup>

Because it is has been suggested that exposure to amniotic fluid progressively damages exposed intestine, some have considered sonographic appearance of the fetal bowel as a criterion for delivery (Figs. 14-26D and 14-28B). Several<sup>165-168</sup> but not all<sup>169</sup> investigators have shown that bowel dilatation is associated with increased risk of postnatal complications, such as atresias, particularly if multiple intra-abdominal loops are involved. There is less evidence that thickened bowel wall is an independent risk factor<sup>170</sup> and dilatation of the fetal stomach is not associated with complications.<sup>171</sup>

Of note, change in the sonographic appearance of fetal bowel is not an indication for early delivery, because it is assumed that damage has already occurred. Several studies suggest that delivery prior to approximately 37 weeks is associated with worse outcomes.<sup>172-176</sup> On the other hand, because of the ongoing risk of in utero demise<sup>164</sup> as well as the theoretic possibility of bowel damage, many centers recommend elective delivery at about 37 weeks<sup>177</sup> even if testing remains reassuring. One study showed that this approach is associated with improved outcomes.<sup>178</sup>

In the past, there was a great deal of controversy regarding the appropriate route for delivery. Although there have been no randomized controlled trials, several retrospective series failed to demonstrate improvement in outcome after cesarean delivery. At the present time, most patients with fetal gastroschisis are allowed to labor.<sup>177</sup>

### Neonatal Management

Immediately after delivery, intravenous hydration and nasogastric decompression should be initiated. The exteriorized bowel is wrapped with warm saline-soaked gauze and then with plastic to prevent evaporative loss. The child is placed in the right lateral decubitus position to prevent kinking of the mesentery.

Repair of the abdominal wall defect can be done either by primary closure or staged closure, with use of a silo (see Fig. 14-29) followed by closure of the fascia and skin. Regions of atretic bowel can be repaired at the time of primary closure or electively, several weeks later. Return of bowel function might be delayed and prolonged hospitalizations are not uncommon. The neonatal death rate is 4% to 8%.<sup>151,152,154</sup>

Long-term outcome for survivors is excellent. The most serious problem is short bowel syndrome (or short gut syndrome), which affects 4% to 10% of children with gastroschisis. Relatively minor gastrointestinal problems may occur, though often growth, neurodevelopment, and life satisfaction are similar to that reported in the general population.<sup>177</sup>

### Bladder and Cloacal Exstrophy/OEIS Complex

There is a spectrum of abnormalities involving the lower abdomen and genitourinary tract ranging from epispadias at the mild end through bladder exstrophy to cloacal exstrophy/OEIS complex at the severe end.<sup>179,180</sup> The prevalence of bladder and cloacal exstrophy is 3 and 0.5 per 100,000, respectively.<sup>181,182</sup>

### Embryology

Approximately 6 weeks after conception, development of the urorectal septum divides the cloaca into the urogenital sinus anteriorly and the hindgut posteriorly (see Fig. 14-9). Simultaneously, the infraumbilical abdominal wall is formed by lateral to medial extension of mesoderm between the ectoderm and the cloaca; if this process is deficient, the cloacal membrane can rupture anteriorly. If rupture of the cloacal membrane occurs after the urorectal septum has reached the urogenital membrane, the result is *bladder exstrophy*, which in the male is accompanied by epispadias (Fig. 14-30A and B). If rupture of the cloacal membrane occurs prior to complete descent of the urorectal septum, the result is *cloacal exstrophy*, involving anterior herniation of bladder and small bowel, preventing normal midline fusion of the hindgut, bladder plate, and genital structures.<sup>180</sup> Exteriorized cecum and terminal ileum lie in the midline between the two hemibladders and hemiphalli (Fig. 14-30C). The distal hindgut ends in a blind pouch. Spinal abnormalities such as hemivertebrae, sacral hypogenesis, and dysraphism are commonly associated with cloacal exstrophy. The acronym *OEIS complex* is sometimes used; some suggest that OEIS is similar or identical to cloacal exstrophy.<sup>183</sup>

### Sonographic Diagnosis

Sonographic diagnosis of bladder exstrophy is based on persistent nonvisualization of the bladder in a fetus with normal amniotic fluid volume (Fig. 14-31A). The fetal bladder normally starts to refill within several minutes after voiding; thus, a prolonged period of nonvisualization would suggest an abnormality. In most cases of exstrophy, a small soft tissue mass can be seen at the lower abdominal wall inferior to the umbilical cord insertion, representing redundant bladder mucosa (Fig. 14-31B).

The diagnosis of cloacal exstrophy should be suspected in the second or third trimester if a ventral wall defect is associated with persistent nonvisualization of the bladder; there may also be hemivertebrae with kyphoscoliosis or evidence of lumbosacral meningomyelocele.<sup>184</sup> The prolapsed terminal ileum may have a characteristic



“elephant trunk” appearance<sup>185</sup> (see Fig. 14-32). The sonographic findings are variable,<sup>186</sup> and there are often additional abnormalities.<sup>187</sup>

In the first trimester, a cystic mass can sometimes be identified, prior to rupture of the cloacal membrane.<sup>188</sup> There also appears to be an association between increased nuchal translucency and cloacal exstrophy.<sup>189</sup>

Karyotype with microarray<sup>190</sup> should be considered, in part to ascertain fetal sex, because it is often difficult to determine by ultrasound imaging. This information may be useful for antenatal counseling.<sup>191</sup>

### Neonatal Management

The newborn should have its exposed organs moistened with sterile saline solution and covered with a sterile plastic wrap to prevent fluid loss, trauma, and infection. Surgical correction of bladder exstrophy can be done either as a primary repair or in a staged fashion.<sup>192</sup> After repair, the majority of patients with bladder exstrophy are continent.<sup>193</sup>

Surgical repair of the various manifestations of cloacal exstrophy is far more complex, requiring a multidisciplinary approach. Long-term complications including urinary incontinence are common; of particular concern are psychosocial issues related to gender assignment and sexual identity, an area of current interest and investigation. Genetically male infants reared as males may have phallic inadequacy,<sup>194</sup> but attempts at reassignment of female gender to genetic males have proved problematic.<sup>195</sup> Most urologists now recommend that 46,XY infants be raised as males.<sup>196</sup>

### Pentology of Cantrell

Pentology of Cantrell can be thought of as a very high ventral wall defect including a cleft of the distal sternum with some degree of ectopia cordis (Fig. 14-33B), an anterior diaphragmatic defect, a high omphalocele, a pericardial defect, and cardiac malformation. Cases in which some but not all of these features are present can be considered incomplete forms of this condition.<sup>197</sup> The diagnosis can be made by sonography as early as the first trimester if there is ectopia cordis, and there is a reported association with an enlarged nuchal translucency<sup>198</sup> (Fig. 14-33A). Because of the variability in presentation and the small number of cases in the literature, it is best to individualize the prognosis, which can sometimes be favorable (see Fig. 14-33).

### Limb–Body Wall Complex/Amniotic Band Syndrome

This group of disruptive processes is referred to by many names, including *amniotic band disruption sequence*, *body stalk anomaly*, and *short umbilical cord syndrome*. The pathophysiology of these disorders is not known, nor is it established whether they are related.<sup>199,200</sup> Mild cases of amniotic band syndrome involve only limb amputations; more severe forms also manifest craniofacial deformities. The terms *limb–body wall complex* and *body stalk anomaly* refer to severe cases in which there is thoracoabdominoschisis, severe kyphoscoliosis, and abnormally short umbilical cord, in addition to other defects.<sup>201</sup>

The diagnosis of limb–body wall complex has been made as early as the first trimester (see Fig. 14-34); the findings were kyphoscoliosis and large abdominal wall defect, often in association with enlarged nuchal translucency.<sup>202</sup> This particular condition is lethal and should be differentiated from other ventral wall defects, in particular gastroschisis, which has a better prognosis, as do mild cases of amniotic band disruption sequence. Karyotype is usually normal, but may be useful when counseling for future pregnancies. Labor complications are common and cesarean delivery may be necessary for those patients who continue the pregnancy.<sup>203</sup>

### Urachal Cyst

The urachus is an embryologic remnant of the allantois, which connects the urogenital sinus and later the bladder with the proximal umbilical cord.<sup>204</sup> The urachus normally atrophies to become the median umbilical ligament. Incomplete atrophy of the urachus results in a urachal cyst, visible by ultrasound imaging as a cystic structure at the ventral aspect of the fetus, communicating with the fluid-filled bladder (Fig. 14-35A). The umbilical arteries are splayed on either side of the urachal cyst and bladder (Fig. 14-35B). Although not a true ventral wall defect, a urachal cyst may resemble an omphalocele. It often resolves in the second half of pregnancy<sup>205</sup> but a partially everted bladder may be seen.<sup>206,207</sup> MRI may be helpful in establishing the diagnosis,<sup>208</sup> which is important because the prognosis for urachal cyst is better than that for omphalocele. The treatment is postnatal surgical resection.

### ACKNOWLEDGMENTS

The contributions of several sonographers and sonologists in obtaining and interpreting many of these images are greatly appreciated. In the prenatal diagnosis unit at Massachusetts General Hospital we have a team approach. It is often difficult or impossible to determine who obtained a particular image.

I also want to acknowledge the critical review of the manuscript by Ilona Goldfarb, MD, and Cassandra Kelleher, MD.

Finally, I would like to thank all of those who have taught me ultrasound over the years, and in particular, Beryl Benacerraf, MD.

### REFERENCES

- Mitchell B, Sharma R: *Embryology: An Illustrated Colour Text*, Edinburgh, 2005, Elsevier/Churchill Livingstone.
- Moore KL, Persaud TVN, editors: *The Developing Human: Clinically Oriented Embryology*, ed 6, Philadelphia, 1998, WB Saunders.
- Malinger G, Levine A, Rotmensch S: The fetal esophagus: anatomical and physiological ultrasonographic characterization using a high-resolution linear transducer. *Ultrasound Obstet Gynecol* 24:500–505, 2004.
- Blaas HG, Eik-Nes SH, Kiserud T, Hellevik LR: Early development of the abdominal wall, stomach and heart from 7 to 12 weeks of gestation: a longitudinal ultrasound study. *Ultrasound Obstet Gynecol* 6:240–249, 1995.
- Hertzberg BS: Sonography of the fetal gastrointestinal tract: anatomic variants, diagnostic pitfalls, and abnormalities. *AJR Am J Roentgenol* 162(5):1175–1182, 1994.
- Leigh MW, Pittman JE, Carson JL, et al: Clinical and genetic aspects of primary ciliary dyskinesia/Kartagener syndrome. *Genet Med* 11(7):473–487, 2009.
- Applegate KM, Goske MJ, Pierce G, Murphy D: Situs revisited: imaging of the heterotaxy syndrome. *Radiographics* 19:837–852, 1999.
- Salomon LJ, Baumann C, Delezoide AL, et al: Abnormal abdominal situs: what and how should we look for? *Prenat Diagn* 26:282–285, 2006.
- Sase M, Miwa I, Sumi M, et al: Gastric emptying cycles in human fetus. *Am J Obstet Gynecol* 193:1000–1004, 2005.
- Al-Salem AH, Abdulla MR, Kothari MR, Naga MI: Congenital pyloric atresia, presentation, management, and outcome: a report of 20 cases. *J Pediatr Surg* 49:1078–1082, 2014.
- Rizzo G, Capponi A, Arduini D, Romanini C: Prenatal diagnosis of gastroesophageal reflux by color and pulsed Doppler ultrasonography in a case of congenital pyloric atresia. *Ultrasound Obstet Gynecol* 6:290–292, 1995.
- McKelvey A, Stanwell J, Smeulders N, et al: Persistent non-visualisation of the fetal stomach: diagnostic and prognostic implications. *Arch Dis Child Fetal Neonatal Ed* 95(6):F439–F442, 2010.



13. Rothenberg SS: Esophageal atresia and tracheoesophageal fistula malformations. In Holcomb GW, Murphy JP, Ostlie DJ, editors: *Ashcraft's Pediatric Surgery*, ed 6, Philadelphia, 2014, Elsevier.
14. Pedersen R, Calzolari E, Husby S, Garne E, EUROCAT Working group: Oesophageal atresia: prevalence, prenatal diagnosis and associated anomalies in 23 European regions. *Arch Dis Child* 97(3):227–232, 2012.
15. Stringer MD, McKenna KM, Goldstein RB, et al: Prenatal diagnosis of esophageal atresia. *J Pediatr Surg* 30(9):1258–1263, 1995.
16. Brantberg A, Blaas K, Haugen SE, Eik-Nes SH: Esophageal obstruction-prenatal detection rate and outcome. *Ultrasound Obstet Gynecol* 30(2):180–187, 2007.
17. de Jong EM, de Haan MA, Gischler SJ, et al: Pre- and postnatal diagnosis and outcome of fetuses and neonates with esophageal atresia and tracheoesophageal fistula. *Prenat Diagn* 30(3):274–279, 2010.
18. Sparey C, Jawaheer G, Barrett AM, Robinson SC: Esophageal atresia in the Northern Region Congenital Anomaly Survey, 1985–1997: prenatal diagnosis and outcome. *Am J Obstet Gynecol* 182:427–431, 2000.
19. Choudhry M, Boyd PA, Chamberlain PF, Lakhoo K: Prenatal diagnosis of tracheo-oesophageal fistula and oesophageal atresia. *Prenat Diagn* 27(7):608–610, 2007.
20. Borsellino A, Zaccara A, Nahom A, et al: False-positive rate in prenatal diagnosis of surgical anomalies. *J Pediatr Surg* 41(4):826–829, 2006.
21. Fallon SC, Ethun CG, Olutoye OO, et al: Comparing characteristics and outcomes in infants with prenatal and postnatal diagnosis of esophageal atresia. *J Surg Res* 190:242–245, 2014.
22. Kunisaki SM, Bruch SW, Hirschl RB, et al: The diagnosis of fetal esophageal atresia and its implications on perinatal outcome. *Pediatr Surg Int* 30(10):971–977, 2014.
23. Solt I, Rotmensch S, Bronshtein M: The esophageal “pouch sign”: a benign transient finding. *Prenat Diagn* 30:845–848, 2010.
24. Ethun CG, Fallon SC, Cassidy CI, et al: Fetal MRI improves diagnostic accuracy in patients referred to a fetal center for suspected esophageal atresia. *J Pediatr Surg* 49(5):712–715, 2014.
25. Garabedian C, Verpillat P, Czerkiewicz I, et al: Does a combination of ultrasound, MRI, and biochemical amniotic fluid analysis improve prenatal diagnosis of esophageal atresia? *Prenat Diagn* 34(9):839–842, 2014.
26. Wang B, Tashiro J, Allan BJ, et al: A nationwide analysis of clinical outcomes among newborns with esophageal atresia and tracheoesophageal fistulas in the United States. *J Surg Res* 190(2):604–612, 2014.
27. Aguayo P, Ostlie DJ: Duodenal and intestinal atresia and stenosis. In Holcomb GW, Murphy JP, Ostlie DJ, editors: *Ashcraft's Pediatric Surgery*, ed 6, Philadelphia, 2014, Elsevier.
28. Hemming V, Rankin J: Small intestinal atresia in a defined population: occurrence, prenatal diagnosis and survival. *Prenat Diagn* 27:1205–1211, 2007.
29. Choudhry MS, Rahman N, Boyd P, Lakhoo K: Duodenal atresia: associated anomalies, prenatal diagnosis and outcome. *Pediatr Surg Int* 25:727–730, 2009.
30. Malone FD, Crombleholme TM, Nores JA, et al: Pitfalls of the “double bubble” sign; a case of congenital duodenal duplication. *Fetal Diagn Ther* 12:298–300, 1997.
31. Syngelaki A, Chelemen T, Dagklis T, et al: Challenges in the diagnosis of fetal non-chromosomal abnormalities at 11–13 weeks. *Prenat Diagn* 31:90–102, 2011.
32. Rossi AC, Prefumo F: Accuracy of ultrasonography at 11–14 weeks of gestation for detection of fetal structural anomalies. A systematic review. *Obstet Gynecol* 122(6):1160–1167, 2013.
33. Lawrence MJ, Ford WD, Furness ME, et al: Congenital duodenal obstruction: early antenatal ultrasound diagnosis. *Pediatr Surg Int* 16:342–345, 2000.
34. Cohen-Overbeek TE, Grijseels EW, Niemeijer ND, et al: Isolated or non-isolated duodenal obstruction: perinatal outcome following prenatal or postnatal diagnosis. *Ultrasound Obstet Gynecol* 32(6):784–792, 2008.
35. Torfs CP, Christianson RE: Anomalies in Down syndrome individuals in a large population-based registry. *Am J Med Genet* 77:431–438, 1998.
36. Brantberg A, Blaas HG, Salvesen KA, et al: Fetal duodenal obstruction: increased risk of prenatal sudden death. *Ultrasound Obstet Gynecol* 20(5):439–446, 2002.
37. Escobar MA, Ladd AP, Grosfeld JL, et al: Duodenal atresia and stenosis: long-term follow-up over 30 years. *J Pediatr Surg* 39(6):867–2004.
38. Vincoff NS, Callen PW, Smith-Bindman R, Goldstein RB: Effect of ultrasound transducer frequency on the appearance of the fetal bowel. *J Ultrasound Med* 18(12):799–803, 1999.
39. Harrison KL, Martinez D, Mason G: The subjective assessment of echogenic fetal bowel. *Ultrasound Obstet Gynecol* 16:524–529, 2000.
40. Sepulveda W, Sebire NU: Opinion. Fetal echogenic bowel: a complex scenario. *Ultrasound Obstet Gynecol* 16:510–514, 2000.
41. Publications Committee, Society for Maternal Fetal Medicine, Odibo AO, Goetzinger KR: Isolated echogenic bowel diagnosed on second-trimester ultrasound. *Contemp OB/GYN*, Aug 1, 2011. Available at <<http://contemporaryobgyn.modernmedicine.com>>.
42. Agathokleous M, Chaveeva P, Poon LC, et al: Meta-analysis of second-trimester markers for trisomy 21. *Ultrasound Obstet Gynecol* 41(3):247–261, 2013.
43. Reddy UM, Abuhamad AZ, Levine D, Saade GR, Fetal Imaging Workshop Invited Participants: Fetal imaging: executive summary of a joint Eunice Kennedy Shriver National Institute of Child Health and Human Development, Society for Maternal-Fetal Medicine, American Institute of Ultrasound in Medicine, American College of Obstetricians and Gynecologists, American College of Radiology, Society for Pediatric Radiology, and Society of Radiologists in Ultrasound Fetal Imaging Workshop. *J Ultrasound Med* 33(5):745–757, 2014.
44. Scotet V, Dugueperoux I, Audrezet MP, et al: Focus on cystic fibrosis and other disorders evidenced in fetuses with sonographic finding of echogenic bowel: 16-year report from Brittany, France. *Am J Obstet Gynecol* 203(6):592, e1–e6, 2010.
45. Picone O, Teissier N, Cordier AG, et al: Detailed in utero ultrasound description of 30 cases of congenital cytomegalovirus infection. *Prenat Diagn* 34(6):518–524, 2014.
46. Guerra B, Simonazzi G, Puccetti C, et al: Ultrasound prediction of symptomatic congenital cytomegalovirus infection. *Am J Obstet Gynecol* 198:380.e1–380.e7, 2008.
47. Goetzinger KR, Cahill AG, Macones GA, Odibo AO: Echogenic bowel on second-trimester ultrasonography: evaluating the risk of adverse pregnancy outcome. *Obstet Gynecol* 117(6):1341–1348, 2011.
48. Mailath-Pokorny M, Klein K, Klebermass-Schrehof K, et al: Are fetuses with isolated echogenic bowel at higher risk for an adverse pregnancy outcome? Experience from a tertiary referral center. *Prenat Diagn* 32:1295–1299, 2012.
49. Strocker AM, Sniijders RJ, Carlson DE, et al: Fetal echogenic bowel: parameters to be considered in differential diagnosis. *Ultrasound Obstet Gynecol* 16:519–523, 2000.
50. Al-Kouatly HB, Chasen ST, Streltsoff J, Chervenak FA: The clinical significance of fetal echogenic bowel. *Am J Obstet Gynecol* 185:1035–1038, 2001.
51. Saha E, Mullins EW, Paramasivam G, et al: Perinatal outcomes of fetal echogenic bowel. *Prenat Diagn* 32:758–764, 2012.
52. Buitert HD, Holswilder-Olde Scholtenhuis MA, Bouman K, et al: Outcome of infants presenting with echogenic bowel in the second trimester of pregnancy. *Arch Dis Child Fetal Neonatal Ed* 98(3):F256–F259, 2013.
53. Nyberg DA, Mack LA, Patten RM, Cyr DR: Fetal bowel: normal sonographic findings. *J Ultrasound Med* 6:3–6, 1987.
54. Wax JR, Hamilton T, Cartin A, et al: Congenital jejunal and ileal atresia. *J Ultrasound Med* 25:337–342, 2006.
55. Amat S, Czerkiewicz I, Benoist JF, et al: Isolated hyperechoic fetal colon before 36 weeks' gestation reveals cystinuria. *Ultrasound Obstet Gynecol* 38(5):543–547, 2011.
56. Sweeney B, Surana R, Puri P: Jejunioileal atresia and associated malformations: correlation with the timing of the in utero insult. *J Pediatr Surg* 36:774–776, 2001.

57. Festen S, Brevoord JC, Goldhoorn GA, et al: Excellent long-term outcome for survivors of apple peel atresia. *J Pediatr Surg* 37(1):61–65, 2002.
58. Shorter J, Georges A, Perenyi A, Garrow E: A proposed classification system for familial intestinal atresia and its relevance to the understanding of the etiology of jejunoileal atresia. *J Pediatr Surg* 41:1822–1825, 2006.
59. Yoo SJ, Park KW, Cho SY, et al: Definitive diagnosis of intestinal volvulus in utero. *Ultrasound Obstet Gynecol* 13(3):200–203, 1999.
60. Molvarec A, Bábinszki A, Kovács K, et al: Intrauterine intestinal obstruction due to fetal midgut volvulus: a report of two cases. *Fetal Diagn Ther* 22(1):38–40, 2007.
61. Kim SH, Kim SH: Congenital chloride diarrhea: antenatal ultrasonographic findings in siblings. *J Ultrasound Med* 20(10):1133–1136, 2001.
62. Rubesova E: Fetal bowel anomalies: US and MR assessment. *Pediatr Radiol* 42(Suppl 1):S101–S106, 2012.
63. Surana J, Puri P: Small intestinal atresia: effect on fetal nutrition. *J Pediatr Surg* 29:1250–1252, 1994.
64. Zangheri G, Andreani M, Ciriello E, et al: Fetal intra-abdominal calcifications from meconium peritonitis: sonographic predictors of postnatal surgery. *Prenat Diagn* 27(10):960–963, 2007.
65. Tibboel D, Gaillard JL, Molenaar JC: The importance of mesenteric vascular insufficiency in meconium peritonitis. *Hum Pathol* 17(4):411–416, 1986.
66. Nam SH, Kim SC, Kim DY, et al: Experience with meconium peritonitis. *J Pediatr Surg* 42(11):1822–1825, 2007.
67. Gilliland A, Carlan SJ, Greenbaum LD, et al: Undescended testicle and meconium-filled hemiscrotum: prenatal ultrasound appearance. *Ultrasound Obstet Gynecol* 20(2):200–202, 2002.
68. Dirkes K, Crombleholme TM, Craig SD, et al: The natural history of meconium peritonitis diagnosed in utero. *J Pediatr Surg* 30(7):979–982, 1995.
69. Zerbini M, Gentilomi GA, Gallinella G, et al: Intra-uterine parvovirus B19 infection and meconium peritonitis. *Prenat Diagn* 18(6):599–606, 1998.
70. McDuffie RS, Bader T: Fetal meconium peritonitis after maternal hepatitis A. *Am J Obstet Gynecol* 180:1031–1032, 1999.
71. Bischoff A, Frischer J, Dickie BH, Pena A: Anorectal malformation without fistula: a unique defect with unique characteristics. *Pediatr Surg Int* 30:763–766, 2014.
72. Cuschieri A, EUROCAT Working Group: Descriptive epidemiology of isolated anal anomalies: a survey of 4.6 million births in Europe. *Am J Med Genet* 103(3):207–215, 2001.
73. Cuschieri A, EUROCAT Working Group: Anorectal anomalies associated with or as part of other anomalies. *Am J Med Genet* 110(2):122–130, 2002.
74. Mundt E, Bates MD: Genetics of Hirschsprung disease and anorectal malformations. *Semin Pediatr Surg* 19:107–117, 2010.
75. Khalil A, Cooke PC, Mantovani E, et al: Outcome of first-trimester fetal abdominal cysts: cohort study and review of the literature. *Ultrasound Obstet Gynecol* 43:413–419, 2014.
76. Brantberg A, Blaas HG, Haugen SE, et al: Imperforate anus: a relatively common anomaly rarely diagnosed prenatally. *Ultrasound Obstet Gynecol* 28(7):904–910, 2006.
77. Pohl-Schickinger A, Henrich W, Degenhardt P, et al: Echogenic foci in the dilated fetal colon may be associated with the presence of a rectourinary fistula. *Ultrasound Obstet Gynecol* 28:341–344, 2006.
78. Moon MH, Cho JY, Kim JH, et al: In-utero development of the fetal anal sphincter. *Ultrasound Obstet Gynecol* 35(5):556–559, 2010.
79. Vijayaraghavan SB, Prema AS, Suganyadevi P, et al: Sonographic depiction of the fetal anus and its utility in the diagnosis of anorectal malformations. *J Ultrasound Med* 30(1):37–45, 2011.
80. Elchalal U, Yanai N, Valsky DV, et al: Application of 3-dimensional ultrasonography to imaging the fetal anal canal. *J Ultrasound Med* 29(8):1195–1201, 2010.
81. Ochoa JH, Chiesa M, Vildoza RP, et al: Evaluation of the perianal muscular complex in the prenatal diagnosis of anorectal atresia in a high-risk population. *Ultrasound Obstet Gynecol* 39:521–527, 2012.
82. Bischoff A, Leavitt MA, Breech L, et al: Hydrocolpos in cloacal malformations. *J Pediatr Surg* 45:1241–1245, 2010.
83. Winkler NS, Kennedy AM, Woodward PJ: Cloacal malformation: embryology, anatomy, and prenatal imaging features. *J Ultrasound Med* 31:1843–1855, 2012.
84. Bischoff A, Levitt MA, Lim FY, et al: Prenatal diagnosis of cloacal malformations. *Pediatr Surg Int* 26(11):1071–1075, 2010.
85. Shono T, Taguchi T, Suita S, et al: Prenatal ultrasonographic and magnetic resonance imaging findings of congenital cloacal anomalies associated with meconium peritonitis. *J Pediatr Surg* 42(4):681–684, 2007.
86. Livingston JC, Elicevik M, Breech L, et al: Persistent cloaca: a 10-year review of prenatal diagnosis. *J Ultrasound Med* 31(3):403–407, 2012.
87. Capito C, Belarbi N, Paye Jaouen A, et al: Prenatal pelvic MRI: additional clues for assessment of urogenital obstructive abnormalities. *J Pediatr Urol* 10(1):162–166, 2014.
88. Calvo-Garcia M, Kline-Fath B, Levitt MA, et al: Fetal MRI clues to diagnose cloacal malformations. *Pediatr Radiol* 41(9):1117–1128, 2011.
89. Weichert J, Hartge D, Germer U, et al: Persistent right umbilical vein: a prenatal condition worth mentioning? *Ultrasound Obstet Gynecol* 37:543–548, 2011.
90. Foo D, Wong K, Lan CL, Tam P: Impact of prenatal diagnosis on choledochal cysts and the benefits of early excision. *J Pediatr Child Health* 45:28–30, 2009.
91. Simchen MJ, Toi A, Bona M, et al: Fetal hepatic calcifications: prenatal diagnosis and outcome. *Am J Obstet Gynecol* 187:1617–1622, 2002.
92. Hyett J: Intra-abdominal masses: prenatal differential diagnosis and management. *Prenat Diagn* 28:645–655, 2008.
93. Isaacs H, Jr: Fetal and neonatal hepatic tumors. *J Pediatr Surg* 42:1797–1803, 2007.
94. Avni F, Masseur A, Cassart M: Tumours of the fetal body: a review. *Pediatr Radiol* 39:1147–1157, 2009.
95. Shin JC, Tsao PN, Huang SF, et al: Antenatal diagnosis of congenital hepatoblastoma in utero. *Ultrasound Obstet Gynecol* 16(1):94–97, 2000.
96. Devonald K, Ellwood D, Colditz PB: The variable appearances of fetal gallstones. *J Ultrasound Med* 11(11):579–585, 1992.
97. Stringer MD, Lim P, Cave M, et al: Fetal gallstones. *J Pediatr Surg* 31:1589–1591, 1996.
98. Suma V, Marini A, Bucci N, et al: Fetal gallstones: sonographic and clinical observations. *Ultrasound Obstet Gynecol* 12:439–441, 1998.
99. Shen O, Rabinowitz R, Yagel S, Gal M: Absent gallbladder on fetal ultrasound: prenatal findings and postnatal outcome. *Ultrasound Obstet Gynecol* 37:673–677, 2011.
100. Dreux S, Boughanim M, Lepinard C, et al: Relationship of non-visualization of the fetal gallbladder and amniotic fluid digestive enzymes analysis to outcome. *Prenat Diagn* 32(5):423–426, 2012.
101. Yoon PW, Bresee JS, Olney RS, et al: Epidemiology of biliary atresia: a population-based study. *Pediatrics* 99:376–382, 1997.
102. Chalouhi G, Muller F, Dreux S, et al: Prenatal non-visualization of fetal gallbladder: beware of biliary atresia! *Ultrasound Obstet Gynecol* 38(2):237–238, 2011.
103. Saada J, Parant O, Kessler S, et al: Prenatal diagnosis and outcome of congenital splenic cyst: report of two cases. *Prenat Diagn* 26:9–10, 2006.
104. Ji E, Lee EK, Kwon TH: Isolated echogenic foci in the left upper quadrant of the fetal abdomen: are they significant? *J Ultrasound Med* 23:483–488, 2004.
105. Schmider A, Henrich W, Reles A, et al: Etiology and prognosis of fetal ascites. *Fetal Diagn Ther* 18:230–236, 2003.
106. Nose S, Usui N, Soh H, et al: The prognostic factors and the outcome of primary isolated fetal ascites. *Pediatr Surg Int* 27(8):799–804, 2011.
107. Zelop C, Benacerraf B: The causes and natural history of fetal ascites. *Prenat Diagn* 14:941–946, 1994.
108. El Bishry G: The outcome of isolated fetal ascites. *Eur J Obstet Gynecol* 137:43–46, 2008.
109. Favre R, Dreux S, Dommergues M, et al: Nonimmune fetal ascites: a series of 79 cases. *Am J Obstet Gynecol* 190(2):407–412, 2004.



110. Heling KS, Chaoui R, Kirchmair F, et al: Fetal ovarian cysts: prenatal diagnosis, management and postnatal outcome. *Ultrasound Obstet Gynecol* 20(1):47–50, 2002.
111. Ben-Ami I, Kogan A, Fuchs N, et al: Long-term follow-up of children with ovarian cysts diagnosed prenatally. *Prenat Diagn* 30(4):342–347, 2010.
112. Cesca E, Midrio P, Boscolo-Berto R, et al: Conservative treatment of complex neonatal ovarian cysts: a long-term follow-up analysis. *J Pediatr Surg* 48(3):510–515, 2013.
113. Nemeč U, Nemeč SF, Bettelheim D, et al: Ovarian cysts on prenatal MRI. *Eur J Radiol* 81(8):1937–1944, 2012.
114. Galinier P, Carfagna L, Juricic M, et al: Fetal ovarian cysts management and prognosis: a report of 82 cases. *J Pediatr Surg* 43(11):2004–2009, 2008.
115. Bagolan P, Giorlandino C, Nahom A, et al: The management of fetal ovarian cysts. *J Pediatr Surg* 37(1):25–30, 2002.
116. Laje P, Flake A, Adzick NS: Prenatal diagnosis and postnatal resection of intraabdominal enteric duplications. *J Pediatr Surg* 45:1554–1558, 2010.
117. Winderl L, Silverman R: Prenatal identification of a completely cystic internal sacrococcygeal teratoma (type IV). *Ultrasound Obstet Gynecol* 9:425–428, 1997.
118. Sumi A, Sato Y, Kakui K, et al: Prenatal diagnosis of anterior sacral meningocele. *Ultrasound Obstet Gynecol* 37(4):493–496, 2011.
119. Picone O, Laperelle J, Sonigo P, et al: Fetal magnetic resonance imaging in the antenatal diagnosis and management of hydrocolpos. *Ultrasound Obstet Gynecol* 30:105–109, 2007.
120. Sauvat F, Sarnacki S, Brisse H, et al: Outcome of suprarenal localized masses diagnosed during the perinatal period. *Cancer* 94(9):2474–2480, 2002.
121. Moon SB, Shin HB, Seo JM, Lee SK: Clinical features and surgical outcome of a suprarenal mass detected before birth. *Pediatr Surg Int* 26(3):241–246, 2010.
122. Acharya S, Jayabose S, Kogan SJ, et al: Prenatally diagnosed neuroblastoma. *Cancer* 80(2):304–310, 1997.
123. Hero B, Simon T, Spitz R, et al: Localized infant neuroblastomas often show spontaneous regression: results of the prospective trials NB95-S and NB97. *J Clin Oncol* 26(9):1505–1510, 2008.
124. Calzolari E, Bianchi F, Dolk H, Milan M, EUROCAT Working Group: Omphalocele and gastroschisis in Europe: a survey of 3 million births 1980–1990. *Am J Med Genet* 58:187–194, 1995.
125. Barisic I, Clementi M, Häusler M, et al, Euroscan Study Group: Evaluation of prenatal ultrasound diagnosis of fetal abdominal wall defects by 19 European registries. *Ultrasound Obstet Gynecol* 18(4):309–316, 2001.
126. Stoll C, Alembik Y, Dott B, Roth MP: Omphalocele and gastroschisis and associated malformations. *Am J Med Genet A* 146A(10):1280–1285, 2008.
127. Benjamin B, Wilson G: Anomalies associated with gastroschisis and omphalocele: analysis of 2825 cases from the Texas Birth Defects Registry. *J Pediatr Surg* 49:514–519, 2014.
128. Byron-Scott R, Haan E, Chan A, et al: A population-based study of abdominal wall defects in south Australia and western Australia. *Paediatr Perinat Epidemiol* 12(2):136–151, 1998.
129. Salihi H, Pierre-Louis B, Druschel C, Kirby R: Omphalocele and gastroschisis in the state of New York, 1992–1999. *Birth Defects Res A Clin Mol Teratol* 67:630–636, 2003.
130. Brantberg A, Blaas HG, Haugen SE, Eik-Nes SH: Characteristics and outcome of 90 cases of fetal omphalocele. *Ultrasound Obstet Gynecol* 26(5):527–537, 2005.
131. Iacovella C, Contro E, Ghi T, et al: The effect of the contents of exomphalos and nuchal translucency at 11–14 weeks on the likelihood of associated chromosomal abnormality. *Prenat Diagn* 32(11):1066–1070, 2012.
132. Radhakrishna U, Nath SK, McElreavey K, et al: Genome-wide linkage and copy number variation analysis reveals 710 kb duplication on chromosome 1p31.3 responsible for autosomal dominant omphalocele. *J Med Genet* 49(4):270–276, 2012.
133. Chen CP, Lin CJ, Chen YY, et al: 3q26.31–q29 duplication and 9q34.3 microdeletion associated with omphalocele, ventricular septal defect, abnormal first-trimester maternal serum screening and increased nuchal translucency: prenatal diagnosis and aCGH characterization. *Gene* 532(1):80–86, 2013.
134. Wilkins-Haug L, Porter A, Hawley P, Benson CB: Isolated fetal omphalocele, Beckwith-Weidemann syndrome, and assisted reproductive technologies. *Birth Defects Res A Clin Mol Teratol* 85(1):58–62, 2009.
135. Weksberg R, Shuman C, Beckwith JB: Beckwith-Weidemann syndrome. *Eur J Hum Genet* 18:8–14, 2010.
136. Hurst J, Firth H, Chitty L: Review: syndromic associations with congenital anomalies of the fetal thorax and abdomen. *Prenat Diagn* 28:676–684, 2008.
137. *Online Mendelian Inheritance in Man (OMIM)*. Available at <http://www.ncbi.nlm.nih.gov/omim>.
138. Lakasing L, Cicero S, Davenport M, et al: Current outcome of antenatally diagnosed exomphalos: an 11 year review. *J Pediatr Surg* 41(8):1403–1406, 2006.
139. Biard JM, Wilson RD, Johnson MP, et al: Prenatally diagnosed giant omphaloceles: short- and long-term outcomes. *Prenat Diagn* 24:434–439, 2004.
140. Kagan KO, Staboulidou I, Syngelaki A, et al: The 11–13-week scan: diagnosis and outcome of holoprosencephaly, exomphalos and megacystis. *Ultrasound Obstet Gynecol* 36:10–14, 2010.
141. Khalil A, Arnaoutoglou C, Pacilli M, et al: Outcome of fetal exomphalos diagnosed at 11–14 weeks of gestation. *Ultrasound Obstet Gynecol* 39(4):401–406, 2012.
142. Daltro P, Fricke BL, Kline-Fath BM, et al: Prenatal MRI of congenital abdominal and chest wall defects. *AJR Am J Roentgenol* 184(3):1010–1016, 2005.
143. Castilla EE, Mastroiaco P, Orioli IM: Gastroschisis: international epidemiology and public health perspectives. *Am J Med Genet C Semin Med Genet* 148C:162–179, 2008.
144. Suver D, Lee S, Shekherdimian S, Kim S: Left-sided gastroschisis: higher incidence of extraintestinal congenital anomalies. *Am J Surg* 195:663–666, 2008.
145. McClellan EB, Shew SB, Lee SS, et al: Liver herniation in gastroschisis: incidence and prognosis. *J Pediatr Surg* 46(11):2115–2118, 2011.
146. Rankin J, Dillon E, Wright C: Congenital anterior abdominal wall defects in the north of England, 1986–1996: occurrence and outcome. *Prenat Diagn* 19:662–668, 1999.
147. Opitz JM, Pysher TJ: Invited editorial comment: further reflections on gastroschisis. *Am J Med Genet C Semin Med Genet* 148C(3):192–198, 2008.
148. Feldkamp M, Carey J, Sadler T: Development of gastroschisis: review of hypotheses, a novel hypothesis, and implications for research. *Am J Med Genet A* 143A:639–652, 2007.
149. Rasmussen S, Frias J: Non-genetic risk factors for gastroschisis. *Am J Med Genet C Semin Med Genet* 148C(3):199–212, 2008.
150. Kohl M, Wiesel A, Schier F: Familial recurrence of gastroschisis: literature review and data from the population-based birth registry “Mainz Model.” *J Pediatr Surg* 45:1907–1912, 2010.
151. Brantberg A, Blaas HG, Salvesen KA, et al: Surveillance and outcome of fetuses with gastroschisis. *Ultrasound Obstet Gynecol* 23:4–13, 2004.
152. Fillingham A, Rankin J: Prevalence, prenatal diagnosis and survival of gastroschisis. *Prenat Diagn* 28:1232–1237, 2008.
153. Kronfli R, Bradnock T, Sabharwal A: Intestinal atresia in association with gastroschisis: a 26-year review. *Pediatr Surg Int* 26:891–894, 2010.
154. Bradnock TJ, Marven S, Owen A, et al: Gastroschisis: one year outcomes from national cohort study. *BMJ* 343:d6749, 2011.
155. Durfee SM, Benson CB, Adams CR, et al: Postnatal outcome of fetuses with the prenatal diagnosis of gastroschisis. *J Ultrasound Med* 32(3):407–412, 2013.
156. Ruano R, Picone O, Bernardes L, et al: The association of gastroschisis with other congenital anomalies: how important is it? *Prenat Diagn* 31(4):347–350, 2011.
157. Mastroiaco P, Lisi A, Castilla EE, et al: Gastroschisis and associated defects: an international study. *Am J Med Genet* 143A(7):660–671, 2007.

158. Opitz JM: Invited comment: gastroschisis. *Am J Med Genet A* 143A:635–638, 2007.
159. Stevenson RE, Rogers R, Chandler J, et al: Escape of the yolk sac: a hypothesis to explain the embryogenesis of gastroschisis. *Clin Genet* 75:326–333, 2009.
160. Netta DA, Wilson RD, Visintainer P, et al: Gastroschisis: growth patterns and a proposed prenatal surveillance protocol. *Fetal Diagn Ther* 22(5):352–357, 2007.
161. South A, Stutey K, Meinzen-Derr J: Meta-analysis of the prevalence of intrauterine fetal death in gastroschisis. *Am J Obstet Gynecol* 209:114, e1–e13, 2013.
162. Lausman AY, Langer JC, Tai M, et al: Gastroschisis: what is the average gestational age of spontaneous delivery? *J Pediatr Surg* 42(11):1816–1821, 2007.
163. Kunz L, Gilbert W, Towner D: Increased incidence of cardiac anomalies in pregnancies complicated by gastroschisis. *Am J Obstet Gynecol* 193:1248–1252, 2005.
164. Overton TG, Pierce MR, Gao H, et al: Antenatal management and outcomes of gastroschisis in the UK. *Prenat Diagn* 32(13):1256–1262, 2012.
165. Nick AM, Bruner JP, Moses R, et al: Second-trimester intra-abdominal bowel dilation in fetuses with gastroschisis predicts neonatal bowel atresia. *Ultrasound Obstet Gynecol* 28(6):821–825, 2006.
166. Huh N, Hirose S, Goldstein R: Prenatal intraabdominal bowel dilation is associated with postnatal gastrointestinal complications in fetuses with gastroschisis. *Am J Obstet Gynecol* 202:396, e1–e6, 2010.
167. Contro E, Fratelli N, Okoye B, et al: Prenatal ultrasound in the prediction of bowel obstruction in infants with gastroschisis. *Ultrasound Obstet Gynecol* 35(6):702–707, 2010.
168. Ghiozoli M, James C, David AL, et al: Gastroschisis with intestinal atresia—predictive value of antenatal diagnosis and outcome of postnatal treatment. *J Pediatr Surg* 47(2):322–328, 2012.
169. Badillo A, Hendrick H, Wilson RD, et al: Prenatal ultrasonographic gastrointestinal abnormalities in fetuses with gastroschisis do not correlate with postnatal outcomes. *J Pediatr Surg* 43(4):647–653, 2008.
170. Goetzinger KR, Tuuli MG, Longman RE, et al: Sonographic predictors of postnatal bowel atresia in fetal gastroschisis. *Ultrasound Obstet Gynecol* 43(4):420–425, 2014.
171. Alfaraj MA, Ryan G, Langer JC, et al: Does gastric dilation predict adverse perinatal or surgical outcome in fetuses with gastroschisis? *Ultrasound Obstet Gynecol* 37(2):202–206, 2011.
172. Ergün O, Barksdale E, Ergün FS, et al: The timing of delivery of infants with gastroschisis influences outcome. *J Pediatr Surg* 40(2):424–428, 2005.
173. Charlesworth P, Njere I, Allotey J, et al: Postnatal outcome in gastroschisis: effect of birth weight and gestational age. *J Pediatr Surg* 42(5):815–818, 2007.
174. Boutros J, Regier M, Skarsgard ED, Canadian Pediatric Surgery Network: Is timing everything? The influence of gestational age, birth weight, route, and intent of delivery on outcome in gastroschisis. *J Pediatr Surg* 44(5):912–917, 2009.
175. Cain MA, Salemi JL, Paul Tanner J, et al: Perinatal outcomes and hospital costs in gastroschisis based on gestational age at delivery. *Obstet Gynecol* 124(3):543–550, 2014.
176. Overcash RT, DeUgarte DA, Stephenson FL, et al: University of California Fetal Consortium: Factors associated with gastroschisis outcomes. *Obstet Gynecol* 124(3):551–557, 2014.
177. Lepigeon K, Van Mieghem T, Vasseur Maurer S, et al: Gastroschisis—what should be told to parents? *Prenat Diagn* 34(4):316–326, 2014.
178. Baud D, Lausman A, Alfaraj MA, et al: Expectant management compared with elective delivery at 37 weeks for gastroschisis. *Obstet Gynecol* 121(5):990–998, 2013.
179. Keppler-Noreuil KM: OEIS complex (omphalocele-exstrophy-imperforate anus-spinal defects): a review of 14 cases. *Am J Med Genet* 99:271–279, 2001.
180. Phillips T: Spectrum of cloacal exstrophy. *Semin Pediatr Surg* 20:113–118, 2011.
181. Jayachandran D, Bythell M, Ward Platt M, Rankin J: Register based study of bladder exstrophy-epispadias complex: prevalence, associated anomalies, prenatal diagnosis and survival. *J Urol* 186:2056–2061, 2011.
182. Martinez-Frias ML: Exstrophy of the cloaca and exstrophy of the bladder: two different expressions of a primary developmental field defect. *Am J Med Genet* 99:261–269, 2001.
183. Carey J: Exstrophy of the cloaca and the OEIS complex: one and the same. *Am J Med Genet* 99:270, 2001.
184. Meizner I, Levy A, Barnhard Y: Cloacal exstrophy sequence; an exceptional ultrasound diagnosis. *Obstet Gynecol* 86:446–450, 1995.
185. Clements M, Chalmers D, Meyers M, Vemulakonda V: Prenatal diagnosis of cloacal exstrophy: a case report and review of the literature. *Urology* 83(5):1162–1164, 2014.
186. Vasudevan PC, Cohen MC, Whitby EH, et al: The OEIS complex: two case reports that illustrate the spectrum of abnormalities and a review of the literature. *Prenat Diagn* 26(3):267–272, 2006.
187. Austin PF, Homsy YL, Gearhart JP, et al: The prenatal diagnosis of cloacal exstrophy. *J Urol* 160(3 Pt 2):1179–1181, 1998.
188. Mallman M, Reutter H, Geipel A, et al: Early prenatal diagnosis of the OEIS complex with different appearance in early compared with late pregnancy before spontaneous rupture of the cloacal membrane. *Prenat Diagn* 34(8):1–3, 2014.
189. Keppler-Noreuil KM, Gorton S, Foo F, et al: Prenatal ascertainment of OEIS complex/cloacal exstrophy—15 new cases and literature review. *Am J Med Genet A* 143A(18):2122–2128, 2007.
190. El-Hattab AW, Skorupski JC, Hsieh MH, et al: OEIS complex associated with chromosome 1p36 deletion: a case report and review. *Am J Med Genet A* 152A(2):504–511, 2010.
191. Goyal A, Fishwick J, Hurrell R, et al: Antenatal diagnosis of bladder/cloacal exstrophy: challenges and possible solutions. *J Pediatr Urol* 8(2):140–144, 2012.
192. Pierre K, Borer J, Phelps A, Chow J: Bladder exstrophy: current management and postoperative imaging. *Pediatr Radiol* 44:768–786, 2014.
193. Ebert AK, Schott G, Bals-Pratsch M, et al: Long-term follow-up of male patients after reconstruction of the bladder-exstrophy-epispadias complex: psychosocial status, continence, renal and genital function. *J Pediatr Urol* 6(1):6–10, 2010.
194. Woo L, Thomas J, Brock J: Cloacal exstrophy: a comprehensive review of an uncommon problem. *J Pediatr Urol* 6:102–111, 2010.
195. Reiner W, Gearhart J: Discordant sexual identity in some genetic males with cloacal exstrophy assigned to female sex at birth. *N Engl J Med* 350(4):333–341, 2004.
196. Diamond DA, Burns JP, Mitchell C, et al: Sex assignment for newborns with ambiguous genitalia and exposure to fetal testosterone: attitudes and practices of pediatric urologists. *J Pediatr* 148(4):445–449, 2006.
197. van Hoorn JH, Moonen RM, Huysentruyt CJ, et al: Pentalogy of Cantrell: two patients and a review to determine prognostic factors for optimal approach. *Eur J Pediatr* 167(1):29–35, 2008.
198. Hsieh YY, Lee CC, Chang CC, et al: Prenatal sonographic diagnosis of Cantrell's pentalogy with cystic hygroma in the first trimester. *J Clin Ultrasound* 26(8):409–412, 1998.
199. Martinez-Frias ML, Bermejo E, Rodriguez-Pinilla E: Body stalk defects, body wall defects, amniotic bands with and without body wall defects, and gastroschisis: comparative epidemiology. *Am J Med Genet* 92:13–18, 2000.
200. Hunter A, Seaver L, Stevenson R: Limb-body wall defect: is there a defensible hypothesis and can it explain all the associated anomalies? *Am J Med Genet A* 155:2045–2059, 2011.
201. Smrcek JM, Germer U, Krokowski M, et al: Prenatal ultrasound diagnosis and management of body stalk anomaly: analysis of nine singleton and two multiple pregnancies. *Ultrasound Obstet Gynecol* 21(4):322–328, 2003.
202. Daskalakis G, Sebire NJ, Jurkovic D, et al: Body stalk anomaly at 10–14 weeks of gestation. *Ultrasound Obstet Gynecol* 10(6):416–418, 1997.



203. Costa ML, Couto E, Furlan E, et al: Body stalk anomaly: adverse maternal outcomes in a series of 21 cases. *Prenat Diagn* 32(3):264–267, 2012.
204. Tolaymat LL, Maher JE, Kleinman GE, et al: Persistent patent urachus with allantoic cyst: a case report. *Ultrasound Obstet Gynecol* 10(5):366–368, 1997.
205. Shukunami K, Tsuji T, Kotsuji F: Prenatal sonographic features of vesicoallantoic cyst. *Ultrasound Obstet Gynecol* 15:545–546, 2000.
206. Lugo B, McNulty J, Emil S: Bladder prolapse through a patent urachus: fetal and neonatal features. *J Pediatr Surg* 41:E5–E7, 2006.
207. Matsui F, Matsumoto F, Shimada K: Prenatally diagnosed patent urachus with bladder prolapse. *J Pediatr Surg* 42:E7–E10, 2007.
208. Fuchs F, Picone O, Levailant JM, et al: Prenatal diagnosis of a patent urachus cyst with the use of 2D, 3D, 4D ultrasound and fetal magnetic resonance imaging. *Fetal Diagn Ther* 24(4):444–447, 2008.

akusher-lib.ru

# Fetal Genitourinary Tract

*Anthony O. Odibo, Jeffrey M. Dicke*

## SUMMARY OF KEY POINTS

- Normal renal function is fully established by the 9th week of gestation.
- It is preferable to describe the findings in the fetal renal pelvis, calyces, ureter, and bladder in cases of urinary tract dilation, rather than using nonspecific terms such as pyelectasis, caliectasis, and hydronephrosis.
- Renal cystic anomalies may be a manifestation of underlying genetic disorders.
- Ultrasound findings in cases of lower urinary tract obstruction (LUTO) are more predictive of poor renal function than serial biochemical analyses of fetal urine.
- Although inability to visualize a kidney in its normal location is typically associated with either renal agenesis or ectopia, an abnormal or nonvisualized normal kidney remains a possibility.
- In sonographic terms, dysplasia is nonspecific and refers to a variety of findings.
- Over 50% of all congenital abdominal masses found in the neonate originate in the kidney with the most common fetal renal tumor being mesoblastic nephroma.
- Prominent adrenal glands suggest either renal agenesis, congenital adrenal hyperplasia (CAH), or the presence of a de novo neoplastic process.
- Disorders of sexual differentiation are heterogeneous and may be secondary to hormonal defects or unidentified genetic diseases.
- Fetal ovarian cysts have an excellent prognosis as the majority resolve in the postnatal period spontaneously.

## OUTLINE

### Embryology, 504

### Normal Fetal Urinary Tract, 504

### Obstructive Urinary Tract Abnormalities, 504

Transient Dilation, 506

Ureteropelvic Junction Obstruction, 506

Ureterovesical Junction Obstruction, 509

Duplex Collecting System/Ureterocele, 509

Vesicoureteral Reflux, 511

Lower Urinary Tract Obstruction, 512

Urethral Atresia, 515

Congenital Megalourethra, 515

Cloacal Malformation, 515

Prune-Belly Syndrome, 515

Megacystis-Microcolon-Intestinal Hypoperistalsis Syndrome, 515

Management of Fetal Renal Pelvic Dilatation After Birth, 516

### Nonobstructive Fetal Urinary Tract Anomalies, 517

Nonobstructive Megaureter, 517

Empty Renal Fossa, 518

Unilateral Renal Agenesis, 519

Aberrant Cephalad Migration, 520

Renal Fusion Abnormalities, 520

### Dysplastic Kidneys, 521

### Miscellaneous Cystic Renal Disorders, 523

Glomerulocystic Kidneys, 523

Medullary Cystic Dysplasia, 523

### Unclassified Renal Cystic Diseases, 523

Multicystic Dysplastic Kidney, 523

### Renal Tumors, 525

### Nonobstructive Fetal Bladder Abnormalities, 526

Absent or Nonvisualized Bladder, 526

Epispadias, Bladder Exstrophy, and Cloacal Exstrophy, 526

### Bilateral Single Ectopic Ureters, 528

### Fetal Adrenal Glands, 529

Normal Adrenal Glands, 529

Adrenal Disorders, 530

### Fetal Genital Anomalies, 531

Disorders of Sexual Development, 532

### Fetal Ovarian Cysts, 532

### Hydrocolpos/Hydrometrocolpos, 534



Congenital abnormalities of the kidneys and urinary tract (CAKUT) affect 1 in 500 live births and constitute about 20% of all major fetal anomalies,<sup>1,2</sup> and autopsy evidence suggests an even higher prevalence.<sup>3</sup> Although antenatal diagnosis of urinary tract malformations appears to be improving secondary to improved resolution of ultrasound equipment, there are relatively high false positive rates. This is compounded by the lack of a consensus on terminology and diagnostic criteria for cases of antenatal urinary tract dilatation.

## EMBRYOLOGY

The urogenital system consists of two structurally and functionally different components—the urinary system and the genital system. Both develop from a common ridge of mesodermal tissue, the intermediate mesoderm, along the posterior wall of the abdominal cavity.

Human embryos develop three sets of excretory organs or kidney systems during intrauterine life.<sup>4</sup> The embryonic kidneys, which form in a cranial to caudal sequence, in order of appearance are the pronephros, the mesonephros, and the metanephros. The pronephros and the mesonephros both regress in utero, and the metanephros ultimately becomes the permanent kidneys<sup>5,6</sup> (Fig. 15-1A and B). The mesonephros serves as an excretory organ for the embryo whereas the definitive kidney begins its development, then regresses by the 4th month. Some elements of the mesonephros are retained in the mature urogenital system as part of the reproductive tract.<sup>6</sup>

The metanephros forms in the sacral region as a pair of structures called the metanephric diverticulum or ureteric bud. It emanates from the distal portion of the mesonephric duct and comes in contact with and penetrates the metanephric mesenchymal blastema (metanephric mesoderm) at approximately the 28th day.<sup>5,6</sup>

The ureteric bud and metanephric mesoderm exert reciprocal inductive effects toward each other, and the proper differentiation of these structures depends on these inductive signals. The metanephric mesoderm induces the ureteric bud to branch, and the ureteric bud induces the metanephric mesoderm to condense and undergo mesenchymal-epithelial conversion. The nephron, which consists of the glomerulus, proximal tubule, loop of Henle, and distal tubule, is thought to derive from the metanephric mesoderm, whereas the collecting system, consisting of collecting ducts, calyces, pelvis, and ureter, is formed from the ureteric bud.<sup>6</sup>

The division of the ureteric bud results in the eventual pelvicalyceal patterns and their corresponding renal lobules. The first few divisions of the ureteric bud give rise to the renal pelvis, major and minor calyces, and collecting tubules. Thereafter, the first generations of collecting ducts are formed. When the ureteric bud first invades the metanephric mesoderm, its expanded end forms an ampulla that will eventually give rise to the renal pelvis. By the 6th week, the ureteric bud has bifurcated at least four times, yielding 16 branches. These branches then coalesce to form two to four major calyces extending from the renal pelvis. By the 7th week, the next four generations of branches also fuse, forming the minor calyces. By the 32nd week, approximately 11 additional generations of bifurcation have resulted in approximately 1 to 3 million branches, which will become the collecting duct tubules. In humans, although renal maturation continues to take place postnatally, nephrogenesis is completed before birth.<sup>6</sup> The kidney moves cephalad from its pelvic position to the lumbar region by the 6th to 9th week of gestation.

Initially, the excretory ducts of both systems enter a common cavity, the cloaca.<sup>4</sup> The urorectal septum develops during the 4th to 6th weeks and separates the cloaca into an anterior urogenital sinus and the rectum posteriorly. The urogenital sinus gives rise to the bladder superiorly and the membranous urethra inferiorly.<sup>7</sup> Initially the bladder is

continuous with the allantois, but when the lumen of the allantois is obliterated, a thick fibrous cord, the urachus, remains and connects the apex of the bladder with the umbilicus. The genital ridges can be seen medial to the mesonephros and these form the gonads, which differentiate into male and female testis and ovaries, respectively, by the 8th week.

## NORMAL FETAL URINARY TRACT

With the use of transvaginal transducers, the fetal kidneys can be demonstrated at approximately 11 weeks, and they can be visualized by 12 weeks using transabdominal probes (Fig. 15-2). During the first trimester, the kidneys appear as hyperechoic oval structures at both sides of the spine with echogenicity comparable to that of the liver or spleen. The bladder can be seen in most fetuses from the 9th week of gestation (Fig. 15-3). The echogenicity of the fetal kidneys progressively decreases, and by the third trimester, the cortical echogenicity should be less than that of the liver or spleen. Corticomedullary (CMD) differentiation begins at about 14 to 15 weeks and should always be demonstrated in fetuses older than 18 weeks (Fig. 15-4B). Growth and appropriate size of the fetal kidneys can be evaluated by measuring renal length and comparing it to normal charts. The normal kidney grows at an average rate of 1.1 mm per gestational week. During the second and third trimesters, the kidneys are easily identified by imaging the dorsolumbar spine and scanning on either side in parasagittal and transverse axial sections (Fig. 15-4A). Urine distending the renal pelvis may help in their identification. Under normal conditions, the fetal ureters are not visible.<sup>8-10</sup>

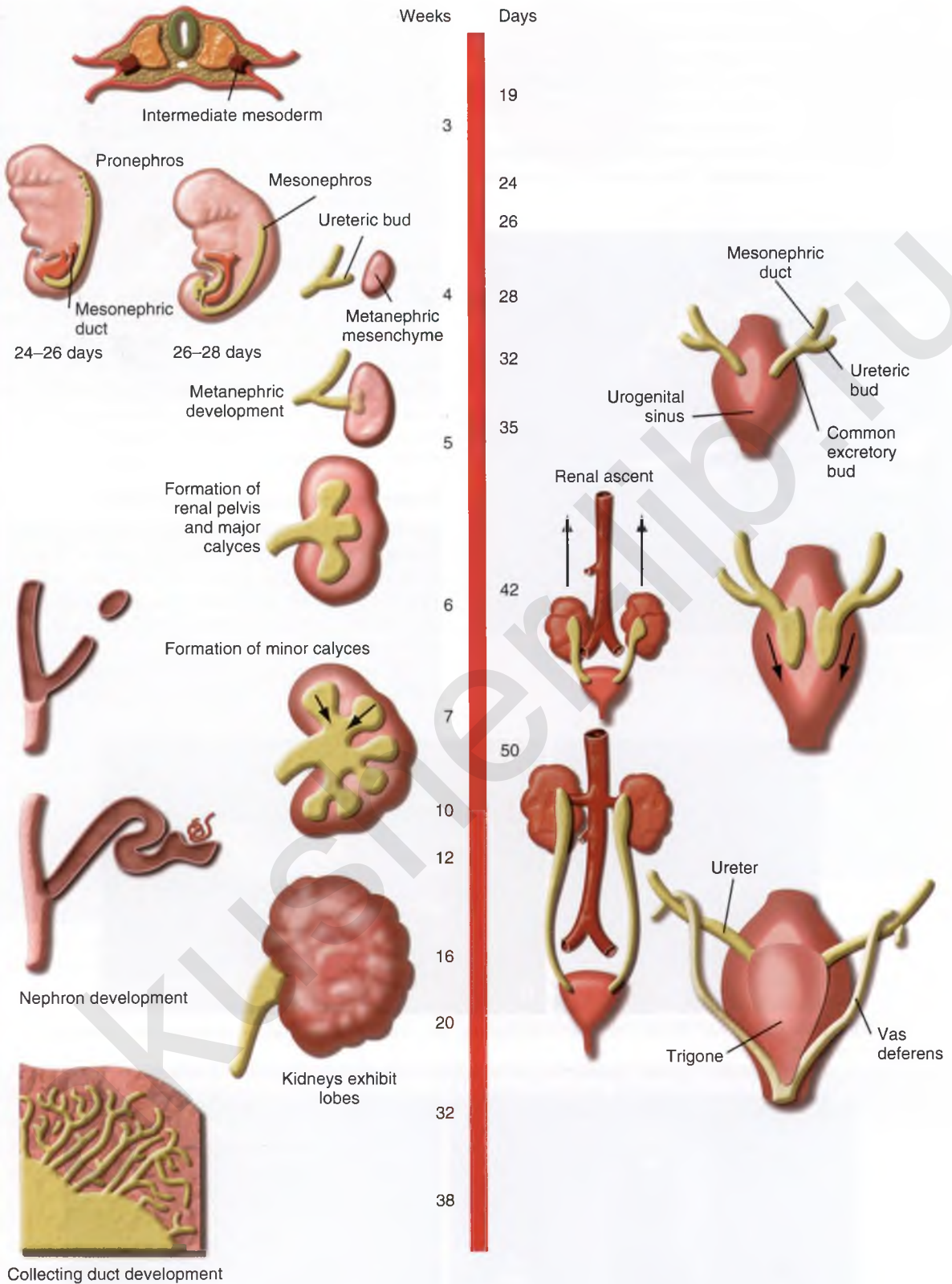
Production of urine by the kidneys begins during the 9th week of embryonic life. At this stage, the urine in the bladder allows visualization as a fluid-filled structure within the fetal pelvis (Fig. 15-5).

During the second and third trimester, the bladder will empty and refill continuously every 25 to 30 minutes. This cycle can be monitored during the sonographic examination. Toward the end of the pregnancy, this cycle decreases, especially in female fetuses, possibly from hormonal influence on the fetal bladder neck. The position of the fetal bladder is easily identified, because it lies between the umbilical arteries within the fetal pelvis. These arteries are readily seen with the use of color Doppler imaging.<sup>8,9</sup> The normal thickness of the bladder wall is about 2 mm, and the ideal position to measure this is at the level of the umbilical arteries.

In addition to visualization of the bladder and normal kidneys, the assessment of the urinary tract (UT) should include an evaluation of the amniotic fluid volume. After 14 weeks, two thirds of the normal amniotic fluid is produced by fetal urination and one third comes from pulmonary fluid. A normal volume of amniotic fluid is mandatory for proper development of the fetal lung.<sup>11</sup>

## OBSTRUCTIVE URINARY TRACT ABNORMALITIES

Urinary tract dilation is one of the most common sonographic prenatal diagnoses, affecting 1% to 5% of all pregnancies. The condition is most commonly diagnosed by measuring the anteroposterior (AP) diameter of the renal pelvis on a transverse scan of the fetal abdomen (Figs. 15-6 and 15-7). The exact incidence is confounded by the different terms used to describe this condition in the literature, including hydronephrosis, pyelectasis, pelviectasis, and pelvicaliectasis. In an attempt to limit the use of these confusing terms, this chapter will use the term *urinary tract dilation* and be more specific when the underlying renal abnormality is known, as recently suggested in a Consensus Statement endorsed by the major fetal and postnatal renal imaging societies.<sup>12</sup> The proposed classification system suggests describing



**A** Kidney development      **B** Ureter and bladder development

**FIG 15-1** The timeline of urogenital system development in the kidney (**A**) and ureter and bladder (**B**). (Modified from Park JM: Normal and anomalous development of the urogenital system. In Walsh PC: Campbell's Urology, 8th ed. Philadelphia, WB Saunders, 2002, p 1737. Copyright © 2002 Saunders, an imprint of Elsevier; and Larsen WJ: Human Embryology. New York, Churchill Livingstone, 1997. Illustration by James A. Cooper, MD, San Diego, CA.)



findings on renal ultrasound examination as shown in Table 15-1 and Figure 15-8 and classifying normal renal findings as in Table 15-2. The panel went on to propose stratifying prenatal risks and management schemes based on findings as shown in Figure 15-9. Examples of sonographic features of common findings associated with urinary tract dilation are shown in Figures 15-8 and 15-10A and B.

In the low-risk group, other than one prenatal follow-up sonogram, no postnatal follow-up is recommended. This approach is in contrast



**FIG 15-2** First trimester kidneys (arrows) appear as hyperechoic structures beside the spine with echogenicity comparable to that of the liver or spleen.

to high-risk groups, which require closer and more frequent evaluation. The proposed classification system builds on that previously proposed by the Society for Fetal Urology (Fig. 15-11A and B), with the advantage of being endorsed by other professional organizations, including the Society for Maternal-Fetal Medicine, the American Institute for Ultrasound in Medicine, and the American College of Radiologists. Prospective studies are needed to evaluate the effectiveness of the classification system in streamlining management of these abnormalities. The common causes, and their incidence, of urinary tract dilation are shown in Table 15-3.<sup>13</sup>

### Transient Dilation

The majority of fetuses with an antenatal diagnosis of renal dilation have normal renal findings postnatally. Transient dilation is thought to result from narrowing or natural folds within the urinary tract during the early developmental phase, which eventually resolve. Because this is a retrospective diagnosis, it is difficult to differentiate from other causes of urinary tract dilation. In general, the fetuses with transient dilation tend to have AP diameters of less than 6 mm in the second trimester and less than 8 mm in the third trimester.<sup>14-16</sup>

### Ureteropelvic Junction Obstruction

The hallmark of ureteropelvic junction (UPJ) obstruction is the finding of a dilated renal pelvis and calyces without dilation of the ureters. This condition affects 1 in 2000 births and is responsible for 10% to 30% of all cases of antenatal renal dilation.<sup>16,17</sup> The cause of UPJ obstruction remains unknown, but it is observed more commonly in male fetuses.

The threshold measurement for diagnosis on axial views of the kidney is 7 mm for mild dilation (see Fig. 15-6), between 7 and 15 mm

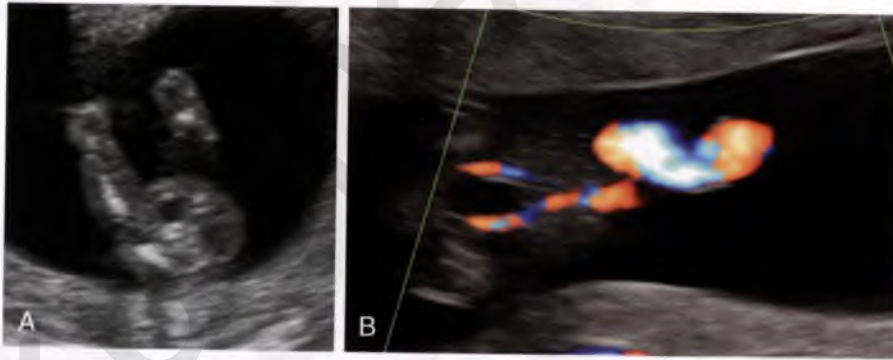


**FIG 15-3** Axial view of first trimester fetal bladder (A); first trimester bladder delineated by umbilical arteries (B).

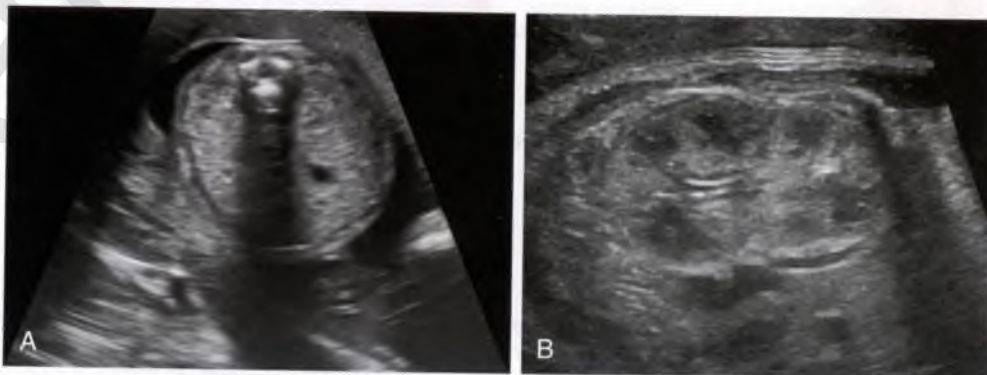


**FIG 15-4** Axial view of normal-appearing second trimester kidneys examined with the spines at the ideal position (A); normal corticomedullary differentiation in a normal third trimester kidney, demonstrating the difference between the hypoechoic medulla and the echogenic cortex (B).



FIG 15-5 Sagittal view of a first trimester fetal bladder (arrow).



FIG 15-6 Transverse view of unilateral dilated renal pelvis with no evidence of dilated calyces. LT, left; RT, right.



A



B

FIG 15-7 Bilateral mild dilatation. **A**, Illustration demonstrating the method for measuring the degree of dilatation. A transverse axial plane of section of the fetal abdomen is obtained, and an anteroposterior measurement of the renal pelvis is obtained. **B**, Transverse sonographic scan through both kidneys (K) demonstrating a mildly distended renal pelvis and the method of measuring the renal pelvis (arrows). Ab, fetal abdomen; Sp, spine. (Illustration by James A. Cooper, MD, San Diego, CA.)

TABLE 15-1 Ultrasound Parameters Included in the Urinary Tract Dilatation Classification System

Ultrasound Parameters	Measurement/Findings	Note
Anteroposterior renal pelvic diameter (APRPD)	AP in mm	Measured on transverse image at the maximal diameter of intrarenal pelvis (Fig. 15-7)
Calyceal dilation: central (major calyces)	Yes/no	Subjective assessment
Calyceal dilation: peripheral (minor calyces)	Yes/no	
Parenchymal thickness	Normal/abnormal	
Parenchymal appearance	Normal/abnormal	
Ureter	Normal/abnormal	Evaluate echogenicity, corticomedullary differentiation, and for cortical cysts
Bladder	Normal/abnormal	Dilation of ureter is considered abnormal prenatally, although transient visualization of the ureter is considered normal postnatally
		Evaluate wall thickness for the presence of ureterocele and for a dilated posterior urethra

Modified from Nguyen HT, Benson CB, Bromley B, et al: Multidisciplinary consensus on the classification of prenatal and postnatal urinary tract dilation (UTD classification system). *J Pediatr Urol* 10(6):982-998, 2014.



## UTD Classification System

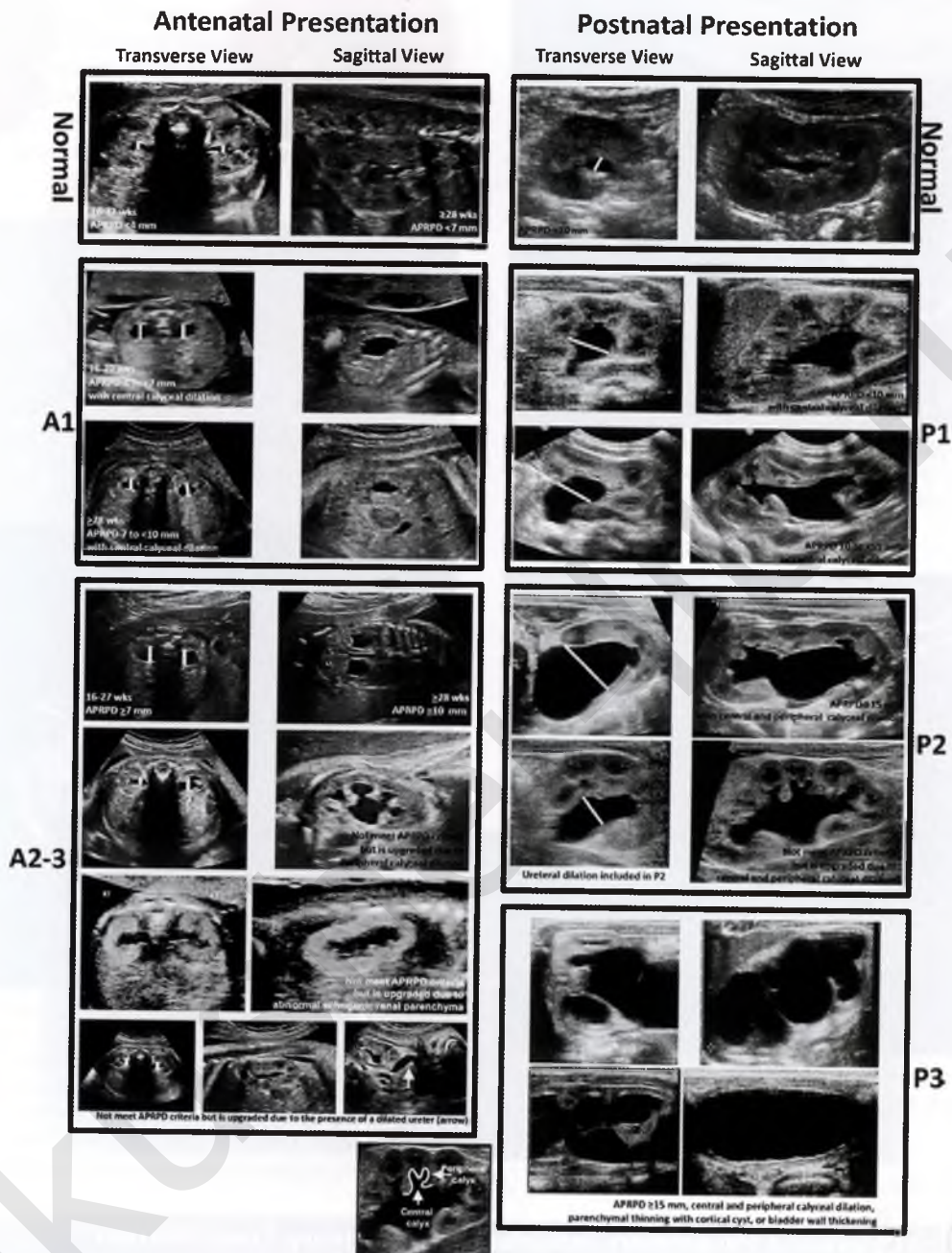


**FIG 15-8** The urinary tract dilation (UTD) classification system, which describes the appearance of the urinary tract based on antenatal and postnatal presentation. Antenatal presentation (*left column*) is divided into normal, A1 and A2-3, and measurements between 16 and 27 weeks and 28 or more weeks of gestation. A normal urinary tract is one with no urinary tract abnormalities and anteroposterior renal pelvic diameter (APRPD) measuring less than 4 mm between 16 and 27 weeks' gestation and less than 7 mm at 28 or more weeks of gestation. A1 describes a normal urinary tract with 4 to less than 7 mm pelvic dilation at 16 to 27 weeks' gestation or 7 to less than 10 mm at 28 or more weeks of gestation with or without central calyceal dilation. UTD A2-3 is for fetuses with APRPD of 7 mm or more between 16 and 27 weeks' gestation or 10 mm or greater at 28 or more weeks of gestation, peripheral calyceal dilation, ureteral dilation, renal parenchymal, or bladder abnormalities. The postnatal presentation (*right column*) is divided into normal, P1, P2, and P3. Measurements are more reliable if taken 48 hours after birth or later. A normal urinary tract is one with no urinary tract abnormalities and APRPD less than 10 mm. P1 describes a normal urinary tract with APRPD 10 to less than 15 mm or central calyceal dilation. P2 describes APRPD 15 mm or more or peripheral calyceal dilation. P3 describes additional ureteral dilation, abnormal renal echogenicity, or cysts or bladder abnormalities regardless of APRPD measurement. (From Chow JS, Benson CB, Lebowitz RL: The clinical significance of an empty renal fossa on prenatal sonography. *J Ultrasound Med* 24(8):1049-1054, 2005.)

**TABLE 15-2 Normal Values for Urinary Tract Dilatation Classification System**

Ultrasound Findings	TIME AT PRESENTATION		
	16 to 27.9 Weeks	≥28 Weeks	Postnatal (>48 Hours)
Anteroposterior renal pelvic diameter	<4 mm	<7 mm	<10 mm
Calyceal dilation			
Central	No	No	No
Peripheral	No	No	No
Parenchymal thickness	Normal	Normal	Normal
Parenchymal appearance	Normal	Normal	Normal
Ureter(s)	Normal	Normal	Normal
Bladder	Normal	Normal	Normal
Unexplained oligohydramnios	No	No	NA

Modified from Nguyen HT, Benson C, Bromley B, et al: Multidisciplinary consensus on the classification of prenatal and postnatal urinary tract dilation (UTD classification system). *J Pediatr Urol* 10(6):982-998, 2014.  
N/A, not applicable.

for moderate dilation, and greater than 15 mm for marked dilation by 32 weeks' gestation. The more dilated the system, the more likely it is that renal function will be compromised after birth. In addition to measurement of the renal pelvis, it is important to determine and to document whether the central or peripheral calyces are dilated. Evaluation of the kidneys should also include assessment of the appearance of the cortices; thinned, hyperechogenic renal cortices with cysts often represent obstructive dysplasia and impaired function (Fig. 15-12). Although there is inconsistent correlation between the antenatal renal appearance and postnatal function, the presence of cysts commonly indicates the presence of dysplasia and compromised renal function.<sup>18-22</sup>

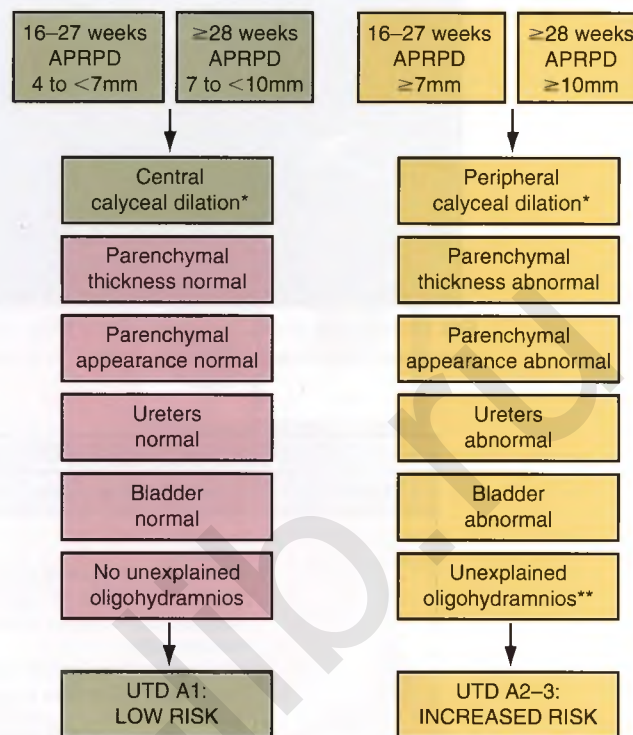
The differential diagnosis of UPJ obstruction includes reflux, transient dilation, multicystic dysplastic kidney (MCDK), and ureterovesical junction (UVJ) obstruction. Less common differential diagnoses of UPJ obstruction are megacalycoses due to medullary hypoplasia in which the calyces are more dilated than the renal pelvis; infundibular stenosis with no medullary hypoplasia, but calyceal dilation still present; and isolated cysts within the kidney.

Associated renal or extrarenal anomalies are present in 12% to 25% of cases of UPJ obstruction.<sup>23</sup> Once diagnosed in the second trimester, follow-up at or after 32 weeks is recommended to exclude cases with transient dilatation that may have resolved by this time (<7 mm dilated). Conflicting reports have been published regarding the association of isolated mild renal pelvic dilation and aneuploidy, but the overall evidence suggests that although this association is weak, it is significant and should be discussed with patients.<sup>24-26</sup> Patients should be informed of the overall good prognosis for fetuses with UPJ obstruction. Of those cases that are persistent in the postnatal period, 19% to 25% may require some form of surgical intervention.<sup>27,28</sup>

### Ureterovesical Junction Obstruction

UVJ obstruction is responsible for 5% to 10% of all cases of urinary tract dilation. In about 25% of cases, the contralateral kidney is also affected. The diagnosis of UVJ obstruction is based on the demonstration of a dilated ureter in the presence of a dilated renal pelvis and a normal bladder.<sup>29-32</sup> Peristaltic waves can often be seen, and they modify the caliber of the ureter (Fig. 15-13). The dilatation may increase in utero, but it usually decreases after birth.

### PRENATAL PRESENTATION



\*Central and peripheral calyceal dilation may be difficult to evaluate early in gestation

\*\*Oligohydramnios is suspected to result from a urological cause

**FIG 15-9** Urinary tract dilation (UTD) management scheme. APRPD, anteroposterior renal pelvic diameter. (Adapted from Nguyen HT, Benson C, Bromley B, et al: Multidisciplinary consensus on the classification of prenatal and postnatal urinary tract dilation [UTD classification system]. *J Pediatr Urol* 10(6):982-998, 2014.)

The underlying cause of UVJ obstruction appears to be a localized dysfunction in a region of the lower ureter. In most instances, it is not possible to differentiate between dilation secondary to UVJ obstruction and that occurring secondary to high-grade vesicoureteral reflux (VUR). A clue to the diagnosis is variability in the diameter of the renal pelvis during one single examination, which favors a diagnosis of VUR. It is also important to distinguish the usually tortuous dilated ureter from loops of bowel. Another common cause of a dilated ureter is a ureterocele (discussed later).

The prognosis for UVJ obstruction is generally good, and the degree of ureteric dilation may offer some clue to the long-term prognosis and the need for postnatal surgery.<sup>33,34</sup>

### Duplex Collecting System/Ureterocele

Renal pelvic dilation secondary to a ureterocele or ectopic implantation of the ureter causes 5% to 7% of antenatal urinary tract dilation (Fig. 15-14). Renal duplication can occur without dilatation, but is more readily demonstrated once dilation has developed (Fig. 15-15). Most commonly the ureter draining the upper pole moiety has an ectopic insertion located inferior and medial to the normal bladder insertion site. Often an ectopic ureterocele is also seen within the bladder (Fig. 15-14C). Dilatation of the lower pole moiety most commonly occurs because of reflux. Duplex kidneys are thought to arise from an additional ureteric bud from the mesonephric duct.<sup>35</sup>

A ureterocele is visualized as a septum or cyst within the bladder, although the ectopic extravascular insertion may be difficult to diagnose



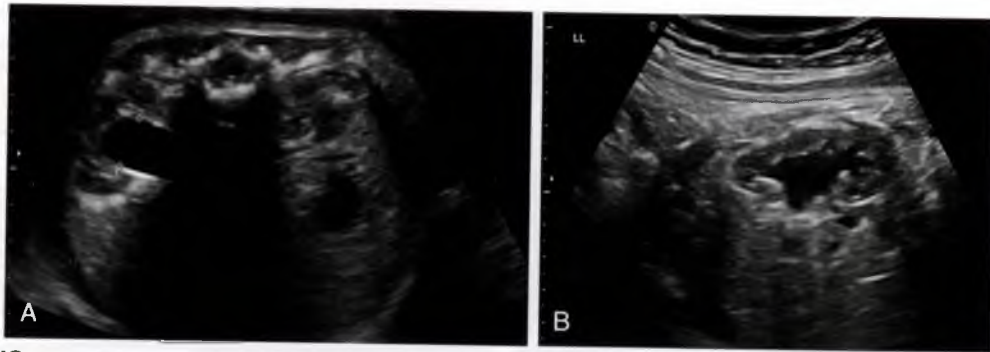


**FIG 15-10** Transverse view of unilateral dilated renal pelvis with no evidence of dilated calyces (**A**); sagittal view showing unilateral dilated renal pelvis with both central and peripheral dilation of the calyces (**B**).

SOCIETY OF FETAL UROLOGY GRADING SYSTEM OF CONGENITAL HYDRONEPHROSIS		
Grade	Central renal complex	Renal parenchymal thickness
0	Intact	Normal
I	Mild splitting of pelvis (dilation)	Normal
II	Moderate splitting of pelvis and calyces, but complex, confined within renal border	Normal
III	Marked splitting, pelvis dilated outside renal borders and calyces dilated	Normal
IV	Further pelvicalyceal dilation	Thinned

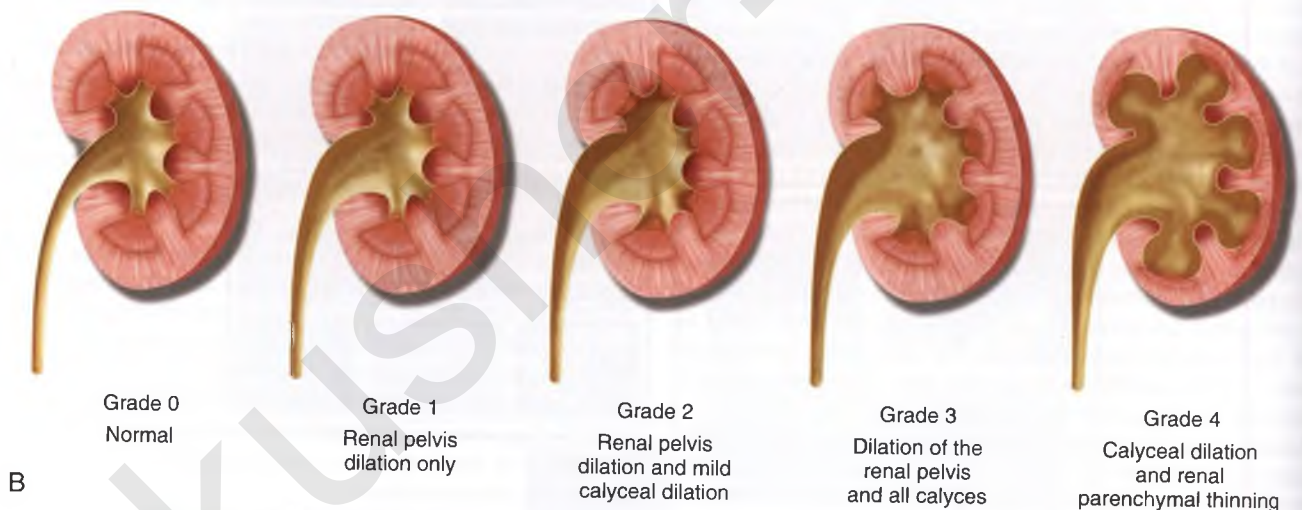


**FIG 15-11** Society of Fetal Urology (SFU) grading system of congenital hydronephrosis. **A**, Description. **B**, Illustration demonstrating the FSU ultrasound grading system of hydronephrosis. (Illustration by James A. Cooper, MD, San Diego, CA.)

**TABLE 15-3 Etiology of Urinary Tract Dilatation**

Cause	Incidence
Transient dilatation	41-88%
Ureteropelvic junction (UPJ) obstruction	10-30%
Vesicoureteral reflux (VUR)	10-20%
Ureterovesical junction (UVJ) obstruction	5-10%
Duplex collecting system/ureterocele	5-7%
Multicystic dysplastic kidney	4-6%
Lower urinary tract obstruction (LUTO)	1-2%

in utero<sup>36-38</sup> (Fig. 15-14C). In some cases, the renal parenchyma of the obstructed side may be thinned and dysplastic. Although most cases of ureterocele are visible on prenatal ultrasound examinations, sonologists should be aware that a full bladder may sometimes compress the cyst and prevent visualization. A ureterocele may also prolapse into the urethra and result in acute LUTO.

The differential diagnosis of ureterocele includes UVJ obstruction and VUR. It should be remembered that 50% of duplex collecting systems have coexisting VUR in the lower pole moiety. The prognosis is generally good but will depend on the degree of associated renal dysplasia affecting each pole. In the prenatal period, follow-up ultrasound examinations to document worsening urinary tract dilatation are

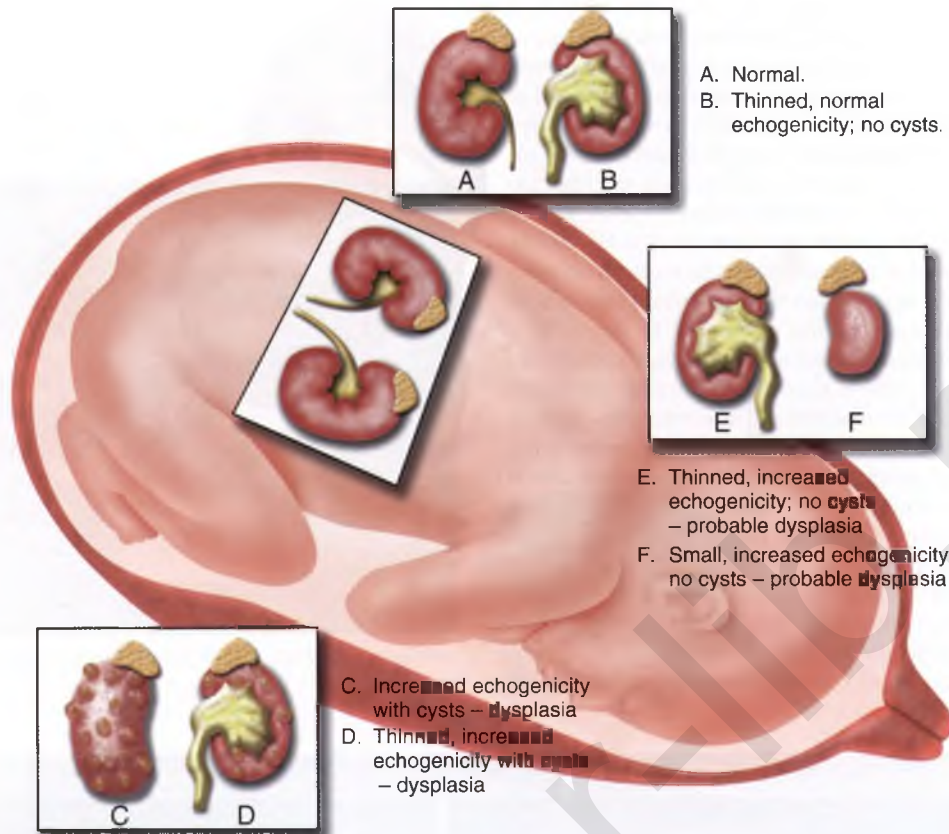


**FIG 15-12** Urinary tract obstruction produces a varied response from the kidneys. **A**, The kidney may remain normal in distal obstruction, without reflux. **B**, Pelvocaliectasis may attenuate the parenchymal thickness. **C**, The kidney may suffer cystic dysplasia (parenchymal cysts), become fibrotic (increased echogenicity), and cease to function (lack of pelvocaliectasis). **D**, Alternatively, it may undergo cystic dysplasia with parenchymal cysts and increased echogenicity but continue to have pelvocaliectasis and a thinned parenchyma. If no cysts are visible but the parenchyma is of greatly increased echogenicity, either with **(E)** or without **(F)** pelvocaliectasis, dysplasia is probably, but not invariably, present. (Illustration by James A. Cooper, MD, San Diego, CA.)

indicated. Postnatal evaluation with further testing for residual renal function and reflux is recommended.

### Vesicoureteral Reflux

VUR constitutes 10% to 20% of all diagnosed cases of antenatal urinary tract dilation. This diagnosis can be challenging to make prenatally and should be suspected in the presence of varying degrees of renal pelvis dilation with an associated either unilateral or bilateral dilated ureter (Fig. 15-16A and B). Proposed causes for VUR include transient bladder outlet obstruction that resolves prior to delivery, high voiding pressure resulting in distortion of the vesicoureteric junction, and delayed maturation of the vesicoureteric junction.<sup>39,40</sup> There also appears to be a strong familial predisposition, raising the possibility of a genetic cause in some cases.<sup>41</sup>

The diagnosis of VUR is important to confirm, as up to 40% of affected infants will develop renal scarring and long-term damage if undetected. The finding of a normal postnatal renal ultrasound examination does not exclude the diagnosis of VUR, and a micturating cystourethrogram may be indicated to completely rule out the diagnosis.<sup>42</sup>

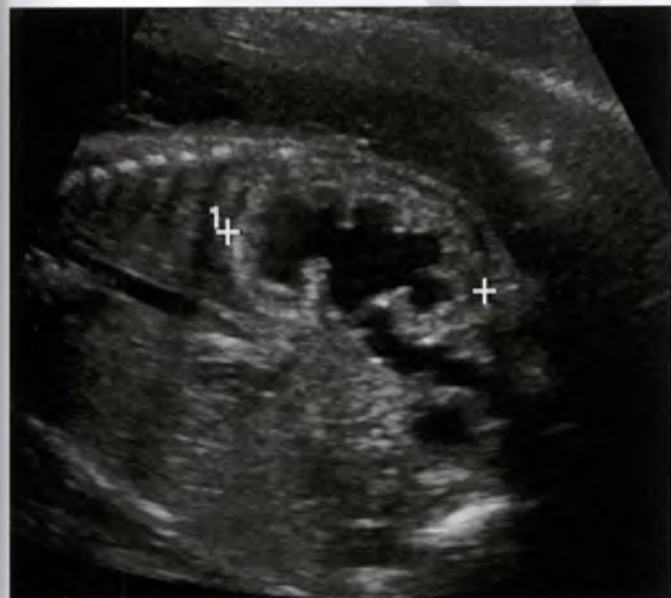


**FIG 15-13** Hydroureteronephrosis. There is dilation of the renal pelvis and calyces, as well as of the ureter in this sagittal image.



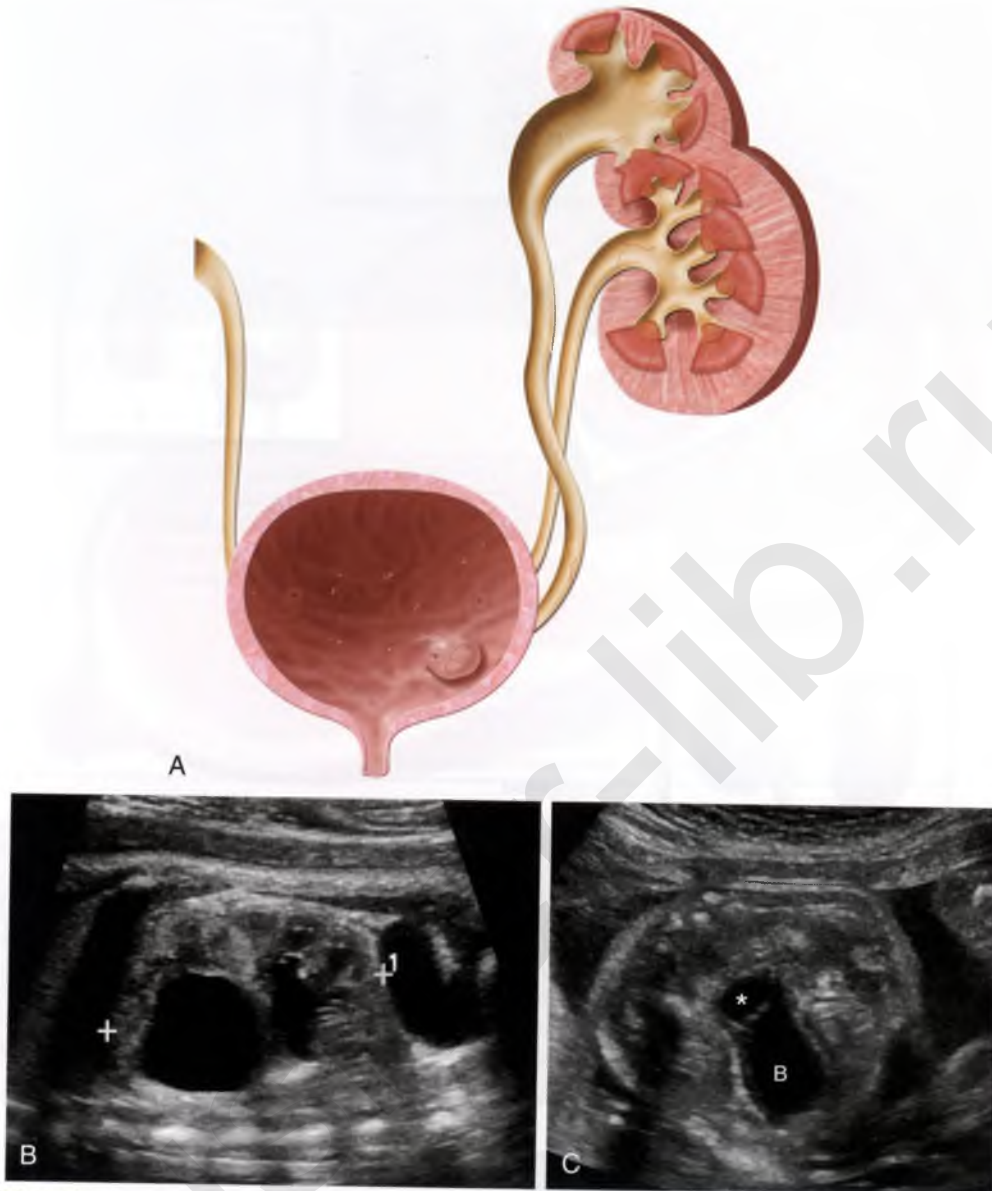


**FIG 15-14** Renal duplication with obstructed upper pole and ureterocele. **A**, Illustration demonstrating duplication of the collective system. Typically the upper pole moiety is obstructed, and the lower pole moiety often demonstrates reflux. The ureter from the upper pole moiety inserts more medially and caudally into the bladder than the ureter from the lower pole. This is referred to as the Meyer-Weigert rule. Dilatation of the submucosal portion of the ureter results in a ureterocele. **B**, Sagittal scan through the kidney demonstrating a dilated upper pole and normal lower pole; the dilated ureter is also seen. **C**, Sagittal scan through the bladder (B) displaying the ureterocele (*asterisk*). (Illustration by James A. Cooper, MD, San Diego, CA).

### Lower Urinary Tract Obstruction

The most common cause of severe bladder outlet obstruction is a *posterior urethral valve* (PUV) (Fig. 15-17). PUVs are membranes within the posterior aspect of the urethra. This condition affects male fetuses and typically presents with an enlarged bladder and dilated urethra, producing the classic keyhole sign seen on ultrasound imaging (Figs. 15-17A and 15-18). The ureters and renal pelves are usually also dilated. With worsening obstruction, the bladder wall becomes hypertrophied with development of trabeculations. Renal parenchymal destruction and dysplasia may result from back-pressure, resulting in atrophic changes. Other findings in severe cases include

severe oligohydramnios, perinephric urinomas, and urinary ascites (Fig. 15-19).

The oligohydramnios seen in LUTO can result in phenotypic changes in the newborn, including Potter facies and contractures of the extremities. The most important consequence of oligohydramnios is the development of pulmonary hypoplasia, a significant contributor to infant mortality and morbidity risks.

Prenatal management involves differentiating bladder enlargement secondary to PUV from other causes of LUTO and from causes of nonobstructive bladder enlargement (Table 15-4). The finding of massive bladder distention associated with oligohydramnios in a male

fetus strongly suggests PUV. Careful assessment can identify fetuses with potential to benefit from prenatal intervention.

Features of poor prognosis in cases of LUTO include early diagnosis, bilateral marked dilatation, persistently obstructed bladder, oligohydramnios, and secondary lung hypoplasia. Bilateral renal dilatation



**FIG 15-15** Sagittal view of a duplicated kidney demonstrating mild dilatation of both poles.

and LUTO have an increased risk of associated chromosomal anomalies, and, therefore, evaluation of fetal chromosomes may be warranted. The finding of associated hyperechogenic and cystic renal parenchyma is frequently associated with poor renal outcomes, with a positive predictive value of 59%, and negative predictive value of 56% regarding postnatal renal function. Conversely, although the presence of renal cortical cysts suggests a poor prognosis, normal renal cortical echogenicity does not exclude dysplasia. A systematic review including 13 articles and 215 women showed amniotic fluid volume and renal cortical appearance on ultrasound imaging to have only modest screening accuracy for predicting postnatal outcome (Table 15-5).<sup>43</sup>

The role of measuring urinary electrolytes in the fetal urine obtained through transabdominal vesicocentesis to predict renal function is controversial. The process involves serial drainage of the fetal bladder with urine sent for biochemical analyses (Table 15-6). The initial urine sample obtained may not be reliable for prognosticating renal function as it may have been stagnant over a long time. Furthermore, there are discrepancies in the predictive value of urine biochemistry in published studies on LUTO owing to small sample size, variations in cutoff values used, gestational age at interrogation, and sampling frequency in published studies.<sup>44-48</sup> Fetuses with renal damage show decreased urinary concentrating ability, especially of sodium and calcium.<sup>49-53</sup> Measurements of  $\beta_2$ -microglobulin in the fetal urine has been suggested as demonstrating a better predictive accuracy, but a

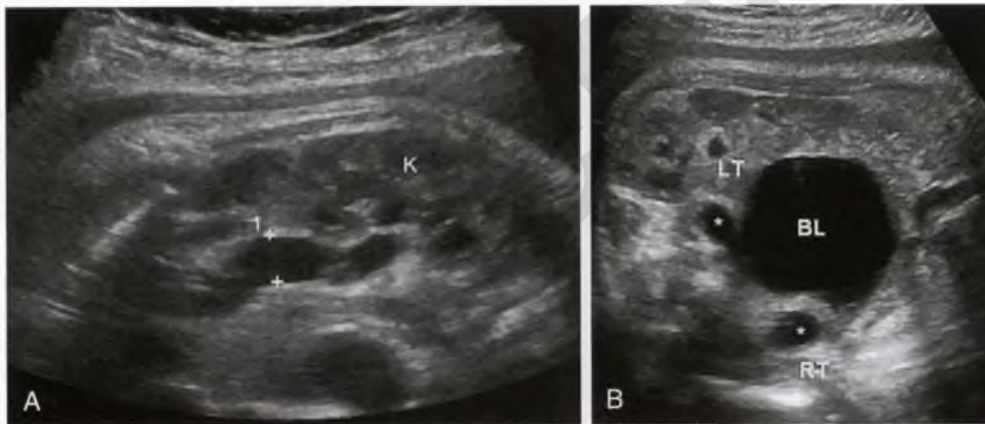


**FIG 15-16** Vesicoureteral reflux (VUR). **A**, Sagittal image of kidney (K) without renal pelvic dilation but with a dilated ureter (*calipers*). **B**, Axial image through the bladder (BL) demonstrating dilated left (LT) and right (RT) ureters (*asterisks*). The finding of varying degrees of renal pelvic dilation with associated ureteric dilatation both unilaterally and bilaterally should raise the suspicion for VUR.

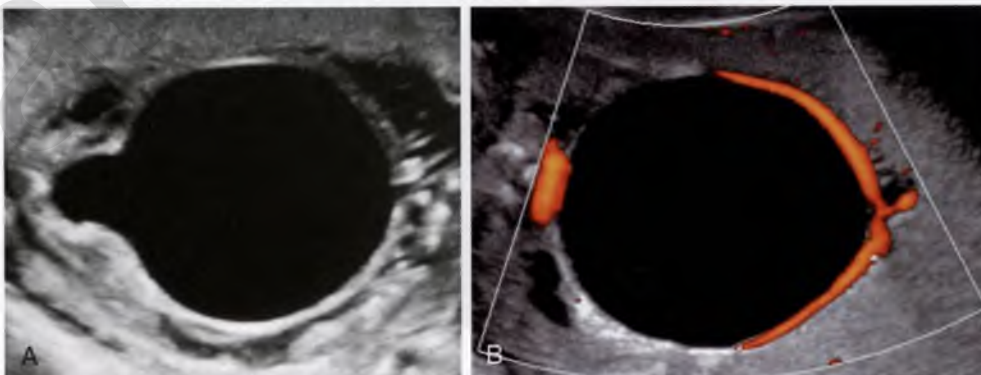


**FIG 15-17** Posterior urethral valves. **A**, Enlarged bladder with classic keyhole appearance. **B**, Confirmation that this large fluid-filled structure represents the bladder by demonstration of umbilical arteries using color flow Doppler sonography.



systematic review including 23 articles and 572 women found this protein to be less accurate than measurement of urinary sodium and calcium.<sup>54</sup>

The goals of prenatal intervention are to avoid further renal damage and to prevent pulmonary hypoplasia. Vesicoamniotic shunting to divert urine from the obstructed fetal bladder into the amniotic cavity

has been the primary prenatal intervention used for several years. However, the outcomes following vesicoamniotic shunting and the long-term results have not been convincing.<sup>55-57</sup> The only randomized controlled trial evaluating this technique (the PLUTO [Percutaneous shunting in Lower Urinary Tract Obstruction] trial) was stopped early because of poor recruitment. Although the trial suggested a trend toward improved survival in the group that received shunting, the relative risk (RR) was not statistically significant (RR 1.88; confidence interval [CI] 0.71-4.96).<sup>57</sup> The PLUTO trial was limited by a significant number of crossovers in the treatment arms; therefore, the authors performed an “as treated” analysis, which showed significant survival benefit from vesicoamniotic shunting. The long-term outcomes from the study are still pending.

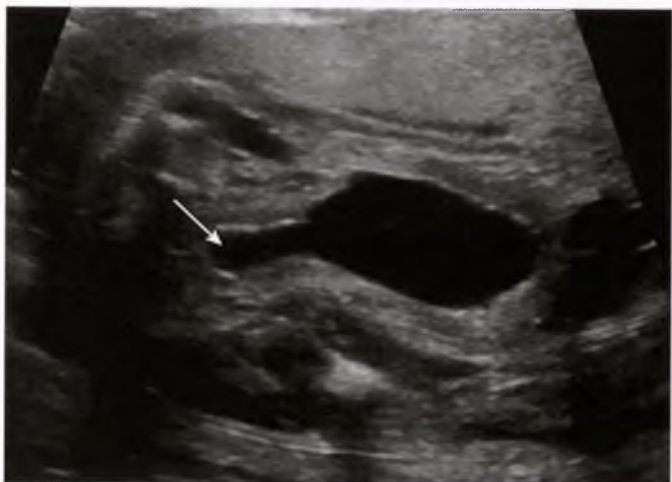


**FIG 15-18** Posterior urethral valves with thick-walled bladder and dilated urethra (arrow).

**TABLE 15-4 Causes of Enlarged Bladder**

Posterior urethral valves
Anterior urethral valves
Urethral atresia
Congenital megalourethra
Prolapsed ureterocele
Megacystis megaureter (vesicoureteral reflux)
Megacystis-microcolon-intestinal hypoperistalsis syndrome
Cloacal malformation

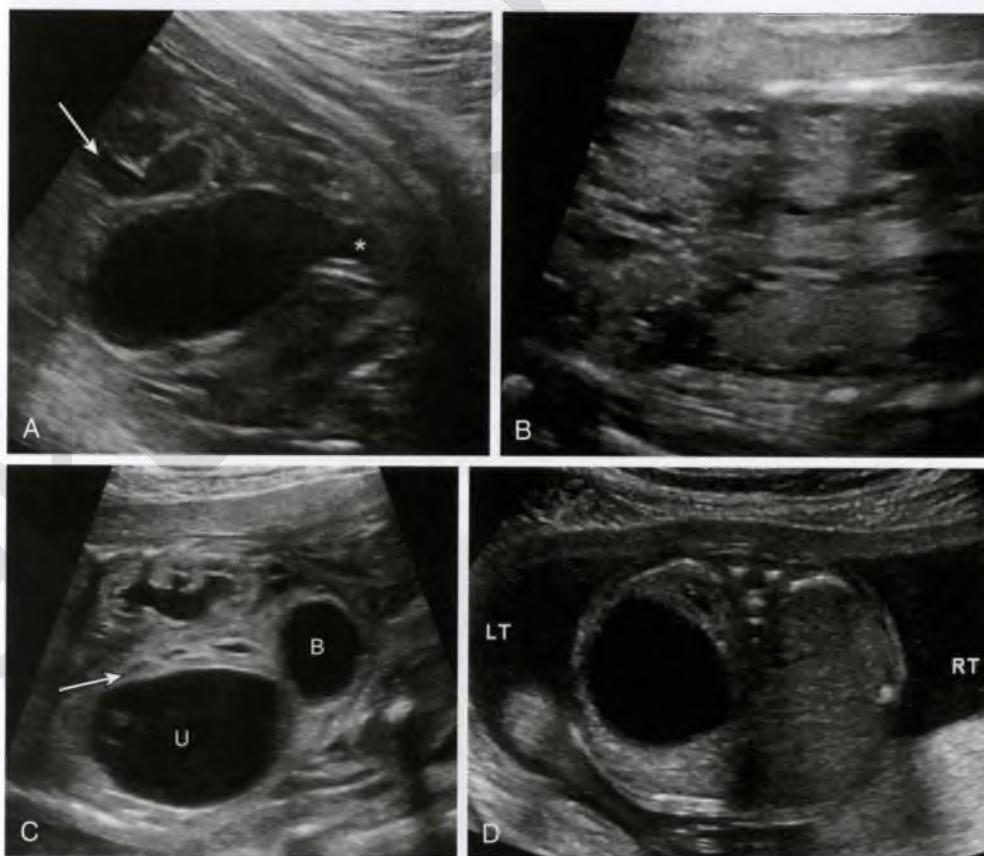


**FIG 15-19** Posterior urethral valves. **A**, Dilated bladder and urethra (asterisk) with dilated ureter (arrow). **B**, Cystic dysplasia resulting from longstanding severe obstruction. **C**, Urinoma (U) resulting from rupture of the renal collecting system with severe obstruction and pressure. The kidney (arrow) is compressed medially and the decompressed, normal-sized bladder (B) is also seen. **D**, Axial image of a large, left (LT) urinoma. RT, right.

**TABLE 15-5 Antenatal Sonographic Screening and Detection of Poor Postnatal Renal Outcome**

Criteria	Sensitivity	Specificity	AUC
Oligohydramnios	0.63 (0.51-0.74)	0.76 (0.65-0.85)	0.74
Renal cortex appearance	0.57 (0.37-0.76)	0.84 (0.71-0.94)	0.78
Gestational age at diagnosis <24 weeks	0.48 (0.26-0.70)	0.82 (0.66-0.92)	0.68 ( <i>P</i> = 0.14)

AUC, area under the curve.

Modified from Morris R, Malin G, Khan K, Kilby M: Antenatal ultrasound to predict postnatal renal function in congenital lower urinary tract obstruction: systematic review of test accuracy. *Br J Obstet Gynaecol* 116:1290-1299, 2009.

**TABLE 15-6 Favorable Prognostic Features in Lower Urinary Tract Obstruction**

Features	Levels/Findings
Sodium	<100 mg/dL
Chloride	<90 mg/dL
Osmolality	<200 mg/dL
Calcium	<8 mg/dL
$\beta_2$ -Microglobulin	<4 mg/dL
Total protein	<20 mg/dL
Amniotic fluid volume	Normal
Renal cortex appearance	Not cystic or echogenic
Gestational age at diagnosis	>24 weeks

Data taken from Morris et al,<sup>43</sup> Glick et al,<sup>44</sup> Nicolaides et al,<sup>45</sup> Mandelbrot et al,<sup>46</sup> Johnson et al,<sup>47</sup> and Muller et al.<sup>48</sup>

Recent case reports have suggested the feasibility of fetoscopic placement of transurethral stents in fetuses with bladder outlet obstruction, although at this time the series are too small for reliable information on outcomes.<sup>58</sup>

### Urethral Atresia

Urethral atresia has a sonographic appearance similar to that of PUV and should be considered in female fetuses with bladder outlet obstruction. Unlike PUV, the obstruction is usually complete and may result in megacystis detected during the first trimester (Fig. 15-20). The condition often has a poor prognosis.<sup>59</sup>

### Congenital Megalourethra

Congenital megalourethra is a rare condition affecting male infants, and it is usually associated with a dilated and elongated penile urethra that may appear sausage-shaped in continuity with a distended bladder (Fig. 15-21A through C). The proposed cause is delayed apoptosis at the penile meatus; this has also been referred to as "anterior urethral valves," although the condition is not actually caused by valves. This process can lead to abnormal development or hypoplasia of the penile erectile tissue. Other sonographic features are similar to those seen in PUV.<sup>60,61</sup> In some cases, the obstruction resolves spontaneously and the outcome can be favorable.<sup>62,63</sup>

### Cloacal Malformation

Cloacal malformation is a rare cause of bladder outlet obstruction affecting 1 in 50,000 pregnancies. It is caused by failure of development



**FIG 15-20** Megacystis, early second trimester (case of urethral atresia). Frontal view through the fetal head and abdomen. The abdomen is filled by the distended urinary bladder.

of the urorectal fold that usually separates the rectum from the genital tract. Consequently, a convergence of the gastrointestinal and genitourinary tracts occurs, with a common opening in the perineum. The condition is seen predominantly in females and can result in the collection of urine in the uterus and vagina (hydrometrocolpos) as well as bladder outlet obstruction and dilated ureters<sup>64-66</sup> (Fig. 15-22). Because of the complex embryologic anomalies involved, cloacal malformation can present with multiple phenotypes and associated anomalies including ureteral ectopia, bladder duplication, renal agenesis, sacral agenesis, open neural tube defects, and vertebral anomalies. The finding of ultrasound features suggestive of PUV in a female fetus should increase the suspicion for cloacal malformations. Transient ascites may be present from chemical irritation of the peritoneum by urine. It may be followed by intra-abdominal calcifications. Depending on the degree of bladder outlet obstruction, profound oligohydramnios may be present.

### Prune-Belly Syndrome

Prune-belly syndrome (PBS) refers to an abnormally lax abdominal wall secondary to extensive stretching during early development. Historically, the condition was thought to result from primary partial or complete absence of the abdominal muscles, although it is currently thought that it is more likely a secondary result of overdistention due to bladder dilation that, in some cases, may have resolved spontaneously. The ultrasound features are very similar to those of PUV, but in PBS, the bladder distention and urethral dilation are not as marked. In addition, similar to PUV the condition is more common in male fetuses; therefore, diligent evaluation is required to distinguish these anomalies, as the therapeutic implications are significantly different prenatally.<sup>67-69</sup> The prognosis is often poor, similar to that of PUV, secondary to severe pulmonary hypoplasia if oligohydramnios was present.

### Megacystis-Microcolon-Intestinal Hypoperistalsis Syndrome

Megacystis-microcolon-intestinal hypoperistalsis syndrome (MMIHS) is an autosomal recessive condition occurring more commonly in females. It presents with evidence of a functional small bowel obstruction, a microcolon with intestinal malrotation, a markedly enlarged bladder, and bilateral hydronephrosis. The bladder finding is not secondary to a physical obstruction, as the condition is characterized by



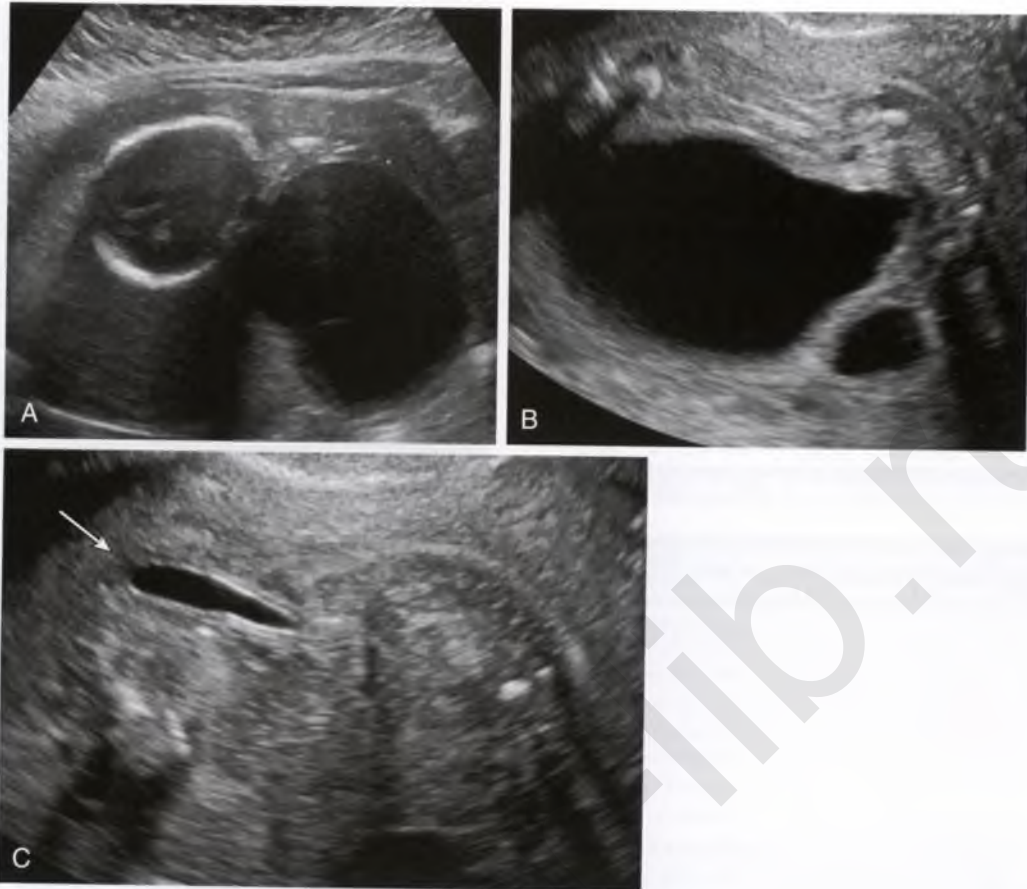


**FIG 15-21** Congenital megalourethra. **A**, Breech fetus with severe oligohydramnios and markedly distended urinary bladder. These sonographic findings are similar to those seen with bladder outlet obstruction due to posterior urethral valves. **B**, Coronal view of dilated urinary bladder with dilation of the prostatic urethra. **C**, Targeted transvaginal sonographic images reveal dilated, elongated penile urethra (*arrow*).

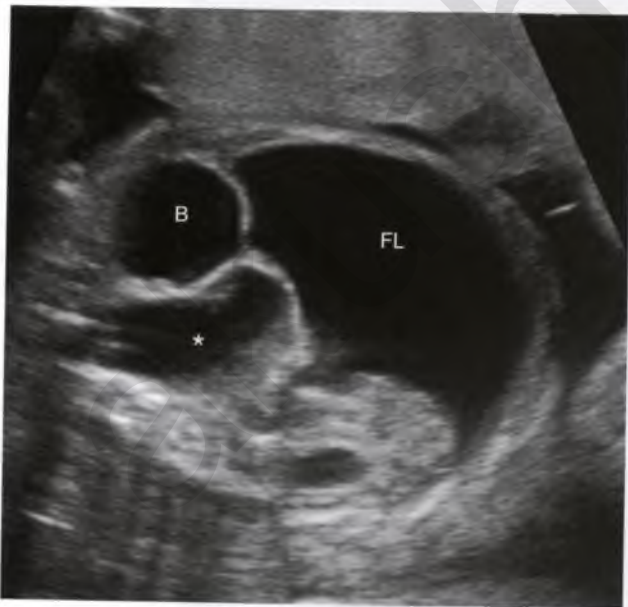


**FIG 15-22** Cloacal malformation. Cloacal malformation, related to convergence of the genital, urinary, and intestinal contents, appears as a central pelvic cystic mass (*asterisk*) containing fluid and dependent layering echoes. This structure is located posterior to the urinary bladder (B). There is a large volume of free intraperitoneal fluid (FL) present, presumed to be due to reflux of urine and meconium through the fallopian tubes. This may result in irritation and chemical peritonitis.

normal amniotic fluid volume and even polyhydramnios in late pregnancy. The underlying cause is poorly understood, but myogenic, neurogenic, and even hormonal mechanisms have been proposed.<sup>70-72</sup> There may be associated anomalies of other organ systems, including omphalocele, cleft lip/palate, and cardiac defects, and the condition is associated with a poor prognosis that becomes apparent in the newborn period. The finding of an enlarged bladder with normal amniotic fluid volume suggests the differential diagnosis of MMIHS after excluding cloacal malformation.

### Management of Fetal Renal Pelvic Dilation After Birth

Dilation of the renal pelvis is often the initial finding in abnormalities of the fetal urinary tract. Although there is generally a direct relationship between fetal renal pelvic dilation and obstructive processes of the urinary tract, there is considerable overlap with nonobstructive disorders. It should be appreciated that renal pelvic dilation detected prenatally often resolves spontaneously after birth with no correction required. In a series from our institution, 140 of 342 (40.9%) fetuses with renal pelvic dilation had nonobstructive hydronephrosis. In these cases, renal pelvic dilation detected prenatally was confirmed postnatally, but ultimately regressed without therapy.<sup>73</sup>

Similarly, in a study of 350 infants with antenatally detected urinary tract abnormalities born in two Nottingham teaching hospitals in the United Kingdom, 170 of 350 (48.6%) were classified as “non-specific dilatation” (NSD). The majority of these (133/170) were categorized as NSD1. NSD1 referred to those fetuses with a renal pelvic diameter

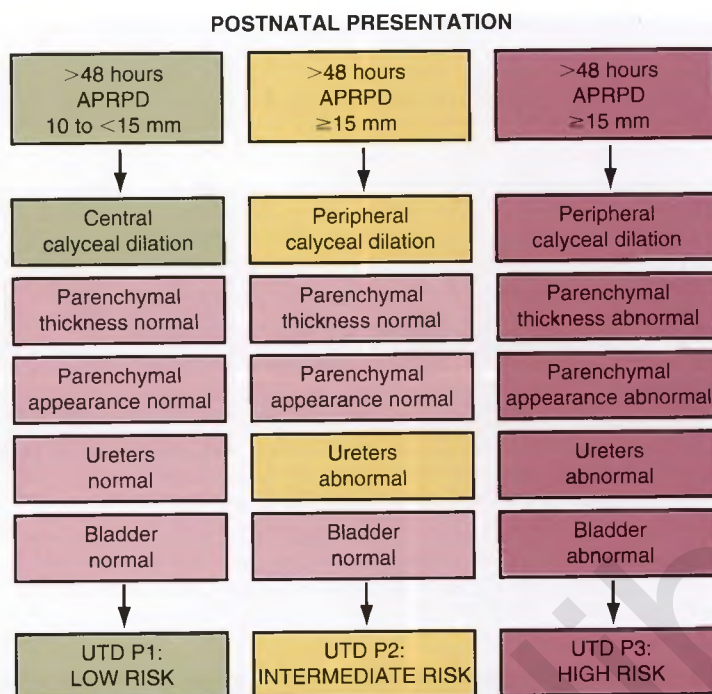


**FIG 15-23** Urinary tract dilation (UTD) risk stratification: postnatal presentation for UTD P1 (low risk), UTD P2 (intermediate risk), and UTD P3 (high risk). Note: stratification is based on the most concerning ultrasound finding. For example, if the anteroposterior renal pelvic diameter (APRPD) is in the UTD P1 range, but there is peripheral calyceal dilation, the classification is UTD P2. Similarly, the presence of parenchymal abnormalities denotes UTD P3 classification, regardless of APRPD measurement.

less than 10 mm in the AP diameter, no caliectasis or hydroureter, and normal renal cortex and size on renal ultrasound examination performed 4 to 6 weeks after birth. Infants in this group were exempt from further follow-up unless presenting with signs or symptoms of a urinary tract infection. Infants in the NSD2 group were those with a renal pelvis greater than 10 mm in the AP diameter. These infants subsequently underwent a voiding cystourethrogram (VCUG) or radionuclide renal scan to rule out reflux and renal drainage abnormalities, respectively. If normal, renal ultrasound examination was repeated within the first year of life. If renal pelvic dilatation was less than 10 mm, these infants were discharged from care with no further evaluation unless they developed symptoms of a urinary tract abnormality. The authors concluded that a large percentage of fetuses with renal pelvic dilatation can be served by a single postnatal renal ultrasound examination and that expectant management is appropriate and operative intervention is often unnecessary.<sup>14</sup>

It is important that information relevant for the proper postnatal management of the newborn be transmitted to the pediatric team. In the majority of cases, no significant disease is observed postnatally, and the prenatal dilation represents transient or physiologic hydronephrosis. However, a variety of findings seen in the neonate after birth may suggest an abnormality of the urinary tract (Fig. 15-23). After birth, some conditions require immediate confirmation and therapeutic maneuvers in order to protect renal function and prevent problems such as urinary tract infection, stone formation, and pain. These conditions include obstructive PUVs or the presence of an ectopic ureterocele that has prolapsed into the urethra, leading to oligouria or anuria and necessitating immediate treatment.<sup>57</sup>

However, extensive evaluation is not always necessary and, in addition to time and expense, can result in discomfort and radiation exposure, as well as the consequences of false positive diagnoses and stress

for the family. There is therefore some controversy as to which infants require radiologic evaluation and prophylactic antibiotics. In some cases, a workup should be planned but can be done on a less urgent basis. Ultrasound imaging is the least invasive and most common method of postnatal imaging. However, ultrasound examinations can only provide anatomic, not functional, evaluation, and findings are altered by bladder filling and hydration status. Because infants are relatively dehydrated at birth, later ultrasound evaluation (on the second day of life or later) is more accurate in assessing renal tract dilation. A normal ultrasound examination in the week after birth is not sufficient to verify the absence of disease and therefore later follow-up is often recommended (Fig. 15-24).<sup>12</sup>

Historically, all patients with renal tract dilation have been treated with prophylactic antibiotic therapy after birth until a final diagnosis and a final therapeutic decision are made. However, studies have not consistently demonstrated a benefit of antibiotics in preventing urinary tract infection. Therefore, the universal use of antibiotics is controversial,<sup>74,75</sup> particularly in low-risk infants.

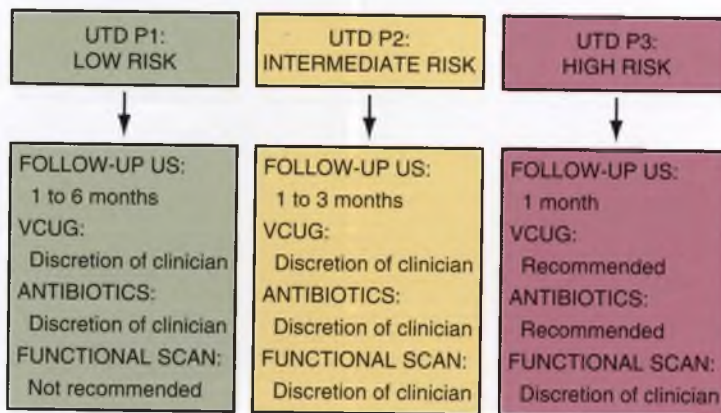
## NONOBSTRUCTIVE FETAL URINARY TRACT ANOMALIES

### Nonobstructive Megaureter

The fetal ureters are not visible sonographically unless dilated. The normal ureteral diameter in children is usually less than 5 mm. A ureteral diameter greater than 7 mm is considered a megaureter and can be obstructive or nonobstructive. Megaureter is considered primary when obstructive processes have been excluded. Nonrefluxing primary megaureter is the most common cause of primary megaureter in the neonate.<sup>76</sup> In this condition, the ureter is enlarged in the absence



## RISK-BASED MANAGEMENT, POSTNATAL DIAGNOSIS



The choice to utilize prophylactic antibiotics or recommend voiding cystourethrogram will depend on the suspected underlying pathology

**FIG 15-24** Risk-based management for urinary tract dilation (UTD) that persists into the postnatal period. US, ultrasound; VCUG, voiding cystourethrogram. (Adapted from Nguyen HT, Benson C, Bromley B, et al: Multidisciplinary consensus on the classification of prenatal and postnatal urinary tract dilation [UTD classification system]. *J Pediatr Urol* 10(6):982-998, 2014.)

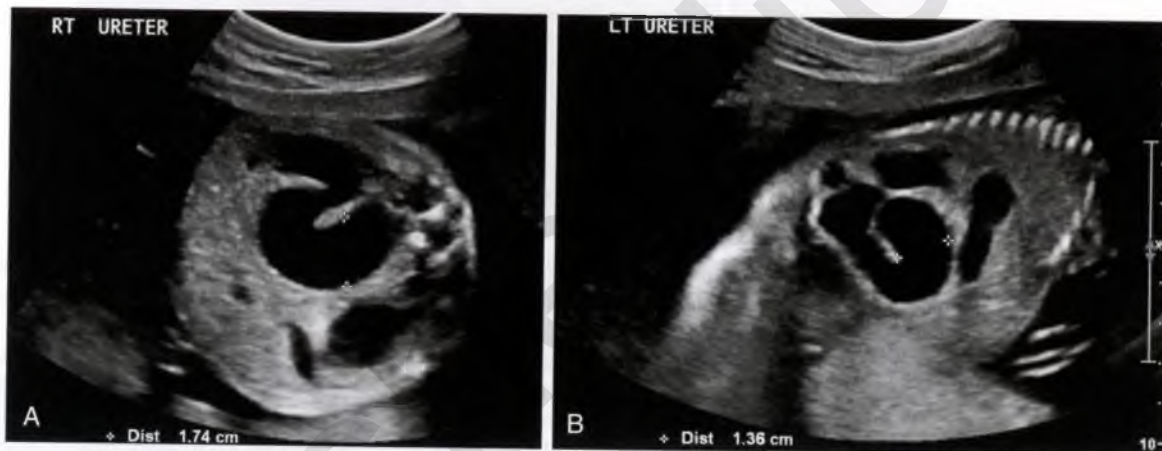


**FIG 15-25** Bilateral megaureter. **A** and **B**, Axial images through the abdomen of a fetus with dilated, tortuous ureters.

of reflux or obstruction, and the bladder and bladder outlet are normal. It occurs four times more frequently in males than in females and is bilateral in 25% of cases. Proposed causes include abnormal peristalsis, delayed patency, and sustained folding of the fetal ureter.<sup>77</sup> The most characteristic sonographic finding is a dilated tortuous ureter running from the kidney to the bladder (Fig. 15-25). Peristalsis may be observed. Care should be taken to differentiate a dilated ureter from fluid-filled bowel loops. Renal pelvic dilation may be mild or absent with megaureter. If associated with a duplex collecting system, an ectopic ureterocele may be noted (see Fig. 15-14). Postnatal evaluation of prenatally suspected megaureter involves a VCUG to exclude reflux and radionuclide scanning to assess renal function and rule out obstruction. Patients with nonobstructive, nonrefluxing megaureter are typically asymptomatic with normal renal function and require no therapy.<sup>78</sup>

### Empty Renal Fossa

The inability to visualize a kidney in one or both renal fossas raises a number of diagnostic possibilities that vary in prognosis and diagnostic difficulty. Nonvisualization of both kidneys, in conjunction with anhydramnios and prolonged inability to identify the fetal bladder, is

characteristic of bilateral renal agenesis (Fig. 15-26). This condition occurs in 0.1 to 0.3 per 1000 births.<sup>79</sup> The diagnosis may be more challenging than expected as a result of the lack of an acoustic window, fetal position, and potential confusion resulting from the presence of the adrenal gland oriented longitudinally in the renal fossa (Fig. 15-27). Fetal adrenal glands are large relative to their adult sizes and may appear similar in contour to the fetal kidney. Visualization of the fetal kidneys in the midtrimester may also be obscured by the presence of bowel in the renal fossa and the lack of perinephric fat, which serves to highlight the renal contours in the third trimester. Diagnostic maneuvers that may be helpful include color Doppler interrogation of the renal arteries and an inability to demonstrate them on a coronal view of the fetal retroperitoneum (Fig. 15-28); fetal magnetic resonance imaging (MRI) may also be useful. A reliable diagnosis, although challenging, is important for parental counseling. Currently, bilateral renal agenesis is considered a lethal disorder, not only because of the absence of functioning kidneys but also secondary to the pulmonary hypoplasia that results from anhydramnios. The demonstration of amniotic fluid in the first trimester does not exclude a diagnosis of bilateral renal agenesis because the fluid at this stage in pregnancy is dialysate of the fetal and placental membranes. If this diagnosis is

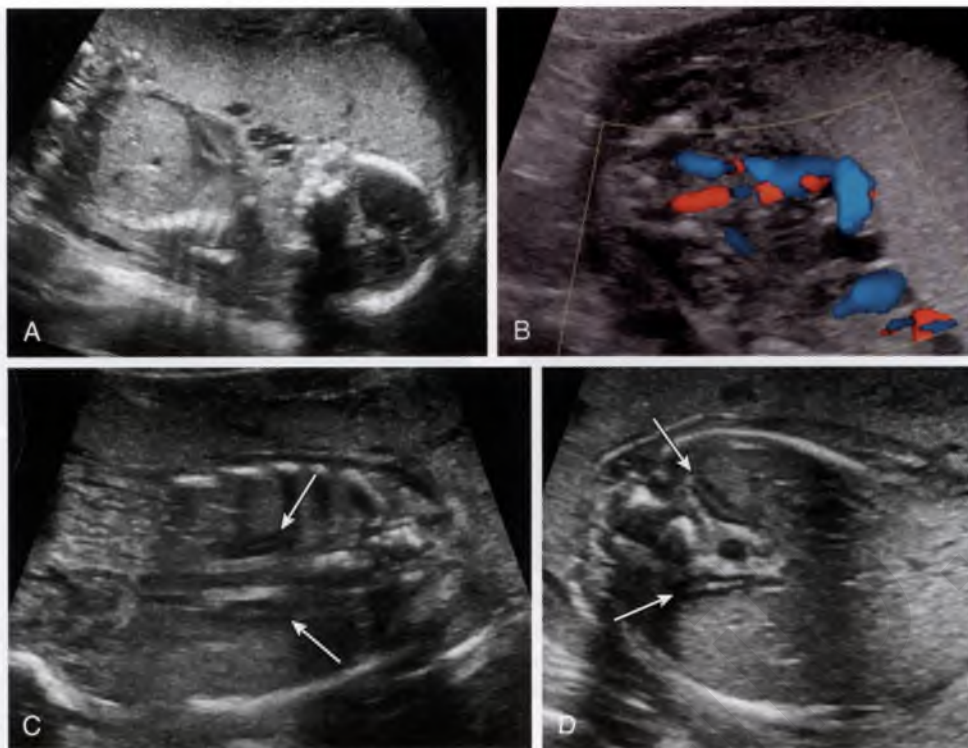


**FIG 15-26** Bilateral renal agenesis. **A**, Anhydramnios. **B**, Empty bladder, demonstrated using color Doppler sonography. Coronal (**C**) and axial (**D**) images through the fetal abdomen demonstrating elongation owing to absence of the kidneys bilaterally, the so-called “lying down adrenal” sign.

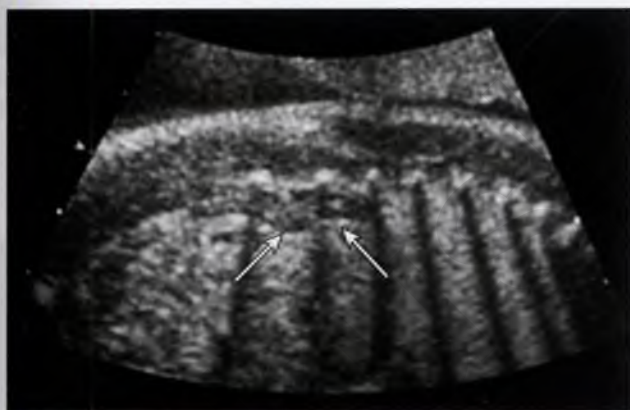


**FIG 15-27** The sagittal view showing elongated adrenal gland (arrows) demonstrating the “lying down adrenal” sign.



**FIG 15-28** Bilateral renal agenesis. Absence of the renal arteries as demonstrated by color Doppler imaging.

entertained, it is recommended to document the presence of both maternal and paternal kidneys as there is a heritable component to many renal disorders and an affected fetus may be the first indication of risk.<sup>80</sup>

### Unilateral Renal Agenesis

Unilateral renal agenesis is three to four times more common than bilateral absence and should be suspected when only one kidney is identified and the contralateral fossa is empty, typically filled with bowel.<sup>79</sup> A thorough search is warranted, as the kidney may be present but ectopic. Hypertrophy of the single identified kidney suggests unilateral agenesis, as enlargement occurs in 90% or more of fetuses with a single functioning kidney (Fig. 15-29).<sup>81,82</sup> Although compensatory nephrogenesis may benefit the fetus, epidemiologic studies indicate

that individuals born with a single functioning kidney are at risk for renal dysfunction and hypertension in early adulthood.<sup>83</sup> As agenesis of one or both kidneys is associated with up to a 30% risk of other genetic syndromes or anomalies, care should be taken to exclude other abnormalities.<sup>84</sup>

In one series of 93 fetuses presumed to have unilateral renal agenesis, 10 (11%) were subsequently found to have a normally positioned kidney. Seven were dysplastic, one was neoplastic, and two were normal. This series illustrates the fact that although inability to visualize a kidney in its normal location is typically associated with either renal absence or ectopia, an abnormal or nonvisualized normal kidney remains a possibility.<sup>64</sup>



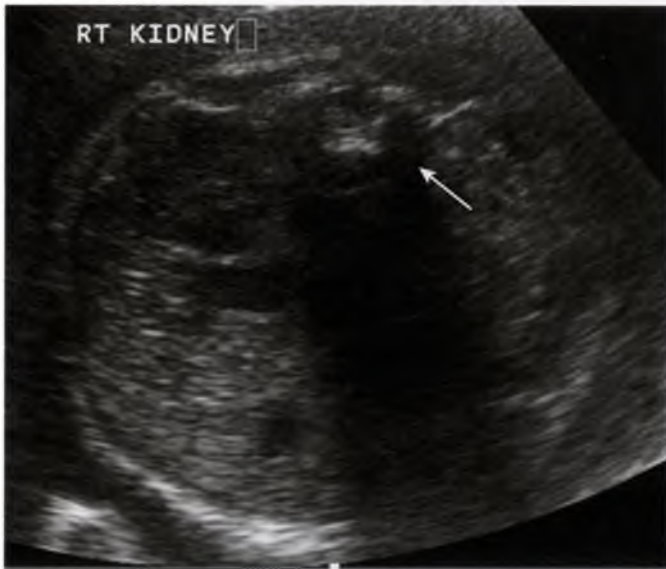


**FIG 15-29** Unilateral renal agenesis. Absence of the left kidney with compensatory hypertrophy on the right (RT).

### Aberrant Cephalad Migration

Aberrant cephalad migration of the kidneys during early embryologic development may result in renal ectopia. The absence of compensatory hypertrophy in cases of a unilateral empty renal fossa suggests a present but displaced kidney. An unascended or pelvic kidney is estimated to occur in 1:2200 to 1:3000 live births and is the most common manifestation of renal ectopia.<sup>85</sup> Visualization may be challenging because of the presence and sonographic similarity of bowel. The pelvic kidney is typically proximate to the bladder and may be midline or lateral to midline with no right or left dominance (Fig. 15-30). It may be irregular in contour and smaller than normal. The blood supply is variable and feeding vessels arise distal to the aortic bifurcation.<sup>86</sup>

### Renal Fusion Abnormalities

Ectopic location of the kidneys is also a feature of renal fusion abnormalities. These typically present as *horseshoe* kidney or crossed fused renal ectopia.

#### Horseshoe Kidney

Horseshoe kidney is the most common fusion defect, with an estimated incidence of 1 in 400 births and a male preponderance of 2:1. This condition results from abnormal fusion and ascent of the kidneys. In most cases, fusion occurs at the lower poles but it may involve the upper poles or both lower and upper poles. Depending on the position of the kidneys, fusion may be symmetric or asymmetric. The tissue connecting the kidneys is referred to as the isthmus. It is thought that normal ascent of the kidneys is precluded by inability of the kidneys to traverse the inferior mesenteric artery at the level of the isthmus. The distinguishing feature of the horseshoe kidney, the isthmus, is the most reliable sonographic clue to the diagnosis (Fig. 15-31). Visualization of the isthmus and its connection to the lower poles as well as the medial orientation of the lower poles are characteristic findings of this abnormality. However, depending on the thickness of the isthmus, clear identification may not be possible. Other sonographic features that may be observed in cases of horseshoe kidneys include low-lying location, bent or curved contour, elongation of the lower pole, and ill-defined inferior margin of the kidney. The vascular supply is not uniform and may derive from the aorta, the iliac arteries, and less

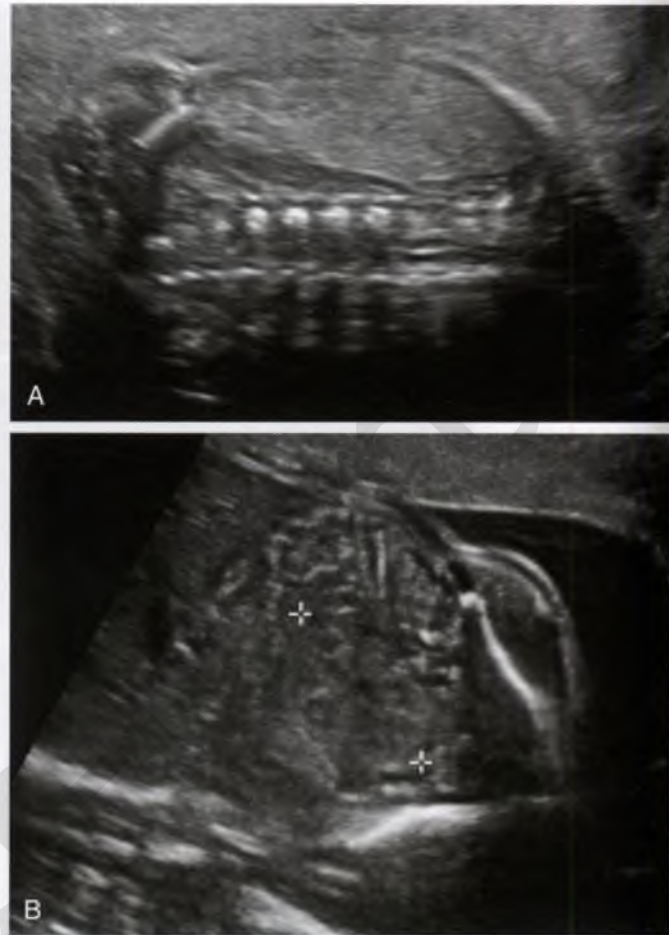


**FIG 15-30** Unilateral pelvic kidney. **A**, Empty left renal fossa on this coronal image, with a "lying down adrenal" sign. **B**, Further imaging demonstrates a kidney in the fetal pelvis (*calipers*).



**FIG 15-31** Horseshoe kidney. Demonstration of the isthmus is the most reliable sonographic clue to the diagnosis.



commonly the inferior mesenteric artery or the median sacral artery. Despite its relative frequency, prenatal diagnosis is uncommon.<sup>87,88</sup>

### Crossed Fused Renal Ectopia

*Crossed fused renal ectopia* is much less common than horseshoe kidney and is detected in 1:2000 to 1:7000 individuals in postmortem series. This condition results from fusion of one kidney to the other with the ureter crossing the midline to insert appropriately into the bladder. There are multiple varieties of crossed fused kidneys, depending on the site of fusion. The typical sonographic finding, in addition to an empty renal fossa, is a single bilobed mass-like reniform structure. Although the vascular supply may be variable, usually two renal arteries are present, one in the expected location and the other positioned more inferiorly to the crossed kidney. The difficulty in prenatal diagnosis is reflected in the fact that 20% to 30% of postnatally diagnosed cases are detected incidentally. In the absence of other malformations, individuals with crossed fused renal ectopia typically remain asymptomatic. Overall, the clinical prognosis is similar for horseshoe kidney and crossed fused ectopia.<sup>86,87,89</sup>

### DYSPLASTIC KIDNEYS

Renal dysplasia is a histologic, not sonographic, diagnosis reflecting either abnormal early development or disturbed terminal maturation.

In sonographic terms, dysplasia is nonspecific and generally refers to a variety of findings, including kidneys that are echogenic or bright, abnormal in size and structure, and with or without identifiable cysts of varying sizes (Fig. 15-32). Changes may be unilateral or bilateral and associated with normal or reduced amniotic fluid volume.

Obstruction of the urinary tract is a common antecedent of renal dysplasia, typically associated with MCDKs. Nonobstructive processes are diverse and include heritable conditions, other genetic syndromes, nongenetic sporadic occurrences, and exposure to certain drugs that are renal teratogens. These conditions are not necessarily exclusive and in some cases may be additive.

*Polycystic kidney disease* refers to two disorders, *autosomal recessive polycystic kidney disease (ARPKD)* and *autosomal dominant polycystic kidney disease (ADPKD)*. The designations ARPKD and ADPKD are preferred to their former monikers, infantile and adult-onset polycystic kidney disease, respectively. This reflects the fact that there can be considerable overlap in age at presentation as well as a better understanding of the genetic basis of these conditions.<sup>90</sup>

ARPKD has an incidence of approximately 1 in 20,000 live births.<sup>91</sup> It is a single gene disorder resulting from mutations in *PKHD1*, a large gene on chromosome 6p12, which encodes for the complex protein fibrocystin/polyductin.<sup>92</sup> Expression of fibrocystin occurs in the primary cilia as well as the basal body of renal and bile duct cells. Histologically, it is characterized by dilatation of the collecting ducts,

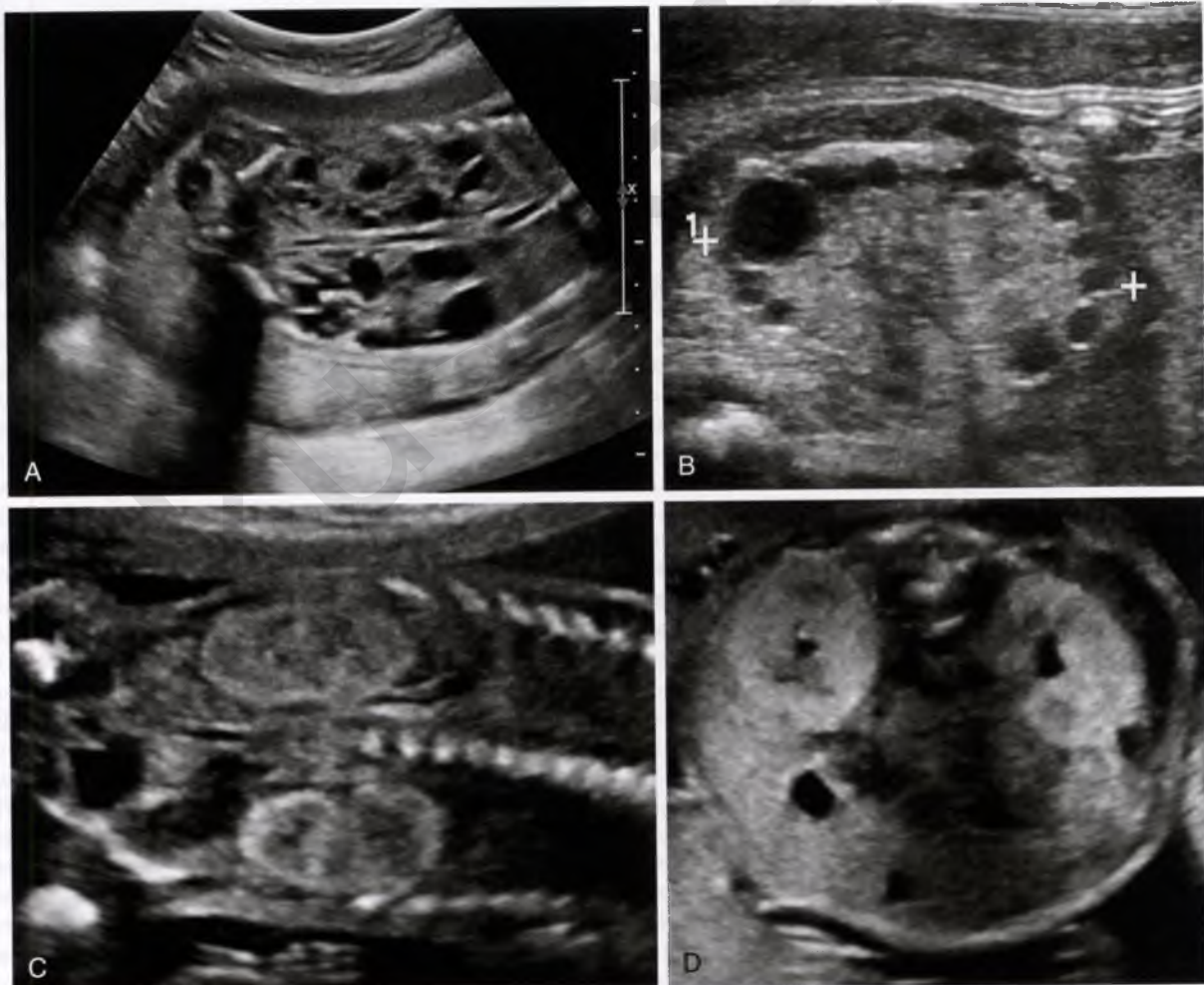


**FIG 15-32 A-D,** Renal dysplasia. Variable appearance of renal dysplasia, which can include kidneys that are echogenic or bright, abnormal in size and structure, and with or without identifiable cysts of varying sizes.



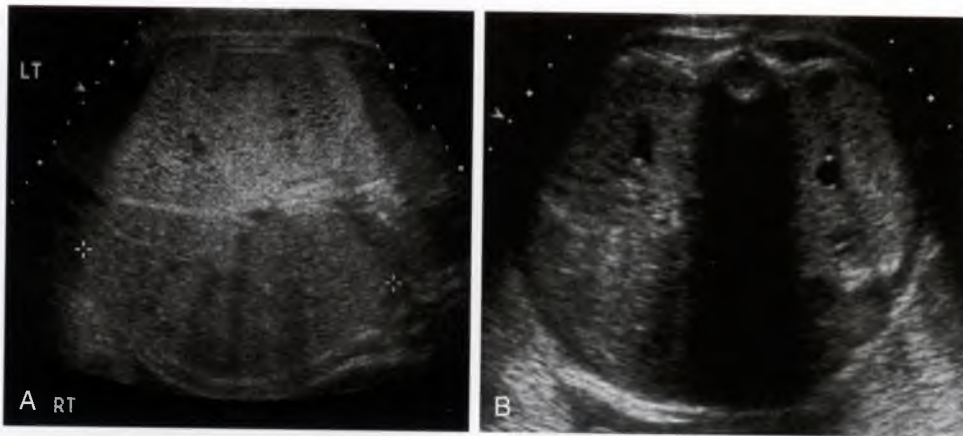


**FIG 15-33** Autosomal recessive polycystic kidney disease. Typical appearance of bilaterally enlarged, hyperechoic kidneys with lack of corticomedullary differentiation seen in coronal (A) and axial (B) views. LT, left; RT, right.

glomerular and cortical tubule lesions, and renal cortical necrosis. This results in multiple small (1-2 mm) peripherally positioned cysts involving the collecting ducts with preservation of the renal pelvis and ureters. In contrast, in ADPKD there are typically fewer, larger cysts that develop within all areas of the nephron or collecting ducts. Concomitant hepatic changes associated with ARPKD include portal fibrosis and biliary dysgenesis. The age of onset is variable, with four subtypes, categorized as perinatal, neonatal, infantile, and juvenile. The perinatal subtype is the most common, accounting for about 40% of cases. It is characterized by fetal renal failure and congenital hepatic fibrosis in 40% to 50%. Perinatal mortality rate is high owing to respiratory failure as a result of oligohydramnios-induced pulmonary hypoplasia.<sup>93</sup>

Ultrasound manifestations of ARPKD typically include bilaterally enlarged, hyperechoic kidneys with lack of CMD differentiation (Fig. 15-33). The bright appearance of the kidneys results from the multiple tissue-fluid interfaces of the numerous microcysts, even though the cysts themselves are too small to be discretely visualized. In contrast to ADPKD, kidney size in ARPKD does not correlate with renal function.<sup>94</sup> In a first pregnancy with sonographic features of ARPKD and subsequent neonatal death, histopathologic examination of the kidneys and liver should be performed to confirm or refute the diagnosis of ARPKD.<sup>95</sup>

It should be appreciated that the typical sonographic features of ARPKD may not develop until beyond 24 weeks of gestation. Failure to make the diagnosis in the first or second trimester does not preclude its later onset. For pregnancies known to be at risk, molecular genetic studies on DNA from chorionic villi or amniocytes can be used for prenatal diagnosis when the causative mutations have been identified.<sup>94</sup>

For individuals who are not diagnosed until late in pregnancy or after birth, more than half will require renal transplantation prior to 20 years of age. Complications of congenital hepatic fibrosis, such as esophageal varices and cholangitis, may present during childhood or later and may be remote from the time of renal transplantation.<sup>96</sup>

*Adult type polycystic kidney disease* with autosomal dominant inheritance is much more common than ARPKD, with a carrier frequency of the abnormal gene of approximately 1 in 1000 in the general population. It is the most common cause of heritable cystic renal disease in children and adults. Mutations in the *PKD1*, *PKD2*, and *PKD3* genes are found in most individuals with ADPKD. *PKD1* encodes for the polycystin-1 protein and is identified in approximately 85% of

individuals with ADPKD. *PKD2* encodes for polycystin-2 and is seen in less severe cases with later onset. Penetrance is nearly 100% if life span allows. However, because of variable expressivity and the 10% incidence of spontaneous mutation, the family history is negative in nearly 50% of cases.<sup>97</sup>

Normally, nephrogenesis begins during the 9th week of gestation and proceeds from the inner to outer cortex until the 36th week when this process is complete. The number of nephrons is a function not only of gestational age but also of fetal growth. Low birth weight is associated with reduced nephron mass and number of glomeruli. This is thought to be a significant contributing factor to the considerable differences in onset and variability of renal compromise in affected families. ADPKD is characterized by normal initial nephron and collecting duct development with their later cystic dilatation, resulting in subsequent loss of adjacent normal anatomy. Disturbed epithelial cell maturation results in the development of variable size cysts within the cortex and medulla, which progressively increase in size, typically allowing detection in early childhood. Although the onset of renal failure is usually not until the fifth or sixth decade of life, cyst formation begins in the fetal to neonatal period. Associated cysts in the central nervous system, pancreas, spleen, and liver have also been described.<sup>98,99</sup>

The ultrasound presentation of ADPKD in the fetus was detailed by Brun and associates<sup>100</sup> in a retrospective multicenter study involving 27 fetuses with a diagnosis of ADPKD. Ultrasound image parameters evaluated included amniotic fluid volume, renal and bladder size, the presence or absence of renal cysts, renal parenchymal echogenicity, and the state of CMD differentiation. Characteristic findings included moderately enlarged (1-2 standard deviations above the mean) kidneys with hyperechoic cortex and hypoechogenic medulla, resulting in increased CMD differentiation (Fig. 15-34). Cortical echogenicity was thought to be due to the presence of multiple microcysts in the renal cortex. The amniotic fluid volume was normal in most cases, and renal findings were usually observed in the third trimester.<sup>100</sup> The reported experience with prenatal detection of ADPKD is otherwise limited and includes cases of both normal-appearing kidneys and diffusely enlarged and hyperechoic kidneys. The prognosis for fetuses diagnosed with ADPKD in utero is similarly lacking. However, available evidence suggests that in the absence of oligohydramnios, the immediate outcomes are favorable. Risk factors for childhood onset of hypertension and renal failure are thought to include an affected mother or sibling or parental new mutation.<sup>90,101,102</sup>



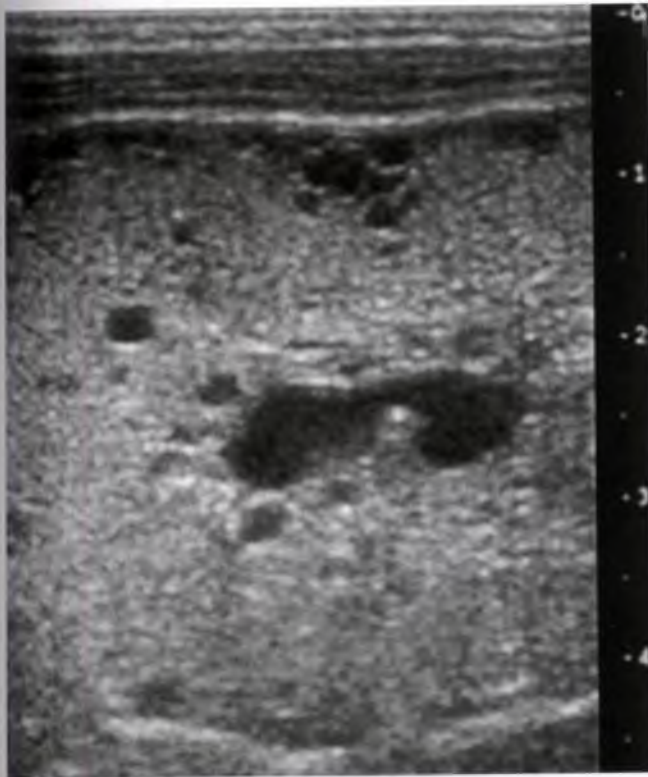


**FIG 15-34** Autosomal dominant polycystic kidney disease (ADPKD), glomerulocystic form in a neonate. Sagittal scan through the enlarged kidney, which appears hyperechoic with multiple tiny cysts, mostly peripheral. The father was affected by ADPKD.

Although isolated hyperechogenicity of the fetal kidneys may be secondary to either ARPKD or ADPKD, it is a nonspecific finding. Other reported diagnoses associated with isolated hyperechogenic kidneys include diffuse cortical cysts, cystic dysplasia, nephrocalcinosis, and tubular dysgenesis. There are also cases in which no diagnosis is established postnatally and the children remain symptom free. In some cases, the kidneys become normal appearing and in some there is persistent unexplained hyperechogenicity<sup>103-105</sup> (Table 15-7).

The finding of hyperechogenic fetal kidneys in association with extrarenal malformations has been reported in a number of genetic conditions, including Bardet-Biedl, Meckel-Gruber, Ivemark II, Jarcho-Levin, Beckwith-Wiedemann, and Beemer syndromes, as well as in trisomy 13 (Figs. 15-35 and 15-36).<sup>106</sup> If the diagnosis of a syndrome can be established, this is helpful in determining prognosis. Large hyperechogenic kidneys should prompt consideration of invasive testing for chromosomal microarray analysis.

## MISCELLANEOUS CYSTIC RENAL DISORDERS

(Table 15-8)

### Glomerulocystic Kidneys

Glomerulocystic kidneys (GLCKs) are defined as kidneys that contain cysts that correspond to distended Bowman spaces on histologic examination. From 5% to 10% of the spaces must be affected in order to establish such a diagnosis. Glomerular cysts are not specific to one simple disorder, but they can be present with several types of renal cystic diseases, both inherited and sporadic (Table 15-9).

On sonographic examination, classic GLCKs appear as enlarged hyperechoic kidneys (usually more than 4 standard deviations for the

gestation) and they usually lose the normal CMD differentiation. The most suggestive feature is the presence of subcapsular cortical cysts (Fig. 15-37A and B); these cysts can develop in utero or after birth. When present, the diagnosis is straightforward. This finding may help to characterize various syndromes in association with GLCKs when other malformations coexist. The prognosis will be based on associated findings and on the volume of amniotic fluid.<sup>107-110</sup>

### Medullary Cystic Dysplasia

Medullary cystic dysplasia is characterized by cystic changes in the kidney involving primarily the medullary tubules. Similar to GLCKs, medullary cystic dysplasia is not a specific clinical condition and may be a feature of many syndromes. It may also coexist with glomerulocystic changes (see Table 15-9). Tubular and interstitial fibrosis may develop progressively. The renal findings seen in medullary cystic dysplasia are the typical renal histologic changes seen in the Meckel-Gruber syndrome. The medullary cystic changes develop very early in the pregnancy and may be obvious as early as the end of the first trimester. The demonstration of anomalies of the central nervous system and of the extremities (polydactyly) renders the diagnosis even more certain. On sonography, the kidneys are enlarged, a pseudo-CMD differentiation is present as early as the end of the first trimester, and the medulla is very prominent. This pattern as demonstrated at this early stage is very typical<sup>111</sup> (see Fig. 15-35). A recent case report suggests a possible role of *HNFI1B* genetic mutation in some cases of medullary renal cysts.<sup>112</sup>

Cystic dysplasia is also common in Bardet-Biedl syndrome (renal cystic disease, retinitis pigmentosa, polydactyly, and hypogonadism). The renal lesions are not concentrated in the medullary areas but are more diffuse. The sonographic pattern is that of diffuse hyperechoic, slightly or markedly enlarged kidneys. Cysts may be present in utero or develop after birth. Polydactyly is a classic associated finding in utero. The other abnormalities of Bardet-Biedl syndrome develop later in childhood.<sup>111-115</sup>

## UNCLASSIFIED RENAL CYSTIC DISEASES

Macrocysts of the kidney may be encountered in cases of tuberous sclerosis. The cysts have specific histopathologic features that include eosinophilic epithelium. Other evidence of the disease, such as cardiac rhabdomyomas and intracerebral lesions, may be present in utero. Several other syndromes may also have features that include renal microcysts or macrocysts (e.g., Ivemark syndrome) (see Fig. 15-36).<sup>90,116,117</sup>

### Multicystic Dysplastic Kidney

MCDK is one of the most common renal disorders (Fig. 15-38). The sonographic findings in patients with MCDK are usually straightforward: unilateral involvement with noncommunicating cysts of variable size, variable amount of hyperechogenic stroma, no normal cortex or medulla, irregular renal contours, and no identifiable collecting system (Fig. 15-39). The cysts can be large, presenting as a large fetal abdominal mass, or on the contrary, microcystic MCDK may develop in the upper part of a duplex system or be located in an ectopic position. The size of the cysts may decrease in utero or after birth. Therefore, the entire MCDK may “disappear” and give the appearance of renal agenesis. Unilateral involvement carries a good prognosis, although there may be an anomaly affecting the contralateral kidney (UPJ obstruction). The condition can be associated with other system's malformations. When MCDK is an isolated finding, there is no increased risk of chromosomal anomaly. Cases with bilateral involvement (about 1 out of 15 cases) are associated with severe oligohydramnios and



TABLE 15-7 Causes of Bilateral Hyperechoic Kidneys

	Corticomedullary Differentiation	Isolated Malformation	Polymalformative
Obstructive dysplasia	—	++	—
Hereditary cystic diseases			
ADPKD	+ or —	+++	(+)
ARPKD	— or reversed	+++	
GCD	—	+	+++
MCD	+		+++
Syndromes with other abnormalities			
Overgrowth syndromes			
Beckwith-Wiedemann	+		
Perlman	+		
Zellweger	+		++
Ivemark	+ or —		++
Diabetes and renal cysts	+ or —		++
Bardet-Biedl	+ or —		++
Meckel-Gruber	+ or —		++
Nonhereditary fetal diseases			
Renal vein thrombosis	+ or	++	
Infection	+	++	+
Intoxication	+	++	
Metabolic diseases (undescribed)	+ or reversed	++	
Maternal diseases	+	++	
Chromosomal anomalies	+ or —		+++
Congenital nephrotic syndromes	+ or —	++	
Nephrostomatosis	+ or —	++	
Normal variant	+	++	

ADPKD, autosomal-dominant polycystic kidney disease; ARPKD, autosomal-recessive polycystic kidney disease; GCD, glomerulocystic disease; MCD, medullary cystic disease.

Data from the following sources:

- Thomas IF, Smith DW: Oligohydramnios: cause of the non-renal features of Potter's syndrome including pulmonary hypoplasia. *J Pediatr* 84:811, 1974.
- Onen A, Jayanthi VR, Koff SA: Long-term follow-up of prenatally detected severe bilateral newborn hydronephrosis initially managed nonoperatively. *J Urol* 168:1118, 2002.
- Jaswon MS, Dobbie L, Puri S, et al: Prospective study of outcome in antenatally diagnosed renal pelvis dilatation. *Arch Dis Child Fetal Neonatal Ed* 80:F35, 1999.
- John U, Kahler C, Schulz S, et al: The impact of fetal renal pelvic diameter on postnatal outcome. *Prenat Diagn* 24:591, 2004.
- Chitty LS, Griffin DR, Johnson P, et al: The differential diagnosis of enlarged hyperechogenic kidneys with normal or increased liquor volume: report of five cases and review of the literature. *Ultrasound Obstet Gynecol* 1:115, 1991.
- Carr MC, Benacerraf BR, Estroff JA, et al: Prenatally diagnosed bilateral hyperechoic kidneys with normal amniotic fluid: postnatal outcome. *J Urol* 153:442, 1995.
- Blane CE, Barr M, DiPietro MA, et al: Renal obstructive dysplasia: ultrasound diagnosis and therapeutic implications. *Pediatr Radiol* 21:274, 1991.
- Campos A, Figueroa ET, Gunasekaran S, et al: Early presentation of tuberous sclerosis as bilateral renal cysts. *J Urol* 149:1077, 1993.
- Winyard P, Chitty L: Dysplastic and polycystic kidneys: diagnosis, associations and management. *Prenat Diagn* 21:924, 2001.
- Rabelo EA, Oliveira EA, Silva GS, et al: Predictive factors of ultrasonographic involution of prenatally detected multicystic dysplastic kidney. *BJU Int* 95(6):868-871, 2005.
- Rabelo EA, Oliveira EA, Diniz JS, et al: Natural history of multicystic kidney conservatively managed: a prospective study. *Pediatr Nephrol* 19:1102, 2004.
- Oliveira EA, Diniz JS, Vilasboas AS, et al: Multicystic dysplastic kidney detected by fetal sonography: conservative management and follow-up. *Pediatr Surg Int* 17:54, 2001.
- Matsell DG: Renal dysplasia: new approaches to an old problem. *Am J Kidney Dis* 32:535, 1998.
- Blazer S, Zimmer EZ, Zelikovic I, et al: Natural history of fetal renal cysts detected in early pregnancy. *J Urol* 162:812, 1999.
- McHugh K, Stringer DA, Hebert D, et al: Simple renal cysts in children: diagnosis and follow-up with US. *Radiology* 178:383, 1991.
- Kolatsi-Joannou M, Bingham C, Ellard S, et al: Hepatocyte nuclear factor-1b: a new kindred with renal cysts and diabetes and gene expression in normal human development. *J Am Soc Nephrol* 12:2175, 2001.
- Bingham C, Hattersley AT: Renal cysts and diabetes syndrome resulting from mutations in hepatocyte nuclear factor-1b. *Nephrol Dial Transplant* 19:2703, 2004.

pulmonary hypoplasia and carry a poor prognosis (Fig. 15-40A and B).<sup>118-121</sup>

## RENAL TUMORS

Over 50% of all congenital abdominal masses found in the neonate originate in the kidney. In the fetus, the most common renal tumor is the mesoblastic nephroma (Fig. 15-41). This appears as a solid tumor that is sometimes difficult to differentiate from the adjacent renal parenchyma. The tumor can appear partially cystic. In utero, associated polyhydramnios is typical, whereas hypertension develops after birth. Cases of fetal renal Wilms tumor have been reported as solid or partially cystic tumors. The prognosis is usually good. Bilateral involvement of the kidneys suggests nephroblastomatosis, a condition associated with multiple benign renal nodular lesions.

Patients with Beckwith-Wiedemann syndrome, congenital aniridia, and Perlman and Drash syndromes are at risk of developing renal tumors. The main differential diagnosis of a cystic renal tumor includes MCDK.<sup>122-125</sup> Solid masses adjacent to the kidney, such as neuroblastoma and subdiaphragmatic bronchopulmonary sequestration (BPS) (see Chapter 12), should be differentiated from true renal masses.

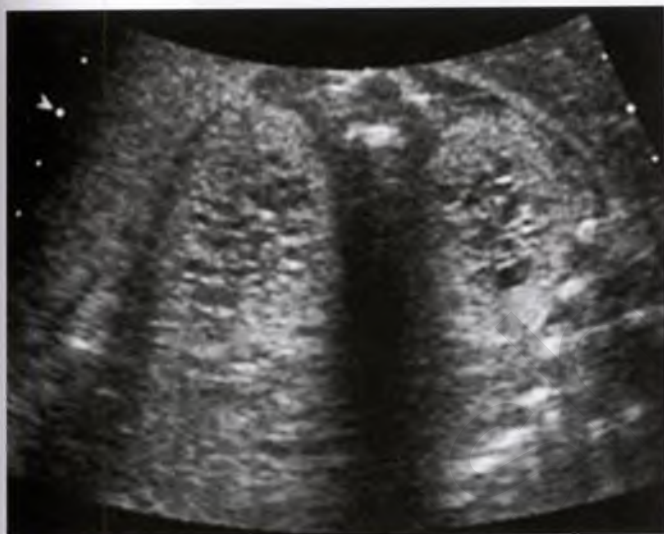


**FIG 15-35** Medullary cystic dysplasia, Meckel-Gruber syndrome. Transverse scan of the fetal abdomen. Both kidneys display an abnormal pattern: diffusely cystic changes involving the entire kidney. (An occipital encephalocele was also present, which is not shown.)

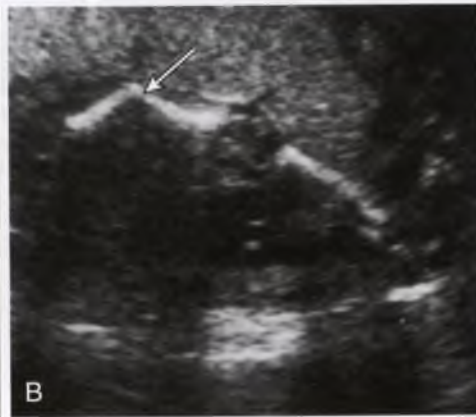


**FIG 15-36** Ivemark II syndrome, second trimester. **A**, Sagittal scan through the hyperechoic kidney, corticomedullary differentiation. **B**, Associated limb deformity: an angulated femur is visible (arrow).

## TABLE 15-8 Differential Diagnosis of Fetal Renal Cysts

### Unilateral Single Cysts

- Simple renal cyst
- Unilateral dominant cystic disease
- Cystic tumor
- Nonrenal cyst
- Urinoma

### Unilateral Multiple Cysts

- Multicystic dysplastic kidney (MCDK)
- Unilateral obstructive dysplasia
- Unilateral dominant cystic disease

### Bilateral Multiple Cysts

- Bilateral MCDKs (oligohydramnios)
- Bilateral obstructive dysplasia (urinary tract dilation)
- Autosomal dominant polycystic kidney disease
- Autosomal recessive polycystic kidney disease (cysts usually not visualized)
- Subcortical cysts (glomerulocystic kidneys)
- Syndromes with cystic dysplasia
- Meckel-Gruber medullary cysts
- Tuberous sclerosis (macrocyts)
- Ivemark II syndrome
- Bardet-Biedl syndrome (cortical cysts)

## TABLE 15-9 Causes of Glomerulocystic Kidneys

- Glomerulocystic kidney disease
  - Autosomal-dominant polycystic kidney disease in young infants
  - Dominant glomerulocystic kidney disease in older patients
  - Sporadic nonsyndromal glomerulocystic kidney disease
  - Familial hypoplastic glomerulocystic disease
- Glomerulocystic kidneys in heritable syndromes
  - Tuberous sclerosis
  - Orofaciodigital syndrome type 1
  - Trisomy 13
  - Short rib polydactyly syndromes
  - Jeune syndrome (asphyxiating thoracic dystrophy)
  - Zellweger syndrome
  - Familial nephronophthisis
- Glomerular cysts in dysplastic kidneys
  - Diffuse cystic dysplasia
  - Renal-hepatic-pancreatic dysplasia (Ivemark II syndrome)



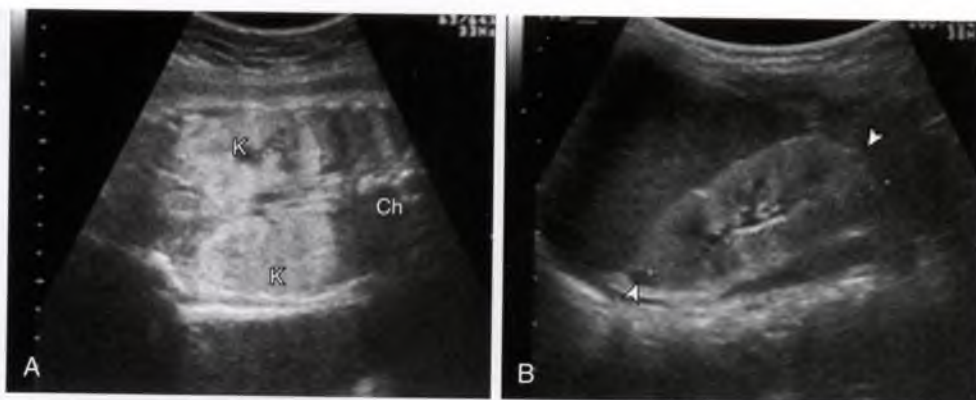


**FIG 15-37** Glomerulocystic kidney in a “diabetes and renal cyst syndrome.” **A**, In utero, third trimester. Front view through both kidneys (K), which appear enlarged and hyperechoic without corticomedullary differentiation. Ch, chest. **B**, At birth, sagittal scan through the right kidney. Small peripheral cysts have now appeared (arrowheads).

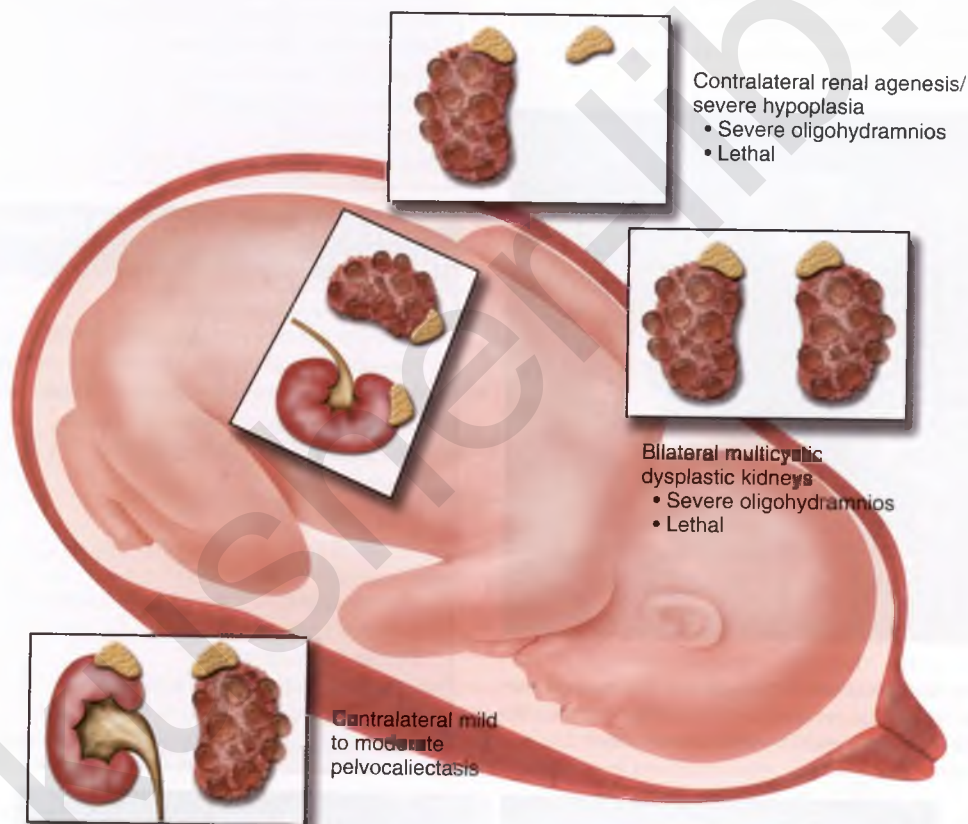


**FIG 15-38** The multicystic dysplastic kidney is essentially nonfunctional. Attention must be focused on the contralateral kidney, because it is the only potentially functional kidney. (Illustration by James A. Cooper, MD, San Diego, CA.)

## NONOBSTRUCTIVE FETAL BLADDER ABNORMALITIES

### Absent or Nonvisualized Bladder

Fetal urine production begins at 8 to 10 weeks of gestation, and visualization of the bladder in the pelvis is typically possible from 11 to 12 weeks' gestational age. Persistent inability to identify the bladder beyond 15 weeks' gestation is a pathologic finding.<sup>8</sup> The presence of normal amniotic fluid volume in the absence of a visible bladder

indicates either that the urine produced is unable to reach the bladder or that the bladder is unable to hold the urine.

### Epispadias, Bladder Exstrophy, and Cloacal Exstrophy

Epispadias, bladder exstrophy, and cloacal exstrophy represent a spectrum of urologic abnormalities of progressive severity. The reported incidence ranges from 1:117,000 for epispadias to 1:30,000 to 50,000 for bladder exstrophy, to 1:250,000 for cloacal exstrophy.<sup>126</sup>

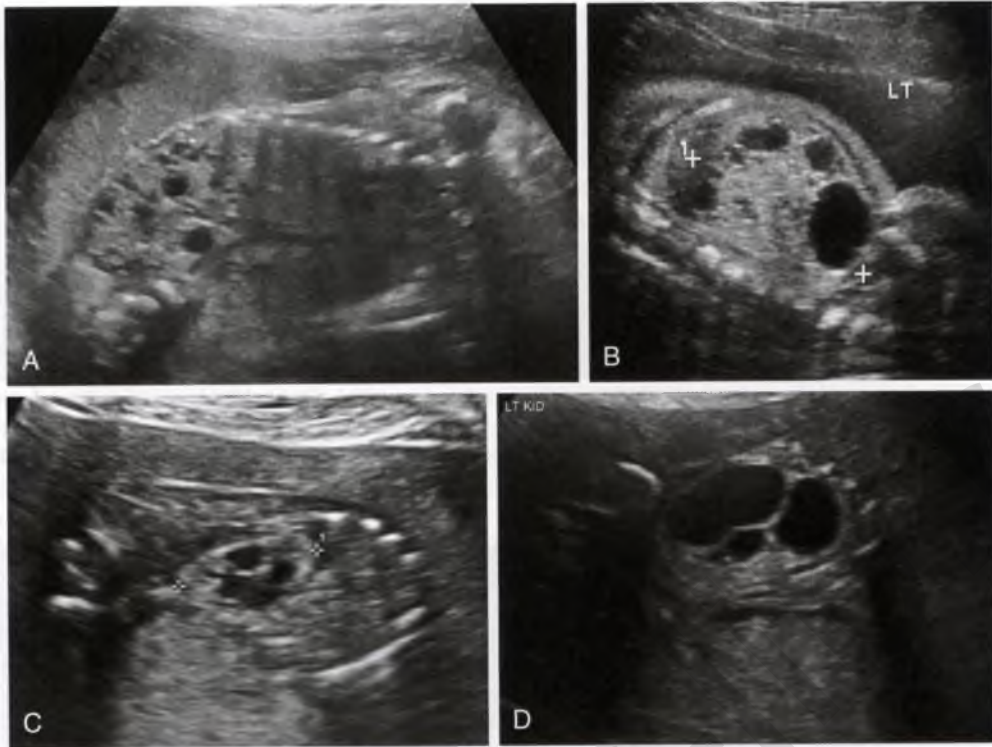


**FIG 15-39** Multicystic dysplastic kidney (MCDK). Images **A-D** demonstrate variable appearance in second trimester fetuses. Features include noncommunicating cysts of variable size, variable amount of hyperechoic stroma, no normal cortex or medulla, irregular renal contours, and no identifiable collecting system. The abnormal MCDK is delineated by the calipers in **B** and **C**. LT, left. (**C** and **D**, Courtesy Department of Obstetrics and Gynecology, Yale University School of Medicine, New Haven, CT.)

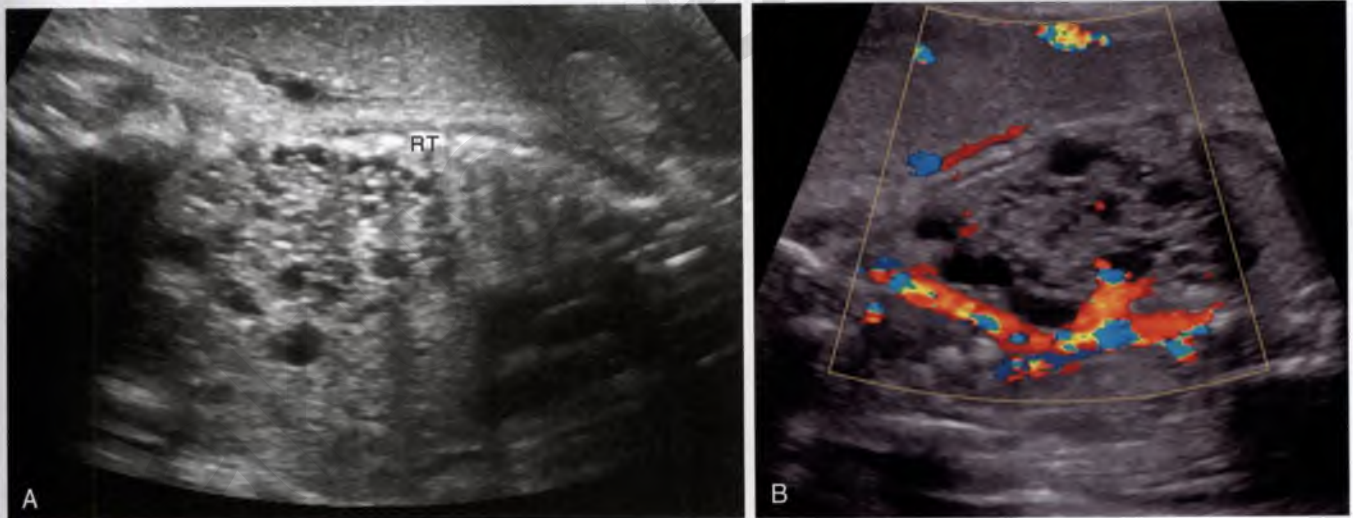


**FIG 15-40** Multicystic dysplastic kidney. **A**, Sagittal image of the right (RT) kidney reveals multiple scattered small cysts. **B**, Coronal image with color Doppler interrogation shows flow at the renal hilum. The fluid-filled spaces at the periphery of the kidney are nonvascular and represent cortical cysts.

### Epispadias

In males, epispadias is characterized by a broad, short penis, a gap in the pubic symphysis, and dorsal chordee. The scrotum is normal, and the testes are typically descended with normal function. Ejaculation may be abnormal secondary to the abnormal posterior urethra. In females, the clitoris is divided and the vagina is displaced anteriorly. The absence of normal pelvic muscle support can result in uterine prolapse, although fertility is unaffected. A deficient bladder neck leads to constant urinary leakage. This may be manifest prenatally by a small

or absent bladder, inferiorly displaced umbilicus, and, in males, abnormal genitalia.<sup>127</sup>

### Bladder Exstrophy

The integrity of the fetal ventral wall depends on migration of mesenchymal cells between the abdominal ectoderm and the cloaca. This process is initiated in the 4th week of gestation, and its failure results in a lack of muscle and connective tissue in the infraumbilical abdominal wall. It should be suspected when there is persistent



nonvisualization of the bladder in the setting of normal amniotic fluid volume and absence of other urinary tract abnormalities. The key sonographic features suggestive of bladder exstrophy include absent bladder in the pelvis, a soft tissue mass (the exstrophied bladder) adjacent to the lower abdominal wall, low umbilical cord insertion, abnormal external genitalia (small phallus and anteriorly deviated scrotum), and separation of the iliac crests<sup>128</sup> (Fig. 15-42A and B). Competing conditions that may obscure the diagnosis of bladder exstrophy include other ventral wall defects, such as omphalocele, gastroschisis, and cloacal exstrophy. The accuracy of prenatal diagnosis using ultrasound is lacking, with reported detection rates of 10% to 25%.<sup>129,130</sup> Given the imprecision in sonographic detection, MRI has more recently been advocated as a useful adjunct in evaluation of suspected cases. It is less affected by maternal habitus and fluid volume and allows better resolution of the soft tissue and genitalia.<sup>131</sup> Prenatal detection is important for counseling and planning surgical treatment. Ideally, bladder and abdominal wall closure is performed within the first 48 hours after birth. Additionally, parents should be prepared for the potential long-term morbid conditions of urinary incontinence, reduced fertility, and need for staged genitourinary reconstructive procedures.<sup>132</sup>

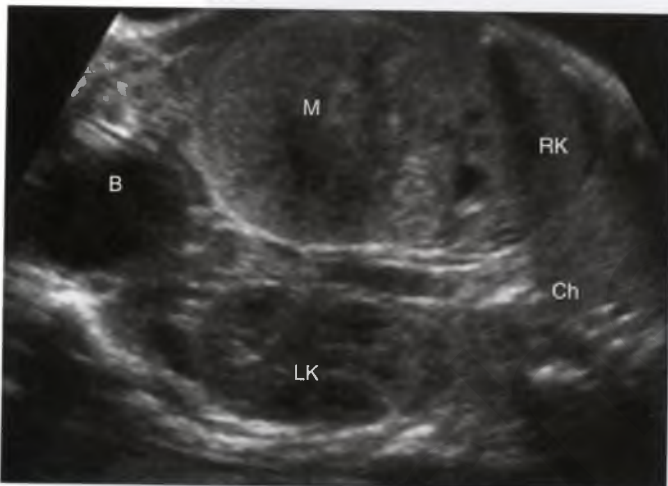


**FIG 15-41** Mesoblastic nephroma, third trimester. Sagittal scan of the fetal trunk. A large round solid mass (M) has developed in the lower pole of the right kidney (RK). B, bladder; Ch, chest; LK, left kidney.

### Cloacal Exstrophy

Inability to visualize the bladder is also a sentinel feature of cloacal exstrophy, a rare combination of anorectal and urogenital malformations with a reported incidence of 1:200,000 to 400,000.<sup>133</sup> Cloacal exstrophy is in the spectrum of the OEIS complex (omphalocele, cloacal exstrophy, imperforate anus, and spinal anomalies).<sup>134</sup> Other features reported in association with cloacal exstrophy include a cystic anterior abdominal wall mass, presumed to represent a persistent cloacal membrane, abnormal external genitalia, renal anomalies (hydronephrosis, agenesis, and MCDK), lower extremity defects, widened pubic arches, and single umbilical artery.<sup>135</sup> Given its rarity, uniform diagnostic criteria are lacking and prenatal diagnosis is uncommon. A high index of suspicion should be maintained when evaluating any fetal ventral wall defect in which the bladder is not visualized in the pelvis. In a recent retrospective review of eight patients with cloacal exstrophy, the diagnosis was missed in four fetuses using sonography but confirmed in all eight cases with fetal MRI. In addition to nonvisualization of the bladder, the MRI findings allowing a confident diagnosis of cloacal exstrophy included a protruding lower abdominal/pelvic contour and absence of meconium filling of the rectum and colon, a manifestation of the hindgut anomaly. Meconium distention of the rectum is typically observed by 21 weeks of gestation, so failure of detection with MRI after this time strongly suggests cloacal exstrophy<sup>136</sup> (Figs. 15-43 and 15-44). As with bladder exstrophy, prenatal detection is essential for planning the location, route, and tertiary site of delivery. Parents should be counseled that even though postnatal survival rates are near 90%, this achievement is obtained at the cost of multiple corrective procedures and a high risk of urinary and fecal incontinence.<sup>135</sup>

### BILATERAL SINGLE ECTOPIC URETERS

Ectopic ureters typically occur in the setting of renal duplex collecting systems, which are more common in females. Ectopic ureters associated with a single renal pelvis are more likely in males. Aberrant ureteric bud development is the underlying disorder that results in ectopic implantation, which may be at the bladder neck, prostate, or posterior urethra. In females, the ureters may communicate with the urethra or vaginal vault. Regardless of gender or site of implantation, the end result is that urine produced by the kidneys can bypass the bladder, which does not fill, whereas normal amniotic fluid volume can be maintained. Although rare, this diagnosis should be entertained when

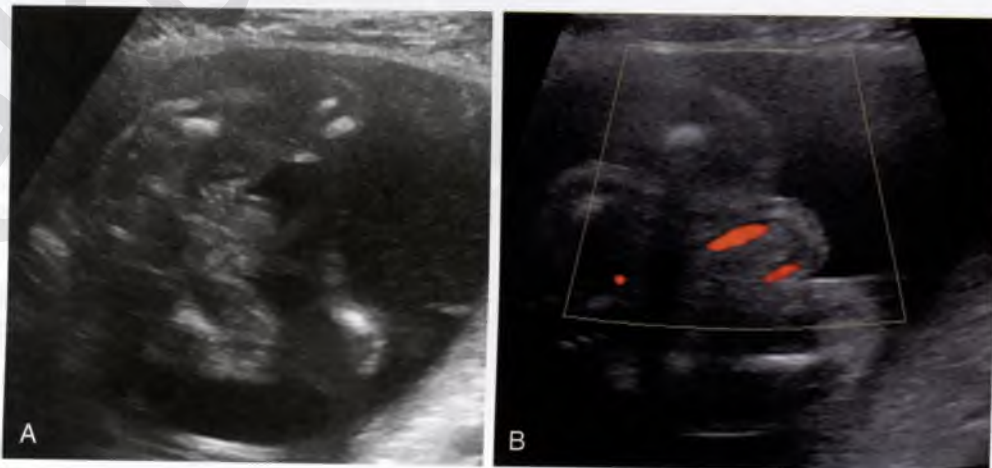


**FIG 15-42** Bladder exstrophy. **A**, Axial view of lower abdomen showing absent bladder in the pelvis and a soft tissue mass (the exstrophied bladder) in the anterior lower abdomen. **B**, Nonvisualization of fetal bladder in the pelvis is aided by color Doppler demonstration of the umbilical arteries.

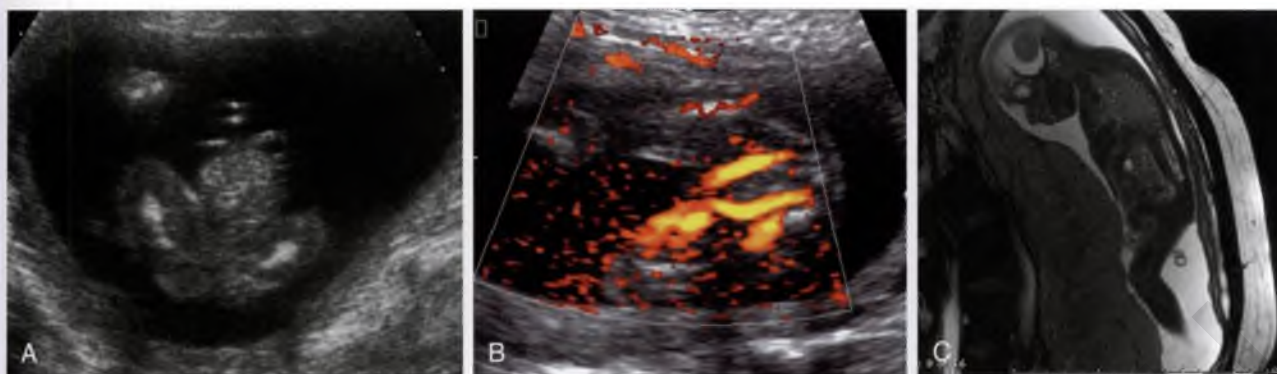


**FIG 15-43** Cloacal extrophy. **A**, Axial view of lower abdomen showing mass in the lower anterior abdomen. **B**, Nonvisualization of fetal bladder in the pelvis confirmed by color Doppler identification of umbilical arteries. **C**, Fetal magnetic resonance imaging aids the diagnosis of cloacal extrophy with demonstration of exteriorized bladder.

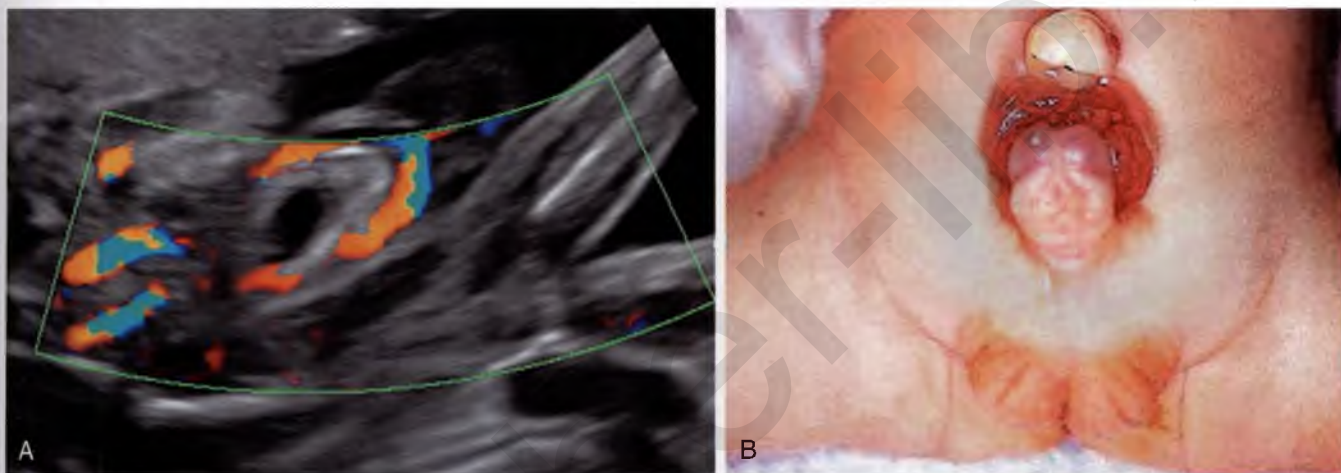


**FIG 15-44** Cloacal extrophy. **A**, Exteriorized fetal bladder can occasionally be demonstrated using color Doppler imaging. **B**, Postnatal photograph confirms cloacal extrophy.

there is nonvisualization of the bladder with none of the accompanying features of bladder or cloacal extrophy. The lack of normal filling and emptying of the bladder compromises bladder development, which typically necessitates reimplantation and reconstructive procedures. There is a significant residual risk of incontinence and renal impairment. Ureteric reimplantation has been shown to preserve renal function with postsurgical improvement determined by the degree of renal dysplasia.<sup>137,138</sup>

## FETAL ADRENAL GLANDS

### Normal Adrenal Glands

The fetal adrenal glands are easily demonstrated, especially using transvaginal transducers, by the end of the first trimester. They appear as pyramidal hypoechoic structures at the superior aspect of the hyperechoic kidney (Fig. 15-45). At that stage, their size is approximately half that of the kidney. Progressively, during the second trimester, CMD differentiation is observed with a hypoechoic cortex and hyperechoic medulla. The shape is that of a triangular structure on the superior aspect of the kidney. The size of the gland increases but relatively less than the kidney. During the third trimester, the appearance of the fetal adrenal gland is very similar to that of the neonatal adrenal glands (Fig. 15-46A and B). In cases of renal agenesis, the adrenal gland is more prominent and may be elongated, giving the so-called “lying



**FIG 15-45** Fetal adrenal glands. First trimester image demonstrating normal fetal adrenal glands superior to the fetal kidneys (arrows).



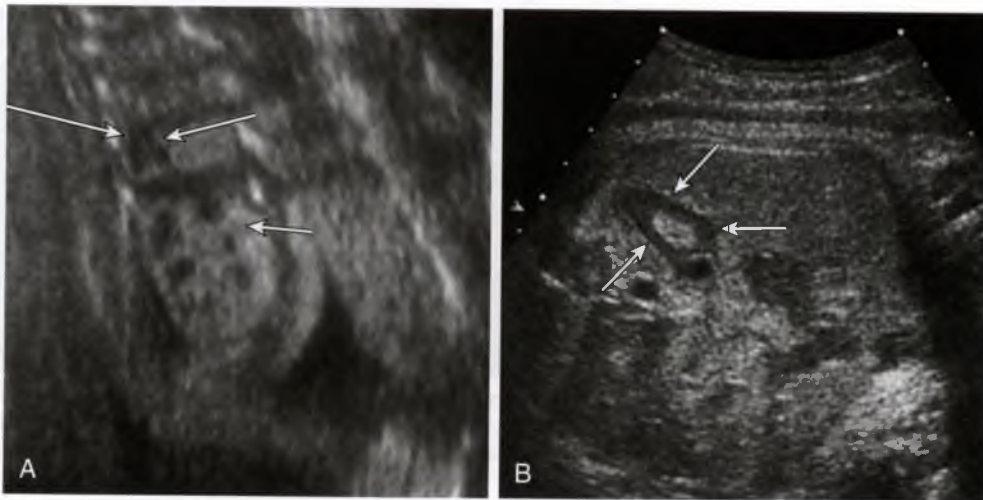


**FIG 15-46** Normal fetal adrenal gland. **A**, Second trimester, coronal view. The triangular adrenal gland is visible (arrows) above the kidney (short arrow). **B**, Third trimester, transverse view. The right adrenal gland is visible (arrows) with normal cortico (hypoechoic)-medullary (hyperechoic) differentiation.

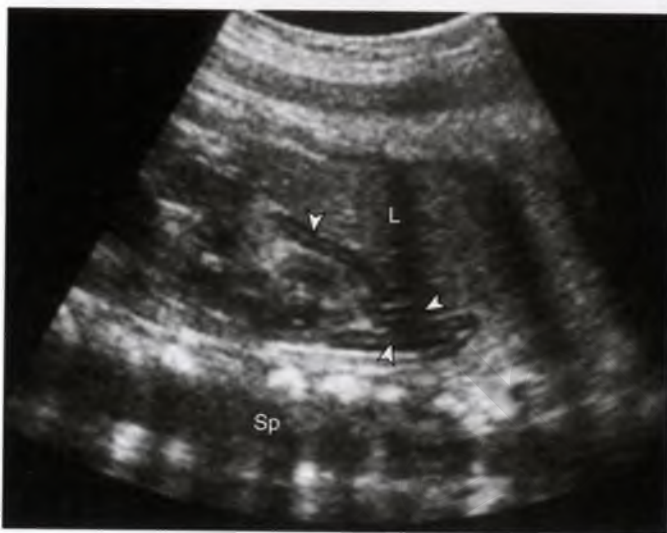


**FIG 15-47** Adrenogenital syndrome, third trimester. Sagittal scan through the right flank demonstrating the hypertrophied adrenal gland (arrowheads). L, liver; Sp, spine.

down adrenal sign”) (see Fig. 15-24). This should not be misinterpreted as a dysplastic kidney.<sup>139-141</sup>

## Adrenal Disorders

### Adrenogenital Syndrome

Adrenogenital syndrome (AGS) usually occurs secondary to CAH and the adrenal glands may enlarge as early as the second trimester. They may display a cerebriform wrinkled pattern (Fig. 15-47). The condition is associated with disorders of sexual differentiation in the female fetus (see later). Fetal MRI may be needed to differentiate cases of AGS from neuroblastoma; in the former, T2-weighted images will display isointense or hypointense signals, whereas in the latter the signals are hyperintense. Several authors have proposed using maternal corticosteroid therapy, once the condition has been ascertained, in order to reduce the virilization of the female fetus, although this treatment is controversial.<sup>142-146</sup>



**FIG 15-48** Adrenal hemorrhage. Fetus with bilaterally enlarged adrenal gland secondary to adrenal hemorrhage.

### Adrenal Masses

Cystic or solid masses in the region of the adrenal gland may be secondary to benign cystic enlargement, hemorrhage, CAH, or adrenal tumors (Figs. 15-48 through 15-50).

### Neuroblastoma

Neuroblastoma should be considered when a mass is seen in the suprarenal region, regardless of the specific characteristics of the mass. Neuroblastoma may present with a cystic, solid, or more complex appearance (see Fig. 15-50). Color Doppler imaging may demonstrate increasing vascularization of the hyperechogenic aspects of the mass. The prognosis of antenatal neuroblastoma is excellent even when hepatic metastases are present. Furthermore, some cases of spontaneous involution have been reported. Large adrenal cysts may develop in association with the Beckwith-Wiedemann syndrome. These cysts may bleed, in which case their appearance will become more complex. Extra-adrenal origins of a mass in this region, such as

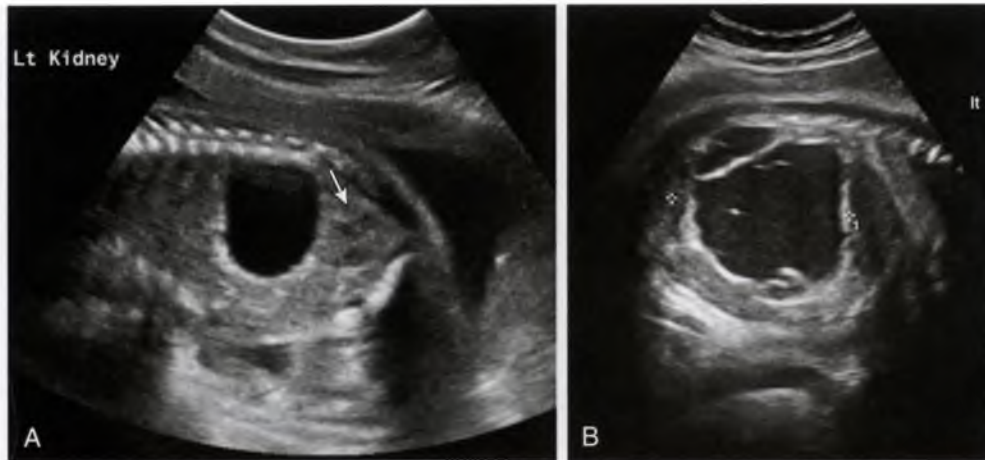


**FIG 15-49** Adrenal cyst. **A**, Sagittal image of the left (Lt) fetal kidney (*arrow*) demonstrating a large cyst in the adrenal gland superior to the kidney at 27 weeks' gestation. **B**, The same fetus at 34 weeks' gestation, demonstrating interval evolution of the cyst. (Courtesy Department of Obstetrics and Gynecology, Yale University School of Medicine, New Haven, CT.)

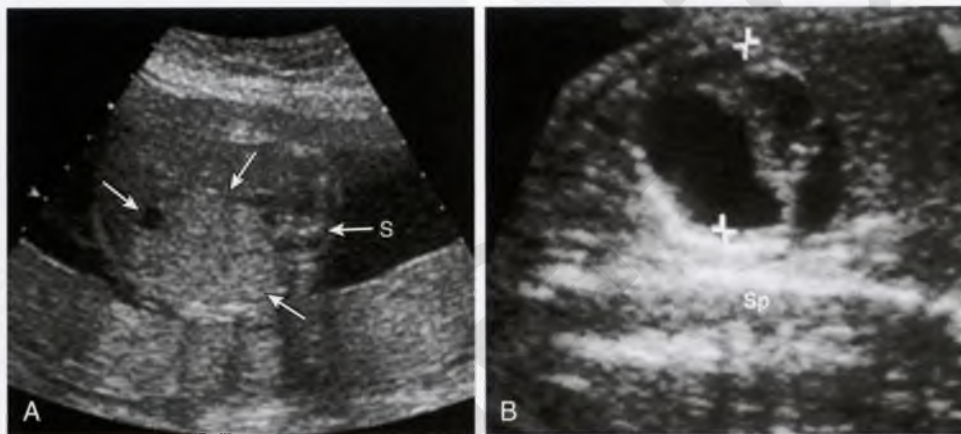


**FIG 15-50** Neuroblastoma. **A**, Transverse axial scan of the fetal abdomen in a second trimester fetus. A large paraspinal solid mass (*arrows*) with a single cystic component is seen. This was a neuroblastoma at birth. S, spine. **B**, Partially cystic mass (between calipers) corresponding to the neuroblastoma. Sp, spine.

### TABLE 15-10 Differential Diagnosis of Adrenal Masses

Neuroblastoma
Adrenal hemorrhage
Adrenal neoplasms
Adrenal cysts—isolated or associated with multicystic dysplastic kidneys or Beckwith-Wiedemann syndrome
Subdiaphragmatic bronchopulmonary sequestration

subdiaphragmatic pulmonary sequestration, should also be included in the differential diagnosis (Table 15-10).<sup>142,147-160</sup>

### FETAL GENITAL ANOMALIES

Current expertise and ultrasound technology allow a confident diagnosis of fetal gender at 13 weeks' gestation or later in 99% to 100% of cases with normal external genitalia. Determination of fetal sex is possible at less than 13 weeks but accuracy is variable and it should not be relied upon to guide pregnancy management at this stage. In the

late first and early second trimesters, gender determination is based primarily upon the sagittal sign. When scanned in the sagittal plane, the normal penis points upward, whereas the clitoris is oriented downward. Subsequently, identification of fetal sex depends upon visualization of the scrotum and penis in males and labia in females, which present as either two or more parallel lines (Fig. 15-51). Adjunctive findings that may be useful in uncertain cases include presence or absence of testicular descent, penile/scrotal size, origin and direction of the urinary stream, and visualization of the uterus.<sup>161-163</sup>

Three-dimensional sonography has also proved useful in characterizing genital abnormalities. This is a function of the improved spatial resolution and detailed surface rendering afforded by this modality.<sup>164</sup> The critical period for sexual development appears to be 8 to 12 weeks of gestation. This is suggested by reports of normal-appearing genitalia at 13 to 15 weeks with subsequent abnormalities of size and structure that appear to evolve as pregnancy progresses. This supports the notion that some genital malformations change throughout pregnancy rather than always occurring following a single nonprogressive insult.<sup>165</sup>

*Transient clitoromegaly* and *hypertrophy of the labia* have also been reported. In one reported series of 62,145 pregnancies, there were four fetuses with isolated clitoromegaly detected at 15 to 16 weeks' gestation. A diagnosis of hypospadias was initially entertained. On follow-up



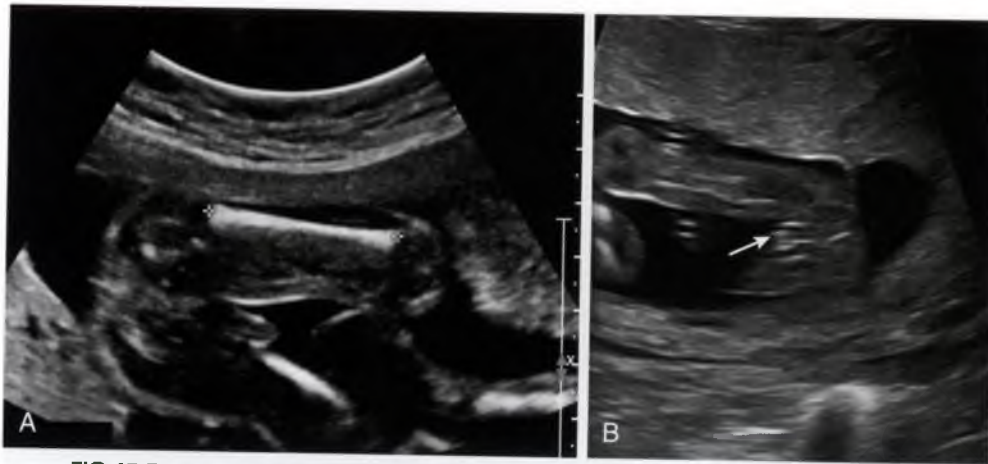


**FIG 15-51** Normal fetal genitalia, **A**, Male. **B**, Female; parallel lines indicate labia (arrow).

at 22 to 26 weeks, the clitoromegaly was resolved. The three fetuses with isolated hypertrophy of the labia minora had normal-appearing female genitalia at 15 weeks with suspected ambiguous genitalia noted at 21 to 23 weeks. Repeat examinations revealed gradual resolution of the hypertrophy with normal-appearing genitalia at 26 to 32 weeks. All cases had a normal female karyotype and normal external genitalia at birth. It was speculated that transient changes in the size of the clitoris correlate with changes in hormone production by the immature adrenal glands.<sup>166</sup>

### Disorders of Sexual Development

In addition to the genital abnormalities associated with bladder and cloacal exstrophy discussed earlier, other genital malformations include hypospadias, virilization syndromes (clitoromegaly, fused labia), incomplete masculinization of male genitalia (micropenis), and discordance between fetal phenotype and karyotype (Fig. 15-52). They are a heterogeneous group of disorders with different defects in hormones or their effects. Multiple as yet unidentified disease genes are implicated.

*Hypospadias* refers to abnormal location of the urethral orifice, which may be along the penile shaft, in the margin of the scrotum, or in the perineum. It reflects failure of development of the anterior urethra and has a reported incidence of 1:250 to 1:5000 live births. Associated genitourinary anomalies are seen in up to 40% of children with this diagnosis, and nongenitourinary anomalies occur in 7% to 10%. The prenatal sonographic features observed with hypospadias include loss of the pointed tip of the penis, which appears instead as a pointed cone; abnormal ventral curvature of the penis (chordee), presumed secondary to a strand of connective tissue acting as a bowstring between the meatus and glans; a small penile shaft with two parallel echogenic lines representing the remains of the dorsal hood; and the tulip sign, which results from severe curvature of the penis between the two scrotal folds (Fig. 15-53). This represents a severe form of hypospadias. Using power or color Doppler to demonstrate the origin of the urinary stream during bladder emptying can also allow a diagnosis in some cases of hypospadias.<sup>167,168</sup>

In a known genetic female with abnormal external genitalia or a fetus with genital ambiguity (or disorder of sexual development) and unknown karyotype, identification of a normal uterus suggests a likely diagnosis of a virilized female. The absence of a uterus is consistent with an undervirilized male. Transverse scanning through the pelvis at the level of the fetal bladder should reveal a rounded echogenic uterus positioned between the hypoechoic rectum and bladder. Nomograms



**FIG 15-52** Disorder of sexual differentiation, third trimester. Scan through the scrotum. The two hemiscrotums are separated by a penis that is too short (arrowhead) (split scrotum sign).

of uterine width and circumference are available from 19 through 38 weeks' gestation.<sup>169</sup>

The most common cause of female virilization is *congenital adrenal hyperplasia* (CAH). Most cases of CAH are from 21-hydroxylase deficiency (CYP21 CAH). Definitive prenatal diagnosis of CYP21 CAH is possible in families with a previously affected child if the causative mutations have been identified. Although complex, fewer than 12 mutations represent more than 90% of the mutant alleles, and phenotype does not necessarily predict genotype. This is an autosomal recessive condition with a 25% chance for an affected child in each pregnancy; affected females are at risk for genital virilization. Maternal treatment with steroids early in the first trimester may ameliorate the effects of CYP21 CAH on female genital anatomy. However, the appropriateness, ethics, and outcomes of the prenatal treatment of CAH with dexamethasone remain controversial.<sup>170,171</sup>

### FETAL OVARIAN CYSTS

With improved ultrasound imaging, greater numbers of ovarian cysts are being diagnosed prenatally. These cysts are secondary to maternal



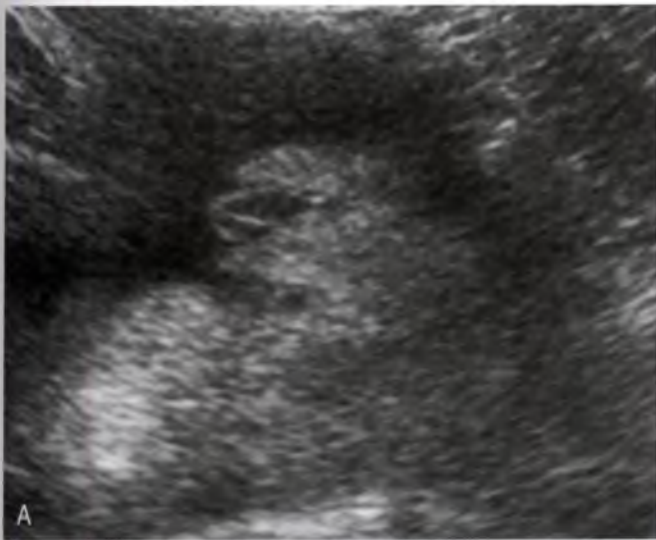


**FIG 15-53** Hypospadias, third trimester. **A**, The classic tulip sign. **B**, The penis (*arrow*) appears shortened and the tip is broad without the normal pointed appearance.

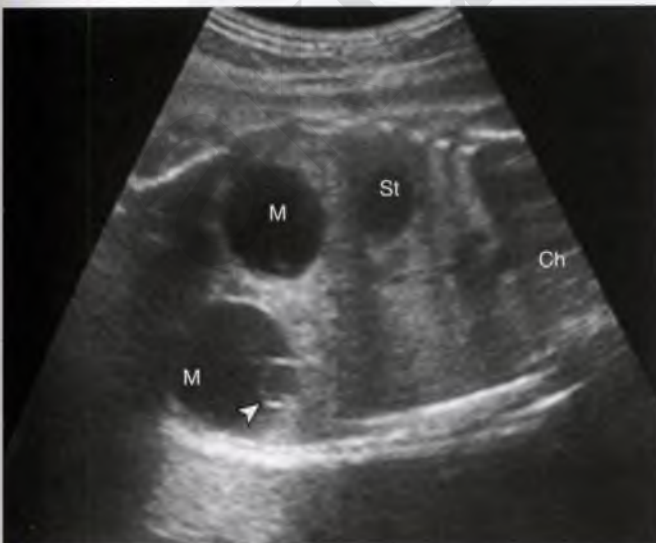


**FIG 15-54** Bilateral ovarian cysts, third trimester. Frontal view of the fetal trunk demonstrating two cystic masses (M). In one of them, a smaller cyst is visible (daughter cyst sign) (*arrowhead*). Ch, chest; St, stomach.

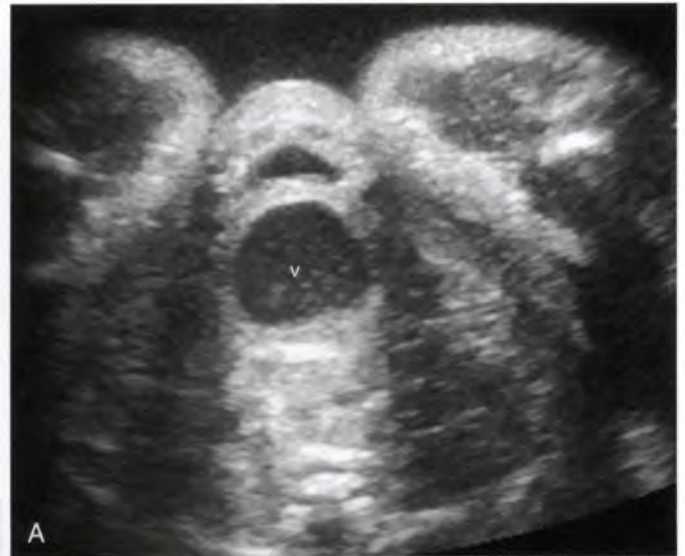


**FIG 15-55** Hydrometrocolpos. **A**, Transaxial image of the distended fluid-filled vagina (v). **B**, Sagittal sonographic image of the pelvis in this female fetus demonstrates fluid within the dilated vagina (v) and uterus (ut), located posterior to the normal-appearing urinary bladder (B). A normal volume of amniotic fluid is present.

hormonal stimulation. They can be unilateral or bilateral, they may vary in size, and multiple cysts can occur on the same side (Fig. 15-54). The most common cysts appear as anechoic smooth-walled, avascular cysts that may be functional follicles. However, more complex solid ovarian cysts may be encountered, although rarely. Hemorrhage may occur within these cysts and the larger ones are at risk of torsion. Differential diagnoses of ovarian cysts include duplication cysts, urachal cysts, hydrocolpos, mesenteric cysts, or meconium pseudocysts. Very rarely, a lymphangioma or teratoma may present with features suggesting an ovarian cyst.<sup>172-180</sup> When the diagnosis is unclear, fetal MRI may be helpful. In a series of 56 fetuses who underwent MRI for suspected anomalies, MRI changed the final diagnosis in 4 of 6 with intra-abdominal cysts, with findings including meconium pseudocysts, mesenteric cysts, hydrometrocolpos, and chylous ascites.<sup>181</sup>



Most fetal ovarian cysts resolve spontaneously, either in the antenatal period or in the early postpartum period. The role of surgical intervention, even in the postnatal period, is controversial, as many of these cysts will resolve spontaneously. Very large cysts with potential for torsion may be an indication for either prenatal aspiration or postnatal surgery.

### HYDROCOLPOS/HYDROMETROCOLPOS

Malformations of the female lower genital tract resulting in obstruction of the lower half of the vagina can result in fluid accumulation within

the vagina (hydrocolpos) or in the vagina and uterus (hydrometrocolpos) (Fig. 15-55A and B). It may be secondary to cloacal malformation (see earlier) or rarely may be due to a persistent urogenital sinus (Fig. 15-56A through D).<sup>182-186</sup> Some cases of hydrocolpos may resolve spontaneously, and, therefore, it is important to exclude any associated anomalies to allow appropriate counseling and planning for postnatal management. The possibility of persistent urogenital sinus should be considered when a presacral cystic mass is seen with either clear fluid (urine) or turbid fluid-debris level thought to be due to cervical or vaginal secretions. Fetal MRI may be useful in differentiating isolated hydrocolpos from that associated with cloacal malformations.<sup>187</sup>



**FIG 15-56** Persistent urogenital sinus. **A**, Large fluid-filled structure in the pelvis (*asterisk*) representing the markedly dilated vagina, posterior to the bladder (B). **B**, At the superior aspect of the fluid-filled pelvic mass (*asterisk*), the thick-walled oval structure represents the uterus (ut). Findings indicate hydrometrocolpos. **C**, Transaxial image through the upper abdomen reveals free intraperitoneal fluid (fl), presumed to be due to reflux of urine and vaginal secretions through the fallopian tubes. Normal fluid-filled stomach (st). **D**, Image of external genitalia shows normal labia in this female fetus.

## REFERENCES

- Elder JS: Antenatal hydronephrosis. Fetal and neonatal management. *Pediatr Clin North Am* 44(5):1299–1321, 1997.
- Song R, Yosypiv IV: Genetics of congenital anomalies of the kidney and urinary tract. *Pediatr Nephrol* 26:353–364, 2011.
- Gupta T, Kapoor K, Sharma A, Huria A: The frequencies of the urinary anomalies which were detected in a foetal autopsy study. *J Clin Diagn Res* 6(10):1615–1619, 2012.
- Sadler TW, editor: *Langman's Medical Embryology*, ed 11, Philadelphia, 2009, Lippincott Williams & Wilkins.
- Moore KL, Persaud TVN, Torchia MG: *The Developing Human; Clinically Oriented Embryology*, ed 9, Philadelphia, 2011, WB Saunders.
- Park JM: Normal and anomalous development of the urogenital system. In Walsh PC, editor: *Campbell's Urology*, ed 8, Philadelphia, 2002, WB Saunders.
- Larson WJ: *Human Embryology*, London, 2001, Churchill Livingstone.
- Rosati P, Guaniglia L: Transvaginal assessment of fetal urinary tract in early pregnancy. *Ultrasound Obstet Gynecol* 7:95, 1996.
- Chamberlain PF, Manning FD, Morrison I, et al: Circadian reflux in bladder volume in the term human fetus. *Obstet Gynecol* 64:657, 1984.
- Cohen ML, Cooper J, Eisenberg P, et al: Normal length of fetal kidneys. *AJR Am J Roentgenol* 157:545, 1991.
- Thomas IF, Smith DW: Oligohydramnios: cause of the non-renal features of Potter's syndrome including pulmonary hypoplasia. *J Pediatr* 84:811, 1974.
- Nguyen HT, Benson C, Bromley B, et al: Multidisciplinary consensus on the classification of prenatal and postnatal urinary tract dilation (UTD classification system). *J Pediatr Urol* 10(6):982–998, 2014.
- Nguyen HT, Herndon CDA, Cooper C, et al: The Society for Fetal Urology consensus statement on the evaluation and management of antenatal hydronephrosis. *J Pediatr Urol* 6:212–231, 2010.
- Mallik M, Watson AR: Antenatally detected urinary tract abnormalities: more detection but less action. *Pediatr Nephrol* 23(6):897–904, 2008.
- Maizels M, Wang E, Sabbagha RE, et al: Late second trimester assessment of pyelectasis (SERP) to predict pediatric urological outcome is improved by checking additional features. *J Matern Fetal Neonatal Med* 19(5):295–303, 2006.
- Sairam S, Al-Habib A, Sasson S, Thilaganathan B: Natural history of fetal hydronephrosis diagnosed on mid-trimester ultrasound. *Ultrasound Obstet Gynecol* 17(3):191–196, 2001.
- Karnak I, Woo LL, Shah SN, et al: Results of a practical protocol for management of prenatally detected hydronephrosis due to ureteropelvic junction obstruction. *Pediatr Surg Int* 25(1):61–67, 2009.
- Anderson N, Claudice-Engle T, Allau R, et al: Detection of obstruction uropathy in the fetus. *AJR Am J Roentgenol* 164:719, 1995.
- Stocks A, Richards D, Freutzen B, et al: Correlation of prenatal renal pelvic antero-posterior diameter with postnatal outcome. *J Urol* 155:1050, 1996.
- Maizels M, Reisman ME, Slom LS: Grading nephroureteral dilatation detected in the first year of life: correlation with obstruction. *J Urol* 148:609, 1992.
- Kaefer M, Peters CA, Petik AB, et al: Increased renal echogenicity: a US sign for differentiating between obstructive and nonobstructive etiologies of in utero bladder distension. *J Urol* 158:1026, 1997.
- Chudleigh T: Mild pyelectasis. *Prenat Diagn* 21:916, 2001.
- Bosman G, Reuss A, Nijman JM, et al: Prenatal diagnosis, management and outcome of fetal uretero-pelvic junction obstruction. *Ultrasound Med Biol* 17:117–120, 1991.
- Coco C, Jeanty P: Isolated fetal pyelectasis and chromosomal abnormalities. *Am J Obstet Gynecol* 193:732–738, 2005.
- Carbone JF, Tuuli MG, Dicke JM, et al: Revisiting the risk for aneuploidy in fetuses with isolated pyelectasis. *Prenat Diagn* 31:566–570, 2011.
- Orzechowski KM, Berghella V: Isolated fetal pyelectasis and the risk of Down syndrome: a meta-analysis. *Ultrasound Obstet Gynecol* 42:615–621, 2013.
- Dhillon HK: Prenatally diagnosed hydronephrosis: the Great Ormond Street experience. *Br J Urol* 81(Suppl 2):39–44, 1998.
- Palmer LS, Maizels M, Cartwright PC, et al: Surgery versus observation for managing obstructive grade 3 to 4 unilateral hydronephrosis: a report from the Society for Fetal Urology. *J Urol* 159:222, 1998.
- McLellan DL, Retik AB, Bauer SB, et al: Rate and predictors of spontaneous resolution of prenatally diagnosed primary nonrefluxing megaureter. *J Urol* 168(5):2177–2180, 2002.
- Shukla AR, Cooper J, Patel RP, et al: Prenatally detected primary megaureter: a role for extended follow-up. *J Urol* 173:1353, 2005.
- Zhou Q, Cardoza JD, Barth R: Prenatal ultrasound of congenital renal malformations. *AJR Am J Roentgenol* 173:1371, 1999.
- Gunn TR, Dennot MD, Mora J, et al: Antenatal diagnosis of urinary tract abnormalities after 28 weeks gestation. *Am J Obstet Gynecol* 172:479, 1995.
- Liu HY, Dhillon HK, Yeung CK, et al: Clinical outcome and management of prenatally diagnosed megaureters. *J Urol* 152(2 Pt 2):614–617, 1994.
- Baskin LS, Zderic SA, Snyder HM, et al: Primary dilated megaureter: long term follow up. *J Urol* 152:618–621, 1994.
- Abuhamad AZ, Horton CE, Evans AT: Renal duplication anomalies in the fetus: clues to prenatal diagnosis. *Ultrasound Obstet Gynecol* 7:174–177, 1996.
- Jee LD, Rickwood AM, Williams MP, Anderson PA: Experience with duplex system anomalies detected by prenatal ultrasonography. *J Urol* 149(4):808–810, 1993.
- Vergani P, Centi P, Locatelli A, et al: Accuracy of prenatal ultrasonographic diagnosis of duplex renal system. *J Ultrasound Med* 18(7):463–467, 1999.
- Austin PE, Cain MP, Casale AJ, et al: Prenatal outlet obstruction secondary to ureterocele. *Urology* 52:1132, 1998.
- Koff SA: Relationship between dysfunctional voiding and reflux. *J Urol* 148:1703–1705, 1992.
- Avni EF, Sopolman CC: The origins of vesico-ureteric reflux in male newborns: further evidence in favour of a transient urethral obstruction. *Br J Urol* 78:454–457, 1996.
- Puri P, Cascio S, Lakshmandass G, et al: Urinary tract infection and renal damage in sibling vesicoureteral reflux. *J Urol* 160:1028–1030, 1998.
- Gloor JM, Ramsey PS, Ogburn PL, et al: The association of isolated mild fetal hydronephrosis with postnatal vesicoureteral reflux. *J Matern Fetal Neonatal Med* 12:196, 2002.
- Morris R, Malin G, Khan K, Kilby M: Antenatal ultrasound to predict postnatal renal function in congenital lower urinary tract obstruction: systematic review of test accuracy. *Br J Obstet Gynaecol* 116:1290–1299, 2009.
- Glick PL, Harisson MR, Golbus MS, et al: Management of the fetus with congenital hydronephrosis. II. Prognostic criteria and selection for treatment. *J Pediatr Surg* 20:376, 1985.
- Nicolaides KH, Cheng HH, Snijders RJ, Moniz CF: Fetal urine biochemistry in the assessment of obstructive uropathy. *Am J Obstet Gynecol* 166(3):932–937, 1992.
- Mandelbrot L, Dumez Y, Muller F, et al: Prenatal prediction of renal function in fetal obstructive uropathies. *J Perinat Med* 19:283, 1991.
- Johnson MP, Bukowski TP, Kithier K, et al: Fetal urine albumin/globulin ratio in the in utero evaluation of obstructive uropathies. *Am J Hum Genet* 51:259, 1992 (abstract).
- Muller F, Bernard MA, Benkirane A, et al: Fetal urine cystatin C as a predictor of postnatal renal function in bilateral uropathies. *Clin Chem* 45(12):2292–2293, 1992.
- Spitzer A: The current approach to the assessment of fetal renal function: fact or fiction. *Pediatr Nephrol* 10:230, 1996.
- Brussières L, Laborde K, Souberbielle JC, et al: Fetal urinary insulin like growth factor 1 and binding protein 3 in bilateral obstructive uropathies. *Prenat Diagn* 15:1047, 1995.
- McLorie G, Farhat W, Klouwy A, et al: Outcome analysis of vesicoamniotic shunting in a comprehensive population. *J Urol* 166(3):1036–1040, 2001.



52. Makino Y, Kobayashi H, Kyono K, et al: Clinical results of fetal obstructive uropathy treated by vesico-amniotic shunting. *Urology* 55:118, 2000.
53. Carr MC: Prenatal management of urogenital disorders. *Urol Clin North Am* 31:389, 2004.
54. Morris RK, Quinlan-Jones E, Kilby MD, Khan KS: Systematic review of accuracy of fetal urine analysis to predict poor postnatal renal function in cases of congenital urinary tract obstruction. *Prenat Diagn* 27(10):900–911, 2007.
55. Biard JM, Johnson MP, Carr MC, et al: Long-term outcomes in children treated by prenatal vesicoamniotic shunting for lower urinary tract obstruction. *Obstet Gynecol* 106:503–508, 2005.
56. Ethun CG, Zamora IJ, Roth DR, et al: Outcomes of fetuses with lower urinary tract obstruction treated with vesicoamniotic shunt: a single-institution experience. *J Pediatr Surg* 48(5):956–962, 2013.
57. Morris RK, Malin GL, Quinlan-Jones E, et al: Percutaneous vesicoamniotic shunting versus conservative management for fetal lower urinary tract obstruction (PLUTO): a randomised trial. *Lancet* 382:1496–1506, 2013.
58. Ruano R, Yoshizaki CT, Giron AM, et al: Fetal cystoscopic placement of transurethral stent in a fetus with urethral stenosis. *Ultrasound Obstet Gynecol* 44(2):238–240, 2014.
59. Reinberg Y, Chelimsky G, Gonzalez R: Urethral atresia and the prune-belly syndrome. Report of 6 cases. *Br J Urol* 72:112–114, 1993.
60. Sepulveda W, Berry SM, Romero R, et al: Prenatal diagnosis of megalourethra. *J Ultrasound Med* 12:761–766, 1993.
61. Amsalem H, Fitzgerald B, Keating S, et al: Congenital megalourethra: prenatal diagnosis and postnatal/autopsy findings in 10 cases. *Ultrasound Obstet Gynecol* 37:678–683, 2011.
62. Wax JR, Pinette MG, Landes A, et al: Prenatal sonographic diagnosis of congenital megalourethra with in utero spontaneous resolution. *J Ultrasound Med* 28(10):1385–1388, 2009.
63. Nijagal A, Sydorak RM, Feldstein VA, et al: Spontaneous resolution of prenatal megalourethra. *J Pediatr Surg* 39(9):1421–1423, 2004.
64. Odibo AO, Turner GW, Borgida AF, et al: Late prenatal ultrasound features of hydrometrocolpos secondary to cloacal anomaly: case reports and review of the literature. *Ultrasound Obstet Gynecol* 9:419–421, 1997.
65. Witters I, Meylaerts L, Peeters H, et al: Fetal hydrometrocolpos, uterus didelphys with low vaginal and anal atresia: difficulties in differentiation from a complex cloacal malformation: a case report. *Genet Couns* 23(4):513–517, 2012.
66. Cilento BG, Jr, Benacerraf BR, Mandell J: Prenatal diagnosis of cloacal malformation. *Urology* 43:386–388, 1994.
67. Tonni G, Ida V, Alessandro V, Bonasoni MP: Prune-belly syndrome: case series and review of the literature regarding early prenatal diagnosis, epidemiology, genetic factors, treatment, and prognosis. *Fetal Pediatr Pathol* 31(1):13–24, 2013.
68. Hoshino T, Ihara Y, Shirane H, Ota T: Prenatal diagnosis of prune belly syndrome at 12 weeks of pregnancy: case report and review of the literature. *Ultrasound Obstet Gynecol* 12(5):362–366, 1998.
69. Papantoniou N, Papoutsis D, Daskalakis G, et al: Prenatal diagnosis of prune-belly syndrome at 13 weeks of gestation: case report and review of literature. *J Matern Fetal Neonatal Med* 23(10):1263–1267, 2010.
70. White SM, Chamberlain P, Hitchcock R, et al: Megacystis-microcolon-intestinal hypoperistalsis syndrome: the difficulties with antenatal diagnosis. Case report and review of the literature. *Prenat Diagn* 20:697–700, 2000.
71. Hidaka N, Kawamata K, Chiba Y: Megacystis-microcolon-intestinal hypoperistalsis syndrome: in utero sonographic appearance and the contribution of vesicocentesis in antenatal diagnosis. *J Ultrasound Med* 25:765–769, 2006.
72. Chen CP, Wang TY, Chuang CY: Sonographic findings in a fetus with megacystis-microcolon-intestinal hypoperistalsis syndrome. *J Clin Ultrasound* 26:217–220, 1998.
73. Dicke JM, Blanco VM, Yan Y, et al: The type and frequency of fetal renal disorders and management of renal pelvis dilatation. *J Ultrasound Med* 25:973, 2006.
74. Estrada CR, Peters CA, Retik AB, Nguyen HT: Vesicoureteral reflux and urinary tract infection in children with a history of prenatal hydronephrosis—should voiding cystourethrography be performed in cases of postnatally persistent grade II hydronephrosis? *J Urol* 181(2):801–806, 2009.
75. Alconcher L, Tombesi M: Mild antenatal hydronephrosis: management controversies. *Pediatr Nephrol* 19:819–820, 2004.
76. Keating MA, Escala J, Snyder HM, et al: Changing concepts in management of primary obstructive megaureter. *J Urol* 142:636, 1989.
77. Shokeir AA, Nijman RJ: Primary megaureter: current trends in diagnosis and treatment. *BJU Int* 86(7):861–868, 2000.
78. Merlini E, Spina P: Primary non-refluxing megaureters. *J Pediatr Urol* 1:409, 2005.
79. Dias T, Sairam S, Kumarasiri S: Ultrasound diagnosis of fetal renal abnormalities. *Best Pract Res Clin Obstet Gynaecol* 28:403, 2014.
80. McPherson E: Renal anomalies in families of individuals with congenital solitary kidney. *Genet Med* 16:215, 2007.
81. Cho JY, Moon MH, Lee YH, et al: Measurement of compensatory hyperplasia of the contralateral kidney: usefulness for differential diagnosis of fetal unilateral empty renal fossa. *Ultrasound Obstet Gynecol* 34:515, 2009.
82. Van Vuuren SH, van der Doef R, Cohen-Overbeek TE, et al: Compensatory enlargement of a solitary functioning kidney during fetal development. *Ultrasound Obstet Gynecol* 40:665, 2012.
83. Lankadeva YR, Singh RR, Tare M, et al: Loss of a kidney during fetal life: long-term consequences and lessons learned. *Am J Physiol Renal Physiol* 306:F791, 2014.
84. Deshpande C, Hennkam RC: Genetic syndromes and prenatally detected renal anomalies. *Semin Fetal Neonatal Med* 13:171, 2008.
85. Cinman NM, Okeke Z, Smith AD: Pelvic kidney: associated disease and treatment. *J Endourol* 21(8):836–842, 2007.
86. Oh KY, Holznagel DE, Ameli JR, et al: Prenatal diagnosis of renal developmental anomalies associated with an empty renal fossa. *Ultrasound Q* 26:233, 2010.
87. Glodney B, Petersen J, Hoffman KJ, et al: Kidney fusion anomalies revisited: clinical and radiological analysis of 209 cases of crossed fused ectopia and horseshoe kidney. *BJU Int* 103:224, 2009.
88. Strauss S, Dushnitsky T, Peer A, et al: Sonographic features of horseshoe kidney: review of 34 patients. *J Ultrasound Med* 19:27, 2000.
89. Nursal GN, Buyukdereli G: Unfused renal ectopia: a rare form of congenital renal anomaly. *Ann Nucl Med* 19(6):507–510, 2005.
90. Winyard P, Chitty L: Dysplastic and polycystic kidneys: diagnosis, associations and management. *Prenat Diagn* 21:924, 2001.
91. Zerres K, Rudnik-Schoneborn S, Steinkamm C, et al: Autosomal recessive polycystic kidney disease. *J Mol Med* 76:303, 1998.
92. Rossette S, Harris PC: Genotype-phenotype correlations in autosomal dominant and autosomal recessive polycystic kidney disease. *J Am Soc Nephrol* 18:1374, 2007.
93. Guay-Woodford LM, Muecher G, Hopkins SD: The severe perinatal form of autosomal recessive polycystic kidney disease maps to chromosome 6p21.1-p12: implications for genetic counseling. *Am J Hum Genet* 56:1101, 1995.
94. Guay-Woodford LM, Bissler JJ, Braun MC, et al: Consensus expert recommendations for the diagnosis and management of autosomal recessive polycystic kidney disease: report of an international conference. *J Pediatr* 165(3):611–617, 2014.
95. Sherwani RK, Kumar A, Rahman K, Rabbani T: Autosomal recessive polycystic kidney disease: the importance of autopsy of suspected cases and genetic counseling. *BMJ Case Rep* 2010:2843, 2010.
96. Denamur E, Delezoide AL, Alberti C, et al: Genotype-phenotype correlations in fetuses and neonates with autosomal recessive polycystic kidney disease. *Kidney Int* 77:350, 2010.
97. Avni FE, Garel L, Cassart M, et al: Perinatal assessment of hereditary cystic renal diseases: the contribution of sonography. *Pediatr Radiol* 36:405, 2006.
98. Orskov B, Christensen KB, Feldt-Rasmussen B, et al: Low birth weight is associated with earlier onset of end-stage renal disease in Danish

- patients with autosomal dominant polycystic kidney disease. *Kidney Int* 81:919, 2012.
99. Chapman A: The fetal environment: a critical phase that determines future renal outcomes in autosomal dominant polycystic kidney disease. *Kidney Int* 81:814, 2012.
  100. Brun M, Maugey-Laulomb B, Eurin D, et al: Prenatal sonographic patterns in autosomal dominant polycystic kidney disease: a multicenter study. *Ultrasound Obstet Gynecol* 24:55, 2004.
  101. MacDermot KD, Saggat-Malik AK, Economides DL, Jeffery S: Prenatal diagnosis of autosomal dominant polycystic kidney disease (PKD1) presenting in utero and prognosis for very early onset disease. *J Med Genet* 35(1):13–16, 1998.
  102. Fick GM, Johnson AM, Strain JD, et al: Characteristics of very early onset autosomal dominant polycystic kidney disease. *J Am Soc Nephrol* 3:1863, 1993.
  103. Tsatsaris V, Gagnadoux MF, Aubry MC, et al: Prenatal diagnosis of bilateral isolated fetal hyperechogenic kidneys. Is it possible to predict long term outcome? *Br J Obstet Gynaecol* 109:1388, 2002.
  104. Mashiach R, Davidovits M, Eisenstein B, et al: Fetal hyperechogenic kidney with normal amniotic fluid volume: a diagnostic dilemma. *Prenat Diagn* 25:553, 2005.
  105. Guerriero S, Gerada M, Piras S, et al: Bilateral fetal hyperechogenic kidneys associated with normal amniotic fluid: an ethical dilemma or normal variant? *Prenat Diagn* 26:190, 2006.
  106. Chaumoitre K, Brun M, Cassart M, et al: Differential diagnosis of fetal hyperechogenic cystic kidneys unrelated to renal tract anomalies: a multicenter study. *Ultrasound Obstet Gynecol* 28:911, 2006.
  107. Bernstein J: Glomerulocystic kidney disease—nosological considerations. *Pediatr Nephrol* 7:464, 1993.
  108. Woolf AS, Feather SA, Bingham C: Recent insights into kidney diseases associated with glomerular cysts. *Pediatr Nephrol* 17:229, 2002.
  109. Guay-Woodford LM, Galliani CA, Musulman-Mroczek E, et al: Diffuse renal cystic disease in children: morphologic and genetic correlations. *Pediatr Nephrol* 12:173, 1998.
  110. Avni FE, Hall M: Renal cystic diseases in children: new concepts. *Pediatr Radiol* 40(6):939–946, 2010.
  111. Ickowicz V, Eurin D, Maugery Laulom B, et al: Meckel Gruber syndrome: sonographic pathologic correlation. *Ultrasound Obstet Gynecol* 27:296, 2006.
  112. Mourri AB, Cassart M, Hall M, Avni FE: The case of HNF-1beta mutation with medullary cysts. *JBR-BTR* 97(1):39–41, 2014.
  113. Cassart M, Eurin D, Didier F, et al: Antenatal renal sonographic anomalies and postnatal follow-up of renal involvement in Bardet-Biedl syndrome. *Ultrasound Obstet Gynecol* 24:51, 2004.
  114. Dar P, Sachs GS, Carter SM, et al: Prenatal diagnosis of Bardet-Biedl syndrome by targeted second-trimester sonography. *Ultrasound Obstet Gynecol* 17:354, 2001.
  115. Dippell J, Varlam DE: Early sonographic aspects of kidney morphology in Bardet-Biedl syndrome. *Pediatr Nephrol* 12:559, 1998.
  116. Campos A, Figueroa ET, Gunasekaran S, et al: Early presentation of tuberous sclerosis as bilateral renal cysts. *J Urol* 149:1077, 1993.
  117. Murakami A, Gomi K, Tanaka M, et al: Unilateral glomerulocystic kidney disease associated with tuberous sclerosis complex in a neonate. *Pathol Int* 62:209–215, 2012.
  118. Mesrobian H, Rushton HG, Bulas D: Unilateral renal agenesis may result from in utero regression of multicystic renal dysplasia. *J Urol* 150:793, 1993.
  119. Rabelo EA, Oliveira EA, Silva GS, et al: Predictive factors of ultrasonographic involution of prenatally detected multicystic dysplastic kidney. *BJU Int* 95:868, 2005.
  120. Rabelo EA, Oliveira EA, Diniz JS, et al: Natural history of multicystic kidney conservatively managed: a prospective study. *Pediatr Nephrol* 19:1102, 2004.
  121. Oliveira EA, Diniz JS, Vilasboas AS, et al: Multicystic dysplastic kidney detected by fetal sonography: conservative management and follow-up. *Pediatr Surg Int* 17:54, 2001.
  122. Leclair MD, El Ghoneini A, Audry G, et al: The outcome of prenatally diagnosed renal tumors. *J Urol* 173:186, 2005.
  123. Bove KE: Wilms tumor and related abnormalities in the fetus and newborn. *Semin Perinatol* 23:310, 1999.
  124. Irsutti M, Puget C, Bauwin C, et al: Mesoblastic nephroma: prenatal US and MRI features. *Pediatr Radiol* 30:147, 2000.
  125. Neri G, Martini-Neri ME, Katz BE, Opitz JM: The Perlman syndrome: familial renal dysplasia with Wilms tumor, fetal gigantism and multiple congenital anomalies. *Am J Med Genet A* 161A(11):2691–2696, 2013.
  126. Yiee J, Wilcox D: Abnormalities of the fetal bladder. *Semin Fetal Neonatal Med* 13(3):164–170, 2008.
  127. Wilcox D, Chitty L: Non-visualisations of the fetal bladder: aetiology and management. *Prenat Diagn* 21:977, 2001.
  128. Gearhart J, Ben-Chaim J, Jeffs R, et al: Criteria for the prenatal diagnosis of classic bladder exstrophy. *Obstet Gynecol* 85:961, 1995.
  129. Jayachandran D, Bythell M, Platt MW, et al: Register based study of bladder exstrophy-epispadias complex: prevalence, associated anomalies, prenatal diagnosis and survival. *J Urol* 186:2056, 2011.
  130. Goyal A, Fishwick J, Hurrell R, et al: Antenatal diagnosis of bladder/cloacal exstrophy: challenges and possible solutions. *J Pediatr Urol* 8:140, 2012.
  131. Goldman S, Szejnfeld PO, Rondon A, et al: Prenatal diagnosis of bladder exstrophy by fetal MRI. *J Pediatr Urol* 9:3, 2013.
  132. Cacciarri A, Pilu G, Mordenti M, et al: Prenatal diagnosis of bladder exstrophy: what counseling? *J Urol* 161:259, 1999.
  133. Hendren WH: Urogenital sinus and cloacal malformations. *Semin Pediatr Surg* 5:72, 1996.
  134. Carey J, Greenbaum B, Hall B: The OEIS complex (omphalocele, exstrophy, imperforate anus, spinal defects). *Birth Defects Orig Artic Ser* 14(6B):253–263, 1978.
  135. Austin PF, Hornsby YL, Gearhart JP, et al: The prenatal diagnosis of cloacal exstrophy. *J Urol* 160:1179, 1998.
  136. Calvo-Garcia MA, Kline-Fath BM, Rubio EI, et al: Fetal MRI of cloacal exstrophy. *Pediatr Radiol* 43:593, 2013.
  137. Wakhlu A, Dalela D, Tandon RK, et al: The single ectopic ureter. *Br J Urol* 82:246, 1998.
  138. Ahmed S, Barker A: Single system ectopic ureters: a review of 12 cases. *J Pediatr Surg* 27:491, 1992.
  139. Avni FE, Maugey-Laulom B, Cassart M, et al: The fetal genitourinary tract. In Callen PW, editor: *Ultrasound in Obstetrics and Gynecology*, Philadelphia, 2002, WB Saunders, pp 670–671.
  140. Brohnestein M, Tsidomy D, Diamant M, et al: Transvaginal US measurement of the adrenal glands at 12 to 17 weeks of gestation. *Am J Obstet Gynecol* 169:1205, 1993.
  141. Chang CH, Yu CH, Cheng FM, et al: Assessment of fetal adrenal gland volume using 3D-US. *Ultrasound Med Biol* 28:1383, 2002.
  142. Maki E, Oh K, Rogers S, Sohaey R: Imaging and differential diagnosis of suprarenal masses in the fetus. *J Ultrasound Med* 33:895–904, 2014.
  143. Saada J, Grebille AG, Aubry MC, et al: US in prenatal diagnosis of congenital adrenal hyperplasia. *Prenat Diagn* 24:627, 2004.
  144. Cassart M, Massez A, Donner C, et al: US diagnosis of fetal adrenal hyperplasia. *Prenat Diagn* 25:1059, 2005.
  145. Rubenstein SC, Benacerraf BR, Retik AB, et al: Fetal suprarenal masses: sonographic appearance and differential diagnosis. *Ultrasound Obstet Gynecol* 5:164, 1995.
  146. Luca JL, Rousseau T, Durand C, et al: Diagnostic and therapeutic dilemma with large prenatally detected cystic adrenal masses. *Fetal Diagn Ther* 17:11, 2002.
  147. Schwarzler P, Bernard JP, Senat MV, et al: Prenatal diagnosis of fetal adrenal masses: differentiation between hemorrhage and solid tumor by color Doppler sonography. *Ultrasound Obstet Gynecol* 13:351, 1999.
  148. Gocmen R, Basaran C, Karcaaltincaba M, et al: Bilateral hemorrhagic adrenal cysts in an incomplete form of Beckwith-Wiedemann syndrome: MRI and prenatal US findings. *Abdom Imaging* 30:786, 2005.
  149. Yamagawa I, Obata K, Saito H: Prenatally detected cystic neuroblastoma. *Pediatr Surg Int* 13(2–3):215–217, 1998.
  150. Izbizky G, Elias D, Gallo A, et al: Prenatal diagnosis of fetal bilateral adrenal carcinoma. *Ultrasound Obstet Gynecol* 26:669, 2005.



151. Merrot T, Walz J, Anastasescu R, et al: Prenatally detected cystic adrenal mass associated with Beckwith-Wiedemann syndrome. *Fetal Diagn Ther* 19:465, 2004.
152. Hosoda Y, Miyano T, Kimura K, et al: Characteristics and management of patients with fetal neuroblastoma. *J Pediatr Surg* 27:623, 1992.
153. Lin JN, Lin GJ, Hung IJ, Hsueh C: Prenatally detected tumor mass in the adrenal gland. *J Pediatr Surg* 34:1620, 1999.
154. Haffa AJ, Many A, Hartoor J, et al: Prenatal US diagnosis of metastatic neuroblastoma. *Prenat Diagn* 13:73, 1993.
155. Liyanage IS, Katoch D: US prenatal diagnosis of liver metastases from adrenal neuroblastoma. *J Clin Ultrasound* 20:401, 1992.
156. Morganti VJ, Anderson NG: Simple adrenal cysts in fetus, resolving in neonate. *J Ultrasound Med* 10:521, 1991.
157. Patti G, Fiocca G, Latini T, et al: Prenatal diagnosis of bilateral adrenal cysts. *J Urol* 150:1189, 1993.
158. Saylor RL, Cohn SL, Morgan ER, et al: Prenatal detection of neuroblastoma by fetal US. *Am J Pediatr Hematol Oncol* 16:356, 1994.
159. Strouse PJ, Boweman RA, Schlenizer AE: Antenatal findings of fetal adrenal hemorrhage. *J Clin Ultrasound* 23:442, 1995.
160. Dighe M, Moshiri M, Phillips G, et al: Fetal genitourinary anomalies—a pictorial review with postnatal correlation. *Ultrasound Q* 27:7–21, 2011.
161. Odeh M, Grinin V, Kais M, et al: Sonographic fetal sex determination. *Obstet Gynecol Surv* 64:50, 2009.
162. Zalel Y, Pinhas-Hamiel O, Lipitz S, et al: The development of the fetal penis—an in utero sonographic evaluation. *Ultrasound Obstet Gynecol* 17(2):129–131, 2001.
163. Johnson P, Maxwell D: Fetal penile length. *Ultrasound Obstet Gynecol* 15:308, 2000.
164. Naylor CS, Carlson D, Santulli T, et al: Use of three-dimensional ultrasonography for prenatal diagnosis of ambiguous genitalia. *J Ultrasound Med* 20:1365, 2001.
165. Pinhas-Hamiel O, Zalel Y, Smith E, et al: Prenatal diagnosis of sex differentiation disorders: the role of fetal ultrasound. *J Clin Endocrinol Metab* 87:4547, 2002.
166. Zimmer EZ, Blazer S, Blumenfeld Z, et al: Fetal transient clitoromegaly and transient hypertrophy of the labia minora in early and mid pregnancy. *J Ultrasound Med* 31:409, 2012.
167. Meizner I, Mashiach R, Shalev J, et al: The “tulip sign”: a sonographic clue for in-utero diagnosis of severe hypospadias. *Ultrasound Obstet Gynecol* 19:250, 2002.
168. Odeh M, Ophir E, Bornstein J: Hypospadias mimicking female genitalia on early second trimester sonographic examination. *J Clin Ultrasound* 36:581, 2008.
169. Soriano D, Lipitz S, Seidman DS, et al: Development of the fetal uterus between 19 and 38 weeks of gestation: in-utero ultrasonographic measurements. *Hum Reprod* 14:215, 1998.
170. Chitty LS, Chatelain P, Wolfenbutter KP, et al: Prenatal management of disorders of sex development. *J Pediatr Urol* 8:576, 2012.
171. Clayton P, Miller WL, Oberfeld SE, et al: Joint LWPES/ESPE CAH working group, 2002 consensus statement on 21-hydroxylase deficiency from the Lawson Wilkins Pediatric Endocrine Society and the European Society for paediatric endocrinology. *J Clin Endocrinol Metab* 87:4048, 2002.
172. Bryant AE, Laufer MR: Fetal ovarian cysts: incidence, diagnosis and management. *J Reprod Med* 49:329–337, 2004.
173. Comparetto C, Giudici S, Coccia ME, et al: Fetal and neonatal ovarian cysts: what's their real meaning? *Clin Exp Obstet Gynecol* 32:123, 2005.
174. Foley PT, Ford WD, McEwing R, et al: Is conservative management of prenatal and neonatal ovarian cysts justifiable? *Fetal Diagn Ther* 20:454, 2005.
175. Awad J, Azar G, Soubra M: US diagnosis of urachal cyst in utero. *Acta Obstet Gynecol Scand* 73:156, 1994.
176. Crombleholme TM, Craigo SD, Gaomal S, et al: Fetal ovarian cyst decompression to prevent torsion. *J Pediatr Surg* 32:1447, 1997.
177. D'Addario V, Vompe G, Kurjak A, et al: US diagnosis and perinatal management of complicated and uncomplicated fetal ovarian cyst. *J Perinat Med* 18:375, 1990.
178. Garel L, Filiatrault D, Brandt M, et al: Antenatal diagnosis of ovarian cysts. *Pediatr Radiol* 21:182, 1991.
179. Hee-Jung L: Daughter cysts sign: a US finding of ovarian cyst in children. *AJR Am J Roentgenol* 174:1013, 2000.
180. Perrotin F, Roy F, Potin J, et al: US diagnosis and prenatal management of fetal ovarian cysts. *J Gynecol Obstet Biol Reprod (Paris)* 29:161, 2000.
181. Gupta P, Sharma R, Kumar S, et al: Role of MRI in fetal abdominal cystic masses detected on prenatal sonography. *Arch Gynecol Obstet* 281:519–526, 2010.
182. Odibo AO, Turner GW, Borgida AF, et al: Late prenatal ultrasound features of hydrometrocolpos secondary to cloacal anomaly: case reports and review of the literature. *Ultrasound Obstet Gynecol* 9:419–421, 1997.
183. Geipel A, Berg C, Germer U, et al: Diagnostic and therapeutic problems in a case of prenatally detected fetal hydrocolpos. *Ultrasound Obstet Gynecol* 18:169, 2001.
184. Ogunyemi D: Prenatal sonographic diagnosis of bladder outlet obstruction caused by a ureterocele associated with hydrocolpos and imperforate hymen. *Am J Perinatol* 18:15, 2001.
185. Manzella A, Filho PB: Hydrocolpos, uterus didelphys and septate vagina in association with ascites: antenatal sonographic detection. *J Ultrasound Med* 17:465, 1998.
186. Taori K, Krishnan V, Sharbidre KG, et al: Prenatal sonographic diagnosis of fetal persistent urogenital sinus with congenital hydrocolpos. *Ultrasound Obstet Gynecol* 36:641–643, 2010.
187. Picone O, Laperelle J, Sonigo P, et al: Fetal magnetic resonance imaging in the antenatal diagnosis and management of hydrocolpos. *Ultrasound Obstet Gynecol* 30:105–109, 2007.

# Ultrasound Features of Fetal Syndromes

*Kathryn Johnson Gray, Louise Wilkins-Haug*

## SUMMARY OF KEY POINTS

- Congenital anomalies can occur in isolation or be indicative of a more extensive underlying process.
- The presence of a congenital anomaly should prompt a thorough evaluation for other anomalies and consideration of additional advanced fetal imaging.
- When an underlying global process is suspected, genetic testing is indicated and a geneticist or genetic counselor should be involved.
- With advances in molecular diagnostics, fetal syndromes are more readily diagnosed by use of both chromosomal microarray and next-generation sequencing technologies.
- When fetal syndromes are diagnosed prenatally, a multidisciplinary team should assist in counseling and care coordination for expectant parents.
- Confirmation of an underlying genetic alteration leading to the observed fetal anomalies can both assist in diagnosis as well as provide information crucial for future reproductive planning.

## OUTLINE

### Maternal Infections, 542

- Fetal Cytomegalovirus Infection, 542
- Fetal Parvovirus B19 Infection, 543
- Fetal Rubella Syndrome, 544
- Fetal Syphilis, 545
- Fetal Toxoplasmosis Syndrome, 546
- Fetal Varicella Zoster, 547

### Teratogens, 548

- Fetal Alcohol Syndrome/Fetal Alcohol Effects, 548
- Fetal Valproic Acid Syndrome, 550
- Fetal Warfarin Syndrome, 551
- Maternal Diabetes/Caudal Regression Syndrome, 551

### Central Nervous System, 553

- Aicardi Syndrome, 553
- Meckel Syndrome, 554
- Lissencephaly, 556
- Septo-optic Dysplasia, 557
- Tuberous Sclerosis, 558
- L1 Syndrome, 560

### Cranium/Face, 561

- Craniosynostoses, 561
- Facial Anomalies, 566

### Musculoskeletal System, 573

- Skeletal Dysplasias
- Other Lethal Skeletal Dysplasias, 580
- Vertebral Anomalies, 583
- Upper Extremity Anomalies, 585
- Lower Extremity Anomalies, 589

### Thorax, 590

- Congenital High Airway Obstruction Syndrome, 590

- Cornelia de Lange Syndrome, 592
- Donnai-Barrow Syndrome, 592
- Fryns Syndrome, 592
- Pallister-Killian Syndrome, 593
- Scimitar Syndrome, 594

### Heart, 594

- 22q11.2 Deletion Syndrome, 595
- Alagille Syndrome, 596
- CHARGE Syndrome, 597
- Heterotaxy Syndromes, 598
- Holt-Oram Syndrome, 601
- Noonan Syndrome, 601
- Pentalogy of Cantrell, 603
- Tuberous Sclerosis, 605

### Gastrointestinal System/Abdominal Wall, 605

- Gastrointestinal System Disorders, 605
- Abdominal Wall Defects, 607

### Genitourinary Tract, 611

- Renal Tract Anomalies, 611
- Genital Anomalies, 613

### Abnormal Fetal Movement, 613

- Antley-Bixler Syndrome, 613
- Caudal Regression Syndrome, 613
- Congenital Ichthyosis, 613
- Congenital Myasthenic Syndromes, 614
- Congenital Myotonic Dystrophy, Type 1, 614
- Fetal Akinesia, 615
- Freeman-Sheldon Syndrome, 617
- Prader-Willi Syndrome, 617



**Fetal Overgrowth, 618**

- Bannayan-Riley-Ruvalcaba Syndrome, 618
- Beckwith-Wiedemann Syndrome, 607
- Klippel-Trenaunay Syndrome, 619
- Megalencephaly-Polymicrogyria-Polydactyly-Hydrocephalus Syndrome, 619
- Perlman Syndrome, 620
- Proteus Syndrome, 620
- Simpson-Golabi-Behmel Syndrome, 621
- Sotos Syndrome, 622
- Weaver Syndrome, 622

**Fetal Growth Restriction, 623**

- Russell-Silver Syndrome, 623

Seckel Syndrome, 623

**Microdeletion Syndromes, 624**

- Deletion 4p (Wolf-Hirschhorn Syndrome), 624
- Deletion 5p (Cri du Chat Syndrome), 625
- Deletion 11q (Jacobsen Syndrome), 625
- Deletion 22q11.2 (DiGeorge Syndrome), 626

**Metabolic Syndromes, 626**

- Neu-Laxova Syndrome, 626
- Smith-Lemli-Opitz Syndrome, 626
- Zellweger Syndrome, 627

**Other Malformations, 628**

- Amniotic Band Sequence, 628
- VACTERL Association, 631

Prenatally, a congenital anomaly is suspected when images of a fetal organ differ from the expected development for a given gestational age. A congenital anomaly can result from a malformation (an intrinsically abnormal developmental process), deformation (normal development with extrinsic forces), disruption (breakdown of previously normal tissue), or dysplasia (an abnormal organization of cells within tissues which may disrupt more than one organ) (Fig. 16-1). Whenever one congenital anomaly is present, a thorough search for other anomalies and unusual findings (i.e., accelerated or restricted fetal growth, abnormal amniotic fluid levels, altered fetal movements) should be undertaken. Additional imaging modalities may be helpful in completing the full fetal assessment including three-dimensional (3D) ultrasound studies, Doppler interrogations, and fetal magnetic resonance imaging (MRI).

The presence of congenital anomalies should prompt consideration of underlying global disorders, especially when several imaging findings are present. Multiple findings may be the result of a sequence, syndrome, or association. In a sequence, a group of anomalies is caused by an initial malformation, deformation, or disruption (i.e., amniotic band sequence). In a syndrome, a group of anomalies is the result of an underlying genetic cause and is pathogenetically related (i.e., Down syndrome). In an association, a given set of anomalies occurs together more frequently than can be explained by chance and the particular anomalies are not known to be the result of a sequence or syndrome (i.e., VACTERL association [vertebral anomalies, anal atresia, cardiac anomalies, tracheoesophageal fistula or esophageal atresia, renal/urinary anomalies, and limb defect]).

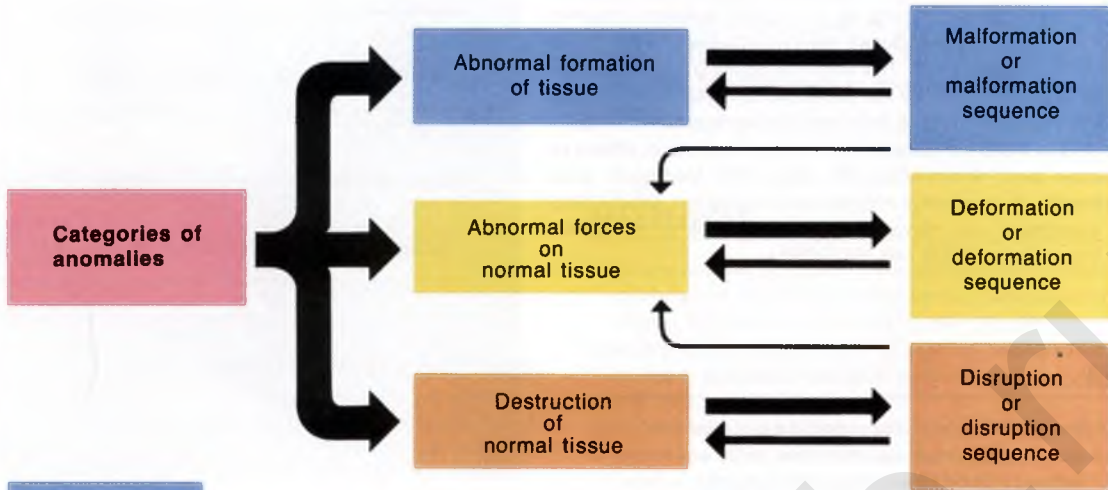
As molecular diagnostic technologies have become more refined and accessible, fetal syndromes are more readily diagnosed in both prenatal and postnatal settings. Prenatally, when a congenital anomaly is seen, chromosomal microarray is now recommended as the first-line test. In addition to aneuploidy, chromosomal microarray allows detection of microdeletion and microduplication syndromes and leads to the identification of approximately 5% more cytogenetic abnormalities

than can be seen on conventional karyotype alone (Fig. 16-2). However, many syndromes are single gene disorders and cytogenetic testing by both karyotype and chromosomal microarray will be normal. For many of these disorders, individual gene testing and gene panel testing is now available. Cost and time to obtain fetal DNA results prenatally still remain a significant hurdle for many syndromes suspected on prenatal imaging. The prenatal diagnostician should work closely with neonatal care providers to assure completion of a genetic workup.

In the following pages, we review fetal syndromes that are potentially detectable based on prenatal imaging findings and group them by prominent features (either the body system affected or some other hallmark such as altered fetal growth or movement). The review is not exhaustive but serves to highlight fetal syndromes commonly encountered by sonologists and sonographers and presents relevant imaging findings and genetics. Fetal syndromes often come to initial clinical attention based on screening prenatal ultrasound imaging; further imaging with 3D sonography and fetal MRI (especially for evaluation of the central nervous system [CNS]) can aid in delineation of additional features. Other specialties, including genetics, maternal-fetal medicine, and pediatric subspecialties (i.e., cardiology, surgery), can then assist with specialized testing, obstetric care, and postpartum planning for patients continuing with their pregnancies. These providers can give a clear overview of the anticipated process to the parents and convey the time and complexities of reaching a specific diagnosis for the fetus or child.

Given the rapid evolution in genetic testing, involvement of the genetics team is particularly important to assure that the most appropriate diagnostic testing is performed either in the prenatal or postnatal period. For many single gene disorders, multiple causative mutations within one gene have been identified. At times, the mutation may be unique or "private" to the family themselves. Completion of genetic studies provides not only confirmation of the diagnosis but an opportunity for the family to utilize the information in future reproductive planning.

**Errors of Morphogenesis**



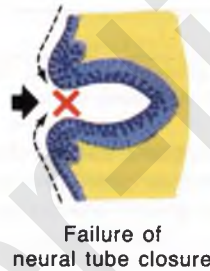
**Malformation**

Etiology

- Chromosomal
- Genetic
- Teratogenic
- Unknown

Morphogenic error

Developing structure  
↓  
Primary structural defect



Myelomeningocele (malformation)

Malformation. Primary structural defect resulting from error in tissue formation

**Deformation**

Etiology

- Extrinsic (fetal constraint)
- Intrinsic (fetal akinesia)

Abnormal force

Normally developed structure  
↓  
Altered structure or position



Clubfoot (deformation)

Deformation. Alteration in shape or position of normally developed structure

**Disruption**

Etiology

- Vascular
- Compressive
- Tearing

Abnormal force

Normally developed structure  
↓  
Tissue destruction



Limb reduction deficit (disruption)

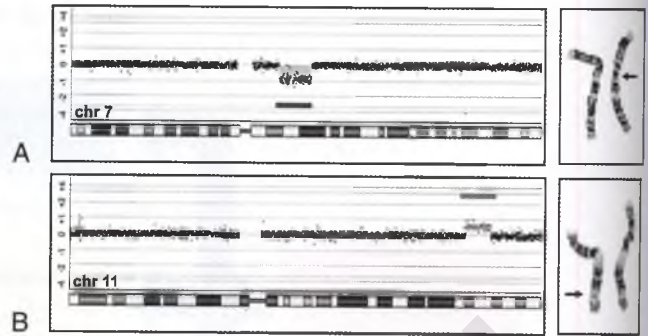
Disruption. Destruction of previously normally developed structure

JOHN A. CRAIG, MD  
©CIBA-GEIGY

**FIGURE 16-1** Errors of morphogenesis. (From Nyhan WL: Structural abnormalities: a systematic approach to diagnosis. Clin Symp 42(2):1-32, 1990, Plate 1, used with permission ©CIBA-GEIGY.)



**FIGURE 16-2** Examples of genomic imbalances detected by a chromosomal microarray but not by karyotyping. **A**, A 10.9-Mb deletion, including more than 60 genes. The deletion includes the Williams-Beuren syndrome region at chromosome region 7q11. The arrow is pointing to the deleted chromosome that was observed by retrospective analysis of G-banded slides. **B**, A 7.2-Mb duplication on the long arm of chromosome 11. Again, the arrow is pointing to the chromosome that has the duplication shown by the darker G-positive band. (From Miller DT, Adam MP, Aradhya S, et al: Consensus statement: chromosomal microarray is a first-tier clinical diagnostic test for individuals with developmental disabilities or congenital anomalies. *Am J Hum Genet* 86(5):749-764, 2010.)



## REFERENCES

Hillman SC, McMullan DJ, Hall G, et al: Use of prenatal chromosomal microarray: prospective cohort study and systematic review and meta-analysis. *Ultrasound Obstet Gynecol* 41(6):610-620, 2013.

Miller DT, Adam MP, Aradhya S, et al: Consensus statement: chromosomal microarray is a first-tier clinical diagnostic test for individuals with developmental disabilities or congenital anomalies. *Am J Hum Genet* 86(5):749-764, 2010.

## MATERNAL INFECTIONS

### Fetal Cytomegalovirus Infection

#### Definition

Fetal cytomegalovirus (CMV) infection is a congenital disorder characterized by hydrops, ascites, and ventriculomegaly caused by transplacental transmission of CMV to the fetus. The double-stranded DNA herpes group virus causes a mild infection or a mononucleosis-type illness in young healthy adults, chronic disease in older adults, and mild to severe congenital infection. Congenital infection is mostly caused by maternal primary infection.

#### Synonym

Fetal cytomegalovirus infection is also known as congenital cytomegalovirus infection.

#### Etiology

Cytomegalovirus (a double-stranded DNA herpes group virus) is the cause of the infection.

#### Incidence

Congenital CMV infection occurs in approximately 1% of all deliveries and is the most common congenital infection. Intrauterine transmission of CMV takes place in approximately 40% of infections, and approximately 10% of liveborn infants have symptomatic disease at the time of birth and later.

#### Diagnosis

CMV infection, as well as other congenital infections, should be suspected whenever nonimmune hydrops is found. Other suggestive findings include intracranial calcifications and intracranial hemorrhage, microcephaly, brain atrophy, abnormal periventricular echogenicities, intraparenchymal foci, ventriculomegaly, intraventricular adhesions, periventricular pseudocysts, sulcation and gyral abnormal patterns, hypoplastic corpus callosum, cerebellar and cisterna magna abnormalities, signs of striatal artery vasculopathy, splenomegaly, chorioretinitis, occlusion of the foramen ovale, signs of right-sided heart overload from the premature closure, ascites, hyperechoic bowel, fetal growth restriction, and oligohydramnios. Most features can be found by sonography beginning at approximately 20 weeks'

gestation. Whenever maternal infection is confirmed, polymerase chain reaction (PCR) testing of amniotic fluid should be performed. PCR testing of amniocentesis samples should be performed after a 6-week interval following the diagnosis of maternal infection and is most sensitive after 21 weeks' gestation. The diagnosis can also be made by histologic study of typical inclusion bodies in biopsy or autopsy specimens. Focal sonographic periventricular increased echogenicity associated with mild ventriculomegaly, without any abnormalities of the cerebral and cerebellar organogenesis or cephalic biometry alteration in the third trimester of pregnancy, should be considered a marker of encephalitis following CMV infection. Fetal MRI is a useful adjunct in the evaluation of intrauterine infection with CMV.

#### Pathogenesis

The exact mode of transplacental passage is uncertain. The virus replicates in fetal tissues, producing inflammation, tissue necrosis, and organ dysfunction. CMV hepatitis in the neonate can present with an intense inflammatory response involving the portal triads. In these cases, lobular disarray, degeneration of hepatocytes, and cholestasis are also seen. The cause of ascites in congenital CMV infection is not certain. Contributing factors may include low serum protein levels due to hepatic dysfunction and portal obstruction resulting from periportal inflammation.

#### Associated Anomalies

Isolated ascites is an uncommon finding in fetuses with CMV infection but may occur. Cardiovascular, gastrointestinal (GI), musculoskeletal, and ocular lesions may be found in association with the classic features. Petechiae, sensorineural hearing loss, and poor intellectual development may also occur after birth.

#### Differential Diagnosis

Because ascites is often the first manifestation of hydrops, the differential diagnosis for fetal ascites is essentially the same as with generalized hydrops, which includes many congenital infections. Conditions that present with intracranial calcifications (such as tuberous sclerosis), hyperechoic bowel (cystic fibrosis and Down syndrome), and hepatomegaly (primary liver disease or extramedullary hematopoiesis) should be considered.

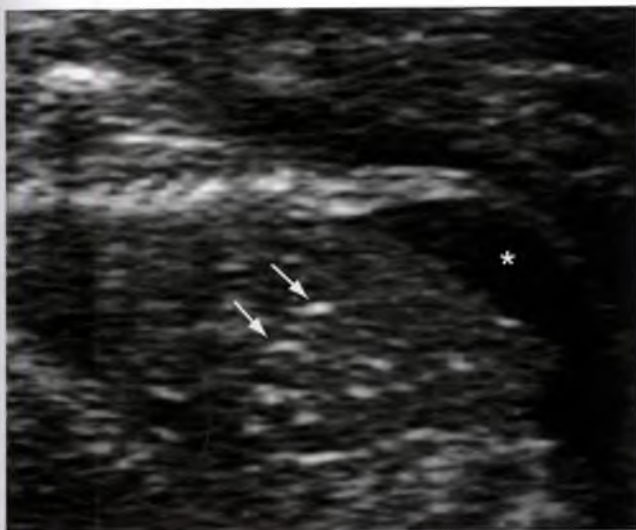


**FIG 16-3** Sonogram of a second trimester fetus with proven cytomegalovirus infection. Hepatic calcifications (arrows) are seen as well as fetal ascites (asterisk).

### Prognosis

In general, neonates with symptomatic CMV infection do poorly, with a neonatal mortality rate of 5%, and 50% to 60% of survivors suffer severe long-term neurologic morbidity. CMV hepatitis is reversible in survivors, but intellectual disability, motor deficits, and hearing loss are expected long-term sequelae. Late sequelae, such as sensorineural hearing loss and neurodevelopmental disorders, occur in 10% to 15% of infants lacking symptoms at birth. Pediatric neurologic morbidity is related to the degree of antenatal ventriculomegaly and, when greater than 15 mm, is associated with an increase in abnormal neurologic development. A normal ultrasound examination does not exclude the possibility of symptoms in the newborn or long-term complications.

### Recurrence Risk

Given that viral infection confers immunity in most patients, there is only a small theoretical risk of reinfection in another pregnancy.

### Management

Termination of pregnancy can be offered before viability. If continuation of the pregnancy is chosen, follow-up with ultrasound examina-

tions every 2 to 4 weeks is recommended to monitor for growth restriction, hydrops, and other fetal manifestations. Antiviral medications have not been shown to decrease the rate of perinatal transmission. Trials are under way for treatment of pregnant women with CMV infection early in pregnancy with hyperimmunoglobulin therapy.

### REFERENCES

- Daiminger A, Bader U, Enders G: Pre- and periconceptual primary cytomegalovirus infection: risk of vertical transmission and congenital disease. *Br J Obstet Gynaecol* 112(2):166–172, 2005.
- Graham E, Duhl A, Ural S, et al: The degree of antenatal ventriculomegaly is related to pediatric neurological morbidity. *J Matern Fetal Med* 10(4):258–263, 2001.
- Guibaud L, Attia-Sobol J, Buenerd A, et al: Focal sonographic periventricular pattern associated with mild ventriculomegaly in foetal cytomegalic infection revealing cytomegalic encephalitis in the third trimester of pregnancy. *Prenat Diagn* 24(9):727–732, 2004.
- Liesnard C, Donner C, Brancart F, et al: Prenatal diagnosis of congenital cytomegalovirus infection: prospective study of 237 pregnancies at risk. *Obstet Gynecol* 95(6 Pt 1):881–888, 2000.
- Malinger G, Lev D, Zahalka N, et al: Fetal cytomegalovirus infection of the brain: the spectrum of sonographic findings. *AJNR Am J Neuroradiol* 24(1):28–32, 2003.
- Moinuddin A, McKinstry RC, Martin KA, Neil JJ: Intracranial hemorrhage progressing to porencephaly as a result of congenitally acquired cytomegalovirus infection—an illustrative report. *Prenat Diagn* 23(10):797–800, 2003.
- Ortiz JU, Ostermayer E, Fischer T, et al: Severe fetal cytomegalovirus infection associated with cerebellar hemorrhage. *Ultrasound Obstet Gynecol* 23(4):402–406, 2004.
- Picone O, Teissier N, Cordier AG, et al: Detailed in utero ultrasound description of 30 cases of congenital cytomegalovirus infection. *Prenat Diagn* 34(6):518–524, 2014.
- Picone O, Vauloup-Fellous C, Cordier AG, et al: A series of 238 cytomegalovirus primary infections during pregnancy: description and outcome. *Prenat Diagn* 33(8):751–758, 2013.
- Sheffield JS, Boppana SB: Cytomegalovirus infection in pregnancy. *UpToDate* 2014. Available at: <<http://www.uptodate.com/home>>.
- Soper DE: Congenital cytomegalovirus infection: an obstetrician's point of view. *Clin Infect Dis* 57(Suppl 4):S171–S173, 2013.
- Wagner N, Kagan KO, Haen S, et al: Effective management and intrauterine treatment of congenital cytomegalovirus infection: review article and case series. *J Matern Fetal Neonatal Med* 27(2):209–214, 2014.

## Fetal Parvovirus B19 Infection

### Definition

Infection with parvovirus B19 causes erythema infectiosum and is a common childhood illness characterized by a “slapped cheek” facial appearance and a lacy erythematous rash on the trunk and extremities. Patients may have systemic symptoms prior to the appearance of the rash, including arthropathy.

### Synonym

Fetal parvovirus B19 infection is also known as fifth disease.

### Etiology

Acute maternal parvovirus B19 viremia leads to transplacental passage of the B19 virus and subsequent fetal infection.

### Incidence

Acute parvovirus B19 infection occurs in 3% to 4% of pregnant women, with the highest infection rates in school teachers and day care workers. Approximately 35% to 53% of pregnant women have immunity from a prior infection.

### Pathogenesis

The interval between maternal infection and fetal hydrops is about 3 weeks, and 93% of cases of fetal hydrops occur within 8 weeks of maternal diagnosis. Acute infection can lead to fetal loss or hydrops fetalis. Hydrops occurs because parvovirus B19 preferentially infects rapidly dividing cells and is cytotoxic to fetal red blood cell precursors, leading in some cases to severe fetal anemia and subsequent hydrops. Parvovirus B19 can also infect myocardial cells and cause myocarditis;



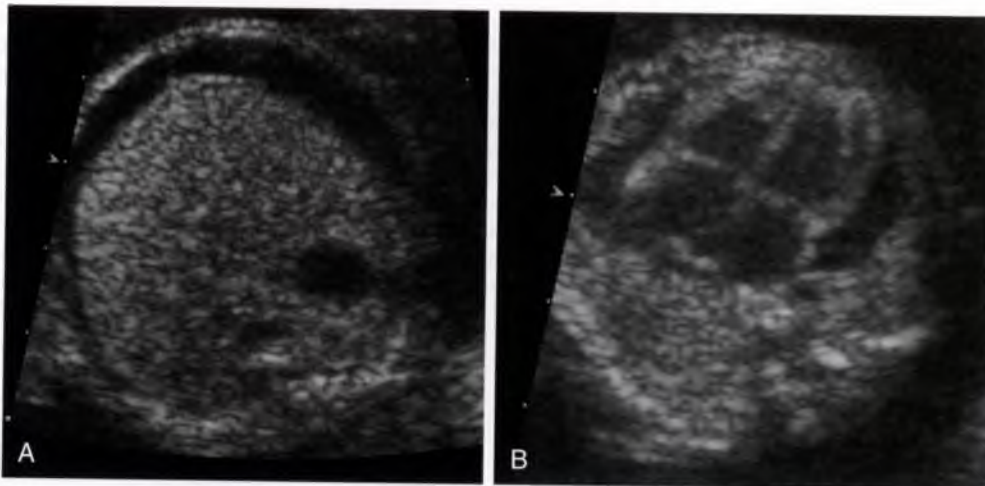


**FIG 16-4** Parvovirus infection. Ascites (**A**) and pericardial effusions (**B**) in a fetus with anemia due to parvovirus infection. Fetal ascites is often the initial sonographic finding in parvovirus infection.

this infection may also initiate apoptosis in cells. The risk of hydrops is greater if infection occurs in the first half of pregnancy. Hydrops can either lead to rapid fetal death or resolve spontaneously (although the rate of spontaneous resolution is uncertain).

### Associated Anomalies

In case reports, other congenital abnormalities have been noted, including ocular abnormalities, hydrocephalus, cleft lip/palate, joint webbing, musculoskeletal anomalies, hepatocellular damage, myocarditis, congenital cardiomyopathy, and myositis.

### Diagnosis

Acute maternal parvovirus infection can be diagnosed by positive IgM serologic findings; IgM can be detected 10 days after infection and may persist for 3 months or longer. IgM can be falsely negative, however, and failure to detect IgM antibodies therefore does not rule out B19 infection. Parvovirus B19 IgG develops several days after IgM and indicates past infection. Maternal B19 viremia can also be confirmed by PCR with improved sensitivity. Fetal parvovirus infections can be confirmed by PCR for B19 DNA in amniotic fluid.

### Differential Diagnosis

Differential diagnosis includes other conditions leading to nonimmune hydrops in the fetus.

### Prognosis

Risk of fetal death is largely limited to parvovirus B19 infections diagnosed in the first half of pregnancy (13% in first trimester, 9% from weeks 13 to 20, and <1% after 20 weeks). Intrauterine transfusion of hydropic fetuses improves prognosis. In addition to fetal anemia, severe fetal thrombocytopenia can occur and lead to exsanguination at the time of intrauterine red blood cell transfusion. Children who survive

fetal hydrops generally do well; an increased risk of developmental delay has been reported, but this has not been demonstrated in all studies.

### Recurrence Risk

There is virtually no recurrence risk because pathogenesis occurs with primary maternal parvovirus B19 infection.

### Management

Pregnant women exposed to parvovirus should have serologic testing for B19 IgM and IgG; positive IgG indicates maternal immunity, and the fetus should be protected. A positive IgM antibody indicates acute infection. Fetal intervention prior to 18 to 20 weeks is often not feasible, and transfusions this early in gestation are associated with an increased risk for fetal loss. Women diagnosed after 20 weeks should receive weekly ultrasound examinations to assess for fetal anemia and hydrops for at least 8 weeks after infection. If severe anemia is detected, intrauterine fetal blood transfusion is indicated.

## REFERENCES

- Chauvet A, Dewilde A, Thomas D, et al: Ultrasound diagnosis, management and prognosis in a consecutive series of 27 cases of fetal hydrops following maternal parvovirus B19 infection. *Fetal Diagn Ther* 30(1):41-47, 2011.
- Dijkmans AC, de Jong EP, Dijkmans BA, et al: Parvovirus B19 in pregnancy: prenatal diagnosis and management of fetal complications. *Curr Opin Obstet Gynecol* 24(2):95-101, 2012.
- Mari G, Norton ME, Stone J, et al: Society for Maternal-Fetal Medicine (SMFM) Clinical Guideline #8: the fetus at risk for anemia—diagnosis and management. *Am J Obstet Gynecol* 212(6):697-710, 2015.
- Riley LE, Fernandes CJ: Parvovirus B19 infection during pregnancy. *UpToDate* 2014. Available at: <<http://www.uptodate.com/home>>.

## Fetal Rubella Syndrome

### Definition

Fetal rubella syndrome is a congenital disorder resulting from primary maternal infection with the rubella virus. It is characterized by deafness, mental retardation, congenital cataract, heart defects, and other

structural anomalies found with variable severity and frequency. The rate of congenital infection with acute rubella during pregnancy is higher than 90% in the first 12 weeks of pregnancy, approximately 60% in weeks 13 to 17, 25% in weeks 18 to 24, and increases again during the last month of pregnancy.

### Synonyms

Synonyms for fetal rubella syndrome are fetal rubella effects, congenital rubella syndrome, and German measles.

### Etiology

Fetal rubella is caused by an RNA togavirus, which is the only member of the genus *Rubivirus*. The fetus is infected by transplacental transmission followed by hematogenous spread.

### Recurrence Risk

There is no recurrence risk of fetal rubella syndrome.

### Incidence

Cases of fetal rubella syndrome are rare in the United States since 2004 following comprehensive vaccination; however, reinfection after vaccination is possible. There were 13 cases reported in the United States between 2001 and 2004. It remains a clinical issue in other parts of the world.

### Diagnosis

The most frequent sonographic findings are cardiac malformations (in particular, septal defects), eye defects (cataracts, microphthalmia, and retinopathy), microcephaly, hepatomegaly, splenomegaly, and growth restriction. The risk of congenital defects is limited to maternal infection during the first 16 weeks of pregnancy. Sensorineural hearing loss and developmental delay are also associated with congenital rubella syndrome. The confirmation of fetal infection can be made by isolating rubella viral RNA from amniotic fluid samples and testing using PCR.

### Associated Anomalies

Occasionally, the following anomalies can be associated with the classic findings of fetal rubella syndrome: renal disorders, hypospadias, cryptorchidism, meningocele, glaucoma, patent ductus arteriosus, and peripheral pulmonary stenosis.

### Differential Diagnosis

Other conditions associated with congenital hepatomegaly and cataracts should be considered. This includes other congenital infections (TORCH [toxoplasmosis, other infections, rubella, cytomegalovirus,

herpes simplex]), fetal anemia, fetal liver tumors, chondrodysplasia punctata, Neu-Laxova syndrome (NLS), Smith-Lemli-Opitz (SLO) syndrome, and Walker-Warburg syndrome.

### Prognosis

Spontaneous abortion and intrauterine death may occur. The postnatal impact of intrauterine infection varies from absence of any defect to all the anomalies mentioned earlier with variable severity. The virus may remain for years in body tissues, causing complications of chronic infection (such as diabetes mellitus from chronic viropathy of the pancreas).

### Management

Termination of pregnancy should be discussed when fetal infection is detected during the first trimester, owing to the severity of the condition in this group. After viability, monthly ultrasound examinations for growth and follow-up of the anomalies are recommended.

### Prevention

Women found to be rubella nonimmune during pregnancy should be offered vaccination postpartum prior to discharge from the hospital. Breastfeeding is not a contraindication to vaccination.

## REFERENCES

- Best JM: Rubella. *Semin Fetal Neonat Med* 12(3):182–192, 2007.
- Migliucci A, Di Fraja D, Sarno L, et al: Prenatal diagnosis of congenital rubella infection and ultrasonography: a preliminary study. *Minerva Ginecol* 63(6):485–489, 2011.
- O'Neill JF: The ocular manifestations of congenital infection: a study of the early effect and long-term outcome of maternally transmitted rubella and toxoplasmosis. *Trans Am Ophthalmol Soc* 96:813–879, 1998.
- Riley LE: Rubella in pregnancy. *UpToDate* 2014. Available at: <<http://www.uptodate.com/home>>.
- Tang JW, Aarons E, Hesketh LM, et al: Prenatal diagnosis of congenital rubella infection in the second trimester of pregnancy. *Prenat Diagn* 23(6):509–512, 2003.

## Fetal Syphilis

### Definition

Fetal syphilis is caused by fetal infection with the spirochete *Treponema pallidum*, which readily crosses the placenta leading to fetal infection.

### Synonym

A synonym for fetal syphilis is congenital syphilis.

### Etiology

Maternal infection with *T. pallidum* leads to transplacental transmission of the virus and resultant fetal infection.

### Incidence

Incidence in 2008 was 10.1 cases per 100,000 liveborn infants with many cases found in women without prenatal care. The risk of transmission is higher for primary and secondary syphilis (50%) than for early latent (40%) and late (10%) syphilis. Transmission can occur at any gestational age. The frequency of vertical transmission increases as gestation advances but severity decreases with infection later in pregnancy.

### Diagnosis

In women with positive syphilis testing, clinical findings concerning for congenital syphilis include growth restriction, as well as liver and placental findings. Signs of liver dysfunction include hepatomegaly and ascites, which can lead to nonimmune hydrops. The placenta is typically large and edematous. Silver-staining of the placenta following delivery is positive for spirochetes. Fetal serologic tests are positive for antitreponemal IgM.

### Associated Anomalies

Clinical findings in neonates may include the following:

- Early congenital syphilis: hepatomegaly, syphilitic rhinitis (“snuffles”), maculopapular rash, generalized lymphadenopathy, and skeletal abnormalities.
- Late congenital syphilis (generally a result of gumma formation in various tissues): facial features (frontal bossing, saddle nose, short maxilla), eye findings (interstitial keratitis, glaucoma, corneal scarring, optic atrophy), sensorineural hearing loss, Hutchinson teeth, mulberry molars, perforation of hard palate, rhagades, gummas,





**FIG 16-5** Syphilis. Darkfield micrograph of *Treponema pallidum*, the organism that causes congenital syphilis. (From Centers for Disease Control and Prevention: Sexually Transmitted Diseases, 2016. Available at <http://www.cdc.gov/std/syphilis/images.htm>.)

anterior bowing of shins (“saber shins”), and paroxysmal cold hemoglobinuria.

### Differential Diagnosis

Findings in neonates can resemble other congenital infections.

### Prognosis

The severity of fetal effects depends on the duration of infection as well as the stage of development at the time of infection.

## Fetal Toxoplasmosis Syndrome

### Definition

Toxoplasmosis is caused by infection with the protozoan parasite *Toxoplasma gondii*. Toxoplasmosis is normally asymptomatic in immunocompetent individuals. Acute infections in pregnant women can be transmitted to the fetus and cause severe illness (mental retardation, blindness, and epilepsy). The risk of maternal-fetal transmission increases with gestational age at the time of exposure, whereas the incidence of severe disease decreases.

### Synonym

Fetal toxoplasmosis syndrome is also known as congenital toxoplasmosis.

### Incidence

An estimated 400 to 4000 cases of congenital toxoplasmosis occur annually in the United States. Of the 750 deaths attributed to toxoplasmosis each year, 375 (50%) are believed to be caused by eating contaminated meat, making toxoplasmosis the third leading cause of food-borne deaths in the United States. The incidence of toxoplasmosis acquisition during pregnancy ranges from 1 to 4 per 10,000. Half of fetuses escape the infection, one third have subclinical infection, and about 10% have severe infection.

### Etiology

Fetal toxoplasmosis is caused by transplacental transmission of parasites following maternal primary infection. Transmission from mothers with chronic infection via reactivation is rare but can be caused by immunologic dysfunction. The rate of fetal transmission increases

### Recurrence Risk

Recurrence is likely only if maternal syphilis infection remains untreated.

### Management

All women presenting for prenatal care should be evaluated for syphilis infection. If positive, penicillin treatment should be given; regimens vary according to the chronicity of the disease. If the duration of the disease is unknown, three doses of benzathine penicillin given at weekly intervals is recommended. If maternal syphilis is treated at least 30 days prior to delivery, only 1% to 2% of infants will be infected. This rate is greater than 70% if maternal syphilis remains untreated. If maternal syphilis is diagnosed after 20 weeks' gestation, an ultrasound examination should be obtained to assess for congenital syphilis.

## REFERENCES

- Araujo Junior E, Martins Santana EF, Rolo LC, et al: Prenatal diagnosis of congenital syphilis using two- and three-dimensional ultrasonography: case report. *Case Rep Infect Dis* 2012:478436, 2012.
- Centers for Disease Control and Prevention: Congenital syphilis—United States, 2003–2008. *MMWR Morb Mortal Wkly Rep* 59(14):413–417, 2010.
- De Santis M, De Luca C, Mappa I, et al: Syphilis infection during pregnancy: fetal risks and clinical management. *Infect Dis Obstet Gynecol* 2012:430585, 2012.
- Dobson SR: Congenital syphilis. *UpToDate* 2014. Available at: <<http://www.uptodate.com/home>>.
- Norwitz ER: Syphilis in pregnancy. *UpToDate* 2014. Available at: <<http://www.uptodate.com/home>>.

greatly as the gestational age at time of seroconversion increases, with transmission rates of 25%, 54%, and 65%, in the first, second, and third trimesters, respectively.

### Pathogenesis

The fetus is infected hematogenously through the placenta during parasitemia in the mother. Ocular toxoplasmosis causes irreversible damage to the retina in utero. The fetus and infant mount inflammatory responses that may contribute to ocular damage.

### Diagnosis

The classic triad suggestive of congenital toxoplasmosis includes chorioretinitis, intracranial calcifications, and hydrocephalus. Less common findings include ascites, pericardial and pleural effusions, and intrahepatic densities. However, most infants infected in utero are born with no obvious signs of toxoplasmosis on routine examination, but many develop learning and visual disabilities later in life. If left untreated, congenital toxoplasmosis can be associated with severe and even fatal disease. Other findings include microcephaly, encephalomyelitis, seizures, intellectual disability, ascites, and hepatosplenomegaly. The diagnosis can be made by using PCR to detect of *Toxoplasma gondii* in amniotic fluid, with increased sensitivity later in pregnancy.

### Differential Diagnosis

Other TORCH infections should be considered.

### Prognosis

Approximately 75% of congenitally infected newborns are asymptomatic.



**FIG 16-6** Severe dilatation of posterior horns of the lateral ventricles in a fetus with toxoplasmosis infection. (Courtesy of Julio Cesar Coub, 2006.)

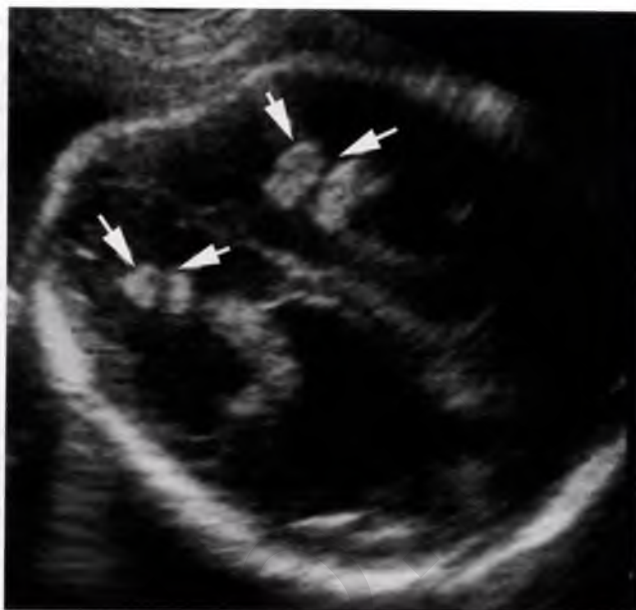


**FIG 16-7** Toxoplasmosis. Intracranial calcifications (arrows) in a fetus with toxoplasmosis infection. (Courtesy of Julio Cesar Coub, 2006.)

### Recurrence Risk

There is typically no recurrence risk.

### Management

Depending on gestational age and whether the fetus is known to be infected, pregnant women have been treated with the antibiotic spiramycin or with sulfadiazine alone or the combination of pyrimethamine and sulfadiazine. Treatment of acute infection during pregnancy has been associated with an approximately 50% reduction in fetal infection.

### Prevention

Toxoplasmosis infection can be prevented in large part by cooking meat to a safe temperature and peeling or thoroughly washing fruits and vegetables before eating. Pregnant women should avoid changing cat litter or, if no one else is available to change the cat litter, use gloves, then wash their hands thoroughly.

### REFERENCES

- Gilbert R, Petersen E: Toxoplasmosis and pregnancy. *UpToDate* 2014. Available at: <<http://www.uptodate.com/home>>.
- Kieffer F, Wallon M: Congenital toxoplasmosis. *Handb Clin Neurol* 112:1099–1101, 2013.
- Lopez A, Dietz VJ, Wilson M, et al: Preventing congenital toxoplasmosis. *MMWR Recomm Rep* 49(RR-2):59–68, 2000.
- Roberts F, Mets MB, Ferguson DJ, et al: Histopathological features of ocular toxoplasmosis in the fetus and infant. *Arch Ophthalmol* 119(1):51–58, 2001.
- Silveira C, Ferreira R, Muccioli C, et al: Toxoplasmosis transmitted to a newborn from the mother infected 20 years earlier. *Am J Ophthalmol* 136(2):370–371, 2003.
- Vidigal PV, Santos DV, Castro FC, et al: Prenatal toxoplasmosis diagnosis from amniotic fluid by PCR. *Rev Soc Bras Med Trop* 35(1):1–6, 2002.

### Fetal Varicella Zoster

#### Definition

Fetal varicella zoster is characterized by abnormalities of multiple organs caused by fetal infection with varicella following maternal chickenpox infection.

#### Synonyms

Fetal varicella zoster is also known as congenital varicella syndrome, varicella embryopathy, and chickenpox.

#### Incidence

The incidence of maternal varicella infection was 1 to 5 in 10,000 pregnancies in the United States in the 1980s but has decreased since vaccination began in 1995. The risk of fetal involvement among all pregnant women infected with varicella varies from 1% to 20%. First trimester varicella infections have been associated with an increased risk of spontaneous abortion. Second trimester varicella infections have been associated with 2% risk of a congenital syndrome character-

ized by limb hypoplasia, cutaneous scars, cataracts, microcephaly, and cortical atrophy.

#### Etiology

Herpesvirus is the etiologic agent.

#### Recurrence Risk

Recurrence risk is less than 1%.

#### Diagnosis

Maternal infection at any time in pregnancy exposes the fetus to a high risk of transplacental contamination and warrants follow-up. The risk of fetal anomalies, however, is the greatest from 8 to 20 weeks' gestation. Sonographic signs of fetal disease include fetal demise, growth restriction, musculoskeletal abnormalities (such as clubfeet and abnormal position of the hands, caused by both necrosis and denervation of the affected tissue), limitation of limb extension due to cicatrices formation, cutaneous scars, limb hypoplasia, chorioretinitis, congenital



cataracts, microphthalmia, hydrops, polyhydramnios, hyperechogenic hepatic foci, cerebral anomalies (such as ventriculomegaly or atrophy and microcephaly), disseminated foci of necrosis and microcalcifications, encephalitis, and echogenic bowel in the second trimester. The placenta can show a multifocal chronic villitis with multinucleated giant cells. Fetal infection can be demonstrated by detection of varicella zoster virus DNA by PCR in fetal blood and amniotic fluid.

### Pathogenesis

Maternal viremia leads to placental infection with subsequent fetal transmission. Direct damage occurs to fetal tissues by the neurotropic varicella virus.

### Associated Anomalies

Congenital anomalies in multiple organs with variable severity can be seen in varicella embryopathy. Among survivors, intellectual disability, seizures, and limitation of movements may develop after birth. The virus may cause serious infections, particularly pneumonia, in adult women.

### Differential Diagnosis

Other viral infections, vascular accidents, and amniotic band syndrome should be considered.

### Prognosis

The severity of fetal involvement varies from dermatologic lesions to lethal disseminated disease. Limited scarring tends to have an excellent prognosis. Fetal brain disruptions, or severe maternal varicella with development of lethal maternal pneumonia and encephalitis, are indicators of an extremely high risk for fetal demise. The rate of fetal demise varies from 39% to 61%. Maternal infection in the first and early second trimester has a higher association with fetal anomalies, whereas third trimester infections have a higher risk for varicella zoster development at the neonatal period. A life-threatening illness may occur in the newborn when delivery occurs within 5 days of the onset of maternal illness.

### Management

Termination of pregnancy can be offered before viability. If continuation of the pregnancy is chosen, ultrasound follow-up is recommended to assess for fetal anomalies, limb contractures, and other signs of fetal compromise. If maternal seroconversion is suspected for varicella zoster, prenatal sonography and MRI may document the extent of tissue damage and assist in counseling. After a therapeutic abortion, fetal infection can be confirmed by detection of varicella zoster viral DNA in fetal tissues and the placenta, as well as by histopathologic findings such as miliary calcified necroses in fetal organs.

### Prevention

Serologic testing and vaccination should be offered to women of child-bearing age, and women should be questioned prior to conception



**FIG 16-8** Varicella zoster infection. The fetal face at autopsy (26 weeks). Note the collapsed cranium, intact skin (very little maceration), disproportionate necrosis of the ocular globes, and flattened midface. (Courtesy of R.R. Lebel, 1992.)

about varicella immunity. Susceptible pregnant patients should be counseled to avoid contact with individuals who have chickenpox. If exposure occurs, varicella zoster immunoglobulin should be administered within 96 hours in an attempt to prevent maternal infection. Susceptible neonates should also receive varicella zoster immunoglobulin. Acyclovir is active against the varicella zoster virus, and treatment is indicated in seriously ill adults and neonates.

### REFERENCES

- Chapman SJ: Varicella in pregnancy. *Semin Perinatol* 22(4):339–346, 1998.
- Hartung J, Enders G, Chaoui R, et al: Prenatal diagnosis of congenital varicella syndrome and detection of varicella-zoster virus in the fetus: a case report. *Prenat Diagn* 19(2):163–166, 1999.
- Petignat P, Vial Y, Laurini R, Hohlfeld P: Fetal varicella-herpes zoster syndrome in early pregnancy: ultrasonographic and morphological correlation. *Prenat Diagn* 21(2):121–124, 2001.
- Riley LE: Varicella-zoster virus infection in pregnancy. *UpToDate* 2014. Available at: <<http://www.uptodate.com/home>>.
- Verstraelen H, Vanzielegheem B, Defoort P, et al: Prenatal ultrasound and magnetic resonance imaging in fetal varicella syndrome: correlation with pathology findings. *Prenat Diagn* 23(9):705–709, 2003.
- Yaron Y, Hassan S, Geva E, et al: Evaluation of fetal echogenic bowel in the second trimester. *Fetal Diagn Ther* 14(3):176–180, 1999.

## TERATOGENS

### Fetal Alcohol Syndrome/Fetal Alcohol Effects

Alcohol use during pregnancy results in a spectrum of adverse outcomes known as fetal alcohol spectrum disorders. Fetal alcohol syndrome (FAS) is one of these disorders. FAS is characterized by specific facial abnormalities and significant impairments in neurodevelopment and physical growth. Children exposed to alcohol (approximately 45 to 50 g of ethanol per day or equivalent)

in utero suffer from growth and mental retardation, physical abnormalities, and immune dysfunction. There is no “threshold,” so some fetuses exhibit signs of fetal alcohol effects at lower exposure. Recommendations for clinicians regarding assessment of thresholds published by the National Institute on Alcohol Abuse and Alcoholism recommend that any woman who reports drinking more than seven drinks per week or more than three drinks on any given day be further assessed for risk of developing alcohol-related problems.

### Synonyms

FAS is one of the fetal alcohol spectrum disorders.

### Incidence

The incidence of FAS ranges from 2 to 30 per 10,000 live births. FAS is the most common cause of intellectual disability in the United States and is thought to occur in 0.5 to 2.0 in 1000 births. The true extent of teratogenic injury from alcohol exposure exceeds the clinically recognized prevalence of FAS, because behavioral and physical teratogenesis may be present in the absence of full expression of the syndrome.

### Etiology/Pathogenesis

FAS is caused by direct toxicity of alcohol and its metabolites that cross the placenta and are not detoxified by the fetal liver. Alcohol is a teratogen and inflicts irreversible damage on the CNS. The rate of alcohol elimination from the fetal compartment is only 3% to 4% that of the maternal rate. Alcohol has fetal effects in all trimesters of pregnancy.

### Diagnosis

The findings include microcephaly, long round philtrum, small micrognathia, cleft palate, suppression of the cupid arch, microphthalmia, microcephaly, dysgenesis of the corpus callosum, malformed ears, atrial septal defect (ASD), ventricular septal defect (VSD), and growth restriction predominantly involving the limbs and occurring early without oligohydramnios. This lack of specificity suggests that the FAS facies may be a common teratogenic expression of exposure to a variety of substances occurring during a defined period of fetal development.

### Differential Diagnosis

Other conditions that involve growth restriction and microcephaly, such as congenital infections and chromosomal anomalies, should be considered.

### Prognosis

Intellectual disability and delayed growth persist postnatally. Most children with FAS have mild to moderate intellectual disability, but this

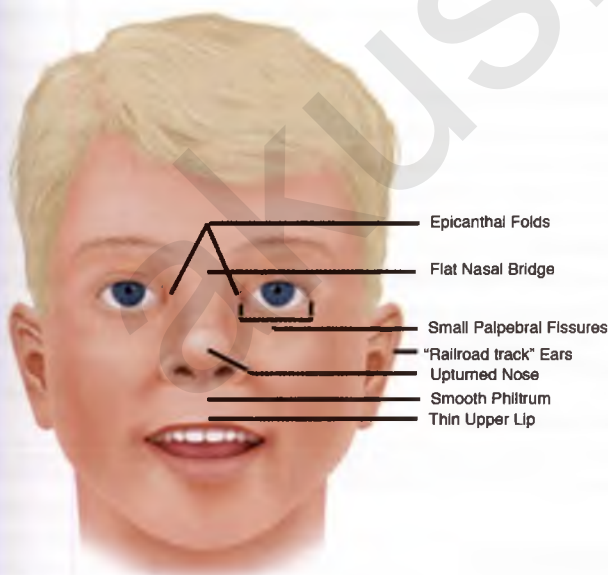


**FIG 16-9** Characteristic facial features in a child with fetal alcohol spectrum disorders. Findings may include a smooth philtrum, thin upper lip, upturned nose, flat nasal bridge and midface, epicanthal folds, small palpebral fissures, and small head circumference. (Courtesy Darryl Leja, NHGRI, National Institutes of Health.)



**FIG 16-10** Characteristic features of an ear of a child with fetal alcohol spectrum disorders. Note the underdeveloped upper part of the ear parallel to the ear crease below ("railroad track" appearance). (Courtesy Darryl Leja, NHGRI, National Institutes of Health.)



**FIG 16-11** Characteristic features of a hand of a child with fetal alcohol spectrum disorders. Note the curved fifth finger (clinodactyly) (*small arrow*) and the upper palmar crease (*large arrow*) that widens and ends between the second and third fingers ("hockey stick" crease). (Courtesy Darryl Leja, NHGRI, National Institutes of Health.)



can vary widely. The severity of intellectual disability appears related to the severity of growth deficits and dysmorphogenesis, such that the more phenotypically affected individuals have lower IQ scores. Hyperactivity is frequently observed. As adults, psychiatric disorders are highly prevalent in individuals with FAS, affecting more than 70% in one series, in which 60% had alcohol or drug dependence, 44% depression, and 40% psychosis.

### Recurrence Risk

Recurrence risk is high (up to 70%) in subsequent pregnancies if mothers continue to drink alcohol.

### Management

The management of these pregnancies should be aimed at reducing alcohol consumption; few programs have had significant efficacy.

## Fetal Valproic Acid Syndrome

### Definition

Fetal valproic acid exposure syndrome results from maternal valproate (an anticonvulsant) use during pregnancy and is characterized by CNS dysfunction, spina bifida, developmental delay, fetal growth restriction, and cardiac anomalies.

### Synonym

Depakote exposure is a synonym for fetal valproic acid syndrome.

### Incidence

Fetal valproic acid syndrome is rare, and the incidence is unknown. Any epileptic pregnant mother has two to three times increased risk for congenital anomalies compared with the general population. If the exposure to valproic acid takes place between the 17th and 30th days after fertilization, the incidence of neural tube defects approaches 1% to 2%. In general, the teratogenic risks are higher with increasing doses of valproic acid, with a significantly higher rate of malformations in doses up to 1000 mg/day.

### Etiology

Exposure to valproic acid is the cause of this syndrome.

### Pathogenesis

The pathogenesis of fetal valproic acid syndrome is unknown.

### Diagnosis

The findings include cardiovascular abnormalities, hypotonia, spina bifida, hypospadias, and limb reduction. The facial appearance can be characterized by an oral cleft, small broad nose, small ears, flat philtrum, a long upper lip with shallow philtrum, and micrognathia/retrognathia. Fetal growth restriction, microcephaly, generalized hypertrichosis sparing palms and soles, coarse face, gum hypertrophy, clubfeet and clubhands, musculoskeletal abnormalities, genital abnormalities, and urogenital defects may also be present. Heart defects have also been reported. In 26% of patients with fetal valproic acid exposure syndrome, cardiovascular abnormalities, most frequently VSDs, aortic or pulmonary stenosis, and persistent ductus arteriosus also occur. Pulmonary hypoplasia is also reported. Epilepsy and intellectual disability may develop after birth.

### Associated Anomalies

Associated anomalies include omphalocele, inguinal hernia, duodenal atresia, and scoliosis. Hyperbilirubinemia, hepatotoxicity, transient

## REFERENCES

- Bertrand J, Floyd RL, Weber MK, National Task Force on FAS/FAE, et al: *Fetal Alcohol Syndrome: Guidelines For Referral and Diagnosis*, Atlanta, 2004, Centers for Disease Control and Prevention.
- Floyd RL, O'Connor MJ, Sokol RJ, et al: Recognition and prevention of fetal alcohol syndrome. *Obstet Gynecol* 106(5 Pt 1):1059–1064, 2005.
- Jouitteau B, Massias C, Sanyas P: [Fetal alcohol syndrome]. *J Radiol* 81(12):1709–1712, 2000.
- Larroque B, Kaminski M: Prenatal alcohol exposure and development at preschool age: main results of a French study. *Alcohol Clin Exp Res* 22(2):295–303, 1998.
- Strömmland K, Mattson SN, Adnams CM, et al: Fetal Alcohol Spectrum Disorders: An International Perspective [Proceedings of Symposia at the 2004 ISBRA Meeting]. *Alcoholism* 29(1121):2005.

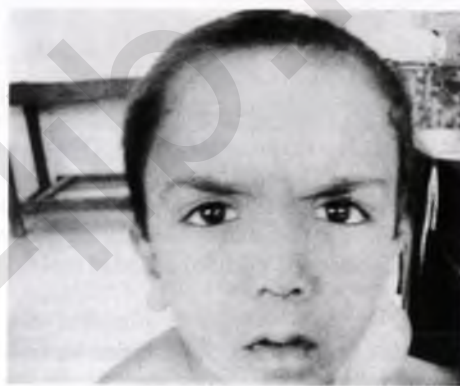


**FIG 16-12** Fetal valproate syndrome. Note low-set ears, slanting forehead, broad nasal bridge, hypertelorism, epicanthal folds, depressed nasal bridge, long philtrum, upturned nose, thin upper lip, and small mouth. (From Kulkarni ML, Zaheeruddin M, Shenoy N, Vani HN: Fetal valproate syndrome. *Indian J Pediatr* 73(10):937-939, 2006.)

hyperglycinemia, afibrinogenemia, and fetal or neonatal distress may be found.

### Differential Diagnosis

Neural tube defects of alternative origin should be considered. However, the clinical history in the presence of spina bifida and cardiac anomaly should suggest the diagnosis.

### Prognosis

Fetuses with major anomalies have a poor prognosis. Metabolic disturbances may also complicate the neonatal period. Affected children can die in infancy, and the surviving patients can have intellectual disability.

### Recurrence Risk

If the mother is exposed to valproic acid in a second pregnancy, the teratogenic effect is likely to be similar.

## REFERENCES

- Janas MS, Arroe M, Hansen SH, Graem N: Lung hypoplasia—a possible teratogenic effect of valproate. Case report. *APMIS* 106(2):300–304, 1998.
- Kozma C: Valproic acid embryopathy: report of two siblings with further expansion of the phenotypic abnormalities and a review of the literature. *Am J Med Genet* 98(2):168–175, 2001.

Stoll C, Audeoud F, Gaugler C, et al: Multiple congenital malformations including generalized hypertrichosis with gum hypertrophy in a child exposed to valproic acid in utero. *Genet Couns* 14(3):289–298, 2003.

ten Berg K, van Oppen AC, Nikkels PG, et al: Complex cardiac defect with hypoplastic right ventricle in a fetus with valproate exposure. *Prenat Diagn* 25(2):156–158, 2005.

## Fetal Warfarin Syndrome

### Definition

Fetal warfarin syndrome is characterized by specific bone and cartilage abnormalities in the fetus, including nasal hypoplasia, limb hypoplasia, and stippled epiphyses. It is caused by fetal exposure to warfarin between weeks 6 and 12 of gestation.

### Synonyms

Fetal warfarin syndrome has also been described as warfarin embryopathy and coumadin exposure.

### Incidence

A wide range has been reported, but the best estimate is that less than 10% of exposed fetuses will have embryopathy. The teratogenic effect is dose-dependent, with greater safety if the dose is less than 5 mg/day.

### Etiology

Warfarin freely crosses the placenta and is a known teratogen, with the highest risk between weeks 6 and 12 of gestation.

### Pathogenesis

The pathogenesis is unknown. Some hypotheses suggest that the drug interferes with post-translational modification of calcium-binding proteins essential for the development of bony structures.

### Diagnosis

Common sonographic findings include developmental abnormalities of bone and cartilage, specifically nasal and limb hypoplasia and stippled epiphyses.

### Associated Anomalies

CNS abnormalities have been more rarely reported and include microcephaly, optic atrophy, intellectual disability, hypotonia, and spasticity.

### Differential Diagnosis

Differential diagnosis includes other disorders affecting the bone and cartilage, specifically chondrodysplasia punctata.

### Prognosis

Because warfarin freely crosses the placenta, it can cause fetal bleeding at any gestational age. The most serious fetal complications are related to cerebral hemorrhage. Data on long-term survivors are lacking.

### Recurrence Risk

The recurrence risk is unknown. Fetal warfarin syndrome is related to warfarin exposure in subsequent pregnancy.

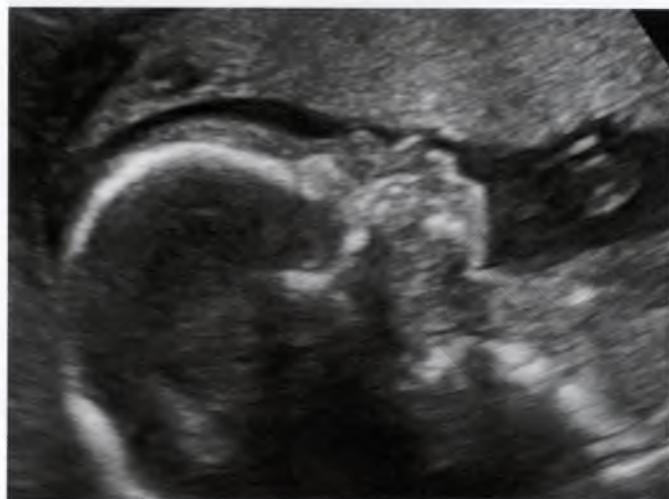


**FIG 16-13** Profile of a fetus with nasal hypoplasia, as is seen with fetal warfarin syndrome.

### Management

When detected prior to viability, termination of the pregnancy can be offered. If the pregnancy continues, no alteration in management is needed. If warfarin is continued throughout the pregnancy, it should be discontinued at 34 to 36 weeks' gestation and an alternative agent should be used for anticoagulation to minimize the risk of fetal bleeding at the time of delivery.

## REFERENCES

- Bauer KA: Use of anticoagulants during pregnancy and postpartum. *UpToDate* 2014. Available at: <<http://www.uptodate.com/home>>.
- Chan KY, Gilbert-Barness E, Tiller G: Warfarin embryopathy. *Pediatr Pathol Mol Med* 22(4):277–283, 2003.
- Gupta P, Kumar S, Roy KK, et al: Prenatal diagnosis of warfarin embryopathy using three-dimensional ultrasound. *Int J Gynaecol Obstet* 111(2):184–185, 2010.
- Howe AM, Lipson AH, de Silva M, et al: Severe cervical dysplasia and nasal cartilage calcification following prenatal warfarin exposure. *Am J Med Genet* 71(4):391–396, 1997.
- Tongsong T, Wanapirak C, Piyamongkol W: Prenatal ultrasonographic findings consistent with fetal warfarin syndrome. *J Ultrasound Med* 18(8):577–580, 1999.

## Maternal Diabetes/Caudal Regression Syndrome

### Definition

Caudal regression syndrome is a rare congenital defect, characterized by the absence of the sacrum, variable defects of portions of lumbar spine, and anomalies in other systems.

### Synonyms

Caudal dysplasia sequence and sacral agenesis are other terms that have been used to describe caudal regression syndrome.

### Incidence

The incidence of caudal regression syndrome is 0.25 to 1 per 10,000 normal pregnancies. This risk is 200 to 250 times higher in diabetic pregnancies.

### Etiology

The cause is unknown, but caudal regression syndrome is associated with maternal diabetes in 16% of the affected fetuses.



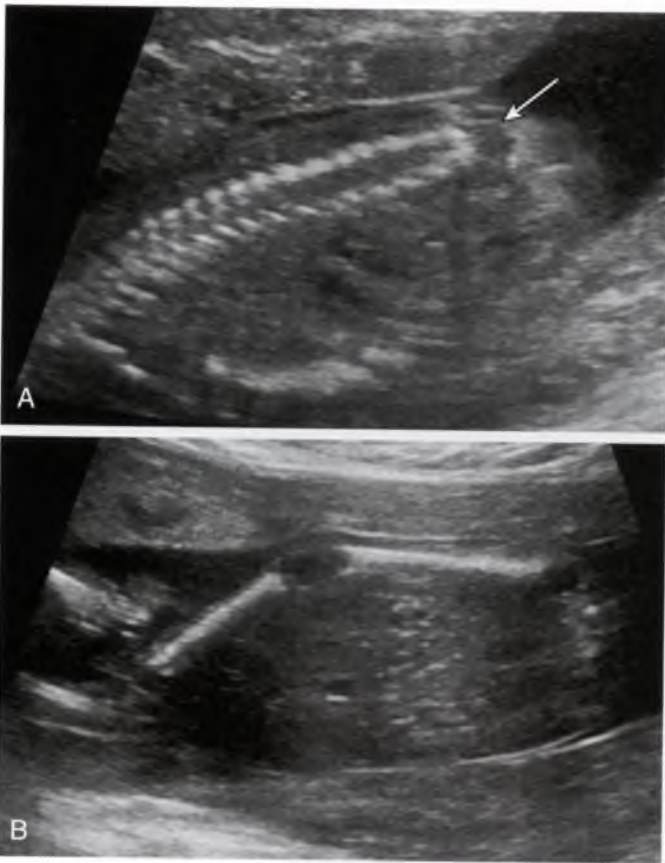


**FIG 16-14** Caudal regression syndrome associated with poorly controlled maternal diabetes. **A**, Absent distal sacral spine (*arrow*); **B**, fixed extension of the lower extremity.

### Recurrence Risk

This anomaly is not thought to be hereditary, and the recurrence risk is very small, although it is higher in diabetics.

### Diagnosis

The sonographic findings are variable, and depend on the extent and severity of the defect. It ranges from complete absence of the sacrum associated with abnormalities of the lumbar spine and lower extremities (such as clubfeet and contractions of the knees and hips) to abnormalities of the sacrum without associated defects. The most typical findings are the absence of a few vertebrae, the shield-like appearance of the fused or approximated iliac wings, and decreased interspace between the femoral heads. Some sonographic planes of section will intersect the fetus at such an angle that no spine is visible, a very striking and probably pathognomonic finding. Decreased movement of the legs is frequently observed. First trimester diagnosis may be difficult because of incomplete ossification of the sacrum at that time. A short crown-rump length and abnormal appearance of the yolk sac have been proposed as early sonographic signs of caudal regression syndrome.

### Genetics

The genetics of caudal regression syndrome is unknown.

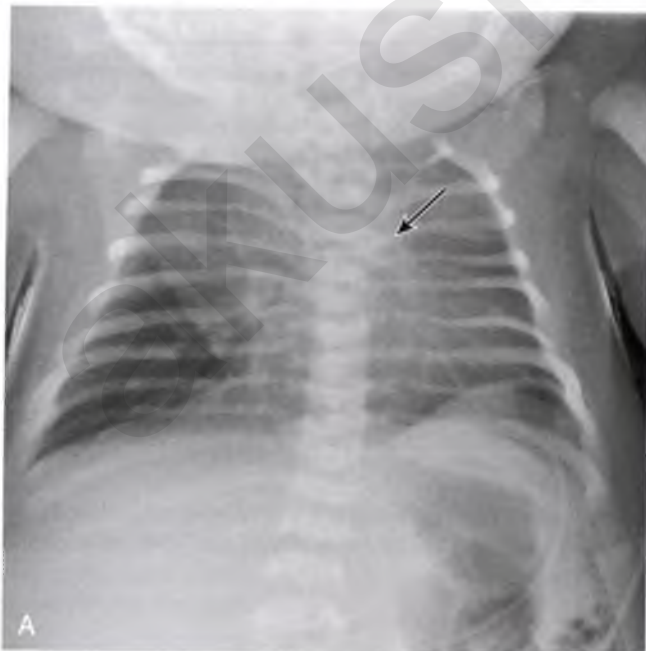


**FIG 16-15** Caudal regression syndrome associated with poorly controlled maternal diabetes. Postnatal radiographs demonstrate vertebral segmentation abnormality (**A**) (*arrow*) and absent sacrum (**B**) (*arrow*).



**FIG 16-16** Caudal regression syndrome. The lack of sacrum allows the iliac wings to be approximated, giving them a shield-like appearance (arrow).

### Pathogenesis

This syndrome is thought to be due to disrupted maturation of the caudal portion of the spinal cord complex before 4 weeks' gestation, leading to motricity deficits and neurologic impairment, varying from incontinence of urine and feces to complete neurologic loss.

## CENTRAL NERVOUS SYSTEM

Characteristic CNS abnormalities are seen in a majority of genetic syndromes, and, thus, an exhaustive list of associated syndromes is beyond the scope of this chapter. CNS abnormalities can be seen in all regions of the brain and include Chiari malformation, holoprosencephaly, lissencephaly, polymicrogyria, cerebellar hypoplasia, agenesis of the corpus callosum, hydrocephalus, neural tube defects, and CNS tumors. Many of these abnormalities and associated conditions are discussed in more detail in Chapter 9, Ultrasound Evaluation of the Fetal Central Nervous System. In this chapter, several syndromes with prominent CNS findings will be reviewed in greater detail, including Aicardi syndrome, Meckel syndrome (MKS), lissencephaly-associated syndromes (Miller-Dieker, Walker-Warburg, Baraitser-Winter, Norman-Roberts, microlissencephaly, and Neu-Laxova syndromes), septo-optic dysplasia, tuberous sclerosis, and L1 syndrome.

### Aicardi Syndrome

#### Definition

Aicardi syndrome is a neurodegenerative disorder first described in 1965, characterized by cerebral atrophy, intracerebral calcification of the basal ganglia, chronic cerebrospinal fluid lymphocytosis, and negative serologic investigations for common prenatal infections. It was classically characterized by agenesis of the corpus callosum, chorioretinal lacunae, and infantile spasms.

#### Incidence

More than 100 cases have been reported. It is seen only in females and 47,XXY males.

### Associated Anomalies

Anomalies of the central nervous, musculoskeletal, genitourinary, cardiac, respiratory, and GI systems may be found in association.

### Differential Diagnosis

Sirenomelia is the main alternative diagnosis and was thought to be the most severe form of caudal regression syndrome previously; it is now considered a separate entity. Fusion of the lower extremities is generally seen in sirenomelia.

### Prognosis

Prognosis depends on the severity of the spinal defect and associated anomalies, but the vast majority of survivors require urologic and orthopedic intervention. Severe forms are commonly associated with cardiac, renal, and respiratory problems, which are responsible for early neonatal death.

## REFERENCES

- Bashiri A, Sheizaf B, Burstein E, et al: Three dimensional ultrasound diagnosis of caudal regression syndrome at 14 gestational weeks. *Arch Gynecol Obstet* 280(3):505–507, 2009.
- Benacerraf BR: Caudal regression syndrome and sirenomelia. In Benacerraf BR, editor: *Ultrasound of Fetal Syndromes*, New York, 1998, Churchill Livingstone, p 250.
- Jaffe R, Zeituni M, Fejgin M: Caudal regression syndrome. *Fetus Spinal Anomalies* 7561:1–3, 1991.
- Kokrdova Z: Caudal regression syndrome. *J Obstet Gynaecol* 33(2):202–203, 2013.

### Etiology

The disorder is thought to be caused by an X-linked dominant de novo gene mutation with lethality in 46,XY males. The causative gene has not been identified.

### Genetics

The genetics of Aicardi syndrome are unknown.

### Diagnosis

The diagnosis is based on clinical features, including chorioretinal lacunae, brain MRI findings (corpus callosum dysgenesis, cerebral asymmetry, periventricular and intracortical gray matter heterotopia, choroid plexus cysts, choroid plexus papillomas, ventriculomegaly), and skeletal findings (abnormal vertebrae and missing ribs). Increased levels of interferon- $\alpha$  can be found in fetal blood and cerebrospinal fluid.

### Associated Anomalies

Other features include characteristic facial features, GI difficulties, small hands, vascular malformations, skin pigmentary lesions, and increased incidence of tumors. Infrequently, there is associated cleft lip and palate.

### Differential Diagnosis

Consider other causes of dysgenesis of the corpus callosum, including infectious causes.

### Prognosis

Survival is highly variable, with mean age of death at about 8 years old. Patients have profound intellectual disability and severe global



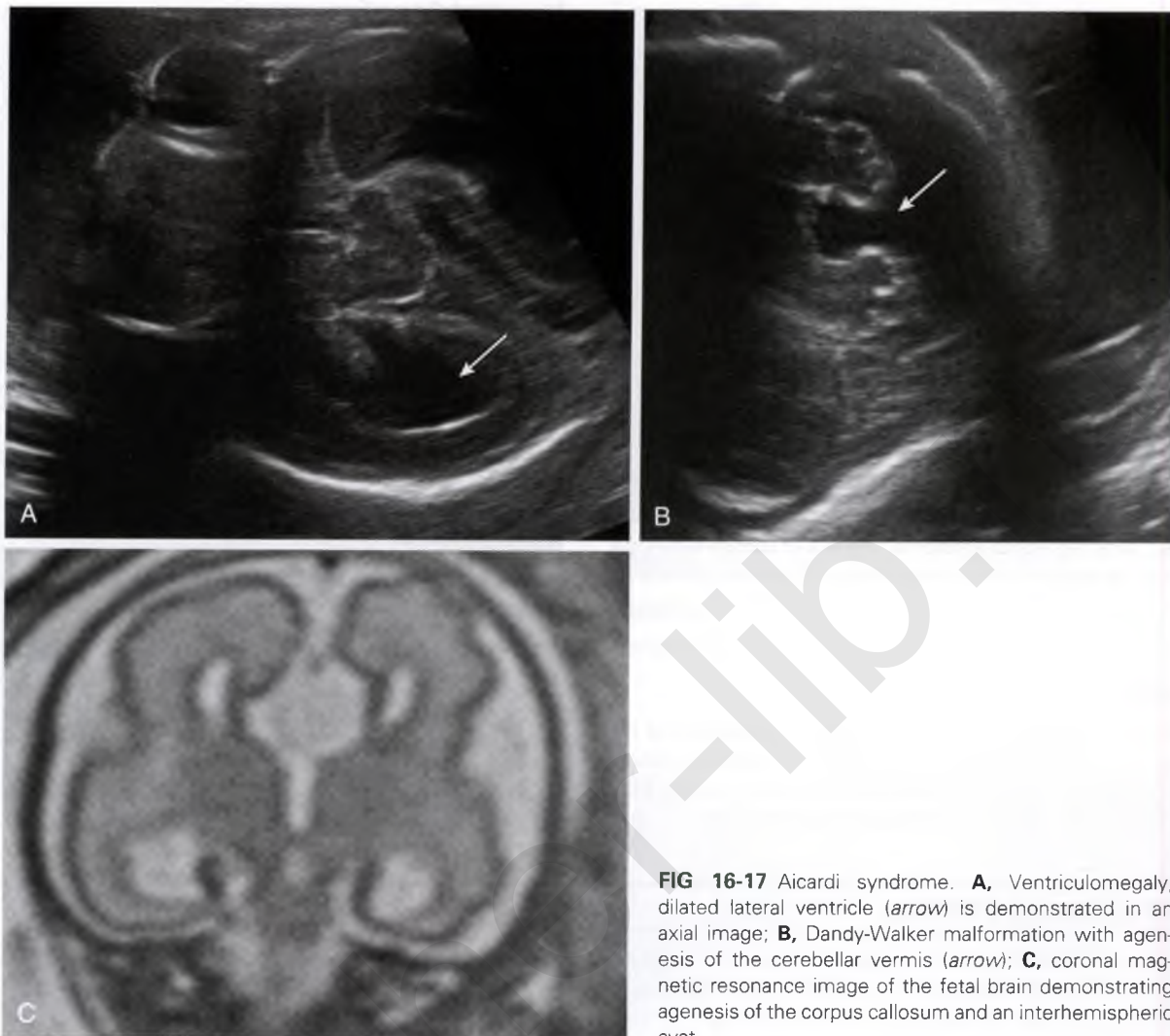


**FIG 16-17** Aicardi syndrome. **A**, Ventriculomegaly; dilated lateral ventricle (*arrow*) is demonstrated in an axial image; **B**, Dandy-Walker malformation with agenesis of the cerebellar vermis (*arrow*); **C**, coronal magnetic resonance image of the fetal brain demonstrating agenesis of the corpus callosum and an interhemispheric cyst.

developmental delay. Medically refractory epilepsy with a variety of seizure types develops over time. Multiple antiepileptic drugs are generally required for seizure control. Costovertebral defects can lead to scoliosis. Constipation and other GI problems are frequent.

### Recurrence Risk

The recurrence risk is less than 1%.

### REFERENCES

Ali M, Highet LJ, Lacombe D, et al: A second locus for Aicardi-Goutieres syndrome at chromosome 13q14-21. *J Med Genet* 43(5):444-450, 2006.

Bromley B, Krishnamoorthy KS, Benacerraf BR: Aicardi syndrome: prenatal sonographic findings. A report of two cases. *Prenat Diagn* 20(4):344-346, 2000.

Le Garrec M, Doret M, Pasquier JC, et al: Prenatal diagnosis of Aicardi-Goutieres syndrome. *Prenat Diagn* 25(1):28-30, 2005.

Neidich JA, Nussbaum RL, Packer RJ, et al: Heterogeneity of clinical severity and molecular lesions in Aicardi syndrome. *J Pediatr* 116(6):911-917, 1990.

Sutton VR, Van den Veyver IB: Aicardi syndrome. In Pagon RA, Adam MP, Ardinger HH, et al, editors: *GeneReviews*, Seattle, 1993-2016, University of Washington.

### Meckel Syndrome

#### Definition

Meckel syndrome (MKS) is a lethal ciliopathy characterized by occipital encephalocele, postaxial polydactyly of the hands and feet, and renal cystic dysplasia. It is commonly associated with ductal plate malformations of the liver.

#### Synonyms

Dysencephalia splanchnocystica and Meckel-Gruber syndrome are synonyms for MKS.

#### Incidence

The prevalence of MKS in Finland is estimated to be 1 in 9000. In U.S. and European populations estimates are 1 in 13,250 to 1 in 140,000. MKS is the most common syndromic form of neural tube defects and polydactyly. MKS includes approximately 5% of all neural tube defects.

#### Etiology

MKS is a ciliopathy, and the proteins encoded by the genes implicated in the disorder encode for proteins involved in primary ciliary function.

### Genetics

The disorder is genetically heterogeneous. The earliest implicated genes include *MKS1* and *MKS3*. Polydactyly is commonly found with *MKS1* mutations and is rare with *MKS3* mutations. Milder CNS phenotypes are seen with *MKS3* mutations. The list of involved genes now includes at least 13 genes, *MKS1* through *10*, *TMEM231*, *TMEM237*, and *C5orf42*. Inheritance is autosomal recessive with significant phenotypic variability. Many of the same genes are also involved in Joubert syndrome.

### Recurrence Risk

There is a 25% recurrence risk for MKS.

### Diagnosis

The disorder can be detected prenatally as early as 11 to 14 weeks. Cystic dysplastic kidneys are seen in almost all cases of MKS

(95-100%). The kidneys initially develop microscopic cysts that destroy the parenchyma and enlarge the organ up to 10 or 20 times. Occipital cephalocele is present in 60% to 80%. Maternal serum or amniotic fluid alpha-fetoprotein (AFP) level may be normal, as a membrane may cover the cephalocele. Other CNS findings include Dandy-Walker malformation and hydrocephalus. Postaxial polydactyly is present in 55% to 75% of fetuses. Other limb anomalies, such as bowing and shortening, may also be present. Liver histologic examination commonly demonstrates ductal plate malformations. Unfortunately, the first sonographic finding is often oligohydramnios, which makes the diagnosis more difficult to establish. Oligohydramnios is caused by



**FIG 16-18** Meckel syndrome: occipital encephalocele (arrow). (Courtesy of Marcos V. Sanchez, 2005. Available at thefetus.net.)

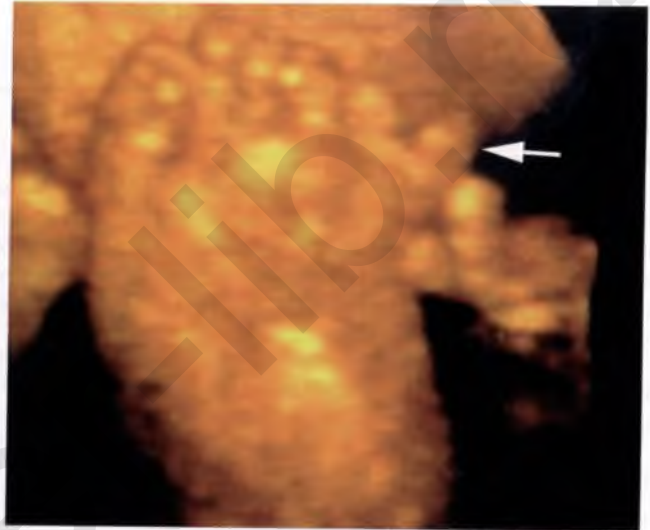


**FIG 16-20** Meckel syndrome: polydactyly (arrow). (Courtesy of Marcos V. Sanchez, 2005. Available at thefetus.net.)



**FIG 16-19** Meckel syndrome: cystic dysplastic kidneys. (Courtesy of Marcos V. Sanchez, 2005. Available at thefetus.net.)



**FIG 16-21** A fetus with Meckel syndrome. Note the small posterior encephalocele, the large abdominal distention due to the bilateral cystic kidneys, and the postaxial polydactyly.



renal dysfunction and develops early in the second trimester when the kidneys replace extracellular diffusion as the main source of amniotic fluid. Some cases of MKS have normal amniotic fluid; thus, the presence of normal fluid does not exclude the diagnosis.

### Differential Diagnosis

Conditions that can present with similar findings include trisomy 13 and 18, Joubert syndrome, Bardet-Biedl syndrome, and Smith-Lemli-Opitz syndrome. Karyotype and molecular genetic testing can assist in clarifying the diagnosis.

### Prognosis

MKS is a lethal disorder. Most infants are stillborn or die hours or days after birth. A few have survived to a few months of age.

## REFERENCES

- Consugar MB, Kubly VJ, Lager DJ, et al: Molecular diagnostics of Meckel-Gruber syndrome highlights phenotypic differences between MKS1 and MKS3. *Hum Genet* 121(5):591–599, 2007.
- Logan CV, Abdel-Hamed Z, Johnson CA: Molecular genetics and pathogenic mechanisms for the severe ciliopathies: insights into neurodevelopment and pathogenesis of neural tube defects. *Mol Neurobiol* 43(1):12–26, 2011.
- Mittermayer C, Lee A, Brugger PC: Prenatal diagnosis of the Meckel-Gruber syndrome from 11th to 20th gestational week. *Ultraschall Med* 25(4):275–279, 2004.
- Nizard J, Bernard JP, Ville Y: Fetal cystic malformations of the posterior fossa in the first trimester of pregnancy. *Fetal Diagn Ther* 20(2):146–151, 2005.
- Shaheen R, Ansari S, Mardawi EA, et al: Mutations in TMEM231 cause Meckel-Gruber syndrome. *J Med Genet* 50(3):160–162, 2013.

## Lissencephaly

### Definition

Lissencephaly is a cerebral developmental disorder, with agyria of the brain, which may be accompanied by pachygyria, minimal or no hydrocephalus, a wide cortical mantle, and characteristic dysmorphic features. The reduced or absent brain gyri are caused by disturbed neuronal migration in the neocortex. Miller in 1963 and Dieker in 1969 provided the first descriptions.

### Synonyms

See later discussion of specific syndromes.

### Incidence

Incidence is uncertain, but estimates range from 11.7 to 40 cases per 1 million births.

### Etiology

Many of the causative genes for lissencephaly have now been identified (see later).

### Pathogenesis

Lissencephaly is due to abnormal cortical development in which migration of neurons from the ventricular zone (a region close to the lateral ventricles) have slow or arrested migration to the cortical plate, leading to reduced folding or stranded neurons. Lissencephaly is now classified into types including the following.

**Classic Types.** Classic type lissencephaly is characterized by abnormally thick, four-layer cerebral cortex without other major brain anomalies. It is caused by mutations in 4 genes: *PAFA*, *HIB1* (*LIS1*), *DCX*, and *TUBA1A*.

**Miller-Dieker Syndrome.** Miller-Dieker syndrome (classic lissencephaly plus) is characterized by severe, classic lissencephaly, as well as facial dysmorphism (high forehead, micrognathia, short nose with anteverted nares, protuberant upper lip, bitemporal narrowing). Severe developmental delay and intellectual disability are also present. Other associated anomalies include omphalocele, cleft palate, and genital anomalies. Miller-Dieker syndrome results from chromosomal deletions at 17p13.3.

**Cobblestone Cortical Malformation.** Cobblestone cortical malformation was previously known as type 2 lissencephaly and is distinct from classic lissencephaly. The cortex appears irregular or pebbled and is thinner. There may also be irregularity in the gray-white matter boundary, dilated ventricles, white matter abnormalities, brainstem hypoplasia, and cerebellar abnormalities. Although this group is genetically heterogeneous, it is most commonly due to defects in

$\alpha$ -dystroglycan O-glycosylation. Known causative genes include *POMT1*, *POMT2*, *POMGNT1*, *FKRP*, *FKTN*, *ISPD*, and *LARGE*. The three associated phenotypes are Walker-Warburg syndrome, muscle-eye-brain disease, and Fukuyama congenital muscular dystrophy (ranging from most to least severe).

**Walker-Warburg Syndrome.** Walker-Warburg syndrome is a congenital muscular dystrophy characterized by eye anomalies and cerebral malformations. A wide variety of eye and cerebral findings have been reported including: microphthalmia, buphthalmos, congenital glaucoma, cataract, optic nerve hypoplasia, persistent hyaloid artery, Dandy-Walker malformation, hydrocephalus, cephalocele, microcephaly, and agenesis of the corpus callosum. Most affected newborns die within the first year of life. No psychomotor development occurs.

**Muscle-Eye-Brain Disease.** Muscle-eye-brain disease is a milder congenital muscular dystrophy in which ambulation may be acquired. Eye findings are common. The cerebral cortex demonstrates frontoparietal pachygyria, the cerebellar vermis is hypoplastic, and the brainstem is usually hypoplastic.

**Fukuyama Congenital Muscular Dystrophy.** Fukuyama congenital muscular dystrophy is the most mild of the three phenotypes. Ambulation is often acquired. Eye findings are variable and often mild. Brain findings are variable, but typically less severe than the other phenotypes.

**X-Linked Lissencephaly With Ambiguous Genitalia.** Males affected with X-linked lissencephaly have severe developmental delay, small or ambiguous genitalia, and seizures. Microcephaly, feeding difficulties, and growth failure are also present. Death in the first year is common. It is caused by mutations in the gene *ARX*.

**Baraitser-Winter Syndrome.** Baraitser-Winter syndrome is a rare syndrome with anterior-predominant pachygyria and characteristic facial features (hypertelorism, broad nose, ptosis, ridged metopic suture, arched eyebrows). Other common features include iris or retinal coloboma, sensorineural deafness, microcephaly, polyhydramnios, increased nuchal translucency, congenital heart defects, and renal tract anomalies. Intellectual disability and epilepsy are common. Caused by gain-of-function mutations in the genes *ACTB* and *ACTG1*.

**Lissencephaly With Cerebellar Hypoplasia.** Lissencephaly with anterior-predominant pachygyria and severe abnormalities of the cerebellum, brainstem, and hippocampus is caused by mutations in *TUBA1A* and *RELN* (Norman-Roberts syndrome).

**Microlissencephaly.** Microlissencephaly is lissencephaly with head circumference at birth of less than three standard deviations. It is caused by mutations in the *NDE1* gene.

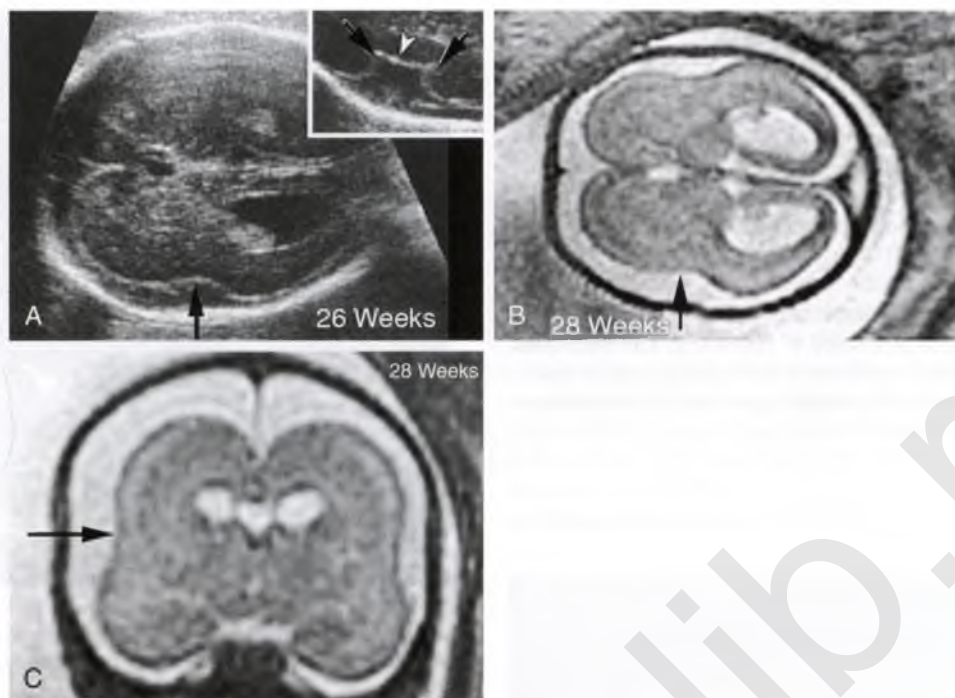


**FIG 16-22** Abnormal sylvian fissure/insula at 26 weeks. **A**, Axial ultrasound image at 26 weeks in a fetus with lissencephaly associated with Miller-Dieker syndrome shows a shallow, flat sylvian fissure/insula (arrow) with absence of angularity at the insular margins. Inset shows the expected appearance of the sylvian fissure/insula in a 26-week normal fetus. Infolding of the operculum should be seen with acute angles (black arrows in inset) at the margins of the insula (white arrowhead in inset) at 24.5 weeks' gestation. Axial (**B**) and coronal (**C**) T2-weighted magnetic resonance images at 28 weeks in the same fetus with Miller-Dieker syndrome showing a shallow sylvian fissure (arrow). The brain has an hourglass or figure-of-eight appearance on the axial image. Also note the agyria, large subarachnoid space, and mildly dilated occipital horns. (From Fong KW, Ghai S, Toi A, et al: Prenatal ultrasound findings of lissencephaly associated with Miller-Dieker syndrome and comparison with pre- and postnatal magnetic resonance imaging. *Ultrasound Obstet Gynecol* 24:716, 2004, used with permission.)

**Neu-Laxova Syndrome.** NLS is a lethal lissencephaly disorder inherited in an autosomal-recessive manner, characterized by growth restriction, microcephaly, agenesis of the corpus callosum, cerebellar hypoplasia, facial dysmorphism, hydrops, ichthyosis, extremity contractures, and syndactyly. It is due to an inborn error of serine metabolism, with causative mutations in the gene *PHGDH*.

### Recurrence Risk

Recurrence risk is dependent on the particular lissencephaly syndrome.

### Diagnosis

Sonographic diagnosis is difficult prior to the late second trimester, when the characteristic cerebral anomalies can be noted. The progressive microcephaly and failure of development of both sulci and gyri (which normally become well defined by 26 to 28 weeks) are suggestive of lissencephaly. Specific lissencephaly-related syndromes are difficult to differentiate prenatally. First-line genetic investigations involve

chromosomal microarray, followed by next-generation sequencing multigene panels or exome sequencing.

### Prognosis

Prognosis varies depending on the particular disorder.

### REFERENCES

- Asano Y, Minagawa K, Okuda A, et al: A case of Walker-Warburg syndrome. *Brain Dev* 22(7):454–457, 2000.
- Blin G, Rabbe A, Ansquer Y, et al: First-trimester ultrasound diagnosis in a recurrent case of Walker-Warburg syndrome. *Ultrasound Obstet Gynecol* 26(3):297–299, 2005.
- Fry AE, Cushion TD, Pilz DT: The genetics of lissencephaly. *Am J Med Genet C Semin Med Genet* 166C(2):198–210, 2014.
- Ghai S, Fong KW, Toi A, et al: Prenatal US and MR imaging findings of lissencephaly: review of fetal cerebral sulcal development. *Radiographics* 26(2):389–405, 2006.
- Stutterd CA, Leventer RJ: Polymicrogyria: a common and heterogeneous malformation of cortical development. *Am J Med Genet C Semin Med Genet* 166C(2):227–239, 2014.

## Septo-Optic Dysplasia

### Definition

Septo-optic dysplasia is a syndrome characterized by anomalies of cerebral midline structures, such as absence of the septum pellucidum,

congenital optic nerve dysplasia, and panhypopituitarism, leading to multiple endocrine defects (diabetes insipidus, hypogonadotropic hypogonadism, hypothyroidism, adrenal insufficiency, abnormal thyrotropin-releasing hormone test, gonadotropin-releasing hormone



test, and gonadotropin hormone–releasing hormone test). Septo-optic dysplasia may represent a mild form of holoprosencephaly.

### Synonym

Septo-optic dysplasia is also known as de Morsier syndrome.

### Incidence

The incidence is estimated at 1 in 10,000 newborns.

### Etiopathology

Environmental factors such as viral infections, medications, and vascular disruption have been postulated to play a role. The implicated genes (see later) are involved in embryonic development and are essential for formation of the eyes, the pituitary gland, and forebrain structures such as the optic nerves.

### Genetics

Mutations in *HESX1*, *OTX2*, and *SOX2* are thought to be causative in a small subset of patients.

### Recurrence Risk

The recurrence risk is unknown, depending on the cause.

### Clinical Findings

- CNS: seizures, mental retardation, atrophy of the optic nerve, dilatation of the suprasellar cistern, empty sella, cortical atrophy and dystrophic corpus callosum, and anterior cephalocele.
- Face: hypotelorism, microphthalmia, visual impairment with nystagmus, unilateral or bilateral optic disk hypoplasia with double rim appearance (choroidal pigment in the outer margin and pale nerve tissue in the inner), variable visual loss, coloboma, strabismus, astigmatism, bilateral cleft lip and palate, high arched palate, and flat nasal bridge.
- Endocrine system: low growth rate and short stature. The most common problem is growth hormone deficiency (93%), followed by adrenocorticotropic hormone (ACTH) deficiency (57%), hypothyroidism (53%), diabetes, and gonadotropin deficiency. Hypothalamic dysfunction is the basic origin of these endocrine abnormalities. Septo-optic dysplasia is responsible for approximately 4% of all growth hormone deficiencies in children.

### Diagnosis

Absence of the cavum septum pellucidum (CSP) is the most common finding. Sometimes, the standard sonographic views of the brain, obtained along the axial planes at midgestation, will fail to identify this absence. Absence of the CSP may not be detected because of the close proximity of the walls of the lateral ventricles, which are typically normal in size and may generate an artifact resembling a normal CSP. MRI is helpful for demonstration of hypoplastic optic tracts, allowing more definitive diagnosis. Hypotelorism, enlarged cerebral ventricles,



**FIG 16-23** Second trimester sonogram of the fetal head in a patient with septo-optic dysplasia. Absence of the septum pellucidum and communication of the frontal horns of the lateral ventricles (arrows) is seen.

communicating lateral ventricles, and bilateral cleft lip and palate have also been recognized prenatally.

### Differential Diagnosis

Several variants with associated schizencephaly, dysgenesis of the corpus callosum, or microphthalmos, as well as incomplete forms, have been described. Lobar holoprosencephaly may also resemble septo-optic dysplasia.

### Prognosis

The variable degree of intellectual disability (from minimal to severe), as well as the presence of multiple endocrine dysfunctions, affects the prognosis for each infant. Hyperthermia (in case of fever), dehydration (fever and diabetes insipidus), and other endocrine dysfunctions should be investigated and corrected.

### REFERENCES

- McMahon CL, Braddock SR: Septo-optic dysplasia as a manifestation of valproic acid embryopathy. *Teratology* 64(2):83–86, 2001.
- Orrico A, Galli L, Zappella M, et al: Septo-optic dysplasia with digital anomalies associated with maternal multidrug abuse during pregnancy. *Eur J Neurol* 9(6):679–682, 2002.
- Pilu G, Tani G, Carletti A, et al: Difficult early sonographic diagnosis of absence of the fetal septum pellucidum. *Ultrasound Obstet Gynecol* 25(1):70–72, 2005.

## Tuberous Sclerosis

### Definition

Tuberous sclerosis is characterized by abnormalities of the skin (facial angiofibromas, hypochromic patches), brain (cortical tubers, subependymal nodules and giant cell astrocytomas, seizures, intellectual disability), kidneys (cysts, renal cell carcinomas, angiomyolipomas), heart (rhabdomyomas, arrhythmias), and lungs (lymphangioliomyomatosis).

### Synonyms

Tuberous sclerosis is also called Bourneville sclerosis and Bourneville disease.

### Incidence

The incidence of tuberous sclerosis is up to 1 in 5800 births. Onset occurs in the first decade of life.

### Etiology

Tuberous sclerosis is transmitted through autosomal-dominant inheritance. Two thirds of affected individuals have a de novo mutation. The expression is highly variable.

### Pathogenesis

Tubers are the expression of an early disorder of embryogenesis. The greater the number of tubers, the greater the number of neurologic impairments. They can be found throughout the cerebral hemispheres, including in the subependymal region located in the walls of lateral ventricles and on the surface of the basal ganglia. They may extend into the ventricles including in the foramen of Monro area and can cause obstruction and hydrocephalus. They may also appear in the cortical gyri and sulcus terminalis. Tuberous sclerosis induces a reduction of the number of neurons, which are substituted by “monster” multinucleated giant neurons. The overgrowth of the fibrillary astrocytes can result in malignant astrocytomas. The sclerosis induces a demyelination, as well as calcium deposition in the glia and the blood vessels, which go through hyaline degeneration.

### Clinical Findings

Tuberous sclerosis can present with a wide variety of signs that involve many organs as a consequence of the multifactorial origin of this genetic disorder (Table 16-1).

### Diagnosis

The diagnosis is usually suggested by the discovery of cardiac tumors, which resemble small uterine myomas (round, usually well-delineated homogeneous masses). Between 51% and 86% of cardiac rhabdomyomas are seen in patients with tuberous sclerosis. Occasionally, the finding of a rhabdomyoma during routine second trimester ultrasound examination may lead to the recognition that the mother is affected. Cardiac rhabdomyomas increase prenatally, may regress in early infancy, remain unchanged during childhood, and regress in

adolescence. The rhabdomyomas may cause rhythm disruptions (Wolff-Parkinson-White syndrome, supraventricular tachycardia, paroxysmal arrhythmias), as well as obstructions or regurgitation. Renal angiofibromas have not been recognized prenatally, although this may simply be a matter of time. Some recent unpublished reports have demonstrated that the periventricular subependymal nodules may also be detected prenatally. 2D Doppler echocardiography is a useful, non-invasive method to diagnose fetal cardiac rhabdomyomas and to monitor their influence on fetal cardiac function. However, it does not help to determine which fetuses affected by rhabdomyomas have tuberous sclerosis. Some studies report that 39% of prenatal suspected cardiac rhabdomyomas will be diagnosed at birth as a tuberous sclerosis syndrome. Family history remains the strongest predictor of the syndrome in prenatal counseling, whereas size of the cardiac tumor cannot reliably be used. The presence of more than one rhabdomyoma is more likely to be associated with tuberous sclerosis than a single identified lesion. MRI can be performed to assess for the associated malformations.



**FIG 16-24** Tuberous sclerosis. Cardiac rhabdomyoma is demonstrated as a large, solid echogenic mass (arrow) in the left cardiac ventricle of this fetus with tuberous sclerosis.

**TABLE 16-1 Main Aspects of Tuberous Sclerosis**

Classic triad (<50% of cases)	
	Facial lesions
	Convulsions
	Mental retardation
Central nervous system	
	Cortical hamartomas
	Lesion of white substance*
	Subependymal hamartomas (95%)
	Typical localization: alongside lateral ventricle walls
	Astrocytoma of subependymal giant cells*
	Localization: foramen of Monro
	Obstructive hydrocephaly
Kidney	
	Cysts
	Angiolipoma
Cardiovascular	
	Rhabdomyoma
	Aneurysm, stenosis, and vascular ectopia
Liver	
	Leiomyoma
	Adenoma

\*No reports of intrauterine visualization.



**FIG 16-25** The typical café-au-lait spot of tuberous sclerosis. (Courtesy of Philippe Jeanty, 1999. Available at thefetus.net.)



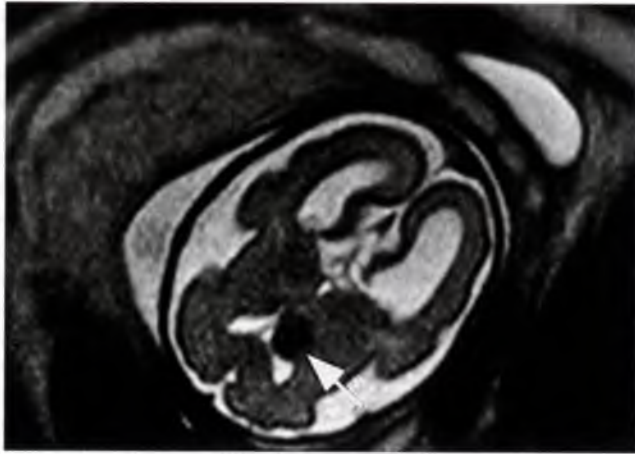


**FIG 16-26** Axial view (T2-weighted) in a fetus of 26 weeks' gestation showing a typical subependymal nodule (arrow). (Courtesy of Heron Werner, 2005. Available at thefetus.net.)

### Genetics

Tuberous sclerosis is caused by defects or mutations in one of two genes, *TSC1* and *TSC2*. *TSC1* produces a protein called hamartin. *TSC2* produces a protein called tuberlin. These proteins act as tumor suppressors, which are agents that regulate cell proliferation and differentiation. At least 1% of patients with tuberous sclerosis have somatic mosaicism for *TSC1* or *TSC2*.

## L1 Syndrome

### Definition

L1 syndrome includes a spectrum of phenotypes (see following synonyms) and is generally characterized by severe hydrocephalus, adducted thumbs, spasticity, and severe intellectual disability.

### Synonyms

Synonyms for L1 syndrome include X-linked hydrocephalus with stenosis of the aqueduct of Sylvius (HSAS), MASA (mental retardation, aphasia, spastic paraplegia, adducted thumbs) syndrome, SPG1 (X-linked complicated hereditary spastic paraplegia type 1), and X-linked corpus callosum agenesis.

### Incidence

The incidence is 1 in 30,000 births, accounting for 5% to 10% of males with congenital hydrocephalus not associated with another syndrome.

### Pathogenesis

Mutations in the *L1CAM* gene are thought to lead to the clinical phenotype. *L1CAM* is an adhesion surface protein involved in transmembrane signaling and is essential for the development and function of neurons.

### Diagnosis

Clinical findings include hydrocephalus with or without stenosis of the aqueduct of Sylvius, as well as corpus callosum agenesis or dysgenesis, cerebellar hypoplasia, small brainstem, and bilateral absence of the pyramids. Bilateral absence of the pyramids on MRI or at autopsy is pathognomonic. Prenatally, hydrocephalus can be seen, but is often not seen prior to 20 to 24 weeks' gestation, and sometimes is not seen even in the third trimester of pregnancy.

### Differential Diagnosis

The predominant prenatal finding is rhabdomyomas. Other cardiac tumors, such as a fibroma, should also be considered.

### Recurrence Risk

Recurrence risk is generally low in cases of new mutations, but up to 1% to 2% due to gonadal mosaicism, 50% if a parent is affected.

### Prognosis

As long as hydrops is not present from the presence of the rhabdomyomas, the prognosis depends on other complications of the disorder. CNS tumors are the leading cause of morbidity and fatality. Renal disease is the second leading cause of early death. Because of the wide variability of expression, an accurate prediction of a child's phenotype is difficult to infer from the status of the parent. Genetic evidence indicates that the degree of intellectual disability depends on the particular genetic alteration present.

## REFERENCES

- D'Addario V, Pinto V, Di Naro E, et al: Prenatal diagnosis and postnatal outcome of cardiac rhabdomyomas. *J Perinat Med* 30(2):170–175, 2002.
- Gamzu R, Achiron R, Hegesh J, et al: Evaluating the risk of tuberous sclerosis in cases with prenatal diagnosis of cardiac rhabdomyoma. *Prenat Diagn* 22(11):1044–1047, 2002.
- Kivelitz DE, Muhler M, Rake A, et al: MRI of cardiac rhabdomyoma in the fetus. *Eur Radiol* 14(8):1513–1516, 2004.
- Northrup H, Koenig MK, Au KS: Tuberous sclerosis complex. In Pagon RA, Adam MP, Ardinger HH, et al, editors: *GeneReviews*, Seattle, 1993–2016, University of Washington.

### Genetics

L1 syndrome is caused by mutations in *L1CAM* gene. Inheritance is X-linked recessive.

### Recurrence Risk

Recurrence risk is 50% for women who are carriers of an *L1CAM* mutation.

### Associated Anomalies

Hirschsprung disease has been seen in some individuals with L1 syndrome.

### Differential Diagnosis

Other syndromic and nonsyndromic causes of hydrocephalus should be excluded.

### Prognosis

The phenotype can range from mild to severe even within the same family.

### Management

A multidisciplinary team is required for optimal management. Head imaging should be performed. Surgical treatment is often required to relieve hydrocephalus. Regular neurologic, developmental evaluation and follow-up are needed. Surgery for adducted thumbs is generally not indicated.

## REFERENCE

- Schrander-Stumpel C, Vos YJ: L1 syndrome. In Pagon RA, Adam MP, Ardinger HH, et al, editors: *GeneReviews*, Seattle, 1993–2016, University of Washington.

**TABLE 16-2 Distinguishing Clinical Features in the *FGFR*-Related Craniosynostosis Syndromes**

Disorder	Thumbs	Hands	Great Toes	Feet	Genetic Basis
Crouzon syndrome	Normal	Normal	Normal	Normal	<i>FGFR2</i>
Crouzon syndrome with acanthosis nigricans (AN)	Normal	Normal	Normal	Normal	<i>FGFR3</i>
Apert syndrome	Occasionally fused to fingers	Soft tissue ± bone syndactyly	Occasionally fused to toes	Soft tissue ± bone syndactyly	<i>FGFR2</i>
Pfeiffer syndrome	Broad, medially deviated	Variable brachydactyly	Broad, medially deviated	Variable brachydactyly	<i>FGFR1</i> (5% of type 1); <i>FGFR2</i> (most)
Muenke syndrome	Normal	± Carpal fusion	± Broad	± Tarsal fusion	<i>FGFR3</i>
Jackson-Weiss syndrome	Normal	Variable	Broad, medially deviated	Abnormal tarsals	<i>FGFR2</i>
Beare-Stevenson syndrome	Normal	Normal	Normal	Normal	< <i>FGFR2</i>
<i>FGFR2</i> -related isolated coronal synostosis	Normal	Normal	Normal	Normal	<i>FGFR2</i>

Adapted from Robin NH, Falk MJ, Haldeman-Englert CR: *FGFR*-related craniosynostosis syndromes. GeneReviews. Seattle, University of Washington, June 2011.

## CRANIUM/FACE

### Craniosynostoses

Craniosynostosis has been reported in over 150 genetic disorders and is found in 1 per 2000 to 2500 live births. Many of the craniosynostoses are caused by mutations in one of the *FGFR* genes, including Apert syndrome, Beare-Stevenson syndrome, Crouzon syndrome, Crouzon syndrome with acanthosis nigricans, *FGFR2*-related isolated coronal synostosis, Jackson-Weiss syndrome, Muenke syndrome, and Pfeiffer syndrome. Although Muenke syndrome and *FGFR2*-related isolated coronal synostosis are characterized by coronal craniosynostosis only, the others have related facial features and extremity findings. *FGFR*-related craniosynostoses have been associated with advanced paternal age. Syndromic craniosynostoses involving other genes include Antley-Bixler syndrome (caused by mutations in the *POR* gene), Carpenter syndrome (caused by mutations in *RAB23*), and Saethre-Chotzen syndrome (caused by mutations in *TWIST1*).

In general, management of the craniosynostoses should include involvement of a multidisciplinary craniofacial clinic at a pediatric

medical center, as a series of staged surgical procedures is often required for treatment and generally involves craniotomy and fronto-orbital advancement. Surgical correction of limb defects may also be needed, depending on the particular anomalies. Early treatment can decrease the risk of secondary complications, such as hydrocephalus and intellectual disability. If proptosis is severe, ophthalmologic lubrication can prevent exposure keratopathy. The prognosis for each affected individual is most dependent on the particular anomalies present and less on the specific craniosynostosis syndrome.

A few of the more common disorders are discussed in more detail above (Table 16-2).

## REFERENCES

- Dicus Brookes C, Golden BA, Turvey TA: Craniosynostosis syndromes. *Atlas Oral Maxillofac Surg Clin North Am* 22(2):103–110, 2014.
- Jezela-Stanek A, Krajewska-Walasek M: Genetic causes of syndromic craniosynostoses. *Eur J Paediatr Neurol* 17(3):221–224, 2013.

### Antley-Bixler Syndrome

**Definition.** Antley-Bixler syndrome is a sterol biosynthesis disorder characterized by craniosynostosis of the coronal and lambdoidal sutures, brachycephaly with frontal bossing, and facial dysmorphism (proptosis, downslanting palpebral fissures, severe depression of the nasal bridge, choanal stenosis or atresia, small mouth, high-arched narrow palate, low-set protruding ears). Hydrocephalus can be present. Limb anomalies include radiohumeral synostosis, bowing of the ulnas and femurs, slender hands and feet, contractions of the proximal interphalangeal joints, advanced bone age, and fractures.

**Synonym.** Antley-Bixler syndrome is also known as trapezoidocephaly-multiple synostosis syndrome.

**Etiology.** Caused by cytochrome P450 oxidoreductase (*POR*) deficiency, Antley-Bixler syndrome is the most severe end of the phenotypic spectrum of *POR* deficiency.

**Incidence.** The incidence is unknown. Since *POR* mutations were first reported in 2004, approximately 50 affected individuals have been reported. More mildly affected individuals are likely underreported.

**Pathogenesis.** The mechanism by which *POR* deficiency leads to multiple malformations remains under investigation. Ambiguous genitalia result from disordered steroidogenesis. Recently, cytochrome P450 activity in bone has been implicated in normal bone development, and, thus, *POR* deficiency may disrupt proper bone formation.

**Diagnosis.** Malformations that may be detected on prenatal ultrasound examination include abnormal skull shape, facial dysmorphism, skeletal abnormalities (bowed femora, bilateral radioulnar synostosis), and ambiguous genitalia. During pregnancy, low maternal estriol may be found on serum screening. Maternal urine may also have increased fetal steroids, including the pregnenolone metabolite epiallopregnanediol and the androgen metabolite androsterone. *POR* deficiency can be diagnosed in affected infants by the detection of urinary sterol or steroid abnormalities, including increased pregnenolone and progesterone metabolites and an elevated ratio of metabolites associated with deficiency of 17-hydroxylase and 21-hydroxylase. Serum concentrations of pregnenolone, progesterone, 17-OH pregnenolone, and 17-OH progesterone may be elevated at baseline or following



ACTH stimulation. Some cases are found on newborn screening (NBS), but NBS is not sensitive enough to detect all cases.

**Genetics.** Antley-Bixler syndrome is caused by mutations in the gene encoding cytochrome P450 reductase (*POR*). Inheritance is autosomal recessive.

**Recurrence Risk.** Recurrence risk is 25%.

**Associated Anomalies.** Congenital heart disease, renal anomalies, abnormalities of the female genitalia, and signs of congenital adrenal hyperplasia are also present. Some degree of intellectual disability is often seen, but intelligence can also be normal.

**Differential Diagnosis.** Other forms of congenital adrenal hyperplasia as well as other craniosynostosis syndromes should be considered.

**Prognosis.** Prognosis improves with age. In infancy, respiratory complications can lead to early death.

**Management.** Multidisciplinary evaluation is needed. Airway management is a primary concern owing to choanal atresia/stenosis.

Functional adrenal studies should be performed and hydrocortisone replacement therapy initiated if low cortisol levels are found. Genital abnormalities are often treatable and should be addressed.

## REFERENCES

- Cragun D, Hopkin RJ: Cytochrome P450 oxidoreductase deficiency. In Pagon RA, Adam MP, Ardinger HH, et al, editors: *GeneReviews*, Seattle, 1993–2016, University of Washington.
- Panda SP, Guntur AR, Polusani SR, et al: Conditional deletion of cytochrome p450 reductase in osteoprogenitor cells affects long bone and skull development in mice recapitulating Antley-Bixler syndrome: role of a redox enzyme in development. *PLoS ONE* 8(9):e75638, 2013.
- Reisch N, Idkowiak J, Hughes BA, et al: Prenatal diagnosis of congenital adrenal hyperplasia caused by P450 oxidoreductase deficiency. *J Clin Endocrinol Metab* 98(3):E528–E536, 2013.

## Apert Syndrome

**Definition.** Apert syndrome is characterized by craniosynostosis, midface and orbital hypoplasia, and bilateral syndactyly of the hands and feet. These findings are accompanied by variable degrees of mental retardation in 50% of cases.

**Incidence.** The incidence of Apert syndrome is 1 per 100,000 live births. It is seen in 4% to 5% of craniosynostosis cases.

**Synonyms.** Apert syndrome is also known as acrocephalosyndactyly type 1 and Apert-Crouzon disease.

**Etiology.** Apert syndrome has autosomal dominant inheritance. Most of the cases are sporadic, resulting from de novo mutations. The disorder is associated with advanced paternal age.

**Sonographic Findings.** Brachycephaly and acrocephaly, high forehead, flat occiput, craniosynostosis involving the coronal sutures, flat face, and hypertelorism are seen. Other ultrasound findings include agenesis of the corpus callosum, mild ventriculomegaly, and fusion of the cervical vertebrae at the level of C5–C6. In the extremities, syndactyly of both bone and soft tissue is seen, involving the second, third, and fourth fingers. Polyhydramnios (caused by the decreased fetal swallowing) and increased nuchal translucency in the first trimester have also been reported.

**Diagnosis.** Typical findings include bicoronal synostosis of the coronal sutures, flattened occiput, a wide, steep forehead, hypoplastic

orbits with exophthalmos and hypertelorism, short nose with depressed nasal bridge, large ears, high palate (occasional cleft palate), and dental crowding. Hydrocephalus is rare. Hearing loss is common. Symmetric syndactyly of the limbs (“mitten-like” hands and feet) is present at least from the second to fourth digits in both the bony and soft tissue. Cardiovascular and genitourinary anomalies are present in 10% of patients.

**Genetics.** Caused by mutations in the *FGFR2* genes, most commonly substitutions S252W and P253R. Genetic molecular studies are recommended for the fetus (by chorionic villus sampling or amniocentesis) and for parents when Apert syndrome is suspected. Inheritance is autosomal dominant with complete penetrance.

**Differential Diagnosis.** Other syndromes with craniosynostosis such as Crouzon, Pfeiffer, Carpenter, and Saethre-Chotzen syndromes should be considered. Molecular genetic studies can exclude these disorders. The pattern of syndactyly is the most helpful for the diagnosis of Apert syndrome.

**Recurrence Risk.** Most mutations are de novo and the recurrence risk is low. If one of the parents carries the disorder, the recurrence risk is 50%.

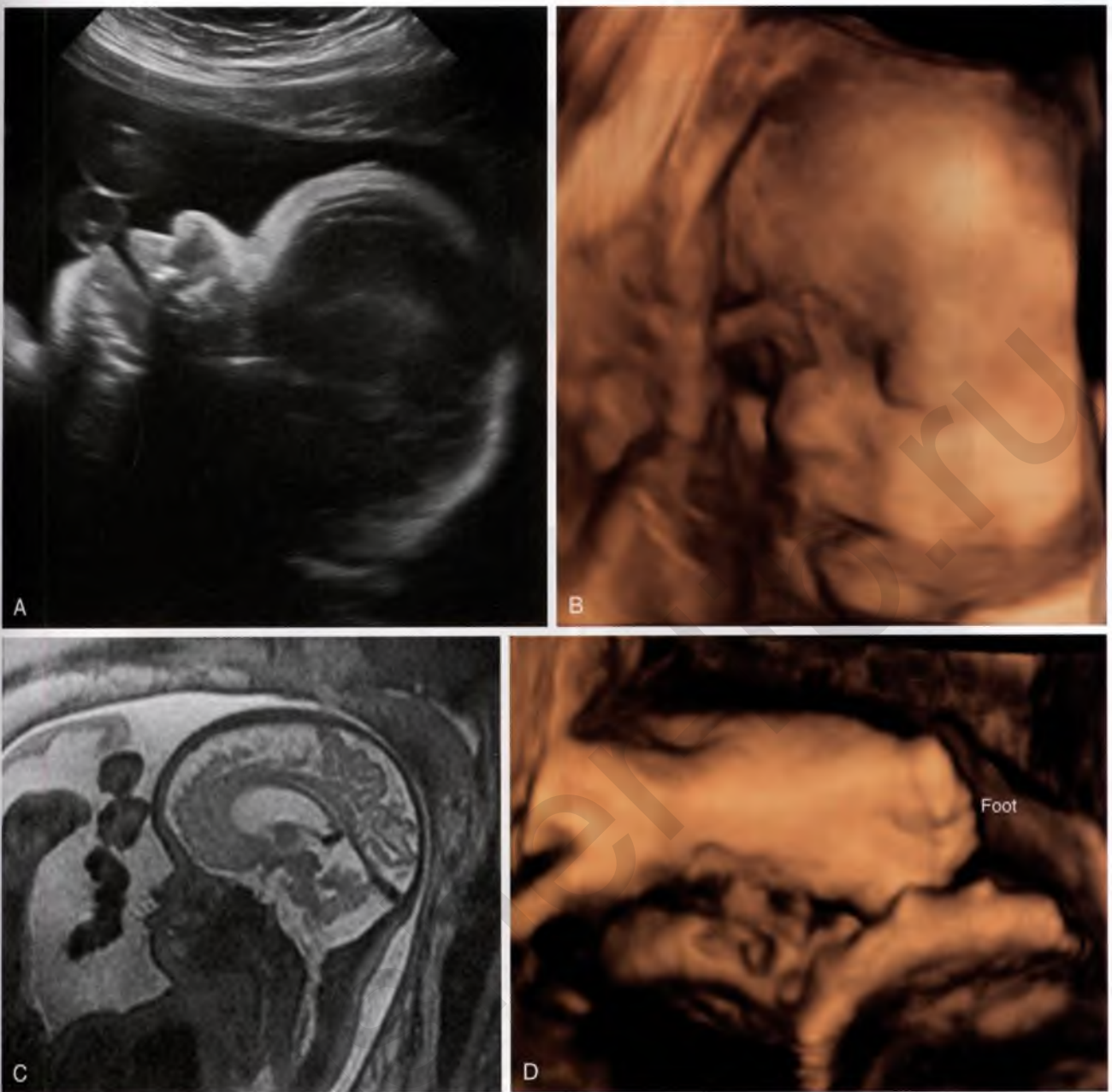


**FIG 16-27** Apert syndrome. Ultrasound images demonstrating frontal bossing and midface hypoplasia on two-dimensional (2D) (A) and 3D (B) images, as well as by magnetic resonance imaging (C). Ultrasound image also demonstrated syndactyly of the foot (D), which is characteristic of Apert syndrome.

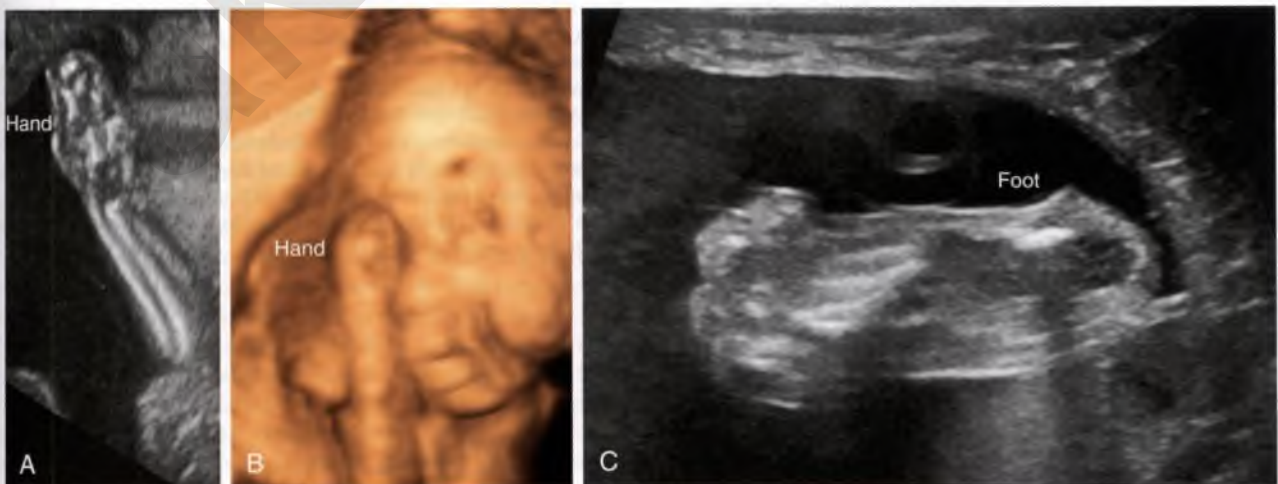


**FIG 16-28** Apert syndrome. Syndactyly of the hand demonstrated with two-dimensional (2D) (A) and 3D (B) ultrasound images. Syndactyly of the foot is also present (C).





**FIG 16-29** Newborn with Apert syndrome. Note appearance of the head, with frontal bossing (**A** and **B**), and syndactyly of the hand (**C**) and foot (**D**).

## REFERENCES

- Blank CE: Apert's syndrome (a type of acrocephalosyndactyly)—observations on a British series of thirty-nine cases. *Ann Hum Genet* 24:151–164, 1960.
- Erickson JD, Cohen MM, Jr: A study of parental age effects on the occurrence of fresh mutations for the Apert syndrome. *Ann Hum Genet* 38(1):89–96, 1974.
- Esser T, Rogalla P, Bamberg C, Kalache KD: Application of the three-dimensional maximum mode in prenatal diagnosis of Apert syndrome. *Am J Obstet Gynecol* 193(5):1743–1745, 2005.
- Ferreira JC, Carter SM, Bernstein PS, et al: Second-trimester molecular prenatal diagnosis of sporadic Apert syndrome following suspicious ultrasound findings. *Ultrasound Obstet Gynecol* 14(6):426–430, 1999.
- Kaufmann K, Baldinger S, Pratt L: Ultrasound detection of Apert syndrome: a case report and literature review. *Am J Perinatol* 14(7):427–430, 1997.
- Parent P, Le Guern H, Munck MR, Thoma M: Apert syndrome, an antenatal ultrasound detected case. *Genet Couns* 5(3):297–301, 1994.
- Park WJ, Theda C, Maestri NE, et al: Analysis of phenotypic features and FGFR2 mutations in Apert syndrome. *Am J Hum Genet* 57(2):321–328, 1995.
- Robin NH, Falk MJ, Haldeman-Englert CR: FGFR-related craniosynostosis syndromes. In Pagon RA, Adam MP, Ardinger HH, et al, editors: *GeneReviews*, Seattle, 1993–2016, University of Washington.
- Skidmore DL, Pai AP, Toi A, et al: Prenatal diagnosis of Apert syndrome: report of two cases. *Prenat Diagn* 23(12):1009–1013, 2003.
- Tunte W, Lenz W: [The frequency and mutation-rate of the Apert syndrome]. *Humangenetik* 4(2):104–111, 1967.

### Carpenter Syndrome

**Definition.** Carpenter syndrome is characterized by craniosynostosis with preaxial polydactyly of the feet. Hand anomalies include brachydactyly, syndactyly, and aplasia or hypoplasia of the middle phalanges.

**Synonym.** Acrocephalopolysyndactyly type II is another name for Carpenter syndrome.

**Incidence.** Carpenter syndrome is rare. Approximately 70 cases have been described.

**Etiology/Pathogenesis.** RAB23 is a member of the RAB guanine triphosphatase (GTPase) family of vesicle transport proteins and acts as a negative regulator of hedgehog signaling. Abnormal hedgehog signaling may lead to much of the clinically recognized phenotype.

**Diagnosis.** Unlikely other syndromic craniosynostoses, in which coronal sutures are most frequently affected, in Carpenter syndrome, fusion of the midline sutures (metopic and sagittal) is common. In severe cases, this leads to cloverleaf skull. On prenatal ultrasound examination, reported features include cystic hygroma, abnormal skull shape, bowed femora, polydactyly, and complex heart defects.

**Genetics.** Carpenter syndrome is caused by mutations in *RAB23*. The inheritance is autosomal recessive. A subtype of Carpenter

syndrome with lateralization defects is thought to be caused by mutations in *MEGF8*.

**Recurrence Risk.** Recurrence risk is 25%.

**Associated Anomalies.** Obesity, umbilical hernia, hearing loss, cryptorchidism, and cardiac defects are often present. Craniosynostosis leads to distinctive facial features. The degree of intellectual disability varies.

**Differential Diagnosis.** Features overlap with Greig cephalopolysyndactyly syndrome. Molecular genetic testing can clarify the diagnosis.

**Prognosis.** Phenotype is extremely variable, even within the same family. Life expectancy is shortened.

### REFERENCES

- Haye D, Collet C, Sembely-Taveau C, et al: Prenatal findings in carpenter syndrome and a novel mutation in *RAB23*. *Am J Med Genet A* 164(11):2926–2930, 2014.
- Twigg SR, Lloyd D, Jenkins D, et al: Mutations in multidomain protein *MEGF8* identify a Carpenter syndrome subtype associated with defective lateralization. *Am J Hum Genet* 91(5):897–905, 2012.

### Crouzon Syndrome

**Definition.** Crouzon syndrome is an *FGFR*-related craniosynostosis characterized by premature fusion of the coronal and frontosphenoidal sutures leading to brachycephaly and a prominent forehead. Facial dysmorphism (proptosis from orbital and midface hypoplasia, external strabismus, mandibular prognathism) is present and extremities are normal.

**Incidence.** The incidence of Crouzon syndrome is 1.6 per 100,000 live births. It is seen in 4.5% of craniosynostosis cases.

**Diagnosis.** Sonographic findings include brachycephaly, midface hypoplasia, and a wide anterior cranial base. Hands and feet are normal. Exophthalmos is always present. About 20% of patients develop optic atrophy. Dental crowding and an open bite are common.

**Genetics.** Caused by mutations in *FGFR2* (except for Crouzon syndrome with acanthosis nigricans, which is caused by mutations in *FGFR3*, seen in ~5% of individuals with Crouzon syndrome). Inheritance is autosomal dominant with complete penetrance and variable expressivity.

**Recurrence Risk.** Recurrence risk is 50% if one parent carries the causative mutation. Occasionally it appears de novo.

**Associated Anomalies.** Progressive hydrocephalus is seen in 30% of cases and can lead to tonsillar herniation. Sacroccygeal tail can also be seen. Cardiovascular anomalies and cleft lip and palate have been reported but are rare.

**Differential Diagnosis.** Other *FGFR*-related craniosynostoses should be considered, including Crouzon syndrome with acanthosis nigricans (should consider if choanal atresia is present).

**Prognosis.** Intellect is generally normal, hearing loss is common, and complications related to hydrocephalus can be life threatening if not treated appropriately.

### REFERENCE

- Robin NH, Falk MJ, Haldeman-Englert CR: *FGFR*-related craniosynostosis syndromes. In Pagon RA, Adam MP, Ardinger HH, et al, editors: *GeneReviews*, Seattle, 1993–2016, University of Washington.

### Pfeiffer Syndrome

**Definition.** Pfeiffer syndrome is characterized by bilateral coronal craniosynostosis, midface hypoplasia, syndactyly of hands and feet, and congenitally enlarged thumbs. Conductive hearing loss is present in more than 80% of patients. The syndrome is divided in three clinical subtypes, with diagnostic and prognostic implications:

- Type I: classic appearance with craniosynostosis (leading to turri-brachycephaly), broad thumbs, and syndactyly. This form is compatible with life, and patients often have normal intelligence.
- Type II: cloverleaf skull, ocular proptosis, broad thumbs, variable visceral anomalies, elbow ankylosis, choanal atresia, and CNS involvement (hydrocephalus). Intellectual disability is common, and this form usually results in early death.
- Type III: craniosynostosis, severe ocular proptosis without cloverleaf skull, elbow ankylosis, and variable visceral anomalies. Affected

fetuses have severe neurologic compromise (including hydrocephalus and tonsillar herniation), with poor prognosis and early death.

**Synonym.** Pfeiffer syndrome is also known as acrocephalosyndactyly type 5.

**Incidence.** The incidence is 1 per 100,000 for all types combined.

**Genetics.** Pfeiffer syndrome is genetically heterogeneous and is caused by mutations in either *FGFR2* or *FGRF1* (type I). Frequently, no mutation can be identified. Type I has autosomal dominant inheritance with complete penetrance and variable expressivity. Most mutations in type II and III are de novo and associated with advanced paternal age.

**Recurrence Risk.** Recurrence risk is 50% if a parental mutation is present. If the mutation is de novo, recurrence risk is very low.

**Diagnosis.** Sonographic signs of Pfeiffer syndrome include craniofacial anomalies (brachycephaly, acrocephaly, craniosynostosis of the



coronal suture, hypertelorism, small nose, and low nasal bridge) and hands and feet anomalies (partial syndactyly of second and third fingers and second, third, and fourth toes, broad thumb, and big toe).

**Associated Anomalies.** Choanal atresia, tracheomalacia and bronchomalacia, cloverleaf skull, fused vertebra, Arnold-Chiari malformation, hydrocephalus, and imperforate anus are associated with this syndrome. After birth, seizures and intellectual disability may be seen.

**Differential Diagnosis.** Saethre-Chotzen and Jackson-Weiss syndromes should be considered in the differential diagnosis.

**Prognosis.** The prognosis depends on the severity of associated anomalies, in particular the severity of the CNS compromise. Type I

generally has a good prognosis. Types II and III are not compatible with life, and death occurs early.

## REFERENCES

- Nazzaro A, Della Monica M, Lonardo F, et al: Prenatal ultrasound diagnosis of a case of Pfeiffer syndrome without cloverleaf skull and review of the literature. *Prenat Diagn* 24(11):918–922, 2004.
- Robin NH, Falk MJ, Haldeman-Englert CR: FGFR-related craniosynostosis syndromes. In Pagon RA, Adam MP, Ardinger HH, et al, editors: *GeneReviews*, Seattle, 1993–2016, University of Washington.

### Saethre-Chotzen Syndrome

**Definition.** Saethre-Chotzen syndrome is characterized by coronal synostosis (unilateral or bilateral), facial asymmetry, ptosis, and characteristic ear appearance (small pinna with a prominent crus). Often present is 2-3 syndactyly of the hand.

**Synonyms.** Synonyms include acrocephalosyndactyly type III and Robinow-Sorauf syndrome (a mild variant).

**Incidence.** Incidence is 1 in 25,000 to 50,000 individuals.

**Diagnosis.** A clinical diagnosis can be made based on craniosynostosis (usually of the coronal sutures), brachycephaly, low frontal hairline, ptosis, facial asymmetry, small ears, and limb anomalies (2-3 syndactyly of the hand, brachydactyly, hallux abnormalities).

**Genetics.** Saethre-Chotzen syndrome is caused by mutations in *TWIST1*; sequencing and deletion/duplication analysis should be performed. Mutations have also been reported in *FGFR2*. Inheritance is autosomal dominant with incomplete penetrance and variable expressivity.

## Facial Anomalies

### Branchiooculofacial Syndrome

**Definition.** Branchiooculofacial syndrome (BOFS) is characterized by branchial skin defects (thin skin, erythematous lesions, erosions), ocular anomalies (microphthalmia, anophthalmia, coloboma, nasolacrimal duct stenosis/atresia), and facial anomalies (hypertelorism, broad nasal tip, upslanted palpebral fissures, cleft lip ± cleft palate, upper lip pits, lower facial weakness). Ear anomalies are common.

**Incidence.** BOFS is rare. Fewer than 100 well-described cases have been reported.

**Diagnosis.** Diagnosis is made on the clinical constellation of branchial skin defect, ocular anomaly, and characteristic facial appearance.

**Genetics.** BOFS is caused by mutations in the gene *TFAP2A*. Inheritance is autosomal dominant. De novo mutations are present in 50% to 60% of affected individuals. Penetrance is complete.

**Recurrence Risk.** If one parent also carries the causative mutation, recurrence risk is 50%. It is significantly less if the mutation is de novo.

**Associated Anomalies.** Associated anomalies include short stature, parietal foramina, radioulnar synostosis, cleft palate, maxillary hypoplasia, hypertelorism, congenital heart disease, and segmentation defects of the vertebrae.

**Differential Diagnosis.** Many features are shared with Muenke syndrome, and, thus, genetic evaluation should also include analysis of the *FGFR2* and *FGFR3* genes. Pfeiffer syndrome and Jackson-Weiss syndrome should also be considered.

**Prognosis.** Intelligence is often normal, although mild to moderate intellectual and developmental delay has been reported. Conductive and sensorineural hearing loss may be present.

## REFERENCE

- Gallagher ER, Ratisoontorn C, Cunningham ML: Saethre-Chotzen syndrome. In Pagon RA, Adam MP, Ardinger HH, et al, editors: *GeneReviews*, Seattle, 1993–2016, University of Washington.

**Recurrence Risk.** Recurrence risk is 50% if a parental mutation is found.

**Associated Anomalies.** Other anomalies include thymic anomalies, renal anomalies, hypoplastic teeth, dysplastic nails, premature hair graying, and defects in hearing and vision.

**Prognosis.** Intellect is generally normal. Feeding difficulties, as well as cosmetic, visual, hearing, and speech issues are often present.

## REFERENCES

- Lin AE, Milunsky JM: Branchiooculofacial syndrome. In Pagon RA, Adam MP, Ardinger HH, et al, editors: *GeneReviews*, Seattle, 1993–2016, University of Washington.
- Milunsky JM, Maher TM, Zhao G, et al: Genotype-phenotype analysis of the branchio-oculo-facial syndrome. *Am J Med Genet A* 155A(1):22–32, 2011.

### Frontonasal Dysplasia

**Definition.** Frontonasal dysplasia is characterized by a broad forehead, widow's peak hairline, ocular hypertelorism, and abnormal nostrils (notched or completely divided) with absence of the nasal tip. A midline defect in the frontal bone (cranium bifidum) is also commonly seen.

**Synonyms.** Synonyms include median cleft face syndrome, fronto-nasal malformation, and frontorhiny.

**Incidence.** Incidence is unknown. Frontonasal dysplasia is rare; at least 100 cases have been reported in the literature.

**Pathogenesis.** Frontonasal dysplasia is due to malformation of the frontonasal elevation. The implicated genes (*ALX1*, *ALX3*, and *ALX4*) encode transcription factors that regulate development of the eyes, nose, and mouth.

**Diagnosis.** The diagnosis is based on the constellation of eye, forehead, and nose findings described earlier.

**Genetics.** The disorder is genetically heterogeneous, with autosomal recessive, autosomal dominant, and X-linked forms of inheritance all reported. The autosomal recessive form is associated with mutations in *ALX1* and *ALX3*. The autosomal dominant form is associated with *ALX4* gene mutations.

**Recurrence Risk.** The recurrence risk is dependent on mode of inheritance.

**Prognosis.** Most individuals have normal intellectual development. Overall prognosis depends on the severity of the malformations and whether or not surgical intervention can improve breathing and feeding issues.

**Management.** Multistage craniofacial surgery is generally needed; for less severe malformations, surgery is often performed at age 6 to 8 and can have excellent cosmetic results.

### Goldenhar Syndrome

**Definition.** Goldenhar syndrome is characterized by hemifacial microsomia, epibulbar dermoids, preauricular appendages, ear hypoplasia, transverse facial clefts, asymmetry of the skull, and spinal anomalies (vertebral segmentation errors).

**Incidence.** Incidence is 1 in 3500 to 1 in 26,000 live births. Male-to-female ratio is 3:2.

**Synonyms.** Synonyms include oculo-auriculo-vertebral dysplasia, hemifacial microsomia, craniofacial microsomia, Goldenhar-Gorlin's syndrome, and facio-auriculo-vertebral dysplasia.

**Etiology.** Goldenhar syndrome is caused by developmental abnormalities of the first and second branchial arches.

**Diagnosis.** Findings are similar to Treacher Collins syndrome (see later) except that they are unilateral leading to significant facial asymmetry. Other features include dystopia, microtia, choanal atresia, cleft palate ± lip, jaw malocclusion, vertebral anomalies, cardiac anomalies, genitourinary anomalies, and CNS involvement.

**Pathogenesis.** Possible fetal hemorrhage in the region of the first and second branchial arches when the blood supply of these arches switches from the stapedia artery to the external carotid artery.

**Genetics.** Genetics for Goldenhar syndrome are unknown. Most cases are thought to be sporadic, although both autosomal recessive and autosomal dominant inheritance have been reported. Transmission is linked in some cases to a region on chromosome 14q32.

**Differential Diagnosis.** Treacher Collins syndrome, Kaufman syndrome (oculocerebrofacial syndrome), acrofacial dysostosis, CHARGE syndrome (coloboma of the eye, heart defects, atresia of the choanae,

### REFERENCES

- Jones KL: Frontonasal dysplasia sequence. In Jones KL, editor: *Smith's Recognizable Patterns of Human Malformation*, ed 6, Philadelphia, 2006, Elsevier Saunders, pp 1268–1269.
- Li C, Slavotinek A, Chudley AE: Manitoba oculotrichoanal syndrome. In Pagon RA, Adam MP, Ardinger HH, et al, editors: *GeneReviews*, Seattle, 1993–2016, University of Washington.
- Twigg SR, Versnel SL, Nurnberg G, et al: Frontorhiny, a distinctive presentation of frontonasal dysplasia caused by recessive mutations in the *ALX3* homeobox gene. *Am J Hum Genet* 84(5):698–705, 2009.
- Uz E, Alanay Y, Aktas D, et al: Disruption of *ALX1* causes extreme microphthalmia and severe facial clefting: expanding the spectrum of autosomal-recessive *ALX*-related frontonasal dysplasia. *Am J Hum Genet* 86(5):789–796, 2010.

retarded mental and growth development, genital anomalies, and ear anomalies), VACTERL, and Nager syndrome should be considered.

**Prognosis.** Treatment is generally cosmetic with multiple reconstructions required in some cases. Airway and vertebral complications have been reported.

**Recurrence Risk.** Recurrence risk is minimal unless an autosomal dominant or autosomal recessive inheritance pattern is suggested.

**Management.** Malar and orbital reconstructions are generally needed and are often performed after age 6. Structural anomalies of the eyes and ears can be corrected with plastic surgery.

### REFERENCES

- Alfi D, Lam D, Gateno J: Branchial arch syndromes. *Atlas Oral Maxillofac Surg Clin North Am* 22(2):167–173, 2014.
- De Catte L, Laubach M, Legein J, Goossens A: Early prenatal diagnosis of oculoauriculo-vertebral dysplasia or the Goldenhar syndrome. *Ultrasound Obstet Gynecol* 8(6):422–424, 1996.
- Kita D, Munemoto S, Ueno Y, Fukuda A: Goldenhar's syndrome associated with occipital meningoencephalocele—case report. *Neurol Med Chir* 42(8):354–355, 2002.
- Martinelli P, Maruotti GM, Agangi A, et al: Prenatal diagnosis of hemifacial microsomia and ipsilateral cerebellar hypoplasia in a fetus with oculoauriculo-vertebral spectrum. *Ultrasound Obstet Gynecol* 24(2):199–201, 2004.
- Witters I, Schreurs J, Van Wing J, et al: Prenatal diagnosis of facial clefting as part of the oculo-auriculo-vertebral spectrum. *Prenat Diagn* 21(1):62–64, 2001.

### Gorlin Syndrome

**Definition.** Gorlin syndrome is characterized by the development of jaw keratocysts and multiple basal cell carcinomas, as well as a characteristic facial appearance with macrocephaly, prominent forehead, coarse facial features, and facial milia.

**Synonym.** Gorlin syndrome has also been referred to as nevoid basal cell carcinoma syndrome (NBCCS).

**Incidence.** Incidence is estimated to be as high as 1 in 18,976.

**Pathogenesis.** Mutations in *PTCH1* lead to alterations in the hedgehog signaling pathway leading to neoplastic cell growth.

**Diagnosis.** Prenatally, cranial and cerebral malformations can be seen, including macrocephaly and ventriculomegaly. Diagnosis is based on major clinical criteria including calcification of the falx, jaw

keratocyst, palmar/plantar pits, and multiple basal cell carcinomas, as well as minor criteria.

**Genetics.** Gorlin syndrome results from mutations in the gene *PTCH1*. Inheritance is autosomal dominant. From 20% to 30% of mutations are de novo. Penetrance is complete; expressivity can be variable.

**Recurrence Risk.** If a parental mutation is present, recurrence risk is 50%.

**Associated Anomalies.** Most individuals have skeletal anomalies (bifid ribs, wedge-shaped vertebrae) and ectopic calcification (in the falx). Cardiac and ovarian fibromas can be seen. Children can develop medulloblastoma (5%). Other anomalies include lymphomesenteric or pleural cysts, cleft lip/palate, polydactyly, and ocular anomalies.



**Differential Diagnosis.** When macrocephaly is detected prenatally, the differential diagnosis includes several overgrowth syndromes, such as Sotos syndrome and Beckwith-Wiedemann syndrome (BWS).

**Prognosis.** Life expectancy is not changed. Cosmetic issues with multiple skin tumors and their removal can lead to social difficulties and can affect quality of life.

**Management/Prevention.** Radiotherapy can lead to the development of thousands of basal cell carcinomas and should be avoided if possible. X-ray exposure should be limited. Direct sun exposure should be avoided.

### Hallerman-Streiff Syndrome

**Definition.** Hallerman-Streiff syndrome is characterized by brachycephaly with frontal bossing, micrognathia, beaked nose, eye anomalies (microphthalmia, cataracts), dental anomalies, hypotrichosis, skin atrophy (especially of the face), and short stature.

**Incidence.** The syndrome is rare, with approximately 150 cases reported.

**Diagnosis.** Diagnosis is based on the clinical criteria described earlier.

**Genetics.** Generally thought to be sporadic, in some cases, the syndrome has been associated with mutations in *GJA1* with autosomal recessive inheritance.

**Recurrence Risk.** Recurrence risk is unknown, but thought to be low.

### Nager Syndrome

**Definition.** Nager syndrome is characterized by preaxial limb anomalies (radial hypoplasia/absence, thumb hypoplasia/absence, triphalangeal thumbs, radioulnar synostosis) and facial anomalies (malar hypoplasia, downward slanting palpebral fissures, lower eyelid coloboma, severe micrognathia).

**Synonym.** Nager syndrome is also known as preaxial acrofacial dysostosis.

**Incidence.** Incidence is unknown, but the syndrome is rare.

**Diagnosis.** Diagnosis is based on the clinical criteria described earlier, including craniofacial and limb malformations. Prenatally, severe micrognathia and upper limb anomalies may be seen.

**Genetics.** The genetic basis is heterogeneous. Recent reports suggest that haploinsufficiency of the gene *SF3B4* leads to the phenotype in families with suggested autosomal dominant inheritance, as well as many individuals with de novo mutations. Autosomal recessive inheritance has also been suggested in some cases.

**Recurrence Risk.** Recurrence risk depends on mode of inheritance.

### Oral-Facial-Digital Syndrome, Type I

**Definition.** Oral-facial-digital syndrome, type I (OFD1), is characterized by anomalies in multiple areas, including the mouth (lobed tongue, tongue lesions, cleft palate, dental anomalies), face (hypertelorism, alae nasi hypoplasia, median cleft, micrognathia), digits (brachydactyly, syndactyly, polydactyly of the hands, duplicated great toe), brain (intracerebral cysts, cerebellar agenesis, agenesis of the corpus callosum), and kidneys (polycystic kidneys).

**Synonym.** OFD1 is also known as Papillon-Léage-Psaume syndrome.

### REFERENCES

- Athar M, Li C, Kim AL, et al: Sonic hedgehog signaling in basal cell nevus syndrome. *Cancer Res* 74(18):4967–4975, 2014.
- Evans DG, Farndon PA: Nevoid basal cell carcinoma syndrome. In Pagon RA, Adam MP, Ardinger HH, et al, editors: *GeneReviews*, Seattle, 1993–2016, University of Washington.
- Evans DG, Howard E, Giblin C, et al: Birth incidence and prevalence of tumor-prone syndromes: estimates from a UK family genetic register service. *Am J Med Genet A* 152A(2):327–332, 2010.

**Differential Diagnosis.** Many features overlap with oculodentodigital dysplasia (ODDD) and other progeroid syndromes.

**Prognosis.** Intellectual disability is present in approximately 15%. Upper airway obstruction can be significant and can lead to cardiac failure and early death.

**Management.** Initial management is focused on airway issues; later management includes cosmetic surgical procedures.

### REFERENCES

- Abrams CK, Scherer SS: Gap junctions in inherited human disorders of the central nervous system. *Biochim Biophys Acta* 1818(8):2030–2047, 2012.
- Robotta P, Schafer E: Hallermann-Streiff syndrome: case report and literature review. *Quintessence Int* 42(4):331–338, 2011.

**Differential Diagnosis.** Facial anomalies are similar to those seen with Treacher Collins syndrome. Differential diagnosis should include Miller syndrome.

**Prognosis.** Upper airway issues can be significant, requiring tracheostomy. Hearing loss, vision loss, and hand anomalies can affect development and quality of life.

### REFERENCES

- Czeschik JC, Voigt C, Alanay Y, et al: Clinical and mutation data in 12 patients with the clinical diagnosis of Nager syndrome. *Hum Genet* 132(8):885–898, 2013.
- Petit F, Escande F, Jourdain AS, et al: Nager syndrome: confirmation of *SF3B4* haploinsufficiency as the major cause. *Clin Genet* 86(3):246–251, 2014.
- Trainor PA, Andrews BT: Facial dysostoses: etiology, pathogenesis and management. *Am J Med Genet C Semin Med Genet* 163C(4):283–294, 2013.

**Incidence.** Almost all affected individuals are female, although males with OFD1 have also been described.

**Pathogenesis.** OFD1 is due to dysfunction of primary cilia.

**Diagnosis.** Many individuals are diagnosed at birth based on the characteristic anomalies. Some cases are diagnosed after polycystic kidney disease is found.

**Genetics.** The syndrome is due to mutations in the *OFD1* gene. Inheritance is X-linked dominant. Approximately 75% of individuals have no family history of OFD1. Penetrance is high, with highly variable expressivity.

**Recurrence Risk.** Recurrence risk is 50% in pregnancies of a female with OFD1. The risk is low if no maternal mutation is present.

**Differential Diagnosis.** Differential diagnosis includes the other oral-facial-digital syndromes, types 2 to 9, as well as other disorders with cystic renal disease, and Meckel-Gruber syndrome.

**Prognosis.** Up to 50% of individuals have intellectual disability, but generally mild. Seizure disorder can be present.

**Management.** Surgery for oral and facial anomalies is often needed. Renal disease should be monitored.

## REFERENCE

Toriello HV, Franco B: Oral-facial-digital syndrome type I. In Pagon RA, Adam MP, Ardinger HH, et al, editors: *GeneReviews*, Seattle, 1993–2016, University of Washington.

### Pierre Robin Sequence

**Definition.** The Pierre Robin sequence consists of the occurrence of three anomalies together: cleft palate, micrognathia, and glossoptosis. These anomalies are found together in multiple syndromes.

**Synonyms.** Pierre Robin sequence is also called cleft palate-micrognathia-glossoptosis, Pierre Robin syndrome, and Robin anomalad.

**Incidence.** Incidence is 1 in 8500 to 1 in 14,000 births. One half of patients with Pierre Robin sequence have an underlying syndrome.

**Etiology.** Inheritance is autosomal-recessive, with a few X-linked cases. Some authors suggest a prenatal and neonatal brainstem dysfunction as a neuroembryologic hypothesis to explain the onset of some cases of Pierre Robin sequence.

**Diagnosis.** Micrognathia is most visible on prenatal ultrasound imaging. Isolated cleft palate is more difficult to detect prenatally. Polyhydramnios may be seen as a result of swallowing difficulty.

**Genetics.** This disorder is heterogeneous; it can be monogenic, chromosomal, or related to teratogens. The cause is unknown in some cases. Multiple forms of inheritance are involved, including autosomal dominant, autosomal recessive, and X-linked.

**Differential Diagnosis.** Differential diagnosis includes syndromes that involve Pierre Robin sequence, such as Stickler syndrome, as well as fetal alcohol syndrome.

**Associated Anomalies.** Other anomalies depend on the exact diagnosis. Cardiac abnormalities are common with an incidence approaching 20%.

**Prognosis.** Upper airway obstruction, neonatal respiratory distress, and feeding problems are common issues.

**Associated Syndromes.** See Table 16-3 for a complete list of associated syndromes.

**Stickler Syndrome.** Stickler syndrome is characterized by ocular findings (myopia, cataract, retinal detachment) and hearing loss (conductive and sensorineural) in addition to Pierre Robin sequence. Joint issues are also common (hypermobility, spondyloepiphyseal dysplasia, precocious osteoarthritis). Mutations in one of five genes are often present: *COL2A1*, *COL11A1*, and *COL11A2* (autosomal dominant inheritance; *COL2A1* most common, at 80–90%), as well as *COL9A1* and *COL9A2* (autosomal recessive; rare). Penetrance is complete but significant phenotypic variability occurs even within families. From 20% to 30% of patients with Pierre Robin sequence may have Stickler syndrome.

**Cerebrocostomandibular Syndrome.** Cerebrocostomandibular syndrome (CCMS) is characterized by costovertebral anomalies (dorsal rib defects) in addition to Pierre Robin sequence. Rib defects often lead to a bell-shaped thorax and can result in flail chest. Other anomalies include growth retardation, scoliosis, dental anomalies, feeding issues, and conductive hearing loss. Severity is highly variable, although

**TABLE 16-3 Selected Syndromes and Chromosomal Anomalies Associated With Pierre Robin Sequence**

Condition	OMIM	Causative Gene	Inheritance Pattern	Additional Features
<b>Primary Skeletal Dysplasias</b>				
Campomelic dysplasia	114290	<i>SOX9</i>	Autosomal dominant	Short stature, campomelia, hearing loss, scoliosis
Stickler syndrome	108300, 604841, 184840	<i>COL2A1</i> , <i>COL11A1</i> , <i>COL11A2</i>	Autosomal dominant	Myopia, retinal detachment, hearing loss, mild short stature
Spondyloepiphyseal dysplasia congenita	183900	<i>COL2A1</i>	Autosomal dominant	Short spine, pectus carinatum, myopia, normal hands and feet
Kniest dysplasia	156550	<i>COL2A1</i>	Autosomal dominant	Short trunk, kyphosis, lumbar lordosis, short limbs, reduced joint mobility
Marshall syndrome	154780	<i>COL11A1</i>	Autosomal dominant	Hypoplastic nasal bones, congenital cataracts, myopia, sensorineural hearing loss
Otospondylomegaepiphyseal dysplasia	277610, 215150	<i>COL11A2</i>	Autosomal dominant	Sensorineural hearing loss, enlarged painful joints, short stature, short limbs
Diastrophic dysplasia	222600	<i>SLC26A2</i>	Autosomal recessive	Short stature, short limbs, joint contractures, talipes equinovarus, kyphoscoliosis
Osteopathia striata with cranial sclerosis	300373	<i>WTX</i>	X-linked dominant	Macrocephaly, frontal bossing, hearing loss, skull base sclerosis, linear metaphyseal bands
Otopalatodigital syndrome type II	304120	<i>FLNA</i>	X-linked semidominant	Frontal bossing, short thumbs and halluces, bowed long bones, conductive hearing loss

Continued



**TABLE 16-3 Selected Syndromes and Chromosomal Anomalies Associated With Pierre Robin Sequence—cont'd**

Condition	OMIM	Causative Gene	Inheritance Pattern	Additional Features
<b>Multiple Congenital Anomaly Syndromes</b>				
Catel-Manzke syndrome	302380	Unknown	Probably autosomal recessive	Clinodactyly of index finger due to accessory ossicle between metacarpal and proximal phalanx, congenital cardiac defects
Toriello-Carey syndrome	217980	Unknown	Possibly autosomal recessive	Agensis corpus callosum, telecanthus, developmental delay
Treacher Collins syndrome	154500	<i>TCOF1</i>	Autosomal dominant	Downslanting palpebral fissures, lower eyelid colobomas, zygomatic hypoplasia
Nager preaxial acrofacial dysostosis	154400	<i>SF3B4</i>	Autosomal dominant	Downslating palpebral fissures, absence of medial third lower lid lashes, conductive hearing loss, radial ray defects
Miller postaxial acrofacial dysostosis	263750	<i>DHODH</i>	Autosomal recessive	Lower lid ectropion, cupped ears, hearing loss, bilateral absence of fifth fingers, supernumerary nipples
Mandibulofacial dysostosis Guion-Almeida type	610536	<i>EFTUD2</i>	Autosomal dominant	Microcephaly, developmental delay, dysplastic ears, preauricular tags, choanal atresia
Auriculocondylar syndrome	602483, 614669	<i>GNAI3</i> , <i>PLCB4</i>	Autosomal dominant	"Question mark" ears, small mouth, prominent cheeks, anomalies of the temporomandibular joint and condyle
Cerebrocostomandibular syndrome	117650	Unknown	Autosomal dominant and recessive reported	Narrow thorax, rib anomalies, conductive hearing loss, growth restriction
Cerebrocostomandibular-like syndrome	606973	<i>COG1</i>	Autosomal recessive	Costovertebral defects, microcephaly, growth restriction, developmental delay, brain anomalies, cryptorchidism
Talipes, ASD, PRS, and persistence of left superior vena cava (TARP)	311900	<i>RBM10</i>	X-linked recessive	Talipes, congenital cardiac defects, persistence of left superior vena cava
Distal arthrogyriposis-PRS (Illium syndrome)	208155	Unknown	Autosomal recessive	Joint contractures, autonomic instability, "whistling face," nervous system classification
PRS, cleft mandible, limb anomalies (Richieri-Costa-Pereira syndrome)	268305	Unknown	Autosomal recessive	Short stature, hypoplastic thumbs, talipes, laryngeal malformations
Andersen-Tawil syndrome	170390	<i>KCNJ2</i>	Autosomal dominant	Cardiac arrhythmias, periodic paralysis, low-set ears, short stature, digital anomalies
PRS + oligodactyly	172880	Unknown	Probably autosomal dominant	Oligodactyly
Fetal alcohol syndrome	—	N/A	Teratogenic	Microcephaly, growth and developmental delay, short palpebral fissures
<b>Neuromuscular Conditions</b>				
Congenital myotonic dystrophy	160900	<i>DMPK</i>	Autosomal dominant	Severe hypotonia, respiratory insufficiency
Carey-Fineman-Ziter syndrome	254940	Unknown	Probably autosomal recessive	Hypotonia, Moebius anomaly, growth delay, feeding difficulties, scoliosis
<b>Chromosomal Abnormalities</b>				
Trisomy 18	—	Unknown	Sporadic chromosomal	Microcephaly, severe growth and cognitive impairment, prominent occiput, cardiac defects, low-set ears, short sternum, overlapping flexed fingers, prominent calcaneus
22q11 microdeletion	188400/192430	<i>TBX1</i>	Autosomal dominant chromosomal	Upslanting palpebral fissures, prominent tubular nose, conotruncal heart defects, renal and endocrine abnormalities, neuropsychiatric problems
17q24 translocations and microdeletions	261800	<i>SOX9</i>	Autosomal dominant chromosomal	Isolated PRS
17q21.31q24.3 inversion and deletion	—	<i>SOX9</i>	Autosomal dominant chromosomal	PRS with hypoploastic scapula and bilateral clubfeet
2q33 microdeletion	608148	<i>SATB2</i>	Autosomal dominant chromosomal	Growth restriction, feeding difficulties, downslating palpebral fissures, prominent nose, dental anomalies, behavioral problems, developmental delay
4q terminal deletion	—	Unknown	Autosomal dominant chromosomal	Cardiac defects, mild developmental delay, but can be normal, stiff hypoplastic fifth fingers with hooked or volar nails

**TABLE 16-3 Selected Syndromes and Chromosomal Anomalies Associated With Pierre Robin Sequence—cont'd**

Condition	OMIM	Causative Gene	Inheritance Pattern	Additional Features
1q duplication	—	Unknown	Autosomal dominant chromosomal	Bilateral fixed flexion deformities of fingers, cardiac and brain anomalies
Partial trisomy 11q	—	Unknown	Autosomal dominant chromosomal	Developmental delay, congenital heart defects
t(1;2)(p34;q33)	613857	<i>FAF1</i>	Chromosomal	PRS in father and son with translocation disrupting <i>FAF1</i> at 1p34
20p12.3 microdeletion	112261	<i>BMP2</i>	Autosomal dominant chromosomal	Long philtrum, digital anomalies, hypotonia
22q12 microdeletion	—	<i>MN1</i>	Autosomal dominant chromosomal	Developmental delay, features of NF2 and Toriello-Carey due to contiguous gene deletion

ASD, atrial septal defect; PRS, Pierre Robin sequence; OMIM, Online Mendelian Inheritance in Man.

From Tan TY, Kilpatrick N, Farlie P: Developmental and genetic perspectives on Pierre Robin sequence. *Am J Med Genet C Semin Med Genet* 163C:295-305, 2013, Table 1.



**FIG 16-30** Micrognathia. Profile of a fetus shows mild micrognathia.



**FIG 16-31** Severe micrognathia in a fetus with Nager syndrome. This can result in severe airway compromise at birth.



**FIG 16-32** Micrognathia in a fetus with Pierre Robin sequence.



prognosis is often poor. This disorder is very rare, with slightly over 80 cases reported. Genetics are unknown, although possible defects in sonic hedgehog signaling have been implicated.

## REFERENCES

- Abadie V, Morisseau-Durand MP, Beyler C, et al: Brainstem dysfunction: a possible neuroembryological pathogenesis of isolated Pierre Robin sequence. *Eur J Pediatr* 161(5):275–280, 2002.
- Hsieh YY, Chang CC, Tsai HD, et al: The prenatal diagnosis of Pierre-Robin sequence. *Prenat Diagn* 19(6):567–569, 1999.

- James PA, Aftimos S: Familial cerebro-costo-mandibular syndrome: a case with unusual prenatal findings and review. *Clin Dysmorphol* 12(1):63–68, 2003.
- Lee W, McNie B, Chaiworapongsa T, et al: Three-dimensional ultrasonographic presentation of micrognathia. *J Ultrasound Med* 21(7):775–781, 2002.
- Robin NH, Moran RT, Ala-Kokko L: Stickler syndrome. In Pagon RA, Adam MP, Ardinger HH, et al, editors: *GeneReviews*, Seattle, 1993–2016, University of Washington.
- Tan TY, Kilpatrick N, Farlie PG: Developmental and genetic perspectives on Pierre Robin sequence. *Am J Med Genet C Semin Med Genet* 163C(4):295–305, 2013.

## Treacher Collins Syndrome

**Definition.** Treacher Collins syndrome is characterized by deficient generation of the lower two thirds of the face, including hypoplasia of the zygoma, maxilla, and mandible.

**Synonyms.** Treacher Collins syndrome is also known as mandibulofacial dysostosis and Treacher Collins-Franceschetti syndrome.

**Etiology.** The syndrome is due to abnormal development of the first and second branchial arches.

**Incidence.** Incidence is 1 in 50,000 live births.

**Diagnosis.** Affected individuals have maxillary and mandibular hypoplasia, choanal atresia/stenosis, downward slanting palpebral fissures, notching of the lower eyelid, sparse or absent eyelashes, microtia/absent external ear, middle ear hypoplasia, cleft palate ± lip, and dental anomalies.

**Genetics.** Three causative genes have been found: *TCOF1* and *POLR1D* (autosomal dominant inheritance; most common) as well as *POLR1C* (autosomal recessive; only 1% of cases). Sixty percent of cases result from de novo mutations. Significant phenotypic variability is seen, even within families. Penetrance is high, but cases of nonpenetrance have been reported.

**Pathogenesis.** Mutations in the preceding genes lead to abnormal production of ribosomal RNA important in the development of the first and second branchial arches, leading structural facial anomalies.

**Recurrence Risk.** Recurrence risk is 50% for the autosomal dominant genes if a parental mutation is present, low if mutation is de novo, and 25% for the autosomal recessive form.

**Differential Diagnosis.** Differential diagnosis includes the other mandibulofacial dysostoses, such as Toriello syndrome, Bauru syndrome, Hedera-Toriello-Petty syndrome, and Guion-Almeida syndrome. Treacher Collins syndrome also shares some features of Nager syndrome, Miller syndrome, Goldenhar syndrome, and craniofacial microsomia.

**Prognosis.** Intelligence is normal. Middle ear hypoplasia causes conductive deafness (40–50% of individuals). Vision loss can also occur (37%). Speech issues are common.

**Management.** Intervention may be needed for the airway and feeding issues.

## REFERENCES

- Alfi D, Lam D, Gateno J: Branchial arch syndromes. *Atlas Oral Maxillofac Surg Clin North Am* 22(2):167–173, 2014.
- Katsanis SH, Jabs EW: Treacher Collins syndrome. In Pagon RA, Adam MP, Ardinger HH, et al, editors: *GeneReviews*, Seattle, 1993–2016, University of Washington.

## Van der Woude Syndrome

**Definition.** Van der Woude syndrome (VWS) is included in a spectrum of *IRF6*-related disorders ranging from isolated cleft lip/palate and popliteal pterygium syndrome. VWS is characterized by lower lip pits, cleft lip and palate, cleft uvula, and hypodontia.

**Synonym.** VWS has been classified as types 1 and 2.

**Incidence.** Incidence is 1 in 40,000 to 1 in 100,000 births. VWS is the most common form of syndromic clefting, accounting for 2% of all cases of cleft lip and palate.

**Pathogenesis.** *IRF6* (interferon regulatory factor 6) is a transcription factor involved in orofacial development.

**Diagnosis.** Prenatal ultrasound examination can detect a cleft lip ± cleft palate, but is likely to miss an isolated cleft palate and lip pits.

**Genetics.** VWS type 1 is caused by mutations in the *IRF6* gene; type 2 is caused by mutations in the *GRHL3* gene (5% of all VWS cases). Inheritance is autosomal dominant. Penetrance is high but can be incomplete. De novo mutations have been reported.

**Recurrence Risk.** If a parental mutation is present, recurrence risk is 50%.

**Differential Diagnosis.** Bartsocas-Pappas syndrome (popliteal pterygium syndrome, lethal type), Kabuki syndrome, BOFS, and



**FIG 16-33** Coronal ultrasound image showing unilateral cleft lip (arrow) in a fetus with van der Woude syndrome.

isolated cleft lip and palate are considered in the differential diagnosis.

**Prognosis.** Multiple surgeries are often needed to treat lip pitting and can lead to scarring and decreased ability to open the mouth. Psychomotor development is generally normal.

### X-linked Opitz G/BBB Syndrome

**Definition.** X-linked Opitz G syndrome (XLOS) is characterized by facial anomalies (hypertelorism, prominent forehead, widow's peak, broad nasal bridge, anteverted nares), laryngoatracheoesophageal defects, and genitourinary anomalies (hypospadias, cryptorchidism, bifid scrotum).

**Incidence.** Incidence is 1 in 50,000 to 1 in 100,000 males.

**Pathogenesis.** Mutations in *MID1* lead to altered mTORC1 signaling, which is thought to affect the development of ventral midline anatomic structures.

**Diagnosis.** Diagnosis is most often based on clinical findings with abnormalities in ventral midline structures, as described previously. Prenatally, those cases associated with congenital heart defects and cleft lip are more likely to be detected.

**Genetics.** XLOS is due to mutations in *MID1*. Inheritance is X-linked. Many individuals are the only ones known to be affected within their families. Penetrance is high; wide phenotypic variability is seen even within families.

**Recurrence Risk.** If the mother is a carrier, there is a 50% chance of transmitting the disease-causing mutation in each pregnancy. Sons who inherit the mutation will be affected. Daughters will be carriers with isolated hypertelorism.

## MUSCULOSKELETAL SYSTEM

### Skeletal Dysplasias

Overall, skeletal dysplasias are seen in 2.4 per 10,000 births, and of these, 0.95 to 1.5 per 10,000 live births are lethal skeletal dysplasias. As a group, there are more than 450 skeletal dysplasias and the specific disorder can be difficult to determine based on prenatal ultrasound findings alone. A genetic cause has been identified for more than 50% of skeletal dysplasias; many are due to de novo mutations. Those with autosomal recessive inheritance often occur without a family history.

In the prenatal setting, particular emphasis should be given to identifying those disorders with neonatal or infantile lethality. Specific details should be obtained on prenatal ultrasound examination if a skeletal dysplasia is suspected, including length and appearance of long bones, facial features, spine, and extremity anomalies, as well as femur/foot ratio. Measurements that can assist in predicting neonatal lethality include chest circumference/abdominal circumference ratio and femur length/abdominal circumference ratio.

Of the lethal skeletal dysplasias, the most common are thanatophoric dysplasia (TD) and osteogenesis imperfecta (type 2), followed by achondrogenesis. Together, these three disorders represent 40% to 60% of all lethal skeletal dysplasias. Other relatively common lethal skeletal dysplasias include campomelic dysplasia, hypophosphatasia congenita, and short-rib polydactyly syndromes. Lethal disorders seen more rarely include atelosteogenesis, rhizomelic chondrodysplasia

## REFERENCES

- Alfi D, Lam D, Gateno J: Branchial arch syndromes. *Atlas Oral Maxillofac Surg Clin North Am* 22(2):167–173, 2014.
- Schutte BC, Saal HM, Goudy S, Leslie E: IRF6-related disorders. In Pagon RA, Adam MP, Ardinger HH, et al, editors: *GeneReviews*, Seattle, 1993–2016, University of Washington.

**Associated Anomalies.** Other anomalies include cleft lip/palate (50%), congenital heart defects, imperforate or ectopic anus, and midline brain defects.

**Differential Diagnosis.** FG syndrome, craniofrontonasal dysplasia, and Mowat-Wilson syndrome should be considered.

**Prognosis.** Intellectual disability and developmental delay are seen in 50% of affected males. Prognosis depends on the severity of the associated anomalies.

**Management.** A multidisciplinary team is needed to manage the multiple anomalies.

## REFERENCES

- Cheng YK, Huang J, Law KM, et al: Prenatal diagnosis of maternally inherited X-linked Opitz G/BBB syndrome by chromosomal microarray in a fetus with complex congenital heart disease. *Clin Chim Acta Int J Clin Chem* 436:140–142, 2014.
- Liu E, Knutzen CA, Krauss S, et al: Control of mTORC1 signaling by the Opitz syndrome protein MID1. *Proc Natl Acad Sci U S A* 108(21):8680–8685, 2011.
- Meroni G: X-linked Opitz G/BBB syndrome. In Pagon RA, Adam MP, Ardinger HH, et al, editors: *GeneReviews*, Seattle, 1993–2016, University of Washington.

punctata, and fibrochondrogenesis. The most common nonlethal skeletal dysplasia is achondroplasia. These disorders are each reviewed in more detail in this section.

## REFERENCES

- Glanc P, Chitayat D: Prenatal diagnosis of the lethal skeletal dysplasias. *UpToDate* 2014. Available at: <<http://www.uptodate.com/home>>.
- Goncalves L, Jeanty P: Fetal biometry of skeletal dysplasias: a multicentric study. *J Ultrasound Med* 13(12):977–985, 1994.
- Krakow D, Lachman RS, Rimoin DL: Guidelines for the prenatal diagnosis of fetal skeletal dysplasias. *Genet Med* 11(2):127–133, 2009.
- Lachman RS, Rappaport V: Fetal imaging in the skeletal dysplasias. *Clin Perinatol* 17(3):703–722, 1990.
- Orioli IM, Castilla EE, Barbosa-Neto JG: The birth prevalence rates for the skeletal dysplasias. *J Med Genet* 23(4):328–332, 1986.
- Rahemtullah A, McGillivray B, Wilson RD: Suspected skeletal dysplasias: femur length to abdominal circumference ratio can be used in ultrasonographic prediction of fetal outcome. *Am J Obstet Gynecol* 177(4):864–869, 1997.
- Taybi H, Lachman RS: *Radiology of Syndromes, Metabolic Disorders, and Skeletal Dysplasias*, ed 3, Chicago, 1990, Year Book Medical Publishers, p 761.
- van Ravenswaaij-Arts CM, Losekoot M: [From gene to disease; achondroplasia and other skeletal dysplasias due to an activating mutation in the fibroblast growth factor]. *Ned Tijdschr Geneesk* 145(22):1056–1059, 2001.



### Thanatophoric Dysplasia

**Definition.** TD is the most common lethal skeletal dysplasia and is characterized by severe rhizomelia, small thorax, normal trunk length, normal bone mineralization, no fractures, thickened redundant skin, and platyspondyly (flattened vertebral bodies). TD is divided into two subtypes:

- Type I: TD1 is the more common form. The femurs have a “telephone receiver” shape, and frontal bossing and midface hypoplasia are present. Cloverleaf skull is not seen. The hands and feet are normal, but the fingers are short.
- Type II: TD2 is the less common form. Femurs are straight with flared metaphyses, and a cloverleaf skull is present (due to craniosynostosis of the lambdoid and coronal sutures).

**Incidence.** Incidence is 1 in 20,000 births.

**Etiology.** Mutations in *FGFR3* are gain-of-function mutations that lead to a constitutively active protein. This leads to chondrocyte proliferation and premature maturation of bone.

**Genetics.** TD1 is caused most frequently by mutations in the fibroblast growth factor receptor 3 gene (*FGFR3*); the most common mutations are R248C and Y373C. TD2 is also caused by mutations in *FGFR3*, specifically the mutation *K650E*. Inheritance is autosomal dominant. Because the disorder is lethal, new diagnoses are generally the result of de novo mutations. Advanced paternal age has been associated with an increased risk.

**Recurrence Risk.** Recurrence risk is low because most mutations are de novo; germline mosaicism remains a possibility but has not been reported in individuals without signs of skeletal dysplasia.

**Diagnosis.** Prenatal findings include severe rhizomelia (seen as early as 12-14 weeks) and a hypoplastic thorax. Craniofacial dysmorphisms include macrocephaly, frontal bossing, midface hypoplasia, and cloverleaf skull. Other features include brachydactyly, platyspondyly, hypotonia, and redundant skinfolds. Other brain anomalies may be seen including polymicrogyria, deep and transverse temporal sulci, and temporal lobe enlargement. Polyhydramnios is seen in approximately 50% of cases. Increased nuchal translucency may be present.

**Differential Diagnosis.** The differential diagnosis includes other types of short-limbed dwarfism and disorders with a cloverleaf skull (such as Apert, Crouzon, Pfeiffer, and Carpenter syndromes). The features can closely resemble homozygous achondroplasia with autosomal recessive inheritance; it can be distinguished from TD by the presence of positive carrier status for heterozygous *FGFR3* mutations in each parent in the case of achondroplasia.

**Prognosis.** In general, affected infants die shortly after birth of respiratory insufficiency due to a small thorax and lung hypoplasia.

**Management.** The option of pregnancy termination should be offered before viability. Sonographic evaluation of hydrocephalus is recommended because it can lead to malpresentation and difficult delivery. If massive hydrocephalus has developed, cephalocentesis or

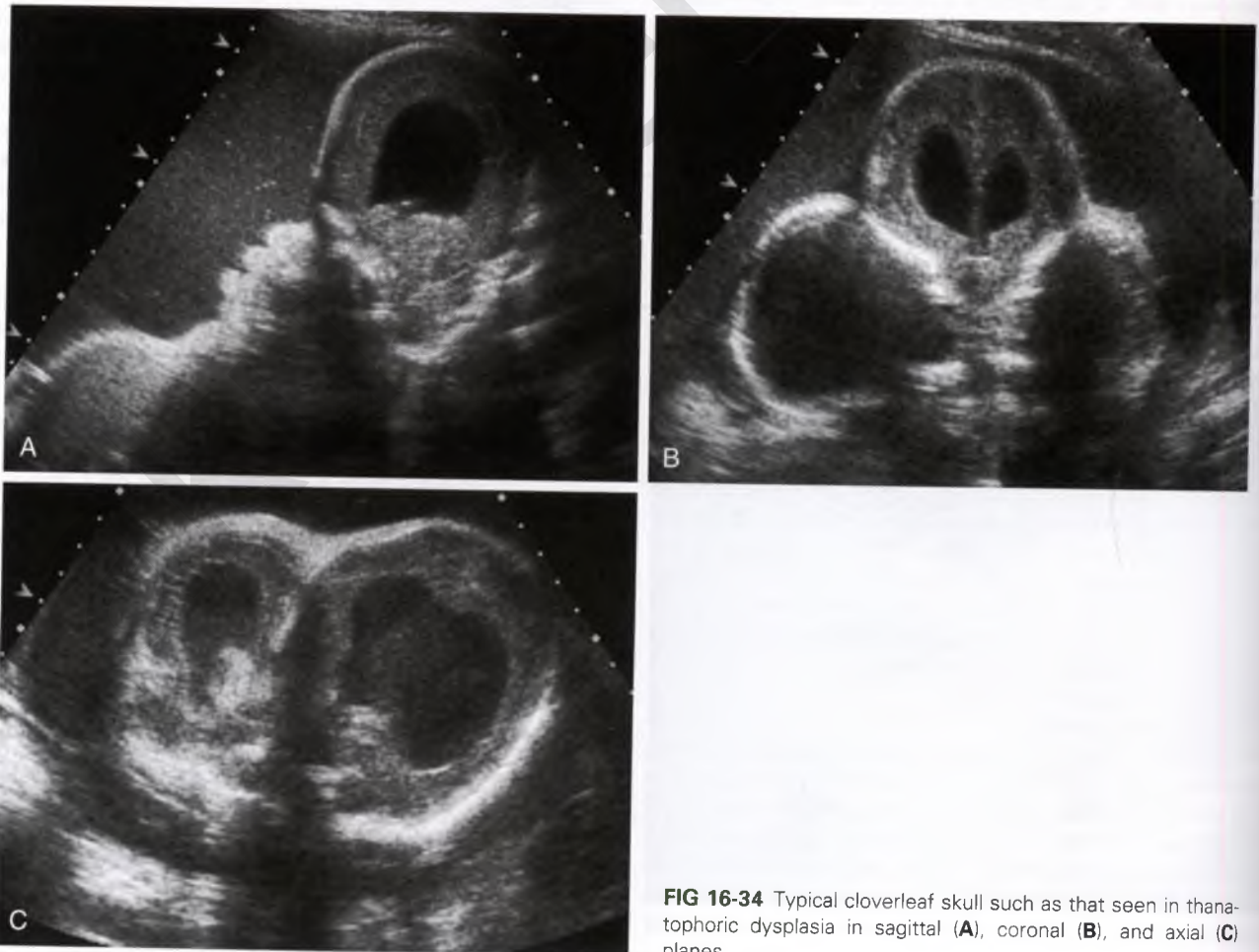


**FIG 16-34** Typical cloverleaf skull such as that seen in thanatophoric dysplasia in sagittal (A), coronal (B), and axial (C) planes.



**FIG 16-35** Thanatophoric dysplasia. **A**, Markedly short femur with telephone receiver morphologic appearance; **B**, axial images demonstrating small thorax with short ribs; **C**, frontal bossing.

elective cesarean delivery should be considered to avoid maternal trauma.

## REFERENCES

- Brodie SG, Kitoh H, Lachman RS, et al: Platspondylic lethal skeletal dysplasia, San Diego type, is caused by FGFR3 mutations. *Am J Med Genet* 84(5):476–480, 1999.
- Chen CP, Chern SR, Shih JC, et al: Prenatal diagnosis and genetic analysis of type I and type II thanatophoric dysplasia. *Prenat Diagn* 21(2):89–95, 2001.
- Escobar LF, Bixler D, Padilla LM: Quantitation of craniofacial anomalies in utero: fetal alcohol and Crouzon syndromes and thanatophoric dysplasia. *Am J Med Genet* 45(1):25–29, 1993.
- Karczeski B, Cutting GR: Thanatophoric dysplasia. In Pagon RA, Adam MP, Ardinger HH, et al, editors: *GeneReviews*, Seattle, 1993–2016, University of Washington.
- Kitoh H, Lachman RS, Brodie SG, et al: Extra pelvic ossification centers in thanatophoric dysplasia and platspondylic lethal skeletal dysplasia-San Diego type. *Pediatr Radiol* 28(10):759–763, 1998.
- Langer LO, Jr, Yang SS, Hall JG, et al: Thanatophoric dysplasia and cloverleaf skull. *Am J Med Genet Suppl* 3:167–179, 1987.
- van der Harten HJ, Brons JT, Dijkstra PF, et al: Some variants of lethal neonatal short-limbed platspondylic dysplasia: a radiological ultrasonographic, neuropathological and histopathological study of 22 cases. *Clin Dysmorphol* 2(1):1–19, 1993.
- Wilcox WR, Tavormina PL, Krakow D, et al: Molecular, radiologic, and histopathologic correlations in thanatophoric dysplasia. *Am J Med Genet* 78(3):274–281, 1998.
- Yamaguchi K, Honma K: Autopsy case of thanatophoric dysplasia: observations on the serial sections of the brain. *Neuropathology* 21(3):222–228, 2001.
- Yuce MA, Yardim T, Kurtul M, et al: Prenatal diagnosis of thanatophoric dwarfism in second trimester. A case report. *Clin Exp Obstet Gynecol* 25(4):149–150, 1998.

## Osteogenesis Imperfecta

**Definition.** Osteogenesis imperfecta (OI) is a heterogeneous group of genetic disorders (classically divided in four types: I, II [congenital], III, and IV) characterized by severe bone fragility, leading to abnormal ossification and multiple fractures. The clinical features range from perinatal lethality (type II) to severe skeletal deformities to those with minimal features. The four types are described as follows:

- Type I: classic nondeforming OI with blue sclerae. Deformities are not seen prenatally.

- Type II: perinatal lethal OI. This is the most severe form and can be seen prenatally.
- Type III: progressively deforming OI. Some features can be seen prenatally.
- Type IV: common variable OI with normal sclerae. Deformities are not generally seen prenatally.

**Synonyms.** OI is also called brittle bone disease.

**Incidence.** The incidence is 6 to 7 per 100,000 for all types of OI, with types I and IV representing more than one half of all cases. Types II and III each have an incidence of 1 to 2 per 100,000.



**Etiology.** *COL1A1* and *COL1A2* encode for type I collagen (found in skin, ligaments, tendons, demineralized bone, and dentine). Defective production of type I collagen leads to decreased bone mineralization and bone fragility.

**Genetics.** OI is due to mutations in *COL1A1* or *COL1A2*. Inheritance is autosomal dominant. Approximately 60% of cases of type I and IV OI are caused by de novo mutations, whereas almost 100% of cases of type II and III OI are caused by de novo mutations. Penetrance is complete, but expression can vary significantly.

**Recurrence Risk.** Recurrence risk depends on whether the mutation was inherited or de novo. Gonadal mosaicism may be present in 3% to 5% of cases with apparent de novo mutations. Less commonly, OI can also be autosomal recessive.

**Diagnosis.** Type II is the most severe form and affected individuals usually die in utero or shortly after birth from severe fractures and pulmonary hypoplasia. Key prenatal findings include severe micromelia (femur length more than 3 standard deviations [SD] below the mean), small thorax, normal head circumference, short

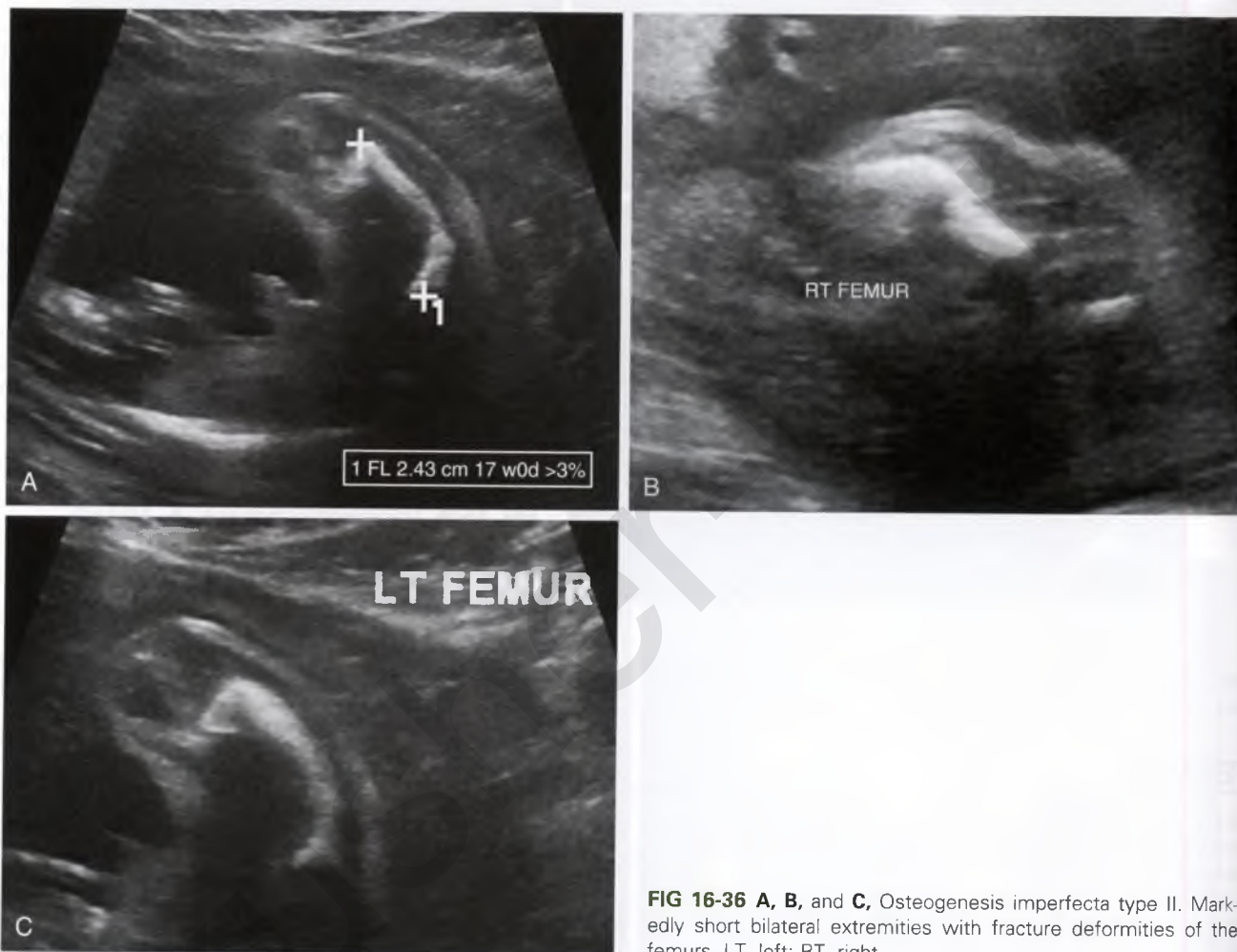


**FIG 16-36 A, B, and C,** Osteogenesis imperfecta type II. Markedly short bilateral extremities with fracture deformities of the femurs. LT, left; RT, right.

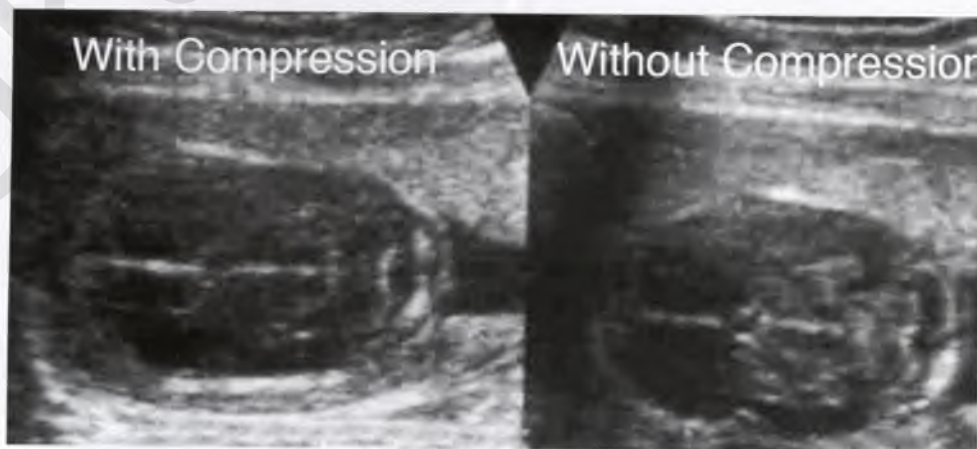


**FIG 16-37** The skull demonstrates markedly decreased echogenicity and is readily compressible even with moderate transducer pressure (left).



**FIG 16-38** Frontal x-ray scans of the fetus. Note the poor mineralization and the numerous fractures.

trunk, decreased bone mineralization (including decreased ossification of the skull), and multiple bone fractures. Multiple fractures may lead the long bones to appear angulated. Both cortices of a bone are often seen. Some findings can be seen as early as 13 to 15 weeks' gestation.

### Achondrogenesis

**Definition.** Achondrogenesis is a heterogeneous group of lethal skeletal dysplasias characterized by severe micromelia, small thorax, short trunk, decreased bone mineralization (particularly of the vertebrae, sacrum, and pubic bones), and occasional fractures. The most common types are described here:

- Type 1: includes type 1A and type 1B. Deficient bone mineralization also affects the calvarium.
- Type 2: similar to type 1, with less severe mineralization deficits.

**Synonyms.** Synonyms include type 1A, Houston-Harris type; type 1B, Fraccaro type; type 2, Langer-Saldino type.

**Incidence.** Incidence is 0.9 to 0.23 per 10,000 births. Type 1 represents 20% of cases; type 2 represents 80% of cases.

**Etiology.** In type 1A, *TRIP11* mutations lead to defects in Golgi-mediated glycosylation and altered transport of multiple cellular proteins. In type 1B, mutations in *SLC26A2* impair activity of the sulfate transporter in chondrocytes and fibroblasts leading to defective cartilage matrix assembly. In type 2, *COL2A1* mutations lead to structural abnormalities in type 2 collagen.

**Genetics.** Type 1 is inherited in autosomal recessive fashion; type 1A is caused by mutations in *TRIP11*, and type 1B is caused by mutations in *SLC26A2* (*DTDST*). Type 2 is an autosomal dominant condition caused by de novo mutations in *COL2A1*.

The other types of OI may not be detected prenatally. Type I is characterized by blue sclerae and normal stature. The first fractures generally occur in infancy. Progressive hearing loss is present in 50% of adults. Type III is apparent at birth; fractures may be caused just by handling the infant. Rib fractures can lead to pulmonary failure in the first few weeks or months of life. Those who survive generally need assistance for mobility and are extremely short. Hearing loss often begins in the teenage years. Type IV is characterized by mildly short stature, adult-onset hearing loss, and normal-to-gray sclerae; phenotype is the most variable. Dentinogenesis imperfecta is common.

**Differential Diagnosis.** The differential diagnosis includes hypophosphatasia (infantile form), achondrogenesis, and other short-limbed dwarfisms.

**Prognosis.** Type II OI is uniformly lethal. The other forms develop after birth and are characterized by progressive deformities of the long bones and short stature.

**Management.** Owing to the uniformly fatal outcome, termination of pregnancy should be offered when type II is diagnosed early in pregnancy and palliative care provided if delivery is undertaken. If continuation of the pregnancy is chosen, cesarean delivery is often recommended for nonlethal OI for prevention of fetal and maternal trauma.

### REFERENCES

- Morgan JA, Marcus PS: Prenatal diagnosis and management of intrauterine fracture. *Obstet Gynecol Surv* 65(4):249–259, 2010.
- Steiner RD, Adsit J, Basel D: COL1A1/2-related osteogenesis imperfecta. In Pagon RA, Adam MP, Ardinger HH, et al, editors: *GeneReviews*, Seattle, 1993–2016, University of Washington.
- Young ID, Thompson EM, Hall CM, Pembrey ME: Osteogenesis imperfecta type IIA: evidence for dominant inheritance. *J Med Genet* 24(7):386–389, 1987.

**Recurrence Risk.** Recurrence risk depends on the mode of inheritance. Type 1 has a 25% recurrence risk. The recurrence risk for type 2 is low.

**Diagnosis.** Type 1 is characterized by severe micromelia, facial dysmorphism (flat face), decreased skull, vertebral, and pelvic bone ossification, short thin ribs, and short long bones with deformity. Other features include short fingers and toes (seen more in type 1B), protuberant abdomen, abundant soft tissue (which can lead the fetus to appear hydroptic), and short neck with thickened tissue. Skull is normally sized. Polyhydramnios is present in 25% of affected fetuses. Breech presentation is common.

Type 2 presents with similar findings but the mineralization deficit is less severe and the long bones less short. Fingers and toes may appear normal.

**Differential Diagnosis.** The differential diagnosis includes other lethal chondrodysplasias. Cartilage histologic examination can assist in distinguishing between the subtypes of achondrogenesis. OI (specifically types II and III) and hypophosphatasia also present with bone demineralization, but the limb shortening is not usually as severe. Abnormal mineralization and shortened trunk length distinguish it from TD in which these are normal.

**Prognosis.** The disorder is perinatally lethal with death occurring prenatally or shortly after birth.



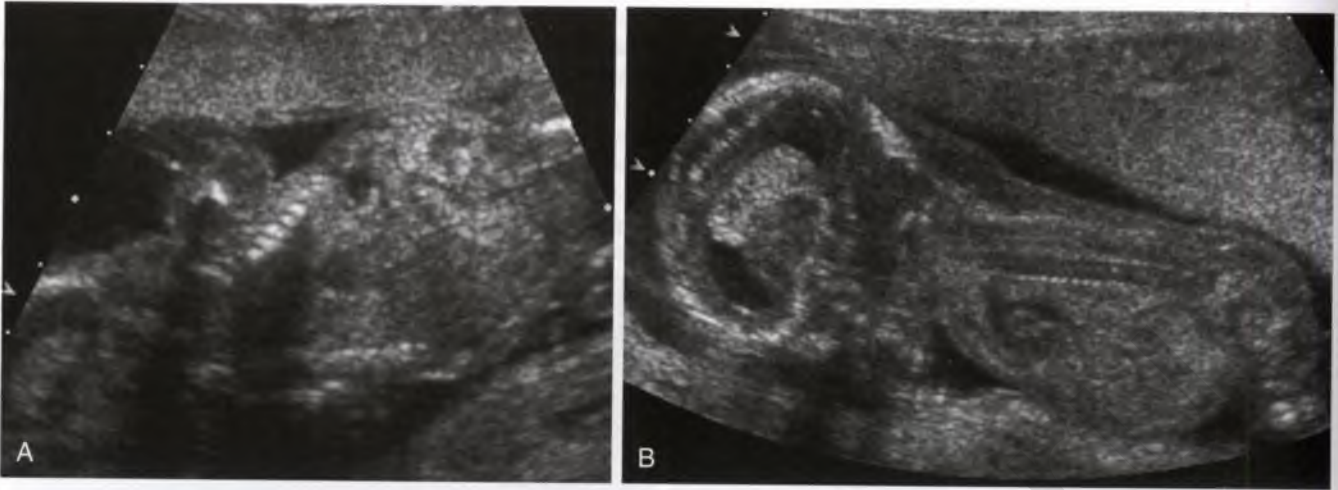


**FIG 16-39** Achondrogenesis. **A**, Coronal image of the fetus with a markedly small thorax; **B**, diffuse lack of bony mineralization, with particular involvement of the spinal vertebrae.

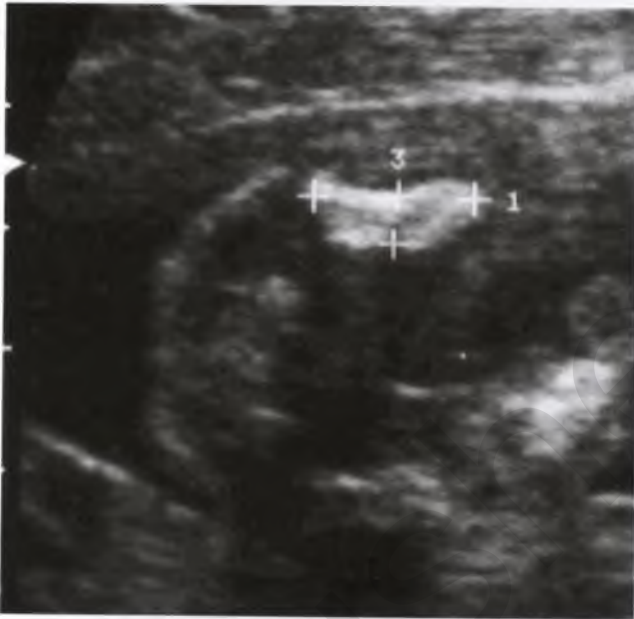


**FIG 16-40** The appearance of transparent bones in which both cortices can be seen.



**FIG 16-41** Micromelia with the arms failing to join in front of the chest.



**FIG 16-42** Achondrogenesis. The appearance of the fetus at 19 weeks.

## REFERENCES

- Bonafe L, Mittaz Crettol L, Ballhausen D, Superti-Furga A: Achondrogenesis type 1B. In Pagon RA, Adam MP, Ardinger HH, et al, editors: *GeneReviews*, Seattle, 1993–2016, University of Washington.
- Grigelioniene G, Geiberger S, Papadogiannakis N, et al: The phenotype range of achondrogenesis 1A. *Am J Med Genet A* 161A(10):2554–2558, 2013.
- Mahony BS, Filly RA, Cooperberg PL: Antenatal sonographic diagnosis of achondrogenesis. *J Ultrasound Med* 3(7):333–335, 1984.
- Meizner I, Barnhard Y: Achondrogenesis type I diagnosed by transvaginal ultrasonography at 13 weeks' gestation. *Am J Obstet Gynecol* 173(5):1620–1622, 1995.

Ozere S, Yuksel A, Tukul T: Prenatal sonographic diagnosis of type I achondrogenesis with a large cystic hygroma. *Ultrasound Obstet Gynecol* 13(1):75–76, 1999.

Smits P, Bolton AD, Funari V, et al: Lethal skeletal dysplasia in mice and humans lacking the golgin GMAP-210. *N Engl J Med* 362(3):206–216, 2010.

Vissing H, D'Alessio M, Lee B, et al: Glycine to serine substitution in the triple helical domain of pro-alpha 1 (II) collagen results in a lethal

perinatal form of short-limbed dwarfism. *J Biol Chem* 264(31):18265–18267, 1989.

Wenstrom KD, Williamson RA, Hoover WW, Grant SS: Achondrogenesis type II (Langer-Saldino) in association with jugular lymphatic obstruction sequence. *Prenat Diagn* 9(7):527–532, 1989.

## Campomelic Dysplasia

**Definition.** Campomelic dysplasia (derived from the Greek word for “bent limb”) is a skeletal dysplasia characterized by bowing and shortening of the long bones, club feet, and distinctive facial features including Pierre Robin sequence with cleft palate.

**Synonyms.** Campomelic dysplasia is also known as campomelic syndrome and campomelic dwarfism.

**Incidence.** Incidence is 1 in 40,000 to 1 in 80,000 births.

**Etiology.** *SOX9* regulates chondrocyte differentiation by regulating the expression of several genes, including the collagen genes *COL2A1* and *COL11A2*. It also functions as a testes-determining gene downstream of *SRY*.

**Genetics.** Campomelic dysplasia is due to mutations in *SOX9*. Inheritance is autosomal dominant; most individuals have de novo mutations, although cases of parental diagnosis following identification of an affected child have been reported.

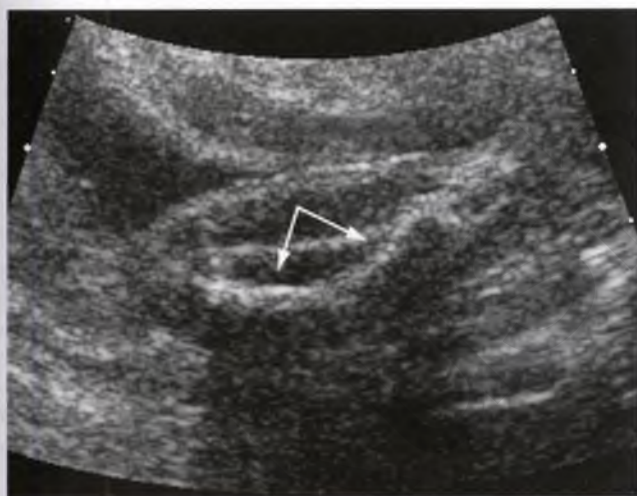


**FIG 16-43** Campomelic dysplasia. Bowing of the femur (arrows). Note the gentle curve that differentiates this entity from the more acute angles seen in fetuses with osteogenesis imperfecta.

**Recurrence Risk.** Recurrence risk is low if the parents are unaffected, although germline mosaicism has been reported.

**Diagnosis.** The most striking feature is anterior bowing of the long bones, particularly the femur and tibia. Other features seen on ultrasound imaging include 11 pairs of ribs, a bell-shaped narrow chest, relatively large head, Pierre Robin sequence with cleft palate, flat face with high forehead, laryngotracheomalacia, cervical spine anomalies, scoliosis, scapular hypoplasia, ambiguous genitalia (or normal female genitalia in a 46,XY individual), dislocated hips, clubfeet, and hydrocephalus. Cardiac and renal anomalies have also been reported. Polyhydramnios may be present.

**Differential Diagnosis.** The differential diagnosis includes OI types II and III, hypophosphatasia, other disorders leading to congenital bowing of the long bones, TD, and spondyloepiphyseal dysplasia.

**Prognosis.** Most cases (>75%) are lethal owing to respiratory insufficiency caused by airway instability or cervical spine instability. Survivors may have respiratory issues, hearing loss, and progressive scoliosis. Intellectual abilities are generally normal.

## REFERENCES

- Akiyama H, Lefebvre V: Unraveling the transcriptional regulatory machinery in chondrogenesis. *J Bone Miner Metab* 29(4):390–395, 2011.
- Cordone M, Lituania M, Zampatti C, et al: In utero ultrasonographic features of campomelic dysplasia. *Prenat Diagn* 9(11):745–750, 1989.
- Khajavi A, Lachman R, Rimoin D, et al: Heterogeneity in the campomelic syndromes. Long- and short-bone varieties. *Radiology* 120(3):641–647, 1976.
- Lee FA, Isaacs H, Jr, Strauss J: The “campomelic” syndrome. Short life-span dwarfism with respiratory distress, hypotonia, peculiar facies, and multiple skeletal and cartilaginous deformities. *Am J Dis Child* 124(4):485–496, 1972.
- Unger S, Scherer G, Superti-Furga A: Campomelic dysplasia. In Pagon RA, Adam MP, Ardinger HH, et al, editors: *GeneReviews*, Seattle, 1993–2016, University of Washington.
- Vidal VP, Chaboissier MC, de Rooij DG, Schedl A: Sox9 induces testis development in XX transgenic mice. *Nat Genet* 28(3):216–217, 2001.
- Wagner T, Wirth J, Meyer J, et al: Autosomal sex reversal and campomelic dysplasia are caused by mutations in and around the *SRY*-related gene *SOX9*. *Cell* 79(6):1111–1120, 1994.

## Hypophosphatasia Congenita

**Definition.** Hypophosphatasia congenita is characterized by severe micromelia, small thorax, normal head circumference, normal trunk length, decreased bone mineralization, and occasional fractures. The cranium is compressible from deficient mineralization.

**Synonyms.** Hypophosphatasia congenita is also called perinatal lethal hypophosphatasia.

**Prevalence.** Hypophosphatasia congenita is seen in 1 in 100,000.

**Etiology.** Hypophosphatasia congenita is associated with reduced activity of serum alkaline phosphatase.

**Genetics.** Hypophosphatasia congenita is due to mutations in *ALPL*, the gene encoding alkaline phosphatase, tissue-nonspecific isozyme (TNSALP). Inheritance is autosomal recessive. Significant phenotypic variability can occur.

**Recurrence Risk.** Recurrence risk is 25% if both parents are found to be mutation carriers. Carriers can be asymptomatic (with only biochemical abnormalities) or may have mild clinical features.

**Diagnosis.** The perinatal lethal form of hypophosphatasia is generally diagnosed on prenatal ultrasound imaging. Features include a small thorax, short bowed limbs, flail chest, and poorly mineralized



skull. Fetal radiographs demonstrate a generalized deficiency in ossification, with tubular bones that appear short, thin, and bowed.

**Differential Diagnosis.** In the prenatal period, the differential includes OI type II, campomelic dysplasia, and chondrodysplasias with defective bone mineralization.

**Prognosis.** Pregnancies may end in stillbirth. Liveborn infants most frequently die of pulmonary insufficiency. Hypercalcemia is common and can lead to apnea and seizures.

## REFERENCES

Hofmann C, Girschick H, Mornet E, et al: Unexpected high intrafamilial phenotypic variability observed in hypophosphatasia. *Eur J Hum Genet* 22(10):1160–1164, 2014.

Mornet E, Nunes ME: Hypophosphatasia. In Pagon RA, Adam MP, Ardinger HH, et al, editors: *GeneReviews*, Seattle, 1993–2016, University of Washington.

Sergi C, Mornet E, Troeger J, Voigtlaender T: Perinatal hypophosphatasia: radiology, pathology and molecular biology studies in a family harboring a splicing mutation (648+1A) and a novel missense mutation (N400S) in the tissue-nonspecific alkaline phosphatase (TNSALP) gene. *Am J Med Genet* 103(3):235–240, 2001.

## Short Rib–Polydactyly Syndromes

**Definition.** Short rib–polydactyly syndromes (SRPSs) are heterogeneous group of lethal skeletal dysplasias typically divided into four subgroups. General findings include severe micromelia, small thorax with short ribs, a trident aspect of the acetabular roof, normal head circumference, normal bone mineralization, and polydactyly. Cardiac and genitourinary abnormalities may be seen. The SRPSs are divided into five subtypes, types I through V. Two related syndromes with a milder phenotype include Ellis–van Creveld syndrome (EVC) and Jeune syndrome. Features of the subtypes can overlap, making diagnosis challenging.

**Synonyms.** Synonyms include type I, Saldino–Noonan syndrome; type II, Majewski syndrome; type III, Verma–Naumoff syndrome; type IV, Beemer–Langer syndrome; and type V.

**Prevalence.** Prevalence is unknown; the syndrome is rare.

**Etiology.** All SRPSs are classified as ciliopathies because of dysfunction of the primary cilium.

**Genetics.** SRPSs are due to mutations in genes affecting primary cilium function, including mutations affecting the dynein motor (*DYNC2H1*), intraflagellar transport complexes (*IFT80*, *IFT122*, *IFT43*, *WDR35*, *WDR19*, *TTC21B*), and basal body (*NEK1*, *EVC*, *EVC2*). Other genes identified include *WDR34* and *WDR60* that also are important for primary cilium function. Inheritance is autosomal recessive.

**Diagnosis.** The most striking ultrasound finding is a very narrow chest with short limbs. The limbs, however, are not as short as those of other lethal conditions such as TD, achondrogenesis, and OI type II.

**Differential Diagnosis.** The differential diagnosis should include the range of SRPSs.

**Prognosis.** There is a phenotypic spectrum, and although many affected infants die, some do survive.

## REFERENCES

Baujatz G, Huber C, El Hokayem J, et al: Asphyxiating thoracic dysplasia: clinical and molecular review of 39 families. *J Med Genet* 50(2):91–98, 2013.

El Hokayem J, Huber C, Couve A, et al: *NEK1* and *DYNC2H1* are both involved in short rib polydactyly Majewski type but not in Beemer Langer cases. *J Med Genet* 49(4):227–233, 2012.

Huber C, Cormier-Daire V: Ciliary disorder of the skeleton. *Am J Med Genet C Semin Med Genet* 160C(3):165–174, 2012.

Huber C, Wu S, Kim AS, et al: *WDR34* mutations that cause short-rib polydactyly syndrome type III/severe asphyxiating thoracic dysplasia reveal a role for the NF- $\kappa$ B pathway in cilia. *Am J Hum Genet* 93(5):926–931, 2013.

McInerney-Leo AM, Schmidts M, Cortes CR, et al: Short-rib polydactyly and Jeune syndromes are caused by mutations in *WDR60*. *Am J Hum Genet* 93(3):515–523, 2013.

## Other Lethal Skeletal Dysplasias

### Atelosteogenesis, Type 2

Atelosteogenesis, type 2 is a rare lethal skeletal dysplasia characterized by rhizomelia, normal head circumference, hitchhiker thumbs, ulnar deviation of fingers, small thorax, protuberant abdomen, facial dysmorphism (flat midface, micrognathia), cleft palate, clubfeet, and a gap between the first and second toes. Death occurs from pulmonary

hypoplasia and tracheobronchomalacia. It is due to mutations in *SLC26A2* (*DTDST*). Inheritance is autosomal recessive.

## REFERENCE

Bonafe L, Mittaz-Crettol L, Ballhausen D, Superti-Furga A: Atelosteogenesis type 2. In Pagon RA, Adam MP, Ardinger HH, et al, editors: *GeneReviews*, Seattle, 1993–2016, University of Washington.

## Fibrochondrogenesis

Fibrochondrogenesis is a rare lethal skeletal dysplasia characterized by short long bones with irregular metaphyses that appear stippled from peripheral spurs and extra-articular calcifications (dumbbell-shaped long bones). Other features include small thorax, normal head circumference, normal hands and feet, flat facies, decreased skull mineralization, and vertebrae with platyspondyly and midline clefts. It is due to mutations in *COL11A1*. Inheritance is autosomal recessive. Carriers of causative mutations can have myopia and early-onset hearing loss.

## REFERENCES

Bekdache GN, Begam MA, Chedid F, et al: Fibrochondrogenesis: prenatal diagnosis and outcome. *J Obstet Gynaecol* 33(7):663–668, 2013.

Tompson SW, Bacino CA, Safina NP, et al: Fibrochondrogenesis results from mutations in the *COL11A1* type XI collagen gene. *Am J Hum Genet* 87(5):708–712, 2010.

### Rhizomelic Chondrodysplasia Punctata, Type I

Rhizomelic chondrodysplasia punctata, type I is a rare skeletal dysplasia with prevalence less than 100,000 births; the classic type is a peroxisome biogenesis disorder characterized by rhizomelia (humerus shorter than femur), epiphyseal and metaphyseal abnormalities (punctate calcifications), vertebral clefting, and congenital cataracts. Other common features include severe postnatal growth deficiency, seizures, and severe intellectual disability. Some children die in the neonatal period; lifespan is generally less than 10 years. It is due to mutations

in *PEX7*, a gene that encodes the receptor for some peroxisomal matrix enzymes. Inheritance is autosomal recessive.

### REFERENCE

Braverman NE, Moser AB, Steinberg SJ: Rhizomelic chondrodysplasia punctata type I. In Pagon RA, Adam MP, Ardinger HH, et al, editors: *GeneReviews*, Seattle, 1993–2016, University of Washington.

### Achondroplasia

**Definition.** Achondroplasia is a relatively common nonlethal skeletal dysplasia characterized by rhizomelia, macrocephaly, and characteristic facial features (frontal bossing and flat midface). Other features include redundant skinfolds on limbs, short fingers, bowed legs, and exaggerated lumbar lordosis.

**Incidence.** Incidence is 1 in 26,000 to 28,000 live births.

**Etiology.** The *FGFR3* mutation, p.Gly380Arg, seen in achondroplasia leads to constitutive activation of *FGFR3*. This results in inhibition of chondrocyte proliferation and differentiation and negatively regulates bone growth.

**Genetics.** Achondroplasia is due to a mutation in *FGFR3*, specifically p.Gly380Arg. Inheritance is autosomal dominant; 80% of mutations are de novo and are exclusively inherited from the father. Advanced paternal age increases the risk of de novo mutations.

**Recurrence Risk.** Recurrence risk is low if both parents have average stature. If one parent is affected, recurrence risk is 50%. If both parents are affected, the risk to offspring is as follows: 25% will have average stature, 50% will have achondroplasia, and 25% will have homozygous achondroplasia (which is lethal).

**Diagnosis.** Prenatally, a shortened femur in comparison to the head circumference can be seen in the second trimester; femur length is often at the 3rd percentile or less by 25 weeks' gestation (see Fig. 16-46). Fetuses with normal interval growth in femoral length during the second trimester are expected to be unaffected. The craniofacial features, including macrocephaly, frontal bossing, and flat midface, can also be seen. Occasionally more subtle anomalies, such as the trident hand (an increased space between the third and fourth digit) or the lack of widening of the lumbar canal, can also be identified.

**Differential Diagnosis.** The differential diagnosis includes TD, hypochondroplasia, achondrogenesis, OI type II, and diastrophic dysplasia.

**Prognosis.** Developmental milestones are often delayed, but intelligence is normal. Craniocervical junction compression increases the



FIG 16-44 Achondroplasia. Frontal bossing.

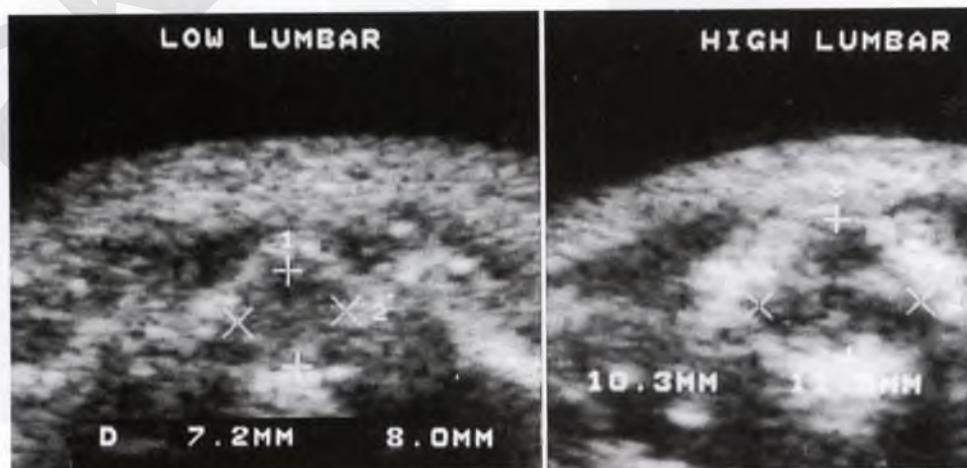
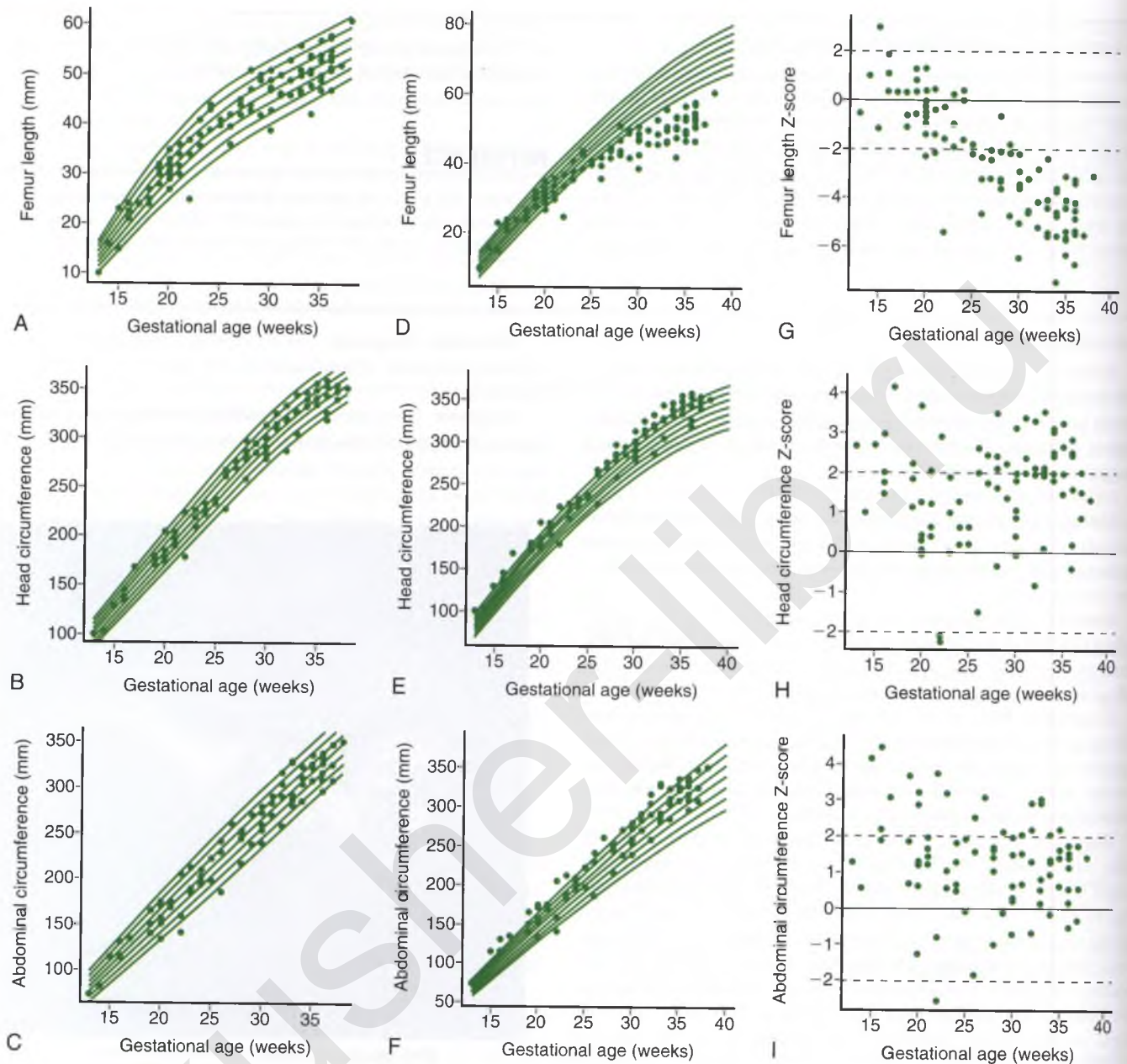


FIG 16-45 Achondroplasia. Lack of widening of the spinal canal.





**FIG 16-46** Fetal size charts for femur length (A), head circumference (B), and abdominal circumference (C) against gestational age in fetuses with achondroplasia. Note the curvature in the femur length chart as growth declines in the third trimester. Comparison with normal fetuses is demonstrated by overlaying measurements from affected fetuses on charts of fetuses of normal size (D-F, respectively) and by plots of Z-scores showing the deviation from the normal range (G-I, respectively). (From Chitty LS, Griffin DR, Meaney C, et al: New aids for the non-invasive prenatal diagnosis of achondroplasia: dysmorphic features, charts of fetal size and molecular confirmation using cell-free fetal DNA in maternal plasma. *Ultrasound Obstet Gynecol* 37(3):283-289, 2011, Fig. 1.)

risk of death in infancy as a result of central apnea (risk ~ 7.5%). Obesity is a common problem that often begins in childhood. Spinal stenosis at L1-L4 is the most common medical complaint in adulthood.

**Management.** Medical issues require ongoing surveillance, and guidelines have been established (see Trotter and Hall, 2005). Strong support groups exist, including the Little People of America, Inc.

## REFERENCES

- Chitty LS, Griffin DR, Meaney C, et al: New aids for the non-invasive prenatal diagnosis of achondroplasia: dysmorphic features, charts of fetal size and molecular confirmation using cell-free fetal DNA in maternal plasma. *Ultrasound Obstet Gynecol* 37(3):283-289, 2011.
- Le Merrer M, Rousseau F, Legeai-Mallet L, et al: A gene for achondroplasia-hypochondroplasia maps to chromosome 4p. *Nat Genet* 6(3):318-321, 1994.

- Moeglin D, Benoit B: Three-dimensional sonographic aspects in the antenatal diagnosis of achondroplasia. *Ultrasound Obstet Gynecol* 18(1):81–83, 2001.
- Patel MD, Filly RA: Homozygous achondroplasia: US distinction between homozygous, heterozygous, and unaffected fetuses in the second trimester. *Radiology* 196(2):541–545, 1995.
- Pauli RM: Achondroplasia. In Pagon RA, Adam MP, Ardinger HH, et al, editors: *GeneReviews*, Seattle, 1993–2016, University of Washington.

- Trotter TL, Hall JG: American Academy of Pediatrics Committee on Genetics: Health supervision for children with achondroplasia. *Pediatrics* 116(3):771–783, 2005.
- Velinov M, Slaugenhaupt SA, Stoilov I, et al: The gene for achondroplasia maps to the telomeric region of chromosome 4p. *Nat Genet* 6(3):314–317, 1994.

## Vertebral Anomalies

### Klippel-Feil Syndrome

**Definition.** Klippel-Feil syndrome (KFS) is characterized by a classic triad of short neck, low posterior hairline, and fusion of cervical vertebrae. Different classification schemes for subtypes have been proposed. KFS1 and KFS3 are autosomal dominant disorders, whereas KFS2 is autosomal recessive.

**Incidence.** Incidence is 1 in 40,000 to 42,000 live births. A slight female predominance has been reported.

**Etiology.** The implicated genes encode for proteins in the bone morphogenetic protein family, which is involved in regulating the differentiation of bone and cartilage.



**FIG 16-47** Second trimester sonogram of a fetus with Klippel-Feil syndrome. Persistent retroflexion of the head on the neck should raise suspicion for this diagnosis.

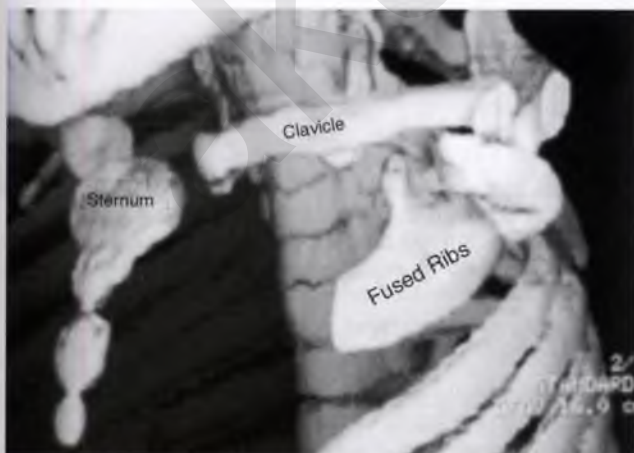


**FIG 16-48** Reformatted computer tomographic scan of a 2-year-old child with Klippel-Feil syndrome. Note the fused ribs. (Courtesy of Ian Suchet, 2002. Available at thefetus.net.)

**Genetics.** KFS1 is due to mutations in the *GDF6* gene, and KFS3 is due to mutations in the *GDF3* gene; both have autosomal dominant inheritance. KFS2 is due to mutations in *MEOX1* and has autosomal recessive inheritance.

**Recurrence Risk.** Recurrence risk depends on the mode of inheritance and presence of parental mutations.

**Diagnosis.** The short neck may be associated with opisthotonos (retroflexion of the head), and disorganization of the cervical vertebrae is potentially recognizable. Other associated anomalies include ocular malformations, cleft lip and palate, oligodontia, craniofacial asymmetry, maxillary constriction and velopharyngeal insufficiency, persistent trigeminal artery, congenital heart defects, and urogenital anomalies. Some cases occurring with situs inversus totalis have been reported.

**Differential Diagnosis.** The differential diagnosis includes other disorders with vertebral anomalies.

**Prognosis.** Complications result from vertebral fusion and include cord compression syndrome, cervical instability, and motility impairment.

### VACTERL Association

See separate entry at the end of this chapter.



**FIG 16-49** A child with Klippel-Feil syndrome. Note the opisthotonic position, low-set ears, and micrognathia.



## REFERENCES

- Barbosa V, Maganzini AL, Nieberg LG: Dento-skeletal implications of Klippel-Feil syndrome [a case report]. *N Y State Dent J* 71(1):48–51, 2005.
- Bayrakli F, Guclu B, Yakicier C, et al: Mutation in MEOX1 gene causes a recessive Klippel-Feil syndrome subtype. *BMC Genet* 14:95, 2013.
- Chacon-Camacho O, Camarillo-Blancarte L, Pelaez-Gonzalez H, et al: Klippel-Feil syndrome associated with situs inversus: description of a new case and exclusion of GDF1, GDF3 and GDF6 as causal genes. *Eur J Med Genet* 55(6–7):414–417, 2012.
- Dickerman RD, Colle KO, Mittler MA: Intramedullary inflammatory mass dorsal to the Klippel-Feil deformity: error in development or response to an abnormal motion segment? *Spinal Cord* 42(12):720–722, 2004.
- Erol M, Caksen H, Tan O, et al: Report of a girl with Klippel-feil syndrome and Poland anomaly. *Genet Couns* 15(4):469–472, 2004.
- Giampietro PF, Raggio CL, Blank RD, et al: Clinical, genetic and environmental factors associated with congenital vertebral malformations. *Mol Syndromol* 4(1–2):94–105, 2013.
- Klippel M, Feil A: The classic: a case of absence of cervical vertebrae with the thoracic cage rising to the base of the cranium (cervical thoracic cage). *Clin Orthop Relat Res* 109:3–8, 1975.
- McGaughran JM, Oates A, Donnai D, et al: Mutations in PAX1 may be associated with Klippel-Feil syndrome. *Eur J Hum Genet* 11(6):468–474, 2003.
- Paksoy Y, SEker M, Kalkan E: Klippel-Feil syndrome associated with persistent trigeminal artery. *Spine* 29(9):E193–E196, 2004.
- Tracy MR, Dormans JP, Kusumi K: Klippel-Feil syndrome: clinical features and current understanding of etiology. *Clin Orthop Relat Res* 424:183–190, 2004.

## Spondylocostal Dysostosis

**Definition.** Spondylocostal dysostosis (SCDO) is characterized by multiple segmentation defects of the vertebrae and rib abnormalities, leading to a short trunk, short neck, and scoliosis.

**Prevalence.** SCDO is rare; SCDO associated with *DLL3* mutations is the most common.

**TABLE 16-4 Some Syndromes That Include Multiple Segmentation Defects of the Vertebrae (Spondylocostal Dysostosis and Spondylothoracic Dysostosis Excluded)**

Syndromes/Disorders	OMIM	Gene	Syndromes/Disorders	OMIM	Gene
Acrofacial dysostosis*	263750		Klippel-Feil*	148900	<i>GDF6, PAX1</i> <sup>†</sup>
Alagille syndrome	118450	<i>JAG1, NOTCH2</i>	Larsen syndrome	150250	<i>FLNB</i>
Anhalt*	601344		Lower mesodermal agenesis*		
Atelosteogenesis III	108721	<i>FLNB</i>	Maternal diabetes mellitus*		
Campomelic dysplasia	211970	<i>SOX9</i>	MURCS association*	601076	
Casamassima-Morton-Nance*	271520		Multiple pterygium syndrome	265000	<i>CHRNA3</i>
Caudal regression*	182940		OEIS syndrome*	258040	
Cerebro-facio-thoracic dysplasia*	213980		Phaver*	261575	
CHARGE syndrome	214800	<i>CHD7</i>	RAPADILINO syndrome ( <i>RECQL4</i> -related disorders)	266280	<i>RECQL4</i>
“Chromosomal”			Robinow ( <i>ROR2</i> -related disorders)	180700	<i>ROR2</i>
Currarino	176450	<i>HLXB9</i>	Rolland-Desbuquois*	224400	
Atelosteogenesis, type II (de la Chapelle syndrome)	256050	<i>SLC26A2</i>	Rokitansky sequence*	277000	<i>WNT4</i>
DiGeorge/deletion 22q11.2/velocardiofacial syndrome	188400		Silverman-Handmaker type of dyssegmental dysplasia (DDSH)	224410	<i>HSPG2</i>
Dysspondylochondromatosis*			Simpson-Golabi-Behmel syndrome	312870	<i>GPC3</i>
Femoral hypoplasia-unusual facies*	134780		Sirenomelia*	182940	
Fibrodysplasia ossificans progressiva	135100	<i>ACVR1</i>	Spondylarcarpotarsal synostosis	272460	<i>FLNB</i>
Fryns-Moerman*			Thakker-Donnai*	227255	
Goldenhar/oculo-auriculo-vertebral spectrum*	164210		Toriello*		
Holmes-Schimke*			Urioste*		
Incontinentia pigmenti	308310	<i>IKBKG</i>	VATER/VACTERL*	192350	
Kabuki syndrome*	147920	<i>MLL2</i>	Verloove-Vanhorick*	215850	
McKusick-Kaufman syndrome	236700	<i>MKKS</i>	Wildervanck*	314600	
KBG syndrome*	148050	<i>ANKRD11</i>	Zimmer*	301090	

\*Underlying cause not known.

<sup>†</sup>Possible associations reported: *PAX1* (McGaughran JM, Oates A, Donnai D, et al: Mutations in *PAX1* may be associated with Klippel-Feil syndrome. *Eur J Hum Genet* 11:468–474, 2003.) and *WNT4* (Philibert P, Bignon-Laubert A, Rouzier R, et al: Identification and functional analysis of a new *WNT4* gene mutation among 28 adolescent girls with primary amenorrhea and müllerian duct abnormalities: a French collaborative study. *J Clin Endocrinol Metab* 93:895–900, 2008.)

CHARGE, coloboma of the eye, heart defects, atresia of the choanae, retarded mental and growth development, genital anomalies, and ear anomalies; OEIS, omphalocele, bladder exstrophy, imperforate anus, and spinal defects; MURCS, müllerian duct aplasia, congenital renal dysplasia, and cervical somite anomalies; RAPADILINO, radial ray defect, patellae hypoplasia or aplasia and cleft or highly arched palate, diarrhea and dislocated joints, little size and limb malformations, and long, slender nose and normal intelligence; VATER/VACTERL, vertebral anomalies, anal atresia, cardiac anomalies, tracheoesophageal fistula or esophageal atresia, renal/urinary anomalies, and limb defects.

From Turnpenny PD, Young E; ICVS (International Consortium for Vertebral Anomalies and Scoliosis): Spondylocostal Dysostosis, Autosomal Recessive. 2009 Aug 25 (Updated 2013 Jan 17). In Pagon RA, Adam MP, Ardinger HH, et al (eds): GeneReviews.® Seattle, University of Washington, 1993–2016, Table 2.

**Etiology.** The causative genes identified to date all encode key proteins in the Notch-signaling pathway, which is essential for vertebral development.

**Genetics.** SCDO is due to mutations in one of four genes: *DLL3*, *MESP2*, *LFNG*, *HES7*. Inheritance is autosomal recessive.

**Recurrence Risk.** Recurrence risk is 25% if both parents are mutation carriers.

**Diagnosis.** Diagnosis is based on radiologic features including vertebral segmentation defects and rib abnormalities. These features can be seen prenatally as early as the late first trimester.

**Differential Diagnosis.** The differential diagnosis includes other rarer conditions with similar vertebral anomalies as well as

syndromes associated with multiple vertebral segmentation defects (Table 16-4).

**Prognosis.** The size of the thorax can compromise respiratory function in neonates and can lead to pulmonary hypertension. Males have increased risk for inguinal hernia. Neurologic complications are rare.

## REFERENCE

Turnpenny PD, Young E, Icvas: Spondylocostal dysostosis, autosomal recessive. In Pagon RA, Adam MP, Ardinger HH, et al, editors: *GeneReviews*, Seattle, 1993–2016, University of Washington.

## Upper Extremity Anomalies

If an upper limb anomaly is noted, particular attention should be given to evaluating for spine, renal, and cardiac anomalies. If the defect is in an isolated forearm, it is rare for further problems to be found. If bilateral upper limb anomalies are noted and the karyotype is normal, there is a high incidence of genetic syndromes, several of which are reviewed later.

### Adams-Oliver Syndrome

**Definition.** Adams-Oliver syndrome (AOS) is characterized by aplasia cutis congenital of the scalp vertex and terminal transverse limb defects (amputations, syndactyly, brachydactyly, oligodactyly).

**Incidence.** Incidence is estimated at 1 in 225,000.

**Etiology.** The implicated genes encode for proteins implicated in embryonic development. Some are thought to affect pericyte function leading to the observed anomalies.

**Genetics.** The genetic cause is heterogeneous, and includes heterozygous mutations in *ARHGAP31* and *RBPJ* (autosomal dominant inheritance) as well as biallelic mutations in *DOCK6* and *EOGT* (autosomal recessive inheritance). Recently, heterozygous mutations in *NOTCH1* were also implicated in AOS.

**Recurrence Risk.** Recurrence risk depends on mode of inheritance and presence of parental mutations.

**Diagnosis.** Prenatally, transverse limb defects may be detected sonographically. Other commonly observed features in affected individuals include vascular anomalies (pulmonary hypertension, portal hypertension, cutis marmorata, venous ectasia, thrombophilia) and congenital heart defects (both right- and left-sided).

**Differential Diagnosis.** The differential diagnosis includes other causes of transverse limb defects.

**Prognosis.** Prognosis depends on the associated anomalies, which can range from mild to severe. Pulmonary hypertension can be life threatening.

## REFERENCES

Chang L, Nosedá M, Higginson M, et al: Differentiation of vascular smooth muscle cells from local precursors during embryonic and adult arteriogenesis requires Notch signaling. *Proc Natl Acad Sci U S A* 109(18):6993–6998, 2012.

Patel MS, Taylor GP, Bharya S, et al: Abnormal pericyte recruitment as a cause for pulmonary hypertension in Adams-Oliver syndrome. *Am J Med Genet A* 129A(3):294–299, 2004.

Stittrich AB, Lehman A, Bodian DL, et al: Mutations in *NOTCH1* cause Adams-Oliver syndrome. *Am J Hum Genet* 95(3):275–284, 2014.

### Cornelia de Lange Syndrome

**Definition.** Cornelia de Lange syndrome (CdLS) is characterized by facial dysmorphism (synophrys, arched eyebrows, long eyelashes, small upturned nose, small widely spaced teeth, micrognathia), growth restriction and microcephaly (prenatal onset), hirsutism, and upper limb reduction defects (phalangeal abnormalities, oligodactyly).

**Synonym.** It is also known as Brachmann-de Lange syndrome.

**Incidence.** Estimates range from 1 in 10,000 to 1 in 100,000. The milder form is likely underdiagnosed.

**Diagnosis.** Diagnosis is based on clinical findings. Other features may include cardiac septal defects, cleft palate, GI dysfunction, hearing loss, myopia, and cryptorchidism. Congenital diaphragmatic hernia (CDH) can occur (1%).

**Genetics.** Implicated genes include *NIPBL* (60% of cases) as well as *SMC1A* and *SMC3* (5% and <1% of cases, respectively). Inheritance of *NIPBL*- and *SMC3*-related CdLS is autosomal dominant; *SMC1A*-related CdLS is X-linked. Most *NIPBL* mutations are de novo. In general, the phenotype associated with mutations in *SMC1A* and *SMC3* is milder. Phenotypic expression in families is relatively consistent. Penetrance is complete.

**Recurrence Risk.** Recurrence risk depends on the implicated gene. Germline mosaicism is increased with *NIPBL*-related CdLS and recurrence is estimated to be 1.5%.

**Differential Diagnosis.** Other disorders to consider include partial duplication of 3q, deletions of 2q31, Fryns syndrome, and FAS.

**Prognosis.** Intellectual disability is generally present. Autistic and self-destructive tendencies are common. Life expectancy is generally normal, although an increased mortality rate has been reported related to aspiration, apnea, congenital heart disease, volvulus, and postsurgical complications.

**Management.** Management guidelines have been published and involve multidisciplinary care for both medical and developmental issues.

## REFERENCES

Deardorff MA, Clark DM, Krantz ID: Cornelia de Lange syndrome. In Pagon RA, Adam MP, Ardinger HH, et al, editors: *GeneReviews*, Seattle, 1993–2016, University of Washington.

Kline AD, Krantz ID, Sommer A, et al: Cornelia de Lange syndrome: clinical review, diagnostic and scoring systems, and anticipatory guidance. *Am J Med Genet A* 143A(12):1287–1296, 2007.



### Ectrodactyly-Ectodermal Dysplasia-Clefting Syndrome

**Definition.** Ectrodactyly-ectodermal dysplasia-clefting (EEC) syndrome is characterized by abnormalities in ectodermal structures (skin, hair, teeth, nails, sweat glands) as well as cleft lip  $\pm$  palate and limb defects (ectrodactyly and syndactyly of the hands and feet).

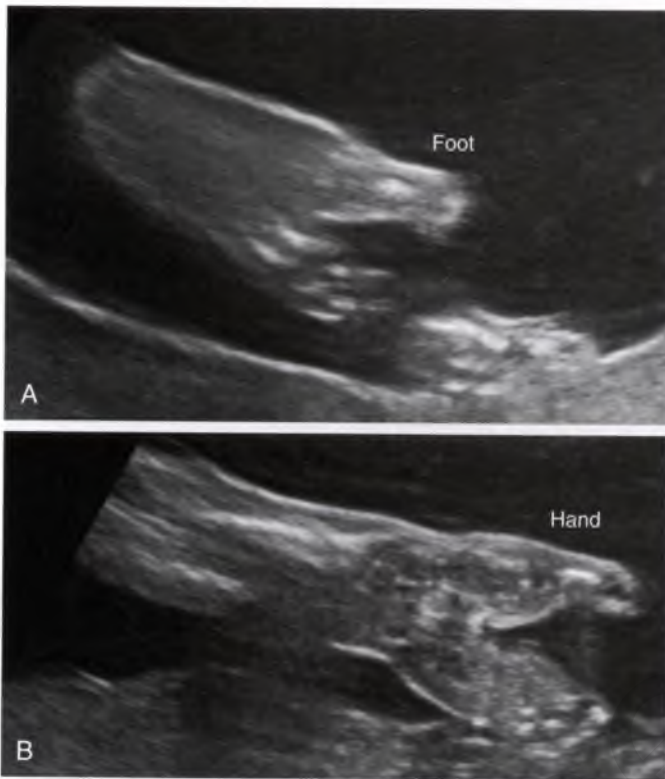


**FIG 16-50** Ectrodactyly-ectodermal dysplasia-clefting (EEC) syndrome. Ectrodactyly of the lower (A) and upper (B) extremities. Sonographic findings of ectrodactyly, especially in association with cleft lip  $\pm$  palate, should prompt evaluation for EEC syndrome.

### Fanconi Anemia

**Definition.** Fanconi anemia (FA) is characterized by structural anomalies, bone marrow failure, and an increased risk of malignancy. Anomalies can include most organ systems, including musculoskeletal, renal, cardiac, GI, skin, and CNS. Absence of physical anomalies does not rule out the disorder.

**Incidence.** Incidence is approximately 1 in 360,000 births.

**Genetics.** Molecular genetic testing is complicated because at least 15 genes have been implicated. Diagnosis is based on chromosomal fragility testing. Inheritance is generally autosomal recessive, except for mutations in *FANCB*, which are X-linked.

**Recurrence Risk.** Recurrence risk depends on mode of inheritance. Risk is 25% for autosomal recessive FA if both parents are mutation carriers.

**Diagnosis.** The diagnosis should be considered prenatally if abnormal thumbs or radial ray defects are noted. Multiple other major congenital malformations may be present.

### Holt-Oram Syndrome

**Definition.** Holt-Oram syndrome (HOS) is characterized by congenital heart disease and anomalies of the upper limbs (specifically anomalies of the carpal, radial, or thenar bones). It is the most common

**Incidence.** Incidence is unknown; the disorder is rare.

**Etiology.** The *TP63* gene encodes for a transcription factor crucial in the development of limbs and ectodermal-derived tissues.

**Genetics.** EEC syndrome is due to mutations in *TP63*. Inheritance is autosomal dominant. Significant intra- and interfamilial phenotypic variability exists.

**Recurrence Risk.** Recurrence risk is 50% if a parental mutation is identified.

**Diagnosis.** Prenatally, ectrodactyly and syndactyly of the hands and feet, as well as cleft lip/palate may be detected. The hands may have a “lobster claw” appearance. Renal anomalies may also be present.

**Differential Diagnosis.** The differential includes other syndromes caused by *TP63* mutations, in particular ankyloblepharon-ectodermal defects-cleft lip/palate syndrome.

**Prognosis.** Correction of orofacial clefting and hand and foot anomalies may be complicated by the presence of ectodermal dysplasia. Corrective surgery should be performed in centers that perform a greater number of complex repairs.

### REFERENCES

- Allen LM, Maestri MJ: Three-dimensional sonographic findings associated with ectrodactyly ectodermal dysplasia clefting syndrome. *J Ultrasound Med* 27(1):149–154, 2008.
- Clements SE, Techanukul T, Coman D, et al: Molecular basis of EEC (ectrodactyly, ectodermal dysplasia, clefting) syndrome: five new mutations in the DNA-binding domain of the TP63 gene and genotype-phenotype correlation. *Br J Dermatol* 162(1):201–207, 2010.
- Gun I, Kizilaslan C, Atalay MA: Familial ectrodactyly-ectodermal dysplasia-clefting syndrome. *Int J Gynaecol Obstet* 119(1):86–87, 2012.
- Rios LT, Araujo Junior E, Caetano AC, et al: Prenatal diagnosis of EEC syndrome with “lobster claw” anomaly by 3D ultrasound. *J Clin Imaging Sci* 2:40, 2012.

**Differential Diagnosis.** The differential includes other conditions with radial ray defects, including chromosomal disorders, VACTERL, and thrombocytopenia-absent radius (TAR) syndrome.

**Prognosis.** The cumulative incidence of bone marrow failure is 90% by age 40 to 50. The risk of hematologic malignancy (mostly acute myelogenous leukemia) is 10% to 30% and of nonhematologic malignancy is 25% to 30%.

### REFERENCES

- Alter BP, Kupfer G: Fanconi anemia. In Pagon RA, Adam MP, Ardinger IH, et al, editors: *GeneReviews*, Seattle, 1993–2016, University of Washington.
- Merrill A, Rosenblum-Vos L, Driscoll DA, et al: Prenatal diagnosis of Fanconi anemia (Group C) subsequent to abnormal sonographic findings. *Prenat Diagn* 25(1):20–22, 2005.

heart-hand syndrome. All individuals have an abnormal carpal bone. Cardiac conduction disease is also common.

**Synonyms.** HOS has also been called heart-hand syndrome.

**Incidence.** Incidence is estimated at 1 in 100,000 live births.

**Etiology.** The *TBX5* gene encodes for a T-box transcription factor important in cardiogenesis and limb development.

**Genetics.** The majority of affected individuals (70%) have a mutation in *TBX5*. Inheritance is autosomal dominant; 85% of affected individuals have a de novo mutation. Significant phenotypic variability is seen. Penetrance is complete for upper limb anomalies.

**Recurrence Risk.** Recurrence risk is 50% if one parent is affected. It is low risk if there has been a prior de novo mutation.

**Diagnosis.** Congenital heart defects are present in 75% of individuals with HOS. The cardiac lesions include ASDs (30-60%) and

VSDs, patent ductus arteriosus, endocardial cushion defect, hypoplasia of the left ventricle, and conduction disturbances (atrioventricular block that usually presents as first-degree heart block but can progress to complete heart block  $\pm$  atrial fibrillation). Radial ray aplasia can vary from a difficult to diagnose triphalangeal thumb to a more obvious clubhand to absence of the thumb.

**Differential Diagnosis.** The differential diagnosis includes other disorders with radial ray aplasia, such as Duane-radial ray syndrome, Townes-Brocks syndrome, TAR syndrome, FA, VACTERL association, and other heart-hand syndromes.

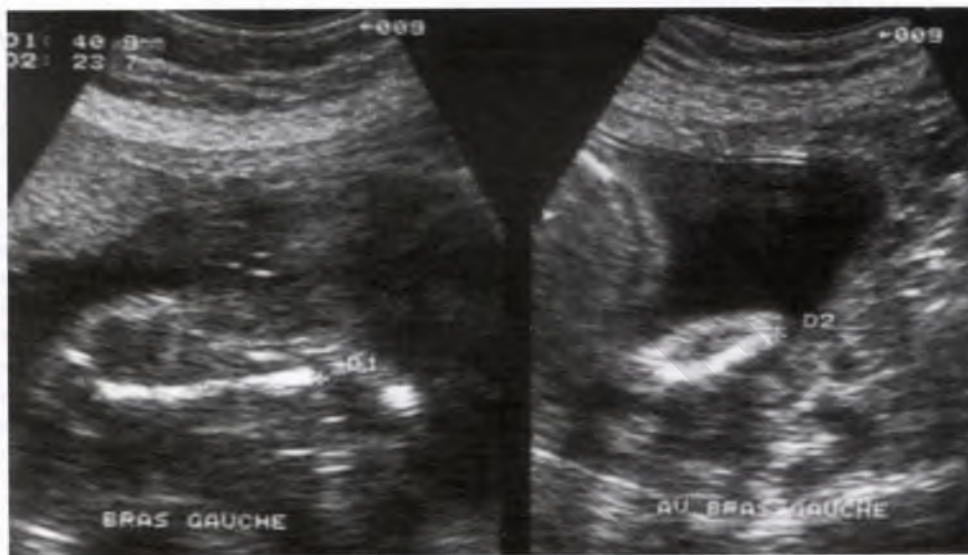


**FIG 16-51** Holt-Oram syndrome. Scan of the right forearm at 22 weeks' gestation. The scan showed an isolated ulna with clubbed arm. (Courtesy of Fabrice Cullier, 2003. Available at thefetus.net.)



**FIG 16-52** Scan of the left forearm at 24 weeks' gestation. The scan showed the ulna alone. (Courtesy of Fabrice Cullier, 2003. Available at thefetus.net.)



**FIG 16-53** Profile of the left forearm of the fetus at 24 weeks' gestation. The thumb is in the same plane as the fingers and is triphalangeal. (Courtesy of Fabrice Cullier, 2003. Available at thefetus.net.)



**Prognosis.** Outcome is mainly related to the severity of the cardiac and orthopedic disability. Cardiac conduction disease can be progressive, and electrocardiogram should be performed at least annually.

## REFERENCES

- Bonnet D, Terrett J, Pequignot-Viegas E, et al: [Gene localisation in 12q12 in Holt-Oram atrio-digital syndrome]. *Arch Malad Coeur Vaiss* 88(5):661–666, 1995.
- Brons JT, van Geijn HP, Wladimiroff JW, et al: Prenatal ultrasound diagnosis of the Holt-Oram syndrome. *Prenat Diagn* 8(3):175–181, 1988.
- Campbell CE, Casey G, Goodrich K: Genomic structure of TBX2 indicates conservation with distantly related T-box genes. *Mamm Genome* 9(1):70–73, 1998.
- Li QY, Newbury-Ecob RA, Terrett JA, et al: Holt-Oram syndrome is caused by mutations in TBX5, a member of the Brachyury (T) gene family. *Nat Genet* 15(1):21–29, 1997.

- McDermott DA, Fong JC, Basson CT: Holt-Oram syndrome. In Pagon RA, Adam MP, Ardinger HH, et al, editors: *GeneReviews*, Seattle, 1993–2016, University of Washington.
- Newbury-Ecob RA, Leavage R, Raeburn JA, Young ID: Holt-Oram syndrome: a clinical genetic study. *J Med Genet* 33(4):300–307, 1996.
- Sletten LJ, Pierpont ME: Variation in severity of cardiac disease in Holt-Oram syndrome. *Am J Med Genet* 65(2):128–132, 1996.
- Smith J: Brachyury and the T-box genes. *Curr Opin Genet Dev* 7(4):474–480, 1997.
- Weber M, Wenz W, van Riel A, et al: [The Holt-Oram syndrome. Review of the literature and current orthopedic treatment concepts]. *Z Orthop Ihre Grenzgeb* 135(4):368–375, 1997.
- Wilson GN: Correlated heart/limb anomalies in Mendelian syndromes provide evidence for a cardiomeic developmental field. *Am J Med Genet* 76(4):297–305, 1998.

## Roberts Syndrome

**Definition.** Roberts syndrome is characterized by prenatal growth restriction, microcephaly, cleft lip ± palate, and limb anomalies (bilateral tetrphocomelia or hypomelia) with upper limbs more severely affected than the lower. Other features include hand anomalies (thumb aplasia or hypoplasia, syndactyly, clinodactyly), elbow and knee contractures, and facial dysmorphism (micrognathia, hypertelorism, shallow orbits leading to exophthalmos, beaked nose, ear malformations).

**Synonyms.** Pseudothalidomide syndrome.

**Prevalence.** The prevalence is unknown; this syndrome is rare. Approximately 150 affected individuals have been reported.

**Etiology.** The unique cytogenetic abnormality, called premature centromere separation, which disrupts chromatid pairing, is responsible for the multiple observed structural anomalies. *ESCO2* encodes for a protein that is essential for cohesion at heterochromatic regions.

**Genetics.** Roberts syndrome is due to mutations in *ESCO2*. Cytogenetic testing can confirm the diagnosis. The presence of premature centromere separation is diagnostic. One negative cytogenetic analysis does not exclude the diagnosis. Inheritance is autosomal recessive, and parental consanguinity is common. Wide phenotypic variability is seen.

**Recurrence Risk.** Recurrence risk is 25% if both parents are mutation carriers.

**Diagnosis.** Prenatally, the presence of growth restriction with symmetric bilateral limb anomalies (tetrphocomelia or hypomelia) and facial dysmorphism should prompt consideration of the diagnosis. Other associated anomalies include congenital heart defects, diaphragmatic defects, splenic agenesis, umbilical cord cyst, GI obstruction, renal anomalies, and genitourinary anomalies.

**Differential Diagnosis.** The differential diagnosis should include Baller-Gerold syndrome, FA, TAR syndrome, tetra-amelia syndrome, and HOS.

**Prognosis.** Significant intellectual disability is present in most individuals. Stillbirth is common, and survival beyond infancy is infrequent, although more mildly affected individuals can survive into adulthood. The prognosis depends on the severity of the anomalies present.

## REFERENCES

- Dulnuan DJ, Matsuoka M, Uketa E, et al: Antenatal three-dimensional sonographic features of Roberts syndrome. *Arch Gynecol Obstet* 284(1):241–244, 2011.
- German J: Roberts' syndrome. I. Cytological evidence for a disturbance in chromatid pairing. *Clin Genet* 16(6):441–447, 1979.
- Gordillo M, Vega H, Jabs EW: Roberts syndrome. In Pagon RA, Adam MP, Ardinger HH, et al, editors: *GeneReviews*, Seattle, 1993–2016, University of Washington.
- Jones KL: Roberts-SC: Phocomelia. In Jones KL, editor: *Smith's Recognizable Patterns of Human Malformation*, ed 5, Philadelphia, 1997, WB Saunders, pp 298–299.
- Paladini D, Palmieri S, Lecora M, et al: Prenatal ultrasound diagnosis of Roberts syndrome in a family with negative history. *Ultrasound Obstet Gynecol* 7(3):208–210, 1996.
- Robins DB, Ladda RL, Thieme GA, et al: Prenatal detection of Roberts-SC phocomelia syndrome: report of 2 sibs with characteristic manifestations. *Am J Med Genet* 32(3):390–394, 1989.
- Stioui S, Privitiera O, Brambati B, et al: First-trimester prenatal diagnosis of Roberts syndrome. *Prenat Diagn* 12(2):145–149, 1992.

## Thrombocytopenia–Absent Radius Syndrome

**Definition.** TAR syndrome is characterized by bilateral absence of the radii with both thumbs present and thrombocytopenia. The thrombocytopenia is transient and may be present at birth or develop in the first few weeks of life. Other features include other skeletal anomalies, congenital heart defects, and genitourinary anomalies. Thumbs are generally normal size but may be wider and flatter than usual and have limited function.

**Synonyms.** TAR syndrome is also known as radial aplasia thrombocytopenia syndrome.

**Prevalence.** Prevalence is estimated at 1 in 100,000 to 200,000.

**Etiology.** The *RBM8A* gene encodes for RNA-binding protein 8A, and its deficiency is thought to lead to tissue-specific developmental consequences.

**Genetics.** TAR syndrome is due to deletion of an at least 200-kb region at chromosome 1q21.1, involving at least 12 known genes. Deletion of the gene *RBM8A* may be largely responsible for the phenotype. Inheritance is autosomal recessive, and, most commonly, individuals have compound heterozygosity of *RBM8A* pathogenic variants (one *RBM8A* hypomorphic mutation and a null mutation due to 1q21.1 deletion). The deletion occurs de novo in 25% to 50% of affected individuals.

**Recurrence Risk.** Recurrence risk is 25% if both parents are found to be mutation carriers.

**Diagnosis.** The diagnosis is based on clinical features, specifically absence of the bilateral radii with normal thumbs with thrombocytopenia (generally present in the first few weeks of life). Prenatally, absent radii may be observed as early as the late first trimester.

**Differential Diagnosis.** The differential diagnosis should include HOS, Roberts syndrome, FA, Duane-radial ray syndrome, VACTERL, and Townes-Brocks syndrome.

**Prognosis.** Although thrombocytopenia is generally transient, it can lead to life-threatening bleeding. Cow milk allergy is common and

can exacerbate the thrombocytopenia. Orthopedic intervention is needed to maximize limb function.

## REFERENCES

- Azemi M, Kolgeci S, Grajcevi-Uka V, et al: Thrombocytopenia absent radius (TAR) syndrome. *Med Arh* 65(3):178–181, 2011.
- Toriello HV: Thrombocytopenia absent radius syndrome. In Pagon RA, Adam MP, Ardinger HH, et al, editors: *GeneReviews*, Seattle, 1993–2016, University of Washington.

## Townes-Brocks Syndrome

**Definition.** Townes-Brocks syndrome (TBS) is characterized by the triad of imperforate anus, dysplastic ears (preauricular tags, microtia, overfolded superior helices), and thumb anomalies (preaxial polydactyly, triphalangeal or hypoplastic thumbs). Other features include impaired renal function (with or without renal malformations), eye anomalies, hearing loss, congenital heart disease, foot malformations, and genitourinary malformations.

**Prevalence.** Prevalence is estimated at 1 in 250,000; these numbers are complicated by significant overlap with VACTERL.

**Genetics.** TBS is due to mutations in *SALL1*. Inheritance is autosomal dominant. Approximately 50% of affected individuals have de novo mutations. Phenotype can be highly variable.

**Recurrence Risk.** Recurrence risk is 50% if one of the parents is affected.

**Diagnosis.** The diagnosis is made clinically based on the presence of imperforate anus (84%), dysplastic ears (87%), and typical thumb malformations with normal radius (89%). Only 67% of affected

patients have all three features of the classic triad. Prenatally, thumb anomalies may be detected; imperforate anus and ear anomalies are more challenging to detect.

**Differential Diagnosis.** The differential diagnosis should include hemifacial microsomia, Duane-radial ray syndrome, and VACTERL association.

**Prognosis.** Immediate surgical intervention is needed for imperforate anus. Orthopedic surgery may be required for thumb anomalies. Renal impairment and hearing loss can both be severe. Intellectual disability is present in 10% of cases.

## REFERENCES

- Kohlhase J: Townes-Brocks syndrome. In Pagon RA, Adam MP, Ardinger HH, et al, editors: *GeneReviews*, Seattle, 1993–2016, University of Washington.
- Miller EM, Hopkin R, Bao L, Ware SM: Implications for genotype-phenotype predictions in Townes-Brocks syndrome: case report of a novel *SALL1* deletion and review of the literature. *Am J Med Genet A* 158A(3):533–540, 2012.

## Lower Extremity Anomalies

If a unilateral leg anomaly is noted, usually other abnormalities are not present. If there are bilateral symmetric anomalies of the lower extremities, skeletal dysplasias should be considered. A few other syndromes leading to prominent lower extremity anomalies exist, including femoral hypoplasia–unusual facies syndrome and sirenomelia. Both are associated with maternal diabetes.

## Femoral Hypoplasia–Unusual Facies Syndrome

**Definition.** Femoral hypoplasia–unusual facies syndrome (FHUFS) is characterized by femoral hypoplasia (or aplasia) and facial dysmorphisms including micrognathia, cleft palate, hypertelorism, long philtrum, and low-set ears. Other associated features include skeletal, renal, neural, and genital anomalies.

**Synonym.** FHUFS is also called femoral-facial syndrome.

**Prevalence.** FHUFS is rare; it is described more often in females.

**Genetics.** Genetics are unknown; most reported cases are sporadic.

**Recurrence Risk.** Recurrence risk is unknown, but low. FHUFS is strongly associated with maternal diabetes.

**Diagnosis.** Prenatally, short femurs and other skeletal anomalies can be observed as early as the early second trimester, although prenatal detection can be difficult.

**Differential Diagnosis.** The differential diagnosis includes other syndromes with femoral hypoplasia, including caudal regression syndrome and campomelic dysplasia.

## REFERENCES

- Figuerola C, Plasencia W, Eguiluz I, et al: Prenatal diagnosis and tridimensional ultrasound features of bilateral femoral hypoplasia–unusual facies syndrome. *J Matern Fetal Neonatal Med* 22(10):936–939, 2009.
- Nowaczyk MJ, Huggins MJ, Fleming A, Mohide PT: Femoral-facial syndrome: prenatal diagnosis and clinical features. Report of three cases. *Am J Med Genet A* 152A(8):2029–2033, 2010.
- Silvas E, Rypens F, Jovanovic M, et al: Prenatal diagnosis of femoral-facial syndrome: report of two cases. *Birth Defects Res A Clin Mol Teratol* 97(12):770–773, 2013.

## Sirenomelia

**Definition.** Sirenomelia is characterized by fusion of the lower extremities and is associated with renal agenesis, absence of the sacrum, rectum, and bladder. Renal agenesis leads to oligohydramnios with

resultant Potter sequence. Other features include spinal column defects, upper limb anomalies, congenital heart defects, and CNS anomalies. It was previously thought to represent a severe form of caudal regression syndrome, but is now considered to be a separate entity.



**Synonyms.** Sirenomelia is also known as mermaid syndrome.

**Prevalence.** Prevalence is estimated at 0.98 per 100,000. Ten to fifteen percent of cases are seen in twin births.

**Etiology.** Sirenomelia is thought to be caused by an alteration in early vascular development leading to “vitelline arterial steal,” in which blood flow is diverted from the caudal region of the embryo to the placenta, resulting in multiple defects of the lower extremities.

**Genetics.** Genetics are unknown; the syndrome is thought to be sporadic.

**Recurrence Risk.** Recurrence risk is unknown, but low.

**Diagnosis.** The diagnosis of sirenomelia is based on the presence of fusion of the lower extremities associated with other skeletal and lumbar spine deformities, bilateral renal agenesis (leading to severe oligohydramnios and pulmonary hypoplasia), and heart and abdominal wall defects. The defect varies from simple cutaneous fusion of the limbs to absence of all long bones but one femur. The defect of the feet is proportional with the defect of the long bones. Because the legs are fused, the rotation of the legs does not occur and they remain in their fetal position.

**Differential Diagnosis.** Caudal regression syndrome is the main consideration in the differential diagnosis, and it usually presents with milder deformities compared to sirenomelia and normal amniotic fluid volume.

**Prognosis.** Sirenomelia is a lethal condition owing to renal agenesis and its complications. Exceptional cases that lack renal agenesis may survive.



**FIG 16-54** Sirenomelia. The fused lower extremity and the flipper-like deformity of the foot are characteristic of sirenomelia.

## REFERENCES

Benacerraf BR: Caudal regression syndrome and sirenomelia. In Benacerraf BR, editor: *Ultrasound of Fetal Syndromes*, New York, 1998, Churchill Livingstone, pp 250–254.

Jones KL: Sirenomelia sequence. In Jones KL, editor: *Smith's Recognizable Patterns of Human Malformation*, ed 5, Philadelphia, 1998, WB Saunders, p 634.

Orioli IM, Amar E, Arteaga-Vazquez J, et al: Sirenomelia: an epidemiologic study in a large dataset from the International Clearinghouse of Birth Defects Surveillance and Research, and literature review. *Am J Med Genet C Semin Med Genet* 157C(4):358–373, 2011.

Stevenson RE, Jones KL, Phelan MC, et al: Vascular steal: the pathogenetic mechanism producing sirenomelia and associated defects of the viscera and soft tissues. *Pediatrics* 78(3):451–457, 1986.

## THORAX

### Congenital High Airway Obstruction Syndrome

#### Definition

Congenital high airway obstruction syndrome (CHAOS) is characterized by obstruction of the fetal upper airways and can be partial or complete.

#### Etiology

CHAOS is caused by atresia or stenosis of the larynx or trachea.

#### Pathogenesis

Tracheal atresia is caused by deficient recanalization of the upper airways at 10 weeks' gestation.

#### Incidence

Incidence is unknown.

#### Diagnosis

Prenatally, bilaterally enlarged hyperechoic lungs, dilated airways, and flattened or inverted diaphragm can be seen. The enlarged lungs

compress the fetal heart, causing it to be displaced centrally and become small and dysfunctional. This can lead to fetal ascites and nonimmune hydrops.

#### Genetics

CHAOS is mostly sporadic, although some genetic syndromes are associated.

#### Recurrence Risk

Recurrence risk depends on association with other possible syndromes (see later discussion).

#### Differential Diagnosis

CHAOS is sometimes misdiagnosed as a bilateral congenital cystic adenomatoid malformation (CCAM). It should also be differentiated from extrinsic causes of tracheolaryngeal obstruction, such as cervical teratoma, vascular rings, and lymphatic malformations.

#### Prognosis

The disorder in general is incompatible with life if unrecognized during the prenatal period.

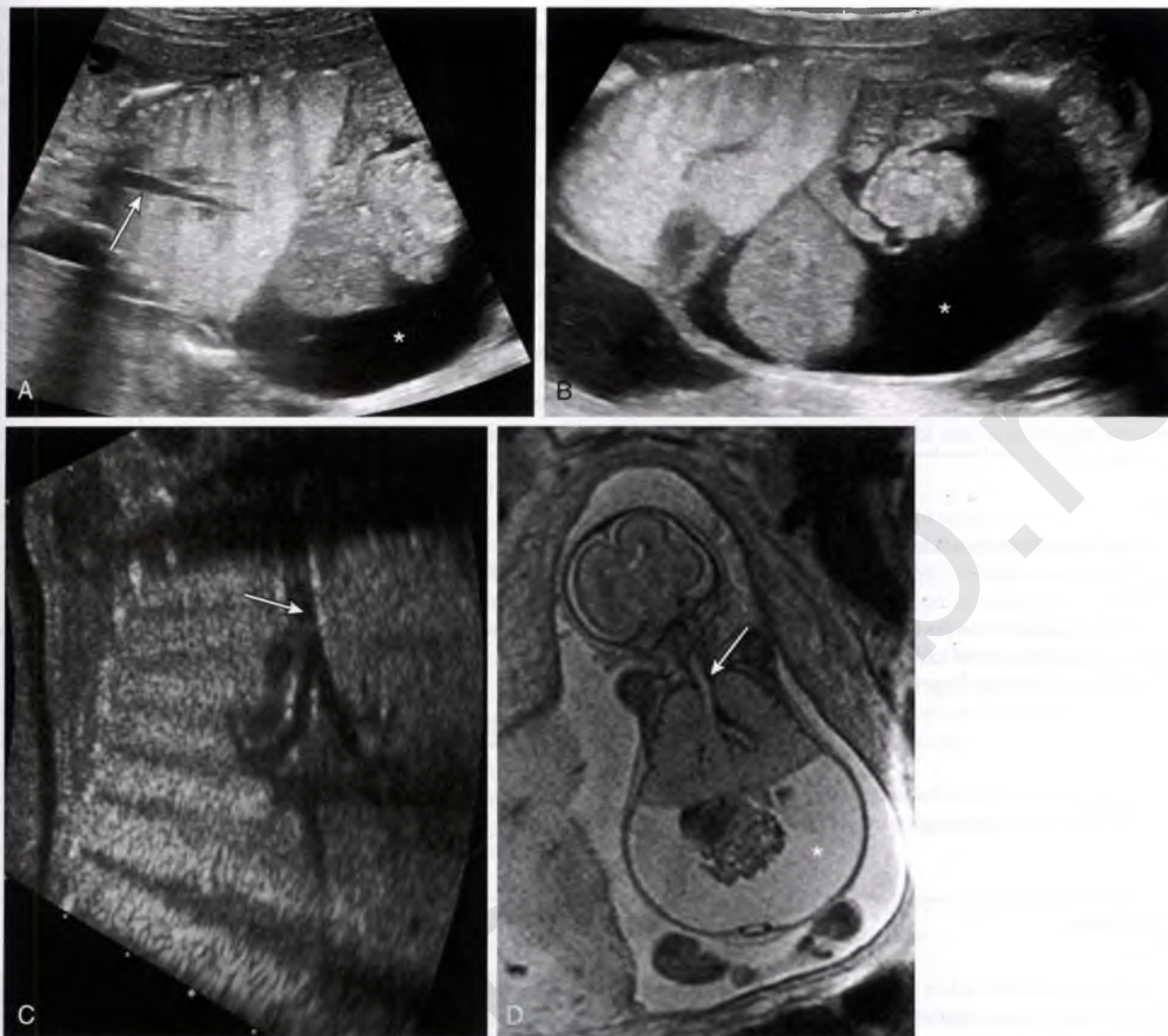


**FIG 16-55** Congenital high airway obstruction syndrome (CHAOS). Coronal (**A** and **C**) and sagittal (**B**) images demonstrate dilated fluid-filled trachea (*arrow*), enlarged hyperechoic bilateral lungs, and hydrops with ascites (*asterisk*). **D**, Coronal magnetic resonance image demonstrates the same findings of a dilated trachea (*arrow*) and ascites (*asterisk*).

### Management

If CHAOS is diagnosed prior to delivery, incomplete obstruction is present, and fetal hydrops has not occurred, an EXIT (ex utero intrapartum treatment) procedure (to establish a fetal airway prior to cessation of fetomaternal circulation) can be performed for delivery.

### Associated Syndromes

CHAOS can occur as part of Fraser syndrome, cri du chat syndrome (5p deletion), short rib–polydactyly syndrome, and 22q11.2 deletion syndrome.

### REFERENCES

- Artunc Ulkumen B, Pala HG, Nese N, et al: Prenatal diagnosis of congenital high airway obstruction syndrome: report of two cases and brief review of the literature. *Case Rep Obstet Gynecol* 2013;728974, 2013.
- Hamid-Sowinska A, Ropacka-Lesiak M, Breborowicz GH: Congenital high airway obstruction syndrome. *Neuro Endocrinol Lett* 32(5):623–626, 2011.



### Cornelia de Lange Syndrome

CdLS is discussed in detail under “Upper Extremities.” It is a rare cause of CDH; 1% to 8% of patients with CdLS have a CDH.

### Donnai-Barrow Syndrome

#### Definition

Donnai-Barrow syndrome is characterized by distinct facial features (hypertelorism, widow’s peak, depressed nasal bridge, posteriorly rotated ears, enlarged fontanelle), ocular findings (myopia, vision loss, iris coloboma, retinal detachment), sensorineural hearing loss, corpus callosum agenesis, CDH (50%), and omphalocele (50%). CDH and omphalocele occur together in one third of cases.

#### Synonym

Donnai-Barrow syndrome is also known as faciooculoacousticorenal (FOAR) syndrome.

#### Incidence

Incidence is unknown; mutant alleles of *LRP2* are thought to be rare.

#### Pathogenesis

The gene, *LRP2*, encodes for the protein megalin. When megalin function is abnormal, proximal renal tubule reuptake of megalin ligands is prevented, leading to excess spillage of low-molecular-weight proteins in the urine.

#### Diagnosis

Diagnosis is based on the clinical features described previously, as well as a distinctive low-molecular-weight proteinuria.

### Genetics

Donnai-Barrow syndrome is due to mutations in the gene *LRP2*. Phenotypic variability even within families is observed. Inheritance is autosomal recessive.

### Recurrence Risk

Recurrence risk is 25% if both parents are mutation carriers.

### Differential Diagnosis

Other conditions with similar features include Pallister-Killian syndrome, Fryns syndrome, acrocallosal syndrome, and craniofrontonasal syndrome.

### Prognosis

Perinatal death is common owing to congenital malformations. Progressive vision loss is common. All individuals have sensorineural hearing loss. Intellectual disability is mild to moderate. Seizures often develop.

### Management

Management includes surgical repair of CDH and omphalocele, treatment of vision and hearing loss, and medical treatment of seizures.

### REFERENCE

Kantarci S, Donnai D, Noonan KM, Pober BR: Donnai-Barrow syndrome. In Pagon RA, Adam MP, Ardinger HH, et al, editors: *GeneReviews*, Seattle, 1993–2016, University of Washington.

### Fryns Syndrome

#### Definition

Fryns syndrome is characterized by diaphragmatic defects (diaphragmatic hernia), facial dysmorphism (hypertelorism, broad/flat nasal bridge, long philtrum, low-set ears, tented upper lip, macrostomia, micrognathia), distal digital nail hypoplasia, and pulmonary hypoplasia. Other anomalies include ocular findings (cloudy corneas, microphthalmia), orofacial clefting, and renal dysplasia.

#### Incidence

Incidence is estimated at 7 per 100,000 live births in France, and 1% to 10% of patients with CDH.

#### Genetics

No specific gene has been implicated. Inheritance is autosomal recessive.

#### Recurrence Risk

Recurrence risk is 25%.

#### Diagnosis

Diagnosis is based on the clinical findings described earlier. The phenotypic variability makes sonographic diagnosis a challenge. Prenatally, CDH and facial dysmorphism may be seen. Development of polyhydramnios late in the second trimester and normal growth or overgrowth of the fetus are also expected.



**FIG 16-56** Axial sonographic image through the chest in fetus with left congenital diaphragmatic hernia. Fluid-filled stomach (S), bowel (B) and portion of the liver (L) are shown on the left, with displacement of the heart (H) toward the right. It is estimated that 1% to 10% of fetuses with congenital diaphragmatic hernia have Fryns syndrome.

### Differential Diagnosis

The differential diagnosis includes chromosomal disorders, Pallister-Killian syndrome (mosaic tetrasomy 12p), Donnai-Barrow syndrome, Zellweger syndrome (deficiency of peroxisomal enzyme), Matthew-Wood syndrome, and CdLS.

### Associated Anomalies

Other anomalies include those of the skeletal, cardiac, central nervous, GI, and genitourinary systems.

### Prognosis

The majority of affected infants are stillborn or die in early neonatal period. Severe intellectual and developmental delay is often reported in those who survive.

## Pallister-Killian Syndrome

### Definition

Pallister-Killian syndrome is characterized by CDH, craniofacial dysmorphism (brachycephaly, high broad forehead, hypertelorism, low-set ears, broad nasal bridge, anteverted nares, long philtrum), short neck, short and broad hands, streaks of skin hyperpigmentation, and CNS anomalies. Seizures are common in infancy.

### Synonyms

Pallister-Killian syndrome is also known as tetrasomy 12p and Teschler-Nicola/Killian syndrome.

### Incidence

Human autosomal tetrasomies are rare. Among them, tetrasomy 12p is undoubtedly the most common.



**FIG 16-57** Pallister-Killian syndrome. Postmortem examination demonstrates a flat facial appearance with dysmorphic, low-set ears. (Courtesy of Fabrice Cuillier, 2003. Available at thefetus.net.)

## REFERENCES

- Ayme S, Julian C, Gambarelli D, et al: Fryns syndrome: report on 8 new cases. *Clin Genet* 35(3):191–201, 1989.
- Barthe B, Cohen H, Saada P: [Prenatal diagnosis of a case of Fryns' syndrome]. *J Gynecol Obstet Biol Reprod* 24(1):57–62, 1995.
- Fryns JP: Prenatal diagnosis and long survival of Fryns syndrome. *Prenat Diagn* 15(1):97–98, 1995.
- Gadow EC, Lippold S, Serafin E, et al: Prenatal diagnosis and long survival of Fryns' syndrome. *Prenat Diagn* 14(8):673–676, 1994.
- Ramsing M, Gillissen-Kaesbach G, Holzgreve W, et al: Variability in the phenotypic expression of Fryns syndrome: a report of two sibships. *Am J Med Genet* 95(5):415–424, 2000.
- Slavotinek A: Fryns syndrome. In Pagon RA, Adam MP, Ardinger HH, et al, editors: *GeneReviews*, Seattle, 1993–2016, University of Washington.

### Genetics

Pallister-Killian syndrome is due to tissue-specific mosaic distribution of a supernumerary isochromosome that consists of two copies of the short arm of chromosome 12, 12p. The chromosomal abnormality is observed in either a mosaic or a nonmosaic state for specific tissues, such as bone marrow and skin fibroblasts. The additional isochromosome 12p is readily seen in skin fibroblasts and is detectable in amniotic fluid and chorionic villi. Testing of peripheral blood lymphocytes is generally negative so the diagnosis can be missed. This syndrome is associated with advanced maternal age.

### Recurrence Risk

Recurrence risk is low; cases are sporadic.

### Etiology

Pallister-Killian syndrome is caused by maternal premeiotic or meiotic error with centromere misdivision.

### Diagnosis

The most common prenatal findings include CDH, short limbs, CNS anomalies and ventriculomegaly, craniofacial dysmorphism, increased nuchal translucency, fetal hydrops, and polyhydramnios. Fetal growth is generally normal. Postnatal growth deceleration is commonly seen. The diagnosis can be confirmed by amniocentesis or chorionic villus sampling. Postnatal diagnosis is challenging given tissue mosaicism and the lack of isochromosome 12p in the peripheral blood.

### Differential Diagnosis

Other diagnoses to consider include chromosomal disorders, Fryns syndrome, chondrodysplasia of Robinow, acrocallosal syndrome, and VATER (vertebrae, anal atresia, tracheoesophageal fistula, renal or kidney anomalies) association.

### Associated Anomalies

A wide range of other anomalies can be seen including those involving the cardiac, musculoskeletal, GI, genitourinary, and cutaneous systems.

### Prognosis

The prognosis is generally poor, but more mild cases have been reported. Less severely affected individuals have severe intellectual disability, seizures, and developmental delay. Hearing loss is also common. Vertebral and joint deformities are often present, and older individuals have muscular atrophy.



## REFERENCES

- Chiesa J, Hoffer M, Rousseau O, et al: Pallister-Killian syndrome [i(12p)]: first pre-natal diagnosis using cordocentesis in the second trimester confirmed by in situ hybridization. *Clin Genet* 54(4):294–302, 1998.
- Gilgenkrantz S, Droulle P, Schweitzer M, et al: Mosaic tetrasomy 12p. *Clin Genet* 28(6):495–502, 1985.
- Langford K, Hodgson S, Seller M, Maxwell D: Pallister-Killian syndrome presenting through nuchal translucency screening for trisomy 21. *Prenat Diagn* 20(8):670–672, 2000.
- Mathieu M, Piussan C, Thepot F, et al: Collaborative study of mosaic tetrasomy 12p or Pallister-Killian syndrome (nineteen fetuses or children). *Ann Genet* 40(1):45–54, 1997.

- Paladini D, Borghese A, Arienzo M, et al: Prospective ultrasound diagnosis of Pallister-Killian syndrome in the second trimester of pregnancy: the importance of the fetal facial profile. *Prenat Diagn* 20(12):996–998, 2000.
- Pober BR, Russell MK, Ackerman KG: Congenital diaphragmatic hernia overview. In Pagon RA, Adam MP, Ardinger HH, et al, editors: *GeneReviews*, Seattle, 1993–2016, University of Washington.
- Wilkins A, Liu H, Park K, et al: Novel clinical manifestations in Pallister-Killian syndrome: comprehensive evaluation of 59 affected individuals and review of previously reported cases. *Am J Med Genet A* 158A(12):3002–3017, 2012.

## Scimitar Syndrome

### Definition

Scimitar syndrome is characterized by right lung hypoplasia and abnormal venous drainage to the inferior vena cava. Cardiac dextro-position and abnormal pulmonary blood supply from the descending aorta are commonly seen. Other congenital heart defects and CDH are also seen.

### Synonym

Scimitar syndrome is also called pulmonary venolobar syndrome.

### Etiology

The partial anomalous pulmonary venous return is due to a connection failure between the right pulmonary veins and the left atrium during fetal development. It is thought to be a developmental disorder of the entire lung bud early in embryogenesis.

### Incidence

Incidence is 2 in 100,000.

### Diagnosis

Scimitar syndrome is a complex form of partially anomalous pulmonary venous return. Classically, the scimitar sign is seen on chest radiograph, referring to a half crescent created by the descent of the anomalous pulmonary vein and is seen adjacent to the junction of the diaphragm and right heart border. The diagnosis can be confirmed by angiography or MRI. Prenatally, the majority of congenital heart defects are detected, but abnormal pulmonary veins are difficult to detect. A fetal echocardiogram by experienced providers allows prenatal detection.

### Genetics

Gene locus for total anomalous pulmonary venous return has been mapped to 4q12, but the genetics specific to scimitar syndrome are not known.

### Recurrence Risk

Recurrence risk is unknown.

### Differential Diagnosis

Other forms of anomalous pulmonary venous return should be considered.

### Associated Anomalies

Other anomalies include bronchogenic cysts, horseshoe lung, accessory diaphragm, and hernias.

### Prognosis

Clinical presentation depends on the shunt volume. The infantile form frequently presents with pulmonary hypertension and is detected based on failure to thrive, respiratory issues, or congestive heart failure. Ultimate prognosis is dependent on the severity of the anomalies.

### Management

Surgical correction is often required, and pulmonary hypertension in infancy is an indication for repair.

## REFERENCES

- Korkmaz AA, Yildiz CE, Onan B, et al: Scimitar syndrome: a complex form of anomalous pulmonary venous return. *J Card Surg* 26(5):529–534, 2011.
- Midyat L, Demir E, Askin M, et al: Eponym. Scimitar syndrome. *Eur J Pediatr* 169(10):1171–1177, 2010.

## HEART

Congenital heart defects are common and prenatal diagnosis should prompt a detailed fetal survey to look for other anomalies and genetic testing should be offered. Septal and valvular defects are the most frequent anomalies. Similar structural defects are linked to more than one genetic locus and variable cardiac lesions can be seen even within families, making diagnosis of possible underlying genetic causes challenging. Chromosomal disorders, including aneuploidies, Turner syndrome, and microdeletion and microduplication syndromes (especially

22q11.2 deletion) should be considered when prenatal cardiac lesions are detected. Many other syndromes caused by single gene defects are also associated with congenital heart defects, some of which are reviewed here.

## REFERENCE

- Nemer M: Genetic insights into normal and abnormal heart development. *Cardiovasc Pathol* 17(1):48–54, 2008.

## 22q11.2 Deletion Syndrome

### Definition

22q11.2 deletion syndrome is characterized by congenital heart disease (74%; conotruncal malformations most common), palate abnormalities (69%; velopharyngeal incompetence, submucosal or overt cleft palate, bifid uvula), characteristic facial features, learning difficulties (70–90%), and immune deficiency (77%). Other findings include hypocalcemia, feeding problems, constipation, structural GI anomalies, and renal anomalies.

### Synonym

Synonyms include DiGeorge syndrome, velocardiofacial syndrome, conotruncal anomaly face syndrome, autosomal dominant Opitz G/BBB syndrome, Sedlackova syndrome, and Cayler cardiofacial syndrome.

### Etiology

Most cases are due to a 3 Mb deletion at chromosome 22q11.2, generally caused by a nonallelic meiotic recombination event during spermatogenesis or oogenesis. This region is flanked by low copy number repeats leading to abnormal interchromosomal exchanges.

### Incidence

Incidence is 1 in 4000 to 1 in 6395 births, although this figure may be an underestimate.

### Diagnosis

Prenatally, the diagnosis is most commonly made because of the presence of a cardiac defect. Conotruncal defects are most common, such as tetralogy of Fallot, interrupted aortic arch, VSD, and truncus

arteriosus. The disorder should be suspected in individuals with the combination of congenital heart disease, palate abnormalities, characteristic facial features, and learning difficulties.

### Genetics

A microdeletion at chromosome 22q11.2 can be detected by fluorescence in situ hybridization, multiplex ligation-dependent probe amplification (MLPA), or chromosomal microarray. Inheritance is autosomal dominant. Approximately 93% of deletions are de novo; 7% have an affected parent. The gene, *TBX1*, found within the deleted region, is thought to be responsible for many of the typical features including cardiac anomalies. Penetrance of the disorder is complete with marked variability in phenotype.

### Recurrence Risk

Recurrence risk is 50% with a known parental mutation.

### Associated Anomalies

Other anomalies include laryngotracheoesophageal anomalies, growth hormone deficiency, autoimmune disorders, seizures, CNS abnormalities, skeletal abnormalities, and ocular abnormalities.

### Differential Diagnosis

Other disorders to consider include SLO syndrome, Alagille syndrome, VATER association, CHARGE syndrome, and Goldenhar syndrome.

### Prognosis

Prognosis depends on the extent of anomalies. Congenital heart defects are the major cause of fatality. Developmental delay and intellectual disability are common. Autism spectrum disorders and schizophrenia

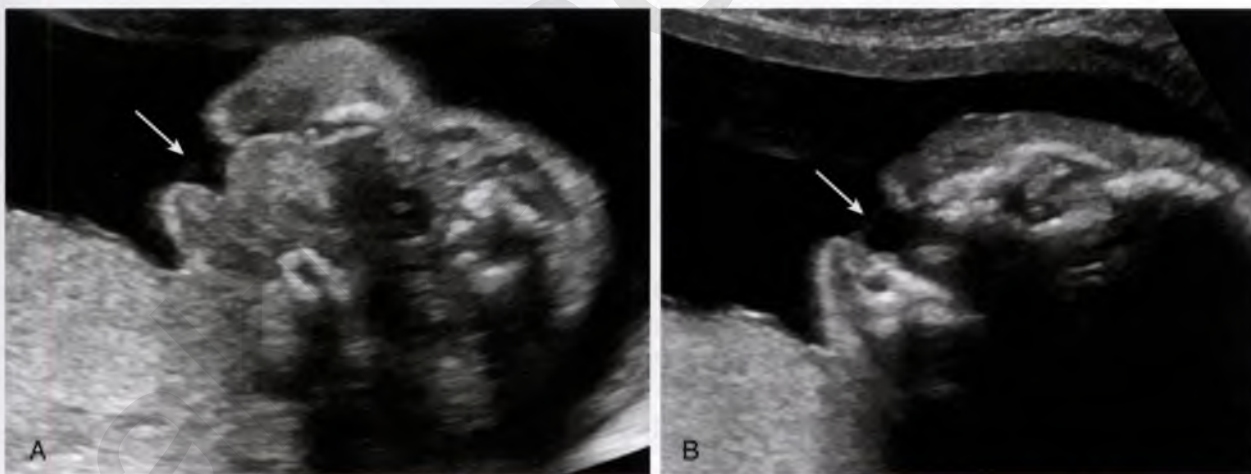


**FIG 16-58** The 22q11.2 deletion syndrome. Unilateral cleft lip (A) and palate (B) in a fetus with congenital heart disease (double outlet right ventricle, not shown).

are frequent (20% and 25%, respectively), and other psychiatric issues are common (such as attention deficit disorder and anxiety).

### Management

Clinical guidelines for affected individuals have been established (Bassett and associates, 2011).

## REFERENCES

- Bassett AS, McDonald-McGinn DM, Devriendt K, et al: Practical guidelines for managing patients with 22q11.2 deletion syndrome. *J Pediatr* 159(2):332–339.e331, 2011.
- Devriendt K, Fryns JP, Mortier G, et al: The annual incidence of DiGeorge/velocardiofacial syndrome. *J Med Genet* 35(9):789–790, 1998.
- McDonald-McGinn DM, Emanuel BS, Zackai EH: 22q11.2 deletion syndrome. In Pagon RA, Adam MP, Ardinger HH, et al, editors: *GeneReviews*, Seattle, 1993–2016, University of Washington.



## Alagille Syndrome

### Definition

Alagille syndrome is characterized by biliary hypoplasia (manifesting as neonatal cholestasis), cardiovascular anomalies (most commonly pulmonary artery stenosis), vertebral abnormalities (butterfly vertebrae), characteristic facies (broad forehead, pointed mandible, bulbous nose tip), and ocular anomalies (posterior embryotoxon).

### Synonyms

Synonyms include Alagille-Watson syndrome, cholestasis with peripheral pulmonary stenosis, arteriohepatic dysplasia, hepatic ductular hypoplasia, and jagged 1 syndrome.

### Incidence

Incidence is 1 in 30,000 to 1 in 50,000 live births. The disorder likely remains underdiagnosed.

### Etiology

This multisystem autosomal dominant disorder has variable penetrance.

### Genetics

Alagille syndrome is due to mutations in *JAG1* (89%) or *NOTCH2* (1-2%). The phenotype is extremely variable even within the same family. Inheritance is autosomal dominant. Approximately 50% to 70% of mutations are de novo, and 30% to 50% are inherited.

### Recurrence Risk

Recurrence risk is 50% with known parental mutation. If a de novo mutation is present in another child, recurrence risk is low but slightly increased from germline mosaicism.

### Diagnosis

The diagnosis is based on clinical features including bile duct paucity, cholestasis, cardiac defect (most commonly peripheral pulmonary artery stenosis), skeletal abnormalities, ocular abnormalities, and characteristic facial features. Other significant anomalies include those of the kidney, neurovasculature, and pancreas. Prenatally, facial dysmorphism, cardiac anomalies, skeletal anomalies, and growth restriction may be seen.

### Differential Diagnosis

Other disorders to consider include other causes of neonatal cholestasis, disorders of intrahepatic cholestasis (Byler syndrome, Aagenaes syndrome), and other syndromes with pulmonary vascular system anomalies (chromosomal disorders, Noonan syndrome, Watson syndrome).  $\alpha_1$ -Antitrypsin deficiency may present as neonatal cholestasis with a paucity of intrahepatic bile ducts.

### Prognosis

Mortality rate is 10% as a result of cardiac disease, liver disease, and vascular accidents. Vascular accidents are a result of vascular anomalies such as basilar artery aneurysms, internal carotid artery anomalies, middle cerebral artery aneurysm, aortic aneurysms and coarctations, and internal carotid artery anomalies.

### Management

This disorder should be suspected in all infants with cholestasis. Given the multisystem involvement, multidisciplinary care is needed.



**FIG 16-59** Alagille syndrome. Enlarged main pulmonary artery (arrow). (Courtesy Francis Duchatel, 2002. Available at thefetus.net.)



**FIG 16-60** Alagille syndrome. Thickened and stenotic pulmonary valve. (Courtesy Francis Duchatel, 2002. Available at thefetus.net.)

## REFERENCES

- Albayram F, Stone K, Nagey D, et al: Alagille syndrome: prenatal diagnosis and pregnancy outcome. *Fetal Diagn Ther* 17(3):182-184, 2002.
- Gauthier F, Hadchouel M: [Congenital disorders of the biliary ducts]. *Revue Prat* 50(19):2142-2145, 2000.
- Harendza S, Hubner CA, Glaser C, et al: Renal failure and hypertension in Alagille syndrome with a novel *JAG1* mutation. *J Nephrol* 18(3):312-317, 2005.
- Ho NC, Lacbawan F, Francomano CA, Ho V: Severe hypodontia and oral xanthomas in Alagille syndrome. *Am J Med Genet* 93(3):250-252, 2000.
- Kamath BM, Spinner NB, Emerick KM, et al: Vascular anomalies in Alagille syndrome: a significant cause of morbidity and mortality. *Circulation* 109(11):1354-1358, 2004.

Lykavieris P, Hadchouel M, Chardot C, Bernard O: Outcome of liver disease in children with Alagille syndrome: a study of 163 patients. *Gut* 49(3):431–435, 2001.

Martin SR, Garel L, Alvarez F: Alagille's syndrome associated with cystic renal disease. *Arch Dis Child* 74(3):232–235, 1996.

Spinner NB, Leonard LD, Krantz ID: Alagille syndrome. In Pagon RA, Adam MP, Ardinger HH, et al, editors: *GeneReviews*, Seattle, 1993–2016, University of Washington.

## CHARGE Syndrome

### Definition

**CHARGE** is a mnemonic for a syndrome characterized by coloboma of the eye, heart defects, atresia of the choanae, retarded mental and growth development, genital anomalies, and ear anomalies with or without deafness.

### Incidence

Incidence is 1 in 8500 to 1 in 10,000 births.

### Genetics

CHARGE syndrome is due to mutations in *CHD7*, which encodes the chromodomain helicase DNA binding protein. Mutations are found in 65% to 70% of patients with clinical features of CHARGE. Not finding a mutation does *not* rule out CHARGE syndrome. Inheritance is autosomal dominant. Penetrance in those with *CHD7* mutations is 100%.

### Recurrence Risk

Most cases are the only cases reported within a family. The empiric recurrence risk is 1% to 2%. If one of the parents has CHARGE or a known *CHD7* mutation, the recurrence risk is 50%.

**TABLE 16-5 Major Characteristics of CHARGE\***

Finding	Includes	Frequency
Coloboma of the eye	Coloboma of the iris, retina, choroids, disc, not including colobomas of the eyelid; microphthalmos (small eyes) or cryptophthalmos (absent eye)	80-90%
Choanal atresia or stenosis	Unilateral or bilateral, bony or membranous; unilateral atresia or stenosis may be difficult to diagnose	50-60%
Cranial nerve dysfunction or anomaly	I: Lack of smell (anosmia) IX/X: Swallowing difficulties VII: Facial palsy (unilateral or bilateral)	Frequent 70-90% 40%
Characteristic CHARGE ear	Short, wide ear with little or no lobe, "snipped off" helix, prominent antihelix that is discontinuous with the tragus, triangular concha, decreased cartilage, often stick out, usually asymmetric Middle ear: ossicular malformations seen on MRI Malformed inner ear (Mondini defect) with deformed cochlea and vestibules seen on MRI	Frequent Frequent 80-90%

MRI, magnetic resonance imaging scan.

\*These are very common in CHARGE and relatively rare in other conditions.

Reproduced with permission from the Charge Syndrome Foundation, available at <http://www.chargesyndrome.org/index.asp>.

### Pathogenesis

*CHD7* is essential for the formation of multipotent migratory neural crest cells that differentiate into different tissues including craniofacial and heart structures, and it regulates genes involved in neural crest cell guidance. *CHD7* mutations are thought to disrupt this process leading to features of the CHARGE syndrome.

### Diagnosis

The diagnosis is based on several associated malformations including colobomas (iris, retina-choroid, disk), choanal atresia/stenosis, cranial nerve dysfunction (anosmia, facial palsy, impaired hearing, swallowing problems), abnormal outer ears, hypogonadotropic hypogonadism, developmental delay, cardiovascular malformations (including conotruncal anomalies, atrioventricular canal defects, and aortic arch anomalies), growth deficiency, orofacial clefts, and tracheoesophageal fistula (see Table 16-5). Specific anomalies seen on temporal bone imaging (hypoplastic semicircular canals) can assist with the diagnosis. The diagnosis may be suspected prenatally from the presence of major anomalies that fit the CHARGE criteria; however, in many cases a cardiac defect is the only anomaly detected prenatally.

### Differential Diagnosis

Other disorders to consider include 22q11.2 deletion syndrome, VACTERL association, Kabuki syndrome, renal coloboma syndrome (*PAX2* mutations), cat-eye syndrome, Joubert syndrome, branchio-oto-renal syndrome, and retinoic embryopathy.

### Prognosis

Mortality rate in the first 2 years of life is 20% to 25%. Choanal atresia is a threat to life because young infants cannot establish the habit of mouth breathing. Feeding difficulties are common. Both hearing and vision loss are frequent. Motor development is often markedly delayed. Prognosis is dependent on the severity of the associated malformations.

### Management

Because of the multiple complex malformations, clinical management requires coordinated multidisciplinary care.

## REFERENCES

- Cyran SE, Martinez R, Daniels S, et al: Spectrum of congenital heart disease in CHARGE association. *J Pediatr* 110(4):576–578, 1987.
- Hall BD: Choanal atresia and associated multiple anomalies. *J Pediatr* 95(3):395–398, 1979.
- Koletzko B, Majewski F: Congenital anomalies in patients with choanal atresia: CHARGE-association. *Eur J Pediatr* 142(4):271–275, 1984.
- Lalani SR, Hefner MA, Belmont JW, Davenport SLH: CHARGE syndrome. In Pagon RA, Adam MP, Ardinger HH, et al, editors: *GeneReviews*, Seattle, 1993–2016, University of Washington.
- Schulz Y, Wehner P, Opitz L, et al: *CHD7*, the gene mutated in CHARGE syndrome, regulates genes involved in neural crest cell guidance. *Hum Genet* 133(8):997–1009, 2014.
- Tellier AL, Cormier-Daire V, Abadie V, et al: CHARGE syndrome: report of 47 cases and review. *Am J Med Genet* 76(5):402–409, 1998.



## Heterotaxy Syndromes

### Definition

This set of syndromes is due to errors of lateralization of the primary field. This leads to either a fetus with a predominant right-sidedness and an isomeric left side (asplenia: a fetus whose left side is a mirror image of its right side) or left-sidedness and an isomeric right side (polysplenia: a fetus whose right side is a mirror image of its left side). These fetuses are usually recognized because of the associated cardiac anomalies.

### Synonym

Heterotaxy syndromes include Ivemark syndrome, cardioplenic syndrome, and asplenia-polysplenia syndrome

### Incidence

The incidence is very low, estimated at 1 in 10,000 to 20,000 live births.

### Etiology

The cause of most laterality defects remains unknown. A small proportion can be explained by a monogenic cause, including the subset related to primary ciliary dyskinesia.

### Genetics

More than 80 genes are required for visceral asymmetry, including the genes *DNAH5* and *DNAI1*. A subset of individuals with heterotaxy have primary ciliary dyskinesia (PCD); at least 6% of individuals with PCD have heterotaxy. Most PCD is inherited in an autosomal recessive manner. The inheritance of heterotaxy in general most often

demonstrates autosomal recessive inheritance; autosomal dominant and X-linked inheritance has also been reported.

### Diagnosis

Prenatally, the diagnosis is usually made by the recognition of the cardiac anomalies, in particular, the presence of atrioventricular septal defect, mesocardia (the axis of the interventricular septum being almost anteroposterior) with an endocardial cushion defect, an intrahepatic segment of the umbilical vein that is also oriented anteroposteriorly, and an odd-looking stomach. The abnormal lobation of the lungs is difficult to recognize and is generally only recognized when a sliver of pleural fluid is infiltrated between the lobes. Another typical finding is the interruption of the inferior vena cava with azygos continuation. This includes an inferior vena cava that is posterior in the upper abdomen (instead of curving anteriorly to enter the right atrium) and the abrupt decrease in size of the inferior vena cava near the diaphragm. An enlarged azygos arch joining the superior vena cava can also be recognized. Doppler study of the splenic artery has been suggested as an aid in diagnosis. Other findings include agenesis of the corpus callosum with pachygyria and hydrocephalus.

### Differential Diagnosis

Other conditions including cardiac anomalies should be considered including trisomy 18.

### Associated Anomalies

Associated defects include CNS anomalies, cleft lip  $\pm$  palate, GI anomalies, and diaphragmatic hernia (Table 16-6).

TABLE 16-6 Major Defects Seen in Cases With Laterality Defects

	All Laterality Defects (n = 517)		Heterotaxy (n = 378)		Situs Inversus Totalis (n = 139)		Fisher's Exact Test, Two-sided P value <sup>a</sup>
		%		%		%	
<b>Congenital heart defects, total cases</b>	425	82.2	365	96.6	60	43.2	0.001
<i>Single ventricle, total</i>	61	11.58	53	14.0	8	5.8	
DIRV, DILV	25	4.8	22	5.8	3	2.2	
Single ventricle indeterminate, unspecified	36	7.0	31	8.2	5	3.6	
<i>Conotruncal</i>	204	39.5	179	47.4	25	18.0	
Truncus arteriosus	4	0.8	4	1.1	0	0	
TOF	20	3.9	16	4.2	4	2.9	
d-loop TGA (includes TGA with VSD)	72	13.9	62	16.4	10	7.2	
Double outlet right ventricle	108	20.9	97	25.7	11	7.9	0.001
<i>l-loop TGA, not single ventricle</i>	36	7.0	26	6.9	10	7.2	
<i>AVCD (AVSD), complete</i>	190	36.8	183	48.4	7	5.0	0.001
<i>Left-sided obstructive defects</i>	26	5.0	22	6.3	2	1.4	
Aortic stenosis	10	1.9	10	2.6	0	0	
Coarctation	2	0.4	2	0.5	0	0	
Hypoplastic left heart syndrome	14	2.7	12	3.2	2	1.4	
<i>Right-sided defects</i>	173	33.5	153	40.5	20		
Ebstein anomaly	2	0.4	1	0.3	1	0.7	
Pulmonary stenosis	82	15.9	73	19.3	9	6.5	0.001
Pulmonary atresia with intact septum	16	3.1	14	3.7	2	1.4	
Non-TOF pulmonary atresia with VSD	73	14.1	65	17.2	8	5.8	0.001
<i>TAPVR</i>	121	23.4	118	31.2	3	2.2	0.001
<i>PAVPR</i>	34	6.6	33	8.7	1	0.7	0.001
<i>Ventricular septal defects, total</i>	63	12.2	45	11.9	18	12.9	0.001
VSD membranous	25	4.8	15	4.0	10	7.2	
VSD malalignment-type	38	7.4	30	7.9	8	5.8	

TABLE 16-6 Major Defects Seen in Cases With Laterality Defects—cont'd

	All Laterality Defects (n = 517)		Heterotaxy (n = 378)		Situs Inversus Totalis (n = 139)		Fisher's Exact Test, Two-sided P value <sup>a</sup>
		%		%		%	
<i>Atrial septal defects</i>	119	23.0	100	26.5	19	13.7	0.001
ASD secundum	82	15.9	68	18.0	14	10.1	
ASD NOS	30	5.8	25	6.6	5	3.6	
ASD other	7	1.4	7	1.9	0	0.0	
<i>Absent right AV valve (e.g., tricuspid atresia)</i>	9	1.7	8	2.1	1	0.7	
<i>Absent left AV valve (e.g., mitral atresia)</i>	26	5.0	20	5.3	6	4.3	
<i>Vena cava, OS (e.g., interrupted IVC)</i>	161	31.1	153	40.5	8	5.8	0.001
<i>SVC/persistent left or bilateral</i>	145	28.0	137	36.2	8	5.8	0.001
<b>Visceral defects, total cases<sup>a,b</sup></b>	517		378		139		
<i>Situs inversus totalis</i>	163	31.5	24	6.3	139	100.0	
<i>Situs ambiguus, right isomerism</i>	66	12.8	66	17.5	0	0.0	
<i>Situs ambiguus, left isomerism</i>	70	13.5	70	18.5	0	0.0	
<i>Situs ambiguus, sidedness unclear, or NOS</i>	169	32.7	169	44.7	0	0.0	
<i>Heterotaxy NOS</i>	104	20.1	104	27.5	0	0.0	
<i>Spleen anomalies</i>	240	46.4	230	60.8	10	7.2	
Asplenia (absent spleen)	149	28.8	144	38.1	5	3.6	
Polysplenia	77	14.9	72	19.0	5	3.6	
Right-sided spleen	14	2.7	14	3.7	0	0.0	
<i>Malrotation</i>	147	28.4	136	36.0	11	7.9	
<i>Extracardiac defects, total cases</i>	41		33		8		
<i>Central nervous system, all</i>	7	1.4	5	1.3	2	1.4	
Neural tube defects, all	2	0.4	2	0.5	0	0.0	
Anencephaly and craniorachischisis	1	0.2	1	0.3	0	0.0	
Spina bifida	1	0.2	1	0.3	0	0.0	
Central nervous system, not NTD	5	1.0	3	0.8	2	1.4	
Holoprosencephaly	1	0.2	1	0.3	0	0.0	
Hydrocephaly	1	0.2	1	0.3	0	0.0	
Dandy-Walker malformation	3	0.6	1	0.3	2	1.4	
<i>Craniosynostosis</i>	1	0.2	1	0.3	0	0.0	
<i>Orofacial clefts</i>	5	1.0	5	1.3	0	0.0	
Cleft lip ± cleft palate	2	0.4	2	0.5	0	0.0	
Cleft palate	3	0.6	3	0.8	0	0.0	
<i>Anotia/microtia</i>	4	0.8	2	0.5	2	1.4	
<i>Esophageal atresia</i>	3	0.6	3	0.8	0	0.0	
<i>Bowel atresia/all</i>	7	1.4	7	1.9	0	0.0	
Intestinal atresia/stenosis	2	0.4	2	0.5	0	0.0	
Anorectal atresia/stenosis	5	1.0	5	1.3	0	0.0	
<i>Diaphragmatic hernia</i>	4	0.8	3	0.8	1	0.7	
<i>Sacral agenesis or caudal dysplasia</i>	5	1.0	3	0.8	2	1.4	
<i>Omphalocele</i>	3	0.6	3	0.8	0	0.0	
<i>Hypospadias second/third degree</i>	1	0.2	1	0.3	0	0.0	
<i>Bilateral renal agenesis or hypoplasia</i>	2	0.4	1	0.3	1	0.7	
<i>Cloacal extrophy</i>	2	0.4	2	0.5	0	0.0	
<i>Biliary atresia</i>	2	0.4	2	0.5	0	0.0	
<i>Transverse limb deficiency</i>	1	0.2	0	0.0	1	0.7	
<i>Intercalary limb deficiency</i>	1	0.2	0	0.0	1	0.7	

<sup>a</sup>For all extracardiac defects, the Chi square test, *P* value was 0.3207, not significant; we did not calculate this for individual defect types because of small numbers.

<sup>b</sup>For heterotaxy or situs inversus totalis, there were no cases of encephalocele, anophthalmos/microphthalmos, cataracts, choanal atresia, duodenal atresia/stenosis, gastroschisis, or bladder exstrophy.

ASD, atrial septal defect; AV, atrioventricular; AVCD (AVSD), atrioventricular canal defect (atrioventricular septal defect); DILV, double inlet left ventricle; DIRV, double inlet right ventricle; IVC, inferior vena cava; NOS, not otherwise specified; NTD, neural tube defect; OS, other specified; SVC, superior vena cava; T/PAPVR, total/partial anomalous pulmonary venous return; TGA, transposition of the great arteries; TOF, tetralogy of Fallot; VSD, ventricular septal defect.

(From Lin AE, Krikov S, Riehle-Colarusso T, et al: Laterality defects in the National Birth Defects Prevention Study (1998–2007): birth prevalence and descriptive epidemiology. *Am J Med Genet Part A* 164A:2581–2591, 2014, Table IV.)



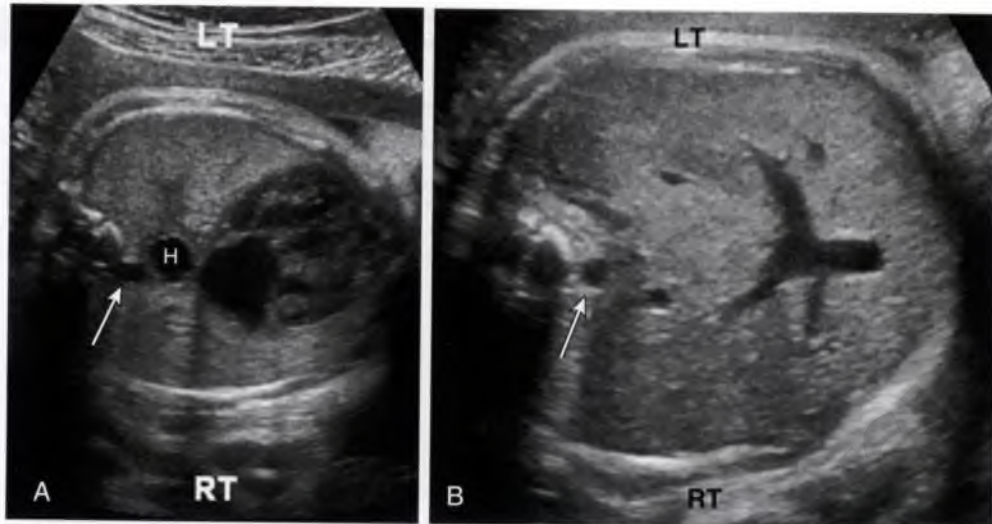


**FIG 16-61** Heterotaxy. Axial image through the fetal chest (**A**) and upper abdomen (**B**) demonstrating right isomerism/asplenia with complex congenital heart abnormality and right-sided descending aorta (*arrow*), hiatal hernia (H), midline liver, and absent spleen. LT, left; RT, right.

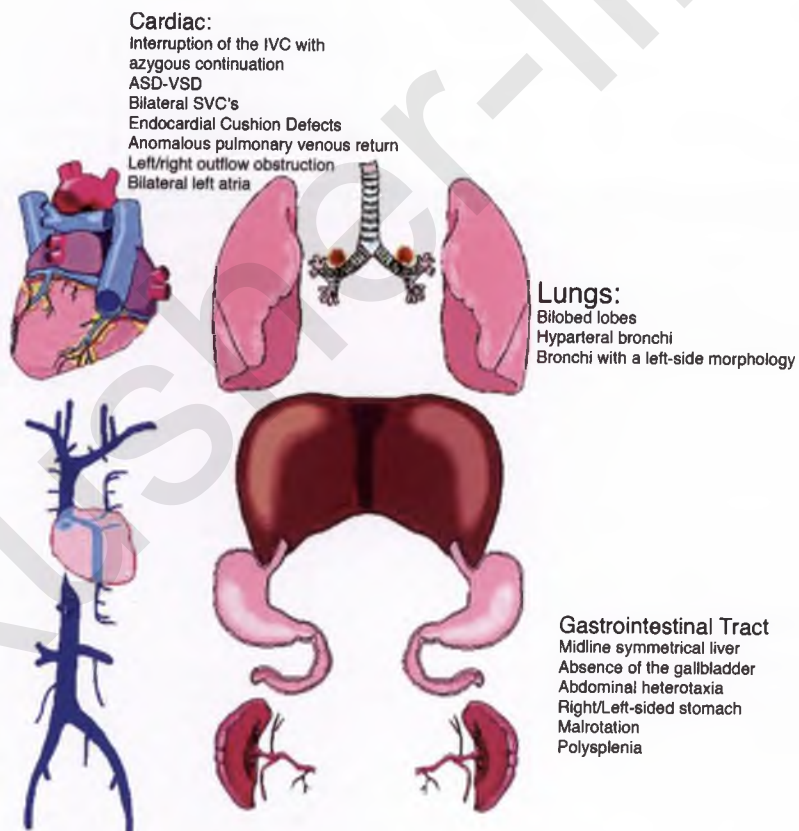


**FIG 16-62** Schematic drawing of the findings in polysplenia. ASD, atrial septal defect; IVC, inferior vena cava; SVC, superior vena cava; VSD, ventricular septal defect. (Courtesy of Philippe Jeanty, 1999. Available at thefetus.net.)

**Prognosis**

Asplenia tends to be a more severe disease from cyanotic heart lesions and superimposed infections. Although morbidity and mortality rates in the neonatal period are determined mainly by the cardinal cardiac defects, the visceral anomalies influence the long-term outcome.

**Management**

Treatment of the infant is dictated by the cardiac defects.

**REFERENCES**

Abuhamad AZ, Robinson JN, Bogdan D, Tannous RJ: Color Doppler of the splenic artery in the prenatal diagnosis of heterotaxic syndromes. *Am J Perinatol* 16(9):469–473, 1999.

Berg C, Geipel A, Smrcek J, et al: Prenatal diagnosis of cardioplenic syndromes: a 10-year experience. *Ultrasound Obstet Gynecol* 22(5):451–459, 2003.

Cesko J, Hajdu J, Marton T, et al: [Familial heterotaxy syndrome. Case report and review of the international literature]. *Orv Hetil* 139(46):2775–2778, 1998.

Lin AE, Krikov S, Riehle-Colarusso T, et al: Laterality defects in the national birth defects prevention study (1998–2007): birth prevalence and descriptive epidemiology. *Am J Med Genet A* 164(10):2581–2591, 2014.

Marton T, Cesko J, Hajdu J, et al: [Heterotaxy syndrome, analysis of 13 cases and review of the literature]. *Orv Hetil* 143(6):299–301, 2002.

Noack F, Sayk F, Ressel A, et al: Ivemark syndrome with agenesis of the corpus callosum: a case report with a review of the literature. *Prenat Diagn* 22(11):1011–1015, 2002.

Zariwala MA, Knowles MR, Leigh MW: Primary ciliary dyskinesia. In Pagon RA, Adam MP, Ardinger HH, et al, editors: *GeneReviews*, Seattle, 1993–2016, University of Washington.

**Holt-Oram Syndrome**

See discussion under “Upper Extremity.”

**Noonan Syndrome****Definition**

Noonan syndrome is characterized by short stature, characteristic facial features (low-set ears, hypertelorism, depressed nasal bridge, macrocephaly), and congenital heart defects. Other findings included a broad or webbed neck, unusual chest shape, coagulation defects, lymphatic dysplasia, undescended testes, spinal deformity, and eye findings (strabismus, amblyopia, nystagmus, cataracts, fundal changes). Developmental delay and intellectual disability are associated but variable.

**Synonyms**

Noonan syndrome is also known as Turner syndrome with normal XX or pseudo-Turner syndrome.

**Incidence**

Incidence is 1 in 1000 to 1 in 2500 live births.

**Etiology**

Noonan syndrome is due to mutations in genes in the RAS-MAPK signaling pathway.

**Genetics**

Genes implicated in Noonan syndrome include *PTPN11* (50%), *SOS1* (10%), *RAF1* (10%), and *KRAS* (< 2%). Other genes implicated in fewer than 1% of cases include *NRAS*, *BRAF*, *MAP2K1*, and *RIT1*. Inheritance is autosomal dominant, with frequent de novo mutations. An affected parent is found in 30% to 75% of families. Penetrance is difficult to estimate; expressivity is variable, with many affected adults diagnosed only after the birth of a more severely affected infant.

**Recurrence Risk**

Recurrence risk is 50% if one of the parents is affected.

**Diagnosis**

Prenatally, an increased nuchal translucency in the setting of normal chromosome studies may be seen in the first trimester. Other features that may be observed in the second trimester include dysmorphic facial features, congenital heart defects, pleural effusions, renal anomalies, polyhydramnios, and hydrops. Congenital heart disease is present in 50% to 80% of affected individuals. The most common heart defects are pulmonary valve stenosis (20–50%) and hypertrophic cardiomyopathy (20–30%); others include ASD, VSD, peripheral pulmonary artery stenosis, aortic coarctation, and tetralogy of Fallot. With prenatal imaging, cardiac defects, especially pulmonary stenosis and cardiomyopathy, tend to be noted less frequently and often not until the third

**TABLE 16-7 Management Guidelines in Noonan Syndrome**

	At Diagnosis	After Diagnosis	If Symptomatic
General	Complete physical and neurologic examination; medical genetics consultation to confirm diagnosis, consider molecular genetic testing and genetic counseling	Yearly complete physical and neurologic examination; return to geneticist if genotype negative or for multisystem assessment; genetic counseling at adolescence or when a young adult	Orchiopexy by age 1 year for cryptorchidism; if lymphedema, refer to specialty clinic; brain and cervical spine MRI if intracranial pressure increases; electroencephalogram and referral to neurologist if seizures suspected
Developmental	Multidisciplinary developmental assessment	Developmental screening yearly for children aged 5 to 18 years	Neuropsychologist testing if screening abnormal; referral to early intervention if delays detected before age 3 years; individual education plan for children aged 5 to 18 years with delays
Dental	First dental assessment between age 1 year and 2 years	Yearly dental assessment	—

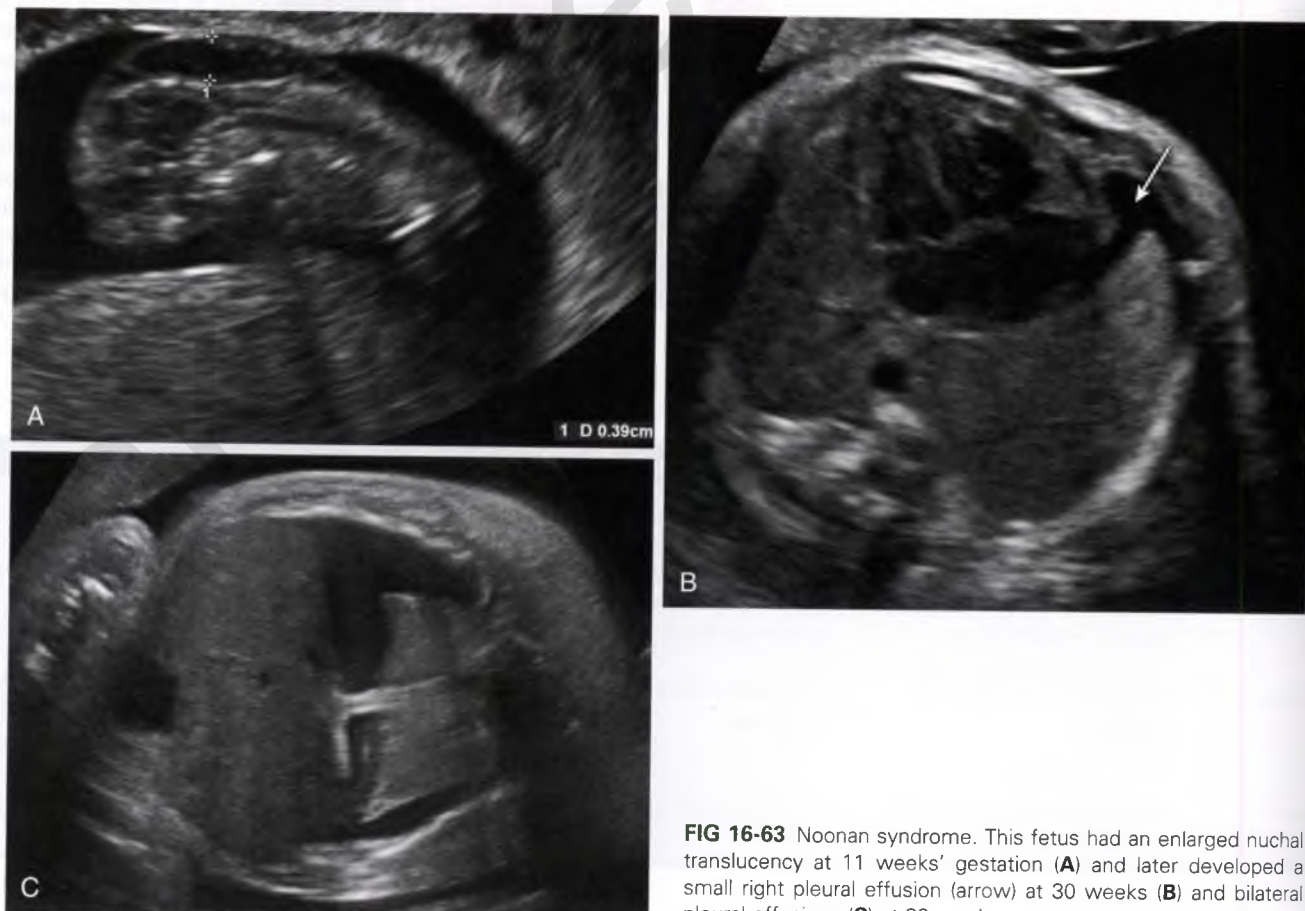
Continued



TABLE 16-7 Management Guidelines in Noonan Syndrome—cont'd

	At Diagnosis	After Diagnosis	If Symptomatic
Growth and feeding	Plot growth on curves for Noonan syndrome	Plot growth on curves for Noonan syndrome three times per year until age 3 years, then yearly	Refer to gastroenterologist for feeding problems or recurrent vomiting, or if evidence of growth failure without comorbid cause exists; thyroid function tests if signs or symptoms of hypothyroidism
Cardiovascular	Cardiac examination, electrocardiogram, echocardiogram	Follow up on the basis of initial findings. If initial assessment normal, repeat every 5 years	—
Ophthalmologic	Baseline eye examination	Repeat every 2 years, sooner if indicated	—
Audiologic	Baseline audiology examination	Repeat if recurrent otitis media or speech delay	Refer to ear, nose, and throat specialist for recurrent otitis media or serous otitis; hearing aids or classroom interventions for hearing loss
Hematologic	Complete blood cell count with differential, and prothrombin time or activated partial thromboplastin time	Repeat complete blood cell count with differential and prothrombin time or activated partial thromboplastin time if aged 6 to 12 months at initial screen; preoperatively: complete blood cell count with differential and prothrombin time or activated partial thromboplastin time, second tier (in consultation with hematologist) factor IX, XI, and XII concentrations, von Willebrand factor, platelet aggregation	Prothrombin time or activated partial thromboplastin time if bleeding abnormal or persistent, refer to hematologist; complete blood cell count with differential for splenomegaly; complete blood cell count with differential and liver function studies for hepatosplenomegaly
Renal	Kidney ultrasound	—	—
Skeletal	Clinical assessment of spine with radiology if indicated by examination	Repeat spinal examination yearly through adolescence; radiology and referral to orthopedic specialist if abnormal	—

From Roberts AE, Allanson JE, Tartaglia M, et al: Noonan syndrome. *Lancet* 381:333-342, Table 3, used with permission.



**FIG 16-63** Noonan syndrome. This fetus had an enlarged nuchal translucency at 11 weeks' gestation (**A**) and later developed a small right pleural effusion (arrow) at 30 weeks (**B**) and bilateral pleural effusions (**C**) at 32 weeks.

trimester. Birth weight is generally normal with short stature most evident later, especially at the time of puberty.

### Differential Diagnosis

An increased nuchal translucency in the first trimester is associated with Turner syndrome and aneuploidy; Noonan syndrome should be considered in the presence of an increased nuchal translucency with normal chromosome studies. Other RASopathies (syndromes with mutations in the RAS-MAPK signaling pathway) can be associated with similar findings both prenatally and in infancy, including cardio-faciocutaneous and Costello syndromes. Aarskog syndrome can present with similar facial features and short stature. Molecular genetic testing can aid in diagnosis.

### Prognosis

Life expectancy is generally normal for those without major complications of heart disease. Feeding difficulties are often present in infants. Hearing loss is common. Developmental delay is variable; intelligence is generally in the normal range, but mild learning difficulties may be present.

### Management

Guidelines for management have been established (Table 16-7).

## REFERENCES

- Achiron R, Heggesh J, Grisaru D, et al: Noonan syndrome: a cryptic condition in early gestation. *Am J Med Genet* 92(3):159–165, 2000.
- Allanson JE, Roberts AE: Noonan syndrome. In Pagon RA, Adam MP, Ardinger HH, et al, editors: *GeneReviews*, Seattle, 1993–2016, University of Washington.
- Aoki Y, Niihori T, Banjo T, et al: Gain-of-function mutations in RIT1 cause Noonan syndrome, a RAS/MAPK pathway syndrome. *Am J Hum Genet* 93(1):173–180, 2013.
- Bradley E, Kean L, Twining P, James D: Persistent right umbilical vein in a fetus with Noonan's syndrome: a case report. *Ultrasound Obstet Gynecol* 17(1):76–78, 2001.
- Joo JG, Beke A, Toth-Pal E, et al: Successful pregnancy in a Noonan syndrome patient after 3 unsuccessful pregnancies from severe fetal hydrops: a case report. *J Reprod Med* 50(5):373–376, 2005.
- Nisbet DL, Griffin DR, Chitty LS: Prenatal features of Noonan syndrome. *Prenat Diagn* 19(7):642–647, 1999.
- Picone O, Benachi A, Mandelbrot L, et al: Thoracoamniotic shunting for fetal pleural effusions with hydrops. *Am J Obstet Gynecol* 191(6):2047–2050, 2004.
- Rauen KA: The RASopathies. *Ann Rev Genomics Hum Genet* 14:355–369, 2013.

## Pentalogy of Cantrell

### Definition

Pentalogy of Cantrell is characterized by five anomalies: deficiency of the anterior diaphragm, midline supraumbilical abdominal wall defect, defect in the diaphragmatic pericardium, intracardiac abnormalities, and lower sternum defect. It was first described in 1958.

### Synonyms

Synonyms include thoracoabdominal ectopia cordis, ectopia cordis, and Cantrell-Heller-Ravitch syndrome.

### Incidence

Pentalogy of Cantrell is very rare. Incidence is estimated at 5.5 per 1 million live births. There is a 2:1 male-to-female ratio.

### Etiology/Pathogenesis

The defects appear to originate from the 3rd week of life with a mesodermal origin, specifically abnormal migration of the splanchnic and somatic mesoderm with premature breakage of the chorion or vitelline sac at days 14 to 18 of gestation.

### Genetics

Most cases are sporadic. X-linked inheritance has been suggested in some families.

### Recurrence Risk

Recurrence risk is unknown. No recurrence has been recorded. One set of monozygotic twins concordant for the syndrome has been reported.

### Diagnosis

Prenatally, the diagnosis can be made as early as the first trimester. Classic findings include complete disruption of the anterior chest and abdominal wall. The finding of cardiac activity outside the chest in association with an omphalocele is diagnostic. Karyotype analysis is recommended to exclude chromosomal anomalies. Ascites and pleural

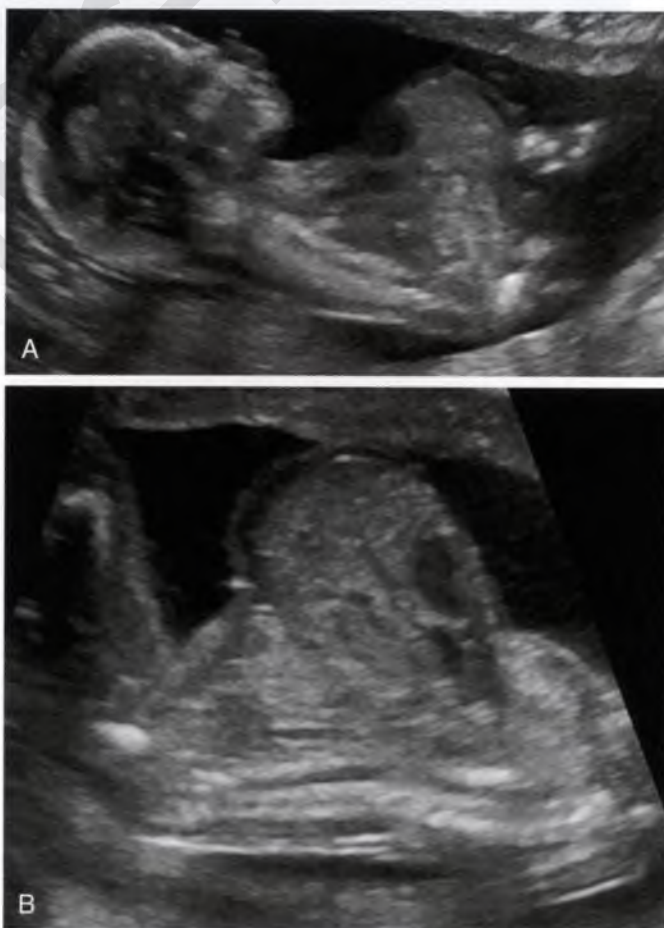


**FIG 16-64** Pentalogy of Cantrell. Fetus with midline thoracoabdominal defect with partially externalized heart and large upper omphalocele at 16 weeks' (A) and 19 weeks' (B) gestation. The fetus also had a conotruncal heart defect (double outlet right ventricle).



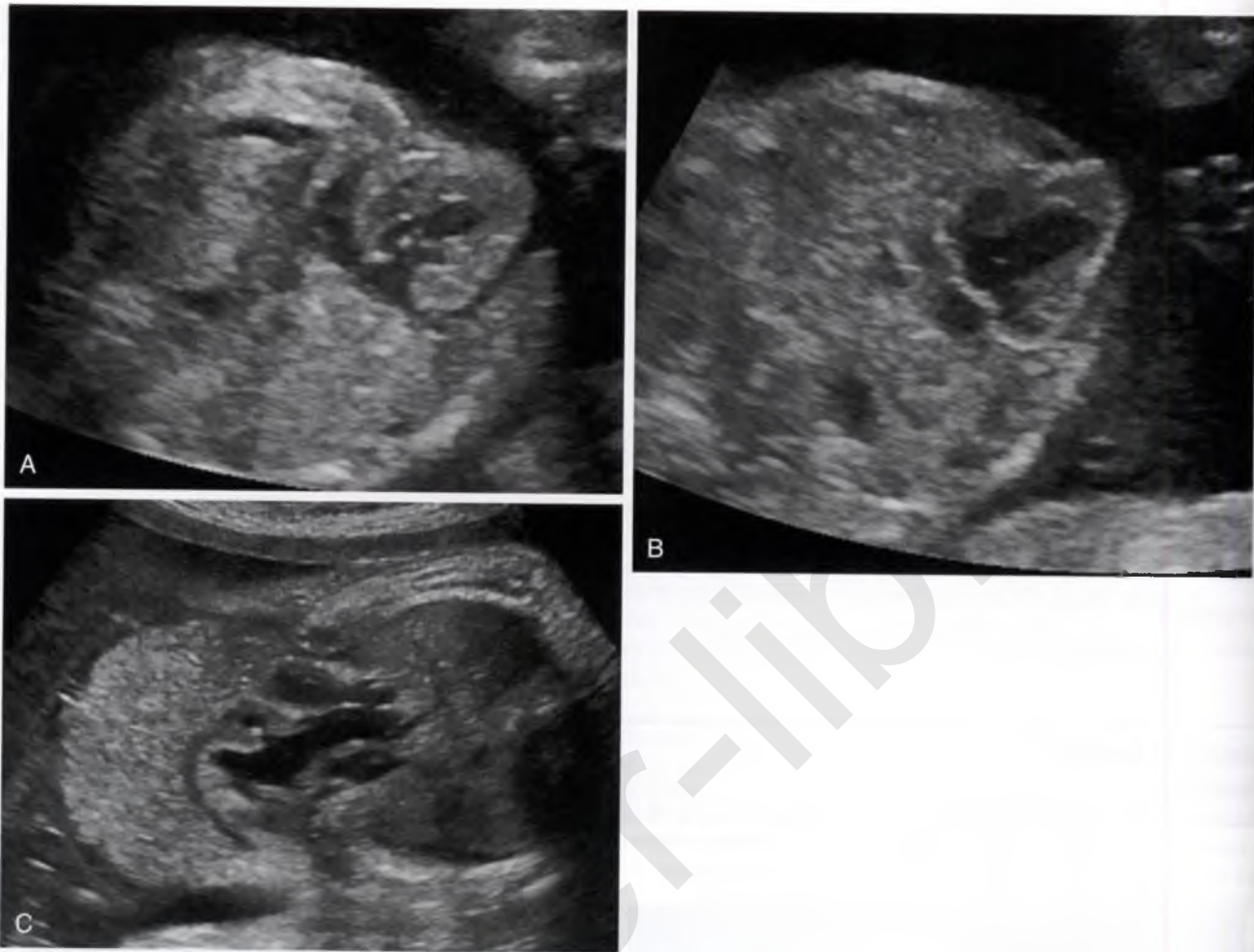


**FIG 16-65** Pentalogy of Cantrell. At 24 weeks' gestation (**A** and **B**), the partially exteriorized heart is demonstrated in these views of the fetal chest. At 35 weeks (**C**), the large upper omphalocele is demonstrated in this axial view of the fetal chest.



**FIG 16-66** Sonogram of an embryo at 10 weeks' gestation with pentalogy of Cantrell. (Courtesy of Fernando Maia, 2005. Available at thefetus.net.)



**FIG 16-67** Color Doppler sonogram in the same patient with pentalogy of Cantrell. (Courtesy of Fernando Maia, 2005. Available at thefetus.net.)

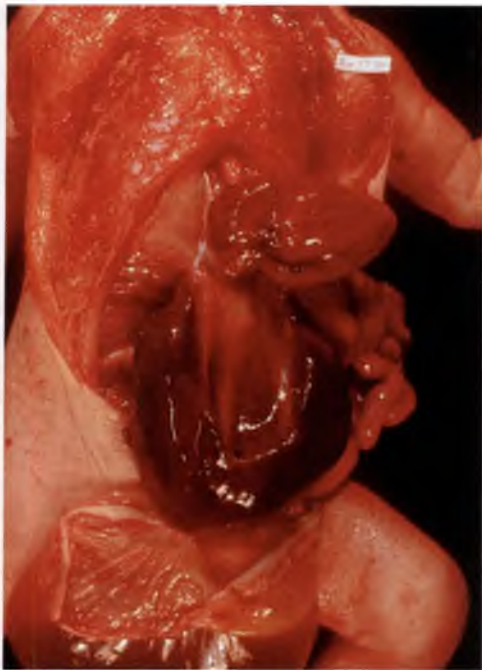


**FIG 16-68** Postmortem view of a fetus with pentalogy of Cantrell. (Courtesy of Heron Werner, 2005. Available at thefetus.net.)

effusion may occur from compression of the contents of both the chest and abdomen.

### Associated Anomalies

Other anomalies include craniofacial anomalies, CNS anomalies, skeletal anomalies, dermatologic anomalies, spina bifida, anencephaly, hydrocephalus, and clubfeet.

### Tuberous Sclerosis

See discussion under “Central Nervous System.” Cardiac rhabdomyomas (seen as well-delineated homogeneous masses) may be seen prenatally; 51% to 86% of patients with cardiac rhabdomyomas have tuberous sclerosis.

## GASTROINTESTINAL SYSTEM/ABDOMINAL WALL

### Gastrointestinal System Disorders

#### Cystic Fibrosis

**Definition.** Cystic fibrosis (CF) is a complex multisystem disorder affecting the respiratory tract, exocrine pancreas, intestine, hepatobiliary system, exocrine sweat glands, and male genital tract.

**Incidence.** Incidence is 1 in 3200 live births in persons of northern European heritage; 1 in 15,000 African Americans; and 1 in 31,000 Asian Americans.

**Diagnosis.** Prenatally, the diagnosis is generally suspected because of the presence of fetal echogenic bowel (owing to intestinal obstruction from abnormal meconium). The risk of CF in a pregnancy with moderate echogenic bowel may be 2% to 3% and, if severe, may be 5% to 20%. Newborns can be diagnosed by an abnormal sweat chloride

### Differential Diagnosis

Differential diagnosis includes isolated thoracic cardiac ectopy, ectopia cordis associated with amniotic band syndrome, body-stalk abnormality, isolated omphalocele, BWS, chromosomal abnormalities.

### Prognosis

Survival is rare, and cases presenting a complete extrusion of heart and abdominal contents have an extremely poor prognosis. The prognosis for individuals with milder forms depends on the extent of the anomalies, including size of the abdominal wall defect and extent of the cardiac defect. Congenital heart disease is a source of major morbidity in infants surviving the neonatal period.

### Management

After delivery, repair of the omphalocele should not be delayed. Repair of the sternal, diaphragmatic, and pericardial defects can be attempted at the same time. Surgical correction is often difficult secondary to hypoplasia of the thoracic cage and inability to enclose the ectopic heart. Respiratory insufficiency secondary to pulmonary hypoplasia can be present.

## REFERENCES

- Carmi R, Boughman JA: Pentalogy of Cantrell and associated midline anomalies: a possible ventral midline developmental field. *Am J Med Genet* 42(1):90–95, 1992.
- Mallula KK, Sosnowski C, Awad S: Spectrum of Cantrell’s pentalogy: case series from a single tertiary care center and review of the literature. *Pediatr Cardiol* 34(7):1703–1710, 2013.
- Pollio E, Sica C, Pacilio N, et al: [Pentalogy of Cantrell: first trimester prenatal diagnosis and association with multicystic dysplastic kidney]. *Minerva Ginecol* 55(4):363–366, 2003.
- Thamboo TP, Chan NH: Pentalogy of Cantrell with a double-outlet left ventricle. *Pathology* 37(1):87–89, 2005.

test, which is positive in more than 90% of individuals with CF. Newborn screening for CF has also now been implemented in most of the United States.

**Genetics.** CF is caused by mutations in the *CFTR* gene. Inheritance is autosomal recessive.

**Recurrence Risk.** Recurrence risk is 25% if both parents are carriers.

**Differential Diagnosis.** The most common other disorders presenting with fetal echogenic bowel include aneuploidy and CMV infection.

**Prognosis.** From 15% to 20% of infants with CF present with meconium ileus. Pulmonary disease is the major cause of long-term morbidity and even death. Lower airway inflammation and chronic endobronchial infection progress to end-stage fibrotic lung disease. Most individuals also have pancreatic insufficiency, and most males are infertile. Overall median survival time is 36.5 years.

**Management.** The prenatal finding of echogenic bowel should prompt evaluation for fetal aneuploidy, maternal CF carrier testing, and CMV infection. If these studies return negative, pregnancy surveillance should be increased given the association of echogenic bowel with fetal growth restriction and stillbirth.





**FIG 16-69** Cystic fibrosis. Axial image through the abdomen of a fetus with echogenic bowel (arrow). Second trimester echogenic bowel may represent cystic fibrosis. Genetic counseling to discuss inheritance, the impact of ethnicity on testing, and the appropriate genetic evaluations should be facilitated.

## REFERENCES

- Aboujaoude R, Alvarez J, Ganesh V, Apuzzio J: Is testing for cytomegalovirus and cystic fibrosis indicated in members of a nonwhite pregnant population in whom the fetus has an echogenic bowel? *Am J Perinatol* 23(5):319–323, 2006.
- Al-Kouatly HB, Chasen ST, Streltsoff J, Chervenak FA: The clinical significance of fetal echogenic bowel. *Am J Obstet Gynecol* 185(5):1035–1038, 2001.
- Ameratunga DM, Said JM, Reidy K, Palma-Dias R: Perinatal outcomes following the ultrasound diagnosis of echogenic bowel: an Australian perspective. *Fetal Diagn Ther* 31(3):179–184, 2012.
- Corteville JE, Gray DL, Langer JC: Bowel abnormalities in the fetus—correlation of prenatal ultrasonographic findings with outcome. *Am J Obstet Gynecol* 175(3 Pt 1):724–729, 1996.
- Cystic Fibrosis Foundation: Patient Registry: *Annual Data Report to the Center Directors 2014*, Bethesda, MD, 2006, Cystic Fibrosis Foundation. Available at: <www.cff.org>.
- Ghose I, Mason GC, Martinez D, et al: Hyperechogenic fetal bowel: a prospective analysis of sixty consecutive cases. *Br J Obstet Gynaecol* 107(3):426–429, 2000.
- Mailath-Pokorny M, Klein K, Klebermass-Schrehof K, et al: Are fetuses with isolated echogenic bowel at higher risk for an adverse pregnancy outcome? Experiences from a tertiary referral center. *Prenat Diagn* 32(13):1295–1299, 2012.
- Slotnick RN, Abuhamad AZ: Prognostic implications of fetal echogenic bowel. *Lancet* 347(8994):85–87, 1996.

## Epidermolysis Bullosa With Pyloric Atresia

**Definition.** Epidermolysis bullosa with pyloric atresia (EB-PA) is characterized by fragility of the skin and mucous membranes with blistering with minimal or no trauma, congenital pyloric atresia, and genitourinary anomalies (dysplastic/multicystic kidney, hydronephrosis/hydronephrosis, ureterocele, duplicated renal collecting system, absent bladder).

**Synonym.** EB-PA is also known as Carmi syndrome.

**Etiology.** Mutations in the implicated genes lead to deficiency of either the  $\alpha 6\beta 3$  integrin complex or the interacting protein, plectin. These proteins are necessary for epidermal integrity. The association with pyloric atresia is not well understood.

**Incidence.** EB-PA is very rare. The EB-PA subtype of EB may represent 15% of all cases of EB.

**Genetics.** Three genes have been implicated in the disorder: *ITGB4* (80%), *ITGA6* (5%), and *PLEC1* (15%). Inheritance is autosomal recessive. Carrier status of both parents should be confirmed because

germline mosaicism and uniparental isodisomy are possible. Penetrance is complete.

**Recurrence Risk.** If both parents are mutation carriers, recurrence risk is 25%.

**Diagnosis.** Prenatally, suspicion of pyloric atresia may be initially raised based on identification of an enlarged stomach bubble. Intra-gastric sediment can suggest a possible fetal abrasive skin lesion condition. Polyhydramnios and high amniotic fluid AFP levels (>20 multiples of the median) are often seen.

**Associated Anomalies.** Other anomalies include localized absence of the skin (aplasia cutis congenita), hypotrichosis, dystrophic nails, contractures, and dilated cardiomyopathy.

**Differential Diagnosis.** Other disorders to consider include other subtypes of epidermolysis bullosa and isolated pyloric atresia.

**Prognosis.** The clinical course is usually severe and often lethal in the neonatal period. Affected infants may develop sepsis with severe electrolyte abnormalities as a result of extensive skin blistering and

erosion. Infants who survive generally have less severe cutaneous manifestations and require repair of the pyloric atresia.

## REFERENCES

Chung HJ, Uitto J: Epidermolysis bullosa with pyloric atresia. *Dermatol Clin* 28(1):43–54, 2010.

Maurice P, Eyrolle-Guignot D, Dhombres F, et al: The key role of ultrasound examination in the prenatal diagnosis of epidermolysis bullosa with pyloric atresia. *Prenat Diagn* 33(9):908–909, 2013.

Pfendner EG, Lucky AW: Epidermolysis bullosa with pyloric atresia. In Pagon RA, Adam MP, Ardinger HH, et al, editors: *GeneReviews*, Seattle, 1993–2016, Washington.

### Megacystis-Microcolon-Intestinal Hypoperistalsis Syndrome

**Definition.** Megacystis-microcolon-intestinal hypoperistalsis syndrome (MMIHS) is characterized by a prenatally distended urinary bladder and functional intestinal obstruction.

**Etiology.** *ACTG2* encodes for the protein  $\gamma 2$  enteric actin and is thought to be important for cell integrity, structure, and motility. It associates with the actin cytoskeletal filament network. Mutations in *ACTG2* lead to dysfunction of enteric smooth muscle.

**Genetics.** Many cases are caused by heterozygous *ACTG2* mutations. Genetic heterogeneity may exist. Most cases are de novo, although less severely affected parents with disease-causing *ACTG2* mutations have now been reported.

**Recurrence Risk.** For de novo cases, recurrence risk is estimated at approximately 1% because of the risk of germline mosaicism. Recurrence risk is 50% with a known parental mutation.

**Incidence.** MMIHS is rare. More than 230 cases have been described in the literature.

**Diagnosis.** Prenatal findings include megacystis, hydronephrosis, dilated stomach, and dilated small intestine. Polyhydramnios can also be seen. Newborns are found to have dilated bladders without structural obstruction, dilated small intestine, and intestinal hypoperistalsis with diminished caliber of the colon. Renal function is preserved.

**Differential Diagnosis.** The differential should include other disorders leading to fetal megacystis, such as posterior urethral valves.

**Prognosis.** Death is common in infancy as a result of feeding issues and complications.

**Management.** Extensive surgical operations are required including transplantation of multiple organs, including the small bowel. Survival rate after multivisceral transplantation is only 12% to 20%. Most survivors are dependent on total parenteral nutrition and urinary catheterization.

## REFERENCES

Thorson W, Diaz-Horta O, Foster J, 2nd, et al: De novo *ACTG2* mutations cause congenital distended bladder, microcolon, and intestinal hypoperistalsis. *Hum Genet* 133(6):737–742, 2014.

Tuzovic L, Anyane-Yeboah K, Mills A, et al: Megacystis-microcolon-intestinal hypoperistalsis syndrome: case report and review of prenatal ultrasonographic findings. *Fetal Diagn Ther* 36(1):74–80, 2014.

Wangler ME, Gonzaga-Jauregui C, Gambin T, et al: Heterozygous de novo and inherited mutations in the smooth muscle actin (*ACTG2*) gene underlie megacystis-microcolon-intestinal hypoperistalsis syndrome. *PLoS Genet* 10(3):e1004258, 2014.

### Abdominal Wall Defects

#### Beckwith-Wiedemann Syndrome

**Definition.** BWS is a growth disorder originally characterized by the classic triad of macrosomia, macroglossia, and omphalocele. Other features include visceromegaly, embryonal tumors, neonatal hypoglycemia, ear creases/pits, and renal abnormalities.

**Incidence.** Incidence is estimated at 1 in 13,700, but this figure is likely an underestimate given that some individuals have a more mild phenotype and remain undiagnosed.

**Etiology.** The condition is sporadic in approximately 85% of cases. Assisted reproductive technology increases the risk of imprinting disorders, including BWS.

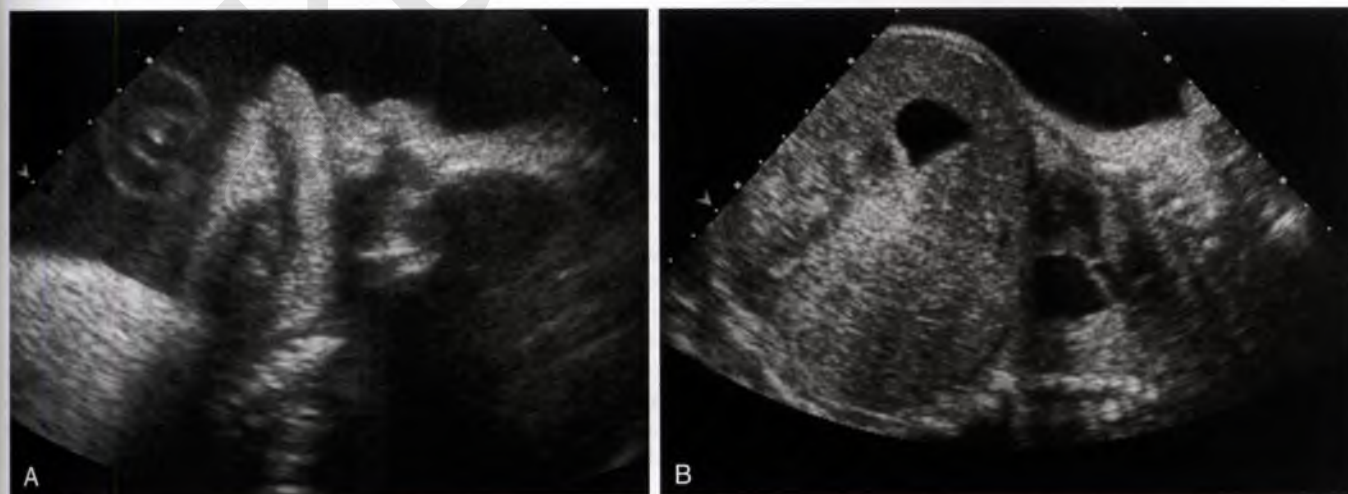


**FIG 16-70** Beckwith-Wiedemann syndrome (BWS). Macroglossia (A) and hepatomegaly (B) are visualized in this fetus with macrosomia and BWS.



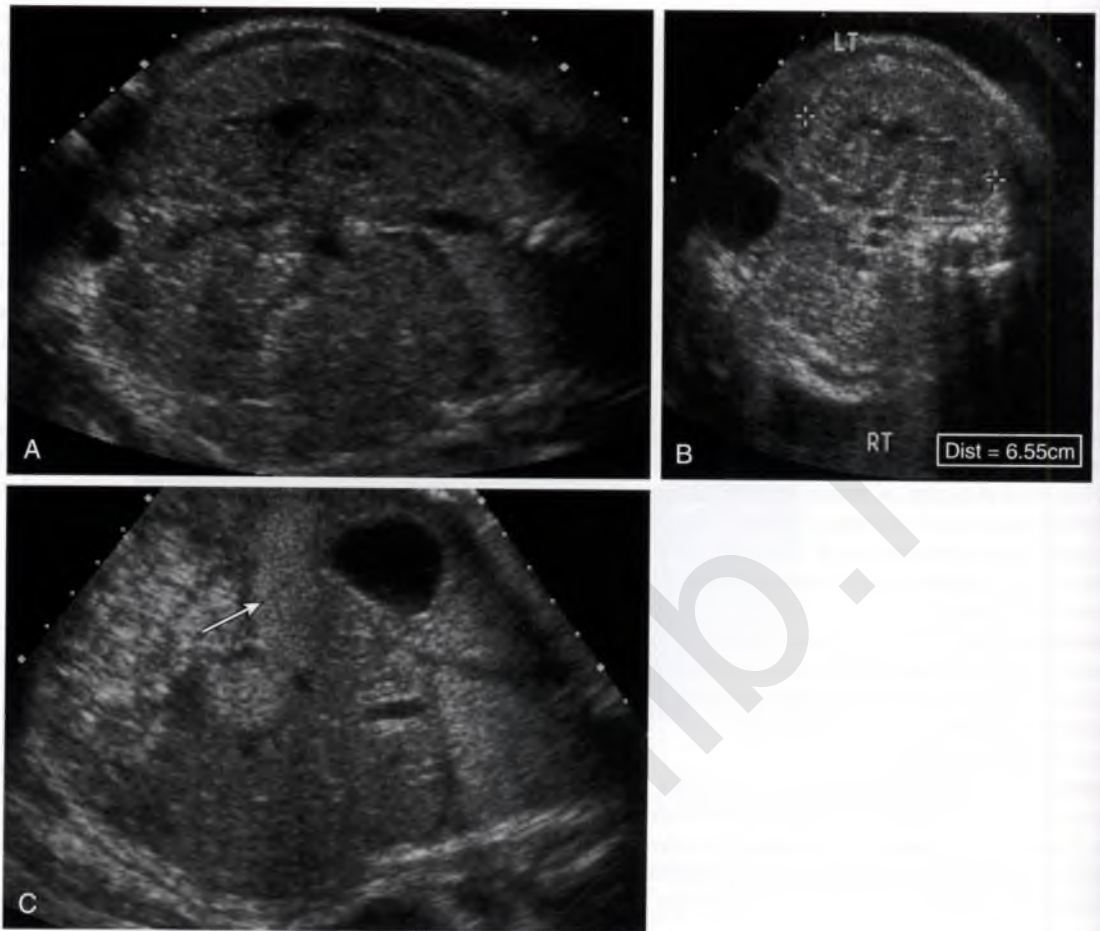


**FIG 16-71** Organomegaly is characteristic of Beckwith-Wiedemann syndrome. In this fetus, nephromegaly (A) and an enlarged pancreas (B and C) (arrow) are seen. LT, left; RT, right.



**FIG 16-72** Beckwith-Wiedemann syndrome. The earlobe groove (arrow) can be recognized with detailed examination.

**Genetics.** BWS is due to epigenetic and genomic alterations at chromosome 11p15. These alterations include loss of methylation on the maternal chromosome at imprinting center 2 (IC2; 50% of individuals); paternal uniparental disomy at chromosome 11p15 (20%); gain of methylation on the maternal chromosome at imprinting center 1 (IC1; 5%). Sequence analysis of *CDKN1C* identifies mutations in 40% of families with the disorder and in 5% to 10% of cases without a family history. Overall, 85% of individuals with BWS have a negative family history, and 15% have a family history consistent with autosomal dominant inheritance. Penetrance is incomplete and expressivity is variable.

**Recurrence Risk.** Recurrence risk depends on the underlying mechanism leading to BWS.

**Diagnosis.** Prenatal findings include macrosomia, macroglossia, omphalocele, polyhydramnios, long umbilical cord, and an enlarged placenta. Many of these features are not present until the late second trimester. Renal anomalies may be present and include medullary dysplasia, duplicated collecting system, cystic changes, and nephromegaly. Embryonic tumors may present early in life, including Wilms tumor and hepatoblastoma, as well as neuroblastoma, adrenocortical carcinoma, and rhabdomyosarcoma. Hemihyperplasia can often be seen at birth, but may become less pronounced as a child grows.

**Differential Diagnosis.** The differential diagnosis includes other growth disorders such as Simpson-Golabi-Behmel syndrome, Perlman syndrome, Costello syndrome, Sotos syndrome, and Proteus syndrome, as well as diabetic fetopathy.

**Prognosis.** Previously, the neonatal mortality rate was as high as 20%, but this is likely lower now. Recognition of associated issues has improved prognosis. Preterm delivery is a common complication due to polyhydramnios and gestational hypertension. Development is usually normal, and prognosis is generally favorable after childhood.

**Management.** If severe macrosomia and adrenal cysts are present, cesarean delivery may be needed. Neonatal hypoglycemia should be monitored and treated. Macroglossia can lead to feeding difficulties and airway obstruction. Screening should be performed for embryonic tumors with serum AFP levels and abdominal ultrasound examination until age 8; overall risk for tumor development in children is 7.5%. Tumor development may vary by specific underlying genetic cause of the child's BWS. Omphalocele should be repaired.

## REFERENCES

- Borer JG, Kaefer M, Barnewolt CE, et al: Renal findings on radiological followup of patients with Beckwith-Wiedemann syndrome. *J Urol* 161(1):235–239, 1999.
- Clericuzio CL, Chen E, McNeil DE, et al: Serum alpha-fetoprotein screening for hepatoblastoma in children with Beckwith-Wiedemann

syndrome or isolated hemihyperplasia. *J Pediatr* 143(2):270–272, 2003.

- Fahmy J, Kaminsky CK, Parisi MT: Perlman syndrome: a case report emphasizing its similarity to and distinction from Beckwith-Wiedemann and prune-belly syndromes. *Pediatr Radiol* 28(3):179–182, 1998.
- Hamada H, Fujiki Y, Obata-Yasuoka M, et al: Prenatal sonographic diagnosis of Beckwith-Wiedemann syndrome in association with a single umbilical artery. *J Clin Ultrasound* 29(9):535–538, 2001.
- Merrot T, Walz J, Anastasescu R, et al: Prenatally detected cystic adrenal mass associated with Beckwith-Wiedemann syndrome. *Fetal Diagn Ther* 19(6):465–469, 2004.
- Reish O, Lerer I, Amiel A, et al: Wiedemann-Beckwith syndrome: further prenatal characterization of the condition. *Am J Med Genet* 107(3):209–213, 2002.
- Shuman C, Beckwith JB, Smith AC, Weksberg R: Beckwith-Wiedemann syndrome. In Pagon RA, Adam MP, Ardinger HH, et al, editors: *GeneReviews*, Seattle, 1993-2016, University of Washington.
- Wangler MF, Chang AS, Moley KH, et al: Factors associated with preterm delivery in mothers of children with Beckwith-Wiedemann syndrome: a case cohort study from the BWS registry. *Am J Med Genet A* 134A(2):187–191, 2005.
- Williams DH, Gauthier DW, Maizels M: Prenatal diagnosis of Beckwith-Wiedemann syndrome. *Prenat Diagn* 25(10):879–884, 2005.

## Cloacal Exstrophy Sequence

**Definition.** Cloacal exstrophy is a complex abdominal wall defect characterized by omphalocele, bladder exstrophy, and imperforate anus. Other anomalies include renal malformations, spinal defects, single umbilical artery, and limb defects.

**Synonym.** Cloacal exstrophy is also known as OEIS complex (omphalocele, bladder exstrophy, imperforate anus, and spinal defects).

**Incidence.** Incidence is 1 in 200,000 to 1 in 400,000, with a female-to-male ratio of approximately 2:1.

**Etiology.** Cloacal exstrophy is thought to result from an early embryologic defect involving the caudal eminence.

**Genetics.** Cloacal exstrophy likely has a heterogeneous cause. Occasionally affected infants have a chromosomal abnormality.

**Recurrence Risk.** Recurrence risk is unknown.

**Diagnosis.** Prenatally, findings include a large intraumbilical anterior midline defect, omphalocele, absent bladder, and polyhydramnios. Genital abnormalities include division of the scrotum or labia and separation or absence of the phallic or clitoral halves. In males, the testes are frequently undescended. In females, vaginal duplication and vaginal agenesis are common.

**Associated Anomalies.** Other defects seen less commonly include esophageal atresia with tracheoesophageal fistula, duodenal atresia, and Chiari I malformation.

**Differential Diagnosis.** Differential diagnosis includes related anomalies within the exstrophy-epispadias spectrum such as bladder exstrophy.

**Prognosis.** Survival increased dramatically after corrective surgery was introduced, with current survival greater than 90%. Comorbid conditions include complications with urinary and bowel function as well as gender assignment.

**Management.** Postnatal management requires a multidisciplinary team and includes multiple surgical procedures. Quality-of-life issues predominate. Gender should be determined by karyotype if not obvious on examination. Plain films of the chest, spine, and pelvis should be obtained. Screening for renal and spinal anomalies should be performed.

## REFERENCES

- Arlen AM, Smith EA: Disorders of the bladder and cloacal anomaly. *Clin Perinatol* 41(3):695–707, 2014.
- Feldkamp ML, Botto LD, Amar E, et al: Cloacal exstrophy: an epidemiologic study from the International Clearinghouse for Birth Defects Surveillance and Research. *Am J Med Genet C Semin Med Genet* 157C(4):333–343, 2011.

## Miller-Dieker Syndrome

See “Central Nervous System.” This syndrome presents with lissencephaly, as well as other anomalies, including rare cases with omphalocele.

## Pentalogy of Cantrell

See “Heart.” This syndrome is associated with abdominal wall defects, most commonly omphalocele.

## Prune-Belly Syndrome

**Definition.** Prune-belly syndrome (PBS) is a rare disorder characterized by deficient abdominal wall muscles, urinary tract malformations, and cryptorchidism in boys.

**Synonym.** PBS is also called Eagle-Barrett syndrome and triad syndrome.

**Incidence.** Incidence is 1 in 35,000 to 1 in 50,000 live births; PBS is most often seen in males and rarely in females (3-5%). It is seen more often in infants born to younger mothers, in twin gestations, and in pregnancies conceived by assisted reproductive technology.

**Etiology.** Many theories to explain the disorder have been proposed and two predominate. The first proposes that urethral atresia and stenosis of the posterior urethral valves lead to severe bladder outlet obstruction. The second proposes that developmental arrest of the lateral plate mesoderm in weeks 6 to 7 of pregnancy leads to deficiency of the muscles of the abdominal wall and defective development of the urinary tract.



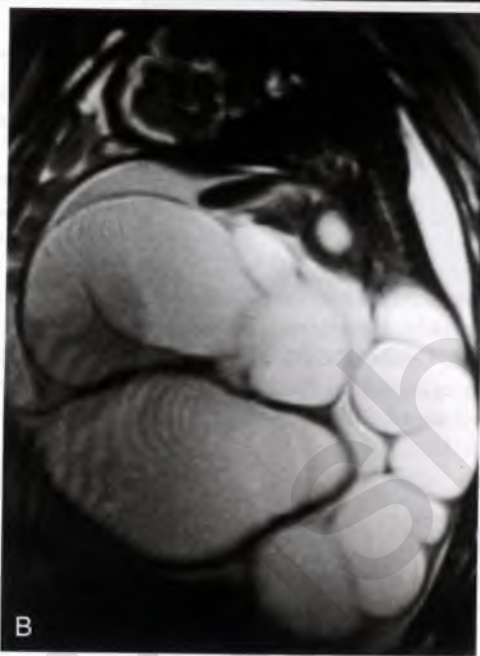
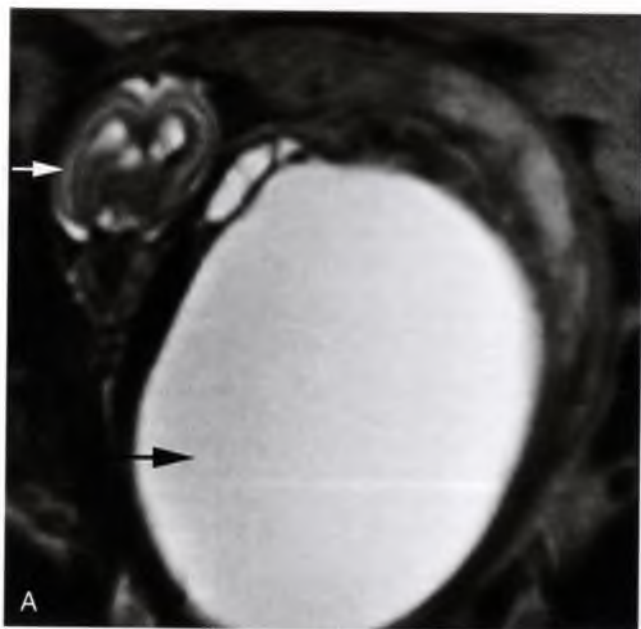


**FIG 16-73 A**, Sagittal T2 magnetic resonance imaging scan demonstrates high signal from a markedly dilated urinary bladder (*black arrow*). Note the size discrepancy of the fetal head (*white arrow*) at 26 weeks' gestation. **B**, Coronal T2 magnetic resonance imaging scan demonstrates marked dilatation of the fetal ureter. (Courtesy of Heron Werner, 2005. Available at thefetus.net.)

**Genetics.** Genetics are unknown, but PBS likely has a heterogeneous cause. Occasionally it has been reported in association with aneuploidy as well as with abnormalities of *HNF1*.

**Recurrence Risk.** Recurrence risk is unknown, but low.

**Diagnosis.** Prenatally, the diagnosis should be suspected in fetuses with very large abdominal masses. In PBS, the abdominal mass is megacystis (an enlarged bladder); oligohydramnios can be present if lower urinary tract obstruction is severe. Other findings include hyper-echogenic kidneys, Potter facies, pulmonary hypoplasia, gastric dilatation, short bowel, microileum, microcolon, malrotation of the



**FIG 16-74** Postmortem neonatal photograph demonstrating a markedly enlarged abdomen with redundant skin. (Courtesy of Heron Werner, 2005. Available at thefetus.net.)

intestines, imperforate anus, arthrogryposis, clubfeet, and cardiac defects.

**Differential Diagnosis.** The differential diagnosis includes other urinary tract anomalies, such as posterior urethral valves and MMIHS.

**Prognosis.** Prognosis depends on the severity of renal dysfunction, duration and degree of oligohydramnios, and presence of pulmonary hypoplasia. Outcome is favorable in cases with normal amniotic fluid volume.

**Management.** Prenatal management in cases with severe lower urinary tract obstruction is controversial. Fetal intervention aimed at relief of bladder outlet obstruction and restoration of amniotic fluid volume may be beneficial in select cases, but evidence is limited. Postnatal management aims to preserve renal function and prevent urinary tract infection. Abdominal wall reconstruction for both aesthetics and function is often necessary. Orchiopexy is performed to correct intra-abdominal testes. Because extraurinary anomalies are common, a thorough evaluation, especially for cardiac defects, should be performed.

## REFERENCES

- Bonilla-Musoles F, Machado LE, Bailao LA, et al: Abdominal wall defects: two- versus three-dimensional ultrasonographic diagnosis. *J Ultrasound Med* 20(4):379–389, 2001.
- Clayton DB, Brock JW, 3rd: Lower urinary tract obstruction in the fetus and neonate. *Clin Perinatol* 41(3):643–659, 2014.
- Hassett S, Smith GH, Holland AJ: Prune belly syndrome. *Pediatr Surg Int* 28(3):219–228, 2012.
- Hoshino T, Ihara Y, Shirane H, Ota T: Prenatal diagnosis of prune belly syndrome at 12 weeks of pregnancy: case report and review of the literature. *Ultrasound Obstet Gynecol* 12(5):362–366, 1998.
- Leeners B, Sauer I, Funk A: [Prune belly syndrome—diagnosis and therapeutic possibilities]. *Zeitschr Geburtshilfe Neonatol* 203(4):183–186, 1999.
- Leeners B, Sauer I, Schefels J, et al: Prune-belly syndrome: therapeutic options including in utero placement of a vesicoamniotic shunt. *J Clin Ultrasound* 28(9):500–507, 2000.
- Muller Brochut AC, Thomann D, Kluge W, et al: Fetal megacystis: experience of a single tertiary center in Switzerland over 20 years. *Fetal Diagn Ther* 36(3):215–222, 2014.
- Perez-Brayfield MR, Gatti J, Berkman S, et al: In utero intervention in a patient with prune-belly syndrome and severe urethral hypoplasia. *Urology* 57(6):1178, 2001.

Saliu HM, Tchuinguem G, Aliyu MH, Kouam L: Prune belly syndrome and associated malformations. A 13-year experience from a developing country. *West Indian Med J* 52(4):281–284, 2003.

Tonni G, Ida V, Alessandro V, Bonasoni MP: Prune-belly syndrome: case series and review of the literature regarding early prenatal diagnosis, epidemiology, genetic factors, treatment, and prognosis. *Fetal Pediatr Pathol* 31(1):13–24, 2013.

## GENITOURINARY TRACT

### Renal Tract Anomalies

Mild abnormalities of the kidneys and urinary tract are seen in approximately 5 in 1000 births. Many anomalies are isolated and some, such as autosomal recessive polycystic kidney disease, have a known genetic cause (see Chapter 15, The Fetal Genitourinary Tract). Complete renal agenesis is incompatible with extrauterine life and the resultant oligohydramnios can lead to Potter sequence that includes pulmonary hypoplasia and musculoskeletal abnormalities. Other renal tract anomalies are associated with fetal syndromes, and a few notable examples are reviewed here.

### Fraser Syndrome

**Definition.** Fraser syndrome is characterized by cryptophthalmos, cutaneous syndactyly of the hands and feet, and anomalies of the respiratory and urogenital tracts (ambiguous genitalia and renal agenesis).

**Synonym.** Fraser syndrome is also known as cryptophthalmos-syndactyly syndrome.

**Incidence.** Incidence is 0.043 per 10,000 liveborn infants and 1.1 per 10,000 stillbirths.

**Etiology.** The proteins encoded by *FRAS1* and *FREM* form a complex expressed in basement membranes during embryonic development; this complex is involved in epithelial-mesenchymal integrity. *GRIPI* encodes a scaffolding protein that interacts with *FRAS1/FREM* protein complexes and helps to localize the complex to the basal side of cells.

**Genetics.** The genetic cause is heterogeneous and includes mutations in *FRAS1*, *FREM2*, or *GRIPI*. Inheritance is autosomal recessive with marked intrafamilial variability.

**Recurrence Risk.** Recurrence risk is 25% if both parents are found to be mutation carriers.

**Diagnosis.** The diagnosis is based on the combination major and minor characteristics, where three major, or two major and two minor, or one major and three minor diagnostic criteria are present. The

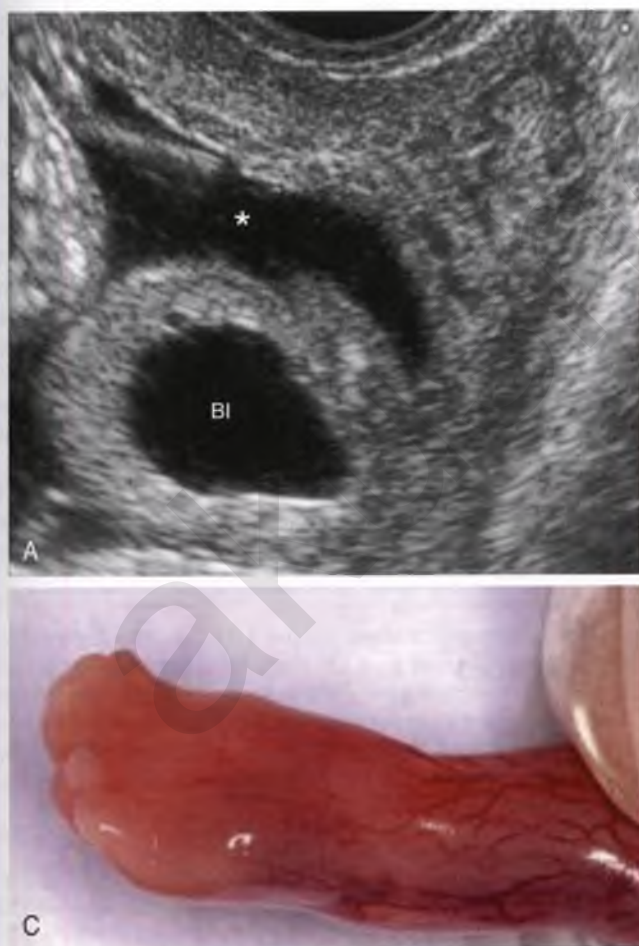


**FIG 16-75** A case of Fraser syndrome diagnosed at 16 weeks' gestation. Megacystis, syndactyly, and oligohydramnios were seen. **A**, Sonogram demonstrating megacystis and ascites (asterisk). **B** and **C**, Neonatal images. Note the distention of the abdominal wall and the postmortem feet with syndactyly between the first, second, and third digits. (Courtesy of Fabrice Cuillier, 2005. Available at thefetus.net.)





**FIG 16-76** Sonogram of another fetus with laryngeal atresia and Fraser syndrome. Bilateral enlarged hyperechogenic lungs, fluid-filled bronchi (arrows), and ascites (asterisk) were present.

major criteria include syndactyly, cryptophthalmos, urinary tract anomalies, ambiguous genitalia, laryngeal or tracheal anomalies, and positive family history. The minor criteria include anorectal defects, dysplastic ears, abnormal skull ossification, umbilical anomalies, and nasal anomalies. Other features include cleft lip  $\pm$  palate; skeletal anomalies; cardiac malformations; and anal atresia. Many of these anomalies can be seen prenatally, but the specific diagnosis may be difficult to determine until after birth.

**Differential Diagnosis.** Other syndromes with syndactyly, renal agenesis, and laryngeal anomalies include cutis aplasia, Nager acrofacial

dysostosis, and Pallister-Hall syndrome, but they are all distinct from Fraser syndrome.

**Prognosis.** The syndrome is fatal if laryngeal atresia or bilateral renal agenesis is present. If cryptophthalmos is present, even surgical repair will yield very poor vision (i.e., 20/200 and 20/360) in the rare correctable cases.

## REFERENCES

- Berg C, Geipel A, Germer U, et al: Prenatal detection of Fraser syndrome without cryptophthalmos: case report and review of the literature. *Ultrasound Obstet Gynecol* 18(1):76–80, 2001.
- Lesniewicz R, Sulik M, Midro AT: [Microphthalmos and hypertelorism as diagnostic index in ultrasound diagnosis of Fraser syndrome]. *Ginekol Pol* 76(2):147–152, 2005.
- Okumus N, Onal EE, Turkyilmaz C, et al: Resuscitation failure due to Fraser syndrome in a newborn undiagnosed in the prenatal period. *Resuscitation* 65(2):221–223, 2005.
- Prasun P, Pradhan M, Goel H: Intrafamilial variability in Fraser syndrome. *Prenat Diagn* 27(8):778–782, 2007.
- Schanze D, Kayserili H, Satkin BN, et al: Fraser syndrome due to mutations in GRIP1—clinical phenotype in two families and expansion of the mutation spectrum. *Am J Med Genet A* 164A(3):837–840, 2014.
- van Haelst MM, Maiburg M, Baujat G, et al: Molecular study of 33 families with Fraser syndrome new data and mutation review. *Am J Med Genet A* 146A(17):2252–2257, 2008.
- van Haelst MM, Scambler PJ, Fraser Syndrome Collaboration Group, Hennekam RC: Fraser syndrome: a clinical study of 59 cases and evaluation of diagnostic criteria. *Am J Med Genet A* 143A(24):3194–3203, 2007.
- Vogel MJ, van Zon P, Brueton L, et al: Mutations in GRIP1 cause Fraser syndrome. *J Med Genet* 49(5):303–306, 2012.

## Meckel Syndrome

See “Central Nervous System.”

## Megacystis-Microcolon-Intestinal Hypoperistalsis Syndrome

See “Gastrointestinal System Disorders.” This syndrome is associated with megacystis (enlarged fetal bladder) in the absence of urinary tract obstruction.

## MURCS Association

**Definition.** MURCS association is an atypical form of Mayer-Rokitansky-Kuster-Hauser (MRKH) syndrome. MURCS stands for müllerian duct aplasia (MU), congenital renal dysplasia (R), and cervical somite anomalies (CS). It is characterized by uterovaginal atresia in females, with associated kidney and skeletal anomalies. Cardiac and otologic anomalies can also be seen.

**Synonym.** MURCS association is also known as MRKH syndrome type 2 or atypical MRKH.

**Incidence.** Incidence is estimated at 1 in 50,000.

**Genetics.** Little is known. A heterogeneous genetic cause has been suggested, with both familial and sporadic cases reported. Some cases of MRKH have been linked to mutations in *LHX1* or *TBX6*. Familial cases appear to demonstrate autosomal dominant inheritance with incomplete penetrance.

**Recurrence Risk.** Recurrence risk is variable depending on cause.

**Diagnosis.** Prenatally, müllerian anomalies are difficult to detect, and the diagnosis may be suspected based on renal and vertebral anomalies.

**Differential Diagnosis.** Other conditions with renal, müllerian, and vertebral anomalies, such as VACTERL, are considered in the differential diagnosis.

**Management.** First-degree relatives of affected patients can have isolated renal anomalies and should undergo screening by renal sonography.

## REFERENCES

- Herlin M, Hojland AT, Petersen MB: Familial occurrence of Mayer-Rokitansky-Kuster-Hauser syndrome: a case report and review of the literature. *Am J Med Genet A* 164A(9):2276–2286, 2014.
- Ledig S, Brucker S, Barresi G, et al: Frame shift mutation of *LHX1* is associated with Mayer-Rokitansky-Kuster-Hauser (MRKH) syndrome. *Hum Reprod* 27(9):2872–2875, 2012.
- Sandbacka M, Laivuori H, Freitas E, et al: *TBX6*, *LHX1* and copy number variations in the complex genetics of Mullerian aplasia. *Orphanet J Rare Dis* 8:125, 2013.

**Perlman Syndrome**

See “Fetal Overgrowth.” Associated renal anomalies include nephromegaly, as well as hyperechogenic kidneys and hydronephrosis.

**Genital Anomalies**

Male genital anomalies are common, particularly hypospadias and epispadias. These anomalies are often isolated but can be seen in association with many different fetal syndromes. Female genital anomalies can include ovarian cysts, vaginal and uterine malformations, and ambiguous genitalia (particularly in the setting of an adrenogenital syndrome, such as 21-hydroxylase deficiency due to *CYP21A2* gene mutations) (see Chapter 15, The Fetal Genitourinary Tract). Patients with disorders of sex development should be evaluated by a multidisciplinary team. Common diagnoses include congenital adrenal hyperplasia, androgen insensitivity, mixed gonadal dysgenesis, clitoral/labial anomalies, hypogonadotropic hypogonadism, and hypospadias. Multi-

system genetic conditions associated with ambiguous genitalia include Antley-Bixler syndrome, campomelic dysplasia, CHARGE syndrome, Denys-Drash syndrome, Fraser syndrome, Pallister-Hall syndrome, Robinow syndrome, SLO syndrome, WAGR syndrome, X-linked lisencephaly with ambiguous genitalia (XLAG), and X-linked Opitz G/BBB syndrome. These conditions should be suggested by their associated clinical findings.

**REFERENCES**

- Adam MP, Fechner PY, Ramsdell LA, et al: Ambiguous genitalia: what prenatal genetic testing is practical? *Am J Med Genet A* 158A(6):1337–1343, 2012.
- Parisi MA, Ramsdell LA, Burns MW, et al: A gender assessment team: experience with 250 patients over a period of 25 years. *Genet Med* 9(6):348–357, 2007.

**ABNORMAL FETAL MOVEMENT****Antley-Bixler Syndrome**

See earlier discussion under “Craniosynostoses.”

**Caudal Regression Syndrome**

See previous discussion under “Teratogens.”

**Congenital Ichthyosis****Definition**

Congenital ichthyosis represents a group of conditions with varying severity; the most severe form is harlequin ichthyosis. In harlequin ichthyosis, infants are often born prematurely and are noted to be encased in hard, thick skin that appears armor-like and severely restricts movement. The thick skin results in deformities of the face, head, and extremities.

**Synonyms**

Congenital ichthyosis is also called harlequin syndrome or harlequin ichthyosis.

**Prevalence**

Prevalence is 1 in 200,000 for all types of congenital ichthyosis; the harlequin ichthyosis phenotype is very rare.

**Etiology**

*ABCA12* encodes for an ATP-binding cassette transporter important for the transport of epidermal lipids and their processing enzymes in the upper layers of the epidermis. Mutations lead to the improper formation of lamellar bodies, thereby preventing formation of lipid bilayers in the stratum corneum and causing hyperkeratosis and abnormal barrier function of the skin.

**Genetics**

Congenital ichthyosis is caused by mutations in several different genes; harlequin ichthyosis is generally caused by mutations in *ABCA12* (>93%). Inheritance is autosomal recessive.

**Recurrence Risk**

Recurrence risk is 25% if both parents are mutation carriers.

**Diagnosis**

The diagnosis is based on skin findings seen at birth. The skin is thick and hard, and plates of cornified skin are often separated by deep fissures. Facial features appear deformed, and microcephaly is often present. Prenatally, facial dysmorphism (fixed open mouth, fringed lip, short nasal bone, hypertrophic palpebral fissures), clenched hands and feet, growth restriction, and hyperechogenic amniotic fluid may be seen. Decreased fetal movement may be reported.

**Differential Diagnosis**

The differential diagnosis includes Sjögren-Larsson syndrome, Netherton syndrome, Gaucher disease, keratitis-ichthyosis-deafness syndrome, trichothiodystrophy, hypohidrotic ectodermal dysplasia, and epidermolytic and superficial epidermolytic ichthyosis.

**Prognosis**

Harlequin ichthyosis is often lethal from respiratory distress, feeding issues, dehydration, electrolyte imbalance, temperature instability, and systemic infection. Children who survive shed the thick skin and then develop intense redness of the skin with scaling (erythroderma).

**REFERENCES**

- Richard G, Bale SJ: Autosomal recessive congenital ichthyosis. In Pagon RA, Adam MP, Ardinger HH, et al, editors: *GeneReviews*, Seattle, 1993–2016, University of Washington.
- Tourette C, Tron E, Mallet S, et al: Three-dimensional ultrasound prenatal diagnosis of congenital ichthyosis: contribution of molecular biology. *Prenat Diagn* 32(5):498–500, 2012.



## Congenital Myasthenic Syndromes

### Definition

Congenital myasthenic syndromes (CMSs) are a group of syndromes characterized by fatigability of skeletal muscle. Affected muscles are generally ocular, bulbar, and limb muscles; smooth muscle and cardiac muscle are not involved. In the subtype with neonatal onset, other findings include eyelid ptosis, feeding issues, apnea, and arthrogryposis multiplex congenita (multiple congenital contractures in different body locations).

### Synonyms

CMSs include congenital myasthenia.

### Prevalence

The CMSs are rare; prevalence is estimated at 2.5 to 12.5 in 1 million.

### Etiology

The implicated genes encode for proteins involved in neuromuscular junction function and different types of alterations in these proteins lead to the observed clinical phenotypes.

### Genetics

These syndromes are due to mutations in one of multiple genes encoding for proteins expressed at the neuromuscular junction. Implicated genes include *CHRNE*, *CHRNA1*, *CHRNB1*, *CHRND* (autosomal dominant or recessive inheritance), as well as *AGRN*, *CHAT*, *COLQ*, *DOK7*, *GFPT1*, *MUSK*, *RAPSN*, and *SCN4A* (autosomal recessive inheritance). There is significant variability in the severity of clinical disease.

### Recurrence Risk

Recurrence risk depends on mode of inheritance. For autosomal recessive subtypes, recurrence is 25% if both parents are carriers. For autosomal dominant subtypes, some are de novo with low recurrence risk; if a parent is affected, the recurrence risk is 50%.

### Diagnosis

The diagnosis of CMS is based on a combination of clinical findings, including skeletal muscle weakness, characteristic electromyographic

findings (decremental response of the compound muscle action potential with low-frequency stimulation), absence of antiacetylcholine receptor and anti-MuSK antibodies in the blood, and failure of symptoms to improve with immunosuppression. Other features include hypotonia, congenital contractures, facial dysmorphism (high-arched palate, elongated face), and waddling gait. Symptoms usually present in the first 2 years of life. Prenatally, there may be maternal reports of decreased fetal movement. Sonographically, lack of fetal mobility and abnormal fetal positioning may be noted. Fixed flexion abnormalities of the joints may be seen. Additionally, increased nuchal translucency and polyhydramnios have been reported.

### Differential Diagnosis

The differential diagnosis includes myasthenia gravis, spinal muscular atrophy, and congenital muscular dystrophies.

### Prognosis

The prognosis depends on the severity of the presentation. Sudden apnea and cyanosis can be seen in neonates. Feeding difficulties and choking spells are common. Muscles are easily fatigued, but cognition, sensation, and coordination are normal.

### Management

Patients with CMS generally benefit from therapy with acetylcholine esterase inhibitors or the potassium channel blocker 3,4-diaminopyridine.

## REFERENCES

- Abicht A, Dusl M, Gallenmuller C, et al: Congenital myasthenic syndromes: achievements and limitations of phenotype-guided gene-after-gene sequencing in diagnostic practice: a study of 680 patients. *Hum Mutat* 33(10):1474–1484, 2012.
- Abicht A, Muller J, Lochmuller H: Congenital myasthenic syndromes. In Pagon RA, Adam MP, Ardinger HH, et al, editors: *GeneReviews*, Seattle, 1993–2016, University of Washington.
- Kalampokas E, Kalampokas T, Sofoudis C, et al: Diagnosing arthrogryposis multiplex congenita: a review. *ISRN Obstet Gynecol* 2012:264918, 2012.
- Lammens M, Moerman P, Fryns JP, et al: Fetal akinesia sequence caused by nemaline myopathy. *Neuropediatrics* 28(2):116–119, 1997.

## Congenital Myotonic Dystrophy, Type 1

### Definition

Congenital myotonic dystrophy, type 1 (congenital DM1), is characterized by hypotonia and severe generalized weakness at birth. Respiratory insufficiency is common. Less severe forms (mild and classic) associated with later onset and milder symptoms also exist.

### Prevalence

Prevalence is 1 in 20,000 for all groups of myotonic dystrophy, type 1.

### Etiology

*DMPK* encodes for myotonin-protein kinase, a serine-threonine protein kinase, that is localized in the heart and skeletal muscle at locations important for intercellular conduction and impulse transmission. The effects of the CTG repeat are complex and still under investigation.

### Genetics

Congenital DM1 is due to expansion of a trinucleotide repeat (CTG) in a noncoding region of the gene *DMPK*. This congenital form is due to a CTG repeat size of more than 1000; more than 50 CTG repeats are associated with disease manifestations. Inheritance is autosomal dominant.

### Recurrence Risk

If a parent has an expanded CTG repeat, there is a 50% chance for each child to inherit the mutant allele. The CTG repeat can expand during gametogenesis, increasing the risk that children will have more severe disease than their affected parents. Expansion is more likely with maternal transmission of the disease.

### Diagnosis

The diagnosis of congenital DM1 is generally suspected on the basis of clinical features in neonates including hypotonia, generalized

weakness (including facial muscle weakness with a tented upper lip), and respiratory insufficiency. CNS findings include cerebral atrophy and ventricular dilation. Prenatally, polyhydramnios, clubfeet, mild ventriculomegaly, and decreased fetal movement are often reported.

### Differential Diagnosis

The differential diagnosis includes other myopathies and congenital muscular dystrophies.

### Prognosis

Congenital DM1 often leads to early death, with average life span of 4 to 5 years. Fatality from respiratory failure is common. Infants who

survive often have gradual improvement in motor function, but develop progressive myopathy and may also have cataracts and cardiac problems. Intellectual disability is present in 50% to 60%.

### REFERENCES

- Bird TD: Myotonic dystrophy type 1. In Pagon RA, Adam MP, Ardinger HH, et al, editors: *GeneReviews*, Seattle, 1993–2016, University of Washington.
- Zaki M, Boyd PA, Impey L, et al: Congenital myotonic dystrophy: prenatal ultrasound findings and pregnancy outcome. *Ultrasound Obstet Gynecol* 29(3):284–288, 2007.

## Fetal Akinesia

### Definition

Fetal akinesia is a heterogeneous group of disorders unified by the hallmark of reduced or absent fetal movement. Labels given to subsets of this group include fetal akinesia deformation sequence (FADS), fetal hypokinesia sequence, Pena-Shokeir syndrome, arthrogryposis multiplex congenita, and multiple pterygia syndrome.

### Incidence

The incidence is unknown; fetal akinesia is rare.

### Etiology

The cause of these disorders is heterogeneous and continues to be elucidated. Implicated defects can be located at any point in the motor system, including the brain, spinal cord, peripheral nerves, neuromuscular junction, skeletal muscle, and connective tissue. Fetal movement begins at 8 weeks' gestation; it begins centrally and moves outward and downward, with all limbs moving by 12 weeks' gestation. Fetal movement is crucial for normal development of the joints and contiguous tissues. The earlier the onset of lack of movement starts and the longer it continues the worse the resulting deformations will be.

### Genetics

A subset of cases of fetal akinesia have an identifiable genetic mutation (see Table 16-8); many cases do not have a genetic cause identified. Lethal multiple pterygium syndrome has recently been linked to biallelic mutations in *CHRNA3*.

### Recurrence Risk

Recurrence risk depends on cause and can range from a low recurrence risk to 25%.

### Diagnosis

Multiple anomalies are associated with fetal akinesia. They include arthrogryposis, pterygia, subcutaneous edema/fetal hydrops, cleft palate, retromicrognathia, lung hypoplasia, rocker-bottom feet, brain anomalies, short umbilical cord, and polyhydramnios (as a result of decreased fetal swallowing). The diagnosis may be made by sonography as early as 12 weeks' gestation because of fetal edema and abnormal limb positioning.

### Differential Diagnosis

The differential diagnosis includes other conditions with multiple congenital contractures, as well as conditions presenting with fetal hydrops (which includes aneuploidy and Turner syndrome in the first trimester).

### Prognosis

Most severe cases result in either stillbirth or death at birth or in the newborn period from pulmonary hypoplasia.



**FIG 16-77** Arthrogryposis multiplex. Fixed flexion deformity of the hips. Bilateral congenital talipes equinovarus is also noted. (Courtesy of S. Manohar, MD, 2004. Available at thefetus.net.)



**FIG 16-78** Postnatal image of a fetus with arthrogryposis multiplex. (Courtesy of S. Manohar, MD, 2004. Available at thefetus.net.)



TABLE 16-8 Genes Associated With Fetal Akinesia

Gene	MIM	Mode of Inheritance	Disease Entity
Genes involved in motor neuron development and survival			
<i>SMN1</i>	600354	AR	SMA, FADS
<i>ERBB3</i>	190151	AR	LCCS2
<i>GLE1</i>	603371	AR	LCCS1, LAAHD
<i>PIP5K1C</i>	606102	AR	LCCS3
<i>UBE1</i>	314370	XL	XL-SMA
Genes encoding components of the neuromuscular junction			
<i>CHRNA1</i>	100690	AR	FADS
<i>CHRND</i>	100720	AR	AMC/CMS with fetal akinesia; FADS
<i>CHRNA3</i>	100730	AR	Lethal and EV MPS
<i>CNTN1</i>	600016	AR	CM with fetal akinesia
<i>DOK7</i>	610285	AR	FADS
<i>SYNE1</i>	608441	AR	AMC with fetal akinesia
<i>RAPSN</i>	601592	AR	AMC, FADS
Genes encoding adult skeletal muscle proteins			
<i>ACTA1</i>	102610	AD	FADS
<i>BIN1</i>	601248	AR	CNM with fetal akinesia
<i>DMPK</i>	605377	AD	FADS/DM
<i>FKBP</i>	606596	AR	WWS with fetal akinesia
<i>LMNA</i>	150330	AR	LGMD1B with fetal akinesia
<i>MTM1</i>	300415	XL	MTM with fetal akinesia
<i>NEB</i>	161650	AR	FADS
<i>RYR1</i>	180901	AR, AD	FADS, CRM with fetal akinesia
<i>TPM2</i>	190990	AR, AD	EV MPS, DA1, DA2B
<i>TNNI2</i>	191043	AD	DA1, DA2B
<i>TNNT3</i>	600692	AD	DA1, DA2B
Genes encoding fetally expressed myostructural proteins			
<i>MYH3</i>	160270	AD	DA2A, DA2B
<i>MYH8</i>	160741	AD	CC-DA7, DA7
<i>MYBPC1</i>	160794	AD	DA1
<i>UTRN</i>	128240		Arthrogyrosis with fetal akinesia
Other genes			
<i>FGFR2</i>	176943	AD	FADS
<i>GBE1</i>	607839	AR	GSD-IV/FADS

AD, autosomal dominant; AMC, arthrogyrosis multiplex congenita; AR, autosomal recessive; CC, Carney complex; CM, congenital myopathy; CMS, congenital myasthenic syndrome; CNM, centronuclear myopathy; CRM, core-rod myopathy; DA, distal arthrogyrosis; DM, myotonic dystrophy; DMPK, dystrophin myotonia protein kinase; EV, Escobar variant; FADS, fetal akinesia deformation sequence; GSD-IV, glycogen storage disease type IV; LAAHD, lethal arthrogyrosis with anterior horn cell disease; LCCS, lethal congenital contracture syndrome; LGMD1B, limb-girdle muscular dystrophy type 1B; MPS, multiple pterygia syndrome; MIM, Mendelian Inheritance in Man; MTM, myotubular myopathy; SMA, spinal muscular atrophy; WWS, Walker-Warburg syndrome; XL, X-linked.

From Ravenscroft G, Sollis E, Charles AK, et al: Fetal akinesia: review of the genetics of the neuromuscular causes. *J Med Genet* 48:793-801, 2011, Table 1.

## REFERENCES

- Abicht A, Muller J, Lochmuller H: Congenital myasthenic syndromes. In Pagon RA, Adam MP, Ardinger HH, et al, editors: *GeneReviews*, Seattle, 1993–2016, University of Washington.
- Cox PM, Brueton LA, Bjelogric P, et al: Diversity of neuromuscular pathology in lethal multiple pterygium syndrome. *Pediatr Dev Pathol* 6(1):59–68, 2003.
- Entezami M, Runkel S, Kunze J, et al: Prenatal diagnosis of a lethal multiple pterygium syndrome type II. Case report. *Fetal Diagn Ther* 13(1):35–38, 1998.
- Hall JG: Pena-Shokeir phenotype (fetal akinesia deformation sequence) revisited. *Birth Defects Res A Clin Mol Teratol* 85(8):677–694, 2009.
- Landau D, Mishori-Dery A, Hershkovitz R, et al: A new autosomal recessive congenital contractural syndrome in an Israeli Bedouin kindred. *Am J Med Genet A* 117A(1):37–40, 2003.
- Paladini D, Tartaglione A, Agangi A, et al: Pena-Shokeir phenotype with variable onset in three consecutive pregnancies. *Ultrasound Obstet Gynecol* 17(2):163–165, 2001.
- Ravenscroft G, Sollis E, Charles AK, et al: Fetal akinesia: review of the genetics of the neuromuscular causes. *J Med Genet* 48(12):793–801, 2011.
- Sergi C, Poeschl J, Graf M, Linderkamp O: Restrictive dermopathy: case report, subject review with Kaplan-Meier analysis, and differential diagnosis of the lethal congenital contractural syndromes. *Am J Perinatol* 18(1):39–47, 2001.

## Freeman-Sheldon Syndrome

### Definition

Freeman-Sheldon syndrome is a distal arthrogryposis syndrome characterized by multiple congenital contractures of both the upper and lower limbs (as well as facial muscles) and is generally considered to be the most severe of the distal arthrogryposis syndromes. Because of facial muscle contractures, the lips appear pursed and a small oral opening is observed. The hands demonstrate camptodactyly with ulnar deviation of the fingers, and clubfeet are present.

### Synonyms

Freeman-Sheldon syndrome is also known as distal arthrogryposis type 2A (DA2A) and whistling-face syndrome.

### Prevalence

The syndrome is rare.

### Etiology

*MYH3* encodes for the embryonic myosin heavy chain and the implicated *MHY3* mutations are predicted to interfere with myosin's catalytic activity, suggesting that defective myofiber force prenatally leads to congenital contractures.

### Genetics

Freeman-Sheldon syndrome is due to mutations in *MYH3*. Inheritance is autosomal dominant. More than 70% of cases are sporadic. Wide phenotypic variability is seen.

### Recurrence Risk

With sporadic mutations, recurrence risk is low. Recurrence risk is 50% with an affected parent.

## Prader-Willi Syndrome

### Definition

Prader-Willi syndrome (PWS) is characterized by severe infantile hypotonia and feeding difficulties. Subsequently, excessive eating in childhood leads to the development of morbid obesity. Other features include developmental delay, cognitive impairment, behavioral issues, hypogonadism, short stature, and characteristic facial features (narrow bifrontal diameter, almond-shaped palpebral fissures, narrow nasal bridge, thin upper lip, downturned mouth).

### Synonym

Prader-Labhart-Willi syndrome is another name for the syndrome.

### Prevalence

Prevalence is 1 in 10,000 to 30,000.

### Etiology

The exact function of the genes within the Prader-Willi critical region are still being investigated.

### Genetics

Abnormal imprinting within the paternally derived Prader-Willi critical region (PWR) on chromosome 15 (15q11.2-q13) can be detected by DNA methylation analysis. Abnormal imprinting can be caused by paternal deletion, maternal uniparental disomy 15, or an imprinting defect. Although DNA methylation can establish the diagnosis, it cannot determine the mechanism; thus, further testing is needed if DNA methylation testing is positive for PWS.

### Diagnosis

The diagnosis is based on clinical features including multiple distal contractures and characteristic facial appearance (small oral opening, hypertelorism, epicanthus, telecanthus, hypoplastic nasal alae, low-set ears, "H-shaped" chin dimple). Other anomalies may include scoliosis, rib anomalies, short stature, dental crowding, spinal bifida occulta, cryptorchidism, and congenital hip dysplasia or dislocation. Prenatally, joint contractures and facial dysmorphism may be appreciated.

### Differential Diagnosis

The differential diagnosis includes other distal arthrogryposis syndromes, in particular distal arthrogryposis type 2B. Molecular genetic testing can assist in confirming the diagnosis.

### Prognosis

Anesthesia complications are common (including malignant hyperthermia, arrhythmias, and difficulties with intubation and IV access), and multiple surgeries are needed. Feeding difficulties and aspiration are common. Intelligence is normal.

## REFERENCES

- Beck AE, McMillin MJ, Gildersleeve HI, et al: Genotype-phenotype relationships in Freeman-Sheldon syndrome. *Am J Med Genet A* 164(11):2808–2813, 2014.
- Hegde SS, Shetty MS, Rama Murthy BS: Freeman-Sheldon syndrome—prenatal and postnatal diagnosis. *Indian J Pediatr* 77(2):196–197, 2010.
- Salati SA, Hussain M: Freeman-sheldon syndrome. *APSP J Case Rep* 4(1):7, 2013.
- Toydemir RM, Rutherford A, Whitby FG, et al: Mutations in embryonic myosin heavy chain (*MYH3*) cause Freeman-Sheldon syndrome and Sheldon-Hall syndrome. *Nat Genet* 38(5):561–565, 2006.

### Recurrence Risk

Recurrence risk depends on the mode of abnormal imprinting. Generally, recurrence risk is less than 1% if the prior child had a deletion or uniparental disomy, 50% with an imprinting defect, and 25% with a parental chromosomal translocation.

### Diagnosis

Ultrasound examination may reveal polyhydramnios, decreased fetal movements, malpresentation, characteristic craniofacial features, large biparietal diameter, slightly enlarged lateral ventricles, hypoplasia of the corpus callosum, abnormal fetal heart rhythm with prolonged inactive periods and diurnal variation of the incidence of heart rate accelerations, and hypoplastic male external genitalia. Fetal size is generally normal. Other features include strabismus; hypopigmented hair, eyes, and skin; hip dysplasia; and scoliosis.

### Differential Diagnosis

The differential diagnosis includes Angelman syndrome, fragile X syndrome, several myopathies and neuropathies, congenital DM1, and *MECP2*-related disorders.

### Prognosis

Severe hypotonia with associated feeding difficulties lead to failure to thrive in early infancy; enteral feeds are commonly needed. Global developmental delay is generally seen. Choking is a reported cause of death in up to 8% of affected individuals. Feeding improves by age 1 to 2 years, and hyperphagia becomes more prevalent in early childhood. After age 8, hyperphagia predominates and obesity is common.



Hyperphagia has been linked to a hypothalamic abnormality leading to lack of satiety. Obesity is a major cause of morbidity and fatality.

### Management

Guidelines for management have been published (Cassidy SB and colleagues, 2012; McCandless SE, 2011).

## REFERENCES

- Carrel AL, Myers SE, Whitman BY, Allen DB: Growth hormone improves body composition, fat utilization, physical strength and agility, and growth in Prader-Willi syndrome: a controlled study. *J Pediatr* 134(2):215–221, 1999.
- Cassidy SB, Lai LW, Erickson RP, et al: Trisomy 15 with loss of the paternal 15 as a cause of Prader-Willi syndrome due to maternal disomy. *Am J Hum Genet* 51(4):701–708, 1992.
- Cassidy SB, Schwartz S, Miller JL, Driscoll DJ: Prader-Willi syndrome. *Genet Med* 14(1):10–26, 2012.
- Driscoll DJ, Miller JL, Schwartz S, Cassidy SB: Prader-Willi syndrome. In Pagon RA, Adam MP, Ardinger HH, et al, editors: *GeneReviews*, Seattle, 1993–2016, University of Washington.

- Fong BF, De Vries JI: Obstetric aspects of the Prader-Willi syndrome. *Ultrasound Obstet Gynecol* 21(4):389–392, 2003.
- Glenn CC, Deng G, Michaelis RC, et al: DNA methylation analysis with respect to prenatal diagnosis of the Angelman and Prader-Willi syndromes and imprinting. *Prenat Diagn* 20(4):300–306, 2000.
- Gunay-Aygun M, Schwartz S, Heeger S, et al: The changing purpose of Prader-Willi syndrome clinical diagnostic criteria and proposed revised criteria. *Pediatrics* 108(5):E92, 2001.
- Hiroi H, Kozuma S, Hayashi N, et al: A fetus with Prader-Willi syndrome showing normal diurnal rhythm and abnormal ultradian rhythm on heart rate monitoring. *Fetal Diagn Ther* 15(5):304–307, 2000.
- L'Hermine AC, Aboura A, Brisset S, et al: Fetal phenotype of Prader-Willi syndrome due to maternal disomy for chromosome 15. *Prenat Diagn* 23(11):938–943, 2003.
- McCandless SE, Committee on Genetics: Clinical report—health supervision for children with Prader-Willi syndrome. *Pediatrics* 127(1):195–204, 2011.
- Purvis-Smith SG, Saville T, Manass S, et al: Uniparental disomy 15 resulting from “correction” of an initial trisomy 15. *Am J Hum Genet* 50(6):1348–1350, 1992.
- Schinzel A: Approaches to the prenatal diagnosis of the Prader-Willi syndrome. *Hum Genet* 74(3):327, 1986.

## FETAL OVERGROWTH

Congenital overgrowth refers to a newborn weight greater than the 97th percentile and is caused by a heterogeneous group of conditions. A subset of these conditions are overgrowth syndromes and include chromosomal disorders as well as the following syndromes: Bannayan-Riley-Ruvalcaba, Beckwith-Wiedemann, Klippel-Trenaunay, megalencephaly-polymicrogyria-polydactyly-hydrocephalus (MPPH), Perlman, Proteus, Simpson-Golabi-Behmel, Sotos, and Weaver syndromes. Of these syndromes, the ones with the most striking degree of prenatal overgrowth are Beckwith-Wiedemann, MPPH, Perlman,

Simpson-Golabi-Behmel, and Sotos syndromes. Each of these syndromes is described in further detail in this section.

## REFERENCES

- Verloes A, Massart B, Dehalleux I, et al: Clinical overlap of Beckwith-Wiedemann, Perlman and Simpson-Golabi-Behmel syndromes: a diagnostic pitfall. *Clin Genet* 47(5):257–262, 1995.
- Vora N, Bianchi DW: Genetic considerations in the prenatal diagnosis of overgrowth syndromes. *Prenat Diagn* 29(10):923–929, 2009.

## Bannayan-Riley-Ruvalcaba Syndrome

### Definition

Bannayan-Riley-Ruvalcaba syndrome (BRRS) is the most severe disorder in the *PTEN*-related overgrowth spectrum. It is characterized by macrocephaly, lipomatosis, intestinal hamartomatous polyposis, and pigmented penile macules. Developmental delay is common. Capillary malformations can be present, but are generally isolated.

### Prevalence

The prevalence is unknown, but the syndrome is likely underdiagnosed.

### Etiology

Mutations in *PTEN* (a tumor suppressor gene) lead to absent or decreased *PTEN* protein resulting in uninhibited phosphorylation of AKT1. This results in abnormal cell proliferation.

### Genetics

The syndrome is due to mutations in *PTEN*. Inheritance is autosomal dominant.

### Recurrence Risk

Recurrence risk is 50% with an affected parent.

### Diagnosis

Diagnosis is based on the cardinal features described earlier. Official diagnostic criteria have not been set. Other features can include macrocephaly at birth, myopathy of the proximal muscles, joint hyperextensibility, scoliosis, and pectus excavatum.

### Differential Diagnosis

The differential diagnosis postnatally includes other hamartoma syndromes and *PTEN*-related disorders (such as Cowden syndrome).

### Prognosis

Developmental delay and intellectual disability are common (~50% of individuals).

## REFERENCES

- Eng C: *PTEN* hamartoma tumor syndrome (PHTS). In Pagon RA, Adam MP, Ardinger HH, et al, editors: *GeneReviews*, Seattle, 1993–2016, University of Washington.
- Mirzaa G, Conway R, Graham JM, Dobyns WB: PIK3CA-related segmental overgrowth. In Pagon RA, Adam MP, Ardinger HH, et al, editors: *GeneReviews*, Seattle, 1993–2016, University of Washington.

### Beckwith-Wiedemann Syndrome

See “Abdominal Wall Defects.” This is the most common overgrowth syndrome.

### Klippel-Trenaunay Syndrome

#### Definition

Klippel-Trenaunay syndrome (KTS) is characterized by congenital vascular malformations (capillary, venous, or lymphatic) and altered growth of bone and soft tissues (hypertrophy [most common] or hypotrophy [less common] of a small or large body part). Capillary malformations can be located anywhere on the body. The other malformations are generally on the extremities and adjacent regions of the trunk. The vascular malformations are often located in the same body site as the growth disturbance.

#### Synonyms

KTS was previously used synonymously with Klippel-Trenaunay-Weber syndrome and Parkes Weber syndrome. KTS and Parkes Weber syndrome are now considered separate entities, and the use of Klippel-Trenaunay-Weber syndrome is discouraged.

#### Incidence

Incidence is unknown; the syndrome is rare.

#### Etiology

Many hypotheses have been proposed, including multifactorial, polygenic, or a mosaic mutation. A mosaic gene mutation is likely the most plausible, as somatic mutations in components of the PI3K-AKT pathway have been identified in other patchy overgrowth syndromes.

#### Genetics

Genetic factors are unknown; it generally occurs sporadically. It is differentiated from Parkes Weber syndrome by testing for *RASA1* mutations, which are found in Parkes Weber syndrome but not in KTS.

#### Recurrence Risk

Recurrence risk is thought to be low.

#### Diagnosis

The diagnosis is based on the clinical features of vascular malformations and disturbed growth of bony and soft tissues. Other common features include limb anomalies (polydactyly, syndactyly), skeletal malformations (scoliosis, hip dislocation, clubfeet), and autonomic dysfunction. Prenatally, asymmetric limb growth may be detected. Other reports of nonimmune hydrops, polyhydramnios, cardiac failure, and ventriculomegaly attributed to KTS may be associated instead with Parkes Weber syndrome.

#### Differential Diagnosis

The differential includes *PI3KCA*-related segmental overgrowth syndromes (such as CLOVES [congenital, lipomatous overgrowth,

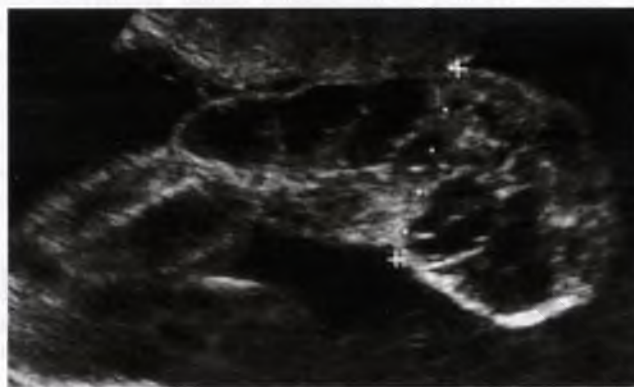


**FIG 16-79** Klippel-Trenaunay syndrome. Sonogram of the leg of a fetus at 20 weeks' gestation with marked edema. (Courtesy of Carlos Alberto Mejia Escobar, 2000. Available at thefetus.net.)

vascular malformations, epidermal nevi and scoliosis/skeletal/spinal anomalies]), Parkes Weber syndrome, and Proteus syndrome.

#### Prognosis

Patients with KTS are at risk for superficial thrombophlebitis, deep venous thrombosis, pulmonary embolism, and infection. Leg length discrepancy is common. Procedures to remove excess girth of soft tissues are possible.

### REFERENCES

- Cakiroglu Y, Doger E, Yildirim Kopuk S, et al: Sonographic identification of Klippel-Trenaunay-Weber syndrome. *Case Rep Obstet Gynecol* 2013:595476, 2013.
- Happle R: Mosaicism in human skin. Understanding the patterns and mechanisms. *Arch Dermatol* 129(11):1460–1470, 1993.
- Heydanus R, Wladimiroff JW, Brandenburg H, et al: Prenatal diagnosis of Klippel-Trenaunay-Weber syndrome: a case report. *Ultrasound Obstet Gynecol* 2(5):360–363, 1992.
- Oduber CE, van der Horst CM, Hennekam RC: Klippel-Trenaunay syndrome: diagnostic criteria and hypothesis on etiology. *Ann Plast Surg* 60(2):217–223, 2008.
- Rebarber A, Roman AS, Roshan D, Blei F: Obstetric management of Klippel-Trenaunay syndrome. *Obstet Gynecol* 104(5 Pt 2):1205–1208, 2004.
- Revencu N, Boon LM, Domp Martin A, et al: Germline mutations in *RASA1* are not found in patients with Klippel-Trenaunay syndrome or capillary malformation with limb overgrowth. *Mol Syndromol* 4(4):173–178, 2013.
- Sahinoglu Z, Uludogan M, Delikara NM: Prenatal sonographic diagnosis of Klippel-Trenaunay-Weber syndrome associated with umbilical cord hemangioma. *Am J Perinatol* 20(1):1–6, 2003.
- Yang JI, Kim HS, Ryu HS: Prenatal sonographic diagnosis of Klippel-Trenaunay-Weber syndrome: a case report. *J Reprod Med* 50(4):291–294, 2005.

### Megalencephaly-Polymicrogyria-Polydactyly-Hydrocephalus Syndrome

#### Definition

MPPH syndrome is characterized by congenital megalencephaly, bilateral perisylvian polymicrogyria, and postaxial polydactyly. It is associated with an increased risk of hydrocephalus.

#### Prevalence

Prevalence is unknown; the syndrome is only recently recognized.

#### Etiology

The implicated genes are involved in the PI3K-AKT signaling pathway. Mutations are gain of function and lead to activation of



this pathway, resulting in uncontrolled cellular proliferation and survival.

### Genetics

MPPH is due to de novo mutations in *PIK3R2*, *AKT3*, and *CCND2*.

### Recurrence Risk

Recurrence risk is thought to be low.

### Diagnosis

The diagnosis of MPPH is based on characteristic brain findings including megalencephaly, ventriculomegaly or hydrocephalus, and cortical brain abnormalities (perisylvian polymicrogyria). Postaxial polydactyly is present in a subset of affected individuals.

### Differential Diagnosis

Many features overlap with megalencephaly-capillary malformation (MCAP) syndrome, but MPPH syndrome lacks vascular malformations, focal somatic overgrowth, and syndactyly. Additionally, overgrowth in MPPH tends to be symmetric; asymmetric overgrowth can be seen in MCAP. Other conditions to be considered include hemi-

megalencephaly, Proteus syndrome, and other disorders due to mutations in the PI3K-AKT pathway.

### Prognosis

Progressive ventriculomegaly can lead to hydrocephalus, and Chiari malformations may be present. Head size can be as large as 10 SD above the mean. An increased risk of malignancy has been reported (~3%).

## REFERENCES

- Mirzaa G, Conway R, Graham JM, Dobyns WB: PIK3CA-related segmental overgrowth. In Pagon RA, Adam MP, Ardinger HH, et al, editors: *GeneReviews*, Seattle, 1993-2016, University of Washington.
- Mirzaa GM, Parry DA, Fry AE, et al: De novo *CCND2* mutations leading to stabilization of cyclin D2 cause megalencephaly-polymicrogyria-polydactyly-hydrocephalus syndrome. *Nat Genet* 46(5):510-515, 2014.
- Mirzaa GM, Riviere JB, Dobyns WB: Megalencephaly syndromes and activating mutations in the PI3K-AKT pathway: MPPH and MCAP. *Am J Med Genet C Semin Med Genet* 163C(2):122-130, 2013.
- Riviere JB, Mirzaa GM, O'Roak BJ, et al: De novo germline and postzygotic mutations in *AKT3*, *PIK3R2* and *PIK3CA* cause a spectrum of related megalencephaly syndromes. *Nat Genet* 44(8):934-940, 2012.

## Perlman Syndrome

### Definition

Perlman syndrome is characterized by prenatal overgrowth, dysmorphic facial features (small upturned nose, small mouth, deep-set eyes, low-set ears, crease over the nasal bridge), visceromegaly, and predisposition to Wilms tumor.

### Prevalence

The syndrome is rare.

### Etiology

*DIS3L2* is important in regulation of mitosis and cell proliferation. The mechanism by which mutations lead to the clinical phenotype of Perlman syndrome is currently under investigation.

### Genetics

Perlman syndrome is due to mutations in *DIS3L2*. Inheritance is autosomal recessive.

### Recurrence Risk

Recurrence risk is 25% if both parents are mutation carriers.

### Diagnosis

Prenatally, polyhydramnios, fetal macrosomia, nephromegaly, and fetal ascites are common. Neonatal findings include macrosomia,

nephromegaly, hepatomegaly, hypotonia, abdominal distention, cryptorchidism, and dysmorphic facial features. Nephroblastomatosis and Wilms tumor are common.

### Differential Diagnosis

The differential diagnosis includes other overgrowth syndromes, particularly Simpson-Golabi-Behmel and Beckwith-Wiedemann syndromes.

### Prognosis

Perlman syndrome has a high mortality rate and occurs both as stillbirths and neonatal deaths; more than 50% of affected individuals die in the neonatal period. Approximately two thirds of survivors develop Wilms tumor. Intellectual disability and developmental delay are common.

## REFERENCES

- Alessandri JL, Cuillier F, Ramful D, et al: Perlman syndrome: report, prenatal findings and review. *Am J Med Genet A* 146A(19):2532-2537, 2008.
- Morris MR, Astuti D, Maher ER: Perlman syndrome: overgrowth, Wilms tumor predisposition and *DIS3L2*. *Am J Med Genet C Semin Med Genet* 163C(2):106-113, 2013.

## Proteus Syndrome

### Definition

Proteus syndrome is characterized by progressive, segmental overgrowth of body tissues, most commonly the skeleton, skin, adipose tissue, and CNS. Most overgrowth occurs postnatally.

### Prevalence

Proteus syndrome is very rare; approximately 120 cases have been reported.

### Etiology

*AKT1* encodes for a tyrosine kinase. The particular mutation (p.Glu17Lys) associated with Proteus syndrome leads to constitutive kinase activation, which is thought to lead to the observed clinical features.

### Genetics

Proteus syndrome is due to mosaic somatic mutations in *AKT1* (p.Glu17Lys). It is thought that germline *AKT1* mutations would be lethal in early development.

### Recurrence Risk

There is no known risk to offspring of an affected individual because the implicated mutation is somatic.

### Diagnosis

It is distinct from other overgrowth syndromes because most overgrowth is postnatal and is distorting and progressive. A few individuals (<5%) may have the prenatal finding of hemimegalencephaly. Distortion of the skeletal system is characteristic (for example, leg length discrepancy of up to 20 cm and scoliosis greater than 90 degrees). Cerebriform connective tissue nevi are present in most individuals and are virtually pathognomonic. Other features include adipose dysregulation, vascular malformations, bullous pulmonary degeneration, and overgrowth of other organs (spleen, liver, thymus, gut).

### Differential Diagnosis

The differential diagnosis includes PTEN hamartoma tumor syndrome, CLOVES syndrome, hemihyperplasia, and KTS.

## Simpson-Golabi-Behmel Syndrome

### Definition

Simpson-Golabi-Behmel syndrome is characterized by pre- and postnatal overgrowth, a characteristic facial appearance (macrocephaly, coarse facial features, macrostomia, macroglossia, palate anomalies), and intellectual disability. Affected individuals are at high risk for the development of embryonal tumors (~10% of individuals), including Wilms tumor, hepatoblastoma, adrenal neuroblastoma, gonadoblastoma, and hepatocellular carcinoma.

### Prevalence

Prevalence is unknown.

### Etiology

*GPC3* and *GPC4* encode for glypicans, which are important in cell growth and division; the exact mechanisms leading to the clinical features of the syndrome remain unknown.

### Genetics

The syndrome is due to mutations in *GPC3* and *GPC4*. Inheritance is X-linked.

### Recurrence Risk

With a maternal mutation carrier, there is a 50% chance of transmitting the mutation to each child. Males who inherit the mutation will be affected. Females will be carriers, although they can exhibit clinical features owing to skewed X-inactivation.

### Diagnosis

The diagnosis is based on clinical features and a family history suggestive of X-linked inheritance, along with molecular genetic testing. The diagnosis should be considered in the setting of macrosomia, characteristic facial features, and associated congenital anomalies. These anomalies can include CNS anomalies, supernumerary nipples, umbilical hernia, diaphragmatic hernia, congenital heart defects, genitourinary defects, GI anomalies, skeletal anomalies (scoliosis, rib anomalies, fused vertebrae, congenital hip dislocation), and hand anomalies (large hands, postaxial polydactyly). Elevated maternal serum AFP (in the absence of abdominal wall or spine defects) has been reported.

### Prognosis

The overall prognosis depends on the location and degree of overgrowth, as well as coexistent complications. Overgrowth progresses rapidly in childhood and leads to severe disfigurement. The risk of tumor development is increased (most commonly ovarian cystadenomas, testicular tumors, and meningiomas), as along with pulmonary problems and risk of thrombophilia (deep venous thrombosis and pulmonary embolism).

## REFERENCE

Biesecker LG, Sapp JC: Proteus syndrome. In Pagon RA, Adam MP, Ardinger HH, et al, editors: *GeneReviews*, Seattle, 1993–2016, University of Washington.

### Differential Diagnosis

The differential diagnosis includes other fetal overgrowth syndromes, including BWS, Weaver syndrome, and Perlman syndrome.

### Prognosis

The intellectual disability can range from mild to severe. Screening for embryonic tumors is generally recommended. The overall prognosis depends on the other anomalies present. Up to 50% of affected males die in the neonatal period.

## REFERENCES

- Day R, Fryer A: Index finger abnormalities in Simpson-Golabi-Behmel syndrome. *Clin Dysmorphol* 14(1):35–36, 2005.
- Golabi M, Leung A, Lopez C: Simpson-Golabi-Behmel syndrome type 1. In Pagon RA, Adam MP, Ardinger HH, et al, editors: *GeneReviews*, Seattle, 1993–2016, University of Washington.
- Hughes-Benzie RM, Tolmie JL, McNay M, Patrick A: Simpson-Golabi-Behmel syndrome: disproportionate fetal overgrowth and elevated maternal serum alpha-fetoprotein. *Prenat Diagn* 14(4):313–318, 1994.
- Konig R, Fuchs S, Kern C, Langenbeck U: Simpson-Golabi-Behmel syndrome with severe cardiac arrhythmias. *Am J Med Genet* 38(2–3):244–247, 1991.
- Li M, Shuman C, Fei YL, et al: *GPC3* mutation analysis in a spectrum of patients with overgrowth expands the phenotype of Simpson-Golabi-Behmel syndrome. *Am J Med Genet* 102(2):161–168, 2001.
- Lin AE, Neri G, Hughes-Benzie R, Weksberg R: Cardiac anomalies in the Simpson-Golabi-Behmel syndrome. *Am J Med Genet* 83(5):378–381, 1999.
- Poetke M, Jamil B, Muller U, Berlien HP: Diffuse neonatal hemangiomatosis associated with Simpson-Golabi-Behmel syndrome: a case report. *Eur J Pediatr Surg* 12(1):59–62, 2002.
- Taniyama T, Kitai N, Iguchi Y, et al: Craniofacial morphology in a patient with Simpson-Golabi-Behmel syndrome. *Cleft Palate Craniofac J* 40(5):550–555, 2003.
- Veugelers M, Cat BD, Muyldermans SY, et al: Mutational analysis of the *GPC3/GPC4* glypican gene cluster on Xq26 in patients with Simpson-Golabi-Behmel syndrome: identification of loss-of-function mutations in the *GPC3* gene. *Hum Mol Genet* 9(9):1321–1328, 2000.
- Yamashita H, Yasuhi I, Ishimaru T, et al: A case of nondiabetic macrosomia with Simpson-Golabi-Behmel syndrome: antenatal sonographic findings. *Fetal Diagn Ther* 10(2):134–138, 1995.



## Sotos Syndrome

### Definition

Sotos syndrome is characterized by pre- and postnatal overgrowth, characteristic facial features, and intellectual disability.

### Synonym

Cerebral gigantism is a synonym.

### Incidence

Incidence is 1 in 14,000 live births.

### Etiology

*NSD1* encodes for a histone methyltransferase involved in transcriptional regulation through histone modification and chromatin remodeling. The mechanism by which *NSD1* mutations lead to the clinical features of Sotos syndrome is not currently known.

### Genetics

Sotos syndrome is due to mutations in *NSD1*. Inheritance is autosomal dominant. More than 95% of mutations are de novo.

### Recurrence Risk

Recurrence risk is low (<1%) if neither parent is a mutation carrier.

### Diagnosis

Sotos syndrome should be considered with overgrowth (>2 SD above the mean) with advanced bone age and characteristic facial features. Facial features include malar flushing, frontal bossing, sparse hair in

the frontotemporal region, downsloping palpebral fissures, long narrow face (triangular shape), and prominent jaw. These features are most apparent between ages 1 and 6. Other associated features include CNS anomalies (ventriculomegaly, midline defects), congenital heart defects, renal anomalies, scoliosis, seizures, and behavioral problems. Maternal preeclampsia occurs in approximately 15% of pregnancies of children with Sotos syndrome.

### Differential Diagnosis

The differential includes other fetal overgrowth syndromes, including BWS, Weaver syndrome, Simpson-Golabi-Behmel syndrome, and Bannayan-Riley-Ruvalcaba syndrome.

### Prognosis

Intellectual disability can range from mild to severe. Developmental delay is common and thought to be due to the overgrowth, as well as hypotonia and poor coordination. Tumors occur in approximately 3% of individuals and include hematologic malignancies, neuroblastoma, and sacrococcygeal teratoma.

## REFERENCES

- Tatton-Brown K, Cole TRP, Rahman N: Sotos syndrome. In Pagon RA, Adam MP, Ardinger HH, et al, editors: *GeneReviews*, Seattle, 1993–2016, University of Washington.
- Tatton-Brown K, Rahman N: The *NSD1* and *EZH2* overgrowth genes, similarities and differences. *Am J Med Genet C Semin Med Genet* 163C(2):86–91, 2013.

## Weaver Syndrome

### Definition

Weaver syndrome is characterized by tall stature, characteristic facial features, and other clinical features (advanced bone age, poor coordination, umbilical hernia, abnormal tone, hoarse cry, camptodactyly of fingers or toes).

### Synonym

*EZH2*-related overgrowth also describes Weaver syndrome.

### Prevalence

Prevalence is unknown; the genetics were recently discovered and more mildly affected individuals are likely to remain undiagnosed.

### Etiology

*EZH2* encodes for a histone methyltransferase involved in regulation of transcription. The mechanisms by which *EZH2* mutations lead to the clinical features of Weaver syndrome are currently unknown.

### Genetics

The syndrome is due to mutations in *EZH2*. Inheritance is autosomal dominant. Many mutations are de novo.

### Recurrence Risk

Recurrence risk is 50% with an affected parent.

### Diagnosis

The diagnosis is based on tall stature (height > 2 SD), characteristic facial appearance (retrognathia, large fleshy ears, “stuck on” appearance of chin with central dimple, hypertelorism, round face and cheeks, broad forehead, and almond-shaped palpebral fissures), and other associated anomalies.

### Differential Diagnosis

The differential diagnosis includes other fetal overgrowth syndromes, including Sotos syndrome, BWS, and Simpson-Golabi-Behmel syndrome.

### Prognosis

Intellect can range from normal to severe intellectual disability. Malignancies may occur more frequently, in particular neuroblastoma and hematologic malignancies.

## REFERENCE

- Tatton-Brown K, Rahman N: *EZH2*-related overgrowth. In Pagon RA, Adam MP, Ardinger HH, et al, editors: *GeneReviews*, Seattle, 1993–2016, University of Washington.

## FETAL GROWTH RESTRICTION

Although fetal growth restriction is relatively common, severe early-onset growth restriction should raise concern for an underlying genetic or metabolic disorder. Underlying chromosomal disorders, including aneuploidy, triploidy, and microdeletion syndromes, should be at the top of the differential diagnosis. Metabolic disorders should also be considered (see later). Many of the single gene disorders discussed in the preceding sections are also associated with growth restriction and should be considered based on other sonographic findings that are present. A few additional syndromes with the hallmark of severe prenatal growth restriction are discussed here, specifically Russell-Silver syndrome (RSS) (characterized by severe growth restriction and normal head circumference) and Seckel syndrome (characterized by growth restriction and severe microcephaly).

### Russell-Silver Syndrome

#### Definition

RSS is characterized by severe fetal growth restriction (with birth weight  $> -2$  SD below the mean), as well as postnatal growth deficiency. Other features include short stature, normal head circumference, clinodactyly of the fifth finger, characteristic facial features (triangular facies with a broad forehead and narrow chin), and asymmetry of the limbs, body, and/or face.

#### Prevalence

Prevalence is estimated at 1 in 100,000.

#### Etiology

The mechanisms by which the identified genetic alterations lead to RSS are not yet fully understood.

#### Genetics

The genetics are heterogeneous, and the disorder most commonly occurs sporadically. Some individuals have hypomethylation of the

paternal IC1 on chromosome 11p15.5 (35-50%). Others have uniparental disomy for chromosome 7 (UPD7; 10%).

#### Recurrence Risk

Recurrence risk is low if RSS in the proband was due to paternal hypomethylation at IC1 or maternal UPD7.

#### Diagnosis

The diagnosis is difficult to make prenatally because growth restriction may be the main presenting feature, is relatively common, and may not be identified until the third trimester. Postnatally, low birth weight, postnatal growth deficiency, normal head circumference, triangular facies, and asymmetry may assist in the diagnosis. Skin pigmentary changes, genitourinary anomalies, and hypoglycemia are also seen.

#### Differential Diagnosis

The differential diagnosis includes other disorders leading to intrauterine growth retardation and short stature, specifically chromosomal disorders and disorders of DNA repair (such as FA and Bloom syndrome).

#### Prognosis

Developmental delay and intellectual disability are common. Early issues with feeding, hypoglycemia, and growth are the most frequent problems. Growth hormone therapy has been shown to improve growth and final height.

## REFERENCE

Saal HM: Russell-Silver syndrome. In Pagon RA, Adam MP, Ardinger HH, et al, editors: *GeneReviews*, Seattle, 1993–2016, University of Washington.

### Seckel Syndrome

#### Definition

Seckel syndrome is part of a primary autosomal recessive microcephaly spectrum of disorders characterized by severe microcephaly in the absence of visceral malformations. The microcephaly begins during the second trimester of gestation, is less than  $-2$  SD at birth, and has a slow rate of increase following birth. Fetal growth restriction and slow postnatal growth are seen in Seckel syndrome.

#### Synonym

Primary autosomal recessive microcephalies and Seckel syndrome spectrum disorders.

#### Prevalence

Seckel syndrome is rare and was likely previously overdiagnosed. Fewer than 50 definitive cases of Seckel syndrome have been reported. Primary microcephaly has an incidence of 1 in 30,000 to 250,000.

#### Etiology

Mutations in the implicated genes are thought to lead to general growth failure and brain growth failure resulting in the observed clinical phenotype.

#### Genetics

Implicated genes in Seckel syndrome include *ATR*, *NIN*, and *ATRIP*, as well as *RBBP8*, *CEP152*, *CENPJ*, *CEP63*, and *PHC1*. Inheritance is autosomal recessive.

#### Recurrence Risk

Recurrence risk is 25% if both parents are carriers.

#### Diagnosis

The diagnosis is based on clinical features, normal brain architecture (with reduced brain volume), and family history suggestive of autosomal recessive inheritance. In addition to severe microcephaly, other findings include brain abnormalities (most commonly reduced brain



volume with normal structure), cognitive impairment, short stature, and craniosynostosis.

### Differential Diagnosis

The differential diagnosis includes all causes of primary and secondary microcephaly, including CNS malformations, associated syndromes, chromosomal disorders, and teratogens (such as alcohol).

### Prognosis

Intellectual disability is generally moderate to severe in Seckel syndrome. Survival has been reported in individuals older than age 50.

## MICRODELETION SYNDROMES

### Deletion 4p (Wolf-Hirschhorn Syndrome)

#### Definition

Wolf-Hirschhorn syndrome (WHS) is characterized by craniofacial features, including “Greek warrior helmet appearance” of the nose and forehead, microcephaly, hypertelorism, high-arched eyebrows, downturned mouth, micrognathia, and malformed ears with pits/tags. All affected individuals have prenatal growth restriction followed by postnatal growth delay. Other common features include seizures, skeletal anomalies, congenital heart defects, hearing loss, urinary tract anomalies, and CNS anomalies.

#### Incidence

Incidence is estimated at 1 in 50,000 births, although WHS is likely underdiagnosed. The female-male ratio is 2:1.

#### Etiology

Deletion of the Wolf-Hirschhorn syndrome critical region (WHSCR) at 4p16 leads to the phenotype of WHS. Candidate genes in this region potentially responsible for the clinical phenotype are *LEMT1* and *WHSC1*. The exact function of each of these genes is not currently well understood.

#### Genetics

The syndrome is due to a chromosomal 4p16.3 deletion that includes the WHSCR (between 1.4 to 1.9 Mb from the 4p terminus). This deletion can be detected by chromosomal microarray. As many as 50% to 60% of individuals have an isolated de novo deletion of 4p16, and 40% to 50% have an unbalanced translocation with both 4p deletion and partial trisomy of a different chromosome arm.

#### Recurrence Risk

Translocations can be de novo or inherited from a parent with a balanced translocation. Recurrence risk depends on the origin of the deletion.

#### Diagnosis

The prenatal diagnosis is suggested by the presence of severe fetal growth restriction, normal amniotic fluid, midline defects, and craniofacial dysmorphisms. The diagnosis can be confirmed antenatally or postnatally by chromosomal microarray.

#### Differential Diagnosis

The differential diagnosis includes Seckel syndrome, CHARGE syndrome, SLO syndrome, Opitz G/BBB syndrome, Williams

## REFERENCE

Verloes A, Drunat S, Gressens P, Passemard S: Primary autosomal recessive microcephalies and seckel syndrome spectrum disorders. In Pagon RA, Adam MP, Ardinger HH, et al, editors: *GeneReviews*, Seattle, 1993–2016, University of Washington.

syndrome, Rett syndrome, Angelman syndrome, and Smith-Magenis syndrome.

### Prognosis

All individuals have developmental delay and intellectual disability, which can vary in severity. Most patients have multiple seizures. Feeding issues are common.

## REFERENCES

- Aslan H, Karaca N, Basaran S, et al: Prenatal diagnosis of Wolf-Hirschhorn syndrome (4p-) in association with congenital hypospadias and foot deformity. *BMC Pregnancy Childbirth* 3(1):1, 2003.
- Battaglia A, Carey JC, South ST, Wright TJ: Wolf-Hirschhorn syndrome. In Pagon RA, Adam MP, Ardinger HH, et al, editors: *GeneReviews*, Seattle, 1993–2016, University of Washington.
- Beaujard MP, Jouannic JM, Bessieres B, et al: Prenatal detection of a de novo terminal inverted duplication 4p in a fetus with the Wolf-Hirschhorn syndrome phenotype. *Prenat Diagn* 25(6):451–455, 2005.
- Boog G, Le Vaillant C, Collet M, et al: Prenatal sonographic patterns in six cases of Wolf-Hirschhorn (4p-) syndrome. *Fetal Diagn Ther* 19(5):421–430, 2004.
- De Keersmaecker B, Albert M, Hillion Y, Ville Y: Prenatal diagnosis of brain abnormalities in Wolf-Hirschhorn (4p-) syndrome. *Prenat Diagn* 22(5):366–370, 2002.
- Dietze I, Fritz B, Huhle D, et al: Clinical, cytogenetic and molecular investigation in a fetus with Wolf-Hirschhorn syndrome with paternally derived 4p deletion. Case report and review of the literature. *Fetal Diagn Ther* 19(3):251–260, 2004.
- Dufke A, Seidel J, Schoning M, et al: Microdeletion 4p16.3 in three unrelated patients with Wolf-Hirschhorn syndrome. *Cytogenet Cell Genet* 91(1–4):81–84, 2000.
- Eiben B, Leipoldt M, Schubbe I, et al: Partial deletion of 4p in fetal cells not present in chorionic villi. *Clin Genet* 33(1):49–52, 1988.
- Sase M, Hasegawa K, Honda R, et al: Ultrasonographic findings of facial dysmorphism in Wolf-Hirschhorn syndrome. *Am J Perinatol* 22(2):99–102, 2005.
- Tachdjian G, Fondacci C, Tapia S, et al: The Wolf-Hirschhorn syndrome in fetuses. *Clin Genet* 42(6):281–287, 1992.
- Verloes A, Schaaps JP, Herens C, et al: Prenatal diagnosis of cystic hygroma and chorioangioma in the Wolf-Hirschhorn syndrome. *Prenat Diagn* 11(2):129–132, 1991.
- Vinals F, Sepulveda W, Selman E: Prenatal detection of congenital hypospadias in the Wolf-Hirschhorn (4p-) syndrome. *Prenat Diagn* 14(12):1166–1169, 1994.

## Deletion 5p (Cri du Chat Syndrome)

### Definition

Cri du chat syndrome (CdCS) is characterized by a high-pitched (“cat-like”) cry, microcephaly, and facial dysmorphisms (broad nasal bridge, epicanthal folds, micrognathia). Other reported features include cardiac defects, renal anomalies, CNS anomalies, preauricular tags, syndactyly, hypospadias, and cryptorchidism.

### Incidence

CdCS is seen in 1 in 1500 to 50,000 live births.

### Etiology

Deletion of particular regions of 5p are thought to be responsible for specific aspects of the clinical phenotype. Genes within 5p15 potentially linked to the clinical features include *CTNND2*, *SEMA5A*, *TERT*, *SRD5A1*, and *TPPP*.

### Genetics

CdCS is due to deletion on the short arm of chromosome 5 (5p-). The deletion can range in size from 5 to 40 Mb and can include the entire p arm or just the region 5p15. The deletion can be an isolated de novo deletion (80%), the result of a familial translocation (12%), a de novo translocation with deletion of 5p and partial trisomy of another chromosomal arm (3%), or the result of mosaicism (3%) or ring chromosomes (2.4%). Eighty percent of the de novo deletions are paternal in origin.

### Recurrence Risk

Recurrence risk depends on the mechanism of the deletion. De novo deletions and de novo translocations are unlikely to recur.

### Diagnosis

The diagnosis is based on clinical features and can be confirmed by karyotype or chromosomal microarray. The cat-like cry is thought to

be due to anomalies of the larynx and epiglottis. Prenatally, CdCS often remains undetected owing to mild and nonspecific sonographic markers. Cases associated with more significant fetal anomalies are more likely to be detected.

### Differential Diagnosis

The differential diagnosis includes other disorders with microcephaly and facial dysmorphisms, in particular other chromosomal disorders. The high-pitched cry is characteristic of CdCS. Chromosomal microarray can aid in confirmation of the diagnosis.

### Prognosis

Affected individuals have severe intellectual and developmental delay. Neonatal issues include poor feeding, hypotonia, and cyanosis. Mortality rate is estimated at 10% in the first year of life; after the first year, survival expectation is high.

## REFERENCES

- Cerruti Mainardi P: Cri du Chat syndrome. *Orphanet J Rare Dis* 1:33, 2006.
- Chen CP, Huang MC, Chen YY, et al: Cri-du-chat (5p-) syndrome presenting with cerebellar hypoplasia and hypospadias: prenatal diagnosis and aCGH characterization using uncultured amniocytes. *Gene* 524(2):407–411, 2013.
- Li DZ, Yi CX: Prenatal diagnosis of Cri du Chat syndrome: four cases report. *J Matern Fetal Neonatal Med* 25(12):2799, 2012.
- Rodriguez-Caballero A, Torres-Lagares D, Rodriguez-Perez A, et al: Cri du chat syndrome: a critical review. *Med Oral Patol Oral Cir Bucal* 15(3):e473–e478, 2010.

## Deletion 11q (Jacobsen Syndrome)

### Definition

Jacobsen syndrome (JS) is characterized by pre- and postnatal growth restriction, characteristic facial features (prominent forehead, trigonocephaly, facial asymmetry, hypertelorism, ptosis, coloboma, downslanting palpebral fissures, epicanthal folds, broad nasal bridge, short nose, V-shaped mouth, small and low-set ears), and abnormal platelet function/thrombocytopenia. Other common anomalies include heart defects, and anomalies of the kidneys, skeletal system, GI tract, genitalia, and CNS.

### Incidence

Incidence is estimated at 1 in 100,000 births. Female-male ratio is 2:1.

### Etiology

The chromosomal region 11q23 includes 342 genes; the minimal region for the JS phenotype is the 11q24.1 qter, which includes 174 genes. Some of these genes have been linked to clinical features of JS.

### Genetics

JS is due to partial deletions in the long arm of chromosome 11. The deletion size ranges from 7 to 20 Mb, extending from 11q23.3 to the telomere. The deletion can be isolated and arise de novo (85% of

individuals) or can be due to an unbalanced translocation that is de novo or inherited as the result of a balanced familial translocation. The diagnosis can be confirmed by karyotype or chromosomal microarray.

### Recurrence Risk

Recurrence risk depends on the mechanism leading to the deletion. De novo chromosomal translocations are unlikely to recur. Recurrence of isolated terminal 11q deletions has been reported. If a parent is affected with JS, the recurrence risk is 50%.

### Diagnosis

The diagnosis is based on the key clinical findings described previously and can be confirmed by genetic testing. The more mild the phenotype, the less likely affected children are to be diagnosed early. The diagnosis is often not made prenatally, and cases detected antenatally tend to be those with more severe congenital malformations. Prenatal diagnosis can be confirmed by chromosomal microarray performed on amniotic fluid or chorionic villi. Smaller deletions may not be appreciated by G-banded karyotypes.

### Differential Diagnosis

The differential diagnosis includes other chromosomal disorders, Turner syndrome, Noonan syndrome, and other causes of thrombocytopenia.



### Prognosis

Prognosis depends on the associated anomalies. Cardiac defects can be severe, requiring surgery shortly after birth. Vision, hearing, immunologic, and hormonal problems are common. Feeding issues are also frequent. Approximately 20% of affected individuals die during the first 2 years of life. Intellectual disability ranges from mild to severe and is associated with the size of the chromosomal deletion. Life expectancy for survivors is unknown.

### Deletion 22q11.2 (DiGeorge Syndrome)

See discussion of DiGeorge syndrome under “Heart.”

## METABOLIC SYNDROMES

Many metabolic syndromes lack any striking prenatal features. Some present with isolated fetal growth restriction or nonimmune hydrops. A few are associated with multiple, characteristic congenital anomalies and are discussed in this section.

### Neu-Laxova Syndrome

#### Definition

NLS is characterized by fetal growth restriction, microcephaly, characteristic facial features (short eyelids, proptosis, gaping mouth), flexion deformities, and skin abnormalities (ichthyosis, hyperkeratosis). Other features include edema of the hands and feet, limb anomalies, brain malformations, and neural tube defects.

#### Prevalence

NLS is rare; more than 70 individuals have been reported to date.

#### Etiology

Several serine-deficiency disorders have been reported and NLS may represent the more severe end of the disease spectrum. High serine levels are necessary during cell proliferation in order to replenish the one-carbon pool required for synthesizing nucleotides and other cellular components. Serine deficiency is thought to lead to the growth issues and malformations seen in NLS.

#### Genetics

NLS is due to defects in enzymes in the L-serine biosynthesis pathway, including the genes *PHGDH*, *PSAT1*, and *PSPH*. Inheritance is autosomal recessive.

### Smith-Lemli-Opitz Syndrome

#### Definition

SLO syndrome was the first genetic syndrome to be identified that had a metabolic cause. It is characterized by pre- and postnatal growth restriction, microcephaly, characteristic facial features (narrow forehead, ptosis, epicanthal folds, short mandible, short nose, anteverted nares, low-set ears), and other congenital anomalies. Common malformations include cleft palate, congenital heart defects, postaxial polydactyly, 2-3 syndactyly of the toes, and genital anomalies. Anomalies in all body systems have been reported (Table 16-9).

#### Incidence

Incidence is 1 in 20,000 to 40,000 live births.

## REFERENCES

- Boehm D, Laccone F, Burfeind P, et al: Prenatal diagnosis of a large de novo terminal deletion of chromosome 11q. *Prenat Diagn* 26(3):286–290, 2006.
- Manolakos E, Orru S, Neroutsou R, et al: Detailed molecular and clinical investigation of a child with a partial deletion of chromosome 11 (Jacobsen syndrome). *Mol Cytogenet* 2:26, 2009.
- Mattina T, Perrotta CS, Grossfeld P: Jacobsen syndrome. *Orphanet J Rare Dis* 4:9, 2009.

### Recurrence Risk

Recurrence risk is 25% if both parents are mutation carriers.

### Diagnosis

Prenatally, growth restriction, microcephaly, facial dysmorphism, joint contractures, skin edema, and CNS anomalies may be seen. Postnatal diagnosis is based on clinical features, a family history suggestive of autosomal recessive inheritance, and confirmation by molecular genetic testing.

### Differential Diagnosis

The differential diagnosis includes other disorders with similar features, in particular chromosomal disorders.

### Prognosis

NLS leads to death in the prenatal or early postnatal period. Discovery of the implicated metabolic pathway may lead to potential therapies in the future.

## REFERENCES

- Acuna-Hidalgo R, Schanze D, Kariminejad A, et al: Neu-Laxova syndrome is a heterogeneous metabolic disorder caused by defects in enzymes of the L-serine biosynthesis pathway. *Am J Hum Genet* 95(3):285–293, 2014.
- Dhillon P, Bofill JA: Neu-Laxova syndrome: a prenatal diagnosis. *J Miss State Med Assoc* 52(10):307–309, 2011.
- Shaheen R, Rahbeeni Z, Alhashem A, et al: Neu-Laxova syndrome, an inborn error of serine metabolism, is caused by mutations in *PHGDH*. *Am J Hum Genet* 94(6):898–904, 2014.

### Etiology

Mutations in *DHCR7* lead to deficiency of the enzyme 7-dehydrocholesterol reductase resulting in defective cholesterol biosynthesis. Cholesterol deficiency during development is thought to lead to the observed clinical phenotype of SLO syndrome.

### Genetics

SLO syndrome is due to mutations in *DHCR7*, leading to deficiency of the enzyme 7-dehydrocholesterol reductase and elevated serum concentrations of 7-dehydrocholesterol (7-DHC). Inheritance is autosomal recessive.

### Recurrence Risk

Recurrence risk is 25% if both parents are mutation carriers.

**TABLE 16-9 Anomalies Associated With Smith-Lemli-Opitz Syndrome**

Anatomic Area	Anomaly	
Limbs	Syndactyly (of the second and third toes in particular)	
	Postaxial polydactyly	
	Short limbs	
	Clinodactyly	
	Dislocated hips	
	Valgus deformity	
	Radial deviation of the hands	
	Ulnar deviation of the fingers	
	Rocker-bottom feet	
	Abnormal palmar creases	
	Digital whorl dermal ridge pattern	
	CNS/Head	Microcephaly
		Trigonocephaly
Agenesis of the corpus callosum		
Seizures		
Demyelination of cerebral hemispheres, cranial nerves, and peripheral nerves		
Hydrocephalus		
Cerebral hypoplasia		
Cardiac	Cerebellar hypoplasia	
	Ventricular septal defect	
	Atrial septal defect	
	Atriomegaly	
	Ventriculomegaly	
Genitourinary	Hypospadias	
	Cryptorchidism	
	Micropenis	
	Bifidum scrotum	
	Hypoplastic scrotum	
	Microurethra	
	Ambiguous genitalia	
	Prominent clitoral hood	
	Redundant labia minora	
	Hypoplastic labia	
	Rudimentary uterus	
	Ureteropelvic junction obstruction	
	Renal hypoplasia	
	Urethral stenosis	
	Cystic renal dysplasia	
Male pseudohermaphroditism		

CNS, central nervous system.

### Diagnosis

The detection of an extremely reduced concentration of cholesterol and abnormal accumulation of serum 7-DHC can confirm the diagnosis in infants and adults. Prenatally, either biochemical or molecular

genetic testing can be performed. Elevated 7-DHC can be found in the amniotic fluid in the second trimester or in chorionic villi in the first trimester; normally, 7-DHC is undetectable in both specimens. Decreased levels of estriol in both the maternal circulation and maternal urine may be decreased, especially in later pregnancy. On prenatal ultrasound images, growth restriction and multiple congenital anomalies may be seen. Increased nuchal translucency, cystic hygroma, and nonimmune hydrops have also been reported.

### Differential Diagnosis

The differential diagnosis includes other disorders with growth restriction and multiple congenital anomalies, in particular aneuploidy (trisomies 13, 18, and 12), other chromosomal disorders, Dubowitz syndrome, Meckel-Gruber syndrome, and Noonan syndrome.

### Prognosis

Prognosis depends on the severity of the malformations, and the clinical spectrum of phenotypes is wide. Intellectual disability is generally moderate to severe. Feeding issues and failure to thrive are common.

### REFERENCES

- Curry CJ, Carey JC, Holland JS, et al: Smith-Lemli-Opitz syndrome-type II: multiple congenital anomalies with male pseudohermaphroditism and frequent early lethality. *Am J Med Genet* 26(1):45–57, 1987.
- Hyett JA, Clayton PT, Moscoso G, Nicolaides KH: Increased first trimester nuchal translucency as a prenatal manifestation of Smith-Lemli-Opitz syndrome. *Am J Med Genet* 58(4):374–376, 1995.
- Kelley RI, Hennekam RC: The Smith-Lemli-Opitz syndrome. *J Med Genet* 37(5):321–335, 2000.
- McGaughran JM, Clayton PT, Mills KA, et al: Prenatal diagnosis of Smith-Lemli-Opitz syndrome. *Am J Med Genet* 56(3):269–271, 1995.
- Nowaczyk MJ, Wayne JS: The Smith-Lemli-Opitz syndrome: a novel metabolic way of understanding developmental biology, embryogenesis, and dysmorphology. *Clin Genet* 59(6):375–386, 2001.
- Nowaczyk MJ, Whelan DT, Hill RE: Smith-Lemli-Opitz syndrome: phenotypic extreme with minimal clinical findings. *Am J Med Genet* 78(5):419–423, 1998.
- Nowaczyk MJM: Smith-Lemli-Opitz syndrome. In Pagon RA, Adam MP, Ardinger HH, et al, editors: *GeneReviews*, Seattle, 1993–2016, University of Washington.
- Opitz JM: RSH/SLO (“Smith-Lemli-Opitz”) syndrome: historical, genetic, and developmental considerations. *Am J Med Genet* 50(4):344–346, 1994.
- Pandya PB, Kondylios A, Hilbert L, et al: Chromosomal defects and outcome in 1015 fetuses with increased nuchal translucency. *Ultrasound Obstet Gynecol* 5(1):15–19, 1995.
- Ryan AK, Bartlett K, Clayton P, et al: Smith-Lemli-Opitz syndrome: a variable clinical and biochemical phenotype. *J Med Genet* 35(7):558–565, 1998.
- Tint GS, Salen G, Batta AK, et al: Correlation of severity and outcome with plasma sterol levels in variants of the Smith-Lemli-Opitz syndrome. *J Pediatr* 127(1):82–87, 1995.
- Waterham HR, Wijburg FA, Hennekam RC, et al: Smith-Lemli-Opitz syndrome is caused by mutations in the 7-dehydrocholesterol reductase gene. *Am J Hum Genet* 63(2):329–338, 1998.

### Zellweger Syndrome

#### Definition

Zellweger syndrome (ZS) is one (and the most severe) of three phenotypes of the peroxisome biogenesis disorders; the others are neonatal adrenoleukodystrophy and infantile Refsum disease. Affected infants present with hypotonia and poor feeding; they are noted to have characteristic facies (flat face, large anterior fontanelle, broad nasal bridge), seizures, and liver cysts with hepatic dysfunction. The long bones

may be noted to have distinctive stippling (chondrodysplasia punctata).

#### Synonym

ZS is also known as cerebrohepatorenal syndrome.

#### Prevalence

Prevalence is estimated at 1 in 50,000.



### Etiology

The implicated *PEX* genes encode for a class of proteins called peroxins that are required for normal peroxisome assembly. Peroxisomes are the site of many anabolic and catabolic pathways, and deficiency in their formation is thought to be responsible for the observed clinical phenotype of ZS.

### Genetics

ZS is due to mutations in 1 of 12 *PEX* genes; approximately 68% of individuals have mutations in *PEX1*. Inheritance is autosomal recessive.

### Recurrence Risk

Recurrence risk is 25% if both parents are mutation carriers.

### Diagnosis

The diagnosis can be determined by biochemical testing. Initial screening is performed with measurement of plasma very long chain fatty acid (VLCFA) levels. Elevated C26:0 and C26:1, as well as increased ratios of C24/C22 and C26/C22, indicate a defect in peroxisomal fatty acid metabolism. Peroxisomal mosaicism can exist with different tissues having disparate biochemical testing results. Molecular genetic testing can assist in confirmation of the diagnosis. Prenatally, growth restriction, decreased fetal movement, and increased nuchal translucency may be noted. Other sonographic features reported include an abnormal head shape, facial dysmorphism, ventriculomegaly, hepatomegaly, and cardiac defects.

### Differential Diagnosis

The differential diagnosis includes other disorders with significant hypotonia, including trisomy 21, PWS, congenital DM1, and spinal muscular atrophy.

## OTHER MALFORMATIONS

### Amniotic Band Sequence

#### Definition

Amniotic band sequence is a set of congenital malformations ranging from minor constriction rings and lymphedema of the digits to complex, bizarre multiple congenital anomalies that are attributed to amniotic bands that stick, entangle, and disrupt fetal parts.

#### Synonyms

Historically, diverse nomenclature has been used to describe the anomalies, including amniotic band syndrome, amniotic band disruption complex, and limb body wall complex.

#### Incidence

Estimates range from 1 in 1200 to 1 in 15,000 live births.

#### Genetics

In general, amniotic band sequence is not thought to have a genetic cause.

#### Recurrence Risk

No increased recurrence risk is expected.

#### Etiology

The cause is not precisely known. Some theories have been suggested including teratogenic, multifactorial, and genetic factors that cause early rupture of the amnion.

### Prognosis

Most infants with ZS do not progress developmentally and die within the first year. Seizures may be difficult to control. Death is due to apnea, respiratory issues, or secondary to infection.

## REFERENCES

- Cuillier F, Cartault F, Lemaire P, et al: [Subependymal pseudocysts in the fetal brain revealing Zellweger syndrome]. *J Gynecol Obstet Biol Reprod* 33(4):325–329, 2004.
- de Graaf IM, Pajkrt E, Keessen M, et al: Enlarged nuchal translucency and low serum protein concentrations as possible markers for Zellweger syndrome. *Ultrasound Obstet Gynecol* 13(4):268–270, 1999.
- Depreter M, Espeel M, Roels F: Human peroxisomal disorders. *Microsc Res Tech* 61(2):203–223, 2003.
- Johnson JM, Babul-Hirji R, Chitayat D: First-trimester increased nuchal translucency and fetal hypokinesia associated with Zellweger syndrome. *Ultrasound Obstet Gynecol* 17(4):344–346, 2001.
- Lee HF, Mak SC, Wu FW, et al: Zellweger syndrome: report of one case. *Acta Paediatr* 42(1):53–56, 2001.
- Steinberg SJ, Elcioglu N, Slade CM, et al: Peroxisomal disorders: clinical and biochemical studies in 15 children and prenatal diagnosis in 7 families. *Am J Med Genet* 85(5):502–510, 1999.
- Steinberg SJ, Raymond GV, Braverman NE, Moser AB: Peroxisome biogenesis disorders, Zellweger syndrome spectrum. In Pagon RA, Adam MP, Ardinger HH, et al, editors: *GeneReviews*, Seattle, 1993–2016, University of Washington.

### Pathogenesis

Rupture of the amnion in early pregnancy leads to entrapment of fetal structures by “sticky” mesodermic bands that originate from the chorionic side of the amnion, followed by disruption. It has been suggested that the bands lead to a decreased blood flow in the constricted limb and subsequent natural amputation. This exogenous mechanistic theory does not explain several features of this syndrome, such as why there are reported cases of amniotic band syndrome with histologically normal and intact amniotic lining; why internal abnormalities such as holoprosencephaly, cerebellar dysplasia, heterotopia, cardiac, and renal abnormalities can be seen; and why monozygotic twins are more often affected than dizygotic twins.

### Diagnosis

The syndrome results in structural anomalies that vary from minor to lethal forms. The most common findings are constriction rings around the digits, arms, and legs; swelling of the extremities distal to the point of constriction; amputation of digits, arms, and legs; asymmetric face; facial clefts; cephalocele; anencephaly; acrania; multiple joint contractures; pterygium; clubfeet, clubhands, and pseudosyndactyly; and microphthalmia, uveal coloboma, corneal metaplasia, and unilateral chorioretinal lacunae. A detailed view of the fetus's face, digits, and body with 3D sonography may assist with the diagnosis.

### Differential Diagnosis

A uterine synechia or septation can simulate an amniotic band.

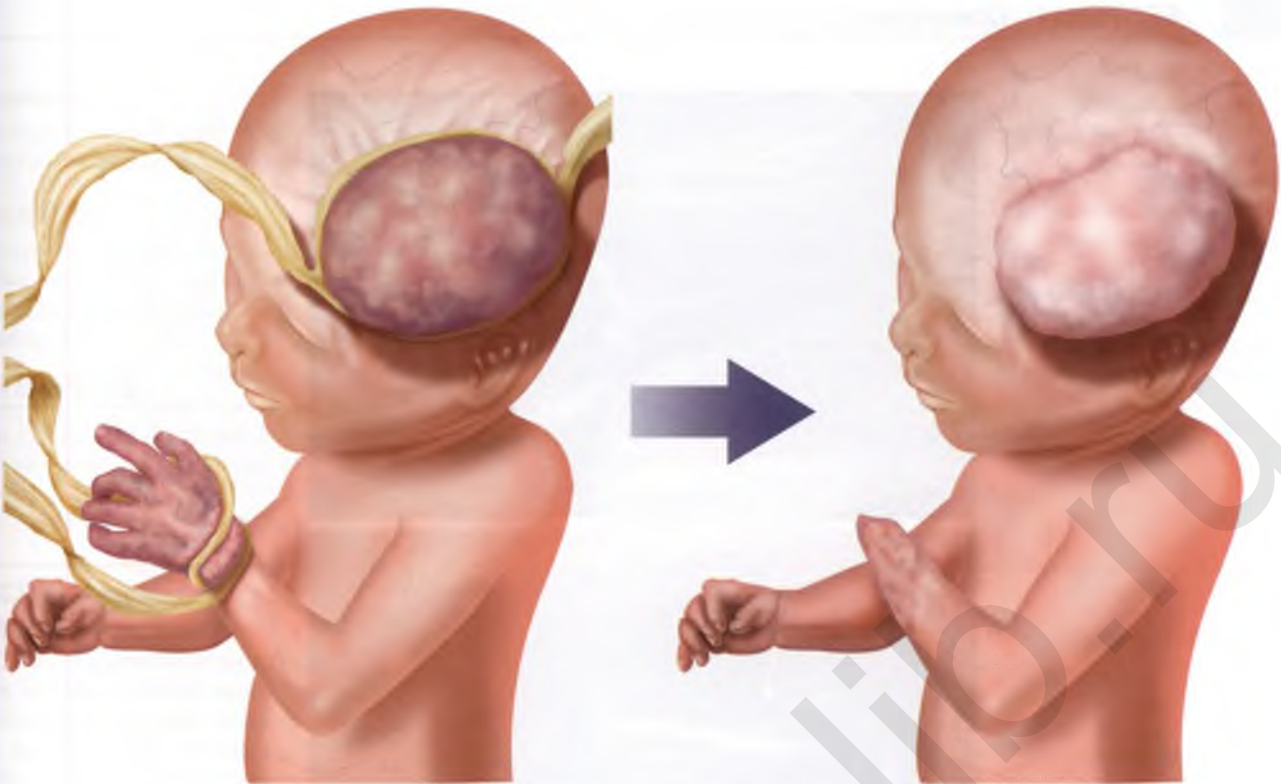


**FIG 16-80** Pathophysiology of amniotic band sequence. Amniotic band wrapping around the extremity and head resulting in nonembryologic abnormalities such as amputation of the distal limb and a noncentral encephalocele. (Illustration by James A. Cooper, MD, San Diego, CA.)

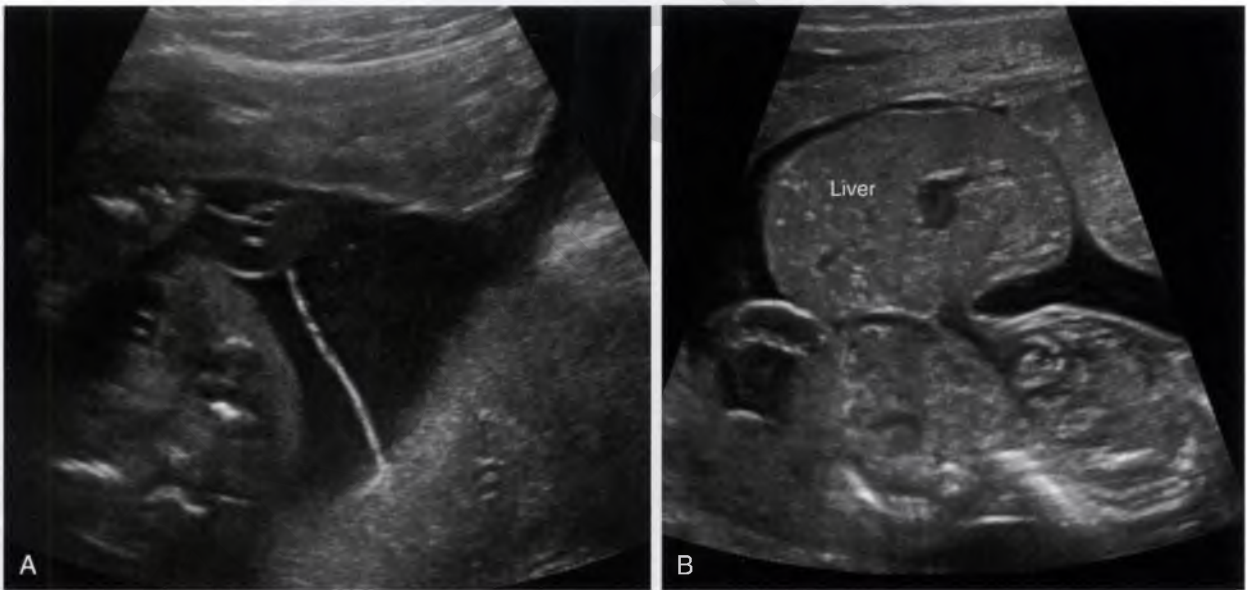


**FIG 16-81** Amniotic band sequence. **A**, Disrupted, discontinuous amniotic membrane. **B**, Nonanatomic abdominal wall defect, with exteriorized liver and bowel. **C**, Upper extremity limb amputation (*arrow*).



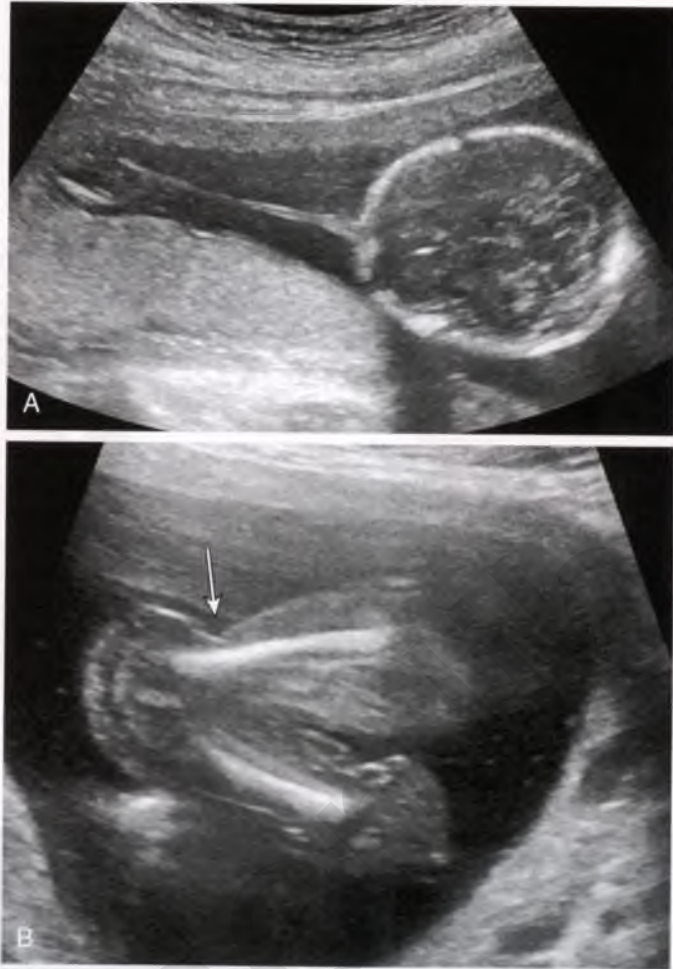


**FIG 16-82** Amniotic band sequence. **A**, Abnormal intrauterine membrane attached to the fetus. **B**, Focal constriction deformity of the thigh.

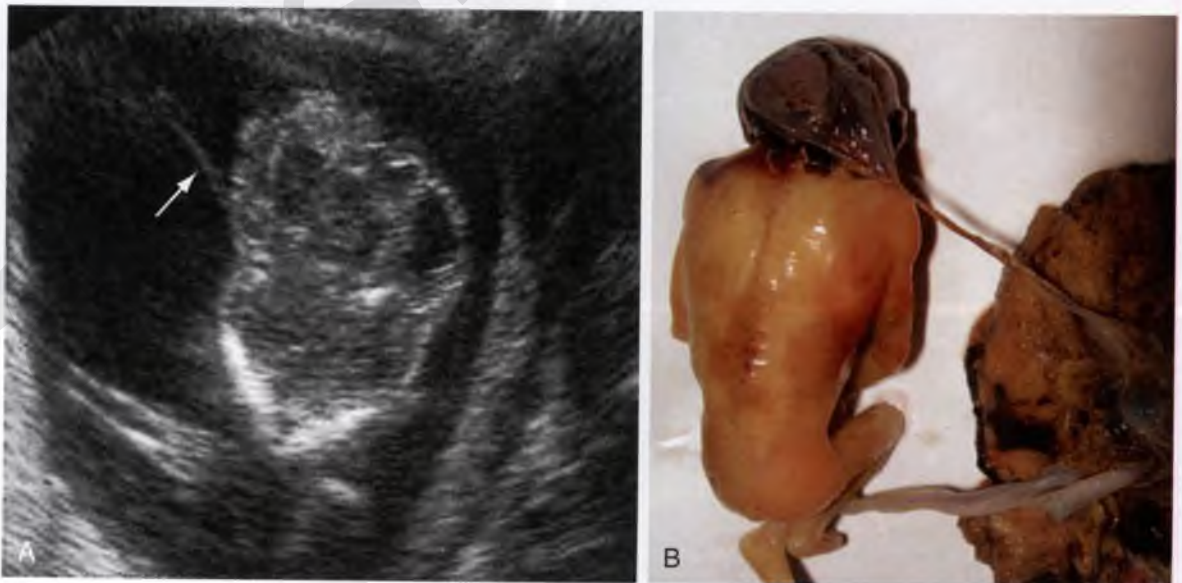


**FIG 16-83** **A**, Amniotic band attached to the fetal head. **B**, Postnatal image showing an amniotic band attached to the skull and the exencephaly. (Courtesy, Vicente Ruiz, 2005. Available at thefetus.net.)

**Prognosis**

The more severe forms are lethal. Mild manifestations sometimes are found just at birth and do not have an impact on survival.

**Management**

Management depends on the extent of the anomalies. Endoscopic release has been reported and may prove beneficial in releasing the constriction band in threatened limb amputation, but this procedure remains controversial.

**REFERENCES**

Chen CP, Chang TY, Lin YH, Wang W: Prenatal sonographic diagnosis of acrania associated with amniotic bands. *J Clin Ultrasound* 32(5):256–260, 2004.

Cincore V, Ninios AP, Pavlik J, Hsu CD: Prenatal diagnosis of acrania associated with amniotic band syndrome. *Obstet Gynecol* 102(5 Pt 2):1176–1178, 2003.

Paladini D, Foglia S, Sglavo G, Martinelli P: Congenital constriction band of the upper arm: the role of three-dimensional ultrasound in diagnosis, counseling and multidisciplinary consultation. *Ultrasound Obstet Gynecol* 23(5):520–522, 2004.

Pedersen TK, Thomsen SG: Spontaneous resolution of amniotic bands. *Ultrasound Obstet Gynecol* 18(6):673–674, 2001.

Sentilhes L, Verspyck E, Eurin D, et al: Favourable outcome of a tight constriction band secondary to amniotic band syndrome. *Prenat Diagn* 24(3):198–201, 2004.

Sherer DM, Lysikiewicz AJ: Doppler flow velocimetry assisted diagnosis of an intrauterine synechia during pregnancy. *Am J Perinatol* 19(8):421–426, 2002.

**VACTERL Association****Definition**

VACTERL is a mnemonic for a nonrandom association of malformations including vertebral anomalies, *a*nal atresia, *c*ardiac anomalies, *t*racheoesophageal fistula or *e*sophageal atresia, *r*enal/urinary anomalies, and *l*imb defect. Patients are considered to have the VACTERL association when three or more organ systems are involved. The associated defects occur with the following frequencies: 50% to 80% tracheoesophageal fistula, 60% to 90% anal atresia, 60% to 80% vertebral anomalies, 40% to 80% cardiac defects, 50% to 80% renal anomalies, and 40% to 50% limb abnormalities.

**Incidence**

VACTERL is seen in 1 in 10,000 to 40,000 live births.

**Etiology**

VACTERL is thought to be due to defective mesodermal development of unknown origin.

**Genetics**

Genetic involvement is unknown; most cases are sporadic.

**Recurrence Risk**

Recurrence risk is estimated at 1%.

**Diagnosis**

The diagnosis of VACTERL can be difficult to make prenatally because many of the features can be difficult to determine sonographically. A small stomach in association with polyhydramnios may suggest



**FIG 16-84** VACTERL association. **A**, Longitudinal image of the fetal spine demonstrating multiple segmentation abnormalities; **B**, four-chamber view of the fetal heart with a ventricular septal defect (VSD) (arrow); **C**, radial ray anomaly, with absent bones of the forearm and hand. VACTERL, vertebral anomalies, anal atresia, cardiac anomalies, tracheoesophageal fistula or esophageal atresia, renal/urinary anomalies, and limb defect.





**FIG 16-85** VACTERL association. Sonogram of a fetus with anal atresia and a dilated segment of large intestine. VACTERL, vertebral anomalies, anal atresia, cardiac anomalies, tracheoesophageal fistula or esophageal atresia, renal/urinary anomalies, and limb defect.

tracheoesophageal fistula. Vertebral anomalies can be subtle. The constellation of limb defects (particularly radial anomalies), renal anomalies, and cardiac defects should raise suspicion. Seeing as there is not a known genetic cause for VACTERL, it remains a diagnosis of exclusion, and postnatal examination is necessary for comprehensive evaluation.

### Differential Diagnosis

The differential diagnosis includes chromosomal disorders, CHARGE syndrome, 22q11 deletion syndrome, Feingold syndrome, Holt-Oram syndrome, Townes-Brockes syndrome, Fanconi anemia, and Pallister-Hall syndrome.

### Prognosis

The prognosis depends on the particular association of anomalies. If surgical correction is achieved, the outcome can be positive. Some

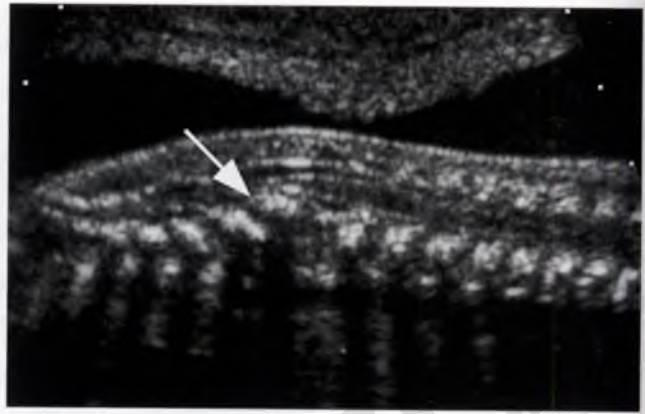


**FIG 16-86** Abnormal vertebrae (arrow) in association with the previously mentioned findings and a radial abnormality (not shown) should arouse suspicion of VACTERL association. VACTERL, vertebral anomalies, anal atresia, cardiac anomalies, tracheoesophageal fistula or esophageal atresia, renal/urinary anomalies, and limb defect.

patients will be affected by their congenital malformations throughout their life. Intellectual ability is generally normal.

### REFERENCES

- Kolker AR, Coombs CJ, Meara JG, et al: Patterns of radial dysmorphology with the VACTERL association in the adriamycin-exposed prenatal rat. *Ann Plast Surg* 45(5):525–530, 2000.
- Kolon TF, Gray CL, Sutherland RW, et al: Upper urinary tract manifestations of the VACTERL association. *J Urol* 163(6):1949–1951, 2000.
- Shaw-Smith C: Oesophageal atresia, tracheo-oesophageal fistula, and the VACTERL association: review of genetics and epidemiology. *J Med Genet* 43(7):545–554, 2006.
- Solomon BD, Baker LA, Bear KA, et al: An approach to the identification of anomalies and etiologies in neonates with identified or suspected VACTERL (vertebral defects, anal atresia, tracheo-esophageal fistula with esophageal atresia, cardiac anomalies, renal anomalies, and limb anomalies) association. *J Pediatr* 164(3):451–457.e451, 2014.

# Evaluation of Hydrops Fetalis

Hector Mendez-Figueroa, Suneet P. Chauhan

## SUMMARY KEY POINTS

- Diagnosis of hydrops fetalis requires two or more of the following sonographic abnormalities: scalp and body wall edema (defined as skin thickness  $>5$  mm), ascites, pleural effusion, pericardial effusion, polyhydramnios, and placental thickening ( $\geq 4$  cm in the second trimester and  $\geq 6$  cm in the third trimester).
- *Immune hydrops* refers to cases in which the underlying condition is due to fetal anemia developing from maternal red blood cell alloimmunization. *Nonimmune hydrops* refers to cases resulting from all other conditions.
- Almost 90% of cases of hydrops are secondary to a nonimmune mechanism.
- For women with a prior history of a fetus or child with alloimmunization, defined as requiring intrauterine transfusion or exchange transfusions after birth, the use of serial maternal titers to identify the fetus at risk is not indicated because these measures are no longer predictive in these circumstances.
- Measurements of the peak systolic velocity (PSV) in the middle cerebral artery (MCA) are highly predictive of fetal anemia and are the preferred method to manage pregnancies at risk for immune hydrops.
- If MCA PSV measurements reach a value greater than 1.5 MoM (multiples of the median), fetal blood sampling via cordocentesis should be performed.
- During fetal transfusions, the blood should be transfused at a rate of 5 to 10 mL/minute, and if feasible, an attempt should be made to reach a final hematocrit of 50% to 65%.
- The most common causes of nonimmune hydrops are cardiovascular conditions, which include arrhythmias, structural abnormalities, and diverse cardiomyopathies.
- A fetal echocardiogram should be part of the initial evaluation of nonimmune hydrops.

## OUTLINE

Background and Definition, 633

Incidence, 635

Immune Hydrops, 635

Mechanism, 635

Management, 638

Prediction of Anemia, 639

Intrauterine Transfusion, 641

Prognosis, 643

Nonimmune Hydrops, 643

Mechanism, 643

Evaluation and Management, 644

Treatment, 647

Prognosis, 648

Maternal Risks From Hydrops, 649

Conclusion, 649

## BACKGROUND AND DEFINITION

Hydrops fetalis has been defined as the pathologic accumulation of excessive fluid within two or more fetal compartments. These features can be detected sonographically and include scalp and body wall edema (defined as skin thickness greater than 5 mm),<sup>1</sup> ascites, pleural effusion, pericardial effusion, presence of polyhydramnios (amniotic fluid index greater than 25 cm or maximum verticle pocket greater than 8 cm),<sup>2</sup> and placental thickening ( $\geq 4$  cm in the second trimester and  $\geq 6$  cm in the third trimester)<sup>3,4</sup> (Figs. 17-1 through 17-8).

The use of this term should be limited to cases that meet the criteria outlined here because the diagnosis is associated with a poor prognosis and the workup for the cause may be extensive. The presence of one but not two of these criteria may be secondary to different causes and

may also be associated with a better outcome than hydrops fetalis. In certain situations, the finding of a single abnormal fluid accumulation may be a sign of progressive and evolving hydrops fetalis and may warrant more frequent imaging and surveillance.

Based on the cause, the condition should be classified either as immune or nonimmune hydrops. Immune hydrops refers to all cases in which the underlying condition is due to fetal anemia developing from red blood cell (RBC) alloimmunization. The term *nonimmune hydrops* was reserved for the cases that resulted from all other conditions. Immune hydrops was probably first described in 1609 when a French midwife delivered a set of twins: the first one was hydropic and stillborn, whereas the second twin was noted to be severely jaundiced and subsequently died, most likely from kernicterus.<sup>5</sup> This association was then again reported in 1932 when Diamond and colleagues



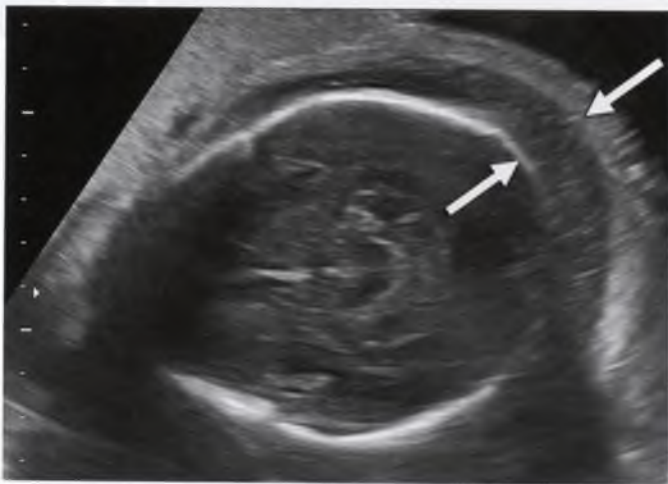


**FIG 17-1** Scalp edema noted (between arrows) at 32 weeks' gestation. Cause: idiopathic. (Courtesy of Anthony Swartz, BS, RT(R), RDMS.)

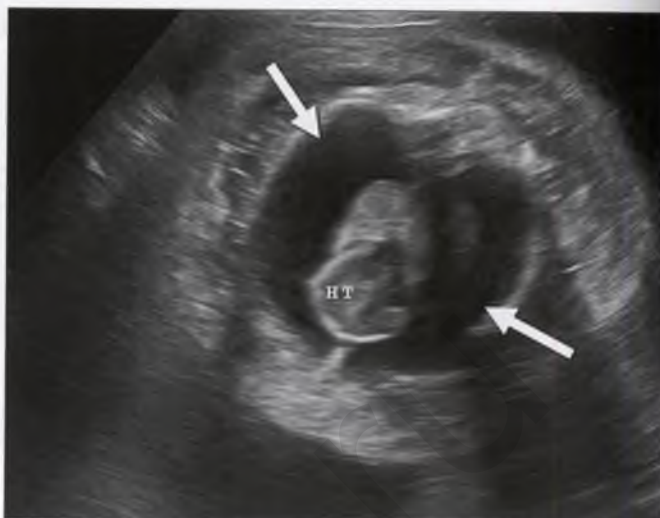


**FIG 17-3** Bilateral pleural effusions (arrows) at 32 weeks' gestation. HT, midline fetal heart. Cause: idiopathic. (Courtesy of Anthony Swartz, BS, RT(R), RDMS.)



**FIG 17-2** Cross-sectional view of the fetal thoracic cavity at 19 weeks' gestation. Note pericardial effusion (arrow). Also note the cardiomegaly. Cause: maternal RhD alloimmunization and resulting hemolytic disease of the fetus/newborn.



**FIG 17-4** Predominantly left-sided pleural effusion (large arrow) at 30 weeks' gestation. Fetal heart (asterisk) is displaced to the right side of the chest. Large left-sided pulmonary sequestration is noted (small arrow). Note extreme polyhydramnios as well. Cause: intrathoracic mass with deviation of mediastinum. (Courtesy of Sharon Pinette, RDMS.)

described a disease characterized by anemia and jaundice that was associated with erythroblastosis and RBC hemolysis.<sup>6</sup> Although the clinical features were described, the cause and pathogenesis were largely unknown. In 1938 Darrow described the concept of an antigen-antibody reaction leading to icterus gravis neonatorum.<sup>7</sup> In 1940, the work by Landsteiner and Weiner led to the discovery of the rhesus (Rh) antigen that was expressed on the surface of RBCs.<sup>8</sup> Later, in 1941 Levine and associates described the pathophysiology of the disease in a case series involving five patients. They observed that Rh-negative women form antibodies to Rh-positive RBCs, and transplacental passage of these antibodies to the fetus can lead to erythroblastosis fetalis.<sup>9</sup>

Prevention of immune hydrops would have to wait decades. William Pollack, working in collaboration with Vincent J. Freda and John G. Gorman, developed a gamma globulin from anti-D serum. This gamma globulin was administered to RhD-negative inmates who then failed to develop anti-D antibodies when exposed to RhD-positive RBCs.<sup>10</sup> At the same time, Finn and colleagues were also investigating

the potential prevention of Rh hemolytic disease. They injected radioactive-labeled Rh-positive RBCs into Rh-negative men; they were able to demonstrate that administration of anti-D gamma globulin not only led to Rh-positive cells being coated by antibodies but also to a much more rapid destruction of these cells.<sup>11</sup> Later, Hamilton treated RhD-negative women following their first delivery and showed that this strategy prevented formation of anti-D antibodies in the second pregnancy and led to improved perinatal outcomes.<sup>12</sup> A subsequent multicenter clinical trial directed by Pollack led to the widespread use



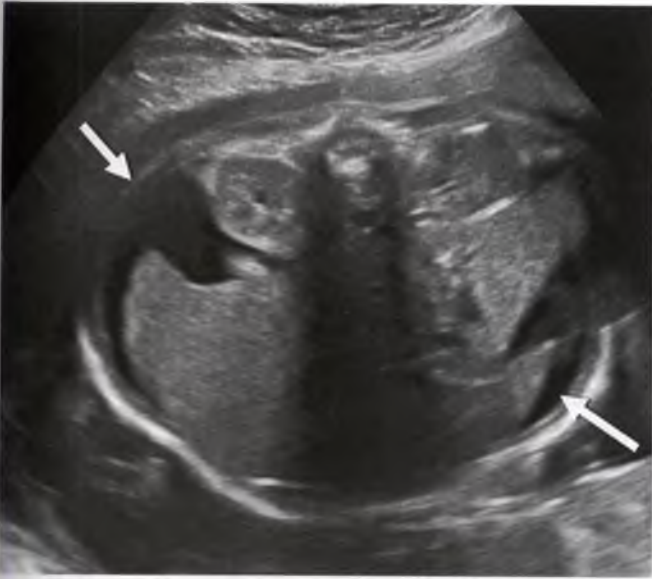


**FIG 17-5** Cross-sectional view of the fetal abdomen at 32 weeks' gestation. Note ascites (arrows). Cause: fetal cytomegalovirus infection.



**FIG 17-6** Cross-sectional view of the fetal abdomen at 19 weeks' gestation. Note ascites (arrow). Cause: trisomy 22. (Courtesy of Sharon Pinette, RDMS.)

of anti-D immune globulin in clinical practice.<sup>13</sup> The work by these pioneers helped the development of the current practice guidelines presently used throughout most of the world.

## INCIDENCE

The true incidence of hydrops fetalis is difficult to quantify. Many studies differ on the definition of cases included in their series as well as the study population. The reported incidence ranges from 1:424<sup>14</sup> to 1:2000<sup>15</sup> live births admitted to a neonatal intensive care unit



**FIG 17-7** Longitudinal section of the fetal abdomen (fetal head on left) at 19 weeks' gestation—same fetus as illustrated in Figure 17-6. Note ascites (arrow). Cause: trisomy 22. (Courtesy of Sharon Pinette, RDMS.)

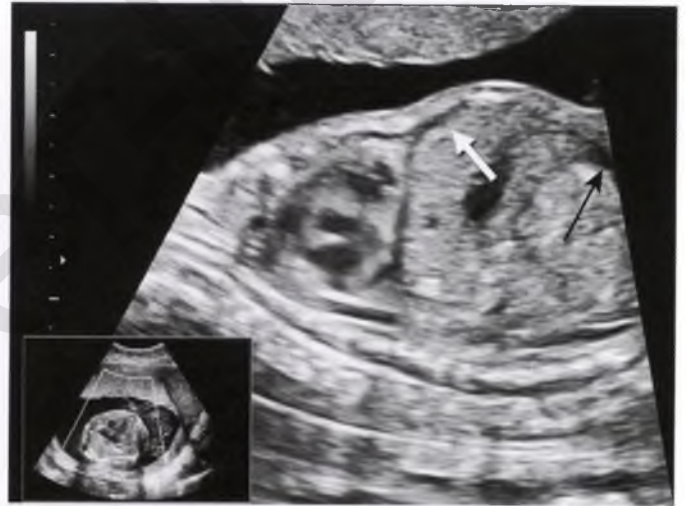


**FIG 17-8** Longitudinal view of the fetal thorax and abdomen at 19 weeks' gestation (head on left of image). Note early ascites (arrows). Cause: maternal RhD alloimmunization and resulting hemolytic disease of the fetus/newborn.

(NICU). The widespread use of anti-D immune globulin has led to a decrease in the overall incidence of immune hydrops over the past few decades. Macafee and coworkers reported that in 1970, 82% of the hydrops cases were secondary to immune hydrops.<sup>16</sup> The incidence of nonimmune hydrops has been reported to range from 1:1500 to 1:3800 births.<sup>17,18</sup> More recent publications have reported a shift in incidence; currently almost 90% of cases of hydrops are secondary to a nonimmune mechanism.<sup>17</sup>

## IMMUNE HYDROPS

### Mechanism

The pathophysiology of immune hydrops is exemplified by RhD isoimmunization. However, several other RBC antigens have been linked to the development of immune hydrops (Table 17-1). The RhD antigen is one of the most immunogenic antigens expressed on the surface of RBCs<sup>19</sup>; other antigens differ in their ability to cause the disease.



**TABLE 17-1 Red Blood Cell Antibodies and Associated Hemolytic Disease of the Fetus and Newborn**

Antigen System	Specific Antigen	Antigen System	Specific Antigen	Antigen System	Specific Antigen
<b>Frequently Associated With Severe Disease</b>					
Kell	-K (K1)				
Rhesus	-D				
	-c				
<b>Infrequently Associated With Severe Disease</b>					
Colton	-Co <sup>a</sup>	MNS	-Mt <sup>a</sup>	Rhesus	-HOFM
	-Co3		-MUT		-LOCR
Diego	-ELO		-Mur		-Riv
	-Di <sup>a</sup>		-Mv		-Rh29
	-Di <sup>b</sup>		-s		-Rh32
	-Wf <sup>a</sup>		-s <sup>d</sup>		-Rh42
	-Wf <sup>b</sup>		-S		-Rh46
Duffy	-Fy <sup>a</sup>		-U		-STEM
Kell	-Js <sup>a</sup>		-V <sup>w</sup>		-Tar
	-Js <sup>b</sup>	Rhesus	-Be <sup>a</sup>	Other	-HJK
	-k (K2)		-C	antigens	-JFV
	-Kp <sup>a</sup>		-Ce		-JONES
	-Kp <sup>b</sup>		-C <sup>w</sup>		-Kg
	-K11		-C <sup>x</sup>		-MAM
	-K22		-ce		-REIT
	-Ku		-D <sup>w</sup>		-Rd
	-Ul <sup>a</sup>		-E		
Kidd	-Jk <sup>a</sup>		-E <sup>w</sup>		
MNS	-En <sup>a</sup>		-Evans		
	-Far		-e		
	-Hil		-G		
	-Hut		-Go <sup>a7</sup>		
	-M		-Hr		
	-Mj <sup>a</sup>		-Hro		
	-Mit		-JAL		
<b>Associated With Mild Disease</b>					
Dombrock	-Do <sup>a</sup>	Gerbich	-Ge2	Scianna	-Sc2
	-Gy <sup>a</sup>		-Ge3	Other	-Vel
	-Hy		-Ge4	antigens	-Lan
	-Jo <sup>a</sup>		-Ls <sup>a</sup>		-At <sup>a</sup>
Duffy	-Fy <sup>b</sup>	Kidd	-Jk <sup>b</sup>		-Jr <sup>a</sup>
	-Fy3		-Jk3		

From Moise KJ. Fetal anemia due to non-Rhesus-D red-cell alloimmunization (level III). *Semin Fetal Neonatal Med* 2008;13:207-214.

Maternal alloimmunization results from the exposure to foreign RhD-positive cells that eventually lead to an immunologic response. The most common cause of this phenomenon is a transplacental passage of fetal cells into maternal circulation, such as during a miscarriage, amniocentesis, trauma, or delivery (Fig. 17-9). Using Kleihauer-Betke stain, as many as 75% of women have some evidence of the presence of fetal RBCs in maternal circulation during pregnancy or delivery.<sup>20</sup>

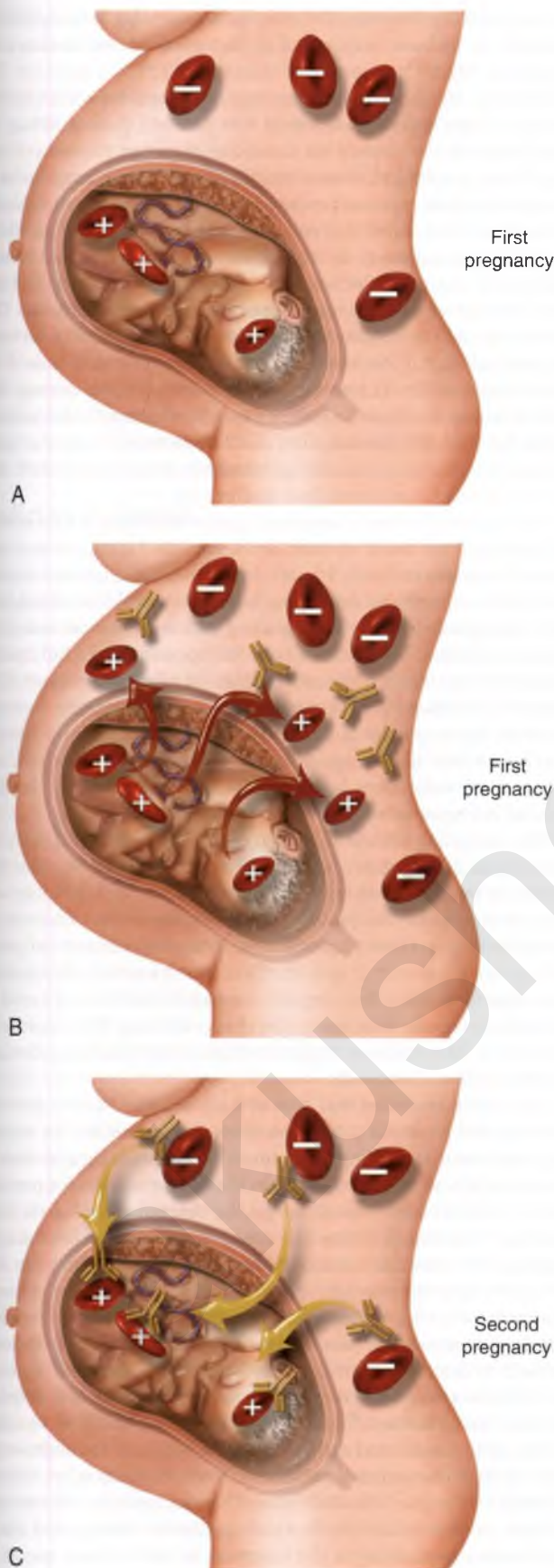
The risk of fetal-maternal hemorrhage also increases with gestational age: 0.01 mL of fetal blood may be detected in 3% of pregnancies the first trimester and 46% during the third trimester.<sup>20</sup> The probability

of alloimmunization is directly proportional to the amount of fetal blood that crosses the placental barrier. It has been estimated that 0.25 mL of fetal blood is the minimum amount required to lead to alloimmunization. For these reasons, delivery poses the greatest risk for Rh sensitization. The proper administration of RhD immune globulin, however, can effectively prevent the formation of maternal antibodies. Transfusion of incompatible blood can also lead to maternal sensitization; this is the most common mechanism explaining alloimmunization from other RBC antigens.

The genetics of the Rh system are complex. The Rh factor is among the largest of the blood groups and contains well over 50 different recognized antigens.<sup>21</sup> Rearrangements in the Rh locus can result in hybrid proteins that can lead to additional antigen expression. Only a small number of these antigens are actually clinically relevant. During pregnancy there are three antigens that can lead to the formation of antibodies and alloimmunization, Rh (D) and Rh (CcEe). These antigens are encoded by two genes located on the short arm of chromosome 1, the RhD and RhCE genes.<sup>22</sup> Each gene contains 10 exons. It has been speculated that through a mechanism involving alternative splicing these two genes could direct the synthesis of different proteins corresponding to different variations in Rh antigens.<sup>23</sup> Fischer and Race have proposed a concept to explain the inheritance of the alleles in the Rh genes.<sup>24</sup> In the majority of patients, three pairs of Rh antigens are inherited from each parent—Cc, Dd, and Ee. An individual can be heterozygous or homozygous for each allele. The Rh-positive or Rh-negative status of a patient is determined by the presence or absence (or possible nonexpression) of the D antigen site. The Rh (CcEe) has fewer alleles and a limited number of mutations reported. The Cc and the Ee alleles are codominant and expressed in a heterozygous fashion. It should also be noted that the symbol “d” simply indicates the absence of D antigen; there is no “d” allele.

The D antigen is a transmembrane protein located on the surface of the erythrocyte that contains several extracellular loops. More than 150 different alleles for the Rh (D) gene have been reported, most likely a byproduct of numerous mutations within the gene.<sup>25</sup> The complete absence of the RhD antigen is called a *negative allele*. The gene frequency varies according to race and ethnicity. Rh-negative individuals are reported in approximately 1% of the Chinese and Japanese populations, whereas the Basque tribe in northern Spain has a reported incidence of approximately 30%.<sup>26</sup> In the patient population of the Americas, the difference among races and various ethnic backgrounds is also noticeable. Caucasians of European descent have an Rh-negative incidence of 15%, whereas Hispanics and African Americans have an incidence closer to 8%. Among several African populations, a variant of Rh (D) gene referred to as the RhD pseudogene (Rh  $\psi$ ) has also been described.<sup>27</sup> This gene contains all the 10 exons normally found on the Rh (D) gene but has a difference in gene expression due to the presence of a stop codon in the intron between exons 3 and 4. Because of this change, the Rh (D) protein is not synthesized, and the patient is phenotypically Rh (D) negative. This gene is detected in more than 60% of Rh-negative black Africans.<sup>27</sup>

After the first exposure to the D antigen, a weak immunologic response is mounted over 6 weeks to a year. The predominant immunoglobulin produced in this first interaction is immunoglobulin (Ig) M. This large protein does not cross the placenta, and therefore the first pregnancy is usually not affected. However, a second exposure to the antigen can cause B lymphocytes to differentiate into plasma cells and proliferate. This amnesic response in the immune system is characterized by the production of IgG almost entirely; these IgG antibodies can cross the placental barrier. Two IgG subclasses have been shown to be produced during this stage, IgG1 and IgG3.<sup>28</sup> Disease severity appears to be lower in cases in which IgG1 is almost exclusively present.



Fetal erythropoiesis begins in the yolk sac by day 21. The Rh antigen can be expressed as early as day 30 of gestation. After the second exposure, there is an increase in the production of IgG antibodies leading to an increase in maternal titers. These antibodies recognize and attach to the foreign antigen on the fetal RBC surface. The IgG antibody lacks the ability to bind complement, and therefore, the antibody-coated fetal RBCs are sequestered by macrophages and are destroyed by the reticuloendothelial system extravascularly. This chain of events leads to the development of fetal anemia.

As the life span of the fetal RBC is reduced, a greater burden is placed on the hematopoietic system. It has been proposed that medullary hematopoiesis is stimulated in the early stages of mild anemia and that recruitment of extramedullary sites occurs only after anemia has progressed and become severe. This is evidenced by the fact that in severe disease, both the liver and the spleen become enlarged because of congestion and increased extramedullary hematopoiesis, causing the release of nucleated RBC precursors (erythroblasts). In a study evaluating umbilical cord samples from 127 pregnancies, Nicolaides and associates showed that significant erythroblastosis was present only when the hemoglobin deficit was greater than 7 g/dL<sup>29</sup> (Fig. 17-10). Severe anemia can lead to decreased oxygen delivery and hypoxia in certain end organs, causing cardiac output to increase as a compensatory mechanism. However, these mechanisms may be inadequate to maintain adequate perfusion. The loss of the buffer function of fetal RBCs also contributes to worsening acid-base disturbances. Soothill and colleagues reported an increase in the lactate concentration in the umbilical artery when hemoglobin levels were below 8 g/dL and an increase in umbilical vein concentration when this level

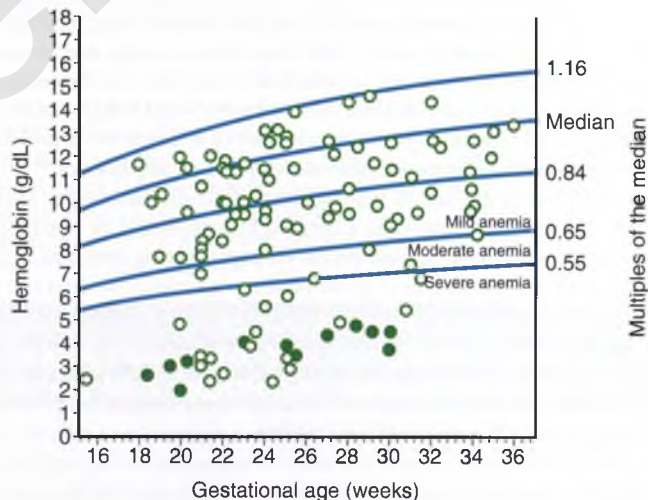


**FIG 17-10** Relationship between fetal hemoglobin and gestational age. (From Mari G, Deter RL, Carpenter RL, et al: Noninvasive diagnosis by Doppler ultrasonography of fetal anemia due to maternal red-cell alloimmunization. Collaborative Group for Doppler Assessment of the Blood Velocity in Anemic Fetuses (Level II-1). *N Engl J Med* 342:9-14, 2000; used with permission.)

**FIG 17-9 A**, Initial pregnancy in which the mother is Rh negative and is carrying a fetus that is Rh positive. **B**, At the time of delivery, the fetal Rh-positive red blood cells enter the maternal circulation and initiate an antibody response. **C**, In a subsequent pregnancy, antibodies enter the fetal circulation, attaching to the red blood cells and resulting in the sequestration and destruction of these cells. (Illustration by James A. Cooper, MD, San Diego, CA.)



dropped to 4 g/dL.<sup>30</sup> This finding implies that disease progression leads to a shift in cellular metabolism to a predominantly anaerobic state.

The exact mechanism leading to fetal hydrops is incompletely understood. It is well known that anemia must be severe before hydrops develops and that fetal hemoglobin must fall below six standard deviations from the mean for that gestational age.<sup>29</sup> Initial studies indicated that low fetal albumin levels leading to decreased colloid pressure and increased extravasation could be a contributing factor leading to hydrops.<sup>31,32</sup> However, more recent studies have shown that hypoalbuminemia is found in only a small percentage of fetuses with hydrops<sup>33</sup> and that drops in albumin levels appear to be a component of the very late stages of the disease.<sup>34</sup> Other factors may also lead to increased vascular permeability facilitating the development of hydrops. Berger and coworkers demonstrated that concentration of ferritin and lipid-peroxidation products were increased, leading to the suggestion that iron overload and free radical damage may contribute to the pathogenesis.<sup>35</sup> Cardiac dysfunction is also common among fetuses affected by severe anemia and could possibly play a role in the disease process. Affected fetuses develop an increase in both biventricular cardiac diameter and umbilical venous pressure.<sup>36,37</sup> The increase in venous pressure may potentially lead to increased fluid extravasation, favoring the development of hydrops. The increase in venous pressure could also lead to an obstruction of lymphatic flow. Interestingly enough, it has also been shown that umbilical venous pressure decreases as early as 24 hours following therapeutic fetal intravascular transfusion.<sup>38</sup>

## Management

Severe fetal anemia that eventually leads to hydrops has direct implications for both fetal survival and long-term neonatal and infant outcomes. Cases of fetal anemia characterized by severe hydrops have a 74% survival rate compared to a 94% survival rate seen in nonhydrops cases.<sup>39</sup> In a longitudinal study evaluating the long-term neurologic outcomes following intrauterine transfusion for RBC alloimmunization, over 95% of the 291 children followed were found to have normal developmental outcomes. However, a history of hydrops was found to be a significant risk factor for neurodevelopmental impairment.<sup>40</sup>

Prevention is the key to management of alloimmunization. This starts at the first prenatal visit; a detailed history should be obtained from all patients. Specifics and details on past obstetric events as well as any previous transfusion of blood products are crucial to determining patients who may be at risk. Initial laboratory workup should include ABO typing with determination of RhD status as well as an antibody screen via a maternal indirect Coombs test. If a patient is found to be RhD negative, it should be determined if she is a candidate for prophylactic Rh immunoglobulin. If the antibody screen is positive, the blood bank should report the identity and the titer of the antibody. Titer levels are used to assess the likelihood of risk that the fetus may become affected. Antibodies that have been associated with hemolytic disease of the newborn are listed in Table 17-1.

A repeat antibody screen for RhD should be done at 24 to 28 weeks. If this screen is negative, the patient is a candidate for anti-D prophylaxis via passive immunoglobulin administration. Although the exact mechanism of action is unknown, this strategy has been shown to be effective. In the United States, it is recommended that a single dose of 300 µg of anti-D immunoglobulin be administered at 28 weeks' gestation.<sup>41</sup> Immune prophylaxis probably works through the antigen clearance hypothesis. In this scenario, the administered immunoglobulin attaches to the RBCs. This interaction favors the removal of the coated cells by the mononuclear phagocytic system, particularly the macrophages, therefore not allowing these antigens to be recognized by the immune system.<sup>42</sup> However, recent studies using several different animal models have shown that this hypothesis does not explain the

entire mechanism of action. Other antigen-presenting cells, capable of initiating an immune response, also play a role in the clearance of D-positive RBCs.<sup>43</sup>

After the administration of the immune prophylaxis at 28 weeks' gestation, some experts recommend that a second dose of 300 µg be administered if the woman has not delivered within 12 weeks of her dose.<sup>44</sup> One prophylactic dose of 300 µg of anti-D immunoglobulin is enough to prevent exposure produced by 30 mL of RhD-positive blood or 15 mL of fetal cells.<sup>45</sup> Current guidelines dictate that if an RhD-negative woman delivers an RhD-positive infant, she should have a quantitative test (i.e., Kleihauer-Betke stain) done to determine the exact amount of anti-D immune globulin to be administered. The result of this test is typically multiplied by a factor of 50 to determine the total amount of fetomaternal hemorrhage. The dose should be administered within 72 hours of delivery, although this strategy has been shown to be effective up to 28 days after delivery.<sup>44</sup> Also, women at risk for RhD alloimmunization should also receive a dose of prophylactic immunoglobulin after any obstetric event or procedure that puts her at risk for maternal-fetal hemorrhage.

Women who have been sensitized against RhD should have maternal antibody titer levels repeated every 4 weeks during the first and second trimesters and every 2 weeks during the third trimester in order to determine the risk of developing hemolytic disease. Maternal-fetal ABO incompatibility may be protective and decreases the risk of D alloimmunization.<sup>21</sup> If a fetus is both RhD positive and ABO incompatible with the mother, this reduces the risk of alloimmunization to about 2%. Variations in the techniques used to determine the antibody level have led to the use of different thresholds to determine when a fetus is at risk for developing anemia. The titer value that is determined to be critical varies from 1:8 to 1:32. Clinicians should be familiar with the reference value used within their facilities.

Paternal testing can also be used to determine the risk of developing fetal anemia. RhD-positive fathers have a probability of being heterozygous. In the past, mathematical modeling along with ethnicity was used to determine the probability of heterozygosity. Advances in genetic testing have now allowed for the direct determination of paternal zygosity. If paternity is assured, this test can be used in the management algorithm of an RhD-negative woman. If the father is found to be heterozygous, the fetus has a 50% chance of being RhD negative. If the father is RhD negative, the fetus will likewise be RhD negative and therefore will not be at risk.

It has been estimated that 40% of RhD-negative women carry an RhD-negative fetus. For this reason, some have advocated for a more direct approach attempting to eliminate excessive testing and anxiety. Direct assessment of fetal blood type can be done via invasive prenatal testing. Amniocentesis can allow for the determination of the fetal genotype.<sup>46</sup> Because genotype may not correlate with the RBC antigen expression in some rare instances, direct fetal blood sampling can also be used to determine the fetal phenotype. However, this technique is associated with a higher complication rate and a greater risk of fetal demise as compared to amniocentesis. Recently, newer noninvasive methods to determine fetal genotype have become available. As early as 1997, it was recognized that cell-free fetal DNA could be detected in the maternal circulation,<sup>47</sup> with reports indicating that it was present in detectable quantities as early as 38 days' gestation.<sup>48</sup> Throughout the years, several companies developed different techniques to identify different loci on the fetal RhD gene. This test became commercially available in Europe and North America. Reports from several European centers specializing in the treatment of RhD disease started to emerge indicating the high accuracy of this test.<sup>49,50</sup> A meta-analysis looking at over 30 articles concluded that the overall accuracy of this test was around 94% with a sensitivity of 95.4% and a specificity of



98.6%.<sup>51</sup> Several European countries, with different patient populations and insurance payment plans, have started to adopt noninvasive RhD testing as part of the management protocol of women at risk for RhD alloimmunization with success.<sup>52</sup> More worldwide widespread use was limited by the concerns of the lack of data regarding cost analysis. A recent cost analysis done in the United States by Hawk and associates concluded that with the current cost of RhD typing, routine antenatal anti-D immunoglobulin prophylaxis was still less costly.<sup>53</sup> It is possible that with more automated techniques and increased competition driven by higher demand, the cost of testing may decrease, leading to the expansion of the acceptance of this test as part of the RhD alloimmunization management protocol. However, some have raised concern that, because cell-free DNA screening does not detect 100% of RhD-positive fetuses, routine use of cell-free DNA to target RhD immune globulin for RhD-negative women would cause increased sensitization compared with routine RhD immune globulin administration. Assays for detecting RhCc, RhE, and Kell typing via cell-free fetal DNA are also currently available.<sup>54</sup>

### Prediction of Anemia

Once a patient has been sensitized, there is a risk for fetal anemia. Several invasive techniques allow for the direct evaluation of fetal hemoglobin and hematocrit. Normally, fetal hemoglobin concentration increases with advancing gestation, and reference ranges for fetal hemoglobin have been established using fetal blood sampling (Table 17-2). Cordocentesis can accurately detect fetal anemia; however, this technique carries with it a risk of pregnancy loss and fetal demise reported to range from 0.9% to 3.2%.<sup>55</sup> Historically, another method used in the prediction of fetal anemia was through amniocentesis. Levels of bilirubin within the amniotic fluid were measured using the AOD<sub>450</sub> assay to predict hemolysis. The values obtained would be later plotted against published nomograms to determine the risk of severe fetal anemia.<sup>56,57</sup> This approach had the downside that in many cases serial amniotic fluid samplings were required to assess the severity and progression of the disease. These two procedures have been relegated to the past by the widespread use of sonographic Doppler evaluation of the middle cerebral artery (MCA).<sup>58</sup>

Advances in ultrasound technology have led to this technique now being the preferred method of prediction of fetal anemia. As mild to moderate anemia develops, the fetus responds with several compensatory mechanisms. The increased demand is thought to lead to increased ventricular output and stroke volume. These changes, along with a decrease in fetal blood viscosity secondary to the loss of RBCs, lead to an increase in flow velocity. Several fetal vessels were interrogated in an attempt to identify an easily accessible window for evaluation of blood flow. Measurements of the peak systolic velocity (PSV) in the MCA have been found to be highly predictive of severe fetal anemia. This vessel has the benefit of being easily identifiable with low intra-observer and interobserver variability. Because this measurement varies across gestational ages, the Collaborative Group for Doppler Assessment of the Blood Velocity in Anemic Fetuses has developed a reference in which the PSV measurement obtained is converted to multiples of the median (MoM) and used to predict the probability of fetal anemia (Table 17-3).<sup>59</sup> Using a hemoglobin concentration of 5 g/dL as a threshold, a cutoff of 1.5 MoM has been found to be highly predictive of severe fetal anemia requiring therapy in RBC alloimmunization affected pregnancies (Figs. 17-10 and 17-11). This approach led to a false positive rate of approximately 12%. Later studies comparing the accuracy of this measurement to serial amniocentesis determined that this sonographic measurement has a better sensitivity and specificity.<sup>60</sup> With the increasing experience and standardization in obtaining this measurement as well as the improvement in ultrasound

**TABLE 17-2 Reference Ranges for Fetal Hemoglobin Concentration as a Function of Gestational Age**

Gestational Age (weeks)	HEMOGLOBIN CONCENTRATION (g/dL)			
	1.0 MoM (Median)	0.55 MoM	0.65 MoM	0.84 MoM
18	10.6	5.8	6.9	8.9
19	10.9	6.0	7.1	9.1
20	11.1	6.1	7.2	9.3
21	11.4	6.2	7.4	9.5
22	11.6	6.4	7.5	9.7
23	11.8	6.5	7.6	9.9
24	12.0	6.6	7.8	10.0
25	12.1	6.7	7.9	10.2
26	12.3	6.8	8.0	10.3
27	12.4	6.8	8.1	10.4
28	12.6	6.9	8.2	10.6
29	12.7	7.0	8.3	10.7
30	12.8	7.1	8.3	10.8
31	13.0	7.1	8.4	10.9
32	13.1	7.2	8.5	11.0
33	13.2	7.2	8.6	11.1
34	13.3	7.3	8.6	11.1
35	13.4	7.4	8.7	11.2
36	13.5	7.4	8.7	11.3
37	13.5	7.5	8.8	11.4
38	13.6	7.5	8.9	11.4
39	13.7	7.5	8.9	11.5
40	13.8	7.6	9.0	11.6

Normal hemoglobin values were 0.84 MoM or greater; mild anemia, between 0.65 and 0.84 MoM; moderate anemia, between 0.55 and 0.64 MoM; and severe anemia, 0.55 MoM or less.

MoM, multiples of the median.

Modified from Mari G, Deter RL, Carpenter RL, et al: Noninvasive diagnosis by Doppler ultrasonography of fetal anemia due to maternal red-cell alloimmunization. Collaborative Group for Doppler Assessment of the Blood Velocity in Anemic Fetuses (level II-1). *N Engl J Med* 2000;342:9-14.

**TABLE 17-3 Expected Peak Velocity of Systolic Blood Flow in the Middle Cerebral Artery as a Function of Gestational Age**

Week of Gestation	PEAK VELOCITY (cm/s)			
	1.00 MoM (Median)	1.29 MoM	1.50 MoM	1.55 MoM
18	23.2	29.9	34.8	36.0
20	25.5	32.8	38.2	39.5
22	27.9	36.0	41.9	43.3
24	30.7	39.5	46.0	47.5
26	33.6	43.3	50.4	52.1
28	36.9	47.6	55.4	57.2
30	40.5	52.2	60.7	62.8
32	44.4	57.3	66.6	68.9
34	48.7	62.9	73.1	75.6
36	53.5	69.0	80.2	82.9
38	58.7	75.7	88.0	91.0
40	64.4	83.0	96.6	99.8

MoM, multiples of the median.

From Mari G, Deter RL, Carpenter RL, et al: Noninvasive diagnosis by Doppler ultrasonography of fetal anemia due to maternal red-cell alloimmunization. *N Engl J Med* 342:9, 2000.



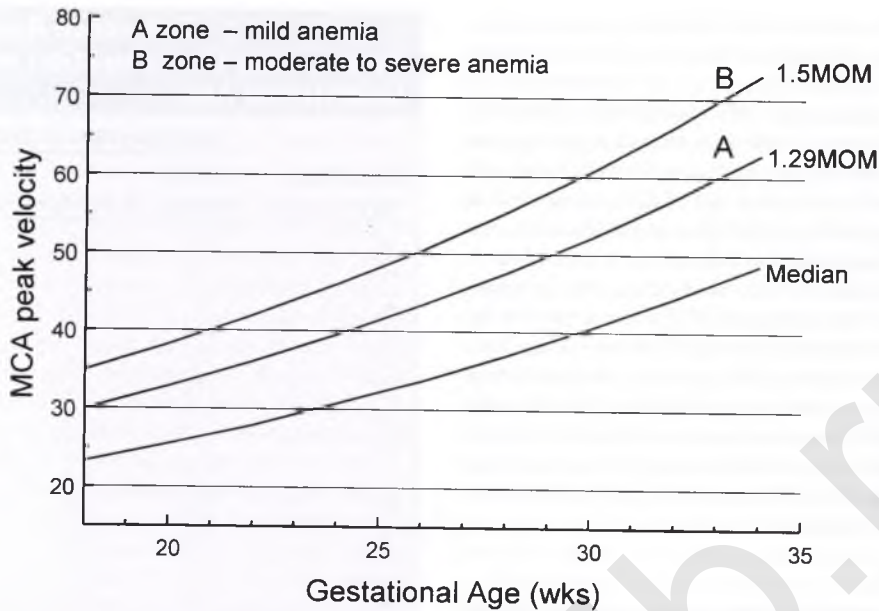


**FIG 17-11** Nomogram for mild anemia (1.29 MoM) and moderate-severe anemia (1.5 MoM). MCA, middle cerebral artery; MoM, multiples of median; zone A values, mild anemia; zone B values, moderate to severe anemia.

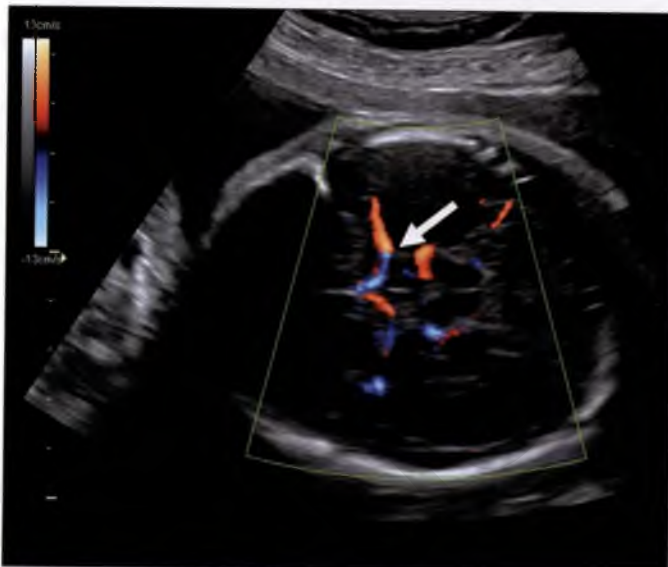


**FIG 17-12** Anterior and middle cerebral artery (arrow) using color flow Doppler sonography for localization. (Courtesy of Anthony Swartz, BS, RT(R), RDMS.)



**FIG 17-13** Middle cerebral artery (MCA) assessment at 19 weeks' gestation. Top image illustrates power Doppler localization of the proximal MCA vessel. Note Doppler gate location. Peak systolic velocity on lower image was measured at 52.42 cm/second; 1.87 MoM for this gestational age. FHR, fetal heart rate; MoM, multiples of the median. (Courtesy of Anthony Swartz, BS, RT(R), RDMS.)

technology, measurement of PSV in the MCA has become the surveillance modality of choice in alloimmunized pregnancies.

The MCA can be easily identified at the base of fetal skull. Color Doppler is utilized to identify the entire circle of Willis (Figs. 17-12 and 17-13). The examiner should interrogate the MCA closest to the transducer. If this is not possible, evaluation of the MCA in the far field may provide reliable results.<sup>61</sup> The 1- to 2-mm Doppler gate should then be placed just distal to the origin of the MCA from the carotid siphon. The ultrasound probe should be manipulated so a 0-degree angle of insonation is obtained. One approach to help achieve this angle is to start by obtaining the view for a biparietal diameter measurement. The probe should then be angled slightly toward the fetal skull and moved sideways in order to "tilt" the fetal head on the

ultrasound screen. This will allow the MCA to be viewed in an almost completely vertical position. Angle correction can sometimes be used if the 0-degree angle insonation cannot be obtained effectively,<sup>62</sup> although this approach is not preferred. Several measurements of the MCA PSV should be obtained, as these can be distorted by fetal movement or breathing. All measurements should have similar values to one another. The best measurement obtained should be used; the values obtained should not be averaged.

MCA PSV can be obtained as early as 16 to 18 weeks' gestation. A multicenter prospective trial has shown that this measurement has a high false positive rate when measured after 35 weeks' gestational age.<sup>63</sup> Measurements should be repeated every 1 to 2 weeks depending on the clinical presentation. If MCA PSV measurements reach a value greater

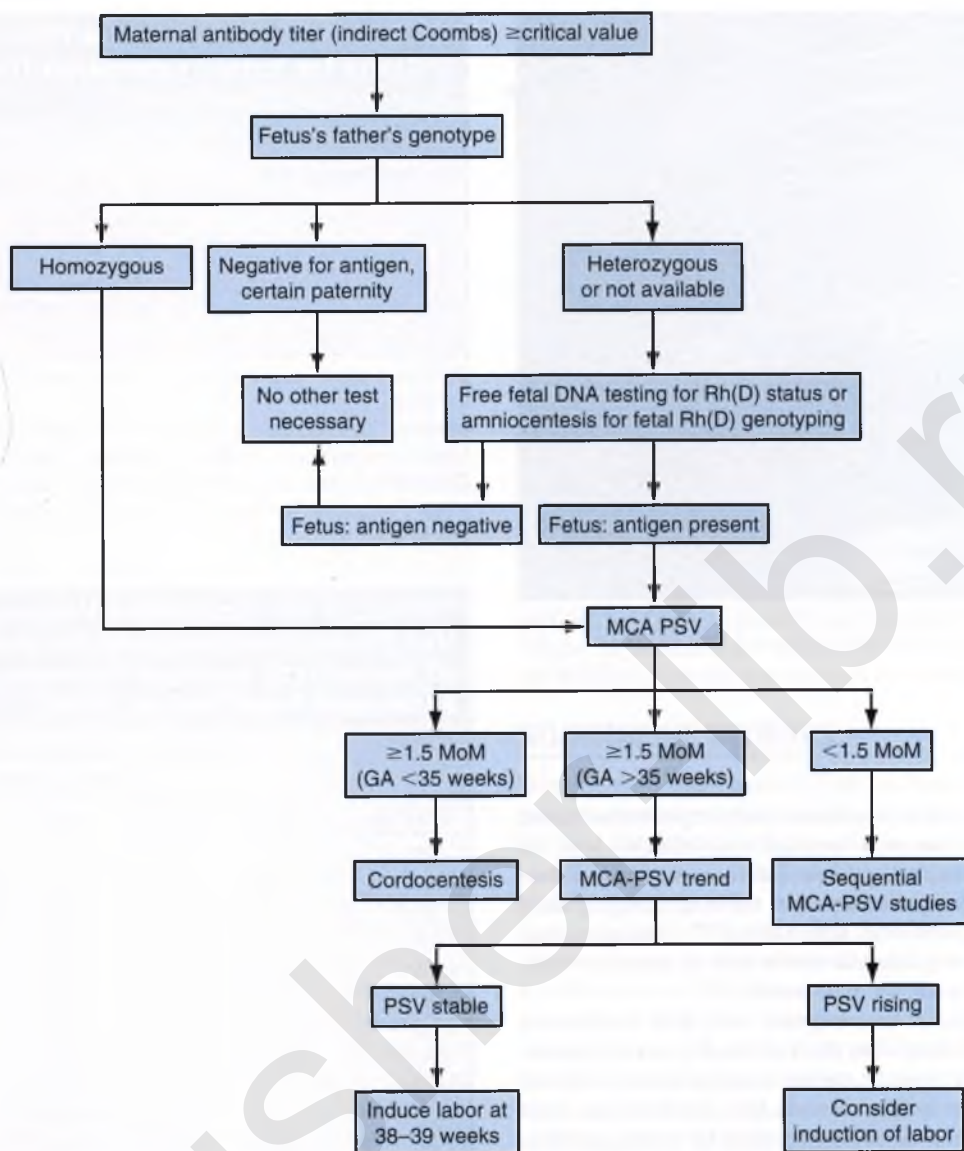


**FIG 17-14** Algorithm for the clinical management of the red blood cell alloimmunized pregnancy. GA, gestational age; MCA, middle cerebral artery; MoM, multiples of the median; PSV, peak systolic velocity. (Modified from Moise KJ Jr, Argoti PS: Management and prevention of red cell alloimmunization in pregnancy: a systematic review (level I). *Obstet Gynecol* 120:1132-1139, 2012.)

than 1.5 MoM, fetal blood sampling via cordocentesis should be performed. Should the fetal hematocrit be found to be below 30%, intrauterine transfusion is indicated. Many experts recommend that if the serial evaluation of MCA PSV remains below the established threshold, monitoring should be continued, with a plan for induction of labor at 37 to 38 weeks. Delivery is also warranted if there is any evidence of fetal compromise. Antenatal testing via nonstress test or biophysical profile should also be instituted starting at 32 weeks' gestation.

Elevated MCA PSV after 35 weeks represents a therapeutic challenge. In the past, some investigators advocated performing amniocentesis to obtain both levels of bilirubin within the amniotic fluid measured using the  $\Delta OD_{450}$  assay as well as testing fetal lung maturity. However, the lack of familiarity with performing fetal lung maturity assays within several referral centers added to the fact that there has been a move toward abandonment of fetal lung maturity testing in well-dated pregnancies<sup>64</sup> has led to the abandonment of the practice of amniocentesis beyond 35 weeks for this indication.

For women with a prior history of an affected fetus or child, defined as a fetus requiring intrauterine transfusion or exchange transfusions after birth, the use of serial maternal titers is no longer indicated because they are no longer predictive after an affected pregnancy. Fetal RhD status can be established; if the fetus is RhD positive, monitoring with serial MCA Doppler tests should commence around 16 to 18 weeks. Figure 17-14 summarizes a proposed protocol for evaluation and management of affected pregnancies.

### Intrauterine Transfusion

Access into the fetal circulation is obtained under ultrasound guidance using a 22-G needle. Venous access is the goal; inadvertent arterial puncture can be associated with vasospasm, bradycardia, and sudden death. If the placenta is anterior, direct puncture at the site of cord insertion may be possible (Fig. 17-15). A free loop of cord or the intrahepatic portion of the umbilical vein can also be used. After gaining access, a sample of fetal blood should be sent for analysis of





**FIG 17-15** Packed red blood cells seen streaming in the fetal umbilical vein (arrow) at the time of an intravascular transfusion at 26 weeks' gestation. The cord insertion into the anterior placenta is located at the asterisk.

fetal ABO and Rh type, direct Coombs test, and complete blood count including platelets, reticulocyte count, and total bilirubin level. To decrease fetal movements during the procedure, an intravenous dose of a paralytic agent such as pancuronium at a dose of 0.2 mg/kg using the estimated fetal weight may be administered.<sup>65,66</sup> Although several centers include the use of furosemide within their treatment protocol, this strategy has not been shown to be beneficial.<sup>67</sup>

Transfused blood should be compatible with both mother and fetus. With a first transfusion, when the fetal blood type is not known, O negative blood is used. Typically, the hematocrit of the unit of blood used is increased to 70% to 80% to reduce the volume of transfused blood to the fetus. The unit should also be tested for cytomegalovirus; hepatitis A, B, and C; and human immunodeficiency virus (HIV) and should also be leukocyte depleted in order to decrease the risk of viral transmission and graft-versus-host disease. Several methods have been proposed to calculate the amount of blood to transfuse. One of simplest methods has been described by Giannina and colleagues.<sup>68</sup> Once the starting hematocrit is known, the estimated fetal weight determined sonographically in grams is multiplied by a fixed coefficient to determine the amount of blood in milliliters required to reach the target fetal hematocrit. A coefficient of 0.02 is used to increase the hematocrit by 10%, and for every 5% above this value the coefficient is increased by 0.01 (i.e., 0.04 to increase by 20%). If, for example, the starting hematocrit is 15% and the estimated fetal weight is 1000 g, then 50 mL of blood would need to be transfused to reach a target hematocrit of 40% (increase by 25% using a coefficient of 0.05) (Tables 17-4 through 17-7).

The ultimate goal of fetal transfusions is not only to correct anemia but also to suppress fetal erythropoiesis. The blood should be transfused at a rate of 5 to 10 mL/minute. Most referral centers attempt to reach a final hematocrit of 50% to 65%. One exception to this rule is the hydropic fetus. A fetus with hydrops is not able to tolerate severe volume overload, and for this reason the hematocrit should not be increased greater than fourfold.<sup>69</sup> A repeat procedure can be done 48 hours later to achieve the target hematocrit.

**TABLE 17-4 Method for Calculating Volume for Fetal Transfusion Using Transfusion Coefficient**

Desired Increment in Hematocrit (%)	Transfusion Coefficient
10	0.02
15	0.03
20	0.04
25	0.05
30	0.06

Estimated fetal weight (g) × transfusion coefficient = volume to transfuse.

Modified from Moise KJ, Whitecar PW: Antenatal therapy for hemolytic disease. In Hadley A, Soothill P (eds): *Alloimmune Disorders of Pregnancy. Anemia, Thrombocytopenia and Neutropenia in the Fetus and Newborn*. Cambridge, UK, Cambridge University Press, 2002.

**TABLE 17-5 Predicted Volume of Packed Red Blood Cells Required for Desired Level of Hematocrit Increase According to Estimated Fetal Weight (EFW)**

EFW (g)	LEVEL OF DESIRED INCREASE IN HEMATOCRIT				
	10%	15%	20%	25%	30%
500	12.5	16.1	19.7	23.2	26.8
600	14.8	19.1	23.4	27.7	32.0
700	17.2	22.2	27.2	32.2	37.2
800	19.5	25.2	31.0	36.7	42.4
900	21.8	28.3	34.7	41.2	47.6
1000	24.2	31.3	38.5	45.7	52.8
1100	26.5	34.4	42.3	50.1	58.0
1200	28.8	37.4	46.0	54.6	63.2
1300	31.2	40.5	49.8	59.1	68.4
1400	33.5	43.5	53.5	63.6	73.6
1500	35.8	46.6	57.3	68.1	78.8
1600	38.1	49.6	61.1	72.5	84.0
1700	40.5	52.7	64.8	77.0	89.2
1800	42.8	55.7	68.6	81.5	94.4
1900	45.1	58.7	72.4	86.0	99.6
2000	47.5	61.8	76.1	90.5	104.8
2100	49.8	64.8	79.9	94.9	110.0
2200	52.1	67.9	83.7	99.4	115.2
2300	54.5	70.9	87.4	103.9	120.4
2400	56.7	73.9	91.0	108.2	125.4
2500	59.0	76.9	94.8	112.7	129.6

From Plecas DV, Chitkara U, Berkowitz GS, et al: Intrauterine intravascular transfusion for severe erythroblastosis fetalis: how much to transfuse (level II-3)? *Obstet Gynecol* 1990;75:965-969.

Prior to the use of intravenous transfusion (IVT), intraperitoneal transfusions were advocated as a method of administering blood to the anemic fetus. With advances in real-time ultrasound technology and the increased experience with intravenous access to the fetal circulation, the use of peritoneal transfusion has fallen into disfavor. One approach that has been advocated has been the use of combined intravenous and intraperitoneal transfusion. This method is used within certain centers to allow an increase in the interval between scheduled

**TABLE 17-6 Predicted Volume of Packed Red Blood Cells Required for Desired Level of Hematocrit Increase According to Gestational Age**

Gestational Age (weeks)	LEVEL OF DESIRED INCREASE IN HEMATOCRIT				
	10%	15%	20%	25%	30%
21	13.1	14.2	15.2	16.3	17.3
22	13.7	15.8	17.9	19.9	22.0
23	14.8	17.9	21.1	24.2	27.3
24	16.5	20.6	24.8	30.0	33.1
25	18.7	23.9	29.1	34.3	39.5
26	21.4	27.7	33.9	40.2	46.4
27	24.7	32.0	39.3	46.6	53.9
28	28.6	36.9	45.3	53.6	61.9
29	33.0	42.4	51.7	61.1	70.5
30	37.9	48.4	58.8	69.2	79.6
31	43.4	54.9	66.4	77.8	89.3
32	49.5	62.0	74.5	87.0	99.5
33	56.0	69.6	83.2	96.7	110.3
34	63.2	77.8	92.4	107.0	121.6

From Plecas DV, Chitkara U, Berkowitz GS, et al: Intrauterine intravascular transfusion for severe erythroblastosis fetalis: how much to transfuse (level II-3)? *Obstet Gynecol* 1990;75:965-969.

fetal transfusions, because it is known that the fetal hematocrit declines approximately 1% per day.<sup>70</sup> This approach allows for a more stable fetal hematocrit between transfusions.<sup>71</sup> Although the decline in fetal hematocrit is more rapid between the first few transfusions, on average a 14-day interval should be used between IVTs. This schedule can be safely continued until around 35 weeks, with a plan for delivery 2 to 3 weeks later. The need for exchange transfusion postnatally has been reported to be decreased with the administration of oral phenobarbital 30 mg three times a day to enhance liver maturation.<sup>72</sup>

Patients who develop severe Rh alloimmunization prior to 20 weeks' gestation may not always be treated with IVT. The small size of the fetal vessels makes this strategy technically difficult. Intrapertoneal transfusion can sometimes be employed, although there is no formula available to calculate the amount of blood to transfuse. The use of suppressive therapy has also been presented as an option for treatment in these patients. Maternal administration of intravenous immunoglobulin (IVIG) has been used in some cases. It is thought that this strategy works by inhibiting the maternal antibody synthesis and by blocking the transport of antibodies transplacentally. Some studies have demonstrated that this strategy, followed by IVT, led to improved survival rate as compared to IVT alone.<sup>73</sup> A case series of patients followed in Sweden showed that this strategy, along with maternal plasma exchange, may be beneficial when used prior to the development of severe fetal anemia.<sup>74</sup> The high cost of this therapy and the limited data should be considered when deciding which treatment modality to employ.

### Prognosis

With the advent of fetal transfusion and the improvements in the NICU, the prognosis of immune hydrops has improved. Because one of the goals of intrauterine transfusions is to suppress hematopoiesis, neonates born after receiving this therapy have suppressed bone marrow function and a decrease in the reticulocyte production. Several

of these newborns may require transfusions after birth, commonly referred to as "top-up" transfusions.

A retrospective review of 208 women who were treated with over 590 transfusions demonstrated that this strategy was associated with an overall survival rate of 86%. The diagnosis of hydrops as well as the need for transfusions prior to 20 weeks' gestation was associated with a lower survival rate. The overall fetal loss rate attributed to the procedure was calculated to be 4.8%.<sup>75</sup> Short-term neonatal outcomes were also reviewed in a study from Scotland that evaluated 116 pregnant women who underwent 457 intrauterine fetal transfusions over a 10-year period. The survival rate quoted in this cohort was 97.4%. After delivery, 33% of neonates required respiratory assistance, 16% had an exchange transfusion, and 54% required a top-up transfusion. The authors quoted a procedure-related loss rate that ranged from 0.8% to 2.3%.<sup>76</sup>

Neurodevelopmental outcomes were evaluated in the LOTUS (long-term neurodevelopmental outcome after intrauterine transfusion for hemolytic disease of the fetus/newborn) study that assessed 291 children followed to median age of 8.2 years. The authors reported a high rate of intact survival, with only 2.1% of the cohort being diagnosed with cerebral palsy. The development of hydrops fetalis was a major risk factor associated with adverse neurodevelopmental outcomes.<sup>40</sup>

## NONIMMUNE HYPDROPS

Nonimmune hydrops fetalis (NIHF) is a heterogeneous condition that may be secondary to multiple causes. Several publications have identified over 100 different conditions that are associated with NIHF; some associations between NIHF and certain pathologic conditions are limited to case reports or small case series. Table 17-8 lists the conditions associated with NIHF that have been reported. It has been reported that up to 60% of cases detected prenatally can have a cause specifically identified<sup>77</sup>; this number increases to 85% when postnatal evaluation is taken into consideration.<sup>78</sup> However, a significant percentage of cases will still not have an identifiable cause. Most reports indicate that cardiovascular causes, which include arrhythmias, structural abnormalities, and diverse cardiomyopathies, are the most common conditions leading to NIHF. Up to 16% of all cases can be explained by a chromosomal cause, whereas hematologic abnormalities contribute to approximately 4% to 12% of NIHF cases.<sup>78,79</sup>

### Mechanism

Owing to the variety of causes, determining the exact mechanism(s) of development of NIHF is challenging. The precise pathophysiologic pathway will depend on the underlying cause, but in some cases this remains unclear. It appears that the underlying process in several conditions can be explained by a dysregulation of fluid movement between the vascular and interstitial spaces, caused by either an increase in interstitial fluid production or a decrease in lymphatic return.<sup>80</sup> Examples of these conditions include structural heart defects leading to an increased right cardiac pressure causing increased central venous pressure; an obstruction of venous or arterial blood flow such as the one caused by obstructive chest masses; inadequate diastolic ventricular filling as seen in fetal arrhythmias; fetal hepatic fibrosis leading to decreased liver function and hypoalbuminemia; or the reduced osmotic pressure exemplified by congenital nephrosis. Severe fetal anemia secondary to a lack of RBC production, blood loss, or increased RBC destruction may lead to high-output cardiac failure causing fluid imbalance leading to hydrops.

Certain congenital infections may also lead to NIHF. Several mechanisms have been proposed and vary by the underlying infectious



**TABLE 17-7 Example Setup for Fetal Blood Sampling and Transfusion**

1. Obtain O-negative, CMV-negative, irradiated packed red blood cells from the blood bank. O-positive blood may be needed when antibodies to the c antigen are present because O-negative, c-negative blood is very rare (prevalence of 0.0001%).
2. Under sterile conditions, open:
  - a. Four paper or cloth drapes or single sterile drape (as used for cesarean delivery)
  - b. Towel clips as needed
  - c. One spinal needle,\* 20 or 22 gauge (22 gauge for transfusions before 24 weeks of gestation or if thrombocytopenia is suspected), prepared with heparin to prevent clot formation
  - d. Sterile ultrasound probe cover
  - e. Sterile ultrasound gel
  - f. A skin preparation solution (Betadine- or chlorhexidine-based solution)
  - g. Eight to ten 1-mL syringes, flushed with heparin to avoid clot formation
  - h. One 1-mL syringe for paralytic agent (atracurium or vecuronium)
  - i. Five to ten 20-mL syringes (for storing blood)
  - j. Four 12-mL syringes
  - k. One 3-mL syringe
  - l. Three needles, 18 or 20 gauge, for drawing blood from blood bank into 20-mL syringes
  - m. One 22- or 25-gauge needle
  - n. A 5.5-inch small-bore extension set with T-connector and Luer adaptor
  - o. Three-way stopcock
3. Fill two 5-mL syringes with physiologic saline solution.
4. Flush 1-mL syringes with heparin; save one unflushed 1-mL syringe for vecuronium (or atracurium).
5. Draw up normal saline to make three saline flushes; remove air bubbles by holding syringes upright and tapping to release bubbles to top; then attach small-bore connection tubing and flush air through.
6. Reconstitute vecuronium with 10 mL of normal saline.
  - a. Draw up 1 mL of vecuronium and 9 mL of normal saline in a 12-mL syringe.
  - b. Transfer 1 mL of vecuronium mixture to an unheparinized 1-mL syringe.
  - c. Mark both the 12-mL and 1-mL syringes containing vecuronium, to avoid confusion.
  - d. Usual dose of vecuronium is 0.1 mg/kg and of atracurium is 0.4 mg/kg.
7. Draw up 2% lidocaine in 3-mL syringe, attached to a 22- or 25-gauge needle, for injection at puncture site for maternal local anesthesia.
8. Care should be taken to maintain sterility when drawing up solutions: Either have an assistant hold the containers of saline, vecuronium, lidocaine, and blood from the blood bank, or use single-operator technique, keeping one hand sterile and one hand unsterile.
9. Attach intravenous connection tubing to unit of packed red blood cells.
10. Attach stopcock, taking care to maintain sterility on one end of the stopcock.
11. Fill 20-mL syringes with blood by opening stopcock.
  - a. Remove any air bubbles that may be present by holding syringe upright and tapping side of syringe to release air bubbles.
12. Have tubes available to send for laboratory studies.
  - a. Remember to include not only initial, midway, and final blood count samples but also any additional tubes for genetic studies, liver function studies, or other tests.

\*Length of needle is determined beforehand by measuring the distance on the ultrasound image from maternal abdominal wall to cord insertion site.

From Society for Maternal-Fetal Medicine (SMFM) clinical guideline #7: Nonimmune hydrops fetalis. *Am J Obstet Gynecol* 2015;212(2):127-139; used with permission.

agent involved. Some pathogens may cause an inflammatory reaction leading to an increased capillary permeability; the microorganism may also attack the liver and cardiac tissue, directly causing fetal hepatitis or myocarditis, or may cause bone marrow suppression such as in the case of parvovirus B19.

Chromosomal abnormalities, such as Turner syndrome (45,X), can cause lymphatic vessel dysplasia and obstruction that can lead to cystic hygroma formation. Fetal structural abnormalities in multiple organ systems such as the musculoskeletal, neurologic, and gastrointestinal systems, have also been associated with the development of hydrops, although the exact mechanism may not always be known.

### Evaluation and Management

Every effort should be made to identify the underlying cause. A detailed maternal history that includes exposures to infectious agents or toxins, the presence of pets, or any unusual travel or eating habits should be

collected and recorded at the time of diagnosis. A detailed pedigree may identify consanguinity, increasing the likelihood of an autosomal recessive disorder. Comprehensive fetal anatomy evaluation via a detailed high-resolution ultrasound may reveal an abnormality causing NIHF. A fetal echocardiogram should also be part of the initial evaluation. Doppler evaluation of the PSV of the MCA will lead to the identification of fetal anemia in some cases of NIHF. Immune hydrops should be excluded by determining maternal blood type and RhD antigen status. To rule out fetal-maternal hemorrhage, a Kleihauer-Betke smear, showing the presence of fetal cells in the maternal peripheral blood, or flow cytometry analysis, estimating the volume of fetal bleeding, may also be indicated.

Maternal serologic antibody titers for congenital infections, especially for parvovirus B19, or direct isolation of viruses and parasites from amniotic fluid with polymerase chain reaction evaluation should be considered. Prenatal diagnostic testing, including karyotype,

TABLE 17-8 Causes and Associations of Nonimmune Hydrops

Cause/Association	Frequency*	Cause/Association	Frequency*
<b>Focal Abnormalities</b>		<b>Pulmonary and Mediastinal</b>	
<b>Cranial</b>		Primary unilateral/bilateral hydrothorax, chylothorax	High
Fetal intracranial hemorrhage	Low	CPAM	
Vein of Galen aneurysm	Low	Macrocystic CPAM	Low
Cerebral tumor	Low	Microcystic CPAM	Low
<b>Thoracic</b>		Extralobar pulmonary sequestration	Low
<b>Cardiac structural defects</b>		Laryngeal atresia (CHAOS)	
AV septal defect, isolated or in association with Down syndrome	Low	Mediastinal teratoma	
AV septal defect in combination with heterotaxia syndrome (sinus ambiguus, left or right atrial isomerism) and bradyarrhythmia	High	Fibrosarcoma	
Tricuspid dysplasia and Ebstein anomaly	Low	Intrathoracic alimentary tract duplication cyst	
Severe obstruction of right ventricular outflow tract by pulmonary stenosis, pulmonary atresia, and premature closure of the ductus arteriosus (occurring spontaneously or induced with indomethacin)	Low	Diaphragmatic hernia	Low
Absent pulmonary valve syndrome (typically combined with tetralogy of Fallot or agenesis of the ductus arteriosus)	Low	Pulmonary lymphangiectasia	
Truncus arteriosus communis with truncal valve insufficiency	Low	<b>Gastrointestinal</b>	
Premature closure of the foramen ovale		Diaphragmatic hernia	Low
Unknown		Meconium peritonitis caused by bowel perforation;	Low
Severe obstruction of left ventricular outflow tract by aortic stenosis and atresia leading to interatrial left-to-right shunt or premature closure of foramen ovale	Low	spontaneous bowel obstruction (various types of atresias of the intestinal tract, volvulus), or infection	
<b>Cardiac tumors</b>		Intestinal hemorrhage caused by bowel perforation	Low
Rhabdomyoma, often associated with tuberous sclerosis	Low	Hepatitis	
Hemangioma		Hepatic fibrosis	
Hamartoma		Hemachromatosis	
Intrapericardial teratoma		Cholestasis	
<b>Cardiomyopathy</b>		Cirrhosis with portal hypertension	
Dilated		Congenital portal dysplasia	
Restrictive		Polycystic disease of liver	
Myocarditis		Giant cell hepatitis	
Myocardial infarction		Torsion of ovarian cyst	
Idiopathic arterial calcification	High	<b>Renal</b>	
<b>Arrhythmias</b>		Congenital nephrosis (Finnish type)	Low
Tachyarrhythmias	High	Urethral obstruction with rupture of bladder	Low
Supraventricular tachycardia		Polycystic kidney diseases (ARCKD, ADCKD)	Low
Atrial flutter		Renal vein thrombosis	
Ventricular tachycardia		<b>Tumor and Vascular Disorders</b>	
Bradyarrhythmias		Teratoma (sacroccoccygeal, mediastinal, intracerebral, intrapericardial)	Low
Sinus bradycardia	Low	Mediastinal fibrosarcoma	
Complete heart block		Disseminated congenital neuroblastoma	
Combined with atrial isomerism and structural defect (see above)	High	Hepatoblastoma	
In presence of maternal autoimmune antibodies (anti-SSA, anti-SSB)	Low	Hamartoma	
		Mesoblastic nephroma	
		AVM	
		Fetal hemangioma (liver, neck, chest)	Low
		Diffuse neonatal hemangiomatosis	High
		Klippel-Trenaunay-Weber syndrome	Low
		Umbilical cord hemangioma	Low
		Chorioangioma	Low
		Vena cava inferior thrombosis	
		Renal vein thrombosis	
		Idiopathic arterial calcification	High

\*Rate of the occurrence of hydrops if the fetus has the respective disease. In the vast majority of cases and associations, the incidence is too low for giving reliable information.

Continued



TABLE 17-8 Causes and Associations of Nonimmune Hydrops—cont'd

Cause/Association	Frequency*	Cause/Association	Frequency*
<b>Generalized Abnormalities</b>			
<b>Hematologic Disorders Causing Fetal Anemia</b>			
<b>Excessive Erythrocyte Loss</b>			
Intrinsic hemolysis or abnormal hemoglobins			
$\alpha$ -Thalassemia	High	Achondroplasia	
Erythrocyte enzyme disorders; glucose-6-phosphate dehydrogenase deficiency, pyruvate kinase deficiency, glucose phosphate isomerase deficiency	Low	Koide osteochondrodysplasia	
Erythrocyte membrane disorders; abnormalities of spectrin	Low	McGuire osteochondrodysplasia	
Extrinsic hemolysis			
Kasabach-Merritt sequence (AVMs) and tumors		Intrauterine dwarfism with thin bones and fractures (Kozlowski-Kann syndrome)	
Hemorrhage			
Fetomaternal hemorrhage	High	Greenberg-Rimoin chondrodysplasia	
Fetal closed-space hemorrhage (bowel, intracranial, tumor)	Low	Lethal chondrodysplasia with Dandy-Walker cyst and multiple congenital anomalies (Moerman-Vandenbergh-Fryns syndrome)	
Twin-to-twin transfusion (including acardiac parasitic twin)	Low	Lethal Kniest-like dysplasia	
<b>Erythrocyte Underproduction</b>		Chondrodysplasia punctata, Conradi-Hunermann variant	
Liver and bone marrow replacement syndromes			
Transient myeloproliferative disorder		Pyknoachondrogenesis	
Congenital leukemia		Wegmann-Jones-Smith syndrome	
Red blood cell aplasia and dyserythropoiesis			
Parvovirus B19 infection	High	Boomerang skeletal dysplasia	
Blackfan-Diamond syndrome	Low	Lethal chondrodysplasia with advanced bone age (Blomstrand syndrome)	
Dyserythropoietic anemia (types I and II)	Low	Herva-Leisti-Kirkman syndrome (contractures, congenital lethal Finnish type)	
<b>Infectious Causes</b>		Congenital infantile cortical hyperostosis (Caffey syndrome)	
Parvovirus B19 infection	High	<b>Metabolic Disorders</b>	
Cytomegalovirus infection	Low	Lysosomal storage diseases	Low
Syphilis	Low	Sphingolipidoses	Low
Toxoplasmosis	Low	Gangliosidosis	
Herpes simplex virus infection	Low	Galactosialidosis	
Adenovirus infection	Low	Farber disease	
Coxsackievirus infection	Low	Gaucher disease (glucocerebrosidase deficiency)	
Varicella	Low	Niemann-Pick disease type A	
Hepatitis A	Low	Mucopolysaccharidoses	
Rubella	Low	Mucopolysaccharidosis type I (Hurler syndrome)	
Respiratory syncytial virus infection	Low	Mucopolysaccharidosis type IVa (Morquio syndrome type A)	
Listeriosis	Low	Mucopolysaccharidosis type VII ( $\beta$ -glucuronidase deficiency)	
Chagas disease	Low	Mucolipidoses	
Leptospirosis	Low	Mucolipidosis type I (sialidosis)	
<b>Skeletal Dysplasias</b>		Mucolipidosis type II (I-cell disease)	
Achondrogenesis types I and IA	Low	Transport defects	
Achondrogenesis, Langer-Saldino		Sialic acid storage disease	
Short rib-polydactyly syndromes		Salla disease	
Saldino-Noonan		Niemann-Pick disease type C	
Majewski		Other lysosomal storage diseases	
Verma-Naumoff		Wolman disease	
Beemer		Carbohydrate-deficient glycoprotein syndrome	Low
Osteogenesis imperfecta type II		Glycogen storage disease type II (Pompe syndrome)	Low
Lethal osteopetrosis		Cardiac glycogen storage disease with normal maltase activity	Low
Asphyxiating thoracic dysplasia (Jeune syndrome)		Carnitine deficiency	Low
		Erythrocyte enzyme disorders	
		Glucose-6-phosphate dehydrogenase deficiency	Low
		Pyruvate kinase deficiency	Low
		Glucose phosphate isomerase deficiency	Low
		Fetal hyperthyroidism (maternal Graves disease)	Low
		Fetal hypothyroidism	Low

TABLE 17-8 Causes and Associations of Nonimmune Hydrops—cont'd

Cause/Association	Frequency*	Cause/Association	Frequency*
<b>Syndromes</b>		<b>Chromosomal Aberrations</b>	
Autosomal dominant inheritance	Low	Trisomy 13	Low
G syndrome (Opitz-Frias syndrome)		Trisomy 15	
Congenital myotonic dystrophy		Trisomy 16	
Cornelia de Lange syndrome		Monosomy X (Turner syndrome)	
Noonan syndrome		Trisomy 18	
Yellow nail syndrome		Trisomy 21 (Down syndrome)	
Tuberous sclerosis (already in utero with rhabdomyomas)		Triploidy	
Autosomal recessive inheritance		Tetraploidy	
Arthrogryposis multiplex congenita		Trisomy 10 mosaicism	
Pena-Shokeir syndrome		46,XX/XY mosaic	
Lethal multiple pterygium syndrome		49,XXXXY	
Neu-Laxova syndrome		Other structural rearrangements	
Recurrent isolated hydrops			
Cryptophthalmia-syndactyly syndrome (Fraser syndrome)		<b>Placental and Umbilical Cord Anomalies</b>	
Cumming syndrome		Chorioangioma	Low
Polysplenia syndrome (left atrial isomerism)		Chorioangioma as part of Beckwith-Wiedemann syndrome	
Orofaciodigital syndrome type II (Mohr syndrome)		Subchorial placental hematoma	
Isolated recurrent cystic hygroma		True knots of the cord	
Elejalda syndrome		Angiomyxoma of the umbilical cord	
McKusick-Kaufman syndrome		Aneurysm of the umbilical artery	
Angio-osteohypertrophy syndrome (Klippel-Feil-Trenaunay syndrome)	Low	Hemorrhagic endovasculitis of the placenta	
Beckwith-Wiedemann syndrome	Low	Chorionic vein thrombosis	
		Placental and umbilical vein thrombosis	
		Umbilical cord torsion	

ADCKD, autosomal dominant chronic kidney disease; ARCKD, autosomal recessive chronic kidney disease; AV, atrioventricular; AVM, arteriovenous malformation; CHAOS, congenital high airway obstruction syndrome; CPAM, congenital pulmonary airway malformation.

fluorescence in situ hybridization (FISH) analysis, or chromosomal microarray may be offered to these patients in an attempt to identify any chromosomal abnormality or pathogenic copy number variant (see Chapter 2). Percutaneous umbilical blood sampling (PUBS) may be part of the diagnostic evaluation in cases of elevated MCA PSV with a negative workup.<sup>81</sup> Diagnostic testing may also allow for specific testing for lysosomal storage disorders, which have been reported to cause as many as 25% of unexplained NIHF<sup>82</sup> (Figs. 17-16 and 17-17). Amniotic fluid level of alpha-fetoprotein should be obtained. After birth, a thorough physical examination of the newborn along with a detailed evaluation of the products of conception could lead to the underlying cause. A detailed histologic evaluation of the placenta may also yield important diagnostic information. Figure 17-18 summarizes the evaluation for cases of NIHF.

## Treatment

The treatment of nonimmune hydrops is determined by the gestational age at which the diagnosis is made, as well as the ability to identify the cause of the NIHF. Appropriate counseling should be offered to parents; NIHF associated with structural anomalies carries a poor prognosis. In some cases, termination of pregnancy may be an option available to the patient. Certain fetal conditions, such as congenital pulmonary airway malformations and twin-to-twin transfusion syndrome, may benefit from fetal intervention. Open fetal surgery may be of benefit in some cases such as sacrococcygeal teratomas or obstructive chest lesions.<sup>83</sup> Intrauterine fetal transfusion may be a therapeutic option if severe fetal anemia is determined to be the cause of NIHF, as in cases of parvovirus B19 infections. Shunt placement for certain obstructive procedures or paracentesis and thoracocentesis may be

both diagnostic and therapeutic in these conditions (Table 17-9) (see Chapter 24).

Antenatal medical treatment has also been described in certain conditions, with some authors reporting complete resolution of hydrops and improved outcomes.<sup>84</sup> Fetal arrhythmias may be converted back to normal sinus rhythm with administration of antiarrhythmic medication to the mother. Several protocols have been described such as the use of sotalol for the treatment of supraventricular tachycardia<sup>85</sup> or the administration of flecainide or digoxin in the treatment of fetal atrial flutter.<sup>86</sup> The dose, indication, and side effects of these medications are listed in Table 17-10. Congenital cytomegalovirus infection has been treated with maternal intravenous administration of hyperimmune globulin (IVIG) with varying results. Some authors have reported the resolution of ascites in fetuses affected with this condition that were treated with IVIG,<sup>87</sup> whereas others have failed to show such promising results.<sup>88</sup> When congenital syphilis was determined to be the cause of NIHF, patients have been treated with a continuous infusion of 18 million U of penicillin G daily for 10 days with resolution of hydrops.<sup>89,90</sup> The use of pyrimethamine, sulfadiazine, and folic acid at 27 weeks in a pregnancy complicated by congenital toxoplasmosis led to the complete resolution of hydrops 4 weeks later.<sup>91</sup>

Once the diagnosis of NIHF has been established, careful fetal surveillance is necessary. A multidisciplinary approach may be required in some cases. Antenatal testing may be indicated, although the precise method and frequency have yet to be established. Serial ultrasonographic evaluation both to evaluate fetal growth and to possibly detect undiscovered structural abnormalities may assist in the management of such pregnancies. Delivery should be done at a tertiary care hospital



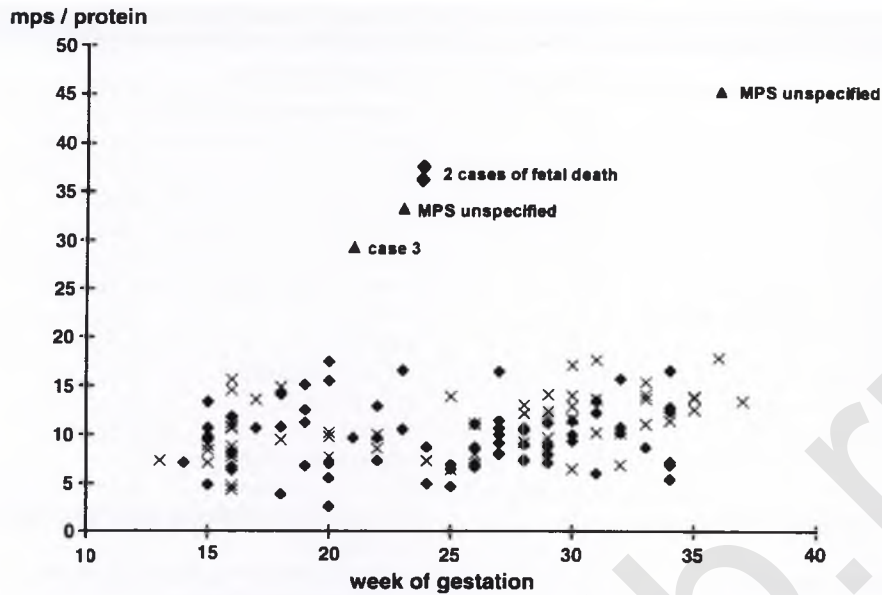


**FIG 17-16** Normal values for amniotic fluid mucopolysaccharides (MPS) corrected for total protein. x marks represent 40 normal control patients; ◆ symbols represent 71 cases of nonimmune hydrops fetalis. Note: in two cases of fetal death elevated levels of MPS were found, although cultured amniocytes for 21 different lysosomal enzymes were normal. Three abnormal cases are depicted. (From Kooper AJ, Janssens PM, de Groot AN, et al: Lysosomal storage diseases in non-immune hydrops fetalis pregnancies. Clin Chim Acta 371:176, 2006; reprinted with permission.)

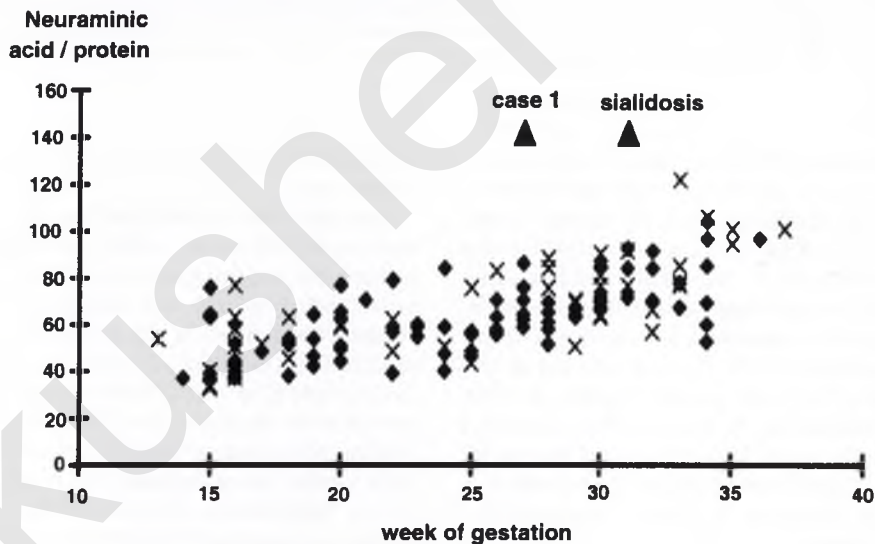


**FIG 17-17** Normal values for amniotic fluid bound and free neuraminic acid corrected for total protein. x marks represent 40 normal control patients; ◆ symbols represent 71 cases of nonimmune hydrops fetalis (NIHF). Two abnormal cases are depicted. (From Kooper AJ, Janssens PM, de Groot AN, et al: Lysosomal storage diseases in non-immune hydrops fetalis pregnancies. Clin Chim Acta 371:176, 2006; reprinted with permission.)

to allow for the appropriate neonatal interventions and a thorough newborn examination, attempting to determine the underlying cause. The timing and the mode of delivery will be determined by a number of factors, most importantly fetal status. With cases of hydrops causing massive fetal fluid retention, difficulty at delivery with risk of dystocia and fetal trauma may prompt the need for a cesarean delivery in cases of NIHF in which fetal survival is possible.

### Prognosis

In cases of NIHF, the prognosis is dependent on the underlying cause. NIHF secondary to treatable causes such as fetal arrhythmia, chylothorax, or infection with parvovirus B19 have a better survival rate. The development of intrauterine therapies such as intrauterine transfusions and minimally invasive fetal surgery have contributed to improved outcomes. The rate of intrauterine survival is also dependent on

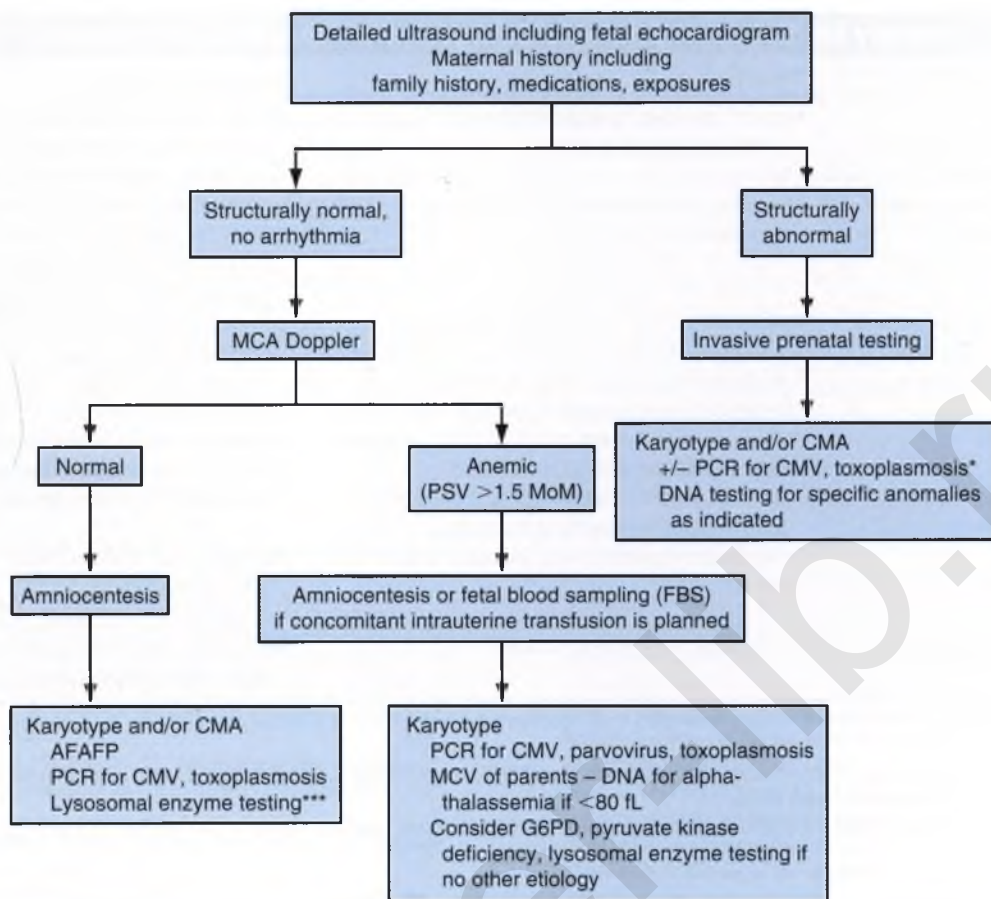


**FIG 17-18** Algorithm for the diagnosis and management of nonimmune hydrops. AFAFP, amniotic fluid alpha-fetoprotein; CMA, chromosomal microarray analysis; CMV, cytomegalovirus; G6PD, glucose-6-phosphate dehydrogenase; MCA, middle cerebral artery; MCV, mean corpuscular volume; PCR, polymerase chain reaction; PSV, peak systolic velocity. (Modified from Norton ME, Chauhan SP, Dashe J, Society for Maternal-Fetal Medicine: Evaluation of non-immune hydrops. *Am J Obstet Gynecol* Dec. 2014 [Epub ahead of print].)

gestational age at diagnosis, with a 31% survival rate if diagnosed prior to 24 weeks and a 48% survival rate if the diagnosis is made later.<sup>17</sup> Among pregnancies that result in a liveborn infant, the neonatal mortality rate has been reported to be as high as 60%.<sup>92</sup> This rate does not appear to have improved over the past couple of decades. This increased survival rate may also be a consequence of increased antenatal detection during the same time period. In a series evaluating 568 newborns with hydrops admitted to a NICU, higher mortality rates were associated with a younger gestational age, a low 5-minute Apgar score, and a need for high levels of support during the first day after birth.<sup>14</sup> The risk of recurrence in future pregnancies will again depend on the underlying cause. Some cases of recurrence in idiopathic NIHF have been reported and are likely due to undiagnosed genetic disorders.<sup>93</sup>

Long-term outcomes will also be dependent on the underlying cause. In a cohort of anemic fetuses secondary to parvovirus B19 infection that were treated with intrauterine transfusion, at a median of 5 years 11% of the children had been diagnosed with neurodevelopmental impairment.<sup>94</sup> In a series of 51 newborns affected with NIHF, the rate of normal development of infants who had survived to 1 year of life was 68%.<sup>95</sup>

## MATERNAL RISKS FROM HYDROPS

There are maternal risks associated with the diagnosis of fetal hydrops. A constellation of symptoms referred to as *mirror syndrome* may

develop in a small percentage of women. This complication is characterized by the combination of symptoms mimicking preeclampsia with edema (90%), hypertension (60%), and proteinuria (40%).<sup>96</sup> Pulmonary edema, which may develop in as many as 21% of women, is another major morbid condition associated with hydrops.<sup>97</sup> Other symptoms include headache, oliguria, and visual disturbances as well as abnormal laboratory values including low platelet count, anemia, and elevated creatinine and liver function test values. The only apparent cure for this condition appears to be delivery. Several case reports have described cases in which the complete resolution of symptoms is seen after the underlying cause of fetal hydrops is either treated or corrected.<sup>98,99</sup>

If polyhydramnios is associated with fetal hydrops, this can lead to other complications including preterm uterine contractions, preterm labor and premature rupture of membranes, maternal discomfort, and respiratory distress. The use of serial amnioreductions may lead to the improvement of symptoms; others have advocated for the use of prostaglandin inhibitors to decrease amniotic fluid production.

## CONCLUSION

In this chapter, the incidence, mechanism, diagnosis, and treatment of both immune and nonimmune hydrops have been presented. Although several advances have been made in the treatment of this disease, it is clear that many questions are still unanswered. With the evolution of



TABLE 17-9 Therapy for Selected Etiologic Categories of Nonimmune Hydrops

Etiologic Category*	Therapy	Recommendation
Cardiac tachyarrhythmia, supraventricular tachycardia, atrial flutter, or atrial fibrillation	Maternal transplacental administration of antiarrhythmic medication(s)	Treatment with antiarrhythmic medication unless gestational age is close to term or there is maternal or obstetric contraindication to therapy
Fetal anemia secondary to parvovirus infection or fetomaternal hemorrhage	Fetal blood sampling followed by intrauterine transfusion	Fetal intrauterine transfusion if anemia is confirmed, unless pregnancy is at an advanced gestation age and risks associated with delivery are considered to be less than those associated with procedure
Fetal hydrothorax, chylothorax, or large pleural effusion associated with bronchopulmonary sequestration	Fetal needle drainage of effusion or placement of thoracoamniotic shunt; if gestational age is advanced, needle drainage before delivery in selected cases	Consider drainage of large unilateral pleural effusion(s) resulting in NIHF, or, if gestational age is advanced, consideration of needle drainage before delivery
Fetal CPAM	<i>Macrocystic type:</i> fetal needle drainage or effusion or placement of thoracoamniotic shunt; <i>microcystic type:</i> maternal administration of corticosteroids, bethamethasone 12.5 mg IM q24h × 2 doses or dexamethasone 6.25 mg IM q12h × 4 doses	Consider drainage of large macrocystic CPAM that has resulted in NIHF; if large microcystic CPAM has resulted in NIHF, suggested management options include maternal corticosteroid administration
TTTS or TAPS	Laser ablation of placental anastomoses or selective termination	Consideration of fetoscopic laser photocoagulation of placental anastomoses for TTTS or TAPS that has resulted in NIHF < 26 weeks
Twin reversed arterial perfusion sequence	Percutaneous radiofrequency ablation	Referral for consideration of percutaneous radiofrequency ablation that has resulted in NIHF

\*For each of these etiologic conditions, it is recommended that treatment be performed at a tertiary care center or a center with expertise in relevant therapy.

CPAM, congenital pulmonary airway malformation; IM, intramuscular; NIHF, nonimmune hydrops fetalis; TAPS, twin anemia-polycythemia sequence; TTTS, twin-twin transfusion sequence.

From Society for Maternal-Fetal Medicine (SMFM) clinical guideline #7: Nonimmune hydrops fetalis. *Am J Obstet Gynecol* 2015;212(2):127-139; used with permission.

TABLE 17-10 Medications Used to Treat Fetal Arrhythmia: Dose, Contraindications, and Side Effects

Medication	Dosage	Contraindications	Side Effects
Sotalol	160 mg PO q12h; may increase to 320 mg q8h	Maternal history of cardiac disease, maternal bradycardia or prolonged QTc interval	Prolongation of maternal QTc interval, potassium and magnesium abnormalities
Flecainide	100 µg q8h	Second- or third-degree AV block	Prolongation of maternal QTc interval, headache, palpitations
Digoxin	500 µg loading PO/IV; then 250 µg q12h PO	Maternal history of cardiac disease	AV block, severe bradycardia, palpitations, visual disturbances
Amiodarone	600 mg PO q8h; then decrease to 200-400 mg per day	Maternal history of cardiac disease, second- or third-degree AV block, prolonged QTc interval	Prolongation of maternal QTc interval, bradycardia, nausea/vomiting

AV, atrioventricular; IV, intravenous; PO, by mouth; q, every.

Data from treatment protocols in Shah A, Moon-Grady A, Bhogal N, et al: Effectiveness of sotalol as first-line therapy for fetal supraventricular tachyarrhythmias. *Am J Cardiol* 2012;109:1614-1618.

diagnostic tests, including more sophisticated DNA testing for genetic disorders, and the advances in minimally invasive fetal surgery, the overall spectrum and prognosis of this disease may change. Continued research is required to determine the best treatment algorithm that can be offered to patients with this diagnosis.

## REFERENCES

- Skoll MA, Sharland GK, Allan LD: Is the ultrasound definition of fluid collections in non-immune hydrops fetalis helpful in defining the underlying cause or predicting outcome? *Ultrasound Obstet Gynecol* 1:309-312, 1991.
- Fleischer AC, Killam AP, Boehm FH, et al: Hydrops fetalis: sonographic evaluation and clinical implications. *Radiology* 141:163-168, 1981.
- Lee AJ, Bethune M, Hiscock RJ: Placental thickness in the second trimester: a pilot study to determine the normal range. *J Ultrasound Med* 31:213-218, 2012.
- Hoddick WK, Mahony BS, Callen PW, Filly RA: Placental thickness. *J Ultrasound Med* 4:479-482, 1985.
- Bowman JM: RhD hemolytic disease of the newborn. *N Engl J Med* 339:1775-1777, 1998.
- Diamond LK, Blackfan KD, Baty JM: Erythroblastosis fetalis and its association with universal edema of the fetus, icterus gravis neonatorum and anemia of the newborn. *J Pediatr* 1:269-309, 1932.
- Darrow RR: Icterus gravis neonatorum. *Arch Path* 25:378, 1938.
- Landsteiner K, Weiner AS: An agglutinable factor in human blood recognized by immune sera for Rhesus blood. *Proc Soc Exp Biol Med NY* 48:223-224, 1940.

9. Levine P, Katzin EM, Burnham L: Isoimmunization in pregnancy: its possible bearing on the etiology of erythroblastosis fetalis. *JAMA* 116:825–827, 1941.
10. Freda VJ, Gorman JG, Pollack W: Successful prevention of experimental Rh sensitization in man with an anti-Rh gamma2-globulin antibody preparation: a preliminary report. *Transfusion* 4:26–32, 1964.
11. Finn R, Clarke CA, Donohoe WT, et al: Experimental studies on the prevention of Rh haemolytic disease. *Br Med J* 1:1486–1490, 1961.
12. Hamilton EG: Prevention of Rh isoimmunization by injection of anti-D antibody. *Obstet Gynecol* 30:812–815, 1967.
13. Pollack W, Gorman JG, Freda VJ, et al: Results of clinical trials of RhoGAM in women. *Transfusion* 8:151–153, 1968.
14. Abrams ME, Meredith KS, Kinnard P, Clark RH: Hydrops fetalis: a retrospective review of cases reported to a large national database and identification of risk factors associated with death. *Pediatrics* 120:84–89, 2007.
15. Trainor B, Tubman R: The emerging pattern of hydrops fetalis—incidence, aetiology and management. *Ulster Med J* 75:185–186, 2006.
16. Macafee CA, Fortune DW, Beischer NA: Non-immunological hydrops fetalis. *J Obstet Gynaecol* 77:226–237, 1970.
17. Sohan K, Carroll SG, De La Fuente S, et al: Analysis of outcome in hydrops fetalis in relation to gestational age at diagnosis, cause and treatment. *Acta Obstet Gynecol Scand* 80:726–730, 2001.
18. Anandakumar C, Biswas A, Wong YC, et al: Management of non-immune hydrops: 8 years' experience. *Ultrasound Obstet Gynecol* 8:196–200, 1996.
19. Mourant AE, Kopec AC, Domaniewska-Sobczak K: *The Distribution of the Human Blood Groups, and Other Polymorphisms*, ed 2, London, 1976, Oxford University Press.
20. Bowman JM, Pollock JM, Penston LE: Fetomaternal transplacental hemorrhage during pregnancy and after delivery. *Vox Sang* 51(2):117–121, 1986.
21. Westhoff CM: The structure and function of the Rh antigen complex. *Semin Hematol* 44:42–50, 2007.
22. Cherif-Zahar B, Mattei MG, Le Van Kim C, et al: Localization of the human Rh blood group gene structure to chromosome region 1p34.3-1p36.1 by in situ hybridization. *Hum Genet* 86:398–400, 1991.
23. Le Van Kim C, Cherif-Zahar B, Raynal V, et al: Multiple Rh messenger RNA isoforms are produced by alternative splicing. *Blood* 80:1074–1078, 1992.
24. Fischer RA, Race RR: Rh gene frequencies in Great Britain. *Nature* 157:48–49, 1946.
25. Flegel WA: Molecular genetics of RH and its clinical application. *Transfus Clin Biol* 13(1–2):4–12, 2006.
26. Wagner FF, Eicher NI, Jorgensen JR, et al: DNB: a partial D with anti-D frequent in Central Europe. *Blood* 100:2253–2256, 2002.
27. Singleton BK, Green CA, Avent ND, et al: The presence of an RHD pseudogene containing a 37 base pair duplication and a nonsense mutation in Africans with the Rh D-negative blood group phenotype. *Blood* 95:12–18, 2000.
28. Pollock JM, Bowman JM: Anti-Rh(D) IgG subclasses and severity of Rh hemolytic disease of the newborn. *Vox Sang* 59:176–179, 1990.
29. Nicolaidis KH, Thilaganathan B, Rodeck CH, Mibashan RS: Erythroblastosis and reticulocytosis in anemic fetuses. *Am J Obstet Gynecol* 159:1063–1065, 1988.
30. Soothill PW, Nicolaidis KH, Rodeck CH, et al: Relationship of fetal hemoglobin and oxygen content to lactate concentration in Rh isoimmunized pregnancies. *Obstet Gynecol* 69:268–271, 1987.
31. Nicolaidis KH, Warenski JC, Rodeck CH: The relationship of fetal plasma protein concentration and hemoglobin level to the development of hydrops in rhesus isoimmunization. *Am J Obstet Gynecol* 152:341–344, 1985.
32. Phibbs RH, Johnson P, Tooley WH: Cardiorespiratory status of erythroblastic newborn infants. II. Blood volume, hematocrit, and serum albumin concentration in relation to hydrops fetalis. *Pediatrics* 53:13–23, 1974.
33. Pasman SA, Meerman RH, Vandenbussche FP, Oepkes D: Hypoalbuminemia: a cause of fetal hydrops? *Am J Obstet Gynecol* 194:972–975, 2006.
34. Weiner CP: Human fetal bilirubin levels and fetal hemolytic disease. *Am J Obstet Gynecol* 166:1449–1454, 1992.
35. Berger HM, Lindeman JH, van Zoeren-Grobden D, et al: Iron overload, free radical damage, and rhesus haemolytic disease. *Lancet* 335:933–936, 1990.
36. Weiner CP, Heilskov J, Pelzer G, et al: Normal values for human umbilical venous and amniotic fluid pressures and their alteration by fetal disease. *Am J Obstet Gynecol* 161:714–717, 1989.
37. Moise KJ, Jr, Carpenter RJ, Jr, Hesketh DE: Do abnormal Starling forces cause fetal hydrops in red blood cell alloimmunization? *Am J Obstet Gynecol* 167:907–912, 1992.
38. Weiner CP, Pelzer GD, Heilskov J, et al: The effect of intravascular transfusion on umbilical venous pressure in anemic fetuses with and without hydrops. *Am J Obstet Gynecol* 161:1498–1501, 1989.
39. Schumacher B, Moise KJ, Jr: Fetal transfusion for red blood cell alloimmunization in pregnancy. *Obstet Gynecol* 88:137–150, 1996.
40. Lindenburg IT, Smits-Wintjens VE, van Klink JM, et al: Long-term neurodevelopmental outcome after intrauterine transfusion for hemolytic disease of the fetus/newborn: the LOTUS study. *Am J Obstet Gynecol* 206:141.e1–141.e8, 2012.
41. American College of Obstetricians and Gynecologists: ACOG Practice Bulletin. Prevention of Rh D alloimmunization. No. 4, May 1999 (replaces educational bulletin No. 147, October 1990). Clinical management guidelines for obstetrician-gynecologists. *Int J Gynaecol Obstet* 66(1):63–70, 1999.
42. Brinc D, Lazarus AH: Mechanisms of anti-D action in the prevention of hemolytic disease of the fetus and newborn. *Hematology Am Soc Hematol Educ Program* 2009:185–191, 2009.
43. Brinc D, Le-Tien H, Crow AR, et al: IgG-mediated immunosuppression is not dependent on erythrocyte clearance or immunological evasion: implications for the mechanism of action of anti-D in the prevention of hemolytic disease of the newborn? *Br J Haematol* 139:275–279, 2007.
44. Bowman JM: Controversies in Rh prophylaxis. Who needs Rh immune globulin and when should it be given? *Am J Obstet Gynecol* 151:289–294, 1985.
45. Pollack W, Ascari WQ, Kochesky RJ, et al: Studies on Rh prophylaxis. 1. Relationship between doses of anti-Rh and size of antigenic stimulus. *Transfusion* 11:333–339, 1971.
46. Bennett PR, Le Van Kim C, Colin Y, et al: Prenatal determination of fetal RhD type by DNA amplification. *N Engl J Med* 329:607–610, 1993.
47. Lo YM, Corbetta N, Chamberlain PE, et al: Presence of fetal DNA in maternal plasma and serum. *Lancet* 350:485–487, 1997.
48. Costa JM, Giovangrandi Y, Ernault P, et al: Fetal RHD genotyping in maternal serum during the first trimester of pregnancy. *Br J Haematol* 119:255–260, 2002.
49. Gautier E, Benachi A, Giovangrandi Y, et al: Fetal RhD genotyping by maternal serum analysis: a two-year experience. *Am J Obstet Gynecol* 192:666–669, 2005.
50. Minon JM, Gerard C, Senterre JM, et al: Routine fetal RHD genotyping with maternal plasma: a four-year experience in Belgium. *Transfusion* 48:373–381, 2008.
51. Geifman-Holtzman O, Grotegut CA, Gaughan JP: Diagnostic accuracy of noninvasive fetal Rh genotyping from maternal blood—a meta-analysis. *Am J Obstet Gynecol* 195:1163–1173, 2006.
52. Wikman AT, Tiblad E, Karlsson A, et al: Noninvasive single-exon fetal RHD determination in a routine screening program in early pregnancy. *Obstet Gynecol* 120:227–234, 2012.
53. Hawk AF, Chang EY, Shields SM, Simpson KN: Costs and clinical outcomes of noninvasive fetal RhD typing for targeted prophylaxis. *Obstet Gynecol* 122:579–585, 2013.
54. Finning K, Martin P, Summers J, Daniels G: Fetal genotyping for the K (Kell) and Rh C, c, and E blood groups on cell-free fetal DNA in maternal plasma. *Transfusion* 47:2126–2133, 2007.
55. Tangshewinsirikul C, Wanapirak C, Piyamongkol W, et al: Effect of cord puncture site in cordocentesis at mid-pregnancy on pregnancy outcomes. *Prenat Diagn* 31:861–864, 2011.



56. Liley AW: Liquor amnii analysis in the management of the pregnancy complicated by resus sensitization. *Am J Obstet Gynecol* 82:1359–1370, 1961.
57. Queenan JT, Tomai TP, Ural SH, King JC: Deviation in amniotic fluid optical density at a wavelength of 450 nm in Rh-immunized pregnancies from 14 to 40 weeks' gestation: a proposal for clinical management. *Am J Obstet Gynecol* 168:1370–1376, 1993.
58. Moise KJ, Jr: Diagnosing hemolytic disease of the fetus—time to put the needles away? *N Engl J Med* 355:192–194, 2006.
59. Mari G, Deter RL, Carpenter RL, et al: Noninvasive diagnosis by Doppler ultrasonography of fetal anemia due to maternal red-cell alloimmunization. Collaborative Group for Doppler Assessment of the Blood Velocity in Anemic Fetuses. *N Engl J Med* 342(1):9–14, 2000.
60. Oepkes D, Seaward PG, Vandebussche FP, et al: Doppler ultrasonography versus amniocentesis to predict fetal anemia. *N Engl J Med* 355:156–164, 2006.
61. Abel DE, Grambow SC, Brancazio LR, Hertzberg BS: Ultrasound assessment of the fetal middle cerebral artery peak systolic velocity: a comparison of the near-field versus far-field vessel. *Am J Obstet Gynecol* 189:986–989, 2003.
62. Ruma MS, Swartz AE, Kim E, et al: Angle correction can be used to measure peak systolic velocity in the fetal middle cerebral artery. *Am J Obstet Gynecol* 200:397.e1–397.e3, 2009.
63. Zimmermann R, Carpenter RJ, Jr, Durig P, Mari G: Longitudinal measurement of peak systolic velocity in the fetal middle cerebral artery for monitoring pregnancies complicated by red cell alloimmunisation: a prospective multicentre trial with intention-to-treat. *Br J Obstet Gynaecol* 109:746–752, 2002.
64. American College of Obstetricians and Gynecologists: ACOG Committee Opinion No. 560: medically indicated late-preterm and early-term deliveries. *Obstet Gynecol* 121(4):908–910, 2013.
65. Copel JA, Grannum PA, Harrison D, Hobbins JC: The use of intravenous pancuronium bromide to produce fetal paralysis during intravascular transfusion. *Am J Obstet Gynecol* 158:170–171, 1988.
66. Moise KJ, Jr, Deter RL, Kirshon B, et al: Intravenous pancuronium bromide for fetal neuromuscular blockade during intrauterine transfusion for red-cell alloimmunization. *Obstet Gynecol* 74:905–908, 1989.
67. Chestnut DH, Pollack KL, Weiner CP, et al: Does furosemide alter the hemodynamic response to rapid intravascular transfusion of the anemic fetal lamb? *Am J Obstet Gynecol* 161:1571–1575, 1989.
68. Giannina G, Moise KJ, Jr, Dorman K: A simple method to estimate volume for fetal intravascular transfusions. *Fetal Diagn Ther* 13:94–97, 1998.
69. Radunovic N, Lockwood CJ, Alvarez M, et al: The severely anemic and hydropic isoimmune fetus: changes in fetal hematocrit associated with intrauterine death. *Obstet Gynecol* 79:390–393, 1992.
70. Berkowitz RL, Chitkara U, Goldberg JD, et al: Intrauterine intravascular transfusions for severe red blood cell isoimmunization: ultrasound-guided percutaneous approach. *Am J Obstet Gynecol* 155:574–581, 1992.
71. Moise KJ, Jr, Carpenter RJ, Jr, Kirshon B, et al: Comparison of four types of intrauterine transfusion: effect on fetal hematocrit. *Fetal Ther* 4:126–137, 1989.
72. Trevett TN, Jr, Dorman K, Lamvu G, Moise KJ, Jr: Antenatal maternal administration of phenobarbital for the prevention of exchange transfusion in neonates with hemolytic disease of the fetus and newborn. *Am J Obstet Gynecol* 192:478–482, 2005.
73. Voto LS, Mathet ER, Zapatero JL, et al: High-dose gammaglobulin (IVIG) followed by intrauterine transfusions (IUTs): a new alternative for the treatment of severe fetal hemolytic disease. *J Perinat Med* 25:85–88, 1997.
74. Gottvall T, Filbey D: Alloimmunization in pregnancy during the years 1992–2005 in the central west region of Sweden. *Acta Obstet Gynecol Scand* 87(8):843–848, 2008.
75. van Kamp IL, Klumper FJ, Meerman RH, et al: Treatment of fetal anemia due to red-cell alloimmunization with intrauterine transfusions in the Netherlands, 1988–1999. *Acta Obstet Gynecol Scand* 83:731–737, 2004.
76. McGlone L, Simpson JH, Scott-Lang C, et al: Short-term outcomes following intrauterine transfusion in Scotland. *Arch Dis Child Fetal Neonatal Ed* 96(1):F69–F70, 2011.
77. Santo S, Mansour S, Thilaganathan B, et al: Prenatal diagnosis of non-immune hydrops fetalis: what do we tell the parents? *Prenat Diagn* 31:186–195, 2011.
78. Bellini C, Hennekam RC, Fulcheri E, et al: Etiology of nonimmune hydrops fetalis: a systematic review. *Am J Med Genet A* 149A(5):844–851, 2009.
79. Norton ME: Nonimmune hydrops fetalis. *Semin Perinatol* 18:321–332, 1994.
80. Bellini C, Hennekam RC: Non-immune hydrops fetalis: a short review of etiology and pathophysiology. *Am J Med Genet A* 158A:597–605, 2012.
81. Berry SM, Stone J, Norton ME, Society for Maternal-Fetal Medicine, et al: Fetal blood sampling. *Am J Obstet Gynecol* 209:170–180, 2013.
82. Gimovsky AC, Luzzi P, Berghella V: Lysosomal storage diseases as an etiology of non-immune hydrops: a systematic review. *Am J Obstet Gynecol* 212(3):281–290, 2015.
83. Bullard KM, Harrison MR: Before the horse is out of the barn: fetal surgery for hydrops. *Semin Perinatol* 19:462–473, 1995.
84. Knilans TK: Cardiac abnormalities associated with hydrops fetalis. *Semin Perinatol* 19:483–492, 1995.
85. Shah A, Moon-Grady A, Bhogal N, et al: Effectiveness of sotalol as first-line therapy for fetal supraventricular tachyarrhythmias. *Am J Cardiol* 109:1614–1618, 2012.
86. Jaeggi ET, Carvalho JS, De Groot E, et al: Comparison of transplacental treatment of fetal supraventricular tachyarrhythmias with digoxin, flecainide, and sotalol: results of a nonrandomized multicenter study. *Circulation* 124:1747–1754, 2011.
87. Nigro G, Adler SP, La Torre R, Best AM: Congenital Cytomegalovirus Collaborating Group. Passive immunization during pregnancy for congenital cytomegalovirus infection. *N Engl J Med* 353(13):1350–1362, 2005.
88. Revello MG, Lazzarotto T, Guerra B, et al: A randomized trial of hyperimmune globulin to prevent congenital cytomegalovirus. *N Engl J Med* 370:1316–1326, 2014.
89. Wendel GD, Jr, Sheffield JS, Hollier LM, et al: Treatment of syphilis in pregnancy and prevention of congenital syphilis. *Clin Infect Dis* 35(Suppl 2):S200–S209, 2002.
90. Galan HL, Yandell PM, Knight AB: Intravenous penicillin for antenatal syphilotherapy. *Infect Dis Obstet Gynecol* 1(1):7–11, 1993.
91. Friedman S, Ford-Jones LE, Toi A, et al: Congenital toxoplasmosis: prenatal diagnosis, treatment and postnatal outcome. *Prenat Diagn* 19(4):330–333, 1999.
92. Czernik C, Proquitt H, Metzke B, Buhner C: Hydrops fetalis—has there been a change in diagnostic spectrum and mortality? *J Matern Fetal Neonatal Med* 24(2):258–263, 2011.
93. Goh SL, Tan JV, Kwek KY, Yeo GS: Recurrent non-immune fetal hydrops: a case report. *Ann Acad Med Singapore* 35(10):726–728, 2006.
94. De Jong EP, Lindenburg IT, van Klink JM, et al: Intrauterine transfusion for parvovirus B19 infection: long-term neurodevelopmental outcome. *Am J Obstet Gynecol* 206:204.e1–204.e5, 2012.
95. Nakayama H, Kukita J, Hikino S, et al: Long-term outcome of 51 liveborn neonates with non-immune hydrops fetalis. *Acta Paediatr* 88:24–28, 1999.
96. Braun T, Brauer M, Fuchs I, et al: Mirror syndrome: a systematic review of fetal associated conditions, maternal presentation and perinatal outcome. *Fetal Diagn Ther* 27:191–203, 2010.
97. Gedikbasi A, Oztarhan K, Gunenc Z, et al: Preeclampsia due to fetal non-immune hydrops: mirror syndrome and review of literature. *Hypertens Pregnancy* 30:322–330, 2011.
98. Goa S, Mimura K, Kakigano A, et al: Normalisation of angiogenic imbalance after intra-uterine transfusion for mirror syndrome caused by parvovirus B19. *Fetal Diagn Ther* 34:176–179, 2013.
99. Livingston JC, Malik KM, Crombleholme TM, et al: Mirror syndrome: a novel approach to therapy with fetal peritoneal-amniotic shunt. *Obstet Gynecol* 110:540–543, 2007.

# Ultrasound Evaluation of the Gravid Cervix

Vincenzo Berghella, Adeb Khalifeh

## SUMMARY OF KEY POINTS

- Transvaginal ultrasound (TVU) for cervical assessment is one of the best techniques for predicting preterm birth (PTB).
- A cervical length (CL) of less than 25 mm between 16 and 24 weeks' gestation is the most reliable threshold for an increased risk of PTB.
- The shorter the cervix and the earlier in gestation the shortening occurs, the higher the risk of PTB.
- TVU is the gold standard for ultrasound cervix measurements because a short cervix can be missed on transabdominal scans.
- Appropriate technique is key to accurate TVU measurement of CL.
- With a dynamic cervix, or in the presence of funneling, practitioners should report the shortest optimally imaged transvaginal ultrasound measurement of closed CL as the one single measurement to guide clinical decisions.
- The same transvaginal CL has very different positive predictive values depending on the a priori individual patient characteristics.
- The predictive value of sonographic CL determination in twins between 24 and 34 weeks' gestation is low.

## OUTLINE

### Ultrasound Examination Techniques, 653

- Transabdominal Ultrasound, 653
- Translabial Ultrasound, 654
- Transvaginal Ultrasound, 655

### Limitations and Pitfalls, 656

- Full Bladder, 656
- Excessive Pressure, 656
- Contraction, 656
- Underdeveloped Lower Uterine Segment, 656

### Clinical Applications, 657

- Transvaginal Ultrasound of the Cervix for Prediction of Preterm Birth, 657

### Dynamic Changes (Spontaneous or After Transfundal Pressure), 660

### Normal Versus Abnormal Cervical Length, 660

### Best Gestational Age and Frequency of Examinations, 661

### Populations, 661

- Singleton Without Prior Spontaneous Preterm Birth (Low Risk), 663
- Singleton With a Prior Spontaneous Preterm Birth (High Risk), 664

Women With Cerclage, 664

Women With Pessary, 664

Twins, 665

Triples, 665

### Three-Dimensional Transvaginal Ultrasound Examination of the Cervix, 665

### What Pathophysiologic Mechanisms Associate a Short Cervical Length With Preterm Birth?, 666

### Clinical Use of Cervical Length for Prevention of Preterm Birth, 667

Asymptomatic Singletons Without Prior Spontaneous Preterm Birth, 667

Asymptomatic Singletons With Prior Spontaneous Preterm Birth, 668

Asymptomatic Multiple Gestations, 668

Preterm Labor, 669

Preterm Premature Rupture of the Membranes, 669

Prediction of Start of Spontaneous Labor, 669

Predicting the Success of Labor Induction and Mode of Delivery, 670

### Conclusions, 670

Ultrasound assessment of the cervix during pregnancy has become an essential part of modern clinical care. Significant advances have been made in understanding the proper role of this sonographic screening test. In this chapter we will review the technique of transvaginal cervical assessment and discuss its expanding role in clinical practice.

## ULTRASOUND EXAMINATION TECHNIQUES

### Transabdominal Ultrasound

In the 1970s, the first attempts at evaluating the cervix used transabdominal ultrasound (TAU). Unfortunately, this technique has



relatively poor reliability and validity because of the following shortcomings: (1) the bladder often needs to be adequately filled to obtain a good image, resulting in elongation of the cervix and masking of any funneling of the internal os; (2) fetal parts can obscure the cervix, especially after 20 weeks; (3) the distance from the probe to the cervix results in degraded image quality; and (4) obesity and manual pressure interfere with the resulting image.<sup>1</sup> Therefore, it is generally suggested that TAU should not be used for assessment of the cervix, even as a screening test, because its sensitivity for prediction of disease (e.g., increased risk for PTB) is unacceptably low (8%)<sup>2</sup> in comparison to TVU. All randomized controlled trials (RCTs) that proved benefit with different treatments for a sonographically detected short cervix used TVU: vaginal progesterone,<sup>3,4</sup> cerclage,<sup>5-9</sup> and pessary.<sup>10,11</sup> The sensitivity of TVU has been shown to be significantly higher than TAU in detecting a short cervix<sup>12-16</sup> (Table 18-1).

As can be seen from the studies described in Table 18-1, it is still unclear if TAU is better done before or after voiding; only two studies report blind results. The cutoff for TAU-detected CL measurement needs to be high (usually >35 mm) to achieve a sensitivity of more than 90% for a shortened cervix by TVU, in which case most patients screened with TAU would need a subsequent TVU to confirm or rule out a short cervix. In 9% to 51% of attempted TAU, CL was not obtainable. Moreover, TVU CL screening has been shown to have superior cost-effectiveness compared to TAU, with TVU associated with slightly

better prevention of PTB, resulting in cost savings of millions of dollars.<sup>17</sup> All major guidelines that have described CL screening have clearly recommended TVU, including the Society for Maternal-Fetal Medicine (SMFM),<sup>18</sup> the American College of Obstetricians and Gynecologists (ACOG),<sup>19</sup> and the Royal College of Obstetricians and Gynaecologists.<sup>20</sup> Given the preponderance of the evidence, TAU is less effective than TVU and should not be used for CL screening.

### Translabial Ultrasound

Translabial (also known as transperineal) ultrasound (TLU) was first described in France in the early 1980s. This technique involves having the woman lie on the examination table with her hips and knees flexed. Adjusting the examination table to place her in a Trendelenburg position can be helpful. A covered transducer (using a probe cover, or glove, and sterile gel) is positioned in a sagittal orientation on the perineum between the labia majora at the level of the vaginal introitus (Fig. 18-1). Elevation of the woman's hips with a cushion or by positioning her hands to achieve a pelvic tilt can be used to improve visualization. Unlike TAU, this technique does not require bladder filling, is not impaired by obscuration by fetal parts, and with the transducer closer to the cervix, achieves close to 100% visualization. Other advantages of this technique are that the transducer does not enter the vagina (so no pressure can be exerted on the cervix thus no alteration in appearance from mechanical effect), it does not require an additional

**TABLE 18-1 Transabdominal Ultrasound in Detection of Short Cervix**

Study*	GA, Week (Mean)	N (TVU CL < 25 mm)	Bladder	Blind	TAU Cutoff (mm)	TA Variation (Longer/Shorter)	Sensitivity	Need TVU (TAU Not Obtainable)
Saul et al, 2008 <sup>12</sup>	14-34 (22)	191 (14)	Postvoid	Yes	≤30	Same	100%	NA
Stone et al, 2010 <sup>13</sup>	18-20	203	Postvoid	No	NA	Shorter	NA	NA
To et al, 2000 <sup>14</sup>	22-24 (23)	149	Prevoid	NA	NA	NA	NA	NA (51%)
Hernandez-Andrade et al, 2012 <sup>15</sup>	6-39 (24)	220 (20)	Prevoid	Yes	≤25 ≤30	Longer	43% 57%	NA
Friedman et al, 2013 <sup>16</sup>	18-24 (20.5)	1217 (76)	Prevoid Postvoid	No	≤36 ≤36	Shorter	96% 96%	60% (6%) NA (17%)

\*These studies are listed in the references at the end of the chapter.

CL, cervical length; GA, gestational age; TAU, transabdominal ultrasound; TVU, transvaginal ultrasound.

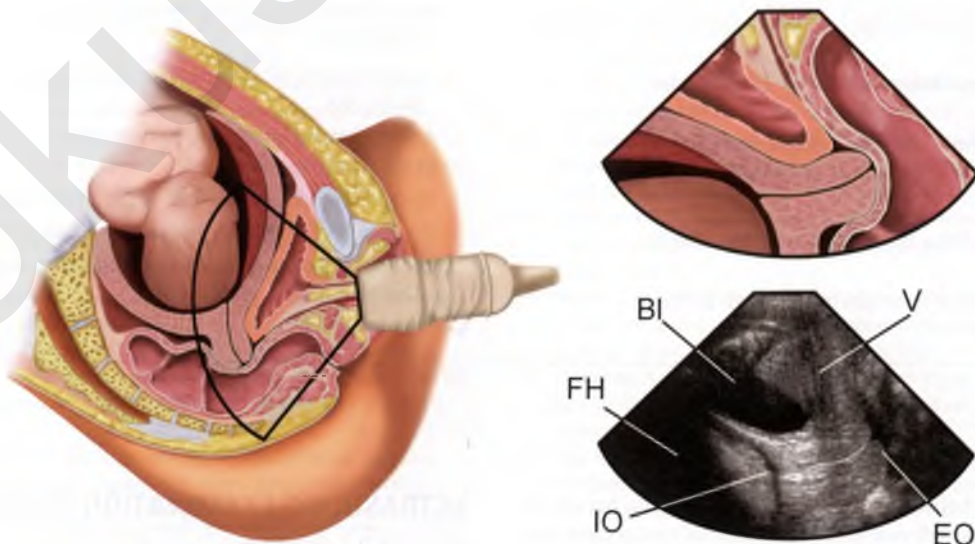


**FIG 18-1** Diagrams and sonogram of the female pelvis demonstrating placement of the ultrasound transducer for translabial imaging of the gravid cervix. BI, bladder; EO, external os; FH, fetal head; IO, internal os; V, vagina. (Illustration by James A. Cooper, MD, San Diego, CA.)

transducer, it can be performed in the setting of ruptured membranes, and it is well accepted by most women. The main drawback of TLU, however, is that gas in the rectum sometimes impedes visualization of the cervix, especially the external os. TLU is also more difficult to master than TVU and has been reported to be an unsatisfactory alternative.<sup>21</sup> However, with experience in using TLU, adequate visualization of the cervix can often be obtained.

### Transvaginal Ultrasound

The first studies of the human cervix using TVU date back to the late 1980s. A clean transvaginal probe covered by a condom is gently inserted into the vagina (Fig. 18-2A and B). The technique shares the advantages of TLU; however, the probe is close to the cervix, without the problem of obscuring bowel gas. Thus, TVU has become the preferred approach for sonographic evaluation of the gravid cervix in virtually all clinical settings (Fig. 18-3A to C). Current

recommendations for the performance of TVU of the cervix are shown in Table 18-2.<sup>22</sup>

The total time for TVU of the cervix is approximately 5 minutes. For optimal results, the following criteria should be sought: the internal os should be either flat or at an isosceles angle with respect to the uterus, the whole length of the cervix should be visualized, a symmetric image of the external os should be obtained, the distance from the surface of the posterior lip to the cervical canal should be equal to the distance from the surface of the anterior lip to the cervical canal, and there should be no increased echogenicity in the cervix (a sign of excessive pressure).<sup>23</sup>

Successful completion of the education program, examination, and continuing image review, all provided by the Perinatal Quality Foundation of the SMFM, is available and is recommended.<sup>22</sup> Ideally, TVU CL assessment should only be performed after this program has been completed.

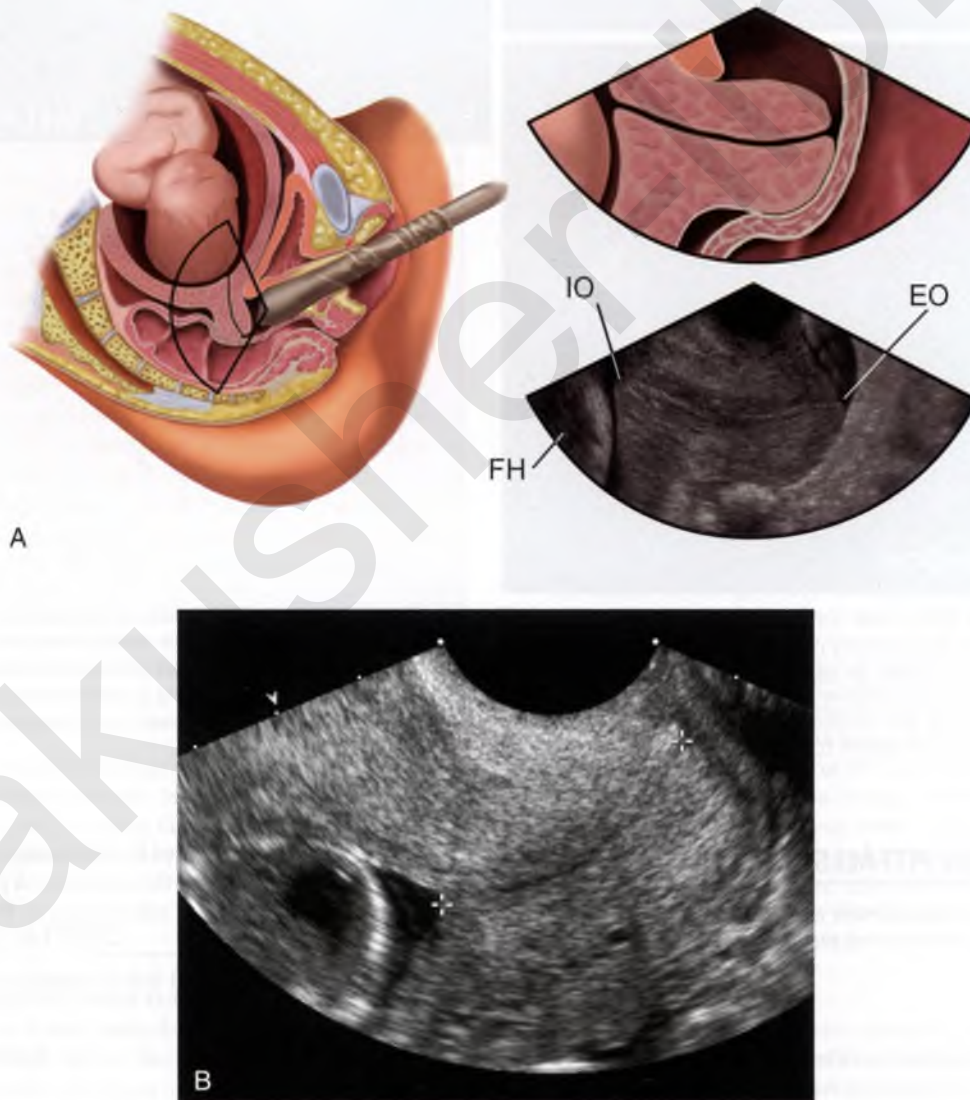


**FIG 18-2 A**, Diagrams and sonogram of the female pelvis demonstrating placement of the ultrasound transducer for transvaginal imaging of the gravid cervix. EO, external os; FH, fetal head; IO, internal os. **B**, Two-dimensional ultrasound image of the cervix in its longest axis in the sagittal view. The internal and external os (*calipers*) and the entire endocervical canal can be clearly seen, and the image is enlarged so that it occupies more than 75% of the screen. (Illustrations by James A. Cooper, MD, San Diego, CA.)



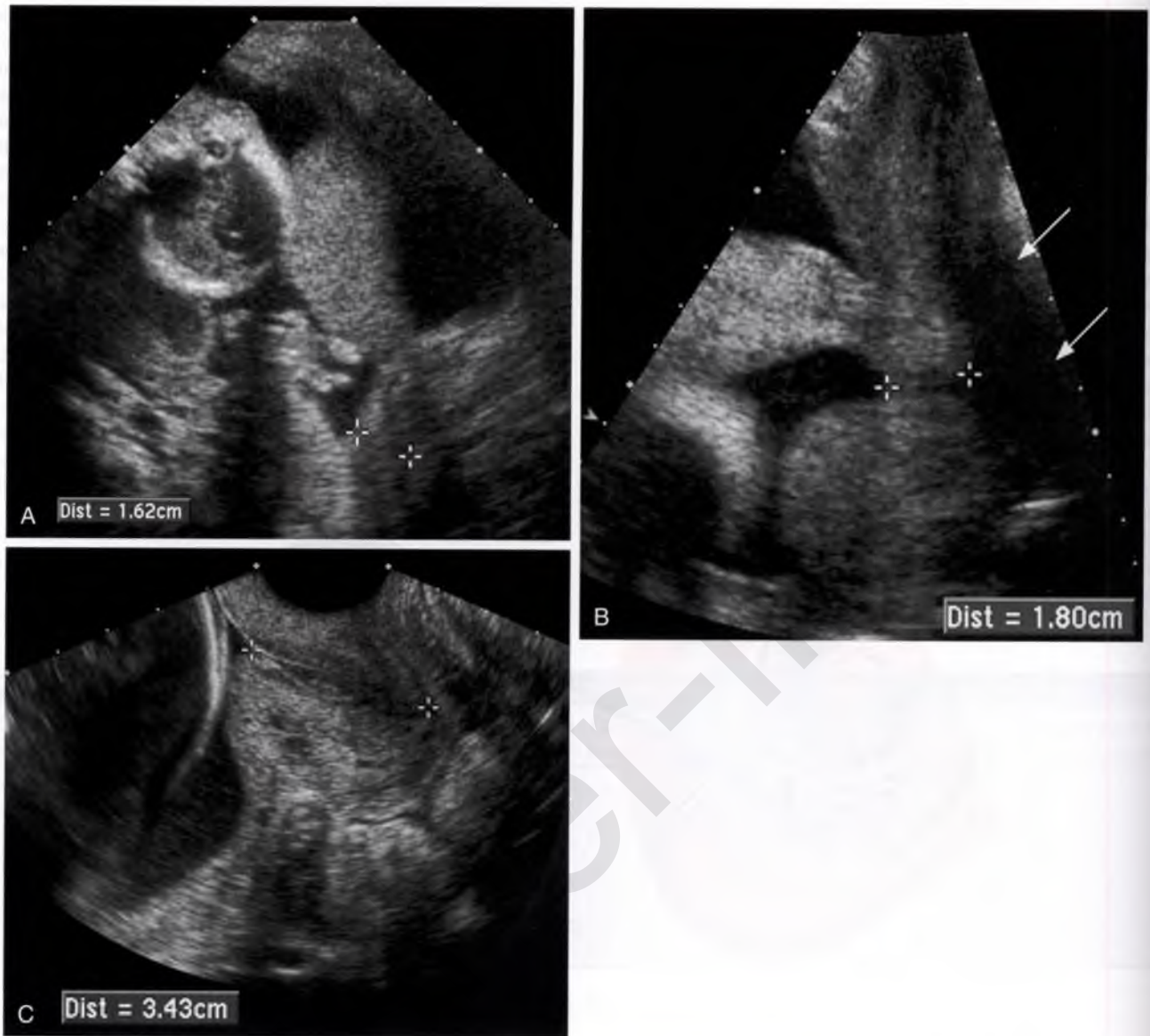


**FIG 18-3** Three methods of imaging the cervix. **A**, Transabdominal sonogram. The cervix, which is distant from the ultrasound transducer, is poorly seen and appears to measure 1.62 cm in length (*calipers*). **B**, Translabial sonogram in the same patient. With this approach, visualization of the cervix is somewhat clearer, but shadowing from air in the rectum (*arrows*) partially obscures the view, resulting in undermeasurement of the cervical length (*calipers*). **C**, Transvaginal sonogram. The cervix is well seen and measures 3.43 cm in length (*calipers*).

## LIMITATIONS AND PITFALLS

Although TVU of the cervix is usually straightforward, an anatomic or technical difficulty is encountered in approximately one fourth of patients.<sup>24</sup>

### Full Bladder

A bladder that is not completely empty of urine can exert pressure on and appear to elongate the cervix or might mask funneling or opening of the internal os.

### Excessive Pressure

Excessive pressure by the examiner with the transvaginal transducer can also mask funneling or opening of the internal os and can elongate

the cervix. This can be recognized by alterations in appearance including asymmetry in thickness of the anterior and posterior walls of the cervical canal and by increased echogenicity of the cervix (Fig. 18-4).

### Contraction

Uterine segment contractions may mimic the appearance of funneling of the internal cervical os. In such cases, there is rounded myometrium around the cervix and a normal cervix distal to the contraction (Fig. 18-5).

### Underdeveloped Lower Uterine Segment

Before 14 weeks, the lower uterine segment is difficult to distinguish from the endocervical canal, because the gestational sac has not reached a sufficient size to completely expand the lower part of the uterus.

**TABLE 18-2 Recommendations for the Technical Performance of Transvaginal Ultrasound Examination of the Cervix**

Measurement is taken on a transvaginal image:

- Transvaginal measurements are the gold standard for ultrasound cervix measurements.
- The short cervix can be missed on transabdominal scans.

The transvaginal image is filled primarily with the cervix, and the field of view is optimized for measurement:

- The cervix occupies approximately 75% of the image.
- The bladder area is visible.

The anterior width of the cervix equals the posterior width:

- The anterior cervical thickness is equal to the posterior cervical thickness.
- The echogenicity is similar for both anterior and posterior portions.
- There is limited concavity created by the transducer.

The maternal bladder is empty:

- The maternal bladder has a variable effect on the cervical length.

The external os is seen:

- The external os is a small triangular area at the inferior portion of the transcervical canal.
- The anterior and posterior portions of the cervix come together at the external os.

The endocervical canal is visible throughout:

- The endocervical canal is a linear echogenicity created by the interface between the anterior and posterior walls of the cervix.
- The canal extends between the internal os and external os.

Caliper placement is correct:

- Calipers are placed where the anterior and posterior walls of the cervix touch at the internal os and external os.
- Calipers do not extend to the outermost edge of the cervical tissue.

Cervix mobility is considered:

- Insert transvaginal probe to view the cervix, withdraw probe until the image blurs to reduce compression from the transducer, then reapply just enough pressure to create best image.
- Apply mild suprapubic or fundal pressure to watch for funneling. Reduce probe pressure while fundal or suprapubic pressure is applied.
- Visualize the cervix for 3-5 minutes and watch for shortening or funneling.

Modified from Perinatal Quality Foundation: Cervix Measurement Criteria. 2015. Available at [www.clear.perinatalquality.org/](http://www.clear.perinatalquality.org/).

Therefore, the measurement of the true CL is difficult before 14 weeks. At other times, particularly between 14 and 18 weeks' gestation, the presence of a contraction can close the lower uterine segment and make the distinction between this structure and the true CL difficult.

## CLINICAL APPLICATIONS

### Transvaginal Ultrasound of the Cervix for Prediction of Preterm Birth

#### Screening Test Criteria

TVU of the cervix is most often used in obstetrics as a screening test for the prediction of PTB.<sup>1</sup> To be clinically beneficial, a screening test must fulfill specific criteria (Table 18-3).<sup>3,5-9,17,24-32</sup>

**Important and Prevalent Condition.** First, a good screening test must evaluate for a clinically important and prevalent condition. PTB occurs in 11.5% of births, or approximately 500,000 pregnancies, per

year in the United States alone.<sup>26</sup> It is the leading cause of perinatal morbidity and fatality in the United States and as such may be the most important pathologic condition in obstetrics. In terms of years of life lost, PTB is one of the most important diseases in all of medicine.

**Technique Well Described.** The technique is well described (see Table 18-2).

**Safe and Acceptable.** TVU of the cervix is very safe. There is no inoculation of bacteria with TVU. In a randomized trial comparing the use of TVU or the nonuse of TVU in the presence of premature preterm rupture of membranes (PPROM), there was no increased risk of infection for mother or fetus with TVU of the cervix compared with no TVU of the cervix.<sup>28</sup> TVU is also well accepted by pregnant women. Pain and severe discomfort are experienced by fewer than 2% of women undergoing TVU, and more than 99% of women would agree to a similar procedure in the future.<sup>32,33</sup>

**Reliable/Reproducible.** The interobserver and intraobserver variability scores of TVU are both less than 10%.<sup>34</sup> This low variability between operators is achieved only after adequate training with supervised scans and with strict adherence to proper technique, as described earlier.

**Recognizable Early Asymptomatic Phase.** The changes of the cervix that are associated with preterm or term labor have been demonstrated by TVU. These changes include initial opening of the internal os, progressive cervical shortening and widening along the endocervical canal from the internal to the external os, and ultimate opening of the external os. The earliest changes at the internal os are almost always asymptomatic and can be detected only by TVU.

**Accuracy of Prediction: Valid Comparison With Manual Examination of the Cervix.** Cervical assessment by manual (digital) examination was a traditional method for prediction of PTB. Digital and transvaginal ultrasound examinations of CL every 2 weeks from 14 to 30 weeks' gestation were compared in one study (with examiners blinded to the results of the alternate technique)<sup>34</sup> and found to both independently predict PTB, but TVU had a much stronger association with PTB than manual examination of the cervix. The mean sonographic CL of the PTB group was significantly shorter than that of the term delivery group, whereas there was no difference in manual cervical measurements between the two groups.<sup>34</sup>

The relative lack of success of the digital examination in predicting PTB is probably due to the fact that it is subjective (interobserver variability of 52%),<sup>35</sup> not accurate for evaluating the internal os (the upper half of the cervix is not measurable by this method),<sup>36</sup> and nonspecific (15% to 16% of primiparous women and 17% to 35% of multiparous women who are delivered at term have cervixes that are 1 cm to 2 cm dilated by manual examination in the late second trimester).<sup>37</sup> Sonographic CL measurements are, on average, 11 mm longer than manual estimations. The majority, about three fourths, of asymptomatic women with funneling of the internal os have a cervix felt to be closed and at least 2 cm long by manual examination.<sup>38</sup> These data demonstrate clear benefits of TVU over manual examination for evaluation of the cervix and prediction of PTB.

#### Measurements

**Cervical Length.** Different cervical parameters have been evaluated as predictors of PTB (Fig. 18-6). CL, as measured from the internal to the external os along the endocervical canal, is the most reproducible and reliable measurement (Figs. 18-2B and 18-7A and B). If the cervical canal is curved, defined as a deviation of the canal of more than 5 mm, the CL can be preferably measured as the sum of two straight lines that essentially follow the curve (Fig. 18-7C).<sup>37</sup> A short CL is usually straight, whereas the presence of a curved cervix generally



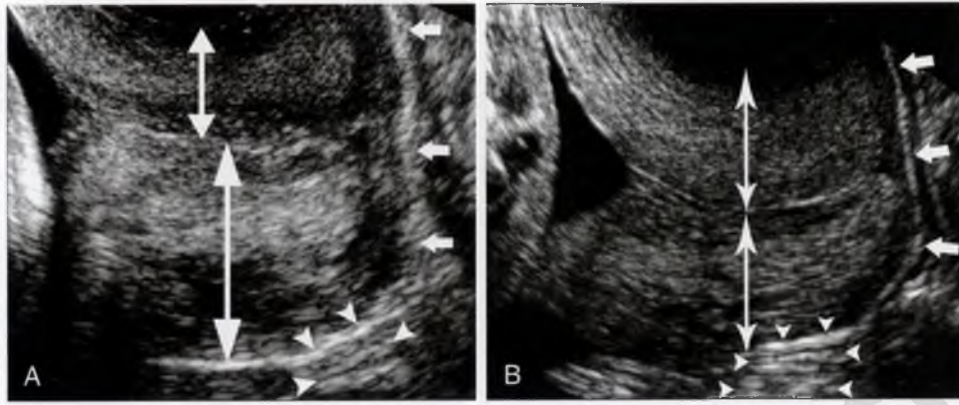


**FIG 18-4** **A**, Ultrasound image of the cervix with excess manual pressure from the transvaginal probe. The anterior lip of the cervix appears significantly thinner than the posterior lip of the cervix (*double-headed arrows*). Small triangular markers (*arrowheads*) show increased echogenicity below the posterior lip of the cervix, an indication of excess pressure. **B**, The anterior and posterior portions of the cervix appear equal in thickness (*double-headed arrows*). The transvaginal transducer should be inserted just enough to adequately visualize and obtain a reliable measurement of cervical length, without altering anatomy. Vaginal mucosa appears hyperechoic (*small short arrows*).



**FIG 18-5** Cervix with lower uterine segment contractions (*asterisks*). Lower uterine segment contractions should be considered whenever the apparent cervical length (CL) measures more than 50 mm, the cervical canal assumes an S shape, or the lower uterine segments (either anteriorly, posteriorly, or both) appear thickened and asymmetric. Lower uterine segment contractions can distort the landmarks of the cervix resulting in inaccurate CL measurement.

signifies a CL of more than 25 mm and, therefore, is a reassuring finding. If the cervical canal is closed, CL is the only parameter that needs to be measured.

**Funneling.** In about 10% of low-risk women<sup>29</sup> and 25% to 33% of high-risk women,<sup>34,38,39</sup> the internal os is open (Fig. 18-8). In this case, the open portion of cervix (funnel length) and internal os diameter (funnel width) can be measured. The percentage of funneling is calculated as funnel length divided by total CL. Total CL is equivalent to the sum of funnel length and functional CL. Functional CL in this case is the closed portion of the endocervical canal only. Functional CL is the sonographic CL used for calculations and predictions, and the term CL, if not otherwise specified, refers to the functional CL.

If funneling is present, the shape can be recorded. A continuous process of funneling has been described, going from a normal T shape, to Y, then V, and finally a U shape (Figs. 18-9 and 18-10).<sup>40</sup> It appears that U-shaped funneling is more likely to be associated with PTB compared with a V-shaped funnel<sup>41</sup>; however, these distinctions are somewhat subjective.

Careful evaluation of the apparent funneling with TVU over several minutes (at least 5) should resolve any question of the morphologic character of the upper cervical canal. In some instances, the depth of a true funnel may be difficult to quantify, because the funneled portion may merge with the lower uterine segment and the characteristic shoulder that depicts the border between lower uterine segment and the true cervix may be flattened. Funneling has been reported to have higher interobserver variability among examiners and different centers than CL.<sup>29</sup>

In spite of these difficulties, funneling has been reported to have better or similar predictive accuracy for PTB than CL.<sup>29,34,38</sup> In one high-risk population, minimal funneling (<25%) noted between 14 and 22 weeks was not associated with a significant increase in PTB, whereas moderate funneling (25-50%) and severe funneling (>50%) were associated with a 50% or more probability of PTB.<sup>34</sup> The fact that less than 25% funneling is not associated with an increased risk of PTB is important, because this is a common finding that should not raise alarm or result in intervention. Funneling has been shown in all

TABLE 18-3 Criteria for Clinical Benefits of Screening Test

Characteristic of Screening Test	Comments
<b>Disease</b>	
Disease is clinically important	PTB: 1 million deaths annually worldwide <sup>25</sup>
Disease is clearly defined	Birth < 37 weeks
Disease prevalence is well known	11.5% in United States; about 10% worldwide <sup>25,26</sup>
Disease natural history is known; recognizable early asymptomatic phase	First cervical changes occur at the internal os <sup>27,31</sup>
<b>Screening</b>	
Screening technique well described	Several articles
Screening is safe and acceptable	RCT on PPRM showing safety <sup>28</sup> ; 99% would have it again; <2% experience severe pain <sup>32,33</sup>
Screening has a reasonable cutoff identified	20 mm is the 5th percentile, 25 mm is the 10% percentile in the general U.S. population <sup>29</sup>
Results are reproducible (reliable)	<10% intraobserver and interobserver variability <sup>34</sup>
Results are accurate (valid)	Better than manual examination; predictive in all populations studied (hundreds of studies)
<b>Intervention, Cost-Effectiveness, and Feasibility</b>	
"Early" intervention is effective	Two RCTs for vaginal progesterone <sup>3-29</sup> ; five RCTs for cerclage <sup>5-9</sup>
Screening and treating abnormal findings is cost-effective	Two cost-effectiveness manuscripts published <sup>17,30</sup>
Facilities for screening are readily available	All pregnancies are offered a sonogram for fetal anatomy screening at around 18-24 weeks
Facilities for treatment are readily available	Vaginal progesterone is easily administered on an outpatient basis

PPROM, premature preterm rupture of membranes; PTB, preterm birth; RCT, randomized controlled trial.

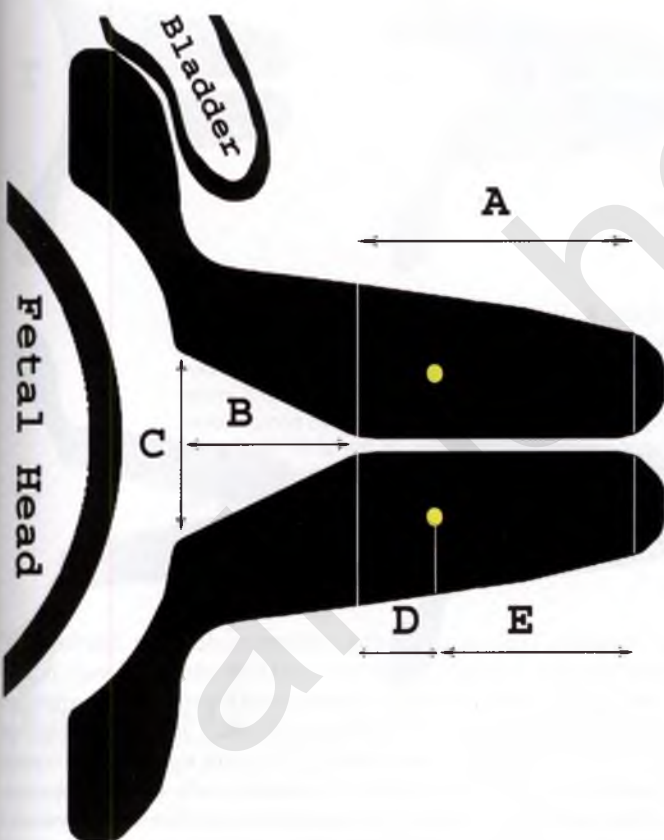


**FIG 18-6** Diagram illustrating major landmarks of the cervix, in the sagittal plane, and adjacent structures. In this example, a cerclage is present, represented by two yellow dots. A indicates the length of closed cervical canal (effective cervical length), B is the funnel length, C is the funnel width, D is the distance from the internal os to the level of cerclage, and E is the distance from the level of cerclage to the external os. In this example, the fetal head is the presenting part and the maternal bladder is seen anteriorly.

studies, not just those focused on high-risk pregnancies, to predict PTB.<sup>29,34,38,39,42-47</sup> If funneling is present, the CL is almost always short (<25 mm). In the presence of a short CL, the presence of funneling may<sup>29,43,46,47</sup> or may not<sup>39,42,44,45</sup> add to the prediction of PTB or adverse perinatal outcome. Compared with a CL less than 25 mm alone, adding funneling can increase the sensitivity for PTB (from 61-74%) without major changes in specificity, and positive and negative predictive values.<sup>43</sup> In addition, the risk of PTB is higher if both a short CL and funneling are detected, compared with a short CL without funneling.<sup>47</sup> On the contrary, the presence of funneling in a woman with a normal ( $\geq 25$  mm) CL does not seem to increase her risk of PTB (see funnel Y in Fig. 18-9).<sup>48</sup>

Given these shortcomings, as well as the fact that almost all intervention trials are based on TVU-detected CL (TVU-CL) alone, we do not recommend recording funneling on ultrasound reports. Following this recommendation will help to avoid confusion, as only CL is needed for clinical care.

**Sludge.** Free-floating echogenic material within the amniotic fluid has been referred to as sludge, or debris. Sludge has been proved to be an independent risk factor for PTB,<sup>49,50</sup> microbial invasion of the amniotic cavity, and histologic chorioamnionitis.<sup>51,52</sup> There are, however, no studies on interventions specific to intra-amniotic sludge or to prevent its consequences when present.

**Other Measurements.** Many parameters other than CL and the presence or absence of a funnel have been studied in relation to PTB,<sup>53</sup> including funnel width, funnel length, endocervical canal dilatation, cervical index (funnel length + 1/function length), anterior and posterior cervical width, cervical angle, cervical canal contour (straight versus curved), cervical position (horizontal versus vertical), lower uterine segment thickness, vascularity, visibility of chorion-amnion membranes at the internal os, cervical gland area,<sup>54</sup> quantitative tissue characterization,<sup>55</sup> and others. None of these parameters has proved more reliable or predictive than CL. Additionally, there is insufficient evidence to assess if the addition of any of these parameters improves the predictive accuracy already provided by CL. Several other measurements may be taken in the presence of a cerclage (Figs. 18-11 through



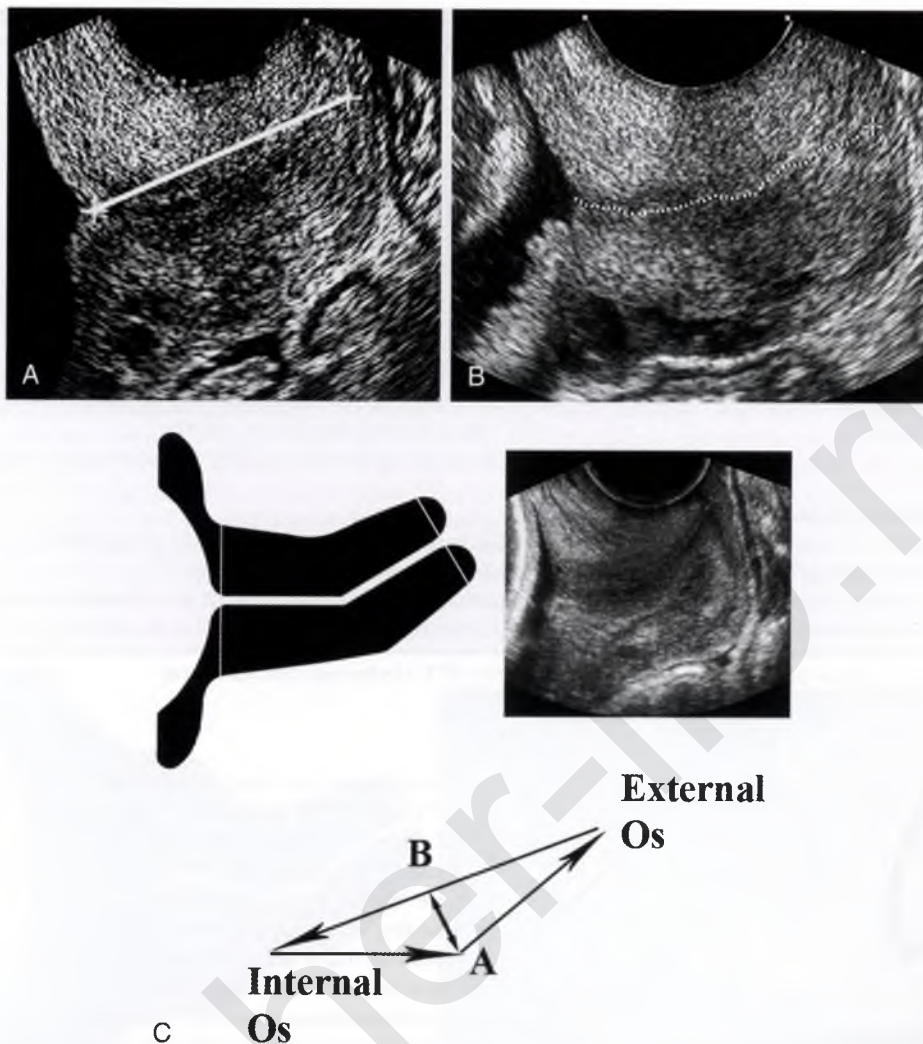


**FIG 18-7** Measurement of the cervix using three techniques. **A**, The cervical length (CL) is measured in a linear fashion from the internal os to the external os because the cervical canal appears straight. **B**, The canal is measured using the manual draw feature of the ultrasound equipment. The draw feature will not always properly draw the cervical canal and might overestimate the CL. **C**, The diagram and the ultrasound image illustrate a curved cervix, which can be measured in a single straight line or by summing two components. The curved cervix can be measured by drawing a line connecting the internal os to the point where the straight canal bends upward and then drawing another line connecting that point to the external os (sum of those two measurements = A). Or a straight line can be drawn from the internal os to the external os (B). If the difference between A and B is more than 5 mm, then the cervical canal should be measured in two steps and summed (A).

18-14). Although some of these measurements may be predictive of PTB, **TVU-CL alone should be reported in all populations in which TVU for prediction of PTB is performed.**

### **DYNAMIC CHANGES (SPONTANEOUS OR AFTER TRANSFUNDAL PRESSURE)**

In less than 5% of transvaginal sonographic examinations, CL may change dynamically during the course of a 5- to 10-minute examination, and in some cases, funneling of the upper cervical canal may appear and resolve. This usually happens if the woman is having contractions. Similarly, the cervix will shorten in response to transfundal pressure (TFP) in approximately 5% of cases.<sup>56</sup> When changes occur, the shortest CL should be recorded. In most cases in which the cervix shortens spontaneously or in response to TFP, it is already abnormal

at baseline. There is conflicting evidence concerning whether TFP increases the screening potential of TVU. In one study, only one of nine patients with an initially normal cervix who had abnormalities after the application of TFP delivered preterm,<sup>34</sup> and adding response to TFP as a screening criteria for PTB did not significantly increase predictive accuracy. In contrast, in a larger study, dynamic changes, either spontaneous or after TFP, significantly improved the predictive accuracy of TVU for PTB.<sup>39</sup> Dynamic changes may indeed improve predictive accuracy; *practitioners should report the shortest optimally imaged CL as the one single measurement to guide clinical decisions.*

### **NORMAL VERSUS ABNORMAL CERVICAL LENGTH**

A normal CL measures 25 to 50 mm at 14 to approximately 30 weeks of gestational age. A measurement of 25 mm is approximately the 10%

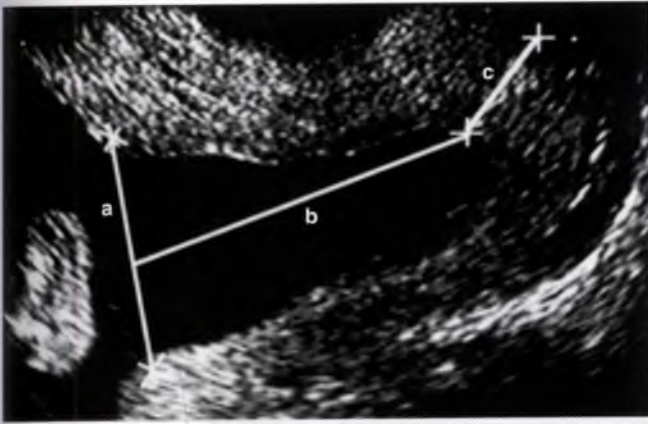


**FIG 18-8** Transvaginal sonogram in a patient with cervical funneling. Funnel width (a) is usually measured by identifying the lower uterine segment notch (or genu) either anteriorly or posteriorly (or both) and drawing a connecting line perpendicular to the axis of the cervical canal. The funnel length (b) is measured by drawing a line connecting the middle of the funnel width to the tip of the funnel. Cervical length is measured from the tip of the funnel to the external os (c).

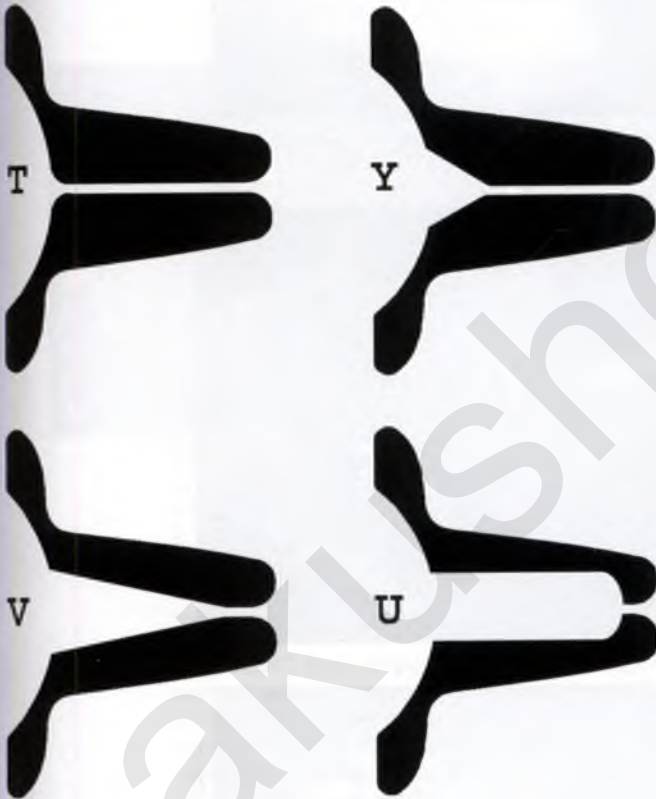


**FIG 18-9** Diagrams of typical shapes of cervical funneling. T represents a closed normal cervix. Y represents a small funnel, which if less than 25%, with residual cervical length of 25 mm or greater, may not be clinically significant. V represents a more significant funnel, extending closer to the external os. U represents the funnel of most concern; in this situation, the cervix can often be dilated clinically as noted by manual examination.

percentile for low-risk (i.e., without a prior spontaneous PTB) singletons<sup>29</sup> and approximately the 25% percentile for high-risk (i.e., with a prior spontaneous PTB) singletons.<sup>34,39</sup> A short CL is less than 25 mm at these gestational ages, with the best prediction for PTB obtained at 16 to 24 weeks. The shorter the CL, the higher the risk of PTB.<sup>29</sup> A

short CL is a better predictor of early PTB than later PTB.<sup>56</sup> A CL greater than 50 mm can be normal but warrants scrutiny, for it may reflect a measurement that includes the lower uterine segment, as often happens before 16 weeks.

## BEST GESTATIONAL AGE AND FREQUENCY OF EXAMINATIONS

Almost all patients, even those at the highest risk, have a normal CL (i.e.,  $\geq 25$  mm) in the first and early second trimesters. Before 14 weeks, measuring CL may be predictive only in very high-risk women, such as those with a prior second trimester loss or history of a large or repeated cervical cone biopsy. In a study of TVU of the cervix in high-risk women, only 5% had a CL less than 25 mm between 10 and 14 weeks, and these women were indeed very high risk based on prior history (i.e., pregnancy losses or major cervical surgery).<sup>57</sup> Sensitivity for the prediction of PTB is very low in this time interval, because most women who eventually deliver preterm typically have cervical shortening detected at 16 weeks or later. An additional drawback of very early screening is that the lower uterine segment is difficult to distinguish from the true cervix in the late first and early second trimesters.

After 30 weeks, the CL progressively shortens in preparation for term labor. CL less than 25 mm, in particular CL measuring 15 to 24 mm, after 30 weeks can be physiologic and not associated with an increased risk of PTB in asymptomatic women. When it occurs, the most common gestational age for short cervix or funneling to develop in women destined to deliver preterm is 18 to 22 weeks.<sup>34,38</sup> Therefore, if a screening program is to include only one CL assessment, it should be done in this time frame. High-risk patients destined to deliver preterm may have earlier cervical changes. The earlier the short CL is detected, the higher the risk of PTB. A cervix length measuring less than 25 mm has been reported to have a positive predictive value of 70% when detected between 14 and 18 weeks, and of 40% when detected between 18 and 22 weeks, in high-risk women.<sup>34</sup> Therefore, it may be that women with the highest risk of PTB (e.g., patients with classic histories of cervical insufficiency, prior second trimester losses, early PTBs, or large cone biopsies) may benefit from early (e.g., 12-14 weeks) TVU of the cervix to determine the need for intervention.

The benefits of repeated TVU examinations and the optimal interval for follow-up TVU assessments have not been clearly established. If a screening program were employed in relatively low-risk women, one TVU measurement of the cervix at approximately 18 to 22 weeks would likely be most effective. It appears that one normal TVU-CL assessment between 14 and 18 weeks and another between 18 and 22 weeks is reassuring and adequate in most high-risk women.<sup>41</sup> In women at very high risk for PTB, such as those with prior second trimester loss or very early spontaneous PTB, some have advocated TVU of the cervix every 2 weeks, at least between 14 and 24 weeks. If the CL measures 25 to 29 mm, the interval can be increased to every week. The fact that TVU at 14 to 22 weeks is at least as predictive of PTB as TVU after 22 weeks is important, because interventions to prevent PTB are most effective when changes predisposing to PTB are detected early in the process.

## POPULATIONS

Numerous studies have evaluated the predictive accuracy of TVU to measure CL for PTB in many different populations.<sup>1</sup> Populations screened include asymptomatic women with singleton (low- or high-risk), twin, and triplet pregnancies, and symptomatic women with preterm labor (PTL) or PPRM. Although the TVU technique in these studies is similar, study population (in particular, prior PTB or not),



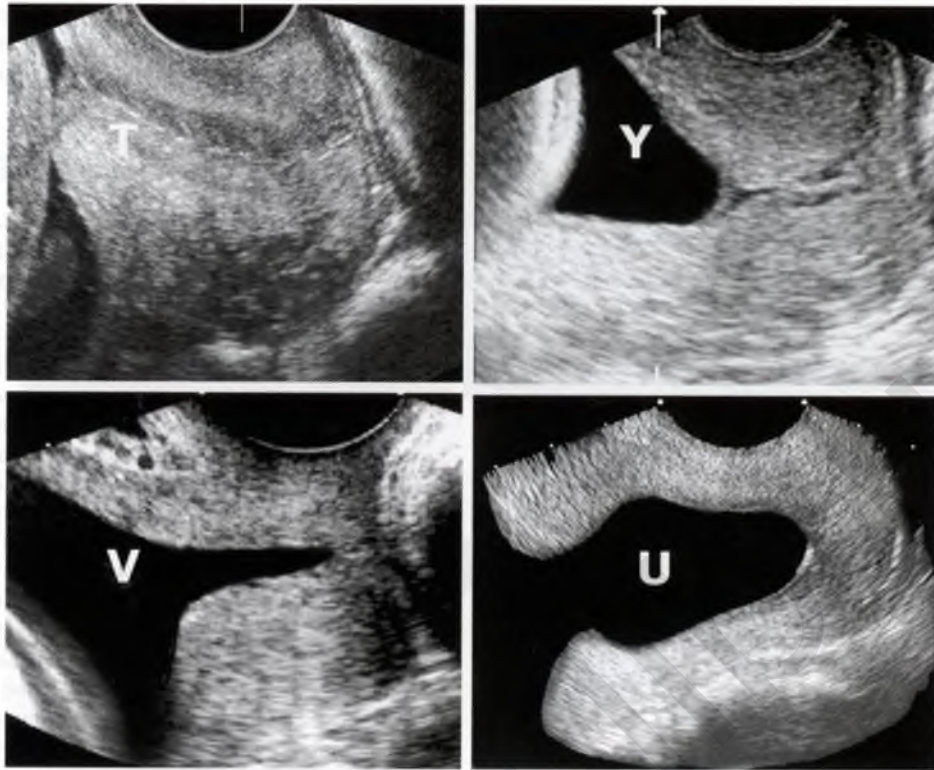


**FIG 18-10** These ultrasound images show the respective funnel shapes, as depicted graphically in Figure 18-9.

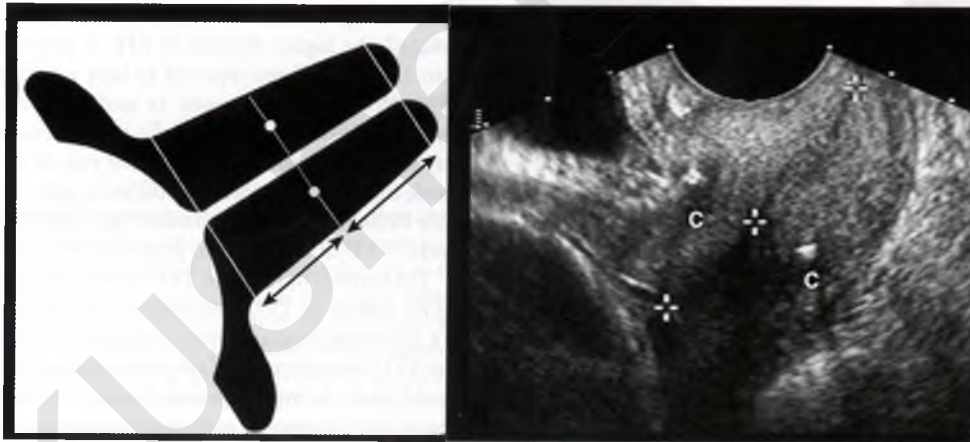


**FIG 18-11** Diagram and sagittal transvaginal ultrasound image of a cervix with cerclage in place. The cerclage (c) is seen as two bright spots, in the anterior and posterior lips of the cervix. In this case, the measurement of the cervix is obtained by summing the distance from the internal os to the level of cerclage and from the level of cerclage to the external os (*calipers*). Note that the orientation of the cervix in this image is not quite horizontal but oblique/vertical, making identification of cervical landmarks more difficult because the ultrasound beam is not perpendicular to the endocervical canal.

gestational age at which TVU was done, frequency of TVU cervical parameters studied, and outcomes vary. In reviewing the available studies, it is important to include those with the best design, that is, those that describe proper technique, blinding of managing physicians to ultrasound results, and the inclusion of large numbers of patients. In most studies, the cervical parameter found to have the best predictive accuracy, as determined by receiver operating characteristic curves, is an TVU-CL less than 25 mm. The screening interval is early in the second trimester, usually between 16 and 24 weeks. The most common

primary outcome is spontaneous PTB at less than 35 weeks' gestation (Table 18-4).<sup>29,39,58-63</sup> It is of utmost importance to recognize that the same TVU-CL measurement confers very different positive predictive values depending on the a priori individual patient characteristics. For example, a CL less than 25 mm is associated with a risk of PTB less than 35 weeks of 18% to 30% in a singleton without prior spontaneous PTB,<sup>29</sup> and a risk of 55% in a singleton with prior spontaneous PTB.<sup>39</sup> Sensitivity and specificity of TVU-CL for prediction of PTB change substantially depending on the population studied (see Table 18-3).

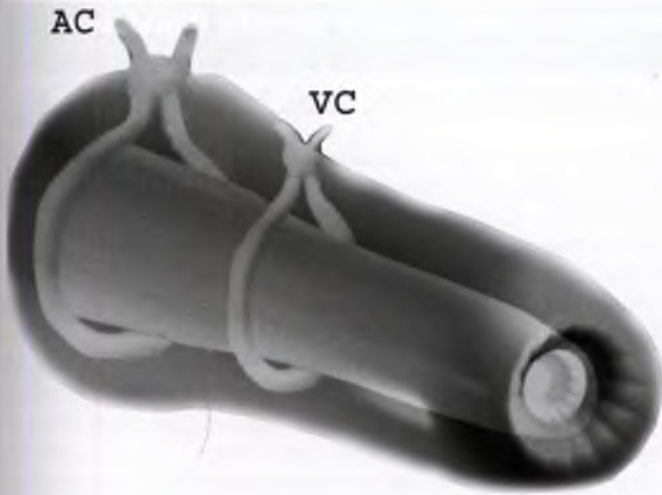


**FIG 18-12** Three-dimensional graphic of the cervix showing the usual locations of abdominal cerclage (AC) and vaginal cerclage (VC) placement. The AC is located high, close to the level of the lower uterine segment, whereas the VC is usually placed close to the middle of the length of the cervix.

### Singleton Without Prior Spontaneous Preterm Birth (Low Risk)

Numerous studies have reported nomograms for CL in either nonselected (mostly low risk, defined as with no prior PTB, and some with prior PTB) or low-risk (with no prior PTB) pregnant women with singleton gestations.<sup>29,64,65</sup> In these women, CL is a continuous variable, with a mean of 35 to 40 mm measured between 14 to 30 weeks, with the lower 10th percentile measuring 25 mm and the upper 10th (90th percentile) measuring 50 mm.<sup>29,65</sup> A progressive and natural shortening of CL is observed after 30 weeks, even in patients destined to deliver at term.<sup>64</sup> There may be a very slight progressive linear reduction of CL before 30 weeks.<sup>66</sup> There seems to be no difference in CL between nulliparous and multiparous women throughout pregnancy, whereas risk factors for PTB such as African origin, age younger than 20 years, low body mass index, and prior miscarriage or PTB are associated with a shorter CL.<sup>66</sup>

In asymptomatic singleton gestations, as in all other groups, the shorter the cervix, the higher the risk of PTB.<sup>1</sup> Using different cutoffs for CL from 15 to 34 mm, the positive predictive values ranged from 6% to 44%.<sup>1</sup> These relatively low values are likely due, at least in part, to the low prevalence of PTB in this population (0.8% to 15%). In one

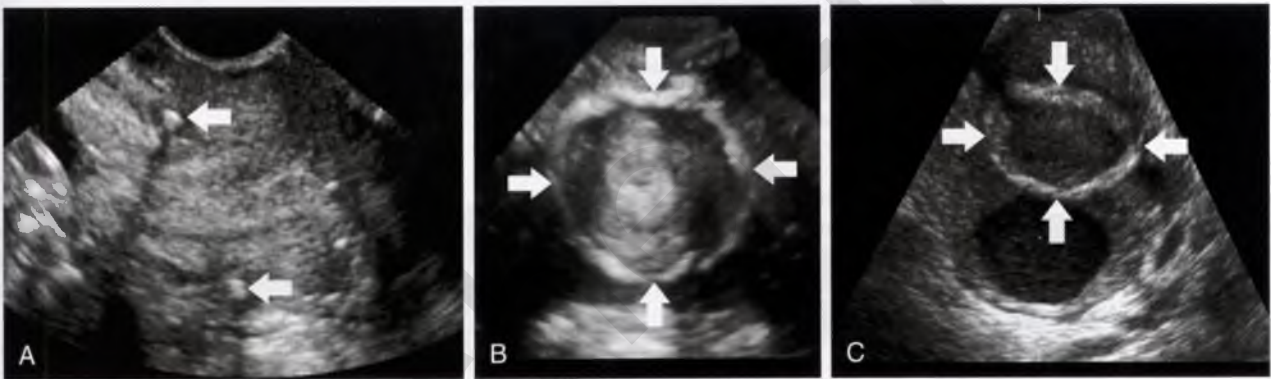


**FIG 18-13** Transvaginal ultrasound images of the cervix with vaginal cerclage. **A**, Two-dimensional (2D) sagittal ultrasound image of the cervix. In this plane of section, the cerclage suture appears as two bright echoes (arrows) within the anterior and posterior cervical stroma, surrounding the endocervical canal. **B**, Three-dimensional (3D) ultrasound-derived image in the axial plane. In this view of the cervix, the vaginal cerclage suture is depicted in its entirety (arrows). **C**, 3D ultrasound-derived image in the axial plane. In this case, the vaginal cerclage suture (arrows) is well visualized and noted to have pulled through, located within the anterior lip of the cervix, anterior to the dilated endocervical canal.

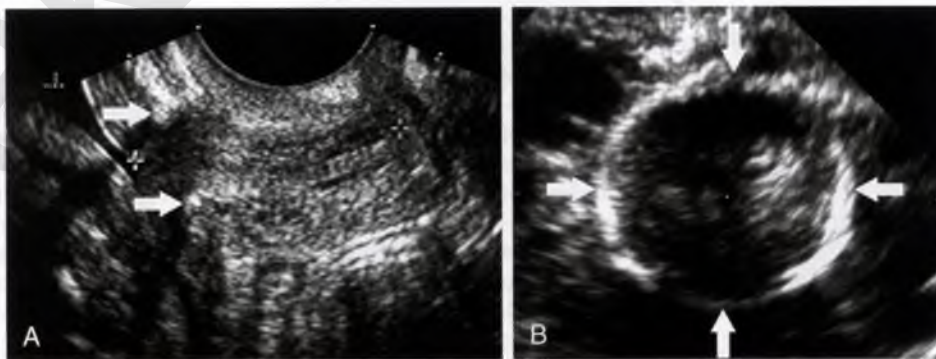


**FIG 18-14** Transvaginal ultrasound images of the cervix with abdominal cerclage. **A**, Two-dimensional (2D) sagittal ultrasound image of the cervix. In this plane of section, the cerclage suture appears as two bright echoes (arrows) placed near the level of the internal os. The cervical length is measured (calipers). **B**, Three-dimensional ultrasound-derived image in the axial plane. Note the cerclage suture is depicted in its entirety (arrows).



**TABLE 18-4 Prediction of Preterm Birth by Transvaginal Ultrasound in Specific Populations of Pregnant Women**

Author*	n	PTB (%)	PTB Defined (wk)	GA Studied (wk)	CL Cutoff (mm)	% Abn	Sens	Spec	PPV	NPV	RR
<b>Asymptomatic</b>											
Singleton: low risk (cross-sectional)											
Iams <sup>27</sup>	2915	4.3	<35	22-25	25	10	37	92	18	97	6.2*
Singleton: prior preterm birth											
Owen <sup>39</sup>	183	26	<35	16-24	25	—	69	80	55	88	4.5
Singleton: prior cone biopsy											
Berghella <sup>58</sup>	109	13	<35	16-24	<25	28	64	78	30	94	4.7
Singleton: müllerian anomaly											
Airoldi <sup>60</sup>	64	11	<35	14-24	<25	16	71	91	50	96	13.5
Singleton: prior D&E											
Visintine <sup>59</sup>	131	30	<35	14-24	<25	51	53	75	48	78	2.2
Twins											
Goldenberg <sup>61</sup>	147	32	<35	22-24	≤25	18	30	88	54	74	3.2
Triplets											
Guzman <sup>62</sup>	47	34	<32	15-20	≤25	<25	8.2	25	100	100	72
		NA									
<b>Symptomatic</b>											
Singletons with preterm labor											
Venditelli <sup>63</sup>	200	41	<37	19-39	<30	64	84	88	54	80	2.8

\*For studies published by these lead authors, see the references listed at the end of the chapter.

% abn, percent abnormal; CL, cervical length; D&E, dilation and evacuation; GA, gestational age; NPV, negative predictive value; PPV, positive predictive value; PTB%, incidence of preterm birth; RR, relative risk compared with those with normal CL, except\*, compared with values higher than the 75th percentile; Sens, sensitivity; Spec, specificity.

of the better-designed, larger studies,<sup>29</sup> the sensitivity was only 37% and the positive predictive value only 18%. This means that the majority (63%) of the few women without risk factors who delivered preterm were not identified by TVU screening, and that 82% of these low-risk patients who were found to have a short CL less than 25 mm at 24 weeks delivered at or after 35 weeks.

### Singleton With a Prior Spontaneous Preterm Birth (High Risk)

There are over 30 different risk factors for PTB.<sup>67</sup> Several studies have assessed the predictive value of TVU-CL in women with some of the most important risk factors, including prior PTB,<sup>39</sup> cone biopsy,<sup>58</sup> two or more voluntary terminations,<sup>59</sup> or müllerian anomaly.<sup>60</sup> As Table 18-4 shows, CL between 14 and 24 weeks is predictive of PTB in all of these high-risk populations. In fact, the more worrisome the obstetric history, the shorter the cervix, because prematurity risk is a continuum.<sup>68</sup> A woman with clinical risk factors for PTB who has a normal (≥25 mm) CL between 18 and 22 weeks has a less than 10% risk of PTB, representing a significant reduction in risk and potentially preventing unnecessary interventions. On the contrary, the sensitivity of TVU-CL to determine which high-risk women will deliver preterm is about 70%, much higher than in low-risk women. The incidence of PTB at less than 35 weeks is often greater than 50% when the additional risk factor of TVU-CL less than 25 mm is discovered before 24 weeks in these high-risk women. The positive predictive values are also much higher in high-risk than in low-risk women (see Table 18-4). PTB within 4 weeks of TVU occurs in about 13% of asymptomatic women with short CL and in none of the pregnancies without such ultrasound findings; thus, steroid therapy for fetal lung maturity is rarely indicated, even in asymptomatic women with a short CL.<sup>43</sup> It is important to note that, at least in high-risk patients, PTB following the detection of a short CL is most often preceded by PPROM (48-68%)

instead of PTL.<sup>34,69</sup> CL less than 10 mm in these women is particularly predictive of PPROM.<sup>70</sup> TVU in women with prior PTB at less than 32 weeks demonstrated that the best predictive accuracy is achieved with serial TVU examinations, assessing the shortest CL after spontaneous or TFP-elicited changes.<sup>39</sup> The sensitivity and positive predictive value reached 69% and 55%, respectively. This was the only blinded multicenter study controlled for quality performed in women at high risk for PTB and, therefore, contains the most reliable and valid predictive data in this population.<sup>39</sup>

### Women With Cerclage

TVU of the cervix has been evaluated in women with history-indicated, ultrasound-indicated, or physical examination-indicated cerclage in place. Most studies have shown that transvaginal cerclage is placed in the middle portion of the cervix in the vast majority of cases (see Fig. 18-13).<sup>71-73</sup> Transabdominal cerclage is instead placed at the level of the internal os (see Fig. 18-14). The higher (closer to the internal os) the cerclage suture is placed, the more effective the prevention of PTB.<sup>74,75</sup> Evaluation of precerclage and postcerclage TVU-CL has shown that CL measurement usually increases after cerclage, and that an increase in CL is associated with a higher rate of term delivery.<sup>76,77</sup>

Studies evaluating the accuracy of TVU for predicting PTB in patients with cerclage<sup>71-73,76</sup> show that TVU-detected cervical parameters are predictive of PTB. CL less than 25 mm and upper cervix (the closed portion located above the level of the cerclage; see Fig. 18-13) less than 10 mm are probably the two best predictive parameters.

### Women With Pessary

Despite the lack of widespread evidence of the benefit of a pessary in preventing PTB,<sup>78</sup> interest in using a pessary has resurfaced as a result of the PECEP trial, an RCT showing a significant decrease in PTB and improved neonatal outcome.<sup>10</sup> Several studies are under way to provide

guidance supporting or refuting the use of a pessary. Some clinicians follow-up CL assessment with TVU without removing the pessary. One study has shown minimal interobserver difference using this method.<sup>79</sup>

### Twins

Despite the significant risks of perinatal morbidity and mortality resulting from PTB in twin pregnancies, the prediction of PTB in twins using traditional clinical means is limited. A CL of 25 mm or less at 24 weeks' gestation has been found to be the best predictor of PTB in twins, including studies evaluating fetal fibronectin and bacterial vaginosis<sup>61</sup> (see Table 18-4). Compared with singleton pregnancies, twin pregnancies that deliver at term have been shown to have a similar TVU-CL at 14 to 19 weeks but a progressively shorter cervix after 20 weeks' gestation.<sup>60</sup> Because cervical shortening can occur after 20 weeks' gestation even in some twin pregnancies destined to deliver at term, TVU of the cervix before 20 to 24 weeks may lead to better prediction of PTB. Unfortunately, the predictive value of sonographic CL determination in twins between 24 and 34 weeks' gestation is low.<sup>81</sup> As with high-risk singletons, a short cervix is a good predictor of PTB in twins. Importantly, fewer than 10% of twin pregnancies with sonographic CL measuring greater than 35 mm between 18 and 26 weeks deliver before 35 weeks.<sup>82</sup> This reassuring finding could allow obstetricians to avoid instituting bed rest or other interventions commonly used in management of twin pregnancies. Unfortunately, sensitivity of TVU-CL to predict which twin gestations will deliver preterm is only 30%. Some multiple gestations likely deliver preterm not primarily because of cervical insufficiency but because of rapid

uterine expansion leading to contractions, a process not well screened by TVU-CL.<sup>1</sup>

### Triplets

Few studies have reported on TVU of the cervix and prediction of PTB in triplet pregnancies. As shown in Table 18-4, sensitivity of TVU-CL to predict which triplet gestations will deliver preterm is low, as in twin gestations, making this screening test relatively ineffective in multiple pregnancies.<sup>62</sup>

## THREE-DIMENSIONAL TRANSVAGINAL ULTRASOUND EXAMINATION OF THE CERVIX

Three-dimensional volume data, including for TVU-CL assessment, can be presented in a variety of orthogonal multiplanar displays in which sagittal, axial, and coronal views of the cervix are shown simultaneously (Fig. 18-15). The multiplanar view allows for visualization of anatomic planes that are not possible with two-dimensional ultrasound imaging (i.e., planes that are perpendicular to the ultrasound beam, such as the coronal view of the cervix). In addition, the three-dimensional multiplanar display makes possible visualization of the true midsagittal plane of the cervix by objectively selecting this plane in the coronal view. The coronal view of the cervix is a unique image obtained only with three-dimensional ultrasound, providing additional information regarding the shape and dimensions of the endocervical canal. Evaluation of the funneled cervix is also improved by using three-dimensional ultrasound, as it can be visualized in all three

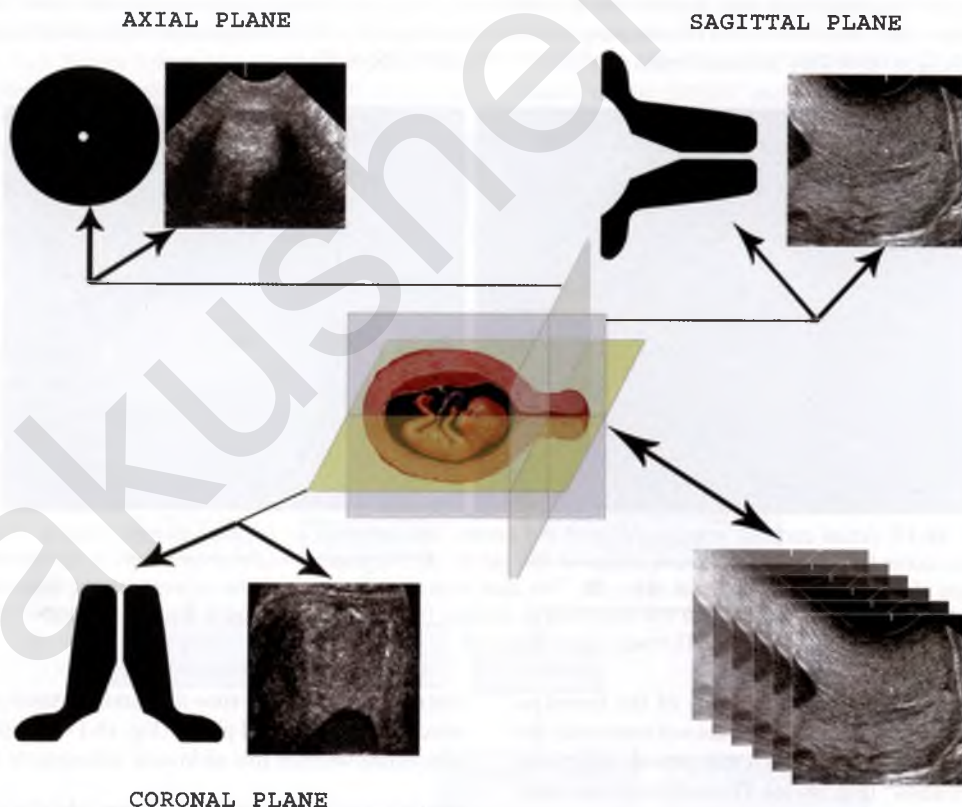


**FIG 18-15** Diagram illustrating three-dimensional volume acquisition of two-dimensional images of the cervix in the sagittal plane and subsequent display of the cervix in three orthogonal planes (sagittal, axial, and coronal). Note that these three planes simultaneously shown are interactively linked to each other in a 90-degree (orthogonal) relationship. The evaluation of the cervix is not limited to the sagittal plane but extends with imaging in the axial and coronal planes. Note that cervical length and funnel length and width are shown both in the sagittal and coronal planes.



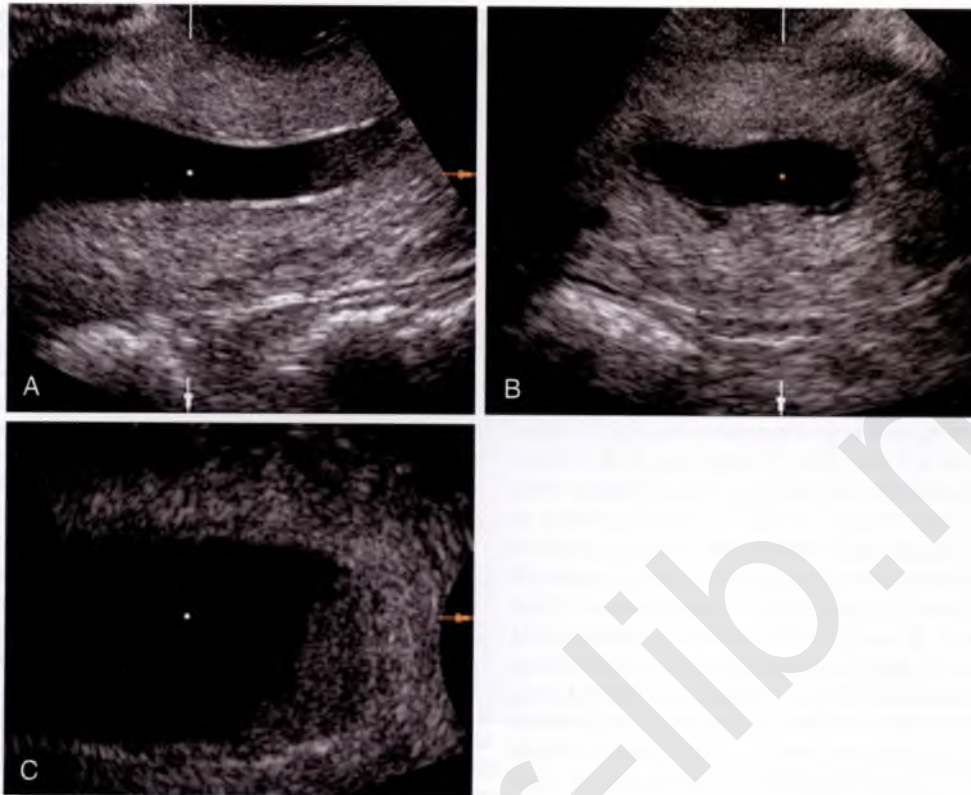


**FIG 18-16** Multiplanar display of the cervix in sagittal (A), axial (B), and coronal (C) planes. Significant funneling of the cervix with low level echoes is referred to as sludge in the dilated endocervical canal. The sludge is best visualized in the coronal plane (C). Note that the width of the funnel as shown in the coronal plane (C) is more than twice its height as shown in the sagittal plane (A).

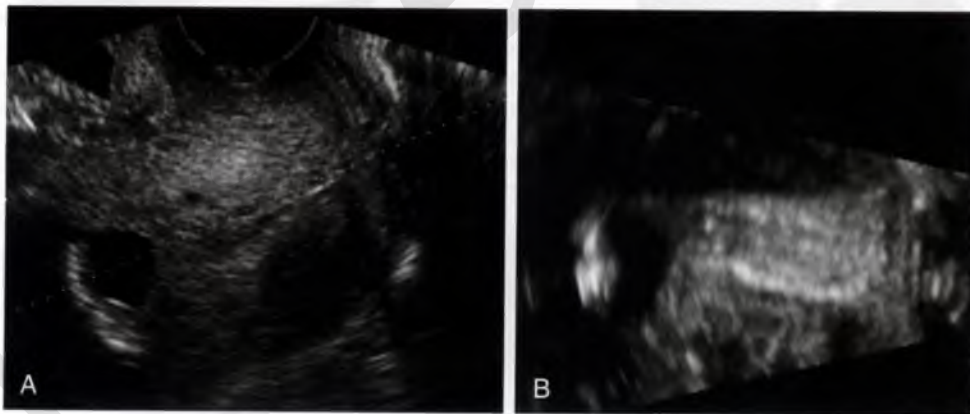


**FIG 18-17** Virtual contrast imaging (VCI) of the cervix, also referred to as thin volume imaging. Two-dimensional (2D) sagittal ultrasound image of the cervix (A) displayed simultaneously with a VCI-derived image of the cervix in the coronal plane (B). This dual view enables the operator to evaluate the cervix in real time in both the sagittal and the true coronal planes. This is done by properly placing the dotted line along the preferred axis in the 2D image, as shown in A.

planes: sagittal, axial, and coronal. Measurements of the funnel or endocervical canal widths in the coronal plane are not necessarily the same as their respective sagittal values, which may provide additional, potentially useful information<sup>83</sup> (Fig. 18-16). Three-dimensional ultrasound makes it possible to obtain an axial plane through the cervix at the level of a cerclage, demonstrating the entire stitch (see Figs. 18-13 and 18-14).<sup>83</sup> This view is not readily obtainable with conventional two-dimensional sonography. Whether three-dimensional ultrasound imaging enhances clinical management in patients with or without cerclage in place is unknown. New display and acquisition methods

enable the operator to view the cervix in multiple slices in operator-selectable distances and planes (Fig. 18-17). Further research is needed to evaluate whether this additional information is of clinical benefit.

### WHAT PATHOPHYSIOLOGIC MECHANISMS ASSOCIATE A SHORT CERVICAL LENGTH WITH PRETERM BIRTH?

Three primary mechanisms have been associated with the development of an asymptomatic short TVU-CL. First, a short CL can be

caused by a specific weakness of the cervix, or cervical insufficiency (this term is preferred rather than “cervical incompetence”).<sup>84</sup> Cervical insufficiency is due in most cases to traumatic or surgical damage. Women with one or more dilatation and evacuation or curettage procedures for termination of pregnancy have a higher incidence of short TVU-CL, as well as an increased risk of PTB.<sup>85</sup> Clinically, it is extremely rare to observe a short TVU-CL due to a maternal congenital disorder or connective tissue disease. It is interesting to note that almost no pregnant women, even those at high risk, have a short CL in the first trimester.<sup>59</sup> It is thought that the early developing intrauterine pregnancy exerts little pressure on the cervix and is unlikely to result in dilatation, even in the setting of cervical insufficiency.

Second, a short CL can develop secondary to an inflammatory or infectious process. There is a strong association between short TVU-CL and infection. High amniotic fluid interleukin 6 (IL-6), later development of chorioamnionitis,<sup>86</sup> and acute inflammatory lesions of the placenta<sup>87</sup> have all been associated with short CL. Women with both a short CL and bacterial vaginosis have a higher incidence of PTB than matched women with a short CL but no bacterial vaginosis.<sup>88</sup> Short CL leading to PTB is often associated with PPRM and not with PTL, providing additional evidence for the role of infection.<sup>89</sup> There is insufficient evidence thus far to determine if infection results in the development of short CL or, alternatively, if this association between infection and short CL occurs because short CL allows ascending infection from the vagina. A short CL can allow easier access of potentially pathologic vaginal organisms into the intrauterine environment, leading to prolonged subclinical chorioamnionitis and subsequent PTB. Women with a normal CL have mechanical and immunologic protection against the ascent of lower vaginal organisms.

Third, studies have shown that the majority of asymptomatic women with CL less than 25 mm before 24 weeks have contractions more often than control subjects with normal CL.<sup>90,91</sup> It is unclear

whether contractions cause the short CL, are a result of the short cervix, or whether these two factors exert interactive effects.

Most probably, the three aforementioned mechanisms, in addition to other factors, act synergistically in some women to contribute, in different ways in each individual, to the development of a short CL.

## CLINICAL USE OF CERVICAL LENGTH FOR PREVENTION OF PRETERM BIRTH

TVU-CL is a predictor of PTB. As with any predictor, an effort to avoid its occurrence is the first step toward prevention. There are limited studies on the primary prevention of short CL. Progesterone therapy has been associated with preventing the development of a short CL,<sup>92</sup> but more studies are needed in this area investigating the impact on reducing PTB.

Algorithms for care using TVU-CL measurements to screen for PTB risk are evolving, particularly as more randomized studies on interventions based on short TVU-CL are published and as professional societies disseminate updated guidelines.<sup>18-20</sup> Included here are the currently recommended evidence-based management schemes.

### Asymptomatic Singletons Without Prior Spontaneous Preterm Birth

An TVU-CL assessment can be offered to *all* pregnant women carrying singletons at 18 to 22 weeks (i.e., the time of the “anatomy” ultrasound examination) including those without prior PTB. Screening based on other risk factors is not recommended, as it has not been sufficiently studied, and because in many populations the large majority of pregnant women have at least one risk factor for PTB (96% in our urban U.S. population).<sup>93</sup>

The algorithm shown in Figure 18-18 has been recommended for clinical use by SMFM<sup>18</sup> and was subsequently endorsed by ACOG.<sup>19</sup>

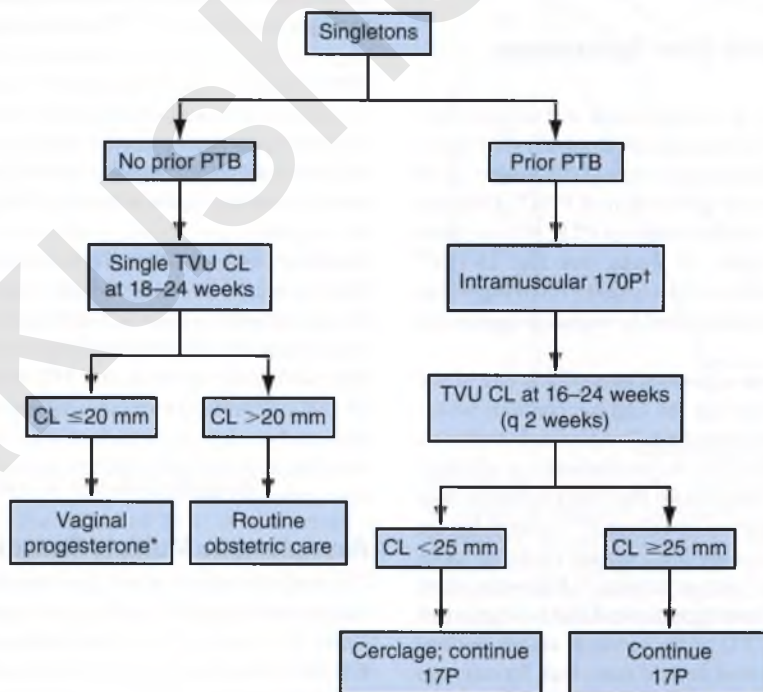


**FIG 18-18** Algorithm for use of progestogens in prevention of preterm birth in clinical care. CL, cervical length; PTB, preterm birth; 17P, 17 $\alpha$ -hydroxyprogesterone caproate; TVU, transvaginal ultrasound. \*For example, daily 200 mg suppository or 90 mg gel from time of diagnosis of short CL to 36 weeks. †250 mg intramuscularly every week from 16 to 20 weeks to 36 weeks. (Adapted from Society for Maternal-Fetal Medicine Publications Committee, with assistance of Vincenzo Berghella: Progesterone and preterm birth prevention: translating clinical trials data into clinical practice. *Am J Obstet Gynecol* 206(5):376-386, 2012.)



The term *universal CL screening* has been used to refer to TVU-CL screening in singleton pregnancies without prior PTB. In general, over 80% to 90% of women accept TVU-CL screening, especially if offered with an opt-out approach, in the absence of a language barrier.<sup>94</sup> Women with a prior term birth tend to have a lower acceptance rate,<sup>95</sup> as they likely are less concerned about the possibility of PTB. Approximately 1% of women carrying singletons without prior PTB who accept TVU screening have a short CL of 20 mm or less before 24 weeks.<sup>94</sup> Vaginal progesterone is recommended to reduce the risk of PTB in an asymptomatic woman with a singleton gestation without a prior PTB found to have TVU-CL of 20 mm or less before or at 24 weeks of gestation.<sup>18,19</sup> This recommendation is based on the reported approximate 45% decreased risk of PTB associated with this intervention found in two separate randomized trials.<sup>3,4</sup> Analyses of this management scheme (see Fig. 18-18) predict that up to 100,000 PTBs could be prevented, 1000 infants saved, and \$13 billion saved annually in the United States.<sup>17,30</sup> Both SMFM and ACOG have therefore stated that implementation of such a screening strategy can be viewed as reasonable and can be considered by individual practitioners, following strict guidelines.<sup>18,19</sup>

Interestingly, in these women found to have short CL, activity restriction, such as bed rest, is *not* recommended, as it is associated with an *increase* in PTB compared to normal levels of activity.<sup>96</sup>

Cerclage has also not been shown to be associated with a significant reduction in PTB in singletons without prior PTB and a short TVU-CL less than 25 mm before 24 weeks, but the nonsignificant 24% reduction deserves further study.<sup>97</sup>

As previously discussed, pessary has been associated with a significant reduction in PTB in singletons without prior PTB and a short TVU-CL less than 25 mm before 24 weeks in one trial,<sup>10</sup> but a subsequent trial failed to confirm these results.<sup>11</sup> Further trials are in progress to assess the efficacy of pessary for prevention of PTB in women with short CL.

### Asymptomatic Singletons With Prior Spontaneous Preterm Birth

Based on randomized trial data, it is recommended that women with singleton pregnancies with prior spontaneous PTB should start intramuscular injections of 17 $\alpha$ -hydroxyprogesterone (17P) weekly at 16 weeks and continue until 36 weeks for prevention of PTB.<sup>98</sup> Although this regimen is associated with a 34% decrease in PTB, 36% of these women nevertheless delivered before 37 weeks (see Fig. 18-18).<sup>98</sup> Another trial reported a lower incidence of recurrent PTB in singletons with prior PTB in those who were randomized to vaginal progesterone 90 mg compared to 17P.<sup>99</sup>

Because cervical insufficiency as a cause of short CL is one of the leading hypotheses, cervical cerclage was the first intervention postulated to be of benefit in this clinical situation. Randomized studies on history-indicated (previously referred to as prophylactic, or elective) cerclage without the use of TVU have shown that this procedure does not prevent PTB in high-risk singleton gestations,<sup>100,101</sup> except for the subgroup of women with three or more prior second trimester losses or PTBs.<sup>102</sup> Nor is it beneficial in twin gestations.<sup>103</sup> Following these disappointing results, researchers have hypothesized that a subgroup of women could be identified with TVU of the cervix in whom cerclage may be beneficial. Cerclage was indeed devised more than 50 years ago for women with both a poor obstetric history characterized by second trimester losses and cervical changes in the current pregnancy.<sup>104,105</sup> The four randomized trials<sup>7,9,106,107</sup> on the efficacy of ultrasound-indicated cerclage have been analyzed in meta-analyses,<sup>108,109</sup> which allowed for larger numbers with more robust statistics and offered careful assessment of different populations of women with short CL. In fact,

**TABLE 18-5 Efficacy of Ultrasound-Indicated Cerclage**<sup>110,111,1136</sup>

Population	Effect of Cerclage on PTB < 35 Weeks
Singleton gestations	
Low risk for PTB (no other risk factors)	No significant difference
Prior PTB at 16-36 weeks	30% decrease
Prior second trimester loss	43% decrease
Twin gestations	No significant difference

PTB, preterm birth.

ultrasound-indicated cerclage has different effects in different populations (Table 18-5).<sup>110,111</sup> In women with singleton gestation and prior PTB or second trimester loss, the use of cerclage (performed if TVU-CL measures less than 25 mm prior to 24 weeks) is associated with a 30% significant decrease in recurrent PTB, and—most importantly—a 36% significant decrease in perinatal morbidity and mortality rates.<sup>112</sup> Based on these data, SMFM,<sup>18</sup> ACOG,<sup>19</sup> and RCOG<sup>20</sup> have all recommended that cerclage be offered to women with singleton gestations, prior spontaneous PTB, and TVU-CL less than 25 mm before 24 weeks.

The randomized trial<sup>107</sup> that showed the most benefit from cerclage included administration of indomethacin to the women studied, and not to the control subjects, raising the possibility that indomethacin may have contributed significantly to the prevention of PTB. Analysis of the effect of indomethacin indeed reveals that it can prevent PTB less than 24 weeks and PPRM in women with short CL.<sup>113</sup> Given that women with short CL are often found to have contractions,<sup>90,91</sup> it is possible that one of the efficacious interventions in this setting is tocolytic therapy.

A short CL has also been associated with infection. Analysis of the use of antibiotics reveals no effect of this therapy on prevention of PTB in women with short CL.<sup>108</sup> Unfortunately, antibiotics have often failed to prevent PTB when used for other risk factors for PTB, such as prior PTB,<sup>114</sup> positive fetal fibronectin,<sup>115</sup> or symptomatic PTL.<sup>116</sup>

An added benefit of screening with TVU to determine CL in this population is that it can be used to avoid performing unnecessary interventions (e.g., cerclage) in high-risk women whose TVU-CL remains normal. About 60% of such high-risk women, who are carrying singleton pregnancies with prior history of spontaneous PTB, maintain a normal CL until after 24 weeks and deliver at term and can thus be spared any intervention. Only about 40% of such high-risk women develop a short CL and are at true risk of PTB, and these women can be offered intervention. Management of singleton gestations with prior spontaneous PTB, even early in gestation, with serial TVU-CL appears to be a safe alternative to a policy of placing history-indicated cerclage in all such women, as confirmed by a meta-analysis studying approximately 400 women included in four randomized trials that addressed this issue.<sup>109</sup>

### Asymptomatic Multiple Gestations

Currently no interventions have been definitively shown to be beneficial in preventing PTB and its consequences in multiple gestations with short CL. Cerclage is not beneficial and may in fact be harmful, but this procedure been evaluated in a total of only 49 twin pregnancies with TVU-CL less than 25 mm before 24 weeks randomized to cerclage or no cerclage.<sup>117</sup> Pessary has been associated with significant reductions in PTB less than 28 weeks and less than 32 weeks as well as with composite poor perinatal outcome in a secondary analysis of an RCT including 133 twin pairs with TVU-CL less than 38 mm before 23 weeks, but more data from dedicated RCTs are needed.<sup>118</sup>



17P caproate has been found to not be beneficial when studied in 175 twin pregnancies (>90% of whom had no prior spontaneous PTB) with TVU-CL 25 mm or less before 24 weeks in a recent meta-analysis.<sup>119</sup> In contrast, vaginal progesterone has been found to have some benefit in preventing either PTB or adverse perinatal outcome in a limited number (<60) of twin pregnancies (>95% of whom had no prior spontaneous PTB) with TVU-CL 25 mm or less before 24 weeks in two meta-analyses,<sup>119,120</sup> but again more data from dedicated RCTs are needed.

In summary, the evidence is insufficient to support TVU-CL screening in all twin pregnancies for PTB prevention. If large, well-designed RCTs confirm the benefits of pessary or vaginal progesterone in twins with short TVU-CL before 24 weeks, then TVU-CL could become an effective screening test for this very high risk population.

### Preterm Labor

TVU of the cervix has been studied extensively as a predictor of PTB in women with symptoms of PTL (see Table 18-4). All studies have reported a statistically significant positive predictive accuracy of TVU-CL for PTB.<sup>121</sup> The presence of sludge (see Fig. 18-16) in women with suspected PTL is associated with intra-amniotic infection and high risk for PTB.<sup>49</sup> TVU-CL is helpful in the clinical management of women with suspected PTL. First, it helps confirm or exclude the diagnosis. The diagnosis of PTL has usually been made between 20 and 36 weeks by documenting regular uterine contractions and cervical change by manual examination. However, more than 70% of women given the diagnosis of PTL deliver at term and thus might receive unnecessary intervention. Women with these clinical findings but TVU-CL 30 mm or greater have less than 1% chance of delivering within 1 week and less than 10% chance of delivering before 35 weeks. Such women therefore are unlikely to benefit from administration of corticosteroids for fetal lung maturity, tocolysis, or other interventions. The diagnosis of PTL should be confirmed by documenting TVU-CL less than 20 mm, and only those women in whom such measurement is confirmed should receive interventions.<sup>121</sup>

A randomized trial studying the use of the algorithm shown in Figure 18-19 for management of women with PTL at 24 to 34 weeks was associated not only with a shorter time in triage, but also with a 65% decrease in PTB less than 37 weeks.<sup>122</sup> We recommend use of this protocol, based primarily on TVU-CL assessment, for management of women with threatened PTL.

The potential utility of repeat measurements of CL following tocolysis for PTL has been studied and found to predict PTB, but not with any more accuracy than the first measurement at presentation. The variation in CL between the first and subsequent measurements seems not to be predictive of PTB, such that the authors of this study concluded that "to repeat ultrasonographic CL measurement after successful tocolysis [may be] useless."<sup>123</sup>

### Preterm Premature Rupture of the Membranes

Several studies have evaluated the utility of TVU of the cervix in women with PPROM. A randomized trial demonstrated the safety of performing TVU in this group, finding that women who had TVU experienced similar incidences of maternal and neonatal infections as did control subjects who did not undergo TVU.<sup>29</sup> The latency from PPROM to delivery is directly correlated with CL; thus, women with shorter CLs have shorter latencies.<sup>124,125</sup> No studies have assessed whether this clinical knowledge affects outcomes.

### Prediction of Start of Spontaneous Labor

TVU of the cervix can also be useful in predicting onset of labor in pregnant women at term.<sup>126,127</sup> Based on TVU-CL measurements at 37

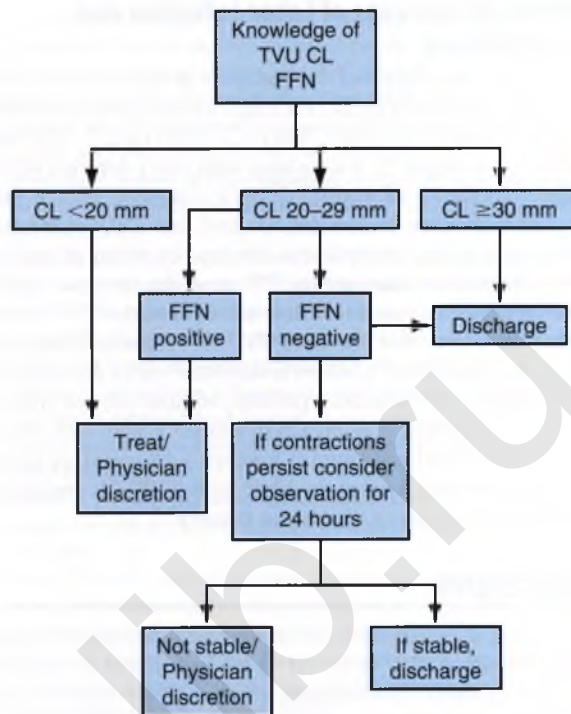


**FIG 18-19** Algorithm for management of women with preterm labor based mainly on cervical length. CL, cervical length; FFN, fetal fibronectin; TVU, transvaginal ultrasound. (Adapted from Ness A, Visintine J, Ricci E, Berghella V: Does knowledge of cervical length and fetal fibronectin affect management of women with threatened preterm labor? A randomized trial. *Am J Obstet Gynecol* 197(4):426.e1-e7, 2007.)

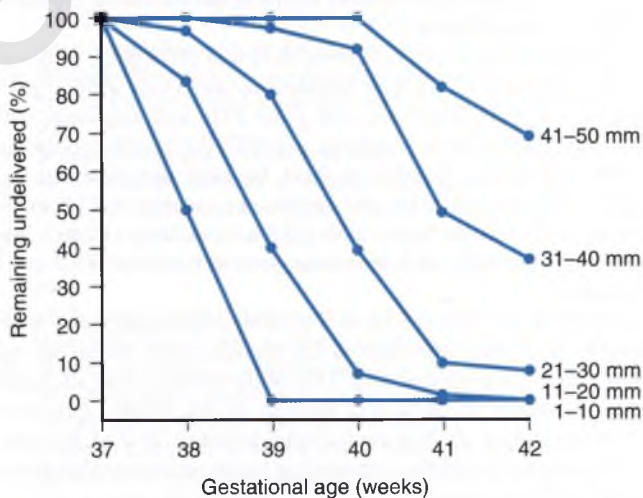


**FIG 18-20** Survival curve estimates of percentages of women not delivered at different gestational ages, according to sonographically measured cervical length at 37 weeks. (From Ramanathan G, Yu C, Osei E, et al: Ultrasound examination at 37 weeks' gestation in the prediction of pregnancy outcome: the value of cervical assessment. *Ultrasound Obstet Gynecol* 22:598, 2003, redrawn with permission.)

weeks, the mean gestational age at delivery increased from 38 weeks for women with CL of 10 mm to 41 weeks for women with CL of 35 mm. There is a 68% chance of delivering after 41 $\frac{7}{8}$  weeks if CL measures greater than 40 mm (Fig. 18-20).<sup>131</sup> CL was also found to be an independent predictor of spontaneous labor in nulliparous women and of vaginal delivery in nulliparous and parous women.<sup>128</sup>



## Predicting the Success of Labor Induction and Mode of Delivery

Several studies have evaluated the predictive accuracy of TVU of the cervix in term gravidas to predict the length of induction and incidence of success (vaginal delivery). Short CL (<30 mm,<sup>129</sup> <28 mm,<sup>130</sup> <26 mm,<sup>131</sup> or wedging<sup>132</sup>) is associated with short duration of labor and higher incidence of vaginal delivery compared with a longer cervix. Although some studies did not find that TVU of the cervix added significantly to the prediction obtained by noting dilatation of the cervix on manual examination,<sup>133,134</sup> most did find that TVU-CL was a better predictor than any Bishop score parameter.<sup>127,129-131</sup> A randomized trial showed that the use of TVU-CL instead of Bishop score for management of labor induction is associated with a decreased need for intracervical prostaglandin treatment, without adverse effects on the success of induction.<sup>135</sup> Women in spontaneous labor with TVU-CL less than 20 mm have been found to have just a 4% incidence of cesarean delivery, whereas women in labor with TVU-CL greater than 40 mm have a 12% chance of cesarean delivery.<sup>127</sup>

## CONCLUSIONS

TVU for cervical assessment is one of the best techniques for predicting PTB. The use of TVU of the cervix has been found to be safe and acceptable to patients. CL measuring less than 25 mm between 16 and 24 weeks of gestation has been shown to be the most reliable threshold associated with an increased risk of PTB. The shorter the cervix and the earlier in gestation the shortening occurs, the higher the risk of PTB. The role of TVU of the cervix has been studied in a wide variety of clinical settings and with different patient populations, consistently finding good prediction of PTB risk. Screening frequency should depend on detailed obstetric history, with serial TVU of the cervix having a better predictive accuracy than a single evaluation, especially in high-risk populations.

The algorithms shown in Figures 18-18 and 18-19 guide evidence-based use of TVU-CL in three populations: singletons without prior spontaneous PTB; singletons with prior PTB; and singletons with threatened PTL. In all these settings, use of TVU-CL, with appropriate intervention if CL is found to be short, has been associated with significant reductions in PTB. The decreased incidence of PTB in the United States seen between 2006 (12.8%) and 2012 (11.5%) may indeed have been due, at least in some part, to the use of TVU in CL screening.

Moreover, TVU-CL can be used to safely avoid unnecessary interventions in women with normal CL measurements. There are still limited data concerning whether TVU of the cervix is clinically useful for the prediction of the start of labor or success of labor induction. Future research on all these clinical applications of TVU of the cervix has the potential to further improve the health outcomes of pregnant women and their babies.

## REFERENCES

- Berghella V, Bega G, Tolosa J, et al: Ultrasound assessment of the cervix. *Clin Obstet Gynecol* 46:947, 2003.
- Hassan SS, Romero R, Berry S, et al: Patients with ultrasonographic cervical length =15 mm have a 50% risk of early spontaneous preterm delivery. *Am J Obstet Gynecol* 182:1458, 2000.
- Fonseca EB, Celik E, Parra M, et al; Fetal Medicine Foundation Second Trimester Screening Group: Progesterone and the risk of preterm birth among women with a short cervix. *N Engl J Med* 357(5):462-469, 2007.
- Hassan SS, Romero R, Vidyadhari D, et al; PREGNANT Trial: Vaginal progesterone reduces the rate of preterm birth in women with a sonographic short cervix: a multicenter, randomized, double-blind, placebo-controlled trial. *Ultrasound Obstet Gynecol* 38(1):18-31, 2011.
- Althuisius SM, Dekker GA, Hummel P, van Geijn HP: Cervical incompetence prevention randomized cerclage trial: emergency cerclage with bed rest versus bed rest alone. *Am J Obstet Gynecol* 189(4):907-910, 2003.
- Rust OA, Atlas RO, Jones KJ, et al: A randomized trial of cerclage versus no cerclage among patients with ultrasonographically detected second-trimester preterm dilatation of the internal os. *Am J Obstet Gynecol* 183(4):830-835, 2000.
- To MS, Alfirevic Z, Heath VC, et al; Fetal Medicine Foundation Second Trimester Screening Group: Cervical cerclage for prevention of preterm delivery in women with short cervix: randomised controlled trial. *Lancet* 363(9424):1849-1853, 2004.
- Owen J, Hankins G, Iams JD, et al: Multicenter randomized trial of cerclage for preterm birth prevention in high-risk women with shortened midtrimester cervical length. *Am J Obstet Gynecol* 201(4):375.e1-375.e8, 2009.
- Berghella V, Odibo AO, Tolosa JE: Cerclage for prevention of preterm birth in women with a short cervix found on transvaginal ultrasound examination: a randomized trial. *Am J Obstet Gynecol* 191(4):1311-1317, 2004.
- Goya M, Pratcorona L, Merced C, et al; Pesario Cervical para Evitar Prematuridad (PECEP) Trial Group: Cervical pessary in pregnant women with a short cervix (PECEP): an open-label randomised controlled trial. *Lancet* 379(9828):1800-1806, 2012.
- Hui SY, Chor CM, Lau TK, et al: Cerclage pessary for preventing preterm birth in women with a singleton pregnancy and a short cervix at 20 to 24 weeks: a randomized controlled trial. *Am J Perinatol* 30(4):283-288, 2013.
- Saul LL, Kurtzman JT, Hagemann C, et al: Is transabdominal sonography of the cervix after voiding a reliable method of cervical length assessment? *J Ultrasound Med* 27(9):1305-1311, 2008.
- Stone PR, Chan EH, McCowan LM, et al; SCOPE Consortium: Transabdominal scanning of the cervix at the 20-week morphology scan: comparison with transvaginal cervical measurements in a healthy nulliparous population. *Aust N Z J Obstet Gynaecol* 50(6):523-527, 2010.
- To MS, Skentou C, Cicero S, Nicolaides KH: Cervical assessment at the routine 23-weeks' scan: problems with transabdominal sonography. *Ultrasound Obstet Gynecol* 15(4):292-296, 2000.
- Hernandez-Andrade E, Romero R, Ahn H, et al: Transabdominal evaluation of uterine cervical length during pregnancy fails to identify a substantial number of women with a short cervix. *J Matern Fetal Neonatal Med* 25(9):1682-1689, 2012.
- Friedman AM, Srinivas SK, Parry S, et al: Can transabdominal ultrasound be used as a screening test for short cervical length? *Am J Obstet Gynecol* 208(3):190.e1-190.e7, 2013.
- Cahill AG, Odibo AO, Caughey AB, et al: Universal cervical length screening and treatment with vaginal progesterone to prevent preterm birth: a decision and economic analysis. *Am J Obstet Gynecol* 202(6):548.e1-548.e8, 2010.
- Society for Maternal-Fetal Medicine Publications Committee, with assistance of Vincenzo Berghella: Progesterone and preterm birth prevention: translating clinical trials data into clinical practice. *Am J Obstet Gynecol* 206(5):376-386, 2012.
- American College of Obstetricians and Gynecologists Committee on Practice Bulletins: ACOG Practice Bulletin No. 130: prediction and prevention of preterm birth. *Obstet Gynecol* 120(4):964-973, 2012.
- Royal College of Obstetricians and Gynecologists: *Cervical Cerclage (Green-top Guideline No. 60)*. May 2011. Available at <www.rcog.org.uk/guidelines/gtg60>.
- Owen J, Neely C, Northern A: transperineal versus transvaginal ultrasonographic examination of the cervix in the midtrimester: a blinded comparison. *Am J Obstet Gynecol* 181:780, 1999.
- Perinatal Quality Foundation: *Cervix Measurement Criteria*. 2015. Available at <www.clear.perinatalquality.org>.
- Burger M, Weber-Rössler T, Willman M: Measurement of the pregnant cervix by transvaginal sonography: an interobserver study and new

- standards to improve the interobserver variability. *Ultrasound Obstet Gynecol* 9:188, 1997.
24. Yost NP, Bloom SL, Twickler DM, et al: Pitfalls in ultrasonic cervical length measurement for predicting preterm birth. *Obstet Gynecol* 93:510, 1999.
  25. Blencowe H, Cousens S, Oestergaard MZ, et al: National, regional, and worldwide estimates of preterm birth rates in the year 2010 with time trends since 1990 for selected countries: a systematic analysis and implications. *Lancet* 379(9832):2162–2172, 2012.
  26. Hamilton BE, Martin JA, Ventura SJ: Births: preliminary data for 2012. *Natl Vital Stat Rep* 62(3):1–20, 2013.
  27. Iams JD: Clinical practice. Prevention of preterm parturition. *N Engl J Med* 370(3):254–261, 2014.
  28. Carlan SJ, Richmond LB, O'Brien WF: Randomized trial of transvaginal ultrasound in preterm premature rupture of membranes. *Obstet Gynecol* 89(3):458–461, 1997.
  29. Iams JD, Goldenberg RL, Meis PJ, et al: The length of the cervix and the risk of spontaneous premature delivery. National Institute of Child Health and Human Development Maternal Fetal Medicine Unit Network. *N Engl J Med* 334(9):567–572, 1996.
  30. Werner EF, Han CS, Pettker CM, et al: Universal cervical-length screening to prevent preterm birth: a cost-effectiveness analysis. *Ultrasound Obstet Gynecol* 38(1):32–37, 2011.
  31. Krebs-Jimenez J, Neubert GA: The microbiological effects of transvaginal sonographic assessment of cervical length. *J Ultrasound Med* 21:727, 2002.
  32. Dutta RL, Economides DL: Patient acceptance of transvaginal sonography in the early pregnancy unit setting. *Ultrasound Obstet Gynecol* 22:503, 2003.
  33. Clement S, Candy B, Heath V, et al: Transvaginal ultrasound in pregnancy: its acceptability to women and maternal psychological morbidity. *Ultrasound Obstet Gynecol* 22:508, 2003.
  34. Berghella V, Tolosa JE, Kuhlman KA, et al: Cervical ultrasonography compared to manual examination as a predictor of preterm delivery. *Am J Obstet Gynecol* 177:723, 1997.
  35. Phelps JY, Higby K, Smyth MH, et al: Accuracy and intraobserver variability of simulated cervical dilatation measurements. *Am J Obstet Gynecol* 173:942, 1995.
  36. Michaels WH, Montgomery C, Karo J, et al: Ultrasound differentiation of the competent from the incompetent cervix: prevention of preterm delivery. *Am J Obstet Gynecol* 154:537, 1986.
  37. Floyd WS: Cervical dilatation in the mid-trimester of pregnancy. *Obstet Gynecol* 18:380, 1961.
  38. Berghella V, Kuhlman K, Weiner S, et al: Cervical funneling: sonographic criteria predictive of preterm delivery. *Ultrasound Obstet Gynecol* 10:161, 1997.
  39. Owen J, Yost N, Berghella V, et al: Mid-trimester transvaginal sonography in women at high risk for spontaneous preterm birth. *JAMA* 286:1340, 2001.
  40. Ziliani M, Azuaga A, Calderon F, et al: Transperineal sonography in second trimester to term pregnancy and early labor. *J Ultrasound Med* 10:481, 1991.
  41. Berghella V: The natural history of cervical funneling in high-risk women. *Obstet Gynecol* 101:120, 2003.
  42. Hasegawa I, Tanaka K, Takahashi K, et al: Transvaginal ultrasonographic cervical assessment for the prediction of preterm delivery. *J Matern Fetal Med* 5(6):305–309, 1996.
  43. Berghella V, Daly SF, Tolosa JE, et al: Prediction of preterm delivery with transvaginal ultrasonography of the cervix in patients with high-risk pregnancies: does cerclage prevent prematurity? *Am J Obstet Gynecol* 181:809, 1999.
  44. To MS, Skentou C, Liao AW, et al: Cervical length and funneling at 23 weeks of gestation in the prediction of spontaneous early preterm delivery. *Ultrasound Obstet Gynecol* 3:200, 2001.
  45. Guzman ER, Walters C, Ananth CV, et al: A comparison of sonographic cervical parameters in predicting spontaneous preterm birth in high-risk singleton gestations. *Ultrasound Obstet Gynecol* 18:204, 2001.
  46. Andrews WW, Copper R, Hauth JC, et al: Second-trimester cervical ultrasound: associations with increased risk for recurrent early spontaneous delivery. *Obstet Gynecol* 95:222, 2000.
  47. Rust OA, Atlas RO, Kimmel S, et al: Does the presence of a funnel increase the risk of adverse perinatal outcome in a patient with a short cervix? *Am J Obstet Gynecol* 192:1060, 2005.
  48. Berghella V, Roman A: Does funneling increase the incidence of preterm birth in women with normal cervical length? *Am J Obstet Gynecol* 193:S147, 2005.
  49. Espinoza J, Gonçalves LF, Romero R, et al: The prevalence and clinical significance of amniotic fluid “sludge” in patients with preterm labor and intact membranes. *Ultrasound Obstet Gynecol* 25(4):346–352, 2005.
  50. Romero R, Kusanovic JP, Espinoza J, et al: What is amniotic fluid “sludge”? *Ultrasound Obstet Gynecol* 30(5):793–879, 2007.
  51. Kusanovic JP, Espinoza J, Romero R, et al: Clinical significance of the presence of amniotic fluid “sludge” in asymptomatic patients at high risk for spontaneous preterm delivery. *Ultrasound Obstet Gynecol* 30(5):793–798, 2007.
  52. Bujold E, Pasquier JC, Simoneau J, et al: Intra-amniotic sludge, short cervix, and risk of preterm delivery. *J Obstet Gynaecol Can* 28(3):198–202, 2006.
  53. Yost NP, Owen J, Berghella V, et al: Second-trimester cervical sonography: features other than cervical length to predict spontaneous preterm birth. *Obstet Gynecol* 103:457, 2004.
  54. Fukami T, Ishihara K, Sekira T, et al: Is transvaginal ultrasonography at midtrimester useful for predicting early spontaneous preterm birth? *J Nippon Med Sch* 70(2):135–140, 2003.
  55. Tekesin I, Hellmeyer L, Heller G, et al: Evaluation of quantitative ultrasound tissue characterization of the cervix and cervical length in the prediction of premature delivery for patients with spontaneous preterm labor. *Am J Obstet Gynecol* 189:532, 2003.
  56. Guzman ER, Rosenberg JC, Houlihan C, et al: A new method using vaginal ultrasound and transfundal pressure to evaluate the asymptomatic incompetent cervix. *Obstet Gynecol* 83:248, 1994.
  57. Owen J, Yost N, Berghella V, et al: Maternal-Fetal Medicine Units Network: Can shortened midtrimester cervical length predict very early spontaneous preterm birth? *Am J Obstet Gynecol* 191(1):298–303, 2004.
  58. Berghella V, Pereira L, Garipey A, et al: Prior cone biopsy: prediction of preterm birth by cervical ultrasound. *Am J Obstet Gynecol* 191:1393, 2004.
  59. Visintine J, Berghella V, Henning D, Baxter J: Cervical length for prediction of preterm birth in women with multiple prior induced abortions. *Ultrasound Obstet Gynecol* 31(2):198–200, 2008.
  60. Airoidi J, Berghella V: Transvaginal ultrasound of the cervix to predict preterm birth in women with uterine anomalies. *Obstet Gynecol* 106:553, 2005.
  61. Goldenberg RL, Iams J, Miodovnik M, et al: The preterm prediction study: risk factors in twin gestation. *Am J Obstet Gynecol* 175:1047, 1996.
  62. Guzman ER, Walters C, O'Reilly-Green C, et al: Use of cervical ultrasonography in prediction of spontaneous preterm birth in triplet gestations. *Am J Obstet Gynecol* 183:1108, 2000.
  63. Venditelli F, Mamelie N, Munoz F, et al: Transvaginal ultrasonography of the uterine cervix in hospitalized women with preterm labor. *Int J Gynecol Obstet* 72:117, 2001.
  64. Andersen HF: Transvaginal and transabdominal ultrasonography of the uterine cervix during pregnancy. *J Clin Ultrasound* 19:77, 1991.
  65. Andersen HF, Nugent CE, Wanty SD, et al: Prediction of risk for preterm delivery by ultrasonographic measurement of cervical length. *Am J Obstet Gynecol* 163:859, 1990.
  66. Heath VCF, Southall TR, Souka AP, et al: Cervical length at 23 weeks of gestation: relation to demographic characteristics and previous obstetric history. *Ultrasound Obstet Gynecol* 12:304, 1998.
  67. Goldenberg RL, McClure EM: The epidemiology of preterm birth. In Berghella V, editor: *Preterm Birth: Prevention and Management*, Oxford, 2010, Wiley-Blackwell, Chap. 4.
  68. Iams JD, Johnson FF, Sonek J, et al: Cervical competence as a continuum: a study of ultrasonographic cervical length and obstetric performance. *Am J Obstet Gynecol* 172:1097, 1995.



69. Odibo AO, Berghella V, Reddy U, et al: Does transvaginal ultrasound of the cervix predict preterm premature rupture of membranes in a high-risk population? *Ultrasound Obstet Gynecol* 18:223, 2001.
70. Odibo AO, Talucci M, Berghella V: Prediction of preterm premature rupture of membranes by transvaginal ultrasound features and risk factors in a high-risk population. *Ultrasound Obstet Gynecol* 20:245, 2002.
71. Quinn MJ: Vaginal ultrasound and cervical cerclage: a prospective study. *Ultrasound Obstet Gynecol* 2(6):410, 1992.
72. Andersen HF, Karimi A, Sakala EP, et al: Prediction of cervical cerclage outcome by transvaginal ultrasonography. *Am J Obstet Gynecol* 171:1102, 1994.
73. Berghella V, Davis G, Wapner RJ: Transvaginal ultrasound of the cervix in pregnancies with prophylactic cerclage. *Am J Obstet Gynecol* 180:S173, 1999.
74. Miroshnichenko G, Visintine JF, Suhag A, et al: Is cerclage height associated with the incidence of preterm birth in women with a history-indicated cerclage? *Am J Perinatol* 28(1):83–86, 2011.
75. Scheib S, Visintine JF, Miroshnichenko G, et al: Is cerclage height associated with the incidence of preterm birth in women with an ultrasound-indicated cerclage? *Am J Obstet Gynecol* 200(5):e12–e15, 2009.
76. Guzman ER, Houlihan C, Vintzileos A, et al: The significance of transvaginal ultrasonographic evaluation of the cervix in women treated with emergency cerclage. *Am J Obstet Gynecol* 175:471, 1996.
77. Althuisius SM, Dekker GA, van Geijn HP, et al: The effect of therapeutic McDonald cerclage on cervical length as assessed by transvaginal ultrasonography. *Am J Obstet Gynecol* 180:366, 1999.
78. Abdel-Aleem H, Shaaban OM, Abdel-Aleem MA: Cervical pessary for preventing preterm birth. *Cochrane Database Syst Rev* 5:CD007873, 2013.
79. Goya M, Pratcorona L, Higuera T, et al: Sonographic cervical length measurement in pregnant women with a cervical pessary. *Ultrasound Obstet Gynecol* 38(2):205–209, 2011.
80. Kushnir O, Izquierdo LA, Smith JF, et al: Transvaginal sonographic measurement of cervical length. Evaluation of twin pregnancies. *J Reprod Med* 40(5):380–382, 1995.
81. Wennerholm UB, Holm B, Mattsby-Baltzer I, et al: Fetal fibronectin, endotoxin, bacterial vaginosis and cervical length as predictors of preterm birth and neonatal morbidity in twin pregnancies. *Br J Obstet Gynecol* 104:1398, 1997.
82. Yang JH, Kuhlman K, Daly S, et al: Prediction of preterm birth by second trimester cervical sonography in twin pregnancies. *Ultrasound Obstet Gynecol* 15:288, 2000.
83. Bega G, Lev-Toaff A, Kuhlman K, et al: Three-dimensional multiplanar transvaginal ultrasound of the cervix in pregnancy. *Ultrasound Obstet Gynecol* 16:351, 2000.
84. American College of Obstetricians and Gynecologists: ACOG Practice Bulletin No. 142: cerclage for the management of cervical insufficiency. *Obstet Gynecol* 123(2 Pt 1):372–379, 2014.
85. Shah PS, Zao J, Knowledge Synthesis Group of Determinants of preterm/LBW births: Induced termination of pregnancy and low birthweight and preterm birth: a systematic review and meta-analyses. *Br J Obstet Gynaecol* 116(11):1425–1442, 2009.
86. Dowd J, Permezel M, Garland S, et al: Is there an interaction between cervical length and cervical microbiology in the pathogenesis of preterm labour? *Aust N Z J Obstet Gynecol* 41:177, 2001.
87. Althuisius SM, Barbe E, Dekker GA, et al: Short cervical length implies high risk of chorioamnionitis. *Am J Obstet Gynecol* 182:S20, 2000.
88. Guzman ER, Shen-Schwarz S, Benito C, et al: The relationship between placental histology and cervical ultrasonography in women at risk for pregnancy loss and spontaneous preterm birth. *Am J Obstet Gynecol* 181:793, 1999.
89. Berghella V, Talucci M, Desai A: Does transvaginal sonographic measurement of cervical length before 14 weeks predict preterm delivery in high-risk pregnancies? *Ultrasound Obstet Gynecol* 21:140, 2003.
90. Berghella V, Iams JD, Newman RB, et al: for the National Institute of Child Health and Human Development Network of Maternal-Fetal Medicine Units: Frequency of uterine contractions in asymptomatic pregnant women with or without a short cervix on transvaginal ultrasound. *Am J Obstet Gynecol* 191(4):1253–1256, 2004.
91. Lewis D, Pelham J, Sawhney H, et al: Most asymptomatic pregnant women with a short cervix on ultrasound are having uterine contractions. *Am J Obstet Gynecol* 185:S144, 2001.
92. O'Brien JM, Defranco EA, Adair CD, et al: Effect of progesterone on cervical shortening in women at risk for preterm birth: secondary analysis from a multinational, randomized, double-blind, placebo-controlled trial. *Ultrasound Obstet Gynecol* 34(6):653–659, 2009.
93. Mella MT, Mackeen AD, Gache D, et al: The utility of screening for historical risk factors for preterm birth in women with known second trimester cervical length. *J Matern Fetal Neonatal Med* 26(7):710–715, 2013.
94. Orzechowski KM, Nicholas SS, Baxter JK, et al: Implementation of a universal cervical length screening program for the prevention of preterm birth. *Am J Perinatol* 31(12):1057–1062, 2014.
95. Orzechowski KM, Boelig R, Nicholas SS, et al: Is universal cervical length screening indicated in women with prior term birth? *Am J Obstet Gynecol* 212(2):234.e1–234.e5, 2015.
96. Grobman WA, Gilbert SA, Iams JD, et al; Eunice Kennedy Shriver National Institute of Child Health and Human Development (NICHD) Maternal-Fetal Medicine Units (MFMU) Network: Activity restriction among women with a short cervix. *Obstet Gynecol* 121(6):1181–1186, 2013.
97. Berghella V, Odibo AO, To MS, et al: Cerclage for short cervix on ultrasonography: meta-analysis of trials using individual patient-level data. *Obstet Gynecol* 106(1):181–189, 2005.
98. Meis PJ, Klebanoff M, Thom E, et al; National Institute of Child Health and Human Development Maternal-Fetal Medicine Units Network: Prevention of recurrent preterm delivery by 17 alpha-hydroxyprogesterone caproate. *N Engl J Med* 348(24):2379–2385, 2003.
99. Maher MA, Abdelaziz A, Ellaithy M, Bazeed MF: Prevention of preterm birth: a randomized trial of vaginal compared with intramuscular progesterone. *Acta Obstet Gynecol Scand* 92(2):215–222, 2013.
100. Lazar P, Gueguen S: Multicentred controlled trial of cervical cerclage in women at moderate risk of preterm delivery. *Br J Obstet Gynecol* 91:731, 1984.
101. Rush RW, McPherson K, Jones L, et al: A randomized controlled trial of cervical cerclage in women at high risk of spontaneous preterm delivery. *Br J Obstet Gynecol* 91:724, 1984.
102. MRC/RCOG Working Party on Cervical Cerclage: Final report of the Medical Research Council/Royal College of Obstetricians and Gynaecologists multicentre randomized trial of cervical cerclage. *Br J Obstet Gynecol* 100:516, 1993.
103. Dor J, Shalev J, Mashiach S, et al: Elective cervical suture of twin pregnancies diagnosed ultrasonically in the first trimester following induced ovulation. *Gynecol Obstet Invest* 13:55, 1982.
104. Shirodkar VN: A new method of operative treatment for habitual abortions in the second trimester of pregnancy. *Antiseptic* 52:299, 1955.
105. McDonald IA: Suture of the cervix for inevitable miscarriage. *J Obstet Gynecol* 64:346, 1957.
106. Rust OA, Atlas RO, Reed J, et al: Revisiting the short cervix detected by transvaginal ultrasound in the second trimester: Why cerclage therapy may not help. *Am J Obstet Gynecol* 185:1098, 2001.
107. Althuisius SM, Dekker GA, Hummel P, et al: Final results of the cervical incompetence prevention randomized cerclage trial (CIPRACT): therapeutic cerclage with bed rest versus bed rest alone. *Am J Obstet Gynecol* 185:1106, 2001.
108. Berghella V, Rust O, Althuisius S, et al: Short cervix on ultrasound: do antibiotics prevent preterm birth? *Am J Obstet Gynecol* 193:S48, 2005.
109. Berghella V, Mackeen AD: Cervical length screening with ultrasound-indicated cerclage compared with history-indicated cerclage for prevention of preterm birth: a meta-analysis. *Obstet Gynecol* 118(1):148–155, 2011.
110. Berghella V, Obido AO, To MS, et al: Cerclage for short cervix on ultrasound: meta-analysis of trials using individual patient-level data. *Obstet Gynecol* 106:181, 2005.

111. Berghella V, Baxter J, Pereira L: Cerclage: should we be doing them? *Contrib Obstet Gynecol* 12:34, 2005.
112. Berghella V, Rafael TJ, Szychowski JM, et al: Cerclage for short cervix on ultrasonography in women with singleton gestations and previous preterm birth: a meta-analysis. *Obstet Gynecol* 117(3):663–671, 2011.
113. Berghella V, Rust O, Althuisius S: Short cervix on ultrasound: does indomethacin prevent preterm birth? *Am J Obstet Gynecol* 195(3):809–813, 2006.
114. Gighangi PB, Ndinya-Achola JO, Ombete J, et al: Antimicrobial prophylaxis in pregnancy: a randomized, placebo-controlled trial with cefetamet-pivoxil in pregnant women with poor obstetrical history. *Am J Obstet Gynecol* 177:680, 1997.
115. Andrews WW, Sibai BM, Thom EA, et al: Randomized clinical trial of metronidazole plus erythromycin to prevent spontaneous preterm delivery in fetal-fibronectin-positive women. *Obstet Gynecol* 101:847, 2003.
116. King J, Flenady V: Prophylactic antibiotics for inhibiting preterm labour with intact membranes. *Cochrane Database Syst Rev* 4:CD000246, 2002.
117. Roman AS, Rebarber A, Pereira L, et al: Efficacy of ultrasound indicated cerclage in multiple gestations. *J Ultrasound Med* 24:763, 2005.
118. Liem S, Schuit E, Hegeman M, et al: Cervical pessaries for prevention of preterm birth in women with a multiple pregnancy (ProTWIN): a multicentre, open-label randomised controlled trial. *Lancet* 382(9901):1341–1349, 2013.
119. Schuit E, Stock S, Rode L, et al; Global Obstetrics Network (GONet) collaboration: Effectiveness of progestogens to improve perinatal outcome in twin pregnancies: an individual participant data meta-analysis. *Br J Obstet Gynaecol* 122(1):27–37, 2015.
120. Romero R, Nicolaides K, Conde-Agudelo A, et al: Vaginal progesterone in women with an asymptomatic sonographic short cervix in the midtrimester decreases preterm delivery and neonatal morbidity: a systematic review and metaanalysis of individual patient data. *Am J Obstet Gynecol* 206(2):124.e1–124.e19, 2012.
121. Berghella V, Ness A, Bega G, et al: Cervical sonography in women with symptoms of preterm labor. *Obstet Gynecol Clin North Am* 32:383, 2005.
122. Ness A, Visintine J, Ricci E, Berghella V: Does knowledge of cervical length and fetal fibronectin affect management of women with threatened preterm labor? A randomized trial. *Am J Obstet Gynecol* 197(4):426.e1–426.e7, 2007.
123. Rozenberg P, Rudant J, Chevret S, et al: Repeat measurement of cervical length after successful tocolysis. *Obstet Gynecol* 104:995, 2004.
124. Rizzo G, Capponi A, Angeline E, et al: The value of transvaginal ultrasonographic examination of the uterine cervix in predicting preterm delivery in patients with preterm premature rupture of membranes. *Ultrasound Obstet Gynecol* 11:23, 1998.
125. Gire C, Faggianelli P, Nicaise C, et al: Ultrasonographic evaluation of cervical length in pregnancies complicated by preterm premature rupture of membranes. *Ultrasound Obstet Gynecol* 19:565, 2002.
126. Rozenberg P, Goffinet F, Hessabi M, et al: Comparison of the Bishop score, ultrasonographically measured cervical length, and fetal fibronectin assay in predicting time until delivery and type of delivery at term. *Am J Obstet Gynecol* 182:108, 2000.
127. Ramanathan G, Yu C, Osei E, et al: Ultrasound examination at 37 weeks' gestation in the prediction of pregnancy outcome: the value of cervical assessment. *Ultrasound Obstet Gynecol* 22:598, 2003.
128. Vankayalapati P, Sethna F, Roberts N, et al: Ultrasound assessment of cervical length in prolonged pregnancy: prediction of spontaneous onset of labor and successful vaginal delivery. *Ultrasound Obstet Gynecol* 31(3):328–331, 2008.
129. Ware V, Raynor BD: Transvaginal ultrasonographic cervical measurement as a predictor of successful labor induction. *Am J Obstet Gynecol* 182:1030, 2000.
130. Pandis GK, Papageorghiou AT, Ramanathan VG, et al: Preinduction sonographic measurement of cervical length in the prediction of successful induction of labor. *Ultrasound Obstet Gynecol* 18:623, 2001.
131. Gabriel R, Darnaud T, Chalot F, et al: Transvaginal sonography of the uterine cervix prior to labor induction. *Ultrasound Obstet Gynecol* 19:254, 2002.
132. Boozarjomehri F, Timor-Tritsch E, Chao CR, et al: Transvaginal ultrasonographic evaluation of the cervix before labor: presence of cervical wedging is associated with shorter duration of induced labor. *Am J Obstet Gynecol* 171:1081, 1994.
133. Chandra S, Crane JM, Hutchens D, et al: Transvaginal ultrasound and digital examination in predicting successful labor induction. *Obstet Gynecol* 98:2, 2001.
134. Watson WJ, Stevens D, Wleter S, et al: Factors predicting successful labor induction. *Obstet Gynecol* 88:990, 1996.
135. Bartha JL, Romero-Carmona R, Martinez-Del-Fresno P, et al: Bishop score and transvaginal ultrasound for preinduction cervical assessment: a randomized clinical trial. *Ultrasound Obstet Gynecol* 25:155, 2005.
136. Saccone G, Rust O, Althuisius S, et al: Cerclage for short cervix in twin pregnancies: systematic review and meta-analysis of randomized trials using individual patient-level data. *Acta Obstet Gynecol Scand* 94(4):352–358, 2015.



# Ultrasound Evaluation of the Placenta, Membranes, and Umbilical Cord

Jodi S. Dashe, Barbara L. Hoffman

## SUMMARY OF KEY POINTS

- Assessment of the relationship between the placenta and the internal cervical os is an essential component of sonography in the second and third trimesters.
- Placenta previa is identified in 1% to 5% of second-trimester sonograms but is present at birth in only 3/1000 births.
- Transvaginal sonography is considered safe regardless of placental location, even in the presence of bleeding.
- Conditions associated with vasa previa include resolved placenta previa or low-lying placenta, velamentous cord insertion, and succenturiate or bilobate placenta.
- Sonographic criteria for detection of placenta accreta include placental lacunae, thinning of the retroplacental myometrium, and irregularity or disruption of the bladder-serosal interface, with bridging vessels between the placenta and the bladder-serosal interface on color Doppler imaging.
- A placental hematoma initially appears isoechoic to the placenta, becoming hypoechoic within 1 week and sonolucent in approximately 2 weeks.
- Targeted sonography is indicated if there are abnormalities of the umbilical cord or its vessels, including umbilical cord cyst, single umbilical artery, or persistent right umbilical vein, to evaluate for the presence of associated fetal anomalies.

## OUTLINE

### Placental Development, 674

Normal Placenta, 676

### Abnormalities of Placental Size and Shape, 677

Abnormal Placental Shape, 677

Abnormal Placental Thickness, 677

### Abnormalities of Placental Location, 678

Placenta Previa, 679

Low-Lying Placenta, 680

### Placental Cord Insertion Abnormalities, 681

Velamentous Cord Insertion, 681

Vasa Previa, 682

### Morbidly Adherent Placenta—Placenta Accreta, 683

Epidemiology and Risk Factors, 684

Sonographic Findings: Second and Third Trimesters, 684

Magnetic Resonance Imaging for Placenta Accreta, 684

First Trimester Placenta Accreta and Cesarean Scar

Pregnancy, 686

### Vascular Abnormalities of the Placenta, 687

Placental Sonolucencies, 687

Placental Calcification, 688

Placental Hematomas, 688

Placental Abruption, 689

### Chorioangioma, 689

### Placental Membrane Abnormalities, 691

Extrachorial Placentation, 691

Uterine Synechia(e), 692

Amniotic Band Sequence, 692

### Umbilical Cord, 693

Normal Development, 693

Remnants and Cysts, 694

Dimensions and Coiling, 695

Vascular Abnormalities of the Umbilical Cord, 695

### Summary, 699

## PLACENTAL DEVELOPMENT

In early human development, the blastocyst typically implants in the upper uterine corpus and contains two cell types. The outer *trophoblast* layer will form the placenta. The inner cell mass or *embryoblast* gives rise to the embryo, amnion, and umbilical cord (Fig. 19-1). Following implantation, trophoblast cells at the embryoblast pole proliferate and become a double layer, each with its own function. The outer

*syncytiotrophoblast* is a multinucleate syncytium that lacks distinct cells. It produces multiple hormones and is responsible for maternal-fetal gas, nutrient, and waste exchange. In contrast, the inner *cytotrophoblasts* have distinct cell membranes, are mitotically active, and serve as stem cells for the syncytiotrophoblast. During its life cycle, a cytotrophoblast first divides and proliferates. Then later, its cell walls disintegrate, and its contents merge into the expanding syncytiotrophoblast. At day 7 after conception, the syncytiotrophoblast at the embryoblast

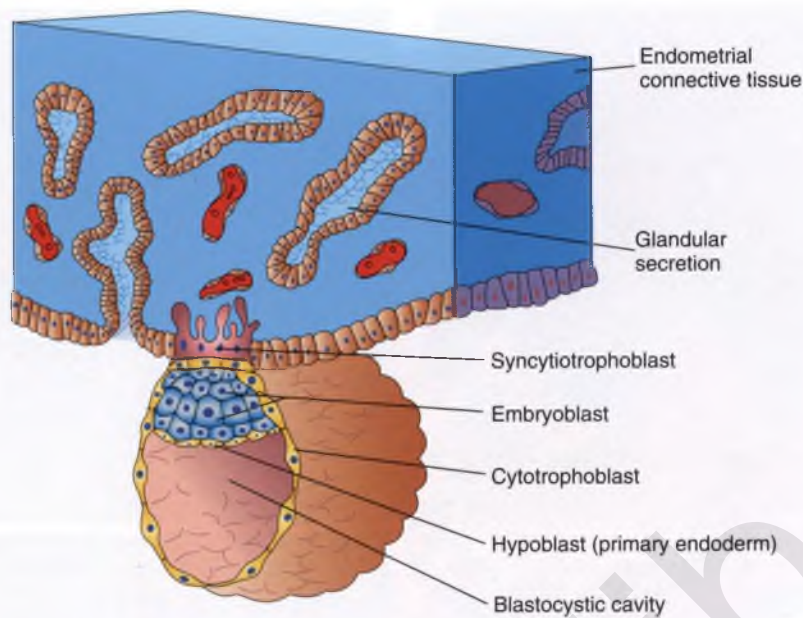


**FIG 19-1** Following blastocyst attachment, the syncytiotrophoblast invades the endometrium, which is hormonally prepared for implantation. (From Moore KL, Persaud TVN, Torchia MG: The first week of human development. In Moore KL, Persaud TVN, Torchia MG [eds]: The Developing Human: Clinically Oriented Embryology, 9th ed. Philadelphia, WB Saunders, 2013, p 37, Fig. 2-19B.)

pole invades the decidua, which is endometrium that has been primed for pregnancy. Following initial invasion, the syncytiotrophoblast grows and spreads to surround the entire conceptus. During invasion, decidual blood vessels and glands are entered, and released blood fills lacunae or lakes within the syncytium (Fig. 19-2). These lacunae eventually form the intervillous spaces. The syncytium is then invaded by cytotrophoblasts, and by definition, *primary villi* are thereby formed. Penetration extends the full thickness of the syncytiotrophoblast, and cytotrophoblasts meet at the bottom to form a circumferential trophoblast shell. Here, the primary villi are anchored.

Following cytotrophoblast invasion, extraembryonic mesenchyme moves into the primary villi to form *secondary villi* (Fig. 19-3). Next, angiogenesis begins within secondary villi, which are then termed *tertiary villi*. During this same time, vasculature from the early umbilical cord fuses with vessels of the *chorionic plate*, that is, the fetal surface of the placenta (Fig. 19-4). The *basal plate* is the opposite side, where the deeper invading trophoblast and the maternal decidua, specifically the decidua basalis, meet.

During the 7th week after menstruation, tertiary villi increase in diameter and develop into immature *intermediate villi*, which are important growth centers for villous tree branching. New branches begin first as syncytial sprouts. They are invaded by cytotrophoblasts and then by mesenchyme. Last, vessels develop within the mesenchyme. With this repeated branching and sprouting, the villous tree begins to attain its final form. Finally, at the beginning of the third trimester, slender mature intermediate villi branch to form *terminal villi*. During terminal villi angiogenesis, capillary growth exceeds villous growth. As a result, capillaries begin to coil and bulge to the periphery of a given villus. This bulging thins the trophoblast layers and creates the small diffusion distance needed for maternal-fetal exchange.

Distinct from these *villous trophoblasts*, some cytotrophoblasts break through the trophoblast perimeter and continue to invade into maternal tissue as *extravillous cytotrophoblasts*. These cells are further classified as *interstitial trophoblasts* and *endovascular trophoblasts*. The

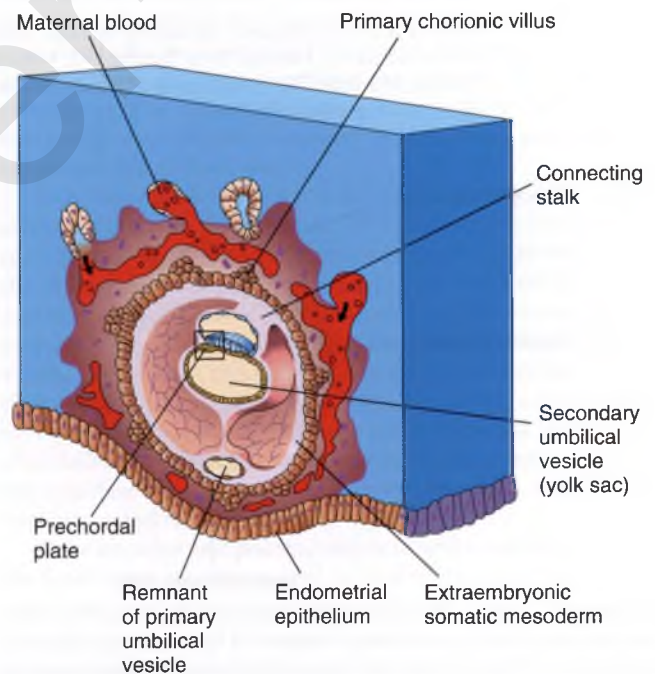


**FIG 19-2** Syncytiotrophoblasts surround the entire conceptus and invade decidual blood vessels and glands. (From Moore KL, Persaud TVN, Torchia MG: Second week of human development. In Moore KL, Persaud TVN, Torchia MG [eds]: The Developing Human: Clinically Oriented Embryology, 9th ed. Philadelphia, WB Saunders, 2013, p 45, Fig. 3-5B.)

endovascular trophoblasts penetrate and plug maternal spiral arteries, which supply the decidua and intervillous space. Later, these cytotrophoblasts reverse their action and work to increase intervillous blood flow. For this, they invade the vascular media layer and replace its smooth muscle with fibrinoid material. This remodeling converts



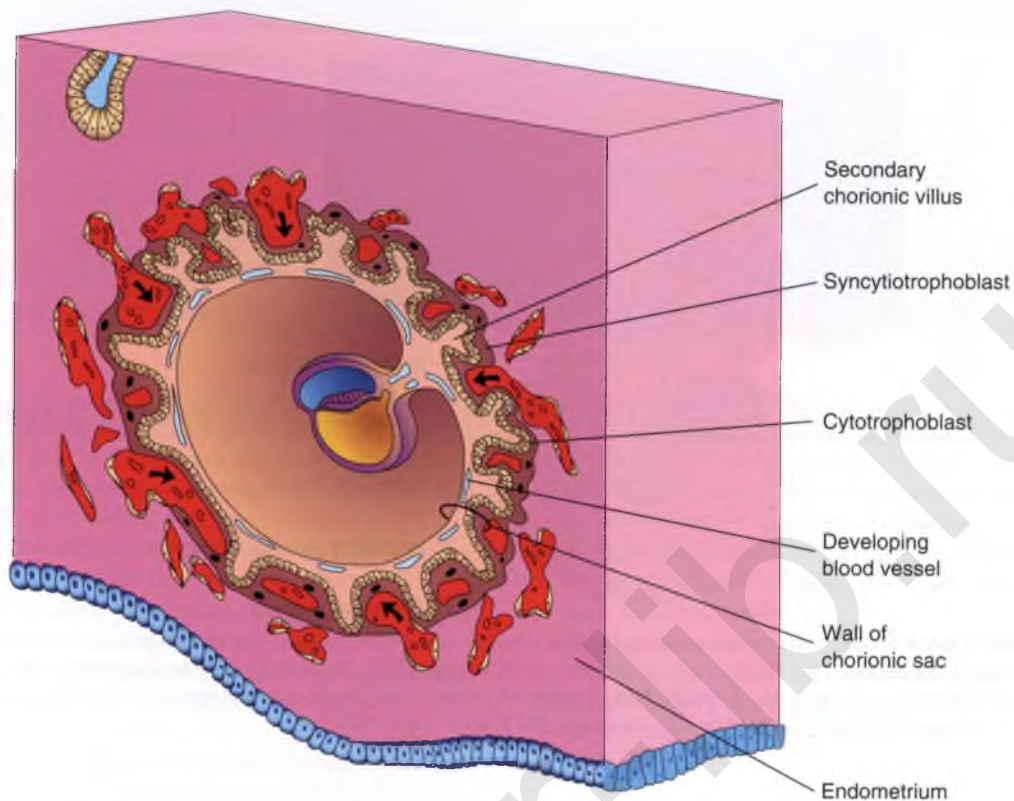


**FIG 19-3** Extraembryonic mesenchyme (*light orange*) moves into the primary villi to form secondary villi. (From Moore KL, Persaud TVN, Torchia MG: Third week of human development. In Moore KL, Persaud TVN, Torchia MG [eds]: *The Developing Human: Clinically Oriented Embryology*, 9th ed. Philadelphia, WB Saunders, 2013, p 68, Fig. 4-14A.)

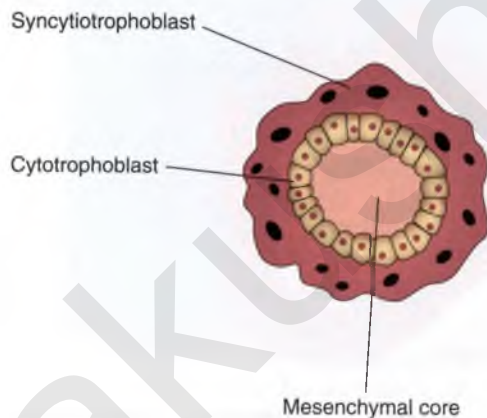


**FIG 19-4** Angiogenesis begins within secondary villi, which are then termed tertiary villi. Concurrently, vessels of the chorionic plate join vessels within these villi and also fuse with vessels from the connecting stalk, which is part of the early umbilical cord. At this stage, the amnion (*blue*) surrounds the embryo. (From Moore KL, Persaud TVN, Torchia MG: Third week of human development. In Moore KL, Persaud TVN, Torchia MG [eds]: *The Developing Human: Clinically Oriented Embryology*, 9th ed. Philadelphia, WB Saunders, 2013, p 68, Fig. 4-14B.)

narrow-lumen, muscular spiral arteries into dilated, low-resistance uteroplacental vessels. In contrast, the interstitial trophoblasts invade the decidua and surround spiral arteries. Their functions are less well understood and may include vessel preparation for endovascular trophoblast remodeling.

Within the mature maternal-fetal circulation, oxygen-carrying maternal erythrocytes first enter the intervillous space via spiral arteries. Here, maternal blood is forced into close contact with terminal villi. Oxygen diffuses through the syncytiotrophoblast and then through the widely spaced but contiguous cytotrophoblast layer into fetal erythrocytes within capillaries of each terminal villous branch. Capillaries coalesce into larger fetal vessels within the main villus. From here, oxygenated fetal blood ultimately drains into the single umbilical vein and back to the fetus.

### Normal Placenta

At term, the typical placenta weighs 470 g, is round to oval with a 22-cm diameter, and has a central thickness of 2.5 cm.<sup>1</sup> It is composed of a placental disk, extraplacental membranes, and a three-vessel umbilical cord. The maternal surface is the *basal plate*, which is divided by clefts into portions—termed *cotyledons*. These clefts mark the site where internal septa originating from the decidua basalis push up into the intervillous space. The fetal surface is the *chorionic plate*, into which the umbilical cord inserts, typically in the center. Large fetal vessels that originate from the cord vessels then spread and branch across the chorionic plate before entering stem villi of the placental parenchyma. When examining the placenta, either following delivery or during fetoscopic surgery—for example, during laser therapy for twin-twin transfusion syndrome—the fetal arteries almost invariably cross over fetal veins. The chorionic plate and its vessels are covered by amnion.

Sonographically, the placenta in the first and early second trimesters appears homogeneous in echotexture and mildly hyperechoic compared with the underlying myometrium. It then becomes more isoechoic with advancing gestation (Fig. 19-5). As examples, after

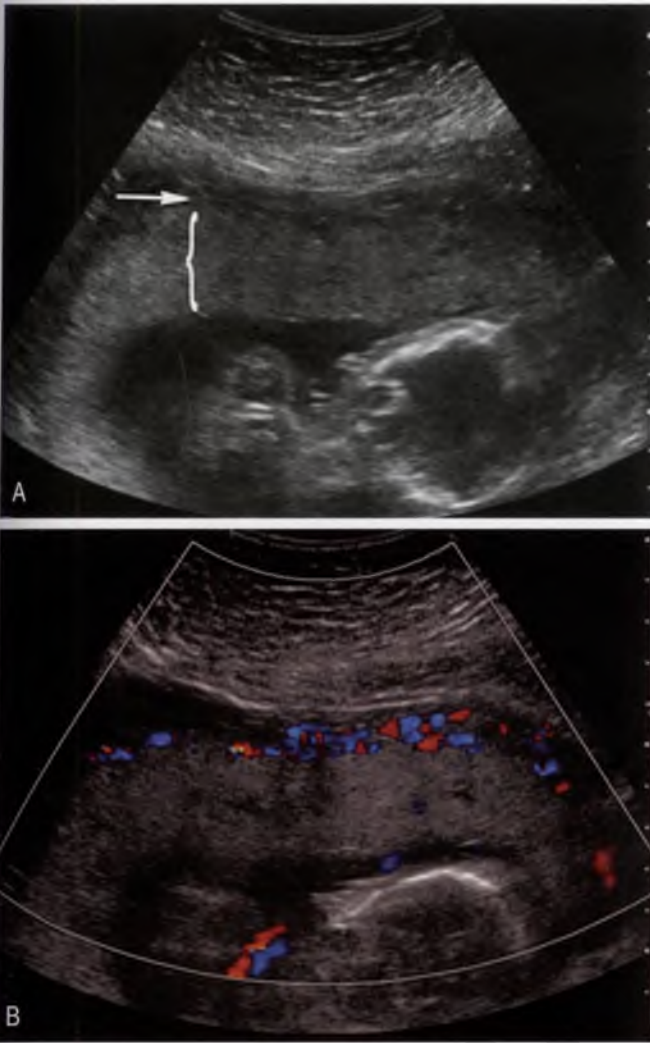


**FIG 19-5** Second-trimester placenta. **A**, The placenta is isoechoic with its adjacent myometrium, its thickness is marked by the bracket, and an arrow points to the retroplacental space. **B**, With color Doppler, vessels are seen spanning the retroplacental space. (Courtesy of Adriana Male, RDMS, Parkland Health and Hospital Systems, Dallas, Texas.)

midpregnancy, it is common to identify small placental sonolucencies, and in the third trimester, the placenta may appear more heterogeneous, with visible calcifications.

The sonographic thickness is usually greater than that of the gross specimen owing to collapse of intervillous spaces as blood drains from the placenta. As a general rule, the placental thickness in millimeters roughly approximates the gestational age in weeks.<sup>2-4</sup> It does not normally exceed 4 cm in the second trimester or 6 cm in the third trimester. The retroplacental “clear” space normally measures less than 1 to 2 cm and, as the name suggests, appears hypoechoic. The retroplacental space is a common location of hematoma development. Inability to visualize the retroplacental space in a woman at risk for placenta accreta raises concern.

## ABNORMALITIES OF PLACENTAL SHAPE AND THICKNESS

### Abnormal Placental Shape

In contrast to the normal architecture described previously, placentas may form as separate disks of nearly equal size. This bilobate or bilobed



**FIG 19-6** This succenturiate lobe has vessels that travel within intervening membranes and connect it to the main placental disk. (Courtesy of Dr. Jaya George, University of Texas Southwestern Medical Center, Dallas, Texas.)

placenta is also known as *placenta duplex*. The cord inserts *between* the two placental lobes, either into a connecting chorionic bridge or into intervening membranes. Sonographic detection of a bilobate placenta that has a chorionic bridge—normal placental tissue connecting the two lobes—is not likely, particularly if not specifically sought. However, if placental lobes are separated by intervening membranes and the cord inserts directly into these membranes, such that the cord insertion is *velamentous*, then sonographic detection may help to avoid cord avulsion at delivery. A placenta containing three or more equal-sized lobes is rare and termed *multilobate*.

A *succenturiate lobe* is an accessory placental lobe that develops away from the main placental disk. The umbilical cord inserts into the main body of the placenta, and prominent vessels may be visible coursing along the intervening membranes (Figs. 19-6 and 19-7). If an accessory placental lobe is suspected, color Doppler sonography may be particularly helpful in identifying the location and path of these vessels. Occasionally, the vessels that connect the main body of the placenta to a succenturiate lobe overlie the cervix, a form of vasa previa. Clinically, an accessory lobe may be retained in the uterus after delivery and cause postpartum uterine atony and hemorrhage. Succenturiate lobe is encountered more frequently with *in vitro* fertilization and twin gestations.<sup>5,6</sup>

There are other rare placental shapes in which varying portions of the fetal membranes are covered by functioning villi. With *placenta membranacea*, all or nearly all of the membranes are covered with villi. This form of abnormal placentation may lead to serious hemorrhage, preterm delivery, and hysterectomy because of associated placenta previa or accreta.<sup>7,8</sup> With *ring-shaped placenta*, the placenta is annular, and a partial or complete ring of placental tissue is present. With *placenta fenestrata*, the central portion of a placenta disk is missing. These variants are not typically visible sonographically.

### Abnormal Placental Thickness

*Placentomegaly*, an abnormally thickened placenta, is diagnosed if the placental thickness exceeds 4 cm in the second trimester or 6 cm in the third trimester (Fig. 19-8). There are numerous causes of placentomegaly, including maternal diabetes, severe maternal anemia, severe fetal growth restriction, aneuploidy, and congenital infections.<sup>9-12</sup> The latter include syphilis, parvovirus infection, cytomegalovirus infection,



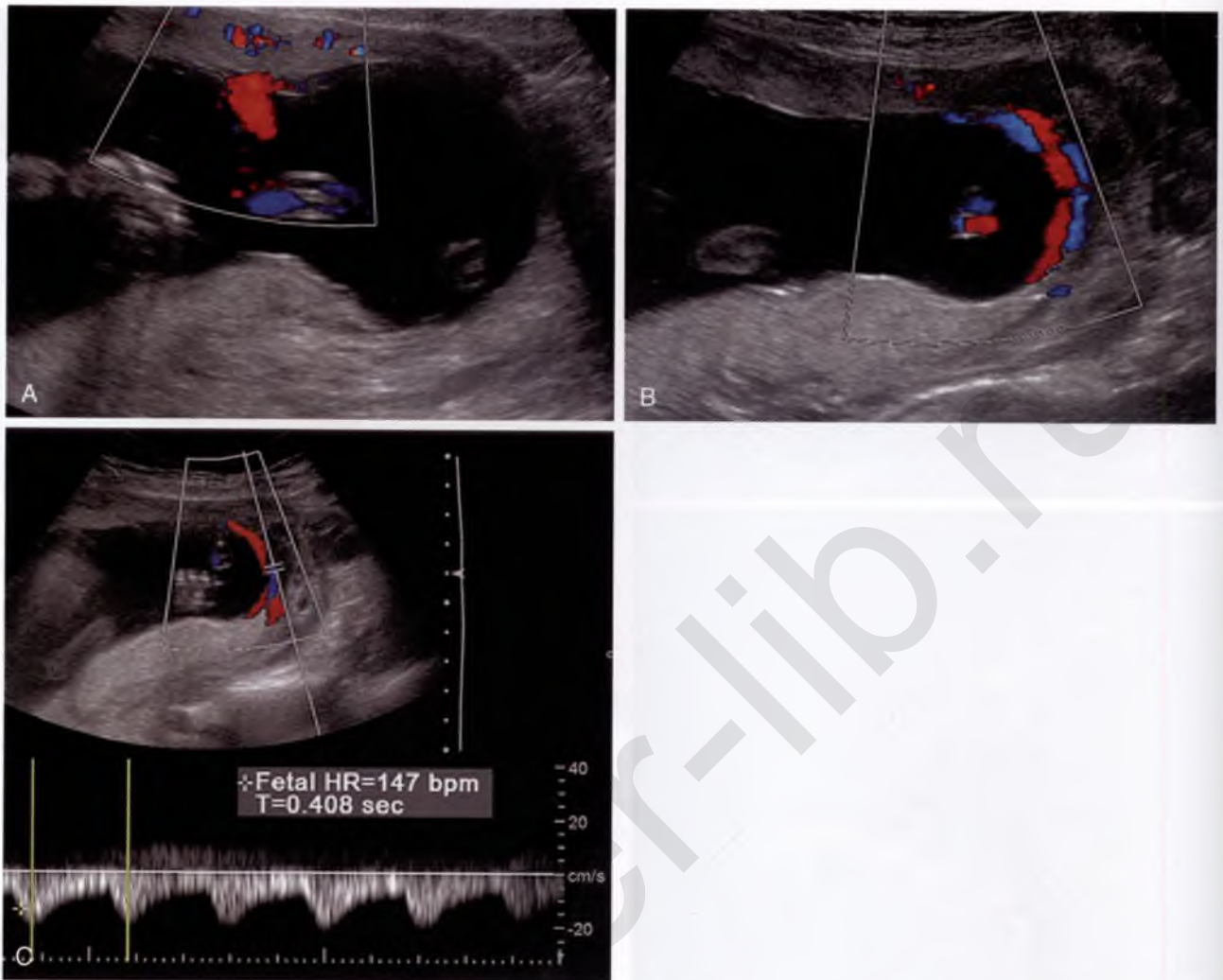


**FIG 19-7** Succenturiate lobe. **A**, In this 20-week gestation, the umbilical cord inserts at the main body of the placenta, which is implanted anteriorly. **B**, Color Doppler sonography shows vessels connecting the main portion of the placenta to a posterior succenturiate lobe. **C**, Spectral Doppler interrogation of the arterial vessels connecting the succenturiate lobe to the placenta demonstrates a normal fetal heart rate (HR), 147 beats per minute (bpm).

toxoplasmosis, herpesvirus infection (rarely), and if at risk, rubella or schistosomiasis. Placentomegaly is a component of hydrops fetalis, and any cause that can result in immune or nonimmune hydrops may present with placentomegaly as a component. In some cases, placentomegaly may result from collections of blood or fibrin within the placenta. Examples include massive perivillous fibrin deposition, intervillous or subchorionic thromboses, and large retroplacental hematomas, which are described later. Neoplasia is a rare cause. Benign vascular lesions include chorioangioma and chorangiomas, also described in subsequent sections.

Gestational trophoblastic disease creates a thick cystic-appearing placenta. Cystic vesicles are also seen with placental mesenchymal dysplasia. Vesicles in this rare condition correspond to dilated stem villi that result from stromal expansion.

A placenta is not generally considered too thin, although focal attenuation may occur if a hematoma develops and subsequently resolves. A pregnancy with severe polyhydramnios may appear to have a thin placenta as a function of compression by fluid. A small placenta associated with a growth-restricted fetus may also appear thinner.

## ABNORMALITIES OF PLACENTAL LOCATION

The placental location may reliably be assessed by 16 weeks' gestation. The location, whether anterior, posterior, left- or right-lateral, or a combination of these, should be noted in the sonogram report. A survey of the uterus for accessory placental tissue—a succenturiate lobe—and an assessment of the placental cord insertion site, if visible, should also be performed and documented. An evaluation of the relationship between the placenta and the internal cervical os is a component of the standard obstetric sonogram that is performed at approximately 18 to 20 weeks.<sup>13</sup>

Transabdominal sonography is typically used to screen for abnormalities of placental location, and if the placenta is either clearly over the cervix or away from the lower uterine segment, its sensitivity and negative predictive value are excellent (Fig. 19-9).<sup>14,15</sup> However, if the lower uterine segment cannot be clearly visualized, transvaginal sonography is the most accurate method—the “gold standard”—for assessing the relationship between the inferior placental edge and the internal cervical os (see Fig. 19-9).<sup>16-18</sup> Transvaginal sonography is

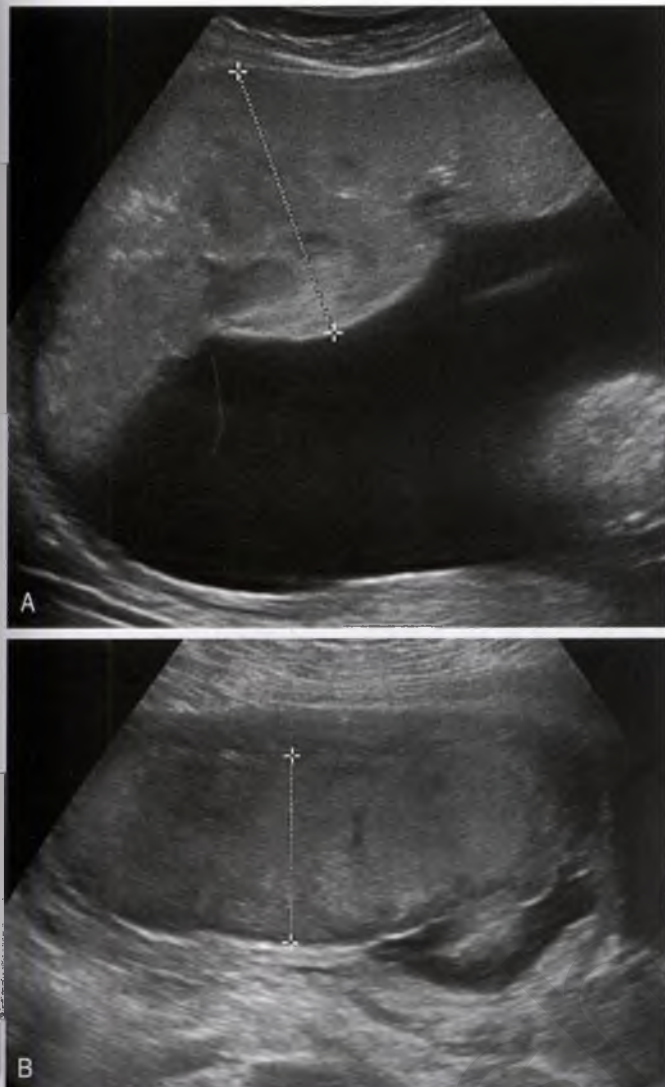


**FIG 19-8** Placentomegaly. **A**, This anterior placenta measured 7.1 cm in thickness at 28 weeks' gestation. The fetus was hydropic in the setting of trisomy 21. **B**, The placental thickness measures 4.6 cm at 20 weeks' gestation. Oligohydramnios was also present, and the maternal serum alpha-fetoprotein level exceeded 18 multiples of the median. Pathologic examination following delivery confirmed a large intervillous thrombus.

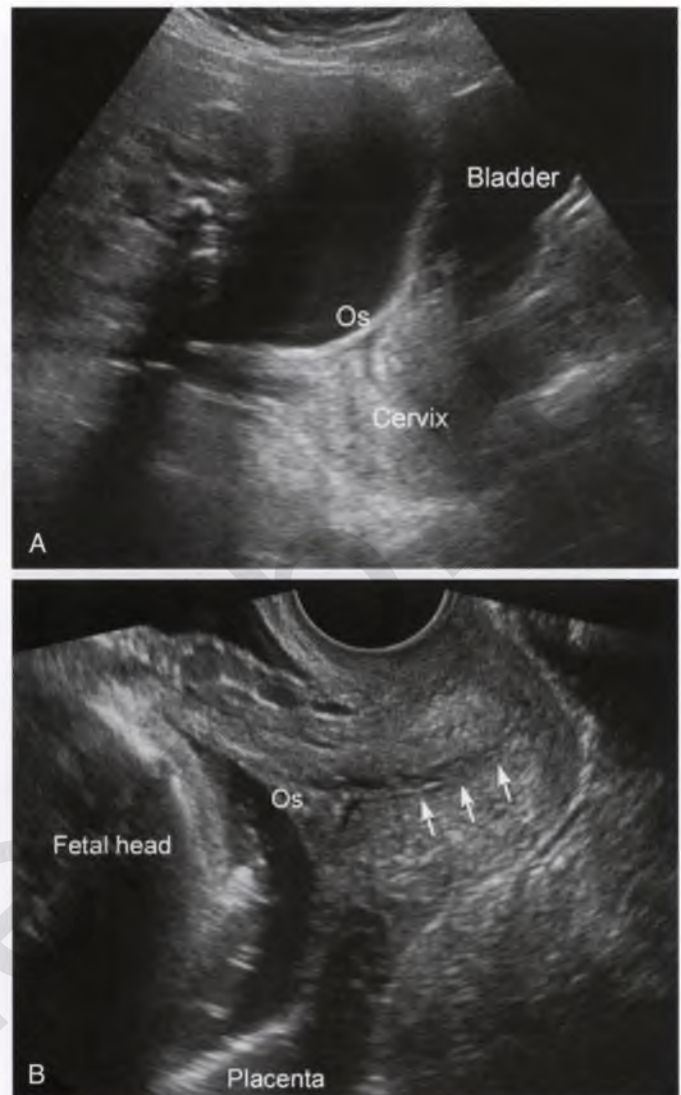


**FIG 19-9** Normal lower uterine segment. **A**, Transabdominal image at 35 weeks demonstrating no evidence of placenta previa or low-lying placenta. **B**, Transvaginal image at 36 weeks, similarly demonstrating no evidence of placenta previa or low-lying placenta. The posterior placental edge is well away from the closed internal cervical os. Arrows depict the endocervical canal.

considered safe regardless of placental location, even in the presence of bleeding.<sup>19</sup> Translabial sonography is less commonly used, but it may be of benefit if transabdominal images are suboptimal and transvaginal sonography is not available or is contraindicated. Abnormalities of placental location include placenta previa and low-lying placenta.

### Placenta Previa

Derived from the Latin *prævia*, for *going before*, placenta previa indicates that the placenta is the presenting part rather than the fetus. Sonographic identification of placenta previa is essential because affected pregnancies are at risk for vaginal bleeding, which is often initially painless—a *herald bleed*—but requires urgent evaluation as hemorrhage may ensue. Women with prior cesarean delivery and placenta previa are at risk for placental invasion, and the risk increases with the number of prior cesarean deliveries.

### Prevalence

Placenta previa complicates approximately 3/1000 singleton births in population-based series.<sup>20-23</sup> Risk factors include older maternal age, multiparity, multifetal gestation, cigarette smoking, and especially prior cesarean delivery.<sup>20,24-26</sup> Previa is present at delivery in fewer than 1/1500 women younger than age 20 but in more than 1% of those older than age 35.<sup>27</sup> It is largely a complication of multiparous women, as only 20% of cases occur in first pregnancies.<sup>24</sup> It is also more common in twins and is found in approximately 4/1000 twin births.<sup>20</sup> Placenta previa is particularly prevalent among dichorionic pregnancies and attributed to two implantation events covering a larger area.<sup>26</sup>

### Terminology

As sonography has replaced physical examination of the cervix in cases of suspected previa, terminology has changed. Largely based on



findings from the clinical “double set-up” examination in preparation for delivery of suspected placenta previa, three general categories were formerly used:

- *Complete placenta previa* referred to a placenta that completely covered the cervix, or more specifically, the internal cervical os.
- *Partial placenta previa* indicated that the placenta partially covered the cervical os. Clinically, this could occur and be detected only when cervical dilatation was present, because one had to visualize the placental edge crossing over the dilated cervix.
- *Marginal placenta previa* indicated that the placental edge just reached the margin of the internal cervical os, generally noted via gentle palpation during double set-up examination.

Sonographically, it is not usually possible to differentiate between the categories of partial and marginal placenta previa, because if the cervix is closed the internal cervical os appears as a “point” (Fig. 19-10). All women in whom the placenta covers the cervix or reaches the cervical os will require cesarean delivery, such that a distinction between

complete, partial, and marginal previa as defined earlier does not change pregnancy management.

Recently, the classification of placenta previa was revised by a workshop that included the National Institute of Child Health and Human Development (NICHD), Society for Maternal-Fetal Medicine, American Institute of Ultrasound in Medicine, American College of Obstetricians and Gynecologists, American College of Radiology, Society for Pediatric Radiology, and Society of Radiologists in Ultrasound.<sup>28,29</sup> Using the new classification, the diagnosis of *placenta previa* is made when the placenta covers or just reaches the internal cervical os, eliminating the terms complete, partial, and marginal. If the inferior placental edge *encroaches* upon the cervix, such that it is within 2 cm of the internal os but does not overlie it, the diagnosis is *low-lying placenta*. If the inferior placental edge is 2 cm or more from the internal cervical os, the placental location is considered normal.

### Placental “Migration”

Most women diagnosed with placenta previa or low-lying placenta in the second trimester will have normal placental location by the end of pregnancy. This apparent “migration” of the placenta away from the lower uterine segment with advancing gestational age has been well described but is not completely understood. Enlargement of the uterus may result in differential growth of the placenta toward the well-vascularized fundus, a phenomenon known as *trophotropism*. Visualization of the lower uterine segment also may become clearer later in gestation, and placental tissue that previously appeared to have implanted over the cervix, particularly with transabdominal sonography alone, may have been merely adjacent to the region of the cervix and may seem, on follow-up, to have moved several centimeters away.

With transabdominal sonography, approximately 5% of pregnancies are thought to have placenta previa in the second trimester.<sup>30</sup> However, when imaged transvaginally, only 1% to 2% are diagnosed with placenta previa in the second trimester.<sup>31-33</sup> Overall, about 90% of previas diagnosed prior to 20 weeks’ gestation resolve before delivery.<sup>24</sup> The later in gestation that previa is identified, the higher the likelihood that it will persist until delivery. Specifically, placenta previa identified at about 24 weeks’ gestation persists in approximately half of cases, whereas previa identified at 32 weeks persists in nearly 75%.<sup>24</sup> The degree to which the placenta overlaps the cervical os increases the likelihood that placenta previa will persist, as does a history of one or more prior cesarean deliveries.

### Management

Persistent placenta previa will require cesarean delivery. Because of the frequent resolution of previa with advancing gestational age, sonography is indicated if a woman with suspected previa develops bleeding. In the absence of bleeding, follow-up sonography is recommended at approximately 32 weeks’ gestation.<sup>29</sup> If there is any question about placental location, transvaginal sonography should be performed. And, because resolved placenta previa is associated with vasa previa, color and spectral duplex Doppler sonographic scans are recommended to evaluate for possible abnormalities of the umbilical cord insertion. If placenta previa or low-lying placenta are found to persist at the 32-week sonogram, transvaginal sonography is recommended at 36 weeks’ gestation.<sup>29</sup>

### Low-Lying Placenta

Placentation is termed *low-lying* if the inferior placental edge *encroaches* upon the cervix, such that it does not overlie but is within 2 cm of the internal os (Fig. 19-11). The prevalence of low-lying placenta is approximately 3/1000 pregnancies at approximately 36 weeks’ gestation,

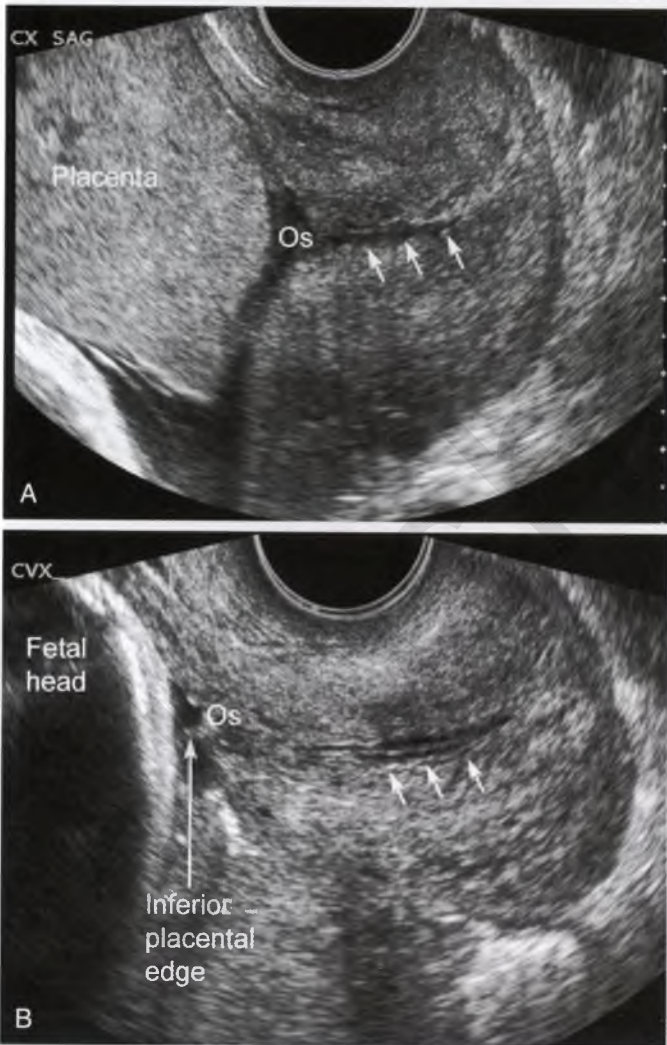


**FIG 19-10** Placenta previa. **A**, In this transvaginal image at 32 weeks’ gestation, the anterior placenta previa completely covers the internal cervical os. **B**, In this image from a different patient, also at 32 weeks’ gestation, the inferior edge of the posterior placenta just reaches the level of the internal cervical os. Whether the placenta partially covers the closed os or just reaches its margin is not a distinction that is technically feasible or clinically helpful. Short arrows depict the endocervical canal in both images.



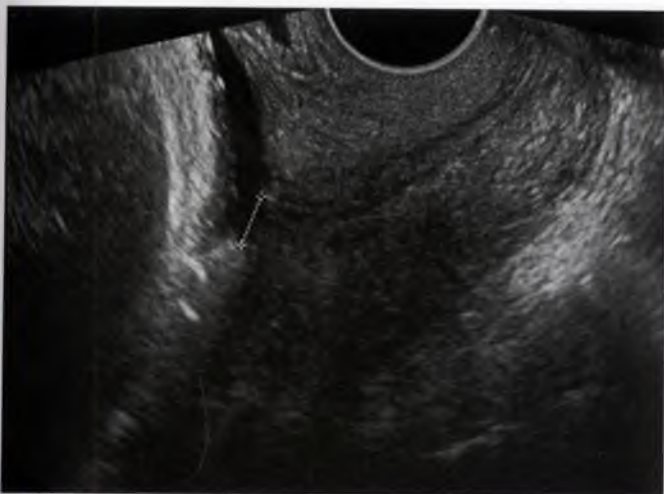


**FIG 19-11** Low-lying placenta. In this transvaginal image at 34 weeks' gestation, the measurement from the inferior edge of the posterior placenta to the internal os is approximately 8 mm.

thus similar to placenta previa.<sup>34</sup> As with placenta previa, a low-lying placenta identified in the early second trimester often resolves prior to delivery. In one series of 1240 pregnancies with low-lying placenta diagnosed between 16 and 24 weeks' gestation, 90% had resolved by 32 weeks and 98% had resolved by delivery.<sup>35</sup>

### Management

If low-lying placenta is identified in the second trimester, a follow-up sonogram is recommended at approximately 32 weeks' gestation. If the placenta is low-lying in the third trimester, transvaginal sonography is recommended: (1) to aid in accurate measurement of the distance from the inferior placental edge to the internal cervical os and (2) to exclude vasa previa. If the placenta is low-lying at 32 weeks' gestation, transvaginal sonography is recommended at 36 weeks.<sup>29</sup>

Unlike placenta previa, low-lying placenta is not a contraindication to vaginal delivery. However, the risks of vaginal bleeding and need for blood transfusion are increased. In studies of women with low-lying placenta who have labored, approximately one third required cesarean delivery specifically for bleeding.<sup>36-38</sup> In two series, vaginal delivery was more likely if the distance from the placental edge to the internal cervical os (as measured by sonography) was between 1 and 2 cm than if the placenta was within 1 cm of the os.<sup>34,38</sup> However, whenever the placenta has implanted in the lower uterine segment, even when greater than 2 cm from the internal cervical os, there is an increased risk of bleeding, and excessive bleeding may occur regardless of whether the patient is delivered vaginally or via cesarean.<sup>36,37</sup>

## PLACENTAL CORD INSERTION ABNORMALITIES

The umbilical cord usually inserts centrally into the placenta (Fig. 19-12). Not uncommonly, however, the cord inserts into the edge of the placenta—a *marginal insertion*, which is also known as a *Battledore placenta* (see Fig. 19-12B). The prevalence of marginal insertion of the umbilical cord is approximately 6% in singleton births and 10% to 15% in twin gestations.<sup>39,40</sup> Marginal cord insertion, usually defined as cord insertion less than 2 cm from the placental edge, may confer a small increase in the risk for adverse pregnancy outcomes. In a population-based series of more than 600,000 singletons, marginal insertion was associated with placental abruption (odds ratio 1.5), placenta previa (odds ratio 1.8), and small-for-gestational age (SGA) neonate (odds ratio 1.2), but not perinatal deaths.<sup>40</sup> Marginal cord

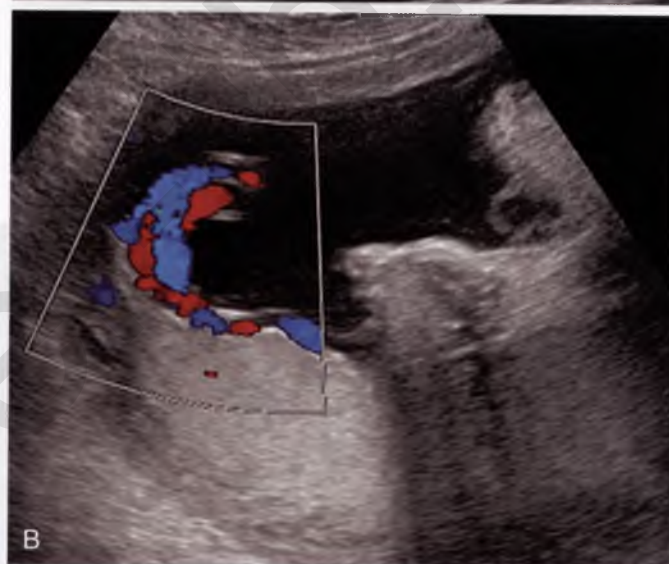
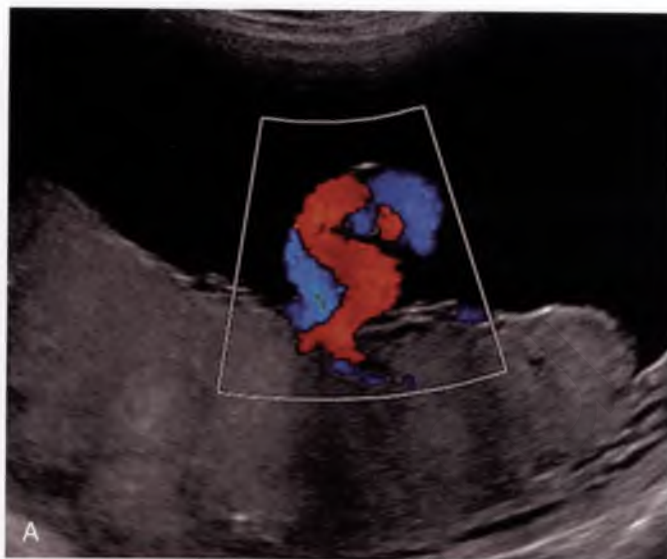


**FIG 19-12** Placental cord insertion. **A**, Central (normal) placental cord insertion. **B**, Marginal cord insertion, also known as *Battledore placenta*.

insertion appears to be particularly common in monozygotic twins, and it has been associated with an increased risk for an SGA newborn in monozygotic but not dizygotic twin pregnancies.<sup>39</sup>

### Velamentous Cord Insertion

With this abnormality, the umbilical cord does not insert directly into the placenta but rather into the membranes usually a short distance away from the placental edge (Fig. 19-13). Sonographically, the umbilical arteries and vein may be visible traversing the membranes along the wall of the uterus, unprotected by Wharton jelly, before inserting at the margin of the placenta (Fig. 19-14). Color Doppler sonography assists with visualization. Theories regarding the development of velamentous cord insertion include trophotropism, described earlier, or an error in initial blastocyst attachment that orients the fetus a distance away from the decidua basalis rather than directly opposite it.<sup>41</sup>

In population-based series, velamentous insertion occurs in approximately 0.5% to 1.5% of singleton births and 6% of twins.<sup>40,42</sup> It is more prevalent in monozygotic twins, particularly in the smaller twin of a monozygotic pair, and it is associated with birth weight discordance.<sup>39</sup> In a population-based review of more than 600,000



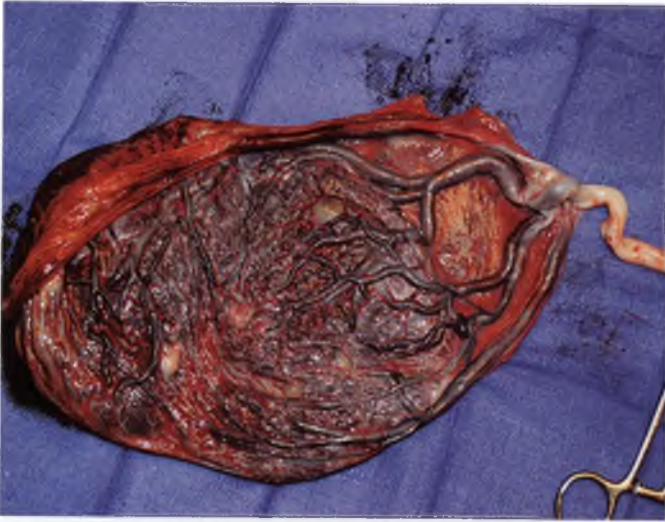


**FIG 19-13** Velamentous cord insertion. In this gross placental specimen, several large vessels are supported only by intervening membranes as they extend from the umbilical cord to the placental disk. (Courtesy of Dr. David Nelson, University of Texas Southwestern Medical Center, Dallas, Texas.)

singleton births, velamentous insertion was associated with an approximately twofold increased risk for placental abruption, SGA neonate, and perinatal death.<sup>40</sup> It has also been reported in 7% of fetal deaths prior to 24 weeks' gestation.<sup>43</sup> The risk for placenta previa is increased, and this is the most common precursor of *vasa previa*, discussed next. Care should be taken at delivery to avoid avulsing the umbilical cord when delivering the placenta, as velamentous insertion is associated with a greater than 10-fold increase in need for manual placental extraction.<sup>42</sup>

### Vasa Previa

In approximately 1/2500 deliveries, fetal vessels course within the membranes that overlie the cervix, a potentially devastating complication termed *vasa previa* (Fig. 19-15).<sup>44-46</sup> *Vasa previa* can develop in two settings: either with a velamentous cord insertion—connecting the umbilical cord to the placenta, or with a succenturiate or bilobed placenta—connecting the two placental lobes.<sup>46</sup> In one review, each of these causes accounted for approximately 50% of prenatally diagnosed *vasa previa* cases.<sup>47</sup> Multiple gestations are a recognized risk factor, and twins comprise 12% to 25% of those with *vasa previa* in published series.<sup>44,48</sup> Pregnancies resulting from assisted reproductive technologies appear to be at particular risk.<sup>49</sup>

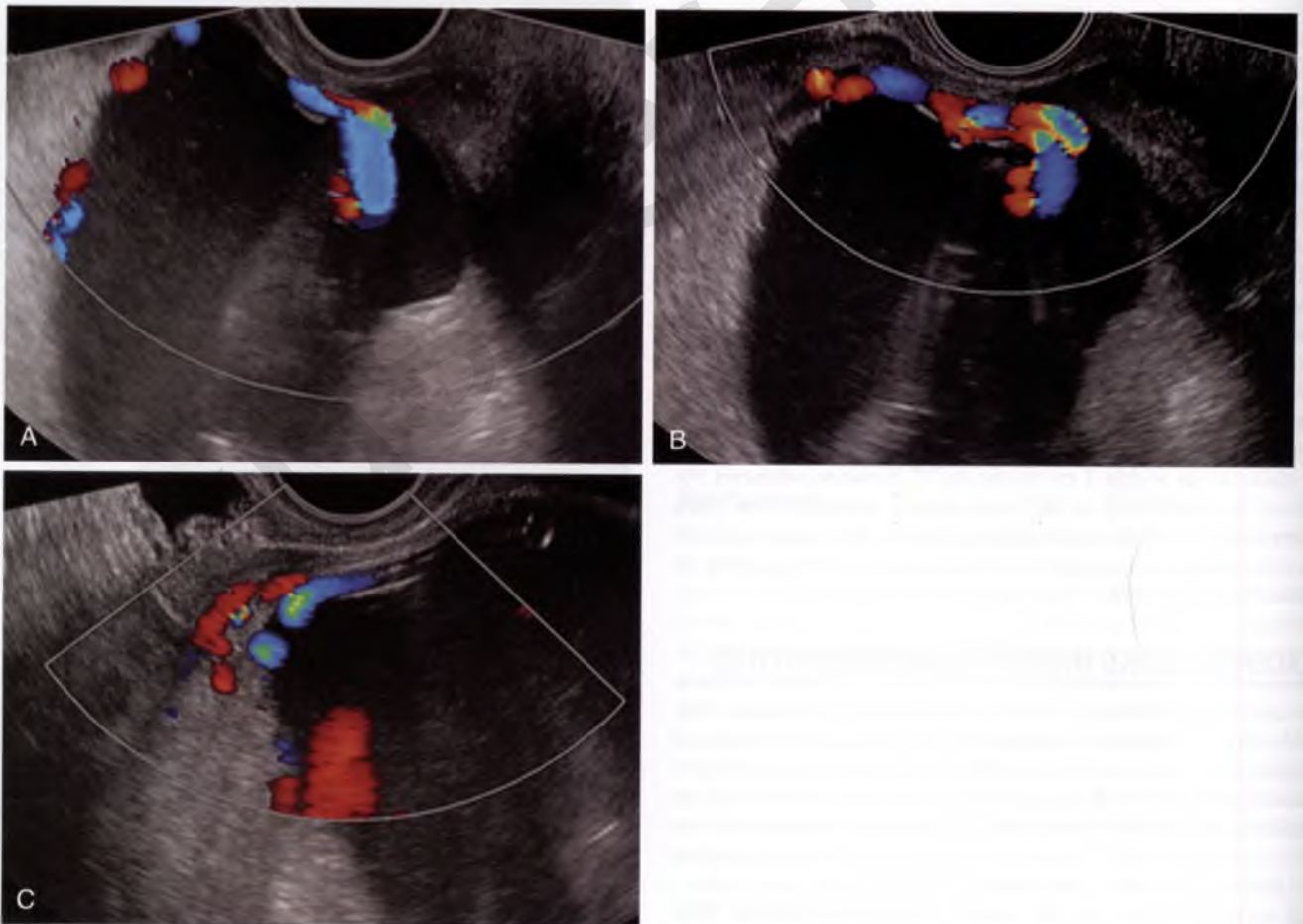


**FIG 19-14** Velamentous cord insertion. **A**, In this transvaginal color Doppler ultrasound image at 22 weeks' gestation, the umbilical cord is seen inserting into the membranes along the anterior wall of the lower uterine segment, a short distance away from the anterior placenta. **B**, The umbilical vessels run along the anterior uterine wall. **C**, The umbilical vessels insert into the inferior margin of the anterior placenta.



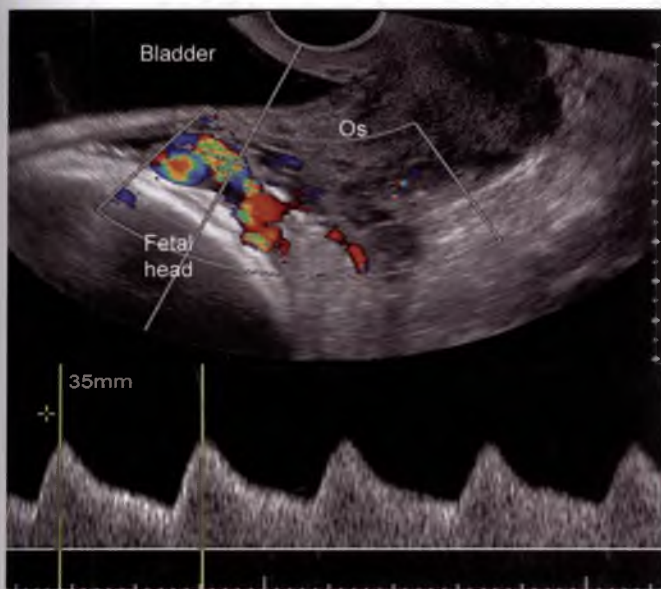


**FIG 19-15** Vasa previa. The placenta is posterior and low-lying, and the umbilical cord insertion is velamentous, directly into the membranes just anterior to the cervix, such that unprotected fetal vessels course directly over the internal os.

There are no standardized criteria for how close the fetal vessels must be to the internal cervical os to constitute vasa previa, and a threshold of “within 2 cm of the os” has been proposed.<sup>48</sup> In one series, all emergent deliveries with vasa previa had a fetal vessel within 2 cm of the internal cervical os.<sup>44</sup>

Vasa previa is potentially catastrophic if unrecognized, because the fetal vessels are prone to compression during labor and because the fetus can quickly exsanguinate when the membranes rupture. With prenatal detection, reported survival rate exceeds 95%.<sup>44,47,48</sup> In the absence of prenatal diagnosis, however, the perinatal mortality rate is as high as 50%.<sup>47</sup>

If the diagnosis is suggested sonographically in the second trimester, up to 25% of cases may resolve prior to delivery.<sup>48</sup> If vasa previa persists, scheduled cesarean delivery is recommended prior to the onset of labor.<sup>50</sup> Some have advocated that this occur prior to 36 weeks’ gestation.<sup>47,48</sup>

Vasa previa should be considered whenever one encounters a low-lying placenta or a resolved placenta previa, as well as in the setting of velamentous cord insertion, succenturiate lobe, or bilobate (bilobed) placenta. Careful sonographic assessment should include color and spectral duplex Doppler evaluation to identify fetal vessels overlying the cervix, which confirms the diagnosis (Fig. 19-16). Routine evaluation of the placental cord insertion site may help to avoid missing this rare but devastating entity. However, it is recognized that even with transvaginal imaging and color Doppler sonography, not all cases of vasa previa will be detected antepartum.<sup>50</sup>

### MORBIDLY ADHERENT PLACENTA— PLACENTA ACCRETA

Disorders of abnormal placental attachment or invasion include three entities, based on the degree to which chorionic villi invade myometrial tissue:

- *Placenta accreta*: implantation of placental villi directly onto myometrial tissue rather than the decidua basalis
- *Placental increta*: invasion of placental villi into the myometrium

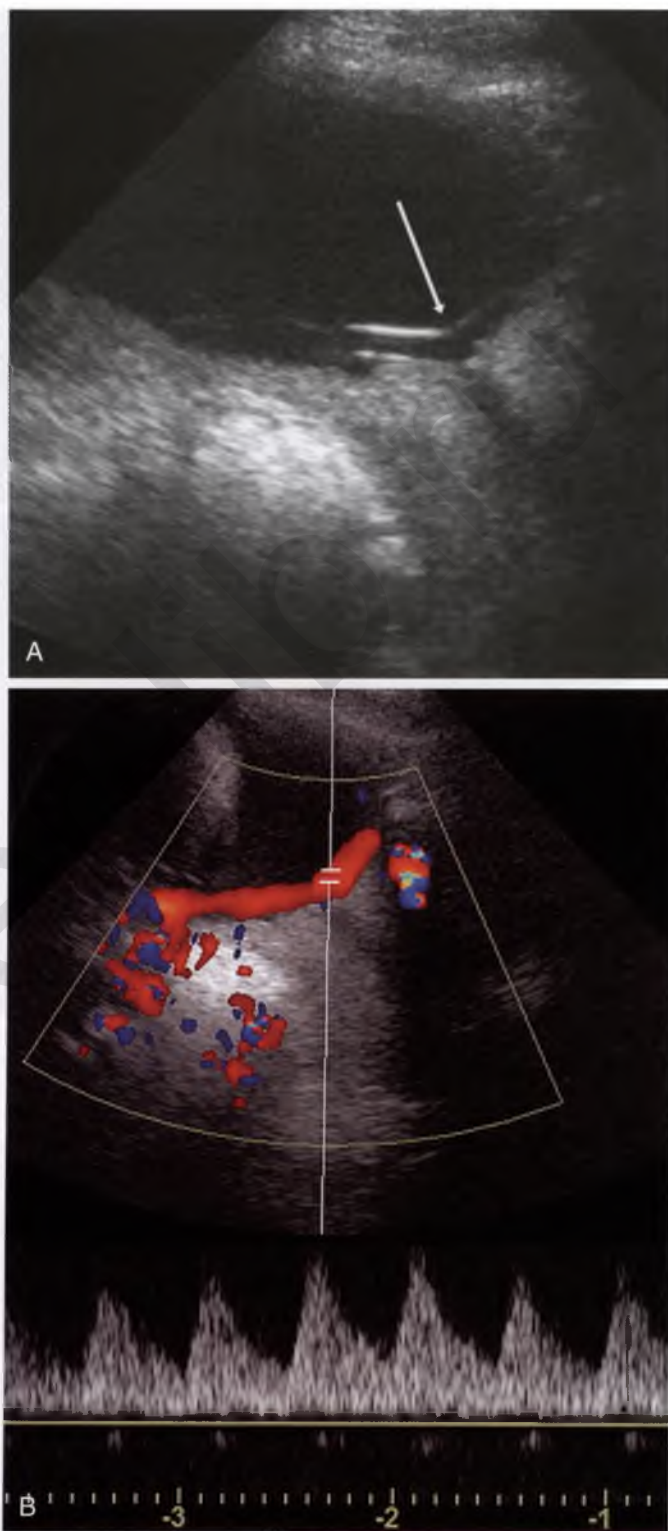


**FIG 19-16** Vasa previa. **A**, A tubular structure (*arrow*) is shown overlying the cervix on this transabdominal sagittal sonographic image. **B**, With color and spectral duplex Doppler interrogation, this structure is shown to be a fetal vessel, confirming vasa previa. In many instances, the unprotected fetal vessel crossing the cervix is not appreciated on gray-scale images and is only detected with careful Doppler evaluation.



- *Placenta percreta*: placental growth through the myometrium, extending to or through the uterine serosa

Clinically, of these three forms of abnormal attachments, placenta accreta is encountered in approximately 75% of cases, whereas increta develops in 15% to 20% and percreta in 5% to 10%.<sup>51</sup> However, *placenta accreta* is also the general term frequently applied to encompass all three of these conditions, a practical consideration in that the distinction is often not made until delivery.<sup>52</sup> Abnormal implantation of the placenta is believed to result from partial or total absence of the decidua basalis and imperfect development of the fibrinoid or Nita-buch layer—the normal physiologic line of cleavage.<sup>27</sup> Involvement of the entire placenta is termed *total accreta*, whereas if not all placental lobules are involved, the condition is called *partial* or *focal placenta accreta*.

At delivery, the placenta fails to separate normally, leading to significantly increased maternal morbidity. Severe hemorrhage may necessitate cesarean hysterectomy and often massive transfusion of blood products with need for intensive care (Fig. 19-17).<sup>52-54</sup> Thus, to minimize both maternal and neonatal morbidity and mortality rates, prenatal detection is important to permit timely coordination of multidisciplinary care and to arrange for maternal transfer to a center with adequate resources.<sup>52,54,55</sup>

### Epidemiology and Risk Factors

The prevalence of placental invasion has increased in recent years in parallel with the rise in cesarean delivery rates.<sup>56</sup> Series from the past decade suggest that the prevalence has increased to 1/500 to 1/900 pregnancies.<sup>57-59</sup>

An overwhelming majority of cases occur in the presence of two factors: placenta previa and prior cesarean delivery. The risk increases sharply with each subsequent cesarean delivery. In the setting of placenta previa, the risk for placental invasion is approximately 3% at the first cesarean delivery, 11% by the second, 40% by the third, and 60% to 70% for subsequent cesarean deliveries.<sup>53</sup> However, in the absence of previa, the risk for placenta accreta is only 0.03% at the initial cesarean and remains less than 1% up to the fifth cesarean.<sup>53</sup> Regardless of whether the placenta previa is anterior or posterior, placental invasion also may develop if the placenta overlies uterine scarring, resulting from prior uterine leiomyoma resection,<sup>60</sup> endometrial ablation,<sup>61-63</sup> or Asherman syndrome.<sup>64</sup>

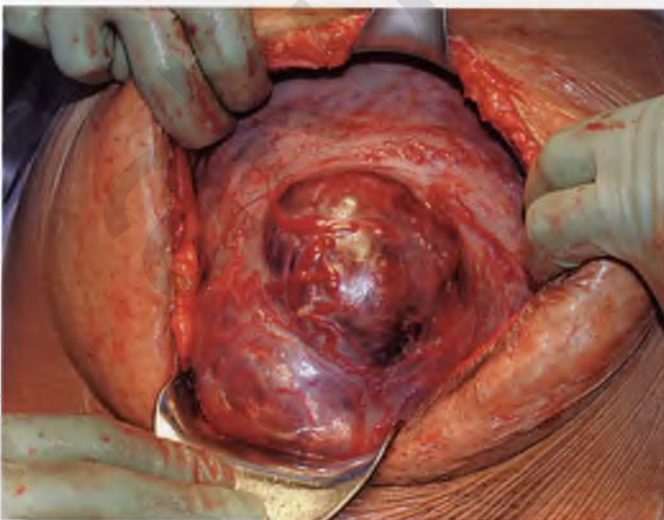


**FIG 19-17** Placenta percreta. At the time of cesarean delivery, the placenta is seen bulging through the attenuated lower uterine segment myometrium and is covered only by uterine serosa.

### Sonographic Findings: Second and Third Trimesters

Sonographic criteria for detection of morbidly adherent placenta or placental invasion include the following:

- Multiple placental *lacunae*. These irregularly shaped hypoechoic vascular spaces may give the placenta a “Swiss cheese” appearance. They contain turbulent flow shown with color Doppler imaging (Fig. 19-18).
- Thinning of the retroplacental myometrium, with the smallest myometrial thickness measuring less than 1 mm in the sagittal plane (Fig. 19-19).
- Irregularity or disruption of the echogenic interface between the maternal bladder and uterine serosa—the *bladder-serosal interface*—on gray-scale imaging.
- Increased vascularity of the bladder-serosal interface, with *bridging vessels* that course from the placenta to the region of the bladder-serosal interface (and sometimes farther into the bladder) shown with color Doppler imaging (Fig. 19-20).
- Loss of the normal linear hypoechoic area between the placenta and the wall of the uterus, called the *retroplacental clear space* (see Fig. 19-19).

Evaluation for suspected placenta accreta is not straightforward and can be quite challenging. In addition to transabdominal scanning, transvaginal sonography should be performed with the patient's bladder partially filled, using both gray-scale and color Doppler sonography.<sup>65</sup> The utility and accuracy of the sonographic findings associated with accreta vary in reported series according to which individual factors were noted, the total number of factors identified, and whether the analysis was prospective or retrospectively performed. In a woman with a prior cesarean delivery and placenta overlying the lower uterine segment, *any* individual sonographic finding heightens the index of suspicion and should prompt investigation for other features of invasion.

Several observations and investigations regarding the sonographic findings of accreta have been reported. Loss of the retroplacental clear space is a common cause of false positive reports and is therefore best used in conjunction with other findings.<sup>66-68</sup> As single factors, lacunae and interruption of the bladder-serosal interface, particularly when color Doppler sonography confirms hypervascularity, appear to have higher positive-predictive values for invasion than other characteristics.<sup>69</sup> Placental lacunae can vary in degree. Finberg and Williams (1992) developed a grading scale for lacunae: grade 1+ for one to three lacunae, usually small; grade 2+ for four to six lacunae, typically larger; and grade 3+ for diffuse lacunae throughout the placenta.<sup>66</sup> More extensive lacunae throughout the placenta have been associated not just with placental invasion but with placenta percreta.<sup>66</sup> Another finding that may be associated with placenta percreta is hypervascularity of the entire bladder-serosal interface shown with three-dimensional (3D) power Doppler sonography.<sup>67</sup>

In a recent meta-analysis of 23 series that included 3700 pregnancies at risk for placenta accreta, the pooled sensitivity of sonography to identify invasion was 91% and the specificity was 97%.<sup>70</sup> However, the reported sensitivity for the individual studies ranged from 60% to 100%, and the specificity ranged from 50% to 100%.<sup>70</sup> Thus, although the overall utility of sonography for suspected placental invasion is good, there is considerable variability in published reports. More recently, investigators have tried to combine the various sonographic findings with clinical parameters, such as number of prior cesarean deliveries, to more accurately predict placental invasion.<sup>58,71</sup>

### Magnetic Resonance Imaging for Placenta Accreta

Magnetic resonance imaging is not recommended for routine evaluation of suspected placental invasion, as its sensitivity and specificity are



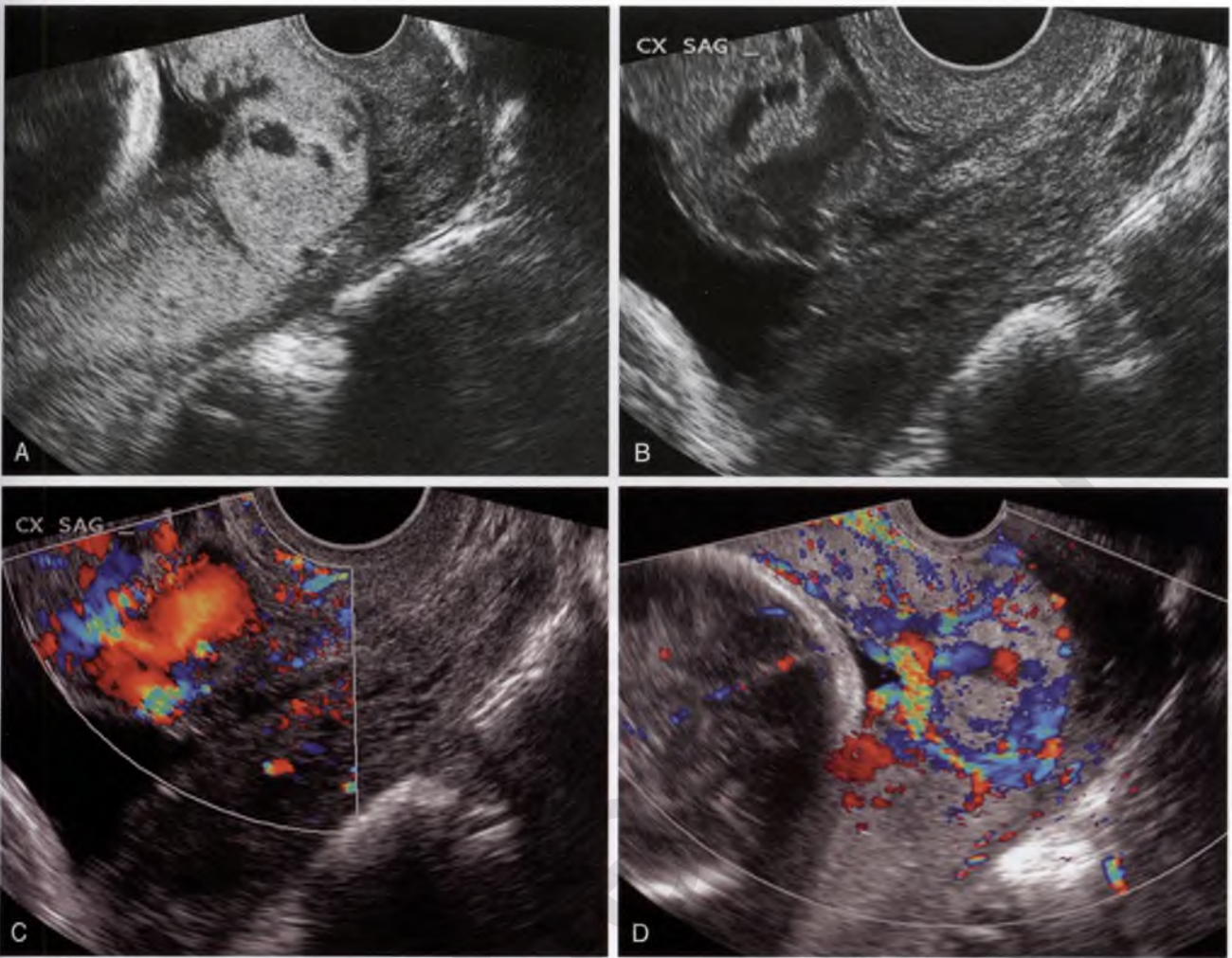


**FIG 19-18** Placental lacunae. **A** and **B**, Transvaginal images in the sagittal plane depict placenta previa with multiple placental lacunae. The images are from two different pregnancies, each at 28 weeks of gestation. **C** and **D**, Color Doppler ultrasound imaging (from the patients shown in **A** and **B**, respectively) demonstrates turbulent flow within these irregularly shaped vascular spaces.

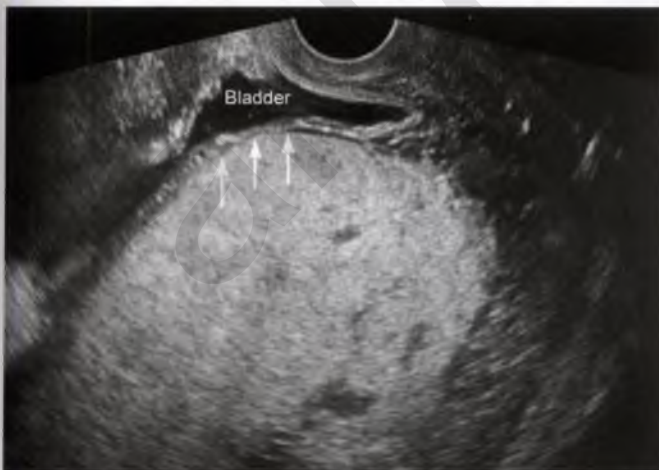


**FIG 19-19** Thinning of retroplacental myometrium. This transvaginal image at 32 weeks of gestation shows the placenta (previa) filling the lower uterine segment, and there is marked attenuation of the retroplacental myometrium (arrows). The smallest myometrial thickness is below 1 mm.

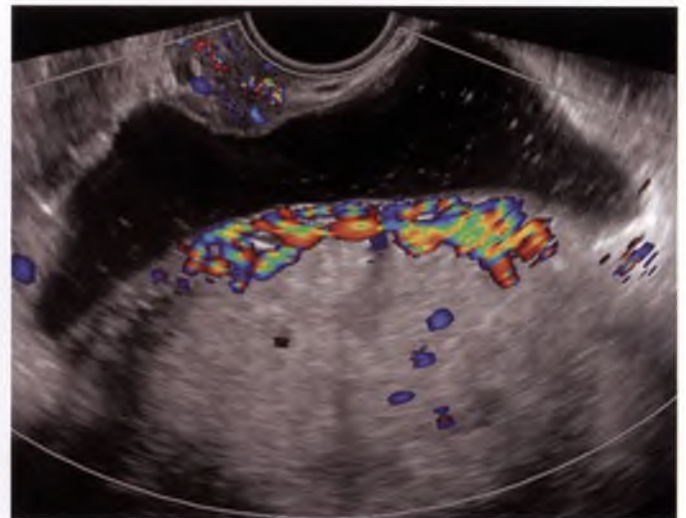


**FIG 19-20** Bridging vessels. This transvaginal sonographic image at 32 weeks' gestation was obtained in the transverse plane and depicts prominent bridging vessels, shown with color Doppler, that course from the placenta to the bladder-serosal interface. They correspond to the irregularities along the bladder-serosal interface visible with gray-scale imaging.



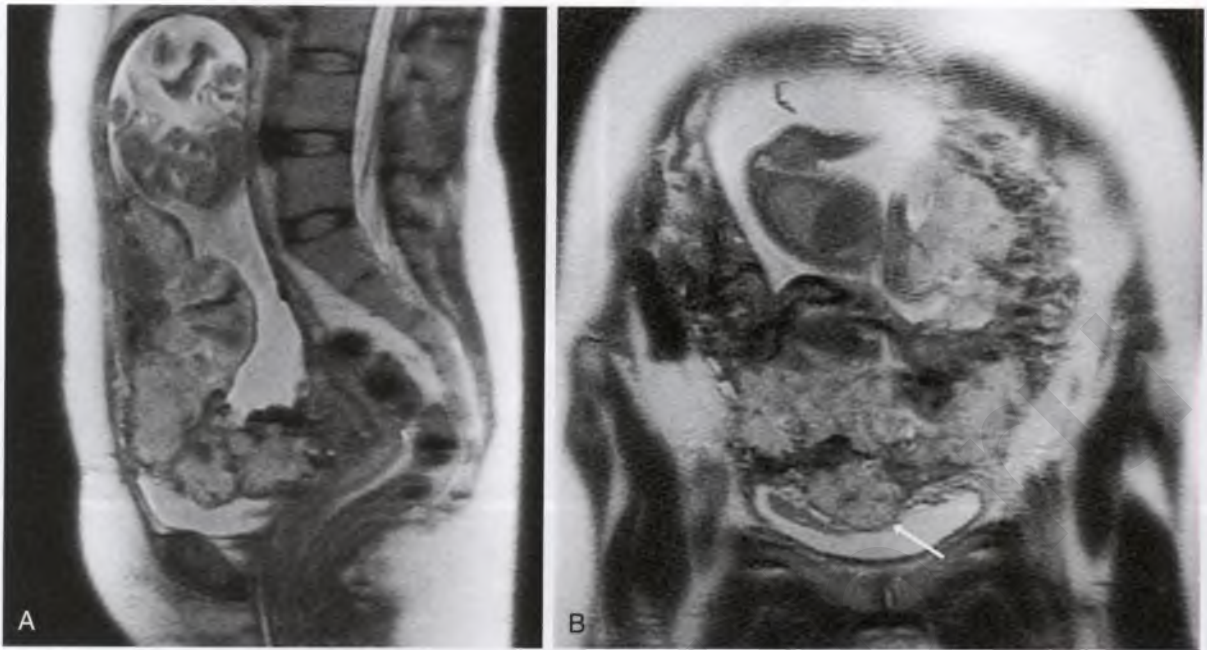


**FIG 19-21** Placenta percreta. Placental invasion with involvement of the maternal bladder wall, indicating placenta percreta, is shown on these sagittal (A) and coronal (B) single shot fast spin echo magnetic resonance images, obtained for purposes of surgical planning. The heterogeneity of the placenta is due to lacunae. Irregularity of the placental interface is noted with extension into the bladder wall (arrow). Intraluminal material within the bladder represents blood clot. (Courtesy of Dr. Liina Poder, University of Texas Southwestern Medical Center, Dallas, Texas.)

similar to sonography, and it has not been shown to affect mode of delivery or need for cesarean hysterectomy.<sup>72,73</sup> It may be useful, however, when ultrasound findings are inconclusive or additional information is needed (Fig. 19-21).<sup>29,72</sup> For example, in a patient with prior uterine surgery, instrumentation, or injury involving the posterior myometrium, sonographic visualization may be limited by fetal position or other factors. In such cases in which concern for possible placental invasion is raised, targeted magnetic resonance imaging might be of benefit.

### First-Trimester Placenta Accreta and Cesarean Scar Pregnancy

The rising prevalence of placental invasion, coupled with increasing use of first-trimester sonography, has led to recognition of placenta accreta in the first trimester. As previously stated, most pregnancies with placental invasion have placenta previa overlying a prior hysterotomy scar. Similarly, it is possible for implantation to occur in the region of the scar tissue at the anterior lower uterine segment—termed *cesarean scar pregnancy*—which may result in early uterine rupture.<sup>74</sup> Multiple investigators have found that cesarean scar pregnancy and placenta accreta share the same pathogenesis and that cesarean scar pregnancy, rather than being a separate entity, may be a precursor to second- or third-trimester placenta accreta.<sup>75-77</sup>

First-trimester sonographic findings of cesarean scar pregnancy include the following.<sup>75,78,79</sup>

- Gestational sac implantation that is low and anterior in the uterus, in the region of the hysterotomy scar. Before 8 weeks, the sac may fill the “niche” of the scar in a triangular configuration, and by 8 weeks, the gestational sac shape may appear more rounded.<sup>78</sup>
- Attenuation of the myometrial layer between the gestational sac and bladder, such that the measured distance from the anterior trophoblastic border to the uterine serosa is 1 to 3 mm (Fig.

19-22).<sup>75</sup> This measurement is comparable to the smallest myometrial thickness reported on sonographic imaging done later in pregnancy.

- Visible irregularities along the placental-myometrial interface.
- Echolucent areas within the placenta, a precursor to the lacunae visible later in gestation (Fig. 19-23).
- Prominent vascularity in the region of the prior hysterotomy scar shown with color Doppler ultrasound imaging.

The utility of these sonographic criteria for prediction of invasion has not as yet been established. In one series of suspected cesarean scar pregnancies that were expectantly managed, 90%—9 of 10 pregnancies—delivered liveborn neonates in the third trimester.<sup>80</sup> However, in each of these cases, the eventual pathologic diagnosis was placenta *percreta*, suggesting that pregnancies that come to attention in the first trimester may have more severe invasion. Concerns have been raised that a higher index of suspicion is required to identify pregnancies with placental invasion in the first trimester.<sup>74</sup>

A caveat in the management of suspected first-trimester placental invasion is that none of the aforementioned sonographic findings differentiates pregnancies that will experience early uterine rupture from those that will result in placenta accreta/percreta but with delivery of a term or near-term infant. It has been hypothesized that the clinical course may depend on factors such as depth and progression of abnormal placental invasion.<sup>76</sup> In some cases, the gestational sac appears to bulge or “balloon” outward from the uterus toward the bladder, which is particularly worrisome (see Fig. 19-22).<sup>81</sup> The sensitivity and positive-predictive value of this sonographic finding have not been established.

Identification of suspected first-trimester invasion poses challenges regarding patient counseling. Regardless of whether a woman decides to continue or terminate the pregnancy, she is at significant risk for hemorrhage and for hysterectomy—although certainly not invariably.



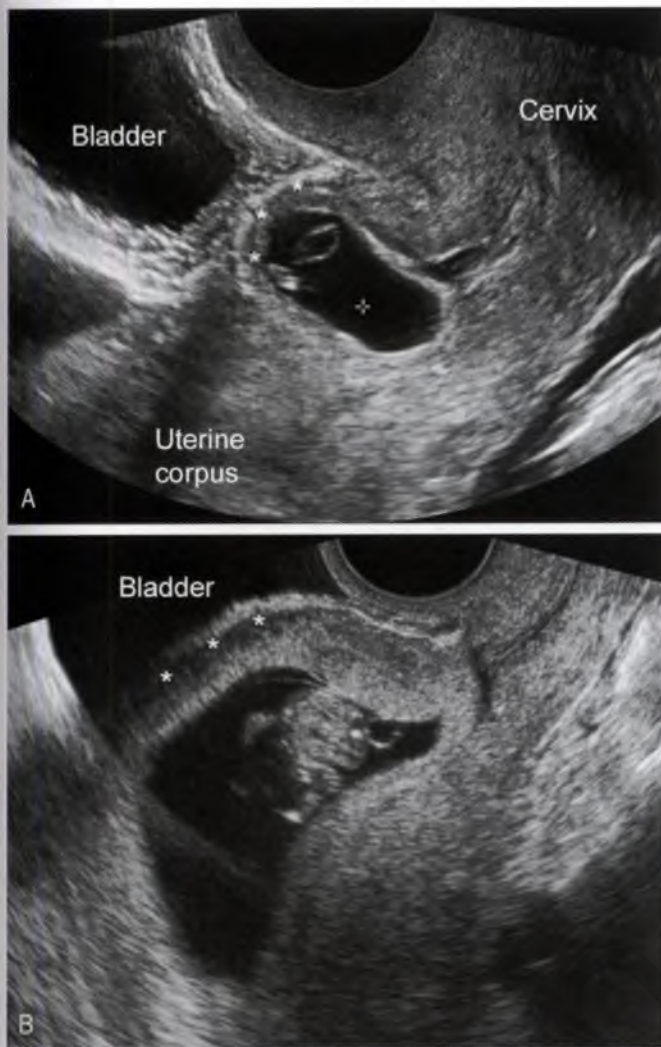


**FIG 19-22** Cesarean scar pregnancy with attenuation of retroplacental myometrium. **A**, In this transvaginal image of a 6-week gestation, the gestational sac is implanted low and anteriorly in the uterus (in the region of the hysterotomy scar) and appears to bulge outwardly; there is no visible myometrial layer (*asterisks*) between the gestational sac and maternal bladder. **B**, This transvaginal sonogram at 11 weeks shows thinning of the myometrial layer (*asterisks*) between the gestational sac and the bladder.

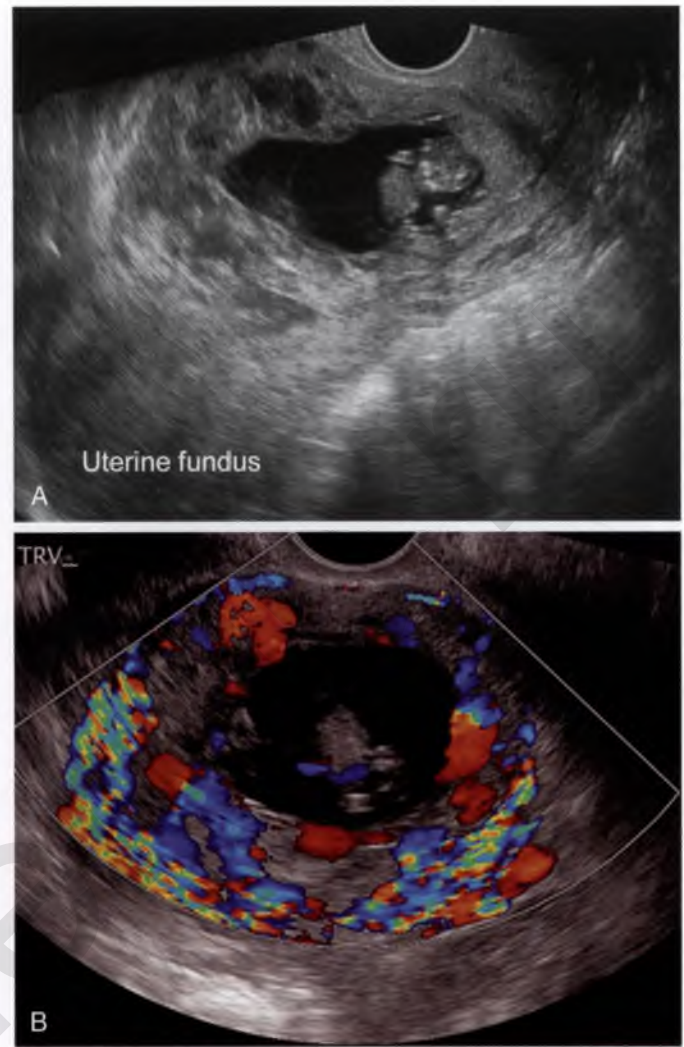


**FIG 19-23** Cesarean scar pregnancy with echolucent placental spaces. **A**, This transvaginal image in the sagittal plane at 10 weeks' gestation depicts numerous hypoechoic areas within the placenta. Not only has the gestational sac implanted inferior and anterior within the lower uterine segment, but also the sac appears to bulge or "balloon" outward from the uterine serosa. **B**, Color Doppler sonographic imaging demonstrates prominent turbulent flow within the echolucent areas. This cesarean scar pregnancy was treated with methotrexate and evacuation of the uterus.

If she continues the pregnancy, she will require close surveillance and coordination of delivery planning. If she elects to terminate, local injection of methotrexate and hysteroscopic-guided procedures have been reported to have the lowest complication rates.<sup>74</sup>

## VASCULAR ABNORMALITIES OF THE PLACENTA

### Placental Sonolucencies

Within the maternal-fetal circulation of the placenta, blood may accumulate abnormally at various points. These abnormalities can mechanically be organized into those that develop from disrupted maternal blood flow and those from altered fetal circulation. Of the two types, maternal blood flow abnormalities are more commonly seen sonographically. They can broadly be grouped as: (1) fibrin collections within the intervillous space, namely, subchorionic and perivillous fibrin deposition; (2) placental infarction, caused by spiral artery

occlusion; (3) intervillous thrombus, created by villous breaks that permit mixing of maternal and fetal blood within the intervillous space; and (4) hematomas. Despite specific histologic differentiation of these entities, the sonographic appearances of these collections are more generic. In some instances, location may best suggest the origin.

Many of these collections appear on ultrasound images as variably sized anechoic or hypoechoic areas typically lacking flow with color Doppler interrogation (Fig. 19-24). These placental sonolucencies often represent sites of fibrin deposition or intervillous thrombus. Less frequently they represent a mature hematoma, as hematomas are typically hypoechoic or anechoic in the acute phase, heterogeneously echogenic in the subacute phase, and anechoic in the chronic phase. Although not the result of vascular disruption, for completeness in this discussion, another sonolucency to consider is the decidual septal cyst. This is an area of focal degeneration within the maternal decidual septa, described earlier, that bulges up from the basal plate.



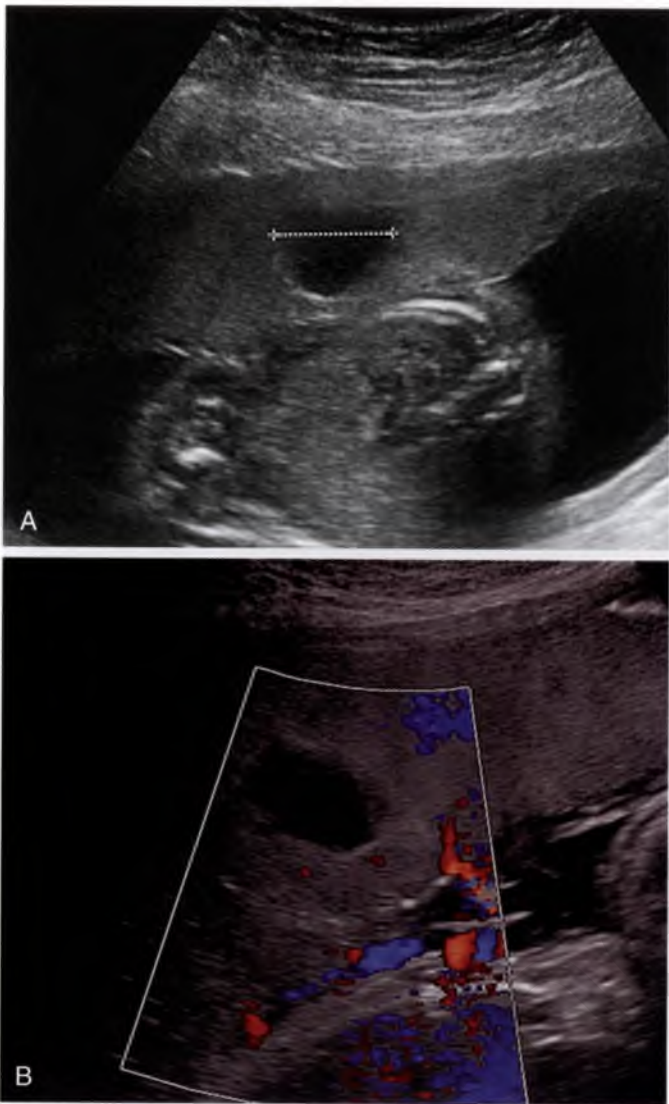


**FIG 19-24** Placental sonolucencies. **A**, A sonolucency measuring 2 cm in diameter is visible within an otherwise homogeneous placenta at 20 weeks' gestation. **B**, Color Doppler sonographic imaging at 34 weeks' gestation demonstrates absence of flow within the hypoechoic cystic space.

Placental lacunae or lakes initially appear similar to placental sonolucencies on gray-scale images but display internal blood flow when color Doppler ultrasound is applied.<sup>82</sup> These lakes are homogeneous, anechoic, avillous vascular spaces in the placenta, surrounded by normal echogenic placental parenchyma. They can be seen within placentas implanted anywhere in the corpus. However, they are especially important when seen in association with placenta previa, as they may be a marker for placental invasion (accreta) in that setting (see Fig. 19-18).

Of the remaining vascular-disruption histologic types, most placental infarcts are initially hypoechoic and difficult to discern sonographically. With time, areas of involvement may calcify, making sonographic detection easier. *Maternal floor infarction* refers to the presence of dense fibrinoid layer within the placental basal plate and is erroneously termed an infarction. These lesions are not reliably imaged but may result in a thicker basal plate and heterogeneous placenta. Massive perivillous fibrin deposition and intervillous

or subchorionic thrombosis in some cases may result in a jelly-like placenta. On ultrasound images, these placentas appear thickened, with patchy hypoechoogenicity and an abnormal echotexture that seems to “wobble.”

As stated, strict correlation between sonographic appearance and ultimate histologic diagnosis is imprecise. And variability in terminology and definitions used by sonologists and pathologists adds to the disparity among studies. In general, small placental sonolucencies or placental “lakes” are clinically insignificant, whereas larger or numerous lesions have been linked to fetal growth restriction.<sup>83</sup>

### Placental Calcification

Calcium salts can be deposited throughout the placenta but are most common at the basal plate. Calcification accrues with advancing gestation, increasing maternal serum calcium levels, and smoking.<sup>84,85</sup> Echogenic foci representing calcifications can easily be seen and recognized sonographically. Grannum and coworkers (1979) created a grading scale from 0 to III that reflected increasing calcification with increasing numeric grade.<sup>86</sup> In the first and second trimesters, the normal homogeneous placenta lacks echogenic foci (grade 0). A grade I placenta displays 1-mm to 4-mm scattered horizontal hyperechoic lines within the placenta but not in its most basal layer. Grade II placentas show these echogenic lines throughout all depths as well as hyperechoic, comma-shaped curves extending from the chorionic plate into the placenta. In grade III placentas, the echogenic lines persist, and the deep hyperechoic indenting curves reach the basal plate (Fig. 19-25).

Such grading criteria are vulnerable to interobserver variability and show limited ability to predict neonatal outcome in low-risk general pregnancy populations.<sup>87-89</sup> However, some investigators note that placental calcification at an early gestational age may be associated with poor uteroplacental blood flow, placental abruption, and some adverse neonatal outcomes, including low birth weight.<sup>90-94</sup>

### Placental Hematomas

The diagnosis of subchorionic or retroplacental hematoma is based on identifying an anechoic or hypoechoic fluid collection behind or adjacent to the gestational sac in the first trimester, or a similar fluid collection behind the placenta or membranes in the second trimester. Hematomas can also occur within the placenta or may be preplacental (Figs. 19-26 and 19-27). They are often identified in the setting of vaginal bleeding, particularly in the first trimester. Initially, a retroplacental hematoma typically is isoechoic or slightly hyperechoic compared to the placenta—so it may at first appear that the placenta is thickened or inhomogeneous. However, the hematoma generally becomes hypoechoic relative to the placenta within 1 week, and by 2 weeks the placental hematoma appears sonolucent.<sup>95</sup> When describing a hematoma, it is suggested that use of the term *hemorrhage* be avoided.

In population-based series, the prevalence of subchorionic hematoma is approximately 2% to 3% in the first or second trimester.<sup>96,97</sup> First-trimester hematoma has been associated with increased risk for adverse pregnancy outcome regardless of whether the sonographic findings are accompanied by vaginal bleeding<sup>98</sup> and regardless of hematoma size.<sup>99</sup> In one series of more than 1000 pregnancies with subchorionic hematoma identified during routine second-trimester ultrasound examination, the finding was associated with a 50% increase in the preterm birth rate and a threefold increase in the placental abruption rate.<sup>97</sup> A meta-analysis of seven series of subchorionic hematoma reported a twofold increase in risk for fetal death and stillbirth, such that approximately 1% of women with hematoma experienced a stillbirth.<sup>100</sup> No specific surveillance protocol has been demonstrated to have clinical utility in reducing rates of adverse outcome in this setting. Importantly, pregnancy outcomes are good



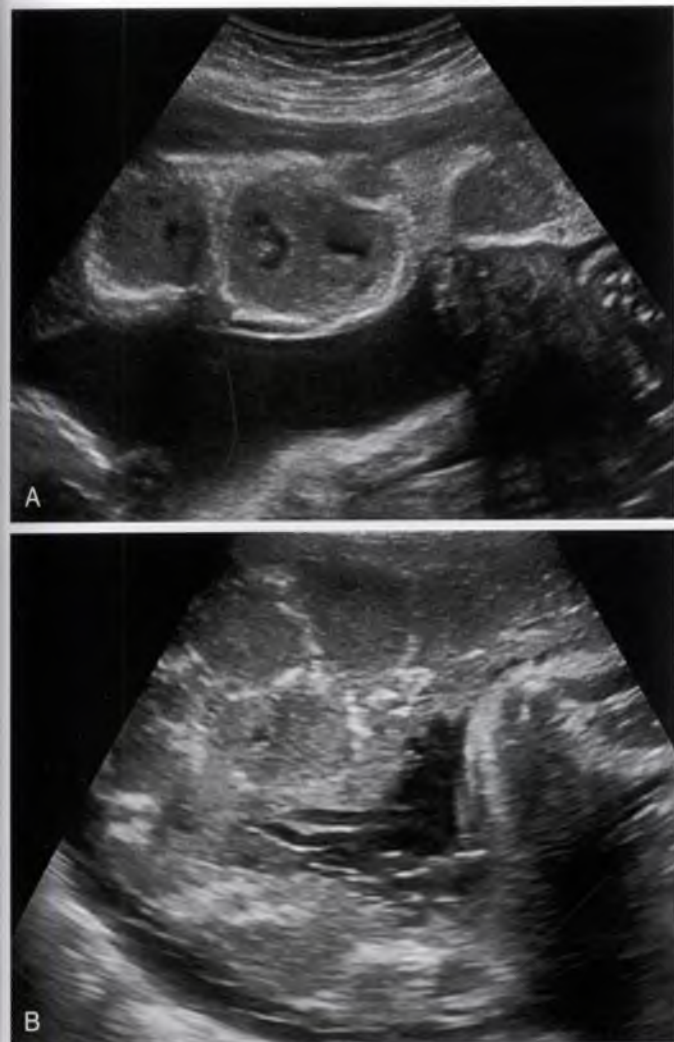


**FIG 19-25** Placental calcifications. **A**, Extensive placental calcifications and small hypoechoic areas are visible in this 32-week gestation. The woman developed preeclampsia, and her fetus was growth restricted. **B**, Placental calcifications may be a normal finding, as in this 36-week gestation. The birth weight was appropriate for gestational age at delivery.

in most of those in whom subchorionic hematoma is an incidental sonographic finding.

### Placental Abruption

Placental abruption, also termed *abruptio placentae*, is defined as the premature separation of a normally implanted placenta. It complicates approximately 1% of pregnancies.<sup>101</sup> Abruption is characterized by hemorrhage into the decidua basalis, resulting in an expanding decidual hematoma that prematurely detaches the placenta from the uterine wall. Risk factors include chronic hypertension, preeclampsia, preterm rupture of membranes, cigarette smoking, cocaine abuse, prior pregnancy complicated by abruption, and maternal trauma.<sup>27</sup> Pregnancies with first- or second-trimester bleeding may be found to have chronic placental abruption at delivery. With these, a retroplacental hematoma and a visible depression at the maternal surface of the placenta are seen during clinical inspection. The risk for abruption is reported to be increased about fivefold—a risk of approximately 5%—in the setting of a visible hematoma.<sup>96,97</sup>

Acute abruption constitutes an obstetric emergency that can lead to fetal death and, without prompt treatment, even maternal cardiovascular collapse. Although sonography is often used to evaluate the cause of third-trimester vaginal bleeding, acute placental abruption is *not* usually a sonographic diagnosis. One study of women being evaluated because of concern for abruption found that fewer than 25% of those with actual abruption at delivery had sonographic evidence of a subchorionic or retroplacental hematoma.<sup>102</sup> Thus, a normal sonogram cannot be used to exclude placental abruption.

There are no established sonographic criteria to define when a retroplacental hematoma is extensive enough to be considered an abruption. That said, use of the term implies that a hematoma has the potential to result in maternal or fetal compromise or has already done so. The sonographic appearance of placental abruption will depend in part on the size and location of the hematoma and, importantly, on the time elapsed between its development and the sonographic examination. Characteristics are shown in Figure 19-28.

### CHORIOANGIOMA

These benign tumors are discrete masses composed of multiple fetal capillaries supported by stroma. Also called *chorangioma*, the incidence of these placental tumors approximates 0.2% to 0.6%.<sup>103,104</sup> In some instances, maternal serum alpha-fetoprotein levels are

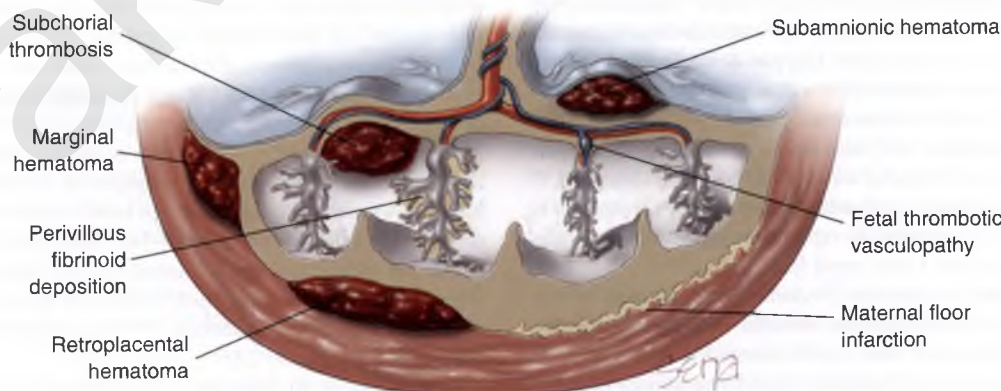


**FIG 19-26** This drawing shows the locations of various placental hematomas. (From Hoffman BL, Cunningham FG: Placental abnormalities. In Cunningham FG, Leveno KL, Bloom SL, et al [eds]: *Williams Obstetrics*, 24th ed. New York, McGraw-Hill, 2014.)





**FIG 19-27** Placental hematoma. **A** and **B**, This patient presented with vaginal bleeding at 18 weeks and was found to have a large preplacental hematoma. The hematoma is similar in echogenicity to the underlying placenta, slightly hypoechoic, in the setting of acute bleeding.

elevated.<sup>105</sup> On ultrasound images, a chorioangioma appears as a well-circumscribed, round, heterogeneous predominantly hypoechoic mass often near the cord insertion site along the fetal surface of the placenta and protrudes into the amniotic cavity (Fig. 19-29).<sup>106</sup> Variations may include tumors with internal septations or calcifications. Increased blood flow may be visible with color Doppler sonography and may help to distinguish these lesions from other placental masses. The differential diagnosis includes hematoma, partial hydatidiform mole, teratoma, tumor metastasis, and leiomyoma. Chorioangiomas with arterial or venous spectral Doppler waveforms have been identified.<sup>107</sup> During obstetric management, surveillance with serial sonograms is recommended to assess for possible rapid tumor growth, which has been reported and associated with rapid fetal decline.<sup>108</sup>

Physiologically, these tumors are predominantly perfused by the fetal circulation. Thus, chorioangioma size and degree of vascularity correlate with the volume of fetal blood shunted to the mass and are thereby predictive of fetal outcome. Small chorioangiomas are usually asymptomatic. Large tumors, typically those measuring more than 4 cm, may be associated with significant arteriovenous shunting resulting in fetal high-output cardiac failure and hydrops.<sup>109</sup> Platelet



**FIG 19-28** Placental abruption. **A**, This patient presented at 16 weeks with vaginal bleeding and pain. The placenta appears thickened and inhomogeneous. The fetus died during the sonogram. **B**, At delivery, more than 90% of the placenta was covered with adherent clot.

sequestration and erythrocyte damage within the mass can also cause fetal microangiopathic anemia and thrombocytopenia. Marked polyhydramnios can develop, and postulated theories include transudate from tumor vessels across the chorionic plate and increased fetal urine production associated with the hyperdynamic cardiac state.<sup>110,111</sup> Hemorrhage, preterm delivery, and fetal growth restriction may also complicate large tumors.<sup>104,112,113</sup> Because of these risks, some have treated large tumors in very preterm pregnancies by interdicting excessive blood flow using vascular occlusion or ablation techniques.<sup>114-117</sup> Successful prenatal intervention may best be achieved in those cases in which the chorioangioma is located remote from the umbilical cord insertion site and not supplied directly by the umbilical artery but rather by its secondary branches.<sup>114,118</sup> Fetal therapy for chorioangioma is discussed in Chapter 24.

In contrast to this focal mass, chorangioma is an increased density of capillaries within villi and is one of the many causes of placentomegaly. Chorangioma is found in approximately 5% of placentas submitted for histologic analysis.<sup>119</sup> Associated conditions include



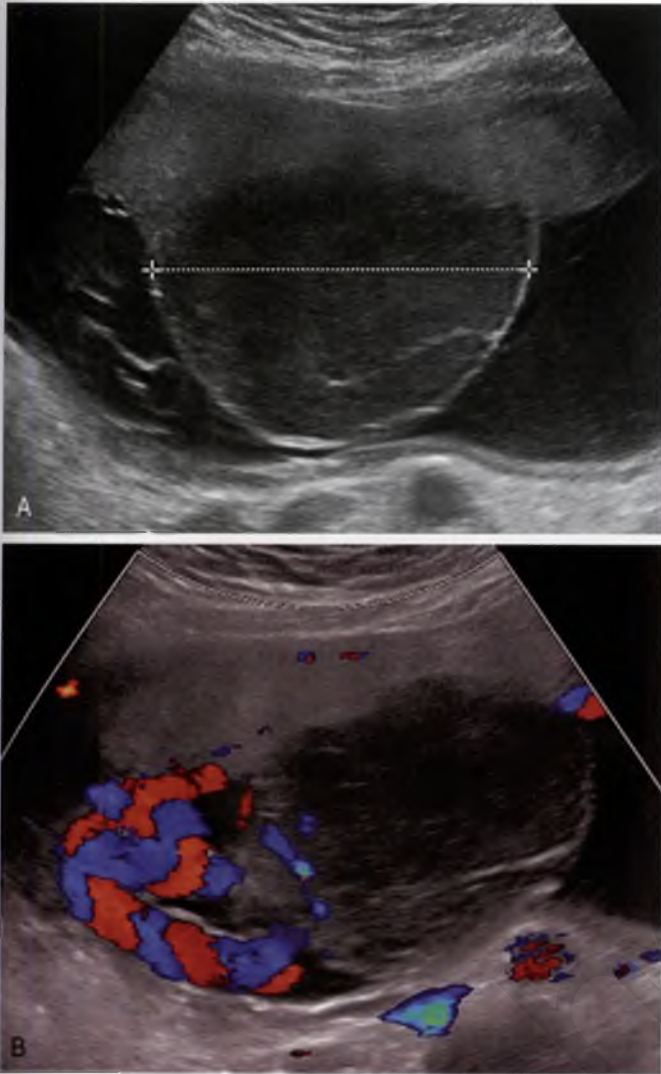


**FIG 19-29** Placental chorioangioma. **A** and **B**, An inhomogeneous mass measuring more than 8 cm in diameter is visible bulging from the fetal surface of the placenta, adjacent to the placental cord insertion, in this 28-week gestation. The pregnancy was followed with frequent surveillance. Pathologic examination following delivery confirmed placental chorioangioma.

preeclampsia, maternal diabetes mellitus, placental abruption, cord anomalies, maternal infection, and pregnancy at high altitude.<sup>120-122</sup>

## PLACENTAL MEMBRANE ABNORMALITIES

In early human development, the inner cell mass develops a small space, the future amniotic cavity, that is lined by amnioblasts and that lies above the embryoblast (Fig. 19-30). With expansion, the amnion eventually surrounds the embryo and sheaths the future umbilical cord (see Figs. 19-3 and 19-4).

In the early first trimester, the amnion and chorion are separated by the exocoelomic cavity, and this relationship is often seen sonographically (see Fig. 4-18). These layers later fuse and line the entire uterine cavity as the chorioamnion or placental membranes. Alterations in this relationship create membranes or bands seen sonographically and listed in Table 19-1. Those related to multifetal gestation and müllerian anomaly are discussed in their respective chapters.

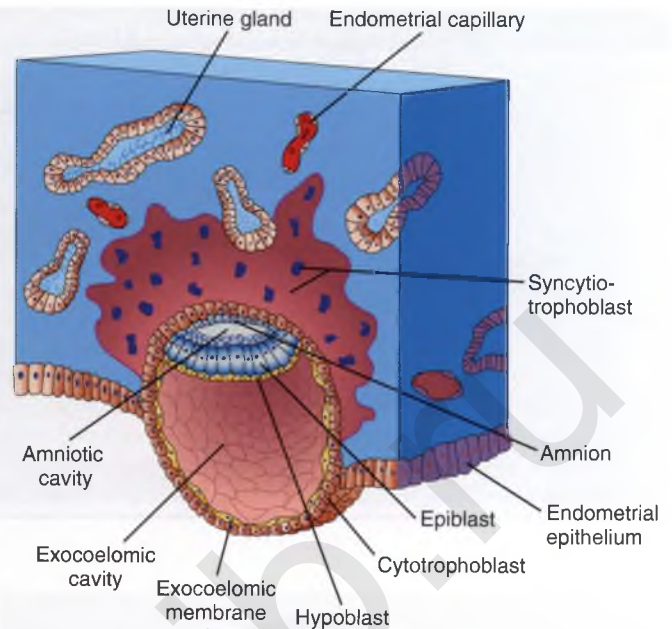


**FIG 19-30** In early human development, the forming amniotic cavity is lined by amnioblasts (labeled amnion) and lies above the embryo's epiblast layer. (From Moore KL, Persaud TVN, Torchia MG: *Second week of human development*. In Moore KL, Persaud TVN, Torchia MG [eds]: *The Developing Human: Clinically Oriented Embryology*, 9th ed. Philadelphia, WB Saunders, 2013, p 42, Fig. 3-1A.)

Placenta-related hemorrhage was discussed earlier in this chapter, whereas extrachorial placentation, uterine synechiae, and amniotic band sequence are described here.

## Extrachorial Placentation

*Extrachorial placentation* is the broader term used to describe both *circummarginate* and *circumvallate placentas*. Both are developmental variants in which the surface area of the chorionic plate is significantly smaller than that of the underlying placenta. This leaves a ring of placenta uncovered by chorionic plate, and hence, *extrachorial*. In this condition, the chorionic plate and its large vessels appear to stop abruptly, well short of the placental edge. From this abrupt line of transition, only amnion and chorionic membranes, without fetal vessels, cover the exposed outer ring of placenta. With *circummarginate* type, a smooth layer of amniochorion extends and covers the exposed peripheral placenta. With *circumvallate* placenta, the amniochorion folds back onto itself at the perimeter before extending across the outer rim of placenta (Fig. 19-31).

As a result, *circummarginate* placenta has no distinct sonographic findings. In contrast, with *circumvallate* placenta, ultrasound may reveal a thin curvilinear sheet or shelf of tissue bounded on each side by amniotic fluid. The sheet or shelf arises from and is attached to the peripheral margin of the placenta (Fig. 19-32). Despite these characteristic findings, the sensitivity of sonography for this diagnosis is poor.<sup>123</sup>

The clinical significance of extrachorial placentation has been debated. Associations between *circumvallate* placenta and adverse outcomes are reported by some but not all investigators and include antepartum bleeding, preterm labor, abruption, and perinatal death.<sup>5,6,124-126</sup> Moreover, it may be that larger rings of exposed placenta are linked with abnormal outcomes.<sup>127</sup> In contrast, these same studies show *circummarginate* placenta to be benign.



TABLE 19-1 Linear Structures and Bands Seen by Ultrasound During Pregnancy

Entity	Sonographic Findings
Normal early separation of the chorion and amnion	Crescent-shaped amnion mirrors the chorion's curvature. Distinct from the fetus. Fuses after 16 weeks' gestation.
Subchorionic hematoma	Echogenic blood lies between the myometrium and chorioamnion. The chorioamnion is seen as a thin linear reflector spanning the cavity. The hemorrhage and apparent band resolve with time.
Uterine synechiae (amniotic sheet)	Broad-based band, 2.5-4.0 mm thick, protrudes into and crosses the cavity. On cross section, appears shelf-like.
Circumvallate placenta	Broad-based curled wedge of tissue extends from one placental edge across to the other, just above the placental surface. On cross section, appears shelf-like.
Amniotic band	Thin wispy strands cross and appear to tether/entangle/distort fetal parts.
Uterine septum	Early intrauterine pregnancy is situated in one horn of a septate or bicornuate uterus. Thick band of echoes, which may be wedge-shaped, extend from uterine fundus in the midline.
Membranes from vanishing twin	Depending on chorionicity, either a thin amnion or thicker chorioamnion spans the cavity.
Placental vessels supported by membranes: Velamentous insertion Succenturiate lobe	On gray-scale ultrasound imaging, vessel walls may appear as bands. Color Doppler interrogation will clarify by showing intraluminal flow.



**FIG 19-31** Circumvallate placenta. Chorionic plate vessels stop abruptly at this ringed perimeter. Here, the amniochorion folds back upon itself to create the characteristic circumferential curled edge. (Courtesy of Dr. Irwin Kerber, University of Texas Southwestern Medical Center, Dallas, Texas.)

### Uterine Synechia(e)

This term refers to one or more linear bands of scar tissue within the uterus. In the setting of an intrauterine pregnancy, it may also be called an amniotic sheet, to indicate that the amnion and chorion layer (like a sheet) cover an intrauterine adhesion. The prevalence of this finding ranges from 0.5% to 1%.<sup>128-131</sup> The most common antecedent is prior uterine surgery such as curettage, which is reported to be 15% to 30% more common in those with synechiae than among control subjects.<sup>129,130</sup>

Sonographically, a thick, linear echogenic structure is seen to extend from one wall of the uterine cavity across to the other (Fig. 19-33). It may appear wider at its base. The fetus moves freely and untethered. There may be color Doppler flow along the sheet, but Doppler findings are considered variable.<sup>128</sup> A uterine synechia may resemble the thick dividing membrane of a dichorionic twin gestation or the linear echoes overlying a resorbed placental hematoma. It may also resemble the curled peripheral edge of a circumvallate placenta, though it can be distinguished from that entity in that its location is not restricted to

the placental margin (see Fig. 19-31). The differential diagnosis of linear structures within the cavity includes both uterine synechia and amniotic band sequence. These entities can be distinguished by ultrasound given that uterine synechiae are prominent, echogenic, and isolated findings, whereas amniotic bands are thin and generally identified after associated fetal anomalies are recognized.

Previously, an amniotic sheet was considered a benign finding, and a goal of ultrasound evaluation was to exclude other conditions. However, in recent series, synechiae have been associated with preterm premature membrane rupture, preterm birth, and placental abruption.<sup>129-131</sup> Other outcomes, including fetal growth restriction and stillbirth, do not appear to be more common, and there is no evidence to support altering prenatal care or surveillance if a uterine synechia is identified.<sup>129,131</sup>

### Amniotic Band Sequence

This rare sequence is caused and characterized by thin bands of amnion that cut across, tether, constrict, or amputate fetal parts. It is also called *amniotic band disruption complex (ABDC)* and *amniotic deformity adhesion and mutilation (ADAM)* complex. At least 80% of reported cases are associated with limb anomalies—primarily limb reduction defects.<sup>132,133</sup> Amputation of a distal extremity or digit(s) is common, and hands are involved more often than feet. Other abnormalities can include nonanatomic clefts of the face, cleft lip/cleft palate, or encephalocele.<sup>134</sup> Umbilical cord involvement is also frequent. In milder cases, a fetal extremity can appear entangled by faint linear echoes that represent bands of amnion. However, extensive defects involving multiple limbs and organ systems also may occur (Fig. 19-34). Severe defects of the spine or ventral wall that accompany amniotic bands suggest *limb-body wall complex*, which is discussed in Chapter 14 (Ultrasound Evaluation of the Fetal Gastrointestinal Tract and Abdominal Wall).

This condition is variably called a *syndrome*, meaning that all of the abnormalities result from the same cause, and a *sequence*, meaning that the abnormal findings developed sequentially from an initial insult. This reflects controversy about the underlying cause. Torpin (1965) proposed a theory implicating early rupture of the amnion, which allowed the embryo-fetus to become entangled in “sticky” mesodermal bands arising from the underlying chorion.<sup>135</sup> Torpin's *extrinsic* theory contrasted with the *intrinsic* theory proposed earlier by Streeter (1930)—namely, that an abnormality of the embryonic germinal disk was the primary insult and that the amniotic bands were secondary.<sup>136</sup> Astute

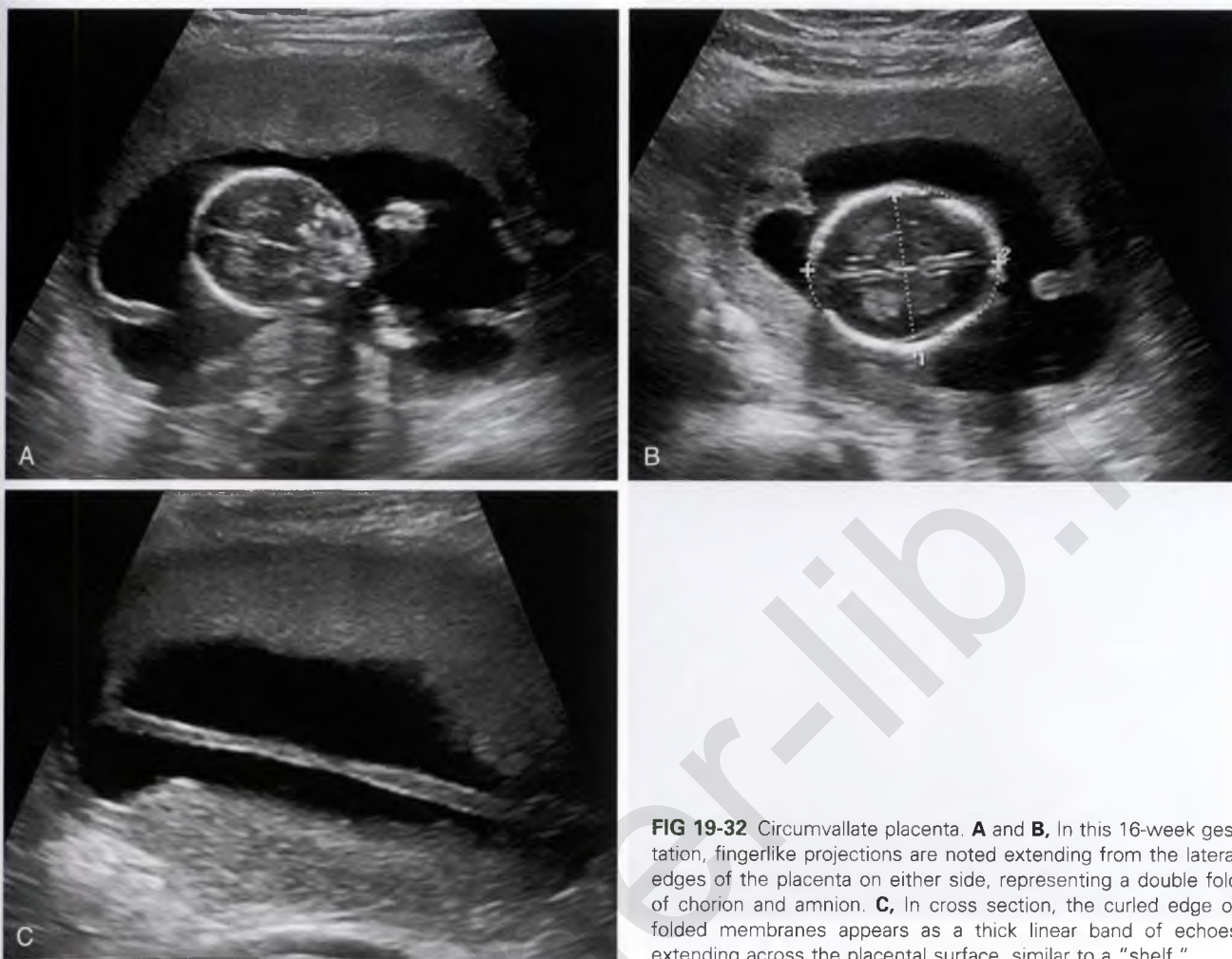


**FIG 19-32** Circumvallate placenta. **A** and **B**, In this 16-week gestation, fingerlike projections are noted extending from the lateral edges of the placenta on either side, representing a double fold of chorion and amnion. **C**, In cross section, the curled edge of folded membranes appears as a thick linear band of echoes extending across the placental surface, similar to a “shelf.”



**FIG 19-33** Uterine synechia (amniotic sheet). A thick linear band of echoes extends anteroposteriorly across the uterine cavity in this 19-week singleton gestation. It has no relationship to the placental location, differentiating it from circumvallate placenta, and it does not involve fetal parts.

observations that amniotic bands cut across transversely rather than diagonally, and that they encircle fetal parts rather than coiling along them, are not fully explained by either theory (Bronshtein and Zimmer, 1997).<sup>137</sup> Nonetheless, most agree that fetal abnormalities associated with amniotic band sequence are disruptions, and the condition is virtually always sporadic.

Not infrequently, fetal morphologic abnormalities associated with amniotic band sequence are more obvious sonographically than the bands themselves (see Fig. 19-34). As with any fetal anomaly, targeted sonography is indicated. Identification of a limb reduction defect or an encephalocele in an atypical location—sites other than the occipital midline—should prompt careful evaluation for amniotic bands. Similarly, edema of a distal extremity or positional deformity of an extremity raises suspicion. With improvements in ultrasound imaging technology and routine first-trimester evaluation, the sequence has been detected in the late first trimester.<sup>133</sup> Counseling regarding prognosis generally depends on the fetal abnormalities visible by ultrasound. Fetal surgery for amniotic band sequence is discussed in Chapter 24 (The Role of Ultrasound in Fetal Procedures).

## UMBILICAL CORD

### Normal Development

Formed during embryogenesis, the umbilical cord contains the omphaloenteric duct, developing from the yolk sac, and the body stalk,



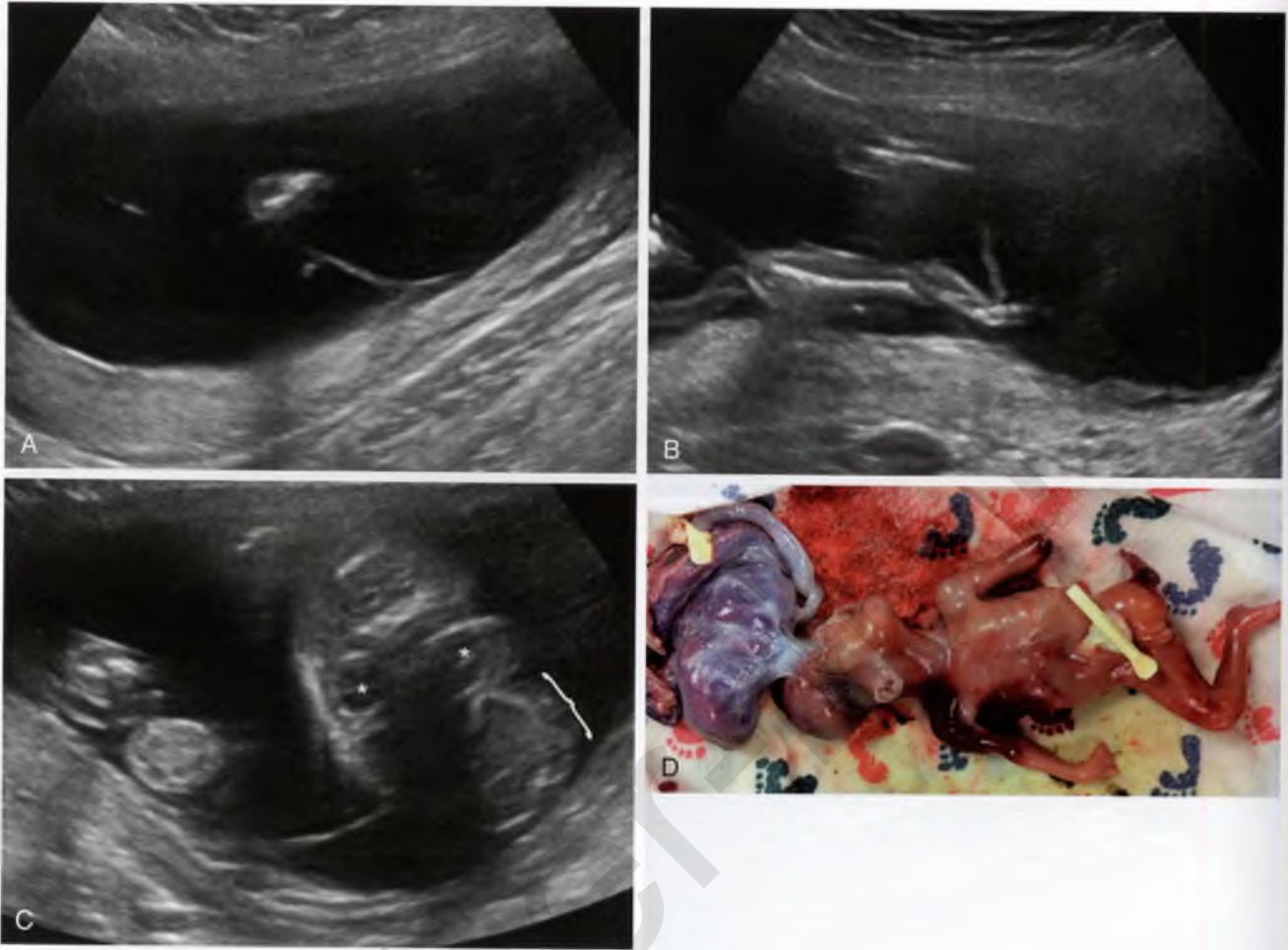


**FIG 19-34** Amniotic band sequence. **A**, A wispy thin, discontinuous linear structure extends from the uterine wall in this singleton pregnancy at 19 weeks' gestation. **B**, The fetal arms appear entangled in these amniotic bands. Further imaging revealed significant disruption of the hands and fingers. **C**, The amniotic bands have resulted in a severe atypical encephalocele (*bracket*). Asterisks mark the orbits. **D**, Gross pathologic specimen of the fetus.

connecting the embryo and placenta (see Fig. 19-4). Within the body stalk, there are two umbilical arteries, which arise initially from the dorsal aorta and, after further development, from the internal iliac arteries. Also within this stalk, the allantois is a diverticulum of the yolk sac, and both umbilical veins arise from coalescing venules that drain the allantois. Ultimately, the extraembryonic portion of the allantois degenerates, the right umbilical vein becomes obliterated, and a single left umbilical vein remains. The omphalomesenteric or vitelline duct connects the primitive intestines with the yolk sac and usually regresses between the 7th and 10th weeks of gestation.

The final umbilical cord contains specialized mucopolysaccharide-rich mesenchyme, Wharton jelly, which surrounds the two umbilical arteries and one umbilical vein. This substance is not typically seen by ultrasound, and the cord is visually identified by its three vessels (Fig. 19-35).

### Remnants and Cysts

Several structures are present within the umbilical cord during fetal development, and their remnants may be seen when the mature cord is cut transversely. Indeed, Jauniaux and colleagues (1989) sectioned 1000 cords, and in one fourth, they found remnants of vitelline duct, allantoic duct, and embryonic vessels.<sup>138</sup> These remnants were

not associated with congenital malformations or perinatal complications. However, because of their small size, most are not identified sonographically.

Cysts occasionally are found along the course of the cord. They are designated histologically according to their origin. True cysts are epithelium-lined remnants of the allantoic or vitelline ducts and tend to be located closer to the fetal insertion site (Fig. 19-36). An allantoic cyst may be associated with a urachal anomaly, and evaluation may identify a persistent communication between the bladder and the umbilical cord—a *patent urachus*. In contrast, more common pseudocysts form from local degeneration of Wharton jelly and occur anywhere along the cord. True cysts and pseudocysts can have a similar sonographic appearance.

Single umbilical cord cysts are identified in approximately 1% of first-trimester sonograms.<sup>139,140</sup> Most are isolated and resolve, and these are not associated with adverse pregnancy outcomes.<sup>140,141</sup> Multiple cysts, in contrast, may confer increased risk for spontaneous abortion or aneuploidy.<sup>139</sup> Cysts persisting into the second or third trimester are associated with an increased risk for fetal abnormalities, particularly omphalocele and patent urachus, and if abnormalities are present, the aneuploidy risk is also increased.<sup>142</sup> Thus, an umbilical cord cyst is an indication for a targeted obstetric sonogram. However,

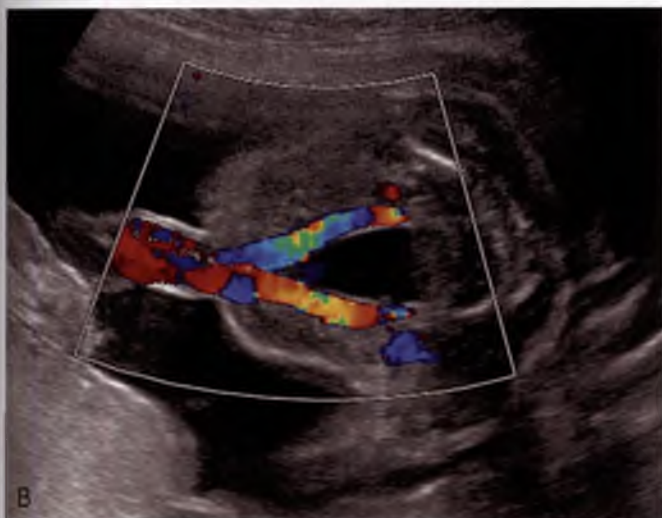


**FIG 19-35** **A**, Normal three-vessel umbilical cord in cross section, comprising two umbilical arteries and a larger umbilical vein. **B**, Color Doppler image of the fetal bladder encircled by the two umbilical arteries, which are a continuation of the superior vesical arteries, confirms that the cord has three vessels.

if no associated anomalies are identified, the prognosis appears to be favorable.

### Dimensions and Coiling

Most umbilical cords are 40 to 70 cm long, and few measure less than 32 cm or greater than 100 cm. Cord length is influenced positively by both amniotic fluid volume and fetal mobility. Short cords may be associated with fetal growth restriction, congenital malformations such as body stalk anomaly, intrapartum distress, and a twofold increased risk for stillbirth.<sup>143,144</sup> Excessively long cords are more likely to be linked with cord entanglement or prolapse and with fetal anomalies, acidemia, and demise.

Antenatal determination of cord length is technically challenging. Although not part of standard sonographic evaluation, cord diameter has been used as a predictive marker for fetal outcomes. The main variable resulting in differing diameters is the Wharton jelly content. Some have linked lean cords with poor fetal growth and large-diameter cords with macrosomia. However, the clinical utility of this parameter is still unclear.<sup>145-148</sup>



**FIG 19-36** Umbilical cord cyst. A 2-cm anechoic cyst is visible eccentric to the cord vessels and within millimeters of the fetal ventral abdominal wall in this 20-week gestation. The differential diagnosis for this finding includes an omphalomesenteric duct cyst, allantoic duct cyst, and amniotic inclusion cyst. Pseudocysts, which are not lined by epithelium and represent focal absence of Wharton jelly, are also common.

Cord coiling characteristics have also been reported, although this too is not part of standard sonographic evaluation. The umbilical vessels usually spiral through the cord in a sinistral (left-twisting) direction.<sup>149</sup> The number of complete coils per centimeter of cord length has been termed the *umbilical coiling index (UCI)*.<sup>150</sup> The reported normal sonographic index is 0.4, which contrasts with the normal value of 0.2 derived by actual cord measurement postpartum (Figs. 19-37 and 19-38).<sup>151</sup>

Most pregnancies with an abnormal UCI have a normal outcome. Some, but not all, pathologic studies of delivered placentas and cords report an increased association of hypo- or hypercoiling and stillbirth, fetal growth restriction, intrapartum distress, and chromosomal or anatomic abnormalities.<sup>152-156</sup> However, sonographically estimated UCI may be less helpful, as it may not correlate with the measured value obtained from the postpartum specimen.<sup>153,157-159</sup> Moreover, cord coiling varies along the length of the cord, and it is more coiled near the fetus, which may affect measurement accuracy.<sup>160</sup>

## Vascular Abnormalities of the Umbilical Cord

### Single Umbilical Artery

A single umbilical artery (SUA), resulting in a two-vessel umbilical cord, is usually identified sonographically when an artery is visible coursing adjacent to the fetal bladder along only one side (Fig. 19-39). A SUA may be visible in the first trimester. It is readily identified during the routine second trimester fetal anatomic survey, and documentation of umbilical cord vessel number is a standard component of this examination.<sup>13</sup> In a cross section of the umbilical cord, only a single artery and the vein are visible (see Fig. 19-39). The diagnosis of suspected SUA should be verified at the level of the fetal bladder, as the two umbilical arteries may occasionally fuse near their placental insertion. Theories regarding the pathogenesis of SUA include primary agenesis or secondary atrophy of one of the two umbilical arteries.<sup>161</sup>

In population-based series, the prevalence of SUA identified during second-trimester sonographic examination is 0.4% to 0.6% in singleton pregnancies or approximately 1/200 births.<sup>162-164</sup> The prevalence is



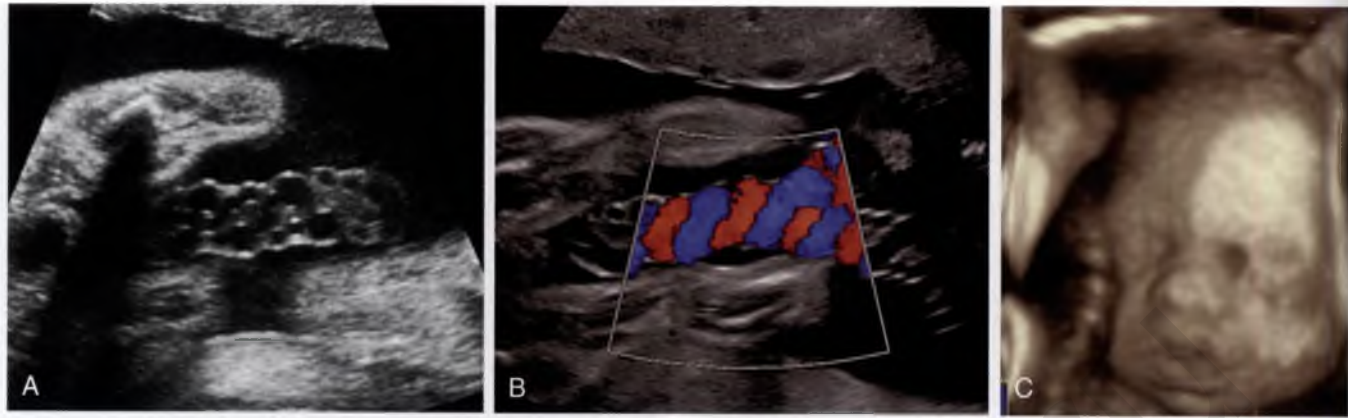


**FIG 19-37** Hypercoiled umbilical cord. **A**, Hypercoiling of the umbilical cord vessels was incidentally noted during a routine second-trimester sonogram. **B**, Color Doppler imaging depicts the coiled loops of cord. **C**, Three-dimensional sonography shows the coiling of this umbilical cord in the third trimester.

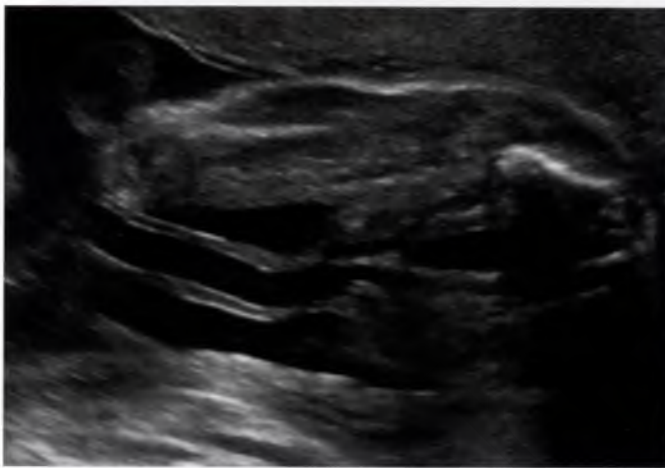


**FIG 19-38** Hypocoiled umbilical cord. The vessels of the umbilical cord appear undercoiled throughout its course. The two umbilical arteries are visible on either side of the larger umbilical vein.



**FIG 19-39** Single umbilical artery, also called two-vessel cord. **A**, In cross section, only one umbilical artery and vein are visible. Because two umbilical arteries may sometimes fuse near the placental cord insertion, suspected single umbilical artery should be confirmed at the level of the fetal bladder. **B**, Color Doppler imaging shows only one umbilical artery adjacent to the fluid-filled bladder.

higher in populations referred for risk factors such as maternal age, abnormal aneuploidy screening, or suspected fetal abnormalities.<sup>165</sup> An important consideration and observation is whether the SUA is *isolated*, namely, whether it occurs without associated major fetal structural abnormalities or aneuploidy. In approximately 80% of cases, SUA is an isolated finding.<sup>162-164</sup>

Of those cases with SUA, the left umbilical artery is absent in approximately 70%,<sup>165</sup> and in some but not all reports, absence of the left umbilical artery is more strongly linked with structural anomalies and aneuploidy.<sup>166,167</sup> Tobacco use is associated with a twofold increased risk.<sup>164</sup> The prevalence of SUA in one fetus in a twin pregnancy is approximately 2%, with no relation to chorionicity, thus affecting 1% of twin fetuses overall.<sup>168</sup>

SUA has been consistently associated with an increased risk for congenital abnormalities—in particular, cardiac and renal anomalies. In population-based series, the risk for cardiac anomalies in nonaneuploid fetuses with an SUA is 7%, and the risk for renal anomalies approximates 5%, most commonly with renal pelvis dilatation.<sup>162-164</sup> This amounts to a 20-fold increase in the risk for cardiac anomalies and a threefold increase in the risk for renal anomalies in singleton



pregnancies.<sup>163</sup> Targeted sonographic evaluation is recommended when an SUA is identified. It is somewhat controversial whether fetal echocardiography is also indicated, particularly if the finding appears isolated.<sup>162,169</sup>

When SUA is seen in association with fetal morphologic abnormalities, the aneuploidy risk is considerably increased. With one major structural anomaly and SUA, the aneuploidy risk is approximately 4%, increasing to as much as 50% if more than one major anomaly is present.<sup>170</sup> Among aneuploid fetuses, approximately 15% have an SUA.<sup>165</sup> The most common chromosomal abnormality associated with SUA is trisomy 18, followed by trisomies 13 and 21 and triploidy.<sup>165,170</sup> Importantly, in the absence of associated anomalies, multiple investigators have reported that the risk for aneuploidy is *not* increased with isolated SUA.<sup>165,167,170</sup>

An association between isolated SUA and fetal growth restriction has been well described but remains controversial. Several recent series have identified an approximate twofold increase in the prevalence of low birth weight (at or below the 10th percentile for gestational age) with isolated SUA.<sup>163,164</sup> However, other researchers have found no increase in rates of fetal growth impairment.<sup>166,171,172</sup> A recent systematic review of more than 900 pregnancies with isolated SUA found that affected infants weighed approximately 50 g less than those with three-vessel umbilical cords, a difference that did not reach statistical—or clinical—significance.<sup>173</sup> The authors of this meta-analysis concluded that serial sonograms for growth assessment should not be routine practice.<sup>173</sup>

### Persistent Right Umbilical Vein

As noted earlier, the vein in the fully developed umbilical cord is normally the left umbilical vein. The right umbilical vein is present early but then atrophies in most cases. When the right umbilical vein persists, the left umbilical vein atrophies—such that the cord has three vessels. This variant is appreciated on views through the fetal abdomen but not the umbilical cord. In a transverse image of the fetal abdomen at the level at which the abdominal circumference is measured, the intrahepatic persistent right umbilical vein is visible lateral and to the right, rather than to the left, of the fetal gallbladder and it courses toward, rather than away from, the left side of the fetal stomach (Fig. 19-40).

As an isolated sonographic finding, an intrahepatic persistent right umbilical vein would not be apparent at birth unless specifically sought. In sonographic series, the reported prevalence approximates 1 in 1000.<sup>174,175</sup> Associated anomalies, particularly cardiovascular and renal abnormalities, have been described in 25% to 40% of cases.<sup>174-176</sup> It is plausible that because anomalies associated with persistent right umbilical vein may be more obvious during a screening sonogram than the venous variant, the reported prevalence may be underestimated. Nonetheless, targeted sonographic evaluation is recommended if a persistent right umbilical vein is identified. If the anomaly is isolated, it is not associated with aneuploidy, and the fetal prognosis is considered excellent.<sup>174-176</sup>

### Umbilical Vein Varix

An umbilical vein varix is a focal dilatation of the umbilical vein within the fetal abdomen. Thus, the umbilical *cord* is normal. A varix is diagnosed based on the transverse diameter measurement of the umbilical vein at its widest point, which is typically just within the fetal abdominal wall. The caliber of the vein normally increases with advancing gestational age, from approximately 3 mm at 15 weeks to 8 mm by term.<sup>177</sup> The image is obtained with a transverse sonographic view of the abdomen (Fig. 19-41). In most research studies and case reports, varix is diagnosed when the measurement is 9 mm or greater or if the

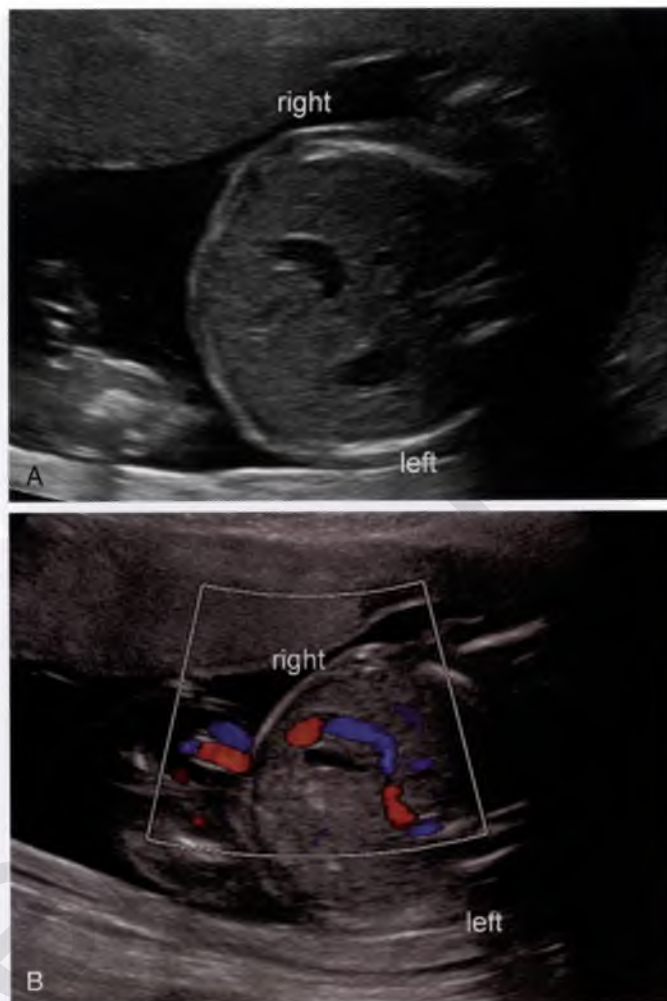


**FIG 19-40** Persistent right umbilical vein. **A**, In this transverse view of the fetal abdomen at 19 weeks, the J-shaped intrahepatic umbilical vein courses toward (rather than away from) the left side of the fetal stomach. **B**, Color Doppler sonography reveals the course of the persistent right umbilical vein, located lateral and to the right of the gallbladder.

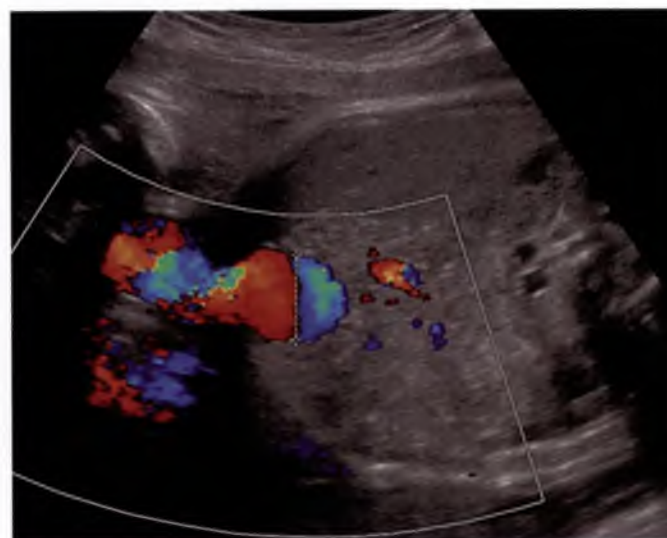


**FIG 19-41** Umbilical vein varix. Color Doppler sonography depicts focal enlargement of the intra-abdominal umbilical vein in this 36-week gestation. The diameter of the vein measured 17 mm.



measurement of the extrahepatic portion of the umbilical vein is at least 50% larger than the intrahepatic portion.<sup>178-182</sup>

The reported prevalence of umbilical vein varix ranges from approximately 1/400 to 1/2000 pregnancies, with the diagnosis typically made in the third trimester.<sup>178,180,182</sup> Umbilical vein varix is associated with major fetal anomalies in approximately 5% to 10%, and minor aneuploidy markers in another 10% to 15%.<sup>178,180,182</sup> The aneuploidy risk is increased when structural anomalies or minor markers are visible, with trisomy 21 the most commonly reported. These findings are in contrast to early studies, which reported a strong association between umbilical cord varix and major abnormalities, as well as fetal demise.<sup>177,183</sup> However, in recent series, at least 80% of cases were found to be isolated, and good outcomes have been consistently described.<sup>178,179,182</sup> This may reflect greater awareness of this finding and improved visualization with modern sonographic equipment.

It is believed that the extrahepatic portion of the vein within the abdomen represents the weakest part of the umbilical circulation.<sup>182</sup> This weakness may account for dilatation of the umbilical vein observed in cases of hydrops fetalis and other conditions with fetal volume overload or heart failure, such as alloimmunization, twin-twin transfusion syndrome, and twin-reversed arterial perfusion sequence.<sup>178,180,182</sup> Because of the association with other abnormalities, targeted sonographic evaluation is recommended. Fetal surveillance has also been advocated, although evidence that this results in improved pregnancy outcomes is lacking.

### Knots, Nuchal Cords, and Cord Entanglement

A knot or "true knot" in the umbilical cord is occasionally encountered by ultrasound, although it is more likely to be an unexpected finding at delivery (Fig. 19-42). The prevalence at birth approximates 1%.<sup>184,185</sup> Factors associated with cord knots include longer umbilical cord and multiparity. In population-based series, a knot in the umbilical cord is associated with a 4- to 10-fold increase in the risk for fetal death.<sup>184,185</sup> In case reports, color Doppler, power Doppler, and 3D or 4D sonography have been used to improve image quality in suspected cases.<sup>186-189</sup> Based on expert opinion, fetal surveillance has been suggested if this finding is incidentally discovered, but there is no evidence to support a specific modification to prenatal care.<sup>187-190</sup> Focal redundancy of the umbilical cord vessels has been termed a *false knot* (Fig. 19-43). This redundancy of cord vessels is of no clinical significance.

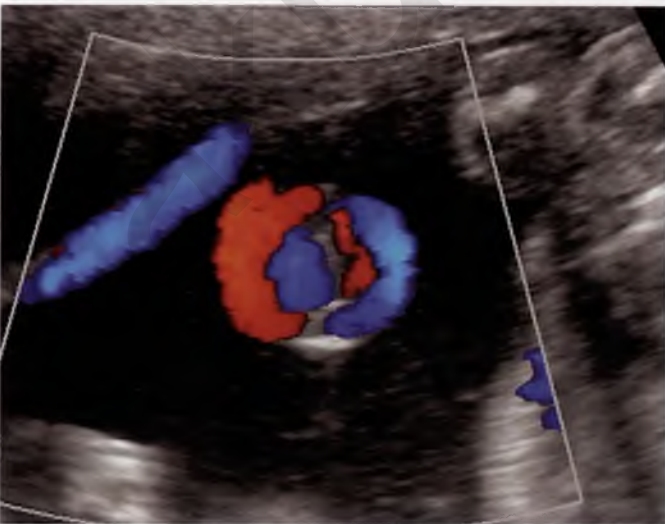


**FIG 19-42** Umbilical cord knot suggested by color Doppler sonography at 22 weeks' gestation.

Nuchal cord is present in approximately 15% to 30% of births, and it is not considered a complication of either pregnancy or delivery. If sought, it is often identified by in utero ultrasound. However, prenatal detection of a nuchal cord is not associated with adverse fetal outcome, and no form of surveillance is recommended.

Umbilical cord entanglement is frequently identified when scanning monochorionic, monoamniotic twins, and it is invariably encountered at delivery (Fig. 19-44). In one recent series, all monoamniotic twin gestations had sonographic evidence of cord entanglement when this finding was specifically sought (Fig. 19-45).<sup>191</sup> Cord entanglement is no longer believed to be a major contributor to perinatal morbidity or mortality risks in these rare pregnancies.<sup>192</sup> Rather, adverse outcomes in monoamniotic pregnancies are more commonly attributable to other complications such as twin-reversed arterial perfusion sequence, to prematurity, or to associated anomalies. Surveillance is commonly instituted once viability is reached.



**FIG 19-43** Knotting and coiling of the umbilical cord. **A**, A false knot is shown and the cord segment toward the right of this is hypocooled. **B**, A complex true knot is shown and the cord segment toward the right of this is hypercoiled.



**FIG 19-44** Umbilical cords from a monoamniotic-monoamniotic twin pair after cesarean delivery show marked entanglement. (Courtesy of Dr. Seth Hawkins, University of Texas Southwestern Medical Center, Dallas, Texas.)



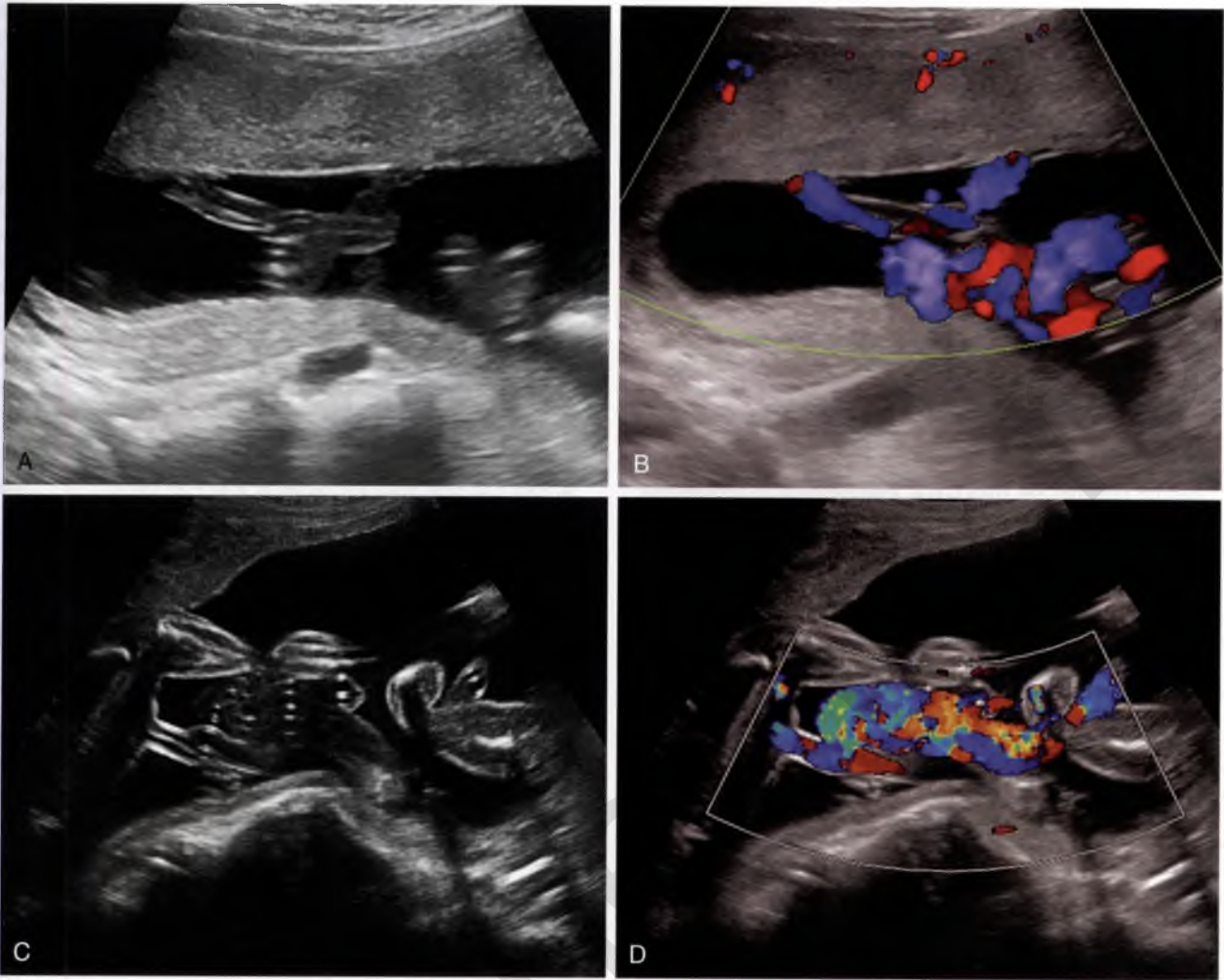


**FIG 19-45** Cord entanglement. **A**, In this monochorionic-monoamniotic twin gestation at 20 weeks, there is cord entanglement near the level of the placental cord insertion sites—which are in close proximity to one another. **B**, Color Doppler sonography may help facilitate visualization of cord entanglement. **C**, Cord entanglement is also apparent near the insertion of the umbilical cord at the fetal ventral abdominal wall. **D**, Again, color Doppler sonography demonstrates the two entwined cords. The infants were delivered by cesarean at 32 weeks, without incident.

## SUMMARY

Evaluation of the placenta and umbilical cord is an important component of obstetric sonography. Assessment of the relationship between the placenta and the internal cervical os is essential in the second and third trimesters. Conditions associated with vasa previa include resolved placenta previa or low-lying placenta, velamentous cord insertion, and succenturiate or bilobate placenta. Sonographic criteria for detection of placenta accreta include placental lacunae, thinning of the retroplacental myometrium, and irregularity or disruption of the bladder-serosal interface, with bridging vessels between placenta and the bladder-serosal interface on color Doppler imaging. Targeted sonography is indicated if there are abnormalities of the umbilical cord or its vessels, including umbilical cord cyst, SUA, or persistent right umbilical vein, to evaluate for the presence of associated fetal anomalies. Finally, and importantly, transvaginal sonography is frequently key to accurate placental assessment and is considered safe regardless of placental location, even in the presence of bleeding.

## REFERENCES

1. Benirschke K, Burton GJ, Baergen RN: Macroscopic features of the delivered placenta. In Benirschke K, Burton GJ, Baergen RN, editors: *Pathology of the Human Placenta*, ed 6, Berlin, Germany, 2012, Springer, pp 13–15.
2. Elchalal U, Ezra Y, Levi Y, et al: Sonographically thick placenta: a marker for increased perinatal risk—a prospective cross-sectional study. *Placenta* 21(2–3):268–272, 2000.
3. Hoddick WK, Mahony BS, Callen PW, et al: Placental thickness. *J Ultrasound Med* 4(9):479–482, 1985.
4. Tongsong T, Boonyanurak P: Placental thickness in the first half of pregnancy. *J Clin Ultrasound* 32(5):231–234, 2004.
5. Suzuki S, Igarashi M: Clinical significance of pregnancies with succenturiate lobes of placenta. *Arch Gynecol Obstet* 277(4):299–301, 2008.
6. Suzuki S, Igarashi M, Inde Y, et al: Abnormally shaped placentae in twin pregnancy. *Arch Gynecol Obstet* 281(1):65–69, 2010.
7. Pereira N, Yao R, Guilfoil DS, et al: Placenta membranacea with placenta accreta: radiologic diagnosis and clinical implications. *Prenat Diagn* 33(13):1293–1296, 2013.



8. Ravangard S, Henderson K, Fuller K: Placenta membranacea. *Arch Gynecol Obstet* 288(3):709–712, 2013.
9. Degani SM: Sonographic findings in fetal viral infections: a systematic review. *Obstet Gynecol Surv* 61(5):329–336, 2006.
10. Dombrowski MP, Wolfe HM, Saleh A, et al: The sonographically thick placenta: a predictor of increased perinatal morbidity and mortality. *Ultrasound Obstet Gynecol* 2(4):252–255, 1992.
11. Jauniaux E, Hustin J: Chromosomally abnormal early ongoing pregnancies: correlation of ultrasound and placental histological findings. *Human Pathol* 29(11):1195–1199, 1998.
12. Porat S, Fitzgerald B, Wright E, et al: Placental hyperinflation and the risk of adverse perinatal outcome. *Ultrasound Obstet Gynecol* 42(3):315–321, 2013.
13. American Institute of Ultrasound in Medicine: AIUM practice guideline for the performance of obstetric ultrasound examinations. *J Ultrasound Med* 32(6):1083–1101, 2013.
14. Olive EC, Roberts CL, Nassar N, et al: Test characteristics of placental location screening by transabdominal ultrasound at 18–20 weeks. *Ultrasound Obstet Gynecol* 28:944, 2006.
15. Quant HS, Friedman AM, Wang E, et al: Transabdominal ultrasonography as a screening test for second-trimester placenta previa. *Obstet Gynecol* 123:628, 2014.
16. Bhide A, Thilaganathan B: Recent advances in the management of placenta previa. *Curr Opin Obstet Gynecol* 16:447, 2004.
17. Oppenheimer LW, Farine D: A new classification of placenta previa: measuring progress in obstetrics. *Am J Obstet Gynecol* 201:227, 2009.
18. Oyelese Y, Smulian JC: Placenta previa, placenta accreta, and vasa previa. *Obstet Gynecol* 107:927, 2006.
19. Timor-Tritsch IE, Yunis RA: Confirming the safety of transvaginal sonography in patients suspected of placenta previa. *Obstet Gynecol* 81:742, 1993.
20. Ananth CV, Demissie K, Smulian JC, et al: Placenta previa in singleton and twin births in the United States, 1989 through 1998: a comparison of risk factor profiles and associated conditions. *Am J Obstet Gynecol* 188:275, 2003.
21. Faiz AS, Ananth CV: Etiology and risk factors for placenta previa: an overview and meta-analysis of observational studies. *J Matern Fetal Neonatal Med* 13(3):175–190, 2003.
22. Martin JA, Hamilton BE, Sutton PD, et al: Births: final data for 2003. *Natl Vital Stat Rep* 54(2):1–116, 2005.
23. Rosenberg T, Pariente G, Sergienko R, et al: Critical analysis of risk factors and outcome of placenta previa. *Arch Gynecol Obstet* 284:47–51, 2011.
24. Dashe JS, McIntire DD, Ramus RM, et al: Persistence of placenta previa according to gestational age at ultrasound detection. *Obstet Gynecol* 99:692–697, 2002.
25. Usta IM, Hobeika EM, Musa AA, et al: Placenta previa-accreta: risk factors and complications. *Am J Obstet Gynecol* 193:1045–1049, 2005.
26. Weis MA, Harper LM, Roehl KA, et al: Natural history of placenta previa in twins. *Obstet Gynecol* 120:753–758, 2012.
27. Obstetrical hemorrhage. In Cunningham FG, Leveno KJ, Bloom SL, et al, editors: *Williams Obstetrics*, ed 24, New York, 2014, McGraw-Hill, pp 793–806.
28. Dashe JS: Toward consistent terminology of placental location. *Semin Perinatol* 37:375, 2013.
29. Reddy UM, Abuhamad AZ, Levine D, et al; Fetal Imaging Workshop Invited Participants: Fetal imaging: executive summary of a joint Eunice Kennedy Shriver National Institute of Child Health and Human Development, Society for Maternal-Fetal Medicine, American Institute of Ultrasound in Medicine, American College of Obstetricians and Gynecologists, American College of Radiology, Society for Pediatric Radiology, and Society of Radiologists in Ultrasound Fetal Imaging Workshop. *Obstet Gynecol* 123(5):1070–1082, 2014.
30. Townsend RR, Laing FC, Nyberg DA, et al: Technical factors responsible for “placental migration”: sonographic assessment. *Radiology* 160:105, 1986.
31. Becker Rh, Vonk R, Mende BC, et al: The relevance of placental location at 20–23 gestational weeks for prediction of placenta previa at delivery: evaluation of 8650 cases. *Ultrasound Obstet Gynecol* 17:496, 2001.
32. Lauria MR, Smith RS, Treadwell MC, et al: The use of second-trimester transvaginal sonography to predict placenta previa. *Ultrasound Obstet Gynecol* 8:337, 1996.
33. Taipale P, Hilesmaa V, Ylostalo P: Diagnosis of placenta previa by transvaginal sonographic screening at 12–16 weeks in a nonselected population. *Obstet Gynecol* 89:364, 1997.
34. Vergani P, Ornaghi S, Pozzi I, et al: Placenta previa: distance to internal os and mode of delivery. *Am J Obstet Gynecol* 201:266.e1–266.e5, 2009.
35. Heller HT, Mullen KM, Gordon RW, et al: Outcomes of pregnancies with a low-lying placenta diagnosed on second-trimester sonography. *J Ultrasound Med* 33:691, 2014.
36. Bhide A, Prefumo F, Moore J, et al: Placental edge to internal os distance in the late third trimester and mode of delivery in placenta praevia. *Br J Obstet Gynaecol* 110:860, 2003.
37. Matsubara S, Ohkuchi A, Kikkawa M, et al: Blood loss in low-lying placenta: placental edge to cervical internal os distance of less vs. more than 2 cm. *J Perinat Med* 36:507, 2008.
38. Bronsteen R, Valice R, Lee W, et al: Effect of a low-lying placenta on delivery outcome. *Ultrasound Obstet Gynecol* 33:204, 2009.
39. Kent EM, Breathnach FM, Gillan JE, et al: Placental cord insertion and birthweight discordance in twin pregnancies: results of the national prospective ESPRIT Study. *Am J Obstet Gynecol* 205:376.e1, 2011.
40. Ebbing C, Kiserud T, Johnsen SL, et al: Prevalence, risk factors, and outcomes of velamentous and marginal cord insertions: a population-based study of 634,741 pregnancies. *PLoS ONE* 8:e70380, 2013.
41. Benirschke K, Burton GJ, Baergen RN: Anatomy and pathology of the umbilical cord. In Benirschke K, Burton GJ, Baergen RN, editors: *Pathology of the Human Placenta*, ed 6, Berlin, Germany, 2012, Springer, pp 309–375.
42. Esakoff TF, Cheng YW, Snowden JM, et al: Velamentous cord insertion: is it associated with adverse perinatal outcomes? *J Matern Fetal Neonatal Med* 28(4):409–412, 2015.
43. Pinar H, Goldenberg RL, Koch MA, et al: Placental findings in singleton stillbirths. *Obstet Gynecol* 123:325, 2014.
44. Bronsteen R, Whitten A, Balasubramanian M, et al: Vasa previa: clinical presentations, outcomes, and implications for management. *Obstet Gynecol* 122:352, 2013.
45. Oyelese KO, Tuner M, Lees C, et al: Vasa previa: an avoidable obstetric tragedy. *Obstet Gynecol Surv* 54:138, 1999.
46. Catanzarite V, Maida C, Thomas W, et al: Prenatal sonographic diagnosis of vasa previa: ultrasound findings and obstetric outcome in ten cases. *Ultrasound Obstet Gynecol* 18:109, 2001.
47. Oyelese Y, Catanzarite V, Prefumo F, et al: Vasa previa: the impact of prenatal diagnosis on outcomes. *Obstet Gynecol* 103:937, 2004.
48. Rebarber A, Dolin C, Fox NS, et al: Natural history of vasa previa across gestation using a screening protocol. *J Ultrasound Med* 33:141, 2014.
49. Schachter M, Tovbin Y, Arieli S, et al: In vitro fertilization is a risk factor for vasa previa. *Fertil Steril* 78:642, 2002.
50. Gagnon R1, Morin L, Bly S, et al; Society of Obstetricians and Gynaecologists of Canada: Clinical Practice Guideline: guidelines for the management of vasa previa. *J Obstet Gynaecol Can* 31(8):748–760, 2009.
51. Miller DA, Chollet JA, Goodwin TM: Clinical risk factors for placenta previa-placenta accreta. *Am J Obstet Gynecol* 177:210, 1997.
52. American College of Obstetricians and Gynecologists: ACOG Committee Opinion No. 529: placenta accreta. *Obstet Gynecol* 120:207, 2012.
53. Silver RM, Landon MB, Rouse DJ, et al: Maternal morbidity associated with multiple repeat cesarean deliveries. *Obstet Gynecol* 107:1226, 2006.
54. Eller AG, Bennett MA, Sharshiner M, et al: Maternal morbidity in cases of placenta accreta managed by a multidisciplinary care team compared with standard obstetric care. *Obstet Gynecol* 117:331, 2011.
55. Abuhamad A: Morbidly adherent placenta. *Semin Perinatol* 37:359, 2013.
56. Flood KM, Said S, Geary M, et al: Changing trends in peripartum hysterectomy over the last 4 decades. *Am J Obstet Gynecol* 220:632.e1, 2009.
57. Wu S, Kicherginsky M, Hibbard JU: Abnormal placentation: twenty-year analysis. *Am J Obstet Gynecol* 192:1458, 2005.

58. Weiniger CF, Einav S, Deutsch L, et al: Outcomes of prospectively-collected consecutive cases of antenatal-suspected placenta accreta. *Int J Obstet Anesth* 22:273, 2013.
59. Koai E, Kadpawat A, Gebb J, et al: Clinical outcomes of anterior compared with posterior placenta accreta. *Obstet Gynecol* 123(Suppl 1):60S, 2014.
60. Mathiesen E, Hohenwarter M, Basir Z, et al: Placenta increta after hysteroscopic myomectomy. *Obstet Gynecol* 122:478, 2013.
61. Hare AA, Olah KS: Pregnancy following endometrial ablation: a review article. *J Obstet Gynaecol* 25:108, 2005.
62. Hamar BD, Wolff EF, Kodaman PH, et al: Premature rupture of membranes, placenta increta, and hysterectomy in a pregnancy following endometrial ablation. *J Perinatol* 26:135, 2006.
63. Roux I, Das M, Fernandez H, et al: Pregnancy following endometrial ablation: a report of 3 cases. *J Reprod Med* 58:173, 2013.
64. Al-Serehi A, Mhoyan A, Brown M, et al: Placenta accreta: an association with fibroids and Asherman syndrome. *J Ultrasound Med* 27:1623, 2008.
65. Twickler DM, Lucas ML, Balis AB, et al: Color flow mapping for myometrial invasion in women with a prior cesarean delivery. *J Matern Fetal Med* 9(6):330–335, 2000.
66. Finberg HJ, Williams JW: Placenta accreta: prospective sonographic diagnosis in patients with placenta previa and prior cesarean section. *J Ultrasound Med* 11:333, 1992.
67. Cali G, Giambranco L, Puccio G, et al: Morbidly adherent placenta: evaluation of ultrasound diagnostic criteria and differentiation of placenta accreta from percreta. *Ultrasound Obstet Gynecol* 41:406, 2013.
68. Comstock CH, Love JJ, Bronsteen RA, et al: Sonographic detection of placenta accreta in the second and third trimesters of pregnancy. *Am J Obstet Gynecol* 190:1135, 2004.
69. Comstock CH, Bronsteen RA: The antenatal diagnosis of placenta accreta. *Br J Obstet Gynaecol* 121:171, 2014.
70. D'Antonio F, Iacovella C, Bhide A: Prenatal identification of invasive placentation using ultrasound: systemic review and meta-analysis. *Ultrasound Obstet Gynecol* 42:509, 2013.
71. Rac MWF, Dashe JS, Wells CE, et al: Ultrasound predictors of placental invasion: the Placenta Accreta Index. *Am J Obstet Gynecol* 212(3):343.e1–343.e7, 2015.
72. Warshak CR, Eskander R, Hull AD, et al: Accuracy of ultrasonography and magnetic resonance imaging in the diagnosis of placenta accreta. *Obstet Gynecol* 108:573, 2006.
73. McLean LA, Heilbrun ME, Eller AG, et al: Assessing the role of magnetic resonance imaging in the management of gravid patients at risk for placenta accreta. *Acad Radiol* 18(9):1175–1180, 2011.
74. Timor-Tritsch IE, Monteagudo A: Unforeseen consequences of the increasing rate of cesarean deliveries: early placenta accreta and cesarean scar pregnancy. A review. *Am J Obstet Gynecol* 207(1):14–29, 2012.
75. Moschos E, Wells CE, Twickler DM: Biometric sonographic findings of abnormally adherent trophoblastic implantations on cesarean delivery scars. *J Ultrasound Med* 33:475, 2014.
76. Sinha P, Mishra M: Cesarean scar pregnancy: a precursor of placenta percreta/accreta. *J Obstet Gynaecol* 32:621, 2012.
77. Timor-Tritsch IE, Monteagudo A, Cali G, et al: Cesarean scar pregnancy and early placenta accreta share a common histology. *Ultrasound Obstet Gynecol* 43(4):383–395, 2014.
78. Timor-Tritsch IE, Monteagudo A, Santos R, et al: The diagnosis, treatment, and follow-up of cesarean scar pregnancy. *Am J Obstet Gynecol* 207(1):44.e1–44.e13, 2012.
79. Ballas J, Pretorius D, Hull AD, et al: Identifying sonographic markers for placenta accreta in the first trimester. *J Ultrasound Med* 31:1835, 2012.
80. Timor-Tritsch IE, Monteagudo A, Cali G, et al: Cesarean scar pregnancy is a precursor of morbidly adherent placenta. *Ultrasound Obstet Gynecol* 44(3):346–353, 2014.
81. Moschos E, Sreenarasimhaiah S, Twickler DM: First-trimester diagnosis of cesarean scar ectopic pregnancy. *J Clin Ultrasound* 36:504, 2008.
82. Jauniaux E, Moscoso G, Campbell S, et al: Correlation of ultrasound and pathologic findings of placental anomalies in pregnancies with elevated maternal serum  $\alpha$ -fetoprotein. *Eur J Obstet Gynecol Reprod Biol* 37(3):219–230, 1990.
83. Brown DL, DiSalvo DN, Frates MC, et al: Placental surface cysts detected on sonography: histologic and clinical correlation. *J Ultrasound Med* 21(6):641–646, 2002.
84. Brown HL, Miller JM, Jr, Khawli O, et al: Premature placental calcification in maternal cigarette smokers. *Obstet Gynecol* 71(6):914–917, 1988.
85. Fox H, Sebire NJ: Macroscopic abnormalities of the placenta. In Fox H, Sebire NJ, editors: *Pathology of the Placenta*, ed 3, Philadelphia, 2007, WB Saunders, pp 95–145.
86. Grannum PA, Berkowitz RL, Hobbins JC: The ultrasonic changes in the maturing placenta and their relation to fetal pulmonary maturity. *Am J Obstet Gynecol* 133(8):915–922, 1979.
87. Hill LM, Breckle R, Ragozzino MW, et al: Grade 3 placentation: incidence and neonatal outcome. *Obstet Gynecol* 61(6):728–732, 1983.
88. Moran M, Ryan J, Higgins M, et al: Poor agreement between operators on grading of the placenta. *J Obstet Gynaecol* 31(1):24–28, 2011.
89. Sau A, Seed P, Langford K: Intraobserver and interobserver variation in the sonographic grading of placental maturity. *Ultrasound Obstet Gynecol* 23(4):374–377, 2004.
90. Chen KH, Chen LR, Lee YH: Exploring the relationship between preterm placental calcification and adverse maternal and fetal outcome. *Ultrasound Obstet Gynecol* 37(3):328–334, 2011.
91. Chen KH, Chen LR, Lee YH: The role of preterm placental calcification in high-risk pregnancy as a predictor of poor uteroplacental blood flow and adverse pregnancy outcome. *Ultrasound Med Biol* 38(6):1011–1018, 2012.
92. McKenna D, Tharmaratnam S, Mahsud S, et al: Ultrasonic evidence of placental calcification at 36 weeks' gestation: maternal and fetal outcomes. *Acta Obstet Gynecol Scand* 84(1):7–10, 2005.
93. Patterson RM, Hayashi RH, Cavazos D: Ultrasonographically observed early placental maturation and perinatal outcome. *Am J Obstet Gynecol* 147(7):773–777, 1983.
94. Proud JG: Third trimester placental grading by ultrasonography as a test of fetal wellbeing. *BMJ* 294(6588):1641–1644, 1987.
95. Nyberg DA, Cyr DR, Mack LA, et al: Sonographic spectrum of placental abruption. *AJR Am J Roentgenol* 148:161, 1987.
96. Nagy S, Bush M, Stone J, et al: Clinical significance of subchorionic and retroplacental hematomas detected in the first trimester of pregnancy. *Obstet Gynecol* 102:94, 2003.
97. Norman SM, Odibo AO, Macones GA, et al: Ultrasound-detected subchorionic hemorrhage and the obstetric implications. *Obstet Gynecol* 116:311, 2010.
98. Ball RH, Ade CM, Schoenborn JA, et al: The clinical significance of ultrasonographically detected subchorionic hemorrhages. *Am J Obstet Gynecol* 174:996, 1996.
99. Maso G, D'Ottavio G, De Seta F, et al: First-trimester intrauterine hematoma and outcome of pregnancy. *Obstet Gynecol* 105:339, 2005.
100. Tuuli MG, Norman SM, Odibo AO, et al: Perinatal outcomes in women with subchorionic hematoma. *Obstet Gynecol* 117:1205, 2011.
101. Ananth CV, Berkowitz GS, Savitz DA, et al: Placental abruption and adverse perinatal outcomes. *JAMA* 282:1646, 1999.
102. Glantz C, Purnell L: Clinical utility of sonography in the diagnosis and treatment of placental abruption. *J Ultrasound Med* 21:837, 2002.
103. Guschmann M, Henrich W, Entezami M, Dudenhausen JW: Chorioangioma—new insights into a well-known problem. I. Results of a clinical and morphological study of 136 cases. *J Perinat Med* 31(2):163–169, 2003.
104. Wou K, Chen MF, Mallozzi A, et al: Pregnancy outcomes and ultrasonographic diagnosis in patients with histologically-proven placental chorioangioma. *Placenta* 32(9):671–674, 2011.
105. Khong TY, George K: Maternal serum alpha-fetoprotein levels in chorioangiomas. *Am J Perinatol* 11(03):245–248, 1994.
106. Zalel Y, Weisz B, Gamzu R, et al: Chorioangiomas of the placenta: sonographic and Doppler flow characteristics. *J Ultrasound Med* 21(8):909–913, 2002.



107. Taori K, Patil P, Attarde V, et al: Chorioangioma of placenta: sonographic features. *J Clin Ultrasound* 36(2):113–115, 2008.
108. Prapas N, Liang RI, Hunter D, et al: Color Doppler imaging of placental masses: differential diagnosis and fetal outcome. *Ultrasound Obstet Gynecol* 16(6):559–563, 2000.
109. Al Wattar BH, Hillman SC, Marton T, et al: Placenta chorioangioma: a rare case and systematic review of literature. *J Matern Fetal Neonatal Med* 27(10):1055–1063, 2013.
110. Jauniaux E, Ogle R: Color Doppler imaging in the diagnosis and management of chorioangiomas. *Ultrasound Obstet Gynecol* 15(6):463–467, 2000.
111. Wehrens XH, Offermans JP, Snijders M, et al: Fetal cardiovascular response to large placental chorioangiomas. *J Perinat Med* 32(2):107–112, 2004.
112. Sepulveda W, Alcalde JL, Schnapp C, et al: Perinatal outcome after prenatal diagnosis of placental chorioangioma. *Obstet Gynecol* 102(5 Pt 1):1028–1033, 2003.
113. Zanardini C, Papageorgiou A, Bhide A, et al: Giant placental chorioangioma: natural history and pregnancy outcome. *Ultrasound Obstet Gynecol* 35(3):332–336, 2010.
114. Jones K, Tierney K, Grubbs BH, et al: Fetoscopic laser photocoagulation of feeding vessels to a large placental chorioangioma following fetal deterioration after amnioreduction. *Fetal Diagn Ther* 31(3):191–195, 2012.
115. Lau TK, Leung TY, Yu SCH, et al: Prenatal treatment of chorioangioma by microcoil embolisation. *Br J Obstet Gynaecol* 110(1):70–73, 2003.
116. Nicolini U, Zuliani G, Caravelli E, et al: Alcohol injection: a new method of treating placental chorioangiomas. *Lancet* 353(9165):1674–1675, 1999.
117. Quintero RA, Reich H, Romero R, et al: In utero endoscopic devascularization of a large chorioangioma. *Ultrasound Obstet Gynecol* 8(1):48–52, 1996.
118. Sepulveda W, Wong AE, Herrera L, et al: Endoscopic laser coagulation of feeding vessels in large placental chorioangiomas: report of three cases and review of invasive treatment options. *Prenat Diagn* 29(3):201–206, 2009.
119. Ogino S, Redline RW: Villous capillary lesions of the placenta: distinctions between chorangioma, chorangiomatosis, and chorangiosis. *Human Pathol* 31(8):945–954, 2000.
120. Amer HZ, Heller DS: Chorangioma and related vascular lesions of the placenta—a review. *Fetal Pediatr Pathol* 29(4):199–206, 2010.
121. Evers IM, Nikkels PGJ, Sikkema JM, et al: Placental pathology in women with type 1 diabetes and in a control group with normal and large-for-gestational-age infants. *Placenta* 24(8–9):819–825, 2003.
122. Gupta R, Nigam S, Arora P, et al: Clinico-pathological profile of 12 cases of chorangiosis. *Arch Gynecol Obstet* 274(1):50–53, 2006.
123. Harris RD, Wells WA, Black WC, et al: Accuracy of prenatal sonography for detecting circumvallate placenta. *AJR Am J Roentgenol* 168(6):1603–1608, 1997.
124. Benson RC, Fujikura T: Circumvallate and circummarginate placenta. Unimportant clinical entities. *Obstet Gynecol* 34(6):799–804, 1969.
125. Wentworth P: Circumvallate and circummarginate placentas. Their incidence and clinical significance. *Am J Obstet Gynecol* 102(1):44–47, 1968.
126. Sebire NJ, Sepulveda W: Correlation of placental pathology with prenatal ultrasound findings. *J Clin Pathol* 61(12):1276–1284, 2008.
127. Rolschau J: The relationship between some disorders of the umbilical cord and intrauterine growth retardation. *Acta Obstet Gynecol Scand* 72:15–21, 1978.
128. Ozkavukcu E, Haliloglu N: Gray-scale and color Doppler US findings of amniotic sheets. *Diagn Interv Radiol* 18:298–302, 2012.
129. Gun I, Muhcu M, Mungen E, et al: Effect of an amniotic sheet on pregnancy outcomes. *J Ultrasound Med* 32(5):807–813, 2013.
130. Nelson LD, Grobman WA: Obstetric morbidity associated with amniotic sheets. *Ultrasound Obstet Gynecol* 36:324–327, 2010.
131. Tuuli MG, Shanks A, Bernhard L, et al: Uterine synechiae and pregnancy complications. *Obstet Gynecol* 119(4):810–814, 2012.
132. Martinez-Frias ML, Bermejo E, Pinilla ER: Body stalk defects, body wall defects, amniotic bands with and without body wall defects, and gastroschisis: comparative epidemiology. *Am J Med Genet* 92:13–18, 2000.
133. Barzilay E, Harel Y, Haas J, et al: Prenatal diagnosis of amniotic band syndrome—risk factors and ultrasonic signs. *J Matern Fetal Neonatal Med* 28(3):281–283, 2015. [Epub 2014 May 22].
134. Obdejn MC, Offringa PJ, Bos RR, et al: Facial clefts and associated limb anomalies: description of three cases and a review of the literature. *Cleft Palate Craniofac J* 47(6):661–667, 2010.
135. Torpin R: Amniochorionic mesoblastic fibrous strings and amniotic bands: associated constricting fetal malformations or fetal death. *Am J Obstet Gynecol* 91:65–75, 1965.
136. Streeter GL: Focal deficiencies in fetal tissues and their relation to intrauterine amputation. *Contrib Embryol* 22:1, 1930.
137. Bronshtein M, Zimmer EZ: Do amniotic bands amputate fetal organs? *Ultrasound Obstet Gynecol* 10:309–311, 1997.
138. Jauniaux E, De Munter C, Vanesse M, et al: Embryonic remnants of the umbilical cord: morphologic and clinical aspects. *Hum Pathol* 20(5):458–462, 1989.
139. Ghezzi F, Raio L, Di Naro E, et al: Single and multiple umbilical cord cysts in early gestation: two different entities. *Ultrasound Obstet Gynecol* 21:215–219, 2003.
140. Gilboa Y, Kivilevitch Z, Katorza E, et al: Outcomes of fetuses with umbilical cord cysts diagnosed during nuchal translucency examination. *J Ultrasound Med* 30(11):1547–1551, 2011.
141. Hannaford K, Reeves S, Wegner E: Umbilical cord cysts in the first trimester: are they associated with pregnancy complications? *J Ultrasound Med* 32(5):801–806, 2013.
142. Zangen R, Boldes R, Yaffe H, et al: Umbilical cord cysts in the second and third trimesters: significance and prenatal approach. *Ultrasound Obstet Gynecol* 36(3):296–301, 2010.
143. Berg TG, Rayburn WF: Umbilical cord length and acid-base balance at delivery. *J Reprod Med* 40(1):9–12, 1995.
144. Krakowiak P, Smith EN, de Bruyn G, et al: Risk factors and outcomes associated with a short umbilical cord. *Obstet Gynecol* 103(1):119–127, 2004.
145. Barbieri C, Cecatti JG, Krupa F, et al: Validation study of the capacity of the reference curves of ultrasonographic measurements of the umbilical cord to identify deviations in estimated fetal weight. *Acta Obstet Gynecol Scand* 87(3):286–291, 2008.
146. Cromi A, Ghezzi F, Di Naro E, et al: Large cross-sectional area of the umbilical cord as a predictor of fetal macrosomia. *Ultrasound Obstet Gynecol* 30(6):861–866, 2007.
147. Raio L, Ghezzi F, Di Naro E, et al: Sonographic measurement of the umbilical cord and fetal anthropometric parameters. *Eur J Obstet Gynecol Reprod Biol* 83(2):131–135, 1999.
148. Raio L, Ghezzi F, Di Naro E, et al: Umbilical cord morphologic characteristics and umbilical artery Doppler parameters in intrauterine growth-restricted fetuses. *J Ultrasound Med* 22(12):1341–1347, 2003.
149. Lacro RV, Jones KL, Benirschke K: The umbilical cord twist: origin, direction, and relevance. *Am J Obstet Gynecol* 157(4 Pt 1):833–838, 1987.
150. Strong TH, Jr, Jarles DL, Vega JS, et al: The umbilical coiling index. *Am J Obstet Gynecol* 170(1 Pt 1):29–32, 1994.
151. Sebire NJ: Pathophysiological significance of abnormal umbilical cord coiling index. *Ultrasound Obstet Gynecol* 30(6):804–806, 2007.
152. Chitra T, Sushanth YS, Raghavan S: Umbilical coiling index as a marker of perinatal outcome: an analytical study. *Obstet Gynecol Int* 2012:213689, 2012.
153. de Laat MW, Franx A, Nikkels PGJ, et al: Prenatal ultrasonographic prediction of the umbilical coiling index at birth and adverse pregnancy outcome. *Ultrasound Obstet Gynecol* 28(5):704–709, 2006.
154. de Laat MW, Meij JJC, Visser GH, et al: Hypercoiling of the umbilical cord and placental maturation defect: associated pathology? *Pediatr Dev Pathol* 10(4):293–299, 2007.
155. Ernst LM, Minturn L, Huang MH, et al: Gross patterns of umbilical cord coiling: correlations with placental histology and stillbirth. *Placenta* 34(7):583–588, 2013.

156. Jessop FA, Lees CC, Pathak S, et al: Umbilical cord coiling: clinical outcomes in an unselected population and systematic review. *Virchows Arch* 464(1):105–112, 2014.
157. Qin Y, Lau TK, Rogers MS: Second-trimester ultrasonographic assessment of the umbilical coiling index. *Ultrasound Obstet Gynecol* 20(5):458–463, 2002.
158. Predanic M, Perni SC, Chasen ST, et al: Assessment of umbilical cord coiling during the routine fetal sonographic anatomic survey in the second trimester. *J Ultrasound Med* 24(2):185–191, 2005.
159. Kurita M, Hasegawa J, Mikoshiba T, et al: Ultrasound evaluation of the amount of Wharton's jelly and the umbilical coiling index. *Fetal Diagn Ther* 26(2):85–89, 2009.
160. Blickstein I, Varon Y, Varon E: Implications of differences in coiling indices at different segments of the umbilical cord. *Gynecol Obstet Invest* 52(3):203–206, 2001.
161. Fox H, Sebire NJ: Pathology of the umbilical cord. In Fox H, Sebire NJ, editors: *Pathology of the Placenta*, ed 3, Philadelphia, 2007, WB Saunders, pp 473–509.
162. Defigueiredo D, Dagklis T, Zidere V, et al: Isolated single umbilical artery: need for specialist echocardiography? *Ultrasound Obstet Gynecol* 36:553, 2010.
163. Hua M, Odibo AO, Macones GA, et al: Single umbilical artery and its associated findings. *Obstet Gynecol* 115(5):930, 2010.
164. Murphy-Kaulbeck L, Dodds L, Joseph KS, et al: Single umbilical artery risk factors and pregnancy outcomes. *Obstet Gynecol* 116(4):843, 2010.
165. Lubusky M, Dhaifalal I, Prchazka M, et al: Single umbilical artery and its siding in the second trimester of pregnancy: relation to chromosomal defects. *Prenat Diagn* 27:327, 2007.
166. Abuhamad AZ, Shaffer W, Mari G, et al: Single umbilical artery: does it matter which artery is missing? *Am J Obstet Gynecol* 173:728, 1995.
167. Geipel A, Germer U, Welp T, et al: Prenatal diagnosis of single umbilical artery: determination of the absent side, associated anomalies, Doppler findings, and perinatal outcome. *Ultrasound Obstet Gynecol* 15:114, 2000.
168. Stout MJ, Odibo AO, Longman R, et al: The incidence of isolated single umbilical artery in twins and adverse pregnancy outcomes. *Prenat Diagn* 33:269, 2013.
169. Prefumo F, Guven MA, Carvalho JS: Single umbilical artery and congenital heart disease in selected and unselected populations. *Ultrasound Obstet Gynecol* 35:552, 2010.
170. Dagklis T, Defigueiredo D, Staboulidou I, et al: Isolated single umbilical artery and fetal karyotype. *Ultrasound Obstet Gynecol* 36:291, 2010.
171. Predanic M, Perni SC, Friedman A, et al: Fetal growth assessment and neonatal birth weight in fetuses with an isolated single umbilical artery. *Obstet Gynecol* 105:1093, 2005.
172. Bombrys AE, Neiger R, Hawkins S, et al: Pregnancy outcome in isolated single umbilical artery. *Am J Perinatol* 25:239, 2008.
173. Voskamp BJ, Fleurke-Rozema H, Oude-Rengerink K, et al: Relationship of isolated single umbilical artery to fetal growth, aneuploidy, and perinatal mortality: systematic review and meta-analysis. *Ultrasound Obstet Gynecol* 42(6):622–628, 2013.
174. Weichert J, Hartge D, Germer U, et al: Persistent right umbilical vein: a prenatal condition worth mentioning? *Ultrasound Obstet Gynecol* 37:543, 2011.
175. Martinez R, Gamez F, Bravo C, et al: Perinatal outcome of ultrasound prenatal diagnosis of persistent right umbilical vein. *Eur J Obstet Gynecol Reprod Biol* 168:36, 2013.
176. Wolman I, Gull I, Fait G, et al: Persistent right umbilical vein: incidence and significance. *Ultrasound Obstet Gynecol* 19:562, 2002.
177. Mahoney BS, McGahan JP, Nyberg DA, et al: Varix of the fetal intra-abdominal umbilical vein: comparison with normal. *J Ultrasound Med* 11:73, 1992.
178. Byers BD, Goharkhay N, Mateus J, et al: Pregnancy outcome after ultrasound diagnosis of fetal intra-abdominal umbilical vein varix. *Ultrasound Obstet Gynecol* 33(3):282–286, 2009.
179. Weissmann-Brenner A, Simchen MJ, Moran O, et al: Isolated fetal umbilical vein varix—prenatal sonographic diagnosis and suggested management. *Prenat Diagn* 29:229, 2009.
180. Mankuta D, Nadjari M, Pomp G: Isolated fetal intra-abdominal umbilical vein varix: clinical importance and recommendations. *J Ultrasound Med* 30:273, 2011.
181. Cohen Y, Har-Tov J, Fait G, et al: Ultrasonographic evidence of intra-abdominal umbilical vein dilatation: is it a true varix? *Ultrasound Med Biol* 38:412, 2012.
182. Lee SW, Kim MY, Kim JE, et al: Clinical characteristics and outcomes of antenatal fetal intra-abdominal umbilical vein varix detection. *Obstet Gynecol Sci* 57:181, 2014.
183. Sepulveda W, Mackenna A, Sanchez J, et al: Fetal prognosis in varix of the intrafetal umbilical vein. *J Ultrasound Med* 17:171, 1998.
184. Airas U, Heinonen S: Clinical significance of true umbilical knots: a population-based analysis. *Am J Perinatol* 19:127, 2002.
185. Sornes T: Umbilical cord knots. *Acta Obstet Gynecol Scand* 79:157, 2000.
186. Ramon y Cajal CL, Martinez RO: Four-dimensional ultrasonography of a true knot of the umbilical cord. *Am J Obstet Gynecol* 195:896, 2006.
187. Scioscia M, Fornale M, Bruni F, et al: Four-dimensional and Doppler sonography in the diagnosis and surveillance of a true cord knot. Case report. *J Clin Ultrasound* 39:157, 2011.
188. Rodriguez N, Angarita AM, Casasbuenas A, et al: Three-dimensional high-definition flow imaging in prenatal diagnosis of a true umbilical cord knot. *Ultrasound Obstet Gynecol* 39:245, 2012.
189. Abuhamad A: Three-dimensional ultrasound with color Doppler imaging of an umbilical cord true knot. Picture of the month. *Ultrasound Obstet Gynecol* 43:360, 2014.
190. Stempel LE: Beyond the pretty pictures: giving obstetricians just enough (umbilical) cord to hang themselves. *Am J Obstet Gynecol* 195:888, 2006.
191. Dias T, Mahsud-Dornan S, Bhide A, et al: Cord entanglement and perinatal outcome in monoamniotic twin pregnancies. *Ultrasound Obstet Gynecol* 35:201, 2010.
192. Rossi AC, Prefumo F: Impact of cord entanglement on perinatal outcome of monoamniotic twins: a systematic review of the literature. *Ultrasound Obstet Gynecol* 41:131, 2013.



# Amniotic Fluid Volume in Fetal Health and Disease

Everett F. Magann, Adam T. Sandlin

## SUMMARY OF KEY POINTS

- The pathways influencing amniotic fluid volume (AFV) are dynamic and complex and are not completely understood.
- The balance of maintaining the overall AFV occurs at three key areas: fetal urine production and fetal swallowing, the intramembranous pathway, and the osmotic fluid gradient created between the mother and the fetus.
- There are several published curves that attempt to define a normal AFV.
- Abnormal fluid volumes should be defined as specific high or low values across gestation that are linked with adverse pregnancy outcomes.
- The single deepest pocket measurement for estimation of the AFV is the preferred technique for assessment during the ultrasound evaluation.

## OUTLINE

Amniotic Fluid Physiology and Dynamics, 704

Determination of Amniotic Fluid Volume, 706

Potential Difficulties in Amniotic Fluid Volume Estimation Using Ultrasound, 707

Normal Amniotic Fluid Volume in Singleton Pregnancies, 708

Amniotic Fluid Volume and Pregnancy Outcomes, 710  
Oligohydramnios, 711

Pulmonary Hypoplasia, 711

Assessment of Amniotic Fluid Volume in the High-Risk Patient, 712

Polyhydramnios, 712

Fetal Growth Restriction and Amniotic Fluid Volume, 714

Amniotic Fluid Volume in Twin Pregnancies, 714

Conclusions, 715

Amniotic fluid provides an ideal setting for the developing fetus by providing an environment that protects from trauma, provides a source of water, allows for normal fetal movements essential for anatomic development, and contributes to the development of the fetal lungs.<sup>1</sup> The amniotic fluid volume (AFV) can reflect fetal well-being, and changes in the volume may indicate maternal or fetal disease processes. Therefore, the assessment of the AFV is an essential component to the sonographic evaluation of the gravid patient.

## AMNIOTIC FLUID PHYSIOLOGY AND DYNAMICS

Once thought to be a static collection of fluid with turnover once per day, the AFV is now recognized to be a complex system involving multiple dynamic pathways that influence the inflow and outflow of fluid and solutes within the amniotic space. The physiologic processes that influence the AFV are complex and not yet completely understood. In order to appreciate the AFV, knowledge of the pathways for potential amniotic fluid movement and the regulatory mechanisms involved need to be considered.

Several potential variables influence the overall AFV. Most influential are fetal urine production and fetal swallowing.<sup>2</sup> Others include secretion of fetal lung fluid, the intramembranous pathway (movement of water and solutes between amniotic fluid and fetal blood and

the placenta), the transmembranous pathway (movement of water and solutes across the surface area of the amnion and chorion), secretions by the fetal oronasal cavities, and movement of water across the highly permeable fetal skin during early gestation.<sup>2</sup> Amniotic fluid consists primarily of water (98-99%).<sup>2</sup> In early pregnancy, amniotic fluid is isotonic with maternal or fetal plasma and contains a small amount of proteins.<sup>2</sup> Although amniotic fluid is present in early gestation prior to fetal urine production, not much is known regarding the dynamics of amniotic fluid early in human pregnancy. However, there is likely an active transport of solutes across the amnion into the amniotic space with water moving passively down an osmotic gradient.<sup>2</sup> A transudate of plasma may also occur across nonkeratinized fetal skin or from the mother across the uterine decidua and the placental surface, which may contribute to the AFV in early pregnancy<sup>1</sup> (Fig. 20-1).

Much more is known about the dynamics of the AFV in the latter half of pregnancy. Fetal skin keratinizes at approximately 22 to 25 weeks' gestation, preventing further movement of water across the fetal skin.<sup>2</sup> As a result of an increasing production of dilute fetal urine, amniotic fluid osmolality and sodium concentrations decrease as the gestational age increases.<sup>2</sup> Ultimately amniotic fluid osmolality reaches 250 to 260 mOsm/mL at term.<sup>2</sup> Fetal osmolality ( $\approx$ 278 mOsm/mL) remains close to maternal osmolality (280 mOsm/mL), thereby

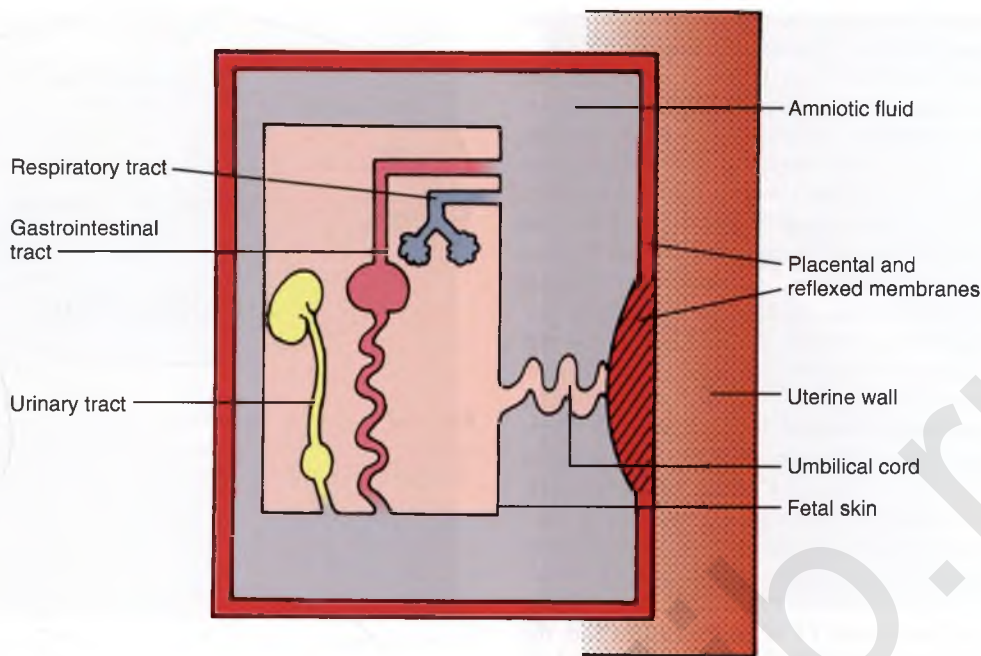


**FIG 20-1** The major fetal and maternal amniotic structures involved in the formation and reabsorption of amniotic fluid. (From Wallenburg HCS: The amniotic fluid. *J Perinatal Med* 5:193, 1977.)

limiting the amount of water transfer between the fetal and maternal circulations under normal conditions.<sup>3</sup>

Fetal urine production is the primary source of amniotic fluid in the second half of pregnancy. This is supported by the near complete absence of amniotic fluid in the setting of renal agenesis or fetal urinary tract obstruction. Fetal urine first enters the amniotic space at 8 to 11 weeks' gestation and continually increases throughout gestation.<sup>4</sup> Fetal urine production per kilogram of fetal body weight at 25 weeks' gestation is approximately 110 mL/kg per 24 hours, and it increases to approximately 190 mL/kg per 24 hours at 39 weeks' gestation.<sup>5</sup> Based on sonographic studies of the fetal bladder measured at regular intervals, the human fetal urine output at term is estimated to be 700 to 900 mL/day.<sup>2</sup> In order to contribute to the regulation of the AFV, the fetus is able to respond to changes in fluid status by adjusting urine flow.<sup>1</sup> Thurlow and Brace<sup>6</sup> observed fetal ovine hypoxia to be associated with increased urine flow, as opposed to the often associated chronic fetal hypoxia and low AFV. Similarly, Gagnon and associates<sup>7</sup> found the reduction in overall AFV in the setting of chronic severe placental insufficiency in sheep was due to an increase in the intramembranous absorption of amniotic fluid, not a decrease in fetal urinary production. This finding suggests that human regulation of the AFV is mediated by other mechanisms (e.g., intramembranous absorption) in addition to changes in fetal urine production at times of fetal hypoxia.<sup>7</sup>

Fetal swallowing plays a key role in maintaining a stable AFV. In humans, the fetus begins to swallow around the same time that fetal urine first enters the amniotic space, at 8 to 11 weeks' gestational age.<sup>2</sup> An estimated 210 to 760 mL/day is swallowed by the near term fetus.<sup>8</sup> In the ovine fetus, hypoxia has been shown to suppress fetal swallowing,<sup>9</sup> whereas decreases in amniotic fluid osmolality and increases in fetal plasma osmolality will increase fetal swallowing.<sup>10</sup> In primates, esophageal ligation leads to the development of hydramnios; however, the AFV returns to normal before delivery.<sup>11</sup> It is thought the maintenance of a constant AFV despite esophageal ligation in the presence of continued urine production is a result of increasing intramembranous

absorption.<sup>12</sup> Based on these studies, it seems the human fetus is able to alter its swallowing to some degree under various conditions; however, it is unlikely that this represents the major regulatory mechanism by which the human fetus maintains its AFV.

Secretion of fetal lung fluid into the amniotic cavity is well established. This concept is supported by the fact that phospholipids are present in the amniotic fluid that can be used as tests for fetal lung maturity. These phospholipids are of pulmonary origin and are not present in substantial quantities in the fetal urine. Ligation of the trachea in utero in other animal species results in expansion of the fetal lung seemingly due to the continued production of fetal lung fluid.<sup>2</sup> Fetal lung fluid secretion allows for pulmonary expansion serving to promote fetal lung development.<sup>1</sup> Near term fetal sheep demonstrate an outflow of lung fluid of 200 to 400 mL/day.<sup>13</sup> Approximately half of the secreted lung fluid enters the amniotic fluid, and the remainder is swallowed as it exits the trachea,<sup>9</sup> resulting in a net secretion of 100 to 200 mL/day. Secretion flow is likely the result of active transport of chloride ions across the epithelial lining of the developing lungs.<sup>2</sup> The fetal glottis serves to prevent backflow of amniotic fluid into the trachea; thus, there appears to be little osmotic exchange between amniotic fluid and fetal plasma in the lung.<sup>3</sup> Secretion of lung fluid into the amniotic fluid is likely a main contributor to the AFV, although factors that regulate fetal lung fluid secretion are poorly understood, and the exact amount secreted into the amniotic cavity in the human fetus has not yet been quantified.

An excess of approximately 400 mL is present within the amniotic cavity after considering the volume of fetal urine production and secreted lung fluid less the amount removed via fetal swallowing.<sup>3</sup> Furthermore, as gestation advances, fetal urine production as well as secreted lung fluid increases. The process by which this excess volume is compensated to maintain AFV balance is referred to as the *intramembranous pathway*. Based on studies in the near term ovine fetus, it is estimated that approximately 200 to 500 mL/day of amniotic fluid is absorbed via the intramembranous pathway.<sup>14</sup> Studies in other animal species have demonstrated that the AFV returns to a homeostatic state



even after large volumes of fluid are infused into the amniotic fluid cavity or after esophageal ligation.<sup>1</sup> This finding suggests there is a continuous flow of water and solutes from the amniotic fluid into the fetal circulation. The osmotic gradient between the fetal circulation and the amniotic fluid appears to influence the intramembranous movement of water and solutes across the fetal vessels on the surface of the placenta into the fetal circulation. However, in one ovine study, it was demonstrated that only approximately 35% of the intramembranous movement of fluid depends on the osmotic difference between the amniotic fluid and the fetal circulation.<sup>15</sup> Consequently, there must be other nonpassive mechanisms that contribute to this pathway.

The maternal fluid status can influence the fluid balance between the fetal circulation and the AFV. At times of maternal dehydration, the intramembranous pathway likely plays a role in correcting the fetal volume status. With maternal dehydration, the maternal serum osmolality increases, resulting in water movement from the fetal circulation to the maternal circulation. This results in a fetal dehydration state causing increased fetal osmolality and promoting movement of water from the amniotic fluid back into the fetal circulation in order to restore the fetal intravascular volume, leading to a decrease in the AFV.<sup>3</sup> The reverse is also true. As demonstrated by Magann and colleagues, intravenous maternal hydration with 1 L of fluid increased both the actual and sonographically estimated AFV in the human fetus, with an average increase in the actual AFV of 188 mL.<sup>16</sup> Similarly, Kilpatrick and coworkers showed that in a patient with a low AFV, maternal hydration with 2 L of water can increase the human fetal amniotic fluid index (AFI) by up to 31%.<sup>17</sup> There is little evidence to support the movement of fluid via the transmembranous pathway as a major contributor to the overall AFV. Studies in sheep suggest that only 10 mL/day is absorbed by the uterus in late gestation in the setting of normal osmolality.<sup>18</sup> Given the large surface area of the amnion and chorion, it is clear why membrane permeability has been proposed as a regulator of the AFV. However, very little is known regarding the permeability and filtration characteristics of the membranes as they relate to amniotic fluid dynamics.

The amount of fluid secreted by the fetal oronasal cavities is small and not considered a main contributor to the AFV. Studies in sheep demonstrate that approximately 25 mL/day is secreted by the fetal oronasal cavities in late gestation.<sup>19</sup> Based on information regarding transepidermal water loss in the preterm infant, it is generally believed there is movement of water across the fetal skin before 22 to 25 weeks' gestation, which contributes to the AFV in the first half of pregnancy. It seems reasonable to assume there may be a relationship between fetal weight and the AFV because a larger fetus would presumably produce more urine output. However, neonatal birth weight has not been shown to be correlated with either a dye-determined or an ultrasound-estimated AFV.<sup>20</sup> In addition, no clinical correlation has been shown between the AFI and estimated human fetal weight<sup>21</sup> (Fig. 20-2).

## DETERMINATION OF AMNIOTIC FLUID VOLUME

How does one measure the AFV during pregnancy? The true AFV can be measured by dye-dilution techniques utilizing amniocentesis or can be directly measured at the time of cesarean delivery.<sup>22-24</sup> However, these methods are obviously not practical for routine clinical use. Alternatively, the AFV is commonly estimated with the use of ultrasound techniques. In the literature, four techniques have been described to estimate the AFV: the AFI<sup>25-27</sup>; the single deepest pocket (SDP), also referred to as the deepest vertical pocket (DVP) or maximal vertical pocket (MVP)<sup>28,29</sup>; the two-diameter pocket<sup>30</sup>; and subjective assessment.<sup>31,32</sup> The two methods most commonly used are the AFI and DVP. The two-diameter pocket measurement (horizontal and vertical

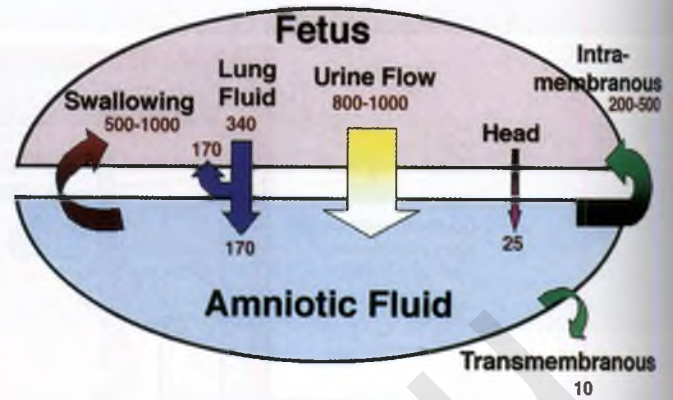


**FIG 20-2** Summary of the flow of fluids into and out of the amniotic space in late gestation. (From Brace RA: Physiology of amniotic fluid volume regulation. Clin Obstet Gynecol 40:286, 1997.)

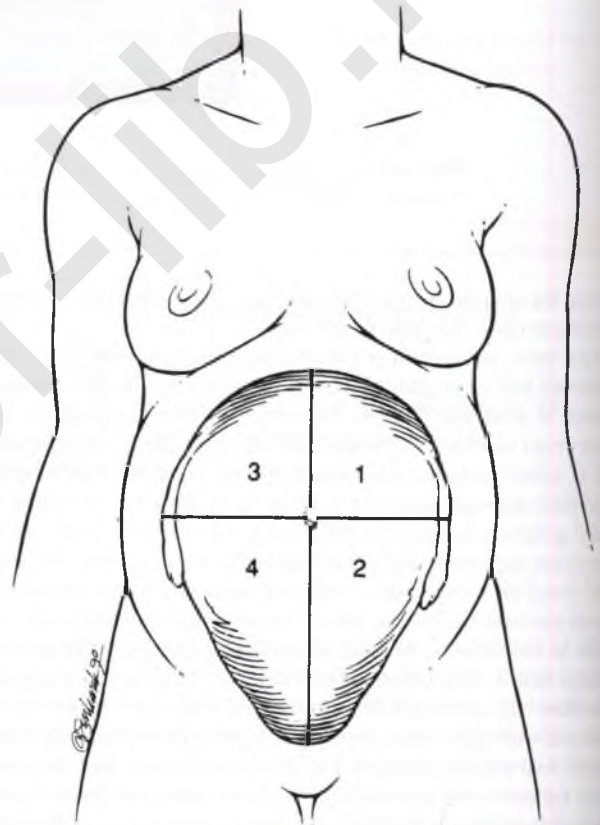


**FIG 20-3** Diagram of the division of the uterus into four equal quadrants for determination of the amniotic fluid index (AFI). With the patient supine and the ultrasound transducer perpendicular to the table, the vertical depth (measured in centimeters) of the largest amniotic fluid pocket free of umbilical cord in each quadrant is measured. AFI is calculated by summing these four measurements. (From Gabbe SG, Niebyl JR, Simpson JL: Obstetrics: Normal and Problem Pregnancies, 2nd ed. New York, Churchill Livingstone, 1991.)

dimensions of the maximum vertical pocket are multiplied together to obtain a single value, in  $\text{cm}^2$ ) was shown to not be a better predictor of AFV than the AFI and is no longer widely used.<sup>33</sup> As originally described by Phelan and associates, in order to calculate the AFI, the abdomen is divided into four quadrants in which the umbilicus divides the upper and lower halves and the linea nigra divides the right and left halves (Fig. 20-3).<sup>34</sup> With the patient supine, the linear (or





**FIG 20-4** Normal amniotic fluid volume assessed by measurement of the largest single pocket of fluid. In this 22-week gestation, the largest vertical pocket of amniotic fluid, devoid of umbilical cord, is 24 mm.

curvilinear) transducer is placed along the maternal anterior abdominal wall and held perpendicular to the floor. The maximum vertical pocket of fluid (usually reported in centimeters) is measured in each of the four quadrants, and the AFI (in centimeters) equals the sum of these four measurements.<sup>25,34</sup> The DVP is simply the largest single vertical pocket of fluid that is at least 1 cm in width, obtained following the same criteria described here<sup>29,31</sup> (Fig. 20-4).

Studies have demonstrated that the dye-determined amniotic fluid calculation and direct measurement at the time of cesarean delivery have good concordance ( $r = 0.99$ ) and either can be used to determine actual AFV.<sup>35</sup> It has been shown that both the AFI and the DVP technique can reliably identify normal AFVs. Unfortunately, most studies have demonstrated poor reliability for ultrasound-estimated AFVs to predict actual low or high volumes.<sup>22-24,30,36,37</sup> Subjective assessment (visual interpretation without ultrasound measurements) of AFV has been compared with dye-determined or directly measured AFV, and studies have shown no difference in the accuracy of subjective compared to objective assessment (visual interpretation with ultrasound measurements) in the correct determination of AFV.<sup>38</sup> Likewise, when comparing subjective assessment of AFV in the second and third trimesters and objective assessment with dye-determined fluid volumes, neither operator experience nor sonographic technique was found to affect the accuracy of ultrasound estimates of the AFV<sup>31</sup> (Figs. 20-5 and 20-6).

Traditionally, pockets filled with umbilical cord have not been used in measurement of the AFV. The use of color Doppler ultrasound can help detect umbilical cord, which may be present within an apparent pocket of amniotic fluid. Thus, it has been suggested that color Doppler be applied during evaluation of the AFV to identify segments of umbilical cord that may not be appreciated on standard gray-scale ultrasound images (Fig. 20-7) in order to improve detection of low AFV.<sup>39</sup> However, the use of color Doppler in the sonographic estimation of AFV has been shown to result in overdiagnosis of low AFV (oligohydramnios).<sup>40</sup> In a study by Magann and colleagues, the use of color Doppler inappropriately diagnosed 21% of women with low AFV who actually had normal dye-determined AFVs.<sup>41</sup> In addition, color



**FIG 20-5** Longitudinal sonogram in a second trimester gestation with normal amniotic fluid. Subjective evaluation of normal amniotic fluid depends on the relationship between amniotic fluid and the space occupied by the fetus and placenta.

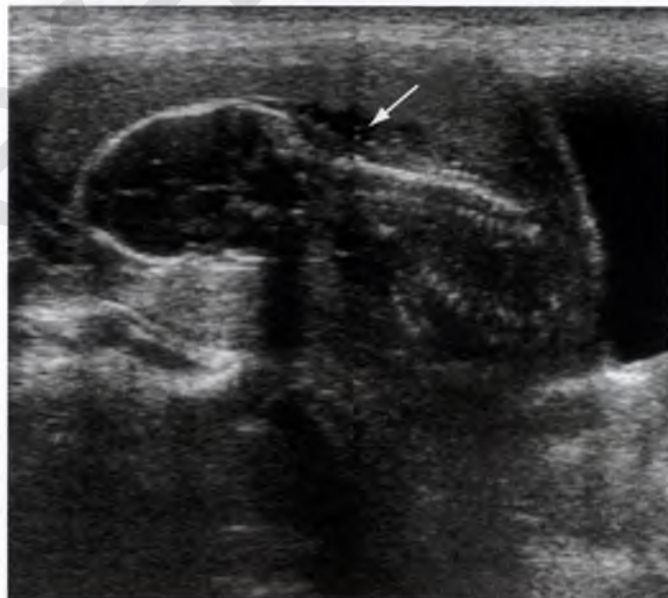


**FIG 20-6** Sonogram of a fetus with renal agenesis. Virtually no amniotic fluid is seen. The fetus is "crowded" within the uterus. The only relatively anechoic space is occupied by the umbilical cord (arrow).

Doppler did not identify any more pregnancies with true dye-determined low AFVs compared with traditional gray-scale ultrasound imaging.<sup>41</sup>

### POTENTIAL DIFFICULTIES IN AMNIOTIC FLUID VOLUME ESTIMATION USING ULTRASOUND

Determining an estimated AFV either objectively or subjectively is generally straightforward. However, a few potential pitfalls are worth mentioning. Maternal positioning, whether supine or at a 45-degree semierect position, does not appear to influence the measurement of



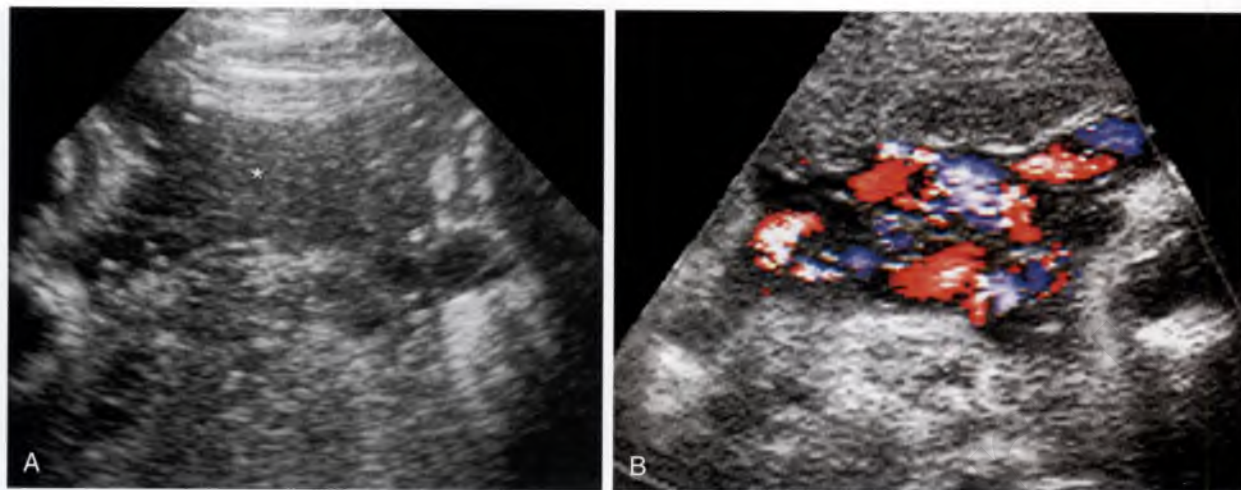


**FIG 20-7** **A**, Apparent amniotic fluid pocket (*asterisk*) in a third trimester pregnancy. **B**, Color Doppler interrogation reveals that this pocket is entirely filled with umbilical cord.

the AFV.<sup>42</sup> However, as demonstrated by Fok and coworkers,<sup>43</sup> fetal positioning can influence the calculation of the AFI, although it does not appear to influence the DVP measurement (Fig. 20-8). Fetal movements do not appear to alter the assessment of AFV, nor does the choice of the transducer, whether curvilinear or sector.<sup>44</sup>

Excessive pressure with the transducer while scanning can negatively influence the estimation of AFV. Flack and associates demonstrated that excess pressure on the maternal abdomen resulted in a 21% decrease in calculated AFI measurement.<sup>45</sup> It is important to remember that maternal adipose tissue tends to scatter the ultrasound beam, which may result in artificial echoes suggested within pockets of amniotic fluid. Thus, obese women may appear to have reduced volume of amniotic fluid as a result of these artifactual echoes (Fig. 20-9). It may help to use a lower frequency transducer when assessing the AFV in these patients. Also, measurements of amniotic fluid pockets may be made in varying locations by different examiners; this too can lead to variation in estimates of AFV (Fig. 20-10).

## NORMAL AMNIOTIC FLUID VOLUME IN SINGLETON PREGNANCIES

In order to establish what constitutes an abnormal AFV, methods for assessing normal amniotic fluid for singleton pregnancies must be determined. Based on published studies in the literature, there are multiple accepted definitions of an abnormally low or high AFV. An abnormally low AFV (referred to as *oligohydramnios*) has been defined as any one of the following: a total volume less than 200 mL<sup>22</sup> or less than 500 mL,<sup>23,24</sup> a value below the 5th percentile for gestational age,<sup>46</sup> an SDP less than 2 cm,<sup>28,47,48</sup> an AFI less than 5 cm,<sup>25-27,48,49</sup> or a subjectively low AFV.<sup>31</sup> An increased AFV (referred to as *polyhydramnios*) can be defined as any one of the following: a total volume greater than 2000 mL,<sup>30</sup> a value above the 95th<sup>27</sup> or 97th percentiles for gestational age, an SDP greater than or equal to 8 cm,<sup>50</sup> an AFI greater than or equal to 24 cm<sup>51</sup> or greater than 25 cm,<sup>52</sup> or a subjectively increased AFV.<sup>31</sup>

Several studies have attempted to define normal AFVs across gestation. The AFV deemed normal is to a certain degree dependent upon the gestational age at which it was measured. There are multiple published reference curves demonstrating changes in AFV across gestation and a few notable studies evaluating either dye-determined or directly measured AFVs. Queenan and colleagues,<sup>53</sup> in 1972, used dye-determined methods to assess the AFVs of 187 patients across gestation

from 15 to 16 weeks to 41 to 42 weeks. They demonstrated an increase in AFV as pregnancy advanced from the 15th to the 20th week, and then AFV remained relatively constant from the 20th through the 41st week. Their study showed that the AFV peaked at 33 to 34 weeks' gestation, then gradually decreased until term, decreasing at a greater rate after 41 weeks.<sup>53</sup> Brace and Wolf<sup>54</sup> in 1989 derived normal values from a compilation of 705 pregnancies from 12 previously published studies<sup>53,55-65</sup> with gestational ages ranging from 8 to 43.2 weeks. They reported a peak AFV of 931 mL at 33.8 weeks with a decrease in the AFV thereafter (Fig. 20-11). Using polynomial regression and log transformation of the data, the authors found no statistically significant change in the AFV from 22 to 39 weeks' gestation, with an average volume of 777 mL and a range of 630 to 817 mL.<sup>54</sup> They showed a decrease in the AFV after 40 weeks by 8% per week.<sup>54</sup> Magann and coworkers, in 1997, measured the AFVs of 144 singleton pregnancies between 15 and 40 weeks also using a single dye-dilution technique with analysis performed in the same laboratory; the AFV was found to increase across gestation with a peak at 40 weeks.<sup>56</sup> In 2014, Sandlin and associates<sup>67</sup> modeled AFVs across gestation in normal singleton pregnancies using the statistical method *quantile regression* (QR). In their study, 379 women with singleton pregnancies were evaluated and their amniotic volumes were calculated by either dye-dilution technique or direct measurement at the time of cesarean delivery between 16 and 41 weeks' gestation.<sup>67</sup> These authors were then able to derive a normative chart for AFVs across each week of gestation (16-41 weeks) at the 5th, 25th, 50th, 75th, and 95th percentiles (Table 20-1).<sup>67</sup> The authors point out in their study that the use of quantile regression enabled them to relax the stringent assumptions of standard regression models and overcome several of those limitations, thereby allowing them to more appropriately estimate values at the extremes of a distribution (e.g., below the 5th and above the 95th percentiles). Because those values are labeled as abnormal, this is where clinical interest and concern lie—the relationship of abnormal amniotic fluid values and their subsequent association with perinatal outcome.<sup>67</sup>

Given that the actual AFV can only be directly calculated by amniocentesis with dye-dilution techniques or directly measured at the time of cesarean delivery, in clinical practice, the AFV is estimated by ultrasound evaluation using the AFI, the DVP, or subjective assessment. An often-cited reference for normal ultrasound-estimated AFV is an article by Moore and Cayle,<sup>27</sup> published in 1990, in which the authors attempted to define the normal AFI in pregnancy. They evaluated the





**FIG 20-8** **A**, Sonogram of the fundic portion of the uterus in a second trimester pregnancy. Although this single large amniotic fluid pocket simulates polyhydramnios, it was the only area of amniotic fluid. **B**, Sonogram of the same patient in the mid- to lower uterine segment. No amniotic fluid is seen in this scan. If amniotic fluid volume had to be assessed on the basis of this image alone, it would be interpreted as oligohydramnios.

AFI, as described by Rutherford and colleagues,<sup>25</sup> in 791 patients with normal pregnancies between 16 and 44 weeks. Using polynomial regression and logarithmic transformation, they found the mean AFI curve to rise beginning at 16 weeks, peak at 27 weeks, plateau until 33 weeks, and then decline until 42 weeks. They observed that the AFI decreased by 12% per week after 40 weeks<sup>27</sup> (Table 20-2). In 2000, Magann and coworkers<sup>48</sup> performed a prospective study to determine normal values for sonographically measured AFI, SDP, and two-diameter pocket in normal human pregnancy. They recruited 50 patients at every gestational age between 14 and 41 weeks, for a total of 1400 patients. The data were analyzed using linear regression and logarithmic transformation, and they found that when AFI is used to define fluid status across gestation, it increases from 14 to 31 weeks and then declines thereafter; when SDP or two-diameter pocket is used, the AFV increases from 14 to 20 weeks' gestation, plateaus



**FIG 20-9** Sonogram in a moderately obese patient. Artifactual echoes within the amniotic fluid make the actual amniotic fluid less apparent.

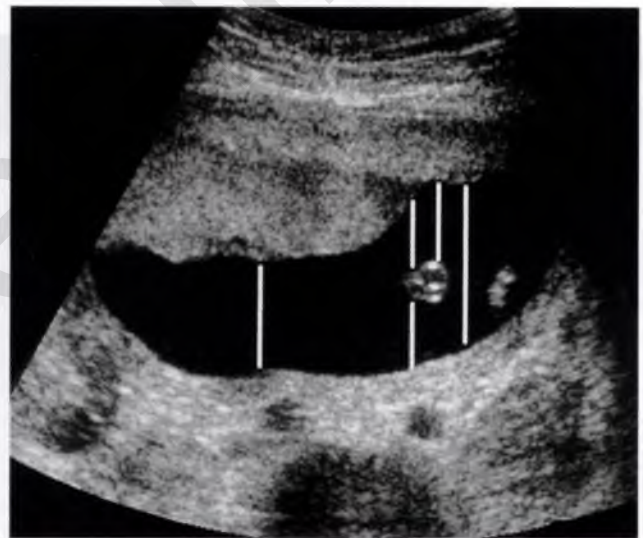


**FIG 20-10** Sonogram of a second trimester pregnancy. Measurements of this amniotic fluid pocket might be made in a variety of locations by different examiners, and some examiners may choose not to use this pocket for measurement.

between 20 and 37 weeks, and then gradually declines thereafter through the 41st week. If one were to consider the individual cases in the study by Magann and coworkers<sup>48</sup> but use the curve reported by Moore and Cayle,<sup>27</sup> one would find that 36% of the patients in the study by Magann and coworkers<sup>48</sup> who had normal outcomes would have been labeled as having abnormally low or high AFVs. In 2007, Machado and associates<sup>68</sup> evaluated the AFIs of 2868 pregnant women. Using multiple linear regression and quadratic polynomial adjustments, they found the AFIs across gestation to be essentially constant between 20 and 33 weeks' gestation, decreasing after 33 weeks, with the most significant decrease after the 38th week of gestation.<sup>68</sup> Lei and Wen<sup>69</sup> constructed an AFI curve by gestational week based on data from 5496 Chinese women. The 5th, 50th, and 95th percentiles of this study were different from the curves of both Moore and Cayle<sup>27</sup> and Magann and coworkers<sup>48</sup> across gestation. The curves of both Lei and



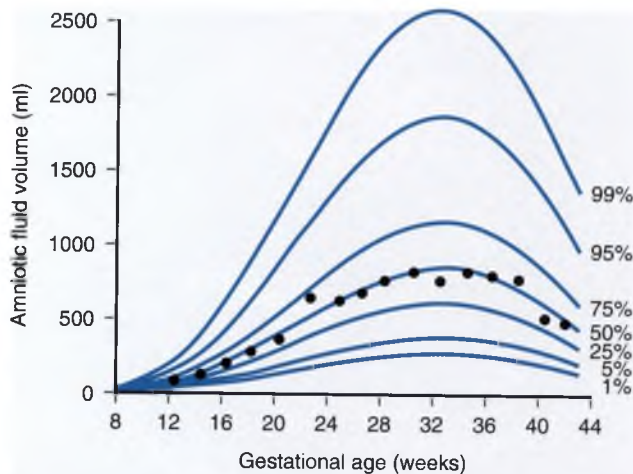


**FIG 20-11** Nomogram shows amniotic fluid volumes as a function of gestational age on a linear scale. Dots are means for each 2-week interval. Percentiles are calculated from polynomial regression equation and standard deviation of residuals. (From Brace RA, Wolf EJ: Normal amniotic fluid volume changes throughout pregnancy. *Am J Obstet Gynecol* 161:386, 1989.)

**TABLE 20-1 Amniotic Fluid Volume Percentile Values in Relation to Gestational Age by Second-Order Quantile Regression**

Weeks of Gestation	AMNIOTIC FLUID VOLUME PERCENTILE				
	5th	25th	50th	75th	95th
16	134.0	334.5	377.1	503.2	694.7
17	132.3	322.0	389.6	552.2	937.2
18	130.9	311.1	401.9	602.0	1233.7
19	129.9	301.7	414.0	652.1	1584.8
20	129.2	293.7	425.8	701.8	1986.6
21	128.9	286.9	437.2	750.4	2430.0
22	128.9	281.4	448.3	797.2	2900.5
23	129.2	277.0	459.0	841.5	3378.4
24	129.8	273.7	469.2	882.5	3839.9
25	130.8	271.4	478.9	919.5	4258.8
26	132.1	270.2	488.1	951.9	4609.3
27	133.8	270.0	496.7	979.1	4868.0
28	135.8	270.8	504.7	1000.5	5016.9
29	138.3	272.6	512.1	1015.9	5045.3
30	141.1	275.4	518.8	1024.8	4951.1
31	144.4	279.3	524.8	1027.1	4741.3
32	148.1	284.4	530.0	1022.8	4430.5
33	152.3	290.6	534.5	1012.0	4040.0
34	157.0	298.0	538.2	994.8	3594.8
35	162.3	306.8	541.1	971.6	3121.4
36	168.2	317.0	543.2	942.8	2644.7
37	174.7	328.8	544.5	909.0	2186.7
38	182.0	342.3	545.0	870.7	1764.2
39	190.0	357.7	544.7	828.7	1389.0
40	198.2	375.2	543.5	783.6	1067.1
41	207.9	395.0	541.5	736.2	800.0

Amniotic fluid volumes are in milliliters.

From Sandlin AT, Ounpraseuth ST, Spencer HJ, et al: Amniotic fluid volume in normal singleton pregnancies: modeling with quantile regression. *Arch Gynecol Obstet* 289:967-972, 2014, used with permission.

**TABLE 20-2 Amniotic Fluid Index Values in Normal Pregnancy**

Weeks of Gestation	AMNIOTIC FLUID INDEX PERCENTILE					n
	2.5th	5th	50th	95th	97.5th	
16	73	79	121	185	201	32
17	77	83	127	194	211	26
18	80	87	133	202	220	17
19	83	90	137	207	225	14
20	86	93	141	212	230	25
21	88	95	143	214	233	14
22	89	97	145	216	235	14
23	90	98	146	218	237	14
24	90	98	147	219	238	23
25	89	97	147	221	240	12
26	89	97	147	223	242	11
27	85	95	146	226	245	17
28	86	94	146	228	249	25
29	84	92	145	231	254	12
30	82	90	145	234	258	17
31	79	88	144	238	263	26
32	77	86	144	242	269	25
33	74	83	143	245	274	30
34	72	81	142	248	278	31
35	70	79	140	249	279	27
36	68	77	138	249	279	39
37	66	75	135	244	275	36
38	65	73	132	239	269	27
39	64	72	127	226	255	12
40	63	71	123	214	240	64
41	63	70	116	194	216	162
42	63	69	110	175	192	30

Amniotic fluid index values are obtained by measuring the vertical depth of the largest clear amniotic fluid pocket in each of four equal uterine quadrants. The values from each quadrant are measured in millimeters and added together.

From Moore TR, Cayle JE: The amniotic fluid index in normal human pregnancy. *Am J Obstet Gynecol* 162:1168, 1990.

Wen<sup>69</sup> and Magann and coworkers<sup>48</sup> reported AFIs less at each gestational age than in the curve of Moore and Cayle.<sup>27</sup>

These findings suggest that what may be considered normal AFV at any point during gestation is likely different depending on the population being investigated. Thus, population-specific curves should be considered in order to more appropriately define normal AFV. Despite many years of investigation and several reported studies, there has yet to be a clearly defined, widely accepted normal estimated value for AFV at each week of gestation; therefore, what truly constitutes abnormal AFV cannot be precisely determined. Whether the AFV decreases in late gestation, remains steady throughout most of the third trimester, or increases throughout gestation with a peak at term has not been clearly established. Ideally, normal AFV should be defined as a value between established high and low volume cutoffs, at which associations with adverse pregnancy outcomes are clearly linked.

## AMNIOTIC FLUID VOLUME AND PREGNANCY OUTCOMES

There are few investigations evaluating intrapartum and perinatal outcomes within 72 hours of the true dye-determined AFV calculations.

In one study,<sup>30</sup> no differences were observed between groups with oligohydramnios, normal AFV, or polyhydramnios and complications including risk of meconium-stained amniotic fluid, variable decelerations influencing delivery, or low 5-minute Apgar scores. In another study, 100 unlabored women had AFV determined by dye-dilution technique just before elective cesarean delivery, and oligohydramnios was not predictive of low umbilical artery pH at delivery.<sup>70</sup> In a third analysis, intrapartum and perinatal outcomes including fetal heart rate variability, variable decelerations, late decelerations, fetal labor intolerance, need for amnioinfusion, fetal growth restriction (FGR), birth weight, mode of delivery, umbilical artery pH less than 7.2, and neonatal intensive care unit (NICU) admission were evaluated in 74 pregnancies with dye-determined AFV and with delivery within 72 hours.<sup>71</sup> The dye-determined fluid volumes labeled as oligohydramnios, normal, and polyhydramnios were not predictive of adverse intrapartum or neonatal outcomes.<sup>71</sup>

### Oligohydramnios

An increased risk for adverse pregnancy and neonatal outcomes such as nonreactive nonstress tests (NSTs), fetal heart rate decelerations, meconium staining, cesarean delivery for labor intolerance, and low Apgar scores have been shown in women with an AFI of 5 cm or less in several studies.<sup>25,49,72</sup> However, not all of the studies are consistent, and furthermore, not all investigators agree that an AFI of 5 cm or less is associated with adverse pregnancy outcomes. In other studies evaluating both low-risk<sup>73</sup> and at-risk patients,<sup>74-77</sup> oligohydramnios was not linked with adverse pregnancy or perinatal outcomes. It is imperative that estimates of AFV be accurate and correlate with outcomes for them to be useful in management of at-risk pregnancies; thus, contradictory studies regarding the cutoff for oligohydramnios and its relationship to intrapartum and perinatal outcomes make interpretation and decision making difficult for the practitioner.

In a study by Casey and colleagues,<sup>49</sup> which evaluated adverse outcomes after 34 weeks' gestation in pregnancies with oligohydramnios, after correction for fetal malformations and congenital syndromes, there was no difference between pregnancies with an AFI 5 cm or less and those with an AFI greater than 5 cm in the risk of cesarean delivery for fetal labor intolerance, umbilical cord arterial pH of less than 7, NICU admissions, seizures in the first 24 hours after delivery, or neonatal death. It is important to note that in studies comparing pregnancies with AFIs 5 cm or less and those greater than 5 cm, many of the intrapartum outcomes evaluated, such as fetal heart rate tracing influencing delivery, cesarean delivery for fetal labor intolerance, and Apgar scores, are subjective measures. The only two objective assessments are the presence or absence of meconium staining and umbilical cord arterial pH. In a meta-analysis by Chauhan and coworkers,<sup>78</sup> increased risk of cesarean deliveries for fetal labor intolerance and Apgar score less than 7 at 5 minutes was demonstrated in the group with AFI 5 or less cm compared to those with AFI greater than 5 cm; however, no difference between these two groups was observed in the risk of neonatal acidosis (umbilical cord arterial pH < 7.0), an objective outcome. Chamberlain and associates<sup>28</sup> evaluated 7582 referred high-risk patients and the relationship of a single DVP measurement, after correction for major congenital anomalies, as a predictor of perinatal mortality rate. The perinatal mortality rates were 1.97/1000 (~0.2%) for a DVP greater than 2 cm to less than 8 cm, 37.74/1000 (~3.8%) for a DVP 1 cm or greater to 2 cm or less, and 109.4/1000 (~11%) for a DVP less than 1 cm.

In 2008, a Cochrane review compared the use of the AFI measurement to the DVP measurement as a screening test for the prediction of adverse pregnancy outcome.<sup>79</sup> In this review, no significant differences were identified in the primary outcomes of NICU admissions or

perinatal deaths. However, there were more women with a diagnosis of oligohydramnios, more labor inductions, and more cesarean deliveries for a nonreassuring fetal heart rate tracing when using the AFI. There were no differences in the number of nonreassuring fetal heart rate tracings, assisted vaginal deliveries with or without a nonreassuring fetal heart rate tracing, umbilical artery pH of less than 7.1, Apgar score of less than 7 at 5 minutes, presence of meconium, or NICU admissions.<sup>79</sup> The authors of the review concluded that DVP was the better measurement because the use of the AFI increased the diagnosis of oligohydramnios and labor inductions without improvement in peripartum outcomes.<sup>79</sup> Likewise, a 2009 meta-analysis of randomized controlled trials comparing the AFI to the DVP during antepartum fetal surveillance concluded that the DVP measurement is the method of choice in the assessment of AFV.<sup>80</sup>

The cause of oligohydramnios can generally be divided into one of three categories: fetal anatomic abnormalities (e.g., bladder outlet obstruction, renal agenesis), premature rupture of membranes (PROM), or a reflection of a maternal or fetal disease state as a result of uteroplacental insufficiency (e.g., hypertensive disorders such as preeclampsia, FGR, postterm pregnancy). Oligohydramnios can also result from maternal exposure to medications such as angiotensin-converting enzyme (ACE) inhibitors, angiotensin receptor blockers (ARBs),<sup>81</sup> or nonsteroidal agents such as indomethacin.<sup>82</sup> Once low AFV is identified, a targeted sonographic examination should be performed to evaluate for fetal anomalies as well as fetal growth assessment. A detailed maternal history and physical examination should be obtained to evaluate for specific conditions that can be associated with oligohydramnios (e.g., hypertensive disorders, PROM). Depending on the gestational age, antenatal testing should be considered (e.g., fetal NST, biophysical profile [BPP]) along with consultation with a maternal-fetal medicine specialist. Serial ultrasound evaluations for fetal growth (every 3-4 weeks) and for AFV assessment (e.g., weekly when less than 41 weeks' gestational age, twice weekly after 41 weeks or if FGR) as well as Doppler flow studies (e.g., umbilical artery Doppler flow) (particularly in the setting of FGR) are warranted. Pregnancies complicated by prolonged oligohydramnios from an early gestational age can result in fetal deformations (e.g., Potter sequence or oligohydramnios sequence) and fetal pulmonary hypoplasia, which can be lethal. Unfortunately, treatment for oligohydramnios (e.g., amnioinfusion) has not been shown to improve neonatal outcomes. Oligohydramnios at term is generally considered an indication for delivery.

### Pulmonary Hypoplasia

Patients with prolonged oligohydramnios from any cause, including renal causes or preterm PROM (PPROM), are at increased risk for pulmonary hypoplasia, which is frequently fatal. It has long been known that amniotic fluid is important for normal development of the fetal lungs. What has been less clear is how oligohydramnios interferes with the normal developmental process. During human gestation, there are five main stages of fetal lung development: embryonic, from approximately the 3rd to the 6th week; pseudoglandular, from the 5th to the 17th week; canalicular, from the 16th to the 26th week; sacular, from the 24th to the 36th week; and alveolar, from the 32nd week to term and beyond (see Chapter 12). By the 16th week of gestation, all of the branches of the tracheobronchial tree, up to the terminal bronchioles, are established.<sup>83</sup> Oligohydramnios that results in pulmonary hypoplasia, which is characterized by inadequate development of pulmonary acini and restricted vascularization, normally must occur during the canalicular stage of development.

Several theories have been postulated as to the basis for pulmonary hypoplasia in patients with severe oligohydramnios, including abnormal fetal breathing, increased pressure on the fetal thorax, and



abnormal pulmonary fluid egress.<sup>83</sup> Abnormalities of fetal breathing are unlikely to be the cause, because normal fetal breathing movements are documented to occur in animals as well as in humans with oligohydramnios-related pulmonary hypoplasia. Compression of the fetal thorax is also an unlikely cause because pressure within the amniotic sac in patients with oligohydramnios is low. Normally, the pressure in the amniotic space is between 1 and 14 mm Hg. When oligohydramnios is present and the membranes are intact, the intra-amniotic pressure is 1 mm Hg or less.<sup>84,85</sup> It has been postulated that fetal lung fluid acts as an internal stent for the developing surrounding lung.<sup>86</sup> Normally, the upper airways produce resistance to the egress of fluid out of the trachea. In the presence of oligohydramnios and low amniotic pressure, it is theorized that the pressure gradient results in the loss of this lung fluid.<sup>85</sup> In addition, work by Harding, Hooper, and Dickson<sup>87</sup> in sheep has demonstrated that the rise in pulmonary airway pressure relative to amniotic sac pressure may be caused by increased spinal flexion and resulting increased abdominal and thoracic pressure in the fetus with oligohydramnios. In a 1996 study, Kilbride, Yeast, and Thi-beault<sup>88</sup> evaluated patients who experienced PPRM at less than 29 weeks' gestation. Most patients did not experience a change in amniotic fluid status over time; however, as many as 20% of patients did. Although the prognosis was poor and the likelihood of pulmonary hypoplasia was high in the group in which the amniotic fluid pockets were less than 1 cm, there was no association between moderate oligohydramnios (1- to 2-cm pockets) and pulmonary hypoplasia. Thus, on the basis of this study, it is inappropriate to group all patients with an AFI less than 5 cm together in an attempt to prognosticate on the development of pulmonary hypoplasia.

In one review of 11 studies, the reported incidence of pulmonary hypoplasia secondary to midtrimester PPRM ranged widely from 1% to 48%.<sup>89</sup> Another review of six studies on PPRM before 24 weeks reported an incidence of pulmonary hypoplasia of 19% ( $n = 120$ ).<sup>90</sup> These percentages do not represent the true natural history, given the limitations inherent in these reviews that summarize only retrospective cohorts reported from tertiary care centers. The wide range in prevalence is partly explained by the absence of uniform pathologic and clinical definitions. Histologic findings form the basis of the diagnosis of pulmonary hypoplasia, but complete autopsy data were often not available.

Amnioinfusion has been proposed as a means to potentially improve outcomes in cases of PPRM by preventing pulmonary hypoplasia, limiting fetal deformation abnormalities, increasing time to delivery interval, and improving fetal BPP through reduction in risk of umbilical cord compression. However, at this time there is no solid evidence to support this practice.<sup>91</sup> A large randomized trial is under way to determine whether there is benefit from serial amnioinfusions in the setting of PPRM.<sup>92</sup>

### Prediction of Pulmonary Hypoplasia in the Setting of Oligohydramnios

Prediction of pulmonary hypoplasia after midtrimester PPRM is important for optimal management. Once midtrimester PPRM has occurred, an assessment of the probability of pulmonary hypoplasia is important both for clinical decision making and for counseling of patients. Previous studies have shown that gestational age at the time of rupture of the membranes is strongly associated with the occurrence of pulmonary hypoplasia. Other factors that have been associated with pulmonary hypoplasia are the duration of the rupture of the membranes and the degree of oligohydramnios.<sup>93</sup>

Sonography has been proposed as potentially useful in the prediction of lethal pulmonary hypoplasia. Prediction of lethal pulmonary hypoplasia has been attempted based on fetal thoracic circumference

(TC) and sagittal lung length or transverse lung diameter measurements, as well as cardiac/thoracic circumference (CC/TC) and thoracic/abdominal circumference (TC/AC) ratios. However, in one study, TC, CC/TC, and TC/AC measurements failed to provide an acceptable prenatal prediction of lethal pulmonary hypoplasia in either the total study group or the subset with PPRM. In the latter, the clinical parameters provided better prediction than biometric parameters, whereas the combination of clinical, biometric, and Doppler findings were most accurate. Doppler velocimetry was used to detect changes in pulmonary artery waveforms that may be useful in the prediction of pulmonary hypoplasia.<sup>94</sup> In general, fetal two-dimensional biometric indices are late indicators of pulmonary hypoplasia, with a sensitivity and specificity not satisfactory for use in clinical management. Data on the predictive value of the presence or absence of fetal breathing movements are contradictory. Furthermore, the applicability of three-dimensional sonography, computed tomography, and magnetic resonance imaging for accurate measurement of fetal lung volume in the prediction of pulmonary hypoplasia still needs to be determined.

### ASSESSMENT OF AMNIOTIC FLUID VOLUME IN THE HIGH-RISK PATIENT

One question that often arises is how frequently one should perform semiquantitative assessment of AFI during antepartum testing in the high-risk patient. Wing and colleagues<sup>95</sup> and Lagrew and coworkers<sup>96</sup> evaluated this issue. Wing and colleagues concluded that for patients at less than 41 weeks of gestation undergoing antepartum testing, weekly assessment of AFI is probably adequate if the initial measurement is in the normal range ( $\geq 8$  cm) because the risk of developing oligohydramnios within 4 days is only 1.7% and within 7 days only 2.2%. As they stated in their report, "for patients at less than 41 weeks of gestation whose initial AFI measurement is in the low-normal range (5 to 8 cm), twice-weekly assessment is justified on the basis of a higher risk for an AFI 5 cm or less within 4 days (12.3%). For all patients at 41 or more weeks of gestation, twice-weekly AFI assessments are recommended regardless of the initial measurement." In 1992, Lagrew and coworkers<sup>96</sup> addressed the issue of frequency of AFV assessment. They concluded that there is minimal risk ( $<0.5\%$ ) of oligohydramnios within 4 days after a normal AFI; therefore, AFI measurements in patients less than 41 weeks of gestation should be performed weekly. It should be noted that these evaluations were done using AFI calculations, and no similar data are available using DVP measurements.

### Polyhydramnios

The incidence of polyhydramnios (also referred to as *hydramnios*) ranges from 0.2% to 2.0%.<sup>97</sup> The degree of polyhydramnios can be described using the terms *mild*, *moderate*, and *severe*. Mild polyhydramnios has been defined as an AFI of 25 to 30 cm<sup>98,99</sup> or a DVP of 8 cm or greater,<sup>100</sup> moderate polyhydramnios as an AFI of 30.1 to 35 cm<sup>98,99</sup> or a DVP of 12 cm or greater,<sup>100</sup> and severe polyhydramnios as an AFI of 35.1 cm or greater<sup>98,99</sup> or a DVP of 16 cm or greater<sup>100</sup> (Figs. 20-12 and 20-13).

Idiopathic polyhydramnios accounts for approximately 50% to 60% of cases.<sup>50,101</sup> The remaining cases typically fall into one of the following categories: congenital anomalies and genetic disorders (8-45%), maternal diabetes (5-26%), multiple gestations (8-10%), fetal anemia (1-11%), and other (e.g., hydrops fetalis, Bartter syndrome, and congenital viral infections).<sup>100-110</sup> The mechanism by which idiopathic polyhydramnios develops is not known. Membrane-bound water channels, called *aquaporins*, may play a role in the development of polyhydramnios, but the exact physiology is not yet understood.<sup>111-113</sup>





**FIG 20-12** Sonogram of a patient with marked polyhydramnios. The fetus is surrounded and virtually floating in the amniotic fluid.



**FIG 20-13** Sonogram of a patient with esophageal atresia and polyhydramnios showing absence of the fetal stomach (*arrow*) and increased amniotic fluid (*asterisk*).

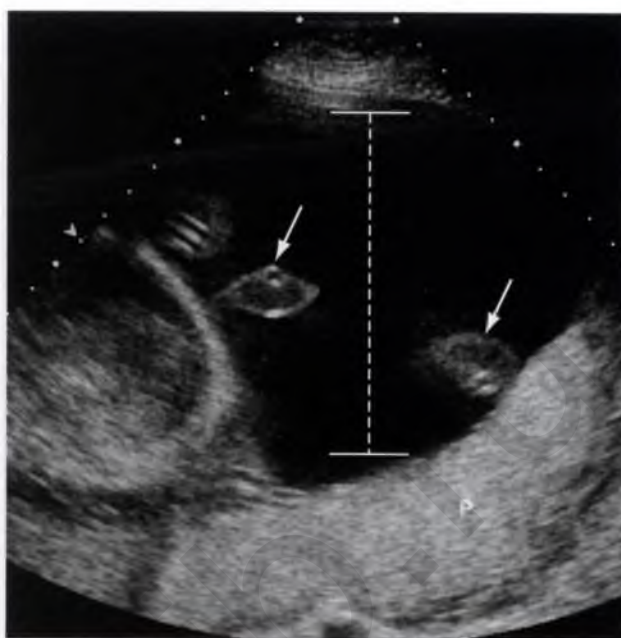


**FIG 20-14** Sonogram of a pocket of amniotic fluid in a patient with hydrops fetalis and polyhydramnios. Two small segments of umbilical cord (*arrows*) are seen traversing the measured pocket of amniotic fluid. The placenta (P), which appears normal to prominent in this case, is, in fact, abnormally thickened.

The proposed mechanism of polyhydramnios associated with maternal diabetes is related to fetal polyuria due to increased osmotic diuresis as a result of fetal hyperglycemia.<sup>120</sup> Poorer glucose control has been shown to correlate with higher amniotic glucose concentration and higher AFI.<sup>121</sup> There may also be an increase in fetal urinary output in macrosomic fetuses (which are often seen in diabetic pregnancies).<sup>121</sup> The incidence of polyhydramnios in mothers with pregestational diabetes after 24 weeks' gestational age has been shown to be 18.8%.<sup>122</sup> In the setting of gestational diabetes, the incidence of polyhydramnios ranges from 8% to 20%<sup>123</sup> and is found up to 30 times more often than in nondiabetic pregnancies.<sup>124</sup>

As with oligohydramnios, sonographic evaluation of amniotic fluid in the setting of polyhydramnios has not been found to be very accurate in reflecting actual AFV.<sup>37</sup> The predictive ability of AFI and DVP to identify polyhydramnios above the 95th or 97th percentile has been shown to be 33% and 46%, respectively.<sup>46</sup> Using color flow Doppler sonography in the assessment of amniotic fluid does not increase ability to detect polyhydramnios via sonography.<sup>125</sup> Ultrasound imaging is often challenging in the setting of polyhydramnios. Excessive fetal movement, due to the large amount of intrauterine fluid, may make it very difficult to obtain the necessary images. In addition, the fetus may be positioned deep within the uterus and thus far from the maternal anterior abdominal wall and far from the transducer. Therefore, depth settings often need to be adjusted to better visualize fetal anatomy. Another consideration when scanning a patient with polyhydramnios is that, as the uterus expands because of increasing fluid volume, the placental thickness may appear to decrease. Thus, an abnormally thickened placenta (e.g., related to fetal hydrops) may measure within normal limits (Figs. 20-14 and 20-15).

Pregnancies complicated by polyhydramnios are at increased risk for adverse outcomes, including perinatal fatality.<sup>123,126-128</sup> This increased perinatal mortality risk is reported both in pregnancies complicated by idiopathic polyhydramnios as well as those in which polyhydramnios is related to fetal structural anomalies.<sup>97</sup> The presence of

Increasing severity of polyhydramnios correlates with an increased risk of perinatal death and congenital abnormalities.<sup>114-116</sup> Up to 31% of pregnancies with severe polyhydramnios (AFI  $\geq$  35 cm) have a major congenital anomaly.<sup>104</sup> The most common structural anomalies associated with polyhydramnios are central nervous system (28%), cardiac (22%), or gastrointestinal malformations (14%).<sup>117</sup> The risk of fetal aneuploidy in those fetuses found to have an anomaly by sonography is 10%.<sup>104</sup> In those fetuses without sonographic evidence of an anomaly, the risk of aneuploidy is only 1%.<sup>104</sup> The most common aneuploidies associated with polyhydramnios are trisomy 21, trisomy 18, and trisomy 13, although other chromosomal abnormalities can also occur.<sup>118,119</sup> There is not a significant difference in the reported risk of fetal aneuploidy with increasing severity of polyhydramnios.<sup>104</sup>



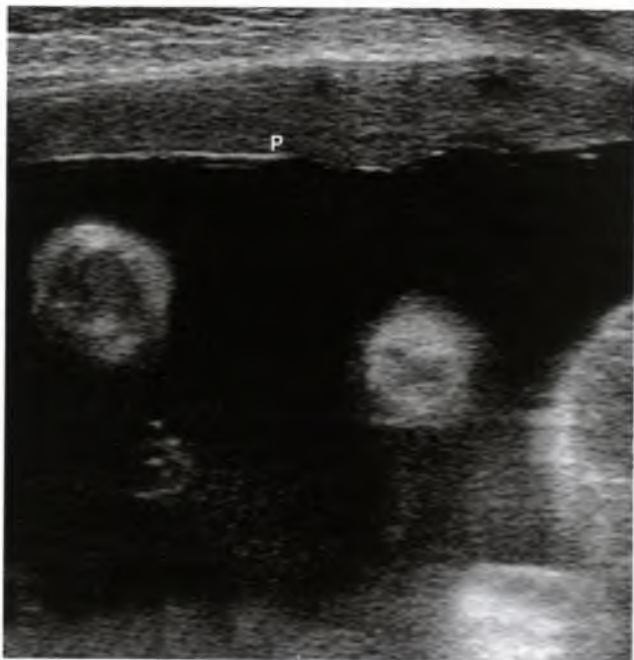


**FIG 20-15** Sonogram in a patient with marked polyhydramnios. The placenta (P) becomes thin as the uterus expands from the increased amniotic fluid volume.

polyhydramnios in a pregnancy complicated by diabetes does not, however, appear to result in additional increased risk of perinatal fatality; rather, it is primarily the poorly controlled diabetes and underlying maternal disease process that is related to adverse pregnancy outcomes in diabetic pregnancies.<sup>97</sup> A review of all cases of idiopathic polyhydramnios found an overall twofold to fivefold increased risk of perinatal mortality.<sup>123</sup>

Once polyhydramnios is detected by ultrasound, a targeted sonographic examination should be performed to evaluate for possible fetal morphologic anomalies or fetal hydrops. In addition, maternal glucose screen should be administered, if not already performed, to assess for maternal diabetes.<sup>97</sup> If a structurally abnormal fetus is identified, evaluation for fetal aneuploidy should be offered. Ultrasound surveillance for fetal growth and AFV assessment is warranted. The form of antepartum fetal surveillance in the setting of idiopathic polyhydramnios depends in part upon the gestational age.<sup>97</sup> Symptomatic polyhydramnios has been treated with large volume amnioreduction or medical therapy (e.g., indomethacin) or a combination of the two.<sup>97</sup> A multidisciplinary team approach, including maternal-fetal medicine specialists, neonatologists, genetic counselors, and possibly pediatric surgeons or pediatric cardiologists, is recommended for management and treatment of a pregnant patient with significant polyhydramnios.<sup>97</sup>

### Fetal Growth Restriction and Amniotic Fluid Volume

In the setting of FGR due to uteroplacental insufficiency, it is hypothesized that hypoxemia leads to decreased perfusion of the fetal kidneys, due to shunting of fetal blood flow to the brain, heart, and adrenal glands, thus resulting in decreased urine output and oligohydramnios. It has been shown that when oligohydramnios is present in the setting of FGR, the perinatal mortality rate is increased 47-fold.<sup>28</sup> Thus, in the setting of FGR, fetal surveillance with either NST or BPP is recommended twice weekly in conjunction with weekly AFV assessment and Doppler flow studies (e.g., uterine artery Doppler). FGR complicates approximately 3% to 6% of cases with polyhydramnios.<sup>126,128,129</sup> The

finding of polyhydramnios with FGR has been referred to as an “ominous combination” and raises high suspicion for underlying major fetal anomalies, chromosomal abnormalities, or both.<sup>119</sup> In a study of 39 fetuses with polyhydramnios and FGR, Sickler and associates found major anomalies in 92% including chromosomal abnormalities in 38%.<sup>119</sup> The overall mortality rate in this group of 39 fetuses with both polyhydramnios and FGR was 59%.<sup>119</sup>

Umbilical artery Doppler interrogation in the setting of polyhydramnios but without FGR is not routinely indicated. In some cases, polyhydramnios may resolve during the pregnancy. In these cases, the fetuses are not at increased risk of intrauterine or neonatal death compared to those with persistent or worsening hydramnios.<sup>130</sup> There does appear to be a distinction between acute versus chronic development of polyhydramnios.<sup>102</sup> Queenan and Gadow describe acute polyhydramnios as “a rampant fulminating process terminating in spontaneous labor, usually before the end of the second trimester.”<sup>99,102</sup> In their study of six cases with acute polyhydramnios diagnosed before 24 weeks’ gestation, all six resulted in perinatal death.<sup>102</sup>

### Amniotic Fluid Volume in Twin Pregnancies

The assessment of AFV as part of the sonographic evaluation is as important in twin pregnancies as it is in singleton pregnancies, both for the detection of fetal anomalies and for the evaluation of those at risk for adverse pregnancy outcomes. Additionally, twin pregnancies can be complicated by discordant growth or other unique conditions, such as twin-to-twin transfusion syndrome. The increased risk of anomalies and adverse outcomes in twins and higher order multiple pregnancies emphasize the importance of accurate assessment of AFV. In twin pregnancies, chorionicity and amnionicity are significant factors in the risks of associated perinatal morbidity and mortality.

### Normal Amniotic Fluid Volume in Twins

As with singletons, in order to understand and identify twins with abnormal AFV, it is helpful to review and recognize normal AFV in this setting. Only one study to date has defined AFV in twins, reporting findings in 45 third trimester diamniotic twin pregnancies.<sup>131</sup> Of the 45 twin pairs evaluated, none was found to have fetal anomalies, growth restriction, discordant growth, or evidence of twin-to-twin transfusion syndrome. The AFV was determined by amniocentesis with dye-dilution techniques.<sup>132</sup> The mean AFV for each twin was 877 mL, with 90% of the volumes between 215 and 2500 mL.<sup>131</sup> These volumes were very similar to the calculated normal volumes of fluid in singleton pregnancies.<sup>53,54,66</sup>

### Ultrasound Estimation of Amniotic Fluid Volume in Twins

As with singletons, ultrasound is used to estimate AFV in twins. Although some investigators have advocated the use of summated AFI technique to estimate volumes in twins,<sup>133-135</sup> such methods will fail to identify many twin pregnancies complicated by discordant or abnormal AFVs. The technique estimates AFV by identifying and measuring the single DVP in each of the four quadrants of the maternal abdomen (divided vertically into right and left by the linea nigra and horizontally into upper and lower by the umbilicus [the same technique used to estimate AFV in singletons]) and summing those four measurements to determine the AFI in centimeters. This calculation is done without taking membrane placement into consideration. An analysis to assess the accuracy of the summated AFI in 62 normal diamniotic twin pregnancies in which AFV had been determined by dye-dilution technique revealed that summated AFI would have classified 58 of the 62 twin pairs (93.5%) as having normal fluid when only 32 pairs (51.6%) actually had normal fluid based on dye-dilution technique.<sup>136</sup> Additionally, 10 of the 62 twin pairs had oligohydramnios determined by



dye dilution in both sacs, but the summated AFI incorrectly identified 80% of these as having normal AFV for both twins.<sup>136</sup> Clearly, ultrasound evaluation must include documentation of the intertwin membrane and address AFV measurement on either side in order to identify those twin pregnancies with abnormal AFV (oligohydramnios or polyhydramnios). Other ultrasound techniques<sup>136-138</sup> have been used to estimate amniotic fluid for each twin. Gerson and colleagues<sup>137</sup> identified the dividing intertwin membrane and then measured the largest pocket of amniotic fluid in each sac, both above and below the level of the fetal diaphragm (a two-quadrant measurement). Hill and coworkers<sup>138</sup> located the dividing membrane and used the longitudinal axis of the fetus to divide each amniotic sac into right and left halves and the horizontal axis of the fetal diaphragm into upper and lower halves (a four-quadrant measurement). Magann and associates<sup>136</sup> identified the dividing membrane by ultrasound and measured the DVP of fluid in each of the four quadrants of the maternal abdomen as used for AFI calculation in singleton pregnancies (another two-quadrant measurement). Only the study by Magann and associates<sup>136</sup> was compared to dye-dilution technique, which revealed 35 twins with low fluid, 48 with normal fluid, and 7 with high fluid volumes. The two-quadrant Magann technique identified 98% of those with normal fluid but only 20% of those with low volumes.<sup>136</sup>

The subjective estimation of AFV in twins (visual assessment without measurements) was found to be as accurate as objective numeric determination (with use of AFI or DVP) in correctly identifying those with normal fluid, oligohydramnios, or polyhydramnios confirmed by dye-dilution technique.<sup>137</sup> Now, though not validated by dye-determined studies, for twins and higher order multiples, the DVP of fluid (in centimeters) in each amniotic sac is used to estimate AFV following the same approach as in singleton pregnancies.<sup>28</sup> Using this technique, DVP of 2 cm or less is defined as oligohydramnios and greater than 8 cm is defined as polyhydramnios, with measurements in between deemed normal AFV (Figs. 20-16 and 20-17).

### Amniotic Fluid Volume and Pregnancy Outcomes in Twins

It is important to address whether AFV considered abnormal by ultrasound is correlated with adverse pregnancy outcome. There is limited information regarding estimated AFV in twins in relation to pregnancy outcome. In one study correlating dye-determined AFV and delivery outcome within 48 hours, there was no significant association between oligohydramnios, normal fluid volume, or polyhydramnios and neonatal outcomes.<sup>139</sup> Another study evaluated 299 normal dichorionic diamniotic and mono chorionic diamniotic twin pregnancies followed by serial sonograms. The last recorded estimated AFV based on SDP was correlated with intrapartum and neonatal outcomes.<sup>140</sup> Pregnancies with polyhydramnios in one sac were more likely to have an abnormal fetal heart rate tracing and more likely, based on that, to undergo cesarean delivery.<sup>140</sup> In addition, fetuses with polyhydramnios were more likely to have 5-minute Apgar scores less than 7, umbilical artery pH less than 7, respiratory distress syndrome, and transient tachypnea of the newborn compared with fetuses with oligohydramnios or normal fluid volume.<sup>140</sup> Other authors have also observed an increased risk of early gestational age at delivery, increased perinatal loss, and increased neonatal fatality associated with polyhydramnios in twin pregnancies.<sup>141,142</sup> As with singletons, once abnormal AFV is detected in a twin or high order multiple pregnancy, further evaluation should be performed to assess for possible conditions, such as PROM, twin-to-twin transfusion syndrome (Fig. 20-18), structural anomalies, abnormalities of fetal growth, or maternal conditions such as hypertensive disease or diabetes. Consultation with a maternal-fetal medicine specialist is recommended in patients carrying a multiple pregnancy with abnormal fluid volumes.

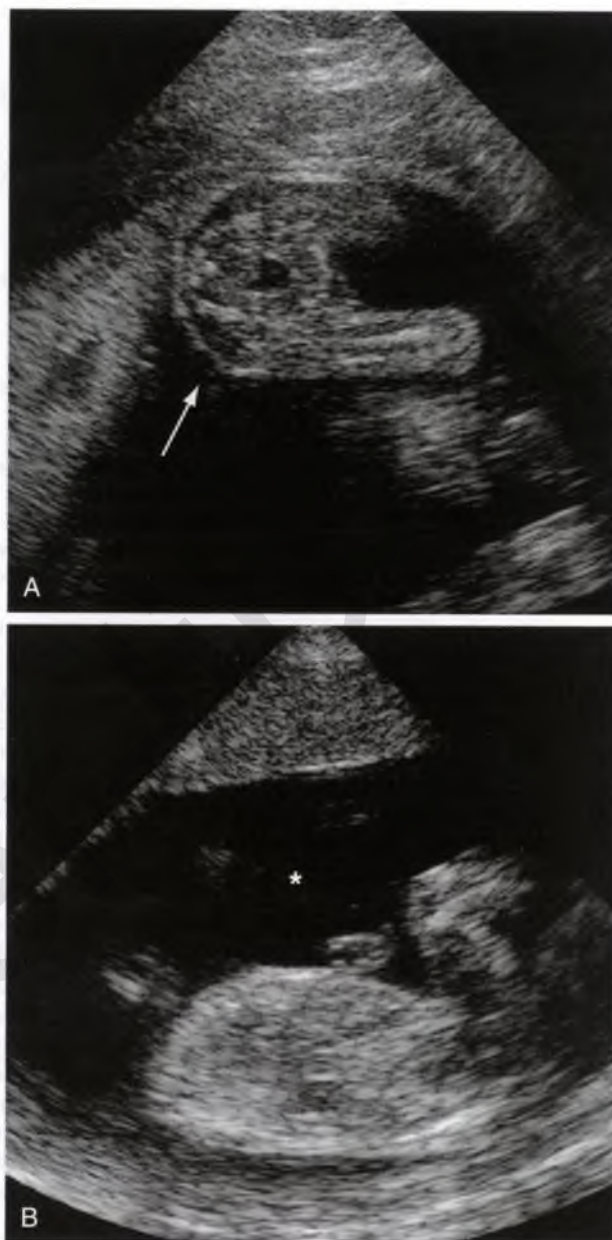


**FIG 20-16** Sonogram of a patient with a mono chorionic twin pregnancy with twin-to-twin transfusion syndrome. **A**, The donor fetus in the oligohydramniotic sac (arrow) is “stuck” to the anterior uterine wall. **B**, The recipient fetus is in a polyhydramniotic sac (asterisk). Often the dividing amniotic membrane cannot be identified.

### CONCLUSIONS

It is helpful to understand the dynamics of amniotic fluid and recognize normal fluid volume in singleton and twin pregnancies. Various techniques for ultrasound assessment of AFV have been described. There are significant implications of abnormal AFV, low or high, detected sonographically. Although AFV dynamics are multifaceted and not fully understood, the regulatory balance of AFV is concentrated at three main levels: fetal urine production and fetal swallowing, the intramembranous pathway, and the osmotic fluid gradient generated by the maternal-fetal relationship. Normal values and ranges for AFV are difficult to define. Efforts have been made to establish cutoff values for abnormal high and low volumes (polyhydramnios and





**FIG 20-17** Sonogram from a patient with a diamniotic dichorionic twin pregnancy. Subjective evaluation revealed normal amniotic fluid in each gestational sac on either side of the amniotic membrane (arrow).

oligohydramnios, respectively) determined based on correlation with adverse pregnancy outcomes. Two main techniques are used to numerically estimate AFV by ultrasound: AFI and DVP. It has been found that, of these, DVP is the preferred method. There are potential pitfalls in this assessment, and both techniques can be unreliable when correlated with actual AFV. Often, subjective assessment is used in the initial determination of fluid status.

Assessment of amniotic fluid is used as a vital sign for fetal well-being. AFV evaluation is an essential component of the BPP in antenatal testing.<sup>29</sup> Abnormalities in AFV may be a reflection of the status of the uteroplacental unit. Thus, an obstetric ultrasound examination must include attention to amniotic fluid. A working knowledge and basic understanding of the physiology that maintains balance of intrauterine amniotic fluid is essential in order to promptly identify abnormalities in this process, which may result from maternal or fetal conditions. Importantly, normal AFV cannot by itself assure good perinatal outcome; additional information regarding the patient's history, physical examination, fetal status, and the remainder of the sonographic evaluation of the fetus is necessary to complete the picture.

## REFERENCES

1. Beall MH, van den Wijngaard JP, van Gemert MJ, Ross MG: Amniotic fluid dynamics. *Placenta* 28(8-9):816-823, 2007.
2. Modena AB, Fieni S: Amniotic fluid dynamics. *Acta Biomed* 75(Suppl 1):11-13, 2004.
3. Moore TR: Amniotic fluid dynamics reflect fetal and maternal health and disease. *Obstet Gynecol* 116:759-765, 2010.
4. Abramovich DR, Page KR: Pathways of water transfer between liquor amnii and the feto-placental unit at term. *Eur J Obstet Gynecol* 3:155-158, 1973.
5. Lotgering FK, Wallenberg HC: Mechanisms of production and clearance of amniotic fluid. *Semin Perinatol* 10(2):94-102, 1986.
6. Thurlow RW, Brace RA: Swallowing, urine flow, and amniotic fluid response to prolonged hypoxia in the ovine fetus. *Am J Obstet Gynecol* 189:601-608, 2003.
7. Gagnon R, Harding R, Brace RA: Amniotic fluid and fetal urinary responses to severe placental insufficiency in sheep. *Am J Obstet Gynecol* 186:1076-1084, 2002.
8. Prichard JA: Deglutition by normal and anencephalic fetuses. *Obstet Gynecol* 25:289-297, 1965.
9. Brace RA, Wlodek ME, Cock ML, Harding R: Swallowing of lung liquid and amniotic fluid by the ovine fetus under normoxic and hypoxic conditions. *Am J Obstet Gynecol* 171:764-770, 1994.
10. Ross MG, Nijland MJ: Fetal swallowing: relation to amniotic fluid regulation. *Clin Obstet Gynecol* 40:352-365, 1997.
11. Minei LJ, Suzuki K: Role of fetal deglutination and micturition in the production and turnover of amniotic fluid in the monkey. *Obstet Gynecol* 48:177-181, 1976.
12. Matsumoto LC, Cheung CY, Brace RA: Effect of esophageal ligation on amniotic fluid volume and urinary flow rate in fetal sheep. *Am J Obstet Gynecol* 182:699-705, 2000.

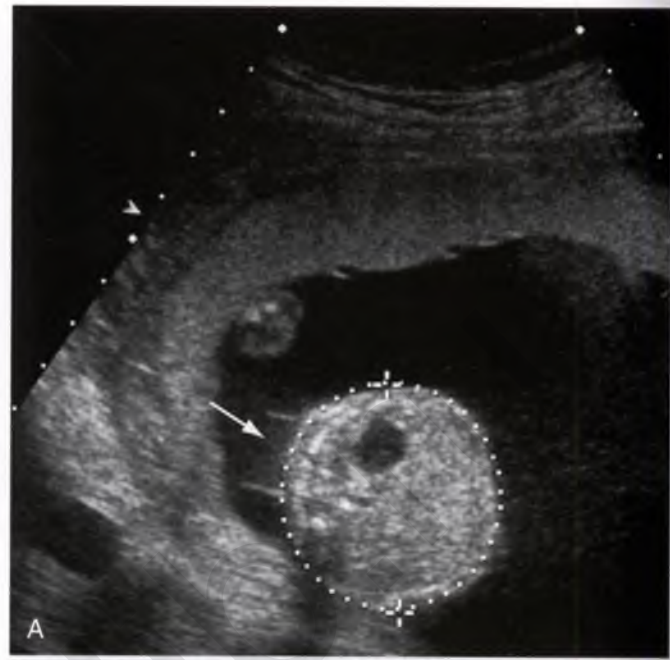


**FIG 20-18 A**, Sonogram of the fetal abdomen and surrounding amniotic fluid in a case of twin-to-twin transfusion syndrome. At first glance the fluid surrounding the donor abdomen appears to reside within its amniotic sac. In fact, there is only a small amount of hyperechogenic fluid (arrow) seen within the amniotic sac that enshrouds the fetus. **B**, Sonogram of the two amniotic sacs in a pregnancy with twin-to-twin transfusion syndrome. The amniotic fluid (arrow) surrounding the donor twin (Do) is more echogenic than the fluid in the recipient sac (Re).

13. Adamson TM, Brodecky V, Lambert TF, et al: The production and composition of lung fluid in the in-utero foetal lamb. In Comline RS, Cross KW, Dawes GS, et al, editors: *Foetal and Neonatal Physiology*, Cambridge, England, 1973, Cambridge University Press, pp 208–216.
14. Gilbert WM, Brace RA: The missing link in amniotic fluid volume regulation: intramembranous absorption. *Obstet Gynecol* 74:748–754, 1989.
15. Faber JJ, Anderson DF: Absorption of amniotic fluid by amniochorion in sheep. *Am J Physiol Heart Circ Physiol* 282(3):H850–H854, 2002.
16. Magann EF, Doherty DA, Chauhan SP, et al: Effect of maternal hydration on amniotic fluid volume. *Obstet Gynecol* 101:1261–1265, 2003.
17. Kilpatrick SJ, Safford KL, Pomeroy T, et al: Maternal hydration increases maternal amniotic fluid index. *Obstet Gynecol* 78:1098–1102, 1991.
18. Anderson DF, Faber JJ, Parks CM: Extraplacental transfer of water in the sheep. *J Physiol* 406:75–84, 1988.
19. Brace RA: Amniotic fluid volume and its relationship to fetal fluid balance: review of experimental data. *Semin Perinatal* 10:102–112, 1988.
20. Magann EF, Doherty DA, Chauhan SP, et al: Is there a relationship to dye determined or ultrasound estimated amniotic fluid volume adjusted percentiles and fetal weight adjusted percentiles? *Am J Obstet Gynecol* 190:1610–1614, 2004.
21. Owen P, Osman I, Farrell T: Is there a relationship between fetal weight and amniotic fluid index? *Ultrasound Obstet Gynecol* 20:61–63, 2002.
22. Horsager R, Nathan L, Leveno KJ: Correlation of measured amniotic fluid volume and sonographic predictions of oligohydramnios. *Obstet Gynecol* 83:955–958, 1994.
23. Magann EF, Nolan TE, Hess LW, et al: Measurement of amniotic fluid volume: accuracy of ultrasonography techniques. *Am J Obstet Gynecol* 167:1533–1537, 1992.
24. Dildy GA, III, Lira N, Moise KJ, Jr, et al: Amniotic fluid volume assessment: comparison of ultrasonographic estimates versus direct measurements with a dye-dilution technique in human pregnancy. *Am J Obstet Gynecol* 167:986–994, 1992.
25. Rutherford SE, Phelan JP, Smith CV, Jacobs N: The four-quadrant assessment of amniotic fluid volume: an adjunct to antepartum fetal heart rate testing. *Obstet Gynecol* 70:353–356, 1987.
26. Baron C, Morgan MA, Garite TJ: The amniotic fluid volume assessed intrapartum on perinatal outcome. *Am J Obstet Gynecol* 173:167–174, 1995.
27. Moore TR, Cayle JE: The amniotic fluid index in normal human pregnancy. *Am J Obstet Gynecol* 162:1168–1174, 1990.
28. Chamberlain PF, Manning FA, Morrison I, et al: Ultrasound evaluation of amniotic fluid volume, I: the relationship of marginal and decreased amniotic fluid volumes to perinatal outcomes. *Am J Obstet Gynecol* 150:245–249, 1984.
29. Manning FA, Platt LD, Sipos L: Antepartum fetal evaluation: development of a fetal biophysical profile. *Am J Obstet Gynecol* 136:787–795, 1980.
30. Magann EF, Morton ML, Nolan TE, et al: Comparative efficacy of two sonographic measurements for the detection of aberrations in the amniotic fluid volume and the effects of amniotic fluid volume on pregnancy outcomes. *Obstet Gynecol* 83:959–962, 1994.
31. Magann EF, Perry KG, Jr, Chauhan SP, et al: The accuracy of ultrasound evaluation of amniotic fluid volume in singleton pregnancies: the effect of operator experience and ultrasound interpretative technique. *J Clin Ultrasound* 25:249–253, 1997.
32. Hallak M, Kirshon B, O'Brian Smith E, et al: Subjective ultrasonographic assessment of amniotic fluid depth: comparison with the amniotic fluid index. *Fetal Diagn Ther* 8(4):256–260, 1993.
33. Chauhan SP, Magann EF, Perry KG, Jr, Morrison JC: Intrapartum amniotic fluid index and two-diameter pocket are poor predictors of adverse neonatal outcome. *J Perinatol* 17:221–224, 1997.
34. Phelan JP, Smith CV, Broussard P, Small M: Amniotic fluid volume assessment with the four-quadrant technique at 36–42 weeks' gestation. *J Reprod Med* 32(7):540–542, 1987.
35. Magann EF, Whitworth NS, Files JC, et al: Dye-dilution techniques using aminohippurate sodium: do they accurately reflect amniotic fluid volume? *J Matern Fetal Neonatal Med* 11:167–170, 2002.
36. Chauhan SP, Magann EF, Morrison JC, et al: Ultrasonographic assessment of amniotic fluid does not reflect actual amniotic fluid volume. *Am J Obstet Gynecol* 177:291–296, 1997.
37. Magann EF, Nevils BG, Chauhan SP, et al: Low amniotic fluid volume is poorly identified in singleton and twin pregnancies using the 2 × 2 cm pocket technique of the biophysical profile. *South Med J* 92:802–805, 1999.
38. Magann EF, Chauhan SP, Whitworth NS, et al: Subjective versus objective evaluation of amniotic fluid volume of pregnancies of less than 24 weeks' gestation: how can we be accurate? *J Ultrasound Med* 20:191–195, 2001.
39. Magann EF, Sandlin AT, Ounpraseuth ST: Amniotic fluid and the clinical relevance of the sonographically estimated amniotic fluid volume. *J Ultrasound Med* 30:1573–1585, 2011.
40. Bianco A, Rosen T, Kuczynski E, et al: Measurement of the amniotic fluid index with and without color Doppler. *J Perinat Med* 27:245–249, 1999.
41. Magann EF, Chauhan SP, Barrilleaux S, et al: Ultrasound estimate of amniotic fluid volume: color Doppler overdiagnosis of oligohydramnios. *Obstet Gynecol* 98:71–74, 2001.
42. Tressler T, Bernazzoli M, Hole J, Martinez F: The effects of maternal position on the amniotic fluid index. *J Ultrasound Med* 25(4):445–447, 2006.
43. Fok WY, Chan IY, Lau TK: The influence of fetal position on amniotic fluid index and single deepest pocket. *Ultrasound Obstet Gynecol* 28:162–165, 2006.
44. Del Valle GO, Bateman L, Gaudier FL, Sanchez-Ramos L: Comparison of three types of ultrasound transducers in evaluating the amniotic fluid index. *J Reprod Med* 39(11):869–872, 1994.
45. Flack NJ, Dore C, Southwell D, et al: The influence of operator transducer pressure on ultrasonographic measurements of amniotic fluid volume. *Am J Obstet Gynecol* 171(1):218–222, 1994.
46. Magann EF, Doherty DA, Chauhan SP, et al: How well do the amniotic fluid index and single deepest pocket indices (below the 3rd and 5th and above the 95th and 97th percentiles) predict oligohydramnios and hydramnios? *Am J Obstet Gynecol* 190:164–169, 2004.
47. Morris JM, Thompson K, Smithey J, et al: The usefulness of ultrasound assessment of amniotic fluid in predicting adverse outcome in prolonged pregnancy: a prospective blinded observational study. *Br J Obstet Gynaecol* 110:989–994, 2003.
48. Magann EF, Sanderson M, Martin JN, Chauhan S: The amniotic fluid index, single deepest pocket, and two-diameter pocket in normal human pregnancy. *Am J Obstet Gynecol* 182:1581–1588, 2000.
49. Casey BM, McIntire DD, Bloom SL, et al: Pregnancy outcomes after antepartum diagnosis of oligohydramnios at or beyond 34 weeks' gestation. *Am J Obstet Gynecol* 182:909–912, 2000.
50. Chamberlain PF, Manning FA, Morrison I, et al: Ultrasound evaluation of amniotic fluid volume. II. The relationship of increased amniotic fluid volume of perinatal outcome. *Am J Obstet Gynecol* 150:250–254, 1984.
51. Carlson DE, Platt LD, Medearis AL, Horenstein J: Quantifiable polyhydramnios: diagnosis and management. *Obstet Gynecol* 75:989–993, 1990.
52. Phelan JP, Ahn MO, Smith CV, et al: Amniotic fluid index measurements during pregnancy. *J Reprod Med* 32(8):601–604, 1987.
53. Queenan JT, Thompson W, Whitfield CR, Shah SI: Amniotic fluid volumes in normal pregnancies. *Am J Obstet Gynecol* 114:34–38, 1972.
54. Brace RA, Wolf EJ: Normal amniotic fluid volume changes throughout pregnancy. *Am J Obstet Gynecol* 161:382–388, 1989.
55. Abramovich DR: The volume of amniotic fluid in early pregnancy. *J Obstet Gynaecol Br Commonw* 75(7):728–731, 1968.
56. Charles D, Jacoby HE, Burgess F: Amniotic fluid volumes in the second half of pregnancy. *Am J Obstet Gynecol* 93:1042–1047, 1965.
57. Gadd RL: The volume of the liquor amnii in normal and abnormal pregnancies. *J Obstet Gynaecol Br Commonw* 73:11–22, 1966.



58. Gillibrand PN: Changes in amniotic fluid volume with advancing pregnancy. *J Obstet Gynaecol Br Commonw* 76:527–529, 1969.
59. Haswell GL, Morris JA: Amniotic fluid volume studies. *Obstet Gynecol* 42:725–732, 1973.
60. Marsden D, Huntingford PJ: An appraisal of the Coomassie blue dilution technique for measuring the volume of liquor amnii in late pregnancy. *J Obstet Gynaecol Br Commonw* 72:65–68, 1965.
61. Nelson MM: Amniotic fluid volumes in early pregnancy. *J Obstet Gynaecol Br Commonw* 79:50–53, 1972.
62. Rhodes P: The volume of liquor amnii in early pregnancy. *J Obstet Gynaecol Br Commonw* 73:23–26, 1966.
63. Sinha R, Carlton M: The volume and composition of amniotic fluid in early pregnancy. *J Obstet Gynaecol Br Commonw* 77:211–214, 1970.
64. van Otterlo LC, Wladimiroff JW, Wallenburg HC: Relationship between fetal urine production and amniotic fluid volume in normal pregnancy and pregnancy complicated by diabetes. *Br J Obstet Gynaecol* 84:205–209, 1977.
65. Wagner G, Fuchs F: The volume of amniotic fluid in the first half of human pregnancy. *J Obstet Gynaecol Br Emp* 69:131–136, 1962.
66. Magann EF, Bass D, Chauhan SP, et al: Amniotic fluid volume in normal singleton pregnancies. *Obstet Gynecol* 90:524–528, 1997.
67. Sandlin AT, Ounpraseuth ST, Spencer HJ, et al: Amniotic fluid volume in normal singleton pregnancies: modeling with quantile regression. *Arch Gynecol Obstet* 289:967–972, 2014.
68. Machado MH, Cecatti JC, Krupa F, Faundes A: Curve of amniotic fluid index measurements in low-risk pregnancy. *Acta Obstet Gynecol Scand* 86:37–41, 2007.
69. Lei H, Wen SW: Normal amniotic fluid index by gestational week in a Chinese population. Central-South China Fetal Growth Study Group. *Obstet Gynecol* 92(2):237–240, 1998.
70. Magann EF, Chauhan SP, Martin JN, Jr: Is amniotic fluid volume status predictive of fetal acidosis at delivery? *Aust N Z J Obstet Gynaecol* 43(2):129–133, 2003.
71. Magann EF, Doherty DA, Chauhan SP, et al: Dye-determined amniotic fluid volume and intrapartum/neonatal outcome. *J Perinatol* 24(7):423–428, 2004.
72. Shmoys SM, Sivkin M, Dery C, et al: Amniotic fluid index: an appropriate predictor of perinatal outcome. *Am J Perinatol* 7:266–269, 1990.
73. Zhang J, Troendle J, Meikle S, et al: Isolated oligohydramnios is not associated with adverse perinatal outcomes. *Br J Obstet Gynaecol* 111:220–225, 2004.
74. Magann EF, Chauhan SP, Kinsella MJ, et al: Antenatal testing among 1001 patients at high risk: the role of ultrasonographic estimate of amniotic fluid volume. *Am J Obstet Gynecol* 180:1330–1336, 1999.
75. Barrilleaux PS, Magann EF, Chauhan SP, et al: Amniotic fluid index as a predictor of adverse perinatal outcome in the HELLP syndrome. *J Reprod Med* 52:293–298, 2007.
76. Ott WJ: Reevaluation of the relationship between amniotic fluid volume and perinatal outcome. *Am J Obstet Gynecol* 192:1803–1809, 2005.
77. Magann EF, Kinsella MJ, Chauhan SP, et al: Does an amniotic fluid index of  $\leq 5$  cm necessitate delivery in high-risk pregnancies? A case-control study. *Am J Obstet Gynecol* 180(6 Pt 1):1354–1359, 1999.
78. Chauhan SP, Sanderson M, Hendrix NW, et al: Perinatal outcome and amniotic fluid index in the antepartum and intrapartum periods: a meta-analysis. *Am J Obstet Gynecol* 181:1473–1478, 1999.
79. Nabhan AF, Abdelmoula YA: Amniotic fluid index versus single deepest vertical pocket as a screening test for preventing adverse pregnancy outcome. *Cochrane Database Syst Rev* (3):CD006593, 2008.
80. Nabhan AF, Abdelmoula YA: Amniotic fluid index versus single deepest vertical pocket: a meta-analysis of randomized controlled trials. *Int J Gynaecol Obstet* 104(3):184–188, 2009.
81. Bullo ML, Tschumi S, Bucher BS, et al: Pregnancy outcome following exposure to angiotensin-converting enzyme inhibitors or angiotensin receptor antagonists: a systematic review. *Hypertension* 60(2):444–450, 2012.
82. Antonucci R, Zaffanello M, Puxeddu E, et al: Use of non-steroidal anti-inflammatory drugs in pregnancy: impact on the fetus and newborn. *Curr Drug Metab* 13(4):474–490, 2012.
83. Lauria MR, Gonik B, Romero R: Pulmonary hypoplasia: pathogenesis, diagnosis, and antenatal prediction. *Obstet Gynecol* 86:466, 1995.
84. Hill LM: Oligohydramnios: sonographic diagnosis and clinical implications. *Clin Obstet Gynecol* 40:314, 1997.
85. Nicolini U, Fisk NM, Rodeck CH, et al: Low amniotic pressure in oligohydramnios—is this the cause of pulmonary hypoplasia? *Am J Obstet Gynecol* 161(5):1098, 1989.
86. Adzick NS, Harrison MR, Glick PL, et al: Experimental pulmonary hypoplasia and oligohydramnios: relative contributions of lung fluid and fetal breathing movements. *J Pediatr Surg* 19:658, 1984.
87. Harding R, Hooper SB, Dickson KA: A mechanism leading to reduced lung expansion and lung hypoplasia in fetal sheep during oligohydramnios. *Am J Obstet Gynecol* 163:1904, 1990.
88. Kilbride HW, Yeast J, Thibeault DW: Defining limits of survival: lethal pulmonary hypoplasia after midtrimester premature rupture of membranes. *Am J Obstet Gynecol* 175:675, 1996.
89. Grisaru-Granovsky S, Eitan R, Kaplan M, Samueloff A: Expectant management of midtrimester premature rupture of membranes: a plea for limits. *J Perinatol* 23(3):235–239, 2003.
90. Waters TP, Mercer BM: The management of preterm premature rupture of the membranes near the limit of fetal viability. *Am J Obstet Gynecol* 201(3):230–240, 2009.
91. van Teeffelen S, Pajkrt E, Willekes C, et al: Transabdominal amnioinfusion for improving fetal outcomes after oligohydramnios secondary to preterm prelabour rupture of membranes before 26 weeks. *Cochrane Database Syst Rev* (8):CD009952, 2013.
92. van Teeffelen AS, van der Ham DP, Willekes C, et al: Midtrimester preterm prelabour rupture of membranes (PPROM): expectant management or amnioinfusion for improving perinatal outcomes (PPROMEXIL-III trial). *BMC Pregnancy Childbirth* 14:128, 2014.
93. van Teeffelen AS, van der Ham DP, Oei SG, et al: The accuracy of clinical parameters in the prediction of perinatal pulmonary hypoplasia secondary to midtrimester prelabour rupture of fetal membranes: a meta-analysis. *Eur J Obstet Gynecol Reprod Biol* 148(1):3–12, 2010.
94. Laudy JA, Tibboel D, Robben SG, et al: Prenatal prediction of pulmonary hypoplasia: clinical, biometric, and Doppler velocity correlates. *Pediatrics* 109(2):250–258, 2002.
95. Wing DA, Fishman A, Gonzalez C, et al: How frequently should the amniotic fluid index be performed during the course of antepartum testing? *Am J Obstet Gynecol* 174:33, 1996.
96. Lagrew DC, Pircon RA, Nageotte M, et al: How frequently should the amniotic fluid index be repeated? *Am J Obstet Gynecol* 167:1129, 1992.
97. Sandlin AT, Chauhan SP, Magann F: Clinical relevance of sonographically estimated amniotic fluid volume: polyhydramnios. *J Ultrasound Med* 32:851–863, 2013.
98. Lazebnik N, Hill LM, Guzik D, et al: Severity of polyhydramnios does not affect the prevalence of large-for-gestational age newborn infants. *J Ultrasound Med* 15:385–388, 1996.
99. Lazebnik N, Many A: The severity of polyhydramnios, estimated fetal weight and preterm delivery are independent risk factors for the presence of congenital malformations. *Gynecol Obstet Invest* 48:28–32, 1999.
100. Hill LM, Breckle R, Thomas ML, Fries JK: Polyhydramnios: ultrasonically detected prevalence and neonatal outcome. *Obstet Gynecol* 69:21–25, 1987.
101. Ben-Chetrit A, Hochner-Celnikier D, Ron M, Yagel S: Hydramnios in the third trimester of pregnancy: a change in the distribution of accompanying fetal anomalies as a result of early ultrasonographic prenatal diagnosis. *Am J Obstet Gynecol* 162:1344–1345, 1990.
102. Queenan JT, Gadow EC: Polyhydramnios: chronic versus acute. *Am J Obstet Gynecol* 108:349–355, 1970.
103. Phelan JP, Martin GI: Polyhydramnios: fetal and neonatal implications. *Clin Perinatol* 16:987–994, 1989.

104. Dashe JS, McIntire DD, Ramus RM, et al: Hydramnios: anomaly prevalence and sonographic detection. *Obstet Gynecol* 100:134–139, 2002.
105. Ledger WF: Maternal infection with adverse fetal and newborn outcomes. In Ledger WF, editor: *Infection in the Female*, Philadelphia, 1986, Lea & Febiger, p 197.
106. Murray SR: Hydramnios: a study of 846 cases. *Am J Obstet Gynecol* 88:65–67, 1964.
107. Stoll CG, Alembik Y, Dott B: Study of 156 cases of polyhydramnios and congenital malformations in a series of 118,265 consecutive births. *Am J Obstet Gynecol* 165:586–590, 1991.
108. Shani H, Sivan E, Cassif E, Simchen MJ: Maternal hypercalcemia as a possible cause of unexplained fetal polyhydramnios: a case series. *Am J Obstet Gynecol* 199(4):410.e1–410.e5, 2008.
109. Dorleijn DM, Cohen-Overbeek TE, Groenendaal F, et al: Idiopathic polyhydramnios and postnatal findings. *J Matern Fetal Neonatal Med* 22:315–320, 2009.
110. Panting-Kemp A, Nguyen T, Castro L: Substance abuse and polyhydramnios. *Am J Obstet Gynecol* 187:602–605, 2002.
111. Zhu X, Jiang S, Hu Y, et al: The expression of aquaporin 8 and aquaporin 9 in fetal membranes and placenta in term pregnancies complicated by idiopathic polyhydramnios. *Early Hum Dev* 86(10): 657–663, 2010.
112. Mann SE, Ricke EA, Torres EA, Taylor RN: A novel model of polyhydramnios: amniotic fluid volume is increased in aquaporin 1 knockout mice. *Am J Obstet Gynecol* 192:2041–2046, 2005.
113. Mann SE, Dvorak N, Gilbert H, Taylor RN: Steady-state levels of aquaporin 1 mRNA expression are increased in idiopathic polyhydramnios. *Am J Obstet Gynecol* 194:884–887, 2006.
114. Pri-Paz S, Khalek N, Fuchs KM, Simpson LL: Maximal amniotic fluid index as a prognostic factor in pregnancies complicated by polyhydramnios. *Ultrasound Obstet Gynecol* 39:648–653, 2012.
115. Bundgaard A, Anderson BR, Rode L, et al: Prevalence of polyhydramnios at a Danish hospital: a population-based study. *Acta Obstet Gynecol Scand* 86:1427–1431, 2007.
116. Damato N, Filly RA, Goldstein RB, et al: Frequency of fetal anomalies in sonographically detected polyhydramnios. *J Ultrasound Med* 12(1):11–15, 1993.
117. Martinez-Frias MJ, Bermejo E, Rodriguez-Pinilla E, Frias JL: Maternal and fetal factors related to abnormal amniotic fluid. *J Perinatol* 19:514–520, 1999.
118. Landy HJ, Isada NB, Larsen JW: Genetic implications of idiopathic hydramnios. *Am J Obstet Gynecol* 157:114–117, 1987.
119. Sickler GK, Nyberg DA, Sohaey R, Luthy DA: Polyhydramnios and fetal intrauterine growth restriction: ominous combination. *J Ultrasound Med* 16:609–614, 1997.
120. Nobile de Santis MS, Radaelli T, Taricco E, et al: Excess of amniotic fluid: pathophysiology, correlated diseases and clinical management. *Acta Biomed* 75(Suppl 1):53–55, 2004.
121. Xu ZM, Wu LF: Correlation between amniotic fluid glucose concentration and amniotic fluid volume and neonatal birth weight in pregnancy complicated by gestational diabetes mellitus [in Chinese]. *Zhonghua Fu Chan Ke Za Zhi* 41(11):724–728, 2006.
122. Idris N, Wong SF, Thomae M, et al: Influence of polyhydramnios on perinatal outcome in pregestational diabetic pregnancies. *Ultrasound Obstet Gynecol* 36:338–343, 2010.
123. Magann EF, Chauhan SP, Doherty DA, et al: A review of idiopathic hydramnios and pregnancy outcomes. *Obstet Gynecol Surv* 62:795–802, 2007.
124. Lufkin EG, Nelson RL, Hill LM, et al: An analysis of diabetic pregnancies at Mayo Clinic, 1950–79. *Diabetes Care* 7(6):539–547, 1984.
125. Zlatnik G, Olson G, Bukowski R, Saade GR: Amniotic fluid index measured with the aid of color flow Doppler. *J Matern Fetal Neonatal Med* 13:242–245, 2003.
126. Biggio JR, Jr, Wenstrom KD, Dubard MB, Cliver SP: Hydramnios prediction of adverse perinatal outcome. *Obstet Gynecol* 94:773–777, 1999.
127. Maymon E, Ghezzi F, Shoham-Vardi I, et al: Isolated hydramnios at term gestation and the occurrence of peripartum complications. *Eur J Obstet Gynecol Reprod Biol* 77:157–161, 1998.
128. Magann EF, Doherty DA, Lutgendorf MA, et al: Peripartum outcomes of high-risk pregnancies complicated by oligo- and polyhydramnios: a prospective longitudinal study. *J Obstet Gynecol Res* 32:268–277, 2010.
129. Eydoux P, Choiset A, Le Porrier N, et al: Chromosomal prenatal diagnosis: study of 936 cases of intrauterine abnormalities after ultrasound assessment. *Prenat Diagn* 9:255–269, 1989.
130. Golan A, Worman I, Sagi J, et al: Persistence of polyhydramnios during pregnancy: its significance and correlation with maternal and fetal complications. *Gynecol Obstet Invest* 37:18–20, 1994.
131. Magann EF, Whitworth NS, Bass JD, et al: Amniotic fluid volume of third-trimester diamniotic twin pregnancies. *Obstet Gynecol* 85(6):957–960, 1995.
132. Charles D, Jacoby HE: Preliminary data on the use of sodium aminohippurate to determine amniotic fluid volumes. *Am J Obstet Gynecol* 95:266–269, 1966.
133. Watson WJ, Harlass FE, Menard MK, et al: Sonographic assessment of amniotic fluid in normal twin pregnancy. *Am J Perinatol* 12(2):122–124, 1995.
134. Chau AC, Kjos SL, Kovacs BW: Ultrasonographic measurement of amniotic fluid volume in normal diamniotic twin pregnancies. *Am J Obstet Gynecol* 174(3):1003–1007, 1996.
135. Porter TE, Dildy GA, Blanchard JR, et al: Normal values for amniotic fluid index during uncomplicated twin pregnancy. *Obstet Gynecol* 87(5 Pt 1):699–702, 1996.
136. Magann EF, Chauhan SP, Martin JN, Jr, et al: Ultrasonic assessment of the amniotic fluid volume in diamniotic twins. *J Soc Gynecol Investig* 2(4):609–613, 1995.
137. Gerson A, Free SM, Jr, Russino J, et al: Amniotic fluid index in twin gestation. *Ultrasound Obstet Gynecol* 10(2):98–102, 1997.
138. Hill LM, Krohn M, Lazebnik N, et al: The amniotic fluid index in normal twin pregnancies. *Am J Obstet Gynecol* 182(4):950–954, 2000.
139. Magann EF, Whitworth NS, Rhodes PG, et al: Effect of amniotic fluid volume on neonatal outcome in diamniotic twin pregnancies. *South Med J* 91(10):942–945, 1998.
140. Magann EF, Doherty DA, Ennen CS, et al: The ultrasound estimation of amniotic fluid volume in diamniotic twin pregnancies and prediction of peripartum outcomes. *Am J Obstet Gynecol* 196(6):570.e1–570.e6, 2007.
141. Orhan A, Kurzal RB, Istwan NB, et al: The impact of hydramnios on pregnancy outcome in twin gestations. *J Perinatol* 25(1):8–10, 2005.
142. Varma TR, Bateman S, Patel RH, et al: The relationship of increased amniotic fluid volume to perinatal outcome. *Int J Gynaecol Obstet* 27(3):327–333, 1988.



# Antepartum Fetal Surveillance and the Role of Ultrasound

*Sarah Ellestad, Sarah Wheeler, Jeffrey A. Kuller*

## SUMMARY OF KEY POINTS

- The goal of antepartum testing is to prevent fetal death.
- Antepartum testing is most commonly performed in pregnancies identified as high risk due to maternal conditions or following the identification of fetuses at risk for intrauterine compromise so that intervention and timely delivery can prevent progression to stillbirth.
- Antepartum surveillance may also be used to confirm the well-being of the normal fetus so as to prevent unnecessary intervention and iatrogenic prematurity.
- Real-time ultrasonography, including assessment of fetal heart rate patterns and umbilical artery Doppler velocimetry, is a component of antepartum surveillance.
- Surveillance techniques include fetal kick counts, nonstress test (NST), contraction stress test (CST), biophysical profile (BPP), modified biophysical profile, and umbilical artery Doppler velocimetry.

## OUTLINE

Assessment of Fetal Movement, 720

Nonstress Test, 721

Contraction Stress Test, 724

Biophysical Profile, 726

Modified Biophysical Profile, 729

Umbilical Artery Doppler Velocimetry, 730

Conclusions, 730

Antepartum fetal assessment is used to assess the risk of fetal death in pregnancies complicated by maternal medical problems or fetal compromise.<sup>1</sup> Multiple techniques can be utilized to assess fetal status, including fetal kick counts, nonstress test (NST), contraction stress test (CST), biophysical profile (BPP), modified BPP, and umbilical artery Doppler velocimetry. All of these techniques are aimed at identifying hypoxic or acidemic fetuses with the intention of providing an opportunity to intervene before permanent damage or death results. As such, antenatal surveillance can be used to screen for fetal compromise when it is suspected (i.e., maternal report of decreased fetal movement) or anticipated (cyanotic maternal heart disease). Ultrasound can be particularly valuable because it provides a real-time view of fetal activity and assessment of the intrauterine environment. Acute events, however, such as abruption or cord accident, cannot be predicted by such techniques.

Serial antepartum surveillance using one or multiple fetal assessment techniques is the standard of care for pregnancies complicated by maternal or fetal complications. There is little evidence from randomized controlled trials that antepartum testing actually decreases the risk of fetal death, and some evidence suggests that it may actually be harmful as a result of increases in the rate of iatrogenic prematurity.<sup>2</sup> Nevertheless, antenatal testing remains a mainstay of prenatal care to assess fetal well-being for a wide range of maternal and fetal indications (Table 21-1). The primary measure of antepartum testing efficacy is the false negative rate, which is defined as the incidence of fetal death within 1 week of a normal test result. Among the aforementioned

antepartum testing techniques, false negative rates range from a low of 0.4/1000 for CSTs to a high of 3.2/1000 for NSTs.<sup>3</sup> However, the high false positive rate of various testing protocols (up to 50% with the NST), defined as an abnormal test result in the setting of an uncompromised fetus, limits the utility of interpreting a test in isolation without considering the clinical situation or utilizing subsequent surveillance measures<sup>3</sup> (Table 21-2).

## ASSESSMENT OF FETAL MOVEMENT

*Quickening*, or the time at which fetal movement is first perceptible to the mother, typically occurs at about 19 to 20 weeks.<sup>4</sup> With advancing gestation, fetal movement becomes more pronounced and peaks at approximately 38 weeks. Periods of active movement generally last about 40 minutes whereas quiet periods last about 20 minutes.<sup>5</sup> The fetus is most active between 9:00 PM and 1:00 AM, which correlates with falling maternal glucose levels.<sup>5</sup>

Fetal physiology studies performed in the setting of growth-restricted fetuses demonstrate that fetal movement decreases with increasing hypoxia.<sup>6</sup> Thus, maternal assessment of fetal movement is a potentially simple and inexpensive method of monitoring fetal well-being. Physicians routinely inquire about fetal activity as part of the standard prenatal visit.<sup>7</sup> In the low-risk pregnancy, this technique is often the only form of fetal surveillance that is performed.

Numerous protocols can be used for quantifying normal movement; however, there are no high-quality studies indicating a superior

**TABLE 21-1 Indications for Antepartum Fetal Surveillance Testing****Maternal Conditions**

- Pregestational diabetes mellitus
- Hypertension
- Systemic lupus erythematosus
- Chronic renal disease
- Antiphospholipid syndrome
- Hyperthyroidism (poorly controlled)
- Hemoglobinopathies (sickle cell, sickle cell–hemoglobin C, or sickle cell–thalassemia disease)
- Cyanotic heart disease

**Pregnancy-Related Conditions**

- Gestational hypertension
- Preeclampsia
- Decreased fetal movement
- Gestational diabetes mellitus (poorly controlled or medically treated)
- Oligohydramnios
- Fetal growth restriction
- Late-term or postterm pregnancy
- Isoimmunization
- Previous fetal demise (unexplained or recurrent risk)
- Monochorionic multiple gestation (with significant growth discrepancy)

Data from Liston R, Sawchuck D, Young D: Fetal health surveillance: antepartum and intrapartum consensus guideline. Society of Obstetrics and Gynaecologists of Canada, British Columbia Perinatal Health Program. *J Obstet Gynaecol Can* 29:S3-S56, 2007 [published erratum appears in *J Obstet Gynaecol Can* 29:909, 2007].

**TABLE 21-2 Risk of Stillbirth Within 1 Week of a Normal Test**

Antenatal Test	Risk of Stillbirth/1000
NST (once a week) <sup>a</sup>	3.2
NST (twice a week) <sup>b</sup>	1.9
BPP <sup>c</sup>	0.8
Modified BPP <sup>d</sup>	0.8
CST <sup>e</sup>	0.4

BPP, biophysical profile; CST, contraction stress test; NST, nonstress test.

<sup>a</sup>Freeman RK, Anderson G, Dorchester W: A prospective multi-institutional study of antepartum fetal heart rate monitoring. II. Contraction stress test versus nonstress test for primary surveillance. *Am J Obstet Gynecol* 143(7):778-781, 1982.

<sup>b</sup>Boehm FH, Salyer S, Shah DM, Vaughn WK: Improved outcome of twice weekly nonstress testing. *Obstet Gynecol* 67(4):566-568, 1986.

<sup>c</sup>Manning FA, Morrison I, Harman CR, et al: Fetal assessment based on fetal biophysical profile scoring: experience in 19,221 referred high-risk pregnancies. II. An analysis of false-negative fetal deaths. *Am J Obstet Gynecol* 157(4 Pt 1):880-884, 1987.

<sup>d</sup>Miller DA, Rabello YA, Paul RH: The modified biophysical profile: antepartum testing in the 1990s. *Am J Obstet Gynecol* 174(3):812-817, 1996.

methodology or parameters for normal amounts of fetal movement.<sup>8</sup> Most often, women are advised to do “kick counts” by lying on their side and counting the number of fetal movements. The perception of 10 distinct movements in 2 hours is commonly regarded as reassuring.<sup>9,10</sup> Once 10 movements have been recognized by the mother, the count may be discontinued. Kick counts can be repeated as often as

daily. It may, however, be just as useful to encourage the mother to report any change from what she perceives as “normal.”

Multiple factors other than deteriorating fetal status can affect maternal perceptions of movement, including gestational age, placental location, medications, maternal activity, position, and obesity.<sup>11,12</sup> However, decreased fetal movement has been associated with an increased risk of stillbirth.<sup>11</sup> Further evaluation, therefore, is always warranted once decreased maternal perception of fetal movement is reported both to exclude potentially reversible factors that may be responsible and to ensure fetal well-being.

There is only one randomized controlled trial evaluating formal fetal movement counting. During this study, over 68,000 low-risk women were enrolled and randomized to regular fetal movement evaluation (intervention group) or routine care (control group). The antepartum death rate was statistically equal in both groups, 2.9/1000 in the intervention group versus 2.7/1000 in the control group.<sup>13</sup> Reporting compliance was a major limitation of this study and may have affected the results. Only 46% of women in the intervention group were compliant in reporting decreased fetal movement. In contrast, a prospective cohort study performed in Norway found that providing written information about fetal activity, including a definition of what constitutes decreased fetal movement, as well as an invitation to monitor fetal movements via kick charts, reduced the incidence of stillbirth by almost 50% in women who presented with a complaint of decreased fetal movement (odds ratio [OR] 0.51, 95% confidence interval [CI] 0.32-0.81).<sup>14</sup> There have been no randomized controlled trials evaluating fetal movement counting in women with high-risk pregnancies. A systematic review published in the Cochrane Database concluded that there is insufficient evidence to recommend routine fetal movement counting to prevent stillbirth.<sup>15</sup>

**NONSTRESS TEST**

The NST is the most common screening test used in antepartum surveillance. A cardiotocograph, or external fetal monitor, is used to simultaneously record the fetal heart rate (FHR) and maternal uterine activity with Doppler ultrasound transducers that are placed on the maternal abdomen. NST interpretation is based on the premise that a healthy, well-oxygenated fetus will demonstrate accelerations of the heart rate with movement. During an NST, the uterus is quiescent (hence the term *nonstress*) and the FHR is evaluated for a period of up to 20 minutes, although it may be extended for up to 40 minutes to allow for variations in the fetal sleep-wake cycle. The FHR pattern, including baseline heart rate, variability, and the presence or absence of accelerations and decelerations are evaluated in NST interpretation (Figs. 21-1 and 21-2). These parameters reflect a fetus’s ability to adapt effectively to the intrauterine environment and can give the provider information about fetal well-being.

The FHR baseline is regulated by the autonomic nervous system. The parasympathetic innervation of the heart is mediated by the vagus nerve and is responsible for a chronotropic effect that slows down the FHR, as well as an oscillatory effect that alters R wave intervals, resulting in the heart rate variability. The sympathetic nervous system, on the other hand, releases norepinephrine when stimulated, which accelerates the FHR and improves inotropy, or contractility.<sup>16</sup> The FHR baseline is the average number of beats per minute (rounded to 0 or 5) over a 10-minute period. Periods of marked variability (amplitude of the FHR greater than 25 beats per minute above the baseline) should not be used to determine the baseline. Additionally the baseline should be identifiable for at least 2 minutes during the NST, although the 2 minutes may not be contiguous.<sup>17</sup> Most clinicians do not use a computerized model to determine baseline and instead “eyeball” the



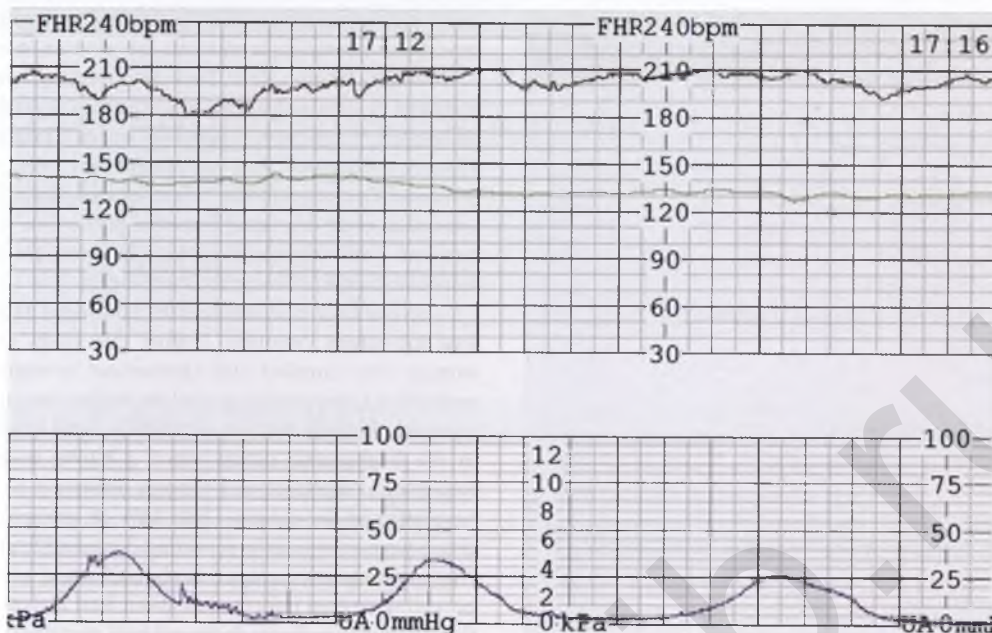


**FIG 21-1** Fetal heart rate (FHR) tracings demonstrating fetal tachycardia with a baseline fetal heart rate (top line) of about 200 beats per minute (bpm). The green line demonstrates maternal pulse; the bottom tracing shows uterine activity (UA).

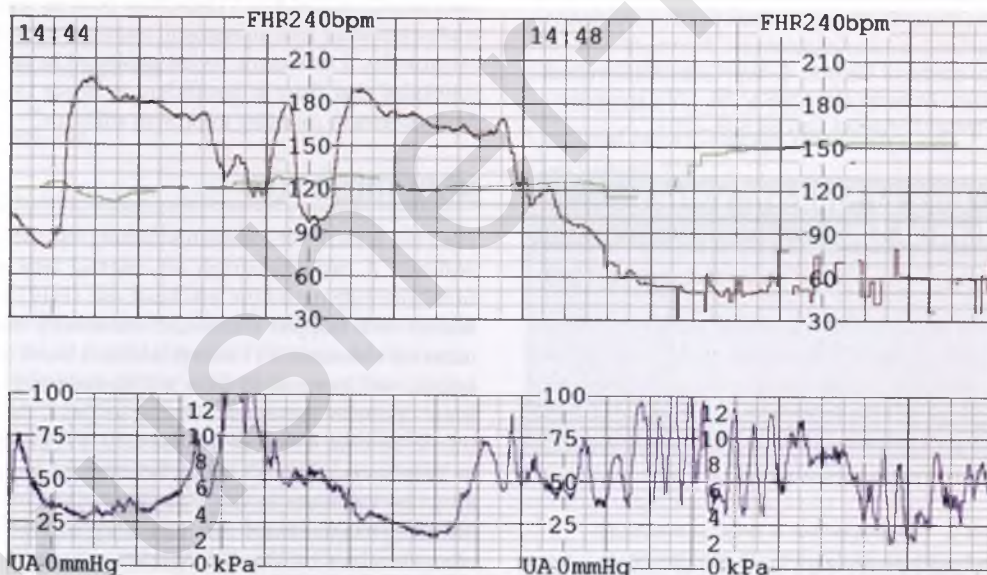


**FIG 21-2** Fetal terminal bradycardia, with an initial fetal heart rate (FHR) of about 180 bpm (beats per minute) that decreases to 60 bpm at the end of the tracing. The green line shows maternal pulse; the bottom tracing shows uterine activity (UA).

tracing, leading to subjectivity in interpretation. Additionally, the baseline may be indeterminate, meaning the NST cannot be interpreted. The normal baseline FHR ranges from 110 to 160 beats per minute; the baseline is usually in the higher end of the normal range early in gestation and decreases as gestation advances.<sup>18</sup>

Variability refers to the expected fluctuations in the baseline FHR that are irregular in amplitude and frequency and are quantified as the amplitude of the peak-to-trough in beats per minute.<sup>17</sup> Variability can be absent, minimal, moderate, or marked (Fig. 21-3). Moderate variability, in which the amplitude ranges between 6 and 25 beats per minute, is considered reassuring.<sup>1</sup> FHR variability is rare before 24 weeks but should be present after 28 weeks. Absence of variability in the third trimester should be considered abnormal until further

evaluation. Tracings demonstrating minimal variability (amplitude less than 6 beats per minute) or absent variability (amplitude range is undetectable) warrant further investigation, especially when the gestational age is in the mid- to late third trimester.

Accelerations are defined as a visually abrupt increase in FHR with onset to peak less than 30 seconds. In a fetus that is 32 weeks' gestation or greater, the acceleration should peak at least 15 beats per minute above the baseline and persist for at least 15 seconds from baseline to baseline. In a fetus younger than 32 weeks the peak of the acceleration should be at least 10 beats per minute above baseline and persist for at least 10 seconds.

Decelerations are classified as late, early, or variable (Fig. 21-4) and differ in their onset, nadir, and recovery in relation to uterine

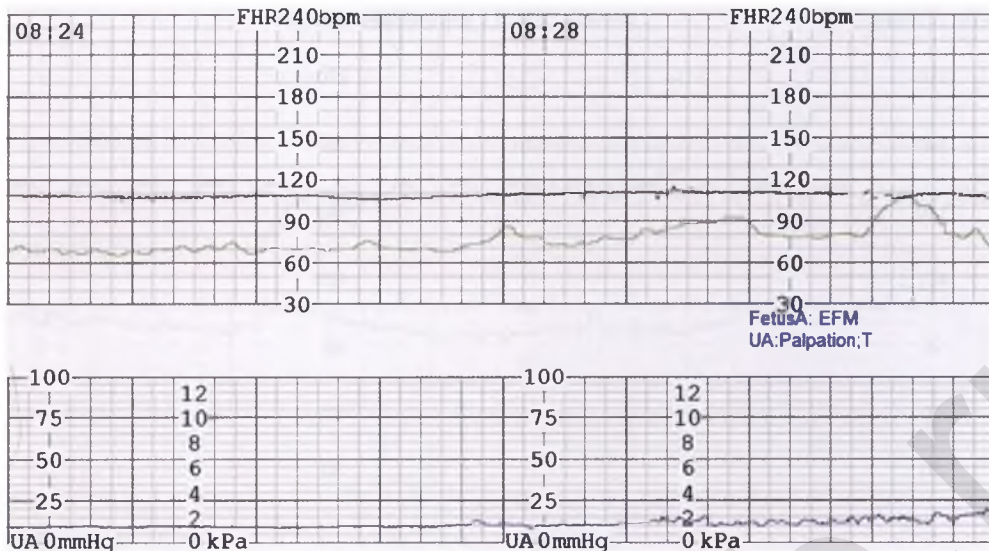


**FIG 21-3** Fetal heart rate (FHR) tracing (*top line*) with a heart rate of 110 bpm (beats per minute) and a nearly flat line consistent with minimal variability. Absence of variability is abnormal and requires further evaluation. EFM, electronic FHR monitoring; UA, uterine activity. The green line shows maternal pulse. The bottom tracing shows uterine activity (UA).

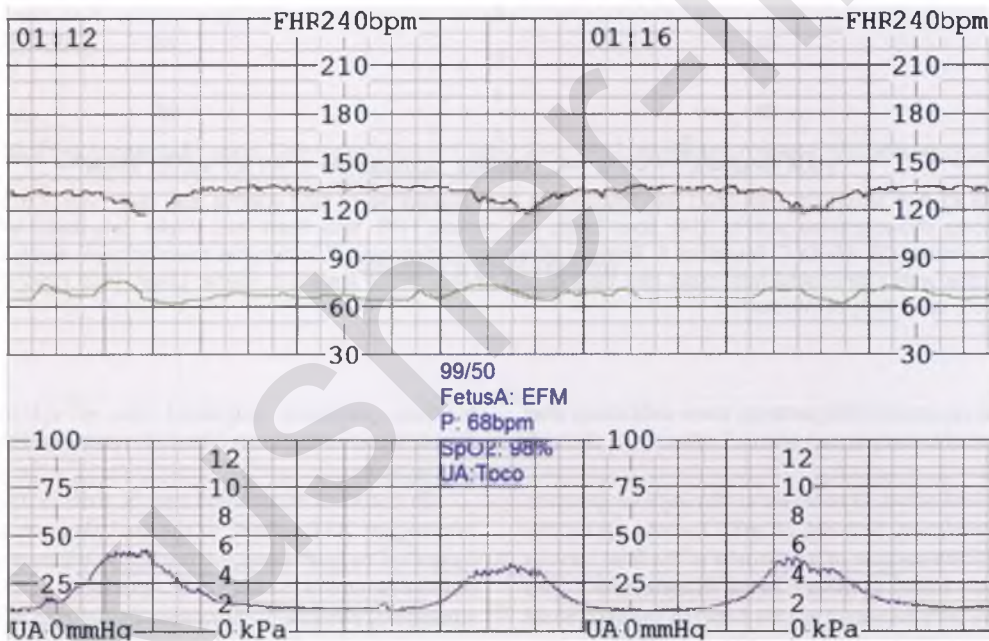


**FIG 21-4** Fetal heart rate (FHR) tracing demonstrating early decelerations, in which the FHR (*top line*) decreases gradually with a nadir at the same time as the uterine contraction (*lower green line*). EFM, electronic FHR monitoring; SpO<sub>2</sub>, oxygen saturation as measured by pulse oximetry; UA, uterine activity. The green line shows maternal pulse. The bottom tracing shows uterine activity (UA).

contractions. Each type of deceleration has a different cause (hypoxemia, head compression, and cord compression, respectively). Correct identification of the type of deceleration can therefore impact FHR interpretation and management.

A sinusoidal FHR is relatively rare and is defined as a smooth, sine wave–like undulating pattern in the FHR baseline with a cycle frequency of 3 to 5/minute that persists for over 20 minutes (Fig. 21-5). This pattern is highly associated with fetal anemia. It is considered abnormal and requires prompt attention. Given the association with fetal anemia, assessment by measurement of the peak systolic velocity of the fetal middle cerebral artery (MCA) using Doppler velocimetry is warranted in the absence of a known cause (see Chapter 22).

Ultimately, the NST is interpreted as “reactive” or “nonreactive.” A reactive NST is defined as the presence of at least two accelerations of the FHR 15 beats per minute or greater above the baseline for a minimum of 15 seconds within a 20-minute period of monitoring. A nonreactive NST lacks the appropriate number of accelerations or doesn’t meet criteria for acceleration but does not demonstrate absence of variability or decelerations. In 2008, the Eunice Kennedy Shriver National Institute of Child Health and Human Development in conjunction with the American College of Obstetricians and Gynecologists and the Society for Maternal-Fetal Medicine published recommendations for the terminology and interpretation of FHR tracings and described a new three-tiered system. Although the emphasis



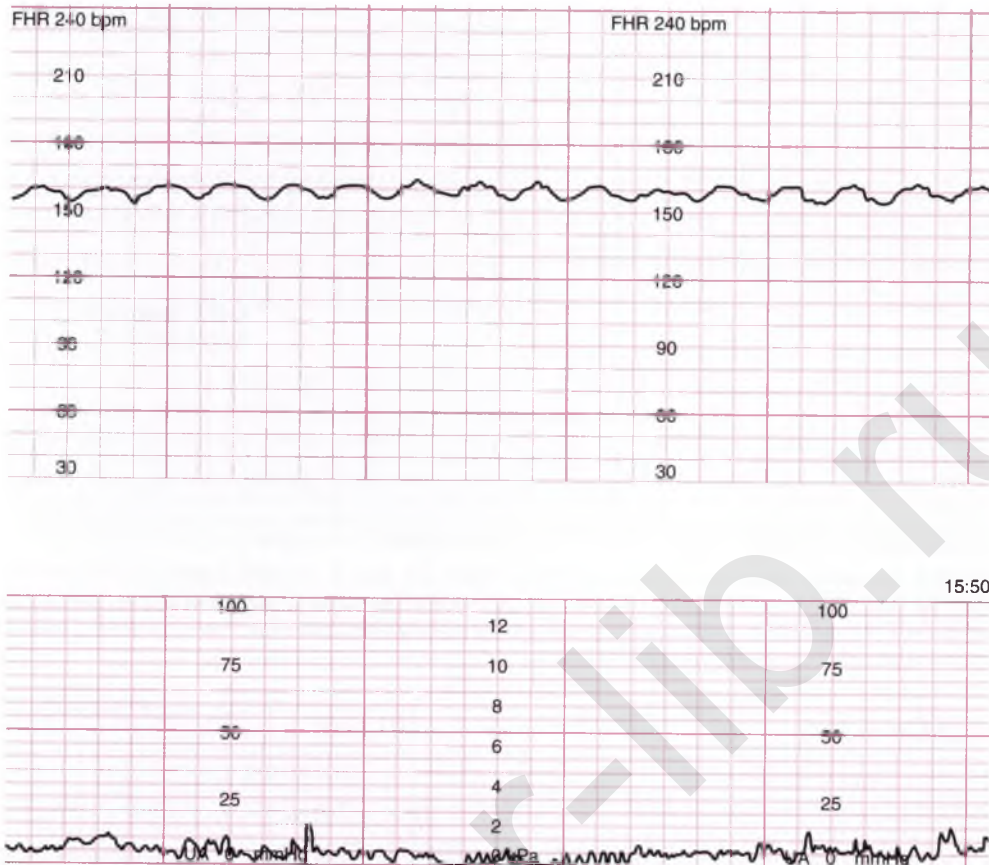


**FIG 21-5** A sinusoidal fetal heart rate tracing (*top line*), suggestive of fetal anemia (see text). The bottom tracing shows uterine activity (UA). bpm, beats per minute; FHR, fetal heart rate. (From Catanzarite VA, Schrimmer DB, Madia C, Mendoza A: Prenatal sonographic diagnosis of intracranial haemorrhage: report of a case with a sinusoidal fetal heart rate tracing, and review of the literature. *Prenat Diagn* 15(3):229-235, 1995, used with permission.)

in this report is on intrapartum FHR patterns, these definitions may also be extrapolated to the antepartum setting<sup>19</sup> (Figs. 21-6 through 21-8 and Table 21-3).

Maturation of the fetal nervous system occurs throughout gestation and affects NST interpretation. Between 24 and 28 weeks, up to 50% of NSTs will not be reactive because of immaturity of the fetal nervous system, which limits the utility of the test in the midtrimester.<sup>20</sup> This number of nonreactive tests decreases to 15% between the gestational ages of 28 and 32 weeks.<sup>21,22</sup> Frequency and amplitude of FHR accelerations increase with advancing gestational age, which contributes to the decrease in nonreactive NSTs as gestational age increases.<sup>23,24</sup>

Despite widespread use of the NST, there are limited data to support its efficacy in the prevention of stillbirth. A Cochrane review reported that performing an NST had no significant effect on the rate of stillbirth or any measure of perinatal morbidity.<sup>25</sup> However, the trials included in this meta-analysis were conducted in the early 1980s, when testing was first being introduced and may not reflect how these tests are utilized and interpreted today.<sup>25</sup> Likewise, the use of sonography as an adjunct to fetal assessment as well as advances in neonatal care have changed since the studies included in the meta-analysis were performed.

Traditionally, the NST was performed on a weekly basis. Starting in 1981, Boehm and associates began increasing the frequency of testing to twice a week in women with at-risk pregnancies and found that the rate of stillbirth after a reactive NST decreased to 1.9/1000 compared

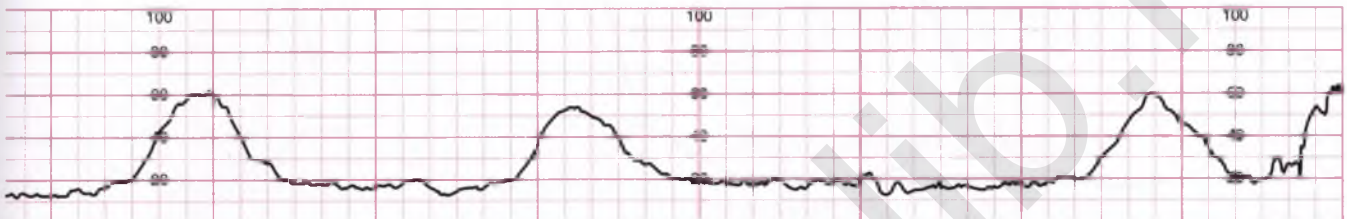
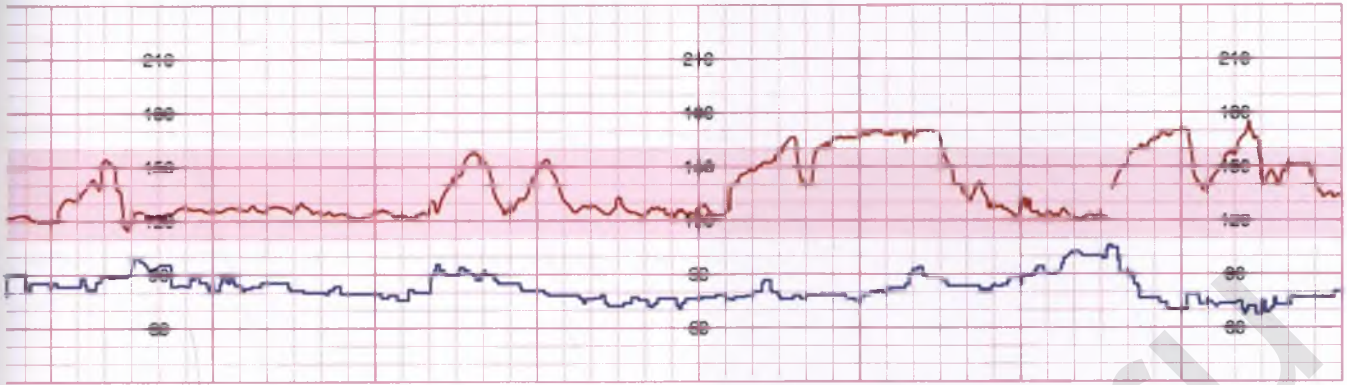
to their previously published rate of 6.1/1000.<sup>26</sup> Twice weekly testing remains the most common recommendation in most clinical circumstances.

Vibroacoustic stimulation may be used to decrease the number of nonreactive NSTs related to the fetal sleep cycle. Using an artificial larynx on or just above the maternal abdomen and delivering short bursts of sound to the fetus over 1 to 5 seconds, fetal movement may be stimulated, potentially shortening the waiting period before an acceleration is produced without compromising the test's validity.<sup>27-29</sup> A 2014 systematic review found that the use of vibroacoustic stimulation shortened the mean overall testing time by almost 7 minutes  $-6.93$  minutes, (95% CI 12.09 minutes to  $-1.76$  minutes) and reduced the frequency of nonreactive NSTs by 40% (OR 0.62, 95% CI 0.48-0.81).<sup>29</sup>

## CONTRACTION STRESS TEST

A CST evaluates the FHR using cardiocography during uterine contractions, which cause transient decreased oxygenation. Therefore, this test assesses the fetal oxygenation status during periods of "stress."<sup>27</sup> Contractions can occur spontaneously or can be induced via nipple stimulation or intravenous oxytocin administration. The goal of a CST is to identify the fetus at risk for compromise by observing the fetus in the presence of (reversible) stress before permanent damage occurs.<sup>30</sup> Once three contractions in a 10-minute period are achieved, the CST is characterized as negative if no late or significant variable

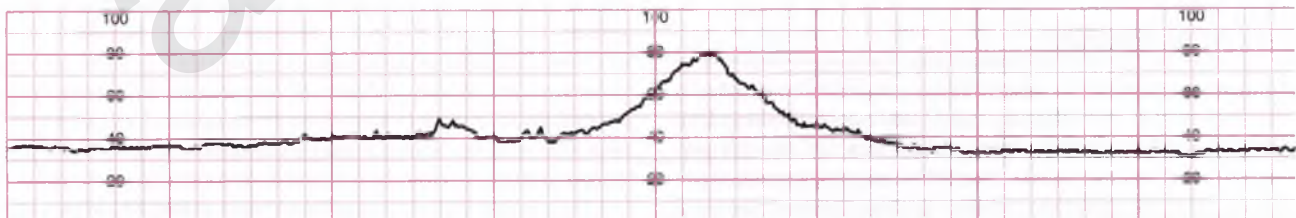
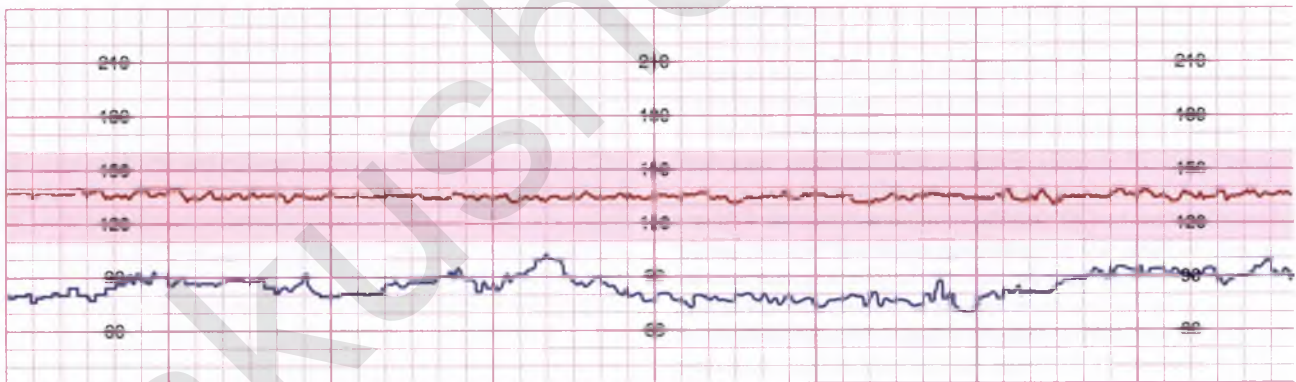
## Category I FHR Tracing



FHR Baseline = 125 BPM  
 Moderate Variability  
 No Decelerations  
 Several Accelerations

**FIG 21-6** Category I tracing. See classification in Table 21-3. BPM, beats per minute; FHR, fetal heart rate. (Personal file of Dr. Leo Brancazio, Duke University.)

## Category II FHR Tracing

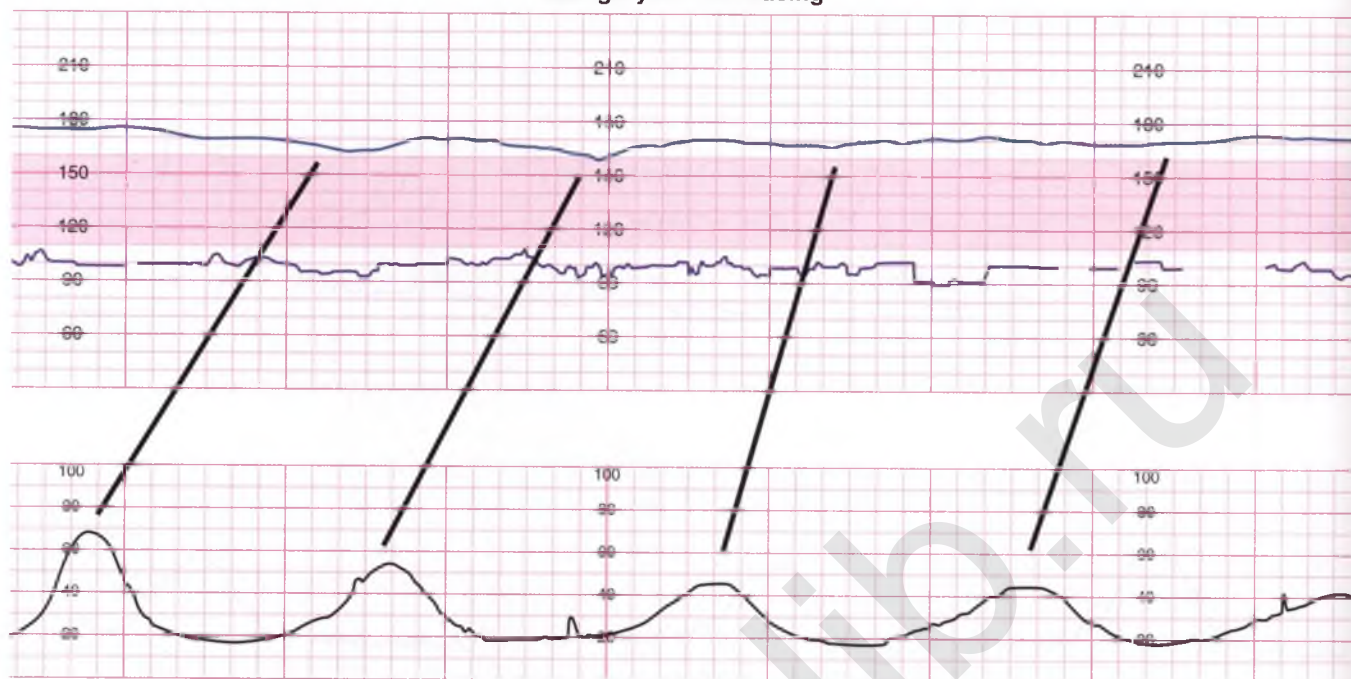


FHR Baseline = 135 BPM  
 Minimal Variability  
 No Accelerations  
 No Decelerations

**FIG 21-7** Category II tracing. See Table 21-3. BPM, beats per minute; FHR, fetal heart rate. (Personal file of Dr. Leo Brancazio, Duke University.)



## Category III FHR Tracing



FHR Baseline = 175 BPM  
 Absent Variability  
 No Accelerations  
 Recurrent Late Decelerations

**FIG 21-8** Category III tracing. See Table 21-3. BPM, beats per minute; FHR, fetal heart rate. (Personal file of Dr. Leo Brancazio, Duke University.)

decelerations are noted. A positive CST is defined by the presence of late decelerations following 50% or more of the contractions and necessitates further evaluation.<sup>9</sup> CST results can be additionally categorized as equivocal-suspicious (intermittent late decelerations or significant variable decelerations), equivocal (FHR decelerations that occur in the presence of contractions more frequent than every 2 minutes or lasting longer than 90 seconds), and unsatisfactory (fewer than three contractions in 10 minutes or an uninterpretable tracing).<sup>7</sup>

Contraindications to CST include conditions that contraindicate contractions and labor and preclude a vaginal delivery or increase the risk of preterm delivery, uterine rupture, or bleeding and include preterm labor, preterm premature rupture of membranes (PPROM), a history of extensive uterine surgery, classical cesarean delivery, or known placenta previa. A CST may also be used to help determine mode of delivery in situations of potential or suspected fetal compromise including PPROM or fetal growth restriction.

## BIOPHYSICAL PROFILE

A BPP integrates ultrasound observations and cardiocography. A BPP is a noninvasive and relatively quick method of assessing fetal well-being that utilizes multiple components that can be independently affected by fetal hypoxemia. The BPP score may provide more in-depth information regarding severity or chronicity of the fetal oxygen state. It is composed of four acute biophysical components and one chronic biophysical component. Each of the acute components, which include the NST, fetal breathing, fetal movement, and fetal tone, is controlled by a discrete regulatory center in the central nervous system (CNS). These centers begin functioning at different gestational ages.<sup>31</sup> Tone, controlled by a center in the cortex-subcortical area, is the

earliest physical activity to appear and can first be observed at about 8 weeks' gestational age. Next is fetal movement, which is regulated by a center in the cortex nuclei and appears at about 9 weeks' gestation. Breathing movements can be visualized at about 21 weeks and are controlled by a center in the ventral surface of the fourth ventricle. The last of the acute biophysical activities to appear is FHR reactivity, which isn't present until the late second trimester or early third trimester and is regulated in the posterior hypothalamus and medulla.<sup>32</sup> Fetal breathing movements and FHR reactivity, therefore, are more gestational age dependent than tone and movement, both of which should be present early in the first trimester.

To perform a BPP, real-time ultrasound is used to observe the fetus over a maximum period of 30 minutes and either 2 points or 0 points are awarded based on the presence or absence of each parameter. A maximum of 10 points can be achieved during the BPP. Points are awarded for fetal movement if two or more discrete body or limb movements are observed within 30 minutes. Fetal tone is defined as one or more episodes of extension with return to flexion in a limb or opening and closing of the hand (Video 21-1). Fetal breathing is defined as an episode of chest wall movements that are sustained for more than 20 seconds (Video 21-2). Points are also awarded for a reactive NST and an amniotic fluid index (AFI) of 5 cm or more or a deepest vertical pocket (DVP) of at least 2 cm (Fig. 21-9, Table 21-4).

The *gradual hypoxia concept* is a theory that the biophysical activities that appear first embryologically are the last to disappear with worsening hypoxia; the activities that are the most sensitive to hypoxia are those that develop last. The more components of the BPP that are absent, the higher the incidence of acidemia.<sup>32-35</sup> Fetal breathing center neurons and the cardioregulatory neurons controlling the coupling of fetal movement and heart rate acceleration are most susceptible to

**TABLE 21-3 Three-Tiered Fetal Heart Rate Interpretation System****Category I**

Category I fetal heart rate (FHR) tracings that include *all* of the following:

- Baseline rate: 110-160 beats per minute (bpm)
- Baseline FHR variability: moderate
- Late or variable decelerations: absent
- Early decelerations: present or absent
- Accelerations: present or absent

**Category II**

Category II tracings include all FHR tracings not categorized as category I or category III. Category II tracings may represent an appreciable fraction of those encountered in clinical care. Examples of category II FHR tracings include any of the following:

**Baseline Rate**

- Bradycardia not accompanied by absent baseline variability
- Tachycardia

**Baseline FHR Variability**

- Minimal baseline variability
- Absent baseline variability not accompanied by recurrent decelerations
- Marked baseline variability

**Accelerations**

- Absence of induced accelerations after fetal stimulation

**Periodic or Episodic Decelerations**

- Recurrent variable decelerations accompanied by minimal or moderate baseline variability
- Prolonged deceleration  $\geq 2$  minutes but  $< 10$  minutes
- Recurrent late decelerations with moderate baseline variability
- Variable decelerations with other characteristics, such as slow return to baseline, "overshoots," or "shoulders"

**Category III**

Category III FHR tracings include either:

- Absent baseline FHR variability and any of the following:
  - Recurrent late decelerations
  - Recurrent variable decelerations
  - Bradycardia
- Sinusoidal pattern

Macones GA, Hankins GD, Spong CY, et al: The 2008 National Institute of Child Health and Human Development workshop report on electronic fetal monitoring: update on definitions, interpretation, and research guidelines. *Obstet Gynecol* 112(3):661-666, 2008.

changes in fetal oxygenation. The centers regulating fetal movement are more resistant to changes in fetal status, and the center regulating fetal tone is the most resistant. Thus, there is a predictable response in the loss of biophysical activities to hypoxemia with loss of fetal breathing movements and FHR acceleration/NST reactivity first, followed by decreased fetal movement and finally loss of tone.<sup>32</sup> This predictable response helps to estimate not only the presence of hypoxemia but also the duration and severity. This is further demonstrated in a study that looked at the relationship between fetal biophysical scores and cord blood gases and acid-base measurements in nonlabored fetuses within 3 hours of a cesarean delivery. As expected, the first manifestations of fetal hypoxemia and acidemia were loss of FHR reactivity and

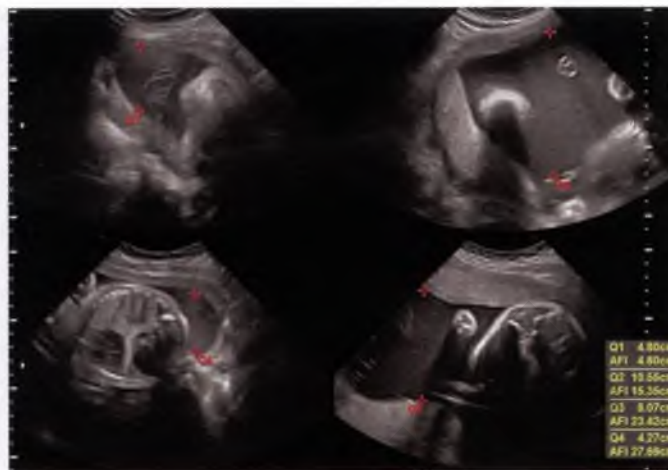


**FIG 21-9** Determination of the amniotic fluid index, with measurement of the deepest vertical pocket in each of the four quadrants of the uterus.

breathing movements; fetal movements and tone were subsequently compromised with increasing degrees of hypoxemia, acidemia, and hypercapnia<sup>31</sup> (Figs. 21-10 through 21-13).

Figure 21-14 displays the inverse relationship between increasingly abnormal BPP scores and presence of fetal distress, admission to neonatal intensive care unit (NICU), fetal growth restriction, low 5-minute Apgar scores, and low cord pH. Likewise, Figure 21-15 demonstrates the linear relationship between lower BPP scores and perinatal morbidity and mortality rates, and Figure 21-16 shows the inverse relationship noted between the last BPP score before delivery and incidence of cerebral palsy.<sup>36</sup> These three figures, which all demonstrate the exponential and highly significant relationship between the BPP in closest proximity to delivery and umbilical venous pH and perinatal morbidity and mortality, provide further proof that the last BPP reflects the presence and degree of acidemia, that acidemia is a manifestation of asphyxia, and that asphyxia can contribute to death or fetal damage.<sup>37</sup>

The chronic component of the BPP is the amniotic fluid volume. Points are awarded if one or more pockets of fluid without umbilical cord or fetal small parts measuring at least 2 cm in the vertical axis are noted.<sup>38</sup> Alternatively a formal AFI can be performed by dividing the uterus into four quadrants and adding up the single deepest pocket in each quadrant (see Fig. 21-9). The range of normal for an AFI is based on gestational age; however, points are awarded for an AFI over 5 cm.<sup>39</sup> In the setting of placental dysfunction, a decrease in amniotic fluid volume takes about 15 days to progress from normal to barely abnormal; the average time to reach severe oligohydramnios is about 23 days in fetuses with growth restriction.<sup>40</sup>

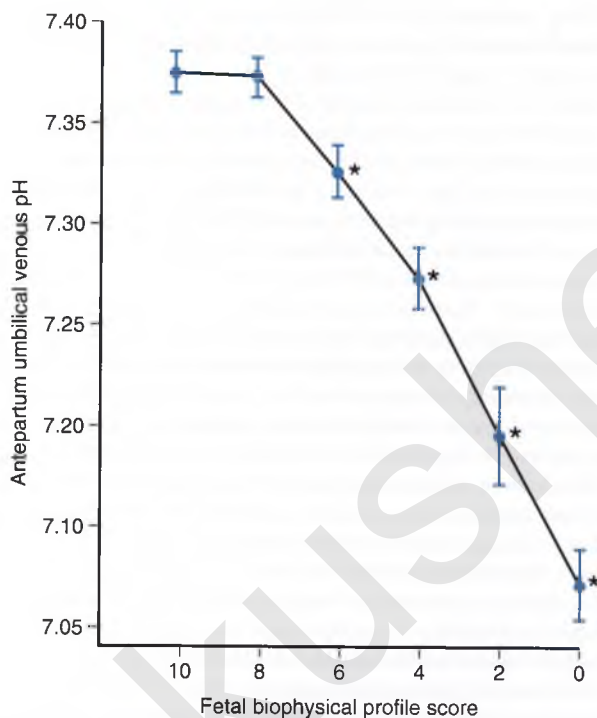
A normal BPP score (8/10 or 10/10) effectively rules out the presence of hypoxemia. However, an abnormal score does not necessarily prove that hypoxemia is present. The more components that are absent, and the longer period of time those variables are absent, the higher the likelihood that pathologic change exists. The fetus has adaptive responses to states of low oxygen, which include decreasing activity, increased oxygen extraction, increased fetal hemoglobin (with increased oxygen-carrying capacity), and redistribution of blood flow to increase perfusion to the fetal brain, heart, and adrenals.<sup>41</sup> In some cases of chronic fetal disease, such as growth restriction, biophysical variables may initially be absent but can subsequently reappear. As such, the presence of certain components of the BPP does not guarantee that the fetus is not hypoxic and may explain why stillbirths still occur following a "normal" BPP.<sup>41</sup> The false negative rate, or risk of



TABLE 21-4 Fetal Biophysical Profile Scoring

Variable	Score 2	Score 0
Fetal breathing movements	Presence of at least 30 seconds of sustained fetal breathing movements in 30 minutes of observation.	Less than 30 seconds of fetal breathing movements in 30 minutes.
Fetal movements	Three or more gross body movements in 30 minutes of observation. Simultaneous limb and trunk movements are counted as a single movement.	Two or less gross body movements in 30 minutes of observation.
Fetal tone	At least one episode of motion of a limb from a position of flexion to extension and a rapid return to flexion.	Limb in a position of semi- or full-extension with no return to flexion with movement; absence of fetal movement is counted as absent tone.
Fetal activity	Presence of two or more fetal heart rate accelerations of at least 15 beats per minute and lasting at least 15 seconds and associated with fetal movement in 40 minutes.	No acceleration or less than two accelerations of the fetal heart rate in 40 minutes of observation.
Qualitative amniotic fluid volume	A pocket of amniotic fluid that measures at least 1 cm in two perpendicular planes.	Large pocket of amniotic fluid measures less than 1 cm in two perpendicular planes.
Maximal score	10	
Minimal score		0

From Manning FA, Platt LD, Sipos L: Antepartum fetal evaluation: development of a fetal biophysical profile score. *Am J Obstet Gynecol* 136:787, 1980.



**FIG 21-10** The relationship between fetal umbilical venous pH ( $\pm$  SD [standard deviation]) by cordocentesis and the fetal biophysical profile score. The correlation was linear, inverse, and very significant ( $r^2 = 0.912$ ;  $P < 0.01$ ). (From Manning FA: Dynamic ultrasound-based fetal assessment: the fetal biophysical profile score. *Clin Obstet Gynecol* 38(1):26-44, 1995.)

fetal death within a week of a normal test result, ranges between 0.4 and 0.6/1000 live births, a rate that is about 10% of the observed perinatal mortality rate in any high-risk study population.<sup>42,43</sup> These deaths may also be due to acute events that cannot be anticipated such as a cord prolapse, abruption, or accidental cord compression.

The amniotic fluid volume component of the BPP greatly influences BPP interpretation and pregnancy management. With a BPP of 8/10 or 10/10 (including 2 points for amniotic fluid), the risk of developing fetal asphyxia within 1 week with no intervention is low (about

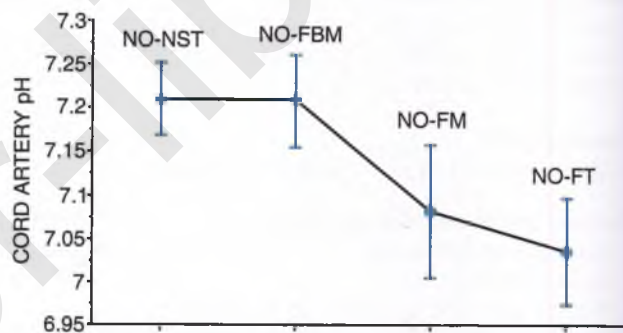


**FIG 21-11** Relationship between cord artery pH and absent fetal biophysical activities. The pH tends to be lower in the absence of movements or tone compared with nonreactive nonstress testing or absence of breathing. Results are expressed in means (95% error bars). NO-FBM, absent fetal breathing; NO-FM, absent fetal movements; NO-FT, absent fetal tone; NO-NST, nonreactive nonstress test. (From Vintzileos AM, Fleming AD, Scorza WE, et al: Relationship between fetal biophysical activities and umbilical cord blood gas values. *Am J Obstet Gynecol* 165(3):707-713, 1991.)

1/1000). When the BPP is 6/10 or 8/10 (with no points awarded for amniotic fluid) the risk of developing fetal asphyxia within 1 week without intervention is increased, from 20/1000 to 30/1000 to more than 50/1000. A 6/10 score, which includes 2 points for amniotic fluid, is considered equivocal, and management depends on gestational age and the indication for testing. The possibility of developing fetal asphyxia cannot be excluded with an equivocal test result, and the test should be repeated within 24 hours in the setting of prematurity; if the fetus is at or near term, delivery may be recommended. A score of 0/10 to 4/10 is more ominous and is associated with a 115/1000 to 550/1000 risk of fetal asphyxia within 1 week if no intervention occurs.<sup>44</sup>

Management, however, must be individualized. A low biophysical score warrants immediate investigation for factors other than hypoxia that may be present, such as prolonged fetal sleep cycles, maternal sedative medications, fetal anomalies, and maternal disease. If confounding factors are absent, a low score increases the risk for fetal acidemia and the likelihood of fetal compromise and death. It is important to note that BPP score does not dictate or predict delivery mode.

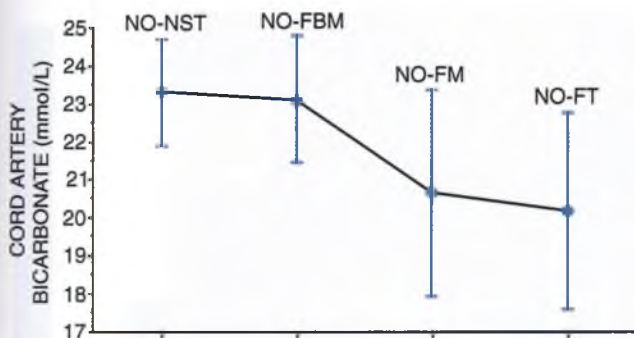


**FIG 21-12** Relationship between cord artery bicarbonate level and absent fetal biophysical activities. The bicarbonate level tends to be lower in the absence of movements or tone compared with nonreactive nonstress testing and absence of breathing. Results are means expressed in millimoles per liter (95% error bars). NO-FBM, absent fetal breathing; NO-FM, absent fetal movements; NO-FT, absent fetal tone; NO-NST, nonreactive nonstress test. (From Vintzileos AM, Fleming AD, Scorza WE, et al: Relationship between fetal biophysical activities and umbilical cord blood gas values. *Am J Obstet Gynecol* 165(3):707-713, 1991.)

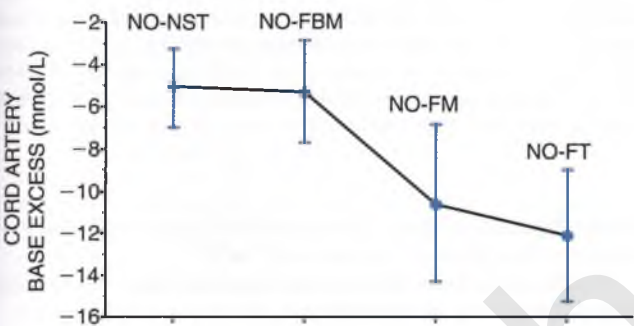


**FIG 21-13** Relationship between cord artery base excess and absent fetal biophysical activities. The base excess tends to be lower in the absence of movements or tone compared with nonreactive nonstress testing and absence of breathing. Results are means expressed in millimoles per liter (95% error bars). NO-FBM, absent fetal breathing; NO-FM, absent fetal movements; NO-FT, absent fetal tone; NO-NST, nonreactive nonstress test. (From Vintzileos AM, Fleming AD, Scorza WE, et al: Relationship between fetal biophysical activities and umbilical cord blood gas values. *Am J Obstet Gynecol* 165(3):707-713, 1991.)

**Modified Biophysical Profile**

Performing a full BPP requires a trained sonographer and a clinician trained to interpret an NST and can take up to 50 minutes, including 30 minutes for the ultrasound examination and 20 minutes for the NST. Given the resources needed to perform a complete BPP, modifications were proposed. In 1989 Clark and colleagues<sup>27</sup> first introduced the modified BPP, which combines the NST and the AFI. The original study used vibroacoustic stimulation after 5 minutes of the NST if spontaneous accelerations were absent. A second stimulus was administered if no accelerations were noted in 10 minutes. Once two accelerations were noted, the NST was discontinued. The AFI was measured via the four quadrant technique. The NST, using vibroacoustic stimulation if needed, served as an indicator of short-term fetal oxygenation status, whereas the AFI served as an indicator of long-term fetal renal perfusion and uteroplacental function.<sup>45</sup> Today the modified BPP is often performed using a traditional NST along with an amniotic fluid assessment via formal AFI or DVP. The modified BPP is considered

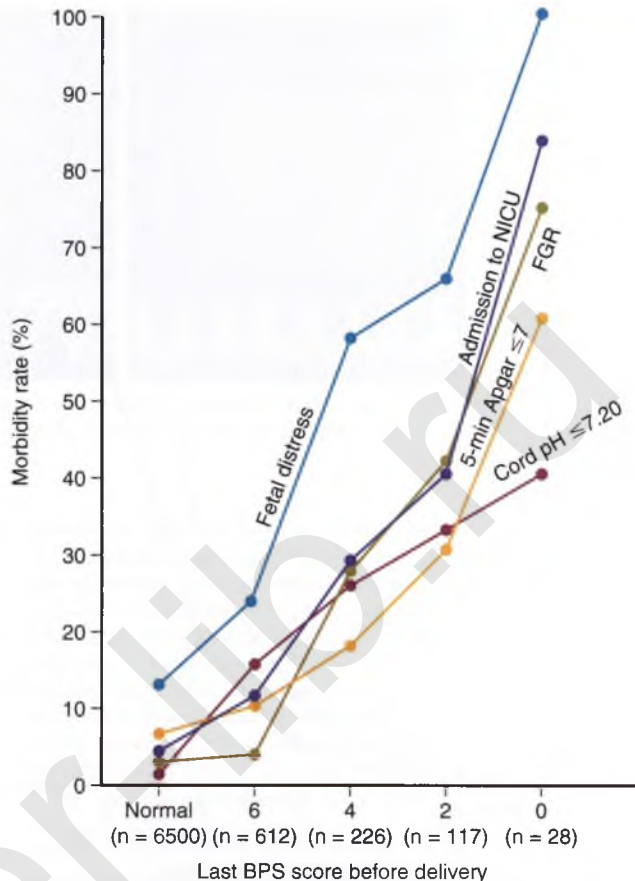


**FIG 21-14** Relationship between perinatal morbidity rate measured by five outcome variables and last biophysical profile scoring (BPS) result before delivery. A significant inverse linear correlation is observed for each variable. FGR, fetal growth restriction; NICU, neonatal intensive care unit. (Modified from Manning FA, Harman CR, Morrison I, et al: Fetal assessment based on fetal biophysical profile scoring. IV. An analysis of perinatal morbidity and mortality. *Am J Obstet Gynecol* 162(3):703-709, 1990.)

normal if the DVP is over 2 cm or AFI is at least 5 cm and the NST is reactive. If either of these parameters is not met, further investigation including a full BPP is indicated.

In a review of 26,257 tests among 12,620 high-risk patients, the predictive value of the four ultrasound components of the BPP (when normal) was found to be equivalent to that of the full BPP (including the NST).<sup>46</sup> This observation was demonstrated in a subsequent prospective study evaluating the use of NST only when values for one or more of the ultrasound components was abnormal and was found to reduce the need for NSTs in 95% of cases.<sup>47</sup> An NST should always be performed if any of the ultrasound components is abnormal. However, a BPP score of 8/10 is as accurate as a score of 10/10 for the prediction of fetal well-being, as long as points are not deducted for fluid.<sup>48</sup>

There is a paucity of studies comparing the full BPP to the modified BPP. In the single trial comparing the two, no difference was noted in neonatal outcomes between the groups.<sup>49</sup> Comparing the modified BPP as the primary testing method and the complete BPP as the backup test, antepartum fetal death was 6.75 times less common in high-risk women who were tested than in their nontested counterparts. However, the modified BPP is associated with a high rate of false positive results (60%), which led to iatrogenic prematurity in 1.5% of women tested before term.<sup>49</sup> Despite the limited data, the modified



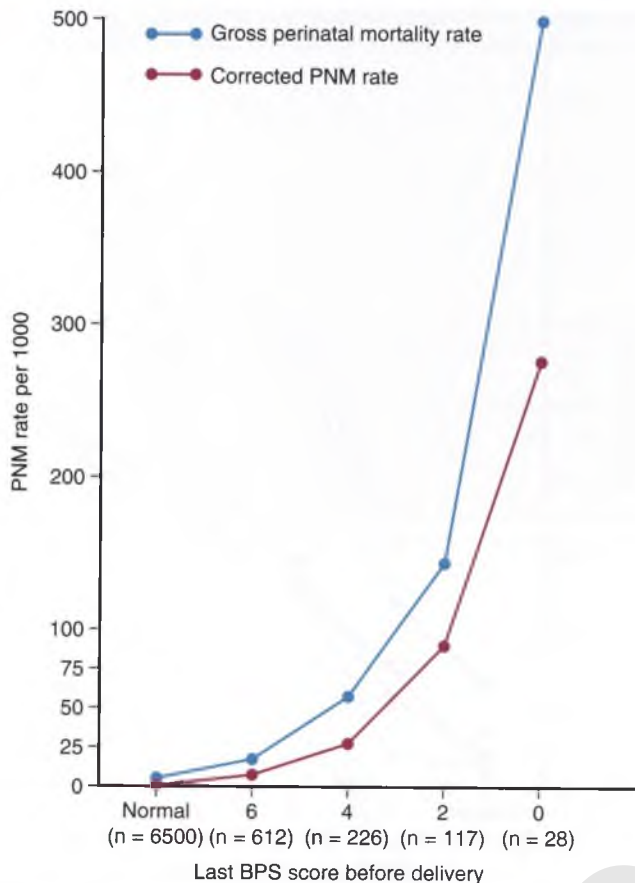


**FIG 21-15** Relationship between perinatal mortality (PNM) rate, either total or corrected for major anomaly, and the last biophysical profile scoring (BPS) result. The relationship is exponential and yields a highly significant correlation with  $\log_{10}$  conversion. (From Manning FA, Harman CR, Morrison I, et al: Fetal assessment based on fetal biophysical profile scoring. IV. An analysis of perinatal morbidity and mortality. *Am J Obstet Gynecol* 162(3):703-709, 1990.)

BPP is widely utilized for fetal surveillance as it requires less expertise and is less time consuming than a full BPP yet provides additional information over an NST alone.

### UMBILICAL ARTERY DOPPLER VELOCIMETRY

Doppler velocimetry can be used to observe flow velocity waveforms in the fetal umbilical arteries. In the normal fetus, high-velocity systolic and diastolic flow is noted within the umbilical artery such that the ratio between systolic and diastolic flow is low (Fig. 21-17). Increased resistance in placental vasculature may create impedance to flow resulting in diminished diastolic flow such that the ratio of systolic to diastolic flow is high.<sup>50-52</sup> In the setting of growth restriction, studies have shown that a systolic/diastolic ratio two standard deviations above the mean for a given gestational age is abnormal, warrants close surveillance, and consideration of antenatal steroids or delivery depending on gestational age.<sup>53</sup>

As flow resistance increases, absent or reversed diastolic flow can be observed (see Fig. 21-17). Both of these findings are ominous and increase the risk for perinatal fatality. Demonstration of absent or reversed end-diastolic flow in the umbilical artery, therefore, requires further investigation and consideration of delivery depending on the gestational age and clinical context.<sup>54,55</sup> The addition of Doppler interrogation of the umbilical artery to standard antepartum testing in the

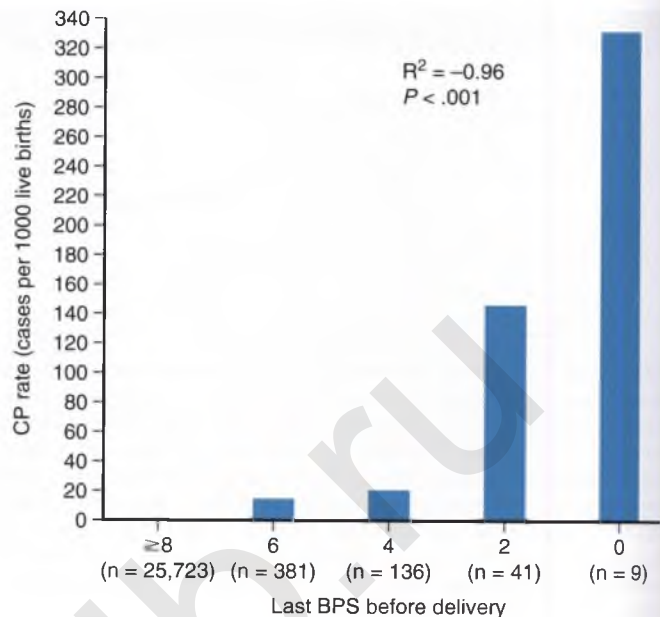


**FIG 21-16** The relationship between the fetal biophysical profile score (BPS) and cerebral palsy (CP) rate is inverse, exponential, and highly significant ( $R^2 = -0.965$ ;  $P < 0.001$ ). Infants were followed for 5 years after birth. (From Manning FA, Bondaji N, Harman CR, et al: Fetal assessment based on fetal biophysical profile scoring. VIII. The incidence of cerebral palsy in tested and untested perinates. *Am J Obstet Gynecol* 178(4):696-706, 1998.)

setting of fetal growth restriction is associated with a reduction in the rate of perinatal death by as much as 29%.<sup>56,57</sup>

Doppler technology is further discussed in Chapter 22, The Role of Doppler Ultrasound in Obstetrics.

### CONCLUSIONS

Despite limited scientific evidence supporting the use of antenatal testing to decrease the perinatal mortality rate, antenatal surveillance is considered standard of care in the management of pregnancies affected by maternal or fetal disease. As such, future research investigating the effectiveness of antenatal testing techniques is unlikely to take the form of randomized controlled trials, and recommendations will continue to be based largely on consensus and expert opinion.

However, antenatal testing does provide an opportunity to evaluate the health of both the mother and the fetus on a more frequent basis and allows the provider an opportunity to educate the mother on findings and expectations regarding the pregnancy, her health, and the well-being of her fetus. Because of the high rate of false positive findings with each of the testing methods described, providers should be prepared to interpret the findings in the context in which they are undertaken, which includes the test indication, fetal gestational age, and whether the condition at present is temporary or reversible.

As a general rule, because the goal of antepartum fetal surveillance is to prevent fetal death, testing should not be performed in pregnancies that are previsible or complicated by lethal abnormalities unless other circumstances apply. Frequency and duration of surveillance will depend on the indication and chronicity of the maternal and fetal condition. Abnormal test results may be followed up with a subsequent test (i.e., a nonreactive test may be followed by a BPP) and may provide an opportunity to increase maternal/fetal surveillance, administer steroids, and help plan for delivery.

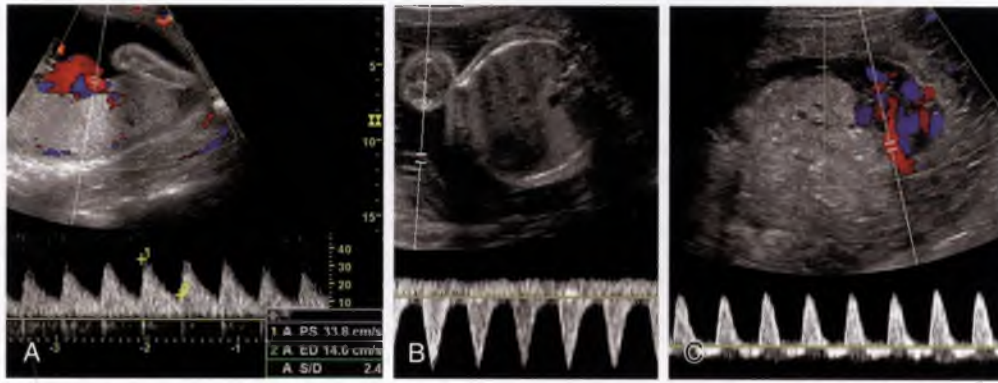


**FIG 21-17** Umbilical artery Doppler velocimetry. **A**, Normal umbilical artery Doppler waveform with diastolic flow present. Systolic/diastolic (S/D) ratio 2.4. **B**, Absent diastolic flow. **C**, Reversed end-diastolic flow.

## REFERENCES

- American College of Obstetricians and Gynecologists: ACOG Practice Bulletin No. 106: intrapartum fetal heart rate monitoring: nomenclature, interpretation, and general management principles. *Obstet Gynecol* 114(1):192–202, 2009.
- Thacker SB, Berkelman RL: Assessing the diagnostic accuracy and efficacy of selected antepartum fetal surveillance techniques. *Obstet Gynecol Surv* 41(3):121–141, 1986.
- Freeman RK, Anderson G, Dorchester W: A prospective multi-institutional study of antepartum fetal heart rate monitoring. II. Contraction stress test versus nonstress test for primary surveillance. *Am J Obstet Gynecol* 143(7):778–781, 1982.
- Andersen HF, Johnson TR, Jr, Flora JD, Jr, Barclay ML: Gestational age assessment. II. Prediction from combined clinical observations. *Am J Obstet Gynecol* 140(7):770–774, 1981.
- Patrick J, Campbell K, Carmichael L, et al: Patterns of gross fetal body movements over 24-hour observation intervals during the last 10 weeks of pregnancy. *Am J Obstet Gynecol* 142(4):363–371, 1982.
- Bekedam DJ, Visser GH: Effects of hypoxemic events on breathing, body movements, and heart rate variation: a study in growth-retarded human fetuses. *Am J Obstet Gynecol* 153(1):52–56, 1985.
- American College of Obstetricians and Gynecologists: ACOG Practice Bulletin No. 145: antepartum fetal surveillance. *Obstet Gynecol* 124(1):182–192, 2014.
- Pearson JF, Weaver JB: Fetal activity and fetal wellbeing: an evaluation. *Br Med J* 1(6021):1305–1307, 1976.
- American College of Obstetricians and Gynecologists: ACOG Practice Bulletin No. 9, October 1999 (replaces Technical Bulletin No. 188, January 1994). Antepartum fetal surveillance. Clinical management guidelines for obstetrician-gynecologists. *Int J Gynaecol Obstet* 68(2):175–185, 2000.
- Moore TR, Piacquadio K: A prospective evaluation of fetal movement screening to reduce the incidence of antepartum fetal death. *Am J Obstet Gynecol* 160(5 Pt 1):1075–1080, 1989.
- Neldam S: Fetal movements as an indicator of fetal well-being. *Dan Med Bull* 30(4):274–278, 1983.
- O'Neill E, Thorp J: Antepartum evaluation of the fetus and fetal well being. *Clin Obstet Gynecol* 55(3):722–730, 2012.
- Grant A, Elbourne D, Valentin L, Alexander S: Routine formal fetal movement counting and risk of antepartum late death in normally formed singletons. *Lancet* 2(8659):345–349, 1989.
- Tveit J, Saastad E, Bordahl PE, et al: *The epidemiology of decreased fetal movements. Proceedings of the Norwegian Perinatal Society Conference*, Oslo, Norway, November 2006.
- Mangesi L, Hofmeyr GJ: Fetal movement counting for assessment of fetal wellbeing. *Cochrane Database Syst Rev* (1):CD004909, 2007.
- Parer JT: Fetal heart rate. In Creasy RK, Resnik R, editors: *Maternal fetal medicine*, ed 4, Philadelphia, 1999, WB Saunders.
- Macones GA, Hankins GD, Spong CY, et al: The 2008 National Institute of Child Health and Human Development workshop report on electronic fetal monitoring: update on definitions, interpretation, and research guidelines. *J Obstet Gynecol Neonatal Nurs* 37(5):510–515, 2008.
- Wheeler T, Murrills A: Patterns of fetal heart rate during normal pregnancy. *Br J Obstet Gynaecol* 85(1):18–27, 1978.
- Macones GA, Hankins GD, Spong CY, et al: The 2008 National Institute of Child Health and Human Development workshop report on electronic fetal monitoring: update on definitions, interpretation, and research guidelines. *Obstet Gynecol* 112(3):661–666, 2008.
- Bishop EH: Fetal acceleration test. *Am J Obstet Gynecol* 141(8):905–909, 1981.
- Lavin JP, Jr, Miodovnik M, Barden TP: Relationship of nonstress test reactivity and gestational age. *Obstet Gynecol* 63(3):338–344, 1984.
- Druzin ML, Fox A, Kogut E, Carlson C: The relationship of the nonstress test to gestational age. *Am J Obstet Gynecol* 153(4):386–389, 1985.
- Sadovsky G, Nicolaidis KH: Reference ranges for fetal heart rate patterns in normoaeamic nonanaemic fetuses. *Fetal Ther* 4(2–3):61–68, 1989.
- Park MI, Hwang JH, Cha KJ, et al: Computerized analysis of fetal heart rate parameters by gestational age. *Int J Gynaecol Obstet* 74(2):157–164, 2001.
- Grivell RM, Alfirevic Z, Gyte GM, Devane D: Antenatal cardiotocography for fetal assessment. *Cochrane Database Syst Rev* (12):CD007863, 2012.
- Boehm FH, Salyer S, Shah DM, Vaughn WK: Improved outcome of twice weekly nonstress testing. *Obstet Gynecol* 67(4):566–568, 1986.
- Clark SL, Sabey P, Jolley K: Nonstress testing with acoustic stimulation and amniotic fluid volume assessment: 5973 tests without unexpected fetal death. *Am J Obstet Gynecol* 160(3):694–697, 1989.
- Smith CV, Phelan JP, Platt LD, et al: Fetal acoustic stimulation testing. II. A randomized clinical comparison with the nonstress test. *Am J Obstet Gynecol* 155(1):131–134, 1986.
- Tan KH, Smyth RM, Wei X: Fetal vibroacoustic stimulation for facilitation of tests of fetal wellbeing. *Cochrane Database Syst Rev* (12):CD002963, 2013.
- Wyatt SN, Rhoads SJ: A primer on antenatal testing for neonatal nurses: part 2: tests of fetal well-being. *Adv Neonatal Care* 6(5):228–241, 2006.
- Vintzileos AM, Feinstein SJ, Lodeiro JG, et al: Fetal biophysical profile and the effect of premature rupture of the membranes. *Obstet Gynecol* 67(6):818–823, 1986.
- Vintzileos AM, Gaffney SE, Salinger LM, et al: The relationship between fetal biophysical profile and cord pH in patients undergoing cesarean section before the onset of labor. *Obstet Gynecol* 70(2):196–201, 1987.
- Vintzileos AM, Fleming AD, Scorza WE, et al: Relationship between fetal biophysical activities and umbilical cord blood gas values. *Am J Obstet Gynecol* 165(3):707–713, 1991.
- Vintzileos AM, Campbell WA, Nochimson DJ, Weinbaum PJ: The use and misuse of the fetal biophysical profile. *Am J Obstet Gynecol* 156(3):527–533, 1987.



35. Vintzileos AM, Gaffney SE, Salinger LM, et al: The relationships among the fetal biophysical profile, umbilical cord pH, and Apgar scores. *Am J Obstet Gynecol* 157(3):627-631, 1987.
36. Manning FA, Bondaji N, Harman CR, et al: Fetal assessment based on fetal biophysical profile scoring. VIII. The incidence of cerebral palsy in tested and untested perinates. *Am J Obstet Gynecol* 178(4):696-706, 1998.
37. Manning FA: Fetal biophysical profile: a critical appraisal. *Clin Obstet Gynecol* 45(4):975-985, 2002.
38. Chamberlain PF, Manning FA, Morrison I, et al: Ultrasound evaluation of amniotic fluid volume. I. The relationship of marginal and decreased amniotic fluid volumes to perinatal outcome. *Am J Obstet Gynecol* 150(3):245-249, 1984.
39. Phelan JP, Ahn MO, Smith CV, et al: Amniotic fluid index measurements during pregnancy. *J Reprod Med* 32(8):601-604, 1987.
40. Nicolaides KH, Peters MT, Vyas S, et al: Relation of rate of urine production to oxygen tension in small-for-gestational-age fetuses. *Am J Obstet Gynecol* 162(2):387-391, 1990.
41. Martin CB, Jr: Normal fetal physiology and behavior, and adaptive responses with hypoxemia. *Semin Perinatol* 32(4):239-242, 2008.
42. Manning FA, Morrison I, Harman CR, et al: Fetal assessment based on fetal biophysical profile scoring: experience in 19,221 referred high-risk pregnancies. II. An analysis of false-negative fetal deaths. *Am J Obstet Gynecol* 157(4 Pt 1):880-884, 1987.
43. Dayal AK, Manning FA, Berck DJ, et al: Fetal death after normal biophysical profile score: an eighteen-year experience. *Am J Obstet Gynecol* 181(5 Pt 1):1231-1236, 1999.
44. Manning FA: Fetal biophysical profile. *Obstet Gynecol Clin North Am* 26(4):557-577, 1999.
45. Rutherford SE, Phelan JP, Smith CV, Jacobs N: The four-quadrant assessment of amniotic fluid volume: an adjunct to antepartum fetal heart rate testing. *Obstet Gynecol* 70(3 Pt 1):353-356, 1987.
46. Manning FA, Platt LD, Sipos L: Antepartum fetal evaluation: development of a fetal biophysical profile. *Am J Obstet Gynecol* 136(6):787-795, 1980.
47. Manning FA, Menticoglou S, Harman CR, et al: Antepartum fetal risk assessment: the role of the fetal biophysical profile score. *Baillieres Clin Obstet Gynaecol* 1(1):55-72, 1987.
48. Manning FA: Antepartum fetal surveillance. *Curr Opin Obstet Gynecol* 7(2):146-149, 1995.
49. Miller DA, Rabello YA, Paul RH: The modified biophysical profile: antepartum testing in the 1990s. *Am J Obstet Gynecol* 174(3):812-817, 1996.
50. Giles WB, Trudinger BJ, Baird PJ: Fetal umbilical artery flow velocity waveforms and placental resistance: pathological correlation. *Br J Obstet Gynaecol* 92(1):31-38, 1985.
51. Reuwer PJ, Bruinse HW, Stoutenbeek P, Haspels AA: Doppler assessment of the fetoplacental circulation in normal and growth-retarded fetuses. *Eur J Obstet Gynecol Reprod Biol* 18(4):199-205, 1984.
52. Erskine RL, Ritchie JW: Umbilical artery blood flow characteristics in normal and growth-retarded fetuses. *Br J Obstet Gynaecol* 92(6):605-610, 1985.
53. Devoe LD, Gardner P, Dear C, Faircloth D: The significance of increasing umbilical artery systolic-diastolic ratios in third-trimester pregnancy. *Obstet Gynecol* 80(4):684-687, 1992.
54. Karsdorp VH, van Vugt JM, van Geijn HP, et al: Clinical significance of absent or reversed end diastolic velocity waveforms in umbilical artery. *Lancet* 344(8938):1664-1668, 1994.
55. Nicolaides KH, Bilardo CM, Soothill PW, Campbell S: Absence of end diastolic frequencies in umbilical artery: a sign of fetal hypoxia and acidosis. *BMJ* 297(6655):1026-1027, 1988.
56. Giles W, Bisits A: Clinical use of Doppler ultrasound in pregnancy: information from six randomised trials. *Fetal Diagn Ther* 8(4):247-255, 1993.
57. Alfirevic Z, Stampalija T, Gyte GM: Fetal and umbilical Doppler ultrasound in normal pregnancy. *Cochrane Database Syst Rev* (8):CD001450, 2010.

# Role of Doppler Sonography in Obstetrics

Malgorzata Mlynarczyk, Letty Romary, Alfred Z. Abuhamad

## SUMMARY OF KEY POINTS

- Absent or reverse flow during diastole in the umbilical artery represents an advanced stage of placental compromise and is associated with more than 70% of placental arterial obliteration.
- In the presence of fetal hypoxemia, central redistribution of blood flow occurs, resulting in an increased blood flow to the brain, heart, and adrenals and a reduction in flow to the peripheral and placental circulations, known as the *brain-sparing effect*.
- Middle cerebral artery (MCA) peak systolic velocities (PSVs) are increased in the presence of fetal anemia. The greater velocity results from decreased blood viscosity and increased cardiac output.
- Pulsed Doppler velocimetry of the uterine artery should be obtained immediately after the vessel crosses the hypogastric artery and before it divides into the uterine and cervical branches. Abnormal uterine artery circulation has been associated with fetal growth restriction (FGR), preeclampsia, preterm delivery, and nonreassuring fetal status in labor.
- Doppler flow studies of the inferior vena cava and ductus venosus in the fetus provide information with regard to right ventricular preload, myocardial compliance, and right ventricular end-diastolic pressure.
- Inferior vena cava Doppler waveforms are triphasic in shape, with the first phase corresponding to ventricular systole, the second phase to early diastole, and the third phase to late diastole or the atrial kick. Ductus venosus Doppler waveforms are biphasic in shape, with the first phase corresponding to ventricular systole, the second phase to early diastole, and the nadir of the second phase to late diastole or the atrial kick.
- Reversed flow in the ductus venosus during atrial systole may be due to worsening placental disease, impaired cardiac function secondary to metabolic compromise, congenital heart defects, redistribution of hepatoportal blood flow through the liver, or a combination of these factors.
- To obtain accurate Doppler indices in fetal echocardiography, the sample volume is placed distal to the respective valves, the insonating angle should be within 0 to 20 degrees of the direction of blood flow, Doppler waveforms should be obtained during fetal apnea, and multiple measurements should be made.
- Doppler waveforms across the atrioventricular valves are bicuspid in shape. The first peak (E wave) corresponds to early ventricular filling of diastole, the second peak (A wave) corresponds to atrial systole or the atrial kick, with the E/A ratio being an index of ventricular preload and compliance.
- Doppler waveforms across the semilunar valves are uniphasic in shape. PSV and the time to peak velocity (TPV) increase with advancing gestation. These Doppler indices reflect ventricular contractility, arterial pressure, and afterload.
- Umbilical artery Doppler surveillance should be initiated when a growth-restricted fetus is considered viable. Abnormal Doppler waveforms of the umbilical artery have been associated with adverse perinatal outcome.
- Obtaining umbilical artery Doppler screening routinely in low-risk pregnancies has not been shown to improve outcome.

## OUTLINE

Physical Principles, 733

Fetal Arterial Doppler, 734

Umbilical Artery, 734

Middle Cerebral Artery, 735

Uterine Artery, 736

Fetal Venous Doppler, 738

Fetal Cardiac Doppler, 744

Optimizing the Image, 744

Fetal Doppler and Fetal Growth Restriction, 745

## PHYSICAL PRINCIPLES

The Doppler effect, first reported by Christian Doppler in 1842,<sup>1</sup> describes the apparent variation in frequency of a light or a sound wave as the source of the wave approaches or moves away relative to an observer. The traditional example that is given to describe this physical phenomenon is the apparent change in sound level of a train

as it approaches and then departs a station. The sound seems higher in pitch as the train approaches the station and seems lower in pitch as the train departs the station. The actual sound of the train is constant, it is the apparent change in sound pitch to a stationary observer that describes the Doppler effect. This apparent change in sound pitch (Doppler effect), or what is also termed the *frequency shift*, is proportional to the speed of movement of the sound-emitting source. In



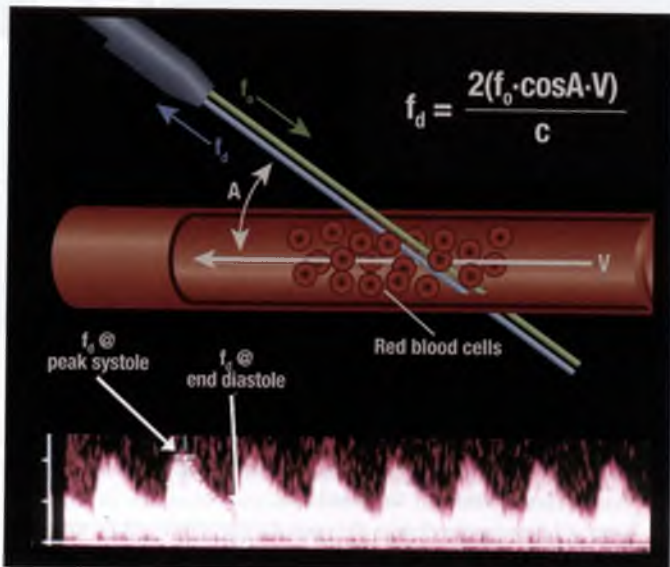


**FIG 22-1** The Doppler effect ( $f_d$ ) is dependent on the initial frequency of the ultrasound transducer ( $f_0$ ), the velocity of flow ( $V$ ) of the blood within a vessel, and the cosine of the angle ( $A$ ) that the ultrasound beam makes with the direction of blood flow. The frequency shift ( $f_d$ ) is displayed as a time-dependent plot within a cardiac cycle and is inversely proportional to the constant ( $c$ ), which reflects a constant related to the medium in which the sound is traversing.

clinical applications, when an ultrasound beam with a certain frequency is used to insonate a blood vessel, the reflected frequency or frequency shift is directly proportional to the speed with which the red blood cells are moving (blood flow velocity) within that particular vessel. This frequency shift of the returning signal is displayed in a graphic form as a time-dependent plot. In this display, the vertical axis represents the frequency shift, and the horizontal axis represents the temporal change of this frequency shift as it relates to the events of the cardiac cycle (Fig. 22-1). This frequency shift is highest during systole, when the blood flow is at its fastest, and lowest during end diastole, when the blood flow is at its slowest in the peripheral circulation. Given that the velocity of flow in a particular vascular bed is inversely proportional to the downstream impedance to flow, the frequency shift therefore derives information on the downstream impedance to flow of the vascular bed under study. The frequency shift is also dependent on the cosine of the angle that the ultrasound beam makes with the direction of blood flow in the targeted blood vessel (see formula in Fig. 22-1). When the sound beam is parallel to the blood vessel of interest and thus the moving red blood cells, the entire Doppler shift is measured. However, when an angle exists between the direction of flow and the sound beam, the measured velocity is less than the true velocity.<sup>2</sup> The degree to which the velocity is accurately measured depends on the angle of incidence (cosine  $Q$ ). At an angle of 0 degrees, the measured velocity is equal to the true velocity. When the sound beam is perpendicular to the direction of flow (90 degrees), the measured velocity is zero, because the cosine of 90 degrees is zero.<sup>2</sup> Thus, ideally, one wants to measure the velocity with as small an angle as possible.

Given that the insonating angle is difficult to measure in clinical practice, indices that rely on ratios of frequency shifts were developed to quantitate Doppler waveforms. By relying on ratios of frequency shifts, these Doppler indices are thus independent of the effects of the insonating angle of the ultrasound beam. Doppler indices that are commonly used in obstetric practice are shown in Figure 22-2.

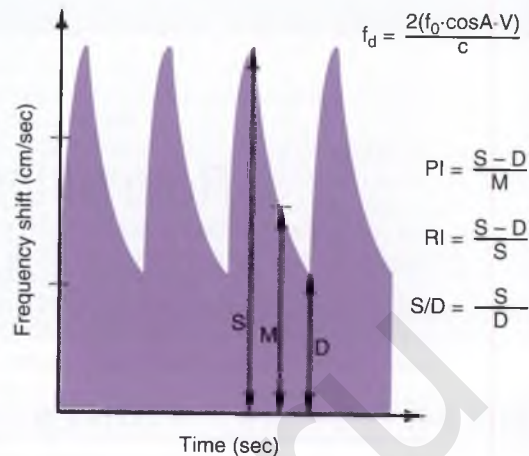


**FIG 22-2** Doppler indices commonly used in obstetric imaging.  $c$ , constant related to the medium in which the sound is traversing;  $D$ , diastole;  $M$ , mean;  $PI$ , pulsatility index;  $RI$ , resistance index;  $S$ , systole.

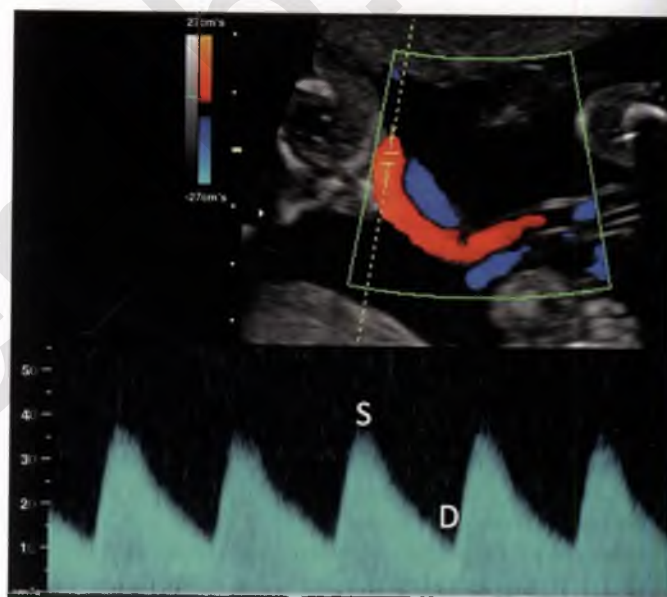


**FIG 22-3** Doppler waveforms of the umbilical artery in a normal fetus in the third trimester of pregnancy. Note the increased end-diastolic velocity ( $D$ ), consistent with a low impedance circulation.  $S$ , peak systole.

## FETAL ARTERIAL DOPPLER

### Umbilical Artery

The umbilical arterial circulation is normally a low-impedance circulation, with an increase in the amount of end-diastolic flow with advancing gestation.<sup>3,4</sup> Umbilical arterial Doppler waveforms reflect the status of the placental circulation, and the increase in end-diastolic flow that is seen with advancing gestation is a direct result of an increase in the number of tertiary stem villi that takes place with placental maturation (Fig. 22-3).<sup>5,6</sup> Diseases that obliterate small muscular arteries in placental tertiary stem villi result in a progressive decrease in end-diastolic flow in the umbilical arterial Doppler waveforms until absent, and then reverse flow during diastole is noted (Fig. 22-4).<sup>7,8</sup> Reversed diastolic flow in the umbilical arterial circulation represents an advanced stage of placental compromise and is associated with more than 70% of placental arterial obliteration.<sup>9-12</sup> The notation of absent or reversed end-diastolic flow in the umbilical artery is commonly associated with

severe FGR and oligohydramnios.<sup>13,14</sup> Only in pregnancies with suspected FGR does the use of umbilical artery Doppler sonography reduce the number of perinatal deaths and unnecessary obstetric interventions.<sup>15,16</sup>

Doppler waveforms of the umbilical arteries can be obtained from any segment along the umbilical cord. Waveforms obtained from the placental end of the cord show more end-diastolic flow and thus lower ratio values (resistive index [RI], systole/diastole [S/D] ratio) than waveforms obtained from the abdominal cord insertion.<sup>17</sup> There are differences in Doppler indices of arterial waveforms obtained from different anatomic locations of the same umbilical cord, but they are generally minor and have no significance in clinical practice

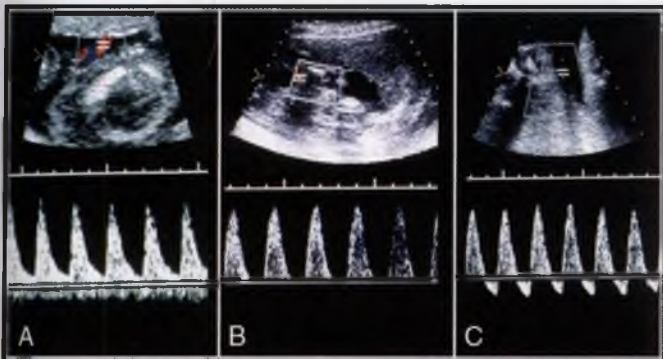


FIG 22-4 Abnormal umbilical artery Doppler waveforms; decreased end-diastolic velocity (A), absent end-diastolic velocity (B), reversed end-diastolic velocity (C).

(Tables 22-1 through 22-3).<sup>3,4</sup> In 2013, the International Society for Ultrasound in Obstetrics and Gynecology (ISUOG) recommended taking Doppler measurements from a free loop of cord for the sake of simplicity and consistency.<sup>18</sup>

### Middle Cerebral Artery

The MCA is the most accessible cerebral vessel to ultrasound imaging in the fetus, and it carries more than 80% of cerebral blood flow.<sup>19</sup> The cerebral circulation is normally a high-impedance circulation with continuous forward flow throughout the cardiac cycle.<sup>20</sup> In the presence of fetal hypoxemia, central redistribution of blood flow occurs, resulting in increased blood flow to the brain (Fig. 22-5), heart, and adrenals and a reduction in flow to the peripheral and placental circulations. This blood flow redistribution is known as the *brain-sparing effect* and plays a major role in fetal adaptation to oxygen deprivation.<sup>20-22</sup>

The right and left middle cerebral arteries represent major branches of the circle of Willis in the fetal brain. The circle of Willis, which is supplied by the internal carotid and vertebral arteries, can be imaged with color flow Doppler sonography in a magnified axial plane of the fetal head obtained at the base of the skull, at the level of the thalami and wings of sphenoid bone (Fig. 22-6). In this plane, the proximal and distal middle cerebral arteries are seen in their long axis, with their course almost parallel to the ultrasound beam. As such, the insonating beam, which is parallel to the vessel and thus has an angle of insonation of 0 degrees, will result in a measured velocity that accurately reflects the true velocity of blood in this vessel ( $\cos 0 = 1$ ). MCA Doppler waveforms, obtained from the proximal third portion of the vessel, immediately after its origin from the circle of Willis, have shown the best reproducibility (Tables 22-4 and 22-5 and Fig. 22-7).<sup>22</sup>

TABLE 22-1 Reference Values for Serial Measurements of the Umbilical Artery Systolic-Diastolic Ratio

Gestation (weeks)	SYSTOLIC-DIASTOLIC RATIO, BY PERCENTILE								
	2.5th	5th	10th	25th	50th	75th	90th	95th	97.5th
19	2.73	2.93	3.19	3.67	4.28	5.00	5.75	6.26	6.73
20	2.63	2.83	3.07	3.53	4.11	4.80	5.51	5.99	6.43
21	2.51	2.70	2.93	3.36	3.91	4.55	5.22	5.67	6.09
22	2.43	2.60	2.83	3.24	3.77	4.38	5.03	5.45	5.85
23	2.34	2.51	2.72	3.11	3.62	4.21	4.82	5.22	5.61
24	2.25	2.41	2.62	2.99	3.48	4.04	4.63	5.02	5.38
25	2.17	2.33	2.52	2.88	3.35	3.89	4.45	4.83	5.18
26	2.09	2.24	2.43	2.78	3.23	3.75	4.30	4.66	5.00
27	2.02	2.17	2.35	2.69	3.12	3.63	4.15	4.50	4.83
28	1.95	2.09	2.27	2.60	3.02	3.51	4.02	4.36	4.67
29	1.89	2.03	2.20	2.52	2.92	3.40	3.89	4.22	4.53
30	1.83	1.96	2.13	2.44	2.83	3.30	3.78	4.10	4.40
31	1.77	1.90	2.06	2.36	2.75	3.20	3.67	3.98	4.27
32	1.71	1.84	2.00	2.29	2.67	3.11	3.57	3.87	4.16
33	1.66	1.79	1.94	2.23	2.60	3.03	3.48	3.77	4.06
34	1.61	1.73	1.88	2.16	2.53	2.95	3.39	3.68	3.96
35	1.57	1.68	1.83	2.11	2.46	2.87	3.30	3.59	3.86
36	1.52	1.64	1.78	2.05	2.40	2.80	3.23	3.51	3.78
37	1.48	1.59	1.73	2.00	2.34	2.74	3.15	3.43	3.69
38	1.44	1.55	1.69	1.95	2.28	2.67	3.08	3.36	3.62
39	1.40	1.51	1.64	1.90	2.23	2.61	3.02	3.29	3.54
40	1.36	1.47	1.60	1.85	2.18	2.56	2.96	3.22	3.48
41	1.33	1.43	1.56	1.81	2.13	2.50	2.90	3.16	3.41

From Acharya G, Wilsgaard T, Bernsten GKR, et al: Reference ranges for serial measurements of umbilical artery Doppler indices in the second half of pregnancy. *Am J Obstet Gynecol* 192:937, 2005.



**TABLE 22-2 Resistance Index of the Umbilical Artery Between 20 and 40 Weeks of Gestation**

Gestation (weeks)	RESISTANCE INDEX, BY PERCENTILE		
	5th	50th	95th
20	0.567	0.690	0.802
21	0.557	0.680	0.793
22	0.548	0.671	0.784
23	0.539	0.663	0.776
24	0.530	0.655	0.768
25	0.522	0.646	0.760
26	0.514	0.639	0.752
27	0.506	0.631	0.745
28	0.498	0.623	0.737
29	0.490	0.615	0.730
30	0.482	0.608	0.723
31	0.474	0.600	0.715
32	0.465	0.592	0.707
33	0.457	0.584	0.700
34	0.449	0.576	0.692
35	0.440	0.567	0.684
36	0.431	0.559	0.675
37	0.422	0.550	0.667
38	0.412	0.540	0.657
39	0.402	0.530	0.648
40	0.390	0.519	0.637

From Merz E (ed): *Ultrasonography in Obstetrics and Gynecology*, vol 1. Stuttgart, Thieme, 2005, pp 469-480, 614.

**TABLE 22-3 Pulsatility Index of the Umbilical Artery Between 20 and 40 Weeks of Gestation**

Gestation (weeks)	PULSATILITY INDEX, BY PERCENTILE		
	5th	50th	95th
20	0.940	1.216	1.505
21	0.913	1.189	1.476
22	0.890	1.165	1.450
23	0.869	1.142	1.427
24	0.849	1.122	1.405
25	0.831	1.102	1.385
26	0.813	1.084	1.365
27	0.798	1.065	1.346
28	0.780	1.048	1.327
29	0.764	1.031	1.308
30	0.748	1.014	1.290
31	0.732	0.997	1.272
32	0.716	0.980	1.254
33	0.700	0.963	1.236
34	0.684	0.946	1.218
35	0.668	0.928	1.199
36	0.651	0.910	1.180
37	0.634	0.891	1.160
38	0.615	0.872	1.139
39	0.595	0.851	1.117
40	0.573	0.828	1.093

From Merz E (ed): *Ultrasonography in Obstetrics and Gynecology*, vol 1. Stuttgart, Thieme, 2005, pp 469-480, 614.

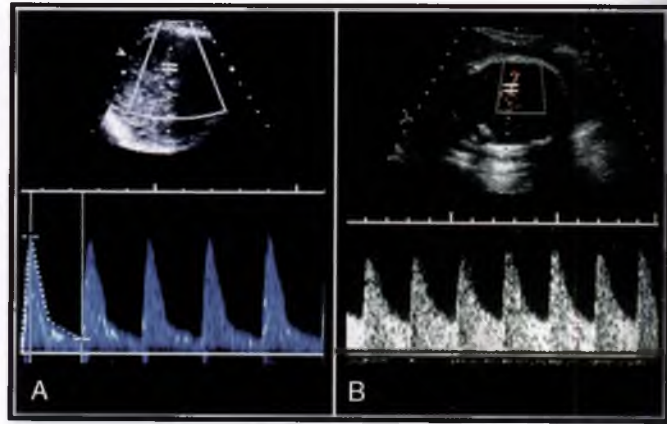


**FIG 22-5** Doppler waveforms of the middle cerebral artery in a normal fetus (A) and in a hypoxic fetus (B). Note the increase in end-diastolic velocity in fetus B resulting from a low-impedance cerebral circulation as part of the brain-sparing reflex.

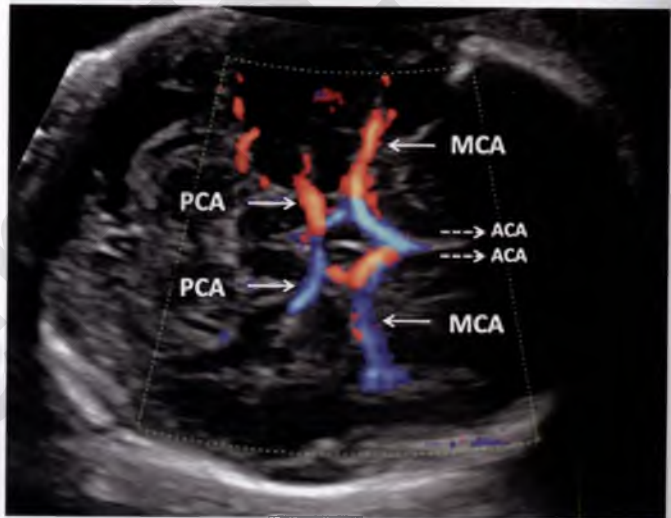


**FIG 22-6** Circle of Willis shown on color Doppler imaging. ACA, anterior cerebral artery; MCA, middle cerebral artery; PCA, posterior cerebral artery. (From *Ultrasound in Obstetrics & Gynecology: A Practical Approach*. Available at [www.openultrasound.com](http://www.openultrasound.com). Used with permission.)

MCA evaluation is often used to assess well-being in the fetus with suspected growth restriction (see later) as well as fetuses with hemolytic disease due to Rh isoimmunization or parvovirus B19 infection (see Chapters 6 and 17) (Fig. 22-8). In cases of isoimmunization, MCA PSVs are increased in relation to decreased fetal hemoglobin, decreased blood viscosity, and increased cardiac output (Table 22-6). Care should be taken to optimize Doppler settings to reliably evaluate flow in the vessel and to accurately measure PSV in the MCA (Fig. 22-9). In the case of FGR, hemoglobin is typically unaffected, and it is speculated that the increase in MCA blood flow with subsequent increased diastolic waveforms on Doppler is a result of elevated fetal blood pressures. PSV above 1.50 multiples of the median (MoM) in fetuses at risk have been reported to have sensitivity of 100% in cases of red blood cell isoimmunization and other causes of fetal anemia.<sup>23,24</sup>

### Uterine Artery

Pregnancy is associated with physiologic changes at the level of the uterine vasculature, resulting in a progressive decrease in impedance with advancing gestation.<sup>25</sup> This maternal adaptation to pregnancy is

TABLE 22-4 Reference Values for the Resistance Index of the Middle Cerebral Artery

Gestation (weeks)	RESISTANCE INDEX, BY PERCENTILE			Gestation (weeks)	RESISTANCE INDEX, BY PERCENTILE		
	5th	50th	95th		5th	50th	95th
18	0.544	0.687	0.787	31	0.652	0.798	0.907
19	0.574	0.708	0.808	32	0.645	0.792	0.902
20	0.592	0.727	0.828	33	0.636	0.783	0.894
21	0.608	0.744	0.846	34	0.625	0.773	0.885
22	0.622	0.758	0.861	35	0.612	0.761	0.873
23	0.633	0.771	0.874	36	0.597	0.747	0.86
24	0.643	0.782	0.886	37	0.579	0.73	0.844
25	0.651	0.79	0.895	38	0.56	0.712	0.826
26	0.656	0.796	0.902	39	0.539	0.692	0.807
27	0.659	0.801	0.907	40	0.515	0.669	0.785
28	0.661	0.803	0.91	41	0.489	0.644	0.761
29	0.66	0.803	0.911	42	0.462	0.618	0.735
30	0.657	0.801	0.91				

From Bahlmann F, Reinhard I, Krummenauer F, et al: Blood flow velocity waveforms of the fetal middle cerebral artery in a normal population: reference values from 18 weeks to 42 weeks of gestation. *J Perinat Med* 30:490, 2002.

TABLE 22-5 Reference Values for Umbilical Artery (UA) and Middle Cerebral Artery (MCA) Resistance Indices, as Well as Their Ratio, by Percentile

Gestation (weeks)	UA RESISTANCE INDEX			MCA RESISTANCE INDEX			RATIO		
	5th	50th	95th	5th	50th	95th	5th	50th	95th
24	0.615	0.717	0.828	0.778	0.867	—	0.696	0.809	0.968
25	0.605	0.707	0.819	0.789	0.881	—	0.676	0.791	0.955
26	0.594	0.697	0.810	0.795	0.892	—	0.658	0.775	0.945
27	0.583	0.687	0.802	0.798	0.898	—	0.642	0.761	0.937
28	0.572	0.678	0.793	0.797	0.901	—	0.628	0.750	0.932
29	0.562	0.668	0.785	0.793	0.900	—	0.616	0.740	0.929
30	0.551	0.658	0.776	0.786	0.897	—	0.606	0.732	0.928
31	0.540	0.648	0.767	0.776	0.891	—	0.597	0.726	0.929
32	0.530	0.638	0.759	0.764	0.883	—	0.590	0.722	0.931
33	0.519	0.629	0.750	0.750	0.872	—	0.585	0.719	0.936
34	0.508	0.619	0.742	0.734	0.860	—	0.581	0.717	0.941
35	0.498	0.609	0.733	0.717	0.846	—	0.578	0.717	0.949
36	0.487	0.599	0.724	0.698	0.831	—	0.576	0.718	0.957
37	0.476	0.589	0.716	0.677	0.814	—	0.575	0.720	0.967
38	0.465	0.580	0.707	0.655	0.795	—	0.576	0.724	0.978
39	0.455	0.570	0.699	0.632	0.776	—	0.577	0.728	0.991
40	0.444	0.560	0.690	0.607	0.755	—	0.580	0.734	1.004
41	0.433	0.550	0.681	0.582	0.734	—	0.583	0.740	1.018
42	0.423	0.540	0.673	0.556	0.711	—	0.588	0.747	1.034

From Kurmanavicius J, Florio I, Wisser J, et al: Reference resistance indices of the umbilical, fetal middle cerebral and uterine arteries at 24-42 weeks of gestation. *Ultrasound Obstet Gynecol* 10:112, 1997.

thought to result from the trophoblastic invasion of the maternal spiral arterioles in the first half of pregnancy.<sup>26</sup> The invaded maternal spiral arterioles are rendered maximally dilated and minimally responsive to the sympathetic and parasympathetic systems. This adaptation is intended to ensure a sustained increase in blood flow to the uterus during pregnancy.

The uterine circulation can be assessed by Doppler velocimetry of the uterine arteries. Each uterine vessel can be demonstrated by color Doppler as it crosses over the hypogastric artery and vein just before it enters the uterus at the uterine-cervical junction (Fig. 22-10). Pulsed Doppler velocimetry of the uterine artery should be obtained

immediately after the vessel crosses the hypogastric artery and before it divides into the uterine and cervical branches. The presence of a notch in the waveform and an increase in the impedance index after 22 weeks of gestation characterizes an abnormal uterine circulation (Fig. 22-11 and Tables 22-7 and 22-8).<sup>27</sup> A substantial risk of complication is noted in pregnancies that show an abnormal uterine circulation in the late second and third trimesters.<sup>28,29</sup> Pregnancy complications include FGR, preeclampsia, preterm delivery, and nonreassuring fetal status in labor.<sup>28,29</sup>

Women with abnormal serum analyte screening results, such as elevated alpha-fetoprotein, inhibin, human chorionic gonadotropin,



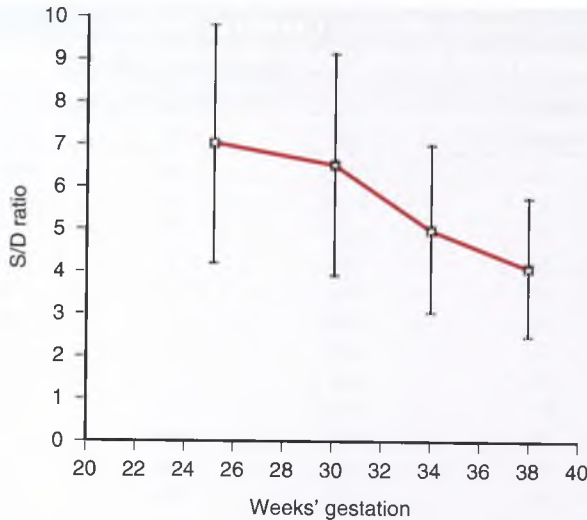


**FIG 22-7** Middle cerebral artery Doppler systole/diastole (S/D) ratios. (Modified from Woo JSK, Liang ST, Chan FY, et al: Middle cerebral artery Doppler flow velocity. *Obstet Gynecol* 70:613, 1987. Used with permission from the American College of Obstetricians and Gynecologists.)

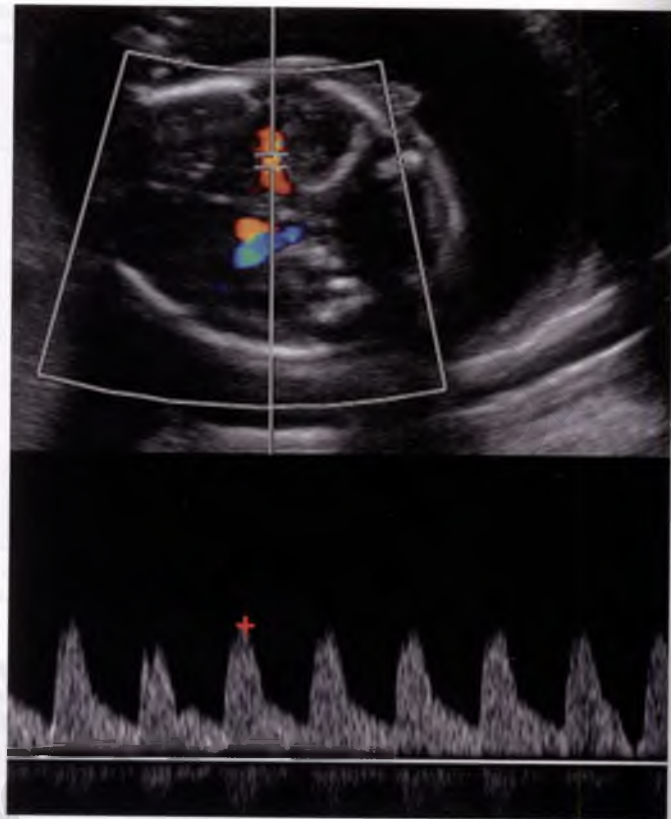


**FIG 22-8** Doppler imaging and measurement of peak systolic velocity in the fetal middle cerebral artery.

**TABLE 22-6** Threshold of Peak Velocity of Systolic Blood Flow in the Middle Cerebral Artery Above Which Mild, Moderate, and Severe Anemia Occur

Gestation (weeks)	PEAK VELOCITY THRESHOLD (cm/sec)		
	Severe Anemia	Moderate Anemia	Mild Anemia
18	29.9	34.8	36.0
20	32.8	38.2	39.5
22	36.0	41.9	43.3
24	39.5	46.0	47.5
26	43.3	50.4	52.1
28	47.6	55.4	57.2
30	52.2	60.7	62.8
32	57.3	66.6	68.9
34	62.9	73.1	75.6
36	69.0	80.2	82.9
38	75.7	88.0	91.0
40	83.0	96.6	99.8

From Mari G, Deter RL, Carpenter RL, et al: Non-invasive diagnosis by Doppler ultrasonography of fetal anemia due to maternal red-cell alloimmunization. Collaborative Group for Doppler Assessment of the Blood Velocity in Anemic Fetuses. *N Engl J Med* 342:9, 2000.

or decreased free estradiol are potential candidates for uterine artery Doppler assessment. The combination of an abnormal analyte in the presence of abnormal uterine artery Doppler has been associated with markedly increased risk of preeclampsia, FGR, placental abruption, and fetal demise.<sup>23,30,31</sup>

Although in general, uterine artery Doppler studies are better at predicting early preeclampsia than term preeclampsia,<sup>32</sup> the use of this parameter alone has low predictive value for the development of preeclampsia. At this time, there is insufficient evidence to support the utility of uterine artery Doppler studies as a screening tool for pre-

eclampsia, as randomized clinical trials have failed to find any improvement in maternal or fetal outcomes.<sup>33</sup>

## FETAL VENOUS DOPPLER

Doppler waveforms obtained from the central venous circulation in the fetus reflect the physiologic status of the right ventricle. Specific information with regard to right ventricular preload, myocardial compliance, and right ventricular end-diastolic pressure can be derived from Doppler flow studies of the inferior vena cava and ductus venosus in the fetus.<sup>34-39</sup>

After 15 weeks of gestation, the umbilical vein normally has continuous monophasic blood flow but becomes pulsatile with fetal breathing or in pathologic cases, such as in severe FGR or fetal hydrops. In general, umbilical venous flow is assessed qualitatively as either continuous (monophasic) or pulsatile<sup>40</sup> (Fig. 22-12).

Inferior vena cava Doppler waveforms can be obtained from a coronal plane of the chest and abdomen. In this view, the inferior vena cava can be imaged as it enters into the right atrium, joined by the ductus venosus and the left hepatic vein (Fig. 22-13). The inferior vena cava can be studied at two locations: at the inlet into the right atrium or in the segment between the entrance of the hepatic vein and the ductus venosus. A good correlation coefficient exists between these two measurement sites, and the location that provides the smallest angle of insonation with the vector of blood flow should be chosen.<sup>38</sup> Inferior vena cava Doppler waveforms are triphasic in shape, with the first phase corresponding to ventricular systole, the second phase to early diastole, and the third phase to late diastole or the atrial kick (Fig. 22-14).

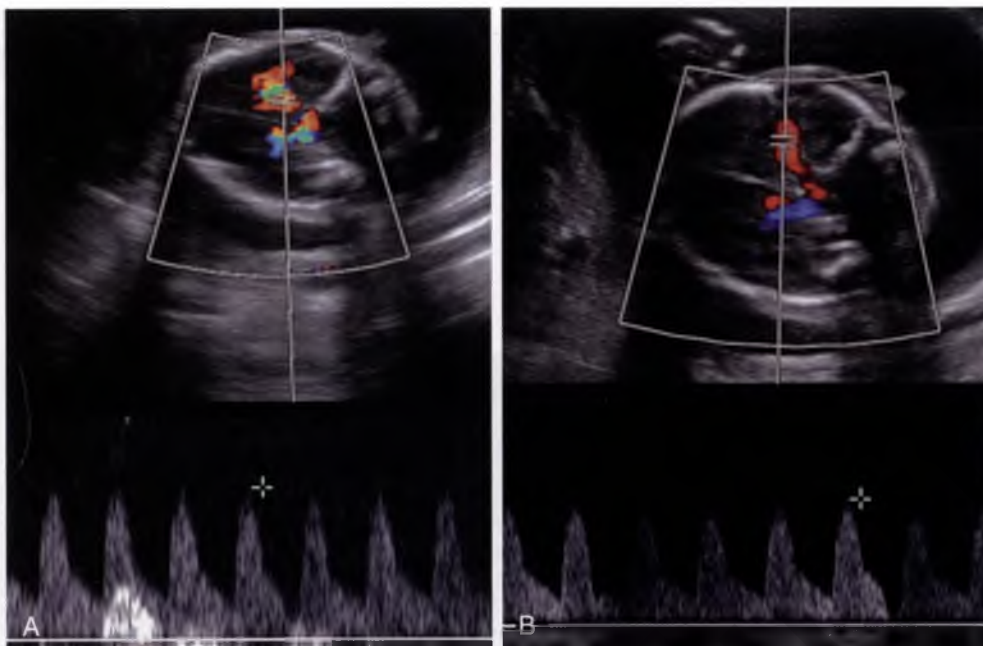


**FIG 22-9** Color and spectral Doppler imaging of fetal middle cerebral artery (MCA) with measurement of peak systolic velocity (PSV). **A**, PSV measured 39 cm/second. Because of suboptimal technique with high gain and low scale settings and incorrect placement of sample gate, the peak velocity was erroneously undermeasured. **B**, With improved technique, including adjustments in gain, scale, angle of insonation, and sample gate placement, true peak velocity in the MCA was obtained and found to be 46.5 cm/second.

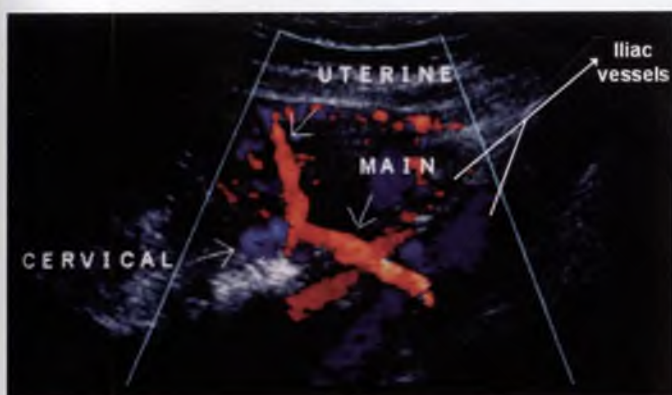


**FIG 22-10** Color Doppler imaging in the lateral lower uterine segment showing the main uterine artery as it crosses over the hypogastric iliac vessels before it enters the uterus and then divides into a uterine branch and a cervical branch.

Ductus venosus Doppler waveforms can be obtained from a transverse view through the fetal abdomen at the same anatomic plane as the abdominal circumference (Fig. 22-15). By superimposing color flow Doppler image on the gray-scale image, the ductus venosus can be identified as it branches from the portal vein. High-velocity turbulent flow with color aliasing is commonly seen within the ductus venosus given its narrow lumen. The presence of aliasing on color flow Doppler image helps in identifying the ductus venosus in early gestation. Adjusting gain and scale settings allows the ductus venosus to be optimally visualized (Fig. 22-16). Ductus venosus Doppler waveforms are biphasic in shape, with the first phase corresponding to ventricular systole, the second phase to early diastole, and the nadir of the second phase to late diastole or the atrial kick (Fig. 22-17 and Tables 22-9 through 22-12).

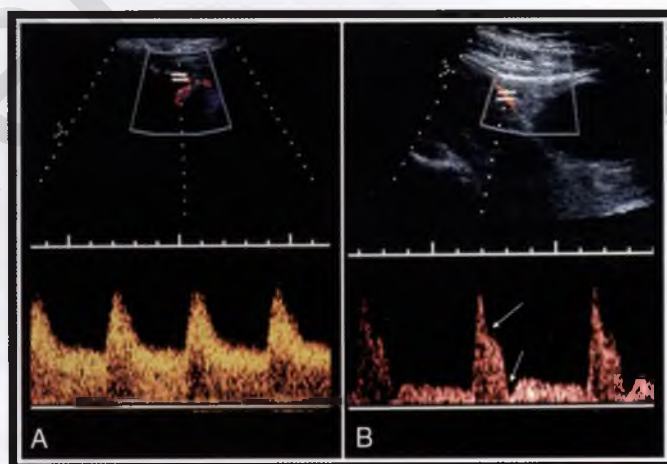


**FIG 22-11** Doppler waveforms of the uterine artery obtained in the late second trimester of pregnancy showing normal uterine circulation (**A**) with increased end-diastolic velocity implying low-impedance circulation and abnormal uterine artery circulation (**B**) with a waveform notch (top arrow) and low end-diastolic velocity (high impedance) (lower arrow).

Blood flow through the umbilical vein carrying oxygenated blood to the fetus can be assessed either within the fetal abdomen or within the amniotic fluid (Table 22-13).

Reversed flow in the ductus venosus results from a decline and subsequent reversal in forward flow velocity during atrial systole. It may be due to worsening placental disease, impaired cardiac function secondary to metabolic compromise, congenital heart defects, redistribution of hepatoportal blood flow through the liver, or a combination of these factors<sup>25</sup> (Fig. 22-18).

*Text continued on p. 744*



**TABLE 22-7 Resistance Index of the Uterine Artery**

Gestation (weeks)	RESISTANCE INDEX, BY PERCENTILE		
	5th	50th	95th
18	0.222	0.447	0.659
19	0.204	0.429	0.641
20	0.194	0.419	0.630
21	0.186	0.411	0.622
22	0.180	0.405	0.615
23	0.175	0.400	0.610
24	0.171	0.395	0.605
25	0.167	0.391	0.601
26	0.163	0.387	0.597
27	0.160	0.384	0.593
28	0.157	0.380	0.590
29	0.154	0.378	0.587
30	0.152	0.375	0.584
31	0.150	0.372	0.581
32	0.147	0.370	0.578
33	0.145	0.368	0.576
34	0.144	0.366	0.574
35	0.142	0.364	0.571
36	0.140	0.362	0.569
37	0.139	0.360	0.567
38	0.137	0.358	0.566
39	0.136	0.357	0.564
40	0.135	0.355	0.562

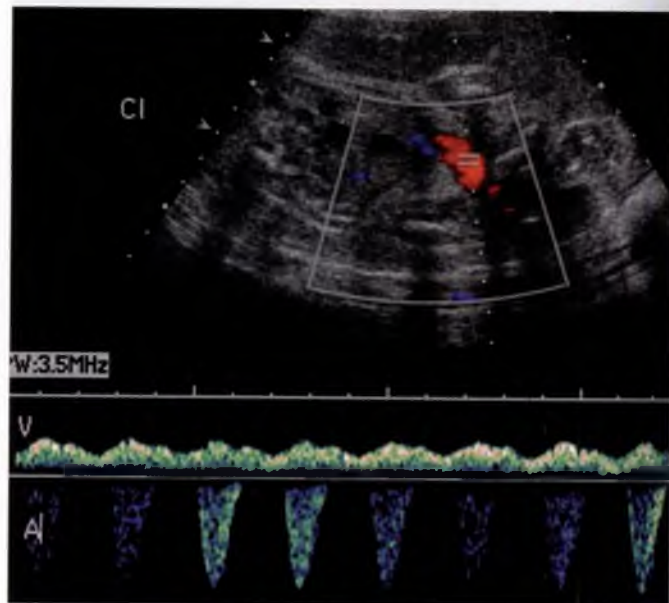
**TABLE 22-8 Pulsatility Index of the Uterine Artery**

Gestation (weeks)	PULSATILITY INDEX, BY PERCENTILE		
	5th	50th	95th
18	0.509	0.888	1.407
19	0.460	0.838	1.356
20	0.436	0.812	1.328
21	0.420	0.795	1.309
22	0.407	0.781	1.293
23	0.397	0.769	1.280
24	0.388	0.759	1.268
25	0.381	0.751	1.258
26	0.374	0.743	1.248
27	0.369	0.736	1.239
28	0.363	0.729	1.230
29	0.358	0.722	1.222
30	0.354	0.716	1.214
31	0.349	0.711	1.207
32	0.345	0.705	1.199
33	0.341	0.700	1.192
34	0.337	0.695	1.185
35	0.333	0.690	1.178
36	0.330	0.684	1.171
37	0.326	0.679	1.164
38	0.322	0.674	1.157
39	0.318	0.669	1.150
40	0.313	0.663	1.143

From Merz E (ed): Ultrasonography in Obstetrics and Gynecology, vol 1. Stuttgart, Thieme, 2005, pp 469-480, 614.

From Merz E (ed): Ultrasonography in Obstetrics and Gynecology, vol 1. Stuttgart, Thieme, 2005, pp 469-480, 614.

**FIG 22-12** Abnormal flow with phasicity in the umbilical vein (V) sampled near the cord insertion (CI) at the fetal anterior abdominal wall. Note absent diastolic flow in the umbilical artery (A) in this fetus with fetal growth restriction.



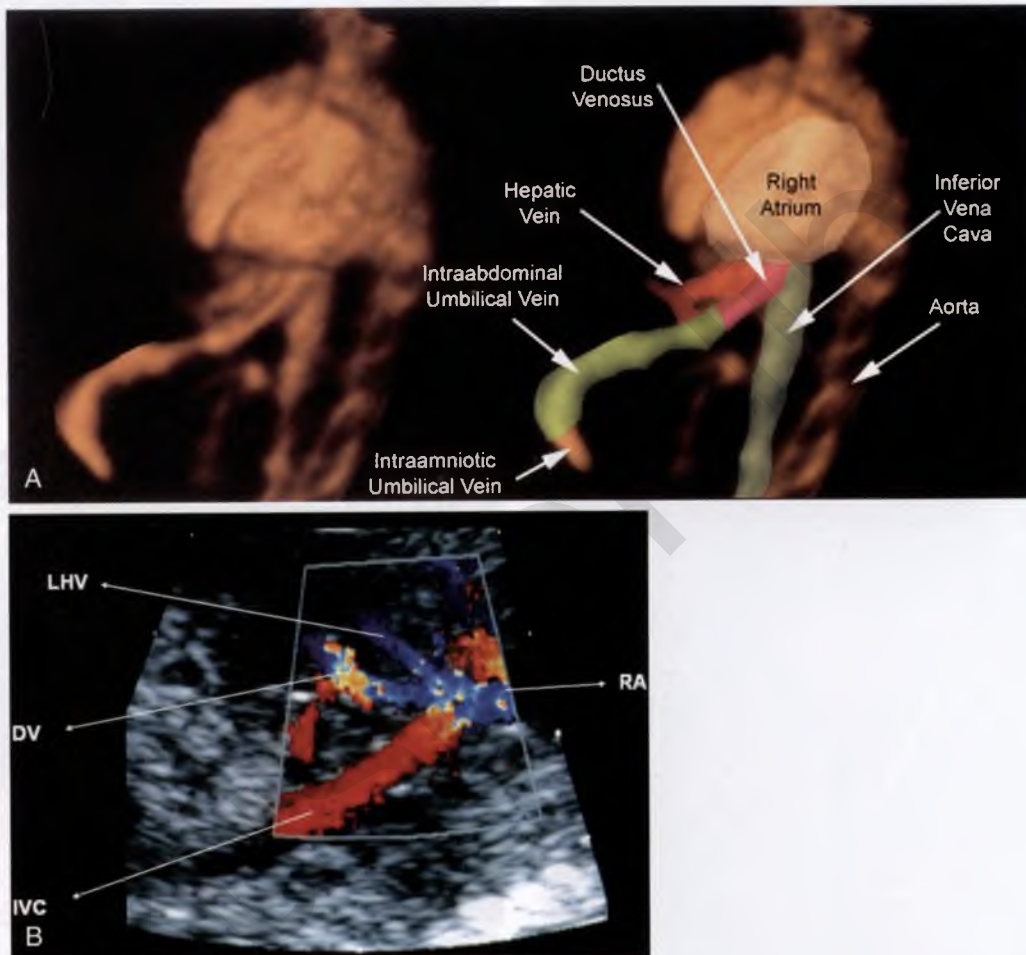


**FIG 22-13 A**, Three-dimensional B flow image from a 17-week fetus illustrating the relationships of the venous system, heart, and aorta. **B**, Color Doppler sonogram of a coronal plane of the fetal abdomen and chest showing the inferior vena cava (IVC), joined by the ductus venosus (DV) and the left hepatic vein (LHV) as it enters the right atrium (RA). (A from DeVore GR: Pulsed Doppler examination of the fetal heart. In Goldberg BB, McGahan JP [eds]: *Fetal Ductus Venosus in Atlas of Ultrasound Measurements*, 2nd ed. Philadelphia, Mosby/Elsevier, 2006.)



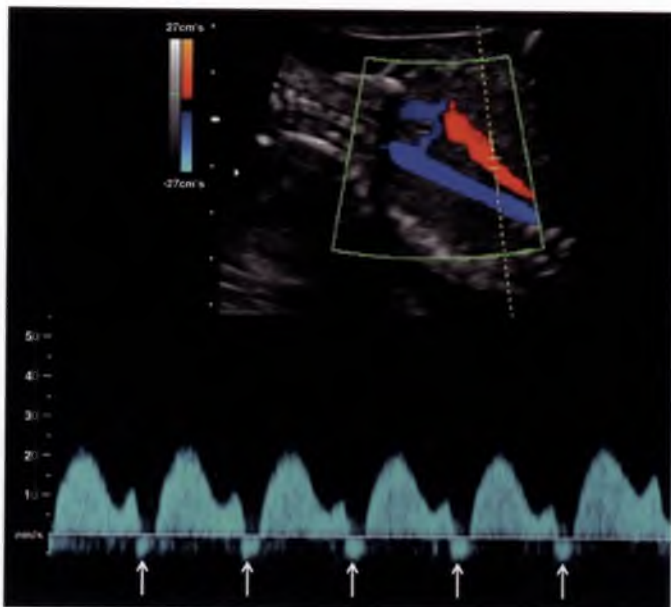


**FIG 22-14** Doppler waveforms of the inferior vena cava in a normal fetus in the third trimester of pregnancy. Note the presence of reversed flow (arrows) during the atrial contraction phase of diastole.

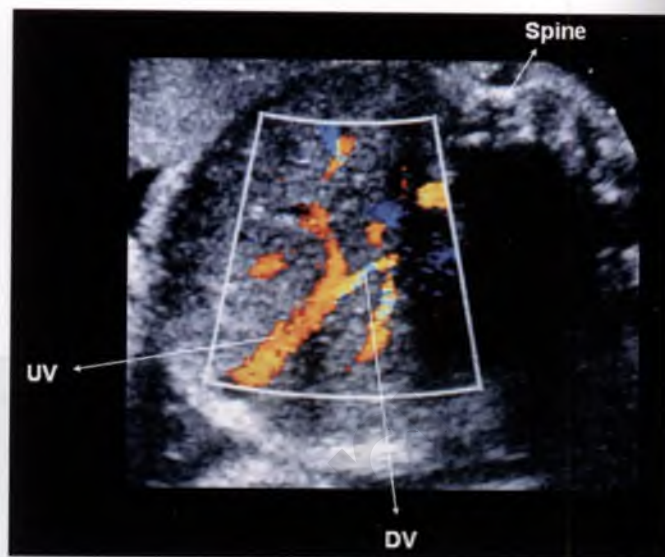


**FIG 22-15** Color Doppler sonogram of a transverse plane of the fetal abdomen showing the umbilical vein (UV) and the ductus venosus (DV). Note the presence of turbulence (with aliasing) on color Doppler in the ductus venosus.

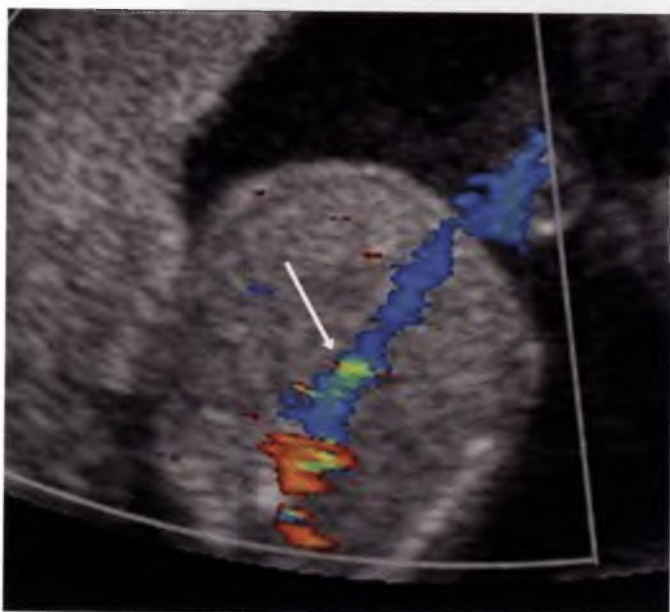


**FIG 22-16** High scale settings best reveal high-velocity flow with aliasing in the ductus venosus (arrow) on this transaxial color Doppler ultrasound image through the fetal upper abdomen.

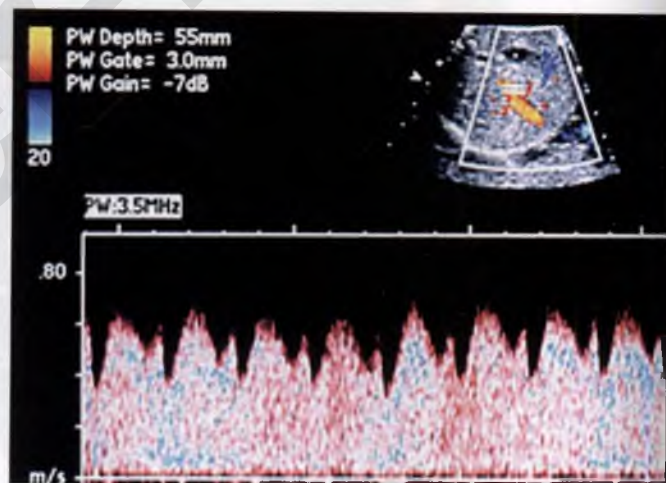


**FIG 22-17** Doppler waveforms of the ductus venosus in a normal fetus in the third trimester of pregnancy. Note the presence of forward flow within the ductus venosus throughout the cardiac cycle.

**TABLE 22-9 Ductus Venosus Preload Index: a/S**

Gestation (weeks)	PRELOAD INDEX, BY PERCENTILE		
	5th	50th	95th
20	0.342	0.508	0.674
21	0.341	0.507	0.673
22	0.341	0.507	0.673
23	0.340	0.506	0.672
24	0.339	0.505	0.671
25	0.339	0.505	0.671
26	0.338	0.504	0.670
27	0.338	0.504	0.670
28	0.337	0.503	0.669
29	0.336	0.502	0.668
30	0.336	0.502	0.668
31	0.335	0.501	0.667
32	0.335	0.501	0.667
33	0.334	0.500	0.666
34	0.333	0.499	0.665
35	0.333	0.499	0.665
36	0.332	0.498	0.664
37	0.332	0.498	0.664
38	0.331	0.497	0.663
39	0.330	0.496	0.662
40	0.330	0.496	0.662

a, atrial systolic peak blood flow velocity; S, systolic peak blood flow velocity.

From Baschat AA: Relationship between placental blood flow resistance and precordial venous Doppler indices. Ultrasound Obstet Gynecol 22:561, 2003.

**TABLE 22-10 Ductus Venosus Peak Velocity Index: (S - a)/D**

Gestation (weeks)	PEAK VELOCITY INDEX, BY PERCENTILE		
	5th	50th	95th
20	0.381	0.580	0.779
21	0.380	0.579	0.779
22	0.380	0.579	0.778
23	0.379	0.578	0.777
24	0.678	0.578	0.777
25	0.378	0.577	0.776
26	0.377	0.576	0.776
27	0.377	0.576	0.775
28	0.376	0.575	0.774
29	0.375	0.575	0.774
30	0.375	0.574	0.773
31	0.374	0.573	0.773
32	0.374	0.573	0.772
33	0.373	0.572	0.771
34	0.372	0.572	0.771
35	0.372	0.571	0.770
36	0.371	0.570	0.770
37	0.371	0.570	0.769
38	0.370	0.569	0.768
39	0.369	0.569	0.768
40	0.369	0.568	0.767

a, atrial systolic peak blood flow velocity; D, diastolic peak blood flow velocity; S, systolic peak blood flow velocity.

From Baschat AA: Relationship between placental blood flow resistance and precordial venous Doppler indices. Ultrasound Obstet Gynecol 22:561, 2003.

**TABLE 22-11 Ductus Venosus Pulsatility Index: (S - a)/TAMX**

Gestation (weeks)	PULSATILITY INDEX, BY PERCENTILE		
	5th	50th	95th
20	0.410	0.643	0.875
21	0.409	0.642	0.874
22	0.408	0.641	0.873
23	0.407	0.640	0.872
24	0.406	0.639	0.871
25	0.405	0.638	0.870
26	0.404	0.637	0.869
27	0.403	0.636	0.868
28	0.402	0.635	0.867
29	0.401	0.634	0.866
30	0.400	0.633	0.865
31	0.399	0.632	0.864
32	0.398	0.631	0.863
33	0.397	0.630	0.862
34	0.396	0.629	0.861
35	0.395	0.628	0.860
36	0.394	0.627	0.859
37	0.393	0.626	0.858
38	0.392	0.625	0.857
39	0.391	0.624	0.856
40	0.390	0.623	0.855

a, atrial systolic peak blood flow velocity; S, systolic peak blood flow velocity; TAMX, time-averaged maximum velocity.

From Baschat AA: Relationship between placental blood flow resistance and precordial venous Doppler indices. Ultrasound Obstet Gynecol 22:561, 2003.

**TABLE 22-12 Ductus Venosus S/a Ratio**

Gestation (weeks)	S/a RATIO, BY PERCENTILE		
	5th	50th	95th
20	1.331	2.161	2.991
21	1.329	2.159	2.989
22	1.327	2.157	2.987
23	1.324	2.154	2.984
24	1.322	2.152	2.982
25	1.320	2.150	2.980
26	1.318	2.148	2.978
27	1.315	2.145	2.975
28	1.313	2.143	2.973
29	1.311	2.141	2.971
30	1.308	2.138	2.968
31	1.306	2.136	2.966
32	1.304	2.134	2.964
33	1.301	2.131	2.961
34	1.299	2.129	2.959
35	1.297	2.127	2.957
36	1.295	2.125	2.955
37	1.292	2.122	2.952
38	1.290	2.120	2.950
39	1.288	2.118	2.948
40	1.285	2.115	2.945

a, atrial systolic peak blood flow velocity; S, systolic peak blood flow velocity.

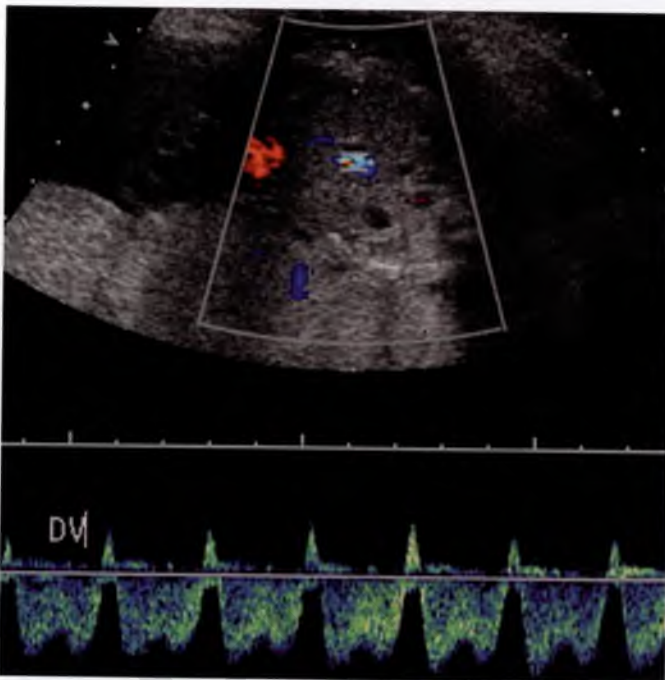
From Baschat AA: Relationship between placental blood flow resistance and precordial venous Doppler indices. Ultrasound Obstet Gynecol 22:561, 2003.



TABLE 22-13 Umbilical Vein Blood Flow Mean Velocity

Gestation (weeks)	MEAN VELOCITY (cm/sec), BY PERCENTILE			Gestation (weeks)	MEAN VELOCITY (cm/sec), BY PERCENTILE		
	5th	50th	95th		5th	50th	95th
20	5.70	7.90	10.70	31	7.04	9.67	13.02
21	5.82	8.06	10.91	32	7.17	9.83	13.23
22	5.94	8.22	11.12	33	7.29	9.99	13.44
23	6.07	8.38	11.33	34	7.41	10.16	13.66
24	6.19	8.54	11.54	35	7.53	10.32	13.87
25	6.31	8.71	11.76	36	7.65	10.48	14.08
26	6.43	8.87	11.97	37	7.78	10.64	14.29
27	6.56	9.03	12.18	38	7.90	10.80	14.50
28	6.68	9.19	12.39	39	8.02	10.96	14.71
29	6.80	9.35	12.60	40	8.14	11.12	14.92
30	6.92	9.51	12.81				

From Barbera A, Galan HL, Ferrazzi E, et al: Relationship of umbilical vein blood flow to growth parameters in the human fetus. *Am J Obstet Gynecol* 181:174, 1999.



**FIG 22-18** Abnormal spectral Doppler waveform of the ductus venosus (DV) with reversed a wave flow resulting from decline and subsequent reversal in forward flow during atrial systole in this fetus with severe fetal growth restriction.

## FETAL CARDIAC DOPPLER

### Optimizing the Image

Adequate imaging of the fetal heart is essential for accurate Doppler measurements. Several steps can improve ultrasound imaging when faced with suboptimal scanning conditions. Resort to the echocardiography settings on the ultrasound equipment as the first step in optimizing the image. The echocardiography settings allow for enhanced image contrast, tissue characterization, and a faster frame rate, which improve cardiac imaging. Other steps include minimizing the depth on the display monitor, insonating the heart through an angle that

avoids shadowing by the fetal ribs and sternum, adjusting the focal zones to the area of interest, and most importantly enlarging the area of interest (zoom), which allows visualization of details within the heart. These simple steps result in adequate visualization of the fetal heart in most conditions. When adding color Doppler to the gray-scale image, select high-velocity scales given that the velocity of cardiac blood flow is higher than that of the peripheral fetal circulation. By adjusting the filters to a high setting and by directing the angle of insonation of the ultrasound beam parallel to the direction of blood flow, the color Doppler image is optimized, and wall motion artifact is significantly reduced.

Doppler indices in fetal echocardiography are quantitative parameters and, for the majority, are angle dependent. To obtain accurate Doppler indices in fetal echocardiography, the sample volume is placed distal to the respective valves, the insonating angle should be within 0 to 20 degrees of the direction of blood flow, Doppler waveforms should be obtained during fetal apnea, and multiple measurements should be obtained. Color Doppler is used to direct placement of the sample volume; placing the sample volume at the brightest colors of the blood flow segment will ensure the best measurements. Figure 22-19 shows Doppler indices commonly used in fetal echocardiography.

The fetal circulation is different from the adult circulation in many aspects. The fetal circulation is in parallel rather than in series, and the right ventricular cardiac output is greater than the left ventricular cardiac output.<sup>41,42</sup> The progressive development of organs during gestation influence blood distribution and vascular impedance.<sup>41</sup> With advancing gestation, ventricular compliance is increased, total peripheral resistance is decreased, preload is increased, and combined cardiac output is increased.<sup>41</sup> Compliance of the left side of the fetal heart increases more rapidly than compliance of the right side of the fetal heart with advancing gestation.<sup>41</sup> The pulmonary vascular resistance is high in the fetus, and the pulmonary arterial pressure is almost systemic.<sup>43,44</sup> Flow to the pulmonary vascular bed is maintained at a low rate, with a noted increase toward the end of gestation.<sup>42,43</sup> Cardiac output in the fetus is mainly affected by preload and ventricular compliance.<sup>41</sup> Right-to-left shunts at the level of the foramen ovale and ductus arteriosus have a significant impact on cardiac flow patterns and affect the distribution of blood and oxygen to various organs. Flow across the foramen ovale contributes to the majority of blood entering the left ventricle, and more than two thirds of right ventricular output is directed to the ductus arteriosus.<sup>42,45</sup> This shunting mechanism

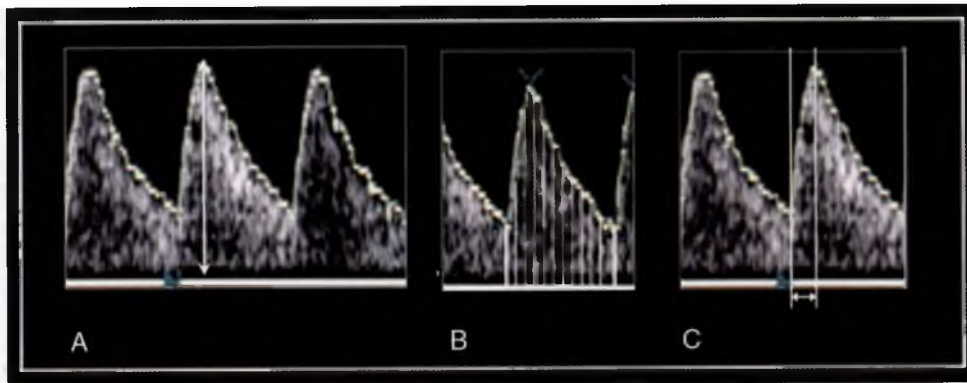


**FIG 22-19** Doppler indices that are commonly used in fetal echocardiography: peak-systolic velocity (A), time-velocity integral (B), and time-to-peak velocity (C).

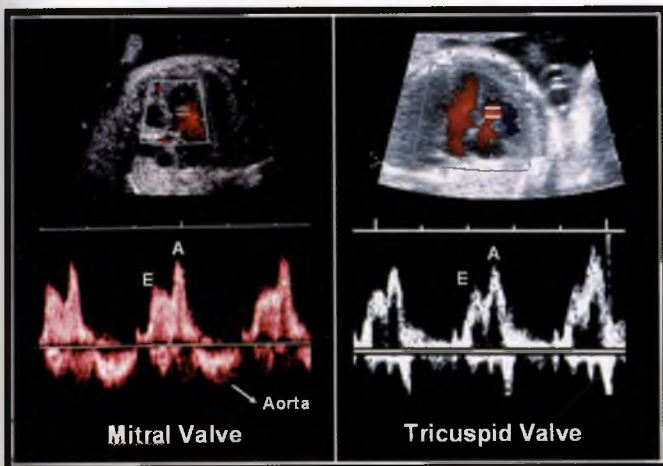


**FIG 22-20** Doppler waveforms obtained across the mitral and tricuspid valves. Owing to the proximity of the mitral and aortic valves, a portion of the aortic outflow is noted during systole (arrow, aorta). A, A wave; E, E wave.

ensures the delivery of blood with high oxygen content to the coronary and cerebral circulations.

Doppler waveforms across the atrioventricular valves are bicuspid in shape (Fig. 22-20). The first peak (E wave) corresponds to early ventricular filling of diastole, and the second peak (A wave) corresponds to atrial systole or the atrial kick. Unlike in postnatal life, the velocity of the A wave is higher than that of the E wave in the fetus.<sup>41,46</sup> This highlights the importance of the role that atrial systole plays in cardiac filling in the fetus. The E/A ratio increases with advancing gestation and reflects ventricular diastolic function.<sup>41,46</sup> E and A velocity peaks are higher in the right ventricle, and this right ventricular dominance is noted from the first trimester.<sup>41,46,47</sup> Shifting to left ventricular dominance starts in utero toward the end of gestation.<sup>41</sup> The E/A ratio is an index of ventricular preload and compliance (Table 22-14).<sup>41</sup>

Doppler waveforms across the semilunar valves are uniphasic in shape (Fig. 22-21). Indices most commonly used for the semilunar Doppler waveforms include the PSV and the TPV. PSV and TPV increase with advancing gestation across the semilunar valves.<sup>41,45,48-51</sup> PSV is higher across the aorta than across the pulmonary artery owing to a decreased afterload and a smaller diameter across the aorta.<sup>41,45,48-51</sup> These Doppler indices reflect ventricular contractility, arterial pressure, and afterload (Table 22-15).

**TABLE 22-14 Mitral and Tricuspid Valve E/A Ratios**

Gestation (weeks)	MITRAL VALVE E/A RATIO, BY PERCENTILE			TRICUSPID VALVE E/A RATIO, BY PERCENTILE		
	2.5th	50th	97.5th	2.5th	50th	97.5th
20	0.40	0.59	0.77	0.47	0.65	0.83
21	0.42	0.60	0.79	0.49	0.66	0.84
22	0.43	0.62	0.80	0.50	0.68	0.85
23	0.45	0.63	0.82	0.52	0.69	0.86
24	0.46	0.65	0.83	0.53	0.70	0.87
25	0.48	0.66	0.84	0.54	0.71	0.88
26	0.49	0.68	0.86	0.55	0.72	0.89
27	0.50	0.69	0.87	0.56	0.73	0.90
28	0.52	0.70	0.88	0.57	0.74	0.90
29	0.53	0.71	0.89	0.58	0.74	0.91
30	0.54	0.73	0.90	0.58	0.75	0.91
31	0.55	0.74	0.91	0.59	0.75	0.92
32	0.56	0.75	0.92	0.59	0.76	0.92
33	0.57	0.76	0.93	0.60	0.76	0.92
34	0.58	0.76	0.93	0.60	0.76	0.92
35	0.59	0.77	0.94	0.60	0.76	0.92
36	0.59	0.78	0.95	0.60	0.76	0.92
37	0.60	0.79	0.95	0.60	0.76	0.92
38	0.61	0.79	0.96	0.60	0.76	0.92

A, A wave velocity; E, E wave velocity.

From DeVore GR: Pulsed Doppler examination of the fetal heart. In Goldberg BB, McGahan JP (eds): Atlas of Ultrasound Measurements, 2nd ed. Philadelphia, Mosby Inc/Elsevier, 2006.

## FETAL DOPPLER AND FETAL GROWTH RESTRICTION

Arterial Doppler abnormalities, at the level of the umbilical and middle cerebral arteries (brain-sparing reflex), confirm the presence of hypoxemia in the growth-restricted fetus and present early warning signs (see Table 22-5).<sup>52-55</sup> Once arterial centralization occurs, however, no clear trend is noted in the observational period, and thus, arterial redistribution may not be helpful for the timing of the delivery.<sup>52</sup> On the other hand, the presence of reversed end-diastolic flow in the umbilical arteries is a sign of advanced fetal compromise, and strong consideration should be given for delivery except for extreme prematurity. Cesarean



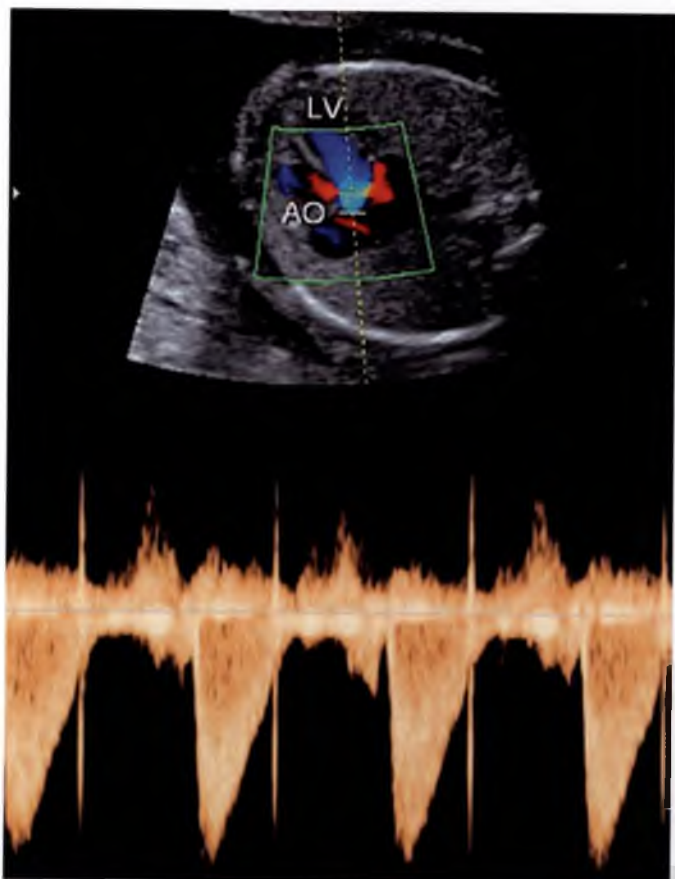


**FIG 22-21** Doppler waveforms obtained across the aortic valve. AO, aorta; LV, left ventricle.

delivery should be given preference in this setting because labor may cause further fetal compromise.

For best results, umbilical artery Doppler surveillance should be initiated when a growth-restricted fetus is considered viable.<sup>56</sup> Absent or reversed end-diastolic flow in the umbilical artery is the only vessel abnormality that has been definitely associated with adverse perinatal outcome.<sup>56,57</sup> Doppler studies of the ductus venosus, MCA, and other vessels have some prognostic value for FGR, but they have not been sufficiently evaluated in randomized trials to recommend routine use in clinical practice.<sup>57</sup>

The current literature suggests that venous Doppler abnormalities in the inferior vena cava and ductus venosus and abnormal fetal heart rate monitoring, even in its computerized version, follow arterial Doppler abnormalities and are thus associated with a more advanced stage of fetal compromise.<sup>52-56,58</sup>

Furthermore, in the majority of severely growth-restricted fetuses, sequential deterioration of arterial and venous Doppler precedes biophysical profile score deterioration.<sup>53</sup> At least one third of fetuses show early signs of circulatory deregulation 1 week before biophysical profile deterioration, and in most cases, Doppler deterioration precedes biophysical profile deterioration by 1 day.<sup>53</sup>

The occurrence of such abnormal late stage changes of vascular adaptation by the growth-restricted fetus appears to be the best predictor of perinatal death, independent of gestational age and weight.<sup>55</sup> In a longitudinal study of the use of Doppler in growth-restricted fetuses, all intrauterine deaths and all neonatal deaths, with the exception of one case, had late Doppler changes at the time of delivery, whereas only a few of the surviving fetuses showed such changes.<sup>55</sup> These findings have been confirmed by a large prospective multicenter study that

**TABLE 22-15 Peak or Maximum Velocity of the Aorta and Main Pulmonary Artery**

Gestation (weeks)	AORTA PEAK VELOCITY (cm/sec), BY PERCENTILE			PULMONARY ARTERY PEAK VELOCITY (cm/sec), BY PERCENTILE		
	2.5th	50th	97.5th	2.5th	50th	97.5th
20	29	62	95	23	53	80
21	30	63	96	24	54	81
22	32	65	98	25	56	82
23	33	66	99	27	57	84
24	34	67	100	28	58	85
25	36	68	101	29	59	86
26	37	70	103	30	61	87
27	38	71	104	31	62	89
28	40	72	105	32	63	90
29	41	74	107	34	64	91
30	42	75	108	35	65	92
31	44	76	109	36	67	93
32	45	77	110	37	68	95
33	46	79	112	38	69	96
34	48	80	113	39	70	97
35	49	81	114	41	72	98
36	50	82	115	42	73	100
37	52	84	117	43	74	101
38	53	85	118	44	78	102

From DeVore GR: Pulsed Doppler examination of the fetal heart. In Goldberg BB, McGahan JP (eds): *Atlas of Ultrasound Measurements*, 2nd ed. Philadelphia, Mosby Inc/Elsevier, 2006.

demonstrated that, prior to 27 weeks of gestation, gestational age is the most important factor determining neonatal outcome in growth-restricted infants delivered before 33 weeks of gestation. However, after 27 weeks, abnormality of ductus venosus becomes a very important cardiovascular predictor of neonatal complications.<sup>59</sup> Despite these findings, there is insufficient evidence to recommend using ductus venosus Doppler as a routine screening tool in growth-restricted fetuses.

This sequential deterioration of the hypoxic, growth-restricted fetus is rarely seen at gestations beyond 34 weeks.<sup>60,61</sup> Indeed, normal umbilical artery Doppler findings are common in growth-restricted fetuses in late gestations, and cerebroplacental ratios also have poor correlation with outcome of growth-restricted fetuses at greater than 34 weeks of gestation.<sup>62</sup> Therefore, caution should be exercised when Doppler is used in the clinical management of fetuses with FGR beyond 34 weeks of gestation.

The largest to date prospective observational trial (PORTO study) recently demonstrated the presence of not one but multiple potential patterns of Doppler deterioration in FGR pregnancies.<sup>57</sup> None of the patterns were particularly predominant in either the entire cohort of growth-restricted fetuses or in those that required delivery prior to 34 weeks.<sup>63</sup> These findings have not been confirmed by an interventional trial.

The pathophysiology of FGR has not been fully described because recent studies have highlighted the presence of significant variation in fetal adaptation to hypoxemia. The pattern of incremental deterioration of arterial Doppler abnormalities, followed by venous Doppler abnormalities, and then followed by abnormal fetal heart tracings and biophysical profile abnormalities is not seen in approximately 20% of preterm fetuses.<sup>52</sup> Furthermore, only 70% of fetuses with FGR show

significant deterioration of all vascular beds by the time they are delivered, and about 10% show no significant circulatory change by delivery time.<sup>53</sup> In a prospective, observational study, more than 50% of fetuses with FGR delivered because abnormal fetal heart rate tracings did not have venous Doppler abnormalities.<sup>55</sup> In view of these findings, the universal introduction of venous Doppler into the clinical management of the growth-restricted fetus should await the results of randomized trials on this subject. Subanalysis of the TRUFFLE study (Trial of Randomized Umbilical and Fetal Flow in Europe) (a prospective, multicenter randomized trial) suggests that when an abnormality of the ductus venosus is used as one of the main criteria for delivery of a growth-restricted fetus, the neonatal morbidity and time interval from diagnosis to delivery are related to the presence and severity of maternal hypertensive conditions.<sup>64</sup>

FGR is associated with several changes at the level of the fetal heart involving preload, afterload, ventricular compliance, and myocardial contractility. An increase in afterload is seen at the level of the right ventricle owing to increased placental impedance.<sup>65</sup> A decrease in afterload is noted at the level of the left ventricle owing to decreased cerebral impedance associated with the brain-sparing reflex.<sup>65</sup> These changes in afterload result in a redistribution of the cardiac output from right to left ventricle.<sup>65</sup> Preload is reduced at both atrioventricular valves owing to hypovolemia and decreased filling associated with FGR.<sup>49,60,66,67</sup> This decrease in preload is reflected by a decrease in the E/A ratio, decreased atrial peak, and decreased time velocity integral at the mitral and tricuspid valves.<sup>49,66,67</sup>

Evidence of reduced myocardial contractility in the presence of severe FGR has also been reported. Ventricular ejection force, an index of ventricular systolic function that is independent of preload and afterload, is decreased at the level of the right and left ventricles in FGR.<sup>68</sup> Growth-restricted fetuses with reduced ventricular ejection force have a shorter time to delivery, a higher incidence of nonreassuring fetal heart rate tracing, and a lower pH at birth when compared with control subjects.<sup>68</sup> A significant correlation between the severity of fetal acidosis at cordocentesis and ventricular ejection force values validates the association of this index and the severity of fetal compromise.<sup>68</sup> Myocardial cell damage, demonstrated by elevated levels of cardiac troponin T, is seen in some fetuses with severe growth restriction.<sup>65</sup> This advanced stage of fetal compromise is associated with signs of increased systemic venous pressure, a change in the distribution of cardiac output, a rise in right ventricle afterload, and a high incidence of tricuspid regurgitation.<sup>65</sup> These findings suggest that Doppler abnormalities in the proximal venous system of the growth-restricted fetus result from fetal myocardial cell damage and increased systemic venous pressure.<sup>65</sup>

The fetal heart plays a central role in the adaptive mechanisms for hypoxemia and placental insufficiency. As discussed in this chapter, longitudinal data on the hemodynamic sequence of the natural history of FGR show that the umbilical artery and MCA are the first variables to become abnormal.<sup>69</sup> These arterial Doppler abnormalities are followed by abnormalities in the right cardiac diastolic indices, followed by the right cardiac systolic indices, and finally, by both left diastolic and systolic cardiac indices.<sup>69</sup> Preserving the left systolic function as the last variable to become abnormal ensures an adequate left ventricular output, which supplies the cerebral and coronary circulations.

Several of the Doppler changes seen in association with FGR in the peripheral circulation are directly related to the adaptation of the fetal heart. The current management of FGR involves the use of Doppler at the peripheral arterial circulation (middle cerebral and umbilical arteries), at central venous vessels (ductus venosus and inferior vena cava), and with cardiocography. Adding cardiac Doppler may improve management of the fetus with FGR, but studies are lacking on the prospective clinical evaluation of the FGR with cardiac Doppler.

However, it is becoming more obvious that those changes in the central venous circulation reflect an advanced stage of fetal compromise, commonly associated with myocardial dysfunction and damage.

## REFERENCES

- Doppler C: Uber das farbige Licht der Dopplersterne und einiger anderer Gestirne des Himmels. [On the coloured light of double stars and certain other stars of the heavens]. *Royal Bohemian Society* 2:465, 1842.
- Edelman SK, editor: *Understanding Ultrasound Physics*, ed 3, Woodlands, TX, 2004, Education for the Sonographic Professional.
- Fleischer A, Schulman H, Farmakides G, et al: Umbilical artery waveforms and intrauterine growth retardation. *Am J Obstet Gynecol* 151:502, 1985.
- Ott WJ: The diagnosis of altered fetal growth. *Obstet Gynecol Clin North Am* 15:237, 1988.
- Giles WB, Trudinger BJ, Baird PJ: Fetal umbilical artery flow velocity waveforms and placental resistance: pathological correlation. *Br J Obstet Gynecol* 92:31, 1985.
- Manning FA: Intrauterine growth restriction. Diagnosis, prognostication, and management based on ultrasound methods. In Manning FA, editor: *Fetal Medicine: Principles and Practice*, Norwalk, CT, 1995, Appleton & Lange, pp 87–94.
- Hadlock FP, Deter RL, Harrist RB, et al: A date-independent predictor of intrauterine growth retardation: femur length/abdominal circumference ratio. *AJR Am J Roentgenol* 141:979, 1993.
- Trudinger BJ, Stevens D, Connelly A, et al: Umbilical artery flow velocity waveforms and placental resistance: the effect of embolizations of the umbilical circulation. *Am J Obstet Gynecol* 157:1443, 1987.
- Brown HL, Miller JM, Jr, Gabert HA, et al: Ultrasonic recognition of the small-for-gestational-age fetus. *Obstet Gynecol* 69:631, 1987.
- Creasy RK, Resnick R: Intrauterine growth retardation. In Creasy RK, Resnick R, editors: *Maternal Fetal Medicine: Principles and Practice*, Philadelphia, 1984, WB Saunders.
- Kingdom JC, Burrell SJ, Kaufmann P: Pathology and clinical implications of abnormal umbilical artery Doppler waveforms. *Ultrasound Obstet Gynecol* 9:271, 1997.
- Morrow RJ, Adamson SL, Bull SB, et al: Effect of placental embolization on the umbilical arterial velocity waveform in fetal sheep. *Am J Obstet Gynecol* 161:1055, 1989.
- Bernstein IM, Horbar JD, Badger GJ, et al: Morbidity and mortality among very-low-birth weight neonates with intrauterine growth restriction. *Am J Obstet Gynecol* 182:198, 2000.
- Copel JA, Reed KL: *Doppler Ultrasound in Obstetrics and Gynecology*, New York, 1995, Raven Press, pp 187–198.
- Westergaard HB, Langhoff-Roos J, Lingman G, et al: A critical appraisal of the use of umbilical artery Doppler ultrasound in high risk pregnancies: use of meta-analyses in evidence-based obstetrics. *Ultrasound Obstet Gynecol* 17:466–476, 2001.
- Alfirevic Z, Stampalija T, Gyte GM: Fetal and umbilical Doppler ultrasound in high-risk pregnancies. *Cochrane Database Syst Rev* (11):CD007529, 2013.
- Trudinger BJ: Doppler ultrasonography and fetal well being. In Reece EA, Hobbins JC, Mahoney M, editors: *Medicine of the Fetus and Mother*, Philadelphia, 1992, JB Lippincott.
- Bhide A, Acharya G, Bilardo CM, et al: ISUOG practice guidelines: use of Doppler ultrasonography in obstetrics. *Ultrasound Obstet Gynecol* 41(2):233–239, 2013.
- Veille JC, Hanson R, Tatum K: Longitudinal quantitation of middle cerebral artery blood flow in normal human fetuses. *Am J Obstet Gynecol* 169:1393, 1993.
- Mari G, Deter RL: Middle cerebral artery flow velocity waveforms in normal and small-for-gestational age fetuses. *Am J Obstet Gynecol* 166:1262, 1992.
- Soothill PW, Ajayi RA, Campbell S, et al: Relationship between fetal academia at cordocentesis and subsequent neurodevelopment. *Ultrasound Obstet Gynecol* 2:80, 1992.



22. Mari G, Abuhamad AZ, Brumfield J, et al: Doppler ultrasonography of the middle cerebral artery peak systolic velocity in the fetus: reproducibility of measurement. *Am J Obstet Gynecol* 85:abstract 669, 2001.
23. Hoffman C, Galan H: Assessing the "at risk" fetus: Doppler ultrasound. *Current Opin Obstet Gynecol* 21:161-166, 2009.
24. Hanif F, Drennan K, Mari G: Variable affecting the middle cerebral artery peak systolic velocity in anemic and IUGR fetuses. *Am J Perinatol* 24:501-505, 2007.
25. Robertson WB, Brosens I, Dixon HG: Uteroplacental vascular pathology. *Eur J Obstet Gynecol Reprod Biol* 5:47, 1975.
26. Pijnenborg R, Bland JM, Robertson WB, et al: Uteroplacental arterial changes related to interstitial trophoblast migration in early pregnancy. *Placenta* 4:397, 1983.
27. Arduini D, Rizzo G, Boccolini MR, et al: Functional assessment of uteroplacental and fetal circulations by means of color Doppler ultrasonography. *J Ultrasound Med* 9:249, 1990.
28. Hernandez-Andrade E, Brodzski J, Lingman G, et al: Uterine artery score and perinatal outcome. *Ultrasound Obstet Gynecol* 19:438, 2002.
29. Lees C, Parra M, Missfelder-Lobos H, et al: Individualized risk assessment for adverse pregnancy outcome by uterine artery Doppler at 23 weeks. *Obstet Gynecol* 98:369, 2001.
30. Dugoff L, Hobbins JC, Malone FD, et al: First-trimester maternal serum PAPP-A and free-beta subunit human chorionic gonadotropin concentrations and nuchal translucency are associated with obstetric complications: a population-based screening study (the FASTER Trial). *Am J Obstet Gynecol* 191:1446-1451, 2004.
31. Dugoff L, Lynch AM, Cioffi-Ragan D, et al: FASTER Trial Research Consortium: first trimester uterine artery Doppler abnormalities predict subsequent intrauterine growth restriction. *Am J Obstet Gynecol* 193:1208-1212, 2005.
32. Myatt L, Clifton RB, Roberts JM, et al: The utility of uterine artery Doppler velocimetry in prediction of preeclampsia in a low-risk population. *Obstet Gynecol* 120(4):815-822, 2012.
33. American College of Obstetricians and Gynecologists, Task Force on Hypertension in Pregnancy: Hypertension in pregnancy. Report of the American College of Obstetricians and Gynecologists' Task Force on Hypertension in Pregnancy. *Obstet Gynecol* 122(5):1122-1131, 2013.
34. Hecher K, Hackelöer B: Cardiotocogram compared to Doppler investigation of the fetal circulation in the premature growth-retarded fetus: longitudinal observations. *Ultrasound Obstet Gynecol* 9:152, 1997.
35. Huisman TWA, Stewart PA, Wladimiroff JW: Flow velocity waveforms in the fetal inferior vena cava during the second half of normal pregnancy. *Ultrasound Med Biol* 17:679, 1991.
36. Reed KL, Appleton CP, Anderson CF, et al: Doppler studies of vena cava flows in human fetuses: insights into normal and abnormal cardiac physiology. *Circulation* 81:498, 1990.
37. Reuss ML, Rudolph AM, Dae MW: Phasic blood flow patterns in the superior and inferior venae cavae and umbilical vein of fetal sheep. *Am J Obstet Gynecol* 145:70, 1983.
38. Rizzo G, Arduini D, Romanini C: Inferior vena cava flow velocity waveforms in appropriate- and small-for-gestational-age fetuses. *Am J Obstet Gynecol* 166:1271, 1992.
39. Rizzo G, Capponi A, Talone PE, et al: Doppler indices from inferior vena cava and ductus venosus in predicting pH and oxygen tension in umbilical blood at cordocentesis in growth retarded fetuses. *Ultrasound Obstet Gynecol* 7:401, 1996.
40. Mari G, Hanif F: Fetal Doppler: umbilical artery, middle cerebral artery, and venous system. *Semin Perinatol* 32(4):253-257, 2008.
41. Chang CH, Chang FM, Yu CH, et al: Systemic assessment of fetal hemodynamics by Doppler ultrasound. *Ultrasound Med Biol* 26:777, 2000.
42. Mielke G, Norbert B: Cardiac output and central distribution of blood flow in the human fetus. *Circulation* 103:1662, 2001.
43. Mielke G, Benda N: Blood flow velocity waveforms of the fetal pulmonary artery and the ductus arteriosus: reference ranges from 13 weeks to term. *Ultrasound Obstet Gynecol* 15:213, 2000.
44. Hong Y, Choi J: Doppler study on pulmonary venous flow in the human fetus. *Fetal Diagn Ther* 14:86, 1999.
45. Brezinka C: Fetal hemodynamics. *J Perinat Med* 29:371, 2001.
46. Harada K, Rice MJ, Shiota T, et al: Gestational age and growth related alternations in fetal right and left ventricular diastolic filling patterns. *Am J Cardiol* 79:173, 1997.
47. Ben-Ami M, Peleg D, Haddad S, et al: Normal cardiac flow velocities at 14-16 weeks gestation measured by transvaginal ultrasound. *Ultrasound Obstet Gynecol* 19:47, 2002.
48. Severi FM, Rizzo G, Bocchi C, et al: Intrauterine growth retardation and fetal cardiac function. *Fetal Diagn Ther* 15:8, 2000.
49. Rizzo G, Arduini D, Romanini C: Doppler echocardiographic assessment of fetal cardiac function. *Ultrasound Obstet Gynecol* 2:434, 1992.
50. Groenenberg IAL, Stijnen T, Wladimiroff JW: Flow velocity waveforms in the fetal cardiac outflow tract as a measure of fetal well-being in intrauterine growth retardation. *Pediatr Res* 27:379, 1990.
51. Machado MVL, Chita SC, Allan LD: Acceleration time in the aorta and pulmonary artery measured by Doppler echocardiography in the midtrimester normal human fetus. *Br Heart J* 58:15, 1987.
52. Baschat AA, Gembruch U, Reiss I, et al: Relationship between arterial and venous Doppler and perinatal outcome in fetal growth restriction. *Ultrasound Obstet Gynecol* 16:407, 2000.
53. Baschat AA, Gembruch U, Harman CR: The sequence of changes in Doppler and biophysical parameters as severe fetal growth restriction worsens. *Ultrasound Obstet Gynecol* 18:571, 2001.
54. Hecher K, Bilardo CM, Stigter RH, et al: Monitoring of fetuses with intrauterine growth restriction: a longitudinal study. *Ultrasound Obstet Gynecol* 18:564, 2001.
55. Ferrazzi E, Bozzo M, Rigano S, et al: Temporal sequence of abnormal Doppler changes in the peripheral and central circulatory systems of the severely growth-restricted fetus. *Ultrasound Obstet Gynecol* 19:140, 2002.
56. Berkley E, Chauhan SP, Abuhamad A: Doppler assessment of the fetus with intrauterine growth restriction. *Am J Obstet Gynecol* 206:300, 2012.
57. Unterscheider J, Daly S, Geary MP, et al: Optimizing the definition of intrauterine growth restriction: the multicenter prospective PORTO Study. *Am J Obstet Gynecol* 208:290, 2013.
58. Pardi G, Cetin I, Marconi AM, et al: Diagnostic value of blood sampling in fetuses with growth retardation. *N Engl J Med* 328:692, 1993.
59. Baschat AA, Cosmi E, Bilardo CM, et al: Predictors of neonatal outcome in early-onset placental dysfunction. *Obstet Gynecol* 109:253, 2007.
60. Hecher K, Campbell S, Doyle P, et al: Assessment of fetal compromise by Doppler ultrasound investigation of the fetal circulation. Arterial, intracardiac, and venous blood flow velocity studies. *Circulation* 91:129, 1995.
61. Harrington K, Thompson MO, Carpenter RG, et al: Doppler fetal circulation in pregnancies complicated by pre-eclampsia or delivery of a small for gestational age baby: 2. Longitudinal analysis. *Br J Obstet Gynaecol* 106:453, 1999.
62. Bahado-Singh RO, Kovanci E, Jeffers A, et al: The Doppler cerebroplacental ratio and perinatal outcome in intrauterine growth restriction. *Am J Obstet Gynecol* 180:750, 1999.
63. Unterscheider J, Daly S, Geary MP, et al: Predictable progressive Doppler deterioration in IUGR: does it really exist? *Am J Obstet Gynecol* 209:539, 2013.
64. Lees C, Marlow N, Arabin B, et al: Perinatal morbidity and mortality in early-onset fetal growth restriction cohort outcomes of the trial of randomized umbilical and fetal flow in Europe (TRUFFLE). *Ultrasound Obstet Gynecol* 42:400, 2013.
65. Makikallio K, Vuolteenaho O, Jouppila P, et al: Ultrasonographic and biochemical marker of human fetal cardiac dysfunction in placental insufficiency. *Circulation* 105:2058, 2002.
66. Reed KI, Anderson CF, Shenker L: Changes in intracardiac Doppler blood flow velocities in fetuses with absent umbilical artery diastolic flow. *Am J Obstet Gynecol* 157:774, 1987.
67. Forouzan I, Graham E, Morgan MA: Reduction of right atrial peak systolic velocity in growth-restricted discordant twins. *Am J Obstet Gynecol* 175:1033, 1996.
68. Rizzo G, Capponi A, Rinaldo D, et al: Ventricular ejection force in growth-retarded fetuses. *Ultrasound Obstet Gynecol* 5:247, 1995.
69. Figueras F, Puerto B, Martinez JM, et al: Cardiac function monitoring of fetuses with growth restriction. *Eur J Obstet Gynecol Reprod Biol* 110:159, 2003.

# Role of Magnetic Resonance Imaging in Obstetrics

*Sherelle Laifer-Narin, Diane M. Twickler*

## SUMMARY OF KEY POINTS

- Magnetic resonance imaging (MRI) does not use ionizing radiation, and no known biologic risks are associated with this imaging modality.
- MRI is an important tool for the evaluation of maternal complications in pregnancy, including the evaluation of atypical advanced ectopic pregnancies, suspected appendicitis, pelvic masses, hepatic and genitourinary diseases, and placenta accreta.
- In the fetus, MRI is a useful adjunct to the sonographic diagnosis of suspected central nervous system (CNS) lesions, particularly isolated mild ventriculomegaly.
- MRI may provide additional information for certain fetal thoracic lesions, can aid in predicting prognosis in diaphragmatic hernias, and can provide additional information in the setting of complex fetal genitourinary abnormalities.
- MRI studies add important information for the potential fetal surgery candidate and may direct crucial decisions for delivery management, as with the ex utero intrapartum treatment (EXIT) procedure.
- MRI has been found to be useful in the diagnosis of abnormal placental implantation in cases with an equivocal diagnosis on ultrasound imaging.
- Advances in MRI technology continue to allow for better resolution of fetal structures, and it is likely that this technique will have increasing application in prenatal diagnosis and evaluation of fetal abnormalities.

## OUTLINE

**Safety, 749**

**Technique, 750**

T2-Weighted Imaging, 750

T1-Weighted Imaging, 750

Balanced Steady-State Free Precession, 750

Diffusion-Weighted Imaging, 751

Other Magnetic Resonance Acquisitions, 751

**Maternal Imaging, 751**

**Fetal Imaging, 752**

Anomalies of the Central Nervous System, 752

Anomalies of the Face, Neck, and Thorax, 755

Abnormalities in the Fetal Abdomen, 762

Tumors, 763

Monochorionic Twins, 765

Abnormal Placentation, 765

Emerging Concepts, 768

**Conclusions, 769**

The role of MRI in managing the obstetric patient is increasingly expanding. Although sonography is the primary imaging modality for evaluation of the pregnant patient, MRI has been in use for the past 30 years and is now considered an established adjunct imaging modality for obstetric management. Maternal obesity, oligohydramnios, fetal positioning, and fetal ossification can hamper ultrasound evaluation. Advantages of MRI include lack of ionizing radiation, superior soft tissue contrast, wide field of view imaging, and image acquisition in multiple true orthogonal planes. Various sequences allow us to discern soft tissue, fluid, hemorrhage, fat, and meconium. Additional sequences allow us to identify regions of hypoxia/ischemia. Limitations of MRI include maternal anxiety and claustrophobia, maternal habitus, and fetal motion when evaluating for anomalies. In this chapter we address the utility of MRI as an adjunctive second-line imaging modality in evaluating the symptomatic pregnant patient, the fetus, and the abnormally adherent placenta.

## SAFETY

No known biologic risks are associated with MRI. No delayed sequelae from MRI examination have been encountered, and it is expected that the potential risk for any such delayed sequelae is extremely small or nonexistent. MRI utilizes no ionizing radiation, although concerns include exposure to fluctuating electromagnetic fields, high sound intensity levels, and effects on fetal heart rate patterns during the procedure. Several animal and tissue studies have been conducted to determine the biologic effects of electromagnetic fields with conflicting reports. An early study looked at the long-term effects of repetitive exposure to a static 1.5-tesla (T) magnetic field on human lung fibroblasts.<sup>1</sup> Study and control group proliferations were similar, indicating no adverse effect from repetitive MR exposure.

Few human studies on risks of MRI and early development have been completed. A large epidemiologic retrospective study compared



spontaneous abortion rates, infertility rates, incidence of low birth weight, and premature delivery among nurses and technologists working with MRI before and after employment.<sup>2</sup> There were no increased incidences of adverse outcomes in the MR-exposed group. Two studies reported follow-up on children exposed to echo-planar MR in utero. The first by Baker and associates completed a 3-year follow-up on 20 children with no demonstrable increase in the occurrence of disease or disability.<sup>3</sup> These patients were imaged with a 0.5-T superconductive magnet from 21 weeks to term. In the second case-controlled prospective observational study of 20 infants exposed to echo-planar imaging, pediatric assessments completed on these infants at 9 months of age were normal.<sup>4</sup>

In reference to the sound intensity and exposure, one study assessed the sound level experienced by the fetal ear during an MR procedure by having a volunteer swallow a microphone connected to a thin lead and filling the stomach with a liter of fluid to represent an amniotic sac.<sup>5</sup> There was at least 30-dB attenuation in intensity from the body surface to within the fluid-filled stomach, which reduced the acoustic sound pressure down from the dangerous threshold of 120 dB to an acceptable level of less than 90 dB. This level is lower than the 135 dB experienced when vibroacoustic stimulation is used. No evidence of hearing loss was found in one study after 450 babies were exposed to this noise intensity from vibroacoustic stimulation.<sup>6</sup>

Studies have also looked at fetal heart rate patterns during MR procedures and reported no change in heart rate patterns or incidence of fetal movements.<sup>7</sup> Recommendations from the latest document from the American College of Radiology concerning safe practices for MRI have determined that MRI can be performed in pregnancy if the data are needed to affect the care of the fetus or mother during pregnancy.<sup>8</sup> Because of the potential for dissociation of the chelate molecule in the amniotic fluid, MRI contrast agents should not be routinely administered. The longer the chelate molecule remains in a protected space such as the amniotic sac, the greater the potential for dissociation of the potentially toxic gadolinium ion, which can lead to nephrogenic systemic fibrosis in at-risk adults.<sup>8</sup> Gadolinium is listed as a category C drug in pregnancy based on Food and Drug Administration classifications, implying that it should be administered only if potential benefits warrant use of the drug despite potential risks. It is recommended that women undergoing MRI during pregnancy provide informed written consent documenting that they understand the potential risks and benefits of the procedure.

## TECHNIQUE

Fetal and maternal studies are generally performed on a 1.5-T magnet or less, and it is recommended that informed consent be obtained for all patients in the settings of either institutional review board (IRB)-approved protocols or as a clinically indicated procedure. In addition, all women complete a written MRI safety screening questionnaire including information regarding metallic implants, pacemakers, or other metal- or iron-containing devices that may impact the study.<sup>8</sup> Iron supplementation may rarely cause artifact in the colon but does not usually affect the fetal resolution. Portable devices and monitors must be evaluated using U.S. Food and Drug Administration labeling criteria to prevent ferrous objects from entering unsafe zones within the MRI areas.<sup>8</sup> Anxiolytics are not routinely administered because significant maternal anxiety is a very rare event (less than 1% in our population), but in those unique circumstances, short-acting benzodiazepines may be administered. The recommended weight limit is approximately 400 pounds (but dependent on body habitus) on most closed current MR units; therefore, the extremely obese woman may not be a candidate for MRI.

Women are placed feet first in the supine or left lateral decubitus position. A torso coil is used in most circumstances, with the occasional use of either the body or cardiac coil, depending on maternal size, fetal size, and area of interest. A triplanar balanced steady-state free precession (bSSFP) sequence through the entire maternal uterus is initially obtained for localization purposes and planning subsequent sequences, which have a large field of view (350-400 mm), using 6-mm slice thickness with 3-mm interslice gap.

## T2-Weighted Imaging

T2-weighted image acquisitions are utilized to define fetal anatomy and dysmorphic features that have certain tissue characteristics based on a specific spin echo sequence using relatively long repetition time (TR) and long echo time.

Half-Fourier single shot RARE (rapid acquisition with relaxation enhancement) has become the mainstay of maternal pelvic and fetal imaging because of its high tissue resolution and rapid acquisition times. This ultrafast single shot imaging has an average acquisition time of less than 1 second, depending on imaging parameters. Other names for this sequence include single shot fast spin echo (SSFSE) and half-Fourier acquisition single shot turbo spin echo (HASTE). Specifics of the sequence vary, but for the single shot acquisition one signal and one measurement is acquired, the TR range is 800 to 1100 ms, echo time is 60 to 90 ms, flip angle is 130 to 150 degrees with 0- to 2-mm gap, and field of view is 300 to 350 mm.<sup>9</sup>

Fetal images may be obtained contiguously or interleaved, both having distinct advantages. Fetal movement degrades MR images, and contiguous slices may allow for better visualization of some contiguous structures in some slices, even if movement occurs during other slices in the acquisition. The interleave method allows for improved signal-to-noise ratio by obtaining every other image with an interslice gap and repeating process to include that missed gap; this prevents excitation of adjacent and consecutive sections.<sup>10,11</sup>

## T1-Weighted Imaging

The use of T1-weighted gradient echo sequences provides additional information, owing to very short T1 relaxation times and allowing for improved visualization of subacute blood, fat, and proteinaceous fluid as well as fetal liver and meconium. Hyperintense pituitary and thyroid glands can also be seen. Late in gestation the fetal bones have a hypointense appearance. The images are less sensitive in defining some solid organ anatomy because of less tissue contrast.

In the setting of obstetric imaging, T1-weighted sequences are utilized to assess for the presence and distribution of T1 hyperintense meconium, to determine the size and location of the fetal liver, and to evaluate fetal or maternal hemorrhage or fat-containing lesions. Some T1-weighted sequences require more than one single shot with short TR (range 7.7-112 ms), echo time (4.2-5 ms), and flip angle (130-150 degrees). T1-weighted sequences may be obtained by single shot T1-weighted sequences or three-dimensional (3D) imaging techniques, with or without fat suppression. Because of improved signal-to-noise ratio, breath-hold T1-weighted gradient recalled echo sequences are generally used. T1-weighted breath-hold images are acquired with 5.5-mm slice thickness and 10% (0.5-mm) gap with field of view range of 300 to 350 mm.<sup>12,13</sup>

## Balanced Steady-State Free Precession

bSSFP acquisitions have manufacturer acronyms such as True-FISP and FIESTA (fast imaging with steady-state precession and fast imaging employing steady-state acquisition) and are complex in terms of how they derive their contrast, the result of which is high T2 weighting in fluid and high T1 weighting in tissue.<sup>14</sup> Vessels are displayed quite well,



especially when surrounded by dense tissue such as liver parenchyma or the vertebral disk spaces.<sup>15</sup> Tissue contrast tends to be quite good, with slice thickness for bSSFP in the range of 5 to 6 mm and field of view ranging from 260 to 300 mm.<sup>14</sup>

### Diffusion-Weighted Imaging

Diffusion-weighted imaging (DWI) is based on echo-planar imaging that produces images of water diffusion; this diffusion of water may be restricted in certain disease states, such as hypoxic edema (ischemia) of the brain. Diffusion anisotropy has the potential to characterize premyelination structures and can identify the corpus callosum and other white matter tracts, which will be discussed in Emerging Concepts.<sup>12,14,15</sup>

### Other Magnetic Resonance Acquisitions

Many other acquisitions can be applied, some of which will be discussed in Emerging Concepts and are briefly reviewed. Short tau inversion recovery (STIR) images may provide improved resolution of tissue characteristics when the water contents of structures are similar. Additional sequences such as fluid attenuated inversion recovery (FLAIR), hydrography, blood oxygen level–dependent (BOLD) imaging, and certain echo-planar imaging may be performed as needed.<sup>16</sup>

## MATERNAL IMAGING

In an effort to image the pregnant patient with abdominal pain rapidly and efficiently, the MRI protocol includes multiplanar T2-weighted SSFSE images (with and without fat saturation) of the abdomen and pelvis, gradient echo sequences, and a single plane T1-weighted sequence.

A wide range of pathologic conditions can cause abdominal pain in the pregnant patient. Clinical diagnosis is often challenging because of nonspecific leukocytosis, compression and displacement of organs by the gravid uterus, and nonspecific nausea and vomiting.<sup>17</sup> It is important to differentiate obstetric from nonobstetric causes of the acute abdomen in an effort to minimize maternal and fetal morbidity and mortality risks.<sup>18</sup> Conditions that necessitate surgical intervention must be identified.

Ectopic pregnancy continues to be the leading obstetric cause of death in early pregnancy.<sup>19</sup> MRI has been shown to be useful in delineating unusual implantation sites, including pregnancies implanted in the interstitium, cervix, cesarean scar, and rudimentary horn of an anomalous uterus, and within the peritoneal cavity (Fig. 23-1). T1-weighted sequences can depict blood products, and the presence of hemoperitoneum and hematosalpinx are highly suggestive of ectopic pregnancy in a patient with a positive pregnancy test and no intrauterine gestational sac. The large field of view and multiplanar capability of MRI allow exact delineation of advanced first trimester and second trimester ectopic pregnancies, which might not be appreciated on ultrasound imaging. Late presentation of ectopic pregnancy can be catastrophic and fatal because of risk of rupture and hemorrhage. The late presentation of an advanced cesarean scar pregnancy that has grown cephalad might mimic a normal intrauterine pregnancy. Demonstration of myometrial tissue surrounding a gestational sac without continuity to the cervix can help discriminate between a pregnancy in a bicornuate uterus versus a rudimentary horn pregnancy.<sup>20</sup>

Acute appendicitis is the most common nonobstetric cause for surgical intervention during pregnancy. Early diagnosis is essential, as surgical delay is associated with increased risk of appendiceal perforation, leading to an increased rate of maternal morbidity and fetal loss<sup>19</sup> (Fig. 23-2). Other gastrointestinal causes of abdominal pain include inflammatory and infectious bowel disease, bowel obstruction, and

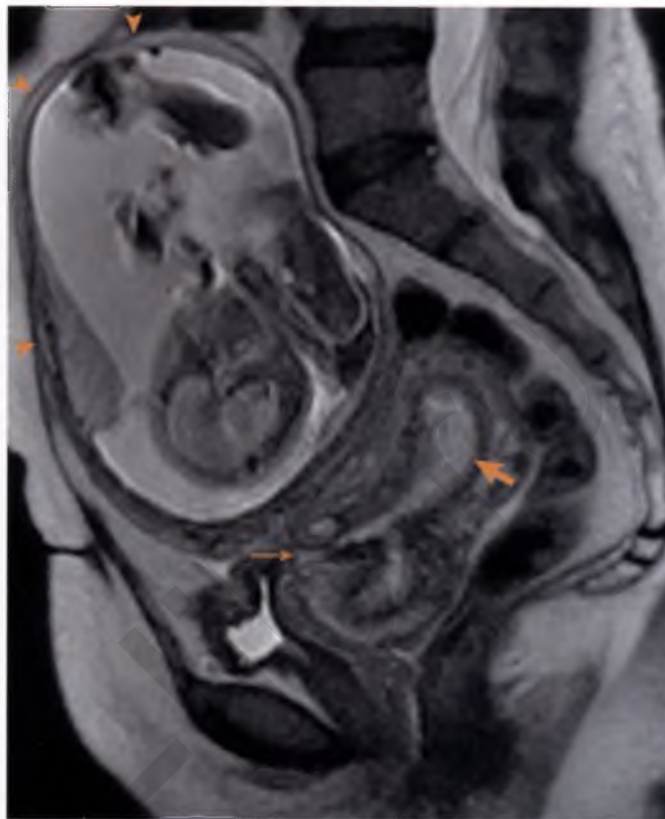


**FIG 23-1** Rudimentary horn ectopic pregnancy at 19 weeks' gestation. Sagittal T2-weighted imaging demonstrates ectopic pregnancy implanted within a noncommunicating rudimentary horn of an anomalous uterus (*arrowheads*). The unicornuate endometrial cavity is empty (*bold arrow*) and there is a previous cesarean scar (*small arrow*).

diverticulitis (Fig. 23-3). Symptoms (abdominal pain, nausea, vomiting) are similar to those that occur with normal pregnancy. Comprehensive cross-sectional imaging is essential for evaluation, and MRI is preferable to computed tomography because of lack of ionizing radiation.

Physiologic dilatation of the urinary tract occurs in up to 90% of pregnant patients. MR urography can differentiate obstructive hydronephrosis caused by renal calculi from physiologic hydronephrosis if renal enlargement, perinephric fluid, and abrupt caliber change of the ureter are demonstrated (Fig. 23-4).

Hepatobiliary causes of abdominal pain include HELLP syndrome (hemolysis, elevated liver enzymes, low platelet count) and acute fatty liver of pregnancy, hepatitis, gallbladder disease, and pancreatitis. MRI and MR cholangiopancreatography can be useful in demonstrating choledocholithiasis and pseudocysts in the patient suspected of having pancreatitis.

Gynecologic causes of pain during pregnancy include ovarian cysts, masses, and torsion and uterine abnormalities, such as leiomyomas and congenital müllerian anomalies. Fluid, solid components, septations, nodularity, edema, hemorrhage, and fat content can be seen on MRI. If a primary pelvic mass is suspicious for malignancy, MRI can depict ascites, peritoneal implants, and lymphadenopathy.

The hypercoagulable state of pregnancy, venous compression by the gravid uterus, and hormone-induced venodilatation put the pregnant patient at increased risk for venous thromboembolic disease, most of



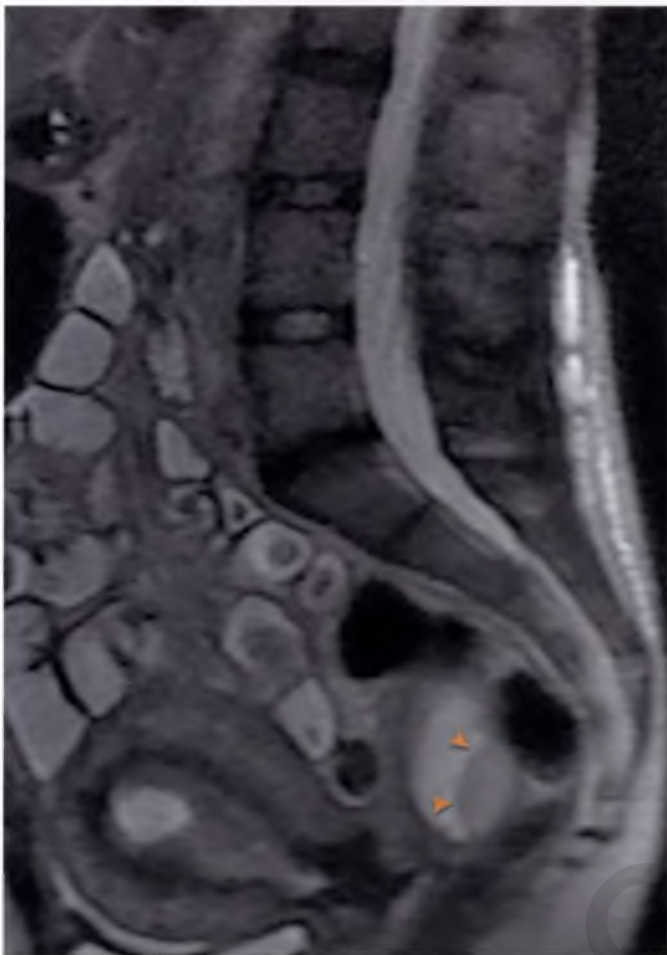


**FIG 23-2** Ruptured appendicitis at 6 weeks' gestation. Sagittal T2-weighted imaging demonstrates complex fluid collection with fluid-debris level (arrowheads) consistent with abscess in the cul-de-sac. Surgery confirmed ruptured appendicitis with resultant abscess; intra-uterine fetal demise occurred 3 days later.

which occurs in the lower extremities. However, thrombosis can also develop in the hepatic, mesenteric, gonadal, and pelvic veins, and these sites can be demonstrated by MRI.

## FETAL IMAGING

Fetal MRI has emerged as an accepted and essential adjunct imaging modality for prenatal diagnosis. Not only does fetal MRI provide additional information useful in patient counseling and management, it also helps determine mode of delivery, location of delivery (community versus tertiary center, labor and delivery room versus operating room), multidisciplinary involvement (pre-, peri-, and postnatal), and decisions regarding fetal intervention. These issues include in utero procedures as well as requirement for airway establishment during delivery.

The fetal MRI examination is conducted to evaluate the fetus within the gravid uterus. Detailed analysis is performed, including placental location, cervical length, amniotic fluid volume, placental cord insertion, and fetal anatomic evaluation. Imaging may be focused on a specific region of interest, but the entire fetus is typically evaluated. Imaging begins with a triplanar scout sequence (axial, coronal, and sagittal to the mother), followed by three-plane orthogonal

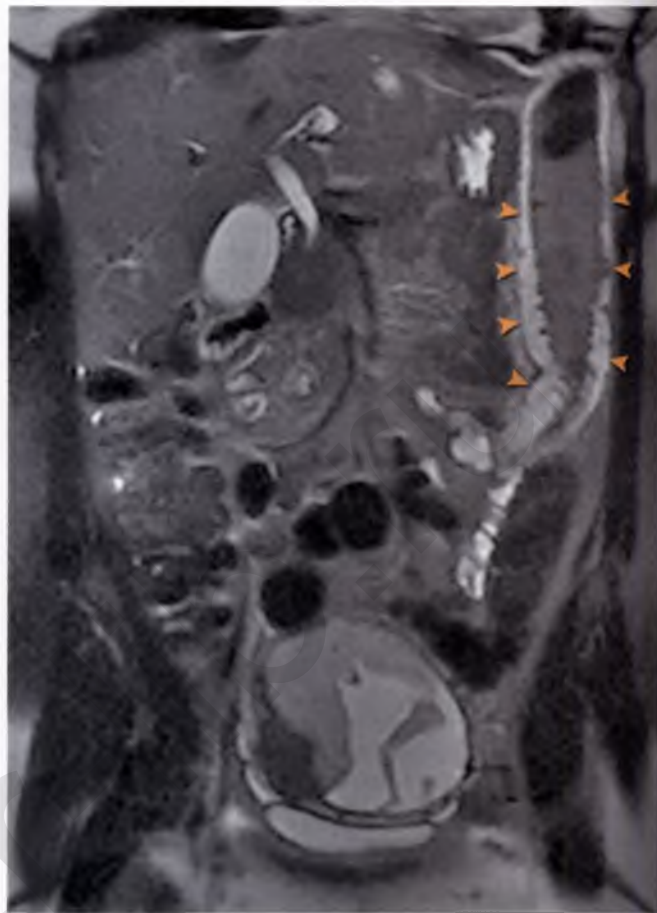


**FIG 23-3** Community-acquired *Clostridium difficile* colitis at 16 weeks' gestation with severe crampy lower abdominal pain. Coronal T2-weighted imaging with fat saturation demonstrates diffuse descending colonic wall thickening (arrowheads).

imaging of normal and pathologic fetal anatomy. Multiplanar T2-weighted images, as noted earlier, are the mainstay of fetal imaging sequences with bSSFP, T1-weighted images, DWI, and other acquisitions applied, depending upon clinical circumstances.

## Anomalies of the Central Nervous System

In 1997, Levine and colleagues reported the utility of MRI as an adjunctive modality for CNS anomalies suspected at ultrasound examination (Fig. 23-5). MRI not only corroborated ultrasound findings but also demonstrated additional findings that could alter patient counseling and management.<sup>21</sup> The goal of MRI is to perform an anatomic survey documenting normal intracranial structures and to identify and characterize abnormalities in order to provide a comprehensive, precise diagnosis. In a study evaluating the utility of MRI with respect to gestational age, it was found that if an MRI examination was performed prior to 24 weeks' gestational age, decisions influenced the continuation or termination of a pregnancy, particularly in the United States. Management decisions that occurred if an MRI examination was performed after 24 weeks of gestation were those relating to delivery location, mode of delivery, and postnatal care.<sup>22</sup> Major CNS indications for referral to fetal MRI include ventriculomegaly, midline defects, posterior fossa abnormalities, and neural tube defects. Additional indications include, but are not limited to, cortical abnormalities, encephaloclastic abnormalities, cystic masses, and tumors (Table 23-1).

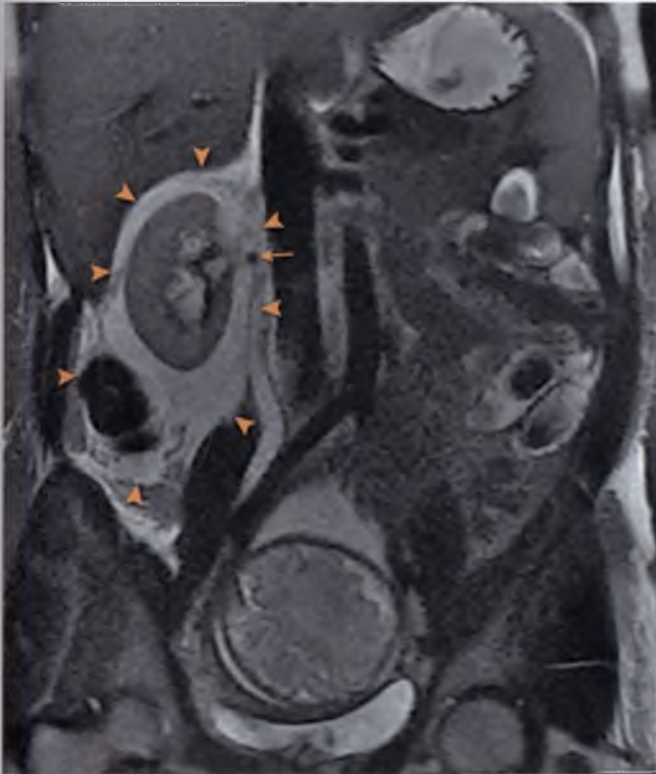


**FIG 23-4** Forniceal rupture at 32 weeks' gestation. Coronal T2-weighted imaging with fat saturation demonstrates an obstructing right ureteropelvic junction (UPJ) calculus (*arrow*) with large amount of retroperitoneal perinephric fluid (*arrowheads*). In addition, the right ureter distal to the calculus is dilated, related to the gravid state.

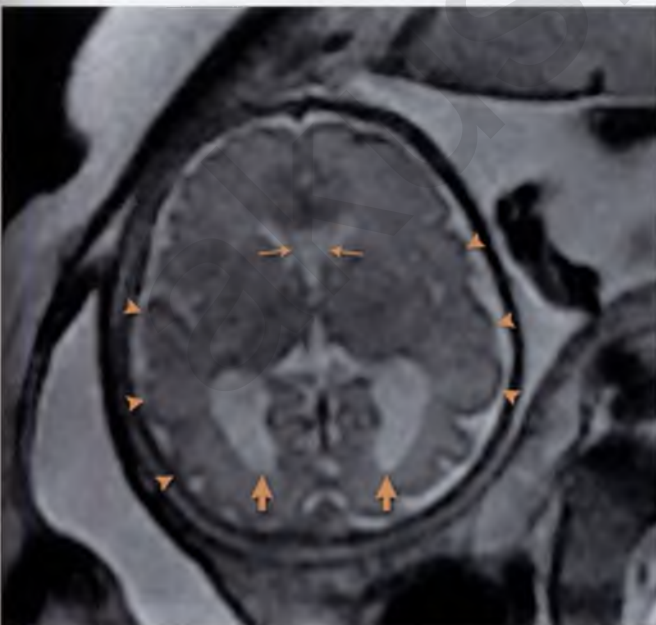


**FIG 23-5** Normal fetal brain at 34 weeks' gestation. Axial balanced steady-state image demonstrates normal lateral ventricles (*bold arrows*), cavum septum pellucidum (*small arrows*), and cortical sulci (*arrowheads*).

### TABLE 23-1 Summary of Fetal Magnetic Resonance Imaging Indications

#### Brain and Spine

Congenital anomalies of the brain suspected or not adequately assessed by sonography

- Ventriculomegaly
- Agenesis of the corpus callosum
- Holoprosencephaly
- Posterior fossa anomaly
- Cerebral cortical malformations

Vascular abnormalities of the brain suspected or not adequately assessed by sonography

- Vascular malformations
- Hydranencephaly
- Infarction
- Monochorionic twin pregnancy complications

Congenital anomalies of the spine suspected or not adequately assessed by sonography

- Neural tube defect
- Sacrococcygeal teratoma
- Caudal regression/sacral agenesis
- Sirenomelia
- Vertebral anomaly

#### Skull, Face, and Neck

Masses of the face and neck suspected or not adequately assessed by sonography

- Venolymphatic malformation
- Hemangioma
- Goiter
- Teratoma
- Micrognathia

#### Thorax

Masses in the thorax suspected or not adequately assessed by sonography

- Congenital pulmonary airway malformations (including congenital cystic adenomatoid malformation, pulmonary sequestration, and congenital lobar emphysema)
- Congenital diaphragmatic hernia
- Laryngeal obstruction

Volumetric assessment of fetal lung parenchyma, particularly in fetuses at risk for pulmonary hypoplasia secondary to oligohydramnios, chest mass, or skeletal dysplasia

#### Abdomen, Retroperitoneum, and Pelvis

Abdominal or pelvic mass suspected or not adequately assessed by sonography

- Abdominopelvic cyst
- Tumors such as hemangiomas, neuroblastomas, sacrococcygeal teratomas, and suprarenal or renal masses
- Complex genitourinary anomalies, including cloacal malformation
- Renal anomalies, particularly those associated with severe oligohydramnios
- Bowel anomalies such as megacystis microcolon

#### Complications of Monochorionic Twins Fetal Surgery Assessment

Modified from American College of Radiology (ACR) and the Society for Pediatric Radiology (SPR): ACR-SPR Practice Parameter for the Safe and Optimal Performance of Fetal Magnetic Resonance Imaging (MRI). 2014. Available at <http://www.acr.org/guidelines>.



Ventriculomegaly is defined as dilatation of the lateral ventricle greater than 10 mm at the level of the atria and is one of the most common indications for fetal MRI. Ventriculomegaly may be isolated or may be associated with an underlying cause including obstruction from congenital aqueductal stenosis, dysmorphic appearance such as agenesis of the corpus callosum, intracranial hemorrhage, or syndromal ventriculomegaly, as part of a complex malformation<sup>23</sup> (Fig. 23-6). MRI has been shown to be useful in fetuses with ventriculomegaly, allowing for assessment of degree of enlargement, search for underlying cause, and presence/absence of additional findings<sup>22,24</sup> (Fig. 23-7). Because the prognosis is related to the presence of additional abnormalities,<sup>25</sup> prenatal detection of associated anomalies is essential. Sonographically occult findings can include agenesis of the corpus callosum, cortical malformations, cerebellar abnormalities, and destructive changes.<sup>26</sup>

Corpus callosal agenesis is a disorder of prosencephalic midline development.<sup>27</sup> The corpus callosum can be visualized on midline sagittal MRI after 20 weeks' gestational age. Fetal MRI has been able to delineate a normal corpus callosum in 20% of cases referred for suspected callosal agenesis and has detected occult abnormalities including gyral abnormalities, posterior fossa abnormalities, brainstem anomalies, and periventricular nodular heterotopia in up to 63% of cases<sup>28</sup> (Figs. 23-8 and 23-9).

Holoprosencephaly is a complex anomaly of the prosencephalon manifested by lack of cleavage of midline structures. This malformation is classified into subtypes representing a continuum of midline nonseparation. In decreasing order of severity, they include alobar, semilobar, lobar, and middle interhemispheric variant types of holoprosencephalies<sup>29</sup> (Figs. 23-10 and 23-11).

Fetal MRI can help distinguish an abnormal from a normal posterior fossa and can aid in determining true defects from normal variants. Prognosis and neurodevelopmental outcome depend on the

degree of vermian dysplasia and presence of additional supratentorial anomalies (Figs. 23-12 and 23-13). Diagnoses of Dandy-Walker malformation, vermian agenesis, and brainstem anomalies portend a poor prognosis; cerebellar hypoplasia is associated with an uncertain prognosis; and mega cisterna magna, Blake pouch cyst, and retrocerebellar arachnoid cyst are associated with a good neurologic prognosis<sup>30,31</sup> (Fig. 23-14).

Although neural tube defects such as myelomeningocele are easily visualized and diagnosed on ultrasound imaging, MRI can depict degree of cerebellar herniation and ventriculomegaly and the level and length of dysraphic defect and can detect associated anomalies including callosal agenesis, cerebellar dysplasia, spinal cord abnormalities (split cord malformation), and masses<sup>32</sup> (Fig. 23-15). In a study following the outcomes of 36 fetuses with spina bifida, it was found that worsening cerebellar herniation on MRI was significantly associated with childhood seizure activity, high risk of bladder dysfunction, and lack of independent ambulation, which are findings important for prenatal counseling.<sup>33</sup>

Disorders of cortical formation are an important cause of developmental delay and epilepsy. Malformations can occur at different stages of cortical maturation, resulting in abnormalities that reflect the time of insult. Recognition of normal cortical development as well as abnormal morphologic features is essential for accurate diagnosis. These abnormalities include microcephaly, hemimegalencephaly, lissencephaly, heterotopias, polymicrogyria, and schizencephaly<sup>34,35</sup> (Figs. 23-16 through 23-18). Glenn and associates reported a high degree of accuracy for diagnosis of polymicrogyria and schizencephaly by fetal MRI, with 100% specificity achieved for polymicrogyria, schizencephaly, and heterotopia if malformation was identified, in later gestations, in at least two planes.<sup>36</sup>

When encephaloclastic changes of the fetal brain are seen, one must suspect acquired injury for which the primary cause is ischemia

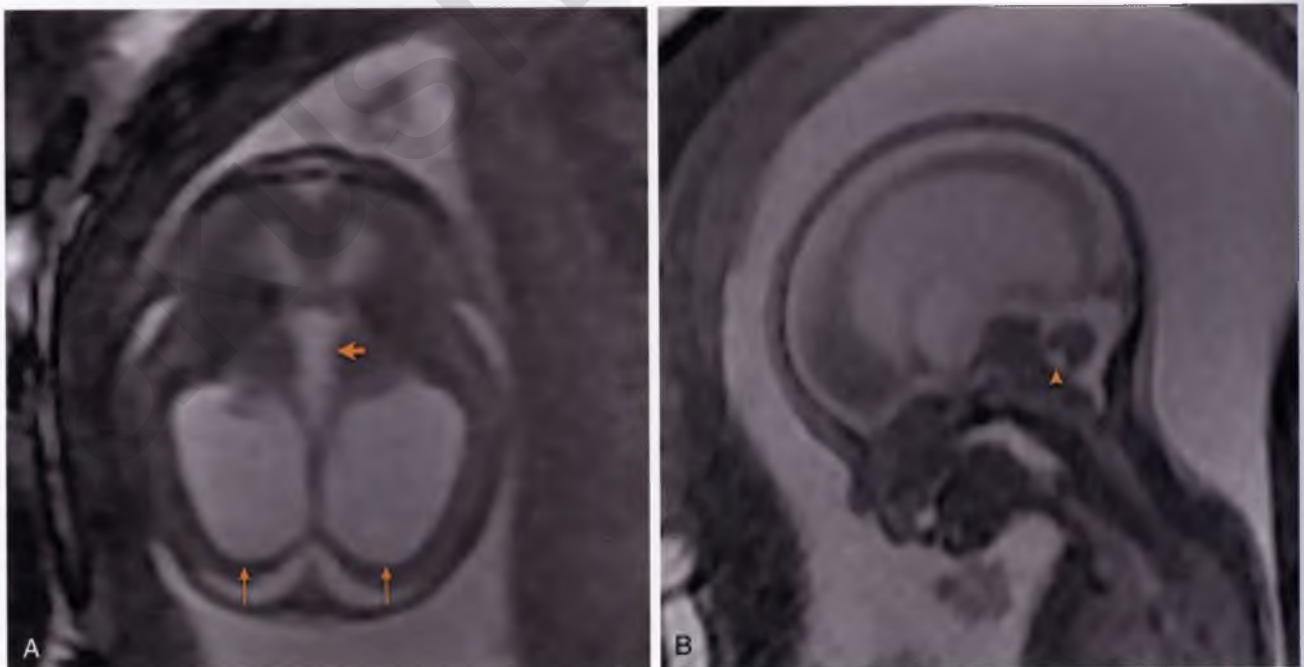


**FIG 23-6** Ventriculomegaly secondary to aqueductal stenosis at 20 weeks' gestation. Axial (**A**) and sagittal (**B**) balanced steady-state images demonstrate dilated lateral ventricles measuring 17 to 19 mm in diameter (small arrows), dilated third ventricle (bold arrow), and normal size fourth ventricle (arrowhead in B), consistent with aqueductal stenosis.

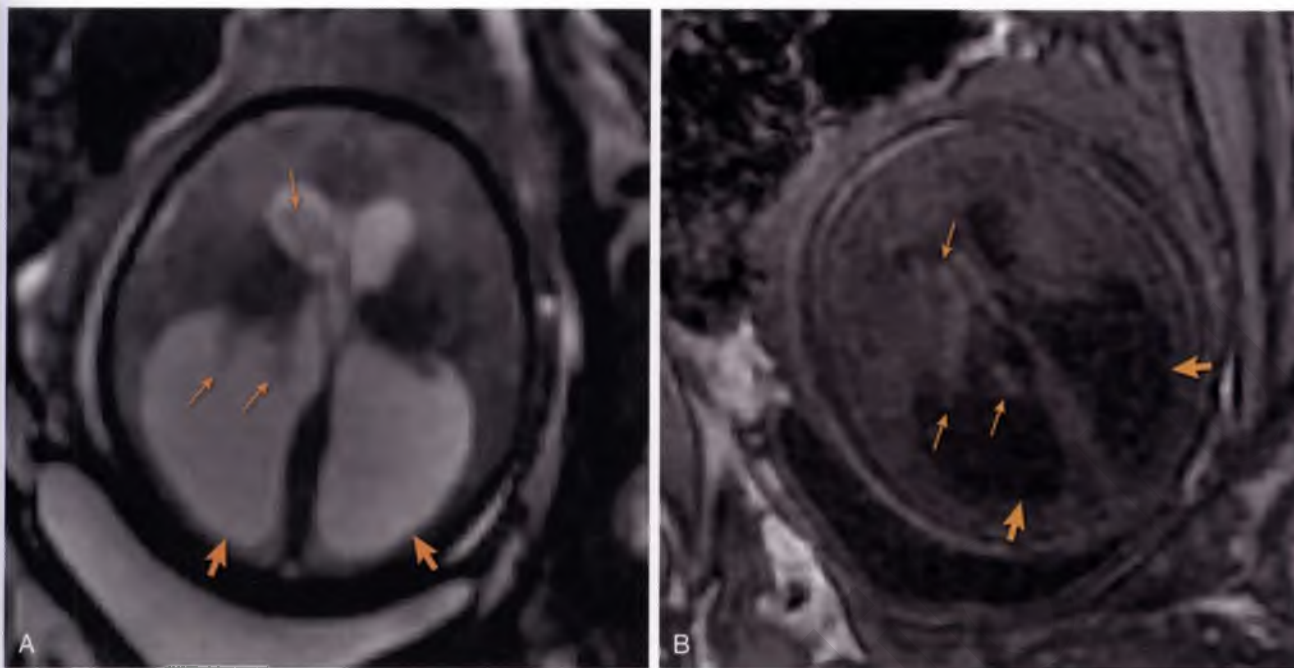


**FIG 23-7** Intracranial hemorrhage causing new-onset hydrocephalus at 34 weeks' gestation. **A**, Axial balanced steady-state image with dilated lateral ventricles (*bold arrows*) and thrombus shown in right lateral ventricle (*small arrows*). **B**, Axial T1-weighted imaging bright signal in right germinal matrix and in dilated right lateral ventricle (*small arrows*) consistent with hemorrhage.

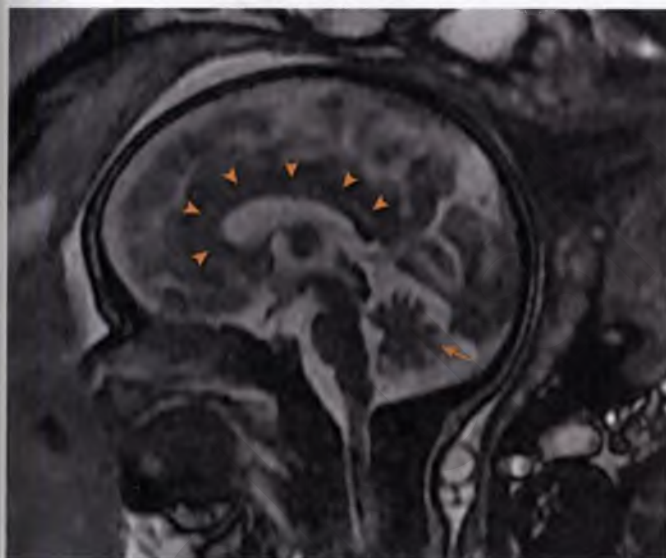


**FIG 23-8** Normal corpus callosum at 34 weeks' gestation. Sagittal balanced steady-state image demonstrates normal midline structures—corpus callosum (*arrowheads*), fourth ventricle, and cerebellar vermis (*arrow*).

(Fig. 23-19). The cause of fetal brain damage may include maternal, fetal, placental, infectious, toxic/metabolic, or mechanical/traumatic conditions (Fig. 23-20). Fetal MRI demonstrates not only chronic structural encephaloclastic changes, including ventriculomegaly, parenchymal defects, porencephaly, and volume loss, but also acute changes such as recent hemorrhage and ischemia (Fig. 23-21). The workup can be extensive and includes searching for an underlying cause.<sup>37,38</sup>

Differential diagnosis of intracranial cystic lesions includes primary arachnoid cysts; encephaloclastic lesions resulting from hemorrhage, trauma, or infection; gliopendymal cysts; schizencephaly; and cystic neoplasms. Arachnoid cysts are composed of a fibrous connective tissue wall, whereas gliopendymal cysts have an ependymal lining. The prognosis of fetuses with an arachnoid cyst depends on the presence or absence of associated intracranial anomalies and aneuploidy.<sup>39</sup> It is important to recognize normal fetal anatomy and not mistake enlargement of the cavum septum pellucidum, cavum vergae, or cavum velum interpositum for pathologic cysts<sup>40-42</sup> (Fig. 23-22).

### Anomalies of the Face, Neck, and Thorax

The EXIT procedure is performed to secure the airway in a fetus with airway obstruction. During the EXIT procedure, the fetal head is partially delivered through a cesarean incision while remaining attached via the umbilical cord to the placental circulation, during which time a fetal airway is established. The key tenet of the EXIT procedure is maintenance of uterine relaxation and uterine volume to prevent placental detachment and preserve uteroplacental blood flow. Once the airway is established and ventilation can be performed, the umbilical cord is clamped and cut and the infant is fully delivered. The EXIT procedure, as described, is referred to as the EXIT-to-airway procedure. Additional indications have led to adjunct procedures, including EXIT-to-resection, EXIT-to-ECMO (extracorporeal membrane oxygenation), and EXIT-to-separation procedures.<sup>43</sup> With sonographically suspected airway obstruction, MRI is particularly helpful in defining the presence or absence of free egress of amniotic fluid into the hypopharynx and bright signal of fluid in the trachea.

The two most common giant neck masses are cystic lymphangiomas (also known as *lymphovenous malformations*) and teratomas (Fig. 23-23). Cystic lymphangiomas present as septated, fluid-filled masses. They are most commonly posterolateral in location. Cervicofacial teratomas are typically anterior, large, and bulky, with cystic and solid

*Text continued on p. 761*



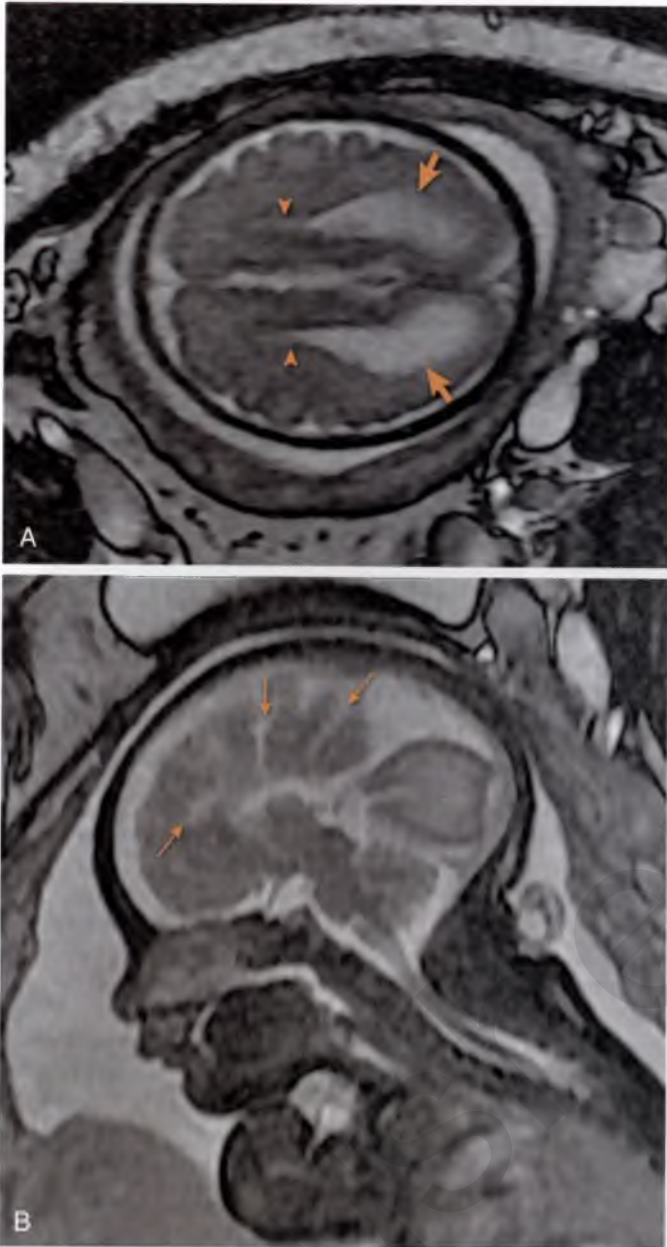


**FIG 23-9** Agenesis of the corpus callosum at 31 weeks' gestation. Axial (**A**) and sagittal (**B**) balanced steady-state images demonstrate wide separation of the frontal horns of the lateral ventricles (*arrowheads*) and colpocephaly (*bold arrows*), sometimes referred to as the *teardrop appearance* with radial orientation of the gyri (*small arrows*).

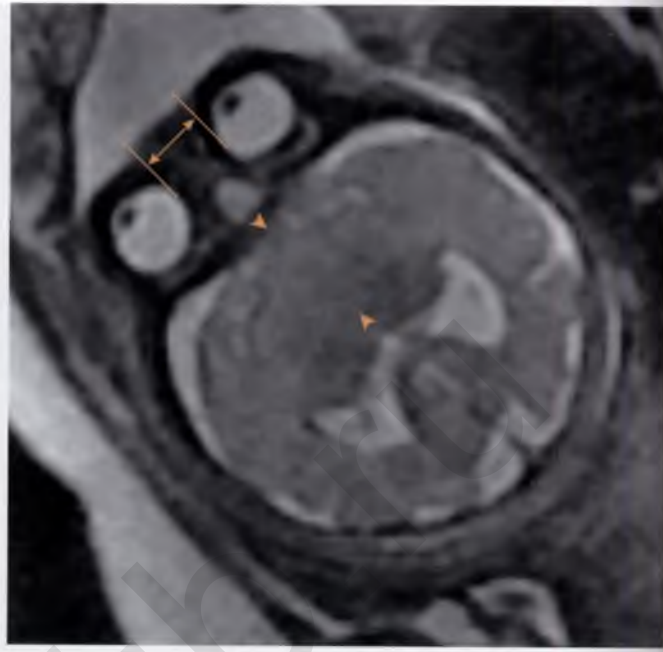


**FIG 23-10** Semilobar holoprosencephaly at 36.5 weeks' gestation. Oblique axial balanced steady-state image demonstrates interdigitation (*arrowheads*) of the cortex of the frontal lobes, absent anterior horns of the lateral ventricles (*double-headed arrow*), and subtle hypotelorism (*double-headed arrow*), consistent with semilobar holoprosencephaly.

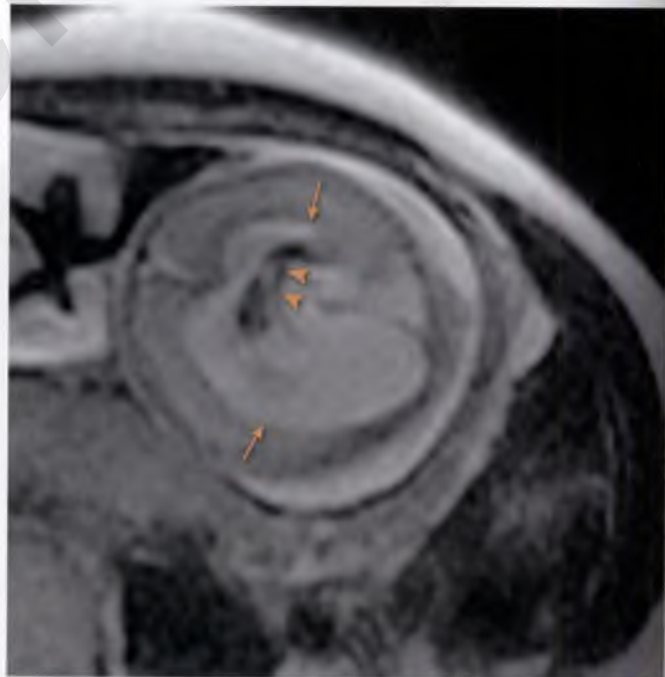


**FIG 23-11** Holoprosencephaly spectrum at 23.5 weeks' gestation. Axial T2-weighted imaging demonstrates bilateral ventriculomegaly (*arrows*) and flow void artifact across the midline (*arrowheads*) confirming communication of the ventricles, with falx present anteriorly and posteriorly.

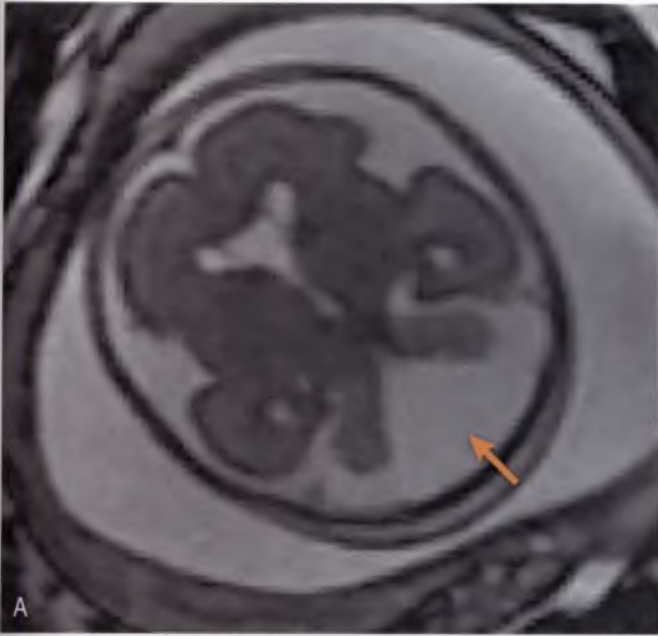


**FIG 23-12** Dandy-Walker malformation at 24.5 weeks' gestation. Axial (**A**) and sagittal (**B**) balanced steady-state images demonstrate the fourth ventricle communicating with cisterna magna (*arrow*), and marked hypoplastic, raised vermis (*arrowhead*) with tentorial elevation.

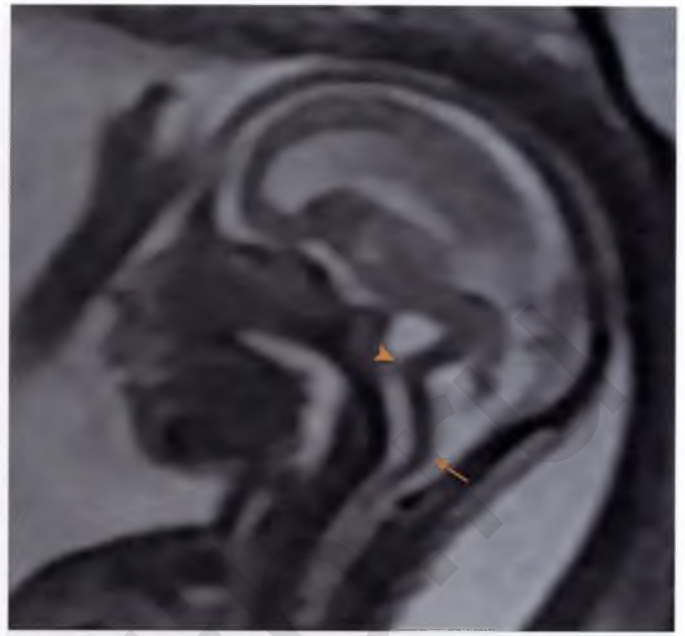


**FIG 23-13** Pontocerebellar hypoplasia at 20 weeks' gestation. Sagittal balanced steady-state image demonstrates abnormally thin brainstem, hypoplastic pons, anterior kinking of the brainstem at the level of the fourth ventricle (*arrowhead*), and posterior kinking at the pontomesencephalic junction (*arrow*), consistent with pontocerebellar hypoplasia.

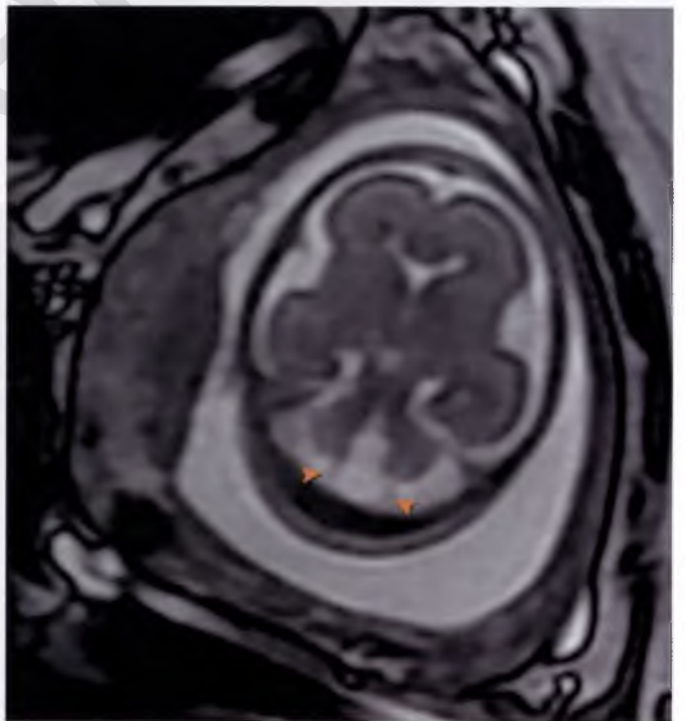


**FIG 23-14** Blake pouch cyst at 23 weeks' gestation. Axial balanced steady-state image demonstrates retrocerebellar cystic lesion with a limiting membrane ballooning out from the fourth ventricle consistent with a Blake pouch cyst (*arrowheads*). Postnatal magnetic resonance findings were normal.



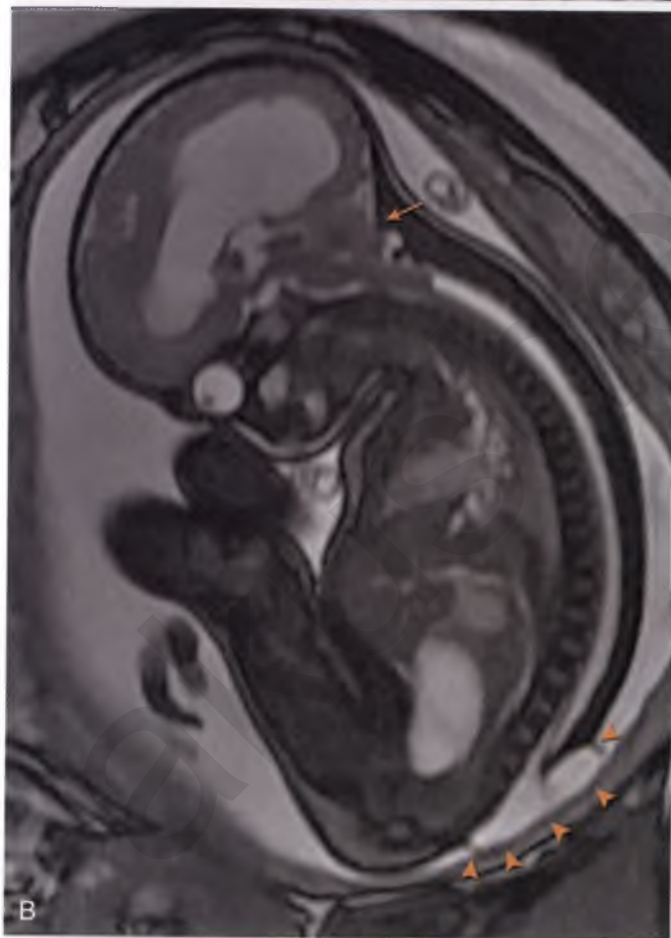
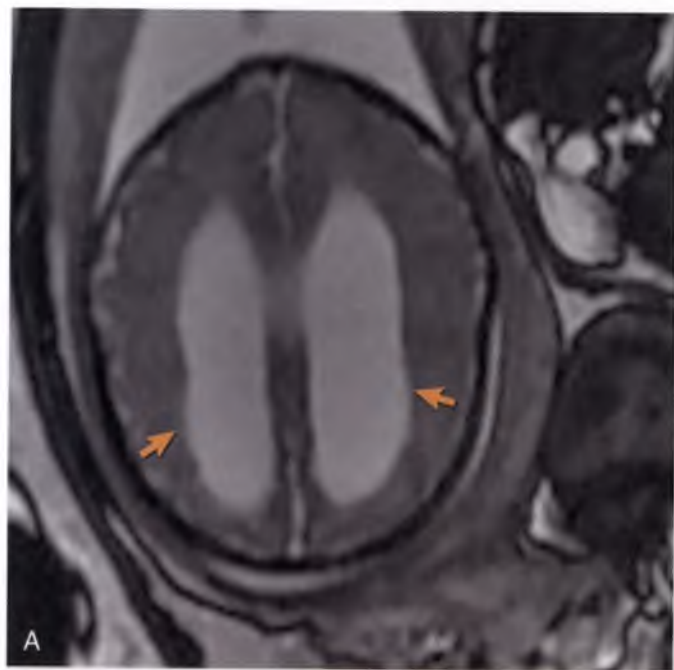


**FIG 23-15** Chiari II malformation at 32 weeks' gestation. Axial (**A**) and sagittal (**B**) balanced steady-state images demonstrate ventriculomegaly (*bold arrows*), downward herniation of cerebellar tonsils (*small arrow*), spina bifida defect with tethered cord, and lumbosacral myelomeningocele (*arrowheads*).

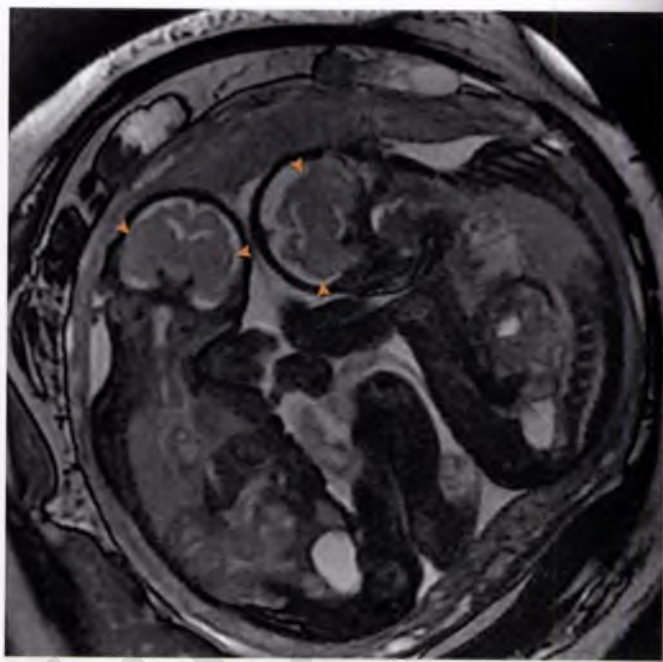


**FIG 23-16** Abnormal cortical formation at 29 weeks in monozygotic twin gestation. Coronal balanced steady-state image demonstrates abnormal sulcation (*arrowheads*), difficult to detect by ultrasound imaging. Head measurements were markedly small, consistent with microcephaly.

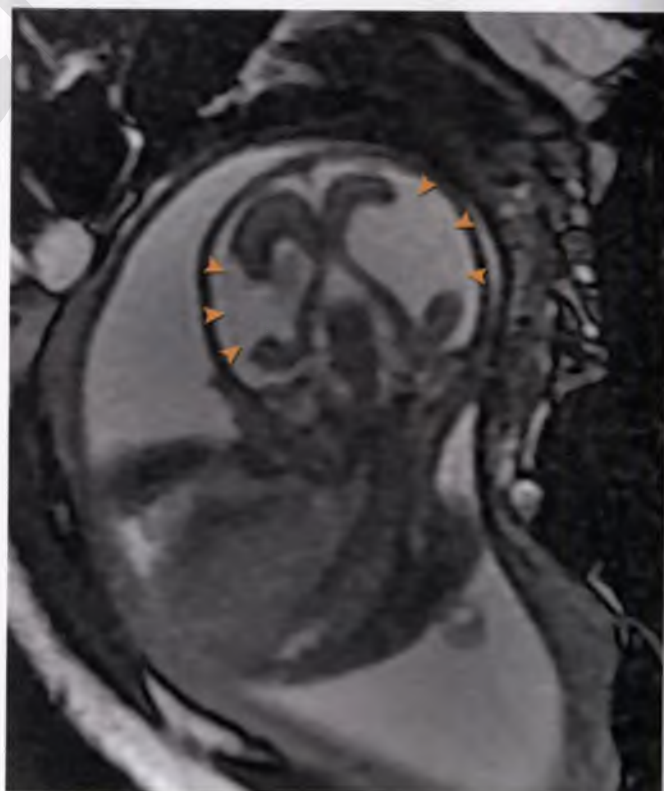


**FIG 23-17** Bilateral open lip schizencephaly at 21.5 weeks' gestation. Coronal balanced steady-state image demonstrates large bilateral schizencephalic defects (*arrowheads*) lined with gray matter.

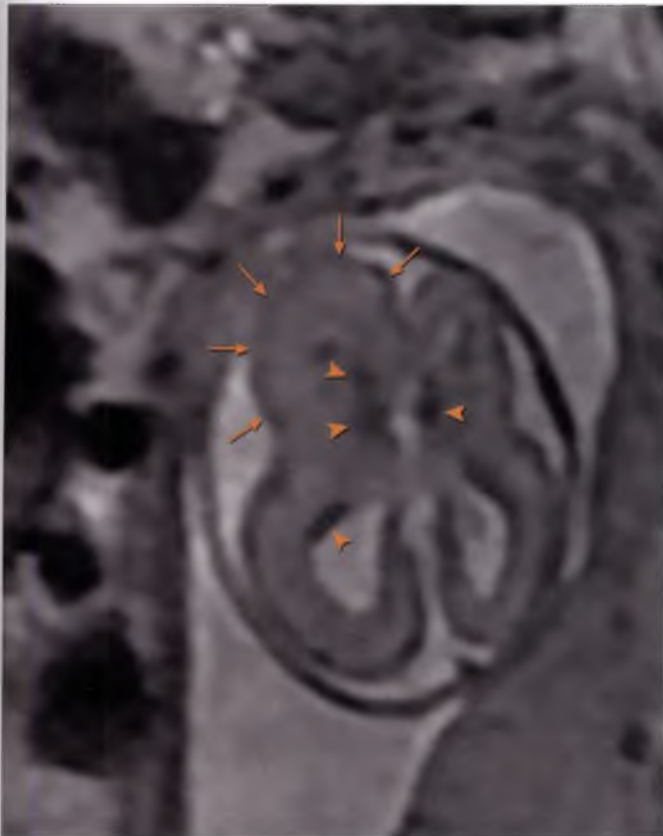


**FIG 23-18** Hemimegalencephaly at 19.5 weeks' gestation in a patient referred for ventriculomegaly. Axial T2-weighted imaging demonstrates asymmetric cerebral hemispheres, with increased cortical thickness (arrows) and pachygyria involving the right cerebral hemisphere. The right lateral ventricle is mildly dilated and there are multiple subependymal and cortical low signal intensity foci (arrowheads).

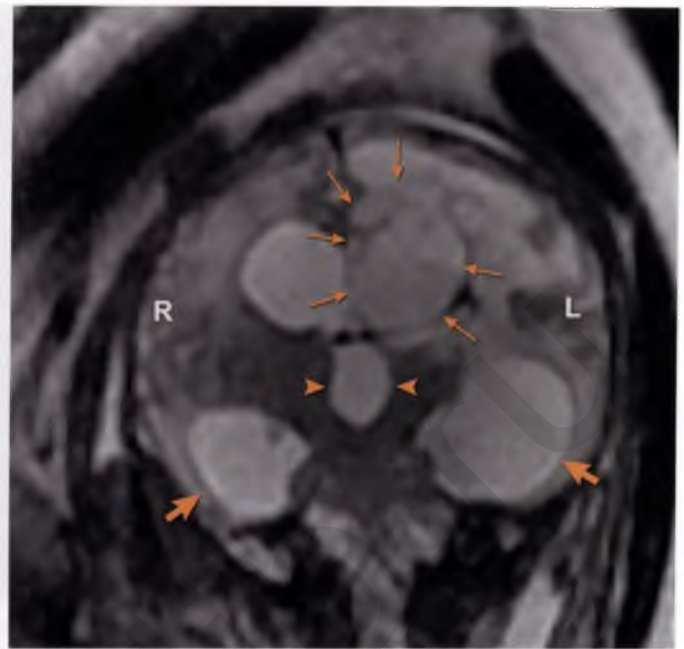


**FIG 23-19** Grade IV hemorrhage with encephaloclastic changes at 35 weeks' gestation. Coronal balanced steady-state image demonstrates left germinal matrix hemorrhage with extension into the left lateral ventricle. There is intraventricular clot (small arrows), marked ventriculomegaly (bold arrows), and enlarged third ventricle (arrowheads). Loss of cerebral cortex in the bilateral, left (L) greater than right (R), hemispheres, consistent with infarcts and encephalomalacia noted involving the left cortex.

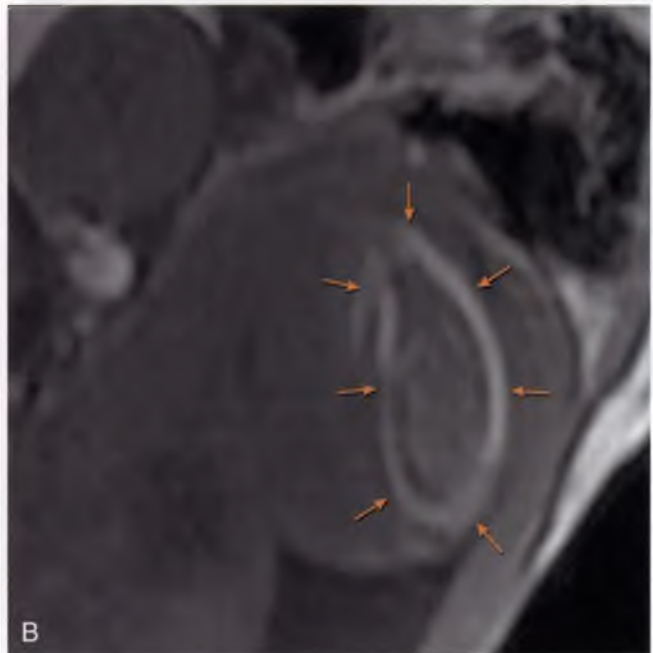


**FIG 23-20** **A** and **B**, Large intracranial hemorrhage at 21 weeks' gestation in a patient with cytomegalovirus infection. Axial balanced steady-state image (**A**) and T1-weighted imaging (**B**) demonstrate large hematoma (arrows) compressing the lateral ventricle.



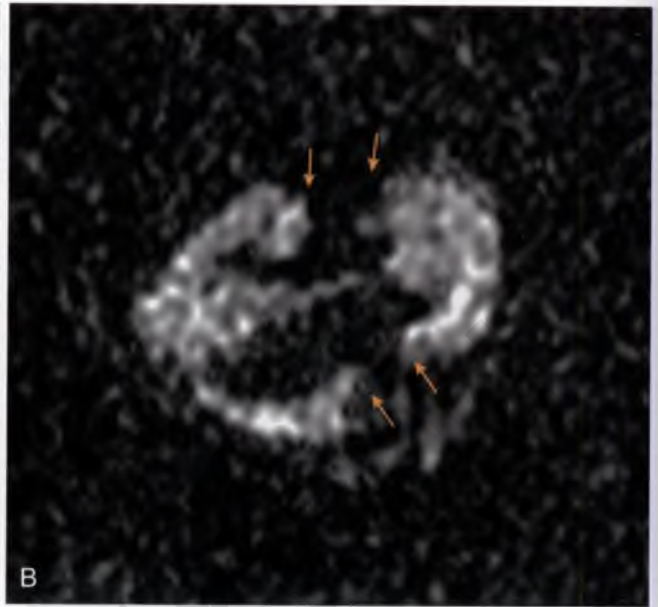
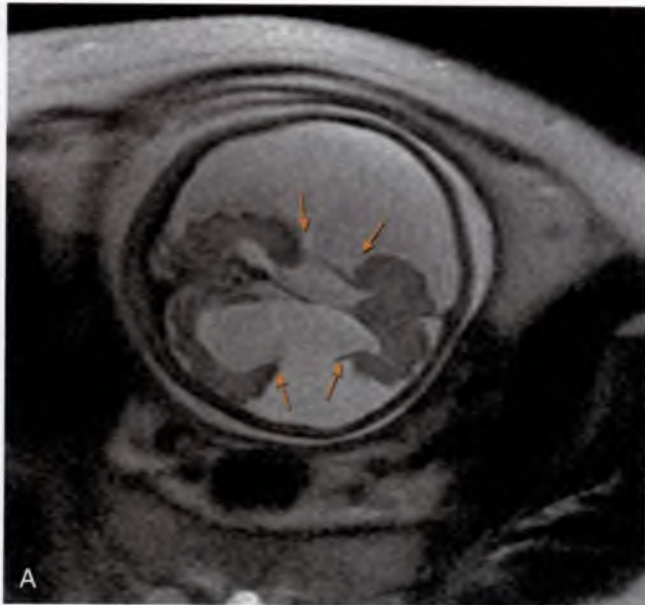


**FIG 23-21** Schizencephaly, cerebral volume loss, and diffuse restricted diffusion at 33 weeks' gestation in a fetus with hypoplastic left side of heart. **A**, Note generous extra-axial fluid collections bilaterally, secondary to parenchymal volume loss with bilateral open lip schizencephaly (*arrows*). **B**, Diffusion-weighted imaging shows global restriction, consistent with diffuse ischemia.

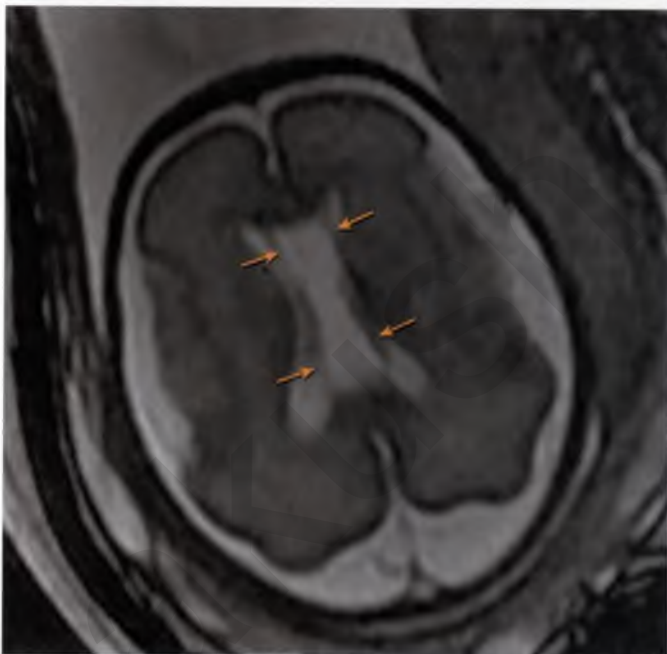


**FIG 23-22** Cavum septum pellucidum et vergae at 24.5 weeks' gestation in a patient referred for suspicion of a dilated third ventricle. Axial balanced steady-state image demonstrates fluid separating the leaflets of the septum pellucidum (*arrows*), with posterior extension to the splenium of the corpus callosum.

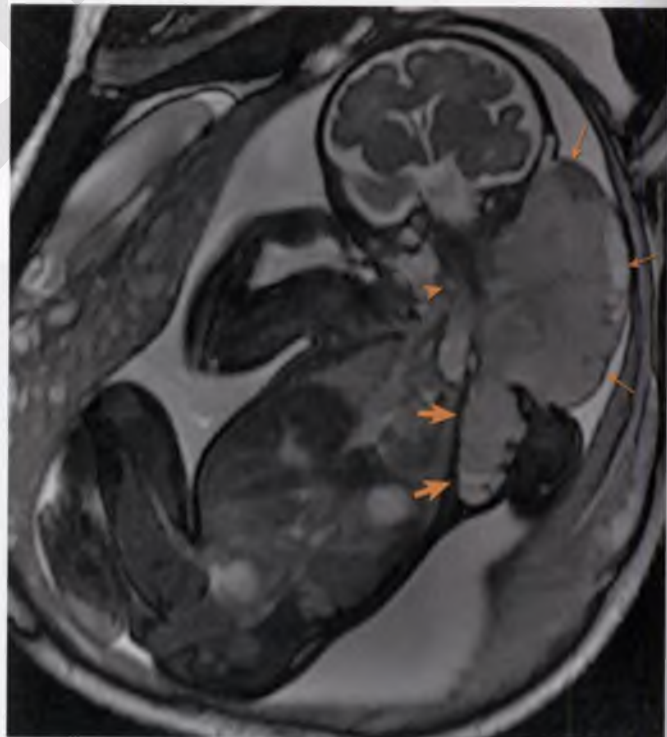


**FIG 23-23** Venolymphatic malformation at 31 weeks' gestation. Coronal balanced steady-state image demonstrates extensive multi-loculated neck mass (*arrows*) with subcutaneous and deep muscular tissue involvement, extending cephalad to the skull base and periauricular region, medially involving the retropharynx (*arrowhead*) and prevertebral and paravertebral spaces, and caudally to the shoulder joint and thoracic inlet (*bold arrows*). The airway was compressed but patent.

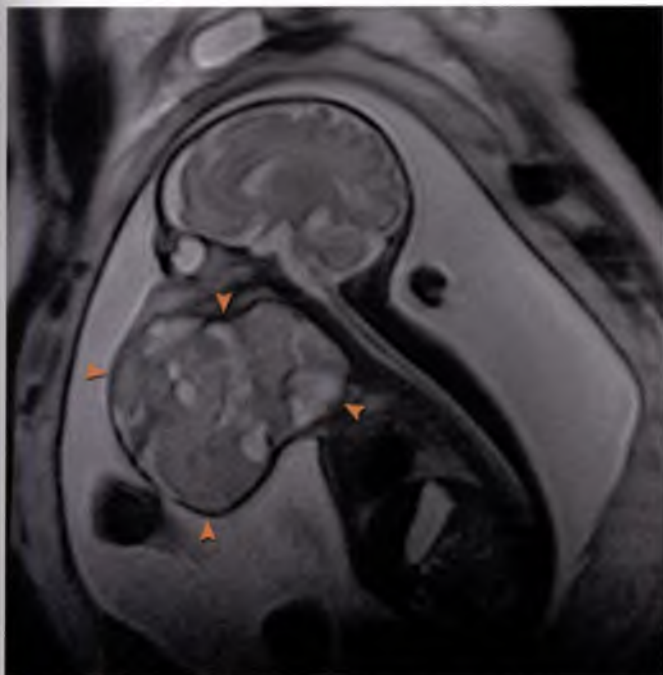


**FIG 23-24** Large oropharyngeal teratoma at 32 weeks' gestation. Sagittal T2-weighted imaging demonstrates a mixed cystic and solid mass (arrowheads) involving the mandible, maxilla, and oropharynx with airway obstruction, necessitating an EXIT (ex utero intrapartum treatment) procedure at delivery.

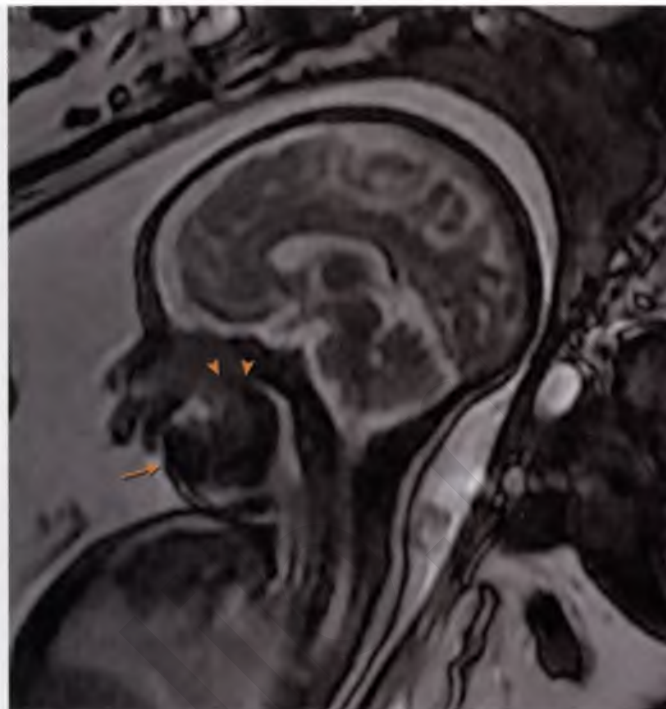


**FIG 23-25** Pierre Robin syndrome at 37 weeks' gestation. Sagittal balanced steady-state image demonstrates retrognathia and micrognathia (arrow) and isolated cleft palate (arrowheads). Polyhydramnios was also present.

elements (Fig. 23-24). Epignathus teratomas arise from the hard or soft palate and present as a fungating mass extending out of the oral cavity.

Micrognathia, characterized by mandibular hypoplasia and a small chin, is a feature of several congenital syndromes (Fig. 23-25). If severe micrognathia is seen in association with polyhydramnios and an absent stomach, sagittal MR images may be useful in demonstrating not only micrognathia but also glossoptosis, retroposition of the tongue, and abnormal positioning of the glottis, with resultant airway obstruction.

Tracheolaryngeal airway obstruction is life threatening, with a reported mortality rate of 80% to 100% if unrecognized prior to delivery. Causes may be intrinsic, including tracheolaryngeal web or atresia, or extrinsic due to tumor or vascular ring. Obstruction of the airway leads to hyperexpanded lungs, flattened/everted hemidiaphragms, fetal hydrops, and ascites, a constellation of findings known as congenital high airway obstruction syndrome (CHAOS)<sup>44</sup> (Fig. 23-26).

MRI has altered the approach to the fetus with a cervicofacial anomaly. In utero detection of airway obstruction can allow for planning of an EXIT procedure in fetuses diagnosed with giant neck masses, severe micrognathia, or tracheolaryngeal obstruction, thereby avoiding neonatal hypoxia and asphyxia.<sup>45,46</sup> Mortality rate in infants undergoing EXIT is reported at 8%, whereas the rate in those treated without EXIT with similar diagnoses ranges from 10% to 57%. Without EXIT, there may be increased neonatal morbidity and developmental delay due to hypoxia.<sup>47</sup> Additionally, MRI can detect the site of fetal tracheolaryngeal obstruction in CHAOS, allowing for more effective airway establishment.<sup>45,48</sup>

The presence of polyhydramnios and nonvisualization of the stomach bubble suggest esophageal atresia, although these signs are nonspecific and have been reported in normal fetuses, along with a

wide variety of conditions, including CNS, tracheopharyngeal, thoracic, and neuromuscular abnormalities; congenital heart disease; aneuploidies; twins; and diabetes.<sup>49</sup> MRI has correctly identified the presence or absence of esophageal atresia based on the observation of a dilated esophageal pouch as a positive predictor<sup>50</sup> (Fig. 23-27).

The use of dynamic cine MRI performed in the sagittal plane can be useful in documenting isolated cleft palate,<sup>51</sup> assessing foregut duplication cyst of the tongue and determining airway patency,<sup>52</sup> and visualizing a blind-ending, dilated esophageal pouch during swallowing to reach a reliable diagnosis of esophageal atresia.<sup>53</sup>

Congenital diaphragmatic hernia (CDH) is the principal indication for fetal thoracic MRI. Numerous articles have compared ultrasound imaging with MRI in predicting outcomes and survival in fetuses with CDH based on calculation of lung volume and degree of liver herniation, the major prognostic factors in the setting of CDH, as postnatal morbidity and death are primarily due to pulmonary hypoplasia and pulmonary hypertension.<sup>54-60</sup> MRI can depict herniated intrathoracic contents in a fetus with CDH. Liver is well demarcated on T1-weighted images, and discrimination of large versus small bowel can be performed because of T1 bright appearance of meconium in large bowel<sup>13</sup> (Fig. 23-28).

Congenital lung lesions encompass a spectrum of abnormalities, including congenital pulmonary airway malformation (CPAM), bronchopulmonary sequestration (BPS), and congenital lobar overinflation (CLO). CPAMs account for approximately one half of all lesions and contain either macrocystic or microcystic components (Fig. 23-29). Blood supply to a CPAM is via the pulmonary artery and vein. BPS accounts for approximately one third of lesions and consists of non-functioning bronchopulmonary tissue with systemic arterial blood supply. The majority of BPSs are supradiaphragmatic (85%-90%), with 10% to 15% found in an infradiaphragmatic location. Of all BPS



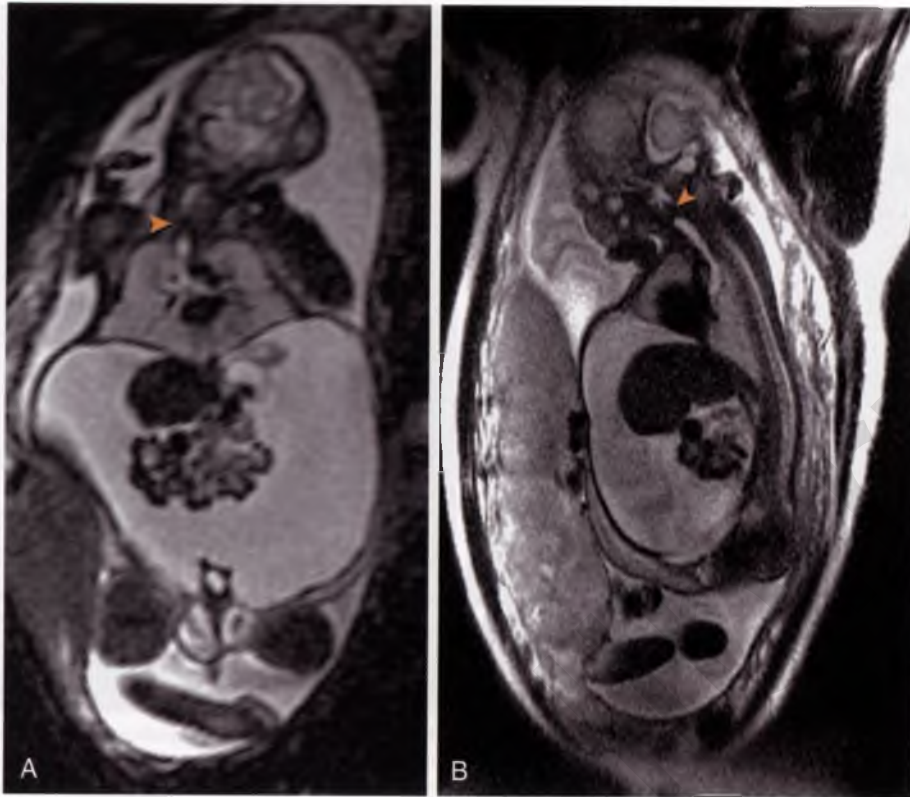


**FIG 23-26** Congenital high airway obstruction syndrome (CHAOS) at 23 weeks' gestation. T2-weighted coronal (A) and sagittal (B) images demonstrate bright lungs, bell-shaped thorax, and large volume of ascites. The dilated fluid-filled trachea can be seen distal to the laryngeal obstruction (*arrowhead*).



**FIG 23-27** Esophageal atresia at 34 weeks' gestation. Coronal balanced steady-state image demonstrates blind-ending, dilated, tubular, fluid-filled structure consistent with dilated esophagus (*arrow*).

masses, three fourths will be hybrid lesions, with components of both CPAM and sequestration. CLO results from bronchial obstruction of a main or lobar bronchus, either from mucous plug or extrinsic compression due to vessel or mass (Fig. 23-30). Macrocystic CPAMs tend to be more heterogeneous, multilocular, and cystic in appearance with architectural distortion (see Fig. 23-29). Microcystic CPAMs are homogeneous but also demonstrate architectural distortion. BPS lesions appear homogeneous, without architectural distortion and, if a feeding vessel is visualized, can be diagnosed with confidence. Hybrid lesions demonstrate features common to both CPAM and BPS. CLO appears uniformly hyperintense on T2-weighted imaging secondary to fluid overdistention of pulmonary segments and lobes.<sup>61-63</sup> MRI plays a complementary role to ultrasound imaging, confirming or providing alternate diagnoses.

### Abnormalities in the Fetal Abdomen

Abnormalities in the fetal abdomen are an infrequent indication for MRI evaluation. Fetal abdominal disease encompasses abnormalities of the hepatobiliary system, gastrointestinal tract, genitourinary tract, and abdominopelvic masses.

Hyperintense T1 signal within bowel loops can indicate the presence of meconium, which is usually seen in the distal ileum or colon. T2 hyperintense bowel dilatation usually indicates proximal small bowel dilatation, whereas T1 hyperintense bowel dilatation typically represents distal ileal or colonic obstruction<sup>64</sup> (Fig. 23-31). However, a 2010 study demonstrated proximal jejunal atresia in nine cases of suspected ileal atresia, revealing the imprecision of determining the exact site of obstruction by imaging.<sup>65</sup>

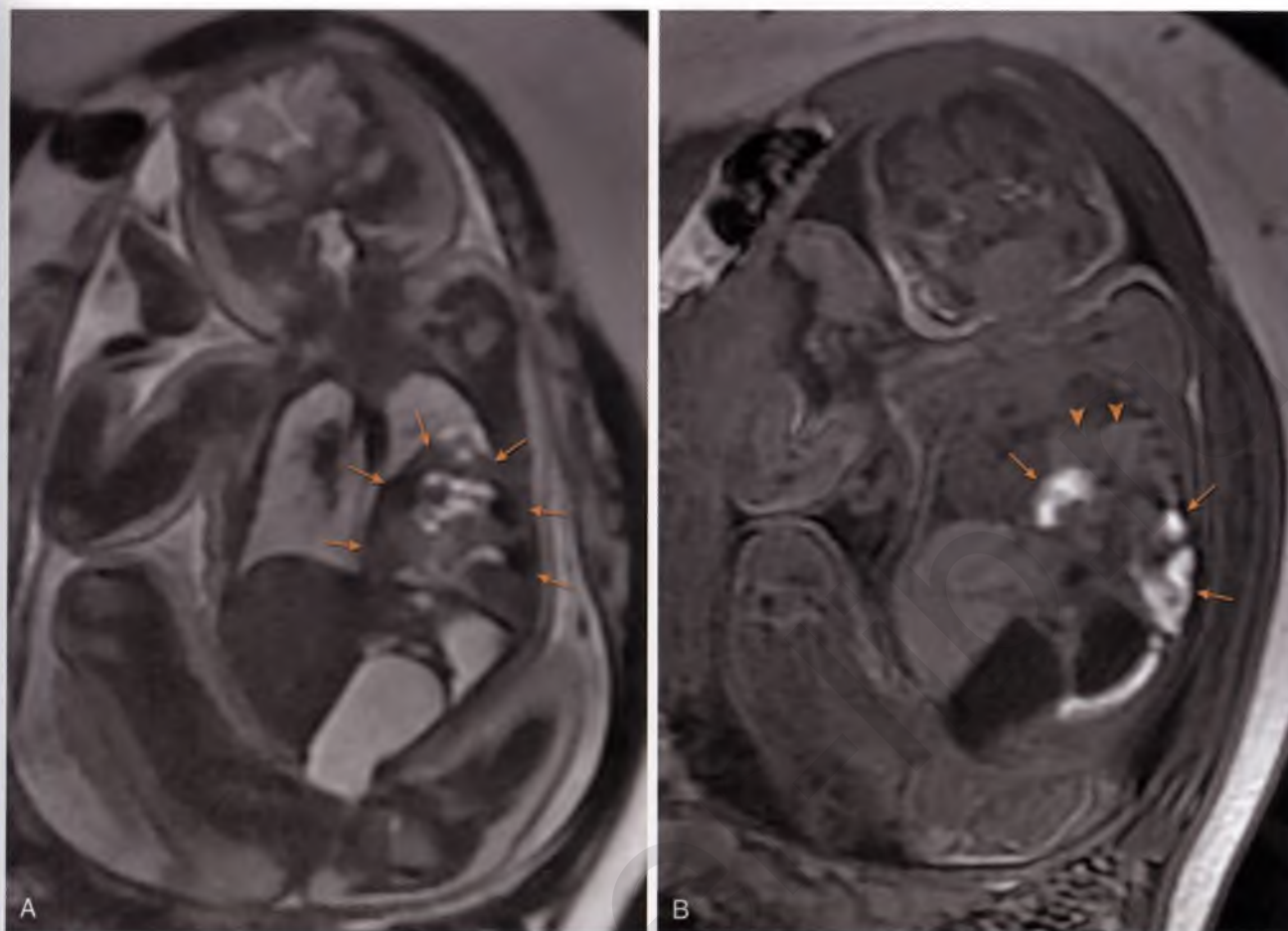


**FIG 23-28** Congenital diaphragmatic hernia (CDH) at 35.5 weeks' gestation. Coronal T2-weighted imaging (**A**) and T1-weighted imaging (**B**) demonstrate a large left-sided CDH (arrows) containing left lobe of liver and small and large bowel. The fluid-filled stomach is not herniated, located within the abdomen. T1-weighted imaging demonstrates herniated left lobe of liver (arrowheads) and large bowel segments containing high signal meconium (arrows).

Genitourinary anomalies are well demonstrated on MRI, and imaging is not hindered by oligohydramnios. Renal cystic disease, duplication of the collecting system, hydronephrosis, megacystis-microcolon-intestinal hypoperistalsis syndrome, and cloacal exstrophy with two characteristic hemibladders can be visualized by fetal MRI.<sup>66</sup>

Cystic masses within the abdominal cavity may be categorized according to location: upper abdominal, lower abdominal, and retroperitoneal. Most fetal abdominopelvic masses occur in the lower abdomen and are urogenital or gynecologic in origin, including ovarian cysts and hydrometrocolpos (Figs. 23-32 and 23-33). Upper abdominal cysts include choledochal, mesenteric, hepatic, and splenic cysts. Retroperitoneal masses include lymphangiomas, adrenal cysts, and adrenal neuroblastomas. MRI has shown benefit in evaluating cystic abdominal masses with respect to both improved tissue characterization and anatomic localization.<sup>67</sup>

Abdominal wall defects include gastroschisis, omphalocele, cloacal exstrophy, limb body wall complex (LBWC), and pentology of Cantrell. Recognition of common features of each entity and potential pitfalls is essential for proper diagnosis. Ruptured omphalocele may mimic gastroschisis, congenital hernia of the umbilical cord may mimic omphalocele, and dilated vagina may be mistaken for normal urinary bladder in cases of cloacal malformation.<sup>68</sup> MRI is of benefit in

visualizing omphalocele sac content, size of anterior abdominal wall defect, quantity of extruded bowel, suggestion of bowel atresia, and presence of additional anomalies<sup>69</sup> (Fig. 23-34). Omphalocele may be isolated, or part of a severe anomaly, such as cloacal exstrophy, LBWC, or pentology of Cantrell. Fetal MRI is particularly helpful in defining and assessing the more complex lesions. Differentiation of treatable abdominal wall defects from lethal entities can help guide appropriate counseling and management.<sup>70</sup>

### Tumors

Teratomas are the most common fetal neoplasm, with the sacrococcygeal region being the most common site (Fig. 23-35). However, these tumors can also occur in the head, neck, chest, abdomen, and pelvis (Fig. 23-36). They are typically bulky and heterogeneous, with mixed solid and cystic appearance. Sacrococcygeal tumors can become very large and vascular, leading to atrioventricular shunting, high-output cardiac failure, and hydrops, with a reported fetal mortality rate of 50%.<sup>71</sup> In a study of prognostic factors predictive of outcome in fetuses with sacrococcygeal teratomas, a tumor volume/fetal weight ratio (TFR) lower than 0.12 before 24 weeks' gestation predicted an uncomplicated perinatal course with 100% survival. A TFR higher than 0.12 had an increased risk of complications and perinatal demise.<sup>72</sup>



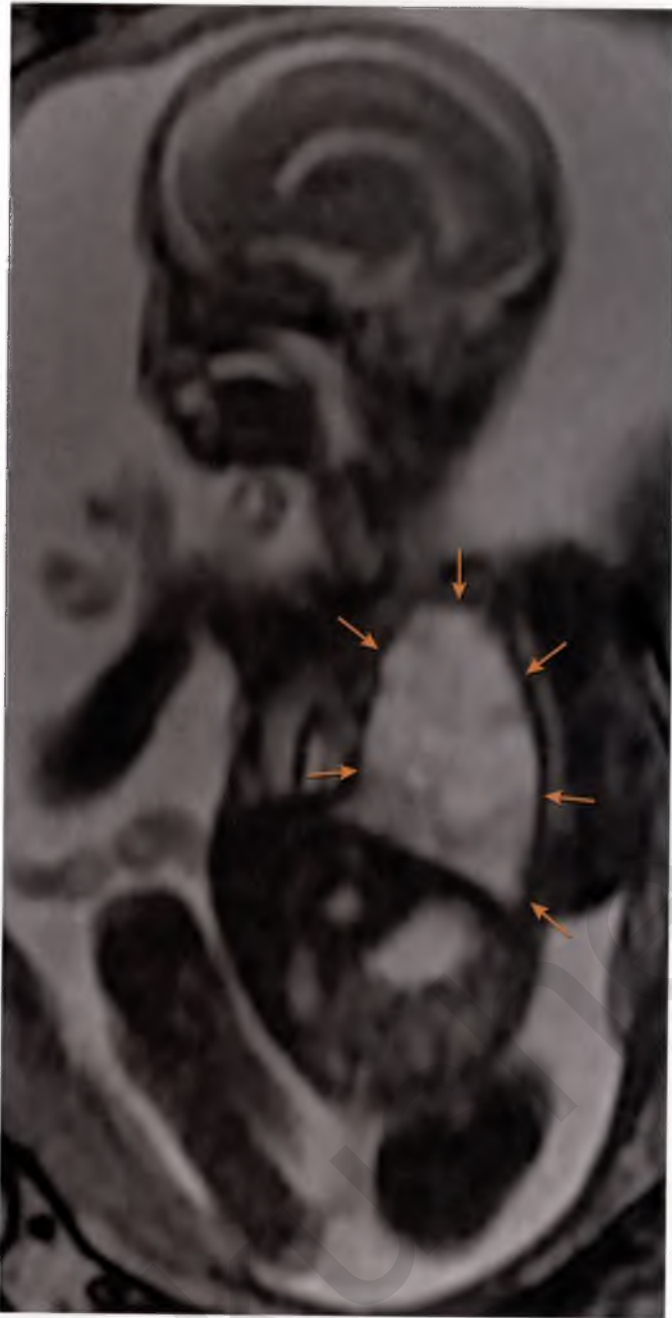


**FIG 23-29** Congenital pulmonary airway malformation (CPAM) at 20 weeks' gestation. Coronal balanced steady-state image demonstrates a large macrocystic, multilocular mass occupying the left hemithorax (arrows).



**FIG 23-30** Congenital lobar overinflation at 26 weeks' gestation. Coronal T2-weighted imaging demonstrates expanded, hyperintense right mid-upper lobe (arrows) compared with normal-appearing right lower lobe and left lung. Postnatal computed tomography confirmed congenital lobar emphysema likely due to right middle lobe bronchial atresia.



**FIG 23-31** Meconium ileus at 32.5 weeks' gestation. Coronal T1-weighted imaging demonstrates high signal intensity dilated distal loop of small bowel (arrows). Infant tested positive for cystic fibrosis.

Lymphangiomas are malformations of the lymphatic system that belong to the spectrum of venolymphatic malformations. Lymphangiomas can occur anywhere and are classified into simple, cavernous, and cystic forms. MRI can depict size and extent of lymphangiomas.<sup>73</sup> Those with a vascular component are called *hemangiolympangiomas* and may be associated with Klippel-Trenaunay syndrome if there is soft tissue hypertrophy of the affected limb and one or more port wine stains found on physical examination<sup>74</sup> (Fig. 23-37).

### Monochorionic Twins

A distinct spectrum of complications may affect monochorionic twin pregnancies, many due to vascular anastomoses in the shared placenta. These complications include twin-twin transfusion syndrome (TTTS), twin anemia-polycythemia sequence, selective fetal growth restriction

(sFGR), and neurologic damage following spontaneous death of a co-twin. In addition, interventions may be performed, including selective reduction or laser ablation of inter-twin vascular connections in the shared placenta with risk of subsequent neurologic sequelae in the surviving twin. Historically, it was thought that injury occurred as a result of transfusion of thromboplastic proteins from the dead twin into the survivor's circulation (twin embolization syndrome) resulting in disseminated intravascular coagulation. More recently, the proposed mechanism is thought to be related to blood loss from the survivor into the placental territory of a dead co-twin through vascular anastomoses in the shared monochorionic placenta.<sup>75,76</sup> This can lead to hypotension and underperfusion of the living twin with resultant ischemia and infarction of susceptible organs, with intracranial injury most apparent.<sup>77</sup> A study evaluating CNS findings in surviving fetuses following spontaneous co-twin demise identified abnormalities on MRI in 33% of cases; these observations included polymicrogyria, intracranial hemorrhage, and ventriculomegaly<sup>78</sup> (Fig. 23-38). More recently, DWI has been shown to detect acute ischemic cerebral lesions in a surviving fetus within 3 to 4 days of co-twin demise. This was seen following spontaneous intrauterine fetal demise (IUFD), fetal death after treatment for TTTS, and following selective termination.<sup>79,80</sup>

The use of MRI in the evaluation of conjoined twins was first reported in 1986<sup>81</sup> (Fig. 23-39). MRI can accurately depict the shared fetal anatomy, organ fusion, and associated malformations, allowing identification of conjoined twin pairs who may be amenable to post-natal surgical separation.

### Abnormal Placentation

*Abnormal placentation* refers to abnormal placental adherence to the myometrium and is classified according to depth of invasion. In placenta accreta, chorionic villi are attached directly to the myometrium without normal intervening decidua basalis. Chorionic villi partially invade the myometrium in placenta increta, and chorionic villi penetrate the myometrium to the level of the serosa or beyond in placenta percreta.<sup>18,82</sup> The proposed pathogenesis is twofold. Scarring from a variety of processes, including prior cesarean delivery, uterine surgery, myomectomy, or curettage, leads to a defect in the decidua basalis, with concomitant local hypoxia posing an increased risk for placental invasion. This defect in the decidua basalis and excessive trophoblast invasion lead to development of placenta accreta.<sup>83</sup> In 2005, Wu and coworkers reported a 20-year analysis of abnormal placentation, finding that the incidence of placenta accreta had risen from 1/2500 deliveries in 1982 to 1/533 deliveries.<sup>84</sup> This correlated with the rising cesarean delivery rate and increased incidence of placenta previa. The most important risk factors for placenta accreta were found to be prior cesarean delivery, placenta previa, and advanced maternal age.<sup>84</sup> In a study by Miller and associates, 9.3% of women with placenta previa had placenta accreta, but placenta accreta occurred in only 0.005% of women without placenta previa.<sup>85</sup> Silver and colleagues found that maternal morbidity increases with increasing number of prior cesarean deliveries, with risk of abnormal placentation following the first cesarean delivery of 3%, increasing to 40% following the third cesarean delivery, and 67% following the fifth cesarean delivery.<sup>86</sup>

Some published series require histopathologic proof for confirming the diagnosis of placenta accreta, and others will employ clinical criteria, as histologic examination may be unreliable because of sampling error or there may be incidental positive findings in asymptomatic cases. Clinical criteria include difficult manual removal of the placenta and continued bleeding from the implantation site after placental delivery. In a cohort of 111 cases of abnormal placentation, clinical criteria were used in 35 of the 111 (31.5%) to diagnose placenta accreta.<sup>84</sup>



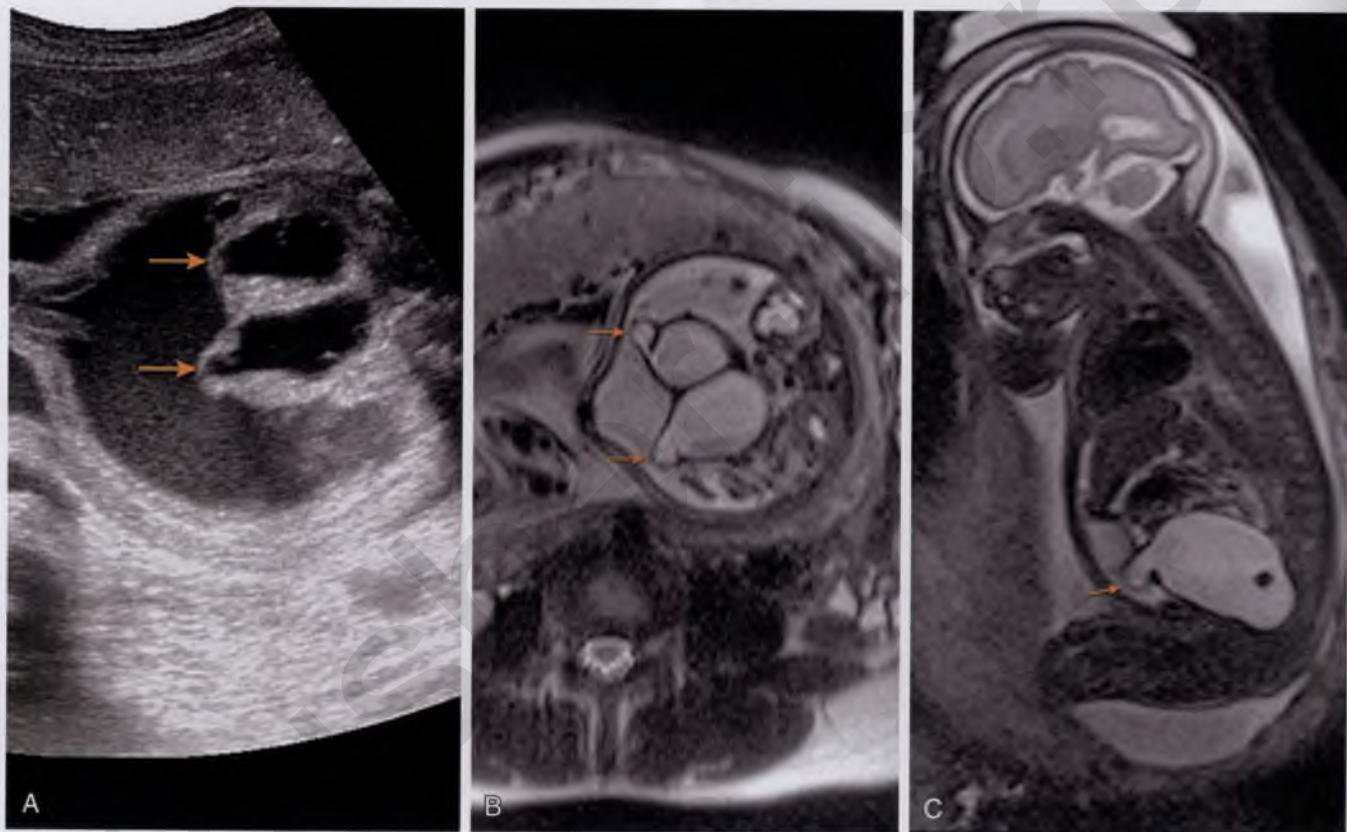


**FIG 23-32** Hydrometrocolpos with uterine duplication in complex cloacal malformation at 31 weeks' gestation. Axial ultrasound image (**A**) and axial (**B**) and sagittal (**C**) magnetic resonance images are shown. Dilated proximal fallopian tubes (*arrows*) communicate with fluid-filled duplicated endometrial cavities. Complex pelvic ascites is adjacent to hydrometrocolpos.

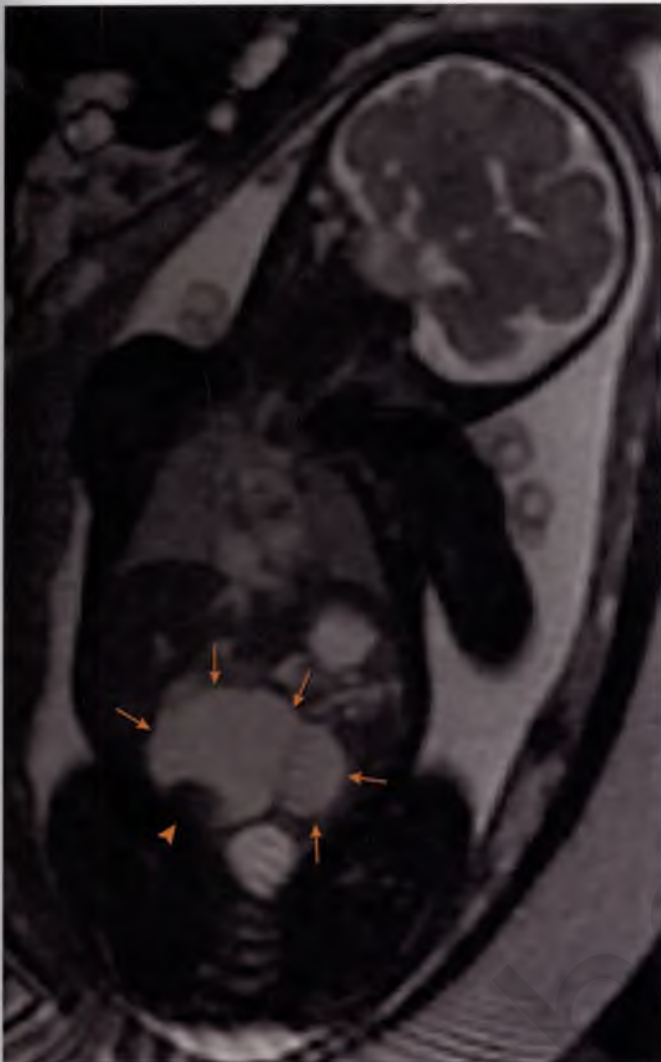


**FIG 23-33** Left ovarian and fallopian tube torsion and infarction at 32 weeks' gestation. Coronal balanced steady-state image demonstrates large pelvic cystic mass (arrows) with septation and solid nodule (arrowhead).

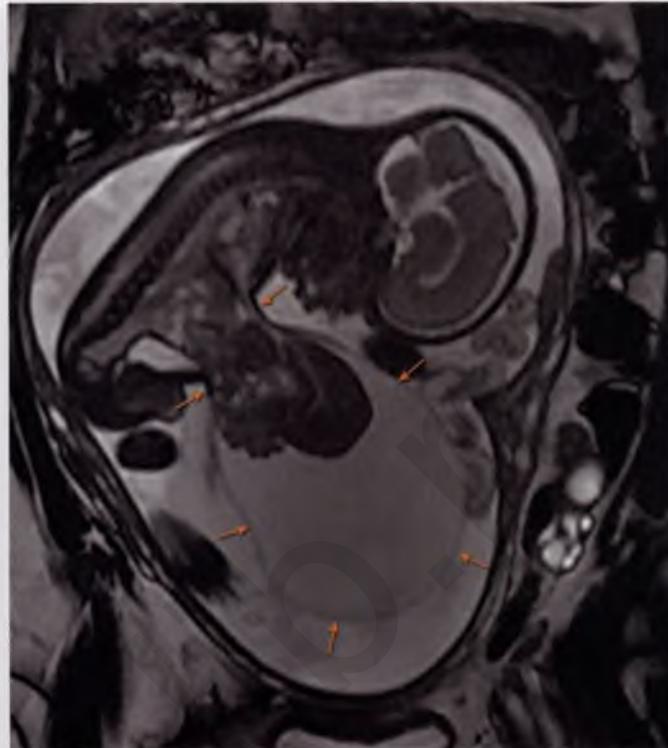


**FIG 23-34** Giant omphalocele at 29 weeks' gestation. Sagittal balanced steady-state image demonstrates giant omphalocele (arrows) containing liver, bowel, and large volume of ascites.

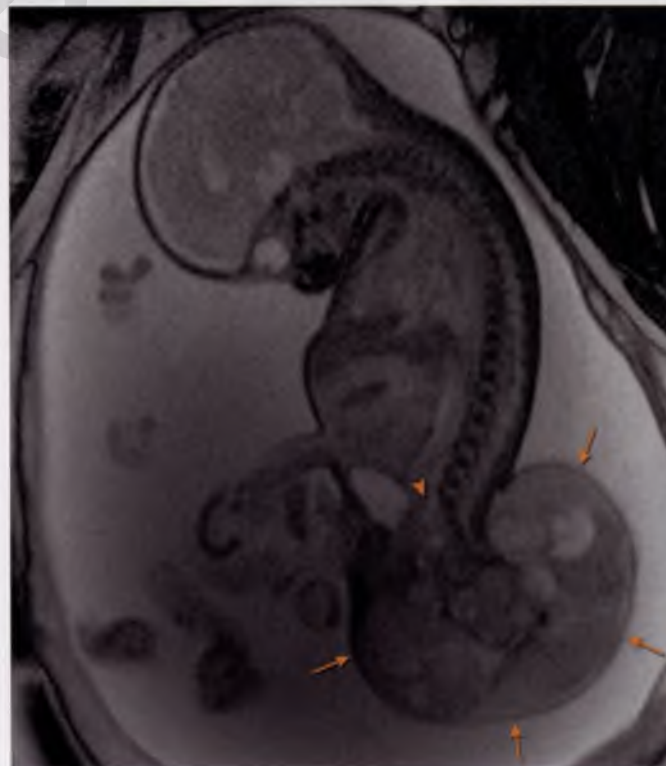


**FIG 23-35** Sacrococcygeal teratoma at 26 weeks' gestation. Sagittal T2-weighted imaging demonstrates a large complex exophytic cystic and solid sacrococcygeal mass (arrows) with minimal intrapelvic extension in the presacral region (arrowhead).



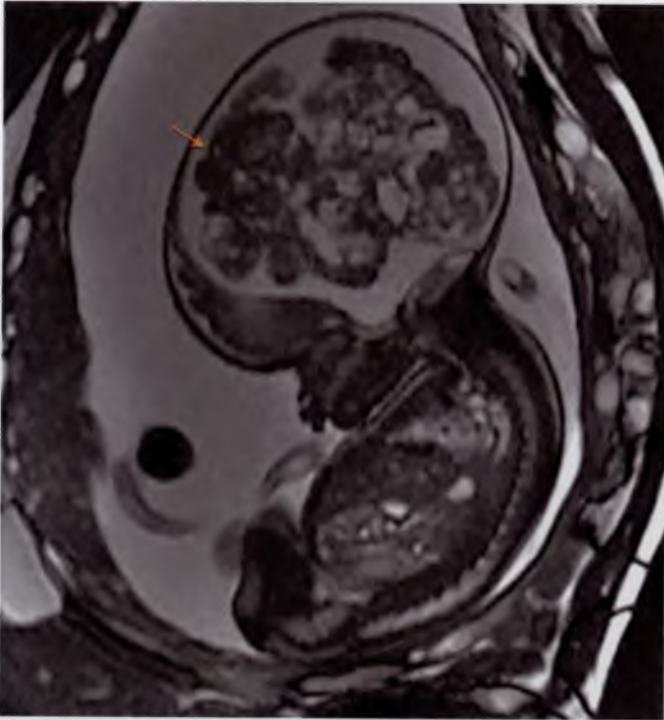


**FIG 23-36** Large intracranial teratoma at 32 weeks' gestation. Sagittal balanced steady-state image demonstrates complex cystic and solid intracranial mass (*arrow*) expanding the cerebral hemisphere. Pathologic examination demonstrated malignant immature teratoma.

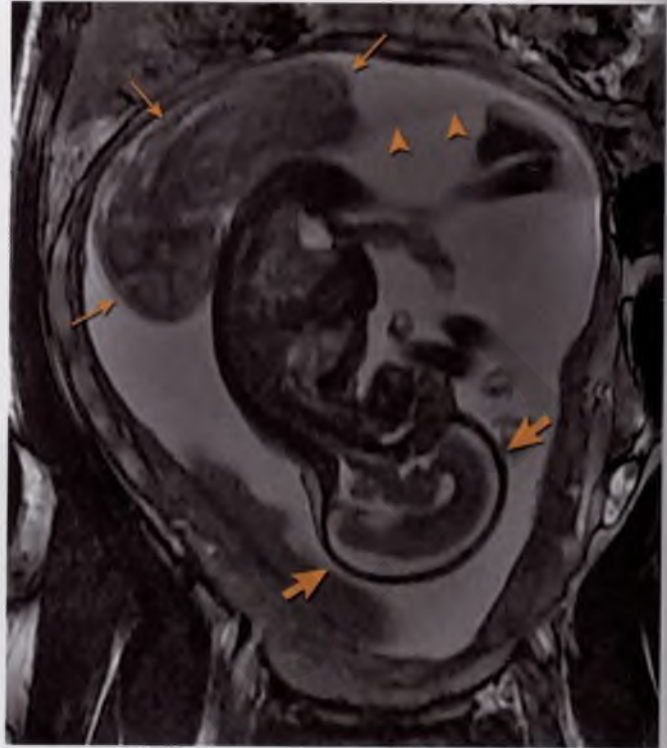


**FIG 23-38** Monozygotic diamniotic twins at 23.5 weeks' gestation, status post demise of twin B. Coronal balanced steady-state image performed 3 weeks following co-twin demise demonstrates mass-like appearance of the stuck demised twin B (*small arrows*), thin intertwin membrane (*arrowheads*), and no evidence of intracranial hemorrhage or ischemia in surviving twin A (*bold arrows*).

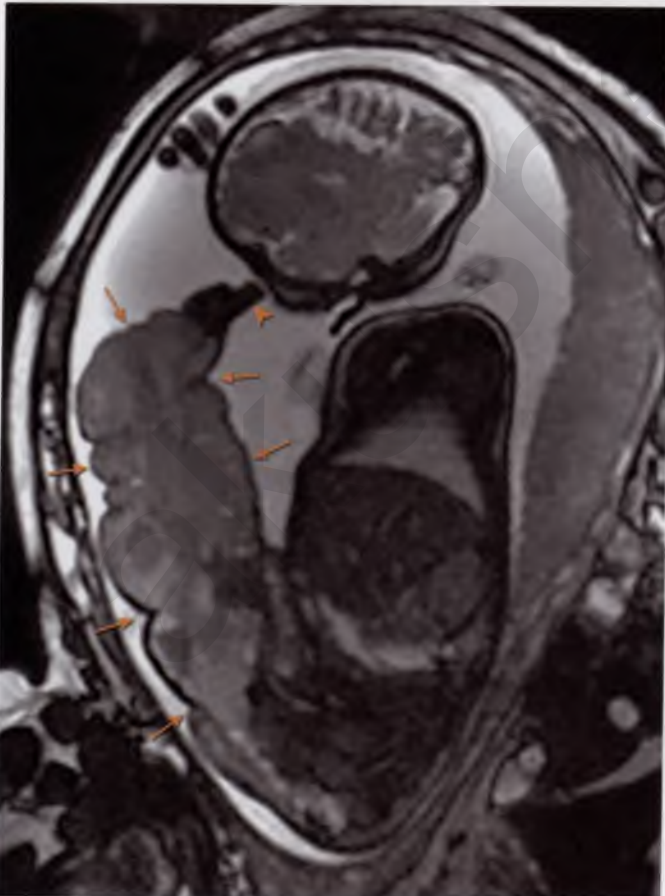


**FIG 23-37** Klippel-Trénaunay syndrome at 37 weeks' gestation. Sagittal balanced steady-state image demonstrates large venolymphatic malformation involving nearly the entire lower extremity (*arrows*) sparing the toes (*arrowhead*), with intrapelvic extension.

Abnormal placental adherence can result in catastrophic, life-threatening hemorrhage; therefore, the diagnosis of this potentially morbid condition is of utmost importance. Multidisciplinary planning has been shown to reduce maternal morbidity.<sup>18</sup> Prenatal MRI diagnosis of placenta percreta was first reported in 1992, with placenta previa and loss of the myometrial contour at the lower uterine segment detected by MRI.<sup>87</sup> Our placental MRI protocol consists of sagittal, coronal, and axial T2-weighted RARE and gradient echo images to image the entire gravid uterus, and one T1-weighted sequence in the sagittal plane, with the maternal bladder partially full.

Lax and coworkers found that the most useful criteria for diagnosing abnormal placentation using MRI were uterine bulging, heterogeneous signal intensity within the placenta, and T2 dark intraplacental bands<sup>88</sup> (Figs. 23-40 through 23-43). MRI has been shown to be useful in the determination of abnormal placental implantation in cases with equivocal diagnoses on ultrasound imaging.

Although reports in the medical literature question the accuracy and cost effectiveness of MRI for abnormal placentation,<sup>89,90</sup> many conclude that predelivery confirmed diagnosis of placenta accreta is associated with decreased maternal hemorrhagic morbidity.<sup>91,92</sup> More recently, MRI was shown to accurately delineate topographic extension into the parametrial regions and to identify cervicotrigonal vascular hyperplasia, significant prognostic details informing surgical approach and dissection.<sup>93</sup>

### Emerging Concepts

As MRI acquisition times shorten and technology allows for improved resolution of structures without degradation due to motion, fetal imaging may progress in three potential directions. One is volume



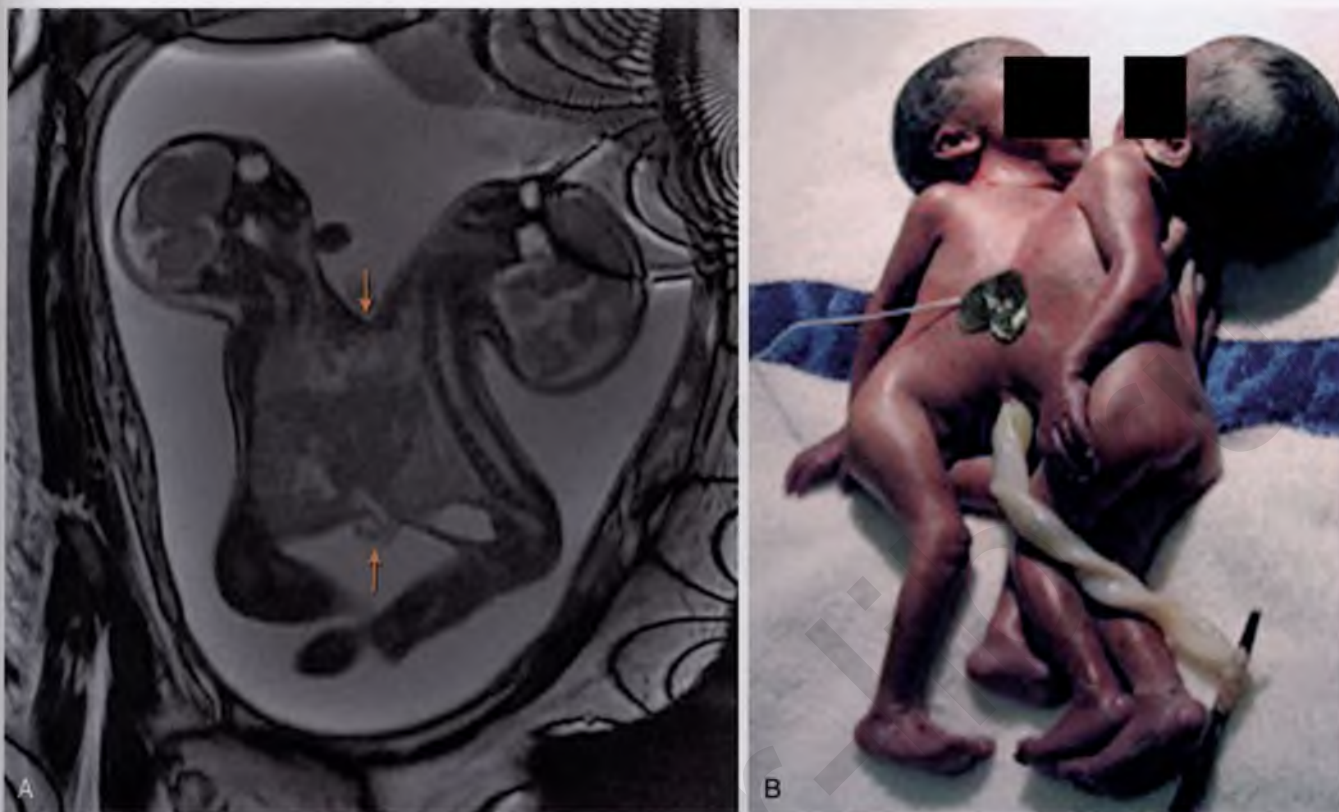


**FIG 23-39 A and B,** Thoraco-omphalopagus conjoined twins at 28 weeks' gestation. Coronal balanced steady-state image demonstrates fusion of the anterior chest and abdominal wall (arrows), with shared liver and heart. Separation could not be performed. Twins expired soon after birth.

acquisition and 3D postprocessing. This technique is similar to advances in spiral computed tomography with multiple channel detectors, in which one large high-resolution image can be processed in any plane of section. Applying this to imaging detailed fetal anatomy of interest requires faster acquisition times, ability to correct for fetal motion, and improved field of view options. New vendors have been developing these systems. Studies have looked at combined orthogonal views that create a volume of the fetal brain with subsequent postprocessing of improved images that correct for motion and limited resolution.<sup>93,94</sup> One study described actual alterations of development in the fetal brain in the setting of mild ventriculomegaly, based on 3D volumetric and surface analysis.<sup>94</sup>

The second direction is dynamic, real-time MRI for evaluation of the fetal heart and other moving structures. A feasibility study reviewed MRI examinations of the chest to delineate certain components of fetal cardiac anatomy.<sup>95</sup> They found that bSSFP acquisitions such as True-FISP and FIESTA were helpful in defining certain atrial, ventricular, conotruncal, and venous relationships. This technique must be coupled with an acquisition that captures the anatomy in some predictable fashion when the fetal heart rate is 120 to 160 beats per minute.

Finally, many of the already established acquisitions that assess physiologic functions commonly referred to as functional MRI (fMRI) may be explored in the fetus. This approach includes spectroscopy for investigating brain and pulmonary maturity, which has been addressed in small series.<sup>96,97</sup> As discussed previously, DWI and apparent diffusion coefficient (ADC) have been used for evaluating the fetal CNS<sup>12,14,98-100</sup> and placental hypoxemia/ischemia.<sup>101</sup> DWI and ADC mapping of the fetal brain have the added advantage of providing diffusion tensor and white matter tract imaging.<sup>98-100</sup> Fetal tractography

with diffusion tensor imaging (DTI) has been used to delineate fetal sensorimotor tracts and corpus callosum as they develop in utero.<sup>102</sup> BOLD MRI has also been employed in the sheep model to demonstrate changes in fetal tissue oxygenation and display the fetal brain-sparing mechanism.<sup>103</sup> Recently, sophisticated postprocessing techniques and fMRI have been adapted to correlate macroscopic scale activations in the fetal brain with gestational age in vivo. This fMRI study was able to demonstrate the heterogeneous development of emerging human brain networks of the fetus in utero.<sup>104</sup>

In spite of new and exciting advances, these emerging technologies are still in experimental stages and should undergo rigorous investigations before their clinical applications become established.

## CONCLUSIONS

In summary, MRI is emerging as an important tool for the evaluation of maternal complications in pregnancy, including the evaluation of atypical advanced ectopic pregnancies, suspected appendicitis, pelvic masses, hepatic and genitourinary diseases, and placenta accreta. In the fetus, it is an important adjunct to the sonographic diagnosis of suspected CNS lesions, in particular, isolated ventriculomegaly. Fetal MRI may provide additional information for certain intrathoracic lesions, aid in predicting prognosis in CDHs, and help delineate complex genitourinary abnormalities. MRI studies add important information in the care of potential fetal surgery candidates and may direct crucial decisions for delivery management, such as use of the EXIT procedure. Evaluation of the fetal heart, brain function, and fetal-placental physiology are possible and may become clinically applicable as new and improved technologies emerge.



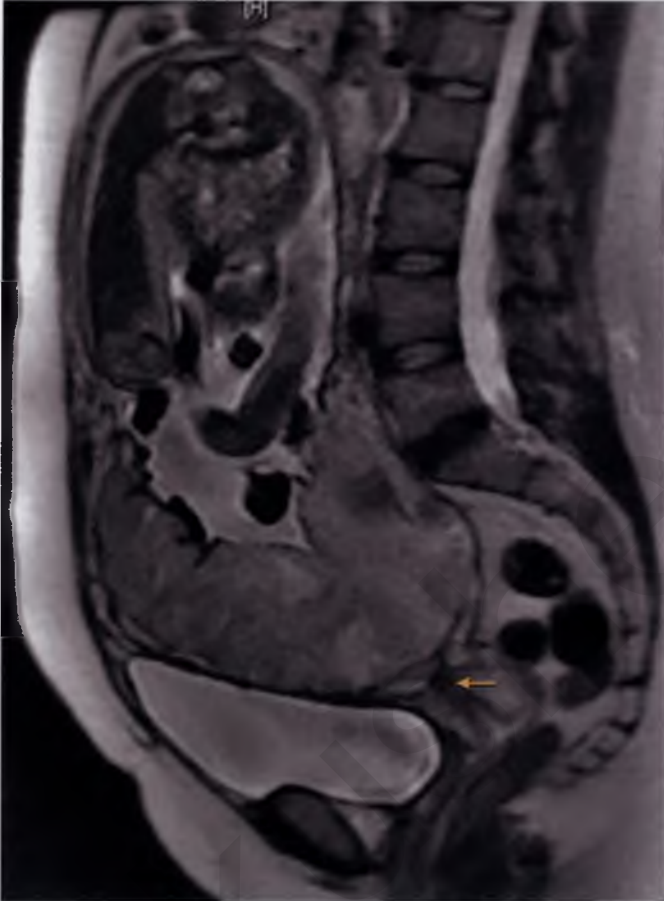


**FIG 23-40** Central placenta previa at 34 weeks' gestation, history of one prior cesarean delivery. Sagittal T2-weighted imaging demonstrates a central placenta previa covering the internal os of the cervix (*arrow*). The placenta is homogeneous in signal intensity, normal in thickness, with an intact myometrial margin.

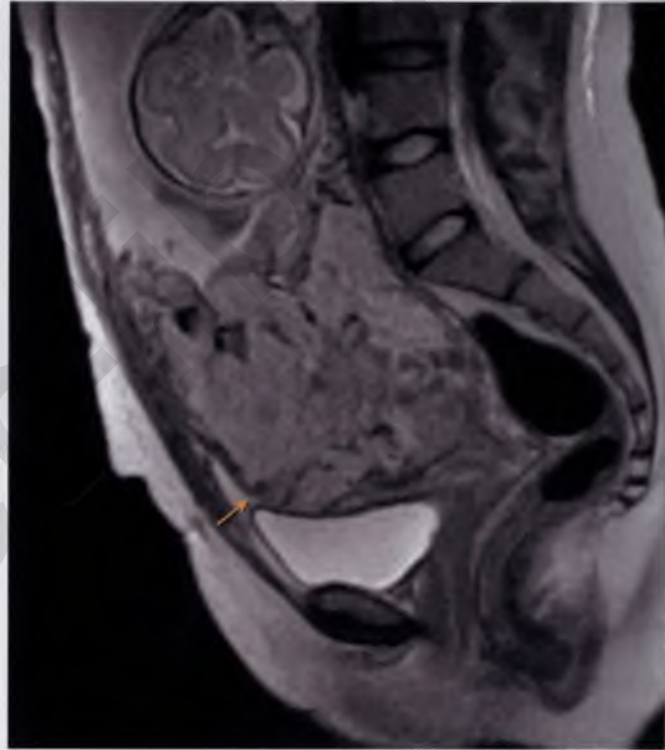


**FIG 23-41** Placenta accreta at 25 weeks' gestation, history of two prior cesarean deliveries. Sagittal T2-weighted imaging demonstrates a central placenta previa. The placenta demonstrates heterogeneous signal intensity, with disordered T2-weighted dark intraplacental bands, with loss of normal placental-myometrial interface and bulging contour (*arrow*).

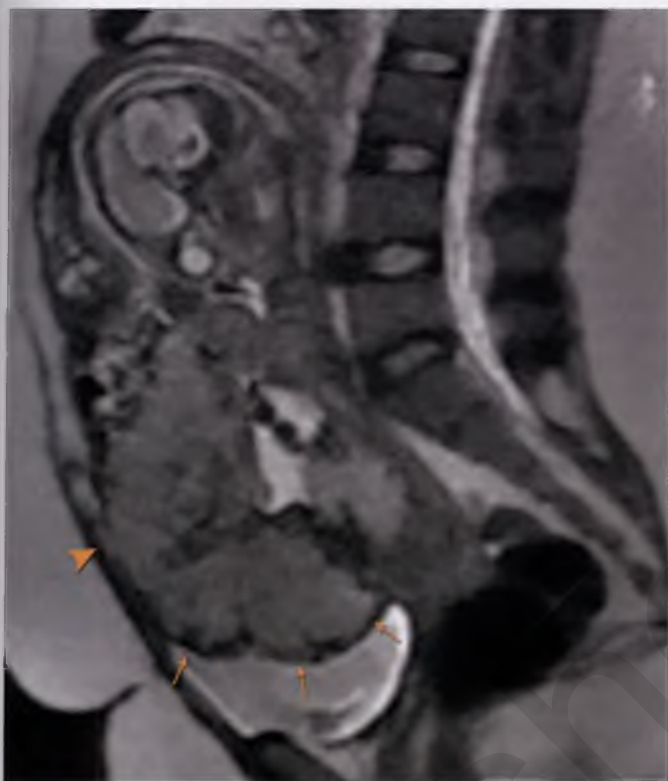


**FIG 23-42** Placenta percreta at 27 weeks' gestation, history of two prior cesarean deliveries. Sagittal T2-weighted imaging demonstrates a thickened heterogeneous placenta with lobulation (*arrows*), mass effect and thickened dark nodular contour at the interface with the urinary bladder, and loss of the normal myometrial margin anteriorly (*arrowhead*).

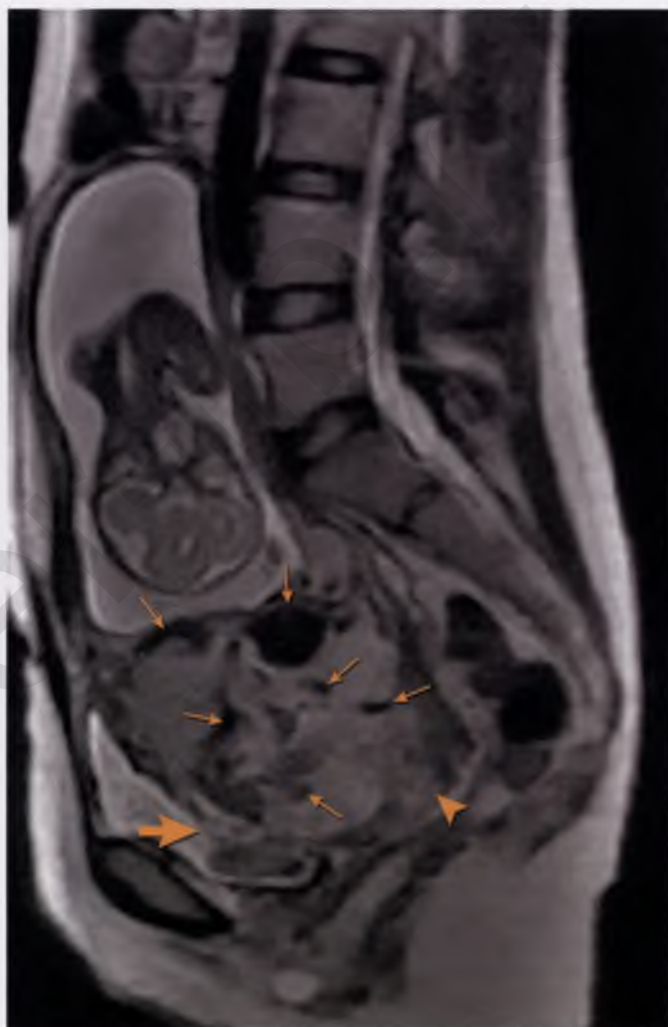


**FIG 23-43** Placenta percreta at 21 weeks' gestation, history of two prior cesarean deliveries, presenting with vaginal bleeding. Sagittal T2-weighted imaging demonstrates a markedly thickened, heterogeneous central placenta previa. There are intraplacental dark bands (*small arrows*), lobulation and mass effect with extension through the myometrium and superior urinary bladder surface (*bold arrow*), and involvement of the cervix (*arrowhead*).



## REFERENCES

1. Wiskirchen J, Groenewaller EF, Kehlbach R, et al: Long-term effects of repetitive exposure to a static magnetic field (1.5 T) on proliferation of human fetal lung fibroblasts. *Magn Reson Med* 41(3):464–468, 1999.
2. Kanal E: Pregnancy and the safety of magnetic resonance imaging. *Magn Reson Imaging Clin North Am* 2(2):309–317, 1994.
3. Baker PN, Johnson IR, Harvey PR, et al: A three-year follow-up of children imaged in utero with echo-planar magnetic resonance. *Am J Obstet Gynecol* 170(1 Pt 1):32–33, 1994.
4. Clements H, Duncan KR, Fielding K, et al: Infants exposed to MRI in utero have a normal paediatric assessment at 9 months of age. *Br J Radiol* 73(866):190–194, 2000.
5. Glover P, Hykin J, Gowland P, et al: An assessment of the intrauterine sound intensity level during obstetric echo-planar magnetic resonance imaging. *Br J Radiol* 68(814):1090–1094, 1995.
6. Arulkumaran S, Skurr B, Tong H, et al: No evidence of hearing-loss due to fetal acoustic stimulation test. *Obstet Gynecol* 78(2):283–285, 1991.
7. Vadeyar SH, Moore RJ, Strachan BK, et al: Effect of fetal magnetic resonance imaging on fetal heart rate patterns. *Am J Obstet Gynecol* 182(3):666–669, 2000.
8. Kanal E, Barkovich AJ, Bell C, et al: ACR guidance document for safe MR practices: 2007. *AJR Am J Roentgenol* 188(6):1447–1474, 2007.
9. Pedrosa I, Zeikus EA, Levine D, Rofsky NM: MR imaging of acute right lower quadrant pain in pregnant and nonpregnant patients. *Radiographics* 27(3):721–743, discussion 743–753, 2007.
10. Yamashita Y, Namimoto T, Abe Y, et al: MR imaging of the fetus by a HASTE sequence. *AJR Am J Roentgenol* 168(2):513–519, 1997.
11. Levine D, Barnes PD, Sher S, et al: Fetal fast MR imaging: reproducibility, technical quality, and conspicuity of anatomy. *Radiology* 206(2):549–554, 1998.
12. Brugger PC, Stuhr F, Lindner C, Prayer D: Methods of fetal MR: beyond T2-weighted imaging. *Eur J Radiol* 57(2):172–181, 2006.
13. Zizka J, Elias P, Hodik K, et al: Liver, meconium, haemorrhage: the value of T1-weighted images in fetal MRI. *Pediatr Radiol* 36(8):792–801, 2006.
14. McKenzie C, Levine D: Current techniques and future directions for fetal MR imaging. In Levine D, editor: *Atlas of Fetal MRI*, Boca Raton, FL, 2005. CRC Press, pp 175–192.
15. Abele TA, Lee SL, Twickler DM: MR imaging quantitative analysis of fetal Chiari II malformations and associated open neural tube defects: balanced SSFP versus half-Fourier RARE and interobserver reliability. *J Magn Reson Imaging* 38(4):786–793, 2013.
16. American College of Radiology (ACR) and the Society for Pediatric Radiology (SPR): *ACR-SPR Practice Parameter for the Safe and Optimal Performance of Fetal Magnetic Resonance Imaging (MRI)*. 2014. Available at <<http://www.acr.org/guidelines>>.
17. Spalluto LB, Woodfield CA, DeBenedictis CM, Lazarus E: MR imaging evaluation of abdominal pain during pregnancy: appendicitis and other nonobstetric causes. *Radiographics* 32(2):317–334, 2012.
18. Leyendecker JR, DuBose M, Hosseinzadeh K, et al: MRI of pregnancy-related issues: abnormal placentation. *AJR Am J Roentgenol* 198(2):311–320, 2012.
19. Woodfield CA, Lazarus E, Chen KC, Mayo-Smith WW: Abdominal pain in pregnancy: diagnoses and imaging unique to pregnancy—review. *AJR Am J Roentgenol* 194(6 Suppl):WS14–WS30, 2010.
20. Tsafir A, Rojansky N, Sela HY, et al: Rudimentary horn pregnancy: first-trimester prerupture sonographic diagnosis and confirmation by magnetic resonance imaging. *J Ultrasound Med* 24(2):219–223, 2005.
21. Levine D, Barnes PD, Madsen JR, et al: Fetal central nervous system anomalies: MR imaging augments sonographic diagnosis. *Radiology* 204(3):635–642, 1997.
22. Levine D, Barnes PD, Robertson RR, et al: Fast MR imaging of fetal central nervous system abnormalities. *Radiology* 229(1):51–61, 2003.
23. Dill P, Poretti A, Boltschauer E, Huisman TA: Fetal magnetic resonance imaging in midline malformations of the central nervous system and review of the literature. *J Neuroradiol* 36(3):138–146, 2009.
24. Benacerraf BR, Shipp TD, Bromley B, Levine D: What does magnetic resonance imaging add to the prenatal sonographic diagnosis of ventriculomegaly? *J Ultrasound Med* 26(11):1513–1522, 2007.
25. Gaglioti P, Oberio M, Todros T: The significance of fetal ventriculomegaly: etiology, short- and long-term outcomes. *Prenat Diagn* 29(4):381–388, 2009.
26. Glenn OA, Barkovich AJ: Magnetic resonance imaging of the fetal brain and spine: an increasingly important tool in prenatal diagnosis, part 1. *AJNR Am J Neuroradiol* 27(8):1604–1611, 2006.
27. Volpe P, Campobasso G, De Robertis V, Rembouskos G: Disorders of prosencephalic development. *Prenat Diagn* 29(4):340–354, 2009.
28. Glenn OA, Goldstein RB, Li KC, et al: Fetal magnetic resonance imaging in the evaluation of fetuses referred for sonographically suspected abnormalities of the corpus callosum. *J Ultrasound Med* 24(6):791–804, 2005.
29. Hahn JS, Barnes PD: Neuroimaging advances in holoprosencephaly: refining the spectrum of the midline malformation. *Am J Med Genet C Semin Med Genet* 154C(1):120–132, 2010.
30. Adamsbaum C, Moutard ML, Andre C, et al: MRI of the fetal posterior fossa. *Pediatr Radiol* 35(2):124–140, 2005.
31. Patek KJ, Kline-Fath BM, Hopkin RJ, et al: Posterior fossa anomalies diagnosed with fetal MRI: associated anomalies and neurodevelopmental outcomes. *Prenat Diagn* 32(1):75–82, 2012.
32. Glenn OA, Barkovich J: Magnetic resonance imaging of the fetal brain and spine: an increasingly important tool in prenatal diagnosis: part 2. *AJNR Am J Neuroradiol* 27(9):1807–1814, 2006.
33. Chao TT, Dashe JS, Adams RC, et al: Central nervous system findings on fetal magnetic resonance imaging and outcomes in children with spina bifida. *Obstet Gynecol* 116(2 Pt 1):323–329, 2010.
34. Abdel Razek AA, Kandell AY, Elsorogy LG, et al: Disorders of cortical formation: MR imaging features. *AJNR Am J Neuroradiol* 30(1):4–11, 2009.
35. Fogliarini C, Chaumoitte K, Chapon F, et al: Assessment of cortical maturation with prenatal MRI: part II: abnormalities of cortical maturation. *Eur Radiol* 15(9):1781–1789, 2005.
36. Glenn OA, Cuneo AA, Barkovich AJ, et al: Malformations of cortical development: diagnostic accuracy of fetal MR imaging. *Radiology* 263(3):843–855, 2012.
37. Prayer D, Brugger PC, Kasprian G, et al: MRI of fetal acquired brain lesions. *Eur J Radiol* 57(2):233–249, 2006.
38. Girard N, Gire C, Sigaudy S, et al: MR imaging of acquired fetal brain disorders. *Childs Nerv Syst* 19(7–8):490–500, 2003.
39. Chen CP: Prenatal diagnosis of arachnoid cysts. *Taiwan J Obstet Gynecol* 46(3):187–198, 2007.
40. Bronshtein M, Weiner Z: Prenatal diagnosis of dilated cava septi pellucidi et vergae: associated anomalies, differential diagnosis, and pregnancy outcome. *Obstet Gynecol* 80(5):838–842, 1992.
41. Vergani P, Locatelli A, Piccoli MG, et al: Ultrasonographic differential diagnosis of fetal intracranial interhemispheric cysts. *Am J Obstet Gynecol* 180(2 Pt 1):423–428, 1999.
42. Eisenberg VH, Zalel Y, Hoffmann C, et al: Prenatal diagnosis of cavum velum interpositum cysts: significance and outcome. *Prenat Diagn* 23(10):779–783, 2003.
43. Digne MK, Peterson SE, Dubinsky TJ, et al: EXIT procedure: technique and indications with prenatal imaging parameters for assessment of airway patency. *Radiographics* 31(2):511–526, 2011.
44. Courtier J, Poder L, Wang ZJ, et al: Fetal tracheolaryngeal airway obstruction: prenatal evaluation by sonography and MRI. *Pediatr Radiol* 40(11):1800–1805, 2010.
45. MacArthur CJ: Prenatal diagnosis of fetal cervicofacial anomalies. *Curr Opin Otolaryngol Head Neck Surg* 20(6):482–490, 2012.
46. Morris LM, Lim FY, Elluru RG, et al: Severe micrognathia: indications for EXIT-to-airway. *Fetal Diagn Ther* 26(3):162–166, 2009.
47. Lazar DA, Olutoye OO, Moise KJ, Jr, et al: Ex-utero intrapartum treatment procedure for giant neck masses—fetal and maternal outcomes. *J Pediatr Surg* 46(5):817–822, 2011.
48. Shimabukuro F, Sakumoto K, Masamoto H, et al: A case of congenital high airway obstruction syndrome managed by ex utero intrapartum



- treatment: case report and review of the literature. *Am J Perinatol* 24(3):197–201, 2007.
49. Houben CH, Curry JJ: Current status of prenatal diagnosis, operative management and outcome of esophageal atresia/tracheo-esophageal fistula. *Prenat Diagn* 28(7):667–675, 2008.
  50. Ethun CG, Fallon SC, Cassady CI, et al: Fetal MRI improves diagnostic accuracy in patients referred to a fetal center for suspected esophageal atresia. *J Pediatr Surg* 49(5):712–715, 2014.
  51. Kazan-Tannus JF, Levine D, McKenzie C, et al: Real-time magnetic resonance imaging aids prenatal diagnosis of isolated cleft palate. *J Ultrasound Med* 24(11):1533–1540, 2005.
  52. Houshmand G, Hosseinzadeh K, Ozolek J: Prenatal magnetic resonance imaging (MRI) findings of a foregut duplication cyst of the tongue: value of real-time MRI evaluation of the fetal swallowing mechanism. *J Ultrasound Med* 30(6):843–850, 2011.
  53. Salomon LJ, Sonigo P, Ou P, et al: Real-time fetal magnetic resonance imaging for the dynamic visualization of the pouch in esophageal atresia. *Ultrasound Obstet Gynecol* 34(4):471–474, 2009.
  54. Lazar DA, Ruano R, Cass DL, et al: Defining “liver-up”: does the volume of liver herniation predict outcome for fetuses with isolated left-sided congenital diaphragmatic hernia? *J Pediatr Surg* 47(6):1058–1062, 2012.
  55. Debus A, Hagelstein C, Kilian AK, et al: Fetal lung volume in congenital diaphragmatic hernia: association of prenatal MR imaging findings with postnatal chronic lung disease. *Radiology* 266(3):887–895, 2013.
  56. Walleyo A, Debus A, Kehl S, et al: Periodic MRI lung volume assessment in fetuses with congenital diaphragmatic hernia: prediction of survival, need for ECMO, and development of chronic lung disease. *AJR Am J Roentgenol* 201(2):419–426, 2013.
  57. Nawapun K, Eastwood M, Sandaite I, et al: The correlation between the observed-to-expected total fetal lung volume with intra-thoracic organ herniation on magnetic resonance images in fetuses with isolated left-sided congenital diaphragmatic hernia. *Ultrasound Obstet Gynecol* 46(2):162–167, 2015.
  58. Ruano R, Lazar DA, Cass DL, et al: Fetal lung volume and quantification of liver herniation by magnetic resonance imaging in isolated congenital diaphragmatic hernia. *Ultrasound Obstet Gynecol* 43(6):662–669, 2014.
  59. Bebbington M, Victoria T, Danzer E, et al: Comparison of ultrasound and magnetic resonance imaging parameters in predicting survival in isolated left-sided congenital diaphragmatic hernia. *Ultrasound Obstet Gynecol* 43(6):670–674, 2014.
  60. Zamora JJ, Olutoye OO, Cass DL, et al: Prenatal MRI fetal lung volumes and percent liver herniation predict pulmonary morbidity in congenital diaphragmatic hernia (CDH). *J Pediatr Surg* 49(5):688–693, 2014.
  61. Recio Rodriguez M, Martinez de Vega V, Cano Alonso R, et al: MR imaging of thoracic abnormalities in the fetus. *Radiographics* 32(7):E305–E321, 2012.
  62. Pacharn P, Kline-Fath B, Calvo-Garcia M, et al: Congenital lung lesions: prenatal MRI and postnatal findings. *Pediatr Radiol* 43(9):1136–1143, 2013.
  63. Barth RA: Imaging of fetal chest masses. *Pediatr Radiol* 42(Suppl 1):S62–S73, 2012.
  64. Saguintaah M, Couture A, Veyrac C, et al: MRI of the fetal gastrointestinal tract. *Pediatr Radiol* 32(6):395–404, 2002.
  65. Colombani M, Ferry M, Garel C, et al: Fetal gastrointestinal MRI: all that glitters in T1 is not necessarily colon. *Pediatr Radiol* 40(7):1215–1221, 2010.
  66. Caire JT, Ramus RM, Magee KP, et al: MRI of fetal genitourinary anomalies. *AJR Am J Roentgenol* 181(5):1381–1385, 2003.
  67. Gupta P, Sharma R, Kumar S, et al: Role of MRI in fetal abdominal cystic masses detected on prenatal sonography. *Arch Gynecol Obstet* 281(3):519–526, 2010.
  68. Nakagawa M, Hara M, Shibamoto Y: MRI findings in fetuses with an abdominal wall defect: gastroschisis, omphalocele, and cloacal exstrophy. *Jpn J Radiol* 31(3):153–159, 2013.
  69. Sugai Y, Hosoya T, Kurachi H: MR imaging of fetal omphalocele: a case report. *Magn Reson Med Sci* 7(4):211–213, 2008.
  70. Aguirre-Pascual E, Epelman M, Johnson AM, et al: Prenatal MRI evaluation of limb-body wall complex. *Pediatr Radiol* 44(11):1412–1420, 2014.
  71. Woodward PJ, Sohaey R, Kennedy A, Koeller KK: From the archives of the AFIP: a comprehensive review of fetal tumors with pathologic correlation. *Radiographics* 25(1):215–242, 2005.
  72. Rodriguez MA, Cass DL, Lazar DA, et al: Tumor volume to fetal weight ratio as an early prognostic classification for fetal sacrococcygeal teratoma. *J Pediatr Surg* 46(6):1182–1185, 2011.
  73. Rha SE, Byun JY, Kim HH, et al: Prenatal sonographic and MR imaging findings of extensive fetal lymphangioma: a case report. *Korean J Radiol* 4(4):260–263, 2003.
  74. Goncalves LF, Rojas MV, Vitorello D, et al: Klippel-Trenaunay-Weber syndrome presenting as massive lymphangiohemangioma of the thigh: prenatal diagnosis. *Ultrasound Obstet Gynecol* 15(6):537–541, 2000.
  75. Fusi L, McParland P, Fisk N, et al: Acute twin-twin transfusion: a possible mechanism for brain-damaged survivors after intrauterine death of a monozygotic twin. *Obstet Gynecol* 78(3 Pt 2):517–520, 1991.
  76. Benirschke K: Intrauterine death of a twin: mechanisms, implications for surviving twin, and placental pathology. *Semin Diagn Pathol* 10(3):222–231, 1993.
  77. Hu LS, Caire J, Twickler DM: MR findings of complicated multifetal gestations. *Pediatr Radiol* 36(1):76–81, 2006.
  78. Jelin AC, Norton ME, Bartha AI, et al: Intracranial magnetic resonance imaging findings in the surviving fetus after spontaneous monozygotic cotwin demise. *Am J Obstet Gynecol* 199(4):398.e1–e5, 2008.
  79. Hoffmann C, Weisz B, Yinon Y, et al: Diffusion MRI findings in monozygotic twin pregnancies after intrauterine fetal death. *AJNR Am J Neuroradiol* 34(1):212–216, 2013.
  80. Weisz B, Hoffmann C, Ben-Baruch S, et al: Early detection by diffusion-weighted sequence magnetic resonance imaging of severe brain lesions after fetoscopic laser coagulation for twin-twin transfusion syndrome. *Ultrasound Obstet Gynecol* 44(1):44–49, 2014.
  81. Turner RJ, Hankins GD, Weinreb JC, et al: Magnetic resonance imaging and ultrasonography in the antenatal evaluation of conjoined twins. *Am J Obstet Gynecol* 155(3):645–649, 1986.
  82. Baughman WC, Corteveille JE, Shah RR: Placenta accreta: spectrum of US and MR imaging findings. *Radiographics* 28(7):1905–1916, 2008.
  83. Abuhamad A: Morbidly adherent placenta. *Semin Perinatol* 37(5):359–364, 2013.
  84. Wu S, Kocherginsky M, Hibbard JU: Abnormal placentation: twenty-year analysis. *Am J Obstet Gynecol* 192(5):1458–1461, 2005.
  85. Miller DA, Chollet JA, Goodwin TM: Clinical risk factors for placenta previa-placenta accreta. *Am J Obstet Gynecol* 177(1):210–214, 1997.
  86. Silver RM, Landon MB, Rouse DJ, et al: Maternal morbidity associated with multiple repeat cesarean deliveries. *Obstet Gynecol* 107(6):1226–1232, 2006.
  87. Thorp JM, Jr, Councell RB, Sandridge DA, Wiest HH: Antepartum diagnosis of placenta previa praecox by magnetic resonance imaging. *Obstet Gynecol* 80(3 Pt 2):506–508, 1992.
  88. Lax A, Prince MR, Mennitt KW, et al: The value of specific MRI features in the evaluation of suspected placental invasion. *Magn Reson Imaging* 25(1):87–93, 2007.
  89. Lam G, Kuller J, McMahon M: Use of magnetic resonance imaging and ultrasound in the antenatal diagnosis of placenta accreta. *J Soc Gynecol Invest* 9(1):37–40, 2002.
  90. McLean LA, Heilbrun ME, Eller AG, et al: Assessing the role of magnetic resonance imaging in the management of gravid patients at risk for placenta accreta. *Acad Radiol* 18(9):1175–1180, 2011.
  91. Warshak CR, Ramos GA, Eskander R, et al: Effect of predelivery diagnosis in 99 consecutive cases of placenta accreta. *Obstet Gynecol* 115(1):65–69, 2010.
  92. Tikkanen M, Paavonen J, Loukovaara M, Stefanovic V: Antenatal diagnosis of placenta accreta leads to reduced blood loss. *Acta Obstet Gynecol Scand* 90(10):1140–1146, 2011.



93. Palacios-Jaraquemada JM, Bruno CH, Martin E: MRI in the diagnosis and surgical management of abnormal placentation. *Acta Obstet Gynecol Scand* 92(4):392–397, 2013.
94. Rousseau F, Glenn OA, Iordanova B, et al: Registration-based approach for reconstruction of high-resolution in utero fetal MR brain images. *Acad Radiol* 13(9):1072–1081, 2006.
95. Gorincour G, Bourliere-Najean B, Bonello B, et al: Feasibility of fetal cardiac magnetic resonance imaging: preliminary experience. *Ultrasound Obstet Gynecol* 29(1):105–108, 2007.
96. Fenton BW, Lin CS, Macedonia C, et al: The fetus at term: in utero volume-selected proton MR spectroscopy with a breath-hold technique—a feasibility study. *Radiology* 219(2):563–566, 2001.
97. Kok RD, van den Berg PP, van den Bergh AJ, et al: Maturation of the human fetal brain as observed by 1H MR spectroscopy. *Magn Reson Med* 48(4):611–616, 2002.
98. Bartha AI, Yap KR, Miller SP, et al: The normal neonatal brain: MR imaging, diffusion tensor imaging, and 3D MR spectroscopy in healthy term neonates. *AJNR Am J Neuroradiol* 28(6):1015–1021, 2007.
99. Guimiot F, Garel C, Fallet-Bianco C, et al: Contribution of diffusion-weighted imaging in the evaluation of diffuse white matter ischemic lesions in fetuses: correlations with fetopathologic findings. *AJNR Am J Neuroradiol* 29(1):110–115, 2008.
100. Kim DH, Chung S, Vigneron DB, et al: Diffusion-weighted imaging of the fetal brain in vivo. *Magn Reson Med* 59(1):216–220, 2008.
101. Yeh BM: Has the time arrived to image placental perfusion? *Radiology* 241(3):633–634, 2006.
102. Kasprian G, Brugger PC, Weber M, et al: In utero tractography of fetal white matter development. *Neuroimage* 43(2):213–224, 2008.
103. Sorensen A, Pedersen M, Tietze A, et al: BOLD MRI in sheep fetuses: a non-invasive method for measuring changes in tissue oxygenation. *Ultrasound Obstet Gynecol* 34(6):687–692, 2009.
104. Jakab A, Schwartz E, Kasprian G, et al: Fetal functional imaging portrays heterogeneous development of emerging human brain networks. *Front Hum Neurosci* 8:852, 2014.

# Role of Sonography in Fetal Procedures

*Ramen H. Chmait, Paulo Nassar de Carvalho, Robert H. Ball*

## SUMMARY OF KEY POINTS

- Sonography has transformed the field of fetal therapy and serves as the widely available, necessary diagnostic and intraoperative guidance tool.
- The potential benefits of open maternal-fetal surgery must be weighed against the potential maternal and fetal risks, which have the potential of complicating the index pregnancy and subsequent pregnancies.
- Minimally invasive fetal surgery is associated with much lower maternal risks and is the preferred surgical approach for most fetal conditions amenable to in utero therapy.
- Monochorionic diamniotic twin pregnancies are associated with significant morbidity and mortality risks, and close surveillance with serial sonograms is warranted.
- Prenatal repair of myelomeningocele (MMC) is associated with improved neurologic outcomes and increased likelihood of an ability to ambulate without need for orthotics.
- The role of fetal therapy in severe congenital diaphragmatic hernia (CDH) remains under investigational protocols.
- The finding of fetal hydrops should be investigated carefully for underlying conditions that are potentially treatable in utero, such as anemia, congenital pulmonary airway malformation (CPAM), primary pleural effusion, sacrococcygeal teratoma (SCT), and chorioangioma.
- The field of fetal therapy is rapidly evolving. With further improvement of surgical equipment and prenatal diagnostic modalities, access to the fetal-placental unit via minimally invasive methods will likely become increasingly refined and provide a conduit for additional novel treatments of the fetus.

## OUTLINE

Open Maternal-Fetal Surgery, 776

Minimally Invasive Maternal-Fetal Surgery, 776

Ex Utero Intrapartum Therapy, 777

Conditions Amenable to Fetal Therapy, 778

Complicated Monochorionic Twins, 778

Myelomeningocele, 783

Congenital Diaphragmatic Hernia, 785

Congenital Pulmonary Airway Malformation, 788

Pleural Effusion, 789

Fetal Cardiac Interventions, 789

Lower Urinary Tract Obstruction, 790

Sacrococcygeal Teratoma, 791

Amniotic Band Syndrome, 791

Chorioangioma, 792

Summary, 793

Intrauterine fetal transfusion for severe fetal anemia secondary to Rh hemolytic disease was the first invasive prenatal therapy performed in humans. It is difficult for current practitioners to imagine that initial efforts in the 1960s were performed in the absence of ultrasound guidance.<sup>1</sup> Abdominal palpation and intrauterine and intraperitoneal instillation of contrast agent followed by fluoroscopy were used to perform the first fetal transfusions. Sonography has transformed the field of fetal therapy and serves as the ubiquitous diagnostic and intraoperative guidance tool.

An accurate detailed anatomic diagnosis is critical in determining the appropriateness of fetal surgical intervention. Fetal malformations that are not isolated or are associated with aneuploidy or a syndrome have generally been excluded as candidates for intervention. However, over the last few years, with the development of less invasive therapeutic options as well as increased accommodation for parental choice,

this paradigm has shifted (e.g., pleuroamniotic shunting for effusions and hydrops in a fetus with trisomy 21). Great effort should be made to confirm both the accurate diagnosis of a malformation and to determine if it is isolated or if other, possibly subtle associated abnormalities are present. In addition to targeted obstetric sonography, ancillary techniques to ensure full and accurate assessment include fetal echocardiography, magnetic resonance imaging (MRI), and genetic studies such as karyotyping and chromosomal microarray analysis. Counseling of patients and their families regarding the fallibility of the process, explaining that abnormalities initially believed to be isolated may not ultimately prove to be so, is a must.

In addition to its role as the primary tool for fetal diagnosis, sonography is routinely used during fetal interventions, both for instrument guidance and to monitor the fetus. In the following sections, fetal conditions amenable to in utero therapy as well as the role of



sonography in the diagnosis and treatment of various fetal abnormalities will be highlighted.

## OPEN MATERNAL-FETAL SURGERY

Maternal laparotomy/hysterotomy was historically the primary approach to fetal therapy (Fig. 24-1). Over time there has been a shift away from this technique toward minimally invasive fetal interventions. The development of small-diameter endoscopes has enabled surgical access into the womb with less perturbation to the pregnancy. Still, maternal laparotomy/hysterotomy remains the primary surgical approach for in utero repair of MMC and is one treatment option for fetal lung lesions and teratomas.<sup>2</sup>

Early experience with open maternal-fetal surgery was plagued by significant immediate postoperative complications, including maternal pulmonary edema related to use of multiple tocolytics, intraoperative blood loss, and refractory preterm labor.<sup>3</sup> With refinement of surgical technique, anesthesia, and immediate postoperative care, the risks of open maternal-fetal surgery have decreased, although they still remain high compared to minimally invasive approaches. In 2011, the results of a randomized controlled trial comparing prenatal versus postnatal surgical repair of MMC (MOMS [Management of Myelomeningocele Study] trial) were published.<sup>2</sup> In 78 patients who underwent open fetal surgery, the rate of maternal pulmonary edema was 6%, blood transfusion 9%, and preterm delivery before 30 weeks' gestation 13%. The postprocedure rate of oligohydramnios was 21%, and the rate of placental abruption was 6%. With respect to maternal risk, uterine dehiscence at the time of delivery was noted in 10% of cases, with an additional 25% of cases described as having a very thin lower uterine segment. There were no maternal deaths or uterine ruptures. The procedure also has significant impact on future pregnancies, with a 28% risk of subsequent uterine dehiscence or rupture.<sup>4</sup> All patients who undergo open maternal-fetal surgery require cesarean delivery before the onset of labor for the index pregnancy and all future pregnancies. As an *American College of Obstetricians and Gynecologists Committee Opinion* states, "Maternal-fetal surgery is a major procedure for the woman and her fetus, and it has significant implications and complications that occur acutely, postoperatively, for the duration of the pregnancy, and in subsequent pregnancies."<sup>5</sup>

Patients contemplating open maternal-fetal surgery undergo lengthy discussion about the risks of the procedure, with an emphasis on differentiating the risks to the mother, the fetus, and the pregnancy.



**FIG 24-1** Photograph of operative laparotomy and hysterotomy in a Rhesus monkey. This early work paved the way for the ability to perform such procedures safely in the mother carrying a fetus with a variety of malformations.

The risks to the mother are similar to those for any major abdominal surgery, although in this case, there is no direct physical benefit to her. General anesthesia risks are relatively increased owing to the high levels of inhalational anesthetics required to achieve uterine quiescence.<sup>6</sup> In addition, there are risks associated with aggressive tocolytic therapy and bed rest in pregnant women, who are in a hypercoagulable state. The risks to the fetus are primarily vascular instability and hypoperfusion intraoperatively, leading to organ injury or death, and prematurity due to postoperative complications. The risks to the pregnancy are primarily preterm labor and preterm premature rupture of membranes (PPROM) resulting in preterm delivery. Infectious complications are rare, except when PPRM leads to prolonged latency. As mentioned previously, an important additional discussion point is that all subsequent deliveries, as well as the index pregnancy, must be via cesarean delivery. Data regarding future fertility are reassuring, with no documented increased incidence of infertility.<sup>7</sup> Another potential risk in subsequent pregnancies is placenta accreta; the site of a hysterotomy performed for fetal surgery in the second trimester is not the same as a lower segment cesarean delivery. Thus, placental implantation in a subsequent pregnancy is more likely to overlie the uterine scar, increasing the risk of accreta, and this factor must be considered in the sonographic evaluation of a subsequent pregnancy.

Sonography is used for guidance before the hysterotomy procedure in open maternal-fetal cases. Once general anesthesia and intubation of the patient have been initiated, and the sterile field is established, sonography is used to assess fetal lie, fetal location within the uterus, and position of the placenta. If needed, transabdominal manipulation is used to position the fetus such that the fetal surgical site is near the fundus. Laparotomy is then performed and the sonography transducer, covered in a sterile sleeve, is placed directly on the surface of the uterus. The location and edge of the placenta are identified, because this information is critical in determining where to safely enter the uterus. Generally, one wants to make the uterine incision as far from the placental edge as possible. Once the incision is made, and the amniotic fluid drains, the uterus shrinks. If the placental edge is too close to the uterine incision, there is a risk of bleeding and abruption, which cannot readily be controlled and, if significant, will usually necessitate immediate delivery for maternal safety.

Sonography is also used for transuterine monitoring of the fetal heart during the surgical repair of the MMC (Fig. 24-2). Following completion of the fetal intervention, the membranes and myometrium are closed with several layers of suture. A catheter is left in the uterine cavity to allow lactated Ringer solution to be infused together with antibiotics. Sonography is used to determine the volume of "amniotic" fluid instilled to achieve a low-normal level, aiming to minimize stress on the suture line.

Postoperative management generally involves 24 hours of intravenous tocolysis with magnesium sulfate as well as maintenance with oral indomethacin for a total of 48 hours. Antibiotic "prophylaxis" is continued for 24 hours. Typically, ultrasound monitoring to evaluate the fetus, amniotic fluid volume, cervical length, and ductal patency is performed daily. Hospital discharge generally occurs 4 to 5 days after surgery. If the patient is stable without complications, long-term monitoring with follow-up sonograms usually involves weekly evaluation.

## MINIMALLY INVASIVE MATERNAL-FETAL SURGERY

Minimally invasive fetal surgery generally refers to all invasive fetal interventions performed without the need for hysterotomy. Depending on the indications and goals of the procedure, minimally invasive fetal therapy may be performed under ultrasound guidance alone, such as





**FIG 24-2** Chorioamniotic separation noted, with amniotic fluid seen on either side of the membrane (arrow), following fetal procedure.



**FIG 24-3** EXIT (ex utero intrapartum therapy) procedure. Photograph obtained following reversal of fetal tracheal occlusion for congenital diaphragmatic hernia demonstrates intubation of the neonate while placental umbilical circulation is maintained.

**TABLE 24-1 List of Fetal Conditions Amenable to Minimally Invasive Fetal Treatment**

Condition	Procedure
<b>Needle and Shunts</b>	
Alloimmunization	Transfusion
Bronchopulmonary sequestration	Interstitial ablation of feeding vessel
Congenital pulmonary airway malformation	Thoracoamniotic shunt or sclerotherapy
Critical aortic stenosis	Balloon valvuloplasty
Iatrogenic preterm premature rupture of fetal membranes	Amniopatch
Lower urinary tract obstruction	Vesicoamniotic shunt
Pleural effusion	Thoracoamniotic shunt
Pericardial teratoma with effusion	Pericardioamniotic shunt
Symptomatic polyhydramnios	Amnioreduction
<b>Operative Fetoscopy</b>	
Amniotic band syndrome	Lysis of constriction bands
Chorioangioma	Ablation of feeding vessels
Congenital diaphragmatic hernia	Tracheal occlusion
Myelomeningocele	Fetoscopic patch or closure
Twin reversed arterial perfusion sequence	Umbilical cord occlusion
Twin-twin transfusion syndrome	Laser photocoagulation of communicating vessels
Vasa previa (type II)	Laser occlusion of vasa previa
Sacroccygeal teratoma	Interruption of vascular supply

needle or shunt placement procedures, or may require a combined approach with both sonography and endoscopy, also known as operative fetoscopy (Table 24-1).

Ultrasound-guided needle interventions include intrauterine transfusion (IUT) and amnioreduction. Shunts are used when indicated for chronic drainage of abnormal, fluid-filled fetal cavities, organs, and cysts. A wide variety of fetal conditions have been

surgically managed via operative fetoscopy.<sup>8,9</sup> This technique, which utilizes a 3.3-mm or smaller endoscope, is associated with significantly lower risk of preterm birth, neonatal morbidity, and maternal morbidity as compared to open fetal surgery.<sup>3</sup> There is a lower rate of preterm labor and of PPRM. The length of hospitalization and time until return to normal maternal activity are also shorter. In addition, patients who have undergone minimally invasive fetal therapy do not require cesarean delivery for the index pregnancy or for future pregnancies.

Minimally invasive procedures are performed under local or regional anesthesia. Depending on the gestational age and the protocols of the medical center, the procedure may be performed in the surgical operating room, labor and delivery unit, or ultrasound examination suite. Operative fetoscopy requires simultaneous utilization of ultrasound and fetoscopic imaging. Access to the amniotic cavity is achieved with thin-walled semiflexible plastic cannulas and either a plastic blunt-ended obturator using the Seldinger technique or sharp trocars. Specifics have been reviewed in several texts.<sup>8</sup> Ultrasound imaging is used to identify an appropriate entry point and then to direct the instrument into the amniotic cavity, avoiding the placenta and the fetus and maternal organs such as bowel and bladder. The obturator/trocar is replaced by the fetoscope. Sonography is still used to direct the scope within the uterus, because its field and depth of view can be relatively limited. At the conclusion of the procedure, the sheath is removed. As the puncture is only 1 to 3 mm in size, the uterine wall spontaneously closes with minimal risk of amniotic fluid leak from the insertion site. In many cases, little or no tocolytic medication is needed, and patients are generally discharged from the hospital within 24 hours following the procedure.

## EX UTERO INTRAPARTUM THERAPY

The ex utero intrapartum therapy (EXIT) procedure is a specialized surgical procedure performed at the time of delivery. It was first developed in the early 1990s to permit the controlled reversal of tracheal occlusion performed in utero for the treatment of severe CDH (Fig. 24-3).<sup>10</sup> This procedure is utilized in cases in which prenatal ultrasound findings predict significant neonatal airway compromise, resulting from lesions such as large oral or neck masses, or congenital



high airway obstruction syndrome (CHAOS). Maternal general endotracheal anesthesia with high levels of an inhalational agent is provided to maintain uterine quiescence. The fetal head and neck are delivered through a low transverse uterine incision, protecting the umbilical cord and maintaining uteroplacental blood flow for an extended period of time. This allows for the performance of a surgical procedure or life-saving intervention while the fetus continues to be oxygenated and ventilated through placental support. The EXIT procedure has been used to perform fetal bronchoscopy, laryngoscopy, tracheostomy, cannulation for extracorporeal membrane oxygenation (ECMO), and even resection of a lung mass or lobectomy.<sup>11</sup>

Once the uterus is exposed, intraoperative ultrasound assessment is required to confirm placental location and fetal position. The hysterotomy is performed, avoiding placental margins along the lower uterine segment. Preventing complete decompression of the uterus is important to reduce the likelihood of placental separation. This can be achieved by keeping the lower part of the fetal body within the uterus and by performing continuous amnioinfusion with a catheter. The EXIT procedure is not a simple variation of a cesarean delivery and should be carried out in specialized centers. The presence of a complete multidisciplinary team is required to perform appropriate preoperative evaluation, including discussion of the fetal diagnosis, counseling, and planning for the EXIT procedure. The intraoperative team includes an anesthesiologist, maternal-fetal medicine specialist, pediatric surgical subspecialist(s), and operating room nursing assistants. Neonatologists and a second complete operative team should be prepared to receive the newborn in the event that corrective measures performed while still on umbilical circulation are unsuccessful.<sup>11</sup>

## CONDITIONS AMENABLE TO FETAL THERAPY

### Complicated Monochorionic Twins

Monochorionic twin gestations are associated with a high risk of significant perinatal morbidity and mortality as compared to dichorionic twins and singletons.<sup>12,13</sup> This increased risk is partially attributed to the unique placental vascular communications present in monochorionic twin gestations. Because the circulatory systems communicate, the death of one monochorionic twin may result in acute hypotension in the survivor; this hemodynamic instability may result in subsequent death or injury to the co-twin.<sup>14</sup> A systematic review of 28 primary studies, including over 4500 twin pregnancies with in utero demise of one twin, reported that the rate of monochorionic versus dichorionic co-twin demise was 12% versus 4%, and the rate of neurologic abnormality in the surviving co-twin was 18% versus 1%, respectively.<sup>15</sup> Placental vascular communications are also thought to be important factors in the development of twin-twin transfusion syndrome (TTTS), twin anemia-polycythemia sequence (TAPS), and twin reversed arterial perfusion (TRAP) sequence.

Placental share is an additional factor with significant impact on perinatal outcomes in monochorionic twins. Marked unequal partitioning of the placental mass may be manifest clinically by selective fetal growth restriction (sFGR). Finally, the risk of structural anomalies is increased in monochorionic twins, including in particular those involving the central nervous system as well as cardiac and gastrointestinal tract abnormalities. Over 80% of such anomalies are discordant (only one twin affected).<sup>16,17</sup> Some of these anomalies are associated with a high risk of fetal demise if managed expectantly. Even without the previously described complications, monochorionic twins are at an increased risk of neurodevelopment impairment. In one study, Ortibus and colleagues prospectively followed 136 monochorionic twin pregnancies from the first trimester through infancy.<sup>18</sup> After excluding pregnancies complicated by TTTS, discordant growth,

intrauterine fetal demise (IUID), and prematurity (birth before 32 weeks' gestation), the authors found that the 160 remaining infants had a 7% risk of neurodevelopmental impairment and a 0.6% risk of cerebral palsy.

Complications affect approximately 20% of monochorionic twins, and, thus, accurate diagnosis and close surveillance of these pregnancies are recommended.<sup>19</sup> Chorionicity should be established as early as possible in the pregnancy.<sup>20</sup> First and early second trimester ultrasound examination has been shown to be highly accurate in determining chorionicity and should be performed to allow for appropriate triage and management of the pregnancy.<sup>21</sup> Close surveillance of monochorionic twins should include frequent sonograms, typically performed every 2 weeks, to monitor amniotic fluid volumes and fetal bladders.<sup>22,23</sup> Cervical length assessment and Doppler interrogation should be performed, if necessary. If TTTS, TAPS, TRAP, sFGR, or discordant structural anomalies are suspected, the patient should be referred to an experienced center.

### Twin-Twin Transfusion Syndrome

TTTS occurs in approximately 10% of monochorionic twins.<sup>19</sup> Most experts believe that TTTS develops in monochorionic twin pairs as a result of unbalanced net flow of blood through vascular communications in the shared placenta.<sup>24,25</sup> A series of pathophysiologic changes ensue from the net shunting of blood from one twin (donor) to the other twin (recipient), resulting in hypovolemia and oliguria in one, and volume overload and polyuria in the other (Fig. 24-4A). These hemodynamic derangements result in a cascade of physiologic changes<sup>26,27</sup> leading to donor twin oligohydramnios, recipient twin polyhydramnios, and characteristic anatomic and arteriovenous flow alterations that can be identified by sonography with Doppler.<sup>28-30</sup> Without intervention, early severe TTTS has a very high rate of perinatal injury or death.<sup>31</sup>

The diagnosis of TTTS is based on the following in utero ultrasound-based criteria: (1) monochorionicity and (2) single maximal vertical pocket (MVP) of amniotic fluid less than 2.0 cm on one side of the dividing membrane, and MVP of more than 8.0 cm on the other side.<sup>28</sup> Once the diagnosis has been established, the syndrome may be staged according to the Quintero staging system (Table 24-2). The establishment of diagnostic criteria and the classification of TTTS by Quintero and associates<sup>28</sup> have allowed researchers to compare outcome data following various therapeutic interventions and to predict perinatal survival after treatment.<sup>32</sup>

The perinatal mortality rate of expectantly managed TTTS has been reported to be as high as 95%.<sup>31</sup> Of the various treatment approaches that have been considered for TTTS, those with the best-reported outcomes are serial amniocenteses and selective laser photocoagulation of communicating vessels (SLPCV) via operative fetoscopy (Fig. 24-4B). Serial amniocentesis (or amnioreduction) involves drainage of amniotic fluid from the polyhydramniotic recipient sac using vacuum-assisted devices attached to an 18- to 20-gauge spinal needle. The volume of amniotic fluid that should be withdrawn has not been standardized, although usually the MVP of amniotic fluid in the recipient sac is reduced to approximately 8 cm or less. Serial amniocenteses serve to significantly reduce the amount of amniotic fluid in the recipient sac, thereby diminishing overall uterine distention.

SLPCV is performed via operative fetoscopy, allowing direct visualization of the vessels on the placental surface. Once mapping of vascular communications has been performed, those vessels are occluded using laser energy (Figs. 24-5 and 24-6). The basic principle of SLPCV is that the causative inter-twin vascular communications are ablated, thus treating the underlying pathogenic cause of this syndrome.<sup>33</sup> With laser surgery, the circulations in a shared placenta are



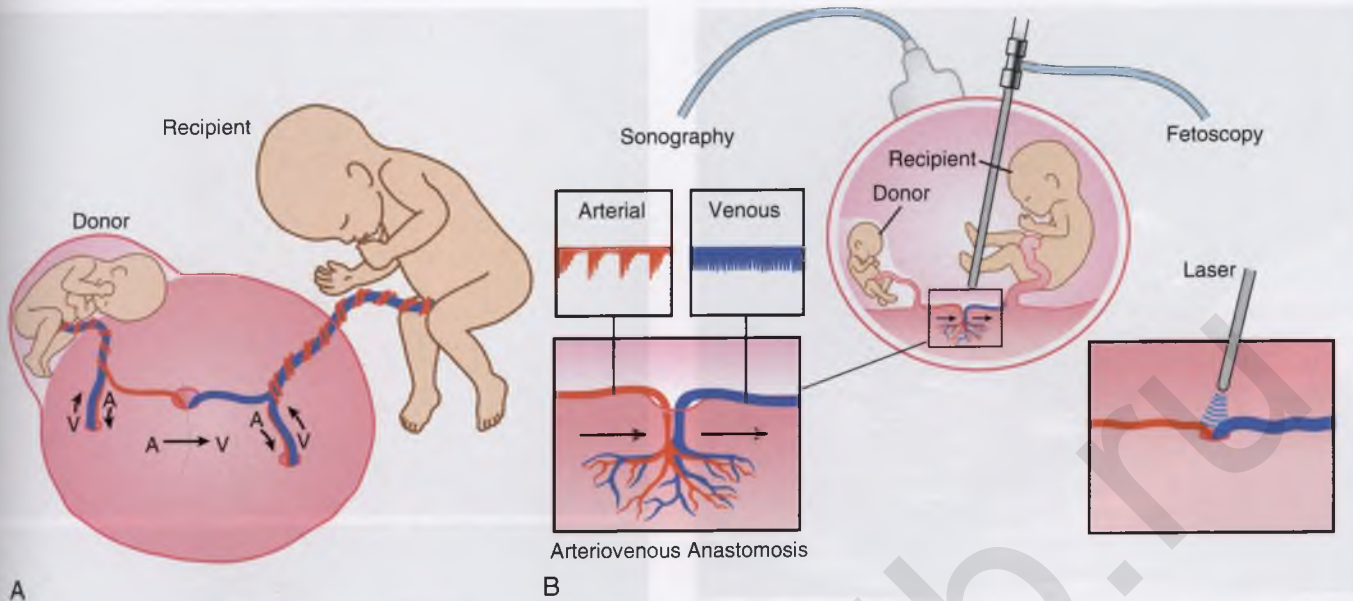


**FIG 24-4 A**, Monochorionic twin placenta, demonstrating arteriovenous vascular (A → V) connection. **B**, Diagram illustrating sonographic guidance for laser ablation for twin-twin transfusion syndrome. Doppler interrogation is used to identify arterial and venous connections, and laser energy is applied to the site of anastomosis.

**TABLE 24-2 Staging of Twin-Twin Transfusion Syndrome**

Stage	Polyhydramnios/ Oligohydramnios*	Persistently Empty Bladder in Donor	Abnormal Doppler <sup>†</sup>	Hydrops	Demise
I	X				
II	X	X			
III	X	X	X		
IV				X	
V					X

\*Polyhydramnios is defined as deepest vertical pocket 8 cm or greater; oligohydramnios is defined as deepest vertical pocket 2 cm or less.

<sup>†</sup>At least one of the following: (1) umbilical artery absent/reserved end-diastolic flow, (2) absent/reversed end-diastolic flow in the ductus venosus, (3) pulsatile umbilical venous flow.

Modified from Quintero RA, Morales WJ, Allen MH, et al: Staging of twin-twin transfusion syndrome. *J Perinatol* 19:550, 1999; and Taylor MJO, Jolly M, Wee L, et al: Validation of the Quintero staging system for twin-twin transfusion syndrome. *Obstet Gynecol* 100:1257, 2002.

divided, functionally converting it to a dichorionic twin pregnancy, with improved perinatal outcomes.<sup>34</sup>

After the introduction of laser ablation as a treatment option for TTTS, the Eurofetus group conducted a randomized controlled trial that compared serial amniocentesis to SLPCV.<sup>35</sup> Pretrial power analysis projected the need for a total of 172 patients to demonstrate a significant difference in outcomes between the two treatment arms. However, after enrollment of 142 patients, interim analysis revealed that the perinatal survival rate of at least one twin was 51% (36/70) in the amnioreduction arm versus 76% (55/72) in the laser therapy arm. Based on this statistically significant difference, the study was halted. In addition, in the laser group, pregnancy duration was approximately 4 weeks longer (33 weeks vs. 29 weeks,  $P = 0.003$ ). The amnioreduction group had a significantly higher rate of neurologic complications (14% vs. 6%,  $P = 0.02$ ), and this difference persisted at the 6-month follow-up evaluation.

Most subsequent studies have confirmed that SLPCV is the optimal treatment for TTTS.<sup>36</sup> Intervention with laser surgery has resulted in survival rates for at least one twin ranging from 65% to 93% and dual survival rates ranging from 18% to 62%.<sup>37</sup> Although several factors may influence perinatal outcomes in laser-treated TTTS patients, one

important consideration is disease severity.<sup>38</sup> Knowledge of perinatal outcomes of TTTS pregnancies treated with laser, stratified by Quintero stage, may facilitate patient selection and counseling. In a series of 682 consecutive cases of TTTS treated via SLPCV, there was a 91% perinatal survival rate of at least one twin and 67% survival rate of both twins.<sup>39</sup> Of note, perinatal survival of at least one fetus has been reported to be independent of Quintero stage, whereas dual twin survival does appear to differ based on stage. This is predominantly because stage III pregnancies are associated with decreased donor twin survival (Table 24-3), particularly in those with growth restriction of the donor. These pregnancies are nearly twice as likely as those without growth restriction to suffer in utero demise of the donor.<sup>40</sup> The average gestational age at delivery following laser surgery is approximately 33 weeks, with 10% delivering between 24 and 28 weeks' gestation.<sup>41</sup> The laser surgical technique has undergone recent modifications that may further improve perinatal outcomes.<sup>42,43</sup>

The surgical goal of SLPCV is to completely occlude all placental vascular connections between the twin pair. A missed or inadequately lasered vessel, referred to as a residual anastomosis (RA), may be associated with adverse perinatal outcomes such as persistent or reversed TTTS or TAPS.<sup>44-46</sup> Pathologic confirmation of complete ablation of





**FIG 24-5** Laser for twin-twin transfusion syndrome. Fetoscope can be seen adjacent to twin A in the polyhydramniotic sac. The placenta is posterior.

vascular communications can be ascertained via ex vivo placental injection studies in cases without placental maceration related to IUFD.<sup>44</sup> RA after SLPCV has been reported to be as low as 4%<sup>47</sup> to 5%,<sup>48</sup> although some studies have reported frequencies of RA ranging from 32%<sup>44-46</sup> to as high as 75%<sup>49</sup> of cases. In a 2014 trial investigating laser coagulation of the entire vascular equator, the rate of RA was still 19%.<sup>50</sup> The wide range of RA rates in these studies has been attributed to the laser technique employed and to the method of placental evaluation.<sup>45</sup>

Despite evidence that SLPCV improves neonatal survival and reduces morbidity, cerebral injury is not fully prevented. Periventricular infarction, hemorrhagic injury, and ischemic white matter damage have been detected prenatally in fetuses treated with laser surgery for TTTS.<sup>51</sup> The incidence of cerebral damage may be underestimated, because neurodevelopmental impairment and intellectual disability may only manifest several months or years after birth.<sup>52,53</sup> Thus, a major concern for clinicians and parents is the rate of neurologic impairment in survivors. A systematic review found that the risk of neurodevelopmental impairment after laser therapy for TTTS is about 11%.<sup>54</sup> Cerebral palsy was the most frequent diagnosis, accounting for about 40% of abnormal neurologic outcomes.<sup>54</sup> In a cohort of 100 TTTS survivors treated with in utero laser surgery, formal neurodevelopmental testing, performed at 2 years of age, revealed normal range mean Battelle Developmental Inventory, 2nd edition (BDI-2)<sup>11</sup> scores of 101.3 (standard deviation [SD] = 12.2) for the entire cohort.<sup>55</sup> The overall rate of neurodevelopmental impairment, defined as blindness, deafness, cerebral palsy, or BDI-2 score less than 70, was 4%.<sup>55</sup>

### Selective Fetal Growth Restriction

sFGR, defined as one twin with an estimated fetal weight (EFW) below the 10th percentile for gestational age, is reported to occur in at least 10% of monochorionic twin pairs.<sup>56</sup> It is important to note that significant growth discordance with or without amniotic fluid discordance is not required for the diagnosis of sFGR. sFGR appears to be distinct from TTTS, although there may be significant overlap in these conditions.<sup>57</sup> It is believed that sFGR develops because of unequal

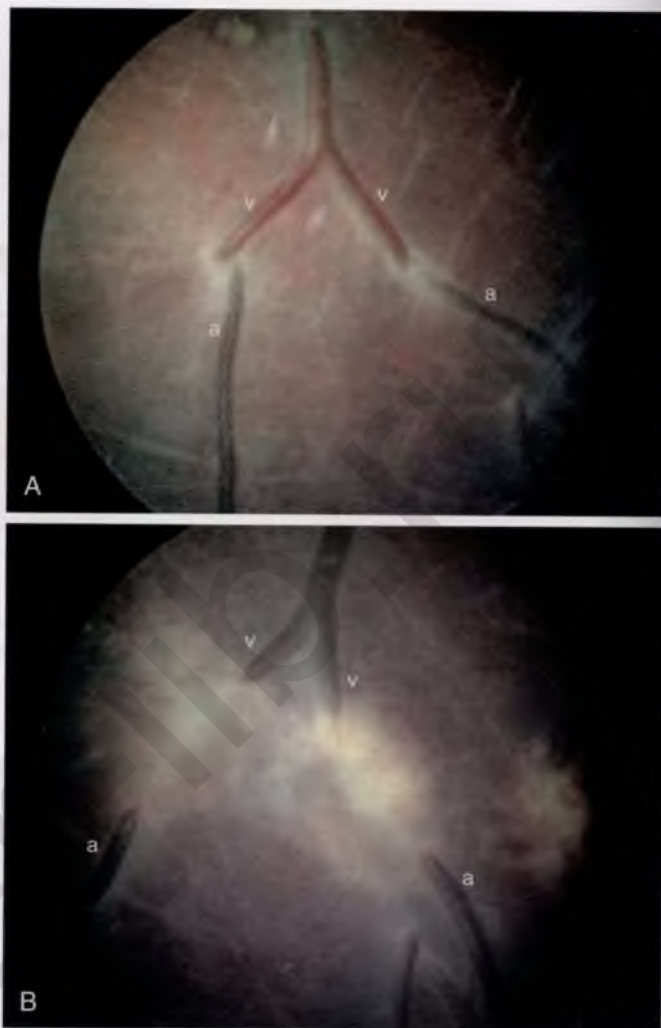


**FIG 24-6** Fetoscopic image of the fetal surface of a monochorionic twin placenta in the region of the vascular equator. Two placental arteries (a) from the donor twin communicate with placental veins (v) of the recipient twin, shown before (A) and after (B) laser photocoagulation.

**TABLE 24-3 Stage-Based Perinatal Survival After Laser Surgery for Twin-Twin Transfusion Syndrome**

	Stage I (n = 114)	Stage II (n = 177)	Stage III (n = 328)	Stage IV (n = 63)
At least 1 survivor	92%	93%	88%	92%
Dual survival	79%	76%	59%*	68%

\*Decreased dual twin survival in Quintero stage III patients predominantly from decreased donor twin survival in cases complicated by severe growth restriction.

Modified from Chmait RH, Kontopoulos EV, Korst LM, et al: Stage-based outcomes of 682 consecutive cases of twin-twin transfusion syndrome treated with laser surgery: the USFetus experience. *Am J Obstet Gynecol* 204(5):393.e106, 2011.

placental share, with the sFGR fetus perfusing a smaller portion of the single shared placenta.<sup>58</sup>

Although disproportion in placental territories allocated to monochorionic twin pairs appears to be the primary contributor to sFGR, the presence of vascular communications plays an important role in



perinatal outcome.<sup>56</sup> There is increased likelihood of spontaneous in utero demise of the sFGR fetus, which may result in concomitant demise or severe neurologic handicap of the co-twin.<sup>15</sup> Following demise of the sFGR twin, sudden redistribution of blood flow via placental vascular connections can lead to acute hypotension in the surviving co-twin. Thus, the larger (appropriately grown for gestational age, AGA) twin may face an increased risk of neurodevelopmental impairment related to co-twin demise or prematurity.<sup>59</sup> One observational study monitored 84 consecutive monochorionic twin pairs with discordant amniotic fluid that did not meet criteria for TTTS and showed a 60% (23/38 fetuses) overall survival rate in the subgroup that met criteria for sFGR.<sup>60</sup> In another study of 17 pregnancies with sFGR that were managed expectantly, the survival rate of the sFGR twin was 59%.<sup>61</sup> The rate of short-term intracranial injury (including periventricular leukomalacia, intraventricular hemorrhage, and ventriculomegaly) in this group of patients was 14%. In a separate review, the overall incidence of severe cerebral injury in survivors of pregnancies complicated by sFGR was found to be approximately 8%.<sup>59</sup> Factors associated with poor neurologic outcomes included abnormal umbilical artery Doppler waveforms, intrauterine co-twin demise, and earlier gestational age at birth.<sup>59</sup>

The understanding of the pathophysiologic changes of sFGR has advanced significantly in recent years. A staging system based on umbilical artery Doppler findings was proposed by Gratacos and colleagues in 2007 and is now used by some centers.<sup>56</sup> The authors classified monochorionic twin pregnancies complicated by sFGR into three categories based on umbilical artery Doppler waveforms of the sFGR twin, as follows: type I with persistent forward diastolic flow; type II with persistent absent or reversed end-diastolic flow (AREDF); and type III with intermittent absent or reversed end-diastolic flow (iAREDF). These three groups are associated with different patterns of placental anastomoses and with different clinical courses, which can influence prenatal monitoring and management.

In type I sFGR, the median age at diagnosis is approximately 20 weeks' gestation. In utero deterioration is not common in this group. Once this diagnosis is made, umbilical artery Doppler findings in the sFGR twin usually remain normal until delivery.<sup>58</sup> It is reasonable to maintain close surveillance with weekly sonograms with Doppler, and to escalate follow-up as necessary. There appears to be no benefit from fetal intervention in this group, and it is reasonable to plan delivery at 34 to 35 weeks' gestation in the absence of obstetric indications for earlier delivery.<sup>62</sup>

At this time, the optimal treatment strategy for monochorionic twin pregnancies complicated by sFGR type II, with persistent AREDF in the umbilical artery, is not clear. Expectant management requires close monitoring of the pregnancy with sonography or fetal heart rate monitoring, often in the hospital setting, from 24 weeks' gestation until delivery, aiming to prolong the pregnancy yet intending to deliver the twins prior to demise of the growth-restricted fetus. The umbilical artery Doppler findings cannot be used to predict imminent fetal demise. Doppler interrogation of the ductus venosus (DV) appears to be the best adjunct for fetal surveillance, as is done in singleton pregnancies complicated by FGR.<sup>62</sup> Observation of absent or reversed a-wave flow on DV waveforms should prompt the clinician to consider delivery or fetal intervention, depending on gestational age. If the DV waveform remains normal, the patient can be followed once or twice a week. Expectant management is associated with a very high (nearly 100%) rate of prematurity, with risk of neurologic injury to the AGA twin. Intervention may be considered in cases of type II sFGR, particularly when the diagnosis is made prior to viability. One therapeutic option is to perform operative fetoscopic ablation of all inter-twin vascular communications, thereby creating a "functionally"

dichorionic twin gestation.<sup>61</sup> The surgical intervention is similar to the laser technique used for treatment of TTTS, although the procedure may be technically more difficult. Quintero and coworkers performed a feasibility study that showed a trend toward decreased rate of neurologic deficits in the AGA twin (14% rate of neurologic injury in the expectantly managed group versus 0% in the SLPCV group).<sup>61</sup> Chalouhi and associates found that SLPCV resulted in a survival rate of 52% in sFGR twins and 74% in AGA twins.<sup>63</sup> As an alternative to fetoscopic SLPCV, umbilical cord occlusion (UCO) or radiofrequency ablation (RFA) of the sFGR twin has been offered.<sup>58</sup> These techniques aim to protect the AGA twin from potential injury or death resulting from spontaneous in utero demise of the sFGR co-twin. These approaches, by definition, result in demise of the sFGR fetus. Selective reduction in these circumstances has resulted in survival rates of the AGA co-twin of 74%.<sup>63</sup>

Type III sFGR is characterized by iAREDF in the umbilical artery of the sFGR twin. The umbilical artery Doppler waveform pattern displays cyclic changes during diastole, such that there is alternating positive AREDF.<sup>62</sup> This unique Doppler waveform suggests the presence of a large arterioarterial (AA) anastomosis within the shared placenta, coursing between the twins' cord insertion sites.<sup>64</sup> Outcomes of pregnancies with evidence of type III sFGR may be difficult to predict.<sup>56</sup> Unexpected IUFD has been reported in approximately 15% of cases, with sudden death documented hours after a normal Doppler ultrasound examination.<sup>65</sup> Another study has reported that the AGA twin has an elevated risk of postnatal white matter lesions, even if the smaller twin is born alive.<sup>66</sup> Thus, management of these pregnancies is challenging. Fetoscopic laser ablation of vascular connections has been attempted in this population, but the results were not favorable compared to expectant management.<sup>67</sup> SLPCV could not be completed in over 10% of cases owing to technical difficulties, and overall perinatal survival rate was 64% in the laser group compared to 86% in those managed expectantly. However, it should be noted that the prevalence of leukomalacia in the larger infant was 1/17 (5.9%) in the laser group versus 4/28 (14.3%) in the expectantly managed group.<sup>67</sup>

Late-onset sFGR, referring to the development of growth restriction of one twin after 26 weeks' gestation, is another previously described subgroup of complicated monochorionic twin gestations.<sup>68</sup> The prevalence of late-onset sFGR among monochorionic twin pairs has been reported by Lewi and colleagues to be 6.3% in a cohort of 208 pregnancies.<sup>68</sup> Mean gestational age at delivery was 35 weeks and 38% of infants met postnatal diagnostic criteria for TAPS. There was one intrauterine death.<sup>68</sup>

### Twin Anemia-Polycythemia Sequence

TAPS is an atypical form of TTTS that also appears to be caused by a net transfer of blood from one monochorionic twin to the other. TAPS is characterized by large inter-twin hemoglobin differences in the absence of oligohydramnios and polyhydramnios. This condition may develop spontaneously (2-6% of monochorionic twins) or as a result of residual vascular communications following laser surgery (2-13% of monochorionic twins who have had laser).<sup>44,69-72</sup> Unlike TTTS, which is likely due to more acute hemodynamic imbalances, the pathogenesis of TAPS has been attributed to chronic net transfusion from one twin to the other, presumably at a slow enough rate to allow for hemodynamic equilibration.<sup>73,74</sup> TAPS may result in severe anemia in one twin and polycythemia in the other (Fig. 24-7). Placental pathologic studies have shown that pregnancies complicated by TAPS have relatively few, small-caliber (<1 mm) arteriovenous communications as compared to larger arteriovenous communications seen in placentas from pregnancies affected by classic TTTS.<sup>74</sup>



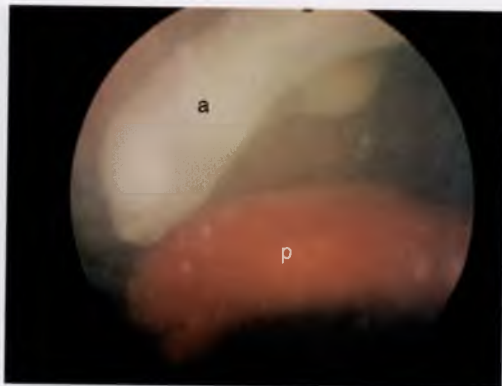


**FIG 24-7** Fetoscopic image demonstrating striking discordance in coloration between monozygotic twin fetuses with TAPS (twin anemia polycythemia syndrome). The red foot belongs to the polycythemic (p) twin and the pale white foot belongs to the anemic (a) twin.

Although there is not consensus in the literature, the antenatal definition of TAPS usually requires that the middle cerebral artery (MCA) peak systolic velocity (PSV) measures greater than 1.5 multiples of the median (MoM) in the anemic twin and less than 1.0 MoM in the polycythemic twin, and that the pregnancy is not affected by oligohydramnios or polyhydramnios.<sup>69</sup> An antenatal staging system has been proposed, and although it has not been validated clinically, it is useful to facilitate communication between practitioners.<sup>74</sup> Stage 1 is defined as MCA PSV measurement greater than 1.5 MoM in one twin and less than 1.0 MoM in the other, without evidence of fetal compromise. Stage 2 is defined as MCA PSV greater than 1.7 MoM in one twin and less than 0.8 MoM in the other, also without signs of fetal compromise. Stage 3 requires fulfillment of stage 1 or 2 criteria, with additional finding of critically abnormal Doppler waveforms (defined as AREDF in the umbilical artery, pulsatile flow in the umbilical vein, or reversed a-wave flow in the DV) in the anemic twin. Stage 4 includes hydropic changes in the anemic twin, whereas stage 5 is defined as demise, preceded by TAPS, of one or both twins. Postnatal diagnostic criteria and classification, described by the same investigators, requires an inter-twin hemoglobin difference of more than 8 g/dL and at least one of the following: reticulocyte count ratio more than 1.7 and placental pathologic findings of only small (<1 mm diameter) inter-twin vascular communications.<sup>74</sup>

Given the relatively low prevalence and lack of clinical awareness of this condition, the natural history of TAPS is unclear and decision making regarding antenatal treatment is controversial. Case series have reported expectant management with timed delivery,<sup>69,75-77</sup> intrauterine fetal transfusion,<sup>78</sup> and fetoscopic laser treatment.<sup>77-82</sup> Favorable outcomes have been described in pregnancies with uncomplicated TAPS using expectant management or other conservative measures, particularly in those diagnosed in the third trimester. Spontaneous resolution of TAPS has also been reported.<sup>83</sup> However, TAPS may progress and result in perinatal death or neurologic injury.<sup>72,76</sup> Polycythemia can lead to vascular sludging, which may lead to cerebral venous thrombosis resulting in intraventricular hemorrhage and parenchymal infarction, and fetal anemia may affect cerebral oxygenation resulting in hypoxic-ischemic cerebral injury.<sup>76</sup> Timed delivery, on the other hand, must be weighed against the risks of prematurity. Although survival rates of 75% can be obtained with expectant management, it has been suggested that treatment with IUT or laser surgery can increase survival to over 90%.<sup>74</sup> A recent 2014 study has reported that neurodevelopmental impairment and cognitive delay were found in almost 20% of children surviving posttreatment for TAPS, with the lowest cognitive scores detected in the subgroup of TAPS survivors

treated with IUT.<sup>84</sup> It is not known whether survivors of spontaneously resolved TAPS face a similar risk for neurodevelopmental impairment or cognitive delay.

IUT has been suggested as a temporizing, symptomatic treatment of the anemic twin in a pair affected by TAPS. However, there is concern that transfused blood may worsen symptoms in the recipient (polycythemic) twin, which might then develop iatrogenic complications related to hyperviscosity, such as limb necrosis.<sup>72</sup> Two cases have exhibited spontaneous placental vascular thromboses, possibly because of hyperviscosity in the polycythemic twin.<sup>82</sup> Thus, IUT (without definitive laser surgery) may exacerbate the risk of vascular thromboses and other complications. The use of intrauterine partial exchange transfusion may help reduce the risk of severe polycythemia complications.<sup>85</sup> On the other hand, partial exchange transfusion in the neonate has been associated with suboptimal coagulation with subsequent disseminated intravascular coagulation, so this procedure is not without risk.<sup>76</sup>

Fetoscopic laser surgery is the only definitive treatment for TAPS. Laser surgery may be beneficial in pregnancies complicated by TAPS, particularly in high-risk cases in which additional ultrasound findings suggest fetal compromise. However, laser surgery may be technically more challenging in TAPS than in TTTS given the absence of polyhydramnios, absence of a “stuck” twin, slack inter-twin membrane, and difficulty visualizing the very small communicating vessels. Nevertheless, reports of fetoscopic laser treatment for TAPS have indicated that this intervention can be effective.<sup>77-82,86</sup> Further research is needed to establish selection criteria for in utero treatment of TAPS, possibly based on the presence of coexisting amniotic fluid discordance; Doppler waveform abnormalities in the umbilical artery, umbilical vein, or DV; sFGR; hydrops fetalis; cervical insufficiency; or gestational age at onset.

### Twin Reversed Arterial Perfusion Sequence

TRAP sequence affects approximately 1% of monozygotic twins, or about 1 in 35,000 pregnancies.<sup>87</sup> The presence of direct artery-to-artery and vein-to-vein placental anastomoses allows one fetus (pump twin) to perfuse the other anomalous fetus, typically referred to as an acardiac fetus (perfused twin). The term *acardiac fetus* is at times a misnomer, as the perfused twin may rarely have a rudimentary heart. The perfused twin is supplied with blood flowing in a reversed direction (the umbilical artery delivers blood to the perfused twin and the umbilical vein carries blood away, toward the placenta). Because of the direct artery-to-artery anastomosis, the deoxygenated blood from the pump twin is carried to the perfused twin through that twin's umbilical artery or arteries. The perfused twin, typically with no functional beating heart, has severe maldevelopment of cephalic, thoracic, and upper extremity structures, which is not compatible with postnatal survival.

Ultrasound diagnosis of TRAP sequence can be made in the first and early second trimesters, particularly with the aid of color and spectral Doppler techniques.<sup>88</sup> Note that the lack of a beating heart within the perfused twin may be misinterpreted as co-twin demise. In some cases, the presence of a rudimentary heart may be confusing. In this setting, it is important to interrogate the cord insertion site at the anterior abdominal wall of the anomalous fetus to assess for reversal of flow direction in the umbilical artery (Fig. 24-8).

The risk of pump twin demise is as high as 50% to 75% due to the hemodynamic burden and volume overload.<sup>89</sup> Risk factors for poor perinatal outcome include polyhydramnios in the pump twin, critically abnormal Doppler waveforms, hydrops, or a large perfused anomalous twin measuring greater than 50% of the pump twin's estimated weight.<sup>90</sup> If at least one of these factors is present between 16



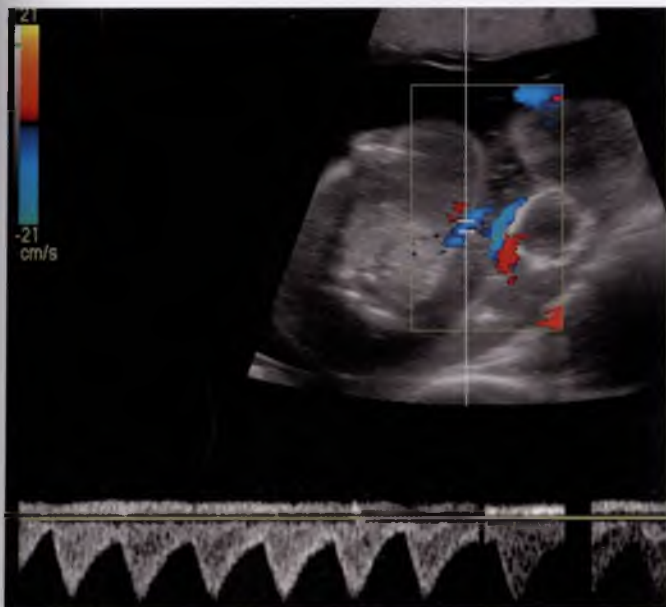


**FIG 24-8** Twin reversed arterial perfusion (TRAP) sequence. Transaxial ultrasound image of the acardiac twin at the level of the umbilical cord insertion. Color and spectral Doppler interrogation demonstrates reversed pulsatile arterial flow (in blue), directed away from the transducer toward the acardiac fetus. This Doppler ultrasound finding is pathognomonic of TRAP sequence.

and 26 weeks' gestation, the patient should be offered the option of intervention to achieve UCO of the perfused twin. In one study of 74 cases complicated by TRAP sequence, high-risk factors were defined as at least one of the following ultrasound findings: (1) abdominal circumference of the perfused twin equal to or greater than that of the pump twin, (2) polyhydramnios (maximum vertical pocket > 8 cm), (3) abnormal Doppler waveform in the pump twin, (4) hydrops of the pump twin, or (5) monoamniotic twins.<sup>90</sup> The perinatal survival rate for the high-risk pump twins in those patients who did not elect to undergo UCO was 43%.<sup>90</sup> Current reported perinatal survival rates of high risk pump twins who have undergone UCO is approximately 80% to 90%.<sup>91,92</sup>

A variety of techniques have been used to achieve UCO of the acardiac twin. Fetoscopic UCO is one common approach, and can be performed using a variety of surgical techniques, such as umbilical cord laser photocoagulation, laser of the placental vascular communications, and suture ligation.<sup>90</sup> Similar results can be achieved with bipolar electrocautery<sup>93</sup> and intrafetal RFA<sup>94,95</sup> (Fig. 24-9). Each approach is particularly suited to a given clinical circumstance, and the UCO modality is usually dictated by technical considerations, availability of instrumentation, and surgeon preference.<sup>96,97</sup>

### Twins With Discordant Structural Anomalies

Monochorionic twins may be affected by discordant structural anomalies. Patients with monochorionic twins discordant for a severe congenital anomaly, particularly those at significant risk of in utero demise, should be offered the option of selective reduction by UCO. Treatment via intravascular potassium chloride (KCl) injection is the primary method for selective reduction in dichorionic twins<sup>98</sup> but is contraindicated in monochorionic twin gestations for two reasons.<sup>99</sup> First, vascular communications within the monochorionic placenta may serve as a conduit for passage of the injected agent to the co-twin. Second, following reduction, acute exsanguination or hypotension of the

co-twin via the connections in the shared placenta can result in neurologic injury or death. Thus, in these cases, UCO can be performed in a similar fashion to that described for TRAP sequence. As there are potential complications, including injury to the co-twin, those monochorionic twin pregnancies with discordant anomalies for whom UCO is considered require careful assessment and counseling of the risks and benefits particular for each case.<sup>100</sup>

### Myelomeningocele

Spina bifida is one of the most common birth defects in the United States,<sup>101</sup> occurring in approximately 1 in 1500 liveborn infants annually.<sup>5</sup> Spina bifida occurs when the embryonic neural plate fails to complete its development and does not fully close along its length. Failure of the posterior neuropore to close can result in meningocele (only the meninges protrude through the spinal defect) or MMC (both neural and meningeal elements protrude).<sup>102,103</sup> Both lesions are referred to by the generic term spina bifida, with MMC being the more common type. Infants born with MMC require neurosurgical closure within the first days of life, and face lifelong disabilities, including varying degrees of sensorimotor paralysis below the level of the lesion, as well as bladder and bowel incontinence, musculoskeletal deformities, and spinal cord tethering at the site of surgical repair. For most individuals with MMC, lifelong support, rehabilitation, and medical interventions are likely.<sup>104-106</sup>

The combination of maternal serum alpha-fetoprotein (MSAFP) screening and routine use of obstetric ultrasound imaging in the second trimester has resulted in approximately a 90% detection rate of MMC.<sup>107</sup> Sonography typically reveals spinal dysraphism with splayed vertebral arches. The spina bifida lesion may appear flat with no overlying sac or may have a thin-walled sac filled with cerebrospinal fluid covering the placode. The sac may contain neural elements that can be seen on sonography (see Chapter 9, Fig. 9-7). Search for associated intracranial ultrasound findings is critical for maximizing in utero sonographic detection of spina bifida. The cisterna magna may appear obliterated and the cerebellum banana-shaped because of downward herniation of this structure into the upper cervical spinal canal (Chiari II malformation). A characteristic lemon-shaped calvarium may be seen, with inward scalloping of the frontal bones. Dilatation of the lateral cerebral ventricles is another common finding. Finally, equinovarus (clubfoot) deformity of one or both lower extremities can be found in fetuses with spina bifida.<sup>107</sup>

MMC leads to injury and loss of spinal cord tissue at and below the level of the lesion. Abnormal spinal cord development may explain some of the neurologic deficits associated with MMC. However, mounting evidence suggests that intrauterine trauma and toxic exposure to amniotic fluid may contribute to the newborn's neurologic impairment.<sup>108-110</sup> The "two-hit hypothesis" of spinal cord injury in MMC has been shown in a variety of animal models, including sheep, rhesus monkey, pig, rabbit, rat, mouse, chick, and duck.<sup>111</sup> The majority of these experiments have involved surgically created MMC, in which a multilevel laminectomy and dural opening are performed midgestation. Later in pregnancy, repair of the lesion is performed in one set of animals, whereas the lesion is left unrepaired in the others. The control group is then compared to the study group. The theoretical advantage of fetal repair of MMCs is that the neural tube is covered and protected many months before the expected delivery date. The basis for anticipating improved neurologic function is that coverage and restoration of the dysplastic neural placode within the spinal canal isolate it from amniotic fluid and prevent ongoing injury.

In animal models, prenatal correction of iatrogenic MMC has led to the birth of offspring with preserved motor function and sphincter control. Reversal of cerebellar herniation has also been noted in sheep



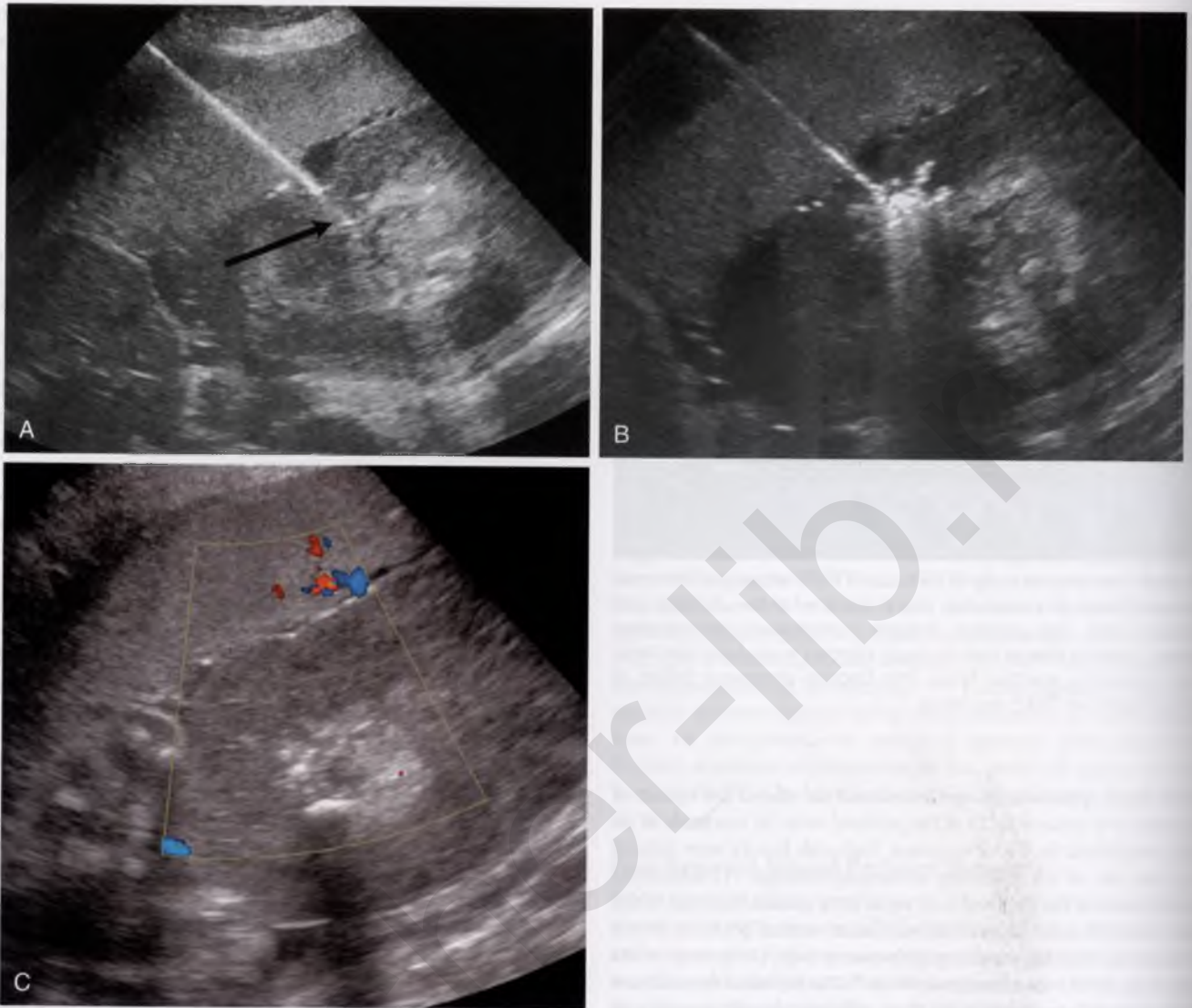


**FIG 24-9** Radiofrequency ablation of acardiac fetus. **A**, Device is deployed into fetal abdomen at level of cord insertion (*arrow*). **B**, Bright reflection from gas bubbles created during radiofrequency ablation procedure. **C**, Color Doppler confirms absent flow in acardiac fetus following procedure.

that underwent intrauterine operations. Mueli and colleagues surgically created a spinal cord lesion in fetal sheep at 75 days of gestation that simulated an MMC lesion.<sup>112-114</sup> Following delivery, pathologic evaluation of the exposed spinal cord in the control group resembled a human spina bifida lesion. These animals were incontinent and had loss of sensation and motor function below the level of the lesion. Other animals with surgically created spina bifida lesions were treated using a myocutaneous flap at 100 days of gestation. These animals subsequently had near-normal motor function and bowel and bladder control. In another animal experiment, hindbrain herniation mimicking Chiari II malformation was surgically created prenatally by establishing leakage of spinal cord fluid at the level of the distal cord. Fetal repair subsequently reversed this hindbrain herniation.<sup>115</sup>

Encouraged by results in animal models, investigators began to repair MMC in human fetuses. Owing to technologic constraints, the surgical approach adopted has been open in utero repair (Figs. 24-10 and 24-11).<sup>116</sup> This procedure requires general anesthesia of the mother to maintain uterine quiescence, maternal laparotomy, hysterotomy,

and neurosurgical closure of the fetal MMC. In 1999, Tulipan and coworkers reported outcomes of 26 of their first 28 cases of in utero MMC repair in humans, comparing them to historic MMC control subjects treated with postnatal surgical repair.<sup>117,118</sup> Intrauterine MMC repair was associated with reduced incidence of moderate to severe hindbrain herniation (4% vs. 50%) and reduced occurrence of shunt-dependent hydrocephalus (58% vs. 92%). However, the average level of lower extremity function closely matched the average anatomic level of the MMC lesion in both groups. Similar findings were noted by other investigators.<sup>119</sup> In 2003, the National Institutes of Health (NIH) funded a multicenter randomized controlled trial of open in utero surgical repair of fetal MMC versus standard neonatal repair. The results of this MOMS trial were published in 2011.<sup>2</sup> Inclusion criteria specified a singleton gestation with upper level of the MMC lesion between T1 and S1, evidence of hindbrain herniation, gestational age at surgery between 19.0 and 25.9 weeks, normal karyotype, absence of anomalies unrelated to the MMC, absence of severe kyphosis, and maternal body mass index less than 35. Prenatal repair resulted in



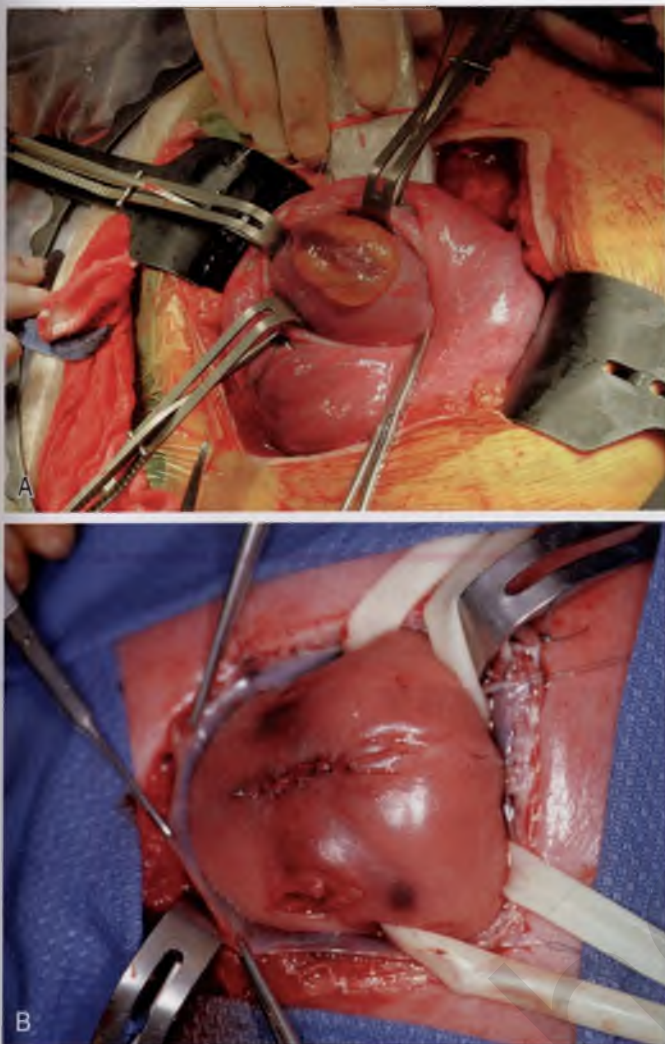


**FIG 24-10** Photograph of a fetus with lumbar myelomeningocele before (A) and after (B) in utero repair.

reduced need for ventriculoperitoneal shunting at 12 months of age, decrease in the rate of hindbrain herniation at 12 months, doubling of the ability to ambulate without the assistance of orthotics, and level of sensorimotor function two or more levels better than expected based on anatomic level of the defect. However, open in utero repair was associated with significant risks, including higher rates of preterm birth, fetal intraoperative bradycardia, oligohydramnios, placental abruption, maternal pulmonary edema, and maternal transfusion and a 35% risk of uterine thinning or dehiscence.

A fetoscopic approach for in utero correction of open spina bifida was first reported in 1997 by Bruner and colleagues.<sup>120</sup> By 2011, a total of 19 surgeries with complete in utero treatment of MMC had been attempted by Verbeek and colleagues.<sup>121</sup> With growing experience, Kohl and his team have demonstrated that fetoscopic treatment of MMC may achieve perinatal outcomes similar to those reported in the MOMS trial, which involved the open fetal surgical approach.<sup>122,123</sup> Pedreira and associates have reported on four cases treated fetoscopically using a simplified surgical technique to achieve watertight closure, taking advantage of the unique healing characteristics of the fetus (Fig. 24-12).<sup>124</sup> Because of the decreased maternal risks with operative fetoscopy as compared to open fetal surgery, it is highly likely that if neurodevelopmental outcomes of MMC are found to be comparable, this

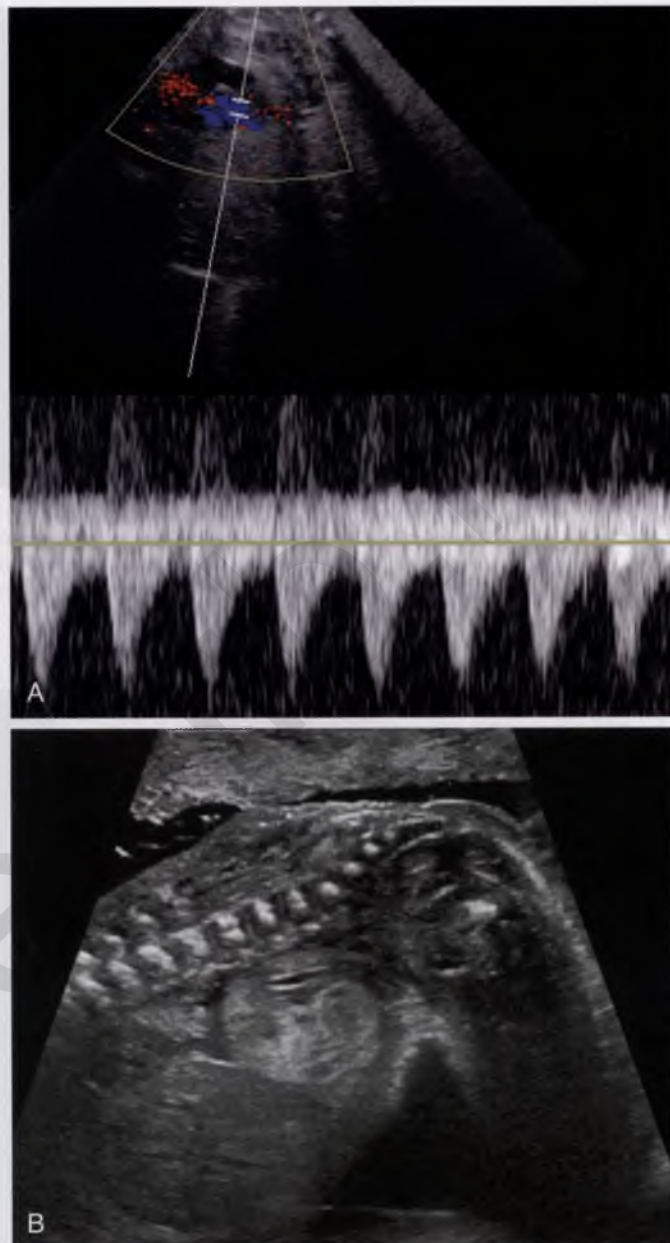


**FIG 24-11** Open fetal myelomeningocele repair. A, Intraoperative monitoring of fetal cardiac activity. B, Intraoperative evaluation of fetal spine following in utero repair.

surgical approach will replace open maternal-fetal surgery for this condition.

### Congenital Diaphragmatic Hernia

CDH is a sporadic birth defect that occurs in 1 in 2500 to 3000 pregnancies.<sup>125</sup> Approximately 80% of CDHs are left-sided, 15% are right-sided, and 5% are bilateral. About 50% to 60% are isolated abnormalities and the remaining cases are associated with genetic syndromes and other anomalies.<sup>126</sup> With CDH, the diaphragmatic defect results in herniation of abdominal organs into the thoracic cavity, causing displacement and compression of the fetal lungs. The abnormal in utero lung development is clinically manifest after birth by neonatal respiratory insufficiency and pulmonary hypertension.<sup>127</sup> The natural history of isolated CDH depends on the degree of pulmonary compromise



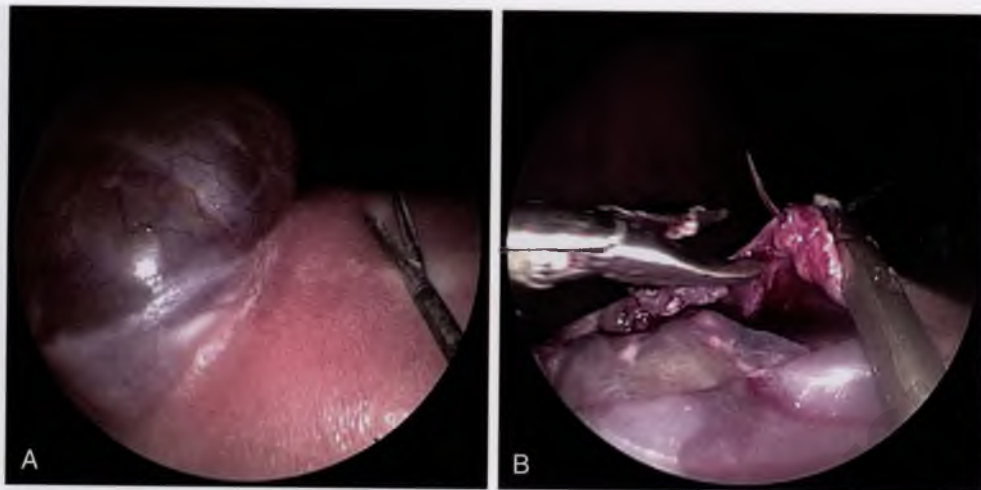


**FIG 24-12** Images from fetoscopic fetal myelomeningocele repair. Fetal surgery is performed under maternal general anesthesia using minimally invasive technique with three trocars and partial carbon dioxide insufflation. **A**, The fetal lumbosacral myelomeningocele is seen through the fetoscope. **B**, After dissection of the neural placode, the surrounding skin is closed over with a cellulose patch using a single continuous stitch. (Courtesy of Dr. Denise Pedreira.)

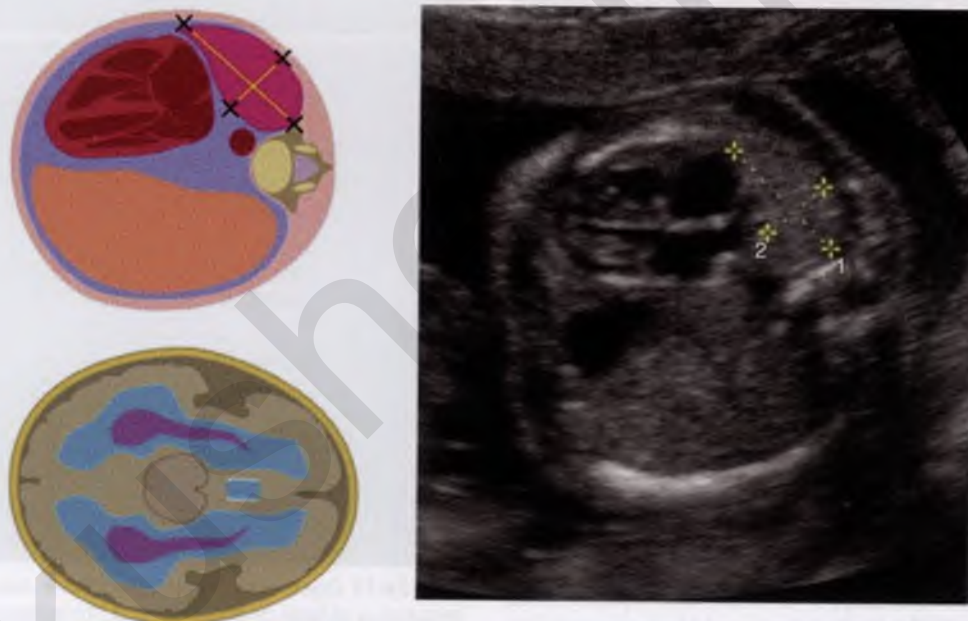


**FIG 24-13** Illustration of the method for measuring lung-to-head ratio (LHR) in a fetus with left congenital diaphragmatic hernia (CDH). The measurement of the right lung (in a fetus with typical left CDH) uses a transverse axial plane of section through the fetal thorax at the level of the four-chamber view of the fetal heart. The ultrasound section should be symmetric so that a single rib is seen on each side. The longest axis of the right lung is measured (in millimeters) and is multiplied by the longest perpendicular measurement (in millimeters). This product ( $\text{mm}^2$ ) is then divided by the measurement of the head circumference (in millimeters), obtained at the level of the standard biparietal diameter view, to obtain the LHR.

present at birth. Overall, perinatal mortality risk has remained high despite advances in neonatal intensive care.<sup>126,128-131</sup> Of liveborn cases with prenatally diagnosed CDH, the pulmonary hypoplasia is lethal in 30% to 40%.<sup>129</sup> Thus, the goal of prenatal assessment of CDH is twofold: (1) determine if the CDH is isolated and (2) assess the degree of mass effect upon the developing lungs.

A variety of indirect measures have been used to more precisely determine the prognosis of fetuses with CDH. In addition to identifying herniation of liver into the thorax, the area of the contralateral lung

and its relationship to the head circumference (lung-to-head ratio, LHR) has been assessed as a prognostic indicator. LHR was first proposed by Metkus and coworkers in 1996 as a sonographic parameter to predict neonatal outcome in fetuses with CDH.<sup>132</sup> LHR is calculated by dividing the product of the largest perpendicular diameters of the contralateral lung on a transaxial image at the level of the four-chamber view of the heart (lung area, in  $\text{mm}^2$ ) by the head circumference (in mm) (Fig. 24-13). The margins of the contralateral lung may also be traced manually to provide a more accurate determination of lung



area. Division of the calculated lung area by the head circumference, used as an internal control, was suggested to provide a gestational age-independent measure of CDH severity.<sup>132</sup> However, use of LHR as a predictor for neonatal outcomes and as a sonographic criterion for surgical intervention in CDH has come into question.<sup>133,134</sup> Peralta and associates, in a study of 650 normal fetuses with gestational ages of 12 to 32 weeks, demonstrated that LHR increases with advancing gestation, indicating that this parameter is not independent of gestational age.<sup>135</sup> Jani and colleagues proposed the use of observed versus expected (o/e) LHR to correct for the effect of gestational age.<sup>133</sup> However, o/e LHR was able to identify only 46% of CDH fetuses that did not survive, with an attendant 10% false positive rate.<sup>133</sup> Others have suggested that the suboptimal performance of LHR may be related to variability in ultrasound technique and methodology used to calculate this ratio.<sup>136</sup>

Another reason why LHR is a problematic measure is related to its mathematical formula.<sup>137</sup> The lung area (numerator) is measured in mm<sup>2</sup> (area), whereas the head circumference (denominator) is measured in mm (length). This results in a first-degree polynomial equation, which, in the case of LHR, has a persistent positive slope.<sup>137</sup> LHR increases with advancing gestation. The same holds true for o/e LHR.<sup>138</sup> Using mathematical modeling, a gestational age-independent sonographic index of lung size, the quantitative lung index (QLI), was developed by Quintero and coworkers.<sup>137</sup> This calculation involves the division of two second-degree polynomials:

$$QLI = LA / (HC/10)^2$$

where LA is the traced lung area (in mm<sup>2</sup>) of the contralateral lung at the level of the four-chamber view of the heart and HC is the head circumference (in mm).<sup>137</sup> The 50th percentile of QLI is approximately 1.0 from 16 to 32 weeks of gestation, whereas a small lung (<1st percentile) is defined as QLI less than 0.6<sup>137</sup> (Fig. 24-14).

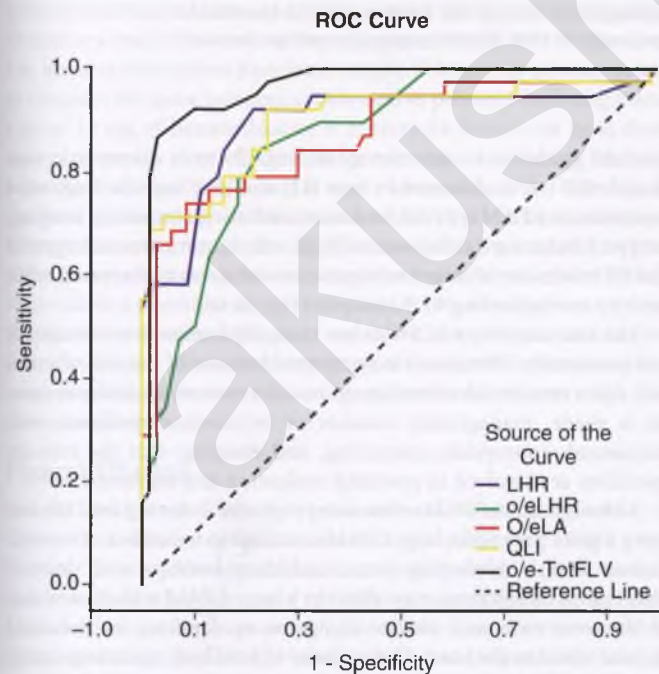


**FIG 24-14** Receiver operating characteristic (ROC) curve for prediction of neonatal death using the quantitative lung index (QLI), observed versus expected contralateral lung area (O/eLA), lung-to-head ratio (LHR), observed versus expected lung-to-head ratio (o/eLHR), and observed versus expected total lung volume (o/e-TotFLV).

Other methods to evaluate lung size include measuring total lung volume using MRI or three-dimensional (3D) sonography.<sup>139</sup> Although these modalities provide enhanced visualization of lung fields, they have not been shown to provide more accurate prognosis compared to standard 2D sonography. Liver herniation is consistently associated with higher postnatal mortality rate; thus, quantification of the degree of liver herniation is another method that has been used to predict outcome.<sup>140,141</sup>

Using the previously described prenatal assessment techniques, fetal intervention has been proposed for severe forms of isolated CDH, defined as LHR less than 1.0, o/e LHR less than 25%, or QLI less than 0.6.<sup>138,139</sup> Mild to moderate CDH is not considered an indication for in utero surgery at this time because of the relatively high survival rates with postnatal care.<sup>139</sup> In the past, prenatal surgical intervention emulated postnatal surgery for CDH, intending anatomic repair of the diaphragm. The procedure was shown to be feasible in the fetus, except when the liver was herniated. Acute reduction of the liver back into the fetal abdomen resulted in kinking of the DV and obstruction of blood flow from the umbilical vein. Therefore, fetuses with “liver up”—that is, those that would most benefit from in utero repair, were not candidates for fetal surgery. Based on observations made regarding lung growth in fetuses with congenital high airway obstruction, the concept of iatrogenic reversible fetal tracheal occlusion (to promote pulmonary development) was proposed and carefully investigated. In 2003, a randomized clinical trial conducted in the United States compared tracheal occlusion via open fetal surgery to expectant management.<sup>142</sup> Entry criteria for the study included LHR 1.4 or less. The study did not show a benefit of in utero surgery over standard postnatal care. However, a post-hoc analysis of the data suggested that a more restrictive LHR of less than 1.0 might have been more appropriate, because survival rate in this subgroup of CDH fetuses was only 33% compared to nearly 100% in fetuses with LHR greater than 1 in both the surgical and expectant management groups.<sup>142</sup> Since then, the approach to in utero management of CDH has undergone a paradigm shift, with abandonment of all open fetal surgery techniques (whether to correct the defect or perform external tracheal occlusion<sup>143</sup>) in favor of ultrasound-guided, fetoscopic tracheal occlusive procedures.

Tracheal occlusion has been offered as a prenatal intervention for severe CDH in the hopes of improving perinatal survival.<sup>144,145</sup> Animal and human studies have shown that the lungs of CDH fetuses have morphologic abnormalities,<sup>146,147</sup> manifest by fewer alveoli with increased interstitial tissue<sup>148</sup> and decreased number but excessively muscularized intrapulmonary arteries<sup>149,150</sup> as well as impaired lung mechanics.<sup>151</sup> The concept of prenatal tracheal occlusion is based on experimental data suggesting there is accelerated lung growth following this intervention owing to mechanical stretching forces from the increased hydrostatic lung fluid pressure.<sup>152</sup> However, despite a gross increase in lung mass, sustained fetal tracheal occlusion results in histologic abnormalities in the lung, including oligomacroleoalveolar development<sup>153</sup> and decreased number of type II alveolar cells.<sup>154</sup> Therefore, intermittent tracheal occlusion was proposed to better emulate normal fetal lung growth and maturation, which appear to be related to both tonic stretching forces due to in utero pulmonary fluid secretion as well as cyclic stretching forces from intermittent fetal breathing activity.<sup>155,156</sup>

The current clinical strategy is to perform tracheal occlusion between weeks 26 and 28, followed by removal of the occlusion at 34 weeks' gestation,<sup>143,145</sup> although there is some controversy regarding optimal timing and duration of occlusion.<sup>157</sup> Insertion of the tracheal occlusive device is performed under combined ultrasound and fetoscopic guidance. The endoscope is introduced into the amniotic cavity and is advanced into the fetal mouth and through the pharynx, larynx,



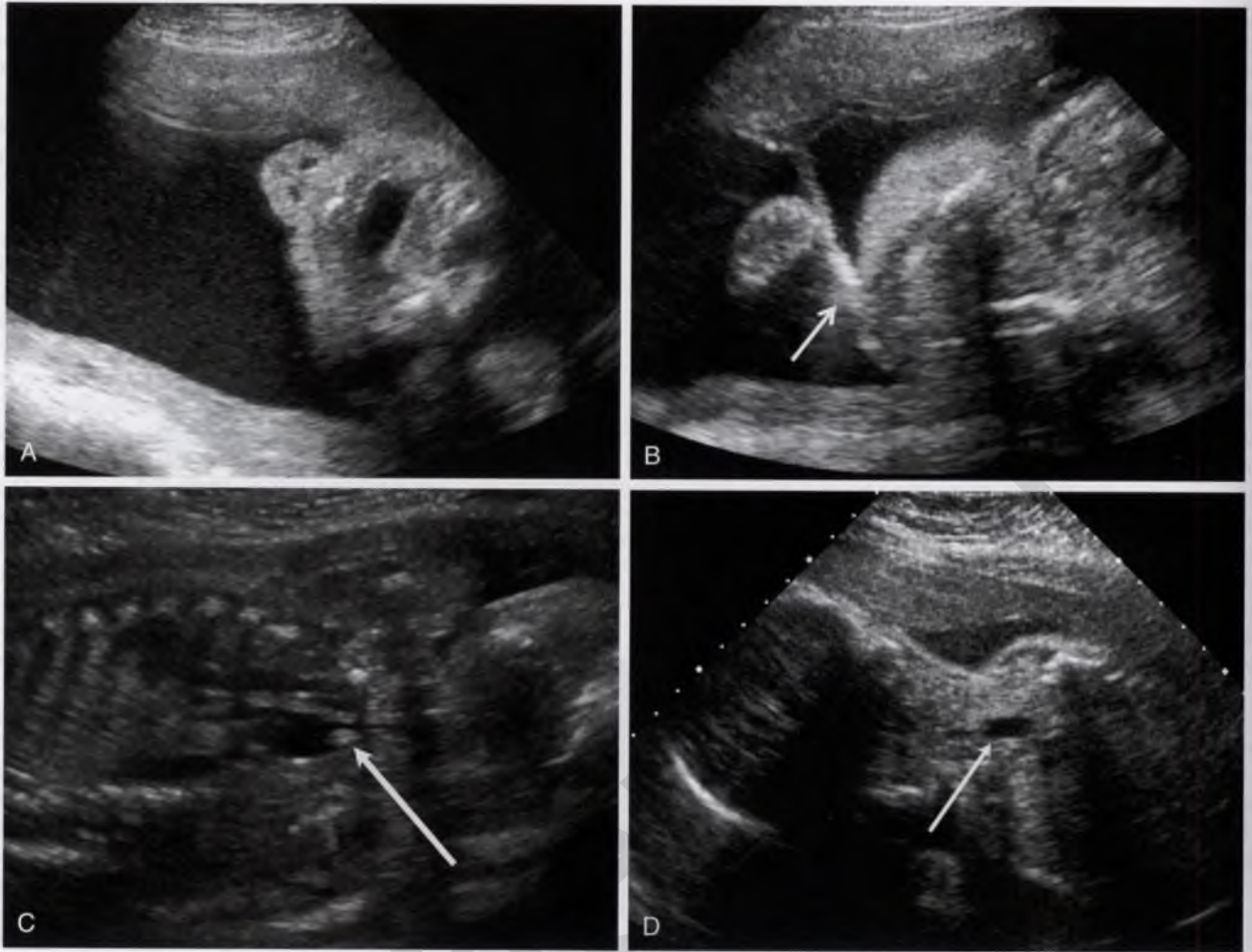


**FIG 24-15** Tracheal balloon occlusion for congenital diaphragmatic hernia. **A**, Fetal mouth is identified. **B**, Device is seen adjacent to fetal mouth (arrow). **C**, Device is seen in fetal trachea deploying balloon (arrow). **D**, Balloon is seen in fetal trachea (arrow).

past the epiglottis, and into the fetal trachea. Once the carina is identified, the device is deployed (Fig. 24-15). Two tracheal occlusive devices have been utilized: a detachable balloon<sup>158</sup> and a modified 8-mm Z-stent.<sup>159</sup> Removal of the tracheal occlusive device is performed at approximately 34 weeks' gestation via fetoscopic retrieval or at the time of delivery via EXIT procedure. Studies of fetuses with severe isolated CDH have demonstrated significant improvement in survival rates in those who underwent fetoscopic tracheal occlusion compared with control subjects.<sup>144,160</sup> Additional trials, including one being conducted by the fetal endoscopic tracheal occlusion (FETO) task group in Europe, are ongoing. Interpretation and applicability of the results of these trials must take into account the inclusion criteria, local resources, and postnatal care provided to these infants.

### Congenital Pulmonary Airway Malformation

CPAM, previously termed congenital cystic adenomatoid malformation, is an abnormality of lung development characterized by hamartomatous overgrowth of the terminal bronchioles with subsequent suppression and lack of differentiation of normal alveoli.<sup>161</sup> CPAMs are classified into three major types.<sup>162</sup> Type I CPAM is defined as a distinct, thin-walled cyst that measures greater than 2 cm in diameter and is lined with ciliated pseudostratified columnar epithelium. In contrast, types II and III lesions consist of multiple microcysts lined by

cuboidal epithelium (each cyst measuring <2 cm in diameter in type II and <0.5 cm in diameter in type III) and may contain large solid components. CPAM type can be determined using ultrasound imaging, as type I lesions are composed of large echolucent cysts and types II and III lesions are of mixed echogenicity with areas of increased echogenicity corresponding to microcysts (Fig. 24-16).

The vast majority of CPAMs are clinically benign, both prenatally and postnatally. They are usually resected because of the risk of infection and a remote risk of malignant transformation. Once the diagnosis is made, management consists of in utero surveillance with ultrasound, appropriate counseling, and ensuring that the relevant specialists are involved in postnatal evaluation and treatment.

Although most CPAMs remain asymptomatic during fetal life and carry a good prognosis, large CPAMs can lead to a number of complications in the developing fetus, including hydrops and death.<sup>163</sup> Hydrops can result from mass effect by a large CPAM with obstruction of the vena cava and cardiac compression, resulting in decreased venous return to the heart. The presence of fetal hydrops in association with CPAM is the most important prognostic factor. In the absence of hydrops, live birth rates are reported to be higher than 95%.<sup>164</sup> However, the presence of hydrops carries a grave prognosis, with risk of perinatal mortality close to 100% without fetal intervention.<sup>165</sup> Thus, fetal therapy is indicated when hydrops develops in the second or early third





**FIG 24-16** Ultrasound images of three types of congenital pulmonary airway malformations (CPAM). **A**, Type I CPAM (macrocystic) with several cysts measuring greater than 2 cm in diameter. **B**, Type II CPAM (mixed macrocysts and microcysts) with several distinct small cysts measuring less than 2 cm in diameter (*calipers*), surrounded by hyperechoic, solid-appearing tissue that represents the microcystic component. **C**, Type III CPAM (microcystic), a hyperechoic, solid-appearing lesion (*calipers*) with no sonographically resolvable distinct cysts. H, heart.

trimester.<sup>165</sup> In an attempt to predict which fetuses with CPAM are at risk of developing hydrops, calculation of the ratio of the lesion volume (in cubic centimeters) divided by the head circumference (in centimeters) (CPAM volume ratio [CVR]) has been proposed.<sup>166</sup> When the calculated CVR is greater than 1.6, there is approximately 80% risk for subsequent development of fetal hydrops.

If fetal hydrops develops before 32 to 34 weeks' gestation, fetal intervention can be lifesaving. Fetal treatment for large type I CPAMs involves percutaneous aspiration and drainage via thoracoamniotic shunt placement.<sup>167</sup> In general, prognosis is favorable. Types II and III CPAMs are composed of multiple microcysts with solid components and are not amenable to aspiration or thoracoamniotic shunting. Historically, these lesions have been treated with open maternal-fetal surgery, fetal thoracotomy, and tumor resection, resulting in resolution of hydrops and a fetal survival rate of approximately 50%.<sup>168</sup> However, less invasive alternatives have been sought.<sup>169</sup> Maternal administration of steroids (the same protocol as that used to promote fetal lung maturity, or 12 mg of betamethasone  $\times$  2, every 24 hours) has been demonstrated to be very effective in preventing or reversing hydrops secondary to large CPAMs and is now widely offered.<sup>170-172</sup> Percutaneous laser ablation, coil embolization, and RFA have all been utilized in attempts to reduce tumor size. Of these modalities, percutaneous laser ablation may be associated with the lowest procedure-related risk.<sup>170</sup> Percutaneous sclerotherapy of semisolid CPAMs has also been successfully performed, with subsequent reduction in tumor size and resolution of hydrops.<sup>173</sup> Since the recognition of the effectiveness of maternal corticosteroids, however, such surgical interventions are much less commonly required.

### Pleural Effusion

Isolated fetal pleural effusion (also referred to as hydrothorax) is uncommon, with a reported incidence of 1/10,000 to 1/15,000 pregnancies.<sup>174</sup> Prenatal sonographic diagnosis is made by identification of anechoic fluid adjacent to and partially surrounding the lung. When pleural effusions are large and unilateral, they can exert mass effect with significant mediastinal shift, which can secondarily lead to hydrops, an independent risk factor for perinatal death.<sup>175</sup> Prognosis largely depends on the underlying cause of the fetal hydrothorax. There is a significant association between fetal pleural effusions and aneuploidy as well as other structural abnormalities.<sup>176</sup> Thus, detailed anatomic survey and fetal genetic testing should be offered.<sup>177</sup> Unilateral

fetal hydrothorax appears to more often occur sporadically and is associated with a more favorable prognosis than bilateral effusions. Unilateral hydrothorax may be caused by congenital malformation of the thoracic duct or the pulmonary lymphatic system.<sup>178</sup> Hydrothorax resulting from lymphatic malformations may be supported by the finding of an elevated lymphocyte count ( $>80\%$ ) in aspirated pleural fluid (fetal chylothorax).<sup>174</sup> Large unilateral hydrothorax with associated mass effect can progress to bilateral pleural effusions and subsequent hydrops fetalis, thereby complicating the clinical picture. Determination of whether a hydroptic fetus has a primary pleural effusion or pleural fluid from generalized hydrops can be challenging. In cases of fetal hydrops with large asymmetric pleural effusions and evidence of associated mass effect with mediastinal shift and eversion of the hemidiaphragm, many authors will assume that the larger pleural effusion is the primary cause.<sup>179</sup>

Fetal intervention in the setting of hydrothorax is typically reserved for cases that develop secondary hydrops and has been shown to improve survival rate in this group.<sup>180,181</sup> Perinatal survival rate of hydroptic fetuses with a dominant pleural effusion treated with thoracoamniotic shunting is approximately 50%.<sup>179</sup> Some authors offer fetal treatment in cases considered high risk for developing hydrops, such as those with rapidly enlarging effusions, polyhydramnios, significant mediastinal shift, or evidence of cardiac compromise,<sup>182</sup> evidenced by fetal echocardiography documenting abnormal ventricular filling.<sup>183</sup> Several different therapeutic modalities for management of fetal hydrothorax have been described, including repeated thoracenteses, thoracoamniotic shunting, maternal blood injection into the fetal pleural cavity, and pleurodesis. Of these, the most commonly employed technique is thoracoamniotic shunting.<sup>184</sup>

### Fetal Cardiac Interventions

An emerging area of fetal therapy is in the treatment of congenital heart defects. Some cardiac defects are structurally simple, but because of the dynamics of fetal growth and circulation, progressive abnormal development of the great vessels, outflow tracts, and ventricles can ensue, resulting in a poorly functioning heart after birth. An example of this is critical aortic stenosis, which may progress to hypoplastic left heart syndrome (HLHS). It has been speculated that in utero reversal of aortic valve stenosis can prevent progression to ventricular hypoplasia. At present, the standard postnatal treatment for a single-ventricle heart, such as HLHS, is staged palliative surgery (Norwood





**FIG 24-17** Aortic valvuloplasty. Needle device is in the left ventricle with tip at the aortic valve.

operation, followed by Fontan procedure). The goal of fetal cardiac intervention for critical aortic stenosis with evolving HLHS is to alter left-sided heart physiology and promote ventricular growth in utero to allow for postnatal survival with healthy biventricular circulation.<sup>184</sup>

There is increasing experience with ultrasound-guided fetal cardiac catheterization and valvular balloon dilatation. In most cases, this procedure can be done using a percutaneous approach. An 18- to 19-gauge needle is introduced into the fetal left cardiac ventricle using real-time ultrasound guidance (Fig. 24-17 and Video 24-1). A balloon angioplasty catheter is passed over a wire that has been advanced across the stenotic valve. Once it is determined that the angioplasty balloon is in the appropriate position at the level of the aortic valve annulus, it is inflated under ultrasound guidance. After balloon inflation, the wire and balloon are removed, and the fetus is closely monitored for bradycardia or pericardial effusion. The multidisciplinary team at Boston Children's/Brigham and Women's Hospital reported successful valvular dilation in approximately 80% of cases. Of the technically successful cases, over 30% have biventricular circulation after birth, with another 8% converted to biventricular circulation after initial univentricular palliation.<sup>184</sup>

Experience in fetuses with HLHS with restrictive or intact atrial septum is more limited, as is experience with intervention for pulmonary atresia or stenosis with intact ventricular septum. However, further research will determine optimal patient selection, timing, and technique of intervention for different types of potentially correctable fetal heart defects. As noted earlier, these procedures are performed percutaneously, and, therefore, maternal and pregnancy risk profile is relatively low. This advantage may allow for a lower threshold for innovative intervention and may expand the indications, even if the success rate is variable.

### Lower Urinary Tract Obstruction

Fetal urethral abnormalities resulting in lower urinary tract obstruction (LUTO) are associated with significant morbidity and mortality risks. LUTO occurs in approximately 1/5000 to 1/8000 male fetuses. The most common cause of LUTO is posterior urethral valves in males<sup>185</sup> and urethral atresia in females.<sup>186</sup> Complete obstruction leads to progressively severe oligohydramnios and then anhydramnios.

**TABLE 24-4 Fetal Urine Prognostic Thresholds\***

	Good Prognosis	Poor Prognosis
Sodium	<90 mmol/L	>100 mmol/L
Chloride	<90 mmol/L	>100 mmol/L
Osmolality	<180 mOsm/L	>200 mOsm/L
Total protein	<20 mg/dL	>40 mg/dL
$\beta_2$ -Microglobulin	<6 mg/L	>10 mg/L

\*Thresholds are based on urine obtained between 18 and 24 weeks estimated gestational age. Values that fall between good and poor prognosis are considered "gray zone" with expectation for moderate or greater postnatal renal impairment, but potential for postnatal pulmonary survival.

Depending upon the gestational age when this occurs, pulmonary hypoplasia often ensues. In addition, vesicoureteral reflux and elevated back-pressure affecting the renal parenchyma can cause cystic dysplasia and renal failure. Untreated, LUTO leads to hydronephrosis, renal dysplasia, and perinatal death in up to 90% of patients.<sup>187</sup> Death is attributed to pulmonary hypoplasia and renal dysplasia.

Aiming to reconstitute amniotic fluid volume and decompress the high-pressure urinary system, vesicoamniotic shunt placement into the distended fetal bladder has, for several years, been offered to patients with LUTO and secondary oligohydramnios. With experience, it has been recognized that case selection is critical. In some fetuses with irreversible renal damage, pulmonary growth could be salvaged, but the morbidity of neonatal renal failure with need for long-term dialysis and eventual renal transplantation became evident. This has led to attempts to better predict fetal and thus neonatal renal function and to identify those for whom shunting might benefit pulmonary as well as renal outcome. It was hypothesized that the best method to assess renal function would involve sampling fetal urine with analysis of urinary electrolytes and other analytes. Evaluation of urinary electrolytes appears to be most predictive when two or three sequential vesicocenteses are performed several days apart, in fetuses in whom bladder refilling and normal-appearing renal parenchyma are shown by sonography (Table 24-4).<sup>188</sup> Nicolini and Spelzini suggested modifying the algorithm of assessing patients with LUTO by performing a single cordocentesis.<sup>189</sup> This may allow determination of fetal karyotype and assessment of fetal urinary function based on serum  $\beta_2$ -microglobulin level with one diagnostic procedure.

Percutaneous ultrasound-guided vesicoamniotic shunt placement in fetuses with LUTO and secondary oligohydramnios is offered to those with normal karyotype, no sonographic or biochemical evidence of renal cystic dysplasia, and no additional major structural anomalies (Fig. 24-18). Data regarding short- and long-term outcomes following fetal intervention demonstrate improved survival rate but relatively high rates of renal and pulmonary morbidity. An overview by Clark and associates of 16 studies including 342 fetuses reported a 73% intact survival rate, with increased overall perinatal survival rate after bladder drainage via vesicocentesis or vesicoamniotic shunt compared to no intervention.<sup>190</sup> A multinational randomized clinical trial comparing treatment versus expectant management could not be completed because of difficulties with recruitment.<sup>191</sup> A case series of 20 pregnancies complicated by LUTO with well documented in utero findings and subsequent 5-year follow-up revealed that children treated with vesicoamniotic shunting had normal neurodevelopment. However, in the 18 survivors, 6 had acceptable renal function, 4 had mild renal insufficiency, and 6 required dialysis and eventual transplantation.<sup>192</sup> In



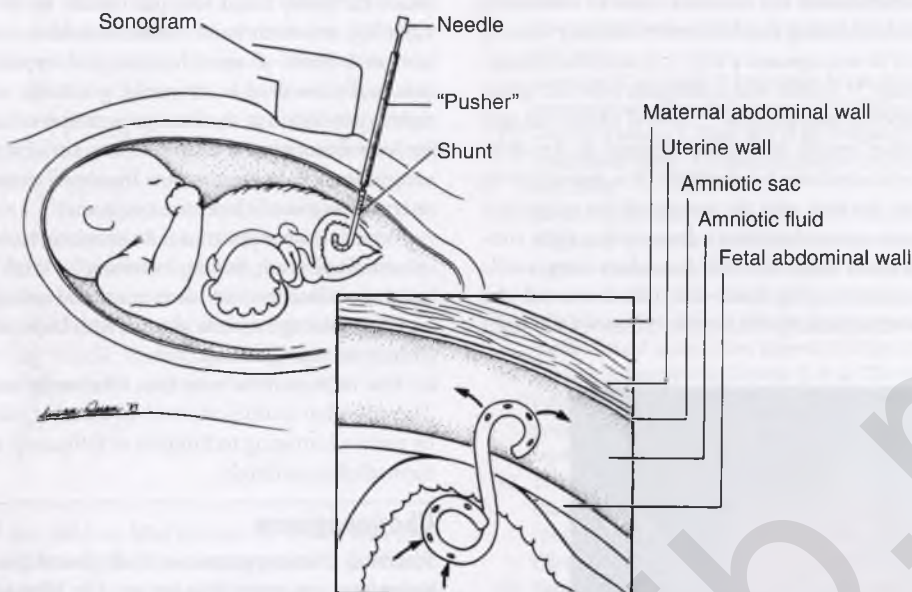


**FIG 24-18** Placement and deployment of a fetal bladder shunt. The double pigtail catheter is pushed off the needle so that one end is within the fetal bladder and the other end is in the amniotic space. (From Adzick NS, Flake AW, Harrison MR: Recent advances in prenatal diagnosis and treatment. *Pediatr Clin North Am* 32:1103, 1985.)

addition, many were lagging in growth and had persistent pulmonary issues. Similar experience is reported by other centers, with chronic renal insufficiency in one half to two thirds of survivors, despite having had favorable fetal urine profiles as a prerequisite for in utero intervention.

Shunt-related complications occur in approximately 40% of cases.<sup>193</sup> The shunt may withdraw into the fetal abdomen, resulting in iatrogenic urinary ascites, or pull out of the fetal bladder or out of the fetus entirely. Replacement of the shunt is associated with additional risk of fetal demise, chorioamnionitis, PPRM, miscarriage, or preterm delivery, leading to a total perinatal loss rate of approximately 4% per procedure. Effective and reliable treatment is likely to change the course of the disease in utero and possibly provide a more favorable outlook for these pregnancies. Thus, several alternative treatment approaches to obstructive uropathy have been proposed. One refinement, aiming to reduce the risk of catheter dislodgement, is the development of a novel double-disk/double pigtail catheter shunt.<sup>194</sup> Another treatment approach is fetal cystoscopy with endoscopic fulguration of the posterior urethral valves.<sup>195</sup> With cystoscopy, it may be possible to correct the outlet obstruction and allow normal bladder cycling for the remainder of the pregnancy. This approach has compared favorably to vesicoamniotic shunting, but there remains concern regarding the potential for additional injury to the fetus and possible subsequent fistula formation.

### Sacroccocygeal Teratoma

SCTs are cystic and solid tumors arising from the area of the coccyx. The SCTs relevant to this discussion of fetal therapy are large, predominantly solid, and highly vascularized. Large SCTs with marked blood flow can lead to high-output cardiac overload, hydrops, and death. Assessment of tumor size, growth rate, and fetal cardiac function allow for identification of those fetuses at risk for decompensation. Fetuses with large SCTs and secondary heart failure with hydrops before viability have a dismal prognosis, with nearly 100% mortality rate, and are considered candidates for fetal intervention.<sup>196</sup>

Attempts have been made to perform either definitive resection or devascularization of the tumor in hopes of allowing cardiac recovery. Tumor resection via open maternal-fetal surgery has been associated with suboptimal outcomes, with inherent major fetal and maternal risks.<sup>197</sup> Various minimally invasive treatment approaches aimed at interrupting blood supply to the SCT have been attempted, including coiling, embolization, sclerotherapy, monopolar cautery, laser ablation, and RFA. A 2014 review identified 34 cases of fetal SCT treated via a minimally invasive approach; the overall survival rate was 44%, with 30% survival rate in cases with and 67% survival rate in cases without evidence of secondary cardiac decompensation.<sup>198</sup> An additional 12 cases were treated via an open maternal-fetal surgical approach, and the survival rate was 50%.<sup>198</sup> Long-term outcomes have not been reported in detail.

### Amniotic Band Syndrome

Amniotic band syndrome (ABS) is a sporadic congenital anomaly thought to result from amnion rupture followed by attachment of fibrous amniotic strands to the fetus. Adherence to or entanglement of the fetus in amniotic remnants may lead to fetal deformation, malformation, or disruption.<sup>199</sup> Estimates of ABS incidence range from 1 in 1200 to 1 in 15,000 live births.<sup>200</sup>

Depending both on the degree of adherence of the amniotic band as well as its location along the fetus, outcomes can vary widely. ABS may result in minor single digit abnormalities, distal extremity amputations, and craniofacial or thoracoabdominal destructive eviscerations. Constriction of extremities is the most common form of ABS and causes edema distal to the constricted site, amputation, and other deformities (Fig. 24-19).<sup>201</sup> Amputations occur as a result of progressive adherence and strangulation of the extremity as the fetus grows and develops.<sup>202</sup> Animal studies have shown that in utero band release can restore normal circulation and function to the extremity.<sup>203</sup>

Similar to animal models, release of the amniotic band constriction in human fetuses results in reduction of distal limb edema, restoration of limb structure and function, and avoidance of amputation.



Quintero and coworkers performed the first two cases of minimally invasive surgery to release constricting bands in utero, utilizing scissors under endoscopic guidance in one case and a YAG (yttrium-aluminum-garnet) laser fiber in another.<sup>201</sup> Hüsler and colleagues reported seven cases using the same transecting instruments.<sup>204</sup> Several additional case series have described similar results with improvement in structure and function after fetoscopic amniotic band release. It is important to note that constrictions can develop over the course of the pregnancy as the fetus grows. One case report describes a fetus with a tight constricting band of the right lower extremity with secondary distal swelling, whereas a loose nonconstricting band was noted around the normal-contoured left lower extremity. Fetoscopic release of the right

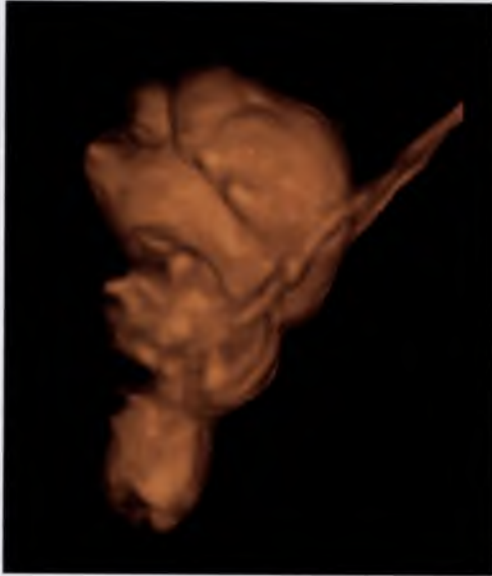


**FIG 24-19** Amniotic band syndrome affecting fetus at 22 weeks 4 days. Ultrasound image with three-dimensional surface rendering demonstrates effects of a tight constricting amniotic band around the fetal forearm with marked distal swelling of the wrist and hand. (Modified from Assaf R, Llanes A, Chmait R: In utero release of constriction amniotic bands via blunt dissection. *Fetal Pediatr Pathol* 31(1):25-29, 2012.)

lower extremity band was performed at 29 weeks' gestation.<sup>205</sup> The right leg, on which band release was done in utero, had normal function at 2 years of age. However, the opposite (left) leg, which was minimally involved at 29 weeks' gestation, subsequently developed a tight constriction as the fetus grew, and residual deficits in that extremity were documented at age 2. Thus, serial sonographic surveillance is recommended to monitor for the development of constriction bands over the course of the entire pregnancy.

Fetal demise may occur if an amniotic band incorporates a segment of umbilical cord, thereby resulting in cord compression. Therefore, another indication for amniotic band release is for cases in which bands involve the umbilical cord, with hopes of preventing fetal demise from cord strangulation.<sup>206</sup>

It is important to note that ABS rarely involves just one fetal part. There is often multifocal involvement that may or may not be detected by prenatal imaging techniques or fetoscopy, and the patient should be counseled accordingly.

### Chorioangioma

Placental chorioangiomas are abnormal proliferations of chorionic tissue and are present in up to 1% of placentas.<sup>207</sup> Most placental chorioangiomas are small and not associated with risk to the fetus. Large chorioangiomas, those that measure greater than 4 cm in diameter, can have significant fetal consequences, including polyhydramnios, microangiopathic hemolytic fetal anemia, high-output cardiac failure resulting in nonimmune hydrops, and fetal growth restriction.<sup>208</sup> Large chorioangiomas are associated with a 40% risk of intrauterine demise.<sup>209</sup> Fortunately, large chorioangiomas are rare with a reported incidence of 1:3500 to 1:9000 pregnancies.<sup>207</sup>

On ultrasound imaging, placental chorioangioma appears as a well-circumscribed, vascularized, solid mass bulging along the fetal surface of the placenta. Color flow Doppler sonography is a useful tool to assess for tumor vascularity (Fig. 24-20A). More vascular and hypoechoic tumors are associated with greater risk of pregnancy complications, whereas nonvascular and hyperechoic lesions tend to have more favorable outcomes.<sup>207</sup>

Because large chorioangiomas are associated with poor perinatal outcomes, fetal therapy has been proposed in cases with evidence of high-output cardiac compromise or hydrops. Fetal anemia is not

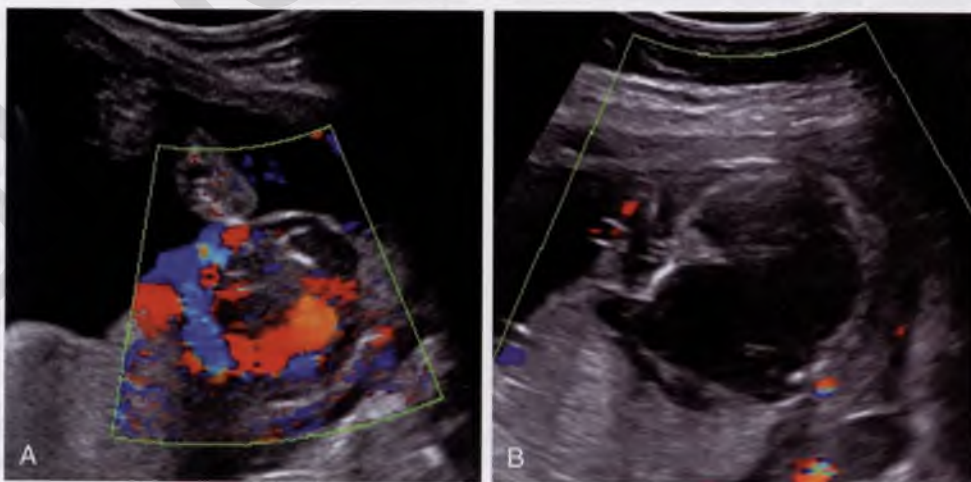


**FIG 24-20** Placental chorioangioma. **A**, Color Doppler sonography at 25 weeks' gestation reveals a large, markedly vascular, well-circumscribed mass protruding from the fetal surface of the placenta. **B**, Sonogram performed at 29 weeks' gestation, following laser photocoagulation of the feeding vessels. The chorioangioma has decreased in size, appears predominantly cystic, with no demonstrable internal flow shown by color Doppler interrogation.



uncommon in these patients. Thus, monitoring of MCA PSV and other ultrasound markers of fetal anemia is recommended. IUT may improve outcomes in cases with significant anemia. Development of severe polyhydramnios is also not uncommon. Amnioreduction may help ameliorate maternal symptoms and reduce the risk of preterm labor. However, the drop in intrauterine pressure from amniotic fluid decompression may result in increased tumor perfusion, thereby promoting fetal deterioration.<sup>210</sup> Definitive treatment aiming to interrupt blood supply to the chorioangioma has been attempted using a variety of approaches (Fig. 24-20B).<sup>211</sup> Ultrasound-guided percutaneous treatment options include alcohol injection, embolization, and interstitial laser therapy. Endoscopic methods include suture ligation and laser photocoagulation of feeding vessels. Endoscopic occlusion of feeding vessels to the chorioangioma has been associated with an 80% survival rate in one small series.<sup>211</sup>

## SUMMARY

Sonography has allowed the field of fetal therapy to evolve and provides diagnostic information as well as intraoperative guidance. Although open maternal-fetal surgery was the primary method of accessing the fetus with initial attempts at fetal surgical intervention, this approach is associated with significant maternal and fetal risks. Minimally invasive fetal surgery is associated with much lower maternal risks and is currently the preferred surgical approach for most fetal conditions amenable to in utero therapy. Such interventions typically are performed under ultrasound guidance. With further improvement of surgical equipment and prenatal diagnostic modalities, access to the fetal-placental unit via minimally invasive methods will likely become increasingly refined and provide a conduit for additional novel treatments of the fetus.

## REFERENCES

- Liley AW: Intrauterine transfusion of foetus in haemolytic disease. *Br Med J* 2(5365):1107–1109, 1963.
- Adzick NS, Thom EA, Spong CY, et al: A randomized trial of prenatal versus postnatal repair of myelomeningocele. *N Engl J Med* 364(11):993–1004, 2011.
- Golombek K, Ball RH, Lee H, et al: Maternal morbidity after maternal-fetal surgery. *Am J Obstet Gynecol* 194(3):834–839, 2006.
- Wilson RD, Lemerand K, Johnson MP, et al: Reproductive outcomes in subsequent pregnancies after a pregnancy complicated by open maternal-fetal surgery (1996–2007). *Am J Obstet Gynecol* 203(3):209.e1–209.e6, 2010.
- American College of Obstetricians and Gynecologists: ACOG Committee Opinion No. 550: maternal-fetal surgery for myelomeningocele. *Obstet Gynecol* 121(1):218–219, 2013.
- Van de Velde M, De Buck F: Fetal and maternal analgesia/anesthesia for fetal procedures. *Fetal Diagn Ther* 31(4):201–209, 2012.
- Farrell JA, Albanese CT, Jennings RW, et al: Maternal fertility is not affected by fetal surgery. *Fetal Diagn Ther* 14(3):190–192, 1999.
- Deprest J, Jani J, Lewi L, et al: Fetoscopic surgery: encouraged by clinical experience and boosted by instrument innovation. *Semin Fetal Neonatal Med* 11(6):398–412, 2006.
- Quintero R, Morales W: Operative fetoscopy: a new frontier in fetal medicine. *Contemp Ob Gyn* 44:45–68, 1999.
- Schulman SR, Jones BR, Slotnick N, et al: Fetal tracheal intubation with intact uteroplacental circulation. *Anesth Analg* 76(1):197–199, 1993.
- Moldenhauer JS: Ex utero intrapartum therapy. *Semin Pediatr Surg* 22(1):44–49, 2013.
- Victoria A, Mora G, Arias F: Perinatal outcome, placental pathology, and severity of discordance in monochorionic and dichorionic twins. *Obstet Gynecol* 97(2):310–315, 2001.
- Dube J, Dodds L, Armson BA: Does chorionicity or zygosity predict adverse perinatal outcomes in twins? *Am J Obstet Gynecol* 186(3):579–583, 2002.
- Larroche JC, Droulle P, Delezoide AL, et al: Brain damage in monozygous twins. *Biol Neonate* 57(5):261–278, 1990.
- Ong SS, Zamora J, Khan KS, et al: Prognosis for the co-twin following single-twin death: a systematic review. *Br J Obstet Gynaecol* 113(9):992–998, 2006.
- Boyle B, McConkey R, Garne E, et al: Trends in the prevalence, risk and pregnancy outcome of multiple births with congenital anomaly: a registry-based study in 14 European countries 1984–2007. *Br J Obstet Gynaecol* 120(6):707–716, 2013.
- Glinianaia SV, Rankin J, Wright C: Congenital anomalies in twins: a register-based study. *Hum Reprod* 23:1306–1311, 2008.
- Ortibus E, Lopriore E, Deprest J, et al: The pregnancy and long-term neurodevelopmental outcome of monochorionic diamniotic twin gestations: a multicenter prospective cohort study from the first trimester onward. *Am J Obstet Gynecol* 200(5):494.e1–494.e8, 2009.
- Lewi L, Lewi P, Diemert A, et al: The role of ultrasound examination in the first trimester and at 16 weeks' gestation to predict fetal complications in monochorionic diamniotic twin pregnancies. *Am J Obstet Gynecol* 199(5):493.e1–493.e7, 2008.
- Bajoria R, Kingdom J: The case for routine determination of chorionicity and zygosity in multiple pregnancy. *Prenat Diagn* 17(13):1207–1225, 1997.
- Carroll SG, Soothill PW, Abdel-Fattah SA, et al: Prediction of chorionicity in twin pregnancies at 10–14 weeks of gestation. *Br J Obstet Gynaecol* 109(2):182–186, 2002.
- Reddy UM, Abuhamad AZ, Levine D, et al: Fetal imaging: Executive summary of a Joint Eunice Kennedy Shriver National Institute of Child Health and Human Development, Society for Maternal-Fetal Medicine, American Institute of Ultrasound in Medicine, American College of Obstetricians and Gynecologists, American College of Radiology, Society for Pediatric Radiology, and Society of Radiologists in Ultrasound Fetal Imaging Workshop. *Am J Obstet Gynecol* 210(5):387–397, 2014.
- Society for Maternal-Fetal Medicine, Simpson LL: Twin-twin transfusion syndrome. *Am J Obstet Gynecol* 208(1):3–18, 2013.
- Quintero R, Quintero L, Bornick P, et al: The donor-recipient (D-R) score: *in vivo* endoscopic evidence to support the hypothesis of a net transfer of blood from donor to recipient in twin-twin transfusion syndrome. *Prenat Neonat Med* 5:84–91, 2000.
- Bajoria R, Wigglesworth J, Fisk NM: Angioarchitecture of monochorionic placentas in relation to the twin-twin transfusion syndrome. *Am J Obstet Gynecol* 172(3):856–863, 1995.
- Mahieu-Caputo D, Meulemans A, Martinovic J, et al: Paradoxical activation of the renin-angiotensin system in twin-twin transfusion syndrome: an explanation for cardiovascular disturbances in the recipient. *Pediatr Res* 58(4):685–688, 2005.
- Wieacker P, Wilhelm C, Prompeler H, et al: Pathophysiology of polyhydramnios in twin transfusion syndrome. *Fetal Diagn Ther* 7(2):87–92, 1992.
- Quintero R, Morales W, Allen M, et al: Staging of twin-twin transfusion syndrome. *J Perinatol* 19:550–555, 1999.
- Chang YL, Chmait RH, Bornick PW, et al: The role of laser surgery in dissecting the etiology of absent or reverse end-diastolic velocity in the umbilical artery of the donor twin in twin-twin transfusion syndrome. *Am J Obstet Gynecol* 195(2):478–483, 2006.
- Ishii K, Chmait RH, Martinez JM, et al: Ultrasound assessment of venous blood flow before and after laser therapy: approach to understanding the pathophysiology of twin-twin transfusion syndrome. *Ultrasound Obstet Gynecol* 24(2):164–168, 2004.
- Saunders NJ, Snijders RJ, Nicolaides KH: Therapeutic amniocentesis in twin-twin transfusion syndrome appearing in the second trimester of pregnancy. *Am J Obstet Gynecol* 166(3):820–824, 1992.
- Kontopoulos EV, Quintero RA, Chmait RH, et al: Percent absent end-diastolic velocity in the umbilical artery waveform as a predictor of intrauterine fetal demise of the donor twin after selective laser



- photocoagulation of communicating vessels in twin-twin transfusion syndrome. *Ultrasound Obstet Gynecol* 30(1):35–39, 2007.
33. Quintero R, Morales W, Mendoza G, et al: Selective photocoagulation of placental vessels in twin-twin transfusion syndrome: evolution of a surgical technique. *Obstet Gynecol Surv* 53(12 Suppl):S97–S103, 1998.
  34. Lencen R, Paupe A, Ciarlo G, et al: Neonatal outcome in preterm monochorionic twins with twin-to-twin transfusion syndrome after intrauterine treatment with amnioreduction or fetoscopic laser surgery: comparison with dichorionic twins. *Am J Obstet Gynecol* 196(5):450.e1–450.e7, 2007.
  35. Senat MV, Deprest J, Boulvain M, et al: Endoscopic laser surgery versus serial amnioreduction for severe twin-to-twin transfusion syndrome. *N Engl J Med* 351(2):136–144, 2004.
  36. Rossi AC, D'Addario V: Laser therapy and serial amnioreduction as treatment for twin-twin transfusion syndrome: a meta-analysis and review of literature. *Am J Obstet Gynecol* 198(2):147–152, 2008.
  37. Ahmed S, Luks FI, O'Brien BM, et al: Influence of experience, case load, and stage distribution on outcome of endoscopic laser surgery for TTTS—a review. *Prenat Diagn* 30(4):314–319, 2010.
  38. Skupski DW, Luks FI, Walker M, et al: Preoperative predictors of death in twin-to-twin transfusion syndrome treated with laser ablation of placental anastomoses. *Am J Obstet Gynecol* 203(4):388.e311, 2010.
  39. Chmait RH, Kontopoulos EV, Korst LM, et al: Stage-based outcomes of 682 consecutive cases of twin-twin transfusion syndrome treated with laser surgery: the USFetus experience. *Am J Obstet Gynecol* 204(5):393.e1–393.e6, 2011.
  40. Van Winden KR, Quintero RA, Kontopoulos EV, et al: Perinatal survival in cases of twin-twin transfusion syndrome complicated by selective intrauterine growth restriction. *J Matern Fetal Neonatal Med* 28(13):1549–1553, 2015.
  41. Chmait RH, Korst LM, Llanes A, et al: Perioperative characteristics associated with preterm birth in twin-twin transfusion syndrome treated by laser surgery. *Am J Obstet Gynecol* 209(3):264.e1–264.e8, 2013.
  42. Slaghekke F, Lopriore E, Lewi L, et al: Fetoscopic laser coagulation of the vascular equator versus selective coagulation for twin-to-twin transfusion syndrome: an open-label randomised controlled trial. *Lancet* 383(9935):2144–2151, 2014.
  43. Chmait RH, Kontopoulos EV, Quintero RA: Sequential laser surgery for twin-twin transfusion syndrome. *Am J Perinatol* 31(Suppl 1):S13–S18, 2014.
  44. Lopriore E, Slaghekke F, Middeldorp JM, et al: Residual anastomoses in twin-to-twin transfusion syndrome treated with selective fetoscopic laser surgery: localization, size, and consequences. *Am J Obstet Gynecol* 201(1):66.e1–66.e4, 2009.
  45. Lopriore E, Middeldorp JM, Oepkes D, et al: Residual anastomoses after fetoscopic laser surgery in twin-to-twin transfusion syndrome: frequency, associated risks and outcome. *Placenta* 28(2–3):204–208, 2007.
  46. Lewi L, Jani J, Cannie M, et al: Intertwin anastomoses in monochorionic placentas after fetoscopic laser coagulation for twin-to-twin transfusion syndrome: is there more than meets the eye? *Am J Obstet Gynecol* 194(3):790–795, 2006.
  47. Quintero RA, Martinez JM, Lopez J, et al: Individual placental territories after selective laser photocoagulation of communicating vessels in twin-twin transfusion syndrome. *Am J Obstet Gynecol* 192(4):1112–1118, 2005.
  48. Chmait RH, Assaf SA, Benirschke K: Residual vascular communications in twin-twin transfusion syndrome treated with sequential laser surgery: frequency and clinical implications. *Placenta* 31(7):611–614, 2010.
  49. De Paepe ME, Friedman RM, Poch M, et al: Placental findings after laser ablation of communicating vessels in twin-to-twin transfusion syndrome. *Pediatr Dev Pathol* 7(2):159–165, 2004.
  50. Slaghekke F, Lewi L, Middeldorp JM, et al: Residual anastomoses in twin-twin transfusion syndrome after laser: the Solomon randomized trial. *Am J Obstet Gynecol* 211(3):285.e1–285.e7, 2014.
  51. Lopriore E, van Wezel-Meijler G, Middeldorp JM, et al: Incidence, origin, and character of cerebral injury in twin-to-twin transfusion syndrome treated with fetoscopic laser surgery. *Am J Obstet Gynecol* 194(5):1215–1220, 2006.
  52. Escobar GJ, Littenberg B, Petitti DB: Outcome among surviving very low birthweight infants: a meta-analysis. *Arch Dis Child* 66(2):204–211, 1991.
  53. Ornstein M, Ohlsson A, Edmonds J, et al: Neonatal follow-up of very low birthweight/extremely low birthweight infants to school age: a critical overview. *Acta Paediatr Scand* 80(8–9):741–748, 1991.
  54. Rossi AC, Vanderbilt D, Chmait RH: Neurodevelopmental outcomes after laser therapy for twin-twin transfusion syndrome: a systematic review and meta-analysis. *Obstet Gynecol* 118(5):1145–1150, 2011.
  55. Vanderbilt DL, Schrager SM, Llanes A, et al: Predictors of 2-year cognitive performance after laser surgery for twin-twin transfusion syndrome. *Am J Obstet Gynecol* 211(4):388.e1–388.e7, 2014.
  56. Gratacos E, Lewi L, Munoz B, et al: A classification system for selective intrauterine growth restriction in monochorionic pregnancies according to umbilical artery Doppler flow in the smaller twin. *Ultrasound Obstet Gynecol* 30(1):28–34, 2007.
  57. Grubbs BH, Benirschke K, Korst LM, et al: Role of low placental share in twin-twin transfusion syndrome complicated by intrauterine growth restriction. *Placenta* 32(8):616–618, 2011.
  58. Valsky DV, Eixarch E, Martinez JM, et al: Selective intrauterine growth restriction in monochorionic diamniotic twin pregnancies. *Prenat Diagn* 30(8):719–726, 2010.
  59. Inklaar MJ, van Klink JM, Stolk TT, et al: Cerebral injury in monochorionic twins with selective intrauterine growth restriction: a systematic review. *Prenat Diagn* 34(3):205–213, 2014.
  60. Huber A, Diehl W, Zikulnig L, et al: Perinatal outcome in monochorionic twin pregnancies complicated by amniotic fluid discordance without severe twin-twin transfusion syndrome. *Ultrasound Obstet Gynecol* 27(1):48–52, 2006.
  61. Quintero RA, Bornick PW, Morales WJ, et al: Selective photocoagulation of communicating vessels in the treatment of monochorionic twins with selective growth retardation. *Am J Obstet Gynecol* 185(3):689–696, 2001.
  62. Valsky DV, Eixarch E, Martinez JM, et al: Selective intrauterine growth restriction in monochorionic twins: pathophysiology, diagnostic approach and management dilemmas. *Semin Fetal Neonatal Med* 15(6):342–348, 2010.
  63. Chalouhi GE, Marangoni MA, Quibel T, et al: Active management of selective intrauterine growth restriction with abnormal Doppler in monochorionic diamniotic twin pregnancies diagnosed in the second trimester of pregnancy. *Prenat Diagn* 33(2):109–115, 2013.
  64. Gratacos E, Lewi L, Carreras E, et al: Incidence and characteristics of umbilical artery intermittent absent and/or reversed end-diastolic flow in complicated and uncomplicated monochorionic twin pregnancies. *Ultrasound Obstet Gynecol* 23(5):456–460, 2004.
  65. Ishii K, Murakoshi T, Takahashi Y, et al: Perinatal outcome of monochorionic twins with selective intrauterine growth restriction and different types of umbilical artery Doppler under expectant management. *Fetal Diagn Ther* 26(3):157–161, 2009.
  66. Gratacos E, Carreras E, Becker J, et al: Prevalence of neurological damage in monochorionic twins with selective intrauterine growth restriction and intermittent absent or reversed end-diastolic umbilical artery flow. *Ultrasound Obstet Gynecol* 24(2):159–163, 2004.
  67. Gratacos E, Antolin E, Lewi L, et al: Monochorionic twins with selective intrauterine growth restriction and intermittent absent or reversed end-diastolic flow (type III): feasibility and perinatal outcome of fetoscopic placental laser coagulation. *Ultrasound Obstet Gynecol* 31(6):669–675, 2008.
  68. Lewi L, Gucciardo L, Huber A, et al: Clinical outcome and placental characteristics of monochorionic diamniotic twin pairs with early- and late-onset discordant growth. *Am J Obstet Gynecol* 199(5):511.e1–511.e7, 2008.
  69. Lopriore E, Middeldorp JM, Oepkes D, et al: Twin anemia-polycythemia sequence in two monochorionic twin pairs without oligo-polyhydramnios sequence. *Placenta* 28(1):47–51, 2007.
  70. Nakayama S, Ishii K, Kawaguchi H, et al: Perinatal outcome of monochorionic diamniotic twin pregnancies managed from early



- gestation at a single center. *J Obstet Gynaecol Res* 38(4):692–697, 2012.
71. Lewi L, Jani J, Blickstein I, et al: The outcome of mono chorionic diamniotic twin gestations in the era of invasive fetal therapy: a prospective cohort study. *Am J Obstet Gynecol* 199(5):514.e1–514.e8, 2008.
  72. Robyr R, Lewi L, Salomon LJ, et al: Prevalence and management of late fetal complications following successful selective laser coagulation of chorionic plate anastomoses in twin-to-twin transfusion syndrome. *Am J Obstet Gynecol* 194(3):796–803, 2006.
  73. Lopriore E, Oepkes D: Fetal and neonatal haematological complications in mono chorionic twins. *Semin Fetal Neonatal Med* 13(4):231–238, 2008.
  74. Slaghekke F, Kist WJ, Oepkes D, et al: Twin anemia-polycythemia sequence: diagnostic criteria, classification, perinatal management and outcome. *Fetal Diagn Ther* 27(4):181–190, 2010.
  75. Sainz JA, Romero C, Garcia-Mejido J, et al: Analysis of middle cerebral artery peak systolic velocity in mono chorionic twin pregnancies as a method for identifying spontaneous twin anaemia-polycythemia sequence. *J Matern Fetal Neonatal Med* 27(11):1174–1176, 2014.
  76. Lopriore E, Slaghekke F, Kersbergen KJ, et al: Severe cerebral injury in a recipient with twin anemia-polycythemia sequence. *Ultrasound Obstet Gynecol* 41(6):702–706, 2013.
  77. Weingertner AS, Kohler A, Kohler M, et al: Clinical and placental characteristics in four new cases of twin anemia-polycythemia sequence. *Ultrasound Obstet Gynecol* 35(4):490–494, 2010.
  78. Gucciardo L, Lewi L, Vaast P, et al: Twin anemia polycythemia sequence from a prenatal perspective. *Prenat Diagn* 30(5):438–442, 2010.
  79. Assaf SA, Benirschke K, Chmait RH: Spontaneous twin anemia-polycythemia sequence complicated by recipient placental vascular thrombosis and hydrops fetalis. *J Matern Fetal Neonatal Med* 24(3):549–552, 2011.
  80. Diehl W, Glosemeyer P, Tavares De Sousa M, et al: Twin anemia-polycythemia sequence in a case of monoamniotic twins. *Ultrasound Obstet Gynecol* 42(1):108–111, 2013.
  81. Ishii K, Hayashi S, Mabuchi A, et al: Therapy by laser equatorial placental dichorionization for early-onset spontaneous twin anemia-polycythemia sequence. *Fetal Diagn Ther* 35(1):65–68, 2014.
  82. Abdel-Sattar M, Platt LD, DeVore G, et al: Treatment of complicated spontaneous twin anemia-polycythemia sequence via fetoscopic laser ablation of the vascular communications. *Fetal Diagn Ther* 38(3):233–237, 2014.
  83. Lopriore E, Hecher K, Vandenbussche FP, et al: Fetoscopic laser treatment of twin-to-twin transfusion syndrome followed by severe twin anemia-polycythemia sequence with spontaneous resolution. *Am J Obstet Gynecol* 198(2):e4–e7, 2008.
  84. Slaghekke F, van Klink JM, Koopman HM, et al: Neurodevelopmental outcome in twin anemia-polycythemia sequence after laser surgery for twin-twin transfusion syndrome. *Ultrasound Obstet Gynecol* 44(3):316–321, 2014.
  85. Genova L, Slaghekke F, Klumper FJ, et al: Management of twin anemia-polycythemia sequence using intrauterine blood transfusion for the donor and partial exchange transfusion for the recipient. *Fetal Diagn Ther* 34(2):121–126, 2013.
  86. Groussolles M, Sartor A, Connan L, et al: Evolution of middle cerebral artery peak systolic velocity after a successful laser procedure for iatrogenic twin anemia-polycythemia sequence. *Ultrasound Obstet Gynecol* 39(3):354–356, 2012.
  87. James WH: A note on the epidemiology of acardiac monsters. *Teratology* 16(2):211–216, 1977.
  88. Bornstein E, Monteagudo A, Dong R, et al: Detection of twin reversed arterial perfusion sequence at the time of first-trimester screening: the added value of 3-dimensional volume and color Doppler sonography. *J Ultrasound Med* 27(7):1105–1109, 2008.
  89. Moore TR, Gale S, Benirschke K: Perinatal outcome of forty-nine pregnancies complicated by acardiac twinning. *Am J Obstet Gynecol* 163(3):907–912, 1990.
  90. Quintero RA, Chmait RH, Murakoshi T, et al: Surgical management of twin reversed arterial perfusion sequence. *Am J Obstet Gynecol* 194(4):982–991, 2006.
  91. Bebbington M: Selective reduction in complex mono chorionic gestations. *Am J Perinatol* 31(Suppl 1):S51–S58, 2014.
  92. Lee H, Bebbington M, Crombleholme TM: North American Fetal Therapy Network: The North American Fetal Therapy Network Registry data on outcomes of radiofrequency ablation for twin-reversed arterial perfusion sequence. *Fetal Diagn Ther* 33(4):224–229, 2013.
  93. Nicolini U, Poblete A, Boschetto C, et al: Complicated mono chorionic twin pregnancies: experience with bipolar cord coagulation. *Am J Obstet Gynecol* 185(3):703–707, 2001.
  94. Livingston JC, Lim FY, Polzin W, et al: Intrafetal radiofrequency ablation for twin reversed arterial perfusion (TRAP): a single-center experience. *Am J Obstet Gynecol* 197(4):399.e1–399.e3, 2007.
  95. Morel O, Malartic C, Barranger E: Radiofrequency ablation for twin-reversed arterial perfusion sequence: the unknown cord occlusion delay calls for long term neonatal follow-up of the surviving twins. *Am J Obstet Gynecol* 197(5):557–558, author reply 558, 2007.
  96. Bebbington M: Selective reduction in multiple gestations. *Best Pract Res Clin Obstet Gynaecol* 28(2):239–247, 2014.
  97. Lee H, Wagner AJ, Sy E, et al: Efficacy of radiofrequency ablation for twin-reversed arterial perfusion sequence. *Am J Obstet Gynecol* 196(5):459.e1–459.e4, 2007.
  98. Evans MI, Andriole S, Britt DW: Fetal reduction: 25 years' experience. *Fetal Diagn Ther* 35(2):69–82, 2014.
  99. Nobili E, Paramasivam G, Kumar S: Outcome following selective fetal reduction in mono chorionic and dichorionic twin pregnancies discordant for structural, chromosomal and genetic disorders. *Aust N Z J Obstet Gynaecol* 53(2):114–118, 2013.
  100. Chmait RH, Quintero RA: Operative fetoscopy in complicated mono chorionic twins: current status and future direction. *Curr Opin Obstet Gynecol* 20(2):169–174, 2008.
  101. Waitzman NJ, Romano PS, Scheffler RM: Estimates of the economic costs of birth defects. *Inquiry* 31(2):188–205, 1994.
  102. Sadler TW: Embryology of neural tube development. *Am J Med Genet C Semin Med Genet* 135C(1):2–8, 2005.
  103. Shaer CM, Chescheir N, Schulkin J: Myelomeningocele: a review of the epidemiology, genetics, risk factors for conception, prenatal diagnosis, and prognosis for affected individuals. *Obstet Gynecol Surv* 62(7):471–479, 2007.
  104. Oakeshott P, Hunt GM: Long-term outcome in open spina bifida. *Br J Gen Pract* 53(493):632–636, 2003.
  105. Davis BE, Daley CM, Shurtleff DB, et al: Long-term survival of individuals with myelomeningocele. *Pediatr Neurosurg* 41(4):186–191, 2005.
  106. Tomlinson P, Sugarman ID: Complications with shunts in adults with spina bifida. *BMJ* 311(7000):286–287, 1995.
  107. Cameron M, Moran P: Prenatal screening and diagnosis of neural tube defects. *Prenat Diagn* 29(4):402–411, 2009.
  108. Sival DA, Begeer JH, Staal-Schreinemachers AL, et al: Perinatal motor behaviour and neurological outcome in spina bifida aperta. *Early Hum Dev* 50(1):27–37, 1997.
  109. Meuli M, Meuli-Simmen C, Hutchins GM, et al: The spinal cord lesion in human fetuses with myelomeningocele: implications for fetal surgery. *J Pediatr Surg* 32(3):448–452, 1997.
  110. Drewek MJ, Bruner JP, Whetsell WO, et al: Quantitative analysis of the toxicity of human amniotic fluid to cultured rat spinal cord. *Pediatr Neurosurg* 27(4):190–193, 1997.
  111. George TM, Fuh E: Review of animal models of surgically induced spinal neural tube defects: implications for fetal surgery. *Pediatr Neurosurg* 39(2):81–90, 2003.
  112. Meuli M, Meuli-Simmen C, Hutchins GM, et al: In utero surgery rescues neurological function at birth in sheep with spina bifida. *Nat Med* 1(4):342–347, 1995.
  113. Meuli M, Meuli-Simmen C, Yingling CD, et al: Creation of myelomeningocele in utero: a model of functional damage from spinal



- cord exposure in fetal sheep. *J Pediatr Surg* 30(7):1028–1032, discussion 1032–1023, 1995.
114. Meuli M, Meuli-Simmen C, Yingling CD, et al: In utero repair of experimental myelomeningocele saves neurological function at birth. *J Pediatr Surg* 31(3):397–402, 1996.
  115. Paek BW, Farmer DL, Wilkinson CC, et al: Hindbrain herniation develops in surgically created myelomeningocele but is absent after repair in fetal lambs. *Am J Obstet Gynecol* 183(5):1119–1123, 2000.
  116. Deprest JA, Flake AW, Gratacos E, et al: The making of fetal surgery. *Prenat Diagn* 30(7):653–667, 2010.
  117. Tulipan N, Bruner JP, Hernanz-Schulman M, et al: Effect of intrauterine myelomeningocele repair on central nervous system structure and function. *Pediatr Neurosurg* 31(4):183–188, 1999.
  118. Tulipan N, Hernanz-Schulman M, Lowe LH, et al: Intrauterine myelomeningocele repair reverses preexisting hindbrain herniation. *Pediatr Neurosurg* 31(3):137–142, 1999.
  119. Sutton LN, Adzick NS, Bilaniuk LT, et al: Improvement in hindbrain herniation demonstrated by serial fetal magnetic resonance imaging following fetal surgery for myelomeningocele. *JAMA* 282(19):1826–1831, 1999.
  120. Bruner JP, Tulipan NE, Richards WO: Endoscopic coverage of fetal open myelomeningocele in utero. *Am J Obstet Gynecol* 176(1 Pt 1):256–257, 1997.
  121. Verbeek RJ, Heep A, Maurits NM, et al: Fetal endoscopic myelomeningocele closure preserves segmental neurological function. *Dev Med Child Neurol* 54(1):15–22, 2012.
  122. Kohl T: Percutaneous minimally-invasive fetoscopic surgery for spina bifida aperta. Part I: surgical technique and perioperative outcome. *Ultrasound Obstet Gynecol* 44(5):515–524, 2014.
  123. Degenhardt J, Schurg R, Winarno A, et al: Percutaneous minimal-access fetoscopic surgery for spina bifida aperta. Part II: maternal management and outcome. *Ultrasound Obstet Gynecol* 44(5):525–531, 2014.
  124. Pedreira DA, Zanon N, de Sa RA, et al: Fetoscopic single-layer repair of open spina bifida using a cellulose patch: preliminary clinical experience. *J Matern Fetal Neonatal Med* 27(16):1613–1619, 2014.
  125. Kotecha S, Barbato A, Bush A, et al: Congenital diaphragmatic hernia. *Eur Respir J* 39(4):820–829, 2012.
  126. Gallot D, Coste K, Francannet C, et al: Antenatal detection and impact on outcome of congenital diaphragmatic hernia: a 12-year experience in Auvergne, France. *Eur J Obstet Gynecol Reprod Biol* 125(2):202–205, 2006.
  127. de Buys Roessingh AS, Dinh-Xuan AT: Congenital diaphragmatic hernia: current status and review of the literature. *Eur J Pediatr* 168(4):393–406, 2009.
  128. Stege G, Fenton A, Jaffray B: Nihilism in the 1990s: the true mortality of congenital diaphragmatic hernia. *Pediatrics* 112(3 Pt 1):532–535, 2003.
  129. Colvin J, Bower C, Dickinson JE, Sokol J: Outcomes of congenital diaphragmatic hernia: a population-based study in Western Australia. *Pediatrics* 116(3):e356–e363, 2005.
  130. Hedrick HL, Danzer E, Merchant A, et al: Liver position and lung-to-head ratio for prediction of extracorporeal membrane oxygenation and survival in isolated left congenital diaphragmatic hernia. *Am J Obstet Gynecol* 197(4):422.e1–422.e4, 2007.
  131. Datin-Dorriere V, Rouzies S, Taupin P, et al: Prenatal prognosis in isolated congenital diaphragmatic hernia. *Am J Obstet Gynecol* 198(1):80.e1–80.e5, 2008.
  132. Metkus AP, Filly RA, Stringer MD, et al: Sonographic predictors of survival in fetal diaphragmatic hernia. *J Pediatr Surg* 31(1):148–151, 1996.
  133. Jani J, Nicolaides KH, Keller RL, et al: Observed to expected lung area to head circumference ratio in the prediction of survival in fetuses with isolated diaphragmatic hernia. *Ultrasound Obstet Gynecol* 30(1):67–71, 2007.
  134. Peralta CF, Cavoretto P, Csapo B, et al: Lung and heart volumes by three-dimensional ultrasound in normal fetuses at 12–32 weeks' gestation. *Ultrasound Obstet Gynecol* 27(2):128–133, 2006.
  135. Peralta CF, Jani J, Cos T, et al: Left and right lung volumes in fetuses with diaphragmatic hernia. *Ultrasound Obstet Gynecol* 27(5):551–554, 2006.
  136. Jani JC, Peralta CF, Nicolaides KH: Lung-to-head ratio: a need to unify the technique. *Ultrasound Obstet Gynecol* 39(1):2–6, 2012.
  137. Quintero RA, Quintero LF, Chmait R, et al: The quantitative lung index (QLI): a gestational age-independent sonographic predictor of fetal lung growth. *Am J Obstet Gynecol* 205(6):544.e1–544.e8, 2011.
  138. Quintero RA, Kontopoulos EV, Quintero LF, et al: The observed vs. expected lung-to-head ratio does not correct for the effect of gestational age on the lung-to-head ratio. *J Matern Fetal Neonatal Med* 26(6):552–557, 2013.
  139. Ruano R, Ali RA, Patel P, et al: Fetal endoscopic tracheal occlusion for congenital diaphragmatic hernia: indications, outcomes, and future directions. *Obstet Gynecol Surv* 69(3):147–158, 2014.
  140. Cannie M, Jani J, Chaffiotte C, et al: Quantification of intrathoracic liver herniation by magnetic resonance imaging and prediction of postnatal survival in fetuses with congenital diaphragmatic hernia. *Ultrasound Obstet Gynecol* 32(5):627–632, 2008.
  141. Lazar DA, Ruano R, Cass DL, et al: Defining “liver-up”: does the volume of liver herniation predict outcome for fetuses with isolated left-sided congenital diaphragmatic hernia? *J Pediatr Surg* 47(6):1058–1062, 2012.
  142. Harrison MR, Keller RL, Hawgood SB, et al: A randomized trial of fetal endoscopic tracheal occlusion for severe fetal congenital diaphragmatic hernia. *N Engl J Med* 349(20):1916–1924, 2003.
  143. Quintero RA: *Diagnostic and Operative Fetoscopy*, New York, 2002, Parthenon Publishing.
  144. Jani JC, Nicolaides KH, Gratacos E, et al: Severe diaphragmatic hernia treated by fetal endoscopic tracheal occlusion. *Ultrasound Obstet Gynecol* 34(3):304–310, 2009.
  145. Ruano R, Duarte SA, Pimenta EJ, et al: Comparison between fetal endoscopic tracheal occlusion using a 1.0-mm fetoscope and prenatal expectant management in severe congenital diaphragmatic hernia. *Fetal Diagn Ther* 29(1):64–70, 2011.
  146. Roubliova X, Verbeek E, Wu J, et al: Pulmonary vascular morphology in a fetal rabbit model for congenital diaphragmatic hernia. *J Pediatr Surg* 39(7):1066–1072, 2004.
  147. Hellmeyer L, Ballast A, Tekesin I, et al: Evaluation of the development of lung hypoplasia in the premature lamb. *Arch Gynecol Obstet* 271(3):231–234, 2005.
  148. Lipsett J, Cool JC, Runciman SI, et al: Morphometric analysis of preterm fetal pulmonary development in the sheep model of congenital diaphragmatic hernia. *Pediatr Dev Pathol* 3(1):17–28, 2000.
  149. O'Toole SJ, Irish MS, Holm BA, et al: Pulmonary vascular abnormalities in congenital diaphragmatic hernia. *Clin Perinatol* 23(4):781–794, 1996.
  150. Ting A, Glick PL, Wilcox DT, et al: Alveolar vascularization of the lung in a lamb model of congenital diaphragmatic hernia. *Am J Respir Crit Care Med* 157(1):31–34, 1998.
  151. Jani JC, Flemmer AW, Bergmann F, et al: The effect of fetal tracheal occlusion on lung tissue mechanics and tissue composition. *Pediatr Pulmonol* 44(2):112–121, 2009.
  152. DiFiore JW, Fauza DO, Slavin R, et al: Experimental fetal tracheal ligation and congenital diaphragmatic hernia: a pulmonary vascular morphometric analysis. *J Pediatr Surg* 30(7):917–923, discussion 923–924, 1995.
  153. Davey MG, Hooper SB, Cock ML, et al: Stimulation of lung growth in fetuses with lung hypoplasia leads to altered postnatal lung structure in sheep. *Pediatr Pulmonol* 32(4):267–276, 2001.
  154. De Paepe ME, Papadakis K, Johnson BD, et al: Fate of the type II pneumocyte following tracheal occlusion in utero: a time-course study in fetal sheep. *Virchows Arch* 432(1):7–16, 1998.
  155. Wild YK, Piasecki GJ, De Paepe ME, et al: Short-term tracheal occlusion in fetal lambs with diaphragmatic hernia improves lung function, even in the absence of lung growth. *J Pediatr Surg* 35(5):775–779, 2000.
  156. Davey MG, Hedrick HL, Bouchard S, et al: Temporary tracheal occlusion in fetal sheep with lung hypoplasia does not improve postnatal lung function. *J Appl Physiol* 94(3):1054–1062, 2003.



157. Kohl T, Gembruch U, Tchatcheva K, Schaible T: Current consequences of prenatal diagnosis of congenital diaphragmatic hernia by Deprest et al (*J Ped Surg* 2006;41:423-430). *J Pediatr Surg* 41(7):1344-1345, author reply 1345-1346, 2006.
158. Deprest J, Nicolaidis K, Done E, et al: Technical aspects of fetal endoscopic tracheal occlusion for congenital diaphragmatic hernia. *J Pediatr Surg* 46(1):22-32, 2011.
159. Sosa-Sosa C, Bermudez C, Chmait RH, et al: Intraluminal tracheal occlusion using a modified 8-mm Z-stent in a sheep model of left-sided congenital diaphragmatic hernia. *J Matern Fetal Neonatal Med* 25(11):2346-2353, 2012.
160. Ruano R, Yoshisaki CT, da Silva MM, et al: A randomized controlled trial of fetal endoscopic tracheal occlusion versus postnatal management of severe isolated congenital diaphragmatic hernia. *Ultrasound Obstet Gynecol* 39(1):20-27, 2012.
161. Wilson RD, Hedrick HL, Liechty KW, et al: Cystic adenomatoid malformation of the lung: review of genetics, prenatal diagnosis, and in utero treatment. *Am J Med Genet A* 140(2):151-155, 2006.
162. Stocker JT, Madewell JE, Drake RM: Congenital cystic adenomatoid malformation of the lung. Classification and morphologic spectrum. *Hum Pathol* 8(2):155-171, 1977.
163. Adzick NS: Management of fetal lung lesions. *Clin Perinatol* 30(3):481-492, 2003.
164. Cavoretto P, Molina F, Poggi S, et al: Prenatal diagnosis and outcome of echogenic fetal lung lesions. *Ultrasound Obstet Gynecol* 32(6):769-783, 2008.
165. Witlox RS, Lopriore E, Oepkes D: Prenatal interventions for fetal lung lesions. *Prenat Diagn* 31(7):628-636, 2011.
166. Crombleholme TM, Coleman B, Hedrick H, et al: Cystic adenomatoid malformation volume ratio predicts outcome in prenatally diagnosed cystic adenomatoid malformation of the lung. *J Pediatr Surg* 37(3):331-338, 2002.
167. Wilson RD: In utero therapy for fetal thoracic abnormalities. *Prenat Diagn* 28(7):619-625, 2008.
168. Adzick NS: Management of fetal lung lesions. *Clin Perinatol* 36(2):363-376, 2009.
169. Baud D, Windrim R, Kachura JR, et al: Minimally invasive fetal therapy for hydropic lung masses: three different approaches and review of the literature. *Ultrasound Obstet Gynecol* 42(4):440-448, 2013.
170. Morris LM, Lim FY, Livingston JC, et al: High-risk fetal congenital pulmonary airway malformations have a variable response to steroids. *J Pediatr Surg* 44(1):60-65, 2009.
171. Curran PF, Jelin EB, Rand L, et al: Prenatal steroids for microcystic congenital cystic adenomatoid malformations. *J Pediatr Surg* 45(1):145-150, 2010.
172. Peranteau WH, Wilson RD, Liechty KW, et al: Effect of maternal betamethasone administration on prenatal congenital cystic adenomatoid malformation growth and fetal survival. *Fetal Diagn Ther* 22(5):365-371, 2007.
173. Lee FL, Said N, Grikscheit TC, et al: Treatment of congenital pulmonary airway malformation induced hydrops fetalis via percutaneous sclerotherapy. *Fetal Diagn Ther* 31(4):264-268, 2012.
174. Longaker MT, Laberge JM, Dansereau J, et al: Primary fetal hydrothorax: natural history and management. *J Pediatr Surg* 24(6):573-576, 1989.
175. Weber AM, Philipson EH: Fetal pleural effusion: a review and meta-analysis for prognostic indicators. *Obstet Gynecol* 79(2):281-286, 1992.
176. Ruano R, Ramalho AS, Cardoso AK, et al: Prenatal diagnosis and natural history of fetuses presenting with pleural effusion. *Prenat Diagn* 31(5):496-499, 2011.
177. Waller K, Chaithongwongwatthana S, Yamasmit W, et al: Chromosomal abnormalities among 246 fetuses with pleural effusions detected on prenatal ultrasound examination: factors associated with an increased risk of aneuploidy. *Genet Med* 7(6):417-421, 2005.
178. Yinon Y, Kelly E, Ryan G: Fetal pleural effusions. *Best Pract Res Clin Obstet Gynaecol* 22(1):77-96, 2008.
179. Yinon Y, Grisaru-Granovsky S, Chaddha V, et al: Perinatal outcome following fetal chest shunt insertion for pleural effusion. *Ultrasound Obstet Gynecol* 36(1):58-64, 2010.
180. Picone O, Benachi A, Mandelbrot L, et al: Thoracoamniotic shunting for fetal pleural effusions with hydrops. *Am J Obstet Gynecol* 191(6):2047-2050, 2004.
181. Knox EM, Kilby MD, Martin WL, et al: In-utero pulmonary drainage in the management of primary hydrothorax and congenital cystic lung lesion: a systematic review. *Ultrasound Obstet Gynecol* 28(5):726-734, 2006.
182. Rustico MA, Lanna M, Coviello D, et al: Fetal pleural effusion. *Prenat Diagn* 27(9):793-799, 2007.
183. Yonemoto H, Itoh S, Nakamura Y, et al: Hemodynamic evaluation of a prenatal thoracoamniotic shunt for fetal pleural effusion. *Early Hum Dev* 82(6):411-414, 2006.
184. McElhinney DB, Tworetzky W, Lock JE: Current status of fetal cardiac intervention. *Circulation* 121(10):1256-1263, 2010.
185. Reuss A, Wladimiroff JW, Niermeijer MF: Antenatal diagnosis of renal tract anomalies by ultrasound. *Pediatr Nephrol* 1(3):546-552, 1987.
186. Kumar S, Fisk NM: Distal urinary obstruction. *Clin Perinatol* 30(3):507-519, 2003.
187. Nakayama DK, Harrison MR, de Lorimier AA: Prognosis of posterior urethral valves presenting at birth. *J Pediatr Surg* 21(1):43-45, 1986.
188. Johnson MP, Bukowski TP, Reitleman C, et al: In utero surgical treatment of fetal obstructive uropathy: a new comprehensive approach to identify appropriate candidates for vesicoamniotic shunt therapy. *Am J Obstet Gynecol* 170(6):1770-1776, discussion 1776-1779, 1994.
189. Nicolini U, Spelzini F: Invasive assessment of fetal renal abnormalities: urinalysis, fetal blood sampling and biopsy. *Prenat Diagn* 21(11):964-969, 2001.
190. Clark TJ, Martin WL, Divakaran TG, et al: Prenatal bladder drainage in the management of fetal lower urinary tract obstruction: a systematic review and meta-analysis. *Obstet Gynecol* 102(2):367-382, 2003.
191. Morris RK, Malin GL, Quinlan-Jones E, et al: Percutaneous vesicoamniotic shunting versus conservative management for fetal lower urinary tract obstruction (PLUTO): a randomised trial. *Lancet* 382(9903):1496-1506, 2013.
192. Biard JM, Johnson MP, Carr MC, et al: Long-term outcomes in children treated by prenatal vesicoamniotic shunting for lower urinary tract obstruction. *Obstet Gynecol* 106(3):503-508, 2005.
193. Coplen DE: Prenatal intervention for hydronephrosis. *J Urol* 157(6):2270-2277, 1997.
194. Quintero RA, Gomez Castro LA, Bermudez C, et al: In utero management of fetal lower urinary tract obstruction with a novel shunt: a landmark development in fetal therapy. *J Matern Fetal Neonatal Med* 23(8):806-812, 2010.
195. Quintero RA, Hume R, Smith C, et al: Percutaneous fetal cystoscopy and endoscopic fulguration of posterior urethral valves. *Am J Obstet Gynecol* 172(1 Pt 1):206-209, 1995.
196. Langer JC, Harrison MR, Schmidt KG, et al: Fetal hydrops and death from sacrococcygeal teratoma: rationale for fetal surgery. *Am J Obstet Gynecol* 160(5 Pt 1):1145-1150, 1989.
197. Hedrick HL, Flake AW, Crombleholme TM, et al: Sacrococcygeal teratoma: prenatal assessment, fetal intervention, and outcome. *J Pediatr Surg* 39(3):430-438, discussion 430-438, 2004.
198. Van Mieghem T, Al-Ibrahim A, Deprest J, et al: Minimally invasive therapy for fetal sacrococcygeal teratoma: case series and systematic review of the literature. *Ultrasound Obstet Gynecol* 43(6):611-619, 2014.
199. Heifetz SA: Strangulation of the umbilical cord by amniotic bands: report of 6 cases and literature review. *Pediatr Pathol* 2(3):285-304, 1984.
200. Bianchi DW, Crombleholme TM, D'Alton ME: *Fetology: Diagnosis and Management of the Fetal Patient*, New York, 2000, McGraw-Hill.
201. Quintero RA, Morales WJ, Phillips J, et al: In utero lysis of amniotic bands. *Ultrasound Obstet Gynecol* 10(5):316-320, 1997.
202. Soldado F, Aguirre M, Peiro JL, et al: Fetal surgery of extremity amniotic bands: an experimental model of in utero limb salvage in fetal lamb. *J Pediatr Orthop* 29(1):98-102, 2009.
203. Crombleholme TM, Dirkes K, Whitney TM, et al: Amniotic band syndrome in fetal lambs. I: Fetoscopic release and morphometric outcome. *J Pediatr Surg* 30(7):974-978, 1995.



204. Hüsler MR, Wilson RD, Horii SC, et al: When is fetoscopic release of amniotic bands indicated? Review of outcome of cases treated in utero and selection criteria for fetal surgery. *Prenat Diagn* 29(5):457–463, 2009.
205. Assaf R, Llanes A, Chmait R: In utero release of constriction amniotic bands via blunt dissection. *Fetal Pediatr Pathol* 31(1):25–29, 2012.
206. Derderian SC, Iqbal CW, Goldstein R, et al: Fetoscopic approach to amniotic band syndrome. *J Pediatr Surg* 49(2):359–362, 2014.
207. Amer HZ, Heller DS: Chorangioma and related vascular lesions of the placenta—a review. *Fetal Pediatr Pathol* 29(4):199–206, 2010.
208. Sepulveda W, Wong AE, Herrera L, et al: Endoscopic laser coagulation of feeding vessels in large placental chorioangiomas: report of three cases and review of invasive treatment options. *Prenat Diagn* 29(3):201–206, 2009.
209. Hadi HA, Finley J, Strickland D: Placental chorioangioma: prenatal diagnosis and clinical significance. *Am J Perinatol* 10(2):146–149, 1993.
210. Jones K, Tierney K, Grubbs BH, et al: Fetoscopic laser photocoagulation of feeding vessels to a large placental chorioangioma following fetal deterioration after amnioreduction. *Fetal Diagn Ther* 31(3):191–195, 2012.
211. Lim FY, Coleman A, Polzin W, et al: Giant chorioangiomas: perinatal outcomes and techniques in fetoscopic devascularization. *Fetal Diagn Ther* 37(1):18–23, 2015.

akusher-lib.ru

# Obstetric Ultrasound Imaging and the Obese Patient

Beryl Benacerraf

## SUMMARY OF KEY POINTS

- Obesity is epidemic and a significant public health problem.
- Obese women are at increased risk of maternal complications of pregnancy compared to women of normal weight.
- Fetuses of obese gravidas are at increased risk of malformations compared to those of normal weight women.
- Ultrasound imaging of obese patients is hampered by acoustic noise, artifacts, and thicker anterior abdominal wall, all of which degrade the image.
- Although ultrasound examinations of obese gravidas often are repeated in order to obtain adequate images, fetal anatomic evaluation is frequently suboptimal despite several attempts.
- There are several ways to optimize the image quality while scanning obese patients.

Over 60% of the population of the United States is considered overweight, and more than one third is obese, making obesity a significant public health problem.<sup>1,2</sup> In 2005, the World Health Organization estimated that 1.6 billion adults worldwide were overweight and 400 million were frankly obese (body mass index [BMI]  $\geq 30$ ).<sup>3</sup> This worldwide epidemic shows no sign of abating and continues to increase, especially in the United States. A growing body of evidence shows that obese patients have a higher risk of a multitude of health problems, including heart disease, type 2 diabetes, hypertension, stroke, “metabolic syndrome,” arthritis, cancer, respiratory problems, sleep apnea, pregnancy complications, and more (Table 25-1).<sup>4</sup> The National Institutes of Health and the World Health Organization define obesity according to the BMI (in kg/m<sup>2</sup>). A BMI of 18 to 24.9 is normal, and a BMI of 25 to 29.9 is overweight. Classes I, II, and III obesity are defined as BMIs of 30 to 34.9, 35 to 39.9, and 40 or higher, respectively.<sup>5</sup>

Obese women have an increased risk for adverse pregnancy outcomes that impact both the mother and the fetus.<sup>2,3,5-22</sup> Sebire and associates described 287,213 patients, of which 39% were obese, and reported that several maternal complications increased with the degree of obesity.<sup>6</sup> Table 25-1 lists the most common maternal and fetal complications associated with maternal obesity. In addition, an increased risk of fetal malformations has been associated with obesity,<sup>7-10</sup> and fetal anomalies such as neural tube defects, cardiac anomalies, anal atresia, and limb reduction abnormalities are reported to be significantly more common with obese patients compared to the normal weight population (Table 25-2).<sup>10</sup>

Uhden and colleagues reported that the relative risk of heart defects is 2.04 in fetuses of obese compared to normal weight women.<sup>11</sup> Watkins and coworkers also demonstrated that obese compared to average weight women have an elevated risk of fetal anomalies such as spina bifida (odds ratio [OR] 3.5; 95% confidence interval [CI] 1.2-10.3), omphalocele (OR 3.3; 95% CI 1.0-10.3), and heart defects (OR 2.0; 95% CI 1.2-3.4), as well as multiple anomalies (OR 2.0; 95% CI 1.0-3.8).<sup>7</sup> In a study evaluating risk factors for fetal malformations,

Waller and associates showed that patients who had infants with spina bifida, heart defects, anorectal atresia, hypospadias, limb reduction defects, diaphragmatic hernia, and omphalocele were significantly more likely to be obese, with ORs between 1.33 and 2.10.<sup>8</sup> A meta-analysis of 12 studies demonstrated that the OR for having a fetus with a neural tube defect was 1.22, 1.70, and 3.11 for overweight, obese, and severely obese patients compared to normal weight patients, indicating that the risk rises with increasing obesity.<sup>9</sup>

Obese gravidas require more medical resources than normal weight patients and often present difficult technical problems for the medical personnel providing their care.<sup>12</sup> High BMI patients have been reported to require more interventions and care of all types, including obstetric ultrasound examinations, medications, telephone calls to providers, and prenatal visits with physicians compared to women of normal weight.<sup>12</sup>

In addition to requiring more numerous ultrasound examinations, the examinations required to detect fetal anomalies and pregnancy complications are often more technically challenging in obese compared to thinner patients.<sup>13-22</sup> The quality of the ultrasound examination done on an obese patient is technically inferior when compared to the same scan done on slimmer patients owing to the distance traversed by the sound beam and the density of adipose tissue. Hence, the quality of the ultrasound image relates inversely to the distance that the beam must travel to reach the fetus. The ultrasound beam is absorbed, dispersed, and attenuated in adipose tissue, limiting the image quality in evaluation of the fetus.<sup>13-22</sup> The ultrasound image is further degraded with each centimeter that it penetrates through the body to reach the fetus. As a result, the most obese patients who are at the highest risk of maternal and fetal complications also have the poorest quality imaging by ultrasound. Over time, advances in ultrasound technology have resulted in improved image quality even in the more challenging patients. Preprocessing and postprocessing filters, speckle-reduction filters, compound imaging, and tissue harmonic imaging have all contributed to improved image quality.<sup>2,3</sup> Despite



these new tools, the ultrasound image in obese gravidas often remains fuzzy and noisy and suffers from excessive backscatter and artifacts (Fig. 25-1).

A number of studies have compared the ability to evaluate the fetus and detect fetal anomalies in obese versus normal weight women. Stothard and colleagues showed that although the risk of many fetal anomalies is significantly higher in obese compared with normal weight patients, a fetal anatomic survey was not completed at the time of the first ultrasound detailed scan in more than 50% of obese women.<sup>10</sup> Dashe and associates evaluated the quality of second trimester ultrasound studies done at 18 to 24 weeks on a cohort of 10,112 patients, 34% of whom were overweight and 26% of whom were obese.<sup>13</sup> The following 10 anatomic views were evaluated for adequacy: cerebral ventricles, posterior fossa, midline face (profile), four-chamber view of the heart, spine, ventral wall, cord vessels, stomach, kidneys, and bladder. Table 25-3 lists the relationship between successful scans and obesity class, showing a steady decline in scan quality with increasing BMI.<sup>13</sup> Maxwell and coworkers compared patients with a BMI of 30 or higher (average 35.7) with those having a BMI lower than 25 and found that 26% of the anatomic surveys in obese women were

incomplete compared to 2.5% of those in women with a normal BMI.<sup>15</sup> Uhden and colleagues also reported that the percentage of poor ultrasound images rose from 6.4% to 17.4% when comparing normal weight to obese patients, whereas the prevalence of heart defects was higher (relative risk = 2.04) in obese and overweight women when compared to normal weight patients.<sup>11</sup>

Several other investigators have also reported that poor fetal anatomic visualization increases with maternal BMI, although the imaging improves with advancing gestational age in most patients.<sup>19</sup> Hence, it is recommended that obese gravidas be imaged later in gestation to avoid excessive repeat ultrasound examinations to complete the fetal survey.<sup>22</sup> In one study of 7140 patients, maternal BMI was inversely proportional to the rate of completion of anatomic surveys, and the number of scans required to obtain satisfactory images increased directly with BMI. Delaying the initial survey until 20 weeks (rather than 18 weeks) has been reported to increase the chance that the fetal anatomic survey can be completed in a single ultrasound examination.<sup>21</sup>

Hendler and associates evaluated the rate of poor visualization of specific fetal parts on ultrasound scans and found that it correlated linearly with the degree of the patient's obesity and was significantly worse in the obese group for both the fetal spine (43% vs. 29%) and heart (37% vs. 19%).<sup>16</sup> Although visualization of cardiac anatomy improved when the scan was repeated at 21 weeks' gestation, the heart was still inadequately imaged in 20% of the obese population even after multiple scans.<sup>16</sup>

Fuchs and coworkers reported on several factors associated with successful completion of ultrasound scans in overweight and obese patients, including having 10 additional minutes for the scan, moving the fetus so that the back was in posterior or lateral position, having a more experienced person perform the scan, and body habitus that

**TABLE 25-1 Risks Associated With Maternal Obesity**

Maternal Risks	Fetal Risks
Cardiovascular disease	Congenital anomalies
Hypertension	Lower detection of fetal anomalies
Recurrent miscarriage	Macrosomia
Gestational diabetes	Inaccurate fetal weight estimate
Preeclampsia	Preterm birth
Cesarean delivery	Stillbirth and neonatal death
Postpartum hemorrhage	
Wound infection	
Thromboembolism	
Maternal death	

**TABLE 25-2 Fetal Anomalies Associated With Maternal Obesity**

Anomaly	OR (95% CI)
Anal atresia	1.48 (1.12-1.97)
Cardiac defects	1.30 (1.12-1.51)
Hydrocephalus	1.68 (1.19-2.36)
Limb reduction	1.34 (1.03-1.73)
Neural tube defect	1.87 (1.62-2.15)

CI, confidence interval; OR, odds ratio.

Modified from Stothard KJ, Tennant PWG, Bell R, Rankin J: Maternal overweight and obesity and the risk of congenital anomalies. A systematic review and meta-analysis. *JAMA* 301(6):636-650, 2009.

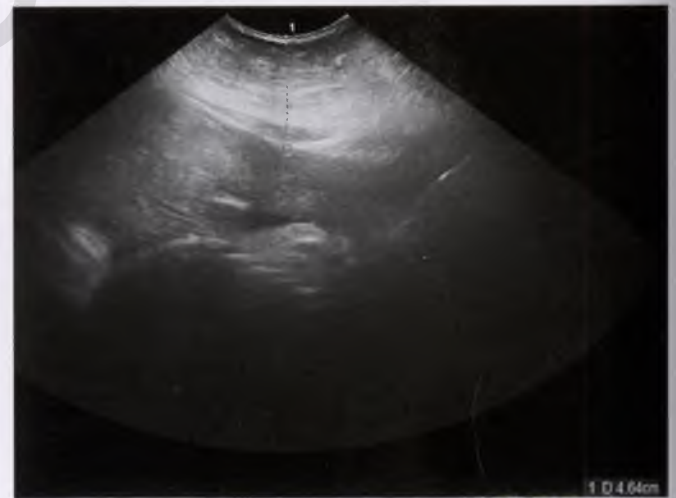


**FIG 25-1** This is an attempt at imaging a third trimester fetus in an obese patient. Note the very echogenic adipose tissue in the anterior abdominal wall that attenuates the sound before it reaches the fetus.

**TABLE 25-3 Percentage of Patients in Whom the Fetal Anatomic Survey Was Completed by BMI Category**

	Normal Weight (BMI < 25)	Overweight (BMI 25-29)	Class I Obesity (BMI 30-34)	Class II Obesity (BMI 35-39)	Class III Obesity (BMI ≥ 40)
Dashe et al <sup>13</sup>	72%	68%	57%	41%	30%
Thornburg et al <sup>17</sup>	79%	76%	72%	61%	49%

BMI, body mass index (in kg/m<sup>2</sup>).



included a thinner maternal abdominal wall thickness.<sup>18</sup> Another study found that sonologists with more than 20 years' experience were more likely to complete a successful fetal ultrasound scan on obese patients (adjusted OR 3.27; 95% CI 1.15-9.25) compared to their less experienced colleagues, suggesting that experience also plays a role in obtaining satisfactory images on challenging patients as well as perhaps in confidence in reporting on suboptimal examinations.<sup>20</sup>

Several studies have evaluated the use of ultrasound in screening for Down syndrome in obese gravidas.<sup>22-24</sup> As the maternal BMI increases, it takes significantly more time to obtain a nuchal translucency measurement, and the failure rate of obtaining an adequate measurement increases.<sup>22</sup> Tsai and colleagues studied 5690 patients and reported that the degree of obesity hampered performance of the genetic sonogram.<sup>23</sup> This study also showed that the chance of finding one or more ultrasound markers for aneuploidy screening differed significantly among BMI groups (16% in normal, 13% in overweight, 15% in class I, 12% in class II, and 10% in class III obese women,  $P < 0.02$ ), indicating that obese women are less likely to have soft signs identified by ultrasound.<sup>23</sup>

The FaSTER trial was a large prospective cohort study performed to compare a variety of first and second trimester screening strategies for Down syndrome. A secondary analysis of this study reported on the detection of anomalies in obese gravidas.<sup>24</sup> Cardiac anomalies were identified with a higher sensitivity and specificity in women with a BMI lower than 25 compared to obese women. In a logistic regression model, maternal obesity diminished the likelihood that fetal malformations would be identified sonographically (OR 0.7; 95% CI 0.6-0.9;  $P = 0.001$ ).<sup>24</sup>

In patients in whom fetal anatomy is poorly visualized because of increased maternal abdominal wall thickness, the American Institute of Ultrasound in Medicine guidelines suggest that the report of the sonographic examination should document the nature of the technical limitation.<sup>25</sup> Although a follow-up examination may be helpful and should be performed in 2 to 4 weeks, in some cases the fetal anatomy is still not optimally visualized. In such cases, it is suggested that further follow-up is recommended only if clinically indicated.<sup>26</sup>

There is evidence that high maternal BMI is also associated with a reduced accuracy of the sonographic fetal weight estimate. Fox and associates demonstrated that maternal BMI is associated with an increased absolute error and absolute percent error in sonographic fetal weight calculation, even after controlling for birth weight.<sup>27</sup> It has been suggested that customized fetal growth curves may improve the accuracy of fetal weight estimates and better predict fetal growth restriction in obese patients.<sup>28</sup>

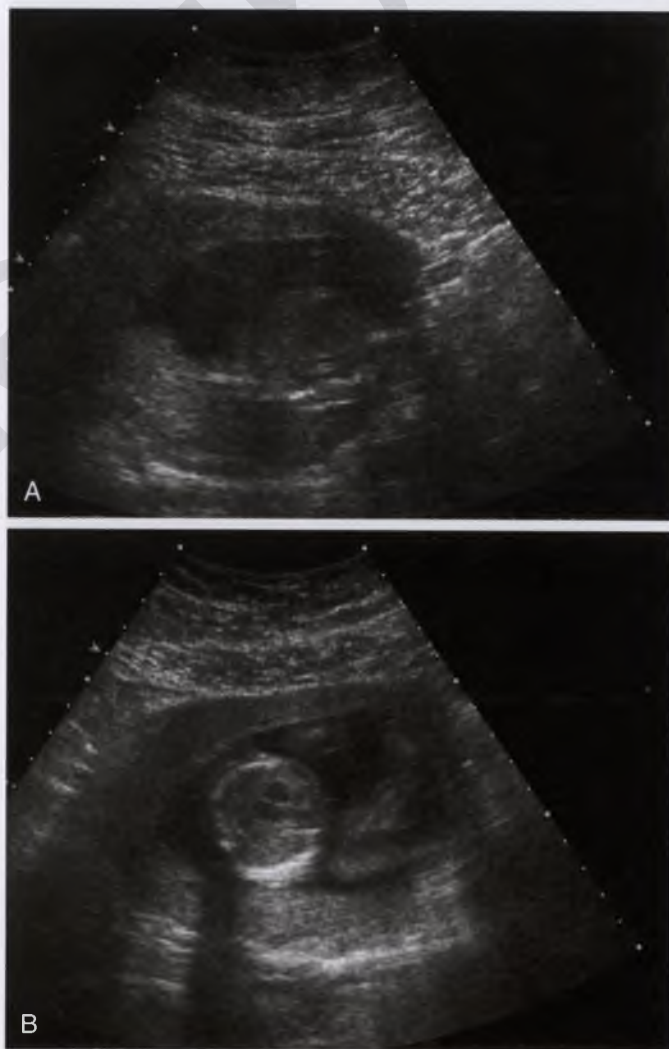
As noted earlier, a number of advances in ultrasound technology have improved image quality and include speckle-reduction filters, tissue harmonic imaging, and other noise-reducing methods to enhance the penetration of the sound beam and clarity of the image.<sup>29,30</sup> Nonetheless, the distance between the transducer and the fetus remains the greatest obstacle to adequate fetal imaging in the obese patient.

Table 25-4 lists several strategies that can help improve imaging in these circumstances.<sup>31</sup> Use of different transducers, including sector probes with smaller footprint and narrower field of view, as well as lower frequency, may improve tissue penetration and, thus, image quality. Ultrasound equipment allows selecting preset parameters optimized for challenging patients, including maternal obesity. Use of the umbilicus as an acoustic window requires traversal of less adipose tissue between the transducer and the uterus and fetus. Unfortunately, this window is generally small, thus limiting the improved visualization to a small portion of the uterus (Fig. 25-2). One can also lift the panniculus and scan beneath it, just over the pubic symphysis. This approach affords access to the lower uterine segment but again results

#### TABLE 25-4 Techniques to Improve Ultrasound Image Quality in Obese Gravidas

1. Transducer selection: smaller footprint (sector); narrow field of view; lower frequency
2. Use of preset parameters optimized for obesity
3. Improve signal-to-noise ratio
  - a. Compound imaging, speckle-reduction filters, preprocessing and postprocessing, and tissue harmonics
4. Transvaginal ultrasound with external manipulation of fetus
5. Use of umbilicus as acoustic window
6. Patient positioning
  - a. Sitting while imaging above panniculus
  - b. Modified Sims position with imaging from flank or groin
7. Full maternal bladder

Modified from Benacerraf BR: The use of obstetrical ultrasound in the obese gravida. *Semin Perinatol* 37:345-347, 2013; Benacerraf BR: A technical tip on scanning obese gravidas. *Ultrasound Obstet Gynecol* 35:615-616, 2010.



**FIG 25-2** Transabdominal scan of a 16-week fetus in a severely obese patient. **A**, The fetal chest is seen from the midabdomen through the panniculus. **B**, The fetal chest of the same fetus is seen through the umbilicus. Note that the ultrasound beam is severely degraded in A. In B, there is less adipose tissue and a clearer image of the fetal heart when imaging through the umbilical area.



in limited visualization of the body and fundus of the uterus. Alternatively, one can scan the patient in a sitting position and scan directly above the panniculus, in the midabdomen, pushing the panniculus down. Because the mid- to upper abdomen has less adipose tissue than the lower abdomen, this approach allows scanning through a decreased distance between the skin surface and the fetus. Filling the patient's bladder will raise the fundus of the uterus to a more cephalad position and may improve visualization by allowing scanning through a thinner portion of the anterior abdominal wall.

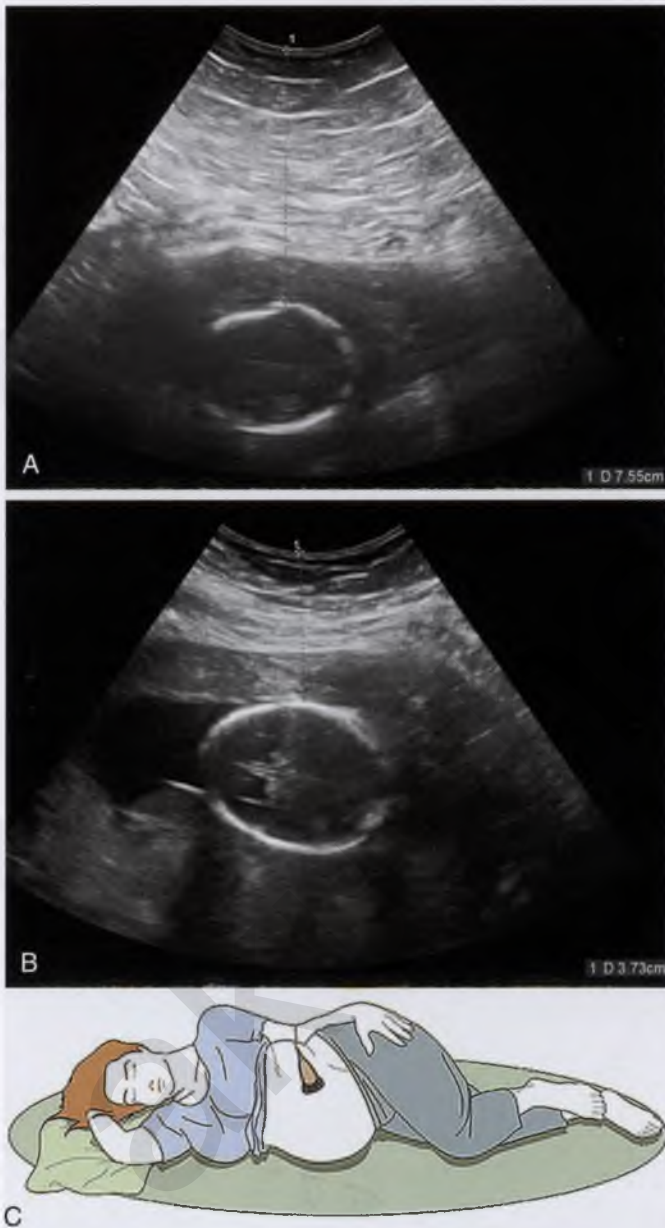


**FIG 25-3** Scan of the fetal head at 17 weeks in a severely obese patient. **A**, Image of the fetal head when the patient is lying on her back with the transducer on the surface of the maternal belly. Note that the transducer is 7.5 cm from the uterine wall. When the same patient is placed in the modified Sims position, the distance is reduced to 3.7 cm and the quality of the image is improved (**B**). **C**, Drawing of a patient in the modified Sims position, showing the panniculus on the table and the position of the transducer on the flank. (From Benacerraf BR: The use of obstetrical ultrasound in the obese gravida. *Semin Perinatol* 37:345-347, 2013, used with permission.)

Especially in the early second trimester, scanning the obese patient transvaginally can provide images that are produced with a higher frequency transducer at a shorter distance to the fetus than when using the traditional transabdominal methods. One can also attempt to manipulate the fetal position using the free hand on the maternal abdomen to shift the fetal presenting part during the transvaginal scan so as to better visualize all the fetal anatomy. Lastly, use of a modified Sims position (Fig. 25-3C) allows the examiner to scan the fetus through the mother's flank or groin, which typically have less tissue, and therefore less depth of penetration is required when compared to the anterior abdominal wall.<sup>32</sup> In the modified Sims position, the patient is placed on her side and further rotated ventrally so that the panniculus lies on the ultrasound table. Figure 25-3 shows the effect of the narrower distance between the transducer and the fetal part when using the modified Sims position. It is important to try this position on both sides because one side is typically better than the other, but the optimal side is unpredictable and varies for each patient and fetal position.

In conclusion, obesity is a rapidly growing public health problem and is epidemic in the United States. Maternal obesity results in a significantly elevated risk for adverse outcome for both mother and fetus, including a higher frequency of fetal anomalies. Obese patients present a difficult technical problem for the ultrasound examiner because sound penetrates adipose tissue poorly and produces images limited by noise and artifact, often requiring repeat examinations to adequately assess fetal anatomy. Scans performed later in gestation may be useful to complete the fetal anatomic survey, and special techniques such as patient positioning or transvaginal scanning can enhance the sonographic image quality in these patients.

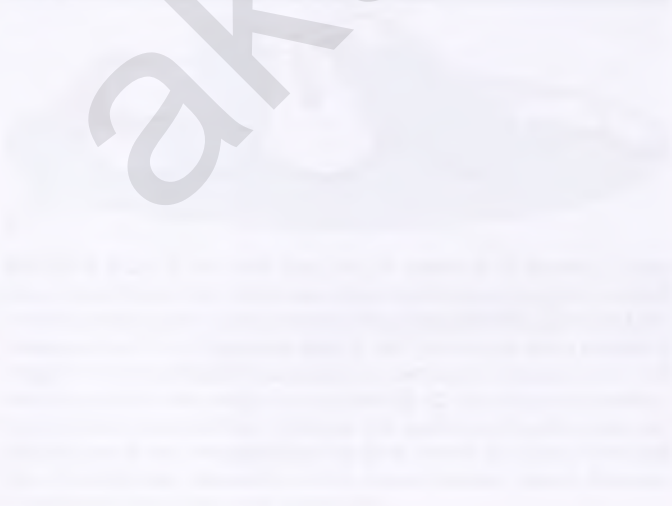
## REFERENCES

1. Department of Health and Human Services, Centers for Disease Control and Prevention: *Overweight & Obesity: Data & Statistics*. Available at: <[www.cdc.gov/nccdphp/dnpa/obesity/consequences.htm](http://www.cdc.gov/nccdphp/dnpa/obesity/consequences.htm)>, 2015.
2. Paladini D: Sonography in obese and overweight pregnant women: clinical, medicolegal and technical issues. *Ultrasound Obstet Gynecol* 33:720-729, 2009.
3. Weichert J, Hartge DR: Obstetrical sonography in obese women: a review. *J Clin Ultrasound* 39:209-216, 2011.
4. Reece EA: Perspectives on obesity, pregnancy and birth outcomes in the United States: the scope of the problem. *Am J Obstet Gynecol* 198:23-27, 2008.
5. National Institutes of Health, National Heart, Lung and Blood Institute: *How Are Overweight and Obesity Diagnosed?* Available at: <<http://www.nhlbi.nih.gov/health/health-topics/topics/obe/diagnosis.html>>, 2012.
6. Sebire NJ, Jolly M, Harris JP, et al: Maternal obesity and pregnancy outcome: a study of 287,213 pregnancies in London. *Int J Obes Relat Metab Disord* 25(8):1175-1182, 2001.
7. Watkins ML, Rasmussen SA, Honein MA, et al: Maternal obesity and risk for birth defects. *Pediatrics* 111:1152-1158, 2003.
8. Waller DK, Shaw GM, Rasmussen SA, et al: National Birth Defects Prevention Study: prepregnancy obesity as a risk factor for structural birth defects. *Arch Pediatr Adolesc Med* 161(8):745-750, 2007.
9. Rasmussen SA, Chu SY, Kim SY, et al: Maternal obesity and risk of neural tube defects: a metaanalysis. *Am J Obstet Gynecol* 198:611-619, 2008.
10. Stothard KJ, Tennant PWG, Bell R, Rankin J: Maternal overweight and obesity and the risk of congenital anomalies. A systematic review and meta-analysis. *JAMA* 301(6):636-650, 2009.
11. Uhdén M, Knippel AJ, Stressig R, et al: Impact of maternal obesity and maternal overweight on the detection rate of fetal heart defects and the image quality of prenatal echocardiography. *Ultraschall Med* 32(Suppl 2):E108-E114, 2011.

12. Chu SY, Bachman DJ, Callaghan WM, et al: Association between obesity during pregnancy and increased use of health care. *N Engl J Med* 358:1444–1453, 2008.
13. Dashe JS, McIntire D, Twickler DM: Maternal obesity limits the ultrasound evaluation of fetal anatomy. *J Ultrasound Med* 28:1025–1030, 2009.
14. Hendler I, Blackwell SC, Bujold E, et al: Suboptimal second-trimester ultrasonographic visualization of the fetal heart in obese women: should we repeat the examination? *J Ultrasound Med* 24:1205–1209, 2005.
15. Maxwell C, Dunn E, Tomlinson G, Glanc P: How does maternal obesity affect the routine fetal anatomic ultrasound? *J Matern Fetal Neonat Med* 23(10):1187–1192, 2010.
16. Hendler I, Blackwell SC, Bujold E, et al: The impact of maternal obesity on midtrimester sonographic visualization of fetal cardiac and craniospinal structures. *Int J Obes Relat Metab Disord* 28:1607–1611, 2004.
17. Thornburg LL, Miles K, Ho M, et al: Fetal anatomic evaluation in the overweight and obese gravida. *Ultrasound Obstet Gynecol* 33:670–675, 2009.
18. Fuchs F, Houllier M, Voulgaropoulos A, et al: Factors affecting feasibility and quality of second-trimester ultrasound scans in obese pregnant women. *Ultrasound Obstet Gynecol* 41:40–46, 2013.
19. Khoury FR, Ehrenberg HM, Mercer BM: The impact of maternal obesity on satisfactory detailed anatomic ultrasound image acquisition. *J Matern Fetal Neonat Med* 22:337–341, 2009.
20. Chung JH, Pelayo R, Hatfield TJ, et al: Limitations of the fetal anatomic survey via ultrasound in the obese obstetrical population. *J Matern Fetal Neonatal Med* 25:1945–1949, 2012.
21. Lantz ME, Chisholm CA: The preferred timing of second-trimester obstetric sonography based on maternal body mass index. *J Ultrasound Med* 23:1019–1022, 2004.
22. Thornburg LL, Mulconry M, Post A, et al: Fetal nuchal translucency thickness evaluation in the overweight and obese gravida. *Ultrasound Obstet Gynecol* 33:665–669, 2009.
23. Tsai LJ, Ho M, Pressman EK, Thornburg L: Ultrasound screening for fetal aneuploidy using soft markers in the overweight and obese gravida. *Prenatal Diagn* 9:821–826, 2010.
24. Aagaard-Tillery KM, Flint Porter T, Malone FD, et al: Influence of maternal BMI on genetic sonography in the FaSTER trial. *Prenat Diagn* 30:14–22, 2010.
25. American Institute of Ultrasound in Medicine: AIUM practice guideline for the performance of obstetric ultrasound examinations. *J Ultrasound Med* 32(6):1083–1101, 2013.
26. Reddy UM, Abuhamad AZ, Levine D, et al; Fetal Imaging Workshop Invited Participants: Fetal imaging: executive summary of a joint Eunice Kennedy Shriver National Institute of Child Health and Human Development, Society for Maternal-Fetal Medicine, American Institute of Ultrasound in Medicine, American College of Obstetricians and Gynecologists, American College of Radiology, Society for Pediatric Radiology, and Society of Radiologists in Ultrasound Fetal Imaging Workshop. *Obstet Gynecol* 123(5):1070–1082, 2014.
27. Fox NS, Bhavsar V, Saltzman DH, et al: Influence of maternal body mass index on the clinical estimation of fetal weight in term pregnancies. *Obstet Gynecol* 113:641–645, 2009.
28. Gupta M, Lauring J, Kunselman AR, et al: Fetal growth restriction may be underestimated in obese patients. *Obstet Gynecol* 123(Suppl 1):98S–99S, 2014.
29. Paladini D, Vassallo M, Tartaglione A, et al: The role of tissue harmonic imaging in fetal echocardiography. *Ultrasound Obstet Gynecol* 23:159–164, 2004.
30. Tranquart F, Grenier N, Eder V, Pourcelot L: Clinical use of ultrasound tissue harmonic imaging. *Ultrasound Med Biol* 25:889–894, 1999.
31. Benacerraf BR: The use of obstetrical ultrasound in the obese gravida. *Semin Perinatol* 37:345–347, 2013.
32. Benacerraf BR: A technical tip on scanning obese gravidas. *Ultrasound Obstet Gynecol* 35:615–616, 2010.



Gynecology



Faded text in the upper right quadrant of the page, likely bleed-through from the reverse side.

Faded text in the middle right quadrant of the page, likely bleed-through from the reverse side.

Faded text in the lower right quadrant of the page, likely bleed-through from the reverse side.

akusher-lib.ru

# Normal Anatomy of the Female Pelvis and Transvaginal Sonography

Jill E. Langer

## SUMMARY OF KEY POINTS

- Transabdominal sonography (TAS) and transvaginal sonography (TVS) are often complementary, providing different diagnostic information. TAS provides a wider field of view and better visualization of superficial structures and large pelvic masses but has limited resolution. The transvaginal approach allows the probe to be placed closer to the “target organs,” providing higher resolution imaging, but has a limited field of view.
- Because of the ability to use higher frequency probes, TVS usually provides the best anatomic detail. Therefore, TVS is considered the optimal sonographic technique with the highest diagnostic yield and should be incorporated into the sonographic examination of the female pelvis unless there are reasons that the transvaginal approach should be avoided.
- Not all patients are appropriate candidates for transvaginal examination. The examination should not be performed on any patient who does not or cannot willingly consent to the procedure, as well as on most virginal patients and those who experience marked discomfort with probe insertion.
- The appearance of the normal endometrium and ovary varies significantly throughout the menstrual cycle in women of reproductive age. It is important to be cognizant of the expected changes in order to avoid misinterpreting physiologic changes as pathologic.
- Transperineal, translabial, and transrectal sonography should be considered alternative approaches for imaging the female pelvis and are particularly useful for evaluation of the postmenopausal uterus, the cervix, and the lower urinary tract.

## OUTLINE

Indications and Contraindications, 805  
 Protocols, 807  
 Patient and Probe Preparation, 808  
 Imaging Technique, 808  
 Pelvic Anatomy, 811  
 Vascular Anatomy, 816

The Uterus, 821  
 The Ovaries, 826  
 The Fallopian Tube, 827  
 The Urinary Bladder, Distal Ureters, and Urethra, 829  
 The Rectosigmoid Colon, 829  
 Conclusions, 832

Pelvic sonography is considered the initial imaging tool of choice for assessing suspected gynecologic disorders in patients of all ages. Sonography offers the advantages of widespread availability, low cost, and lack of exposure to ionizing radiation and is often the only imaging examination necessary for diagnosis of uterine, ovarian, and adnexal disease. In addition, sonography is extremely useful in the evaluation of pathologic changes affecting the pelvic portions of the urinary system, gastrointestinal tract, and musculoskeletal structures that may mimic the clinical presentation of gynecologic disease. In many ultrasound laboratories, the standard protocol for ultrasound examination of the female pelvis begins with TAS using the filled urinary bladder as the acoustic window, followed by TVS after emptying the bladder and placing the patient in the lithotomy position.<sup>1,2</sup> The two imaging techniques are complementary, often providing different diagnostic information. TAS provides a wider field of view than the transvaginal approach and provides better visualization of superficial structures and structures remote from the vagina. However, by placing the probe closer to the “target organs,” the transvaginal approach requires less depth of penetration and bypasses the attenuating soft tissues

overlying the pelvic organs, allowing utilization of a higher frequency probe, which provides higher resolution and anatomic detail of the uterus, ovaries, and adnexa (Fig. 26-1). The normal sonographic anatomy described in this chapter reflects a combined transabdominal and transvaginal approach and is weighted, as in clinical practice, to emphasize the positive attributes of both TVS and TAS.

## INDICATIONS AND CONTRAINDICATIONS

High-resolution TVS has been widely available since the mid-1980s and is considered an integral part of gynecologic as well as early obstetric sonographic examinations.<sup>1,2</sup> TVS typically provides more anatomic detail of the uterus, endometrium, ovaries, and adnexa than does TAS. This is because the probe is placed closer to the organs of interest and requires less depth of penetration; therefore, a higher frequency probe with ensuing higher resolution can be utilized (Figs. 26-2 and 26-3).

An additional advantage of TVS is the capability of using the probe tip to assess pelvic structures for tenderness. By applying gentle



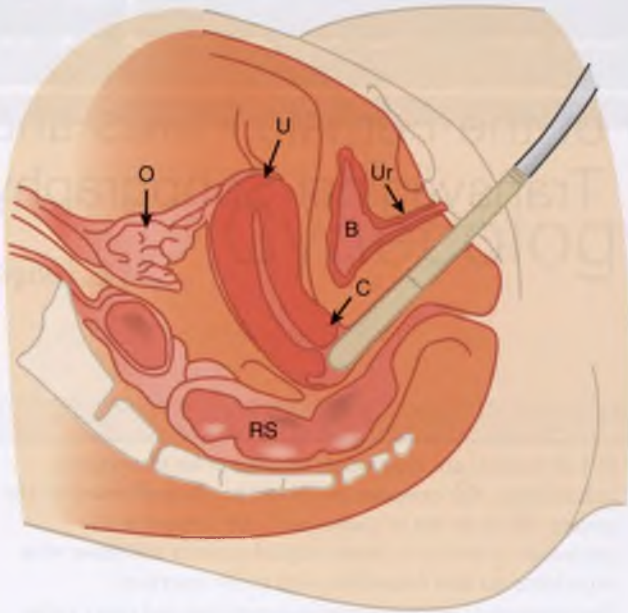


**FIG 26-1** Diagrammatic representation of the transvaginal ultrasound examination. Insertion of the probe into the vaginal canal allows the transducer to be placed in close proximity to the pelvic organs, bypassing the overlying soft tissues. Because less depth of soft tissue penetration is required, a higher frequency transducer can be utilized, providing better resolution in comparison to the transabdominal approach. B, urinary bladder; C, cervix; O, ovary; RS, rectosigmoid colon; U, uterine body; Ur, urethra.

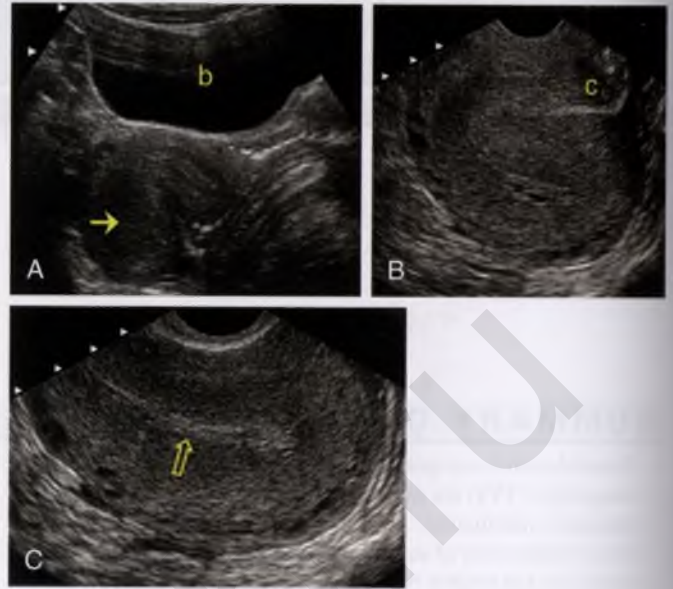


**FIG 26-2** Improved visualization of the uterus with transvaginal imaging. **A**, Longitudinal transabdominal sonogram of a retroflexed uterus performed through a full urinary bladder (b). The endometrial canal (arrow) in the body of the uterus is not well seen as it lies parallel to the ultrasound beam. **B**, Transvaginal sonogram of the same patient. The cervix (c) is interposed between the transvaginal probe and the body of the uterus. This gives suboptimal visualization of the myometrium and endometrial canal. **C**, Transvaginal sonogram of the body and fundus of the uterus after the probe has been repositioned beyond the cervix and angled posteriorly. The probe now lies immediately adjacent to the retroflexed uterus, providing much improved visualization of the endometrium (open arrow).

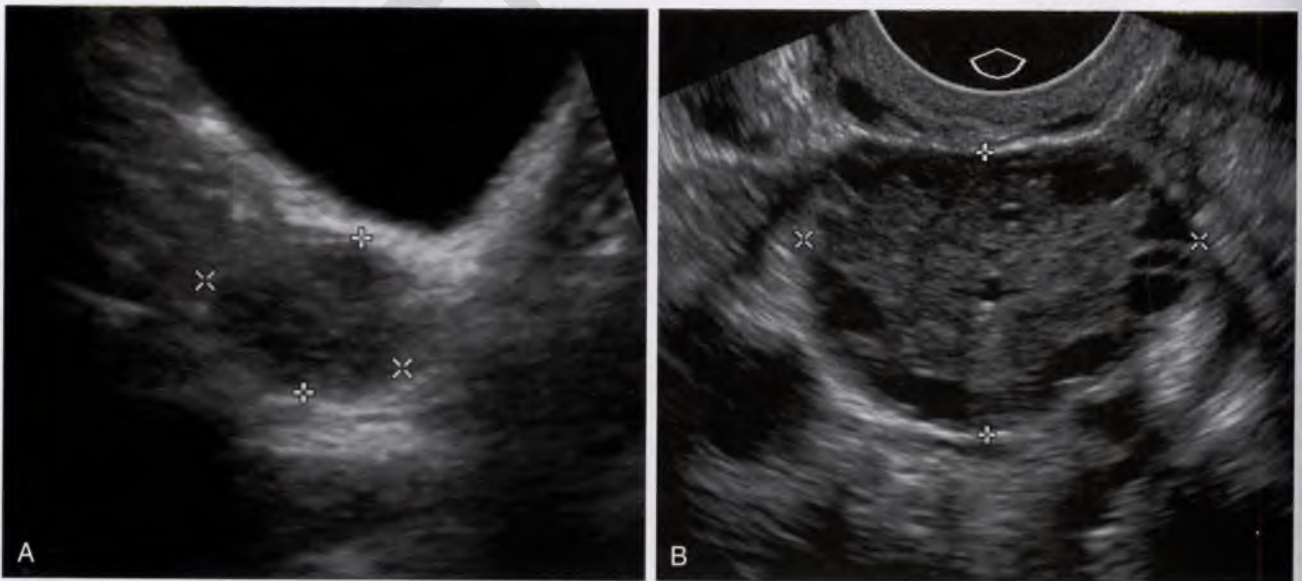


**FIG 26-3** Improved characterization of ovarian morphologic appearance with transvaginal imaging. **A**, Longitudinal transabdominal scan of the right ovary (calipers) provides little anatomic detail. **B**, Transvaginal scan of the right ovary (calipers) in the sagittal plane demonstrates multiple small peripheral anechoic follicles and central echogenic stroma in this patient with polycystic ovary syndrome.



pressure with the transducer tip to pelvic structures, it is possible to localize the region of tenderness with greater specificity than with TAS or bimanual examination. Hence, TVS is considered the optimal sonographic technique for imaging the female pelvis and should be incorporated into the sonographic examination in all situations for which it will provide additional clinically useful diagnostic information, barring contraindications to the transvaginal approach (see later).<sup>1-8</sup>

Indications for pelvic sonography include but are not limited to the following<sup>1</sup>:

- Evaluation of pelvic pain and pelvic masses
- Evaluation of endocrine abnormalities, including polycystic ovaries
- Evaluation of dysmenorrhea, amenorrhea, abnormal vaginal bleeding, and delayed menses
- Evaluation, monitoring, and treatment of infertility patients
- Evaluation of pelvic anatomy in the setting of a limited clinical examination
- Evaluation of suspected pelvic infection
- Further characterization of a pelvic abnormality noted on another imaging study
- Evaluation of congenital uterine and lower genital tract anomalies
- Evaluation of excessive bleeding, pain, or signs of infection after pelvic surgery, delivery, or abortion
- Localization of an intrauterine contraceptive device
- Screening for malignancy in high-risk patients
- Evaluation of incontinence or pelvic organ prolapse
- Evaluation for possible ectopic pregnancy
- Evaluation of a first trimester gestation for viability, growth, and anomalies
- Evaluation of the placenta, cervix, and other pelvic structures in second and third trimester gestations
- Evaluation of fetal anatomy in second and third trimester gestations
- Guidance for interventional or surgical procedures

However, not all patients are appropriate candidates for TVS. The transvaginal examination should not be performed in any patient who does not or cannot willingly consent to the procedure. There may be cultural, religious, or social reasons why TVS is inappropriate. In addition, TVS is rarely recommended in premenarchal or virginal patients, and if deemed necessary, it should be performed only after careful discussion with the individual and parent or guardian, as appropriate.<sup>1,2</sup> If a patient experiences anxiety or discomfort at the time of attempted probe insertion (e.g., in the setting of a narrow introitus or vaginal abnormality such as atrophic or inflammatory vaginitis), termination of the transvaginal portion of the examination is recommended. It may be helpful to allow the patient to insert the probe herself. In many postmenopausal women, TVS is required to adequately image the endometrium and ovaries, because the TAS examination may be compromised by a variety of senescent changes, including decreased urinary bladder capacity, increased body habitus, an atrophic and ill-defined endometrium, and small ovarian size. Fortunately, postmenopausal patients tolerate the transvaginal examination well, with an overall patient acceptance rate that is only slightly less than that in women of reproductive age.<sup>3</sup> Transrectal sonographic imaging may be performed as an alternative to TVS to image the uterus and adnexal structures in postmenopausal women with their consent. Transperineal and translabial scanning can be used in patients who are not candidates for the transvaginal approach and is also useful for evaluation of pelvic organ prolapse, as well as of the cervix and the lower urinary tract<sup>1</sup> (Fig. 26-4). TVS may also be contraindicated in some second and third trimester obstetric patients with active bleeding or ruptured membranes.

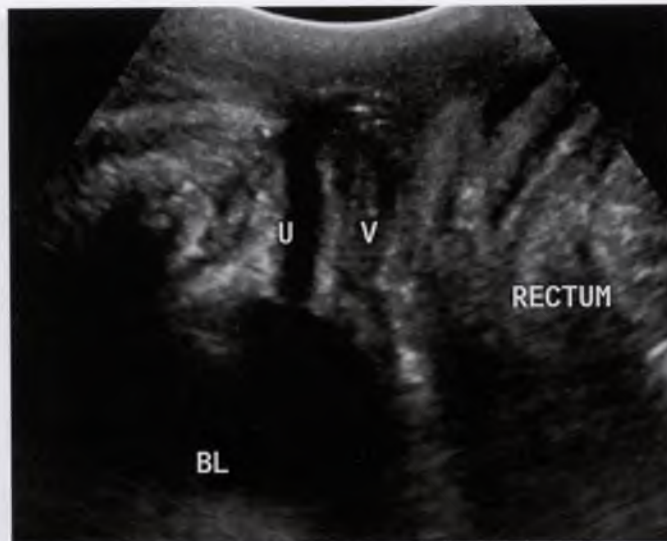


**FIG 26-4** Transperineal image of the urethra. Longitudinal image obtained by placing the probe on the perineum shows a normal urethra (U), which appears as a nearly anechoic linear channel arising from the bladder cephalad and parallel to the vagina (V) in this patient with symptoms concerning for lower urinary tract disease. BL, urinary bladder.

Although TVS offers superior resolution to TAS, TVS may be compromised by sound attenuation (e.g., by large or calcified leiomyomas in the lower uterus) or by positioning of the ovaries or other lesions high in the pelvis beyond the field of view of the transvaginal probe. Large uterine size and fixation of the uterus to the anterior abdominal wall by adhesions, such as after cesarean delivery, can also limit the ability of TVS to assess the entire uterus for pathologic change or to perform accurate measurements. In these situations, TAS provides a wider field of view than the transvaginal approach and thus allows better visualization of structures in the upper pelvis or in a superficial location. Furthermore, TAS can provide a more panoramic view of the entire pelvis, which is helpful in the setting of a large pelvic mass (Fig. 26-5). TAS also allows assessment of related intra-abdominal disease and structures, such as quantification of free intraperitoneal fluid in the hepatorenal space and paracolic gutters, hydronephrosis in the setting of a large pelvic mass or malignancy, and, more rarely, identification of peritoneal implants.

## PROTOCOLS

Protocols for pelvic sonography vary between institutions and can be tailored according to the specific clinical indication. In some institutions, it is routine to perform a complete transabdominal pelvic sonogram using the distended urinary bladder as an acoustic window, followed by a complete transvaginal pelvic sonogram with an empty bladder. In other institutions, women are not asked to fill their bladders before routine pelvic sonograms, but initially have a limited transabdominal examination, irrespective of the fullness of the urinary bladder, to screen for large pelvic masses and to measure the uterus. Subsequently, the patient is asked to void and a complete transvaginal sonogram is performed. At other sites, patients initially undergo TVS with an empty bladder, because this examination alone will provide diagnostic imaging in the majority of cases.<sup>1,9</sup> In this scenario, if TVS does not provide adequate imaging, most commonly because one or both of the ovaries are not visualized or there is incomplete visualization of an enlarged uterus or pelvic mass, TAS with an empty or partially filled urinary bladder is then performed.<sup>9</sup> In a small minority of



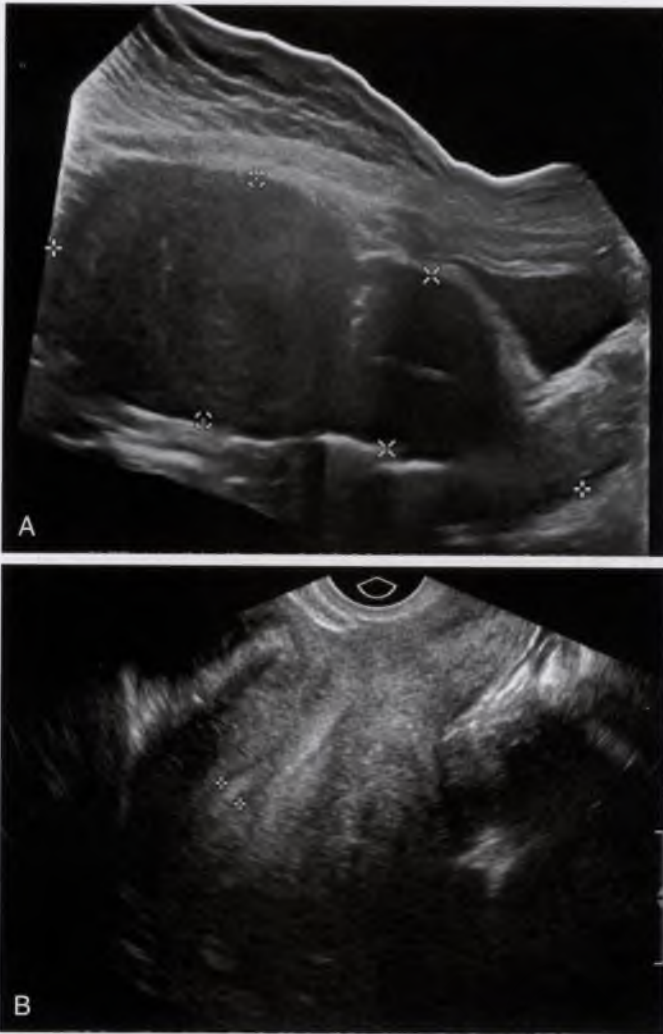


**FIG 26-5** Pelvic mass only visible on transabdominal sonography. **A**, Longitudinal midline extended field of view transabdominal sonogram of the uterus demonstrates a large fundal leiomyoma (calipers with central dot) extending to the level of the umbilicus. Measurement of the uterus includes the large leiomyoma (calipers). **B**, Longitudinal transvaginal image does not image the leiomyoma, as it was located above the uterine fundus, beyond the field of view of the transvaginal probe. Calipers show endometrium.

patients, the combination of these two examinations will still fail to visualize an ovary or the entire pelvic anatomy, and the patient is then asked to fill her bladder and the transabdominal examination is repeated with a distended bladder.

Patients who undergo serial pelvic sonography for specific targeted indications, such as follicle monitoring, are often only examined by TVS. When pelvic sonography is performed in emergent clinical situations, TAS may be initially and quickly performed in the setting of an empty or incompletely filled bladder to assess for the presence of hemoperitoneum, a large pelvic mass, or other pathologic features, and TVS is then performed if considered necessary as guided by the clinical scenario (Fig. 26-6).

## PATIENT AND PROBE PREPARATION

As with all ultrasound applications, it is standard practice to use the highest possible transducer frequency that allows visualization of the

target organs.<sup>1,2</sup> During TAS, visualization of the pelvic organs is typically limited by sound attenuation by the intervening anterior abdominal wall and subcutaneous and preperitoneal fat, as well as fat in the mesentery and omentum. As a result of this attenuation and the distance of the area of interest from the anterior abdominal wall, it is often not possible to use transducers with frequencies above 6 MHz for TAS, unless the patient is very thin. TVS is typically performed using a probe of 7.5 MHz or higher frequency, taking advantage of the ability to place the probe closer to the pelvic organs because of fewer intervening structures and resulting in less sound attenuation.

The patient should void immediately before the transvaginal examination so that the urinary bladder is as empty as possible. This will improve visualization of the reproductive organs, especially the adnexal structures, which may be displaced out of the pelvis when the bladder is distended, and will reduce patient discomfort. The sonologist or sonographer should obtain a pertinent history from the patient, explain the rationale for performing the TVS as well as how the examination is performed, and obtain verbal consent before beginning the examination.<sup>1,2</sup> If a male sonologist or sonographer is to perform the examination, a female staff member (an aide, nurse, or other staff member) should be present in the room for the entire transvaginal examination to act as a chaperone. Consideration of having a chaperone present for all TVS, even if performed by a female, should be in accordance with local policy and is recommended in some institutions.<sup>1,10</sup> The patient should be positioned as comfortably as possible in the lithotomy position using either a gynecologic examination table with stirrups or by placing cushions or folded linens underneath the buttocks to elevate and abduct the hip region. The patient should be appropriately covered and draped, and the examination should be conducted with the same respect for privacy afforded patients during the performance of a bimanual pelvic examination.<sup>2</sup>

To prevent the spread of infectious disease, the transvaginal probe should be appropriately disinfected using high-level disinfection protocols between uses according to the manufacturers' and Occupational Safety and Health Administration (OSHA) recommendations. Following disinfection, the probe is wiped clean, and either a small amount of transducer coupling gel is placed inside a probe cover or a pregelled probe cover is placed over the probe. Because of concern for latex allergies, many laboratories use nonlatex probe covers for all patients. Care is taken to minimize air bubbles over the transducer face when applying the probe cover, and if they are noted, the probe cover should be readjusted. The final step in the process of probe preparation is to lubricate the tip of the covered probe with a sterile, nonspermicidal lubricant. Individual packets are preferred over large multiuse containers to minimize the potential for contamination of the gel and reduce the risk of transmission of infection. The sonographer should wear gloves while preparing the probe and performing the examination.<sup>1,2</sup>

## IMAGING TECHNIQUE

The patient, the sonographer, or the physician may introduce the transvaginal transducer, preferably under real-time monitoring. After insertion, the sonologist should position the probe to optimize imaging of the pelvic organs, usually by placement of the probe in the anterior or lateral vaginal fornix and by the application of gradually applied firm pressure against the vaginal wall as tolerated by the patient. The orientation of the image is controlled by probe rotation and angulation (Fig. 26-7). Before recording any images, many sonologists will perform a pelvic survey by slowly sweeping the ultrasound beam in a long-axis orientation from the midline through the adnexa continuing out to the pelvic sidewalls on each side. The probe is then rotated 90 degrees counterclockwise into the short axis, and the beam is swept from the



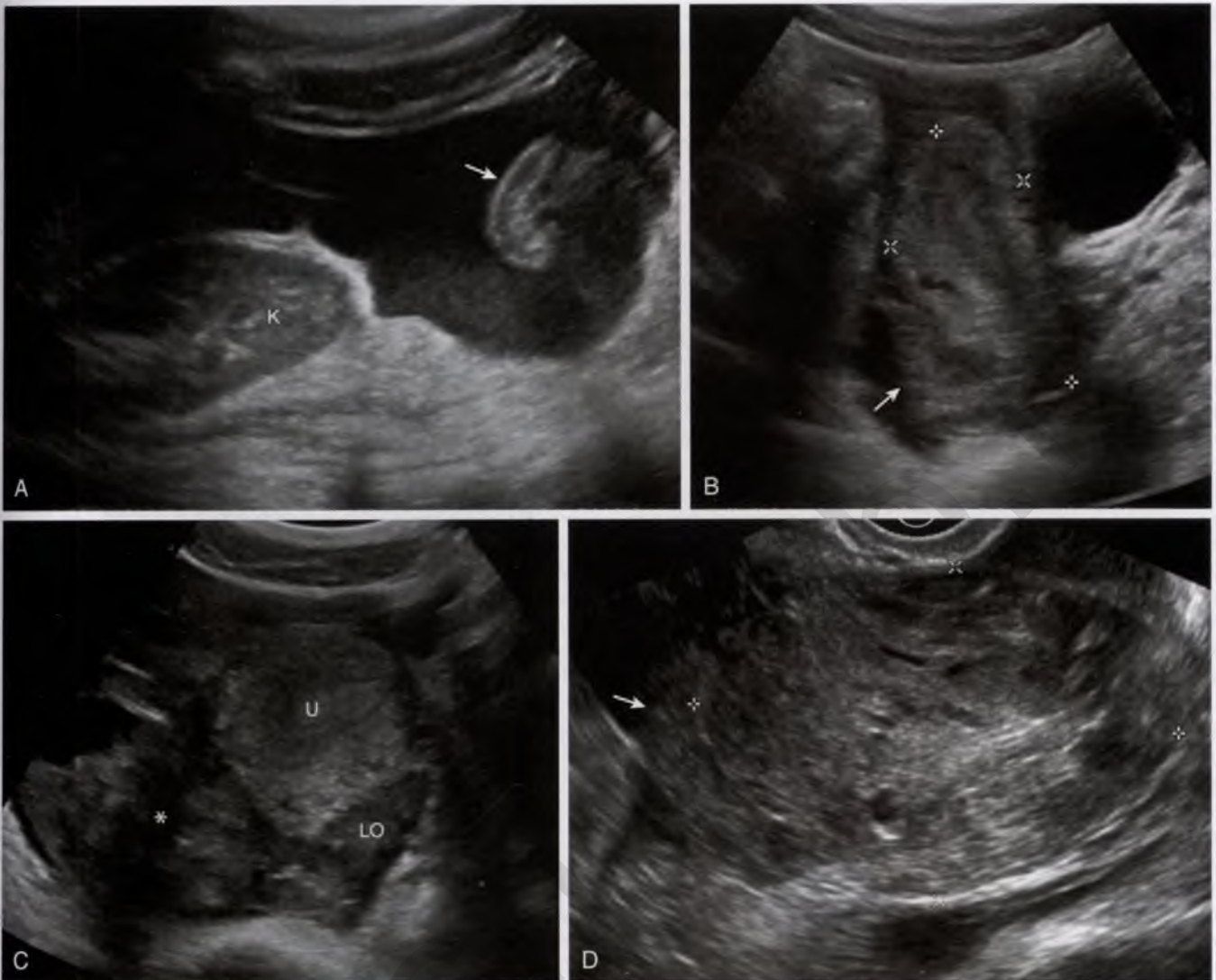


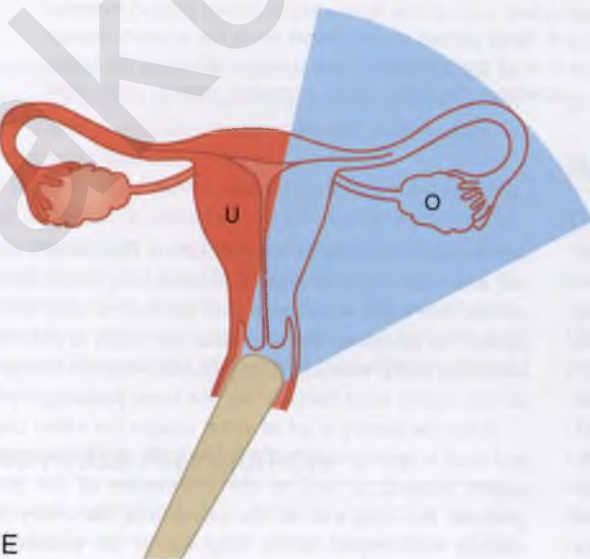
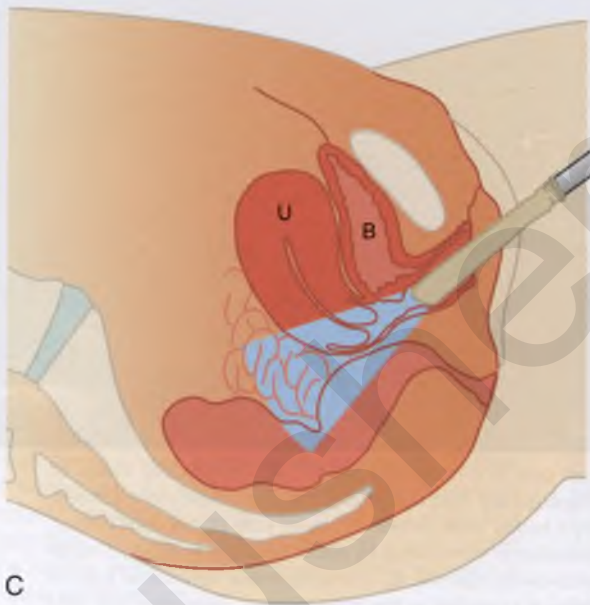
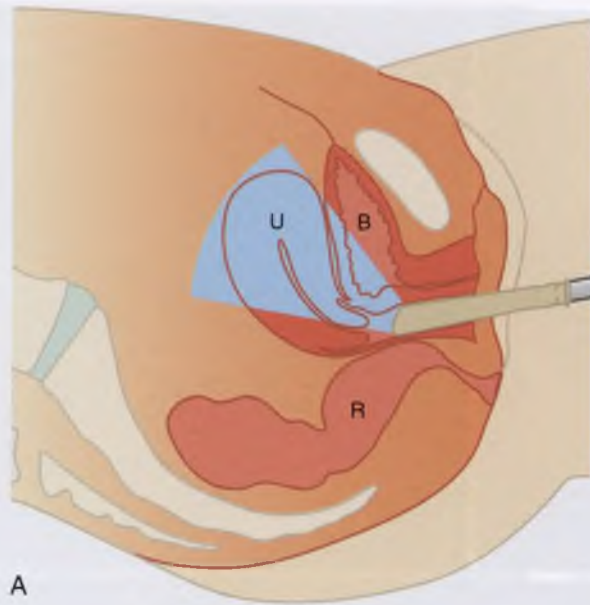
**FIG 26-6** Hemoperitoneum from a ruptured ovarian cyst in a nongravid patient. **A**, Longitudinal image of the right flank demonstrates a large amount of intraperitoneal fluid containing low-level dependent echoes, most consistent with hemoperitoneum surrounding a bowel loop (*arrow*). K, lower pole of the right kidney. **B**, Longitudinal scan of the pelvis shows the uterus (*calipers*) surrounded by pelvic fluid and echogenic material representing intraperitoneal hemorrhage in the cul-de-sac (*arrow*). **C**, Transabdominal transverse scan of the pelvis shows a large amount of echogenic material (*asterisk*) in the right adnexa, obscuring the right ovary. LO, left ovary; U, uterus. **D**, Transvaginal longitudinal scan of the right adnexa shows altered morphologic appearance of the right ovary from a ruptured cyst. Note clotted blood (*arrow*) along the superior aspect of the ovary (*calipers*). The patient was stable at the time of the ultrasound examination, allowing the transvaginal scan to be performed to confirm the suspected diagnosis of a ruptured ovarian cyst with hemoperitoneum.

cervix to the fundus of the uterus. The probe is then angled to each side of the pelvis, and scanning is performed by sweeping both superiorly and inferiorly through each adnexal region. The survey quickly ascertains the relative positions of the uterus and ovaries and identifies any obvious disease. Additionally, the probe can be advanced or withdrawn, which will move adjacent pelvic viscera and displace bowel and allow structures to be placed in the focal zone of the transducer or moved out of regions with near-field artifact. In response to gentle pressure with the transvaginal probe, the pelvic organs should normally slide over one another. Any restriction to normal motion may indicate the presence of adhesions.<sup>11</sup> Visualization of the pelvic anatomy can

also be facilitated by applying pressure on the patient's anterior abdominal wall with the sonologist's nonscanning hand, thereby pushing a mobile ovary or a mass down into the field of view of the transvaginal probe.<sup>2</sup> In addition, the bimanual approach is extremely helpful in localizing pelvic tenderness or pain, allowing the sonographer to focus on the region most likely to harbor some pathologic problem.

After the survey, a set of static images (or video clips) is obtained and each is appropriately labeled to indicate the anatomic structure or region imaged, as well as the orientation of the probe.<sup>1</sup> In many patients, the long axis of the uterus and the ovary may be slightly oblique with respect to the long axis of the patient's body, and the





probe should be oriented along that same obliquity to image in the uterus and ovary each along its long axis. The long-axis TVS view is usually referred to as a sagittal imaging plane, and the short-axis view as a coronal or transverse imaging plane.<sup>2</sup> At our institution, the imaging protocol includes one or more static sagittal views of the posterior cul-de-sac, cervix (including the endocervical canal from internal to external os), midline uterus with and without the maximum anteroposterior (AP) dimension and length measured, parasagittal right and left uterine body, midline sagittal endometrium with and without the maximum AP dimension measured, and right and left ovaries with and without the maximum AP dimension and length of each measured. Coronal or transverse static images include posterior cul-de-sac; cervix; uterus at the fundal, midbody, and lower uterine segment levels with and without the maximum width measured; midbody and fundal endometrium; and right and left ovaries with and without the maximum width measured (Fig. 26-8).

Additionally, any disease or variant of normal must be assessed and appropriate additional images recorded. Most laboratories now include cine clip acquisition in addition to static images. Color Doppler, power Doppler, and pulsed Doppler are often added to the protocol depending upon the clinical situation and abnormality demonstrated on grayscale imaging. The use of three-dimensional (3D) sonography also has become standard in many laboratories (Fig. 26-9). By capturing a volume of data, 3D imaging permits a display of any desired plane through the uterus, cervix, ovaries, and adnexa and optimizes assessment of the entire endometrial canal. 3D imaging is particularly useful for the assessment of intrauterine device (IUD) positioning and submucosal myomas, as well as uterine fundal contour and morphologic appearance in the setting of suspected congenital anomalies<sup>1,12-14</sup> (Fig. 26-10).

## PELVIC ANATOMY

The pelvis, so-called because of its resemblance to a basin, is divided into two structurally continuous compartments, the true (or lesser) pelvis and the false (or greater) pelvis, by an oblique plane passing from the sacral promontory, the arcuate and pectineal lines, and the superior margin of the symphysis pubis (Fig. 26-11). The circumference of this plane is called the linea terminalis, or pelvic brim.<sup>15</sup> The true pelvis is the lower portion and is bounded anteriorly by the pubis and pubic rami, posteriorly by the sacrum and coccyx, laterally by the fused ilium and ischium, and inferiorly by the muscles of the pelvic floor. The false pelvis is bounded laterally by the flanged portions of the iliac bones, the base of the sacrum posteriorly, and the abdominal wall anteriorly and laterally. In the absence of masses in the nongravid patient, the uterus, ovaries, adnexa, and collapsed urinary bladder are located in the true pelvis.<sup>16</sup> As the urinary bladder fills, the dome of the bladder extends into the false pelvis and displaces the loops of small bowel superiorly, providing an acoustic window for transabdominal imaging. Intracavitary probes (transvaginal and transrectal) allow visualization of the pelvic viscera from within the true pelvis.

Translabial and transperineal sonography view the true pelvis from the pelvic floor.

The anterior surface of the uterus is covered with peritoneum to the level of the upper cervix. The peritoneal space anterior to the uterus and posterior to the urinary bladder is the vesicouterine pouch or anterior cul-de-sac (Figs. 26-11 and 26-12). This space is usually empty, but it may contain loops of small bowel. Posteriorly, the peritoneal reflection extends to the posterior fornix of the vagina (Fig. 26-13), forming the posterior cul-de-sac or rectouterine pouch, which is the peritoneal space posterior to the uterus and anterior to the rectosigmoid colon.<sup>16</sup> On transvaginal imaging, a small amount of free fluid is often demonstrated in the posterior cul-de-sac in normal women of menstruating age, likely from fluid released at ovulation. However, the presence of fluid in the anterior cul-de-sac or lateral pelvic recesses, a large amount of fluid in the posterior cul-de-sac, and the presence of pelvic fluid in nonovulatory female patients all raise concern for intraperitoneal disease (Fig. 26-14).

Laterally, the peritoneal reflection forms the broad ligaments, which extend from the lateral aspect of the uterus to the lateral pelvic side walls bilaterally (Fig. 26-15). The broad ligaments divide the pelvic cavity into anterior and posterior compartments. The free border of the broad ligaments contains the fallopian tubes.<sup>16</sup> The broad ligaments may be identified sonographically when they are outlined by free intraperitoneal fluid (Fig. 26-16). The ovary is attached to the posterior layer of the broad ligament by reflections of peritoneum referred to as the mesovarium (see Fig. 26-12). The superior margin of the portion of the broad ligament containing the fallopian tube is referred to as the mesosalpinx. The superior margin of the broad ligament lateral to the fimbriated end of the fallopian tube is the suspensory ligament of the ovary (infundibulopelvic ligament), through which the ovarian vessels and nerves course.<sup>17</sup> The round ligaments arise at the uterine cornua, anterior to the fallopian tubes in the broad ligaments, and extend anterolaterally to run beneath the inguinal ligament and insert into the fascia of the labia majora. The ovarian (utero-ovarian) ligaments arise from the uterine cornua posterior to the fallopian tubes and attach to the inferior extremity of the ovary. In the absence of free intraperitoneal fluid, the fallopian tubes, mesovarium, mesosalpinx, and ovarian and round ligaments are not usually identified sonographically (Fig. 26-17). The suspensory ligament of the ovary is usually not directly visible. However, the ovarian artery within the suspensory ligament of the ovary is often identified with color Doppler on TAS or TVS<sup>18,19</sup> (Fig. 26-18). The base of the lateral margin of the broad ligament is continuous with the dense connective tissue of the pelvic floor, which unites with the supravaginal portion of the cervix. The lower medial margin of the broad ligament is widely attached to the connective tissues adjacent to the cervix known as the parametrium. The uterosacral ligaments extend posterolaterally from the supravaginal cervix, encircle the rectum, and insert into the fascia over the sacrum. The uterosacral ligaments form the lateral boundaries of the rectouterine pouch.<sup>20</sup>

*Text continued on p. 816*

**FIG 26-7** Orientation of the probe during transvaginal scanning. **A**, Diagram of the longitudinal axis imaging plane of the anteverted uterus. The probe is then moved in this orientation through the uterus and adnexa laterally out to each sidewall to image the entire pelvis in the longitudinal plane. B, urinary bladder; R, rectum; U, uterus. **B**, Corresponding transvaginal sonogram in the sagittal plane demonstrating the corpus of the uterus as depicted in A. bo, bowel. **C**, Diagram of the longitudinal plane used to image the cervix and posterior cul-de-sac (rectouterine pouch). The probe is oriented in the longitudinal plane and has been slightly withdrawn more proximally within the vaginal canal and angled inferiorly and posteriorly. B, bladder; U, uterus. **D**, Corresponding transvaginal image of **C** demonstrates the cervix (cx) and the endocervical canal (arrows). **E**, Diagram of the short-axis or coronal imaging plane. The probe has been rotated 90 degrees counterclockwise from the longitudinal plane in **A** and manually steered to the patient's left to obtain the coronal view of the left adnexa as depicted in the diagram. O, ovary; U, uterus. **F**, Corresponding coronal short-axis view of the left ovary (calipers).



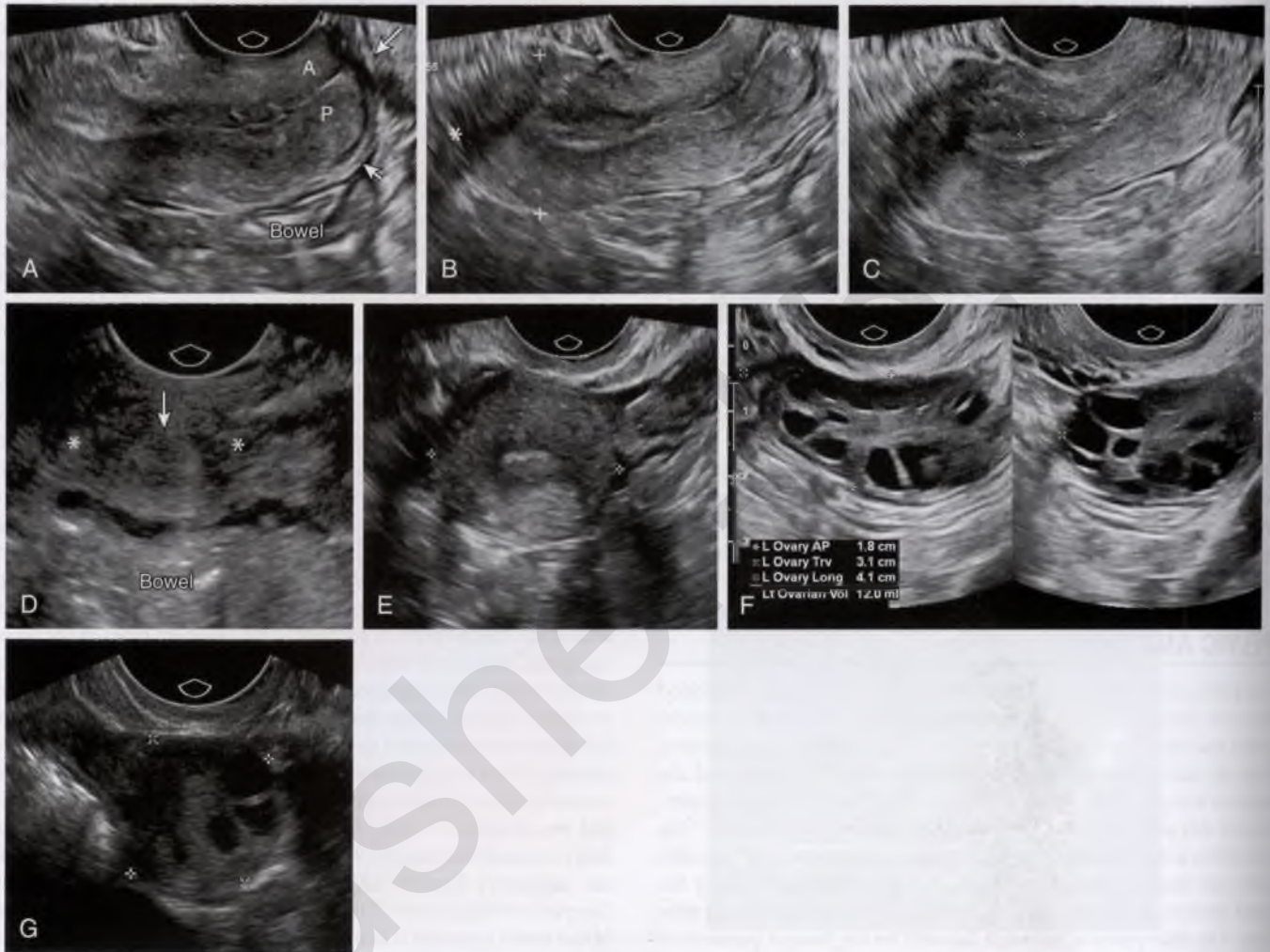


**FIG 26-8** Representative images from a transvaginal sonogram in a single patient. **A**, Longitudinal axis view of the cervix and posterior cul-de-sac. Bowel loops are noted in the cul-de-sac. A, anterior lip of the cervix; P, posterior lip of the cervix. Long arrow indicates the external os. Short arrow indicates the posterior vaginal fornix. **B**, Longitudinal axis midline view of the uterus with measurements of uterine size (*calipers*). **C**, Midline longitudinal axis view of the uterus with measurements of the endometrium (*calipers*). Note that the endometrium is visible throughout the entire length of the uterus and can be seen to be continuous with the endocervical canal. **D**, Coronal or short-axis view of the cervix. The outer wall of the cervix is marked by the calipers (*asterisks*). Solid arrow indicates the central echogenic endocervical canal, which is surrounded by the hypoechoic fibrous cervical stroma. Note fluid-filled loop of bowel posterior to cervix in the cul-de-sac. **E**, Coronal or short-axis view of the uterus (*calipers*). Note central echogenic endometrium and surrounding hypoechoic subendometrial halo. **F**, Sagittal and coronal (short-axis) view of the left ovary (*calipers*). **G**, Coronal (*short axis*) view of the right ovary (*calipers*) demonstrating numerous small anechoic follicles.



**FIG 26-9** Three-dimensional (3D) sonography of the uterus. Note typical 2D sagittal image of a retroverted, retroflexed uterus (*top left*) with the 3D rendered image in the coronal plane (*top right*). e, endometrium. The 3D coronal view has been rotated showing the triangular echogenic endometrial canal (e) (*bottom left*). Arrow points to the cornual region (C) of the endometrial cavity. Postoperative gross specimen of the uterus, tubes, and ovaries from a different patient (*bottom right*) showing an appearance comparable to the coronal image seen on the bottom left.

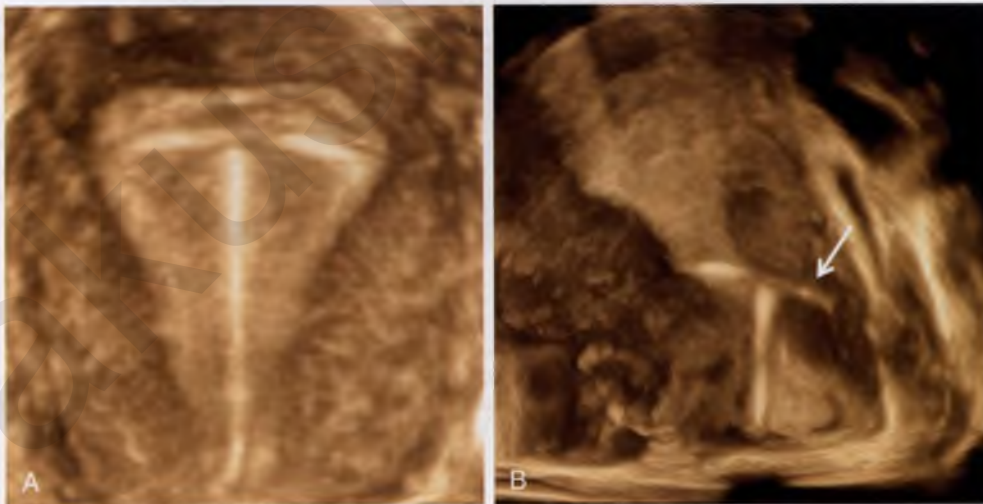
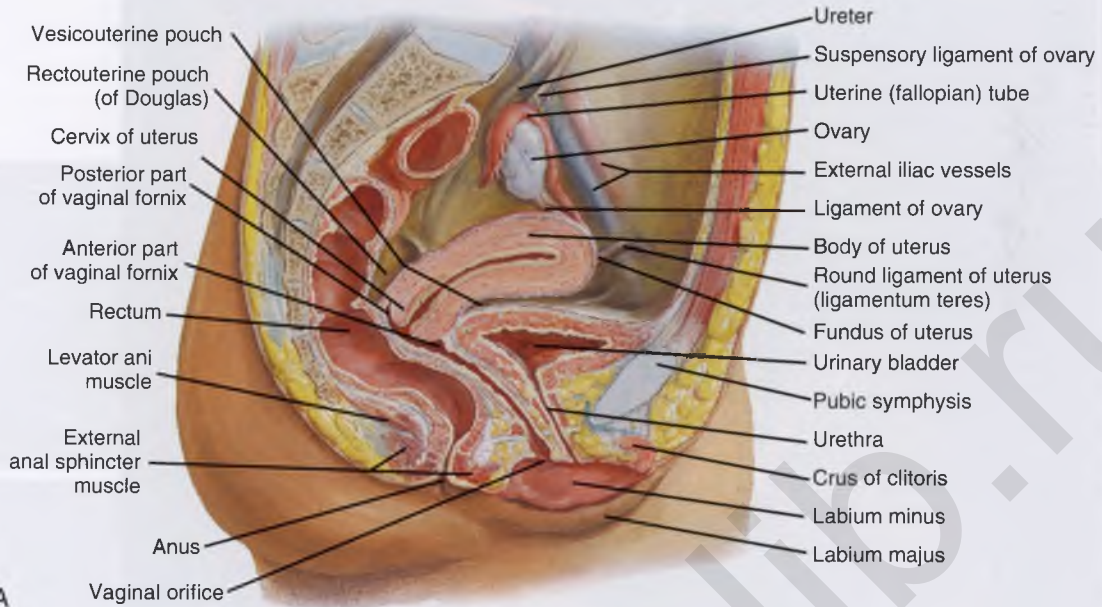


**FIG 26-10 A**, Three-dimensional (3D) coronal image of the uterus demonstrating an intrauterine device (IUD) in satisfactory position within the endometrial canal. **B**, 3D coronal image in a different patient shows inferior displacement of an IUD into the lower uterine and endocervical canal with penetration of the left arm into the myometrium (*arrow*).



**Topography of the Female Pelvic Viscera: Median and Paramedian Sagittal Section Diagrams**

**Median sagittal section**



**Paramedian sagittal section**

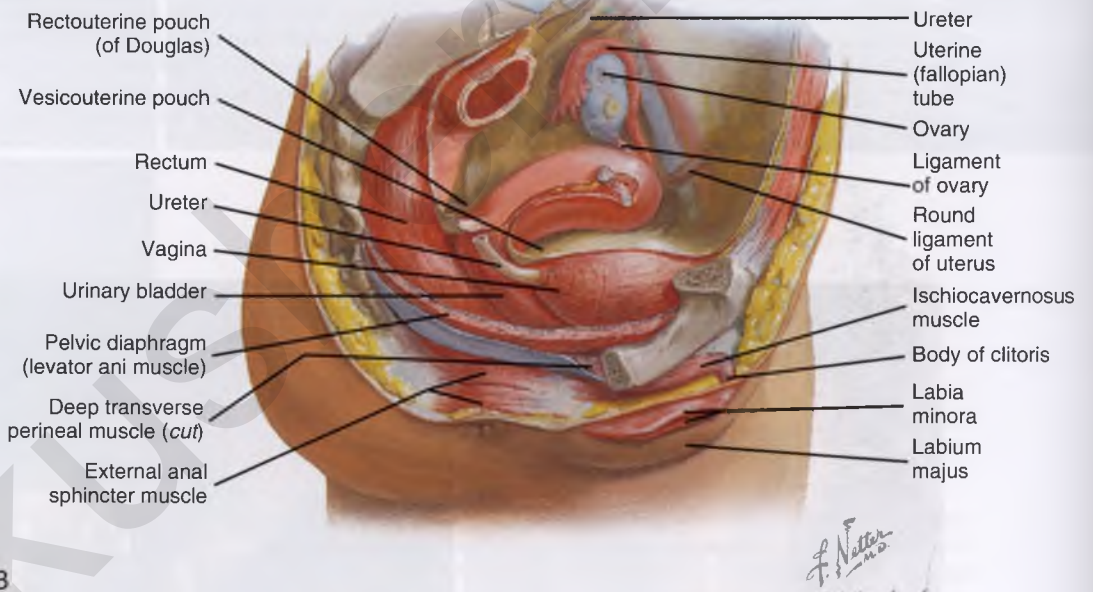
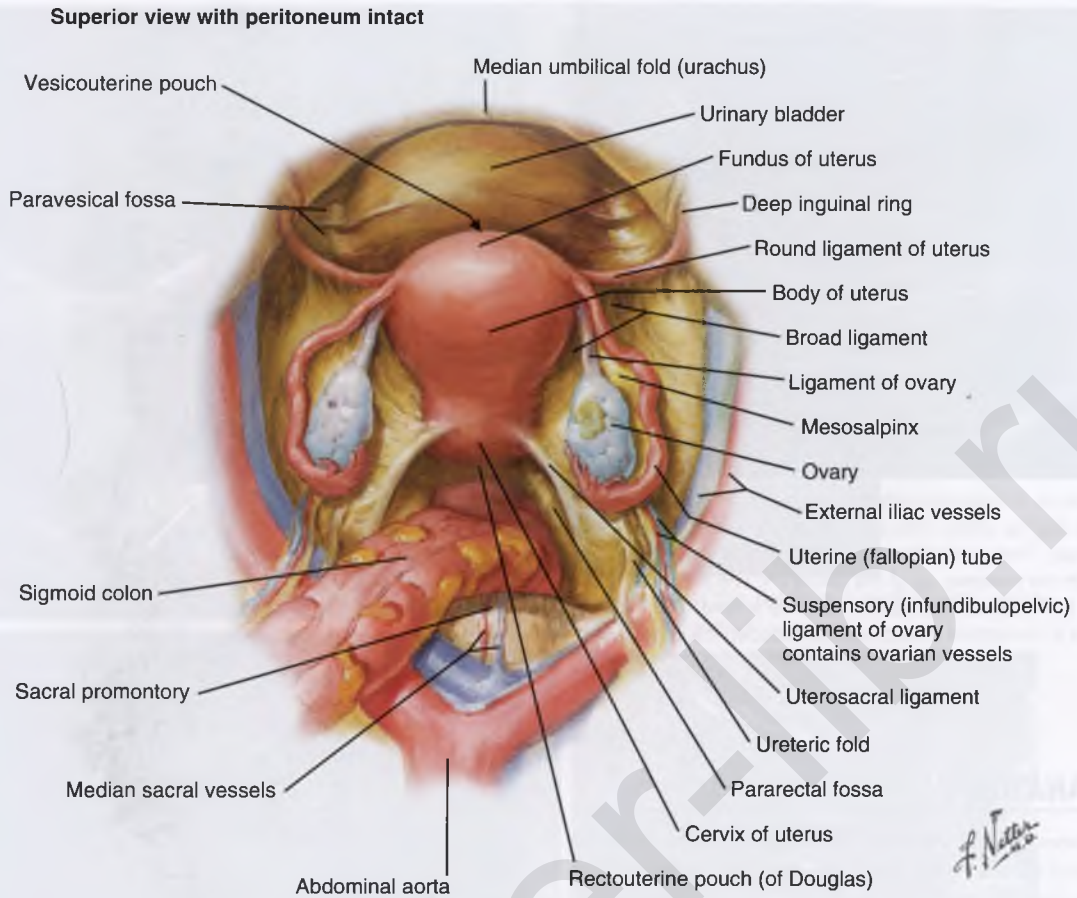


**FIG 26-11** Median (A) and paramedian (B) sagittal section diagrams of the female pelvis demonstrating the relationship of the uterus, urinary bladder, rectum, and adnexal structures. (Copyright Elsevier, Inc. Netterimages.com.)



**Superior view with peritoneum and uterus removed**

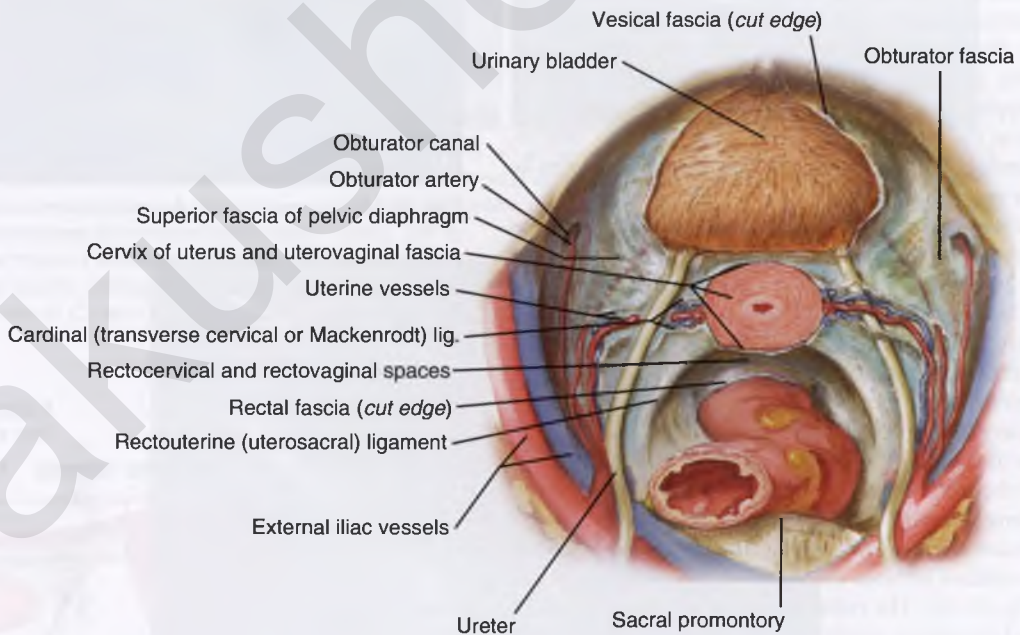


**FIG 26-12** Diagram of the female pelvis (superior view). (Copyright Elsevier, Inc. Netterimages.com.)



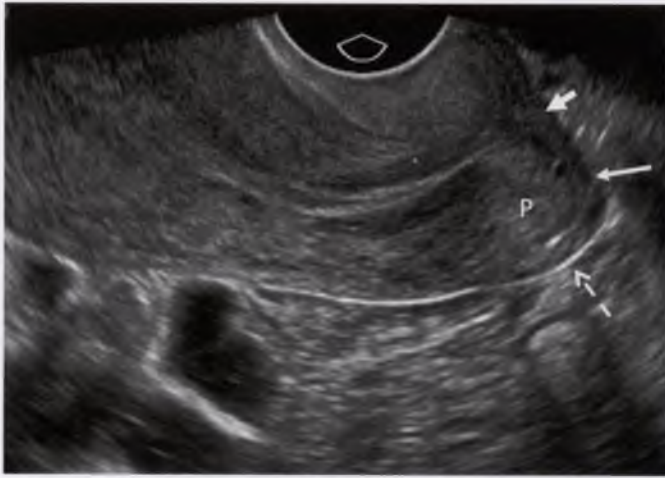


**FIG 26-13** Posterior cul-de-sac/posterior vaginal fornix. Transvaginal sonogram in the sagittal plane through the cervix with bowel in the posterior cul-de-sac. The posterior wall of the vagina (*long arrow*) is seen merging with the posterior lip of the cervix (P). The posterior fornix is demonstrated by a thin echogenic line (*dashed arrow*). The external cervical os is seen at the end of the echogenic endocervical canal (*short, thick arrow*).

## VASCULAR ANATOMY

The aorta bifurcates into the common iliac arteries, which enter the pelvis anterior and medial to the psoas muscles. The common iliac arteries bifurcate into the external and internal iliac (or hypogastric) arteries approximately at the level of the L5/S1 disk. The external iliac artery is larger than the internal iliac artery and lies just medial to the psoas muscle, exiting the pelvis via the femoral canal to supply the lower extremity. The internal iliac arteries supply the pelvic viscera, walls of the pelvis, perineum, and gluteal region.<sup>17</sup> It is the anterior division that supplies branches to the bladder, uterus, cervix, and vagina. Anterior to the internal iliac arteries are the ureters, ovaries, and fimbriated ends of the fallopian tubes. The internal iliac veins lie posterior to their respective arteries.

The uterine artery ascends in a tortuous course lateral to the uterus in the broad ligament to the junction of the fallopian tube and the uterus (see Fig. 26-19). From the cornua of the uterus, the uterine artery gives rise to a branch that courses laterally to reach the hilum of the ovary, where it anastomoses with the ovarian artery, and another branch supplies the fallopian tube. The uterine artery also supplies the cervix via multiple branches, some of which anastomose with branches of the vaginal artery to form the azygos arteries of the vagina, one of which is anterior to and the other posterior to the vagina. The uterine arteries provide the main arterial supply to the uterus via multiple branches that pierce the uterine wall and then divide into the anterior and posterior arcuate arteries, which anastomose extensively with each other across the midline between the middle and outer layers of the myometrium (Fig. 26-20). The radial arteries arise from the arcuate arteries and travel centrally to supply the rich capillary network in the deeper layers of the myometrium and the endometrium (Figs. 26-20 and 26-21). The radial arteries give rise to the straight and spiral arteries of the endometrium. The straight arteries supply the basalis layer of the endometrium. The spiral arteries supply the superficial two thirds of the endometrium and become longer and more tortuous as the endometrium thickens in the secretory phase of the menstrual cycle (Fig. 26-22). Blood flow is generally detectable in the uterine

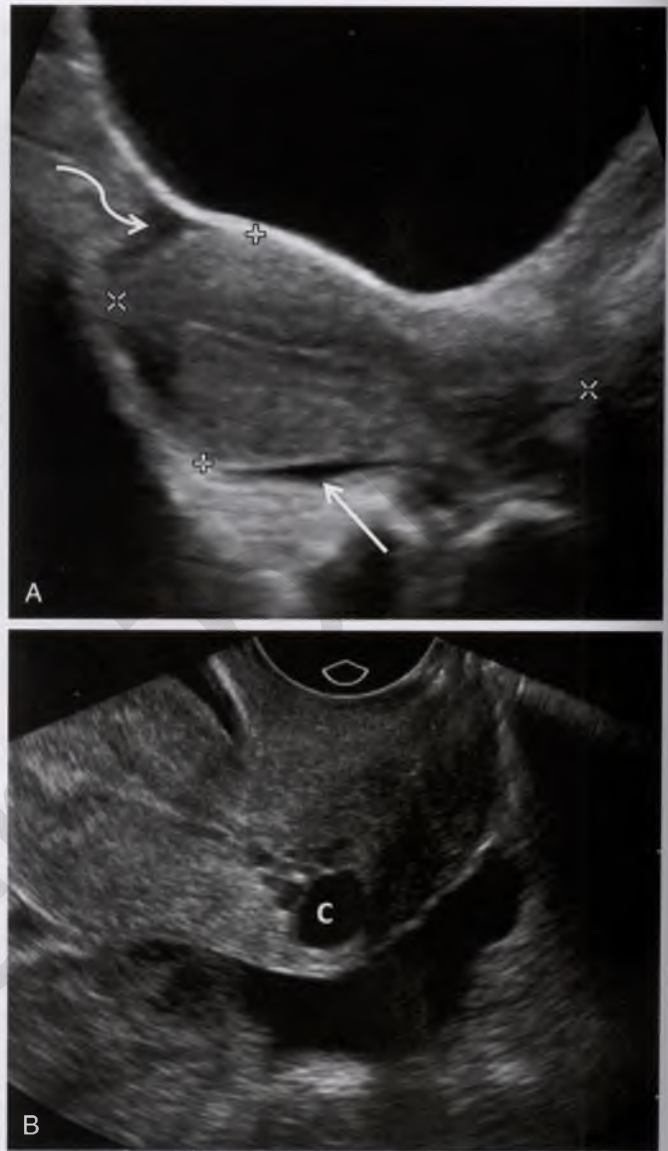


**FIG 26-14** Free pelvic fluid. **A**, Longitudinal transabdominal sonogram of the uterus (*calipers*) shows a small amount of fluid in the anterior (*curved arrow*) and posterior cul-de-sac (*straight arrow*). **B**, Longitudinal transvaginal scan in a different patient shows anterior and posterior cul-de-sac free fluid. A nabothian cyst (C) is visible in the cervix.

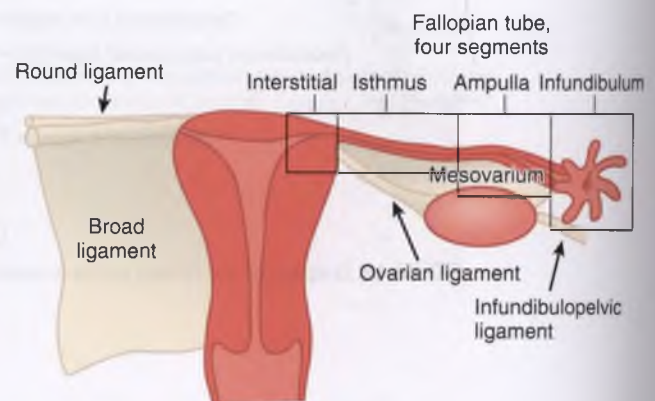


**FIG 26-15** Diagram of the ovary, uterus, and adjacent peritoneal reflection and ligaments.

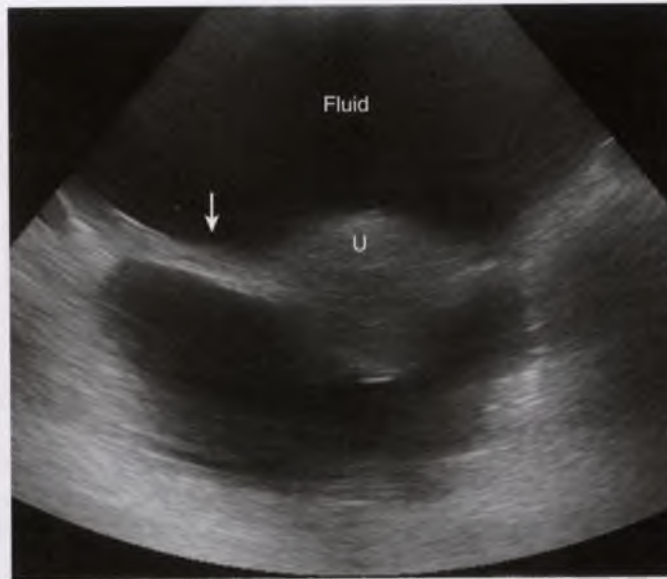


**FIG 26-16** The broad ligament. Transabdominal transverse image of the pelvis in a patient with ascites showing the broad ligament (*arrow*) on the right outlined by fluid. U, uterus.

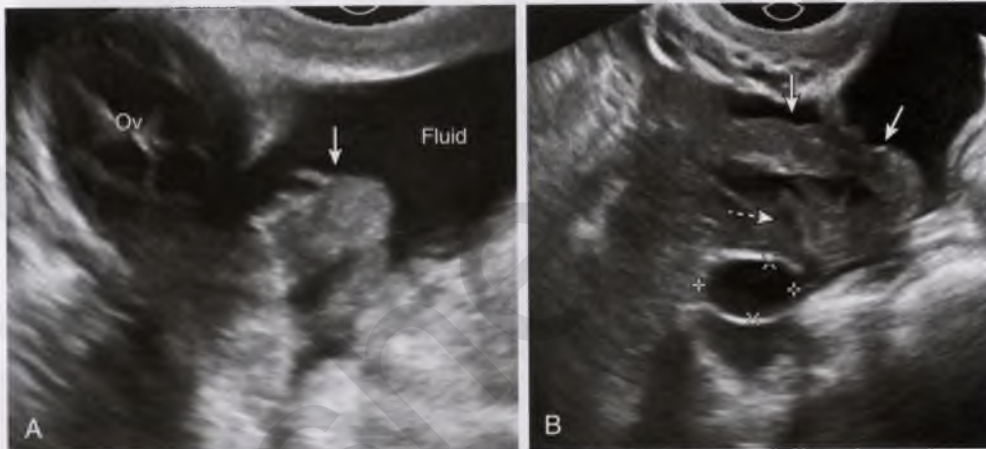


**FIG 26-17** The fallopian tube. **A**, Sagittal image of the left adnexa showing the fallopian tube (*arrow*) outlined by pelvic fluid, adjacent to the left ovary (Ov). **B**, Sagittal image obtained in a plane just medial to that of **A** shows the fallopian tube (*arrows*) including the fimbria (*dashed arrow*). A paratubal cyst (*calipers*) is also seen adjacent to the fallopian tube.

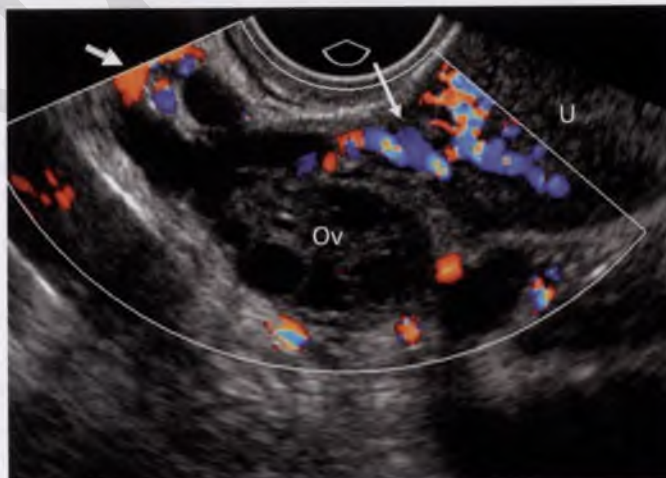


**FIG 26-18** Suspensory ligament and ovarian artery. Oblique longitudinal transvaginal sonogram of the left adnexa showing the ovarian artery (*short arrow*), which lies within the laterally and superiorly located suspensory ligament, and the ovarian branches of the uterine artery (*long arrow*), which lie medially in the broad ligament. Ov, ovary; U, uterus.



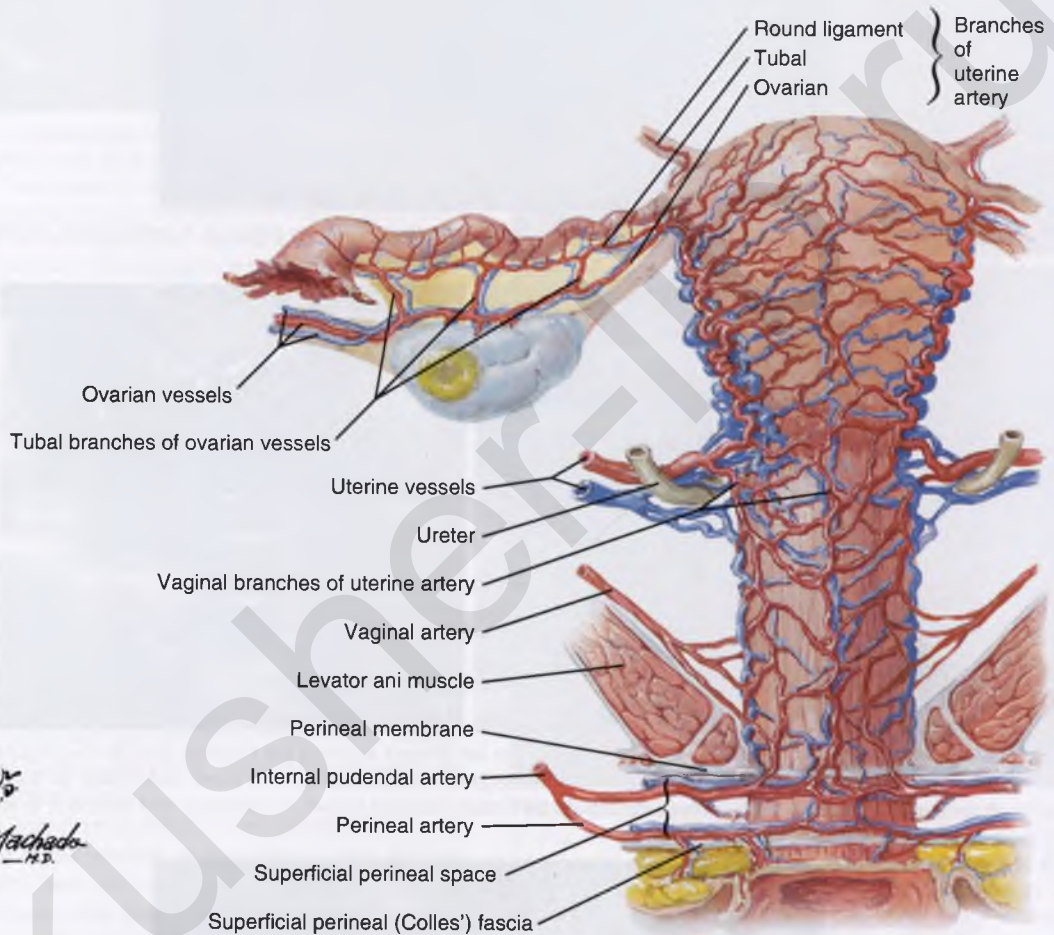


**FIG 26-19** Diagram of the ovarian, uterine, and vaginal arteries and veins and the ipsilateral ureter. (From Netter FH: Interactive Atlas of Human Anatomy. Plate 379B. Summit, NJ, CIBA-Geigy Co., 1995. Copyright 1981, 1990, 1995, and 1998, by Novartis. Reprinted with permission from Clinical Symposia, Vol. 33/1; 42/2; Netter Collection, Vol. 2 & Interactive Atlas, illustrated by Frank H. Netter, MD, and John A. Craig, MD. All rights reserved.)

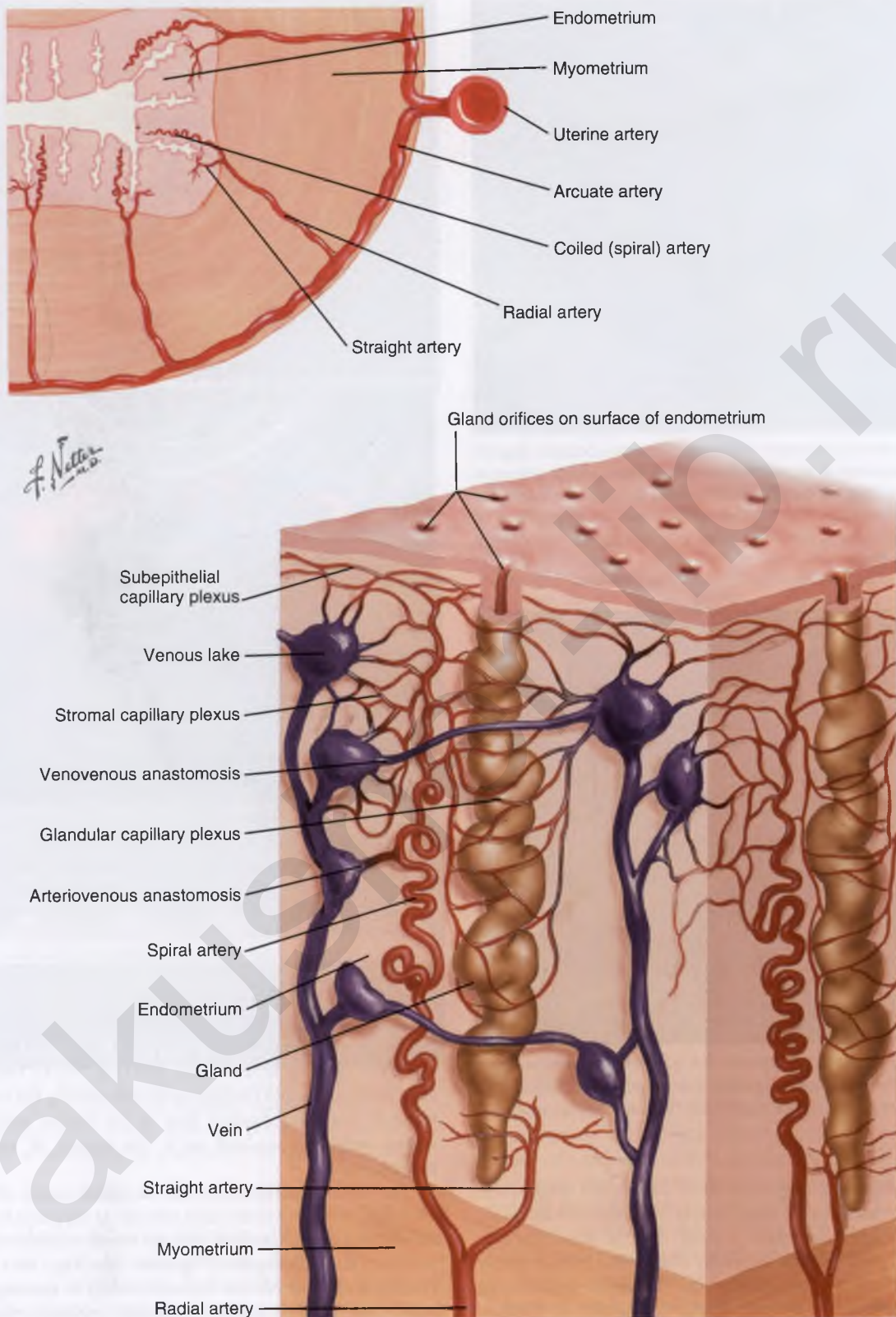


**FIG 26-20** Diagram of a uterine cross section and deep section showing the uterine artery, arcuate plexus, and radial, straight, and spiral arteries. (Copyright Elsevier, Inc. Netterimages.com.)





**FIG 26-21** Uterine radial artery. Transvaginal color Doppler sagittal image in a patient with a retroverted uterus. A radial artery (*arrow*) is demonstrated coursing perpendicularly from the arcuate arterial plexus toward the endometrium. The thickness and trilaminar appearance of the endometrium indicate that the patient is in the periovulatory stage of the menstrual cycle.

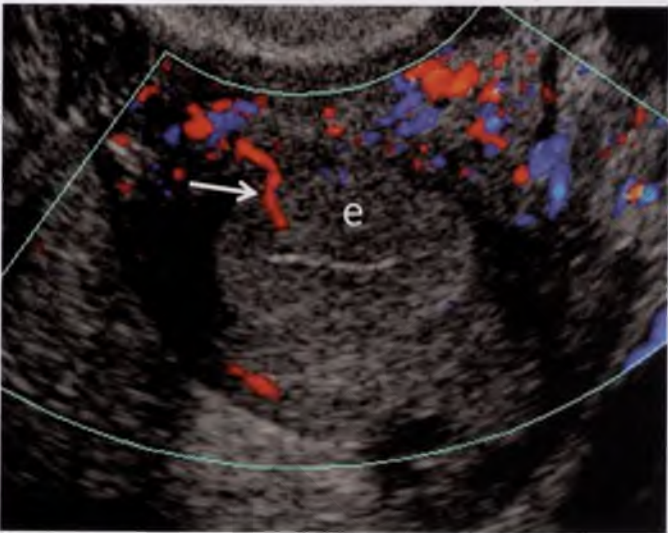


**FIG 26-22** Spiral artery. Transvaginal color Doppler short-axis or transverse view of the uterus demonstrating flow within a spiral artery (*arrow*) within the relatively homogeneous thick echogenic secretory endometrium (e).

arteries on Doppler sonography in women of all ages, but visualization of the radial arteries becomes progressively more difficult following menopause.<sup>21</sup> Endometrial spiral arterial flow is generally seen throughout the menstrual cycle in healthy women, but is most readily detected in the secretory phase of the cycle.<sup>21-23</sup> However, endometrial arterial flow is only detectable on Doppler sonography in approximately 30% of women 1 to 5 years after menopause, and in one study, no Doppler-detectable endometrial blood flow was found in women who were more than 5 years postmenopausal.<sup>21</sup>

The arcuate venous plexus accompanies the arcuate arteries and is frequently identified sonographically running between the outer one third and inner two thirds of the myometrium on gray-scale or color Doppler imaging (Fig. 26-23). Spectral Doppler waveforms of the

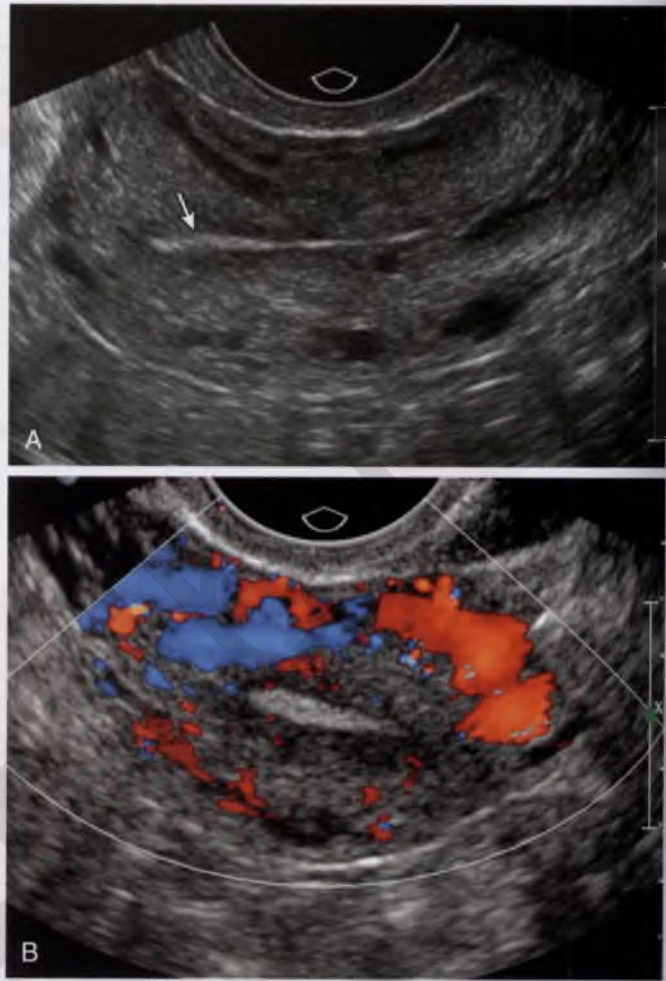


**FIG 26-23** Arcuate venous plexus. **A**, Longitudinal gray-scale image of the uterus shows linear/tubular and circular anechoic regions representing the arcuate venous plexus in the uterine body separating the outer one third of the myometrium from the inner two thirds. Note the thin echogenic, early proliferative appearance of the endometrium (*arrow*). **B**, Transverse color Doppler image shows flow within these veins.

normal uterine artery in the nongravid premenopausal woman typically have a high-resistance waveform pattern, with an early diastolic notch and relatively little diastolic flow (Fig. 26-24). The arterial waveform pattern does not change significantly during the menstrual cycle. However, increased diastolic flow in the uterine artery is observed during pregnancy as well as in the setting of endometritis or malignancy.

The ovarian arteries arise from the lateral margin of the aorta at a level slightly inferior to the renal arteries. At the pelvic brim, they cross the external iliac artery and vein and course medially within the suspensory (infundibulopelvic) ligament (see Figs. 26-12 and 26-19). Ovarian arterial blood flow varies according to the stage of the menstrual cycle likely because of hormonally mediated changes in vessel wall compliance, resulting in increased blood flow to the ovary in the late follicular and early luteal phases.<sup>19</sup> Hence, in the first half of the menstrual cycle or in the nonovulating ovary, a spectral tracing from the ovarian artery will demonstrate relatively low peak systolic velocity (PSV) and end-diastolic velocity (EDV). However, at the time of ovulation the arterial waveform from the ovulating ovary will change and both PSV and EDV will increase with a resultant decrease in resistive



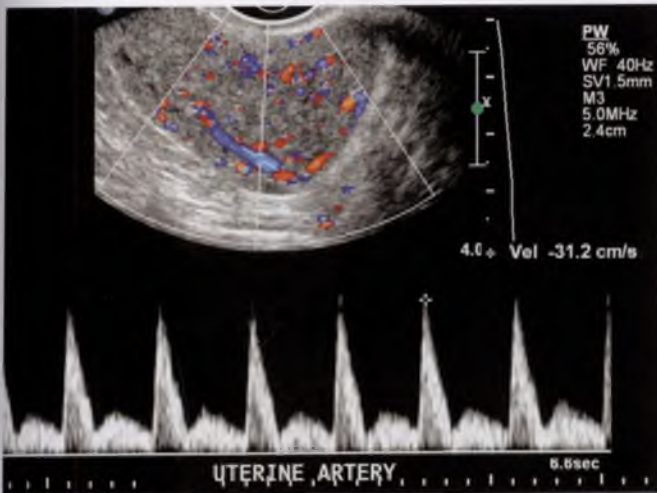


**FIG 26-24** Normal uterine artery. A uterine artery is seen flowing toward the fundus (away from the transducer) and demonstrates a typical high-resistance waveform pattern with a sharp systolic upstroke and thin, pointed systolic peak with relatively little diastolic flow and prominent early diastolic notch.

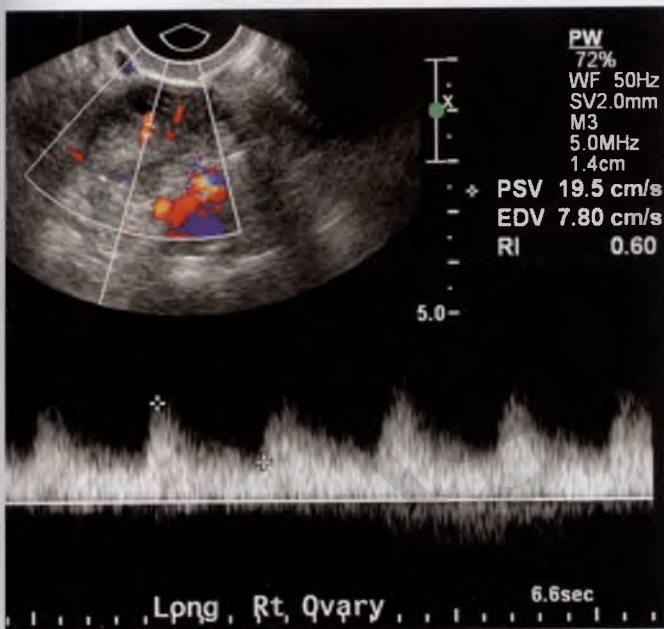


**FIG 26-25** Ovarian artery. Spectral Doppler waveform from the right ovarian artery obtained just prior to ovulation reveals spectral broadening, slight rounding of the systolic peak, and pronounced diastolic flow consistent with a low-resistance waveform. The resistive index (RI) is 0.60.

index (RI) (Fig. 26-25). Following menopause, both PSV and EDV in the ovarian artery will decrease. Often no diastolic flow will be observed, yielding an RI of 1.0 (Fig. 26-26).<sup>23</sup> The ovarian veins ascend out of the pelvis adjacent to the ovarian artery, with the right ovarian vein draining into the inferior vena cava just below the renal vein and the left ovarian vein emptying into the left renal vein.<sup>17</sup>

## THE UTERUS

The uterus consists of two major parts: the body (or corpus) and the cervix. The corpus is predominantly muscular, whereas the cervix is

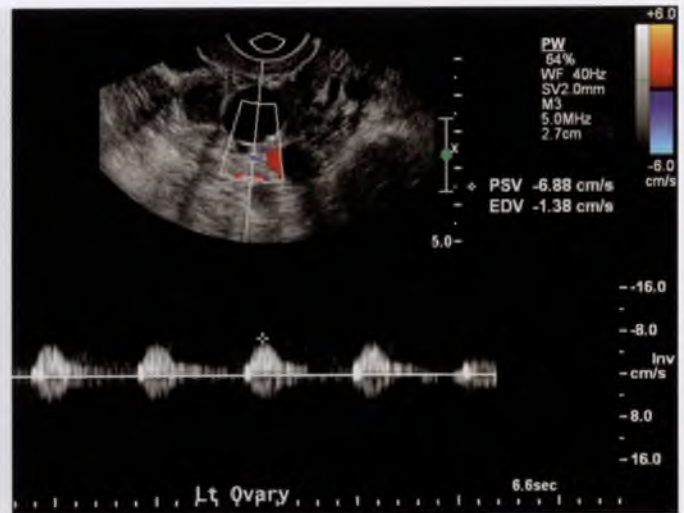


**FIG 26-26** Spectral Doppler waveform of the postmenopausal ovary. Spectral Doppler tracing from the left ovary of a postmenopausal woman. Note low peak systolic velocity (PSV) and complete absence of end diastolic flow. The resistive index (RI) is 1.00.

composed predominantly of collagenous and elastic tissue and has only 10% smooth muscle. The isthmus is a narrow portion or “waisting” of the uterus that corresponds to the approximate position of the internal os and demarcates the boundary between the lower uterine segment of the corpus and the cervix. The anterior surface of the corpus is almost flat, whereas the posterior surface is convex. The fallopian tubes emerge from the cone-shaped cornua of the uterus, situated at the junction between the superior and lateral uterine margins. The fundus of the uterus is the superior portion of the uterus above the level of the insertion of the fallopian tubes<sup>24</sup> (see Fig. 26-9).

The overall uterine length is measured on a midline sagittal image from the tip of the serosal surface of the fundus to the distal aspect of the cervix (i.e., the external os). The AP dimension of the uterus is measured on the same sagittal image from its outer anterior to outer posterior wall, in a plane perpendicular to the longitudinal axis. The maximum width is measured outer wall to outer wall on the transverse or coronal view.<sup>1,24,25</sup> Uterine size varies with age as well as with parity in the reproductive age patient. The uterus measures approximately 6 to 8.5 cm in length in nulliparous women and 8 to 10.5 cm in multiparous women.<sup>25-27</sup> The AP diameter ranges from 2 to 4 cm in nulliparas and 3 to 5 cm in multiparas,<sup>26</sup> whereas the width of the corpus measures approximately 3 to 5 cm in nulliparous women and 4 to 6 cm in multiparas.<sup>25-27</sup> Following menopause, the uterus atrophies with the most rapid decline in uterine size occurring within the first 10 years. In women who are more than 5 years postmenopausal, the uterus typically measures 3.5 to 7.5 cm in length, 1.7 to 3.3 cm in AP dimension, and 2 to 4 cm in width.<sup>26,27</sup> The uterus is typically pear-shaped, with the body twice the size of the cervix during the reproductive years. In the postmenopausal and pediatric patient, the uterus is more tubular in configuration, with the body and cervix nearly equivalent in length.<sup>24</sup>

Uterine position is highly variable and changes with varying degrees of distention of the urinary bladder. The cervix is anchored at the angle of the bladder by the parametrium and is less freely movable than the corpus and fundus. Uterine position is described in relation to the angle of the long axis of the uterine body with the long axis of the cervix (flexion) and the long axis of cervix to the long axis of the vagina



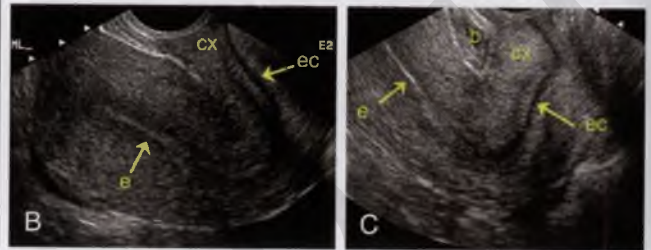
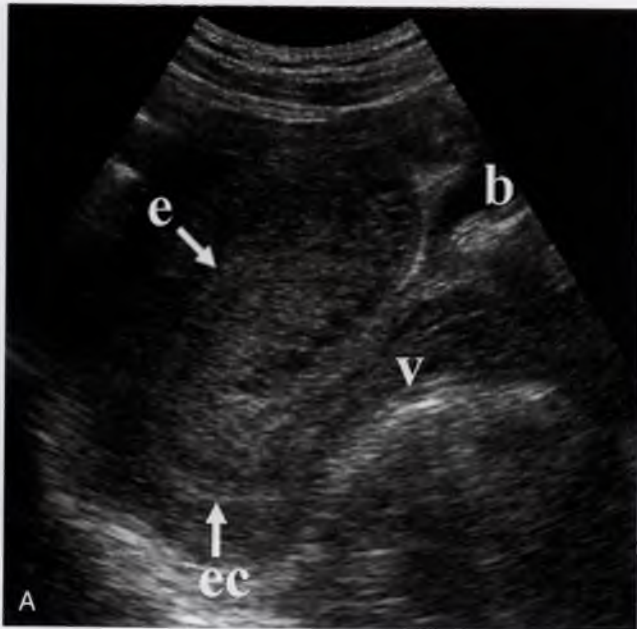


**FIG 26-27** Anteverted uterus. **A**, Transabdominal sonogram in the midline sagittal plane through the uterus. The bladder (b) is almost completely empty. **B**, Transvaginal midsagittal scan of an anteverted uterus. **C**, Transvaginal scan of the cervix and lower uterine segment. The bladder (b) is almost empty. The endocervical (ec) and endometrial (e) canals form an angle of approximately 90 degrees in all three images at the level of the internal os. cx, cervix; v, vagina.

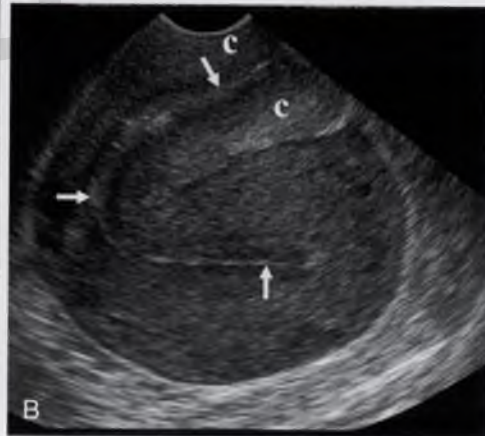


**FIG 26-28** Retroverted uterus. Transabdominal (**A**) and transvaginal (**B**) sonograms of a retroverted uterus. The uterine body is bent backward or posteriorly at the level of the internal os of the cervix (c), well over 90 degrees. On the transabdominal image, the cervix is tilted upward with respect to the vagina, indicating anteversion. In B, when the bladder is emptied to perform the transvaginal examination, the cervix points slightly posteriorly, indicating a change to retroversion. Note the endometrial and endocervical canals (arrows). b, bladder.

(version).<sup>28</sup> The most common position on TAS, with a distended urinary bladder, is anteversion without flexion (Fig. 26-11B). Anteversion (Fig. 26-27), retroflexion (Figs. 26-2 and 26-28), retroversion (see Fig. 26-28), and tilting of the uterus to the right or the left are considered to be normal variants in position, unless the uterus is displaced by pelvic disease.

The anteverted or anteverted uterus is usually well imaged on TAS because it lies in a superficial location, just behind the acoustic window

of the urinary bladder, and is oriented perpendicular to the ultrasound beam. When the uterus is retroverted or retroflexed, it is often difficult to evaluate by TAS and ideally is imaged with the transvaginal probe<sup>28</sup> (see Figs. 26-2 and 26-28). TAS of the retroverted and retroflexed uterus requires the sound beam to travel deeper into the pelvis and along a path parallel to the length of the uterus, as compared to the anteverted or anteverted uterus, resulting in marked attenuation of sound, which limits evaluation of the endometrium and may cause the



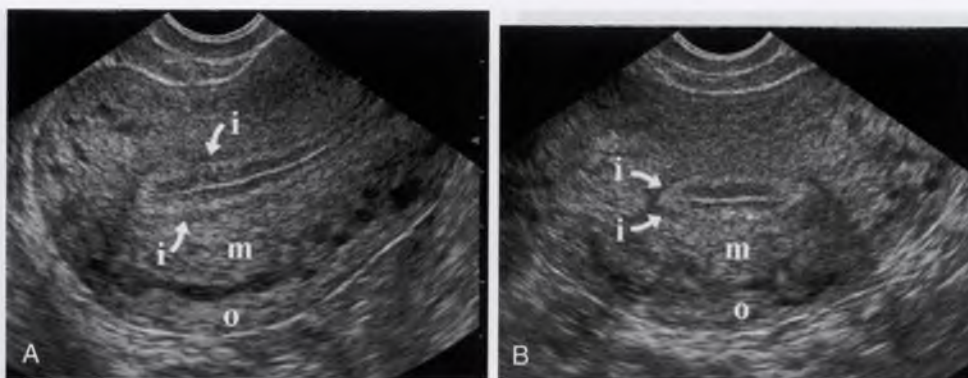


**FIG 26-29** Myometrial layers. Transvaginal longitudinal (A) and transverse (coronal) (B) sonograms demonstrating the three layers of the myometrium: the outer (o), intermediate (m), and hypoechoic inner (i) layers (arrows).

fundal myometrium to appear more hypoechoic and simulate the appearance of a fundal myoma or other disease. The transvaginal approach allows the probe to be positioned immediately adjacent to the body of the retroverted or retroflexed uterus, without intervening structures and at a perpendicular imaging plane, providing better visualization of the endometrium and the fundal myometrium than the transabdominal technique. When the uterus is retroflexed, the cervix may be interposed between the probe and the body of the uterus. To improve uterine visualization with the transvaginal probe, one must position the probe around the cervix and angle it posteriorly so that the probe now lies immediately adjacent to the body and fundus of the uterus (see Fig. 26-28).

The myometrium of the uterus is composed of bundles of smooth muscle fibers, intermixed with connective tissue, blood vessels, lymphatics, and nerves, and is divided into three zones: the inner, intermediate or middle myometrium, and outer myometrium<sup>3,26</sup> (Fig. 26-29). The outer layer of the myometrium consists of longitudinally oriented muscle fibers that course over the fundus and converge at the cervix and cornua. The outer layer is separated from the intermediate or middle layer by the arcuate vessels. The intermediate layer is usually the thickest of the three layers and its muscle layer consists of spiral bands extending from cornua to cervix, which interdigitate in the midsagittal plane. The inner myometrium is the thinnest layer and has both longitudinal and circular muscle fibers. The inner layer may be extremely hypoechoic. When it is observed to be hypoechoic, it has been termed the subendometrial halo (Fig. 26-30) and is believed to correspond to the markedly hypointense junctional zone observed on T2-weighted magnetic resonance (MR) sequences.<sup>23</sup> However, the hypoechoic subendometrial halo is not visualized in all patients and may not be circumferentially intact in many patients, appearing as an incomplete or fragmented hypoechoic subendometrial band of tissues. The thickness and echogenicity of the subendometrial halo do not appear to vary significantly during the menstrual cycle. The inner myometrial myometrium and endometrial mucosa both arise from the paramesonephric ducts, whereas the remainder of the myometrium is mesenchymal in origin. The inner myometrial-endometrial junction (EMJ) is histologically unique in the human body in that it lacks a submucosal layer.<sup>29</sup>

The nongravid uterus is not quiescent but demonstrates transient myometrial contractions and organized wave-like activity in the inner myometrium. These wave patterns change their frequency, intensity, and directionality throughout the phases of the menstrual cycle. Waves travel from cervix to fundus in the periovulatory phase of the menstrual cycle, presumably in an effort to promote sperm transport within the endometrial canal, and are reversed in the menstrual phase.<sup>30</sup> Uncoordinated or absent wave activity has been associated

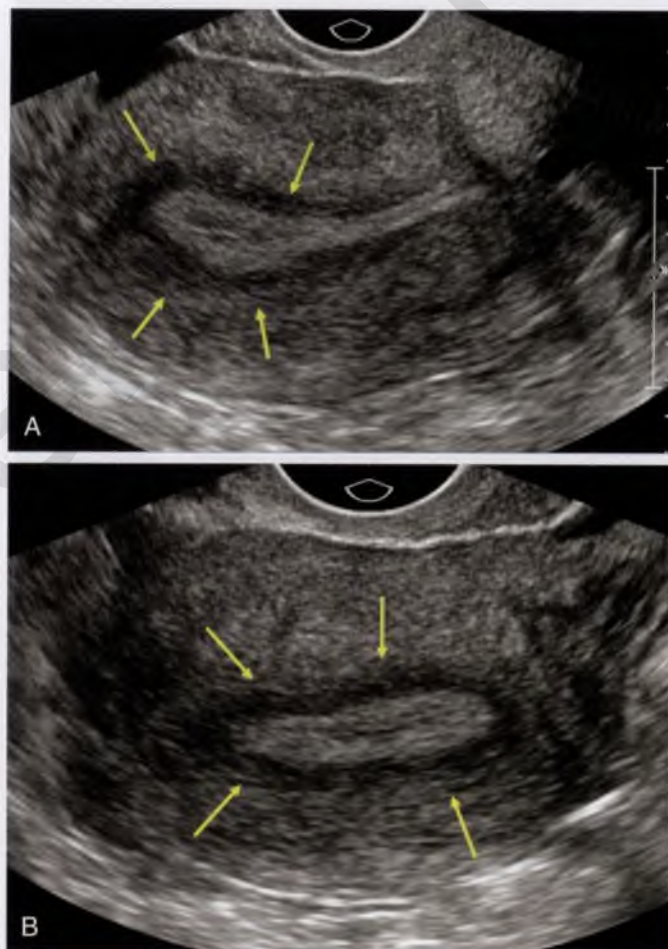


**FIG 26-30** The inner myometrium. Transvaginal longitudinal (A) and transverse (coronal) (B) gray-scale images demonstrating the hypoechoic inner myometrium (arrows), which has been termed the subendometrial halo.

with higher rates of infertility, and wave activity can be suppressed by oral contraceptives.<sup>31</sup>

The endometrium is composed of a superficial layer (zona functionalis) and a deeper basalis layer. The thickness and sonographic appearance of the endometrium change cyclically during the menstrual cycle.<sup>32-34</sup> In the menstrual and very early proliferative phase, the endometrium is thin, usually under 4 mm, and appears brightly echogenic and homogeneous (Fig. 26-31). Throughout the mid to late



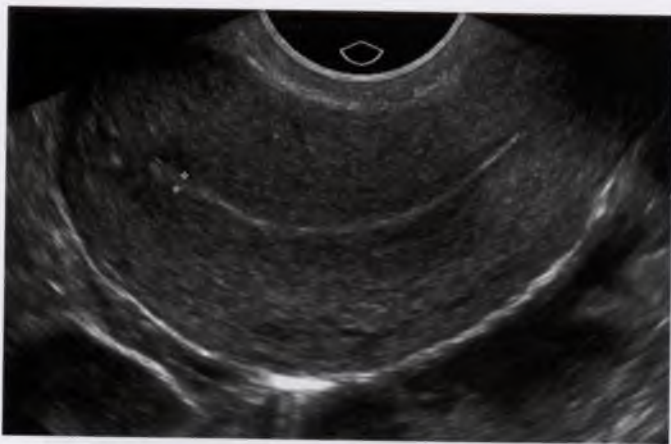


**FIG 26-31** Early proliferative phase endometrium. The endometrium (*calipers*) appears as a thin, echogenic, and slightly irregular line in this patient on day 5 of the menstrual cycle.



**FIG 26-32** Periovulatory endometrium. Transvaginal longitudinal sonogram demonstrates the normal trilaminar appearance of the endometrium (*calipers*) in the late proliferative phase of the cycle. The basal layer of the endometrium is echogenic, but the more superficial functional layer has become hypoechoic as a result of estrogen effects. The central echogenic line (*arrows*) represents the interface where the endometrium lining the anterior and posterior walls of the uterine cavity meet.

proliferative phase of the cycle (days 5 to 14) the functionalis layer of the endometrium increases in thickness under the influence of estrogen and becomes more hypoechoic compared to the basalis layer, such that the endometrium develops a trilaminar or striated appearance, typically measuring 12 to 13 mm (normal range 10-16 mm) at ovulation<sup>33</sup> (Fig. 26-32). During the secretory phase (days 15 to 28), the functional layer becomes thickened, soft, and edematous under the influence of progesterone (Fig. 26-33). A glycogen-rich fluid is secreted by the glandular epithelium, and the spiral arteries become tortuous. The resultant effect is that the functional layer increases in echogenicity to become once again isoechoic to the basalis layer.<sup>32,33</sup> At the end of the secretory stage, the endometrium may measure up to 16 to 18 mm in thickness and is homogeneous in echotexture.

Endometrial thickness is best assessed on TVS, and by convention is reported as the sum of the measurement of both the anterior and posterior layers of the endometrium at the thickest segment on a midline longitudinal image.<sup>35,36</sup> It is critical that the measurement be made on a midline sagittal image, as imaging obliquely or too close to the uterine cornua will result in an overestimation of endometrial thickness. If the endometrium can be shown to be continuous with the endocervical canal, the sonographer can be certain that the imaging



**FIG 26-33** Secretory endometrium. Transvaginal sonogram in the sagittal plane on day 19 of the menstrual cycle shows a uniformly echogenic endometrium (*calipers*) measuring 10.2 mm. The functional layer of the endometrium has become isoechoic with the basal layer, and the trilaminar appearance is therefore no longer evident.



**FIG 26-34** Endometrial polyp. The central echogenic line representing the interface of the anterior and posterior endometrial layers of the proliferative endometrium with its characteristic trilaminar appearance is interrupted by an oval echogenic lesion (*arrow*), which proved to be a benign endometrial polyp. This is sometimes referred to as the "bead on a string" sign.

plane is midline. If the endometrium appears triangular or bulbous rather than symmetric, or oval or cigar-shaped in configuration, the imaging plane is likely off-axis and not midline.

The central thin echogenic line represents the interface between the two layers of the endometrium and should be continuous. Disruption of the central echogenic white line or heterogeneity of the endometrium may indicate an underlying intracavitary lesion, such as a polyp, myoma, or adhesion (Fig. 26-34). The subjacent hypoechoic subendometrial halo just peripheral to the endometrium represents the innermost layer of the myometrium and should not be included in the endometrial measurement.<sup>35</sup> A small amount of hypoechoic fluid or mucus within the endometrial cavity may be a normal finding, but should not be included in the endometrial thickness measurement (Fig. 26-35). Larger amounts of fluid or retained echogenic blood clots are considered abnormal and raise suspicion for underlying disease or obstructed menstrual flow, such as may be seen with adhesions or cervical stenosis. In women taking oral contraceptives or using other





**FIG 26-35** Endometrial fluid. Transvaginal longitudinal sonogram of a retroverted, retroflexed uterus shows a small amount of anechoic fluid in the uterine cavity (*asterisk*). The endometrial thickness measurement is determined by measuring the anterior and posterior endometrial layers individually, as shown by the "+" and "x" electronic calipers. These two numbers are then summed to obtain the double thickness measurement.



**FIG 26-36** Normal postmenopausal endometrium. The endometrium (*calipers*) is atrophic, appearing as a thin white line measuring under 1 mm in a patient who has been postmenopausal for 10 years. The hypoechoic tissue subjacent to the endometrium represents the inner compact layer of myometrium and is referred to as the subendometrial halo. The subendometrial halo should not be included in the measurement of the endometrial thickness. Note that the cervix (length indicated by *asterisks*) is approximately equal in size to the uterine body and the uterine body is more tubular in configuration, as is commonly seen following menopause, rather than pear-shaped, which is the typical configuration of the uterus during the reproductive years.

hormonal contraceptives, such as progesterone-bearing IUDs, the endometrium is generally thin throughout the month.

The postmenopausal endometrium is typically atrophic, from lack of estrogen stimulation, and appears on ultrasound imaging as a thin, homogeneous echogenic line that measures less than 3 mm in most postmenopausal women<sup>37</sup> (Fig. 26-36). It has been shown that the measurement of the endometrium obtained by TVS corresponds within 1 mm of that measured on pathologic examination,<sup>25,36</sup> allowing TVS to play an important role in diagnostic evaluation of women with suspicion for endometrial cancer.<sup>36-38</sup> In a postmenopausal woman

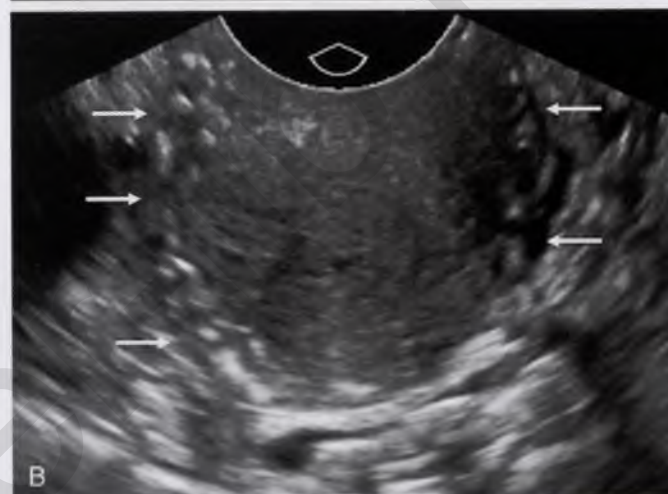


**FIG 26-37** Arcuate artery calcifications. Longitudinal (**A**) and transverse (**B**) images from a transvaginal ultrasound examination performed on a postmenopausal woman showing calcification of the arcuate vessels (*arrows*) in the typical location along the periphery of the uterus.

who presents with vaginal bleeding, endometrial cancer is considered to be extremely unlikely when the endometrium is homogeneous, regular, and measures less than 4 to 5 mm in maximal diameter, provided that the endometrium is completely visualized on the TVS. If the endometrium exceeds 4 to 5 mm in a postmenopausal woman with vaginal bleeding, endometrial sampling is usually obtained to evaluate for possible malignant or premalignant endometrial changes. However, the threshold for recommending endometrial biopsy in the asymptomatic postmenopausal woman is somewhat more controversial, and is reported to range from 8 to 11 mm.<sup>38</sup>

Calcified uterine arcuate vessels are commonly noted in elderly postmenopausal women, especially those with diabetes, vascular disease, hypertension, or hypercalcemia.<sup>39</sup> These vessels appear as peripheral linear reflectors in a circumferential pattern in the superficial myometrium (i.e., between the outer and inner layers of the myometrium, see earlier) (Fig. 26-37).

The cervix is best visualized and assessed by TVS. However, the probe often has to be partially withdrawn and angled posteriorly or anteriorly for optimal visualization, depending on the orientation of the uterus.<sup>28</sup> The endocervical canal is continuous with the endometrial canal, appearing as a thin, echogenic stripe (Figs. 26-8A, 26-13, and 26-27). Fluid or mucus is sometimes seen in the endocervical canal,



particularly in the preovulatory period. Color Doppler imaging can be useful to distinguish mucus from small endocervical polyps, which are common findings. Subjacent to the endocervical canal is a hypoechoic band that represents the fibrous cervical stroma and is continuous with the subendometrial halo or inner layer of the myometrium. The outer wall of the cervix is similar in echogenicity to the outer myometrium (Figs. 26-13 and 26-28). Numerous cervical glands extend from the endocervical mucosa into the adjacent connective tissue of the cervix.<sup>40</sup> Occlusion of the cervical glands results in the formation of retention cysts, known as nabothian cysts, which lie close to the endocervical canal. They may be single or multiple. Nabothian cysts typically contain simple fluid and are asymptomatic. Uncommonly, nabothian cysts may be complicated by hemorrhage or infection or grow to large size<sup>28</sup> (see Fig. 26-14). The cervix extends inferiorly into the upper vagina and is surrounded by the anterior, posterior, and the two lateral fornices of the vaginal canal (Figs. 26-8A and 26-13). Occasionally, air can be seen in the vaginal fornices surrounding the cervix on TAS. The vagina is seen on ultrasound imaging as a hypoechoic tubular structure with an echogenic lumen that curves inferiorly over the muscular perineal body at the introitus (see Figs. 26-4 and 26-27).

## THE OVARIES

The normal ovary is ellipsoid in shape and is variable in both location and orientation, depending upon the age and parity of the patient as well as the degree of bladder distention. In the nulliparous adult female, the ovaries are situated in the ovarian fossa (also known as the fossa of Waldeyer), which is adjacent to the lateral pelvic side wall and is bounded by the obliterated umbilical artery anteriorly, the ureter and internal iliac artery posteriorly, and the external iliac vein superiorly<sup>16</sup> (see Fig. 26-12). The inferior aspect of the ovary is slightly smaller than the superior or tubal aspect and is bound to the uterine cornua by the ovarian ligament, which lies within the broad ligament. The lateral surface of the ovary is in contact with the parietal peritoneum lining the ovarian fossa, and most of the medial surface is covered by the fallopian tube (Fig. 26-38). The anterior border of the

ovary is attached to the mesovarium, through which the vascular channels and nerves pass into the ovarian hilum.<sup>16</sup>

Ovarian volume is calculated by measuring the ovary in three dimensions (length, width, and depth) on two orthogonal planes and using the formula for the prolate ellipse ( $L \times W \times D/2$ ). Ovarian size depends upon age, menstrual status, pregnancy status, body habitus, and phase of the menstrual cycle.<sup>41-43</sup> In premenopausal women, the mean ovarian volume is 9.8 mL (with 5% and 95% confidence intervals of 2.5 and 21.9 mL), with the highest volumes found in the preovulatory phase and the lowest volumes in the luteal phase.<sup>41</sup> Normal ovarian volume decreases after the age of 30 years. In one large study, mean ovarian volume significantly decreased in each decade up to age 60 years, measuring 6.6 mL in women under 30 years of age, 6.1 mL in women 30 to 39 years old, 4.8 mL at ages 40 to 49 years, 2.6 mL at ages 50 to 59 years, 1.98 mL at ages 60 to 69 years, and 1.85 mL over age 70 years. The authors found a statistically significant increased ovarian size in tall women but no relationship to weight.<sup>42</sup> Despite the small size of the postmenopausal ovary, the majority are detectable by TVS.<sup>42,43</sup>

The normal ovary in women of reproductive age has a variable appearance over the course of the menstrual cycle.<sup>44</sup> Developing and immature follicles can be seen throughout the entire menstrual cycle and appear as anechoic, unilocular, sharply marginated cysts, measuring from 2 to 9 mm (Figs. 26-8F and 26-38). By days 8 to 12 of the menstrual cycle, one or more dominant follicles will grow to a diameter of approximately 20 to 25 mm and then rupture at ovulation, releasing the oocyte.<sup>44</sup> Up to 80% of patients have a second nondominant follicle that becomes almost as large as the dominant follicle. The preovulatory dominant follicle may have a slightly complex appearance, with the oocyte and its supporting structures appearing as a ring-like structure within the follicle (the cumulus oophorus) (Fig. 26-39). Following ovulation, the corpus luteum evolves from the remnant of the mature follicle through a process of cellular hypertrophy and increased vascularization of the cyst wall. Therefore, a corpus luteum is typically visible in the secretory phase of the menstrual cycle and in the first few weeks of early pregnancy. On sonographic imaging, the corpus luteum

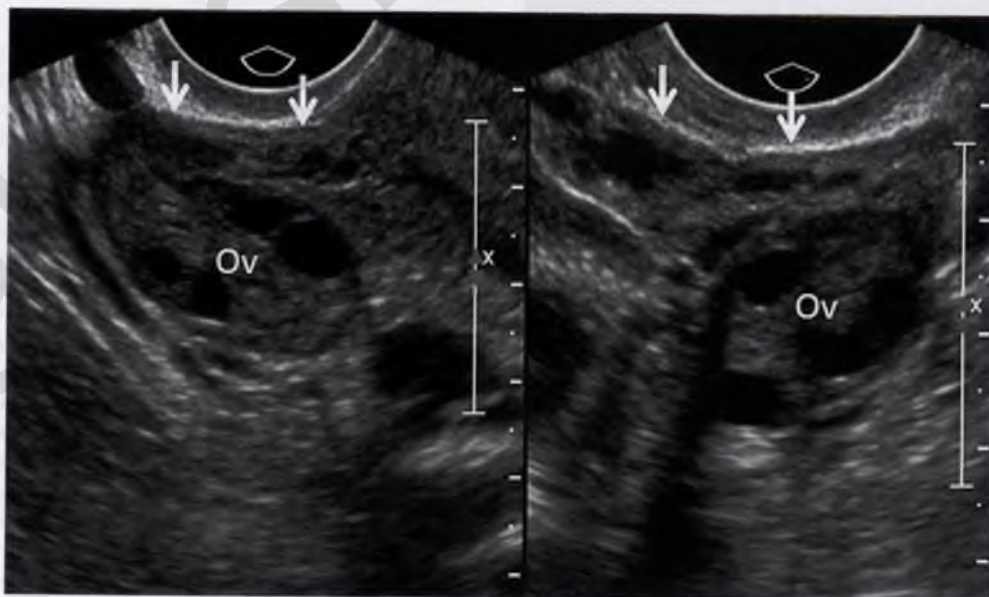


**FIG 26-38** Normal ovary. Transvaginal gray-scale images displayed in split-screen format (longitudinal orientation on the right and the coronal or transverse orientation on the left) show a normal left ovary (Ov). Note the distal fallopian tube (arrows) overlying the ovarian surface. Multiple small subcentimeter anechoic follicles are noted in the ovarian parenchyma, although most are relatively peripheral.



typically has a relatively thick, homogeneously echogenic wall, the inner margin of which may be slightly irregular with a crenulated appearance. On color Doppler, the wall of the corpus luteum often demonstrates a circumferential ring of arterial flow with a low resistance spectral Doppler waveform.<sup>45-47</sup> Internal echoes are common, reflecting variable amounts of internal hemorrhage that occurred at the time of ovulation, and occasionally a corpus luteum may be filled with homogeneous low level echoes mimicking a solid mass. However, there is usually evidence of enhanced through transmission because of the fluid content and there will be no central vascularity (Fig. 26-40). Typically the corpus luteum is under 3.0 cm in maximal dimension, but rarely it may become larger.<sup>45,46</sup> If pregnancy does not occur, the corpus luteum gradually involutes and atrophies to become the corpus albicans, which is typically not sonographically identifiable. Small echogenic foci, measuring 1 to 3 mm, may be noted in the periphery of otherwise normal appearing ovaries in approximately half of women undergoing TVS, particularly in the perimenopausal age group. These foci often demonstrate ring down artifact and are a benign finding,



**FIG 26-39** Dominant follicle. Transvaginal longitudinal sonogram of the right ovary (*calipers*) shows a dominant anechoic follicle with a peripheral ring representing the cumulus oophorus (*arrow*).

likely related to the presence of tiny cysts, possibly cholesterol or hemosiderin deposition, and less likely tiny calcifications. These tiny echogenic foci may come and go underneath the surface epithelium and should not raise concerns or result in follow-up imaging.<sup>48</sup>

In the postmenopausal patient, ovarian size decreases correlating with hormonal status and length of time since menopause. Mean postmenopausal ovarian volumes have been reported to range from 1.2 to 5.8 mL, with an ovarian volume of greater than 8 mL considered abnormal in all cases.<sup>41,49</sup> Some authors have suggested that a unilateral ovarian size twice that of the opposite side, regardless of the size, should also be considered abnormal.<sup>41</sup> Even though folliculogenesis has ceased, the postmenopausal ovaries are not as quiescent as initially thought. Small simple adnexal cysts, measuring as large as 3 cm, have been reported in up to 15% of postmenopausal women; most of these spontaneously regress on serial sonographic examinations.<sup>46,50,51</sup> These simple cysts, seen early in menopause, most likely represent an occasional ovulatory event or an atretic follicle. However, any anechoic cystic lesion in a postmenopausal ovary should generally be referred to as a cyst.<sup>46</sup> In late menopause, although ovulation is rare, smaller cysts less than or equal to 1 cm have been reported in up to 21% of women.<sup>50,51</sup> TVS will detect these cysts more readily than TAS because of the higher resolution of the higher frequency transvaginal probe (Fig. 26-41). These simple-appearing cysts, measuring less than 1 cm in maximal diameter, do not need further follow-up, and whether or not they are described in the final report can be left to the discretion of the interpreting physician.<sup>46</sup>

## THE FALLOPIAN TUBE

The fallopian tubes are variable in length, measuring approximately 7 to 12 cm. Each tube is situated in the superior free margin of the broad ligament and is covered by peritoneum. The fallopian tube is narrowest in the interstitial or intramural portion as it travels through the muscular wall of the uterus to open into the cornual region of the endometrial cavity. The interstitial portion of the fallopian tube measures approximately 1 cm in length and can be visualized with TVS in the superior right and left lateral corpus of the uterus as a fine, echogenic line arising from the angular, most lateral cephalad edge of the endometrial canal and running somewhat obliquely through the uterine wall toward the serosal surface (Fig. 26-42). Using 3D sonography, one

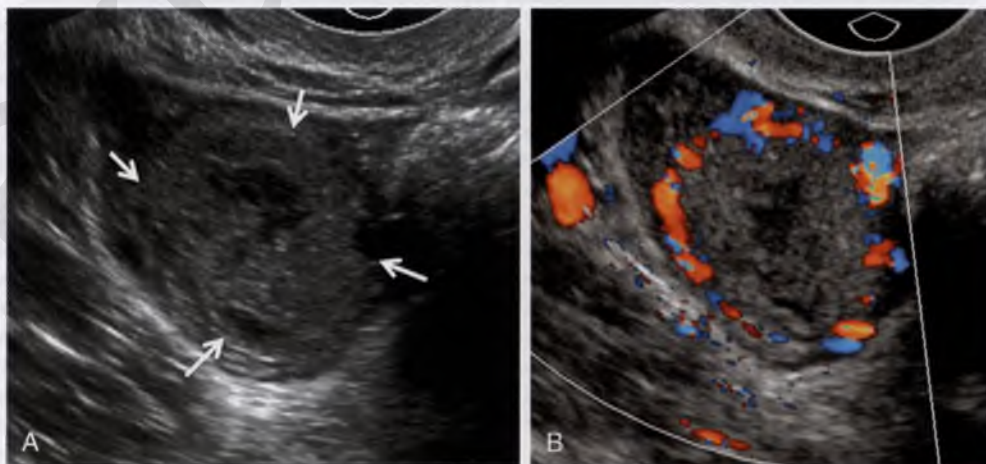


**FIG 26-40** Corpus luteum. **A**, Transvaginal sonogram demonstrating a slightly echogenic lesion within the right ovary (*arrows*), with a complex cystic central component and thick homogeneous wall. **B**, Color Doppler imaging shows markedly increased blood flow in a peripheral ring-like pattern, sometimes described as a "ring of fire," a characteristic appearance of the corpus luteum.



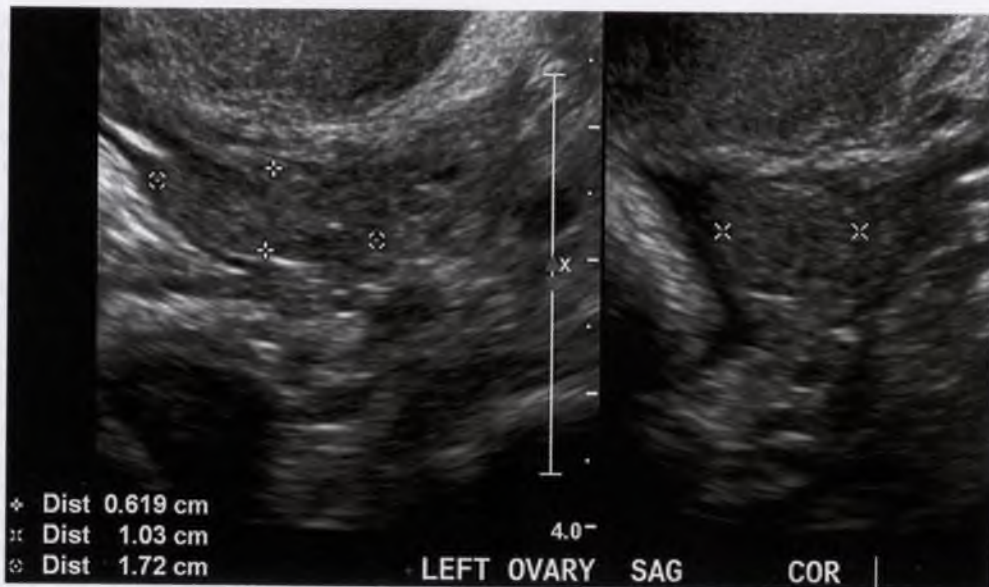


**FIG 26-41** The postmenopausal ovary. Transvaginal gray-scale images displayed in split-screen format (longitudinal orientation on the right and coronal or transverse orientation on the left) show the typical appearance of a postmenopausal ovary (*calipers*). The ovarian volume is less than 2 mL and no clear follicles are seen.

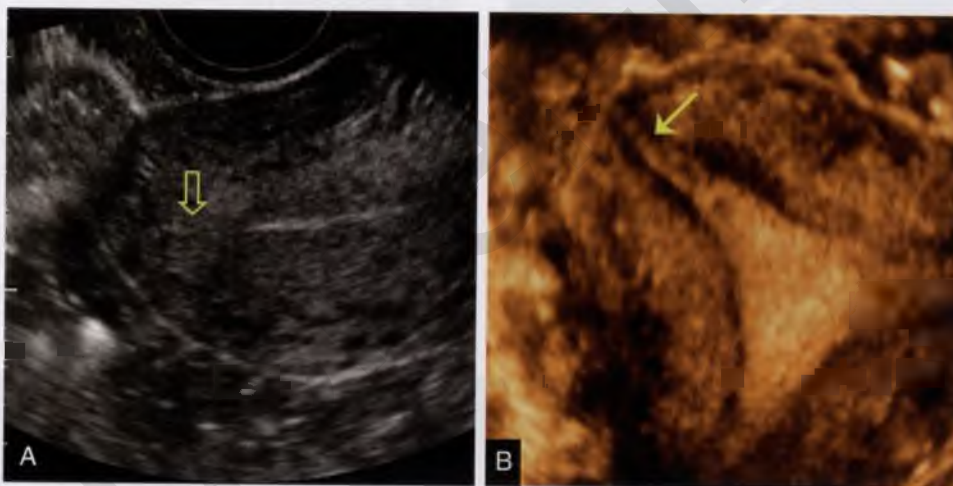


**FIG 26-42** Interstitial portion of the fallopian tube. **A**, Transverse transvaginal scan of the uterine fundus showing a thin echogenic line extending from the cornual portion of the endometrium toward the serosal surface of the uterus representing the interstitial portion of the fallopian tube (*open arrow*). **B**, Three-dimensional (3D) coronal view of the uterine fundus showing the echogenic, triangular endometrial canal and the interstitial portion of one fallopian tube (*arrow*) extending to the serosal surface. On 3D sonography, this portion of the tube appears thicker than its true size.

can often visualize the interstitial portion of the fallopian tube on a superior coronal view.<sup>12</sup> The isthmus is the narrow segment of the tube immediately adjacent to the uterine wall. As the tube extends laterally, it widens forming the ampullary and infundibular regions. The infundibulum is funnel-shaped, terminates as the fimbriated end of the tube, and opens into the peritoneal cavity. The isthmus, ampulla, and infundibulum are usually not visualized on either TAS or TVS unless there is tubal disease or free fluid in the lateral pelvic recess (see Fig. 26-17). The vascular supply of the fallopian tube comes from the vascular arch formed by the anastomosis of the uterine and ovarian arteries.

Part of the cranial end of the paramesonephric duct (which normally forms the uterus, fallopian tube, and fibromuscular wall of the

vagina) may persist as a vesicular appendage to the fallopian tube referred to as a hydatid cyst of Morgagni or a paratubal cyst. Sonographically, paratubal cysts usually appear as small, unilocular, round thin-walled anechoic structures and are most easily seen when surrounded by free intraperitoneal fluid (Figs. 26-17B and 26-43). The mesonephric ducts, which form the efferent ductules, epididymis, ductus deferens, seminal vesicles, and ejaculatory ducts in male fetuses, may persist as rudimentary, blind tubules in women. Mesonephric duct remnants may appear as parovarian cysts in the loose connective tissue adjacent to the ovary. Closer to the uterus, the mesonephric duct may persist as a Gartner duct cyst along the lateral wall of the uterus and vagina, superior to the hymen<sup>16,24,52</sup> (Fig. 26-44).



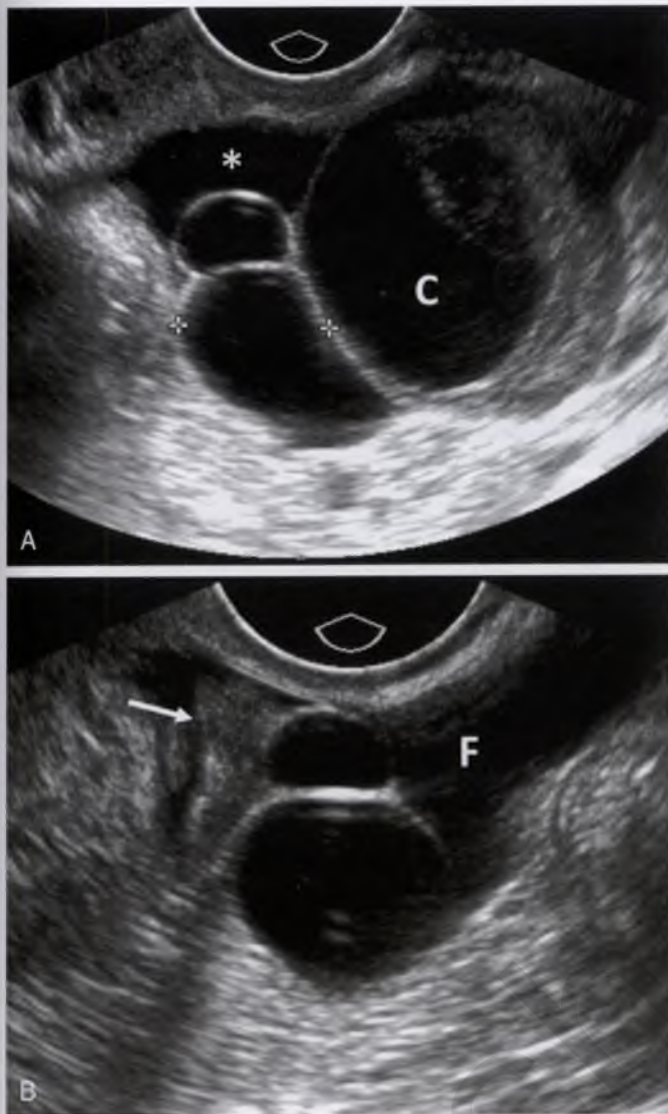


**FIG 26-43** Paratubal cyst. **A**, Transvaginal sonogram shows a bilobed cystic structure (*calipers*) abutting a hemorrhagic cyst (C) within the adjacent ovary. Note small amount of free fluid anteriorly (asterisk). **B**, An image obtained slightly more lateral than the plane of image in A demonstrates that the bilobed cyst abuts the fallopian tube (*arrow*), which is outlined by pelvic fluid (F). Although the bilobed configuration is slightly atypical, this lesion proved to be a paratubal cyst.

## THE URINARY BLADDER, DISTAL URETERS, AND URETHRA

The appearance of the urinary bladder depends on the degree of distention. The distended bladder will be round on a superior transverse imaging plane. More inferiorly, the pelvic musculature and bones cause the bladder to be square in the transverse plane (Fig. 26-45). The bladder wall is homogeneously echogenic and should be uniform in thickness, measuring less than 3 mm when well distended. The ureteric and urethral orifices are visualized at the base and neck of the bladder, respectively. In the upper pelvis, the ureter lies anterior to the internal iliac artery and posterior to the ovary. More inferiorly, the ureter courses anteromedially to lie within the inferomedial portion of the broad ligament, where it is in close proximity to the uterine artery. The ureter then runs anteriorly, situated in front of the lateral fornices of

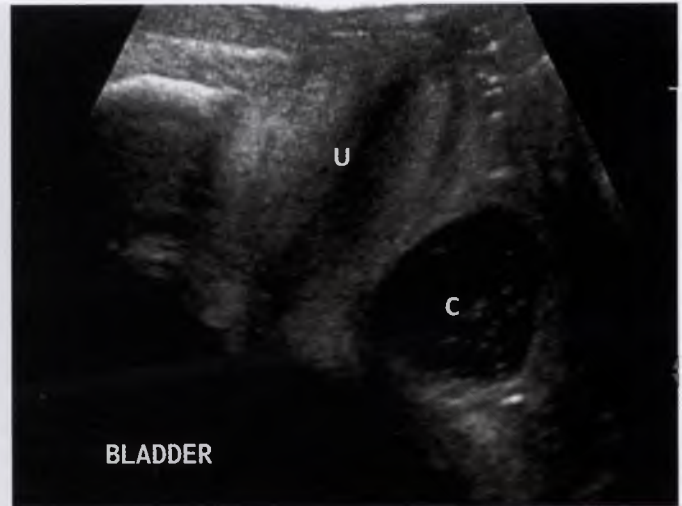


**FIG 26-44** Gartner duct cyst. A transperineal sonogram shows a minimally complicated Gartner duct cyst (C) within the connective tissue adjacent to the vagina. U, urethra.

the vagina, about 2 cm lateral to the supravaginal cervix, and then passes medially to enter the trigone of the bladder anterior to the vagina (Fig. 26-46). The relationship of the ureter to the ovary, cervix, uterine artery, and vagina is of clinical importance because pelvic disease may obstruct the ureter, resulting in secondary hydronephrosis. The distal portion of the ureter just proximal to the ureteral orifice is often well seen on TAS through the distended bladder. The distal ureter and ureterovesical junction (UVJ) can also be well seen on TVS if the bladder is partially distended. Hence, TVS is an excellent means of searching for UVJ stones, especially in the pregnant patient (Fig. 26-47). The presence of a ureteral jet in the bladder on color Doppler imaging as urine is expelled by the peristalsing ureter into the bladder is a normal finding on both TAS and TVS and indicates that the ureter is at least partially patent.

TVS enables better visualization of the trigone and posterior wall of the urinary bladder, as well as the urethra in comparison to TAS. To visualize the urethra, the probe is placed at the introitus or just partially inserted into the vagina and directed upward (Fig. 26-48). Surrounding the inner echogenic layer of the mucosa, there is a thin layer of smooth muscle and then an outer sheath of striated muscle. The longitudinally oriented smooth muscle is thicker anteriorly in the middle third of the urethra. The paraurethral glands of Skene lie posterior to the urethra near the UVJ and empty through the paraurethral duct near the external urethral orifice. Urethral diverticula are distended and/or obstructed urethral mucous glands and are found posterior and lateral to the urethra anywhere along its length. They may be a source of pelvic pain and recurrent urinary tract infection and can be easily documented on TVS. They may be round or horseshoe-shaped, partially encircling the urethra (Fig. 26-49). Although these diverticula are usually anechoic, internal echoes may be observed, either diffuse or layering. This non-specific finding may be secondary to infection or debris from stasis or chronic inflammation. Echogenic shadowing calculi may also be observed in urethral diverticula as stasis predisposes to calculus formation as well as infection.

## THE RECTOSIGMOID COLON

The sigmoid colon begins at the inlet of the true pelvis and is extremely variable in length. It has a mesentery, and its course is variable, looping



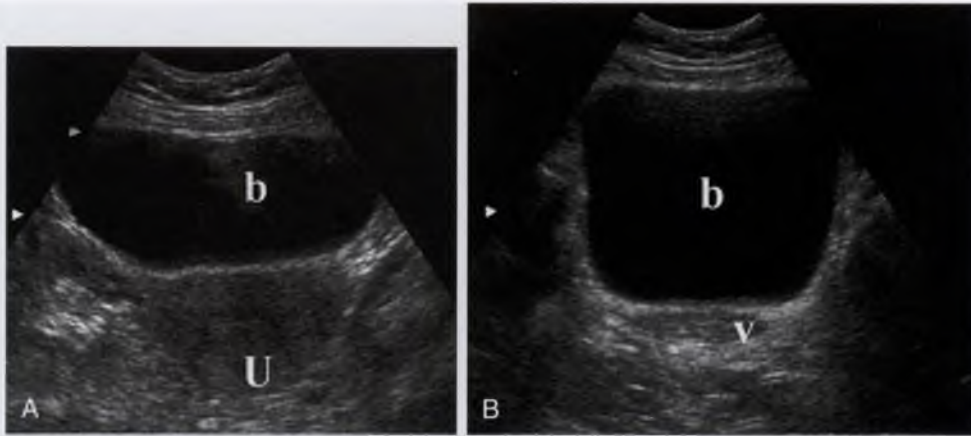


**FIG 26-45** Normal urinary bladder. **A**, Transverse transabdominal sonogram of the urinary bladder at the level of the corpus of the uterus (U). At this level, the bladder (b) has a rounded or oval configuration. **B**, Transverse transabdominal sonogram of the urinary bladder at the level of the vagina (v). At this level, the bladder (b) has a square configuration. The normal bladder wall is thin, echogenic, and regular, measuring less than 3 mm in thickness.

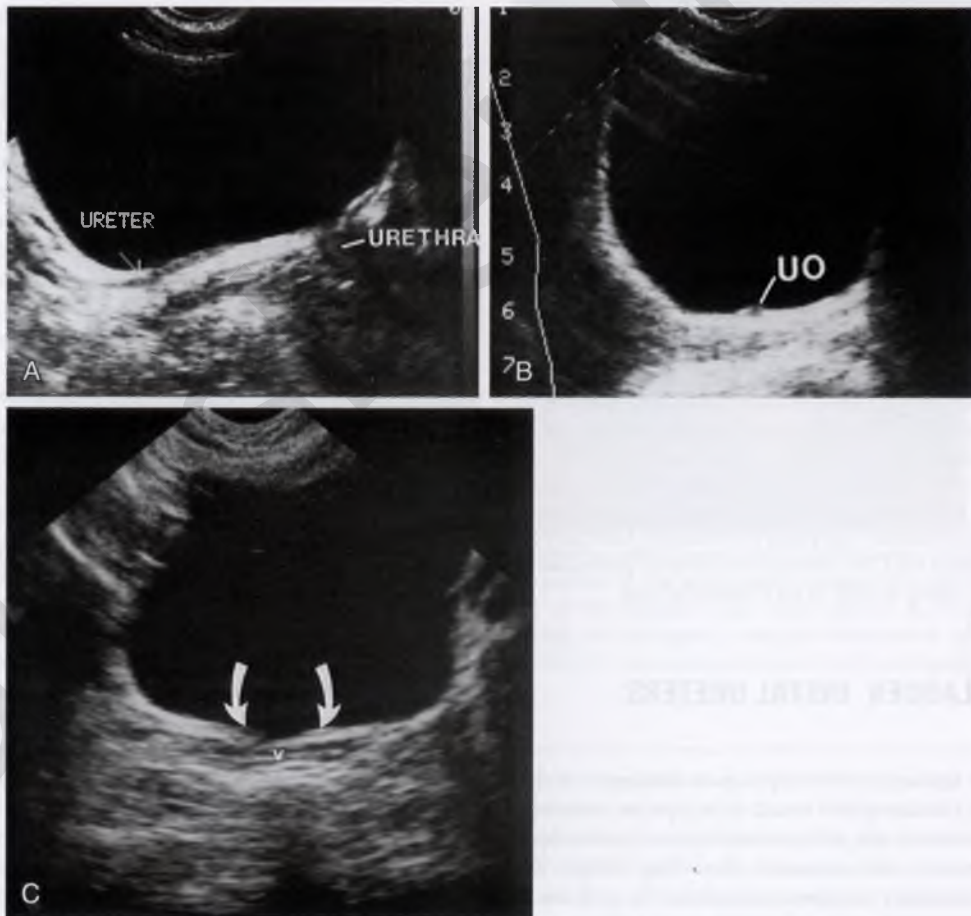


**FIG 26-46** **A**, Longitudinal transabdominal sonogram of the right ureter and urethra. **B**, Longitudinal transabdominal sonogram of the right ureteric orifice (UO). **C**, Transverse transabdominal sonogram of both ureteric orifices (curved arrows). v, vagina.

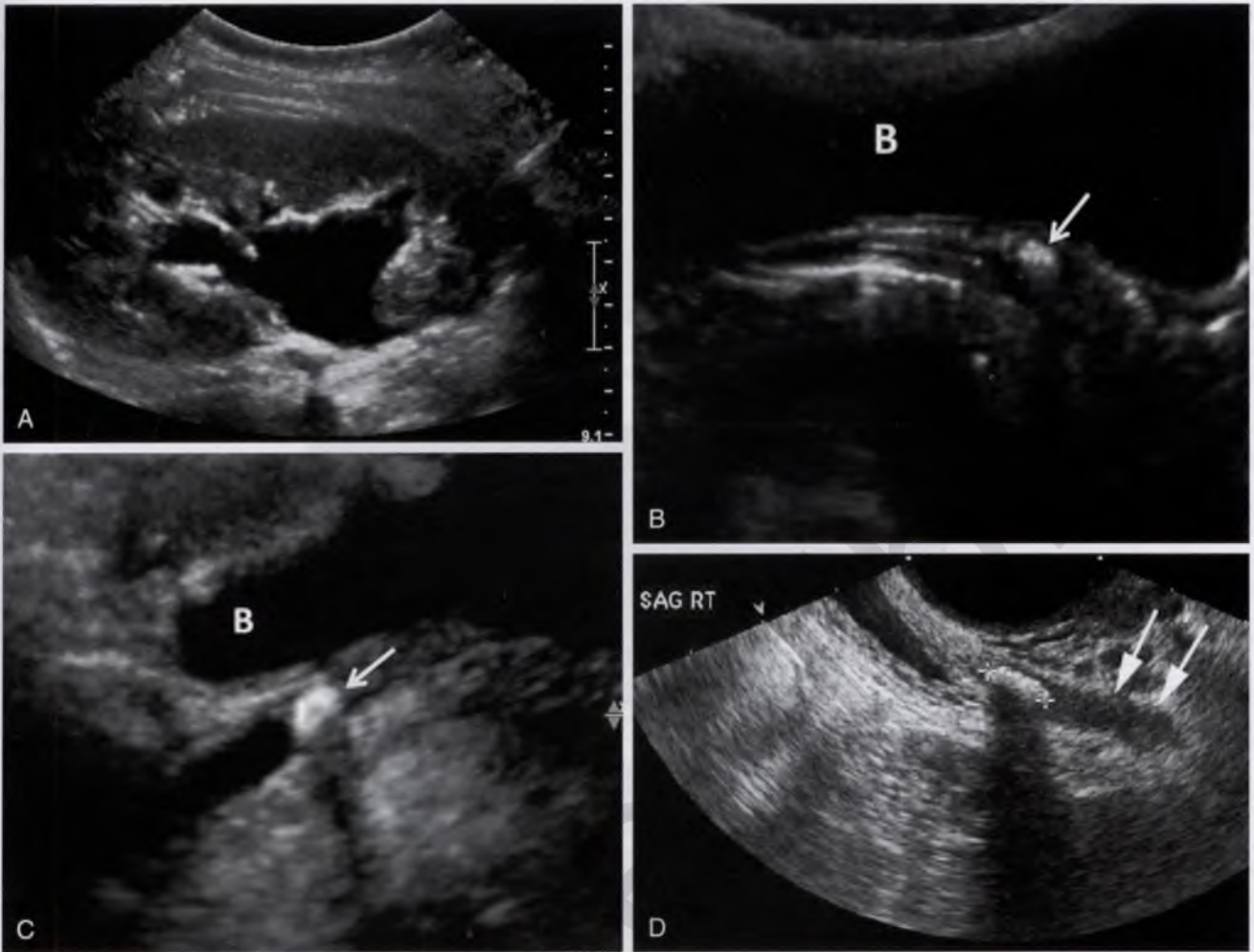


**FIG 26-47** Distal ureteral calculus. **A**, Longitudinal image of the left kidney demonstrates moderate hydronephrosis. **B**, Transverse transabdominal sonogram (TAS) of the urinary bladder shows an echogenic calculus (arrow) in the distal left ureter at the ureterovesicular junction (UVJ) posterior to the bladder (B). **C**, Longitudinal TAS shows the distal left ureteral calculus (arrow) with posterior acoustic shadowing. The distal left ureter is dilated proximal to the calculus. Note how the distal ureter courses ventrally to enter the bladder (B). **D**, Longitudinal transvaginal image in a different patient shows an obstructing ureteral calculus (calipers) at the UVJ that was not evident on TAS. Note the obstructed, dilated ureter (arrows) proximal to the echogenic shadowing calculus.

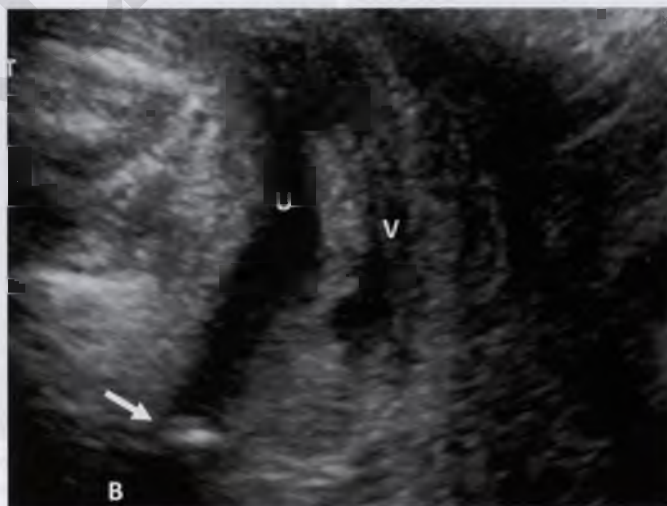


**FIG 26-48** Urethra. Longitudinal image of the urethra obtained with minimal insertion of the probe into the vaginal canal shows the anechoic tubular urethra (U) above the vagina (V). A small air bubble (arrow) is noted in the proximal urethra, just beyond the bladder neck. B, bladder.



either to the left or right before ascending on the left to join the descending colon. The rectum begins at the third sacral vertebra and is fixed in position. The rectosigmoid colon usually contains gas and fecal material that cast an acoustic shadow and may make identification or differentiation from pelvic masses difficult. Often, differentiation between a pelvic mass and the rectosigmoid colon can be made on real-time imaging if peristalsis can be documented or if the characteristic appearance of the bowel wall can be identified (Fig. 26-50). Differentiation between bowel contents and a mass is not usually a problem if the transvaginal approach is used. The sigmoid colon is best imaged with the transvaginal probe directed posteriorly toward the adnexa and gently pushed deeper into the pelvis. The sigmoid colon should be examined if the patient's symptoms cannot be explained by examination of the rest of the pelvic organs.

The pelvic organs can be examined via the transrectal approach in patients for whom a transvaginal scan is not possible. Using a conventional transvaginal probe, one can obtain images of the uterus, ovaries, and adnexa that have superior resolution compared with the transabdominal approach (Fig. 26-51). This technique is not commonly used, but should be considered in the appropriate patient. Verbal consent should be obtained and the probe should be inserted gently using generous lubrication.

## CONCLUSIONS

The sonographic appearance of the female reproductive tract changes dramatically over the course of a lifetime and throughout the menstrual cycle in women of reproductive age. A thorough understanding

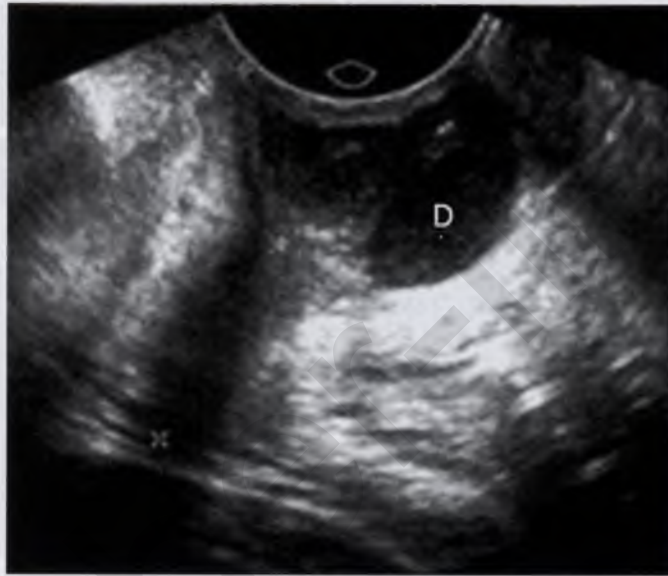


**FIG 26-49** Urethral diverticulum. Longitudinal image obtained with minimal insertion of the probe into the vaginal canal demonstrating a urethral diverticulum (D) containing echogenic fluid and small stones posterior to the urethra (calipers).

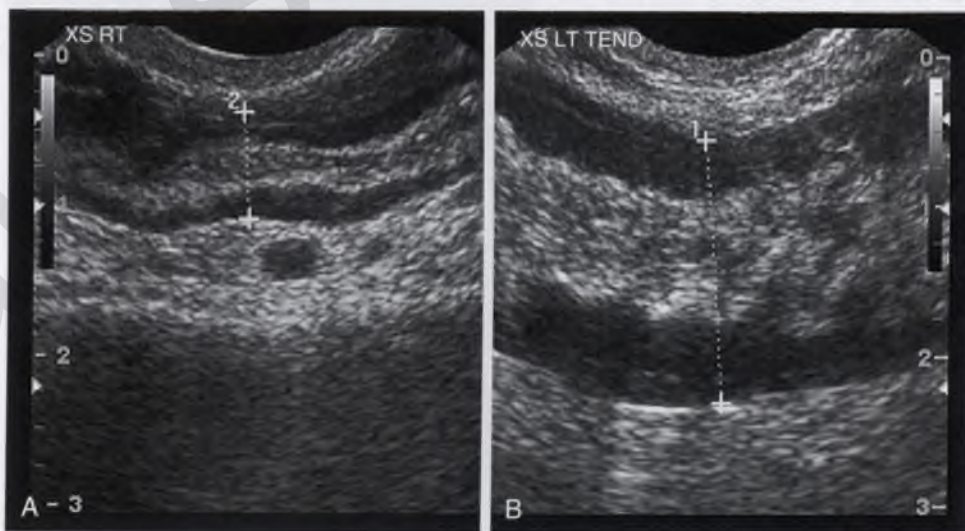


**FIG 26-50** Rectosigmoid colon. **A**, A transverse transvaginal scan through a section of normal sigmoid colon to the right of the midline. The overall thickness is 0.71 mm (calipers 2) compared with the abnormal segment in **B**. **B**, A scan in a similar plane, obtained to the left of the midline showing a thick-walled loop of bowel in a patient with inflammatory bowel disease. The overall thickness is 1.7 cm. The muscularis layer (hypoechoic) and the submucosa (echogenic) are thicker in the abnormal, inflamed segment than in the normal segment. The inflamed segment was also focally tender when compressed with the transvaginal probe.

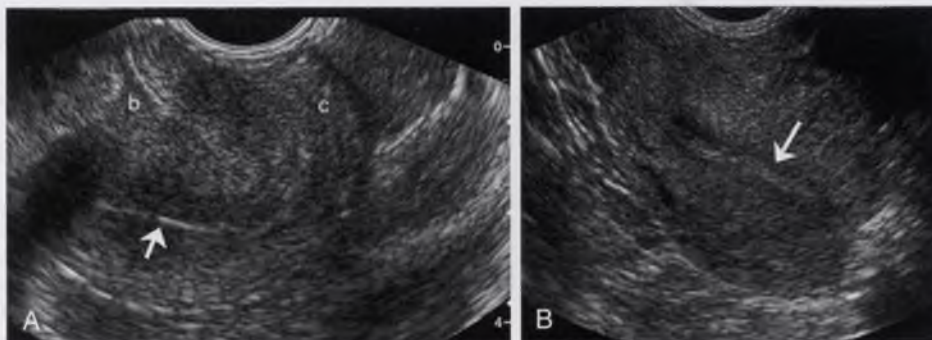


**FIG 26-51** Transrectal scan. Longitudinal transrectal scan of an anteverted uterus (A) and a retroverted uterus (B). The bladder (b) is almost empty. The endometrium (arrows) is thin in both patients. c, cervix.

of how hormonal changes affect the sonographic appearance of the uterus and ovaries is critical in differentiating normal physiologic change from pelvic disease. In addition, the experienced sonographer should be aware of the normal sonographic appearance of surrounding structures as pelvic sonography may be extremely useful in the evaluation of disease affecting the pelvic portions of the urinary system, gastrointestinal tract, and musculoskeletal structures that may mimic gynecologic disease.

## REFERENCES

- American Institute of Ultrasound in Medicine (AIUM); American College of Radiology (ACR); American College of Obstetricians and Gynecologists (ACOG); Society for Pediatric Radiology (SPR); Society of Radiologists in Ultrasound (SRU): AIUM practice guideline for the performance of ultrasound of the female pelvis. *J Ultrasound Med* 33(6):1122–1130, 2014.
- Bohm-Velez M, Mendelson EB: Transvaginal sonography: applications, equipment and technique. In Nyberg DA, Hill LM, Bohm-Velez M, Mendelson EB, editors: *Transvaginal Sonography*, St. Louis, 1992, Mosby, pp 1–20.
- Lyons EA, Gratton D, Hamington C: Transvaginal sonography of normal pelvic anatomy. *Radiol Clin North Am* 30:663–675, 1992.
- Freimanis MG, Jones AF: Transvaginal ultrasound. *Radiol Clin North Am* 30:955–976, 1992.
- Tessler FN, Schiller VL, Perella RR, et al: Transabdominal versus transvaginal pelvic sonography: prospective study. *Radiology* 170:553–556, 1989.
- Mendelson EB, Bohm-Velez M, Joseph N, Neiman HL: Gynecologic imaging: comparison of transabdominal and transvaginal sonography. *Radiology* 166:321–324, 1988.
- Leibman AJ, Kruse B, McSweeney MB: Transvaginal sonography: comparison with transabdominal sonography in the diagnosis of pelvic masses. *AJR Am J Roentgenol* 151:89–92, 1988.
- Coleman BG, Arger PH, Grumbach K, et al: Transvaginal and transabdominal sonography; prospective comparison. *Radiology* 168:639–643, 1988.
- Benacerraf BR, Shipp TD, Bromley B: Is a full urinary bladder still necessary for pelvic sonography? *J Ultrasound Med* 19(4):237–241, 2000.
- Stagno SJ, Forster H, Belinson J: Medical and osteopathic boards' positions on chaperones during gynecologic examinations. *Obstet Gynecol* 94:352–354, 1999.
- Zimmer EZ, Timor-Tritsch IE, Rottem S: The technique of transvaginal sonography. In Timor-Tritsch IE, Rottem S, editors: *Transvaginal Sonography*, ed 2, New York, 1991, Elsevier, p 61.
- Bega G, Lev-Toaff AS, O'Kane P, et al: Three-dimensional ultrasonography in gynecology: technical aspects and clinical applications. *J Ultrasound Med* 22:1249–1269, 2003.
- Lev-Toaff AS, Pinheiro LW, Bega G, et al: Three-dimensional multiplanar sonohysterography: comparison with conventional two-dimensional sonohysterography and x-ray hysterosalpingography. *J Ultrasound Med* 20:295–306, 2001.
- Benacerraf BR, Shipp TD, Bromley B: Which patients benefit from a 3D reconstructed coronal view of the uterus added to standard routine 2D pelvic sonography? *AJR Am J Roentgenol* 190:626–629, 2008.
- Osteology. In Goss CM, editor: *Gray's Anatomy; Anatomy of the Human Body*, ed 29, Philadelphia, 1973, Lea & Febiger, pp 95–286.
- The Urogenital System. In Goss CM, editor: *Gray's Anatomy; Anatomy of the Human Body*, ed 29, Philadelphia, 1973, Lea & Febiger, pp 1265–1339.
- The Arteries. In Goss CM, editor: *Gray's Anatomy; Anatomy of the Human Body*, ed 29, Philadelphia, 1973, Lea & Febiger, pp 561–667.
- Fleischer AC, Kepple DM, Vasquez J: Conventional and colour Doppler transvaginal sonography in gynecologic infertility. *Radiol Clin North Am* 30:693, 1992.
- Schiller VL, Grant EG: Doppler ultrasonography of the pelvis. *Radiol Clin North Am* 30:735, 1992.
- Muscles and fascia. In Goss CM, editor: *Gray's Anatomy; Anatomy of the Human Body*, ed 29, Philadelphia, 1973, Lea & Febiger, pp 371–526.
- Kurjak A, Kupesic S: Ovarian senescence and its significance on uterine and ovarian perfusion. *Fertil Steril* 64:532, 1995.
- Kupesic S, Kurjak A: Uterine and ovarian perfusion during the periovulatory period assessed by transvaginal color Doppler. *Fertil Steril* 60:439, 1993.
- Scoutt LM, Flynn SD, Luthringer DJ, McCarthy SM: Junctional zone of the uterus: correlation of MR imaging and histologic examination of hysterectomy specimens. *Radiology* 179:403–407, 1991.
- Cunningham FG, MacDonald PC, Gant NF, et al: Anatomy of the reproductive tract in women. In Cunningham FG, MacDonald PC, Gant NF, et al, editors: *Williams Obstetrics*, ed 19, Norwalk, CT, 1993, Appleton & Lange, p 57.
- Platt JF, Bree RL, Davidson D: Ultrasound of the normal non-gravid uterus: correlation with gross and histopathology. *J Clin Ultrasound* 18:15–19, 1990.
- Merz E, Mirio-Tesanic D, Bahlmann F, et al: Sonographic size of uterus and ovaries in pre- and postmenopausal women. *Ultrasound Obstet Gynecol* 7:38–42, 1996.
- Miller EI, Thomas RH, Lines P: The atrophic postmenopausal uterus. *J Clin Ultrasound* 5:261–263, 1977.
- Fleischer AC, Kepple DM: Benign conditions of the uterus, cervix and endometrium. In Nyberg DA, Hill LM, Bohm-Velez M, Mendelson EB, editors: *Transvaginal Sonography*, St. Louis, 1992, Mosby, pp 21–41.
- Naftalin J, Jurkovic D: The endometrial-myometrial junction: a fresh look at a busy crossing. *Ultra Obstet Gynecol* 34:1–11, 2009.
- Lyons EA, Taylor PJ, Zheng XH, et al: Characterization of subendometrial myometrial contraction throughout the menstrual cycle in normal fertile women. *Fertil Steril* 55:771–774, 1991.
- Van Gestel I, Ijland MM, Hoogland HJ, Evers JL: Endometrial wave-like activity in the non-pregnant uterus. *Hum Reprod Update* 9(2):131–138, 2003.



32. Templeton A: Transvaginal sonographic assessment of follicular and endometrial growth in spontaneous and clomiphene citrate cycles. *Fertil Steril* 56:208–212, 1991.
33. Bakos O, Lundkvist O, Bergh T: Transvaginal sonographic evaluation of endometrial growth and texture in spontaneous ovulatory cycles—a descriptive study. *Hum Reprod* 8:799–806, 1993.
34. Dickey RP: Ultrasonography of the endometrium. In Rizk B, editor: *Ultrasonography in Reproductive Medicine and Infertility*, New York, 2010, Cambridge University Press, pp 97–102.
35. Fleischer A, Kalemeris G, Machin J, et al: Sonographic depiction of normal and abnormal endometrium with histopathologic correlation. *J Ultrasound Med* 5:445–452, 1986.
36. Bennett GL, Andreotti R, Lee SI, et al: ACR appropriateness criteria on abnormal vaginal bleeding. *J Am Coll Radiol* 8:460–468, 2011.
37. Breijer MC, Peeters JA, Opmeer BC, et al: Capacity of endometrial thickness measurement to diagnose endometrial carcinoma in asymptomatic PM women; a systematic review and meta-analysis. *Ultrasound Obstet Gyneol* 40:621, 2012.
38. Smith Birdman R, Weiss E, Feldstein V: How thick is too thick? When endometrial thickness should prompt biopsy in postmenopausal woman without vaginal bleeding. *Ultrasound Obstet Gyneol* 24:558–565, 2004.
39. Occhipinti K, Kutcher R, Rosenblatt R: Sonographic appearance and significance of arcuate artery calcification. *J Ultrasound Med* 10:97–100, 1991.
40. Aboulghar M, Rizk B: Ultrasonography of the cervix. In Rizk B, editor: *Ultrasonography in Reproductive Medicine and Infertility*, New York, 2010, Cambridge University Press, pp 103–112.
41. Cohen HL, Tice HM, Mandel FS: Ovarian volumes measured by US: bigger than we think. *Radiology* 177:189, 1990.
42. Pavlik EJ, DePriest PD, Gallion HH, et al: Ovarian volume related to age. *Gynecol Oncol* 77:410–412, 2000.
43. Fleischer AC, McKee MS, Gordon AN, et al: Transvaginal sonography of post-menopausal ovaries with pathologic correlation. *J Ultrasound Med* 9:637, 1990.
44. Ritchie WGM: Sonographic evaluation of normal and induced ovulation. *Radiology* 161:1–10, 1986.
45. Brown DL: A practical approach to the ultrasound characterization of adnexal masses. *Ultrasound Q* 23:87–105, 2007.
46. Levine D, Brown DL, Andreotti RF, et al: Management of asymptomatic ovarian and other adnexal cysts imaged at US: Society of Radiologists in Ultrasound Consensus Conference Statement. *Radiology* 256(3):943–954, 2010.
47. Zaidi J, Jurkovic D, Campbell S, et al: Luteinized unruptured follicle: morphology, endocrine function and blood flow changes during the menstrual cycle. *Hum Reprod* 10:44–49, 1995.
48. Brown DL, Frates MC, Muto MG, Welch WR: Small echogenic foci in the ovaries; correlation with sonographic findings. *J Ultrasound Med* 23:307–313, 2004.
49. Aviram R, Gassner G, Markovitch O, et al: Volumes of normal ovaries, ovaries with benign lesions and ovaries with cancer in menopausal women: is there an optimal cut-off value to predict malignancy? *J Clin Ultrasound* 36(1):1–5, 2008.
50. Wolf SI, Gosink BB, Felderson MR, et al: The prevalence of simple adnexal cysts in the postmenopausal woman. *Radiology* 180:65–71, 1991.
51. Greenlee RT, Kessel B, Williams CR, et al: Prevalence, incidence and natural history of simple ovarian cysts among women > 55 years old in a large cancer screening trial. *Am J Obstet Gynecol* 202:373.e1–373.e9, 2010.
52. Moore KL: The urogenital system: the urinary and genital systems. In Moore KL, editor: *The Developing Human*, ed 3, Philadelphia, 1982, WB Saunders, p 255.

# Abnormal Uterine Bleeding: The Role of Ultrasound

Maryam Rezvani, Thomas C. Winter

## SUMMARY OF KEY POINTS

- Abnormal uterine bleeding is most commonly due to dysfunctional anovulatory bleeding in premenopausal women and endometrial atrophy in postmenopausal women.
- Approximately 90% of endometrial cancer occurs after age 50, with the most common symptom being abnormal vaginal bleeding.
- Transvaginal sonography (EVS) is the initial step in the workup of postmenopausal bleeding; however, if the endometrium is not adequately visualized EVS must be followed with biopsy or additional imaging.
- Saline infusion sonohysterography (SIS) is a simple, low-cost, minimally invasive procedure with a high level of diagnostic accuracy.
- SIS is more sensitive than EVS for the detection of focal endometrial abnormalities and rivals hysteroscopy in the identification and characterization of focal lesions.
- SIS can be used to triage patients with abnormal uterine bleeding to the appropriate biopsy technique.
- Tamoxifen, a selective estrogen receptor modulator (SERM), induces endometrial proliferation, which can take the form of hyperplasia, polyp, cancer, or cystic atrophy.

## OUTLINE

### Evolution of Endometrial Assessment, 835

- Transvaginal Sonography, 836
- Saline Infusion Sonohysterography, 836
- Preprocedure Considerations, 837
- Examination Technique, 837
- Challenges, 837

### Abnormal Uterine Bleeding, 838

- Postmenopausal Bleeding, 838
- Premenopausal Bleeding, 839

### Endometrial Pathology, 839

- Endometrial Atrophy, 839
- Endometrial Hyperplasia, 840
- Endometrial Polyps, 840
- Endometrial Carcinoma, 842
- Tamoxifen, 842

### Summary, 844

Abnormal uterine bleeding accounts for up to 20% of all gynecologic visits. Once pregnancy has been excluded, the most likely cause of uterine bleeding in premenopausal women is dysfunctional anovulatory bleeding. However, as women get older, organic pathologic conditions such as endometrial polyps, submucous myomas, endometrial hyperplasia, and even frank endometrial carcinoma become more likely. The Surveillance Epidemiology and End Results (SEER) database reports that the incidence of endometrial carcinoma is 25.1/100,000 women per year.<sup>1</sup> The incidence of endometrial cancer increases with age, with the median age at diagnosis being 62 years.<sup>1</sup> The SEER program reports that 5.6% of new cases occur in women age 35 to 44 years, 18.4% in women age 45 to 54 years, 33.9% in women age 55 to 64 years, 23.4% in women age 65 to 74 years, and 12.6% in women age 75 to 84 years, with the remaining 6.1% at the extremes of the age spectrum.<sup>1</sup> Therefore, in postmenopausal women who are not on hormonal replacement therapy, any vaginal bleeding is considered to be secondary to endometrial cancer until proved otherwise, although the incidence of malignancy in such patients ranges from 2% to 10%, depending upon risk factors.

Nonetheless, the vast majority of patients with abnormal vaginal bleeding will have either dysfunctional uterine bleeding in association with episodes of anovulation that can best be managed hormonally or expectantly with reassurance (premenopausal women), or endometrial atrophy (postmenopausal women). The utility of ultrasound to distinguish such patients from those with organic pathologic conditions in a safe, painless, and convenient manner is clear.

## EVOLUTION OF ENDOMETRIAL ASSESSMENT

Endometrial curettage was first described in 1843, and for many years it was the gold standard for evaluation of the endometrium, becoming the most common hospital-based operation performed on women worldwide. However, in the mid-1900s, it was realized that the technique missed endometrial lesions in approximately 10% of cases; of these, 80% were polyps.<sup>2</sup> In the 1970s, vacuum-suction curettage devices allowed endometrial sampling to be performed without anesthesia in an office setting. Subsequently, cheaper, smaller, and less painful plastic catheters with their own internal pistons to generate



suction became popular (e.g., Pipelle device, Unimar, Wilton, CT). They were found to have similar efficacy but better patient acceptance. Still, the Pipelle catheter was found to sample as little as 4% of the surface area of the endometrium and, therefore, had limited ability to identify malignancy confined to a polyp or localized to less than 50% of the endometrial surface.<sup>3,4</sup> Thus, focal endometrial abnormalities such as polyps, focal hyperplasia, or carcinoma involving small areas of the uterine cavity may go undetected with undirected endometrial sampling, whether by curettage or various types of suction aspirations.

### Transvaginal Sonography

Pelvic sonography is considered the first-line imaging modality of the uterus. Transabdominal imaging can be helpful in the setting of large leiomyomas or a globally enlarged uterus. However, the mainstay of endometrial evaluation is transvaginal sonography (EVS) with higher frequency transducers and, hence, better resolution. In premenopausal women, the examination should be performed early in the proliferative phase at about days 4 through 6 of the menstrual cycle. Postmenopausal women can be examined any time unless they are on cyclic hormone replacement, in which case imaging should be performed about 5 to 10 days after the last progestin tablet.<sup>5</sup>

The endometrium should be evaluated in both the sagittal and transverse planes. Measurement of endometrial thickness is obtained in the midline sagittal plane perpendicular to the long axis of the endometrium at the site of maximal thickness. By convention, endometrial thickness is measured to include both the anterior and posterior layers (double layer thickness) (Fig. 27-1).<sup>5</sup> Fluid in the endometrial cavity should not be included in the measurement; rather, the single layer thickness of the anterior plus the posterior layer of the endometrium should be measured and summed. If the endometrium is not adequately visualized in its entirety, it should be reported as nonmeasurable and incompletely visualized. Poor visualization of the endometrium has been reported in 10% to 24% of cases and may be due to uterine position, distortion by leiomyomas or adenomyosis, or distortion of the endometrial-myometrial interface from endometrial carcinoma.<sup>5,6</sup>

In the setting of intracavitary disease, the endometrial thickness measurement should include the lesion.<sup>5</sup> A three-dimensional (3D) coronal view of the uterus has been found to be a useful adjunct to two-dimensional (2D) sonography in patients with suspected

endometrial abnormalities (Fig. 27-2). One study reported that additional information was obtained from the 3D coronal reconstruction in 39% of patients with an endometrial thickness of 5 mm or more.<sup>7</sup> The presence and location of leiomyomas were more confidently diagnosed, in particular those in a submucosal location.<sup>7</sup> Intracavitary fluid is quantified by measuring its maximal thickness in the sagittal plane.<sup>5</sup>

### Saline Infusion Sonohysterography

Sonohysterography, hysterosonography, EVS with fluid contrast augmentation, saline-infused sonography, and saline infusion sonohysterography (SIS) are the many appellations used to describe the instillation of sterile saline into the endometrial cavity during EVS to better evaluate the endometrium and fallopian tubes. Echogenic contrast agents such as air bubbles may be used, especially when evaluating

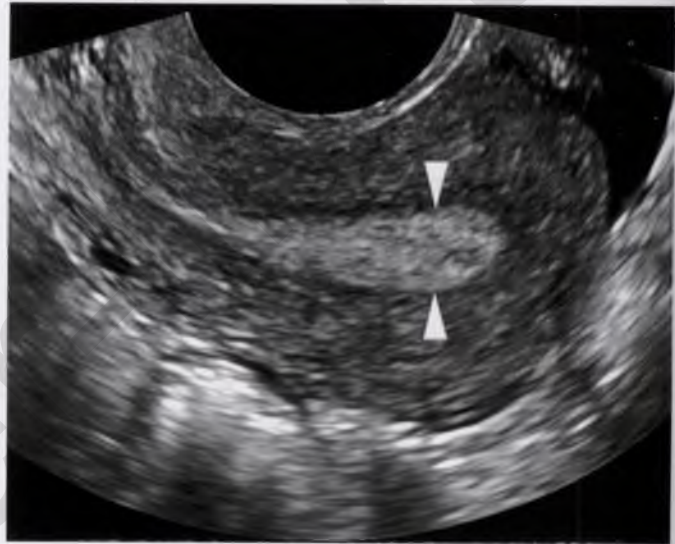


**FIG 27-1** A 25-year-old woman referred for sonographic evaluation for oligomenorrhea. Longitudinal transvaginal sonographic image of the retroverted uterus shows a normal homogeneous endometrial echo complex measuring 8 mm in thickness. Standard measurement of the endometrium is performed at its thickest part (arrowheads) in the mid-sagittal plane.

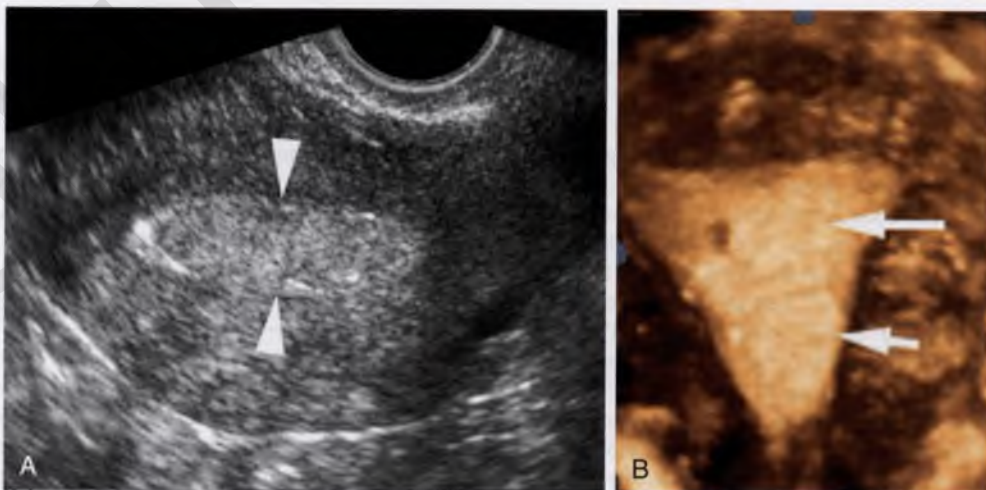


**FIG 27-2** A 62-year-old woman with postmenopausal bleeding. **A**, Transvaginal sonography shows homogeneous echogenic thickening of the endometrial echo complex (arrowheads). **B**, Coronal three-dimensional image shows two subtle hyperechoic intracavitary masses (arrows). The additional information allowed triage to hysteroscopically guided biopsy and removal, confirming endometrial polyps.



for patency of the fallopian tubes. An examination performed with particular attention to the fallopian tubes is known as *sonosalpingography*. SIS is a simple, low cost, minimally invasive procedure with a high level of diagnostic accuracy. Specific advantages over hysterosalpingography are the lack of ionizing radiation and the ability to more accurately characterize masses in the endometrial cavity.<sup>8</sup>

### Preprocedure Considerations

The SIS examination should be scheduled close to days 4 through 7 of the menstrual cycle in premenopausal women to decrease the possibility of false positive results because of the common normal irregularity and increased thickness of the secretory phase endometrium,<sup>9</sup> as well as to avoid the possibility of performing the examination in a pregnant patient. However, in a patient with dysfunctional uterine bleeding it may not be possible to optimally time the examination. In these patients, a course of medroxyprogesterone acetate 10 mg daily for 10 days may be considered with the procedure timed to the withdrawal bleeding. The SIS patient should be advised to take a nonsteroidal anti-inflammatory drug (NSAID) approximately 30 minutes prior to her procedure to reduce discomfort. If this has not been done, an NSAID can be administered and the examination delayed by 30 minutes. The benefits of premedication outweigh the short delay. Prophylactic antibiotics may be prescribed if pelvic inflammatory disease is suspected or if the patient requires systemic prophylaxis for bacterial endocarditis.<sup>8</sup>

### Examination Technique

A calm, quietly confident demeanor and the use of familiar language without negative connotations can be very helpful in overcoming patient apprehension about the procedure.<sup>10</sup> Including a female attendant in the room regardless of physician gender is recommended. Written informed consent is obtained from the patient, at which time the procedure is explained to the patient and all her questions are answered. Preparing patients for the possibility of cramping during speculum and catheter placement improves their tolerance of any discomfort.<sup>8</sup>

The urinary bladder should be emptied before proceeding in order to optimize patient comfort and image quality. The examination is performed with the patient in the lithotomy position with the buttocks positioned past the edge of the table. Elevation of the pelvis with a pillow or by having the patient place her hands under her hips can improve the angle of the vaginal vault, making the pelvis more accessible. Avoiding sudden movements and unnecessary noise as well as keeping instruments out of the patient's view will help to maintain a calm atmosphere. Initial physical examination should be performed to exclude genital inflammation, determine the position of the cervix, and estimate the appropriate size and type of speculum to be used. A warm speculum is placed in the vagina to localize the cervix, which is then cleansed with antiseptic solution. Abdominal pressure on the uterus just above the pubic symphysis may help bring a posterior cervix into view. A variety of catheters may be employed to infuse fluid, but we will describe one of the easiest systems for the beginner, the dedicated balloon-tipped catheter.<sup>11</sup> Before inserting the catheter, the lumen should be flushed with saline to remove all air. The catheter is then passed into the uterine cavity past the internal os (Fig. 27-3) but with care not to touch the fundus, which can cause pain and elicit a vasovagal response. As much air as possible should be removed from the balloon, which is then filled with saline; otherwise posterior structures will be obscured by shadowing from air in the balloon. With experience, the balloon may be inflated within the cervix itself to decrease pain and to successfully perform studies in which one is unable to pass the catheter all the way through the cervix into the endometrial cavity.<sup>12</sup> The speculum is carefully removed without dislodging the catheter.

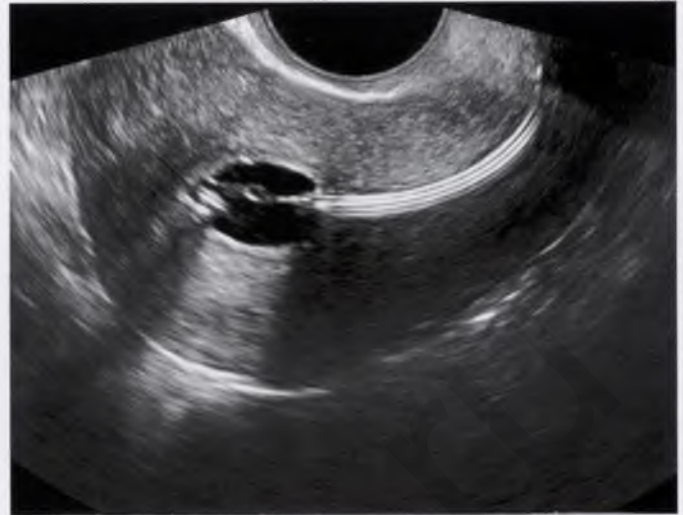


**FIG 27-3** A 28-year-old woman with menorrhagia. Longitudinal transvaginal sonography of the uterus obtained during a normal saline infusion sonohysterographic examination shows insertion of the catheter and inflation of the balloon just past the internal cervical os. The balloon is inflated with saline to avoid shadowing and obscuration of the posterior uterine wall by gas.



**FIG 27-4** A 33-year-old woman with menometrorrhagia actively bleeding at the time of the examination. Longitudinal transvaginal sonography of the retroverted uterus obtained during saline infusion sonohysterography shows the balloon (arrowhead) dislodging echogenic clot (arrow) in the endometrial cavity.

The vaginal transducer is introduced and positioned for longitudinal imaging of the uterus. The uterine cavity is distended with sterile saline under direct visualization. A slow rate of saline infusion will reduce cramping. Once adequate distention is achieved, multiplanar 2D EVS, with Doppler interrogation if necessary, as well as a 3D volume acquisition of the uterus is performed. Once the upper uterus has been satisfactorily evaluated, the balloon is deflated and additional sterile saline injected for evaluation of the lower uterine segment.<sup>8</sup>

### Challenges

Blood in the endometrial cavity may cause confusion. Direct visualization of the cavity during gentle catheter manipulation and saline flushes can be helpful in differentiating mobile blood products (Fig. 27-4) from a true endometrial abnormality. Both the stenotic and



patulous cervix can be a challenge. Cervical stenosis may be encountered in a nulliparous patient, a patient who has previously had cone biopsies or loop electrosurgical excision procedure, or in perimenopausal and postmenopausal patients.<sup>8</sup> A metal stilet introduced through the catheter may increase stiffness sufficiently to allow passage of the catheter into the uterine cavity. Alternatively, a small diameter sound may be used to probe the cervix, determine cervical orientation, straighten the cervix, and remove adhesions. Although not routinely used while performing SIS, a single tooth tenaculum may be used at the 12 o'clock position if the uterus is markedly flexed to put gentle traction on the cervix and straighten the uterus, allowing passage of the catheter.<sup>8</sup> If a tenaculum is used, the speculum should be replaced at the conclusion of the procedure to check for cervical bleeding. The uterine cavity may be difficult to distend if fluid escapes via a patulous cervix or patent fallopian tubes. Appropriate catheter position should be confirmed, and slow injection of saline with minimal pressure may help reduce spillage from the fallopian tubes. A balloon system or 8-Fr pediatric Foley catheter should be used if the cervix is incompetent or patulous.<sup>8</sup> Although there are theoretical concerns regarding the possibility of spreading adenocarcinoma into the peritoneal cavity or in causing endometriosis with SIS, neither of these considerations has proved to be relevant in practice.<sup>13-15</sup>

as bleeding that occurs outside the expected window in women on sequential hormone replacement therapy (HRT) or any bleeding in a postmenopausal woman not on HRT.<sup>16</sup> Most common are benign causes, including endometrial atrophy, polyps, hyperplasia, and uterine leiomyomas. However, approximately 7% to 14% of women with postmenopausal bleeding will have endometrial cancer (range 1-25% depending on age and risk factors; see later discussion).<sup>16,17</sup> Women with recurrent bleeding are a particularly high-risk group.<sup>18</sup> Furthermore, more than 90% of endometrial cancer occurs after age 50, with the most common symptom by far being abnormal vaginal bleeding.<sup>16</sup> This statistic alone warrants evaluation of all women with postmenopausal bleeding.

Following clinical evaluation, EVS is the initial step in the workup of a postmenopausal woman with abnormal bleeding (Fig. 27-5). Ultrasound is better tolerated and more often diagnostic (>95%) compared with endometrial biopsy (EMB). The false negative rate for endometrial cancer following in-office biopsy is 5% to 15%; the rate can be reduced to 2% to 6% but only if dilation and curettage (D&C) is performed.<sup>17</sup> Even with D&C, only 60% of the endometrium may be sampled and focal lesions may be missed.<sup>19</sup> Up to 28% of endometrial biopsies may be nondiagnostic or insufficient.<sup>17</sup> Cervical stenosis and patient intolerance may prevent EMB, and even when technically successful, an inadequate specimen may be obtained in 5% to 15% of patients.<sup>16</sup> Blind biopsy is further limited by its decreased sensitivity for focal endometrial abnormalities. Although reliable for the detection of endometrial cancer occupying more than 50% of the uterine cavity, EMB can miss up to 33% of malignancies occupying a smaller area.<sup>4</sup> Unfortunately, just under half of endometrial cancers have been reported to occupy more than 50% of the uterine cavity.<sup>4,20</sup>

## ABNORMAL UTERINE BLEEDING

### Postmenopausal Bleeding

Postmenopausal vaginal bleeding is extremely common and is estimated to occur in up to 55% of postmenopausal women. The Society of Radiologists in Ultrasound (SRU) defines postmenopausal bleeding

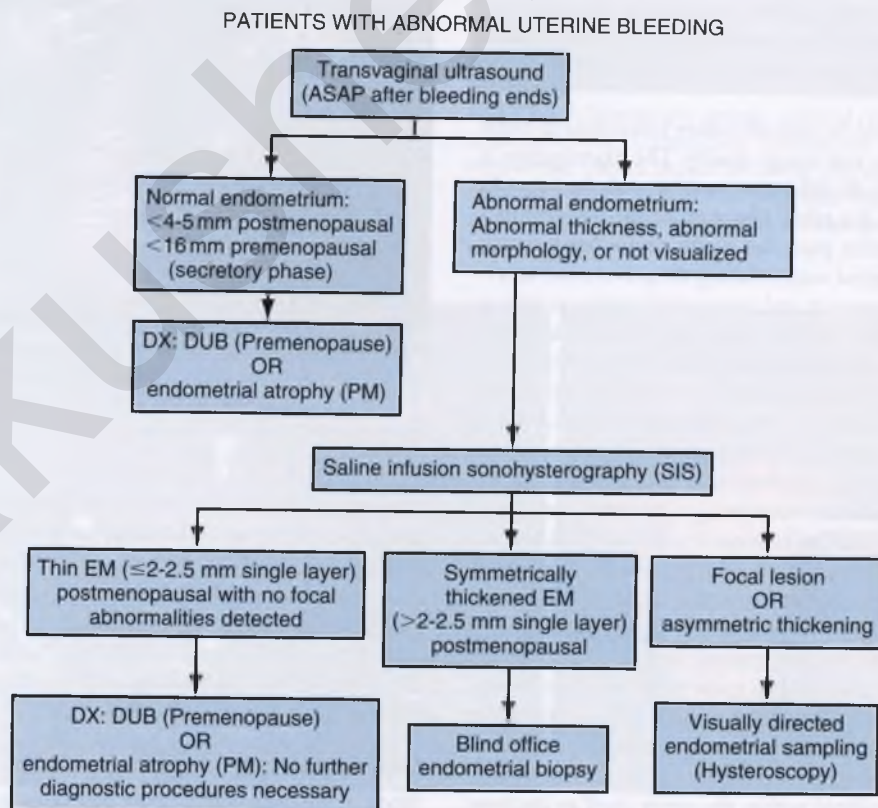


**FIG 27-5** Algorithm for evaluation and management of patients with abnormal uterine bleeding. ASAP, as soon as possible; DUB, dysfunctional uterine bleeding; DX, diagnosis; EM, endometrium; PM, postmenopausal; SIS, saline-infused sonohysterogram.



Endometrial carcinoma is rare when the endometrium is adequately visualized, thin, and homogeneous on EVS. In fact, when the endometrial thickness measures less than 4 to 5 mm on EVS, the negative predictive value for endometrial carcinoma is 99% to 100% if the endometrium is adequately visualized in its entirety. In such patients, the cause of vaginal bleeding is most likely endometrial atrophy, and no further evaluation is needed with either biopsy or additional imaging unless symptoms persist or worsen. The SRU consensus statement recommends using an endometrial thickness threshold of 5 mm or less, whereas the ACOG (American College of Obstetricians and Gynecologists) committee opinion is that the threshold should be 4 mm or less.<sup>21,22</sup> Both societies recommend reporting the endometrium thickness on EVS as a double thickness measurement of the thickest segment of the endometrial echo complex (usually in the fundus) obtained in the midline sagittal plane and agree that further evaluation is necessary if the complex is indistinct, heterogeneous, or focally thickened. Nondiagnostic transvaginal studies occur in 2.8% to 10% of patients and are likely because of factors such as the orientation of the uterus, prior surgery, obesity, and coexisting adenomyosis or leiomyomas.<sup>20,23</sup> Alternative evaluation should be performed if the endometrium is not visualized in its entirety, given the 15% incidence of endometrial cancer in this patient population.<sup>23</sup>

Approximately 50% of cases of premenopausal and postmenopausal abnormal uterine bleeding are caused by focal abnormalities of the endometrium.<sup>24</sup> SIS is more sensitive than EVS for the detection of focal endometrial abnormalities and rivals hysteroscopy in the identification and characterization of focal lesions.<sup>24,25</sup> Furthermore, SIS can be used to triage patients with abnormal uterine bleeding to the appropriate biopsy technique. EMB or D&C is considered adequate for evaluation of a diffuse process, whereas hysteroscopy is recommended for focal abnormalities due to the risk of sampling error with EMB and D&C for focal disease as described previously. Because of the increased sensitivity of SIS for the detection of focal endometrial abnormalities, it may also be helpful in the case of discordant EVS and EMB results. One study found that 14% of patients with abnormal vaginal bleeding had abnormalities on SIS despite a normal appearance of the endometrium on EVS.<sup>26</sup>

When using an endometrial thickness threshold of 5 mm, the sensitivity of EVS for endometrial cancer is 96%, with the positive predictive value increasing as the thickness of the endometrium increases.<sup>16-18</sup> This compares with a sensitivity of greater than 85% for EMB.<sup>16</sup> If the threshold for endometrial thickness is decreased to 4 mm, there is no significant change in the sensitivity of EVS for detecting endometrial cancer. However, specificity decreases and there will be more false positive diagnoses.<sup>16</sup> However, this opinion was not uniformly shared by all participants at the SRU consensus panel on postmenopausal bleeding, with the dissenters recommending 4 mm as a threshold.<sup>22</sup> All agree that the use of HRT increases the false positive rate at either threshold.

Although much energy has been devoted to determining the threshold endometrial thickness in a postmenopausal woman with vaginal bleeding, there is no consensus on the normal endometrial thickness in a postmenopausal woman without vaginal bleeding. However, the latter scenario is not infrequently encountered due to the widespread use of EVS for evaluation of the female pelvis. If the threshold of greater than 5 mm that is recommended by the SRU for women with postmenopausal vaginal bleeding is applied to asymptomatic women, the false positive rate and consequently the number of biopsies performed in normal women would be unacceptable.<sup>27</sup> Although there is no standardized cutoff for endometrial thickness in a postmenopausal woman without vaginal bleeding, all agree it should be higher than 5 mm in this patient population with low pretest probability of endometrial cancer.<sup>21</sup>

When applying a decision analysis approach to determine the endometrial thickness in asymptomatic postmenopausal women at which the risk of endometrial cancer approaches that of symptomatic postmenopausal women with vaginal bleeding and an endometrial thickness more than 5 mm, the result has been reported to be over 11 mm.<sup>28</sup> An endometrial thickness over 11 mm in an asymptomatic postmenopausal woman carries an endometrial cancer risk of 6.7%, comparable to that of 7.3% in a postmenopausal woman with vaginal bleeding and an endometrial thickness greater than 5 mm.<sup>28</sup> This threshold would result in biopsy of only 0.25% of women to detect 87% of occult endometrial cancers.<sup>28</sup> For the more conservative endometrial thickness threshold of 4 mm recommended by ACOG for symptomatic postmenopausal women, the corresponding normal endometrial thickness in asymptomatic postmenopausal women is considered to be less than 10 mm, with an endometrial thickness more than 10 mm in an asymptomatic postmenopausal woman carrying a 5.8% risk of endometrial cancer.<sup>28</sup>

EVS is not recommended as a screening tool for endometrial cancer in asymptomatic postmenopausal women, but this analysis provides some guidance on how to manage the thickened endometrium incidentally observed in a postmenopausal woman without bleeding on an ultrasound scan performed for other reasons. However, the decision to biopsy the endometrium will no doubt include overall assessment of the patient, including risk factors for endometrial cancer.

### Premenopausal Bleeding

Dysfunctional uterine bleeding in a nonpregnant premenopausal woman occurs as menorrhagia, metrorrhagia, or menometrorrhagia. There is no widely accepted threshold for abnormal endometrial thickness in premenopausal women, although typically diffuse homogeneous thickening greater than 16 mm in the secretory phase is used (there is no accepted threshold value in the proliferative phase). However, a thickened endometrium in the late secretory phase of the menstrual cycle is often normal, so routine studies ideally should be performed in the early proliferative phase to minimize false positive results. The sensitivity and specificity of EVS for detecting endometrial disease in the premenopausal population using a cutoff value of more than 16 mm are not optimal at 67% and 75%, respectively.<sup>29,30</sup> In the setting of a diffusely thickened endometrium or persistent bleeding unresponsive to hormonal therapy, SIS is indicated because of its ability to detect abnormalities in patients with normal EVS and to differentiate focal from diffuse processes, allowing triage to the appropriate biopsy technique.<sup>26</sup> Focal abnormalities such as asymmetric thickening, cystic change, and the hyperechoic line sign should be further evaluated regardless of endometrial thickness and be triaged to hysteroscopy for direct visualization and biopsy.<sup>19</sup> The hyperechoic line sign is indicative of a focal intracavitary process and is thought to represent the echogenic endometrium abutting the intracavitary mass or the interface between the mass and surrounding endometrium. Overall, SIS is better tolerated and more often technically successful in premenopausal women than in postmenopausal women.<sup>34</sup>

## ENDOMETRIAL PATHOLOGY

### Endometrial Atrophy

Endometrial atrophy is the most common cause of postmenopausal bleeding, representing 50% to 75% of cases.<sup>31</sup> Atrophy of the functional, more superficial, layer of the endometrium occurs in response to a prolonged hypoestrogenic state. Only a thin basalis layer remains at the endometrial/myometrial junction, leaving the underlying myometrial vessels exposed. Menopause is the most common cause of endometrial atrophy; other causes include prolonged oral contraception.



EVS typically demonstrates a thin uniform endometrium measuring less than 5 mm (Fig. 27-6). There may be cystic dilatation of the endometrial glands that may cause pseudo-widening of the endometrium, an appearance often seen in women taking tamoxifen (see later). The single layer thickness of the endometrium should be less than 2.5 mm on SIS in patients with endometrial atrophy without areas of focal thickening or irregularity.

### Endometrial Hyperplasia

Endometrial hyperplasia accounts for 4% to 8% of cases of postmenopausal bleeding.<sup>32</sup> Unopposed estrogen stimulation leads to a proliferation of endometrial glands. Unlike normal proliferative phase endometrium, there is a higher gland-to-stroma ratio and the glands are irregular in size and shape.<sup>33</sup> Endometrial hyperplasia can be seen with chronic anovulatory states, unopposed exogenous estrogen exposure, tamoxifen use, obesity, and estrogen-secreting ovarian tumors.<sup>32</sup> There are four categories of endometrial hyperplasia based on the glandular and stromal architecture and the presence of nuclear atypia. The presence of nuclear atypia in the hyperplastic endometrium increases the risk of coexisting foci of endometrial carcinoma and the future development of malignancy. The incidence of endometrial cancer in simple hyperplasia without atypia is 1%, and in simple atypical hyperplasia it is 8%.<sup>33</sup> Complex hyperplasia without atypia has a cancer incidence of 3%, whereas complex atypical hyperplasia has a cancer incidence of 29%.<sup>33</sup> Unfortunately, the pathologic diagnosis of atypia is not easy and has a low level of interobserver agreement. Often women with atypical hyperplasia have coexistent foci of endometrial carcinoma. Up to one third of cases of endometrial cancer are preceded by hyperplasia.<sup>33</sup>

In patients with endometrial hyperplasia, ultrasound demonstrates thickening of the endometrial echo complex, which is typically diffuse, echogenic, and homogeneous, with a well-defined myometrial interface (Fig. 27-7). There may be foci of cystic change, which correspond to dilated endometrial glands (Fig. 27-8). Focal endometrial thickening (Fig. 27-9) and areas of heterogeneity are less common and better demonstrated with SIS. Generally accepted thresholds for abnormal endometrial thickening are greater than 5 mm for postmenopausal

women not on HRT and more than 16 mm for premenopausal women in the secretory phase of the menstrual cycle, although there is some controversy over these numbers, as discussed earlier. Additionally, focal endometrial thickening or heterogeneity is considered abnormal even if below these thresholds for endometrial thickening.

### Endometrial Polyps

Endometrial polyps are hyperplastic growths consisting of dense fibrous tissue or smooth muscle with disorganized endometrial glands. Polyps can be asymptomatic or cause dysfunctional uterine bleeding in premenopausal women and account for up to 30% of postmenopausal bleeding.<sup>32</sup> Polyps may spontaneously resolve, particularly when small (<1 cm) and occurring in asymptomatic postmenopausal women.<sup>34</sup> Polyps can be hyperplastic, atrophic, or rarely, functional.



**FIG 27-7** A 32-year-old woman with bleeding and cramping. Longitudinal transvaginal sonography of the uterus obtained during saline infusion sonohysterogram demonstrates diffuse thickening of the endometrium (arrowheads) consistent with endometrial hyperplasia.

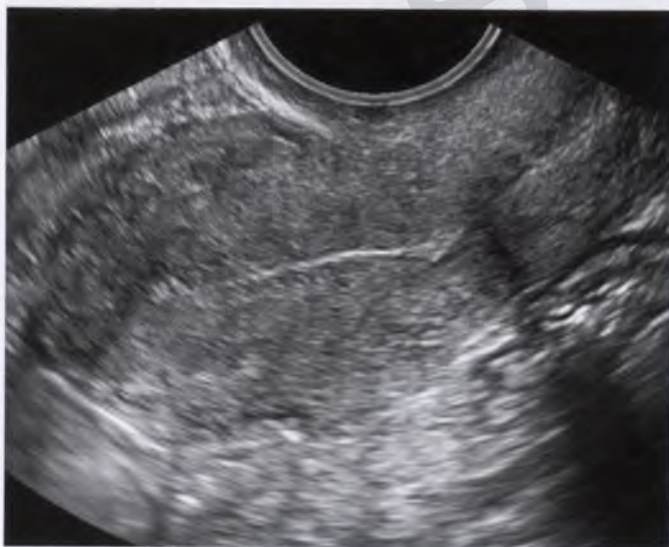


**FIG 27-6** Longitudinal transvaginal sonography of the uterus shows a uniformly thin endometrial stripe measuring 1 mm in thickness. When adequately visualized, a thin endometrium less than 4 to 5 mm essentially excludes malignancy in a postmenopausal woman with vaginal bleeding.

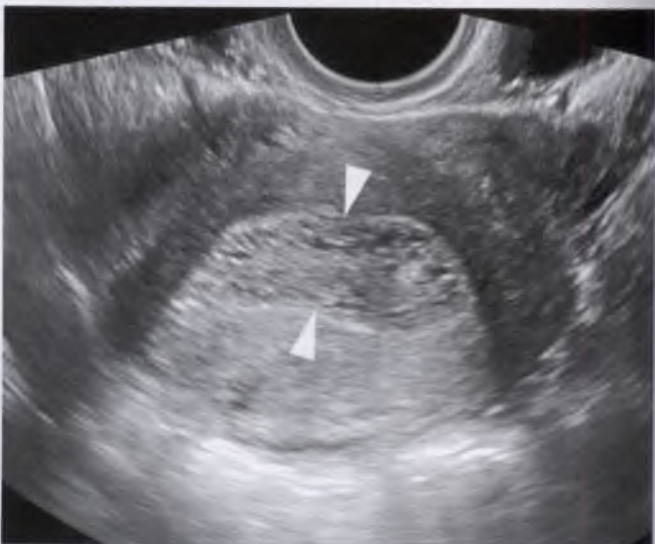


**FIG 27-8** A 41-year-old woman with menorrhagia. Transverse transvaginal sonography shows diffuse thickening of the endometrium (arrowheads) with internal areas of cystic change resulting in the typical "swiss cheese" appearance of endometrial hyperplasia.



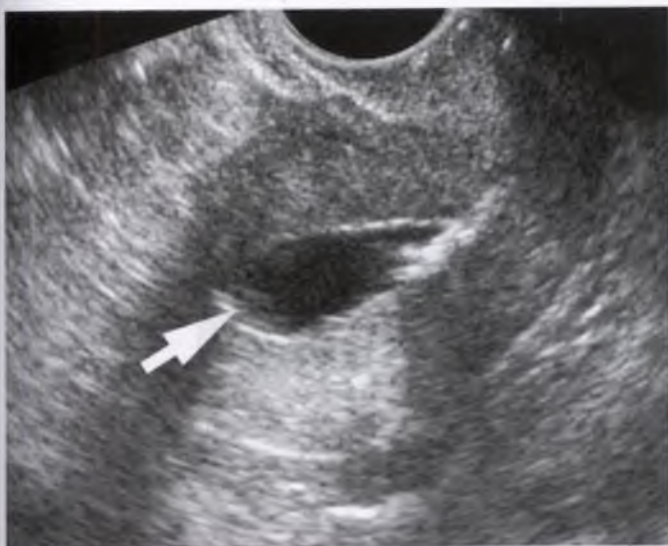


**FIG 27-9** A 57-year-old woman with postmenopausal bleeding and transvaginal sonography (EVS) showing a possible endometrial polyp, later shown to be endometrial hyperplasia at hysteroscopy. Longitudinal EVS of the uterus obtained during saline infusion sonohysterography demonstrates plaque-like focal thickening (arrow) of the fundal endometrium with internal cystic change.

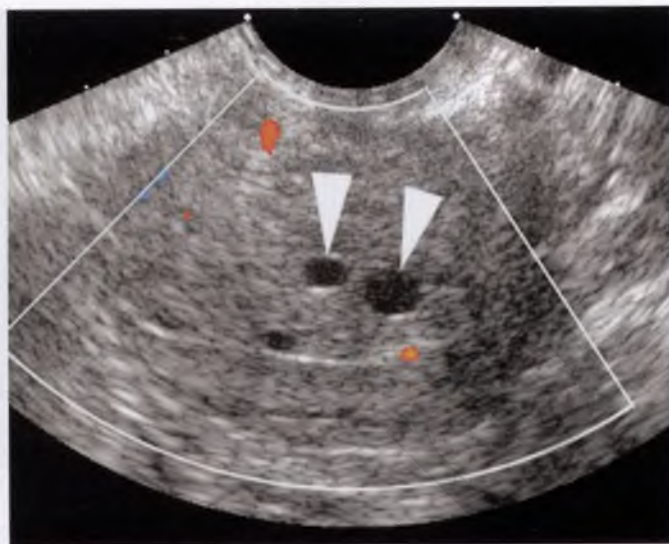


**FIG 27-10** A 57-year-old woman with postmenopausal bleeding and negative endometrial biopsy. Transverse color Doppler image of the uterus shows endometrial thickening with several anechoic internal cysts (arrowheads) corresponding to dilated endometrial glands in a polyp. Hysterectomy confirmed a 2-cm endometrial polyp attached to the right uterine cornu. Endometrial biopsy is unreliable for detection of focal endometrial disease, thus making sonographic evaluation an essential part of the workup of postmenopausal bleeding.

Atrophic polyps occur in postmenopausal women and are composed of atrophic but dilated glands. Rarely endometrial polyps harbor atypia (3.1-4.7%) or foci of malignancy (0.8-1.4%). The likelihood of neoplastic polyps is higher in women with symptomatic bleeding and in those who are postmenopausal.<sup>34</sup> Although 8% to 36% of postmenopausal women on tamoxifen develop endometrial polyps, it is unclear whether there is an associated increased risk of malignancy.<sup>34</sup> Endometrial polyps can be sessile or pedunculated, are multiple in 20% of women, and are reported to range from 1 mm to a few centimeters in size. Women on tamoxifen tend to have larger and multiple polyps. Large size is defined as greater than 1 cm, and a polyp is considered pedunculated if the maximum transverse diameter of the lesion is larger than its diameter at the level of the endometrium.<sup>5,34</sup> Pedunculated polyps have a vascular fibrous stalk. They most commonly arise in the uterine cornua or fundus and rarely can prolapse through the cervix. Intralesional cysts represent dilated endometrial glands.

Ultrasound demonstrates diffuse or focal echogenic thickening of the endometrial echo complex.<sup>35</sup> One study found 79% of polyps to be hyperechoic, with the remainder having variable echogenicity, and 59% will have internal cystic spaces<sup>19</sup> (Fig. 27-10). The endometrial-myometrial interface is typically intact, with the polyp forming an acute angle with the endometrium.<sup>35</sup> Color Doppler imaging can be helpful by demonstrating the vascular pedicle (Fig. 27-11), seen in just under half of polyps.<sup>35</sup> A single feeding artery is typically seen in functional polyps, whereas half of polyps, usually the atrophic type, show no flow on color Doppler imaging.

SIS is particularly helpful in demonstrating focal endometrial lesions with an otherwise normal endometrial thickness elsewhere in the uterine cavity, whereas diffuse endometrial thickening on EVS is nonspecific and may be caused by focal lesions as well as by diffuse disease (Fig. 27-12). The majority of polyps have a narrow attachment to the endometrium, although less commonly they may be sessile or broad-based (Fig. 27-13).<sup>19</sup> SIS is useful not only for triaging patients with endometrial thickening seen on EVS to hysteroscopically guided

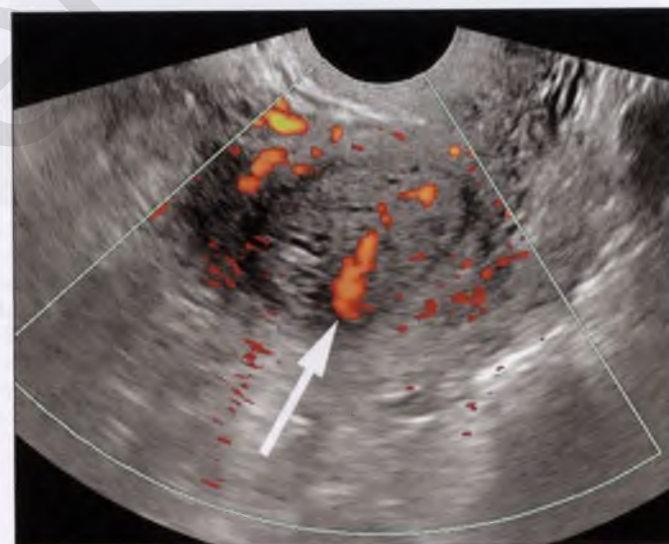


**FIG 27-11** A 68-year-old woman with postmenopausal bleeding. Transverse power Doppler image of the uterus shows cystic endometrial thickening with a single vascular pedicle (arrow) consistent with a focal abnormality, specifically an endometrial polyp. As is often the case with focal endometrial abnormalities, blind endometrial biopsy was negative, but a benign polyp was diagnosed on hysteroscopic polypectomy.

biopsy for removal of focal endometrial abnormalities but also for differentiating endometrial from myometrial lesions such as submucosal leiomyomas (Fig. 27-14).<sup>32</sup> The broad attachment to the myometrium and the intact overlying rim of endometrium help to distinguish submucosal leiomyomas from other focal endometrial processes.<sup>19</sup> Leiomyomas are also more likely to be hypoechoic compared to the endometrium as well as to the myometrium.



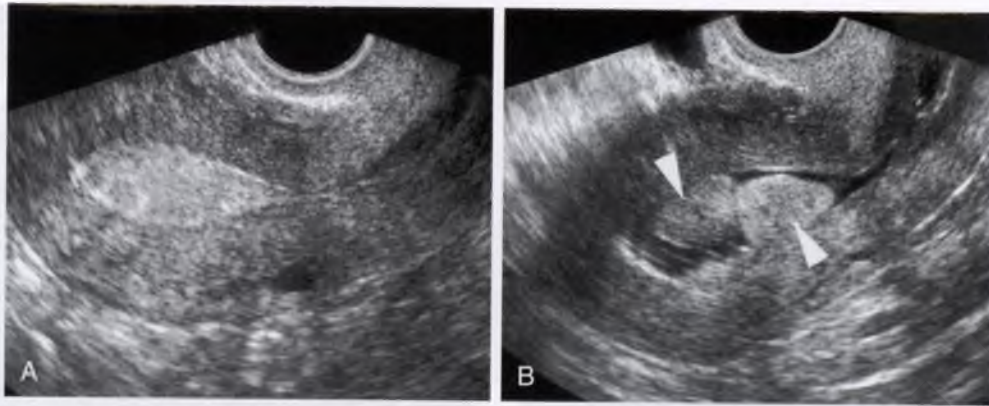


**FIG 27-12** A 62-year-old woman with postmenopausal bleeding. **A**, Transvaginal longitudinal ultrasound image of the uterus shows diffuse echogenic thickening of the endometrium. **B**, Longitudinal saline infusion sonohysterography (SIS) shows two echogenic polypoid masses (*arrowheads*) with otherwise normal thin endometrium. SIS is helpful in triaging patients with diffuse endometrial thickening to blind biopsy or, in the case of a focal abnormality as shown here, to hysteroscopic removal.



**FIG 27-13** A 39-year-old woman referred for saline infusion sonohysterography (SIS) to evaluate possible filling defect seen on conventional hysterosalpingogram (HSG). Longitudinal SIS image of the uterus shows focal posterior endometrial thickening (*arrow*). The maximum diameter of the lesion is smaller than its base, consistent with a sessile polyp. Subsequent hysteroscopic removal of the lesion confirmed a 5-mm benign polyp. SIS is helpful both for demonstrating small abnormalities that may be missed on transvaginal sonography (EVS), as well as for confirming normal endometrium in the remainder of the uterine cavity. SIS can detect abnormalities missed on EVS in 14% to 24% of cases.<sup>6,26</sup>

## Endometrial Carcinoma

Endometrial carcinoma is defined as cancer occurring above the level of the internal cervical os involving the upper two thirds of the uterus. It is the most common of the gynecologic cancers and represents 95% of uterine malignancies and 6% of all cancers in women. It is the fourth most common cancer in women.

Endometrial carcinoma most commonly presents with abnormal uterine bleeding, allowing early diagnosis and treatment. EVS is the best and most commonly used imaging modality for the detection of endometrial cancer. EVS is readily available and can virtually exclude endometrial cancer in women with a thin endometrium. Endometrial

carcinoma is most common in the sixth and seventh decades of life, with more than 90% occurring after age 50. Women under age 40 constitute only about 5% of cases. The majority of patients (75-80%) are diagnosed with stage I disease, which has an overall 5-year survival rate of 80% to 85% and a cancer-specific survival rate of 90% to 95%.<sup>17</sup> Risk factors for endometrial cancer include estrogen HRT, obesity, polycystic ovary syndrome, chronic anovulation, tamoxifen, nulliparity, early menarche, late menopause, hypertension, and diabetes mellitus. The majority of cases are of endometrioid histology, which is associated with chronic estrogen exposure, a common theme noted among the risk factors.

EVS typically demonstrates diffuse endometrial thickening (Fig. 27-15) or an endometrial mass. The thickened endometrial echo complex is most often hyperechoic but may have areas of decreased echogenicity. The myometrial interface can be well defined with an intact subendometrial halo if no myometrial invasion has occurred. However, focal or diffuse disruption of the subendometrial halo or extension of the echogenic endometrial lesion into the more hypoechoic underlying myometrium is concerning for myometrial invasion. Doppler evaluation has not been found to be helpful, as there is significant overlap of findings (such as resistive index and pulsatility index measurements) seen with benign and malignant endometrial thickening. Mass-like lesions may be homogeneous or heterogeneous and often have an irregular surface. Polypoid masses may be superficially attached to the endometrium and otherwise expand the uterine cavity. Occasionally endometrial cancer may appear as an ill-defined and poorly visualized endometrial echo complex, which may be misinterpreted as poor visualization because of technical factors. If the endometrium is not adequately visualized in a postmenopausal woman with abnormal vaginal bleeding, additional evaluation should be performed to exclude endometrial cancer given the 15% incidence of endometrial cancer in this population<sup>23</sup> (Fig. 27-16). Findings suggestive of endometrial cancer on SIS include irregular endometrial thickening, endometrial heterogeneity, an irregular focal endometrial mass with or without myometrial invasion or irregular vascularity on color Doppler, and a rigid or poorly distensible uterine cavity.<sup>36</sup>

## Tamoxifen

Tamoxifen, a selective estrogen receptor modulator (SERM), is used to treat breast cancer or as prophylaxis to prevent breast cancer in high-risk patients. Although an antiestrogen agent in breast tissue, tamoxifen and other SERMs bind to estrogen receptors at the uterine



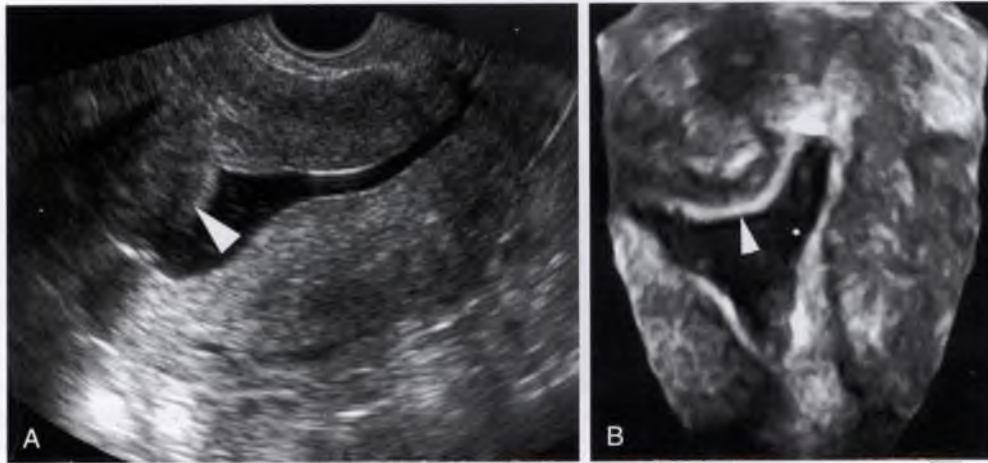


**FIG 27-14** **A**, Longitudinal image of the uterus obtained during saline infusion sonohysterography (SIS) shows a hypoechoic submucosal mass (*arrowhead*) protruding into the uterine cavity at the fundus. **B**, Coronal three-dimensional (3D) image better demonstrates the thin layer of overlying echogenic endometrium (*arrowhead*), further confirming the submucosal location of this leiomyoma. If available, 3D volume acquisition of the uterus should be performed routinely with SIS.

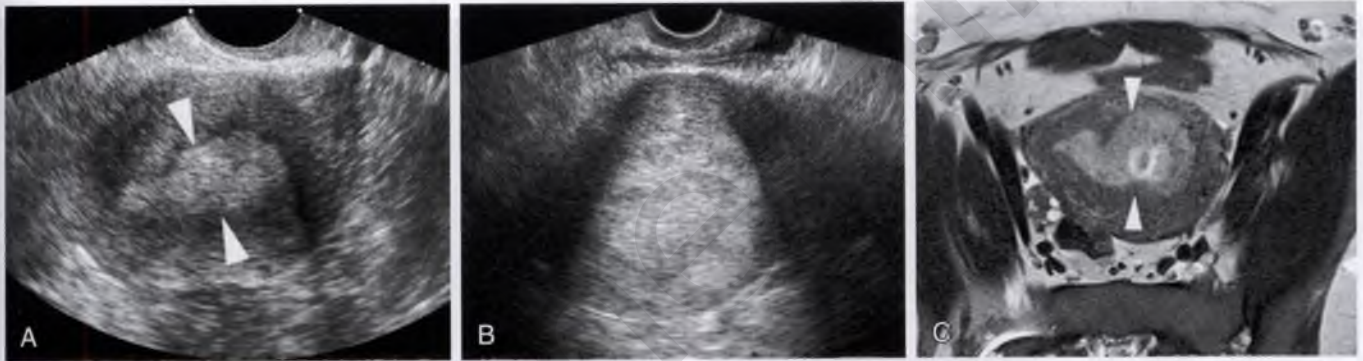


**FIG 27-15** A 26-year-old premenopausal obese woman with dysfunctional uterine bleeding. **A**, Transverse transvaginal sonography (EVS) image of the uterus demonstrates irregular and asymmetric echogenic thickening of the endometrial echo complex (*arrowheads*). Dilatation and curettage (D&C) was performed, showing chronic endometritis but no evidence of malignancy. **B**, EVS performed 2 years later in the setting of continued abnormal bleeding shows increased endometrial thickening with an ill-defined endometrial-myometrial interface. Given the results from prior D&C, magnetic resonance imaging was performed. **C**, Axial oblique T2-weighted image of the uterus shows mass-like irregular thickening of the endometrium (*arrowheads*) with less than 50% thickness myometrial invasion. Hysterectomy confirmed stage 1A endometrial carcinosarcoma.

level and have a paradoxical effect in the uterus, inducing endometrial proliferation, which can take the form of hyperplasia, polyp, cancer, or cystic atrophy. Not only can these endometrial abnormalities coexist, but tamoxifen is also associated with adenomyosis, enlargement of leiomyomas, and ovarian cysts. Tamoxifen “mucosa” or cystic atrophy differs from endometrial atrophy seen in postmenopausal women not on tamoxifen both on hysteroscopic and histologic evaluation.<sup>37</sup> Scattered protuberances are seen in the background of hypervascularized and atrophic endometrium. Microscopically, cystic spaces within a fibrous stroma are lined by atrophic endometrium. The exact location of the cysts is controversial; the two main theories being within the endometrium at the endometrial/myometrial junction, within the inner myometrium (subendometrium) or both.<sup>37,38</sup> Up to 50% of women develop endometrial abnormalities while on tamoxifen therapy, usually in the first 36 months of treatment. Most patients are asymptomatic and in this population no surveillance

imaging is recommended. Symptomatic patients typically have abnormal uterine bleeding. Further investigation of the bleeding is undertaken when the endometrium is more than 5 mm in a postmenopausal woman.

Tamoxifen-induced proliferation of the endometrium has a non-specific sonographic appearance of endometrial thickening with cystic dilation of the endometrial glands. This may represent endometrial hyperplasia, polyps, or carcinoma, as well as the pseudo-thickening of cystic endometrial atrophy (Fig. 27-17).<sup>29</sup> In this patient population, metastatic breast cancer (Fig. 27-18) should always be considered in the differential diagnosis. Polyps tend to be multiple and larger in women taking tamoxifen, with a median size of 2.9 cm (range of 0.3-11 cm).<sup>39</sup> Following discontinuation of tamoxifen, endometrial thickening slowly decreases at a rate of approximately 1.3 mm per year. Therefore, the endometrium may remain thickened for 6 to 12 months following discontinuation of tamoxifen therapy.<sup>40</sup>



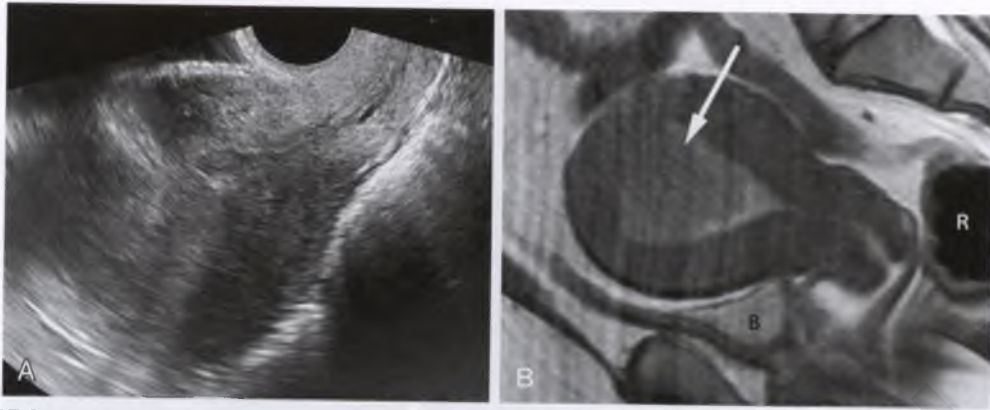


**FIG 27-16** A 43-year-old premenopausal nulliparous woman with history of endometrial hyperplasia, obesity, and hypertension now with abnormal bleeding. **A**, Longitudinal transvaginal sonographic image of the uterus demonstrates a poorly visualized endometrial stripe. It could not be determined if this was due to technical factors or true endometrial disease, and therefore, a magnetic resonance imaging scan was performed. **B**, Sagittal T2-weighted image of the uterus shows a polypoid endometrial mass (*arrow*), hypointense relative to the normal high signal intensity endometrium. The mass-myometrial interface at the uterine fundus is ill defined, concerning for invasion; however, this is less than 50% of the myometrial thickness. Stage 1A endometrial cancer was confirmed at hysterectomy. B, bladder; R, rectum.

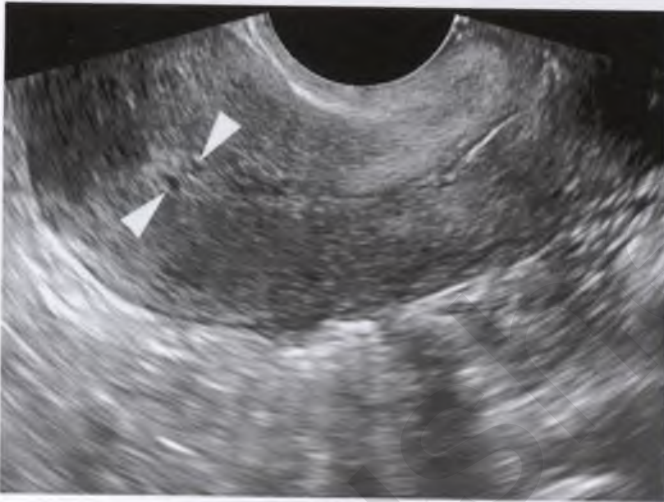


**FIG 27-17** A 43-year-old woman with breast cancer and chemotherapy-induced ovarian failure now with abnormal uterine bleeding. Longitudinal transvaginal sonographic image of the uterus shows a thin endometrial stripe with small cysts (*arrowheads*) at the endometrial-myometrial junction, typically seen in cystic endometrial atrophy induced by tamoxifen. This sonographic appearance could mimic a small focal endometrial polyp with cysts.

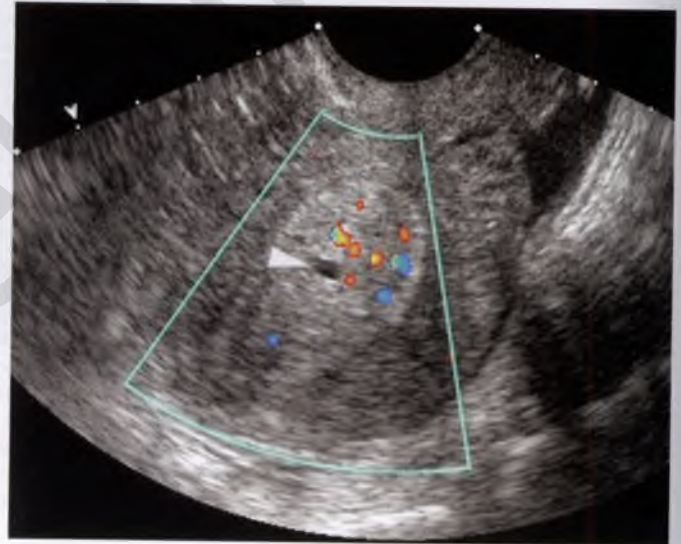


**FIG 27-18** A 50-year-old woman with breast cancer on tamoxifen therapy with intermittent vaginal bleeding. Transverse color Doppler transvaginal sonographic image of the uterus shows endometrial thickening with internal cystic change (*arrowhead*) and diffusely increased vascularity. This appearance is nonspecific and may represent endometrial hyperplasia, polyp, or carcinoma, particularly in the setting of tamoxifen therapy. Although much less common, metastatic breast cancer can have this appearance. Endometrial biopsy was negative; however, the patient underwent hysterectomy with the goal of inducing surgical menopause prior to initiation of an aromatase inhibitor. Final surgical disease demonstrated poorly differentiated metastatic breast cancer.

## SUMMARY

Abnormal uterine bleeding is most commonly due to dysfunctional anovulatory bleeding in premenopausal women and endometrial atrophy in postmenopausal women. However, endometrial assessment is mandatory to exclude focal endometrial disease and endometrial carcinoma. The latter is of particular concern in the symptomatic postmenopausal population. EVS provides noninvasive high-resolution imaging of the endometrium, allowing triage of patients to medical treatment, blind endometrial sampling, or direct hysteroscopic visualization with sampling or removal of focal disease. The high negative predictive value of EVS essentially excludes significant disease when a thin distinct endometrial echo is seen. If the endometrium is abnormal

or not adequately visualized with EVS, SIS can help stratify patients into the following categories: (1) no anatomic abnormality, (2) diffuse endometrial abnormality that may then be evaluated with blind endometrial sampling, or (3) focal endometrial abnormality that must be evaluated under direct visualization. Such an ultrasound-based approach will not only help exclude endometrial carcinoma but will also identify the source of any bleeding and allow for better clinical management.



## REFERENCES

- National Cancer Institute: *Surveillance Epidemiology and End Results (SEER) Program: Cancer Stat Fact Sheets: Endometrial Cancer*. November 26, 2014. Available at <<http://seer.cancer.gov/statfacts/html/corp.html>>.
- Word B, Gravlee LC, Wideman GL: The fallacy of simple uterine curettage. *Obstet Gynecol* 12(6):642–648, 1958.
- Rodriguez MH, Platt LD, Medearis AL, et al: The use of transvaginal sonography for evaluation of postmenopausal ovarian size and morphology. *Am J Obstet Gynecol* 159(4):810–814, 1988.
- Guido RS, Kanbour-Shakir A, Rulin MC, et al: Pipelle endometrial sampling. Sensitivity in the detection of endometrial cancer. *J Reprod Med* 40(8):553–555, 1995.
- Leone FP, Timmerman D, Bourne T, et al: Terms, definitions and measurements to describe the sonographic features of the endometrium and intrauterine lesions: a consensus opinion from the International Endometrial Tumor Analysis (IETA) group. *Ultrasound Obstet Gynecol* 35(1):103–112, 2010.
- Kazandi M, Aksehirli S, Cirpan T, et al: Transvaginal sonography combined with saline contrast sonohysterography to evaluate the uterine cavity in patients with abnormal uterine bleeding and postmenopausal endometrium more than 5 mm. *Eur J Gynaecol Oncol* 24(2):185–190, 2003.
- Benacerraf BR, Shipp TD, Bromley B: Which patients benefit from a 3D reconstructed coronal view of the uterus added to standard routine 2D pelvic sonography? *AJR Am J Roentgenol* 190(3):626–629, 2008.
- Lindheim SR, Sprague C, Winter TC, 3rd: Hysterosalpingography and sonohysterography: lessons in technique. *AJR Am J Roentgenol* 186(1):24–29, 2006.
- Wolman I, Groutz A, Gordon D, et al: Timing of sonohysterography in menstruating women. *Gynecol Obstet Invest* 48(4):254–258, 1999.
- Lang E, Hatsiopolou O, Koch T, et al: Can words hurt? Patient-provider interactions during invasive procedures. *Pain* 114(1–2):303–309, 2005.
- Dessole S, Farina M, Capobianco G, et al: Determining the best catheter for sonohysterography. *Fertil Steril* 76(3):605–609, 2001.
- Spielloch RL, Winter TC, Schouweiler C, et al: Optimal catheter placement during sonohysterography: a randomized controlled trial comparing cervical to uterine placement. *Obstet Gynecol* 111(1):15–21, 2008.
- Alcazar JL, Errasti T, Zornoza A: Saline infusion sonohysterography in endometrial cancer: assessment of malignant cells dissemination risk. *Acta Obstet Gynecol Scand* 79(4):321–322, 2000.
- Berry E, Lindheim SR, Connor JP, et al: Sonohysterography and endometrial cancer: incidence and functional viability of disseminated malignant cells. *Am J Obstet Gynecol* 199(3):240, 2008.
- Takac I: Saline infusion sonohysterography and the risk of malignant extrauterine spread in endometrial cancer. *Ultrasound Med Biol* 34(1):7–11, 2008.
- Goldstein RB, Bree RL, Benson CB, et al: Evaluation of the woman with postmenopausal bleeding: Society of Radiologists in Ultrasound-Sponsored Consensus Conference statement. *J Ultrasound Med* 20(10):1025–1036, 2001.
- Barwick TD, Rockall AG, Barton DP, et al: Imaging of endometrial adenocarcinoma. *Clin Radiol* 61(7):545–555, 2006.
- Gull B, Karlsson B, Milsom J, et al: Can ultrasound replace dilation and curettage? A longitudinal evaluation of postmenopausal bleeding and transvaginal sonographic measurement of the endometrium as predictors of endometrial cancer. *Am J Obstet Gynecol* 188(2):401–408, 2003.
- Baldwin MT, Dudiak KM, Gorman B, et al: Focal intracavitary masses recognized with the hyperechoic line sign at transvaginal US and characterized with hysterosonography. *Radiographics* 19(4):927–935, 1999.
- Goldstein SR: Sonography in postmenopausal bleeding. *J Ultrasound Med* 31(2):333–336, 2012.
- American College of Obstetricians and Gynecologists: ACOG Committee Opinion No. 426: the role of transvaginal ultrasonography in the evaluation of postmenopausal bleeding. *Obstet Gynecol* 113(2 Pt 1):462–464, 2009.
- Doubilet PM: Society of Radiologists in Ultrasound Consensus Conference statement on postmenopausal bleeding. *J Ultrasound Med* 20(10):1037–1042, 2001.
- Burbos N, Musonda P, Crocker SG, et al: Management of postmenopausal women with vaginal bleeding when the endometrium cannot be visualized. *Acta Obstet Gynecol Scand* 91(6):686–691, 2012.
- de Kroon CD, de Bock GH, Dieben SW, et al: Saline contrast hysterosonography in abnormal uterine bleeding: a systematic review and meta-analysis. *Br J Obstet Gynaecol* 110(10):938–947, 2003.
- van Dongen H, de Kroon CD, Jacobi CE, et al: Diagnostic hysteroscopy in abnormal uterine bleeding: a systematic review and meta-analysis. *Br J Obstet Gynaecol* 114(6):664–675, 2007.
- Laifer-Narin S, Ragavendra N, Parmenter EK, et al: False-normal appearance of the endometrium on conventional transvaginal sonography: comparison with saline hysterosonography. *AJR Am J Roentgenol* 178(1):129–133, 2002.
- Breijer MC, Peeters JA, Opmeer BC, et al: Capacity of endometrial thickness measurement to diagnose endometrial carcinoma in asymptomatic postmenopausal women: a systematic review and meta-analysis. *Ultrasound Obstet Gynecol* 40(6):621–629, 2012.
- Smith-Bindman R, Weiss E, Feldstein V: How thick is too thick? When endometrial thickness should prompt biopsy in postmenopausal women without vaginal bleeding. *Ultrasound Obstet Gynecol* 24:558–565, 2004.
- Shi AA, Lee SI: Radiological reasoning: algorithmic workup of abnormal vaginal bleeding with transvaginal sonography and sonohysterography. *AJR Am J Roentgenol* 191(6 Suppl):S68–S73, 2008.
- Smith P, Bakos O, Heimer G, et al: Transvaginal ultrasound for identifying endometrial abnormality. *Acta Obstet Gynecol Scand* 70(7–8):591–594, 1991.
- Nalaboff KM, Pellerito JS, Ben-Levi E: Imaging the endometrium: disease and normal variants. *Radiographics* 21(6):1409–1424, 2001.
- Davis PC, O'Neill MJ, Yoder IC, et al: Sonohysterographic findings of endometrial and subendometrial conditions. *Radiographics* 22(4):803–816, 2002.
- Giuntoli RL, Zacur HA: *Classification and diagnosis of endometrial hyperplasia*. UpToDate: Nov. 24, 2015. Available at <<http://www.uptodate.com/contents/classification-and-diagnosis-of-endometrial-hyperplasia>>.
- Lee SC, Kaunitz AM, Sanchez-Ramos L, et al: The oncogenic potential of endometrial polyps: a systematic review and meta-analysis. *Obstet Gynecol* 116(5):1197–1205, 2010.
- Bhaduri M, Tomlinson G, Glanc P: Likelihood ratio of sonohysterographic findings for discriminating endometrial polyps from submucosal fibroids. *J Ultrasound Med* 33(1):149–154, 2014.
- Laifer-Narin SL, Ragavendra N, Lu DS, et al: Transvaginal saline hysterosonography: characteristics distinguishing malignant and various benign conditions. *AJR Am J Roentgenol* 172(6):1513–1520, 1999.
- Ascher SM, Imaoka I, Lage JM: Tamoxifen-induced uterine abnormalities: the role of imaging. *Radiology* 214(1):29–38, 2000.
- Goldstein SR: Unusual ultrasonographic appearance of the uterus in patients receiving tamoxifen. *Am J Obstet Gynecol* 170(2):447–451, 1994.
- Cohen I: Endometrial pathologies associated with postmenopausal tamoxifen treatment. *Gynecol Oncol* 94(2):256–266, 2004.
- Fishman M, Boda M, Sheiner E, et al: Changes in the sonographic appearance of the uterus after discontinuation of tamoxifen therapy. *J Ultrasound Med* 25(4):469–473, 2006.



# Ultrasound Evaluation of the Uterus

Liina Pöder

## SUMMARY OF KEY POINTS

- Sonography is the imaging modality of choice for evaluation of the myometrium, with magnetic resonance imaging (MRI) reserved as a problem-solving technique.
- Many müllerian duct anomalies can be accurately diagnosed with sonography, and three-dimensional (3D) imaging of the fundal contour is diagnostic in differentiating the bicornuate uterus (>1 cm fundal cleft between the two horns) and the septate uterus.
- Adenomyosis presents most commonly in middle-aged multiparous women with uterine tenderness, dysmenorrhea, and menorrhagia and most commonly appears on ultrasound images as an ill-defined or poorly marginated area within the myometrium or thickening of the hypoechoic subendometrial halo. The most specific findings are myometrial cysts and echogenic linear or nodular extension of the endometrium into the subjacent myometrium.
- Leiomyoma is the most common uterine neoplasm. Symptoms are primarily related to location and size. Although most leiomyomas are sharply marginated, well-circumscribed hypoechoic masses, leiomyomas may be isoechoic or echogenic relative to the myometrium.
- There is overlap in the sonographic and MRI appearance of leiomyomas and adenomyosis/adenomyomas, and the entities may coexist.
- Lipoleiomyomas are typically extremely echogenic and sharply marginated with posterior attenuation.
- Leiomyosarcomas may be difficult to differentiate from degenerating leiomyomas on both sonography and MRI.
- Patients with gestational trophoblastic disease (GTD) most commonly present with an echogenic endometrial mass containing numerous small cysts and demonstrating increased vascularity. Fetal parts may be seen in partial moles or coexistent twin pregnancy. Myometrial invasion can be seen with persistent disease or choriocarcinomas, but on imaging may be difficult to differentiate from increased vascularity and “pseudoinvasion” from the placental bed, arteriovenous malformations (AVMs), or retained products of conception (RPOC).
- Uterine AVMs are most often traumatic in origin but may also be congenital or diagnosed in the setting of persistent GTD and RPOC.
- Sonography may be helpful in the diagnosis of endocervical polyps. However, the sonographic appearances of cervical leiomyoma and carcinoma overlap.

## OUTLINE

### Imaging, 847

- Guidelines, 847
- Techniques, 847
- Anatomy, 848

### Congenital Malformations, 852

### Benign Uterine Conditions, 857

- Adenomyosis, 857
- Leiomyomas, 858
- Lipomatous Uterine Tumors, 866

### Malignant Conditions, 866

- Gestational Trophoblastic Disease, 866
- Uterine Sarcomas, 868

### Iatrogenic Processes, 871

- Arteriovenous Malformations, 871
- Intrauterine Contraceptive Devices, 872
- The Postpartum and Postabortive Uterus, 872

### Cervical Cysts and Polyps, 878

### Conclusions, 878

Sonography is clearly the modality of choice for imaging the female pelvis, including the uterus and adnexal structures. In our clinical laboratory, a combination of transabdominal pelvic scanning as well as transvaginal examination is performed in most patients. This approach allows the examiner to evaluate the true pelvis in its entirety with a wide field of view on transabdominal imaging, as well as to

assess specific structures using high-resolution images obtained on transvaginal scanning. Primary evaluation with ultrasound in conjunction with clinical information is often sufficient for diagnosis and patient management and will help optimize recommendations for further imaging as necessary. When ultrasound evaluation fails to provide adequate information or does not answer the clinical question,

further evaluation with MRI, computed tomography (CT) scanning, hystero-graphy, or saline infusion sonography (SIS) can be performed. MRI of the uterus is discussed in detail in Chapter 36.

In this chapter, we discuss ultrasound evaluation of the normal uterus, anatomic variants, and benign and malignant conditions. A discussion of the normal and abnormal endometrium in the patient who presents with abnormal uterine bleeding is presented in Chapter 27.

## IMAGING

### Guidelines

The American Institute of Ultrasound in Medicine (AIUM) guidelines for imaging of the uterus have been developed to assist physicians in performing sonographic studies of the female pelvis.<sup>1</sup> Knowing the potential, but also the limitations, of ultrasound helps us to maximize the probability of detecting most significant abnormalities. As with any clinical test, ultrasound examination of the pelvis should be performed only if there is a valid clinical reason. Following the AIUM guidelines, the indications for pelvic sonography include, but are not limited to, the following:

1. Evaluation of pelvic pain
2. Evaluation of pelvic masses
3. Evaluation of endocrine abnormalities, including polycystic ovaries
4. Evaluation of dysmenorrhea (painful menses)
5. Evaluation of amenorrhea
6. Evaluation of abnormal bleeding
7. Evaluation of delayed menses
8. Follow-up of a previously detected abnormality
9. Evaluation, monitoring, and/or treatment of infertility patients
10. Evaluation in the presence of a limited clinical examination of the pelvis
11. Evaluation for signs or symptoms of pelvic infection
12. Further characterization of a pelvic abnormality noted on another imaging study
13. Evaluation of congenital uterine and lower genital tract anomalies
14. Evaluation of excessive bleeding, pain, or signs of infection after pelvic surgery, delivery, or abortion

15. Localization of an intrauterine contraceptive device
16. Screening for malignancy in high-risk patients
17. Evaluation of incontinence or pelvic organ prolapse
18. Guidance for interventional or surgical procedures; and
19. Preoperative and postoperative evaluation of pelvic structures<sup>1</sup>

### Techniques

All relevant anatomic structures in the pelvis should be identified first by transabdominal technique, and then more detailed evaluation of the deep pelvic structures should be performed using the transvaginal technique. In specific situations when transvaginal evaluation cannot be performed or tolerated, transrectal or transperineal evaluation can be very useful.

The transducer should be selected to operate at the highest clinically appropriate frequency that will allow adequate visualization of deep pelvic structures. For transabdominal evaluation, a 3.5-MHz or higher transducer is employed. Curved linear array transducers, as well as sector transducers with a smaller footprint, are most often employed. For transabdominal evaluation, the bladder should be adequately distended to displace bowel superiorly out of the true pelvis and to provide an acoustic window to visualize the uterus and adnexa (Fig. 28-1).

For transvaginal evaluation, the urinary bladder should be emptied and the patient placed in a comfortable position but with her pelvis tilted either with the use of stirrups or by the placement of padding under the patient to elevate the hips. The patient or the sonographer, depending upon the patient's preference, may introduce the vaginal transducer with real-time monitoring. For transvaginal evaluation, the AIUM recommends using probe frequencies of 5 MHz or higher (Fig. 28-2). If a male sonologist is performing the examination, a female member of the staff should be present as a chaperone. However, in some clinical situations, a chaperone is helpful and recommended even for a female sonologist.

The vagina, uterus, and the urinary bladder are used as reference points for identification of the remaining normal and abnormal pelvic structures. The uterine size, shape, and orientation should be assessed and documented in both sagittal (long-axis) and transverse (axial or short-axis) planes. The endometrium, myometrium, and cervix should be carefully evaluated, and their appearance documented. The uterine

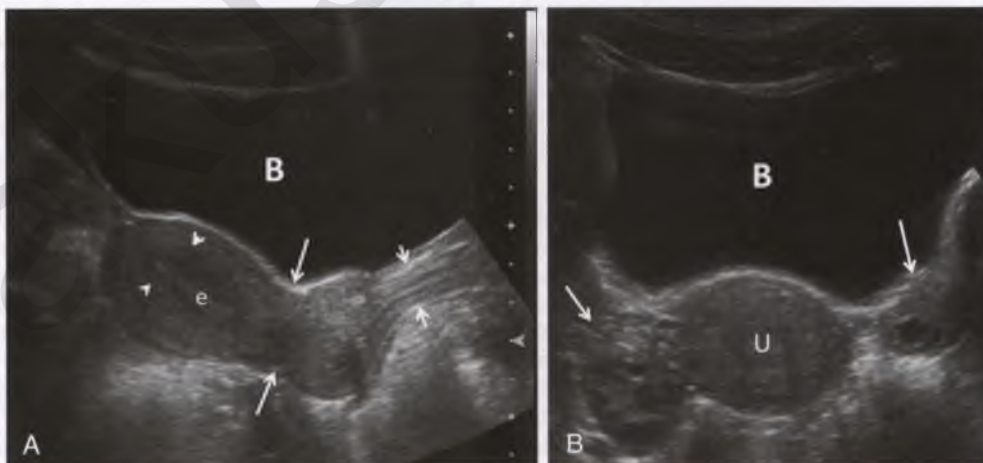


**FIG 28-1** Transabdominal gray-scale ultrasound images of the normal uterus. **A**, Sagittal imaging plane. Note indentation below the lower uterine segment indicating the level of the internal os (*long arrows*), the striated appearance of the vagina (*short arrows*), the linear homogeneously echogenic endometrium (e), and the surrounding hypoechoic subendometrial halo (*arrowheads*). Note the acoustic window provided by the distended urinary bladder (B). **B**, Transverse imaging plane. Note the bladder (B), right and left ovaries (*arrows*), and uterus (U).



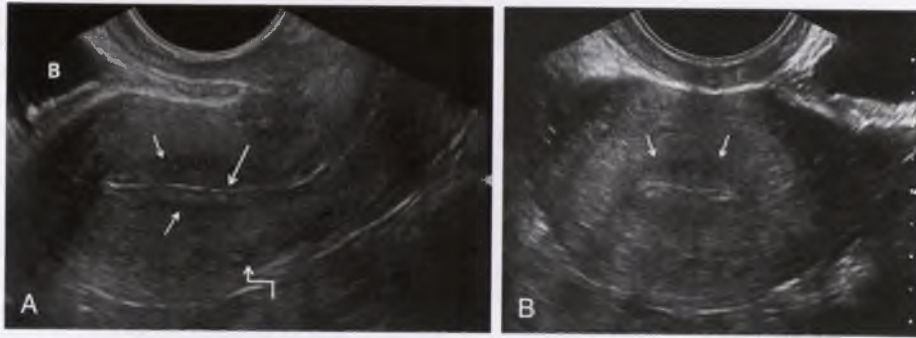


**FIG 28-2** Transvaginal gray-scale ultrasound images of the normal uterus. **A**, Sagittal imaging plane. Note thin brightly echogenic line (*long arrow*) representing artifact or mucus between the echogenic anterior and posterior layers of the endometrium and the subjacent hypoechoic subendometrial halo (*short arrows*). The anechoic tubular arcuate vessels separating the outer from the intermediate layer of the myometrium are faintly visualized (*crooked arrow*). **B**, bladder. **B**, Transverse imaging plane. The hypoechoic subendometrial halo (*arrows*) can be seen surrounding the echogenic endometrium. Note significantly improved resolution and visualization of the normal zonal anatomy in these higher frequency transvaginal images in comparison to the lower frequency transabdominal images (Fig. 28-1). However, the transabdominal images have a larger field of view, providing a better overview of pelvic structures.

length is measured in long axis from the fundus to the external os of the cervix, and the anteroposterior dimension is measured on the same image perpendicular to the long axis. The width is measured on either a transaxial or coronal imaging plane. If the volume of the uterine corpus is assessed, the cervical component should be excluded.<sup>1</sup> Myometrial masses and contour abnormalities should be recorded in two different planes and their locations recorded.<sup>1</sup> Assessment of the endometrium is performed primarily in the sagittal (or sometimes coronal) plane. Variations of the normal appearance of the endometrium during different phases of the menstrual cycle and with hormonal supplementation should be considered (Fig. 28-3) and have been described in detail in preceding chapters. Doppler evaluation of the uterus and endometrium can be of added value. 3D imaging is increasingly available and can also provide valuable additional information, particularly by providing a coronal image of the fundal contour of the uterus in women with suspected uterine congenital malformations and to localize leiomyomas.

SIS, or as it is often referred to, sonohysterography, is an innovative technique used to evaluate a variety of endometrial and myometrial processes that involve the endometrial canal. The most common indications for SIS include, but are not limited to, evaluation of the following:

1. Abnormal uterine bleeding
2. Uterine cavity, especially with regard to uterine leiomyomas, polyps, and synechiae
3. Abnormalities detected on transvaginal sonography, including focal or diffuse endometrial or intracavitary abnormalities
4. Congenital abnormalities of the uterus
5. Infertility
6. Recurrent pregnancy loss

SIS is contraindicated in women who could be pregnant or have an active infection. Because the normal secretory endometrium may be thick and simulate endometrial disease, the examination should be scheduled in premenopausal women during the follicular phase of the menstrual cycle, after menstrual flow has ceased but prior to ovulation, no later than the 10th day of the menstrual cycle. Active vaginal bleeding is not generally a contraindication but can make imaging challenging or even nondiagnostic.<sup>2</sup>

At our institution, we perform a preliminary transabdominal and transvaginal sonogram before SIS. After the procedure is explained to

the patient, the external os is cleansed before catheterization of the cervical canal using aseptic technique. A sonohysterography catheter (flushed with saline to remove any air bubbles) is then advanced into the endometrial canal. Once in the endometrial canal, the balloon is inflated (preferably with saline rather than air to avoid shadowing) so that the catheter does not become dislodged. However, some clinicians prefer to use a catheter without a balloon. The speculum is removed, and the transvaginal probe is reinserted adjacent to the catheter. Under ultrasound guidance, the balloon is gently retracted to occlude the internal os. Sterile saline should be administered under real-time sonography. The amount of saline introduced is variable, often between 5 and 30 mL. Normal anatomy and abnormal findings should be documented in two separate imaging planes using a high-frequency transvaginal probe, and the endometrium should be fully evaluated from one cornua to the other (Fig. 28-4). Additional techniques such as color Doppler and 3D imaging may be helpful in evaluating both normal and abnormal findings.

## Anatomy

The uterus is a hollow organ in which the myometrium is firmly adherent to a thin internal layer of endometrium. Externally the uterus is embedded between the two layers of the broad ligament. Anatomically, the uterus lies between the bladder anteriorly and the rectosigmoid colon posteriorly. The uterus is divided into two major parts, the body or corpus and the cervix. The most superior aspect of the uterus is referred to as the fundus and the area where the fallopian tubes enter into the uterus is referred to as the cornua. Anterior to the fallopian tubes are the round ligaments, one on each side, which extend anterolaterally, coursing through the inguinal canals and inserting onto the fascia of the labia majora. The uterus has a dual arterial blood supply. The majority of the blood supply comes from the uterine arteries, which arise from the internal iliac arteries, and a minor source of blood supply is the ovarian arteries.

The uterus is most often anteverted and anteflexed (Fig. 28-5), but it may also be retroflexed (Fig. 28-6) or retroverted (Fig. 28-7). Descriptions of flexion refer to the relationship of the body of the uterus to the cervix at the level of the internal os (usually the angle is about 270 degrees), whereas version refers to the cervical relationship to the vagina. The cervix of the uterus is fixed in the midline. However, the body of the uterus can be mobile, and uterine position and orientation

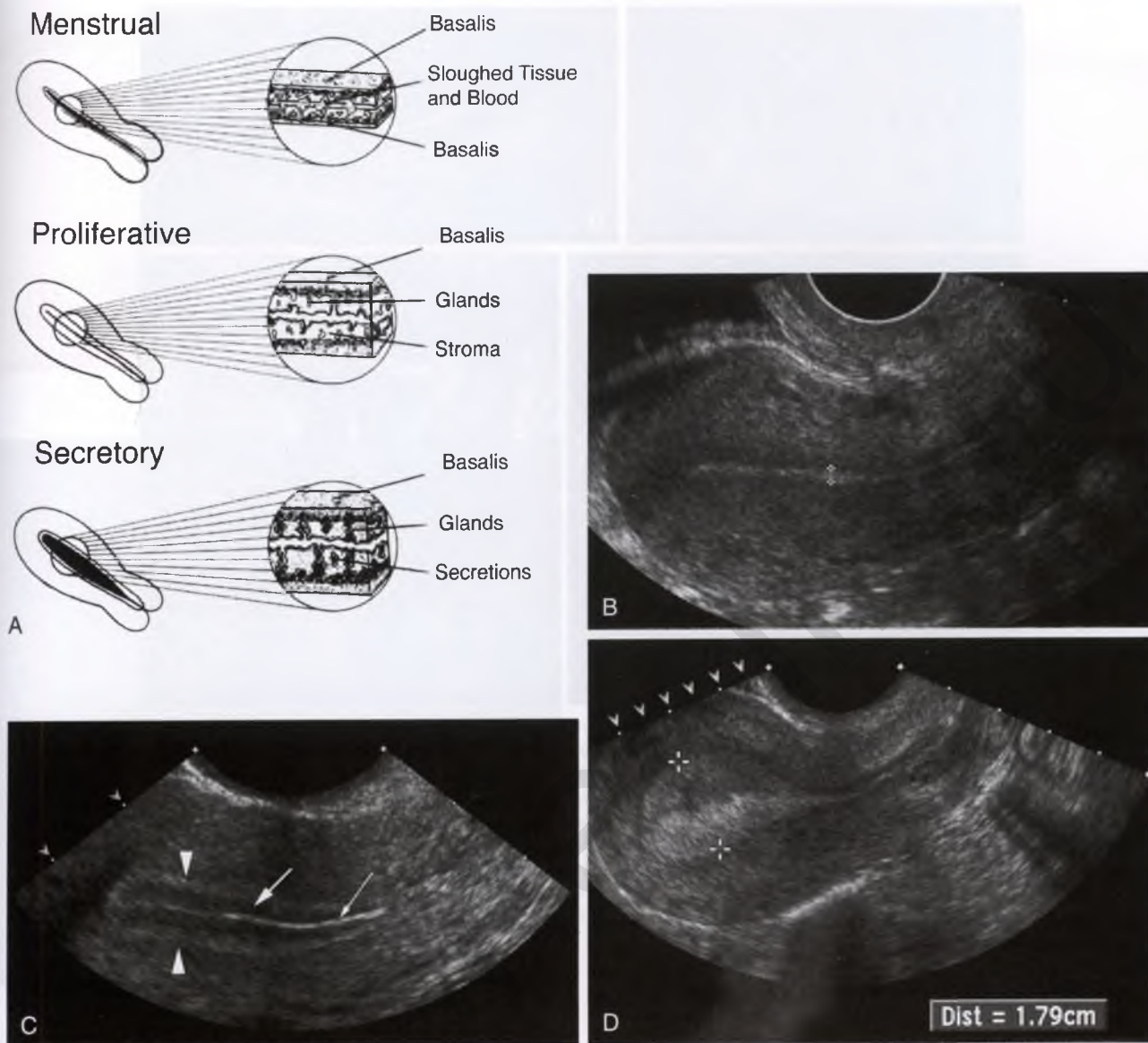


**FIG 28-3 A**, Diagram depicting normal development of the endometrium during the menstrual, proliferative, and secretory phases. In the menstrual phase, the endometrium appears as a thin, irregular interface. The central echogenicity probably arises from sloughed tissue and blood. In the proliferative phase, the endometrium is relatively hypoechoic, likely a reflection of the straight and orderly arrangement of the glandular elements. The central thin, echogenic line is likely a specular reflection from the endometrial surfaces. In the secretory phase, the endometrium achieves its maximum thickness and echogenicity. This appearance is from the distended and tortuous glands, which contain secretions. **B**, Postmenstrual transvaginal sagittal image of the uterus demonstrating the normal thin homogeneously echogenic early proliferative endometrium (*calipers*). **C**, Transvaginal sagittal image of the periovulatory endometrium. A three-layered endometrium is seen, giving the endometrium a striated appearance: the collapsed endometrial lumen is demonstrated by the very thin central echogenic line (*thin arrow*). The surrounding hypoechoic layer representing the edematous functionalis endometrium (*thick arrow*) and an outer hyperechoic layer representing the basal endometrium (*arrowheads*) are seen. **D**, Transvaginal sagittal image of the secretory endometrium. In the secretory stage of the menstrual cycle, the endometrium (*calipers*) becomes thick and more homogeneously echogenic. (A from Fleischer AC, Kalemeris GC, Entman SS: Sonographic depiction of the endometrium during normal cycles. *Ultrasound Med Biol* 12:271, 1986, Pergamon Journals Ltd. Reprinted by permission of Elsevier Science. Copyright 1986 by World Federation of Ultrasound in Medicine and Biology.)



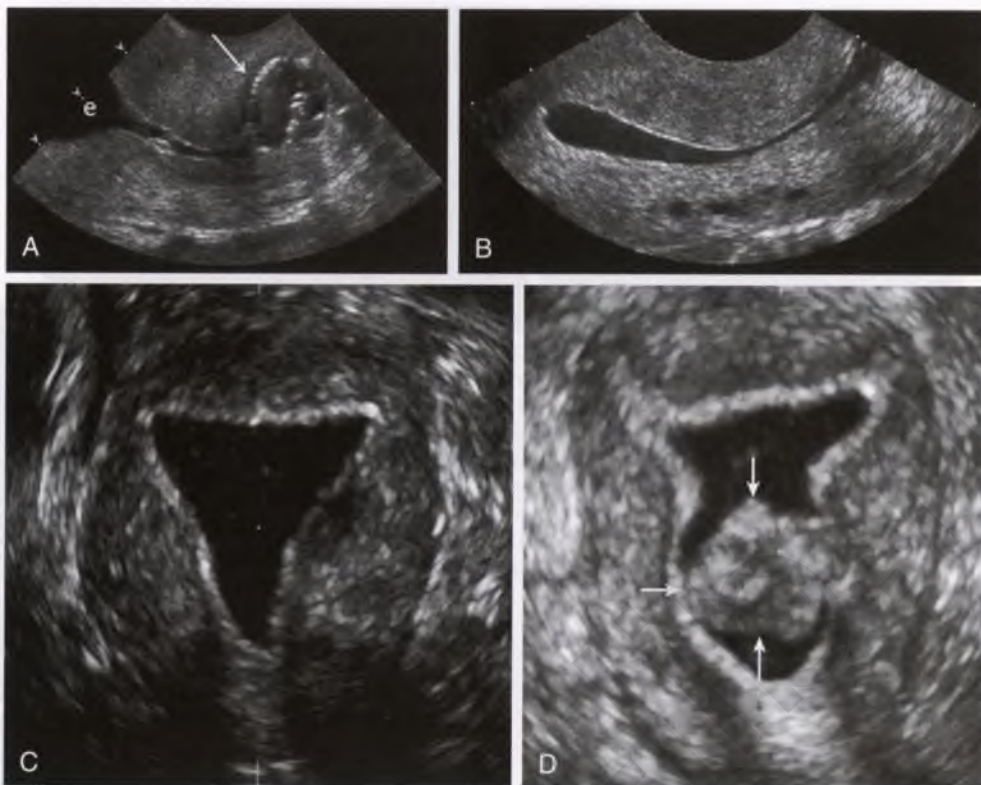


**FIG 28-4** Saline-infused sonohysterogram. **A**, Transvaginal sagittal image of the cervix demonstrating the catheter balloon (*arrow*) positioned in the lower endocervical canal. Anechoic fluid is in the upper endocervical canal and lower endometrial cavity (*e*). **B**, Transvaginal sagittal image after saline infusion. The normal thin echogenic endometrium is well seen circumferentially. The endometrial cavity is filled with anechoic fluid. Note several small, round anechoic structures in a linear configuration in the posterior wall of the myometrium. These are the arcuate vessels and would fill in with color Doppler. **C**, A coronal three-dimensional reconstruction after saline infusion, demonstrating the normal regular, thin, echogenic endometrium without any intracavitary abnormalities. **D**, In comparison, a coronal three-dimensional reconstruction after saline infusion revealed a 100% intracavitary leiomyoma (*arrows*), separate from the thin, regular echogenic endometrium.

may change with varying degrees of bladder and rectal distention. Retroversion and retroflexion are not infrequent in the nongravid state. In such cases the fundus of the uterus is positioned in the sacral hollow. During pregnancy the uterus enlarges and physiologically undergoes reduction by the 14th to 16th weeks of gestation. The fundus of the uterus then rises into the false pelvis. If this fails to happen, the uterus becomes “trapped” in the sacral hollow, often referred to as “incarcerated.” In cases of incarceration of the uterus, the cervix is drawn upward either against or above the symphysis pubis, resulting in distortion of the bladder and urethra as the gestation progresses. The posteriorly positioned fundus can cause pressure on the rectum. Typically, patients present between the 13th to 17th weeks of pregnancy with symptoms of bladder outlet obstruction. A history of multiple trips to the emergency room for bladder outlet obstruction should raise suspicion.

A constellation of three findings on sonography is diagnostic of an incarcerated uterus:

1. The pregnancy is deep within the cul-de-sac.
2. The maternal urinary bladder lies anterior rather than inferior to the uterine corpus and marked bladder distention is noted.
3. A soft tissue structure (the cervix) is seen between the bladder and pregnancy. This appearance can be misconstrued as an empty uterus associated with an ectopic or abdominal pregnancy.

Failure to recognize an incarcerated uterus can result in compromise of the uterine circulation, leading to spontaneous abortion or even uterine rupture. If recognized early, manual uterine repositioning is usually possible (Fig. 28-8).

The shape and size of the uterus vary throughout life, affected mostly by hormonal status. The mean measurement of the prepubertal uterus is 2.8 cm in length and 0.8 cm in maximum anteroposterior dimension, with the cervix accounting for two thirds of the total length and contributing to the pear-shaped appearance (Fig. 28-9).<sup>3</sup> It is important to remember that in the immediate postdelivery state, the neonatal uterus can be slightly larger owing to the effects of residual maternal hormones. For the same reason, the echogenic endometrium is well seen and a small amount of fluid can be present in the endometrial cavity.

From birth until 4 years of age, the uterus decreases in size. At approximately 8 years of age, the uterus starts to grow preferentially in the fundus. The uterus continues to grow for several years after menarche until it reaches the mean dimensions of a reproductive age uterus, which are approximately 7 cm long and 4 cm wide. Parity increases the size of the uterus, with a multiparous uterus measuring approximately 8.5 cm by 5.5 cm.<sup>4</sup>

Following menopause, the uterus decreases in size. The decrease in size is related to the number of years since menopause,<sup>4</sup> although the



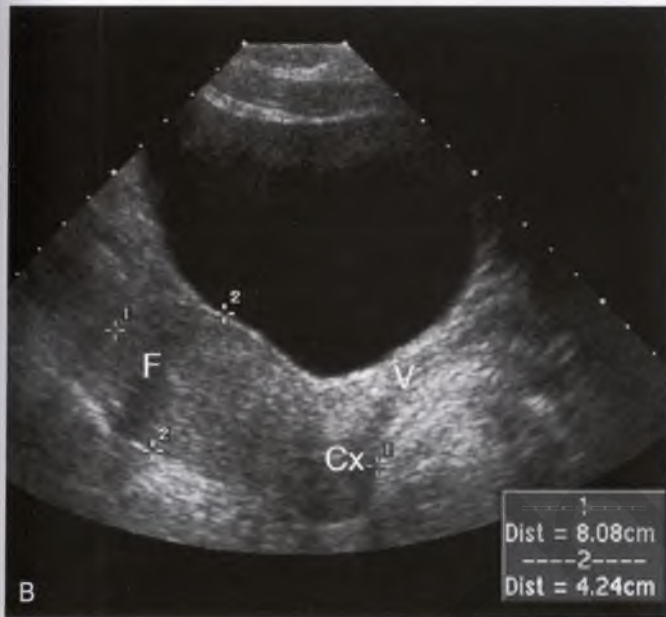


**FIG 28-5 A**, Illustration demonstrating an anteverted, anteflexed normal uterus. The cervix is pointing slightly more posterior in relationship to the vagina, and the fundus is flexed anterior in relation to the cervix. **B**, Midline sagittal sonogram demonstrating anteversion of the cervix (Cx) to the vagina (V). A distended urinary bladder slightly displaces the fundus (F) posteriorly. Standard measurements of the uterine size are made from fundus to cervix (*calipers 1*) and from anterior to posterior uterine wall (*calipers 2*) on sagittal transabdominal view. (A from James A. Cooper, MD, San Diego, CA.)

reduction in size is believed to be most rapid during the first decade following menopause. The length of the normal postmenopausal uterus has been reported to range from 3.5 to 6.5 cm and the anteroposterior dimension from 1.2 to 1.8 cm.<sup>5</sup>

The normal myometrium is composed of three layers. The innermost layer, immediately adjacent to the endometrium, is the thinnest and is relatively compact histologically. This layer is also both hypovascular and hypoechoic when compared to the echogenic endometrium and surrounding middle layer of the myometrium. This layer is often referred to as the subendometrial halo and may not always be visualized sonographically. Sometimes, small extremely echogenic foci, usually less than a few millimeters in size and without posterior shadowing, are seen in the inner myometrium at the endometrial/myometrial interface. These foci are thought to represent dystrophic calcifications due to previous intrauterine instrumentation and have

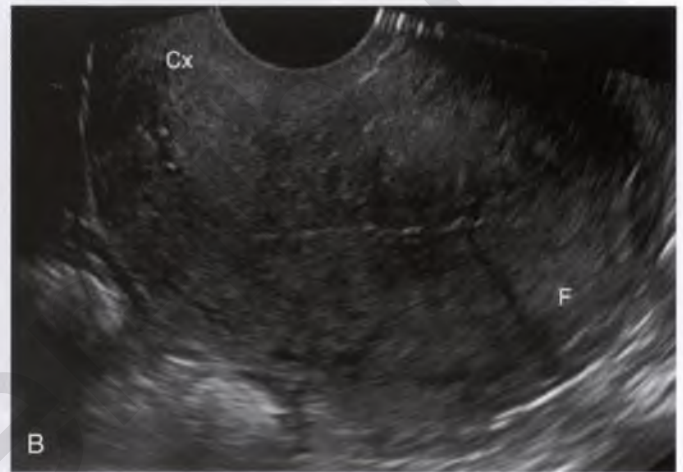
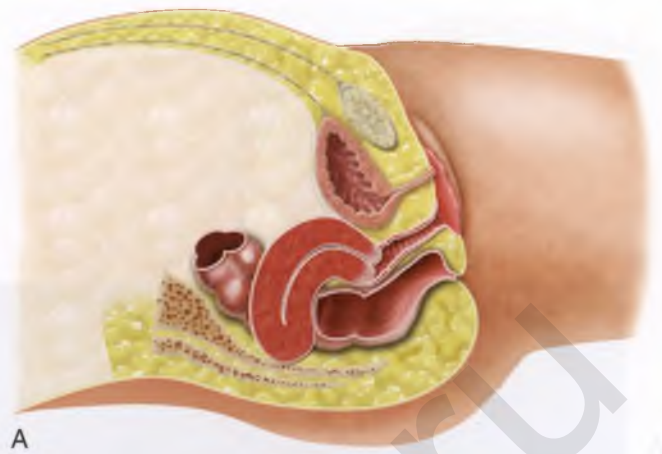


**FIG 28-6 A**, Illustration demonstrating a retroflexed uterus. The cervix is in conventional position in relationship to the vagina. However, the uterine fundus is flexed posteriorly at the level of the internal os in relation to the cervix. **B**, Midline sagittal transvaginal sonogram demonstrating uterine retroflexion. Uterine fundus (F) is positioned posterior and retroflexed in relation to the cervix (Cx). Note angulation between the echogenic endocervical canal and thin echogenic endometrium (owing to the flexion). (A from James A. Cooper, MD, San Diego, CA.)

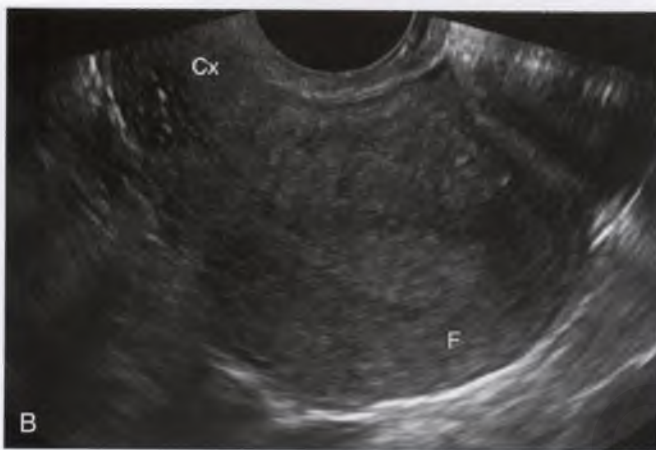
no clinical significance. The middle or intermediate layer lies between the subendometrial halo and the arcuate vessels. This is the thickest myometrial layer and is normally uniform and intermediate in echogenicity. The outer layer lies peripheral to or above the arcuate vessels. This layer is relatively thin and slightly less echogenic compared to the intermediate layer in most patients. The cervix is measured from the internal os, identified by narrowing or “waisting” of the uterus at the junction of the lower uterine segment with the cervix to the lips of the external os, which can be seen to project into the lumen of the vagina. The central endocervical canal is echogenic and continuous with the endometrium. The surrounding fibrous cervical stroma is quite hypoechoic and is continuous with the subendometrial halo, if present. The outer cervical muscular layer is continuous with and similar in echogenicity to the intermediate layer of the myometrium (Fig. 28-10).

The arcuate vessels separate the outer layer from the intermediate layer of the myometrium. The arcuate veins are larger than the arcuate arteries and are potentially compressible with excessive probe or manual pressure. The arcuate vessels (particularly the veins) can be prominent and mimic cystic changes. This potential misinterpretation can easily be clarified by using color Doppler imaging (Fig. 28-11).





A



B

**FIG 28-7** **A**, Illustration demonstrating a retroverted uterus; the cervix is angled slightly posterior in relation to the vagina, and the fundus is bent slightly posterior in relation to the cervix, indicating retroflexion as well. **B**, Midline sagittal transvaginal sonogram demonstrating posterior displacement of the fundus (F) and posterior angulation of the cervix (Cx). (A from James A. Cooper, MD, San Diego, CA.)

The arcuate arteries branch into radial arteries that penetrate the intermediate layer and reach the level of the inner layer. The arcuate arteries may calcify in postmenopausal women, and this process can be seen earlier in diabetic patients. This change is considered part of the normal aging process (Fig. 28-12).

## CONGENITAL MALFORMATIONS

The incidence of congenital müllerian duct anomalies is estimated to be approximately 0.5% in the general population. However, they are more often diagnosed during workup for infertility, frequent miscarriages, or menstrual disorders. Embryologically, the two paired müllerian ducts ultimately develop into the fallopian tubes, uterus, cervix, and the upper two thirds to four fifths of the vagina. The lower one fifth to one third of the vagina and the ovaries have a separate embryologic origin. Uterine malformations arise from three different causes: failure of development of the müllerian ducts, failure of fusion of the müllerian ducts, or failure of resorption of the median septum (Fig. 28-13). There is a strong association of upper urinary tract anomalies with congenital uterine malformations. These anomalies have been reported to be most common in patients with hypoplasia or agenesis, occurring in as many as 30% to 40% of patients. Ipsilateral renal agenesis and ectopic pelvic kidney are most common.

Early developmental failure of the müllerian ducts can result in agenesis or hypoplasia of the proximal two thirds of the vagina, cervix, and uterus, being part of the Mayer-Rokitansky-Küster-Hausler (MRKH) syndrome. This syndrome is an extreme form of müllerian duct anomaly with complete agenesis of the proximal vagina and anomalous cervix and uterus, and patients usually present in early puberty with primary amenorrhea.<sup>6</sup> The ovaries are normal but the fallopian tubes may be closed and the uterus is often anomalous. The vaginal aplasia can vary from complete absence to a blind-ending pouch. Associated renal anomalies are common, in particular absence or ectopia of the kidney. Because there can be subtypes of MRKH syndrome as well as overlap with other rare müllerian duct hypoplasia/aplasia syndromes, it is important to describe findings rather than trying to fit them into a strict category. MRI is usually the most helpful imaging modality for diagnosis of this entity given the complex spectrum of findings. Most important is communication with the clinical team regarding the relevance of findings and preoperative planning.

Arrested development of the müllerian ducts can also cause uterine agenesis or hypoplasia. This abnormality may present as vaginal, cervical, fundal, tubal, or combined agenesis or hypoplasia.

Complete or partial agenesis of a unilateral müllerian duct leads to development of a unicornuate uterus with a single fallopian tube (Fig. 28-13).<sup>6</sup> The unicornuate uterus accounts for approximately 20% of all müllerian duct anomalies. In some cases, a rudimentary horn on the opposite side can be seen. This rudimentary horn may or may not communicate with the endometrial cavity in the normal side. If there is no communication between the endometrial cavities of the rudimentary and normal horns, retrograde menstruation may occur, leading to the development of endometriosis. Ectopic pregnancies may also rarely occur in the rudimentary horn. Such ectopic pregnancies can lead to massive hemorrhage as they can grow to relatively large size before rupturing. Therefore, if a rudimentary horn is documented, surgical resection is usually recommended. The poorest fetal survival among all müllerian duct anomalies has been reported with the unicornuate uterus. Spontaneous abortion has been reported to occur in 34%, preterm labor in 20%, and intrauterine demise in 10%.<sup>6,7</sup> The live birth rate is estimated to be only 50%.<sup>7</sup> The unicornuate uterus seems to be the most difficult müllerian duct anomaly to confidently diagnose on sonography because it can be confused and misdiagnosed as a small uterus. Looking for the contralateral rudimentary horn, which can be filled with blood, may sometimes help. The rudimentary horn may have a distended and dystrophic appearance and should not be mistaken for an adnexal mass. MRI is considered the study of choice in resolving these complicated situations. Recently 3D ultrasound has been reported to be useful in diagnosis, allowing visualization on the coronal imaging plane of a single asymmetric endometrial cavity that is laterally deviated, with or without a rudimentary horn. Forty percent of cases are reported to have renal anomalies, typically ipsilateral to the rudimentary horn, most often renal agenesis or pelvic kidney.<sup>6</sup>

Complete failure of fusion of the müllerian ducts leads to development of two separate uteri, each with its own cervix, termed *uterus didelphys* (Fig. 28-13). This is a relatively rare anomaly accounting for fewer than 5% of all müllerian duct anomalies. The endometrial cavities of each hemiuterus do not communicate. A longitudinal or oblique vaginal septum is common, but not always present. An oblique septum may be obstructive and such patients will present with hematocolpos, dysmenorrhea, pelvic mass, vaginal discharge, or pelvic pain. The vaginal septum may also lead to dyspareunia and even rarely vaginal dystocia during vaginal delivery. If no obstruction is present, most patients are asymptomatic and uterus didelphys is an incidental finding. Patients with uterus didelphys usually successfully carry pregnancies to term, and infertility is an uncommon presentation.<sup>6</sup> On



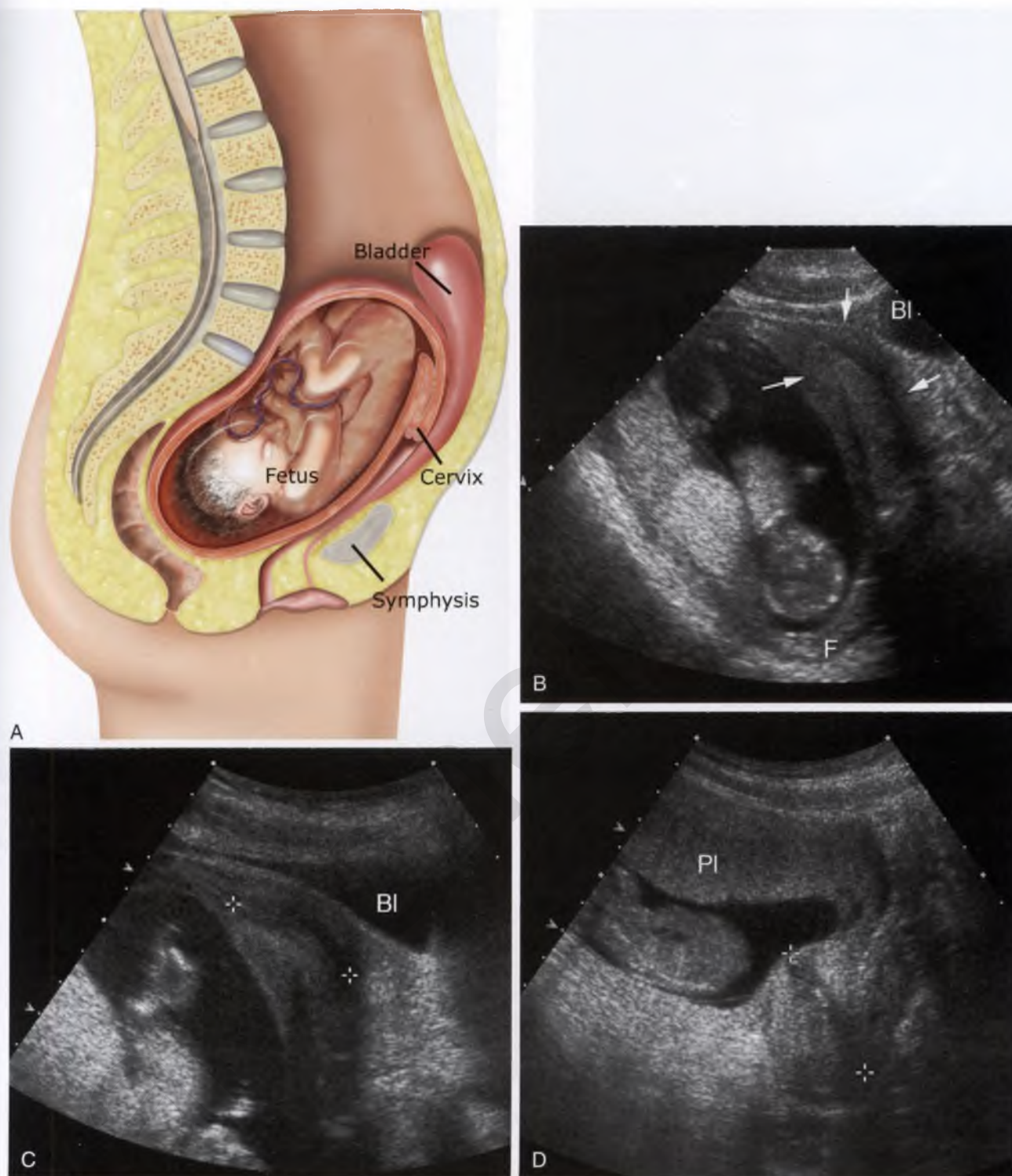


**FIG 28-8** **A**, Illustration demonstrating an incarcerated uterus. If a retroflexed uterus fails to reduce and the gestation progresses, the fundus will become incarcerated deep in the pelvis within the sacral hollow. The cervix will be drawn anteriorly and superiorly and the bladder will be displaced superiorly. **B**, Transabdominal sagittal image of an incarcerated uterus in a patient with a 14-week-old gestation. The patient presented with inability to empty the urinary bladder. The uterine fundus (F) is trapped in the sacral hollow. The cervix (arrows) is drawn anteriorly and superiorly and can be misconstrued as an empty uterus, thereby suggesting an ectopic or transabdominal pregnancy. Bl, bladder. **C**, Sagittal view of the same patient demonstrating the degree to which the bladder (Bl) is drawn superiorly. Note abnormal position of the cervix (calipers). **D**, Following manual reduction, note normal physiologic relationship of the uterus and cervix (calipers). The placenta (Pl) is located anteriorly although it appeared posterior in location when the uterus was incarcerated. (A from James A. Cooper, MD, San Diego, CA.)



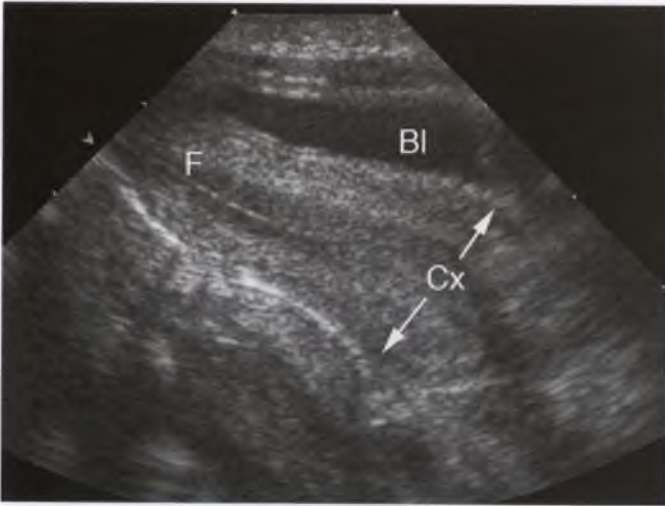


**FIG 28-9** Transabdominal sagittal view of the normal prepubertal uterus. The cervix (Cx) is significantly more prominent than the body or fundus (F) of the uterus. Bl, bladder.

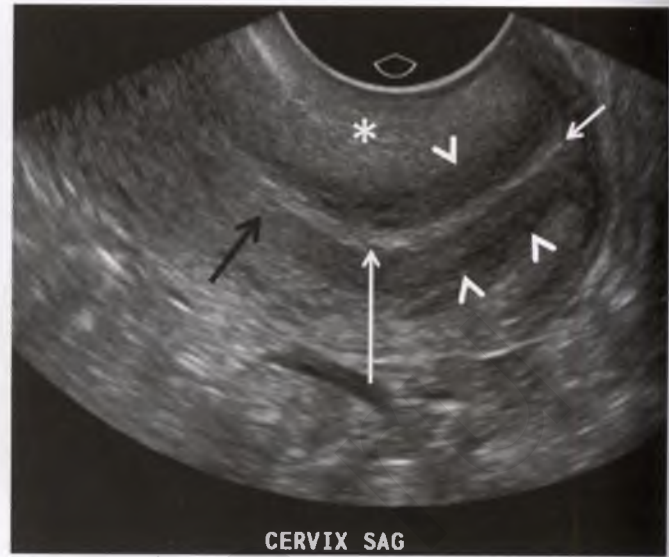


**FIG 28-10** Normal sonographic zonal anatomy of the cervix. Note central linear echogenic endocervical canal (*long white arrow*), subcent hypoechoic fibrous cervical stroma (*arrowheads*), outer muscular layer of intermediate echogenicity (*asterisk*), external os (*short white arrow*) between the lips of the cervix, and internal os (*black arrow*) at the level of narrowing or constriction between the body of the uterus and the cervix.

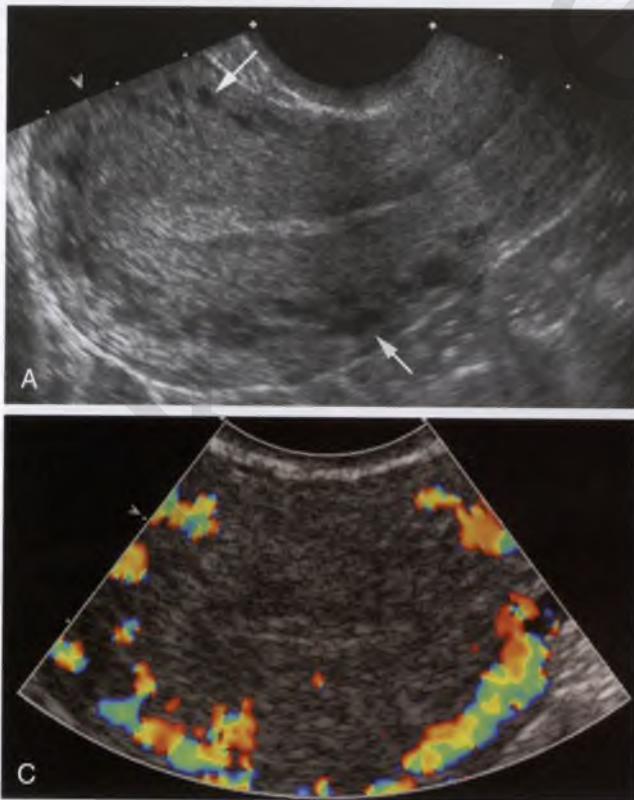


**FIG 28-11** Transvaginal sagittal (A) and transverse (B) sonograms of the uterus demonstrating prominent anechoic round areas (*arrows*) between the outer third and inner myometrium. These are the arcuate vessels, which can mimic cystic changes. C, These cystic appearing spaces are confirmed to be arcuate vessels by applying color Doppler.

ultrasound images, the two widely separated fundal horns with a deep fundal cleft, two uterine cavities, and two separate cervixes can be identified. However, the vaginal septum is better evaluated on physical examination and with MRI or CT (Fig. 28-14), although occasionally 3D ultrasound imaging may be helpful. Unilateral renal agenesis is often present, particularly in the setting of obstructed uterus didelphys.<sup>6</sup>

A rare syndrome that can be seen in the setting of uterus didelphys is obstructed hemivagina and ipsilateral renal anomaly (OHVIRA); some cases do not fit the classic definition. An absent kidney in the expected anatomic location should trigger a search for an ectopic or

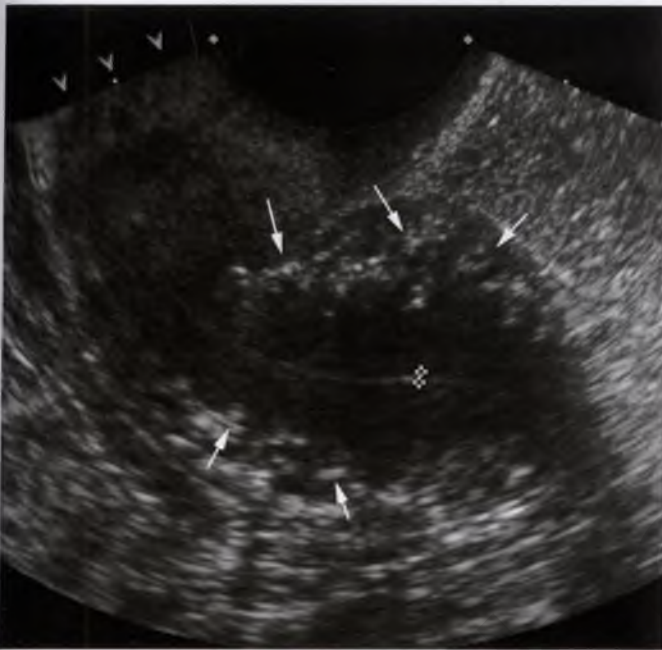


**FIG 28-12** Transvaginal sagittal view of small retroverted and retroflexed uterus in a postmenopausal woman demonstrating arcuate artery calcifications (arrows). Calipers show the endometrium.

possibly a dysplastic/atrophic kidney. If obstructed hemivagina is seen, this finding should also trigger a search for possible ectopic insertion of a ureter.<sup>8,9</sup> Obstructed hemivagina and ipsilateral renal agenesis syndrome should be redefined as ipsilateral renal anomalies: cases of symptomatic atrophic and dysplastic kidney with ectopic ureter to obstructed hemivagina.

Partial fusion of the two müllerian ducts with incomplete fusion at the fundus leads to formation of a bicornuate uterus and a single cervix (Fig. 28-13). The bicornuate uterus is estimated to account for approximately 10% of all müllerian duct anomalies. The fundal contour of the bicornuate uterus is concave, and the two horns are divergent. MRI criteria based on this appearance are an intercornual distance greater than 4 cm and a fundal cleft depth 1 cm or more between the horns.<sup>6</sup> Patients with bicornuate uterus have few reported obstetric problems, and most cases are discovered incidentally. However, an increased incidence of cervical incompetence has been reported.<sup>10</sup> Decreased size of the uterine cavity has also been reported to be associated with poor fetal outcome.<sup>11</sup> Sonographically, in a bicornuate uterus, the endometrial cavities are widely separated, and a deep indentation in the fundal contour is obvious. Imaging of the fundal contour requires obtaining an image in a coronal plane, which is often easiest with transabdominal pelvic ultrasound if the uterus is anteverted and anteflexed or with 3D transvaginal imaging. MRI is often recommended for definitive diagnosis. The bicornuate uterus should be distinguished from a uterine didelphys, and a single cervix should be documented to confirm the diagnosis of a bicornuate uterus (Fig. 28-15). However, if two endocervical canals are present, such as in the bicornuate bicollis uterus, identification of a vaginal septum can be the only way to discriminate between a bicornuate bicollis and didelphys uterus. Unfortunately, one fourth of bicornuate uterus cases have been reported to have a vaginal septum as well, which makes them indistinguishable from didelphys.<sup>6</sup> MRI is the optimal imaging technique for evaluation of vaginal septa. Often in these complex cases with overlapping appearances, it is best to describe what is seen on MRI rather than to attempt to categorize.

Failure of resorption of the septum after complete fusion of the müllerian ducts leads to formation of a septate uterus (Fig. 28-13), which is the most common type of müllerian duct anomaly,

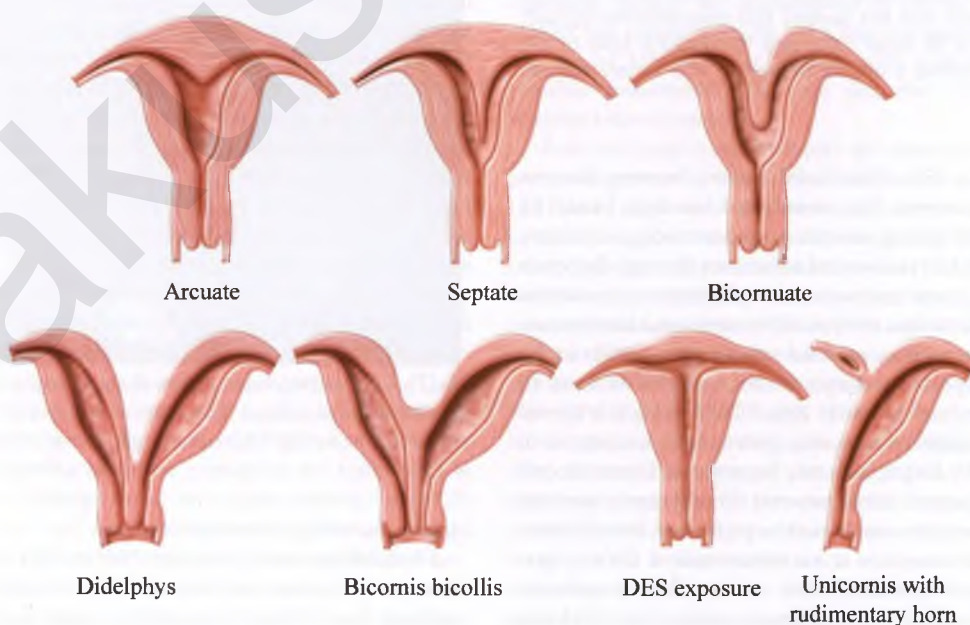


**FIG 28-13** Most common uterine anomalies. DES, diethylstilbestrol. (Illustration by James A. Cooper, MD, San Diego, CA.)



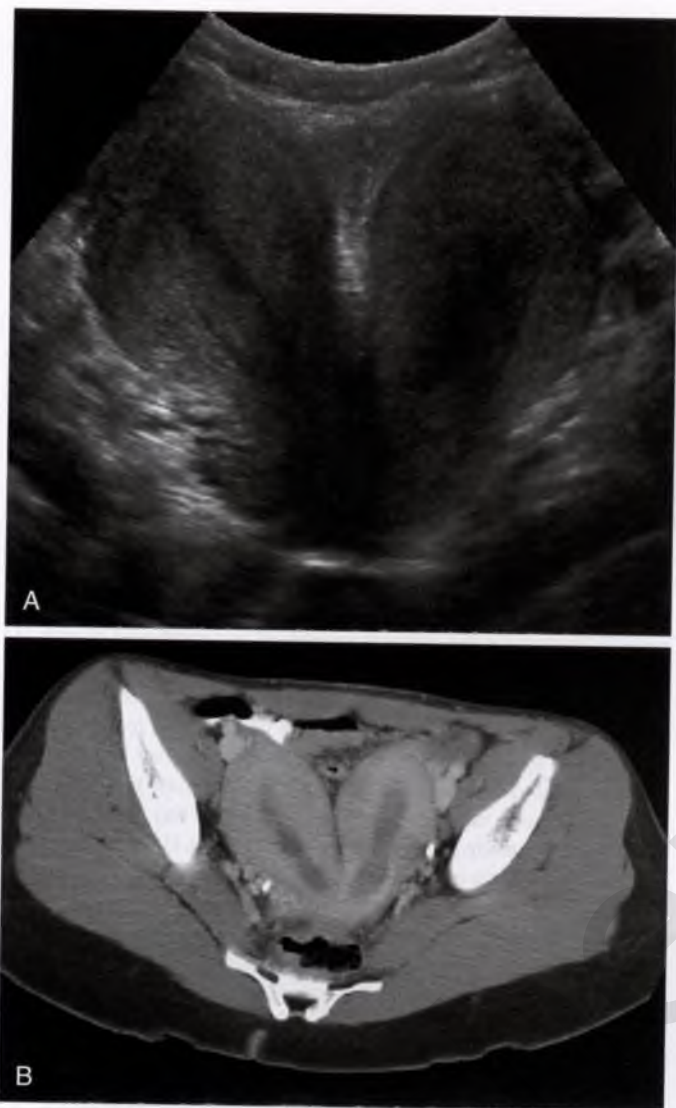


**FIG 28-14** **A**, Coronal transvaginal view of a didelphys uterus with completely separate right and left cavities and deep intervening cleft between the two horns. **B**, Axial computed tomography scan of the same patient demonstrating a uterine didelphys with widely splayed uterine horns.

accounting for close to 55%. The fundal contour between the two endometrial cavities is convex, flat, or indented less than 1 cm. The septum may be partial (if partial resorption has occurred) or complete, extending to the internal cervical os and sometimes through the cervix to the external os. The septum can contain fibrous or myometrial tissue. The endometrial cavities are typically symmetric. Many women with a septate uterus experience repeated miscarriages, usually in the first trimester, with a reported incidence of miscarriage of 65% and an incidence of premature birth of nearly 20%.<sup>11</sup> Confirming this type of anomaly is clinically important because metroplasty is reported to improve fetal survival.<sup>6,12</sup> Metroplasty may be performed hysteroscopically in women with a septate uterus, whereas surgical repair/resection in a patient with a bicornuate uterus must be performed transabdominally, although surgical correction is less often required. On sonography, the smooth fundal contour (either convex, flat, or indented <1 cm) is diagnostic, but requires obtaining an image of the fundus in the coronal plane, which can be difficult on transvaginal imaging and is more easily accomplished with 3D imaging or occasionally with



**FIG 28-15** A coronal three-dimensional image demonstrating a heart-shaped bicornuate uterus. Fundal indentation is well seen (arrow), as well as the widely divergent horns (asterisks) with a single cervix and endocervical canal (arrowhead). (Courtesy of Dr. Beryl R. Benacerraf, Boston, MA.)

transabdominal imaging if the uterus is anteverted and anteflexed. There is less divergence between the two endometrial cavities, which are usually separated by a very thin septum (Fig. 28-16). The septum can extend all the way to the external os or even upper vagina.<sup>6</sup> If the septum does not extend to the internal cervical os, it should be described as a partial septate uterus. Because of superior multiplanar imaging capability, MRI is generally considered the most definitive imaging modality for distinguishing a septate from a bicornuate uterus as obtaining a true coronal image through the uterine fundus is routinely possible on MRI. It is the depth of the fundal notch between the two uterine horns that is the primary diagnostic criterion rather than the composition of the septum. Evaluation of associated renal anomalies and for the presence of a vaginal septum is also easily accomplished with MRI. However, advances in the use of 3D ultrasound have made it possible to visualize the fundal contour in many patients, and 3D sonography is replacing MRI in some centers for at least initial evaluation of uterine congenital anomalies.

An arcuate configuration of the uterus is a normal variant in which the thickened fundal portion of the myometrium slightly indents the endometrial canal, creating a heart-shaped endometrial cavity (Fig. 28-17). This variant occurs when there is near complete resorption of the uterovaginal septum. The external contour of the uterus is normal, either convex or flat. There is a single uterine cavity, and as such, there is little effect on pregnancy outcome, although a high prevalence (12%) of arcuate uterus has been reported in women who have repeated second trimester miscarriages.<sup>13</sup>

Diethylstilbesterol, in use from 1940 to 1970 to prevent miscarriage, was reported to cause uterine anomalies in the female fetus, specifically resulting in a T-shaped endometrial cavity and hypoplastic uterus. Patients with this anomaly are at increased risk for spontaneous abortions, preterm deliveries, and ectopic pregnancies.<sup>6</sup> Sonography will





**FIG 28-16** Coronal three-dimensional image of a septate uterus. Note two separate, but close endometrial cavities, thin hypoechoic septum extending to the level of the internal os, and smooth convex fundal contour without indentation between the two horns. (Courtesy of Dr. Beryl R. Benacerraf, Boston, MA.)

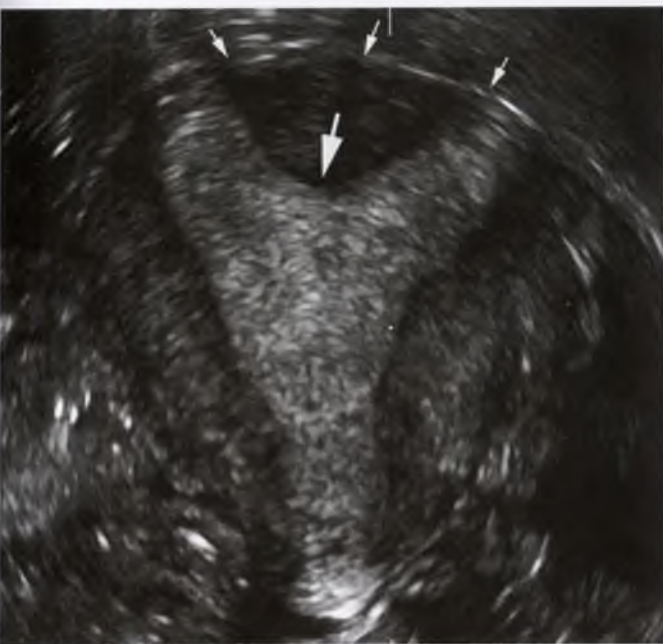


**FIG 28-17** Coronal three-dimensional image of an arcuate uterus with a small myometrial indentation into the fundal aspect of the endometrium (*large arrow*). The outer serosal contour of the uterus is smooth and outwardly convex (*small arrows*).

reveal a small uterus with an irregular T-shaped appearance to the endometrial cavity. 3D sonography with multiplanar capabilities can be of assistance in evaluation of the internal and external contours in these cases. Transvaginal sonography remains the primary imaging modality, although MRI is used as a problem-solving technique in more challenging cases.<sup>14</sup>

In conclusion, the visualization of the fundal contour is paramount, looking for a cleft larger or smaller than 1 cm in differentiating fusion anomalies (didelphys and bicornuate) from resorption anomalies (septate and arcuate). 3D imaging can be very effective, but if inconclusive, MRI is helpful for definitive diagnosis.

## BENIGN UTERINE CONDITIONS

### Adenomyosis

Although often overlooked, adenomyosis is a common condition, reported in up to 70% of hysterectomy specimens. Adenomyosis is characterized by migration of endometrial glands and stroma from the stratum basale into the myometrium. This often occurs in association with reactive hyperplasia of the surrounding myometrial smooth muscle, which interdigitates with the ectopic endometrial tissue. The ectopic endometrial glands tend to be found at least 2 to 3 mm below the endometrial-myometrial junction. Two widely accepted theories for the cause of adenomyosis are that it either results from a defect in or absence of the basement membrane at the endometrial-myometrial junction or that it is related to endometrial migration through lymphatic or vascular channels. Possible risk factors include uterine trauma such as childbirth or uterine instrumentation, chronic endometritis, and hyperestrogenism.<sup>3,4,15,16</sup>

Adenomyosis is most prevalent among middle-aged women who have had children and is much less commonly seen in nulliparous or postmenopausal patients. Although many patients are completely asymptomatic, common presenting symptoms include uterine tenderness, dysmenorrhea, menorrhagia, and uterine enlargement. These symptoms are nonspecific and are very similar to the symptoms seen in patients with uterine leiomyomas, pelvic congestion syndrome, endometriosis, endometrial polyps, and endometrial carcinoma. Given the marked differences in prognosis and therapy between these entities, accurate diagnosis is extremely important. Symptoms can be extremely debilitating, and misdiagnosis can prolong the time course before appropriate care is instituted. Therapeutic regimens such as gonadotropin-releasing hormone inhibitors, oral contraceptives, nonsteroidal anti-inflammatory drugs, oral contraceptives, and endometrial ablation are available, but are not always fully effective.<sup>3,4,15,16</sup> An emerging therapy for adenomyosis is uterine artery embolization (UAE), but reported results from this treatment are inconsistent and the use of UAE to treat patients with symptomatic adenomyosis remains controversial. The only definitive treatment at this time remains hysterectomy.<sup>17</sup>

Both sonography and MRI play an important role in the diagnosis and management of women with adenomyosis. Imaging is also used to evaluate response to treatment and progression of the disease. For optimal diagnosis, transvaginal sonography should be performed using high-frequency transducers, between 5 to 10 MHz. The reported sensitivity and specificity of transvaginal sonography for identifying adenomyosis range from 53% to 89% and 67% to 98%, respectively, and overall accuracy is reported to range from 68% to 86%. The sensitivity of MRI is reported to range from 78% to 88% and specificity from 67% to 93%.<sup>4,16</sup> Although MRI and sonography are reported to have similar accuracy in diagnosing this condition, sonography is most often the first imaging study obtained in patients with the symptoms described previously.<sup>3,4,15</sup> However, MRI is considered to have better specificity and accuracy, particularly in women with associated disorders,<sup>18</sup> and it is also important to recognize that leiomyomas and adenomyosis often coexist (>60%), making accurate and specific diagnosis of the cause of symptoms more difficult.

The imaging features of adenomyosis derive from the presence of the ectopic endometrial glands within the myometrium, as well as the



surrounding stromal reaction of densely packed smooth muscle cells. This process often results in globular enlargement of the uterus without a discrete mass or contour deformity. Although focal adenomyomas can develop, they are rare and are unlikely to cause a contour abnormality, as leiomyomas often do. The previously described sonographic zonal anatomy of the uterus is altered in patients with adenomyosis. The subendometrial halo becomes thicker and more irregular, either diffusely or focally. Poor definition of the endometrial-myometrial junction with pseudo-widening of the endometrial echo complex is caused by heterotopic endometrial tissue extending from the stratum basale. The subjacent myometrium may become heterogeneous with areas of increased or decreased echogenicity. Tiny punctate echogenic foci may be noted in the involved area. Hypoechoic striations may radiate throughout the involved parenchyma and extend posteriorly, believed to be edge shadowing due to the extensive smooth muscle hypertrophy. Although this shadowing is very similar to shadowing caused by leiomyomas, areas of adenomyosis lack distinct margins and mass effect and are more irregular and less rounded, as opposed to leiomyomas, which are typically round and sharply marginated. Small anechoic cysts, which on pathologic examination correspond to dilated endometrial glands, are often observed in the subendometrial myometrium, particularly during the secretory stage of the menstrual cycle. Hyperechoic foci, either linear or nodular, may extend directly from the endometrium into the myometrium and are believed to represent foci of ectopic endometrial tissue (Fig. 28-18). Color Doppler examination can also be helpful in differentiating adenomyosis from leiomyomas. Areas of adenomyosis often demonstrate diffuse hypervascularity throughout the lesion, whereas peripheral rather than internal blood flow is most commonly observed on color Doppler interrogation of leiomyomas.

Focal adenomyosis, or adenomyoma, presents with a more atypical appearance (see Fig. 28-18) and is visualized as a focal mass with poorly defined margins, in contrast to leiomyomas, which have distinct margins. Occasionally a focal adenomyoma is primarily cystic in appearance and may sometimes be found on MR to be filled with blood products. It is important to differentiate between adenomyomas and leiomyomas. At surgery, leiomyomas can often be easily separated and removed from the adjacent myometrium, whereas adenomyomas are not easily separated from the surrounding myometrium because of the surrounding smooth muscle hypertrophy. Therefore, adenomyosis or adenomyomas cannot be focally excised for cure.

Sonography has a reported sensitivity of 80% to 87% and a specificity of 94% to 98% in differentiating between adenomyosis and leiomyomas. The most specific ultrasound findings are the small anechoic myometrial cysts (seen best in the second half of the menstrual cycle) and the echogenic linear striations or nodules extending from the endometrium into the subjacent myometrium. Myometrial contractions can cause heterogeneity of the myometrium and apparent thickening of the subendometrial halo on ultrasound images and the junctional zone on MRI, thereby mimicking adenomyosis. When difficulties arise in sonographic diagnosis, MRI can be helpful in achieving a more definitive diagnosis. However, focal adenomyomas may be difficult to differentiate from leiomyomas with both imaging modalities.<sup>4,16</sup> In particular, on the rare occasions when an adenomyoma protrudes into the endometrial cavity, it will appear identical to a intracavitary polyp or pedunculated submucosal or intracavitary leiomyoma. Some authors consider polypoid adenomyomas a separate entity from adenomyosis.<sup>19</sup>

Endometrial abnormalities, such as hyperplasia and carcinoma, are reported to occur more often in patients with adenomyosis.<sup>3,15</sup> Rarely, an adenocarcinoma has been reported to arise from within a focus of adenomyosis. Adenocarcinoma would be very difficult to distinguish on any imaging modality from typical adenomyosis without

**TABLE 28-1 Features of Adenomyosis**

Diffusely globular uterus with smooth external uterine contour
Asymmetric globularity
Myometrial cystic areas/echogenic foci
Pseudo-thickening of the endometrium
Diffuse increased internal vascularity
Striated edge shadows/"venetian blind" shadowing without a discrete mass
Focal ill-defined mass
Features that help to differentiate from leiomyomas
Smooth external contour of uterus
Minimal mass effect on serosa/endometrium relative to the size of the lesion
Lack of calcification
Ill-defined margins
Central versus peripheral vascularity

malignancy (see Fig. 28-18). A more common scenario would be an endometrial carcinoma extending into foci of adenomyosis. In cases in which adenomyosis coexists with endometrial cancer, it is very difficult to determine whether the cancer is insinuating into preexisting areas of adenomyosis or if there are areas of true myometrial invasion. This distinction is crucial because myometrial invasion is an important prognostic indicator. However, it cannot always be achieved on imaging and can even be very difficult to determine on histopathologic examination (Table 28-1).<sup>20</sup>

### Leiomyomas

Leiomyomas (fibroids or myomas) are benign smooth muscle neoplasms with varying amounts of fibrous tissue and are the most common uterine neoplasm, reported in 20% to 30% of women over 30 years of age. Leiomyomas are more common in African-American women. Other risk factors include obesity, early age of onset of menstruation, and a diet rich in red meat. There may be a genetic predisposition. These tumors are usually multiple, causing enlargement of the uterus with a lobular serosal contour unlike adenomyosis, which results in globular but smooth-contoured uterine enlargement.

Leiomyomas most commonly present with a palpable pelvic mass, uterine enlargement, pelvic pain, anemia, and dysfunctional uterine bleeding. Symptoms are largely related to location and size. The vast majority of leiomyomas are intramural, submucosal (including intracavitary), or subserosal in location. Subserosal leiomyomas may be exophytic or pedunculated (Fig. 28-19). Intramural leiomyomas are most common, but are least likely to be symptomatic. On rare occasions, an exophytic leiomyoma will project into the broad ligament (intraligamentous). In these instances, the leiomyoma may clinically and radiologically simulate an ovarian mass (Fig. 28-20). A leiomyoma can also arise in the cervix (see later). An unusual form of leiomyoma is the parasitic leiomyoma, a pedunculated subserosal myoma that, if in close contact with an adjacent structure, can parasitize the blood supply and even become detached from the uterus. This classification of leiomyomas is relevant because symptoms and treatment vary according to their location and subtype.<sup>21</sup> However, when leiomyomas are large, they may be difficult to classify according to this scheme (Fig. 28-21).

Growth of leiomyomas is dependent on estrogen levels. Rapid growth in pregnancy is reported in about 50% of patients (Fig. 28-22). When rapidly growing, leiomyomas can outgrow their blood supply, resulting in degeneration or infarction.<sup>21</sup> Leiomyomas are associated with increased risk of early pregnancy failure, especially in women with multiple gestations.<sup>22</sup> Leiomyomas located in the cervix and lower uterine segment can interfere with vaginal delivery and should be



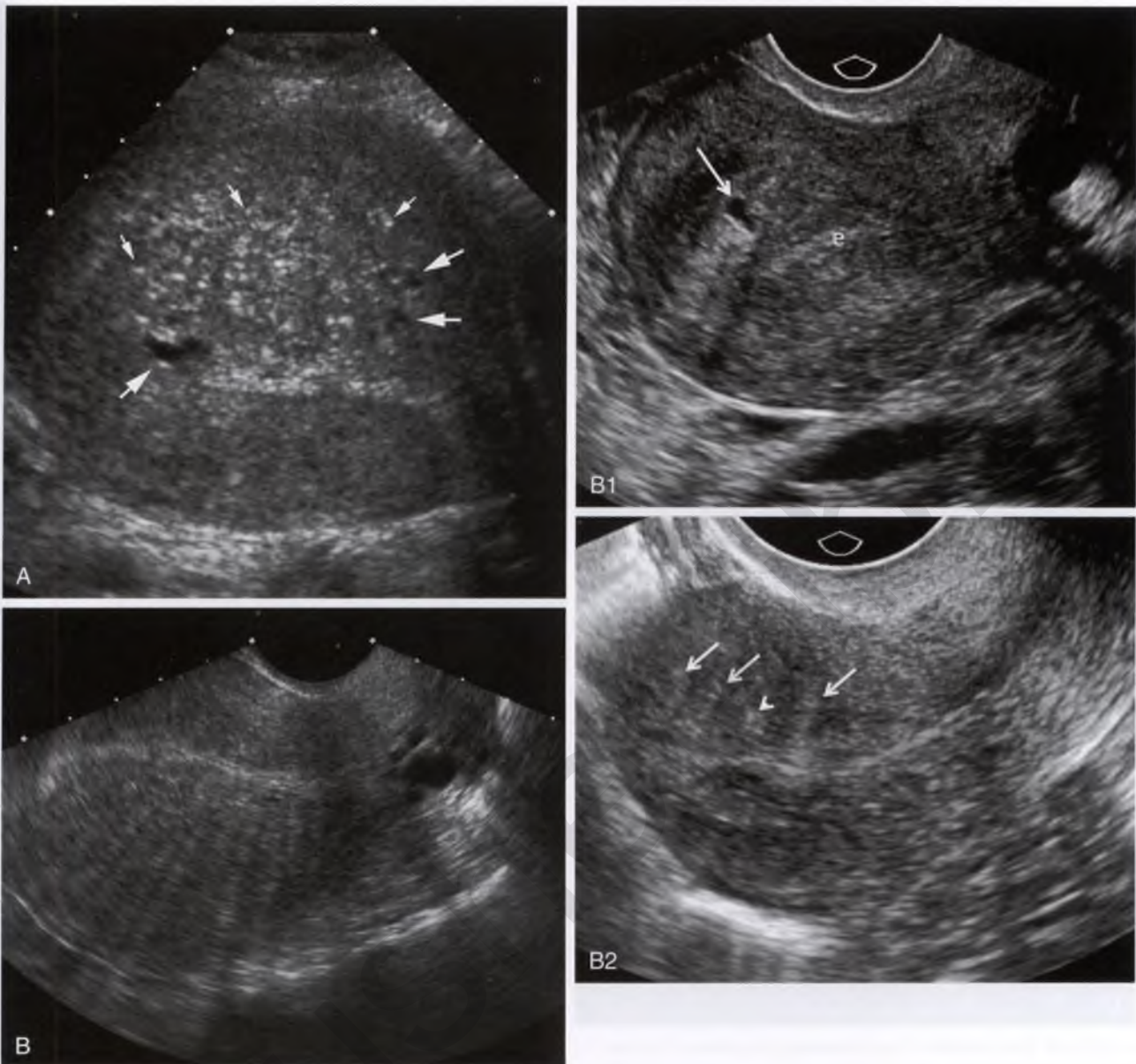


**FIG 28-18** Adenomyosis: spectrum of appearances. **A**, Enlarged uterus with typical features of adenomyosis. Multiple bright echogenic foci are seen throughout the myometrium (*small arrows*) in addition to numerous subendometrial myometrial anechoic cysts (*large arrows*). **B**, Sagittal sonogram of the uterus demonstrating numerous thin hypoechoic, "venetian blind" or "comb-like" striations in the posterior myometrium. Although a similar pattern of striations may be seen with leiomyomas, the absence of a focal mass, the increased thickness of the posterior wall of the uterus compared to the anterior wall, and the presence of several small subendometrial myometrial cysts make this more characteristic of adenomyosis. **B1**, Sagittal transvaginal sonographic image demonstrating heterogeneity of the myometrium and two adjacent small myometrial cysts (*arrow*) with increased through transmission. Such myometrial cysts are believed to be a very specific finding for adenomyosis. *e*, endometrium. **B2**, Sagittal transvaginal sonographic image demonstrating heterogeneity of the myometrium, which is also relatively hypoechoic. Note several echogenic linear striations extending from the endometrium into the myometrium (*arrows*) and one nodular echogenic area (*arrowhead*) in the subendometrial tissue. A similar pattern of endometrial tissue extending into the myometrium can be seen on magnetic resonance imaging (MRI) and is believed to be another relatively specific finding for adenomyosis.

*Continued*



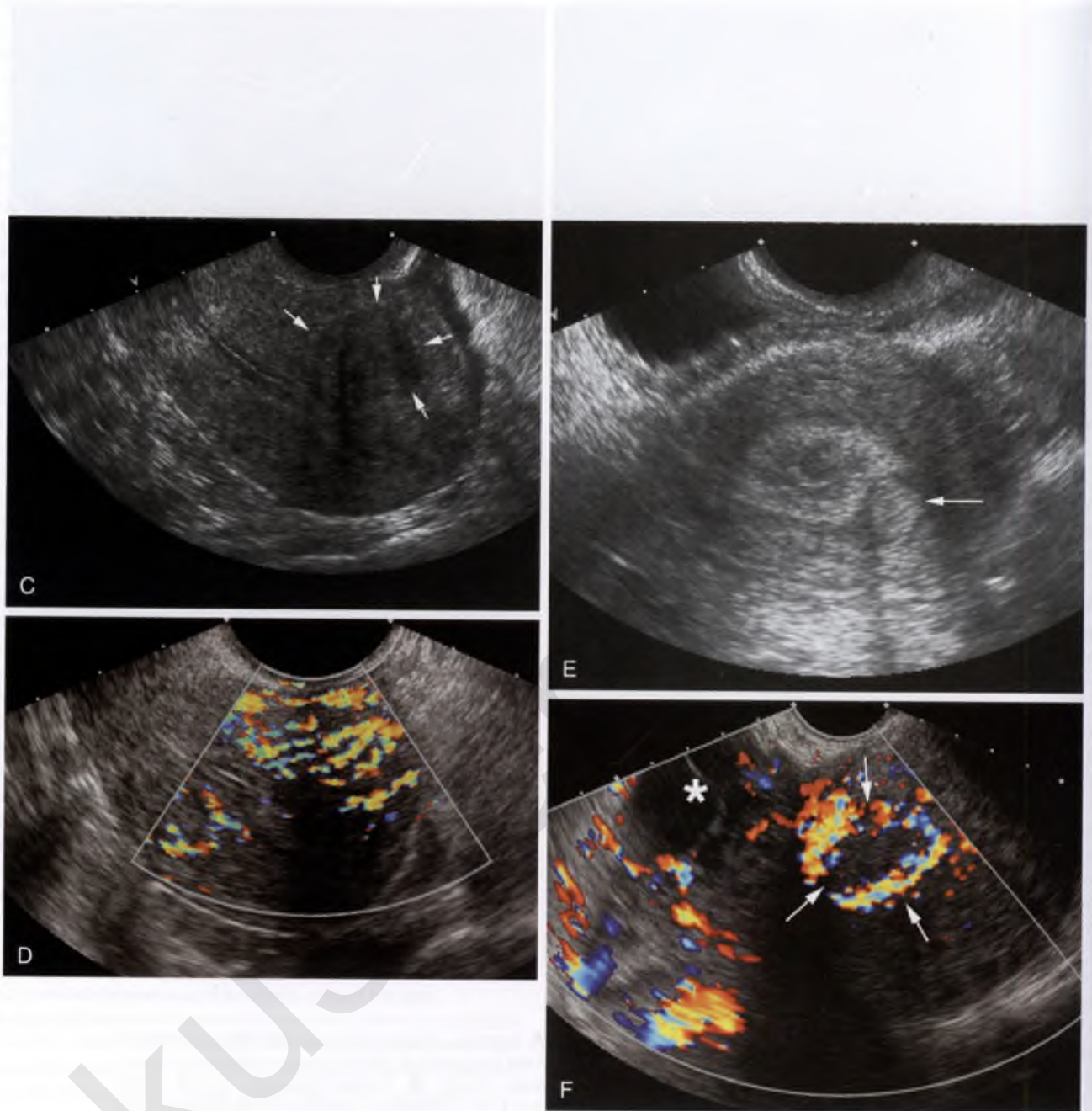


**FIG 28-18, cont'd C**, Transvaginal sonogram in a patient with a focal hypoechoic adenomyoma (*arrows*). On gray-scale imaging it can be very difficult to differentiate a focal adenomyoma from an intramural leiomyoma. **D**, Color Doppler image of the same patient in C, demonstrating increased vascularity within the adenomyoma. Such increased vascularity would be atypical for a leiomyoma. **E**, Another patient with an adenomyoma. In this case the adenomyoma is hyperechoic (*arrow*), indenting but separate from the endometrium. **F**, Transvaginal color Doppler image of a patient with an adenosarcoma arising in the background of adenomyosis with sarcomatous overgrowth. Note intense peripheral vascularity (*arrows*) surrounding a mass thought to represent an adenomyoma arising in the background of diffuse adenomyosis. A large cystic and solid mass (*asterisk*) is seen on the right, which was thought to be of ovarian origin.

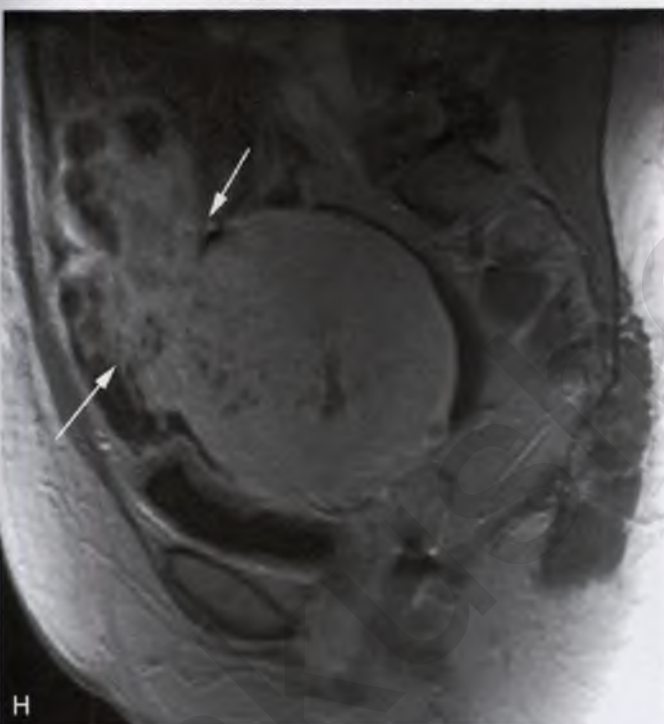
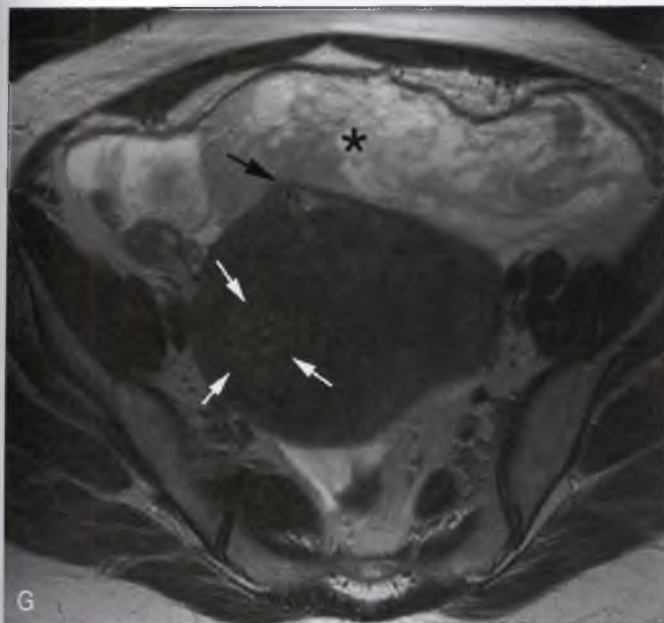


**FIG 28-18, cont'd G,** Axial T2 weighted MRI image better demonstrates the extent of the adenomyosis (diffuse low signal intensity of the myometrium) as well as the more focal adenomyoma (*white arrows*) with numerous small hyperintense foci. A small subtle area of serosal breakthrough is noted (*black arrow*), which represents "expelling" of the adenocarcinoma depicted as a large high T2W signal heterogeneous mass noted anteriorly (*asterisk*). **H,** Sagittal postcontrast T1W image demonstrates tumor extending from the uterine wall through the serosal surface into the anterior pelvis (*arrows*). The final pathologic image demonstrated endometrial stromal sarcoma with heterogeneous differentiation, FIGO stage III (International Federation of Gynecology and Obstetrics).

monitored during pregnancy. Conversely, leiomyomas may precipitously decrease in size and even infarct following delivery as estrogen levels drop. As estrogen levels decline in older women, leiomyomas typically regress and thus are rarely symptomatic in postmenopausal patients.<sup>21</sup>

Leiomyomas are readily recognized on sonography, although the sonographic appearance is variable. In the past, the diagnosis of leiomyomas was often suggested on ultrasound images if the uterus was heterogeneously enlarged, especially if the contour was lobular. However, in today's ultrasound practice, most leiomyomas are readily identified as focal, sharply marginated myometrial masses, and a diffusely heterogeneous enlarged uterus is more likely to indicate adenomyosis. Leiomyomas may be hypoechoic, isoechoic, or echogenic relative to the myometrium, although the majority are hypoechoic. The surrounding myometrium can become compressed and form a pseudocapsule, which can be readily identified on ultrasound images as well as MRI (Fig. 28-23). Occasionally compressed lymphatics and vessels can create a thin hypoechoic rim around intramural leiomyomas (Fig. 28-21A). Although small leiomyomas are typically homogeneous, leiomyomas larger than 3 cm in diameter are often heterogeneous (Fig. 28-24). As leiomyomas increase in size, they tend to outgrow their blood supply, which leads to degeneration: hyaline, myxoid, cystic, or hemorrhagic (Fig. 28-25). Degenerated leiomyomas have a more atypical appearance on sonography and MRI (Fig. 28-26).<sup>21,22</sup> Degeneration may result in edema with cystic spaces, echogenic hemorrhagic areas, and dystrophic calcification. Dystrophic calcification occurs predominantly in postmenopausal patients. The calcifications can be curvilinear and peripheral or clump-like and will demonstrate dense posterior shadowing. Many leiomyomas demonstrate areas of acoustic attenuation even if they do not contain obvious calcifications. The posterior shadowing may be dense or striated (comb-like). This attenuation is believed to be caused by the transitional zone between apposed tissues of different acoustic properties such as fibrous tissue and smooth muscle, as well as refraction from the edges of whorls and bundles of smooth muscle.<sup>23</sup> This characteristic shadowing is very helpful in differentiating an exophytic leiomyoma from an adnexal or ovarian mass. However, the smooth muscle hypertrophy associated with adenomyosis may also cause a striated pattern of posterior shadowing and a similar appearance (Fig. 28-27). Edge refraction at the interface of the leiomyoma with the normal surrounding myometrium is common and may help to identify a leiomyoma that is isoechoic to the normal myometrium. Peripheral blood flow is commonly observed on color or power Doppler images; it is much less common to detect internal vascularity in a benign leiomyoma with color Doppler imaging.

Submucosal leiomyomas may present with menorrhagia, menometrorrhagia, and even anemia, requiring definitive treatment with resection. Submucosal leiomyomas can have varying degrees of intracavitary extension. Both size and the degree to which a leiomyoma projects into the endometrial cavity will determine the likelihood of successful hysteroscopic resection. Leiomyomas with 50% or greater intracavitary extension are more easily resected via hysteroscopy. Until recently, sonohysterography was considered the best modality to determine the degree of intracavitary extension of a leiomyoma (Fig. 28-28). More recently, 3D sonography has proved to be useful as well (Fig. 28-29).

Transvaginal imaging may be limited if the leiomyomas are large or pedunculated. In this situation, transabdominal imaging may improve visualization. MRI is a valuable modality to evaluate large or atypical leiomyomas, as the multiplanar capability and larger field of view are particularly useful.



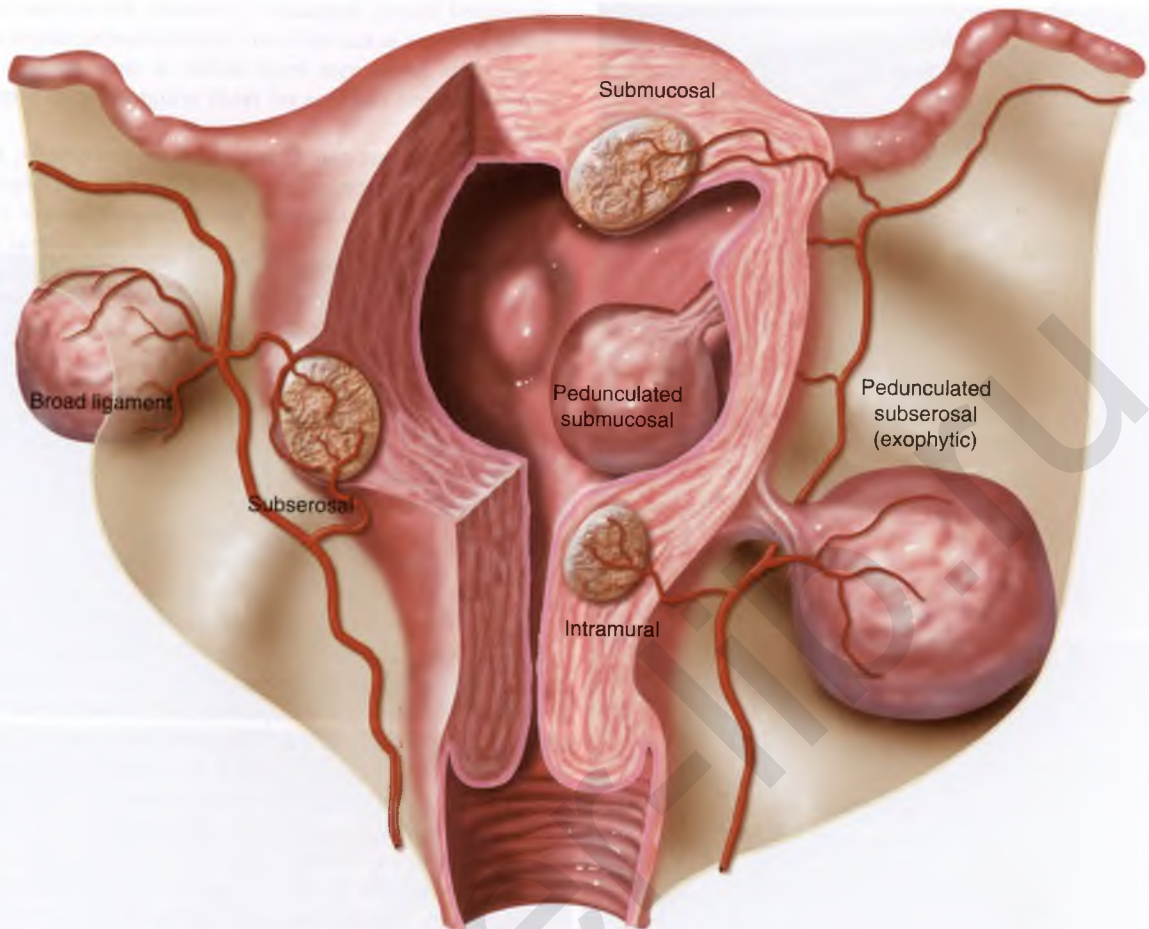


**FIG 28-19** Common locations of leiomyomas. (Illustration by James A. Cooper, MD, San Diego, CA.)



**FIG 28-20** Transverse abdominal sonogram. A left adnexal solid mass (*asterisk and calipers*) is seen. Although the location would make one think of an ovarian mass, it was in fact a broad ligament myoma. Ut, uterus.

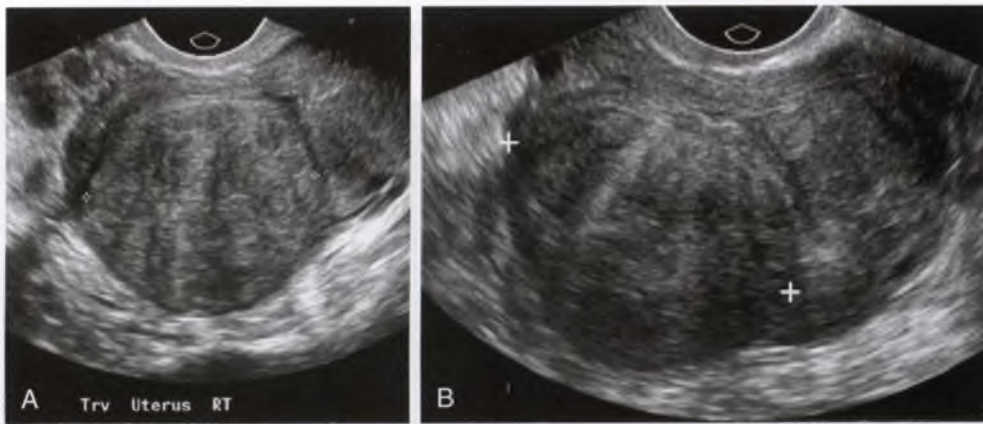


**FIG 28-21** Classification of large leiomyomas. **A** and **B**, When leiomyomas are large, they may appear to be intramural as well as either submucosal or subserosal in location. In these two patients, the leiomyomas (*calipers*) appear to have their epicenter in the myometrium, hence they are predominately intramural in location. However, they both extend beyond the serosal contour of the uterus, giving the uterus a lobular configuration. Thus, they both appear to have a subserosal component. These large masses are somewhat heterogeneous in echotexture. Note the thin peripheral hypoechoic rim partially encompassing the leiomyoma in **A**, likely representing compressed lymphatics or vessels. The lesion in **B** demonstrates several linear areas of shadowing, likely due to dense fibrous or collagenous material within the leiomyoma.

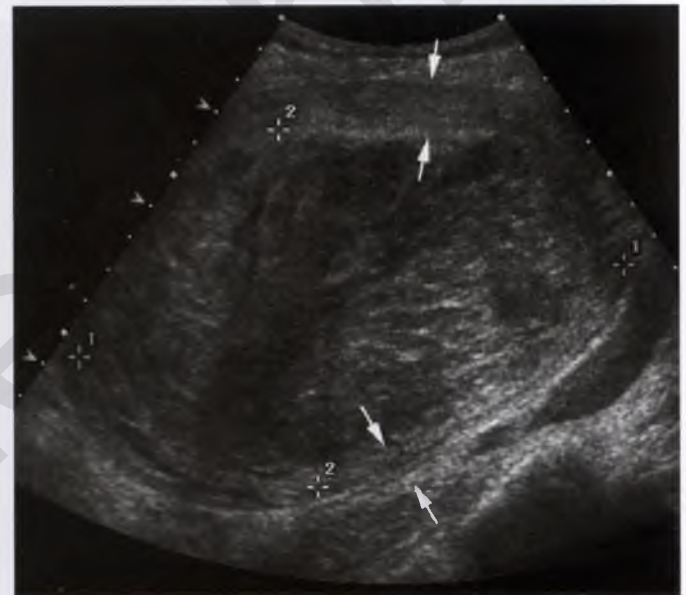


**FIG 28-23** Large uterine myoma (*calipers*). Surrounding compressed myometrium (*arrows*) has created a pseudocapsule.

**FIG 28-22** **A**, Longitudinal sonogram in a pregnant patient at 18 weeks' gestational age. An anterior lower uterine segment leiomyoma (*arrows*) is seen. It does not obstruct the cervix (demarcated by *calipers*). Bl, bladder. **B**, Well-circumscribed, heterogeneous leiomyomas (*arrows*) in the anterior wall of the uterus in another pregnant patient.



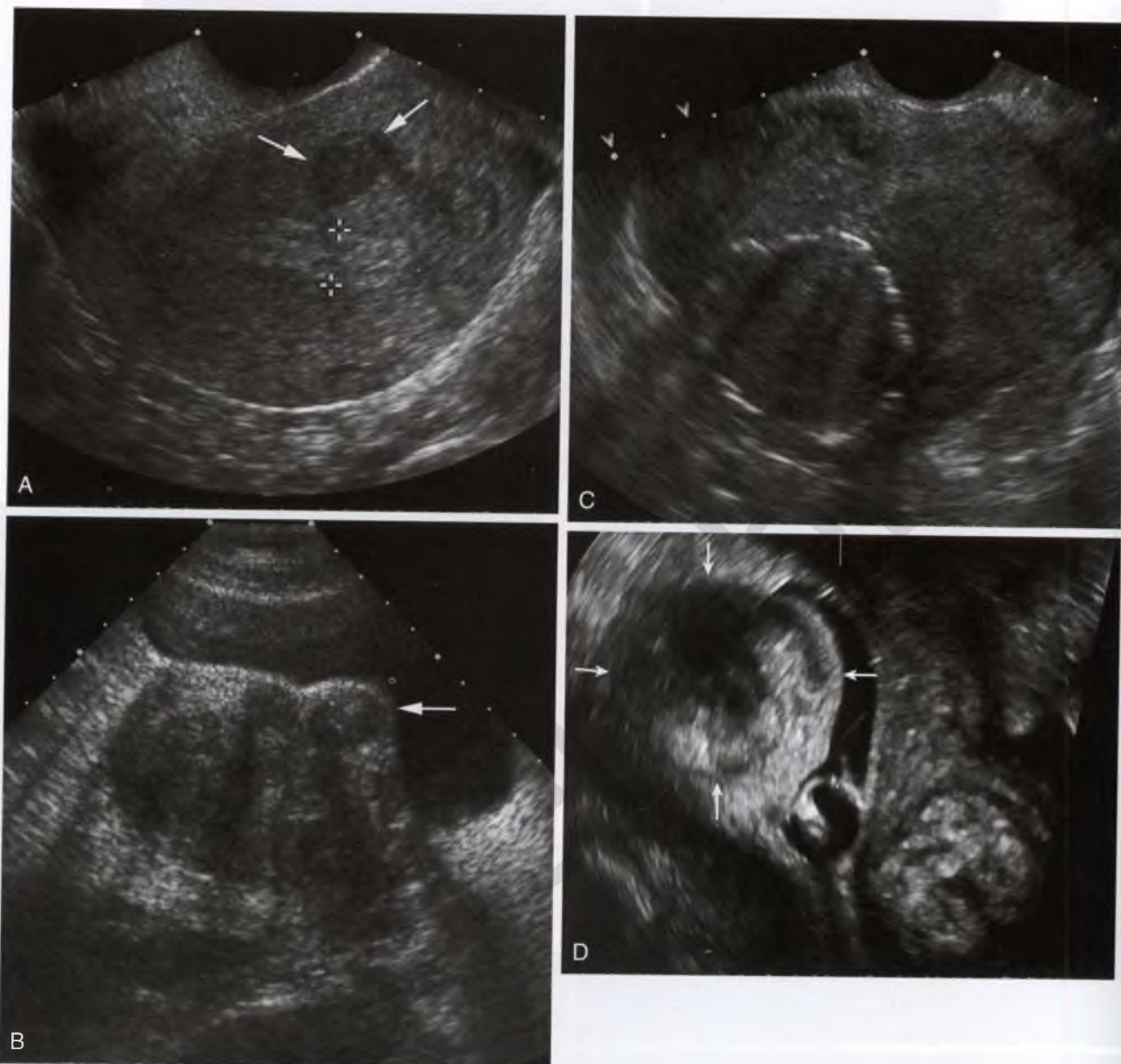


**FIG 28-24** Variable appearance of uterine leiomyomas. **A**, Sagittal transvaginal sonogram demonstrating a small, round, well-circumscribed hypoechoic intramural leiomyoma (*arrows*) separate from the endometrium (*calipers*) in a patient with a retroflexed uterus. **B**, Longitudinal transabdominal sonogram in a patient with multiple uterine leiomyomas. The normal morphologic appearance of the uterus is markedly distorted. The myometrium is heterogeneous and the endometrium could not be identified. An anterior subserosal leiomyoma (*arrow*) distorting the serosal contour projects into the urinary bladder. **C**, Transvaginal sonogram of a leiomyoma demonstrating peripheral echogenic thin rim calcification. **D**, Coronal three-dimensional reconstruction after saline infusion demonstrates a heterogeneous but predominantly echogenic submucosal leiomyoma (*arrows*) with a near 50% intracavitary component.

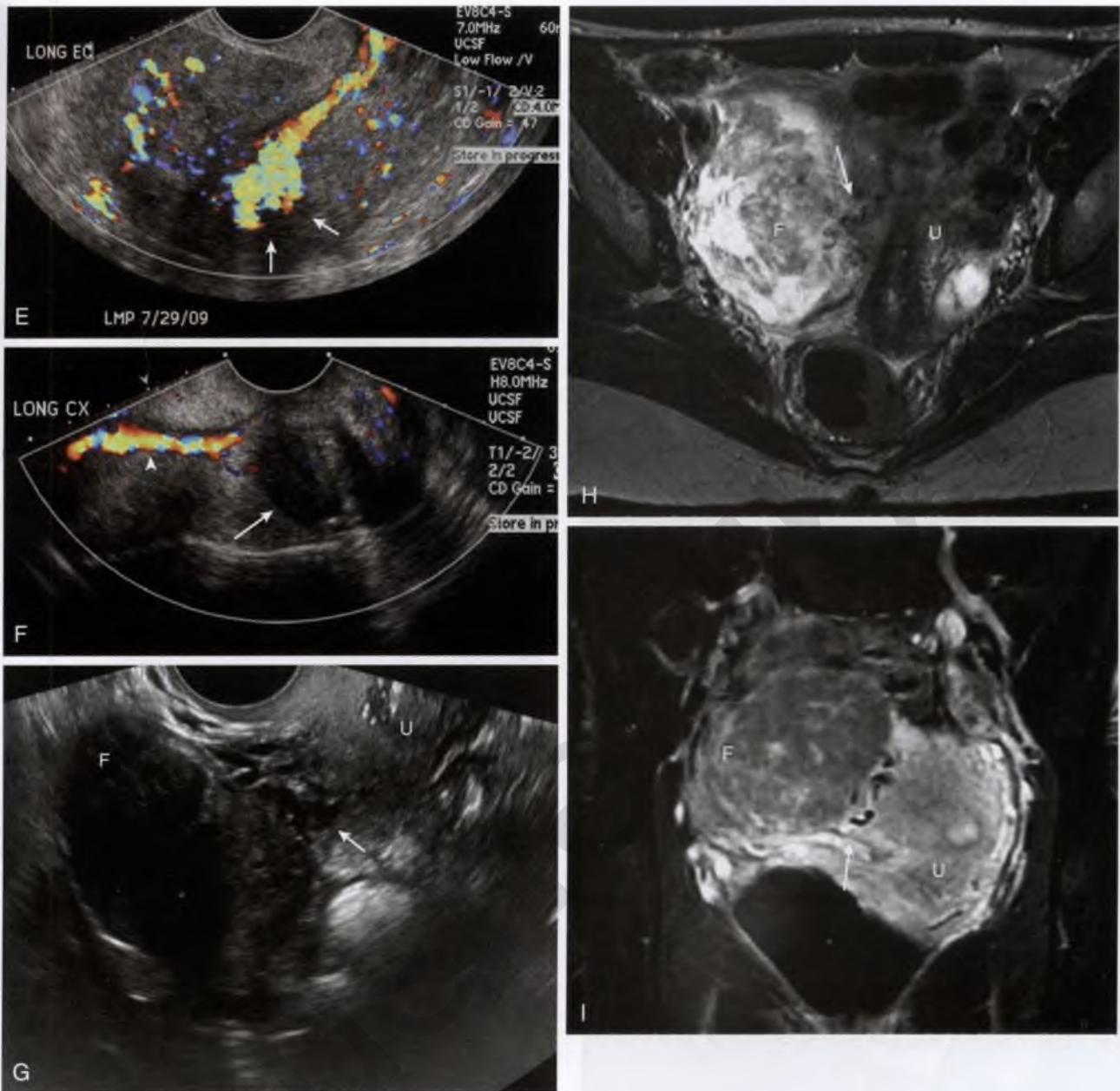


**FIG 28-24, cont'd** **E**, Transvaginal sagittal view of the uterus demonstrating a hypervascular stalk (*arrows*) arising from the posterior wall of the uterus and extending through the endometrial canal into the endocervical canal (right side of image). **F**, The hypervascular stalk (*arrowhead*) is connected to a well-demarcated, rounded, hypoechoic mass (*arrow*) with posterior shadowing that splays the endocervical canal, consistent with a prolapsed leiomyoma. Without the color Doppler demonstration of the vascular stalk, these findings could mimic a cervical leiomyoma. **G**, Transvaginal transverse view of a hypoechoic, slightly lobular shadowing pedunculated leiomyoma (F) in right adnexa. Uterus (U) is medial to the leiomyoma. Tubular anechoic structures (*arrow*) between the leiomyoma and the uterus represent vessels in the bridging pedicle. The bridging vascular pedicle sign is often better seen on magnetic resonance imaging (MRI) and has been reported to be present in more than 70% of pedunculated leiomyomas. **H**, Axial T2-weighted (T2W) MRI image of the right pedunculated leiomyoma (F), demonstrating black (T2 dark) squiggly flow voids of vessels within the pedicle (*arrow*). U, uterus. **I**, Coronal T2W with fat saturation MRI image demonstrating the pedunculated right leiomyoma (F), medially displaced uterus (U), and T2 dark flow voids (*arrow*) in the vascular pedicle.



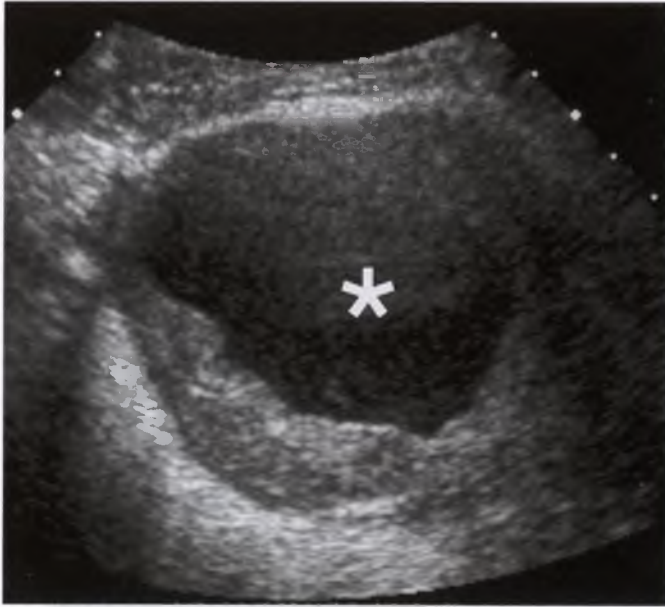


**FIG 28-25** Marked cystic degeneration with large anechoic fluid component (*asterisk*) of a large intramural leiomyoma.

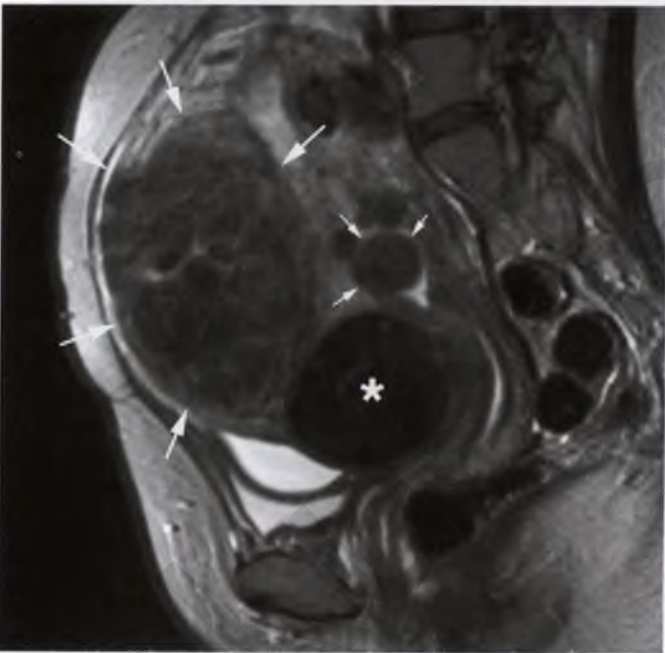


**FIG 28-26** Sagittal T2-weighted (T2W) magnetic resonance image demonstrating various different but common appearances of leiomyomas: small submucosal leiomyoma impressing the endometrial canal with typical low T2W signal (*small arrows*), large anterior intramural leiomyoma (*large arrows*) with internal edema and degeneration (*white areas*), and anterior lower uterine segment leiomyoma (*asterisk*) with extremely low T2W signal consistent with internal blood products/hemosiderin from “red degeneration.”

### Lipomatous Uterine Tumors

Lipomatous tumors of the uterus are rare benign neoplasms and are readily recognized on ultrasound images. The histologic spectrum includes pure lipomas, lipoleiomyomas, fibrolipomas, and myolipomas (Fig. 28-30).<sup>24</sup> A lipoleiomyoma is characterized histologically by

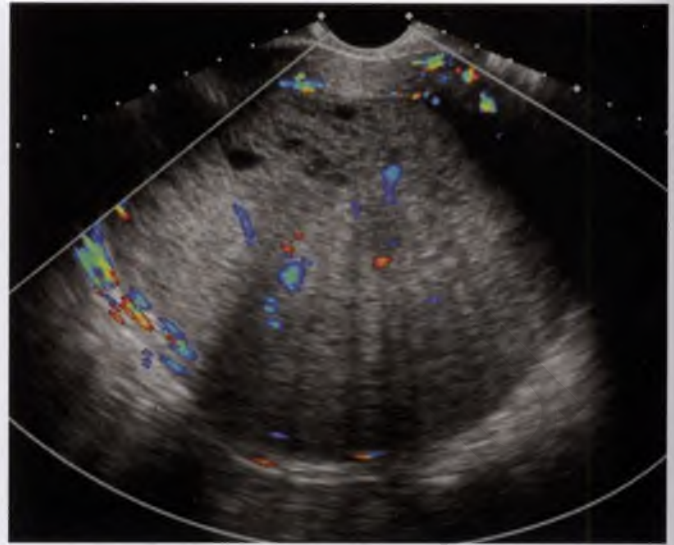


**FIG 28-27** Large relatively echogenic leiomyoma demonstrating small anechoic rounded areas of cystic change anteriorly as well as “venetian blind” shadowing. Both of these features are quite similar to ultrasound findings of adenomyosis.

the presence of mature lipocytes as well as smooth muscle cells and fibrous tissue. Sonographically, these lesions are characteristically extremely echogenic and located within the myometrium. However, occasionally cellular leiomyomas can be extremely echogenic. The margins are typically sharp, but can be lobular. Posterior attenuation may be observed owing to the fat content. Usually there will be no demonstrable color Doppler flow. Lipomatous lesions are usually asymptomatic and do not require surgery. Because mixed lesions can have a more heterogeneous appearance and less characteristic appearance on ultrasound images, MRI can be used to confirm the presence of macroscopic fat within the lesion and therefore confirm that they are benign.

## MALIGNANT CONDITIONS

### Gestational Trophoblastic Disease

GTD is a spectrum of rare diseases characterized by the presence of abnormal trophoblastic proliferation that includes genetically abnormal conceptions with neoplastic potential (i.e., complete hydatidiform moles [CHMs] and partial hydatidiform moles [PHMs] as well as gestational trophoblastic neoplasms [GTNs] or persistent trophoblastic neoplasia [PTN]) including invasive moles and choriocarcinomas (Fig. 28-31A). Risk factors for GTD include extremes of maternal age (under the age of 20 and over the age of 35 years, especially over the age of 50 years) as well as history of prior molar pregnancy. In addition, GTD is much more common in women of Asian origin. The presence of a highly sensitive biomarker, beta-human chorionic gonadotropin (hCG), as well as the availability of effective chemotherapeutic regimens has dramatically improved survival rates.<sup>25</sup>

The most common type of GTD is the CHM. CHMs constitute 80% of GTD, with an incidence of approximately 0.5 to 1 per 1000.<sup>26</sup> Patients most commonly present with vaginal bleeding, sometimes with passage of vesicles, and with markedly elevated serum hCG levels. As the diagnosis is now most often made earlier in the first trimester, hyperemesis and an enlarged uterus for dates are less commonly observed. The genetic material in a CHM is entirely paternal in origin. Most CHMs have a 46,XX diploid karyotype secondary to fertilization of a genetically empty egg by two haploid sperm. At pathologic



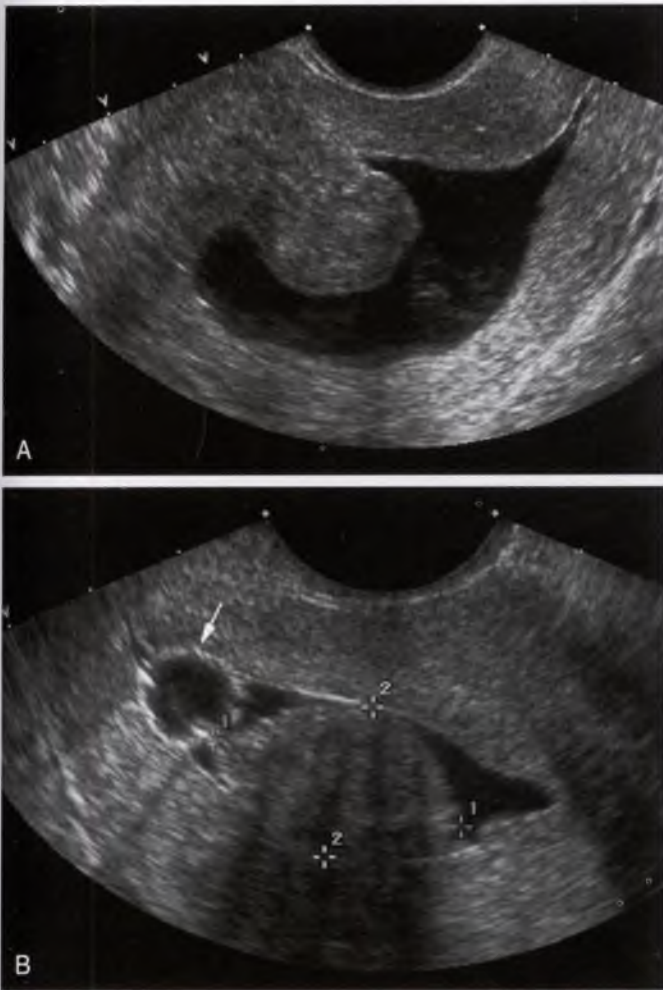


**FIG 28-28** Saline infusion sonohysterography (SIS) in two patients with submucosal, predominantly intracavitary leiomyomas. **A**, Sagittal view from a sonohysterogram demonstrating a myoma that is isoechoic to the myometrium projecting into the uterine cavity that is distended with anechoic fluid. More than 50% of the submucosal leiomyoma is intracavitary. Note overlying echogenic thin layer of endometrium, which helps to differentiate a submucosal leiomyoma from a broad-based endometrial polyp. This leiomyoma was resected hysteroscopically. **B**, Sonohysterogram of another patient with a submucosal leiomyoma (*calipers*) projecting into the uterine cavity. Note parallel hypoechoic regular bands extending from the anterior surface of the leiomyoma posteriorly, so-called “venetian blind” shadowing. The distended balloon filled with anechoic fluid (*arrow*) is seen as well on this image.

examination, no fetal tissue will be identified. The risk of developing PTN is estimated to be approximately 20% following evacuation. However, it is not possible to predict which CHMs will develop persistent disease by either imaging or pathologic characteristics, although women over the age of 40 years and with hCG levels greater than 100,000 mIU/mL, excessive uterine enlargement, theca lutein cysts larger than 6 cm in diameter, and repetitive molar pregnancies seem to be at higher risk for invasion.<sup>27</sup> Hence, women with CHMs are counseled not to become pregnant for a full year following evacuation and are followed carefully with serum hCG levels.

PHMs are the second most common type of GTD.<sup>26</sup> Patients with PHMs typically have less trophoblastic proliferation, milder symptoms, and lower hCG levels. Most PHMs have a 69,XXY or 69,XXY triploid karyotype and will have fetal tissue identified on pathologic



**FIG 28-29** Three-dimensional image of a submucosal intracavitary leiomyoma (*asterisk*) indenting the echogenic endometrium. (Courtesy of Dr. Beryl R. Benacerraf, Boston, MA.)

examination. These patients are estimated to have a risk of approximately 5% for developing PTN.

Sonography is the primary imaging modality used for diagnosis, and many cases are detected incidentally during first trimester ultrasound examinations. MRI is reserved for problem solving, primarily for assessing the extent of uterine invasion and residual disease before and after treatment. However, it can be difficult on both MRI and sonography to accurately identify myometrial invasion. Distinction between CHM versus PHM is important, given the higher invasive potential of CHM.<sup>26</sup>

The typical ultrasound appearance of CHM in the late first or second trimester is an enlarged uterus with the endometrial cavity distended by an echogenic, vascular mass containing clusters of tiny cysts (hydropic villi), sometimes described as the “snowstorm” or “cluster of grapes” appearance. There are no visible fetal parts. The presence of theca lutein cysts in the ovaries may help confirm the diagnosis. However, in today’s practice, theca lutein cysts are infrequently visualized, most likely because patients are imaged and diagnosed at an earlier gestational age. Early in the first trimester, there is a spectrum of sonographic findings ranging from a thickened endometrium without a discrete mass or cystic areas to the more classic appearance of an echogenic endometrial mass with the so-called “cluster of grapes” multicystic appearance (Fig. 28-31B, C1, and C2). Classically, color or power Doppler imaging will reveal increased vascularity within the endometrium or mass. However, not all molar pregnancies will demonstrate increased vascularity on Doppler





interrogation (Fig. 28-31B and C2). Early in the first trimester, a CHM may not be distinguishable from a normal or failed early pregnancy (Fig. 28-31C and Fig. 28-32), and correlation with serum hCG levels is paramount as well as genotyping of the products of conception if evacuated.<sup>28</sup> Interestingly, detection of CHM at an earlier gestational age does not appear to change the incidence of postmolar GTNs.<sup>29</sup> This supports the concept that the diagnosis should not be reached in haste but only after careful correlation with imaging, laboratory, and clinical findings.

PHM has a similar ultrasound appearance to CHM, except that either normal or abnormal appearing fetal parts will be also identified (Fig. 28-33). However, there is a spectrum of disease, and CHM has been reported to occur in conjunction with a normal live twin fetus (Fig. 28-31D and E). The presence of myometrial invasion or retained endometrial tissue on the first follow-up examination after evacuation has been reported to be predictive of risk of GTN or PTN (Fig. 28-34).<sup>30</sup>

Dedicated pelvic MRI is superior to sonography for the detection of myometrial invasion and is used to assess for myometrial invasion as well as extrauterine extension. The appearance of CHM on MRI is described as T1-weighted hypointense, T2-weighted hyperintense tissue/mass with disruption of the junctional zone and enhancing multicystic tissue within the enlarged uterus (Fig. 28-31F and G). However, hypervascularity in the myometrial wall is not predictive of invasive disease and can be seen with normal implantation, RPOC, and AVM.

### Uterine Sarcomas

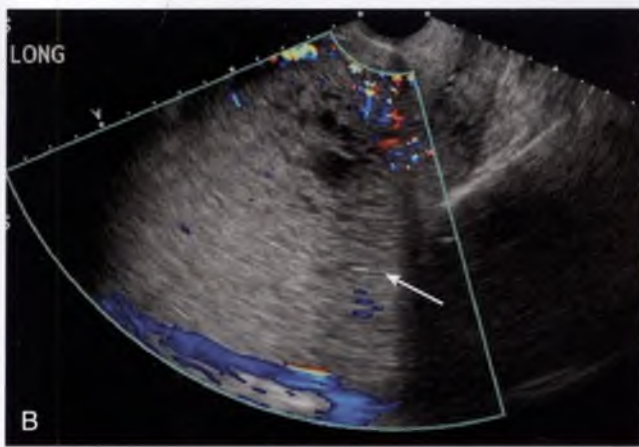
Although leiomyomas are most often benign lesions, leiomyosarcomas do rarely occur. The cause of leiomyosarcomas remains uncertain. Although in some cases it is postulated that leiomyosarcomas develop secondary to degeneration of a preexisting leiomyoma, most leiomyosarcomas are believed to arise independently rather than from a preexisting leiomyoma.<sup>31</sup> Uterine sarcomas are typically extremely aggressive malignancies with poor prognosis. However, early diagnosis can improve survival rates, and therefore, attention to imaging clues is crucial. Clinically, rapid growth of a leiomyoma in a perimenopausal or postmenopausal woman raises the possibility of sarcomatous change or degeneration. Ultrasound findings suggestive of malignancy include rapid change in size, indistinct or infiltrative margin, unusually complex echo pattern, and internal vascularity, especially if the distribution of the vessels is irregular. However, these findings are neither sensitive nor specific, and there may be no significant sonographic difference between a rapidly growing or degenerating myoma and a sarcoma. The internal architecture can change markedly and the amount of solid tissue can even increase in degenerating myomas, although such features raise concern for malignancy. MRI can be obtained to confirm the avid enhancement of solid components. However, MRI findings are also nonspecific, and if there are no prior studies, it is very difficult to determine if solid components in a degenerated myoma represent residual viable benign leiomyoma tissue versus a newly developing leiomyosarcoma, and surgical resection may be indicated. Other signs of malignant degeneration include local

**FIG 28-30** Spectrum of lipoleiomyomas. **A**, Sonogram demonstrating a well-marginated 1.5-cm focal hyperechoic anterior myometrial mass (arrows) that was a lipoleiomyoma. **B**, Transabdominal sonogram demonstrating a large 5-cm lipoleiomyoma. This mass is less echogenic and more heterogeneous than the lipoleiomyoma in A, but it also demonstrates some posterior linear shadowing. **C**, Transvaginal sonogram of a 7-cm extremely hyperechoic mass (asterisk) arising from the lower uterine segment posteriorly with marked posterior attenuation due to the fat content. This mass was also a lipoleiomyoma.

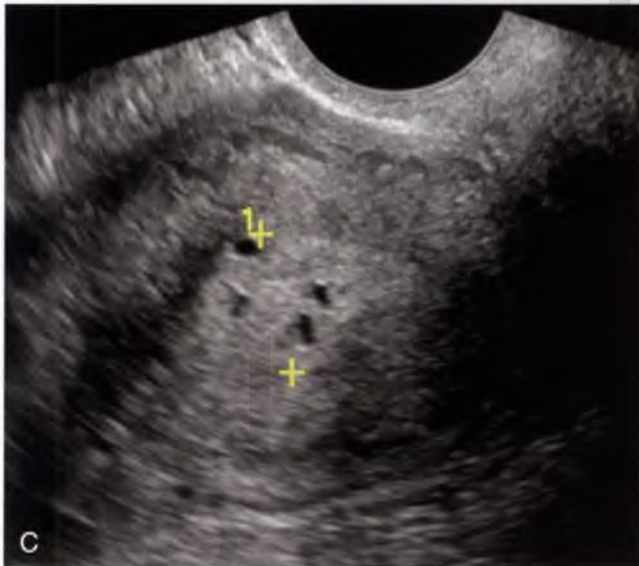




A



B

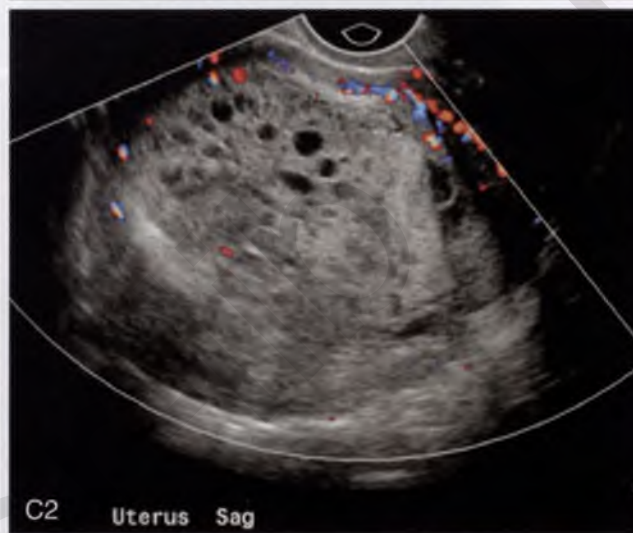


C



C1

Uterus Sag



C2

Uterus Sag



D

**FIG 28-31** **A**, Schematic demonstrating the spectrum of gestational trophoblastic neoplasia. **B**, Transvaginal longitudinal image from a first trimester sonogram demonstrates that the endometrial cavity is distended and filled with echogenic, cystic material (*arrow*). No significant internal color Doppler flow is present. However, internal vascularity can be difficult to detect on Doppler imaging and is usually better demonstrated on magnetic resonance imaging (MRI). There were no visible fetal parts, and dilatation and curettage procedure confirmed complete hydatidiform mole (CHM). **C**, Transvaginal longitudinal image from a first trimester sonogram in another patient demonstrates decidual cysts in the endometrium (*calipers*). This patient had a normal intrauterine pregnancy. Suspicious ultrasound findings should be correlated with human chorionic gonadotropin levels before the final diagnosis. **C1**, Transvaginal sagittal image demonstrating a large mass measuring 5.85 × 4.98 cm distending the endometrial cavity with numerous cysts, the classic “cluster of grapes” appearance of a molar pregnancy. **C2**, Transvaginal color Doppler image of the same patient as in C1 does not demonstrate significant vascularity within the CHM, although a small amount of peripheral blood flow is present. **D**, Transabdominal image of 20-week twin gestation with CHM (*arrows*) and normal twin (*arrowheads*). (**C1** and **C2**, Courtesy Department of Obstetrics and Gynecology and Department of Radiology and Biomedical Imaging, Yale University School of Medicine, New Haven, CT.)





**FIG 28-31, cont'd E**, Three-dimensional sonogram demonstrating normal fetus (F) with CHM (*arrowheads*) twin gestation. **F**, Axial T2-weighted MRI image demonstrates an enlarged uterus and endometrial cavity filled with high signal cystic areas (*arrow*) with central low signal more solid-appearing tissue (*arrowhead*). **G**, Axial postcontrast fat-suppressed MRI image confirms central more solid enhancing core (*arrowhead*) and surrounding lacelike enhancement of cystic tissue (*arrow*). No extrauterine extension is seen.



**FIG 28-32** Hydropic degeneration of the placenta. This patient presented with vaginal bleeding in the late first trimester. The placenta is enlarged, echogenic, and vascular, with numerous anechoic to hypoechoic cystic areas, which raised concern for a molar pregnancy. However, upon histologic and genetic analysis, findings were consistent with hydropic degeneration of the placenta with no evidence of a molar pregnancy. (Courtesy Department of Obstetrics and Gynecology, Yale University School of Medicine, New Haven, CT.)

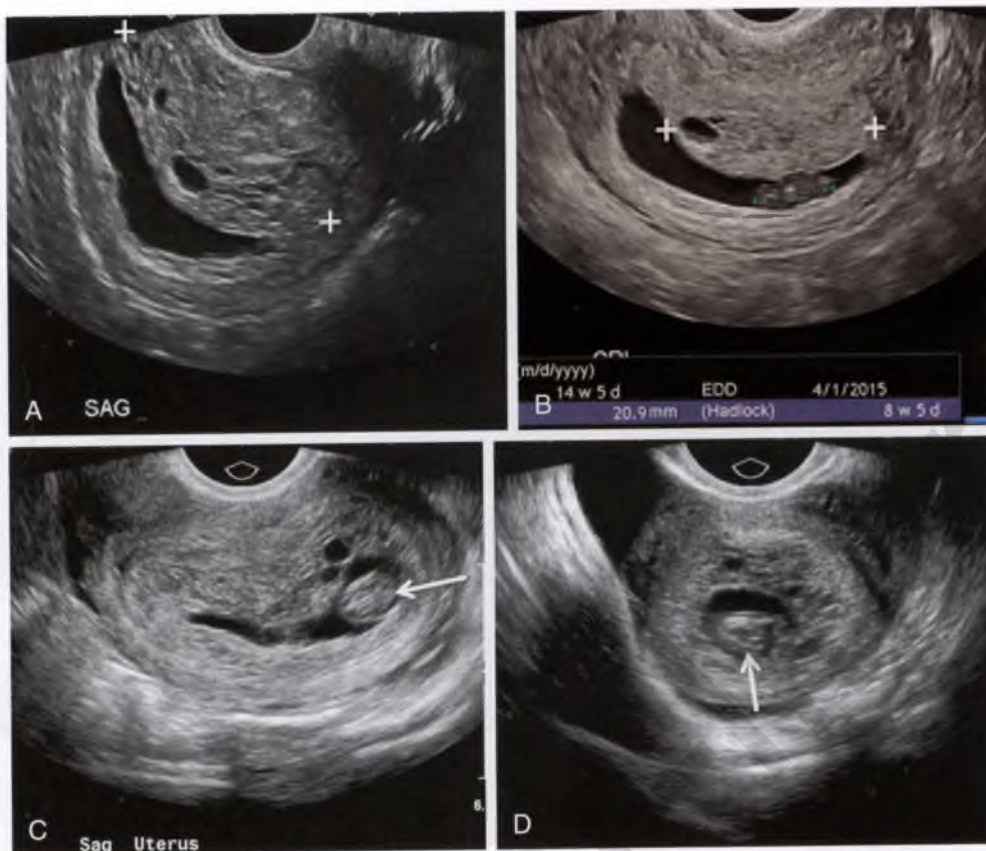


**FIG 28-33** Partial molar pregnancy. **A** and **B**, Gray-scale images from a woman presenting in the first trimester for gestation dating. There is an intrauterine gestational sac containing an embryo (dotted blue-green line in B). The crown-rump length corresponds to an estimated gestational age of 8 weeks 5 days. Note anterior echogenic trophoblastic tissue with numerous cysts (white calipers). Histologic and genetic analysis revealed a partial hydatidiform mole. **C** and **D**, In a second patient with a partial hydatidiform mole, note relative thickening of the trophoblastic tissue anterior to the embryo (arrows). The abnormal tissue also contains numerous small cysts. (Courtesy Department of Obstetrics and Gynecology and Department of Radiology and Biomedical Imaging, Yale University School of Medicine, New Haven, CT.)

invasion and distant metastases, which are more readily detected on MRI or CT than on sonography (Fig. 28-35).

## IATROGENIC PROCESSES

### Arteriovenous Malformations

AVMs consist of multiple communications between the arterial and venous systems without an intervening capillary network. These lesions can be congenital, but are more often iatrogenic as a result of intrauterine instrumentation or are secondary to trauma, malignancy, or infection. Specific causes include miscarriage, therapeutic abortion, dilatation and curettage, cesarean delivery, carcinoma of the cervix or endometrium, uterine infection, trophoblastic disease, leiomyomas, endometriosis, and uterine surgery.<sup>32</sup> Acquired AVMs consist of multiple small arteriovenous fistulas (AVFs). Patients most often present with excessive or dysfunctional uterine bleeding, and sonography is often the first imaging study performed. Color and duplex Doppler sonography have very characteristic findings. Serpiginous cystic areas or a tangle of tubular anechoic blood vessels can be seen on gray-scale sonography; they fill in with avid flow on color or power Doppler imaging. High-velocity, low-resistance (increased end-diastolic velocity) waveforms in the feeding artery and pulsatile high-velocity flow in the draining vein are seen on spectral Doppler. These Doppler characteristics overlap in appearance with the Doppler findings in patients

with GTD and RPOC, both of which histologically may also be characterized by small AVFs. Therefore, when these imaging findings are seen, GTD and RPOC should always be excluded by measuring the serum hCG level (Fig. 28-36A and B).<sup>33,34</sup>

Pseudoaneurysms (PSAs) may also develop as a complication of intrauterine procedures. They can be distinguished from AVMs by color and spectral Doppler imaging. A PSA will appear on gray-scale imaging as an anechoic cystic structure. On color Doppler, swirling blood flow with a “yin-yang” pattern will be observed.<sup>33</sup> A “to-and-fro” pattern with flow heading toward the PSA during systole and away from the PSA during diastole will be noted in the neck of the PSA on spectral Doppler interrogation.

Knowing that uterine curettage or surgical trauma can cause uterine vascular abnormalities such as PSAs and AVFs is useful when imaging patients with such clinical history and abnormal vaginal bleeding. Recognizing these lesions on imaging is important because treatment is quite different than for other causes of dysfunctional uterine bleeding. These abnormalities can be treated safely with transcatheter arterial embolization and may be worsened by uterine curettage. Acquired AVMs are reportedly easier to treat than congenital AVMs because they usually have only one or two feeding arteries. In addition, they are generally not fed by extrauterine vessels and lack a nidus, unlike congenital lesions.<sup>33</sup> In our experience, iatrogenic AVFs that develop following uterine instrumentation such as dilatation and



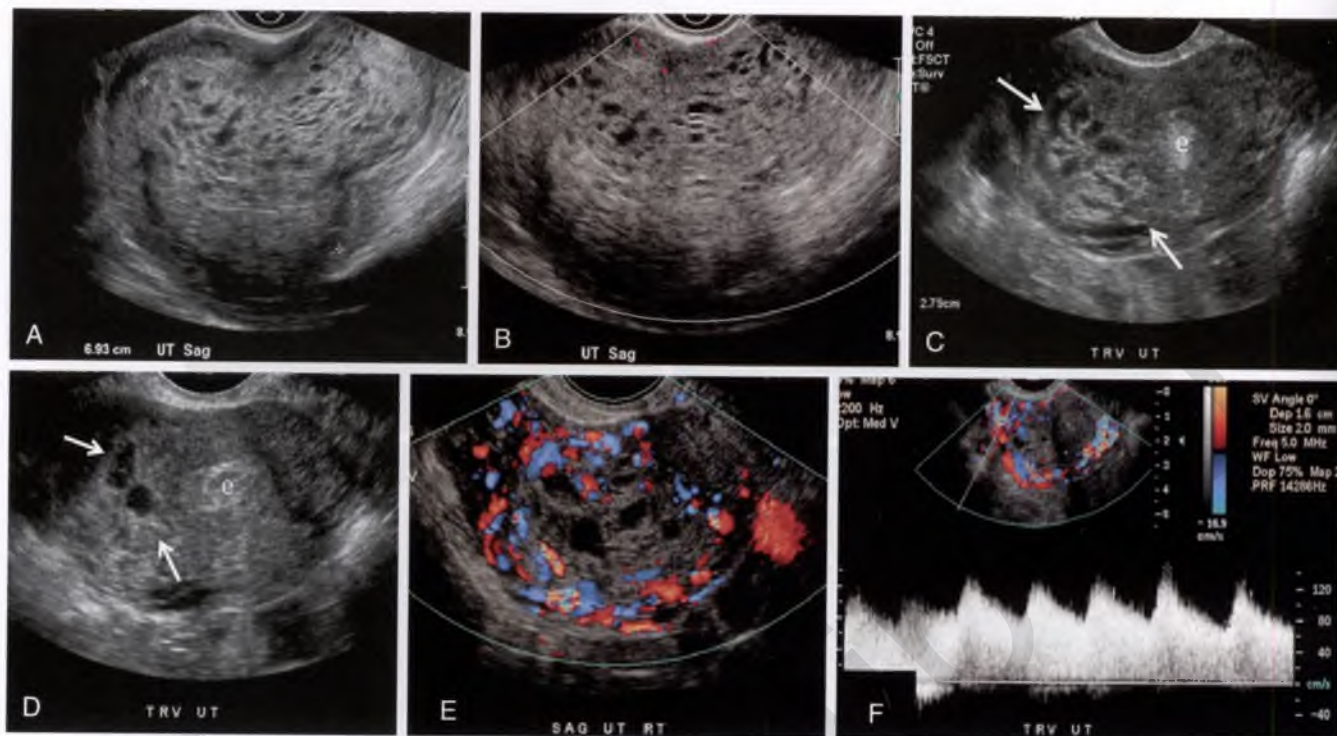


**FIG 28-34** Persistent trophoblastic neoplasia (invasive mole). **A**, Sagittal gray-scale image of the uterus from a woman presenting with vaginal bleeding in the first trimester. The endometrial cavity is markedly distended by a lobular echogenic mass (*calipers*) measuring 6.93 cm containing numerous small cysts. Although the surrounding myometrium is thinned, there is no evidence of myometrial invasion. No gestational sac was identified. Findings are most consistent with a complete hydatidiform mole. **B**, Color Doppler imaging did not reveal increased vascularity within the molar tissue. Although increased vascularity is a common finding in molar pregnancies, the absence of significant Doppler-detected blood flow does not exclude the diagnosis. **C** and **D**, Six months following treatment, the patient returned with elevated serum human chorionic gonadotropin levels. Transverse gray-scale images reveal a complex myometrial mass (*arrows* and *calipers* in **C**; *arrows* in **D**) containing numerous cystic spaces and clearly separate from the endometrium (e). The endometrium (e) appeared normal. **E**, Sagittal color Doppler image reveals increased flow within the mass and in the surrounding myometrium. **F**, Spectral Doppler image demonstrates the classic "trophoblastic" waveform of gestational trophoblastic neoplasia characterized by increased peak systolic and end-diastolic velocity with a low resistive index (0.50). Findings are most consistent with recurrent, invasive gestational trophoblastic neoplasia.

urettage (D&C) rarely require treatment and most often resolve on their own. If they do not resolve and have developed a nidus, they can be difficult to treat, even with multiple attempts with UAE. In such instances, the nidus may need to be treated directly (Fig. 28-36C and D).

### Intrauterine Contraceptive Devices

Contemporary intrauterine devices (IUDs) for contraception are easily visualized with transabdominal and transvaginal sonography as brightly echogenic structures with dense posterior shadowing located within the endometrial cavity. Transvaginal sonography is commonly used to evaluate placement as well as complications such as migration into the myometrium.<sup>35</sup> 3D sonography has been used with great success to improve visibility in technically challenging situations, as well as to confirm the specific type of IUD (Fig. 28-37), and is now considered state of the art for evaluating IUD placement at most institutions.<sup>36</sup> It is important that the reconstructed image is of the actual IUD and not from the shadow from the IUD.

If an IUD is not seen on sonography and history confirms placement, a pelvic radiograph should be obtained to exclude perforation and expulsion into the peritoneal cavity. Blood products as well as products of conception can obscure visualization of an IUD.

Occasionally, an IUD is seen associated with an intrauterine pregnancy. Although IUDs can be easily identified during the first trimester, they are rarely visualized in the second or third trimester of pregnancy. If removal is under consideration, the relationship of the IUD to the gestational sac, whether superior or inferior to the sac, becomes important.

It is not often that sonography is used to evaluate for Essure device placement, because tubal occlusion is usually confirmed with hysterosalpingography. However, ultrasound findings can comment on the proper anatomic placement in the ostia of the fallopian tubes (Fig. 28-37F and G).

### The Postpartum and Postabortive Uterus

Not infrequently, the sonologist is asked to evaluate a woman presenting with bleeding or pain in the first trimester or after delivery or therapeutic abortion. The question most commonly asked is whether or not there are RPOC or a large hematoma within the uterine cavity. A basic knowledge of the normal postpartum uterus is necessary to accurately diagnose pathologic conditions.

The normally enlarged gravid uterus begins to decrease in size several days after delivery.<sup>37</sup> The uterus rapidly decreases in size during the first 1 to 2 postpartum weeks and is usually back to its

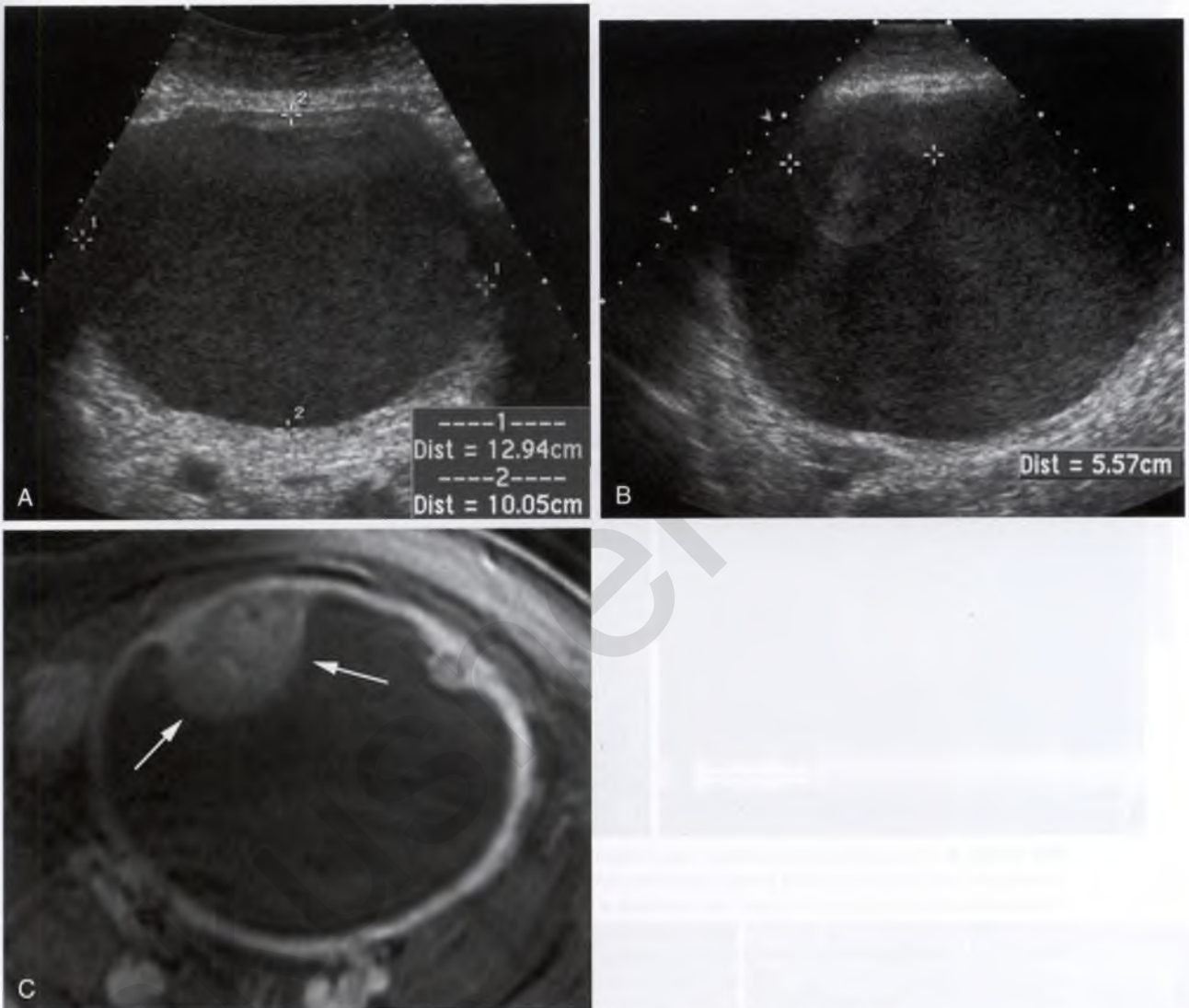


**FIG 28-35** Leiomyosarcoma. Postmenopausal woman with history of stable degenerating leiomyoma. **A**, Transabdominal sonogram demonstrating cystic degeneration of a leiomyoma (*calipers*). Note low level homogeneous internal echoes and increased through transmission. **B**, Transabdominal sonogram 2 years later demonstrates a new mural nodule (*calipers*). **C**, Axial T1-weighted with fat saturation postcontrast magnetic resonance image demonstrates enhancement of the mural nodule (*arrows*). Surgical removal and pathologic examination revealed low-grade sarcoma without myometrial invasion.



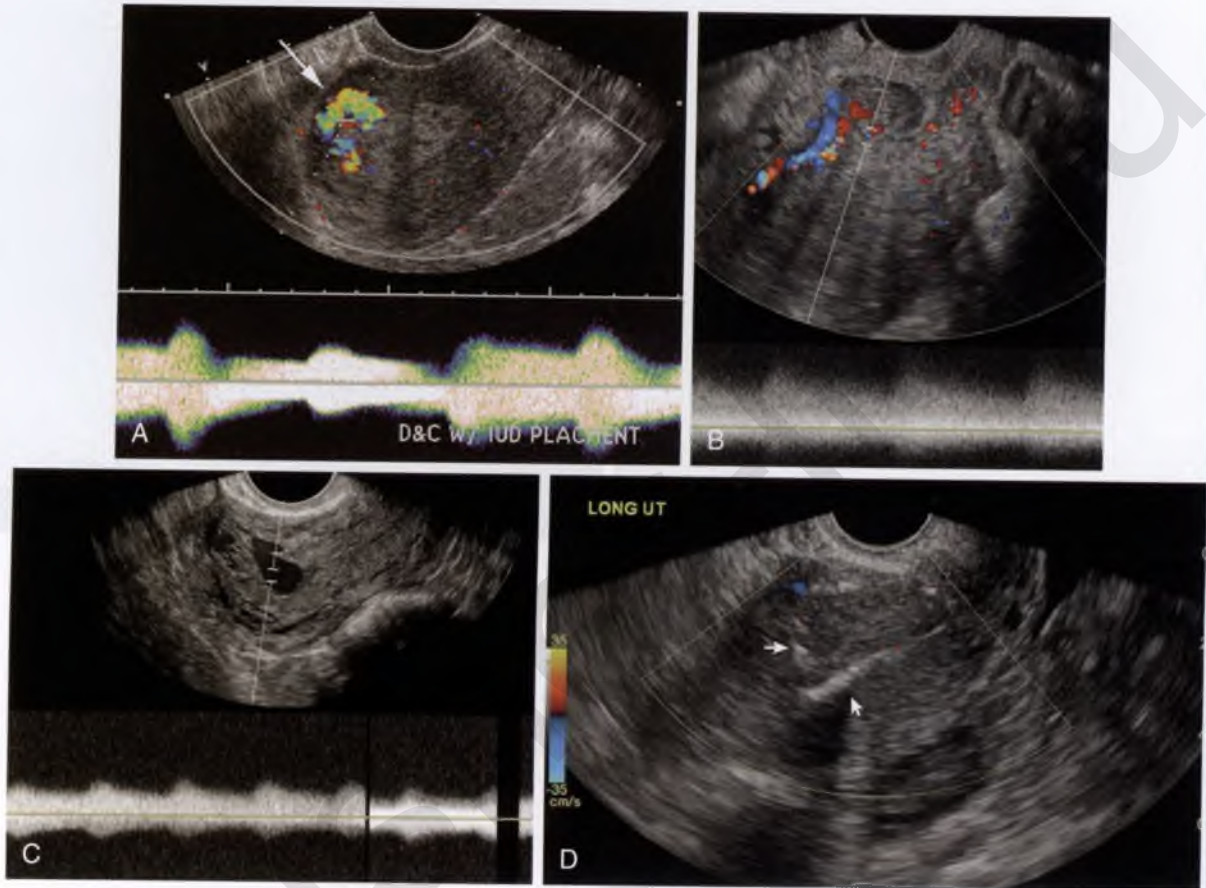


**FIG 28-36** **A**, Intrauterine arteriovenous malformations (AVMs). This patient presented after dilatation and curettage (D&C) and intrauterine device placement with prolonged heavy bleeding for 1 week. Transvaginal image with color and spectral Doppler demonstrates a large fundal iatrogenic AVM (*arrow*) with characteristic low-resistance arterial flow pattern with increased systolic and diastolic flow. Gestational trophoblastic disease was excluded by negative human chorionic gonadotropin levels. **B**, Exactly similar Doppler appearance in a different patient with retained products of conception (RPOC). **C**, Transvaginal sonogram of 23-year-old woman who presented with an AVM from previous D&C with persistent vaginal bleeding following uterine artery embolization  $\times 2$ . Persistent dominant vascular nidus was noted in the anterior myometrium demonstrating a high-velocity low-resistance spectral Doppler waveform. **D**, After direct treatment of the nidus as well as repeat uterine artery embolization the AVM is no longer present and the vaginal bleeding resolved. Note echogenic embolization material in the anterior wall of the uterus and endometrial canal (*arrows*).

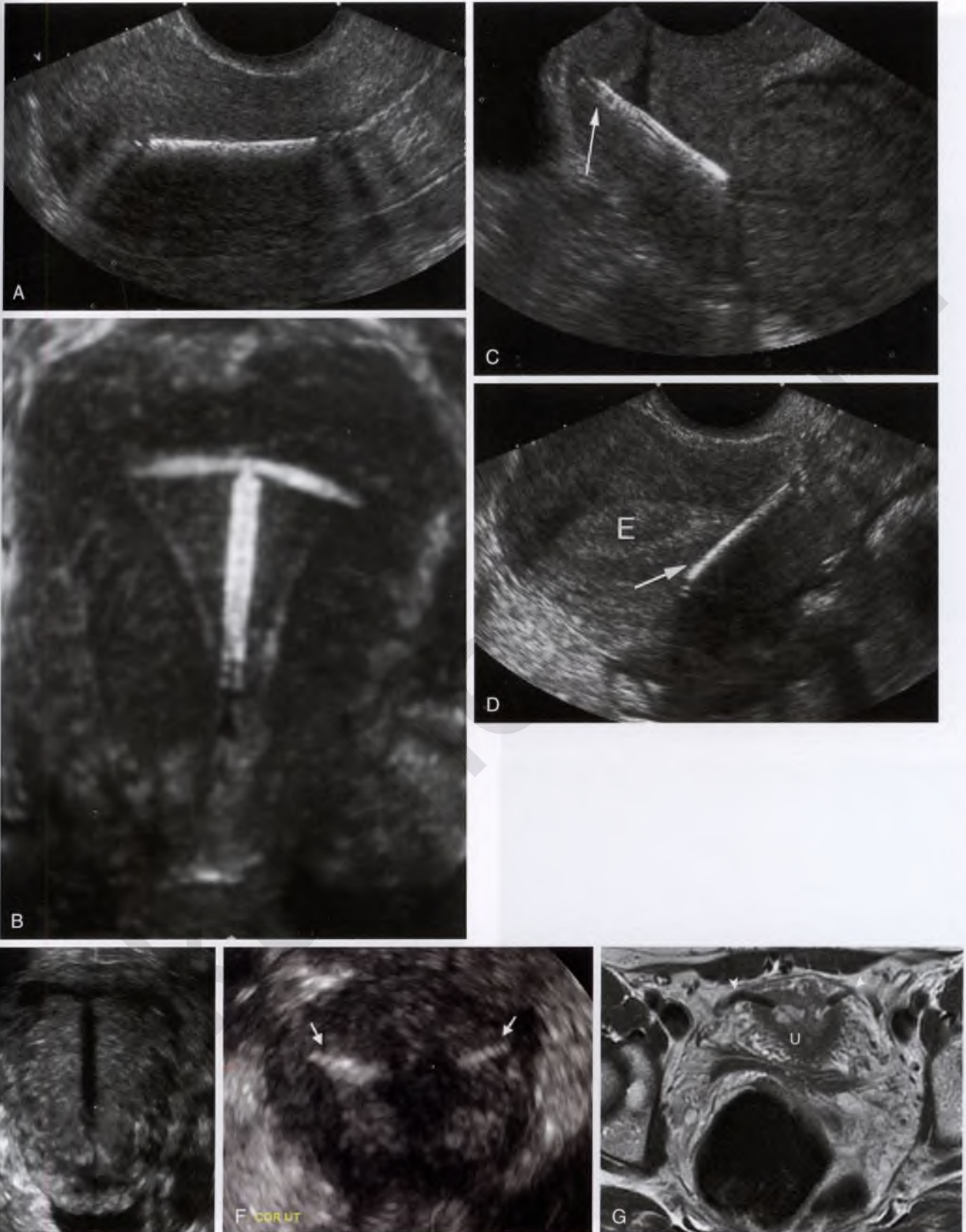


**FIG 28-37** Intrauterine contraceptive devices. **A**, Transvaginal sagittal image demonstrating proper central position in the uterine fundus of an intrauterine device (IUD), which is linear and echogenic with dense posterior shadowing. **B**, Three-dimensional (3D) coronal sonogram demonstrating central positioning in the uterine fundus of an IUD. **C**, Transvaginal sonogram in a patient with a retroverted uterus demonstrating penetration of an IUD into the cervix (*arrow*). **D**, Transvaginal sonogram of an IUD extending into the posterior myometrium (*arrow*). **E**, endometrium. **E**, 3D coronal sonogram demonstrating reconstruction from the shadow (black contour rather than white as expected) of an IUD, which can lead to misinterpretation of the true location of the IUD. **F**, Linear, echogenic Essure devices (*arrows*) in proper position in both the right and left ostia of the fallopian tubes, seen on this 3D sonogram. **G**, Extension of the Essure devices (*arrowheads*) into the proximal portion of the fallopian tubes was confirmed on this T2-weighted axial magnetic resonance image. U, uterus.



nongravid size by 6 to 8 weeks postpartum.<sup>37-39</sup> The endometrium returns to its pregravid state by 3 to 6 weeks postpartum.<sup>37</sup> Small amounts of fluid and echogenic material (likely representing blood clot) may be seen in the normal postpartum endometrial cavity (Fig. 28-38).<sup>37,40</sup> Brightly echogenic foci, likely secondary to air, can also be seen within the endometrial cavity and may persist for several weeks postpartum (Fig. 28-39), particularly following cesarean delivery.<sup>37,41</sup>



**FIG 28-38** Transabdominal sagittal sonogram in a patient 3 days postpartum presenting with more than expected residual postpartum bleeding. Fluid and tissue (arrows) are seen in the endometrial cavity, consistent with hemorrhage. There was no evidence of retained products of conception.



**FIG 28-39** Transabdominal sagittal sonogram in a patient 1 week after cesarean delivery. Linear echogenic focus with dirty shadowing (arrow) consistent with air is seen within the endometrial cavity in the fundus. The endometrium was thin and normal. Air in the endometrial cavity can be a normal finding up to 2 weeks following cesarean delivery and can also be seen normally after vaginal delivery.

The thickness of the postpartum endometrium is variable, ranging in one study from a mean value of 15.8 mm on day 1 to a mean of 5.5 mm on day 28.<sup>42</sup>

Several studies have evaluated endometrial thickness as a potential sign of RPOC.<sup>37,43-50</sup> Although there does not appear to be a cutoff value above which RPOC are certain, if the endometrium is extremely thin, it is unlikely that there are RPOC. One study found that in the absence of an endometrial mass or when the endometrial thickness was less than 10 mm, RPOC were extremely unlikely.<sup>37,50</sup> Thus, sonography appears to be more useful in excluding the diagnosis than in accurately making the diagnosis. A focal echogenic mass is suggestive of RPOC (Fig. 28-40A and B).<sup>37,43,51</sup> This appearance, however, is not a specific or reliable sign, because hemorrhage or blood clot may also be echogenic.<sup>37</sup> Doppler sonography has proved useful in some cases to assist in the diagnosis of RPOC.<sup>37,52</sup> Although flow within a focal

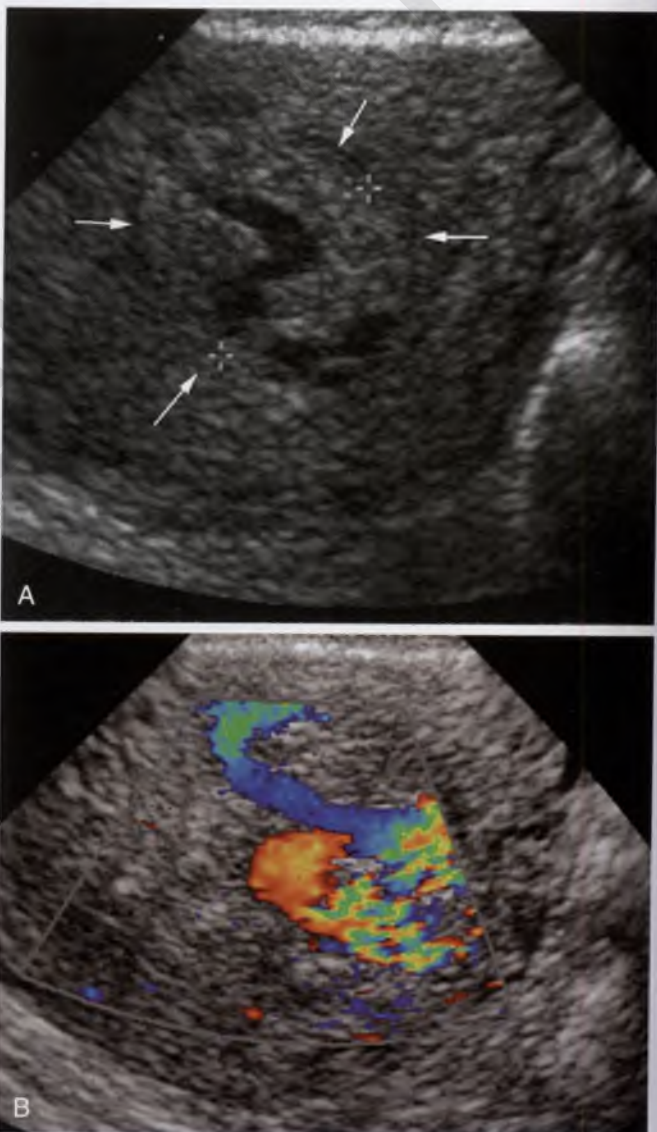


**FIG 28-40 A**, Sonogram from a patient with persistent bleeding following a first trimester therapeutic abortion. Tissue and fluid (arrows) representing retained products of conception (RPOC) are seen within the distended endometrial cavity (calipers). **B**, Doppler imaging of the same patient demonstrates markedly increased vascularity within the tissue consistent with RPOC.





**FIG 28-41** **A**, Sagittal sonogram from a patient presenting with bleeding 1 week postpartum. Tissue (*arrows*) was seen within the endometrial cavity, which is distended, measuring 15 mm. **B**, Corresponding color Doppler imaging demonstrated no evidence of blood flow within the tissue (*arrows*). This represented blood clots without retained products of conception.

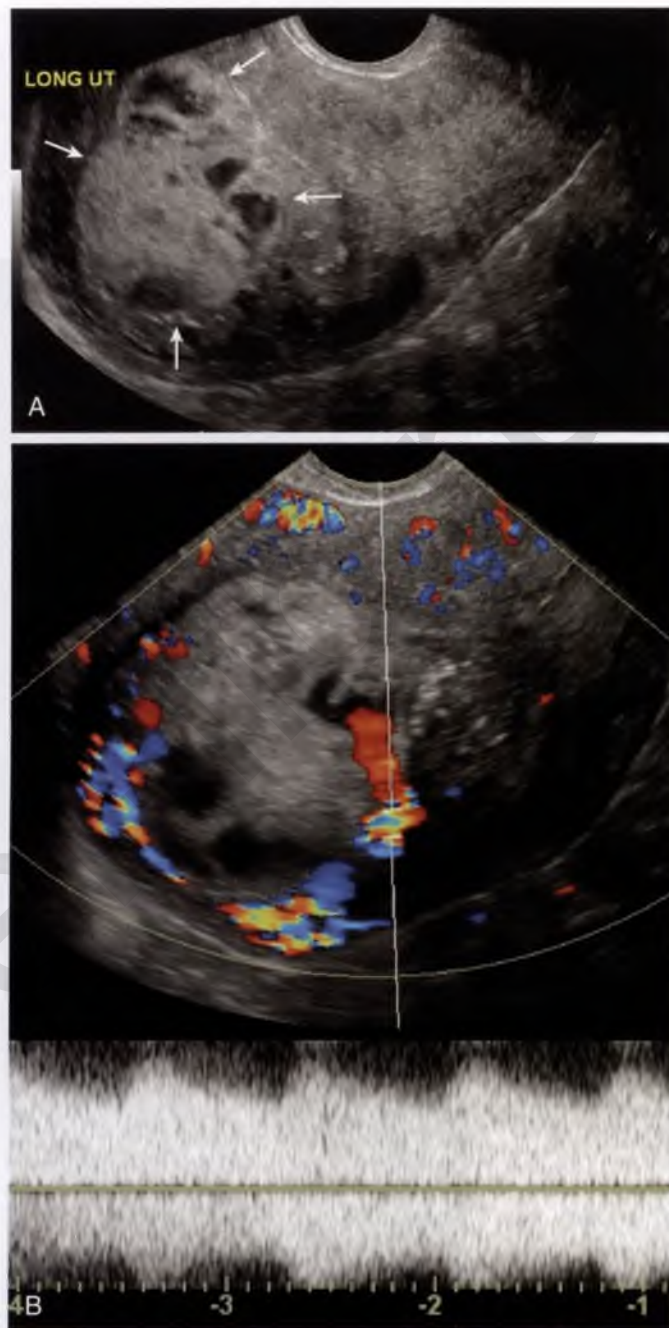


**FIG 28-42** Transvaginal sagittal sonogram from a patient presenting with continuous vaginal bleeding 2 months after delivery. **A**, A complex predominantly hyperechoic solid mass (*arrows*) was seen within the uterine fundus. **B**, Doppler evaluation demonstrates high-velocity low-resistance flow. This was retained placental tissue.

intracavitary mass is suggestive of RPOC in the appropriate clinical setting, the absence of flow does not exclude the diagnosis.<sup>37,50</sup> Placental tissue may persist for months after delivery and be a source of persistent hemorrhage (Fig. 28-41A and B). If the placental tissue is quite sizeable, there is usually an element of placenta accreta (Fig. 28-42A and B).

In all cases of persistent vaginal bleeding in the postgravid state, when a large amount of tissue is seen within the endometrial cavity, the diagnosis of GTD should be considered, although it is much less likely than RPOC (Fig. 28-3A and B). Clinical correlation as well as correlation with serum hCG levels is often diagnostic in excluding GTD, as the hCG level is much higher with GTD than with RPOC.

In summary, we have found at our institution that there is significant overlap in the gray-scale and Doppler findings of RPOC and AVMs as well as GTD. MRI is not generally useful in differentiating between these entities. Statistically, RPOC is by far the most common of the three. Hence, every case should be addressed individually and correlated both with the patient's symptoms as well as serum hCG levels.



## CERVICAL CYSTS AND POLYPS

The normal zonal anatomy of the cervix is well appreciated on transvaginal imaging. The endocervical canal and mucosa typically appear as a central echogenic linear stripe that is continuous with the echogenic endometrium in the body of the uterus. The endocervical canal is generally thin and homogeneous in appearance without variation in thickness along its length, although small cystic areas are occasionally observed, likely representing dilated glands. The subjacent fibrous cervical stroma appears as a markedly hypoechoic band of variable thickness and is continuous with the subendometrial halo in the body of the uterus. Hormonal stimulation does not appear to affect the appearance of the fibrous cervical stroma. The outer muscular cervical layer is intermediate in echogenicity and is continuous with the middle and outer layers of the myometrium (see Fig. 28-10). Nabothian cysts, retention cysts that develop secondary to obstruction of the cervical glands or crypts, are common incidental findings and are usually asymptomatic. They can be found anywhere along the length of the endocervical canal and can vary in size and number. On ultrasound images, nabothian cysts are most commonly anechoic, well-circumscribed, and avascular with increased through transmission, consistent with the sonographic appearance of simple cysts (Fig. 28-43), but internal echoes may be observed owing to mucus, debris, and rarely infection.

Endocervical polyps are most common in premenopausal women over the age of 20 years who have been pregnant. The exact cause is not known, but chronic inflammation and elevated estrogen levels have been reported to be predisposing factors. Patients may present with vaginal bleeding, although many are asymptomatic. On ultrasound images, an endoluminal cervical mass will be identified. The presence of vascularity or a vascular stalk will differentiate endocervical polyps from debris, blood clot, or a mucous plug (Fig. 28-44). If large, an endocervical polyp may obstruct the endocervical canal, resulting in hydrometrocolpos, or may prolapse into the vagina. Cervical leiomyomas appear on ultrasound images as well-circumscribed masses of variable echogenicity and are typically relatively avascular. They most commonly arise from the muscular layer and, hence, are most commonly exophytic and separate from the endocervical canal (Fig.

28-45). However, the sonographic appearance of cervical leiomyomas is nonspecific and may mimic the sonographic appearance of cervical carcinoma.

Ultrasound imaging does not play a significant role in the screening, diagnosis, or staging of cervical carcinoma. Screening and diagnosis are performed effectively with Pap (Papanicolaou) smear and cone biopsy, with subsequent staging performed clinically according to the International Federation of Gynecology and Obstetrics (FIGO) staging system (see Chapter 36). If further imaging is required, it is usually performed with MRI to assess extent of local disease and lymph node involvement, or with CT to assess for lymphadenopathy and distant metastases. However, sonography may occasionally be the first imaging modality performed in a patient who presents with vaginal bleeding or pelvic pain and can also be used to assess complications. On ultrasound images, cervical cancer will appear as a mass of variable echogenicity. Although tumors may be well defined and sharply marginated, especially if small and early stage, cervical cancers will often infiltrate and obliterate the normal zonal anatomy of the cervix, and in particular distort the endocervical canal, which is where cervical cancers originate. Differentiating a small, well-circumscribed cervical cancer from a cervical leiomyoma on ultrasound imaging is extremely difficult, although increased vascularity and heterogeneity favor the diagnosis of a cervical cancer. Larger masses may obstruct the endocervical canal, resulting in hydro- or hematometrocolpos, and irregularity of the outer margin suggests parametrial invasion (Fig. 28-46).

## CONCLUSIONS

Sonography remains the first-line and most valuable imaging modality for the evaluation of uterine anatomy, as well as most benign and malignant processes of the myometrium. However, imaging findings should always be correlated with the clinical scenario. If the ultrasound findings remain equivocal, MRI is recommended as the next imaging modality of choice in most cases. Correlation of imaging findings between the two modalities and expertise of the reader remain paramount for achieving an accurate diagnosis.



**FIG 28-43** Nabothian cysts. Note numerous anechoic cysts of varying sizes along the length of the cervix, several demonstrating increased through transmission.

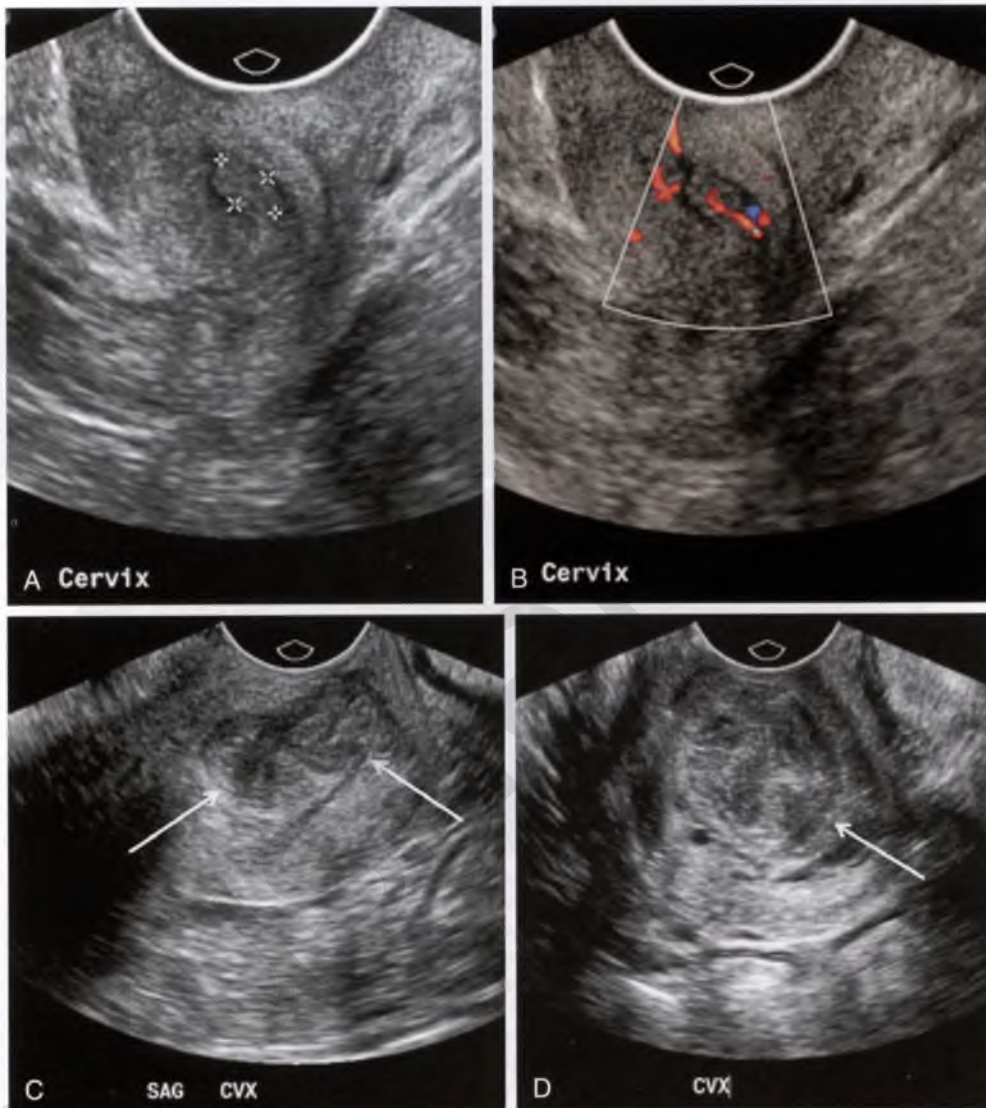


**FIG 28-44** Endocervical polyps. **A**, Transvaginal gray-scale image of the cervix demonstrates a small mass (*calipers*) within the endocervical canal. The differential diagnosis includes blood clot, mucous plug, and debris as well as endocervical polyp. **B**, Corresponding color Doppler image reveals internal vascularity and a feeding vessel, confirming that this is a soft tissue mass, most likely an endocervical polyp rather than blood clot or mucous plug. **C** and **D**, Sagittal and transverse transvaginal gray-scale images of the cervix from another patient with a large, slightly heterogeneous endocervical polyp (*arrows*) distending the endocervical canal.



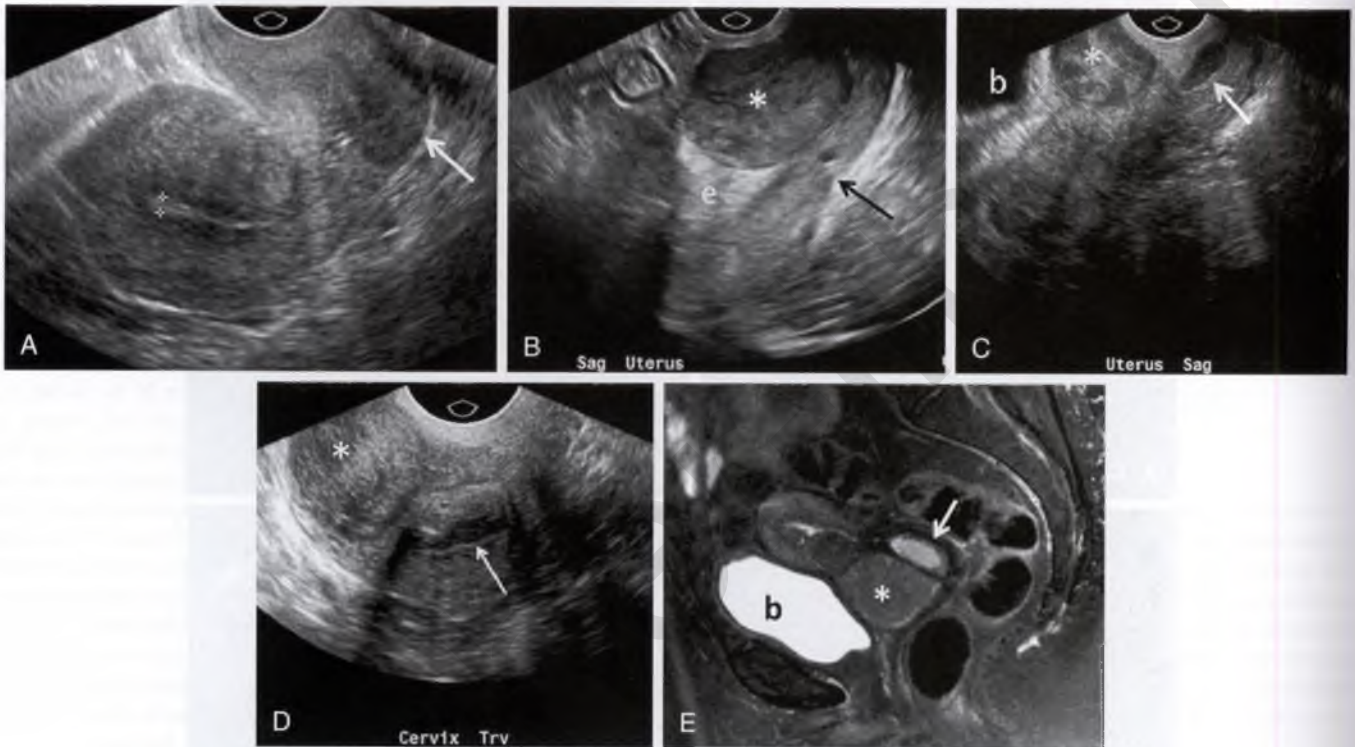


**FIG 28-45** Cervical leiomyomas. **A**, Note hypoechoic mass (*arrow*) arising within the posterior wall of the cervix but separate from the endocervical canal, which appears normal, suggesting that this is not a cervical carcinoma but a lesion arising from the muscular layer of the cervix. Note normal endometrium (*calipers*). **B**, Large exophytic mass (*asterisk*) arising from the anterior wall of the cervix but extending into the lower uterine segment in a second patient with a cervical leiomyoma. There is a small anechoic nabothian cyst in the posterior wall of the cervix, just below the level of the internal os (*arrow* at indentation between the lower uterine segment and upper cervix). *e*, endometrium. **C** and **D**, Sagittal and transverse transvaginal gray-scale images from a third patient with an exophytic cervical leiomyoma (*asterisks*) that is clearly separate from the endocervical canal, which is distended with anechoic fluid (*arrows*). This cervical leiomyoma also extends into the lower uterine segment. *b*, bladder. **E**, Sagittal T2-weighted fat saturation magnetic resonance image of the same patient as in C and D demonstrates similar findings. Low signal intensity cervical leiomyoma (*asterisk*) extends into the lower uterine segment; endocervical canal is distended with high signal intensity fluid (*arrow*). *b*, bladder.

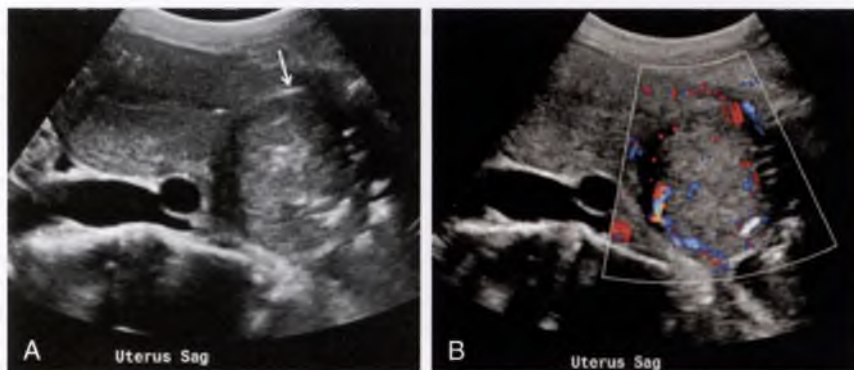


**FIG 28-46** Cervical carcinoma. Sagittal gray-scale (**A**) and color Doppler (**B**) images of the uterus reveal a heterogeneous well-defined, sharply margined vascular cervical mass compressing the iliac vessels posteriorly. The endocervical canal (arrow in **A**) is displaced anteriorly and partially obliterated, suggesting that the mass might have originated from the endocervical canal. There is no evidence of parametrial invasion nor is there extension into either the lower uterine segment or vagina, although the mass is large. However, the sonographic appearance is nonspecific and could be mimicked by a cervical leiomyoma.

## REFERENCES

- American Institute of Ultrasound in Medicine (AIUM); American College of Radiology (ACR); American College of Obstetricians and Gynecologists (ACOG); Society for Pediatric Radiology (SPR); Society of Radiologists in Ultrasound (SRU): AIUM practice guideline for the performance of the ultrasound examination of the female pelvis. *J Ultrasound Med* 33(6):1122–1130, 2014.
- American Institute of Ultrasound in Medicine (AIUM); American College of Obstetricians and Gynecologists; American College of Radiology: AIUM standard for the performance of saline infusion sonohysterography. *J Ultrasound Med* 22(1):121–126, 2003.
- Sample WF, Lippe BM, Gyepes MT: Gray-scale ultrasonography of the normal female pelvis. *Radiology* 125:477, 1977.
- Merz E, Miric-Tesanic D, Bahlmann F, et al: Sonographic size of uterus and ovaries in pre- and postmenopausal women. *Ultrasound Obstet Gynecol* 7:38, 1996.
- Miller EI, Thomas RH, Lines P: The atrophic postmenopausal uterus. *J Clin Ultrasound* 5:261, 1977.
- Behr SC, Courtier JL, Qayyum A: Imaging of mullerian duct anomalies. *Radiographics* 32(6):E233–E250, 2012.
- Reichman D, Laufer MR, Robinson BK: Pregnancy outcomes in unicornuate uteri: a review. *Fertil Steril* 91:1886–1985, 2009.
- Smith NA, Laufer MR: Obstructed hemivagina and ipsilateral renal anomaly (OHVIRA) syndrome: management and follow-up. *Fertil Steril* 87(4):918–922, 2007.
- Schlomer B, Rodriguez E, Baskin L: Obstructed hemivagina and ipsilateral renal agenesis (OHVIRA) syndrome should be redefined as ipsilateral renal anomalies: cases of symptomatic atrophic and dysplastic kidney with ectopic ureter to obstructed hemivagina. *J Pediatr Urol* 11(2):77, e1–6, 2015.
- Gell JS: Mullerian anomalies. *Semin Reprod Med* 21(4):375–388, 2003.
- Protor JA, Haney AF: Recurrent first trimester pregnancy loss is associated with uterine septum but not with bicornuate uterus. *Fertil Steril* 80:1212–1215, 2003.
- Daly DC, Maier D, Soto-Albers C: Hysteroscopic metroplasty: six years' experience. *Obstet Gynecol* 73:201, 1989.
- Saravolos SH, Cocksedge KA, Li TC: Prevalence and diagnosis of congenital uterine anomalies in women with reproductive failure: a critical appraisal. *Hum Reprod Update* 14:415–429, 2008.
- Kubik-Huch RA: Female pelvis. *Eur Radiol* 9:1715, 1999.
- Andreotti RF: The sonographic diagnosis of adenomyosis. *Ultrasound Q* 213:167, 2005.
- Chopra S, Lev-Toaff AS, Ors F, Bergin D: Adenomyosis: common and uncommon manifestations on sonography and magnetic resonance imaging. *J Ultrasound Med* 25:617, 2006.
- Kuligowska E: Pelvic pain: overlooked and underdiagnosed gynecologic conditions. *Radiographics* 25:3, 2005.
- Bazot M: Ultrasonography compared with magnetic resonance imaging for the diagnosis of adenomyosis: correlation with histopathology. *Hum Reprod* 16:2427, 2001.
- Lee EJ: Sonographic findings of uterine polypoid adenomyomas. *Ultrasound Q* 20:2, 2004.
- Tamai K: MRI imaging findings of adenomyosis: correlation with histopathologic features and diagnostic pitfalls. *Radiographics* 25:21, 2005.
- Murase E, Siegelman ES, Outwater EK, et al: Uterine leiomyomas: histopathologic features, MR imaging findings, differential diagnosis, and treatment. *Radiographics* 19:1179, 1999.
- Benson CB, Chow JS, Chang-Lee W, et al: Outcome of pregnancies in women with uterine leiomyomas identified by sonography in the first trimester. *J Clin Ultrasound* 29:261, 2001.
- Kliwer MA, Hertzberg BS, George Y, et al: Acoustic shadowing from uterine leiomyomas: sonographic-pathologic correlation. *Radiology* 196:99, 1995.
- Serafini G, Martinoli C, Quadri P, et al: Lipomatous tumors of the uterus: ultrasonographic findings in 11 cases. *J Ultrasound Med* 15:195, 1996.
- Seckl MJ, Sebire NJ, Fisher RA, et al: Gestational trophoblastic disease: ESMO clinical practice guidelines for diagnosis, treatment and follow up. *Ann Oncol* 24(Suppl 6):vi39–vi50, 2013.
- Benirschke K, Burton GJ, Baergen RN: *Pathology of the Human Placenta*, ed 6, Berlin, 2012, Springer.
- Berkowitz RS, Goldstein DP: Current management of gestational trophoblastic disease. *Gynecol Oncol* 112:654–662, 2009.
- Kani KK, Lee JH, Dighe M, et al: Gestational trophoblastic disease: multimodality imaging assessment with special emphasis on spectrum of abnormalities and value of imaging in staging and management of disease. *Curr Probl Diagn Radiol* 41:1–10, 2012.
- Sun SY, Melamed A, Goldstein DP, et al: Changing presentation of complete hydatidiform mole at the New England Trophoblastic Disease Center over the past three decades: does early diagnosis alter risk for gestational trophoblastic neoplasia? *Gynecol Oncol* 138(1):46–49, 2015.
- Malek M, Moradi B, Mousavi AS, et al: Complementary role of ultrasound in management of gestational trophoblastic disease. *Iran J Radiol* 12(2):e13955, 2015.
- Prayson RA, Hart WR: Pathologic considerations of uterine smooth muscle tumors. *Obstet Gynecol Clin North Am* 22:637, 1995.
- Castro-Aragon I, Aragon I, Urcuyo R, et al: Conservative management of a uterine arteriovenous malformation diagnosed in pregnancy. *J Ultrasound Med* 23:1101, 2004.
- Kwon JH, Kim GS: Obstetric iatrogenic arterial injuries of the uterus: diagnosis with US and treatment with transcatheter arterial embolization. *Radiographics* 22:35, 2002.



34. Polat P, Suma S, Kantarcy M, et al: Color Doppler US in the evaluation of uterine vascular abnormalities. *Radiographics* 22:47, 2002.
35. Mogavero G, Sheth S, Hamper UM: Transvaginal sonography of the nonpregnant uterus. *Radiographics* 13:969, 1993.
36. Valsky DV, Cohen SM, Hochner-Celnikier D, et al: The shadow of the intrauterine device. *J Ultrasound Med* 25:613, 2006.
37. Brown DL: Pelvic ultrasound in the postabortion and postpartum patient. *Ultrasound Q* 21:27, 2005.
38. Wachsberg RH, Kurtz AB, Levine CD, et al: Real-time ultrasonographic analysis of the normal postpartum uterus: technique, variability, and measurements. *J Ultrasound Med* 13:215, 1994.
39. Lavery JP, Shaw LA: Sonography of the puerperal uterus. *J Ultrasound Med* 8:481, 1989.
40. Edwards A, Ellwood DA: Ultrasonographic evaluation of the postpartum uterus. *Ultrasound Obstet Gynecol* 16:640, 2000.
41. Wachsberg RH, Kurtz AB: Gas within the endometrial cavity at postpartum US: a normal finding after spontaneous vaginal delivery. *Radiology* 183:431, 1992.
42. Mulic-Lutvica A, Bekuretsion M, Bakos O, et al: Ultrasonic evaluation of the uterus and uterine cavity after normal, vaginal delivery. *Ultrasound Obstet Gynecol* 18:491, 2001.
43. Cetin A, Cetin M: Diagnostic and therapeutic decision-making with transvaginal sonography for first trimester spontaneous abortion, clinically thought to be incomplete or complete. *Contraception* 57:393, 1998.
44. Alcazar JL, Baldonado C, Laparte C: The reliability of transvaginal ultrasonography to detect retained tissue after spontaneous first-trimester abortion, clinically thought to be complete. *Ultrasound Obstet Gynecol* 6:126, 1995.
45. Rulin MC, Bornstein SG, Campbell JD: The reliability of ultrasonography in the management of spontaneous abortion, clinically thought to be complete: a prospective study. *Am J Obstet Gynecol* 168:12, 1993.
46. Wong SE, Lam MH, Ho LC: Transvaginal sonography in the detection of retained products of conception after first-trimester spontaneous abortion. *J Clin Ultrasound* 30:428, 2002.
47. Nielsen S, Hahlin M: Expectant management of first-trimester spontaneous abortion. *Lancet* 345:84, 1995.
48. Nielsen S, Hahlin M, Oden A: Using a logistic model to identify women with first-trimester spontaneous abortion suitable for expectant management. *Br J Obstet Gynaecol* 103:1230, 1996.
49. Sadan O, Golan A, Girtler O, et al: Role of sonography in the diagnosis of retained products of conception. *J Ultrasound Med* 23:371, 2004.
50. Durfee SM, Frates MC, Luong A, et al: The sonographic and color Doppler features of retained products of conception. *J Ultrasound Med* 24:1181, 2005.
51. Achiron R, Goldenberg M, Lipitz S, et al: Transvaginal duplex Doppler ultrasonography in bleeding patients suspected of having residual trophoblastic tissue. *Obstet Gynecol* 81:507, 1993.
52. Keogan MT, Hertzberg BS, Kliever MA: Low resistance Doppler waveforms with retained products of conception: potential for diagnostic confusion with gestational trophoblastic disease. *Eur J Radiol* 21:109, 1995.

# Evaluation of Pelvic Pain in the Reproductive Age Patient

*Genevieve L. Bennett*

## SUMMARY OF KEY POINTS

- Pelvic pain in the reproductive age patient often presents a diagnostic challenge as there are many causes, including both gynecologic and nongynecologic disorders with overlap in clinical symptoms.
- Pregnancy status must always be determined to exclude a pregnancy-related complication, particularly ectopic pregnancy.
- Pelvic sonography is the well-established first-line imaging method of choice and may require both a transabdominal and transvaginal approach to increase diagnostic accuracy.
- Computed tomography (CT) and magnetic resonance imaging (MRI) may be of added value in evaluation of pelvic pain when ultrasound findings are not definitive.
- Adnexal torsion cannot be excluded in the presence of preserved ovarian blood flow, and gray-scale features along with the clinical picture are more reliable in making this diagnosis.
- Hemorrhagic ovarian cysts demonstrate a wide spectrum of sonographic appearances that may overlap with those of other complex cystic masses, and if greater than 5 cm these cysts may require follow-up imaging to confirm resolution.
- Endometriosis may demonstrate variable sonographic findings and cause both chronic and acute pelvic pain if there are associated complications.
- Most leiomyomas are benign; however, atypical imaging features should prompt further evaluation to exclude the possibility of a malignant uterine neoplasm.
- Focal adenomyosis may mimic myomas sonographically, and MRI can be helpful for more definitive characterization.
- Many nongynecologic causes of pelvic pain, including gastrointestinal and genitourinary disorders, may be identified when ultrasound examination is performed for suspected pelvic disease, and recognition of these disorders may enable prompt diagnosis and eliminate the need for further imaging.

## OUTLINE

### Adnexal Causes of Pelvic Pain, 884

- Adnexal Torsion, 884
- Ruptured or Hemorrhagic Ovarian Cyst, 887
- Pelvic Inflammatory Disease, 891
- Endometriosis, 892
- Peritoneal Inclusion Cyst, 897

### Uterine Causes of Pelvic Pain, 899

- Leiomyomas, 899
- Malignant Uterine Tumors, 903
- Adenomyosis, 904

Malpositioned Intrauterine Device, 906

### Vascular Causes of Pelvic Pain, 906

- Pelvic Congestion Syndrome, 906
- Gonadal Vein Thrombosis, 907

### Nongynecologic Causes of Pelvic Pain, 907

- Acute Appendicitis, 907
- Acute Diverticulitis, 908
- Other Inflammatory Conditions of the Bowel and Mesentery, 910
- Obstructive Uropathy, 912

### Conclusions, 912

Pelvic ultrasound imaging is the well-established first-line imaging method of choice for evaluation of pelvic pain in the reproductive age patient when a gynecologic or obstetric disorder is suspected.<sup>1</sup> Ultrasound imaging is widely available; allows for high-resolution, dynamic real-time evaluation of the uterus, adnexa, and adjacent structures; is relatively low cost; and, importantly, involves no exposure to ionizing radiation. A transvaginal approach should be utilized whenever possible because it yields improved visualization of pelvic anatomy. This approach should be supplemented with transabdominal imaging when uterine or adnexal structures are beyond the field of view of the

transvaginal probe or if an abnormality outside the pelvis is suspected. Occasionally, a transvaginal examination may not be tolerated and only a transabdominal scan can be performed. Duplex and color or power Doppler sonography are essential adjuncts to gray-scale imaging. Although CT may be more useful for evaluation of gastrointestinal or genitourinary disease, because of considerable overlap in clinical symptoms and laboratory findings, these disorders may not initially be suspected, and pelvic sonography should be the first imaging study performed. However, many of these nongynecologic disorders can also be recognized by sonography, and if a diagnosis is established



sonographically, further imaging may not be necessary. In the pregnant patient, ionizing radiation should be avoided when possible, and sonography plays an even greater role.

When a patient complains of pelvic pain, it is critical to establish her pregnancy status as this information will help to narrow the differential diagnosis and direct an appropriate imaging workup. In the pregnant patient with pelvic pain, ectopic pregnancy is often the leading concern, and this important topic is covered in Chapter 33. The primary focus of this chapter is the ultrasound evaluation of pelvic pain in the nonpregnant patient, although the impact of pregnancy on some disorders that cause pelvic pain is discussed when appropriate. Both gynecologic and nongynecologic causes of pelvic pain are reviewed. Disorders that may cause acute or chronic pelvic pain (or both), and conditions that can be medically managed as well as those that require urgent surgical intervention are included. The added value of other imaging modalities in the evaluation of pelvic pain, including CT and MRI, is also addressed.

## ADNEXAL CAUSES OF PELVIC PAIN

### Adnexal Torsion

Adnexal torsion occurs when there is partial or complete rotation of the adnexal structures around their vascular pedicle with associated obstruction of venous outflow and arterial inflow. The true incidence of this disorder is unknown as the diagnosis is made definitively only during surgery. It is estimated that up to 3% of female patients with acute pelvic pain who come to the emergency department have adnexal torsion.<sup>2,3</sup> Adnexal torsion may involve either the ovary or the fallopian tube or both when they twist around the infundibulopelvic ligament and tubo-ovarian ligament. Concomitant ovarian and tubal torsion has been shown to occur in up to 67% of cases.<sup>4</sup> Twisting of the vascular pedicle initially leads to compromise of lymphatic and venous outflow, resulting in diffuse ovarian edema and enlargement. Arterial inflow may initially be sustained because the arteries have thicker, muscular walls and are less collapsible.<sup>5</sup> If left untreated, arterial thrombosis, ischemia, and ultimately infarction and necrosis of the ovary occur. Early diagnosis and surgery are essential to salvage the viable ovary. Predisposing factors for adnexal torsion include an ipsilateral adnexal mass (particularly if larger than 5 cm), pregnancy, ovulation induction, polycystic ovary syndrome, prior pelvic surgery (including tubal ligation), and hypermobility of the adnexal structures (more common in children and adolescents).<sup>3,6,7</sup>

Adnexal torsion may occur at any age, although it occurs predominantly in reproductive age women, most likely because of increased incidence of both physiologic and pathologic ovarian masses. However, up to 24% of cases occur in postmenopausal women.<sup>7</sup> There is a reported higher frequency on the right, perhaps because the sigmoid colon is a relatively fixed structure occupying the left pelvis, which helps to prevent torsion of the left ovary and adnexa. An adnexal mass is reported to be present in 22% to 73% of cases.<sup>6</sup> Large simple cysts and cystic neoplasms such as benign cystic teratomas, hemorrhagic cysts, and cystadenomas are the most commonly associated masses. Large ovaries in the setting of ovarian hyperstimulation are another predisposing factor. The absence of associated ovarian abnormality is more common in premenarchal girls, with 46% of cases of torsion involving normal-appearing ovaries.<sup>3</sup> Potential causes in these patients include increased mobility of the fallopian tubes and mesosalpinx, elongated pelvic ligaments, fallopian tube spasm, strenuous exercise, or abrupt changes in intra-abdominal pressure.<sup>5</sup> Approximately 10% to 25% of cases of adnexal torsion occur during pregnancy, with an incidence of 1:1000 pregnancies, most commonly in the first trimester.<sup>8-10</sup> Torsion is less likely to occur in the setting of pelvic

inflammatory disease (PID), endometriosis, or malignant neoplasms because in these conditions associated adhesions serve to fix the pelvic structures in place.<sup>3</sup>

The clinical presentation of adnexal torsion is variable and may overlap with other causes of acute abdominal or pelvic pain, such as a ruptured ovarian cyst or appendicitis, leading to a diagnostic challenge.<sup>3,11</sup> Classically, patients present with sudden acute onset of intense lower abdominal and pelvic pain, with a palpable painful adnexal mass and peritoneal signs. Additional symptoms may include nausea, vomiting, flank pain, and fever with a slight leukocytosis. A pregnancy test should be performed to exclude the possibility of a pregnancy-related complication such as ectopic pregnancy. The pain may be constant or intermittent, due to intermittent torsion and detorsion of the adnexa, and the intensity of pain experienced may vary with the degree of torsion or traction on the twisted pedicle. When symptoms are intermittent, the diagnosis is even more challenging. A high degree of clinical suspicion is necessary to avoid treatment delay and irreversible damage to the adnexa. Pain that lasts for more than 10 hours is associated with increased likelihood of adnexal necrosis at surgery.<sup>12</sup>

If a patient presents with pelvic pain, and adnexal torsion is suspected, prompt emergent pelvic sonography, including gray-scale, color, and spectral Doppler, is the imaging study of choice. However, as with the clinical diagnosis, the sonographic diagnosis may be challenging because the findings vary with degree and duration of torsion, involvement of the fallopian tube, and the presence of an associated mass.<sup>6,13</sup> The most consistently reported gray-scale ultrasound finding is the presence of a unilaterally enlarged ovary, usually larger than 4 cm, with or without an associated mass.<sup>4,5,7,14-17</sup> (Figs. 29-1 and 29-2). Houry and Abbott found that in a series of 87 cases of torsion, the mean ovarian size was 9.5 cm, with 89% measuring greater than 5 cm.<sup>16</sup> In a study by Chiou and colleagues, an underlying mass was found in 65% of 34 cases of adnexal torsion and a large ovary without a mass in 32% of cases.<sup>7</sup> An additional ultrasound finding is the presence of multiple peripherally located small follicles in the enlarged hypoechoic ovary, the "string of pearls" sign (see Fig. 29-1), which is thought to occur as a result of peripheral displacement of the ovarian follicles secondary to stromal edema and venous congestion,<sup>5</sup> although the reported incidence of this finding varies.<sup>7,14,18</sup> In more longstanding cases, the ovarian stroma may become more heterogeneous in echotexture because of foci of hemorrhage or necrosis. Comparison with the asymptomatic ovary is often helpful in recognizing these findings. An abnormal position of the ovary, which may be located in the midline either superior to the uterus or inferiorly in the pouch of Douglas, or displacement to the contralateral side of the pelvis is an important observation (see Figs. 29-1 and 29-2). The twisted and congested vascular pedicle may appear as an ill-defined adnexal mass adjacent to the torsed ovary. In cross section, it may demonstrate a target appearance with alternating hyperechoic and hypoechoic bands, the so-called "whirlpool" sign<sup>15</sup> (see further discussion later). The amount of associated free fluid around the ovary or in the cul-de-sac is variable, but free fluid is observed in up to 87% of cases.<sup>5</sup>

A more recently described gray-scale sign of ovarian torsion is the *follicular ring sign*. A follicular ring is defined as a perifollicular hyperechoic rim, 1 to 2 mm in thickness, seen surrounding the small (3 to 7 mm) peripheral antral follicles of the torsed ovary<sup>19</sup> (Fig. 29-3). In a series of 15 patients with surgically proven torsion, Sibal observed the follicular ring sign in 12, the whirlpool sign in 7, and absent ovarian blood flow in 7.<sup>19</sup> The follicular ring sign was the only sonographic finding in 4 patients. On microscopic examination, the follicular rings were found to be areas of hemorrhage and edema surrounding the antrum of small follicles. The authors caution that this sign may not



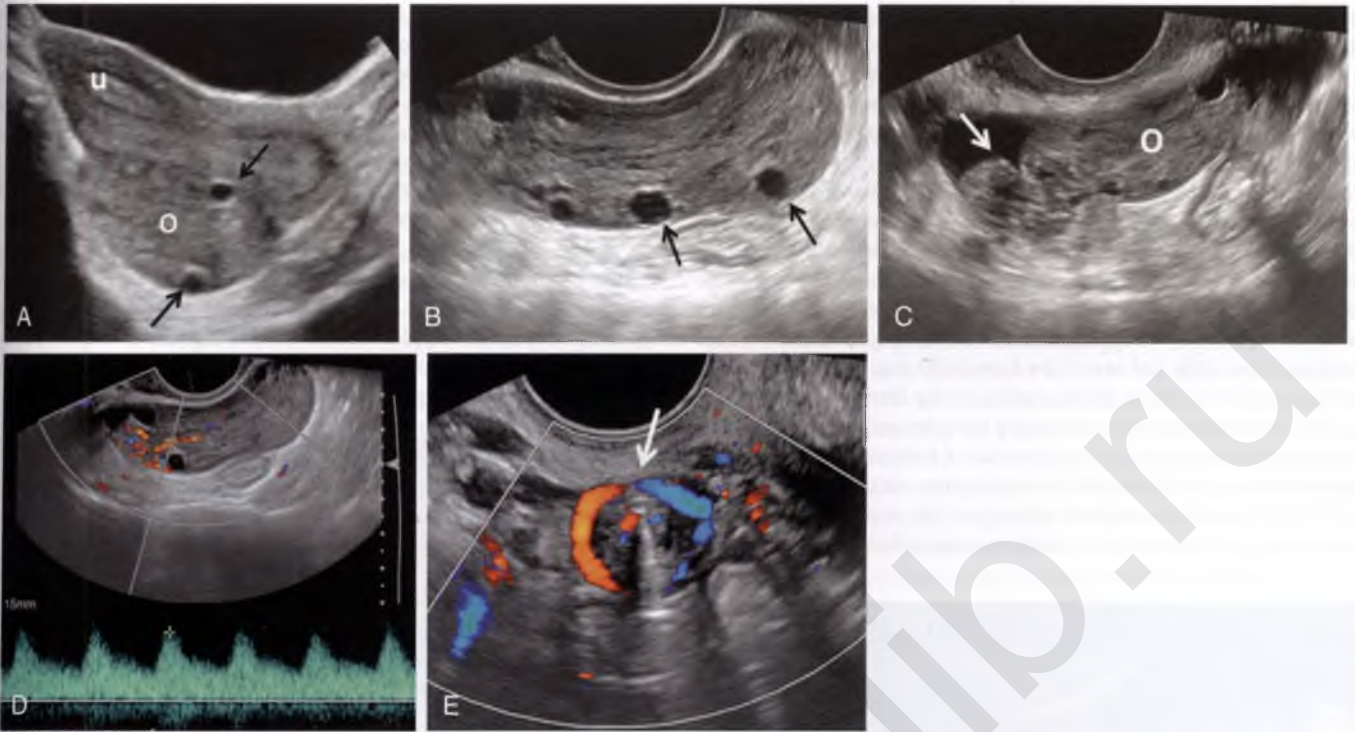


**FIG 29-1** Ovarian torsion without associated mass and viable ovary. **A**, Transabdominal scan demonstrates the enlarged ovary (o) containing multiple peripherally arranged follicles (arrows). The ovary is located posterior to the uterus (u) midline in the cul-de-sac. **B**, At transvaginal evaluation, the ovary is enlarged and edematous with heterogeneous echotexture and peripherally located follicles (arrows), the “string of pearls” sign. **C**, Thickened congested vascular pedicle (arrow) is noted lateral to the ovary (o). There is a small amount of adjacent free fluid. **D**, Arterial flow to the ovary is preserved, shown with color and spectral duplex Doppler sonography. **E**, Whirlpool appearance of vascular pedicle (arrow) on color Doppler sonogram.

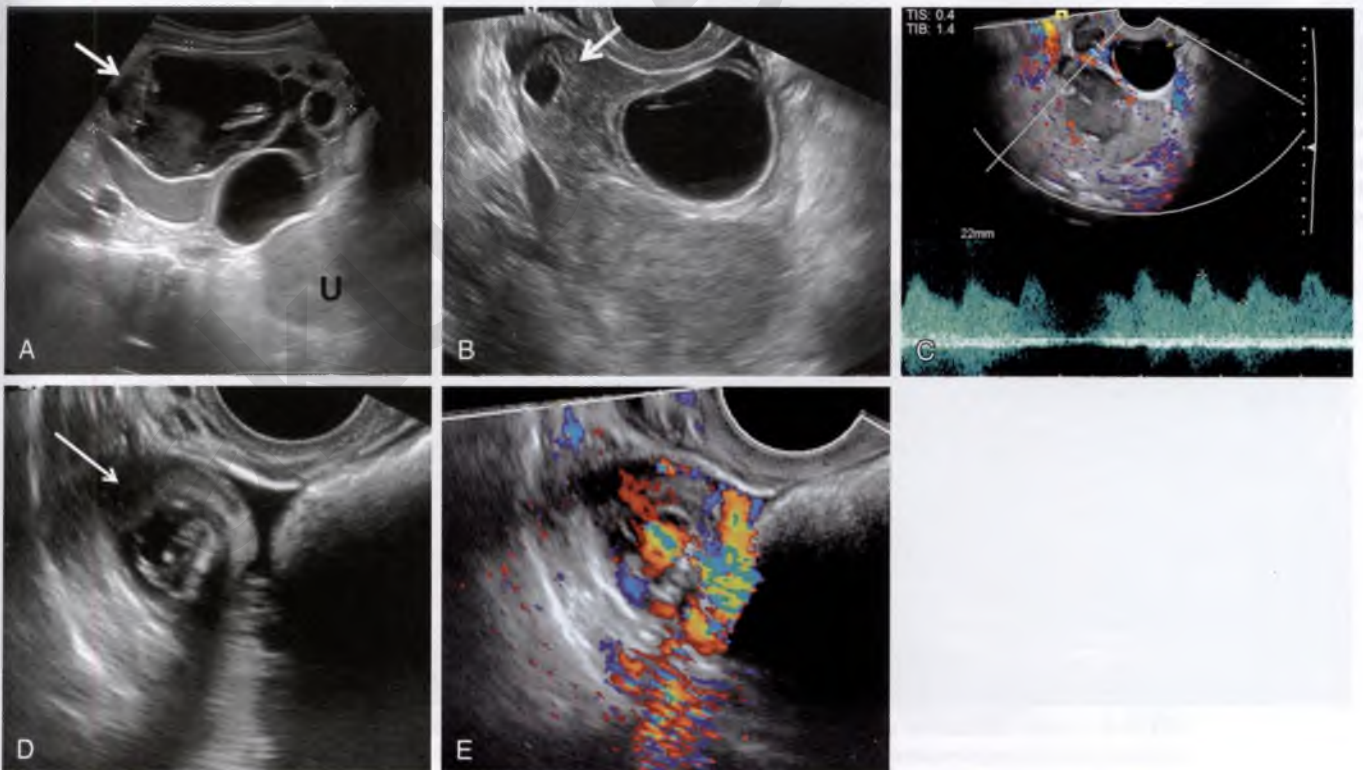


**FIG 29-2** Ovarian torsion with mucinous cystadenoma and viable ovary. **A**, Transabdominal scan demonstrates large multiloculated complex cystic mass (arrow and calipers) located superior to the uterus (U). **B**, Transvaginal scan demonstrates edematous ovarian tissue around the mass with peripheral follicle (arrow) and a small amount of adjacent free fluid. **C**, Arterial and venous flow to the ovary are preserved, shown on color and spectral Doppler sonogram. **D**, Gray-scale image of twisted pedicle with “target” appearance (arrow). **E**, “Whirlpool” appearance of vascular pedicle on color Doppler sonogram.



be seen if the ovary is necrotic or if a large cyst or mass compresses the follicles.

In addition to gray-scale findings, color and spectral Doppler evaluation is an important component of the pelvic ultrasound examination in the assessment of adnexal torsion. As with gray-scale imaging, Doppler findings vary with the degree of torsion, time course, and vascular compromise. Absence of detectable blood flow in the affected ovary allows for a confident diagnosis, with a positive predictive value (PPV) of 94% in one series.<sup>20</sup> However, this is a late finding and suggests that there has already been infarction and that the ovary is no longer viable (Fig 29-4). It may be difficult to detect flow if the ovary is mostly replaced by a large mass, and in this setting an attempt should be made to identify and search for flow in the rim of ovarian parenchyma around the mass. Many reports in the literature have shown that the detection of flow in an ovary on color and spectral Doppler sonography cannot exclude the presence of torsion. The dual arterial supply to the ovary may allow for early preservation of arterial flow, with initial loss of venous flow, although if the torsion is early, intermittent, or only partial, both arterial and venous flow may be preserved

(see Figs 29-1 and 29-2). In a study by Mashiach and associates<sup>21</sup> 13% of women with laparoscopically proven ovarian torsion had normal ovarian blood flow on Doppler. In a study by Chiou and colleagues<sup>7</sup> arterial and venous flow was considered normal in 19% of cases of proven torsion. Bar-On and coworkers<sup>22</sup> reported abnormal ovarian flow on Doppler sonography in only 43.8% of ovarian torsion cases, with a specificity of 91.7%. Shadinger and associates<sup>17</sup> reported preserved arterial flow in 54% and preserved venous flow in 33% of cases in a series of 39 patients with pathologically proven ovarian torsion. Other reports have also demonstrated that Doppler findings can be normal in 45% to 61% of cases of ovarian torsion.<sup>9,23,24</sup> However, analysis of spectral Doppler waveforms may increase sensitivity for the diagnosis of torsion. An arterial waveform with reversal of diastolic flow, a high resistance pattern, may suggest the diagnosis.<sup>25</sup> Recently, an abnormal discontinuous pattern of venous flow has been suggested as a clue to the presence of ovarian torsion when arterial and venous flow is preserved,<sup>26</sup> although this result has not been reproduced in larger studies. In general, the gray-scale findings as well as the clinical picture are thought to be more reliable than Doppler in the diagnosis of adnexal torsion.

A twisted vascular pedicle or "whirlpool sign" is an additional gray-scale and color Doppler finding useful for the diagnosis of adnexal torsion (see Figs. 29-1 and 29-2). The twisted vascular pedicle is the rotation site of the pedicle on itself and appears as a round or beaked mass with concentric alternating hyperechoic and hypoechoic circles or rings on gray-scale sonography.<sup>15,27</sup> The rings are composed of the components of the pedicle, including the broad ligament, fallopian tube, and branches of the ovarian artery and vein. At color Doppler, the twisted vessels in the pedicle appear to be coiled or swirling, as a whirlpool. This finding is best detected when the probe is moved back and forth in a transverse plane along the central axis of the twisted pedicle, which may be located either medial or lateral to the ovary.<sup>27,28</sup> In a study by Lee and colleagues<sup>15</sup> this finding was observed in 88% of cases of torsion. This finding may be a more direct sign of adnexal torsion and may be particularly useful in equivocal cases because it represents the actual site of torsion rather than the secondary effects on the ovary. In a study by Valsky and coworkers<sup>29</sup> there was an increase in true positive cases from 55% to 90% when this sign was observed. The presence of flow in the whirlpool is reportedly a useful predictor of ovarian viability.<sup>15,27</sup>

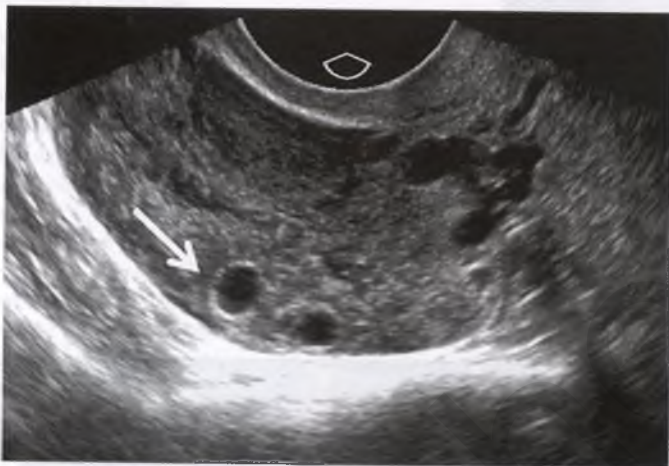


**FIG 29-3** Follicular ring sign in a patient with ovarian torsion. Transvaginal scan demonstrates an enlarged, edematous ovary with peripherally displaced small follicles, several of which have thin echogenic walls (arrow).

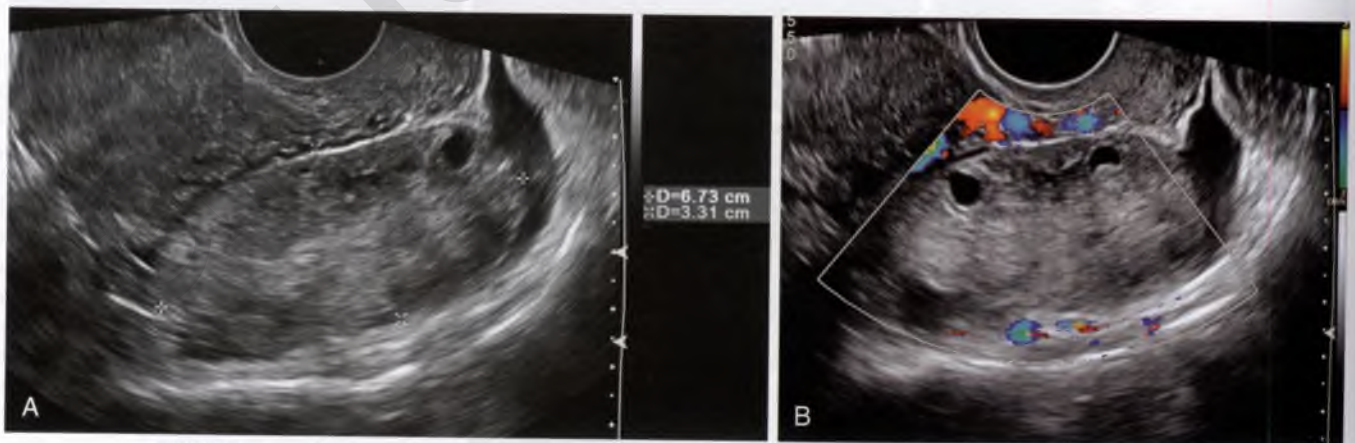


**FIG 29-4** Ovarian torsion with infarcted necrotic ovary. **A**, Transvaginal scan demonstrates an enlarged ovary (calipers) with heterogeneous echotexture and a small amount of adjacent free fluid. **B**, Color Doppler image, optimized with "low flow" settings, demonstrates no flow to the ovary. Note thin echogenic walls of the anterior peripherally displaced follicles, the follicular ring sign. At surgery, the ovary and tube were twisted three times and appeared necrotic. Pathologic examination confirmed hemorrhage, congestion, and infarction of the ovary and fallopian tube.



Although sonography is the primary modality of choice for evaluation of clinically suspected ovarian torsion, CT may be the first study performed in the emergency room setting if ovarian torsion is not initially considered. CT findings have been well described and parallel those observed sonographically, including an enlarged ovary with or without an associated mass, ovarian stromal edema with peripheral follicles, inflammatory stranding in the periovarian fat, a twisted vascular pedicle, a thickened fallopian tube, pelvic free fluid, midline position of the ovary, and deviation of the uterus to the side of the twist<sup>23,30,31</sup> (Fig. 29-5). Lack of enhancement or hematoma may suggest hemorrhagic infarction. In the author's experience, the twisted pedicle may be better appreciated in a nonaxial imaging plane, and multiplanar reformatted images should be reviewed (Fig. 29-6). Recently, in

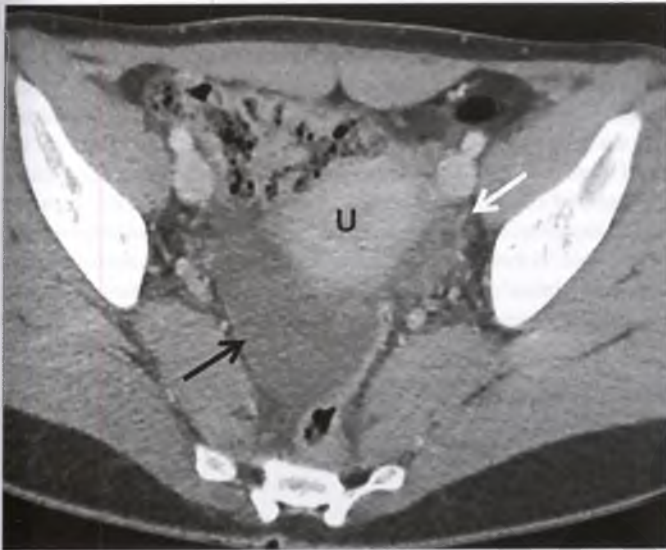


**FIG 29-5** Computed tomography (CT) findings in ovarian torsion with no associated mass. Ovarian torsion in a patient evaluated with contrast-enhanced CT for possible appendicitis. The appendix was normal (not shown); however, the right ovary is enlarged (*black arrow*) and is located posterior to the uterus (U). The left ovary is normal size (*white arrow*) and normally located. Torsion with viable ovary was found at surgery.

2014, it was suggested that CT may be more accurate than ultrasound imaging in detection of ovarian torsion. In one series, CT was performed prior to pelvic ultrasound examination in 70% of cases.<sup>32</sup> In this study, ultrasound imaging was 80% sensitive and 85% to 95% specific for ovarian torsion, whereas CT had a sensitivity of 90% to 100% and specificity of 85% to 90%; however, this was a retrospective study and the results have not been duplicated in larger prospective series. Hence, pelvic sonography remains the first-line imaging test of choice and, importantly, does not expose the patient to radiation or intravenous iodinated contrast agents.

MRI features of ovarian torsion have also been well described and parallel those seen by ultrasound imaging<sup>30,31,33</sup> (Fig. 29-7). MRI may serve as an adjunct to sonography in equivocal cases, enabling better visualization of the twisted pedicle and ovarian edema. MRI is particularly helpful in evaluating the patient with hyperstimulated ovaries in whom the diagnosis of torsion can be particularly challenging because of underlying ovarian enlargement.<sup>34</sup> However, MRI may not be readily available in the emergency setting, and inability to obtain an MRI scan should not result in treatment delay.

Isolated tubal torsion is very rare and usually associated with tubal disease.<sup>35,36</sup> Clinical symptoms are similar to those for ovarian torsion, although imaging features may vary. The most common sonographic appearance is a tubular, dilated fluid-filled structure, often with pointed or "beaked" ends where the twist occurs, in an unusual position in the pelvis and without demonstrable flow in the wall, in association with a normal-appearing ovary (Fig. 29-8). The whirlpool sign may also help with this diagnosis.<sup>37,38</sup>

### Ruptured or Hemorrhagic Ovarian Cyst

Ovarian cysts are common in women of reproductive age, and most are physiologic (functional) cysts. Ovarian cyst rupture and hemorrhage are common physiologic events during the ovarian cycle, involving the follicle or corpus luteum. Although follicular rupture occurs unnoticed in most women, the term *mittelschmerz* (middle pain) is used to describe pain resulting from the release of fluid into the peritoneum with rupture of the normal follicle during ovulation.<sup>39</sup> Hemorrhage into the corpus luteum is common and is due to the increased vascularity of this structure. As the maturing graafian follicle enlarges and the surrounding stromal cells undergo luteinization, the luteinized theca cells become more vascular. During ovulation at midcycle when

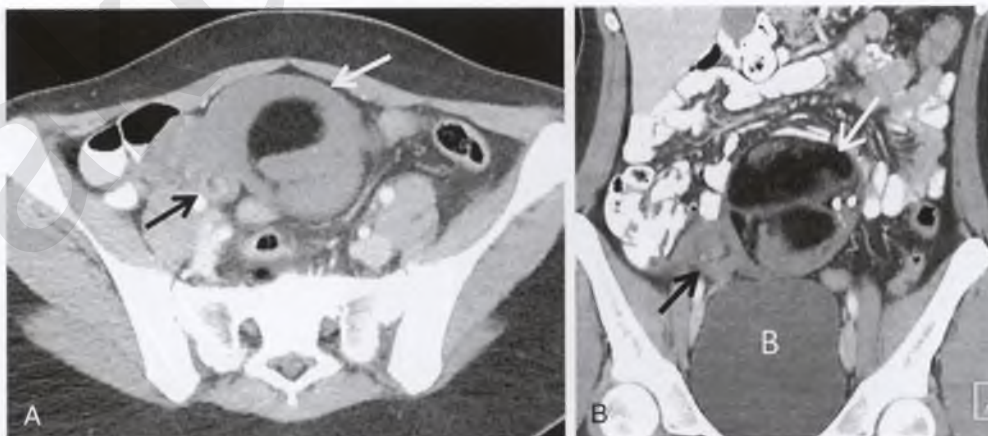


**FIG 29-6** Computed tomography (CT) findings in ovarian torsion associated with mature cystic teratoma. **A**, Axial contrast-enhanced CT image demonstrates large fat-containing mass (*white arrow*) located anteriorly in the midline of the upper pelvis. Note twisted vascular pedicle (*black arrow*). **B**, Coronal reformatted image shows the large mature cystic teratoma (*white arrow*), containing fat and calcifications, in the midline superior to the bladder (B) and the twisted vascular pedicle (*black arrow*).



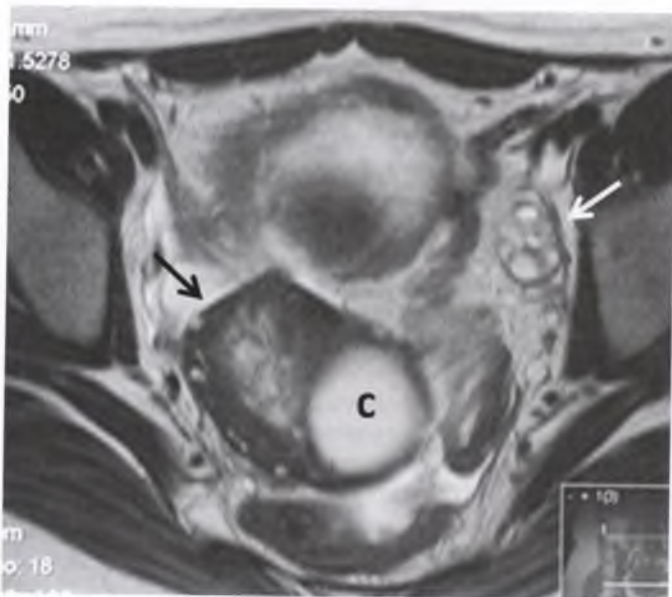


**FIG 29-7** Magnetic resonance imaging findings in ovarian torsion with associated serous cystadenoma. Axial T2-weighted image shows enlarged right ovary (*black arrow*), located in the cul-de-sac at the posterior midline, with T2-weighted hyperintense cyst (C). The ovarian stroma demonstrates heterogeneous signal intensity due to hemorrhage and edema, and there are multiple small peripheral follicles. The left ovary (*white arrow*) is normal in size and appearance.

the follicle ruptures and expels the oocyte, the corpus luteum is formed and the granulosa layer becomes vascularized. The vessels within the wall rupture easily, giving rise to a hemorrhagic cyst.<sup>40</sup> Usually, symptoms are mild and self-limited. However, patients may present to the emergency department with more significant pain if there has been a greater degree of hemorrhage into the cyst or into the peritoneal cavity. Pain is usually sudden in onset, localized to one side of the pelvis, and gradually improves. Peritoneal signs are variable in intensity depending upon the amount of fluid and hemorrhage causing peritoneal irritation. There may be considerable overlap in clinical presentation with other gynecologic and nongynecologic disorders including ovarian torsion, ectopic pregnancy, and acute appendicitis. In one recent series of reproductive age women who presented with right lower quadrant pain and clinical suspicion for appendicitis, 12.8% had gynecologic causes, including 7.2% with cyst rupture, 4.2% with ruptured hemorrhagic corpus luteum, and 1.4% with adnexal torsion.<sup>41</sup> Most of the time, the process is self-limiting, although severe life-threatening hemorrhage may occasionally occur and require urgent surgical intervention. Women with clotting disorders are at a higher risk for severe hemorrhage.<sup>42</sup>

If ovarian cyst rupture or hemorrhage is suspected, sonography is the study of choice. The cyst may not be visualized if it has ruptured and completely decompressed; however, there will generally be free pelvic fluid. Hence, ovarian cyst rupture is often a diagnosis of exclusion if no other cause for the patient's pain is identified. Although variable in appearance, the ruptured or leaking corpus luteum

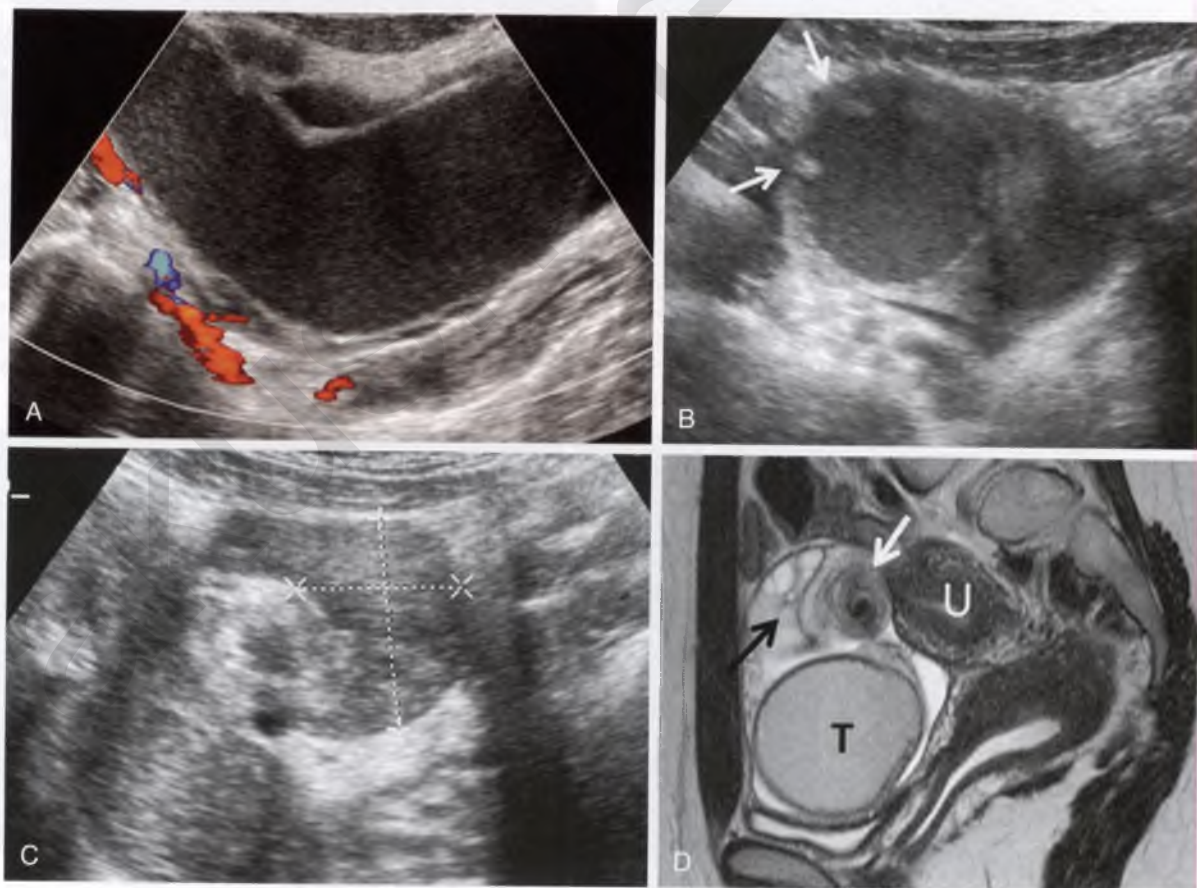


**FIG 29-8** Isolated fallopian tube torsion. **A**, Color Doppler image shows tubular structure filled with complex fluid and no blood flow, corresponding to hematosalpinx. **B**, On cross section, the endosalpingeal folds (*arrows*) are visualized. **C**, The left ovary (*calipers*) was normal in size and echotexture and had normal blood flow (not shown). **D**, Sagittal T2-weighted magnetic resonance image shows the site of the twist (*white arrow*), the normal left ovary (*black arrow*), and the blood-filled dilated fallopian tube (T) anterior to the uterus (U).



classically appears on ultrasound imaging as a small cystic lesion with a crenulated homogeneously hypoechoic wall and low-level internal echoes during the luteal phase of the menstrual cycle.<sup>43</sup> Size is variable, but is typically less than 3 cm. In most cases, there is a peripheral rim of increased vascularity, the “ring of fire” appearance<sup>44</sup> (Fig. 29-9). The sonographic appearance of a hemorrhagic cyst is also quite variable, depending upon when in the evolution of the hemorrhage the patient undergoes imaging. There is a continuum, from acute hemorrhage to clot formation followed by clot retraction. Because of the wide spectrum of appearance, hemorrhagic cysts may mimic other processes and have been referred to as the “great imitator.”<sup>45</sup> However, the characteristic sonographic features have been well described<sup>40,43,46-48</sup> (Fig. 29-10). Size may vary considerably from 2.5 to 10 cm. Acutely, hemorrhage into a cyst has a sonographic pattern of diffuse, homogeneous low-level echoes. A fluid-fluid level may be observed with the dependent echogenic component corresponding to blood. Over time, as red blood cells lyse and fibrin strands form, a reticular pattern of internal echoes is observed (also described as fishnet, cobweb, spider web, or lace-like) (Fig. 29-10B). Fibrin strands produce a network of fine linear echoes and are distinct from true septations in that they are usually innumerable, thinner, and discontinuous, with an irregular fine branching pattern; lack vascularity; and do not extend from wall to wall as a true septation would.<sup>46</sup> An acute clot filling the cyst may appear as dense internal echoes that simulate a solid mass, although lack of blood flow on Doppler imaging and demonstration of increased posterior through transmission are helpful features in suggesting the diagnosis. As the

clot retracts and lyses, it may appear on gray-scale sonography as an echogenic mural component within a cystic lesion and thus may simulate a solid neoplastic mural nodule. However, the retracting clot will often demonstrate concave or straight margins with acute angles, is often triangular, and may have a moth-eaten echotexture<sup>46</sup> (Fig. 29-10C). Lack of Doppler flow is an important feature suggesting mural thrombus as opposed to a tumor nodule, although low-levels of flow in solid tissue may not be detectable by Doppler sonography. Hence, absence of Doppler-detected blood flow is not an entirely reliable feature for a clot in a hemorrhagic cyst. The diagnostic performance of sonography in discriminating hemorrhagic ovarian cysts from other adnexal lesions, including malignancies, has been investigated in a study by Patel and associates,<sup>46</sup> who reported that the reticular or fishnet pattern had a sensitivity of 90%, specificity of 98%, and positive likelihood ratio (LR) of 40 for a hemorrhagic cyst; a retracting clot (solid echoes with a concave margin) was found to have a higher LR (>67) and specificity (100%) but lower sensitivity of 30%, although the combination of fibrin strands, no septations, and smooth wall was found to have an LR of 200, with sensitivity of 90% and specificity of 100%. Approximately 90% of hemorrhagic ovarian cysts will exhibit these features.

For some hemorrhagic ovarian cysts, there is overlap in imaging features with other complex cystic masses, including endometriomas, tubo-ovarian abscesses (TOAs), and cystic ovarian neoplasms, and definitive diagnosis may not be possible at the time of the initial sonogram.<sup>49</sup> The clinical setting is often helpful in focusing the differential

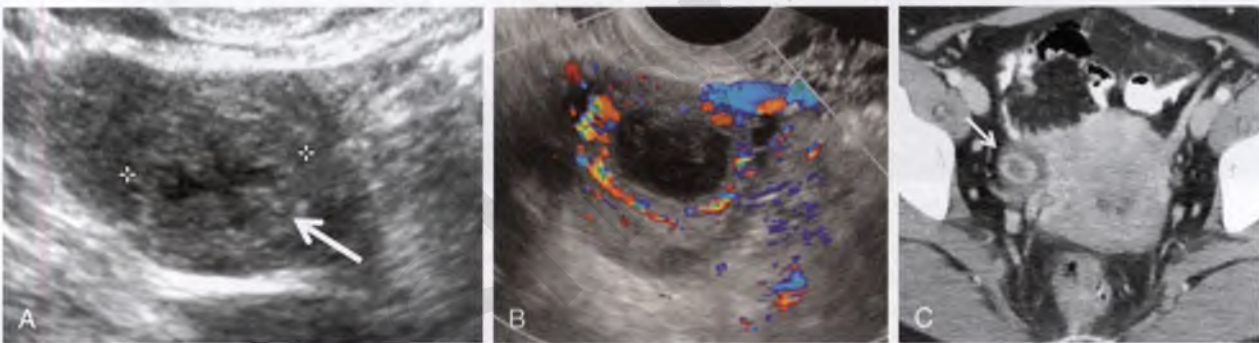


**FIG 29-9** Spectrum of appearances of the corpus luteum. **A**, Cyst with thickened, crenulated wall (arrow and calipers). **B**, Typical “ring of fire” appearance on color Doppler sonogram. **C**, Typical appearance of corpus luteum (arrow) in the right ovary at contrast-enhanced computed tomography. Note enhancement of the wall of the corpus luteum.

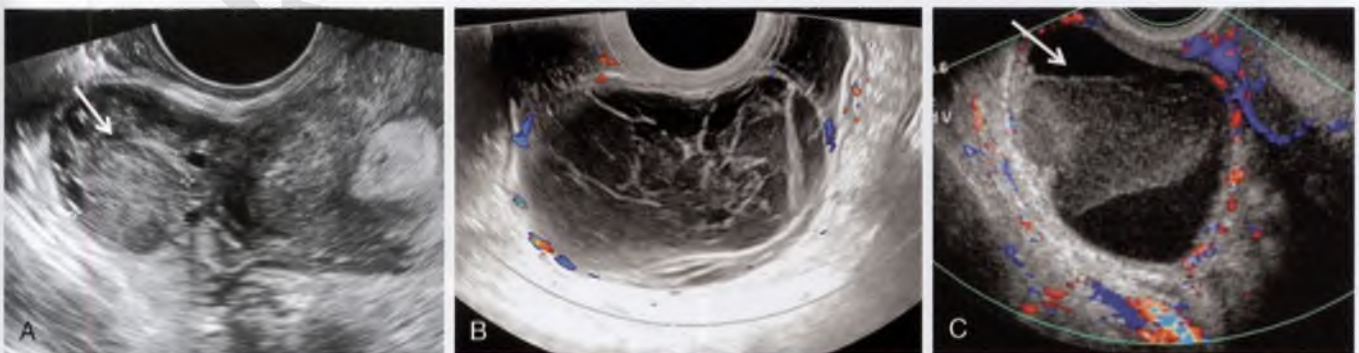


**FIG 29-10** Sonographic spectrum of hemorrhagic ovarian cysts. **A**, Acute hemorrhage may appear as a solid lesion (arrow and calipers) with homogeneous low-level echoes. **B**, Typical fishnet or lace-like appearance representing fibrin strands. No internal vascularity is demonstrated with color Doppler sonography although vascularity is noted in the wall of the cyst. **C**, Retractable clot (arrow) possibly mimicking a solid nodule but recognized as a clot due to straight margins, acute angles, and lack of internal blood flow. Blood flow is shown in the wall of the cyst.



diagnosis. However, if a hemorrhagic cyst is of primary consideration based on imaging features, short-interval follow-up sonography to confirm resolution is recommended because most hemorrhagic cysts typically resolve within 8 weeks.<sup>50</sup> This approach will prevent unnecessary surgical intervention. However, for a classic-appearing hemorrhagic cyst, defined as demonstrating either the reticular fibrin strand or retractile clot patterns, the Society of Radiologists in Ultrasound Consensus Conference Statement for management of asymptomatic ovarian cysts offers the following guidelines.<sup>51</sup> In women of reproductive age, hemorrhagic cysts 3 cm or less need not be described in the sonogram report, and no follow-up is necessary. Hemorrhagic cysts between 3 and 5 cm should be described in the report, but require no follow-up. Hemorrhagic cysts more than 5 cm should undergo short-interval follow-up sonography (6-12 weeks) with imaging optimally performed on days 3 to 10 of the menstrual cycle. In early postmenopause, all suspected hemorrhagic cysts should be described in the report, and short-interval follow-up sonography recommended in 6 to 12 weeks. Because women in late menopause should never develop hemorrhagic ovarian cysts, suspicion for neoplasm is heightened in this setting and surgical evaluation or additional imaging evaluation should be considered.

If a hemorrhagic ovarian cyst ruptures, the cyst may decompress and might not be identified as a discrete finding at sonography. Color Doppler sonography may identify the residual wall of the cyst (Fig. 29-11). A sentinel clot is sometimes identified in the adnexa as a complex mass of mixed echogenicity without blood flow. A variable amount of hemoperitoneum will be observed as free fluid containing low-level echoes, primarily within the pelvis. However, hemoperitoneum may also be noted in the upper abdomen if there has been a large amount of bleeding. Thus, the Morison pouch and the left upper quadrant should be surveyed to assess the amount of intraperitoneal blood. A ruptured ectopic pregnancy could present with similar sonographic and clinical findings; therefore, a human chorionic gonadotropin (hCG) level should always be measured to exclude this possibility. Infected fluid could also mimic the sonographic appearance of hemoperitoneum; therefore, clinical correlation and laboratory findings are important.

CT may occasionally be requested if a ruptured hemorrhagic ovarian cyst is not initially suspected when a patient presents with diffuse abdominal pain. CT findings include a high attenuation adnexal mass compatible with clot and high attenuation peritoneal fluid compatible with hemoperitoneum<sup>52-55</sup> (Fig. 29-12). A rim-enhancing



**FIG 29-11** Ruptured hemorrhagic ovarian cyst. **A**, Color Doppler sonographic image demonstrating the “ring of fire” appearance of a hemorrhagic corpus luteum (*white arrow and calipers*), which is still recognized despite rupture. The ovary is not identified as a discrete structure as it is surrounded by complex material of mixed echogenicity compatible with blood clot (*black arrow*). **B**, Large amount of complex fluid containing echoes (*arrows*) compatible with blood in the cul-de-sac posterior to the uterus (U). **C**, Large amount of hemoperitoneum (*arrows*) in the upper abdomen adjacent to the liver and in the Morison pouch.

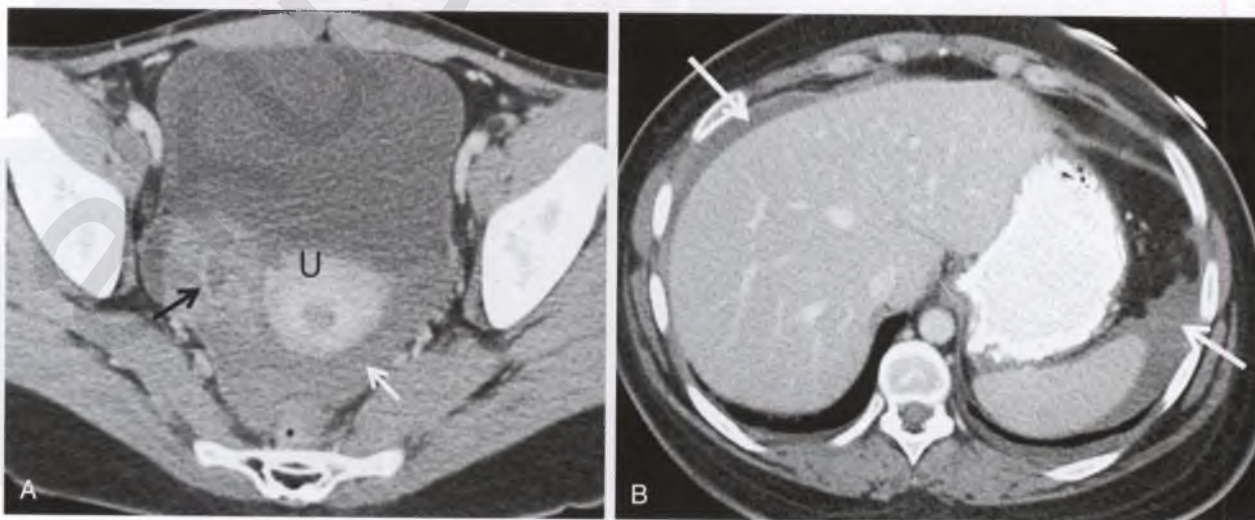


**FIG 29-12** Ruptured hemorrhagic cyst at contrast-enhanced computed tomography (CT). **A**, An irregular, crenulated rim-enhancing cyst (*black arrow*) is visible in the right adnexa surrounded by a high attenuation blood clot. High attenuation fluid compatible with blood (*white arrow*) is present in the cul-de-sac posterior to the uterus (U). **B**, More superior CT image demonstrates blood in the upper abdomen adjacent to the liver and spleen (*arrows*).



ovarian cyst may be identified, and even if the cyst has ruptured, a remnant of the cyst wall may remain visible. If there is active bleeding at the time of the scan, extravasation of contrast material with pooling in the pelvis will be observed.

Other cysts may also rupture, including cystic neoplasms, most commonly mature cystic teratomas. Rupture of ovarian teratomas has been reported to occur in 1% to 4% of cases.<sup>56</sup> Leakage of the liquefied sebaceous contents into the peritoneal cavity results in chemical peritonitis. Chronic leakage from the cyst may result in chronic granulomatous peritonitis.<sup>57</sup> If an adnexal mass is identified that exhibits classic sonographic features of a mature cystic teratoma and the patient has pain, either torsion or rupture of the mass should be considered. A large volume of intraperitoneal fluid, distorted or flattened shape of the mass, and discontinuity of the cyst wall suggest rupture.<sup>57</sup> CT may be helpful for further evaluation, as it may show scattered fat droplets outside the mass, peritoneal fluid, and findings of peritonitis (Fig. 29-13). The peritoneal inflammatory changes may mimic peritoneal carcinomatosis or tuberculous peritonitis, possible diagnostic pitfalls.

### Pelvic Inflammatory Disease

PID refers to a spectrum of disease that occurs when microorganisms ascend from the lower genital tract to infect the uterus, fallopian tubes, and ovaries<sup>58</sup> and is a common cause of emergency room visits and hospitalizations for acute gynecologic disorders.<sup>59</sup> The continuum of infection begins with cervicitis and progresses to endometritis, salpingitis, pyosalpinx, tubo-ovarian complex (TOC), and, ultimately, tubo-ovarian abscess (TOA). One third to one half of cases are due to *Chlamydia trachomatis* or *Neisseria gonorrhoeae*. However, PID is most commonly a polymicrobial infection, and a substantial proportion of cases are nongonococcal and nonchlamydial in origin,<sup>60</sup> involving vaginal flora, anaerobic gram-negative rods, and *Mycoplasma* bacteria. The adnexa may also become secondarily infected from other inflammatory processes, usually gastrointestinal in origin, including appendicitis and diverticulitis. The clinical diagnosis may be challenging, as symptoms and signs vary widely and overlap with other processes

including endometriosis, appendicitis, and ectopic pregnancy. Pelvic pain is the most common presenting symptom, although it may be absent or mild in some patients. On physical examination, cervical motion tenderness as well as uterine and adnexal tenderness are classic findings. There may be associated mucopurulent vaginal discharge, white blood cells on saline microscopy of vaginal secretions, elevated erythrocyte sedimentation rate, and C-reactive protein, leukocytosis, and fever. A delay in treatment may result in significant reproductive and gynecologic morbidity such as infertility, increased risk of ectopic pregnancy, chronic pelvic pain, and recurrent infection. Most patients can be effectively treated as outpatients with broad-spectrum antimicrobial therapy. However, hospitalization may be required for severe cases (including TOAs) or if the diagnosis is in doubt.

Imaging evaluation of patients with suspected PID may be necessary if the symptoms are nonspecific and diagnosis is uncertain, if the patient is not responding to treatment, or if complications such as abscess formation are suspected. If a TOA has formed, imaging may aid in determining the most appropriate method of treatment, with possible options including percutaneous drainage and surgery.

Pelvic ultrasound examination is the first-line imaging method of choice for the evaluation of PID. Ultrasound examination findings vary depending upon the stage of infection, and if PID is early or mild, findings may be nonspecific.<sup>61,62</sup> Patients with endometritis may not exhibit any sonographic imaging findings. A fluid-filled endometrial cavity is suggestive in the clinical setting of fever, vaginal discharge, and uterine tenderness on physical examination (Fig. 29-14). However, intrauterine fluid is a nonspecific finding. Gas in the endometrial cavity will appear on ultrasound imaging as foci of increased echogenicity with associated posterior acoustic shadowing. Although the presence of gas increases concern for possible infection, gas in the endometrial cavity may also be observed postpartum or post instrumentation. Free fluid in the cul-de-sac is also a nonspecific finding, although echoes within the fluid raise suspicion for infection (or hemorrhage). Enlargement and hyperemia of the ovaries with multiple small cysts indicate oophoritis.<sup>63,64</sup>

Findings involving the fallopian tubes are more specific for PID. Although isolated salpingitis may not always be recognizable by sonography, infected fallopian tubes may demonstrate wall thickening and hyperemia.<sup>65</sup> Obstruction at the fimbrial end of the tube due to inflammation will result in a pus-filled dilated tube or pyosalpinx, which



**FIG 29-13** Ruptured mature cystic teratoma. Patient presented to the emergency department with diffuse abdominal pain. There is a fat density mass compatible with mature cystic teratoma in the right adnexa (white arrow). Note focus of fat density separate from the mass (black arrow) and large amount of ascites (asterisks). A ruptured mature cystic teratoma with associated peritonitis was identified at surgery.



**FIG 29-14** Endometritis. Distended endometrial cavity (arrow and callipers) containing complex predominantly hypoechoic fluid in a febrile patient with purulent vaginal discharge.



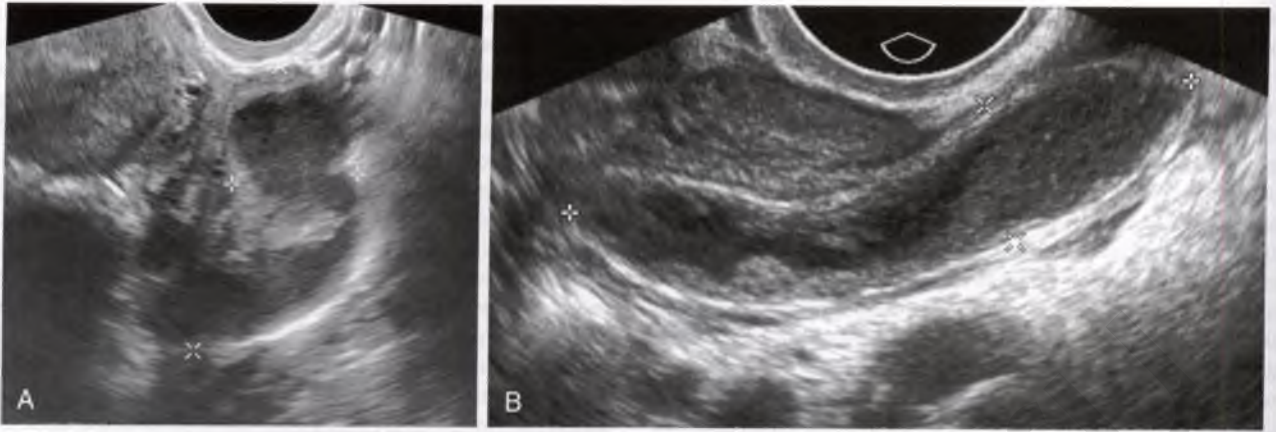


**FIG 29-15** Pyosalpinx. **A**, Distended thick-walled fallopian tube (*calipers*) containing complex fluid compatible with pyosalpinx. **B**, Pitfall: acute appendicitis. Debris-filled tubular structure (*calipers*) in the right adnexa was initially thought to represent pyosalpinx. However, no endosalpingeal folds are identified and this is a blind-ending structure. Computed tomography scan (not shown) confirmed acute appendicitis.

appears as a tubular structure distended with echogenic intraluminal fluid and debris, sometimes with layering echoes indicating a fluid-debris level, and thick hypervascular walls (Fig. 29-15A). Thickened and inflamed endosalpingeal folds may suggest small mural nodules, which give the appearance of a “cogwheel” when imaged in cross section. This finding helps differentiate a pyosalpinx from an inflamed appendix, which is blind-ending and does not have endosalpingeal folds (Fig. 29-15B). If untreated, PID progresses to form a TOC as the inflammation spreads to the adjacent ovary, which becomes enlarged with indistinct contours and increased vascularity, although the ovary remains identifiable as a discrete structure. The inflamed fallopian tube is often adjacent or adherent to the ovary. The final stage is TOA, in which the normal ovary is no longer delineated and an inflammatory mass replaces the ovary and fallopian tube. This appears as a complex multiloculated cystic adnexal mass with internal echoes, layering debris, and thick septations (Fig. 29-16). The mass will be markedly vascular on color Doppler interrogation. The presence of gas in a TOA is very rare. It is estimated that TOAs complicate approximately 10% to 15% of cases of PID.<sup>66</sup> TOA rupture may result in septic shock.

PID most often involves both adnexa, but may occasionally be unilateral. If the process is right-sided, a perforated appendicitis with abscess formation could have a similar appearance, and if left-sided, perforated diverticulitis may give a similar picture. Assessment of patient risk factors for PID is very important in this setting. CT may be required to exclude appendicitis or diverticulitis as the cause of the abscess (Fig. 29-17). CT also may be helpful in detecting complications such as extension of inflammation out of the pelvis and involvement of adjacent structures including the bowel or ureter. A blood-filled fallopian tube (hematosalpinx) in the setting of endometriosis may mimic pyosalpinx and is another diagnostic pitfall. A complex or infected endometrioma may mimic a TOA (see further discussion later). MRI can serve as a useful complementary imaging technique because signal intensity characteristics compatible with chronic blood products will be observed in endometriosis but not in PID. One series evaluating patients with both ultrasound imaging and MRI reported the sensitivity and specificity of MRI for laparoscopically proven PID to be 95% and 89% and of ultrasound imaging to be 81% and 78%, respectively.<sup>67</sup>

Chronic PID may result in obstruction of the ampullary segment of the fallopian tube, causing hydrosalpinx with fluid-filled dilatation of the fallopian tube. Although PID is the most common cause of hydrosalpinx, other causes include tubal ligation, hysterectomy without



**FIG 29-16** Tubo-ovarian abscess. Multiloculated adnexal mass containing complex fluid. No normal ovary was identified.

salpingo-oophorectomy, endometriosis, prior surgery, and malignancy.<sup>65</sup> Hydrosalpinx may be a cause of pelvic pain and infertility. At sonography, a dilated fallopian tube in the absence of infection appears as a C-, U-, or S-shaped anechoic, avascular tubular structure, generally with a thin wall less than 5 mm thick (Fig. 29-18). Small 2 to 3 mm nodules representing the remnants of the endosalpingeal folds may appear as “beads on a string.”<sup>61,68</sup> In one study, hydrosalpinx was diagnosed with the highest likelihood when a tubular mass with small round mural projections or a waist sign was visualized.<sup>69</sup> The incomplete septation sign, due to the distended tube folding on itself, may also be observed but is a less reliable finding. If these features are not observed, hydrosalpinx may be difficult to distinguish from a cystic ovarian neoplasm. Three-dimensional (3D) sonography may increase specificity.<sup>70,71</sup> MRI may be helpful by demonstrating the tubular nature of the mass and intraluminal fluid content.<sup>65</sup> PID may also result in formation of a peritoneal inclusion cyst (discussed later).

## Endometriosis

Endometriosis is defined as the presence of endometrial glands and stroma in ectopic locations outside the uterus.<sup>72,73</sup> Neovascogenesis



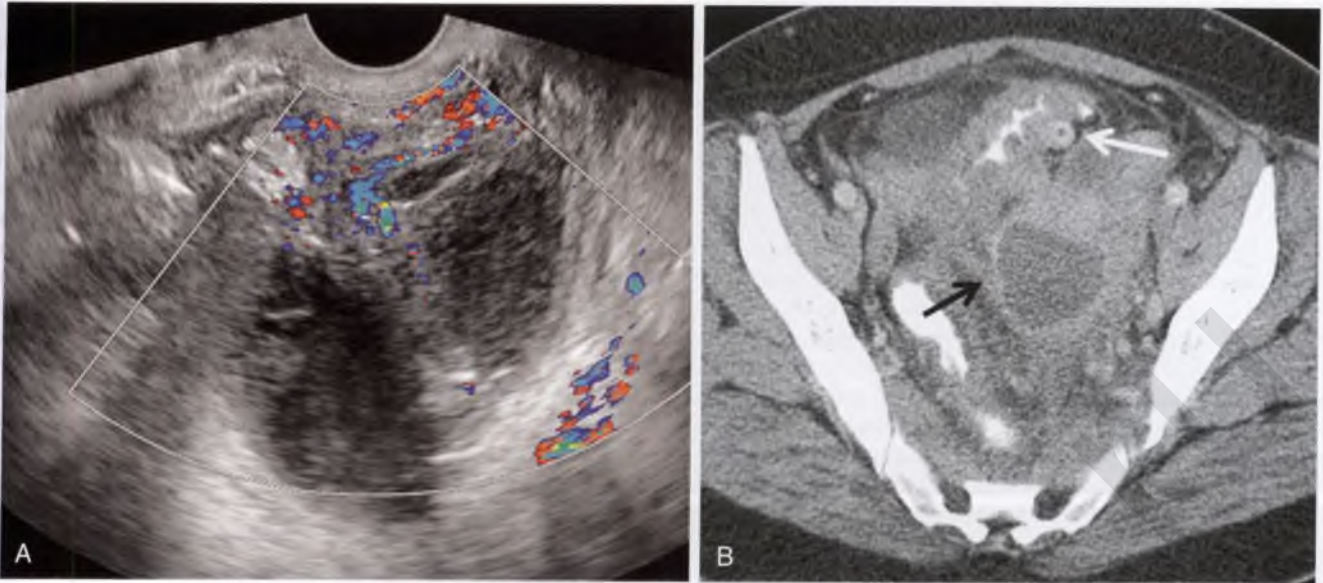


**FIG 29-17** Tubo-ovarian abscess secondary to diverticulitis. **A**, Ultrasound image demonstrates a complex multiloculated pelvic mass with increased peripheral blood flow in a patient with left lower quadrant pain and fever. Note increased echogenicity in the surrounding pelvic fat consistent with inflammation. The patient had no risk factors for pelvic inflammatory disease. **B**, Computed tomography demonstrates the left pelvic abscess (*black arrow*). Note mural thickening of the adjacent sigmoid colon with numerous diverticula (*white arrow*) compatible with diverticulitis, which was the source of the abscess, confirmed at surgery.

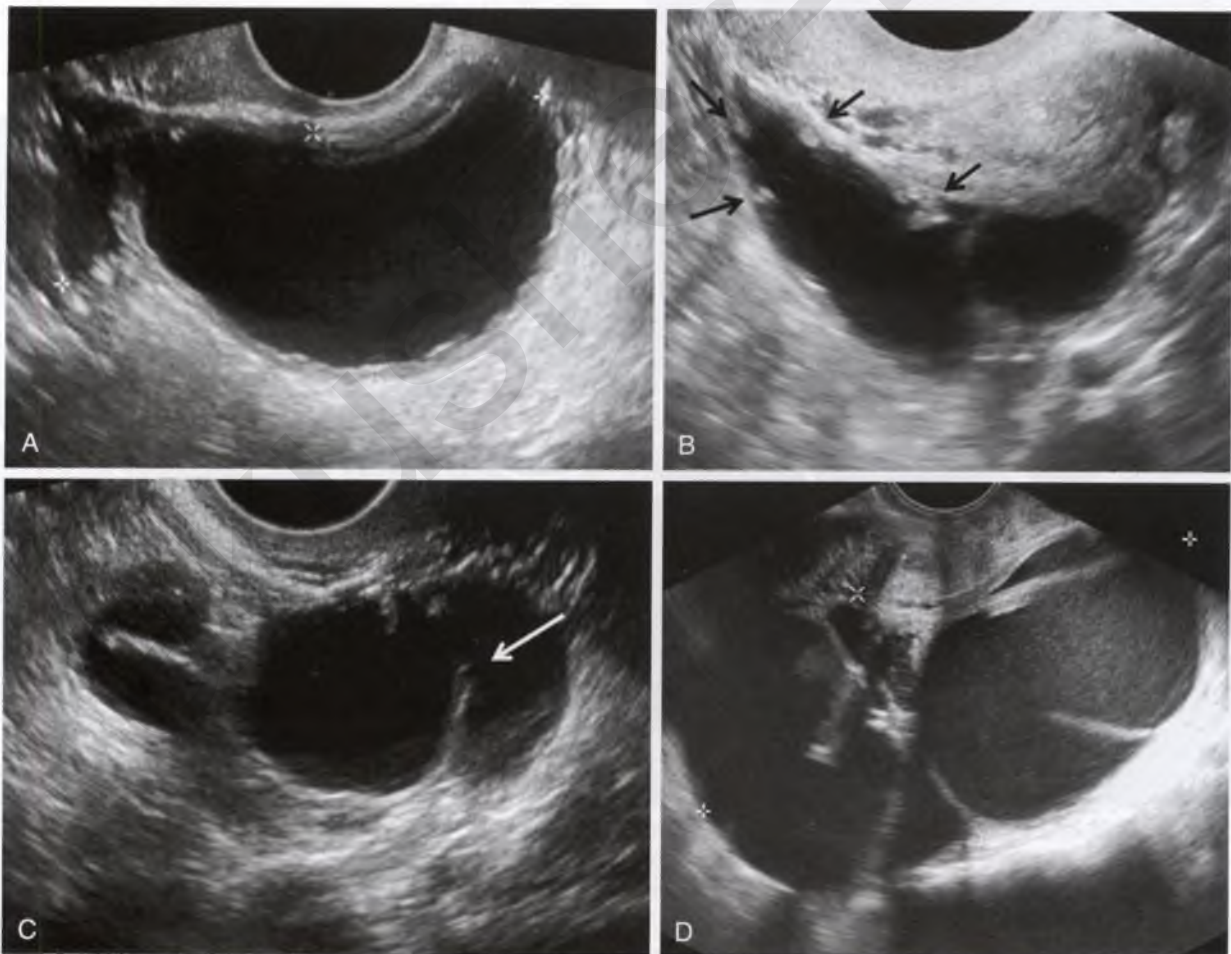


**FIG 29-18** Sonographic spectrum of hydrosalpinx. **A**, Dilated fallopian tube appears as an anechoic fluid-filled, avascular tubular structure (*calipers*). **B**, The endosalpingeal folds (*arrows*) appear as beads on a string. **C**, Incomplete septation (*arrow*) is formed by the tube folding upon itself. **D**, Pitfall: mucinous cystadenoma (*calipers*) appears tubular in configuration with incomplete septations and mimics a distended fallopian tube.



and capillary recruitment are associated with endometriotic lesions at laparoscopy, and there is an associated inflammatory response ultimately progressing to fibrosis.<sup>74</sup> This disorder is associated with a wide variety of symptoms including dysmenorrhea, dyspareunia, chronic pelvic pain, and dysfunctional uterine bleeding.<sup>74</sup> Although pain is usually chronic, complications of endometriosis may result in a more acute presentation. Infertility is an important consequence of endometriosis, due to associated anatomic distortion of the pelvic structures and obstruction of the fallopian tubes. Endometriosis affects up to 10% of women of reproductive age,<sup>75</sup> although in women with pelvic pain, infertility, or both, the prevalence is estimated to be as high as 35% to 50%.<sup>76</sup> Because endometriosis is hormonally responsive, symptoms are often cyclic in nature, and there is repetitive hemorrhage into these lesions. The pathogenesis of endometriosis is complex and remains the subject of debate.<sup>74</sup> Proposed theories include origin of implants from the uterine endometrium, possibly from lymphatic or hematogenous dissemination of endometrial cells or retrograde menstruation. Other theories propose that implants arise from tissues outside the uterus, for example, coelomic metaplasia with transformation of peritoneal tissue to ectopic endometrial tissue or embryonic müllerian rests that develop into endometriotic lesions under the influence of estrogen. A more recent theory suggests that extrauterine stem/progenitor cells originating from bone marrow may differentiate into endometriotic tissue, and this topic is currently an active area of investigation.<sup>77</sup>

The most common sites of endometriotic implantation include the surface of the ovary, uterine suspensory ligaments, uterus or fallopian tube, and the peritoneal surfaces of the pouch of Douglas. Less

common sites of implantation include vagina, bladder, cervix, intestine, cesarean delivery scars, abdominal scars, or the inguinal ligament. Deep pelvic endometriosis is defined as invasive tissue that infiltrates structures at a depth of more than 5 mm from the peritoneal surface and is associated with fibrosis and muscular hyperplasia.<sup>78-80</sup> This preferentially affects the dependent portions of the posterior peritoneal spaces, most commonly the uterosacral ligaments, torus uterinum, rectovaginal pouch, rectum, and rectovaginal septum, with anterior involvement less common. Current treatment options for endometriosis include both medical (primarily hormonal) and surgical management. Diagnostic laparoscopy remains the reference standard for diagnosis and staging of endometriosis, although the role of imaging in endometriosis has continued to evolve. The ovaries are the most common sites of endometriosis and are frequently involved with multiple and bilateral lesions. The classic sonographic appearance of an endometrioma, often referred to as a chocolate cyst because of the presence of thick, dark, degenerated blood products from repetitive cyclic episodes of bleeding, is that of a homogeneous, hypoechoic lesion with low to medium level echoes and no internal vascularity (Fig. 29-19).<sup>81-85</sup> This has often been referred to as a "ground glass" appearance<sup>48</sup> and is highly predictive of an endometrioma, with one retrospective series reporting this appearance in 95% of endometriomas.<sup>84</sup> However, there is a spectrum of sonographic appearances, and in another series, 13 of 87 surgically proven endometriomas were felt to be atypical.<sup>85</sup> In an investigation by Patel and coworkers<sup>84</sup> echogenic mural foci, thought to represent cholesterol deposits, were observed in 36% of endometriomas compared with 6% of nonendometriomas, and septations were found in 45% of endometriomas. In that study, if

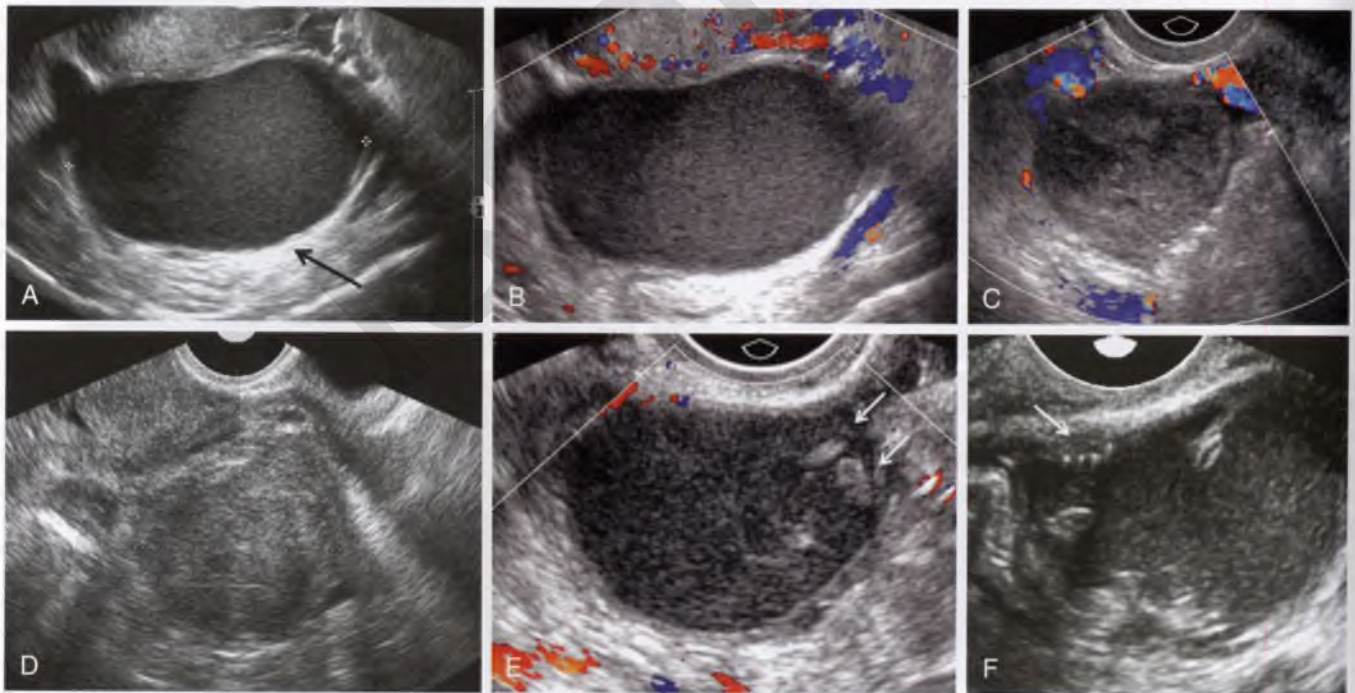


**FIG 29-19** Sonographic spectrum of endometriomas. **A**, Classic appearance of a chocolate cyst (*calipers*) with homogeneous low-level echoes, the ground glass appearance. Posterior acoustic enhancement (*arrow*) confirms a cystic lesion. **B**, No vascularity is demonstrated within the lesion on color Doppler interrogation. **C**, More complex, heterogeneous appearance in another patient as a result of acute hemorrhage into an endometrioma. No internal blood flow is detected on color Doppler sonogram. **D**, Solid appearance of a chronic endometrioma (*calipers*) mimicking a solid adnexal mass. **E**, Avascular mural nodules suggested (*arrows*), representing adherent blood clot. **F**, Complex cystic lesion with possible mural nodules suggested. Appearance simulates an ovarian neoplasm. Echogenic foci along the wall (*arrow*) with comet-tail artifact help suggest the diagnosis of endometrioma.



an adnexal mass had diffuse low-level echoes, as well as hyperechoic mural foci and multilocularity, as well as no evidence of other neoplastic features, it was 32 times more likely to be an endometrioma than any other adnexal mass. Occasionally an endometrioma can mimic a simple ovarian cyst and appear completely anechoic. Other findings include fluid-fluid level, thickened wall, and mural or central calcifications. Avascular mural nodules representing an adherent or retracting blood clot can occasionally be observed, but a clot is less commonly observed in endometriomas than in hemorrhagic ovarian cysts. Rarely, flow within nodular areas has been described, possibly due to endometrial stromal tissue.<sup>43</sup> However, tumor nodules due to malignant degeneration (usually into clear cell or endometrioid carcinoma) of an endometrioma may mimic this appearance and demonstrate Doppler-detected blood flow. Chronic endometriomas may mimic solid masses due to the presence of older blood products and fibrosis.<sup>43</sup> However, typically, there is only perilesional blood flow with no internal vascularity.<sup>86</sup> Doppler waveform analysis is not helpful in diagnosis as low resistance waveforms resembling malignancy can be observed in the wall of an endometrioma.<sup>81</sup>

Ultrasound examination findings of endometriomas may overlap considerably with other adnexal masses including hemorrhagic cysts, TOAs, dermoids, and cystic ovarian neoplasms (Fig. 29-20). In a meta-analysis by Moore and colleagues,<sup>87</sup> the sensitivity of transvaginal sonography for the diagnosis of an endometrioma ranged from 64% to 89% with specificity of 89% to 100%. The most common misdiagnoses were hemorrhagic cysts and dermoids. If a hemorrhagic cyst is a diagnostic consideration, short-interval follow-up ultrasound examination is useful because a hemorrhagic cyst should resolve whereas an endometrioma will persist. If ultrasound findings are not definitive and if ovarian neoplasm is of concern, MRI is the next recommended step.<sup>88-90</sup> As a result of the repeated cycles of bleeding, endometriomas will contain old blood products with high iron and protein concentration creating characteristic findings at MRI with increased signal intensity on T1-weighted images and decreased signal on T2-weighted images, sometimes referred to as *shading*.<sup>91</sup> Mural nodules representing an adherent clot will not enhance on postcontrast subtraction images. An enhancing nodule following the administration of gadolinium is indicative of either malignant degeneration or endometrial stromal tissue. Fat-sensitive images help to identify macroscopic fat in a dermoid (Fig. 29-21). MRI has a greater than 90% sensitivity and specificity for endometriomas.<sup>91</sup>

Endometrial implants involve the fallopian tubes in approximately 6% of women with endometriosis, and adhesions involve the tubes in 26%.<sup>92</sup> Endometriotic implants are most common on the serosal surface, with transmural and mucosal involvement occurring less frequently. Hematosalpinx may be an isolated finding in patients with endometriosis.<sup>89</sup> At sonography, low-level echoes, corresponding to blood products, may be identified in the dilated fallopian tube (Fig. 29-22). This appearance may simulate that of pyosalpinx, and clinical findings are important to differentiate between these entities. MRI may also be helpful by confirming the presence of blood products in the tube.

Endometriotic implants may occur in the anterior abdominal wall, which is the most frequent site of extrapelvic disease. Endometriosis in the abdominal wall is usually found next to a surgical scar or a needle or laparoscopic trocar tract. One of the most common associations is with prior cesarean delivery, reported in 0.03% to 1% of women.<sup>93</sup> In a series of 455 cases of abdominal wall endometriosis, 57% were associated with cesarean delivery scar, and 11% were associated with hysterectomy.<sup>94</sup> Spontaneously occurring implants may be seen adjacent to the umbilicus. Among women with scar endometriosis, only 14% to 26% have concomitant pelvic endometriosis.<sup>95</sup>

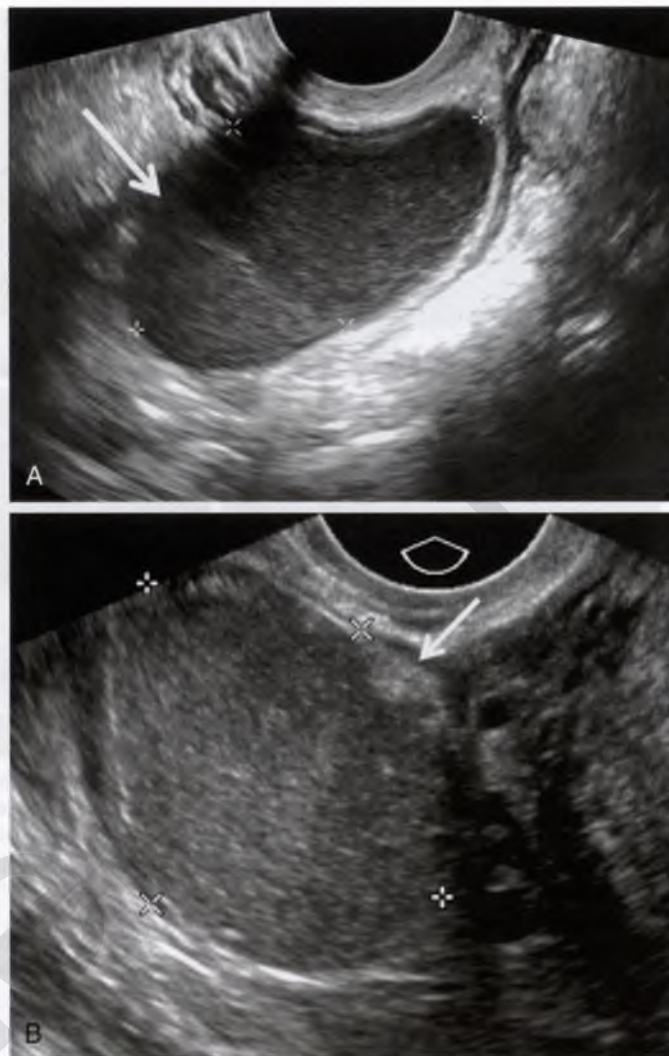


**FIG 29-20** Mimics of endometriomas. **A**, Mucinous cystadenoma (*calipers*) containing layering low-level echoes and fluid-fluid level (*arrow*). Lesion was observed in a postmenopausal patient who underwent surgical evaluation and resection. **B**, Pathologically proved mature cystic teratoma (*calipers*) was originally thought to be an endometrioma with adherent clot (*arrow*). The echogenic mural nodule corresponded to a focus of fat at pathologic examination.

Implants may be confined to the superficial subcutaneous soft tissues but may also involve the rectus muscle. The most widely held theory of pathogenesis states that these implants arise from transportation and direct implantation of endometrial cells during procedures that open the uterus.<sup>96</sup> Women may present with a tender abdominal wall mass adjacent to a scar or with an asymptomatic palpable lump. Pain and swelling may be cyclic, correlating with menstruation. Imaging findings vary depending upon phase of the menstrual cycle, chronicity, number of stromal and glandular elements, and degree of associated bleeding and inflammation.<sup>96</sup> Sonography is usually the first-line imaging study performed, using a high-resolution linear transducer, which will identify a solid, heterogeneous hypoechoic mass with scattered internal echoes, although the appearance is variable<sup>93,97,98</sup> (Fig. 29-23). Areas of cystic change may be observed and the margins may be spiculated with infiltration of adjacent soft tissues.<sup>99,100</sup> Most implants will demonstrate some vascularity at Doppler evaluation.<sup>93,97,99</sup> Differential diagnostic considerations include abdominal wall masses such as desmoid tumor, metastasis, lymphoma, melanoma, hematoma,



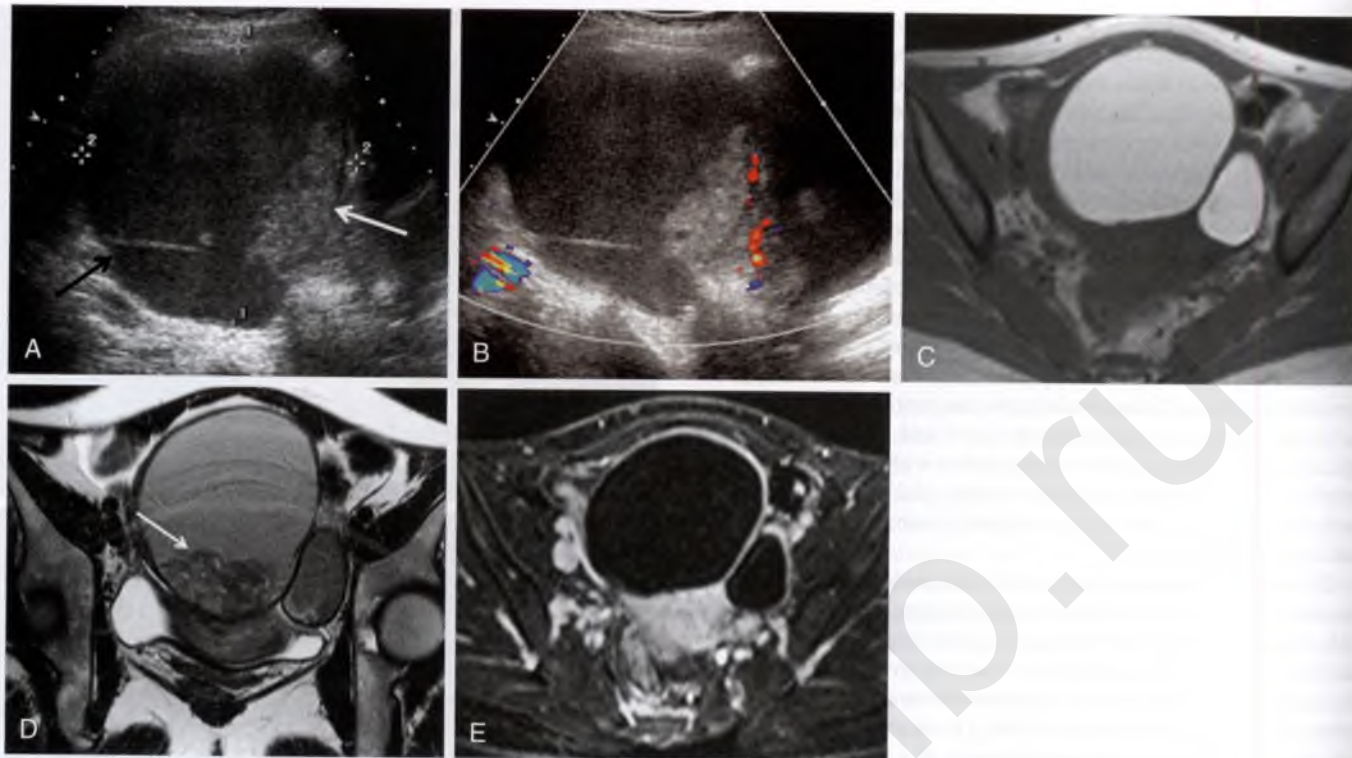


**FIG 29-21** Complex endometrioma mimicking ovarian neoplasm. **A**, A 10-cm complex cystic mass (*calipers*) with septation (*black arrow*) and echogenic, lobulated mural nodule (*white arrow*). **B**, No flow was demonstrated in the nodule with color Doppler interrogation, suggesting the possibility of an adherent blood clot. **C**, Axial T1-weighted magnetic resonance (MR) image demonstrates that the lesion is T1-weighted hyperintense suggesting hemorrhagic content. Note adjacent smaller similar appearing lesion. **D**, Decrease in signal intensity within both lesions on T2-weighted axial MR image represents “shading.” A dependent clot is visible in the larger midline lesion (*arrow*). **E**, Postcontrast subtraction image demonstrates no enhancing solid component. Endometriomas were confirmed at surgery.

suture granuloma, or incisional hernia. Location of the mass next to a scar and history of cyclic pain related to menses suggest the diagnosis. MRI may also be a useful adjunct because it may identify the typical imaging characteristics of hemorrhage as well as avid gadolinium enhancement.<sup>96</sup> The extent of disease may also be better depicted on MRI. Fine-needle aspiration/biopsy with cytologic analysis may help confirm a definitive diagnosis. Wide surgical excision with clear margins to prevent local recurrence is the treatment of choice.

In the past, ultrasound examination was considered most useful for characterization of an adnexal mass as an endometrioma, whereas extraovarian disease and deep pelvic endometriosis was better evaluated with MRI, offering important mapping of extent of disease prior to surgical intervention. However, more recently, an increasing role for sonography in identification of nonovarian disease has been advocated.<sup>101</sup> Gentle probing with the transvaginal ultrasound transducer may identify extraovarian disease, particularly in the deep pelvis.<sup>102,103</sup> Recent studies have shown that sonography may be useful for detecting implants in the bladder, rectovaginal septum, rectum, and sigmoid colon.<sup>104,105</sup> Bazot and associates<sup>106</sup> evaluated a group of women with deep endometriosis and found that sonography had a sensitivity and specificity for detection of disease of 78.5% and 95.2%, respectively, with the highest sensitivity for detecting intestinal and bladder disease. Endometriosis of the uterine serosa, uterosacral ligaments, and retrocervical and retrovaginal spaces may be diagnosed as hypoechoic solid lesions with indistinct margins due to smooth muscle proliferation and prominent fibrotic component<sup>88</sup> (Fig. 29-24). Occasionally, these lesions may also contain cystic spaces. Pelvic adhesions can be

evaluated by moving the transducer back and forth to assess whether the uterus, adnexa, and bowel slide freely. Bowel implants may be more conspicuous after bowel preparation and appear as hypoechoic nodules with variable extension into the bowel wall.<sup>107</sup> A recent meta-analysis showed that transvaginal sonography with or without bowel preparation is an accurate test for noninvasive presurgical detection of deep infiltrating endometriosis of the rectosigmoid with pooled estimates of sensitivity and specificity of 91% and 98%, respectively, and positive and negative predictive value (NPV) of 98% and 95%.<sup>108</sup> Another study reported that transvaginal sonography yields few false positive results but that negative findings are less reliable and that the accuracy of sonography is affected by the location and number of endometriotic lesions.<sup>109</sup>

Although endometriosis most often causes chronic pelvic symptoms, complications may lead to acute pelvic pain. Occasionally an endometrioma may rupture and have a clinical presentation similar to a ruptured hemorrhagic ovarian cyst. On sonography, complex free fluid compatible with hemoperitoneum will be noted in addition to a hemorrhagic-appearing adnexal mass (Fig. 29-25). This occurs more frequently during pregnancy as a result of rapid growth from hormonal stimulation and may become a surgical emergency if there is extensive bleeding.<sup>110</sup> A known history of endometriosis is helpful in establishing the diagnosis. Endometriosis may also be associated with massive hemorrhagic ascites, usually in the setting of pelvic adhesions and ovarian endometriomas.<sup>111</sup> Exudative ascites may result from peritoneal inflammation due to hemoperitoneum following rupture of an endometrioma. An endometrioma may also become superinfected,



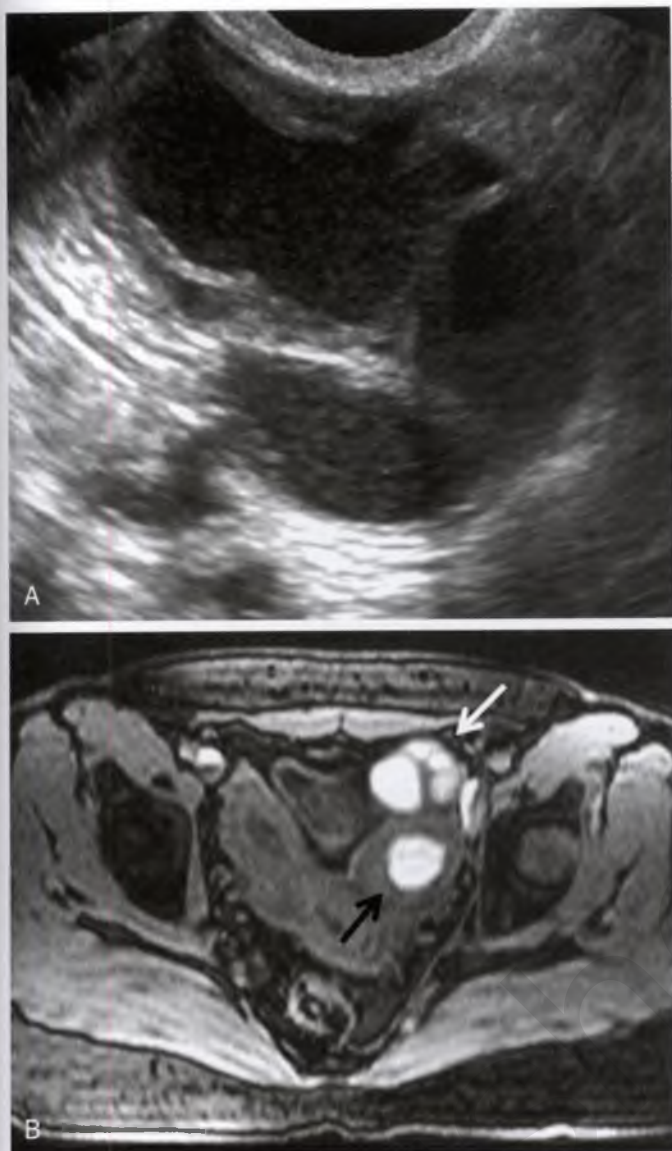


**FIG 29-22** Endometriosis involving fallopian tube with hematosalpinx. **A**, Dilated fallopian tube with low-level intraluminal echoes compatible with blood. **B**, Axial fat-suppressed T1-weighted magnetic resonance image confirms high signal intensity in the tube (*white arrow*) compatible with hematosalpinx. The patient also has a unicornuate uterus with an obstructed left rudimentary horn containing blood (*black arrow*).

clinically mimicking PID. This most commonly occurs after surgical drainage or aspiration.<sup>112</sup> Direct spread from adjacent inflammation or hematogenous spread in a bacteremic patient may also cause superinfection. The sonographic appearance of an infected endometrioma may be identical to an uninfected endometrioma or may appear more complex (Fig. 29-26). Clinical signs of infection are thus crucial in establishing the diagnosis.

During pregnancy, decidualization of an endometrioma may occur as a result of hypertrophy of the ectopic stromal cells, primarily from the effects of progesterone.<sup>113</sup> A decidualized endometrioma increases in size and becomes more complex in appearance, with solid mural nodules or papillary excrescences that may be vascular on Doppler imaging. These changes may mimic a malignant ovarian neoplasm.<sup>114-116</sup> Prior documentation of an endometrioma can be helpful in suggesting this diagnosis, allowing for sonographic surveillance rather than

surgical intervention. MRI may also be useful by demonstrating that the mural nodules have signal intensity and texture similar to the decidualized uterine endometrium.<sup>116,117</sup>

Malignant transformation is a well-described but rare complication of endometriomas, with an estimated incidence of approximately 1%.<sup>118</sup> Women with a history of endometriosis are 4.2 times more likely to develop ovarian cancer than other women, the most common histologic findings being clear cell carcinoma and endometrioid carcinoma arising from glandular elements.<sup>119</sup> Less commonly, endometrial stromal sarcoma can arise from stromal elements.<sup>120</sup> A specific genetic mutation (*ARID1A*) has been implicated in this process.<sup>121</sup> Because of this malignant potential, the Society of Radiologists in Ultrasound Consensus Conference Statement on management of asymptomatic ovarian cysts advised that adnexal masses with classic features of endometriomas be followed at least yearly with serial ultrasound examinations to search for worrisome features, including development of solid vascular components, usually mural based, and rapid interval growth (Fig. 29-27).<sup>51</sup> If such findings are observed, surgical exploration should be recommended. MRI may be helpful to confirm the diagnosis of malignant transformation.<sup>122,123</sup> The frequency of follow-up will vary depending on the patient's age and symptoms. With advancing age, patients may be followed more closely owing to increased incidence of malignant transformation in older women.<sup>124</sup>

### Peritoneal Inclusion Cyst

Peritoneal inclusion cysts are benign fluid-filled lesions lined by mesothelium that occur in the abdomen and pelvis. Although their pathogenesis is a subject of some debate, with both hyperplastic and neoplastic origins proposed, they are generally thought to arise secondary to intra-abdominal inflammation with reactive mesothelial proliferation and impaired absorption of peritoneal fluid. Histologically, mesothelial cells are arranged in a single layer with surrounding reactive stroma and fibrovascular tissue.<sup>125</sup> They occur almost exclusively in premenopausal women with functioning ovaries and a history of abdominal or pelvic surgery or inflammation, including PID, endometriosis, and inflammatory bowel disease. It is believed that the small amount of fluid normally produced by the ovaries and fallopian tubes is loculated by surrounding pelvic adhesions and that absorption of this fluid is impaired by the surrounding fibrous tissue, forming a loculated cystic collection. Although peritoneal inclusion cysts may be incidental findings, they may also be associated with abdominal/pelvic pain or palpable mass. Accurate diagnosis is important to guide patient management. Options for treatment include oral contraceptives to decrease the amount of fluid produced by the ovary, percutaneous drainage, sclerotherapy, or surgical resection.<sup>125</sup> However, these cysts often recur following surgery as new adhesions form. Hence, conservative management is the preferred option in most cases. If mistaken for a cystic ovarian neoplasm, unnecessary or more aggressive therapy may be undertaken.

The imaging features of peritoneal inclusion cysts reflect their pathogenesis, and recognition of these features often allows differentiation from a cystic ovarian mass.<sup>126-128</sup> As the fluid surrounds the ovary, the ovary is entrapped within the cyst and is often identifiable along the cyst wall (Figs. 29-28 and 29-29). Fibrous bands mimicking septations and extending to the ovarian surface may suspend the ovary within the fluid collection, creating a "spoke wheel" or "spider web" appearance. Because these cysts lack a true wall, they typically conform to the shape of the surrounding pelvic organs or peritoneal cavity, becoming irregular in shape with angular margins. They can, however, be ovoid or spherical. Occasionally, features overlap with those of cystic ovarian masses, particularly if the ovary cannot be identified as a discrete structure within the cyst. Rarely, hemorrhage into these lesions



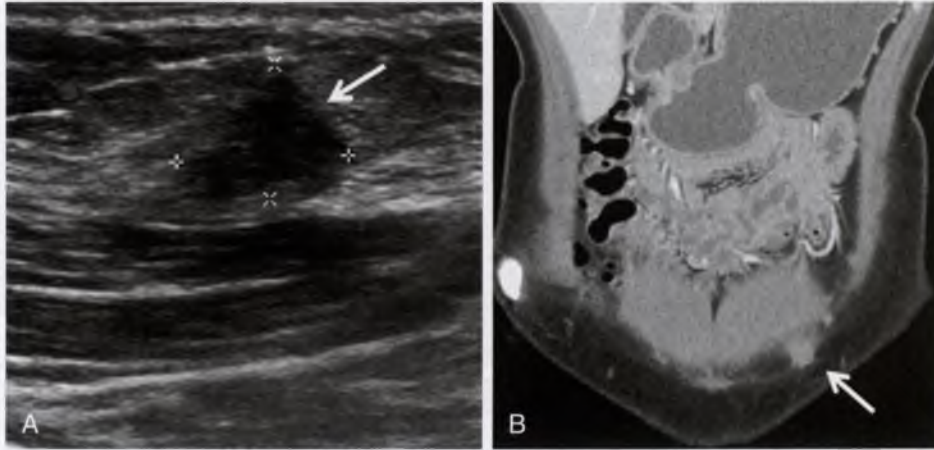


**FIG 29-23** Abdominal wall endometriotic implant. **A**, Hypoechoic, irregularly margined solid nodule (*arrow* and *calipers*) in the subcutaneous soft tissues at the anterior abdominal wall, ventral to the rectus muscle near the surgical scar. The patient, with history of open myomectomy 2 years prior, has a palpable lump. **B**, Coronal computed tomography image demonstrates the nodule (*arrow*) in the subcutaneous soft tissues, corresponding to the finding on ultrasound imaging.



**FIG 29-24** Endometriotic implant at posterior serosal surface of uterus. **A**, Hypoechoic nodule (*arrow* and *calipers*) along the posterior surface of uterus. **B**, Additional hypoechoic implants (*arrow*) are less well defined and have more irregular margins. **C**, Fat-suppressed axial T1-weighted magnetic resonance image showing the hyperintense implants (*arrow*) along the posterior surface of the uterus (U).



**FIG 29-25** Ruptured endometrioma in a patient with acute onset of left lower quadrant pain. **A**, Complex mass (*calipers*) with internal echoes and echogenic focus compatible with clot (*arrow*). **B**, There is associated free fluid (*arrow*) containing echoes, most consistent with hemoperitoneum. **C**, Computed tomography shows the endometrioma (*solid white arrow*). There is a small amount of free fluid (*open arrow*) and pelvic inflammatory changes. There is reactive thickening of an adjacent loop of small bowel (*black arrow*). Ruptured endometrioma was confirmed at surgery.



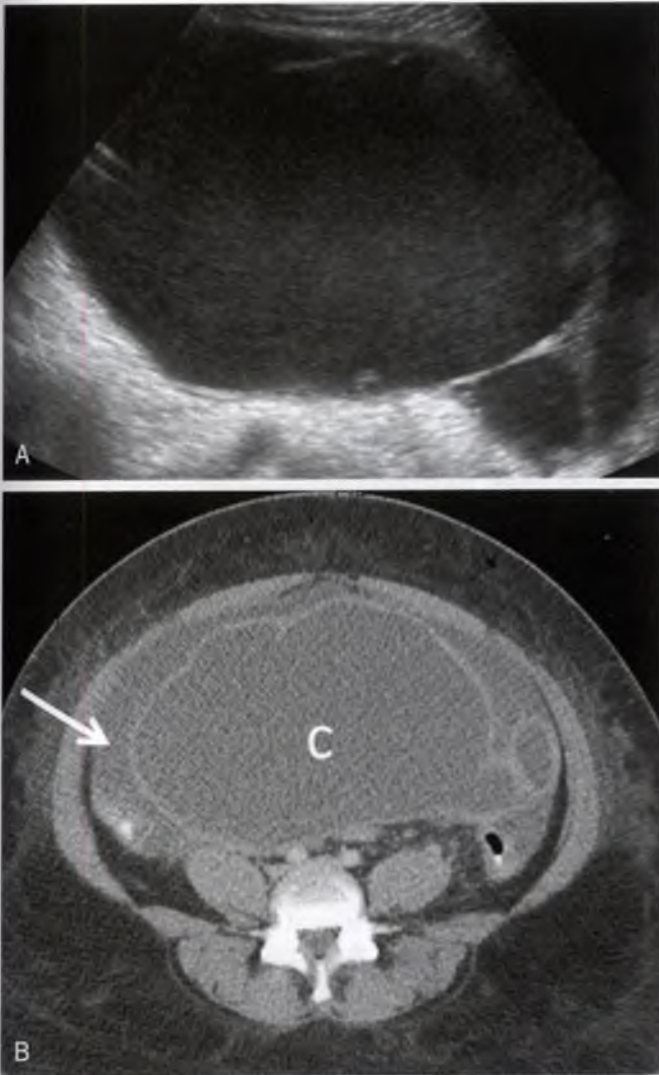


**FIG 29-26** Infected endometrioma with rupture in a patient with abdominal pain and sepsis. **A**, Ultrasound image shows a large complex cystic mass with low-level echoes and incomplete septation. **B**, Computed tomography demonstrates the large cystic mass (C) with incomplete septation anteriorly and associated ascites (arrow). Ruptured endometrioma with superinfection was confirmed at surgery.

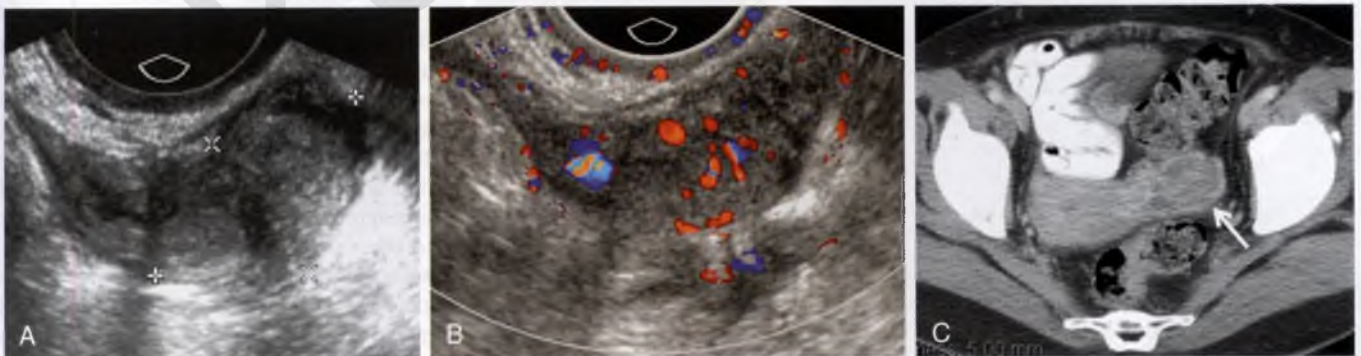


**FIG 29-27** Enlarging solid ovarian mass found on serial sonograms in patient with history of endometriosis. **A**, Transvaginal sonography demonstrates a solid mass (calipers) in the left ovary. **B**, Increased vascularity is demonstrated in the mass with color Doppler sonography, confirming solid nature. **C**, Contrast-enhanced computed tomography scan demonstrates the primarily solid, heterogeneously enhancing left ovarian mass (arrow). Patient underwent surgery and was found to have endometrioid adenocarcinoma with foci of squamous and clear cell differentiation involving the left ovary and fallopian tube arising in a background of endometriosis.

may occur, creating a more complex appearance.<sup>127</sup> The presence of mural nodularity, papillary excrescences, or other solid components should exclude this diagnosis. MRI may allow better appreciation of the shape of the cyst and visualization of the ovary<sup>128</sup> (Fig. 29-28C), confirming the diagnosis. The need for follow-up should be based on patient age and symptoms.

## UTERINE CAUSES OF PELVIC PAIN

### Leiomyomas

Uterine leiomyomas (also termed *fibroids* or *myomas*) are the most common tumor of the female reproductive tract and are found in up to 60% of reproductive age women and in 80% of women during their lifetime.<sup>129</sup> Leiomyomas are benign tumors of smooth muscle origin and have a higher concentration of estrogen and progesterone receptors than normal myometrium.<sup>130</sup> As a result, they grow in response to hormonal stimulation, including during pregnancy, and generally regress after menopause. Although many remain asymptomatic, up to 25% may be associated with symptoms significant enough to warrant treatment.<sup>131</sup> Symptoms include chronic pain, pelvic pressure, dysmenorrhea, infertility, and abnormal vaginal bleeding and vary depending on size, location, and associated complications such as degeneration and infarction.<sup>132</sup> Leiomyomas may undergo various types of degeneration including hyaline, myxomatous, calcific, cystic, fatty, and carneous (red) degeneration.<sup>133</sup> Compression of the ureters by a large myoma may lead to hydronephrosis and flank pain. Uterine leiomyomas are classified by location as intracavitary, submucosal, intramural, subserosal, or exophytic/pedunculated. Recently, a detailed subclassification system to more completely describe the relationship of a leiomyoma to the endometrium and serosa has been described,<sup>134</sup> as these features may impact clinical management. Leiomyomas may occasionally arise outside the uterus in the broad ligament, mimicking an adnexal mass. More unusual manifestations of extrauterine leiomyomas include disseminated peritoneal leiomyomatosis, intravenous leiomyomatosis, and benign metastasizing leiomyomatosis.<sup>135</sup>

Uterine leiomyomas are often suspected upon palpation of an enlarged, lobulated uterus on physical examination with suggestive clinical symptoms. If imaging is required, sonography is the first-line imaging test of choice and is usually sufficient for evaluation. A transabdominal approach is often used to supplement the transvaginal examination when the uterus is enlarged or when location of the leiomyoma prevents adequate sound penetration and visualization. Most



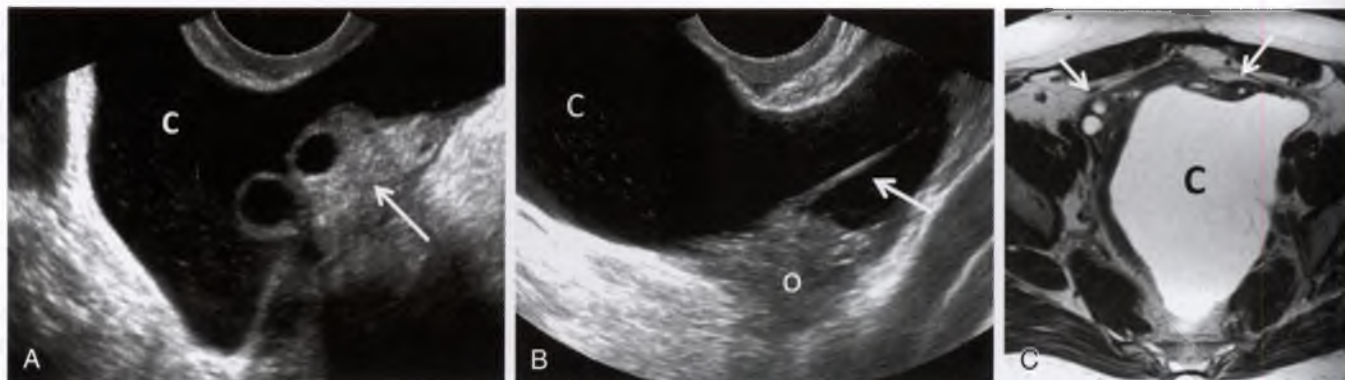


**FIG 29-28** Peritoneal inclusion cyst. **A**, Normal ovary (arrow) identified at the margin of the cyst (c), which contains a small amount of echogenic debris. **B**, A fibrous band (arrow) extends from the ovary (o). The irregular shape of the cyst (c) conforms to adjacent pelvic structures. **C**, T2-weighted axial magnetic resonance image demonstrates both ovaries (arrows) along the anterior wall of the cyst (c).

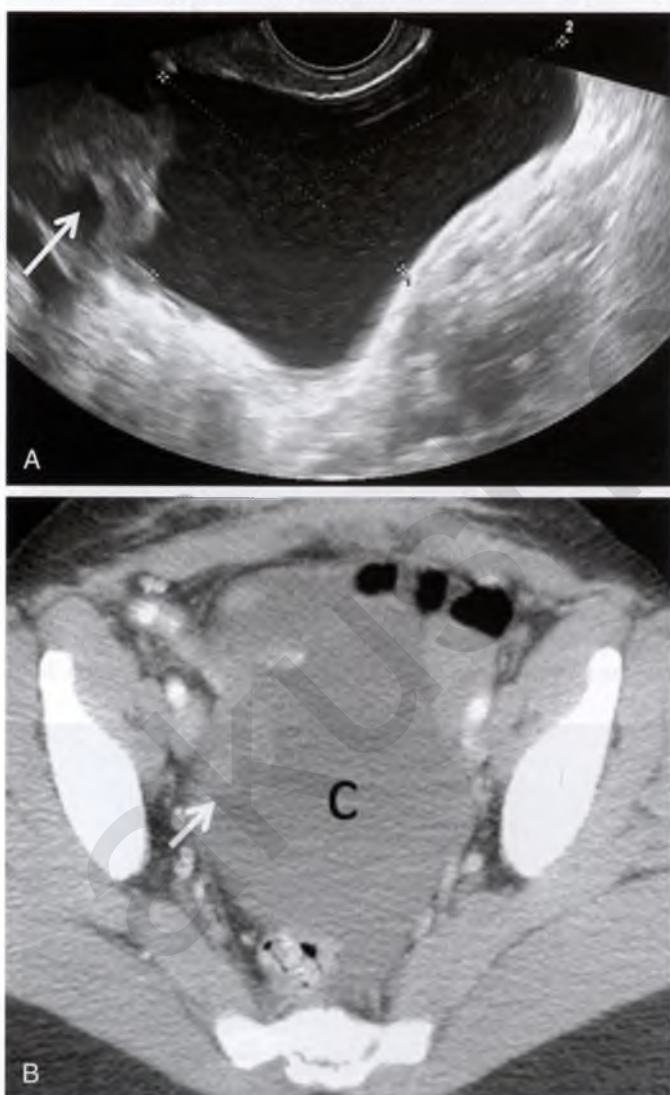


**FIG 29-29** Peritoneal inclusion cyst. **A**, The right ovary (arrow) is noted along the superior wall of the cyst (calipers). Low-level echoes are present in the cyst fluid. **B**, Contrast-enhanced axial computed tomography shows the right ovary (arrow) along the cyst wall. The shape of the cyst (c) conforms to adjacent pelvic structures. The patient had previously undergone hysterectomy for leiomyomas.

often, a leiomyoma appears as a well-defined hypoechoic solid mass arising from the myometrium with a well-defined border or pseudocapsule resulting from compression of adjacent myometrium<sup>136</sup> (Fig. 29-30). However, the echogenicity of the mass varies depending on the relative amount of fibrous tissue and smooth muscle. The amount of fibrous tissue also likely determines the degree of attenuation of the ultrasound beam and posterior acoustic shadowing. As leiomyomas enlarge, they may undergo degeneration or necrosis leading to a heterogeneous appearance with cystic spaces within the lesion. Calcification is more common in older patients and may be present in a peripheral distribution or scattered throughout the lesion. An exophytic or pedunculated myoma may be difficult to differentiate from a solid adnexal mass. Demonstration of a normal ipsilateral ovary and vascular supply derived from the uterus, the *bridging vascular sign*, helps confirm the diagnosis.<sup>137</sup>

### Additional Imaging Modalities

Although a combination of transvaginal and transabdominal sonography is generally sufficient for evaluation of most leiomyomas, supplemental imaging techniques may at times be helpful. If there are multiple large leiomyomas, ultrasound imaging may be very limited owing to associated acoustic attenuation. The endometrium may be obscured, precluding definitive evaluation. Coexisting adenomyosis also may be difficult to diagnose in this setting. Precise mapping of size and location of leiomyomas may be required prior to either surgical or nonsurgical intervention. Sonohysterography is a helpful adjunct for evaluation of submucosal leiomyomas to determine the degree of intracavitary versus intramyometrial extension, which may affect the surgical approach<sup>138</sup> (Fig. 29-31). 3D sonography may also be helpful in this regard. Often, MRI better defines size and location of leiomyomas prior to surgical intervention<sup>139,140</sup> and may also help identify patients who are the most appropriate candidates for uterine artery embolization (UAE) and other treatment options<sup>141-143</sup> (Fig. 29-32). The role of MRI is growing as minimally invasive therapeutic techniques including percutaneous MRI-guided cryoablation and MRI-guided focused sonographic ablation continue to evolve.<sup>144</sup>

### Lipoleiomyoma

An uncommon subtype of leiomyoma is lipoleiomyoma, which has a reported incidence of 0.03% to 0.2%.<sup>145</sup> These tumors contain variable amounts of mesodermal tissue including fat, smooth muscle, and fibrous tissue. They may arise from misplaced embryonic fat cells in the uterus, lipocytic differentiation of primitive connective or



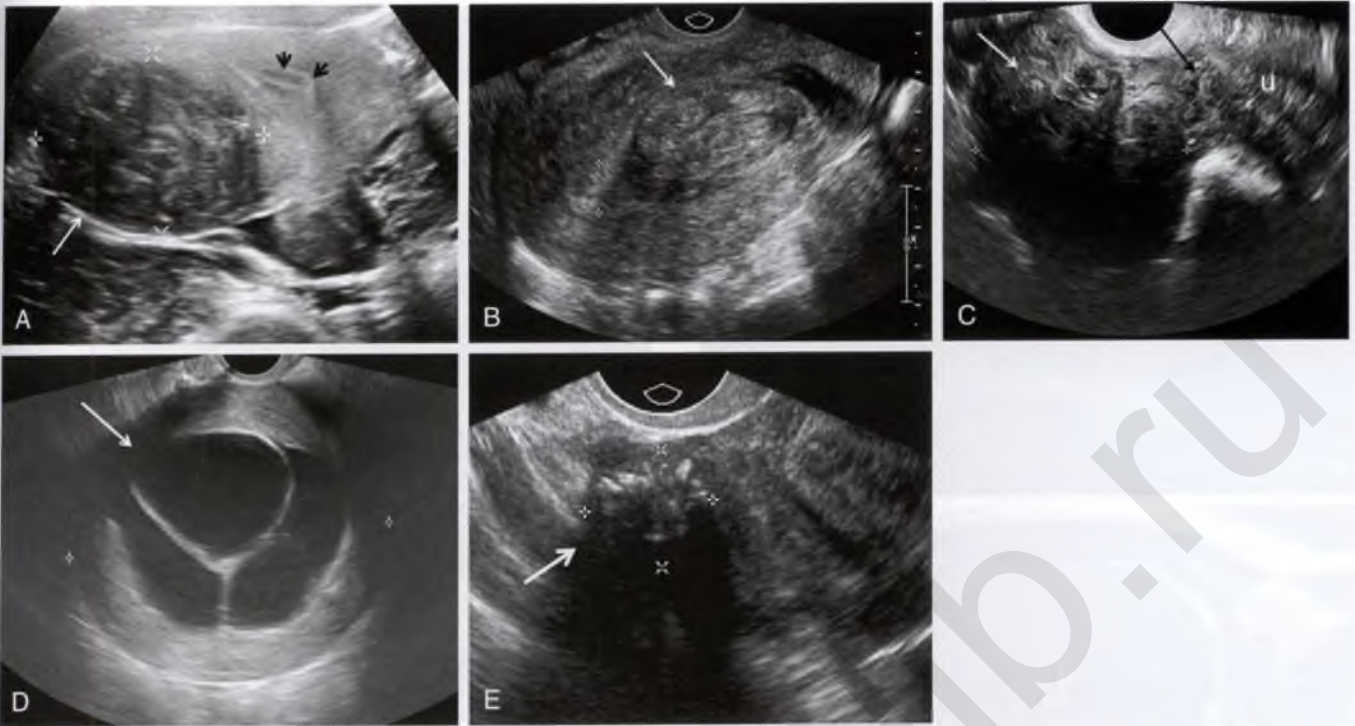


**FIG 29-30** Imaging spectrum of leiomyomas. **A**, Transabdominal scan shows a large heterogeneous intramural leiomyoma (*arrow* and *calipers*) separate from the endometrium (*short black arrows*) and surrounded by a thin rim of myometrium. **B**, Intracavitary submucosal leiomyoma (*arrow*) splaying the endometrium (*calipers*). **C**, Exophytic pedunculated leiomyoma (*white arrow* and *calipers*) arising from the uterine fundus (*u*) mimicking a solid adnexal mass. Note bridging soft tissue pedicle (*black arrow*) connecting the leiomyoma to the uterus. **D**, Leiomyoma with large areas of cystic degeneration (*arrow*) on transverse view of the uterus (*calipers*). **E**, Leiomyoma with echogenic foci (*arrow* and *calipers*) indicating coarse calcifications.

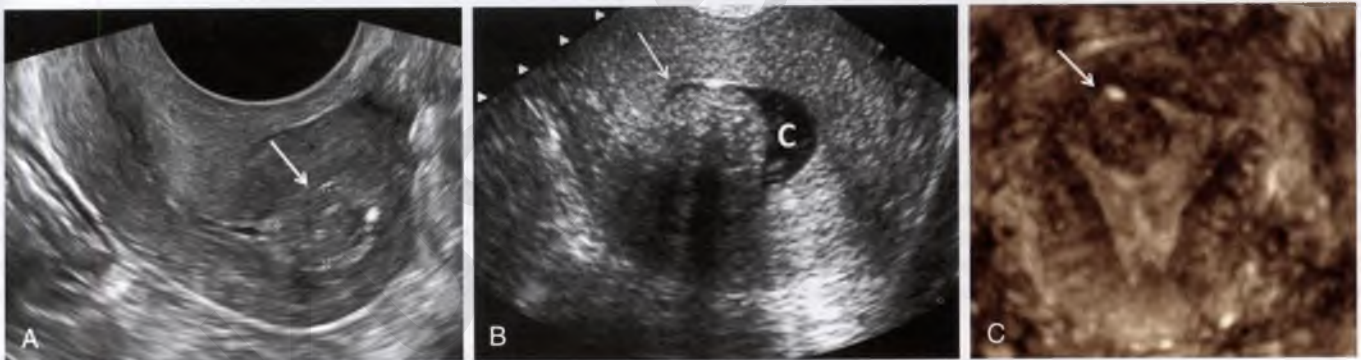


**FIG 29-31** Submucosal leiomyoma. **A**, Transvaginal sonogram demonstrating a submucosal leiomyoma (*arrow* and *calipers*) that is isoechoic to the myometrium and appears to be intracavitary in the fundus of a retroverted uterus. **B**, Sonohysterogram with instilled fluid in the endometrial cavity (*c*) partially outlining the protruding submucosal leiomyoma (*arrow*), which demonstrates posterior acoustic shadowing. **C**, Three-dimensional coronal ultrasound image demonstrates the relationship of the leiomyoma (*arrow*) to the endometrium and confirms that the myoma is predominantly intracavitary.

mesenchymal tissue, or fatty metaplasia of muscle or connective tissue.<sup>146,147</sup> Clinical presentation is generally identical to typical leiomyomas. Imaging characteristics of lipoleiomyomas vary depending upon proportion of fat, muscle, and connective tissue. Because of the fat content in these lesions, they generally appear as hyperechoic masses at sonography, often with posterior attenuation<sup>145,148,149</sup> (Fig. 29-33). A leading differential diagnostic consideration is a mature cystic teratoma of the ovary, which is the most common fat-containing mass in the female pelvis. If the origin of the mass is uncertain, CT or MRI may be performed to confirm the diagnosis.<sup>148-150</sup>

### Acute Complications of Leiomyomas

Although leiomyomas primarily cause chronic symptoms, associated complications may cause acute pelvic pain. Leiomyomas may undergo various types of benign degeneration, the most common being hyaline degeneration consisting of mucopolysaccharide deposits around muscle fibers. An acute form of degeneration is red (carneous) degeneration. This occurs when there is acute infarction of a leiomyoma and is associated with severe acute pelvic pain with local peritoneal symptoms,<sup>151</sup> which may mimic other entities, such as appendicitis (Fig. 29-34). Such degeneration occurs primarily during pregnancy when



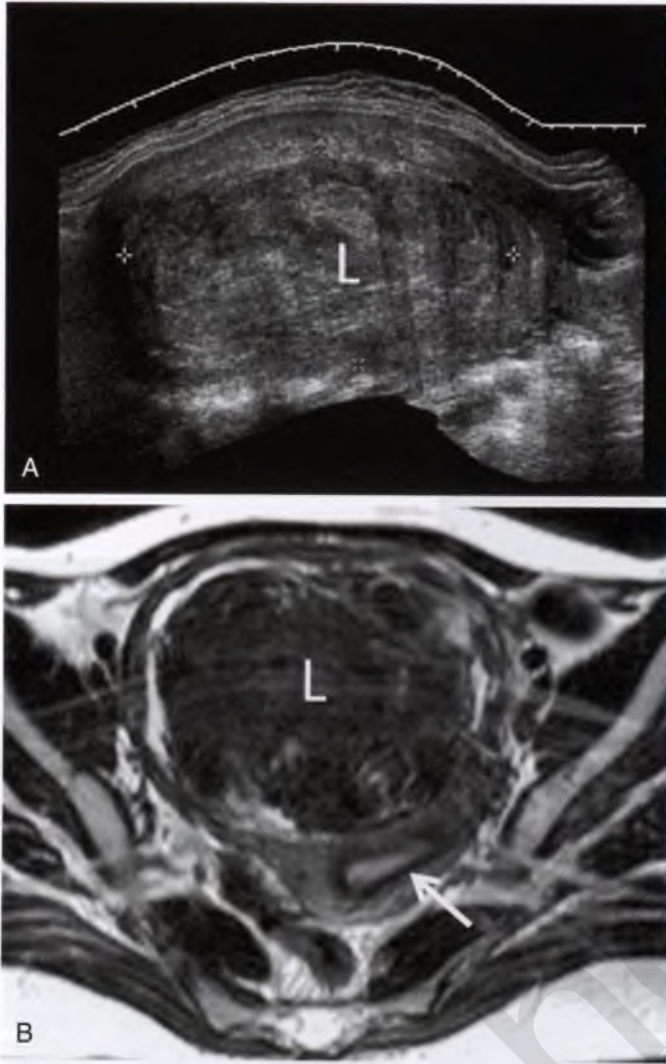


**FIG 29-32** Large intramural leiomyoma. **A**, Extended field of view ultrasound image demonstrates a large (18.3 cm) leiomyoma (L and calipers) occupying most of the uterus. The relationship to the endometrium, which is not visualized, cannot be determined. **B**, T2-weighted axial magnetic resonance image demonstrates that the large leiomyoma (L) is intramural in location. The high signal intensity endometrium (arrow) is delineated, shown to be displaced posteriorly but otherwise unremarkable.

leiomyomas may grow rapidly owing to hormonal stimulation and thus undergo hemorrhagic infarction, or following delivery when hormonal levels rapidly decline. Clinical symptoms and sonographic evidence of degeneration occur in about 5% of pregnant women with known leiomyomas.<sup>152</sup> Rupture of a degenerated leiomyoma is a rare complication that may result in an acute abdomen and potentially life-threatening hemoperitoneum.<sup>152,153</sup>

Leiomyomas may also present with acute pain if they are pedunculated and undergo torsion, mimicking ovarian torsion.<sup>152</sup> Sonography will demonstrate a hypovascular or avascular mass separate from the ovaries, and occasionally a twisted or “beaked” pedicle may be observed. A pedunculated submucosal myoma may protrude into the endometrial cavity on a stalk. These leiomyomas may be expelled from the uterus into the endocervical or vaginal canal and present as an “aborting” or prolapsing mass.<sup>154</sup> In one series, this complication was observed in approximately 2.5% of all leiomyomas.<sup>155</sup> Prolapsing leiomyomas may twist on their vascular pedicle causing infarction and are then at

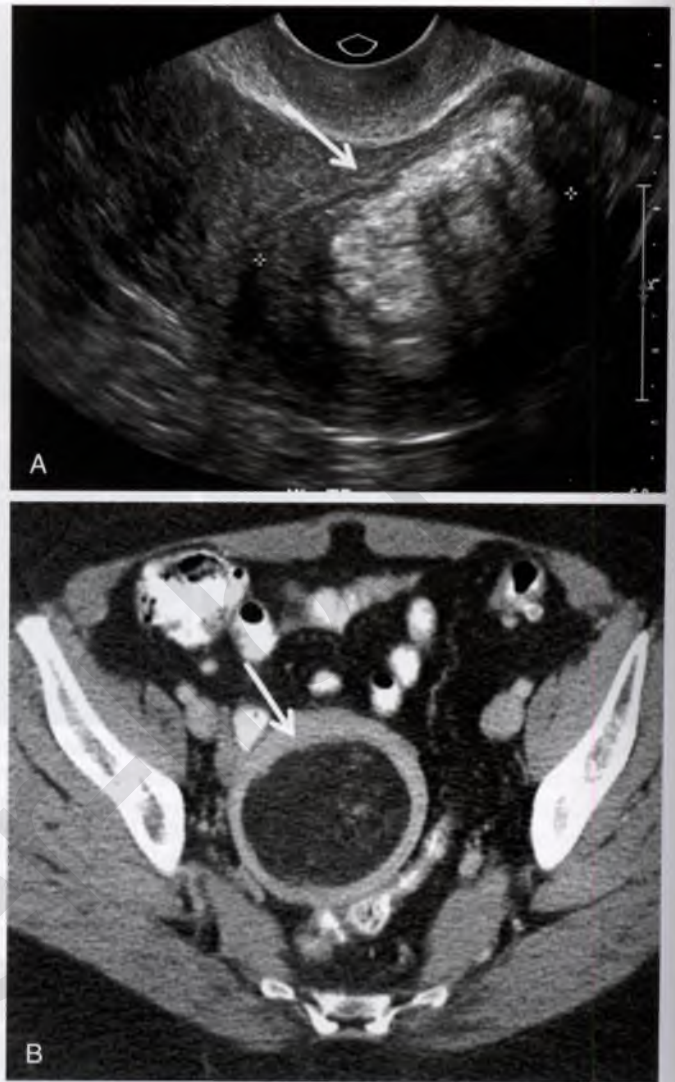


**FIG 29-33** Lipoleiomyoma. **A**, Hyperechoic heterogeneous mass (arrow and calipers) in the uterus with a slightly lobular contour. **B**, Computed tomography confirms the presence of low attenuation fat within the uterine mass (arrow) confirming the diagnosis of intramural lipoleiomyoma.

risk for superinfection. Often, the findings on pelvic examination are limited in this situation because of profuse vaginal bleeding, and pelvic sonography is helpful in establishing the diagnosis. At sonography, a well-circumscribed solid mass is identified in the endocervical canal, with the cervix splayed around the mass, or within the vagina<sup>156</sup> (Fig. 29-35). Slight withdrawal of the transvaginal probe or translabial views may aid in visualization of an intravaginal mass. These masses may be echogenic or heterogeneous owing to associated hemorrhage, edema, and degenerative change. A vascular stalk or pedicle is often demonstrated with targeted color Doppler sonography (Fig. 29-35B). Other intracavitary endometrial masses may also prolapse, including polyps and malignant neoplasms. MRI can be helpful in further evaluation if sonographic findings are equivocal<sup>157,158</sup> (Fig. 29-35C), particularly in determining the extent of myometrial involvement and the thickness of the stalk, which may alter the surgical approach.

Patients may present with pain following UAE. Postembolization syndrome, which occurs in approximately 40% of women following the procedure, consists of fever, pelvic pain, and vaginal discharge, which usually resolves in 24 to 48 hours.<sup>159</sup> The imaging appearance of



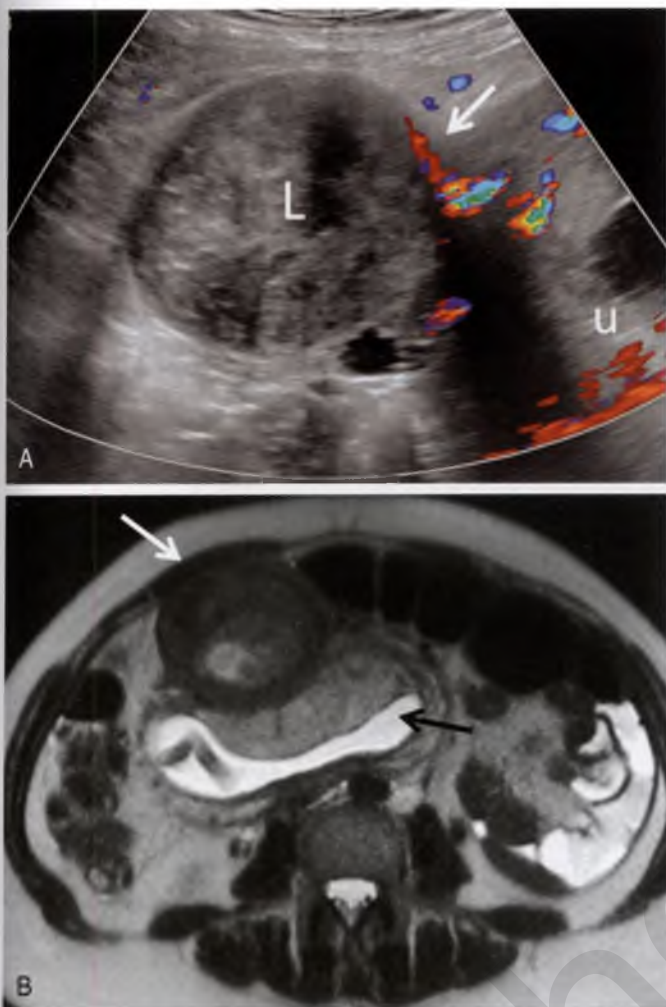


**FIG 29-34** Degenerated exophytic leiomyoma in pregnant patient with right lower quadrant pain, initially evaluated for appendicitis. **A**, Transabdominal ultrasound image demonstrates an exophytic leiomyoma (L) with a bridging vascular sign (*arrow*) confirming origin from the gravid uterus (u). No flow is demonstrated in the leiomyoma owing to hemorrhagic degeneration. **B**, Magnetic resonance imaging was performed to assess for possible appendicitis. Axial T2-weighted image demonstrates heterogeneous, increased signal intensity in the leiomyoma (*white arrow*) owing to degeneration. The exophytic myoma is at the anterior aspect of the gravid uterus (*black arrow*).

leiomyomas after a UAE procedure is variable.<sup>159-162</sup> Air may be seen within a leiomyoma after UAE, thought to be the result of gas filling potential spaces due to tissue infarction and necrosis, and its presence alone does not indicate infection. However, correlation with patient symptoms and clinical findings is critical to promptly diagnose superinfection and to assess for possible development of pyomyoma (suppurative leiomyoma), which may be a life-threatening emergency leading to septic shock and necessitating emergent hysterectomy.<sup>161</sup> Ultrasound findings include a poorly defined mass with internal echoes and reverberation artifacts secondary to the presence of gas<sup>163</sup> (Fig. 29-36). CT can be performed to evaluate for associated complications such as pelvic abscess, uterine rupture, or septic thrombophlebitis of the ovarian vein.

### Malignant Uterine Tumors

Although the diagnosis of uterine leiomyomas is generally straightforward, occasionally there may be concern for a malignant uterine neoplasm, such as leiomyosarcoma, carcinosarcoma (malignant mixed müllerian tumor), endometrial stromal sarcoma, or smooth muscle tumor of uncertain malignant potential (STUMP). Uterine sarcomas are very rare and account for approximately 3% to 6% of uterine cancers.<sup>164,165</sup> They generally occur in older patients who present with abnormal vaginal bleeding, an enlarging pelvic mass, and pelvic pain. Although these symptoms overlap with those of benign leiomyomas, features such as rapid growth of a myoma in a postmenopausal woman not on hormone replacement therapy should raise concern.

Clinical features are important for diagnosis as there is considerable overlap in imaging features of these malignant tumors with benign leiomyomas. Benign leiomyoma variants, such as cellular leiomyomas, may also exhibit concerning atypical imaging features.<sup>166</sup> Sonographic features that raise concern for leiomyosarcoma include a single large dominant myoma with large areas of cystic change/necrosis, ill-defined, infiltrative margins, and increased peripheral and central vascularity with high peak systolic velocity<sup>167-169</sup> (Fig. 29-37).

MRI may help delineate the infiltrative nature and irregular margins of the lesion and may reveal extrauterine extension. Malignant uterine neoplasms also typically have higher signal intensity on T2-weighted images and larger areas of necrosis with regions of increased T1-weighted signal intensity due to hemorrhage, as well as increased contrast enhancement, although there is significant overlap of these features with those of benign leiomyomas.<sup>170-173</sup> More recently, a role for diffusion weighted imaging (DWI) in differentiating benign from malignant uterine tumors has shown promise.<sup>174,175</sup> Unfortunately,

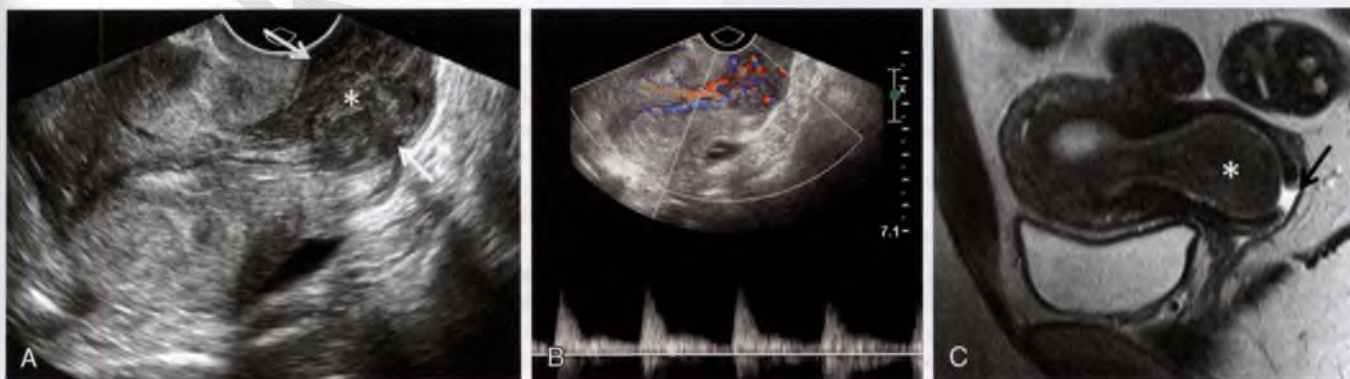


**FIG 29-35** Prolapsing submucosal leiomyoma in patient with pelvic pain and vaginal bleeding. **A**, The prolapsing leiomyoma (*asterisk*) plays the cervix and extends through the endocervical canal into the upper vagina (*arrows*). **B**, Vascular pedicle with arterial flow is demonstrated with color and spectral duplex Doppler sonography. **C**, T2-weighted sagittal magnetic resonance imaging in another patient demonstrates a prolapsing leiomyoma (*asterisk*) spaying the cervix. Note high signal intensity fluid at the level of the open external cervical os (*arrow*).





**FIG 29-36** Infected and infarcted leiomyoma (pyomyoma) in patient with fever, vaginal discharge, and pelvic pain 2 weeks following uterine artery embolization. **A**, Transvaginal sonography demonstrates a large mass in the uterus containing echogenic foci (arrows) with posterior acoustic shadowing and reverberation artifact compatible with gas. **B**, Sagittal reformatted computed tomography image demonstrates the large leiomyoma (arrow) with extensive infarction and foci of gas. The patient underwent emergent hysterectomy shortly after this scan.

despite advanced MRI techniques, there continues to be considerable overlap with benign leiomyomas, particularly for myomas with large areas of degeneration and those of the cellular subtype (Fig. 29-38). Much investigation in this area is currently underway as the role of minimally invasive techniques, including laparoscopic and robotic morcellation and excision of leiomyomas, is increasing, and identification

of neoplasms prior to surgery has become critical to minimize the risk of intraperitoneal dissemination of malignancy.<sup>176</sup>

### Adenomyosis

Adenomyosis is characterized by the presence of ectopic non-neoplastic endometrial glands and stroma within the myometrium surrounded by hypertrophied smooth muscle.<sup>177</sup> The pathogenesis is unknown but may in part be related to absence or defect of the basement membrane at the endometrial-myometrial junction, allowing for abnormal invagination of the basal endometrium into the myometrium.<sup>178</sup> Risk factors include a traumatized endometrial-myometrial interface related to procedures such as curettage; hormonal, genetic, and immunologic factors also play a role.<sup>178</sup> The true incidence of this condition is unknown but it has been estimated to occur in 20% to 30% of the general female population and is found in up to 70% of hysterectomy specimens.<sup>136</sup> An increased incidence in patients with endometriosis has been reported.<sup>179</sup> Symptoms are nonspecific and generally include uterine tenderness and enlargement, dysmenorrhea, and menorrhagia and are more common in older reproductive age women. Adenomyosis may be a diffuse process; however, it may also be focal and limited to one portion of the uterus (adenomyoma). In the past, hysterectomy was considered definitive therapy; however, treatment has evolved to include both medical and surgical therapy, including uterine sparing options such as resection of focal disease, endometrial ablation, UAE, and MR-guided high-frequency sonography.<sup>136</sup>

Sonography is the first-line imaging test of choice to diagnose adenomyosis. The 2D gray-scale sonographic findings of adenomyosis include globally or asymmetrically enlarged uterus, inhomogeneous myometrial echotexture with regions of increased echogenicity corresponding to heterotopic endometrial tissue and decreased echogenicity corresponding to smooth muscle hyperplasia, intramyometrial hypoechoic linear striations radiating throughout the involved parenchyma (“rain shower” or “Venetian blind” appearance), subendometrial echogenic linear striations located near the endometrial-myometrial interface, and thickening of the hypoechoic subendometrial halo (Fig. 29-39).<sup>180-186</sup> Small myometrial cysts may be observed corresponding to dilated glands or hemorrhagic foci. There may be poor definition of the endometrial-myometrial junction with apparent pseudo-widening of the endometrium. In a study by Kepkep and colleagues,<sup>187</sup> subendometrial linear striations had the highest accuracy for the diagnosis. Color and power Doppler sonography often demonstrate diffuse hypervascularity without large feeding vessels. In a meta-analysis of 14 studies including 1898 women who underwent sonography for evaluation of uterine lesions, the pooled sensitivity and specificity of transvaginal sonography for the diagnosis of adenomyosis was 82.5% and 84.6%, respectively.<sup>188</sup> However, detection of adenomyosis at transvaginal sonography may be limited if there are coexisting uterine tumors, such as leiomyomas. In one study, the sensitivity and specificity of transvaginal sonography for diagnosing adenomyosis in patients with leiomyomas was 33.3% and 78%, and in those without leiomyomas was 97.8% and 97.1%, respectively.<sup>189</sup>

More recently, 3D sonographic features of adenomyosis have been described.<sup>186,190</sup> Reconstructed images in the coronal plane demonstrate the subendometrial halo as a hypoechoic zone around the endometrium. In adenomyosis, there is disruption and infiltration of the subendometrial halo by the hyperechoic endometrium. The thickness of the subendometrial halo can be measured at sonography and can be helpful in diagnosing adenomyosis, as has been described for MRI.<sup>186,190</sup>

There is significant overlap between adenomyosis and leiomyomas in terms of clinical symptoms and imaging. In fact, confusion with leiomyomas is one of the most common sonographic pitfalls of



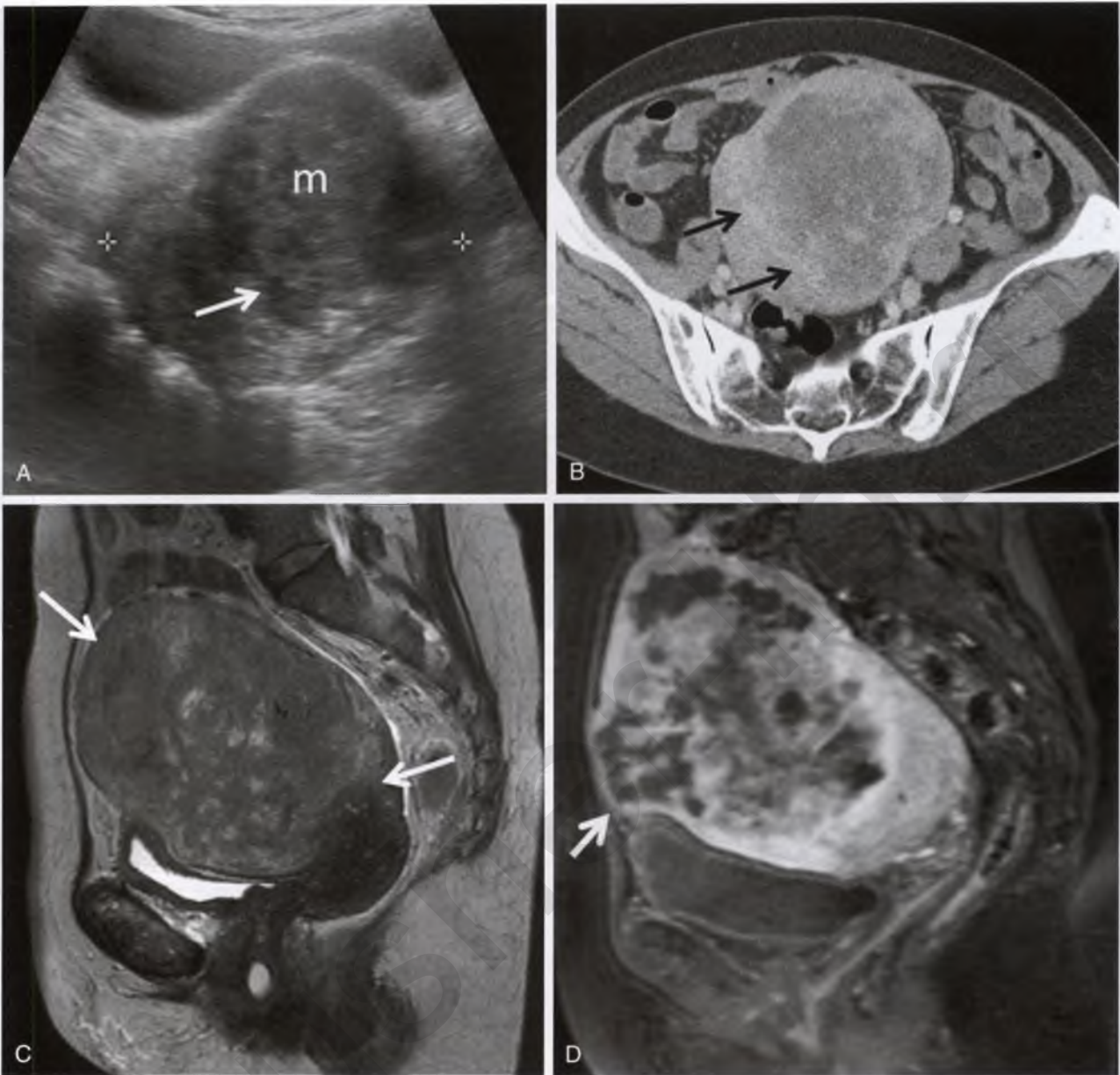


**FIG 29-37** Leiomyosarcoma in postmenopausal patient with pelvic pain and enlarging pelvic mass. **A**, Transabdominal ultrasound image demonstrates large partially exophytic mass (m) arising from the uterus (calipers). The margins of the mass (arrow) appear irregular. **B**, Contrast-enhanced axial computed tomography scan demonstrates infiltrative margins of the mass (arrows) along the border with adjacent myometrium. **C**, T2-weighted sagittal magnetic resonance (MR) image demonstrates heterogeneous increased signal within the large uterine mass (arrows). The margins of the lesion with adjacent myometrium are indistinct and difficult to appreciate, suggesting the infiltrative nature of the mass. **D**, Postcontrast sagittal T1-weighted fat-suppressed MR image demonstrates heterogeneous enhancement of the mass with areas of necrosis, irregular borders, and infiltration of the ventral abdominal wall (arrow).

adenomyosis. However, distinction is important as treatment strategies often differ. This is particularly important in patients for whom surgical intervention with myomectomy is considered. Sonography has a reported sensitivity (80-87%) and specificity (94-98%) in distinguishing the two conditions.<sup>183,191,192</sup> A focal adenomyoma is less well defined than a leiomyoma and does not distort the uterine contour (Fig. 29-40). However, as noted previously, the presence of coexisting leiomyomas may make the identification of adenomyosis more difficult and these processes occur together in up to 63% of cases.<sup>193</sup> MRI has

been shown to be a helpful adjunct to ultrasound examination, with reported accuracy ranging from 85% to 95% and specificity of 67% to 99%.<sup>180,182,186,194-196</sup> On sagittal T2-weighted sequences, MRI findings of adenomyosis include diffuse or focal thickening of the junctional zone to greater than 12 mm, T2-weighted hyperintense foci within the junctional zone, and corresponding high signal on T1-weighted images corresponding to hemorrhage in ectopic endometrial glands. A focal adenomyoma has less mass effect than a leiomyoma and is recognized by the T2-weighted hyperintense foci. Adenomyotic cyst (cystic



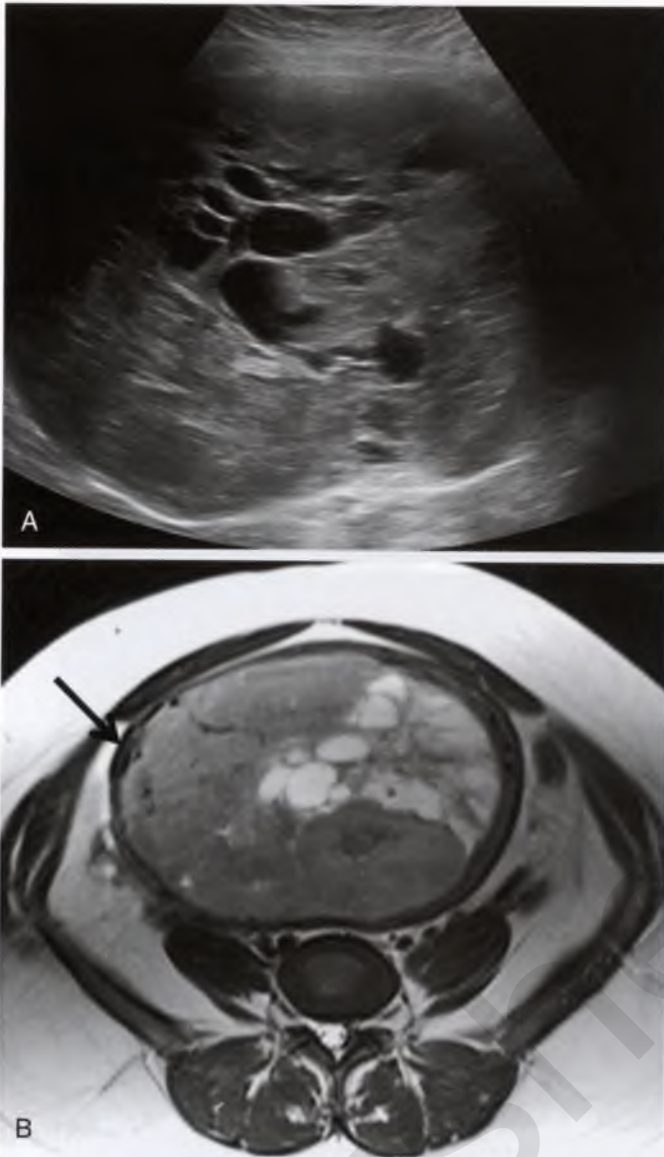


**FIG 29-38** Cellular leiomyoma with imaging features concerning for leiomyosarcoma. **A**, Ultrasound image demonstrates a large dominant mass with irregular, indistinct borders and areas of cystic change within the uterus. **B**, Axial magnetic resonance image demonstrates areas of heterogeneity and increased T2-weighted signal, consistent with necrosis/cystic change. There was questionable invasion of the myometrium (*arrow*). However, benign cellular leiomyoma was found at myomectomy.

adenomyosis) is a rare variant of adenomyosis that appears similar to an endometrioma, with features of an intramyometrial hemorrhagic cystic mass that occasionally is intracavitary.<sup>197,198</sup>

### Malpositioned Intrauterine Device

The intrauterine device (IUD) is one of the most widely used reversible methods of contraception worldwide and the contraceptive method of choice in 5.6% of women in the United States.<sup>199</sup> Ultrasound evaluation is important for verification that an IUD is in the appropriate location and to evaluate for complications. The Copper T-380A (Para-Gard; Barr Pharmaceuticals, Montvale, NJ) IUDs typically have a straight shaft and crossbars that form the shape of a 7 or a T. They are strongly echogenic with associated posterior acoustic shadowing,

and both the side arms and stem are readily visualized (Fig. 29-41). Hormone-containing IUDs are also in widespread use and most commonly contain synthetic progestogen-levonorgestrel within an internal reservoir. The Mirena (Bayer Healthcare Pharmaceuticals, Wayne, NJ) IUD is used most commonly in the United States and has a T-shaped polyethylene frame with side arms that contain barium sulfate. This type of IUD is more difficult to visualize with ultrasound, particularly the crossbars, although the stem will demonstrate characteristic posterior ring-down artifact.<sup>200</sup> The shaft should be centered within the uterine cavity at the miduterus with the crossbars located within the endometrium just below the fundal myometrium.<sup>201</sup> Complications include fragmentation; rotation; migration into the myometrium, lower uterine segment, cervix, or through the myometrium into the peritoneal cavity; and expulsion from the uterus. Inappropriate IUD positioning may result in diminished efficacy as well as pelvic pain and abnormal vaginal bleeding.

In recent years, 3D transvaginal sonography with images reconstructed in the coronal plane has been shown to be an important adjunct to 2D techniques if initial ultrasound findings are equivocal<sup>200,202,203</sup> (see Fig. 29-41). The rendered 3D coronal view is the most useful.<sup>200</sup> On this view, the IUD should be completely visualized with simultaneous depiction of the shaft and the crossbars. If the IUD cannot be visualized in the uterus, abdominal radiograph or noncontrast CT may be helpful for localization.

## VASCULAR CAUSES OF PELVIC PAIN

### Pelvic Congestion Syndrome

Pelvic congestion syndrome (PCS) may be a cause of chronic pelvic pain and results from incompetent valves in the ovarian veins resulting in reflux into pelvic veins, which dilate and become tortuous, forming pelvic varices.<sup>204-207</sup> Venous obstruction, such as a retroaortic left renal vein, compression of the left renal vein by the superior mesenteric artery (nutcracker syndrome), or left iliac vein compression by the right internal iliac artery (May-Thurner syndrome), as well as hormonal factors may contribute to the development of painful pelvic varicosities.<sup>207</sup> Patients most commonly present between the ages of 20 and 40 years with dull pelvic pain, ache, pressure, or heaviness made worse after prolonged periods of standing, while lifting, or during the premenstrual period. Other risk factors include multiparity, retroverted uterus, and pelvic surgery.

Sonography is the first-line imaging choice for assessment of chronic pelvic pain, and PCS may be considered if other more common causes such as endometriosis and leiomyomas have been ruled out. Sonographic findings include multiple dilated veins adjacent to the ovaries and uterus, measuring greater than 5 mm in diameter, and dilated (>5 mm) arcuate veins (especially if observed to cross the myometrium and connect to the pelvic varicosities).<sup>208,209</sup> Dilatation of the ovarian veins more than 6 mm with retrograde flow is a more specific finding, but can be much more difficult to document on ultrasound imaging in large patients. Scanning with the patient in the upright position may help distend the pelvic veins.<sup>210</sup> Velocity of intraluminal flow and diameter of the pelvic varices often increases following Valsalva maneuvers. Polycystic ovarian changes have also been associated with PCS. However, not all patients with pelvic varicosities develop pain. It has been estimated that 40% to 60% of women with pelvic varices and reflux will develop PCS.<sup>204,211,212</sup> Contrast-enhanced MR venography (MRV) can be helpful in establishing the diagnosis, and retrograde reflux into the gonadal veins may be demonstrated utilizing time-resolved MR techniques.<sup>212-214</sup> Using this technique, the pelvic venous system can be imaged in a single breath-hold. Images are obtained after bolus injection of gadolinium with automatic bolus



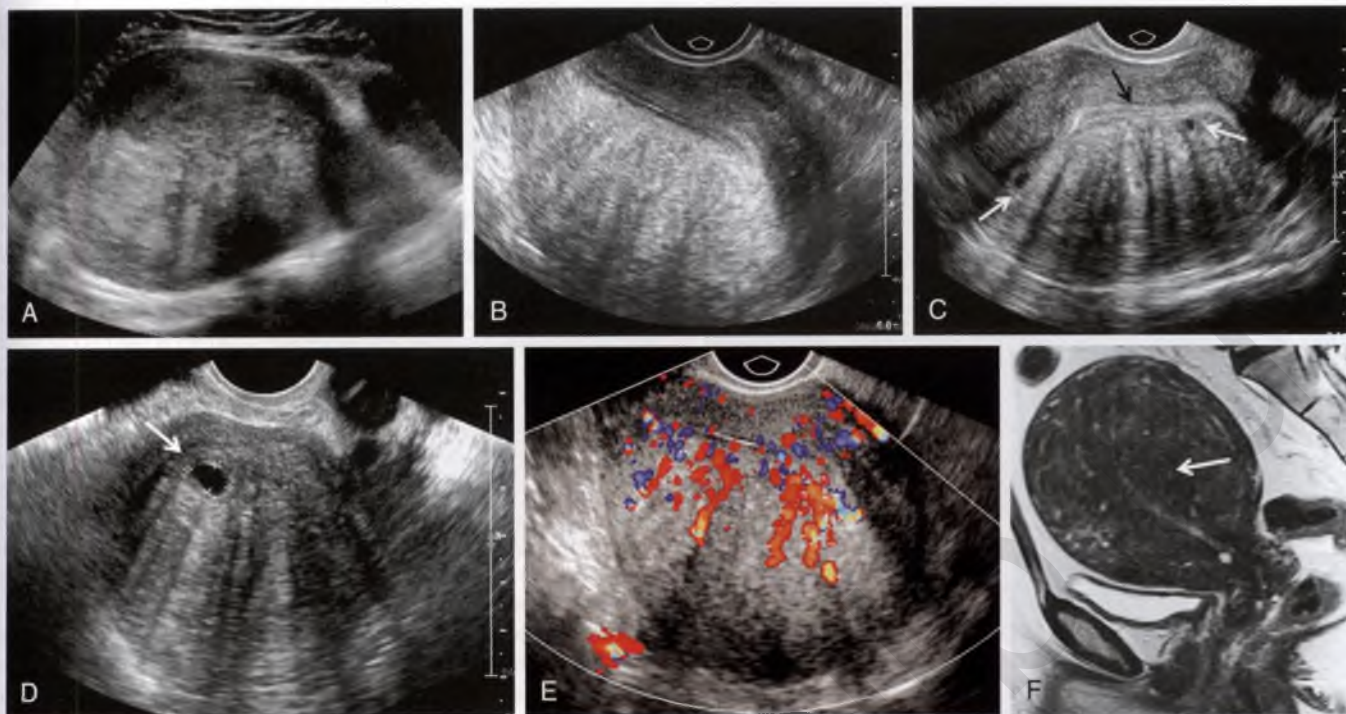


**FIG 29-39** Spectrum of ultrasound findings of adenomyosis. **A**, Transabdominal sagittal ultrasound image demonstrates enlarged, heterogeneous, globular uterus with asymmetric thickening of the posterior myometrium. **B**, Transvaginal sagittal scan from a second patient demonstrates asymmetric thickening of the anterior myometrium, with markedly heterogeneous echotexture, hypoechoic linear striations, and shadowing. Endometrial thickness is measured (*calipers*). The uterus is retroverted. **C**, Transvaginal scan from a third patient demonstrates heterogeneity of the posterior myometrium with small myometrial cysts (*white arrows*) and linear striations. Note linear rays of shadowing in a “comb-like” or “Venetian blind” pattern. The region of abnormal myometrial echotexture is posterior to the endometrium (*black arrow*). **D**, Larger myometrial cyst (*arrow* and *calipers*), with asymmetric thickening, heterogeneity of the myometrium, and “comb-like” shadowing. **E**, Color Doppler sonogram demonstrates diffuse hypervascularity of the asymmetrically thickened posterior myometrium. **F**, Sagittal T2-weighted magnetic resonance image of a different patient with diffuse adenomyosis demonstrating marked diffuse thickening of the junctional zone (*arrow*) and scattered tiny T2-weighted hyperintense foci.

detection and tracking systems (Fig. 29-42). Catheter-directed venography is more invasive and is usually only performed immediately prior to intervention, but it is considered the gold standard for diagnosis. Bilateral ovarian vein embolization with or without direct sclerotherapy of the pelvic varices is the current favored treatment approach.<sup>210,215</sup> Stent placement may be performed for obstructing anatomic abnormalities.

### Gonadal Vein Thrombosis

Patients with thrombosis of the gonadal vein generally present with acute pelvic pain and may also have fever and leukocytosis if there is associated septic thrombophlebitis, which is most common in postpartum patients, in those with PID, or following pelvic surgery. Ovarian vein thrombophlebitis is estimated to occur following less than 0.05% of vaginal deliveries and 1% to 2% of cesarean deliveries.<sup>216</sup> The right gonadal vein is more commonly involved, likely because of increased pressure on the right gonadal vein. The left ovarian vein is felt to be protected owing to retrograde flow from the left renal vein.<sup>13</sup> Ovarian vein thrombosis will appear on ultrasound images as a tubular or serpentine avascular structure, often anechoic to hypoechoic, in the region of the right adnexa and psoas muscle corresponding to the thrombosed vein. Extension into the inferior vena cava may occur. However, these structures may be difficult to visualize at sonography,

particularly in the postpartum setting, because of overlying bowel gas. Contrast-enhanced CT or MRI should generally be performed to establish the diagnosis and evaluate the extent of thrombosis and will show a distended ovarian vein expanded by intraluminal thrombus with a thickened enhancing wall and surrounding inflammation<sup>217</sup> (Fig. 29-43).

### NONGYNECOLOGIC CAUSES OF PELVIC PAIN

Although the primary role of ultrasound examination in a woman presenting with pelvic pain is to evaluate the female reproductive tract, abnormalities of the gastrointestinal or genitourinary tract may occasionally be detected. Recognition of these nongynecologic disorders at ultrasound examination not only enables prompt diagnosis, but may eliminate the need for additional imaging and potentially unnecessary exposure to radiation and intravenous contrast agent.<sup>218-220</sup>

#### Acute Appendicitis

Acute appendicitis is one of the most common nongynecologic causes of acute pelvic pain and the most common gastrointestinal cause of right lower quadrant pain. Classically, patients present with initial periumbilical pain that migrates to the right lower quadrant, rebound tenderness, nausea, vomiting, and leukocytosis. In the adult patient,



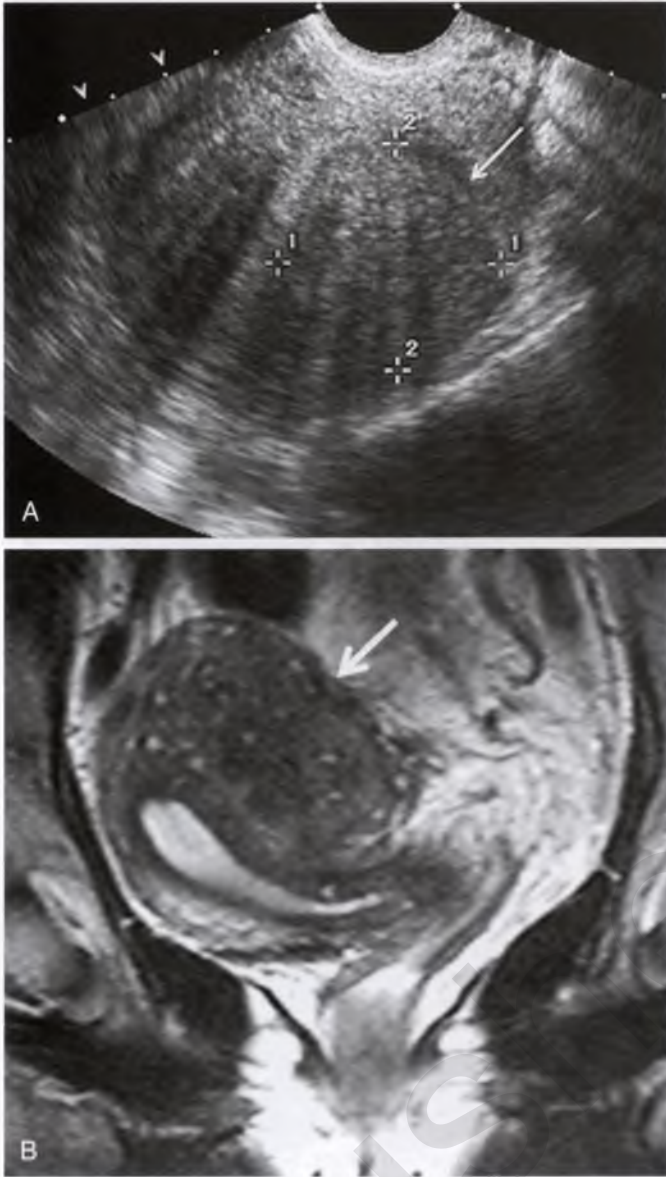


**FIG 29-40** Focal adenomyosis mimicking leiomyoma. **A**, Transvaginal sonogram suggests an ill-defined hypoechoic lesion in the posterior myometrium (*arrow* and *calipers*) without associated mass effect. Note “comb-like” shadowing posterior to this area as well as in the adjacent myometrium, which can be seen with adenomyosis as well as leiomyomas. **B**, Sagittal T2-weighted magnetic resonance image reveals focal adenomyosis (*arrow*) posteriorly. No myoma present.

CT is generally the gold standard for diagnosis and receives the highest ACR Appropriateness Criteria score for evaluation of suspected appendicitis.<sup>221</sup> In a meta-analysis of six prospective studies performed through 2006, CT demonstrated superior sensitivity (91%; 95% confidence interval [CI], 84-95%) and specificity (90%; 95% CI, 85-94%) compared to ultrasound imaging (sensitivity 78%; 95% CI, 67-86%; specificity 83%; 95% CI, 76-88%).<sup>222</sup> A significant decrease in negative appendectomy rates has been shown in reproductive age women who undergo preoperative CT.<sup>223</sup> However, in children, young women, and pregnant women, sonography is often the initial recommended imaging modality in order to reduce radiation exposure. If ultrasound imaging is inconclusive in the nonpregnant patient, CT will generally then be performed; in the pregnant patient, MRI is the next test of choice. A meta-analysis of five case series evaluating MRI for diagnosis

of suspected appendicitis in the pregnant patient yielded a sensitivity of 90.5%, specificity of 98.6%, PPV of 90.4%, and NPV of 99.5%<sup>224</sup> (Fig. 29-44).

At ultrasound examination, the inflamed appendix is best visualized using a high-frequency linear array transducer, typically 7 to 13 MHz, utilizing a graded compression technique at the point of maximal tenderness. The left lateral decubitus position may help visualize a retrocecal appendix. The inflamed appendix appears as a distended, non-compressible, nonperistalsing blind-ending tubular structure with outer wall to outer wall diameter greater than 6 mm<sup>225</sup> (Fig. 29-45). A diameter greater than 6 mm has a reported sensitivity, specificity, NPV, and PPV of 98% for acute appendicitis.<sup>226</sup> If 7 mm is used as the upper limit of normal, there is increased specificity but slightly decreased sensitivity.<sup>218</sup> On cross section, the classic target sign with concentric rings, the multilayered “gut” signature, will be observed. Appendicoliths appear as round, intraluminal echogenic shadowing foci. Mural hyperemia is variable but can be a useful secondary sign. Increased echogenicity and vascularity in the surrounding mesoappendiceal fat suggest inflammation. A periappendiceal abscess will appear as a focal fluid collection and may indicate associated perforation.

The inflamed appendix may occasionally be visualized during a transvaginal pelvic sonogram<sup>227</sup> (Fig. 29-46). Imaging features are similar to those observed on transabdominal scanning, although compression maneuvers cannot be performed. The inflamed appendix must be differentiated from an inflamed fallopian tube, which may at times pose a challenge. However, the appendix will be a blind-ending structure with multilayered gut signature composed of echogenic submucosa and hypoechoic muscularis layers. The inflamed fallopian tube will not be blind-ending and will demonstrate thickened endosalpingeal folds (“cogwheel” morphologic appearance), incomplete septations, and serpentine shape (see Fig. 29-18).

A mucocele of the appendix is an extremely rare condition and refers to dilatation of the appendix with abnormal intraluminal accumulation of mucus.<sup>228,229</sup> There are several subtypes including retention (simple) mucocele, obstruction of the appendix by a benign process such as an endometriotic implant, or other process associated with fibrosis and retention of mucin. Increased mucin production is more commonly due to mucosal hyperplasia than either benign or malignant appendiceal neoplasms (mucinous cystadenomas, adenocarcinomas, or carcinoid tumors). Preoperative diagnosis is essential to prevent rupture and spillage of the contents, which may result in pseudomyxoma peritonei.

A mucocele may be identified sonographically as a blind-ending tubular or oblong structure that is fluid-filled<sup>230,231</sup> (Fig. 29-47). The echogenicity is variable. The onion skin sign has been described, representing layering of the mucin-forming concentric rings.<sup>232</sup> Mural calcification may occasionally be observed. A mucocele could potentially be confused with a dilated fallopian tube or a cystic adnexal mass. Cross-sectional imaging with CT or MRI may be helpful by demonstrating the origin of the mass from the cecum and absence of a normal appendix (Fig. 29-47B). The clinical setting often differs from acute appendicitis with more chronic symptoms of pelvic pain and possibly a palpable mass. However, occasionally a mucocele may become acutely inflamed and present with features similar to acute appendicitis. A greater degree of cystic dilatation of the appendix and mural calcifications may suggest the diagnosis.<sup>233</sup>

### Acute Diverticulitis

Diverticulosis results from either acquired herniations of the submucosa and mucosa into the muscular layer (pseudodiverticula) of the bowel wall or true diverticula containing all bowel layers, which are usually congenital. The incidence of diverticulosis increases with



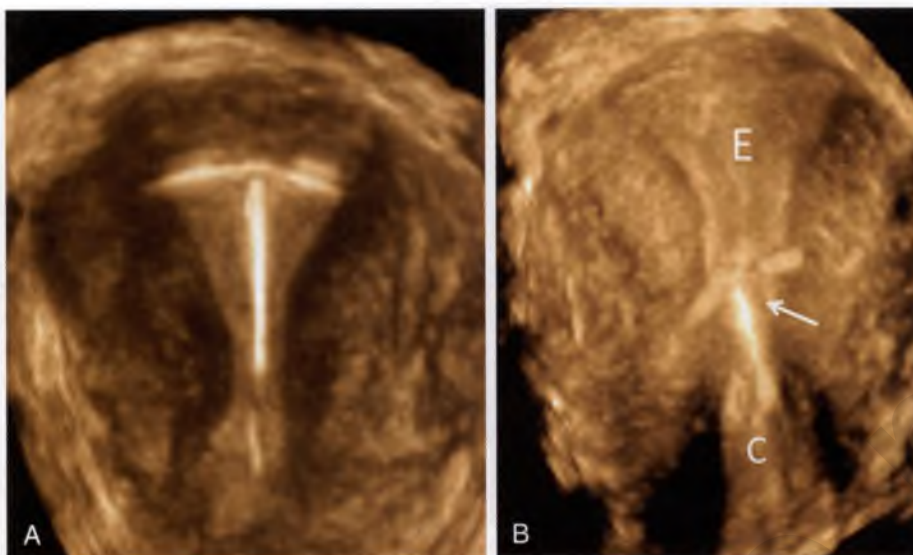


**FIG 29-41** Intrauterine device (IUD) evaluation with three-dimensional (3D) sonography. **A**, The 3D coronal view demonstrates appropriately positioned, intact Copper T IUD within the endometrial cavity. **B**, 3D coronal view demonstrates malpositioned Copper T IUD (*arrow*) located abnormally low in the uterus with side arms embedded in the myometrium. C, cervical canal; E, endometrial canal.

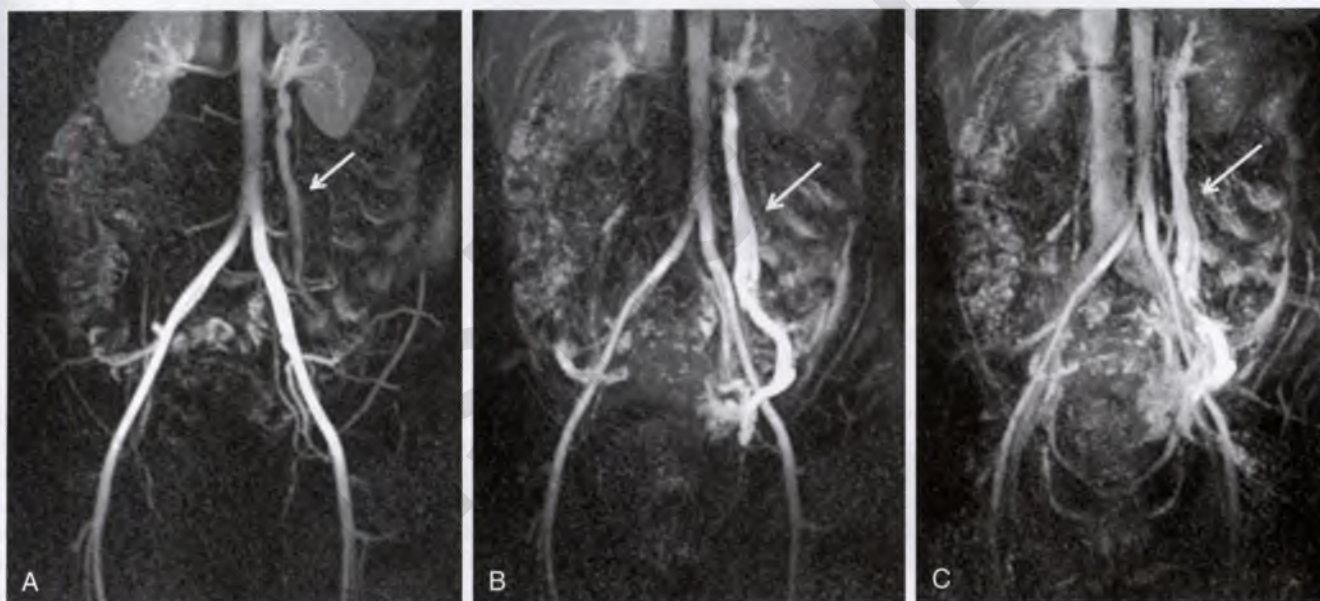


**FIG 29-42** Pelvic congestion syndrome: time-resolved magnetic resonance venography. **A** through **C**, Sequential images demonstrate reflux of contrast agent into the left gonadal vein (*arrow*), which is distended, with associated prominent pelvic varicosities.

advancing age, and it is estimated that diverticulosis is present in 60% of patients older than 80 years.<sup>234</sup> Diverticulitis occurs in 10% to 20% of patients with diverticulosis when a diverticulum becomes obstructed, leading to focal inflammation, diverticular distention, localized ischemia, and ultimately perforation.<sup>235,236</sup> Acute diverticulitis most commonly affects the sigmoid colon. Patients typically present with left lower quadrant pain, fever, and leukocytosis. However, the clinical presentation of acute diverticulitis may mimic that of various pelvic disorders, in particular PID. CT is generally the imaging modality of choice for suspected diverticulitis as it not only establishes the diagnosis but can also reliably identify associated complications such as perforation, abscess and fistula formation, and bowel obstruction.<sup>237</sup>

However, acute diverticulitis may also be reliably diagnosed at sonography with comparable accuracy to CT, and sonography is advocated by some as an alternate first-line imaging modality.<sup>238,239</sup>

To evaluate for diverticulitis, the ultrasound examination is generally performed with a 3.5- to 5.0-MHz probe, which can be supplemented with a high-frequency linear 5- to 12-MHz transducer, using the graded compression technique. Occasionally, the inflamed colonic segment may be visible on transvaginal examination. Ultrasound findings of diverticulitis vary with the degree of inflammation.<sup>240,241</sup> The most common finding is hypoechoic thickening of the colonic wall with a hyperechoic center and variable degrees of hyperemia (Fig. 29-48). An inflamed diverticulum may sometimes be identified





**FIG 29-43** Gonadal vein thrombosis. Coronal reformatted image from contrast-enhanced computed tomography demonstrates distended thrombosed right gonadal vein (*white arrow*) with thrombus extending into the inferior vena cava (*black arrow*).

at the site of maximum tenderness and can contain air, fluid, or occasionally a fecolith. Increased echogenicity and vascularity of the adjacent mesentery and omentum suggest inflammation. An abscess appears as a focal pericolic fluid collection and may contain echogenic foci with dirty shadowing indicating extraluminal air. Diverticulitis in the pelvis may lead to inflammation of the adnexa, mimicking PID (see Fig. 29-17). CT may help confirm the diagnosis and identify complications, in particular perforation and abscess formation, which may require immediate surgical or percutaneous intervention.

### Other Inflammatory Conditions of the Bowel and Mesentery

Epiploic appendagitis is a benign inflammatory process involving the epiploic appendages, which are small finger-like projections of fat covered by serosa on the surface of the large bowel, most numerous in the sigmoid and transverse colon. The cause is believed to be ischemic infarction from torsion or spontaneous thrombosis of the epiploic central draining vein with development of focal inflammation. The patient typically presents with acute-onset pelvic pain and localized tenderness without leukocytosis or fever. This self-limited nonsurgical condition is treated with anti-inflammatory medications and usually resolves in 5 to 7 days.<sup>242</sup> However, the clinical presentation may mimic diverticulitis, appendicitis, or gynecologic disorders, and misdiagnosis



**FIG 29-44** Magnetic resonance image of acute appendicitis in a pregnant patient. Coronal T2-weighted single shot fast spin echo (SSFSE) image demonstrates distended fluid-filled appendix (*white arrows*) located superior to the gravid uterus (*black arrow*) with multiple hypointense filling defects compatible with appendicoliths. Ultrasound examination was indeterminate.

may lead to unnecessary intervention, including surgery. The features at CT have been well described and include an oval pericolic lesion of fat density surrounded by inflammatory changes.<sup>242-245</sup> A central ill-defined round area (central dot sign) corresponds to engorged or thrombosed central vessels or central areas of hemorrhage or fibrosis. There is minimal, if any, thickening of the adjacent colonic wall, which helps to distinguish this entity from primary bowel-related processes. At sonography, a noncompressible hyperechoic ovoid or round solid mass of fatty tissue is identified between the colon and the abdominal wall at the site of maximal tenderness<sup>244-247</sup> (Fig. 29-49). A thin hypoechoic wall may be observed around the mass. Changes to the colonic wall are generally not observed.

Segmental omental infarction can also occur as a result of torsion or spontaneous thrombosis of omental vessels and may present in a similar fashion. Although there are predisposing factors, most cases are idiopathic. These infarctions are usually localized to the right upper and right lower quadrants and may mimic cholecystitis or appendicitis. This is also a benign self-limiting condition. Hazy increased soft tissue density of the omentum or a more discrete fat-density mass is observed on CT, and inflammation in the omentum is disproportionate to any reactive inflammatory changes in the bowel. At ultrasound examination, a hyperechoic mass is identified centered in the omentum in the area of patient discomfort and localized tenderness.<sup>244</sup>



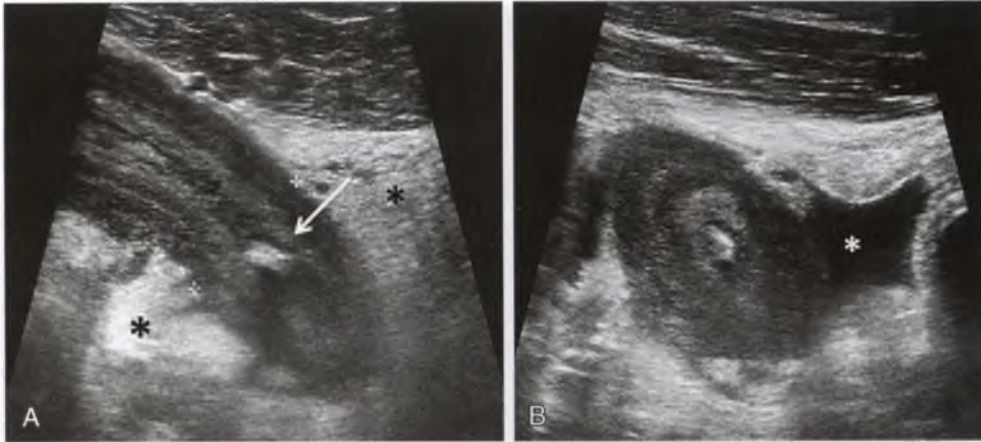


**FIG 29-45** Acute appendicitis. **A**, Targeted ultrasound examination of the right lower quadrant performed with a linear high-resolution transducer shows distended thick-walled appendix (*calipers*) with echogenic, shadowing intraluminal appendicolith (*arrow*). The surrounding periappendiceal fat demonstrates increased echogenicity (*asterisks*) compatible with inflammation. **B**, Transverse image demonstrates periappendiceal fluid (*asterisk*).

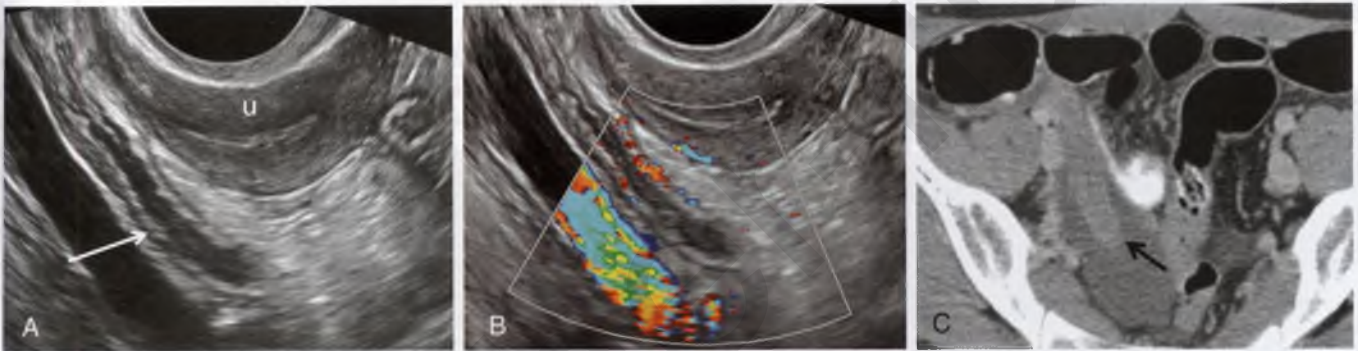


**FIG 29-46** Acute appendicitis detected on transvaginal sonogram. **A**, Patient presented with right pelvic pain and clinically suspected adnexal disease. The tubular, blind-ending appendix is dilated and fluid-filled (*arrow*), located to the right of the uterus (*u*). **B**, Color Doppler sonographic image demonstrates hyperemia in the wall of the inflamed appendix. **C**, Acute appendicitis (*arrow*) was confirmed at computed tomography scan.

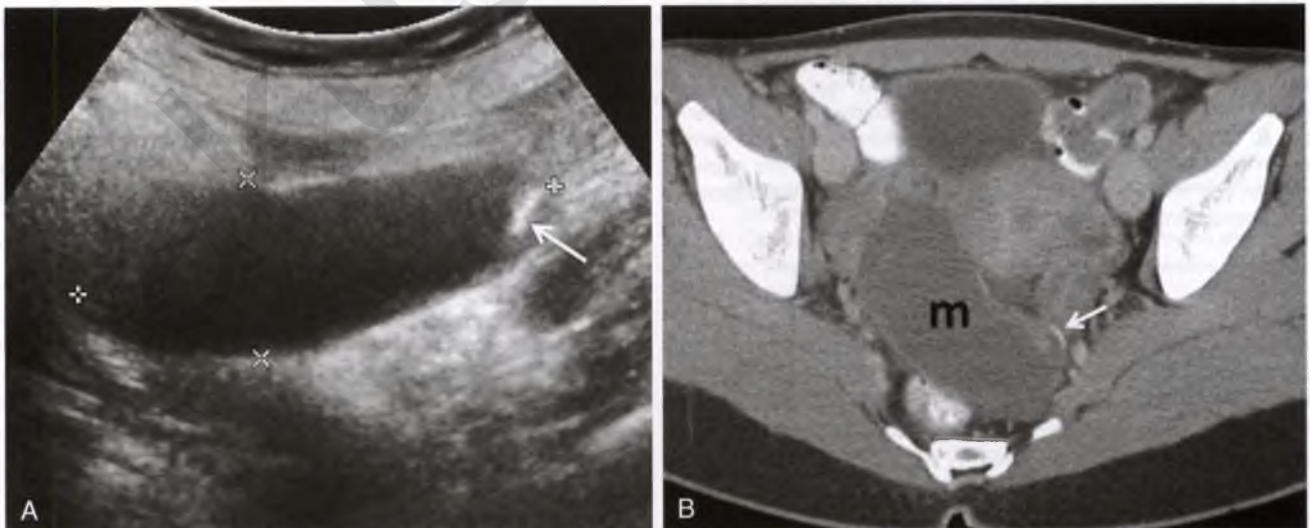


**FIG 29-47** Mucocele of the appendix. **A**, Transabdominal ultrasound image of right lower quadrant demonstrates a markedly dilated, blind-ending tubular structure (*calipers*) with mural calcification at the tip (*arrow*). **B**, Contrast-enhanced axial computed tomography confirms that the mucocele (*m*) originates from the base of the cecum and has mural calcification (*arrow*).



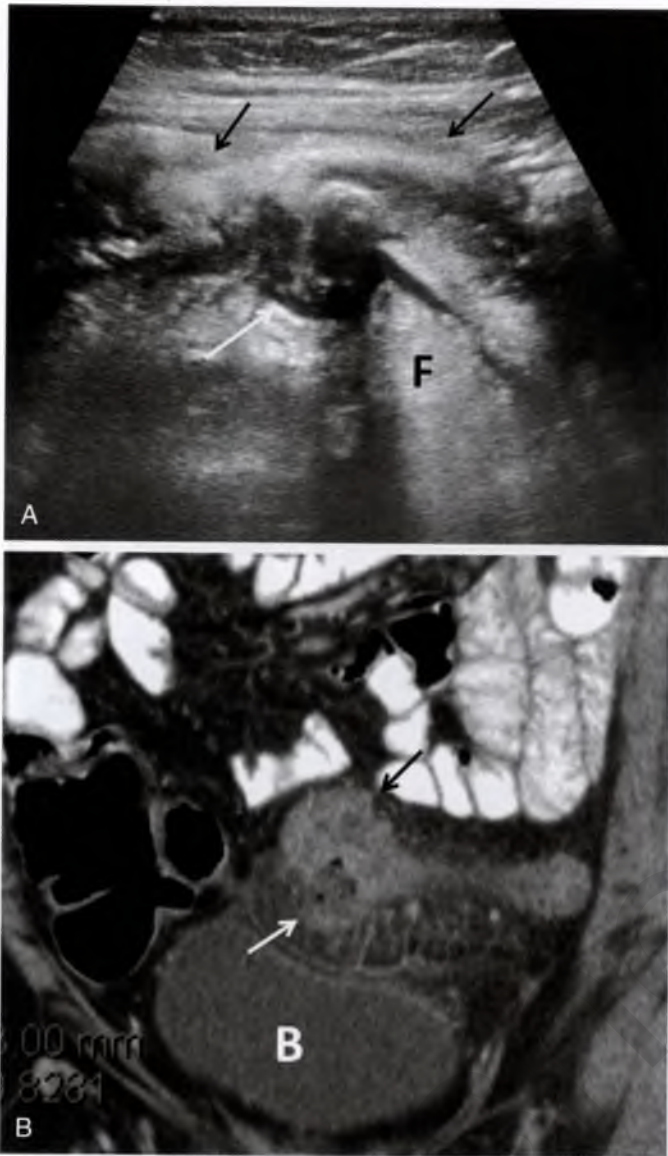


**FIG 29-48** Acute sigmoid diverticulitis in a patient with left pelvic pain. **A**, Evaluation of the left lower quadrant with a linear ultrasound transducer shows thickened sigmoid colon (*black arrows*). There is a focal outpouching with fluid and debris (*white arrow*) representing the inflamed diverticulum. The adjacent inflamed pericolonic fat (F) is hyper-echoic. **B**, Coronal reformatted image from contrast-enhanced computed tomography demonstrates inflamed diverticulum (*white arrow*), with bowel wall thickening (*black arrow*) and stranding in the adjacent pelvic fat consistent with inflammation. B, urinary bladder.

Clinical features of enteritis or colitis may overlap with other pelvic conditions. Inflamed bowel in the setting of enteritis or colitis will demonstrate wall thickening with variable degrees of echogenicity and hyperemia. Decreased peristalsis and increased echogenicity of the mesenteric fat may also be observed. A Meckel diverticulum may appear as a blind-ending pouch-like structure arising from the small bowel, allowing it to be differentiated from the appendix.<sup>248,249</sup>

### Obstructive Uropathy

In general, patients with renal colic present with acute onset of severe colicky flank pain and nausea; 50% of patients will have hematuria on

urinalysis. Although the diagnosis can often be made based on clinical presentation, imaging may be required for confirmation or to exclude other causes of pain and to guide appropriate management (conservative management versus intervention). Intervention is more likely to be required if there is significant hydronephrosis or if the stone is larger than 5 mm.<sup>250,251</sup> In adults, low-dose non-contrast-enhanced renal stone protocol CT is the initial imaging study of choice given the high accuracy for identification and characterization of obstructing ureteral stones as well as associated complications, and this protocol is given the highest score in the ACR Appropriateness Criteria for evaluation of flank pain and suspected kidney stone.<sup>252</sup> The sensitivity and specificity of CT for the diagnosis of kidney stones range from 95% to 96% and 98% to 100% with overall accuracy of 100%.<sup>253,254</sup>

Because the clinical presentation of renal colic may overlap with emergent gynecologic conditions including ovarian torsion or ruptured ovarian cyst, pelvic ultrasound protocols for evaluation of pelvic pain at many institutions include at least limited assessment of the kidneys to evaluate for hydronephrosis, particularly if no cause for the patient's symptoms is identified in the uterus or adnexa. A dilated ureter should be followed as far distal as possible to identify the cause and level of obstruction (Fig. 29-50). A dilated ureter may also be identified as an incidental finding at transvaginal sonography.

The sensitivity of ultrasound for detecting ureteral calculi depends on the size and location of the stone. Proximal stones, near the ureteropelvic junction, and stones in the distal ureter, at a level where the bladder can be used as an acoustic window, are more readily visualized. Detection of distal ureteral stones, close to the level of the ureterovesical junction, can be facilitated by using a transvaginal sonographic approach.<sup>255</sup> However, midureteral stones are often obscured by bowel gas. The reported sensitivity of sonography for obstruction of the collecting system is 73% to 100%.<sup>256</sup> Signs of obstruction include hydronephrosis, hydroureter, and absence of the ureteral jet in the urinary bladder. However, obstructive uropathy cannot be confirmed unless a ureteral stone is visualized, as there are many nonobstructive causes of dilatation of the collecting system.

Sonography is the preferred imaging modality in this evaluation in pregnant patients and children to avoid ionizing radiation.<sup>256</sup> A 2014 analysis of over 2700 patients with flank pain randomized to point-of-care sonography in the emergency department, sonography performed in the radiology department, or CT scan as initial evaluation demonstrated that initial sonography was associated with lower cumulative radiation exposure than initial CT, without significant differences in high-risk diagnoses with complications, serious adverse events, pain scores, return emergency department visits, or hospitalizations.<sup>257</sup> In light of these data, it is likely that sonography will play an even larger role in evaluation of suspected urolithiasis in the nonpregnant patient.

### CONCLUSIONS

Pelvic sonography is the first-line imaging method of choice for evaluation of pelvic pain in the reproductive age patient when a gynecologic disorder is suspected. Sonography often conclusively establishes the diagnosis of ovarian torsion, hemorrhagic ovarian cyst, endometriosis, PID, adenomyosis, complications of leiomyomas, and vascular abnormalities. Furthermore, many nongynecologic causes of pelvic pain including gastrointestinal and genitourinary disorders may be identified at ultrasound examination performed for suspected pelvic abnormalities, and recognition of these disorders may enable prompt diagnosis and eliminate the need for further imaging. When ultrasound findings are equivocal, CT and MRI can be helpful complementary techniques.



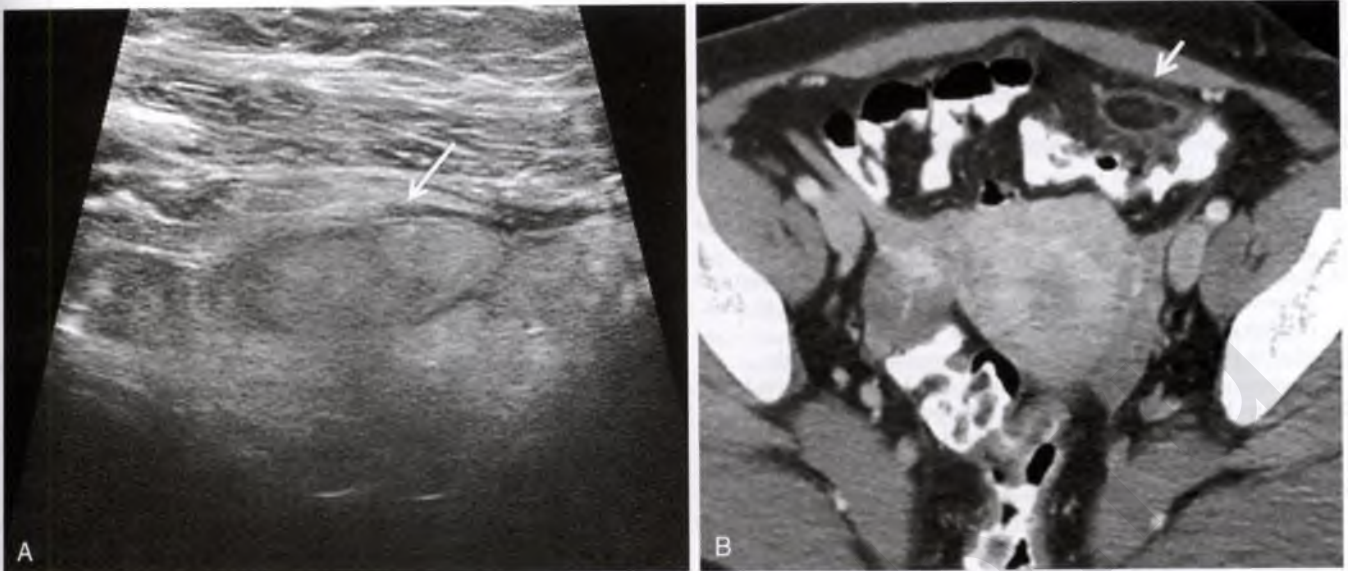


**FIG 29-49** Epiploic appendagitis in patient with left pelvic pain. **A**, High-resolution linear transducer demonstrates an oval hyperechoic mass-like area (arrow) with hypoechoic rim at the point of maximal tenderness. The uterus and adnexa were normal (not shown). **B**, Contrast-enhanced axial computed tomography confirms the diagnosis of epiploic appendagitis. Note rim-enhancing fat-attenuation abnormality at the left lower quadrant (arrow).

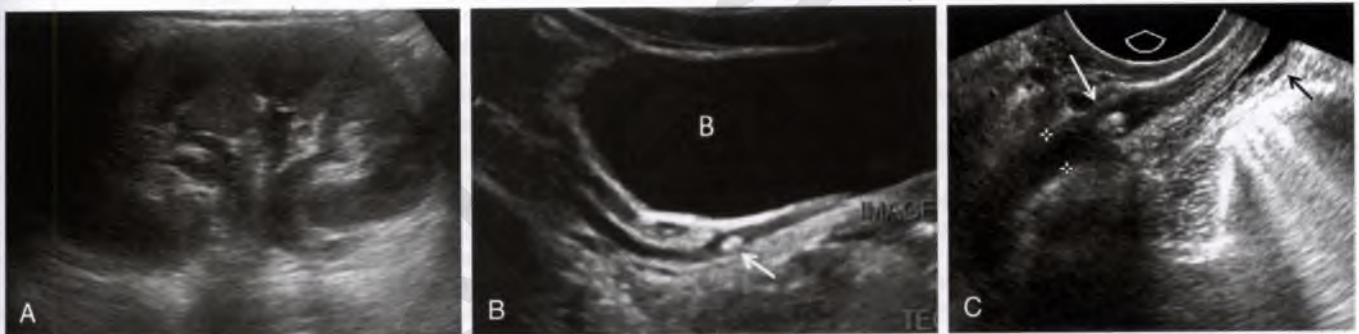


**FIG 29-50** Urolithiasis in patient with right pelvic pain. **A**, Sagittal gray-scale ultrasound image of the right kidney demonstrates mild dilatation of the intrarenal collecting system. The uterus and adnexa were normal (not shown). **B**, Transabdominal scan, using the distended urinary bladder (B) as an acoustic window, demonstrates an echogenic calculus (arrow) in the mildly distended, fluid-filled distal right ureter. **C**, Transvaginal scan demonstrates an echogenic calculus (white arrow) in the dilated distal ureter (calipers) just proximal to the ureterovesical junction. The bladder (black arrow) is decompressed.

## REFERENCES

1. American College of Radiology: *ACR Appropriateness Criteria for Diagnostic Imaging: Acute Pelvic Pain in the Reproductive Age Group*. 2015. Available at <www.acr.org>.
2. Hibbard LT: Adnexal torsion. *Am J Obstet Gynecol* 152:456–461, 1985.
3. Sasaki KJ, Miller CM: Adnexal torsion: review of the literature. *J Minim Invasive Gynecol* 21(2):196–202, 2014.
4. Albayram F, Hamper UM: Ovarian and adnexal torsion: spectrum of sonographic findings with pathologic correlation. *J Ultrasound Med* 20:1083–1089, 2001.
5. Chang HC, Bhatt S, Dogra VS: Pearls and pitfalls in diagnosis of ovarian torsion. *Radiographics* 28:1355–1368, 2008.
6. Cicchiello LA, Hamper UM, Scoutt LM: Ultrasound evaluation of gynecologic causes of pelvic pain. *Obstet Gynecol Clin North Am* 38:85–114, 2011.
7. Chiou SY, Lev-Toaff AS, Masuda E, et al: Adnexal torsion: new clinical and imaging observations by sonography, computed tomography and magnetic resonance imaging. *J Ultrasound Med* 26:1289–1301, 2007.
8. Ginath S, Shalev A, Keidar R, et al: Differences between adnexal torsion in pregnant and nonpregnant women. *J Minim Invasive Gynecol* 19:708–714, 2012.
9. Hasson J, Tsafir Z, Azem F, et al: Comparison of adnexal torsion between pregnant and nonpregnant women. *Am J Obstet Gynecol* 202:536.e1, 2010.
10. Smorgick N, Pansky M, Feingold M, et al: The clinical characteristics and sonographic findings of maternal ovarian torsion in pregnancy. *Fertil Steril* 92(6):1983–1987, 2009.
11. Huchon C, Fauconnier A: Adnexal torsion: a literature review. *Eur J Obstet Gynecol Reprod Biol* 150:8–12, 2010.
12. Mazouni C, Bretelle F, Menard JP, et al: Diagnosis of adnexal torsion and predictive factors of adnexal necrosis. *Gynecol Obstet Fertil* 33:102–106, 2005.
13. Kamaya A, Shin L, Chen B, Desser TS: Emergency gynecologic imaging. *Semin Ultrasound CT MR* 29:353–368, 2008.



14. Graif M, Shalev J, Strauss S, et al: Torsion of the ovary: sonographic features. *AJR Am J Roentgenol* 143:1331–1334, 1984.
15. Lee EJ, Kwon HC, Joo HJ, et al: Diagnosis of ovarian torsion with color Doppler sonography: depiction of twisted vascular pedicle. *J Ultrasound Med* 17:83–89, 1998.
16. Houry D, Abbott JT: Ovarian torsion: a fifteen-year review. *Ann Emerg Med* 38:156–159, 2001.
17. Shadinger LL, Andreotti RF, Kurian RL: Preoperative sonographic and clinical characteristics as predictors of ovarian torsion. *J Ultrasound Med* 27(1):7–13, 2008.
18. Rousseau V, Massicot R, Darwish AA, et al: Emergency management and conservative surgery of ovarian torsion in children: a report of 40 cases. *J Pediatr Adolesc Gynecol* 21:201–206, 2008.
19. Sibal M: Follicular ring sign: a simple sonographic sign for early diagnosis of ovarian torsion. *J Ultrasound Med* 31:1803–1809, 2012.
20. Ben-Ami M, Perlitz Y, Haddad S: The effectiveness of spectral and color Doppler in predicting ovarian torsion. *Eur J Obstet Gynecol Reprod Biol* 104:64–66, 2002.
21. Mashlach R, Melamed N, Gilad N, et al: Sonographic diagnosis of ovarian torsion: accuracy and predictive factors. *J Ultrasound Med* 30:1205–1210, 2011.
22. Bar-On S, Mashlach R, Stockheim D, et al: Emergency laparoscopy for suspected ovarian torsion: are we too hasty to operate? *Fertil Steril* 93:2012–2015, 2010.
23. Hiller N, Appelbaum L, Simanovsky N, et al: CT features of adnexal torsion. *AJR Am J Roentgenol* 189:124–129, 2007.
24. Pena JE, Ufberg D, Cooney N, Denis AL: Usefulness of Doppler sonography in the diagnosis of ovarian torsion. *Fertil Steril* 73:1047–1050, 2000.
25. Fleischer AC, Stein SM, Cullinan JA, Warner MA: Color Doppler sonography of adnexal torsion. *J Ultrasound Med* 14:523–528, 1995.
26. Nizar K, Deutsch M, Filmer S, et al: Doppler studies of the ovarian venous blood flow in the diagnosis of adnexal torsion. *J Clin Ultrasound* 37:436–439, 2009.
27. Vijayaraghavan SB: Sonographic whirlpool sign in ovarian torsion. *J Ultrasound Med* 23:1643–1649, 2004.
28. Navve D, Hershkovitz R, Zetounie E, et al: Medial or lateral location of the whirlpool sign in adnexal torsion. *J Ultrasound Med* 32:1631–1634, 2013.
29. Valsky DV, Esh-Border E, Cohen SM, et al: Added value of the gray-scale whirlpool sign in the diagnosis of adnexal torsion. *Ultrasound Obstet Gynecol* 36:630–634, 2010.
30. Rha SE, Byun JY, Jung SE, et al: CT and MR imaging features of adnexal torsion. *Radiographics* 22:283–294, 2002.
31. Duigenan S, Oliva E, Lee SI: Ovarian torsion: diagnostic features on CT and MRI with pathologic correlation. *AJR Am J Roentgenol* 198:W122–W131, 2012.
32. Swenson DW, Lourenco AP, Beaudoin FL, et al: Ovarian torsion: case-control study comparing the sensitivity and specificity of ultrasonography and computed tomography for diagnosis in the emergency department. *Eur J Radiol* 83:733–738, 2014.
33. Kimura I, Togashi K, Kawakami S, et al: Ovarian torsion: CT and MR imaging appearances. *Radiology* 190(2):337–341, 1994.
34. Cornfeld D, Scoutt L: Torsion of a hyperstimulated ovary during pregnancy: a potentially difficult diagnosis. *Emerg Radiol* 14:331–335, 2007.
35. Gross M, Blumstein SL, Chow LC: Isolated fallopian tube torsion: a rare twist on a common theme. *AJR Am J Roentgenol* 185:1590–1592, 2005.
36. Harmon JC, Binkovitz LA, Binkovitz LE: Isolated fallopian tube torsion: sonographic and CT features. *Pediatr Radiol* 38:175–179, 2008.
37. Vijayaraghavan SB, Senthil S: Isolated torsion of the fallopian tube: the sonographic whirlpool sign. *J Ultrasound Med* 28:657, 2009.
38. Aydin R, Bildirein D, Polat AV: Isolated torsion of the fallopian tube with hydrosalpinx mimicking a multiloculated ovarian cyst: whirlpool sign on preoperative sonography and MRI. *J Clin Ultrasound* 42:45–48, 2014.
39. Bottomley C, Bourne T: Diagnosis and management of ovarian cyst accidents. *Best Pract Res Clin Obstet Gynaecol* 23(5):711–724, 2009.
40. Jain KA: Sonographic spectrum of hemorrhagic ovarian cysts. *J Ultrasound Med* 21:879–886, 2002.
41. Hatipoglu S, Hatipoglu F, Abdullayev R: Acute right lower abdominal pain in women of reproductive age: clinical clues. *World J Gastroenterol* 20(14):4043–4049, 2014.
42. Gupta N, Dadhwal V, Deka D, et al: Corpus luteum hemorrhage: rare complication of congenital and acquired coagulation abnormalities. *J Obstet Gynaecol Res* 33(3):376–380, 2007.
43. Brown DL: A practical approach to the ultrasound characterization of adnexal masses. *Ultrasound Q* 23(2):87–105, 2007.
44. Bourne TH, Hagstrom H-G, Hahlin B, et al: Ultrasound studies of vascular and morphological changes in the human corpus luteum during the menstrual cycle. *Fertil Steril* 65:753–758, 1996.
45. Yoffe N, Bronshtein M, Brandes J, Blumenfeld Z: Hemorrhagic ovarian cyst detection by transvaginal sonography: the great imitator. *Gynecol Endocrinol* 5(2):123–129, 1991.
46. Patel MD, Feldstein VA, Filly RA: The likelihood ratio of sonographic findings for the diagnosis of hemorrhagic ovarian cysts. *J Ultrasound Med* 24:607–614, 2005.
47. Swire MN, Castro-Aragon I, Levine D: Various sonographic appearances of the hemorrhagic corpus luteum cyst. *Ultrasound Q* 20:45–58, 2004.
48. Valentin L: Use of morphology to characterize and manage common adnexal masses. *Best Pract Res Clin Obstet Gynaecol* 18:71–89, 2004.
49. Patel MD: Pitfalls in the sonographic evaluation of adnexal masses. *Ultrasound Q* 28:29–40, 2012.
50. Okai T, Kobayashi K, Ryo E, et al: Transvaginal sonographic appearance of hemorrhagic functional ovarian cysts and their spontaneous regression. *Int J Gynaecol Obstet* 44:47–52, 1994.
51. Levine D, Brown DL, Andreotti RF, et al: Management of asymptomatic ovarian and other adnexal cysts imaged at US: Society of Radiologists in Ultrasound Consensus Conference Statement. *Radiology* 256(3):943–954, 2010.
52. Hertzberg BS, Kliever MA, Paulson EK: Ovarian cyst rupture causing hemoperitoneum: imaging features and the potential for misdiagnosis. *Abdom Imaging* 24:304–308, 1999.
53. Bennett GL, Slywotzky CM, Giovanniello G: Gynecologic causes of acute pelvic pain: spectrum of CT findings. *Radiographics* 22(4):785–801, 2002.
54. Swart JE, Fishman EK: Gynecologic pathology on multidetector CT: a pictorial review. *Emerg Radiol* 15(6):383–389, 2008.
55. Kalish GM, Patel MD, Gunn ML, Dubinsky TJ: Computed tomographic and magnetic resonance features of gynecologic abnormalities in women presenting with acute or chronic pelvic pain. *Ultrasound Q* 23(3):167–175, 2007.
56. Comerci JT, Jr, Licciardi F, Bergh PA, et al: Mature cystic teratoma: a clinicopathologic evaluation of 517 cases and review of the literature. *Obstet Gynecol* 84:22–28, 1994.
57. Park SB, Kim JK, Kim KR, Cho KS: Imaging findings of complications and unusual manifestations of ovarian teratomas. *Radiographics* 28:969–983, 2008.
58. Soper DE: Pelvic inflammatory disease. *Obstet Gynecol* 116:419–428, 2010.
59. Velebil P, Wingo PA, Xia Z, et al: Rate of hospitalization for gynecologic disorders among reproductive-age women in the United States. *Obstet Gynecol* 86(5):764–769, 1995.
60. Haggerty CL, Ness RB: Diagnosis and treatment of pelvic inflammatory disease. *Womens Health* 4:383–397, 2008.
61. Timor-Tritsch IE, Lerner JP, Monteagudo A, et al: Transvaginal sonographic markers of tubal inflammatory disease. *Ultrasound Obstet Gynecol* 12:56–66, 1998.
62. Horror MM, Rodgers SK, Naqvi S: Ultrasound of pelvic inflammatory disease. *Ultrasound Clin* 2(2):297–309, 2007.
63. Cacciatore B, Leminen A, Ingman-Friberg S, et al: Transvaginal sonographic findings in ambulatory patients with suspected pelvic inflammatory disease. *Obstet Gynecol* 80:912–916, 1992.
64. Bulas DI, Ahlstrom PA, Sivit CJ, et al: Pelvic inflammatory disease in the adolescent: comparison of transabdominal and transvaginal sonographic evaluation. *Radiology* 183:435–439, 1992.



65. Rezvani M, Shaaban AM: Fallopian tube disease in the nonpregnant patient. *Radiographics* 31(2):527–548, 2011.
66. Paik CK, Waetjen LE, King G, et al: Hospitalizations for pelvic inflammatory disease and tuboovarian abscess. *Obstet Gynecol* 107:611–616, 2006.
67. Tukey TA, Aronen HJ, Karjalainen PT, et al: MR imaging in pelvic inflammatory disease: comparison with laparoscopy and US. *Radiology* 210(1):209–216, 1999.
68. Benjaminov O, Atri M: Sonography of the abnormal fallopian tube. *AJR Am J Roentgenol* 183(3):737–742, 2004.
69. Patel MD, Acord DL, Young SW: Likelihood ratio of sonographic findings in discriminating hydrosalpinx from other adnexal masses. *AJR Am J Roentgenol* 186(4):1033–1038, 2006.
70. Armstrong L, Fleischer A, Andreotti R: Three-dimensional volumetric sonography in gynecology. An overview of clinical applications. *Radiol Clin North Am* 51:1035–1047, 2013.
71. Timor-Tritsch IE, Monteagudo A, Tsybmal T: Three-dimensional ultrasound inversion rendering technique facilitates the diagnosis of hydrosalpinx. *J Clin Ultrasound* 38:372–376, 2010.
72. Olive DL: Endometriosis. *N Engl J Med* 328:1759–1769, 1993.
73. Guidice LC: Endometriosis. *N Engl J Med* 362(25):2389–2398, 2010.
74. Burney RO, Giudice LC: Pathogenesis and pathophysiology of endometriosis. *Fertil Steril* 98:511–519, 2012.
75. Eskenazi B, Warner ML: Epidemiology of endometriosis. *Obstet Gynecol Clin North Am* 24:235–258, 1997.
76. Meuleman C, Vandenabeele B, Fieuws S, Spiessens C: High prevalence of endometriosis in infertile women with normal ovulation and normospermic partners. *Fertil Steril* 92(19):68–74, 2009.
77. Sasson IE, Taylor HS: Stem cells and the pathogenesis of endometriosis. *Ann N Y Acad Sci* 1127:106–115, 2008.
78. Cornillie FJ, Oosterlynck D, Lauweryns JM, Kononckx PR: Deep infiltrating pelvic endometriosis: histology and clinical significance. *Fertil Steril* 53:978–983, 1990.
79. Koninckx PR, Ussia A, Adamyan L, et al: Deep endometriosis: definition, diagnosis, and treatment. *Fertil Steril* 98:564–571, 2012.
80. Chapron C, Fauconnier A, Vieira M, et al: Anatomical distribution of deeply infiltrating endometriosis: surgical implications and proposition for a classification. *Hum Reprod* 18(1):157–161, 2003.
81. Bhatt S, Kocakoc E, Dogra VS: Endometriosis: sonographic spectrum. *Ultrasound Q* 22:273–280, 2006.
82. Asch E, Levine D: Variations in appearance of endometriomas. *J Ultrasound Med* 26:993–1002, 2007.
83. Kupfer MC, Schwimmer SR, Lebovic J: Transvaginal sonographic appearance of endometriomas: spectrum and findings. *J Ultrasound Med* 11:129–133, 1992.
84. Patel MD, Feldstein VA, Chen DC, et al: Endometriomas: diagnostic performance of US. *Radiology* 210:739–745, 1999.
85. Bennett GL, Slywotzky CM, Cantera M, Hecht EM: Unusual manifestations and complications of endometriosis—spectrum of imaging findings: pictorial review. *AJR Am J Roentgenol* 194(6 Suppl):WS34–WS46, 2010.
86. Alcazar JL, Laparte C, Jurado M, et al: The role of transvaginal ultrasound combined with color velocity imaging and pulsed Doppler in the diagnosis of endometrioma. *Fertil Steril* 67:487–491, 1997.
87. Moore J, Copley S, Morris J, et al: A systematic review of the accuracy of ultrasound in the diagnosis of endometriosis. *Ultrasound Obstet Gynecol* 20:630–634, 2002.
88. Chamie LP, Blasbalg R, Pereira RM, et al: Findings of pelvic endometriosis at transvaginal US, MR imaging and laparoscopy. *Radiographics* 31(4):E77–E100, 2011.
89. Gougoutas CA, Siegelman ES, Hunt J, Outwater EK: Pelvic endometriosis: various manifestations and MR imaging findings. *AJR Am J Roentgenol* 175:353–358, 2000.
90. Kinkel K, Frei KA, Balleyguier C, Chapron C: Diagnosis of endometriosis with imaging: a review. *Eur Radiol* 16:285–298, 2006.
91. Togashi K, Nishimura K, Kimura I, et al: Endometrial cysts: diagnosis with MR imaging. *Radiology* 180(1):73–78, 1991.
92. Jenkins S, Olive DL, Haney AF: Endometriosis: pathogenetic implications of the anatomic distribution. *Obstet Gynecol* 67(3):335–338, 1986.
93. Hensen JH, Van Breda Vriesman AC, Puylaert JB: Abdominal wall endometriosis: clinical presentation and imaging features with emphasis on sonography. *AJR Am J Roentgenol* 186(3):616–620, 2006.
94. Horton JD, Dezee KJ, Ahnfeldt EP, Wagner M: Abdominal wall endometriosis: a surgeon's perspective and review of 445 cases. *Am J Surg* 196(2):207–212, 2008.
95. Aydin O: Scar endometriosis: a gynaecologic pathology often presented to the general surgeon rather than the gynaecologist—report of two cases. *Langenbecks Arch Surg* 392(1):105–109, 2007.
96. Gidwaney R, Badler RL, Yam BL, et al: Endometriosis of abdominal and pelvic wall scars: multimodality imaging findings, pathologic correlation and radiologic mimics. *Radiographics* 32(7):2031–2043, 2012.
97. Park SB, Kim JK, Cho KS: Sonography of endometriosis in infrequent sites. *J Clin Ultrasound* 36:91–97, 2008.
98. Wolf C, Obrist P, Ensinger C: Sonographic features of abdominal wall endometriosis. *AJR Am J Roentgenol* 169:916–917, 1997.
99. Francica G, Giardiello C, Angelone G, et al: Abdominal wall endometriomas near cesarean delivery scars: sonographic and color Doppler findings in a series of 12 patients. *J Ultrasound Med* 22(10):1041–1047, 2003.
100. Francica G, Scarano F, Scotti L, et al: Endometriomas in the region of a scar from cesarean section: sonographic appearance and clinical presentation vary with the size of the lesion. *J Clin Ultrasound* 37(4):215–220, 2009.
101. Benacerraf BR, Groszmann Y: Sonography should be the first imaging examination done to evaluate patients with suspected endometriosis. *J Ultrasound Med* 31:651–653, 2012.
102. Guerriero S, Ajossa S, Gerada M, et al: Diagnostic value of transvaginal “tenderness-guided” ultrasonography for the prediction of location of deep endometriosis. *Hum Reprod* 23:2452–2457, 2008.
103. Saba L, Guerriero S, Sulcis R, et al: MRI and “tenderness guided” transvaginal ultrasonography in the diagnosis of recto-sigmoid endometriosis. *J Magn Reson Imaging* 35:352–360, 2012.
104. Fratelli N, Scioscia M, Bassi E, et al: Transvaginal sonography for preoperative assessment of deep endometriosis. *J Clin Ultrasound* 41:69–75, 2013.
105. Grasso RF, DiGiacomo V, Sedati P, et al: Diagnosis of deep infiltrating endometriosis: accuracy of magnetic resonance imaging and transvaginal 3D ultrasonography. *Abdom Imaging* 35:716–725, 2010.
106. Bazot M, Thomassin I, Hourani R, et al: Diagnostic accuracy of transvaginal sonography for deep pelvic endometriosis. *Ultrasound Obstet Gynecol* 24:180–185, 2004.
107. Chamie LP, Pereira RM, Zanatta A, Serafini PC: Transvaginal US after bowel preparation for deeply infiltrating endometriosis: protocol, imaging appearances, and laparoscopic correlation. *Radiographics* 30(5):1235–1249, 2010.
108. Hudelist G, English J, Thomas AE, et al: Diagnostic accuracy of transvaginal ultrasound for non-invasive diagnosis of bowel endometriosis: systematic review and meta-analysis. *Ultrasound Obstet Gynecol* 37:257–263, 2011.
109. Holland TK, Cutner A, Saridogan E, et al: Ultrasound mapping of pelvic endometriosis: does the location and number of lesions affect the diagnostic accuracy? A multicentre diagnostic accuracy study. *BMC Womens Health* 13:43, 2013.
110. García-Velasco JA, Alvarez M, Palumbo A, et al: Rupture of an ovarian endometrioma during the first trimester of pregnancy. *Eur J Obstet Gynecol Reprod Biol* 76:41–43, 1998.
111. Sait KH: Massive ascites as a presentation in a young woman with endometriosis: a case report. *Fertil Steril* 90:e17–e19, 2008.
112. Kubota T, Ishi K, Takeuchi H: A study of tubo-ovarian and ovarian abscesses, with a focus on cases with endometrioma. *J Obstet Gynaecol Res* 23:421–426, 1997.
113. Miyakoshi K, Tanaka M, Gabionza D, et al: Decidualized ovarian endometriosis mimicking malignancy. *AJR Am J Roentgenol* 171(6):1625–1626, 1998.



114. Sammour RN, Leibovitz Z, Shapiro I, et al: Decidualization of ovarian endometriosis during pregnancy mimicking malignancy. *J Ultrasound Med* 24:1289–1294, 2005.
115. Fruscella E, Testa AC, Ferrandina G, et al: Sonographic features of decidualized ovarian endometriosis suspicious for malignancy. *Ultrasound Obstet Gynecol* 24:578–580, 2004.
116. Machida S, Matsubara S, Ohwada M, et al: Decidualization of ovarian endometriosis during pregnancy mimicking malignancy: report of three cases with a literature review. *Gynecol Obstet Invest* 66:241–247, 2008.
117. Poder L, Coakley FV, Rabban JT, et al: Decidualized endometrioma during pregnancy: recognizing an imaging mimic of ovarian malignancy. *J Comput Assist Tomogr* 32:555–558, 2008.
118. Kawaguchi R, Tsuji Y, Haruta S, et al: Clinicopathologic features of ovarian cancer in patients with ovarian endometrioma. *J Obstet Gynaecol Res* 34:872–877, 2008.
119. Scully RE, Richardson GS, Barlow JF: The development of malignancy in endometriosis. *Clin Obstet Gynecol* 9:381–411, 1966.
120. Brinton LA, Gridley G, Persson I, et al: Cancer risk after a hospital discharge diagnosis of endometriosis. *Am J Obstet Gynecol* 176:572–579, 1997.
121. Wiegand KC, Shah SP, Al-Agha OM, et al: ARID1A mutations in endometriosis-associated ovarian carcinomas. *N Engl J Med* 363:1532–1543, 2010.
122. Tanaka YO, Yoshizako T, Nishida M, et al: Ovarian carcinoma in patients with endometriosis: MR imaging findings. *AJR Am J Roentgenol* 175:1423–1430, 2000.
123. Takeuchi M, Matsuzaki K, Uehara H, Nishitani H: Malignant transformation of pelvic endometriosis: MR imaging findings and pathologic correlation. *Radiographics* 26:407–417, 2006.
124. Kobayashi H, Sumimoto K, Kitanaka T, et al: Ovarian endometrioma-risk factors of ovarian cancer development. *Eur J Obstet Gynecol Reprod Biol* 138:187–193, 2008.
125. Vallerie AM, Lerner JP, Wright JD, Baxi LV: Peritoneal inclusion cysts: a review. *Obstet Gynecol Surv* 64(5):321–334, 2009.
126. Jain KA: Imaging of peritoneal inclusion cysts. *AJR Am J Roentgenol* 174:1559–1563, 2000.
127. Veldhuis WB, Akin O, Goldman D, et al: Peritoneal inclusion cysts: clinical characteristics and imaging features. *Eur Radiol* 23:1167–1174, 2013.
128. Moyle PL, Kataoka MY, Nakai A, et al: Nonovarian cystic lesions of the pelvis. *Radiographics* 30:921–938, 2010.
129. Laughlin SK, Schroeder JC, Baird DD: New directions in the epidemiology of uterine fibroids. *Semin Reprod Med* 28:204–217, 2010.
130. Ciavattini A, Di Giuseppe J, Stortoni P, et al: Uterine fibroids: pathogenesis and interactions with endometrium and endomyometrial junction. *Obstet Gynecol Int* 2013:173184, 2013.
131. Yoon SW, Lee C, Cha SH, et al: Patient selection guidelines in MR-guided focused ultrasound surgery of uterine fibroids: a pictorial guide to relevant findings in screening pelvic MRI. *Eur Radiol* 18:2997–3006, 2008.
132. Parker WH: Etiology, symptomatology, and diagnosis of uterine myomas. *Fertil Steril* 87:725–736, 2007.
133. Ueda H, Togashi K, Konishi I, et al: Unusual appearances of uterine leiomyomas: MR imaging findings and their histopathologic backgrounds. *Radiographics* 19(Spec No):S131–S145, 1999.
134. Munro MG, Critchley HO, Broder MS, et al: Group on Menstrual Disorders; FIGO classification system (PALM-COEIN) for causes of abnormal uterine bleeding in nonpregnant women of reproductive age. *Int J Gynecol Obstet* 113:3–13, 2011.
135. Fasih N, Prasad Shanbhogue AK, Macdonald DB, et al: Leiomyomas beyond the uterus: unusual locations, rare manifestations. *Radiographics* 28(7):1931–1948, 2008.
136. Shwayder J, Sakhel K: Imaging for uterine myomas and adenomyosis. *J Minim Invasive Gynecol* 21:362–366, 2014.
137. Madan R: The bridging vascular sign. *Radiology* 238:371–372, 2006.
138. Cohen LS, Valle RF: Role of vaginal sonography and hysterosonography in the endoscopic treatment of uterine myomas. *Fertil Steril* 73:197–204, 2000.
139. Parker WH: The utility of MRI for the surgical treatment of women with uterine fibroid tumors. *Am J Obstet Gynecol* 206(1):31–36, 2012.
140. Levens ED, Wesley R, Premkumar A, et al: Magnetic resonance imaging and transvaginal ultrasound for determining fibroid burden: implications for research and clinical care. *Am J Obstet Gynecol* 200(5):537.e1–537.e7, 2009.
141. Spielman AL, Keogh C, Forster BB, et al: Comparison of MRI and sonography in the preliminary evaluation for fibroid embolization. *AJR Am J Roentgenol* 187(6):1499–1504, 2006.
142. Rajan DK, Margau R, Kroll RR, et al: Clinical utility of ultrasound versus magnetic resonance imaging for deciding to proceed with uterine artery embolization for presumed symptomatic fibroids. *Clin Radiol* 66(1):57–62, 2011.
143. Omary RA, Vasireddy S, Chrisman HB, et al: The effect of pelvic MR imaging on the diagnosis and treatment of women with presumed symptomatic uterine fibroids. *J Vasc Interv Radiol* 13(11):1149–1153, 2002.
144. Levy G, Hill MJ, Beall S, et al: Leiomyoma: genetics, assisted reproduction, pregnancy and therapeutic advances. *J Assist Reprod Genet* 29:703–712, 2012.
145. Prieto A, Crespo C, Pardo A, et al: Uterine lipoleiomyomas: US and CT findings. *Abdom Imaging* 25:655–657, 2000.
146. Sieinski W: Lipomatous neometaplasia of the uterus. Report of 11 cases with discussion of histogenesis and pathogenesis. *Int J Gynecol Pathol* 8(4):357–363, 1989.
147. Scurry J, Hack M: Leiomyosarcoma arising in a lipoleiomyoma. *Gynecol Oncol* 39(3):381–383, 1990.
148. Dodd GD, III, Budzik RF: Lipomatous tumors of the pelvis in women: spectrum of imaging findings. *AJR Am J Roentgenol* 155:317–322, 1990.
149. Loffroy R, Nezzal N, Mejean N, et al: Lipoleiomyoma of the uterus: imaging features. *Gynecol Obstet Invest* 66:73–75, 2008.
150. Maebayashi T, Takekawa Y, Sasaki J, et al: Radiologic features of uterine lipoleiomyoma. *J Comp Assist Tomogr* 27:162–165, 2003.
151. Griffin Y, Sudigali V, Jacques A: Radiology of benign disorders of menstruation. *Semin Ultrasound CT MR* 31:414–432, 2010.
152. Gupta S, Manyonda IT: Acute complications of fibroids. *Best Pract Res Clin Obstet Gynecol* 23:609–617, 2009.
153. Takai H, Tani H, Matsushita H: Rupture of a degenerated uterine fibroid as a cause of acute abdomen: a case report. *J Reprod Med* 58:72–74, 2013.
154. Dicker D, Feldberg D, Dekel A, et al: The management of prolapsed submucosal fibroids. *Aust N Z J Obstet Gynaecol* 26(4):308, 1986.
155. Ben-Baruch G, Schiff E, Menashe Y, et al: Immediate and late outcome of vaginal myomectomy for prolapsed pedunculated submucosal myoma. *Obstet Gynecol* 72:858, 1988.
156. Sherer DM, Schwartz BM, Otero FJ, et al: Transvaginal sonographic depiction of aborting pedunculated intracavitary uterine leiomyoma. *J Clin Ultrasound* 27:405–408, 1999.
157. Kim JW, Lee CH, Kim KA, Park CM: Spontaneous prolapse of pedunculated uterine submucosal leiomyoma: usefulness of broccoli sign on CT and MR imaging. *Clin Imaging* 32(3):233–235, 2008.
158. Panageas E, Kier R, McCauley TR, McCarthy S: Submucosal uterine leiomyomas: diagnosis of prolapse into the cervix and vagina based on MR imaging. *AJR Am J Roentgenol* 159:555–558, 1992.
159. Verma SK, Gonsalves CF, Baltarowich OH, et al: Spectrum of imaging findings on MRI and CT after uterine artery embolization. *Abdom Imaging* 35(1):118–128, 2010.
160. Ghai S, Rajan DK, Benjamin MS, et al: Uterine artery embolization for leiomyomas: pre and postprocedural evaluation with US. *Radiographics* 25:1159–1176, 2005.
161. Kitamura Y, Ascher SM, Cooper C, et al: Imaging manifestations of complications associated with uterine artery embolization. *Radiographics* 25:S119–S132, 2005.
162. Vott S, Bonilla SM, Goodwin SC, et al: CT findings after uterine artery embolization. *J Comput Assist Tomogr* 24(6):846–848, 2000.
163. Abulafia O, Shah T, Salame G, et al: Sonographic features associated with post-uterine artery embolization pyomyoma. *J Ultrasound Med* 29:839–842, 2010.

164. D'Angelo E, Prat J: Uterine sarcomas: a review. *Gynecol Oncol* 116:131–139, 2010.
165. Sutton G: Uterine sarcomas 2013. *Gynecol Oncol* 130:3–5, 2013.
166. Ip PP, Tse KY, Tam KF: Uterine smooth muscle tumors other than the ordinary leiomyomas and leiomyosarcomas: a review of selected variants with emphasis on recent advances and unusual morphology that may cause concern for malignancy. *Adv Anat Pathol* 17(2):91–112, 2010.
167. Exacoustous C, Romanin ME, Amadio A, et al: Can gray-scale and color Doppler sonography differentiate between uterine leiomyosarcoma and leiomyoma? *J Clin Ultrasound* 35:449–457, 2007.
168. Hata K, Hata T, Maruyama R, Hirai M: Uterine sarcoma: can it be differentiated from uterine leiomyoma with Doppler ultrasonography? A preliminary report. *Ultrasound Obstet Gynecol* 9(2):101–104, 1997.
169. Aviram R, Ochshorn Y, Markovitch O, et al: Uterine sarcomas versus leiomyomas: gray-scale and Doppler sonographic findings. *J Clin Ultrasound* 33(1):10–13, 2005.
170. Tanaka YO, Nishida M, Tsunoda H, et al: Smooth muscle tumors of uncertain malignant potential and leiomyosarcomas of the uterus: MR findings. *J Magn Reson Imaging* 20:998–1007, 2004.
171. Cornfeld D, Israel G, Martel M, et al: MRI appearance of mesenchymal tumors of the uterus. *Eur J Radiol* 74(1):241–249, 2010.
172. Goto A, Takeuchi S, Sugimura K, Maruo T: Usefulness of Gd-DTPA contrast-enhanced dynamic MRI and serum determination of LDH and its isozymes in the differential diagnosis of leiomyosarcoma from degenerated leiomyoma of the uterus. *Int J Gynecol Cancer* 12:354–361, 2002.
173. Shah SH, Jagannathan JP, Krajewski K, et al: Uterine sarcomas: then and now. *AJR Am J Roentgenol* 199:213–223, 2012.
174. Takeuchi M, Matsuzaki K, Nishitani H: Hyperintense uterine myometrial masses on T2-weighted magnetic resonance imaging: differentiation with diffusion-weighted magnetic resonance imaging. *J Comput Assist Tomogr* 33:834–837, 2009.
175. Sato K, Yuasa N, Fujita M, Fukushima Y: Clinical application of diffusion-weighted imaging for preoperative differentiation between uterine leiomyoma and leiomyosarcoma. *Am J Obstet Gynecol* 210:368, 2014.
176. AAGL Advancing Minimally Invasive Gynecology Worldwide: AAGL practice report: morcellation during uterine tissue extraction. *J Minim Invasive Gynecol* 21(4):517–530, 2014.
177. Matalliotakis IM, Kourtis AI, Panidis DK: Adenomyosis. *Obstet Gynecol Clin North Am* 30(1):63–82, 2003.
178. Benagiano G, Habiba M, Brosens I: The pathophysiology of uterine adenomyosis: an update. *Fertil Steril* 98(3):572–578, 2012.
179. Leyendecker G, Bilgicyildirim A, Inacker M, et al: Adenomyosis and endometriosis. Re-visiting their association and further insights into the mechanisms of auto-traumatization. An MRI study. *Arch Gynecol Obstet* 291(4):917–932, 2015.
180. Reinhold C, Tafazoli F, Mehio A, et al: Uterine adenomyosis: transvaginal US and MR imaging features with histopathologic correlation. *Radiographics* 19:S147–S160, 1999.
181. Reinhold C, Atri M, Mehio A, et al: Diffuse uterine adenomyosis: morphological criteria and diagnostic accuracy of transvaginal sonography. *Radiology* 197(3):609–614, 1995.
182. Reinhold C, McCarthy S, Bret PM, et al: Diffuse adenomyosis: comparison of transvaginal US and MR imaging with histopathologic correlation. *Radiology* 199(1):151–158, 1996.
183. Fedele I, Bianchi S, Dorta M, et al: Transvaginal ultrasonography in the diagnosis of diffuse adenomyosis. *Fertil Steril* 58:94–97, 1992.
184. Brosens JJ, de Souza NM, Barker FG, et al: Transvaginal ultrasonography in the diagnosis of adenomyosis uteri: identifying the predictive characteristics. *Br J Obstet Gynaecol* 102:471–474, 1995.
185. Andreotti RF, Fleischer AC: The sonographic diagnosis of adenomyosis. *Ultrasound Q* 21(3):167–170, 2005.
186. Exacoustous C, Manganaro L, Zupi E: Imaging for the evaluation of endometriosis and adenomyosis. *Best Pract Res Clin Obstet Gynaecol* 28:655–681, 2014.
187. Kepkep K, Tuncay YA, Goynumer G, Tural E: Transvaginal sonography in the diagnosis of adenomyosis: which findings are most accurate? *Ultrasound Obstet Gynecol* 30:341–345, 2007.
188. Meredith SM, Sanchez-Ramos L, Kaunitz AM: Diagnostic accuracy of transvaginal sonography for the diagnosis of adenomyosis: systematic review and metaanalysis. *Am J Obstet Gynecol* 201(1):107.e1–107.e6, 2009.
189. Bazot M, Cortez A, Darai E, et al: Ultrasonography compared with magnetic resonance imaging for the diagnosis of adenomyosis: correlation with histopathology. *Hum Reprod* 16(11):2427–2433, 2001.
190. Luciano DE, Exacoustous C, Albrecht L, et al: Three-dimensional ultrasound in diagnosis of adenomyosis: histologic correlation with ultrasound targeted biopsies of the uterus. *J Minim Invasive Gynecol* 20:803–810, 2013.
191. Botsis D, Kassanos D, Antonioc G, et al: Adenomyoma and leiomyoma: differential diagnosis with transvaginal sonography. *J Clin Ultrasound* 26(1):21–25, 1998.
192. Huang RT, Chou CY, Chang CH, et al: Differentiation between adenomyoma and leiomyoma with transvaginal ultrasonography. *Ultrasound Obstet Gynecol* 5(1):47–50, 1995.
193. Bromley B, Shipp TD, Benacerraf B: Adenomyosis: sonographic findings and diagnostic accuracy. *J Ultrasound Med* 19:529–534, 2000.
194. Ascher SM, Jha RC, Reinhold C: Benign myometrial conditions: leiomyomas and adenomyosis. *Top Magn Reson Imaging* 14(4):281–304, 2003.
195. Tamai K, Togashi K, Ito T, et al: MR imaging findings of adenomyosis: correlation with histopathologic features and diagnostic pitfalls. *Radiographics* 25(1):21–40, 2005.
196. Takeuchi M, Matsuzaki K: Adenomyosis: usual and unusual imaging manifestations, pitfalls and problem-solving MR imaging techniques. *Radiographics* 31(1):99–115, 2011.
197. Kataoka ML, Togashi K, Konishi I, et al: MRI of adenomyotic cyst of the uterus. *J Comput Assist Tomogr* 22(4):555–559, 1998.
198. Troiano RN, Flynn SD, McCarthy S: Cystic adenomyosis of the uterus: MRI. *J Magn Reson Imaging* 8(6):1198–1202, 1998.
199. Jones J, Mosher W, Daniels K: Current contraceptive use in the United States, 2006–2010, and changes in patterns of use since 1995. *Natl Health Stat Report* 60:1–25, 2012.
200. Reiner JS, Brindle KA, Khati NJ: Multimodality imaging of intrauterine devices with an emphasis on the emerging role of 3-dimensional ultrasound. *Ultrasound Q* 28(4):251–260, 2012.
201. Peri N, Graham D, Levine D: Imaging of intrauterine contraceptive devices. *J Ultrasound Med* 26:1389–1401, 2007.
202. Lee A, Eppel W, Sam C, et al: Intrauterine device localization by three-dimensional transvaginal ultrasonography. *Ultrasound Obstet Gynecol* 10(4):289–292, 1997.
203. Sakhel K, Benson CB, Platt LD, et al: Begin with the basics. Role of 3-dimensional sonography as a first-line imaging technique in the cost-effective evaluation of gynecologic pelvic disease. *J Ultrasound Med* 32:381–388, 2013.
204. Kuligowska E, Deeds L, Lu K: Pelvic pain: overlooked and underdiagnosed gynecologic conditions. *Radiographics* 25:3–20, 2005.
205. Beard RW, Highman JH, Pearce S, Reginald PW: Diagnosis of pelvic varicosities in women with chronic pelvic pain. *Lancet* 2:946–949, 1984.
206. Liddle AD, Davies AH: Pelvic congestion syndrome: chronic pelvic pain caused by ovarian and internal iliac varices. *Phlebology* 22(3):100–104, 2007.
207. Durham JD, Machan L: Pelvic congestion syndrome. *Semin Intervent Radiol* 30:372–380, 2013.
208. Park SJ, Lim LW, Ko YT, et al: Diagnosis of pelvic congestion syndrome using transabdominal and transvaginal sonography. *AJR Am J Roentgenol* 182:683–688, 2004.
209. Sharma K, Bora MK, Varghese J, et al: Role of transvaginal ultrasound and Doppler in diagnosis of pelvic congestion syndrome. *J Clin Diagn Res* 8(7):5–7, 2014.
210. Freedman J, Ganeshan A, Crowe PM: Pelvic congestion syndrome: the role of interventional radiology in the treatment of chronic pelvic pain. *Postgrad Med J* 86:704–710, 2010.
211. Belenky A, Bartal G, Atar E, et al: Ovarian varices in healthy female kidney donors: incidence, morbidity, and clinical outcome. *AJR Am J Roentgenol* 179(3):625–627, 2002.



212. Ganeshan A, Upponi S, Hon LQ, et al: Chronic pelvic pain due to pelvic congestion syndrome: the role of diagnostic and interventional radiology. *Cardiovasc Intervent Radiol* 30(6):1105–1111, 2007.
213. Pandey T, Shaikh R, Viswamitra S, Jambhekar K: Use of time resolved magnetic resonance imaging in the diagnosis of pelvic congestion syndrome. *J Magn Reson Imaging* 32:700–704, 2010.
214. Kim CY, Miller MJ, Merkle EM: Time resolved MR angiography as a useful sequence for assessment of ovarian vein reflux. *AJR Am J Roentgenol* 193(5):W458–W463, 2009.
215. Lopera J, Suri R, Kroma GM, et al: Role of interventional procedure in obstetrics/gynecology. *Radiol Clin North Am* 51(6):1049–1066, 2013.
216. Brown CE, Stettler RW, Twickler D, et al: Puerperal septic pelvic thrombophlebitis: incidence and response to heparin therapy. *Am J Obstet Gynecol* 181:143–148, 1999.
217. Twickler DM, Setiawan AT, Evans RS, et al: Imaging of puerperal septic thrombophlebitis: prospective comparison of MR imaging, CT and sonography. *AJR Am J Roentgenol* 169:1039–1043, 1997.
218. Baltarowich OH, Scoult LM, Hamper UM: Nongynecologic findings on pelvic ultrasound. Focus on gastrointestinal diseases. *Ultrasound Q* 28:65–85, 2012.
219. Ackerman SJ, Irshad A, Anis M: Ultrasound for pelvic pain II: nongynecologic causes. *Obstet Gynecol Clin North Am* 38:69–83, 2011.
220. Scoult L, Sawyers S, Bokhari J, et al: Ultrasound evaluation of the acute abdomen. *Ultrasound Clin* 2(3):493–523, 2007.
221. American College of Radiology: *ACR Appropriateness Criteria for Diagnostic Imaging: Right Lower Quadrant Pain—Suspected Appendicitis*. 2013. Available at <www.acr.org>.
222. Van Randen A, Bipat S, Zwinderman AH, et al: Acute appendicitis: meta-analysis of diagnostic performance of CT and graded compression US related to prevalence of disease. *Radiology* 249:97–106, 2008.
223. Coursey CA, Nelson RC, Patel MB, et al: Making the diagnosis of acute appendicitis: do more preoperative CT scans mean fewer negative appendectomies? A 10-year study. *Radiology* 254:460–468, 2010.
224. Blumenfeld YJ, Wong AE, Jafari A, et al: MR imaging in cases of antenatal suspected appendicitis—a meta-analysis. *J Matern Fetal Neonatal Med* 24(3):485–488, 2011.
225. Puylaert JB: Ultrasound of acute GI tract conditions. *Eur Radiol* 11(10):1867–1877, 2001.
226. Kessler N, Cyteval C, Gallix B, et al: Appendicitis: evaluation of sensitivity, specificity, and predictive values of US, Doppler US, and laboratory findings. *Radiology* 230:472–478, 2004.
227. Haider Z, Condous G, Ahmed S, et al: Transvaginal sonographic diagnosis of appendicitis in acute pelvic pain. *J Ultrasound Med* 25(9):1243–1244, 2006.
228. Carr NJ, McCarthy WF, Sobin LH: Epithelial noncarcinoid tumors and tumor-like lesions of the appendix. A clinicopathologic study of 184 patients with a multivariate analysis of prognostic factors. *Cancer* 75(3):757–768, 1995.
229. Higa E, Rosai J, Pizzimbono Ca, Wise L: Mucosal hyperplasia, mucinous cystadenoma, and mucinous cystadenocarcinoma of the appendix. A re-evaluation of appendiceal “mucocele.” *Cancer* 32:1525–1541, 1973.
230. Kalu E, Croucher C: Appendiceal mucocele; a rare differential diagnosis of a cystic right adnexal mass. *Arch Gynecol Obstet* 271:86–88, 2005.
231. Papoutsis D, Protopappas A, Belitsos P, et al: Mucocele of the vermiform appendix misdiagnosed as an adnexal mass on transvaginal sonography. *J Clin Ultrasound* 40:522–525, 2012.
232. Caspi B, Cassif E, Auslender R, et al: The onion skin sign: a specific sonographic marker of appendiceal mucocele. *J Ultrasound Med* 23:117, 2004.
233. Bennett GL, Tanpitukpongse TP, Macari M, et al: CT diagnosis of mucocele of the appendix in patient with acute appendicitis. *AJR Am J Roentgenol* 192:W103–W110, 2009.
234. Jacobs DO: Clinical practice: diverticulitis. *N Engl J Med* 357:2057–2066, 2007.
235. Heise CP: Epidemiology and pathogenesis of diverticular disease. *J Gastrointest Surg* 12:1309–1311, 2008.
236. Stollman N, Raskin JB: Diverticular disease of the colon. *Lancet* 363:631–639, 2004.
237. Stoker J, van Randen A, Laméris W, Boermeester M: Imaging patients with acute abdominal pain. *Radiology* 253:31–46, 2009.
238. Helou N, Abdalkader M, Abu-Rustum RS: Sonography: first-line modality in the diagnosis of acute colonic diverticulitis? *J Ultrasound Med* 32:1689–1694, 2013.
239. Laméris W, van Randen A, Bipat S, et al: Graded compression ultrasonography and computed tomography in acute colonic diverticulitis: meta-analysis of test accuracy. *Eur Radiol* 18:2498–2511, 2008.
240. Puylaert JB: Ultrasound of colon diverticulitis. *Dig Dis* 30(1):56–59, 2012.
241. Vijayaraghavan SB: High-resolution sonographic spectrum of diverticulosis, diverticulitis, and their complications. *J Ultrasound Med* 25:75–85, 2006.
242. Almeida AT, Melao L, Viamonte B, et al: Epiploic appendagitis: an entity frequently unknown to clinicians—diagnostic imaging, pitfalls, and look-alikes. *AJR Am J Roentgenol* 193(5):1243–1251, 2009.
243. Singh AJ, Gervais DA, Hahn PF, et al: Acute epiploic appendagitis and its mimics. *Radiographics* 25:1521–1534, 2005.
244. van Breda Vriesman AC, Lohle PN, Coerkamp EG, Puylaert JB: Infarction of omentum and epiploic appendage: diagnosis, epidemiology, and natural history. *Eur Radiol* 9(9):1886–1892, 1999.
245. Rioux M, Langis P: Primary epiploic appendagitis: clinical, US, and CT findings in 14 cases. *Radiology* 191:523–526, 1994.
246. Lee YC, Wang HP, Huang SP, et al: Gray-scale and color Doppler sonographic diagnosis of epiploic appendagitis. *J Clin Ultrasound* 29(3):197–199, 2001.
247. Danse EM, Van Beers BE, Baudrez V, et al: Epiploic appendagitis: color Doppler sonographic findings. *Eur Radiol* 11(2):183–186, 2001.
248. Kuzmich S, Howlett DC, Thust SC: Radiological features of Meckel’s diverticulum and its complications. *Clin Radiol* 64:849–850, 2009.
249. Elsayes KM, Menias CO, Harvin HJ, Francis IR: Imaging manifestations of Meckel’s diverticulum. *AJR Am J Roentgenol* 189:81–88, 2007.
250. Preminger GM, Tiselius HG, Assimos DG, et al: 2007 guideline for the management of ureteral calculi. *J Urol* 178(6):2418–2434, 2007.
251. Coll DM, Varanelli MJ, Smith RC: Relationship of spontaneous passage of ureteral calculi to stone size and location as revealed by unenhanced helical CT. *AJR Am J Roentgenol* 178(1):101–103, 2002.
252. American College of Radiology: *ACR Appropriateness Criteria for Diagnostic Imaging: Acute Onset Flank Pain—Suspicion of Stone Disease (Urolithiasis)*. 2015. Available at <www.acr.org>.
253. Smith RC, Rosenfield AT, Choe KA, et al: Acute flank pain: comparison of non-contrast-enhanced CT and intravenous urography. *Radiology* 194(3):789–794, 1995.
254. Miller OF, Rineer SK, Reichard SR, et al: Prospective comparison of unenhanced spiral computed tomography in the evaluation of acute flank pain. *Urology* 52:982–987, 1998.
255. Laing FC, Benson CB, DiSalvo DN, et al: Distal ureteral calculi: detection with vaginal US. *Radiology* 192(2):545–548, 1994.
256. Moore CL, Scoult L: Sonography first for acute flank pain? *J Ultrasound Med* 31(11):1703–1711, 2012.
257. Smith-Bindman R, Aubin C, Bailitz J, et al: Ultrasonography versus computed tomography for suspected nephrolithiasis. *N Engl J Med* 371(12):1100–1110, 2014.

# Ultrasound Evaluation of the Ovaries

*Douglas L. Brown, Darci J. Wall*

## SUMMARY OF KEY POINTS

- A simple cyst less than 3 cm in the ovary of a premenopausal patient is best termed a follicle and is a normal finding.
- A simple cyst less than 1 cm in the ovary of a postmenopausal patient is considered inconsequential.
- Most ovarian masses are benign and have a typical sonographic appearance that allows accurate diagnosis.
- Many simple and hemorrhagic cysts do not need sonographic follow-up in asymptomatic patients.
- Before diagnosing a simple ovarian cyst, it is important to search carefully for small nodules along the wall.
- A solid area with flow on Doppler imaging is the most important morphologic characteristic of an ovarian mass that raises concern for malignancy.
- The occasional indeterminate appearing ovarian mass can be managed variably by repeat sonography, magnetic resonance imaging (MRI), or surgical evaluation.

## OUTLINE

### Normal and Inconsequential Findings, 920

### Ovarian Cysts With Typical Benign Features, 920

Simple Cysts, 921

Hemorrhagic Cysts, 921

Endometriomas, 922

Mature Cystic Teratomas, 923

### Ovarian Cysts With Typical Malignant Features, 924

### Ovarian Cysts With Indeterminate Features, 925

### Solid Ovarian Masses, 926

### Pitfalls in Evaluating the Ovary, 928

### Ovarian Masses in Pregnancy, 929

### Syndromes and Diseases Associated With Ovarian

### Neoplasms, 929

### Summary, 930

Pelvic sonography, including transvaginal scanning, is the preferred initial imaging modality for evaluation of a suspected ovarian or other adnexal mass.<sup>1</sup> Its high sensitivity and specificity for ovarian malignancy, lack of ionizing radiation, relatively low cost, and wide availability make it an ideal method for evaluation of the ovary. In most patients, sonography is adequate to evaluate an ovarian mass. Scoring systems have been used to characterize ovarian and other adnexal masses sonographically, and they perform reasonably well. However, subjective assessment has been shown to perform as well or better than mathematical scoring systems.<sup>2</sup> Although accurate and timely identification of ovarian malignancy is extremely important, most adnexal masses are benign and most have a typical sonographic appearance. Thus, it is essential to recognize these common benign ovarian masses as frequently as possible and not mistake them for ovarian malignancy. Appropriate sonographic characterization of adnexal masses may help prevent unnecessary follow-up imaging along with its attendant patient anxiety and unnecessary surgery as well as its attendant risks. Detailed sonographic evaluation can prompt referral to gynecologic oncologists for management of adnexal masses that are likely to be malignant. When an adnexal mass has one of the classic benign appearances (to be discussed in this chapter), characterization is complete, although some may warrant sonographic follow-up. If a mass has characteristic malignant findings, imaging for characterization or diagnosis is also typically complete, though further evaluation for staging

may be needed. For masses with indeterminate sonographic findings, management will vary depending upon the clinical circumstances, but options would typically include follow-up sonography, MRI, or surgical evaluation. Standardized terminology<sup>3</sup> and reporting<sup>4</sup> have been suggested for ovarian masses; neither has been widely adopted at this time, but both may be further developed in the future.

In a small minority of patients, additional pelvic imaging with MRI may be helpful when ultrasound fails to clarify the origin of an adnexal mass, when the sonographic features are indeterminate, or when an adnexal mass is inadequately imaged with ultrasound (such as in an obese patient or in one who cannot undergo or declines transvaginal scanning).<sup>1</sup> Although computed tomography (CT) is helpful in staging of patients with known or suspected ovarian malignancy, it does not usually have a significant role in the characterization of adnexal masses.<sup>1</sup> CT may occasionally be helpful if a gastrointestinal origin of an adnexal mass is suspected or to search for a primary neoplasm when ovarian metastases are suspected. Positron emission tomography/CT has little, if any, role at this time in the primary evaluation of ovarian masses,<sup>1</sup> although it too may be helpful to search for a primary neoplasm if ovarian metastases are suspected.

In this chapter, we will review a few normal findings specific to the ovary, discuss sonographic features of benign and malignant ovarian masses, present an approach to assessing indeterminate ovarian masses, and review pitfalls in evaluation of the ovary. When appropriate, the



findings and recommendations of the Society of Radiologists in Ultrasound consensus conference on ovarian and other adnexal cysts have been included in this chapter.<sup>5</sup> Some aspects of ovarian disease will not be discussed or will be mentioned only briefly, as they are covered elsewhere in this text. Ovarian torsion is discussed in Chapter 29, nonovarian adnexal masses including tubo-ovarian abscess in Chapter 31, and polycystic ovary syndrome and ovarian hyperstimulation syndrome in Chapter 32.

## NORMAL AND INCONSEQUENTIAL FINDINGS

Although normal ovarian findings and ultrasound technique is more thoroughly discussed in Chapter 26, a few observations unique to the ovary bear additional mention here (Fig. 30-1). Ovarian follicles typically achieve a size of 2 to 3 cm before ovulation. Hence, simple (unilocular, thin-walled, anechoic) ovarian cysts less than 3 cm in greatest diameter in premenopausal women should generally be considered normal findings.<sup>5</sup> In order to prevent confusion with pathologic findings, it is best not to use the term “cyst” for normal ovarian structures and better to describe them as follicles or to simply report the ovary as normal.<sup>6,7</sup> Simple ovarian cysts less than 1 cm in greatest diameter may be present in postmenopausal women and have been reported in approximately 20% of women 5 or more years following menopause.<sup>8</sup> Hence, simple ovarian cysts less than 1 cm in maximal diameter in a postmenopausal woman generally require no follow-up and are considered inconsequential.<sup>5</sup> The corpus luteum, which typically appears as a thick-walled cystic lesion less than 3 cm in diameter with internal echoes and crenulated wall, should also be recognized as a normal finding in premenopausal women.<sup>5</sup> The wall of the corpus luteum may be quite vascular on Doppler interrogation.

Echogenic foci are a normal finding in many ovaries (Fig. 30-2). Tiny echogenic foci, measuring 1 to 3 mm in width, have no posterior shadowing (although comet-tail artifact may be seen) and may be due to psammomatous calcifications associated with epithelial inclusion cysts, hemosiderin deposition, or bright specular reflections off the back walls of tiny follicles.<sup>9-11</sup> These ovarian echogenic foci are found both in premenopausal and postmenopausal women.<sup>8</sup> They are generally of no significance and may occasionally be helpful in identifying an ovary. Larger echogenic foci in the ovary, usually from isolated calcifications, are also typically benign findings (Fig. 30-3). Echogenic foci 5 mm and larger, some of which may demonstrate posterior acoustic shadowing, seen in otherwise normal ovaries have been attributed to corpus albicans.<sup>12,13</sup> Some association between these foci and



**FIG 30-1** Diagram demonstrating a normal ovary with follicles in various stages of development, from early follicles in the follicular phase of development, through ovulation and subsequent development of the corpus luteum.

adenofibromas has been reported.<sup>14</sup> The pattern of calcifications within the ovary should be examined, as a more extensive peripheral rind of calcifications has been reported in a patient with endosalpinx and serous borderline ovarian neoplasms.<sup>15</sup> Larger coarse ovarian calcifications, in the absence of a mass, are generally benign and can be followed sonographically.<sup>12</sup> Anecdotal evidence suggests that patients with larger or more extensive calcifications in an otherwise normal-appearing ovary should receive additional evaluation or closer follow-up.

## OVARIAN CYSTS WITH TYPICAL BENIGN FEATURES

Ovarian lesions with classic features of simple cysts, hemorrhagic cysts, endometriomas, or dermoids are highly likely to be benign. It is important to recognize the characteristic sonographic features that, when seen, are highly predictive of these benign entities. Reliable characterization of ovarian masses using these sonographic features

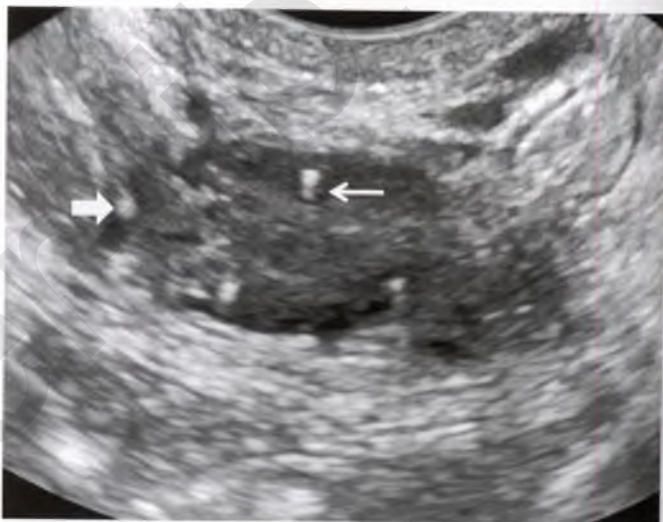


**FIG 30-2** Tiny echogenic foci in the ovary. A 53-year-old postmenopausal patient with several tiny peripheral echogenic foci in each ovary, some with associated comet-tail artifact (*thin arrow*) and some with no distal artifact (*thick arrow*).

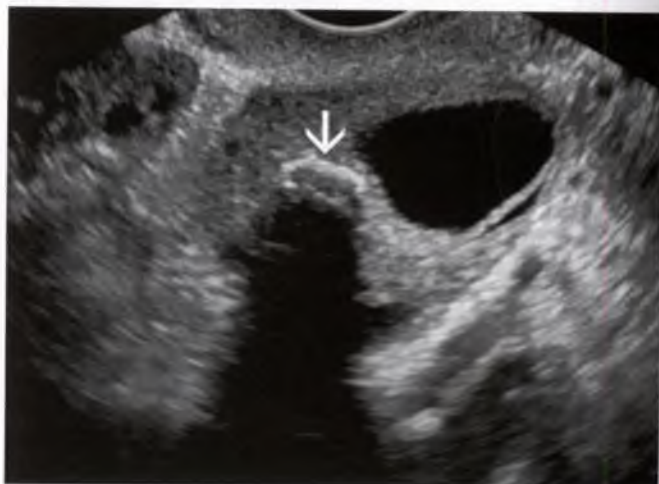


**FIG 30-3** Ovarian calcification. A 9-mm calcification (*arrow*), with posterior acoustic shadowing, is shown within an otherwise normal-appearing ovary. Such calcifications are generally of no clinical significance, but may be followed sonographically.



requires that the mass be fully and adequately visualized by ultrasound. Occasionally, in a patient with a suboptimal ultrasound examination, the interpreting physician will need to decide how to proceed based on available imaging findings and degree of clinical concern. When reporting on adnexal masses seen on pelvic sonograms, it is important to describe specific sonographic features (detailed later) that allow one to determine the likely diagnosis. Use of the word “complex” as a descriptor, with no additional explanation, is problematic as the “catch-all” term is often used for any cystic mass that is not a simple cyst. There are many features that may result in a “complex” sonographic appearance, including a typical reticular pattern suggesting benign hemorrhagic cyst and typical solid nodule worrisome for malignant ovarian carcinoma. Thus, if an ovarian cyst is reported as “complex,” further descriptors detailing those features making it complex should also be provided.<sup>6,7</sup>

### Simple Cysts

As with cysts elsewhere in the body, ovarian cysts with thin walls, anechoic internal contents, posterior acoustic enhancement, and no septations or solid components meet sonographic criteria for simple cysts (Fig. 30-4). Follicular or corpus luteal cysts and serous cystadenomas may appear as simple cysts by sonographic criteria. Simple ovarian cysts occur in 4% to 17% of postmenopausal women and the majority resolve or remain stable on follow-up ultrasound evaluation.<sup>16-21</sup> However, annual follow-up sonography for simple ovarian cysts larger than 1 cm (though some practices may choose to raise this threshold to 3 cm) is recommended in postmenopausal women.<sup>5</sup> In premenopausal women, it is recommended that cysts between 5 and 7 cm in largest diameter be followed yearly by ultrasound examination. The vast majority of simple ovarian cysts are benign.<sup>22-24</sup> With increasing cyst size, however, there is a risk of inadequate assessment of the cyst wall for detection of small solid nodules or papillary formations,<sup>22</sup> which, if present, increase the likelihood of malignancy. The rare occurrence of malignancy in an apparent simple ovarian cyst is more likely in larger cysts, in which small mural nodules may be overlooked.<sup>22</sup> Hence, when evaluating what appears to be a simple cyst, it is important to confirm that the cyst is adequately imaged in its entirety and to carefully assess for small nodules before concluding that it is indeed a simple cyst. Simple cysts measuring larger than 7 cm are still likely benign, though one should consider further imaging evaluation

with MRI to confirm that there is no solid component overlooked by sonography.<sup>5</sup>

### Hemorrhagic Cysts

Fibrin strands and retracting clot are highly specific features of hemorrhagic ovarian cysts (Fig. 30-5).<sup>5,25,26</sup> The fibrin strands are often described as lacy, reticular, fishnet, cobweb, spider web, or sponge-like in appearance.<sup>26,27</sup> Although retractile clot might be confused with a solid mural nodule, it will have no detectable flow by Doppler imaging and typically has scalloped, concave, or straight margins. These features can help differentiate retracting subacute clot from malignant solid tissue, which is usually more round or lobular in configuration and often has demonstrable flow on targeted Doppler imaging.<sup>26,28</sup> Cystic ovarian lesions without detectable internal flow on Doppler imaging and with either the fibrin strand or retractile clot pattern of internal echoes very likely represent hemorrhagic cysts, and typically

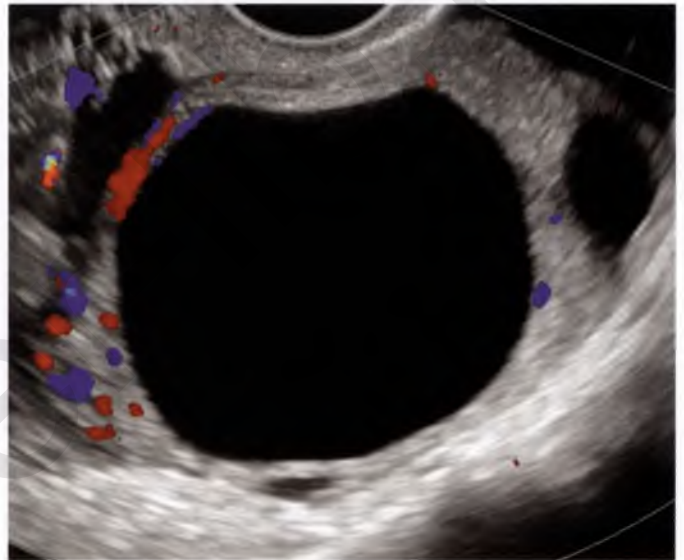


**FIG 30-4** Simple ovarian cyst. Color Doppler ultrasound image of a simple ovarian cyst demonstrates the characteristic findings of anechoic contents, smooth thin wall, no internal vascularity, and posterior acoustic enhancement.

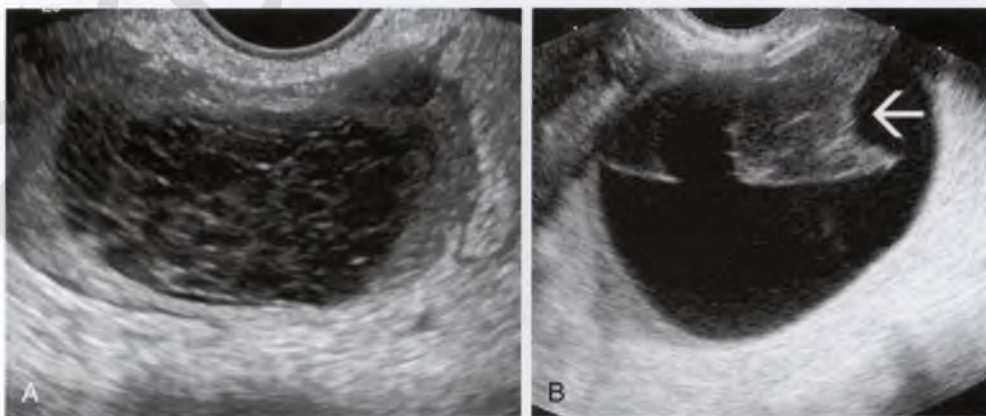


**FIG 30-5** Hemorrhagic ovarian cysts. **A**, This hemorrhagic cyst has a “fishnet” or reticular lace-like pattern of internal echoes due to fibrin strands. Fibrin strands typically appear as thin linear or curvilinear echoes that do not extend across the span of the cyst but appear discontinuous. True internal septations usually course from wall to wall across the cyst. **B**, A hemorrhagic cyst from another patient has a solid-appearing area with a concave margin (*arrow*) due to retractile clot. Color Doppler imaging (not shown) demonstrated no flow in the clot.



resolve within 8 weeks.<sup>27</sup> Such sonographically typical hemorrhagic cysts less than 5 cm in maximal diameter do not generally need follow-up sonography in asymptomatic premenopausal patients.<sup>5</sup> However, sonographically typical hemorrhagic cysts larger than 5 cm, suspected hemorrhagic cysts with atypical morphologic features, and hemorrhagic cysts in perimenopausal or early postmenopausal (1 to 5 years after final menstrual period) women should be reevaluated by follow-up ultrasound evaluation in 6 to 12 weeks to ensure resolution or decrease in size.<sup>5</sup> Women in late postmenopause (greater than 5 years since final menstrual period) would not be expected to develop hemorrhagic ovarian cysts. It is unlikely that one would suspect a hemorrhagic ovarian cyst based on ultrasound criteria in late postmenopause, but if this were to occur, one should consider the possibility of neoplasm and recommend further evaluation with MRI or surgical consultation.<sup>5</sup>

Hemorrhagic ovarian cysts may contain solid-appearing areas due to clot with concave or straight margins and lack of detectable flow by careful Doppler interrogation. There are occasional problematic cases in which apparently solid areas without detectable flow have outwardly convex margins and thus may simulate solid mural neoplastic nodules. Gentle pressure on the cyst with the transvaginal transducer is sometimes helpful, as an intracyst clot may show jiggling or jelly-like motion with this maneuver.<sup>26</sup> If the diagnosis remains uncertain, follow-up ultrasound imaging is often helpful in distinguishing a hemorrhagic cyst (with interval resolution of clot) from an ovarian neoplasm (with persistence, enlargement, or apparent development of internal blood flow). Occasionally a hemorrhagic cyst may simulate a solid lesion with a sonographic appearance of diffuse heterogeneous internal echoes (Fig. 30-6), typically encountered in an acute or subacute stage, before fibrin strands develop.<sup>6,29</sup> Lack of detectable flow by Doppler imaging (using settings optimized to detect low-volume, low-velocity flow) within the apparently solid component, posterior acoustic enhancement, and awareness of this entity in premenopausal women can suggest this possibility. Resolution on follow-up ultrasound examination would confirm the diagnosis of self-limiting hemorrhagic cyst.

The most significant potential complication of a hemorrhagic ovarian cyst is rupture with hemoperitoneum. A ruptured hemorrhagic cyst may be difficult to distinguish from a ruptured ectopic pregnancy, thus necessitating correlation with serum human chorionic

gonadotropin (hCG) level.<sup>30,31</sup> A ruptured ectopic pregnancy typically requires operative management, whereas a ruptured hemorrhagic ovarian cyst can usually be managed expectantly in hemodynamically stable patients.<sup>32-34</sup>

### Endometriomas

Endometriosis occurs when there is endometrial tissue outside the uterus. Most cases are reported in women of childbearing age and a 10-fold increase in prevalence has been reported in patients with an affected first-degree relative.<sup>35</sup> Although some may be asymptomatic, patients most commonly present with pain, which may be cyclic, correlating with their menstrual cycle, or infertility. Some patients with endometriosis will form cysts, termed endometriomas, which are found in up to 44% of women with endometriosis.<sup>36</sup> Most endometriomas are located within the ovary.<sup>37-39</sup> The pathogenesis of intra-ovarian endometriomas may be different than that of endometriosis that occurs as superficial peritoneal implants.<sup>40</sup> Endometriomas are usually readily detectable by ultrasound. Cystic lesions with diffuse low-level internal echoes, sometimes described as “ground glass,” are characteristic, with 95% of endometriomas having this appearance (Fig. 30-7).<sup>26,35,41</sup> Multilocularity and echogenic foci in the wall have been reported to increase the likelihood that a lesion represents an endometrioma<sup>35</sup>; however, neither is required for the diagnosis. In our experience, it is uncommon for endometriomas to be multilocular though there may be multiple adjacent endometriomas that could be difficult to distinguish from multilocularity. Lack of acoustic streaming (movement of echoes inside the cyst during gray-scale or Doppler ultrasound imaging) was initially thought to be predictive of an endometrioma, but subsequent studies have not found absence of acoustic streaming to be reliable for this diagnosis.<sup>42</sup>

Surgical removal is considered for symptomatic endometriomas, for those causing pain and infertility, as well as for those in which malignancy is suspected. Fertility does not always improve following cystectomy, however, as surgery can reduce the number of viable ovarian follicles.<sup>43</sup> Malignancy, typically clear cell carcinoma and less often endometrioid adenocarcinoma, should be suspected in endometriomas that develop solid mural nodules or that rapidly increase in size.<sup>44</sup> MRI can be helpful in assessing endometriomas for enhancing mural nodules and for restricted diffusion in those suspected of

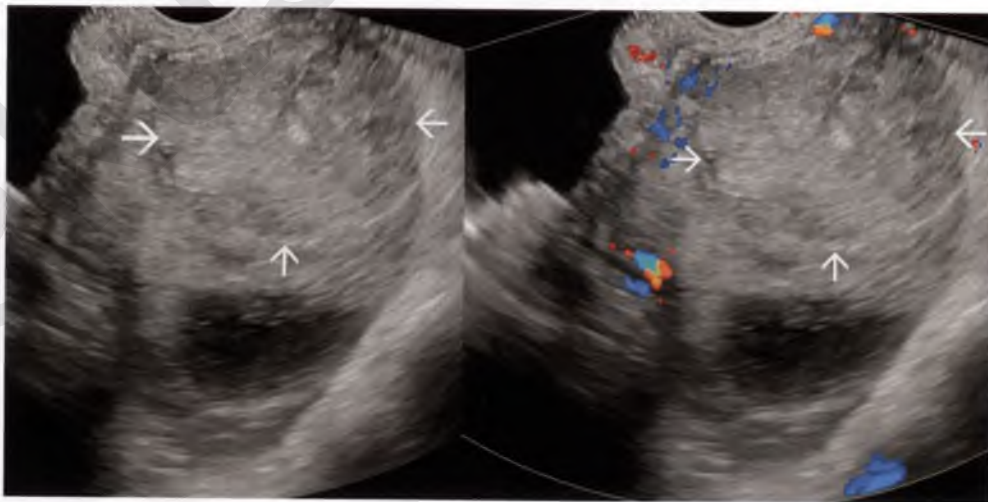


**FIG 30-6** Subacute hemorrhagic ovarian cyst simulating a solid ovarian mass. Dual screen image without and with color Doppler interrogation shows a heterogeneous, predominantly isoechoic, solid-appearing mass (between arrows) within the left ovary of a 41-year-old woman who presented with pelvic pain. Color Doppler imaging (right) shows flow around the periphery of the mass but no flow within it. This lesion resolved on follow-up ultrasound examination.



undergoing malignant transformation.<sup>45</sup> Asymptomatic lesions with typical sonographic appearance of endometriomas can be followed annually with ultrasound.<sup>5</sup>

Given that the sonographic appearance of endometriomas and hemorrhagic cysts occasionally overlap, follow-up sonogram, typically in 6 to 12 weeks, is suggested, particularly if surgical removal of a presumed endometrioma is planned.<sup>5</sup> If the lesion is a hemorrhagic cyst, it will resolve or change on follow-up study. Endometriomas in postmenopausal women may differ in appearance from the typical homogeneous echotexture seen in premenopausal women and may be more heterogeneous with echogenic foci centrally.<sup>46</sup> A small number of endometriomas may contain a small solid-appearing area on ultrasound imaging, and, therefore, it can be difficult to distinguish these endometriomas from malignant lesions.<sup>6,40,41,46,47</sup> Doppler sonographic imaging



**FIG 30-7** Endometrioma. This endometrioma has the classic appearance of a cystic mass with homogeneous low-level internal echoes, sometimes referred to as a “ground glass” appearance. Note posterior acoustic enhancement, suggesting that this is a cystic rather than a solid lesion. There was no internal flow demonstrated by color Doppler imaging (not shown).

is suggested, although it may not resolve the diagnosis as the solid area may be due to focal endometrial tissue with internal blood flow. In such cases, additional evaluation with MRI should be considered.

### Mature Cystic Teratomas

Mature cystic teratomas of the ovary, also termed dermoids, account for up to 20% of ovarian neoplasms. These benign germ cell tumors are composed of at least two of the three germ cell layers (ectoderm, mesoderm, and endoderm). Dermoids are estimated to account for up to 20% of all ovarian tumors found in adult women and are bilateral in 15% to 25% of cases. Most dermoids are asymptomatic and are incidentally detected. However, dermoids may present with symptoms related to large size resulting in compression of adjacent structures. Torsion or rupture of a dermoid may cause significant pain. Several characteristic sonographic appearances have been described, including focal or diffuse hyperechoic component; areas of acoustic shadowing, also known as the “tip of the iceberg” sign; and echogenic lines and dots, also referred to as dermoid “mesh” or “dot-dash” sign. Any combination of these classic sonographic features allows a confident diagnosis of a dermoid (Fig. 30-8).<sup>5,48-54</sup> The hyperechoic component, termed a Rokitansky nodule, typically corresponds to mixed hair and sebaceous material or occasionally to calcification, sometimes related to a bone or tooth.<sup>48,54</sup> The echogenic lines and dots represent hair in fluid.<sup>48,54</sup> Fluid-fluid levels may occur in dermoids but are seen infrequently.<sup>49,53</sup> A dermoid can be confidently suggested if the nondependent fluid is hyperechoic (indicating fat). However, teratomas can display nondependent hypoechoic fluid and thus be difficult to distinguish from other cystic lesions with fluid-fluid levels.<sup>55,56</sup> In such cases, it is important to look for other sonographic features suggesting a dermoid. Floating echogenic globules within a large mass is an uncommon appearance but is reported to be highly predictive of a dermoid.<sup>54,57</sup> Calcifications can occur in dermoids, but calcification alone is not enough to make the definitive diagnosis.<sup>6</sup>

Dermoids can increase in size but tend to do so slowly, with a mean growth rate of 1.8 mm per year in premenopausal women.<sup>58</sup> A serious potential complication of mature cystic teratomas is malignancy—occurring in up to 2% of teratomas, 80% of which are squamous cell carcinoma.<sup>59-63</sup> Additional potential complications include hyperthyroidism resulting from teratomas containing a large amount of thyroid tissue<sup>64</sup>; chemical peritonitis following spontaneous or iatrogenic

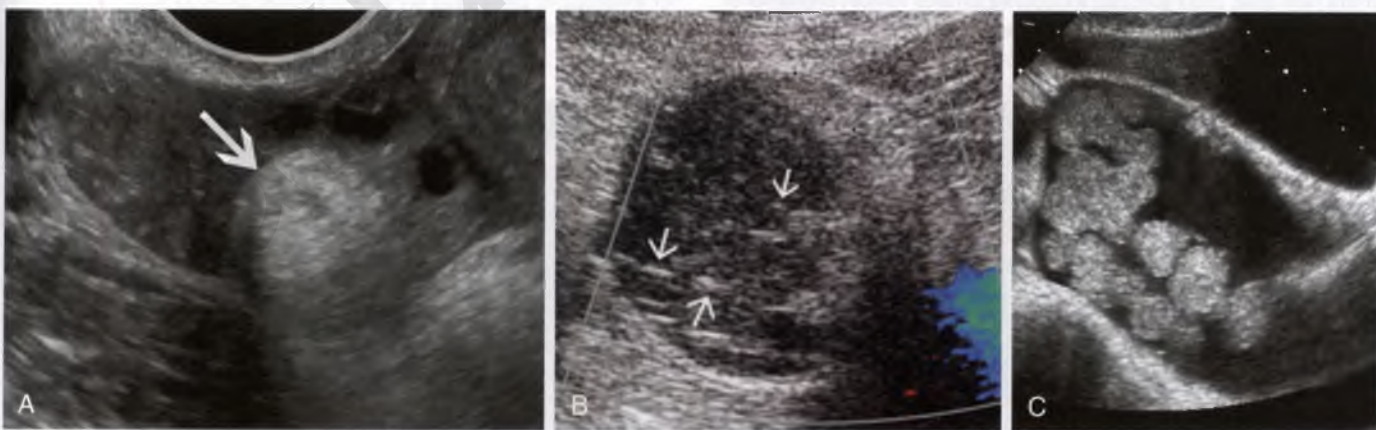


**FIG 30-8** Ovarian dermoids. **A**, This dermoid (arrow) is diffusely hyperechoic. There is adjacent hypoechoic ovarian parenchyma. **B**, Dermoid with hyperechoic lines and dots (some indicated by arrows), also known as dermoid mesh appearance. This morphologic appearance is usually due to the presence of hair within the lesion. This dermoid also has a hyperechoic peripheral component. **C**, Uncommon but pathognomonic appearance of a dermoid containing several spherical structures, some of which are nondependent, thought to represent floating fat balls. These spherical structures contain fat, which allows them to float.



dermoid rupture<sup>65</sup>; and ovarian torsion. Torsion has been reported in 3.5% of dermoids and is more common with larger lesions.<sup>60</sup> Given the possibility of malignant transformation and of interval growth, which could increase the risk of ovarian torsion, annual sonographic follow-up of dermoids should be considered.<sup>5</sup> The reliability of ultrasound in identifying malignant transformation of dermoids is not well established. Features suggestive of malignant transformation include isoechoic branching structures,<sup>66</sup> demonstration of central flow within the mass by Doppler imaging,<sup>67,68</sup> or findings of metastatic disease.

## OVARIAN CYSTS WITH TYPICAL MALIGNANT FEATURES

Ovarian neoplasms, both benign and malignant, are usually classified into one of four general histologic groups: epithelial, sex cord–stromal, germ cell, or metastatic neoplasms.<sup>16,69</sup> There are also borderline epithelial neoplasms that are usually considered malignant, though they confer a better prognosis than frankly malignant lesions, even if peritoneal spread is noted at the time of diagnosis.<sup>16</sup> Borderline tumors tend to occur in younger women. Most ovarian malignancies are epithelial neoplasms and demonstrate a mixture of cystic and solid components. Epithelial neoplasms include several histologic types, including serous, mucinous, endometrioid, and clear cell cystadenocarcinomas. The serous and mucinous forms also have benign counterparts, namely serous and mucinous cystadenomas. There is recent evidence that some epithelial ovarian carcinomas actually arise from the fallopian tube.<sup>70-73</sup> Most ovarian cystadenomas do not undergo malignant degeneration into carcinoma or, if transformation does occur, it is usually into a borderline neoplasm or low-grade malignancy and the rate of transformation is exceedingly slow.<sup>5</sup> Recent studies suggest there may be two types of epithelial ovarian carcinomas. Type I tumors are low-grade neoplasms that present at an early stage with an indolent course and are believed to arise from precursor lesions in the ovary, such as cortical inclusion cysts lined by tubal epithelia (perhaps incorporated into the cyst during ovulation), serous cystadenomas, borderline neoplasms, or endometriosis. Type II tumors are highly aggressive malignancies that present with advanced stage at diagnosis and likely originate from precursors arising in the fimbriated segment of the fallopian tube epithelium.<sup>73-75</sup> Current molecular and genetic research suggests that inactivating mutations of the tumor suppressor gene *TP53* give rise to “p53 signatures” (short segments of fallopian tube epithelium that overexpress p53, a tumor suppressor

protein) in the fimbriated portion of the fallopian tube, which may ultimately transform into serous tubal intraepithelial cancers (STICs). It is now believed that STICs are the likely precursors of all pelvic extrauterine high-grade serous carcinomas either in the fallopian tube or following implantation onto the ovary or peritoneal surfaces.<sup>70-75</sup> *TP53* mutations have been reported in over 90% of high-grade serous carcinomas and *BRCA1/BRCA2* mutations (also tumor suppressor genes that help repair DNA damage) have been found in up to 50% of high-grade serous carcinomas.<sup>75</sup>

Sex cord–stromal neoplasms tend to present as solid ovarian masses<sup>69</sup> but can sometimes have a mixed cystic and solid appearance, especially when large. Germ cell neoplasms and metastatic neoplasms vary in sonographic appearance, some being solid and some mixed cystic and solid. Some specific ovarian neoplasms such as fibromas (the most common sex cord–stromal neoplasm),<sup>76</sup> dysgerminomas (the most common malignant germ cell neoplasm),<sup>77</sup> and many metastases, such as from breast carcinoma,<sup>78</sup> are typically solid masses.

The presence of a solid component, with detectable flow by Doppler imaging, within a cystic ovarian mass is the most important sonographic feature for predicting ovarian malignancy.<sup>5,79</sup> There is also evidence that the larger the solid component within a cystic mass, the higher the risk of malignancy.<sup>80</sup> A small soft tissue component is more typical of borderline or stage I ovarian carcinoma than of advanced ovarian carcinoma.<sup>81</sup> Apart from the characteristic hyperechoic tissue typical of dermoids, the presence of solid nodules (sometimes referred to as papillary projections, excrescences, or vegetations) or more confluent solid tissue with blood flow detected by Doppler imaging is highly likely to indicate malignancy (Figs. 30-9 through 30-11). However, solid components are not a specific finding for ovarian malignancy, as solid mural nodules can be seen in benign cystadenomas and cystadenofibromas. The absence of a solid component makes ovarian malignancy unlikely.<sup>5,6,79</sup> Focal wall thickening in a cystic mass is another sonographic feature worrisome for malignancy.<sup>5</sup>

Irregular or thick (generally defined as >3 mm) septations are also concerning for malignancy, though they are less predictive than solid components.<sup>5</sup> A cystic mass with thin septations and no solid component or a cystic mass with a solid component that has no detectable flow by Doppler imaging (Figs. 30-12 and 30-13) is likely to be a benign ovarian neoplasm, such as a cystadenoma or cystadenofibroma.<sup>5,82</sup> Additional findings of ascites (more than the trace physiologic amount common in premenopausal women), peritoneal implants (Fig. 30-14), or evidence of metastasis are all worrisome findings suggesting malignancy<sup>79</sup> but are not required to prompt suspicion of ovarian cancer.

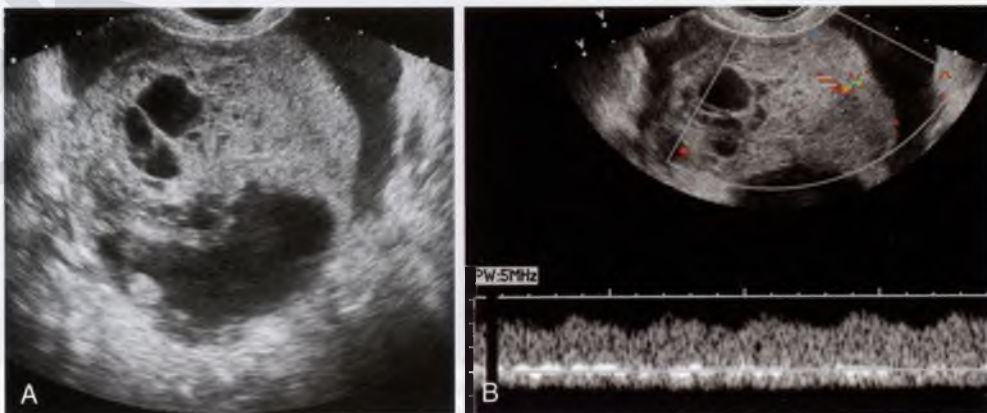


**FIG 30-9** Clear cell cystadenocarcinoma of the ovary. **A**, Mixed cystic and solid mass with a relatively large solid component. **B**, Color and spectral Doppler imaging confirm flow within the solid component of the mass.



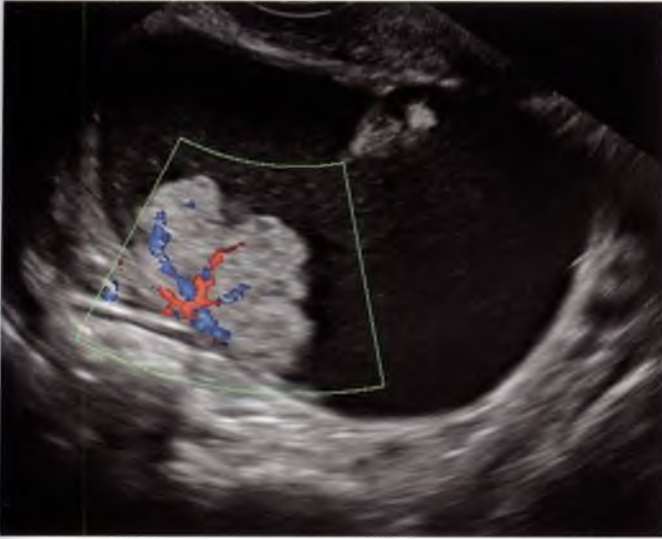


**FIG 30-10** Borderline mucinous neoplasm. The predominantly cystic ovarian mass contains an irregular solid mural nodule that demonstrates internal flow on color Doppler interrogation.

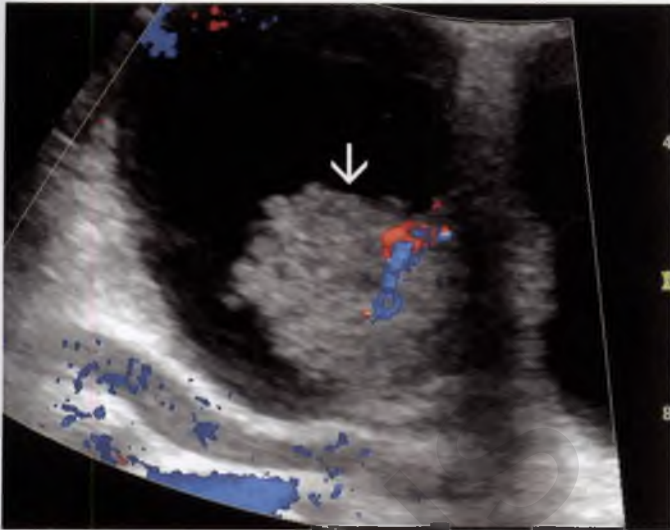


**FIG 30-11** Serous cystadenocarcinoma of the ovary. This predominantly cystic mass contains a solid nodular area (arrow) with irregular margins and flow shown by color Doppler sonography. (Courtesy of Kika Dudiak, MD, Rochester, MN.)

## OVARIAN CYSTS WITH INDETERMINATE FEATURES

The majority of ovarian masses found by sonography are benign, and most demonstrate one of the typical reassuring sonographic patterns discussed earlier. A minority of ovarian masses will be malignant and display characteristic worrisome features. Infrequently, one may encounter an ovarian mass with sonographic morphologic features not characteristic of either a benign or malignant lesion, and, thus, it cannot be definitively diagnosed by ultrasound (i.e., an indeterminate mass). In surgical series, such indeterminate masses have been reported in fewer than 10% of patients.<sup>80,81</sup> The frequency of persistent indeterminate masses in clinical practice is likely less, given that many cystic ovarian lesions resolve spontaneously. The histologic diagnoses of ovarian lesions that tend to be classified as indeterminate masses by sonographic criteria include borderline neoplasms, serous and



**FIG 30-12** Mucinous cystadenoma. This multiloculated cystic mass contains multiple septations with fluid of varying degrees of echogenicity in the locules. This appearance, although not diagnostic, is typical of mucinous cystadenoma.

mucinous cystadenomas/cystadenofibromas, fibromas, and pedunculated uterine leiomyomas.<sup>80,81</sup> There are rare ovarian neoplasms, such as struma ovarii, yolk sac tumors, and others that do not demonstrate characteristic, easily categorized sonographic features.<sup>77,81</sup> At times, laboratory findings such as elevated alpha-fetoprotein level associated with yolk sac tumor or elevated hCG level associated with nongestational ovarian choriocarcinoma may be helpful.<sup>78</sup> The sonographic features more frequently encountered in indeterminate lesions include large mass size, multiple septations, and solid nodules that are small or few in number.<sup>80</sup> For such indeterminate masses, one needs to decide between sonographic follow-up, further assessment with MRI, or surgical evaluation, influenced by the degree of concern based on imaging and clinical findings.<sup>5</sup>

Ovarian cysts that appear unilocular, thin-walled, and anechoic except for a single thin septation or a small calcification in the wall are probably benign and can be followed in a manner similar to that for simple cysts.<sup>5</sup> Cysts that have features suggestive of, but not quite classic for, hemorrhagic cyst, endometrioma, or dermoid can be followed sonographically in 6 to 12 weeks in premenopausal patients.<sup>5</sup> Resolution within this time frame on follow-up ultrasound usually confirms hemorrhagic cyst, whereas lack of change generally excludes a self-limiting lesion such as hemorrhagic cyst.<sup>5</sup> Patients with persistence of such a cyst may benefit from additional imaging with MRI or surgical evaluation.<sup>5</sup>

Ovarian cysts with multiple thin (<3 mm) septations or seemingly solid components, but without detectable flow by color Doppler imaging, are also considered indeterminate masses.<sup>5</sup> Many of them represent benign neoplasms such as serous or mucinous cystadenomas/cystadenofibromas (see Fig. 30-12). Clot within a hemorrhagic cyst can occasionally simulate a solid component in a neoplasm, and, therefore, one should consider a follow-up sonogram in premenopausal patients with this finding, particularly when no flow is detected in the solid-appearing area by targeted Doppler interrogation. Otherwise, patients with such lesions should generally undergo additional imaging with MRI or surgical evaluation.<sup>5</sup> Collision tumors (two adjacent but histologically distinct tumors in the same ovary) can be problematic to recognize and diagnose by ultrasound, but are uncommon. Dermoid and cystadenoma are reported to be the most frequent combination of ovarian collision tumors.<sup>83,84</sup>



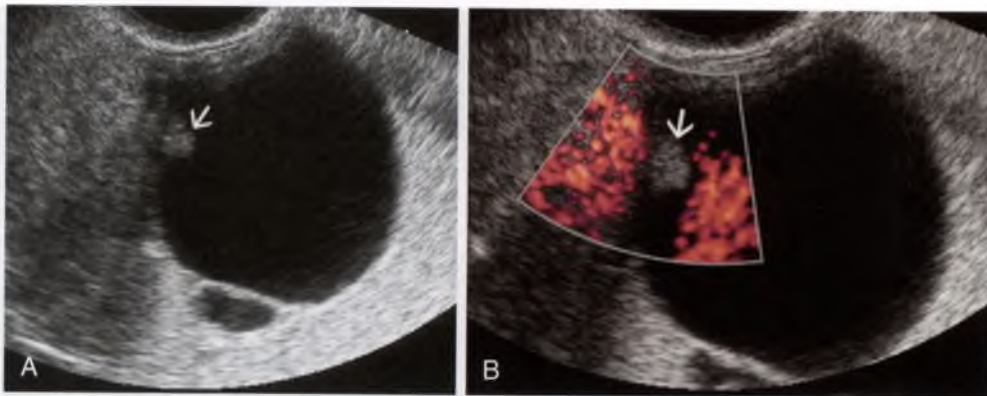


**FIG 30-13** Serous cystadenofibroma. **A**, This predominantly cystic mass contains a small peripheral solid nodule (arrow). **B**, Power Doppler imaging shows no detectable flow in the small solid nodule (arrow). Color pixels in the anechoic fluid of the cystic mass are due to motion artifact.



**FIG 30-14** Peritoneal implants. Sagittal transvaginal ultrasound image demonstrates ascites and confluent solid peritoneal nodules (arrows) in the posterior cul-de-sac. This patient had metastatic serous cystadenocarcinoma of the ovary.

## SOLID OVARIAN MASSES

Solid ovarian masses may be problematic to interpret. Some studies reporting that solid ovarian masses are associated with malignancy have included predominantly solid lesions, defining “solid” as those with up to 20% cystic component.<sup>3,85</sup> The reproducibility of classifying a mass with up to 20% cystic component is not clear, as the authors used a subjective assessment based on two-dimensional images.<sup>3</sup> Other investigators report that the majority of solid adnexal masses are benign, particularly if one considers ovarian lesions that are completely solid and includes the common occurrence of pedunculated uterine leiomyomas simulating solid ovarian masses (in those cases when the ipsilateral ovary is not identified).<sup>6,86,87</sup> Use of color or power Doppler imaging to demonstrate a vascular connection to the uterus can help prevent mistaking a pedunculated leiomyoma for a solid ovarian mass.<sup>88,89</sup> If that is not helpful, MRI is often useful for evaluating a solid adnexal mass of unclear origin.<sup>90</sup> Patients with solid adnexal masses that cannot be confirmed to be pedunculated uterine leiomyomas by means of sonography or MRI will generally need surgical consultation.

When a solid ovarian mass is seen, a sex cord–stromal tumor should be considered. Fibromas or fibrothecomas are the most commonly encountered type and usually occur in women aged 40 to 50 years old.<sup>76</sup> Ovarian fibromas or fibrothecomas typically appear as hypoechoic solid masses,<sup>76</sup> sometimes homogeneous and sometimes heterogeneous (Fig. 30-15). On occasion, they may demonstrate marked posterior acoustic shadowing, which is strongly suggestive of this diagnosis.<sup>91</sup> Other sex cord–stromal tumors, such as granulosa cell tumors and Sertoli-Leydig cell tumors, vary in appearance, some being completely solid and some with variable cystic components.<sup>90,92-94</sup> Of all ovarian masses, sex cord–stromal tumors are most commonly associated with hormone secretion. Granulosa cell tumors most commonly secrete estrogen, and Sertoli-Leydig cell tumors most commonly secrete androgens. Inhibin B levels are often elevated in patients with granulosa cell tumors and may be useful for reaching the diagnosis and for follow-up surveillance after surgery.<sup>95</sup> Patients with estrogen-secreting granulosa cell (or other) neoplasms may demonstrate associated findings due to hormonal effect, such as endometrial thickening or other endometrial abnormalities. Several published reports provide more detailed review of sex cord–stromal tumors.<sup>76,90,92-94</sup>

Most tumors in the surface epithelial group demonstrate cystic components, with variable amounts of solid tissue. Malignant epithelial tumors are infrequently completely solid.<sup>96</sup> Brenner tumors (also known as transitional cell tumors)<sup>97</sup> are uncommon surface epithelial tumors that often differ in appearance from other epithelial tumors; most are solid, and internal calcifications have been described.<sup>98,99</sup> The vast majority of Brenner tumors are benign.<sup>97</sup>

Of the germ cell neoplasms, dermoids are by far the most common type and have been discussed previously. Dermoids may infrequently be mistaken for solid ovarian tumors, but the majority demonstrate a cystic component. Malignant teratomas are rare and usually have a mixed cystic and solid appearance.<sup>90</sup> Most malignant teratomas are primary tumors occurring in young patients, usually younger than 20 years of age.<sup>77</sup> Malignant transformation (most commonly to squamous cell carcinoma) of a mature cystic teratoma is rare, usually occurring in patients older than 45 years of age, in masses larger than 10 cm, and often associated with elevated squamous carcinoma antigen levels.<sup>68,77</sup> It is unclear which sonographic features best predict malignant transformation of a teratoma. Isoechoic branching structures within the mass,<sup>66</sup> evidence of adjacent extension, and Doppler depiction of flow centrally<sup>67</sup> have been reported as features concerning for malignancy.<sup>5</sup> If one encounters a lobulated solid ovarian mass in a 20- to 30-year-old woman (Fig. 30-16), dysgerminoma should be



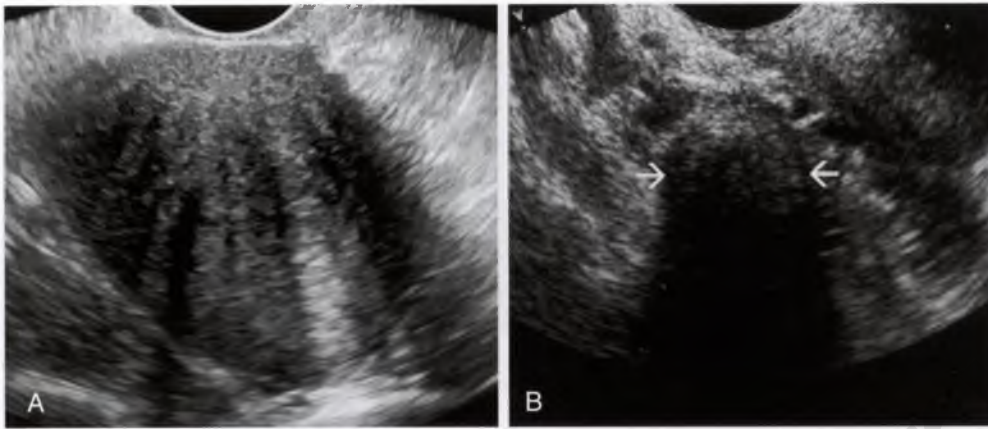


**FIG 30-15** Ovarian fibroma. **A**, This fibroma appears as a slightly heterogeneous, completely solid mass. **B**, This fibroma, from a different patient, appears as a hypoechoic markedly attenuating solid mass (*arrows*). The marked sound attenuation strongly suggests the diagnosis of fibroma. Unlike acoustic shadowing posterior to a calcification or dermoid, there is no echogenic focus or bright reflector at the leading edge of a fibroma.

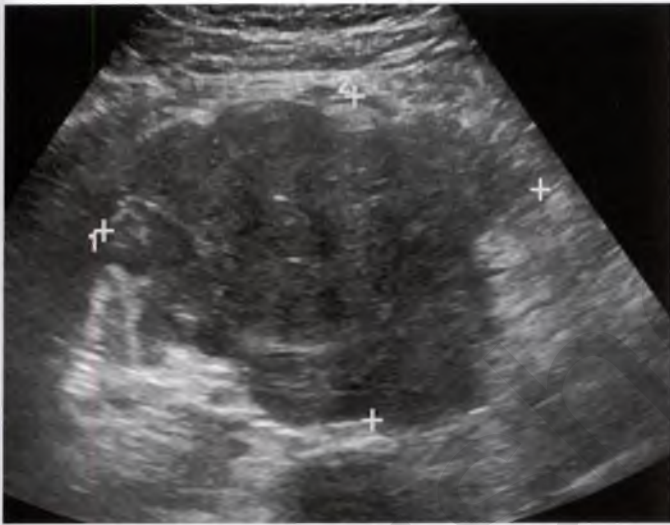


**FIG 30-16** Ovarian dysgerminoma. Completely solid ovarian mass (*calipers*), with an irregular lobulated external contour, seen in a 20-year-old woman. The combination of sonographic appearance and patient age is suggestive of this diagnosis.

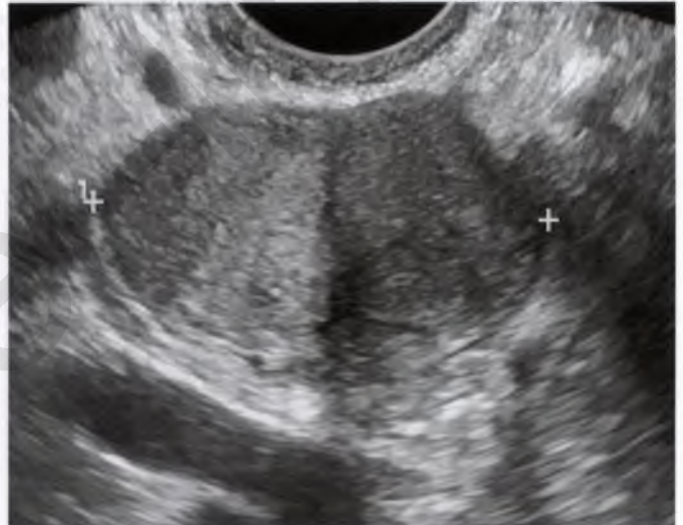


**FIG 30-17** Metastasis to the ovary. This completely solid heterogeneous ovarian mass (*calipers*) was found to be metastasis from a pancreatic neuroendocrine tumor.

strongly considered.<sup>100</sup> It is the most common malignant germ cell neoplasm.<sup>77</sup>

Metastases to the ovary (Fig. 30-17) may occur with various primary malignancies but most commonly are related to breast, colon, or gastric carcinomas.<sup>78,101,102</sup> The finding of bilateral solid ovarian masses is worrisome, though not definitive, for metastases. It is often difficult to distinguish primary ovarian malignancy from metastasis to the ovary.<sup>101</sup> Metastases from breast carcinoma are usually solid masses<sup>78,102</sup> and typically occur only with advanced stage disease.<sup>16</sup> Some authors have found metastases from gastric carcinoma also to be predominantly solid, but this has not been observed by others.<sup>78,102</sup> Metastases from colorectal carcinoma tend to be multiseptated and larger than metastases from other primary tumors.<sup>102</sup> Bilateral ovarian masses are reported to occur most commonly with metastases from gastric carcinoma, compared with other primary tumors.<sup>78</sup>

When evaluating a solid adnexal mass, one needs to consider several possibilities, particularly given that a patient with a solid mass of ovarian origin usually needs surgical evaluation.<sup>86</sup> Many solid masses

of ovarian origin, particularly those occurring in 40- to 50-year-old women, are fibromas or fibrothecomas. These benign ovarian neoplasms are typically treated surgically, in part to confirm the diagnosis. The differential diagnosis for a solid-appearing adnexal mass would include pedunculated uterine leiomyoma, acute or subacute hemorrhagic ovarian cyst (see Fig. 30-6) in which echogenic blood simulates solid tissue (considering this possibility in a premenopausal patient and prompting a short interval follow-up sonogram will usually confirm the diagnosis), and chronic endometrioma in which the degree of internal echogenicity simulates a solid mass (MRI may help confirm the diagnosis of endometrioma in this instance). A pedunculated uterine leiomyoma is the lesion most likely to simulate a solid ovarian mass, and this distinction is most problematic when the ipsilateral ovary is not identified. In such cases, color or power Doppler sonographic evaluation should be used to search for bridging vessels arising from the uterus; if seen, this finding can help confirm pedunculated leiomyomas.<sup>88,89</sup> If the diagnosis of pedunculated uterine leiomyomas cannot be reliably determined by ultrasound, then MRI is



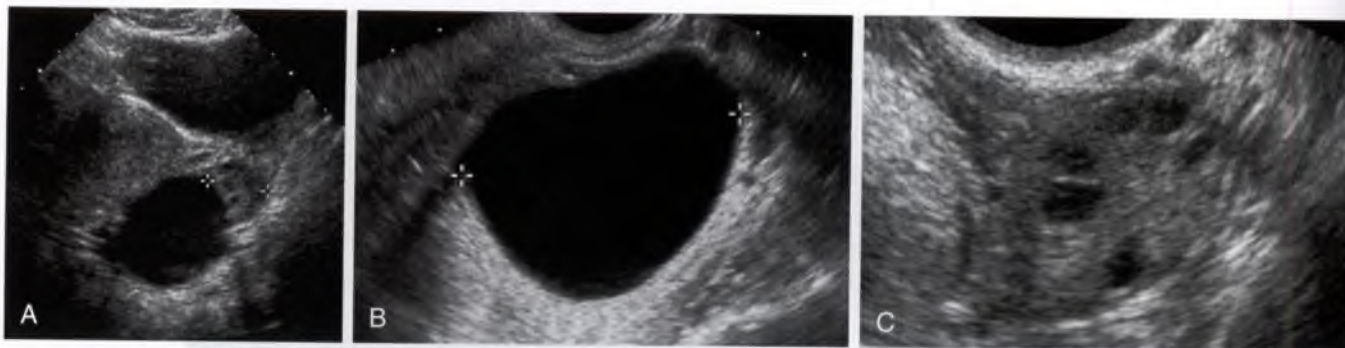


**FIG 30-18** **A**, Transabdominal image of a paraovarian cyst that could be mistaken as arising from the ovary. **B**, Paraovarian cyst. **C**, Normal ovary. On transvaginal imaging (**B** and **C**), the cyst is seen as distinct from the normal ipsilateral ovary.



**FIG 30-19** Peritoneal inclusion peritoneal inclusion cyst. Note the ovary (Ov) suspended among adhesions in the periphery of the pseudocyst.

often helpful. In the setting of bilateral solid ovarian masses, metastases should be considered if there is a known primary malignancy. The remainder of completely solid ovarian masses will likely represent one of various other uncommon neoplasms.

## PITFALLS IN EVALUATING THE OVARY

A few potential pitfalls have been described herein. The possibility of an extraovarian origin of an observed adnexal mass, whether predominantly cystic or solid, should always be considered.<sup>28,103</sup> For example, a paraovarian cyst, which usually appears as a simple unilocular cyst, might be mistaken for an ovarian cyst but can be correctly recognized if seen separate from the ipsilateral ovary (Fig. 30-18). A peritoneal inclusion cyst often has internal septations and can mimic an ovarian neoplasm. Peritoneal inclusion cysts are thought to develop secondary to adhesions around the ovary, resulting in trapping of fluid originating from the ovary during ovulation. They often are irregular in configuration with acute angles and conform to the shape of adjacent structures. The ovary is typically found at the edge of the inclusion cyst (Fig. 30-19) or may appear suspended by septations within the cyst.<sup>104,105</sup> Risk factors for peritoneal inclusion cysts include prior pelvic surgery, endometriosis, trauma, and pelvic inflammatory disease. The possibility of a pedunculated uterine leiomyoma simulating a solid ovarian mass has been discussed.

Another potential pitfall relates to the use of Doppler imaging of the ovary to assess for flow in suspected solid tissue. Optimal Doppler technique (using low-volume, low-velocity settings) is important so that true intrinsic blood flow is detected (Fig. 30-20). However, there is also potential for false positive depiction of flow using Doppler imaging as a result of motion or noise, with possible resultant erroneous diagnosis of suspected malignancy. Distinct linear or curvilinear vessels within tissue shown by color or power Doppler imaging generally represent actual blood flow. However, if only a few isolated pixels of color are shown, this may represent noise/artifact. Therefore, confirmation of an arterial or venous waveform using spectral Doppler interrogation is important before concluding that blood flow is present.<sup>6</sup>

Other potential pitfalls include superior or lateral location of the ovary, such that it is not identified or is poorly visualized on transvaginal scanning.<sup>106</sup> Although transvaginal sonography is most often the optimal approach for imaging an ovarian mass, transabdominal scanning can be helpful and may be necessary in some cases. For example, transabdominal evaluation would be suggested when the ovary is not visualized, when there is high clinical suspicion for an adnexal mass but one is not identified with transvaginal scanning, or when an ovarian mass is so large it cannot be completely evaluated on the small field of view available with the transvaginal approach.<sup>106</sup>

Ovarian tissue situated between two adjacent simple cysts or follicles can simulate a septation and thus falsely raise concern for neoplasm.<sup>28</sup> It might be difficult to differentiate this pseudoseptation from a true intracyst septation, and Doppler depiction of flow is not reliable in making this distinction.<sup>28</sup> Occasionally, a small follicle or cyst may protrude into a larger follicle or cyst, producing a “cyst within a cyst” appearance, which may also simulate a septation. Awareness of these pitfalls/potential mimics and use of short interval follow-up ultrasound evaluation may be helpful and may avert misdiagnosis of ovarian neoplasm.

Sonography of ovarian dermoids can be difficult and problematic.<sup>28,106</sup> They can be overlooked if they consist predominantly of hyperechoic (fatty) tissue as this appearance might be mistaken for gas-filled bowel. Dermoids that are predominantly cystic with only a small peripheral hyperechoic component may be erroneously characterized if only the cystic component is seen and the small hyperechoic component is mistaken for adjacent bowel. Alternatively, a dermoid might be falsely diagnosed if an area of hyperechoic bowel or mesentery is misconstrued as an adnexal mass. Identification of a separate ipsilateral ovary can help avoid this error. Manipulation with the transducer might also prove useful, as bowel may change in shape or peristaltic with extrinsic compression. In some challenging cases, further imaging with MRI or CT might be useful for clarification.



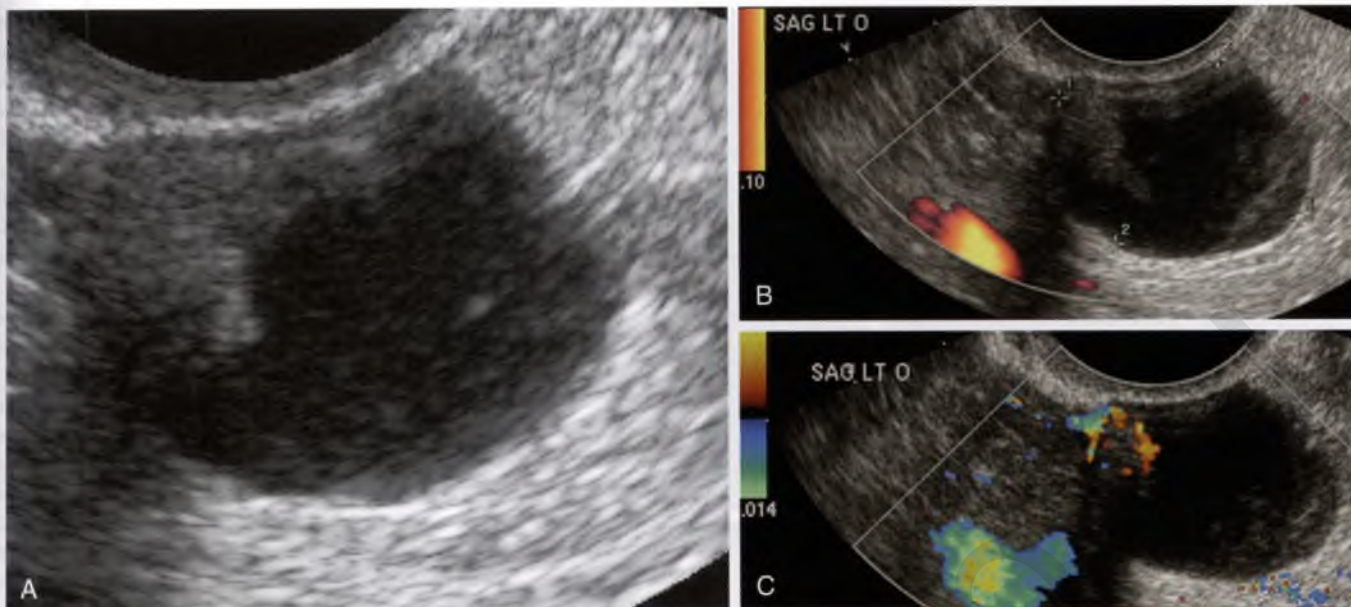


**FIG 30-20** **A**, Cystic ovarian lesion with moderately echogenic, possibly solid mural component. **B**, No convincing blood flow is shown within cystic ovarian lesion on initial power Doppler sonographic images. **C**, Blood flow is shown within solid mural nodule using color Doppler sonography with adjusted settings (including low-scale pulse repetition frequency) optimized to detect low flow.

## OVARIAN MASSES IN PREGNANCY

Many of the same principles discussed earlier regarding sonographic evaluation of ovarian masses also apply during pregnancy. For ovarian masses identified during pregnancy, the risk of malignancy is low and most patients can be managed conservatively with observation and surveillance with follow-up sonograms.<sup>107</sup> Recognition of a few ovarian lesions unique to pregnancy is important to help prevent misdiagnosis.

Theca lutein cysts are most frequently associated with gestational trophoblastic disease, but can also occur with normal singleton or multiple pregnancies and with pregnancies complicated by fetal hydrops. The term *hyperreactio luteinalis* has been used variably, often referring to theca lutein cysts in the absence of ovulation induction<sup>108</sup> and sometimes in the absence of gestational trophoblastic disease. Theca lutein cysts may simulate ovarian neoplasms because they usually appear as a multiseptated cystic mass or multiple adjacent cysts (Fig. 30-21). The bilateral nature of these masses and their known clinical associations usually help suggest the diagnosis.

Decidualized endometriomas are rare but are worth recognizing as they may simulate ovarian malignancy. These lesions are often cystic with small solid components with internal flow detectable by Doppler imaging (Fig. 30-22).<sup>109-111</sup> The endometrial changes that occur in response to progesterone in pregnancy (i.e., decidualization) can also affect ectopic endometrial tissue, resulting in growth of vascularized solid areas within in preexisting endometriomas.<sup>110,112,113</sup> Unfortunately, color Doppler imaging does not reliably distinguish decidualized endometriomas from ovarian malignancy, as both may have detectable flow by Doppler sonography.<sup>113</sup> Awareness of this entity and recommendation for follow-up sonogram, particularly when there is a known history of endometrioma, no other features of malignancy,<sup>109</sup> decrease in size of the mass on follow-up imaging,<sup>110</sup> or MRI showing that the solid tissue has signal characteristics similar to the endometrium<sup>112</sup> can help one suggest the correct diagnosis and possibly obviate the need for surgical evaluation.



**FIG 30-21** Theca lutein cysts. This condition (*calipers*) is likely due to multiple adjacent cysts but can simulate a multiseptated cystic mass. This patient had gestational trophoblastic disease.

Luteoma of pregnancy is a rare benign disorder that has a non-specific sonographic appearance, though most frequently appears solid.<sup>108,114,115</sup> It may be associated with maternal virilization; thus, the presence of hirsutism and elevated serum androgens can help suggest the diagnosis.<sup>108,116</sup>

## SYNDROMES AND DISEASES ASSOCIATED WITH OVARIAN NEOPLASMS

There are a few uncommon syndromes associated with ovarian neoplasms. Some that occur in the setting of an ovarian abnormality



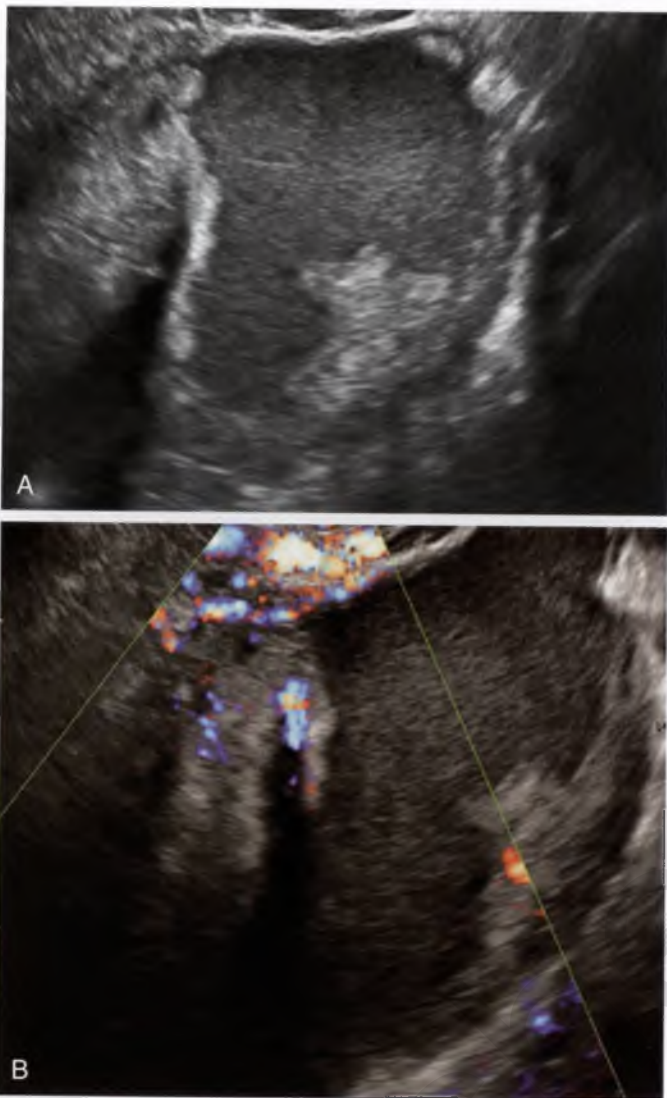


**FIG 30-22** Decidualized endometrioma. **A**, Cystic ovarian mass in a pregnant patient contains diffuse homogeneous low-level internal echoes with an irregular solid-appearing peripheral component. **B**, Color Doppler imaging shows blood flow within the solid area, a finding that is often considered worrisome for malignancy. At surgery, this mass proved to be a decidualized endometrioma. (From Benacerraf BR, Goldstein SR, Groszmann YS: Endometriosis. In Benacerraf BR, Goldstein SR, Groszmann YS [eds]: *Gynecologic Ultrasound: A Problem-Based Approach*. Philadelphia, Elsevier, 2014, Fig. E4-5.)

include Meigs syndrome and ovarian remnant syndrome. Meigs syndrome refers to the rare association of a benign ovarian neoplasm (most frequently a fibroma) with ascites and sometimes with pleural effusion.<sup>117</sup> The presence of ascites may result in increased concern for possible malignancy. Ovarian remnant syndrome refers to the incomplete removal of ovarian tissue following oophorectomy, in association with a pelvic mass and pain.<sup>69</sup> Conditions that result in development of pelvic adhesions are risk factors for this syndrome and one should consider this diagnosis in a patient with the appropriate clinical history and a cystic adnexal mass.<sup>69,118,119</sup>

Other syndromes and diseases may place patients at increased risk for developing ovarian neoplasms. Patients with basal cell nevus (Gorlin syndrome) are at increased risk for ovarian fibromas, which

may be bilateral and calcified.<sup>117</sup> Patients with Peutz-Jeghers syndrome may develop a rare neoplasm known as sex cord tumor with annular tubules (SCTAT).<sup>120</sup> Sonographically, SCTAT may appear as multiple small hyperechoic, possibly calcified masses.<sup>121</sup> There is a reported association with ovarian dermoids in patients with anti-*N*-methyl-D-aspartate receptor encephalitis, a serious and potentially fatal neurologic disease that has been underrecognized.<sup>122</sup> Awareness of the condition and this association should prompt a careful sonographic search, as detection and surgical removal of an ovarian dermoid improve outcomes.

Lynch syndrome and genetic mutations, such as *BRCA1* and *BRCA2*, are associated with increased risk of ovarian carcinoma, though currently there is no convincing evidence supporting the effectiveness of ovarian cancer screening even in these high-risk populations.<sup>123</sup> It is hoped that ongoing studies will provide additional information on the utility and impact of ovarian cancer screening for these patients. Several paraneoplastic syndromes are also associated with ovarian neoplasms.<sup>124</sup> Patients with dermatomyositis are at an increased risk of malignancy, and ovarian carcinoma is one of the most frequently associated cancers.<sup>125</sup> Sonography is used to evaluate these patients for possible ovarian neoplasms.

In women with clinical evidence of hyperandrogenism, sonography is often performed to evaluate for morphologic features of polycystic ovaries, the most common ovarian cause of this condition (discussed in Chapters 32 and 34). Less frequently, ovarian stromal hyperthecosis or androgen-secreting tumors may result in hyperandrogenism. Androgen-secreting lesions such as Sertoli-Leydig cell tumors should be considered in patients with markedly elevated androgen levels or rapid onset or progression of virilizing symptoms.<sup>126</sup> These tumors may be small and difficult to detect by any imaging method. Ovarian stromal hyperthecosis can occur with sonographically normal ovaries but should be considered in patients with suggestive clinical findings and mildly enlarged ovaries.<sup>127</sup>

## SUMMARY

Recognition of normal ovarian sonographic features, such as a dominant follicle and corpus luteum, is important so as not to mistake them for pathologic findings. Most ovarian masses are benign, and the majority demonstrates sufficiently typical sonographic appearances such that they can be reliably characterized by ultrasound. The infrequent ovarian malignancy can also usually be recognized and diagnosed based on typical ultrasound features. A small minority of ovarian masses have indeterminate sonographic findings and generally need to undergo further evaluation by means of follow-up sonography, MRI scan, or surgical evaluation.

## REFERENCES

- Harris RD, Javitt MC, Glanc P, et al: ACR Appropriateness Criteria® clinically suspected adnexal mass. *Ultrasound Q* 29(1):79–86, 2013.
- Van Gorp T, Veldman J, Van Calster B, et al: Subjective assessment by ultrasound is superior to the risk of malignancy index (RMI) or the risk of ovarian malignancy algorithm (ROMA) in discriminating benign from malignant adnexal masses. *Eur J Cancer* 48(11):1649–1656, 2012.
- Timmerman D, Valentin L, Bourne TH, et al: Terms, definitions and measurements to describe the sonographic features of adnexal tumors: a consensus opinion from the International Ovarian Tumor Analysis (IOTA) group. *Ultrasound Obstet Gynecol* 16(5):500–505, 2000.
- Amor F, Alcazar JL, Vaccaro H, et al: GI-RADS reporting system for ultrasound evaluation of adnexal masses in clinical practice: a prospective multicenter study. *Ultrasound Obstet Gynecol* 38(4):450–455, 2011.



5. Levine D, Brown DL, Andreotti RF, et al: Management of asymptomatic ovarian and other adnexal cysts imaged at US: Society of Radiologists in Ultrasound Consensus Conference Statement. *Radiology* 256(3):943–954, 2010.
6. Brown DL, Dudiak KM, Laing FC: Adnexal masses: US characterization and reporting. *Radiology* 254(2):342–354, 2010.
7. Timor-Tritsch IE, Goldstein SR: The complexity of a “complex mass” and the simplicity of a “simple cyst.” *J Ultrasound Med* 24(3):255–258, 2005.
8. Healy DL, Bell R, Robertson DM, et al: Ovarian status in healthy postmenopausal women. *Menopause* 15(6):1109–1114, 2008.
9. Kupfer MC, Ralls PW, Fu YS: Transvaginal sonographic evaluation of multiple peripherally distributed echogenic foci of the ovary: prevalence and histologic correlation. *AJR Am J Roentgenol* 171(2):483–486, 1998.
10. Muradali D, Colgan T, Hayeems E, et al: Echogenic ovarian foci without shadowing: are they caused by psammomatous calcifications? *Radiology* 224(2):429–435, 2002.
11. Brown DL, Frates MC, Muto MG, Welch WR: Small echogenic foci in the ovaries: correlation with histologic findings. *J Ultrasound Med* 23(2):307–313, 2004.
12. Brown DL, Laing FC, Welch WR: Large calcifications in ovaries otherwise normal on ultrasound. *Ultrasound Obstet Gynecol* 29(4):438–442, 2007.
13. Millet J, Much M, Gunabushanam G, et al: Large ovarian calcifications from an unresorbed corpus albicans. *J Ultrasound Med* 31(9):1465–1468, 2012.
14. Brandt KR, Thurmond AS, McCarthy JL: Focal calcifications in otherwise ultrasonographically normal ovaries. *Radiology* 198(2):415–417, 1996.
15. Zeligs KP, Javitt MC, Barner R, Hamilton CA: Atypical ovarian calcifications associated with bilateral borderline ovarian tumors. *J Ultrasound Med* 32(6):1059–1061, 2013.
16. Brown DL: A practical approach to the ultrasound characterization of adnexal masses. *Ultrasound Q* 23(2):87–105, 2007.
17. Conway C, Zalud I, Dilema M, et al: Simple cyst in the postmenopausal patient: detection and management. *J Ultrasound Med* 17(6):369–372, quiz 373–364, 1998.
18. Goldstein SR, Subramanyam B, Snyder JR, et al: The postmenopausal cystic adnexal mass: the potential role of ultrasound in conservative management. *Obstet Gynecol* 73(1):8–10, 1989.
19. Kroon E, Andolf E: Diagnosis and follow-up of simple ovarian cysts detected by ultrasound in postmenopausal women. *Obstet Gynecol* 85(2):211–214, 1995.
20. Levine D, Gosink BB, Wolf SI, et al: Simple adnexal cysts: the natural history in postmenopausal women. *Radiology* 184(3):653–659, 1992.
21. Parsons A: Whither the simple ovarian cyst in postmenopausal women? *Ultrasound Obstet Gynecol* 20(2):112–116, 2002.
22. Ekerhovd E, Wienerroith H, Staudach A, Granberg S: Preoperative assessment of unilocular adnexal cysts by transvaginal ultrasonography: a comparison between ultrasonographic morphologic imaging and histopathologic diagnosis. *Am J Obstet Gynecol* 184(2):48–54, 2001.
23. Modesitt SC, Pavlik EJ, Ueland FR, et al: Risk of malignancy in unilocular ovarian cystic tumors less than 10 centimeters in diameter. *Obstet Gynecol* 102(3):594–599, 2003.
24. Valentin L, Ameys L, Franchi D, et al: Risk of malignancy in unilocular cysts: a study of 1148 adnexal masses classified as unilocular cysts at transvaginal ultrasound and review of the literature. *Ultrasound Obstet Gynecol* 41(1):80–89, 2013.
25. Patel MD, Feldstein VA, Filly RA: The likelihood ratio of sonographic findings for the diagnosis of hemorrhagic ovarian cysts. *J Ultrasound Med* 24(5):607–614, 2005.
26. Valentin L: Use of morphology to characterize and manage common adnexal masses. *Best Pract Res Clin Obstet Gynaecol* 18(1):71–89, 2004.
27. Okai T, Kobayashi K, Ryo E, et al: Transvaginal sonographic appearance of hemorrhagic functional ovarian cysts and their spontaneous regression. *Int J Gynaecol Obstet* 44(1):47–52, 1994.
28. Patel MD: Pitfalls in the sonographic evaluation of adnexal masses. *Ultrasound Q* 28(1):29–40, 2012.
29. Jain KA: Sonographic spectrum of hemorrhagic ovarian cysts. *J Ultrasound Med* 21(8):879–886, 2002.
30. Hertzberg BS, Kliewer MA, Bowie JD: Adnexal ring sign and hemoperitoneum caused by hemorrhagic ovarian cyst: pitfall in the sonographic diagnosis of ectopic pregnancy. *AJR Am J Roentgenol* 173(5):1301–1302, 1999.
31. Hertzberg BS, Kliewer MA, Paulson EK: Ovarian cyst rupture causing hemoperitoneum: imaging features and the potential for misdiagnosis. *Abdom Imaging* 24(3):304–308, 1999.
32. Barnhart KT: Clinical practice. Ectopic pregnancy. *N Engl J Med* 361(4):379–387, 2009.
33. Raziel A, Ron-El R, Pansky M, et al: Current management of ruptured corpus luteum. *Eur J Obstet Gynecol Reprod Biol* 50(1):77–81, 1993.
34. Kim JH, Lee SM, Lee JH, et al: Successful conservative management of ruptured ovarian cysts with hemoperitoneum in healthy women. *PLoS ONE* 9(3):e91171, 2014.
35. Patel MD, Feldstein VA, Chen DC, et al: Endometriomas: diagnostic performance of US. *Radiology* 210(3):739–745, 1999.
36. Busacca M, Vignali M: Ovarian endometriosis: from pathogenesis to surgical treatment. *Curr Opin Obstet Gynecol* 15(4):321–326, 2003.
37. Lee HJ, Park YM, Jee BC, et al: Various anatomic locations of surgically proven endometriosis: a single-center experience. *Obstet Gynecol Sci* 58(1):53–58, 2015.
38. Sznurkowski JJ, Emerich J: Endometriomas are more frequent on the left side. *Acta Obstet Gynecol Scand* 87(1):104–106, 2008.
39. Clement PB: Diseases of the peritoneum. In Kurman RJ, editor: *Blaustein's Pathology of the Female Genital Tract*, ed 5, New York, 2002, Springer-Verlag, pp 729–789.
40. Barbieri RL, Missmer S: Endometriosis and infertility: a cause-effect relationship? *Ann N Y Acad Sci* 955:23–33, discussion 34–36, 396–406, 2002.
41. Guerriero S, Ajossa S, Mais V, et al: The diagnosis of endometriomas using colour Doppler energy imaging. *Hum Reprod* 13(6):1691–1695, 1998.
42. Van Holsbeke C, Zhang J, Van Belle V, et al: Acoustic streaming cannot discriminate reliably between endometriomas and other types of adnexal lesion: a multicenter study of 633 adnexal masses. *Ultrasound Obstet Gynecol* 35(3):349–353, 2010.
43. Psaroudakis D, Hirsch M, Davis C: Review of the management of ovarian endometriosis: paradigm shift towards conservative approaches. *Curr Opin Obstet Gynecol* 26(4):266–274, 2014.
44. Taniguchi F, Harada T, Kobayashi H, et al: Clinical characteristics of patients in Japan with ovarian cancer presumably arising from ovarian endometrioma. *Gynecol Obstet Invest* 77(2):104–110, 2014.
45. McDermott S, Oei TN, Iyer VR, Lee SI: MR imaging of malignancies arising in endometriomas and extraovarian endometriosis. *Radiographics* 32(3):845–863, 2012.
46. Asch E, Levine D: Variations in appearance of endometriomas. *J Ultrasound Med* 26(8):993–1002, 2007.
47. Alcazar JL, Laparte C, Jurado M, Lopez-Garcia G: The role of transvaginal ultrasonography combined with color velocity imaging and pulsed Doppler in the diagnosis of endometrioma. *Fertil Steril* 67(3):487–491, 1997.
48. Bronshtein M, Yoffe N, Brandes JM, Blumenfeld Z: Hair as a sonographic marker of ovarian teratomas: improved identification using transvaginal sonography and simulation model. *J Clin Ultrasound* 19(6):351–355, 1991.
49. Caspi B, Appelman Z, Rabinerson D, et al: Pathognomonic echo patterns of benign cystic teratomas of the ovary: classification, incidence and accuracy rate of sonographic diagnosis. *Ultrasound Obstet Gynecol* 7(4):275–279, 1996.
50. Weerakkody Y, Gaillard F, Knipe H, et al: *Mature (cystic) ovarian teratoma*. Available at <http://radiopaedia.org/articles/mature-cystic-ovarian-teratoma>.
51. Mais V, Guerriero S, Ajossa S, et al: Transvaginal ultrasonography in the diagnosis of cystic teratoma. *Obstet Gynecol* 85(1):48–52, 1995.



52. Malde HM, Kedar RP, Chadha D, Nayak S: Dermoid mesh: a sonographic sign of ovarian teratoma. *AJR Am J Roentgenol* 159(6):1349–1350, 1992.
53. Patel MD, Feldstein VA, Lipson SD, et al: Cystic teratomas of the ovary: diagnostic value of sonography. *Am J Roentgenol* 171(4):1061–1065, 1998.
54. Saba L, Guerriero S, Sulcis R, et al: Mature and immature ovarian teratomas: CT, US and MR imaging characteristics. *Eur J Radiol* 72(3):454–463, 2009.
55. Kim HC, Kim SH, Lee HJ, et al: Fluid-fluid levels in ovarian teratomas. *Abdom Imaging* 27(1):100–105, 2002.
56. Owre A, Pedersen JF: Characteristic fat-fluid level at ultrasonography of ovarian dermoid cyst. *Acta Radiol* 32(4):317–319, 1991.
57. Rao JR, Shah Z, Patwardhan V, et al: Ovarian cystic teratoma: determined phenotypic response of keratocytes and uncommon intracystic floating balls appearance on sonography and computed tomography. *J Ultrasound Med* 21(6):687–691, 2002.
58. Caspi B, Appelman Z, Rabinerson D, et al: The growth pattern of ovarian dermoid cysts: a prospective study in premenopausal and postmenopausal women. *Fertil Steril* 68(3):501–505, 1997.
59. Amerigo J, Nogales FF, Jr, Fernandez-Sanz J, et al: Squamous cell neoplasms arising from ovarian benign cystic teratoma. *Gynecol Oncol* 8(3):277–283, 1979.
60. Comerci JT, Jr, Licciardi F, Bergh PA, et al: Mature cystic teratoma: a clinicopathologic evaluation of 517 cases and review of the literature. *Obstet Gynecol* 84(1):22–28, 1994.
61. Hackethal A, Brueggmann D, Bohlmann MK, et al: Squamous-cell carcinoma in mature cystic teratoma of the ovary: systematic review and analysis of published data. *Lancet Oncol* 9(12):1173–1180, 2008.
62. Hirakawa T, Tsuneyoshi M, Enjoji M: Squamous cell carcinoma arising in mature cystic teratoma of the ovary. Clinicopathologic and topographic analysis. *Am J Surg Pathol* 13(5):397–405, 1989.
63. Westhoff C, Pike M, Vessey M: Benign ovarian teratomas: a population-based case-control study. *Br J Cancer* 58(1):93–98, 1988.
64. Deffleux X, Thubert T, Huchon C, et al: Complications of presumed benign ovarian tumors. *J Gynecol Obstet Biol Reprod (Paris)* 42(8):816–832, 2013.
65. Rubod C, Triboulet JP, Vinatier D: Ovarian dermoid cyst complicated by chemical peritonitis. Case report. *Gynecol Obstet Fertil* 35(7–8):651–653, 2007.
66. Mlikotic A, McPhaul L, Hansen GC, Sinow RM: Significance of the solid component in predicting malignancy in ovarian cystic teratomas—diagnostic considerations. *J Ultrasound Med* 20(8):859–866, 2001.
67. Emoto M, Obama H, Horiuchi S, et al: Transvaginal color Doppler ultrasonic characterization of benign and malignant ovarian cystic teratomas and comparison with serum squamous cell carcinoma antigen. *Cancer* 88(10):2298–2304, 2000.
68. Park JY, Kim DY, Kim JH, et al: Malignant transformation of mature cystic teratoma of the ovary: experience at a single institution. *Eur J Obstet Gynecol Reprod Biol* 141(2):173–178, 2008.
69. Ackerman S, Irshad A, Lewis M, Anis M: Ovarian cystic lesions: a current approach to diagnosis and management. *Radiol Clin North Am* 51(6):1067–1085, 2013.
70. Crum CP, McKeon FD, Xian W: The oviduct and ovarian cancer: causality, clinical implications, and “targeted prevention.” *Clin Obstet Gynecol* 55:24–35, 2012.
71. Crum CP, Herfs M, Ning G, et al: Through the glass darkly: intraepithelial neoplasia, top-down differentiation, and the road to ovarian cancer. *J Pathol* 231:402–412, 2013.
72. Mehra K, Mehrad M, Ning G, et al: STICS, SCOUTs and p53 signatures; a new language for pelvic serous carcinogenesis. *Front Biosci (Elite Ed)* 3:625–634, 2011.
73. Nik NN, Vang R, Shih IeM, Kurman RJ: Origin and pathogenesis of pelvic (ovarian, tubal, and primary peritoneal) serous carcinoma. *Annu Rev Pathol* 9:27–45, 2014.
74. Alcazar JL, Utrilla-Layna J, Minguez JA, Jurado M: Clinical and ultrasound features of type I and type II epithelial ovarian cancer. *Int J Gynecol Cancer* 23(4):680–684, 2013.
75. Kurman RJ, Shih I: Molecular pathogenesis and extraovarian origin of epithelial ovarian cancer—shifting the paradigm. *Hum Pathol* 42:918–931, 2011.
76. Paladini D, Testa A, Van Holsbeke C, et al: Imaging in gynecological disease (5): clinical and ultrasound characteristics in fibroma and fibrothecoma of the ovary. *Ultrasound Obstet Gynecol* 34(2):188–195, 2009.
77. Shaaban AM, Rezvani M, Elsayes KM, et al: Ovarian malignant germ cell tumors: cellular classification and clinical and imaging features. *Radiographics* 34(3):777–801, 2014.
78. Guerriero S, Alcazar JL, Pascual MA, et al: Preoperative diagnosis of metastatic ovarian cancer is related to origin of primary tumor. *Ultrasound Obstet Gynecol* 39(5):581–586, 2012.
79. Brown DL, Doubilet PM, Miller FH, et al: Benign and malignant ovarian masses: selection of the most discriminating gray-scale and Doppler sonographic features. *Radiology* 208(1):103–110, 1998.
80. Valentin L, Ameye L, Savelli L, et al: Adnexal masses difficult to classify as benign or malignant using subjective assessment of gray-scale and Doppler ultrasound findings: logistic regression models do not help. *Ultrasound Obstet Gynecol* 38(4):456–465, 2011.
81. Valentin L, Ameye L, Testa A, et al: Ultrasound characteristics of different types of adnexal malignancies. *Gynecol Oncol* 102(1):41–48, 2006.
82. Goldstein SR, Timor-Tritsch IE, Monteagudo A, et al: Cystadenofibromas: can transvaginal ultrasound appearance reduce some surgical interventions? *J Clin Ultrasound* 43(6):393–396, 2014.
83. Bundy AL, Ritchie WG, Fine C, Brinsko RE: Dermoid tumor and cystadenoma arising in the same ovary. *J Clin Ultrasound* 14(9):727–731, 1986.
84. Kim SH, Kim YJ, Park BK, et al: Collision tumors of the ovary associated with teratoma: clues to the correct preoperative diagnosis. *J Comput Assist Tomogr* 23(6):929–933, 1999.
85. Granberg S, Wikland M, Jansson I: Macroscopic characterization of ovarian tumors and the relation to the histological diagnosis: criteria to be used for ultrasound evaluation. *Gynecol Oncol* 35(2):139–144, 1989.
86. Barney SP, Muller CY, Bradshaw KD: Pelvic masses. *Med Clin North Am* 92(5):1143–1161, 2008.
87. Wang S, Johnson S: Prediction of benignity of solid adnexal masses. *Arch Gynecol Obstet* 285(3):721–726, 2012.
88. Kim SH, Sim JS, Seong CK: Interface vessels on color/power Doppler US and MRI: a clue to differentiate subserosal uterine myomas from extrauterine tumors. *J Comput Assist Tomogr* 25(1):36–42, 2001.
89. Madan R: The bridging vascular sign. *Radiology* 238(1):371–372, 2006.
90. Reiter MJ, Schwoppe RB, Lisanti CJ: Algorithmic approach to solid adnexal masses and their mimics: utilization of anatomic relationships and imaging features to facilitate diagnosis. *Abdom Imaging* 39(6):1284–1296, 2014.
91. Conte M, Guariglia L, Benedetti Panici P, et al: Ovarian fibrothecoma: sonographic and histologic findings. *Gynecol Obstet Invest* 32(1):51–54, 1991.
92. Kim JA, Chun YK, Moon MH, et al: High-resolution sonographic findings of ovarian granulosa cell tumors: correlation with pathologic findings. *J Ultrasound Med* 29(2):187–193, 2010.
93. Van Holsbeke C, Domali E, Holland TK, et al: Imaging of gynecological disease (3): clinical and ultrasound characteristics of granulosa cell tumors of the ovary. *Ultrasound Obstet Gynecol* 31(4):450–456, 2008.
94. Outwater EK, Wagner BJ, Mannion C, et al: Sex cord-stromal and steroid cell tumors of the ovary. *Radiographics* 18(6):1523–1546, 1998.
95. Mom CH, Engelen MJ, Willems PH, et al: Granulosa cell tumors of the ovary: the clinical value of serum inhibin A and B levels in a large single center cohort. *Gynecol Oncol* 105(2):365–372, 2007.
96. Granberg S, Norstrom A, Wikland M: Tumors in the lower pelvis as imaged by vaginal sonography. *Gynecol Oncol* 37(2):224–229, 1990.
97. Seidman JD, Russell P, Kurman RJ: Surface epithelial tumors of the ovary. In Kurman RJ, editor: *Blaustein's Pathology of the Female Genital Tract*, ed 5, New York, 2002, Springer-Verlag, pp 791–904.

98. Dierickx I, Valentin L, Van Holsbeke C, et al: Imaging in gynecological disease (7): clinical and ultrasound features of Brenner tumors of the ovary. *Ultrasound Obstet Gynecol* 40(6):706–713, 2012.
99. Green GE, Mortelet KJ, Glickman JN, Benson CB: Brenner tumors of the ovary: sonographic and computed tomographic imaging features. *J Ultrasound Med* 25(10):1245–1251, quiz 1252–1254, 2006.
100. Youngs DJ, Brown DL: Ovarian mass. In Henningsen C, Kuntz K, Youngs D, editors: *Clinical Guide to Sonography: Exercises for Critical Thinking*, St. Louis, 2014, Elsevier, pp 183–198.
101. Brown DL, Zou KH, Tempany CM, et al: Primary versus secondary ovarian malignancy: imaging findings of adnexal masses in the Radiology Diagnostic Oncology Group Study. *Radiology* 219(1):213–218, 2001.
102. Testa AC, Ferrandina G, Timmerman D, et al: Imaging in gynecological disease (1): ultrasound features of metastases in the ovaries differ depending on the origin of the primary tumor. *Ultrasound Obstet Gynecol* 29(5):505–511, 2007.
103. Henrichsen TL, Brown DL: Approach to imaging the adnexal mass. In Fielding JR, Brown DL, Thurmond AS, editors: *Gynecologic Imaging*, Philadelphia, 2011, Elsevier, pp 427–436.
104. Jain KA: Imaging of peritoneal inclusion cysts. *AJR Am J Roentgenol* 174(6):1559–1563, 2000.
105. Guerriero S, Ajossa S, Mais V, et al: Role of transvaginal sonography in the diagnosis of peritoneal inclusion cysts. *J Ultrasound Med* 23:1193–1200, 2004.
106. Kirby CL, Horrow MM: Pitfalls in gynecologic ultrasound. In Fielding JR, Brown DL, Thurmond AS, editors: *Gynecologic Imaging*, Philadelphia, 2011, Elsevier, pp 21–36.
107. Brady PC, Simpson LL, Lewin SN, et al: Safety of conservative management of ovarian masses during pregnancy. *J Reprod Med* 58(9–10):377–382, 2013.
108. Glanc P, Salem S, Farine D: Adnexal masses in the pregnant patient: a diagnostic and management challenge. *Ultrasound Q* 24(4):225–240, 2008.
109. Barbieri M, Somigliana E, Oneda S, et al: Decidualized ovarian endometriosis in pregnancy: a challenging diagnostic entity. *Hum Reprod* 24(8):1818–1824, 2009.
110. Pateman K, Moro F, Mavrelou D, et al: Natural history of ovarian endometrioma in pregnancy. *BMC Womens Health* 14:128, 2014.
111. Groszmann Y, Howitt BE, Bromley B, et al: Decidualized endometrioma masquerading as ovarian cancer in pregnancy. *J Ultrasound Med* 33:1909–1915, 2014.
112. Poder L, Coakley FV, Rabban JT, et al: Decidualized endometrioma during pregnancy: recognizing an imaging mimic of ovarian malignancy. *J Comput Assist Tomogr* 32(4):555–558, 2008.
113. Proulx F, Levine D: Decidualization of endometrioma in pregnancy. *Ultrasound Q* 30(3):211–212, 2014.
114. Choi JR, Levine D, Finberg H: Luteoma of pregnancy: sonographic findings in two cases. *J Ultrasound Med* 19(12):877–881, 2000.
115. Tannus JF, Hertzberg BS, Haystead CM, Paulson EK: Unilateral luteoma of pregnancy mimicking a malignant ovarian mass on magnetic resonance and ultrasound. *J Magn Reson Imaging* 29(3):713–717, 2009.
116. Masarie K, Katz V, Balderston K: Pregnancy luteomas: clinical presentations and management strategies. *Obstet Gynecol Surv* 65(9):575–582, 2010.
117. Langer JE: Benign ovarian masses. In Fielding JR, Brown DL, Thurmond AS, editors: *Gynecologic Imaging*, Philadelphia, 2011, Elsevier, pp 437–452.
118. Fleischer AC, Tait D, Mayo J, et al: Sonographic features of ovarian remnants. *J Ultrasound Med* 17(9):551–555, 1998.
119. Kho RM, Abrao MS: Ovarian remnant syndrome: etiology, diagnosis, treatment and impact of endometriosis. *Curr Opin Obstet Gynecol* 24(4):210–214, 2012.
120. Banno K, Kisu I, Yanokura M, et al: Hereditary gynecological tumors associated with Peutz-Jeghers syndrome (review). *Oncol Lett* 6(5):1184–1188, 2013.
121. Swanger RS, Brudnicki A: Ultrasound of ovarian sex-cord tumor with annular tubules. *Pediatr Radiol* 37(12):1270–1271, 2007.
122. Acien P, Acien M, Ruiz-Macia E, Martin-Estefania C: Ovarian teratoma-associated anti-NMDAR encephalitis: a systematic review of reported cases. *Orphanet J Rare Dis* 9:157, 2014.
123. Pandharipande PV, Harvey HB, Javitt MC, et al: *American College of Radiology Appropriateness Criteria: Ovarian Cancer Screening*, Rockville, MD, 2012, Agency for Healthcare Research and Quality. Available at <http://www.guideline.gov/content.aspx?id=37950>.
124. Ashour AA, Verschraegen CF, Kudelka AP, Kavanagh JJ: Paraneoplastic syndromes of gynecologic neoplasms. *J Clin Oncol* 15(3):1272–1282, 1997.
125. Hill CL, Zhang Y, Sigurgeirsson B, et al: Frequency of specific cancer types in dermatomyositis and polymyositis: a population-based study. *Lancet* 357(9250):96–100, 2001.
126. Yanushpolsky EH, Brown DL, Smith BL: Localization of small ovarian Sertoli-Leydig cell tumors by transvaginal sonography with color Doppler. *Ultrasound Obstet Gynecol* 5(2):133–135, 1995.
127. Brown DL, Henrichsen TL, Clayton AC, et al: Ovarian stromal hyperthecosis: sonographic features and histologic associations. *J Ultrasound Med* 28(5):587–593, 2009.



# Ultrasound Evaluation of the Fallopian Tube

Mindy M. Horrow

## SUMMARY OF KEY POINTS

- Normal fallopian tubes are difficult to visualize with ultrasound unless surrounded by small amounts of free peritoneal fluid.
- Classic sonographic signs that help distinguish a dilated fallopian tube from other cystic adnexal masses include waist, incomplete septation, cogwheel, and beads on a string signs.
- Acute pyosalpinx is diagnosed on ultrasound examination by the finding of a dilated, tubular adnexal structure filled with complex fluid and a thick, hyperemic wall.
- A tubo-ovarian abscess (TOA) typically presents as a complex adnexal mass with solid and cystic components, thick walls, hyperemia, and an indistinguishable ovary.
- Hematosalpinx secondary to endometriosis appears on ultrasound images as a dilated tubular adnexal structure filled with fine low level echoes.
- Isolated tube torsion is a rare event, often presenting as a dilated fluid-filled tubular structure with a V-shaped configuration or beak-like pointed narrowing at the twisted edge of the tube and is often found in an unusual location.
- The classic clinical presentation of primary fallopian tube malignancy consists of intermittent bloody vaginal discharge, colicky pain relieved by discharge, and a pelvic mass.
- Tube patency can be evaluated sonographically using agitated saline or ultrasound contrast agents.

## OUTLINE

Embryology and Normal Anatomy, 934

Sonographic Signs of Abnormal Fallopian Tubes, 935

Pelvic Inflammatory Disease, 939

Uncommon Tube Infections, 940

Hematosalpinx, 946

Tube Torsion, 946

Malignancy, 946

Evaluation of Tube Patency, 949

Summary, 951

Unlike the uterus and ovaries, the normal fallopian tube is usually not visible on ultrasound images, and, therefore, documentation of the fallopian tube is not a standard requirement for pelvic sonography. Indeed, when visualized, the fallopian tube is usually dilated or thickened and hence abnormal. Further confounding the evaluation of the fallopian tubes is the relative difficulty in distinguishing an abnormal fallopian tube from a complex cystic ovarian mass. The goals of this chapter are to describe the appearance of the normal fallopian tube; review the pathologic processes that result in abnormalities of the tube, both benign and malignant and either acute or chronic; and demonstrate a variety of sonographic findings that can aid the sonographer in correctly distinguishing tube versus ovarian origin of an adnexal mass.

## EMBRYOLOGY AND NORMAL ANATOMY

The fallopian tube serves to connect the ovary to the uterus, allowing passage of the fertilized oocyte into the endometrial cavity. Embryologically, the paired paramesonephric ducts develop from coelomic epithelium during the 5th to 6th weeks of gestation. As the caudal portions fuse to form the uterus, the cranial aspects become the fallopian tubes with the funnel-shaped end remaining open to the

peritoneum. The normal fallopian tubes are 10 to 12 cm long and between 1 to 4 mm in diameter and are located in the mesosalpinx, a fold of the peritoneum within the broad ligament.<sup>1</sup>

The fallopian tube is divided into four anatomic components (Fig. 31-1). The interstitial segment is intramural and found within the uterine cornua near the fundus. The interstitial segment courses from the serosal surface of the uterus through the myometrial wall to open into the endometrial cavity. It is the shortest (2 cm) and narrowest (1 mm) portion of the fallopian tube. The isthmic segment is closest to the uterus with a length of approximately 3.5 cm and a diameter of 2 mm. The ampulla of the tube is the most lateral portion of the fallopian tube as well as the widest and longest section measuring 6 to 7.5 cm in length. The ampulla terminates at the funnel-shaped infundibulum, which has a fimbriated end that drapes over the ovary. Histologically, the plicae or folds of the fallopian tube are more numerous and complex in the ampulla and infundibulum where the ciliated columnar epithelial cells are also more numerous. Peg cells located between the ciliated cells produce the tubular fluid, which provides nutrients for the spermatozoa and oocyte. This fluid progresses toward the lateral end of the fallopian tube near the ovary in the opposite direction of the motion of the cilia and is excreted into the peritoneal cavity, accounting for the frequent finding of a small

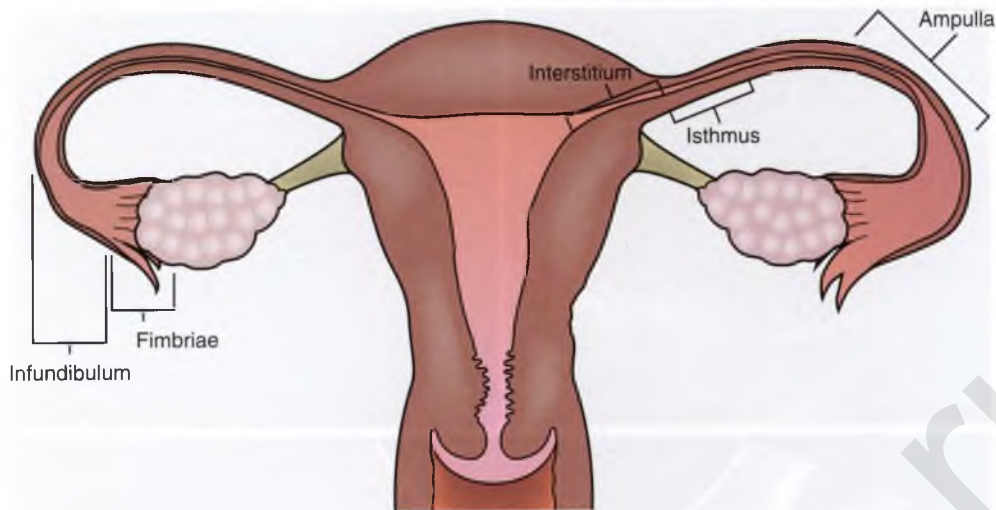


**FIG 31-1** Schematic diagram demonstrating the anatomy of the normal fallopian tube.

amount of simple free fluid in the female pelvis at all stages of the menstrual cycle.<sup>2</sup> The fallopian tube functions to capture the released ovum from the ruptured ovarian follicle and provides a hospitable environment for fertilization and subsequent transfer of the fertilized ovum to the uterus as it grows and differentiates into the blastocyte. The ovum is propelled through the tube toward the uterus by the ciliated epithelium and mucosal plicae as well as muscular contractions in the wall of the tube.

Normal fallopian tubes can occasionally be visualized with transvaginal sonography, especially when there is some fluid in the adnexal regions and minimal pressure is exerted on the probe. The normal fallopian tube appears solid, separate from the ovary and isoechoic to the uterus (Fig. 31-2). The presence of a paratubal cyst, also known as a hydatid of Morgagni, may help localize the tube. These paratubal cysts are usually müllerian remnants of the paramesonephric duct. Most often, they are small, unilocular, simple cysts located at the fimbriated end of the fallopian tube between the tube and the ovary (Video 31-1). An echogenic fat plane between the cyst and the ovary as well as absence of a surrounding rim of ovarian parenchyma serve to differentiate a paratubal cyst from an exophytic ovarian cyst (Fig. 31-3). Simple paratubal cysts are considered a benign finding, and the vast majority of paratubal cysts are of no clinical significance. However, a large paratubal cyst can rupture or serve as a lead point for isolated tube torsion.<sup>3</sup> Rarely, papillary projections in a large (>5 cm) paratubal cyst will indicate malignancy, usually a borderline tumor. Other congenital anomalies of the fallopian tube include hypoplasia, aplasia, ectopic location, and herniation (with the ovary) and are much less common.<sup>4</sup>

## SONOGRAPHIC SIGNS OF ABNORMAL FALLOPIAN TUBES

A variety of sonographic characteristics and signs have been described to help distinguish a dilated fallopian tube from an ovarian mass or other tubular structures in the pelvis such as bowel loops, hydroureter, and varices. Peristalsis, connection to other loops of bowel, as well as the classic striated echopattern or “gut signature” of the bowel wall will serve to distinguish a fluid-filled loop of bowel from a dilated fallopian

tube. A dilated ureter can often be traced to the ureterovesicular junction (UVJ) on transabdominal or transvaginal sonography, and color Doppler should always be used to evaluate any apparent fluid-filled or cystic structure to exclude vascular pathology such as arteriovenous malformations or pelvic varices (Fig. 31-4). Asking the patient to perform a Valsalva maneuver may increase flow in a pelvic varix, making it easier to confirm on color Doppler imaging. Identification of the ovary that is clearly separate from an adnexal mass is the single most helpful finding in distinguishing an abnormal or dilated fallopian tube from a complex cystic ovarian lesion. As the fallopian tube dilates, it often develops an S, U, V, C, or serpiginous shape (Fig. 31-5A and B). The ampullary segment is often wider than the isthmus, and an abrupt transition in diameter between the two segments is often observed (Fig. 31-5C). A waist sign, consisting of diametrically opposed indentations in the wall<sup>5</sup> (Fig. 31-5D), may be observed, usually at the junction of the ampullary portion of the tube with the much wider fimbria. If the dilated tube folds back on itself, the juxtaposition of the two inner walls will create the incomplete septation sign (Fig. 31-5A, E, F, and G), consisting of a linear echogenic protrusion arising from one wall but not reaching the opposite wall. Both cine clips and two-dimensional and three-dimensional reformats can help display the serpiginous nature of the dilated tube (Video 31-2). When the thickened plicae or endosalpingeal folds are visible projecting into the lumen, one may observe numerous 2- to 3-mm echogenic mural-based masses projecting into the lumen of the dilated tube, creating the cogwheel sign (Fig. 31-5H and I) or the beads on a string sign (Fig. 31-5J) as tube markers.<sup>6</sup> These signs are more frequently identified when the tube is only mildly dilated. The wall of the tube is thicker with the cogwheel sign and thinner with the beads on a string sign, with the latter more likely to be seen with chronic inflammation. As the tube becomes increasingly dilated, the thickened plicae are effaced and the hydrosalpinx assumes a more nonspecific cystic appearance with a thin, regular wall. The combination of a tubular shape, waist sign, and visualization of the ovary separate from an adnexal mass has been reported to be the most specific constellation of ultrasound findings to differentiate a dilated fallopian tube from a complex cystic mass of ovarian origin.<sup>5,7</sup> It should be appreciated that visualization of a hydrosalpinx indicates that the tube is blocked, most often secondary to adhesions.



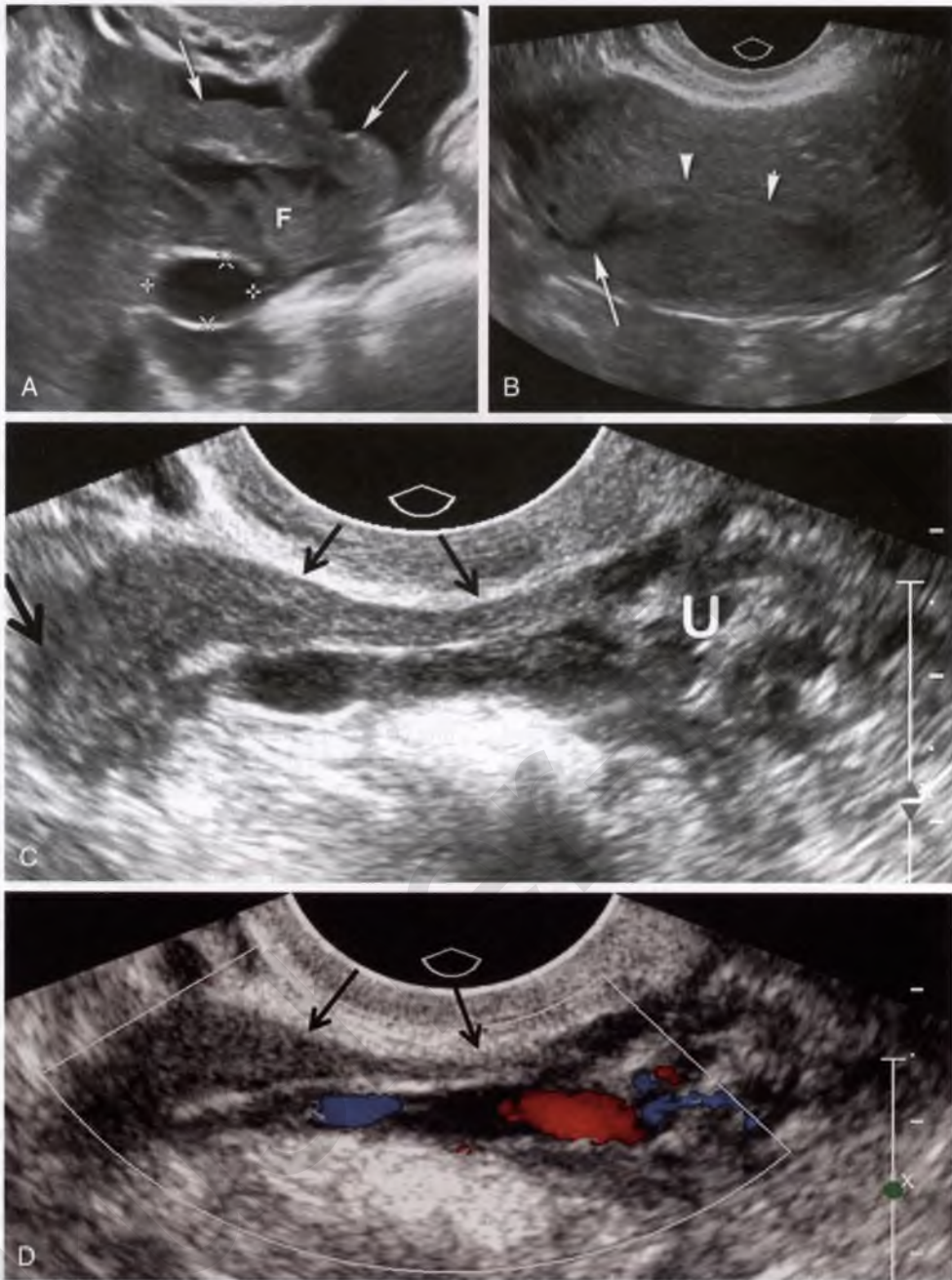


**FIG 31-2** Normal fallopian tubes. **A**, A small amount of anechoic free fluid surrounds the fallopian tube (arrows). Note anechoic paratubal cyst (calipers) adjacent to the fimbriated end (F). **B**, A partial coronal view of the uterine fundus demonstrating a trace amount of fluid (arrow) in the interstitial portion of the right fallopian tube; endometrium is indicated by arrowheads. **C**, Normal fallopian tube (arrows) coursing from the cornua of the uterus (U) above the anechoic uterine vessels to the right adnexa. Note that the more medial isthmic portion (thin arrows) of the tube is the thinnest segment, whereas the fimbriated end (thick arrow), which usually sits above or "caps" the ovary, is the thickest segment. **D**, Color Doppler image of the same patient in C demonstrating the fallopian tube (arrows) above the uterine vessels (blue/red).

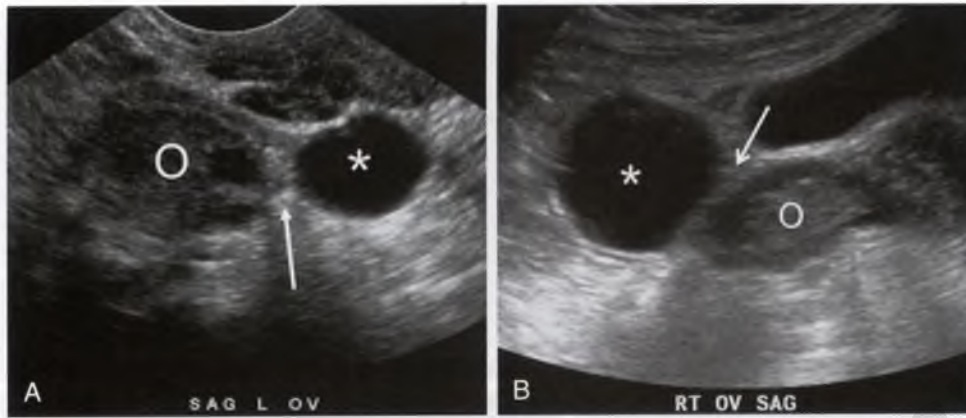


**FIG 31-3** Paratubal cysts. **A** and **B**, Two different patients with paratubal cysts (asterisks). Note echogenic fat plane (arrows) clearly separating the paratubal cysts from the adjacent ovary (O).

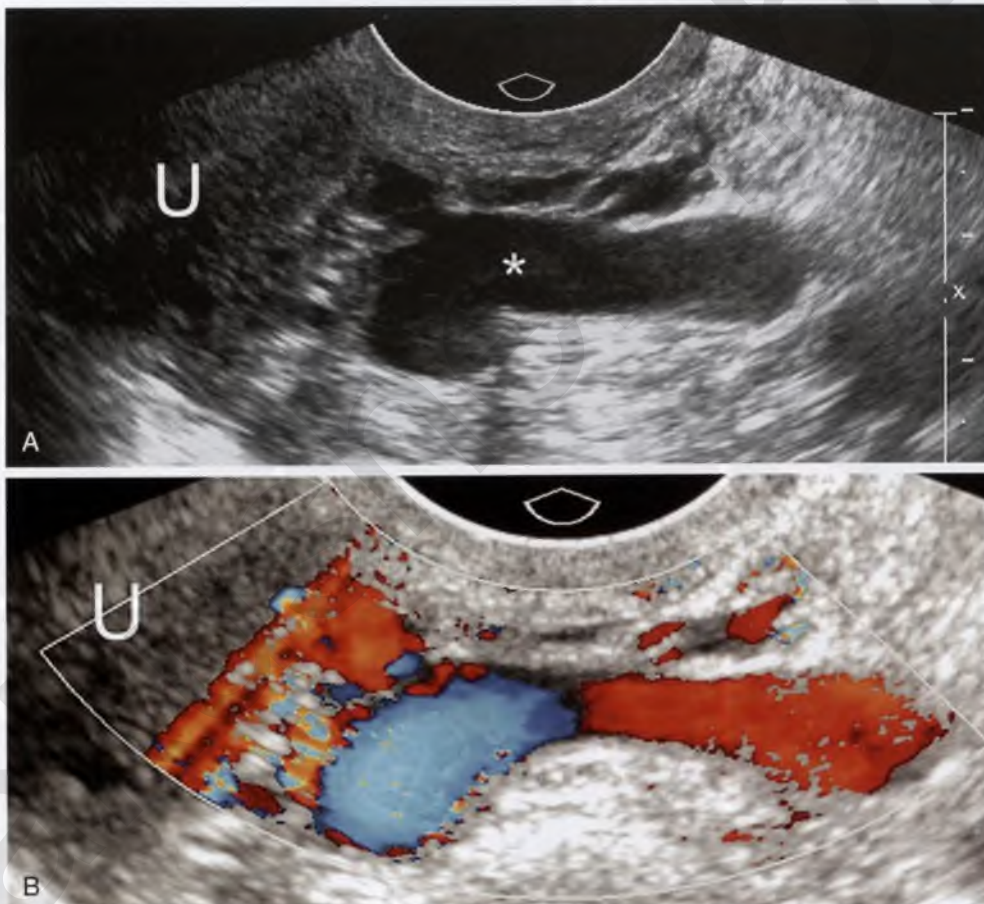


**FIG 31-4** Pelvic varix mimicking hydrosalpinx. **A**, Gray-scale image demonstrating an anechoic serpiginous tubular structure (asterisk) adjacent to the left uterine cornua (U) that could easily be mistaken for a hydrosalpinx. However, color Doppler imaging (**B**) demonstrates that the structure fills in with color, consistent with a pelvic varix. Uterine cornua (U). (From Baltarowich OH, Scoutt LM: Avoiding pitfalls in transvaginal sonography of the female pelvis. *Ultrasound Clin* 5:177-193, 2010, used with permission.)



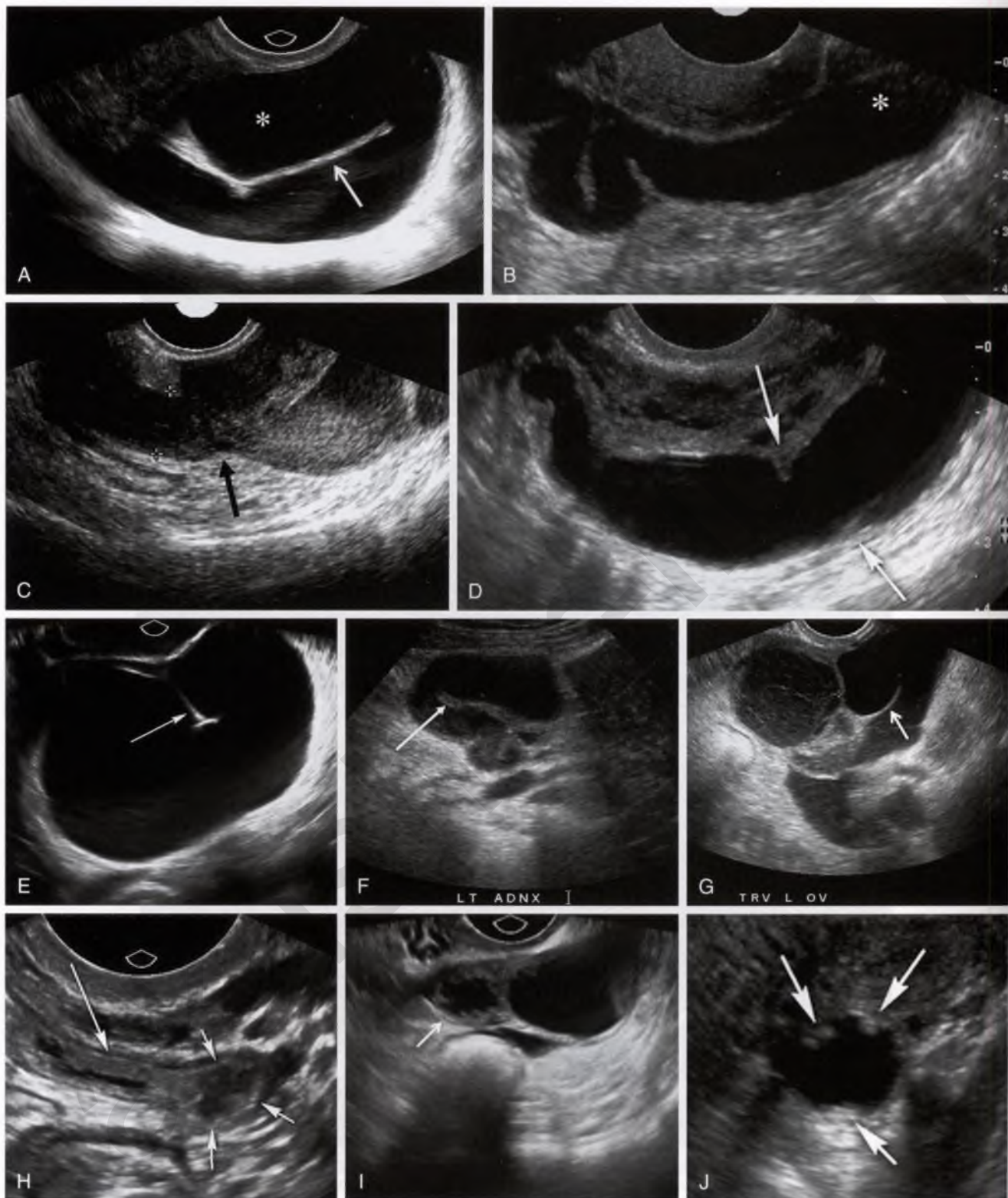


**FIG 31-5** The varied ultrasound image appearance of hydrosalpinx. **A**, Dilated anechoic tubular left adnexal structure in a U shape is consistent with hydrosalpinx. Note that the ampullary end (*asterisk*) anteriorly is wider than the isthmic portion of the tube, which is more posterior on this image. The linear echogenic structure (*arrow*) between the ampullary and isthmic segments represents the two juxtaposed inner walls of the tube as it folds on itself and has been described as the “incomplete septation sign.” Unlike a true septation, the incomplete septation of a folded tube will not extend from wall to wall and the lumen of the tube will remain open around the free edge. This sign helps to differentiate a folded hydrosalpinx from a complex, cystic adnexal mass. **B**, Serpiginous or S-shaped hydrosalpinx. The more lateral ampullary end



**FIG 31-5, cont'd** (*asterisk*) is wider than the isthmus. **C**, Often there is an abrupt transition in diameter (*arrow*) between the wider ampullary portion of the tube and the isthmus (*calipers*) as in this patient with a dilated left fallopian tube containing internal echoes consistent with pyosalpinx. **D**, Waist sign: Note indentations (*arrows*) on opposing sides of the dilated fallopian tube believed to be due to thickening of the endosalpingeal folds. **E**, Incomplete septation sign: Note the thin linear echogenic structure (*arrow*) appearing to protrude into the dilated fallopian tube. This represents the apposition of two segments of the inner wall of the fallopian tube as it folds on itself and, therefore, does not extend across the entire diameter of the dilated fallopian tube. This appearance serves to differentiate a folded fallopian tube from a complex cystic adnexal mass with a true septation that would extend from wall to wall. **F**, Incomplete septation sign (*arrow*) in a second patient with a serpiginous dilated fallopian tube containing low level internal echoes consistent with pyosalpinx. The more dilated ampullary segment is located anteriorly. **G**, Incomplete septation sign (*arrow*) in another patient with pyosalpinx. Note the left ovarian cyst (*calipers*) with fine reticular pattern of internal echoes, likely representing hemorrhage or possibly infection. **H**, Cogwheel sign: Note the slightly dilated, thick-walled tortuous fallopian tube visualized on this image in both long axis (*long arrow*) and in cross section (*short arrows*). Note several mural-based small nodules on cross section representing thickened endosalpingeal folds. This appearance has been termed the cogwheel sign. **I**, Cogwheel sign: Note numerous echogenic, thickened, endosalpingeal folds regularly spaced around the periphery of the dilated fallopian tube in this patient with chronic salpingitis. In cross section (*arrow*), these thickened folds may appear nodular, mimicking cystic ovarian malignancy except that these folds are so regularly spaced and symmetric. **J**, Beads on a string sign: Note the slightly dilated thin-walled fallopian tube in cross section with multiple mural-based echogenic nodules (*arrows*) due to thickening of the endosalpingeal folds, resulting in the appearance of "beads on a string." (J courtesy of Dr. Margarita Revzin, Yale University School of Medicine, New Haven, CT.)

## PELVIC INFLAMMATORY DISEASE

Pelvic inflammatory disease (PID) is usually caused by sexually transmitted organisms that ascend from the vagina and cervix to the upper female genital tract. Approximately 770,000 acute cases are reported yearly in the United States. The number of subacute and chronic cases is unknown. Risk factors for PID include young age, multiple sexual partners, lack of barrier contraception, low socioeconomic class, and smoking.<sup>8-10</sup> The inciting organisms are usually *Chlamydia trachomatis* and *Neisseria gonorrhoeae*, which cause epithelial damage to the tubes, allowing superinfection with polymicrobial opportunistic organisms. The infection initially ascends from the cervix to involve the endometrium causing endometritis and progresses to involve the fallopian tubes resulting in tube inflammation. Tube adhesions may form causing obstruction leading to hydrosalpinx, hematosalpinx, or pyosalpinx. Eventually the infection will spread to the ovary and peritoneum causing uterine serositis, peritonitis, inflammation of the pelvic fat, tubo-ovarian complex (TOC), and finally tubo-ovarian abscess (TOA). Symptoms include pelvic pain, cervical motion tenderness, purulent vaginal discharge (which may be foul smelling), fever, leukocytosis, and elevated erythrocyte sedimentation rate or C-reactive protein level.<sup>11</sup> The degree of pelvic pain is highly variable. Inflammation around the liver can result in right upper quadrant (RUQ) pain, termed Fitz-Hugh-Curtis syndrome. Complications following PID include pelvic abscess, infertility (20%), ectopic pregnancy (9%), and chronic pelvic pain (18%).<sup>12-14</sup>

Because symptoms are insufficient for diagnosis in up to 50% of cases and often overlap with other pelvic conditions such as appendicitis, ruptured or hemorrhagic ovarian cysts, and diverticulitis, imaging is frequently performed. In addition, imaging may be required if the patient is not responding appropriately to antibiotic therapy, particularly if an abscess is suspected. Sonography should be the first imaging study obtained, although occasionally computed tomography (CT) or magnetic resonance imaging (MRI) may be required to assess the full extent of an abscess, especially when rupture is considered likely. Despite the frequent use of ultrasound to assess patients with PID, there are no large trials evaluating the sensitivity and specificity of

sonography for the diagnosis of PID. However, sonography likely has relatively low sensitivity for detecting mild abnormalities and is non-specific for many others. When the fallopian tubes become involved, the specificity of sonography improves.<sup>15,16</sup> Transvaginal sonographic imaging is considered most useful for detecting tube abnormalities and to identify the ovaries, with transabdominal imaging most often used to evaluate large pelvic abnormalities and to assess the full extent of ascites.

Cervicitis is typically occult on ultrasound examination and is diagnosed by direct visualization and culture. Endometritis will appear on ultrasound imaging as indistinct thickening of the endometrium, which is often extremely vascular. The endometrial cavity may be distended with fluid, hemorrhage, and even air, which is characterized on sonography by the presence of echogenic foci with dirty posterior shadowing. However, there is overlap in the sonographic appearance as well as the clinical presentation of endometritis with normal postpartum changes and retained products of conception. In addition, endometritis may develop postpartum or in patients with retained products of conception.

Involvement of the fallopian tube or ovary is the hallmark of PID and results in a variety of sonographic findings. Salpingitis manifests as mild thickening and hyperemia of the tube (Fig. 31-6) and peritubal inflammation. Sonographically, these changes result in a prominent or thick tube that is thus more easily visualized, and hyperemia is typically observed on color Doppler imaging. Increased echogenicity and vascularity in the surrounding pelvic fat is common as a result of inflammation or infection (Fig. 31-7).<sup>17</sup> Small amounts of adjacent complex free fluid may be present and the ovaries may appear enlarged and edematous with an appearance simulating polycystic ovary disease.<sup>18</sup>

Pyosalpinx occurs when adhesions obstruct the fimbriated end of the tube allowing pus to accumulate within the lumen (Fig. 31-8). Fluid debris levels are common, although intraluminal gas is rare. The wall of the tube becomes thick and vascular. Thickening of the endosalpingeal folds may cause the tube wall to appear nodular with numerous 2- to 3-mm nodules projecting into the lumen, the previously described cogwheel sign (see Fig. 31-5). As the infection progresses, the ovary may become adherent to and surrounded by the



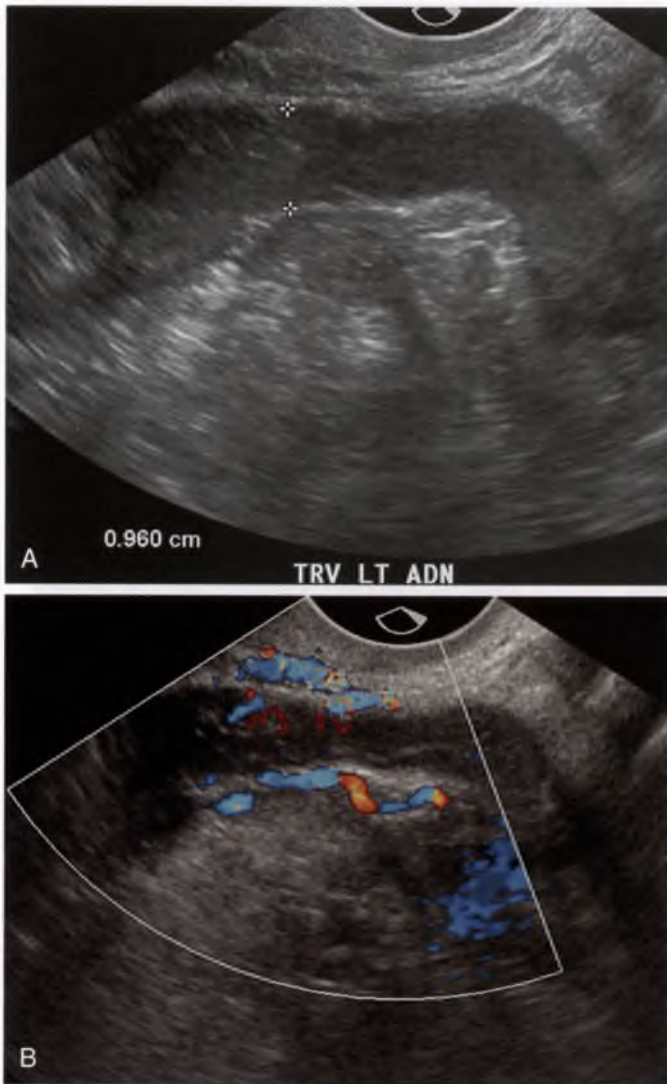


**FIG 31-6** Salpingitis. Note thickened (0.96 cm) left fallopian tube (*calipers*) on gray-scale image (A) in a patient presenting with pelvic pain, fever, and vaginal discharge. Color Doppler image (B) demonstrates increased vascularity in the wall of the tube and in the surrounding inflamed peritubal fat. There is no discernible fluid in the lumen of the tube.

inflamed tube, and eventually pus will pour out of the tube and engulf the ovary. The ovary is initially protected from infection by its thick fibrous capsule. If the ovary (with or without the tube) is clearly distinguishable from the surrounding inflamed and infected tissues, the mass is termed a TOC (Fig. 31-9). Eventually the fibrous capsule will break down and the ovarian parenchyma itself will become infected and necrotic resulting in formation of a TOA and loss of the normal sonographic ovarian architecture. The resulting complex mass is usually multilocular with solid and cystic components, increased vascularity, thickened septa, and sometimes mural nodularity (Figs. 31-10 and 31-11). An acute TOA is usually quite tender on examination. The ovary will not be identifiable within the mass, although the dilated fallopian tube may be at least partially visible (Fig. 31-12). Distinguishing between a TOC and a TOA is clinically important because a TOC will respond better to antibiotic therapy. Clinical findings may not always correlate with the degree of sonographic abnormality. Women with only peritoneal inflammation but without sonographic evidence of pyosalpinx or TOA may be extremely symptomatic owing

to inflammation of the peritoneal surface, whereas patients with recurrent PID and previously damaged tubes may have a very abnormal sonogram but only mild symptoms. Sonographic findings of a TOA are somewhat nonspecific, and endometriomas, ovarian malignancy, and periappendiceal and diverticular abscess may have a very similar appearance<sup>19</sup> (Fig. 31-13). Occasionally acute appendicitis may mimic the clinical presentation of PID and can be diagnosed on transvaginal ultrasound examination. Unilaterality of the right-sided dilated tubular structure, clear separation from the normal ovary, the presence of an appendicolith, and absence of the incomplete septation, waist, or cog-wheel signs can be helpful in differentiating acute appendicitis from a pyosalpinx (Fig. 31-14).

Little is known about the sonographic response to medical therapy for PID, particularly how long it may take for acute abnormalities to resolve.<sup>20</sup> In this author's experience, complex fluid, inflammation and minimally dilated tubes can resolve in several days, whereas a large pyosalpinx or TOA may require weeks to months to resolve. Some reports indicate that patients with a normal sonogram initially may, over time, develop a hydrosalpinx as a result of development of adhesions. Persistent inflammatory masses most likely signify an incompletely treated infection, especially if vascular. Although hydrosalpinx most commonly develops secondary to PID, tube ligation, ovulation induction, tumors, and endometriosis may all lead to hydrosalpinx formation. Occasionally hydrosalpinx occurs after hysterectomy if the fallopian tubes have not been removed.<sup>21</sup>

## UNCOMMON TUBE INFECTIONS

A variety of tube infections occur by routes other than those of ascending sexually transmitted diseases. Tuberculosis reaches and infects the fallopian tubes most commonly via hematogenous or lymphatic routes and occasionally via direct contiguous peritoneal spread. Clinical manifestations include acute and chronic pain, unexplained infertility, and vaginal bleeding. Most commonly the tubes become thick and hyperemic rather than markedly dilated and may progress to a TOA or pelvic abscess (Fig. 31-15).<sup>22</sup>

Tube actinomycosis is most commonly caused by infection of the female genital tract by *Actinomyces israelii*, an opportunistic gram-positive bacterium typically introduced by foreign bodies (such as intrauterine devices [IUDs]), surgery, bowel perforation, and trauma. It is estimated that 25% of IUDs become colonized with *Actinomyces* and that 2% to 4% may develop an infection requiring treatment.<sup>23</sup> The presence of an IUD and pelvic abscess should suggest this diagnosis.<sup>24</sup> Actinomycosis is an aggressive and infiltrative infection, likely due to the proteolytic enzymes produced by the bacteria. The hallmark of this infection is extensive inflammatory infiltration with spread across tissue planes often with fistula and abscess formation (Fig. 31-16). Thus, CT is the modality of choice to determine extent of disease. Treatment involves removal of the IUD, administration of penicillin, and abscess drainage. If the infection is severe, hysterectomy or salpingo-oophorectomy may be required.

Xanthogranulomatous inflammation, which occurs in many organs, most notably in the kidney and gallbladder, has rarely been reported in the female genital tract. It may affect the endometrium, ovary, or fallopian tube.<sup>25</sup> The likely cause is subacute infection with obstruction of the fallopian tube. The characteristic histologic finding of all xanthogranulomatous infections is the presence of lipid-laden macrophages and multinucleated giant cells that replace the destroyed parenchyma of the involved organ. The sonographic and CT appearance of xanthogranulomatous TOA has been reported as a mixed solid and cystic adnexal mass, typically unilateral, with a fairly nonspecific

*Text continued on p. 946*



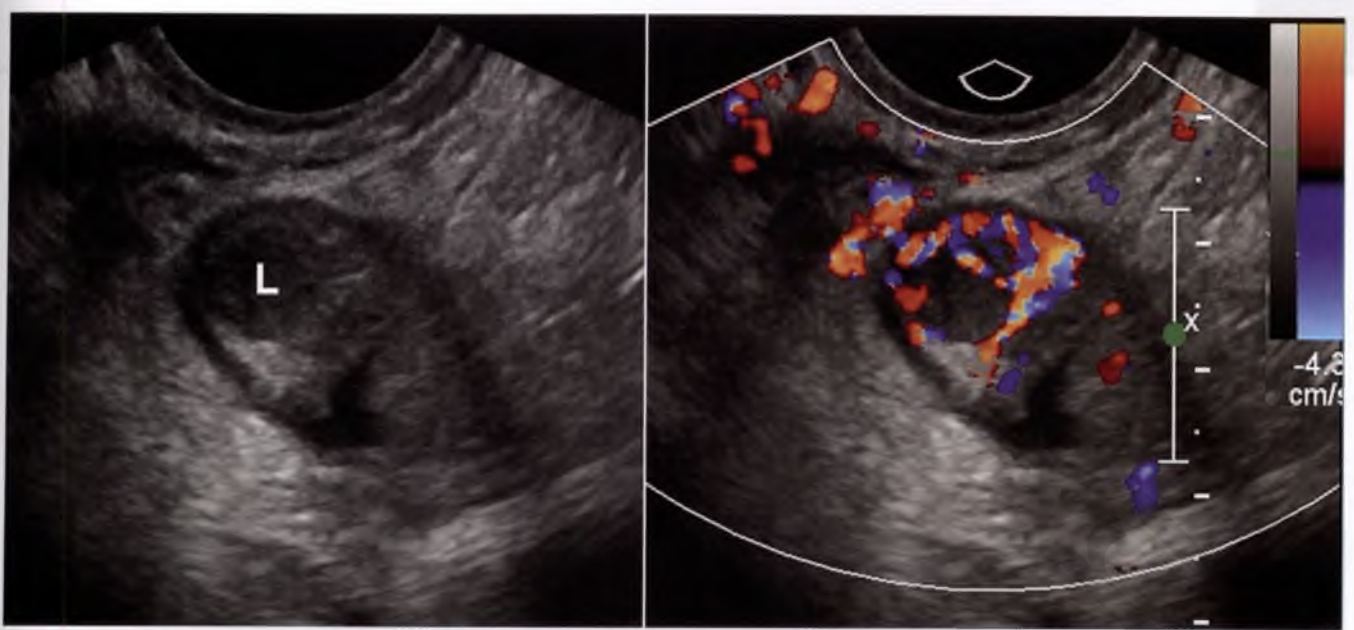


**FIG 31-7** Acute salpingitis: Split screen image of the fallopian tube in cross section on gray-scale (*left*) and color Doppler (*right*). The wall of the fallopian tube is thick and hyperemic with a small amount of complex fluid in the lumen (L). The surrounding fat is echogenic and vascular consistent with inflammation.

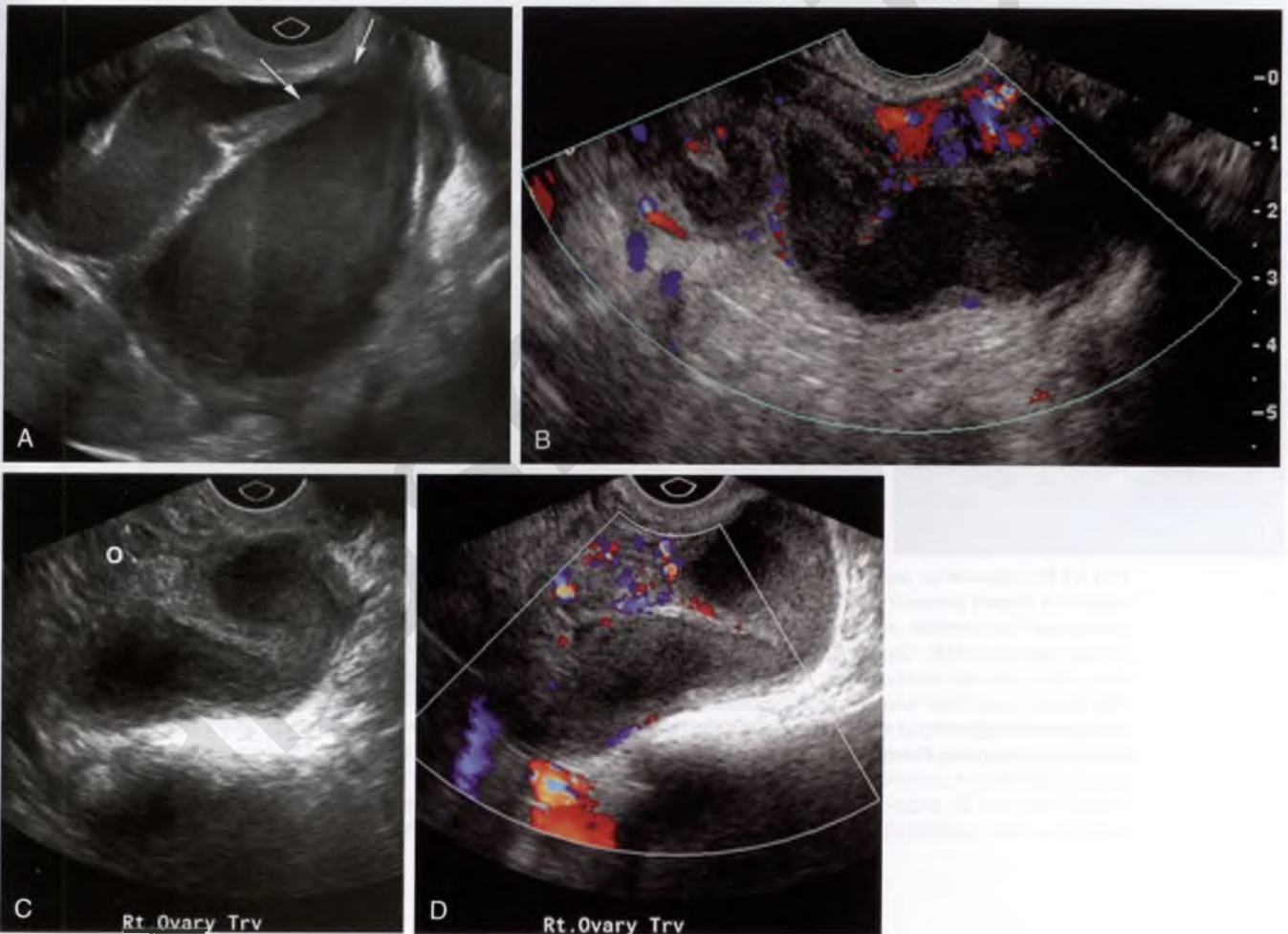


**FIG 31-8** Pyosalpinx. **A**, The left fallopian tube in a patient with pyosalpinx is markedly dilated and filled with echogenic material, consistent with pus, hemorrhage, or debris. Note fluid/fluid level and thick echogenic wall. The tube is curled back upon itself demonstrating the incomplete septation sign and is also focally symmetrically indented, the "waist sign" (*arrows*). **B**, Color Doppler image of the left adnexa in a second patient with pyosalpinx demonstrating a dilated serpiginous tubular structure containing low level intraluminal echoes and increased mural vascularity. Gray-scale (**C**) and color Doppler (**D**) ultrasound images from a third patient with pyosalpinx demonstrating a dilated fallopian tube adherent to the enlarged, edematous right ovary (O). The wall of the tube is thick and hyperemic and the lumen contains internal echoes. Findings are most consistent with pyosalpinx, although hematosalpinx could also result in layering or conglomerate intraluminal echoes within a dilated fallopian tube. (C and D courtesy of Dr. Margarita Revzin, Yale University School of Medicine, New Haven, CT.)



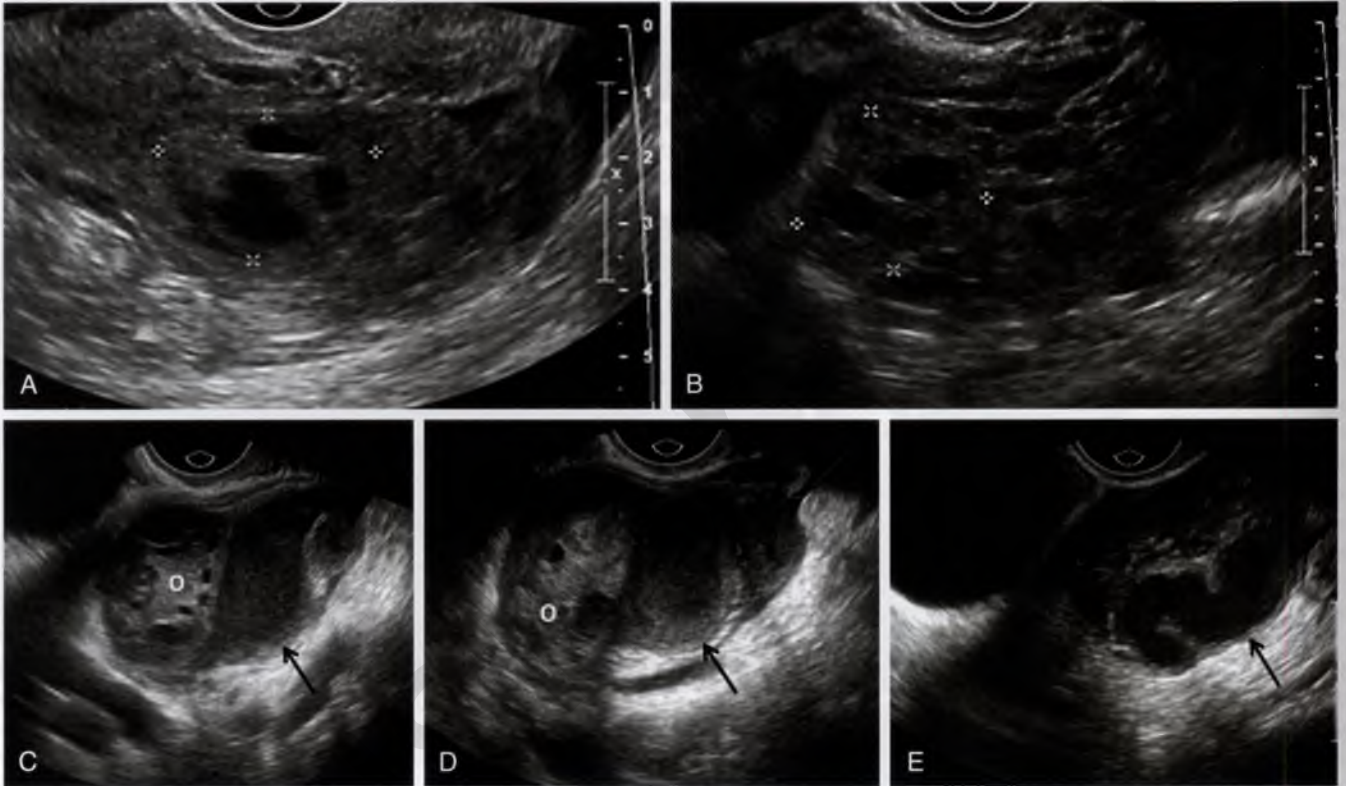


**FIG 31-9** Tubo-ovarian complex. Transverse (**A**) and sagittal (**B**) images demonstrating a complex adnexal mass in a patient presenting with pelvic pain and fever. Note that the ovary (*calipers*) is recognizable and is surrounded by complex inflammatory material suggesting tubo-ovarian complex (TOC) rather than tubo-ovarian abscess (TOA). Sagittal (**C** and **D**) and transverse (**E**) gray-scale images in another patient presenting with pelvic pain and leukocytosis. The ovary (O) is recognizable with its small follicles but is surrounded by the dilated, pus-filled fallopian tube (pyosalpinx) (*arrows*) and complex fluid consistent with TOC. Note increased echogenicity of the adjacent pelvic fat, suggestive of inflammation or infection. (C, D, and E courtesy of Dr. Margarita Revzin, Yale University School of Medicine, New Haven, CT.)

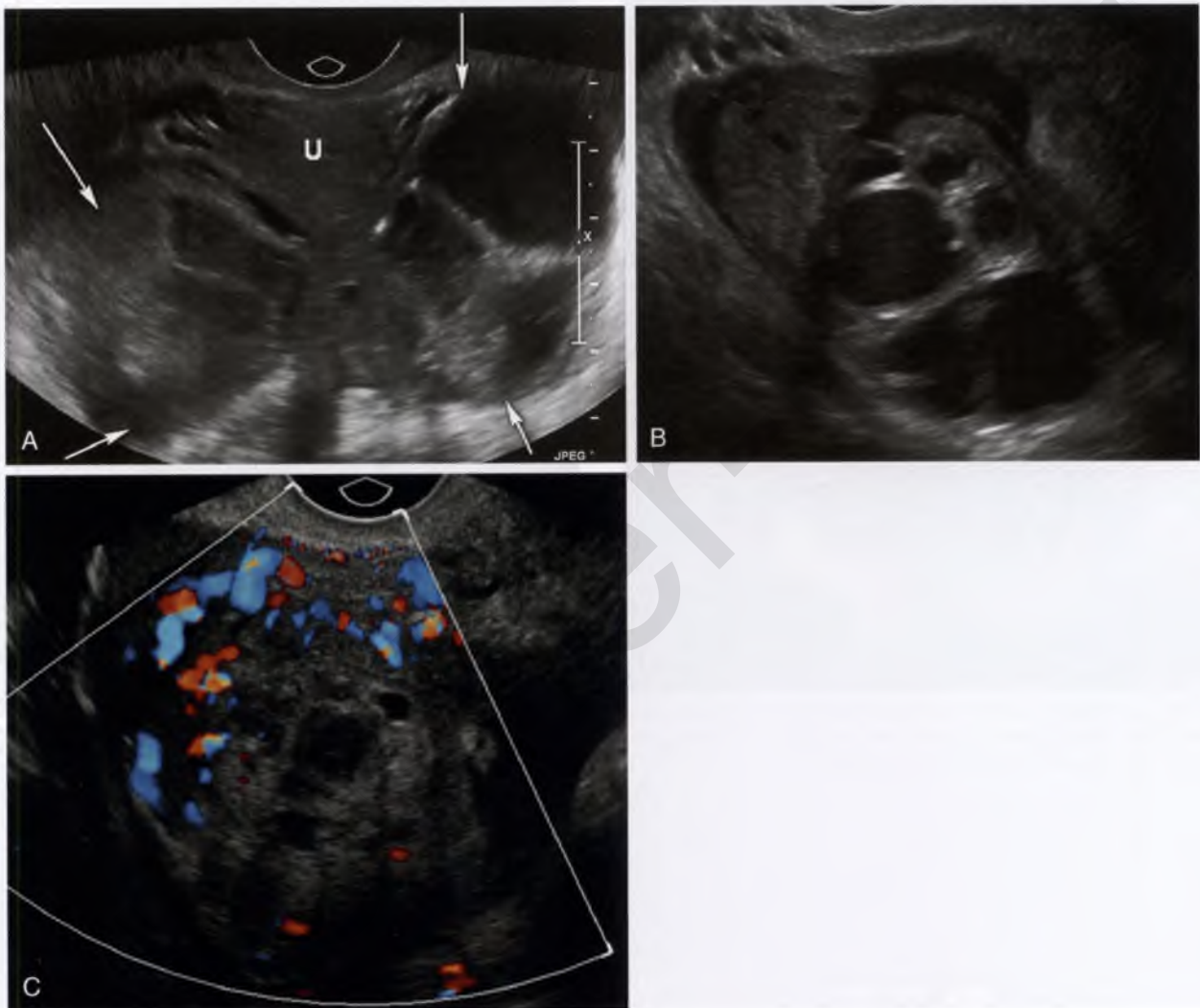


**FIG 31-10** Tubo-ovarian abscess (TOA). **A**, Transverse gray-scale view of the uterus (U) with bilateral TOAs (arrows) demonstrating solid and complex cystic components with ill-defined borders. No normal-appearing ovary could be identified on either side. **B**, Another patient with TOA. Note the complex, multilocular adnexal mass with surrounding free fluid. The ovary and tube are not discretely recognizable. **C**, In a third patient with a TOA, note increased vascularity on color Doppler image of more solid appearing, markedly tender adnexal mass.



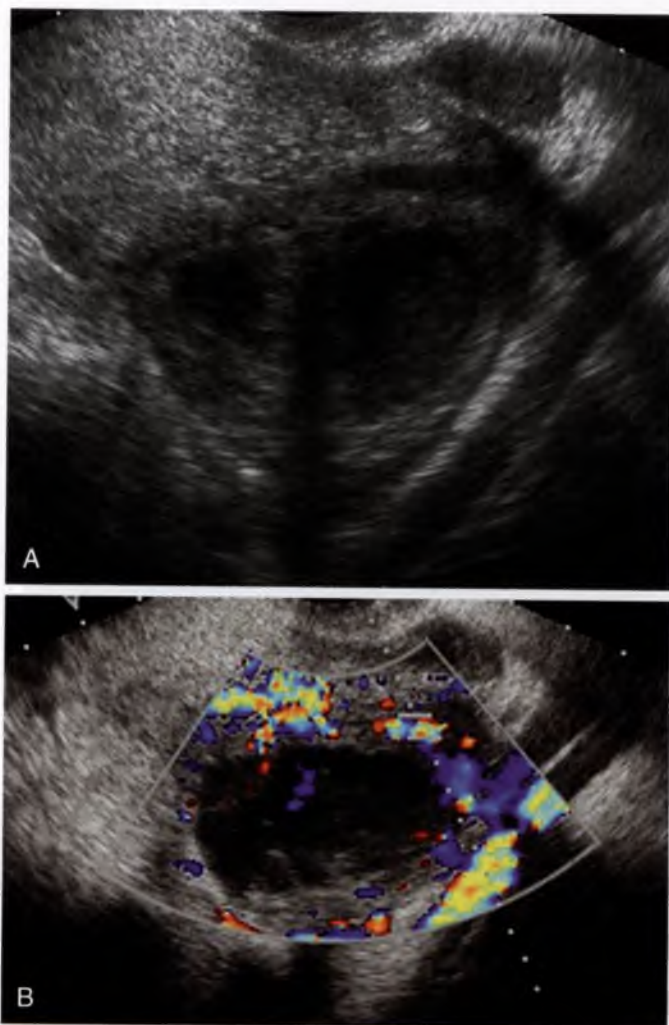


**FIG 31-11** Tubo-ovarian abscess. Gray-scale (**A**) and color Doppler (**B**) transvaginal sonographic images of left adnexal cystic mass with internal echoes and marked peripheral vascularity.

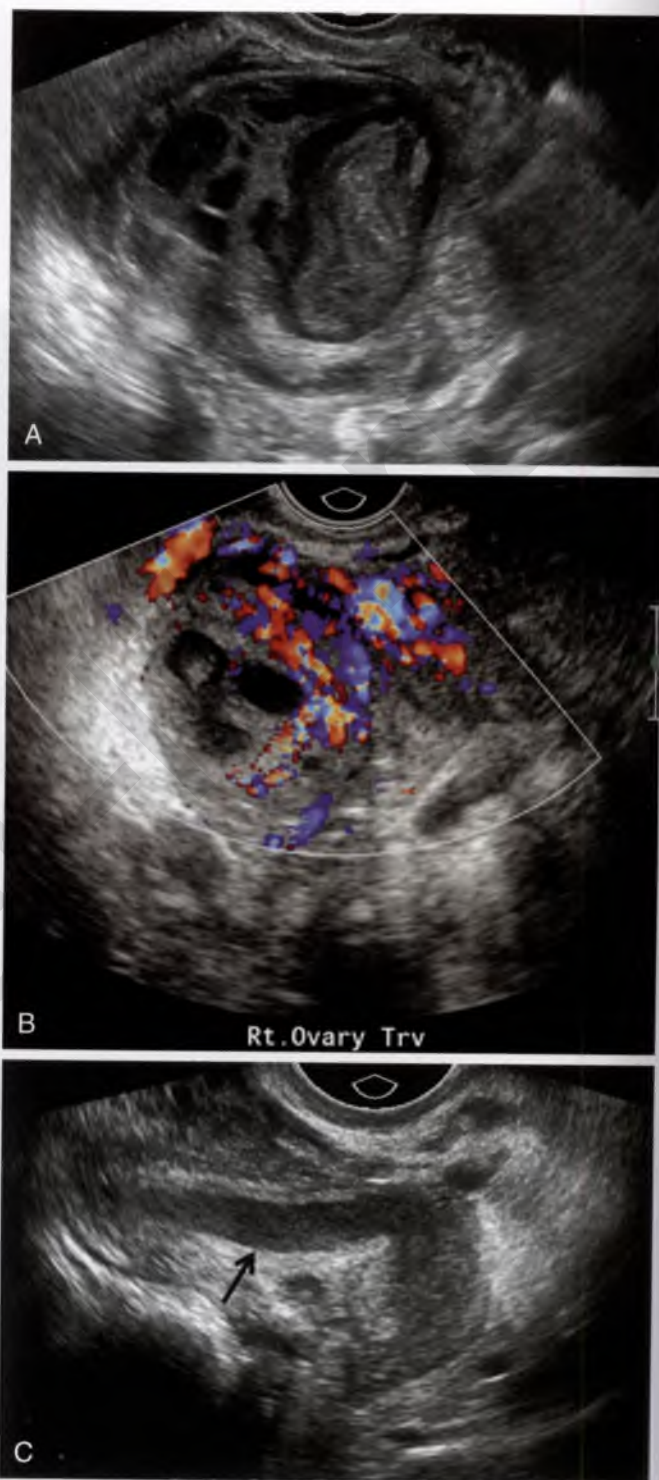


**FIG 31-12** Tubo-ovarian abscess. A 27-year-old woman presented with bilateral pelvic pain and purulent vaginal discharge. **A**, Gray-scale image of the right adnexa demonstrating a complex, tender adnexal mass that was markedly vascular on color Doppler imaging (**B**). **C**, Note mildly dilated thick-walled adjacent pyosalpinx (*arrow*) and increased echogenicity of the adjacent pelvic fat. (Images courtesy of Dr. Margarita Revzin, Yale University School of Medicine, New Haven, CT.)

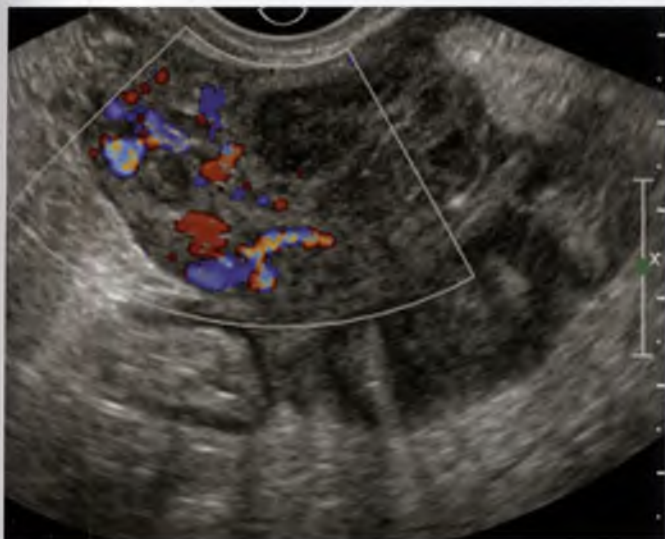


**FIG 31-13** Diverticular abscess. Complex, hypervascular left adnexal mass adjacent to thick-walled bowel loop in a 62-year-old woman who presented with left-sided pelvic pain and fever. At surgery this mass was found to be a diverticular abscess. Diverticular abscess is more likely to occur in older women, be unilateral and left-sided, contain air, and be associated with abnormal loops of bowel. (From Baltarowich OH, Scoutt LM, Hamper UM: Nongynecologic findings on pelvic ultrasound: focus on gastrointestinal diseases. *Ultrasound Q* 28:65-85, 2012, used with permission.)

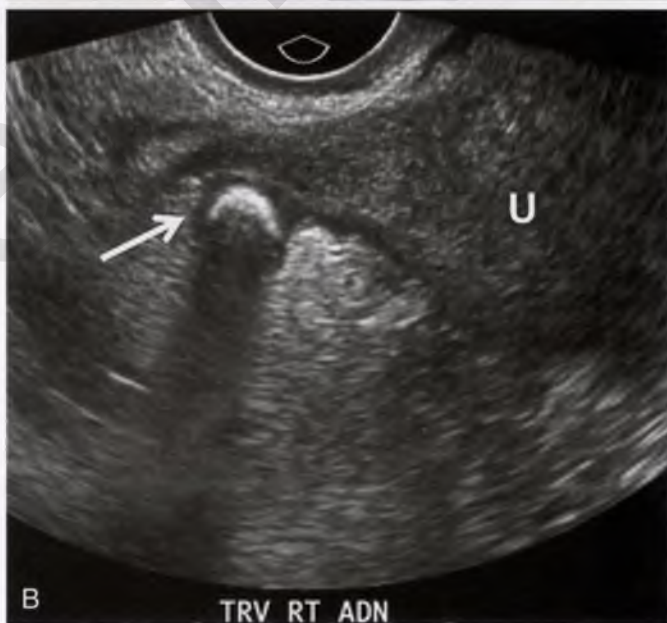
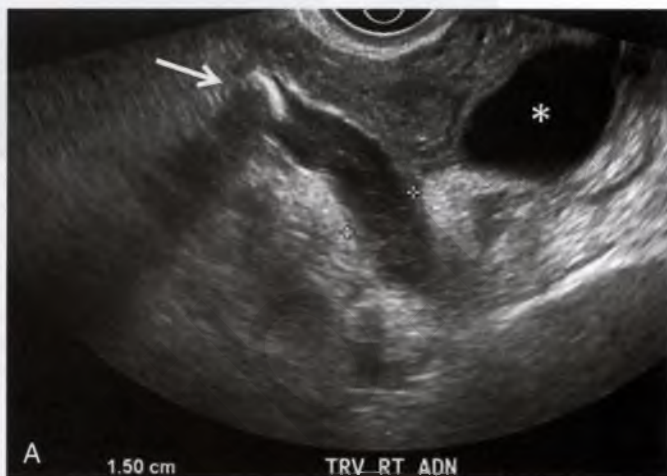


**FIG 31-14** Acute appendicitis. A 37-year-old woman presented with pelvic pain and chills for 2 days. Transvaginal sonographic images of right adnexa (A and B) revealed a tender, fluid-filled tubular structure (*calipers*) measuring 1.5 cm in diameter lateral to the right ovary. Also shown is a sharply marginated echogenic round structure (*arrow*) with dense acoustic shadowing, consistent with appendicolith. Also note increased echogenicity of the adjacent pelvic fat, a nonspecific finding indicative of inflammation or infection. *Asterisk*, right ovarian cyst; U, uterus.



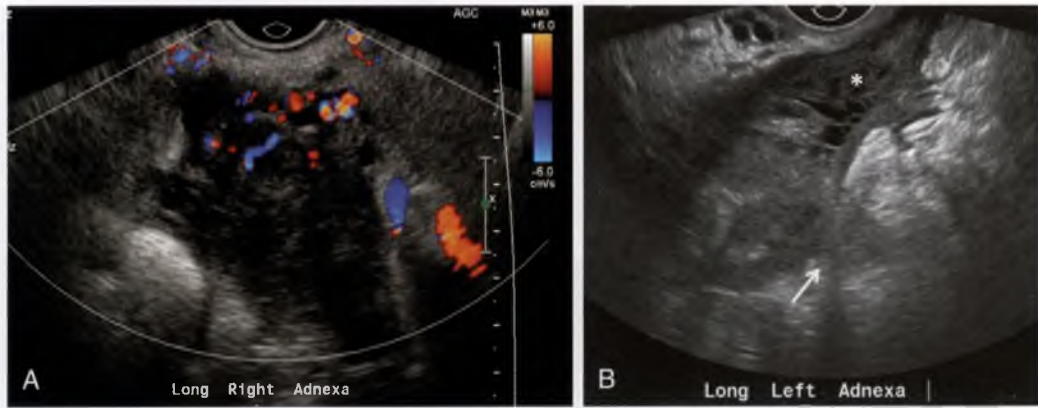


**FIG 31-15** Thirty-year-old woman from southeast Asia presenting with 9 months of unexplained weight loss and pelvic pain. Color Doppler image of the right adnexa (**A**) and gray-scale image of the left adnexa (**B**) demonstrate bilateral hyperemic complex adnexal masses. Note surrounding complex free fluid, best seen in **B** (\*) and infiltration of adjacent pelvic fat (arrow in **B**). Neither fallopian tube or ovary could be discretely identified. Whereas findings are nonspecific and consistent with bilateral tubo-ovarian abscesses, the clinical presentation is atypical for pelvic inflammatory disease because the patient was afebrile and there was no vaginal discharge. CT scan (not shown) demonstrated omental thickening, and biopsy was positive for tuberculosis. CXR (not shown) also demonstrated findings suspicious for tuberculosis. The adnexal masses slowly resolved with anti-TB therapy. (Images courtesy Dr. Manjiri Dighe, University of Washington Medical Center, Seattle, Washington.)

appearance (Fig. 31-17). The differential diagnosis includes endometriosis, PID-related inflammatory mass, and malignancy.<sup>26</sup>

Lastly, a gastrointestinal process that has spread beyond the bowel such as perforated appendicitis or diverticulitis may secondarily infect the fallopian tubes.

## HEMATOSALPINX

In the nonpregnant patient, hematosalpinx is most commonly due to endometriosis but can also occur secondary to PID, adnexal torsion, malignancy, trauma, and uterine anomalies with retrograde menstruation.<sup>19</sup> The sonographic appearance of a hematosalpinx is similar to a pyosalpinx with variable degrees of wall thickening and internal echoes. Echogenicity will be variable depending upon the length of time since the hemorrhage occurred. Layering of the intraluminal echoes may be observed. Endometrial implants on the surface of the tube may cause hydrosalpinx from scarring and fibrosis, whereas luminal implants are more likely to result in hematosalpinx.<sup>27</sup> A hematosalpinx secondary to endometriosis often demonstrates the fine, homogeneous low level internal echoes typical of an endometrioma (Fig. 31-18, Video 31-3). Unlike an acute pyosalpinx, the walls of the tube will be sharply delineated without hyperemia or surrounding inflammation. The presence of blood in the fallopian tube may be easily confirmed on MRI if the sonographic findings are nonspecific.

## TUBE TORSION

Torsion of the fallopian tube without associated ovarian torsion is a rare event and is reported most frequently in adolescent girls. Patients present with nonspecific acute pelvic pain. The diagnosis can be suggested when a painful dilated fallopian tube with a normal ipsilateral ovary is observed.<sup>4</sup> In this author's experience, the tube will often have a tense appearance and be in an unusual location high in the adnexal region or in the midline (Video 31-4). A beaked or pointed appearance of the ends of the twisted dilated tube, which is often in a V- or U-shaped configuration, may be observed (Fig. 31-19). As in ovarian torsion, detection of color flow in the wall of the tube does not exclude the diagnosis of tube torsion. A whirlpool sign may be demonstrated

with coiling of the proximal tube and tube vessels.<sup>28</sup> Tube torsion is usually managed with salpingectomy, though some have suggested a more conservative approach of detorsion and drainage to preserve fertility in girls and young women.<sup>29</sup>

## MALIGNANCY

Previously, primary fallopian tube carcinoma (PFTC) was thought to be the rarest gynecologic malignancy, with an incidence of less than 2%. Risk factors include the *BRCA* mutations as well as nulliparity. PFTC is most common in postmenopausal women. The diagnosis previously required the following characteristics: (a) main tumor arising from endosalpinx, (b) papillary pattern on histologic examination, (c) visible transition between benign and malignant epithelium within the tube, and (d) normal or minimally involved ovary and endometrium (i.e., the tube tumor was required to be larger than any tumor in the ovary or endometrium).<sup>30</sup> However, a recently proposed theory now accepted by many pathologists suggests that most serous ovarian carcinomas actually arise from malignant tube epithelial cells that implant on the ovary.<sup>31</sup> This concept is supported by data from women with *BRCA1* or *BRCA2* mutations who underwent prophylactic salpingo-oophorectomy and were found to have carcinoma in situ or invasive carcinoma of the fallopian tube without ovarian malignancy. Furthermore, the ovary does not intrinsically harbor an epithelial cell of origin as does the fallopian tube. Thus, the true incidence of PFTC may have been significantly underestimated. See Chapter 30, "Ultrasound Evaluation of the Ovaries," for further detail.

Latzko's triad—namely, intermittent bloody vaginal discharge, colicky pain relieved by the discharge, and a pelvic mass—has been described as the classic clinical presentation of PFTC but only occurs in a minority of patients, less than 10%. These symptoms occur as the tumor secretes serous fluid into an obstructed fallopian tube resulting in painful distention of the tube, which intermittently decompresses by discharging fluid into the endometrial cavity or the peritoneum. However, many patients are asymptomatic and the tumor is found incidentally. Approximately 50% of patients present with postmenopausal vaginal bleeding. The imaging findings overlap with primary ovarian carcinoma and depend upon whether the tube is primarily

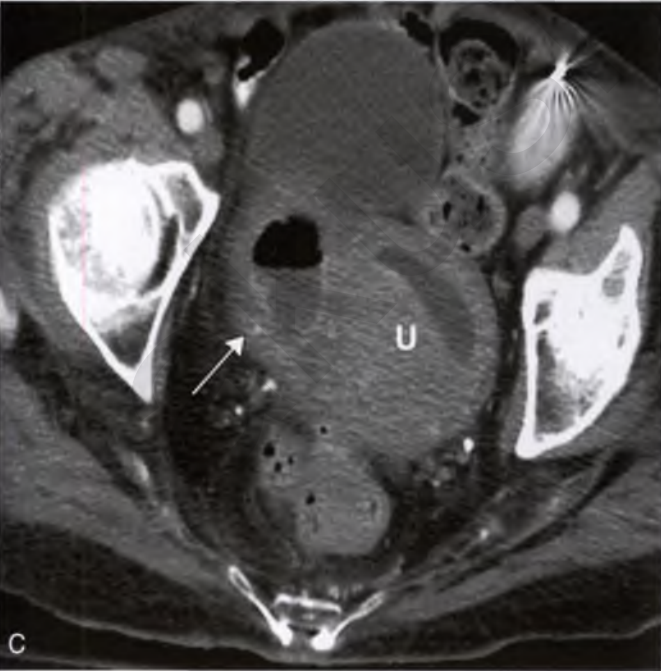
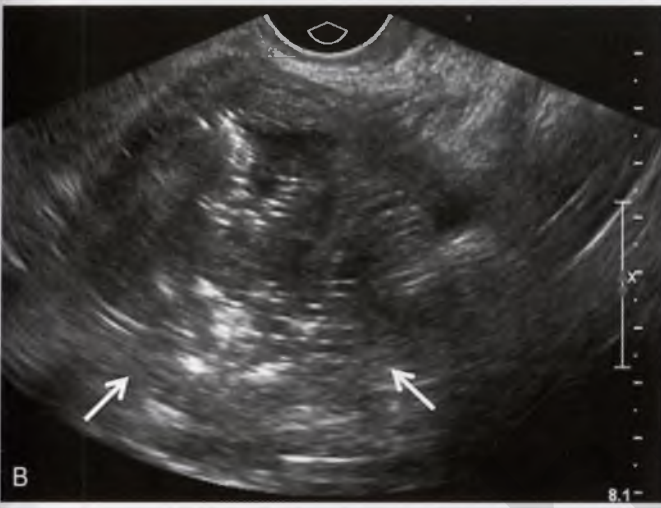


**FIG 31-16** Actinomycosis. Transvaginal sonographic images of the right adnexa (**A** and **B**) in an 82-year-old woman presenting with abdominal discomfort. Note a large mass (*arrows*) adjacent to the uterus (U) containing numerous brightly echogenic foci suggesting microbubbles of gas. Contrast-enhanced axial computed tomographic scan (**C**) confirms the presence of a large gas-containing abscess (*arrow*) in the right adnexa adjacent to the uterus (U). A fistula to the bowel was found at surgery and cultures grew *Actinomyces*. (Images courtesy of Dr. Margarita Revzin, Yale University School of Medicine, New Haven, CT.)



**FIG 31-17** Xanthogranulomatous salpingitis: Note large complex mass with a tubular cystic component posteriorly and a solid component with shadowing echogenic foci adjacent to the normal ovary (O).



**FIG 31-18** Hematosalpinx. Dilated, thin-walled fallopian tube contains fine, homogeneous low level echoes consistent with blood. Posterior enhancement confirms the cystic nature of the lesion. Incomplete septation sign (*arrow*) indicates where the tube has folded on itself.



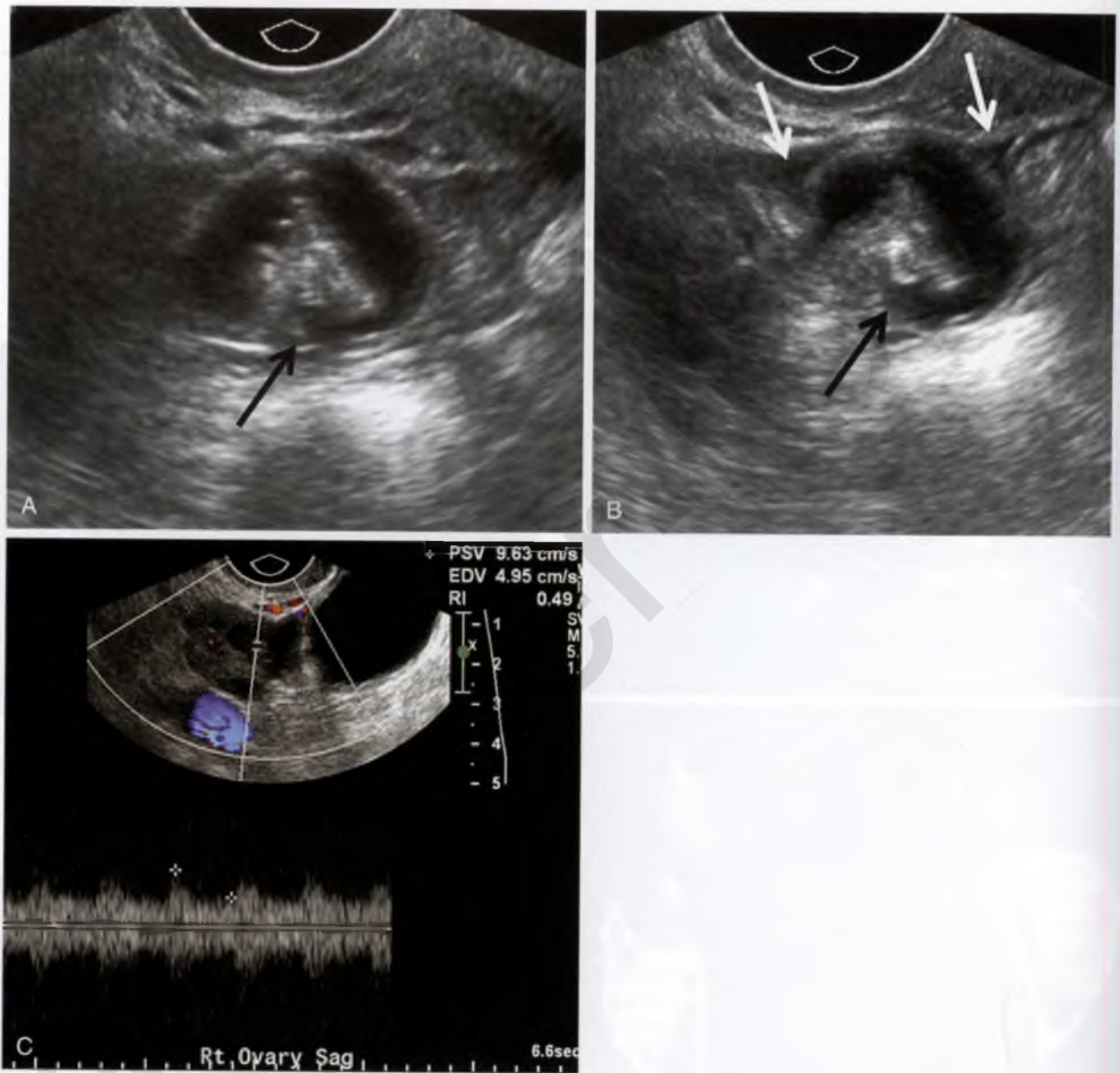


**FIG 31-19** Isolated torsion of the fallopian tube. A 15-year-old girl with acute onset, severe right lower quadrant to midline pelvic pain. **A** and **B**, Note dilated tubular fluid-filled structure in an upside-down U-shaped configuration with a pointed or "beaked" appearance at the medial end (*black arrow*), as a result of twisting or torquing. The twisted fallopian tube was in an abnormal location, situated above the uterus toward the midline. There is a small volume of adjacent free fluid (*white arrows*). **C**, The right ovary appears normal in size and morphologic appearance with normal flow on color and spectral Doppler interrogation.

dilated and fluid-filled, or predominantly thick-walled and solid in appearance (Fig. 31-20).<sup>32</sup> A characteristic observation is a change in sonographic appearance on serial studies as the degree of tube distention varies. Doppler imaging may be useful to differentiate tumor from debris and to detect low resistance flow.<sup>33</sup> CT and MRI should be used for staging.

## EVALUATION OF TUBE PATENCY

Though hysterosalpingography (HSG) has been the traditional imaging modality of choice to evaluate tube patency, newer techniques involving agitated saline and ultrasound contrast agents injected during sonohysterography (SIS) have shown promise as an alternate imaging technique. Although the injection of saline agitated with air bubbles

when performing SIS can confirm tube patency, the bubbles are fairly evanescent. Ultrasound contrast “microbubbles” last longer and can be imaged with real-time cine clips and reconstructed two-dimensional and three-dimensional images to confirm tube patency. Reported correlations with HSG are excellent in several small series.<sup>34</sup> Adding targeted color Doppler interrogation of each tube during directed contrast agent injection can increase the accuracy of SIS for tube patency.<sup>35</sup> It is also generally accepted that accumulation of free fluid in the peritoneal cavity during routine SIS implies patency of at least one fallopian tube.<sup>36</sup> Sonography can also be useful in evaluating patients with mechanical tube occlusion devices, such as Essure, used for contraception. When normally positioned, the portion of the Essure placed in the intramural or interstitial segment of the fallopian tube is easily visualized sonographically (Fig. 31-21). A malpositioned Essure device

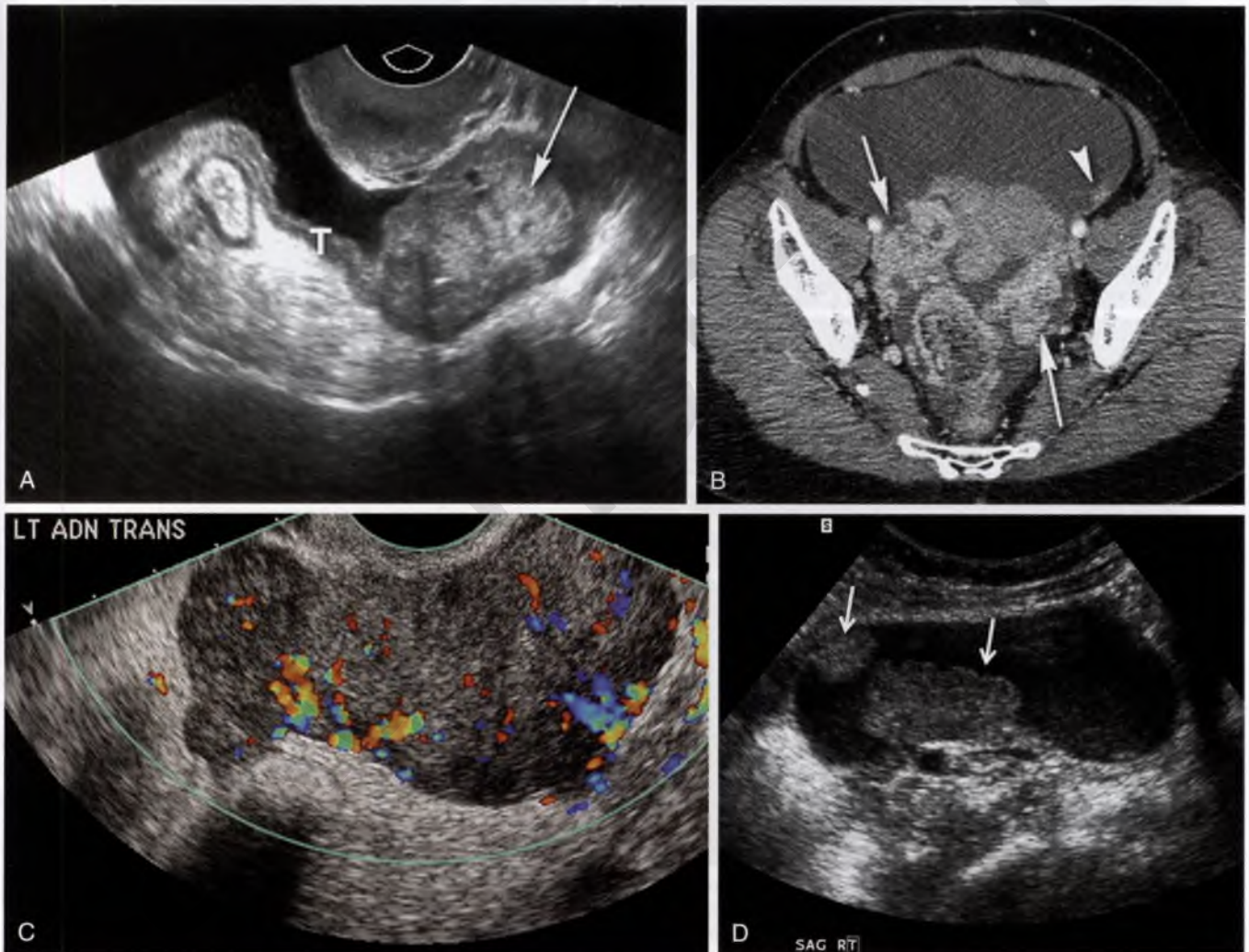


**FIG 31-20** Fallopian tube carcinoma. **A**, Anechoic ascites partially surrounds the hypoechoic left fallopian tube (T), which has an abnormally thick, slightly heterogeneous solid mass-like appearance at the distal end (arrow). **B**, Corresponding axial contrast-enhanced computed tomographic scan demonstrates bilateral abnormal fallopian tubes (arrows), which are thickened, nodular, and enhancing. There is a large amount of surrounding ascites. Note enhancing peritoneal implant (arrowhead). **C**, Color Doppler image demonstrating a solid, vascular left adnexal tubular structure in another patient with primary fallopian tube cancer. **D**, A 43-year-old woman with fallopian tube cancer presented with vaginal bleeding. Transvaginal sonographic image demonstrates right hydrosalpinx containing two solid mural nodules (arrows) highly suggestive of malignancy rather than chronic inflammation as the wall of the fallopian tube is otherwise thin and smooth. (C courtesy of Dr. Douglas Brown, Department of Radiology, Mayo Clinic, Rochester, MN; D courtesy of Dr. Anna Lev-Toaff, Hospital of the University of Pennsylvania, Philadelphia, PA.)



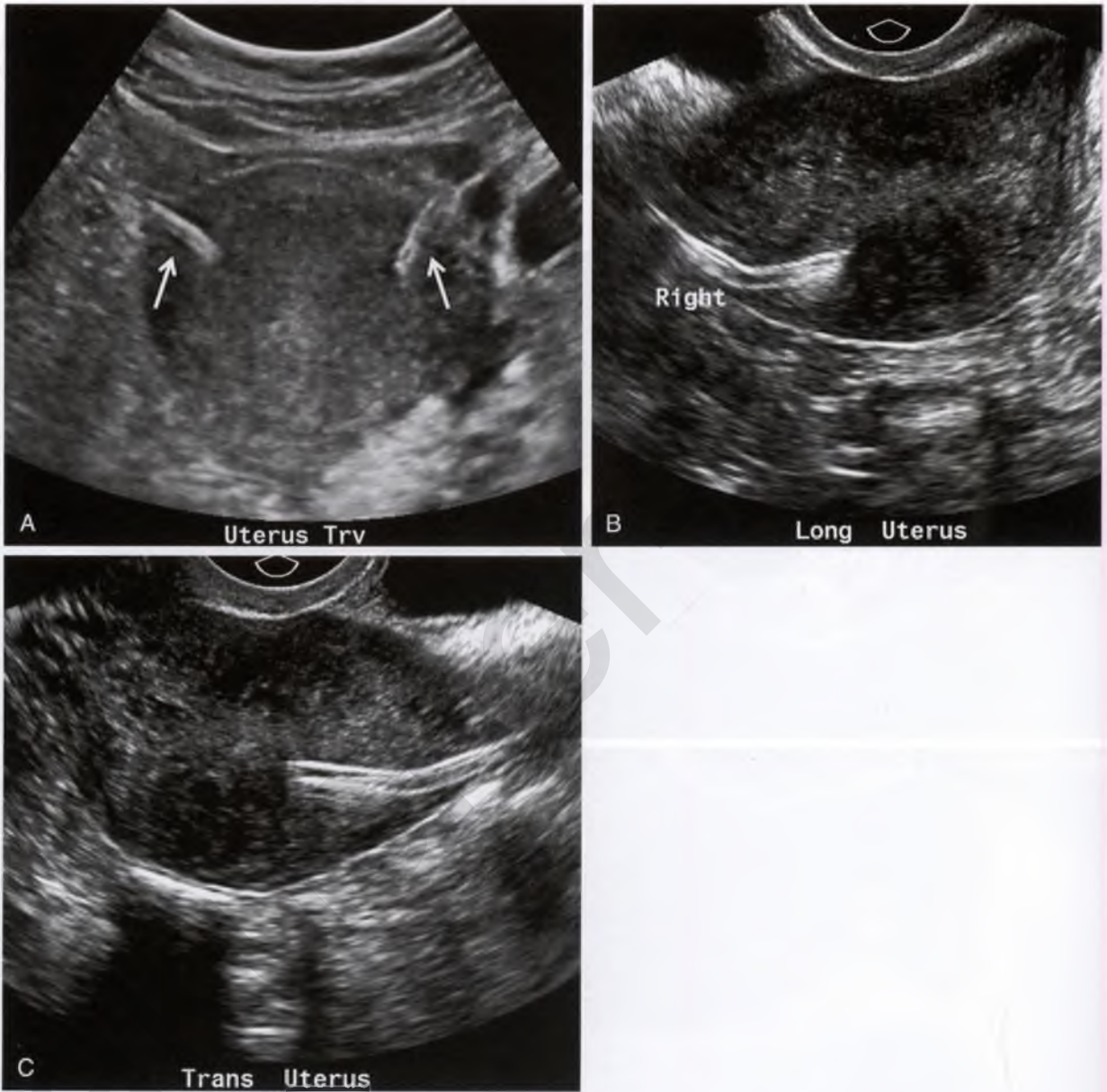


**FIG 31-21** Normal ultrasound appearance of Essure device. **A**, Transabdominal image of the uterus demonstrates Essure microinsert birth control devices. On this coronal view through the uterine fundus, bilateral, slightly curved linear echogenic foci are seen (*arrows*), indicating normal device placement within the interstitial segment of the fallopian tube on each side. On transvaginal sonographic images, the right (**B**) and left (**C**) Essure devices can be seen extending from the interstitial portion of the fallopian tube into the isthmic segment. (Courtesy Department of Obstetrics and Gynecology, Yale University School of Medicine, New Haven, CT.)

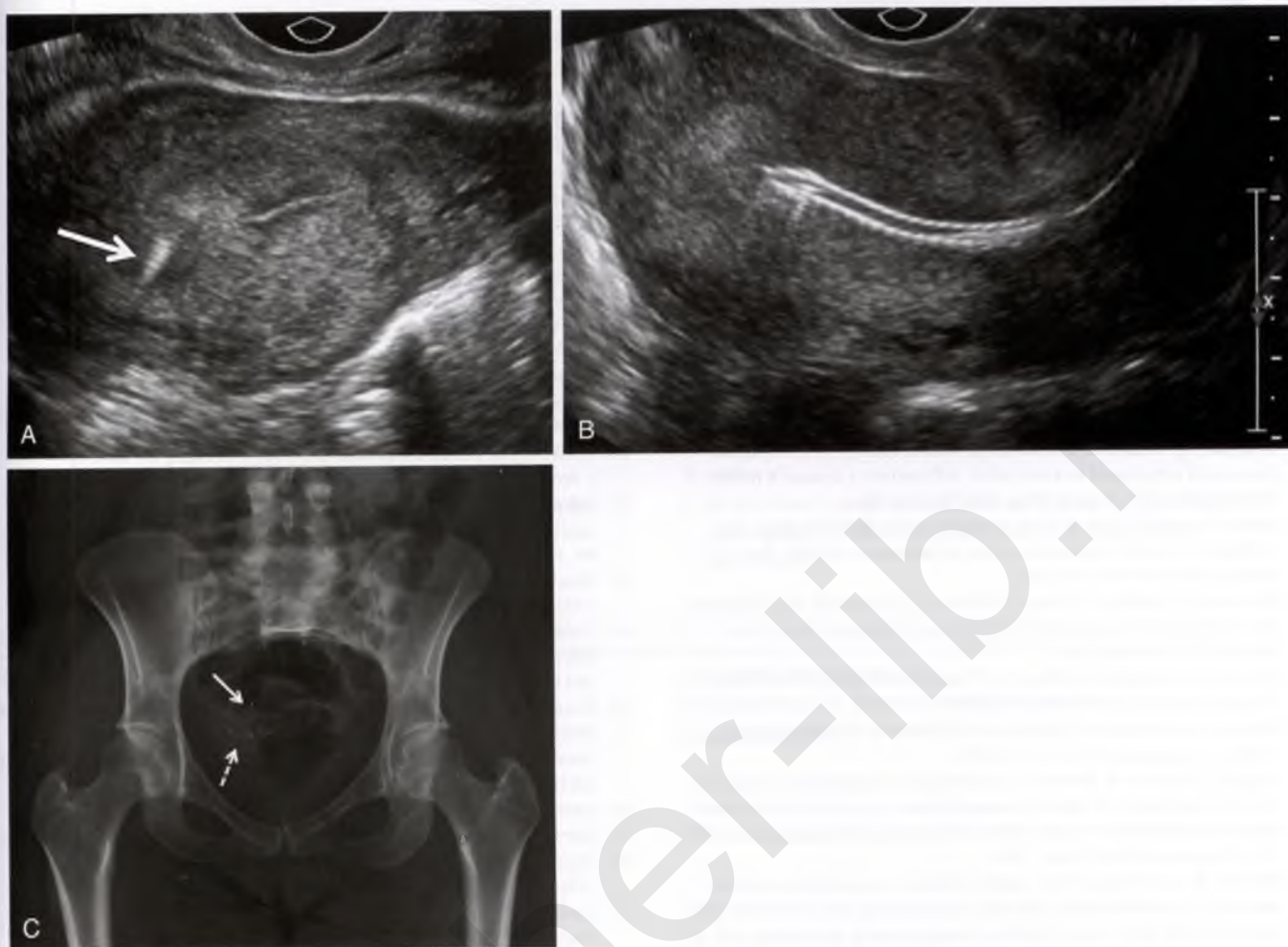


**FIG 31-22** Essure device in abnormal location. **A**, Transverse transvaginal sonographic image of the uterine fundus demonstrating the right Essure device (arrow) in the appropriate location in the interstitial portion of the right fallopian tube. The left device is not visualized on this image. **B**, Midline sagittal transvaginal sonographic image of the uterus demonstrating the left Essure device centrally located within the endometrial cavity. **C**, Radiograph confirms abnormal location of the left Essure device (dotted arrow). Solid arrow, right Essure device. (Courtesy Department of Obstetrics and Gynecology, Yale University School of Medicine, New Haven, CT.)

may also be recognized on sonography (Fig. 31-22).<sup>37</sup> See Chapter 37, “The Role of Ultrasound in Gynecologic Interventions,” for more detail.

## SUMMARY

Both normal and abnormal fallopian tubes can be identified using ultrasound. A dilated fallopian tube, whether a hydrosalpinx, pyosalpinx, or hematosalpinx, will demonstrate a variety of classic sonographic signs that can be used to differentiate a cystic mass of tube origin from ovarian and other pelvic causes. These signs include the waist sign, incomplete septation sign, cogwheel sign, and beads on a string sign and can also be used in other pelvic imaging modalities. However, sonography has the advantage of allowing for more direct correlation with the patient’s pain. In addition, dynamic scanning using compression can help differentiate fallopian tube from ovary. Visualization of subtle tube abnormalities such as mild salpingitis and tube carcinoma can be accomplished using high frequency transvaginal sonography transducers, and evaluation of tube patency using SIS may become more common with the more widespread use of ultrasound contrast agents.

## REFERENCES

1. Moore KL, Persaud TVN: *The Developing Human*, ed 6, Philadelphia, 1998, WB Saunders. chaps. 2 and 13.
2. Standring S, editor: *Gray’s Anatomy: The Anatomical Basis of Clinical Practice*, ed 40, Edinburgh, 2008, Churchill Livingstone, pp 1279–1304. chap. 77, Female Reproductive System.
3. Katre R, Morani AK, Prasad SR, et al: Tumors and pseudotumors of the secondary müllerian system: review with emphasis on cross-sectional imaging findings. *AJR Am J Roentgenol* 195(6):1452–1459, 2010.
4. Merlini L, Anooshiravani M, Vunda A, et al: Noninflammatory fallopian tube pathology in children. *Pediatr Radiol* 12:1330–1337, 2008.
5. Patel MD, Acord DL, Young SW: Likelihood ratio of sonographic findings in discriminating hydrosalpinx from other adnexal masses. *AJR Am J Roentgenol* 186:1033–1038, 2006.
6. Timor-Tritsch IE, Lerner JP, Monteagudo A, et al: Transvaginal sonographic markers of tube inflammatory disease. *Ultrasound Obstet Gynecol* 12:56–66, 1998.
7. Patel MD: Practical approach to the adnexal mass. *Radiol Clin North Am* 1(2):879–899, 2006.
8. Simms I, Rogers P, Charlett A: The rate of diagnosis and demography of pelvic inflammatory disease in general practice: England and Wales. *Int J STD AIDS* 10(7):448–451, 1999.



9. Simms I, Stephenson J: Pelvic inflammatory disease epidemiology; what do we know, and what do we need to know? *Sex Transm Infect* 76(2):80–87, 2000.
10. Washington AE, Aral SO, Wolner-Hanssen P, et al: Assessing risk for pelvic inflammatory disease and its sequelae. *JAMA* 266:2581–2586, 1991.
11. Sweet RL: Treatment of acute pelvic inflammatory disease. *Infect Dis Obstet Gynecol* 2011:561909, 2011.
12. Ness RB, Smith KJ, Chang CC, et al: Prediction of pelvic inflammatory disease among young, single, sexually active women. *Sex Transm Dis* 33(3):137–142, 2006.
13. Westrom L, Joesoef R, Reynolds G, et al: Pelvic inflammatory disease and fertility. A cohort study of 1,844 women with laparoscopically verified disease and 657 control women with normal laparoscopic results. *Sex Transm Dis* 19(4):185–192, 1992.
14. Rosen M, Breitkopf D, Waud K: Tubo-ovarian abscess management options for women who desire fertility. *Obstet Gynecol Surv* 64(10):681–689, 2009.
15. Romosan G, Valentin L: The sensitivity and specificity of transvaginal ultrasound with regard to acute pelvic inflammatory disease: a review of the literature. *Arch Gynecol Obstet* 289:705–714, 2014.
16. Gaitan H, Angel E, Diaz R, et al: Accuracy of five different diagnostic techniques in mild-to-moderate pelvic inflammatory disease. *Infect Dis Obstet Gynecol* 10:171–180, 2002.
17. Romosan G, Bjartling C, Skoog L, Valentin L: Ultrasound for diagnosing acute salpingitis: a prospective observational diagnostic study. *Hum Reprod* 28:1569–1579, 2013.
18. Horrow MM, Rodgers SK, Naqvi S: Ultrasound of pelvic inflammatory disease. *Ultrasound Clin* 2:297–309, 2007.
19. Rezvani M, Shaaban AM: Fallopian tube disease in the nonpregnant patient. *Radiographics* 31:527–548, 2011.
20. Taipale P, Tarjanne H, Ylöstalo P: Transvaginal sonography in suspected pelvic inflammatory disease. *Ultrasound Obstet Gynecol* 6:430–434, 1995.
21. Benjaminov O, Atri M: Sonography of the abnormal fallopian tube. *AJR Am J Roentgenol* 183:737–742, 2004.
22. Kim SH, Kim SH, Yang DM, Kim KA: Unusual causes of tubo-ovarian abscess: CT and MR imaging findings. *Radiographics* 24:1575–1589, 2004.
23. Lely RJ, van Es HW: Case 85: pelvic actinomycosis in association with an intrauterine device. *Radiology* 236(2):492–494, 2005.
24. Triantopoulou C, van der Molen A, van Es AC, Giannila M: Abdominopelvic actinomycosis: spectrum of imaging findings and common mimickers. *Acta Radiol Short Rep* 3(2):1–5, 2014.
25. Jung SE, Lee JM, Lee KY, et al: Xanthogranulomatous oophoritis: MR imaging findings with pathologic correlation. *AJR Am J Roentgenol* 178:749–751, 2001.
26. Zhang XS, Dong HY, Zhang LL, et al: Xanthogranulomatous inflammation of the female genital tract: report of three cases. *J Cancer* 3:100–106, 2012.
27. Kim MY, Rha SE, Oh SN, et al: MR imaging findings of hydrosalpinx: a comprehensive review. *Radiographics* 29:495–507, 2009.
28. Vijayaraghavan SB, Senthil S: Isolated torsion of the fallopian tube: the sonographic whirlpool sign. *J Ultrasound Med* 28:657–662, 2009.
29. Boukaidi SA, Delotte J, Steyaert H, et al: Thirteen cases of isolated tube torsions associated with hydrosalpinx in children and adolescents, proposal for conservative management: retrospective review and literature survey. *J Pediatr Surg* 46:1425–1431, 2011.
30. Pectasides D, Pectasides E, Economopoulos T: Fallopian tube carcinoma: a review. *Oncologist* 11(8):902–912, 2006.
31. Salvador S, Gilks B, Kobel M, et al: The fallopian tube: primary site of most pelvic high-grade serous carcinoma. *Int J Gynecol Cancer* 19(1):58–64, 2009.
32. Shaaban AM, Rezvani M: Imaging of primary fallopian tube carcinoma. *Abdom Imaging* 38(3):608–618, 2012.
33. Huang WC, Yang SH, Yang JM: Ultrasonographic manifestations of fallopian tube carcinoma in the fimbriated end. *J Ultrasound Med* 24:1157–1160, 2005.
34. Strandell A, Bourne T, Bergh C, et al: The assessment of endometrial pathology and tube patency: a comparison between the use of ultrasonography and x-ray hysterosalpingography for the investigation of infertility patients. *Ultrasound Obstet Gynecol* 14(3):200–204, 1999.
35. Jeanty P, Besnard S, Arnold A, et al: Air-contrast sonohysterography as a first step assessment of tube patency. *J Ultrasound Med* 19:519–527, 2000.
36. Panchal S, Nagori C: Imaging techniques for assessment of tube status. *J Hum Reprod Sci* 7:2–12, 2014.
37. Guelfguat M, Gruenberg TR, DiPoce J, Hochshtein JG: Imaging of mechanical tube occlusion devices and potential complications. *Radiographics* 32(6):1659–1673, 2012.

# Sonographic Imaging in Infertility and Assisted Reproduction

Mary C. Frates

## SUMMARY OF KEY POINTS

- Transvaginal sonography (TVS) provides valuable information as part of the initial evaluation of an infertile patient.
- EVS has an essential role in monitoring endometrial thickness and morphology as well as follicular development during hormonal stimulation.
- EVS or transabdominal sonography provides guidance for oocyte retrieval.
- Postretrieval complications such as ovarian hyperstimulation, hemorrhage, and infection are optimally imaged with sonography.

## OUTLINE

### Initial Evaluation, 953

#### Baseline Evaluation, 954

Uterus, 954

Ovary, 956

Fallopian Tube, 958

### Treatment Monitoring, 959

#### Complications of Assisted Reproduction, 962

Conclusion, 963

Infertility can be defined as the inability to conceive a pregnancy after 1 year of unprotected intercourse or after 6 months in a woman over 35 years old. It affects between 6% and 10% of couples in the United States.<sup>1</sup> Because fertility peaks in the third decade and subsequently declines, the age of the female partner is an important variable in the treatment of infertility. The use of sonography, in particular EVS, has become an integral component of the evaluation and treatment of infertility. The transvaginal approach allows high-resolution assessment of the uterus, ovaries, and fallopian tubes. EVS plays a critical role in the diagnosis and treatment of infertile women in combination with serologic testing, physical examination, and careful assessment of medical and surgical history, as well as evaluation of the male partner. Initial baseline ultrasound examination is used primarily to identify structural abnormalities that might affect fertility such as uterine anomalies, endometrial polyps or submucosal leiomyomas, endometrial adhesions/synechiae, or hydrosalpinges. Sonography is also used to assess for possible underlying pathologic processes associated with infertility such as adenomyosis, endometriosis, polycystic ovary syndrome (PCOS), and low antral follicular count. If the baseline pelvic sonogram is inconclusive or noncontributory, further anatomic evaluation can be obtained by means of pelvic magnetic resonance imaging (MRI), hystero-graphy, sonohystero-graphy, or even hysteroscopy and laparoscopy, as indicated. It is estimated that ovulatory defects are the primary cause of infertility in 20% to 40% of infertile women. Structural abnormalities of the female reproductive tract account for approximately 30% of cases; male factors up to 35%; and cervical mucosal, peritoneal, or unexplained abnormalities account for approximately 10% to 15%.<sup>2</sup> Once a treatment plan has been established,

sonography plays an important role in monitoring response, particularly in assessing folliculogenesis and endometrial receptivity. In addition, ultrasound imaging is crucial for guiding infertility treatment such as oocyte retrieval and in assessing posttreatment complications. This chapter will review the role of sonographic imaging in the diagnosis and treatment of women presenting with infertility.

## INITIAL EVALUATION

Part of the initial evaluation of all women with infertility is an assessment of pelvic anatomy. Although high-resolution EVS is the preferred method for imaging the pelvic organs, an initial overview using a transabdominal approach should be performed to evaluate for the possible presence of an enlarged uterus or other pelvic mass. Transvaginal probes are higher frequency than transabdominal transducers and, thus, provide high-resolution images of the uterus, ovaries, and fallopian tubes, but with the tradeoff of reduced penetration and smaller field of view. Masses that extend out of the pelvis cannot be fully imaged or characterized with the transvaginal approach, as they extend beyond the field of view of the transducer. A formal transabdominal sonogram, performed with a distended urinary bladder, or a combination of both transabdominal and transvaginal imaging may be required in some patients. A baseline transvaginal sonographic examination consists of images of the uterus, endometrium, and ovaries, with additional targeted evaluation of any identified abnormality. The reader is referred to individual chapters elsewhere in this textbook about the uterus (Chapter 28), ovaries (Chapter 30), and fallopian tubes (Chapter 31) for additional detail.



## BASELINE EVALUATION

### Uterus

Imaging of a patient with infertility often begins with hysterosalpin-gography (HSG) to assess for uterine anomalies and determine tubal patency. Sonography, including three-dimensional (3D) coronal views, is also a highly accurate initial imaging modality to evaluate for possible structural abnormalities such as congenital uterine anomalies, masses, or adenomyosis<sup>3,4</sup> and is an integral part of the baseline evaluation. At real-time sonography, the uterus should be imaged in both longitudinal (sagittal) and coronal (or transverse) orthogonal planes, with some views including the full length of the cervix. In patients with an enlarged or elongated uterus, it is important to ensure that the entire fundus as well as any exophytic lesion is included. The normal uterus is oval in shape with a curved, slightly convex fundal contour. Uterine malformations are reported to occur in 1% to 7% of infertile patients.<sup>5,6</sup> These malformations are often initially identified at HSG but can be appreciated on the baseline ultrasound image in most affected patients.

A uterine anomaly may be suspected at real-time sonography when, in the transverse plane, the endometrium appears to separate toward the fundus. In this instance, the addition of a 3D coronal view, which provides direct visualization of the fundal contour, the shape of the endometrial cavity, and characterization of any septum between the two uterine horns, can be extremely helpful in categorizing the type of uterine anomaly, which can range from an arcuate configuration (considered by most to be within the range of normal) to uterine didelphys<sup>7-10</sup> (Fig. 32-1A and B). If a uterine anomaly is suspected but cannot be confirmed, repeating the 2D and 3D sonography during the secretory phase of the menstrual cycle, when the endometrium is thick and hyperechoic and thus more visible, may be beneficial. If concern for a uterine anomaly and need for characterization persists, further imaging with pelvic MRI may be helpful. In addition, MRI may provide additional important structural information in patients with complex anomalies (Chapter 36).

Another major component of the baseline sonogram is evaluation of the endometrial pattern and thickness, typically assessed on the midline sagittal long-axis view. The endometrial morphologic appearance and thickness change through the menstrual cycle in response to rising serum estrogen concentrations. During the menstrual phase, the endometrium appears thin, linear, regular, and homogeneously echogenic, typically measuring less than 5 mm in thickness (Fig. 32-2), although in some patients, a more heterogeneous pattern can be seen. Occasionally a small amount of fluid is present in the uterine cavity. This fluid is not included in the reported measurement. Rather, the two endometrial layers (anterior and posterior) are measured separately and added together for reporting purposes (Fig. 32-3). At the baseline study, careful evaluation of the endometrium is necessary to search for intracavitary lesions such as submucosal leiomyomas or endometrial polyps (Fig. 32-4A and B). Focal lesions in the endometrial cavity are typically removed prior to fertility treatment, as resection has been reported to be associated with increased pregnancy rates.<sup>11,12</sup> In a retrospective study of infertility patients with endometriosis published in 2011, Shen and associates reported a clinical pregnancy rate of 49.5% in patients following hysteroscopic polypectomy compared to a pregnancy rate of 29.8% in those without polyps.<sup>11</sup> Medina and colleagues reported in a randomized, prospective study that infertility patients with endometrial polyps undergoing intrauterine insemination were twice as likely to become pregnant if hysteroscopic polypectomy was performed prior to insemination, with a relative risk of 2.1 and a pregnancy rate of 59% in the study group versus 25.4% in the control group.<sup>12</sup> Rarely, other more unusual types

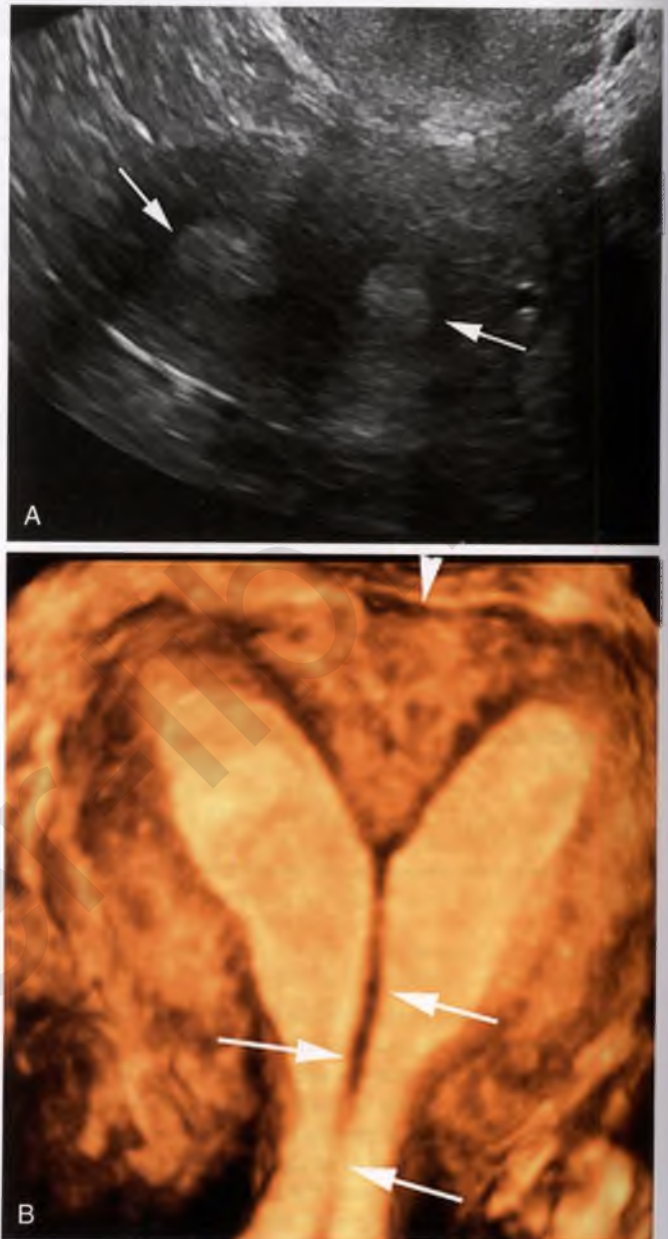


**FIG 32-1** Septate uterus. **A**, Gray-scale axial transvaginal sonogram of the uterus shows a divided echogenic endometrial cavity (arrows). **B**, Three-dimensional rendered coronal image clearly demonstrates a complete thin uterine septum (arrows) dividing the endometrial cavity, extending from the fundus inferiorly into the cervix, below the level of the internal os. Note that the outer serosal contour of the uterine fundus remains smooth, without indentation (arrowhead).

of endometrial diseases, such as unsuspected retained products of conception or osseous metaplasia (Fig. 32-5), are found on baseline imaging; these lesions should also be addressed prior to initiation of fertility treatment.<sup>13</sup> In some patients, sonohysterography may provide further information regarding endometrial disease and is particularly useful in identifying adhesions within the endometrial cavity (Asherman syndrome). Asherman syndrome most commonly occurs following instrumentation such as dilatation and curettage (D&C) but can also occur following intrauterine device placement, uterine artery embolization, radiation therapy, pregnancy, or endometritis. Up to 43% of women with Asherman syndrome will have difficulty



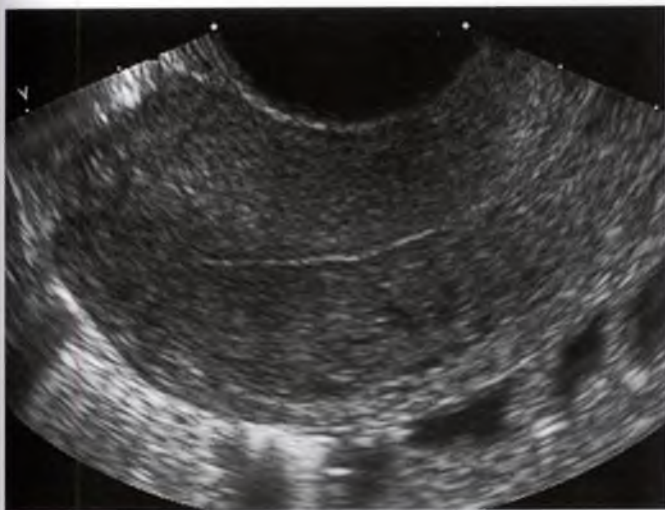


**FIG 32-2** Normal ultrasound appearance of the endometrium during the menstrual phase. Gray-scale transvaginal sagittal image of the uterus demonstrates a thin, linear echogenic endometrium.

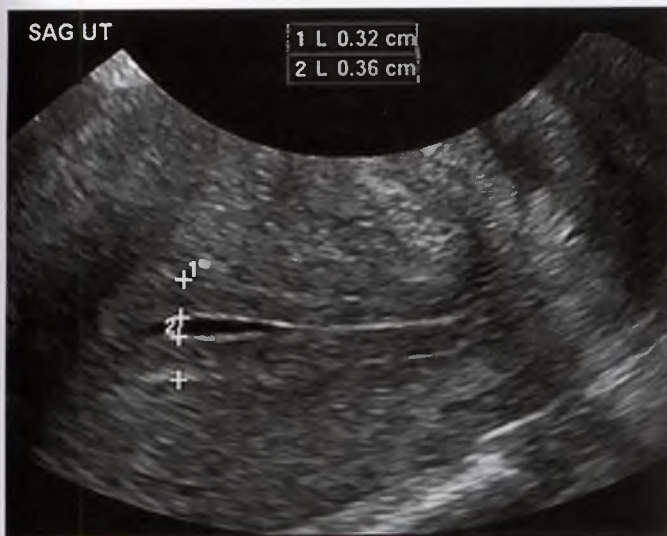


**FIG 32-3** Normal ultrasound appearance of the endometrium during the periovulatory phase. Gray-scale transvaginal sagittal image of the uterus demonstrates the multilayered endometrium, with trace anechoic intrauterine fluid. The measurements of the anterior (1 calipers) and posterior (2 calipers) endometrial layers are summed, resulting in an endometrial thickness of 6.8 mm. The intracavitary fluid is not included in the measurement.

conceiving or will present with recurrent early pregnancy loss. Sonohysterography may also be helpful in identifying and delineating submucosal leiomyomas and polyps (Fig. 32-6).<sup>14</sup>

The myometrium is also evaluated on the baseline sonogram. Abnormalities of the myometrium that may affect fertility include adenomyosis and leiomyomas (also called *fibroids*). Adenomyosis occurs when endometrial glands and stroma burrow into the subjacent myometrium. The classic appearance on EVS is a globular, smooth-contoured, enlarged uterus with asymmetric wall thickening, heterogeneity of the myometrium, thickening of the subendometrial halo, subendometrial myometrial cysts or echogenic nodules or striations, and pencil-thin dark linear radiating striations through the myometrium (Fig. 32-7).<sup>15-17</sup> The presence of adenomyosis is associated with

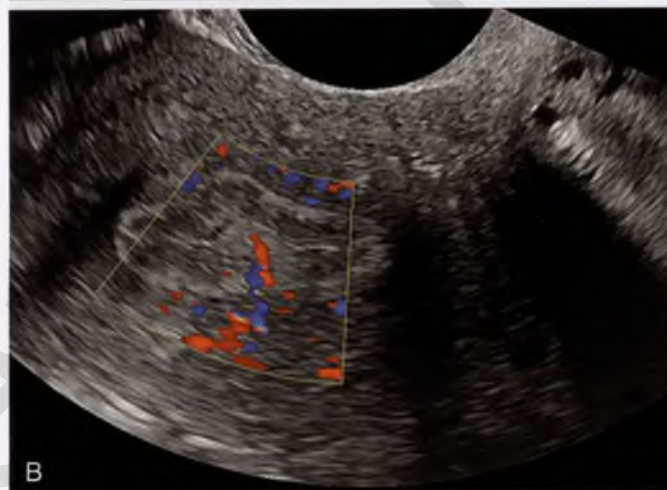
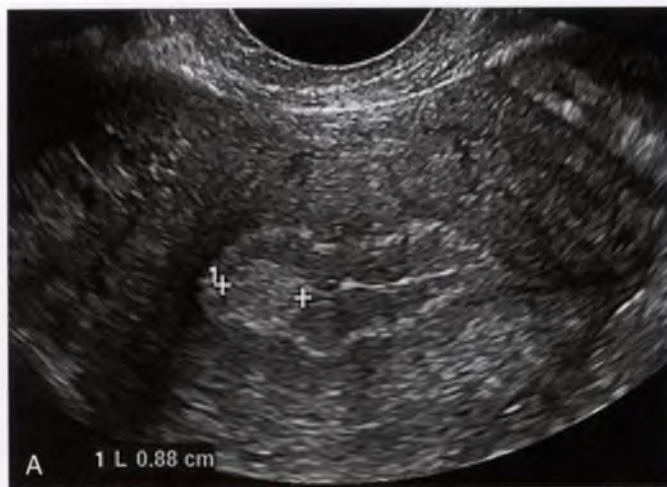


**FIG 32-4** Endometrial polyp. **A**, Coronal gray-scale image of the uterus demonstrates a multilayered appearance of the endometrium (typical of the periovulatory phase of the menstrual cycle) and a focal echogenic lesion (calipers) representing an endometrial polyp. **B**, Sagittal color Doppler image shows a small feeding vessel supplying the polyp.

a significantly lower clinical pregnancy rate,<sup>18-20</sup> with *clinical pregnancy* defined as a pregnancy documented by visualization of a gestational sac or embryo, whereas *chemical pregnancy* indicates a pregnancy diagnosed by documentation of a positive human chorionic gonadotropin (hCG) level. The cause of infertility in patients with adenomyosis is not fully understood but may be related to decreased myometrial contractility, which is necessary to transport the sperm and zygote through the uterus. In addition, adenomyosis has a strong association with endometriosis, particularly in patients less than 36 years of age. Patients with adenomyosis also have an increased risk of early pregnancy loss as compared to patients without adenomyosis.<sup>18-20</sup>

Myomas are found in approximately 20% to 40% of women, with the rate increasing with patient age.<sup>21</sup> The percentage of infertile patients with myomas will likewise vary with age. The classic sonographic appearance of a myoma is a solid mass with well-defined borders. Echogenicity is variable, with most being hypoechoic. Larger myomas are often heterogeneous and may demonstrate a typical swirling pattern, edge refraction, posterior shadowing, and focal areas of calcification on EVS. Identifying and documenting the location of all myomas, particularly in relation to the endometrial cavity and lower uterine segment, are important components of the baseline ultrasound



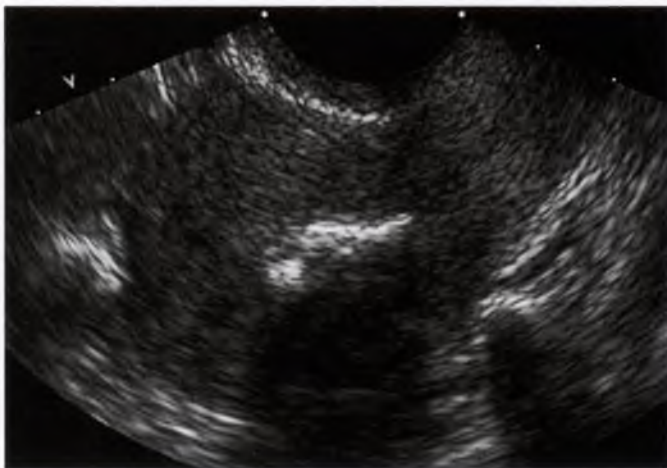


**FIG 32-5** Calcified intrauterine material shown on sagittal gray-scale image of the uterus, incidentally noted on baseline infertility examination. There is angular, echogenic, densely shadowing material, indicating calcification within the endometrial cavity. This does not demonstrate characteristics of submucosal myoma or endometrial polyp. At hysteroscopy, fragments of bone were found and removed, retained since a remote prior pregnancy termination.



**FIG 32-6** Sonohysterogram with endometrial polyp. Sagittal gray-scale transvaginal ultrasound image from a sonohysterogram. The uterus is retroflexed. Instilled anechoic intracavitary sterile saline distends the endometrial cavity and partially outlines a large (2.86 cm) echogenic polyp (*calipers*).

examination. Myomas that deviate or protrude into the endometrial cavity (submucosal) (Fig. 32-8A and B) appear to have a deleterious effect on fertility because of interference with implantation, possibly secondary to pressure effect on the endometrium, which decreases receptivity, and may cause mechanical blockage of the endocervical canal or fallopian tubes. Hence, the possible presence of submucosal myomas should be carefully assessed during the preliminary workup of the infertile patient.<sup>22-25</sup> An increased rate of first trimester pregnancy loss is also found in patients with submucosal myomas,<sup>22,24</sup> and resection of submucosal myomas appears to enhance fertility.<sup>22,23,25</sup> Although the presence of subserosal myomas does not appear to adversely affect conception rates, the effect of intramural myomas on fertility remains unclear.<sup>22,23,26,27</sup> It has been proposed that the presence

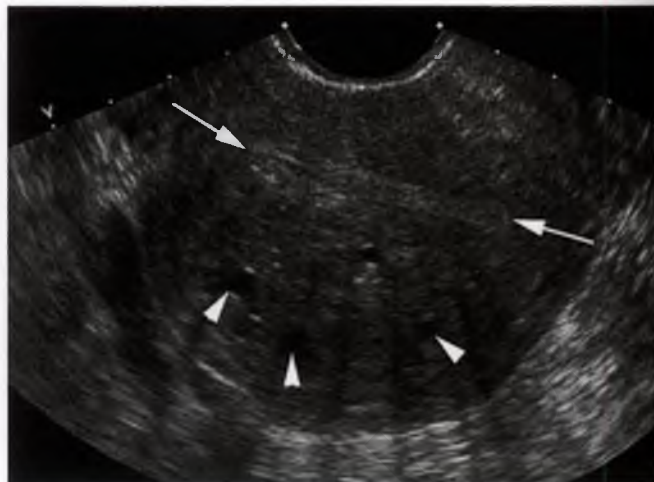


**FIG 32-7** Adenomyosis. Coronal transvaginal gray-scale image demonstrating an enlarged, globular uterus, without focal mass or lobulated contour. The echogenic endometrium is asymmetrically located (*arrows*), indicating thickening of the posterior myometrium. Myometrial heterogeneity with "pencil-thin" radiating dark striations and several small cysts (*arrowheads*) is also noted.

of intramural myomas adversely affects uterine peristalsis, with more frequent peristalsis associated with poor pregnancy rates.<sup>28</sup> Patients with intramural myomas also appear to have higher miscarriage rates.<sup>24</sup> However, it is not clear whether resection of intramural myomas is beneficial.<sup>22,29,30</sup> Because of all this, careful documentation with precise localization of all uterine myomas in the infertile woman is extremely important. Three-dimensional sonography can be helpful in delineation of centrally positioned myomas (Fig. 32-9A and B). If myoma location remains indeterminate, MRI, saline infusion sonohysterography (SIS), HSG, or hysteroscopy should be considered, as these techniques provide the most accurate evaluation of the endometrial cavity and demonstration of possible submucosal myomas.<sup>7</sup> Although myomectomy is the typical treatment option, for some patients with multiple large myomas for whom myomectomy is not an option, uterine artery embolization may have a role (see Chapter 37).<sup>31</sup>

## Ovary

On baseline imaging, the ovaries are routinely evaluated to assess for normal expected findings and to screen for any abnormality. In the first portion of the menstrual cycle, a normal ovary will demonstrate multiple antral follicles, which measure between 2 and 9 mm in maximum diameter (Fig. 32-10). The antral follicle count (AFC) can be correlated with fertility status, response to ovarian stimulation, and success of conception.<sup>32</sup> A low AFC of 4 to 10 follicles between days 2 and 4 of a regular menstrual cycle suggests poor ovarian reserve, which assists in predicting outcome for fertility treatments. Infertile patients over 35 years of age, patients with a single ovary, a prior history of pelvic radiation therapy or chemotherapy, and patients with a family history of early menopause are at increased risk of decreased ovarian reserve. The potential role of 3D sonography in assessing the AFC, aiming to allow for remote evaluation of the ovary via stored 3D imaging, is under investigation.<sup>33,34</sup> Focal ovarian lesions are frequently found at the baseline ultrasound examination. The most common is the residual corpus luteum, a complex thick-walled cyst related to ovulation during the prior menstrual cycle (Fig. 32-11A and B). This is a normal physiologic process, and this "cyst" will spontaneously involute. Additional lesions that might be identified at baseline EVS include endometriomas (Fig. 32-12) and benign ovarian tumors such



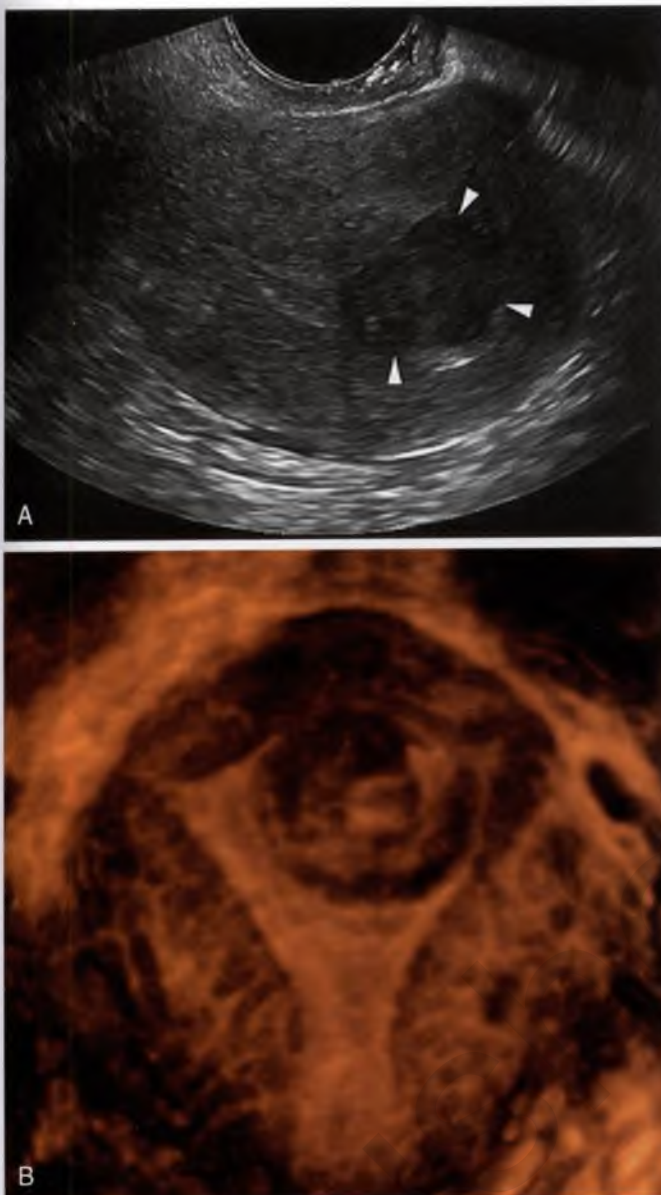


**FIG 32-8** Submucosal leiomyomas. **A**, Sagittal gray-scale transvaginal image of a retroverted uterus shows a hypoechoic round solid mass (*arrowheads*), consistent with a leiomyoma, centrally positioned toward the uterine fundus. Note edge refraction at the inferior surface. **B**, Three-dimensional coronal reconstruction confirms the intracavitary location of this submucosal leiomyoma. Determining the percentage of a submucosal leiomyoma that is intracavitary is important in guiding clinical management. This leiomyoma is amenable to hysteroscopic resection because it is >50% intracavitary.

as dermoid cysts. The ovaries should be assessed for sonographic findings suggestive of PCOS. Patients with PCOS often present with the clinical triad of amenorrhea, hirsutism, and obesity, although clinical presentation is variable. Patients with PCOS are at increased risk of anovulation and thus infertility.<sup>35</sup> In 2003, the Rotterdam Consensus workshop published what was considered the standard sonographic diagnostic criteria for PCOS: 12 or more 2- to 9-mm follicles in each ovary and/or increased ovarian volume measuring more than 10 mL (Fig. 32-13).<sup>36</sup> More recently, it has been noted that with improved image quality and resolution resulting from rapid technologic

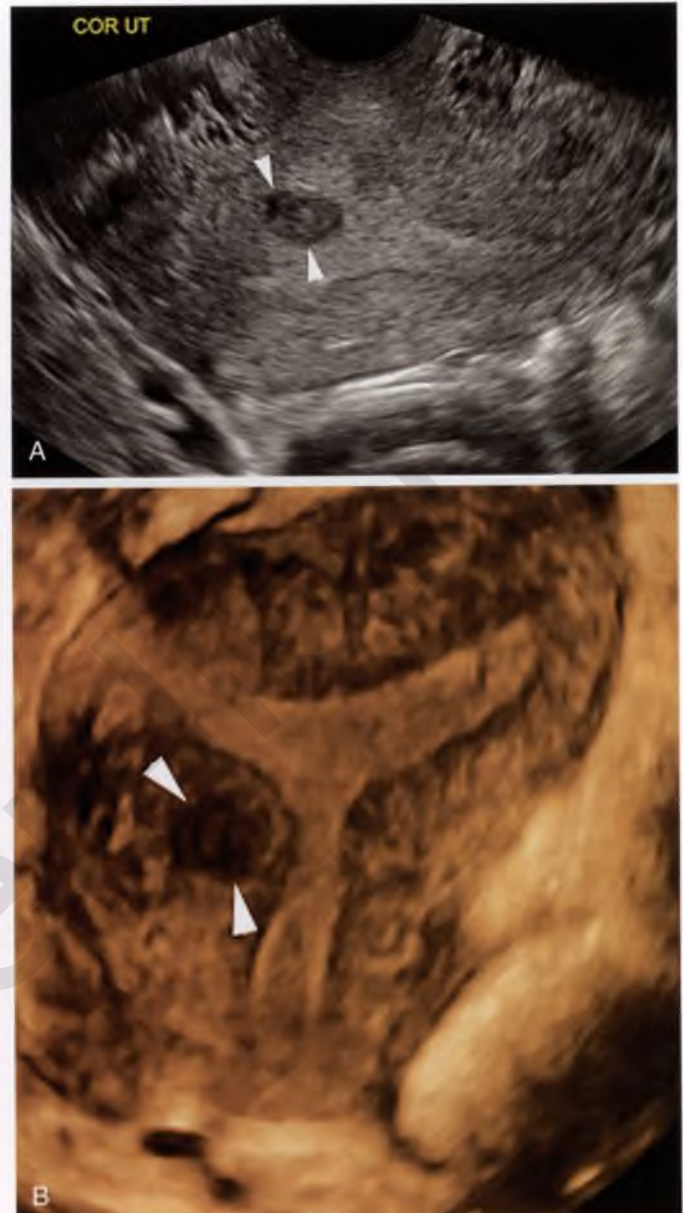


**FIG 32-9** Localization of uterine leiomyoma with three-dimensional sonography. **A**, Coronal gray-scale transvaginal sonographic image of the uterus shows a small hypoechoic leiomyoma (*arrowheads*) in the central portion of the image. On this projection, the leiomyoma appears to be located within the echogenic endometrial cavity. **B**, Three-dimensional coronal reconstruction demonstrates that the small leiomyoma (*arrowheads*) is actually located within the right lateral uterine wall completely surrounded by myometrium and therefore is intramural rather than submucosal.

advancements in sonographic equipment, more than 12 tiny follicles are often seen in healthy women with normal ovaries. Therefore, adhering to the Rotterdam criteria could potentially lead to an overdiagnosis of PCOS.<sup>37,38</sup> A modification of the Rotterdam criteria has been suggested with a threshold of over 25 small follicles necessary for the diagnosis of PCOS in patients imaged with state-of-the-art, high-resolution sonographic equipment.<sup>37,38</sup> At present, this issue has not been settled. The imager is reminded that PCOS is a clinical diagnosis and the sonographic findings should not be used in isolation, as they are neither entirely sensitive nor specific.





**FIG 32-10** Normal ultrasound appearance of the ovary. Coronal gray-scale image of the right ovary on a baseline examination in an infertility patient. There are several antral follicles noted, the largest measuring 7 mm (calipers).

A potential additional role of EVS is to assess mobility of the ovaries. A normal ovary is freely mobile, and pressure on the ovary, either directly with the transvaginal probe or from an anterior approach with the examiner's hand or a transabdominal transducer, will often result in movement of the ovary detectable on real-time imaging. If the ovary remains fixed in position, the presence of adhesions in the pelvis is suggested, possibly related to endometriosis, prior surgery, or prior infection. Such adhesions may affect fertility by potentially preventing "pickup" of the ovum by the open fimbriated end of the fallopian tube.

### Fallopian Tube

The normal fallopian tube is typically not visualized at EVS, although occasionally a collapsed normal tube can be identified (Fig. 32-14), particularly in patients with small amounts of free intraperitoneal fluid. Obstructed fallopian tubes become distended with intraluminal secretions, resulting in hydrosalpinges, which are readily visualized by sonography. A classic hydrosalpinx appears as a tubular, fluid-filled structure with an S, V, or U shape and often a folded configuration (Fig. 32-15) demonstrating the "incomplete septation sign" as the tube folds upon itself. Occasionally small spokes (<3 mm) of similar size or cogwheel-like indentations mimicking small mural nodules can be seen along the wall. The uniformity and regular spacing of these nodules, in addition to the tubal configuration, are critical features in differentiating chronic salpingitis with dilated tube and redundant or inflamed mucosa from a complex, cystic ovarian mass. Tubal patency is most commonly established by means of HSG, where free spillage of contrast material into the peritoneal cavity provides confirmation that the fallopian tube is patent. However, if a hydrosalpinx is visualized at sonography, it can be assumed that the tube is obstructed. The use of intraluminal sonographic contrast material or normal saline agitated with air during sonohysterography, termed *hysterosalpingo-contrast-sonography*, or more commonly abbreviated as HyCoSy, has been proposed as a method of determining tubal patency. Visualization of the brightly echogenic sonographic contrast material or air as it moves through unobstructed tubes and subsequently accumulates in the peritoneal cavity indicates tubal patency.<sup>39-42</sup> The addition of

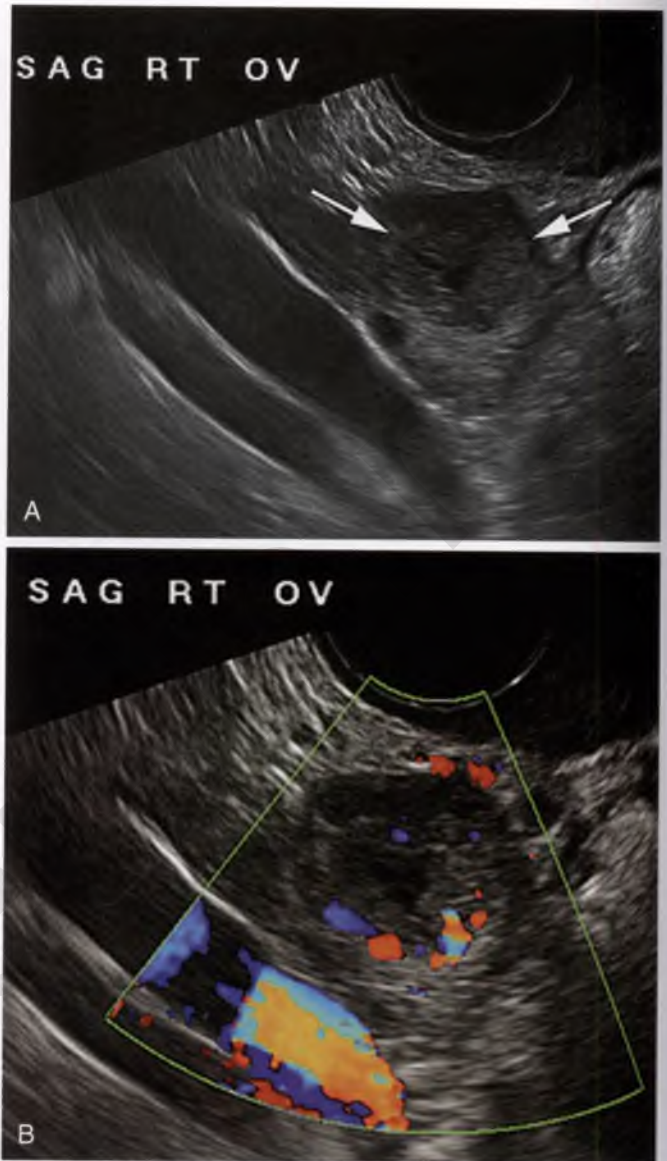


**FIG 32-11** Corpus luteum. **A**, Sagittal gray-scale image of the right ovary, adjacent to the iliac artery and vein, shows a complex, hypoechoic thick-walled cyst (arrows) with the characteristic sonographic appearance of a corpus luteum. There is an adjacent small anechoic follicle posteriorly. **B**, Color Doppler sonographic image shows a prominent ring of peripheral vascularity at the outer edge of the thick-walled cyst, compatible with a corpus luteum.

contrast material (air bubbles) to sonohysterography (i.e., HyCoSy) does appear to provide improved assessment of tubal patency.<sup>42</sup> The further addition of 3D imaging to sonography with contrast injection may be useful.<sup>43</sup> However, all of these techniques are limited by the inability to distinguish unilateral from bilateral tubal patency (as accumulation of contrast material in the peritoneal cavity only indicates that at least one fallopian tube is patent), difficulty in completely visualizing the tube owing to tortuosity, and interference or confusion created by peristalsing bowel. Hence, unless there are comorbid conditions such as endometriosis or pelvic infection, HSG remains the reference standard to screen for fallopian tube patency,<sup>44</sup> as it continues to offer the unique advantage of improved pregnancy rates following the procedure, possibly due to flushing of tubal plugs and luminal debris.<sup>45</sup> Other proposed hypotheses for this phenomenon of improved



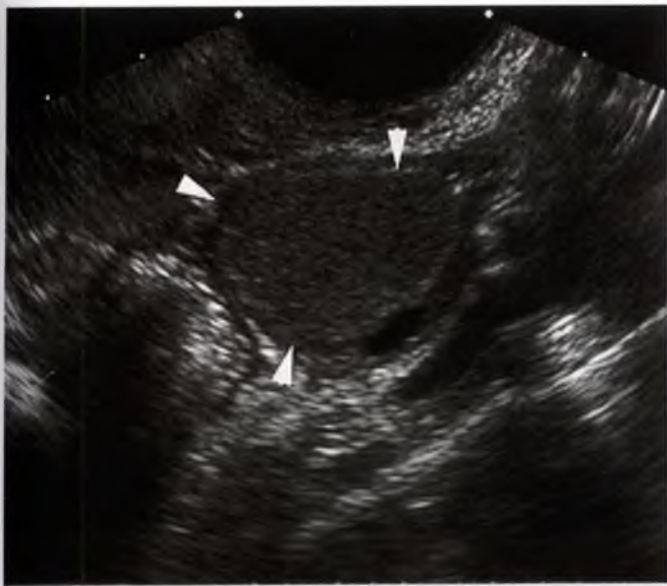


**FIG 32-12** Endometrioma. Coronal gray-scale transvaginal sonographic image of the left ovary demonstrates a complex cyst (*arrowheads*), containing diffuse homogeneous low-level internal echoes, consistent with an endometrioma.



**FIG 32-13** Polycystic ovary syndrome (PCOS). Gray-scale transvaginal sonographic image demonstrating an enlarged right ovary with over 12 small (2- to 9-mm) follicles, located peripherally. The central portion of the ovary has a more solid, echogenic appearance. Similar ovarian morphologic pattern was noted on the left (not shown).

pregnancy rates following HSG include stimulation of tubal ciliary action or alteration of interleukin and prostaglandin production by peritoneal macrophages, which modulate phagocytosis of sperm.<sup>45</sup> Whether oil-soluble media is more effective than water-soluble media remains a matter of debate and ongoing research.<sup>45</sup> If endometriosis or pelvic infection is suspected, then laparoscopy with intraoperative dye test might be considered to assess tubal patency, as full assessment of the pelvis with concomitant treatment could be offered.<sup>44</sup>

When a hydrosalpinx is identified, occlusion of the fallopian tube, which blocks the oocyte from reaching the endometrial cavity, is established. This critical piece of information will impact decision making regarding the type of fertility treatment offered, typically leading to a

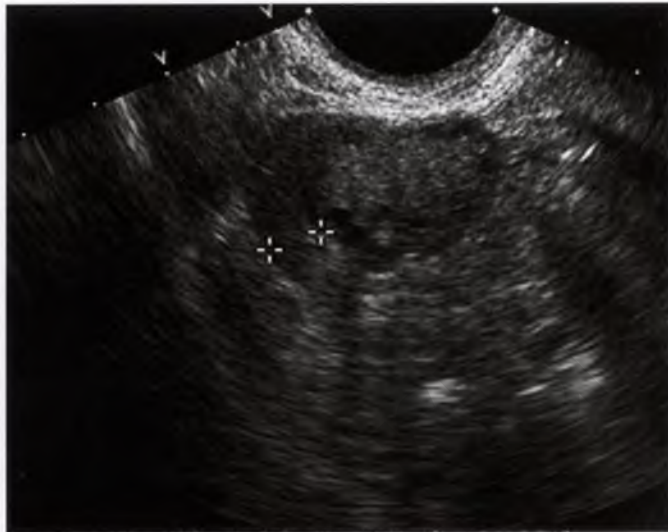


**FIG 32-14** Normal fallopian tube. Coronal gray-scale image of the right ovary shows a small, hypoechoic solid structure (*calipers*) adjacent to the lateral aspect of the ovary, representing a collapsed fallopian tube.

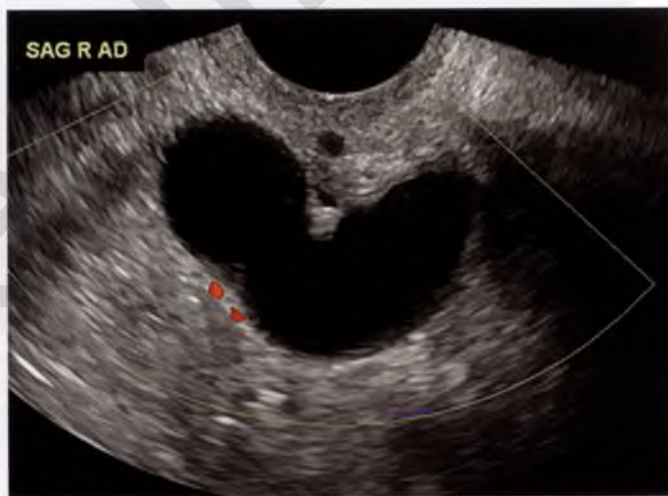


**FIG 32-15** Hydrosalpinx. Sagittal gray-scale image of the right adnexa shows an anechoic, fluid-filled, elongated structure with a waist-like central narrowing consistent with a dilated fallopian tube.

recommendation for in vitro fertilization (IVF). Of note, the presence of hydrosalpinx adversely impacts fertility success rates, not only decreasing the success rate of IVF but also increasing the risk of ectopic pregnancy. Furthermore, components of the fluid within a hydrosalpinx have been shown to be toxic to the developing embryo.<sup>46</sup> Therefore, aspiration or resection of the abnormal tube is sometimes considered in patients with known hydrosalpinx at the time of egg retrieval, with reported increase in subsequent pregnancy rates.<sup>47-49</sup> If internal echoes/debris is identified within a hydrosalpinx, infection must be considered in the appropriate clinical setting.

## TREATMENT MONITORING

Once fertility treatment has been initiated, transvaginal sonographic monitoring of both the endometrium and follicular development begins. Unlike the baseline study, which consists of a complete evaluation of the pelvis in all patients, a sonogram performed for



monitoring purposes is targeted to the endometrium and ovaries or occasionally to the endometrium alone.

The endometrium is evaluated for both thickness and morphologic pattern. Under the influence of hormones given for ovulation induction, the endometrium evolves from a thin (<5 mm) echogenic linear appearance early in the menstrual cycle to a trilaminar or multilayered striated appearance, measuring up to 12 or 14 mm in double-layer thickness during the periovulatory stage (Fig. 32-16). The endometrial thickness typically increases on each subsequent sonogram during the first half of the cycle. Clinical pregnancy rates are reported to be highest when the endometrium measures more than 9 to 10 mm in anteroposterior diameter, whereas an endometrium of under 6 mm correlates with a decreased likelihood of full-term pregnancy<sup>50,51</sup>—although the reason for this difference is unclear. Another study suggests that the combination of both the multilayered pattern and appropriate thickness (7-14 mm) is associated with the best clinical outcomes.<sup>52</sup> Patients undergoing transfer of embryos frozen during a prior stimulated cycle only require targeted endometrial evaluation with attention to morphologic appearance and thickness to determine optimal timing of the transfer procedure. In general, it is preferred to transfer embryos when the endometrium demonstrates a trilaminar appearance and is 7 mm or more in diameter.

Ultrasound plays a critical role in the monitoring of folliculogenesis that occurs during ovulation induction and of controlled ovarian stimulation from parenterally administered gonadotropins or orally administered clomiphene citrate. The choice of treatment is made by a reproductive endocrinology specialist, based upon the most likely cause of the infertility. In general, patients with anovulatory cycles, such as those with PCOS, are treated with clomiphene citrate, whereas patients with hypothalamic pituitary failure, diminished ovarian reserve, or failing ovaries, as well as women with unexplained infertility, might be treated with gonadotropins. Ovarian stimulation is initiated during the first few days of a normal menstrual cycle. Under the influence of stimulating hormones, multiple enlarging follicles can be seen, rather than the typical single dominant follicle created during a natural menstrual cycle. These follicles are monitored intermittently using EVS, thus providing feedback confirming appropriate treatment. Early in the menstrual cycle, patients are typically monitored with blood work and EVS every 3 to 4 days. However, when the follicles are closer to maturation and ovulation, patients are monitored more



**FIG 32-16** Role of ultrasound in monitoring endometrial changes. Sagittal gray-scale image of the endometrium was obtained during a follicular monitoring examination. The endometrial pattern is multilayered or trilaminar, with an anteroposterior diameter thickness measuring 8 mm (calipers), consistent with the periovulatory phase.

frequently, every 1 to 2 days. The reproductive endocrinologist uses the sonographic appearance of the follicles during days 7 through 10 of the menstrual cycle in combination with serum estradiol measurements to predict the most likely time of ovulation. At present, 2D real-time sonography is used for follicular monitoring, but there is increased interest in the possible future role of 3D sonography, which might improve sonographer efficiency as well as decrease measurement error.<sup>53</sup> Once the follicles have reached the optimal size and number ( $\geq 2$  follicles over 18 mm for IVF or a dominant follicle measuring approximately 25 mm following ovulation induction with clomiphene citrate), the patient is given intramuscular hCG, as a substitute for luteinizing hormone, to trigger ovulation (Fig. 32-17A and B).

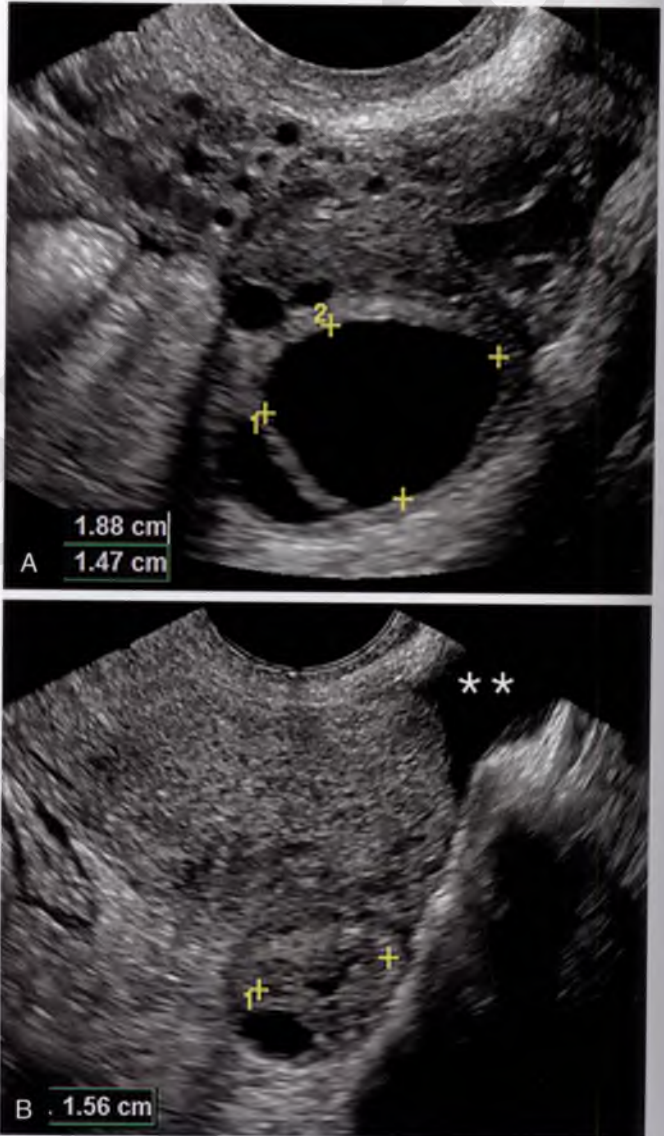


**FIG 32-17** Role of ultrasound in monitoring ovarian follicular development. **A**, Coronal gray-scale image of the left ovary shows two anechoic cysts or follicles. The larger follicle measures approximately 19 x 15 mm (calipers). **B**, Transvaginal sonographic image of the same ovary, 2 days later. The 19-mm anechoic follicle is no longer seen. There is a small complex cyst (calipers) in the same location within the left ovary and new trace volume of free fluid (asterisks). These findings suggest interval ovulation with creation of corpus luteum (calipers), measuring 1.56 cm in diameter.



Careful planning of this stage permits optimal timing for either intrauterine insemination or oocyte retrieval for IVF. Depending on the cause of infertility, the number of follicles recruited may vary, reaching up to 20, with ovulation triggered when at least 4 follicles are 19 to 20 mm or greater in diameter (Fig. 32-18A and B). For patients undergoing IVF, accurate timing of oocyte retrieval is critical. If done too early, aspiration of the follicles will result in retrieval of immature oocytes and no successful fertilization. If done too late, the oocytes will have spontaneously released into the peritoneal cavity and will be lost. Here again, sonography is an essential component of treatment planning and delivery. Oocyte retrieval is performed under real-time ultrasound guidance, allowing for aspiration of each individual measurable follicle in each ovary, in order to retrieve the maximum number of mature oocytes. In the majority of patients, retrieval is performed via a transvaginal approach. However in some, the ovaries are inaccessible transvaginally and are located high in the abdomen owing to a markedly enlarged uterus, prior surgical pexy of the ovaries beyond a pelvic

radiation field, or obesity. In such cases, ultrasound guidance using a transabdominal approach may be required (Fig. 32-19). The ovary demonstrates a very characteristic sonographic appearance following oocyte retrieval. At the time of retrieval, each pierced follicle immediately fills with blood. For several weeks following the procedure, the ovary remains enlarged, with multiple resultant hemorrhagic cysts visible in various stages of evolution and resorption (Fig. 32-20). If conception occurs, one of these cysts will become the corpus luteum of pregnancy.

In efforts to maximize outcomes for assisted fertility, investigators continue to research the potential role of Doppler evaluation of blood flow to the uterus and ovaries. Some Doppler studies have suggested that flow to the endometrium and subendometrium during the early luteal phase is decreased in patients with infertility compared to control subjects.<sup>54-56</sup> More recently, 3D imaging together with power Doppler sonography has been used to evaluate the uterus. However, results in infertile patients remain inconclusive, with reports showing

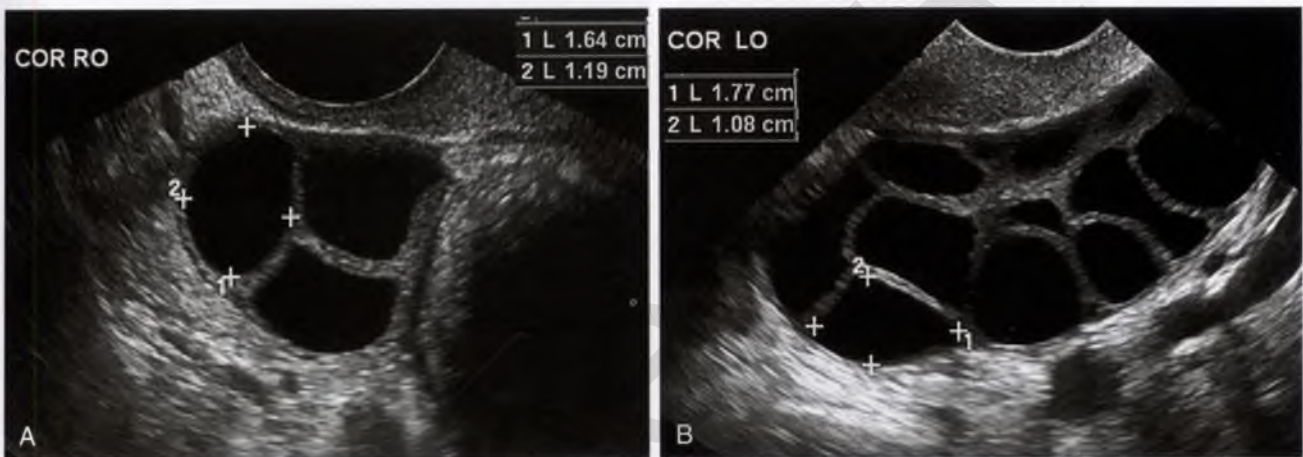


**FIG 32-18** Variable appearance of ovaries on follicular monitoring studies. **A**, Three follicles are shown within the right ovary, measuring up to 16 mm in diameter (*calipers*). **B**, In a different patient, undergoing treatment as an egg donor, the follicular monitoring study shows at least 10 follicles within the left ovary, with an average follicle measuring approximately 18 × 11 mm (*calipers*).



**FIG 32-19** Transabdominal ultrasound guidance for oocyte retrieval. The needle (*arrowheads*) approaches from the patient's left and enters one of several anechoic follicles within the prominent ovary.



**FIG 32-20** Normal appearance of the ovary following oocyte retrieval. Transverse gray-scale image shows multiple small complex cysts at the periphery of the enlarged right ovary, each containing internal echoes indicating blood.



no documented difference in blood flow to the endometrium and subendometrium,<sup>57</sup> no difference in uterine artery or subendometrial flow but decreased flow to the endometrium,<sup>58</sup> and elevated resistive index (RI) and pulsatility index (PI) of the uterine artery and decreased blood flow to the endometrium and subendometrium.<sup>59</sup> Similarly, the reported utility of Doppler parameters of ovarian blood flow is mixed. In one study, higher blood flow in the ovary correlated with more successful pregnancies as compared to patients with less flow,<sup>60</sup> whereas another group found no such difference.<sup>61</sup>

### COMPLICATIONS OF ASSISTED REPRODUCTION

Patients with infertility who undergo assisted reproduction are at risk for several possible complications, including ovarian hyperstimulation syndrome (OHSS), hemorrhage, or infection.<sup>62,63</sup> OHSS is an iatrogenic process that occurs in patients who have undergone ovulation induction with gonadotropins, typically after the administration of hCG. OHSS is estimated to occur in 2% to 10% of patients undergoing assisted reproduction,<sup>63-65</sup> and this complication is more likely to occur in those with higher numbers of developing follicles or high levels of estradiol. OHSS can occur during the luteal phase of the cycle, prior to a positive pregnancy test, or in the early stages of pregnancy. The

primary pathophysiologic process involves increased capillary permeability related to the release of ovarian vasoactive angiogenic substances.<sup>66,67</sup> The imaging findings of OHSS include marked enlargement of the ovaries (>10 cm in diameter) with numerous follicles and associated free intraperitoneal fluid because of third spacing. Pleural effusions can be seen in severely affected patients (Fig. 32-21A through D). The ovaries typically contain multiple complex cysts, representing recently instrumented follicles with hemorrhage. Patients may present with abdominal distention, weight gain, and hemoconcentration from third spacing of fluid. Typically, both ovaries are affected, and their large size may cause them to rise out of the pelvis and be situated near the superior aspect of the uterus. For this reason, a transabdominal imaging approach is usually preferable. Although rare, the markedly enlarged ovaries may, on occasion, undergo torsion or even rupture, which can be difficult to diagnose by sonography because the ovaries are already markedly enlarged with numerous cysts. Hence, it can be difficult to distinguish the typical gray-scale sonographic features found with ovarian torsion. Asymmetry in ovarian size or blood flow and marked tenderness to palpation are important clues to the diagnosis. Remember, however, that pain may also be caused by stretching of the ovarian capsule, hemorrhage into one or more cysts, rupture of one of the cysts, or even ectopic pregnancy. Patients with a large

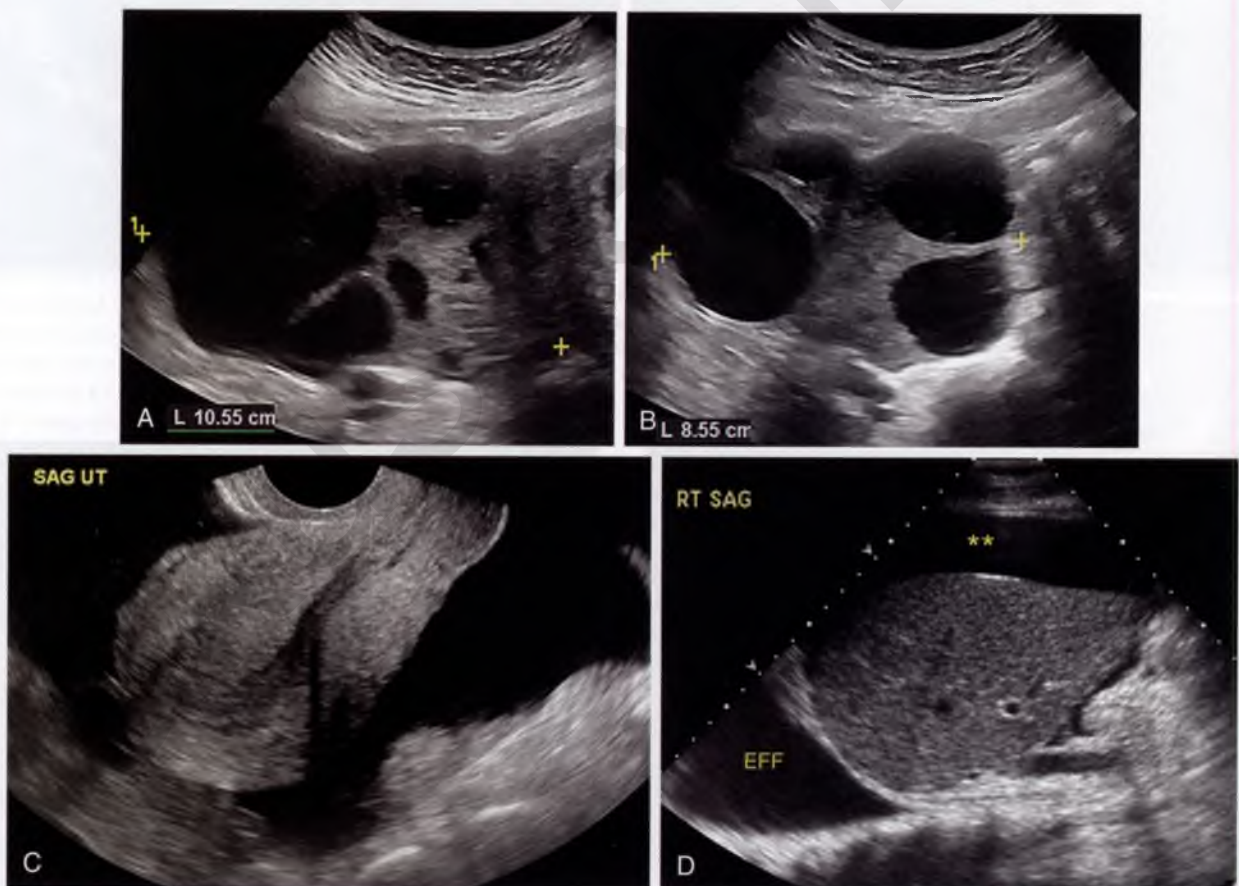


**FIG 32-21** Ovarian hyperstimulation syndrome (OHSS), 2 weeks after oocyte retrieval. **A**, Sagittal transabdominal gray-scale image of the enlarged right ovary (*calipers*), which measures approximately 10.5 cm in diameter and contains multiple cysts. **B**, The enlarged left ovary measures approximately 8.5 cm in diameter and has a similar appearance, with multiple cysts shown on this transabdominal transaxial sonographic image. **C**, Sagittal transvaginal gray-scale image of the uterus shows a large amount of anechoic free fluid in the pelvis. **D**, Sagittal transabdominal gray-scale image of the right upper quadrant demonstrates free intraperitoneal fluid (*asterisks*) anterior to the right lobe of the liver and a right pleural effusion (EFF).



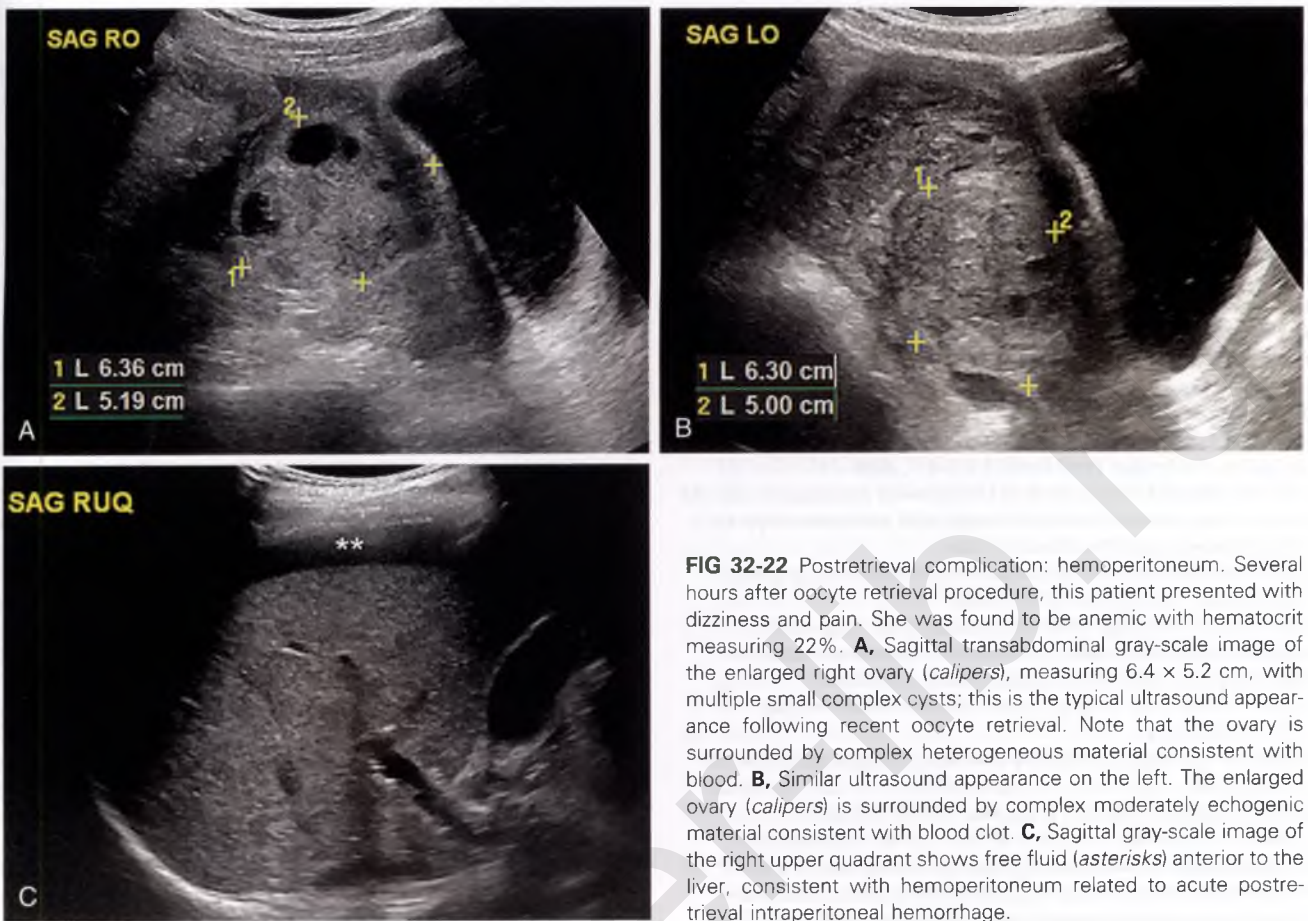


**FIG 32-22** Postretrieval complication: hemoperitoneum. Several hours after oocyte retrieval procedure, this patient presented with dizziness and pain. She was found to be anemic with hematocrit measuring 22%. **A**, Sagittal transabdominal gray-scale image of the enlarged right ovary (*calipers*), measuring 6.4 × 5.2 cm, with multiple small complex cysts; this is the typical ultrasound appearance following recent oocyte retrieval. Note that the ovary is surrounded by complex heterogeneous material consistent with blood. **B**, Similar ultrasound appearance on the left. The enlarged ovary (*calipers*) is surrounded by complex moderately echogenic material consistent with blood clot. **C**, Sagittal gray-scale image of the right upper quadrant shows free fluid (*asterisks*) anterior to the liver, consistent with hemoperitoneum related to acute postretrieval intraperitoneal hemorrhage.

volume of peritoneal or pleural fluid may require therapeutic paracentesis or thoracentesis, and preprocedure sonographic localization or guidance may be useful.

The other potential complications of assisted reproduction, such as hemorrhage and infection, are related to the retrieval procedure. Both are fortunately quite uncommon.<sup>63</sup> During oocyte retrieval, multiple punctures of the vaginal wall and ovary are performed. Typically, the amount of bleeding is quite small, in the range of 10 to 20 mL.<sup>68</sup> If a larger vessel is inadvertently punctured during the procedure, the patient may present in the immediate postretrieval period with evidence of hemorrhage or hemoperitoneum, including dizziness or hypotension. The finding of complex echogenic free fluid in the cul-de-sac or elsewhere in the peritoneal cavity correlates highly with hemoperitoneum and helps differentiate intraperitoneal blood from anechoic free fluid, such as is seen in patients with OHSS (Fig. 32-22A through C). If hemorrhage is suspected, it is important to include sonographic evaluation of the upper abdomen, to assess for intraperitoneal blood not visualized using the transvaginal transducer. Postretrieval infection or tubo-ovarian abscess is a rare complication (Fig. 32-23). Of note, patients with preexisting hydrosalpinges that could harbor subclinical infection are reported to be at increased risk.<sup>69,70</sup>

## CONCLUSION

Infertility continues to be an important health care issue, and the role of sonography in the care of an infertile woman is clearly established.

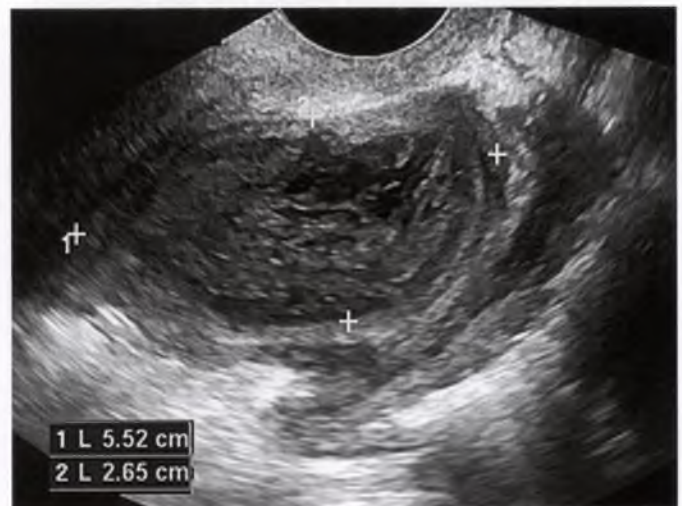


**FIG 32-23** Postretrieval complication: abscess/infection. Sagittal gray-scale image of the enlarged right ovary shows a thick-walled, complex cystic structure with internal echoes (*calipers*) in a patient who presented with fever and pain 1 week after oocyte retrieval. Note a small amount of adjacent echogenic fluid inferiorly. Aspiration of the complex cyst revealed pus, consistent with postretrieval ovarian abscess/infection.



From baseline evaluation to assess for structural abnormality (such as endometrial mass, uterine anomaly, or hydrosalpinx) or low antral follicular count, to monitoring of folliculogenesis, guidance for oocyte retrieval and detection of possible posttreatment complications, sonography, in particular transvaginal sonography, plays an essential role in the diagnosis and clinical management of these patients.

## REFERENCES

- Chandra A, Copen CE, Stephen EH: Infertility and impaired fecundity in the United States, 1982-2010: data from the National Survey of Family Growth. *Natl Health Stat Rep* 67:1-18, 2013.
- Olpin JD, Kennedy A: Secondary infertility in women: radiologic evaluation. *Rep Med Imaging* 4:1-14, 2011.
- Shalev J, Meizner I, Bar-Hava I, et al: Predictive value of transvaginal sonography performed before routine diagnostic hysteroscopy for evaluation of infertility. *Fertil Steril* 73:412-417, 2000.
- Loverro G, Nappi L, Vicino M, et al: Uterine cavity assessment in infertile women: comparison of transvaginal sonography and hysteroscopy. *Eur J Obstet Gynecol Reprod Biol* 100:67-71, 2001.
- Troiano RN, McCarthy SM: Mullerian duct anomalies: imaging and clinical issues. *Radiology* 233:19-34, 2004.
- Saravelos SH, Cocksedge KA, Li TC: Prevalence and diagnosis of congenital uterine anomalies in women with reproductive failure: a critical appraisal. *Hum Reprod Update* 14:415-419, 2008.
- Sadow CA, Sahni VA: Imaging female infertility. *Abdom Imaging* 39(1):92-107, 2014.
- Benacerraf BR, Shipp TD, Bromley B: Which patients benefit from a 3D reconstructed coronal view of the uterus added to standard routine 2D pelvic sonography? *AJR Am J Roentgenol* 190:626-629, 2008.
- Ludwin A, Pitynski K, Ludwin I, et al: Two- and three-dimensional ultrasonography and sonohysterography versus hysteroscopy with laparoscopy in the differential diagnosis of septate, bicornuate, and arcuate uteri. *J Minim Invasive Gynecol* 20(1):90-99, 2013.
- Moini A, Mohammadi S, Hosseini R, et al: Accuracy of 3-dimensional sonography for diagnosis and classification of congenital uterine anomalies. *J Ultrasound Med* 32:923-927, 2013.
- Shen L, Wang Q, Huang W, et al: High prevalence of endometrial polyps in endometriosis-associated infertility. *Fertil Steril* 95:2722-2724, 2011.
- Pérez-Medina T, Bajo-Arenas J, Salazar F, et al: Endometrial polyps and their implication in the pregnancy rates of patients undergoing intrauterine insemination: a prospective, randomized study. *Hum Reprod* 20:1632-1635, 2005.
- Winkelman WD, Frates MC, Fox JH, et al: Secondary infertility and retained fetal bone fragments. *Obstet Gynecol* 122:458-461, 2013.
- Soares SR, Barbosa Dos Reis MM, Camargos AF: Diagnostic accuracy of sonohysterography, transvaginal sonography and hysterosalpingography in patients with uterine cavity diseases. *Fertil Steril* 73:406-411, 2000.
- Sakhel K, Abuhamad A: Sonography of adenomyosis. *J Ultrasound Med* 31:805-808, 2012.
- Bromley B, Shipp TD, Benacerraf B: Adenomyosis: sonographic findings and diagnostic accuracy. *J Ultrasound Med* 19:529-534, 2000.
- Atri M, Reinhold C, Mehio A, et al: Adenomyosis: US features with histologic correlation in an in vitro study. *Radiology* 21:783-790, 2000.
- Vercellini P, Consonni D, Dridi D, et al: Uterine adenomyosis and in vitro fertilization outcome: a systematic review and meta-analysis. *Hum Reprod* 29:964-977, 2014.
- Thalluri V, Tremellen KP: Ultrasound diagnosed adenomyosis has a negative impact on successful implantation following GnRH antagonist IVF treatment. *Hum Reprod* 27:3487-3492, 2012.
- Salim R, Riris S, Saab W, et al: Adenomyosis reduces pregnancy rates in infertile women undergoing IVF. *Reprod Biomed Online* 25(3):273-277, 2012.
- Practice Committee of the American Society for Reproductive Medicine: Myomas and reproductive function. *Fertil Steril* 86(5 Suppl 1):S194-S199, 2004.
- Kroon B, Johnson N, Chapman M, et al: Fibroids in infertility—consensus statement from ACCEPT (Australasian CREI Consensus Expert Panel on Trial Evidence). *Aust N Z J Obstet Gynaecol* 51(4):289-295, 2011.
- Pritts EA, Parker WH, Olive DL: Fibroids and infertility: an updated systematic review of the evidence. *Fertil Steril* 91:1215-1223, 2009.
- Klatsky PC, Tran ND, Caughey AB, Fujimoto VY: Fibroids and reproductive outcomes: a systematic literature review from conception to delivery. *Am J Obstet Gynecol* 198(4):357-366, 2008.
- Somigliana E, Vercellini P, Daguati R, et al: Fibroids and female reproduction: a critical analysis of the evidence. *Hum Reprod* 13:465-476, 2007.
- Garcia Oliveira F, Abdelmassih V, Diamond MP, et al: Impact of subserosal and intramural uterine fibroids that do not distort the endometrial cavity on the outcome of in vitro fertilization-intracytoplasmic sperm injection. *Fertil Steril* 81:582-587, 2004.
- Hart R, Khalaf Y, Yeong CT, et al: A prospective controlled study of the effect of intramural uterine fibroids on the outcome of assisted conception. *Hum Reprod* 16(11):2411-2417, 2001.
- Yoshino O, Hayashi T, Osuga Y, et al: Decreased pregnancy rate is linked to abnormal uterine peristalsis caused by intramural fibroids. *Hum Reprod* 25:2475-2479, 2010.
- Jun SH, Ginsburg ES, Racowsky C, et al: Uterine leiomyomas and their effect on in vitro fertilization outcome: a retrospective study. *J Assist Reprod Genet* 18:139-143, 2001.
- Surrey ES, Minjarez DA, Stevens JM, Schoolcraft WB: Effect of myomectomy on the outcome of assisted reproductive technologies. *Fertil Steril* 83:1473-1479, 2005.
- Firouznia K, Ghanaati H, Sanaati M, et al: Pregnancy after uterine artery embolization for symptomatic fibroids: a series of 15 pregnancies. *AJR Am J Roentgenol* 192:1588-1592, 2009.
- Hendriks DJ, Mol BW, Bancsi LF, et al: Antral follicle count in the prediction of poor ovarian response and pregnancy after in vitro fertilization: a meta-analysis and comparison with basal follicle-stimulating hormone level. *Fertil Steril* 83(2):291-301, 2005.
- Servaes K, Van Schoubroeck D, Welkenhuysen M, et al: How reproducible are 2-dimensional ultrasonographic follicular diameter measurement from stored 3-dimensional files of ovarian scanning? *Gynecol Obstet Invest* 77:163-168, 2014.
- Deb S, Kannamannadiar J, Campbell BK, et al: The interovarian variation in three-dimensional ultrasound markers of ovarian reserve in women undergoing baseline investigation for subfertility. *Fertil Steril* 95:667-672, 2011.
- Lane DE: Polycystic ovary syndrome and its differential diagnosis. *Obstet Gynecol Surv* 61(2):125-135, 2006.
- Rotterdam ESHRE/ASRM-Sponsored PCOS Consensus Workshop Group: Revised 2003 consensus on diagnostic criteria and long-term health risks related to polycystic ovary syndrome. *Fertil Steril* 81(1):19-25, 2004.
- Dewailly D, Lujan ME, Carmina E: Definition and significance of polycystic ovarian morphology: a task force report from the Androgen Excess and Polycystic Ovary Syndrome Society. *Hum Reprod Update* 20(3):334-352, 2014.
- Martins WP, Kollmann M, Raine-Fenning N: Counting ovarian follicles: updated threshold for diagnosis of hyperandrogenic anovulation. *Ultrasound Obstet Gynecol* 44:131-134, 2014.
- Hajishafiqi M, Zobairi T, Zanjani VR, et al: Diagnostic value of sonohysterography in the determination of fallopian tube patency as an initial step of routine infertility assessment. *J Ultrasound Med* 28:1671-1677, 2009.
- Preffumo F, Serafini G, Martinoli C, et al: The sonographic evaluation of tubal patency with stimulated acoustic emission imaging. *Ultrasound Obstet Gynecol* 20:386-389, 2002.
- Fleischer AC, Vasquez JM, Cullinan JA, Eisenberg E: Sonohysterography combined with sonosalpingography: correlation with endoscopic findings in infertility patients. *J Ultrasound Med* 16:381-384, 1997.
- Malik B, Patil S, Boricha BG, et al: A comparative study of the efficacy of sonosalpingography and hysterosalpingogram to test the tubal patency in

- all women with primary and secondary infertility. *Ultrasound Q* 30(2):139–143, 2014.
43. Sladkevicius P, Ohja K, Campbell S, Nargund G: Three-dimensional power Doppler imaging in the assessment of fallopian tube patency. *Ultrasound Obstet Gynecol* 16:644–647, 2000.
  44. Papaioannou S, Sourdrez P, Varma R, et al: Tubal evaluation in the investigation of subfertility: a structured comparison. *Br J Obstet Gynaecol* 111:1313–1321, 2004.
  45. Johnson N, Vandekerckhove P, Watson A, et al: Tubal flushing for subfertility. *Cochrane Database Syst Rev* (2):CD003718, 2005.
  46. Ng EH, Ajonuma LC, Lau EY, et al: Adverse effects of hydrosalpinx fluid on sperm motility and survival. *Hum Reprod* 15(4):772–777, 2000.
  47. Johnson N, van Voorst S, Sowter MC, et al: Surgical treatment for tubal disease in women due to undergo in vitro fertilisation. *Cochrane Database Syst Rev* (20):CD002125, 2010.
  48. Strandell A, Lindhard A, Waldenström U, Thorburn J: Hydrosalpinx and IVF outcome: cumulative results after salpingectomy in a randomized controlled trial. *Hum Reprod* 16:2403–2410, 2001.
  49. Bildirici I, Bukulmez O, Ensari A, et al: A prospective evaluation of the effect of salpingectomy on endometrial receptivity in cases of women with communicating hydrosalpinges. *Hum Reprod* 16:2422–2426, 2001.
  50. Kasius A, Smit JG, Torrance HL, et al: Endometrial thickness and pregnancy rates after IVF: a systematic review and meta-analysis. *Hum Reprod Update* 4:530–541, 2014.
  51. Revel A: Defective endometrial receptivity. *Fertil Steril* 97:1028–1032, 2012.
  52. Zhao J, Zhang Q, Li Y: The effect of endometrial thickness and pattern measured by ultrasonography on pregnancy outcomes during IVF-ET cycles. *Reprod Biol Endocr* 10:100–106, 2012.
  53. Rodríguez M, Guillén JJ, López MJ, et al: Learning curves in 3-dimensional sonographic follicle monitoring during controlled ovarian stimulation. *J Ultrasound Med* 33:649–655, 2014.
  54. Ng EHY, Chan CCW, Tang OS, et al: Endometrial and subendometrial blood flow measured during early luteal phase by three-dimensional power Doppler ultrasound in excessive ovarian responders. *Hum Reprod* 19:924–931, 2004.
  55. Raine-Fenning NJ, Campbell BK, Kendall NR, et al: Endometrial and subendometrial perfusion are impaired in women with unexplained subfertility. *Hum Reprod* 19:2605–2614, 2004.
  56. di Osagie ECO, Seif MW, Aplin JD, et al: Characterizing the endometrium in unexplained and tubal factor infertility: a multiparametric investigation. *Fertil Steril* 82:1379–1389, 2004.
  57. Ng EHY, Chan CCW, Tang OS, et al: Changes in endometrial and subendometrial blood flow in IVF. *Reprod Biomed Online* 18(2):269–275, 2009.
  58. Kim A, Jung H, Choi WJ, et al: Detection of endometrial and subendometrial vasculature on the day of embryo transfer and prediction of pregnancy during fresh in vitro fertilization cycles. *Taiwan J Obstet Gynecol* 53(3):360–365, 2014.
  59. El-Mazny A, Abou-Salem N, Elshenoufy H: Doppler study of uterine hemodynamics in women with unexplained infertility. *Eur J Obstet Gynecol Reprod Biol* 171(1):84–87, 2013.
  60. Mercé LT, Bau S, Barco MJ, et al: Assessment of the ovarian volume, number and volume of follicles and ovarian vascularity by three-dimensional ultrasonography and power Doppler angiography on the HCG day to predict the outcome in IVF/ICSI cycles. *Hum Reprod* 21:1218–1226, 2006.
  61. Giugliano E, Cagnazzo E, Giugliano B, et al: Can Doppler study of the ovarian artery predict the fertility outcome of intrauterine insemination? *J Clin Ultrasound* 42:331–335, 2014.
  62. Baron KT, Babagbemi KT, Arleo EK, et al: Emergent complications of assisted reproduction: expecting the unexpected. *Radiographics* 33(1):229–244, 2013.
  63. Klemetti R, Sevón T, Gissler M, Hemminki E: Complications of IVF and ovulation induction. *Hum Reprod* 20:3293–3300, 2005.
  64. Nastro CO, Teixeira CM, Moroni RM, et al: Ovarian hyperstimulation syndrome: pathophysiology, staging, prediction and prevention. *Ultrasound Obstet Gynecol* 45(4):377–393, 2015.
  65. Papanikolaou EG, Pozzobon C, Kolibianakis EM, et al: Incidence and prediction of ovarian hyperstimulation syndrome in women undergoing gonadotropin-releasing hormone antagonist in vitro fertilization cycles. *Fertil Steril* 85:112–120, 2006.
  66. Gómez R, Soares SR, Busso C, et al: Physiology and pathology of ovarian hyperstimulation syndrome. *Semin Reprod Med* 28:448–457, 2010.
  67. Soares SR: Etiology of OHSS and use of dopamine agonists. *Fertil Steril* 97:517–522, 2012.
  68. Shalev J, Davidi O, Fisch B: Quantitative three dimensional sonographic assessment of pelvic blood after transvaginal ultrasound guided oocyte aspiration: factors predicting risk. *Ultrasound Obstet Gynecol* 23(2):177–182, 2004.
  69. Varras M, Polyzos D, Tsikini A, et al: Ruptured tubo-ovarian abscess as a complication of IVF treatment: clinical, ultrasonographic and histopathologic findings. A case report. *Clin Exp Obstet Gynecol* 30:164–168, 2003.
  70. Matsunaga Y, Fukushima K, Nozaki M, et al: A case of pregnancy complicated by the development of a tubo-ovarian abscess following in vitro fertilization and embryo transfer. *Am J Perinatol* 20:277–282, 2003.



# Ectopic Pregnancy

Oksana H. Baltarowich, Leslie M. Scoutt

## SUMMARY OF KEY POINTS

- The incidence of ectopic pregnancy (EP) in the United States is increasing as a result of an increase in the number of patients with risk factors as well as an increase in diagnosis due to earlier presentation and detection.
- Mortality rate from EP is decreasing because of improved diagnostic techniques and heightened awareness among clinicians and patients.
- The most common predisposing risk factor for EP is tubal abnormality. However, up to 50% of patients with EP have no known risk factors.
- The presence of an extrauterine gestational sac containing a yolk sac or embryo (with or without cardiac activity) is the most specific sonographic finding for EP, whereas an echogenic tubal ring in the adnexa is the most common sonographic finding.
- When sonography is inconclusive, follow-up with both serum human chorionic gonadotropin (hCG) and transvaginal sonography (TVS) should be used to differentiate an intrauterine pregnancy (IUP) from an EP, as either test alone is often insufficient.
- The term *pseudogestational sac* should be avoided, because it implies the presence of an EP and turns attention away from the fact that in the pregnant patient, most intrauterine fluid collections are IUPs that could be harmed by inappropriate therapy.
- The incidence of EPs in unusual locations is increasing. Such EPs are often the result of complications from assisted reproductive techniques (ART) and are associated with higher morbidity and mortality rates compared with tubal EPs.
- The term *cornual pregnancy* has been used variably to describe interstitial EPs (located within the interstitial portion of the fallopian tube as it courses through the myometrium in the cornual portion of the uterus), IUPs located in the angular portion of the endometrial cavity, IUPs in the horn of a bicornuate or septate uterus, or pregnancies in the rudimentary horn of a unicornuate uterus. Hence, the authors recommend that the term *cornual pregnancy* be abandoned because it is confusing. Rather, a more precise, complete anatomic description that clearly states if the pregnancy is within or separate from the endometrial cavity should be provided for any eccentrically located pregnancy in the cornual region of the uterus.

## OUTLINE

**Epidemiology, 967**

**Risk Factors, 967**

**Pathophysiology, 968**

**Clinical Presentation, 969**

**Diagnostic Tests, 969**

Human Chorionic Gonadotropin, 969

Molecular Biomarkers, 970

Transvaginal Sonography, 970

**Sonographic Diagnosis of Ectopic Pregnancy, 971**

Uterine Findings, 971

Adnexal Findings, 972

Cul-de-Sac Findings, 972

Pitfalls, 977

**Ectopic Pregnancies in Unusual Locations, 978**

Interstitial Ectopic Pregnancy, 978

Rudimentary Horn Ectopic Pregnancy, 985

Cervical Ectopic Pregnancy, 986

Myometrial/Cesarean Scar Ectopic Pregnancy, 990

Ovarian Ectopic Pregnancy, 991

Abdominal Ectopic Pregnancy, 991

Retroperitoneal Ectopic Pregnancy, 993

**Chronic Ectopic Pregnancy, 995**

**Posthysterectomy Ectopic Pregnancy, 996**

**Heterotopic Pregnancies, 996**

**Management and Treatment Options, 996**

**Conclusion, 998**

The most accurate definition of an EP is a pregnancy that has implanted in a location other than within the endometrial cavity (Fig. 33-1). In the United States, approximately 2% of all pregnancies are ectopic in location. Worldwide, EP is a significant cause of morbidity and death in women of child-bearing years, especially in countries or areas with poor prenatal care. The mortality rate from EP has decreased in recent

years likely in large part attributable to technologic advances in ultrasound imaging, earlier sonographic imaging and diagnosis, more sensitive hCG tests, and improved treatment with laparoscopy and methotrexate (MTX), along with heightened awareness of the diagnosis among clinicians and patients. However, despite the recent improvements in technology and health care, many cases of EPs are still difficult

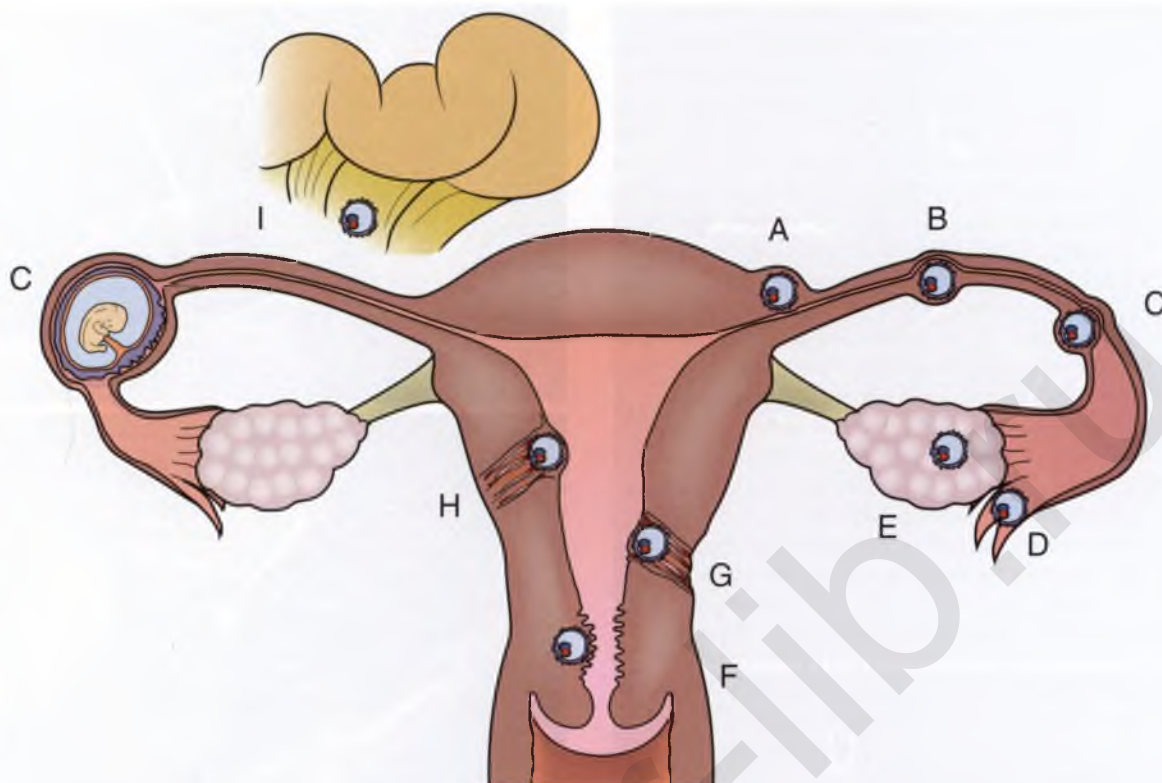


**FIG 33-1** Locations of ectopic pregnancies. Ninety-five percent of ectopic pregnancies occur in the fallopian tube: in the interstitial (A), isthmic (B), ampullary (C, most common), and fimbrial (D) portions. Extratubal ectopic pregnancies may be found in ovarian (E), cervical (F), cesarean scar (G), myometrial scar (H), and abdominal (I) locations.

to diagnose, and some cases elude even the best diagnosticians. Optimal care requires balancing an early but possibly incorrect diagnosis and intervening with the progress of a normal IUP, particularly if it is a desired pregnancy, versus waiting too long to be certain and thus endangering a woman's life from rupture of an EP. This chapter will review the role of sonography in the diagnosis and management of EP, including EPs in unusual locations.

## EPIDEMIOLOGY

According to data from the Centers for Disease Control and Prevention (CDC), the incidence of EP in the United States rose from 0.5% of all pregnancies in the 1970s to 2% in the 1990s.<sup>1,2</sup> This rise has been linked to an increase in the number of patients with risk factors as well as an increase in the number of pregnancies resulting from ART. However, the reported increased incidence of EP is also almost certainly related to earlier presentation of many patients with EP as well as improved diagnostic techniques, including more sensitive assays for hCG and high-resolution TVS. As a result, some very early EPs are now diagnosed that in years past might have spontaneously resolved without coming to medical attention.

Fortunately, the mortality rate associated with EP has progressively decreased in recent years. The EP mortality ratio in the United States decreased from 1.15 deaths per 100,000 live births in 1980 to 1984 to 0.50 death per 100,000 live births in 2003 to 2007. Based on the current average annual rate of decline, the ratio is expected to further decrease to 0.36 death from EP per 100,000 live births by 2013 to 2017.<sup>3</sup> Nonetheless, recent epidemiologic studies suggest that 6% of maternal deaths in the United States are caused by EPs,<sup>4</sup> and EP remains the leading cause of pregnancy-related death during the first trimester.

## TABLE 33-1 Risk Factors for Ectopic Pregnancy

### Major Risk Factors

- Tubal disease
  - Pelvic inflammatory disease: salpingitis
  - Previous ectopic pregnancy
  - Salpingitis nodosa isthmica
  - Tubal sterilization
  - Reconstructive tubal surgery
- In utero exposure to diethylstilbestrol (DES)
- Assisted reproductive technologies (ART)
- Intrauterine devices

### Minor Risk Factors

- Endometriosis
- Early age at first intercourse (<18 years)
- Older maternal age at first pregnancy (>35 years)
- Cigarette smoking
- Previous pelvic/abdominal surgery
- No known risk factors (50% of cases)

## RISK FACTORS

The most common predisposing risk factor for EP is abnormal tubal anatomy, usually tubal scarring, which is most often secondary to salpingitis associated with pelvic inflammatory disease (PID) from sexually transmitted infections (Table 33-1). Salpingitis isthmica



nodosa, which is characterized by nodular thickening of the isthmic portion of the fallopian tube accompanied by multiple diverticula, is found in more than 50% of surgically excised tubal EPs. The diverticula correlate well with the location of the EP implantations.<sup>5</sup> Prior history of EP is also a major risk factor. The rate of recurrent EP is 5% to 20% after a single prior EP, but increases to greater than 30% in women with a history of two consecutive EPs.<sup>6</sup> Other causes of tubal scarring include tubal sterilization, reconstructive tubal surgery, and tubal abnormalities related to diethylstilbestrol (DES) exposure in utero. One study reported the risk of EP within 10 years after tubal sterilization to be 7 per 1000 procedures.<sup>7</sup>

In addition, the incidence of EP is increased in women who have conceived using ART, especially following in vitro fertilization (IVF), even if the fallopian tubes are anatomically normal. Tubal pregnancies may result from inadvertent direct placement of embryos into a diseased tube during embryo transfer (ET). Retrograde migration of a transferred embryo from the uterine cavity into an abnormal tube may also occur.<sup>8</sup> IVF patients are at increased risk of EP because of the high prevalence of tubal damage, the use of ovulation induction therapy, and multiple ETs, which put the patient at risk for heterotopic implantations. The presence of an intrauterine device (IUD) increases the risk for EP by a factor of 2.5. An estimated 25% to 50% of pregnancies conceived with an IUD in place are ectopic, and past IUD use may also pose a small increased risk for EP.<sup>9,10</sup> In general, infertility seems to be a risk factor. There has been no documentation of a clear association between EP and oral contraceptive use, previous elective pregnancy termination, or spontaneous miscarriage.

Other factors with less clear-cut associations have been implicated as risk factors for EP. Epidemiologic studies have shown that cigarette smoking at the time of conception is a risk factor for tubal EP. Possible explanations for this relationship include altered tubal contractility and abnormal ciliary motion from the effect of nicotine or reduced immunity in cigarette smokers, which may affect tubal response to inflammation, as in PID.<sup>11,12</sup> Endometriosis is also associated with higher rates of EP and miscarriage, possibly because endometriosis and other adjacent inflammatory conditions, such as acute or ruptured appendicitis, can secondarily affect the fallopian tube, thereby causing scarring and adhesions. However, more recent studies claim that there is no association between endometriosis and EP.<sup>13</sup> Abnormalities of the zygote and endocrine dysfunction that may affect ovum transport also increase the risk for EP. Age has also been implicated as a risk factor. Women who have their first sexual encounter when younger than 18 years of age or their first pregnancy when older than 35 years of age have a slightly increased risk of tubal pregnancy. Importantly, however, it should be recognized that approximately 50% of patients with EP have no known risk factors.<sup>9</sup>

## PATHOPHYSIOLOGY

Approximately 95% of EPs are located within the fallopian tube (Figs. 33-1 and 33-2): 70% in the ampullary portion of the tube, 12% in the isthmic portion, 11% in the fimbriated end, and 2% to 4% in the interstitial portion.<sup>14</sup> Abnormal locations within the uterus include the cervix, a rudimentary horn, and myometrial scars, including scars following cesarean delivery or myomectomy. Other unusual types of EP include intraovarian, abdominal, retroperitoneal, and mediastinal, as well as chronic and heterotopic (in which there is an ectopic as well as an intrauterine gestation) EPs. EP has also rarely been reported after supracervical hysterectomy and even after total abdominal hysterectomy.

Histologically, the fallopian tube is comprised of mucosal, muscularis, and serosal layers. There is no decidua or decidua basalis as in

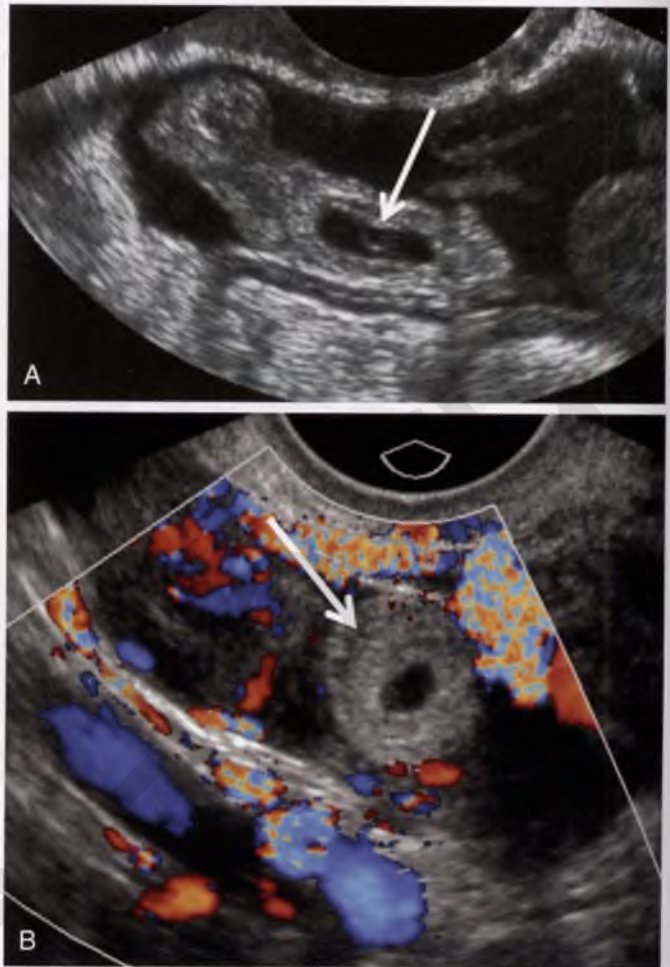


**FIG 33-2** Ectopic pregnancy in the ampullary portion of a fallopian tube. The patient presented with vaginal bleeding and a positive serum human chorionic gonadotropin (hCG). **A**, Transvaginal longitudinal scan of the ampullary portion of the fallopian tube shows that it is surrounded by free pelvic fluid and contains a gestational sac with a yolk sac (arrow). **B**, Transverse color Doppler transvaginal sonogram of the hyperechoic tubal ring of the ectopic gestation shows no demonstrable blood flow in the echogenic ring surrounding the gestational sac (arrow).

the endometrium. The syncytiotrophoblast and cytotrophoblast of the EP invade into the muscularis layer of the fallopian tube and in essence create adherent trophoblastic tissue.<sup>15</sup> As the trophoblastic tissue grows and the tube stretches, it becomes prone to rupture. Some tubal pregnancies are expelled through the fimbriated end of the tube if the trophoblastic tissue is sheered from its attachment to the muscularis layer, resulting in a tubal abortion. Most of these do not survive, but rarely an abdominal pregnancy may result. If the EP implants outside the tube, then the syncytiotrophoblast and cytotrophoblast will invade underlying tissues and the placental tissue becomes extremely difficult to separate from these tissues, resulting in a substantial increased risk of hemorrhage.

In general, it is helpful to consider two broad categories that give rise to ectopic implantation. The first includes conditions that interfere with transport of the fertilized ovum to the endometrial cavity. The second includes conditions that predispose to premature implantation of the fertilized ovum before reaching the endometrial cavity. The fallopian tube should not be viewed as a passive conduit, but rather is part of a complex interactive process involving tubal peristalsis, ciliary



motion, tubal epithelium, and flow of tubal secretions along with the sperm, oocytes, and the conceptus. This all contributes to successful movement of the fertilized ovum through the fallopian tube into the endometrial cavity. This process may become disrupted or altered at many points along the way and result in abnormal implantation.<sup>16</sup> Scarring from prior episodes of salpingitis, tubal sterilization, or tubal reconstructive surgery as well as tubal conditions such as salpingitis isthmica nodosa and abnormalities following in utero DES exposure have been postulated to interfere with transport of the conceptus to the endometrial cavity.<sup>17</sup> Conditions that predispose to premature implantation are less well understood. Previously it was believed that embryos that implant ectopically were likely to have abnormal karyotypes; however, no good data support this theory. A study of 30 surgically excised EPs found no difference in the karyotypes of the chorionic villi from the EPs compared with a control group of IUPs.<sup>18</sup>

## CLINICAL PRESENTATION

Women with EPs most commonly present with symptoms 5 to 8 weeks after the last normal menstrual period. The classic presenting clinical triad of pelvic pain, vaginal bleeding, and an adnexal mass is nonspecific and is found in 20% to 40% of patients with EP. Many patients with pain and vaginal bleeding are not pregnant, and such symptoms are commonly due to hemorrhagic or ruptured ovarian cysts, PID, or dysfunctional uterine bleeding. Even with the addition of a positive pregnancy test and amenorrhea, such signs and symptoms can occur in the setting of a normal IUP, miscarriage, or gestational trophoblastic disease. In fact, it is estimated that 70% to 90% of pregnant women who present with pain or vaginal bleeding in the first trimester and who are clinically suspected of harboring an EP turn out to have an IUP. Clinical findings may also include abdominal or adnexal tenderness. Less common presenting symptoms include referred shoulder pain from irritation of the peritoneal surface under the hemidiaphragm due to free intraperitoneal hemorrhage (Fig. 33-3), cervical motion tenderness, or the urge to defecate secondary to blood collecting in the cul-de-sac. Signs of rupture include hemodynamic instability, orthostatic hypotension, vertigo, loss of consciousness, syncope, or shock from blood loss. EPs in unusual locations may manifest with findings outside the pelvis.

However, tubal EPs can be very difficult to diagnose at an early stage. Nearly a third of cases exhibit no clinical signs and 9% have no symptoms prior to rupture, which can occur at any stage without warning.<sup>19</sup> Frates and associates<sup>20</sup> found that neither sonographic findings nor serum hCG levels were useful predictors of tubal rupture.

Hence, because of the lack of specificity of clinical presentation and physical findings as well as the absence of known risk factors in up to 50% of patients with EPs, clinicians should have a high index of suspicion for EP in any woman of reproductive age who presents with pelvic pain, vaginal bleeding, or symptoms suggestive of blood loss such as syncope or vertigo, even if her pregnancy status is not known. Certainly, any sexually active woman with lower abdominal/pelvic pain and vaginal bleeding after missing a menstrual period should be considered to have an EP until proved otherwise.

## DIAGNOSTIC TESTS

### Human Chorionic Gonadotropin

hCG from the blastocyst is first detectable in maternal serum 6 to 8 days following fertilization. Most current urine pregnancy test kits yield positive results 3 to 4 days after implantation. By 7 days after implantation, which is the time of expected menses, 98% of urine pregnancy tests will be positive. Current pregnancy tests are immuno-

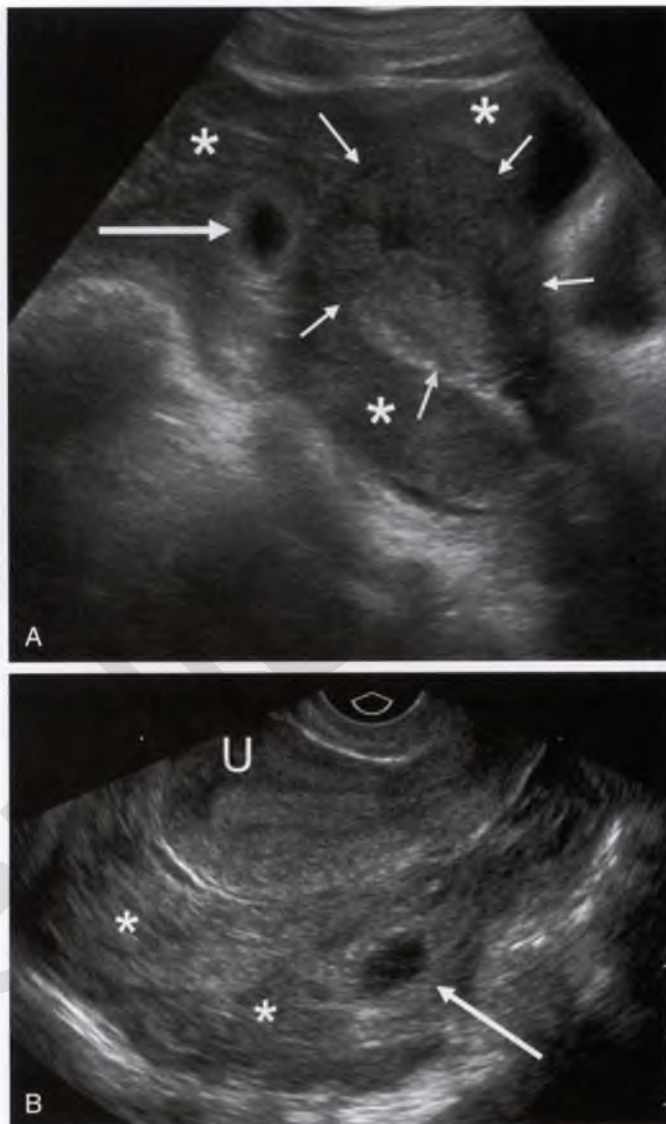


**FIG 33-3** Small ruptured ectopic pregnancy causing large hemoperitoneum. The patient presented with vaginal bleeding and low serum human chorionic gonadotropin (hCG) of 240 mIU/mL and was hemodynamically unstable. **A**, Transabdominal midline longitudinal scan demonstrating the uterus (*small arrows*) surrounded by clotted blood (*asterisks*), which also surrounds a small hyperechoic extrauterine tubal ring of the ectopic gestational sac (*large arrow*). **B**, Transvaginal midline sagittal scan of the empty uterus (*U*) shows clotted blood (*asterisks*) in the cul-de-sac, within which lies the small echogenic ring of the ectopic pregnancy (*arrow*), which, at surgery, was found to have ruptured.

assays of hCG based on monoclonal antibodies to the  $\beta$ -subunit of hCG and are highly sensitive and rapid, with virtually no cross-reactions.<sup>21</sup> If the urine test is negative, suspicion for EP is lowered, but not erased, because a urine pregnancy test will not detect levels of hCG below 25 mIU/mL. Importantly, a quantitative serum hCG test can detect levels approaching zero. If the serum hCG is negative, then an EP is almost certainly excluded, although chronic EP is still possible and rupture of an EP has been reported after the hCG dropped to zero.<sup>22</sup> However, both of these conditions are extremely rare.

There has been much discussion in the literature regarding discriminatory serum hCG levels above which an IUP should be definitively visible by TVS. Levels of 1000 to 2000 mIU/mL (1st International



Reference Preparation [IRP]) were previously used as discriminatory levels for expected visualization of an IUP on TVS. However, most researchers and practitioners now agree that no single serum hCG level should be used to differentiate an IUP from an EP. Rather, analysis of serial hCG levels and follow-up TVS are used to reach the correct diagnosis.<sup>23-25</sup> That said, if the serum hCG level is above 3000 mIU/mL (1st IRP) and the uterus is empty, a normal IUP is unlikely, although there have been anecdotal reports of delivery of a normal pregnancy following an initial TVS demonstrating an empty endometrial cavity with hCG levels as high as 4336 mIU/mL.<sup>26</sup> There are several possible explanations for this shift in discriminatory threshold levels. First, the incidence of multiple gestations has increased, mainly as a result of ART, and hCG levels for a given gestational age would thus be higher in a woman carrying a multiple gestation, compared to a singleton pregnancy, upon which earlier discriminatory numbers were derived. Second, data upon which earlier discriminatory numbers were based came from single institution studies with small patient populations. Third, clinical management and treatment have changed. Now, MTX is often given to treat EPs. If an erroneous, false positive diagnosis of EP is made and an IUP is not recognized, treatment with MTX can result in serious harm to the developing embryo. Hence, the current goal is to achieve 100% specificity with no false positive diagnoses of EP.

In general, the serum hCG level is lower for a given gestational age in the setting of an EP than with an IUP. Hence, when clinical findings are suspicious for possible EP, TVS is indicated even if the serum hCG is very low. Approximately 70% of women with EPs have a slow rise in serum hCG, slower than expected for a normal IUP, or a slow fall in hCG, slower than typical for spontaneous miscarriage.<sup>9</sup> Hence, a sub-optimal increase (i.e., <53% in 48 hours) or plateau of serial hCG values suggests an EP.<sup>9,27-29</sup> Of note, serum hCG levels in some women with EPs may be similar to expected hCG levels in women with normal IUPs. One study revealed that up to 27% of women diagnosed with EP had hCG curves resembling normal IUPs.<sup>30</sup> Others have found that 15% to 20% of EPs have hCG doubling times similar to those for IUPs. In addition, studies have shown that serum hCG levels may increase by only 35% to 66% over 48 hours for some normal IUPs, rather than doubling in that time frame, as has been previously expected.<sup>9,27,29</sup> Furthermore, in 8% of spontaneously resolving EPs, the serum hCG level will fall in a pattern mimicking spontaneous miscarriage. As a result, the use of serum hCG levels alone for follow-up is unreliable for the diagnosis and management of EP.<sup>31</sup>

Using sonography alone for follow-up is also not reliable because some EPs are too small to visualize. Additionally, 6% of apparent miscarriages on ultrasound examination may actually have an underlying EP. A presumed completed miscarriage based on TVS findings of an empty uterus should be treated as a pregnancy of unknown location (PUL) until confirmed as a miscarriage based on serial hCG levels and follow-up TVS. There are reports of patients discharged to home with presumed miscarriage subsequently returning with pain, bleeding, and ruptured EP.

PUL is a descriptive term referring to a pregnancy that is detected biochemically (positive pregnancy test), but not yet visible sonographically or laparoscopically.<sup>32</sup> This term, a temporary descriptor, is used as a holding pattern until the location of the pregnancy is established. The incidence of PULs is dependent not only upon the expertise of the examiners and the adequacy of the sonographic evaluation but also upon gestational age. As women present earlier in pregnancy, more PULs are reported. In 1999 Banerjee and colleagues<sup>33</sup> reported an 8% incidence (135 cases) of PULs in their series of first trimester sonograms. On follow-up, 14% of these turned out to be EPs; 27% developed into normal IUPs; 9% resulted in miscarriages; and 50% resolved

spontaneously. Kirk and Bourne<sup>34</sup> reported that in 8% to 31% of early pregnancies, the gestation will not be visualized on the initial TVS. The vast majority of PULs are eventually found to be IUPs or failed IUPs, and only approximately 7% to 20% are EPs. However, follow-up is very important. There is no reliable method by which to predict which PULs are IUPs and will either progress normally or miscarry and which PULs are EPs and, of these, which EPs will spontaneously resolve and which are likely to rupture.<sup>35</sup> Unfortunately, rupture of EPs has been reported with declining or very low hCG levels, including some rare cases with negative hCG values. It is therefore incorrect to assume that because the hCG level is low, an EP is unlikely or stable or to assume that an EP is too small to visualize and thus not perform a sonogram (see Fig. 33-3).<sup>22,36,37</sup>

## Molecular Biomarkers

Studies are ongoing in attempts to identify diagnostic molecular biomarkers that can reliably distinguish EPs from both normal and abnormal IUPs at an early stage, when the location of the pregnancy is not yet known. These data would be extremely useful in the early diagnosis of EP, obviating the need for multiple follow-up blood tests, ultrasound examinations, and clinic visits, while at the same time decreasing the risk of EP rupture. One of the main challenges in these investigations is that there is no suitable animal model for tubal EP, so research must be performed directly in women. Biomarkers of trophoblastic function, corpus luteal function, angiogenesis, endometrial function, inflammation, muscle damage, and impaired tubal transport are currently being investigated. Although a variety of serum, plasma, and urine biomarkers have been evaluated both independently and in combination, most do not have adequate discriminatory capability to be clinically useful.<sup>38-40</sup> One controlled study of patients with EPs and viable IUPs with hCG levels lower than 1500 mIU/mL demonstrated that a four-marker test, including progesterone, vascular endothelial growth factor (VEGF), inhibin A, and activin A, could predict EP with 100% accuracy. However, additional investigations that include patients with abnormal IUPs are necessary to further assess the utility and reliability of this panel of markers.<sup>41</sup>

## Transvaginal Sonography

In a patient suspected of having an EP, quantitative serum hCG levels and TVS are used in conjunction for diagnosis. It is reasonable to proceed with TVS while the quantitative hCG is being measured or independent of hCG level. Justification for performing TVS prior to obtaining the serum hCG results includes reports that up to 50% of ruptured EPs have extremely low hCG levels (<1000 mIU/mL) and that hCG levels do not necessarily correlate with risk of rupture.<sup>22,36,37</sup>

Although TVS is much more sensitive than transabdominal sonography, most experts recommend that scanning begin with transabdominal pelvic ultrasound, albeit without intentional filling of the bladder.<sup>42</sup> The aim of this limited transabdominal pelvic scan is to obtain an overview of the pelvis; establish the size, location, and position of the uterus; locate an ectopic sac in a high location (Fig. 33-4); and assess for free intraperitoneal fluid, including in the Morison pouch, between the liver and right kidney. This is an excellent method for identifying a large hemoperitoneum that may be missed by TVS. In a supine patient, blood may accumulate in the upper quadrants with only a minimal residual amount of fluid seen in the pelvis. Subsequently, a detailed TVS is performed to provide higher resolution evaluation of the uterus and adnexa.

The yield and reliability of TVS depend upon transducer frequency, patient body habitus, uterine position, presence of leiomyomas, and operator expertise. Optimal transducer frequency for TVS is usually between 5 and 10 MHz. Depth is set such that there is visualization of



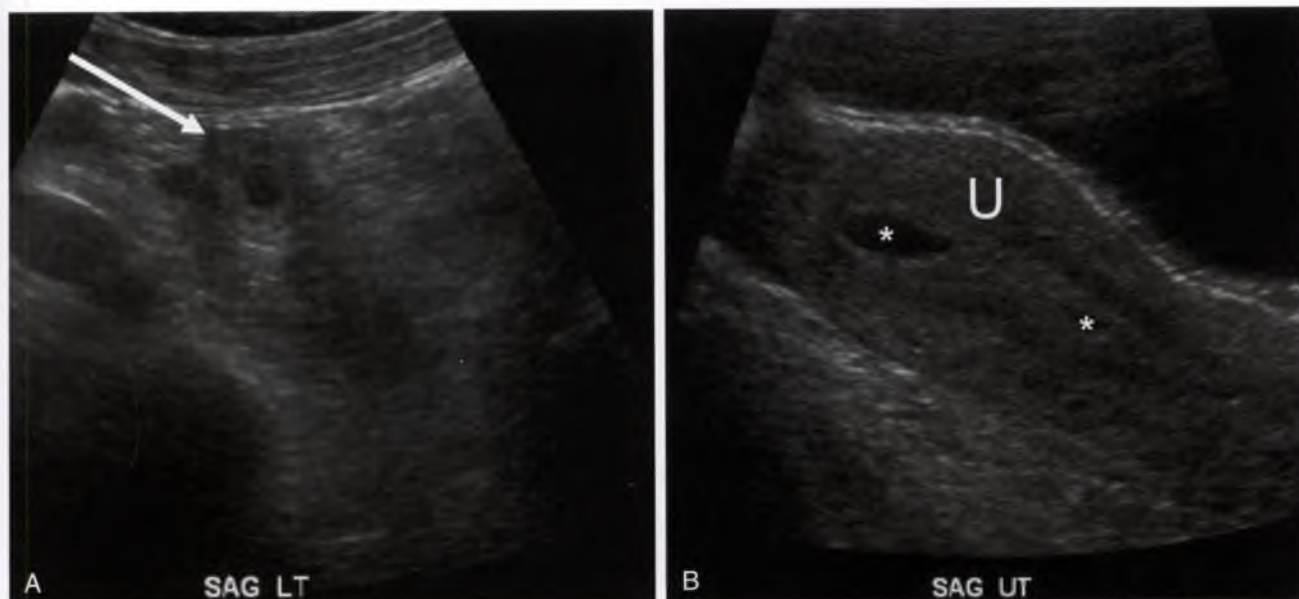


**FIG 33-4** Value of a transabdominal scan in finding an ectopic pregnancy. **A**, Transabdominal longitudinal scan of the pelvis showing the echogenic tubal ring of a small ectopic pregnancy (*arrow*) situated above the uterine fundus (not shown). **B**, Transabdominal midline longitudinal scan of the uterus (U) shows a small amount of anechoic fluid in the endometrial cavity (*asterisks*), indicating a small amount of intrauterine blood. Transvaginal sonography could not image the ectopic sac because of its high location.

pelvic structures 2 to 3 cm beyond the margin of the uterus or ovary, so as not to miss an adjacent or exophytic mass. Overall gain and time gain compensation (TGC) curves are set to optimize the image within the field of view. The object of interest is placed within the focal zone, and the use of multiple focal zones improves resolution. Harmonic imaging and spatial compounding will also improve resolution. Magnification of the area of interest within the uterus or adnexa may improve visualization. Gentle bimanual palpation exerted with one hand on the transvaginal transducer and the other hand pressing on the anterior abdominal wall can be helpful and may serve to identify the area of the patient's pain, where disease is most likely to be found. This maneuver may move structures of interest toward the focal zone such that they are easier to see and will compress bowel, thereby eliminating artifact from air within the bowel lumen. In addition, exerting compression on an adnexal mass and ovary can help differentiate an exophytic corpus luteum, attached to the ovary, from an adjacent EP, which typically move apart, separate from the ovary. Three-dimensional (3D) sonography may be helpful, particularly in evaluation of EPs in unusual locations.

The first structure imaged by ultrasound is the cervix; the endocervical canal should be perpendicular to the ultrasound beam and the walls of the cervix in continuity with the myometrium of the uterine corpus. This positioning allows for evaluation of a possible cervical EP or miscarriage in progress and provides optimal visualization of the cul-de-sac, posterior to the cervix. The cul-de-sac is the most dependent portion of the female pelvis and thus is a common location for EPs or hemoperitoneum. Subsequently, the endometrium, myometrium, and adnexa are thoroughly evaluated. Any fluid within the endometrial cavity is assessed for location, shape, rim, and presence of internal echoes to determine the possibility of an IUP. If an ectopic gestational sac is not identified between the uterus and the ovary, one must scan as far lateral as possible in the pelvis, recognizing that this may result in some discomfort for the patient. Potential "blind spots," where EPs can be located and are difficult to detect include the pelvic

side walls, deep cul-de-sac, above the uterine fundus, and anteriorly between the uterus and bladder. The examination must include targeted evaluation in the region of the patient's pain. Finally, if the hepatorenal space was not checked at the beginning of the examination, one should keep the patient supine and scan, looking for fluid in the Morison pouch.

Color, power, or spectral Doppler sonography may be used to demonstrate blood flow to an EP and to differentiate between vascularized trophoblastic tissue and avascular hematoma. However, Doppler sonography of the endometrium is not advised in order to avoid insonating a possible early IUP that is not yet visible. Color Doppler ultrasound parameters should be optimized for the detection of slow flow. This includes decreasing the scale or pulse repetition frequency (PRF), increasing gain and color saturation, decreasing the wall filter, setting higher color priority, and using a small color box. Spectral Doppler tracings should be obtained to confirm blood flow demonstrated on color Doppler images, as color Doppler sonography is sensitive to motion, which may create color artifact mimicking blood flow.

## SONOGRAPHIC DIAGNOSIS OF ECTOPIC PREGNANCY

### Uterine Findings

In the setting of EP, sonographic findings in the uterus are nonspecific and include absence of an intrauterine gestational sac and fluid in the endometrial canal. If there is no visible intrauterine gestational sac, diagnostic possibilities include EP, very early IUP, failed IUP, or heterotopic pregnancies. At this point, the pregnancy is deemed to be a PUL, and, in current practice, the diagnosis of EP should be based upon positive findings rather than on the absence of an intrauterine gestational sac with serum hCG above a specific discriminatory level. Hence, the search continues. Although the presence of an IUP makes the probability of an EP much less likely, heterotopic pregnancies have



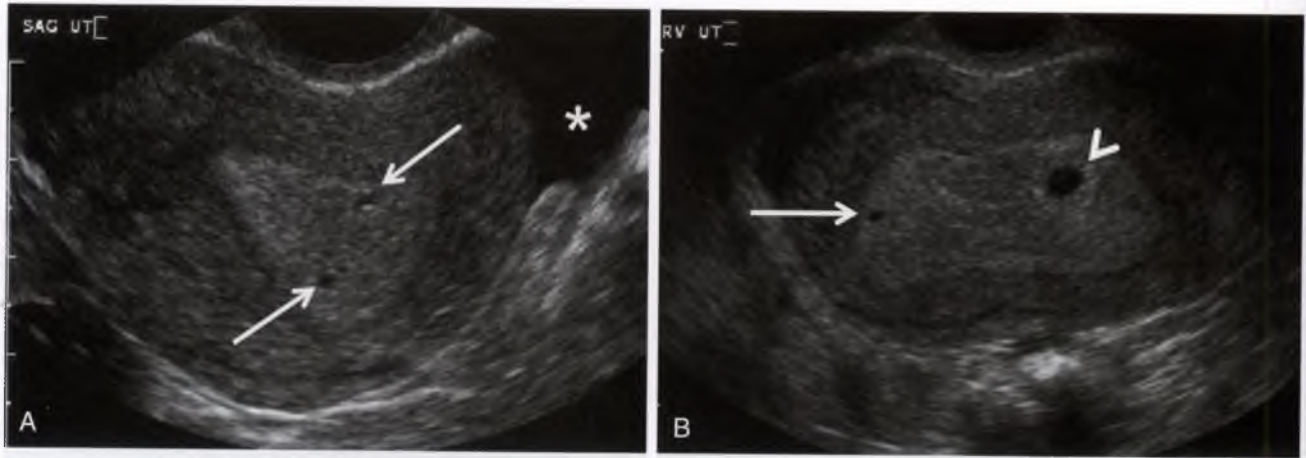


**FIG 33-5** Decidual cysts. **A**, Transvaginal sagittal scan of a retroverted uterus demonstrates two small anechoic cysts (arrows) within the decidual, neither of which has a thick rim (asterisk) adjacent to the uterus. This patient had a tubal ectopic pregnancy (not shown). **B**, Transvaginal transverse scan of another patient shows a small decidual cyst (arrow) and a very early intrauterine gestational sac (intradecidual sac sign) (arrowhead). Note the thicker echogenic rim around the early intrauterine pregnancy.

been reported in 1 out of 4000 pregnancies in the general population, and the incidence is as high as 1 in 100 to 300 pregnancies in women who have undergone ART.<sup>43,44</sup>

Endometrial thickness has not been shown to reliably predict the presence of an EP or the outcome of a PUL.<sup>45</sup> Likewise, decidual cysts have not been proved to be predictive of EPs, despite initial reports that a thin-walled endometrial cyst was associated with a high risk for EP<sup>46-48</sup> (Fig. 33-5). Although Laing and coworkers<sup>49</sup> reported that a thin-walled decidual cyst can be differentiated from an early intrauterine gestational sac with its thicker echogenic wall (intradecidual sac sign) (Fig. 33-5B), most authors rely on the identification of a yolk sac within an endometrial fluid collection to definitively diagnose an intrauterine gestational sac.<sup>50</sup>

In the past, it was thought that intracavitary blood or secretions were relatively common findings in patients with EPs. This fluid, often containing low level echoes, located centrally within the uterine cavity and surrounded by a single echogenic decidual layer, was termed a “pseudogestational sac” or “pseudosac” (Fig. 33-6). Thus, it could be differentiated from a true intrauterine gestational sac, which is either eccentric and embedded in a single layer of the endometrium (intradecidual sign) or surrounded at least partially by two echogenic rims of tissue with an interleaving hypoechoic layer (the double decidual sac sign).<sup>51</sup> However, at present, fluid in the endometrial canal is observed in only 10% to 20% of women with EPs, possibly because of sonographic evaluation at earlier gestational ages. Benson and associates<sup>52</sup> report that in current practice any round or oval well-defined fluid collection in the mid to upper endometrial cavity is statistically more likely to represent an IUP (99.98%) rather than a “pseudosac” associated with an EP (0.02%). Note that an endometrial fluid collection with a tapered or pointed edge is much more likely to be associated with an EP (see Fig. 33-6). In conclusion, the terms “pseudosac” and “pseudogestational sac” should probably be abandoned as they are confusing and of limited use. In current practice, endometrial fluid is infrequently observed in patients with EP.<sup>53,54</sup>

### Adnexal Findings

Visualization of an extrauterine gestational sac containing a yolk sac or an embryo with or without a heartbeat is diagnostic of an EP with

100% positive predictive value (PPV)<sup>55,52</sup> (Fig. 33-7). The next most reliable sonographic finding is an adnexal tubal ring representing an empty gestational sac that appears as a round anechoic fluid collection with a thick echogenic rim. This has also been described as the bagel, donut, or sugar donut sign (Figs. 33-2B, 33-3A, and 33-8). The adnexal tubal ring sign has a 95% PPV for EP and is seen in approximately 50% of cases.<sup>55</sup> The PPV increases if the tubal ring is clearly separate from the ipsilateral ovary (Fig. 33-8B). Color Doppler sonographic imaging may increase the conspicuity of a small tubal ring (Fig. 33-8C). Although some EPs will demonstrate circumferential vascularity, most EPs will demonstrate only segmental or focal vascularity, and some may demonstrate no flow at all on color Doppler ultrasound imaging (Figs. 33-2B and 33-6C). EPs may also appear as a nonspecific adnexal mass representing hemorrhage with blood clot. These masses can be homogeneous, heterogeneous, or complex; may appear either predominantly cystic or solid; and have variable echogenicity ranging from hypo- to hyperechoic, depending upon the time course since hemorrhage occurred (Fig. 33-9). Hemorrhage contained within the fallopian tube (hematosalpinx) will appear tubular or ovoid in shape (Fig. 33-10).<sup>56</sup> Internal vascularity increases the likelihood that the mass represents an EP rather than bland hemorrhage from a ruptured corpus luteum. In the setting of a positive pregnancy test and an empty uterus, any adnexal mass that is clearly not either an intraovarian corpus luteum, paraovarian cyst, or pedunculated myoma has a 92% PPV for EP.<sup>55</sup> EPs are most commonly found situated between the ovary and uterus or in the cul-de-sac, which is the most dependent portion of the female pelvis. Although rare, it is possible to occasionally see twinning in ectopic locations. Possibilities include twin sacs in one fallopian tube, one twin in each tube, monochorionic twins, and conjoined twins (Fig. 33-11).

### Cul-de-Sac Findings

Echogenic free fluid indicative of hemoperitoneum may be the only initial finding in up to 25% of patients with EPs (Fig. 33-12). Hemoperitoneum typically collects in the cul-de-sac as this is the most dependent portion of the female pelvis in the upright position. A pregnant woman with an empty uterus has a 90% probability of EP if

*Text continued on p. 977*

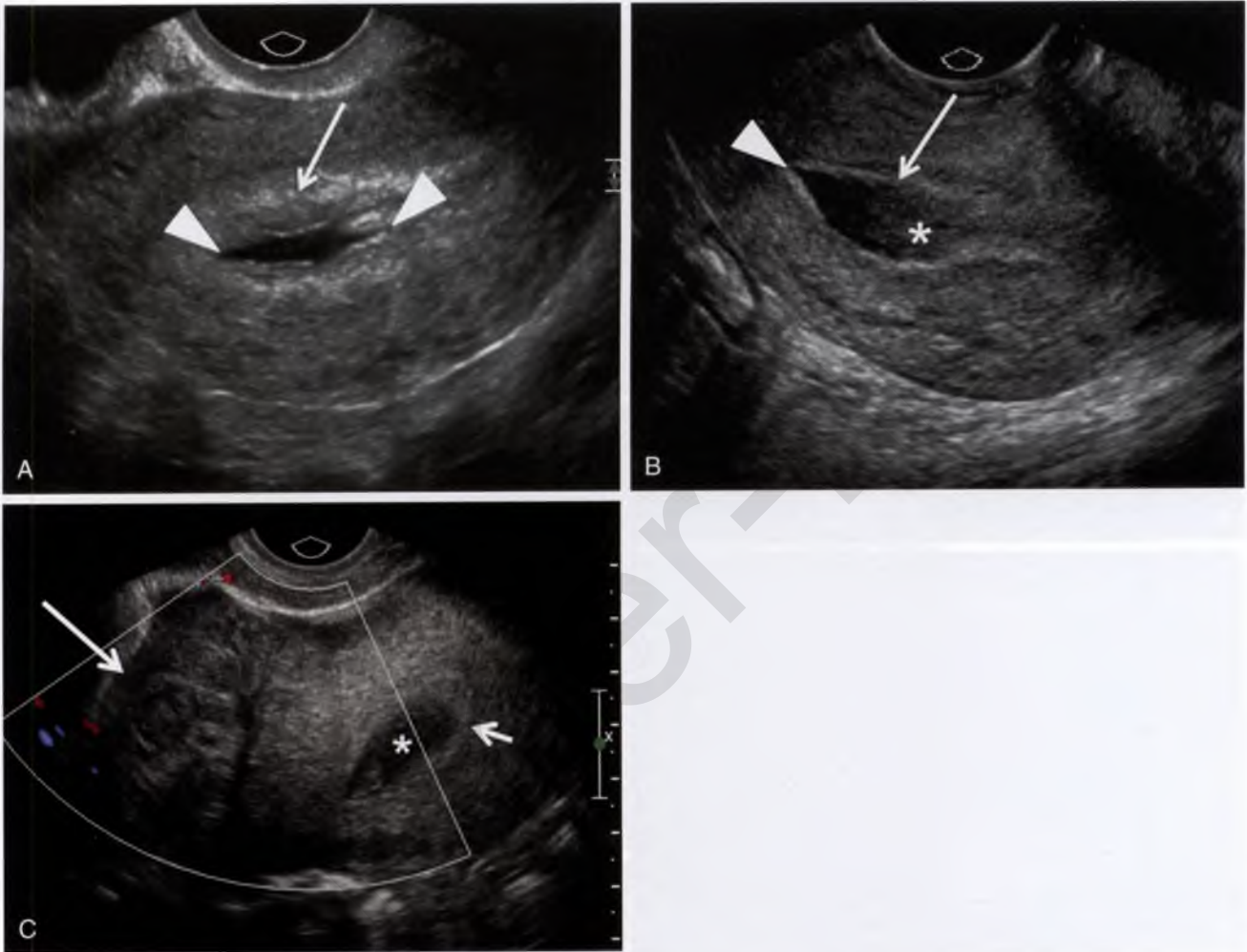


**FIG 33-6** Intrauterine fluid associated with EP, referred to as *pseudogestational sacs*. **A**, Transvaginal sagittal scan of the uterus demonstrating an oblong intrauterine fluid collection with pointed margins (*arrowheads*) surrounded by a single decidual lining (*arrow*). There was an adnexal tubal ectopic pregnancy (not shown). **B**, Transvaginal scan of another patient with fluid in the endometrial canal with pointed edge (*arrowhead*). Intraluminal echoes (*asterisk*) represent blood, surrounded by single thin decidual lining (*arrow*). The patient had an ectopic pregnancy (not shown). **C**, Transvaginal color Doppler scan of a third patient demonstrating a right adnexal ectopic pregnancy adjacent to the uterus surrounded by a large hematoma (*long arrow*). The ectopic pregnancy demonstrates no blood flow on color Doppler interrogation. Fluid-containing low level echoes (*asterisk*) consistent with hemorrhage is noted centrally within the endometrial cavity. The fluid is surrounded by a single echogenic rim of decidual tissue (*short arrow*). This appearance has been referred to as a *pseudogestational sac*. However, most authors now prefer to avoid this potentially confusing terminology and use of this phrase is discouraged.



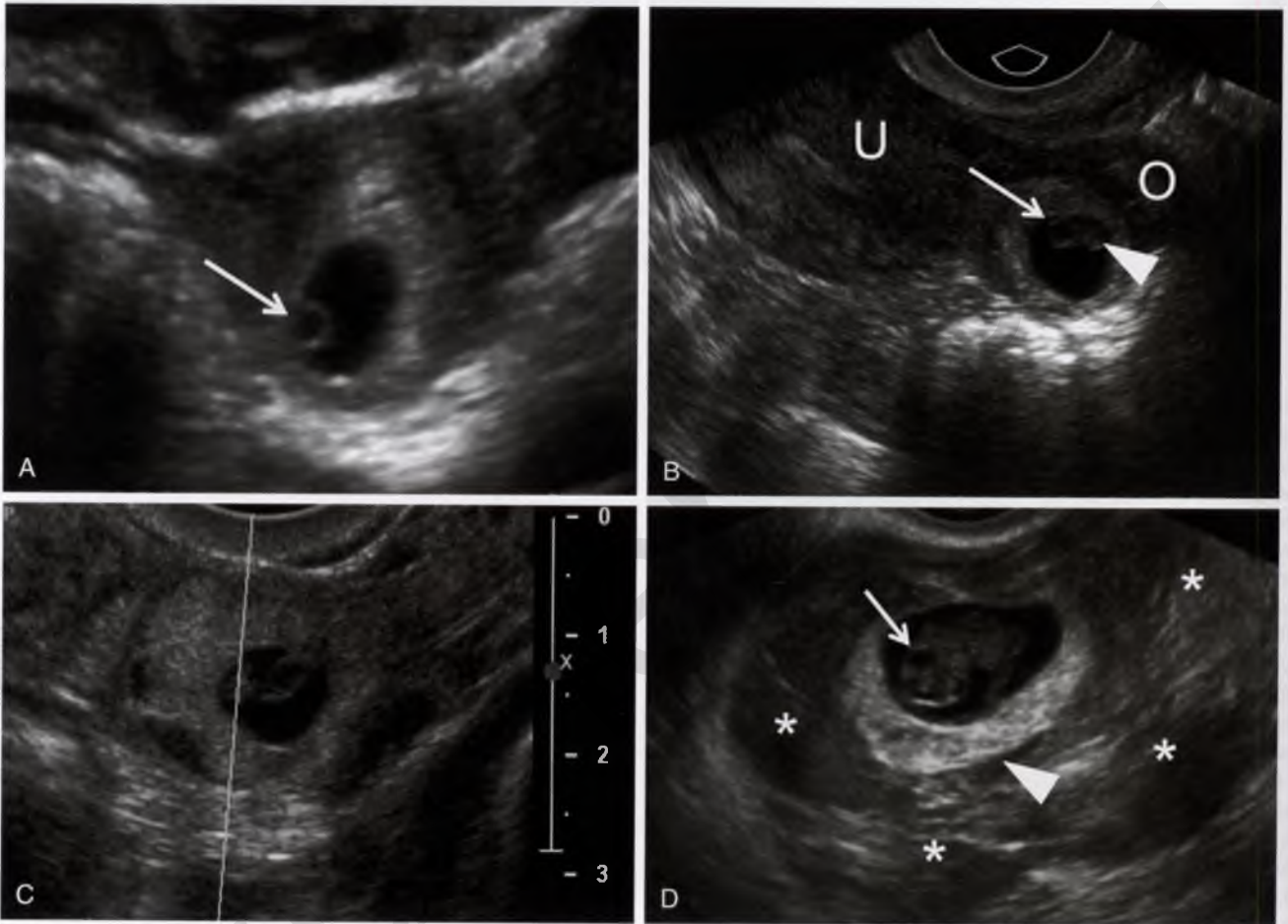


**FIG 33-7** Definitive ultrasound findings of ectopic pregnancy. **A**, Transvaginal scan of an ectopic gestational sac showing a thick hyperechoic rim and a yolk sac (*arrow*) within the anechoic center, but no embryo is seen. **B**, Transvaginal scan of an ectopic gestational sac with a thick hyperechoic rim, situated between the uterus (U) and ovary (O). There is a yolk sac (*arrow*) and an adjacent tiny embryo (*arrowhead*) with no cardiac activity. **C**, Transvaginal scan of an ectopic gestational sac shows a very early embryo with M-mode (tracing of cardiac motion not shown). **D**, Transvaginal scan of the adnexa in a patient with an ectopic gestational sac containing a larger embryo. Cardiac activity was noted on real-time imaging. Note the rhombencephalon (*arrow*) in the posterior fossa. There is a large perigestational hematoma (*asterisks*) that is less echogenic than the trophoblastic tissue at the periphery of the gestational sac (*arrowhead*).

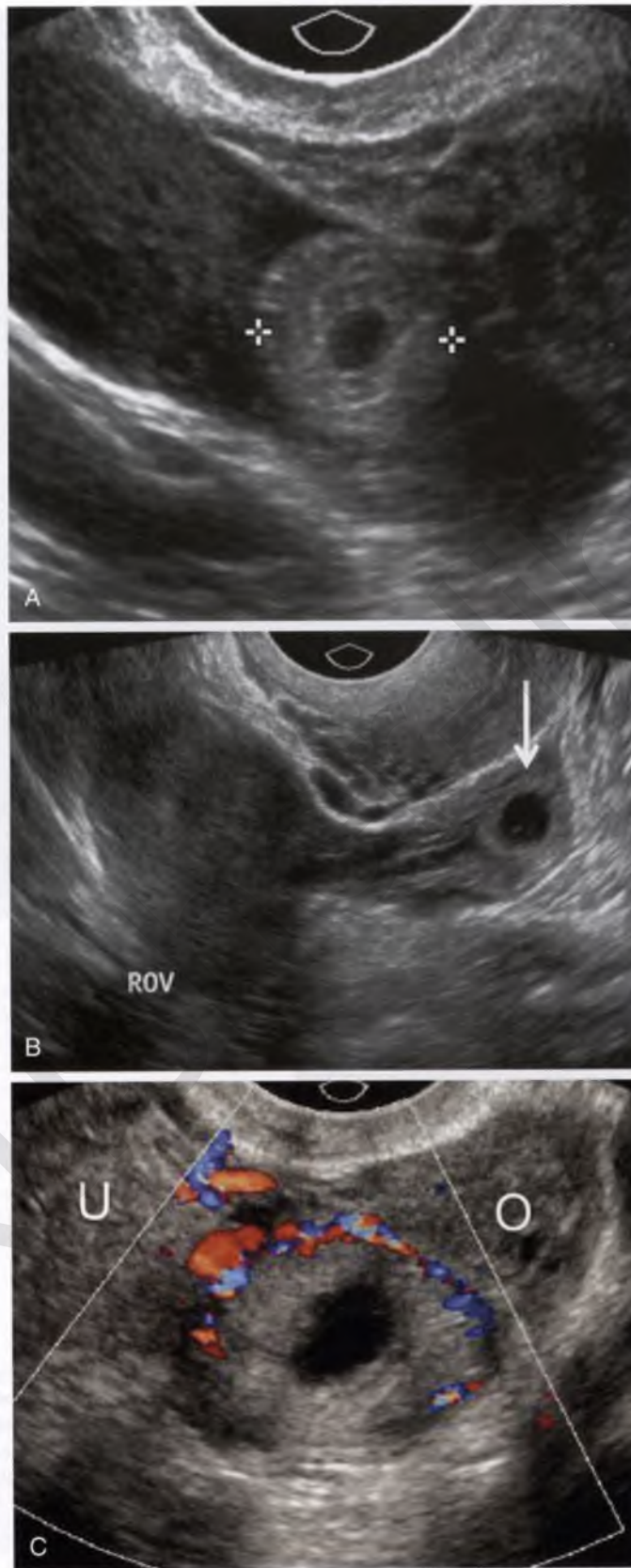


**FIG 33-8** Ectopic pregnancies presenting as tubal rings in three different patients. **A**, Transvaginal scan shows a typical adnexal tubal ring (*between calipers*), also called a “sugar donut” or “bagel” sign, representing an empty ectopic gestational sac with a round anechoic fluid-filled center surrounded by a thick echogenic rim. Note a small amount of adjacent free pelvic fluid. **B**, Transvaginal scan shows the small tubal ring of an ectopic pregnancy (*arrow*) separate from and medial to the right ovary (ROV). **C**, Transvaginal transverse color Doppler scan shows the tubal ring of an ectopic pregnancy located between the uterus (U) and left ovary (O). Note the incomplete color Doppler “ring of fire.”



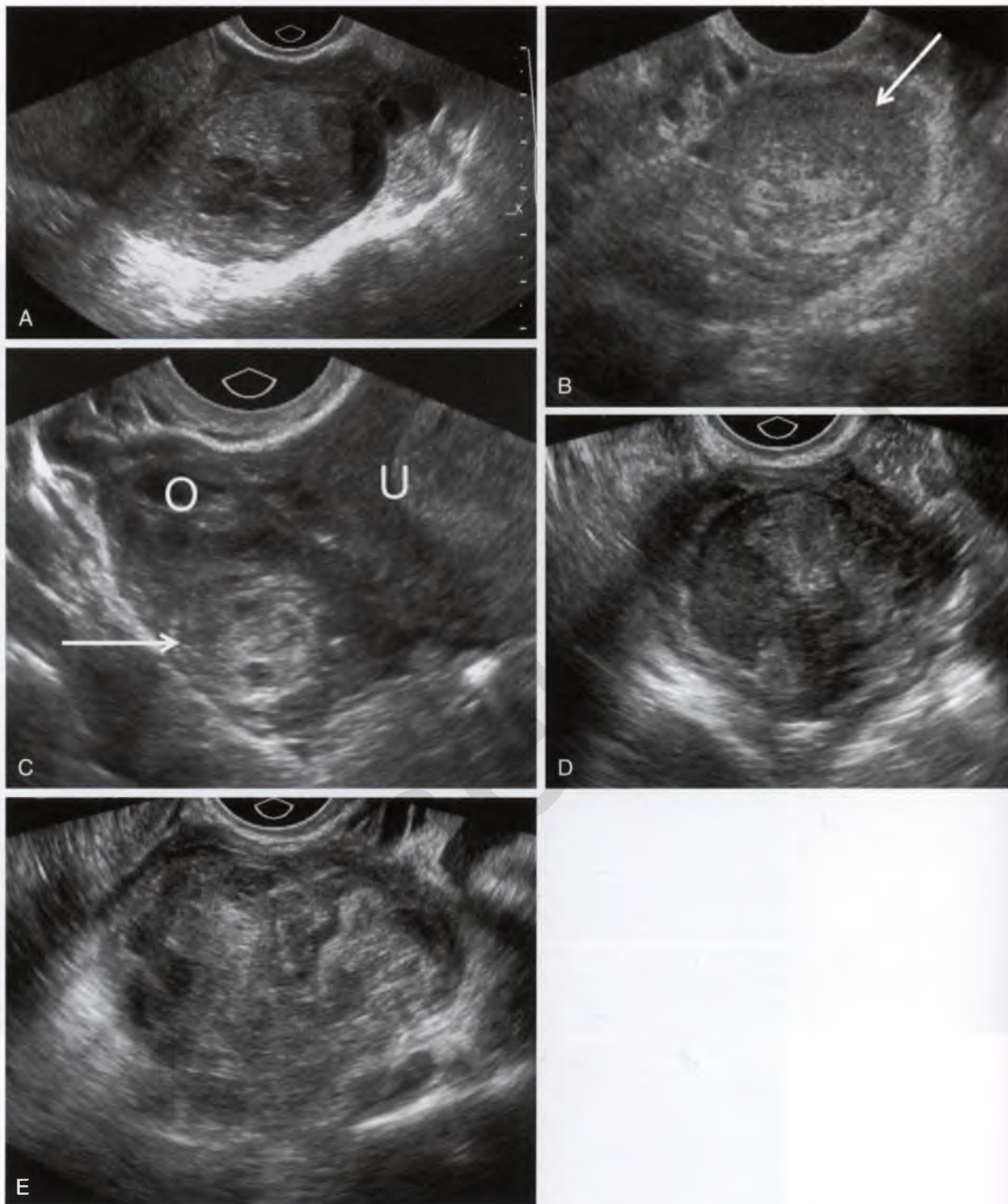


**FIG 33-9** Ectopic pregnancies presenting as nonspecific adnexal masses: varying appearances in five different patients. **A**, Transvaginal scan shows a complex, heterogeneous, predominantly solid-appearing mass. **B**, This ectopic pregnancy is well margined with a relatively homogeneous, echogenic, solid appearance (*arrow*), likely due to blood clot around the ectopic sac within the fallopian tube. **C**, Transvaginal scan shows a complex predominantly solid mass with hyperechoic components (*arrow*) surrounded by more hypoechoic hematoma, representing an ectopic pregnancy situated between the uterus (U) and right ovary (O). **D**, Transvaginal scan shows a large heterogeneous, predominantly cystic mass in the left adnexa. **E**, Transvaginal scan shows a large heterogeneous pelvic mass.



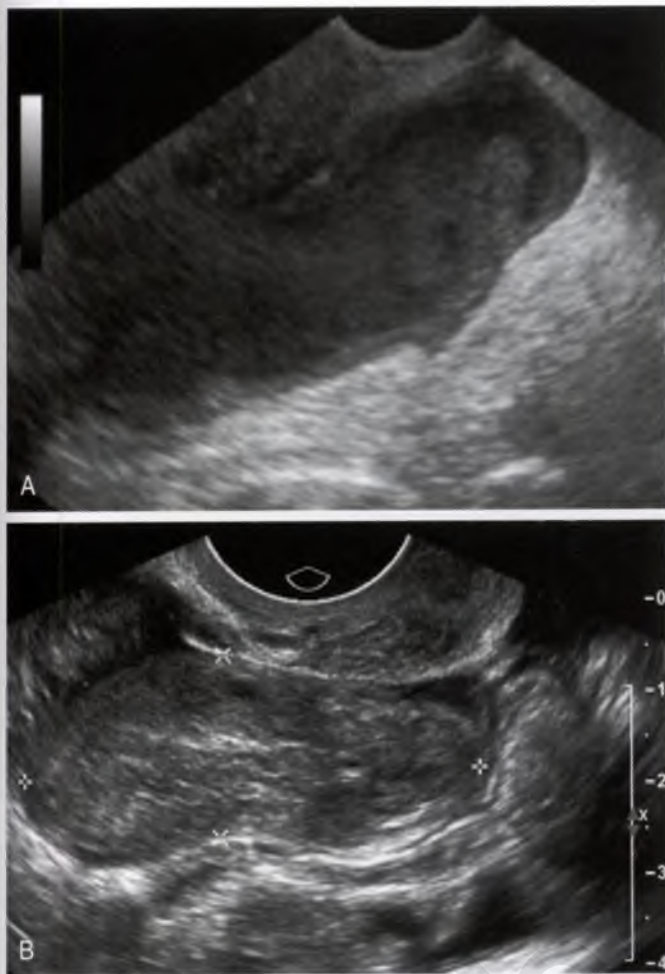


**FIG 33-10** Tubular adnexal masses representing hematosalpinges from ectopic pregnancies. **A**, Transvaginal longitudinal scan demonstrates a distended fallopian tube with intraluminal complex fluid representing blood. Pathologic specimen revealed a tubal ectopic pregnancy. **B**, Transvaginal scan in another patient with an ectopic pregnancy demonstrates a well-margined, tubular heterogeneous structure (*calipers*) consistent with a fallopian tube filled with blood. The gestational sac was not recognizable. A fallopian tube filled with blood (hematosalpinx) will appear oblong on long axis and round on short axis. Smooth well-defined margins and tubular shape help differentiate a tube filled with blood from an adnexal hematoma. (B from Bryan-Rest LL, Scoutt LM: Ectopic pregnancy. In Fielding JR, Brown DL, Thurmond AS (eds): *Gynecologic Imaging*. Philadelphia, Elsevier, 2011, p 335, Fig. 22-4B, used with permission.)

a moderate to large amount of echogenic free peritoneal fluid is found. However, the volume of free fluid has low sensitivity, specificity, and PPV for determining tubal rupture.<sup>20</sup> The amount of free fluid is a good indicator of the risk of hemodynamic instability. Therefore, the upper abdomen should always be assessed as the presence of free fluid in the Morison pouch suggests that there is a relatively large volume and would increase concern for potential hemodynamic instability. When evaluating free fluid, careful attention should be paid to technique as high gain settings can create artifactual echoes. Comparison of cul-de-sac fluid with known anechoic fluid such as urine in the bladder or fluid in an ovarian cyst/follicle at similar depth will help reveal whether echoes are real or artifactual (Fig. 33-12B). One can also look for layering or movement of low-level echoes. It should be

remembered that on occasion acute hemoperitoneum may appear as anechoic fluid. Occasionally, hemoperitoneum in the Morison pouch may appear so echogenic that it approximates the echogenicity of adjacent hepatic parenchyma and may be mistaken for liver because of the silhouette effect (Fig. 33-13). Also, clotted blood may appear echogenic and mass-like, and thus may be difficult to differentiate from loops of bowel (Fig. 33-12D). After the initial clotting stage, fibrinolysis begins and hemoperitoneum will appear heterogeneous, making it more difficult to visualize a small ectopic gestational sac amid amorphous material in the cul-de-sac (see Figs. 33-3 and 33-12B).

### Pitfalls

General limitations in the sonographic diagnosis of EP include lack of operator experience, training, skill, persistence, or lack of attention to details. Patient obesity, leiomyomas, uterine anomalies, retroflexion of the uterus, or hydrosalpinx may also limit sonographic evaluation. Careful and complete patient history should address risk factors such as prior EP, ART, PID, or tubal surgery. If the patient presents at an early gestational age, the EP may be too small to visualize and may fall below the limits of resolution of the ultrasound equipment.

Potential pitfalls in image interpretation include misconstruing fragments of decidua or blood clot within an intrauterine fluid collection as either a yolk sac or embryo, thus leading to a false positive diagnosis of IUP<sup>57</sup> (Fig. 33-14). It can also be very difficult to differentiate an exophytic corpus luteum from an EP (Fig. 33-15), particularly because 80% of EPs will be located ipsilateral to the ovarian corpus luteum (Fig. 33-16). There are several useful points of distinction (Fig. 33-17). A corpus luteum arises from the ovary, and intraovarian EPs are extremely rare (see later). Although a corpus luteum can be exophytic, a peripheral crescent of ovarian parenchyma, termed the “claw sign,” will typically be observed surrounding at least part of the corpus luteum. However, if a mass adjacent to the ovary represents an EP, it will be separate from the ovary with an acute intervening angle between the structures and no “claw sign” (see Fig. 33-17). When prodded with the transvaginal probe or with palpation on the anterior abdominal wall, the EP will typically slide away from the ovary, whereas a corpus luteum will remain attached to and move with the ovary.<sup>58</sup> The tubal ring of an EP is typically thinner and more echogenic than the homogeneous thick wall of the corpus luteum<sup>59,60</sup> (Figs. 33-15A, 33-15C, 33-16A, and 33-17C). However, there is considerable overlap in the echogenicity and thickness of the walls of a corpus luteum and an EP. As a corpus luteum involutes, the inner margin may become crenated or stellate in appearance (Fig. 33-15A and B). Internal echoes are relatively common as a result of hemorrhage and may mimic a yolk sac or embryo (see Fig. 33-15B). Magnified views using harmonic imaging or spatial compounding may be helpful given that definitive identification of a yolk sac or embryo in an adnexal ring-like structure confirms the diagnosis of EP. Both a corpus luteum and an EP can demonstrate marked peripheral vascularity on color Doppler imaging, termed the “ring of fire,” with low-resistance spectral Doppler waveforms with increased diastolic flow. Neither the degree of mural vascularity depicted on color Doppler ultrasound nor the characteristics of flow on spectral Doppler waveforms is helpful in differentiating an EP from a corpus luteum. Although the “ring of fire” sign was initially described as a pattern of color Doppler flow suggestive of EP, subsequent experience has shown that a complete circumferential (360-degree) “ring of fire” is actually more commonly seen with corpora lutea<sup>61</sup> (Figs. 33-15B, 33-15D, and 33-16B). Blood flow in the tubal ring of an EP is more likely to be focal and segmental (Figs. 33-8C and 33-11A).

Other potential sonographic mimickers of EP include degenerated, pedunculated myoma, pelvic abscess, and bowel loops. A painful,



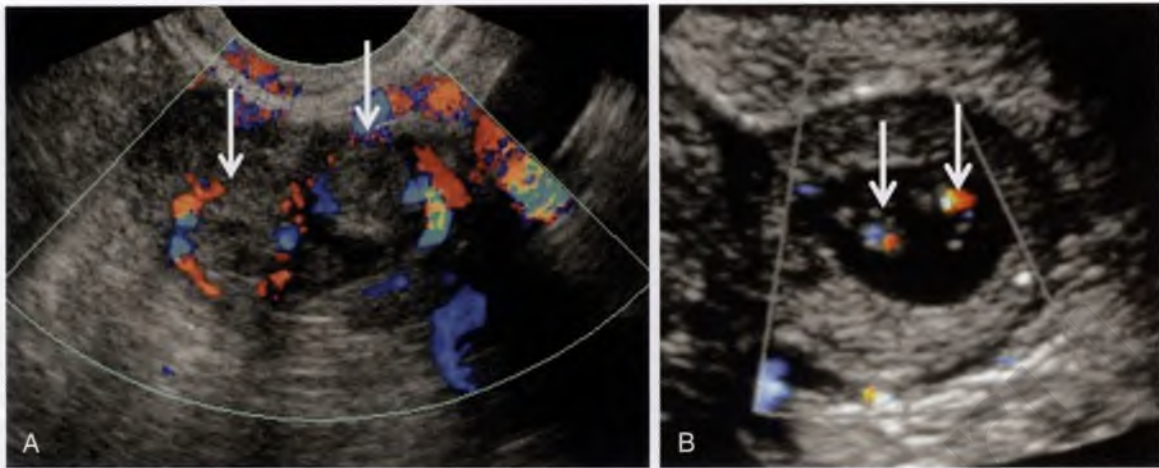


**FIG 33-11** Twin ectopic pregnancies. **A**, Transvaginal color Doppler image of dichorionic diamniotic twin ectopic gestational sacs (arrows), the most common form of twinning resulting from embryo transfer techniques. Note that blood flow shown in the tubal rings is discontinuous, segmental, and focal, rather than a complete 360 degree ring of vascularity, which is more commonly observed with the corpus luteum. **B**, Transvaginal color Doppler scan shows monozygotic twin embryos with central color pixels (arrows) representing cardiac motion in an ectopic tubal pregnancy.

degenerated uterine myoma may have an echogenic rim and a cystic center (Fig. 33-18). Demonstration by Doppler ultrasound of feeding vessels from the uterus establishes the origin of the mass (Fig. 33-18B). A thick-walled abscess with echogenic purulent fluid in the cul-de-sac may mimic an EP (Fig. 33-19). However, most pelvic abscesses will be multilocular and the clinical presentation would include fever and a negative pregnancy test. Bowel loops can potentially mimic a pelvic mass, and, thus, observation of peristalsis is useful in this determination.

## ECTOPIC PREGNANCIES IN UNUSUAL LOCATIONS

As previously stated, the most accurate definition of ectopic (Greek *ektos*, out of place) pregnancy is a pregnancy that has implanted in a location other than the endometrial cavity. Although the vast majority of EPs will implant in the fallopian tube, approximately 4% of EPs are found “out of place” in more unusual locations. These unusual sites of implantation include the interstitial portion of the fallopian tube, cervix, ovary, cesarean incision scar, myometrial scar, abdominal cavity, and even more rarely the retroperitoneum (see Fig. 33-1). Often such EPs are the result of complications from ART, but unusual implantations can also occur spontaneously. These EPs are associated with increased morbidity and mortality rates compared to tubal EPs and are increasing in incidence.<sup>62</sup>

### Interstitial Ectopic Pregnancy

Interstitial EPs account for 2% to 4% of all EPs. Predisposing risk factors include salpingectomy, previous EP, uterine anomalies, and in vitro fertilization with embryo transfer (IVF-ET).<sup>63</sup> Interstitial EPs occur when trophoblastic tissue implants within the interstitial (intramural) portion of the fallopian tube as it courses through the myometrium in the cornual region of the uterus (Figs. 33-20 and 33-21A). Interstitial EPs are found lateral to the round ligament and the uterotubal junction. The terminology for EPs occurring in this region is confusing and has been inconsistently reported in the literature. Because a bulge in the outer contour of the cornual portion of the uterus is typically visualized both sonographically and at surgery, the term *cornual EP* has also been used to describe pregnancies in this area,

and the terms have often been used interchangeably. Other authors use the term *cornual pregnancy* to describe an IUP in the right or left horn (cornu) of a bicornuate or septate uterus (Fig. 33-21D and E). Still others use the term to refer to a pregnancy located in a rudimentary horn in a patient with a unicornuate uterus (Fig. 33-21B and C). Eccentric IUPs located in the superolateral corner of the endometrial cavity at the uterine fundus have also been referred to as cornual pregnancies. However, these pregnancies have a broad interface with the endometrium and, are intrauterine rather than ectopic in location, and in the authors' opinion are best referred to as *angular pregnancies*<sup>64-67</sup> (Fig. 33-21F). Because the term *cornual pregnancy* has been used by different authors to describe a variety of findings ranging from a normal IUP to an IUP in the setting of a congenital uterine anomaly to an EP, the authors suggest avoiding the use of the term altogether. In this text, we use the term *interstitial ectopic pregnancy* to refer to a pregnancy implanted in the interstitial portion of the fallopian tube that lies within the myometrium. We do not use the term *cornual pregnancy*. We use *angular pregnancy* to describe an IUP located in the lateral angle of the endometrial cavity at the uterine fundus where the fallopian tube joins the endometrial cavity. When reporting sonographic findings, we strongly recommend that the location of the pregnancy be precisely described as intrauterine (i.e., within the endometrial cavity) or ectopic (i.e., outside the endometrial cavity). No matter what term is used, it is necessary to reach agreement, provide careful detailed reports, and avoid confusion and miscommunication with clinicians because maternal morbidity, mortality, and treatment of EPs (interstitial EPs and rudimentary horn pregnancies) and IUPs (angular pregnancies and those within bicornuate and septate uteri) are very different.

The primary diagnostic imaging findings of an interstitial EP are eccentric location of the gestational sac within the myometrium and clear separation from the endometrial cavity (Fig. 33-22). A key feature is demonstration of intervening myometrial tissue separating the medial margin of the gestational sac from the echogenic endometrium. The myometrium surrounding the gestational sac will be markedly thin peripherally; and on occasion, there will be no visible myometrial tissue surrounding the lateral margin of the gestational sac, which bulges beyond the superolateral serosal surface of the uterine fundus.

*Text continued on p. 985*

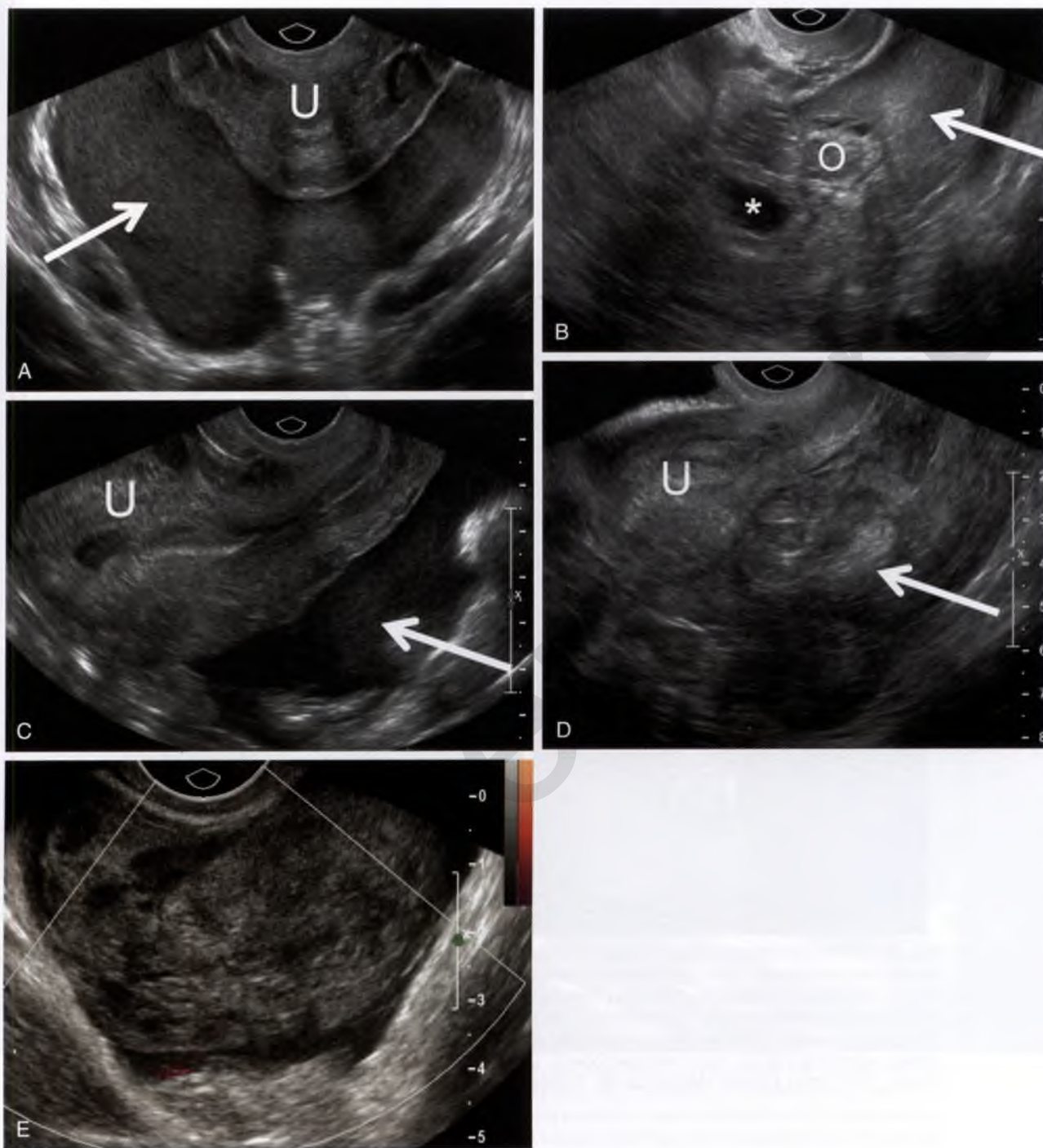


**FIG 33-12** Variable sonographic appearance of hemoperitoneum due to rupture of ectopic pregnancy.

**A**, Transvaginal transverse scan shows homogeneous, low-level echoes representing blood (*arrow*) in the cul-de-sac, posterior to the uterus (U). **B**, Echogenic hemoperitoneum (*arrow*) outlines the ovary (O), which contains several small anechoic follicles, and an ectopic gestational sac (*asterisk*) with an echogenic rim. **C**, Hemoperitoneum, shown posterior to the uterus (U), is nearly anechoic in this patient with a small area of low-level echoes (*arrow*). Note a small amount of fluid in the endometrial cavity. **D**, Transvaginal longitudinal pelvic scan shows complex heterogeneous clotted blood (*arrow*) posterior to the uterus (U) mimicking bowel loops. **E**, Transvaginal transverse power Doppler scan through the cul-de-sac shows complex heterogeneous material with no demonstrable internal blood flow, consistent with clotted blood. Note that there is a small amount of adjacent anechoic free fluid.



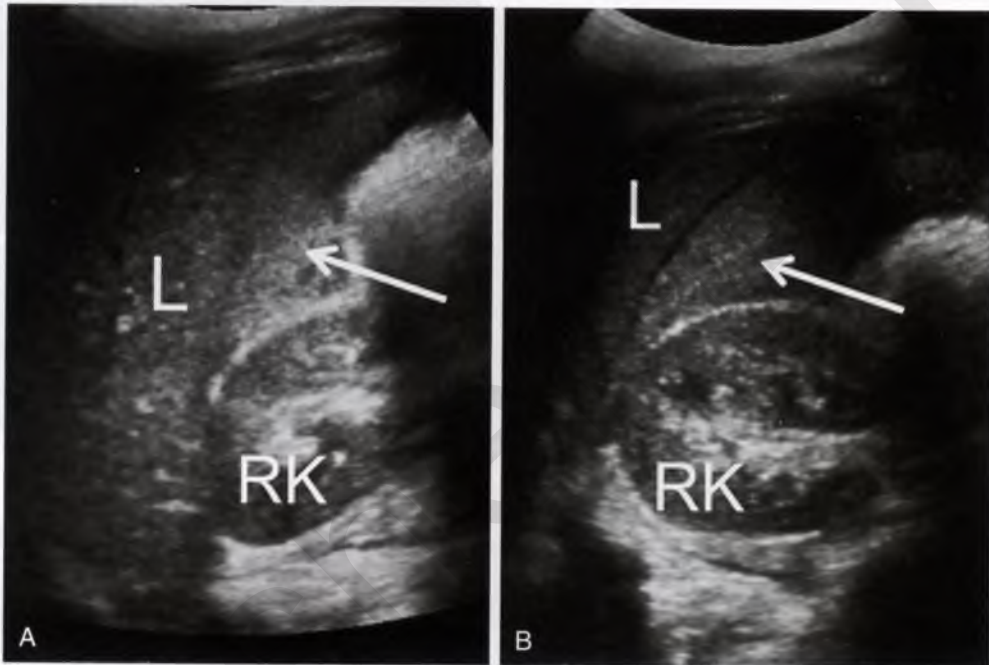


**FIG 33-13** Hemoperitoneum from ruptured ectopic pregnancy may mimic liver parenchyma. **A**, In this patient with hypotension and ruptured ectopic pregnancy (not shown), more than a liter of intraperitoneal blood (*arrow*) accumulated in the Morison pouch, between the right lobe of the liver (L) and the right kidney (RK). This was initially overlooked, mistaken for liver parenchyma owing to similar echogenicity. **B**, Hemoperitoneum (*arrow*) under the liver (L) was eventually correctly recognized when an anechoic stripe was noted, separating liver (L) from hemoperitoneum (*arrow*). RK, right kidney. (Images courtesy of Mindy Horrow, MD, Albert Einstein Medical Center, Philadelphia, PA.)

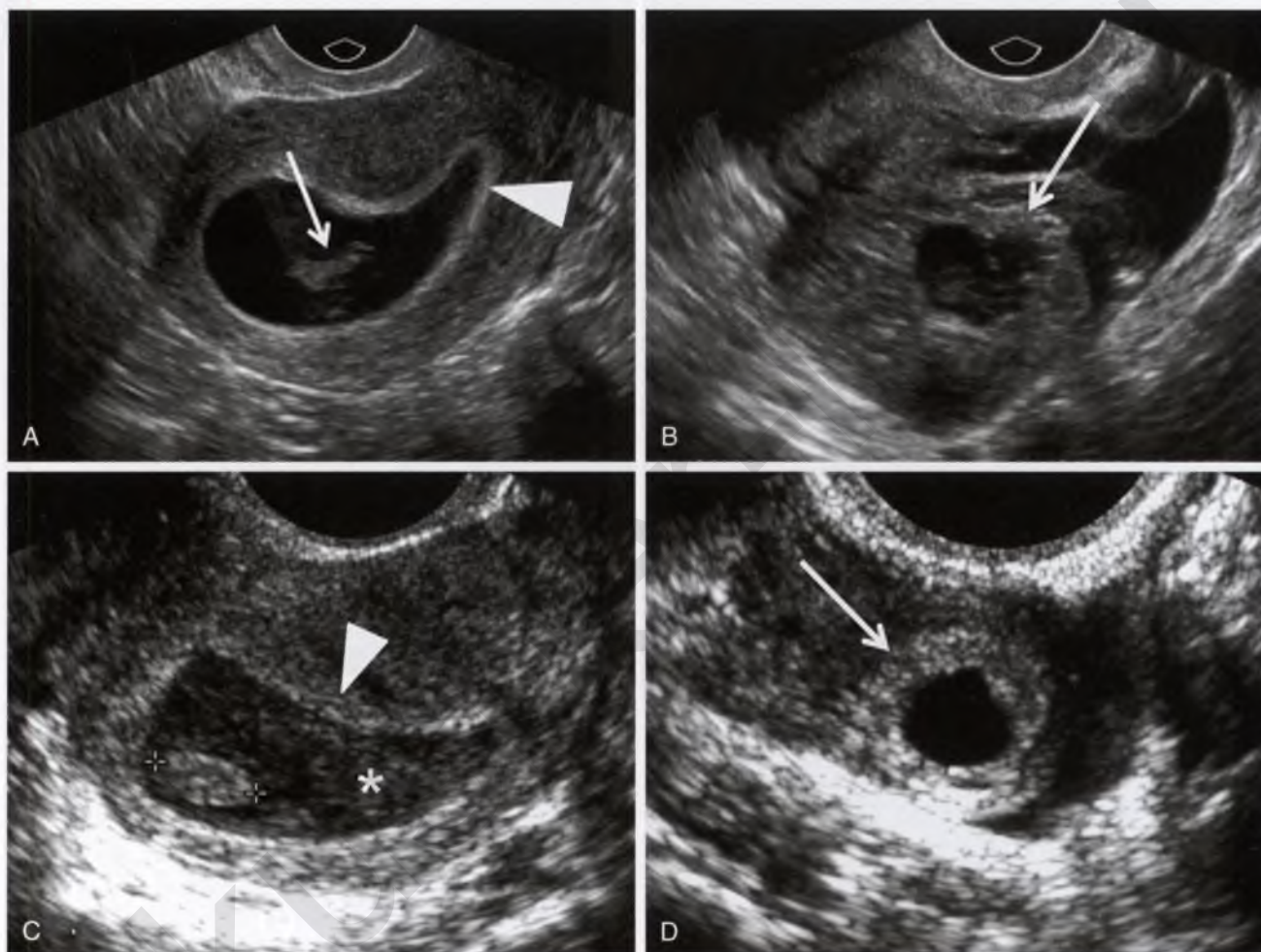


**FIG 33-14** Patients with ectopic pregnancies and intrauterine fluid containing blood clots mimicking embryos. **A**, Transvaginal longitudinal scan of the uterus demonstrates fluid distending the endometrial cavity, surrounded by a single decidual lining (*arrowhead*), containing a small echogenic oblong blood clot (*arrow*) simulating an embryo. **B**, In the same patient shown in **A**, an ectopic pregnancy (*arrow*) was noted on transvaginal view of the adnexa. **C**, In another patient, transvaginal longitudinal scan of the uterus shows internal echoes representing blood in the uterine cavity (*asterisk*) with a small focal blood clot simulating an embryo (*calipers*). Note the single decidual lining of the endometrial cavity (*arrowhead*). **D**, In the same patient shown in **C**, the ectopic adnexal gestational sac (echogenic tubal ring) (*arrow*) is surrounded by echogenic blood.



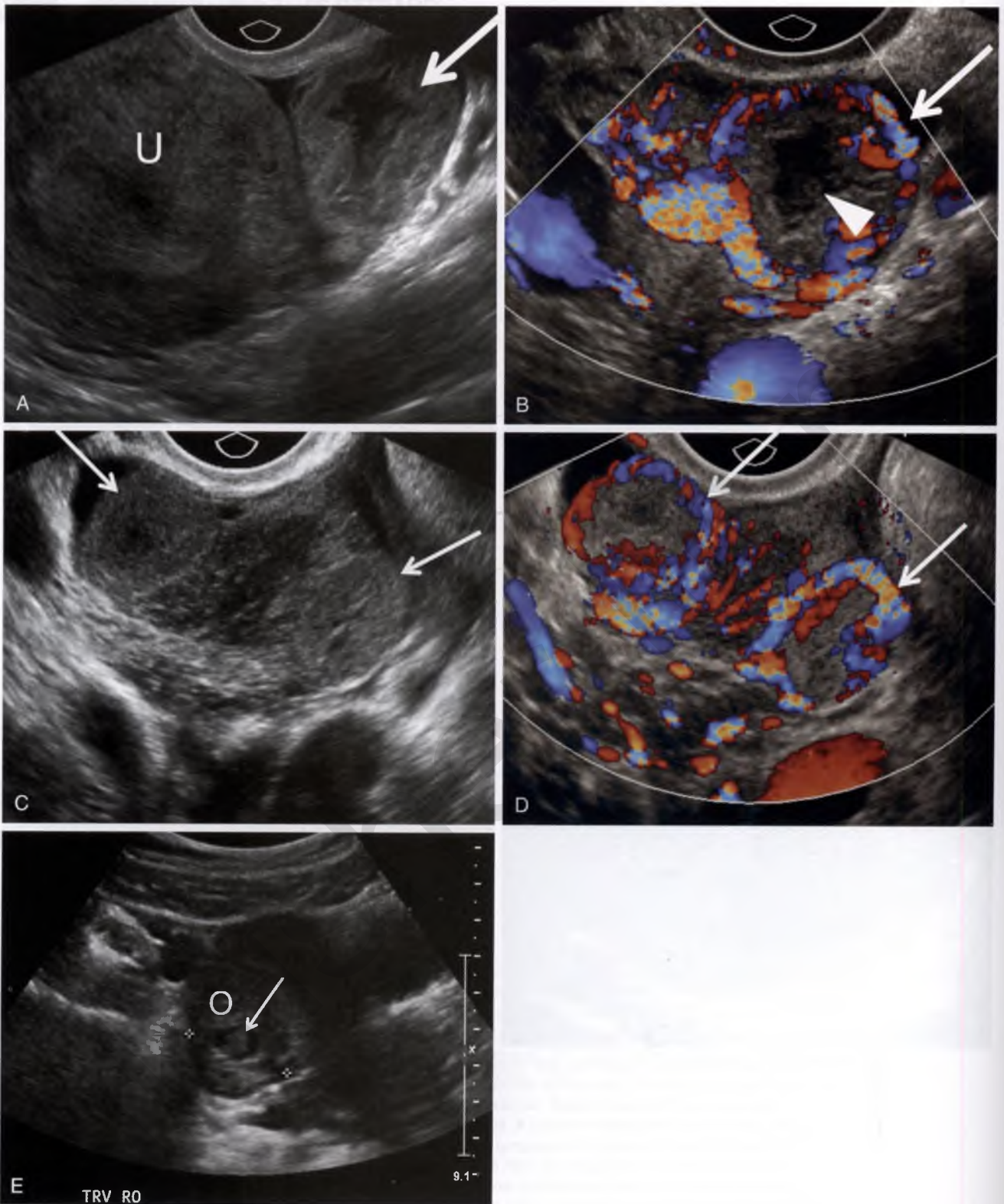


**FIG 33-15** Corpora lutea mimicking ectopic pregnancies. **A**, Transvaginal transverse scan of the uterus (U) and left corpus luteum (*arrow*) with thick, crenated, moderately echogenic rim and irregular cystic center with few internal echoes, mimicking the thick rim of an ectopic pregnancy. There is trace free fluid. **B**, Transvaginal color Doppler scan of A shows circumferential “ring of fire” in the wall of the corpus luteum (*arrow*). Note echoes from hemorrhage within the corpus luteum mimic a yolk sac (*arrowhead*). **C**, Two corpora lutea (*arrows*) with thick, moderately echogenic rims resemble tubal rings of ectopic pregnancy in a patient who underwent ovulation induction. **D**, Transvaginal color Doppler scan of C shows “rings of fire” peripheral to the two corpora lutea (*arrows*). Note that the “rings” of blood flow are continuous and completely circumferential on color Doppler imaging, which is more commonly seen with corpus luteum than with ectopic pregnancy. **E**, This corpus luteum (*calipers*) within the right ovary (O) contains a small echogenic blood clot (*arrow*), resembling an embryo, potentially mimicking an ovarian ectopic pregnancy. The pregnancy test was negative. (B from Cicchiello LA, Hamper UM, Scoutt LM: Ultrasound evaluation of gynecologic causes of pelvic pain. *Ultrasound Clin* 5:209-231, 2010, image 17, p 221, used with permission.)



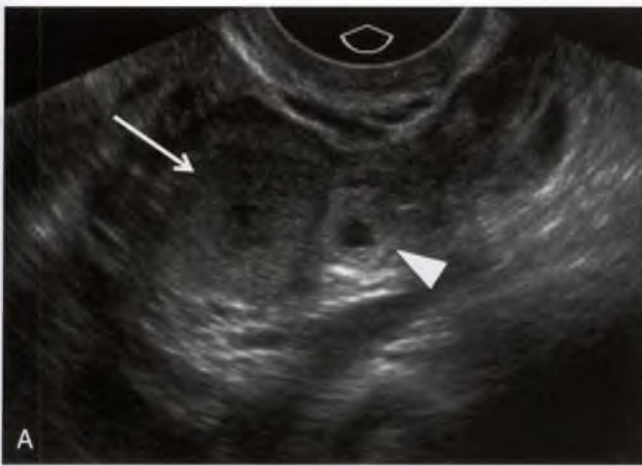


**FIG 33-16** Ectopic pregnancy and ipsilateral corpus luteum with color Doppler ultrasound. **A**, Transvaginal scan of an ectopic gestational sac (*arrowhead*) and the ipsilateral intraovarian corpus luteum (*arrow*). The ring of the ectopic pregnancy is more echogenic than the rim of the corpus luteum. **B**, Transvaginal color Doppler scan showing a circumferential vascular "ring of fire" around the corpus luteum (*arrow*) but no flow around the ectopic sac (*arrowhead*). A ring of fire on color Doppler ultrasound is more commonly seen around a corpus luteum than an ectopic pregnancy.

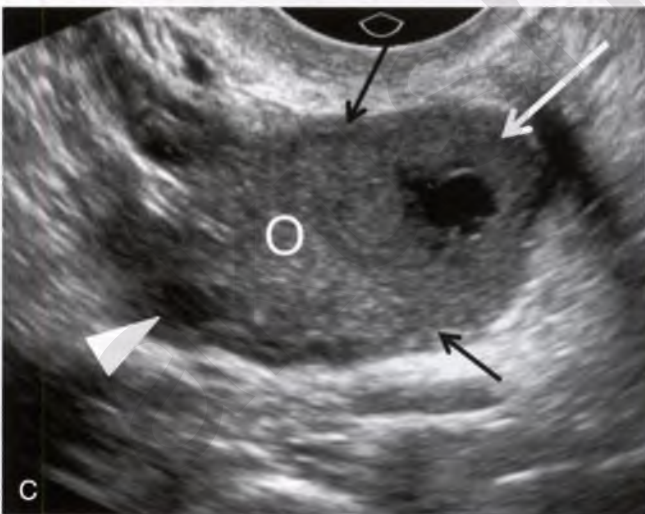
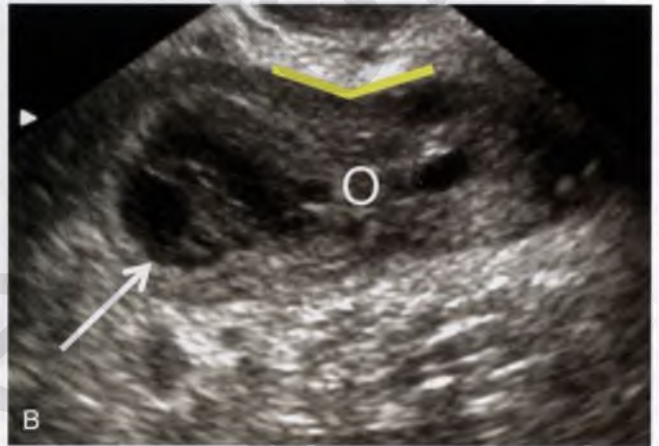
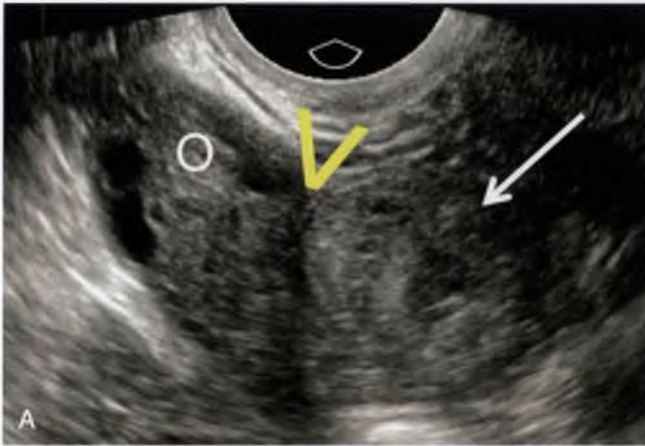


**FIG 33-17** Features used to differentiate an ectopic pregnancy from a corpus luteum. **A**, Transvaginal transverse scan shows that the angle (*narrow V*) between the round ovary (O) and the round heterogeneous mass of the ectopic pregnancy (*arrow*) is acute, because they are adjacent separate structures. When this is observed, the examiner should exert gentle pressure with the transducer or on the anterior abdominal wall to attempt to separate the ectopic pregnancy from the ovary. **B**, Transvaginal transverse scan in another patient demonstrates an obtuse angle (*wide V*) between the corpus luteum (*arrow*), which contains internal hemorrhage, and the ovary (O), because the corpus luteum arises from and is part of the ovary. The exophytic corpus luteum protrudes from the ovary and exhibits the claw sign, with a thin surrounding rim of ovarian parenchyma. In this case, applying pressure would cause the corpus luteum to move with (rather than away from) the ovary. **C**, Transvaginal transverse scan of another patient with a small anechoic ovarian follicle (*arrowhead*) and an exophytic corpus luteum (*white arrow*) arising from the ovary (O). The claw sign is shown (*black arrows*) with crescent of ovarian tissue surrounding part of the corpus luteum. Note that the rim of the corpus luteum is thick but not very echogenic.



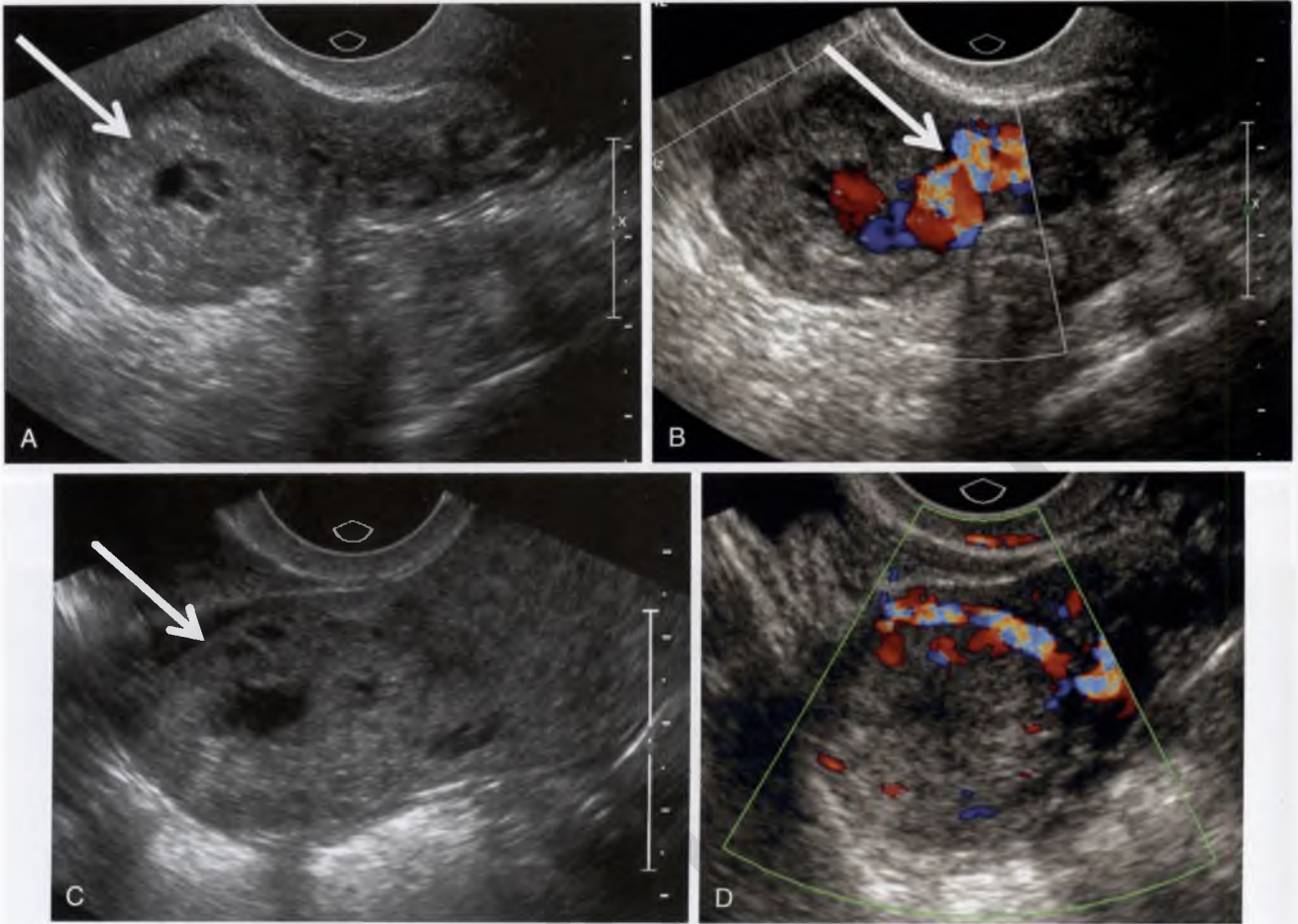


**FIG 33-18** Similar ultrasound appearance of a degenerated pedunculated myoma and an ectopic pregnancy. **A**, Transvaginal scan shows a degenerated pedunculated myoma (*arrow*) simulating an ectopic pregnancy with a thick echogenic rim and a central cystic component. **B**, Transvaginal color Doppler scan of the pedunculated myoma in **A** shows bridging vessels (*arrow*) arising from the uterus, thus establishing the uterine origin of the mass. The pregnancy test was negative. **C**, Transvaginal transverse scan in a second patient shows a similar appearing thick-walled adnexal mass adjacent to the uterus, which represents an ectopic pregnancy (*arrow*). **D**, Transvaginal color Doppler sonogram shows a peripheral ring of vessels, typical of vessels around a gestational sac, in this case an ectopic pregnancy.

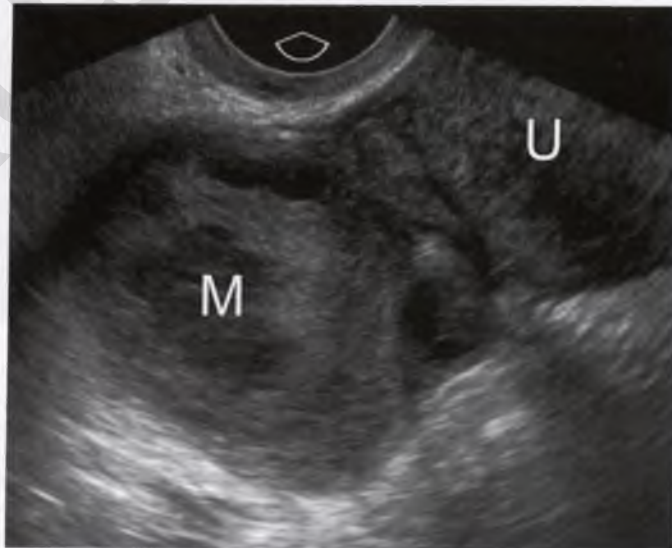


**FIG 33-19** Tubo-ovarian abscess mimicking ectopic pregnancy. Transvaginal transverse scan in a patient with a painful, tender right adnexal mass (**M**) found to be a tubo-ovarian abscess, with a thick echogenic rim and a cystic center with internal echoes, adjacent to the uterus (**U**). The pregnancy test was negative.





**FIG 33-20** Coronal reconstruction of a three-dimensional sonogram of the uterus delineating the interstitial portion of the fallopian tube. The interstitial portion of the fallopian tube (*arrow*) crosses through the myometrium in the cornual portion of the uterine fundus (*asterisks*).

The *interstitial line sign*, namely a thin echogenic line extending from the lateral corner of the endometrium through the myometrium to the ectopic gestational sac or hemorrhagic mass, is believed to represent the proximal lumen of the fallopian tube and is an infrequent but relatively specific finding of an interstitial EP<sup>68,69</sup> (Fig. 33-22B).

There are several important pitfalls in the sonographic diagnosis of interstitial EP and not all eccentric gestational sacs will turn out to be interstitial EPs. Mass effect from leiomyomas or uterine contractions may displace an intrauterine gestational sac into an eccentric location, mimicking an interstitial EP. IUPs in the right or left horn of a bicornuate or septate uterus may also be eccentric in location (Fig. 33-23). However, such pregnancies are intrauterine, located within the endometrial cavity in the uterine horn, and therefore should have a broad interface with surrounding echogenic decidualized endometrium, without intervening hypoechoic myometrium (see Fig. 33-23). An angular pregnancy refers to an eccentrically located but intrauterine gestational sac that implanted into the lateral corner of the endometrial cavity at the uterine fundus near the entrance of the fallopian tube (Fig. 33-24). The distinction between interstitial EPs and eccentric IUPs (whether angular, displaced by myometrial contractions/leiomyomas, or located in the horn of a septate or bicornuate uterus) is more easily made with 3D sonography (with coronal reconstruction) or magnetic resonance imaging (MRI), as it is possible with these imaging techniques to routinely visualize the uterotubal junction, the round ligament, and the interstitial line sign. Specifically, an angular IUP implants in the endometrial cavity medial to the uterotubal junction and round ligament (see Fig. 33-24), whereas an interstitial EP implants lateral to the round ligament. Angular pregnancies are reported to have an increased risk of spontaneous miscarriage, uterine rupture, and abnormal placental implantation. However, the degree of

risk remains controversial, as some reported cases may have been misdiagnosed interstitial EPs.<sup>65,66,70,71,72</sup>

Exophytic subserosal uterine leiomyomas may undergo central cystic degeneration and may mimic a gestational sac. Color Doppler ultrasound imaging will often demonstrate a feeding vessel extending from the uterus to the degenerated leiomyomas, whereas an EP tends to have a peripheral ring of surrounding vessels (see Fig. 33-18). Rarely, highly vascular, intramural myometrial lesions can be mistaken for an interstitial EP, including arteriovenous malformations, hemangiomas, and neoplasms. None of these entities would be expected to be associated with a positive serum hCG except for gestational trophoblastic neoplasia (GTN). A choriocarcinoma or invasive mole located laterally at the fundal myometrium would be especially difficult to differentiate from an interstitial EP, although the serum hCG level would be higher than predicted based on estimated gestational age in a patient with GTN.<sup>73</sup> Duplex Doppler sonography would not be particularly helpful because choriocarcinomas, invasive moles, leiomyosarcomas, and interstitial EPs all tend to demonstrate increased vascularity on color Doppler interrogation with low-impedance, high-velocity arterial waveforms.

Because of the robust blood supply from the surrounding myometrium, an interstitial EP often grows over a longer time period, becoming larger and more vascularized as the trophoblastic tissue invades the surrounding myometrium. Hence, interstitial EPs tend to become symptomatic and rupture later than tubal EPs, usually around 12 weeks' gestational age, potentially resulting in massive hemoperitoneum and hemodynamic instability. The morbidity and mortality rates of interstitial EPs are at least double those of ampullary tubal EPs, with maternal mortality rates approaching 2.2%.

Surgical cornual resection and hysterectomy have been the traditional therapeutic options for interstitial EPs. However, in stable patients, laparoscopic resection with or without ultrasound guidance can be successful. Successful treatment of interstitial EPs with direct injection of MTX into the gestational sac or systemic administration of MTX has also been reported.<sup>74,75</sup> However, the success rate for MTX therapy is lower for interstitial EPs than for ampullary or isthmic tubal EPs.<sup>76,77</sup> If bleeding is profuse, selective uterine artery embolization or vasoconstrictive agents, such as vasopressin, have been successful in controlling hemorrhage. Still, hysterectomy is often necessary for advanced or complicated cases presenting with uterine rupture or significant hemoperitoneum. In stable patients presenting at early gestational ages, successful expectant management of early interstitial EPs has also been reported.<sup>78</sup>

### Rudimentary Horn Ectopic Pregnancy

An unusual form of EP is the development of a gestation in a rudimentary horn attached to a unicornuate uterus, an anomaly that results from incomplete development of one of the müllerian ducts and abnormal fusion of the rudimentary horn with the banana-shaped contralateral, normally developed horn. If the two endometrial cavities are connected, the blastocyst may implant directly into the endometrial cavity of the rudimentary horn. However, in 83% of patients, the rudimentary horn has no direct connection to the endometrial cavity of the normal horn. In such cases, it is postulated that the sperm or fertilized ovum migrates transperitoneally from the contralateral tube to the tube connected to the rudimentary horn and eventually implants into the small endometrial cavity of that rudimentary horn<sup>79</sup> (Fig. 33-21B). If hemorrhage occurs, blood will not be able to exit through the uterine cavity or cervix and will collect in the cul-de-sac or distend the rudimentary horn. If there is a connection to the endometrial cavity of the normal horn, the patient may present with vaginal bleed-



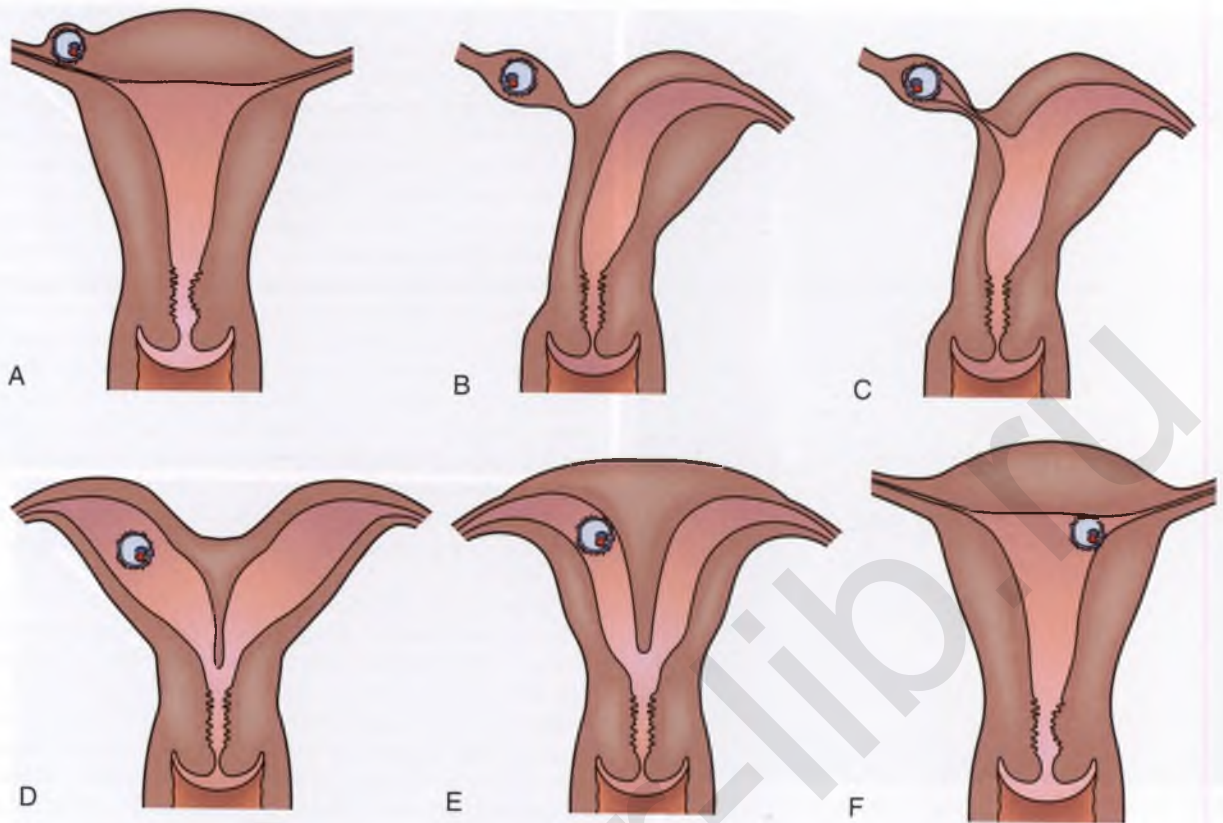


**FIG 33-21** Various locations of implanted gestations near the cornual portion of the uterus. In the past, the term *cornual pregnancy* has been used to describe all of these different types of pregnancies. Therefore, the term is potentially misleading, confusing to sonologists and clinicians, and should not be used. **A**, The gestational sac is implanted in the interstitial portion of the right fallopian tube as it passes through the myometrium in the cornual portion of the uterus, most appropriately termed *interstitial ectopic pregnancy*. **B**, This EP is implanted in a right rudimentary horn, which has no connection to the endometrial cavity, associated with a unicornuate uterus. **C**, This EP is implanted in a right rudimentary horn, which has a direct connection to the endometrial cavity. **D**, The pregnancy is implanted in the right horn of a bicornuate uterus, and is therefore an *intrauterine pregnancy*. **E**, This pregnancy is implanted in the right horn of a septate uterus, and is therefore an *intrauterine pregnancy*. **F**, On the left side of the uterus a pregnancy is implanted in the lateral angle of the endometrial cavity, most appropriately termed an *angular pregnancy*, which is an *intrauterine pregnancy*, not an *ectopic pregnancy*. In summary, the pregnancies depicted in the top row (**A**, **B**, and **C**) are EPs, whereas the pregnancies in the bottom row (**D**, **E**, and **F**) are IUPs.

A pregnancy in this location may be difficult to differentiate from an interstitial EP or a pregnancy in a bicornuate or septate uterus, as all three will present with an eccentric gestational sac. Differentiation is often best accomplished with MRI, which will demonstrate no visible continuity between the endocervical canal and the lumen of the pregnant rudimentary horn, as would be expected in a septate or bicornuate uterus (Fig. 33-25). A 3D sonographic examination may sometimes be helpful.<sup>80</sup>

Rudimentary horn pregnancies have a high rate of spontaneous abortion and fetal growth restriction. They often rupture during the second or third trimester, resulting in fetal demise and significant hemorrhage that can be fatal.<sup>79</sup> Pathologic placentation resulting in a morbidly adherent placenta is common, which further increases the risk of fatal rupture. Hence, if a rudimentary horn is incidentally found, resection is generally recommended to prevent the possibility of ectopic implantation, and pregnancies in rudimentary horns are usually treated with surgical excision or direct injection of potassium chloride (KCl) or MTX. There have been case reports of conservative management and delivery, but these pregnancies were surrounded by thick myometrial tissue and required very close monitoring.<sup>79</sup> Irrespective of pregnancy outcome, ultimately surgical excision of the rudi-

mentary horn is necessary to prevent future implantations and minimize maternal risk.

### Cervical Ectopic Pregnancy

Cervical EPs occur when the fertilized ovum implants directly into the wall of the cervix below the level of the internal cervical os (Fig. 33-26). Risk factors for cervical EP include previous instrumentation, cervical or uterine surgery, abortion, curettage, IVF-ET, uterine anomalies, leiomyomas, synechiae, Asherman syndrome, previous cesarean delivery, IUD placement, and PID. On ultrasound images, the gestational sac will appear eccentric in location, embedded in the wall of the cervix as the trophoblastic tissue invades through the cervical mucosa, usually through a defect in the lining from prior instrumentation or injury (see Fig. 33-26). This is often best appreciated on transverse images where it can be easier to recognize that the gestational sac is located within the wall of the cervix, separate from the endocervical canal, which may be deviated or displaced by the sac. Imaging should include and target both the external and internal ostia. A 3D ultrasound examination can be very helpful in delineating the location of the pregnancy. The gestational sac is typically round or oval with a thick, well-formed echogenic rim (Fig. 33-26A through C). Vascularity in the wall of the

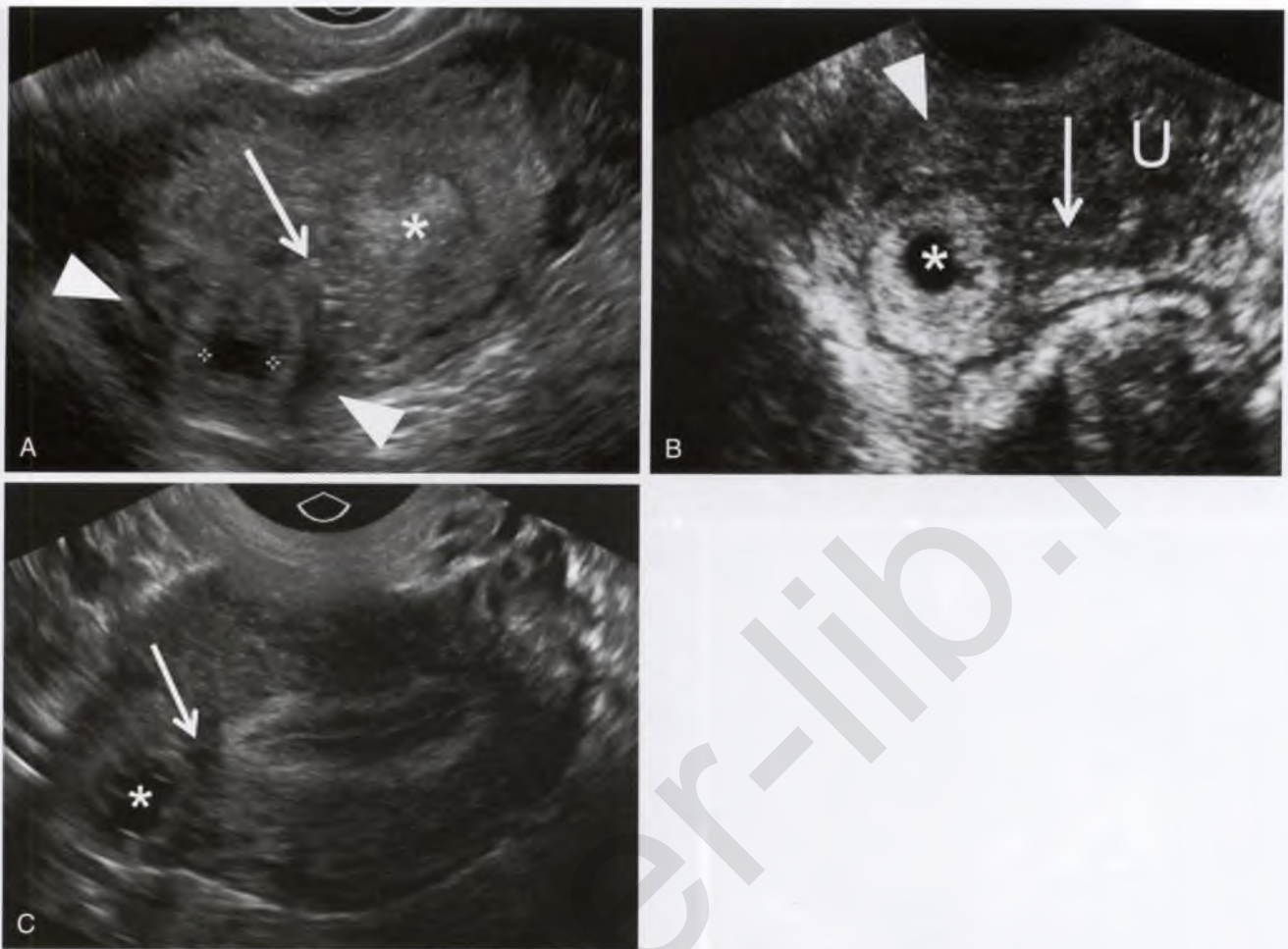


**FIG 33-22** Interstitial ectopic pregnancies. **A**, Transvaginal transverse scan of the uterus shows the eccentrically located interstitial ectopic pregnancy (*calipers*) separate from the endometrial cavity (*asterisk*). Myometrium (*arrow*) clearly separates the medial edge of the gestational sac from the echogenic endometrium (*asterisk*) and surrounds the sac (*arrowheads*). **B**, Transvaginal transverse scan of the uterus (U) in another patient demonstrates the interstitial line sign, a thin echogenic line (*arrow*) extending from the endometrium toward the right-sided interstitial ectopic pregnancy (*asterisk*). Note that the myometrium (*arrowhead*) partially surrounds the gestational sac. **C**, Transvaginal transverse scan of the uterus in a third patient with right-sided interstitial ectopic pregnancy (*asterisk*) demonstrates myometrial tissue (*arrow*) intervening between the edge of the gestational sac and the echogenic endometrium. (**A**, Courtesy Department of Obstetrics and Gynecology, Yale University School of Medicine, New Haven, CT.)

gestational sac and feeding vessels extending from the wall of the cervix to the sac are often appreciated on color Doppler ultrasound imaging. Later in pregnancy, the cervix may appear enlarged, bulbous, and hyperemic on inspection. Ultrasound image will reveal an hourglass-shaped uterus composed of the uterine corpus and disproportionately enlarged cervix with a “waist” at the level of the internal os.<sup>81</sup> However, in current practice, it is unusual to diagnose cervical EPs at such a late stage because most such pregnancies present early in the first trimester.

Distinguishing a cervical pregnancy from an impending or inevitable miscarriage, in which the gestational sac is being evacuated and passing through the endocervical canal, may be difficult (Fig. 33-26D). In patients with an impending miscarriage, the gestational sac will be centrally located within the endocervical canal. The surrounding cervical stroma will be symmetric in thickness, often best appreciated on transverse images. The gestational sac may have an irregular, flattened, or crenated border without surrounding vascularity. The presence of trophoblastic blood flow or embryonic cardiac activity increases the

likelihood that a gestational sac in the cervix is a cervical EP but can sometimes be seen in aborting IUPs. Jurkovic and coworkers<sup>82</sup> described the sliding sign to help differentiate an aborting gestational sac from a cervical EP. When gentle pressure is applied to the cervix by the transvaginal transducer, the aborting gestational sac will slide up and down in the endocervical canal, whereas such movement will not occur with an implanted cervical EP.

Cervical EPs are at risk for rupture and can cause heavy bleeding, often painless and profuse. Because the cervix is composed primarily of fibrous connective tissue with only 15% smooth muscle, contraction of the cervix is usually inadequate to prevent the dilated cervical vessels from hemorrhaging profusely following dilatation and curettage (D&C) or surgical excision of the gestational sac. Therefore, in the past, emergent hysterectomy was typically performed.<sup>83</sup> If, however, the diagnosis of cervical EP is made early in the first trimester, before bleeding has occurred, preservation of future fertility can be achieved by treating with systemic MTX or by direct injection of the embryo and sac with KCl or MTX.<sup>84,85</sup> Surgical debulking or hysteroscopic



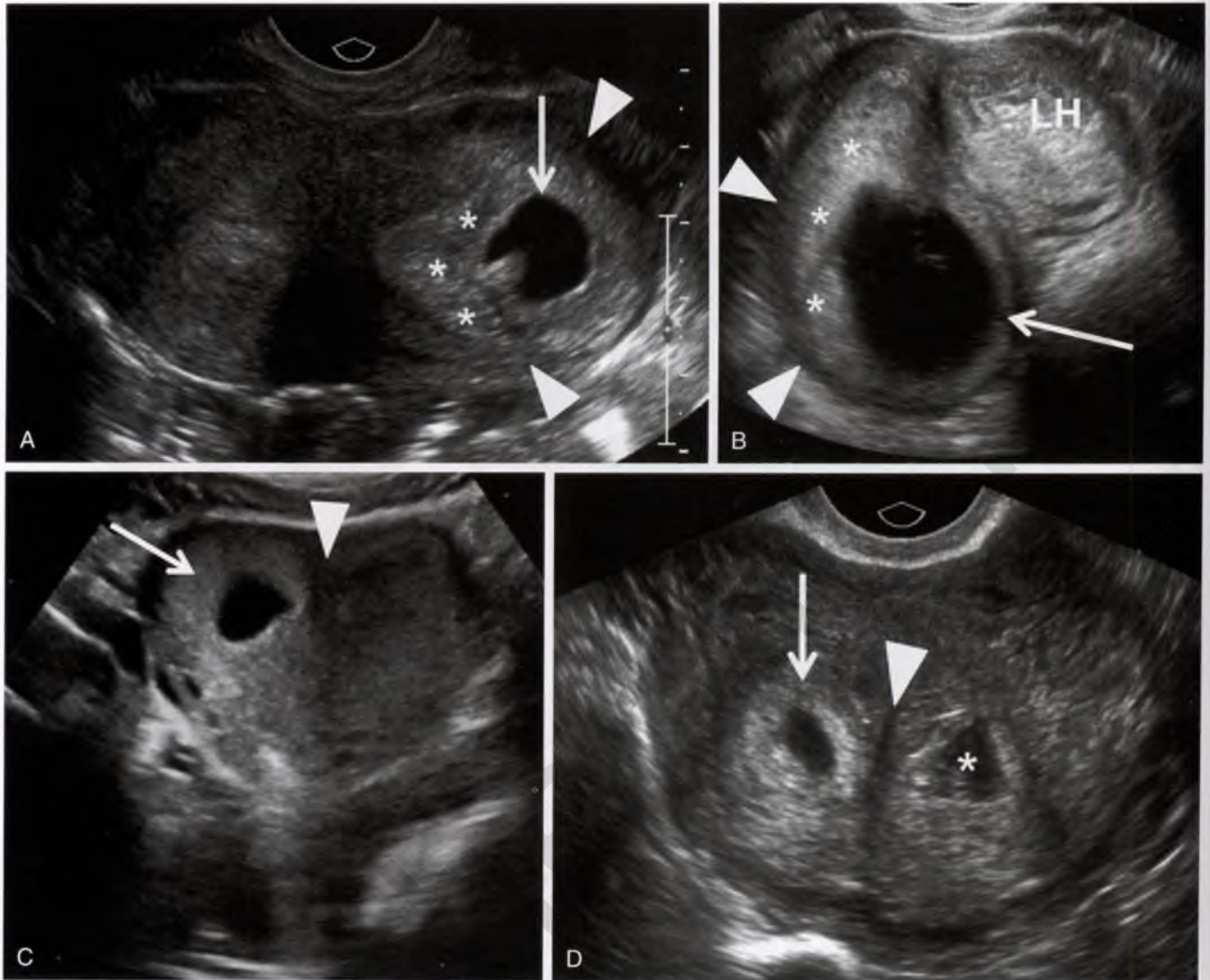


**FIG 33-23** Eccentric intrauterine gestational sacs in bicornuate and septate uteri. **A**, Transvaginal transverse scan of the uterus shows an eccentrically located gestational sac (*arrow*) containing an embryo with a very thin mantle of surrounding myometrium (*arrowheads*). However, this is an intrauterine pregnancy in the endometrial cavity of the left horn of a bicornuate uterus. Note the broad interface with the endometrium (*asterisks*). **B**, Transvaginal transverse scan of the uterus shows an eccentrically located gestational sac (*arrow*) and a thin mantle of surrounding myometrium (*arrowheads*). This is an intrauterine pregnancy in the endometrial cavity of the right horn of a bicornuate uterus. Note the broad interface of the gestational sac with the endometrium (*asterisks*) and the empty left uterine horn (LH). Also note the deep cleft in the contour of the uterine fundus between the two horns, diagnostic of a bicornuate uterus. **C**, Transabdominal coronal scan of a septate uterus shows an eccentrically located gestational sac (*arrow*) in the endometrial cavity of the right cornu. This pregnancy is intrauterine and is located to the right of a thin shadowing septum (*arrowhead*). Note the flat to minimally indented outer contour of the uterine fundus, characteristic of a septate uterus. **D**, Transvaginal transverse scan of the uterus shows an eccentrically located gestational sac (*arrow*) in the endometrial cavity of the right cornu of a septate uterus. This pregnancy is intrauterine and is separated from the endometrial cavity of the left cornu (*asterisk*), which contains echogenic fluid suggesting blood, by a thin shadowing septum (*arrowhead*). (**B**, Courtesy Department of Obstetrics and Gynecology, Yale University School of Medicine, New Haven, CT.)

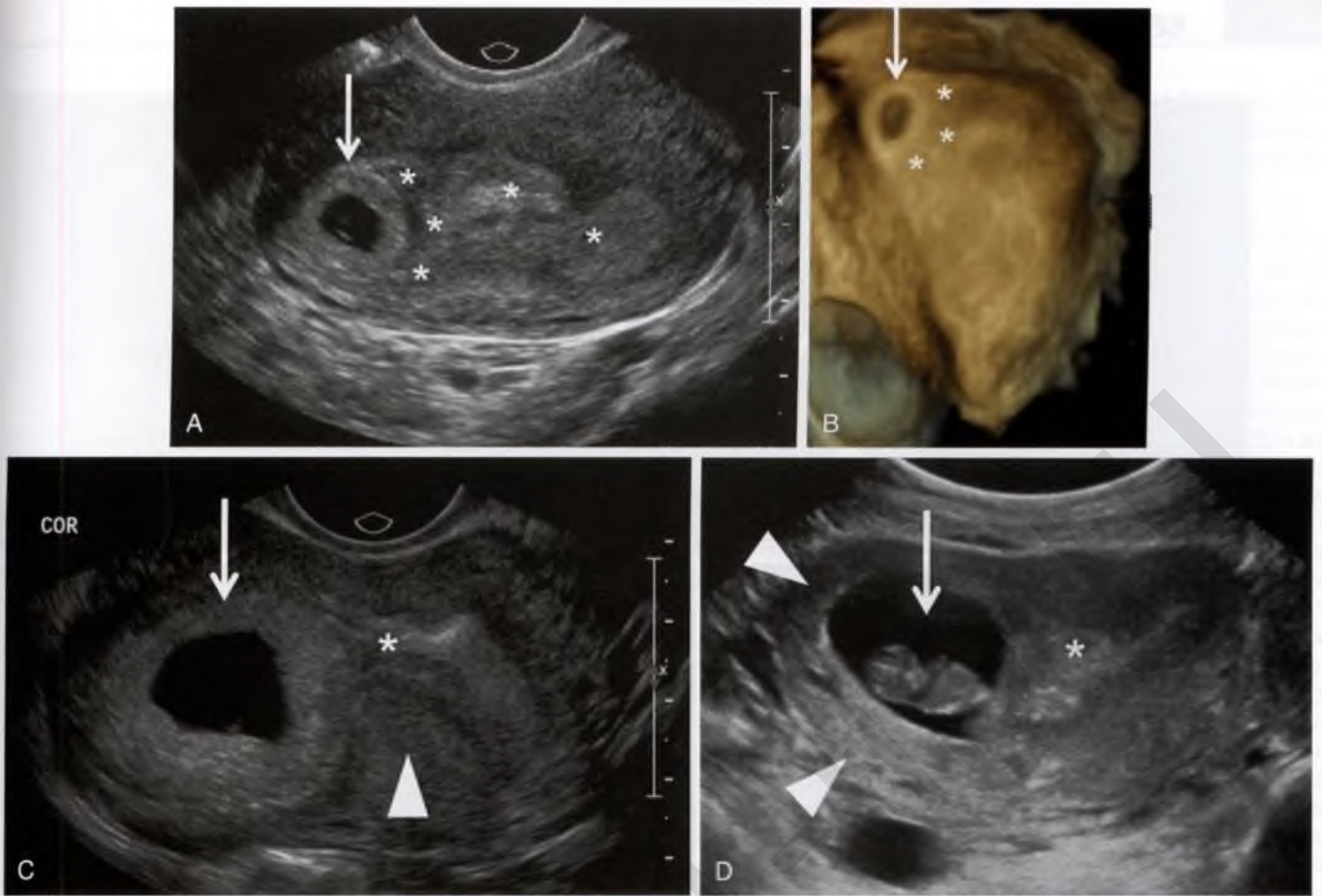


**FIG 33-24** Angular pregnancies implant in the lateral corner or angle of the endometrial cavity in the uterine fundus. **A**, Transvaginal transverse scan of the uterus shows an eccentric gestational sac (*arrow*) implanted in the right lateral corner of the endometrial cavity. The pregnancy is intrauterine and has a broad interface with the endometrium (*asterisks*), which completely surrounds the gestational sac. **B**, Three-dimensional coronal reconstruction of the uterus shows an early gestational sac (*arrow*) in the right lateral corner of the endometrial cavity. The pregnancy is intrauterine and has a broad interface with the endometrium (*asterisks*). **C**, Transvaginal transverse scan of the uterus shows a large empty gestational sac (*arrow*) in the right lateral corner of the endometrial cavity (*asterisk*). A focal uterine contraction (*arrowhead*) is partially responsible for displacing this intrauterine pregnancy laterally toward the right. The patient ultimately had a spontaneous miscarriage without complication. **D**, Transabdominal transverse scan of the uterus shows an embryo (*arrow*) in the right lateral angle of the endometrial cavity (*asterisk*) surrounded by a thick layer of myometrium (*arrowheads*). It is important to recognize that with an angular pregnancy there will be no intervening myometrium between the gestational sac and the endometrium. (**B** and **C**, Department of Obstetrics and Gynecology, Yale University School of Medicine, New Haven, CT.)

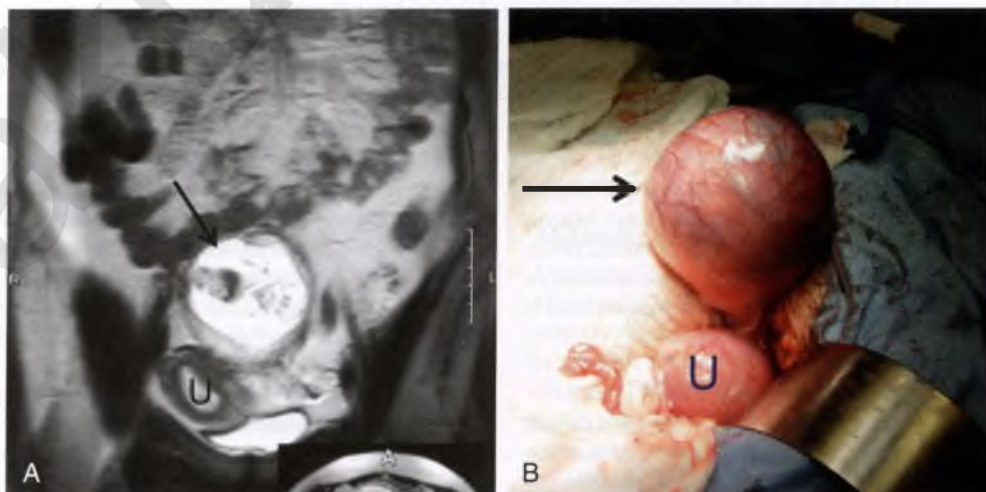


**FIG 33-25** Pregnancy within the rudimentary horn of a unicornuate uterus. **A**, Coronal T2-weighted magnetic resonance image of the pelvis shows the uterus (U) and an adjacent ectopic pregnancy (*arrow*) containing a 10-week fetus. The pregnancy appears attached to the uterus. **B**, Intraoperative photograph showing the uterus (U) and the adjacent ectopic pregnancy (*arrow*), which was located in a rudimentary horn attached to a unicornuate uterus. The ectopic pregnancy was excised without incident.



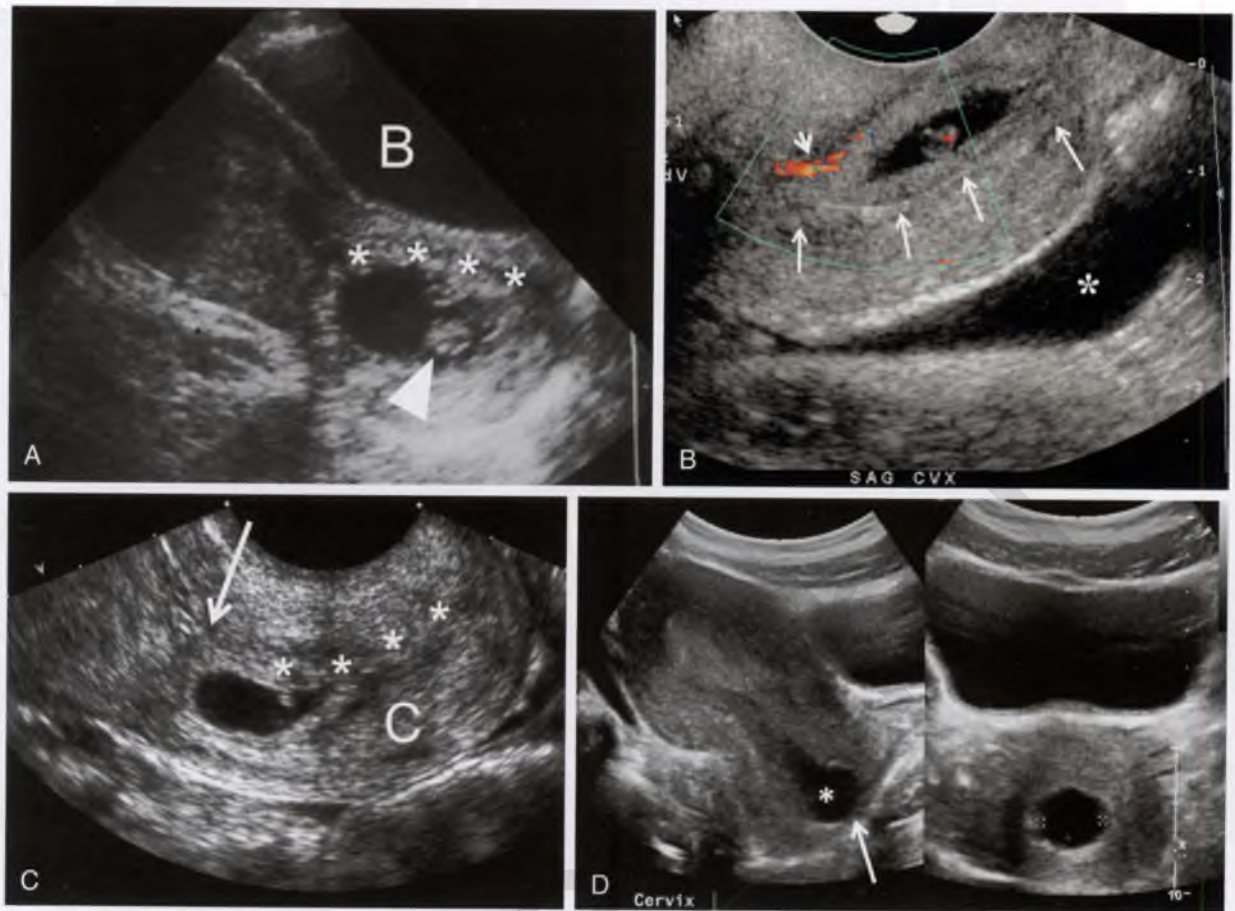


**FIG 33-26** Comparison of cervical ectopic pregnancy and inevitable abortion. **A**, Transabdominal sagittal scan of the uterus shows an ectopic gestational sac containing an embryo (arrowhead) embedded in the posterior wall of the cervix posterior to the endocervical canal (asterisks). (B, bladder.) **B**, Transvaginal sagittal scan of the cervix demonstrates a gestational sac containing an embryo implanted in the anterior cervical wall, adjacent to the echogenic endocervical canal (long arrows). Flow is noted within a feeding vessel (short arrow) in the cervical wall and red pixels in the embryo flickered on real-time imaging indicating cardiac motion. A small amount of free fluid is shown in the cul-de-sac (asterisk). **C**, Transvaginal sagittal scan of the cervix (C) shows an ectopic gestational sac containing an embryo implanted in the posterior cervical wall, deep to the endocervical canal (asterisks) and below the level of the internal cervical os (arrow). **D**, Transabdominal sagittal (left) and transverse (right) scans of the uterus show a spontaneous abortion in progress. This patient presented with vaginal bleeding 1 week after documentation of an intrauterine pregnancy. The gestational sac (asterisk on left and calipers on right) is centrally located within the endocervical canal and appears partially extruded through the external cervical os (arrow on left). The sac appeared to slide back and forth (sliding sac sign) on real-time examination until it was extruded from the cervical canal into the vagina. (B from Bryan-Rest LL, Scoutt LM: Ectopic pregnancy. In Fielding JR, Brown DL, Thurmond AS (eds): *Gynecologic Imaging*. Philadelphia, Elsevier, 2011, p 343, Fig. 22-12C, used with permission.)

resection may be necessary if the gestation is more advanced.<sup>74,85</sup> Bleeding may be controlled by tamponade with a Foley catheter balloon inflated in the endocervical canal, uterine artery embolization, transvaginal ligation of the cervical branches of the uterine arteries, or intracervical vasopressin injection. In current practice, hysterectomy is considered a last resort.

### Myometrial/Cesarean Scar Ectopic Pregnancy

Pregnancies may implant in cesarean delivery scars at the anterior wall of the lower uterine segment (Fig. 33-27). The incidence of cesarean scar EPs has increased in recent years as the rate of cesarean deliveries has increased.<sup>86,87</sup> Cesarean scar EPs have been reported to account for up to 6% of EPs in women with prior cesarean delivery. The risk increases as the number of prior cesarean deliveries increases, and

approximately 72% of cesarean scar pregnancies occur in women who have had more than two cesarean deliveries.<sup>88</sup> In addition, pregnancies can implant into uterine scars following other surgeries such as hysterotomy, myomectomy, D&C, metroplasty, hysteroscopy, manual removal of the placenta, and uterine trauma.<sup>89</sup> These scars are believed to form a “niche” or “diverticulum,” which communicates with the endometrial cavity, allowing the blastocyst to enter and implant. However, the connection or tract may be extremely small, possibly only a microscopic dehiscence.<sup>90</sup> IVF and ET can also lead to myometrial scar EPs, and although rare, even direct myometrial implantation has been reported.

Patients with cesarean scar EPs typically present in the first trimester with painless vaginal bleeding. In general, these pregnancies have poor outcomes with high morbidity and mortality rates due to the risk





**FIG 33-27** Cesarean delivery scar. Prominent cesarean incision scars can serve as a nidus or niche for implantation of ectopic pregnancies. Transvaginal sagittal scan of the uterus shows a triangular fluid collection (*arrow*) in the expected location of a cesarean incision scar, in the anterior wall at the level of the lower uterine segment above the internal cervical os. The apex of the small fluid collection nearly reaches the outer serosal surface of the uterus and the broad base abuts the endometrial cavity. Implantation in this fluid-filled space would result in a cesarean scar ectopic pregnancy that could expand through the myometrial wall, resulting in uterine rupture.

of significant hemorrhage or uterine rupture resulting in hysterectomy in 70% of cases. If growth of the gestation is directed toward the abdominal cavity, uterine dehiscence/rupture and intra-abdominal location of the pregnancy with invasion of placental tissue into adjacent structures (morbidly adherent placenta) becomes likely (Fig. 33-28). If the gestation grows into the endometrial cavity, it is theoretically possible for the pregnancy to progress to term with expectant management (Fig. 33-29). However, term pregnancies arising in cesarean incision scars are at high risk of placenta previa and, almost by definition, morbidly adherent placenta.<sup>91,92</sup> Therefore, the risk of delayed uterine rupture and massive hemorrhage remains and such pregnancies must be carefully monitored. Up to 38% will require hysterectomy at the time of delivery.<sup>91</sup>

On ultrasound imaging, a mass or gestational sac, often triangular and highly vascular, will be observed separate from the endometrial canal extending into the anterior myometrial wall at the lower uterine segment, at the site of the cesarean incision scar just above the internal cervical os. If the sac is large enough, bulging beyond the serosal surface toward the bladder will be observed. It is important to directly search with ultrasound for discontinuity of the anterior uterine surface in the sagittal plane and for trophoblastic tissue situated between the bladder and the anterior uterine wall.<sup>93</sup> Differentiating a cesarean scar EP from a cervical EP depends upon identification of the internal os. A cesarean scar EP implants in the lower uterine segment above the internal os (Fig. 33-29A), whereas a cervical EP implants into the wall of the cervix below the level of the internal os (Fig. 33-26A through C). A 3D ultrasound examination or MRI may be helpful in confirming the diagnosis.

Therapeutic D&C is extremely risky in these patients and may result in massive hemorrhage from inadvertent perforation of the uterus and from invasion of trophoblastic tissue into the myometrium and surrounding tissues. Medical therapy for cesarean scar EPs includes ultrasound-guided injection of KCl or MTX directly into the embryo or the gestational sac, or systemic MTX. Surgical options include

excision with revision of the scar or hysterectomy. Adjunctive uterine artery embolization has been used to control hemorrhage.<sup>94</sup> Combined surgical and medical treatment is recommended by many in the field.<sup>95</sup>

### Ovarian Ectopic Pregnancy

Ovarian EPs have been reported to account for 1% to 3% of all EPs, but in the authors' experience they are extremely rare, likely representing less than 1% of all EPs.<sup>96</sup> It is postulated that ovarian EPs may result either from fertilization occurring within a follicle that has ruptured but failed to extrude the oocyte or from implantation of a fertilized ovum into the ovary. These two types of ovarian EPs have been referred to as primary and secondary, and as intrafollicular and extrafollicular, respectively. Distinction between these two types of ovarian EPs is not feasible and has neither clinical nor therapeutic significance. Risk factors for ovarian EPs include tubal disease, IUD placement, endometriosis, salpingectomy, and ART. Ovarian EPs may occur during ART as the result of reverse migration of transferred embryos following deep deposition into the uterine cavity or if a large volume of culture fluid is used during ET.<sup>97</sup>

The clinical presentation of abdominal or pelvic pain and vaginal bleeding in a pregnant patient mimics that of a tubal EP or of a ruptured or hemorrhagic corpus luteum.<sup>97</sup> TVS demonstrates a thick echogenic, peripherally vascular ring surrounding a cystic area within the ovary, which may mimic the sonographic appearance of a corpus luteum (Fig. 33-30). Because a hemorrhagic corpus luteum is much more common than an ovarian EP, definitive sonographic diagnosis of an ovarian EP requires visualization of a yolk sac or embryo within the echogenic ring. It should be remembered that a small blood clot within a corpus luteum may mimic an embryo. Color or power Doppler ultrasound evaluation may demonstrate hypervascularity of the adjacent ovarian parenchyma (Fig. 33-30B). If a surrounding rim of ovarian tissue is not identified, gentle pressure with the transvaginal probe can be applied. With an ovarian EP, the ovary and gestational sac move together (negative sliding sign), whereas with a tubal EP, the sac slides separately from the adjacent ovary. Still, it may be extremely difficult to differentiate a tubal EP adherent to the ovary from an exophytic ovarian EP, and differentiating an ovarian EP from a hemorrhagic corpus luteum is not always possible.<sup>99</sup> In some instances, 3D ultrasound examination may be helpful. Most often, the diagnosis of a primary ovarian EP is made histologically after laparoscopy, although this too may be difficult.

Early detection of ovarian EPs is important to prevent rupture, abdominal implantation, and the need for more complex surgery. The goal is to preserve as much normal ovarian tissue as possible while protecting the pregnant woman. Hence, the treatment of choice is ovarian wedge resection or laparoscopic cystectomy. Oophorectomy is reserved for more advanced cases. Because laparoscopy is used for both diagnosis and treatment, medical therapy with MTX is usually reserved as a secondary option or in cases of trophoblastic persistence.

### Abdominal Ectopic Pregnancy

Abdominal EPs account for approximately 1.4% of all EPs<sup>100</sup> (Figs. 33-31 and 33-32) and may be classified as primary or secondary. A primary abdominal EP results from intra-abdominal fertilization of an ovum with subsequent direct implantation of the conceptus outside the genital tract. A secondary abdominal EP, which is more common, results from survival of a ruptured tubal or ovarian EP that implants onto the peritoneum, omentum, or abdominal organs (typically bladder and bowel). Implantation on the spleen and in the lesser sac has also been reported.<sup>101-103</sup> An abdominal pregnancy parasitizes blood supply from any vascular surface, which makes this one of the most dangerous types of EP. Such pregnancies are notoriously difficult



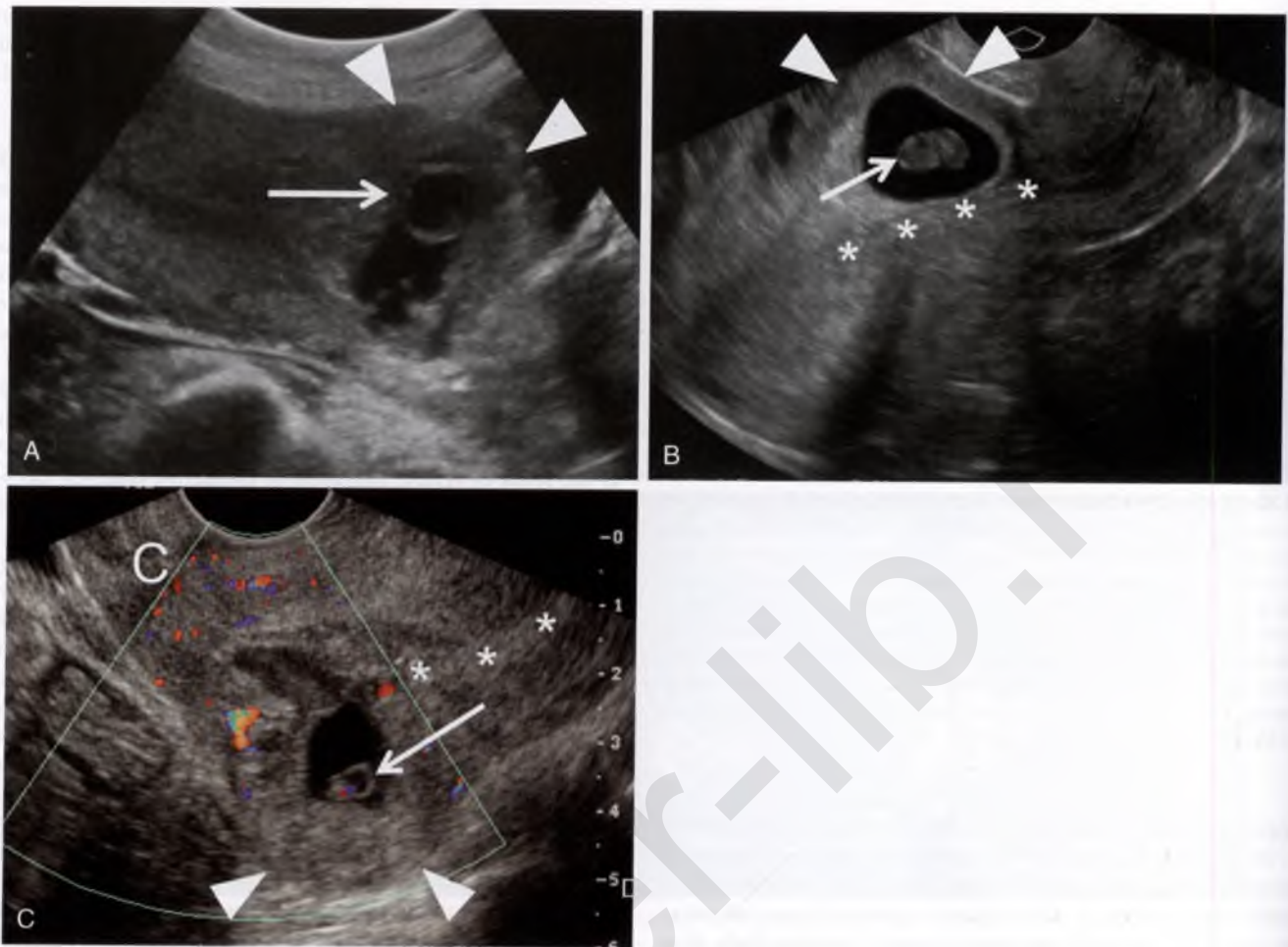


**FIG 33-28** Cesarean scar ectopic pregnancies. **A**, Transabdominal sagittal scan of the uterus shows a gestational sac within the cesarean incision scar (arrow), bulging the lower uterine contour (arrowheads) anteriorly toward the bladder. **B**, Transvaginal sagittal scan of the uterus in a second patient shows an ectopic gestational sac containing an embryo (arrow) within a cesarean incision scar, embedded in the myometrium at the lower uterine segment anterior to the endometrium (asterisks) and bulging the uterine contour (arrowheads) anteriorly toward the abdominal cavity. **C**, Transvaginal sagittal scan with color Doppler ultrasound in a third patient, with a retroverted/retroflexed uterus. There is an ectopic gestational sac containing an embryo with a heartbeat (dot of color) next to the yolk sac (arrow), bulging beyond the serosal surface of the uterine wall (arrowheads), at the level of the cesarean incision scar just above the internal cervical os. Asterisks indicate endometrium; C, cervix. (Courtesy Department of Obstetrics and Gynecology, Yale University School of Medicine, New Haven, CT.)

to diagnose and may not be recognized until the third trimester, often resulting in massive hemorrhage threatening the life of both mother and fetus. Abdominal EP should be considered in the differential diagnosis of an acute abdomen and hemoperitoneum in a woman of reproductive age with no obvious cause. Maternal mortality rate is as high as 20%. Morbidity includes the risks associated with hemorrhage, disseminated intravascular coagulation, bowel obstruction, fistula formation, and adherent placenta. The incidence of full-term abdominal EPs resulting in live births is not known because so few cases have been reported.

Risk factors for abdominal EP include PID, tubal abnormalities, endometriosis, ART, and multiparity. Symptoms are nonspecific and include abdominal pain, painful fetal movements, nausea, and vomiting. Physical examination may detect an abnormal lie of the fetus and a pregnancy that is small for gestational age. Careful history may reveal an episode of pain and vaginal bleeding at 6 to 8 weeks of gestation that resolved, presumably representing the time of tubal rupture.

Abdominal EPs may be missed during ultrasound examinations if the sonographer, concentrating on evaluating the fetus, does not recognize that the uterus is displaced deep in the cul-de-sac resembling the cervix, or that there is no myometrial tissue surrounding the pregnancy. Therefore, it is important to always document the presence of myometrial tissue surrounding the gestational sac and located between the pregnancy and the maternal bladder wall (Fig. 33-31A). In addition, when performing an obstetric sonogram, it is necessary to evaluate the configuration of the lower uterine segment and cervix and to document continuity of the endocervical canal with the endometrial canal/uterine cavity. The walls of the cervix should always be continuous with the myometrium both anteriorly and posteriorly. A clumped appearance of the cervix, a narrow waist in the region of the lower uterine segment, or apparent discontinuity between the cervix and the lower uterine segment should alert the sonographer to the possibility of an abdominal EP (Fig. 33-31B). Abnormal lie of the fetus and oligohydramnios are common ultrasound findings.

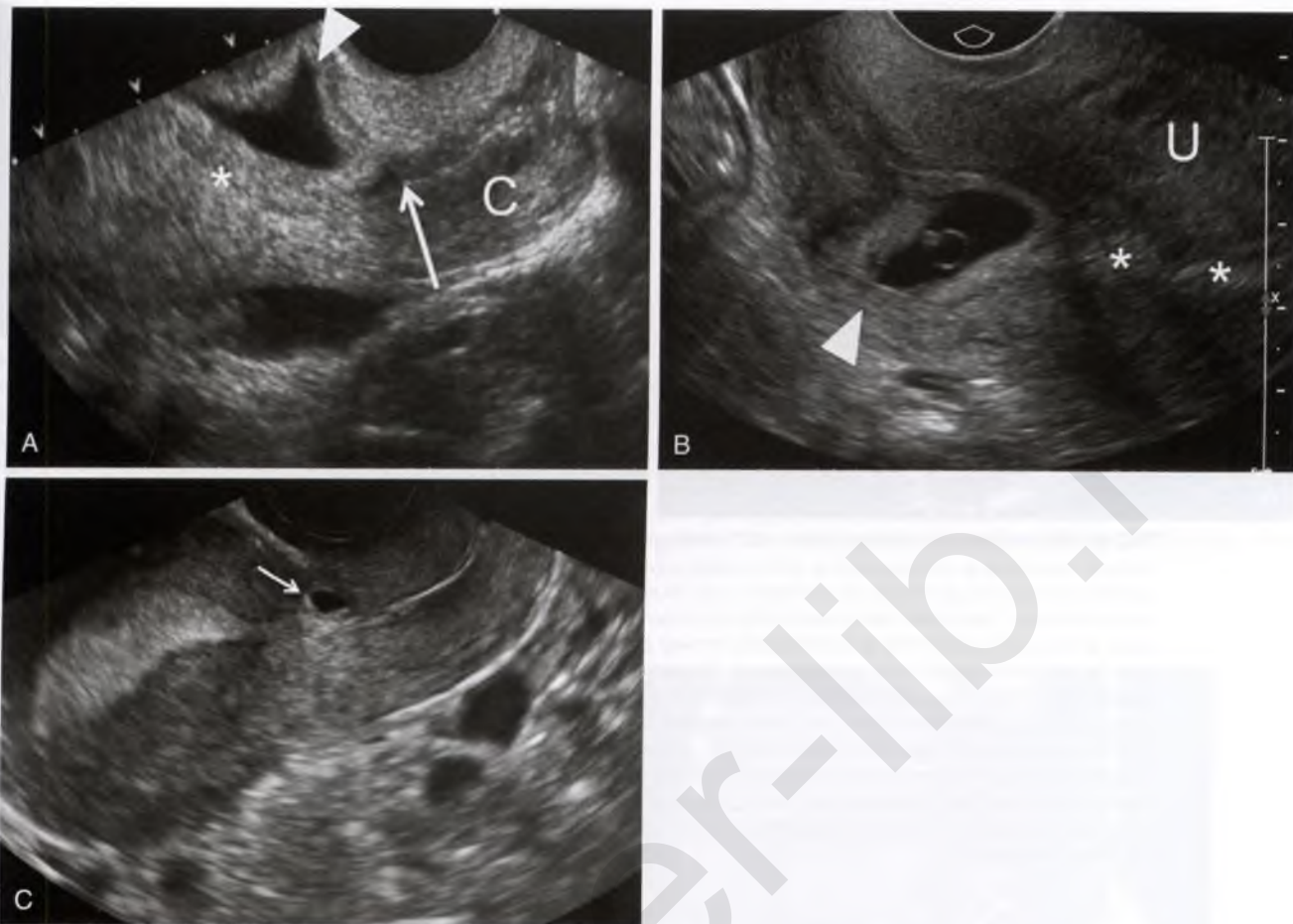


**FIG 33-29** Cesarean scar ectopic pregnancies. **A**, Transvaginal sagittal scan of the lower uterine segment and cervix (C) shows a triangular ectopic gestational sac (*arrowhead*) located in the myometrium at the anterior lower uterine segment above the level of the internal cervical os (*arrow*), bulging slightly into the endometrial cavity (*asterisk*). Very early cesarean scar ectopic pregnancies are often triangular in configuration. **B**, Transvaginal sagittal scan of a patient with a retroverted/retroflexed uterus (U) shows a gestational sac (*arrowhead*), containing a yolk sac and adjacent small embryo, implanted in a cesarean incision scar and growing toward the endometrial cavity (*asterisks*). **C**, Early cesarean scar ectopic pregnancy. The gestational sac (*arrow*) is centered in the anterior myometrial wall at the lower uterine segment above the internal cervical os. It is difficult to predict if the pregnancy will grow toward the endometrial cavity or bulge outward and extend beyond the serosal surface of the uterus. (**B**, Courtesy Anna Lev-Toaff, MD, University of Pennsylvania Hospital, Philadelphia, PA. **C**, Courtesy Department of Obstetrics and Gynecology, Yale University School of Medicine, New Haven, CT.)

Rarely, confirmed abdominal EPs have been allowed to progress into the third trimester (see Fig. 33-32). The fetus is delivered surgically, but removal of the placenta is problematic because of complex vascular attachments or placental invasion into surrounding tissues. Complete removal of the placenta may not be feasible, but resection of as much as possible is recommended because of the substantial risk of secondary infection, hemorrhage, and intestinal obstruction if the placenta is left in situ. Postoperative treatment with MTX has been used to promote involution of residual placental tissue.<sup>103</sup>

### Retroperitoneal Ectopic Pregnancy

EPs in the retroperitoneal space are extremely rare.<sup>104-107</sup> They are difficult to detect and may present with massive retroperitoneal hemorrhage. Although the mechanism of implantation in the retroperitoneal space is not known, possible explanations include iatrogenic manipulation with ART resulting in either retrograde migration of the embryo after ET or uterine perforation and direct placement of the embryo

into the retroperitoneum during ET. Retroperitoneal EPs have been reported in the absence of IVF-ET. In such cases, it is theorized that the embryo initially implants on the posterior peritoneal surface (i.e., an abdominal pregnancy) with subsequent invasion by the trophoblastic tissue through the peritoneal membrane into the retroperitoneal space or through congenital or acquired (perhaps secondary to conditions such as endometriosis) defects in the peritoneal surface. Another theory involves migration of the conceptus through lymphatic channels, a theory supported by Hall and colleagues,<sup>106</sup> who found lymphatic tissue in the excised ectopic mass. Alternatively, migration might occur alongside the retroperitoneal ovarian vessels as they enter or exit the ovary. In support of this last theory, retroperitoneal EPs have been found near the confluence of the left renal and left ovarian veins (Fig. 33-33).

In a symptomatic pregnant patient with a normal laparoscopic examination of the uterus and adnexa, a pregnancy in an extremely unusual location such as the retroperitoneum should be considered,



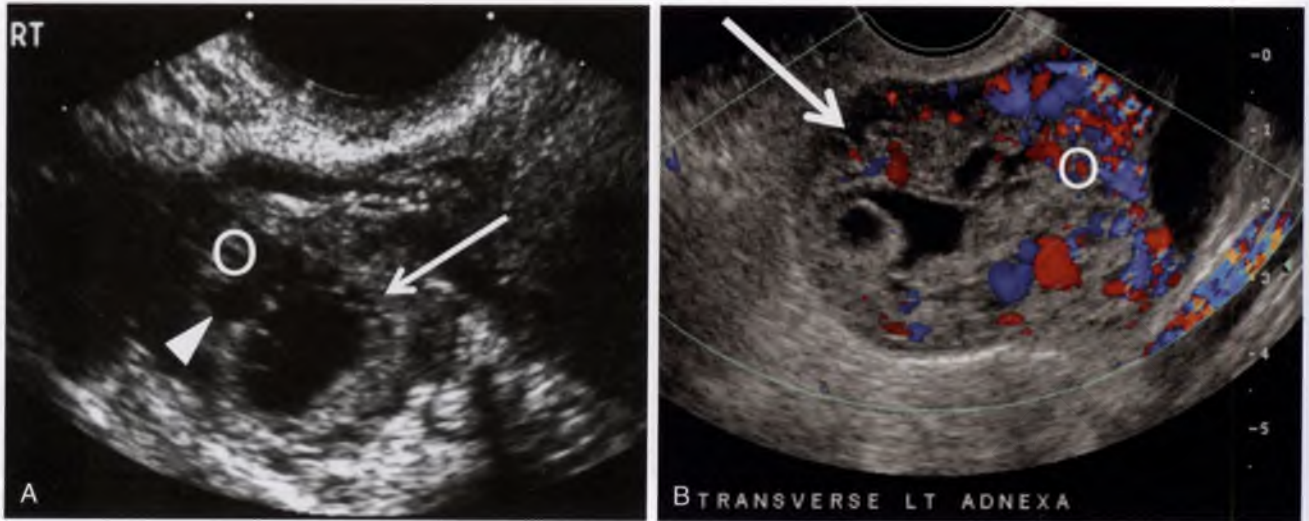


**FIG 33-30** Ovarian ectopic pregnancies. **A**, Transvaginal transverse scan shows an ectopic gestational sac (arrow), containing a yolk sac, arising and bulging outward from the surrounding ovary (O). Chorionic tissue, partially surrounding a follicle (arrowhead), was found to be firmly attached to the ovary, necessitating oophorectomy. This patient had a malpositioned intrauterine device removed 10 days prior, developed pelvic pain, and was found to have a pathologically proved ovarian ectopic pregnancy. **B**, Transvaginal transverse scan with color Doppler ultrasound in another patient shows an ectopic gestational sac (arrow) containing a yolk sac in the left ovary (O). The rim of the ectopic pregnancy is heterogeneous and irregular in thickness, making it difficult to differentiate from ovarian tissue. Note increased vascularity of the ovarian parenchyma, which has been described with ovarian ectopic pregnancies but is not a specific finding. It can be difficult to differentiate an ovarian ectopic pregnancy from a corpus luteum. Given the rarity of ovarian ectopic pregnancies, this diagnosis should not be made on the basis of sonographic findings unless a yolk sac or embryo is clearly documented. (Courtesy Department of Obstetrics and Gynecology, Yale University School of Medicine, New Haven, CT.)

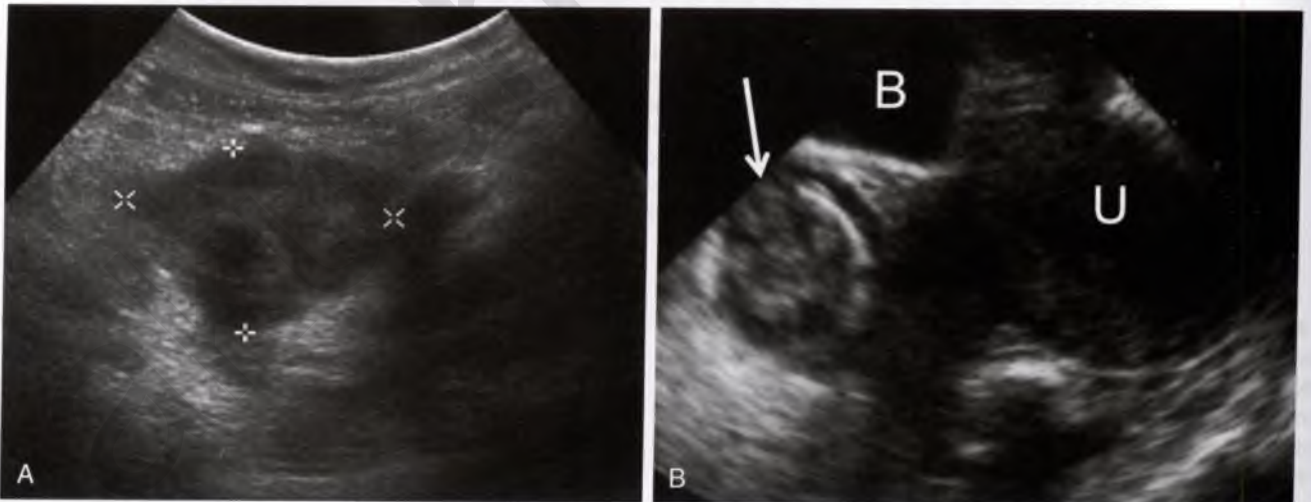


**FIG 33-31** First trimester abdominal ectopic pregnancies. **A**, Transabdominal scan of the left flank just below the kidney in the region of patient's pain shows a very early gestational sac with an ill-defined echogenic rim surrounded by heterogeneous hypoechoic hematoma (calipers), found to be an intraperitoneal or abdominal ectopic pregnancy. **B**, Transvaginal longitudinal scan of the pelvis in another patient shows the head of a 12-week fetus (arrow) far apart from the retroverted/retroflexed uterus (U) and posterior to the maternal urinary bladder (B). The uterus is displaced deep into the cul-de-sac by the developing extrauterine ectopic pregnancy. (A from Bryan-Rest LL, Scutt LM: Ectopic pregnancy. In Fielding JR, Brown DL, Thurmond AS (eds): Gynecologic Imaging. Philadelphia, Elsevier, 2011, p 344, Fig. 22-14B, used with permission.)



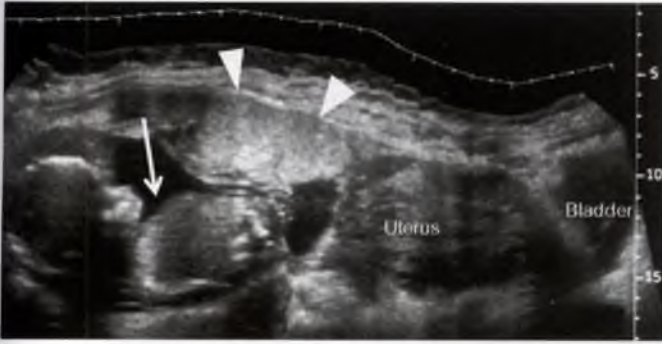


**FIG 33-32** Abdominal pregnancy. Transabdominal longitudinal extended field of view ultrasound image of the abdomen and pelvis of a woman with a term fetus (*arrow*) located in an amniotic sac located well above the uterine fundus. Surgery was performed and resulted in delivery of a live, healthy newborn. Placental tissue is located anteriorly (*arrowheads*) implanted into the peritoneum of the anterior abdominal wall. (From TheFetus.net, used with permission.)

particularly if gestational age is estimated to be longer than 6 weeks and if, based on clinical findings, miscarriage seems unlikely.<sup>107</sup> MRI may be helpful to search for an unusual location of an EP, and in a woman with unexplained hemorrhage, CT scan of the abdomen and pelvis with intravenous contrast may help identify a ring of vessels within the hematoma, which is characteristic of a gestational sac (Fig. 33-33B and C).

### CHRONIC ECTOPIC PREGNANCY

Chronic EP is a form of tubal pregnancy that manifests as a persistent adnexal mass. Active trophoblastic tissue involutes and the wall of the fallopian tube gradually disintegrates. Repeated small hemorrhages create a pelvic hematocele, which is often walled off by adhesions resulting from an inflammatory response. Symptoms are nonspecific, and usually there is a protracted clinical course. Patients complain of persistent, mild pelvic or lower abdominal pain, and rarely dyspareunia or anal pain during defecation. A woman may have missed a period or had either mild irregular or prolonged vaginal bleeding. A tender

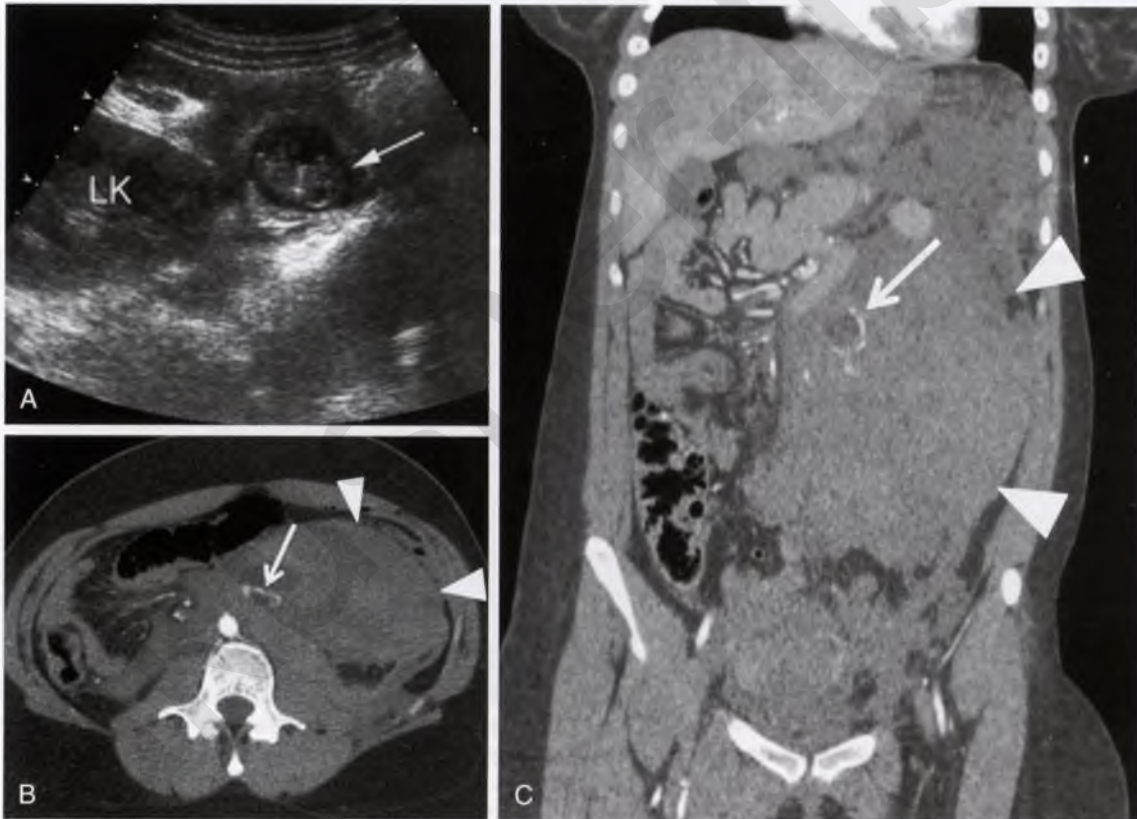


**FIG 33-33** Retroperitoneal ectopic pregnancies located inferior to the left kidney. **A**, Transabdominal coronal image of the left kidney (LK) shows an ectopic gestational sac (*arrow*) containing a live embryo located in the retroperitoneum inferior to the left kidney. **B**, Axial computed tomography (CT) angiogram image through the midabdomen of a second patient with human chorionic gonadotropin level of 28,000 mIU/mL, pregnancy of unknown location (PUL), and dropping hematocrit shows a large left retroperitoneal hematoma (*arrowheads*) and a small cluster of vessels (*arrow*). **C**, Coronal CT angiogram image of the same patient as in B shows the large left retroperitoneal hematoma (*arrowheads*) and a ring of vessels (*arrow*) in the region of the left renal vein. Surgery was performed, and the hematoma was evacuated. The pathologic specimen identified chorionic villi within the blood clot, consistent with retroperitoneal ectopic pregnancy. It is theorized that the ectopic pregnancy migrated cephalad along the course of the left ovarian vein and implanted near the confluence of the left ovarian and left renal veins. (A from Lee JW, Sohn KM, Jung HS: Retroperitoneal ectopic pregnancy. *AJR Am J Roentgenol* 184:1601, 2005, Fig. 1B, used with permission.)



adnexal mass may be palpable. The serum hCG level may be negative or very low. A nonspecific, heterogeneous adnexal mass will be identified on imaging. The natural progression of a chronic EP includes spontaneous resolution, persistence, or rupture.<sup>108</sup> Surgery is often performed for diagnostic purposes, and only when degenerated villi are identified on histologic examination is the definitive diagnosis made.<sup>109,110</sup>

## POSTHYSTERECTOMY ECTOPIC PREGNANCY

Posthysterectomy EPs are the rarest of the unusual EPs. They have been reported after both total and supracervical hysterectomy and may be tubal, ovarian, or abdominal in location.<sup>111</sup> A successful pregnancy following total hysterectomy resulting in a healthy 36-week infant delivered by laparotomy has been reported. In this case, hysterectomy was performed 3 days after coitus resulting in an abdominal pregnancy.<sup>112</sup> Posthysterectomy EPs can be divided into two groups: those presenting early after hysterectomy and those presenting late. In the early type, authors postulate that a fertilized ovum was likely present in the fallopian tube at the time of hysterectomy and spilled into the peritoneal cavity during or immediately after surgery. This type of EP can be avoided if precautions are taken to prevent pregnancy or by pregnancy testing prior to performing a hysterectomy in a sexually active woman of reproductive age. In the late presentation type, which is less common, the EP presents months to years after surgery.<sup>113</sup> Such cases may result from a fistula between the vagina or cervical stump and the peritoneal cavity or fallopian tube, allowing sperm access to an ovum. Impeccable surgical technique and prevention of postoperative pelvic hematomas and infection are the best means of preventing this type of EP.<sup>114</sup>

Patients may present acutely or subacutely with pelvic pain or signs of peritonitis with or without vaginal bleeding. Symptoms are nonspecific and similar to those from pelvic hematoma or infection. Diagnosis depends on obtaining an hCG level. The diagnosis is usually delayed, as the condition is so unexpected in a woman who has undergone hysterectomy. Unfortunately, delay in diagnosis can lead to rupture and hemodynamic instability. Therefore, if at least one ovary has been retained, a pregnancy test should be performed in a woman of reproductive age status posthysterectomy who presents with abdominal/pelvic pain of unknown origin. MRI can be very helpful not only in demonstrating the ectopic gestation, but also in delineating the fistulous tract.

## HETEROTOPIC PREGNANCIES

The incidence of coexistent intrauterine and ectopic pregnancies (Fig. 33-34) in the general population has increased in recent years from an original estimation of 1 in 30,000 pregnancies to 1 in 4000 pregnancies, according to more recent data.<sup>43,115</sup> Risk factors include all those reported for EP and are additive. The risk of heterotopic pregnancies is particularly high for women undergoing ovulation induction or IVF-ET, in whom the incidence has been reported to be as high as 1 in 100<sup>43,44</sup> (Fig. 33-34E and F). The risk increases with the number of embryos transferred, with incidence reported to be as high as 1 in 45 pregnancies if more than four embryos are transferred.

Heterotopic pregnancies remain a diagnostic and therapeutic challenge.<sup>116</sup> Talbot and coworkers<sup>117</sup> found that in 33% of cases, identification of the normal coexistent IUP gave a false assurance that an EP was unlikely and the heterotopic pregnancy was missed with resultant delay in diagnosis. Hence, heightened clinical suspicion, particularly in patients who have undergone ART, is crucial. The presence of an intrauterine gestation with a coexistent extrauterine gestational sac is

diagnostic, whereas an IUP with an adnexal mass, with or without pain and fluid in the cul-de-sac, is concerning. Note that without a good complete clinical history, these findings are much more likely to be misinterpreted as hemoperitoneum due to a ruptured corpus luteum. Persistent pain or increasing hCG levels following spontaneous miscarriage, evacuation of residual products of conception, or elective abortion should raise suspicion of heterotopic pregnancy.

Local injection of KCl or surgical removal of the ectopic gestation allows the IUP to proceed to term in most cases. MTX should be avoided because of the potential risk to the IUP if the pregnancy is desired. Overall, the prognosis for the IUP is good, and approximately 66% of these pregnancies go to term.

## MANAGEMENT AND TREATMENT OPTIONS

Treatment of EP includes surgical, medical, combination, and expectant options. Management depends heavily on imaging features including the size of the ectopic sac, presence of cardiac activity, location, and evidence of tubal rupture or hemoperitoneum. The patient's clinical condition, including hemodynamic stability and comorbid medical conditions, as well as compliance for follow-up are also important factors.

In general, laparotomy and salpingectomy have been replaced with less aggressive surgical approaches utilizing minimally invasive surgery to preserve fertility, such as laparoscopic or hysteroscopic resection of the EP, linear salpingostomy, salpingoscopic removal of the ectopic gestational sac, or even manually milking the gestational sac from the fallopian tube. Laparoscopy is the current standard surgical approach. Laparoscopy is rarely required for diagnosis, but occasionally is helpful in finding an EP when a pregnancy cannot be found on ultrasound imaging (PUL) but the serum hCG level continues to rise. The benefits of laparoscopic surgery compared to laparotomy include lower incidence of postoperative adhesions, less blood loss, and faster recovery. However, laparotomy may still be required if the EP cannot be visualized laparoscopically (usually because of dense adhesions or scar tissue) or in patients who are hemodynamically unstable or who have large EPs of advanced gestational age or interstitial EPs. Wedge resection of an EP located within the myometrium, such as an interstitial or cesarean delivery scar EP, is often performed, in part to repair the underlying myometrial defect to prevent recurrent EPs. In cases of ovarian EPs, wedge resection rather than oophorectomy will help to ensure future fertility. In current practice, hysterectomy is considered a last resort, usually in the setting of uncontrollable hemorrhage.

Medical therapy with systemic MTX is often successful in the treatment of EPs. To determine whether a patient is a candidate for systemic MTX therapy, certain criteria must be met. The patient must be hemodynamically stable without signs or symptoms of active bleeding. Hence, ultrasound examination is extremely important in patient management because the ultrasound finding of extensive hemoperitoneum, which suggests tubal rupture, is a contraindication for MTX therapy and will prompt surgical intervention. The maximal diameter of the ectopic mass should not exceed 3.5 to 5 cm, and no embryonic cardiac activity should be identified. Another relative contraindication to the use of systemic MTX is a serum hCG level higher than 10,000 to 15,000 IU/L. In general, the smaller the EP and the lower the serum hCG level, the more likely that a single dose of MTX will be successful. However, these criteria are not absolute. Various medical disorders are also contraindications to the use of MTX, such as known hypersensitivity to MTX; hepatic, renal, or pulmonary diseases; blood dyscrasias; and immunodeficiency disorders. The patient must be reliable and educated to return for follow-up if signs or symptoms of delayed hemorrhage or rupture develop.



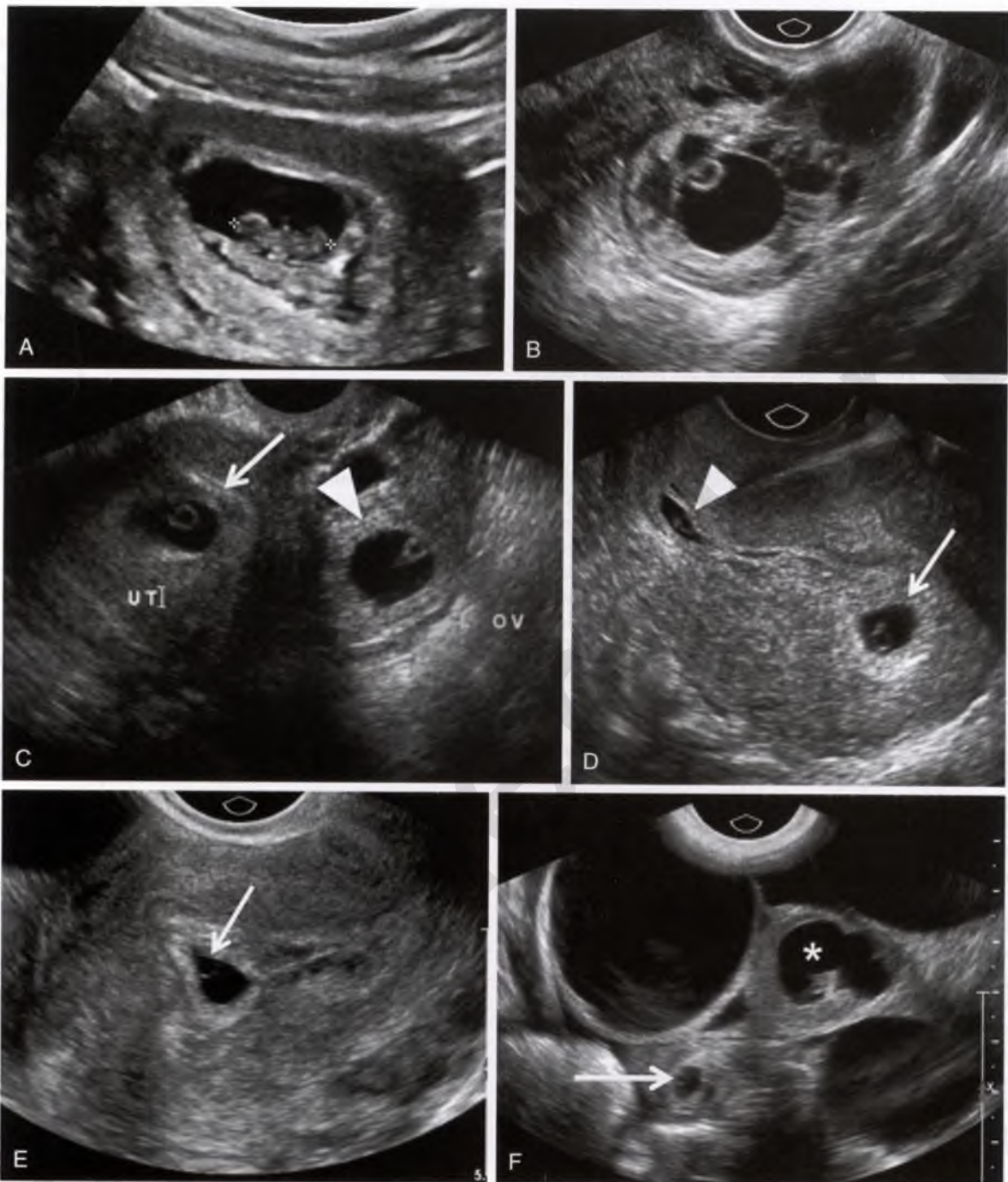


**FIG 33-34** Heterotopic pregnancies. **A**, Transabdominal sagittal scan of the uterus shows a gestational sac containing an embryo (*calipers*). Cardiac motion was observed. **B**, Transvaginal scan of the left adnexa of the same patient as in **A** shows an ectopic pregnancy containing a yolk sac, representing heterotopic pregnancies. The patient had undergone assisted reproductive techniques. **C**, Transvaginal transverse scan of the uterus (UT) and left adnexa (ov) from another patient shows an intrauterine gestational sac (*arrow*) and an ectopic pregnancy in the left adnexa (*arrowhead*), both containing yolk sacs. **D**, Transvaginal longitudinal scan of a retroverted/retroflexed uterus from a third patient shows an intrauterine gestational sac (*arrow*) as well as an ectopic cervical pregnancy (*arrowhead*). Both sacs contain yolk sacs and adjacent tiny embryos. **E**, Transvaginal transverse scan of the uterus of a fourth patient who underwent ovulation induction therapy shows an intrauterine gestational sac containing a yolk sac (*arrow*). **F**, Transvaginal transverse scan of the right adnexa in the same patient as in **E** shows a small ectopic pregnancy with a yolk sac (*arrow*) among several large ovarian cysts due to ovarian hyperstimulation syndrome. One cyst contains clumped echoes indicating blood (*asterisk*). Heterotopic ectopic pregnancies may be difficult to find among multiple ovarian cysts in patients with enlarged ovaries following ovulation induction. (**E** and **F** from Scutt LM, Hamper UM, Angtuaco T: *Ultrasound*. New York, Oxford University Press, 2016 (in press). Used with permission.)



Ultrasound evaluation can serve a role in the follow-up of patients after MTX therapy. Approximately 35% to 60% of patients will present with pelvic pain on days 3 through 7 following administration of MTX because of infarction of the trophoblastic tissue. These patients need to be carefully evaluated with vital signs, hematocrit, and follow-up sonographic examination to assess for interval development of hemoperitoneum to determine if delayed rupture has occurred. If the patient's pain is due to tissue infarction, the pain should resolve within 24 to 48 hours. Following MTX therapy, an adnexal mass may still be seen, and it generally takes longer for the EP to resolve on sonographic imaging than for the serum hCG level to fall to zero. Slight growth of the EP with persistence of color Doppler blood flow is considered within normal limits provided that the hCG level is dropping. However, continued progression of the EP such as development of a sonographically visible yolk sac, embryo, or cardiac activity not previously noted is considered indicative of treatment failure.<sup>118</sup>

Ultrasound-guided direct injection of MTX or KCl into the ectopic sac is another therapeutic option. Direct injection of MTX is believed to destroy the embryo and to infarct the surrounding trophoblastic tissue. A combination of direct intra-amniotic injection of MTX and systemic intramuscular injection is used in selected cases, and a combination of medical and surgical treatment is often indicated in cesarean scar, cervical, and interstitial EPs because of the increased risk of hemorrhage or recurrence. Uterine artery ligation, uterine artery embolization, and balloon tamponade are used adjunctively to control hemorrhage in some cases.

Expectant management of EPs without intervention is increasing. First trimester EPs may resolve spontaneously, and some asymptomatic women with EPs have been successfully followed with serial hCG levels until the level drops to zero. However, patients must be followed closely and advised to immediately return if symptoms of rupture develop, as cases of delayed rupture with hCG levels close to zero have been reported.

Another issue related to medical management of women with EP is treatment of the Rh-negative woman with a first trimester pregnancy loss. It is recommended that providers should administer anti-D immunoglobulin to Rh-negative women in all cases of documented first trimester loss of an established pregnancy, which includes complete abortion and EP.<sup>119,120</sup>

When it is difficult to differentiate between an EP and a failing IUP and follow-up ultrasound examination is nondiagnostic, D&C can be helpful by determining the presence or absence of trophoblastic tissue within the endometrium.<sup>27</sup>

## CONCLUSION

As patients present earlier for diagnosis, clinicians are requesting earlier ultrasound examinations to discriminate between intrauterine and ectopic pregnancies, and in many cases the location of the pregnancy cannot initially be determined. Hence, follow-up serologic testing and TVS are important for management of patients with PULs. Accurate diagnosis and demonstration of EPs are important because management decisions often depend upon size, gestational age, presence or absence of embryonic cardiac activity, and exact location of the EP. In addition, it should be noted that the incidence of EPs, including those in unusual locations, and heterotopic pregnancies is increasing—particularly in patients undergoing ART. Thus, the presence of an IUP does not completely exclude the possibility of a concomitant EP. Furthermore, EPs in unusual locations that historically presented at an advanced gestational age with increased risk of significant hemorrhage are now more likely to be diagnosed earlier, sometimes at screening sonograms when the patient is asymptomatic,

conferring lower risk of uterine rupture and hemodynamic instability. The characteristic imaging features of these unusual ectopic pregnancies have been described, and the management and treatment protocols have evolved. Sonographic evaluation continues to serve an important role in the diagnosis, therapeutic triage, and follow-up of patients with EPs.

## REFERENCES

- Centers for Disease Control and Prevention (CDC): Ectopic pregnancy—United States, 1990-1992. *MMWR Morb Mortal Wkly Rep* 44:46-48, 1995.
- Zane SB, Kieke BA, Jr, Kendrick JS, Bruce C: Surveillance in a time of changing health care practices: estimating ectopic pregnancy incidence in the United States. *Matern Child Health J* 6:227-236, 2002.
- Creanga AA, Shapiro-Mendoza CK, Bish CL, et al: Trends in ectopic pregnancy mortality in the United States: 1980-2007. *Obstet Gynecol* 117(4):837-843, 2011.
- Hoover KW, Tao G, Kent CK: Trends in the diagnosis and treatment of ectopic pregnancy in the United States. *Obstet Gynecol* 115:495-502, 2010.
- Bohm-Velez M, Mendelson EB, Freimanis MG: Transvaginal sonography in evaluating ectopic pregnancy. *Semin Ultrasound CT MR* 11(1):44-58, 1990.
- Lozeau AM, Potter B: Diagnosis and management of ectopic pregnancy. *Am Fam Physician* 72:1707-1714, 2005.
- Peterson H, Xia Z, Hughes J, et al: The risk of ectopic pregnancy after tubal sterilization. *N Engl J Med* 336:762-767, 1997.
- Strandell A, Thorburn J, Hamberger L: Risk factors for ectopic pregnancy in assisted reproduction. *Fertil Steril* 71:282-286, 1999.
- Barnhart KT: Ectopic pregnancy. *N Engl J Med* 361:379-387, 2009.
- Xiong X, Buekens P, Wollast E: IUD use in the risk of ectopic pregnancy: meta-analysis of case-control studies. *Contraception* 52(1):23-34, 1995.
- Coste J, Job-Spira N, Fernandez H: Increased risk of ectopic pregnancy with maternal cigarette smoking. *Am J Public Health* 81(2):199-201, 1991.
- Bouyer J, Coste J, Shojaei T, et al: Risk factors for ectopic pregnancy: a comprehensive analysis based on a large case-control, population-based study in France. *Am J Epidemiol* 157(3):185-194, 2003.
- Bogdanskiene G, Berlingieri P, Grudzinskas JG: Association between ectopic pregnancy and pelvic endometriosis. *Int J Gynaecol Obstet* 92:157-158, 2006.
- Bouyer J, Coste J, Fernandez H, et al: Sites of ectopic pregnancy: a 10 year population-based study of 1800 cases. *Hum Reprod* 17:3224-3230, 2002.
- Green LK, Kott ML: Histopathologic findings in ectopic tubal pregnancy. *Int J Gynecol Pathol* 8(3):255-262, 1989.
- Djahanbakhch O, Ezzati M, Saridogan E: Physiology and pathophysiology of tubal transport: ciliary activity and muscular contractility, relevance to tubal infertility, recent research, and future directions. In Ledger WL, Tan SL, Bahathiq AOS, editors: *The Fallopian Tube in Infertility and IVF Practice*, New York, 2010, Cambridge University Press, pp 18-29.
- Kutluay L, Vicdan K, Turan C, et al: Tubal histopathology in ectopic pregnancies. *Eur J Obstet Gynecol Reprod Biol* 57:91-94, 1994.
- Goddijn M, van der Veen F, Schuring-Bloom GH, et al: Cytogenetic characteristics of ectopic pregnancy. *Hum Reprod* 11:2769-2771, 1996.
- Tay JI, Moore J, Walker JJ: Ectopic pregnancy. *BMJ* 320:916-919, 2000.
- Frates MC, Doubilet PM, Peters HE, et al: Adnexal sonographic findings in ectopic pregnancy and their correlation with tubal rupture and HCG levels. *J Ultrasound Med* 33:697-703, 2014.
- Chard T: Pregnancy tests: a review. *Hum Reprod* 7(5):701-710, 1992.
- Hochner-Celnikier D, Ron M, Goshen R, et al: Rupture of ectopic pregnancy following disappearance of serum beta subunit hCG. *Obstet Gynecol* 79:826-827, 1992.
- Mehta TS, Levine D, Beckwith B: Treatment of ectopic pregnancy: is a human chorionic gonadotropin level of 2,000 mIU/ml a reasonable threshold? *Radiology* 205:569-573, 1997.



24. Condous G, Kirk E, Lu C, et al: Diagnostic accuracy of varying discriminatory zones for the prediction of ectopic pregnancy in women with a pregnancy of unknown location. *Ultrasound Obstet Gynecol* 26:770–775, 2005.
25. Doubilet PM, Benson CB, Bourne T, et al: Diagnostic criteria for nonviable pregnancy early in the first trimester. *N Engl J Med* 369:1443–1451, 2013.
26. Doubilet PM, Benson CB: Further evidence against the reliability of the human chorionic gonadotropin discriminatory level. *J Ultrasound Med* 30:1637–1642, 2011.
27. Practice Committee of American Society for Reproductive Medicine: Medical treatment of ectopic pregnancy. *Fertil Steril* 90(5 Suppl): S206–S212, 2008.
28. Barnhart KT, Sammel MD, Rinaudo PF, et al: Symptomatic patients with an early viable intrauterine pregnancy: HCG curves redefined. *Obstet Gynecol* 104:50–55, 2004.
29. American College of Obstetricians and Gynecologists: ACOG Practice Bulletin No. 94: medical management of ectopic pregnancy. *Obstet Gynecol* 111:1479–1485, 2008.
30. Dillon KE, Sioulas VD, Sammel MD, et al: How and when human chorionic gonadotropin curves in women with an ectopic pregnancy mimic other outcomes: differences by race and ethnicity. *Fertil Steril* 98:911–916, 2012.
31. Barnhart K, Sammel MD, Chung K, et al: Decline of serum human chorionic gonadotropin and spontaneous complete abortion: defining the normal curve. *Obstet Gynecol* 104:975–981, 2004.
32. Barnhart K, van Mello NM, Bourne T, et al: Pregnancy of unknown location: a consensus statement of nomenclature, definitions and outcome. *Fertil Steril* 95:857–866, 2011.
33. Banerjee S, Aslam N, Zosmer N, et al: The expectant management of women with early pregnancy of unknown locations. *Ultrasound Obstet Gynecol* 14:231–236, 1999.
34. Kirk E, Bourne T: Predicting outcomes in pregnancies of unknown location. *Womens Health* 4(5):491–499, 2008.
35. Condous G, Timmerman D, Goldstein S, et al: Pregnancies of unknown location: consensus statement. *Ultrasound Obstet Gynecol* 28:121–122, 2006.
36. Saxon D, Falcone T, Mascha EJ, et al: A study of ruptured tubal ectopic pregnancy. *Obstet Gynecol* 90:46–49, 1997.
37. Galstyan K, Kurzel R: Serum beta-hCG titers do not predict ruptured pregnancy. *Int J Fertil Womens Med* 51(1):14–16, 2006.
38. Attar E: Endocrinology of ectopic pregnancy. *Obstet Gynecol Clin North Am* 31:779–794, 2004.
39. Seeber BE, Barnhart KT: Suspected ectopic pregnancy. *Obstet Gynecol* 107:399–413, 2006.
40. Senapati S, Barnhart KT: Biomarkers for ectopic pregnancy and pregnancy of unknown location. *Fertil Steril* 99(4):1107–1116, 2013.
41. Rausch ME, Sammel MD, Takacs P, et al: Development of a multiple marker test for ectopic pregnancy. *Obstet Gynecol* 117:573–582, 2011.
42. Benacerraf BR: Filling of the bladder for pelvic sonograms: an ancient form of torture. *J Ultrasound Med* 22:239–241, 2003.
43. Maymon R, Shulman A: Controversies and problems in the current management of tubal pregnancy. *Hum Reprod Update* 2:541–551, 1996.
44. Svare J, Norup P, Grove Thomsen S, et al: Heterotopic pregnancies after in-vitro fertilization and embryo transfer: a Danish survey. *Hum Reprod* 8:116–118, 1993.
45. Ellaithy M, Abdelaziz A, Hassan MF: Outcome prediction in pregnancies of unknown location using endometrial thickness measurement: is this of real clinical value? *Eur J Obstet Gynecol Reprod Biol* 168:68–74, 2013.
46. Yeh HC, Goodman JD, Carr L, et al: Intradecidual sign: an US criterion of early intrauterine pregnancy. *Radiology* 161:463–467, 1986.
47. Ackerman TE, Levi CS, Lyons EA, et al: Decidual cyst: transvaginal sonographic sign of ectopic pregnancy. *Radiology* 189(3):727–731, 1993.
48. Chiang G, Levine D, Swire M, et al: The intradecidual sign: is it reliable for diagnosis of early intrauterine pregnancy? *AJR Am J Roentgenol* 183:725–731, 2004.
49. Laing FC, Brown DL, Price JF, et al: Intradecidual sign: is it effective in diagnosis of an early intrauterine pregnancy? *Radiology* 204:655–660, 1997.
50. Levine D: Ectopic pregnancy. *Radiology* 245(2):385–397, 2007.
51. Nyberg DA, Laing FC, Filly RA, et al: Ultrasonographic differentiation of the gestational sac of early intrauterine pregnancy from the pseudogestational sac of ectopic pregnancy. *Radiology* 146:755–759, 1983.
52. Benson CB, Doubilet PM, Peters HE, et al: Intrauterine fluid with ectopic pregnancy. *J Ultrasound Med* 32:389–393, 2013.
53. Doubilet PM, Benson CB: First do no harm ... to early pregnancies. *J Ultrasound Med* 29:685–689, 2010.
54. Doubilet PM, Benson CB: Double sac sign and intradecidual sign in early pregnancy. *J Ultrasound Med* 32:1207–1214, 2013.
55. Brown DL, Doubilet PM: Transvaginal sonography for diagnosing ectopic pregnancy: positive criteria and performance characteristics. *J Ultrasound Med* 13:259–266, 1994.
56. Subramanyam BR, Raghavendra BN, Balthazar EJ, et al: Hematosalpinx in tubal pregnancy: sonographic-pathologic correlation. *AJR Am J Roentgenol* 141:361–365, 1983.
57. Benacerraf BR, Parker-Jones K, Schiff I: Decidual cast mimicking an intrauterine gestational sac and fetal pole in a patient with ectopic pregnancy. *J Reprod Med* 29:498–500, 1984.
58. Blavias M, Lyon M: Reliability of adnexal mass mobility in distinguishing possible ectopic pregnancy from corpus luteum cysts. *J Ultrasound Med* 24:599–603, 2005.
59. Frates MC, Visweswaran A, Laing FC: Comparison of tubal ring and corpus luteum echogenicities: a useful differentiating characteristic. *J Ultrasound Med* 20:27–31, 2001.
60. Stein MW, Ricci ZJ, Novak L, et al: Sonographic comparison of the tubal ring of ectopic pregnancy with the corpus luteum. *J Ultrasound Med* 23:57–62, 2004.
61. Pellerito JS, Troiano RN, Quedens-Case C, et al: Common pitfalls of endovascular color Doppler flow imaging. *Radiographics* 15:37–47, 1995.
62. Molinaro TA, Barnhart KT: Ectopic pregnancies in unusual locations. *Semin Reprod Med* 25(2):123–130, 2007.
63. Agarwal SK, Wisot AL, Garzo G, et al: Cornual pregnancies in patients with prior salpingectomy undergoing in vitro fertilization and embryo transfer. *Fertil Steril* 65:659–660, 1996.
64. Grabor EA: Surgery of the uterus in pregnancy. In Barber AR, Grabor EA, editors: *Surgical Diseases in Pregnancy*, Philadelphia, 1974, WB Saunders, p 390.
65. Jansen RP, Elliott PM: Angular intrauterine pregnancy. *Obstet Gynecol* 58:167–175, 1981.
66. Jansen R, Elliott P: Angular and interstitial pregnancies should not be called “cornual.” *Aust N Z J Obstet Gynaecol* 23(2):123–124, 1983.
67. Mavrelou D, Sawyer E, Helmy S, et al: Ultrasound diagnosis of ectopic pregnancy in the non-communicating horn of a unicornuate uterus (cornual pregnancy). *Ultrasound Obstet Gynecol* 30:765–770, 2007.
68. Jafri SZH, Loginsky SJ, Bouffard JA, et al: Sonographic detection of interstitial pregnancy. *J Clin Ultrasound* 15(4):253–257, 1987.
69. Ackerman TE, Levi CS, Dashefsky SM, et al: Interstitial line: sonographic finding in interstitial (cornual) ectopic pregnancy. *Radiology* 189:83–87, 1993.
70. Tarim E, Ulusan S, Kilicdag E, et al: Angular pregnancy. *J Obstet Gynaecol Res* 30:377–379, 2004.
71. Tanaka Y, Mimura K, Kanagawa T, et al: Three-dimensional sonography in the differential diagnosis of interstitial, angular, and intrauterine pregnancies in a septate uterus. *J Ultrasound Med* 33:2031–2035, 2014.
72. Rankin MB, Dunning A, Arleo EK: Angular pregnancy: a review of cases reported in the literature in the past 80 years. *Obstet Gynecol Cases Rev* 1:3, 2014.
73. Sherer DM, Stimphil R, Hellman M, et al: Transvaginal sonographic findings of isolated intramural uterine choriocarcinoma mimicking an interstitial pregnancy. *J Ultrasound Med* 25:791–794, 2006.
74. Timor-Tritsch IE, Monteagudo A, Matera C, et al: Sonographic evolution of cornual pregnancies treated without surgery. *Obstet Gynecol* 79:1044–1049, 1992.



75. Monteagudo A, Miniur VK, Stephenson C, et al: Nonsurgical management of live ectopic pregnancy with ultrasound-guided local injection: a case series. *Ultrasound Obstet Gynecol* 25:282–288, 2005.
76. Dilbaz S, Katas B, Demir B, Dilbaz B: Treating cornual pregnancy with a single methotrexate injection: a report of 3 cases. *J Reprod Med* 50:141–144, 2005.
77. Barnhart K, Spandorfer S, Coutifaris C: Medical treatment of interstitial pregnancy: a report of three unsuccessful cases. *J Reprod Med* 42:521–524, 1997.
78. Zalel Y, Caspi B, Insler V: Expectant management of interstitial pregnancy. *Ultrasound Obstet Gynecol* 4:238–240, 1994.
79. Nahum GG: Rudimentary horn pregnancy: the 20th century worldwide experience of 588 cases. *J Reprod Med* 47:151–163, 2002.
80. Tsafirir A, Rojansky N, Sela HY, et al: Rudimentary horn pregnancy. *J Ultrasound Med* 24:219–223, 2005.
81. Laughlin CL, Lee TG, Richards RC: Ultrasonographic diagnosis of cervical ectopic pregnancy. *J Ultrasound Med* 2:137–138, 1983.
82. Jurkovic D, Hackett E, Campbell S: Diagnosis and treatment of early cervical pregnancy: a review and a report of two cases treated conservatively. *Ultrasound Obstet Gynecol* 8:373–380, 1996.
83. Leeman LM, Wendland CL: Cervical ectopic pregnancy. *Arch Fam Med* 9:72–77, 2000.
84. Benson CB, Doubilet PM: Strategies for conservative treatment of cervical ectopic pregnancy. *Ultrasound Obstet Gynecol* 8:371–372, 1996.
85. Hung TH, Shau WY, Hsieh TT, et al: Prognostic factors for an unsatisfactory primary methotrexate treatment of cervical ectopic pregnancy: a quantitative review. *Hum Reprod* 13(9):2636–2642, 1998.
86. McKenna DA, Poder L, Goldman M, et al: Role of sonography in the recognition, assessment, and treatment of cesarean scar ectopic pregnancies. *J Ultrasound Med* 27:779–783, 2008.
87. Jurkovic D, Hillaby K, Woelfer B, et al: First-trimester diagnosis and management of pregnancies implanted into the lower uterine segment Cesarean section scar. *Ultrasound Obstet Gynecol* 21:220–227, 2003.
88. Osborn DA, Williams TR, Craig BM: Cesarean scar pregnancy: sonographic and magnetic resonance imaging findings, complications, and treatment. *J Ultrasound Med* 31:1449–1456, 2012.
89. Maymon R, Halperin R, Mendlovic S, et al: Ectopic pregnancies in Cesarean section scars: the 8 year experience of one medical centre. *Hum Reprod* 19:278–284, 2004.
90. Fylstra DL: Ectopic pregnancy within a cesarean scar: a review. *Obstet Gynecol Surv* 57:537–543, 2002.
91. Michaels AY, Washburn EE, Pocius KD, et al: Outcome of Cesarean scar pregnancies diagnosed sonographically in the first trimester. *J Ultrasound Med* 34:595–599, 2015.
92. Timor-Tritsch IE, Khatib N, Monteagudo A, et al: Cesarean scar pregnancies. *J Ultrasound Med* 34:601–610, 2015.
93. Vial Y, Petignat P, Hohlfield P: Pregnancy in a cesarean scar. *Ultrasound Obstet Gynecol* 16:592–593, 2000.
94. Yang MJ, Jeng MH: Combination of transarterial embolization of uterine arteries and conservative surgical treatment for pregnancy in a cesarean section scar. A report of 3 cases. *J Reprod Med* 48:213–216, 2003.
95. Rotas MA, Haberman S, Levgr M: Cesarean scar ectopic pregnancies: etiology, diagnosis, and management. *Obstet Gynecol* 107:1373–1381, 2006.
96. Raziell A, Mordechai E, Schachter M, et al: A comparison of the incidence, presentation, and management of ovarian pregnancies between two periods of time. *J Am Assoc Gynecol Laparosc* 11(2):191–194, 2004.
97. Yovich JL, Turner SR, Murphy AJ: Embryo transfer technique as a cause of ectopic pregnancies in in-vitro fertilization. *Fertil Steril* 44:318–321, 1985.
98. Comstock C, Huston K, Lee W: The ultrasonographic appearance of ovarian ectopic pregnancies. *Obstet Gynecol* 105:42–45, 2005.
99. Ghi T, Banfi A, Marconi R, et al: Three-dimensional sonographic diagnosis of ovarian pregnancy. *Ultrasound Obstet Gynecol* 26:102–104, 2005.
100. Atrash HK, Friede A, Hogue C: Abdominal pregnancy in the United States: frequency and maternal mortality. *Obstet Gynecol* 9:333–337, 1987.
101. Cormio G, Santamato S, Vimercati A, et al: Primary splenic pregnancy. *J Reprod Med* 48(6):479–481, 2003.
102. Delabrousse E, Site O, Le Mouel A, et al: Intrahepatic pregnancy: sonography and CT findings. *AJR Am J Roentgenol* 173:1377–1378, 1999.
103. Martin JN, Sessums JK, Martin RW, et al: Abdominal pregnancy: current concepts of management. *Obstet Gynecol* 71:549–557, 1988.
104. Lee JW, Sohn KM, Jung HS: Retroperitoneal ectopic pregnancy: a case report. *AJR Am J Roentgenol* 184:1600–1601, 2005.
105. Ferland RJ, Chadwick DA, O'Brien JA, et al: An ectopic pregnancy in the upper retroperitoneum following in vitro fertilization and embryo transfer. *Obstet Gynecol* 78:544–546, 1991.
106. Hall JS, Harris M, Levy RC, et al: Retroperitoneal ectopic pregnancy. *J Obstet Gynaecol Br Commonw* 80(1):92–94, 1973.
107. Martinez-Varea A, Hidalgo-Mora JJ, Paya V, et al: Retroperitoneal ectopic pregnancy after intrauterine insemination: case report. *Fertil Steril* 95(7):2433, 2011.
108. Brennan DF, Kwatra S, Kelly M, et al: Chronic ectopic pregnancy: two cases of acute rupture despite negative BhCG. *J Emerg Med* 19:249–254, 2000.
109. Bedi DG, Fagan CJ, Nocera RM: Chronic ectopic pregnancy. *J Ultrasound Med* 3:347–352, 1984.
110. Ugur M, Turan C, Vicdan K, et al: Chronic ectopic pregnancy: a clinical analysis of 62 cases. *Aust N Z J Obstet Gynaecol* 36(2):186–189, 1996.
111. Fylstra DL: Ovarian ectopic pregnancy 6 years after supracervical hysterectomy: a case report. *J Reprod Med* 54:649–651, 2009.
112. Jackson P, Barrowclough IW, France JT, et al: A successful pregnancy following total hysterectomy. *Br J Obstet Gynaecol* 87:353–355, 1980.
113. Fylstra DL: Ectopic pregnancy after hysterectomy: a review and insight into etiology and prevention. *Fertil Steril* 94:431–435, 2010.
114. Villegas E, Gonzalez-Mesa E, Benitez MJ, et al: Tubal ectopic pregnancy two years after laparoscopic supracervical hysterectomy. *BMC Womens Health* 14:69, 2014.
115. DeVoe RW, Pratt JH: Simultaneous intrauterine and extrauterine pregnancy. *Am J Obstet Gynecol* 56(6):1119–1126, 1948.
116. Barrenetxea G, Barinaga-Rementería L, Lopez de Larruzeta A, et al: Heterotopic pregnancy: two cases and a comprehensive review. *Fertil Steril* 87(2):417, 2007.
117. Talbot K, Simpson R, Price N, et al: Heterotopic pregnancy. *J Obstet Gynaecol* 31(1):7–12, 2011.
118. Bixby S, Tello R, Kuligowska E: Presence of a yolk sac on transvaginal sonography is the most reliable predictor of single-dose methotrexate treatment failure in ectopic pregnancy. *J Ultrasound Med* 24:591–598, 2005.
119. Hahn SA, Lavonas EJ, Mace SE, et al, from the American College of Emergency Physicians: Clinical policy: critical issues in the initial evaluation and management of patients presenting to the emergency department in early pregnancy. *Ann Emerg Med* 60:381–390, 2012.
120. American College of Obstetrics and Gynecology: Prevention of Rh D alloimmunization. ACOG Practice Bulletin No: 4, May 1999 (replaces educational Bulletin No: 147, October 1990). Clinical management guidelines for obstetrician-gynecologists. *Int J Gynaecol Obstet* 66(1):63–70, 1999.

# Gynecologic Sonography in the Pediatric and Adolescent Patient

Harriet J. Paltiel, Andrew Phelps

## SUMMARY OF KEY POINTS

- Reproductive tract anomalies may present at different stages of life. Most abnormalities of the external genitalia are obvious at birth, whereas obstructive and nonobstructive lesions of the reproductive tract may be evident at birth or present later during childhood, at puberty, in adolescence, or during adulthood.
- Sonography is used to determine the presence of a uterus and gonadal location in patients with ambiguous genitalia.
- In preadolescent girls with vaginal bleeding, sonography can be used to confirm or exclude a postpubertal appearance of the internal genitalia; to diagnose an estrogen-secreting adrenal or ovarian tumor; and to diagnose a vaginal foreign body or mass.
- In girls with primary amenorrhea, sonography is useful in determining the presence and morphologic appearance of the uterus and ovaries.
- Sonography is a key tool in evaluating pelvic pain in girls, including those with suspected appendicitis.
- In patients with adnexal torsion, the involved ovary is always significantly enlarged, with a median volume 12 times that of the normal contralateral ovary.
- Bleeding into an ovarian cyst in utero or after birth has a high association with long-term ovarian loss.
- Ovarian tumors in the pediatric population are usually benign, with cystic teratomas accounting for more than 90% of all benign ovarian tumors.

## OUTLINE

### Technique, 1001

### Normal Anatomy, 1002

### Normal Gonadal and Reproductive Tract Development, 1002

#### Gonads, 1003

#### External Genitalia and Reproductive Tract, 1003

### Structural Anomalies of the Reproductive Tract, 1004

### Ambiguous Genitalia, 1009

### Prepubertal Bleeding, 1011

#### Precocious Puberty, 1011

#### Vaginal Foreign Body, 1014

#### Vaginal Masses, 1014

### Primary Amenorrhea, 1015

### Pelvic Pain, 1018

#### Adnexal (Ovarian or Tubal) Torsion, 1018

#### Ovarian Cyst, 1018

#### Pelvic Inflammatory Disease, 1019

#### Ectopic Pregnancy, 1019

#### Acute Appendicitis, 1019

#### Genital Hernia, 1020

### Gynecologic Pelvic Masses, 1020

#### Ovarian Masses, 1020

#### Ovarian Tumors, 1020

#### Pregnancy, 1022

### Conclusion, 1022

The most frequent indications for gynecologic ultrasound imaging in the pediatric and adolescent patient are ambiguous genitalia, prepubertal vaginal bleeding, primary amenorrhea, pelvic pain, and pelvic mass. Sonography is the primary imaging modality used in the evaluation of these disorders, with magnetic resonance imaging (MRI) and computed tomography (CT) reserved for further delineation of congenital malformations or tumors.<sup>1-4</sup>

## TECHNIQUE

The pediatric vagina, uterus, and ovaries are best imaged with transabdominal ultrasound when the patient's bladder is full. All girls are

encouraged to drink fluids and not to void in the hour prior to imaging. Teenagers are asked to drink 16 ounces.

Curvilinear, sector, and linear-array ultrasound transducers are usually sufficient for most pelvic ultrasound examinations. In young girls with urogenital malformation, hydrometrocolpos, a labial mass, or anal atresia, a transperineal approach is often useful<sup>5,6</sup> (Fig. 34-1). A transvaginal approach is used to complement the transabdominal examination in sexually active adolescents. In the patient with a complex congenital anomaly, genitography performed with water-soluble contrast material along with ultrasound examination is frequently helpful in identifying and characterizing the vagina, urogenital sinus, or cloaca.



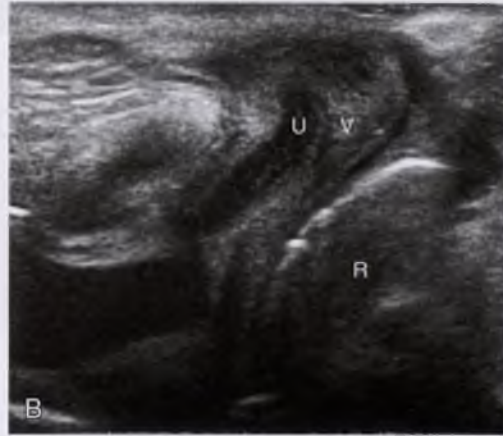
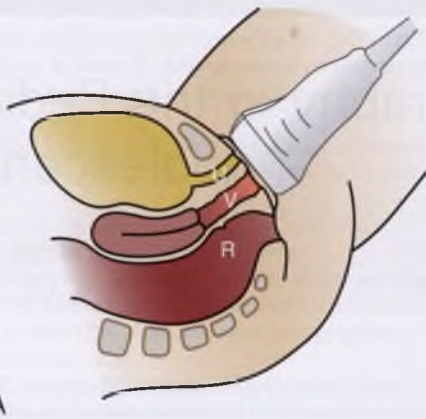


**FIG 34-1** Transducer placement and depiction of normal anatomy using perineal approach. **A**, Diagram demonstrates sagittal orientation of a linear-array transducer on the female perineum. **B**, Corresponding transperineal ultrasound image. R, rectum; U, urethra; V, vagina. (From Paltiel HJ, Phelps A: US of the pediatric female pelvis. *Radiology* 270(3):644-657, 2014, Fig. 1a, used with permission.)

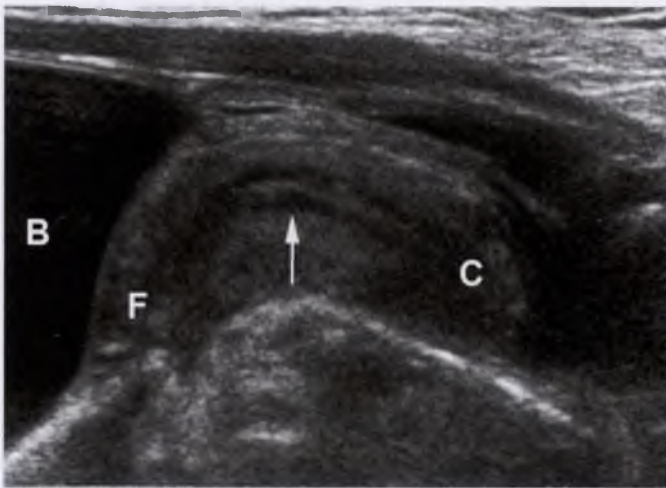


**FIG 34-2** Normal neonatal uterus. Sagittal ultrasound image shows a prominent uterine fundus (F) with echogenic endometrium surrounded by a hypoechoic halo (arrow). B, bladder; C, cervix.

## NORMAL ANATOMY

Uterine and ovarian size and shape are age-dependent and under hormonal influence. Maternal and placental hormonal stimulation lead to a relatively large neonatal uterus and ovaries compared to their size in later infancy, at which point they remain relatively stable in size until a growth spurt occurs at approximately 7 to 8 years of age<sup>7</sup> (Figs. 34-2 and 34-3). Mature ovarian follicles can be identified at all ages owing to the secretion of follicle-stimulating hormone (FSH).<sup>8,9</sup> The prepubertal cervix is greater than or equivalent in thickness to the uterine fundus, and the endometrium is relatively inconspicuous in this age group (Fig. 34-4). Cervical length is approximately twice that of the fundus in the neonate. During childhood, relative cervical length and thickness decrease but uterine fundal length and thickness increase. Average uterine length varies from approximately 2.5 to 4 cm, with thickness less than or equal to 1 cm. Ovarian volume is slightly less than 1 mL. The uterine fundus elongates and thickens during puberty, outstripping the cervix; the endometrium also thickens and undergoes cyclic changes associated with the menstrual cycle.<sup>10</sup>

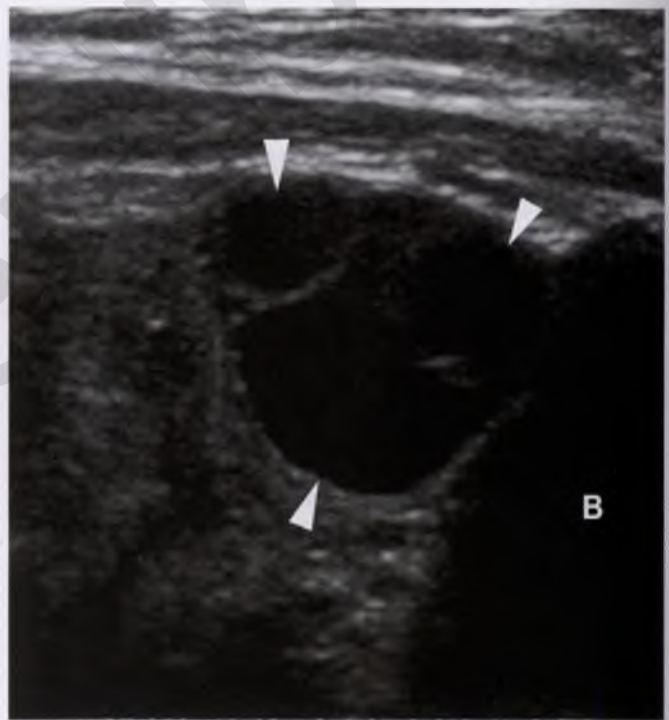


**FIG 34-3** Normal neonatal ovary. Sagittal ultrasound image demonstrates multiple anechoic follicles (arrowheads). B, bladder.

## NORMAL GONADAL AND REPRODUCTIVE TRACT DEVELOPMENT

Development of the female reproductive tract is a complex process that involves cellular differentiation, migration, fusion, and canalization with probable apoptosis (programmed cell death). This integrated sequence of events is associated with many opportunities for abnormal development and structural anomalies. Anomalies of the reproductive tract may present at different time points. Most abnormalities of the external genitalia are obvious at birth, whereas obstructive and non-obstructive lesions of the female reproductive tract may be apparent at birth or only later in childhood, at puberty, in adolescence, or during adulthood.<sup>11</sup>



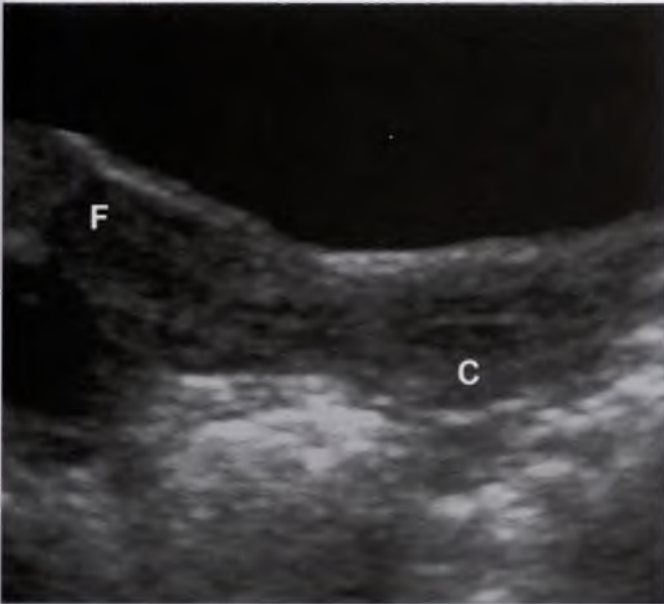


**FIG 34-4** Normal uterus in a 19-month-old girl. Sagittal ultrasound image depicts a fundus (F) that is similar in thickness and length to the cervix (C).

In the first 3 months of embryonic life, the primordia of both the female and male reproductive tracts are present and develop together. The gonads arise after migration of germ cells to the genital ridge, whereas the genital tract evolves from the formation and reshaping of the müllerian (paramesonephric) ducts, urogenital sinus, and vaginal plate.

Biologic differences between males and females are determined genetically during embryonic development. Sex development can be divided into two processes: *sex determination*, the developmental decision that directs the undifferentiated gonad to develop as a testis or ovary; and *sex differentiation*, which occurs once the gonad has developed and is induced by the products of the gonad to establish the phenotypic sex. Factors that affect gene expression influence sex determination, whereas factors that influence sex differentiation include hormones and their receptors.<sup>12</sup>

### Gonads

In the first and second weeks of development, embryos of both sexes differ only in their sex chromosomes. The gonads arise from the bilateral genital ridges, sites of focal mesothelial thickening of the peritoneum, before 5 to 6 weeks of life. A number of genes are required for development of the bipotential gonad. The bipotential gonad becomes an ovary or testis, depending on differentially expressed genes. Both testicular and ovarian development involve sex-specific pathways that appear to act antagonistically to each other. The normal role of the sex-determining region of the Y chromosome (the *SRY* gene) in XY gonads is to tip the balance in favor of the testis-specific pathway. If it is absent or abnormal, the gonad differentiates into an ovary. The presence of two X chromosomes appears to be important for the development of a normal, functioning ovary.<sup>13</sup>

The bipotential gonad begins to develop into either a testis or ovary in XY and XX individuals, respectively, at about 6 weeks of life. Differentiation of the gonads leads to testicular and ovarian hormone production and subsequent induction of anatomic and psychological differences. The first sign of gonadal differentiation occurs in the male with the appearance of Sertoli cells at 6 to 7 weeks of life. Leydig cells

appear at about 8 weeks. At this stage, the only sign of ovarian differentiation is the absence of Sertoli and Leydig cells. At 9 weeks, primordial germ cells begin to differentiate into oogonia followed by normal ovarian development at 12 to 123 weeks of life. In males, testicular cords will form in the absence of germ cells. However, in females, the ovary will not develop in the absence of germ cells.<sup>13</sup>

Testosterone and antimüllerian hormone are secreted by the Leydig and Sertoli cells, respectively, resulting in the differentiation of the genital primordia into the male phenotype. In the absence of a functioning testis, regardless of whether or not an ovary is present, the genital primordia will differentiate into the female phenotype. The presence of a functioning testis is necessary but not sufficient for the development of a male phenotype; normal androgen metabolism is also required.<sup>13</sup>

In adolescence, an increase in adrenal androgen secretion is associated with the appearance of pubic and axillary hair. Estrogen is responsible for breast development; for maturation of the uterus, vagina, and external genitalia; and for the initiation of the menstrual cycle. Excess androgens of either adrenal or ovarian origin may cause acne, hirsutism, clitoromegaly, increased muscle mass, and deepening of the voice.

### External Genitalia and Reproductive Tract

External genital development in the male occurs between the 8th and 12th weeks of life and requires high levels of circulating testosterone, the conversion of testosterone to dihydrotestosterone (DHT) by  $5\alpha$ -reductase in the target organs, and functional androgen receptors. Under the influence of DHT, in the male the urogenital sinus gives rise to the prostate gland; the genital tubercle forms the glans penis; the labiourethral folds form the urethra and ventral shaft of the penis; and the labioscrotal folds fuse to form the scrotum. In the female, or in the absence of testicular tissue secreting biologically active testosterone, functioning androgen receptors, or  $5\alpha$ -reductase, the genital tubercle forms the clitoris; the labiourethral folds form the labia minora; and the labioscrotal folds form the labia majora (Fig. 34-5).<sup>13</sup>

The cell layers involved in the formation of the female reproductive tract include the mesoderm, endoderm, and ectoderm. The mesoderm gives rise to the mesonephros and metanephros. In normal development, the mesonephros involutes, leaving only the wolffian ducts, and the metanephros eventually matures into the kidney. A defect within or insult to these mesodermal structures may ultimately result in congenital anomalies of the gonads, kidneys, and associated ducts. The urogenital sinus arises from the endoderm and gives rise to the bladder and urethra in males and females. In females it also forms the vestibule. The urethral and paraurethral glands in girls and the prostate gland in boys develop as outpouchings of the urethra. Nervous tissue, including sensory epithelium, arises from the ectoderm. Fusion of endoderm and ectoderm is involved in the canalization process; defects lead to fusion failure or obstructive lesions.<sup>11</sup>

During the "indifferent" stage of development, two pairs of genital ducts develop from mesodermal tissue in both males and females: the mesonephric (wolffian) and paramesonephric (müllerian) ducts. The paired wolffian ducts connect the mesonephric kidney to the cloaca. The ureteric bud arises from the wolffian duct at about the 5th week of life and induces differentiation of the metanephros, which eventually becomes the functioning kidney; the mesonephric kidney involutes at 10 weeks. The paramesonephric (müllerian) ducts are identified in both sexes at 6 weeks of life. As they grow, the müllerian ducts lie lateral to the wolffian ducts until they reach the caudal end of the mesonephros where they extend medially to nearly touch in the midline near the cloaca. The urorectal septum forms by the 7th week, separating the urogenital sinus from the rectum. In males, regression of the müllerian ducts begins at 8 weeks of life and is almost complete



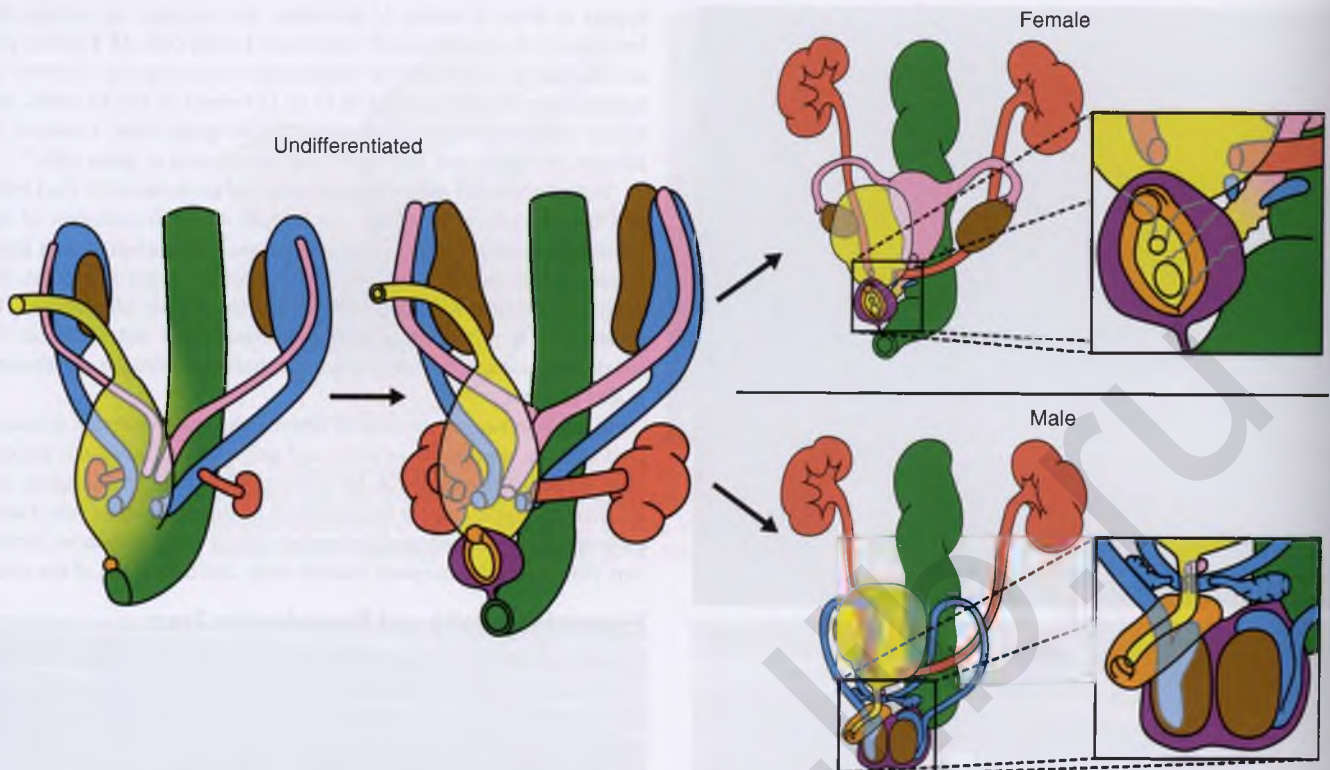


**FIG 34-5** Normal genitourinary development and differentiation. Color coding: blue, mesonephric kidneys and mesonephric (wolffian) ducts (become Gartner ducts in female, vasa deferentia in male); brown, gonads; green, gastrointestinal tract; orange, genital tubercle (becomes clitoris and labia minora in female, phallus in male); pink, paramesonephric (müllerian) ducts (become fallopian tube, uterus, and upper vagina in female, utricle in male); purple, labioscrotal swelling; red, metanephros (permanent kidney and ureter); yellow, urogenital sinus (becomes urinary bladder, urethra, vestibule in female; urinary bladder and urethra in male).

by 10 weeks. In females, the müllerian ducts extend caudally, reaching the urogenital sinus by 9 weeks to form the uterovaginal canal, which inserts into the urogenital sinus at the müllerian tubercle. By the 12th week, the two ducts have completely fused into a single tube, the uterovaginal canal. Two solid evaginations of urogenital sinus origin, the sinovaginal bulbs, grow from the distal müllerian tubercle. Proximal to the sinovaginal bulbs, outgrowths from the distal müllerian ducts result in formation of the vaginal plate. The upper portion of the vagina is formed by vacuolization of the vaginal plate, whereas the lower portion is formed by vacuolization of the sinovaginal bulbs. Canalization begins caudally and proceeds proximally; it is complete by the 5th month of gestation. The distal-most portions of the sinovaginal bulbs form the hymenal tissue which perforates prior to birth (Figs. 34-5 and 34-6). The upper portions of the müllerian ducts form the fallopian tubes.<sup>11</sup>

## STRUCTURAL ANOMALIES OF THE REPRODUCTIVE TRACT

Abnormalities related to lateral fusion, vertical fusion, or resorption, agenesis and/or hypoplasia result in structural anomalies of the reproductive tract. A number of classifications of these anomalies have been proposed, although none is complete.<sup>14</sup> The American Society for Reproductive Medicine (ASRM) system identifies groups with similar clinical manifestations and prognosis, although vaginal anomalies are not included (Table 34-1, Fig. 34-7). The Vagina Cervix Uterus Adnexa—Associated Malformations classification describes abnormalities not covered by the ASRM classification<sup>15</sup> (Table 34-2).



**FIG 34-6** Normal embryologic development of the uterus and vagina. Color coding: pink, paramesonephric (müllerian) ducts; yellow, urogenital sinus.

Vaginal and uterine anomalies may be detected in the neonatal period in children undergoing investigation of multiple congenital anomalies; or in adolescents, during workup of amenorrhea, pelvic or abdominal pain, or mass. An initial ultrasound study is usually sufficient in early childhood, with MRI performed at puberty for a more detailed evaluation. In the patient who first presents in adolescence, MRI is usually done following an abnormal ultrasound examination for a comprehensive assessment of the genitourinary tract.

During development of the uterus, failure of septal resorption between the two embryologic müllerian ducts leads to a septate uterus with two endometrial cavities. The septum can be partial or complete, with extension to the internal cervical os. A single cervix is usually present. The outer fundal contour of the uterus is either normal

**TABLE 34-1 Classification of Müllerian Anomalies According to the ASRM Classification System**

<b>Type I</b>	<b>Müllerian Agenesis or Hypoplasia</b> A. Vaginal (uterus may be normal or exhibit a variety of malformations) B. Cervical C. Fundal D. Tubal E. Combined
<b>Type II</b>	<b>Unicornuate Uterus</b> A. Communicating (endometrial cavity present) B. Noncommunicating (endometrial cavity present) C. Horn without endometrial cavity D. No rudimentary horn
<b>Type III</b>	<b>Uterus Didelphys</b>
<b>Type IV</b>	<b>Uterus Bicornuate</b> A. Complete (division down to internal os) B. Partial
<b>Type V</b>	<b>Septate Uterus</b> A. Complete (septum to internal os) B. Partial
<b>Type VI</b>	<b>Arcuate</b>
<b>Type VII</b>	<b>DES-Related Anomalies</b> A. T-shaped uterus B. T-shaped uterus with dilated horns C. Uterine hypoplasia

ASRM, American Society for Reproductive Medicine; DES, diethylstilbestrol.  
Modified with permission from Buttram VC Jr: Müllerian anomalies and their management. *Fertil Steril* 40(2):159-163, 1983.

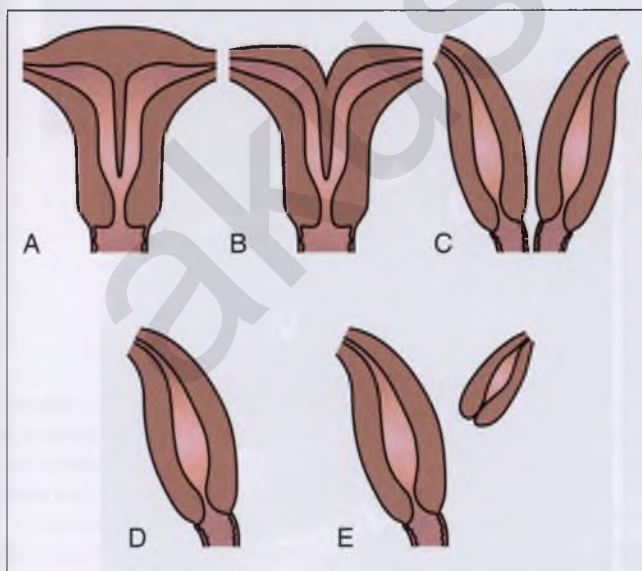


**FIG 34-7** Schematic diagram of common uterine anomalies: A, septate uterus; B, bicornuate uterus; C, didelphys uterus; D, unicornuate uterus; E, unicornuate uterus with remnant noncommunicating horn. (From Paltiel HJ, Phelps A: *US of the pediatric female pelvis*. *Radiology* 270(3):644-657, 2014, Fig. E1, used with permission.)

**TABLE 34-2 VCUAM Classification**

Vagina (V)	0	Normal
	1a	Partial
	1b	Complete hymenal atresia
	2a	Incomplete septate vagina <50%
	2b	Complete septate vagina
	3	Stenosis of the introitus
	4	Hypoplasia
	5a	Unilateral atresia
	5b	Complete atresia
	S1	Sinus urogenitalis (deep confluence)
S2	Sinus urogenitalis (middle confluence)	
S3	Sinus urogenitalis (high confluence)	
C	Cloacae	
+	Other	
#	Unknown	
Cervix (C)	0	Normal
	1	Duplex cervix
	2a	Unilateral atresia/aplasia
	2b	Bilateral atresia/aplasia
	+	Other
	#	Unknown
Uterus (U)	0	Normal
	1	Arcuate
	1b	Septate <50% of the uterine cavity
	1c	Septate >50% of the uterine cavity
	2	Bicornuate
	3	Hypoplastic uterus
	4a	Unilaterally rudimentary or aplastic
	4b	Bilaterally rudimentary or aplastic
	+	Other
	#	Unknown
Adnexa (A)	0	Normal
	1a	Unilateral tubal malformation, ovaries normal
	1b	Bilateral tubal malformation, ovaries normal
	2a	Unilateral hypoplasia/gonadal streak (including tubal malformation if appropriate)
	2b	Bilateral hypoplasia/gonadal streak (including tubal malformation if appropriate)
	3a	Unilateral aplasia
	3b	Bilateral aplasia
	+	Other
	#	Unknown
	Associated malformation (M)	0
R		Renal system
S		Skeleton
C		Cardiac
N		Neurologic
+		Other
#		Unknown

From Oppelt P, Renner SP, Brucker S, et al: The VCUAM (Vagina Cervix Uterus Adnex-associated Malformation) classification: a new classification for genital malformations. *Fertil Steril* 84(5):1493-1497, 2005.

(Figs. 34-7 and 34-8) or flat and broad. A bicornuate uterus results from incomplete fusion of the müllerian ducts. Leave out the part about incomplete development of the uterine horns. The central myometrium may extend to the level of the internal cervical os (bicornuate unicollis) or external cervical os (bicornuate bicollis), and the external surface is indented, typically by more than 1 cm (Fig. 34-9). Complete



nonfusion of both müllerian ducts leads to a didelphys uterus (Fig. 34-10). Both horns are fully developed and nearly normal in size. There are always two cervixes. There may be a transverse or longitudinal vaginal septum. Although a transverse vaginal septum may occur in association with all of the müllerian duplication anomalies, the greatest association is with didelphys uteri. When there is complete or near-complete arrested development of one müllerian duct, a unicornuate uterus develops with a single horn, an ipsilateral round ligament, and fallopian tube. The unicornuate uterus communicates with a single cervix and a normal vagina. In most patients, arrest is incomplete, and a contralateral rudimentary horn with or without functioning endometrium is present (Fig. 34-11). The rudimentary horn may or may not communicate with the developed uterine horn. Sonography may demonstrate two uterine horns of different sizes. Unless functional endometrium within a noncommunicating horn leads to

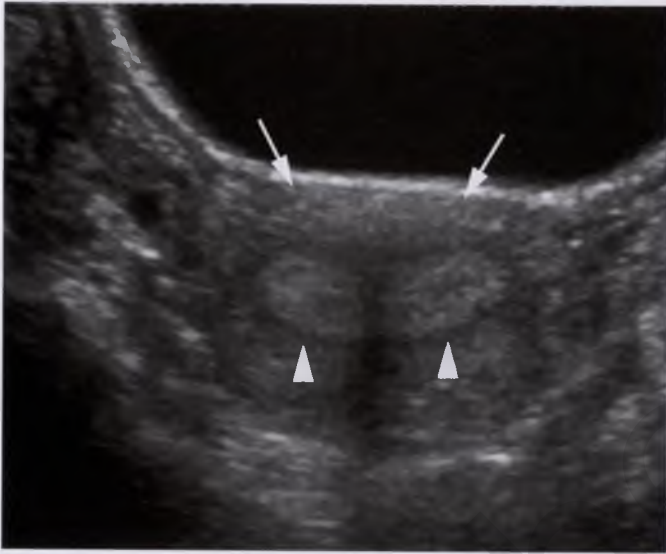


**FIG 34-8** Septate uterus. Transverse ultrasound image of the uterus in a 15-year-old girl with dysmenorrhea reveals two distinct endometrial cavities (*arrowheads*). The external myometrial fundal contour is normal (*arrows*).

hematometra or endometriosis, no treatment is generally required.<sup>11,16,17</sup> However, because of the potential risk of an ectopic pregnancy developing within a rudimentary noncommunicating horn, some advocate surgical resection.

Failure of fusion and canalization of the müllerian ducts and embryologic urogenital sinus lead to a transverse vaginal septum. Septa are generally less than 1 cm in thickness and extend completely or incompletely across the vagina (Fig. 34-12). There is often a small central or eccentric perforation. A complete vaginal septum may occur in the upper (46%), middle (40%), or lower (14%) vagina.<sup>18</sup> The vagina is short or is a blind-ending pouch. The external genitalia appear normal. Girls may present with mucocolpos in infancy or childhood, hematocolpos in adolescence, or pyohematocolpos from



**FIG 34-9** Bicornuate uterus in a 13-year-old girl. Transverse pelvic ultrasound image shows two uterine horns (*asterisks*) with a deep central depression of the external myometrial fundal contour (*arrowhead*). The right kidney was absent (not shown).

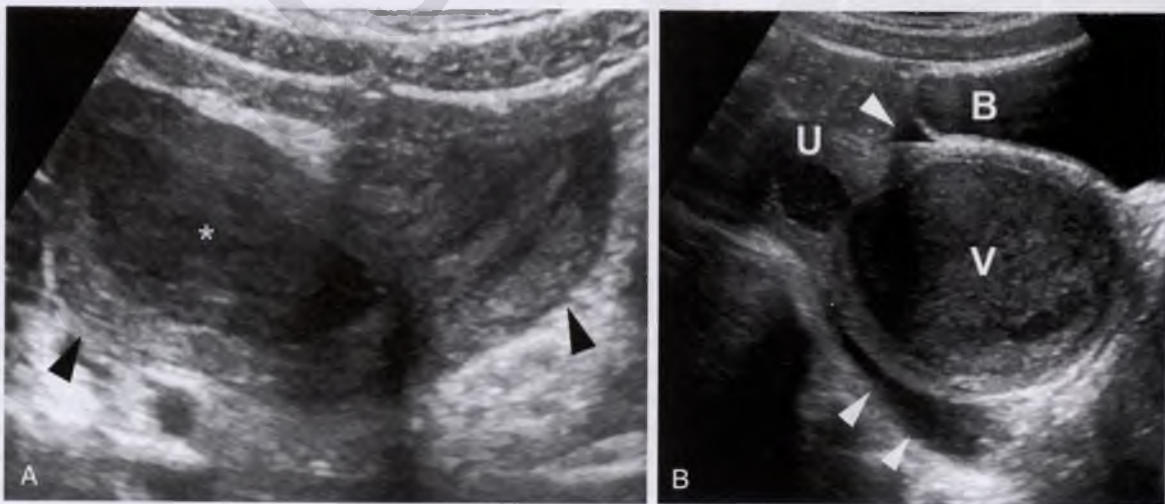


**FIG 34-10** Uterus didelphys in a 12-year-old girl with chronic pelvic pain. **A**, Transverse ultrasound image shows two widely divergent uterine horns (*arrowheads*). The right uterine horn is distended with hypoechoic material consistent with blood (*asterisk*). **B**, Right parasagittal ultrasound image demonstrates an obstructed vagina (V) filled with blood. There is a small amount of free fluid in the cul-de-sac and above the bladder (*arrowheads*). B, bladder; U, uterine fundus. The left vagina was normal (not shown).

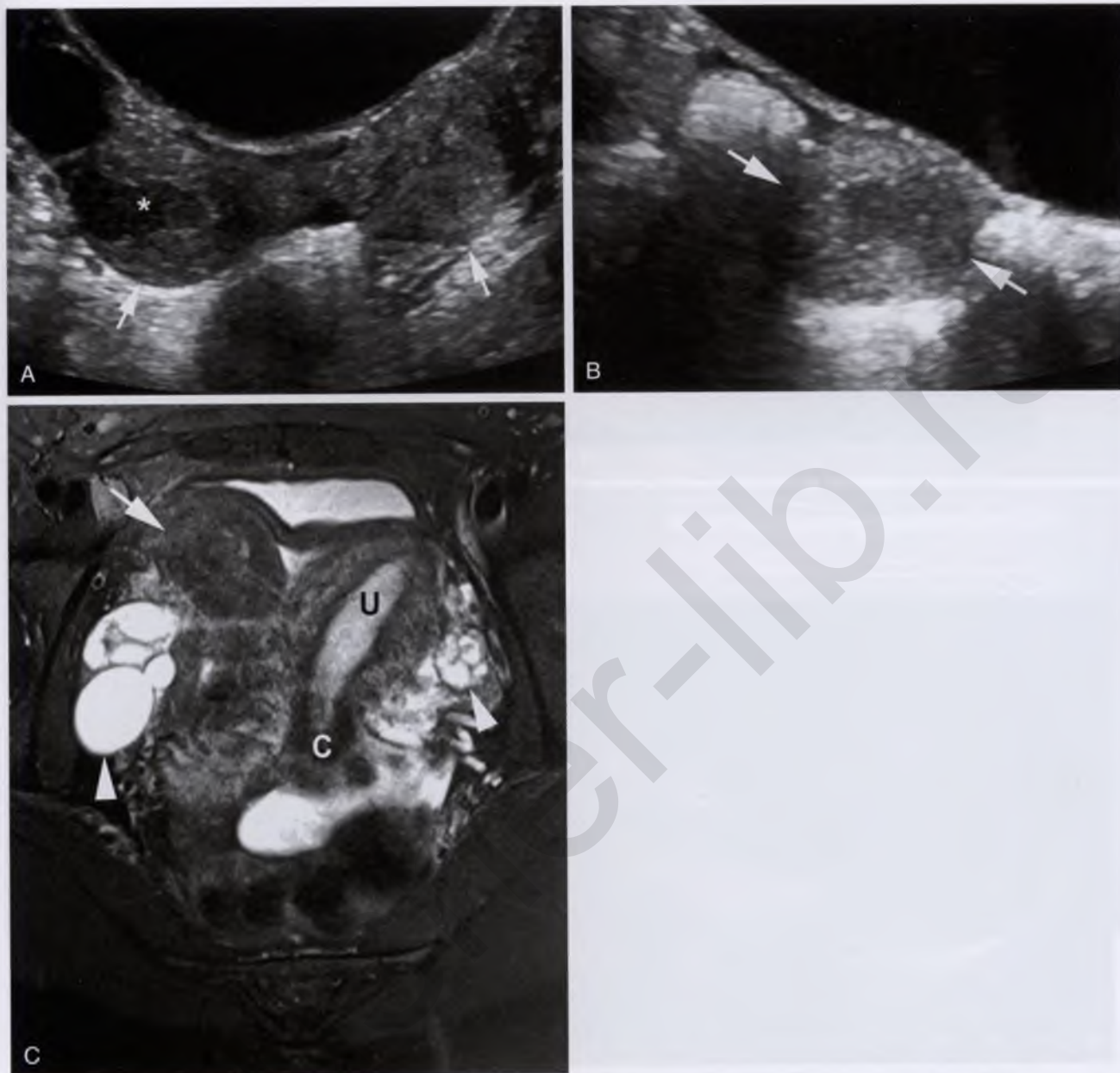


**FIG 34-11** Unicornuate left uterus with an obstructed, rudimentary right hemiuterus in a 13-year-old girl with cyclic pelvic pain. **A**, Transverse ultrasound image reveals two uterine horns (arrows). Hypoechoic fluid distends the right uterine cavity (asterisk). **B**, Sagittal image depicts the truncated right hemiuterus (between arrows). **C**, Coronal T2-weighted magnetic resonance image demonstrates a well-developed left hemiuterus (U) and cervix (C). The smaller right hemiuterine cavity contains low signal intensity material compatible with blood products (arrow). Both ovaries contain normal follicles (arrowheads). The left vagina was normal (not shown). See Videos 34-1 and 34-2.

ascending infection through the small perforation. On imaging studies, it is critical to document the presence of a cervix in order to differentiate between a high vaginal septum and cervical atresia, because treatment and prognosis are very different.<sup>10</sup>

Cervical atresia is rare and occurs in association with absence of the upper vagina. Patients may present with primary amenorrhea, cyclic or chronic abdominal or pelvic pain, or a pelvic mass (Fig. 34-13). The usual treatment is hysterectomy.

Vaginal agenesis (müllerian aplasia, Mayer-Rokitansky-Küster-Hauser syndrome) occurs in approximately 1 in 5000 female births<sup>17</sup> and results in congenital absence of the upper vagina in association

with variable müllerian duct anomalies. There is usually associated cervical and uterine agenesis, although approximately 10% of patients have a rudimentary müllerian structure with or without functional endometrium.<sup>17</sup> Skeletal, renal, and auditory anomalies are common. Affected individuals have a normal female 46,XX karyotype with normal oocyte and ovarian hormonal function. Patients exhibit normal secondary sexual characteristics and a normal perineum on physical examination. Because the hymen and distal vagina are both derived embryologically from the urogenital sinus, the hymen is usually present, along with a small distal vaginal pouch or vaginal dimple. Ultrasound examination is done to identify and characterize any



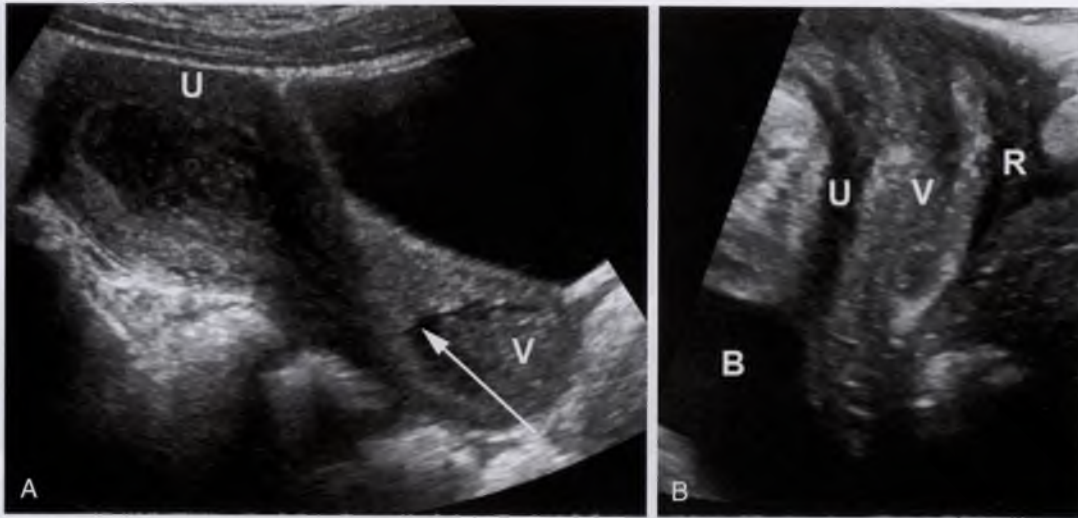


**FIG 34-12** Transverse vaginal septum in a 12-year-old girl with normal external genitalia, primary amenorrhea, and pelvic pain. **A**, Sagittal ultrasound image depicts a fluid-distended uterus (U) and upper vagina (V). The arrow indicates the external cervical os. **B**, Sagittal transperineal image shows a collapsed distal vagina (V). B, bladder; R, rectum; U, urethra.

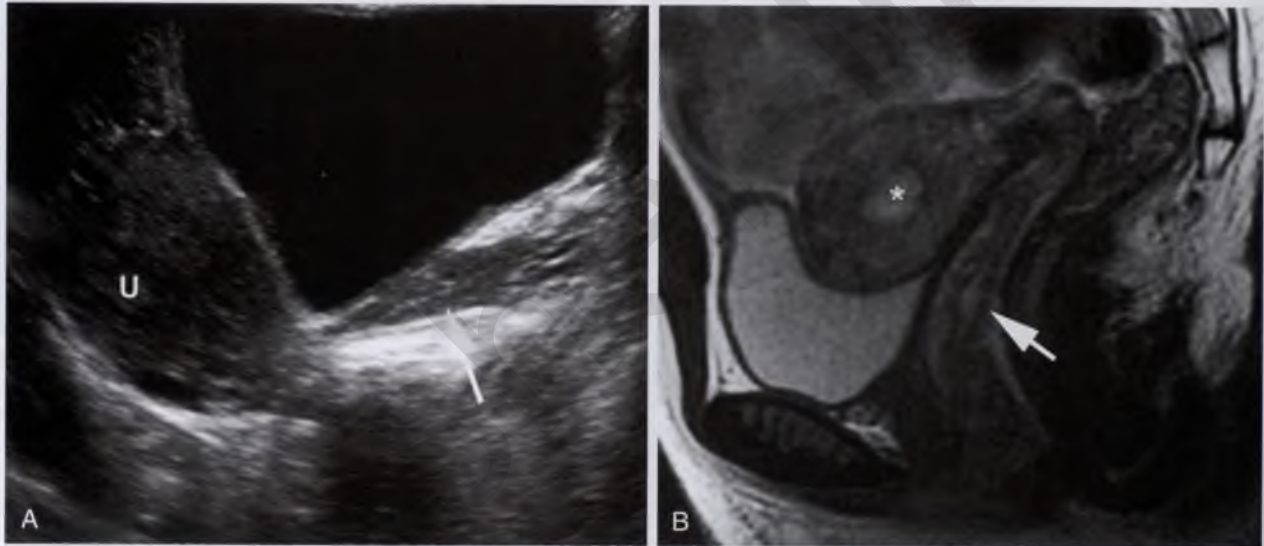


**FIG 34-13** Agenesis of the cervix and upper vagina in a 16-year-old girl with pelvic pain. **A**, Sagittal ultrasound image reveals a uterus (U) without evidence of a cervix or upper vagina. The lower vagina is present (arrow). **B**, Sagittal T2-weighted magnetic resonance image confirms absence of a normal cervix and upper vagina with no communication between the endometrial cavity (asterisk) and the midvaginal canal (arrow).

müllerian tissue; to determine renal presence, position, and morphologic appearance; and to confirm the presence of normal ovaries (Fig. 34-14).

When the lower portion of the vagina fails to develop from the urogenital sinus, distal vaginal atresia occurs and fibrous tissue replaces the absent distal vagina. The upper vagina, cervix, and uterus are normal. Primary amenorrhea is the usual clinical presentation. As the upper vagina becomes distended with blood and secretions, patients may develop cyclic or chronic pain and a pelvic or abdominal mass. Affected individuals have normal secondary sexual characteristics, although a vaginal orifice is absent. Transperineal ultrasound can be used to document absence of the distal vagina and to measure the distance between the proximal vagina and the perineal surface. This technique is especially useful intraoperatively<sup>11</sup> (Fig. 34-15).

An imperforate hymen is the most common anomaly of the female reproductive tract. There are usually no other associated abnormalities. The diagnosis can be made at birth, when a bulge from the associated hydrocolpos or mucocolpos is present, as a result of vaginal secretions related to maternal estrogen stimulation. If not diagnosed at birth, the mucus will eventually be resorbed, and the bulge will resolve. After the onset of menarche, the adolescent patient may be asymptomatic or have a history of cyclic abdominal or pelvic pain.<sup>11</sup> An imperforate hymen can usually be diagnosed by physical examination alone. However, in many patients, a complete physical examination is not performed at birth, and cases in symptomatic adolescents are often initially misdiagnosed.<sup>13</sup> Ultrasound imaging depicts distention of the vagina and uterus with fluid. Echogenic debris within the fluid is due to mucous secretions in infants (Fig. 34-16) and blood in

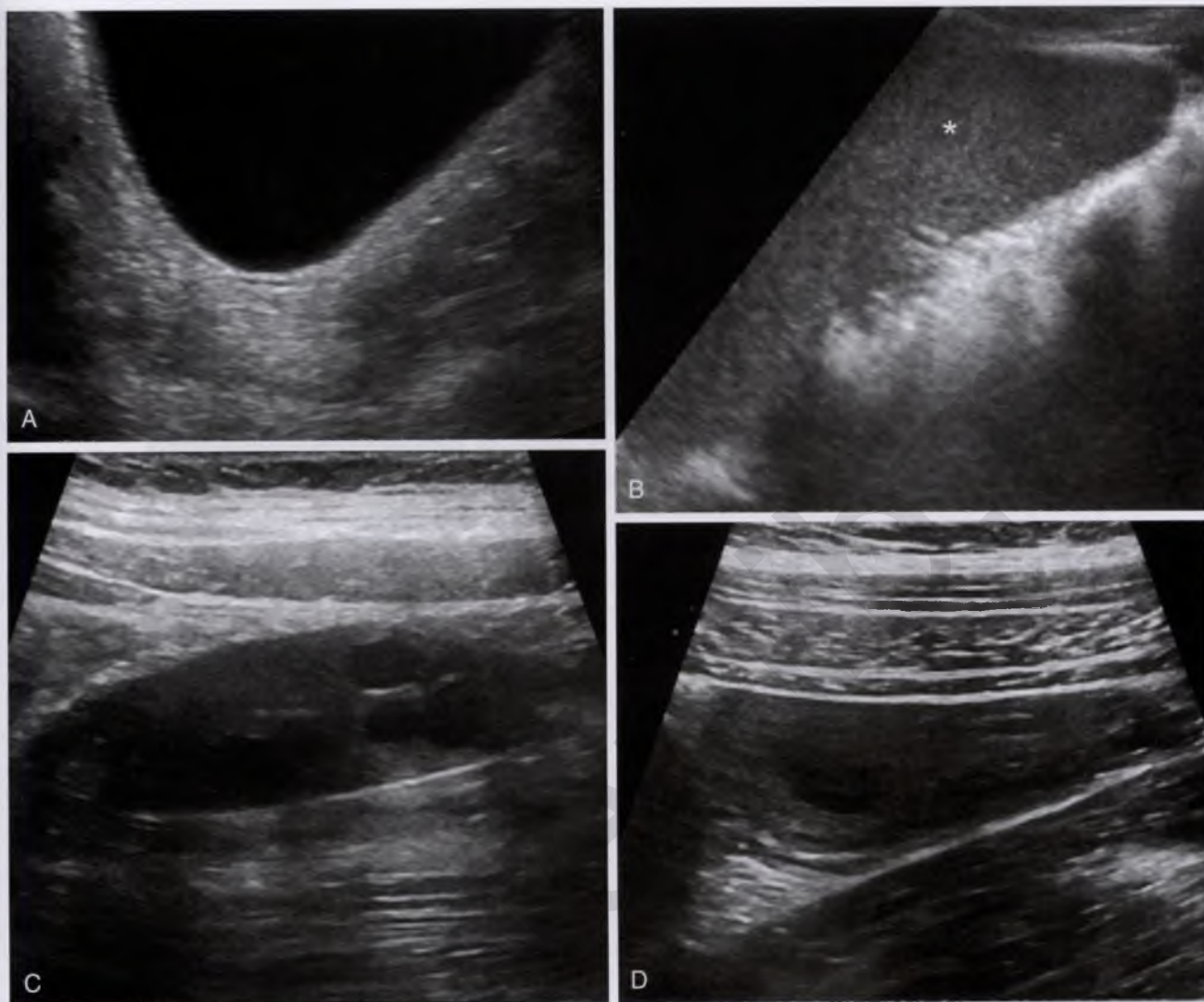


**FIG 34-14** Vaginal agenesis in a 17-year-old girl with primary amenorrhea. **A**, Sagittal midline ultrasound image reveals no evidence of a vagina or uterus. **B**, The left kidney was absent, with an empty renal fossa depicted on a sagittal ultrasound image of the left upper quadrant. The spleen is indicated by an asterisk. Normal right (**C**) and left (**D**) ovaries were identified.

postmenarcheal girls. Ascites may develop following spillage of secretions through the fallopian tubes.

## AMBIGUOUS GENITALIA

Birth of a child with ambiguous genitalia is rare. However, the substantial risk of psychological damage to the patient and family caused by an incorrect or delayed diagnosis necessitates the need for familiarity on the part of health care providers with the various causes as well as approach to diagnosis and management. Any deviation from the normal appearance of the genitalia, such as clitoromegaly or labial fusion, should lead to immediate evaluation.

An International Consensus Conference on Intersex was organized by the Lawson Wilkins Pediatric Endocrine Society and the European Society for Paediatric Endocrinology in 2006 that resulted in a consensus statement proposing the term *disorders of sex development* (DSD) to encompass congenital conditions with atypical development of chromosomal, gonadal, or anatomic sex.<sup>18,19</sup> The DSDs are classified as sex chromosome DSD (karyotype is not the usual 46,XX or 46,XY); 46,XX DSD (chromosomally female); and 46,XY DSD

(chromosomally male) (Table 34-3).<sup>20</sup> Karyotyping, hormonal analysis, and imaging are necessary for adequate delineation of these disorders.

Sonography is used to locate the gonads, to determine the presence or absence of a uterus, and to evaluate the adrenal glands for diffuse enlargement or masses. Retrograde genitography, obtained by injecting contrast material through the urogenital orifice, or voiding cystourethrography will characterize the anatomy of the urethra, vagina (if present), urogenital sinus, and occasionally the cervix. In the presence of a cloacal anomaly, the connections of the genital, urinary, and gastrointestinal tracts to the cloaca can be determined.<sup>21,22</sup>

The most frequent sex chromosome DSD is 45,X (Turner syndrome), which is due to absence of all or part of one of the X chromosomes. Monosomy X is the most common. Characteristic physical features include short stature, low-set ears, webbed neck, and a broad chest. Gonadal dysfunction results in amenorrhea and sterility. The ovaries may not be detected by sonography, and the uterus has a juvenile appearance (Fig. 34-17). Associated conditions include Hashimoto thyroiditis, congenital heart disease, renal anomalies, skeletal abnormalities, and diabetes.



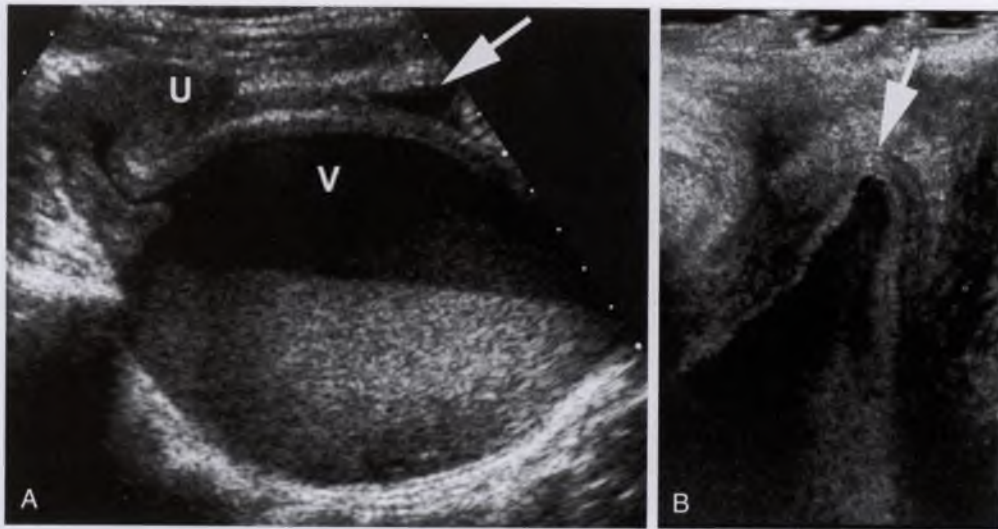


**FIG 34-15** Distal vaginal atresia in a 13-year-old girl with primary amenorrhea and an abdominal mass. **A**, Sagittal ultrasound image demonstrates hydrometrocolpos with marked distention of the vagina (V), with layering internal echoes creating a fluid/fluid level. Note mass effect resulting in marked compression of the urinary bladder (*arrow*) anteriorly. U, uterus. **B**, Sagittal transperineal ultrasound image shows a blind-ending distal vagina (*arrow*) located approximately 1.3 cm from the skin surface.

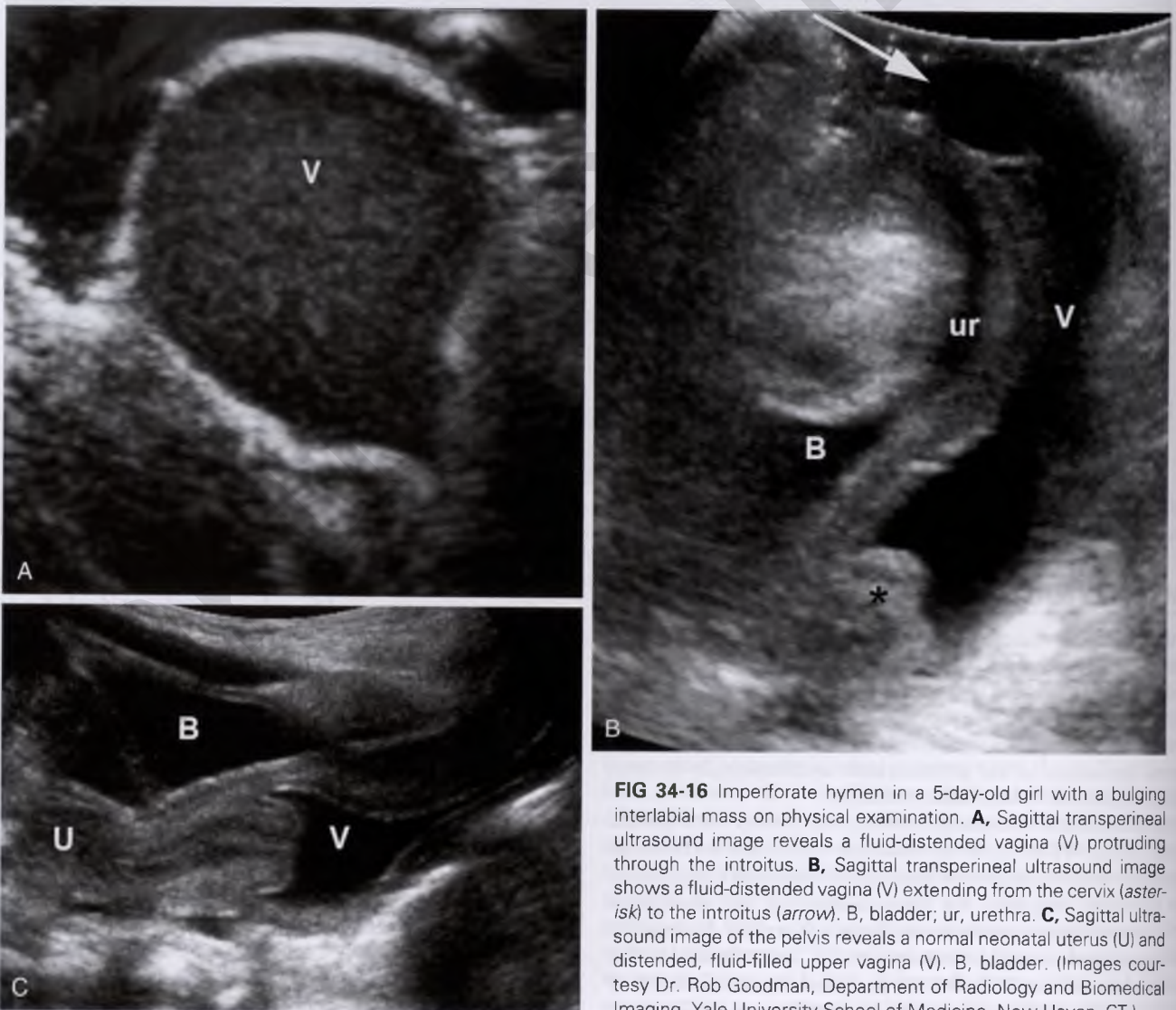


**FIG 34-16** Imperforate hymen in a 5-day-old girl with a bulging interlabial mass on physical examination. **A**, Sagittal transperineal ultrasound image reveals a fluid-distended vagina (V) protruding through the introitus. **B**, Sagittal transperineal ultrasound image shows a fluid-distended vagina (V) extending from the cervix (*asterisk*) to the introitus (*arrow*). B, bladder; ur, urethra. **C**, Sagittal ultrasound image of the pelvis reveals a normal neonatal uterus (U) and distended, fluid-filled upper vagina (V). B, bladder. (Images courtesy Dr. Rob Goodman, Department of Radiology and Biomedical Imaging, Yale University School of Medicine, New Haven, CT.)

TABLE 34-3 A Proposed Classification for Disorders of Sex Development (DSD)

Sex Chromosome DSD	46,XY DSD	46,XX DSD
A: 47,XXY (Klinefelter syndrome and variants)	A: Disorders of gonadal (testicular) development <ol style="list-style-type: none"> <li>1. Complete or partial gonadal dysgenesis (e.g., <i>SRY</i>, <i>SOX9</i>, <i>SF1</i>, <i>WT1</i>, <i>DHH</i>)</li> <li>2. Ovotesticular DSD</li> <li>3. Testis regression</li> </ol>	A: Disorders of gonadal (ovarian) development <ol style="list-style-type: none"> <li>1. Gonadal dysgenesis</li> <li>2. Ovotesticular DSD</li> <li>3. Testicular DSD (e.g., <i>SRY+</i>, <i>dup SOX9</i>, <i>RSP01</i>)</li> </ol>
B: 45,X (Turner syndrome and variants)	B: Disorders in androgen synthesis or action <ol style="list-style-type: none"> <li>1. Disorders of androgen synthesis               <ul style="list-style-type: none"> <li>• Luteinizing hormone receptor mutations</li> <li>• Smith-Lemli-Opitz syndrome</li> <li>• Steroidogenic acute regulatory protein mutations</li> <li>• Cholesterol side-chain cleavage (<i>CYP11A1</i>)</li> <li>• 3<math>\beta</math>-Hydroxysteroid dehydrogenase 2 (<i>HSD3B2</i>)</li> <li>• 17<math>\alpha</math>-Hydroxylase/17,20-lyase (<i>CYP17</i>)</li> <li>• P450 oxidoreductase (<i>POR</i>)</li> <li>• 17<math>\beta</math>-Hydroxysteroid dehydrogenase (<i>HSD17B3</i>)</li> <li>• 5<math>\alpha</math>-Reductase 2 (<i>SRD5A2</i>)</li> </ul> </li> <li>2. Disorders of androgen action               <ul style="list-style-type: none"> <li>• Androgen insensitivity syndrome</li> <li>• Drugs and environmental modulators</li> </ul> </li> </ol>	B: Androgen excess <ol style="list-style-type: none"> <li>1. Fetal               <ul style="list-style-type: none"> <li>• 3<math>\beta</math>-Hydroxysteroid dehydrogenase 2 (<i>HSD3B2</i>)</li> <li>• 21-Hydroxylase (<i>CYP21A2</i>)</li> <li>• P450 oxidoreductase (<i>POR</i>)</li> <li>• 11<math>\beta</math>-Hydroxylase (<i>CYP11B1</i>)</li> <li>• Glucocorticoid receptor mutations</li> </ul> </li> <li>2. Fetoplacental               <ul style="list-style-type: none"> <li>• Aromatase (<i>CYP19</i>) deficiency</li> <li>• Oxidoreductase (<i>POR</i>) deficiency</li> </ul> </li> <li>3. Maternal               <ul style="list-style-type: none"> <li>• Maternal virilizing tumors (e.g., luteomas)</li> <li>• Androgenic drugs</li> </ul> </li> </ol>
C: 45,X/46,XY (mixed gonadal dysgenesis)	C: Other <ol style="list-style-type: none"> <li>1. Syndromic associations of male genital development (e.g., cloacal anomalies, Robinow, Aarskog, hand-foot-genital, popliteal pterygium syndromes)</li> <li>2. Persistent müllerian duct syndrome</li> <li>3. Vanishing testis syndrome</li> <li>4. Isolated hypospadias (<i>CXorf6</i>)</li> <li>5. Congenital hypogonadotrophic hypogonadism</li> <li>6. Cryptorchidism (<i>INSL3</i>, <i>GREAT</i>)</li> <li>7. Environmental influences</li> </ol>	C: Other <ol style="list-style-type: none"> <li>1. Syndromic associations (e.g., cloacal anomalies)</li> <li>2. Müllerian agenesis/hypoplasia (e.g., MURCS association)</li> <li>3. Uterine abnormalities (e.g., MODY5)</li> <li>4. Vaginal atresia (e.g., McKusick-Kaufman syndrome)</li> <li>5. Labial adhesions</li> </ol>
D: 46,XX/46,XY (chimerism)		

DSD, disorders of sex development; MODY5, maturity-onset diabetes of the young type 5; MURCS, müllerian duct aplasia, renal aplasia, and cervicothoracic somite dysplasia.

Revised, with permission, from Hughes IA, Nihoul-Fekété C, Thomas B, Cohen-Kettenis PT: Consequences of the ESPE/LWPES Guidelines for diagnosis and treatment of disorders of sex development. *Best Pract Res Clin Endocrinol Metab* 21(3):351-365, 2007, Table 2.

Most cases of 46,XX DSD result from congenital adrenal hyperplasia. The adrenal glands are enlarged, and there is masculinization of the lower urogenital tract (Fig. 34-18). In patients with a urogenital sinus, reflux of urine into the vagina and uterus can result in hydro-metrocolpos (Fig. 34-19). The ovaries and uterus are normal. Rarer causes of a masculinized but chromosomally normal female include a masculinizing ovarian tumor and maternal androgen ingestion in early pregnancy.

A cloacal malformation occurs when there is interruption of the normal differentiation of the genital, urinary, and gastrointestinal tracts. Cloacal malformations occur only in females, with an incidence of 1 in 40,000 to 50,000 newborns. Failure of the urorectal septum to form or fuse appropriately during embryologic development leads to incomplete separation of these tracts with a common confluence, the cloaca, and a single perineal opening. There is usually concomitant failure of müllerian duct fusion resulting in uterine and proximal vaginal duplication. The urogenital sinus persists, and the lower vagina and hymen do not form normally. In order to prevent bladder outlet obstruction, drainage of pooled urine through the vagina is usually required. A colostomy is performed to decompress the gastrointestinal

tract. Many of these children have additional congenital anomalies necessitating multiple reconstructive operations. Accurate delineation of anatomic abnormalities usually requires genitography or voiding cystourethrography (Figs. 34-20 and 34-21), as well as contrast material-enhanced examination of the distal colostomy limb.<sup>11,21</sup>

## PREPUBERTAL BLEEDING

Vulvovaginitis is the usual cause of prepubertal bleeding. Other causes include precocious puberty, vaginal foreign body, vaginal mass, or genital trauma (either accidental, self-inflicted, or the result of physical or sexual abuse).

## Precocious Puberty

Although the definition of precocious puberty in North American girls is somewhat controversial, the traditional definition of the development of breast or pubic hair in girls younger than 8 years of age is still used by most endocrinologists. Precocious puberty may be central and gonadotropin-dependent or peripheral and gonadotropin-independent. Incomplete forms of precocious puberty include



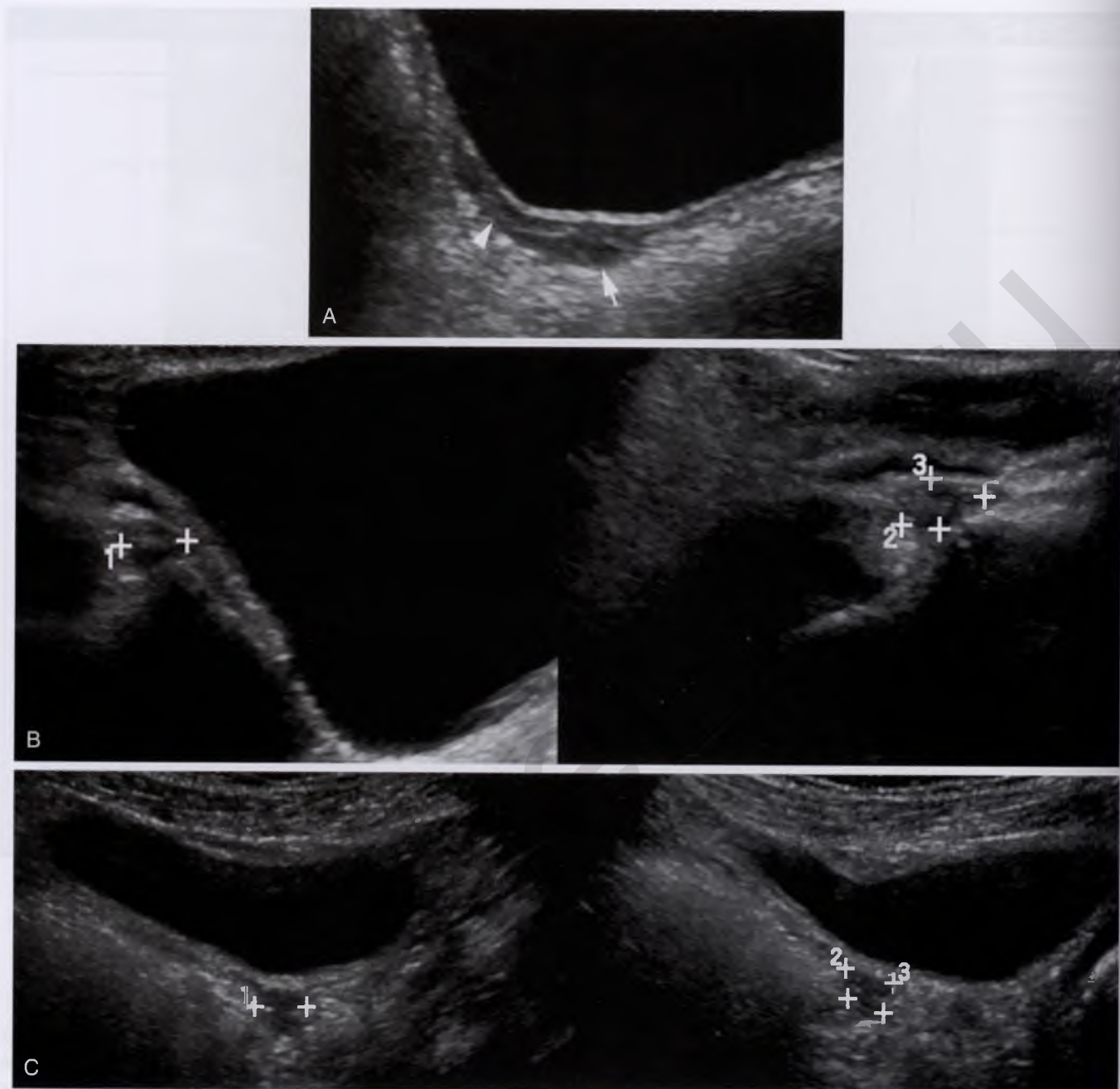


**FIG 34-17** Turner mosaicism in a 14-year-old girl with short stature and premature ovarian insufficiency. **A**, Sagittal ultrasound image shows a juvenile uterine appearance posterior to the distended urinary bladder with relative prominence of the cervix (*arrow*) and a small, underdeveloped fundus (*arrowhead*). Transverse (left side of split screen image) and sagittal (right side of split screen image) ultrasound images demonstrate tiny right (**B**) and left (**C**) ovaries, each with a volume less than 1 mL.

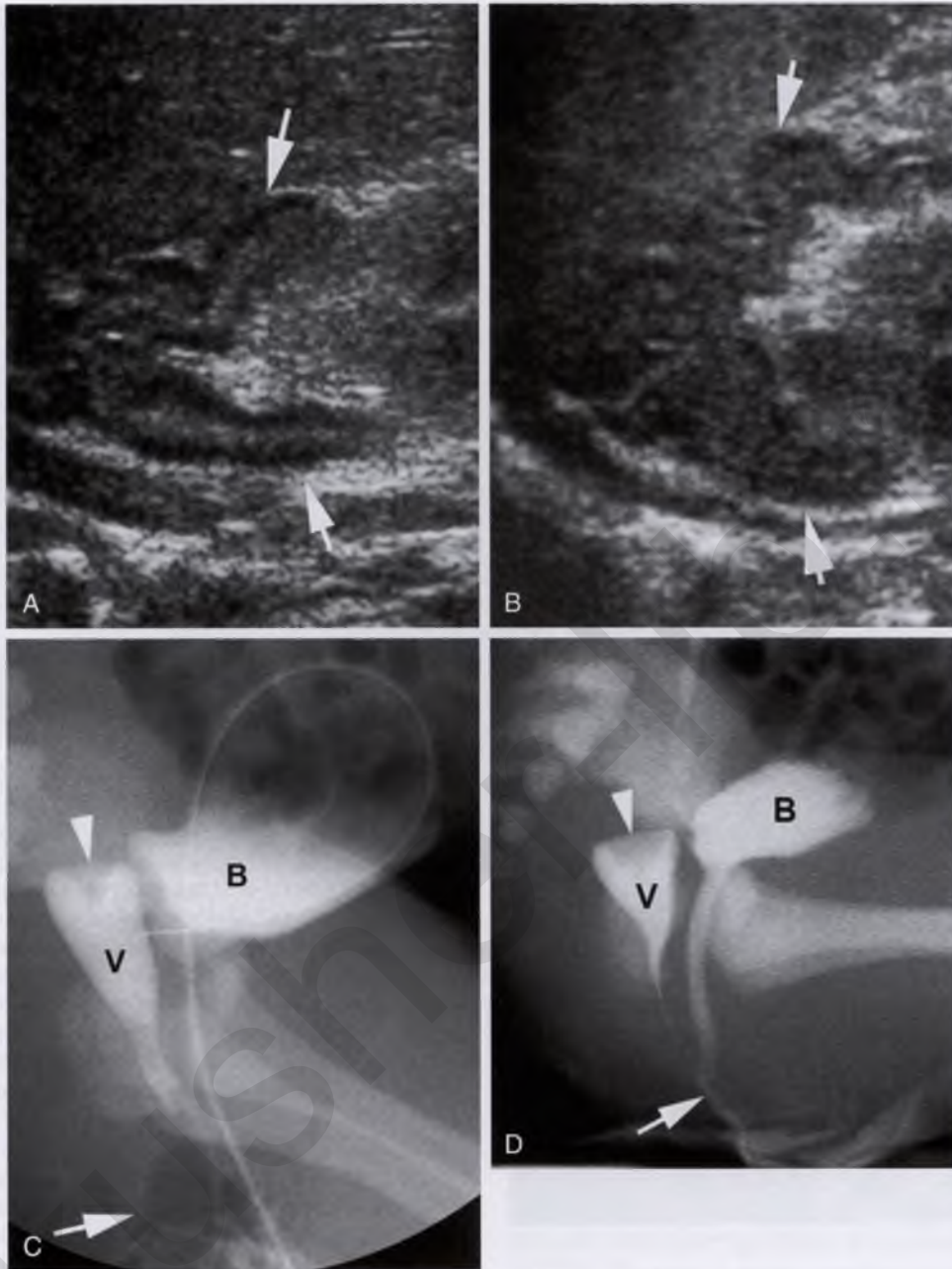


**FIG 34-18** Congenital adrenal hyperplasia in a neonate with clitoromegaly. **A** and **B**, Sagittal ultrasound images reveal large, cerebriform right (**A**) and left (**B**) adrenal glands (*arrows*). The outer cortex is hypoechoic, whereas the central medulla is echogenic. **C**, Sagittal image from retrograde genitography shows a catheter placed through the common perineal channel and coiled within the bladder (**B**). A Foley catheter with air-inflated balloon (*arrow*) was also placed with its tip in the common perineal channel. Injected contrast material outlines the vagina (**V**) with a cervical impression (*arrowhead*) at its apex. **D**, The distal vagina unites with the urethra to form a common perineal channel (*arrow*). **B**, bladder; **V**, vagina; *arrowhead*, cervical impression.



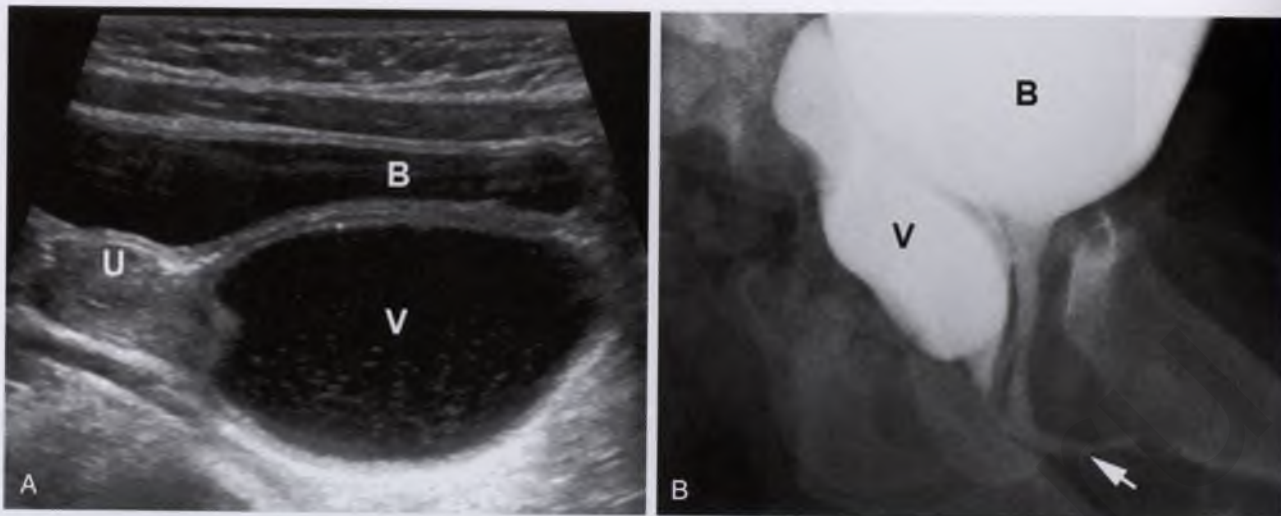


**FIG 34-19** Congenital adrenal hyperplasia in a 13-year-old girl with a single opening on the ventral aspect of an enlarged clitoris. **A**, Sagittal ultrasound image demonstrates a dilated, fluid-filled vagina (V) that compresses the posterior aspect of the bladder (B). The uterus (U) appears normal. **B**, Sagittal image from voiding cystourethrography. There was retrograde filling of the vagina (V) from the bladder (B). The distal vagina and urethra unite to form a common perineal channel (arrow).

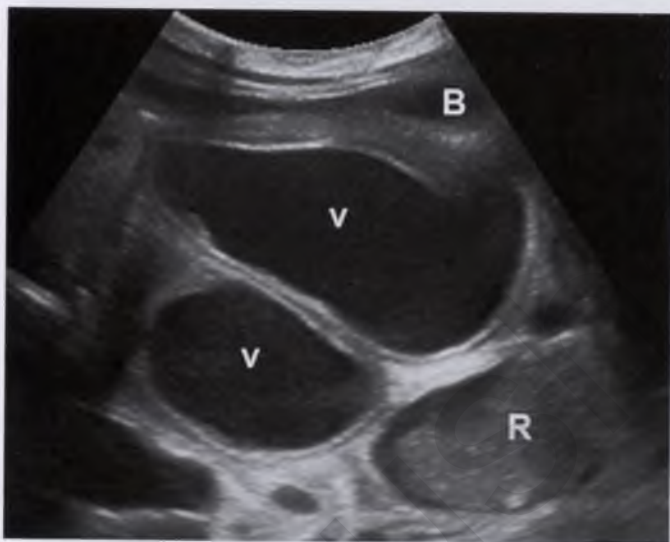


**FIG 34-20** Cloacal malformation in newborn girl. Transverse ultrasound image of the pelvis shows duplicated vaginas (v) filled with fluid. The bladder (B) is anteriorly displaced and compressed. R, rectum. See Video 34-3.

premature thelarche (breast development), premature pubarche (adrenarche; axillary or pubic hair), and isolated premature menarche in the absence of other signs of puberty.<sup>23</sup>

In central precocious puberty, activation of the hypothalamic-pituitary-gonadal axis with secretion of gonadotropin-releasing hormone by the hypothalamus leads to isosexual pubertal development. Central precocious puberty is idiopathic in more than 80% of patients. However, lesions of the hypothalamus, pituitary gland, or adjacent structures have been identified by MRI or CT. Central nervous system abnormalities causing precocious puberty can manifest at any time during childhood, although they are more commonly diagnosed in younger children. Some authors have therefore recommended that any girl younger than 8 years of age with progressive central precocity

undergo central nervous system imaging.<sup>24</sup> Prolonged exposure to sex steroids from any source can also lead to central precocious puberty.<sup>23</sup>

In gonadotropin-independent (peripheral) precocious puberty, serum gonadotropin levels are low. Autonomous estrogen may be produced by an ovarian cyst (Fig. 34-22), ovarian tumor, or, occasionally, an adrenal tumor. These lesions often produce high levels of estrogen, and pubertal development may proceed more quickly than in children with central precocity. Girls exposed to ingested or topical estrogen or androgen can also develop signs of precocity, such as breast development or virilization.<sup>23</sup> Ultrasound is used to determine ovarian size and morphologic features, to detect the presence of an ovarian cyst or estrogen-secreting tumor of the ovary or adrenal gland, and to confirm or exclude a postpubertal appearance of the uterus, because a postpubertal appearance is a sign of abnormal estrogen production. Sonography is also helpful in tracking the effect of medical or surgical therapy.

### Vaginal Foreign Body

The most common vaginal foreign bodies include fibrous material from clothing and carpets and toilet paper. Additional causes include self-exploration and sexual abuse. Patients may present with vaginal discharge, bleeding, urinary symptoms, and abdominal or pelvic pain. Both radiopaque and nonradiopaque objects can appear echogenic on ultrasound examination. There may be a slight indentation on the posterior bladder wall, and distal acoustic shadowing can be present (Fig. 34-23).<sup>2,23</sup>

### Vaginal Masses

Benign vaginal masses include polyps and cysts (Fig. 34-24). Malignant masses are rare and include rhabdomyosarcoma, clear cell carcinoma, and endodermal sinus tumor.<sup>25-29</sup>

Vaginal rhabdomyosarcoma has a bimodal distribution, with the first peak between 2 and 6 years of age and the second between 14 and 18 years of age. It arises in the anterior vaginal wall next to the cervix and can involve the uterus via direct extension from the vagina. The embryonal and botryoid subtypes are the most common. Patients may present with vaginal bleeding and a vaginal, vulvar, or perineal mass. The tumor metastasizes to the liver, lung, lymph nodes, and bone.

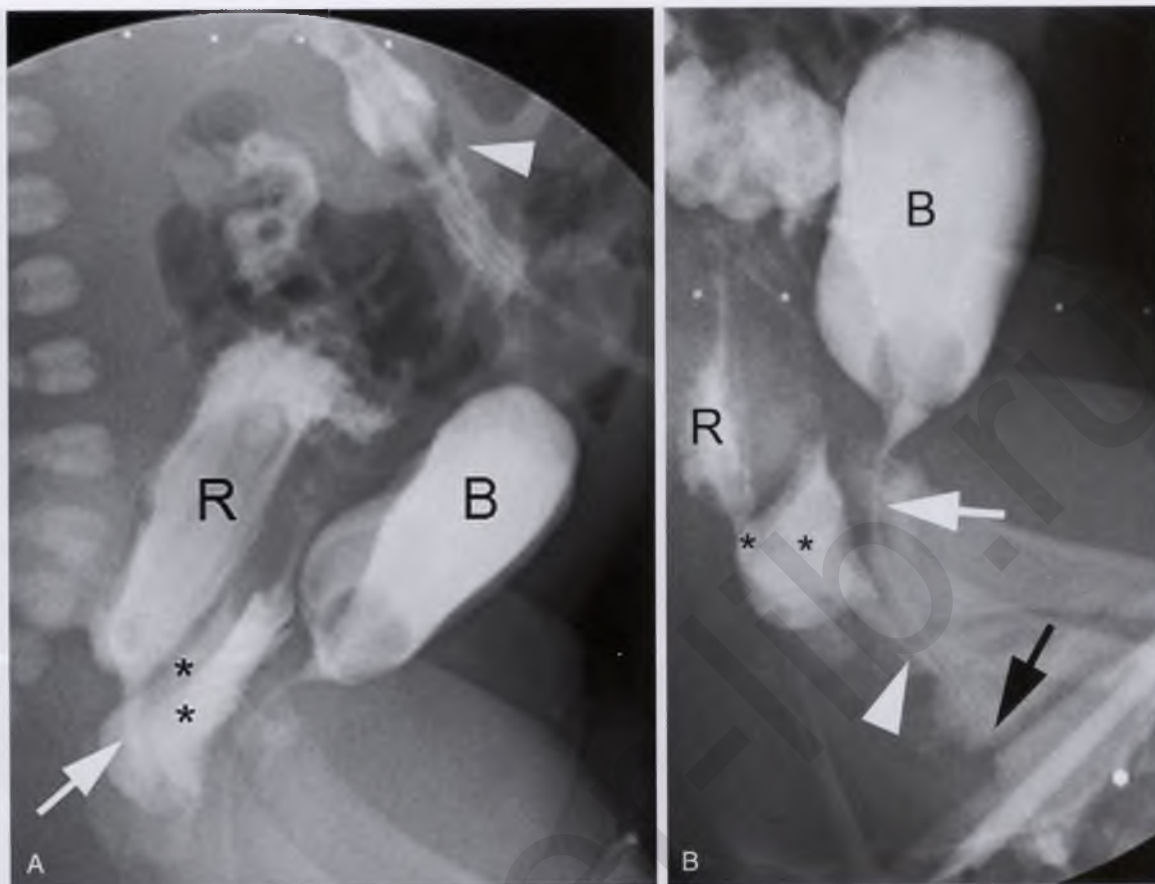


**FIG 34-21** Cloacal malformation in a 12-day-old girl evaluated with fluoroscopy after colostomy. **A**, Sagittal image obtained after contrast material was instilled through a Foley catheter into the bladder (B) and through a balloon catheter into the distal colostomy limb (arrowhead). Contrast material from the rectum (R) fills the duplicated vaginas (asterisks). The narrow distal rectum inserts into a midline septum between the vaginas (arrow). **B**, Sagittal fluoroscopic image shows the distal common vaginal channel (arrowhead) uniting with the urethra (white arrow) to form a common perineal channel (black arrow). B, bladder; R, rectum; asterisks, vaginas.

Sonography is often the first imaging modality used in the investigation of girls with vaginal rhabdomyosarcoma (Fig. 34-25). However, MRI or CT is required to fully assess the extent of pelvic disease, and chest CT is performed to assess for pulmonary metastases.

### PRIMARY AMENORRHEA

Fewer than 10% of girls have menarche before age 11, whereas 90% have begun to menstruate by age 13.75 years.<sup>30,31</sup> The term *primary amenorrhea* refers to the absence of menarche by the age of 15 years. Causes include gonadal dysgenesis (50%); hypothalamic hypogonadism (20%); absence of the vagina, cervix, or uterus (15%); imperforate hymen or transverse vaginal septum (5%); pituitary disease (5%); and other disorders (polycystic ovary syndrome [PCOS], congenital adrenal hyperplasia, and androgen insensitivity) (5%).<sup>32</sup> Ultrasound imaging is usually performed in the initial evaluation of these patients. The need for additional imaging studies is determined by the associated abnormalities.

PCOS affects 6% to 8% of females of reproductive age and is the most common endocrinopathy in premenopausal women.<sup>33</sup> There is no consensus regarding diagnostic criteria and treatment, despite its high prevalence. The Androgen Excess Society criteria for PCOS include (a) hyperandrogenism (hirsutism or hyperandrogenemia) and

(b) ovarian dysfunction (oligoanovulation or polycystic ovaries at ultrasound examination).<sup>34</sup> The diagnosis of PCOS in young adolescents is especially difficult, because mild hyperandrogenemia and transient oligomenorrhea are common in the first years following the onset of menarche.

The ovaries may appear normal or enlarged on ultrasound images, with multiple small follicles (Fig. 34-26). In 2003, the Rotterdam ultrasound criteria defined polycystic ovaries as the presence of 12 or more follicles measuring 2 to 9 mm in diameter or an ovarian volume of more than 10 mL in at least one ovary, as measured at transvaginal sonography.<sup>35</sup> Because most adolescents will undergo transabdominal and not transvaginal sonography, measurement of the number of ovarian follicles is difficult, and volume determinations are usually used as the main sonographic diagnostic criterion for PCOS in adolescents. However, clinical or biochemical evidence of hyperandrogenism is also extremely important in addition to observation of polycystic ovarian morphology (PCOM) in making the diagnosis of PCOS. Recent research and clinical experience have suggested that the number of follicles per ovary required for making the diagnosis of PCOS be increased, partly because of the improvement in technology and the resolution of ultrasound transducers. In 2014, a task force for the Androgen Excess and PCOS Society advised that 25 or more follicles per ovary be observed in women between the ages of 18 and 35 years



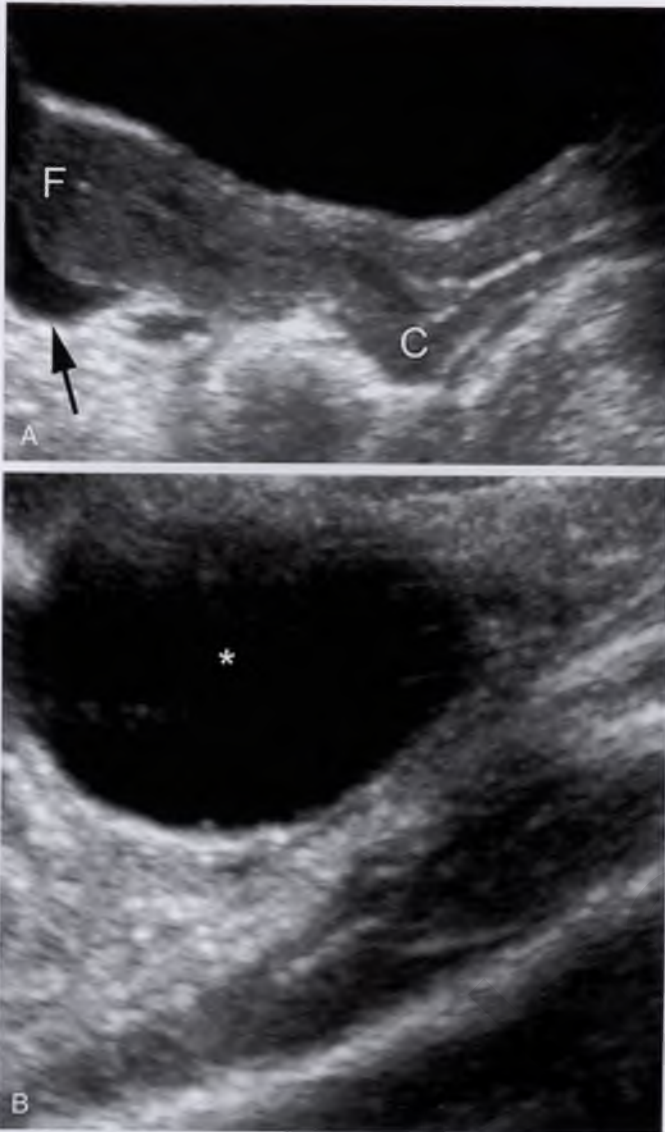


**FIG 34-22** Estrogen-secreting ovarian cyst in a 5-year-old girl with premature breast development and vaginal bleeding. **A**, Sagittal ultrasound image of the pelvis depicts a peripubertal appearance of the uterus, with relative prominence of the uterine fundus (F) compared to the cervix (C). There is a small amount of free pelvic fluid (*arrow*). **B**, Sagittal ultrasound image of the right ovary reveals a large (5 cm diameter) simple cyst (*asterisk*).

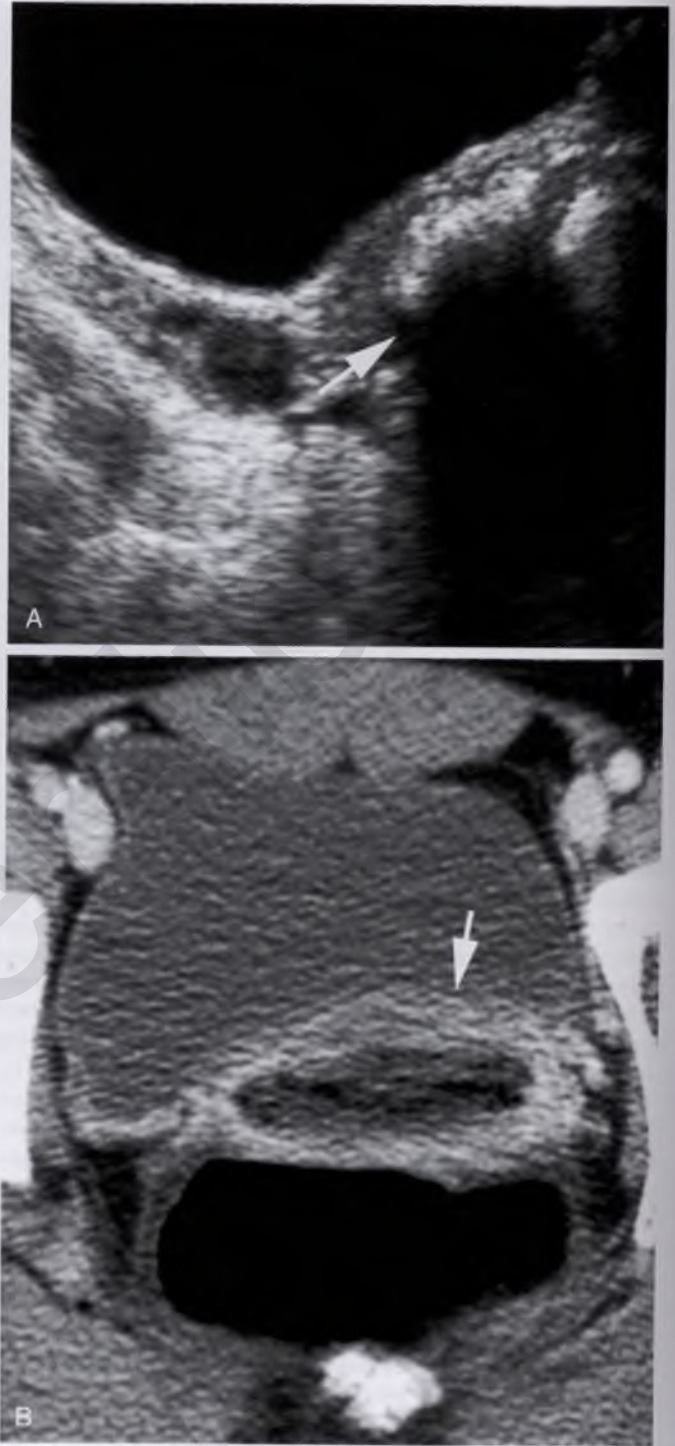


**FIG 34-23** Vaginal foreign body in a 16-year-old girl with chronic abdominal pain. **A**, Sagittal ultrasound image of the pelvis shows echogenic material distending the vaginal lumen with pronounced distal acoustic shadowing (*arrow*). **B**, Axial, intravenous contrast-enhanced computed tomography image of the pelvis reveals thickened, hyperemic vaginal mucosa (*arrow*) with air and debris within the vaginal lumen. A retained tampon was discovered on speculum examination.

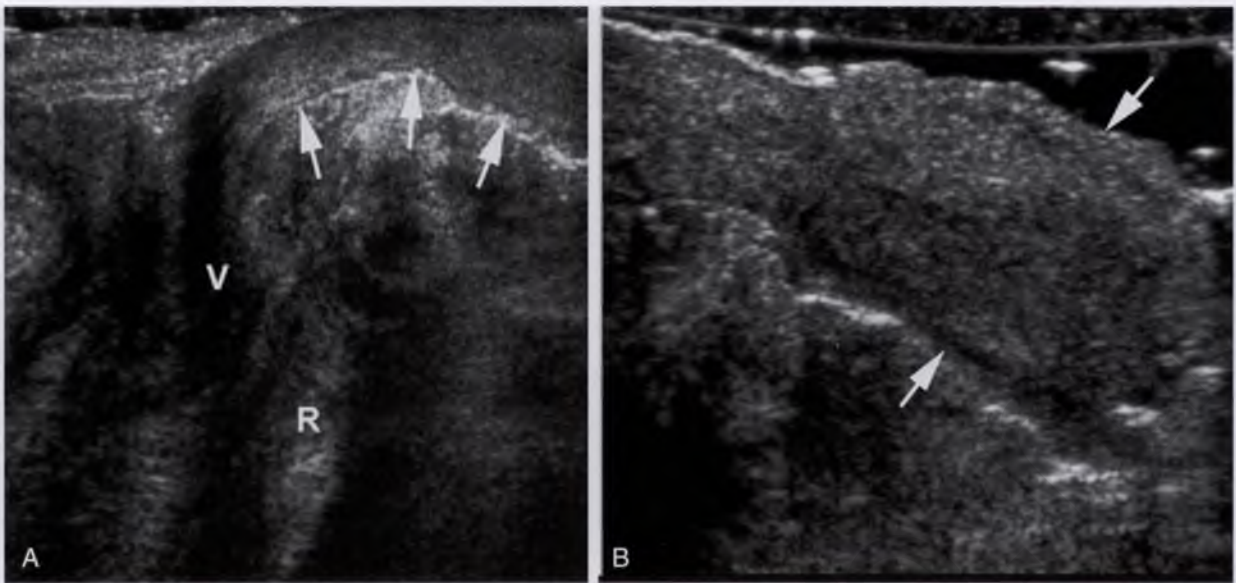


**FIG 34-24** Fibroepithelial polyp in a 17-year-old girl with a mass protruding from the vagina. **A** and **B**, Sagittal transperineal ultrasound images depict a solid mass (*arrows*) extending through the vaginal lumen (V). R, rectum.

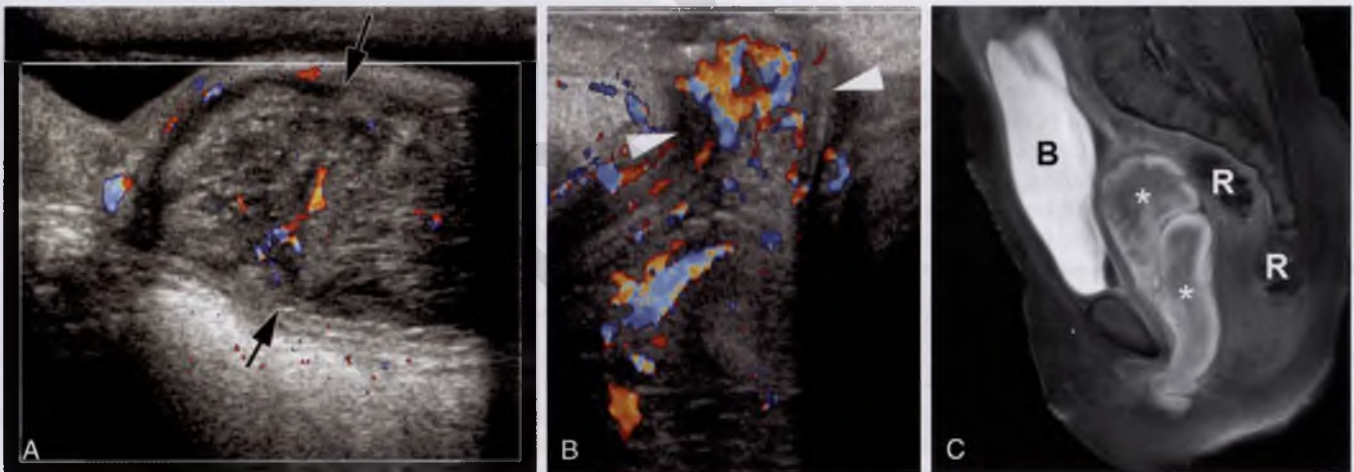


**FIG 34-25** Vaginal rhabdomyosarcoma in a 16-month-old girl. **A**, Sagittal color Doppler ultrasound image of the pelvis shows a solid mass with vascularity filling the vaginal lumen (*between arrows*). **B**, Sagittal transperineal color Doppler ultrasound image demonstrates protrusion of the mass through the introitus (*between arrowheads*). **C**, Sagittal, intravenous contrast-enhanced, fat-suppressed, T1-weighted magnetic resonance image of the pelvis depicts the lobulated solid mass (*asterisks*) between the bladder (B) and rectum (R).





**FIG 34-26** Polycystic ovary syndrome in a 14-year-old girl with obesity, hirsutism, and irregular menstrual periods. Sagittal ultrasound image demonstrates an enlarged right ovary (volume 20.3 mL) with numerous small, intraparenchymal follicles. See Video 34-4.

before making the diagnosis of PCOM, provided the transducer frequency is 8 MHz or higher.<sup>36</sup> Otherwise, ovarian volume of 10 mL or more was the most reliable finding. The task force also advised that PCOM might be inconsequential or representative of very mild PCOS in women without clinical or biochemical evidence of androgen excess.<sup>36</sup> However, these new recommendations have not been adopted by the ASRM.

## PELVIC PAIN

Common causes of pelvic pain in girls include adnexal torsion, hemorrhagic ovarian cyst, pelvic inflammatory disease, ectopic pregnancy, and appendicitis. On rare occasion, the uterus or ovaries may herniate through the canal of Nuck into the labia majora, resulting in a mass with or without associated pain.

### Adnexal (Ovarian or Tubal) Torsion

Partial or complete rotation of the ovary around its vascular pedicle compromises venous and lymphatic drainage and arterial inflow. Torsion is almost always unilateral, and pathologic findings range from massive edema to parenchymal necrosis. Peak incidence of adnexal torsion occurs in adolescence and young adulthood.<sup>37</sup> Ovarian torsion in neonates and premenarcheal girls is unusual as most cases are related to the presence of an ovarian cyst, which is rare in this population. However, torsion of a normal adnexum can occur as a result of hypermobility due to lax supporting ligaments.

The affected ovary is always enlarged, with an average volume 12 times that of the opposite normal ovary.<sup>38</sup> A ratio of torted adnexal volume to normal adnexal volume greater than 20 is predictive of an associated ovarian mass, whereas a ratio less than 20 is predictive of absence of an ovarian mass.<sup>38</sup> The only relatively specific sign of torsion

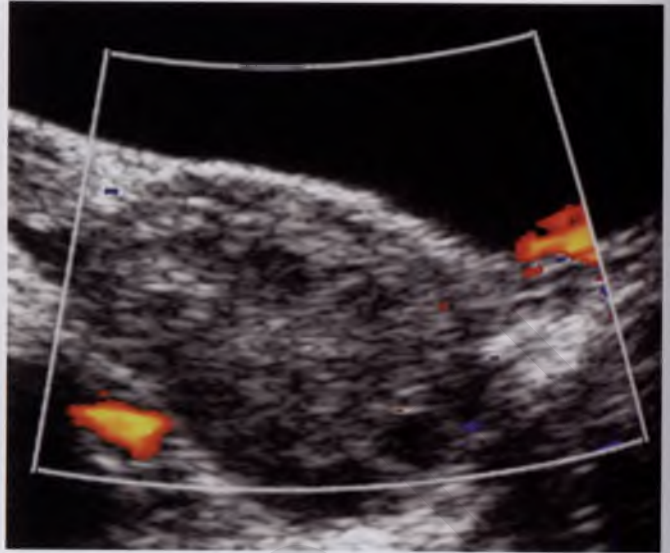


**FIG 34-27** Adnexal torsion in a 14-year-old girl with a 3-day history of progressive right lower quadrant pain. Power Doppler ultrasound image of the right adnexa reveals an enlarged, avascular ovary with mildly enlarged, peripheral follicles. Right ovarian volume was 143 mL, and left ovarian volume was 13.7 mL (not shown). At surgery there was no associated right ovarian mass.

is the presence of multiple mildly enlarged (8-12 mm), peripherally located follicles, thought to be displaced by transudation of fluid into the central ovarian stroma as a result of vascular congestion (Fig. 34-27). Although arterial flow is often absent or reduced, the presence of Doppler detected blood flow does not exclude the diagnosis of ovarian torsion. Isolated torsion of the fallopian tube is rare but can occur in adolescents. On ultrasound image, an anechoic V- or U-shaped tubular structure with a beaked appearance of the ends may be observed, often superior and midline relative to the normal appearing ovary.

### Ovarian Cyst

Ovarian cysts may be functional or nonfunctional. Functional cysts result from gonadotropin stimulation of the ovary and can be of follicular, corpus luteal, or theca luteal origin. Nonfunctional cysts include paraovarian and peritoneal inclusion cysts.

Functional cysts have a bimodal age distribution, with peaks of incidence in the neonatal period and in adolescence. Some functional cysts are hormonally active and cause gonadotropin-independent (peripheral) precocious puberty and, therefore, may present with vaginal bleeding or premature breast development (see Fig. 34-22). Nonfunctional ovarian cysts manifest as nonresolving cystic ovarian masses. Both types of cysts frequently present with either increasing abdominal girth noted by a parent or physician or as an asymptomatic abdominal mass. Additional, less common presentations include acute, severe pain that mimics appendicitis or peritonitis due to hemorrhage, torsion, or perforation; intermittent pain from torsion without complete compromise of the vascular supply; or chronic abdominal pain. Nonspecific symptoms also occur, such as bloating, nausea, vomiting, urinary retention, and frequency. Simple ovarian cysts and hemorrhagic corpus luteal cysts are common in postpubertal girls.

Occasionally, ovarian cysts are detected prenatally. They are usually unilateral, and the majority are thought to result from ovarian stimulation by fetal and maternal gonadotropins. They may be simple or complex by ultrasound imaging and are often displaced cephalad into



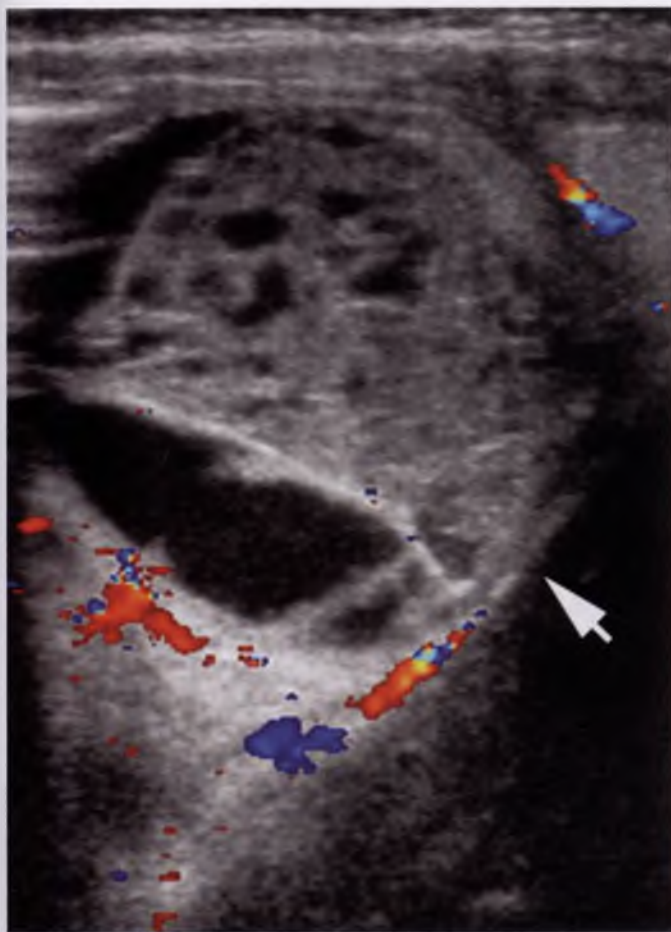


**FIG 34-28** Prenatally detected ovarian cyst complicated by torsion. Sagittal postnatal ultrasound image obtained at 37 days of age shows a left adnexal cyst containing heterogeneous, nonvascular, moderately echogenic material consistent with retracting blood clot (*arrow*). Follow-up ultrasound examination at 6 months of age documented resolution of the cyst. The left ovary could not be identified, in keeping with torsion resulting in infarction and loss of left ovarian parenchyma. The right ovary appeared normal (not shown).

the abdomen, where they may be palpable at birth. Most are asymptomatic, and spontaneous regression occurs after birth. Serial ultrasound studies are performed to document regression, which usually occurs within 3 to 4 months but can take as long as a year.<sup>39</sup>

Bleeding into an ovarian cyst in utero or after birth has a high association with long-term ovarian loss, generally thought to be due to torsion (Fig. 34-28), although some experts believe that ovarian dysgenesis may be the underlying cause.<sup>40,41</sup> The age of the blood within a hemorrhagic ovarian cyst will determine its sonographic features. Fresh blood is hyperechoic relative to the ovarian parenchyma, older blood appears heterogeneous and hypoechoic, but a gelatinous blood clot is anechoic. As the red blood cells lyse, a hemorrhagic cyst may develop a lace-like or reticular pattern of internal echoes as a result of the development of fibrin strands. As the clot coalesces, an echogenic mass with retractile or concave/scalloped margins will be observed. Both of these patterns of internal echoes are very specific for the sonographic appearance of hemorrhagic cysts. Eventually as the clot continues to be resorbed, it will develop a lentiform shape and may become adherent to the cyst wall. The pattern of internal echoes will change over time. Color or power Doppler interrogation will demonstrate no evidence of internal vascularity.

Ultrasound imaging is used to assess whether an ovarian cyst is simple or complex and to determine cyst measurement. Simple cysts or cysts with internal debris suggestive of hemorrhage are managed conservatively, with follow-up imaging performed after 4 to 8 weeks to document regression. If the cyst persists at follow-up but the sonographic features are reassuring, continued observation is appropriate. When a simple ovarian cyst persists, increases in size to more than 5 cm in diameter, or becomes symptomatic, surgery should be considered.<sup>42,43</sup>

### Pelvic Inflammatory Disease

Pelvic inflammatory disease predominantly affects girls of reproductive age and is most often due to an ascending sexually transmitted infection. Common causative organisms include *Chlamydia trachomatis* and *Neisseria gonorrhoeae*, although many infections are polymicrobial. The diagnosis is usually established clinically on the basis of pelvic pain, tenderness, vaginal discharge, elevated white blood cell count, and fever.<sup>44</sup>

Ultrasound findings depend on the stage of the inflammatory process. Early in the course of infection, minimal (if any) imaging abnormalities are detectable. Ultrasound examination is useful in identifying complications of pelvic inflammatory disease, including pyosalpinx and tubo-ovarian abscess. Pyosalpinx appears either as a round or oval periovarian adnexal mass with low-level echoes due to the presence of purulent debris (Fig. 34-29) or as a thick-walled, fluid-filled tubular structure that is often S- or V-shaped. There is a range of ovarian involvement, including enlargement and increased echogenicity; tubo-ovarian complex, consisting of an abnormal adherence and indistinctness of the ovary and fallopian tube surrounded by complex purulent material; and tubo-ovarian abscess that consists of a complex intraovarian or periovarian mass without identifiable ovarian tissue.<sup>45</sup>

### Ectopic Pregnancy

A complete discussion of ectopic pregnancy is beyond the scope of this chapter and is covered in detail in Chapter 33. However, it is important to recognize that ectopic pregnancy may rarely occur in young adolescents, who have the highest reported death rate from this condition. The diagnosis should be considered in the presence of pelvic pain, vaginal bleeding, or a missed menstrual period. Ultrasound examination should be performed, and if an intrauterine pregnancy or ectopic pregnancy is not clearly identified, correlation with serum  $\beta$ -human chorionic gonadotropin (hCG) levels should be obtained.<sup>46</sup> Although no single serum hCG level should be used to definitively differentiate an intrauterine from an ectopic pregnancy, if the serum hCG level is above 3000 mIU/mL (First International Reference Preparation) and the uterus is empty on transvaginal sonography, an ectopic pregnancy should be strongly considered and the patient should be followed carefully with serial hCG levels and transvaginal sonography if clinically stable.<sup>47</sup>

### Acute Appendicitis

Acute appendicitis is the most frequent pediatric surgical emergency. Symptoms of acute appendicitis overlap with a number of other gastrointestinal conditions, including Crohn disease and mesenteric adenitis, as well as acute gynecologic conditions. Patients usually present with right lower quadrant pain, tenderness, and leukocytosis.

The appendix is best imaged with a high-frequency linear-array ultrasound transducer using graded-compression technique. The inflamed appendix appears as a noncompressible, tubular, nonperistalsing, blind-ending structure exhibiting a striated gut wall signature and with an outer-to-outer diameter measuring larger than 6 mm.<sup>48</sup>



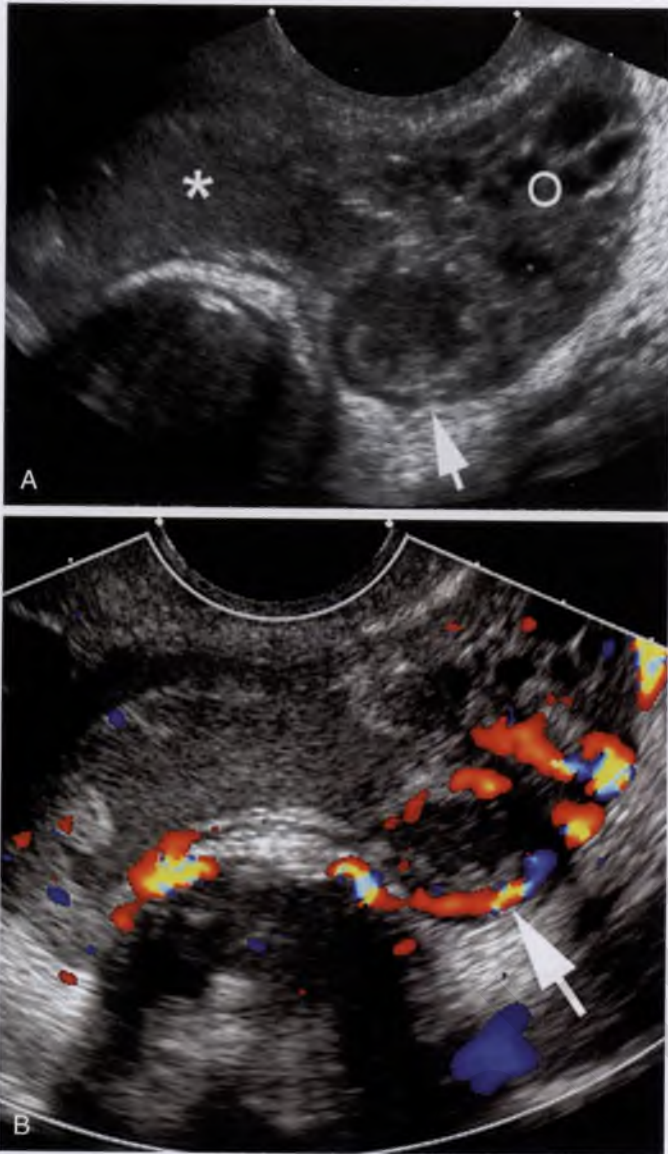


**FIG 34-29** Pyosalpinx in a sexually active 18-year-old girl with gonococcal infection. **A**, Transvaginal ultrasound image demonstrates a thick-walled fallopian tube containing echogenic material and redundant nodular echogenic endothelial surface (arrow) consistent with chronic inflammation, adjacent to the normal left ovary (O). Echogenic fluid is identified within the pelvis (asterisk). **B**, Transvaginal color Doppler ultrasound image reveals hyperemia of the wall of the left fallopian tube (arrow). See Video 34-5.

The appendiceal wall may be hyperemic. Echogenic (with or without acoustic shadowing) intraluminal stones (appendicoliths), increased echogenicity and vascularity of the periappendiceal fat indicative of periappendiceal inflammation, and walled-off fluid collections consistent with abscess formation are also readily depicted sonographically (Fig. 34-30). Advantages of using ultrasound for the diagnosis of appendicitis compared to CT include lack of ionizing radiation, no need for sedation or contrast material, and lower cost.

In our practice, we perform an initial ultrasound examination in children with a suspected diagnosis of acute appendicitis. Cross-sectional imaging with CT or MR is performed only in patients in whom the appendix is not visualized by ultrasound, in patients with a strong clinical suspicion for acute appendicitis and an equivocal

ultrasound study, or in patients with suspected perforated appendix when more complete assessment of inflammatory changes and fluid collections is necessary for management purposes.<sup>49-51</sup>

### Genital Hernia

Inguinal herniation of the uterus or ovaries is a rare condition that may be complicated by torsion, strangulation, and infertility. These indirect, congenital hernias develop when there is a failure of closure of the processus vaginalis between the 36th and 40th weeks of gestation. Abdominal or pelvic contents may herniate through the canal of Nuck into the labia majora (Fig. 34-31).<sup>52</sup> Patients may present with pain or a palpable mass.

## GYNECOLOGIC PELVIC MASSES

Gynecologic masses presenting in girls include ovarian cysts, primary ovarian neoplasms, metastatic ovarian disease, hematocolpos, primary vaginal and uterine neoplasms, and pregnancy.

### Ovarian Masses

Ovarian masses include non-neoplastic cysts as well as benign and malignant ovarian tumors. Most ovarian tumors in children are benign and of germ cell origin.

### Ovarian Tumors

Ovarian tumors may arise from surface epithelium, germ cells, or stroma. The majority develop in the second decade of life, with teratoma (also termed dermoid cyst) being the most common. Teratomas are typically composed of elements of all three germ cell layers, with 90% classified as mature and 10% classified as immature (containing embryonic neural elements) or malignant.<sup>53</sup>

Cystic mature teratomas account for more than 90% of all benign ovarian tumors. They are usually unilateral, although 10% to 20% are bilateral. Most tumors range from 5 to 10 cm in diameter. Ectodermal components predominate, with the sonographic appearance dependent on the relative amounts of calcium, hair, fat, sebum, and serous fluid within the lesion.<sup>29,54,55</sup> The majority are complex in appearance with soft tissue elements composing less than 50% of the mass by volume (Fig. 34-32).

Malignant ovarian tumors are uncommon in the pediatric patient population, accounting for only 1% to 2% of all malignant tumors in children younger than 17 years of age.<sup>56-58</sup> Malignant germ cell neoplasms usually occur in postmenarcheal girls and most often manifest as an asymptomatic abdominal or pelvic mass. They are typically larger than 10 cm in diameter at the time of diagnosis. Intra-abdominal spread occurs to the liver and lymph nodes. Dysgerminoma is the most frequent ovarian malignancy in childhood, and 10% are bilateral. Malignant teratomas contain more than 50% soft tissue elements by volume (Fig. 34-33). Other germ cell tumors may be either homogeneous and echogenic sonographically or complex with cystic areas related to hemorrhage.<sup>29,53-55</sup>

Sex cord-stromal tumors are low-grade malignancies that arise from the Sertoli cells and granulosa theca cells of the embryonic gonad. They usually develop in prepubertal girls and are generally asymptomatic. Sertoli-Leydig cell tumors may cause virilization due to androgen production. Granulosa theca cell tumors may cause isosexual precocity as a result of estrogen production. These tumors appear as heterogeneous masses with cystic foci on ultrasound imaging (Fig. 34-34). Metastases are unusual but may occur within the liver or along the peritoneum.<sup>29,53-55</sup>

The most common epithelial ovarian tumors are serous and mucinous cystadenomas, most of which are large and benign. They do not



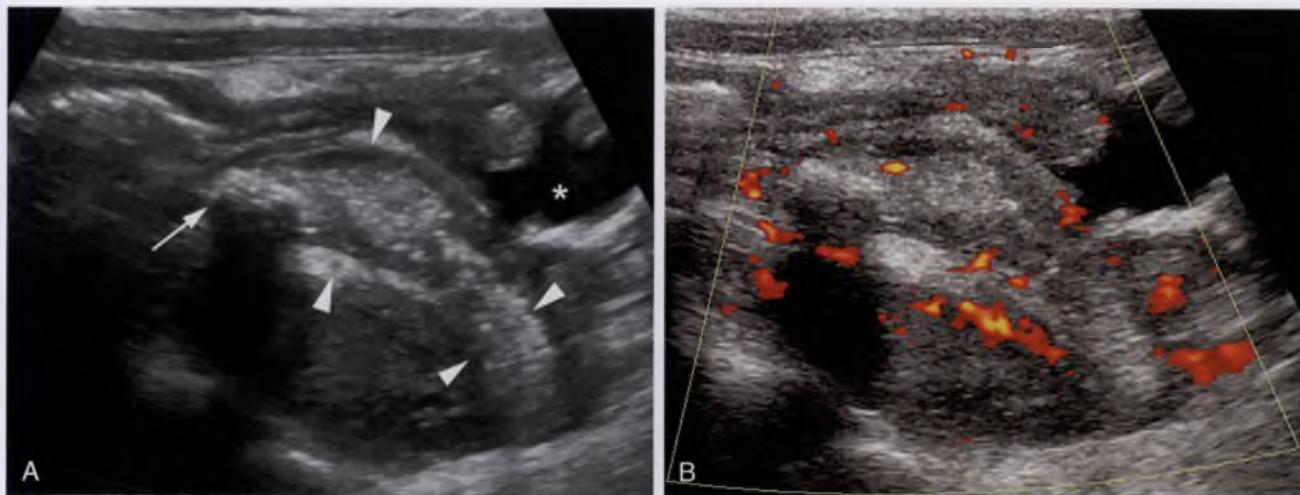


**FIG 34-30** Perforated appendicitis in a 5-year-old girl with abdominal pain. **A**, Sagittal ultrasound image of the right lower quadrant of the abdomen reveals a dilated appendix (*arrowheads*) containing echogenic material as well as a hyperechoic appendicolith at its base (*arrow*), associated with distal acoustic shadowing. There is a small amount of adjacent free fluid (*asterisk*). **B**, Sagittal power Doppler ultrasound image depicts hyperemia of the soft tissues adjacent to the inflamed appendix.

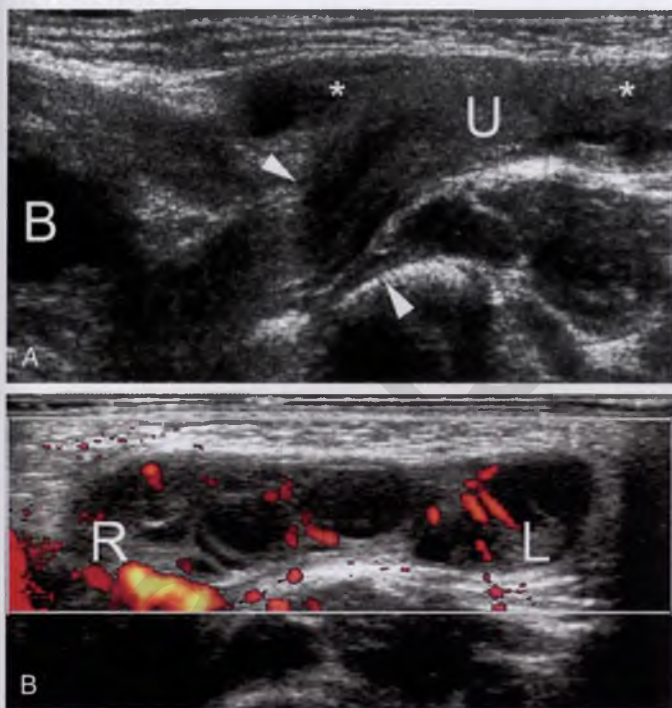


**FIG 34-31** Incarcerated inguinal hernia in a 2-month-old girl. **A**, Transverse ultrasound image of the left groin shows the uterus (U) extending through a fascial defect (*between arrowheads*) into the soft tissues of the left labium majus. The uterus is interposed between the right and left ovaries (*asterisks*). **B**, bladder. **B**, Transverse power Doppler ultrasound image of the left groin demonstrates blood flow to both inguinal ovaries. An incarcerated indirect inguinal hernia was surgically reduced. L, left ovary; R, right ovary. See Video 34-6.



**FIG 34-32** Ovarian dermoid cyst (mature teratoma) in a 17-year-old girl. Sagittal ultrasound image of the right adnexa reveals a complex mass containing cystic (*asterisk*) and solid, echogenic (*arrow*) components.



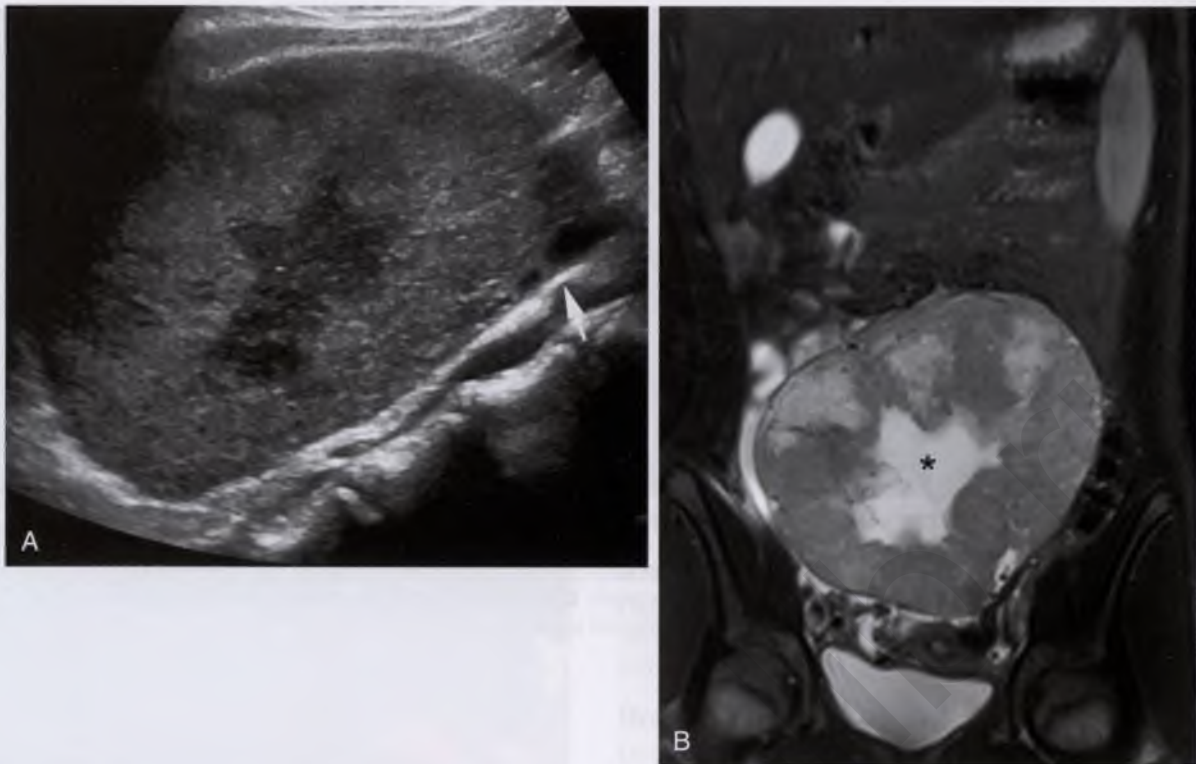


**FIG 34-33** Ovarian dysgerminoma in an 11-year-old girl with abdominal pain, large abdominal mass, and an elevated serum hCG level. **A**, Sagittal ultrasound image demonstrates a large, predominantly solid lesion arising from the right ovary. A few normal-appearing ovarian follicles are noted adjacent to the lower pole of the mass (*arrow*). **B**, Coronal T2-weighted, fat-suppressed magnetic resonance image reveals a 14-cm diameter tumor with central necrosis (*asterisk*). Central geographic hypoechoic area likely represents central necrosis or edema. See Video 34-7.

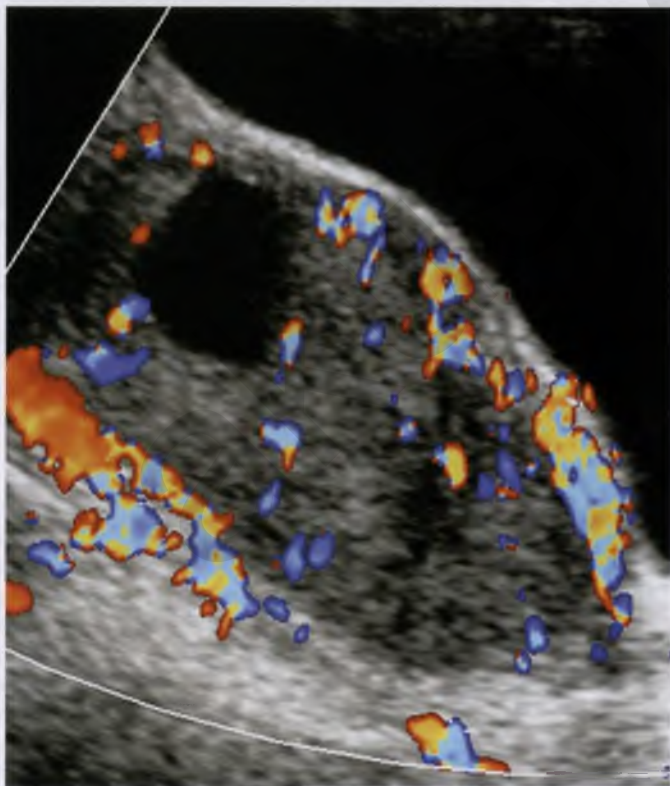


**FIG 34-34** Granulosa cell tumor in a 16-year-old girl undergoing evaluation for primary amenorrhea. Sagittal color Doppler ultrasound image shows a predominantly solid pelvic mass with a prominent anechoic cystic component.

usually develop prior to puberty.<sup>59</sup> A serous cystadenoma is usually a unilocular, thin-walled cystic mass that may contain thin septations and papillary projections; about 20% are bilateral. A mucinous cystadenoma most often presents as a multiloculated cystic mass with thin septations (Fig. 34-35). Papillary projections are identified less frequently, and bilateral ovarian involvement is less common than with serous cystadenomas.<sup>29,54</sup>

Although little has been reported on the subject of metastatic ovarian tumors in children, the ovaries can harbor leukemia,<sup>60</sup> and metastatic spread to the ovaries from neuroblastoma, rhabdomyosarcoma,<sup>61</sup> Burkitt lymphoma,<sup>62</sup> and colon cancer has been documented. Metastatic ovarian involvement is frequently asymptomatic and diagnosed only at autopsy.<sup>63</sup>

### Pregnancy

Pregnancy should always be a diagnostic consideration when a pelvic mass develops in a girl aged 9 years or older. Complications of pregnancy including preeclampsia, placental abruption, and laceration occur more frequently in pediatric patients than in the adult population. There is also an increased need for cesarean delivery in the pregnant pediatric patient.<sup>64</sup>

### CONCLUSION

As the main imaging modality for evaluating the pediatric female pelvis, sonography is useful in depicting ovarian and uterine anatomy; assessing children with ambiguous genitalia; investigating prepubertal bleeding or primary amenorrhea; and in determining the cause of pelvic pain and the origin of pelvic masses.



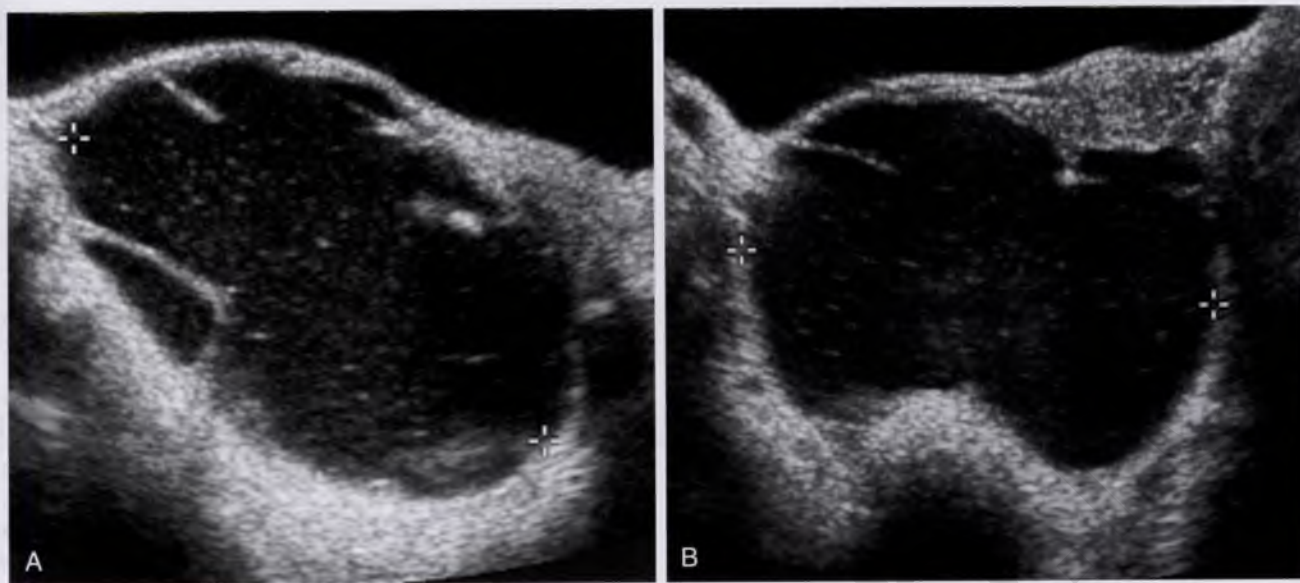


**FIG 34-35** Mucinous cystadenoma in a 15-year-old girl with prolonged vaginal bleeding. Sagittal (**A**) and transverse (**B**) ultrasound images depict a large, cystic mass in the right adnexal region (between cursors). The mass contains multiple septations and echogenic debris.

## REFERENCES

- Garel L, Dubois J, Grignon A, et al: US of the pediatric female pelvis: a clinical perspective. *Radiographics* 21(6):1393–1407, 2001.
- Ziereisen F, Guissard G, Damry N, Avni EF: Sonographic imaging of the paediatric female pelvis. *Eur Radiol* 15(7):1296–1309, 2005.
- Stranzinger E, Strouse PJ: Ultrasound of the pediatric female pelvis. *Semin Ultrasound CT MR* 29(2):98–113, 2008.
- Coley BD: Pediatric gynecologic ultrasound. *Ultrasound Clin* 7(1):107–121, 2012.
- Son JK, Taylor GA: Transperineal ultrasonography. *Pediatr Radiol* 44(2):193–201, 2014.
- Paltiel HJ, Phelps A: US of the pediatric female pelvis. *Radiology* 270(3):644–657, 2014.
- Orsini LE, Salardi S, Pilu G, et al: Pelvic organs in premenarcheal girls: real-time ultrasonography. *Radiology* 153(1):113–116, 1984.
- Cohen HL, Eisenberg P, Mandel F, Haller JO: Ovarian cysts are common in premenarchal girls: a sonographic study of 101 children 2–12 years old. *AJR Am J Roentgenol* 159(1):89–91, 1992.
- Cohen HL, Shapiro MA, Mandel FS, Shapiro ML: Normal ovaries in neonates and infants: a sonographic study of 77 patients 1 day to 24 months old. *AJR Am J Roentgenol* 160(3):583–586, 1993.
- Forrest TS, Elyaderani MK, Muilenburg MI, et al: Cyclic endometrial changes: US assessment with histologic correlation. *Radiology* 167(1):233–237, 1988.
- Laufer M: Structural abnormalities of the female reproductive tract. In Emans SJ, Laufer MR, editors: *Pediatric & Adolescent Gynecology*, ed 6, Philadelphia, 2012, Lippincott Williams & Wilkins.
- Buttram VC, Jr: Müllerian anomalies and their management. *Fertil Steril* 40(2):159–163, 1983.
- Buttram VC, Jr, Gibbons WE: Müllerian anomalies: a proposed classification (an analysis of 144 cases). *Fertil Steril* 32(1):40–46, 1979.
- The American Fertility Society classifications of adnexal adhesions, distal tubal occlusion, tubal occlusion secondary to tubal ligation, tubal pregnancies, müllerian anomalies and intrauterine adhesions. *Fertil Steril* 49(6):944–955, 1988.
- Oppelt P, Renner SP, Brucker S, et al: The VCUAM (Vagina Cervix Uterus Adnex-associated Malformation) classification: a new classification for genital malformations. *Fertil Steril* 84(5):1493–1497, 2005.
- Brody JM, Koelliker SL, Frishman GN: Unicornuate uterus: imaging appearance, associated anomalies, and clinical implications. *AJR Am J Roentgenol* 171(5):1341–1347, 1998.
- Junqueira BL, Allen LM, Spitzer RF, et al: Müllerian duct anomalies and mimics in children and adolescents: correlative intraoperative assessment with clinical imaging. *Radiographics* 29(4):1085–1103, 2009.
- Gibson ED: Transverse upper vaginal septum presenting in pregnancy: a case report and review of the literature. *Aust N Z J Obstet Gynaecol* 43(5):381–383, 2003.
- Lee PA, Houk CP, Ahmed SF, et al: Consensus statement on management of intersex disorders. *Pediatrics* 118(2):e488–e500, 2006.
- Hughes IA, Nihoul-Fekété C, Thomas B, Cohen-Kettenis PT: Consequences of the ESPE/LWPES guidelines for diagnosis and treatment of disorders of sex development. *Best Pract Res Clin Endocrinol Metab* 21(3):351–365, 2007.
- Jaramillo D, Lebowitz RL, Hendren WH: The cloacal malformation: radiologic findings and imaging recommendations. *Radiology* 177(2):441–448, 1990.
- Chavhan GB, Parra DA, Oudjhane K, et al: Imaging of ambiguous genitalia: classification and diagnostic approach. *Radiographics* 28(7):1891–1904, 2008.
- Mansfield MJ: Precocious puberty. In Emans SJ, Laufer MR, editors: *Pediatric & Adolescent Gynecology*, ed 6, Philadelphia, 2012, Lippincott Williams & Wilkins.
- Carel JC, Léger JN: Clinical practice: precocious puberty. *N Engl J Med* 358(22):2366–2377, 2008.
- Tannous WN, Azouz EM, Homsy YL, et al: CT and ultrasound imaging of pelvic rhabdomyosarcoma in children: a review of 56 patients. *Pediatr Radiol* 19(8):530–534, 1989.
- Agrons GA, Wagner BJ, Lonergan GJ, et al: From the archives of the AFIP. Genitourinary rhabdomyosarcoma in children: radiologic-pathologic correlation. *Radiographics* 17(4):919–937, 1997.
- Wexler LH, Meyer WH, Helman LJ: Rhabdomyosarcoma and the undifferentiated sarcomas. In Pizzo PA, Poplack DG, editors: *Principles and Practice of Pediatric Oncology*, ed 5, Philadelphia, 2006, Lippincott Williams & Wilkins.
- Fernandez-Pineda I, Spunt SL, Parida L, et al: Vaginal tumors in childhood: the experience of St. Jude Children's Research Hospital. *J Pediatr Surg* 46(11):2071–2075, 2011.



29. Shah RU, Lawrence C, Fickenscher KA, et al: Imaging of pediatric pelvic neoplasms. *Radiol Clin North Am* 49(4):729–748, 2011.
30. Wu T, Mendola P, Buck GM: Ethnic differences in the presence of secondary sex characteristics and menarche among US girls: the Third National Health and Nutrition Examination Survey, 1988–1994. *Pediatrics* 110(4):752–757, 2002.
31. Chumlea WC, Schubert CM, Roche AF, et al: Age at menarche and racial comparisons in US girls. *Pediatrics* 111(1):110–113, 2003.
32. Reindollar RH, Byrd JR, McDonough PG: Delayed sexual development: a study of 252 patients. *Am J Obstet Gynecol* 140(4):371–380, 1981.
33. Blank SK, Helm KD, McCartney CR, Marshall JC: Polycystic ovary syndrome in adolescence. *Ann N Y Acad Sci* 1135:76–84, 2008.
34. Azziz R, Carmina E, Dewailly D, et al: Position statement: criteria for defining polycystic ovary syndrome as a predominantly hyperandrogenic syndrome: an Androgen Excess Society guideline. *J Clin Endocrinol Metab* 91(11):4237–4245, 2006.
35. Rotterdam ESHRE/ASRM-Sponsored PCOS consensus workshop group: Revised 2003 consensus on diagnostic criteria and long-term health risks related to polycystic ovary syndrome (PCOS). *Hum Reprod* 19(1):41–47, 2004.
36. Dewailly D, Lujou ME, Carmina E, et al: Definition and significance of polycystic ovarian morphology: a task force report for the Androgen Excess and Polycystic Ovarian Syndrome Society. *Hum Repro Update* 20:334–352, 2014.
37. Rossi BV, Ference EH, Zurakowski D, et al: The clinical presentation and surgical management of adnexal torsion in the pediatric and adolescent population. *J Pediatr Adolesc Gynecol* 25(2):109–113, 2012.
38. Servaes S, Zurakowski D, Laufer MR, et al: Sonographic findings of ovarian torsion in children. *Pediatr Radiol* 37(5):446–451, 2007.
39. Kwak DW, Sohn YS, Kim SK, et al: Clinical experiences of fetal ovarian cyst: diagnosis and consequence. *J Korean Med Sci* 21(4):690–694, 2006.
40. Enriquez G, Durán C, Torán N, et al: Conservative versus surgical treatment for complex neonatal ovarian cysts: outcomes study. *AJR Am J Roentgenol* 185(2):501–508, 2005.
41. Ben-Ami I, Kogan A, Fuchs N, et al: Long-term follow-up of children with ovarian cysts diagnosed prenatally. *Prenat Diagn* 30(4):342–347, 2010.
42. Laufer M: Adnexal masses. In Emans SJ, Laufer MR, editors: *Pediatric & Adolescent Gynecology*, ed 6, Philadelphia, 2012, Lippincott Williams & Wilkins.
43. de Silva KS, Kanumakala S, Grover SR, et al: Ovarian lesions in children and adolescents—an 11-year review. *J Pediatr Endocrinol Metab* 17(7):951–957, 2004.
44. Shrier LA: Sexually transmitted infections: chlamydia, gonorrhea, pelvic inflammatory disease, and syphilis. In Emans SJ, Laufer MR, editors: *Pediatric & Adolescent Gynecology*, ed 6, Philadelphia, 2012, Lippincott Williams & Wilkins.
45. Cicchiello LA, Hamper UM, Scoutt LM: Ultrasound evaluation of gynecologic causes of pelvic pain. *Obstet Gynecol Clin North Am* 38(1):85–114, 2011.
46. Vichnin M: Ectopic pregnancy in adolescents. *Curr Opin Obstet Gynecol* 20(5):475–478, 2008.
47. Doubilet PM, Benson CB, Bourne T, et al: Diagnostic criteria for nonviable pregnancy early in the first trimester. *N Engl J Med* 369:1443–1451, 2013.
48. Jeffrey RB, Jr, Laing FC, Townsend RR: Acute appendicitis: sonographic criteria based on 250 cases. *Radiology* 167(2):327–329, 1988.
49. Krishnamoorthi R, Ramarajan N, Wang NE, et al: Effectiveness of a staged US and CT protocol for the diagnosis of pediatric appendicitis: reducing radiation exposure in the age of ALARA. *Radiology* 259(1):231–239, 2011.
50. Thirumoorthi AS, Fefferman NR, Ginsburg HB, et al: Managing radiation exposure in children—reexamining the role of ultrasound in the diagnosis of appendicitis. *J Pediatr Surg* 47(12):2268–2272, 2012.
51. Hennelly KE, Bachur R: Appendicitis update. *Curr Opin Pediatr* 23(3):281–285, 2011.
52. Patel B, Zivin S, Panchal N, et al: Sonography of female genital hernias presenting as labia majora masses. *J Ultrasound Med* 33:155–159, 2014.
53. Amies Oelschlager AM, Sawin R: Teratomas and ovarian lesions in children. *Surg Clin North Am* 92(3):599–613, 2012.
54. Epelman M, Chikwava KR, Chauvin N, Servaes S: Imaging of pediatric ovarian neoplasms. *Pediatr Radiol* 41(9):1085–1099, 2011.
55. Anthony EY, Caserta MP, Singh J, Chen MY: Adnexal masses in female pediatric patients. *AJR Am J Roentgenol* 198(5):W426–W431, 2012.
56. Barber HR: Ovarian cancer. *CA Cancer J Clin* 36(3):149–184, 1986.
57. von Allmen D: Malignant lesions of the ovary in childhood. *Semin Pediatr Surg* 14(2):100–105, 2005.
58. Brookfield KF, Cheung MC, Koniaris LG, et al: A population-based analysis of 1037 malignant ovarian tumors in the pediatric population. *J Surg Res* 156(1):45–49, 2009.
59. Morowitz M, Huff D, von Allmen D: Epithelial ovarian tumors in children: a retrospective analysis. *J Pediatr Surg* 38(3):331–335, 2003.
60. Kim JW, Cho MK, Kim CH, et al: Ovarian and multiple lymph nodes recurrence of acute lymphoblastic leukemia: a case report and review of literature. *Pediatr Surg Int* 24(11):1269–1273, 2008.
61. Young RH, Kozakewich HP, Scully RE: Metastatic ovarian tumors in children: a report of 14 cases and review of the literature. *Int J Gynecol Pathol* 12(1):8–19, 1993.
62. McCarville MB, Hill DA, Miller BE, Pratt CB: Secondary ovarian neoplasms in children: imaging features with histopathologic correlation. *Pediatr Radiol* 31(5):358–364, 2001.
63. Siegel MJ: Female pelvis. In Siegel MJ, editor: *Pediatric Sonography*, ed 4, Philadelphia, 2011, Lippincott Williams & Wilkins.
64. Black AY, Fleming NA, Rome ES: Pregnancy in adolescents. *Adolesc Med State Art Rev* 23(1):123–138, 2012.

# Ultrasound and Magnetic Resonance Imaging in Urogynecology

Milena M. Weinstein, Mark E. Lockhart

## SUMMARY OF KEY POINTS

- Endoanal sonography has an important role in the assessment of the anal sphincter in patients with fecal incontinence.
- Sonography and magnetic resonance imaging (MRI) of the pelvic floor can be useful in evaluation of women with pelvic floor disorders and in assessment of mesh implants.
- There is no strong evidence for *routine* use of pelvic floor sonography in assessment of women with pelvic floor disorders.
- Fistulas and perirectal abscess can be evaluated well by either sonography or MRI prior to therapy.
- Urethral diverticula are well seen by either sonography or MRI, although the direct connection to the urethra is best depicted with MRI.
- Criteria for postintervention and postsurgical evaluation are less well defined for both sonography and MRI.

## OUTLINE

**Pelvic Floor Anatomy and Function, 1026**

**Risk Factors and Indications for Dynamic Pelvic Imaging, 1027**

**Ultrasound Imaging, 1027**

Endoanal Sonography for Anal Incontinence, 1027

Endoanal Sonography for Fistulas and Perianal Abscesses, 1029

Transperineal Sonography of the Anal Sphincter, 1029

Pelvic Floor Sonography, 1030

**Dynamic Pelvic Floor Magnetic Resonance Imaging, 1034**

Technical Considerations, 1034

Anatomy and Magnetic Resonance Imaging Reference Lines, 1036

Abnormal Findings on Magnetic Resonance Imaging, 1036

Limitations of Magnetic Resonance Imaging, 1039

**Summary and Future Direction, 1040**

Pelvic organ prolapse (POP), fecal incontinence, and urinary incontinence in women have been largely ignored from an imaging perspective; recent innovations in both imaging and treatment options have increased attention on the evaluation and management of these conditions. Traditionally, there has been limited research focusing on imaging of female pelvic disorders other than malignancy. This may be in part due to reluctance of women to report this constellation of problems to their clinicians because of embarrassment or because they ascribe these symptoms to a “part of life” that is to be expected with aging and childbirth. However, pelvic floor dysfunction is a significant medical and quality of life issue, and pelvic floor disorders have been reported to affect one in four of all women. Although prevalence increases with age,<sup>1</sup> pelvic floor disorders should not be considered a normal part of aging.

Pelvic floor disorders include POP, urinary incontinence, and anal incontinence. These conditions may manifest with a variety of urinary and defecatory symptoms as well as pain and sexual dysfunction. *Urinary incontinence* (UI) is defined as involuntary leakage of urine.<sup>2</sup> There are two common subtypes—stress urinary incontinence and urgency urinary incontinence. *Stress urinary incontinence* occurs in response to increased intra-abdominal pressure that occurs during exertion, strain, coughing, or sneezing. *Urgency urinary incontinence* occurs at the time of sensation of urgency to urinate. The combination of urinary urgency and frequency is also referred to as *overactive bladder syndrome*.

*Anal incontinence* is the involuntary loss of feces or flatus.<sup>2</sup> The underlying cause of anal incontinence is often an anal sphincter defect following vaginal delivery<sup>3</sup> and less commonly direct trauma, including surgery. However, a variety of other factors can contribute. Neurogenic disorders may result in anal incontinence in the setting of an intact anal sphincter and may be caused by traction neural injury during delivery, as well as by diabetes, certain medications, radiation therapy, and aging. Fecal incontinence is six to eight times more common in women than in men, and the incidence increases with aging. The incidence is highest among multiparous older women, and it is estimated that up to 15% of multiparous women in the United States over the age of 64 years may have fecal incontinence to some degree.

Female pelvic medicine and reconstructive surgery (FPMRS) and urogynecology focus on diagnosis and treatment of pelvic floor disorders. A wide variety of treatment options is available for pelvic floor disorders, ranging from conservative measures, such as pelvic floor muscle training, physical therapy, medications, and supportive devices, to surgical intervention. The lifetime chance of having primary surgery for POP or stress urinary incontinence is estimated to be 20% by the age of 80 years.<sup>4</sup> Many do not seek care, but even the few who seek help may not be effectively treated if multicompartmental disease is not fully appreciated and addressed.<sup>5</sup> Unfortunately, recurrence rate is high, leading to reoperation in 30% of women.<sup>6</sup> Until successful treatment is realized, the impact on a woman's daily quality of life can be



significant. Persistent symptoms such as pain or incontinence can be both debilitating as well as embarrassing and may carry significant psychosocial implications.

Despite ongoing efforts to improve understanding of pelvic floor disorders, the underlying pathophysiologic mechanism is not fully elucidated. Although clinical assessment and examination remain the mainstay of pelvic floor evaluation, imaging has emerged as a potentially useful modality. Indeed, clinicians have begun to avoid using terms such as *cystocele* and *rectocele*, recognizing that the physical examination only identifies prolapse of the vaginal walls—whether anterior and posterior—and cannot identify with certainty the pelvic organs lying behind the vaginal walls. Pelvic floor imaging, however, clarifies the specific anatomy underlying these conditions and potentially helps in understanding the physiologic and pathophysiologic changes. Assessment of anatomy and function using pelvic floor imaging is used increasingly to improve understanding of pelvic floor disorders and hence optimize treatment approaches. However, despite more than 2 decades of imaging research in pelvic floor disorders, imaging still plays a rather limited role in the evaluation of pelvic floor disorders at most institutions.

## PELVIC FLOOR ANATOMY AND FUNCTION

The pelvic floor is a complex structure encompassing an interplay of smooth and striated musculature that, along with both fascia and ligaments, supports and assists in the function of the pelvic floor organs. The main muscles of the pelvic diaphragm are the levator ani muscles, comprising the pubococcygeus, puborectalis, and iliococcygeus muscles. These muscles span the space between the obturator internus muscle laterally, the pubis symphysis anteriorly, and the coccyx posteriorly. The levator hiatus is a funnel-shaped cleft in the muscles of the levator ani

from which exit the urethra, the vagina, and the anal canal.<sup>7</sup> The puborectalis muscle (PRM) is the most inferior (caudal) muscle of the pelvic floor. The two sides of the PRM attach to the two pubic rami anteriorly and merge posterior to the anal canal to form the anorectal angle.<sup>8</sup> The superficial muscles of the pelvic floor make up the *urogenital diaphragm* and include the ischiocavernosus, bulbospongiosus, and transversus perinei superficialis muscles (Fig. 35-1).

Fecal continence is maintained by both constriction of the anal canal as well as anorectal lift of the pelvic floor. The normal anal canal extends proximally from the puborectalis portion of the levator ani muscles to the anal verge, for a distance of approximately 4 cm. The structures surrounding the anal canal are responsible for maintaining fecal continence and include the *internal anal sphincter* (IAS), the *external anal sphincter* (EAS), and the PRM. The EAS encircles the anal canal and is a striated muscle that is under voluntary control. The superficial portion of the EAS muscle is attached posteriorly to the coccyx through the anococcygeal ligament and anteriorly inserts into the perineal body. The deep portion surrounds the anal canal with some integration with the PRM posteriorly and some fibers of this portion interdigitate with the deep transverse perineal muscles. The subcutaneous portion of the EAS is the portion that surrounds the anal canal most distally, approximately 1 cm below the termination of the IAS. The IAS is a smooth muscle, which is under autonomic control and is responsible for 80% of the resting anal sphincter tone. The IAS is created by thickening of the circular smooth muscle in the rectal wall and represents the terminal portion of the inner circular smooth muscle layer of the intestinal tract. The IAS is shorter in length than the EAS, terminating approximately 1 cm distal to the dentate line. The dentate line represents the junction of the subcutaneous and superficial components of the EAS. In addition to these two circular muscle layers, a longitudinal muscle layer extends between the EAS and IAS

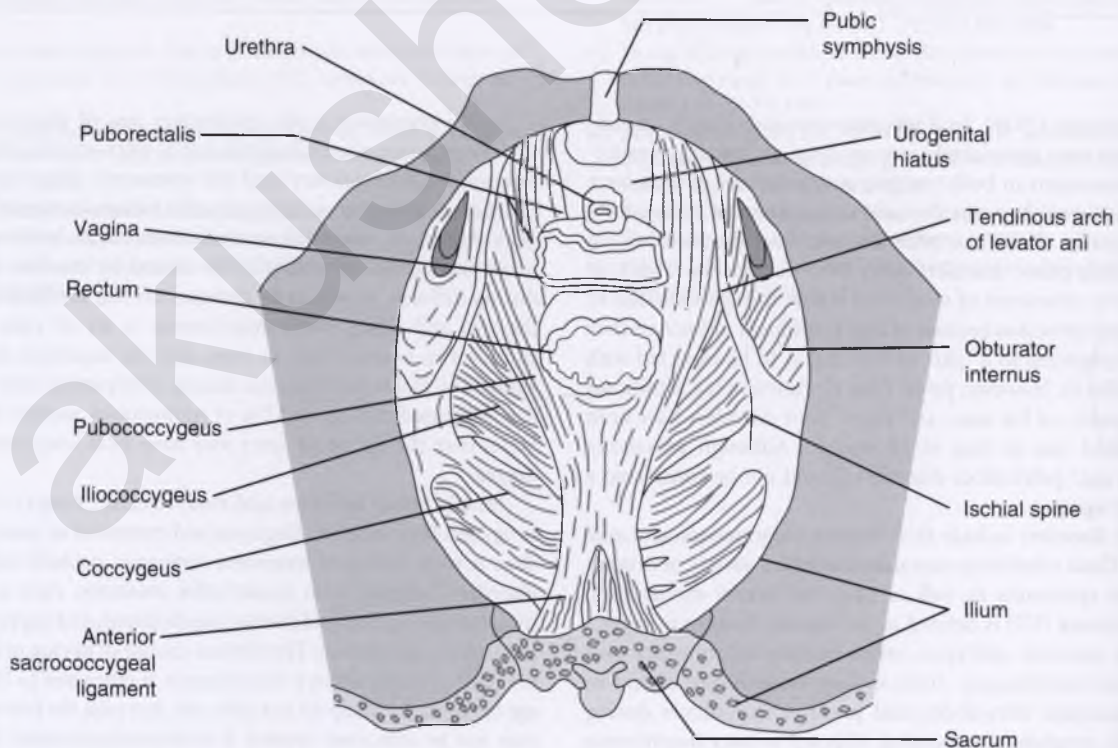


**FIG 35-1** Pelvic floor muscle anatomy. Pelvic floor muscles fill up the “bowl” of the pelvis. The levator ani muscles are composed of the puborectalis, pubococcygeus, and iliococcygeus portions. (Illustration by Rose Katz.)



and serves to anchor the sphincter complex to the fascia of the levator ani as well as to the pelvic side wall.<sup>9</sup>

The perineum separates the anus from the vagina. The central portion of the perineum contains the perineal body, which is the point where the EAS, the bulbospongiosus, and the superficial and deep transverse perineal muscles meet. The presence of a thick perineal body is suggestive of a normal anal sphincter.<sup>10</sup>

The female urethra is a tubular conduit that passes through the retropubic space, perforating the perineal membrane to terminate at its external orifice (external urethral meatus) in the vaginal vestibule directly ventral to the vaginal opening. The normal female urethra is approximately 4 cm long. Urethral continence is maintained by the interplay of multiple structures. The urethral muscle layers are composed of both smooth muscle layers and the striated rhabdosphincter. Dorsally the rhabdosphincter is tightly connected to the ventral portion of the vagina.<sup>11</sup> The proximal urethra and the bladder base are supported by the anterior vaginal wall, which creates a sling-like support that connects laterally to the levator ani muscles at the attachments of the *arcus tendineus fasciae pelvis*. As pelvic floor muscles play an important role in urethral closure for urinary continence, pelvic floor physical therapy targets these muscles to improve their function for management of incontinence and other pelvic floor disorders.<sup>12</sup> In addition to the pelvic floor muscles, another factor important in maintaining urinary continence is the contraction of the smooth and striated muscles within the urethral wall, as well as the ligaments and the fascia that support the bladder and urethra in proper position when intra-abdominal pressure is increased.<sup>13</sup> Urinary continence is preserved by support applied to the bladder neck during pelvic floor contraction, as well as constriction of the urethral lumen.<sup>14,15</sup>

The normal function of the pelvic floor musculature aids in control of both urinary and anal function and also supports the pelvic floor contents. Pelvic floor muscles must perform both voluntary contractions as well as involuntary, or reflex, contractions preceding or at the time of increased abdominal pressure. In response to increased abdominal pressure, the superficial pelvic muscles, such as the anal and urethral sphincters, resist these pressures; and the levator ani muscles support the pelvic floor and counteract this increased pressure by contracting and creating a circular closing of the levator hiatus as well as an upward movement of the pelvic floor and perineum.<sup>14-17</sup> The contraction of the PRM leads to reduction of its two limbs, and this change lifts the anal canal anteriorly, compressing the structures within the levator hiatus against each other as well as the back of the pubic symphysis.<sup>18</sup>

## RISK FACTORS AND INDICATIONS FOR DYNAMIC PELVIC IMAGING

In the surgical literature, there are well-defined risk factors associated with female pelvic floor disorders. Most studies on this topic suggest that pregnancy and childbirth are risk factors for developing pelvic floor dysfunction. Broadly, the trauma of childbirth plays a key role in the development of tears of the pelvic muscles or the EAS/IAS. Symptoms associated with these tears are worsened in the setting of other risk factors such as age, obesity, or poor stool consistency. However, not all women with muscle or sphincter tears will develop incontinence or prolapse. Risk factors for incontinence in women with sphincter tears are Caucasian race, fourth-degree tear during childbirth, increased age, and increased body mass index.<sup>19</sup>

Only in the last 2 decades has cross-sectional imaging played a critical role in characterization of pelvic floor disorders. Surgeons previously based surgery on physical examination and clinical history. As an early adjunct, radiographic defecography was used to confirm

abnormal movement of the pelvic structures, with a positive impact on care. More recently, MRI has been demonstrated to provide exquisite detail of the anatomy of the pelvic floor beyond previous techniques. Further advances with rapid image acquisition have allowed dynamic evaluation of pelvic floor displacement in the setting of strain or evacuation of bowel contents, similar to radiographic defecography. Even more recently, ultrasound has made inroads into pelvic floor imaging and has strengths of its own.

The numerous indications for dynamic pelvic floor imaging range from a bulging mass visualized within the vagina, sensation of pelvic pressure, urinary incontinence, voiding difficulty, anal incontinence, defecatory dysfunction, to postoperative evaluation for complications or recurrent abnormality. In the 2014 ACR Appropriateness Criteria for Pelvic Floor Dysfunction,<sup>20</sup> both transperineal sonography and dynamic MRI are considered “usually appropriate” for symptoms relating to POP, urinary incontinence or dysfunction, and recurrent prolapse after surgical repair. Both “may be appropriate” for anal incontinence, whereas sonography performed with an endorectal probe or MRI with an endorectal coil are highly rated for this indication. For the evaluation of defecatory dysfunction, dynamic MRI or x-ray defecography are considered more appropriate than sonography. However, for evaluation of postoperative complications, standard sonography or MRI may be appropriate, whereas dynamic studies are usually not helpful.

The choice of imaging modality will vary by physician practice pattern and is largely dependent upon surgeon preference and available imaging expertise. Some hospitals may have these studies requested primarily by gastrointestinal surgeons, whereas patients at other sites may be evaluated more often by urogynecologists or gynecologic surgeons. Regardless of the referral source, sonography and MRI are becoming more widely used for evaluation of signs of POP and for workup of urinary and anal incontinence.

Sonography may be performed in the office of the surgeon and is a relatively inexpensive modality. It has been used to explore multiple aspects of pelvic floor dysfunction, including anal and urinary incontinence and POP.<sup>21-23</sup> It is the best means of assessing the integrity of the IAS and EAS. Pelvic floor sonography has been shown to be a superior diagnostic tool in comparison to anal manometry, electromyogram, and conventional defecography.<sup>24</sup> Sonography can also be used to provide biofeedback during pelvic floor training.<sup>16</sup>

MRI may be especially useful in patients who have undergone a failed repair and are being evaluated for further therapy or when there is clinical concern for challenging anatomy or multicompartamental disease. Typically, surgeons make a plan based upon clinical experience, but clinical examination has its limitations in detection and delineation of pelvic floor disorders.<sup>25,26</sup> MRI can directly impact care by refining and improving the surgical plan. In addition, MRI has been clearly shown to detect additional findings beyond clinical examination.<sup>27</sup> Two studies support this concept. In a study reported by Kaufman and associates, MRI changed the surgeon's plan in 41% of complex pelvic surgeries.<sup>28</sup> In another study of 33 patients, the surgeon developed a plan before MRI and revisited the plan afterward. In 67%, the plan was changed based on the imaging findings.<sup>29</sup> A relatively common specific benefit of MRI is the detection of unexpected multicompartamental disease, which substantially improves patient care and has been shown to reduce the rate of reoperation.

## ULTRASOUND IMAGING

### Endoanal Sonography for Anal Incontinence

Endoanal sonography, like endoanal MRI, is well established in evaluation of the anal sphincter complex in women with fecal incontinence



(FI).<sup>30</sup> Fecal incontinence has been reported to affect 9% to 15% of the female population.<sup>31</sup> Social and psychological consequences can be devastating to patients, and many do not discuss fecal incontinence with their providers. Fecal incontinence is usually multifactorial, and risk factors vary from aging, diabetes, neurologic disease, prior anal surgery, and prior obstetric anal sphincter injuries (OASIS). Endoanal sonography is best performed with two-dimensional (2D) ultrasound imaging with a 7- or 10-MHz rotating 360-degree radial array endoanal transducer. The patient is most commonly placed into the left lateral position with the knees bent upward. However, some imagers advocate using the prone or supine lithotomy position. Using a 360-degree radial array transducer, providers can identify the normal anal sphincter complex anatomy and rapidly delineate tears of the anal sphincters.<sup>32</sup>

Using endoanal sonography, multiple layers or rings of differing echogenicity can be identified<sup>33</sup> (Fig. 35-2). The innermost ring is hyperechoic and represents the interface between the transducer and the anal mucosa and submucosal tissues. The underlying markedly hypoechoic ring represents the IAS. The next layer is the intermediate to hyperechoic longitudinal muscle, which is not always distinct on ultrasound imaging and is an extension of the outer longitudinal layer of the rectum. The outermost layer, which is generally echogenic to mixed echogenic, is the EAS. Endoanal axial imaging of the normal anal canal should include at least three characteristic levels. Images of the proximal (cranial) third of the anal canal should include the sling of the PRM, which is visualized posteriorly as a hyperechoic U-shaped structure that closely apportions the posterior portion of the EAS. At this level the EAS will not be observed anteriorly in women. However, the normal IAS will form a complete hypoechoic ring at this level (Fig. 35-2A). In the middle third, the complete rings of both the hypoechoic IAS and echogenic EAS will be seen (Fig. 35-2B). At the level of the

distal anal canal, the normal EAS will extend approximately 1 cm below the IAS (Fig. 35-2C). The anal sphincter thickness has been shown to change with the aging process. The IAS becomes thicker with age, likely because of collagen replacement, whereas the EAS tends to become thinner as the patient ages.

Defects in the anal sphincter complex have been shown to have a strong association with fecal incontinence. Most commonly tears of the anal sphincter are combined and symmetric anterior defects in the EAS and IAS. Isolated EAS defects are also common whereas isolated IAS defects are much less frequent.<sup>34,35</sup> IAS defects usually appear as a hyperechoic disruption of the normally hypoechoic ring of the IAS, whereas EAS tears are seen as hypoechoic, often heterogeneous defects disrupting the continuity of the relatively echogenic EAS. These sonographic changes correspond to the replacement of striated muscle with fibrosis. The extent of the tear is conventionally described as an analogy using the face of a clock, with the 12 o'clock position anterior, the 6 o'clock position posterior above the coccyx, 3 o'clock to the patient's left, and 9 o'clock to the patient's right (Fig. 35-3). In studies in which ultrasound findings have been confirmed by intraoperative findings, the diagnostic accuracy of ultrasound imaging in detecting anal sphincter injury has been reported to have a sensitivity that well exceeds 90%.<sup>36-38</sup> The findings of sonographic anal sphincter defects have been confirmed in multiple studies to correlate with poor sphincter function on anorectal manometry as well as with surgical and histologic findings of sphincter tears.<sup>36,37,39</sup> Endoanal sonography also shows very good interobserver and intraobserver reliability.<sup>40</sup> When added to immediate postpartum clinical assessment, endoanal sonography was shown to enhance recognition of occult anal sphincter tears in postpartum women with second-degree tears who did not have evidence of sphincter tear on clinical examination.<sup>41</sup> Immediate repair of these occult anal sphincter tears reportedly decreased the risk of

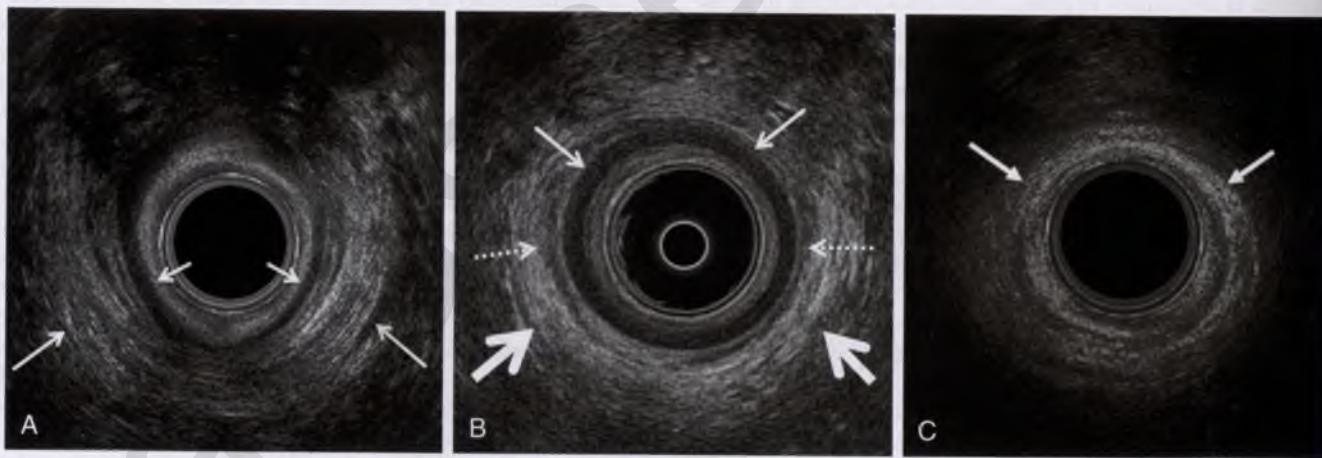


**FIG 35-2** Transverse ultrasound images of the normal anal sphincter. Endoanal ultrasound images at three levels (upper sphincter, midsphincter, and caudal sphincter) at the level of the puborectalis muscle (PRM) shows the internal sphincter, intersphincteric fat, and external sphincter as separate structures. **A**, Endoanal ultrasound image: transverse image of the cephalad (upper) anal sphincter demonstrating the striated relatively echogenic U-shaped sling of the posterior PRM (*long arrows*) and the hypoechoic internal anal sphincter (IAS) (*short arrows*). Note that at this level the external anal sphincter (EAS) is absent. The innermost echogenic ring represents the rectal mucosa and interface with the transducer (central round black structure). **B**, Normal appearance on endoanal ultrasound of the anal sphincters at the midsphincteric level demonstrating the characteristic target or layered appearance. The inner echogenic ring represents the mucosa and interface with the transducer, the IAS is the subjacent markedly hypoechoic ring (*thin arrows*) and the outermost ring represents the EAS (*thick arrows*) and is typically either hyperechoic or of mixed echogenicity. Wispy hypoechoic curvilinear strands with a striated appearance (*dotted arrows*) between the IAS and EAS represent the longitudinal muscle layer. **C**, Endoanal ultrasound image: transverse image of the normal caudal or distal anal sphincter image where the echogenic EAS (*arrows*) extends beyond the IAS representing the superficial portion of the EAS.



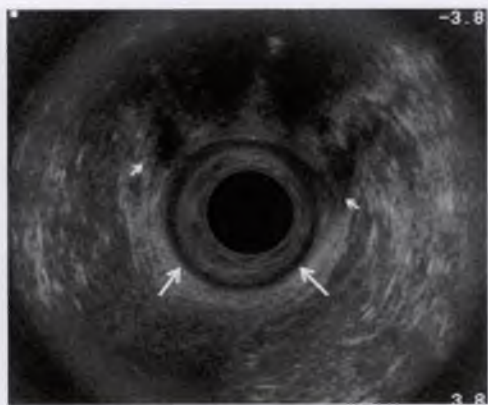


**FIG 35-3** Sphincter tear. Endorectal axial ultrasound image demonstrating an intact hypoechoic internal anal sphincter (arrows), but disruption of the anterior aspect of the external anal sphincter (arrowheads) from the 11 o'clock to the 3 o'clock position.

developing severe postpartum fecal incontinence based on 3 months follow-up examination.

### Endoanal Sonography for Fistulas and Perianal Abscesses

Anorectal abscesses and fistulas usually result from anal gland infections secondary to obstruction from fecal impaction. Approximately 10% are reportedly due to inflammatory bowel disease or direct trauma (including anorectal surgical procedures). A perianal abscess is thought to spread in multiple directions along the path of least resistance and can lead to formation of fistulas. Anorectal fistulas are connections between the perianal skin or vagina and the lumen of the anus or the rectum, although some may be blind ending. For planning surgical intervention, the most important factors for surgeons to know are the location and the size of the abscess, the exact location and number of fistulous tracts, and the relationship of these fistulous tracts to the IAS and EAS. Parks and colleagues<sup>42</sup> described four types of fistula tracts based on their relationship to the sphincteric structures: *intersphincteric*—passes through the IAS and then courses between the muscle layers to the perianal skin; *transsphincteric*—passes through both the IAS and EAS and then through the ischioanal fossa to the skin; *suprasphincteric*—passes above the PRM and then courses through the ischioanal fossa to the skin; and finally *extrasphincteric*—direct communication between perineum and rectum, bypassing the anal canal.

In imaging the fistula tract, the identification of the internal opening can be challenging. The internal opening can appear hypoechoic when acute inflammation is present, or hyperechoic when chronically inflamed or if it contains air.<sup>43</sup> If the external opening of the fistulous tract is visible, injection of hydrogen peroxide into the fistulous opening may improve sonographic identification of the tract as a result of creation of gas bubbles within the fistula (Figs. 35-4 and 35-5).

### Transperineal Sonography of the Anal Sphincter

Although endoanal sonography remains a reference standard in anal sphincter assessment, transperineal sonography can be an effective but less invasive and more accessible modality for evaluation of the anal sphincter.<sup>44</sup> The advantage of transperineal sonography for assessment of the anal sphincter is the possibility of dynamic assessment of the pelvic floor structures without interference of the endocavitary transducer.<sup>45</sup> Transperineal assessment of the anal sphincter complex can be performed in the sagittal and transverse (axial) planes. When 3D

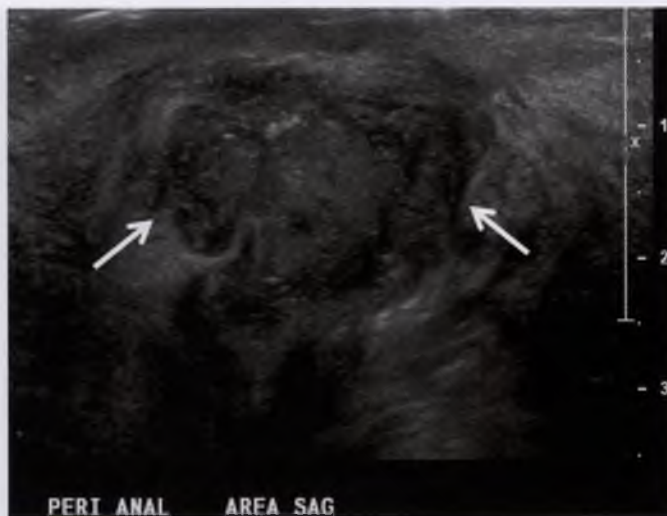


**FIG 35-4** Abscess. Sagittal ultrasound image of the ischioanal fat demonstrates a complex fluid collection (arrows) consistent with perianal abscess.

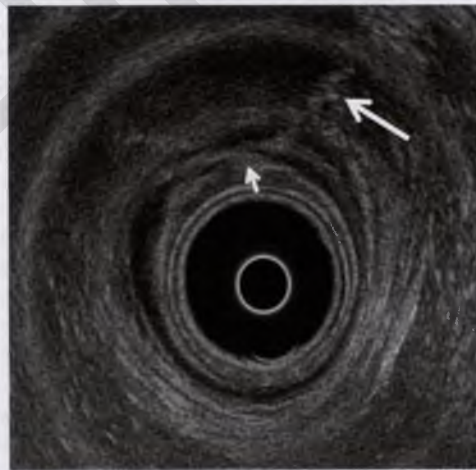


**FIG 35-5** Fistula. Endorectal axial ultrasound image showing disruption of the anterior aspect of the external anal sphincter highlighted by echogenic air bubbles (long arrow). The fistula extends into the intersphincteric space but not through the hypoechoic internal anal sphincter (IAS). However, the IAS appears disrupted anteriorly at the 11 to 12 o'clock position (short arrow).

sonography is used to image the anal sphincter complex, the transducer is oriented toward the anal canal. Postprocessing of the captured 3D volumes then allows detailed evaluation with thin-slice utility (Fig. 35-6).

Using the transperineal technique, the IAS and EAS can be assessed, and the integrity of the PRM can be evaluated. With the transperineal approach, the mucosal folds of the anal canal can be visualized; they are not seen on endoanal imaging because the inserted transducer flattens the folds of the anal mucosa. The stellate-appearing normal folds of the anal mucosa on transperineal imaging have been referred to as the *mucosal star*.<sup>46</sup> Asymmetry in these folds sometimes helps identify disease. Similar to the sonographic findings on endoanal imaging, the appearance of the transverse anal sphincter complex is different, depending on the level of imaging. Some studies suggest that anatomic assessment of the normal anal sphincter is comparable with endoanal and transperineal techniques.<sup>47</sup> Although studies have



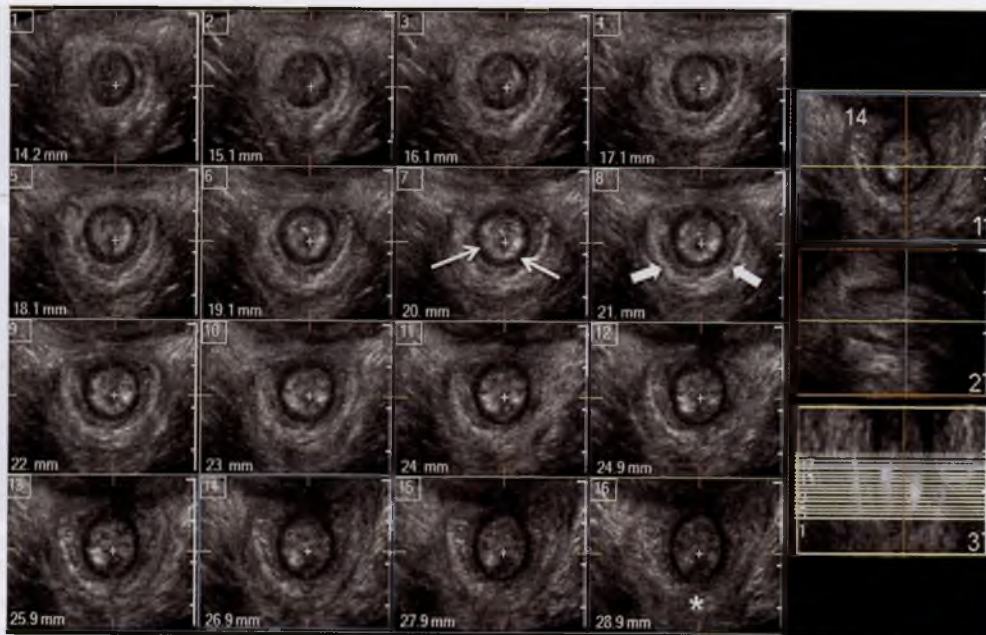


**FIG 35-6** Multiplanar three-dimensional transperineal ultrasound image of the anal canal. Multiple axial images of the anal canal depicting the cross section of the anal canal structures from the caudal (1) to the cranial (16) sections. The cranial images show absence of the anterior portion of the external anal sphincter at the level where the puborectalis muscle sling (*asterisk*) is normally visualized behind the anal canal (*asterisk*). The internal anal sphincter (*thin arrows*) and external anal sphincter (*thick arrows*) are well visualized on the crosshair at the midlevel of the anal canal.

suggested good agreement in detection of anal sphincter defects,<sup>48</sup> others report inferior sensitivity of the transperineal approach.<sup>49</sup> In the authors' experience, endoanal sonography is superior to 2D transperineal sonography, unless 3D transperineal sonography is additionally performed.

### Pelvic Floor Sonography

Over the past 2 decades, many authors have investigated the usefulness of sonographic assessment in women with POP and urinary incontinence or urinary symptoms. Despite the many reported techniques and approaches, pelvic floor sonography still plays a limited role in the investigation of pelvic floor disorders, and thus there are no standardized indications, terminology, and techniques. In this section, the most common techniques and indications will be summarized. The most commonly utilized protocols assess pelvic floor structures and pelvic floor muscle anatomy, integrity, and function as well as dynamic assessment of the pelvic floor structures with the transperineal or translabial approach. Other indications for pelvic floor sonography include assessment of urethral diverticula (sometimes with a transvaginal approach), surgically implanted mesh, and residual urine volume. Many studies have explored the use of 2D and 3D sonography for evaluation of women with pelvic floor symptoms. However, the exact role of pelvic floor sonography is still under investigation.

Women are usually scanned in the dorsal lithotomy position.<sup>50</sup> However, some investigators use the left lateral decubitus position.<sup>51</sup> The most common method for ultrasound evaluation of the pelvic floor is transperineal sonography. Transperineal sonography encompasses two distinct techniques: the translabial technique, which uses a curved array transducer positioned on the labia majora or the perineum,<sup>52</sup> and the transintroital<sup>50</sup> technique, which uses a transvaginal transducer placed on the perineum or just within the vaginal introitus. Depending upon equipment availability, goals, and experience of the sonographer 2D, 3D, or 4D imaging is used. Imaging can

be obtained under resting or dynamic conditions, during maximal strain (Valsalva maneuver), and with pelvic floor muscle contraction (Kegel exercise). Assessment can include a sagittal view of the pelvic floor viscera to localize the urethra, bladder, urethrovesical junction, vaginal walls, uterus, and anorectum, as well as volume imaging to assess pelvic floor hiatus and muscle anatomy, integrity, and function. Evaluation of the urethrovesical angle and anorectal angle can be performed under dynamic conditions.

The midsagittal view of the pelvic floor anatomy helps identify the relative location of the bladder and the urethra, the vagina, and the anorectum (Fig. 35-7). From this view, the posterior urethrovesical and anorectal angles can be assessed. The posterior urethrovesical angle or urethrovesical junction is measured by creating a perpendicular line from the x-axis on the image and following this line to the margin of the bladder base.<sup>53</sup> The anorectal angle is measured at the cross section of the line designating the longitudinal axis of the anal canal and the line along the posterior border of the rectal wall (Fig. 35-8). These measurements can be performed at rest and with dynamic conditions of pelvic floor muscle contraction and strain.<sup>51</sup> The dynamic displacement of the anorectal angle can provide visual biofeedback for PRM and levator ani activity, which can enhance proper muscle biomechanics and is readily accepted by women.<sup>54</sup> In the sagittal view, the perimeter of the PRM is measured as a line that connects the posterior margin of the pubic symphysis and the anorectal angle and is used to assess the dynamic function of the PRM during contraction.<sup>52</sup> Puborectalis activity can be measured as the difference between the "rest" and the "squeeze" measurement. The muscle usually contracts and moves anteriorly and cephalad during contraction.

Transperineal 3D sonography of the pelvic floor has the advantage of improved visualization of the entire pelvic floor hiatus or anal sphincter complex. The 3D images can be captured using either a curvilinear or transvaginal transducer placed on the perineum or labia. To optimize 3D imaging, the sagittal view should include the pubic



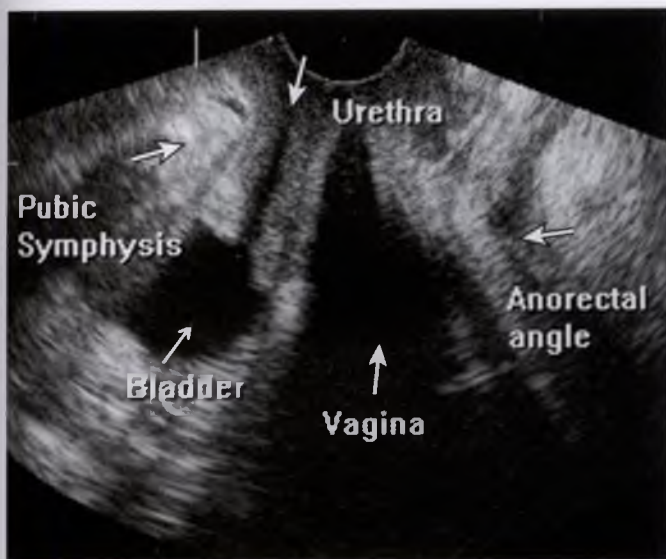


**FIG 35-7** Normal pelvic floor anatomy visualized on the sagittal plane during transperineal ultrasound imaging. Annotated normal sagittal reconstructed image of three-dimensional transperineal ultrasound shows the key structures that are evaluated by this technique. The osseous structures such as the symphysis are echogenic (*white*) whereas the fluid-filled bladder is anechoic (*black*). Gas in the vagina creates posterior shadowing, which may partially obscure structures.



**FIG 35-8** Selection of sagittal imaging plane for hiatus measurement. The hiatal dimensions can be measured in the anteroposterior diameter with a line connecting the pubic symphysis to the anorectal angle. This measurement has been shown to shorten with pelvic floor muscle contraction (Kegel exercises).

symphysis and the anorectal angle because it is on this transverse plane that the pelvic floor hiatus (levator hiatus) is described<sup>8</sup> (Fig. 35-9).

### Pelvic Floor (Levator) Hiatus and Pelvic Floor Musculature

Injury to the levator muscles can be seen either as an avulsion found at the point of muscle insertion onto the inferior pubic ramus or as a tear along muscle fibers. These injuries are possible consequences of overstretching of the levator ani muscles during the second stage of labor when the fetus travels through the birth canal. Levator muscle injuries can occur in 10% to 36% of women at the time of their first delivery. There is no agreement on classification of these muscle

injuries.<sup>55,56</sup> The most common injury related to childbirth is an avulsion injury of the insertion of the puborectalis (or pubvisceralis) muscle onto the pubic ramus<sup>57</sup> (Fig. 35-10).

A variety of studies have assessed pelvic floor morphologic changes related to vaginal delivery and the possible consequences of these changes on future symptoms. Dietz and Lanzarone<sup>58</sup> showed that in a third of women delivering vaginally, avulsions were associated with stress urinary incontinence at 3 months postpartum. Further data from the same group<sup>59</sup> suggest that levator muscle trauma is associated with prolapse of the anterior and apical compartment, but not with bladder dysfunction or urinary incontinence. They also demonstrated that a larger levator hiatus was correlated with POP. Research analyzing a large retrospective cohort suggested that levator ani avulsions are associated with prolapse in women with previous pelvic surgery.<sup>60</sup> Furthermore, some studies suggest that levator avulsion is a predictor of prolapse recurrence after surgical correction of prolapse.<sup>61</sup> Limited reports regarding attempts to surgically repair levator ani muscle avulsions have not been shown to reliably resolve associated pelvic floor disorders or improve symptoms.<sup>61,62</sup> This indicates that restoration of anatomy does not always reconstitute function.

### Urinary Incontinence

Pelvic floor sonography has been used to evaluate women with stress urinary incontinence to assess pelvic floor muscle contraction, urethral anatomy, and bladder neck position before and after incontinence procedures and to evaluate implanted materials used to treat stress urinary incontinence. Sonographic assessment of the anatomy and physiology of the urinary tract can provide insight into the pathophysiology of urinary incontinence. There have been many studies reported using sonography to assess women with urinary incontinence; however, there are no definitive studies on normal female sonographic anatomy of the lower urinary tract. With translabial or transperineal sonography the urethra appears in cross section as a hypoechoic structure surrounded by an echogenic layer representing the urethral muscularis and the sphincter. On sagittal view, the urethra usually courses behind the pubic symphysis. Tunn and coworkers<sup>63</sup> suggested measuring the retrovesical angle with transperineal sonography. This measure evaluates urethral mobility. It is usually performed with Valsalva maneuver. In some patients with urinary incontinence, urethral funneling could be observed during Valsalva maneuver and even at rest. Significant funneling correlates with poor urethral closure pressure, suggesting urethral sphincter deficiency. Khullar and associates<sup>64</sup> reported that women with urgency urinary incontinence and overactive detrusor had significantly thicker bladder walls, as did women with stress urinary incontinence.

Pelvic floor exercises are the mainstay of conservative measures for treatment of urinary incontinence. Bernstein and coworkers showed that pelvic floor muscle thickness and function could be reproducibly assessed by transperineal sonography.<sup>65</sup> He also demonstrated that pelvic floor muscles were thinner in women older than 60 years and in women with stress urinary incontinence compared with continent control subjects. After pelvic floor muscle training, all groups showed increase in muscle thickness, and 60% of women with stress urinary incontinence showed subjective and objective improvement in symptoms. Dietz and coworkers<sup>54</sup> used translabial sonography to provide biofeedback in teaching women to perform proper pelvic floor muscle contraction and showed that translabial sonography is a useful adjunct in pelvic floor muscle training.

### Postintervention Imaging

Since the late 1990s, placement of minimally invasive slings has become a mainstay in surgical treatment of stress urinary incontinence. These



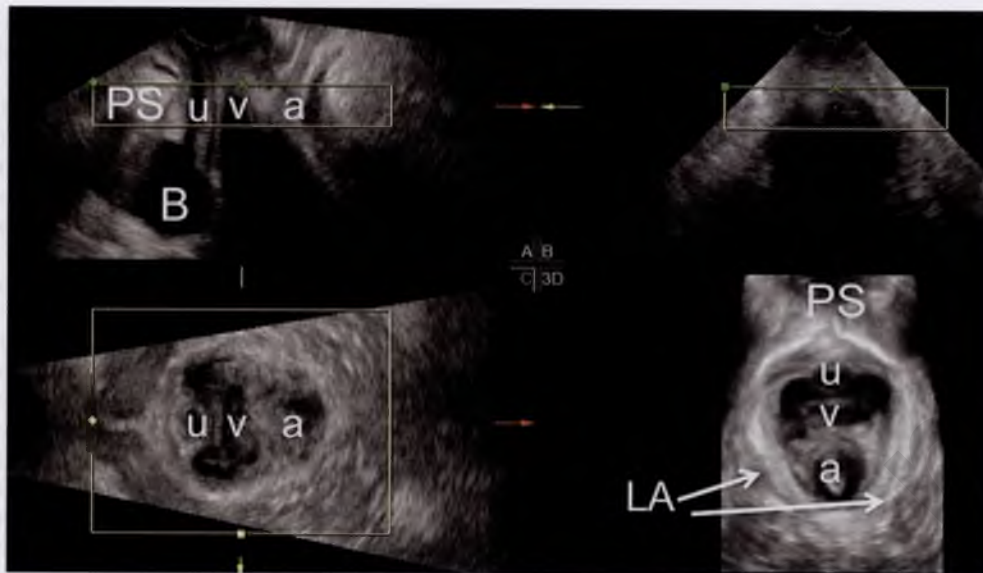


**FIG 35-9** Rendered three-dimensional (3D) image of the normal pelvic floor hiatus demonstrating symmetry of the levator ani muscles. Transperineal pelvic floor 3D sonography: multiplanar view with rendered transverse plane. The four parts of the figure show the midsagittal plane (A), coronal plane (B), axial (transverse) plane (C), and rendered 3D axial (transverse) plane (D). The normal anatomic orientation of pelvic structures is shown in the midsagittal, axial, and rendered planes. The rendered axial image is taken across the plane of "smallest dimension," and the outline of the inferior pubic rami is seen below the pubic symphysis. Rendered reconstruction in an axial plane shows symmetric levator ani muscles (LA and arrows). a, anal sphincter; B, bladder; PS, pubic symphysis; u, urethra; v, vagina.



**FIG 35-10** Three-dimensional (3D) transperineal ultrasound image demonstrating asymmetric hiatus with levator ani muscle avulsion. Rendered 3D transperineal transverse ultrasound image of the pelvic floor hiatus. The pronounced asymmetry of the vagina (v) is easily recognized. This asymmetry is a result of avulsion of the levator ani muscle (arrows) from its attachment at the pubic bone. Contrast this image to the normal appearance of the pelvic floor hiatus in Figure 35-9. a, anal sphincter; u, urethra.

slings are composed of synthetic material, most commonly prolene mesh, that is implanted around the urethra to restore anatomic support.<sup>66</sup> The original retropubic placement of the slings was later modified with an option of using a transobturator placement. The sling is usually placed over the midurethra; however, position may vary. The mesh is highly echogenic and can be easily visualized with pelvic floor sonography (Fig. 35-11). Using pelvic floor sonography, some researchers suggest that sling position along the length of the urethra (i.e., midurethral or in the proximal or distal third of the urethra) is not essential in restoring continence.<sup>67</sup> In one study, Schuettoff and

associates<sup>68</sup> compared assessment of mesh slings with MRI and sonography. They suggested that sonography is most suited for assessment of suburethral and periurethral portions of the sling, whereas MRI is better for evaluating the retropubic portion of the mesh. Pelvic floor sonography can also demonstrate details of the relationship between the suburethral portion of the sling, the urethra, and the symphysis pubis.

For women with stress urinary incontinence and intrinsic sphincter deficiency, different types of urethral bulking agents have been used to improve continence by enhancing urethral coaptation. Transperineal

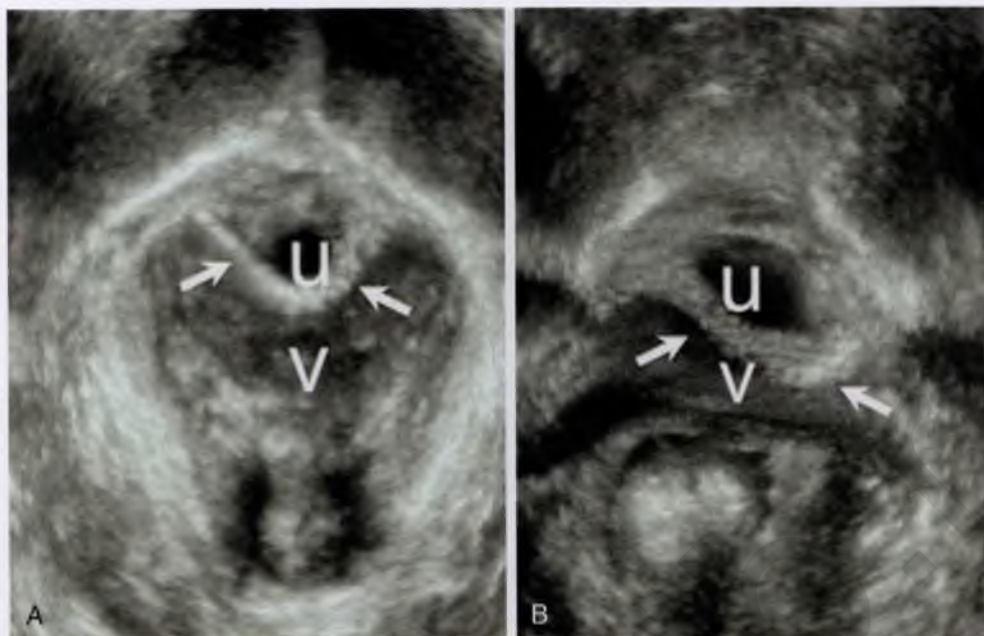


**FIG 35-11** Axial (transverse) images of two types of midurethral synthetic mesh slings (arrows). **A**, A retropubic sling. **B**, A transobturator sling (Monarch) sling. The synthetic mesh is woven and this woven mesh-like quality is easily captured by ultrasound imaging as a highly echogenic structure. The normal anatomic landmarks are annotated on the images: u, urethra; v, vagina.

sonography has been used to optimize and guide placement of the bulking agents. Elia and Bergman found that optimal positioning of the collagen implant was less than 7 mm from the bladder neck.<sup>69</sup> Defreitas and colleagues used 3D transperineal sonography and concluded that circumferential distribution around the urethra achieves better continence than asymmetric distribution of periurethral bulking with collagen.<sup>70</sup> Poon and Zimmern used pelvic floor 3D sonography in their standard algorithm for managing incontinent patients who undergo periurethral collagen injection. In their study, if a patient had no or minimal improvement after periurethral collagen injection and sonography showed low volume retention of collagen or asymmetric distribution, the patient was offered a repeat injection in the area of deficiency. If there is no subsequent improvement in symptoms but a circumferential pattern of distribution is seen on sonography, the injection is considered technically optimal although ineffective, and the patient is offered an alternative treatment.<sup>71</sup>

### Urethral Diverticulum

Female urethral diverticulum can be challenging to diagnose and patients may present with multiple nonspecific urinary symptoms. The most common symptoms are summarized by a triad of the “three Ds”: dysuria, dribbling, and dyspareunia. Patients can also present with recurrent urinary tract infections. Anatomically, a urethral diverticulum is a herniation between the periurethral fibromuscular layer and anterior vaginal wall. Urethral diverticula are thought to be a result of repeated infection and abscess formation within the periurethral and urethral glands (Skene glands), which are usually located in the midurethra along the posterolateral wall near 3 and 9 o'clock. It can be challenging to differentiate diverticula from other vaginal cysts (like Gartner duct cysts and others). Many authors consider MRI a reference standard for diagnostic evaluation of suspected urethral diverticulum (Fig. 35-12). However, pelvic floor sonography is a more accessible technique for such assessment. Transperineal or transvaginal techniques are most commonly used. Information regarding size and

number of diverticula as well as location can be determined by sonography. Characterizing the relationship to the bladder, delineating the ostium of the diverticula and even identifying stones within the lumen of the diverticulum are possible on sonography (Fig. 35-13). However, MRI often helps to delineate the connection to the urethra, which may be difficult to identify with sonography.

### Pelvic Organ Prolapse

Pelvic floor sonography can be used as an adjunct in diagnostic evaluation of women with POP. However, the role of sonography in routine care for women with POP is not yet well defined. In a pilot study, Beer-Gabel and coworkers<sup>51</sup> used dynamic transperineal sonography to identify pelvic floor descent. Assessment of the anorectal angle was comparable to defecography, and rectoceles were easily identified. Dietz and Steensma<sup>72</sup> showed that rectovaginal septal defects could be easily seen on translabial sonography, but a third of women with rectoceles had no detectable sonographic abnormality. Grasso and associates<sup>73</sup> found good to excellent correlation of introital sonographic findings and defecography in evaluation of the anorectal angle, presence of intussusception, and rectocele. Weemhoff and colleagues<sup>74</sup> reported that a pelvic floor sonographic finding of intussusception was predictive of abnormal evacuation proctography. However, prediction of enterocele by sonography was poor compared with evacuation proctography.

POP is clinically measured by a widely accepted technique called the Pelvic Organ Prolapse Quantification (POP-Q)<sup>75</sup> system. In this system the descent of each compartment of prolapse— anterior, posterior, and apical—is measured. A splint-speculum is used to aid in isolation of each of the compartments. This measurement is done while the patient is in the low lithotomy position at maximum Valsalva using the plane of the hymen as a reference. Several studies have attempted to correlate clinical findings on POP-Q to the sonographic findings, but the reference for measurement on sonography is different from the reference that is used in POP-Q. For sonographic



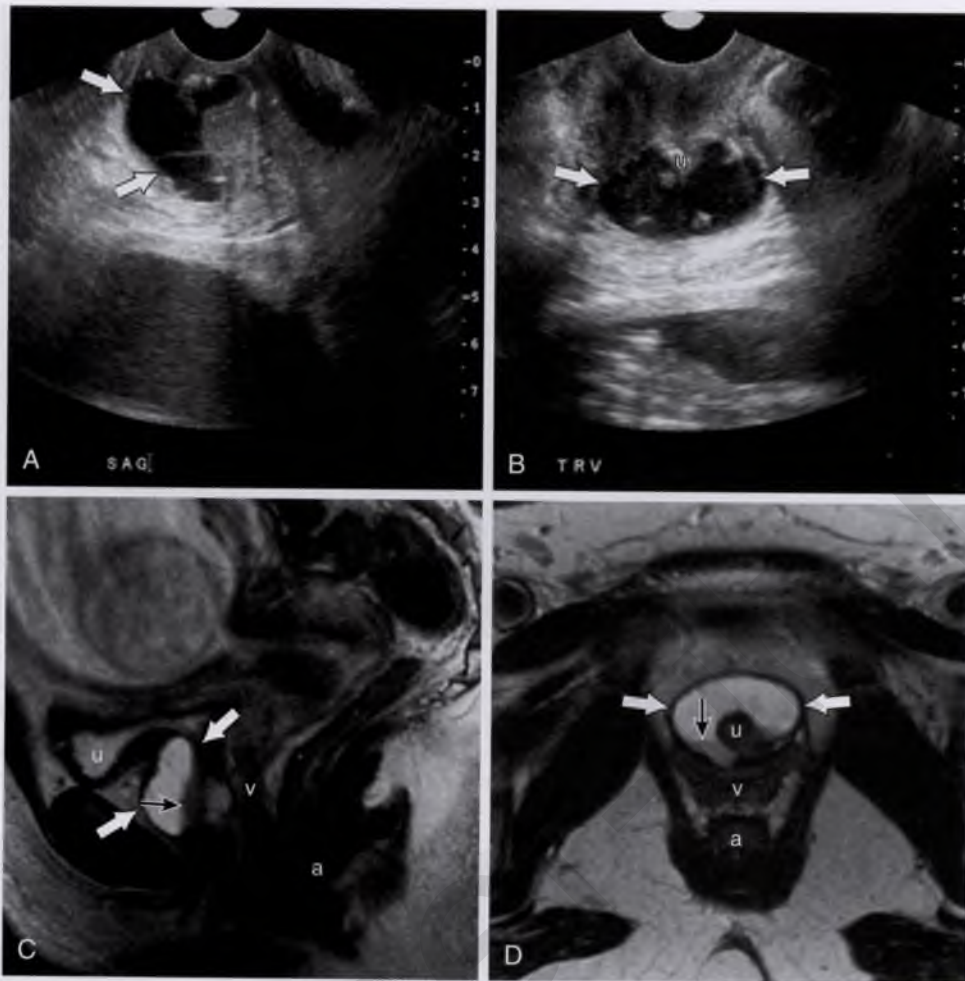


**FIG 35-12** Urethral diverticulum on ultrasound imaging and magnetic resonance imaging. Sagittal (A) and axial (B) gray-scale ultrasound images demonstrate anechoic collection (*white arrows*) surrounding the urethra. Sagittal (C) and axial (D) T2-weighted images of the pelvis show a high signal intensity horseshoe-shaped cystic lesion (*white arrows*) surrounding the urethra (u). Note layering dependent debris (*black arrow*). The location and shape are typical of a urethral diverticulum. a, anal sphincter; v, vagina.

measurements of prolapse, the reference line is usually drawn parallel to the inferoposterior margin of symphysis pubis<sup>76,77</sup> (Fig. 35-14).

Lone and coworkers<sup>78</sup> assessed the relationship between validated POP-Q measures and assessment made by dynamic 2D transperineal sonography. In this study only women with prolapse at or above the hymen were included for analysis. They also adjusted for reference points to minimize the difference between the reference lines used with POP-Q and sonographic measures and found that the proportion of correctly assessed prolapse was around 60% for the anterior and posterior compartments and only 33% for the apical compartment. In addition to difference in reference lines, another possible explanation for this discrepancy is the use of a speculum to examine each compartment in the clinical assessment of prolapse with the POP-Q system.

## DYNAMIC PELVIC FLOOR MAGNETIC RESONANCE IMAGING

As noted in the introductory section, MRI can provide exquisite anatomic and dynamic detail of pelvic floor disorders and is widely used for evaluation of these patients. However, the higher costs of these studies and lack of outpatient office availability can provide barriers to the consideration of MRI relative to ultrasound imaging. There are

also significant differences in the protocols for the acquisition of images and the diagnostic criteria between the two techniques.

### Technical Considerations

Upon arrival to the MRI suite, the patient is dressed in a gown and instructed to empty the bladder and bowel. There is usually an intrinsic short delay until images are obtained which allows partial refilling of the bladder without overdistention. The patient is escorted to the magnet after appropriate safety checks. Approximately 120 mL of sonographic gel is injected into the rectum using two catheter-tipped syringes and a short soft enema tip. This volume of gel distends the rectum, displaces rectal gas, and allows for an evacuation series to be obtained. Larger amounts of gel, up to 200 mL, have been recommended by some experts.<sup>79</sup> However, this may cause overdistention of the rectum. Smaller volumes may leave the patient unable to evacuate the gel during the dynamic part of the evaluation. In our experience, if an evacuation series is not planned, 60 mL of gel will provide adequate distention of the rectum.

The most basic component of the dynamic MRI examination includes a high-resolution anatomic evaluation performed with respiratory gating in the transverse (axial) and coronal planes, centered on the vagina. The images are obtained without fat saturation during



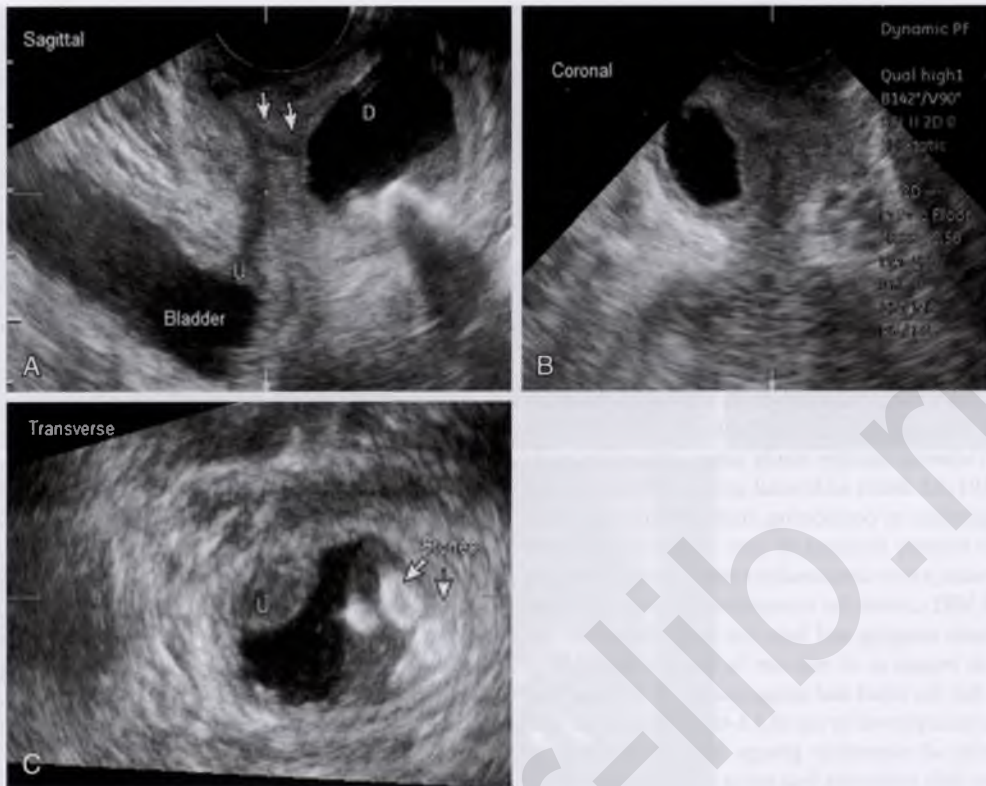


**FIG 35-13** Urethral diverticulum on ultrasound imaging showing sagittal (A), coronal (B), and transverse (C) planes. Multiplanar ultrasound images showing a large diverticulum (D) with multiple echogenic stones (arrows in transverse image) and dependent layering debris. Urethra (u) and fluid-filled anechoic bladder are seen. The hypoechoic diverticular tract is also well visualized on the sagittal image (arrows).

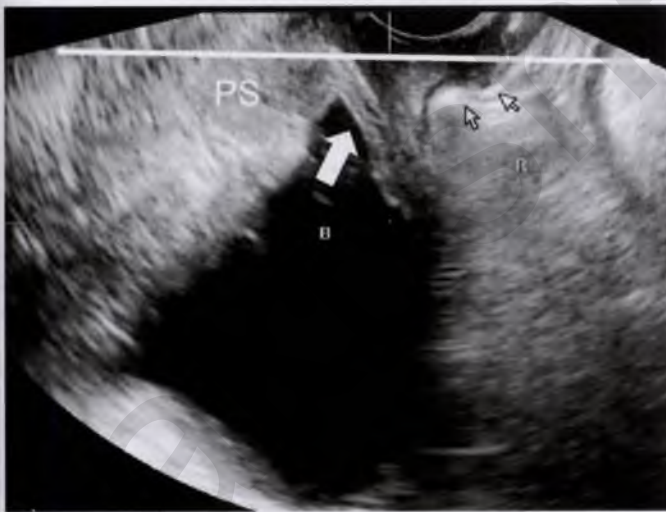


**FIG 35-14** Transperineal ultrasound image in the sagittal plane demonstrating anterior and posterior vaginal wall prolapse (cystocele and rectocele). The thick arrow indicates the cystocele and the two smaller arrows point to the rectocele. The reference line for measurement of prolapse is drawn parallel to the inferior edge of the pubic symphysis. B, bladder; PS, pubic symphysis; R, rectum.

quiet breathing within 4 to 5 minutes. The technologist should ensure that the phased array coil is centered over the low pelvis so that the amount of detected signal at the introitus is not limited. The transverse images should be performed low enough that only the upper thighs are on the lowest images beyond the perineum. Coronal images are centered on the vagina and include the femoral heads laterally with

craniocaudal coverage from the introitus to at least the sacral promontory. The patient should be carefully coached that any movement can degrade the study.

Using the transverse series as a reference, a set of sagittal 10-mm thick images are obtained covering the pelvis between the femoral heads and centered on the lower vagina. From these, a single image can usually be identified that contains the important structures, including the symphysis, urethra, bladder, vagina, rectum, and coccyx. This plane is repeated as a single image in 0.6 to 1.0 second, at rest, and then is subsequently repeated during maximal strain. Balanced steady-state free-precession, half-Fourier acquisition single-shot turbo spin echo, or balanced fast field echo sequences can be used, but one study favors TruFISP technique (true fast imaging with steady-state precession) over half-Fourier acquisition single-shot turbo spin echo.<sup>80</sup> The patient must be adequately coached to strain as if having a bowel movement and to push downward through the pelvis toward the feet. The patient should be reassured that some leakage is expected and even preferred for study quality. If the first strain image appears weak, repeated coaching may be needed. This should be repeated with at least two additional strains if an evacuation series is not performed.<sup>81</sup> Lastly, a cine sequence of the same 10-mm thick slice should be obtained every second for 30 to 60 seconds as the patient evacuates rectal contents into a group of peripads. We instruct the patient to begin when she hears the third sound of the repetitious “knocking” scanner sounds so that we initially have images at rest. Some sites will then repeat the axial high-resolution at-rest images to evaluate recoil or persistence of the displacement of the pelvic structures, but this is not widely performed. If there is concern for obstructed defecation symptoms, the strain sequences are followed by squeeze or Kegel exercise sagittal images to evaluate the anorectal angle.



Uncertainty still remains regarding many aspects of the MRI examination protocol. Intravenous contrast agent is not typically administered. Some investigators recommend intraluminal contrast material to opacify the vagina and small bowel. Although small bowel contrast could aid in detection of an enterocele, it is not widely given because the bowel is well seen without it. Vaginal gel can provide clearer definition of the anterior and posterior vaginal walls in research, but is not widely used as this level of detail is not needed in routine clinical evaluation for surgery.

Most MRI units image the patient in the supine position, which promotes less efficient straining than the seated position on a defecogram commode. However, a small study by Fielding and associates reported no lack of study success using the supine position when there is adequate coaching and strain.<sup>82</sup> Another study showed more laxity in the sitting position, but no difference in detection of clinically relevant abnormalities<sup>83</sup>; whereas another study using orthostatic positioning in an open MRI did detect additional prolapse relative to the supine position.<sup>84</sup> Regardless of positioning, inclusion of evacuation phase cine images has become standard of care. Studies have shown significantly higher sensitivity for abnormalities beyond strain imaging alone,<sup>85</sup> but threshold MRI criteria for evacuation imaging cannot be assumed to mirror strain imaging and have not been defined in the literature. The dynamic images at 10 mm can be easily obtained with any current scanners, but the detail and image quality of the axial and coronal sequences can be improved by use of a 3-tesla (T) scanner over a 1.5-T unit. Evaluation of submuscle groups between the magnet strengths has not been fully evaluated, but using a 3-T magnet could provide benefit in this area as well.

Imaging with an external phased array coil provides poor definition of small tears of the IAS and EAS. These tears can be better imaged with placement of a coil within the anal canal. However, the endoanal coil can distort the pelvic anatomy and is less well tolerated by patients than routine MRI.

## Anatomy and Magnetic Resonance Imaging Reference Lines

### Normal Coronal and Axial Planes

As noted in earlier sections, the pelvic floor is composed of a combination of muscle groups. The three major muscles anchor anteriorly onto the symphysis pubis. The pubovaginalis muscle courses posteriorly around the vagina, whereas the PRM courses posteriorly around the rectum for support. The iliococcygeus muscle forms an oblique sheet of muscle that tracks posterior and cranially to insert broadly onto the inner surface of the iliac wings. Each of these muscles can be separately seen on axial images and should be symmetric right to left. Symmetric thinning may be a normal finding if the normal insertions are intact, and this can be a source of error in MRI interpretation. Typically, the levator muscles will measure 4 to 5 mm in thickness at the level of the midvagina. If the support structures around the vagina are intact, the vagina should have a symmetric appearance on transverse images, often with a butterfly or H shape. The anal sphincter will be best seen on either the axial or coronal series, depending upon its orientation relative to the imaging plane. The circular fibers of the internal sphincter subjacent to the mucosa will be continuous and symmetric. A thin layer of intersphincteric fat coats the IAS and separates it from the EAS muscles, which may be more discontinuous and difficult to fully visualize even in the normal patient.

### Pubococcygeal Line Versus Midpubic Line

Although the pelvic floor is not a linear structure and has more of a bowl shape, a reference point is needed on imaging to allow for the

determination of abnormal from normal. On sagittal imaging, two reference lines are most commonly used<sup>86</sup> (Fig. 35-15). The pubococcygeal line (PCL) is drawn from the inferior edge of the symphysis pubis to the last vertically oriented joint of the coccyx and provides a reference point by which to measure the location and vertical movement of mobile organs. The last vertical joint is chosen because the horizontal tip of the coccyx may move during strain or evacuation, which would alter the measurements. The second most common reference line is the midpubic line. It is drawn on the sagittal view through the pubic bone long axis from the upper anterior pubis through the inferior posterior edge of the pubis, and the line is continued caudally through the anterior pelvic tissues. Proponents of this technique favor its better approximation of the hymen, even though it has only moderate correlation to clinical examination.<sup>87</sup>

### Normal Sagittal Plane

In the sagittal plane, the symphysis, neck of the urinary bladder, bladder neck, cervix, vagina, low rectum, and coccyx should all be visible on a single 10-mm thick image (Fig. 35-15D and E). A series of sagittal images is initially obtained to visualize the entire region and to assess for additional findings, but most of all to localize the optimal plane for dynamic imaging. The normal bladder neck should be no more than 10 mm below the PCL at rest or during strain.<sup>88</sup> The cervix should remain above the PCL at rest and during strain.<sup>89</sup> The posterior plate (posterior wall) of the rectum should nearly parallel the PCL at rest and drop no more than 10 degrees below the PCL with strain.<sup>90</sup> The hiatus should remain normal in size. This is represented as the H-line drawn on sagittal images from the inferior posterior edge of the symphysis to the posterior margin of the circular anal fibers. For evaluation of craniocaudal pelvic descent, the M-line is drawn from these fibers to the PCL such that the line forms a right angle with the PCL. An H-line measuring less than 5 to 6 cm and an M-line less than 2 cm are considered normal.<sup>79,90</sup> The change in urethral angle relative to a vertical reference (urethral rotation) from rest to strain should measure less than 30 degrees.<sup>91</sup>

### Abnormal Findings on Magnetic Resonance Imaging

Pelvic floor disorders are all somewhat interrelated but fall into three main groups: incontinence, obstructed defecation, and prolapse. Incontinence may involve unplanned loss of urine spontaneously or with cough or strain. This is usually related to an anterior compartment abnormality. For anal incontinence, there may be loss of flatus or feces, and this is most typically attributed to posterior compartment or sphincter abnormalities. Obstructed defecation describes the abnormal coordination of muscle relaxation during attempted defecation that prevents adequate emptying of the rectum, whether or not associated with rectocele. Prolapse describes a constellation of clinical findings that most commonly involve a bulge or sensation of fullness in the perineum and vagina. It should be noted that there is significant overlap between the signs/symptoms of incontinence and prolapse in this patient population.

### Anal Incontinence

Incontinence is a multifactorial problem that may specifically involve the anal sphincter complex or can be associated with POP. The imaging of incontinence involves both static and dynamic pelvic floor techniques. With regard to the sphincter, the concentric anal sphincter fibers are most commonly disrupted by prior childbirth, especially if there has been an episiotomy. This disruption can be seen with high-resolution MRI using distention of the sphincter with an endoanal coil. In the short-axis view of the sphincter, a tear will be detected as a focal linear or geographic signal abnormality in the otherwise T2-weighted



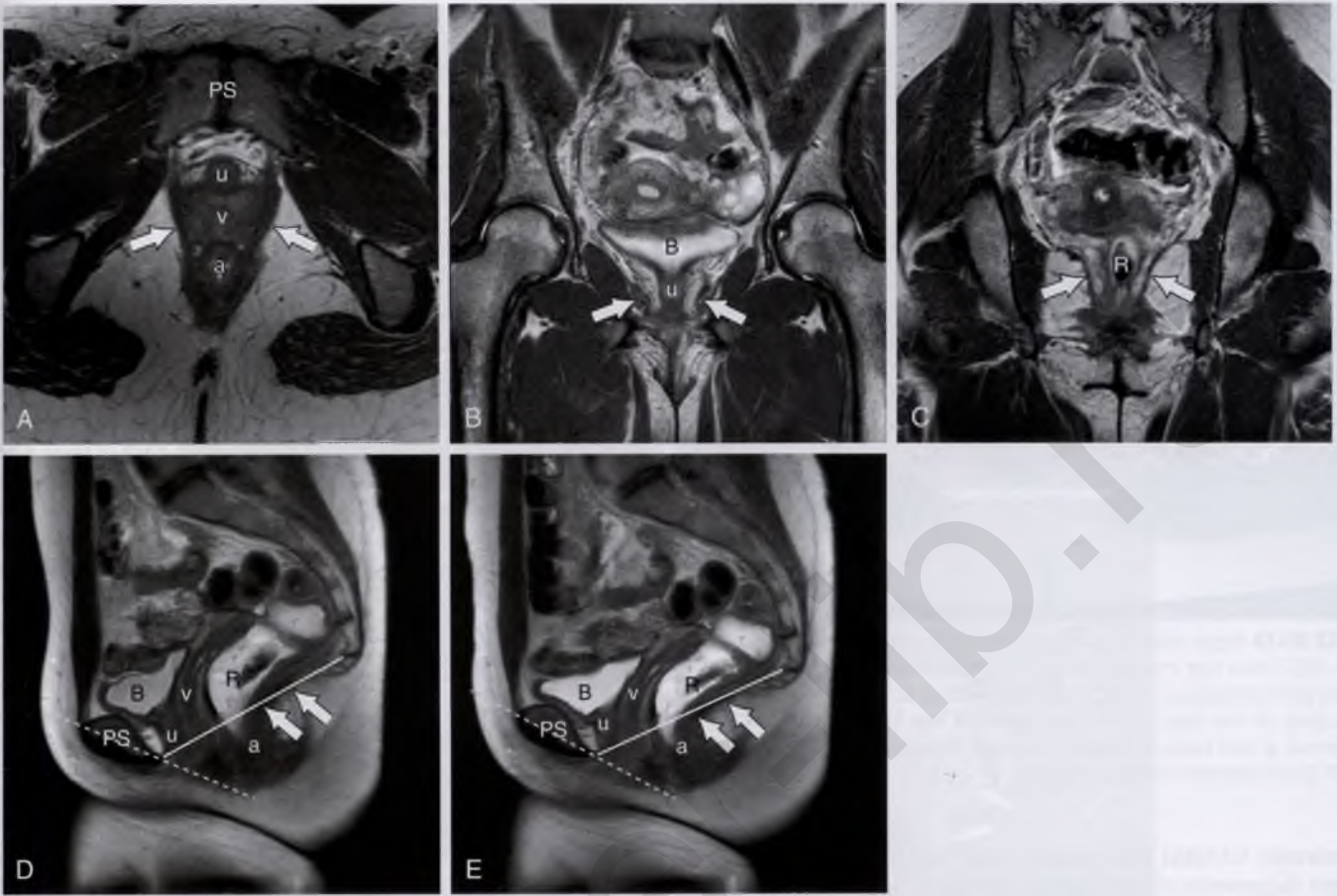


**FIG 35-15** Normal pelvic floor structures on magnetic resonance imaging (MRI). Dynamic T2-weighted MRI of asymptomatic normal subject. **A**, Axial T2-weighted image shows symmetric appearance of bilateral levator muscles (*block arrows*) inserting onto the pubic bones. **B**, Coronal image at the level of the insertion shows symmetric levators as well. **C**, Coronal image at the level of the rectum shows normal levators (*arrows*). **D**, Sagittal T2-weighted image shows normal position of the bladder, vaginal apex, and posterior plate of the rectum (*block arrows*) above the pubococcygeal line (PCL), a representation of the pelvic floor. **E**, With strain, there is little descent of these organs, which remain above the PCL line (*block arrows*). a, anal canal; B, bladder; dotted line, midpubic line; PS, pubic symphysis; R, rectum; u, urethra; v, vagina.

hypointense muscle. However, for standard MRI without an endocoil, the sensitivity and interreader reliability for detecting IAS or EAS tears are low.<sup>92</sup>

On the other hand, research using dynamic MRI has documented a strong correlation between incontinence and tear of the levator muscles at the point where they insert onto the symphysis bone.<sup>93</sup> In this multireader study with good interobserver variability, muscle loss in this region was associated with incontinence. Bilateral partial levator tears correlated with incontinence. Even unilateral disease correlated with symptoms if the tear was complete (Fig. 35-16). If complete, the adjacent paravaginal fat may asymmetrically bulge into the adjacent fat to help identify the abnormality. Focal thinning without bulge may be harder to appreciate, and evaluation should use both axial and coronal images to detect asymmetry of muscle volume. Asymmetric focal thinning of the levator muscles is less challenging to detect than differentiating neuromuscular injury with diffuse muscle atrophy from normal thin muscles. It should be noted that levator atrophy can be present in a subset of nulliparous asymptomatic women, so care should be taken with the diagnosis if thinning is symmetric.<sup>94</sup>

Incontinence is a muscular and neuromuscular abnormality, but osseous structures may contribute to risk. Pelvimetry has been used to predict risk of difficult labor for decades. In a prospective trial, it has

been shown that women with a wide pelvis as measured by intertuberos diameter are at increased risk for urinary incontinence.<sup>95</sup> Similar data suggesting that a wide pelvis is associated with urinary incontinence were again reported in a subsequent study,<sup>96</sup> but another study found no association.<sup>97</sup> A deep sacral curve has been associated with fecal incontinence, possibly due to abnormal pressure on nerves accentuated by this anatomic variation. Most recently, a short anteroposterior diameter of the pelvis on transverse MRI has been shown to be associated with severe levator ani defects.<sup>98</sup> Potential mechanics have been theorized, but the literature in this area is still incomplete and evolving.

### Perianal Fistulas

MRI for the evaluation of perianal fistulas in the setting of inflammatory bowel disease differs in technique and diagnostic considerations in comparison to other anal sphincter imaging. As noted earlier, there are a variety of fistula types to be considered in this disease process, and MRI can provide exquisite detail of fistulous tracts. Dynamic sequences are not required for imaging of perianal fistulas or abscesses, so acquisition times may be longer to provide better signal to noise and spatial resolution. Multiplanar T2-weighted sequences are the mainstay of the technique. A combination of series without fat



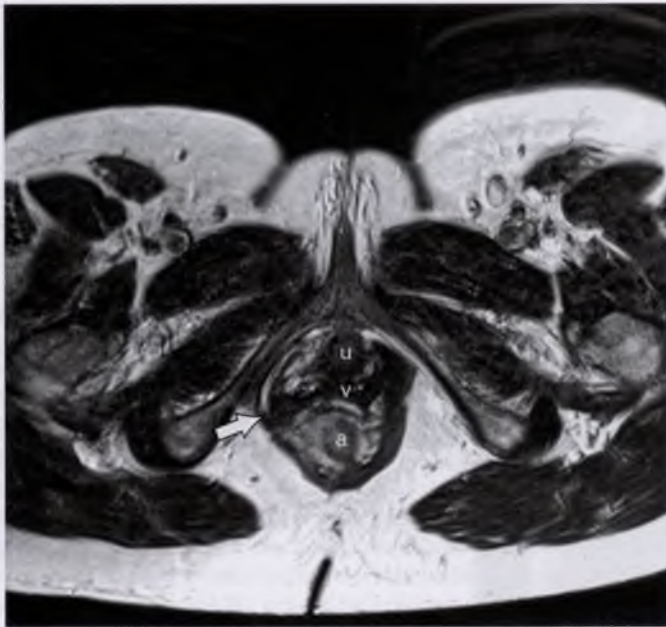


**FIG 35-16** Right levator ani muscle tear with vaginal asymmetry. Axial TruFISP (true fast imaging with steady-state precession) image of the low pelvis shows a normal left levator muscle, but there is asymmetric bulging of the vagina with disruption of the right levator muscles (arrow). a, anal canal; u, urethra; v, vagina. (Courtesy Gaurav Khatri, MD, UT Southwestern Medical Center.)

saturation for better anatomic detail and with fat saturation to highlight the presence of fluid signal is commonly applied. After precontrast T1-weighted images, intravenous contrast is frequently used with subsequent multiplanar T1-weighted sequences to evaluate for enhancement and acute inflammation of the fistulous tracts. Abscesses with high T2-weighted signal intensity fluid and low central T1-weighted signal with surrounding hyperemia are easily identified (Fig. 35-17). Inflammatory tracks into the high pelvis can be well characterized by MRI but may be challenging with sonography.

### Obstructed Defecation

Constipation and incomplete emptying of the rectum is a common presentation of pelvic floor disorders. These patients often present to a gastroenterologist or surgeon who may not be familiar with pelvic floor imaging. The findings on MRI are focused around dyssynergy of pelvic floor relaxation and detection of prolapse. In one series of patients with obstructed defecation symptoms, MRI detected a wide variety of abnormalities, and MRI changed the treatment decision in 20% of symptomatic patients.<sup>99</sup> In one cause of obstructed defecation, the normal relaxation of the anal sphincter is impaired, and there is often paradoxical elevation of the posterior plate with acute angulation of the posterior rectal wall relative to the posterior wall of the anus. This is best visualized on the sagittal strain and evacuation sequences, but there is no universal diagnostic MRI criterion in the literature. The normal anorectal angle range is likely between 94 and 127 degrees, depending on the source in the literature.<sup>79</sup> In general, the normal anorectal angle should increase by 15 to 20 degrees during evacuation. If the angle decreases during evacuation, this is consistent with the diagnosis of obstructed defecation.

Obstructed defecation may be complicated by rectal prolapse. During strain or evacuation attempts, the mucosa or full thickness of the rectal wall may invaginate into the distal lumen of the rectum. MRI provides excellent differentiation between mucosal and full-thickness

intussusceptions.<sup>100</sup> This differentiation is clinically important as full-thickness invagination is more likely to be symptomatic and requires a more extensive surgical procedure for correction. Extension of the prolapsed mucosa into the anal canal may be termed rectal intussusception, and there may be prolapse of the anal mucosa external to the skin in severe cases. However, even mucosal prolapse without extension through the anus can result in incomplete rectal evacuation. Treatment may include stapled transanal resection, transanal Delorme procedure, multicompartimental repair, biofeedback, or conservative management.<sup>99,101</sup>

### Prolapse

Prolapse can occur in any of the three compartments of the pelvis and frequently is multicompartimental (Fig. 35-18). The anterior compartment includes the bladder and urethra. Anterior prolapse includes cystocele, urethral hypermobility, and urethrocele. Each of these is best diagnosed on the sagittal dynamic sequences with strain or evacuation. Cystocele is diagnosed when the bladder neck descends to a level 1 cm or more below the PCL (Fig. 35-19). It is mild when less than 3 cm, moderate when greater than 3 to 6 cm, and severe when greater than 6 cm below the PCL.<sup>102</sup> It is often accompanied by rotation of the urethra from the normal craniocaudal orientation to a more horizontal path beneath the symphysis pubis. Urethrocele is diagnosed as hypermobility of the urethra with movement more than 1 cm below the PCL. Abnormal rotation of the urethra is defined as greater than 30 degrees from baseline angle<sup>103</sup> (Fig. 35-20). Abnormal urethral rotation helps in the diagnosis of anterior compartment prolapse, but it does not alter the management beyond other MRI findings such as bladder descent below the PCL.

Apical compartment prolapse often is concomitant with either anterior or posterior compartment involvement. It is diagnosed on the sagittal dynamic images as prominent descent of the cervix or vagina below the PCL.<sup>104</sup> One study has classified mild apical prolapse as 1 to 2 cm, moderate as 2 to 4 cm, and severe more than 4 cm below the PCL.<sup>80</sup> There may be a combination of elongation of the vagina and anterior rotation of the posterior vaginal wall. When there is a levator muscle tear on axial images as part of apical compartment disease, the vagina may distort and protrude laterally into the paravaginal space. This may be detected as vaginal asymmetry on the axial images. Likewise, an enterocele may protrude into the paravaginal region, representing an apical compartment disorder, or it may also involve the posterior compartment between the vagina and rectum (Fig. 35-21). There is clinical significance of these findings because they may require added complexity of the repair procedure, which may include mesh support.

The posterior compartment includes the rectum and anal sphincter complex. The most common posterior compartment prolapse is the rectocele. When rectal support is compromised, the rectum may bulge anteriorly into the vagina on clinical examination. On sagittal strain or evacuation images, this is represented as a bulge of the anterior rectal wall greater than 2 cm perpendicular beyond the expected course of the anterior wall of the anal sphincter. Some researchers have classified mild rectocele as 2 to 4 cm, moderate 4 to 6 cm, and severe more than 6 cm.<sup>80</sup> Often an anterior rectocele will fill with gas if the patient is supine (Fig. 35-22), but this should not limit its detection.

Posterior compartment laxity is defined as abnormal descent of the rectum during strain. In normal individuals, there should be minimal descent of the posterior plate during strain.<sup>105</sup> When the posterior plate (wall) of the rectum descends more than 15 to 20 degrees below the PCL using the junction of the two lines at the coccyx as the intersection, the diagnosis is suggested.<sup>80</sup> This can be diagnosed also by descent of the circular fibers of the anus. However, a 2014 study found at least



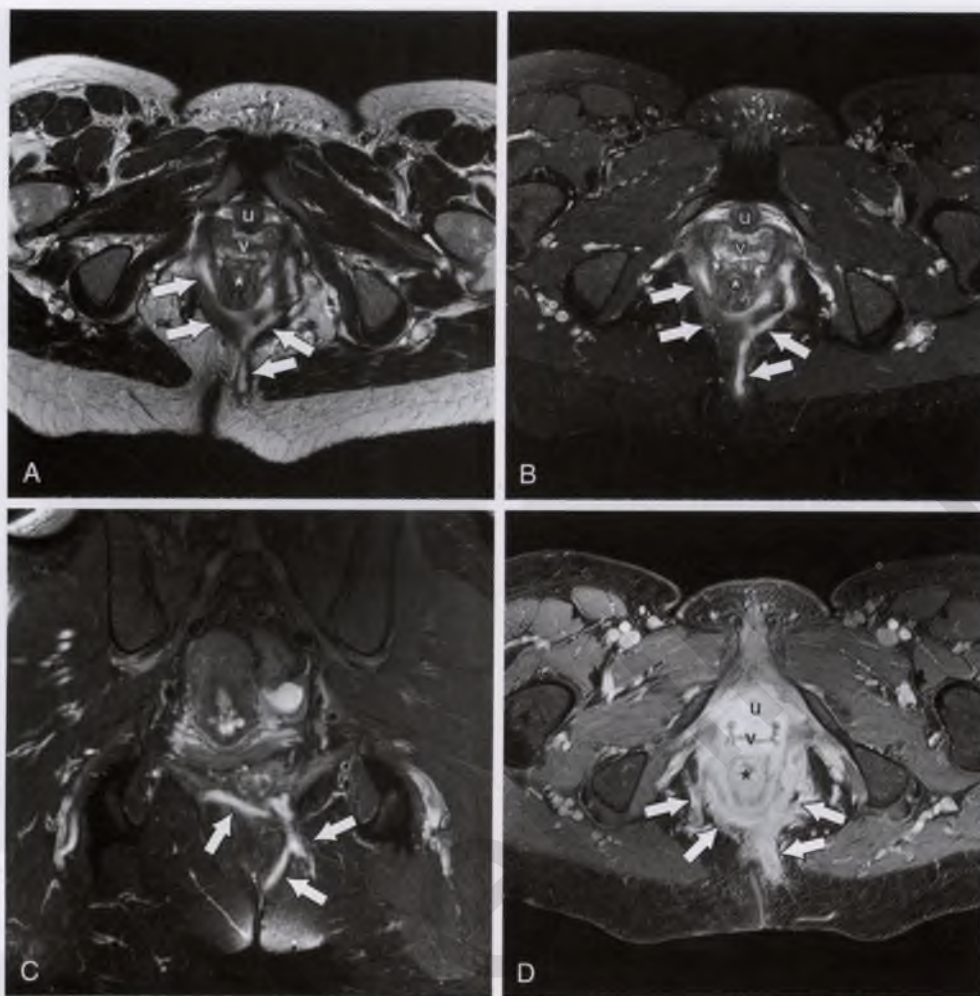


**FIG 35-17** Perianal fistula on magnetic resonance image. Axial T2-weighted images without (**A**) and with (**B**) fat saturation show a complex fistulous tract (*arrows*) partially encircling the internal anal sphincter (*asterisk*) (on T2-weighted sequences, fluid appears bright). The fistula tracks posteriorly, which may be difficult for ultrasound imaging to characterize. Coronal series (**C**) shows the cranial extent of the inflammation, which may also be difficult to detect by ultrasound imaging. On postcontrast T1-weighted series (**D**), there is bright enhancement of the inflammatory tracts without drainable abscess, and the tracts extended to the skin. u, urethra; v, vagina.

moderate posterior descent relative to the PCL in 25% of asymptomatic patients,<sup>106</sup> so the diagnosis should be questioned in the absence of posterior compartmental symptoms or clinical signs.

When the anus descends posteriorly, the pelvic hiatus is enlarged. This pelvic hiatus or the enlargement is represented as the H-line drawn on sagittal images from the inferior posterior edge of the symphysis to the posterior margin of the circular anal fibers. For evaluation of craniocaudal descent of the pelvic floor, the M-line is drawn from these fibers to the PCL such that the line forms a right angle with the PCL. An H-line greater than 6 cm and an M-line greater than 2 cm are considered abnormal for pelvic floor dysfunction.<sup>79</sup> A larger hiatus suggests the need for surgical repair, but the clinical significance depends upon the severity of patient symptoms in association with these imaging findings.

### Limitations of Magnetic Resonance Imaging

Pelvic floor MRI is still a maturing field of imaging, and there are times that the technique may not provide optimal or complete diagnosis of this complex constellation of disorders. Claustrophobia because of the

small imaging acquisition space has been a persistent concern for standard MRI, and open MRI units may not provide equivalent or adequate spatial resolution for visualization of small muscle groups in the deep pelvis. Potentially, premedication of patients with anxiolytics could inhibit full strain effort, but this has not been studied. Furthermore, a medicated patient who is not fully awake and alert may be less attentive to lying still. Motion can not only directly degrade image quality, but it can also result in change of patient position such that the sagittal imaging plane no longer shows all the necessary structures during the strain or evacuation dynamic sequences.

Other limitations lie beyond the patient. Correlation of MRI findings with clinical pelvic examination performed by the gynecologist has been shown to be limited, and when the imaging does not correlate with what the surgeon feels, it lowers confidence. The PCL does not approximate the hymen, which is a landmark for clinical characterization of prolapse. Although the PCL measures downward descent, the clinical examination measures movement of structures anteriorly and inferiorly along the course of the vagina, contributing to differences between imaging and clinical findings. However, the high interobserver





**FIG 35-18** Sagittal magnetic resonance image of multicompartmental prolapse. Sagittal TruFISP (true fast imaging with steady-state precession) image of the pelvis during strain shows descent of all three compartments, a common finding in pelvic organ prolapse. Cystocele (*arrow*) is greater than 2 cm below the pubococcygeal line (*solid line*). Uterovaginal decent is present, and there is abnormal descent of the posterior rectal plate (*dotted line*). B, bladder; PS, pubic symphysis; R, rectum; v, vagina. (Courtesy Gaurav Khatri, MD, UT Southwestern Medical Center.)

variability of clinical examination limits its use as a reference standard. Likewise, there is interobserver variability of the MRI measurements. Thus, the imaging and clinical findings are difficult to align.<sup>92</sup> MRI measurement variability arises from a variety of problems that mostly stem from reader inexperience and training. Muscles are not smooth consistent structures, and muscle irregularity and variations may lead to interreader variability regarding grading of muscle tears. Also, the choice of landmarks for soft tissue structures has shown more variability than for parameters that use osseous landmarks. Despite these problems, there is hope that many of these limitations can be improved with additional training. Beyond the imaging, there is still disagreement among surgeons regarding the best treatments for various forms of POP, including preference for transabdominal versus transvaginal approach. In addition, choice of tissue or mesh for support remains controversial.

## SUMMARY AND FUTURE DIRECTION

Pelvic floor sonography and MRI can be used to evaluate pelvic floor anatomy and function, complementing the clinical assessment of patients with pelvic floor disorders. Pelvic floor imaging techniques have promising utility as an adjunct diagnostic modality for pelvic

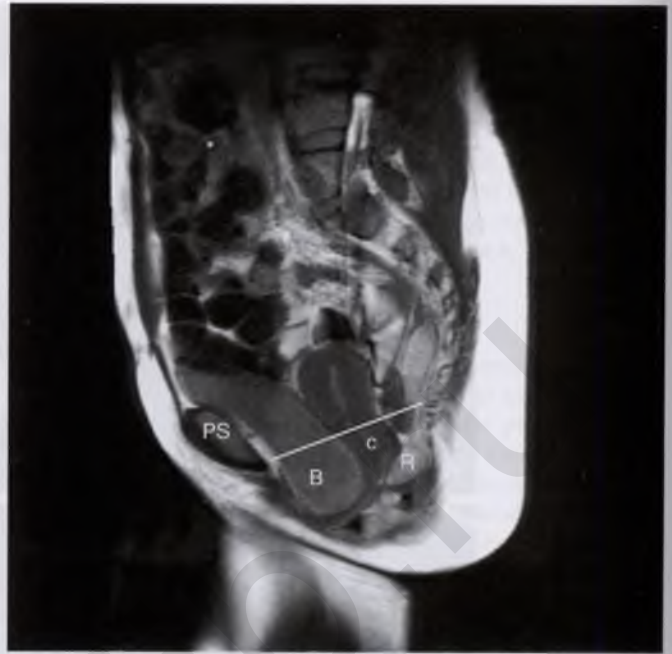


**FIG 35-19** Cystocele on sagittal strain magnetic resonance image. Sagittal T2-weighted image of the pelvis during strain demonstrates anterior compartment descent of the urinary bladder (B) below the pubococcygeal line (*white line*) with some apical component as noted by partial descent of the uterus and cervix (c). PS, pubic symphysis; R, rectum.



**FIG 35-20** Cystocele with urethral rotation on sagittal strain magnetic resonance image. Sagittal T2-weighted image of the pelvis during strain demonstrates multicompartmental descent of the pelvic organs. The urinary bladder (B) is well below the pubococcygeal line (*solid line*). Posterior plate descent (*dotted line*) and rectocele (*thick arrow*) are also present. Of note, there is significant rotation of the urethra with nearly horizontal course (*thin arrow*). PS, pubic symphysis; R, rectum.



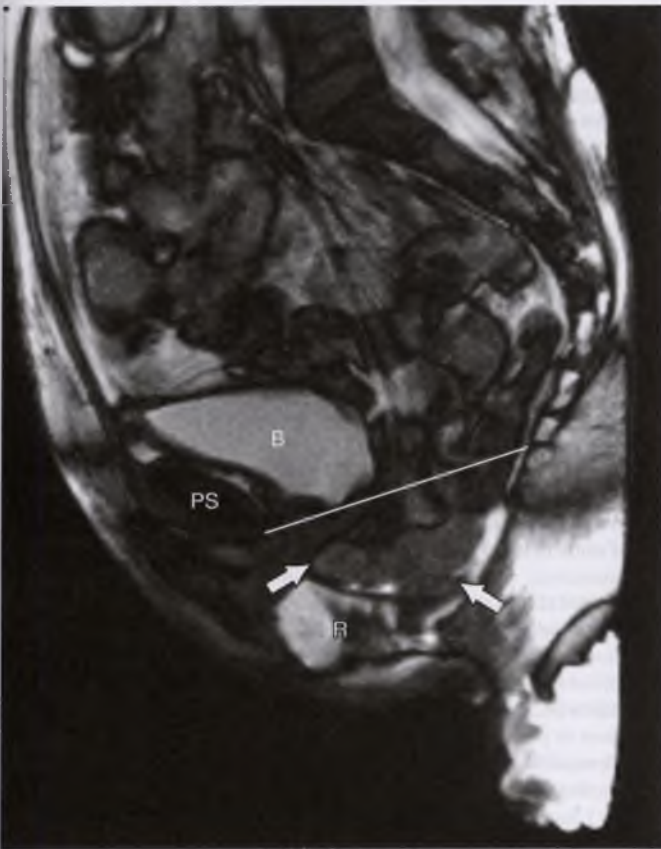


**FIG 35-21** Enterocele on strain magnetic resonance image. Sagittal T2-weighted image of the pelvis during strain shows the protrusion of multiple loops of bowel below the pubococcygeal line (PCL) (white line) between the displaced rectum (R) and urinary bladder (B), consistent with enterocele (arrows). The vagina is not well seen in this plane. PS, pubic symphysis. (Courtesy Gaurav Khatri MD, UT Southwestern Medical Center.)



**FIG 35-22** Rectocele during strain sagittal magnetic resonance imaging (MRI). Sagittal T2-weighted MRI obtained during strain shows abnormal anterior bulge of the anterior wall of the rectum greater than 2 cm from the midaxis of the anal canal (arrows). B, bladder; PS, pubic symphysis; R, rectum.

floor disorders. However, a lack of universal standards has hampered widespread adoption of these imaging techniques.

Endorectal sonography has an important role in assessing the integrity of the IAS and EAS and can be used effectively as a screen for urethral diverticula. Some of the promising applications of pelvic floor sonography include assessment of the integrity of the pelvic floor muscles and biometry. It can be a useful adjunct to pelvic floor muscle training and biofeedback. Other potentially useful applications include investigation of posterior vaginal wall prolapse and assessment of implanted supporting or bulking materials. However, lack of standardized technique, terminology, objective parameters for assessment of pelvic floor disorders, and validation of diagnosis are barriers in the acceptance of pelvic floor sonography as a primary imaging modality in urogynecology. In 2011, an international panel attempted to perform a meta-analysis to analyze the pelvic floor sonographic literature. They deemed the production of a systematic review impossible based on the type and quality of the published literature.<sup>69</sup> They did, however, identify research priorities and advised more coordinated and structured research into internal and external validation of pelvic floor sonography in assessment of pelvic floor disorders.

Over the past 2 decades, MRI has already demonstrated excellent capability to evaluate pelvic floor disorders and has proved to be useful in assisting the surgeon to plan intervention and, thereby, to improve patient outcomes. Continued research including prospective ongoing trials should improve this area further. In addition to recent American

College of Radiology Appropriateness Criteria guidelines, additional practice statements are planned from societies in Europe and North America, and it is hoped that they will provide more standardization of both the acquisition and interpretation of pelvic floor MRI studies. Standardization of the threshold dynamic values and nomenclature is needed. Also, semiautomation of 3D modeling of the pelvic floor structures is only in its early days and may provide additional information with less interobserver and intraobserver variability. Finally, better guidelines for reader/interpreter training may help to reduce variability in the quality of this technique and yield better outcomes for patients.

## REFERENCES

1. Niggard I, Barber MD, Burgio KL, et al: Prevalence of symptomatic pelvic floor disorders in US women. *JAMA* 300(11):1311–1316, 2008.
2. Abrams P, Cardozo L, Fall M, et al: The standardization of terminology in lower urinary tract function: report from the standardization sub-committee of the International Continence Society. *Urology* 61(1):37–49, 2003.
3. Nichols CM, Gill EJ, Nguyen T, et al: Anal sphincter injury in women with pelvic floor disorders. *Obstet Gynecol* 104(4):690–696, 2004.
4. Wu JM, Matthews CA, Conover MM, et al: Lifetime risk of stress urinary incontinence or pelvic organ prolapse surgery. *Obstet Gynecol* 123(6):1201–1206, 2014.
5. Wiskind AK, Creighton SM, Stanton SL: The incidence of genital prolapse after the Burch colposuspension. *Am J Obstet Gynecol* 167(2):399–404, discussion 404–405, 1992.
6. Olsen AL, Smith VJ, Bergstrom JO, et al: Epidemiology of surgically managed pelvic organ prolapse and urinary incontinence. *Obstet Gynecol* 89(4):501–506, 1997.
7. Kruger JA, Heap SW, Murphy BA, Dietz HP: Pelvic floor function in nulliparous women using three-dimensional ultrasound and magnetic resonance imaging. *Obstet Gynecol* 111(3):631–638, 2008.
8. Weinstein MM, Jung SA, Pretorius DH, et al: The reliability of puborectalis muscle measurements with 3-dimensional ultrasound imaging. *Am J Obstet Gynecol* 197(1):68.e1–68.e6, 2007.
9. Chong AK, Hoffman B: Fecal incontinence related to pregnancy. *Gastrointest Endosc Clin North Am* 16(1):71–81, 2006.



10. Oberwalder M, Thaler K, Baig MK, et al: Anal ultrasound and endosonographic measurement of perineal body thickness: a new evaluation for fecal incontinence in females. *Surg Endosc* 18(4):650–654, 2004.
11. Fritsch H, Pinggera GM, Lienemann A, et al: What are the supportive structures of the female urethra? *Neurourol Urodyn* 25(2):128–134, 2006.
12. Lose LG: Simultaneous recording of pressure and cross-sectional area in the female urethra: a study of urethral closure function in healthy and stress incontinent women. *Neurourol Urodyn* 11(2):55–89, 1992.
13. Howard D, Miller JM, Delancey JO, Ashton-Miller JA: Differential effects of cough, Valsalva, and continence status on vesical neck movement. *Obstet Gynecol* 95(4):535–540, 2000.
14. Deindl FM, Vodusek DB, Hesse U, Schüssler B: Activity patterns of pubococcygeal muscles in nulliparous continent women. *Br J Urol* 72(1):46–51, 1993.
15. Peschers UM, Vodusek DB, Fanger G, et al: Pelvic muscle activity in nulliparous volunteers. *Neurourol Urodyn* 20(3):269–275, 2001.
16. Yang JM, Yang SH, Yang SY, et al: Reliability of real-time ultrasound to detect pelvic floor muscle contraction in urinary incontinent women. *J Urol* 182(5):2392–2396, 2009.
17. Sapsford RR, Hodges PW, Richardson CA, et al: Co-activation of the abdominal and pelvic floor muscles during voluntary exercises. *Neurourol Urodyn* 20(1):31–42, 2001.
18. Jung SA, Pretorius DH, Padda BS, et al: Vaginal high-pressure zone assessed by dynamic 3-dimensional ultrasound images of the pelvic floor. *Am J Obstet Gynecol* 197(1):52.e1–52.e7, 2007.
19. Burgio KL, Borello-France D, Richter HE, et al: Risk factors for fecal and urinary incontinence after childbirth: the childbirth and pelvic symptoms study. *Am J Gastroenterol* 102(9):1998–2004, 2007.
20. Pannu HK, Javitt MC, Glanc P, et al: ACR Appropriateness Criteria: pelvic floor dysfunction. *J Am Coll Radiol* 12(2):134–142, 2015.
21. Falk PM, Blatchford GJ, Cali RL, et al: Transanal ultrasound and manometry in the evaluation of fecal incontinence. *Dis Colon Rectum* 37(5):468–472, 1994.
22. Law PJ, Bartram CI: Anal endosonography: technique and normal anatomy. *Gastrointest Radiol* 14(4):349–353, 1989.
23. Law PJ, Kamm MA, Bartram CI: Anal endosonography in the investigation of faecal incontinence. *Br J Surg* 78(3):312–314, 1991.
24. Law PJ, Kamm MA, Bartram CI: A comparison between electromyography and anal endosonography in mapping external anal sphincter defects. *Dis Colon Rectum* 33(5):370–373, 1990.
25. Maglinte DD, Kelvin FM, Fitzgerald K, et al: Association of compartment defects in pelvic floor dysfunction. *AJR Am J Roentgenol* 172(2):439–444, 1999.
26. Kelvin FM, Maglinte DD, Hornback JA, Benson JT: Pelvic prolapse: assessment with evacuation proctography (defecography). *Radiology* 184(2):547–551, 1992.
27. Rentsch M, Paetzel C, Lenhart M, et al: Dynamic magnetic resonance imaging defecography: a diagnostic alternative in the assessment of pelvic floor disorders in proctology. *Dis Colon Rectum* 44(7):999–1007, 2001.
28. Kaufman HS, Buller JL, Thompson JR, et al: Dynamic pelvic magnetic resonance imaging and cystocolpoproctography alter surgical management of pelvic floor disorders. *Dis Colon Rectum* 44(11):1575–1583, 2001.
29. Hetzer FH, Andreisek G, Tzagari C, et al: MR defecography in patients with fecal incontinence: imaging findings and their effect on surgical management. *Radiology* 240(2):449–457, 2006.
30. Haylen BT, de Ridder D, Freeman RM, et al: An International Urogynecological Association (IUGA)/International Continence Society (ICS) joint report on the terminology for female pelvic floor dysfunction. *Neurourol Urodyn* 29(1):4–20, 2010.
31. Whitehead WE, Borrud L, Goode PS, et al: Fecal incontinence in US adults: epidemiology and risk factors. *Gastroenterology* 137(2):512, 517.e1–2, 2009.
32. Gantke B, Schäfer A, Enck P, Lübke HJ: Sonographic, manometric, and myographic evaluation of the anal sphincters morphology and function. *Dis Colon Rectum* 36(11):1037–1041, 1993.
33. Santoro GA, Falco GD: Endoanal and endorectal ultrasonography: methodology and normal pelvic floor anatomy. In Santoro GA, Wiczorek AP, Bartram CI, editors: *Pelvic Floor Disorders: Imaging and Multidisciplinary Approach to Management*, Milan, 2010, Springer, pp 91–102.
34. Oberwalder M, Dinnewitzer A, Baig MK, et al: The association between late-onset fecal incontinence and obstetric anal sphincter defects. *Arch Surg* 139(4):429–432, 2004.
35. Nichols CM, Ramakrishnan V, Gill EJ, Hurt WG: Anal incontinence in women with and those without pelvic floor disorders. *Obstet Gynecol* 106(6):1266–1271, 2005.
36. Deen KI, Kumar D, Williams JG, et al: Anal sphincter defects. Correlation between endoanal ultrasound and surgery. *Ann Surg* 218(2):201–205, 1993.
37. Sultan AH, Kamm MA, Talbot IC, et al: Anal endosonography for identifying external sphincter defects confirmed histologically. *Br J Surg* 81(3):463–465, 1994.
38. Meyenberger C, Bertschinger P, Zala GF, Buchmann P: Anal sphincter defects in fecal incontinence: correlation between endosonography and surgery. *Endoscopy* 28(2):217–224, 1996.
39. Farouk R, Bartolo DC: The use of endoluminal ultrasound in the assessment of patients with faecal incontinence. *J R Coll Surg Edinb* 39(5):312–318, 1994.
40. Gold DM, Halligan S, Kmiot WA, Bartram CI: Intraobserver and interobserver agreement in anal endosonography. *Br J Surg* 86(3):371–375, 1999.
41. Faltin DL, Boulvain M, Floris LA, Irion O: Diagnosis of anal sphincter tears to prevent fecal incontinence: a randomized controlled trial. *Obstet Gynecol* 106(1):6–13, 2005.
42. Parks AG, Gordon PH, Hardcastle JD: A classification of fistula-in-ano. *Br J Surg* 63(1):1–12, 1976.
43. Santoro GA, Murad-Regadas S: Three-dimensional endoanal ultrasonography of the anorectal region. In Shobeiri SA, editor: *Practical Pelvic Floor Ultrasonography*, New York, 2014, Springer, pp 163–184.
44. Valsky DV, Yagel S: Three-dimensional transperineal ultrasonography of the pelvic floor: improving visualization for new clinical applications and better functional assessment. *J Ultrasound Med* 26(10):1373–1387, 2007.
45. Lee JH, Pretorius DH, Weinstein M, et al: Transperineal three-dimensional ultrasound in evaluating anal sphincter muscles. *Ultrasound Obstet Gynecol* 30(2):201–209, 2007.
46. Timor-Tritsch IE, Monteagudo A, Smilen SW, et al: Simple ultrasound evaluation of the anal sphincter in female patients using a transvaginal transducer. *Ultrasound Obstet Gynecol* 25(2):177–183, 2005.
47. Roche B, Deléaval J, Fransioli A, Marti MC: Comparison of transanal and external perineal ultrasonography. *Eur Radiol* 11(7):1165–1170, 2001.
48. Oom DM, West RL, Schouten WR, Steensma AB: Detection of anal sphincter defects in female patients with fecal incontinence: a comparison of 3-dimensional transperineal ultrasound and 2-dimensional endoanal ultrasound. *Dis Colon Rectum* 55(6):646–652, 2012.
49. Roos AM, Abdool Z, Sultan AH, Thakar R: The diagnostic accuracy of transvaginal and transperineal ultrasound for detecting anal sphincter defects: the PREDICT study. *Clin Radiol* 66(7):597–604, 2011.
50. Kleinübing H, Jannini JF, Malafaia O, et al: Transperineal ultrasonography: new method to image the anorectal region. *Dis Colon Rectum* 43(11):1572–1574, 2000.
51. Beer-Gabel M, Teshler M, Barzilai N, et al: Dynamic transperineal ultrasound in the diagnosis of pelvic floor disorders: pilot study. *Dis Colon Rectum* 45(2):239–245, discussion 245–248, 2002.
52. Dietz HP: Pelvic floor ultrasound: a review. *Am J Obstet Gynecol* 202(4):321–334, 2010.
53. Schaefer GN, Koechli OR, Schuessler B, Haller U: Perineal ultrasound for evaluating the bladder neck in urinary stress incontinence. *Obstet Gynecol* 85(2):220–224, 1995.
54. Dietz HP, Wilson PD, Clarke B: The use of perineal ultrasound to quantify levator activity and teach pelvic floor muscle exercises. *Int*



- Urogynecol J Pelvic Floor Dysfunct* 12(3):166–168, discussion 168–169, 2001.
55. Dietz HP: Quantification of major morphological abnormalities of the levator ani. *Ultrasound Obstet Gynecol* 29(3):329–334, 2007.
56. Weinstein MM, Pretorius DH, Jung SA, et al: Transperineal three-dimensional ultrasound imaging for detection of anatomic defects in the anal sphincter complex muscles. *Clin Gastroenterol Hepatol* 7(2):205–211, 2009.
57. DeLancey JO, Kearney R, Chou Q, et al: The appearance of levator ani muscle abnormalities in magnetic resonance images after vaginal delivery. *Obstet Gynecol* 101(1):46–53, 2003.
58. Dietz HP, Lanzarone V: Levator trauma after vaginal delivery. *Obstet Gynecol* 106(4):707–712, 2005.
59. Dietz HP, Steensma AB: The prevalence of major abnormalities of the levator ani in urogynaecological patients. *Br J Obstet Gynaecol* 113(2):225–230, 2006.
60. Model AN, Shek KL, Dietz HP: Levator defects are associated with prolapse after pelvic floor surgery. *Eur J Obstet Gynecol Reprod Biol* 153(2):220–223, 2010.
61. Wong V, Shek K, Rane A, et al: Is levator avulsion a predictor of cystocele recurrence following anterior vaginal mesh placement? *Ultrasound Obstet Gynecol* 42(2):230–234, 2010.
62. Shobeiri SA, Chimpiri AR, Allen A, et al: Surgical reconstitution of a unilaterally avulsed symptomatic puborectalis muscle using autologous fascia lata. *Obstet Gynecol* 114(2 Pt 2):480–482, 2009.
63. Tunn R, Schaer G, Peschers U, et al: Updated recommendations on ultrasonography in urogynecology. *Int Urogynecol J Pelvic Floor Dysfunct* 16(3):236–241, 2005.
64. Khullar V, Salvatore S, Cardozo L, et al: A novel technique for measuring bladder wall thickness in women using transvaginal ultrasound. *Ultrasound Obstet Gynecol* 4(3):220–223, 1994.
65. Bernstein I, Juul N, Grønvall S, et al: Pelvic floor muscle thickness measured by perineal ultrasonography. *Scand J Urol Nephrol Suppl* 137:131–133, 1991.
66. Ulmsten U, Henriksson L, Johnson P, Varhos G: An ambulatory surgical procedure under local anesthesia for treatment of female urinary incontinence. *Int Urogynecol J Pelvic Floor Dysfunct* 7(2):81–85, discussion 85–86, 1996.
67. Ng CC, Lee LC, Han WH: Use of three-dimensional ultrasound scan to assess the clinical importance of midurethral placement of the tension-free vaginal tape (TVT) for treatment of incontinence. *Int Urogynecol J Pelvic Floor Dysfunct* 16(3):220–225, 2005.
68. Schuettoff S, Beyersdorff D, Gauruder-Burmester A, Tunn R: Visibility of the polypropylene tape after tension-free vaginal tape (TVT) procedure in women with stress urinary incontinence: comparison of introital ultrasound and magnetic resonance imaging in vitro and in vivo. *Ultrasound Obstet Gynecol* 27(6):687–692, 2006.
69. Elia G, Bergman A: Periurethral collagen implant: ultrasound assessment and prediction of outcome. *Int Urogynecol J Pelvic Floor Dysfunct* 7(6):335–338, 1996.
70. Defreitas GA, Wilson TS, Zimmern PE, Forte TB: Three-dimensional ultrasonography: an objective outcome tool to assess collagen distribution in women with stress urinary incontinence. *Urology* 62(2):232–236, 2003.
71. Poon CI, Zimmern PE: Role of three-dimensional ultrasound in assessment of women undergoing urethral bulking agent therapy. *Curr Opin Obstet Gynecol* 16(5):411–417, 2004.
72. Dietz HP, Steensma AB: Posterior compartment prolapse on two-dimensional and three-dimensional pelvic floor ultrasound: the distinction between true rectocele, perineal hypermobility and enterocele. *Ultrasound Obstet Gynecol* 26(1):73–77, 2005.
73. Grasso RF, Picicchi S, Quattrocchi CC, et al: Posterior pelvic floor disorders: a prospective comparison using introital ultrasound and colpocystodfecography. *Ultrasound Obstet Gynecol* 30(1):86–94, 2007.
74. Weemhoff M, Kluivers KB, Govaert B, et al: Transperineal ultrasound compared to evacuation proctography for diagnosing enteroceles and intussusceptions. *Int J Colorectal Dis* 28(3):359–363, 2013.
75. Bump RC, Mattiasson A, Bø K, et al: The standardization of terminology of female pelvic organ prolapse and pelvic floor dysfunction. *Am J Obstet Gynecol* 175(1):10–17, 1996.
76. Broekhuis SR, Kluivers KB, Hendriks JC, et al: POP-Q, dynamic MR imaging, and perineal ultrasonography: do they agree in the quantification of female pelvic organ prolapse? *Int Urogynecol J Pelvic Floor Dysfunct* 20(5):541–549, 2009.
77. Santoro GA, Wieczorek AP, Dietz HP, et al: State of the art: an integrated approach to pelvic floor ultrasonography. *Ultrasound Obstet Gynecol* 37(4):381–396, 2011.
78. Lone FW, Thakar R, Sultan AH, Stankiewicz A: Accuracy of assessing Pelvic Organ Prolapse Quantification points using dynamic 2D transperineal ultrasound in women with pelvic organ prolapse. *Int Urogynecol J* 23(11):1555–1560, 2012.
79. Lalwani N, Moshiri M, Lee JH, et al: Magnetic resonance imaging of pelvic floor dysfunction. *Radiol Clin North Am* 51(6):1127–1139, 2013.
80. Hecht EM, Lee VS, Tanpitukpongse TP, et al: MRI of pelvic floor dysfunction: dynamic true fast imaging with steady-state precession versus HASTE. *AJR Am J Roentgenol* 191(2):352–358, 2008.
81. Tumbarello JA, Hsu Y, Lewicky-Gaupp C, et al: Do repetitive Valsalva maneuvers change maximum prolapse on dynamic MRI? *Int Urogynecol J* 21(10):1247–1251, 2010.
82. Fielding JR, Griffiths DJ, Versi E, et al: MR imaging of pelvic floor continence mechanisms in the supine and sitting positions. *AJR Am J Roentgenol* 171(6):1607–1610, 1998.
83. Bertschinger KM, Hetzer FH, Roos JE, et al: Dynamic MR imaging of the pelvic floor performed with patient sitting in an open-magnet unit versus with patient supine in a closed-magnet unit. *Radiology* 223(2):501–508, 2002.
84. Fiaschetti V, Pastorelli D, Squillaci E, et al: Static and dynamic evaluation of pelvic floor disorders with an open low-field tilting magnet. *Clin Radiol* 68(6):e293–e300, 2013.
85. Flusberg M, Sahni VA, Erturk SM, Mortelet KJ: Dynamic MR defecography: assessment of the usefulness of the defecation phase. *AJR Am J Roentgenol* 196(4):W394–W399, 2011.
86. Broekhuis SR, Fütterer JJ, Barentsz JO, et al: A systematic review of clinical studies on dynamic magnetic resonance imaging of pelvic organ prolapse: the use of reference lines and anatomical landmarks. *Int Urogynecol J Pelvic Floor Dysfunct* 20(6):721–729, 2009.
87. Singh K, Reid WM, Berger LA: Assessment and grading of pelvic organ prolapse by use of dynamic magnetic resonance imaging. *Am J Obstet Gynecol* 185(1):71–77, 2001.
88. Yang A, Mostwin JL, Rosenshein NB, Zerhouni EA: Pelvic floor descent in women: dynamic evaluation with fast MR imaging and cinematic display. *Radiology* 179(1):25–33, 1991.
89. Colaiacomo MC, Masselli G, Poletti E, et al: Dynamic MR imaging of the pelvic floor: a pictorial review. *Radiographics* 29(3):e35, 2009.
90. Hoyte L, Schierlitz L, Zou K, et al: Two- and 3-dimensional MRI comparison of levator ani structure, volume, and integrity in women with stress incontinence and prolapse. *Am J Obstet Gynecol* 185(1):11–19, 2001.
91. Comiter CV, Vasavada SP, Barbaric ZL, et al: Grading pelvic prolapse and pelvic floor relaxation using dynamic magnetic resonance imaging. *Urology* 54(3):454–457, 1999.
92. Lockhart ME, Fielding JR, Richter HE, et al: Reproducibility of dynamic MR imaging pelvic measurements: a multi-institutional study. *Radiology* 249(2):534–540, 2008.
93. Morgan DM, Umek W, Stein T, et al: Interrater reliability of assessing levator ani muscle defects with magnetic resonance images. *Int Urogynecol J Pelvic Floor Dysfunct* 18(7):773–778, 2007.
94. Loubeyre P, Copercini M, Petignat P, Dubuisson JB: Levator ani muscle complex: anatomic findings in nulliparous patients at thin-section MR imaging with double opacification. *Radiology* 262(2):538–543, 2012.
95. Handa VL, Lockhart ME, Kenton KS, et al: Magnetic resonance assessment of pelvic anatomy and pelvic floor disorders after childbirth. *Int Urogynecol J Pelvic Floor Dysfunct* 20(2):133–139, 2009.



96. Berger MB, Doumouchtsis SK, DeLancey JO: Bony pelvis dimensions in women with and without stress urinary incontinence. *Neurourol Urodyn* 32(1):37–42, 2013.
97. Stein TA, Kaur G, Summers A, et al: Comparison of bony dimensions at the level of the pelvic floor in women with and without pelvic organ prolapse. *Am J Obstet Gynecol* 200(3):241.e1–241.e5, 2009.
98. Berger MB, Morgan DM, DeLancey JO: Levator ani defect scores and pelvic organ prolapse: is there a threshold effect? *Int Urogynecol J* 25(10):1375–1379, 2014.
99. Elshazly WG, El Nekady AlA, Hassan H: Role of dynamic magnetic resonance imaging in management of obstructed defecation case series. *Int J Surg* 8(4):274–282, 2010.
100. Dvorkin LS, Hetzer F, Scott SM, et al: Open-magnet MR defaecography compared with evacuation proctography in the diagnosis and management of patients with rectal intussusception. *Colorectal Dis* 6(1):45–53, 2004.
101. Ellis CN: Treatment of obstructed defecation. *Clin Colon Rectal Surg* 18(2):85–95, 2005.
102. Kelvin FM, Maglinte DD, Hale DS, Benson JT: Female pelvic organ prolapse: a comparison of triphasic dynamic MR imaging and triphasic fluoroscopic cystocolpoproctography. *AJR Am J Roentgenol* 174(1):81–88, 2000.
103. Bergman A, McCarthy TA, Ballard CA, Yanai J: Role of the Q-tip test in evaluating stress urinary incontinence. *J Reprod Med* 32(4):273–275, 1987.
104. Pannu HK: MRI of pelvic organ prolapse. *Eur Radiol* 14(8):1456–1464, 2004.
105. Goh V, Halligan S, Kaplan G, et al: Dynamic MR imaging of the pelvic floor in asymptomatic subjects. *AJR Am J Roentgenol* 174(3):661–666, 2000.
106. Rosenkrantz AB, Lewis MT, Yalamanchili S, et al: Prevalence of pelvic organ prolapse detected at dynamic MRI in women without history of pelvic floor dysfunction: comparison of two reference lines. *Clin Radiol* 69(2):e71–e77, 2014.

# Role of Magnetic Resonance Imaging in the Evaluation of Gynecologic Disorders

*Priya Bhosale, Catherine Devine, Carly S. Gardner, Aliya Qayyum*

## SUMMARY OF KEY POINTS

- Magnetic resonance imaging (MRI) is a problem-solving tool and has greater accuracy and specificity for characterization of gynecologic masses than sonography or computed tomography (CT), but should generally be performed after pelvic sonography.
- High resolution T2-weighted sequences are the mainstay images for evaluation of nonobstetric gynecologic disorders.
- T1-weighted imaging must be performed with and without fat suppression if characterization of fat or blood products is required.
- The uterine corpus is best assessed in the parasagittal plane.
- The cervix is best assessed in the axial plane.
- MRI is the method of choice for evaluation of congenital uterine anomalies, including associated renal anomalies.
- Water-based gel instilled into the vagina is helpful in cervical and vaginal cancer assessment.
- Gadolinium is helpful in defining the extent and vascularity of tumors.
- Many tumors demonstrate restricted diffusion.
- Staging of gynecologic malignancy is based on the International Federation of Gynecology and Obstetrics (FIGO) system, and cross-sectional imaging is helpful in preoperative planning.

## OUTLINE

### Imaging Techniques, 1046

### Anatomy and Physiology, 1046

Uterus, 1046

Ovaries, 1047

### Congenital Anomalies, 1048

Müllerian Duct Anomalies, 1048

Vaginal Anomalies, 1051

Ovarian Anomalies, 1051

### Leiomyomas, 1051

Definition and Epidemiology, 1051

Clinical Aspects, 1051

Pathophysiology, 1052

Treatment, 1053

Diagnosis, 1053

Imaging Characteristics, 1053

### Adenomyosis, 1056

Definition and Epidemiology, 1056

Clinical Aspects, 1056

Pathophysiology, 1056

Diagnosis, 1056

Imaging Characteristics, 1056

### Endometriosis, 1056

Definition and Epidemiology, 1056

Etiology, 1056

Clinicopathologic Aspects, 1057

Imaging, 1057

### Cervical Cancer, 1057

Epidemiology and Clinical Presentation, 1057

Histopathology, 1059

Diagnosis, 1060

Treatment, 1060

Clinical Staging, 1060

Imaging, 1060

### Endometrial Cancer, 1063

Epidemiology and Clinical Presentation, 1063

Histopathology, 1063

Diagnosis, 1063

Treatment, 1063

Staging, 1064

Imaging, 1064

### Adnexal Masses, 1065

Epidemiology and Clinical Significance, 1065

Imaging Diagnosis and the Role of Magnetic Resonance Imaging, 1066

Differentiation of Benign and Malignant Lesions, 1067

Specific Diagnosis Based on Magnetic Resonance Imaging Findings, 1067

### Conclusion, 1070



This chapter describes the main indications for MRI in the evaluation of nonobstetric gynecologic disorders. In the first two sections, normal anatomy of the female pelvis and common congenital anomalies are discussed. In subsequent sections, the use of MRI in the setting of common benign diseases, namely leiomyomas, adenomyosis, and endometriosis is outlined. Finally, the role of MRI in patients with malignant neoplasms of the reproductive organs is discussed. The main clinical and epidemiologic aspects of gynecologic disease are presented, in addition to the imaging features, in order to emphasize a practical clinical approach to patient management.

## IMAGING TECHNIQUES

Although a detailed discussion of imaging techniques and protocols used in MRI is beyond the scope of this chapter, some of the most important basic concepts with regard to MRI techniques are included to aid in interpretation of images presented herein, targeting those readers unfamiliar with MRI.

T2-weighted images provide the foundation for MRI of the female pelvis. These images are used for evaluation of normal anatomy and detection of most uterine and adnexal abnormalities. T1-weighted images, especially when used in conjunction with fat suppression, are helpful in characterizing the content of adnexal lesions, namely in the identification of blood and fat. When used after the administration of intravenous gadolinium, T1-weighted images also assist in the characterization of some benign and malignant tumors. As a general rule, on T1-weighted images, fat-containing lesions are bright (high signal intensity), whereas water, such as urine in the bladder, is dark (low signal intensity). However, water is bright on T2-weighted images. Therefore, tissues with higher amounts of water, such as tumors and cysts, have high signal intensity on T2-weighted images. Water-based gel instilled into the vagina can be used to distend the vaginal lumen and outline the cervical contour, but this technique is not widely used.<sup>1</sup> Gadolinium-based contrast agents are most commonly used as intravenous contrast media in MRI. Tissues that are infused with gadolinium increase in signal intensity on T1-weighted images when compared with images acquired before contrast administration. Hence, gadolinium is used to increase the contrast between normal and abnormal tissues in the body and to detect vascularity of tissues. For instance, many neoplastic processes enhance more avidly than adjacent normal tissues and thus become more easily visible. Newer techniques such as dynamic multiphase contrast-enhanced MRI (DCE-MRI) and diffusion-weighted imaging (DWI) provide functional information. In DCE-MRI, images are acquired at multiple times following injection of contrast agent, allowing assessment of tissue vascularity and enhancement patterns. DWI does not use intravenous contrast, but displays contrast between tissues based on different rates of diffusion of water molecules. Many malignant tumors are bright on DWI.<sup>2,3</sup>

## ANATOMY AND PHYSIOLOGY

Although it is not within the scope of this chapter to fully discuss the normal anatomy of the female pelvis, a few words regarding specific features on MRI are important. A basic concept that must be remembered is that the patient's hormonal status affects the imaging features of the female reproductive organs, irrespective of the imaging modality.<sup>4-7</sup>

### Uterus

The uterus typically measures from 6 to 9 cm in length in women of reproductive age; the cervix accounts for approximately 30% to 50% of the total uterine length in this age group, but is proportionally larger

before the menarche. Uterine zonal anatomy is best visualized using T2-weighted images, typically acquired in the axial and sagittal planes, and may be described by considering two separate regions, the cervix and the uterine body.

The cervical anatomy is divided into three zones on T2-weighted sequences: the endocervical mucosa centrally, which demonstrates high signal intensity as a result of the presence of mucus within glands; the cervical stroma, which demonstrates low signal intensity owing to the presence of fibrous connective tissue; and the peripherally located smooth muscle, which demonstrates intermediate signal intensity (Fig. 36-1). Varying amounts of mucus may be seen within the endocervical canal, which has a very high signal intensity similar to that of fluid.<sup>5,6,8</sup>

The zonal anatomy of the body of the uterus also consists of three distinct regions on T2-weighted sequences: centrally, the endometrium

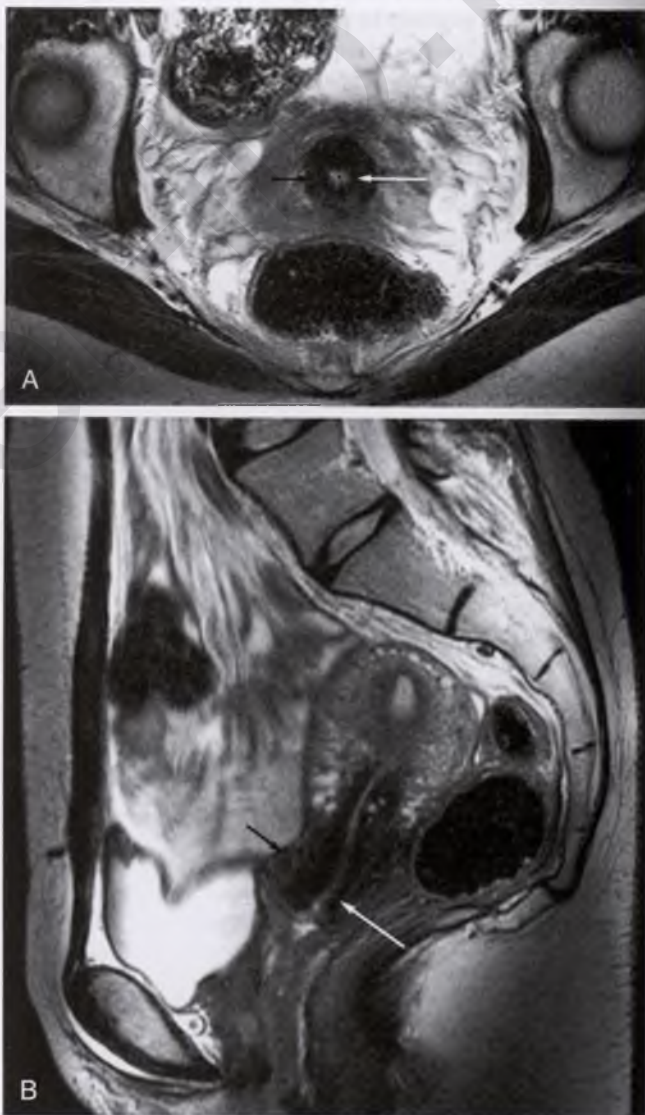


**FIG 36-1** Normal cervix. Axial (**A**) and sagittal (**B**) T2-weighted images demonstrating the normal zonal anatomy of the cervix, composed of an outer rim of smooth muscle (*short black arrow* on **A** and **B**) of intermediate signal intensity, a dark low signal intensity ring of fibrous stroma (*long white arrow* on **A** and **B**), and the high signal intensity endocervical mucosa (*asterisk* on **A**).



demonstrates very high signal intensity; subjacent to the endometrium, the junctional zone, which represents the innermost layer of the myometrium, demonstrates low signal intensity; and the outer myometrium, which demonstrates intermediate signal intensity (Fig. 36-2). At its inferior aspect, the junctional zone is continuous with the low signal intensity fibrous cervical stroma.<sup>8-10</sup>

Identification of the junctional zone is extremely important when evaluating the uterine magnetic resonance zonal anatomy. Studies have shown that the appearance of the zonal anatomy on MRI is influenced by female hormones.<sup>4-6</sup> Normally, the junctional zone should not measure more than 11 mm in thickness in women of reproductive age. In postmenopausal women, women taking oral contraceptives, or in girls before menarche, the zonal anatomy is frequently indistinct and the junctional zone may be very thin.<sup>8</sup>

The MRI appearance of the endometrium is also hormonally influenced and varies with the menstrual cycle. The endometrium becomes progressively thicker between the early follicular (proliferative) phase and ovulation, increasing from 1 to 3 mm in thickness to an average of 8 to 9 mm. The endometrium should not measure more than 15 mm in thickness in women of menstrual age, and typically it measures 11 mm or less in postmenopausal women who are not on hormonal replacement therapy.<sup>11,12</sup> The endometrium is highest in signal intensity during the luteal (secretory) phase.<sup>4,6,8</sup> It is imperative to recognize that the evaluation of endometrium thickness using T2-weighted images may result in overestimation because fluid within the endometrial cavity is also high in signal intensity on T2-weighted sequences (Fig. 36-3).

Unlike the uterine corpus, the cervical zonal anatomy does not demonstrate significant changes during the menstrual cycle. In addition, because the cervix is composed largely of fibrous elastic tissue, enhancement of the cervix following the administration of intravenous

gadolinium differs from enhancement of the uterine corpus. The uterine corpus is a very vascular structure when compared to the cervix and enhances earlier and more avidly than the cervix (Fig. 36-4). This is important because this difference in enhancement pattern may give the appearance of a pseudomass and lead to a misdiagnosis of cervical cancer.

## Ovaries

The normal ovaries demonstrate homogeneous intermediate T1-weighted signal intensity; however, on T2-weighted sequences, an outer high signal intensity cortex and a hypointense central medulla will be observed.<sup>13,14</sup> The ovaries measure approximately 2 × 2 × 3 cm; however, their size fluctuates according to hormonal status, largely because of follicle production and enlargement during the menstrual cycle. The ovaries are most readily identified in women of reproductive age by the presence of such follicles, which appear as small simple cysts of high signal intensity on T2-weighted sequences and low signal intensity on T1-weighted sequences (Fig. 36-5). Primordial follicles are usually smaller, measuring up to 9 mm in diameter, whereas stimulated graafian follicles may reach up to 3 to 5 cm. Other features of these

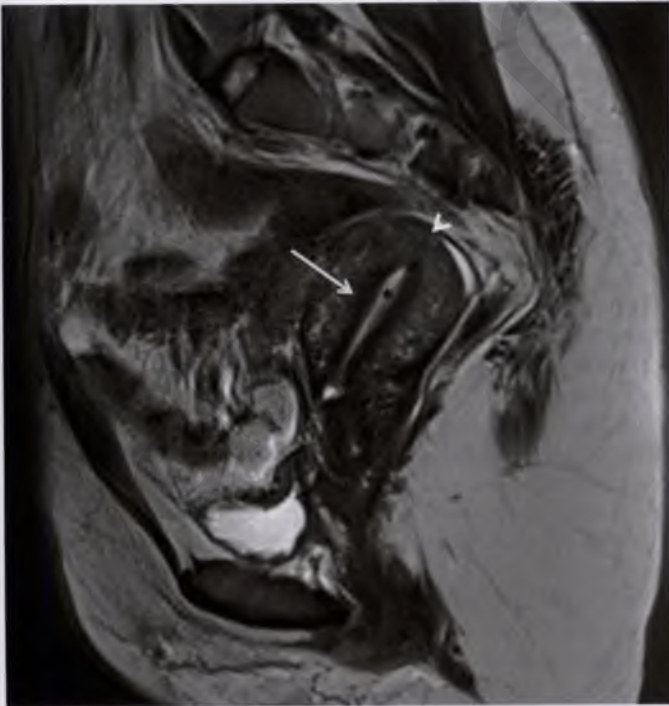


**FIG 36-2** Normal uterus. Sagittal T2-weighted image demonstrating the high signal intensity of the endometrium (*asterisk*) and the zonal anatomy of the uterus, characterized by the low signal intensity (*dark*) junctional zone (*arrow*) subjacent to the endometrium and the intermediate signal intensity outer myometrium (*arrowhead*).

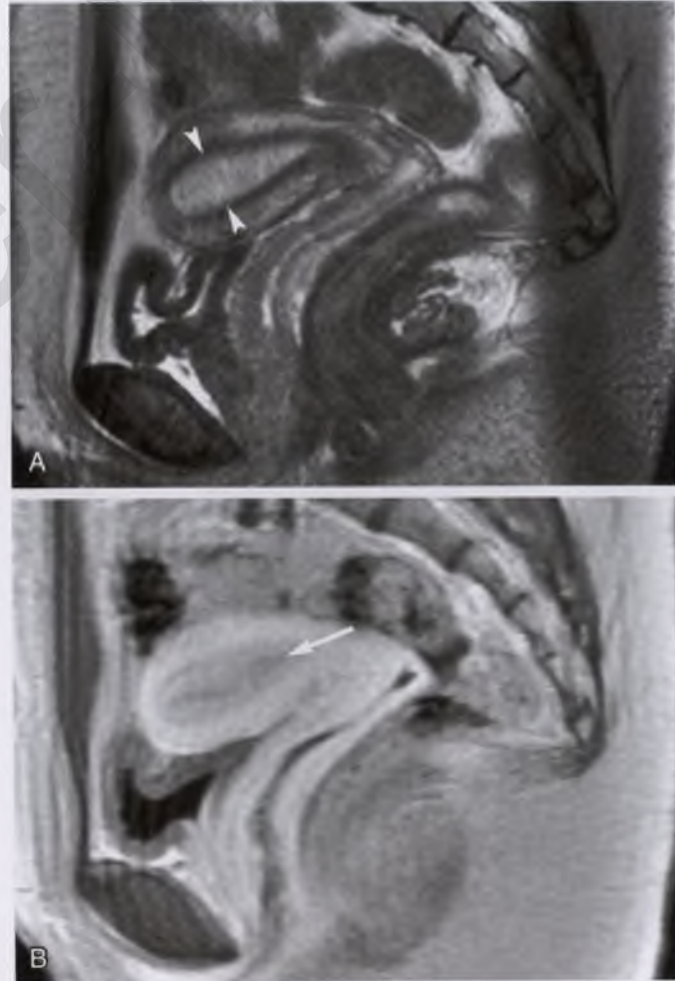


**FIG 36-3** Apparent endometrial thickening. Sagittal T2-weighted (**A**) and postcontrast T1-weighted fat-suppressed (**B**) images. Apparent thickening of the endometrium is seen on the T2-weighted image (*arrowheads* in **A**); however, after administration of gadolinium, while the endometrium enhances, a dark central band of nonenhancing fluid within the cavity becomes evident (*arrow* in **B**).



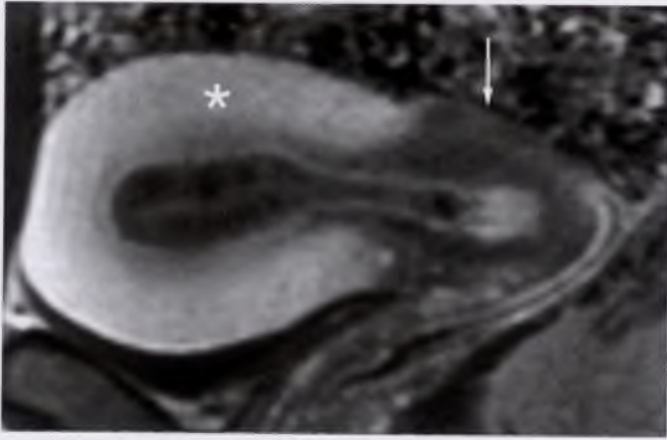


**FIG 36-4** Normal uterus. Gadolinium-enhanced sagittal T1-weighted fat-suppressed image demonstrates the normal difference between enhancement of the myometrium (*asterisk*) and cervical stroma (*arrow*).

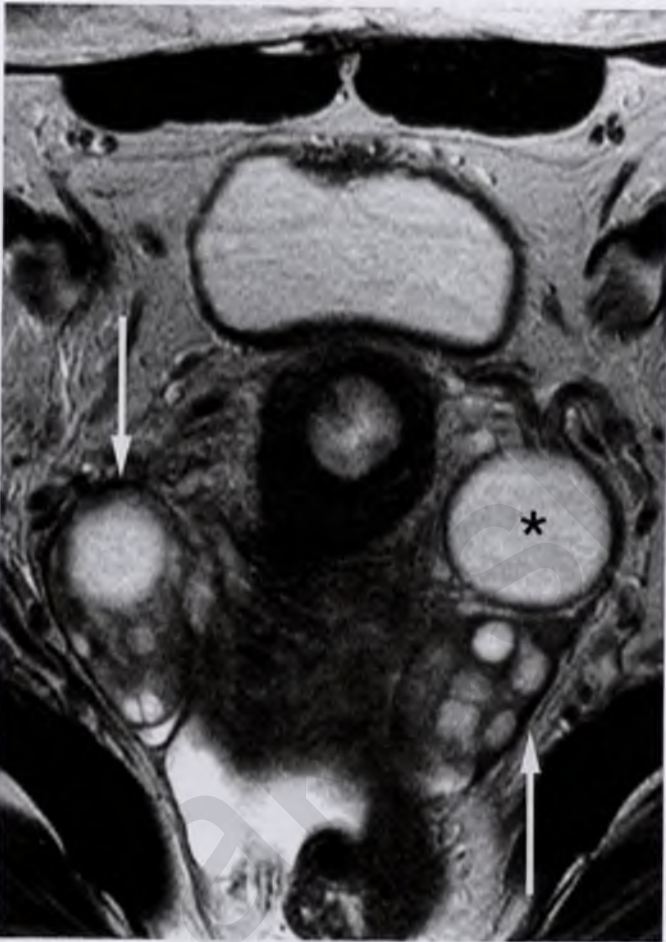


**FIG 36-5** Normal ovaries. Axial T2-weighted image demonstrates the presence of multiple hyperintense follicles in both ovaries (*arrows*), one of which represents the dominant follicle (*asterisk*).

physiologic cysts seen on T2-weighted sequences include imperceptible or thin walls (less than 3 mm) and absence of mural nodules (see Fig. 36-5).<sup>13,14</sup> The number of ovarian follicles decreases following menopause in women who are not taking hormonal replacement therapy. However, simple ovarian cysts are a common incidental finding in postmenopausal women, seen in 14% of women over 55

years of age, and may resolve or remain stable.<sup>10</sup> Ovarian stroma enhances after intravenous contrast agent administration and the use of fat-suppressed sequences helps to identify the ovaries when follicles are not visible. The normal fallopian tubes are not visualized on MRI.<sup>14</sup>

## CONGENITAL ANOMALIES

MRI is the imaging method of choice for evaluation of congenital anomalies of the female reproductive tract. Advantages of MRI include noninvasiveness, lack of ionizing radiation, multiplanar capability enabling visualization of the fundal contour of the uterus, and excellent soft tissue characterization. The use of MRI may reduce the number of invasive procedures and related costs by guiding management decisions.<sup>15</sup>

### Müllerian Duct Anomalies

The müllerian ducts are paired embryologic structures that normally fuse between the 6th and 11th weeks of gestation, forming the uterus, fallopian tubes, cervix, and most of the upper vagina.<sup>16</sup> However, in 0.1% to 10.0% of the general population, either fusion fails to occur or the ducts do not develop normally, resulting in one of the multiple types of anomalies.<sup>17-19</sup> Although müllerian duct anomalies may be asymptomatic depending upon the exact type, they may be associated with primary amenorrhea, infertility, obstetric complications, and endometriosis.<sup>16,17,20,21</sup> It is estimated that as many as 25% of women who present with infertility and miscarriage have müllerian duct anomalies.<sup>22</sup> In addition, 30% to 50% of these women have concurrent renal anomalies, which include renal agenesis, ectopia, fusion, malrotation, and duplication.<sup>16,20,23</sup> Patients suspected of having müllerian duct anomalies are often initially investigated with transvaginal sonography, because it is widely available, safe, and of relatively low cost. Although MRI is considered the reference standard for the evaluation of müllerian duct anomalies with a diagnostic accuracy of almost 100%,<sup>23,29</sup> it is frequently reserved for indeterminate cases or cases in which further information is needed. T2-weighted sequences are the most useful because identification of the zonal anatomy is necessary for complete evaluation and analysis. In addition, the study must include an oblique coronal and axial plane to ensure adequate visualization of the uterine fundal contour.

Although there are many different classifications of müllerian duct anomalies, the American Society for Reproductive Medicine classification is perhaps the most widely used and the best known (Fig. 36-6).<sup>30</sup>

### Agenesis/Hypoplasia

The anomalies within this group result from bilateral nondevelopment or arrested development of the müllerian ducts. Agenesis of the upper vagina and uterus is the most common anomaly in this group and part of the spectrum of the Mayer-Rokitansky-Küster-Hauser syndrome. Patients with this syndrome may present with an atrophic uterus, however, and vaginal abnormalities can range from hypoplasia to agenesis. Urinary system malformations are sometimes associated with the Mayer-Rokitansky-Küster-Hauser syndrome. The second most common anomaly in this class is segmental vaginal agenesis. Isolated agenesis or hypoplasia of the uterus is very rare. In complete uterine agenesis, MRI demonstrates only a short blind-ending vagina, whereas in cases of uterine hypoplasia, the uterus is small and the intercornual diameter of the endometrial cavity is reduced, measuring less than 2.0 cm.

### Unicornuate Uterus

A unicornuate uterus is the consequence of complete arrest or partial development of one müllerian duct in utero. In 90% of cases, partial



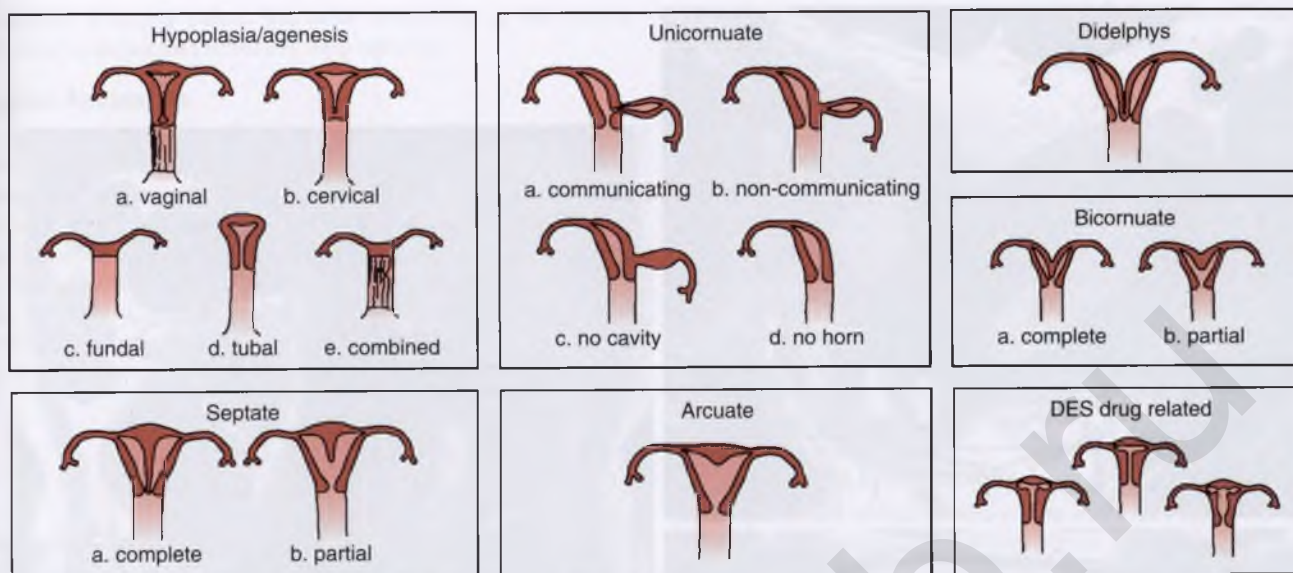


**FIG 36-6** Classification of müllerian duct anomalies used by the American Society for Reproductive Medicine. DES, diethylstilbestrol.

development of the duct occurs, with an ensuing rudimentary horn, which may or may not contain functioning endometrium. The rudimentary horn may be obstructed or may communicate with the main uterine cavity. Clinical associations include very high rates of spontaneous miscarriage, obstetric complications, and endometriosis. A unicornuate uterus will have normal zonal anatomy and has a characteristic banana-shaped configuration. A rudimentary horn can be seen as an adjacent soft tissue mass and may be distinguished from a tumor by virtue of signal intensity characteristics that are similar to myometrium on T2-weighted images. An obstructed (noncommunicating) rudimentary horn may become enlarged as a result of distention from blood products, identified as high signal intensity central material on T1-weighted sequences.

### Uterus Didelphys

Uterus didelphys arises through complete failure of müllerian duct fusion in utero and is characterized by the presence of two separate uteri and cervixes with a vertical septum in the upper vagina. Very rarely, two completely separated vaginas and vaginal orifices may be present. Patients are usually asymptomatic, but hematometocolpos may occur in the presence of an obstructing transverse hemivaginal septum. Clinical complications are similar to those associated with a unicornuate uterus. MRI may be used to readily diagnose uterus didelphys by demonstration of two widely separated uterine horns and two cervixes (Fig. 36-7). The zonal anatomy is preserved. Vaginal septa may not always be identified with MRI, and physical examination may be necessary for confirmation and differentiation from a bicornuate bicollis uterus.

### Bicornuate Uterus

This anomaly is the result of partial failure of fusion of the müllerian ducts. It is characterized by an increased intercornual distance, reportedly measuring wider than 4 cm; a concave external contour of the fundus, measuring more than 1 cm in depth; and a fibrous-muscular septum bisecting the endometrial cavity. The septum may be incomplete, partially dividing the uterine cavity (bicornuate unicollis [Fig. 36-8]), or complete, extending all the way to the external cervical os (bicornuate bicollis). The vagina develops normally. Images obtained

in the oblique coronal plane, along the long axis of the uterus, are useful in assessing the fundal contour. The dividing septum often exhibits signal characteristics similar to myometrium, but may be of low signal intensity inferiorly when fibrous tissue is present.

### Septate Uterus

Septate uterus is the most common müllerian duct anomaly and is thought to result from failure of resorption of a fibrous septum in later stages of development.<sup>16</sup> The result of such failure of resorption is a characteristically small endometrial cavity with a dividing septum, which may be partial or may extend to the external cervical os. Reproductive complications are greatest in this class of müllerian duct anomaly and are attributed to difficulties of implantation. Identification of a convex, flat, or minimally indented fundal contour without a fundal cleft on MRI obtained in the coronal plane (Fig. 36-9) is decisive in distinguishing a septate from a bicornuate uterus. Other diagnostic MRI features include an intercornual distance of less than 4 cm (i.e., not increased) and a thin, dividing, often fibrous septum typically of low T1- and T2-weighted signal intensity, although the septum may have a signal intensity similar to that of myometrium if myometrial smooth muscle is the primary component of the septum. The septum may be partial or complete.

### Arcuate Uterus

This anomaly is recognized by mild indentation of the myometrium into the fundal aspect of the endometrium, attributed to minimally incomplete resorption of the uterovaginal septum. It is classified separately because it is a benign variant without clinical significance. On MRI, the arcuate uterus is typically of normal size with a single endometrial cavity that is minimally indented superiorly by the small non-resorbed septal remnant and may be associated with a small fundal cleft less than 1.0 cm in depth.

### Diethylstilbestrol Exposure

Diethylstilbestrol is a synthetic estrogen that was historically prescribed to prevent miscarriages until 1971. It is estimated that approximately two thirds of patients exposed to this drug while in utero have uterine anomalies. The most common of these anomalies is the classic



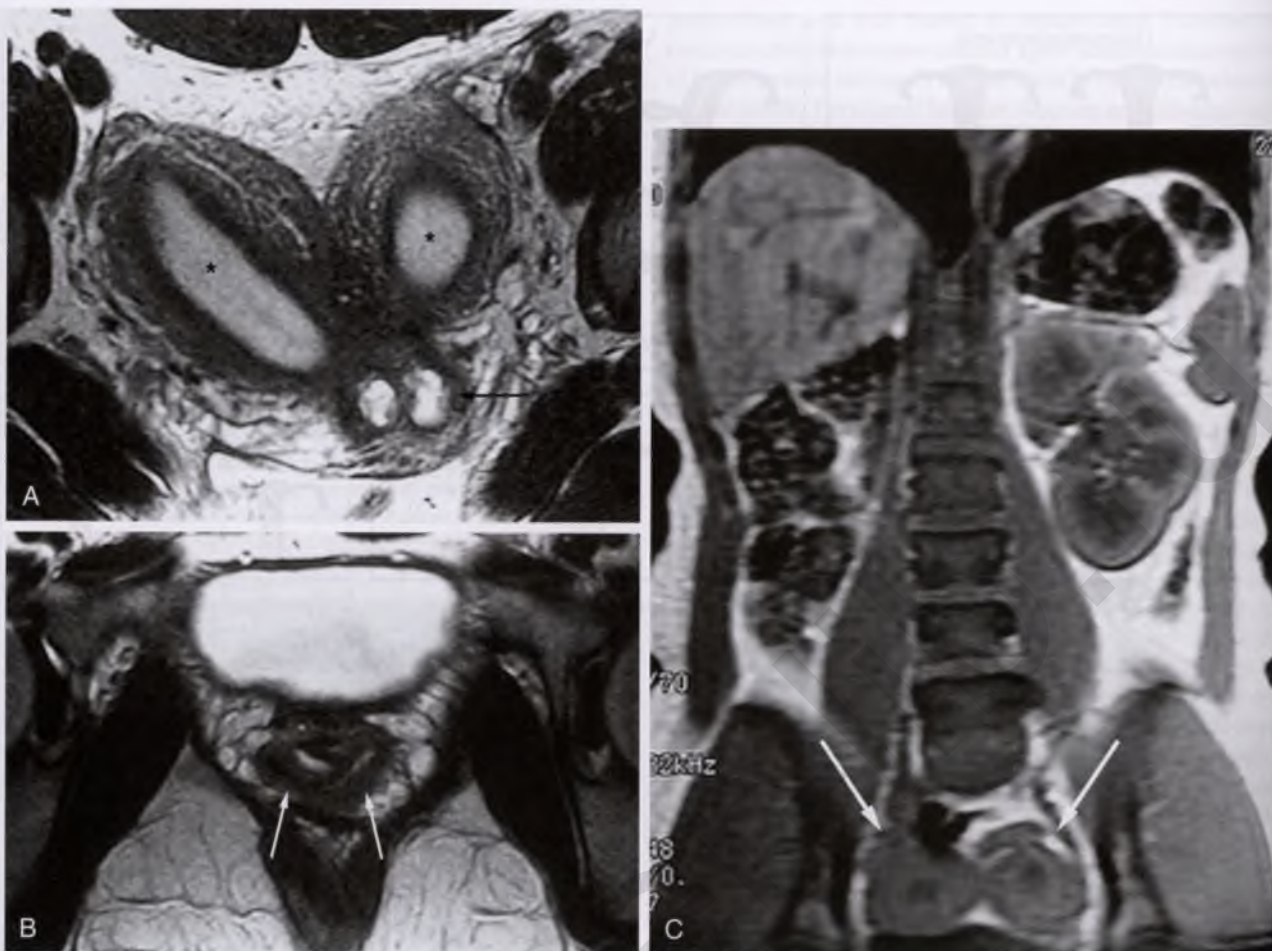


**FIG 36-7** Uterus didelphys. Axial T2-weighted images of the pelvis (**A** and **B**) and coronal T1-weighted image of the abdomen (**C**) demonstrate two separate uteri (*asterisks* on **A** and *arrows* on **C**) and cervix (*black arrow* on **A**), as well as two separate vaginas (*white arrows* on **B**). The right kidney was congenitally absent (**C**).



**FIG 36-8** Bicornuate unicollis uterus. Axial T2-weighted image demonstrates a deep cleft (*double-headed white arrow*) in the uterine fundus widely separating the right and left horns. There is a single cervix (*black arrow*).

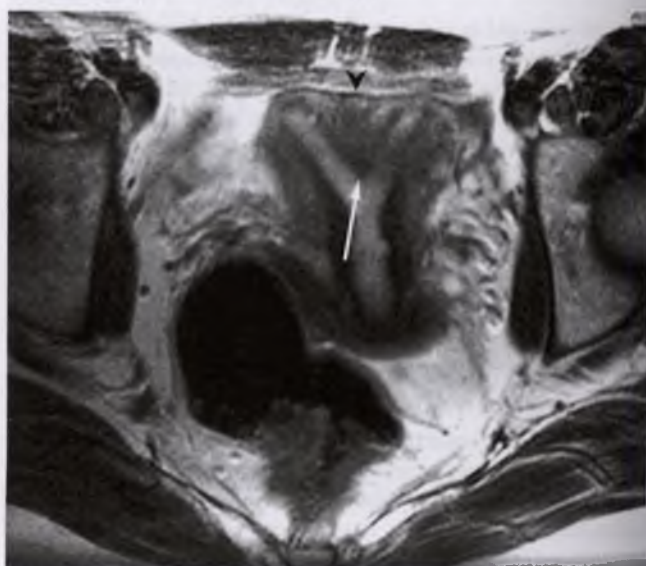


**FIG 36-9** Septate uterus. Axial T2-weighted image demonstrates a partial septum dividing the endometrial cavity (*arrow*) and a flat fundal contour (*arrowhead*).



hypoplastic T-shaped uterus, but other deformities of the uterine horns and endometrial cavity have been reported.

### Vaginal Anomalies

The lower third of the vagina originates from the urogenital sinus rather than the müllerian ducts and is developmentally distinct. Absence of the distal or lower third of the vagina or the presence of a transverse membrane (mimicking an imperforate hymen) results from failure of urogenital sinus development. In both eventualities, the vaginal obstruction causes the vagina and uterus to distend with fluid, referred to as hematometrocolpos when blood products are identified. The upper vagina demonstrates very thin walls, whereas the uterus may have either thin or thick myometrium (Fig. 36-10).

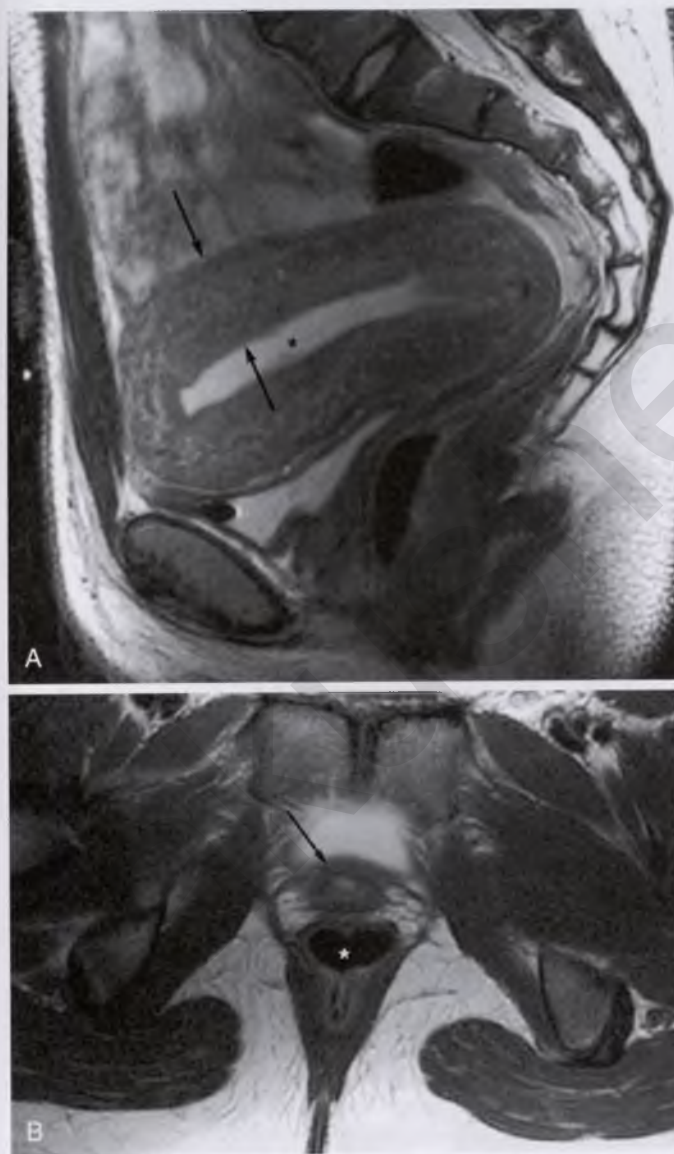


**FIG 36-10** Vaginal agenesis. Sagittal T2-weighted (A) and axial T2-weighted (B) images demonstrate mild distention of the uterine cavity (asterisk on A) and thickening of the myometrium (arrows on A) as well as absence of the vagina between the normal urethra (arrow on B) and rectum (asterisk on B).

Hematometrocolpos is characterized as a heterogeneous collection with high T1- and intermediate or low T2-weighted signal intensity.

### Ovarian Anomalies

The ovaries arise from primitive germ cells that migrate to the embryonic gonadal ridge and subsequently descend into the pelvis. Congenital anomalies of the ovaries are typically associated with chromosomal disorders and include gonadal dysgenesis, commonly occurring with Turner syndrome (45,X karyotype) and Turner syndrome mosaicism (45,X/46XX karyotype). The ovaries of patients with gonadal dysgenesis are absent or seen as fibrous streaks. Fat-suppressed T2-weighted and gadolinium-enhanced T1-weighted sequences are most helpful in the identification of the ovaries.

## LEIOMYOMAS

### Definition and Epidemiology

Leiomyomas are benign tumors arising from uterine smooth muscle cells and occur in more than 80% of African-American women and in approximately 70% of Caucasian women by age 50 years.<sup>31</sup> African-American women are diagnosed with leiomyomas at earlier ages, are more likely to be symptomatic, and are more likely to undergo myomectomies and hysterectomies compared to Caucasian women.<sup>32</sup> Leiomyomas have a significant impact on public health, accounting for at least one third of the 600,000 hysterectomies performed each year in the United States.<sup>33</sup>

### Clinical Aspects

Most patients with leiomyomas are asymptomatic.<sup>31</sup> Clinical symptoms associated with leiomyomas include dysfunctional uterine bleeding, pelvic pressure, and pelvic pain. In addition, there is an association with impaired reproductive function, which may be related to impaired implantation, tubal obstruction, and an increased rate of miscarriage as well as preterm labor.<sup>34,35</sup> Approximately 90% of leiomyomas occur in the uterus, whereas 5% to 10% are cervical in location. Leiomyomas can enlarge during pregnancy, and cervical leiomyomas may cause dystocia.<sup>36,37</sup> A minority of leiomyomas occur in the round and broad ligaments (Fig. 36-11) or adnexa.

Location of the leiomyoma often predicates the symptoms. Uterine leiomyomas are classified as submucosal, intramural, or subserosal (Fig. 36-12). Approximately 5% of leiomyomas are submucosal in location (Fig. 36-13).<sup>37</sup> Submucosal leiomyomas typically present with menometrorrhagia. In addition, a submucosal leiomyoma is more likely to be associated with infertility, dysfunctional uterine bleeding, dysmenorrhea, and anemia. Submucosal leiomyomas are often effectively treated with hysteroscopic resection, depending upon size and intracavitary extent of the mass. Submucosal leiomyomas are distinguished from large intramural leiomyomas based on identification of the lesion's epicenter within the endometrial cavity rather than within the myometrium, and less than 180-degree encirclement by surrounding myometrium.

Subserosal leiomyomas account for approximately 10% to 20% of uterine leiomyomas, are located just under the uterine serosa, and may be pedunculated or sessile (Figs. 36-13 and 36-14). Symptoms are associated with large size owing to mass effect or torsion of a pedunculated lesion. The bridging vascular sign (vessels originating from the uterus and feeding a pelvic mass) is seen in approximately 77% of exophytic leiomyomas and is helpful in differentiating these tumors from solid adnexal masses.<sup>38</sup> Conversely, an ovarian vascular pedicle (identified by the presence of a gonadal vein) may be helpful in establishing that a mass is ovarian in origin. A pedicle is seen in 92% of ovarian masses and 13% of pedunculated subserosal leiomyomas.<sup>39</sup>



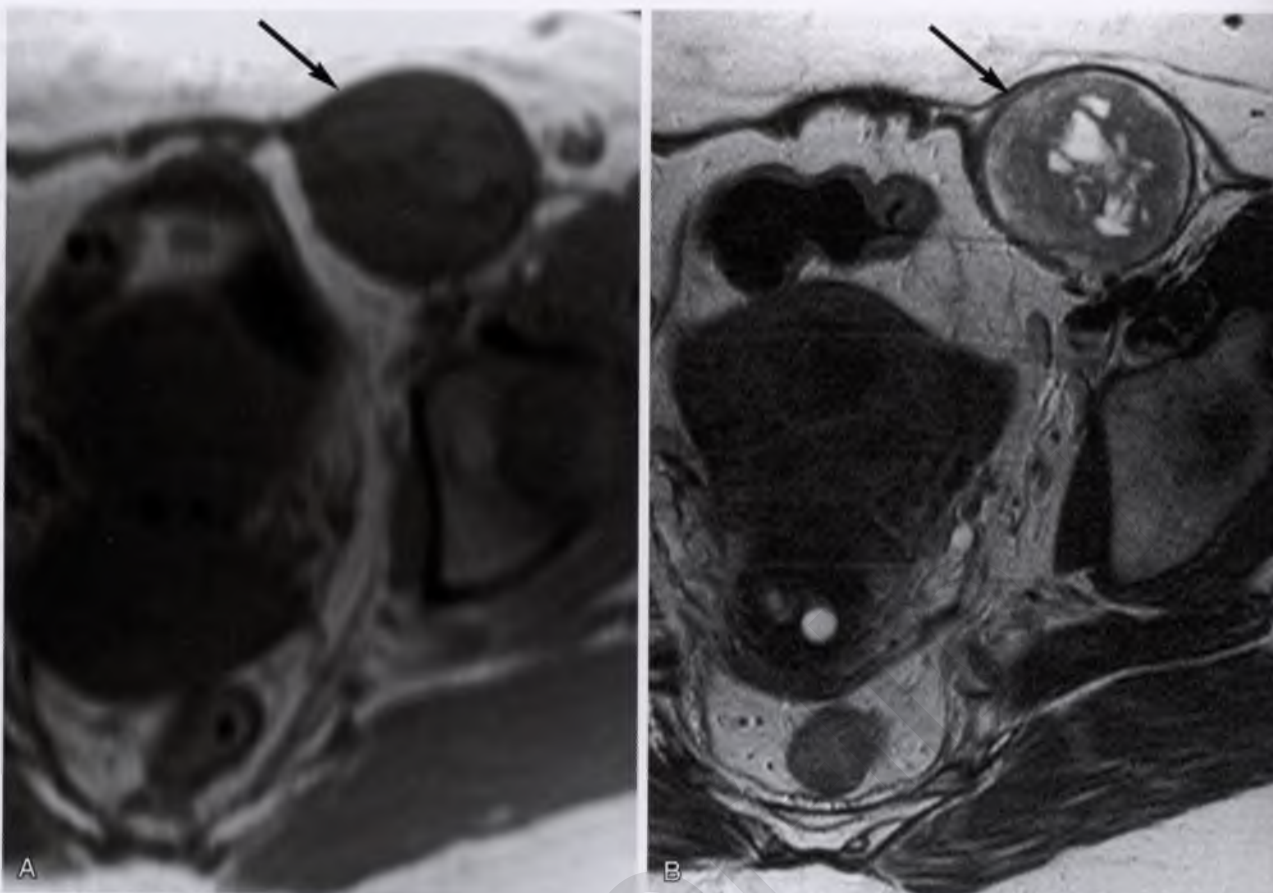


**FIG 36-11** Round ligament leiomyoma. Axial T1-weighted (A) and T2-weighted (B) images demonstrate a round mass (arrows) with the typical appearance of a degenerating leiomyoma, predominantly low signal intensity on both sequences but with central irregular areas of high signal intensity on the T2-weighted image consistent with cystic degeneration. However, the mass is separate from the uterus and has herniated into the left inguinal canal. This mass was surgically proved to be a leiomyoma of the round ligament.

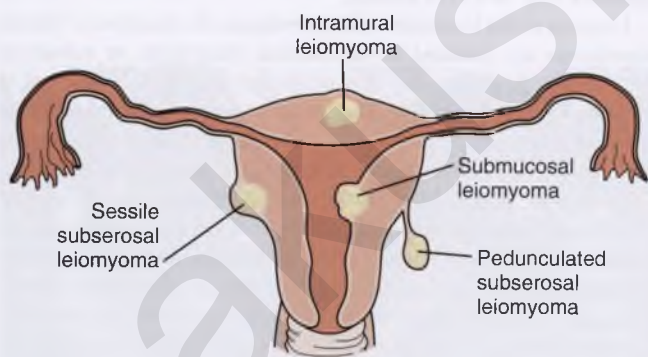


**FIG 36-12** Graphic representation of a sessile subserosal leiomyoma, a pedunculated subserosal leiomyoma, an intramural leiomyoma, and a submucosal leiomyoma.

### Pathophysiology

The pathophysiology of leiomyomas is unknown; however, genetic predisposition and hormonal status are involved in tumor development and growth.<sup>31</sup> Responsiveness of leiomyomas to hormonal stimulation frequently results in enlargement during pregnancy and involution following menopause. Various types of benign degeneration

are common, particularly in large leiomyomas, and include hyaline (most common and present in at least 60% of leiomyomas), cystic, myxoid, fatty, and hemorrhagic degeneration (Fig. 36-15).<sup>40</sup> Imaging-based differentiation between the types of degeneration is usually not possible; however, certain features may favor one or another type. Degeneration within a leiomyoma may make the sonographic diagnosis difficult as a degenerated leiomyoma may have cystic components and, thus, may mimic the sonographic appearance of a complex ovarian mass. In such cases, MRI may be used for diagnosis.<sup>41,42</sup>

Knowledge of atypical locations and presentations, such as benign metastasizing leiomyomas, intravenous leiomyomas, diffuse leiomyomatosis, and peritoneal disseminated leiomyomatosis, is important. Although these uncommon presentations may suggest a malignant process, they are essentially a variation in the growth pattern of this benign lesion.<sup>40</sup> Uterine leiomyosarcomas have been reported to occur in association with leiomyomas.<sup>43</sup> However, genetic studies suggest that these are two different entities arising from separate pathways.<sup>31</sup> Malignant degeneration of a benign leiomyoma into a leiomyosarcoma is considered by most pathologists to be extremely rare, if it occurs at all. Sometimes, the distinction between a leiomyoma and a leiomyosarcoma cannot be reliably made based on MRI characteristics of the primary lesion; however, rapid growth, irregular borders, evidence of extrauterine extension, lymphadenopathy, and metastases are, to different degrees, suggestive of malignancy (Fig. 36-16).





**FIG 36-13** Myomatous uterus. Sagittal T2-weighted image demonstrates a small low signal intensity submucosal leiomyoma (*white arrow*) and distention of the endometrial cavity with intraluminal blood (*asterisk*). Numerous subserosal leiomyomas are noted, including one at the uterine fundus (*black arrow*).

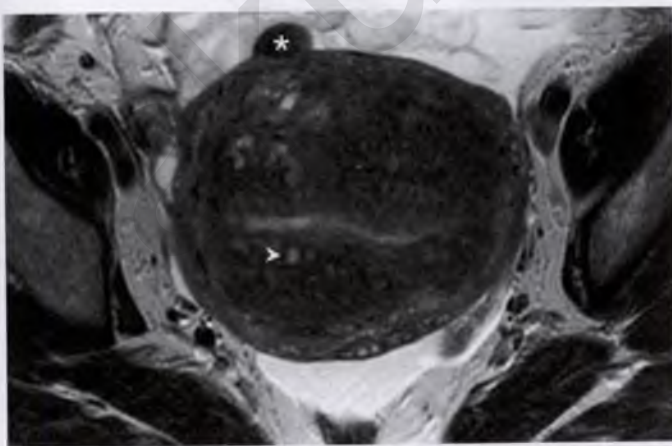


**FIG 36-14** Leiomyoma and adenomyosis. Axial T2-weighted image demonstrates a small low signal intensity subserosal leiomyoma anteriorly (*asterisk*). The junctional zone is markedly thickened and has indistinct margins. Multiple punctate foci of high signal intensity (starry sky appearance) (*arrowhead*), characteristic of adenomyosis, are seen.

## Treatment

The preferred treatment for leiomyomas depends upon their size and location, as well as clinical presentation. The most common therapeutic options are hysterectomy, myomectomy (transabdominal, laparoscopic, or hysteroscopic), myolysis, and uterine artery embolization (UAE).<sup>31,35</sup> Hysterectomy is usually performed in women who have completed childbearing and do not wish to preserve the uterus. Myomectomy is often the choice for those patients who wish to preserve the uterus. In these cases, an abdominal approach is used for multiple large leiomyomas; the laparoscopic approach is appropriate for resection of subserosal and pedunculated lesions, whereas the hysteroscopic technique is preferred for patients with submucosal lesions that are greater than 50% intracavitary. UAE is a newer, safe, and effective technique with the potential to become the treatment of choice for symptomatic uterine leiomyomas.<sup>44</sup> Contraindications to UAE include active pelvic infection, renal insufficiency, and contrast agent allergy. The reported principal advantage of UAE in appropriate candidates is lower morbidity compared to more invasive surgical techniques.

## Diagnosis

The most common indication for MRI of symptomatic patients is to determine the size and location of leiomyomas and to assess for the presence of necrosis or hemorrhage in lesions that appear worrisome on ultrasound imaging, as such factors are essential for guiding appropriate patient management. The initial diagnosis of leiomyoma is typically confirmed and then monitored, as clinically indicated, by pelvic sonography. Ultrasound evaluation may be limited in a number of situations, such as retroverted or retroflexed uterus; uterine or leiomyoma enlargement beyond the sonographic field of view, precluding complete visualization; pedunculated subserosal leiomyomas, which can be difficult to distinguish from adnexal masses; and atypical imaging features. In such cases, MRI is useful as a problem-solving tool and for preprocedural assessment when limited or conservative treatment is planned. Although MRI and sonography have similar overall sensitivity (99% for each) for detection, sonography has a lower reported specificity than MRI (86% and 91%, respectively). Furthermore, MRI is better for determining the total number of lesions.<sup>45</sup> The advantages of MRI over sonography in this application are primarily due to the larger field of view and to significantly improved soft tissue characterization.<sup>45</sup> An additional clinically important benefit of MRI is the ability to readily differentiate leiomyomas from focal adenomyosis, as these two entities are managed differently if uterine preservation is desired.<sup>46,47</sup> Finally, MRI has a role in predicting and monitoring treatment response, especially in patients treated with UAE.<sup>48-50</sup> Pretreatment imaging features predictive of a good response to UAE include submucosal location, small size, avid contrast enhancement (vascularity), and high T2-weighted signal intensity. Conversely, the presence of hemorrhagic degeneration or lack of contrast enhancement before embolization often predicts a poor response. Successful UAE results in hemorrhagic infarction and ultimate reduction in size of both the uterus and any leiomyomas.<sup>48,49,51</sup>

## Imaging Characteristics

On MRI, a simple nondegenerating leiomyoma is depicted as a well-circumscribed, round mass with low signal intensity on both T1- and T2-weighted sequences (see Fig. 36-15).<sup>37</sup> Intramural leiomyomas may demonstrate a high signal intensity pseudocapsule on T2-weighted sequences, which has been attributed to edema and vascular or lymphatic congestion within the surrounding myometrium (Fig. 36-17).<sup>52</sup> Calcifications may be seen as areas of signal void but are generally not well visualized with MRI. Nondegenerating leiomyomas typically show marked enhancement after gadolinium administration, but the use of



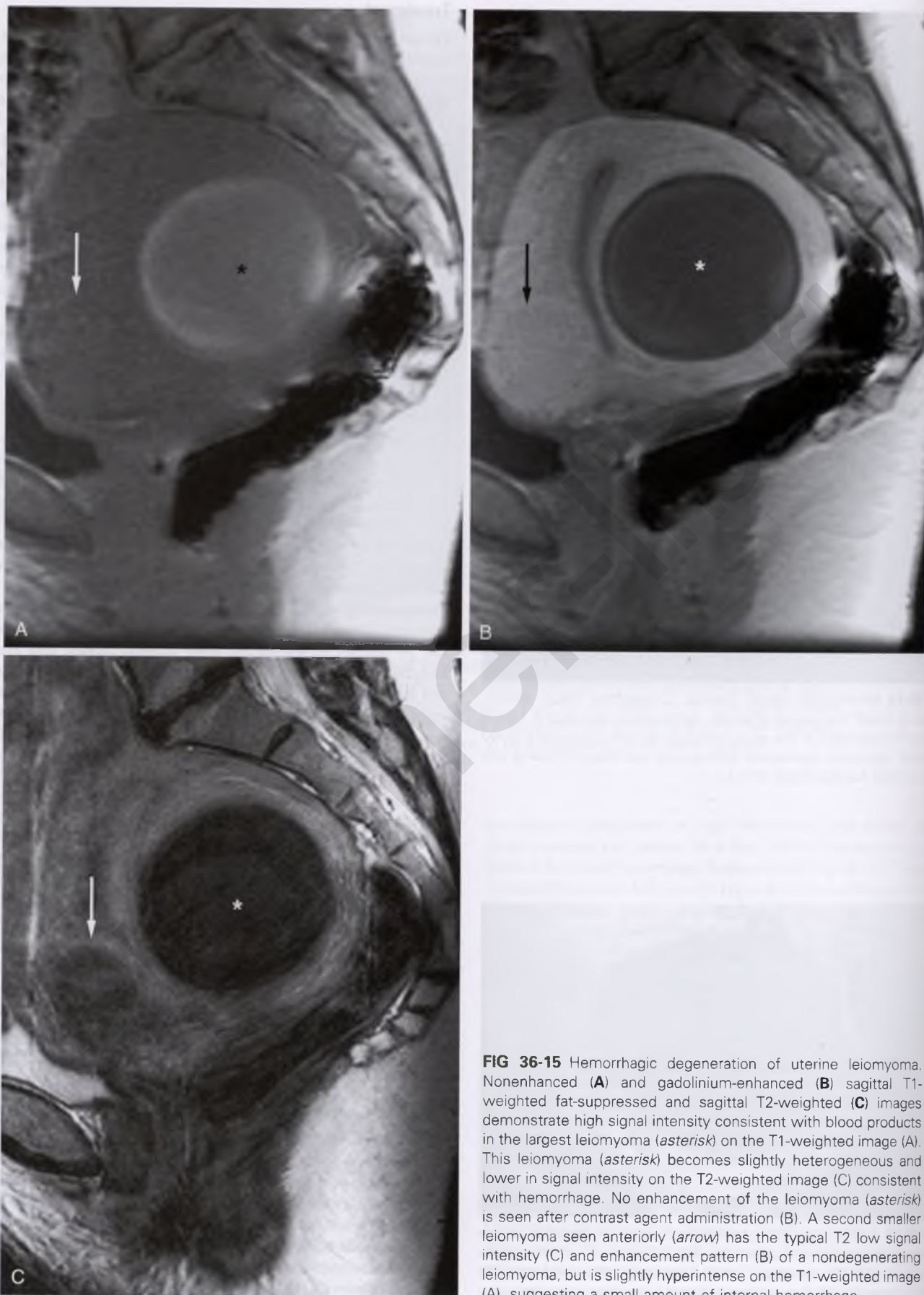


**FIG 36-15** Hemorrhagic degeneration of uterine leiomyoma. Nonenhanced (A) and gadolinium-enhanced (B) sagittal T1-weighted fat-suppressed and sagittal T2-weighted (C) images demonstrate high signal intensity consistent with blood products in the largest leiomyoma (*asterisk*) on the T1-weighted image (A). This leiomyoma (*asterisk*) becomes slightly heterogeneous and lower in signal intensity on the T2-weighted image (C) consistent with hemorrhage. No enhancement of the leiomyoma (*asterisk*) is seen after contrast agent administration (B). A second smaller leiomyoma seen anteriorly (*arrow*) has the typical T2 low signal intensity (C) and enhancement pattern (B) of a nondegenerating leiomyoma, but is slightly hyperintense on the T1-weighted image (A), suggesting a small amount of internal hemorrhage.



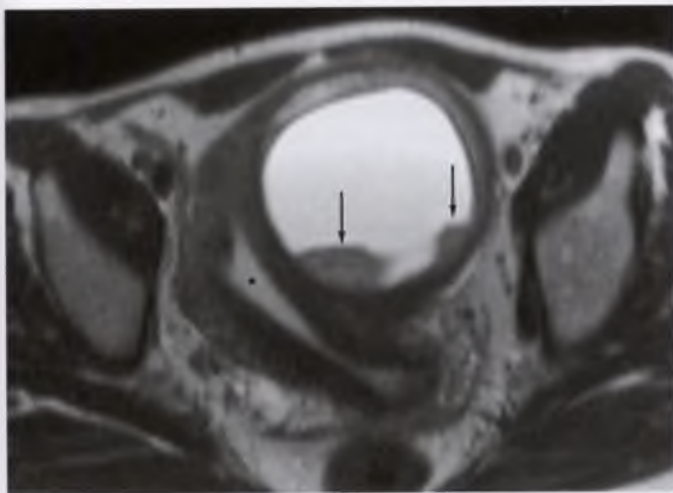


**FIG 36-16** Uterine sarcoma. Axial T2-weighted image. The high signal intensity endometrial cavity (*asterisk*) is displaced by a large cystic (high signal intensity central component) myometrial mass that contains intermediate signal intensity mural nodules (*arrows*) posteriorly; pathologic examination proved the mass to be a uterine sarcoma.

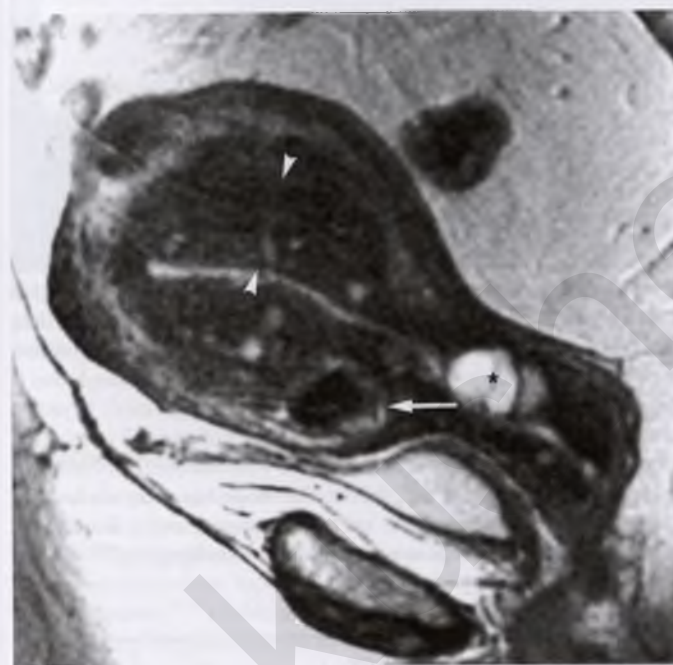


**FIG 36-17** Leiomyomas and adenomyosis. Sagittal T2-weighted image demonstrates a pseudocapsule of high signal intensity around a well-defined myometrial mass (*arrow*) in the anterior wall of the lower uterine segment, diagnostic of a leiomyoma. The low signal intensity junctional zone (*arrowheads*) is diffusely thickened and has the characteristic starry sky appearance with numerous punctate foci of high signal intensity consistent with adenomyosis. *Asterisk*, nabothian cyst.

contrast material is required only for the purpose of determining lesion vascularity when considering UAE (see Fig. 36-15).

As mentioned previously, imaging characteristics of degeneration are nonspecific, but some MRI features may suggest specific types. Leiomyomas with cystic degeneration present with very high signal intensity on T2-weighted sequences (Fig. 36-18).<sup>37</sup> Heterogeneous low T2-weighted signal intensity and a cobblestone or whorled appearance in a leiomyoma is usually associated with hyaline degeneration.<sup>40,37</sup>

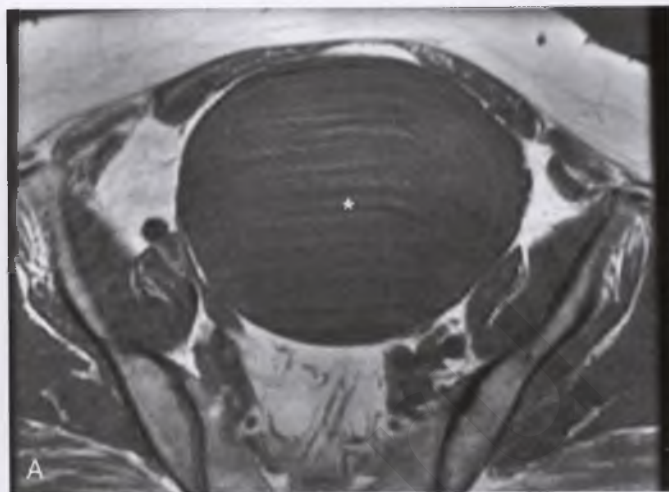


**FIG 36-18** Cystic degeneration of a uterine leiomyoma. Axial T1-weighted (**A**) and sagittal T2-weighted (**B**) images demonstrate a well-circumscribed mass (*asterisks*) arising from the uterus. The lesion demonstrates signal intensity characteristic of a cyst (low signal intensity on T1-weighted images and high signal intensity on T2-weighted images). A few thin septations are seen on the T2-weighted image (B). Pathologic examination proved this to be cystic degeneration of a leiomyoma.

Hemorrhagic degeneration commonly occurs following UAE or as a sequela of rapid lesion enlargement during pregnancy. Hemorrhagic degeneration characteristically manifests as high signal intensity on T1-weighted sequences because of the high proteinaceous content of blood or the presence of methemoglobin (see Fig. 36-15).<sup>40,37</sup> A rim



of low signal intensity on T2-weighted sequences and high signal intensity on T1-weighted sequences may be present and is thought to represent obstructed veins around the lesion.<sup>37</sup> Myxoid degeneration is associated with multiple areas of cystic change and very high T2-weighted signal intensity.<sup>40,37</sup> No specific MRI features have been described that reliably differentiate a leiomyoma from a leiomyosarcoma. However, an irregular, infiltrative, ill-defined border; extrauterine extension; and associated pelvic lymphadenopathy are worrisome features for malignancy, as noted earlier (see Fig. 36-16).

## ADENOMYOSIS

### Definition and Epidemiology

Adenomyosis refers to the presence of intramyometrial endometrial mucosa (both glands and stroma) surrounded by hypertrophied myometrium. Typically, adenomyosis is diagnosed in a multiparous woman in the fourth or fifth decade of life. Although common, the exact prevalence of adenomyosis is difficult to establish. Autopsy and clinical studies on prevalence vary, with a range of 20% to 67% in autopsy studies<sup>53</sup> and 10% to 88% in clinical studies<sup>54-57</sup>; this wide range of reported prevalence is likely a reflection of several factors, including inconsistent pathologic definition of adenomyosis, different uterine specimen processing protocols, and varied patient inclusion criteria.

### Clinical Aspects

The classic clinical scenario is that of a patient who presents with menorrhagia, dysmenorrhea, and metrorrhagia accompanied by an enlarged, smooth-contoured soft uterus that may be tender to palpation. However, one third of patients with adenomyosis are asymptomatic. Both the frequency and severity of symptoms appear to correlate with the extent and depth of myometrial involvement.<sup>53,58,59</sup>

### Pathophysiology

Adenomyosis causes globular enlargement of the uterus with cystic areas, some filled with degraded red blood cells. Adenomyosis may be described as focal, diffuse, or a combination, depending on its distribution within the myometrium. Irrespective of presentation, these lesions have ill-defined margins, unlike leiomyomas, which are sharply marginated with a smooth, regular border.<sup>53</sup>

There are three general hypotheses that attempt to explain the development of adenomyosis.<sup>53</sup> Two hypotheses suggest a process of invagination of the basalis layer of the endometrial mucosa, either between muscle fibers or along the intramyometrial lymphatic system. The third theory suggests that adenomyosis develops as a result of metaplasia from de novo ectopic intramyometrial endometrial tissue. In up to 80% of cases, there are additional uterine pathologic findings, most commonly leiomyomas, but also endometrial polyps, endometrial hyperplasia, and endometrial adenocarcinoma.<sup>53</sup>

### Diagnosis

Although presentation may strongly suggest adenomyosis, clinical diagnosis is not accurate, and imaging is often used prior to treatment selection.

### Imaging Characteristics

Transvaginal sonography is generally the first choice imaging modality in symptomatic patients with adenomyosis. It is widely available, safe, and low cost with good accuracy, similar to that reported for MRI. Reported sensitivity of transvaginal sonography ranges from 57% to 89% and specificity from 65% to 98%.<sup>60-65</sup> However, ultrasound evaluation is somewhat operator dependent, with the best results obtained by experienced examiners. In addition, the accuracy of sonography

decreases in patients who present with large uteri and concurrent leiomyomas. The reported sensitivity and specificity of MRI range from 70% to 86% and 86% to 93%, respectively.<sup>60-62</sup> MRI is generally recommended if sonographic results are equivocal or when additional information is needed, especially for treatment planning.

The diagnosis of adenomyosis on MRI is based on findings identified on T2-weighted sequences. Classically, adenomyosis appears on MRI as focal or diffuse widening of the junctional zone (inner myometrium) or as an ill-defined, hypointense, myometrial mass (see Figs. 36-14 and 36-17). The normal junctional zone in premenopausal women appears as a band of low signal intensity between the endometrium and outer myometrium. Based on the study by Reinhold and associates,<sup>60</sup> identification of a junctional zone wider than 12 mm is diagnostic of adenomyosis, whereas a width of 8 mm or less reliably excludes the condition. For patients with measurements that fall in the indeterminate category (junctional zone measuring between 9 mm and 11 mm), secondary findings including hyperintense punctate foci on T2-weighted images, hyperintense thin parallel lines radiating out from the endometrium into the myometrium (also on T2-weighted images), and ill-defined margins to the areas of low signal intensity (either diffuse or focal thickening of the junctional zone or focal areas within the myometrium near the junctional zone) may help establish the diagnosis (see Fig. 36-14).<sup>47,61,66</sup> The high-signal punctate foci are thought to represent dilated endometrial glands, whereas the striations may represent endometrial invasion into the myometrium.<sup>66</sup>

One of the diagnostic challenges for both sonography and MRI can be differentiating between focal adenomyosis and leiomyoma, because both lesions will be of low signal intensity on T2-weighted MRI sequences and are concomitantly seen in 35% to 55% of patients.<sup>53</sup> This distinction is important, as it helps to determine the choice of expectant, medical, or surgical management. MRI features that suggest the diagnosis of focal adenomyosis include visualization of the characteristic punctate foci of high signal intensity within a lesion that is of low signal intensity on T2-weighted sequences, an ovoid rather than round shape, indistinct margins, absence of a pseudocapsule, minimal mass effect, and continuation with the junctional zone (though this is not essential for diagnosis) (Fig. 36-19).<sup>66,67</sup> Although small hyperintense areas of hemorrhage are occasionally identified on T1-weighted sequences,<sup>68</sup> T1-weighted images, with or without contrast enhancement, are generally not helpful in the diagnosis. The distinction between focal adenomyosis or an adenomyoma from a leiomyoma based on imaging findings may sometimes be challenging.<sup>60,62</sup>

## ENDOMETRIOSIS

### Definition and Epidemiology

Endometriosis refers to the presence of ectopic functional endometrial tissue, which may proliferate in response to hormonal secretion. Caucasian women between 25 and 40 years of age are more commonly affected by this process.<sup>68</sup> Endometriosis affects 5% to 45% of women of reproductive age, but up to 50% of infertile patients.<sup>59,68-70</sup> The overall incidence of endometriosis is 298/100,000 person-years. However, the incidence is five times greater if there is a history of infertility, especially if due to müllerian duct anomalies.<sup>68</sup>

### Etiology

The cause of endometriosis remains unclear; proposed theories include peritoneal seeding from retrograde transport of endometrial cells through the fallopian tubes, development from müllerian remnants, and metaplasia of peritoneal epithelium. These etiologic mechanisms may be complementary, although at present, the theory of retrograde transport of cells seems favored.<sup>71</sup>



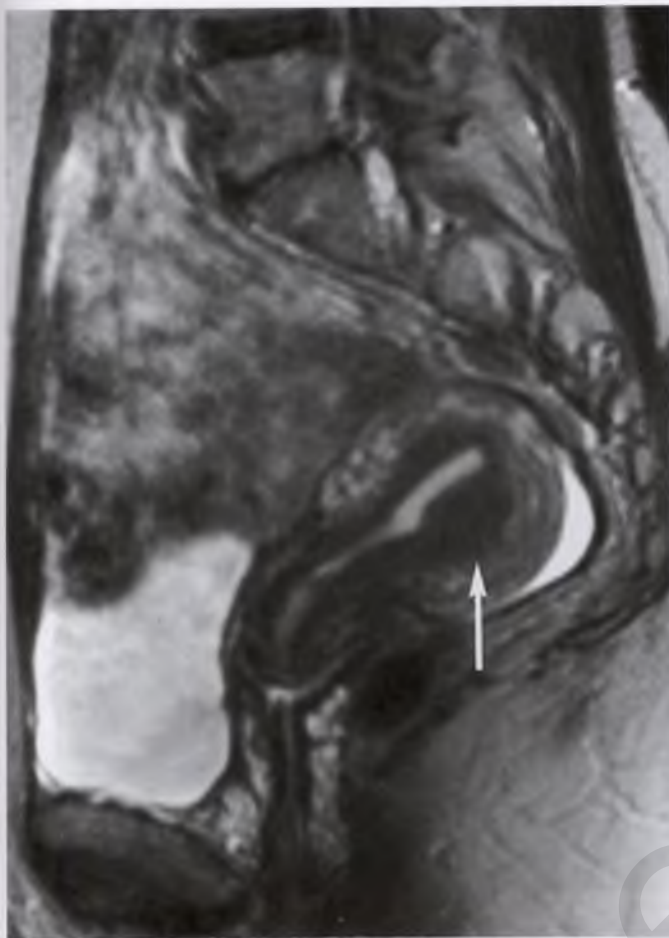


**FIG 36-19** Focal adenomyosis. Sagittal T2-weighted image demonstrates a region of focal thickening of the junctional zone (arrow) with indistinct margins.

### Clinicopathologic Aspects

Typical symptoms of endometriosis include dysmenorrhea, dyspareunia, chronic pelvic pain, and infertility. Although most frequently identified within the pelvis, endometriosis has been described in remote and unusual locations, including the lungs, abdominal wall, and central nervous system.<sup>72-74</sup> Within the pelvis, the sites of involvement in order of decreasing frequency are the ovaries (endometriomas), uterine ligaments, pouch of Douglas, and pelvic peritoneal surfaces. Ovarian involvement is bilateral in 30% to 50% cases.<sup>75</sup>

Endometriomas are one of the most common blood-containing ovarian lesions and are usually found in association with more extensive endometriosis. The ovarian tissue may be partially or completely replaced by the ectopic endometrial tissue, with glands and stroma seen lining the wall of the lesion. A thick, dense fibrous capsule is almost always present at the periphery of an endometrioma. Although endometriomas usually contain old degraded blood products, fresh hemorrhage and clots may also be identified. Adhesions to surrounding structures and internal septations are common and may lead to the misdiagnosis of an ovarian malignancy by sonography.

### Imaging

MRI is usually reserved for cases in which sonography is inconclusive or when there is failure of regression of an ovarian mass seen in the context of endometriosis. Although there are MRI features that suggest

the diagnosis of endometrioma, differentiation of a solitary endometrioma from a hemorrhagic cyst is not always possible based on imaging criteria alone. Often, patients have undergone multiple pelvic ultrasound examinations prior to MRI, and the persistence of a hemorrhagic adnexal mass favors the diagnosis of endometrioma.<sup>76</sup>

The main advantage of MRI over sonography is the ability to confirm the presence of blood within the lesion. Blood products demonstrate high signal intensity on T1-weighted images, which characteristically persists with the application of fat suppression (Fig. 36-20).<sup>77</sup> On T2-weighted sequences, the contents of an endometrioma typically demonstrate low or intermediate signal intensity, depending on the concentration of methemoglobin and other iron products.<sup>78</sup> The loss of signal intensity on T2-weighted images compared to the T1-weighted images is referred to as T2 shading, and may be observed as a diffuse loss of signal intensity or with a layered configuration, with low signal intensity blood products layering dependently within the cyst, sometimes described as the *parfait sign* (Fig. 36-21).<sup>79</sup> A black peripheral rim representing hemosiderin deposition, consequent to recurrent and chronic episodes of hemorrhage, is another typical feature; however, it is not a specific finding of endometrioma (see Fig. 36-21).<sup>76</sup> The fibrous wall of an endometrioma typically is of low signal intensity on both T1- and T2-weighted sequences and may also show contrast enhancement.<sup>80</sup> Although uncommon, malignancy has been reported in association with endometriomas and should be suspected if an enhancing solid nodule or mass is noted within the lesion (Fig. 36-22).<sup>81</sup> In a study by Brinton and colleagues,<sup>43</sup> patients with a longstanding history of ovarian endometriosis had increased risk of ovarian cancer (standardized incidence ratio of 4.2, ranging from 2.0 to 7.7), which is most commonly endometrioid or clear cell type.

In some instances, it may be difficult sonographically to correctly identify an obstructed, blood-filled dilated fallopian tube (hematosalpinx), which often occurs in the setting of endometriosis. This diagnostic dilemma may be resolved with MRI, owing to its large field-of-view and multiplanar imaging capabilities. Endometrial implants are usually hyperintense on both T1- and T2-weighted images (Fig. 36-23); however, small endometrial implants ranging from 2 to 3 mm in diameter are often not detected by any imaging modality. MRI does appear to be fairly accurate for the detection of lesions greater than 1 cm in diameter, and the use of fat-suppressed T1-weighted images reportedly increases the detection of smaller implants.<sup>82,83</sup> Stratton and associates<sup>84</sup> reported a sensitivity and specificity of 69% and 75%, respectively, for detection of endometriosis on MRI using laparoscopy as the standard of reference. Another study reported similar results comparing MRI to laparoscopy; in this series MRI had a diagnostic accuracy of approximately 77%, and statistical analysis demonstrated excellent agreement regarding stage of disease as determined by the two methods ( $\kappa = 0.916$ ,  $P < 0.001$ ).<sup>85</sup> MRI appears to be especially useful for the evaluation of deep pelvic endometriosis and cul-de-sac obliteration (which can be difficult to visualize laparoscopically) with reported sensitivities and specificities ranging from 68% to 94% and 76% to 100%, respectively.<sup>86-88</sup>

## CERVICAL CANCER

### Epidemiology and Clinical Presentation

Cervical carcinoma represents the third most common gynecologic malignancy in the United States. It is diagnosed in 1 in every 154 American women over their lifetime. The American Cancer Society estimates that 12,990 new cases of cervical carcinoma will be diagnosed and that 4,120 cancer related deaths will occur in the United States in 2016.<sup>89</sup> Patients typically present between the third and fourth decades. Most noninvasive cervical cancers are asymptomatic and detected only



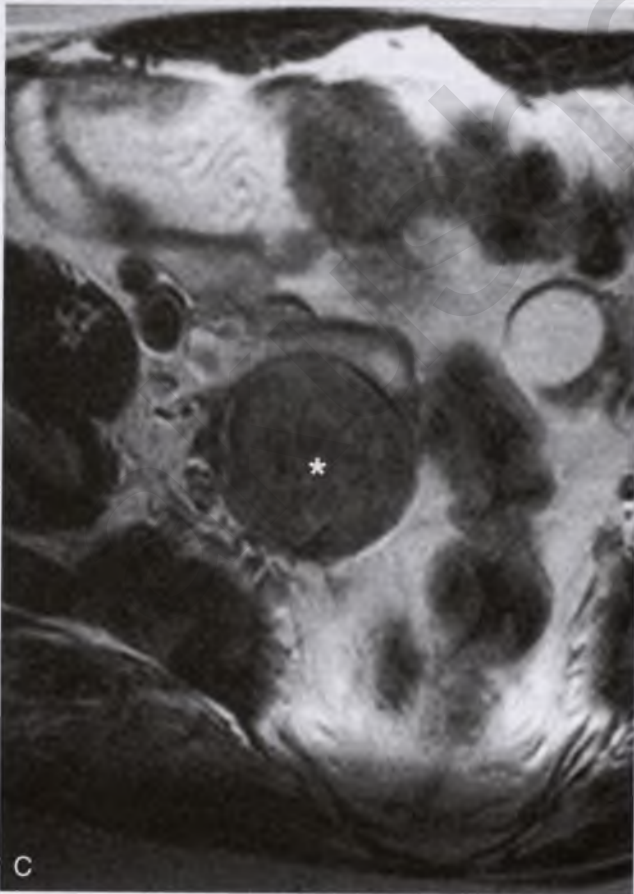
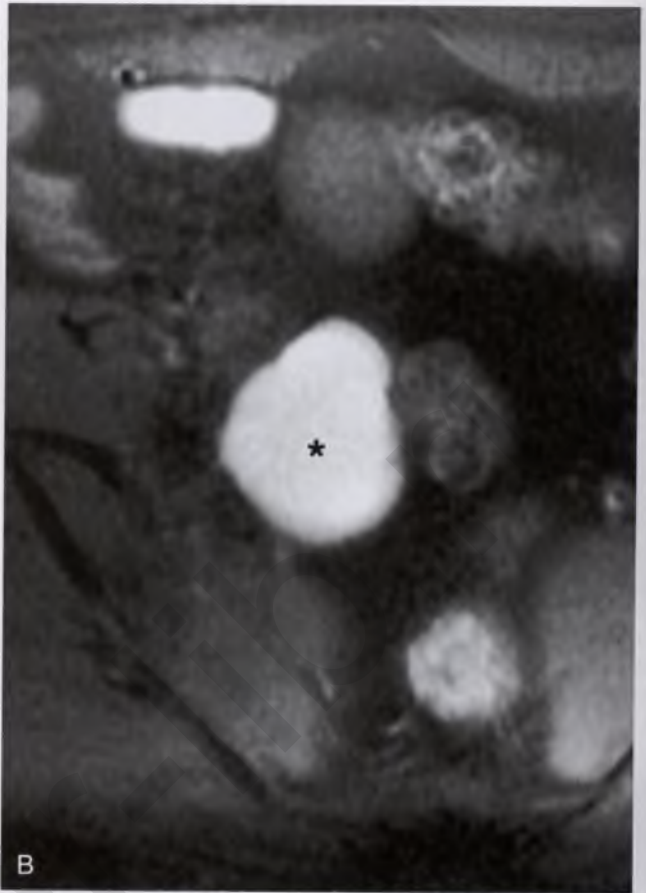
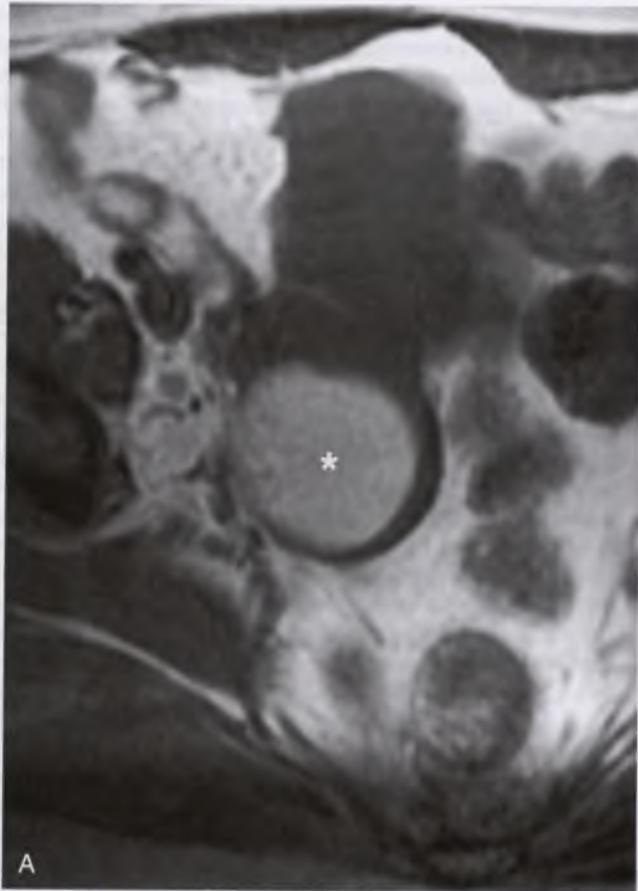


**FIG 36-20** Ovarian endometrioma. Axial T1-weighted images, without (A) and with (B) fat saturation, and axial T2-weighted image (C) demonstrate a right ovarian cystic mass (*asterisk*). The mass is high signal intensity on the T1-weighted image (A) and the high signal intensity persists after fat saturation (B). However, the mass becomes lower in signal intensity on the T2-weighted image (C), consistent with the presence of blood products. The decrease in signal intensity on T2-weighted images compared to T1-weighted images is termed "T2 shading."

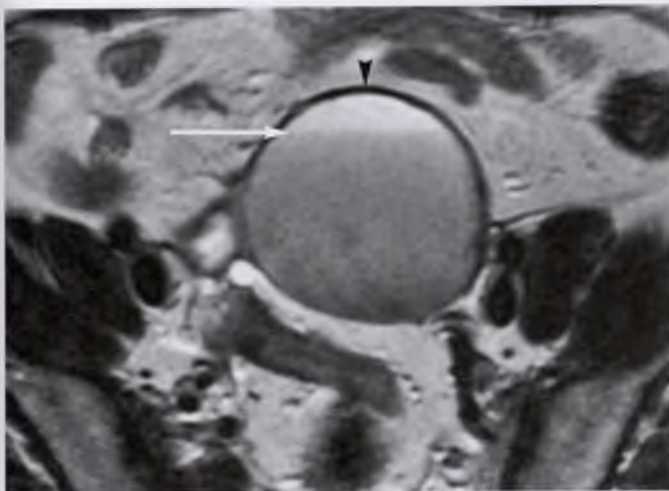


**FIG 36-21** Ovarian endometrioma. Axial T2-weighted image shows a fluid-fluid level (*arrow*) with decreased signal intensity of the dependent portion, darker than the nondependent fluid seen anteriorly. This dependent area demonstrated higher signal intensity on the corresponding T1-weighted image (not shown). The drop in signal intensity between T1- and T2-weighted sequences is termed shading and is believed to be due to the presence of methemoglobin or other iron products. This layering effect has been referred to as the parfait sign and indicates the presence of blood products of varying ages within the endometrioma. Another common finding on magnetic resonance imaging of endometriomas is a very dark peripheral rim (*arrowhead*) due to hemosiderin deposition, also the result of blood degradation.

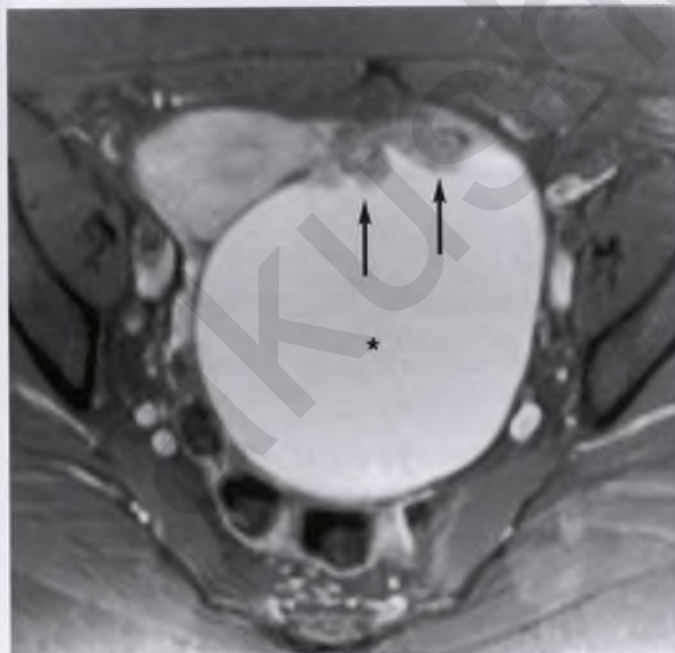


**FIG 36-22** Clear cell carcinoma. Gadolinium-enhanced T1-weighted axial image with fat saturation. A large cystic mass (*asterisk*) that contains fluid of high signal intensity after fat saturation, consistent with blood, is seen within the pelvis. Enhancing mural nodules (*arrows*) anteriorly are suggestive of malignancy, and pathologic examination proved the lesion to be a clear cell carcinoma arising within an endometrioma.

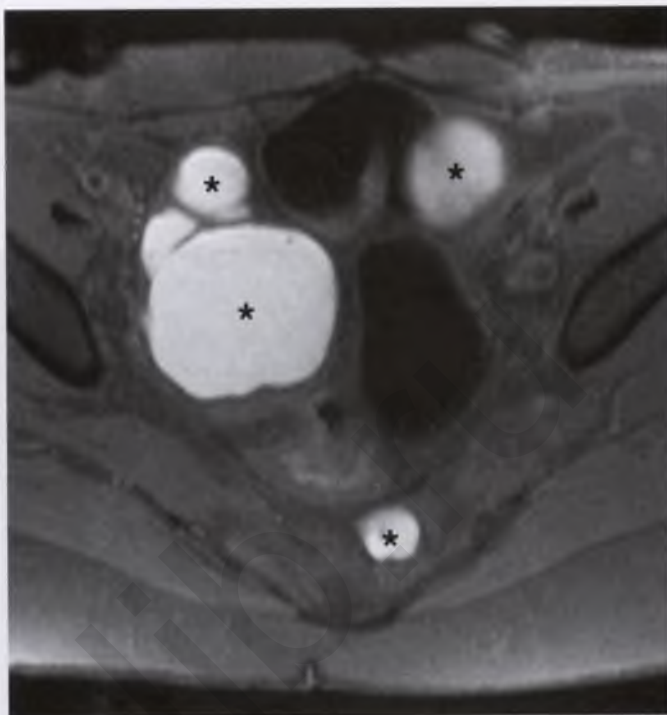


**FIG 36-23** Endometriosis. Axial fat-saturated T1-weighted image of the pelvis demonstrates multiple masses of high signal intensity (*asterisks*), consistent with endometriosis.

by the Papanicolaou (Pap) smear. Patients with invasive cancer typically report a history of intermenstrual or postcoital bleeding but may also be asymptomatic.

Human papillomavirus (HPV) is the most important etiologic factor in cervical cancer. HPV 16 and 18 account for at least two thirds of cervical carcinomas on all continents, followed by HPV 31, 33, 35, 45, 52, and 58 as the next most common types in cancers worldwide. Squamous cell carcinomas are related to HPV infection in more than 99% of cases and the presence of HPV 18 DNA is associated with poor prognosis.<sup>90</sup> Several other risk factors have been reported, including early sexual activity, multiplicity of sexual partners, low socioeconomic status, smoking, and use of oral contraceptives; however, it is unclear if these represent independent risk factors or are directly or indirectly related to HPV infection.<sup>91</sup> HPV vaccination of adolescents was introduced in the United States in 2006 with the goal of decreasing the incidence of HPV-related cervical carcinoma.

### Histopathology

The vast majority of cervical cancers are squamous cell carcinomas arising from foci of dysplasia and atypia at the squamocolumnar junction. The remaining 10% to 15% of cervical cancers arise from the endocervical glands and include adenocarcinoma, adenosquamous carcinoma, adenocystic carcinoma, small cell carcinoma, and lymphoma.<sup>92,93</sup> Adenoma malignum is a very rare subtype of cervical adenocarcinoma (3%) and is associated with Peutz-Jeghers syndrome. It is a multicystic lesion associated with copious watery vaginal discharge and is diagnosed only with deep biopsies of the cervix. Although it is histologically a well-differentiated lesion, in reality, adenoma malignum has very poor prognosis and responds poorly to therapy. The MRI appearance of adenoma malignum may be indistinguishable from a nabothian cyst. It is important to remember that this cancer is exceedingly uncommon and should not be diagnosed based on imaging



findings alone.<sup>94</sup> A few other rare tumors, such as villoglandular tumors, may be seen in the uterine cervix.<sup>95</sup>

There are three patterns of spread of squamous cell carcinoma of the cervix: direct invasion of adjacent organs, which is most common; lymphatic dissemination to pelvic and para-aortic lymph nodes; and rarely, hematogenous spread to the lungs and bones.<sup>96</sup>

### Diagnosis

Imaging has no role in the initial diagnosis of cervical cancer. In the majority of cases, the cancer is detected through Pap smear or exfoliative cytologic tests. The effective use of screening has resulted in a decline in the incidence and mortality rate of invasive squamous cell carcinomas but a relative increase in the incidence of adenocarcinomas.<sup>97-99</sup>

### Treatment

Treatment of cervical cancer largely depends on the stage of disease.<sup>92,100</sup> Patients with microinvasive (stage IA) and early macroinvasive (stage IB1, IIA < 4 cm) disease are usually offered curative surgery—total hysterectomy, with or without lymphadenectomy. If fertility is desired, patients with microinvasive cervical cancer can be treated with cone biopsy. Primary radiotherapy is an alternate option for early macroinvasive disease. For more advanced cases, treatment is usually a combination of surgery, radiotherapy, and chemotherapy.

### Clinical Staging

Staging of cervical cancer is aimed at determining whether or not the tumor is resectable and is currently based on the International Federation of Gynecology and Obstetrics (FIGO) classification system, most recently updated in 2009 (Table 36-1) and unchanged in 2014.<sup>100</sup>

The FIGO classification represents a clinical approach based on findings from physical examination, which may be performed under anesthesia. However, many studies have demonstrated the value of cross-sectional imaging over clinical staging.<sup>101-105</sup> The most recently updated FIGO staging system encourages, but does not mandate, the use of diagnostic imaging techniques to assess the size of the primary tumor. In addition, other investigations, such as cystoscopy, sigmoidoscopy, and intravenous pyelography, are increasingly of historic interest and no longer considered mandatory.

The FIGO staging system is used as a predictor of patient survival,<sup>106,107</sup> but it has limitations. Studies have shown poor correlation between clinical FIGO stage and surgical-pathologic findings. Errors in staging have been reported to be as high as 30% for stage I, 50% for stage II, and 75% for stage III tumors.<sup>93,108,109</sup> These limitations primarily relate to failure in accurately estimating tumor size and in detection of parametrial, pelvic sidewall, bladder, and rectal wall invasion or of metastases to distant organs.<sup>93</sup> In addition, nodal status, known to be one of the most important prognostic factors for patients with cervical carcinoma, is not included even in the most recent revision of the staging system.<sup>93,96,100,108,110</sup>

Accurate staging influences clinical management. Current FIGO guidelines suggest surgical treatment or radiotherapy alone for patients with early disease (i.e., stages IA, IB1, and IIA, with tumor size less than or equal to 4 cm). Patients who have more extensive early disease, stage IB2 (tumor size greater than 4 cm) and stage IIA (upper vaginal involvement), may require radiation and chemotherapy. Furthermore, stage IIB disease (limited extrauterine extension to the parametrium) or greater precludes curative surgical treatment.

### Imaging

MRI is highly accurate for staging cervical cancer, surpassing clinical staging when only stages IIA or greater are considered (73-81% vs.

**TABLE 36-1 Carcinoma of the Uterine Cervix—Federation of Gynecology and Obstetrics (FIGO) Staging**

FIGO Stage	Stage Description
I	Tumor confined to the cervix
IA	Microscopically invasive
IA1	Measured stromal invasion of $\leq 3.0$ mm in depth and extension of $\leq 7.0$ mm
IA2	Measured stromal invasion of $> 3.0$ mm and $\leq 5.0$ mm with an extension of $\leq 7.0$ mm
IB	Clinically visible lesions limited to the cervix
IB1	Clinically visible lesion $\leq 4.0$ cm
IB2	Clinically visible lesion $> 4.0$ cm
II	Cervical carcinoma invades beyond the uterus but not to pelvic wall or lower third of the vagina
IIA	Without parametrial invasion
IIA1	Clinically visible lesion $\leq 4.0$ cm
IIA2	Clinically visible lesion $> 4.0$ cm
IIB	With parametrial invasion
III	Tumor extends to the pelvic wall, involves lower third of vagina, and/or causes hydronephrosis
IIIA	Tumor involves lower third of the vagina with no extension to the pelvic wall
IIIB	Extension to the pelvic wall and/or hydronephrosis/nonfunctioning kidney
IV	Tumor extends beyond the true pelvis or involves mucosa of bladder or rectum
IVA	Invasion of adjacent organs
IVB	Distant metastases

#### Cervical Cancer—5-year relative survival rate by stage

Stage	Survival Rate
All stages	68%
Localized (confined to primary site)	91%
Regional (spread to regional nodes)	57%
Distant (metastases)	16%

Data from Pecorelli S: Revised FIGO staging for carcinoma of the vulva, cervix, and endometrium. *Int J Gynaecol Obstet* 105:103, 2009; and American Cancer Society: *Cancer Facts & Figures 2014*. Atlanta, American Cancer Society, 2014.

53%).<sup>111</sup> T2-weighted sequences are most valuable in the evaluation of cervical cancer. On T2-weighted images, cervical cancer will be identified as a mass of intermediate signal intensity within the normally low signal intensity cervical stroma.<sup>38,93</sup> Dynamic gadolinium-enhanced T1-weighted imaging has been shown to improve detection of cervical cancer and may be especially useful for the evaluation of depth of stromal invasion, parametrial involvement, and bladder wall invasion.<sup>93,105,112</sup> However, the use of single-phase contrast-enhanced T1-weighted images may result in overestimation of disease.<sup>93,104</sup>

### Early Stage Disease

Microinvasive cervical carcinoma (stage IA) cannot be detected by MRI; however, macroinvasive disease (stage IB) can be detected, with an accuracy of 91%.<sup>38,93</sup> In addition, MRI may be used to determine the depth of stromal invasion.<sup>105</sup> In stage IB disease, the low signal intensity cervical stromal ring completely surrounds the tumor (Fig. 36-24).<sup>38,93</sup> Stage II disease is characterized by local extension of tumor beyond the uterus. Stage IIA indicates invasion of the upper two thirds

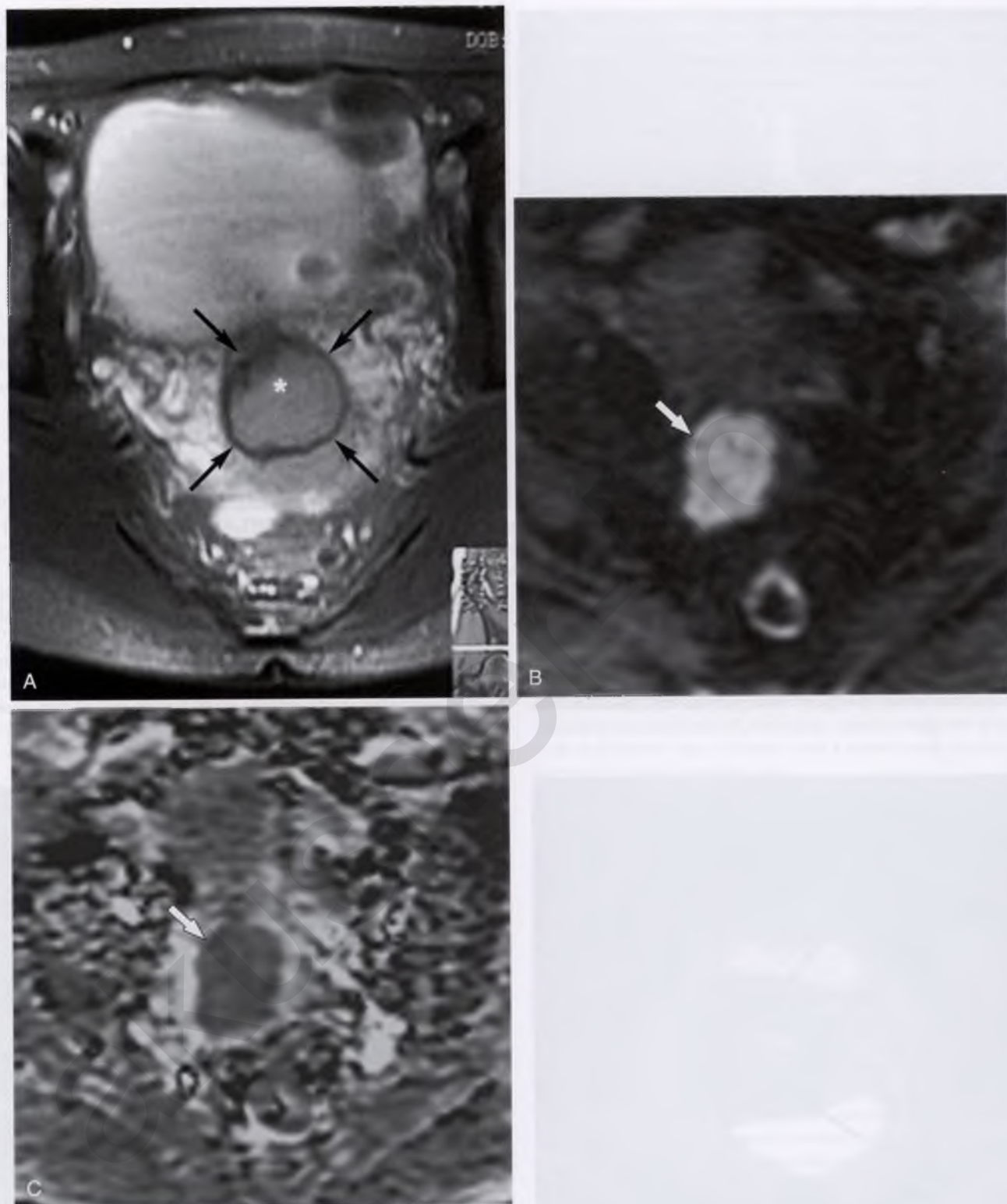


**FIG 36-24** Stage IB cervical cancer. Axial T2-weighted (**A**), diffusion-weighted (**B**), and absolute diffusion coefficient or ADC (**C**) images. T2-weighted image (**A**) shows a mass (*asterisk*) of intermediate signal intensity confined to the cervix, with a preserved peripheral T2-weighted hypointense cervical stromal ring (*arrows* in **A**). Increased signal intensity (*arrow*) on diffusion-weighted image (**B**) and hypointense signal intensity (*arrow*) on the ADC image (**C**) within the mass indicate restricted diffusion.



of the vagina and stage IIB indicates parametrial extension (Fig. 36-25). Vaginal wall extension is best evaluated in the sagittal plane on MRI. Invasion of the vagina should only be diagnosed in the presence of vaginal wall thickening and an increase in the signal intensity of the normally low signal intensity vaginal wall on T2-weighted sequences or avid enhancement of the vagina on DCE-MRI images.<sup>38,93</sup>

### Parametrial Extension

Axial T2-weighted images are used to assess for parametrial invasion. Parametrial extension (stage IIB disease) is diagnosed in the presence of partial or complete disruption of the dark ring of the cervical stroma, associated with an irregular interface between the cervix and adjacent fat (see Fig. 36-25). The presence of a definite bulge of asymmetric high signal tissue is a more specific finding of parametrial invasion. Occasionally, encasement of parametrial vessels may also be seen. Parametrial invasion is demonstrated with an accuracy of 68% to 96% on MRI.<sup>93,105,109</sup> More importantly, MRI has a high negative predictive value for parametrial invasion, ranging from 79% to 100%.<sup>93,109,110,113</sup> The positive predictive value of MRI for parametrial invasion is low, because MRI cannot accurately differentiate benign reactive changes seen adjacent to the cervix from actual tumor invasion.

### Stage III Disease

Invasion of the lower third of the vagina (IIIA) and of the pelvic sidewall (IIIB) (Fig. 36-26) characterizes stage III disease. Pelvic sidewall invasion (stage IIIB) is demonstrated by the loss of fat planes between the tumor and the iliac blood vessels or the muscles of the pelvic sidewall.<sup>93</sup> Increased signal intensity of these muscles may also be observed on T2-weighted sequences (see Fig. 36-26).<sup>93</sup> An important indicator of pelvic sidewall invasion is the presence of hydronephrosis; therefore,

MRI evaluation must include imaging of the upper abdomen, more specifically the kidneys, for assessment of hydronephrosis.<sup>38,93</sup> MRI has an accuracy of approximately 95% in characterizing stage III disease.<sup>113</sup>

### Stage IV Disease

Bladder and rectal invasion are also characterized by loss of fat planes between these organs and the tumor, as well as by increased T2-weighted signal intensity, enhancement, thickening, and irregularity of the bladder and rectal walls (Fig. 36-27).<sup>38,93</sup> MRI has been reported to be 96% accurate in making the diagnosis of bladder and rectal invasion.<sup>113</sup>

### Tumor Size Assessment

Tumor size has been shown to be a significant prognostic factor, and several studies have demonstrated that MRI is an accurate technique for assessing this.<sup>93,108,110,113,114</sup> MRI is far more reliable than clinical examination in assessing tumor size, with reported accuracy approximating 90%.<sup>115</sup>

### Lymph Node Assessment

The latest revision of the FIGO staging system for cervical cancer does not include evaluation of lymph nodes, although it has been shown that lymph node metastases have an impact on prognosis. The presence of nodal metastases has been reported to decrease the 5-year survival rate from 89% to between 48% and 57%.<sup>116</sup>

MRI determination of lymph node involvement is largely dependent on size criteria. A threshold of 1 cm or greater diameter in short axis is generally accepted as indicative of metastatic involvement.<sup>117-119</sup> However, enlarged lymph nodes are a nonspecific finding and may represent merely reactive, hyperplastic lymph nodes in patients with malignancy. Furthermore, small lymph nodes may contain

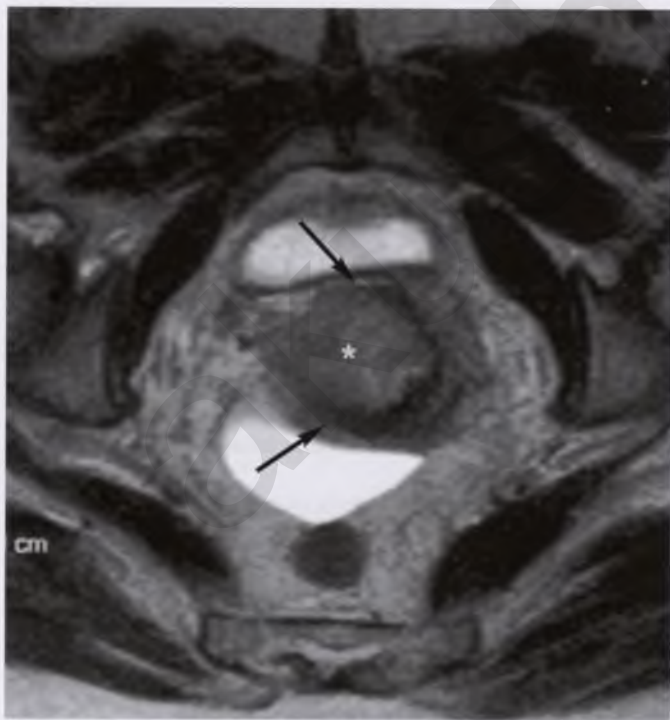


**FIG 36-25** Stage IIB cervical cancer. Axial T2-weighted image. There is interruption of the hypointense ring of cervical stroma (between the arrows) by a large moderately hyperintense cervical mass (asterisk) that bulges into the adjacent fat.

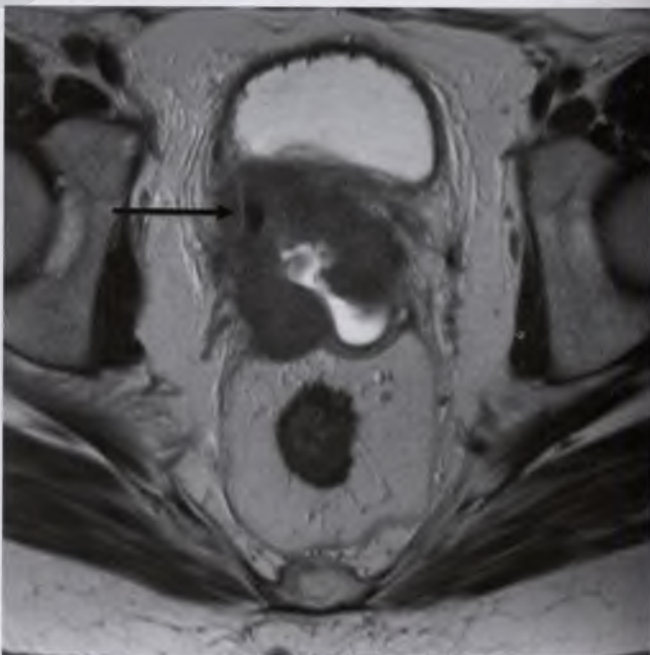


**FIG 36-26** Stage IIIB cervical cancer. Axial T2-weighted image shows an irregular mass extending beyond the cervix into the parametrium bilaterally. Right hydronephrosis was present (not shown) with a stent in the right ureter (arrow). The mass appears to be contiguous with the bladder wall; cystoscopy revealed external mass effect, but no invasion into the bladder.



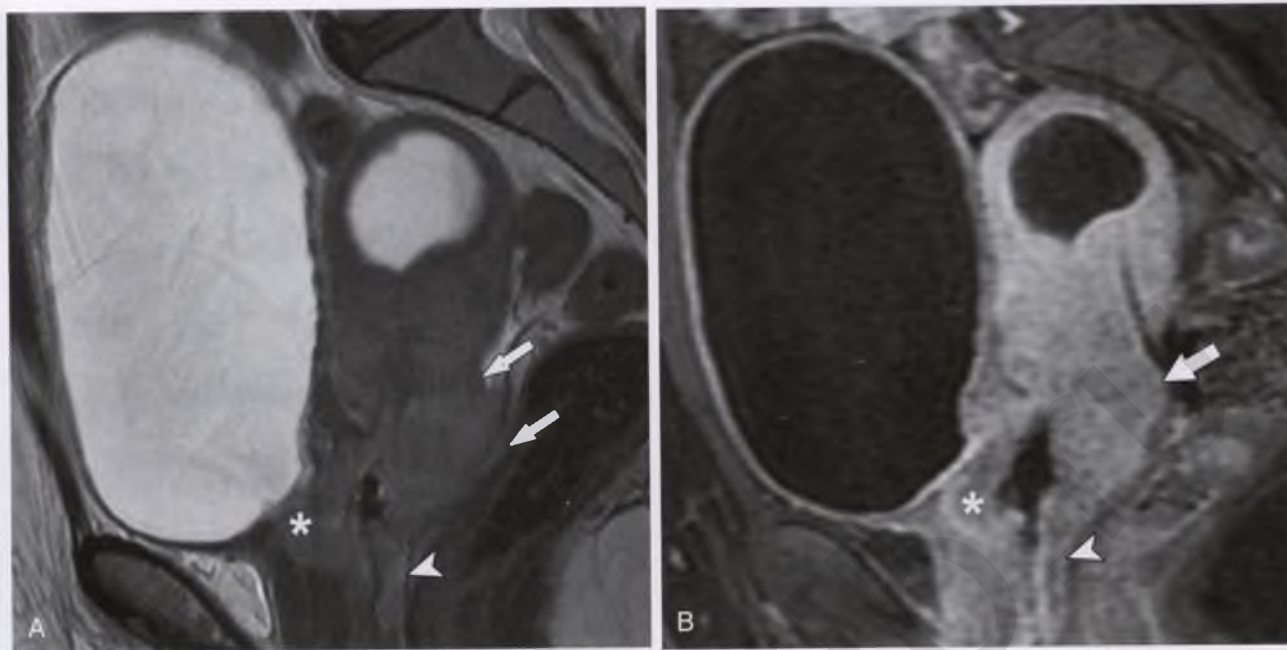


**FIG 36-27** Stage IV cervical cancer. Sagittal T2-weighted image (A) and gadolinium-enhanced fat-saturated T1-weighted image (B) show a large cervical mass extending into the lower uterine segment (arrows) and vagina (arrowhead). The mass also involves the bladder neck (asterisk). Note the distended urinary bladder related to bladder outlet obstruction.

microscopic foci of metastatic disease. The use of lymph node–specific contrast agents, MR lymphography with ultra-small superparamagnetic iron oxide particles, remains under investigation, but sensitivities of 90% to 100% and specificity greater than 95% have been reported for the detection of nodal metastases.<sup>118</sup>

## ENDOMETRIAL CANCER

### Epidemiology and Clinical Presentation

Endometrial cancer is the 10th most common cancer in women and the most common invasive gynecologic malignancy. The American Cancer Society estimates that 60,050 new cases of cancer of the uterine corpus will be diagnosed and that 10,470 cancer related deaths will occur in the United States in 2016.<sup>89</sup> Despite the high incidence compared with other gynecologic malignancies, endometrial cancer has the most favorable prognosis, and most patients with newly diagnosed disease are cured by surgery alone or in combination with adjuvant radiation therapy.<sup>120</sup> Endometrial cancer occurs more frequently in Caucasians and typically presents during the 6th and 7th decades with painless postmenopausal bleeding.<sup>121,122</sup> Many risk factors have been described; most are directly or indirectly related to increased estrogen exposure, including early menarche, late menopause, nulliparity, Stein-Leventhal syndrome (polycystic ovary syndrome), diabetes, and obesity. In addition, a higher incidence of endometrial cancer is associated with adenomatous polyps, breast cancer, and the use of unopposed estrogen therapy.<sup>121-124</sup>

### Histopathology

More than 80% of endometrial cancers are of the endometrioid type, which refers to the presence of endometrial type glands of varying degrees of differentiation. These cancers are subdivided into two groups: type 1 (low grade) and type 2 (high grade). Type 1 endometrial cancers are related to long-term unopposed estrogen therapy; they originate from endometrial hyperplasia and have a more favorable

prognosis. Type 2 cancers account for approximately 10% of endometrial cancers; they are most often seen in association with an atrophic endometrium and have a poorer prognosis. Other histologic types include serous and clear cell carcinomas. Approximately 8% of patients with endometrial cancer present with a synchronous ovarian carcinoma of the same histologic type.<sup>121</sup>

Endometrial carcinoma may present as a localized endometrial lesion, mimicking a polyp, or as diffuse thickening of the endometrium. Tumor spread initially occurs by direct myometrial or cervical extension. Lymphatic invasion is usually limited to the pelvis but may extend to periaortic and aortocaval nodes.<sup>121</sup> Transtubal peritoneal seeding and hematogenous dissemination to the lungs or other sites may occur.<sup>125</sup>

### Diagnosis

The diagnosis of endometrial cancer is based on histologic evaluation of endometrial biopsy specimens, which is highly accurate, especially in symptomatic postmenopausal women. The two most common pathways to diagnosis are immediate endometrial biopsy in a symptomatic woman or transvaginal sonography, followed by biopsy.<sup>121</sup> Estimation of the risk of endometrial cancer following transvaginal sonography in a postmenopausal woman depends upon the presence or absence of vaginal bleeding, the thickness of the endometrial stripe, and the patient's age. In postmenopausal women with vaginal bleeding, an endometrium measuring more than 4 to 5 mm translates to a risk of approximately 7.3%, whereas in the absence of bleeding, a similar risk (6.7%) is seen if the endometrium measures 11 mm or more in thickness.<sup>8</sup> In these two situations, biopsy is warranted. MRI has no role in diagnosing endometrial cancer and is usually reserved as an aid for pretreatment planning.

### Treatment

The primary treatment modality for endometrial cancer is total hysterectomy with bilateral salpingo-oophorectomy and peritoneal fluid



aspiration and washings. In selected cases, omentectomy and retroperitoneal lymph node dissection are performed.<sup>121</sup> Radiation therapy is generally prescribed as an adjuvant treatment to target microscopic metastatic lymphadenopathy. In patients who are not operative candidates because of medical comorbid conditions, radiation therapy may be used with curative purpose. Systemic adjuvant chemotherapy is reported to have results similar to radiation therapy, but with greater toxicity. In patients with more advanced disease, the use of systemic chemotherapy is palliative.<sup>121</sup>

## Staging

Patients with endometrial cancer are staged surgically, usually using the system proposed by FIGO (Table 36-2)<sup>124</sup> or the American Joint Committee on Cancer.<sup>126</sup> Surgical staging provides prognostic information, but is also important for guiding treatment selection.

A poorer prognosis is expected in patients who present with deep myometrial invasion (>50%, stage IB), cervical extension (stage II), and nodal involvement (stage IIIC). Other important prognostic factors include positive peritoneal cytologic findings, poorly differentiated cancer, serous papillary tumor, and clear cell tumors.

Depth of myometrial invasion was found to be the single most important predictor of survival at 5 and 10 years, in a series of 1566 women with endometrial carcinoma.<sup>127</sup> Women with superficial myometrial invasion (invasion of <50% of the myometrial wall thickness, stage IA) have a 3% to 9% incidence of lymph node metastases and a

survival rate of 85% at 5 years. Deep myometrial invasion (invasion of >50% of the myometrial wall thickness, stage IB) is associated with a 20% to 40% risk of nodal disease and a survival rate of only 63% at 5 years.<sup>127</sup> Besides providing prognostic information, staging is also important for treatment selection. For instance, there is evidence that radiation therapy is not indicated in low- or intermediate-risk stage I disease (stage IA and IB) but may be beneficial for patients with more advanced disease and higher risk.<sup>128</sup> Similarly, surgical treatment is dictated by staging, and patients with stage IA disease may not require radical lymphadenectomy, depending on the size and grade of the tumor.<sup>128</sup>

MRI is an accurate tool for endometrial cancer staging, with an overall staging accuracy of approximately 85%.<sup>104,129</sup> The use of gadolinium is an important part of the examination and has been shown to increase the accuracy for assessing depth of myometrial invasion.<sup>104,130-132</sup> The reported accuracy of MRI for identification of deep myometrial invasion varies from 74% to 95%,<sup>129-137</sup> compared with 68% to 73% for transvaginal sonography.<sup>130,138</sup> However, MRI can overestimate depth of myometrial invasion, especially when bulky disease is present that stretches and thins the surrounding myometrium.<sup>134,135</sup> Finally, MRI can also assess cervical extension of tumor (stage II) and extrauterine disease (stages III and IV).

Although imaging evaluation of nodal metastasis has not been reported to be as reliable as surgical sampling, because of the limited accuracy when using size criteria on imaging to characterize and assess for lymph node involvement (see discussion earlier under "Lymph Node Assessment"), results of studies applying ultra-small particles of iron oxide or ultra-small superparamagnetic iron oxide (unavailable in the United States, as its use is not yet approved by the Food and Drug Administration) have been promising. Rockall and coworkers<sup>118</sup> reported excellent sensitivity and specificity for the detection of nodal metastasis on analyses performed per node and per patient, ranging from 82% to 100% and 87% to 97%, respectively. The negative predictive value varied between 96% and 100%.

## Imaging

As mentioned previously, MRI is not used for the diagnosis of endometrial carcinoma, but it is an established part of the imaging evaluation when locally extensive disease is suspected or when physical examination is limited.

Endometrial carcinoma is usually depicted on MRI as an endometrial mass that is iso- or hypointense to normal endometrium on T1-weighted sequences and slightly hyperintense or heterogeneous on T2-weighted sequences. After intravenous gadolinium contrast administration, tumor enhancement is variable, depending upon histologic type and temporal resolution. Endometrial carcinoma is usually hypointense to the myometrium on early phase images. The administration of gadolinium allows vascularized tumors to be distinguished from debris or fluid in the endometrial cavity or endocervical canal. In addition, dynamic gadolinium enhancement facilitates visualization of the junctional zone and the tumor-myometrium interface, as the uterine zonal anatomy may be poorly defined on T2-weighted images in postmenopausal women.

Superficial myometrial invasion (stage IA) is suspected in the presence of interruption of the dark, low signal junctional zone on T2-weighted sequences or subendometrial band of enhancement after contrast administration (Fig. 36-28).<sup>129,130,137</sup> Deep myometrial invasion (stage IB) is characterized if tumor is seen extending into more than 50% of the myometrial thickness, with an intact outer rim (Fig. 36-29).

Cervical extension of tumor (stage II) is best evaluated using sagittal T2-weighted or contrast-enhanced images and may appear as a

**TABLE 36-2 Carcinoma of the Endometrium—Federation of Gynecology and Obstetrics (FIGO) Staging**

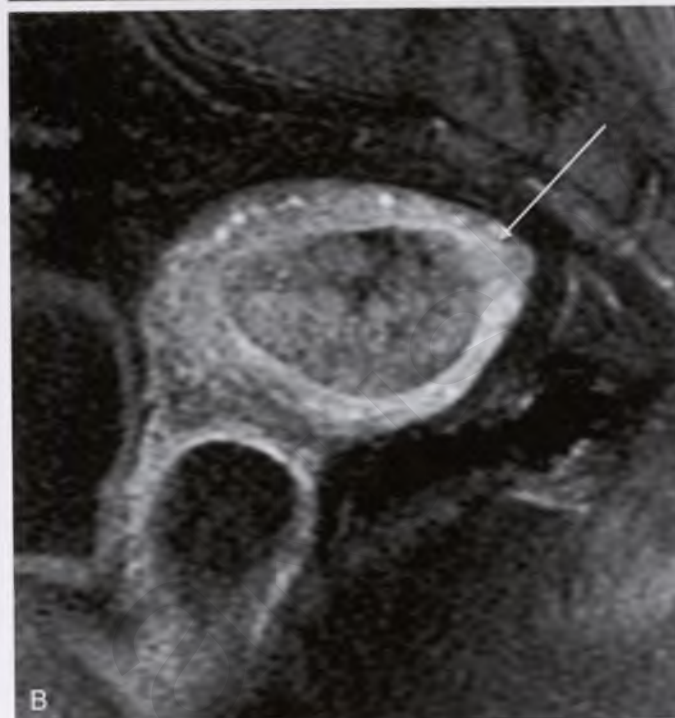
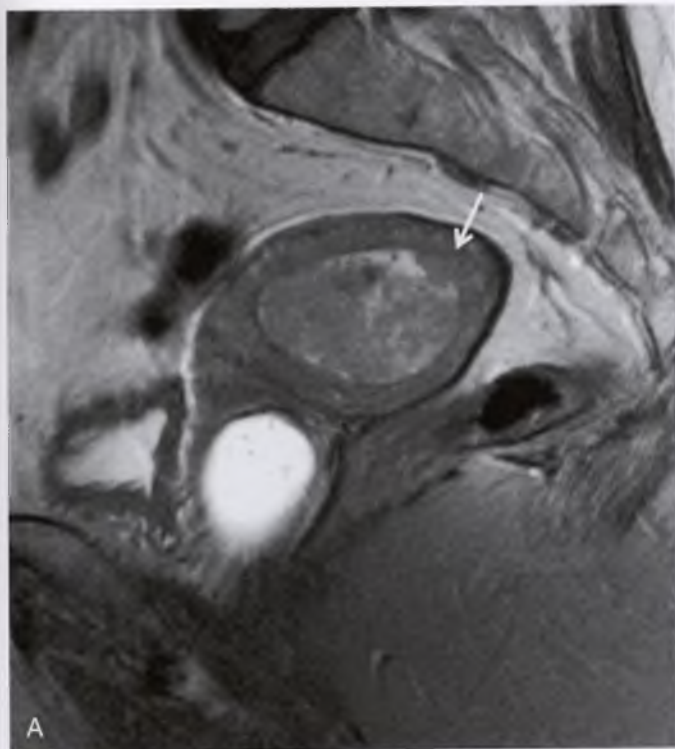
FIGO Stage	Stage Description
0	Carcinoma in situ
I	Limited to the body of the uterus
IA	No or less than 50% myometrial invasion
IB	Equal to or greater than 50% myometrial invasion
II	Cervical stromal involvement Endocervical glandular involvement only is stage I
III	Local or regional spread of the tumor
IIIA	Tumor invades the serosa of the body of the uterus and/or adnexa
IIB	Vaginal or parametrial involvement
IIIC	Pelvic or para-aortic lymphadenopathy
IIIC1	Positive pelvic nodes
IIIC2	Positive para-aortic nodes with or without pelvic nodes
IV	Involvement of rectum and/or bladder mucosa and/or distant metastases
IVA	Bladder or rectal mucosal involvement
IVB	Distant metastases, malignant ascites, peritoneal involvement

Endometrial Cancer—5-year relative survival rate by stage	
Stage	Survival Rate
All stages	82%
Localized (confined to primary site)	95%
Regional (spread to regional nodes)	68%
Distant (metastases)	17%

Data from Pecorelli S: Revised FIGO staging for carcinoma of the vulva, cervix, and endometrium. *Int J Gynaecol Obstet* 105:103, 2009; and American Cancer Society: *Cancer Facts & Figures* 2014. Atlanta, American Cancer Society, 2014.





**FIG 36-28** Stage IA endometrial cancer. Sagittal T2-weighted (A) and sagittal dynamic gadolinium-enhanced fat-saturated T1-weighted (B) images show a tumor filling the endometrial cavity with irregularity at the endometrial-myometrial interface posteriorly (arrows). Additional images were used to diagnose less than 50% myometrial invasion. Pathologic examination confirmed that the tumor invaded 4 mm into a 12-mm thick myometrium.

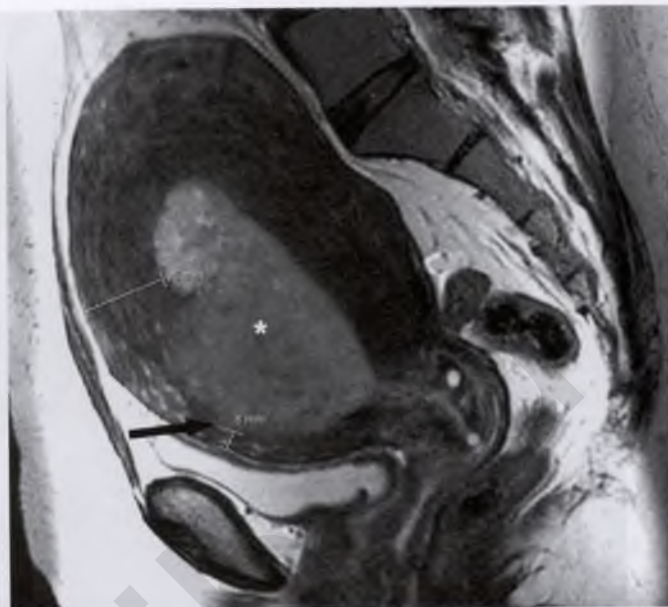


**FIG 36-29** Stage IB endometrial cancer. Sagittal T2-weighted image demonstrates a large hyperintense mass (asterisk) invading through more than 50% of the myometrial wall thickness anteriorly (arrow).

mass expanding the cervical canal (Fig. 36-30). Stage III disease is characterized by extension of tumor beyond the serosa, to the adnexa and parametrium, positive peritoneal cytologic finding, invasion of the vagina, and metastatic pelvic and para-aortic lymph nodes (Fig. 36-31). Stage IV is defined as bladder or rectal invasion and distant metastases. Invasion of the bladder and rectum is suggested by the loss of normal tissue planes, especially fat planes, associated with an increase in signal intensity and thickness of the bladder or rectal walls on T2-weighted images. Contrast administration is also useful to make this diagnosis.

## ADNEXAL MASSES

### Epidemiology and Clinical Significance

It is very common for premenopausal women to develop self-limiting cystic adnexal lesions related to ovulation. In the vast majority of cases these are asymptomatic functional cysts that involute and go undiagnosed; however, approximately 1.5% of women develop a malignant ovarian tumor.<sup>1</sup> Ovarian cancer is the fifth leading cause of cancer-related death among women in the United States and the leading cause of death from gynecologic malignancy. The American Cancer Society estimates that 22,280 new cases of ovarian cancer will be diagnosed and that there will be 14,240 cancer related deaths in the United States in 2016.<sup>89,139</sup> Gynecologic surgery is often prompted by the presence of an adnexal lesion, irrespective of the histologic diagnosis. Approximately 5% to 10% of women in the United States undergo surgery because of a suspected ovarian mass. Imaging plays an important role in lesion characterization, staging, and treatment planning in patients with ovarian cancer.<sup>140</sup>

Many factors must be considered when evaluating a patient with an adnexal mass. They include the patient's age and menopausal status, cancer antigen 125 levels, risk factors, and clinical history. Accurate diagnosis of benign lesions is crucial, as further workup can then be avoided, resulting in reduction of overall health care costs, morbidity, and patient anxiety. Even if resection of a benign lesion is warranted, a less invasive approach, such as laparoscopic surgery, may be used.



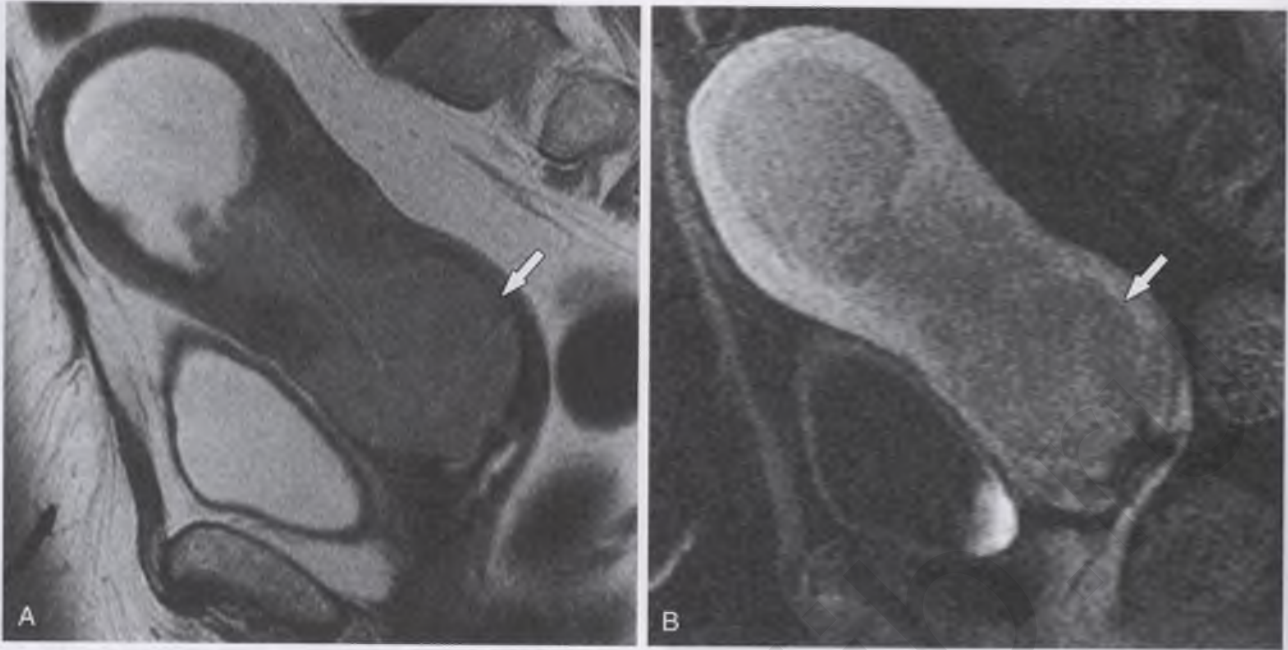


**FIG 36-30** Stage II endometrial cancer. Sagittal T2-weighted (A) and sagittal dynamic gadolinium-enhanced fat-saturated T1-weighted (B) images show a large endometrial cancer invading and distending the cervix (arrows).

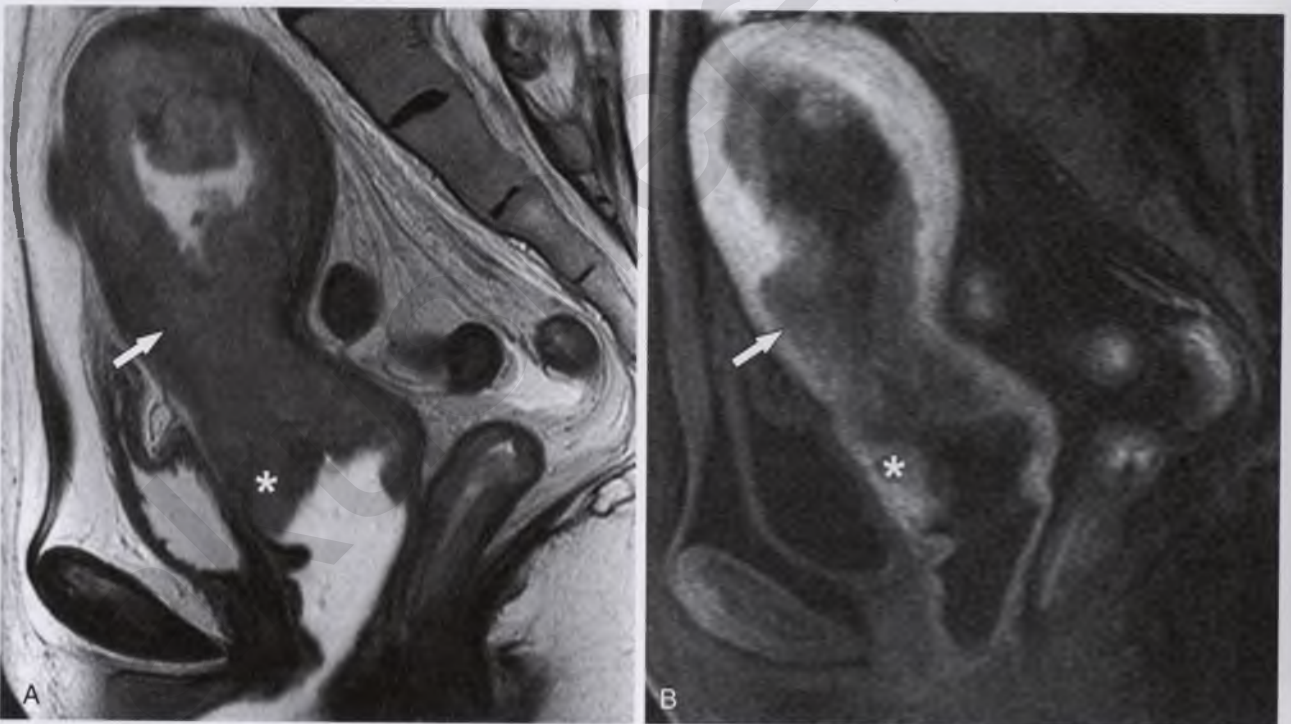


**FIG 36-31** Stage IIIB endometrial cancer. Sagittal T2-weighted (A) and sagittal dynamic gadolinium-enhanced fat-saturated T1-weighted (B) images show an irregular endometrial tumor with greater than 50% myometrial invasion (arrows) and extension into the cervix and upper vagina (asterisks).

Those patients found to have malignant lesions should be referred to gynecologic oncologists, as specialized management has been shown to result in improved survival.<sup>141</sup> In patients with ovarian malignancies, initial surgery can be both diagnostic and therapeutic and is best performed by a surgeon with subspecialized expertise.

### Imaging Diagnosis and the Role of Magnetic Resonance Imaging

Sonography is the primary initial imaging modality for the evaluation of an adnexal mass. The sensitivity and specificity of ultrasound imaging for differentiating benign from malignant adnexal masses



range from approximately 50% to 100% and 46% to 100%, respectively. Ultrasound imaging is particularly useful in distinguishing simple cysts from complex cystic or solid lesions. MRI is beneficial in the evaluation of women with sonographically indeterminate ovarian lesions and low risk for malignancy. In women with indeterminate lesions at high risk of malignancy, imaging should focus on staging the tumor.<sup>142,143</sup>

Advantages of MRI over ultrasound imaging relate to its ability to more precisely identify the composition of soft tissue masses by using differences in tissue relaxation times. MRI is not considered a first-line modality of choice in evaluating adnexal masses because it is expensive, and pelvic sonography often provides all the information necessary to guide patient management. However, MRI is an excellent problem-solving tool, and allows confident diagnosis of many common benign adnexal lesions.<sup>143,144</sup> When an indeterminate mass is seen on ultrasound imaging, contrast-enhanced MRI can diagnose malignancy with a sensitivity and specificity of 100% and 94%, respectively.<sup>142,145</sup> The Radiology Diagnostic Oncology Group study showed that MRI was the most accurate technique in the preoperative evaluation of adnexal masses to assess for possible ovarian malignancy, whereas there was no significant difference between sonography and CT.<sup>146</sup>

### Differentiation of Benign and Malignant Lesions

In general, benign ovarian masses are cystic with thin walls and septa (less than 3 mm); however, there are exceptions to this rule, as will be discussed subsequently. Malignant adnexal masses often manifest internal complexity, referring to the presence of mural nodules, thick septa, solid components, and necrosis. Another feature that suggests malignancy is bilaterality.<sup>81</sup> Malignant tumors are rarely subtle lesions, and peritoneal spread is frequently identified at the time of imaging.<sup>146</sup> Although size has been reported to be a useful feature in differentiating benign from malignant lesions,<sup>147</sup> it is important to remember that even large tumors are more often found to be benign. Although a solid adnexal mass is suggestive of malignancy, and possibly metastasis, not all solid tumors are malignant,<sup>148</sup> and with MRI some benign solid ovarian entities can be diagnosed with adequate accuracy to avoid further workup.

A helpful diagnostic approach is to categorize adnexal masses into one of the following groups: lesions with distinctive features (fat, blood, or fibrous tissue) and a specific diagnosis; cystic, benign-appearing lesions; cystic, malignant-appearing lesions; and predominantly solid lesions.

### Specific Diagnosis Based on Magnetic Resonance Imaging Findings

#### Adnexal Masses With Distinctive Imaging Features (Fat, Blood, or Fibrous Tissue)

Dermoid cysts, also known as benign mature teratomas, are hamartomas that may contain hair, teeth, fat, and mural nodules.<sup>81,149,150</sup> Usually identified during the first 3 decades of life, these lesions are not uncommon but may be missed on pelvic sonogram.<sup>150</sup> In some cases, the ultrasound finding of echogenic fat in the dermoid cyst may simulate adjacent normal structures, such as gas-filled bowel. In contrast, these tumors can be readily identified on MRI because characteristic high signal intensity of fat on T1-weighted images is lost when fat suppression techniques are applied (Fig. 36-32).<sup>81,149</sup>

The two most common adnexal lesions that contain blood are hemorrhagic ovarian cysts and endometriomas. Endometriomas were discussed earlier in this chapter. MRI of hemorrhagic cysts is not commonly performed, because these cysts usually resolve spontaneously, and follow-up sonogram after 6 to 8 weeks is sufficient. As a general

rule, if MRI confirms the presence of blood within an ovarian cyst, no further diagnostic tests are necessary.

Fibromas are the most common sex cord tumors and represent 4% of all ovarian neoplasms. Because of their solid nature, they may be misdiagnosed on sonography as malignant or suspicious lesions or mistaken for exophytic uterine myomas. Classic sonographic features include a markedly hypoechoic solid ovarian mass with attenuation of the sound beam, related to their fibrous composition. On MRI, fibromas demonstrate characteristic morphologic features. Fibromas are composed of bundles of spindle cells resembling fibroblasts, collagen, and hyalinized fibrous tissue and demonstrate low signal intensity on both T2- and T1-weighted sequences and only slight enhancement after gadolinium administration (Fig. 36-33). Ascites may be present in up to 40% of cases, more often when the lesion is large. Meigs syndrome refers to an association with pleural effusions.<sup>81,149,151,152</sup> The malignant potential of fibromas is reported to be less than 1%. Two other ovarian lesions that often manifest foci of low signal intensity on both T2- and T1-weighted MRI sequences are fibrothecoma and cystadenofibroma. Fibrothecoma is a variant of fibroma containing a small population of thecal cells with intracellular lipid. It is similar in MRI appearance to a fibroma, but can be hormonally active and may be associated with endometrial polyps and endometrial hyperplasia.<sup>81,149,151,152</sup> Cystadenofibroma is a variant of serous cystadenoma with very low malignant potential. In most cases, it appears as a multiseptated mass, although small mural nodules may be noted in some.<sup>81,149</sup>

#### Cystic Benign-Appearing Lesions

The most common entity in this category is a physiologic cyst (including follicular cysts). Other possibilities include corpora lutea, theca-lutein cysts, paraovarian cysts, hydrosalpinges, peritoneal inclusion cysts, and cystadenomas. In the vast majority of patients, ultrasound imaging correctly diagnoses and classifies these cysts as benign. However, MRI may provide additional information in the unusual case complicated by infection or hemorrhage.

#### Cystic Malignant-Appearing Lesions

Epithelial tumors represent the most common primary ovarian cancers<sup>81,153</sup>; therefore, they are the most common malignant-appearing cystic adnexal masses. Histologically, these tumors are classified as serous, mucinous, endometrioid, and mesonephroid (clear cell), although recent pathologic analysis suggests that most high-grade serous ovarian tumors actually originate from cells lining the fallopian tube. Most often, these malignancies are cystadenocarcinomas or borderline tumors. Distinguishing these two entities can be difficult because they present with similar imaging features, namely, thick walls or septations and solid mural components (Figs. 36-34 and 36-35).<sup>81</sup> The absence of invasion or metastatic disease favors the diagnosis of a borderline tumor. Ascites is considered a sign of more aggressive disease. In addition, extensive calcifications usually indicate malignancy, particularly in the case of serous tumors. The T1- and T2-weighted signal intensities of cystic areas in a mucinous tumor are often variable, owing to different amounts of mucin within locules.<sup>81</sup>

#### Predominantly Solid Lesions

Predominantly solid lesions of the adnexa may represent primary ovarian lesions, leiomyomas, or nonovarian origin tumors, such as metastases or lymphoma.

The ovary is the most common site of metastasis to the female genital tract. The primary tumors that most commonly spread to the ovaries are endometrial, cervical, gastric, colorectal, and breast cancers.<sup>154</sup> Metastases to the ovaries have no specific appearance but



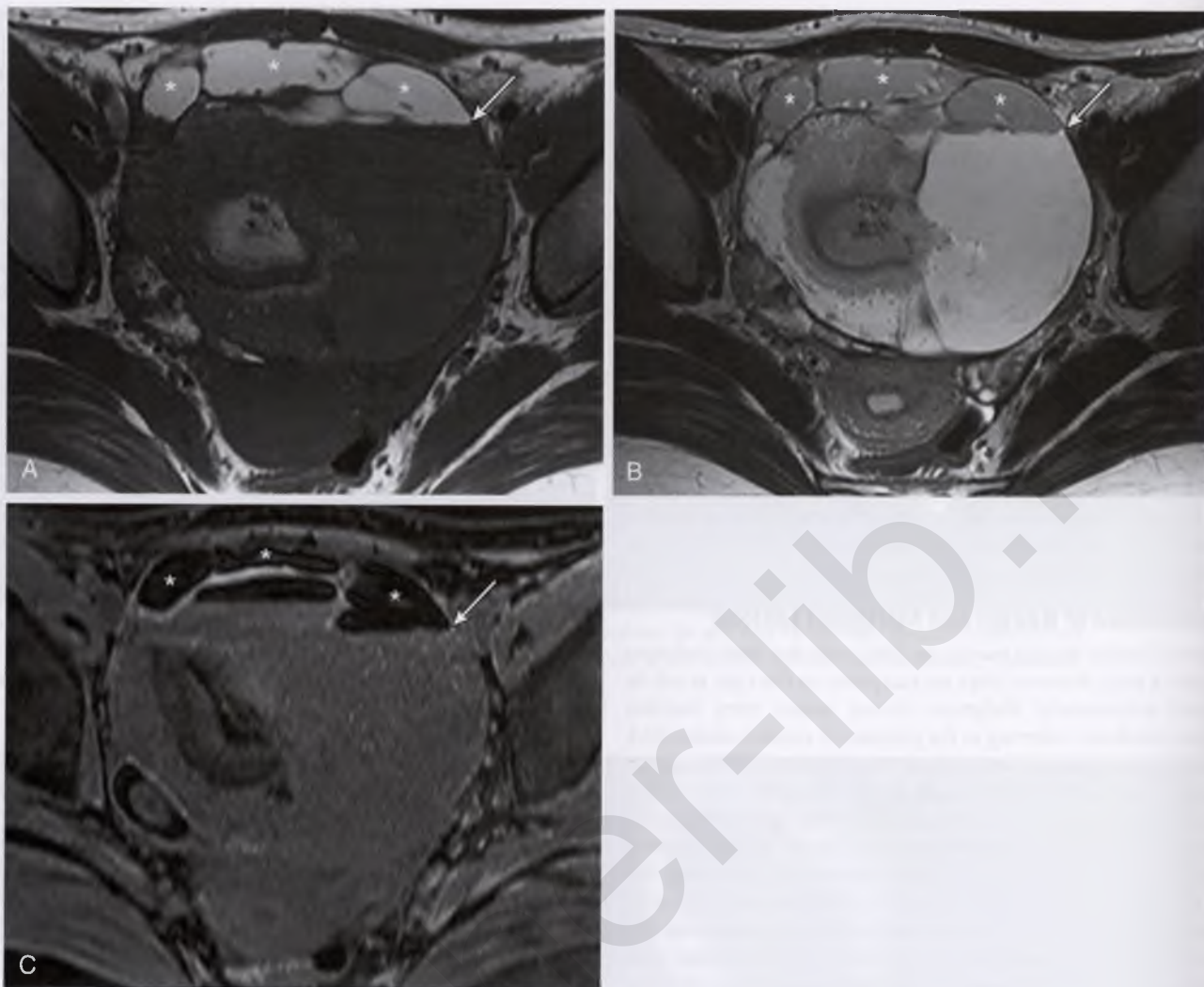


**FIG 36-32** Benign mature cystic teratoma of the ovary. Axial T1-weighted (**A**), T2-weighted (**B**), and fat-saturated T1-weighted (**C**) images. Complex adnexal mass with fat-fluid level (*arrows*). Areas of increased signal intensity (*asterisks*) on T1-weighted (**A**) and T2-weighted (**B**) images and corresponding low signal intensity on fat-saturated T1-weighted image (**C**) are consistent with macroscopic fat, characteristic of a teratoma. (Courtesy of Lisa M. Ho, MD, Duke University, Durham, NC.)

are commonly bilateral masses with marked contrast enhancement. They can be predominantly cystic with necrotic areas or appear primarily solid. The primary tumor is usually clinically apparent with metastatic disease elsewhere (often grade IV).<sup>154-157</sup> Ovarian lymphoma is exceptionally rare but should be suspected in the presence of extensive lymphadenopathy in order to avoid unnecessary surgery.<sup>158</sup>

Primary ovarian tumors can also present as predominantly solid masses; examples include dysgerminomas, granulosa cell tumors, and Sertoli-Leydig cell tumors, also known as androblastomas and arrhenoblastomas. All such tumor types are uncommon, without specific imaging features. They are predominantly solid, though they may demonstrate associated cystic areas (Fig. 36-36). They are most frequently diagnosed in patients younger than 30 years of age, although granulosa cell tumors also have a second peak incidence in postmenopausal women. Dysgerminomas are responsible for one third of all ovarian tumors during pregnancy, and a disproportionate degree of adenopathy, relative to the size and appearance of the ovarian lesion, is sometimes noted.<sup>96</sup> Granulosa cell tumors and Sertoli-Leydig cell tumors are hormonally active, the former producing estrogen and

the latter androgen.<sup>151,159,160</sup> Hence, granulosa cell tumors may be associated with thickening of the endometrium owing to endometrial hyperplasia. Clinical evidence of hormonal effect may help guide the differential diagnosis.

A pedunculated subserosal leiomyoma or a leiomyoma arising from the broad ligament and adnexa may be misdiagnosed as a solid ovarian lesion on ultrasound imaging, as the origin of the lesion can be difficult to determine. In this situation, MRI may prove very helpful in reaching the correct diagnosis given the characteristic appearance of leiomyomas on MRI, as discussed previously, and clear visualization of the pedicle attaching the leiomyoma to the uterine surface.<sup>39,42,54</sup>

### Preoperative Staging

The new revised FIGO staging system adopted in 2014 (Table 36-3) considers fallopian tube, peritoneal, and ovarian tumors as one type of disease and several additional changes in staging were incorporated.<sup>161</sup> Current recommendations include recording histologic type, identifying grade of tumor, and documenting stage IC disease (i.e., evidence of tumor rupture during surgery or positive peritoneal

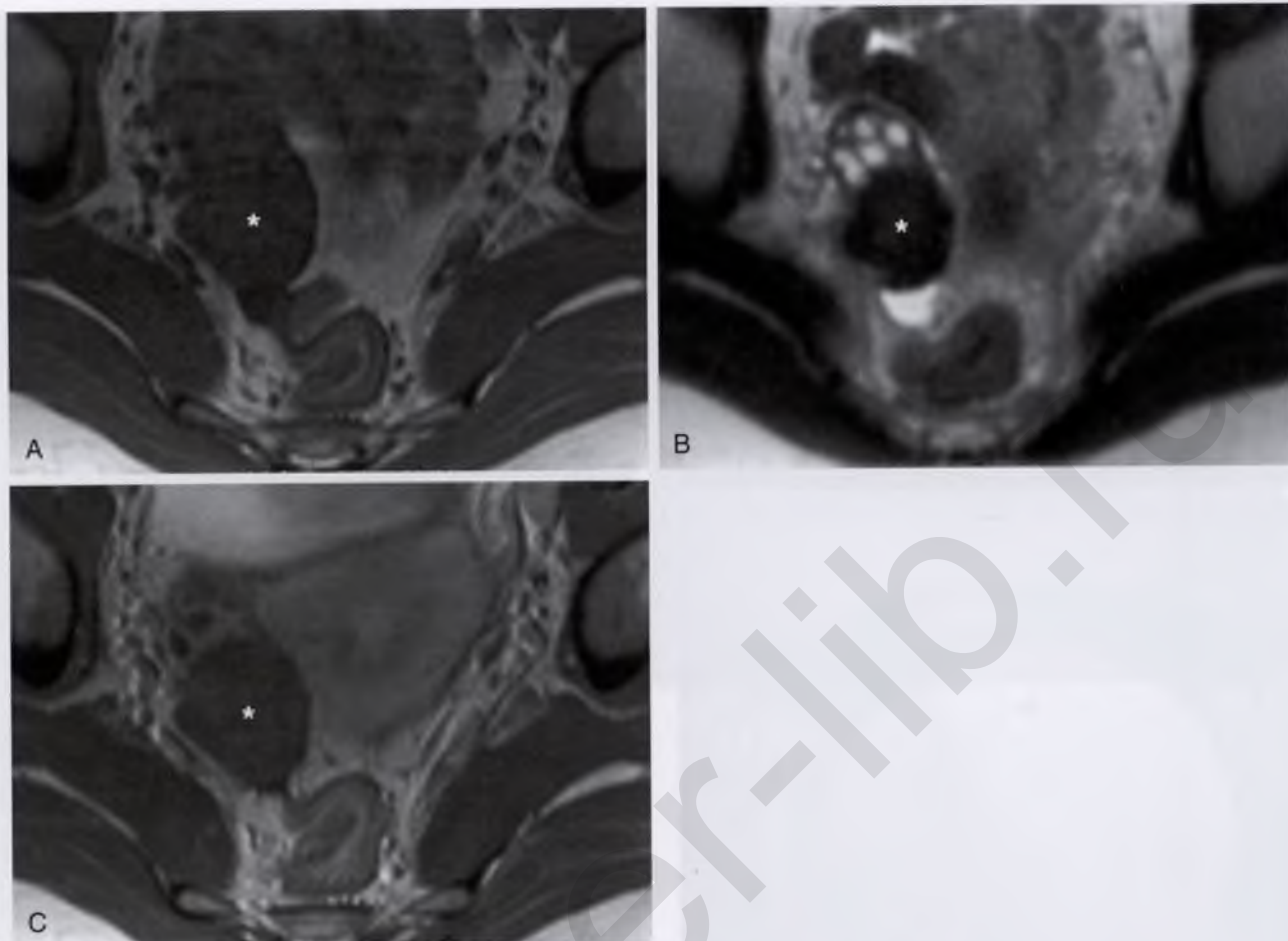


**FIG 36-33** Ovarian fibroma. Axial T1-weighted (A), T2-weighted (B), and gadolinium-enhanced T1-weighted (C) images demonstrate a hypointense solid mass in the right ovary (asterisk). This mass has low signal intensity on both T1-weighted (A) and T2-weighted (B) images and demonstrates only slight enhancement after intravenous gadolinium administration (C), typical for an ovarian fibroma. Note numerous small hyperintense ovarian follicles anteriorly on T2-weighted image (B) that do not enhance following the administration of gadolinium (C).

washings). Lesions with dense adhesions that contain tumor cells are now upgraded to stage II. In stage II disease, tumor involves one or both ovaries or fallopian tubes with direct extension to the uterus or the fallopian tubes (stage IIA) or extends to other pelvic intraperitoneal tissues below the pelvic brim (stage IIB). As such, involvement of the sigmoid colon is now considered stage II disease.<sup>161</sup> The new FIGO system eliminated stage IIC because of recognition of a clear difference in terms of survival between stages II and III disease (A1). The subdivision of stages IIA and IIB remains the same. In stage III disease, tumor involves one or both ovaries with pathologically confirmed spread to the retroperitoneal lymph nodes and involvement of the peritoneum outside the pelvis. FIGO has added stage IIIA disease, which specifically refers to the presence of retroperitoneal adenopathy (A1). Tumor implants along the surface of the liver and spleen are still considered stage IIIC disease. Stage IV disease includes malignant pleural effusion (stage IVA), hepatic or splenic parenchymal metastases, extra-abdominal metastases, inguinal and supraclavicular metastatic lymph nodes, and transmural involvement of visceral structures (stage IVB).

Ovarian cancers most often present at an advanced stage with widespread intraperitoneal metastases. The disease is surgically and pathologically staged; the surgical procedure is most often performed by

laparotomy including total abdominal hysterectomy, bilateral salpingo-oophorectomy, and omentectomy. In addition, biopsy of multiple frequently involved sites is recommended, including the mesentery, diaphragm, peritoneal surfaces, pelvic nodes, and para-aortic nodes.

Although final staging usually results from postoperative histologic findings, this may be modified after imaging analysis. Besides detecting and characterizing adnexal masses as likely malignant, imaging is used to demonstrate metastases, thus preventing understaging. CT and MRI can often detect specific sites of disease that may be unresectable, potentially preventing optimal primary surgical cytoreduction. In such patients, neoadjuvant chemotherapy with interval debulking rather than primary debulking with adjuvant chemotherapy may be utilized.<sup>162,163</sup> Qayyum and associates<sup>164</sup> found that preoperative CT and MRI were equally accurate in the detection of inoperable tumor and prediction of suboptimal debulking in newly diagnosed epithelial ovarian cancer. Imaging sensitivity, specificity, positive predictive value, and negative predictive value were 76%, 99%, 94%, and 96%, respectively. Subdiaphragmatic implants that infiltrate into the liver, serosal involvement of the colon and small bowel, tethering of the mesentery, and implants present in the supracolic omentum and involving the stomach usually require preoperative chemotherapy to make surgical resection feasible.



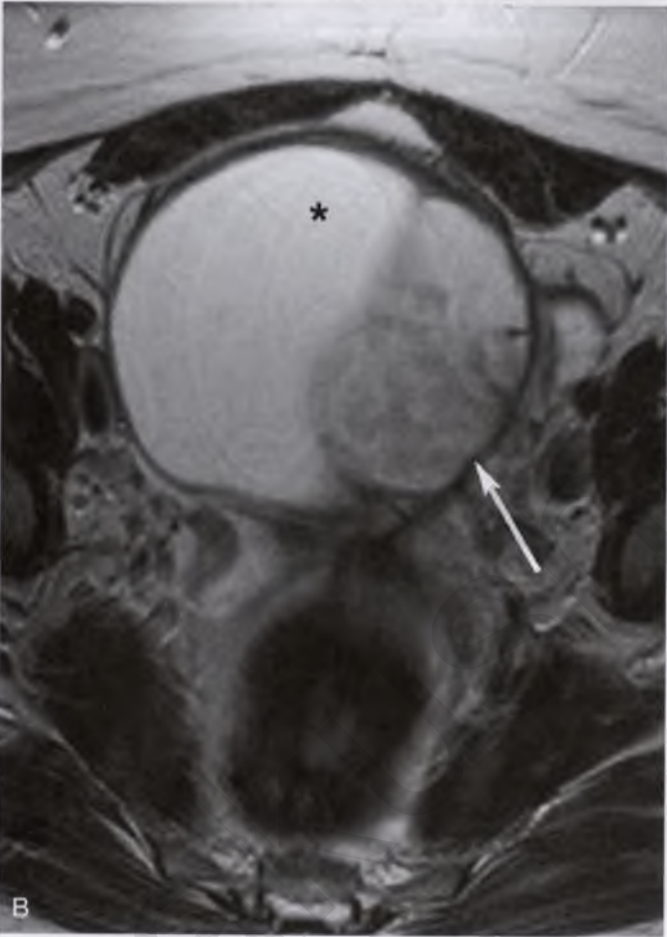
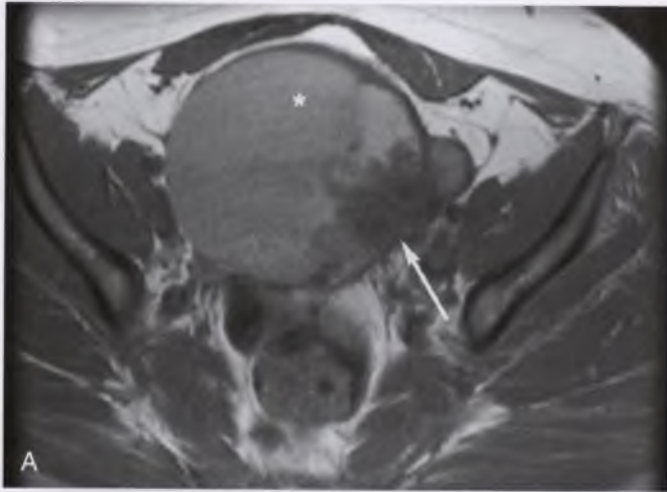


**FIG 36-34** Borderline epithelial ovarian tumor. Axial T1-weighted (A) and T2-weighted (B) images demonstrate a large ovarian mass with solid (arrow) and cystic (asterisk) components. The findings are consistent with a malignant neoplasm, but not specific for any particular histologic finding. Histopathologic analysis confirmed a borderline ovarian cancer. Signal intensity of the cystic component may vary depending on content.

Both CT and MRI have been shown to accurately identify foci of small peritoneal implants, with sensitivities of 95% and 92%, respectively.<sup>165</sup> Similar results were obtained by the Radiology Diagnostic Oncology Group, investigating and comparing the use of Doppler and conventional sonography, CT, and MRI for staging of ovarian cancer.

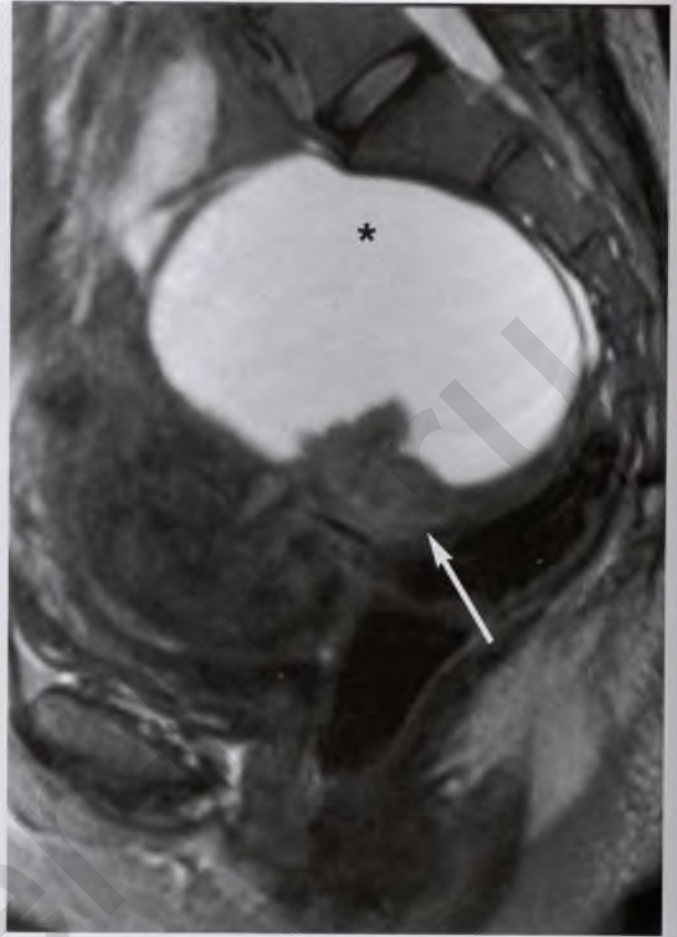


**FIG 36-35** Ovarian serous cystadenocarcinoma. Sagittal T2-weighted image demonstrates a large ovarian mass with solid (papillary projection) (arrow) and cystic (asterisk) components. The findings are consistent with a malignant neoplasm, but are not specific for a particular histologic finding. This tumor is indistinguishable from a borderline tumor (see Fig. 36-34) based on radiologic findings in the absence of metastatic disease. Histopathologic analysis diagnosed an invasive serous adenocarcinoma.

In this study, for differentiating early stage disease (benign lesions, stages I and II cancers) from advanced malignancy (stages III and IV cancers), the specificity of MRI was 88% and the sensitivity 98%. Sonography had the highest specificity (96%) but the lowest sensitivity (75%), whereas CT results were similar to those from MRI (specificity 89% and sensitivity 92%).<sup>146</sup>

## CONCLUSION

In current practice, MRI is commonly used as a problem-solving tool in the evaluation of benign and malignant gynecologic disease. Multiplanar capacity and soft tissue characterization allow for superior imaging assessment of indeterminate gynecologic masses compared with sonography or CT. Future areas of investigation include high-resolution intravoxel incoherent motion (IVIM) MRI, pharmacokinetic analysis, and positron emission tomography/MRI, particularly with respect to assessment of tumor biology and response to cancer therapy.

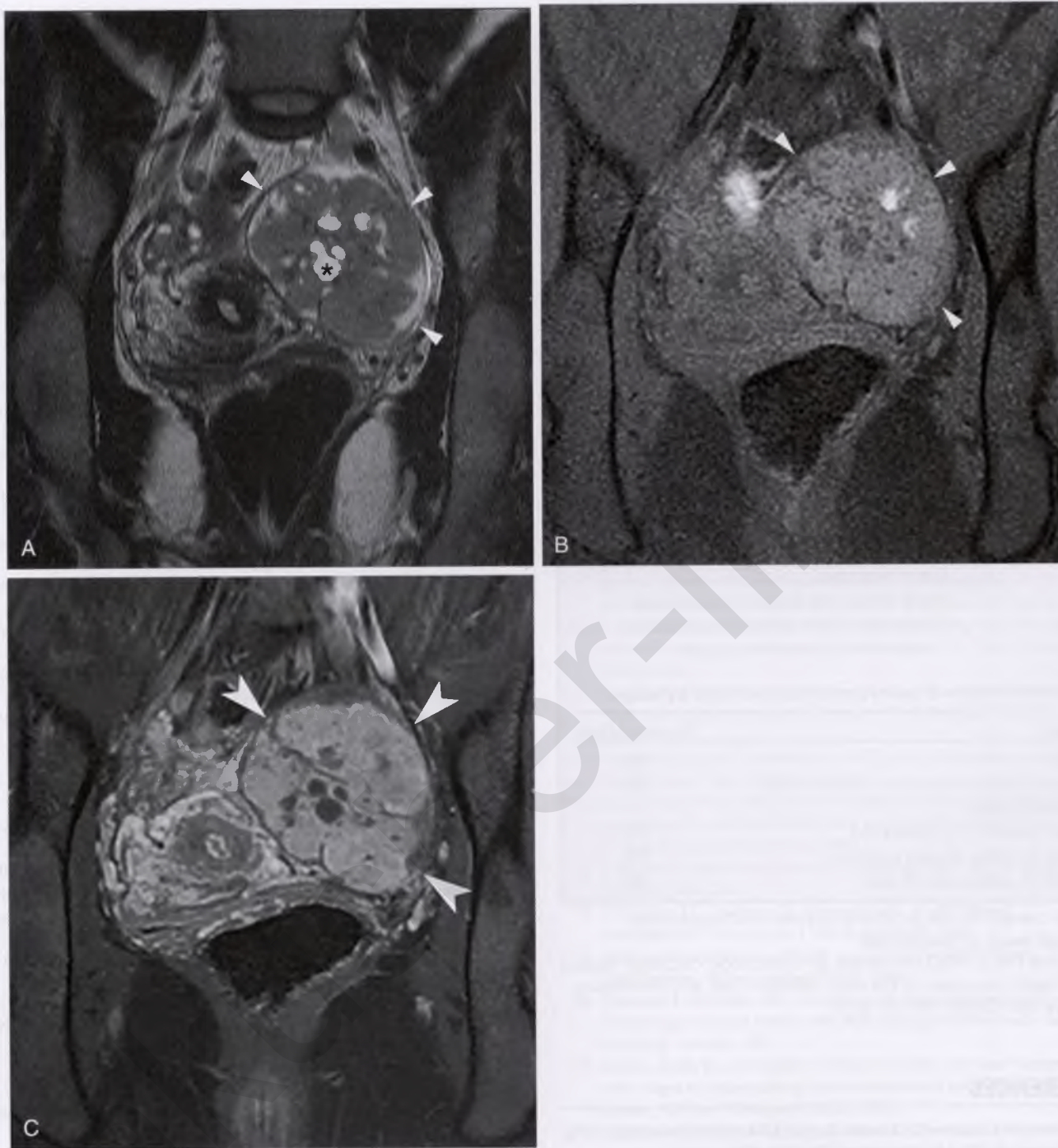


**FIG 36-36** Granulosa cell tumor of the ovary. Coronal T2-weighted (**A**), fat-saturated T1-weighted (**B**), and gadolinium-enhanced fat-saturated T1-weighted (**C**) images show a heterogeneous predominantly solid left ovarian mass (*arrowheads*) with multilocular cystic spaces and enhancement of the solid component (**C**). Several of the small cystic spaces are hyperintense on T1-weighted image (**B**), suggesting that they contain proteinaceous material or blood products.



**TABLE 36-3 Carcinoma of the Ovary/  
Fallopian Tube—Federation of Gynecology  
and Obstetrics (FIGO) Staging**

FIGO Stage	Stage Description
I	Tumor grossly confined to ovaries/fallopian tubes
IA	Unilateral
IB	Bilateral
IC1	Intraoperative tumor rupture
IC2	Preoperative rupture
IC3	With malignant ascites or positive peritoneal washings
II*	Involves one or both ovaries/fallopian tubes
IIA	Direct extension and/or implants on uterus and/or fallopian tubes
IIB	Extension to other pelvic intraperitoneal tissues (below the pelvic brim, e.g., sigmoid)
III	Nodal or extrapelvic peritoneal spread
IIIA1	Positive retroperitoneal lymph node
IIIA2	Microscopic, extrapelvic (above pelvic brim) peritoneal involvement ± positive retroperitoneal lymph node
IIIB/IIIC	Macroscopic, extrapelvic peritoneal involvement ± positive retroperitoneal lymph node (≤2 cm stage IIIB; >2 cm stage IIIC)
IV	Distant metastases
IVA	Pleural effusion with positive cytologic finding
IVB	Hepatic and/or splenic parenchymal metastases; metastases to extra-abdominal organs

**Ovarian Cancer—5-year relative survival rate by stage**

Stage	Survival Rate
Overall	45%
Localized (15% at presentation, confined to ovary/ fallopian tubes)	92%
Distant stage (61% at presentation)	27%
Overall for women 65 years and older	27%
Overall for women under 65 years	58%

\*Major change: IIC (IIA or IIB with positive washings/ascites) removed based on survival data.

Data from Prat J; FIGO Committee on Gynecologic Oncology: Staging classification for cancer of the ovary, fallopian tube, and peritoneum. *Int J Gynecol Obstet* 124:1-5, 2014.

**REFERENCES**

- Brown MA, Mattrey RE, Stamato S, et al: MRI of the female pelvis using vaginal gel. *AJR Am J Roentgenol* 185:1221, 2005.
- Koyama T, Togashi K: Functional MR imaging of the female pelvis. *J Magn Reson Imaging* 25:1101, 2007.
- Sala E, Rockall A, Ranganaraja D, et al: The role of dynamic contrast-enhanced and diffusion weighted magnetic resonance imaging in the female pelvis. *Eur J Radiol* 76:367, 2010.
- Hoad CL, Raine-Fenning NJ, Fulford J, et al: Uterine tissue development in healthy women during the normal menstrual cycle and investigations with magnetic resonance imaging. *Am J Obstet Gynecol* 192:648, 2005.
- Kido A, Togashi K, Nakai A, et al: Oral contraceptives and uterine peristalsis: evaluation with MRI. *J Magn Reson Imaging* 22:265, 2005.
- Togashi K, Nakai A, Sugimura K: Anatomy and physiology of the female pelvis: MR imaging revisited. *J Magn Reson Imaging* 13:842, 2001.
- Kido A, Kataoka M, Koyama T, et al: Changes in apparent diffusion coefficients in the normal uterus during different phases of the menstrual cycle. *Br J Radiol* 83:524, 2010.

- Fielding JR: MR imaging of the female pelvis. *Radiol Clin North Am* 41:179, 2003.
- Brown HK, Stoll BS, Nicosia SV, et al: Uterine junctional zone: correlation between histologic findings and MR imaging. *Radiology* 179:409, 1991.
- Scoutt LM, Flynn SD, Luthringer DJ, et al: Junctional zone of the uterus: correlation of MR imaging and histologic examination of hysterectomy specimens. *Radiology* 179:403, 1991.
- Goldstein RB, Bree RL, Benson CB, et al: Evaluation of the woman with postmenopausal bleeding: Society of Radiologists in Ultrasound-Sponsored Consensus Conference statement. *J Ultrasound Med* 20:1025, 2001.
- Smith-Bindman R, Weiss E, Feldstein V: How thick is too thick? When endometrial thickness should prompt biopsy in postmenopausal women without vaginal bleeding. *Ultrasound Obstet Gynecol* 24:558, 2004.
- Greenlee RT, Kessel B, Williams CR, et al: Prevalence, incidence, and natural history of simple ovarian cysts among women >55 years old in a large cancer screening trial. *Am J Obstet Gynecol* 202:373.e1-373.e9, 2010.
- Togashi K: MR imaging of the ovaries: normal appearance and benign disease. *Radiol Clin North Am* 41:799, 2003.
- Fielding JR: MR imaging of mullerian anomalies: impact on therapy. *AJR Am J Roentgenol* 167:1491, 1996.
- Troiano RN, McCarthy SM: Mullerian duct anomalies: imaging and clinical issues. *Radiology* 233:19, 2004.
- Byrne J, Nussbaum-Blask A, Taylor WS, et al: Prevalence of mullerian duct anomalies detected at ultrasound. *Am J Med Genet* 94:9, 2000.
- Stampe Sørensen S: Estimated prevalence of mullerian anomalies. *Acta Obstet Gynecol Scand* 67:441, 1988.
- Raga F, Bauset C, Remohi J, et al: Reproductive impact of congenital mullerian anomalies. *Hum Reprod* 12:2277, 1997.
- Li S, Qayyum A, Coakley FV, et al: Association of renal agenesis and mullerian duct anomalies. *J Comput Assist Tomogr* 24:829, 2000.
- Qayyum A, Hricak H: Imaging in infertility. *Gynecol Obstet* 6:305, 1999.
- Chan YY, Jayaprakasan K, Tan A, et al: Reproductive outcomes in women with congenital uterine anomalies: a systematic review. *Ultrasound Obstet Gynecol* 38:371-382, 2011.
- Epelman M, Dinan D, Gee MS, et al: Mullerian duct and related anomalies in children and adolescents. *Magn Reson Imaging Clin North Am* 21(4):773-789, 2013.
- Santos XM, Krishnamurthy R, Bercaw-Pratt JL, Dietrich JE: The utility of ultrasound and magnetic resonance imaging versus surgery for the characterization of mullerian anomalies in the pediatric and adolescent population. *J Pediatr Adolesc Gynecol* 25(3):181-184, 2012.
- Fedele L, Dorta M, Brioschi D, et al: Magnetic resonance evaluation of double uteri. *Obstet Gynecol* 74:844, 1989.
- Minto CL, Hollings N, Hall-Craggs M, et al: Magnetic resonance imaging in the assessment of complex mullerian anomalies. *Br J Obstet Gynaecol* 108:791, 2001.
- Mintz MC, Grumbach K: Imaging of congenital uterine anomalies. *Semin Ultrasound CT MR* 9:167, 1988.
- Mintz MC, Thickman DI, Gussman D, et al: MR evaluation of uterine anomalies. *AJR Am J Roentgenol* 148:287, 1987.
- Pellerito JS, McCarthy SM, Doyle MB, et al: Diagnosis of uterine anomalies: relative accuracy of MR imaging, transvaginal sonography, and hysterosalpingography. *Radiology* 183:795, 1992.
- Allen S, Feste JR: Pelvic disease classifications. *Fertil Steril* 51:199, 1989.
- Baird DD, Dunson DB, Hill MC, et al: High cumulative incidence of uterine leiomyoma in black and white women: ultrasound evidence. *Am J Obstet Gynecol* 188:100-107, 2003.
- Eltoukhi HM, Modi MN, Weston M, et al: The health disparities of uterine fibroid tumors for African American women: a public health issue. *Am J Obstet Gynecol* 210:194, 2014.
- Wechter ME, Stewart EA, Myers ER, et al: Leiomyoma-related hospitalization and surgery: prevalence and predicted growth based on population trends. *Am J Obstet Gynecol* 205(5):492.e1-492.e5, 2011.
- Qidwai GI, Caughey AB, Jacoby AF: Obstetric outcomes in women with sonographically identified uterine leiomyomata. *Obstet Gynecol* 107:376, 2006.



35. Manyonda I, Sinthamoney E, Belli AM: Controversies and challenges in the modern management of uterine fibroids. *Br J Obstet Gynaecol* 111:95, 2004.
36. Okamoto Y, Tanaka YO, Nishida M, et al: MR imaging of the uterine cervix: imaging-pathologic correlation. *Radiographics* 23:425, 2003.
37. Murase E, Siegelman ES, Outwater EK, et al: Uterine leiomyomas: histopathologic features, MR imaging findings, differential diagnosis, and treatment. *Radiographics* 19:1179, 1999.
38. Kim JC, Kim SS, Park JY: "Bridging vascular sign" in the MR diagnosis of exophytic uterine leiomyoma. *J Comput Assist Tomogr* 24:57, 2000.
39. Lee JH, Jeong YK, Park JK, et al: "Ovarian vascular pedicle" sign revealing organ of origin of a pelvic mass lesion on helical CT. *AJR Am J Roentgenol* 181:131, 2003.
40. Ueda H, Togashi K, Konishi I, et al: Unusual appearances of uterine leiomyomas: MR imaging findings and their histopathologic backgrounds. *Radiographics* 19:S131, 1999.
41. Inoue H, Aizawa N, Mizuno T, et al: A large degenerated subserous leiomyoma of the uterus: uncommon scintigraphic and ultrasonographic findings. *Ann Nucl Med* 3:55, 1989.
42. Reddy NM, Jain KA, Gerscovich EO: A degenerating cystic uterine fibroid mimicking an endometrioma on sonography. *J Ultrasound Med* 22:973, 2003.
43. Brinton LA, Sakoda LC, Sherman ME, et al: Relationship of benign gynecologic diseases to subsequent risk of ovarian and uterine tumors. *Cancer Epidemiol Biomarkers Prev* 14(12):2929, 2005.
44. Stavropoulos SW, Shlansky-Goldberg R: Embolization of uterine fibroids: patient selection and results of treatment. *J Womens Imaging* 3:153, 2001.
45. Dueholm M, Lundorf E, Hansen ES, et al: Accuracy of magnetic resonance imaging and transvaginal ultrasonography in the diagnosis, mapping, and measurement of uterine myomas. *Am J Obstet Gynecol* 186:409, 2002.
46. Togashi K, Ozasa H, Konishi I, et al: Enlarged uterus: differentiation between adenomyosis and leiomyoma with MR imaging. *Radiology* 171:531, 1989.
47. Togashi K, Nishimura K, Itoh K, et al: Adenomyosis: diagnosis with MR imaging. *Radiology* 166:111, 1988.
48. Jha RC, Ascher SM, Imaoka I, et al: Symptomatic fibroleiomyomata: MR imaging of the uterus before and after uterine arterial embolization. *Radiology* 217:228, 2000.
49. Spies JB, Roth AR, Jha RC, et al: Leiomyomata treated with uterine artery embolization: factors associated with successful symptom and imaging outcome. *Radiology* 222:45, 2002.
50. Kitamura Y, Ascher SM, Cooper C, et al: Imaging manifestations of complications associated with uterine artery embolization. *Radiographics* 25:S119, 2005.
51. Burn PR, McCall JM, Chinn RJ, et al: Uterine fibroleiomyoma: MR imaging appearances before and after embolization of uterine arteries. *Radiology* 214:729, 2000.
52. Mittl RL, Jr, Yeh IT, Kressel HY: High-signal-intensity rim surrounding uterine leiomyomas on MR images: pathologic correlation. *Radiology* 180:81, 1991.
53. Bergeron C, Amant F, Ferenczy A: Pathology and physiopathology of adenomyosis. *Best Pract Res Clin Obstet Gynaecol* 20:511, 2006.
54. Seidman JD, Kjerulff KH: Pathologic findings from the Maryland Women's Health Study: practice patterns in the diagnosis of adenomyosis. *Int J Gynecol Pathol* 15:217, 1996.
55. Curtis KM, Hillis SD, Marchbanks PA, et al: Disruption of the endometrial-myometrial border during pregnancy as a risk factor for adenomyosis. *Am J Obstet Gynecol* 187:543, 2002.
56. Bergholt T, Eriksen L, Berendt N, et al: Prevalence and risk factors of adenomyosis at hysterectomy. *Hum Reprod* 16:2418, 2001.
57. Vercellini P, Parazzini F, Oldani S, et al: Adenomyosis at hysterectomy: a study on frequency distribution and patient characteristics. *Hum Reprod* 10:1160, 1995.
58. Nishida M: Relationship between the onset of dysmenorrhea and histologic findings in adenomyosis. *Am J Obstet Gynecol* 165:229, 1991.
59. Missmer SA, Cramer DW: The epidemiology of endometriosis. *Obstet Gynecol Clin North Am* 30:1, 2003.
60. Reinhold C, McCarthy S, Bret PM, et al: Diffuse adenomyosis: comparison of transvaginal US and MR imaging with histopathologic correlation. *Radiology* 199:151, 1996.
61. Bazot M, Cortez A, Darai E, et al: Ultrasonography compared with magnetic resonance imaging for the diagnosis of adenomyosis: correlation with histopathology. *Hum Reprod* 16:2427, 2001.
62. Dueholm M, Lundorf E, Hansen ES, et al: Magnetic resonance imaging and transvaginal ultrasonography for the diagnosis of adenomyosis. *Fertil Steril* 76:588, 2001.
63. Bazot M, Darai E, Rouger J, et al: Limitations of transvaginal sonography for the diagnosis of adenomyosis, with histopathological correlation. *Ultrasound Obstet Gynecol* 20:605, 2002.
64. Atzori E, Tronci C, Sionis L: Transvaginal ultrasound in the diagnosis of diffuse adenomyosis. *Gynecol Obstet Invest* 42:39, 1996.
65. Vercellini P, Cortesi I, De Giorgi O, et al: Transvaginal ultrasonography versus uterine needle biopsy in the diagnosis of diffuse adenomyosis. *Hum Reprod* 13:2884, 1998.
66. Reinhold C, Tafazoli F, Mehio A, et al: Uterine adenomyosis: transvaginal US and MR imaging features with histopathologic correlation. *Radiographics* 19:S147, 1999.
67. Hricak H, Finck S, Honda G, et al: MR imaging in the evaluation of benign uterine masses: value of gadopentetate dimeglumine-enhanced T1-weighted images. *AJR Am J Roentgenol* 158:1043, 1992.
68. Missmer SA, Hankinson SE, Spiegelman D, et al: Incidence of laparoscopically confirmed endometriosis by demographic, anthropometric, and lifestyle factors. *Am J Epidemiol* 160:784, 2004.
69. Exacoustos C, Manganaro L, Zupi E: Imaging for the evaluation of endometriosis and adenomyosis. *Best Pract Res Clin Obstet Gynaecol* 28:655, 2014.
70. The Practice Committee at the American Society of Reproductive Medicine: Endometriosis and infertility. *Fertil Steril* 81(5):1441, 2004.
71. Vinatier D, Orazi G, Cosson M, et al: Theories of endometriosis. *Eur J Obstet Gynecol Reprod Biol* 96:21, 2001.
72. Chung SY, Kim SJ, Kim TH, et al: Computed tomography findings of pathologically confirmed pulmonary parenchymal endometriosis. *J Comput Assist Tomogr* 29:815, 2005.
73. Dwivedi AJ, Agrawal SN, Silva YJ: Abdominal wall endometriomas. *Dig Dis Sci* 47:456, 2002.
74. Thibodeau LL, Prioleau GR, Manuelidis EE, et al: Cerebral endometriosis. Case report. *J Neurosurg* 66:609, 1987.
75. Carbognin G, Guarise A, Minelli L, et al: Pelvic endometriosis: US and MRI features. *Abdom Imaging* 29:609, 2004.
76. Outwater E, Schiebler ML, Owen RS, et al: Characterization of hemorrhagic adnexal lesions with MR imaging: blinded reader study. *Radiology* 186:489, 1993.
77. Kier R, Smith RC, McCarthy SM: Value of lipid- and water-suppression MR images in distinguishing between blood and lipid within ovarian masses. *AJR Am J Roentgenol* 58:321, 1992.
78. Sugimura K, Takemori M, Sugiura M, et al: The value of magnetic resonance relaxation time in staging ovarian endometrial cysts. *Br J Radiol* 65:502, 1992.
79. Glastonbury CM: The shading sign. *Radiology* 224:199, 2002.
80. Jeong YY, Outwater EK, Kang HK: Imaging evaluation of ovarian masses. *Radiographics* 20:1445, 2000.
81. Wu TT, Coakley FV, Qayyum A, et al: Magnetic resonance imaging of ovarian cancer arising in endometriomas. *J Comput Assist Tomogr* 28:836, 2004.
82. Sugimura K, Okizuka H, Imaoka I, et al: Pelvic endometriosis: detection and diagnosis with chemical shift MR imaging. *Radiology* 188:435, 1993.
83. Takahashi K, Okada S, Ozaki T, et al: Diagnosis of pelvic endometriosis by magnetic resonance imaging using "fat-saturation" technique. *Fertil Steril* 62:973, 1994.
84. Stratton P, Winkel C, Premkumar A, et al: Diagnostic accuracy of laparoscopy, magnetic resonance imaging, and histopathologic



- examination for the detection of endometriosis. *Fertil Steril* 79(5):1078–1085, 2003.
85. Zanardi R, Del Frate C, Zuiani C, Bazzocchi M: Staging of pelvic endometriosis based on MRI findings versus laparoscopic classification according to the American Fertility Society. *Abdom Imaging* 28:733, 2003.
  86. Bazot M, Darai E, Hourani R, et al: Deep pelvic endometriosis: MR imaging for diagnosis and prediction of extension of disease. *Radiology* 232:379, 2004.
  87. Kataoka ML, Togashi K, Yamaoka T, et al: Posterior cul-de-sac obliteration associated with endometriosis: MR imaging evaluation. *Radiology* 234:815, 2005.
  88. Takeuchi H, Kuwatsuru R, Kitade M, et al: A novel technique using magnetic resonance imaging jelly for evaluation of rectovaginal endometriosis. *Fertil Steril* 83:442, 2005.
  89. Siegel RL, Miller KD, Jemal A: Cancer Statistics, 2016. *CA Cancer J Clin* 66:7–30, 2016.
  90. Colombo N, Carinelli S, Colombo A, et al: Cervical cancer: ESMO Clinical Practice Guidelines for diagnosis, treatment and follow-up. *Ann Oncol* 23(Suppl 7):vii27–vii32, 2012.
  91. Tjalma WA, Van Waes TR, Van den Eeden LE, et al: Role of human papillomavirus in the carcinogenesis of squamous cell carcinoma and adenocarcinoma of the cervix. *Best Pract Res Clin Obstet Gynaecol* 19:469, 2005.
  92. National Cancer Institute: *PDQ Cervical Cancer Treatment*, Bethesda, MD, May 28, 2015, National Cancer Institute. Available at: <<http://www.cancer.gov/cancertopics/pdq/treatment/cervical/healthprofessional>>.
  93. Kaur H, Silverman PM, Iyer RB, et al: Diagnosis, staging, and surveillance of cervical carcinoma. *AJR Am J Roentgenol* 180:1621, 2003.
  94. Yamashita Y, Takahashi M, Katabuchi H, et al: Adenoma malignum: MR appearances mimicking nabothian cysts. *AJR Am J Roentgenol* 162:649, 1994.
  95. Matthews-Greer J, Dominguez-Malagon H, Herrera GA, et al: Human papillomavirus typing of rare cervical carcinomas. *Arch Pathol Lab Med* 128:553, 2004.
  96. Cheng X, Cai S, Li Z, et al: The prognosis of women with stage IB1-IBB node-positive cervical carcinoma after radical surgery. *World J Surg Oncol* 18:47, 2004.
  97. Kyndi M, Frederiksen K, Kruger Kjaer S: Cervical cancer incidence in Denmark over six decades (1943–2002). *Acta Obstet Gynecol Scand* 85:106, 2006.
  98. Vizcaino AP, Moreno V, Bosch FX, et al: International trends in incidence of cervical cancer: II. Squamous-cell carcinoma. *Int J Cancer* 86:429, 2000.
  99. Vizcaino AP, Moreno V, Bosch FX, et al: International trends in the incidence of cervical cancer: I. Adenocarcinoma and adenosquamous cell carcinomas. *Int J Cancer* 75:536, 1998.
  100. Pecorelli S, Zigliani L, Odicino F: Revised FIGO staging for carcinoma of the cervix. *Int J Gynaecol Obstet* 105:107, 2009.
  101. Subak LL, Hricak H, Powell CB, et al: Cervical carcinoma: computed tomography and magnetic resonance imaging for preoperative staging. *Obstet Gynecol* 86:43, 1995.
  102. Kim SH, Choi BI, Han JK, et al: Preoperative staging of uterine cervical carcinoma: comparison of CT and MRI in 99 patients. *J Comput Assist Tomogr* 17:633, 1993.
  103. Park W, Park YJ, Huh SJ, et al: The usefulness of MRI and PET imaging for the detection of parametrial involvement and lymph node metastasis in patients with cervical cancer. *Jpn J Clin Oncol* 35:260, 2005.
  104. Hricak H, Hamm B, Semelka RC, et al: Carcinoma of the uterus: use of gadopentetate dimeglumine in MR imaging. *Radiology* 181:95, 1991.
  105. Seki H, Azumi R, Kimura M, et al: Stromal invasion by carcinoma of the cervix: assessment with dynamic MR imaging. *AJR Am J Roentgenol* 168:1579–1585, 1997.
  106. Benedet JL, Odicino F, Maisonneuve P, et al: Carcinoma of the cervix uteri. *J Epidemiol Biostat* 6(1):7, 2001.
  107. Benedet JL, Odicino F, Maisonneuve P, et al: Carcinoma of the cervix uteri. *Int J Gynaecol Obstet* 83:41, 2003.
  108. Narayan K: Arguments for a magnetic resonance imaging-assisted FIGO staging system for cervical cancer. *Int J Gynecol Cancer* 15:573, 2005.
  109. Hricak H, Gatsonis C, Chi DS, et al: Role of imaging in pretreatment evaluation of early invasive cervical cancer: results of the intergroup study American College of Radiology Imaging Network 6651: Gynecologic Oncology Group 183. *J Clin Oncol* 23:9329, 2005.
  110. Follen M, Levenback CF, Iyer RB, et al: Imaging in cervical cancer. *Cancer* 98:2028, 2003.
  111. Thomeer MG, Gerestein C, Spronk S, et al: Clinical examination versus magnetic resonance imaging in the pretreatment staging of cervical carcinoma: systematic review and meta-analysis. *Eur Radiol* 23(7):2005–2018, 2013.
  112. Yamashita Y, Takahashi M, Sawada T, et al: Carcinoma of the cervix: dynamic MR imaging. *Radiology* 182:643, 1992.
  113. Hricak H, Lacey CG, Sandles LG, et al: Invasive cervical carcinoma: comparison of MR imaging and surgical findings. *Radiology* 166:623, 1988.
  114. Horn LC, Bilek K, Fischer U, et al: A cut-off value of 2 cm in tumor size is of prognostic value in surgically treated FIGO stage IB cervical cancer. *Gynecol Oncol* 134:42, 2014.
  115. Tirumani SH, Shanbhogue AK, Prasad SR: Current concepts in the diagnosis and management of endometrial and cervical carcinomas. *Radiol Clin North Am* 51:1087, 2013.
  116. Lai G, Rockall AG: Lymph node imaging in gynecologic malignancy. *Semin Ultrasound CT MR* 31:363, 2010.
  117. Keller TM, Michel SC, Frohlich J, et al: USPIO-enhanced MRI for preoperative staging of gynecological pelvic tumors: preliminary results. *Eur Radiol* 14:937, 2004.
  118. Rockall AG, Sohaib SA, Harisinghani MG, et al: Diagnostic performance of nanoparticle-enhanced magnetic resonance imaging in the diagnosis of lymph node metastases in patients with endometrial and cervical cancer. *J Clin Oncol* 23:2813, 2005.
  119. Harisinghani MG, Barentsz J, Hahn PF, et al: Noninvasive detection of clinically occult lymph-node metastases in prostate cancer. *N Engl J Med* 348:2491, 2003.
  120. National Cancer Institute: *Endometrial Cancer Treatment for Health Professionals (PDQ)*, Bethesda, MD, April 17, 2015, National Cancer Institute. Available at: <<http://www.cancer.gov/cancertopics/pdq/treatment/endometrial/healthprofessional>>.
  121. Amant F, Moerman P, Neven P, et al: Endometrial cancer. *Lancet* 366:491, 2005.
  122. Purdie DM, Green AC: Epidemiology of endometrial cancer. *Best Pract Res Clin Obstet Gynaecol* 15:341, 2001.
  123. Swerdlow AJ, Jones ME: Tamoxifen treatment for breast cancer and risk of endometrial cancer: a case-control study. *J Natl Cancer Inst* 97:375, 2005.
  124. Lacey JV, Jr, Brinton LA, Lubin JH, et al: Endometrial carcinoma risks among menopausal estrogen plus progestin and unopposed estrogen users in a cohort of postmenopausal women. *Cancer Epidemiol Biomarkers Prev* 14:1724, 2005.
  125. Tangitgamol S, Levenback CF, Beller U, et al: Role of surgical resection for lung, liver, and central nervous system metastases in patients with gynecological cancer: a literature review. *Int J Gynecol Cancer* 14:399, 2004.
  126. American Joint Committee on Cancer: Corpus uteri. In Greene FL, Fritz AG, Balch CM, et al, editors: *AJCC Cancer Staging Manual*, ed 6, New York, 2002, Springer-Verlag.
  127. Abeler VM, Kjorstad KE: Endometrial adenocarcinoma in Norway. A study of a total population. *Cancer* 67:3093, 1991.
  128. Pecorelli S: Revised FIGO staging for carcinoma of the vulva, cervix, and endometrium. *Int J Gynaecol Obstet* 105:103, 2009.
  129. Hricak H, Rubinstein LV, Gherman GM, et al: MR imaging evaluation of endometrial carcinoma: results of an NCI cooperative study. *Radiology* 179:829, 1991.
  130. Yamashita Y, Mizutani H, Torashima M, et al: Assessment of myometrial invasion by endometrial carcinoma: transvaginal sonography vs contrast-enhanced MR imaging. *AJR Am J Roentgenol* 161:595, 1993.

131. Sironi S, Colombo E, Villa G, et al: Myometrial invasion by endometrial carcinoma: assessment with plain and gadolinium-enhanced MR imaging. *Radiology* 185:207, 1992.
132. Nasi F, Fiocchi F, Pecchi A, et al: MRI evaluation of myometrial invasion by endometrial carcinoma. Comparison between fast-spin-echo T2w and coronal-FMPSPGR gadolinium-dota-enhanced sequences. *Radiol Med (Torino)* 110:199, 2005.
133. Belloni C, Viganò R, del Maschio A, et al: Magnetic resonance imaging in endometrial carcinoma staging. *Gynecol Oncol* 37:172, 1990.
134. Lien HH, Blomlie V, Trope C, et al: Cancer of the endometrium: value of MR imaging in determining depth of invasion into the myometrium. *AJR Am J Roentgenol* 157:1221, 1991.
135. Sironi S, Taccagni G, Garancini P, et al: Myometrial invasion by endometrial carcinoma: assessment by MR imaging. *AJR Am J Roentgenol* 158:565, 1992.
136. Tsuda H, Murata K, Kawabata M, et al: Preoperative assessment of myometrial invasion of endometrial cancer by MR imaging and intrauterine ultrasonography with a high-frequency probe: preliminary study. *J Ultrasound Med* 16:545, 1997.
137. Ito K, Matsumoto T, Nakada T, et al: Assessing myometrial invasion by endometrial carcinoma with dynamic MRI. *J Comput Assist Tomogr* 18:77, 1994.
138. Arko D, Takac I: High frequency transvaginal ultrasonography in preoperative assessment of myometrial invasion in endometrial cancer. *J Ultrasound Med* 19:639, 2000.
139. American Cancer Society: *Cancer Facts & Figures*, Atlanta, 2014, American Cancer Society, pp 2014.
140. Ovarian Cancer: Screening, Treatment, and Follow-up. *NIH Consensus Statement Online* 12(3):1-30, 1994. Available at: <consensus.nih.gov/1994/1994OvarianCancer096html.htm>.
141. Engelen MJ, Kos HE, Willems PH, et al: Surgery by consultant gynecologic oncologists improves survival in patients with ovarian carcinoma. *Cancer* 106:589, 2006.
142. Sohaib SA, Mills TD, Sahdev A, et al: The role of magnetic resonance imaging and ultrasound in patients with adnexal masses. *Clin Radiol* 60:340, 2005.
143. Iyer VR, Lee SI: MRI, CT, and PET/CT for ovarian cancer detection and adnexal lesion characterization. *AJR Am J Roentgenol* 194:311, 2010.
144. Kinkel K, Lu Y, Mehdizade A, et al: Indeterminate ovarian mass at US: incremental value of second imaging test for characterization—meta-analysis and Bayesian analysis. *Radiology* 236(1):85, 2005.
145. Adusumilli S, Hussain HK, Caoili EM, et al: MRI of sonographically indeterminate adnexal masses. *AJR Am J Roentgenol* 187:732, 2006.
146. Kurtz AB, Tsimikas JV, Tempany CM, et al: Diagnosis and staging of ovarian cancer: comparative values of Doppler and conventional US, CT, and MR imaging correlated with surgery and histopathologic analysis—report of the Radiology Diagnostic Oncology Group. *Radiology* 212:19, 1999.
147. DePriest PD, Shenson D, Fried A, et al: A morphology index based on sonographic findings in ovarian cancer. *Gynecol Oncol* 51:7, 1993.
148. Chang WC, Meux MD, Yeh BM, et al: CT and MRI of adnexal masses in patients with primary nonovarian malignancy. *AJR Am J Roentgenol* 186:1039, 2006.
149. Saini A, Dina R, McIndoe GA, et al: Characterization of adnexal masses with MRI. *AJR Am J Roentgenol* 184:1004, 2005.
150. Bloomfield TH: Benign cystic teratomas of the ovary: a review of seventy-two cases. *Eur J Obstet Gynecol Reprod Biol* 25(3):231, 1987.
151. Jung SE, Rha SE, Lee JM, et al: CT and MRI findings of sex cord-stromal tumor of the ovary. *AJR Am J Roentgenol* 185:207, 2005.
152. Troiano RN, Lazzarini KM, Scoutt LM, et al: Fibroma and fibrothecoma of the ovary: MR imaging findings. *Radiology* 204:795, 1997.
153. Zhang J, Ugnat AM, Clarke K, et al: Ovarian cancer histology-specific incidence trends in Canada 1969–1993: age-period-cohort analyses. *Br J Cancer* 81(1):152, 1999.
154. McCluggage WG, Wilkinson N: Metastatic neoplasms involving the ovary: a review with an emphasis on morphological and immunohistochemical features. *Histopathology* 47:231, 2005.
155. Ha HK, Baek SY, Kim SH, et al: Krukenberg's tumor of the ovary: MR imaging features. *AJR Am J Roentgenol* 164:1435, 1995.
156. Hann LE, Lui DM, Shi W, et al: Adnexal masses in women with breast cancer: US findings with clinical and histopathologic correlation. *Radiology* 216:242, 2000.
157. Kim SH, Kim WH, Park KJ, et al: CT and MR findings of Krukenberg tumors: comparison with primary ovarian tumors. *J Comput Assist Tomogr* 20:393, 1996.
158. Ferrozzi F, Tognini G, Bova D, et al: Non-Hodgkin lymphomas of the ovaries: MR findings. *J Comput Assist Tomogr* 24:416, 2000.
159. Schumer ST, Cannistra SA: Granulosa cell tumor of the ovary. *J Clin Oncol* 21:1180, 2003.
160. Kim SH, Kim SH: Granulosa cell tumor of the ovary: common findings and unusual appearances on CT and MR. *J Comput Assist Tomogr* 26:756, 2002.
161. Prat J, FIGO Committee on Gynecologic Oncology: Staging classification for cancer of the ovary, fallopian tube, and peritoneum. *Int J Gynecol Obstet* 124(1):1-5, 2014.
162. Coakley FV: Staging ovarian cancer: role of imaging. *Radiol Clin North Am* 40:609, 2002.
163. Vergote I, Tropé CG, Amant F, et al: Neoadjuvant chemotherapy or primary surgery in stage IIIC or IV ovarian cancer. *N Engl J Med* 363:943, 2010.
164. Qayyum A, Coakley FV, Westphalen AC, et al: Role of CT and MR imaging in predicting optimal cytoreduction of newly diagnosed primary epithelial ovarian cancer. *Gynecol Oncol* 96:301, 2005.
165. Tempany CM, Zou KH, Silverman SG, et al: Staging of advanced ovarian cancer: comparison of imaging modalities—report from the Radiological Diagnostic Oncology Group. *Radiology* 215:761, 2000.



# Role of Sonography in Gynecologic Interventions

Howard T. Sharp, Thomas C. Winter

## SUMMARY OF KEY POINTS

- Ultrasound (US) has an important role in planning and guiding many gynecologic interventions.
- Prior to endometrial ablation, US may be used to detect focal lesions (e.g., polyps or leiomyomas), assess for tubal disease such as hydrosalpinx, and search for uterine anomalies.
- Whereas magnetic resonance imaging (MRI) remains the gold standard for evaluating patients prior to uterine artery embolization (UAE), US can be used to identify several relative contraindications. Following UAE, US has an important role in assessing post procedural complications such as necrosis or superinfection of the uterus or leiomyomas.
- MRI remains the gold standard for diagnosis and classification of congenital uterine anomalies. However, three dimensional (3D) US can provide important information with significant impact on counseling regarding reproductive prognosis and approach to repair.
- Transabdominal US guidance is extremely useful when accessing the endometrial cavity in patients with cervical stenosis and Asherman syndrome, or when placing brachytherapy devices; direct guidance reduces the risk of uterine perforation or creation of a false channel during instrumentation.
- US is increasingly used to assess for correct placement of Essure microinsert devices in the proximal fallopian tube, although hysterosalpingography still remains the gold standard.
- 3D US is considered the gold standard to document correct IUD placement in the endometrial cavity.
- US guidance can be used to safely guide transvaginal or transabdominal percutaneous biopsies of pelvic masses and drainage of pelvic fluid collections following careful consultation with the referring gynecologist.

## OUTLINE

**Endometrial Ablation, 1077**

**Uterine Artery Embolization, 1078**

**Repair of Congenital Anomalies of the Uterus, 1079**

Agensis, 1080

Lateral Fusion Defects, 1081

Vertical Fusion Defects, 1082

**Guidance for Endometrial Interventions (Cervical Stenosis, Asherman Syndrome), 1082**

**Confirmation of Correct Essure Microinsert Placement for Tubal Sterilization, 1084**

**Malpositioned Intrauterine Device, 1086**

**Pelvic Biopsies and Drainages, 1088**

**Conclusions, 1088**

Gynecologic interventions have undergone significant changes over the past few decades. Procedures once exclusively performed in the operating room under general anesthesia may now be performed under local anesthesia in an office setting. Sonography has been a factor in allowing better preoperative investigation by excluding certain gynecologic disease, and its use in the clinic can guide access that previously required surgical exploration. The goal of this chapter is to describe the information required from ultrasound imaging of the pelvis to assist in gynecologic interventions. This chapter is organized according to gynecologic intervention, in hopes of better

conveying the information that is necessary for a safe and successful procedure. Seven common gynecologic interventions and treated conditions will be covered: endometrial ablation, uterine artery embolization (UAE), repair of congenital anomalies of the uterus, guidance for endometrial interventions for cervical stenosis and Asherman syndrome, confirmation of correct Essure microinsert placement for tubal sterilization, location of malpositioned IUDs, and pelvic biopsies and drainages. Chapters on abnormal uterine bleeding, adnexal masses, ectopic pregnancy, and infertility are presented elsewhere in this textbook and, therefore, are not covered in this chapter.



## ENDOMETRIAL ABLATION

Key questions to consider before endometrial ablation:

- Is an endometrial polyp or mass present?
- Is a leiomyoma present? If so, is it submucosal?
- Is there evidence of tubal disease such as hydrosalpinx?
- Is a uterine anomaly present?

Endometrial ablation is an intervention offered to women who suffer from heavy menstrual bleeding that interferes with normal daily activities enough to warrant intervention, but without a known lesion causing bleeding. Known causes for uterine bleeding such as uterine leiomyomas, endometrial polyps, endometrial cancer or precancerous lesions are more effectively treated by other methods. Furthermore, endometrial ablation in the presence of an endometrial cancer or precancer may lead to a delay in diagnosis.

Historically, endometrial ablation was performed in the operating room under general anesthesia via hysteroscopy. Use of a hysteroscope provides the surgeon with the ability to look into the uterine cavity and manually ablate the endometrium with a ball electrode (rollerball). This procedure causes desiccation of the endometrium in hopes that the endometrium will no longer bleed. Laser energy has also been used, as well as a loop electrode to shave or resect the endometrium. However, these three methods require advanced hysteroscopic skills and may expose the patient to hypotonic fluids to distend the endometrial cavity, thus placing her at risk for hyponatremia which, in some cases, can be associated with life-threatening herniation of the brainstem. Because these surgeries can be difficult to perform, five newer endometrial ablation devices have been approved by the U.S. Food and Drug Administration (FDA). These newer endometrial ablation methods have been approved since 1997 and are often referred to as *global endometrial ablation* (GEA) devices because the endometrial cavity is treated as a whole through a more automated process, rather than by a manual approach that ablates sections of the endometrium with a rollerball, laser, or loop resection. GEA methods employ a variety of modalities to ablate the endometrium, including a thermal balloon, circulated hot fluid, cryotherapy, radiofrequency electrosurgery, and microwave energy. GEA devices allow endometrial ablation to be performed with greater ease in the office, without the risk of fluid overload syndrome that has been associated with traditional hysteroscopic surgery performed with electrolyte-poor fluid. Though rates of amenorrhea have a wide range (14-55%) among GEA methods, patient satisfaction rates are uniformly high, at approximately 85%.<sup>1</sup>

Before considering endometrial ablation, a number of contraindications should be excluded (Table 37-1). Gynecologic ultrasound and particularly saline infusion sonohysterography (SIS) are helpful in assessing for submucosal leiomyomas (Fig. 37-1) and endometrial

polyps, which would be optimally treated with hysteroscopic resection. Excluding such conditions prior to endometrial ablation avoids exposing patients to unnecessary risks of a treatment that will have a lower efficacy as a result of underlying abnormality.

Complications of endometrial ablation may be found on ultrasound examination in the postoperative patient who presents with pain or bleeding. Such complications include infection; uterine perforation; thermal injury to bladder, bowel, or ureter; hematometra (Fig. 37-2); pregnancy-related complications; and the development of subsequent endometrial cancer (not detected with the preoperative biopsy). In a meta-analysis comparing endometrial ablation procedures, the incidence of infectious complications included endometritis



**FIG 37-1** Submucosal, predominantly intracavitary leiomyoma (*asterisk*) well demonstrated by saline infusion sonohysterography on this sagittal transvaginal ultrasound image. Note the thin overlying rim of echogenic endometrium (*arrow*) covering the myoma.



**FIG 37-2** Hematometra following incomplete endometrial ablation. This 51-year-old patient presented with crampy pelvic pain but no bleeding. Transvaginal sagittal image of the uterus demonstrates the endometrial cavity distended with homogeneous hypoechoic material (*asterisk*) that was avascular on color Doppler imaging (not shown). The patient spontaneously bled and decompressed 1 day before her planned cervical dilation.

### TABLE 37-1 Contraindications to Global Endometrial Ablation

Pregnancy or desire to be pregnant in the future
Known or suspected endometrial carcinoma
Premalignant change of the endometrium*
Active pelvic inflammatory disease or hydrosalpinx*
Prior classic cesarean delivery or transmural myomectomy
Uterine anomaly, e.g., septate uterus, bicornuate uterus, or unicornuate uterus
Intrauterine device in place
Submucosal leiomyoma or other endometrial mass
Active urinary tract infection at the time of treatment*

\*Relative contraindications.



(1.4-2.0%), myometritis (0-0.9%), pelvic inflammatory disease (1.1%), and pelvic abscess (0-1.1%).<sup>2</sup>

Pregnancy following ablation has been reported to occur in 0.7% of women who have undergone endometrial ablation and is associated with poor obstetric outcomes.<sup>3</sup> It has been reported as early as 5 weeks after ablation and as late as 12 years postoperatively (following tubal reanastomosis in a planned pregnancy).<sup>4</sup> The chance of pregnancy occurring after endometrial ablation with tubal sterilization is even lower, estimated to be 0.002%, or 1 in 50,000. Though successful pregnancies have been reported, there appears to be a greater risk of complications including preterm birth, intrauterine scarring/uterine chambering (creating separate uterine compartments), and postpartum hemorrhage.<sup>5</sup> It is hypothesized that the risk of preterm birth is in part due to narrowing or chambering of the endometrial cavity, resulting in a smaller area for the gestation. One of the unintended consequences of office endometrial ablation is the inability to perform concomitant tubal sterilization, which could lead to an undesired increased incidence of pregnancy in this population.

Contracture and scarring of the endometrium constitute an expected effect of endometrial ablation. However, when focal areas of normal endometrium persist after a partial ablation, obstructed egress of menses with associated pain may occur. This can manifest as hematometra within the body of the uterine cavity (central hematometra) or at the cornual region. Postablation tubal sterilization syndrome (PATSS) was initially reported in 1993 in a series of six patients presenting with unilateral or bilateral pelvic pain and vaginal spotting subsequent to tubal sterilization and endometrial ablation.<sup>6</sup> The patients were all noted to have scarring of the endometrial cavity with swelling of the proximal portion of one or both fallopian tubes. Symptomatic relief was achieved in five out of six patients with removal of the fallopian tubes. The incidence of PATSS is approximately 6% to 8%, and it usually develops within 2 to 3 years of endometrial ablation. A high index of clinical suspicion is key to the diagnosis of PATSS, as patients typically present with cyclic cramping with or without menses in the setting of prior endometrial ablation and tubal sterilization. The role of sonography in diagnosing PATSS has not been well evaluated. Usually the confirmatory diagnosis is made surgically. However, magnetic resonance imaging (MRI) during periods of symptomatic cramping may be useful using T2-weighted images to look for blood trapped in the uterine cornu.<sup>7</sup> Another concern regarding the scarring of the endometrium that accompanies endometrial ablation is the difficulty with subsequent evaluation of the endometrium with endometrial sampling, sonography, or SIS. The safety of endometrial ablation has not been well studied in women who are at an increased risk of developing endometrial cancer or endometrial hyperplasia. These risks include nulliparity, chronic anovulation, obesity, diabetes mellitus, tamoxifen or selective estrogen receptor modulator (SERM) therapy, and hereditary nonpolyposis colorectal cancer.

Approximately half of the serious complications associated with contraindications to endometrial ablation may be identified preoperatively, as was demonstrated in a series of patient reports entered using the FDA Manufacturer and User Facility Device Experience (MAUDE) database.<sup>8</sup> The initial MAUDE database report described 85 complications in 62 patients. They included major complications, such as 8 cases of thermal bowel injury, 30 cases of uterine perforation, 12 cases requiring emergent laparotomy, and 3 intensive care unit admissions. One patient developed necrotizing fasciitis and eventually underwent vulvectomy, ureterocutaneous ostomy, and bilateral below-the-knee amputations. One of the patients with thermal injury to the bowel died. The contraindications to GEA are summarized in Table 37-1.

Though pelvic ultrasound examination is often performed as part of the preoperative evaluation, a strong case for the use of SIS could be

made as a better modality to exclude contraindications such as submucosal leiomyomas.<sup>9-11</sup> If a polyp is present, endometrial ablation is not necessary, as a simple polypectomy can be performed and bleeding will most often resolve. Likewise, if submucosal leiomyomas are present, hysteroscopic resection of the leiomyoma is indicated; this is an outpatient procedure not associated with the same risk of endometrial scarring as endometrial ablation. Tubal disease such as hydrosalpinx or tubo-ovarian abscess should be treated prior to endometrial ablation to avoid postoperative infectious complications. Lastly, the presence of a uterine septum or other uterine anomaly would make several of the described automated ablation technologies impossible to perform, as the devices may not fit within the endometrial cavity and thus would place the patient at risk for unnecessary anesthesia. Of note, superficial adenomyosis is reasonable to treat with endometrial ablation, although there are reports of decreased efficacy if adenomyosis is extensive.

## UTERINE ARTERY EMBOLIZATION

Key questions to consider for UAE:

- Is the leiomyoma pedunculated?
- Is the leiomyoma submucosal in location?
- Is there leiomyoma growth in a postmenopausal woman?
- Is there concurrent endometrial disease that may be causing bleeding?
- Is adenomyosis present?
- Is there unsuspected adnexal abnormality?

UAE for the treatment of leiomyomas was first described in 1995.<sup>12</sup> In most circumstances, this procedure is performed by interventional radiologists. A 4F or 5F catheter is placed into the uterine arteries via a transcutaneous femoral approach. Polyvinyl alcohol particles or trisacryl gelatin microspheres are injected into the uterine arteries to devascularize the uterus and therefore cause shrinkage of leiomyomas. Supplemental metal coils may be used to assist with vascular occlusion. The patient is usually able to return home within 23 hours of the procedure. There is typically a period of ischemic pain for 2 to 3 hours after embolization, followed by a plateau of pain, and then gradual reduction of pain over the next 2 to 3 days. The advantages of this procedure compared to myomectomy or hysterectomy are a faster recovery and return to normal activities.

Since 1995, there has been considerable progress in the successful performance of UAE. Most initial published reports were case series describing the technique or reports of short-term outcomes.<sup>13,14</sup> Subsequently, larger multicenter series and nonrandomized controlled studies and, finally, randomized clinical trials (RCTs) have been published. Unfortunately, the information from RCTs regarding long-term outcomes is limited owing to short follow-up intervals, although long-term outcomes have been reported in nonrandomized trials. Broder and associates reported up to 5-year follow-up data in an observational study of UAE compared to myomectomy.<sup>15</sup> In the UAE group, there was a higher reoperation rate of 29% (15/51) compared to 3% (1/30) in the myomectomy group ( $P = 0.004$ ). When considering subjective variables, such as worsening of symptoms and being dissatisfied, 39% (20/51) were considered clinical failures in the UAE group compared to 30% (9/30) in the myomectomy group, a nonsignificant difference ( $P = 0.4$ ). Additional 5-year follow-up data were published in a case series by Spies and colleagues.<sup>16</sup> In patients undergoing UAE, they reported a 20% reoperation rate (hysterectomy 13.7%, myomectomy 4.4%, repeat embolization 1.6%) and a 25% chance of failure to control symptoms. Short-term failure (at 12 months) was three times more likely in those with less than the median shrinkage of a dominant leiomyoma. Failure to shrink at the 12-month interval was associated with a five times greater likelihood of long-term failure.



Regarding short-term outcomes, a large multicenter study of over 500 patients undergoing UAE in eight Ontario hospitals reported favorable 3-month outcomes with regard to dominant leiomyoma volume reduction (42%), median leiomyoma life-impact scores, mean menstrual duration, dysmenorrhea, and urinary frequency/urgency.<sup>17</sup>

The EMMY trial (EMbolization vs. hysterectoMY) was a RCT involving 28 Dutch hospitals and compared UAE to hysterectomy. Comparison of safety demonstrated a similar major complication rate of 4.9% for UAE and 2.7% with hysterectomy ( $P = 0.68$ ), but a higher rate of readmission and minor complications in the UAE group (11.1% vs. 0%;  $P = 0.003$  and 58.0% vs. 40.0%;  $P = 0.024$ ; risk ratio 1.45 [1.04–2.02]), respectively.<sup>18</sup> Another multicenter comparative trial of UAE versus myomectomy reported similar clinical findings.<sup>19</sup> A second EMMY publication reported a comparison of the short-term outcomes of pain and time until return to daily activities.<sup>20</sup> Compared to patients undergoing hysterectomy, patients undergoing UAE had significantly less pain during the first 24 hours postoperatively ( $P = 0.012$ ) and returned to work sooner (28.1 vs. 63.4 days). Five RCTs comparing UAE to myomectomy and hysterectomy were also evaluated in a Cochrane review.<sup>21</sup> The review found that outpatient UAE resulted in a similar satisfaction rate compared with hysterectomy and myomectomy, but offered the advantage of a shorter hospital stay and quicker return to activities. However, UAE was associated with a higher minor complication rate and an increased likelihood of surgical intervention within 2 to 5 years of the initial intervention.

The overall complication rate of UAE has been reported to be 5% and is similar when applying the American College of Obstetricians and Gynecologists (ACOG) criteria for perioperative morbidity.<sup>22</sup> Complications range from fever to uterine necrosis and, very rarely, death. Collateral damage to the ovary resulting in premature ovarian failure has also been reported. However, this complication has been reported primarily in patients over age 45 years and may be associated with reduced ovarian reserve.

Pregnancy after UAE remains understudied, with variable complication rates reported. An observational study reported a higher rate of preterm delivery compared to laparoscopic myomectomy (odds ratio 6.2 [1.4, 27.7]).<sup>23</sup> Other studies have raised concerns regarding abnormal placentation (12.5%)<sup>24</sup> and high cesarean delivery rates (88%), but did not report other major risk factors.<sup>25</sup> The effect of UAE on pregnancy is therefore uncertain. However, careful surveillance is required should a patient become pregnant following UAE.

Although MRI has become the standard preprocedural imaging tool in women considering UAE, most women with symptoms first undergo pelvic ultrasound imaging for confirmation of the presence of leiomyomas. Though ultrasound imaging is not as useful as contrast-enhanced MRI in determining leiomyoma characteristics such as tissue viability, ultrasound imaging can be helpful in assessing for pedunculated submucosal and subserosal (Fig. 37-3) leiomyomas, both of which have been associated with an increased risk of complications following UAE.

Pedunculated submucosal (type 0) leiomyomas are defined as being located entirely within the endometrial cavity with no myometrial extension. It should be noted that although leiomyomas may be associated with abnormal uterine bleeding or pelvic pressure symptoms involving the bladder or rectum, leiomyomas are also commonly asymptomatic. Therefore, it is important to exclude other causes of abnormal uterine bleeding (especially endometrial cancer) and to assess for possible endometrial polyps or submucosal leiomyomas. Ultrasound imaging may also detect adenomyosis, which may cause similar symptoms as leiomyomas and, if present, may decrease the efficacy of UAE. Lastly, enlarging leiomyomas, though usually not associated with sarcoma in reproductive age women, are of great concern in postmenopausal women. An increase of more than 20% in

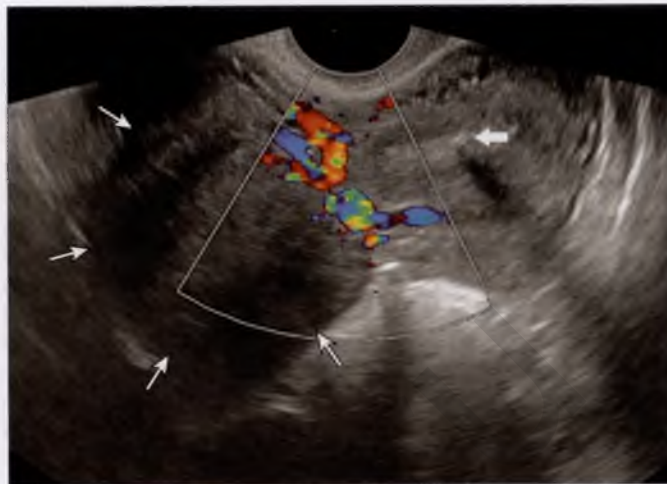


**FIG 37-3** Pedunculated leiomyoma. Transaxial transvaginal color Doppler sonogram of the uterus demonstrating an echogenic focus (large arrow) with associated posterior shadowing within the endometrium, indicating an intrauterine device. Note right-sided hypoechoic solid mass (small arrows) in direct continuity with the myometrium, consistent with a large pedunculated subserosal leiomyoma. Note that color Doppler sonogram imaging can be used to show bridging myometrial vessels.

### TABLE 37-2 Contraindications to Uterine Artery Embolization

Menopause*
Current use of gonadotropin-releasing hormone (GnRH) agonist
Submucosal leiomyoma*
Pedunculated subserosal leiomyoma*
Extensive adenomyosis*
Previous internal iliac artery ligation
Active genitourinary infection*
Malignancy
Pregnancy
Significant immunosuppression

\*Relative contraindications.

measured leiomyoma diameter by ultrasound imaging is considered to represent true growth, not measurement variation.<sup>26</sup> Typically, leiomyomas will reduce in size during menopause. Thus, treatment of leiomyomas with UAE is generally contraindicated in postmenopausal women. The prevalence of sarcomas is approximately 0.2% (1 in 500) in women undergoing hysterectomy or myomectomy for presumed benign leiomyomas; this potential complication has gained attention with recent publicity regarding the dangers of power uterine morcellation.<sup>27</sup> There are currently no ultrasound imaging or MRI features that allow the accurate diagnosis of uterine sarcoma. Contrary to prior belief, rapidly enlarging leiomyomas in reproductive age women have specifically not been found to predict sarcoma.<sup>28</sup> Contraindications to UAE are summarized in Table 37-2.

### REPAIR OF CONGENITAL ANOMALIES OF THE UTERUS

Key questions to consider for repair of congenital anomalies of the uterus:

- Does the patient have two structurally normal kidneys?
- If there is a midline septum, is there notching at the uterine fundus?
- Are two ovaries present?



- Is a vagina present?
- Is there a portion of uterine tissue that may become obstructed?
- Are there one or two cervixes?

The prevalence of congenital anomalies of the reproductive tract is estimated to be as high as 7% in the female population.<sup>29</sup> These anomalies are usually not recognized until they present with pain (obstructed menses), pregnancy complications (fetal malpresentation, preterm labor, recurrent pregnancy loss), or infertility. There are a number of classification systems for müllerian anomalies. The American Fertility Society/American Society of Reproductive Medicine (AFS/ASRM) proposed a standard classification of müllerian anomalies based on vertical fusion defects (Table 37-3 and Fig. 37-4).<sup>30,31</sup> Because of the many variations and complexities associated with these defects, a system known as the Vagina Cervix Uterus Adnexa-associated Malformation (VCUAM) classification system was proposed after being validated in a group of 99 women. (Table 37-4).<sup>32</sup> In 2013, the European Society of Human Reproduction and Embryology (ESHRE) and the European Society for Gynaecological Endoscopy (ESGE) established a common working group and developed a classification system based largely on anatomy that is clinically oriented (Fig. 37-5).<sup>33</sup>

In a review of the clinical implications of uterine anomalies, the frequency of anomalies by type was septate (35%), bicornuate (26%), arcuate (18%), unicornuate (10%), didelphys (8%), and agenesis (3%).<sup>34</sup> Of the developmental defects, there are three categories to consider: agenesis, lateral fusion defects, and vertical fusion defects. Historically, the workup of these anomalies was quite cumbersome and invasive, typically involving hysterosalpingography often with concomitant hysteroscopy, and laparoscopy under general anesthesia. More recently, MRI has become the standard diagnostic imaging modality, obviating the need for these invasive tests. With the refinement and availability of three-dimensional (3D) sonography (Fig. 37-6), some groups have argued that this may become the new gold standard, offering excellent diagnostic imaging at lower cost and with less discomfort than MRI.<sup>35</sup>

## Agenesis

Mayer-Rokitansky-Küster-Hauser (MRKH) syndrome is the absence of the vagina and is usually also associated with uterine and cervical

agenesis. A small subset of patients will also have an obstructed or rudimentary uterus. The ovaries are less likely to be affected. One series of 106 patients reported normal ovaries in 78%, extrapelvic ovaries in 16%, and unilateral, hypoplastic ovaries in 6%.<sup>36</sup> Urologic abnormalities are seen in 25% to 50% of patients including unilateral renal agenesis and pelvic or horseshoe kidney.

**TABLE 37-3 Müllerian Anomalies According to the American Fertility Society Classification System<sup>30</sup>**

Type I: Müllerian agenesis or hypoplasia	
A.	Vaginal (uterus may be normal)
B.	Cervical
C.	Fundal
D.	Tubal
E.	Combined
Type II: Unicornuate uterus	
A1a.	Communicating (no endometrial cavity present)
A1b.	Noncommunicating (endometrial cavity present)
A2.	Horn without endometrial cavity
B.	No rudimentary horn
Type III: Uterus didelphys	
Type IV: Uterus bicornuate	
A.	Complete (division down to internal os)
B.	Partial
C.	Arcuate
Type V: Septate uterus	
A.	Complete (septum to internal os)
B.	Partial
Type VII: Diethylstilbestrol-related anomalies	
A.	T-shaped uterus
B.	T-shaped with dilated horns

From The American Fertility Society classifications of adnexal adhesions, distal tubal occlusion, tubal occlusion secondary to tubal ligation, tubal pregnancies, Müllerian anomalies and intrauterine adhesions. *Fertil Steril* 49(6):944-955, 1988.

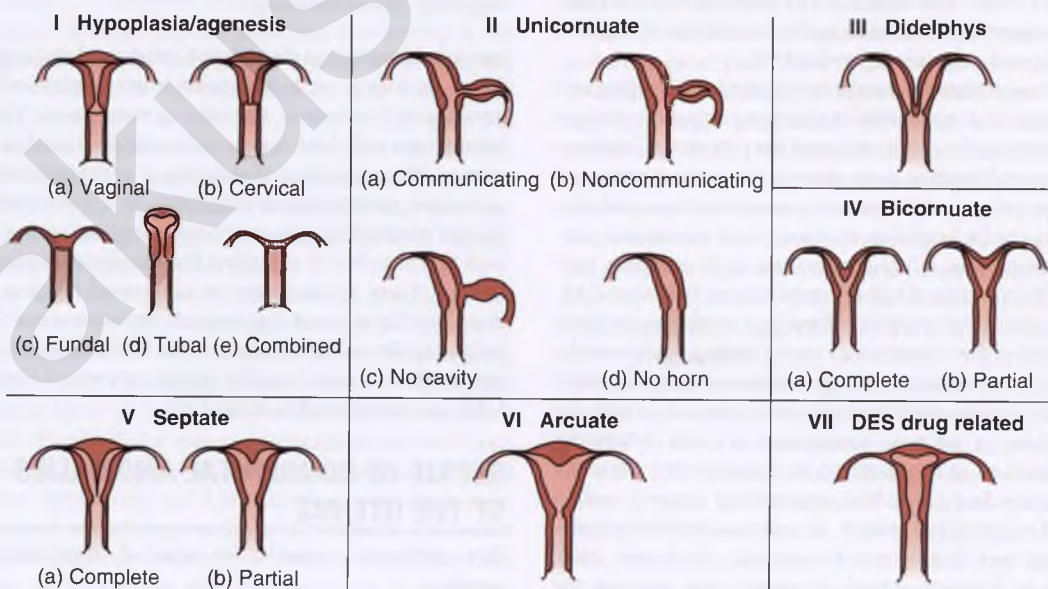


**FIG 37-4** Diagram representing the American Fertility Society/American Society of Reproductive Medicine (AFS/ASRM) classification system for müllerian anomalies.<sup>30,31</sup> DES, diethylstilbestrol.

**TABLE 37-4 The VCUAM Classification System for Genital Malformations: Description of the Individual Malformations Relative to the Organ**

Vagina (V)	0	Normal
	1a	Partial hymenal atresia
	1b	Complete hymenal atresia
	2a	Incomplete septate vagina <50%
	2b	Complete septate vagina
	3	Stenosis of the introitus
	4	Hypoplasia
	5a	Unilateral atresia
	5b	Complete atresia
	S1	Sinus urogenitalis (deep confluence)
	S2	Sinus urogenitalis (middle confluence)
	S3	Sinus urogenitalis (high confluence)
	C	Cloacae
	+	Other
	#	Unknown
	Cervix (C)	0
1		Duplex cervix
2a		Unilateral atresia/aplasia
2b		Bilateral atresia/aplasia
+		Other
#		Unknown
Uterus (U)	0	Normal
	1a	Arcuate
	1b	Septate <50% of the uterine cavity
	1c	Septate >50% of the uterine cavity
	2	Bicornuate
	3	Hypoplastic uterus
	4a	Unilaterally rudimentary or aplastic
	4b	Bilaterally rudimentary or aplastic
	+	Other
	#	Unknown
Adnexa (A)	0	Normal
	1a	Unilateral tubal malformation, ovaries normal
	1b	Bilateral tubal malformation, ovaries normal
	2a	Unilateral hypoplasia/gonadal streak (including tubal malformation if appropriate)
	2b	Bilateral hypoplasia/gonadal streak (including tubal malformation if appropriate)
	3a	Unilateral aplasia
	3b	Bilateral aplasia
	+	Other
	#	Unknown
	associated Malformation (M)	0
	R	Renal system
	S	Skeleton
	C	Cardiac
	N	Neurologic
	+	Other
	#	Unknown

VCUAM, Vagina Cervix Uterus Adnexa-associated Malformation. From Oppelt P, Renner SP, Brucker S, Strissel PL, et al: The VCUAM (Vagina Cervix Uterus Adnex-associated Malformation) classification: a new classification for genital malformations. *Fertil Steril* 84(5):1493-1497, 2005.

Ultrasound evaluation should include assessment for the presence of kidneys, ovaries, uterus, and cervix. In clinical practice, these findings inform counseling about unilateral renal agenesis and surgical repair. Though there is no consensus on the optimal repair for MRKH syndrome, the presence of an obstructed uterus will likely result in symptoms, including pain following menarche, and therefore should be addressed. In general, a nonsurgical treatment (called the Frank procedure) involving creation of a functional vagina with dilators has been fairly successful. Surgical procedures are typically presented as an option for women who have failed dilator therapy. These procedures include the McIndoe procedure (split-thickness graft), Williams vaginoplasty (creation of a vaginal pouch from the labia majora), sigmoid vaginoplasty (resection of a segment of the sigmoid colon brought down to the vagina), and the Vecchietti procedure performed by laparotomy or laparoscopy (a system of traction to gradually create a vagina at the vaginal dimple).

### Lateral Fusion Defects

Lateral fusion defects are the most common types of müllerian defects and result from failure to form one müllerian duct or to resorb the intervening septum, or from failure of migration or fusion of the müllerian ducts.

A *septate uterus* is the most common congenital uterine anomaly, resulting from defective resorption of the tissue between the fused müllerian ducts. The residual septum may extend inferiorly for a portion or for the full length of the uterus, from the fundus to the cervix. The key feature of a septate uterus is a normal smooth external contour at the uterine fundal surface. Septate uteri are often treated, because of the association with recurrent pregnancy loss and preterm labor in 12% to 44% of pregnancies.<sup>37</sup> This anomaly can be treated hysteroscopically as an outpatient procedure with excellent results. There is no need for surgical intervention involving the myometrium, and therefore, patients can subsequently undergo vaginal delivery. Hysteroscopic uterine septum resection may be performed with concomitant laparoscopy to ensure that the uterine fundus is not perforated. Real-time sonography can also be used to guide and monitor such procedures. The plane in which the uterus is imaged should be the same as the plane/axis of the operating instrument; this plane changes with movements that occur during surgery. With experience, these techniques can be mastered, and sonography can be a useful means for guiding such interventions. The arcuate uterus, a subset of septate uterus, has little clinical significance and is therefore not treated surgically.

The *unicornuate uterus* is important to understand for two reasons. First, it is an example of asymmetric lateral fusion: one cavity is usually normal, but small, with an accompanying cervix and fallopian tube. The small endometrial cavity predisposes to preterm birth as well as abnormal fetal lie (e.g., breech), which may lead to cesarean delivery. Second, one müllerian duct may not develop at all, or it may partially develop resulting in a rudimentary horn that may or may not communicate with the myometrium or the endometrial lining of the contralateral uterine horn. If a noncommunicating rudimentary horn has functioning endometrium, it may cycle and slough in response to ovarian hormonal changes and cause chronic pain. The unicornuate uterus may also be associated with an ectopic ovary, which may be an issue in women undergoing ovulation induction or who develop an ovarian neoplasm. Rarely, an ectopic pregnancy can occur in a noncommunicating rudimentary horn. MRI may be a better modality to make this diagnosis and to localize the ovary owing to the larger field of view. A noncommunicating rudimentary horn will usually require surgical removal because of pain and reproductive issues.



The endometrial cavity of a *bicornuate uterus* can have a similar appearance to that of a septate uterus. The primary difference between these anomalies is the indentation of the serosal contour at the fundus of the bicornuate uterus, resulting in two small horns, leading to risks of abnormal fetal lie and preterm birth. The fundal indentation is defined as larger than 1 cm. The clinical significance of notching or an indentation at the fundus (an external contour deformity) is that if repair is performed, it cannot be done with simple hysteroscopic resection, but instead requires laparotomy, with a much lower success rate than that of the septate uterus. Furthermore, future pregnancies would therefore require cesarean delivery because of the high risk of uterine rupture at the repair site. However, most of these patients can conceive and successfully carry a pregnancy, and therefore, surgical repair is seldom required.

*Uterus didelphys* is essentially a double uterus, each with a cervix and often associated with a vaginal septum as well. However, there are several variations, which may involve unilateral findings such as obstructed hemivagina or renal anomalies. These conditions typically require additional imaging with MRI and possibly with hysterosalpingogram (HSG) to evaluate for communication between the endometrial cavities. Surgery is performed for symptomatic patients with a septate vagina and dyspareunia, and often for patients with recurrent miscarriages or preterm birth. Depending upon clinical factors, metroplasty may be considered.

A *longitudinal vaginal septum* is usually associated with uterine anomalies. It may be difficult to detect by ultrasound, as a vaginal transducer may be inadvertently inserted on either side of the septum. One or two cervixes may be present. Alternatively, the septum may originate between two cervixes and fuse into the right or left lateral vaginal wall, concealing one cervix. In the latter case, the septum may result in hemihematocolpos.

### Vertical Fusion Defects

This group of defects results from abnormal fusion of the caudal end of the müllerian duct and the urogenital sinus. With a *transverse vaginal septum*, the external genitalia typically appear normal, whereas the vagina is short because of the transverse septum. Ultrasound imaging may help determine the thickness of the septum in the setting of hematocolpos, which may require treatment by septum resection.

### GUIDANCE FOR ENDOMETRIAL INTERVENTIONS (CERVICAL STENOSIS, ASHERMAN SYNDROME)

Key question to consider for endometrial interventions:

- Can an endometrial stripe be seen?

Ultrasound evaluation and guidance are extremely useful in cases of marked cervical stenosis, which can make it difficult to gain access to the endometrial cavity in patients undergoing endometrial sampling

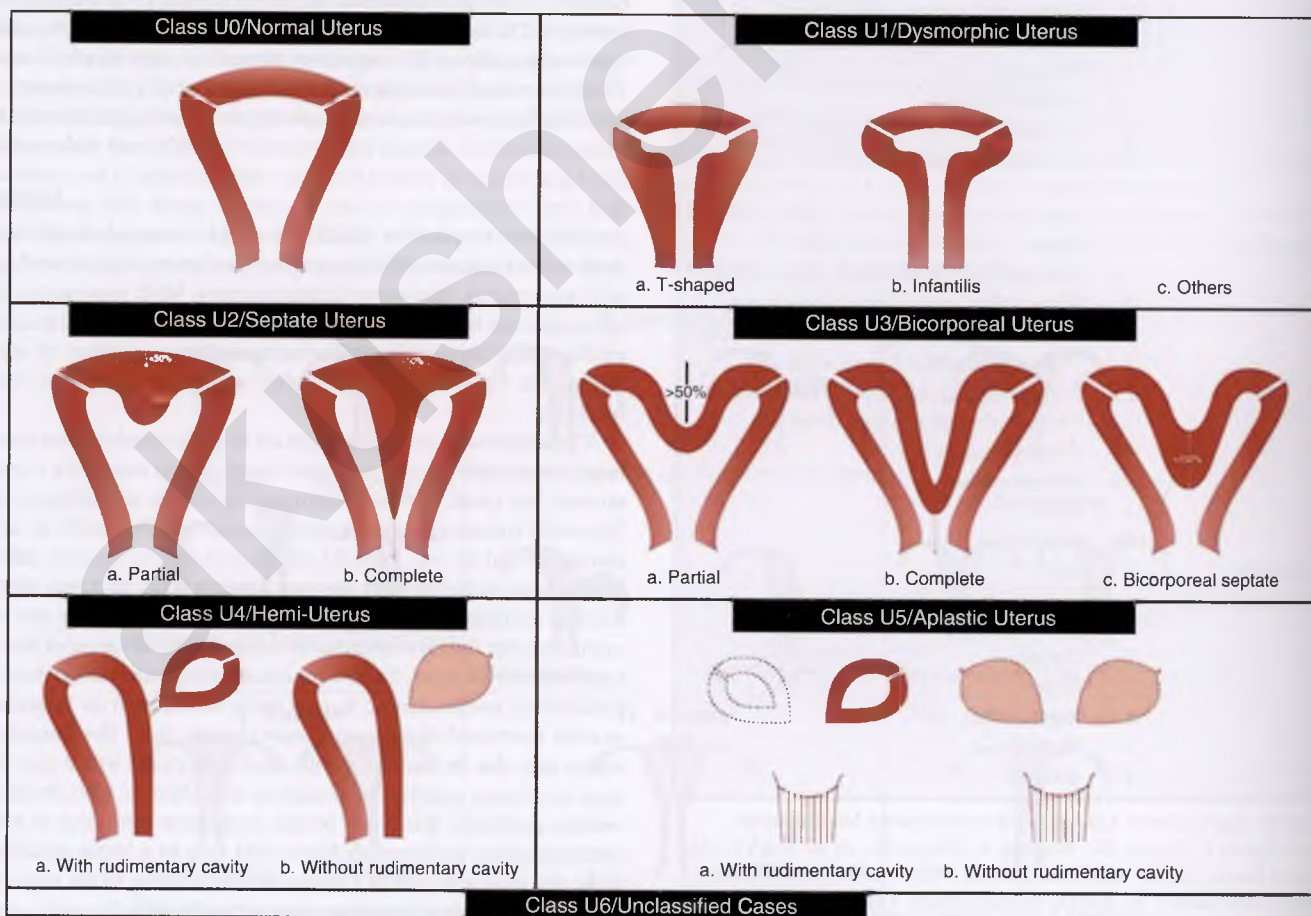


**FIG 37-5** European Society of Human Reproduction and Embryology (ESHRE)/European Society for Gynaecological Endoscopy (ESGE) classification of female genital tract congenital anomalies. **A**, Diagram.

ESHRE/ESGE classification Female genital tract anomalies		ESHRE/ESGE logo	
Uterine anomaly		Cervical/vaginal anomaly	
Main class	Sub-class	Co-existent class	
U0	Normal uterus	C0	Normal cervix
U1	Dysmorphic uterus a. T-shaped b. Infantilis c. Others	C1	Septate cervix
		C2	Double 'normal' cervix
		C3	Unilateral cervical aplasia
U2	Septate uterus a. Partial b. Complete	C4	Cervical aplasia
U3	Bicorporeal uterus a. Partial b. Complete c. Bicorporeal septate	V0	Normal vagina
		V1	Longitudinal non-obstructing vaginal septum
		V2	Longitudinal obstructing vaginal septum
U4	Hemi-uterus a. With rudimentary cavity (communicating or not horn) b. Without rudimentary cavity (horn without cavity/no horn)	V3	Transverse vaginal septum and/or imperforate hymen
		V4	Vaginal aplasia
U5	Aplastic a. With rudimentary cavity (bi- or unilateral horn) b. Without rudimentary cavity (bi- or unilateral uterine remnants/aplasia)		
U6	Unclassified malformations		
U		C	V
Associated anomalies of non-Müllerian origin:			
Drawing of the anomaly			

**B** FIG 37-5, cont'd **B**, Related description. Box provided for sketch of anomaly by interpreting physician. (From Grimbizis GF, Gordts S, Di Spiezio Sardo A, et al: The ESHRE/ESGE consensus on the classification of female genital tract congenital anomalies. Hum Reprod 28(8):2032-2044, 2013.)

or IUD placement.<sup>38</sup> Cervical stenosis may be seen following menopause or may result from cervical trauma such as lacerations, cervical cone biopsy, loop electrosurgical excision procedures (LEEP), or other cervical interventions. The presence of cervical stenosis significantly increases the risk of uterine perforation or creation of a false passage into the uterus during instrumentation to gain access to the endometrial cavity.

For guidance of such procedures, transabdominal sonography is performed through a distended urinary bladder. If necessary, retrograde filling of the bladder with sterile water or saline can be done using a Foley or red rubber catheter and a catheter-tipped syringe. This allows transabdominal sonographic visualization of the endocervical canal and the endometrial cavity to the uterine fundus. A similar approach is employed when real-time intraoperative

ultrasound-guided imaging is provided for placement of brachytherapy devices into the uterus, ensuring that the device is properly centered within the cavity and does not penetrate the myometrium or perforate the uterus (Fig. 37-7). Similarly, in patients with Asherman syndrome (intrauterine adhesions), ultrasound imaging may assist in identification and delineation of the endometrial cavity. This application of real-time ultrasound-guided imaging to minimize endometrial transgression is useful in patients with other conditions as well, including curettage for retained products of conception, pregnancy termination (especially in the setting of a uterine anomaly), hysteroscopic biopsy, and difficult IUD placement. Although rarely indicated, ultrasound-guided endometrial sampling may be performed by traversing the myometrium when severe cervical stenosis precludes conventional access (Fig. 37-8).



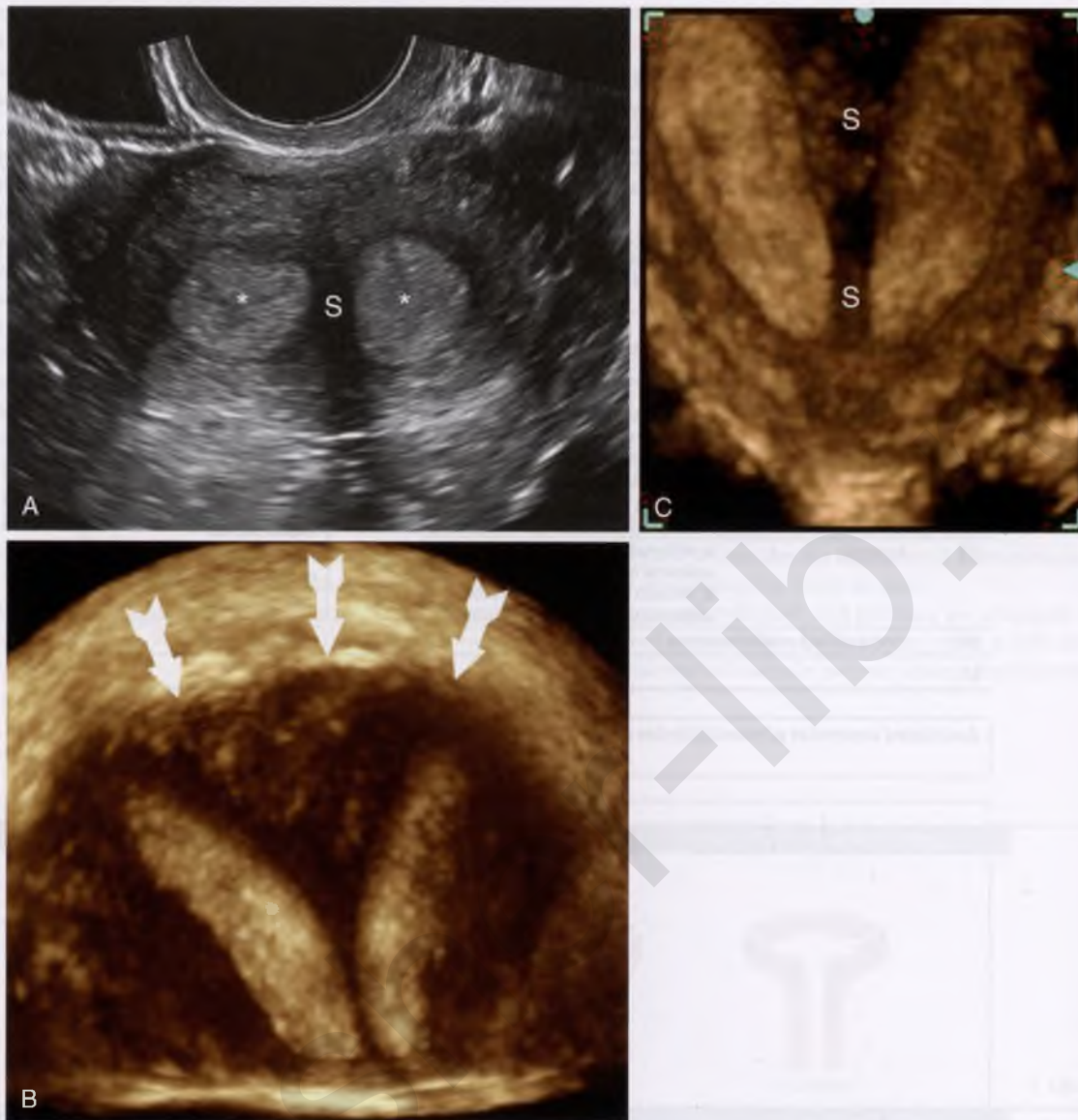


**FIG 37-6** Three different patients with septate uterus. **A**, Two-dimensional (2D) transverse transvaginal ultrasound image shows two portions of the divided endometrial cavity (*asterisks*) with intervening hypoechoic septum (S). **B**, Three-dimensional (3D) sonographic coronal display of a septate uterus demonstrating the important feature used to distinguish this type of anomaly from a bicornuate uterus. Note the preserved, outwardly convex, smooth external uterine contour (*arrows*). **C**, 3D ultrasound coronal image shows the dividing uterine septum (S) extending from the fundus caudally to the cervix.

## CONFIRMATION OF CORRECT ESSURE MICROINSERT PLACEMENT FOR TUBAL STERILIZATION

Key question to consider for confirmation of correct Essure microinsert placement for tubal sterilization:

- Do the reflections of the microinsert cross the outer line/serosa of the uterine wall, and are the proximal ends of both devices visualized medial to the outer line or within the endometrial cavity?

Essure (Bayer AG, Leverkusen, Germany) is a dynamically expanding microinsert device placed within the proximal fallopian tube transcervically, via a hysteroscopic approach, for tubal occlusion. Essure devices are used as a permanent form of birth control as an alternative to laparoscopic tubal ligation. The insert is composed of an inner

stainless steel coil and an outer expanding coil of nitinol (a nickel and titanium alloy). The inner coil contains polyethylene terephthalate fibers, which induce local tissue ingrowth. Optimal placement is defined as having 3 to 8 mm of the device visible at the proximal ostium, which translates to approximately three to eight visible coils (Fig. 37-9). To ensure proper placement, an HSG should be performed 3 months following the insertion procedure. Less invasive means of confirming proper placement include transvaginal ultrasound, SIS, and 3D sonography. However, HSG is still considered the standard of care to assure proper placement, as determined by the FDA.

Verification of proper Essure placement is clinically important. This intervention is effective with a reported 5-year cumulative pregnancy rate of only 2.6 pregnancies per 1000 procedures.<sup>39</sup> However, rarely, expulsion or migration of the device, placement in the endometrium, perforation of the uterus or fallopian tube, and postprocedure

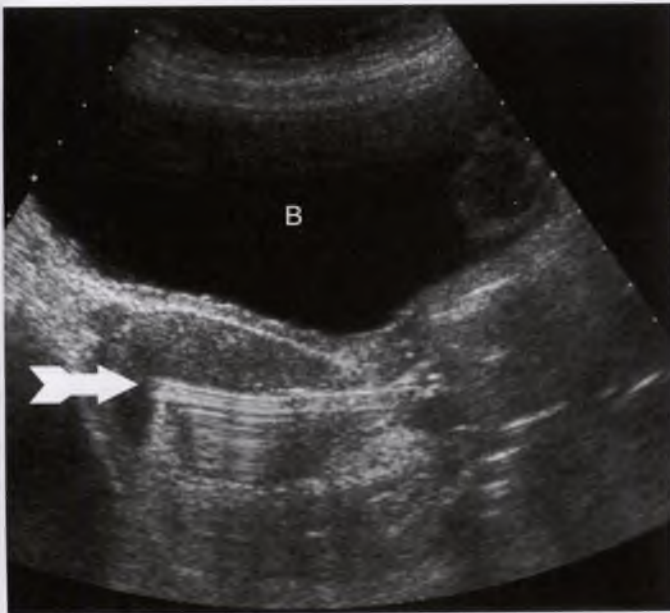


**FIG 37-7** Intraoperative transabdominal sagittal image through a distended urinary bladder (B) showing appropriate placement of a brachytherapy tandem (arrow) centered within the uterus. (Courtesy of Mike Ledwidge, RDMS.)

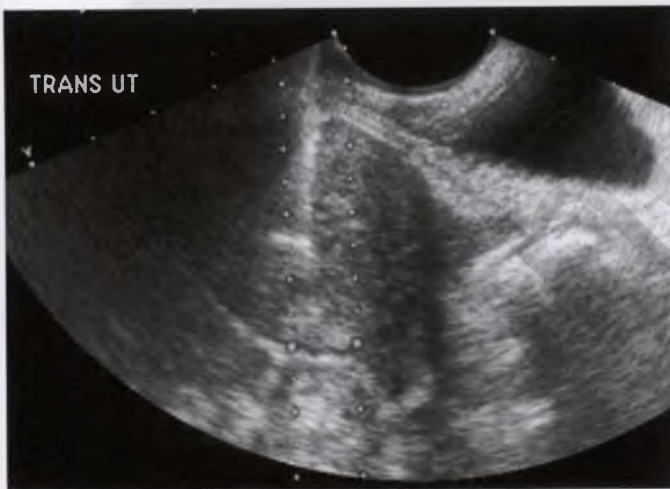


**FIG 37-8** Unusual transuterine approach for endometrial biopsy. Because of marked cervical stenosis, an endometrial biopsy catheter could not be introduced through the cervical canal into the uterus. Real-time transvaginal sonographic guidance was used during sampling of the endometrium, performed after advancing a cutting needle through the uterine serosa and myometrium. Pathologic examination revealed endometrial adenocarcinoma. The echogenic vertical line situated between the guiding dotted lines represents the 18-gauge core biopsy needle.

pregnancy can occur. A systematic review of complications associated with Essure devices found that the most common were malposition, chronic pain, unintended pregnancy, infection, and nickel allergy.<sup>40</sup> The authors also found that complications can involve uterine or tubal perforation or device expulsion or migration and that these complications—along with failure of timely diagnosis of these conditions—were associated with consequences beyond ineffective contraception. In some patients, such complications can result in severe morbidity. Given that patients with pelvic pain after Essure

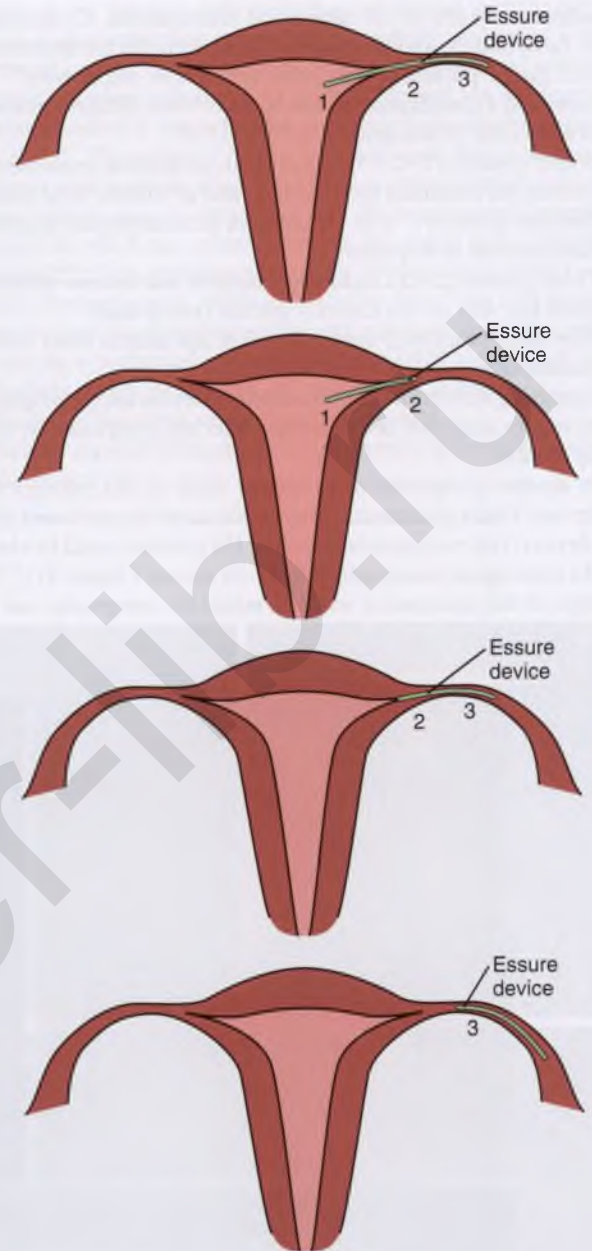


**FIG 37-9** Three-dimensional sonographic classification system for the placement and positioning of Essure microinsert tubal occlusion devices.<sup>41</sup> Perfect position (1 + 2 + 3), proximal position (1 + 2), distal position (2 + 3), and very distal position (3 only).

placement are often evaluated by sonography, one should be familiar with the sonographic findings associated with these devices.

Although sonography is not currently the accepted standard imaging modality to confirm correct Essure placement, investigations are underway to determine the utility and reliability of sonography in this setting. If proved effective, use of sonography could potentially avoid the cost, radiation exposure, and discomfort of conventional fluoroscopic HSG.

One retrospective observational study examined the records of 311 patients who underwent Essure microinsert placement followed 3 months later by 3D sonographic evaluation to verify position. HSG was performed when 3D sonographic findings were inconclusive, or for comparative purposes in a prospective trial. The device was



visualized in 99.6% of 3D ultrasound examinations. Compared to HSG, the sensitivity and specificity of 3D sonography for determining correct Essure placement was 100% and 76.6%, respectively.<sup>41</sup> The authors used a classification system to report four different positions observable with 3D sonography (see Fig. 37-9):

1. Perfect position (1 + 2 + 3): including an intrauterine (endometrial) portion, an interstitial tubal portion, and an isthmic tubal portion
2. Proximal position (1 + 2): including an intrauterine and interstitial tubal portion (suboptimal)
3. Distal portion (2 + 3): including interstitial and isthmic tubal portions, but with no intracavitary portion (suboptimal)
4. Very distal position (3 only): located in the isthmic tubal portion (inadequate)

By identifying abnormally positioned Essure devices using sonography, issues may be addressed and resolved sooner and postprocedure morbidity avoided.

In another prospective observational study of 182 patients who underwent Essure placement, a total of 300 correctly positioned bilateral devices (two microinserts in each of 150 patients) could be identified by transvaginal sonography (Fig. 37-10; also see Chapter 31).<sup>42</sup> The position of the microinserts was determined by sonography, and the

reflection of the device in relation to the outer line (serosal surface) of the uterus was described. The position was considered satisfactory when the specular reflections of the microinserts crossed the outer line of the uterine wall and the proximal ends of both devices were visualized medial to the outer line or within the endometrial cavity. Nine patients had unsatisfactory sonographic identification of the bilateral devices. Compared with HSG as the reference test, the sensitivity and specificity of sonography were 50% and 95%, respectively. The predictive value of a satisfactory transvaginal sonography result was 99%, and the predictive value of an unsatisfactory result was 11%.

## MALPOSITIONED INTRAUTERINE DEVICE

Key questions to consider for malpositioned IUD:

- Is it a copper IUD or progestin-releasing IUD?
- Is it located midline in the endometrial cavity within the uterine body?

A commonly encountered clinical scenario faced by physicians caring for patients with prior insertion of an IUD is that of a missing IUD string. In such cases, it is important to determine if the IUD is present and appropriately positioned within the endometrial cavity. It

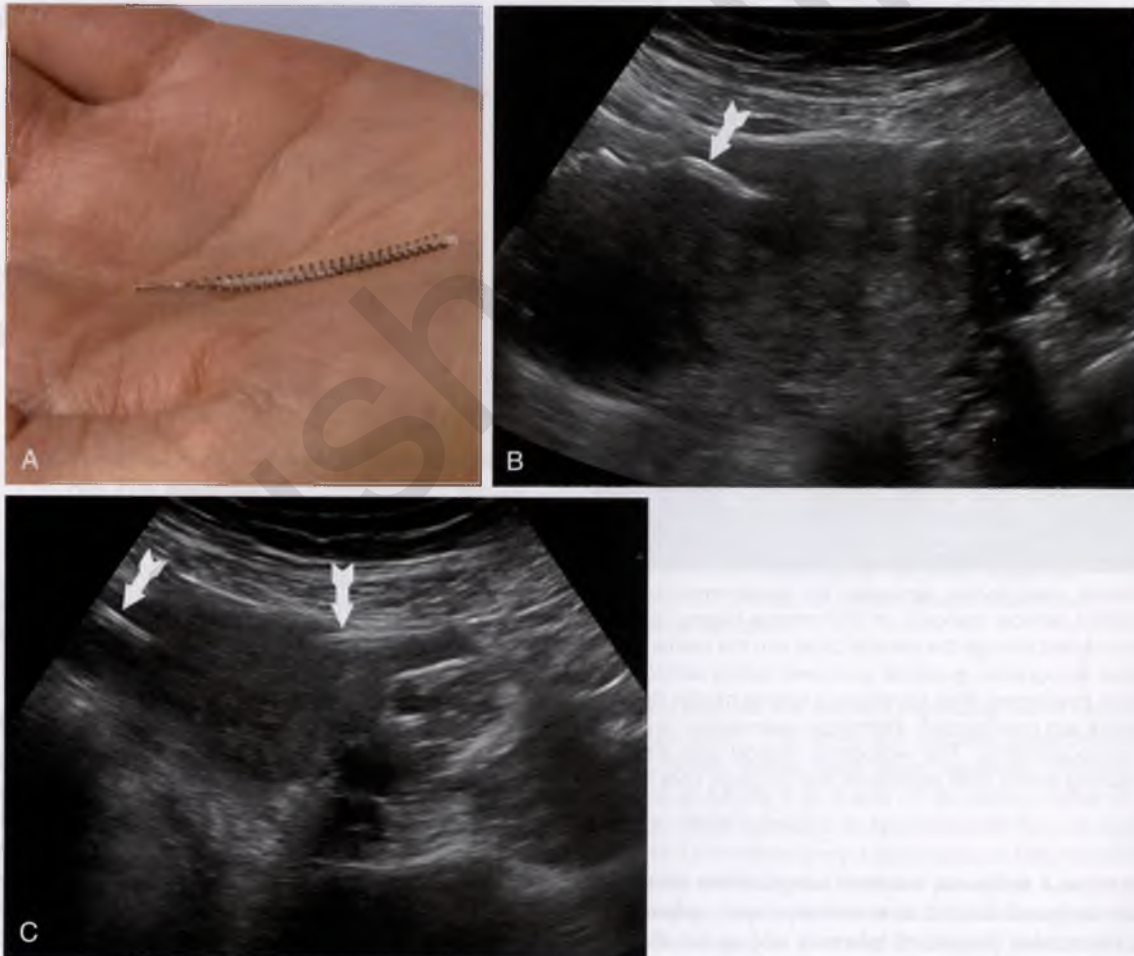


**FIG 37-10** Essure microinserts. **A**, Photographic image from the manufacturer's website (device is placed in a human hand to show scale). **B**, Transabdominal, transverse sonographic image of the uterus showing the right-sided linear echogenic insert (arrow) in the interstitial portion of the fallopian tube, traversing the myometrium. **C**, Additional transabdominal transverse view of the uterus showing both right and left echogenic linear inserts (arrows). (A from Bayer HealthCare Pharmaceuticals: What is Essure? September 2015. Available at [www.essure.com](http://www.essure.com).)

is possible that the string has receded into the endocervical canal or endometrial cavity and the IUD is in place, in which case contraception is still considered effective. If the IUD is not demonstrated by sonography to be within the endometrial cavity, it must be determined if it has become dislodged and expelled or if the IUD has migrated into the myometrium or through it into the pelvic/abdominal cavity, or in rare cases, into the colon or bladder. This can be assessed by radiograph, although occasionally a perforated IUD can be identified by sonography in the cul-de-sac, posterior to the uterus. In such cases, laparoscopic removal of the IUD is necessary. There is controversy regarding management of an IUD that is malpositioned within the endometrial cavity and is either low-lying or has one or both arms partially embedded in the myometrium. Intervention is not always necessary for a malpositioned IUD.<sup>43</sup>

A correctly positioned IUD has its superior portion near the uterine fundus, with its horizontal limbs fully expanded toward the cornual/angular portions of the endometrial cavity (where the interstitial

portion of the fallopian tube joins the endometrial cavity), and its vertical portion extending straight down, centrally positioned within the uterine corpus. The copper IUD (such as Paragard) and synthetic progestin hormone-releasing IUD (such as Mirena) can be identified and distinguished if one is familiar with their basic imaging features (Fig. 37-11). The copper IUD has a central stem that is uniformly echogenic with posterior shadowing from its upper metallic coils and is more conspicuous on ultrasound than the levonorgestrel-releasing Mirena IUD, which has a plastic sleeve on the central stem containing progestin.<sup>44,45</sup> This configuration causes reverberation artifact and acoustic shadowing with visible parallel white lines. This IUD also has echogenic arms due to barium sulfate with echogenic tips. When pelvic sonography is performed and a malpositioned IUD seen (Fig. 37-12), the findings should be reported and described as follows:

- Located in the cervix or lower uterine segment
- Partially expelled with part of the IUD extending through the external cervical os

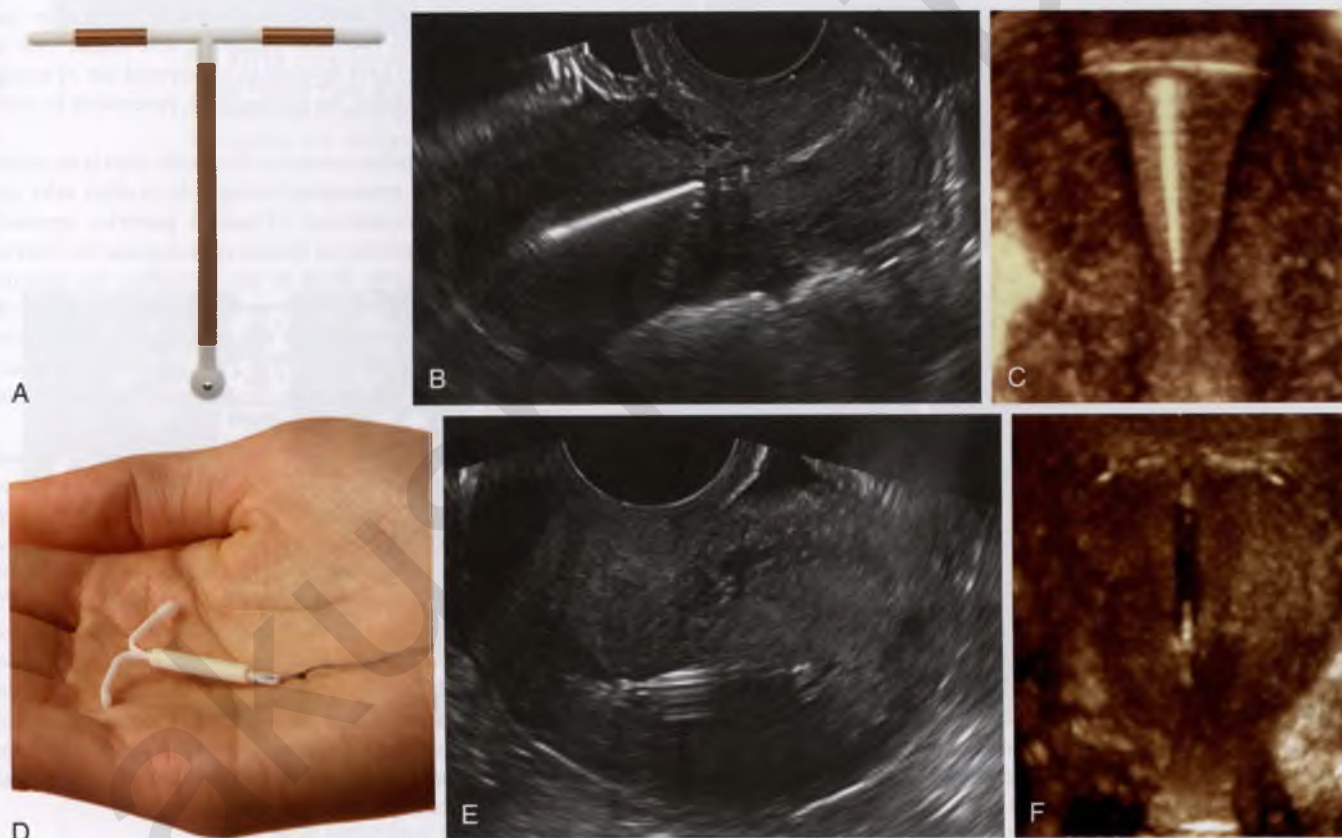


**FIG 37-11** Intrauterine devices (IUDs). **A**, Photograph of a copper IUD from the manufacturer's website. **B**, Transvaginal longitudinal sonographic image of a well-positioned copper IUD showing the characteristic, uniformly echogenic appearance of the linear stem due to the copper coils. **C**, Three-dimensional coronal ultrasound image of a centrally positioned copper IUD. **D**, Photograph of a levonorgestrel (LNG)-releasing IUD from the manufacturer's website. Note the progestin-containing plastic sleeve that surrounds the central stem. **E**, Longitudinal transvaginal ultrasound image of LNG-releasing IUD well positioned within the retroverted, retroflexed uterus. The plastic sleeve adjacent to the central stem results in the characteristic laminated ultrasound appearance with posterior parallel lines and acoustic shadowing. **F**, Three-dimensional coronal ultrasound image of a well-positioned LNG-releasing IUD. Note linear hypoechoic area in the region of the plastic stem. (**A** from Teva Women's Health: What is Paragard? September 2015. Available at <http://www.paragard.com/What-is-Paragard.aspx>. **B** and **E** description of appearance from Stalnaker ML, Kaunitz AM: How to identify and localize IUDs on ultrasound. *OBG Manag* 26(8):40-42, 2014. **D** from Bayer HealthCare Pharmaceuticals: What is Mirena? December 2015. Available at <http://www.mirena-us.com>.)





**FIG 37-12** Malpositioned intrauterine device (IUD). Three-dimensional coronal transvaginal ultrasound image of the uterus shows the abnormally situated echogenic IUD. The IUD is malrotated and inferiorly positioned, in the lower uterine segment, with one of the side arms embedded in the myometrium (*arrow*).

- Malrotated
- Partially or fully embedded in the myometrium
- Extending beyond the uterine serosa or within the pelvic or abdominal cavity

The primary clinical concerns with a malpositioned IUD are potential tissue damage and the risk of pregnancy. The most common presenting symptoms of a malpositioned IUD are pain and bleeding. In this setting, IUD removal will usually result in resolution of symptoms.<sup>46</sup> Interestingly, complete perforation with penetration of an IUD through the myometrium into the peritoneal cavity is often asymptomatic. A woman with a malpositioned copper IUD is at greater risk to become pregnant than one with a malpositioned hormone-containing IUD, which works primarily via hormonal effects on the endometrium, and thus, optimal positioning of the device is less

critical. In a study of 97 women with copper IUDs, the odds ratio for becoming pregnant with a malpositioned IUD compared to a properly positioned IUD was 13.93.<sup>47</sup>

When assessing IUD placement, there are distinct advantages of 3D as compared to 2D sonography, including the enhanced conspicuity of both types of devices and the ability to reconstruct a true coronal imaging plane<sup>44</sup> (Fig. 37-13). 3D sonography is now considered standard care and is routinely performed for assessment of IUD position. Minor inner myometrial penetration of the arms is often seen with this improved technology and is of uncertain but doubtful clinical significance.

## PELVIC BIOPSIES AND DRAINAGES

Key questions to consider for pelvic biopsies and drainages:

- Is it safer and easier to access the target transvaginally or percutaneously?
- If the target is potentially ovarian in origin, has malignancy been considered?

The use of computed tomography (CT) for imaging-guided biopsies and drainages of pelvic masses and collections is well established. However, in the recent past, the many advantages of sonography (less expensive, faster, safer, no radiation exposure, and higher rate of successful tissue sampling) have resulted in widespread use of sonography as the modality of choice for guiding such procedures in many cases.<sup>48-50</sup>

Transvaginal access to pelvic masses or fluid collections is an underutilized approach. Use of transvaginal sonography is often safer and less painful than the conventional CT-guided posterior approach through the region of the piriformis muscle, coursing near the internal iliac vessels and sciatic nerve. Prior to the procedure, the patient's coagulation status is evaluated<sup>51</sup> and moderate sedation is usually administered. A needle guide, attached to a transvaginal sonographic transducer, is used to access the target (Fig. 37-14). A similar approach is used for ovum retrieval in women undergoing assisted reproductive techniques.

Although it has been hypothesized that suspected ovarian masses should not be needled owing to fear of potentially seeding tumor, reported low sensitivity of cytologic tests for the detection of malignancy, and risk of cyst recurrence, more recent investigations have shown that fine needle aspiration biopsy is an acceptable and valuable tool for the evaluation and management of ovarian cysts and masses.<sup>52,53</sup> Ultrasound-guided ovarian biopsy is often useful when patient comorbid conditions render surgery or general anesthesia too risky. A guideline followed by the authors is to never undertake an ovarian biopsy or aspiration until direct approval has been obtained from the gynecologic oncology service. This assures a multidisciplinary team approach to appropriately considering the risks and benefits of all diagnostic and treatment options.

## CONCLUSIONS

In summary, ultrasound imaging has greatly enhanced the ability to safely and effectively perform select gynecologic procedures. This widely available, low-risk modality is ideally suited for evaluating patients and assisting with and guiding many gynecologic interventions.

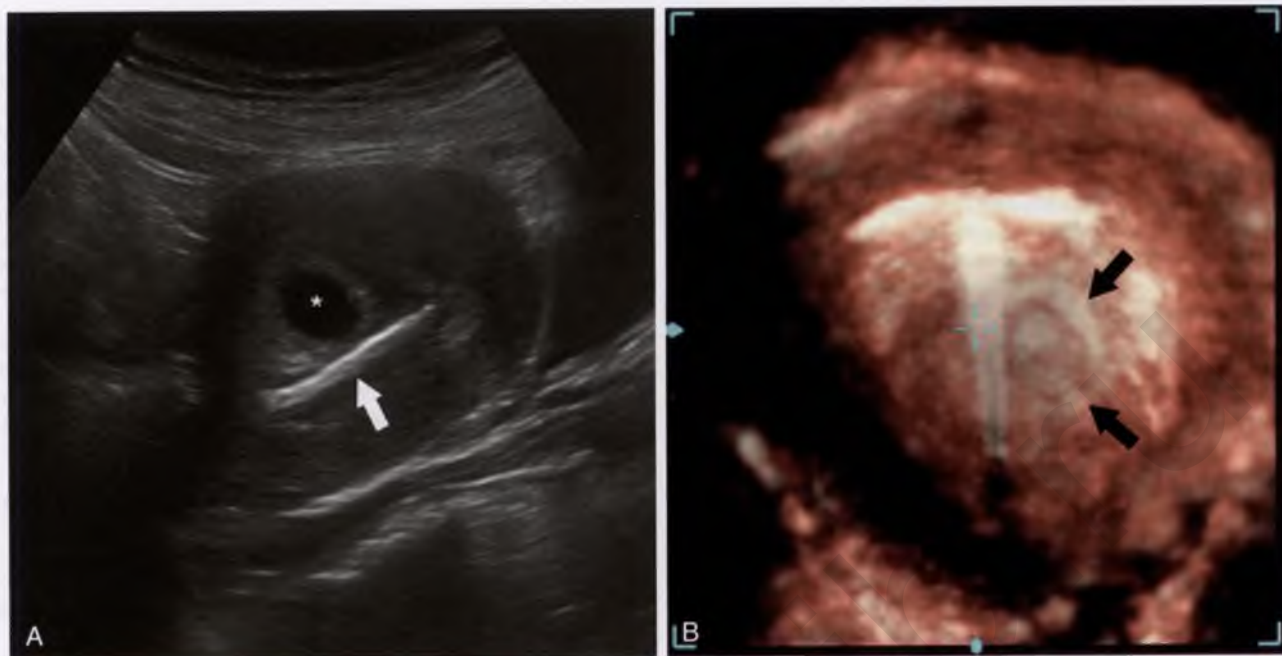


**FIG 37-13** Intrauterine device (IUD) and intrauterine pregnancy. **A**, Longitudinal transabdominal ultrasound image shows linear echogenic IUD stem (*arrow*) directly adjacent to an intrauterine fluid collection (*asterisk*), representing an early gestational sac. **B**, Three-dimensional coronal ultrasound image better delineates the relationship and relative position of the T-shaped IUD to the intrauterine gestational sac (*arrows*).

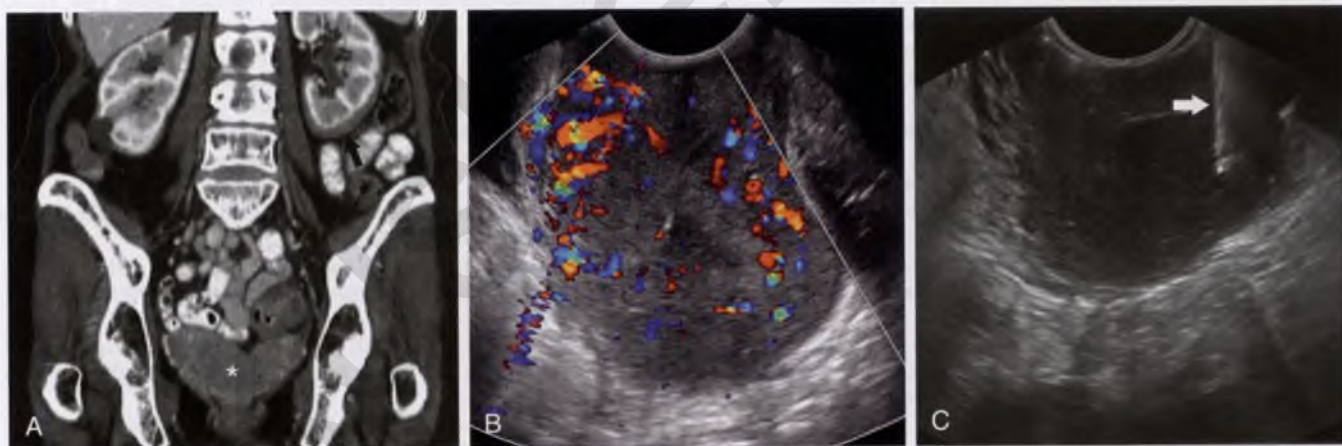


**FIG 37-14** Pelvic lymphoma diagnosed by means of transvaginal ultrasound-guided biopsy. **A**, Reconstructed coronal image from contrast-enhanced computed tomography scan. Note lobulated soft tissue mass (*asterisk*) adjacent to the vaginal cuff. The uterus is surgically absent. It was deemed too difficult to safely obtain a large core tissue sample of this mass via a percutaneous approach. Also note thin rim of lymphomatous tissue surrounding the left kidney (*arrow*). **B**, Transvaginal ultrasound image with color Doppler interrogation shows the moderately echogenic solid pelvic mass with peripheral vascularity. **C**, Using real-time transvaginal sonographic guidance, biopsy of the solid pelvic mass, using an 18-gauge core biopsy needle (*arrow*), was successfully performed without incident.



## REFERENCES

1. Sharp HT: Assessment of new technology in the treatment of idiopathic menorrhagia and uterine leiomyomata. *Obstet Gynecol* 108(4):990–1003, 2006.
2. Lethaby A, Shepperd S, Cooke J, Farquhar C: Endometrial resection and ablation versus hysterectomy for heavy menstrual bleeding. *Cochrane Database Syst Rev* (2):CD000329, 2000.
3. Pugh CP, Crane JM, Hogan TG: Successful intrauterine pregnancy after endometrial ablation. *J Am Assoc Gynecol Laparosc* 7(3):391–394, 2000.
4. Pinette M, Katz W, Drouin M, et al: Successful planned pregnancy following endometrial ablation with the YAG laser. *Am J Obstet Gynecol* 185(1):242–243, 2001.
5. Kir M, Hanlon-Lundberg KM: Successful pregnancy after thermal balloon endometrial ablation. *Obstet Gynecol* 103(5 Pt 2):1070–1073, 2004.
6. Townsend DE, McCausland V, McCausland A, et al: Post-ablation-tubal sterilization syndrome. *Obstet Gynecol* 82(3):422–424, 1993.
7. Turnbull LW, Jumaa A, Bowsley SJ, et al: Magnetic resonance imaging of the uterus after endometrial resection. *Br J Obstet Gynaecol* 104(8):934–938, 1997.
8. Gurtcheff SE, Sharp HT: Complications associated with global endometrial ablation: the utility of the MAUDE database. *Obstet Gynecol* 102(6):1278–1282, 2003.
9. Berridge DL, Winter TC: Saline infusion sonohysterography: technique, indications, and imaging findings. *J Ultrasound Med* 23(1):97–112, quiz 114–115, 2004.
10. Lindheim SR, Sprague C, Winter TC, 3rd: Hysterosalpingography and sonohysterography: lessons in technique. *AJR Am J Roentgenol* 186(1):24–29, 2006.
11. Allison SJ, Horrow MM, Kim HY, Lev-Toaff AS: Saline-infused sonohysterography: tips for achieving greater success. *Radiographics* 31(7):1991–2004, 2011.
12. Ravina JH, Herbretreau D, Ciraru-Vigneron N, et al: Arterial embolisation to treat uterine myomata. *Lancet* 346(8976):671–672, 1995.
13. Hutchins FL, Jr, Worthington-Kirsch R, Berkowitz RP: Selective uterine artery embolization as primary treatment for symptomatic leiomyomata uteri. *J Am Assoc Gynecol Laparosc* 6(3):279–284, 1999.
14. Walker WJ, Pelage JP: Uterine artery embolisation for symptomatic fibroids: clinical results in 400 women with imaging follow up. *Br J Obstet Gynaecol* 109(11):1262–1272, 2002.
15. Broder MS, Goodwin S, Chen G, et al: Comparison of long-term outcomes of myomectomy and uterine artery embolization. *Obstet Gynecol* 100(5 Pt 1):864–868, 2002.
16. Spies JB, Bruno J, Czeyda-Pommersheim F, et al: Long-term outcome of uterine artery embolization of leiomyomata. *Obstet Gynecol* 106(5 Pt 1):933–939, 2005.
17. Pron G, Bennett J, Common A, et al: The Ontario Uterine Fibroid Embolization Trial. Part 2. Uterine fibroid reduction and symptom relief after uterine artery embolization for fibroids. *Fertil Steril* 79(1):120–127, 2003.
18. Hehenkamp WJ, Volkers NA, Donderwinkel PF, et al: Uterine artery embolization versus hysterectomy in the treatment of symptomatic uterine fibroids (EMMY trial): peri- and postprocedural results from a randomized controlled trial. *Am J Obstet Gynecol* 193(5):1618–1629, 2005.
19. Goodwin SC, Bradley LD, Lipman JC, et al: Uterine artery embolization versus myomectomy: a multicenter comparative study. *Fertil Steril* 85(1):14–21, 2006.
20. Hehenkamp WJ, Volkers NA, Birnie E, et al: Pain and return to daily activities after uterine artery embolization and hysterectomy in the treatment of symptomatic uterine fibroids: results from the randomized EMMY trial. *Cardiovasc Intervent Radiol* 29(2):179–187, 2006.
21. Gupta JK, Sinha A, Lumsden MA, Hickey M: Uterine artery embolization for symptomatic uterine fibroids. *Cochrane Database Syst Rev* (5):CD005073, 2012.
22. Spies JB, Spector A, Roth AR, et al: Complications after uterine artery embolization for leiomyomas. *Obstet Gynecol* 100(5 Pt 1):873–880, 2002.
23. Goldberg J, Pereira L, Berghella V, et al: Pregnancy outcomes after treatment for fibromyomata: uterine artery embolization versus laparoscopic myomectomy. *Am J Obstet Gynecol* 191(1):18–21, 2004.
24. Pron G, Mocarski E, Bennett J, et al: Pregnancy after uterine artery embolization for leiomyomata: the Ontario multicenter trial. *Obstet Gynecol* 105(1):67–76, 2005.
25. Carpenter TT, Walker WJ: Pregnancy following uterine artery embolisation for symptomatic fibroids: a series of 26 completed pregnancies. *Br J Obstet Gynaecol* 112(3):321–325, 2005.
26. Moshesh M, Peddada SD, Cooper T, Baird D: Intraobserver variability in fibroid size measurements: estimated effects on assessing fibroid growth. *J Ultrasound Med* 33(7):1217–1224, 2014.
27. Senapati S, Tu FF, Magrina JF: Power morcellators: a review of current practice and assessment of risk. *Am J Obstet Gynecol* 212(1):18–23, 2014.
28. Parker WH, Fu YS, Berek JS: Uterine sarcoma in patients operated on for presumed leiomyoma and rapidly growing leiomyoma. *Obstet Gynecol* 83(3):414–418, 1994.
29. Vallerie AM, Breech LL: Update in Mullerian anomalies: diagnosis, management, and outcomes. *Curr Opin Obstet Gynecol* 22(5):381–387, 2010.
30. Buttram VC, Jr, Gibbons WE: Mullerian anomalies: a proposed classification. (An analysis of 144 cases). *Fertil Steril* 32(1):40–46, 1979.
31. The American Fertility Society classifications of adnexal adhesions, distal tubal occlusion, tubal occlusion secondary to tubal ligation, tubal pregnancies, mullerian anomalies and intrauterine adhesions. *Fertil Steril* 49(6):944–955, 1988.
32. Oppelt P, Renner SP, Brucker S, et al: The VCUAM (Vagina Cervix Uterus Adnex-associated Malformation) classification: a new classification for genital malformations. *Fertil Steril* 84(5):1493–1497, 2005.
33. Grimbizis GF, Gordts S, Di Spiezio Sardo A, et al: The ESHRE/ESGE consensus on the classification of female genital tract congenital anomalies. *Hum Reprod* 28(8):2032–2044, 2013.
34. Grimbizis GF, Camus M, Tarlatzis BC, et al: Clinical implications of uterine malformations and hysteroscopic treatment results. *Hum Reprod Update* 7(2):161–174, 2001.
35. Berger A, Batzer F, Lev-Toaff A, Berry-Roberts C: Diagnostic imaging modalities for mullerian anomalies: the case for a new gold standard. *J Minim Invasive Gynecol* 21(3):335–345, 2014.
36. Fedele L, Bianchi S, Frontino G, et al: Laparoscopic findings and pelvic anatomy in Mayer-Rokitansky-Kuster-Hauser syndrome. *Obstet Gynecol* 109(5):1111–1115, 2007.
37. Heinonen PK: Complete septate uterus with longitudinal vaginal septum. *Fertil Steril* 85(3):700–705, 2006.
38. Hunter RE, Reuter K, Kopin E: Use of ultrasonography in the difficult postmenopausal dilation and curettage. *Obstet Gynecol* 73(5 Pt 1):813–816, 1989.
39. Levy B, Levie MD, Childers ME: A summary of reported pregnancies after hysteroscopic sterilization. *J Minim Invasive Gynecol* 14(3):271–274, 2007.
40. Adelman MR, Dassel MW, Sharp HT: Management of complications encountered with Essure hysteroscopic sterilization: a systematic review. *J Minim Invasive Gynecol* 21(5):733–743, 2014.
41. Legendre G, Levaillant JM, Faivre E, et al: 3D ultrasound to assess the position of tubal sterilization microinserts. *Hum Reprod* 26(10):2683–2689, 2011.
42. Veersema S, Vleugels MP, Timmermans A, Brolmann HA: Follow-up of successful bilateral placement of Essure microinserts with ultrasound. *Fertil Steril* 84(6):1733–1736, 2005.
43. Braaten KP, Benson CB, Maurer R, Goldberg AB: Malpositioned intrauterine contraceptive devices: risk factors, outcomes, and future pregnancies. *Obstet Gynecol* 118(5):1014–1020, 2011.
44. Moschos E, Twickler DM: Does the type of intrauterine device affect conspicuity on 2D and 3D ultrasound? *AJR Am J Roentgenol* 196(6):1439–1443, 2011.
45. Stalnakier ML, Kaunitz AM: How to identify and localize IUDs on ultrasound. *OBG Manag* 26(8):40–42, 2014.
46. Benacerraf BR, Shipp TD, Bromley B: Three-dimensional ultrasound detection of abnormally located intrauterine contraceptive devices which

- are a source of pelvic pain and abnormal bleeding. *Ultrasound Obstet Gynecol* 34(1):110–115, 2009.
47. Inal MM, Ertopcu K, Ozelmas I: The evaluation of 318 intrauterine pregnancy cases with an intrauterine device. *Eur J Contracept Reprod Health Care* 10(4):266–271, 2005.
  48. Dodd GD, 3rd, Esola CC, Memel DS, et al: Sonography: the undiscovered jewel of interventional radiology. *Radiographics* 16(6):1271–1288, 1996.
  49. Yarram SG, Nghiem HV, Higgins E, et al: Evaluation of imaging-guided core biopsy of pelvic masses. *AJR Am J Roentgenol* 188(5):1208–1211, 2007.
  50. Winter TC, Lee FT, Jr, Hinshaw JL: Ultrasound-guided biopsies in the abdomen and pelvis. *Ultrasound Q* 24(1):45–68, 2008.
  51. O'Connor SD, Taylor AJ, Williams EC, Winter TC: Coagulation concepts update. *AJR Am J Roentgenol* 193(6):1656–1664, 2009.
  52. Gupta N, Rajwanshi A, Dhaliwal LK, et al: Fine needle aspiration cytology in ovarian lesions: an institutional experience of 584 cases. *Cytopathology* 23(5):300–307, 2012.
  53. Garcia-Tejedor A, Castellarnau M, Burdio F, et al: Ultrasound guided aspiration of adnexal cysts with a low risk of malignancy: is it a recommendable option? *J Ultrasound Med* 34(6):985–991, 2015.

akusher-lib.ru



# Technical Considerations and Aberrations

akusher-lib.ru

# Artifacts, Pitfalls, and Normal Variants

*Peter W. Callen*

## OUTLINE

An Unfortunate but Common Pitfall, 1093  
 Technical Considerations, 1095  
     Mirror Image Artifact, 1095  
 Pelvis, Gravid and Nongravid Uterus, 1098  
 The First Trimester, 1114  
 The Fetal Head and Neck, 1122

The Fetal Thorax, 1132  
 The Fetal Abdomen, 1135  
 Amniotic Fluid and Membranes, 1143  
 The Fetal Skeleton, 1146  
 Multiple Gestations, 1151

When I began my involvement with diagnostic sonography nearly 4 decades ago, this chapter would have been considered ludicrous. Virtually all of sonography was considered to be either an artifact or a pitfall. Clinicians did not take this modality seriously, and few critical decisions were ever based on the results of the ultrasound examination alone. With time, improvements in both technology and our understanding of normal and abnormal findings made this a useful clinical diagnostic modality. It did not take long for important clinical decisions to be based solely on the results of the ultrasound examination, including surgery, early delivery of the fetus, or even termination of the pregnancy. This evolution, although welcomed by many, has placed a large responsibility on the sonologist. The phrase “*primum non nocere*”—first do no harm—has never been more true.

This chapter is not an attempt to explain the physical principles of sonography or artifact production. It is also unlikely that such a chapter could ever be all-inclusive. I have attempted to find examples of pitfalls, the diagnostic dilemmas that have the potential to lead us to the wrong diagnosis. I have tried to cover both basic potential pitfalls and some of the more esoteric normal variants. Undoubtedly, some readers will find examples here that are so basic as to seem almost insulting. I apologize in advance and will only respond that this chapter is meant

to appeal to a wide audience that includes beginners and seasoned experts. I also do not attempt to give an overly detailed explanation for each example but try to offer what is theorized currently.

If I am able to avoid one false positive diagnosis and prevent unnecessary surgery, termination of a pregnancy, or even 20 weeks of an emotional roller coaster for expectant parents, I have fulfilled my goal.

## AN UNFORTUNATE BUT COMMON PITFALL

I begin this chapter as the subheading suggests, with a common but unfortunate pitfall.

A 34-year-old woman presented to the emergency department complaining of mild pelvic pain with a known history of positive pregnancy test. A quantitative serum  $\beta$ -hCG (human chorionic gonadotropin) revealed a value of 3870 mIU/mL. (This value is nearly double most centers’ “discriminatory zone.”) A diagnostic ultrasound examination revealed no evidence of an intrauterine pregnancy (IUP) or adnexal masses. As a result, the patient was presumed to have an ectopic pregnancy (EP) and was treated with intramuscular methotrexate. A repeat sonogram obtained 1½ weeks later revealed a living IUP. The patient elected to terminate the pregnancy.



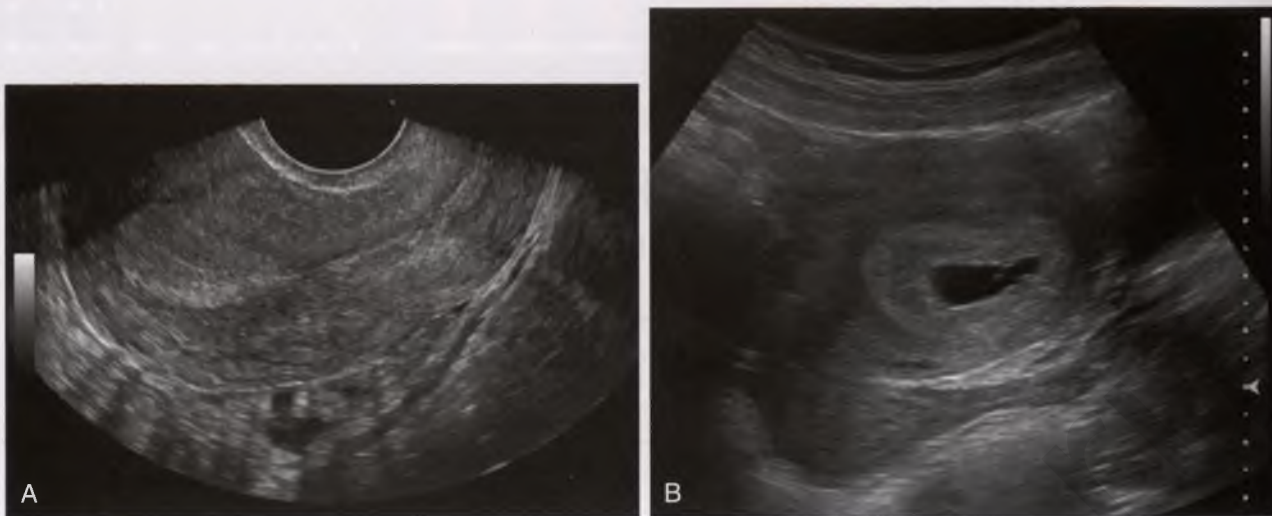


**FIG 38-1** **A**, Transvaginal sonogram obtained at approximately 4.5 weeks demonstrating no evidence of an intrauterine pregnancy. Additional scans revealed normal ovaries without evidence of an adnexal mass. **B**, Transabdominal sonogram obtained 1.5 weeks later revealed a living intrauterine pregnancy.

When a woman of child-bearing age presents to her clinician or emergency room with pelvic pain or bleeding and a positive pregnancy test, clearly the first thought in the diagnostic tree is the possibility of an EP. Most clinicians are aware that the risk of a heterotopic pregnancy (in which both an extrauterine [ectopic] and IUP occur simultaneously) is quite low (1 in 15,000 to 1 in 30,000), although this phenomenon is more common in patients following assisted reproduction. Thus, the goal of sonography is to identify an IUP, making an EP unlikely. Two factors have helped achieve this goal:

1. In the early 1980s, Kadar and others attempted to determine the maternal serum hCG level above which a gestational sac should be consistently seen during sonograms in a patient with a normal IUP. The value was termed the “discriminatory zone.” It should be noted that the values initially reported were significantly higher prior to the advent of transvaginal sonography in use today. Although this upper limit value today is variable at differing institutions, it tends to be between 1500 and 2000 mIU/mL (first IUP).
2. With the advent of high-resolution transvaginal sonography, early pregnancies can now often be identified within the uterus when gestational sacs are as small as 2 to 3 mm.

A noninvasive method of treating EPs with methotrexate became available in the early 1980s. As a result, some clinicians, then and now, treat the patient with methotrexate when both an “empty uterus” at the time of sonography and an elevated  $\beta$ -hCG level (above the discriminatory zone) are present, in an attempt to treat the EP. Unfortunately, some of these patients subsequently have been found to have IUPs, not EPs, on follow-up. It is quite clear that even marked elevations of  $\beta$ -hCG above the discriminatory zone are not always reliable in excluding an intrauterine pregnancy when a gestational sac is not seen at sonography. In these cases, follow-up, rather than immediate treatment, is indicated. Likewise, even in the best of hands and with excellent ultrasound equipment, at 4 to 5 weeks’ gestation an IUP may not be identified sonographically, though the patient may in fact have an IUP. The report should ideally read “An ectopic pregnancy, or a pregnancy too early to be seen within the uterus, cannot be excluded.”

In October 2012, the Society of Radiologists in Ultrasound convened a multispecialty consensus conference to establish criteria on

early first trimester diagnosis of miscarriage and exclusion of a viable IUP when seen in the uterus, as well as to discuss diagnosing and ruling out a viable IUP in a woman with a pregnancy of unknown location. These criteria and an editorial discussion were published in the *New England Journal of Medicine* (Doubilet and associates, 2013; Kaunitz et al 2013). The takeaway points from this panel regarding this pitfall were as follows:

- A single hCG assessment, regardless of level, does not reliably determine a pregnancy’s location or viability (this is because hCG levels in women with nonviable IUPs, viable IUPs, and EP overlap substantially).
- A single hCG level less than 3000 mIU/mL should not elicit treatment for presumed EP because there is a substantial risk that administering methotrexate will damage a normal IUP.
- A single hCG level 3000 mIU/mL or higher in the absence of a sonographically visualized IUP indicates that a viable IUP is possible but unlikely. The most likely diagnosis is failed IUP, so if methotrexate is administered, it is more likely being given unnecessarily to a woman with a failed IUP than to one with an EP. At least one additional hCG level should be measured before initiating treatment for EP.

## REFERENCES

- Kadar N, DeVore G, Romero R: Discriminatory hCG zone: its use in the sonographic evaluation for ectopic pregnancy. *Obstet Gynecol* 58:156–161, 1981.
- Doubilet PM, Benson CB, Bourne T, et al: Diagnostic criteria for nonviable pregnancy early in the first trimester. *N Engl J Med* 369:1443–1451, 2013.
- Kaunitz AM (reviewing Doubilet PM et al, 2013): *Criteria for Diagnosing Early Pregnancy Failure. NEJM Journal Watch, Massachusetts Medical Society*. Available at <<http://www.jwatch.org>>.
- Doubilet PM, Benson CB: Further evidence against the reliability of the human chorionic gonadotropin discriminatory level. *J Ultrasound Med* 30:1637–1642, 2011.

## TECHNICAL CONSIDERATIONS

### Mirror Image Artifact

A mirror image artifact is created when the ultrasound beam is reflected from a strong reflector that is often obliquely oriented and redirects the echoes off a secondary reflector back to the transducer.

The ultrasound computer assumes the sound traveled in a straight line. The mirrored image results in the copy appearing on the same image, though deeper because of the additional time for the mirrored image to return to the transducer. In conventional gray-scale imaging, as well as color Doppler imaging, the mirrored artifact will always be the deeper structure.

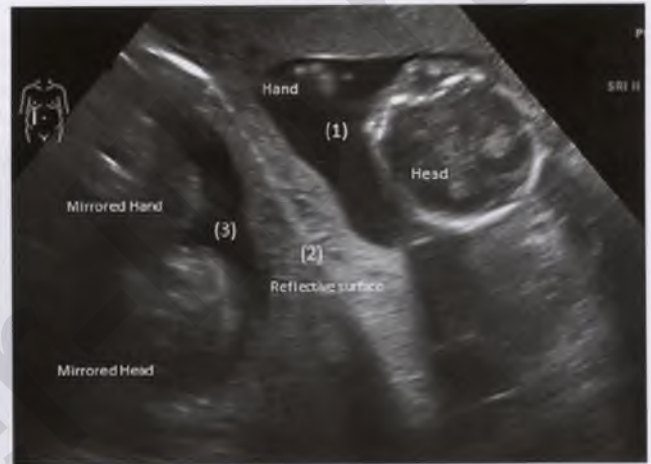
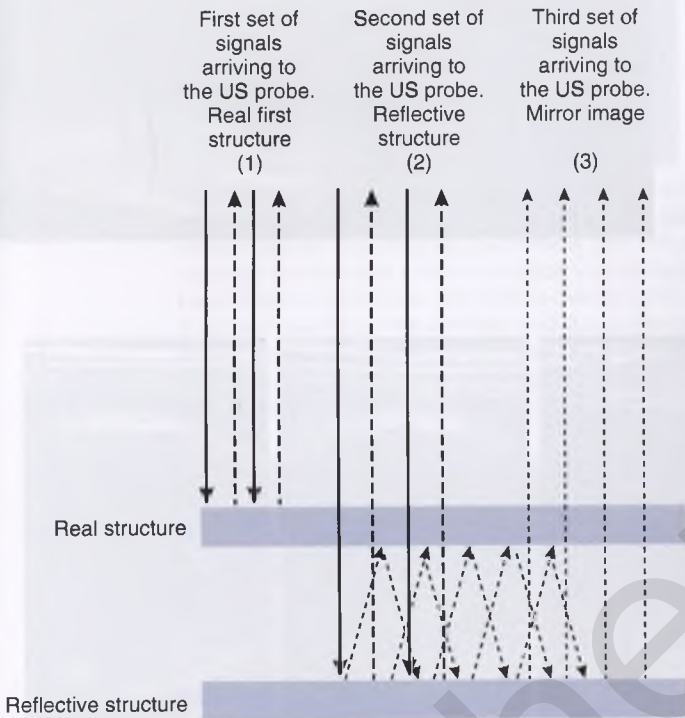


**FIG 38-2** Schematic representation of the mirror image artifact. Ultrasound (US) signals are normally reflected by the structure (fetal head) and by the reflective surface (posterior uterine wall and bowel) arriving on time to the transducer. Some ultrasound signals bounce back and forth between the head and the reflective surface, finally returning to the transducer. Because they arrive later than the original signals, they are represented as another structure behind/deep to the reflective surface. (From Ahn H, Hernandez-Andrade E, Romero R, Ptwardhan M, et al: Mirror artifacts in obstetric ultrasound: case presentation of a ghost twin during the second-trimester ultrasound scan. *Fetal Diagn Ther* 34:248-252, 2013, used with permission.)

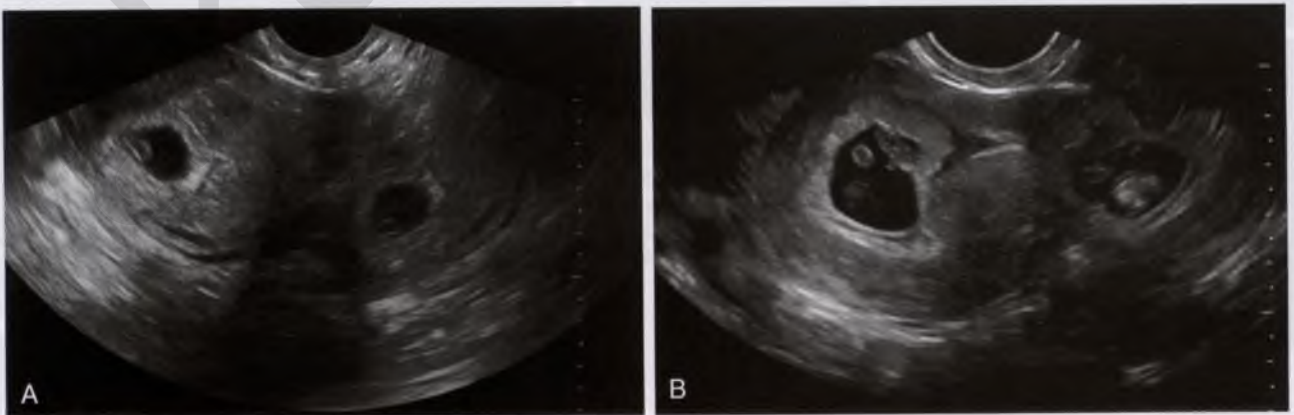


**FIG 38-3 A**, Longitudinal transvaginal sonography demonstrating an intrauterine pregnancy on the left and the mirror image artifact of the image on the right. **B**, Longitudinal transvaginal ultrasound image demonstrating an intrauterine pregnancy on the left and mirror image artifact on the right. (From Malhotra R, Bramante RM, Radomski M, Nelson M: Mirror image artifact mimicking heterotopic pregnancy on transvaginal ultrasound: case series. *West J Emerg Med* 15(6):712-714, 2014, used with permission.)



**FIG 38-4** Sonogram over the inguinal area in a gravid patient at 34 weeks with round ligament varices. Color Doppler imaging demonstrates prominent vessels with venous flow (*arrows*). A mirror image (M) of the varices is seen deep to the vessels.

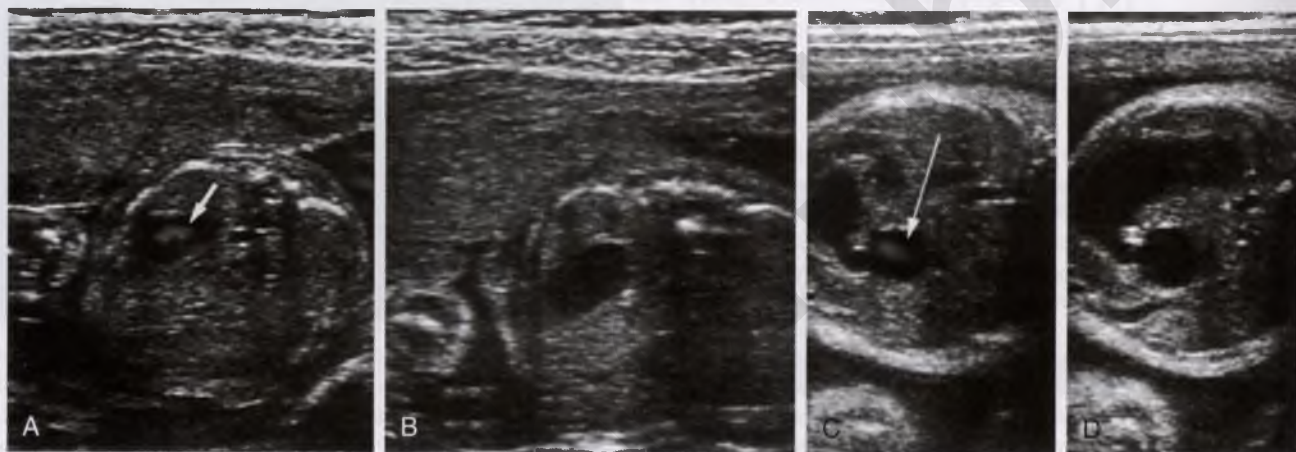
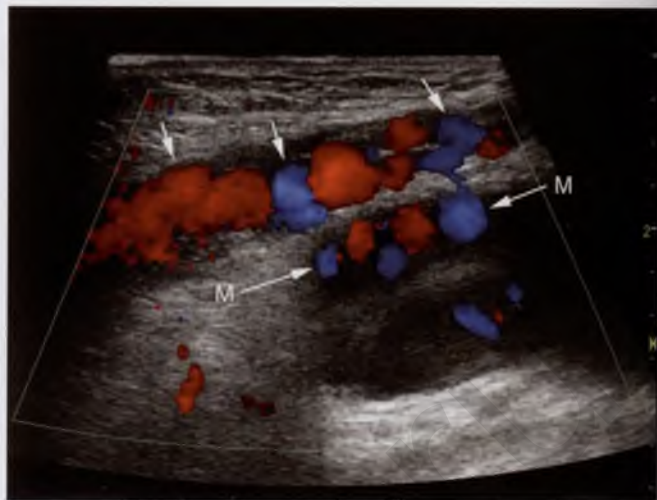


**FIG 38-5** **A** and **C**, Two cases of artifact (*arrows*) appear in the fetal stomach and duodenum. **B** and **D**, If one changes the scanning plane, these echoes will disappear from the area of concern.

**FIG 38-6** Side lobe (gradient) artifact can occur with even the most sophisticated ultrasound scanning equipment. In this case, a side lobe artifact is seen overlying the fetal head (*arrows*). The artifactual nature of these echoes can be confirmed by noting that these echoes are not confined to the head but extend beyond its confines. In addition, changing the scan plane orientation will show the region to be normal.



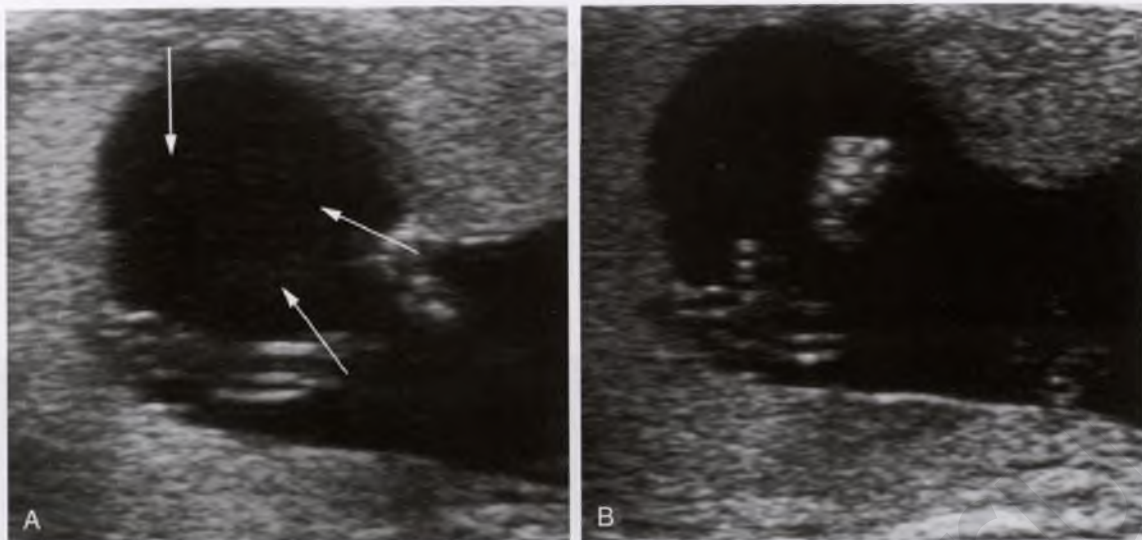


**FIG 38-7** The differentiation of real from artifactual echoes is often problematic during sonographic scanning. A common misconception is that changing to a lower frequency transducer and decreasing the overall system gain or just reducing the system gain will only cause the artifactual echoes alone to disappear. Although it is true that artifactual echoes will not be displayed with these maneuvers, it should be remembered that the real echoes will not be displayed either. **A**, In this patient, numerous low-level echoes (*arrows*) were seen swirling in the amniotic fluid during real-time scanning. Although the origin of the echoes is not known, they may represent shed fetal epithelial cells. **B**, When the system gain was decreased, these real echoes virtually disappeared. Although the hard copy images do not resolve this dilemma, the echoes were clearly seen to be moving and real when the sonologist was performing the scan.

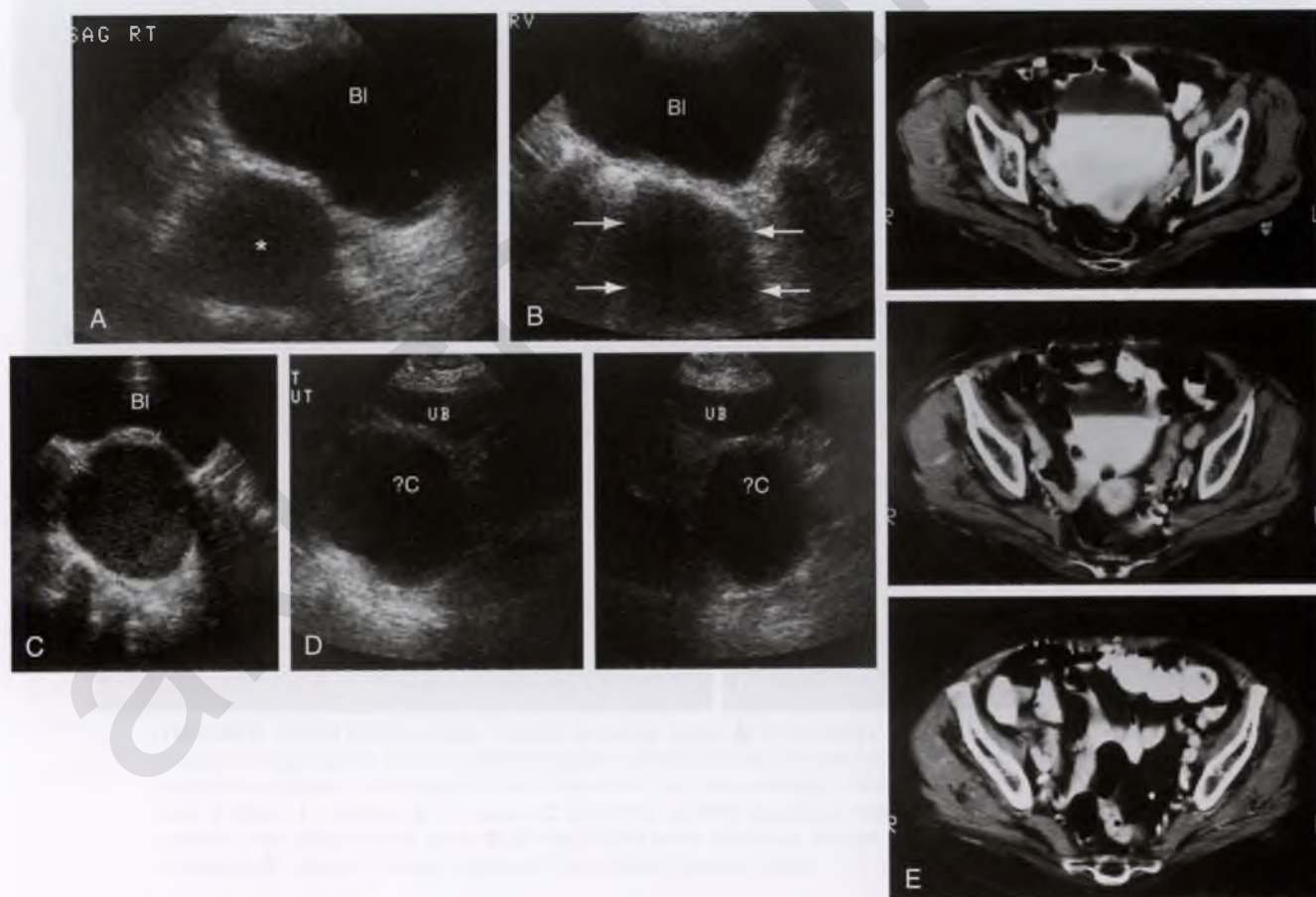


**FIG 38-8** Bowel within the pelvis can masquerade as ovarian cysts. **A**, In this patient, bowel gas and its shadowing create the appearance of a mass (*asterisk*). BI, bladder. **B**, The strong reflection adjacent to the urinary bladder (BI) or the "squared" appearance (*arrows*) to the "cyst" should make one suspicious that bowel gas artifact is causing this appearance. **C**, In a different patient, a true ovarian cyst (*cursors*) has borders on nearly every side and has enhanced through-sound transmission and internal echoes. BI, bladder. **D**, In another patient, two different planes of section demonstrate what appears to be a large pelvic cyst (?C). In fact, this was due to bowel gas artifact. UB, bladder. **E**, Because this appearance was virtually indistinguishable from a pelvic cyst, a computed tomographic scan was performed immediately after the sonogram, confirming the artifactual nature of this "cyst." The scans were normal without evidence of a pelvic mass.



## PELVIS, GRAVID AND NONGRAVID UTERUS

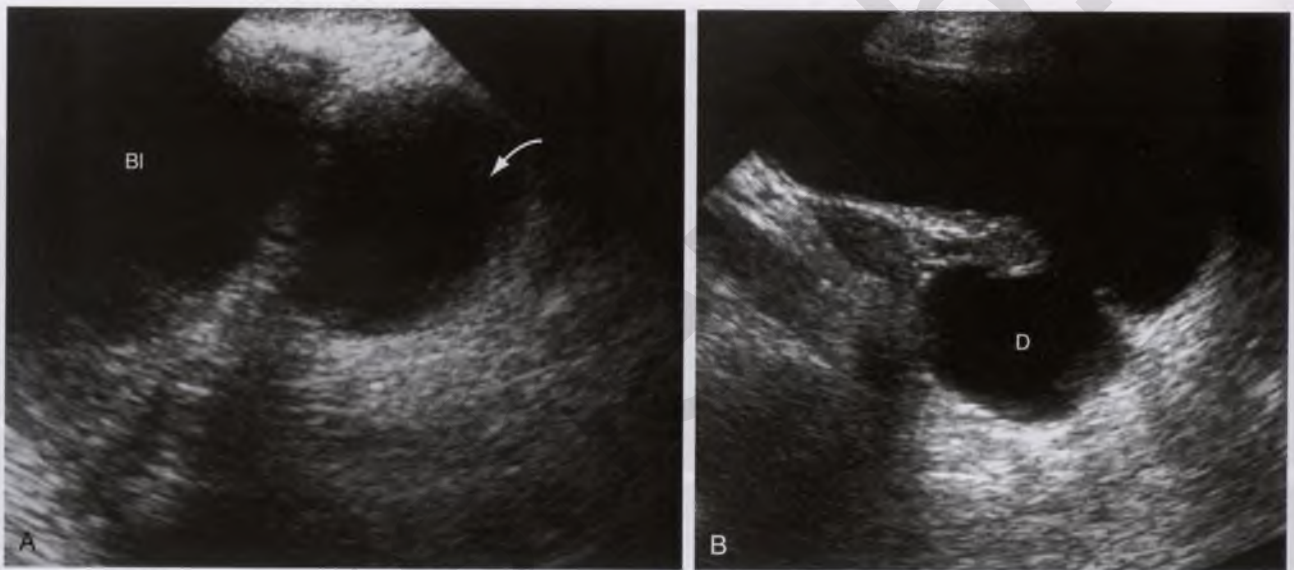


**FIG 38-9** **A**, What appears to be a large pelvic cyst (*arrow*) is seen in this patient. Bl, bladder. **B**, Although the connection to the bladder was not seen in A, this bladder diverticulum (D) is clearly seen in another plane of section.

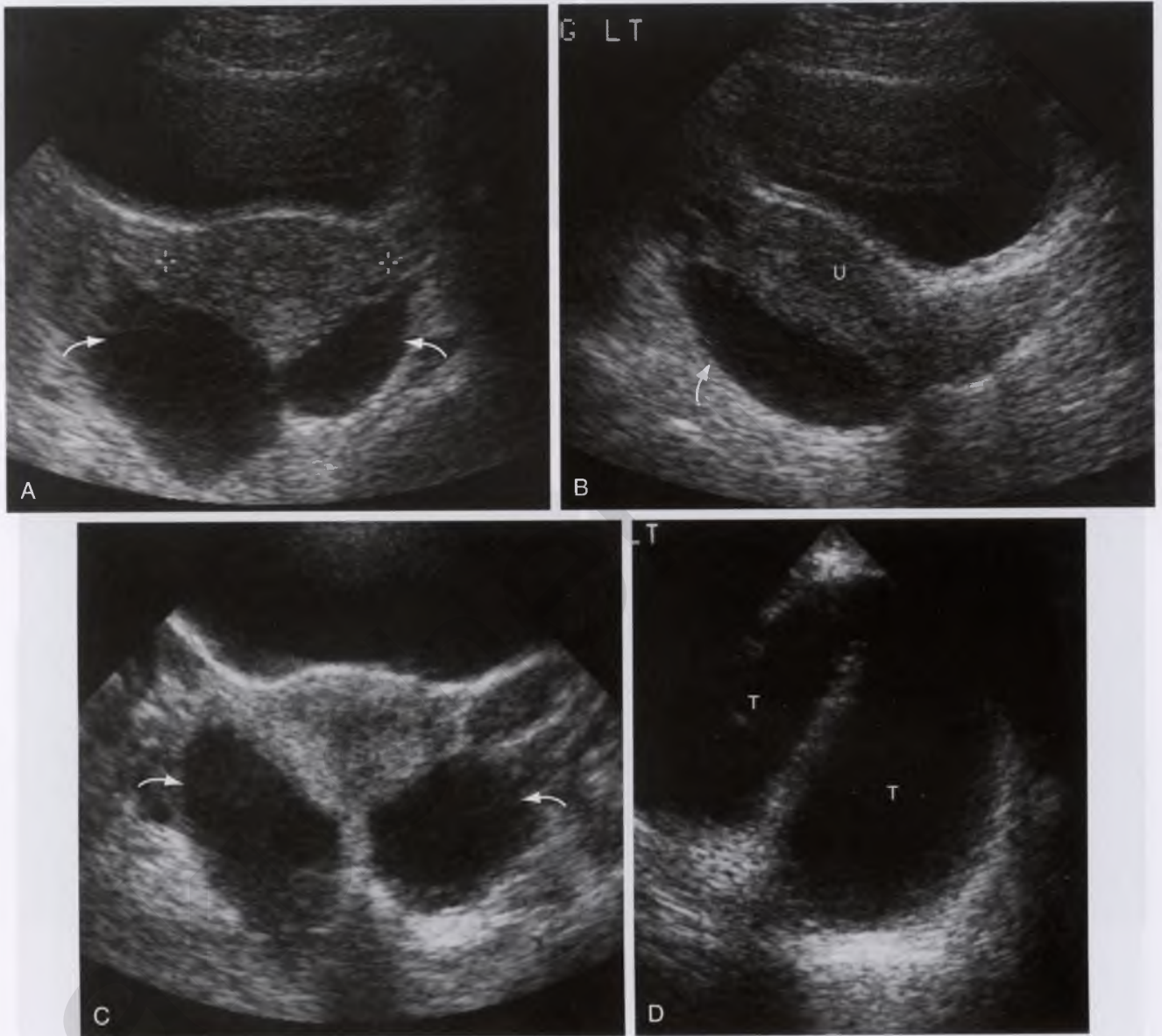


**FIG 38-10** Dilated fallopian tubes simulating ovarian cysts. **A**, A transverse sonogram in this patient demonstrates what appear to be two ovarian cysts (*arrows*) posterior to the uterus ( *cursors*). **B**, A longitudinal sonogram displays the elongated tubular nature of this fluid collection (*arrow*), which is more compatible with a dilated fallopian tube. U, uterus. **C**, In another patient, two large, rounded fluid collections are seen (*arrows*) simulating ovarian cysts. **D**, A longitudinal plane of section through one of these collections demonstrates the tubular (T) retort nature of these dilated fallopian tubes.



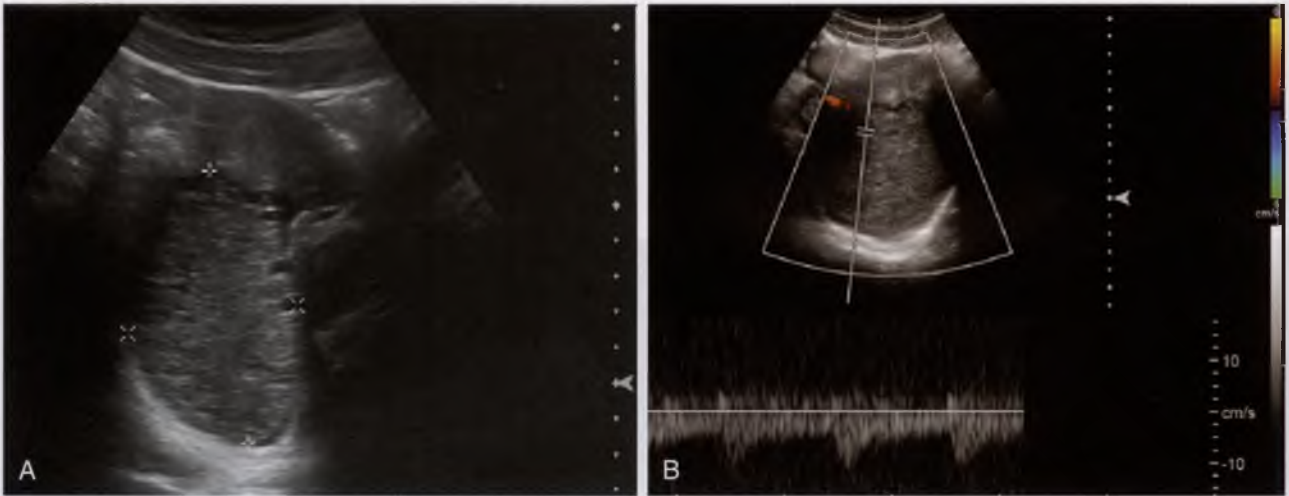


**FIG 38-11** A 19-year-old woman presented with severe pelvic pain and negative pregnancy test. She had been in an emergency room 1 month earlier with the same symptoms. **A**, A pelvic sonogram demonstrates an enlarged ovary with peripheral small cysts. **B**, Doppler sonogram of the ovary demonstrates arterial and venous blood flow. Three hours later an avascular necrotic ovary from ovarian torsion was removed at surgery. Don't be falsely reassured by an apparently normal Doppler sonogram when ovarian torsion is suspected.

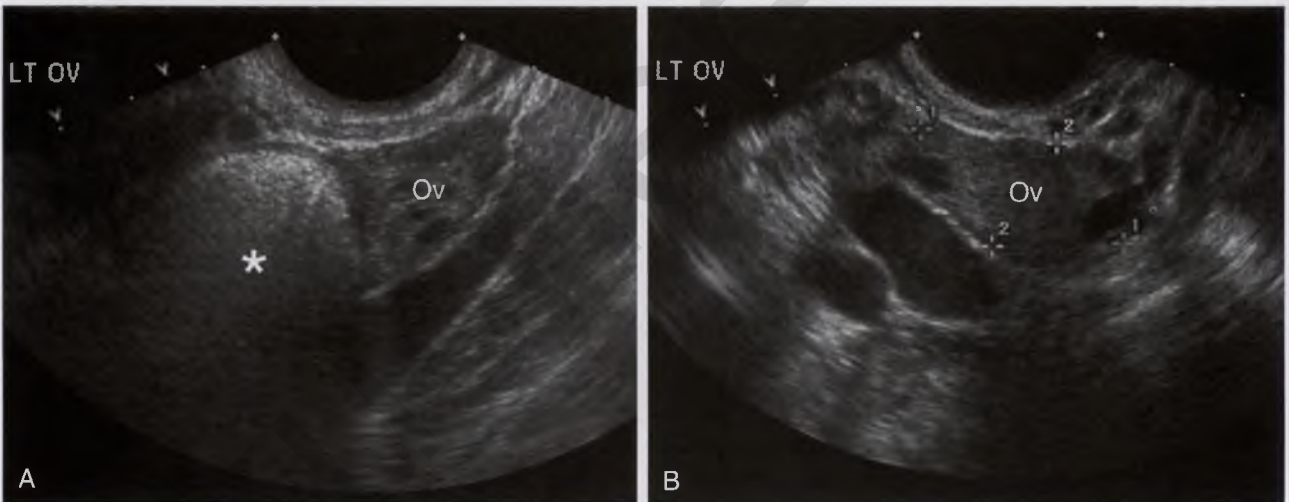


**FIG 38-12** Bowel simulating an ovarian cystic teratoma (dermoid). **A**, A large shadowing mass (*asterisk*) is seen adjacent to or possibly emanating from the ovary (Ov). **B**, Minutes later the normal ovary and adnexal structures are well seen. The bowel, which was the cause of the shadowing, was not seen.



**FIG 38-13** Two round and oval structures are seen in the right adnexa. Although they might be mistaken for abnormal ovaries or paraovarian masses, they represent normal prominent bowel. Typical hypochoic muscularis (*arrows*) is seen.

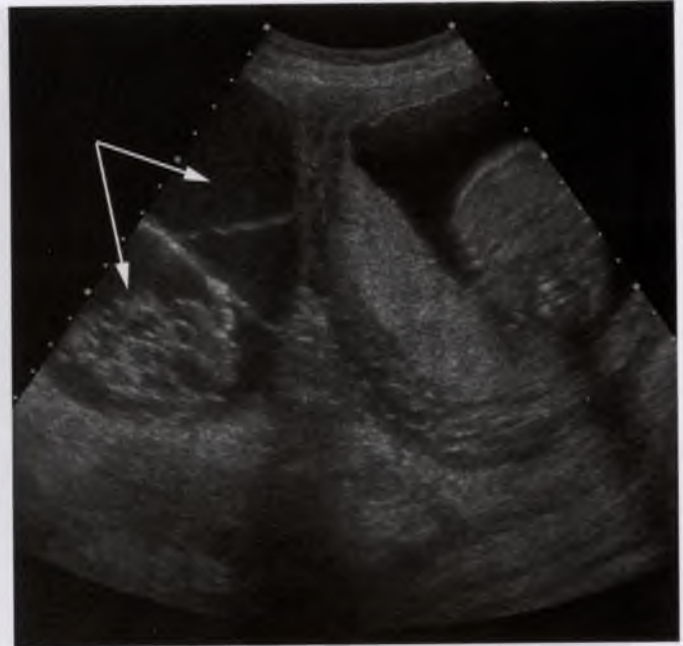


**FIG 38-14** Pregnancy with coexistent ovarian carcinoma. Unfortunately, just because a patient is pregnant does not mean that she cannot have a concomitant ovarian cancer. A multilocular cystic mass (*arrows*) with solid components is seen adjacent to the gravid uterus.

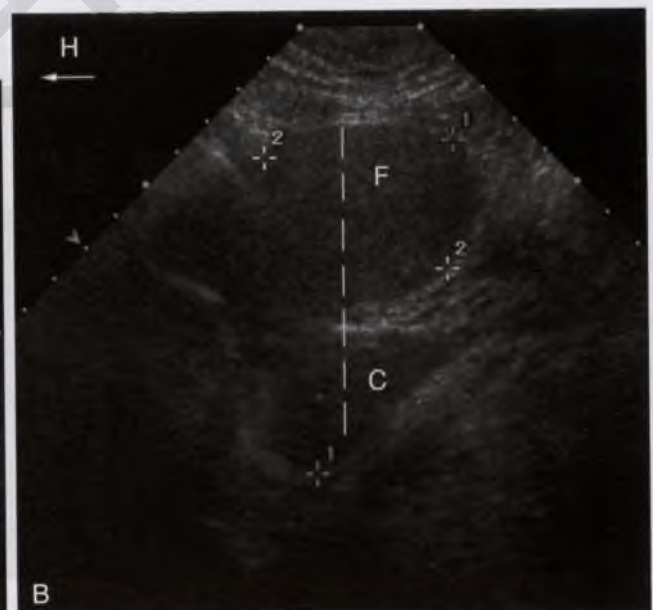
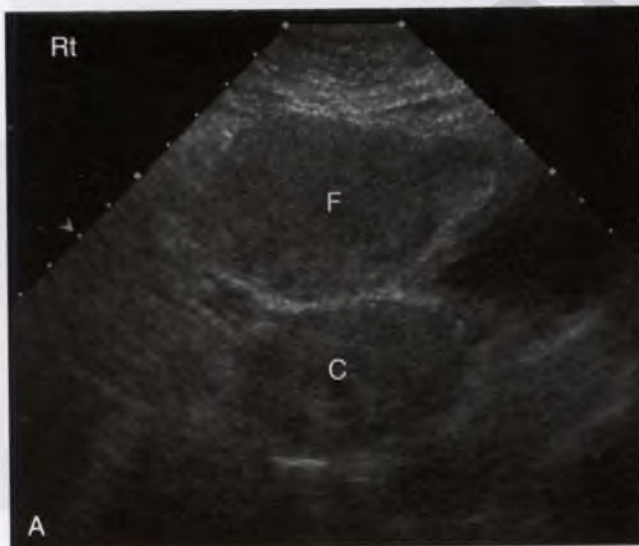


**FIG 38-15 A**, Transverse axial sonogram of the pelvis in a nongravid patient. There appears to be either a duplication of the uterus or the uterus and an adjacent mass (C, F). Rt, right. **B**, A sagittal scan demonstrates that what was seen in the transverse scan was the cervix (C) and fundus (F) of an anteverted uterus. The dashed line represents the plane of section in A. H, head.



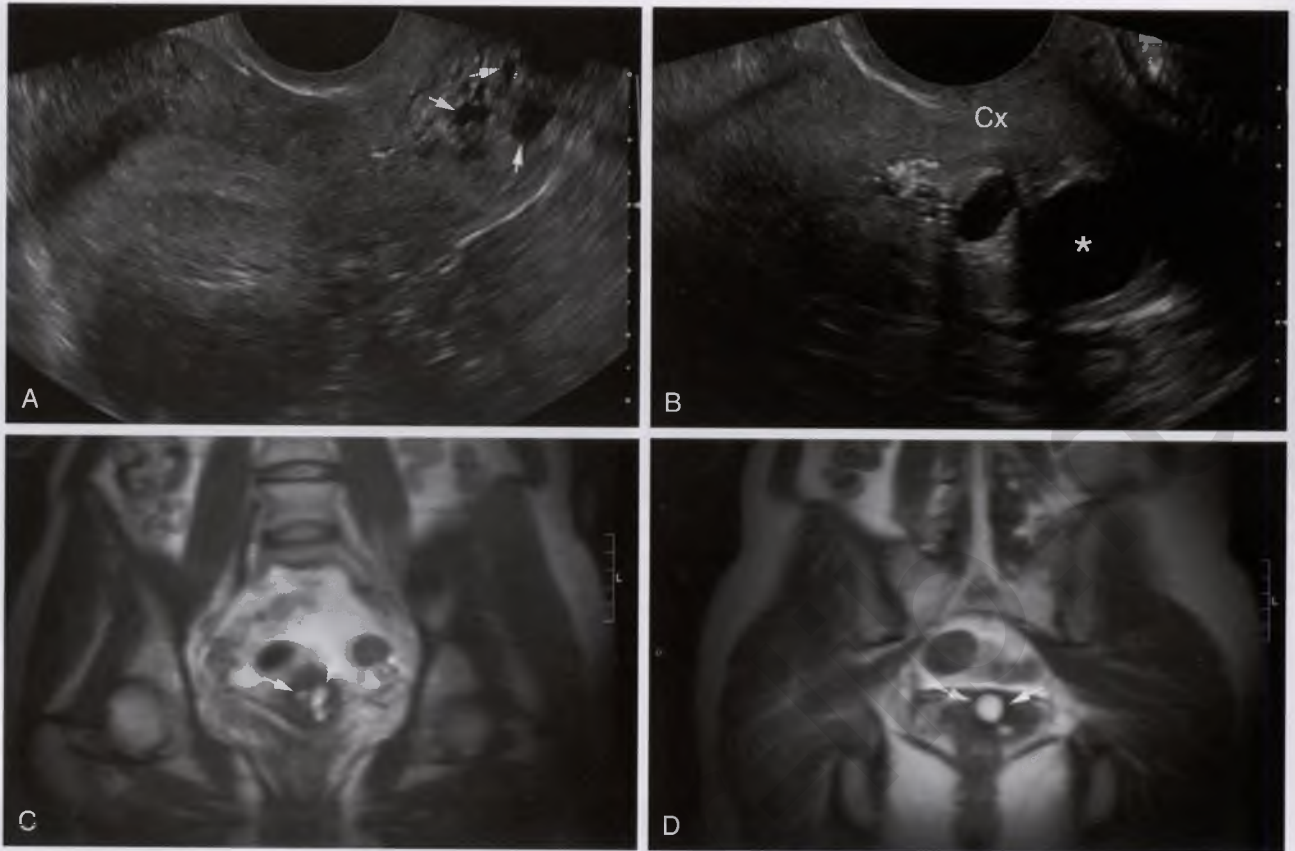


**FIG 38-16** Longitudinal transvaginal sonogram through the cervix of a nongravid uterus. **A** and **B**, Multiple nabothian cysts (*arrows*) are seen in the cervix (Cx). At times these cysts can be quite large (*asterisk*). These retention cysts are quite common and should not be confused with low-implanted gestational sacs or other abnormalities. **C** and **D**, Two coronal T2-weighted magnetic resonance images through the cervix demonstrate multiple, round, T2-weighted hyperintense structures compatible with nabothian cysts (*arrows*).



**FIG 38-17** **A**, Transverse scan through the gravid uterus demonstrates a uterine synechia (*arrow*) crossing the uterine cavity from the anterior to the posterior wall. The singleton fetus moved freely around the synechia. This should not be confused with an amniotic band. **B**, In another patient a uterine synechia (*arrow*) is seen adjacent to the fetal head. **C**, Three-dimensional rendered image of the fetus in **B** demonstrating the synechia (*arrows*).

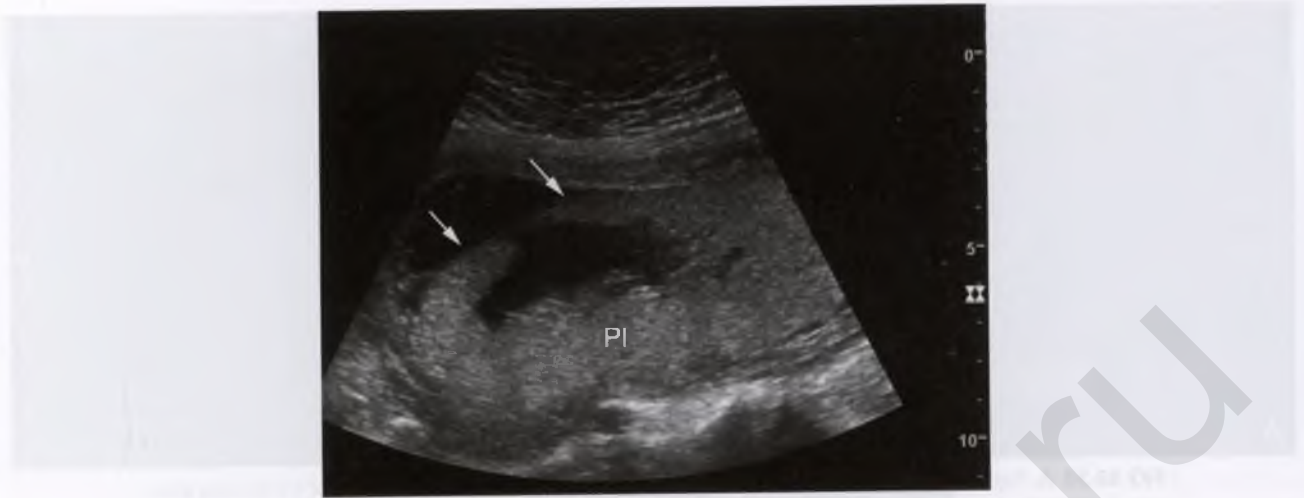


**FIG 38-18** Sonogram of a gravid uterus in the second trimester demonstrating a circumvallate placenta (PI). The infolding of the edge of the placenta (*arrows*) should not be confused with a uterine synechia.

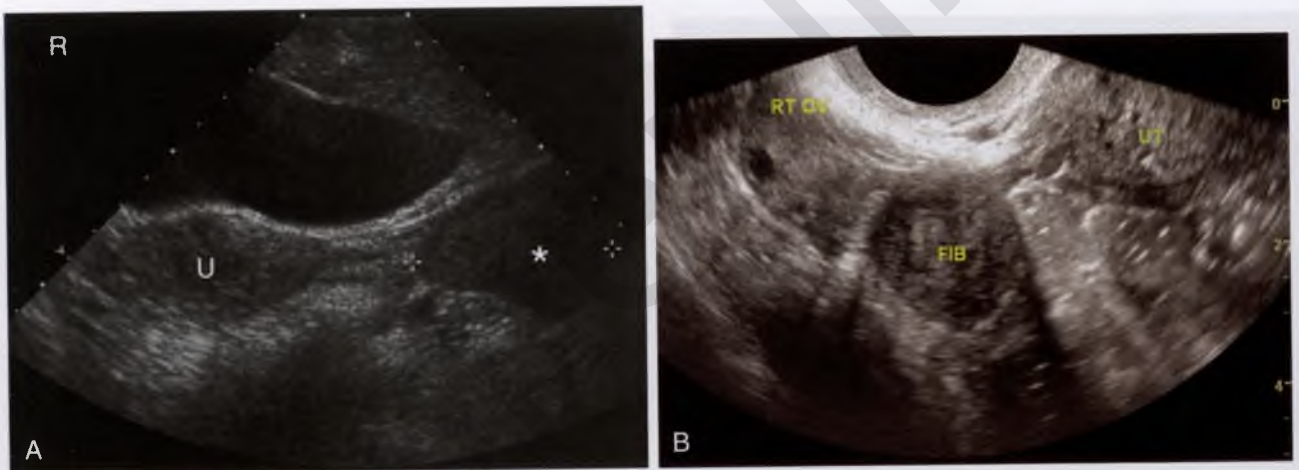


**FIG 38-19 A**, Transverse scan of the pelvis demonstrating a left adnexal solid mass (*asterisk*). Although the anatomic position might suggest an ovarian lesion, the solid nature of the mass should suggest the possibility of a broad ligament myoma, which was ultimately demonstrated on magnetic resonance imaging. U, uterus, R, right. **B**, Coronal transvaginal scan demonstrating a broad ligament myoma (FIB) clearly separate from the uterus (UT) and ovary (RT OV).



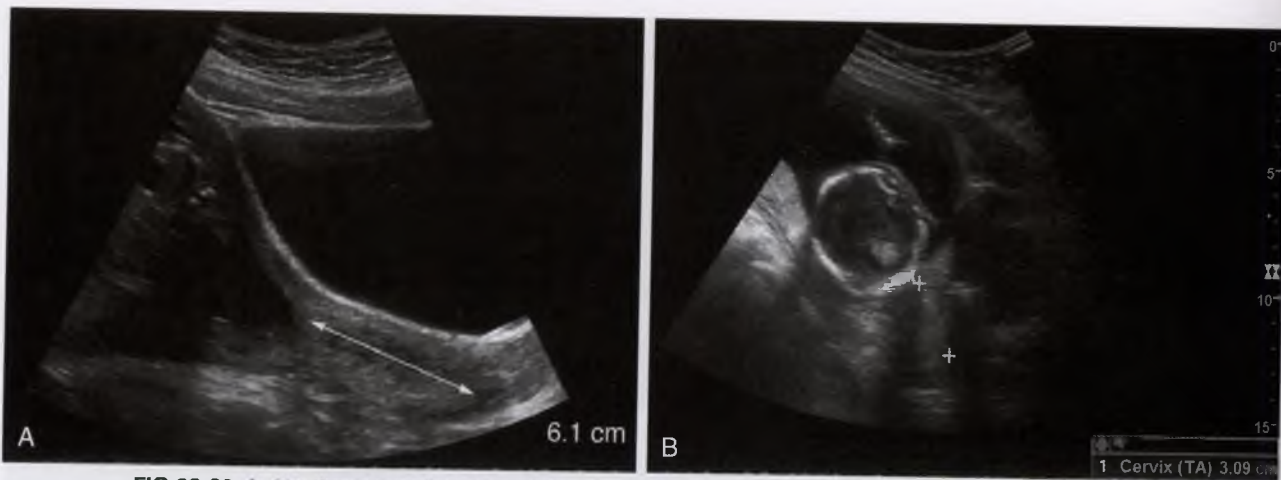


**FIG 38-20** **A**, Significant overdistention of the urinary bladder results in the appearance of a markedly elongated cervix (*double-headed arrow*) measuring 6.1 cm. One is visualizing not only the cervix but the apposed anterior and posterior walls of the lower uterine segment. **B**, Once the patient has emptied her urinary bladder, the true cervical length (*between calipers*) can be accurately measured at 3.09 cm.



**FIG 38-21** A distended urinary bladder has caused the anterior and posterior walls of the lower uterine segment (*arrows*) to come near one another. The trapped amniotic fluid gives the appearance of an incompetent cervix. The cervix was normal in this case.



**FIG 38-22** A myometrial contraction (M) is common in first and second trimester sonograms. This should not be confused with a myoma. Two features help make this distinction: First, in general, myometrial contractions tend to bulge inwardly without affecting the outer contour of the uterus. Uterine myomas tend to bulge inward and outward. Second, myometrial contractions may resolve during the time of scanning.

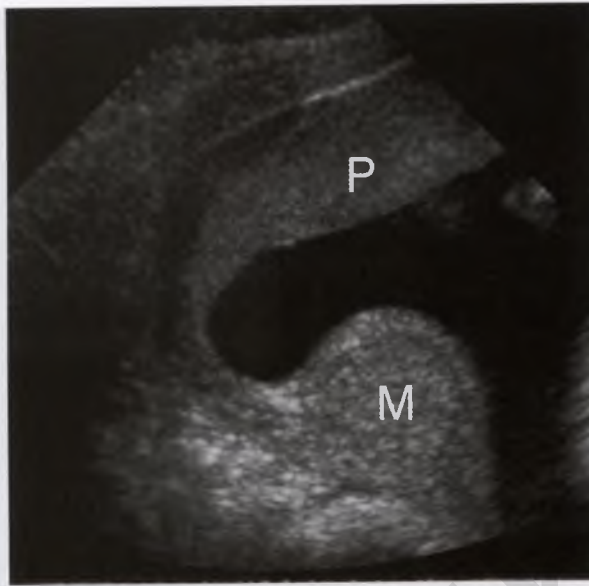


**FIG 38-23** A myometrial contraction (M) in this second trimester pregnancy simulates a myoma. This should not be confused with a succenturiate lobe of the placenta. P, placenta.

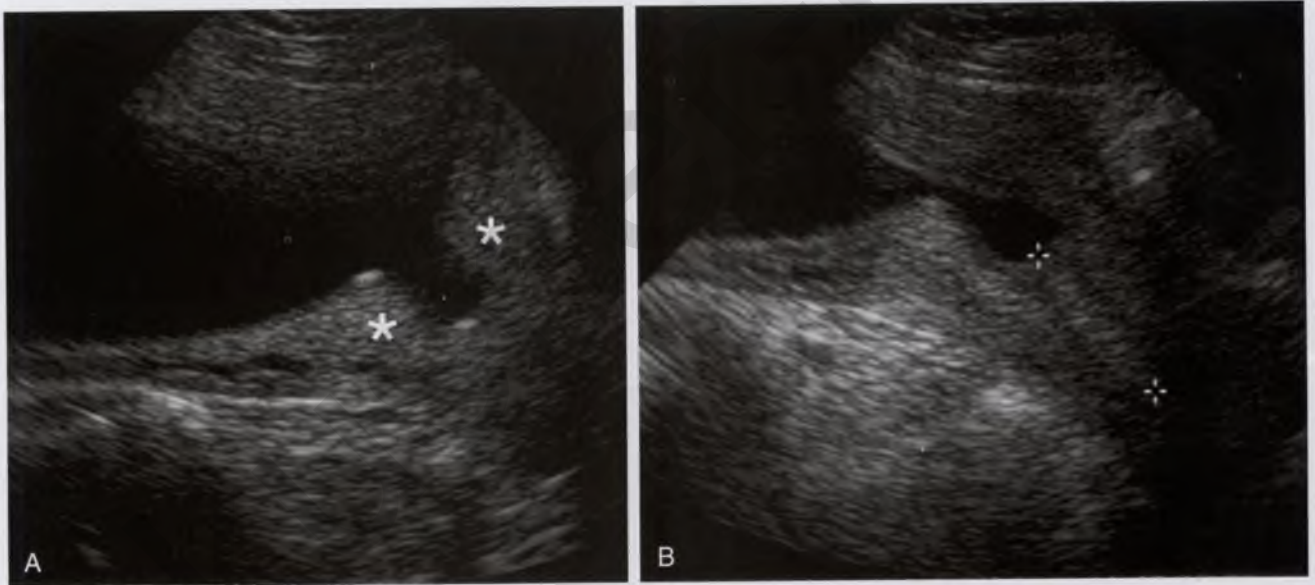


**FIG 38-24** Myometrial contractions of the lower uterine segment are common and may often touch one another. **A**, In this case the contractions (*asterisks*) of the lower uterine segment simulate an open and incompetent cervix. **B**, The normal-appearing cervix, in fact, is well seen (*calipers*) caudal to this contraction.





**FIG 38-25** Myometrial contractions of the lower uterine segment may touch one another (*asterisks*). These opposed contractions have been referred to as “kissing contractions.” In this case, it gives the impression that the placenta (PI) overlies the internal cervical os.



**FIG 38-26** **A**, “Kissing contractions” of the lower uterine segment (*asterisks*). These contractions should not be confused with the cervix (*arrow*). **B**, With time there was partial resolution of the contractions (*asterisks*), so that the true cervical length (3.51 cm) could be measured (*arrow*).



**FIG 38-27** Artifactual short cervix. **A**, Transperineal scan demonstrates a short cervix (*between calipers*) measuring 1.8 cm. Shadowing (*arrows*) from the rectum obscures the remainder of the cervix. **B**, A transvaginal scan in the same patient demonstrates a normal length to the cervix (*between calipers*) of 3.43 cm.

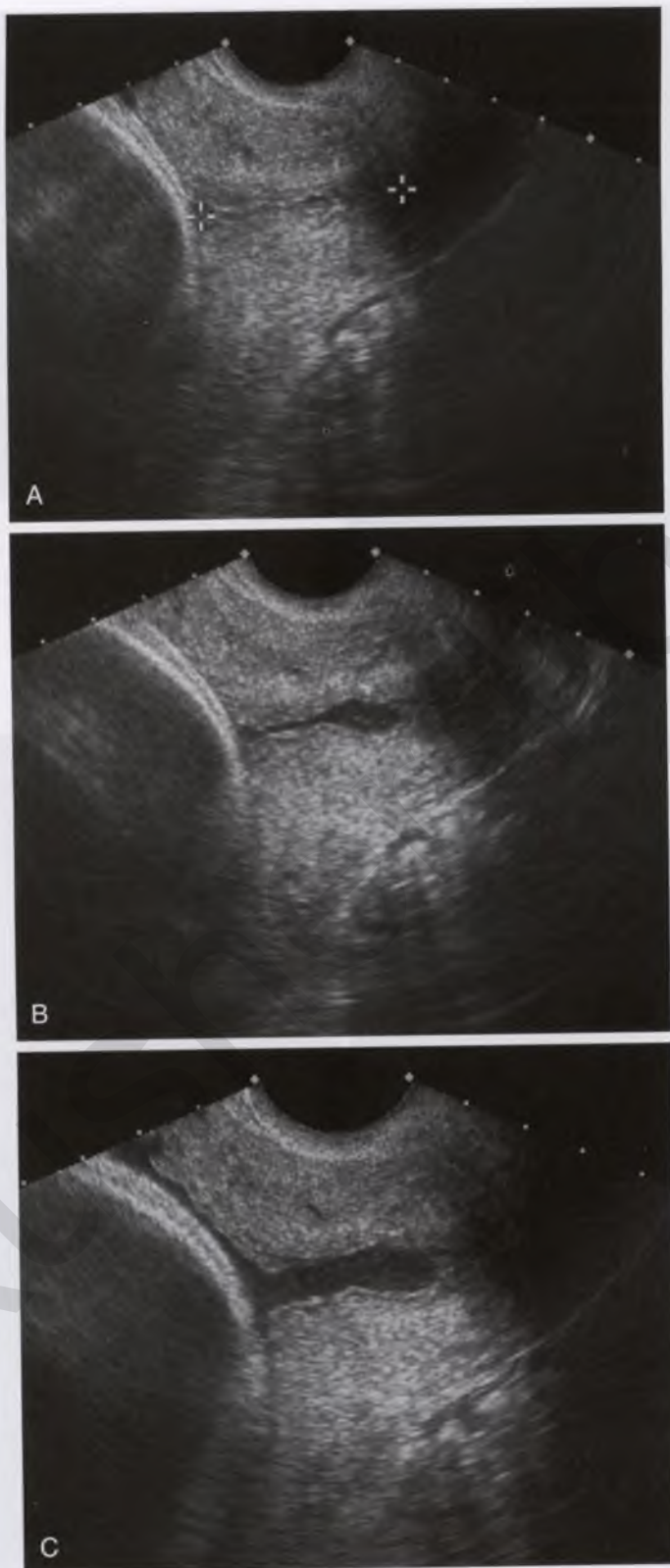


**FIG 38-28** Dynamic changes of cervix. Three transvaginal scans of the cervix (**A** to **C**), taken minutes apart, demonstrate progressive dilatation of the cervix with fluid entering the endocervical canal. This finding should be reported to the referring obstetrician and the residual shortened closed length of the cervix should be reported, as well as the total cervical length.





**FIG 38-29** **A**, A slightly oblique longitudinal scan through the uterus. A small area of placental tissue (*arrow*) appears separate from the major portion of the posterior placenta (PI). This appears to be a succenturiate lobe of the placenta. **B**, When the scan plane is aligned slightly more midline the anterior placental tissue (PI) in **A** can be seen to be continuous with the remainder of the placenta. **C**, A transverse axial plane of section demonstrates continuity between the anterior and posterior placental tissue (PI).

**FIG 38-30** In some patients, the surface area over which the placenta implants may be small. This short insertion site may create the false appearance of a thickened hydropic placenta (P).



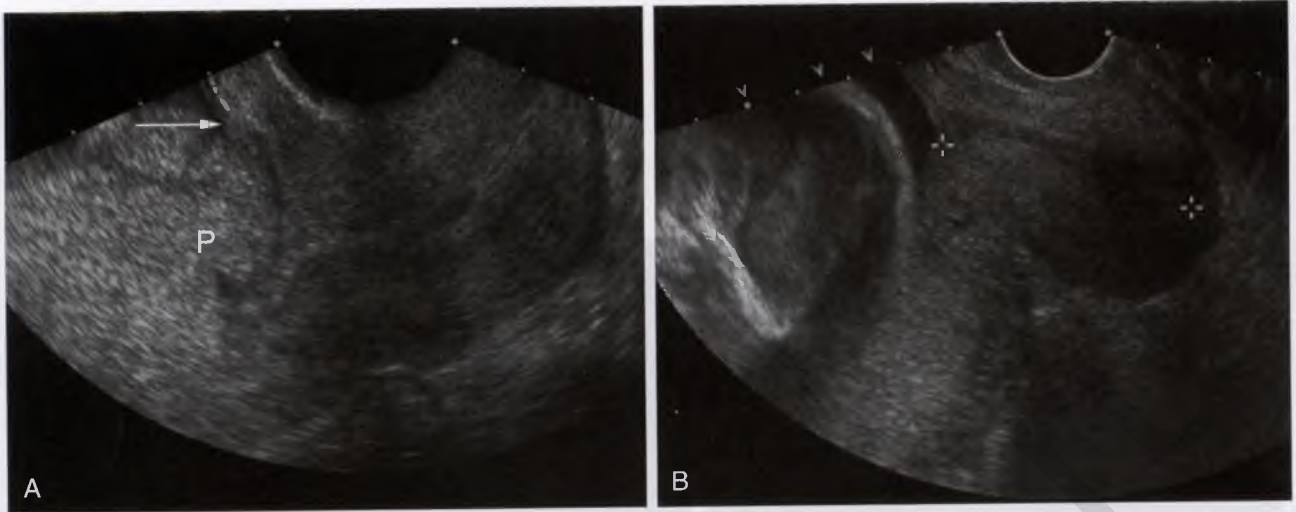


**FIG 38-31** Changing placenta previa. **A**, A transvaginal scan in a patient at 17 weeks demonstrates a complete placenta previa. The leading edge (*arrow*) of the posterior placenta (P) extends across the internal cervical os. **B**, Six weeks later at 23 weeks, the leading edge of the placenta extends to but not beyond the internal cervical os.

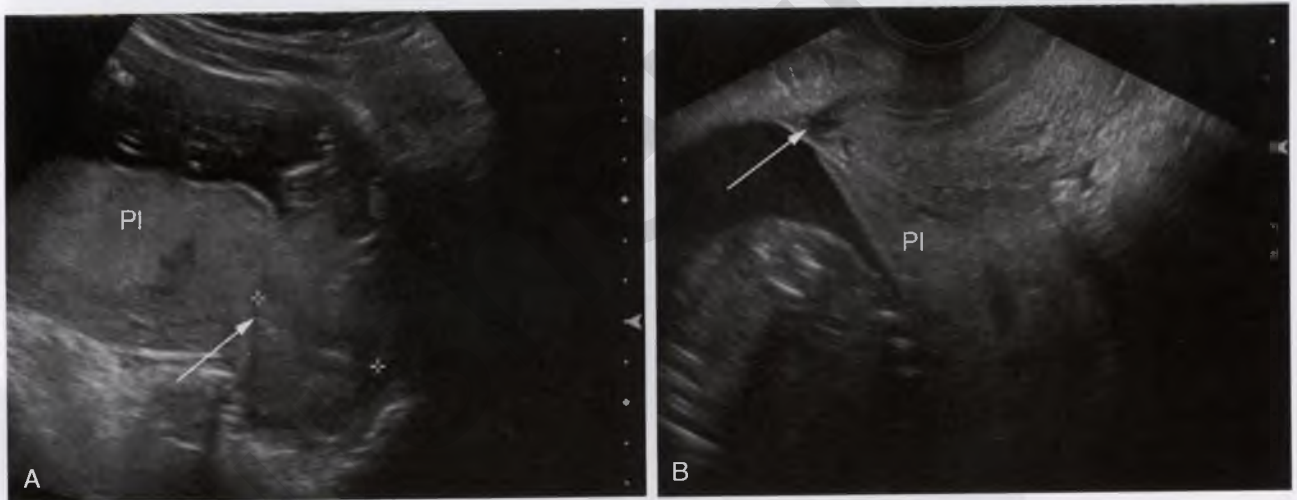


**FIG 38-32** **A**, Transabdominal longitudinal sonogram demonstrating what appears to be complete placenta previa. The placenta (Pl) appears to completely cover the internal cervical os (*arrow*). **B**, Transvaginal sonogram from the same patient demonstrates the placenta (Pl) extends to but does not cover the internal cervical os (*arrow*).



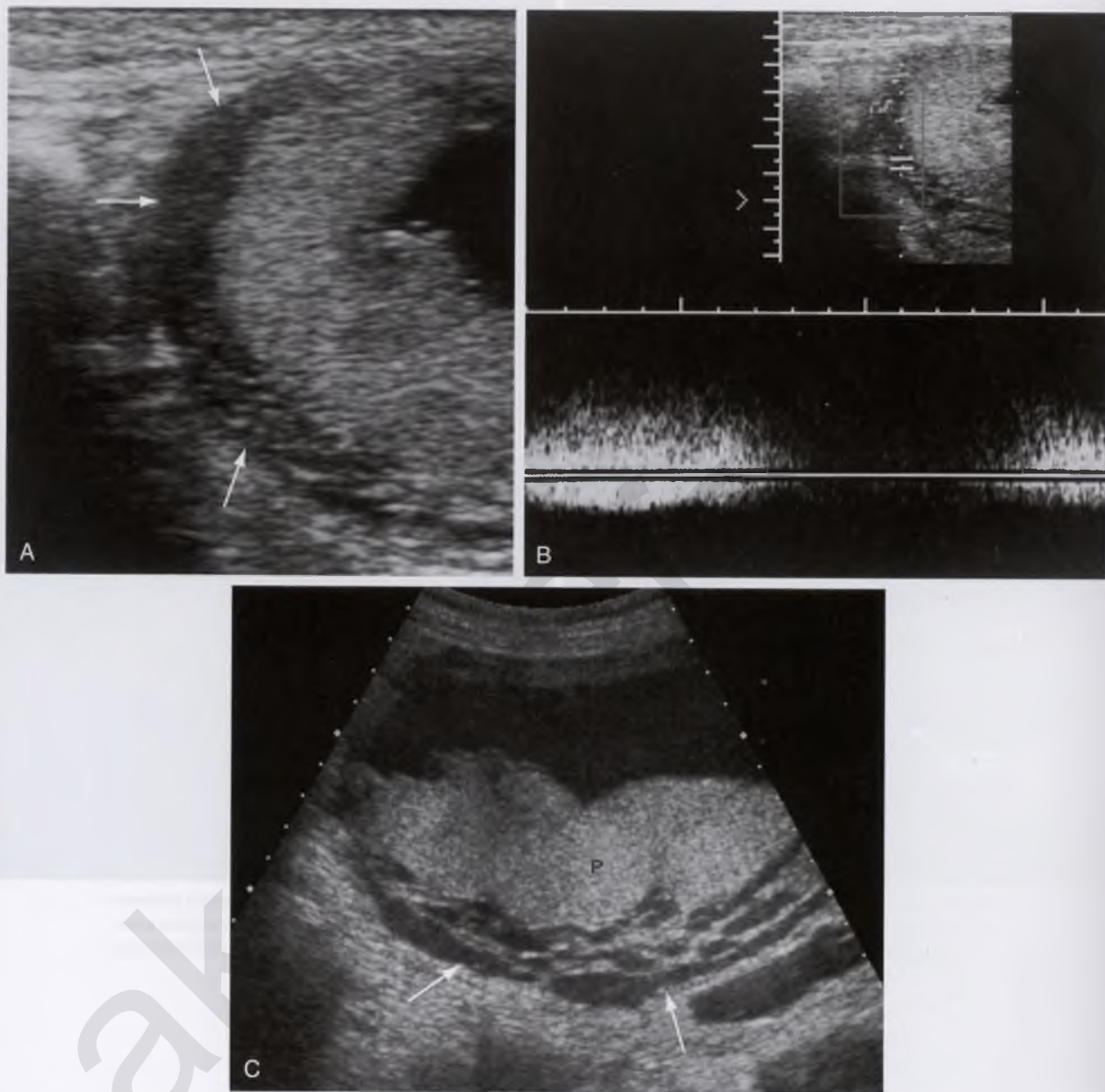


**FIG 38-33** **A**, Veins present in the decidua basalis and myometrium contribute to a hypoechoic region beneath the placenta (*arrows*). This should not be misinterpreted as an abruption. **B**, Doppler interrogation of this region will often confirm the venous nature of this area. **C**, In this case, the veins (*arrows*) deep to the placenta (P) are clearly seen.



**FIG 38-34** A hypoechoic area (*asterisk*) behind the placenta (PI) simulates placental abruption. Rather, this represents a focal myometrial contraction that resolved during the examination.

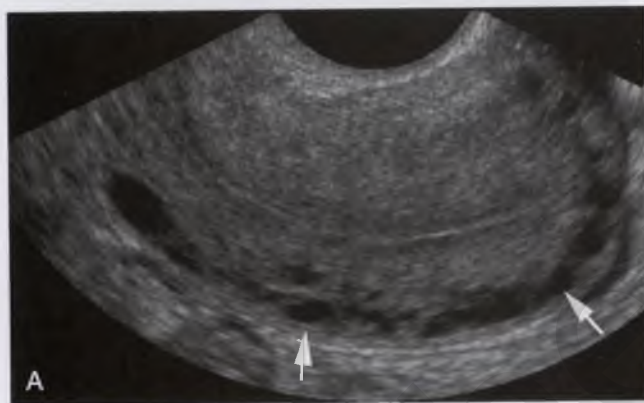


**FIG 38-35** Prominent vessels (*arrows*) at the periphery of the uterus are common in the uterus and should not be mistaken as a precursor to an abruption or as trophoblastic disease. **A**, In this patient, the arcuate vessels (*arrows*) at the periphery of the uterus are quite prominent. **B**, With color Doppler flow imaging, the vascular nature of these structures is well seen.



**FIG 38-36** Transverse scan of the gravid uterus demonstrates the fetal head (H). A calcified structure (*arrows*) is seen adjacent to the fetal head. At first glance, this appears to be another fetus but in fact it represents a calcified myoma.



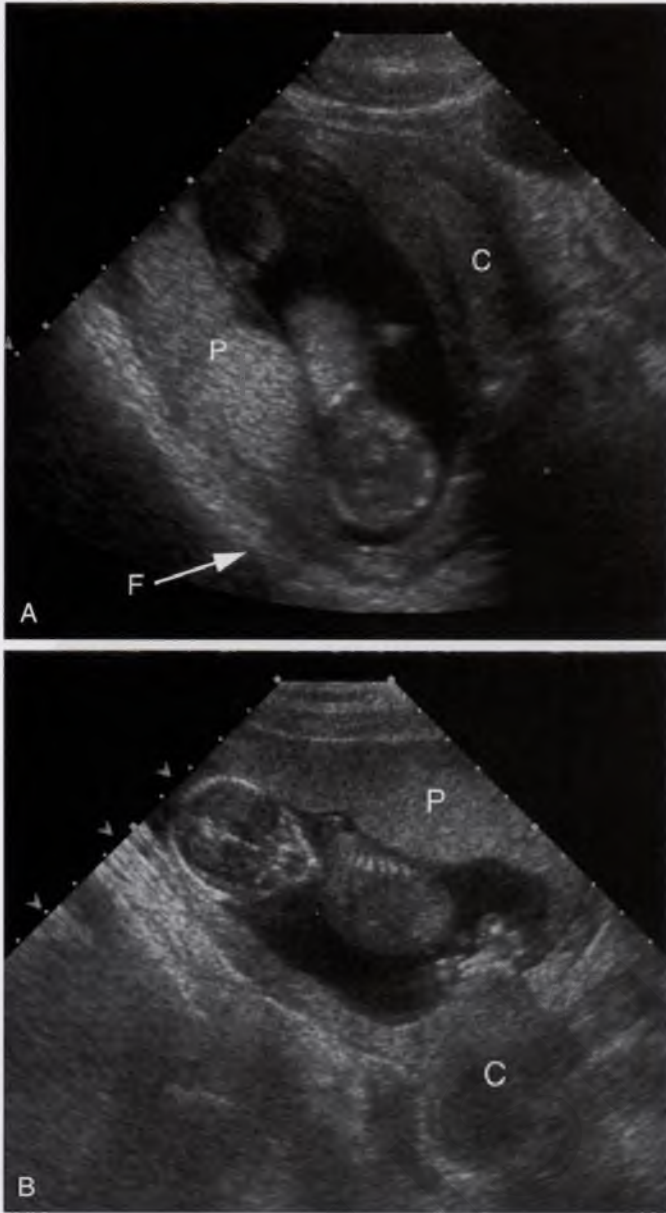


**FIG 38-37** Incarcerated uterus. A persistently retroflexed or retroverted uterus may become “trapped” within the sacral hollow. **A**, Longitudinal scan demonstrating an incarcerated uterus in the early second trimester. What appears to be the lower uterine segment is in fact the fundus (F) that is stuck within the sacral hollow. The cervix (C) is drawn anteriorly and superiorly. The urethra often becomes obstructed, and these patients are often seen in the emergency room with urinary obstruction. P, placenta. **B**, After manual reduction, the cervix (C) and uterus now have a more normal appearance. The placenta (P), which appeared to be posterior in the prerelief scan, is now seen anteriorly.

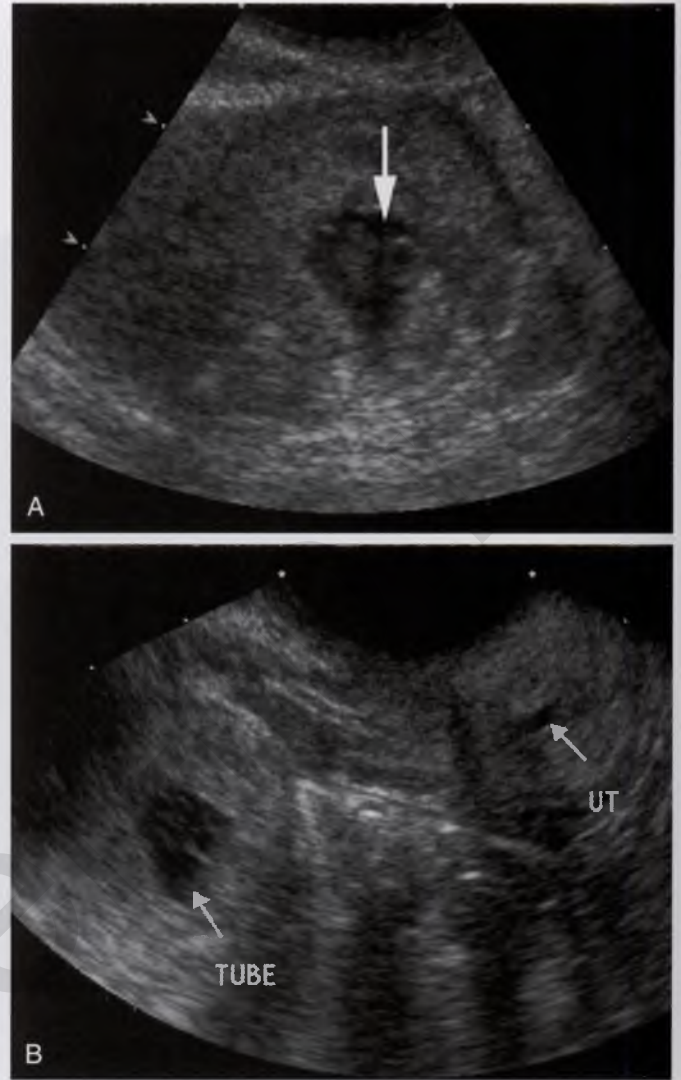


**FIG 38-38** **A**, A transvaginal sonogram demonstrates an embryo and yolk sac (arrow) centrally positioned in what appears to be the uterus. **B**, A transabdominal sonogram of the same patient demonstrates that the pregnancy was in the fallopian tube (TUBE). A small fluid collection representing fluid within the endometrial cavity (decidual cast) of the uterus (UT) is seen. The patient had an ectopic pregnancy.

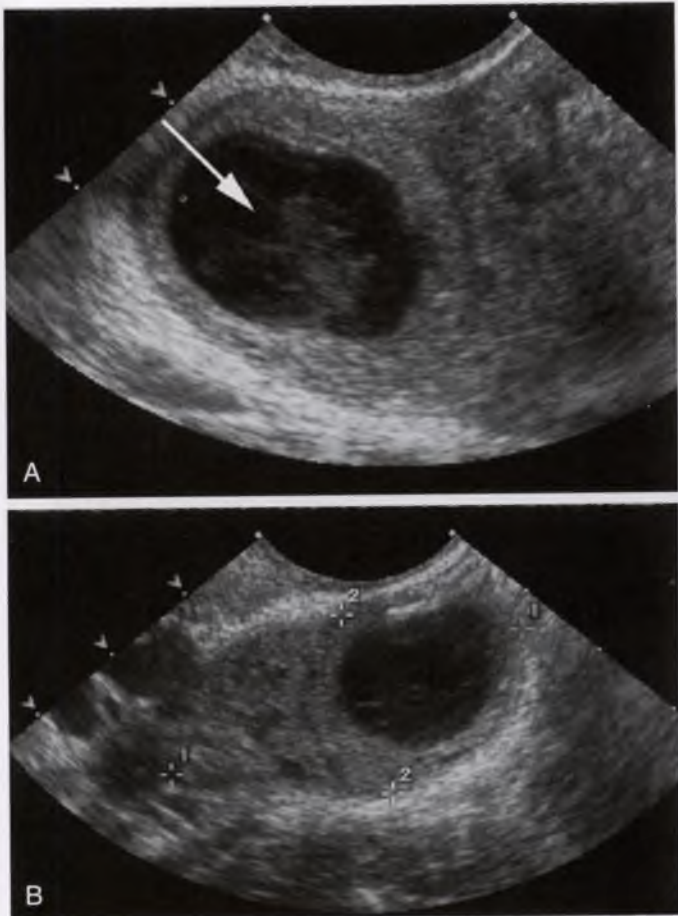


**FIG 38-39** **A**, A transvaginal sonogram demonstrates an ill-defined soft tissue mass (*arrow*) in a cystic fluid collection within the ovary. The uniformly thick wall of the cyst simulates a decidual reaction. This has the appearance of a disorganized embryo within a gestational sac. **B**, An additional scan of the same adnexa demonstrates a more characteristic fishnet appearance of hemorrhage within an ovarian cyst.

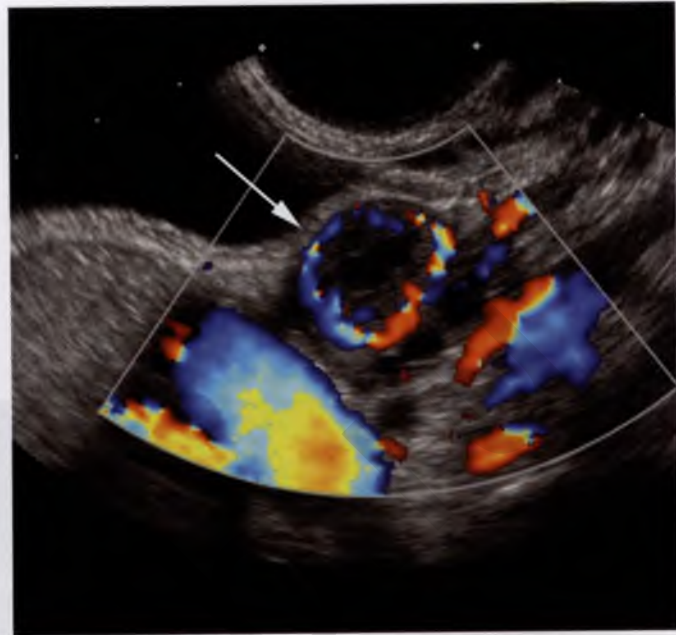


**FIG 38-40** A vascular ring (*arrow*) is seen around a cyst within the adnexa. Although this "ring of fire" was once thought to be characteristic of an ectopic pregnancy, it is recognized that a corpus luteum cyst, as in this case, may produce a similar appearance.



## THE FIRST TRIMESTER

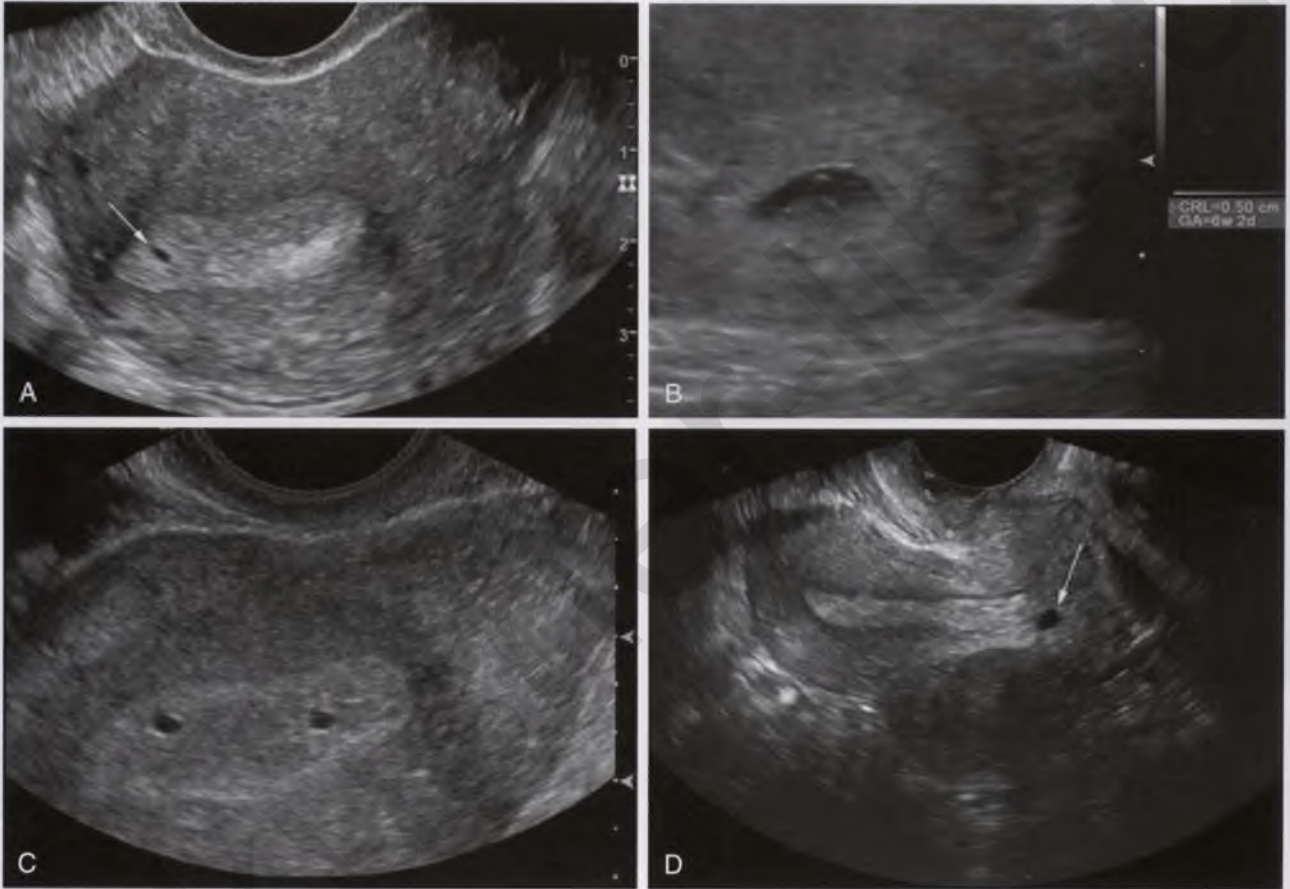


**FIG 38-41** **A**, Very small gestational sac (*arrow*) too early to characterize is seen within the decidualized endometrium. **B**, Two weeks later, normal early intrauterine pregnancy is identified, with embryo visualized. **C**, Two small decidual cysts are seen within the endometrium in a patient with negative pregnancy test. **D**, A small cyst (*arrow*) is seen adjacent to the endometrium. Although this has the appearance of a gestational sac or decidual cyst, it is a nabothian cyst within the cervix.



**FIG 38-42 A**, A sonogram of the gravid uterus in the first trimester demonstrates what appears to be two gestational sacs divided by a thick intertwin membrane (*arrow*). **B**, With slight angulation one can see that the structure dividing the gestational sac was a uterine synechia (*arrow*). E, embryo.



**FIG 38-43** Transvaginal sonogram of an early intrauterine pregnancy and intrauterine device (IUD). The linear structure (*arrow*) seen in the lower uterine segment is an IUD. The relationship of the IUD and the gestational sac should be reported.

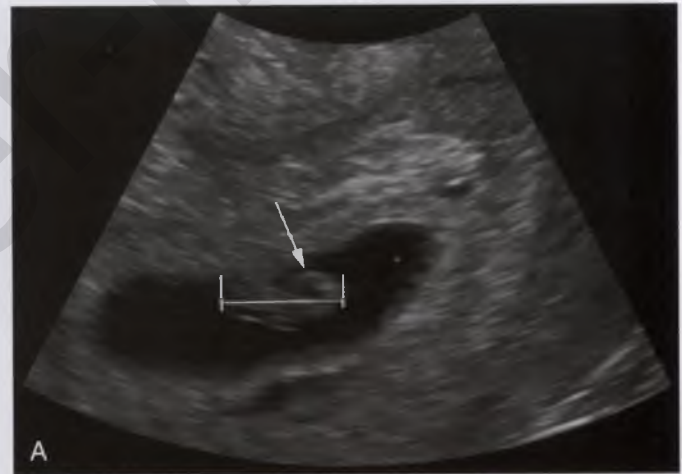


**FIG 38-44 A**, Attempted (and incorrect) measurement of the crown-rump length in a first trimester pregnancy. The measurement includes the embryo toward the left and the yolk sac (*arrow*) toward the right of the image. **B**, In the same pregnancy, the embryonic crown-rump length is correctly measured and does not include the adjacent yolk sac (*arrow*).



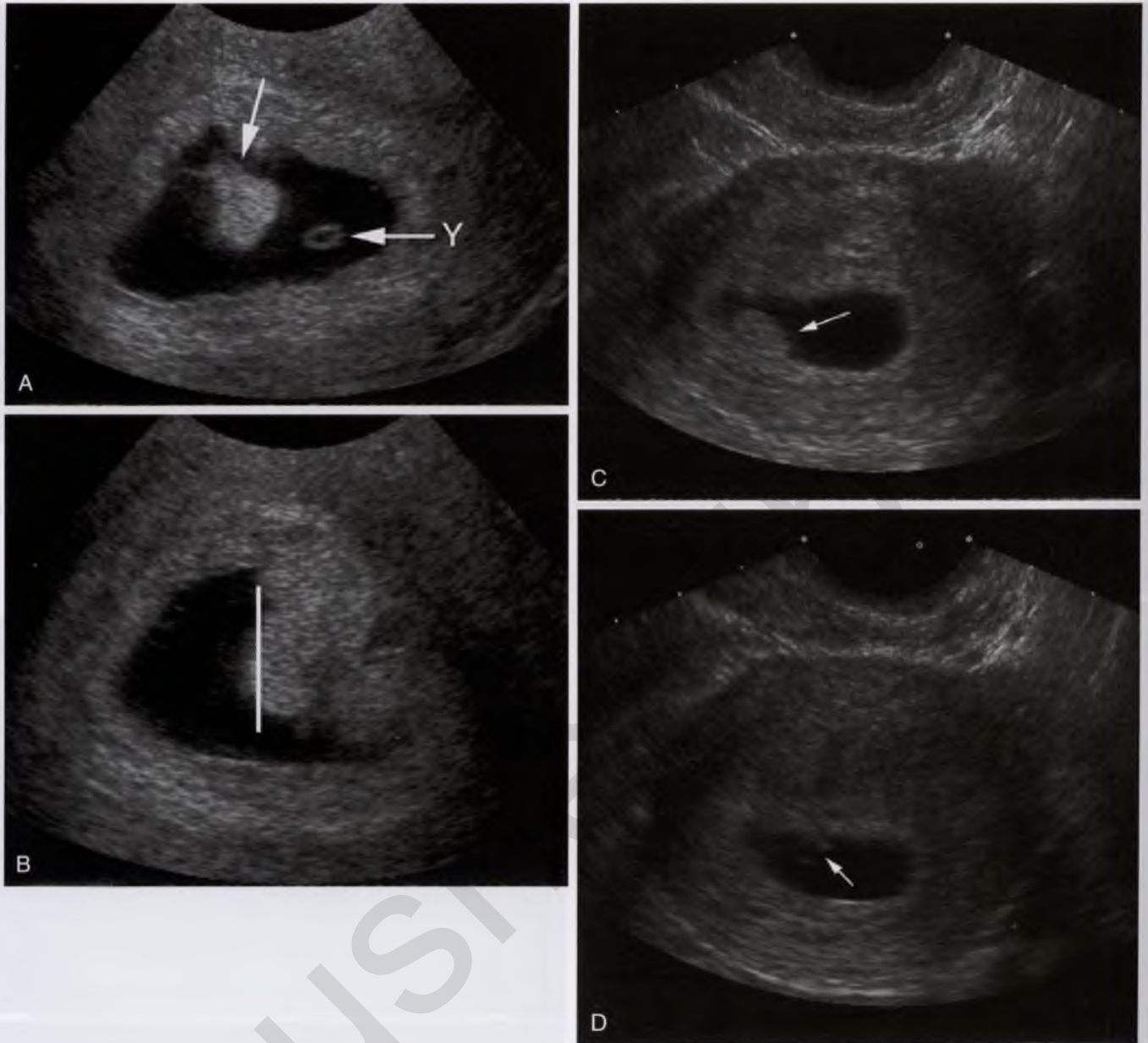


**FIG 38-45** **A**, Longitudinal section through the uterus of a patient presenting with vaginal bleeding during early pregnancy. A yolk sac (Y) is seen in addition to what appears to be an abnormal embryo (*arrow*). **B**, A transverse scan reveals that no embryo is present and that the tissue seen in A was due to partial volume through the developing placenta (*line*). This was a case of early pregnancy failure. **C**, Sonogram of another patient with a first trimester pregnancy at 6 weeks and 2 days. A soft tissue area is seen apparently within the gestational sac simulating a nonviable embryo (*arrow*). **D**, On the opposite side of the gestational sac, a yolk sac and embryo are seen (*arrow*). The patient's pregnancy was subsequently uneventful, and she delivered a normal infant. The structure seen in (C) was a lobular portion of the placenta referred to recently as the "chorionic bump." (Term from Harris RD, Couto C, Karpovsky C, et al: The chorionic bump: a first-trimester pregnancy sonographic finding associated with a guarded prognosis. *J Ultrasound Med* 25:757, 2006; Arleo EK, Troiano RN: Chorionic bump on first-trimester sonography: not necessarily a poor prognostic indicator for pregnancy. *J Ultrasound Med* 34:137-142, 2015.)

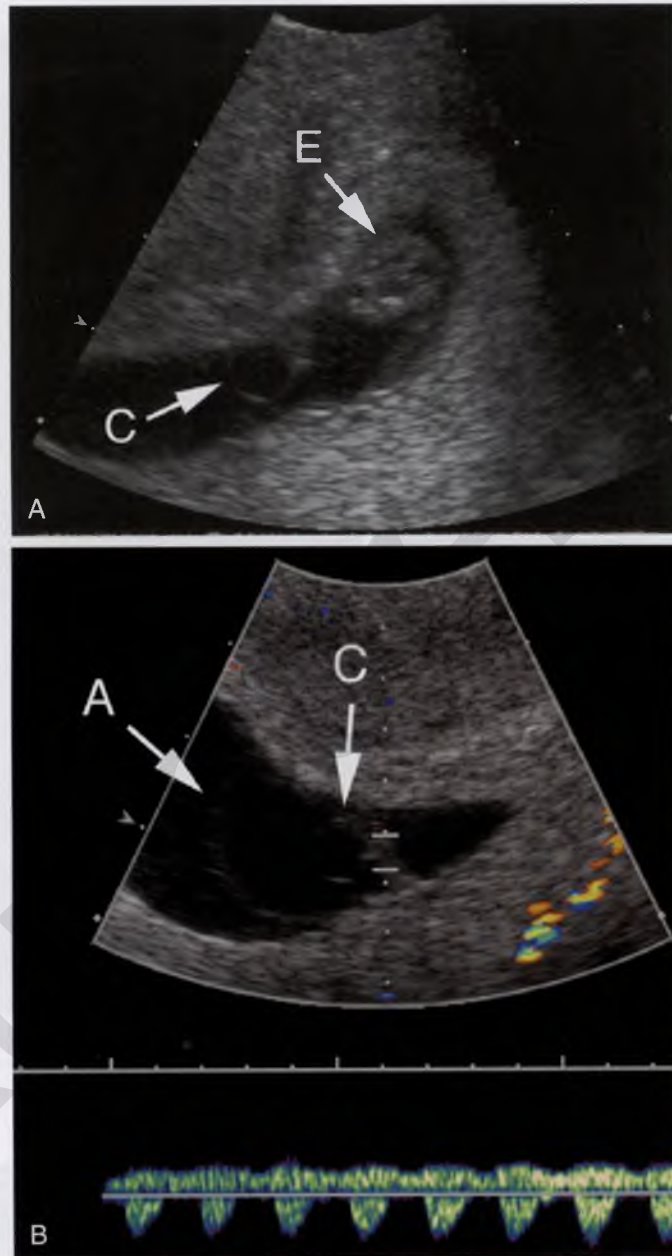


**FIG 38-46** **A**, An umbilical cord cyst (C) is seen in this first trimester pregnancy separate from the embryo (E). **B**, Doppler interrogation of the umbilical cord demonstrates that the cyst (C) is associated with the umbilical cord. A, amnion.



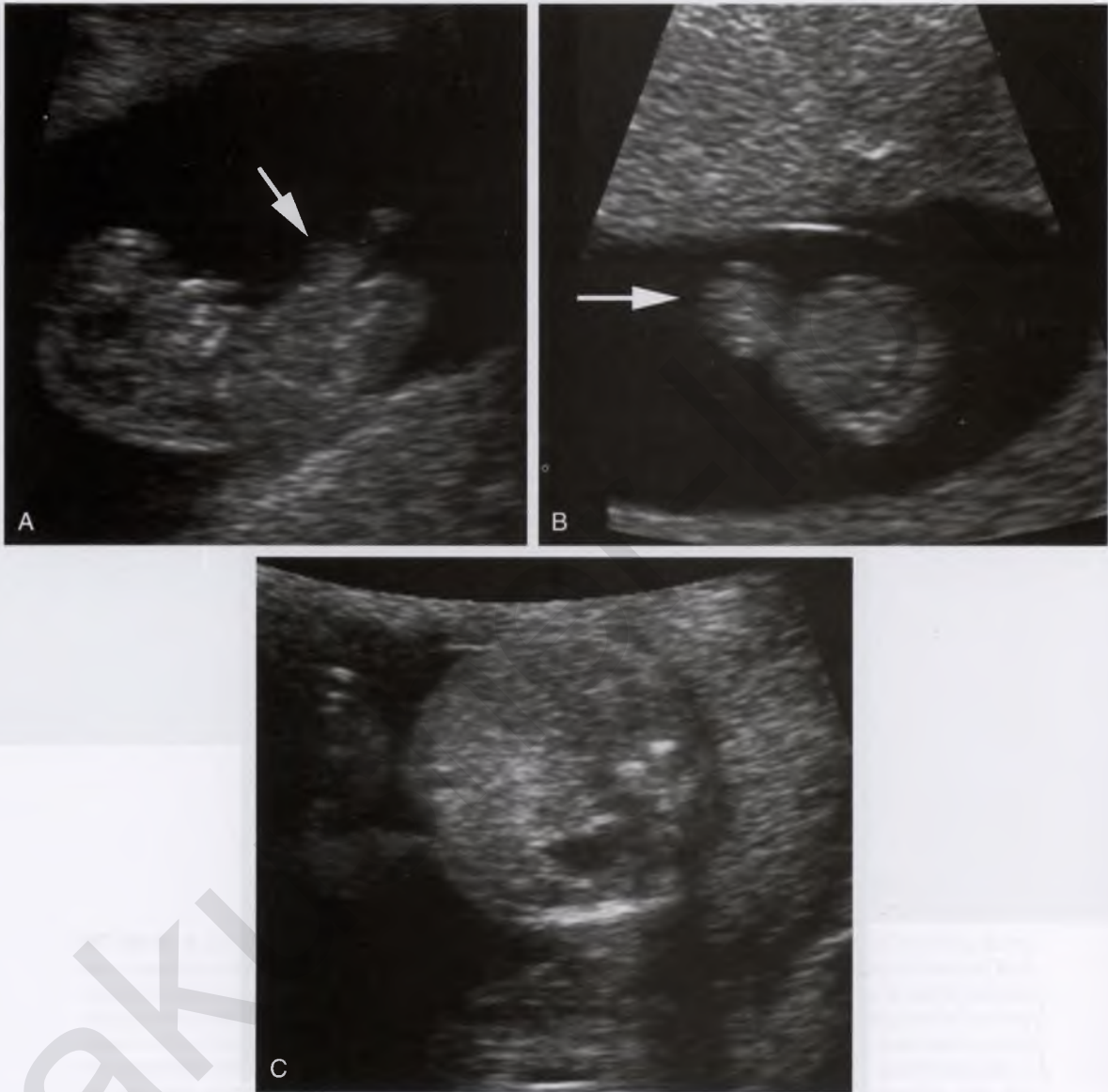


**FIG 38-47** **A**, Sonogram of an embryo demonstrates normal herniation of bowel (*arrow*) into the umbilical cord adjacent to the anterior abdominal wall. **B**, Sonogram of another embryo demonstrates an even larger but normal appearance to the herniated bowel (*arrow*). **C**, A follow-up scan of the patient in B demonstrates a normal anterior abdominal wall without evidence of an anterior abdominal wall defect. If there is any question, a follow-up scan, as was done in this case, should be performed.



**FIG 38-48** The amnion (*arrow*) is frequently identified in first trimester gestations. It apposes the chorion between 12 and 16 weeks' gestation. It should not be mistaken for amniotic band syndrome.



**FIG 38-49** A prominent fluid-filled intracranial area (*arrow*) can be seen in the cranium of the embryo, particularly with transvaginal sonography. This area represents the developing rhombencephalon and should not be mistaken for either hydrocephalus or holoprosencephaly.

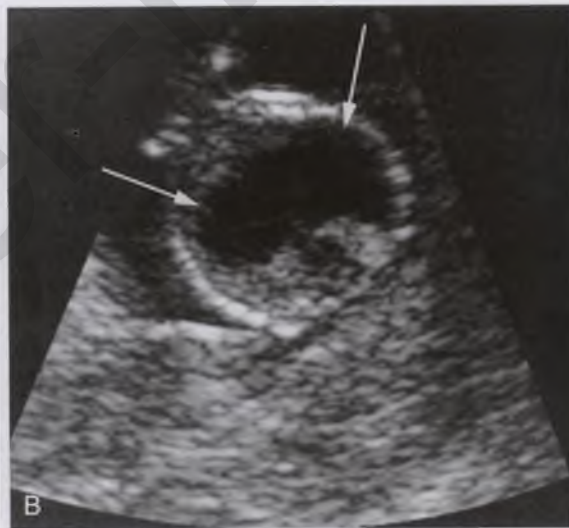


**FIG 38-50** **A**, A transabdominal sonogram of the gravid uterus demonstrated what appeared to be a normal embryo. **B**, A transvaginal sonogram of the same patient done at the time of chorionic villus sampling demonstrates a large monoventricular cavity (*arrows*) consistent with holoprosencephaly. Trisomy 13 was detected.



**FIG 38-51** Although the diagnosis of anencephaly is certainly possible in the first trimester, the likelihood of a false negative diagnosis is high. The angiomatous stroma (**A**, *arrow*) in a case of anencephaly simulates the normal brain in another case (**B**, *arrow*).



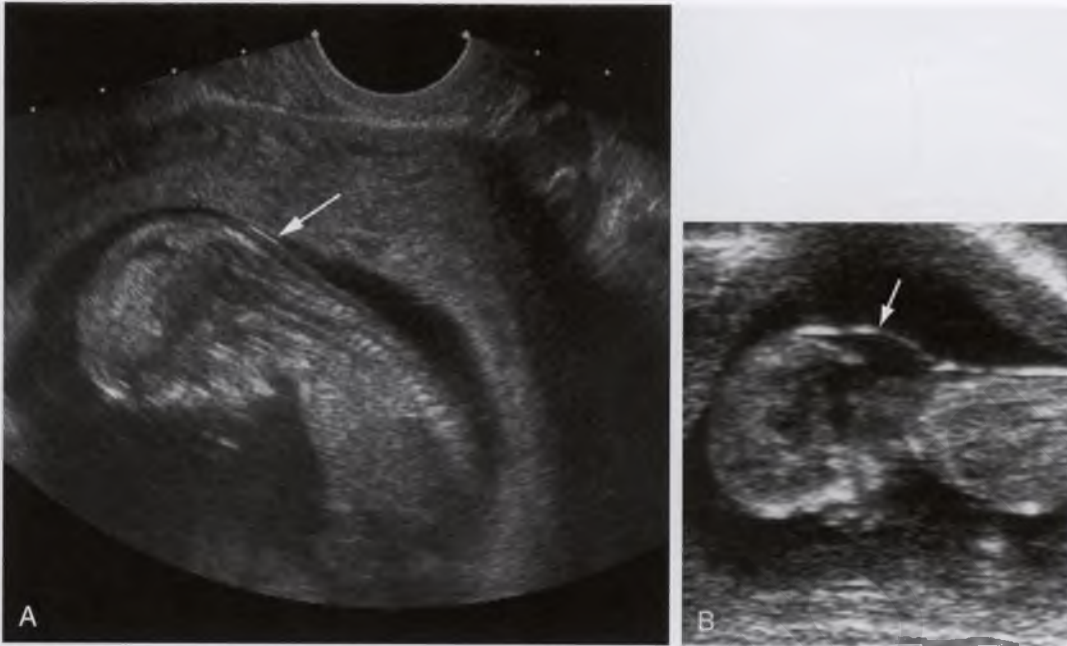


**FIG 38-52** **A**, Normal integument (nuchal translucency) (*arrow*) in an early second trimester fetus. **B**, Normally, the nuchal translucency is measured to determine if it is abnormally increased in thickness. In this fetus, the large rounded configuration to the nuchal translucency (*arrow*) can readily be determined to be abnormal subjectively.

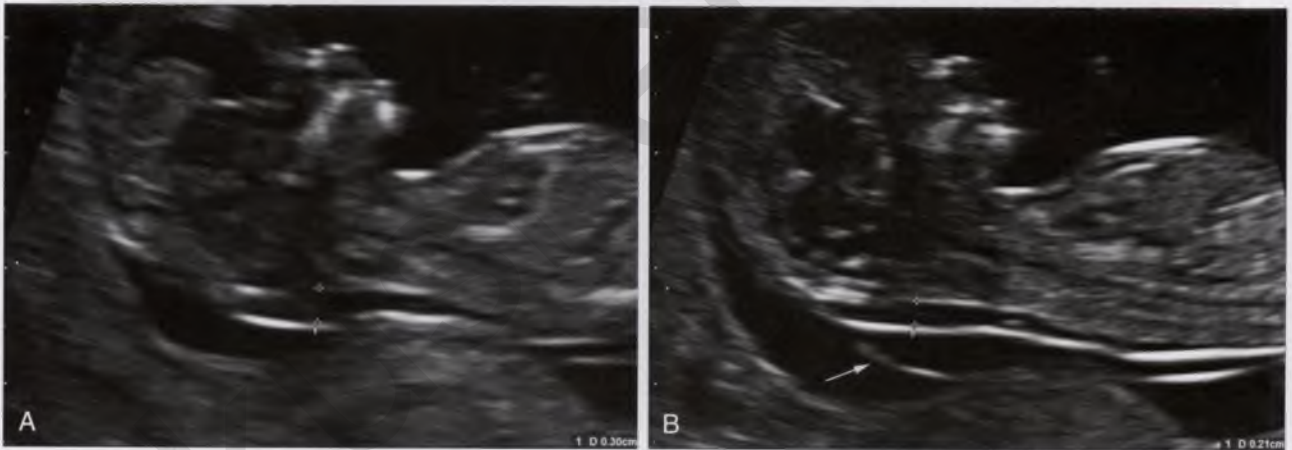


**FIG 38-53** **A**, Erroneous measurement of the nuchal translucency. This abnormal measurement between the calipers extends to the amnion rather than to the integument. **B**, In the same pregnancy, the nuchal translucency is correctly measured and is normal. The amnion (*arrow*) can be seen separate from the fetus.



**FIG 38-54** **A**, On this near sagittal plane of section, the nasal bone (*arrow*) appears to be absent. **B**, In a more midline sagittal scan, the nasal bone (*arrow*) can clearly be seen.

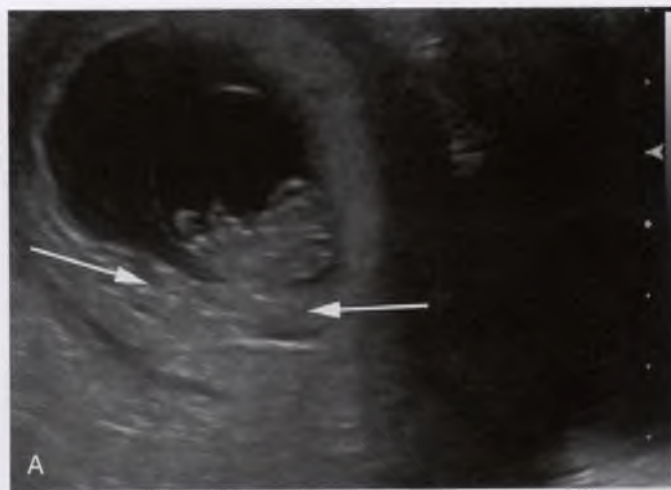


**FIG 38-55** **A**, On many scans through the gravid uterus, there appeared to be a singleton gestation with prominent myometrium posteriorly (*arrows*). **B**, On an oblique plane of section it became clear that there was a dichorionic twin pregnancy with demise of the second twin (*arrows*).



## THE FETAL HEAD AND NECK

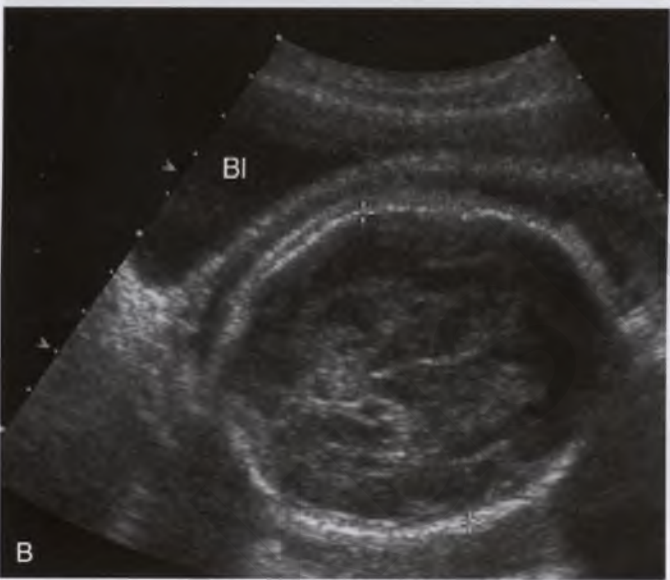


**FIG 38-56** **A**, Sonogram of a third trimester fetus demonstrates what appears to be scalp thickening (*arrow*). **B**, In a slightly wider field of view, it can be clearly seen that what appeared to be fetal scalp was in fact the wall of the maternal urinary bladder. Bl, bladder.

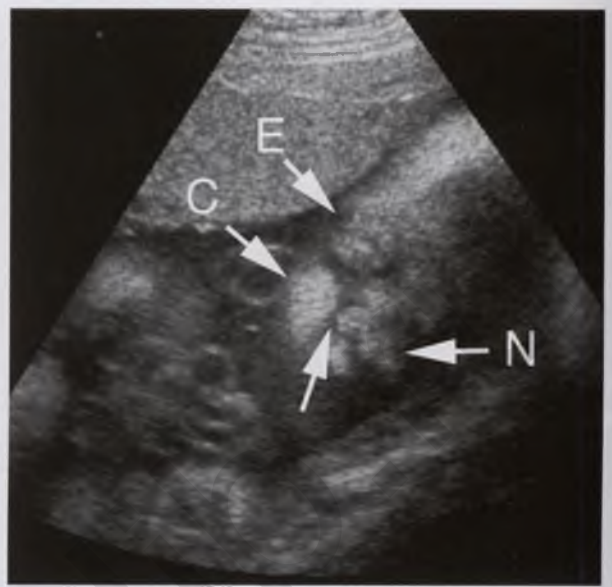
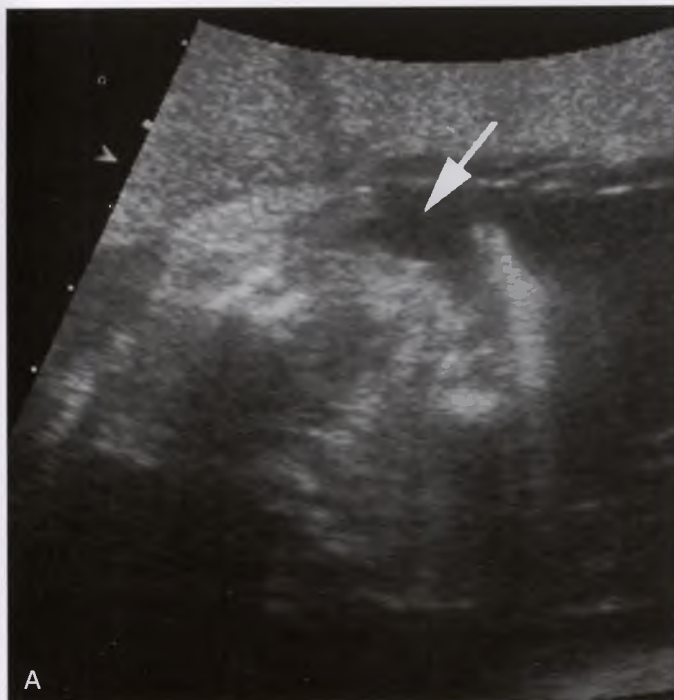
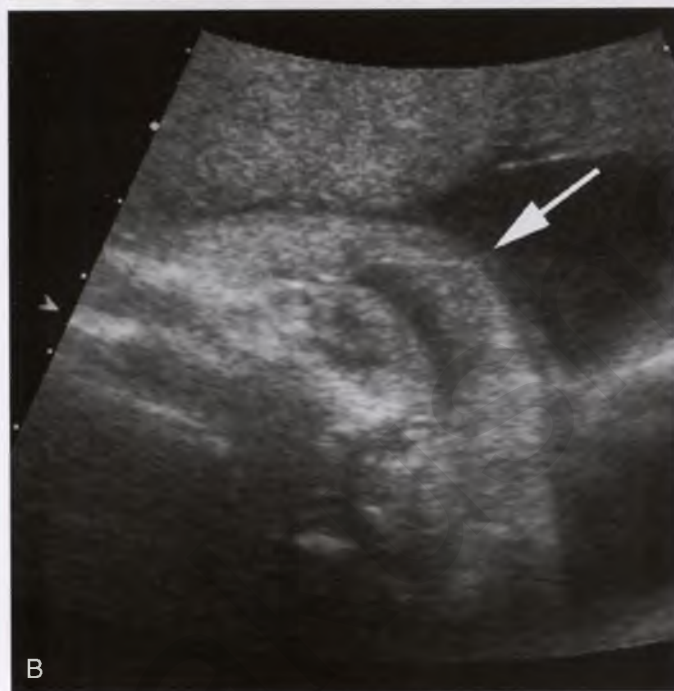


**FIG 38-57** Pseudocleft of the face. The space (*arrow*) between the fetal nose (N) and cheek (C) should not be misinterpreted as a cleft. E, eye.



A



B

**FIG 38-58** Pseudocleft lip. **A**, An angled “oblique” view of the face demonstrates what appears to be a gap in the lip (*arrow*). **B**, Normal-appearing lip (*arrow*) obtained on a slightly different plane of section.



A



B

**FIG 38-59** **A**, Coronal plane of section of the fetal face. Because of a slight compression of the fetal face, the upper lip creates the appearance of a mass (*arrow*). **B**, As the mouth opens wider, the upper lip (*arrow*) appears normal.



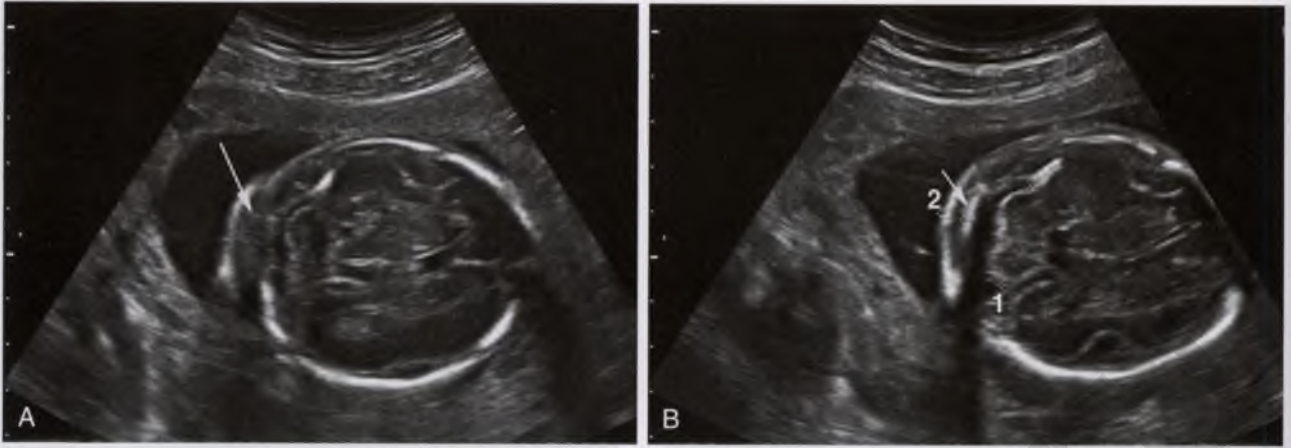


**FIG 38-60** **A**, Transverse axial plane of section of the fetal head at 20 weeks' gestation. The nuchal fold area (*arrow*) appears abnormally prominent. **B**, Normal appearance of the nuchal fold in the same fetus. To accurately measure the nuchal fold the posterior surface of the occipital bone should be imaged (*arrow*). This can often be achieved by scanning from a 30-degree occipital direction. (From Cho JY, Kim KW, Lee YH, Toi A: Measurement of nuchal skin fold thickness in the second trimester: influence of imaging angle and fetal presentation. *Ultrasound Obstet Gynecol* 25:253-257, 2005.)



**FIG 38-61** The nuchal fold (*asterisk*) appears prominent on this sagittal scan through the posterior cervical region. However, this is related to fetal position with extension of the cervical spine.



**FIG 38-62** Normal fetal hair (*arrows*) may be seen commonly in third trimester fetuses and should not be mistaken for a calvarial mass or scalp edema.



**FIG 38-63** Sonogram of the fetal head commonly used for measurement of the biparietal diameter and head circumference. This case has a common variation referred to as dolichocephaly. The importance is that measurement of the biparietal diameter in such fetuses will tend to underestimate gestational age. Dolichocephaly may also be seen in cases of breech presentation, oligohydramnios, and myelomeningocele.



**FIG 38-64** Interaction of the sound beam with the curved surface of the calvarium produces troubling appearances. This fetus appears to have overlapping sutures (*arrow*). In fact, this was an artifact related to refraction of the sound beam. The fetal calvarium was normal when the transducer angle was changed.

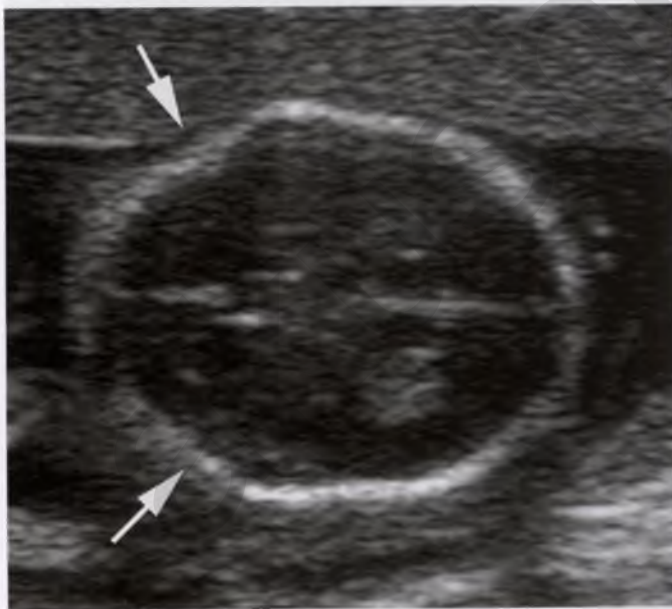


**FIG 38-65** Frontal concave scalloping (*arrows*), the so-called lemon sign, has been described in patients with a myelomeningocele. This may also be a normal finding, as it was in this case.



**FIG 38-66** Projections from the fetal cranium can often be disturbing. In cases of polyhydramnios, the fetal ear (E) can be seen perpendicular to the fetal skull and may simulate an encephalocele, which would be uncommon in this location.



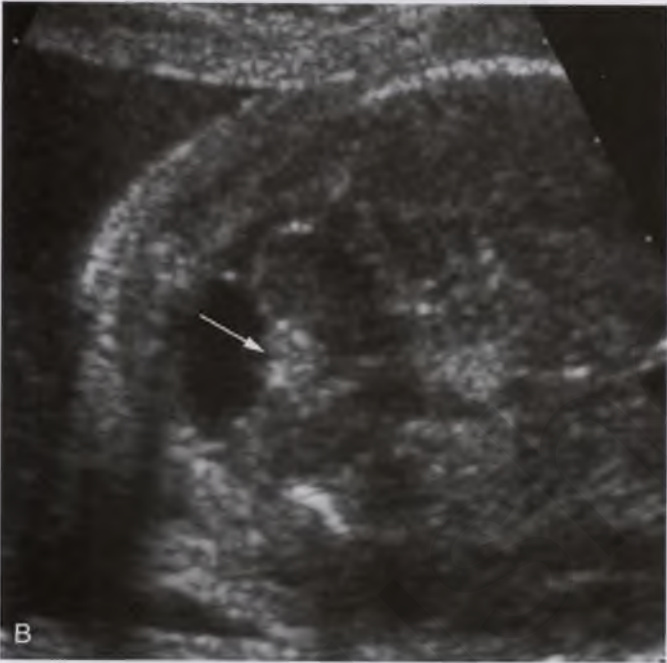


**FIG 38-67** **A**, Sonogram of a fetus at 17 weeks' gestational age. In the posterior fossa, fluid is seen in the midline (*arrow*) and the cerebellar vermis appears to be absent. **B**, A scan of the same patient at 25 weeks reveals a normal vermis (*arrow*), which does not fully form until the middle of the second trimester.

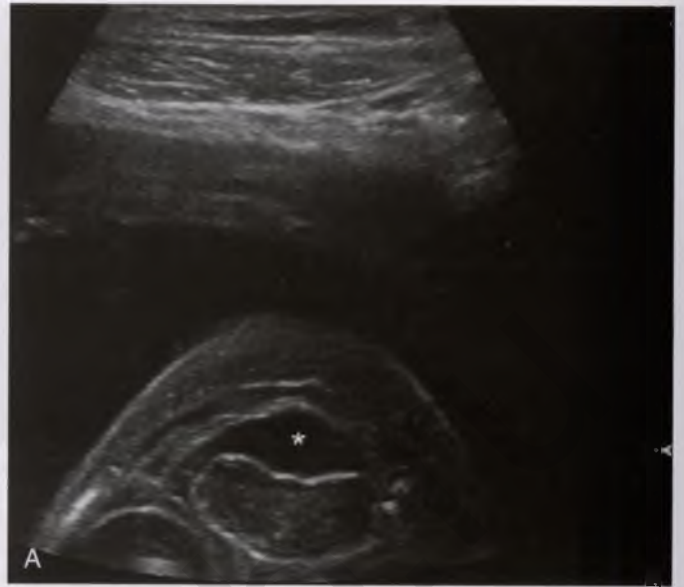


**FIG 38-68** **A**, Steeply angled oblique scan through the posterior fossa makes the cisterna magna (*asterisk*) appear abnormally enlarged. **B**, In a more conventional transverse axial plane of section, the cisterna magna is shown to be normal in size.

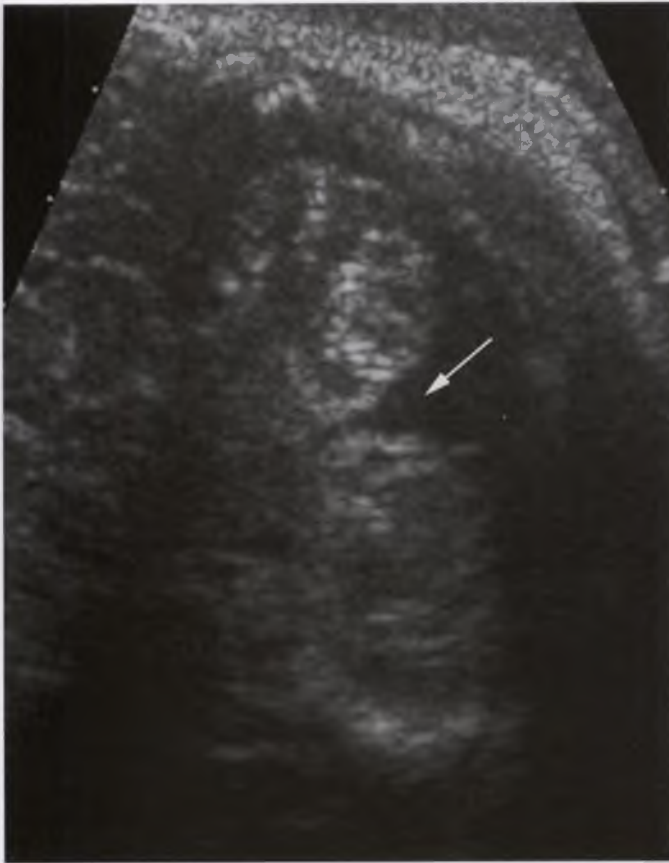


**FIG 38-69** Steep transverse scan through the posterior fossa may contribute to a pitfall. The normal space (*arrow*) between the cerebellar hemispheres (vallecula) may appear overly prominent and simulate vermian agenesis.



**FIG 38-70** Linear echoes (*arrows*) seen in the region of the cisterna magna should not be mistaken for either an arachnoid cyst or a dilated sinus. The exact cause is controversial, although a recent hypothesis is that these echoes may represent the vestigial remnants of Blake pouch. (From Robinson AJ, Goldstein R: The cisterna magna septa: vestigial remnants of Blake's pouch and a potential new marker for normal development of the rhombencephalon. *J Ultrasound Med* 26:83, 2007.)

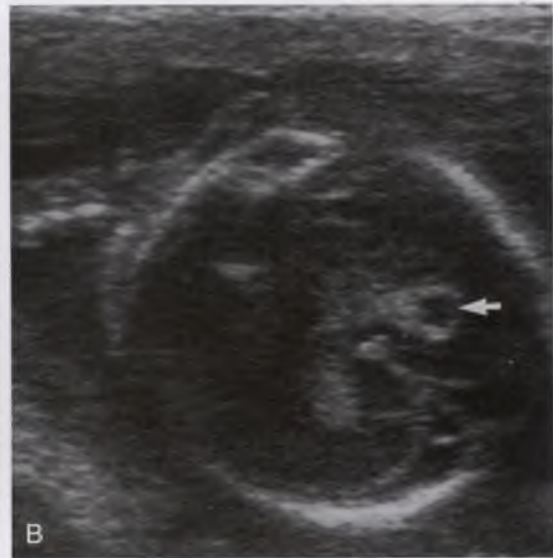
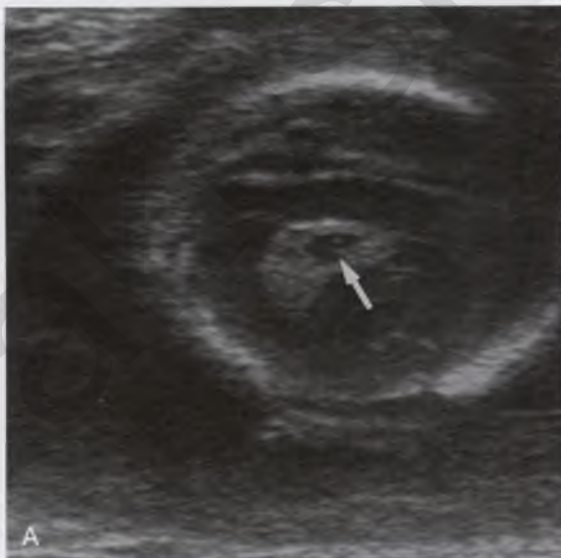


**FIG 38-71 A and B**, The choroid plexus cyst (*arrow*) is a normal variant that has been the subject of much controversy during the past several years. Although most cases are simply normal variants that will resolve by 24 to 26 weeks' gestation, some cases may be associated with other anomalies and trisomy 18.

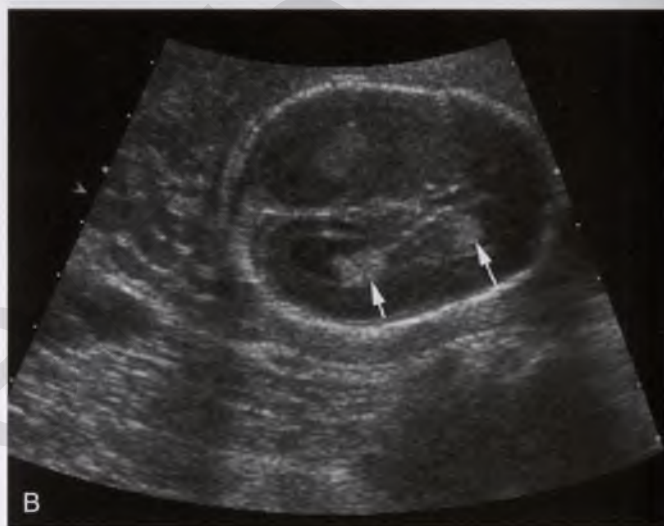




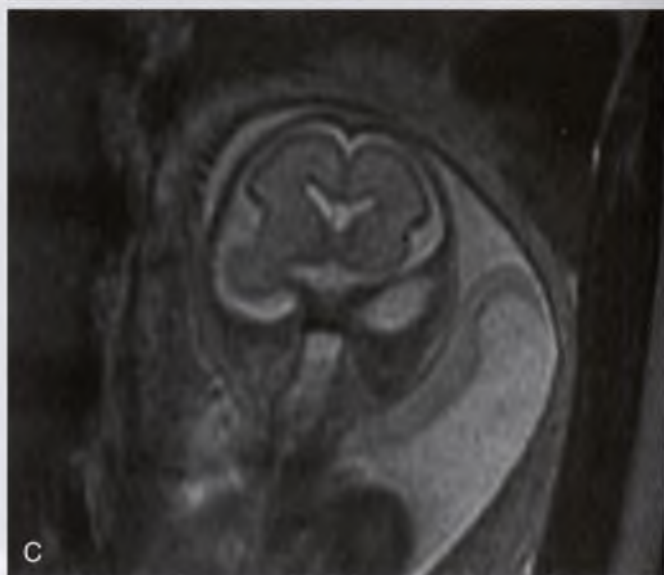
**FIG 38-72** Heterogeneous choroid plexus bilaterally. No defined cysts were seen. The fetus and neonate developed normally.



A



B



C

**FIG 38-73** **A**, Sonogram performed at 18 weeks demonstrated a focal area of increased echogenicity thought to possibly represent intraventricular hemorrhage (*arrow*). **B**, In another plane of section from the same fetus, the area of increased echogenicity was thought to represent normal echogenic choroid plexus (*arrows*). **C**, Because of concern by the patient, she underwent a magnetic resonance imaging scan, which revealed the fetal brain to be normal without intracranial hemorrhage.

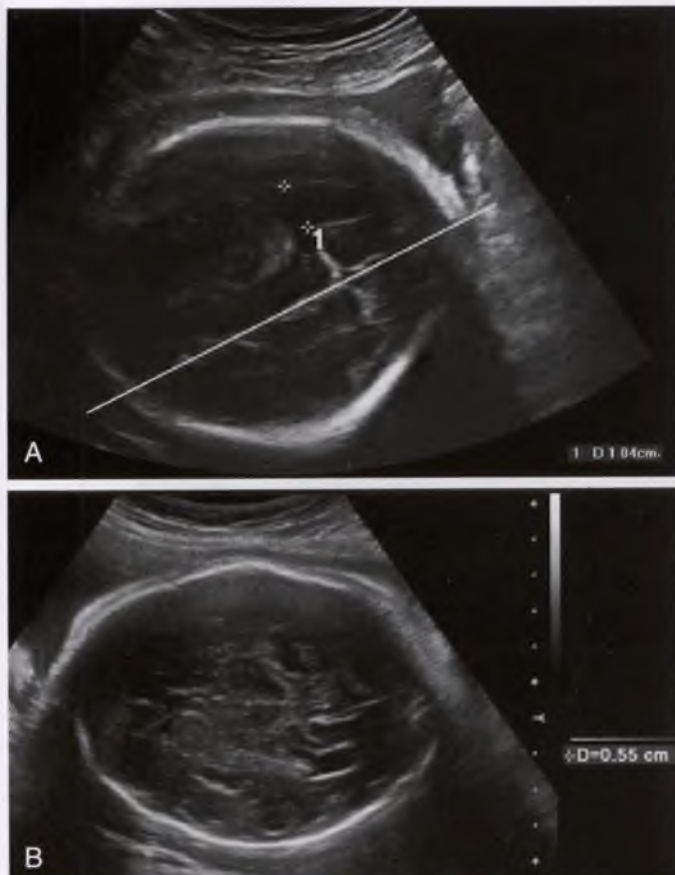


**FIG 38-74** **A**, A patient was referred because a sonogram performed at 31 weeks' gestation revealed a mildly dilated cerebral ventricle. Note that the scan plan is angled (oblique axial) such that the midline (*line*) is off-center. **B**, When the scanning plane was corrected (true transverse axial) such that the brain anatomy appeared symmetric, the lateral ventricle is shown to be of normal size.

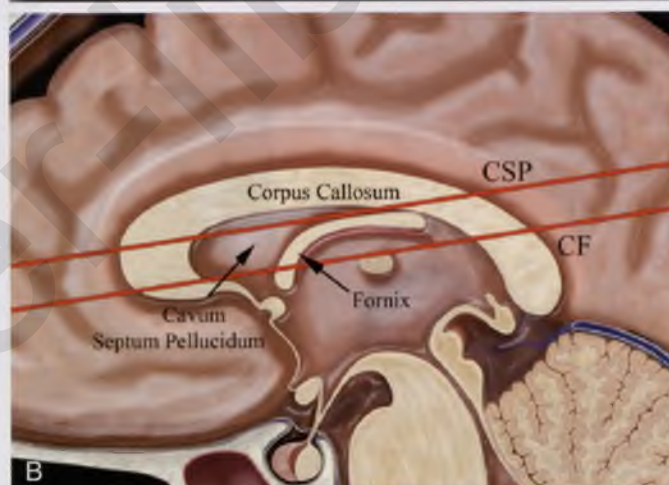


**FIG 38-75** **A**, Transverse axial sonogram of the fetal brain performed at an outside institution at 18 weeks' gestation. The structures between the arrows were interpreted as the normal cavum septi pellucidum. **B**, Midline sagittal illustration demonstrating the relationship of the corpus callosum, cavum septi pellucidum, and the fornix. The planes of section demonstrating the cavum septi pellucidum (CSP) and the columns of the fornix (CF) on corresponding transverse axial planes of section are depicted. **C**, Transverse axial sonogram in an 18-week gestation fetus. The cavum septi pellucidum (*arrow*) appears as a fluid-filled "box" between the frontal horns of the lateral ventricles. (B by James A. Cooper, MD, San Diego, CA.)



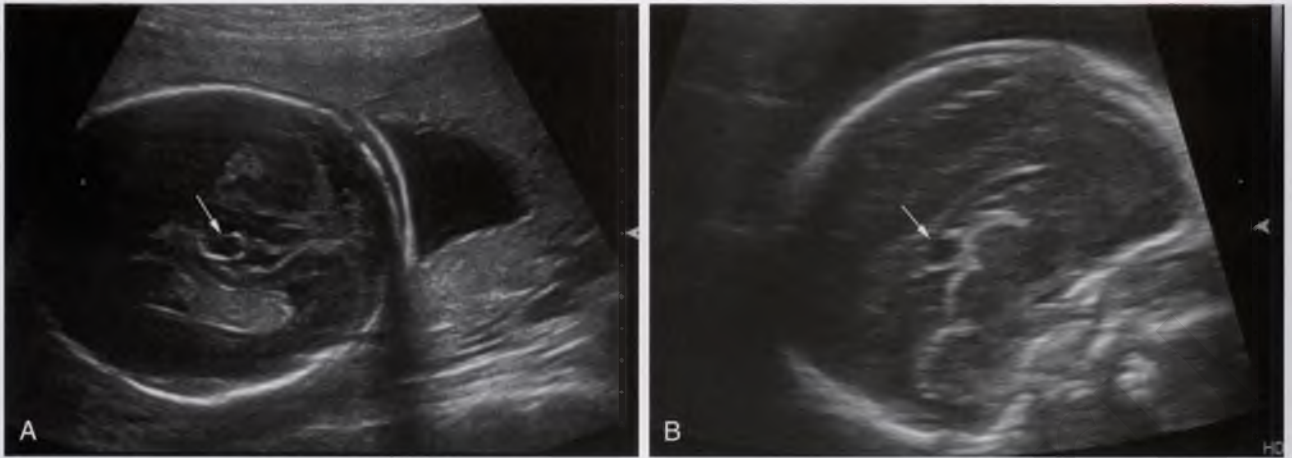


**FIG 38-76** **A**, Cyst of the velum interpositum. A small midline cystic structure (*arrow*) is seen on this transverse axial sonogram. This finding may mimic a dilated third ventricle. **B**, On this sagittal view, the "cyst" (*arrow*) is located anteriorinferior to the splenium of the corpus callosum, superior and posterior to the thalami. It is most often a benign finding. The differential diagnosis of a cyst of the velum interpositum would include dilated cavum vergae or arachnoid cyst of the quadrigeminal cistern.

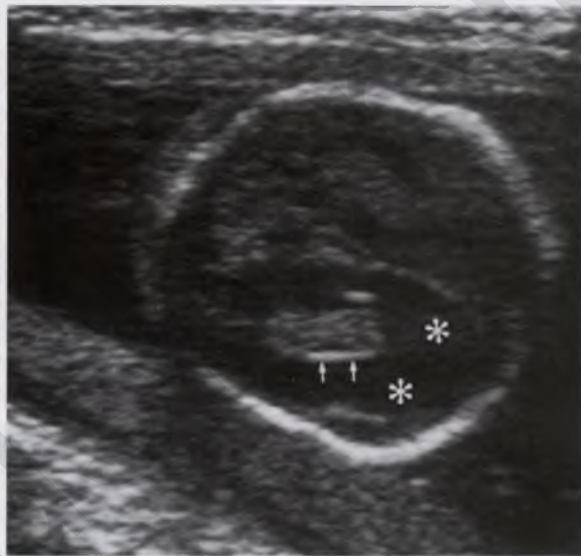


**FIG 38-77** The normal fetal brain is sonolucent (*asterisks*) and may simulate cerebrospinal fluid. This appearance may incorrectly lead to the diagnosis of hydrocephalus. Identification of the lateral ventricular walls (*arrows*) and the choroid plexus within will help resolve this confusion.

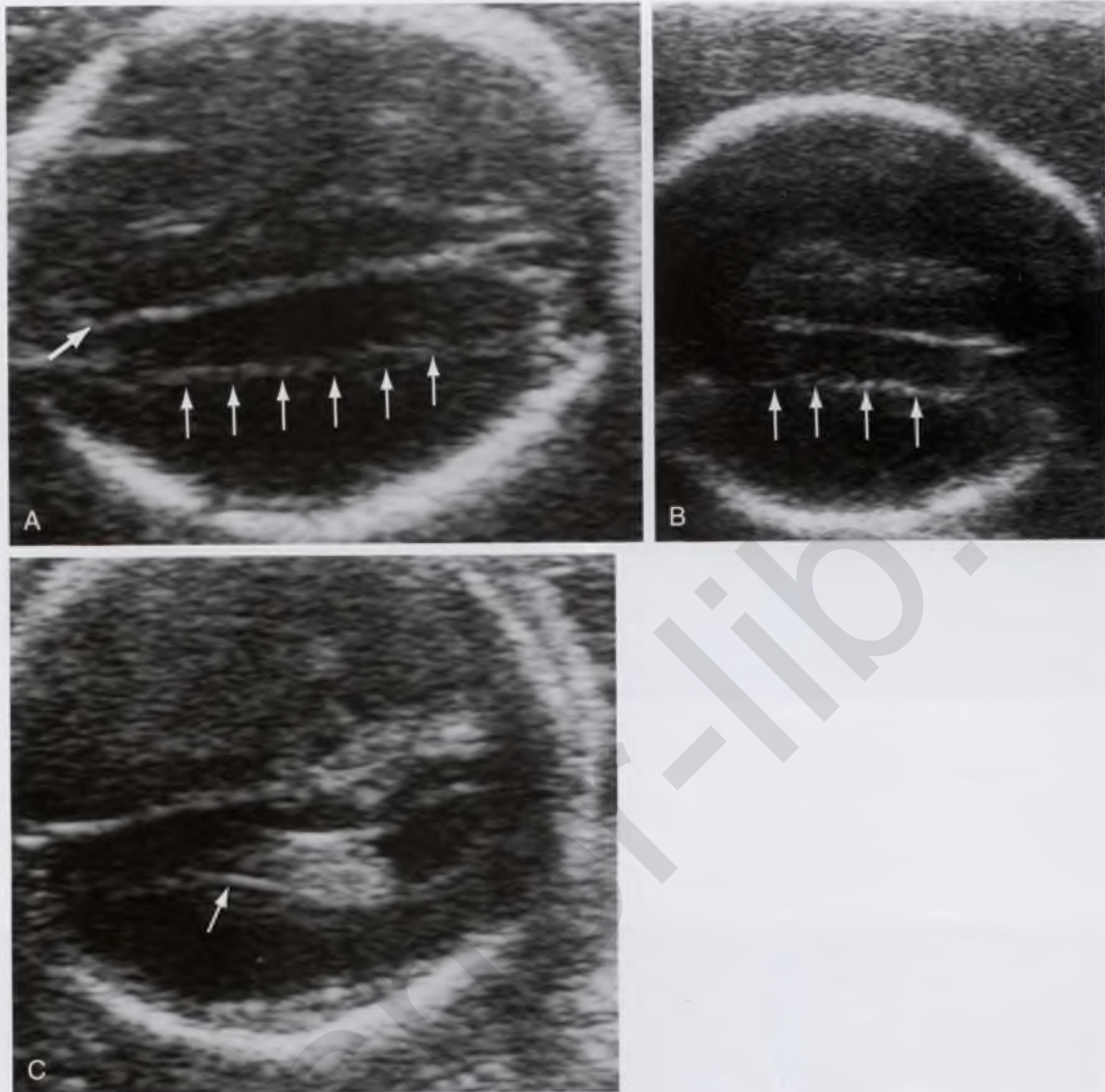


**FIG 38-78** **A** and **B**, Transverse axial plane of section in two normal patients. The paramedian lines (*thin arrows*) paralleling the midline interhemispheric fissure echo (*thick arrow*) are due to deep cerebral medullary white matter veins and not the lateral wall of the lateral ventricle. **C**, The lateral wall of the lateral ventricle (*arrow*) is seen at a slightly more basal level and angling laterally away from the midline.



**FIG 38-79** The hyaloid artery (*arrow*) can often be seen in the second trimester. It disappears between 23 and 28 weeks of gestation and is normally not visible by ultrasound after 29 weeks of gestation.



## THE FETAL THORAX

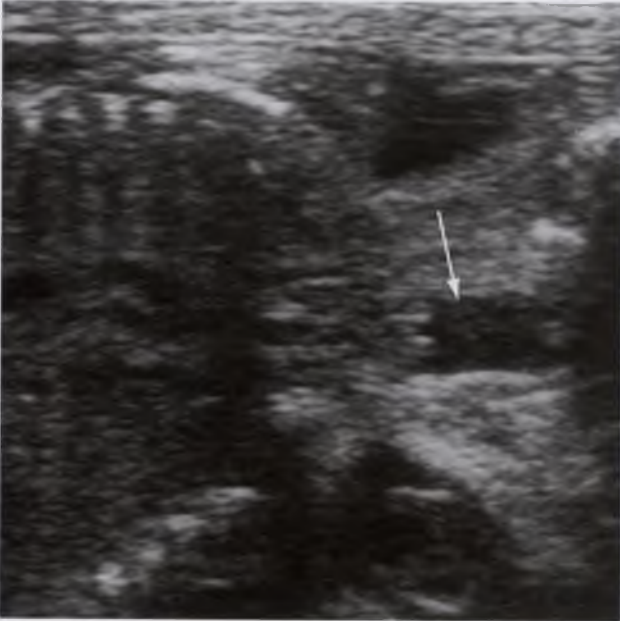


**FIG 38-80** The fetal hypopharynx (*arrow*) may be prominent. It may be seen to fill and empty with fluid during the examination. This should not be mistaken as representing esophageal obstruction.

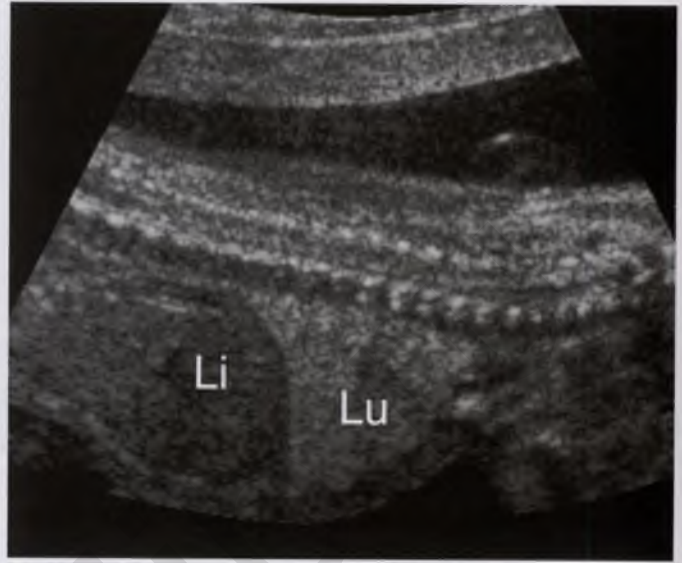


**FIG 38-81** The echogenicity of the fetal lung (Lu) may often be misleading. The lung in this oblique coronal scan appears brightly echogenic compared with the liver (Li); however, this fetus neither is mature nor has lung disease.

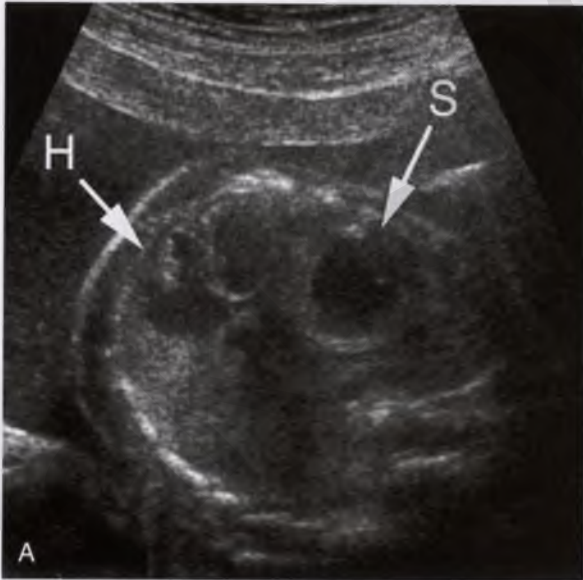


**FIG 38-82 A**, Angled transverse axial plane of section at the level of the fetal heart (H). The fetal stomach (S) is seen at the same level as the heart, raising the possibility of a diaphragmatic hernia. **B**, This sagittal plane of section from the same patient reminds us that the diaphragms (*arrow*) are curved, and a slightly angled transverse plane of section will portray what appears to be a diaphragmatic hernia, although the stomach (S) is, in fact, below the diaphragm.



**FIG 38-83** Soft tissue suggested within the right ventricle may be considered worrisome for either thrombus or neoplasm. In this patient, the normal but prominent moderator band (M) of the right ventricle (RV) is seen. LV, left ventricle.



**FIG 38-84 A**, An apparent defect in the ventricular septum (*arrow*) is seen. This may be due to the origin of the aortic root and the thin membranous septum. **B**, Slight change of the transducer position demonstrates a normal-appearing septum.



**FIG 38-85 A**, The poorly echogenic myocardium (*arrows*) may simulate pericardial fluid. The observation that this area blends imperceptibly with the intraventricular septum should alert one that this is a normal cardiac structure and not pericardial fluid. **B**, The case in A should be contrasted with real pericardial fluid (*arrow*), which contains no echoes.



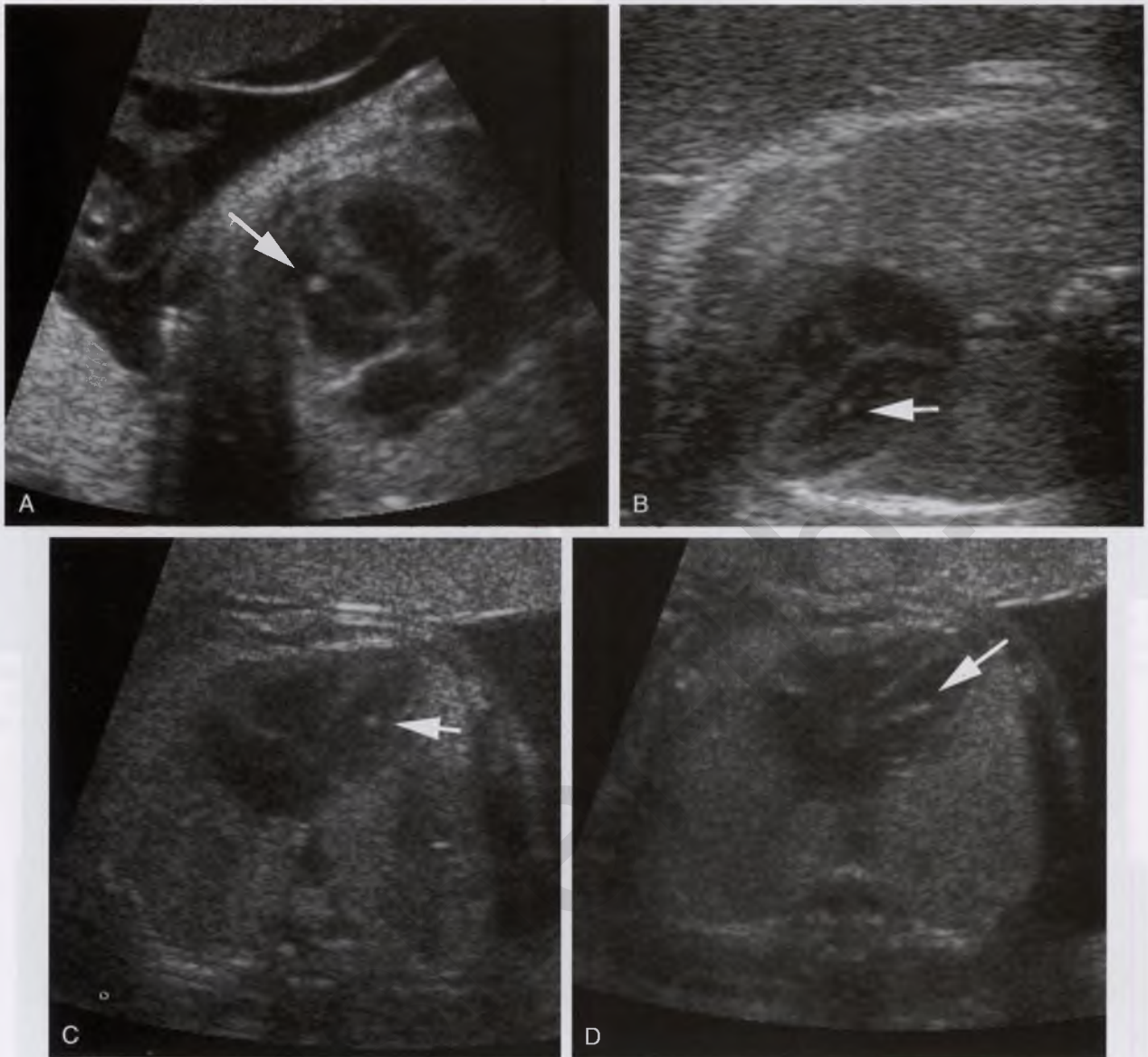


**FIG 38-86** Echogenic intracardiac focus. **A**, A high-amplitude echo (*arrow*) is seen in the left ventricle in this patient. This appearance is believed to be due to reflection from calcification in the papillary muscle. In this case, the echogenic structure was fairly large. The significance of this finding is controversial; in some cases, it is associated with karyotype abnormalities. **B**, A smaller echogenic intracardiac focus (*arrow*) is seen in another patient. **C**, In this patient, a reflection (*arrow*) from the atrioventricular valve is seen. It appears similar to an echogenic intracardiac focus. **D**, The reflection from the surface of the valve (*arrow*) is better seen in another plane of section.

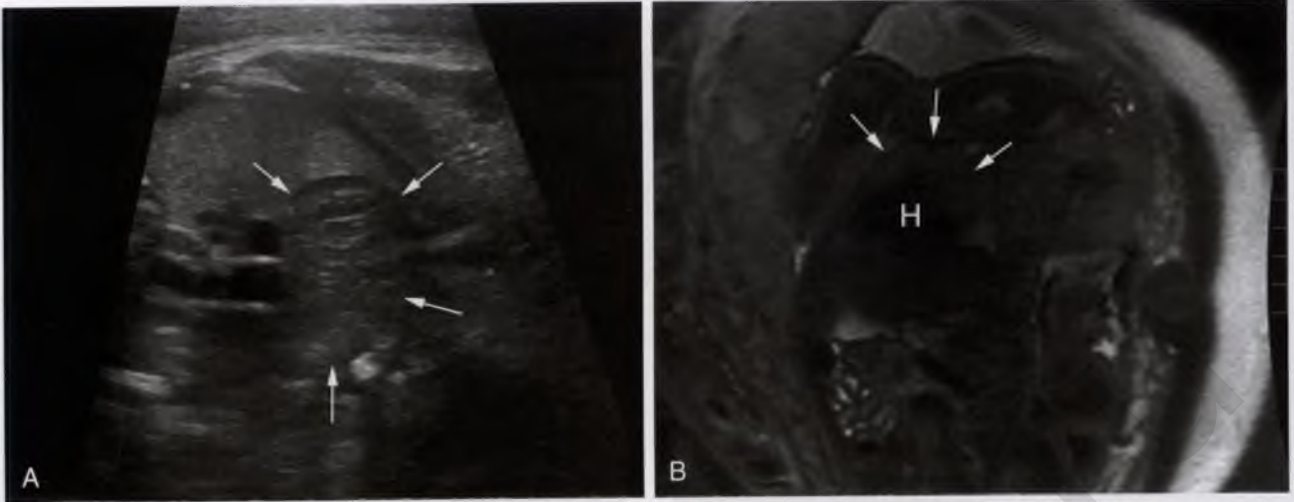


**FIG 38-87** Normal thymus. **A**, The normal thymus (*arrows*) may appear quite prominent in a fetus. It is usually seen as an oval soft tissue structure anterior to the great vessels, as in this case. It should not be misinterpreted as a chest mass. **B**, A magnetic resonance imaging scan of the same patient demonstrates the normal thymus (*arrows*). H, heart.

## THE FETAL ABDOMEN

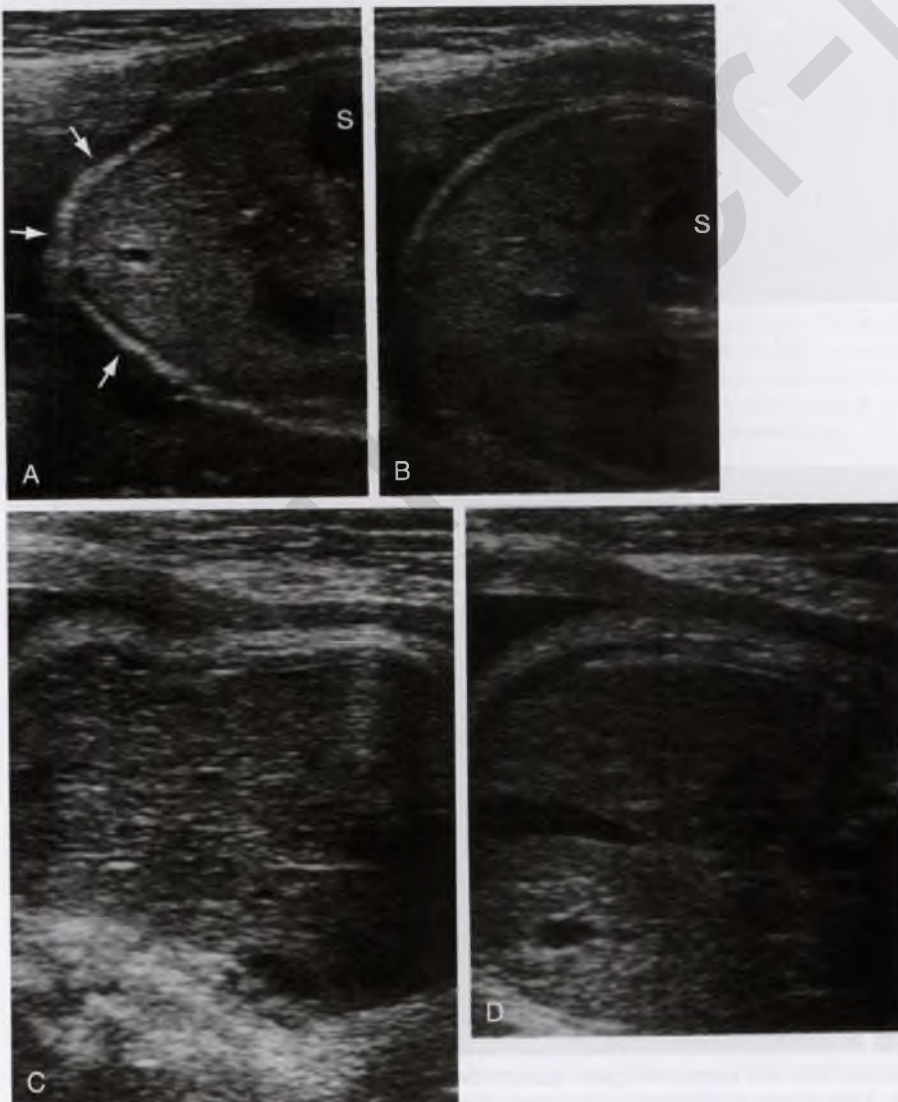


**FIG 38-88** Pseudo-omphalocele in two patients. **A** and **C**, Excessive pressure with the linear array transducer causes deformation of the abdominal wall, simulating an abdominal wall defect. Identification of the normal skin covering this protuberance (*arrows*) and less pressure on the maternal abdomen will usually resolve the confusion. **B** and **D**, Same patients demonstrating normal anterior abdominal wall with light pressure on the maternal abdomen. S, stomach.





**FIG 38-89** Focal laxity of the anterior abdominal wall (*arrow*) is seen in this second trimester sonogram. The anterior abdominal bulge was accentuated when the fetus flexed its thighs. Although this may have the appearance of an anterior abdominal wall defect, it was eccentric and skin covered. The neonate was normal at birth.

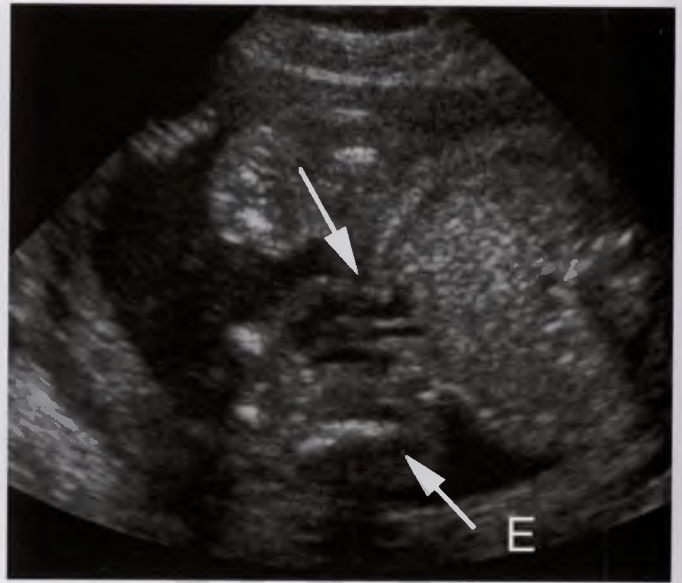


**FIG 38-90** Pseudogastroschisis caused by an extremity (E) adjacent to the umbilical cord insertion site (*arrows*).

**FIG 38-91** Gastroschisis in a second trimester pregnancy. Multiple loops of bowel are seen adjacent to the fetal abdomen within the amniotic fluid. What appears to be dilated bowel is normal colon (*arrow*), which may appear to be prominent although nondilated.

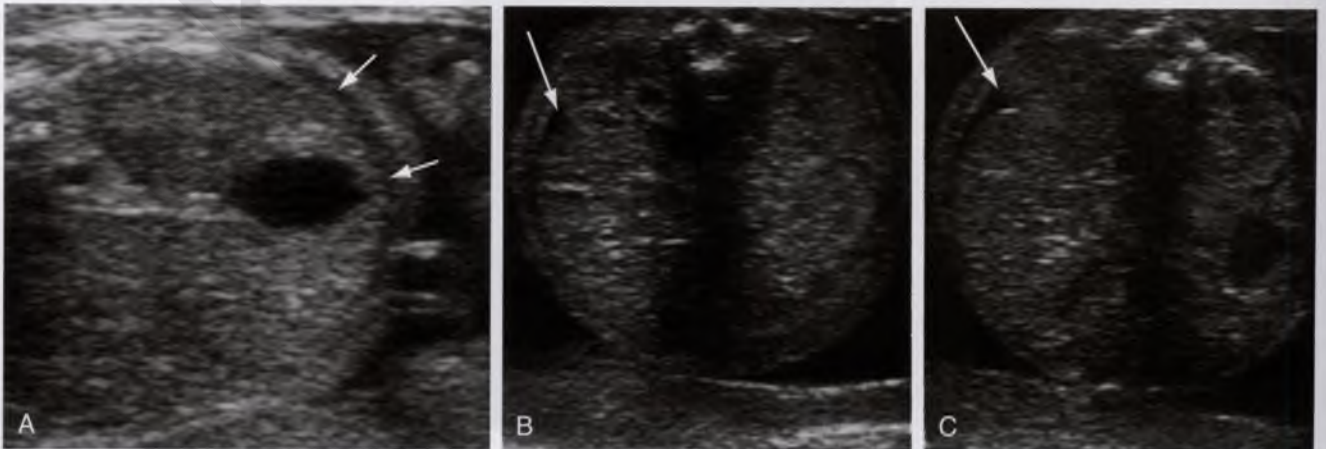
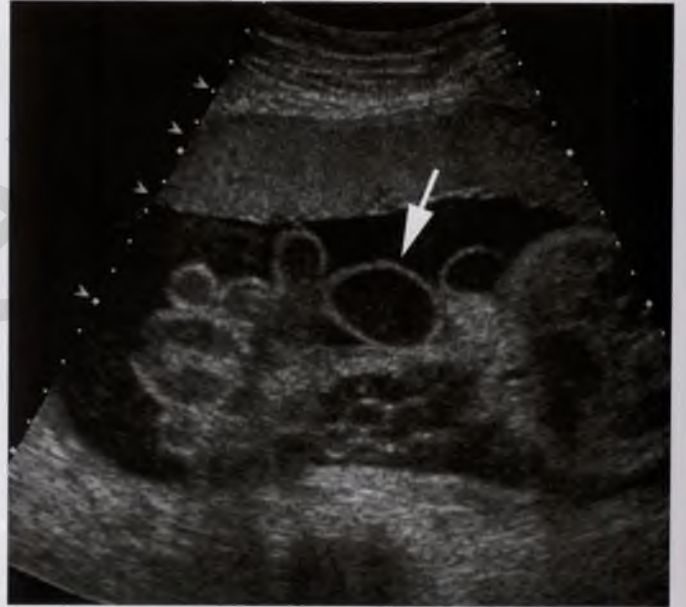


**FIG 38-92** **A**, Pseudoascites resulting from the poorly echogenic appearance of the normal integument (*arrows*). **B** and **C**, A small amount of real ascites is identified in this patient. Notice that the fluid invaginates between the viscera on the right side (*arrows*).



**FIG 38-93** Debris within the fetal stomach (*arrow*). Although occasionally the cause may be known (i.e., swallowed blood from an intrauterine transfusion), most often it is unknown. This is almost always an innocuous finding.

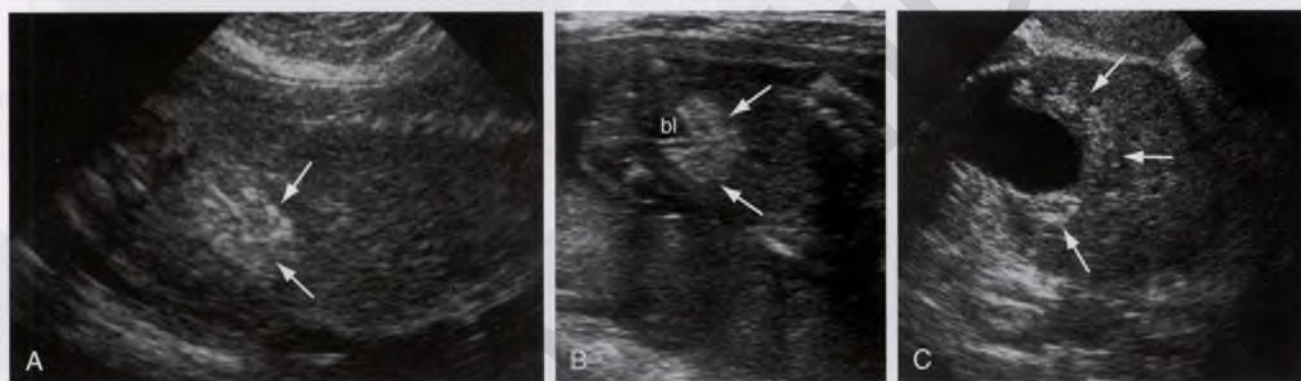


**FIG 38-94** Hyperechogenicity within the fetal abdomen (*arrows*). This finding has received recent attention in the literature as a possible clue to the diagnosis of either cystic fibrosis or aneuploidy. The problem is in differentiating normal from abnormal. **A** and **B**, Normal chromosomes and no evidence of cystic fibrosis. *bl*, bladder. **C**, A case of meconium ileus and cystic fibrosis at birth (*arrows*). To be called echogenic bowel the echogenicity of the bowel should be similar to that of adjacent bone.

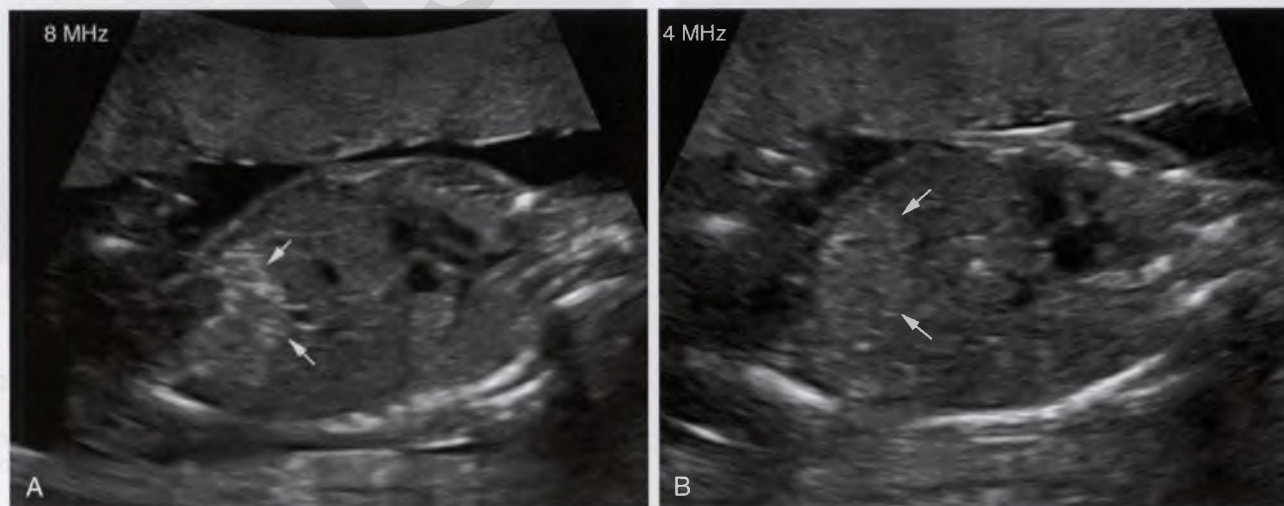


**FIG 38-95** Pseudo-hyperechogenic fetal bowel. **A**, Sonogram of the fetal abdomen obtained with an 8-MHz frequency transducer demonstrates hyperechogenic fetal bowel (*arrows*). The bowel wall is accentuated at this frequency. **B**, Sonogram of the same patient obtained with a 4-MHz frequency transducer demonstrates more normal-appearing fetal bowel (*arrows*). This is a common phenomenon and the sonologist should be aware of the effect of transducer frequency on apparent bowel echogenicity. Caution should be taken before declaring abnormal bowel echogenicity and prompting invasive testing.



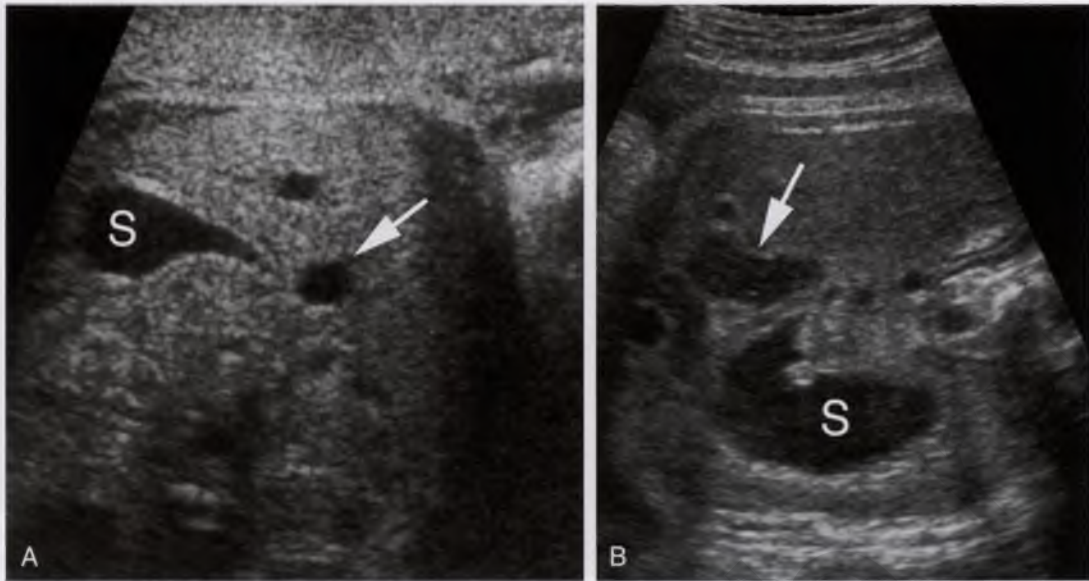


**FIG 38-96** Pseudo-double bubble sign. The double bubble may be seen in cases of duodenal obstruction and has been associated with trisomy 21. **A**, In this case, the fluid-filled structure adjacent to the stomach (S) is the gallbladder (*arrow*) and not the duodenum. **B**, A sonogram of the fetal abdomen in the third trimester demonstrates a prominent segment of colon (*arrow*) adjacent to the fetal stomach (S) and should not be misinterpreted as dilated duodenum.

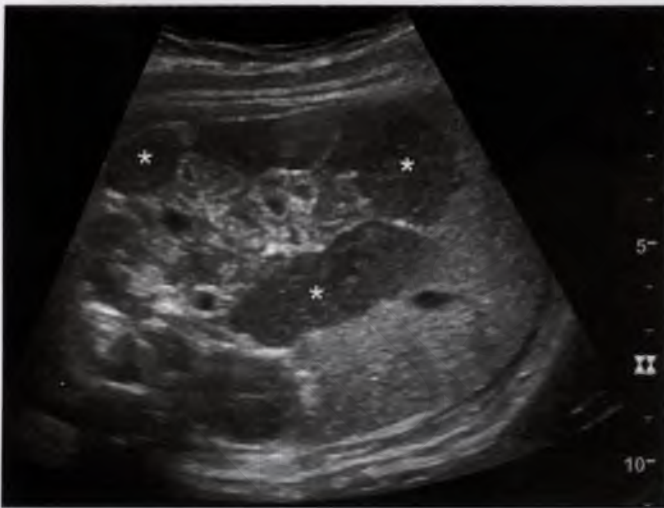


**FIG 38-97** The fetal colon may be quite prominent in the third trimester. The colon (*asterisks*) is prominent but normal in this patient.

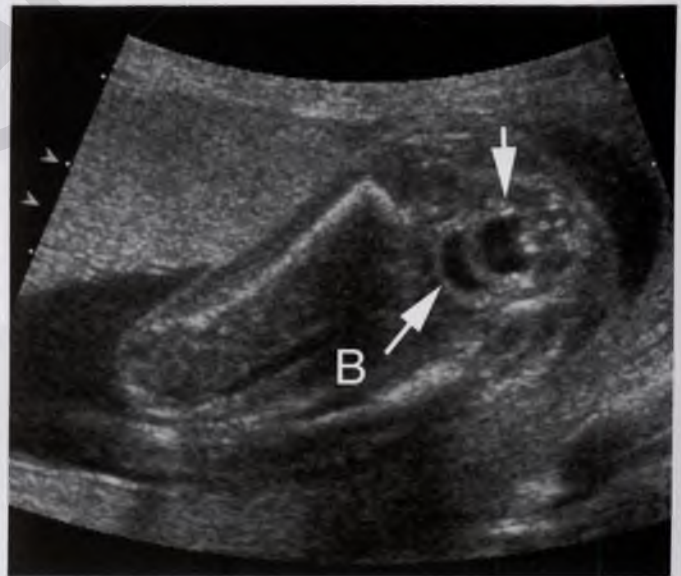


**FIG 38-98** The normal rectum (*arrow*) can occasionally be seen in the second and third trimester fetus. This should not be mistaken for a myelomeningocele or other intrapelvic defect. B, bladder.



**FIG 38-99** In the presence of fetal ascites (A), fluid may enter the lesser sac and result in outlining of the greater omentum (*arrow*). This should not be mistaken for a dilated loop of intestine. L, liver.

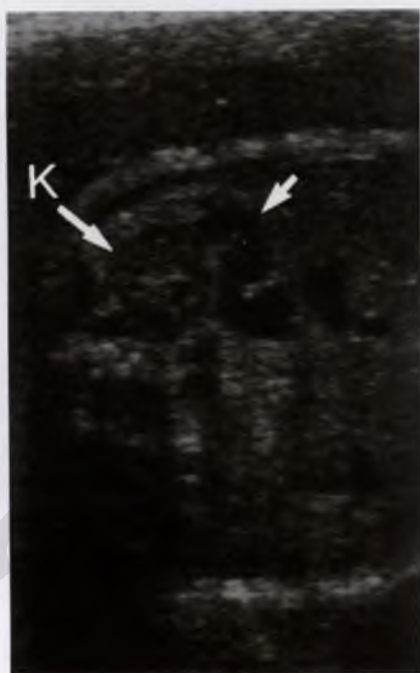


**FIG 38-100** The fetal intestine (*arrow*) may simulate other nonintestinal structures such as a dilated ureter. This is especially true in the second trimester, when the meconium-filled distal small bowel and colon are sonolucent. K, kidney.



**FIG 38-101 A and B**, Fetal gallstones (*arrows*) seen in two third-trimester fetuses. In both cases, the fetus was otherwise normal. This finding does not indicate biliary disease and may resolve before birth.



**FIG 38-102** The normal fetal renal medullary pyramids often appear quite sonolucent (*short arrows*), which may simulate hydronephrosis. This appearance with corticomedullary differentiation is a normal and expected finding. In this case, minimal pelviectasis (*long arrow*) is seen.





**FIG 38-103** An oval paraspinal soft tissue structure is seen simulating the fetal kidney (*arrow*). This structure is the normal adrenal gland, which often is quite prominent in the fetus. The hyperechoic medulla and hypoechoic cortex are well seen.



**FIG 38-104** Splenic cyst. A benign simple small splenic cyst (*arrow*) is seen in this fetus. This is a normal variant and is of no pathologic significance. St, stomach.



**FIG 38-105** Abdominal mass. **A**, Sonogram obtained at 34 weeks' gestation reveals a moderately echogenic mass (*arrow*) at the left upper quadrant of the fetal abdomen. **B**, The mass (M) demonstrates echogenicity similar to that of adjacent bowel (Bo) and appears to be "connected to" and inseparable from the bowel. **C**, Color Doppler ultrasound imaging reveals blood flow within the mass (*arrows*), making it unlikely that this represents bowel. In addition, careful evaluation of part A reveals that the mass abuts the portal vein, thus suggesting that the lesion is of hepatic origin. Postnatal evaluation revealed infantile hepatic hemangioma.



**FIG 38-106** Left congenital diaphragmatic hernia. **A**, Sonogram of a fetus with a left congenital diaphragmatic hernia. Typically this diagnosis is made by observing the fluid-filled stomach within the thorax adjacent to the heart. In this case, bowel loops (Bo) fill the left hemithorax. Electronic calipers are placed measuring the right lung (Lu). These dimensions are needed to calculate the lung-head ratio (LHR), useful in assessing prognosis. **B**, Coronal plane of section of the same fetus demonstrates the stomach (St) normally positioned within the upper abdomen. **C**, The liver (Li) is normally positioned within the abdomen, below the diaphragm (arrows). Lack of herniation of liver into the chest is associated with better prognosis.



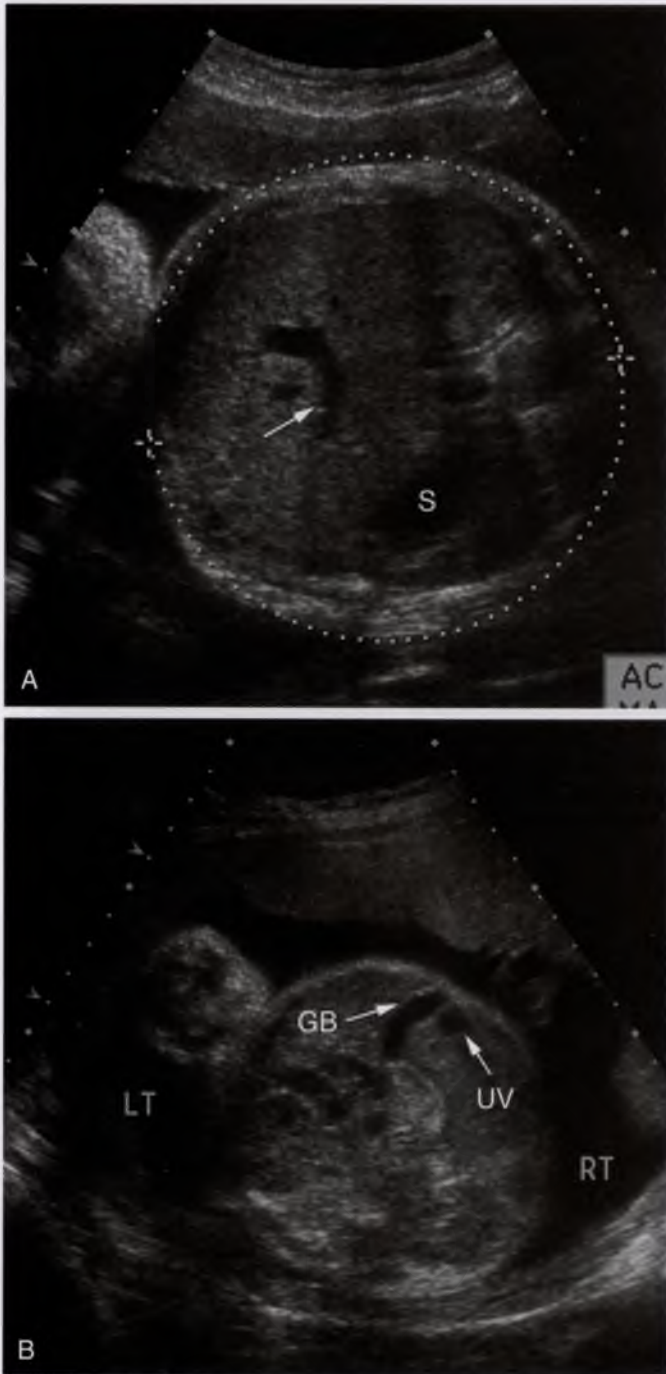


**FIG 38-107** Persistent right umbilical vein. **A**, In this transverse axial scan, the portal vein (*arrow*) is curving toward, rather than away from, the stomach (S). This is a case of persistent right umbilical vein. No other anomalies were detected. **B**, In another case of persistent right umbilical vein, the umbilical vein (UV) is to the right rather than the left of the gallbladder (GB).

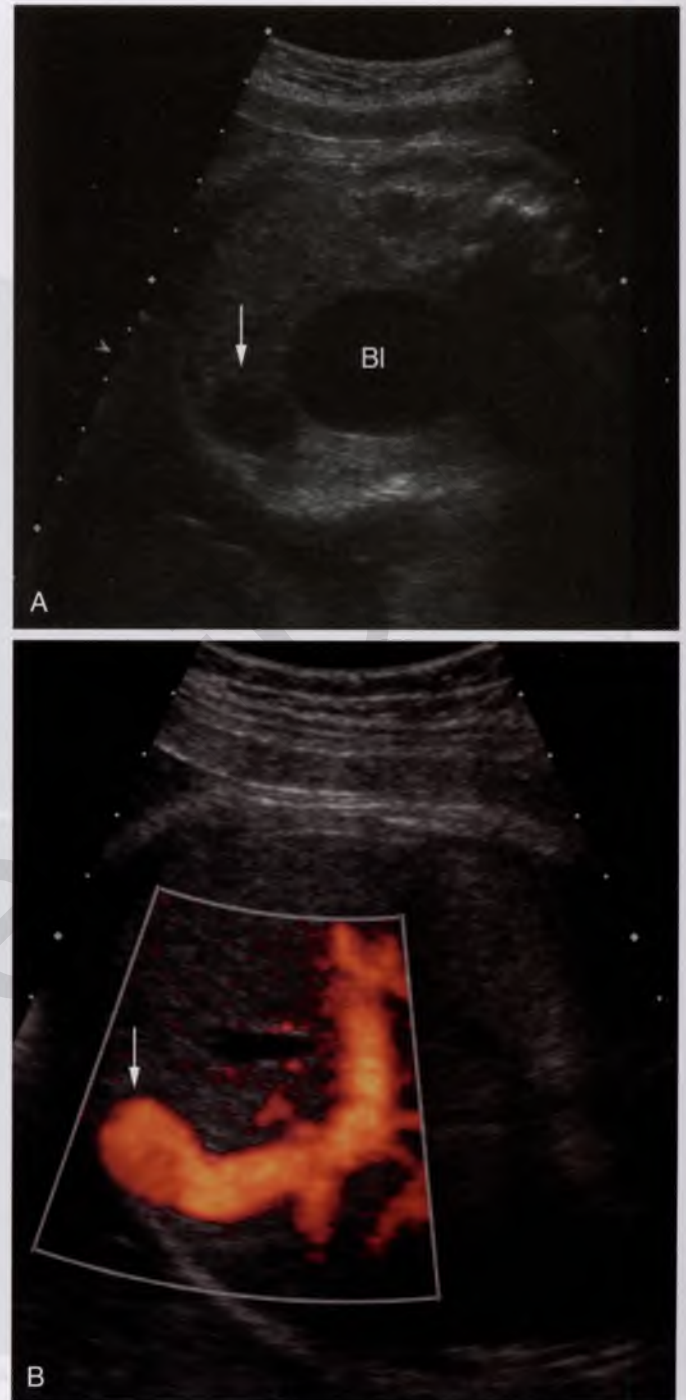


**FIG 38-108** Umbilical vein varix. Initially it was thought that the prognosis in cases of umbilical vein varix was uniformly poor. However, if there are no associated abnormalities, most cases do well. **A**, Umbilical vein varix (*arrow*) seen adjacent to the anterior abdominal wall and the urinary bladder (Bl). **B**, Color Doppler imaging of an umbilical vein varix (*arrow*). In neither case were there associated abnormalities, and the outcomes were normal in both cases.

## AMNIOTIC FLUID AND MEMBRANES

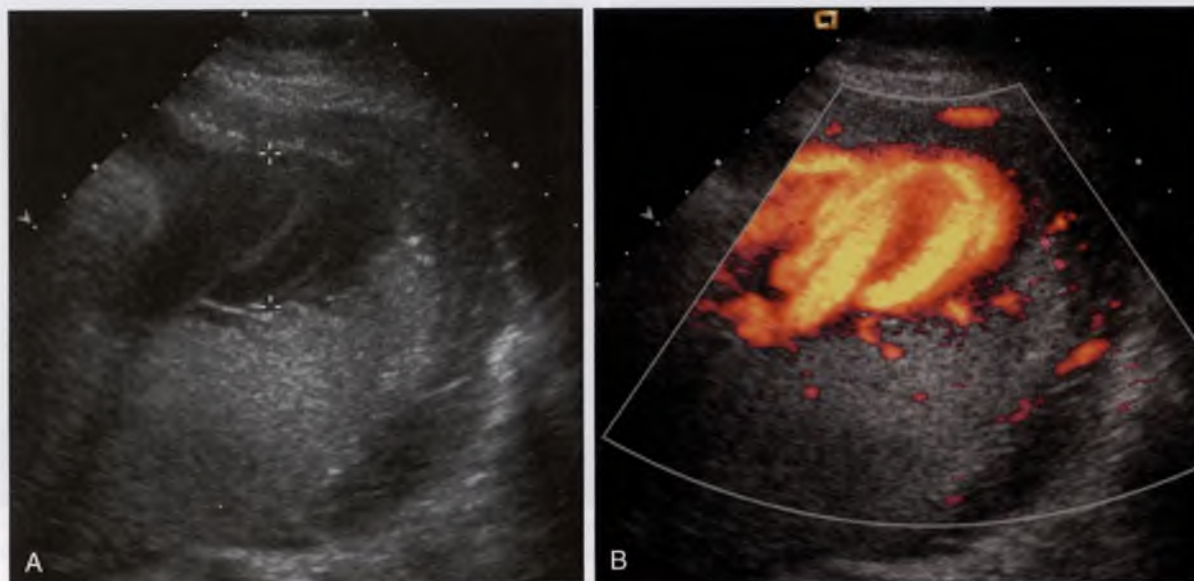


**FIG 38-109** When amniotic fluid volume is assessed, the “pocket” of fluid should be free of umbilical cord. **A**, In this patient, there appears to be a 3-cm pocket of amniotic fluid (*calipers*). **B**, Doppler evaluation of this area revealed that this “pocket” was not amniotic fluid but all umbilical cord.

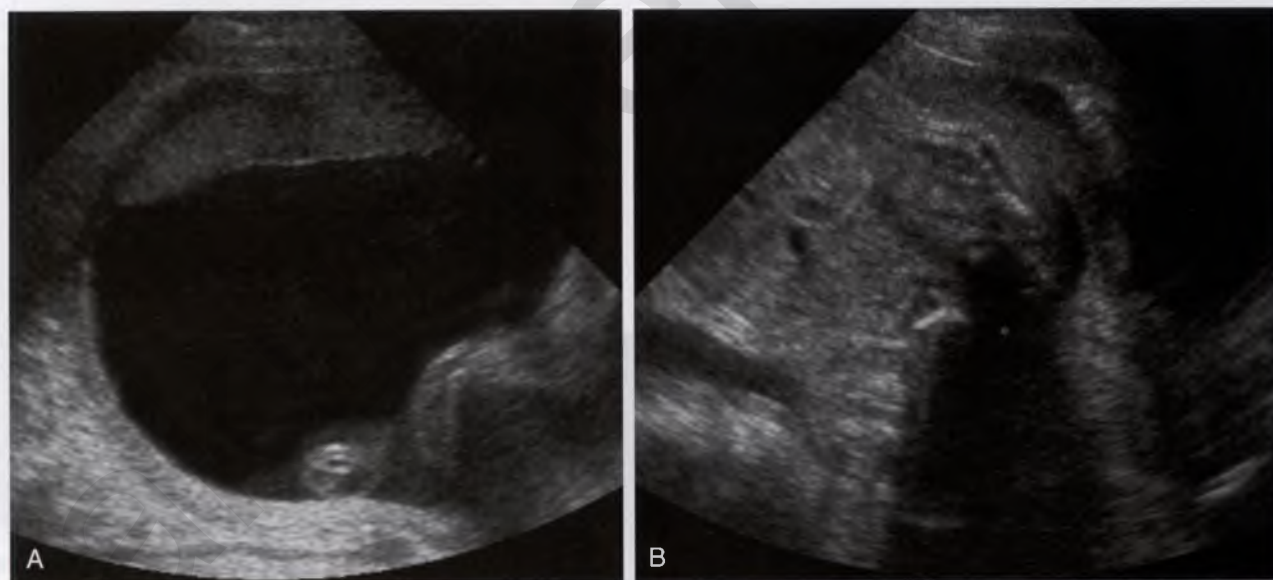


**FIG 38-110** **A**, In this scan of a second trimester pregnancy, a large amniotic fluid pocket is seen, suggesting polyhydramnios. **B**, Little amniotic fluid is seen in a scan near the lower portion of the uterus. The total volume of amniotic fluid was normal. Thus, single views of the gravid uterus may be misleading as to the correct volume of amniotic fluid.



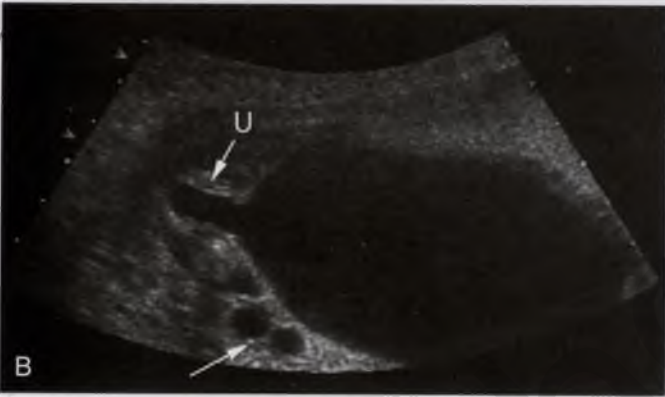
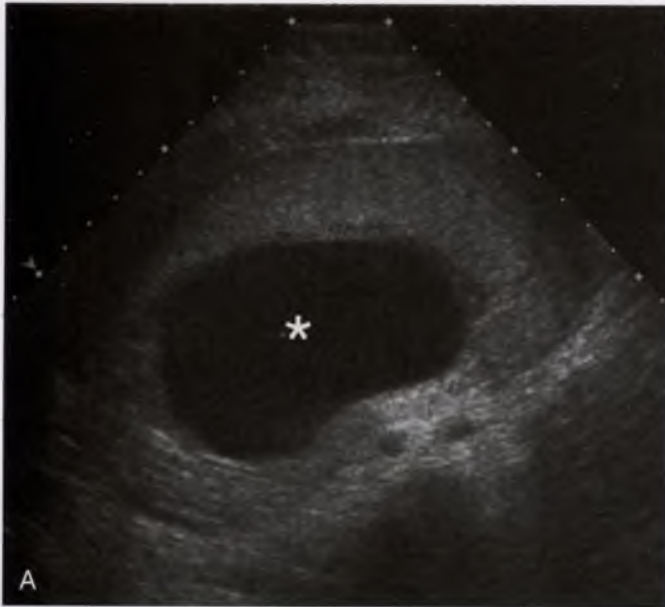


**FIG 38-111** **A**, Large fluid collection (*asterisk*) appears to be amniotic fluid; however, it represents a markedly dilated urinary bladder in a patient with posterior urethral valves. In fact, there was virtually no amniotic fluid. **B**, Another sonogram in the same case demonstrates a dilated posterior urethra (U) and dilated ureters (*arrow*) in addition to the dilated urinary bladder.



**FIG 38-112** In this early second trimester fetus, the amnion (*arrows*) is seen slightly separated from the chorion. This is normal until the 12th to 14th weeks of gestation, at which time the two membranes appose one another.

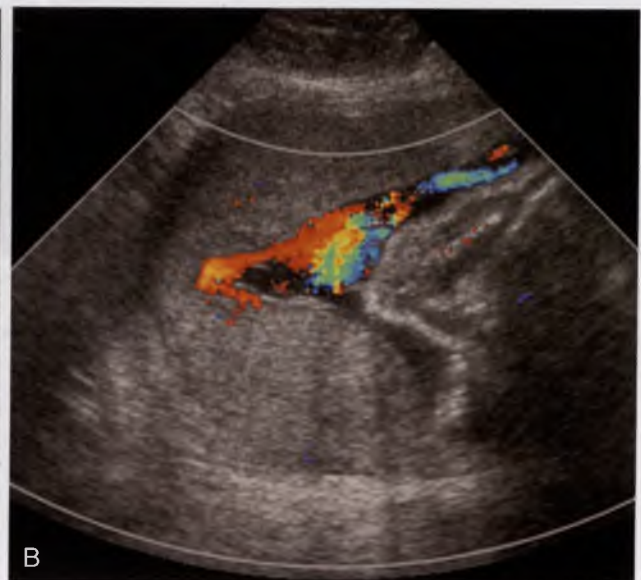
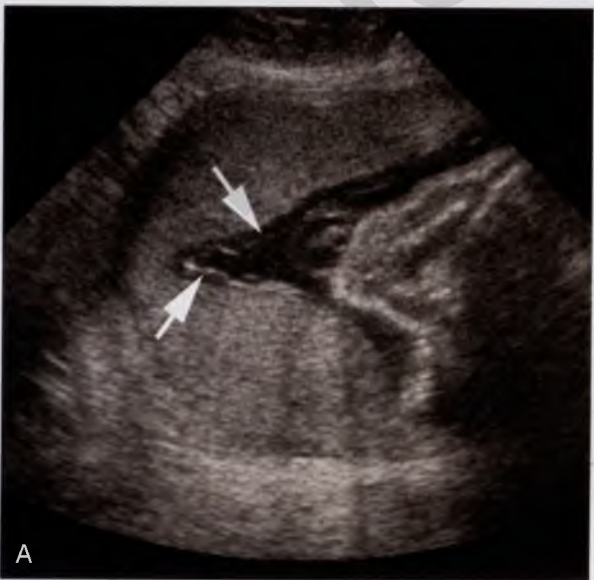


**FIG 38-113** Pseudochoorioamniotic separation. **A**, Apparent chorioamniotic separation is seen with an unapposed amniotic membrane (*arrows*). **B**, Color Doppler imaging reveals that the structure thought to represent membrane was, in fact, umbilical cord.

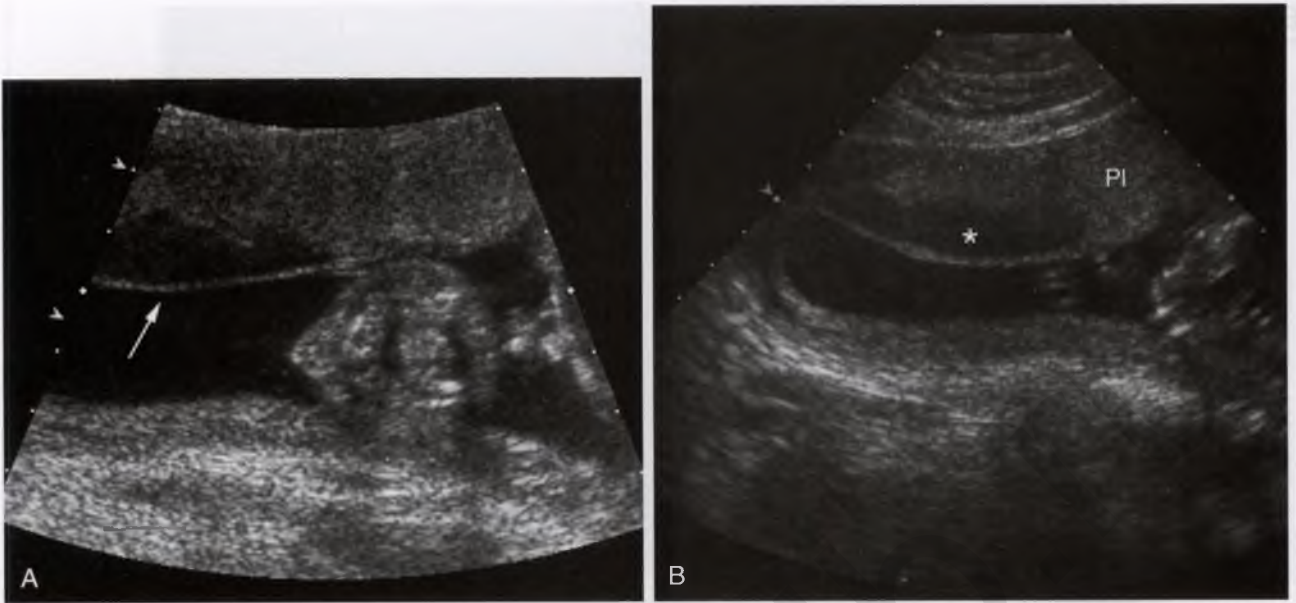


**FIG 38-114** **A**, A linear structure (*arrow*) is seen anteriorly adjacent to the fetal head and placenta. It has the appearance of a free-floating amniotic membrane. **B**, With a larger field of view, the membrane is seen to represent the surface of the placenta (Pl), under which is a hypoechoic area (*asterisk*), likely representing a subchorionic plate hematoma.

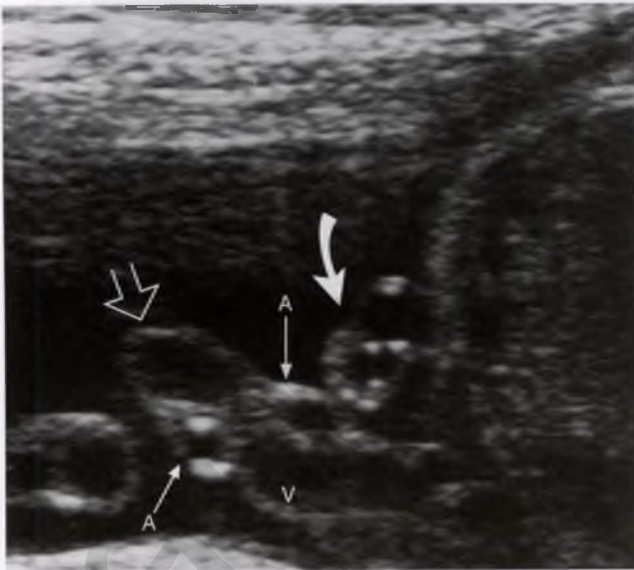


**FIG 38-115** A short-axis view of the umbilical cord should always be obtained when attempting to identify the number of vessels. In this case, the long-axis view (*open arrow*) appears to show two umbilical arteries (A) and one vein (V). In the short-axis view (*curved arrow*), the correct interpretation of a single umbilical artery in a two-vessel cord can be made.



**FIG 38-116** Thick umbilical cord. This patient was noted to have a markedly thickened umbilical cord (*arrows*) with prominent Wharton jelly. The fetus was otherwise normal with normal karyotype and no structural abnormalities. Thickened umbilical cords have been associated with gestational diabetes and karyotype abnormalities but can also be a normal finding, as in this case.



## THE FETAL SKELETON

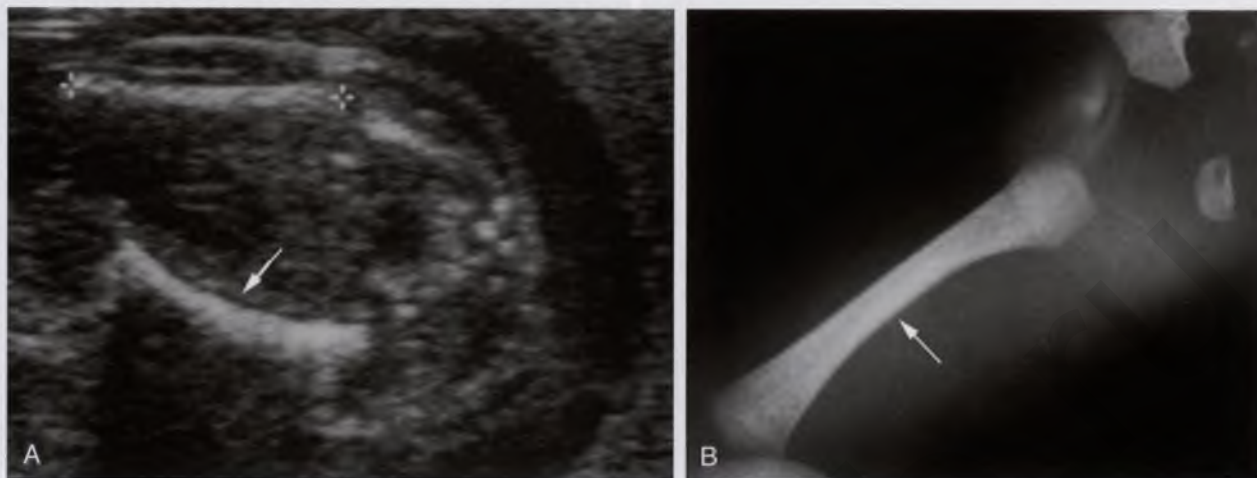


**FIG 38-117** **A**, The normal fetal femur has a medial curve to the metadiaphyseal region. This is seen in the femur farthest from the transducer (*arrow*). The femur closest to the transducer (*cursors*) will demonstrate a straight appearance because the lateral aspect is reflecting the sound and the medial aspect is within its shadow. **B**, Radiograph of a normal neonatal femur demonstrating the normal curved appearance of its medial aspect (*arrow*).

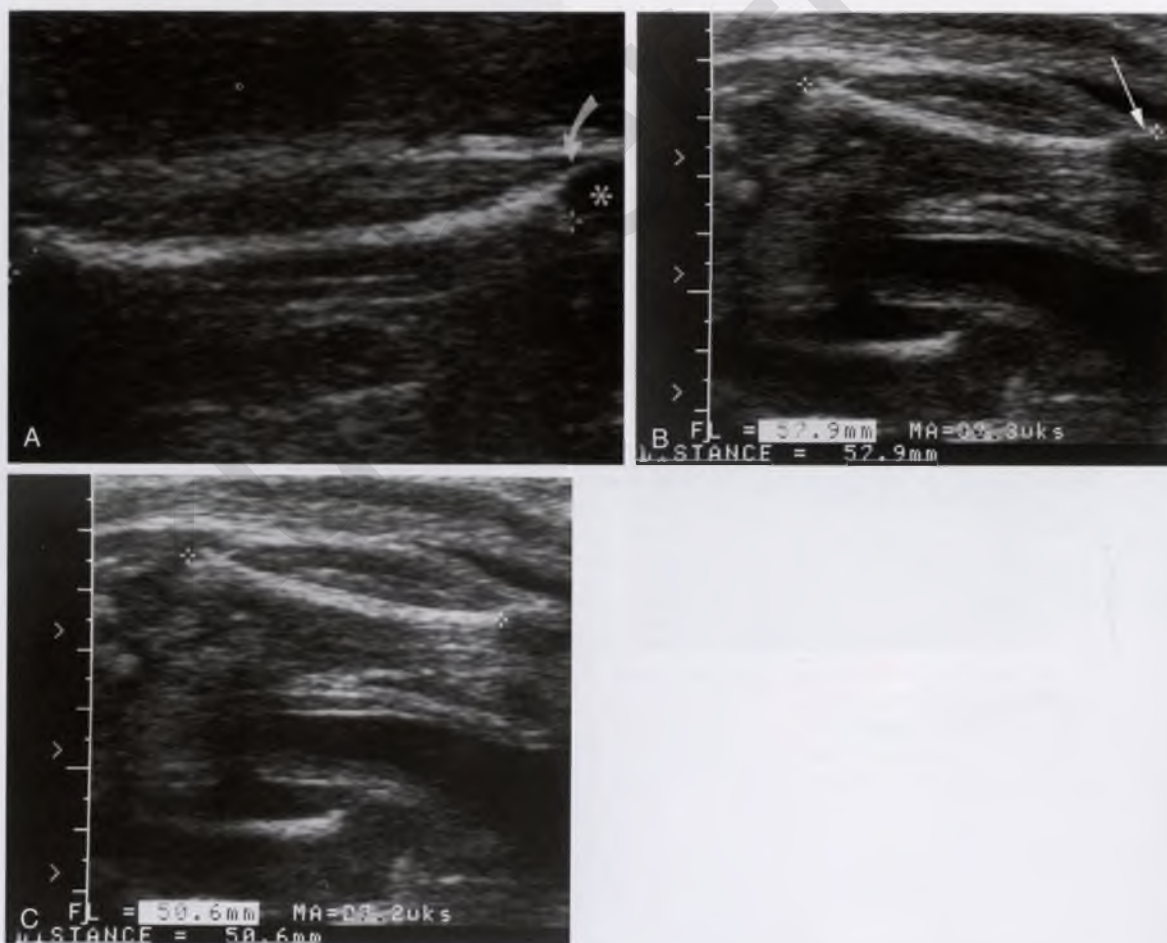


**FIG 38-118** Scans of the fetal femur often demonstrate a linear projection from the distal end. **A**, This projection (*arrow*) is a specular reflection from the distal epiphyseal cartilage (*asterisk*). **B**, The measurement of the femur should not include this reflection (*arrow*). **C**, The measurement should include only the calcified bone. Inclusion of this reflection would have overestimated the gestational age by as much as 3 weeks.

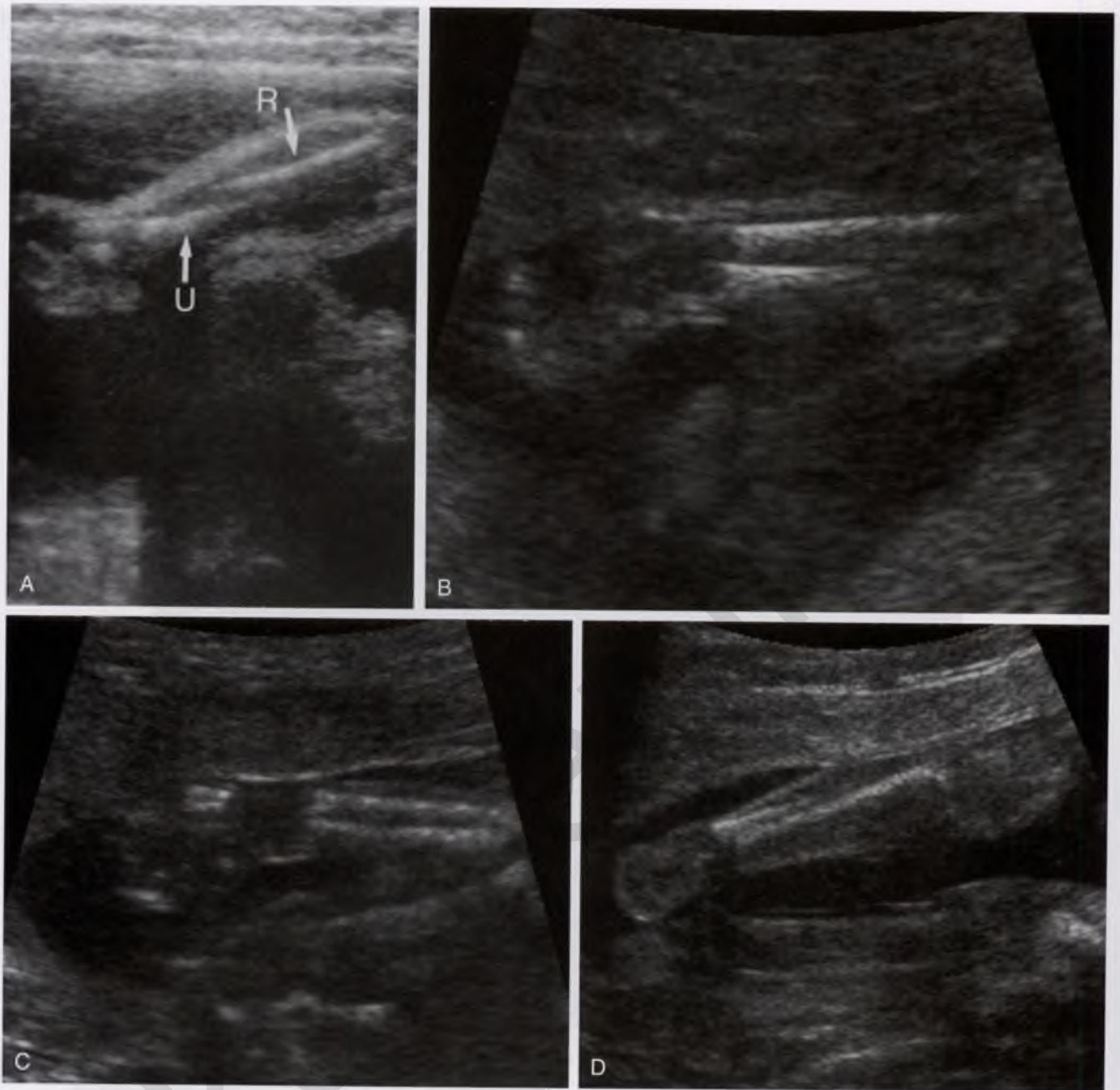
Clinical		LMP = 02 Feb 06	MA = 37w0d	EDD = 09 Nov 06
Ultrasound			MA = 36w3d±16d	EDD = 13-Nov-06
2D		MA ±SD	Mean	
<input type="checkbox"/>	BPD	38w2d±22d	9.41cm	9.37 9.46
<input type="checkbox"/>	HC	37w5d±19d	33.09cm	32.9 33.2
<input type="checkbox"/>	AC	36w3d±21d	32.56cm	32.4 32.6
<input type="checkbox"/>	FL	35w3d±21d	6.92cm	6.97 6.86
<input type="checkbox"/>	CRL			
<input type="checkbox"/>	GS			
<input type="checkbox"/>	HUM			
	HC/AC	1.02 (0.92 - 1.11)	Q1 1.82	EFW 2973±494g (Hadlock) ▼
	FL/AC%	21.2 (20% - 24%)	Q2 3.83	6lb, 9oz ±17oz
	FL/BPD%	73.4 (71% - 87%)	Q3 2.46	LMP% 43.3
	BPD/TTD		Q4 4.30	EFW% 51.2
	CI	83.8 (70% - 86%)	AFI 12.41cm	APTD

Clinical		LMP = 11 Aug 05	MA = 18w5d	EDD = 18 May 06
Ultrasound			MA = 19w0d±SD	EDD = 16-May-06
		MA ±SD	Mean	
<input type="checkbox"/>	BPD	19w3d±12d	4.44cm	4.45 4.42
<input type="checkbox"/>	HC	19w2d±10d	16.60cm	16.3 16.8
<input type="checkbox"/>	AC	19w5d±14d	14.42cm	14.5 14.3 14.3
<input checked="" type="checkbox"/>	FL	18w1d±13d	2.67cm	2.63 2.70
<input type="checkbox"/>	CRL			
<input type="checkbox"/>	GS			
<input type="checkbox"/>	HUM	18w2d±18d	2.60cm	2.54 2.66
	HC/AC	1.15 (1.06 - 1.25)	Q1	EFW 297±40g (Hadlock) ▼
	FL/AC%	****	Q2	0lb, 10oz ±1oz
	FL/BPD%	****	Q3	LMP% ****
	BPD/TTD		Q4	EFW% ****
	CI	74.0 (70% - 86%)	AFI	APTD

**FIG 38-119** Significance of short femoral length. **A**, In the mid to late third trimester, it is not unusual for the femur to be significantly shorter than the other measurements used to estimate gestational age. In this case, the femur is approximately 2 weeks less than the head circumference and menstrual age. The cause of this is uncertain, and the short femur is often attributed to biologic variation or ethnicity. If the bones appear normal morphologically and no anomalies are seen, it is likely a normal variant. This fetus was from white parents of normal height and middle socioeconomic status. **B**, Although the femur can be smaller than other measurements in the third trimester, it is not acceptable for it to be greater than 1 week less than the other measurements in the late first and early to mid second trimesters, as it was in this case (*arrow*). Although this deviation may be nothing more than a temporary growth lag or normal variation at this stage, it may also be a sign of trisomy 21 or an early manifestation of a short-limb skeletal dysplasia. This was a case of trisomy 21. One should not take comfort in comparing the femur measurement to the estimated gestational age by ultrasound imaging. Remember that, unless excluded, the femur measurement is included in the sonographic estimation of gestational age.





**FIG 38-120** Pseudolimb reduction. **A**, Pronation and supination of the forearm may create the appearance that the radius (R) or the ulna (U) is abnormally short (limb reduction abnormality). When both bones are "short" at opposite ends in the same scan, one should be suspicious that this is a technical rather than a real abnormality. **B**, Partial volume of the proximal forearm makes it appear as though the radius and ulna are hypoplastic. **C**, Slight change in transducer angulation reveals that both bones of the forearm are present and normal. **D**, Again, a tomographic plane of section demonstrating only part of the fibula. Both bones of the leg were present and normal.



**FIG 38-121** Pseudo-ulnar hypoplasia. In this three-dimensional rendered image, it appears that the more proximal portion of the ulna is absent (*arrow*). The remainder of the ulna was out of the plane of imaging and was shown on other views to be present and normal.

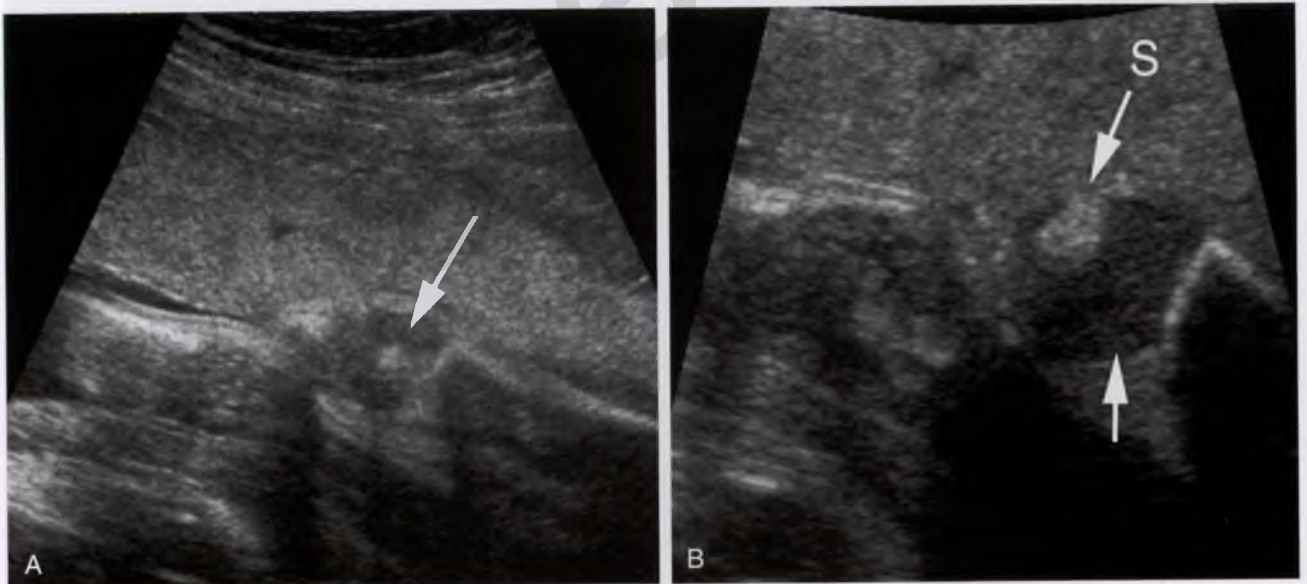


**FIG 38-122** The appearance of the epiphyseal ossification centers is helpful in assessing gestational age. **A**, The synovial tissue is echogenic (*arrow*) and may simulate the appearance of one of these centers, as in this case. The real epiphyseal center would be slightly more proximal. **B**, Synovial tissue (S) is well seen in the same case, without evidence of calcification within the epiphyseal center (*arrow*).



**FIG 38-123** In this case, both hands of the fetus are adjacent to one another. The fingers (*arrows*) from one hand and the fingers (*open arrow*) from the other simulate the appearance of polydactyly.



**FIG 38-124** Apparent missing digits. **A**, Sonogram of the fetal foot appears to show missing second and third digits (*arrow*). This image may suggest missing toes or may mimic the "sandal gap" deformity. **B**, In the same patient, a scan through the foot with slightly different angulation reveals the presence of the second digit. **C**, In an additional view, all remaining digits of the foot were shown (*arrow*). This is another example in which an abnormality is mimicked because not all portions of a fetal body part are included in the same plane of section in a single image.

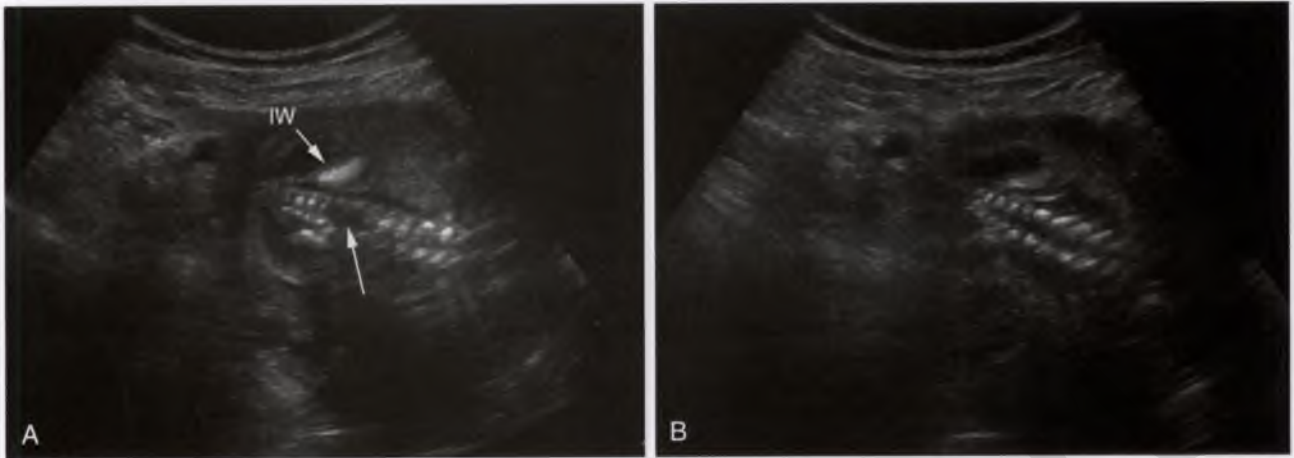


**FIG 38-125** Apparent spinal defect. **A**, Coronal sonogram of the distal spine suggests absent spinal segments (*arrow*) as might be seen with spinal bifida. In fact, this appearance is due to shadowing from the overlying iliac wing (IW). **B**, With slightly different angulation and plane of section, the normal distal spine is better visualized and shown to be intact.

## MULTIPLE GESTATIONS

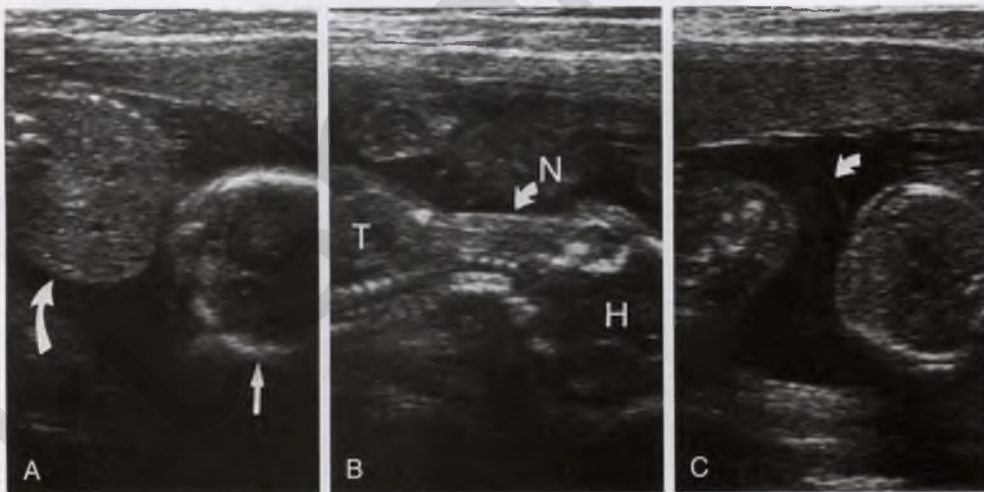


**FIG 38-126** The false negative diagnosis of twins is unusual in the second trimester. If this occurs, it likely results from not "connecting" the fetal head to its body during routine scanning. **A**, In this patient, the fetal head (*straight arrow*) and body (*curved arrow*) are seen in this longitudinal plane of section. Unfortunately, these structures are from different fetuses in this twin pregnancy. **B**, The only way to be absolutely sure of the relation of the head (H) to the body is to demonstrate both structures on the same scan connected to one another through the neck (N). T, thorax. **C**, The dividing membrane (*arrow*) is seen on another plane of section clearly dividing the two fetuses.



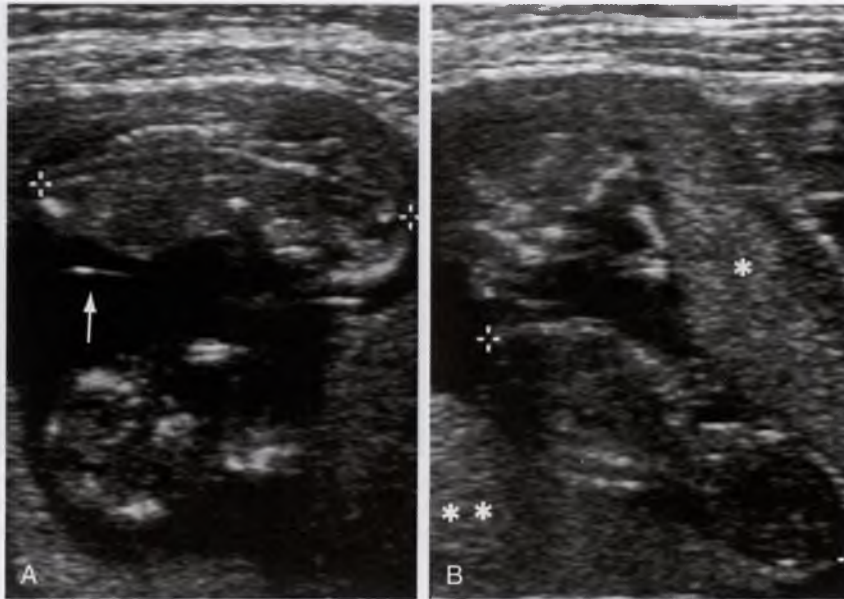


**FIG 38-127** Membrane thickness is often useful in differentiating between monozygotic twins (thin membrane) and dizygotic twins (thick membrane). This method is not always successful, however. **A**, In this twin pregnancy, a scan at 14 weeks' gestation demonstrates a thin membrane (*arrow*) dividing the two gestational sacs. This implies monozygosity. **B**, A longitudinal plane of section at the same time reveals both an anterior placenta (*asterisk*) and a posterior placenta (*double asterisks*).



**FIG 38-128** In this twin gestation, one of the twins was noted to be fixed to the anterior uterine wall. It was initially assumed that this was a monoamniotic twin gestation. Careful inspection reveals that the membrane (*arrow*) dividing the twins can be seen. The anterior fetus is in an oligohydramniotic sac and is smaller than the other twin. This was a case of twin-to-twin transfusion syndrome.

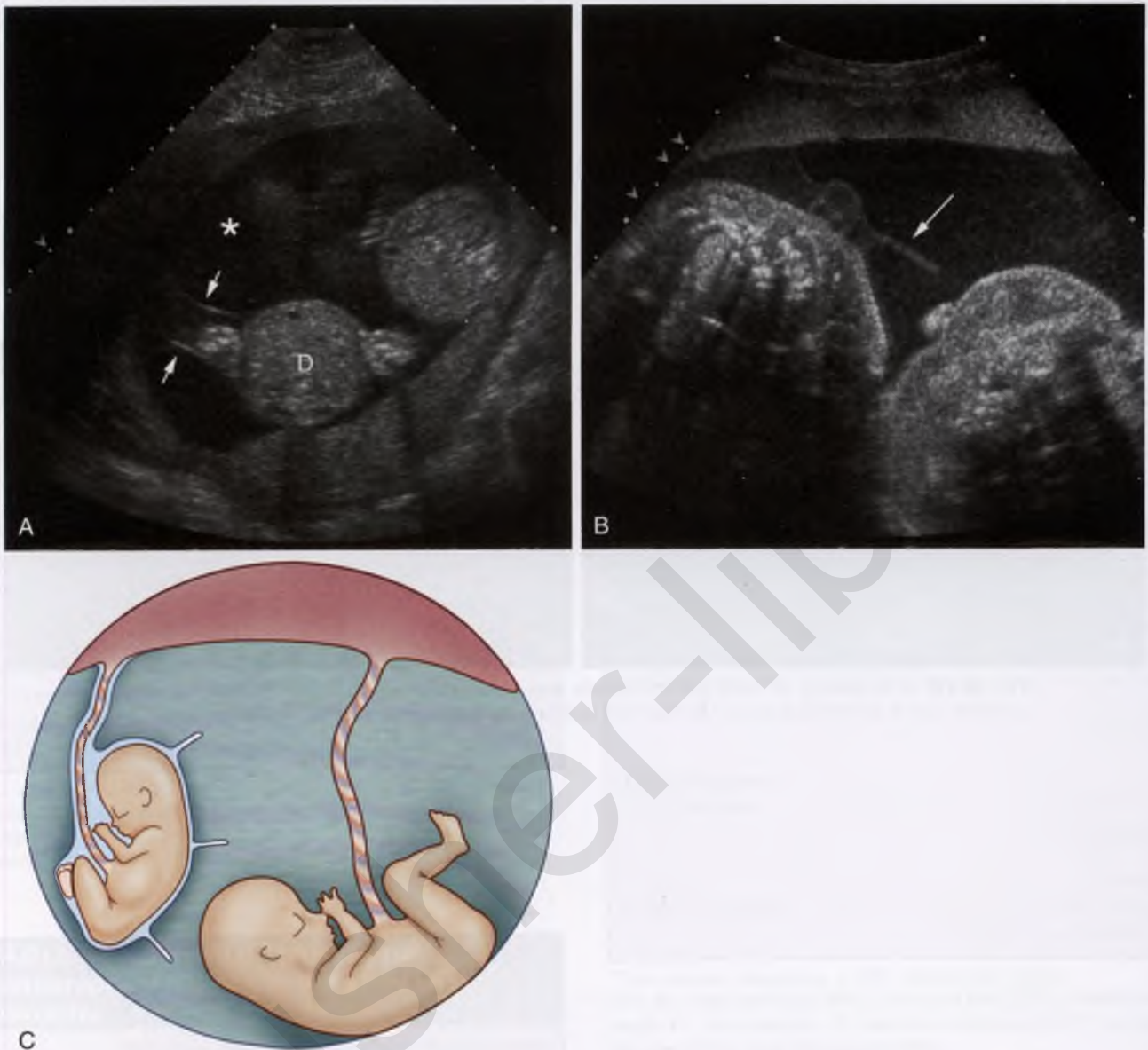


**FIG 38-129** **A**, Monochorionic diamniotic twin pregnancy with twin-to-twin transfusion syndrome. Although it appears as if there is a large amount of fluid (*asterisk*) surrounding the donor twin (D), in fact only a small amount of fluid is seen within the surrounding membrane (*arrows*). **B**, Monochorionic diamniotic twin pregnancy with twin-to-twin transfusion syndrome. Membrane surrounds the donor twin in an oligohydramniotic sac. The membrane has a free edge (*arrow*) projecting into the amniotic fluid surrounding the recipient twin. **C**, Drawing demonstrating the collapsed membrane surrounding the donor twin in an oligohydramniotic sac, similar to what is seen in B.



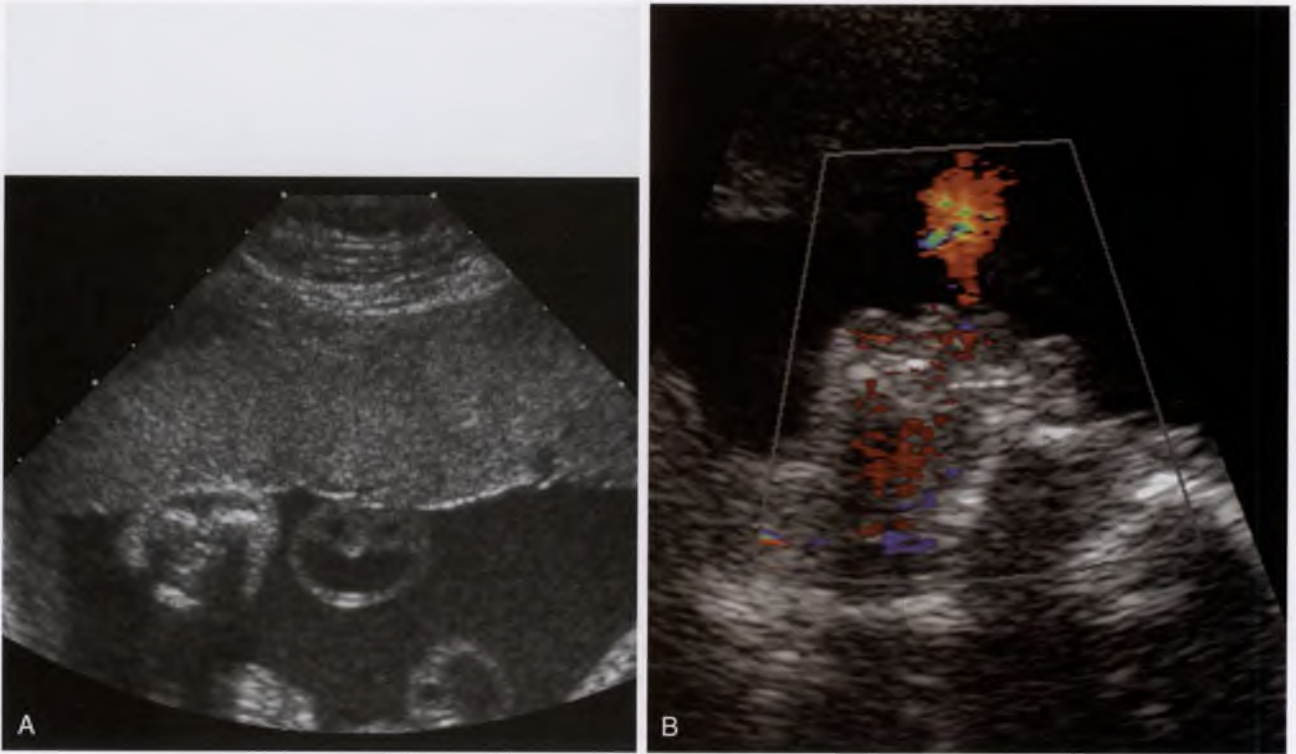


**FIG 38-130** After viewing so many artifacts, pitfalls, and normal variants, you wonder whether: **A**, The umbilical cord is smiling back at you. **B**, The fetus is blowing bubbles.

# Measurements Frequently Used to Estimate Gestational Age and Fetal Biometry

**TABLE A-1 Methods for Determining Menstrual Age**

Clinical or Sonographic Parameter	Variability Estimate (2 SD)
In vitro fertilization*	±1 day
Ovulation induction*	±3 days
Artificial insemination*	±3 days
Single intercourse record*	±3 days
Basal body temperature record*	±4 days
First trimester physical examination	±2 weeks
Second trimester physical examination	±4 weeks
Third trimester physical examination	±6 weeks
First trimester sonographic examination (CRL)	±8% of the estimate
Second trimester sonographic examination (HC, FL)	±8% of the estimate
Third trimester sonographic examination (HC, FL)	±8% of the estimate

CRL, crown-rump length; FL, femur length; HC, head circumference.

\*Indicators of conceptual age (menstrual age = conceptual age + 14 days).

Adapted from Frank P. Hadlock, MD, and James D. Bowie, MD.

**TABLE A-2 Normal Transvaginal Sonographic Findings in the Early First Trimester**

Gestational Age (wk)	Structure First Appears on Ultrasound*	Mean Sac Diameter (mm) <sup>8</sup>	Crown-Rump Length (mm) <sup>10</sup>
5.0	Gestational sac	2	—
5.5	Yolk sac	6	—
6.0	Embryo with heartbeat	10	3
6.5		14	6
7.0	Amnion	18	10
7.5		22	13
8.0		26	16

\*±0.5 week age range for first visibility of each structure.

Superscript numbers in table indicate references at the end of Chapter 4.

**TABLE A-3 Approach to Gestational Age Assignment by Ultrasound on Initial Scan**

Stage of Pregnancy	Basis for GA	Accuracy (wks)*
<b>First Trimester</b>		
Early (5-6 weeks)	Sonographic milestones or MSD	±0.5
Mid to late (6-13 weeks)	CRL	±0.5-1.0
<b>Second Trimester</b>		
If OFD measurable	BPDc or HC	±1.2 (14-20 wks) ±1.9 (20-26 wks)
If OFD not measurable	BPD or FL	±1.4 (14-20 wks) ±2.1-2.5 (20-26 wks)
<b>Third Trimester</b>		
If OFD measurable	BPDc, HC, or FL	±3.1-3.4 (26-32 wks) ±3.5-3.8 (32-42 wks)
If OFD not measurable	FL	±3.1 (26-32 wks) ±3.5 (36-42 wks)

\*Two standard deviations, or 95% confidence interval.

BPD, biparietal diameter; BPDc, corrected BPD; CRL, crown-rump length; FL, femur length; HC, head circumference; MSD, mean sac diameter; OFD, occipitofrontal diameter.



**TABLE A-4 Variability in Predicting Menstrual Age From Sonographic Measurements (14-20 Weeks)**

Parameter	VARIABILITY (2 SD)			
	Hadlock et al*	Rossavik and Fishburne <sup>†</sup>	Persson and Weldner <sup>‡</sup>	Benson and Doubilet <sup>§</sup>
BPD	0.94 wk	1.02 wk	0.92 wk	1.40 wk
HC	0.84 wk	0.92 wk	ND	1.20 wk
AC	1.04 wk	1.12 wk	ND	2.10 wk
FL	0.96 wk	ND	0.98 wk	1.40 wk
BPD, FL	0.80 wk	ND	0.78 wk	ND
HC, FL	0.76 wk	ND	ND	ND

AC, abdominal circumference; BPD, biparietal diameter; FL, femur length; HC, head circumference; ND, no data.

\*Data from Hadlock FP, Harrist RB, Martinez-Poyer J: How accurate is second trimester fetal dating? *J Ultrasound Med* 10:557, 1992.

<sup>†</sup>Data from Rossavik IK, Fishburne JI: Conceptional age, menstrual age, and ultrasound age: a second trimester comparison of pregnancies of known conception date with pregnancies dated from the last menstrual period. *Obstet Gynecol* 73:243, 1989.

<sup>‡</sup>Data from Persson PH, Weldner BM: Reliability of ultrasound fetometry in estimating gestational age in the second trimester. *Acta Obstet Gynecol Scand* 65:481, 1986.

<sup>§</sup>Data from Benson CB, Doubilet PM: Sonographic prediction of gestational age: accuracy of second and third trimester fetal measurements. *Am J Roentgenol* 157:1275, 1991.

**TABLE A-5 Variability in Predicting Menstrual Age in the Second Half of Pregnancy (14-42 Weeks)**

Parameter	VARIABILITY IN WEEKS ( $\pm$ 2 SD)			
	14-20 Weeks	20-26 Weeks	26-32 Weeks	32-42 Weeks
BPD	1.4	2.1	3.8	4.1
Corrected BPD	1.2	1.9	3.3	3.8
HC	1.2	1.9	3.4	3.8
AC	2.1	3.7	3.0	4.5
FL	1.4	2.5	3.1	3.5

AC, abdominal circumference; BPD, biparietal diameter; FL, femur length; HC, head circumference.

Adapted from Benson CB, Doubilet PM: Sonographic prediction of gestational age: accuracy of second and third trimester fetal measurements. *Am J Roentgenol* 157:1275, 1991.

**TABLE A-6 Variability Estimates for Secondary Biometric Parameters**

Parameter	VARIABILITY IN WEEKS ( $\pm$ 2 SD)				
	12-18 Weeks	18-24 Weeks	24-30 Weeks	30-36 Weeks	36-42 Weeks
Binocular distance*	1.8	2.4	3.0	4.0	4.0
Cerebellar diameter <sup>†</sup>	1.0	1.8	2.0	2.4	3.2
Clavicle length <sup>‡</sup>	6.5	6.5	6.5	6.5	6.5
Radius length <sup>§</sup>	1.8	2.2	2.9	3.5	4.1
Ulna length <sup>  </sup>	3.6	3.6	3.6	3.6	3.6
Tibia length <sup>  </sup>	3.5	3.5	3.5	3.5	3.5
Foot length <sup>¶</sup>	1.2	1.7	2.2	2.6	3.1

\*Data from Jeanty P, Cantraine F, Coussaert E, et al: The binocular distance: a new way to estimate fetal age. *J Ultrasound Med* 3:241, 1984.

<sup>†</sup>Data from Hill LM: Transverse cerebellar diameter as a predictor of menstrual age. *Obstet Gynecol* 75:983, 1990.

<sup>‡</sup>Data from Yarkoni S, Schmidt W, Jeanty P, et al: Clavicular measurement: a new biometric parameter for fetal evaluation. *J Ultrasound Med* 4:467, 1985.

<sup>§</sup>Data from Hill LM, Guzik D, Thomas ML, et al: Fetal radius length: a critical evaluation of race as a factor in gestational age assessment. *Am J Obstet Gynecol* 161:193, 1989.

<sup>||</sup>Data from Jeanty P, Rodesch F, Delbeke D: Estimation of fetal age by long bone measurements. *J Ultrasound Med* 3:75, 1984.

<sup>¶</sup>Data from Mercer BM, Sklar S, Shariatmadar A, et al: Fetal foot length as a predictor of gestational age. *Am J Obstet Gynecol* 15:350, 1987.

**TABLE A-7 Gestational Sac Measurement**

Mean Predicted Gestational Sac (cm)	Gestational Age (wk)	Mean Predicted Gestational Sac (cm)	Gestational Age (wk)
1.0	5.0	3.6	8.8
1.1	5.2	3.7	8.9
1.2	5.3	3.8	9.0
1.3	5.5	3.9	9.2
1.4	5.6	4.0	9.3
1.5	5.8	4.1	9.5
1.6	5.9	4.2	9.6
1.7	6.0	4.3	9.7
1.8	6.2	4.4	9.9
1.9	6.3	4.5	10.0
2.0	6.5	4.6	10.2
2.1	6.6	4.7	10.3
2.2	6.8	4.8	10.5
2.3	6.9	4.9	10.6
2.4	7.0	5.0	10.7
2.5	7.2	5.1	10.9
2.6	7.3	5.2	11.0
2.7	7.5	5.3	11.2
2.8	7.6	5.4	11.3
2.9	7.8	5.5	11.5
3.0	7.9	5.6	11.6
3.1	8.0	5.7	11.7
3.2	8.2	5.8	11.9
3.3	8.3	5.9	12.0
3.4	8.5	6.0	12.2
3.5	8.6		

From Hellman LM, Kobayashi M, Fillisti L, et al: Growth and development of the human fetus prior to the twentieth week of gestation. *Am J Obstet Gynecol* 103:789, 1969.



**TABLE A-8 Combined Data Comparing Menstrual Age With Mean Gestational Sac Diameter, Crown-Rump Length, and hCG Levels\***

Menstrual Age (days)	Menstrual Age (wk)	Gestational Sac Size (mm)	Crown-Rump Length (cm)	HCG LEVEL (FIRST IRP)	
				Mean (U/L)	Range (U/L)
30	4.3				
31	4.4				
32	4.6	3		1710	(1050-2800)
33	4.7	4		2320	(1440-3760)
34	4.9	5		3100	(1940-4980)
35	5.0	5.5		4090	(2580-6530)
36	5.1	6		5340	(3400-8450)
37	5.3	7		6880	(4420-10,810)
38	5.4	8		8770	(5680-13,660)
39	5.6	9		11,040	(7220-17,050)
40	5.7	10	0.2	13,730	(9050-21,040)
41	5.9	11	0.3	15,300	(10,140-23,340)
42	6.0	12	0.35	16,870	(11,230-25,640)
43	6.1	13	0.4	20,480	(13,750-30,880)
44	6.3	14	0.5	24,560	(16,650-36,750)
45	6.4	15	0.6	29,110	(19,910-43,220)
46	6.6	16	0.7	34,100	(25,530-50,210)
47	6.7	17	0.8	39,460	(27,470-57,640)
48	6.9	18	0.9	45,120	(31,700-65,380)
49	7.0	19	0.95	50,970	(36,130-73,280)
50	7.1	20	1.0	56,900	(40,700-81,150)
51	7.3	21	1.1	62,760	(45,300-88,790)
52	7.4	22	1.2	68,390	(49,810-95,990)
53	7.6	23	1.3	73,640	(54,120-102,540)
54	7.7	24	1.4	78,350	(58,100-108,230)
55	7.9	25	1.5	82,370	(61,640-112,870)
56	8.0	26	1.6	85,560	(64,600-116,310)
57	8.1	26.5	1.7		
58	8.3	27	1.8		
59	8.4	28	1.9		
60	8.6	29	2.0		
61	8.7	30	2.1		
62	8.9	31	2.2		
63	9.0	32	2.3		
64	9.1	33	2.4		
65	9.3	34	2.5		
66	9.4	35	2.6		
67	9.6	36	2.8		
68	9.7	37	2.9		
69	9.9	38	3.0		
70	10.0	39	3.1		
71	10.1	40	3.2		
72	10.3	41	3.4		
73	10.4	42	3.5		
74	10.6	43	3.7		
75	10.7	44	3.8		
76	10.9	45	4.0		
77	11.0	46	4.1		
78	11.1	47	4.2		
79	11.3	48	4.4		
80	11.4	49	4.6		
81	11.6	50	4.8		
82	11.7	51	5.0		
83	11.9	52	5.2		
84	12.0	53	5.4		

hCG, human chorionic gonadotropin; IRP, International Reference Preparation; U/L, units/liter.

\*Data from Daya S, Woods S: Transvaginal ultrasound scanning in early pregnancy and correlation with human chorionic gonadotropin levels. *J Clin Ultrasound* 19:139, 1991; Hadlock FP, Shah YP, Kanon DJ, et al: Fetal crown rump length: reevaluation of relation to menstrual age (5-18 weeks) with high-resolution real-time US. *Radiology* 182:501, 1992; and Robinson HP: "Gestation sac" volumes as determined by sonar in the first trimester of pregnancy. *Br J Obstet Gynaecol* 82:100, 1975.

Table appears in this form in Nyberg DA, Hill LM, Bohm-Velez M, et al: *Transvaginal Ultrasound*. St. Louis, Mosby-Year Book, 1992.

**TABLE A-9 Predicted Menstrual Age (MA) in Weeks From Crown-Rump Length (CRL) Measurements (cm)\***

CRL	MA	CRL	MA	CRL	MA
0.2	5.7	4.2	11.1	8.2	14.2
0.3	5.9	4.3	11.2	8.3	14.2
0.4	6.1	4.4	11.2	8.4	14.3
0.5	6.2	4.5	11.3	8.5	14.4
0.6	6.4	4.6	11.4	8.6	14.5
0.7	6.6	4.7	11.5	8.7	14.6
0.8	6.7	4.8	11.6	8.8	14.7
0.9	6.9	4.9	11.7	8.9	14.8
1.0	7.2	5.0	11.7	9.0	14.9
1.1	7.2	5.1	11.8	9.1	15.0
1.2	7.4	5.2	11.9	9.2	15.1
1.3	7.5	5.3	12.0	9.3	15.2
1.4	7.7	5.4	12.0	9.4	15.3
1.5	7.9	5.5	12.1	9.5	15.3
1.6	8.0	5.6	12.2	9.6	15.4
1.7	8.1	5.7	12.3	9.7	15.5
1.8	8.3	5.8	12.3	9.8	15.6
1.9	8.4	5.9	12.4	9.9	15.7
2.0	8.6	6.0	12.5	10.0	15.9
2.1	8.7	6.1	12.6	10.1	16.0
2.2	8.9	6.2	12.6	10.2	16.1
2.3	9.0	6.3	12.7	10.3	16.2
2.4	9.1	6.4	12.8	10.4	16.3
2.5	9.2	6.5	12.8	10.5	16.4
2.6	9.4	6.6	12.9	10.6	16.5
2.7	9.5	6.7	13.0	10.7	16.6
2.8	9.6	6.8	13.1	10.8	16.7
2.9	9.7	6.9	13.1	10.9	16.8
3.0	9.9	7.0	13.2	11.0	16.9
3.1	10.0	7.1	13.3	11.1	17.0
3.2	10.1	7.2	13.4	11.2	17.1
3.3	10.2	7.3	13.4	11.3	17.2
3.4	10.3	7.4	13.5	11.4	17.3
3.5	10.4	7.5	13.6	11.5	17.4
3.6	10.5	7.6	13.7	11.6	17.5
3.7	10.6	7.7	13.8	11.7	17.6
3.8	10.7	7.8	13.8	11.8	17.7
3.9	10.8	7.9	13.9	11.9	17.8
4.0	10.9	8.0	14.0	12.0	17.9
4.1	11.0	8.1	14.1	12.1	18.0

\*The 95% confidence interval is  $\pm 8\%$  of the predicted age.  
From Hadlock FP, Shah YP, Kanon DJ, et al: Fetal crown-rump length: reevaluation of relation to menstrual age (5-18 weeks) with high-resolution real-time US. Radiology 182:501, 1992.

**TABLE A-10 Gestational Age (GA) Prediction Based on Head Measurements**

BPD or BPDC* (mm)	Predicted GA (wk)	BPD or BPDC* (mm)	Predicted GA (wk)
20	13.2	59	23.8
21	13.4	60	24.2
22	13.6	61	24.5
23	13.8	62	24.9
24	14	63	25.3
25	14.3	64	25.7
26	14.5	65	26.1
27	14.7	66	26.5
28	14.9	67	26.9
29	15.1	68	27.3
30	15.4	69	27.7
31	15.6	70	28.1
32	15.8	71	28.5
33	16.1	72	29
34	16.3	73	29.4
35	16.6	74	29.9
36	16.8	75	30.3
37	17.1	76	30.8
38	17.3	77	31.2
39	17.6	78	31.7
40	17.9	79	32.2
41	18.1	80	32.7
42	18.4	81	33.2
43	18.7	82	33.7
44	19	83	34.2
45	19.3	84	34.7
46	19.6	85	35.2
47	19.9	86	35.8
48	20.2	87	36.3
49	20.5	88	36.9
50	20.8	89	37.4
51	21.1	90	38
52	21.4	91	38.6
53	21.7	92	39.2
54	22.1	93	39.8
55	22.4	94	40.4
56	22.8	95	41
57	23.1	96	41.6
58	23.5	$\geq 97$	42

BPD, biparietal diameter; BPDC, corrected BPD; OFD, occipitofrontal diameter.

\*BPDC = corrected BPD =  $\sqrt{(\text{BPD} \times \text{OFD})} / 1.265$ .

From Doubilet PM, Benson CB: Improved prediction of gestational age in the late third trimester. J Ultrasound Med 12:647, 1993.



**TABLE A-11 Predicted Menstrual Age for Head Circumference Measurements (8.5-36.0 cm)**

Head Circumference (cm)	Menstrual Age (wk)	Head Circumference (cm)	Menstrual Age (wk)
8.5	13.7	22.5	24.4
9.0	14.0	23.0	24.9
9.5	14.3	23.5	25.4
10.0	14.6	24.0	25.9
10.5	15.0	24.5	26.4
11.0	15.3	25.0	26.9
11.5	15.6	25.5	27.5
12.0	15.9	26.0	28.0
12.5	16.3	26.5	28.6
13.0	16.6	27.0	29.2
13.5	17.0	27.5	29.8
14.0	17.3	28.0	30.3
14.5	17.7	28.5	31.0
15.0	18.1	29.0	31.6
15.5	18.4	29.5	32.2
16.0	18.8	30.0	32.8
16.5	19.2	30.5	33.5
17.0	19.6	31.0	34.2
17.5	20.0	31.5	34.9
18.0	20.4	32.0	35.5
18.5	20.8	32.5	36.3
19.0	21.2	33.0	37.0
19.5	21.6	33.5	37.7
20.0	22.1	34.0	38.5
20.5	22.5	34.5	39.2
21.0	23.0	35.0	40.0
21.5	23.4	35.5	40.8
22.0	23.9	36.0	41.6

**VARIABILITY ESTIMATES ( $\pm 2$  SD)**

12-18 wk	$\pm 1.3$ wk
18-24 wk	$\pm 1.6$ wk
24-30 wk	$\pm 2.3$ wk
30-36 wk	$\pm 2.7$ wk
36-42 wk	$\pm 3.4$ wk

From Hadlock FP, Deter RL, Harrist RB, et al: Fetal head circumference: relation to menstrual age. AJR Am J Roentgenol 138:649, 1982.

**TABLE A-12 Percentile Values for Fetal Head Circumference**

Menstrual Weeks	HEAD CIRCUMFERENCE (CM) BY PERCENTILE				
	3rd	10th	50th	90th	97th
14	8.8	9.1	9.7	10.3	10.6
15	10.0	10.4	11.0	11.6	12.0
16	11.3	11.7	12.4	13.1	13.5
17	12.6	13.0	13.8	14.6	15.0
18	13.7	14.2	15.1	16.0	16.5
19	14.9	15.5	16.4	17.4	17.9
20	16.1	16.7	17.7	18.7	19.3
21	17.2	17.8	18.9	20.0	20.6
22	18.3	18.9	20.1	21.3	21.9
23	19.4	20.1	21.3	22.5	23.2
24	20.4	21.1	22.4	23.7	24.3
25	21.4	22.2	23.5	24.9	25.6
26	22.4	23.2	24.6	26.0	26.8
27	23.3	24.1	25.6	27.1	27.9
28	24.2	25.1	26.6	28.1	29.0
29	25.0	25.9	27.5	29.1	30.0
30	25.8	26.8	28.4	30.0	31.0
31	26.7	27.6	29.3	31.0	31.9
32	27.4	28.4	30.1	31.8	32.8
33	28.0	29.0	30.8	32.6	33.6
34	28.7	29.7	31.5	33.3	34.3
35	29.3	30.4	32.2	34.1	35.1
36	29.9	30.9	32.8	34.7	35.8
37	30.3	31.4	33.3	35.2	36.3
38	30.8	31.9	33.8	35.8	36.8
39	31.1	32.2	34.2	36.2	37.3
40	31.5	32.6	34.6	36.6	37.7

Adapted from Hadlock FP, Deter RL, Harrist RB, et al: Estimating fetal age: computer-assisted analysis of multiple fetal growth parameters. Radiology 152:497, 1984.

**TABLE A-13 Predicted Menstrual Age for Abdominal Circumference Measurements (10-36 cm)**

Abdominal Circumference (cm)	Menstrual Age (wk)	Abdominal Circumference (cm)	Menstrual Age (wk)
10.0	15.6	23.5	27.7
10.5	16.1	24.0	28.2
11.0	16.5	24.5	28.7
11.5	16.9	25.0	29.2
12.0	17.3	25.5	29.7
12.5	17.8	26.0	30.1
13.0	18.2	26.5	30.6
13.5	18.6	27.0	31.1
14.0	19.1	27.5	31.6
14.5	19.5	28.0	32.1
15.0	20.0	28.5	32.6
15.5	20.4	29.0	33.1
16.0	20.8	29.5	33.6
16.5	21.3	30.0	34.1
17.0	21.7	30.5	34.6
17.5	22.2	31.0	35.1
18.0	22.6	31.5	35.6
18.5	23.1	32.0	36.1
19.0	23.6	32.5	36.6
19.5	24.0	33.0	37.1
20.0	24.5	33.5	37.6
20.5	24.9	34.0	38.1
21.0	25.4	34.5	38.7
21.5	25.9	35.0	39.2
22.0	26.3	35.5	39.7
22.5	26.8	36.0	40.2
23.0	27.3		

**VARIABILITY ESTIMATES ( $\pm 2$  SD)**

12-18 wk	$\pm 1.9$ wk
18-24 wk	$\pm 2.0$ wk
24-30 wk	$\pm 2.2$ wk
30-36 wk	$\pm 3.0$ wk
36-42 wk	$\pm 2.5$ wk

From Hadlock FP, Deter RL, Harrist RB, et al: Fetal abdominal circumference as a predictor of menstrual age. AJR Am J Roentgenol 139:367, 1982.

**TABLE A-14 Percentile Values for Fetal Abdominal Circumference**

Menstrual Age (Wks)	ABDOMINAL CIRCUMFERENCE (CM) BY PERCENTILE				
	3rd	10th	50th	90th	97th
14	6.4	6.7	7.3	7.9	8.3
15	7.5	7.9	8.6	9.3	9.7
16	8.6	9.1	9.9	10.7	11.2
17	9.7	10.3	11.2	12.1	12.7
18	10.9	11.5	12.5	13.5	14.1
19	11.9	12.6	13.7	14.8	15.5
20	13.1	13.8	15.0	16.3	17.0
21	14.1	14.9	16.2	17.6	18.3
22	15.1	16.0	17.4	18.8	19.7
23	16.1	17.0	18.5	20.0	20.9
24	17.1	18.1	19.7	21.3	22.3
25	18.1	19.1	20.8	22.5	23.5
26	19.1	20.1	21.9	23.7	24.8
27	20.0	21.1	23.0	24.9	26.0
28	20.9	22.0	24.0	26.0	27.1
29	21.8	23.0	25.1	27.2	28.4
30	22.7	23.9	26.1	28.3	29.5
31	23.6	24.9	27.1	29.4	30.6
32	24.5	25.8	28.1	30.4	31.8
33	25.3	26.7	29.1	31.5	32.9
34	26.1	27.5	30.0	32.5	33.9
35	26.9	28.3	30.9	33.5	34.9
36	27.7	29.2	31.8	34.4	35.9
37	28.5	30.0	32.7	35.4	37.0
38	29.2	30.8	33.6	36.4	38.0
39	29.9	31.6	34.4	37.3	38.9
40	30.7	32.4	35.3	38.2	39.9

Adapted from Hadlock FP, Deter RL, Harrist RB, et al: Estimating fetal age: computer-assisted analysis of multiple fetal growth parameters. Radiology 152:497, 1984.



TABLE A-15 A Comparison of Abdominal Circumference Percentiles Using Sonography

Menstrual Age (wk)	ABDOMINAL CIRCUMFERENCE (cm)					
	10th PERCENTILE			90th PERCENTILE		
	Jeanty et al*	Hadlock et al <sup>†</sup>	Tamura and Sabbagha <sup>‡</sup>	Jeanty et al*	Hadlock et al <sup>†</sup>	Tamura and Sabbagha <sup>‡</sup>
18	10.2	11.5	11.7	13.6	13.5	12.0
20	12.4	13.7	14.2	15.8	16.3	16.7
22	14.6	16.0	14.7	18.0	18.8	19.7
24	16.7	18.1	18.9	20.1	21.3	22.8
26	18.8	20.1	19.8	22.2	23.7	26.7
28	20.8	22.0	23.1	24.2	26.0	27.2
30	22.7	23.9	24.4	26.1	28.3	30.1
32	24.5	25.8	26.7	27.9	30.4	32.4
34	26.2	27.5	28.6	29.6	32.5	33.6
36	27.6	29.2	31.0	31.0	34.4	37.8
38	28.9	30.8	32.8	32.3	36.4	38.5
40	29.9	32.4	33.3	33.3	38.2	41.2

\*Adapted from Jeanty P, Coussaert E, Cantraine F: Normal growth of the abdominal perimeter. *Am J Perinatol* 1:129, 1984.

<sup>†</sup>Adapted from Hadlock FP, Deter RL, Harrist RB, et al: Estimating fetal age: computer-assisted analysis of multiple fetal growth parameters. *Radiology* 152:497, 1984.

<sup>‡</sup>Adapted from Tamura RK, Sabbagha RE: Percentile ranks of sonar fetal abdominal circumference measurements. *Am J Obstet Gynecol* 138:475, 1980.

**TABLE A-16 Gestational Age (GA) Prediction Based on Femur Length (FL)**

FL (mm)	Predicted GA (wk)	FL (mm)	Predicted GA (wk)
10	13.7	45	24.5
11	13.9	46	24.9
12	14.2	47	25.3
13	14.4	48	25.7
14	14.6	49	26.2
15	14.9	50	26.6
16	15.1	51	27.0
17	15.4	52	27.5
18	15.6	53	28.0
19	15.9	54	28.4
20	16.2	55	28.9
21	16.4	56	29.4
22	16.7	57	29.9
23	17.0	58	30.4
24	17.3	59	30.9
25	17.6	60	31.4
26	17.9	61	31.9
27	18.2	62	32.5
28	18.5	63	33.0
29	18.8	64	33.6
30	19.1	65	34.1
31	19.4	66	34.7
32	19.7	67	35.3
33	20.1	68	35.9
34	20.4	69	36.5
35	20.7	70	37.1
36	21.1	71	37.7
37	21.4	72	38.3
38	21.8	73	39.0
39	22.2	74	39.6
40	22.5	75	40.3
41	22.9	76	40.9
42	23.3	77	41.6
43	23.7	≥78	42.0
44	24.1		

From Doubilet PM, Benson CB: Improved prediction of gestational age in the late third trimester. *J Ultrasound Med* 12:647, 1993.

**TABLE A-17 Percentile Values for Fetal Femur Length**

Menstrual Age (wk)	FEMUR LENGTH (CM)				
	3rd	10th	50th	90th	97th
14	1.2	1.3	1.4	1.5	1.6
15	1.5	1.6	1.7	1.9	1.9
16	1.7	1.8	2.0	2.2	2.3
17	2.1	2.2	2.4	2.6	2.7
18	2.3	2.5	2.7	2.9	3.1
19	2.6	2.7	3.0	3.3	3.4
20	2.8	3.0	3.3	3.6	3.8
21	3.0	3.2	3.5	3.8	4.0
22	3.3	3.5	3.8	4.1	4.3
23	3.5	3.7	4.1	4.5	4.7
24	3.8	4.0	4.4	4.8	5.0
25	4.0	4.2	4.6	5.0	5.2
26	4.2	4.5	4.9	5.3	5.6
27	4.4	4.6	5.1	5.6	5.8
28	4.6	4.9	5.4	5.9	6.2
29	4.8	5.1	5.6	6.1	6.4
30	5.0	5.3	5.8	6.3	6.6
31	5.2	5.5	6.0	6.5	6.8
32	5.3	5.6	6.2	6.8	7.1
33	5.5	5.8	6.4	7.0	7.3
34	5.7	6.0	6.6	7.2	7.5
35	5.9	6.2	6.8	7.4	7.8
36	6.0	6.4	7.0	7.6	8.0
37	6.2	6.6	7.2	7.9	8.2
38	6.4	6.7	7.4	8.1	8.4
39	6.5	6.8	7.5	8.2	8.6
40	6.6	7.0	7.7	8.4	8.8

Adapted from Hadlock FP, Deter RL, Harrist RB, et al: Estimating fetal age: computer-assisted analysis of multiple fetal growth parameters. *Radiology* 152:497, 1984.



TABLE A-18 Normal Values (3rd, 50th, 97th Percentiles) of the Lower Limb Bones (mm)

Weeks	FEMUR			TIBIA			FIBULA		
	3rd	50th	97th	3rd	50th	97th	3rd	50th	97th
12	4.4	7.7	11.1	4.4	7.6	10.8	3.6	6.8	10.0
13	7.5	10.9	14.4	5.8	9.2	12.5	5.2	8.5	11.8
14	10.6	14.1	17.6	8.0	11.4	14.8	7.4	10.8	14.2
15	13.6	17.2	20.8	10.6	14.1	17.6	10.0	13.5	17.0
16	16.5	20.3	24.0	13.3	16.9	20.5	12.8	16.4	20.0
17	19.4	23.3	27.2	16.2	19.9	23.5	15.6	19.3	23.0
18	22.3	26.3	30.2	19.0	22.8	26.6	18.4	22.2	26.0
19	25.1	29.2	33.3	21.8	25.7	29.6	21.2	25.1	29.0
20	27.9	32.1	36.3	24.5	28.5	32.5	23.9	27.9	31.8
21	30.6	34.9	39.2	27.2	31.2	35.3	26.4	30.5	34.6
22	33.2	37.6	42.0	29.7	33.8	38.0	28.9	33.1	37.3
23	35.8	40.3	44.8	32.1	36.4	40.6	31.2	35.5	39.8
24	38.3	42.9	47.6	34.4	38.8	43.1	33.5	37.9	42.3
25	40.8	45.5	50.2	36.6	41.0	45.5	35.6	40.1	44.6
26	43.1	48.0	52.8	38.7	43.2	47.8	37.6	42.2	46.8
27	45.4	50.4	55.3	40.7	45.3	49.9	39.6	44.3	49.0
28	47.6	52.7	57.8	42.6	47.3	52.0	41.4	46.2	51.0
29	49.8	55.0	60.1	44.4	49.2	54.0	43.1	48.0	52.9
30	51.8	57.1	62.4	46.1	51.0	55.9	44.8	49.8	54.8
31	53.8	59.2	64.6	47.7	52.7	57.7	46.4	51.5	56.6
32	55.7	61.2	66.7	49.3	54.4	59.5	47.9	53.1	58.3
33	57.5	63.1	68.7	50.8	55.9	61.1	49.3	54.6	59.9
34	59.2	64.9	70.6	52.2	57.5	62.7	50.7	56.1	61.5
35	60.8	66.6	72.4	53.5	58.9	64.3	52.0	57.5	63.0
36	62.3	68.2	74.1	54.8	60.3	65.7	53.2	58.8	64.4
37	63.7	69.7	75.8	56.0	61.6	67.2	54.4	60.1	65.8
38	64.9	71.1	77.3	57.2	62.9	68.5	55.5	61.3	67.1
39	66.1	72.4	78.7	58.3	64.1	69.8	56.6	62.5	68.4
40	67.2	73.6	79.9	59.4	65.2	71.1	57.6	63.6	69.6
41	68.1	74.6	81.1	60.4	66.4	72.3	58.6	64.7	70.8
42	69.0	75.6	82.2	61.4	67.4	73.5	59.5	65.8	72.0

From Chitty LS, Altman DG: Charts of fetal size: limb bones. Br J Obstet Gynaecol 109:919-929, 2002.

TABLE A-19 Length of Fetal Long Bones (mm)

Week No.	HUMERUS			ULNA			RADIUS			FEMUR			TIBIA			FIBULA		
	PERCENTILE			PERCENTILE			PERCENTILE			PERCENTILE			PERCENTILE			PERCENTILE		
	5th	50th	95th	5th	50th	95th	5th	50th	95th	5th	50th	95th	5th	50th	95th	5th	50th	95th
11	—	6	—	—	5	—	—	5	—	—	6	—	—	4	—	—	2	—
12	3	9	10	—	8	—	—	7	—	—	9	—	—	7	—	—	5	—
13	5	13	20	3	11	18	—	10	—	6	12	19	4	10	17	—	8	—
14	5	16	20	4	13	17	8	13	12	5	15	19	2	13	19	6	11	10
15	11	18	26	10	16	22	12	15	19	11	19	26	5	16	27	10	14	18
16	12	21	25	8	19	24	9	18	21	13	22	24	7	19	25	6	17	22
17	19	24	29	11	21	32	11	20	29	20	25	29	15	22	29	7	19	31
18	18	27	30	13	24	30	14	22	26	19	28	31	14	24	29	10	22	28
19	22	29	36	20	26	32	20	24	29	23	31	38	19	27	35	18	24	30
20	23	32	36	21	29	32	21	27	28	22	33	39	19	29	35	18	27	30
21	28	34	40	25	31	36	25	29	32	27	36	45	24	32	39	24	29	34
22	28	36	40	24	33	37	24	31	34	29	39	44	25	34	39	21	31	37
23	32	38	45	27	35	43	26	32	39	35	41	48	30	36	43	23	33	44
24	31	41	46	29	37	41	27	34	38	34	44	49	28	39	45	26	35	41
25	35	43	51	34	39	44	31	36	40	38	46	54	31	41	50	33	37	42
26	36	45	49	34	41	44	30	37	41	39	49	53	33	43	49	32	39	43
27	42	46	51	37	43	48	33	39	45	45	51	57	39	45	51	35	41	47
28	41	48	52	37	44	48	33	40	45	45	53	57	38	47	52	36	43	47
29	44	50	56	40	46	51	36	42	47	49	56	62	40	49	57	40	45	50
30	44	52	56	38	47	54	34	43	49	49	58	62	41	51	56	38	47	52
31	47	53	59	39	49	59	34	44	53	53	60	67	46	52	58	40	48	57
32	47	55	59	40	50	58	37	45	51	53	62	67	46	54	59	40	50	56
33	50	56	62	43	52	60	41	46	51	56	64	71	49	56	62	43	51	59
34	50	57	62	44	53	59	39	47	53	57	65	70	47	57	64	46	52	56
35	52	58	65	47	54	61	38	48	57	61	67	73	48	59	69	51	54	57
36	53	60	63	47	55	61	41	48	54	61	69	74	49	60	68	51	55	56
37	57	61	64	49	56	62	45	49	53	64	71	77	52	61	71	55	56	58
38	55	61	66	48	57	63	45	49	53	62	72	79	54	62	69	54	57	59
39	56	62	69	49	57	66	46	50	54	64	74	83	58	64	69	55	58	62
40	56	63	69	50	58	65	46	50	54	66	75	81	58	65	69	54	59	62

From Jeanty P: Fetal limb biometry (letter). Radiology 147:602, 1983.



TABLE A-20 Reference Values of Major Long Bones

GA (wk)	HUMERUS (mm) <sup>a</sup>			RADIUS (mm) <sup>b</sup>			ULNA (mm) <sup>c</sup>		
	PERCENTILES			PERCENTILES			PERCENTILES		
	5th	50th	95th	5th	50th	95th	5th	50th	95th
12	4.8	8.6	12.3	3.0	6.9	10.8	2.9	6.8	10.7
13	7.6	11.4	15.1	5.6	9.5	13.4	5.8	9.7	13.7
14	10.3	14.1	17.9	8.1	12.0	16.0	8.6	12.6	16.6
15	13.1	16.9	20.7	10.5	14.5	18.5	11.4	15.4	19.4
16	15.8	19.7	23.5	12.9	16.9	20.9	14.1	18.1	22.1
17	18.5	22.4	26.3	15.2	19.3	23.3	16.7	20.8	24.8
18	21.2	25.1	29.0	17.5	21.5	25.6	19.3	23.3	27.4
19	23.8	27.7	31.6	19.7	23.8	27.9	21.8	25.8	29.9
20	26.3	30.3	34.2	21.8	25.9	30.0	24.2	28.3	32.4
21	28.8	32.8	36.7	23.9	28.0	32.2	26.5	30.6	34.8
22	31.2	35.2	39.2	25.9	30.1	34.2	28.7	32.9	37.1
23	33.5	37.5	41.6	27.9	32.0	36.2	30.9	35.1	39.3
24	35.7	39.8	43.8	29.7	34.0	38.2	33.0	37.2	41.5
25	37.9	41.9	46.0	31.6	35.8	40.0	35.1	39.3	43.5
26	39.9	44.0	48.1	33.3	37.6	41.9	37.0	41.3	45.6
27	41.9	46.0	50.1	35.0	39.3	43.6	38.9	43.2	47.5
28	43.7	47.9	52.0	36.7	41.0	45.3	40.7	45.0	49.3
29	45.5	49.7	53.9	38.3	42.6	46.9	42.5	46.8	51.1
30	47.2	51.4	55.6	39.8	44.1	48.5	44.1	48.5	52.8
31	48.9	53.1	57.3	41.2	45.6	50.0	45.7	50.1	54.5
32	50.4	54.7	58.9	42.6	47.0	51.4	47.2	51.6	56.1
33	52.0	56.2	60.5	44.0	48.4	52.8	48.7	53.1	57.5
34	53.4	57.7	62.0	45.2	49.7	54.1	50.0	54.5	59.0
35	54.8	59.2	63.5	46.4	50.9	55.4	51.3	55.8	60.3
36	56.2	60.6	64.9	47.6	52.1	56.6	52.6	57.1	61.6
37	57.6	62.0	66.4	48.7	53.2	57.7	53.7	58.2	62.8
38	59.0	63.4	67.8	49.7	54.2	58.8	54.8	59.3	63.9
39	60.4	64.8	69.3	50.6	55.2	59.8	55.8	60.4	64.9
40	61.9	66.3	70.8	51.5	56.2	60.8	56.7	61.3	65.9

GA, gestational age.

<sup>a</sup>Humerus (mean) =  $-16.24 + 0.76315 \times GA + 0.1683 \times GA^2 - 0.0056212 \times GA^3 + 0.000055666 \times GA^4$ .

<sup>b</sup>Radius (mean) =  $-29.09 + 3.371 \times GA - 0.031 \times GA^2$  (Exacoustos et al, 1991).

<sup>c</sup>Ulna (mean) =  $-34.313 + 3.8685 \times GA - 0.036949 \times GA^2$  (Jeanty et al, 1984).

Derived from compilation of data: Jeanty P, Coussaert E, Cantraine F, et al. A longitudinal study of fetal limb growth. *Am J Perinatol* 1:136, 1984; Merz E, Grubner A, Kern F: Mathematical modeling of fetal limb growth. *J Clin Ultrasound* 17:179, 1989; and Exacoustos C, Rosati P, Rizzo G, Arduini D: Ultrasound measurements of fetal limb bones. *Ultrasound Obstet Gynecol* 1:325, 1991.

From Nyberg DA, McGahan JP, Pretorius DH, Pilu G: *Diagnostic Imaging of Fetal Anomalies*. Philadelphia, Lippincott Williams & Wilkins, 2003.

**TABLE A-21 Gestational Age for Clavicle Length**

Clavicle Length (mm)	GESTATIONAL AGE (WEEKS AND DAYS) BY PERCENTILE		
	5th	50th	95th
11	8 + 3	13 + 6	17 + 2
12	9 + 1	14 + 4	18 + 1
13	10 + 0	14 + 3	19 + 6
14	11 + 6	15 + 2	20 + 5
15	12 + 5	16 + 1	21 + 4
16	12 + 3	18 + 0	21 + 3
17	13 + 2	18 + 5	22 + 2
18	14 + 1	19 + 4	23 + 0
19	16 + 0	19 + 3	24 + 6
20	16 + 6	20 + 2	25 + 5
21	17 + 4	21 + 1	26 + 4
22	17 + 3	22 + 6	26 + 2
23	18 + 2	23 + 5	27 + 1
24	19 + 1	24 + 4	28 + 0
25	21 + 0	24 + 3	29 + 6
26	21 + 5	25 + 1	30 + 5
27	22 + 4	26 + 0	30 + 3
28	22 + 3	27 + 6	31 + 2
29	23 + 2	28 + 5	32 + 1
30	24 + 0	29 + 4	34 + 0
31	25 + 6	29 + 2	34 + 6
32	26 + 5	30 + 1	35 + 4
33	27 + 4	31 + 0	35 + 3
34	27 + 3	32 + 6	36 + 2
35	28 + 1	33 + 5	37 + 1
36	29 + 0	33 + 3	39 + 0
37	30 + 6	34 + 2	39 + 5
38	31 + 5	35 + 1	40 + 4
39	32 + 4	37 + 0	40 + 3
40	32 + 2	37 + 6	41 + 2
41	33 + 1	38 + 4	42 + 0
42	35 + 0	38 + 3	43 + 6
43	35 + 6	39 + 2	44 + 5
44	36 + 5	40 + 1	45 + 4
45	36 + 3	41 + 6	45 + 3

From Yarkoni S, Schmidt W, Jeanty P, et al: Clavicular measurement: a new biometric parameter for fetal evaluation. *J Ultrasound Med* 4:467, 1985.

**TABLE A-22 Comparison of Mean Postpartum and Ultrasonographic Foot Length With Streeter's Pathologic Data (1920)**

Gestational Week	Streeter's Data (mm)	Ultrasonographic Foot Length (mm)	Postpartum Foot Length (mm)
11	7	8	
12	9	9	
13	11	10	
14	14	16	
15	17	16	
16	20	21	
17	23	24	
18	27	27	
19	31	28	
20	33	33	33
21	35	35	
22	40	38	
23	42	42	
24	45	44	
25	48	47	48
26	50	51	
27	53	54	52
28	55	58	
29	57	57	57
30	59	61	60
31	61	62	60
32	63	63	66
33	65	67	68
34	68	68	71
35	71	71	72
36	74	74	74
37	77	75	78
38	79	78	78
39	81	78	80
40	83	82	81
41			82
42			82
43			84

From Mercer BM, Sklar S, Shariatmadar A, et al: Fetal foot length as a predictor of gestational age. *Am J Obstet Gynecol* 156:350, 1987.



TABLE A-23 Fetal Foot Length Percentiles by Menstrual Age\*

Menstrual Age (wk)	N	CV (%)	FETAL FOOT LENGTH PERCENTILES (SMOOTHED)				
			5th	10th	50th	90th	95th
15	18	12.7	1.4	1.5	1.8	2.2	2.3
16	146	10.4	1.6	1.7	2.1	2.5	2.6
17	375	9.7	1.9	2.0	2.4	2.8	2.9
18	613	9.8	2.2	2.3	2.7	3.1	3.2
19	1160	8.9	2.5	2.6	3.0	3.3	3.4
20	929	9.3	2.8	2.9	3.2	3.6	3.7
21	552	8.5	3.1	3.2	3.5	3.9	4.0
22	360	8.9	3.4	3.5	3.9	4.2	4.3
23	222	8.1	3.7	3.8	4.2	4.6	4.7
24	177	7.0	4.0	4.1	4.5	4.9	5.0
25	125	7.1	4.3	4.4	4.8	5.1	5.2
26	123	7.0	4.6	4.7	5.1	5.4	5.5
27	108	6.3	4.8	4.9	5.3	5.7	5.8
28	74	5.4	5.1	5.2	5.6	5.9	6.0
29	66	6.2	5.3	5.4	5.8	6.2	6.3
30	65	5.2	5.6	5.7	6.1	6.4	6.5
31	62	5.7	5.8	5.9	6.3	6.7	6.8
32	65	5.3	6.0	6.1	6.5	6.9	7.0
33	39	4.4	6.3	6.4	6.8	7.1	7.2
34	37	6.8	6.5	6.6	7.0	7.4	7.5
35	24	6.2	6.8	6.9	7.3	7.6	7.7
36	15	5.5	7.0	7.1	7.5	7.9	8.0
37	17	5.3	7.3	7.4	7.7	8.1	8.2

CV, coefficient of variation; N, number of fetuses.

\*Values for percentiles are in centimeters.

From Meiorowitz NB, Ananth CV, Smulian JC, et al: Foot length in fetuses with abnormal growth. J Ultrasound Med 19:201, 2000.

**TABLE A-24 Predicted Menstrual Ages for Transverse Cerebellar Diameters of 14 to 56 mm**

Cerebellum Diameter (mm)	Menstrual Age (wk)	Cerebellum Diameter (mm)	Menstrual Age (wk)
14	15.2	35	29.4
15	15.8	36	30.8
16	16.5	37	30.6
17	17.2	38	31.2
18	17.9	39	31.8
19	18.6	40	32.3
20	19.3	41	32.8
21	20.0	42	33.4
22	20.7	43	33.9
23	21.4	44	34.4
24	22.1	45	34.8
25	22.8	46	35.3
26	23.5	47	35.7
27	24.2	48	36.1
28	24.9	49	36.5
29	25.5	50	36.8
30	26.2	51	37.2
31	26.9	52	37.5
32	27.5	54	38.0
33	28.1	55	38.3
34	28.8	56	38.5

VARIABILITY ESTIMATES ( $\pm 2$ SD)	
12-18 wk	$\pm 1.0$ wk
18-24 wk	$\pm 1.8$ wk
24-30 wk	$\pm 2.0$ wk
30-36 wk	$\pm 2.4$ wk
36-42 wk	$\pm 3.2$ wk

From Hill LM, Guzick D, Fries J, et al: The transverse cerebellar diameter in estimating gestational age in the large-for-gestational-age fetus. *Obstet Gynecol* 75:983, 1990. Reprinted with permission from the American College of Obstetricians and Gynecologists.

**TABLE A-25 Nomogram of the Transverse Cerebellar Diameter According to Percentile Distribution**

Gestational Age (wk)	CEREBELLUM DIAMETER (mm)				
	10th	25th	50th	75th	90th
15	10	12	14	15	16
16	14	16	16	16	17
17	16	17	17	18	18
18	17	18	18	19	19
19	18	18	19	19	22
20	18	19	20	20	22
21	19	20	22	23	24
22	21	23	23	24	24
23	22	23	24	25	26
24	22	24	25	27	28
25	23	21.5	28	28	29
26	25	28	29	30	32
27	26	28.5	30	31	32
28	27	30	31	32	34
29	29	32	34	36	38
30	31	32	35	37	40
31	32	35	38	39	43
32	33	36	38	40	42
33	32	36	40	43	44
34	33	38	40	41	44
35	31	37	40.5	43	47
36	36	29	43	52	55
37	37	37	45	52	55
38	40	40	48.5	52	55
39	52	52	52	55	55

From Goldstein I, Reece A, Pihu G, et al: Cerebellar measurements with ultrasonography in the evaluation of fetal growth and development. *Am J Obstet Gynecol* 156:1065, 1987.



**TABLE A-26 Predicted Biparietal Diameter (BPD) and Week of Gestation From the Inner (IOD) and Outer (OOD) Orbital Distances**

BPD (cm)	Gestation (wk)	IOD (cm)	OOD (cm)	BPD (cm)	Gestation (wk)	IOD (cm)	OOD (cm)
1.9	11.6	0.5	1.3	5.8	24.3	1.6	4.1
2.0	11.6	0.5	1.4	5.9	24.3	1.6	4.2
2.1	12.1	0.6	1.5	6.0	24.7	1.6	4.3
2.2	12.6	0.6	1.6	6.1	25.2	1.6	4.3
2.3	12.6	0.6	1.7	6.2	25.2	1.6	4.4
2.4	13.1	0.7	1.7	6.3	25.7	1.7	4.4
2.5	13.6	0.7	1.8	6.4	26.2	1.7	4.5
2.6	13.6	0.7	1.9	6.5	26.2	1.7	4.5
2.7	14.1	0.8	2.0	6.6	26.7	1.7	4.6
2.8	14.6	0.8	2.1	6.7	27.2	1.7	4.6
2.9	14.6	0.8	2.1	6.8	27.6	1.7	4.7
3.0	15.0	0.9	2.2	6.9	28.1	1.7	4.7
3.1	15.5	0.9	2.3	7.0	28.6	1.8	4.8
3.2	15.5	0.9	2.4	7.1	29.1	1.8	4.8
3.3	16.0	1.0	2.5	7.3	29.6	1.8	4.9
3.4	16.5	1.0	2.5	7.4	30.0	1.8	5.0
3.5	16.5	1.0	2.6	7.5	30.6	1.8	5.0
3.6	17.0	1.0	2.7	7.6	31.0	1.8	5.1
3.7	17.5	1.1	2.7	7.7	31.5	1.8	5.1
3.8	17.9	1.1	2.8	7.8	32.0	1.8	5.2
4.0	18.4	1.2	3.0	7.9	32.5	1.9	5.2
4.2	18.9	1.2	3.1	8.0	33.0	1.9	5.3
4.3	19.4	1.2	3.2	8.2	33.5	1.9	5.4
4.4	19.4	1.3	3.2	8.3	34.0	1.9	5.4
4.5	19.9	1.3	3.3	8.4	34.4	1.9	5.4
4.6	20.4	1.3	3.4	8.5	35.0	1.9	5.5
4.7	20.4	1.3	3.4	8.6	35.4	1.9	5.5
4.8	20.9	1.4	3.5	8.8	35.9	1.9	5.6
4.9	21.3	1.4	3.6	8.9	36.4	1.9	5.6
5.0	21.3	1.4	3.6	9.0	36.9	1.9	5.7
5.1	21.8	1.4	3.7	9.1	37.3	1.9	5.7
5.2	22.3	1.4	3.8	9.2	37.8	1.9	5.8
5.3	22.3	1.5	3.8	9.3	38.3	1.9	5.8
5.4	22.8	1.5	3.9	9.4	38.8	1.9	5.8
5.5	23.3	1.5	4.0	9.6	39.3	1.9	5.9
5.6	23.3	1.5	4.0	9.7	39.8	1.9	5.9
5.7	23.8	1.5	4.1				

From Mayden KL, Tortora M, Berkowitz RL, et al: Orbital diameters: a new parameter for prenatal diagnosis and dating. *Am J Obstet Gynecol* 144:289, 1982.

TABLE A-27 Fetal Thoracic Circumference Measurements\*

Gestational Age (wk)	No.	PREDICTIVE PERCENTILES								
		2.5th	5th	10th	25th	50th	75th	90th	95th	97.5th
16	6	5.9	6.4	7.0	8.0	9.1	10.3	11.3	11.9	12.4
17	22	6.8	7.3	7.9	8.9	10.0	11.2	12.2	12.8	13.3
18	31	7.7	8.2	8.8	9.8	11.0	12.1	13.1	13.7	14.2
19	21	8.6	9.1	9.7	10.7	11.9	13.0	14.0	14.6	15.1
20	20	9.5	10.0	10.6	11.7	12.8	13.9	15.0	15.5	16.0
21	30	10.4	11.0	11.6	12.6	13.7	14.8	15.8	16.4	16.9
22	18	11.3	11.9	12.5	13.5	14.6	15.7	16.7	17.3	17.8
23	21	12.2	12.8	13.4	14.4	15.5	16.6	17.6	18.2	18.8
24	27	13.2	13.7	14.3	15.3	16.4	17.5	18.5	19.1	19.7
25	20	14.1	14.6	15.2	16.2	17.3	18.4	19.4	20.0	20.6
26	25	15.0	15.5	16.1	17.1	18.2	19.3	20.3	21.0	21.5
27	24	15.9	16.4	17.0	18.0	19.1	20.2	21.3	21.9	22.4
28	24	16.8	17.3	17.9	18.9	20.0	21.2	22.2	22.8	23.3
29	24	17.7	18.2	18.8	19.8	21.0	22.1	23.1	23.7	24.2
30	27	18.6	19.1	19.7	20.7	21.9	23.0	24.0	24.6	25.1
31	24	19.5	20.0	20.6	21.6	22.8	23.9	24.9	25.5	26.0
32	28	20.4	20.9	21.5	22.6	23.7	24.8	25.8	26.4	26.9
33	27	21.3	21.8	22.5	23.5	24.6	25.7	26.7	27.3	27.8
34	25	22.2	22.8	23.4	24.4	25.5	26.6	27.6	28.2	28.7
35	20	23.1	23.7	24.3	25.3	26.4	27.5	28.5	29.1	29.6
36	23	24.0	24.6	25.2	26.2	27.3	28.4	29.4	30.0	30.6
37	22	24.9	25.5	26.1	27.1	28.2	29.3	30.3	30.9	31.5
38	21	25.9	26.4	27.0	28.0	29.1	30.2	31.2	31.9	32.4
39	7	26.8	27.3	27.9	28.9	30.0	31.1	32.2	32.8	33.3
40	6	27.7	28.2	28.8	29.8	30.9	32.1	33.1	33.7	34.2

\*Measurements in centimeters.

From Chitkara U, Rosenberg J, Chervenak FA, et al: Prenatal sonographic assessment of the fetal thorax: normal values. Am J Obstet Gynecol 156:1069, 1987.



**TABLE A-28 Percentiles (2.5th, 50th, 97.5th) for Lung Area (Manual Tracing) and Lung Volume From 12 to 32 Gestational Weeks**

Menstrual age (wk)	LEFT LUNG AREA (mm)			RIGHT LUNG AREA (mm)			LEFT LUNG VOLUME (mL)			RIGHT LUNG VOLUME (mL)			TOTAL LUNG VOLUME (mL)		
	2.5th	50th	97.5th	2.5th	50th	97.5th	2.5th	50th	97.5th	2.5th	50th	97.5th	2.5th	50th	97.5th
12	20	36	51	44	58	71	0.63	0.64	0.65	0.59	0.6	0.62	1.37	1.56	1.75
13	26	47	68	42	69	96	0.37	0.57	0.77	0.5	0.75	1	0.85	1.4	1.94
14	36	62	89	48	88	129	0.26	0.69	1.11	0.54	1.06	1.58	0.7	1.65	2.61
15	49	82	114	61	115	169	0.31	0.97	1.64	0.7	1.53	2.36	0.9	2.32	3.74
16	65	104	144	80	148	215	0.49	1.42	2.35	1	2.16	3.33	1.42	3.36	5.31
17	83	130	177	105	186	267	0.79	2.02	3.24	1.42	2.96	4.51	2.25	4.77	7.29
18	103	158	213	134	229	323	1.22	2.76	4.3	1.97	3.92	5.87	3.36	6.52	9.67
19	125	188	252	168	275	383	1.75	3.63	5.51	2.64	5.04	7.44	4.72	8.57	12.4
20	148	220	293	204	325	447	2.38	4.62	6.85	3.43	6.31	9.19	6.31	10.9	15.5
21	172	254	335	243	378	512	3.09	5.71	8.33	4.33	7.73	11.1	8.1	13.5	18.9
22	196	288	380	283	432	580	3.87	6.9	9.92	5.34	9.28	13.2	10.1	16.3	22.6
23	220	323	425	325	486	648	4.71	8.16	11.6	6.45	11	15.5	12.2	19.3	26.5
24	244	358	471	366	541	716	5.58	9.49	13.4	7.64	12.8	17.9	14.4	22.5	30.7
25	268	392	517	406	595	783	6.49	10.9	15.3	8.9	14.7	20.5	16.6	25.8	35
26	290	426	563	445	647	849	7.4	12.3	17.2	10.2	16.7	23.2	18.9	29.2	39.5
27	310	459	609	482	697	913	8.31	13.7	19.1	11.6	18.8	26	21.2	32.7	44.1
28	328	491	653	515	744	973	9.19	15.1	21.1	13	21	29	23.5	36.1	48.7
29	344	521	697	545	787	1029	10	16.6	23.1	14.4	23.2	32	25.7	39.6	53.4
30	358	548	738	569	825	1081	10.8	17.9	25	15.9	25.5	35.1	27.7	42.9	58.1
31	368	573	777	589	858	1127	11.5	19.3	27	17.2	27.7	38.2	29.6	46.2	62.7
32	374	594	814	602	885	1167	12.1	20.5	28.9	18.6	30	41.3	31.3	49.3	67.3

From Peralta CF, Cavoretto P, Csapo B, et al: Assessment of lung area in normal fetuses at 12-32 weeks. *Ultrasound Obstet Gynecol* 26:718-724, 2005; Peralta CF, Cavoretto P, Csapo B, et al: Lung and heart volumes by three-dimensional ultrasound in normal fetuses at 12-32 weeks' gestation. *Ultrasound Obstet Gynecol* 27:128-133, 2006.

**TABLE A-29 Percentiles (10th, 50th, 90th) for Thoracic Diameters From 12 to 41 Weeks of Gestation**

Weeks	THORACIC ANTEROPOSTERIOR DIAMETER (mm)			THORACIC TRANSVERSE DIAMETER (mm)			THORACIC CIRCUMFERENCE (mm)		
	10th	50th	90th	10th	50th	90th	10th	50th	90th
12	11.7	14.2	16.5	11.7	14.2	16.5	11.7	14.2	16.5
13	14.3	17.2	19.8	14.3	17.2	19.8	14.3	17.2	19.8
14	17.1	20.3	23.3	17.1	20.3	23.3	17.1	20.3	23.3
15	19.9	23.4	26.7	19.9	23.4	26.7	19.9	23.4	26.7
16	22.8	26.5	30.2	22.8	26.5	30.2	22.8	26.5	30.2
17	25.8	29.6	33.6	25.8	29.6	33.6	25.8	29.6	33.6
18	28.7	32.6	37.0	28.7	32.6	37.0	28.7	32.6	37.0
19	31.6	35.6	40.5	31.6	35.6	40.5	31.6	35.6	40.5
20	34.2	38.5	43.9	34.2	38.5	43.9	34.2	38.5	43.9
21	36.8	41.4	47.2	36.8	41.4	47.2	36.8	41.4	47.2
22	39.2	44.3	50.4	39.2	44.3	50.4	39.2	44.3	50.4
23	41.5	47.2	53.6	41.5	47.2	53.6	41.5	47.2	53.6
24	43.9	50.0	56.6	43.9	50.0	56.6	43.9	50.0	56.6
25	46.5	52.8	59.5	46.5	52.8	59.5	46.5	52.8	59.5
26	49.1	55.5	62.3	49.1	55.5	62.3	49.1	55.5	62.3
27	51.7	58.2	64.9	51.7	58.2	64.9	51.7	58.2	64.9
28	54.2	60.8	67.4	54.2	60.8	67.4	54.2	60.8	67.4
29	56.6	63.4	69.8	56.6	63.4	69.8	56.6	63.4	69.8
30	58.9	65.9	72.3	58.9	65.9	72.3	58.9	65.9	72.3
31	61.1	68.4	74.9	61.1	68.4	74.9	61.1	68.4	74.9
32	63.2	70.9	77.7	63.2	70.9	77.7	63.2	70.9	77.7
33	65.1	73.2	80.6	65.1	73.2	80.6	65.1	73.2	80.6
34	67.0	75.4	83.4	67.0	75.4	83.4	67.0	75.4	83.4
35	68.8	77.3	85.8	68.8	77.3	85.8	68.8	77.3	85.8
36	70.6	79.0	88.0	70.6	79.0	88.0	70.6	79.0	88.0
37	72.5	80.5	90.0	72.5	80.5	90.0	72.5	80.5	90.0
38	74.3	81.9	91.8	74.3	81.9	91.8	74.3	81.9	91.8
39	75.9	83.1	93.5	75.9	83.1	93.5	75.9	83.1	93.5
40	77.5	84.1	94.9	77.5	84.1	94.9	77.5	84.1	94.9
41	78.8	84.9	95.8	78.8	84.9	95.8	78.8	84.9	95.8

From J Lessoway VA, Schulzer M, Wittmann BK, et al: Ultrasound fetal biometry charts for a North American Caucasian population. J Clin Ultrasound 26:433-453, 1998.



## Measurements Used in Assessing Fetal Weight, Growth, and Body Proportions

**TABLE B-1 Equations for the Estimation of Fetal Weight**

Source	Year	Equation
<b>AC Equations</b>		
Campbell and Wilkin*	1975	$\text{Ln EFW} = -4.564 + 0.282 (\text{AC}) - 0.00331 (\text{AC})^2$
Hadlock et al	1984	$\text{Ln EFW} = 2.695 + 0.253 (\text{AC}) - 0.00275 (\text{AC})^2$
Jordaan	1983	$\text{Log}_{10} \text{EFW} = 0.6328 + 0.1881 (\text{AC}) - 0.0043 (\text{AC})^2 + 0.000036239 (\text{AC})^3$
Warsof et al*	1977	$\text{Log}_{10} \text{EFW} = -1.8367 + 0.092 (\text{AC}) - 0.000019 (\text{AC})^3$
Higginbottom et al	1975	$\text{EFW} = 0.0816 (\text{AC})^3$
<b>FL Equation</b>		
Warsof et al	1986	$\text{Ln EFW} = 4.6914 + 0.151 (\text{FL})^2 - 0.0119 (\text{FL})^3$
<b>AC/FL Equations</b>		
Hadlock et al	1985	$\text{Log}_{10} \text{EFW} = 1.304 + 0.05281 (\text{AC}) + 0.1938 (\text{FL}) - 0.004 (\text{AC}) (\text{FL})$
Warsof et al	1986	$\text{Ln EFW} = 2.792 + 1.08 (\text{FL}) + 0.0036 (\text{AC})^2 - 0.027 (\text{FL}) (\text{AC})$
Woo et al	1985	$\text{Log}_{10} \text{EFW} = 0.59 + 0.08 (\text{AC}) + 0.28 (\text{FL}) - 0.00716 (\text{AC}) (\text{FL})$
<b>AC/BPD Equations</b>		
Warsof et al*	1977	$\text{Log}_{10} \text{EFW} = 1.599 + 0.144 (\text{BPD}) + 0.032 (\text{AC}) - 0.000111 (\text{BPD})^2 (\text{AC})$
Hadlock et al	1984	$\text{Log}_{10} \text{EFW} = 1.1134 + 0.05845 (\text{AC}) - 0.000604 (\text{AC})^2 - 0.007365 (\text{BPD})^2 + 0.000595 (\text{BPD}) (\text{AC}) + 0.1694 (\text{BPD})$
Jordaan*	1983	$\text{Log}_{10} \text{EFW} = -1.1683 + 0.0377 (\text{AC}) + 0.0950 (\text{BPD}) - 0.0015 (\text{BPD}) (\text{AC})$
Hsieh et al	1987	$\text{Log}_{10} \text{EFW} = 2.1315 + 0.0056541 (\text{AC}) (\text{BPD}) - 0.00015515 (\text{BPD}) (\text{AC})^2 + 0.000019782 (\text{AC})^3 + 0.052594 (\text{BPD})$
Woo et al	1985	$\text{Log}_{10} \text{EFW} = 1.63 + 0.16 (\text{BPD}) + 0.00111 (\text{AC})^2 - 0.0000859 (\text{BPD}) (\text{AC})^2$
Vintzileos et al	1987	$\text{Log}_{10} \text{EFW} = 1.879 + 0.084 (\text{BPD}) + 0.026 (\text{AC})$
Shepard et al*	1982	$\text{Log}_{10} \text{EFW} = -1.7492 + 0.166 (\text{BPD}) + 0.046 (\text{AC}) - 0.002546 (\text{BPD})$
<b>AC/BPD/FL Equations</b>		
Woo et al	1985	$\text{Log}_{10} \text{EFW} = 1.54 + 0.15 (\text{BPD}) + 0.00111 (\text{AC})^2 - 0.0000764 (\text{BPD}) (\text{AC})^2 + 0.05 (\text{FL}) - 0.000992 (\text{FL}) (\text{AC})$
Shinozuka et al <sup>†</sup>	1987	$\text{EFW} = 0.23966 (\text{AC})^2 (\text{FL}) + 1.6230 (\text{BPD})^3$
Hadlock et al	1985	$\text{Log}_{10} \text{EFW} = 1.335 - 0.0034 (\text{AC}) (\text{FL}) + 0.0316 (\text{BPD}) + 0.0457 (\text{AC}) + 0.1623 (\text{FL})$
Hsieh et al	1987	$\text{Log}_{10} \text{EFW} = 2.7193 + 0.0094962 (\text{AC}) (\text{BPD}) - 0.1432 (\text{FL}) - 0.00076742 (\text{AC}) (\text{BPD})^2 + 0.001745 (\text{FL}) (\text{BPD})^2$
<b>AC/HC/FL Equations</b>		
Hadlock et al	1984	$\text{Log}_{10} \text{EFW} = 1.326 - 0.00326 (\text{AC}) (\text{FL}) + 0.0107 (\text{HC}) + 0.0438 (\text{AC}) + 0.158 (\text{FL})$
Ott et al*	1986	$\text{Log}_{10} \text{EFW} = 2.0661 + 0.04355 (\text{HC}) + 0.05394 (\text{AC}) - 0.0008582 (\text{HC}) (\text{AC}) + 1.2594 (\text{FL}/\text{AC})$
Combs et al	1993	$\text{EFW} = 0.23718 (\text{AC})^2 (\text{FL}) + 0.03312 (\text{HC})^3$

TABLE B-1 Equations for the Estimation of Fetal Weight—cont'd

Source	Year	Equation
<b>AC/HC/BPD/± FL Equations</b>		
Jordaan	1983	$\text{Log}_{10} \text{EFW} = 2.3231 + 0.02904 (\text{AC}) + 0.0079 (\text{HC}) + 0.0058 (\text{BPD})$
Hadlock et al	1985	$\text{Log}_{10} \text{EFW} = 1.3596 + 0.0064 (\text{HC}) + 0.0424 (\text{AC}) + 0.174 (\text{FL}) + 0.00061 (\text{BPD}) (\text{AC}) - 0.00386 (\text{AC}) (\text{FL})$
<b>Maternal Characteristics Equation</b>		
Nahum et al <sup>†</sup>	2002	$\text{EFW} = \text{Gestational age (d)} \times (9.38 + 0.264 \times \text{fetal sex}^{\ddagger} + 0.000233 \times \text{maternal height [cm]} \times \text{maternal weight at 26.0 wks [kg]} + 4.62 \times \text{third-trimester maternal weight gain rate [kg/d]} \times [\text{parity} + 1])^{\S}$

AC, abdominal circumference; BPD, biparietal diameter; EFW, estimated fetal weight (expressed in grams); FL, fetal length; HC, head circumference; Ln, natural logarithm.

AC, FL, BPD, and HC are expressed in centimeters.

\*The estimated fetal weight for these six algorithms is expressed in kilograms rather than grams.

†The equation of Shinozuka et al has been modified from its original form to include the fetal AC instead of the fetal transverse and anteroposterior abdominal diameters, as were described in the original equation. (Shinozuka N, Okai T, Kohzuma S, et al: Formulas for fetal weight estimation by ultrasound measurements based on neonatal specific gravities and volumes. *J Obstet Gynecol* 157:1140, 1987; Combs CA, Jaekle RK, Rosenn B, et al: Sonographic estimation of fetal weight based on a model of fetal volume. *Obstet Gynecol* 82:365, 1993.)

‡This equation applies only to healthy white mothers who carry term singleton pregnancies. Fetal weight estimates that use this equation should be adjusted systematically for (1) black maternal race (decrement by 161 g), (2) East Asian maternal race (decrement by 291 g), (3) chronic hypertension (decrement by 161 g), (4) pregnancy-induced hypertension/preeclampsia (decrement by 105 g), (5) maternal cigarette smoking (decrement by 17 g per cigarettes smoked per day), and (6) high altitude (decrement by 102 g for every 1000 m in altitude above sea level).

§Fetal sex independently explains approximately 1% of the variance in term fetal weight. It is a significant predictor of birth weight (F test,  $P < 0.001$ ), but it has little overall impact in birth weight predictions. When 0 is entered for fetal sex so that sex is ignored, the mean absolute prediction error does not change, and the median absolute prediction error increases only slightly by 10 g (0.2%). Thus, fetal sex, although potentially useful if available, is nonessential for use of the maternal characteristics equation.

¶Where fetal sex = +1 for male, -1 for female, and 0 when sex is not known; gestational age = days since the onset of the last normal period = the conception age (in days) + 14. (Nahum GG, Stanislaw H: Ultrasonographic prediction of term birth weight: how accurate is it? *Am J Obstet Gynecol* 188:566, 2003.)

From Hill LM: Fetal weight. In Goldberg BB, McGahan JP (eds): *Atlas of Ultrasound Measurements*, 2nd ed. Philadelphia, Mosby/Elsevier, 2006.

TABLE B-2 Neonatal Birth Weight Derived From Gestations Dated by Early Ultrasonography (Male and Female Subjects Combined)

Gestational Age (wk)*	WEIGHT (g) BY PERCENTILE						
	5th	10th	25th	50th	75th	90th	95th
25	450	490	564	660	772	889	968
26	523	568	652	760	885	1016	1103
27	609	660	754	875	1015	1160	1257
28	707	765	870	1005	1162	1322	1430
29	820	884	1003	1153	1327	1504	1623
30	947	1020	1151	1319	1511	1706	1836
31	1090	1171	1317	1502	1713	1928	2070
32	1249	1338	1499	1702	1933	2167	2321
33	1422	1519	1696	1918	2169	2421	2587
34	1608	1714	1906	2146	2416	2687	2865
35	1804	1919	2125	2383	2671	2959	3148
36	2006	2129	2349	2622	2927	3230	3428
37	2210	2340	2572	2859	3177	3493	3698
38	2409	2544	2786	3083	3412	3736	3947
39	2595	2735	2984	3288	3622	3952	4164
40	2762	2904	3155	3462	3798	4127	4340
41	2900	3042	3293	3597	3930	4254	4462
42	3002	3142	3388	3685	4008	4322	4523
43	3061	3195	3432	3717	4026	4324	4515

\*Age to the nearest week. Percentiles listed for 25 weeks, for example, apply to neonates aged 24.5 to 25.4 weeks.

From Doubilet PM, Benson CB, Nadel AS, et al: Improved birth weight table for neonates developed from gestations dated by early ultrasonography. *J Ultrasound Med* 16:241, 1997.



**TABLE B-3 Percentile of Birth Weight in Non-Hispanic White Singleton Infants in California by Sex and Gestational Age**

Gestational Age (completed wk)	10th		50th		90th	
	Male	Female	Male	Female	Male	Female
22	326	314	530	496	736	755
23	376	354	609	569	851	869
24	433	400	699	651	982	996
25	499	454	800	745	1127	1136
26	574	518	913	850	1288	1290
27	662	591	1041	969	1466	1460
28	762	678	1184	1102	1661	1645
29	878	780	1343	1251	1873	1845
30	1007	902	1537	1430	2159	2113
31	1159	1041	1752	1637	2439	2364
32	1348	1219	1979	1861	2727	2619
33	1561	1436	2220	2090	2972	2847
34	1787	1668	2459	2329	3205	3059
35	2030	1918	2694	2562	3415	3250
36	2278	2169	2910	2788	3591	3450
37	2499	2410	3112	2992	3765	3646
38	2696	2587	3292	3161	3931	3802
39	2849	2730	3434	3294	4064	3923
40	2944	2817	3534	3389	4154	4005
41	3018	2873	3598	3450	4214	4040
42	3086	2936	3665	3513	4276	4094
43	3120	2937	3703	3548	4315	4126
44	3120	2966	3712	3554	4330	4136
45	3085	2932	3691	3531	4321	4126
46	3016	2866	3641	3479	4288	4093
47	2916	2771	3563	3400	4231	4040
48	2789	2650	3459	3295	4152	3966

From Williams RL, Creasy RK, Cunningham GC, et al: Fetal growth and perinatal viability in California. *Obstet Gynecol* 59(5):624-632, 1982, Table 3.

**TABLE B-4 Fetal Weight Percentiles in the Third Trimester\***

Gestational Age (wk)	WEIGHT (g) PERCENTILES		
	10th	50th	90th
26	570	860	1320
27	660	990	1470
28	770	1150	1660
29	890	1310	1890
30	1030	1460	2100
31	1180	1630	2290
32	1310	1810	2500
33	1480	2010	2690
34	1670	2220	2880
35	1870	2430	3090
36	2190	2650	3290
37	2310	2870	3470
38	2510	3030	3610
39	2680	3170	3750
40	2750	3280	3870
41	2800	3360	3980
42	2830	3410	4060
43	2840	3420	4100
44	2790	3390	4110

\*From Doubilet PM, Benson CB, Nadel AS, Ringer SA: Improved birth weight table for neonates developed from gestations dated by early ultrasonography. *J Ultrasound Med* 16:241-249, 1997.

**TABLE B-5 Percentiles for Birth Weight by Gestational Age in Boy and Girl Infants as Reported in the INTERGROWTH21 Study**

GA	BOYS						GIRLS					
	Number of Observations	PERCENTILES FOR BIRTH WEIGHT (kg)					Number of Observations	PERCENTILES FOR BIRTH WEIGHT (kg)				
		3rd	10th	50th	90th	97th		3rd	10th	50th	90th	97th
33 weeks	34	1.18	1.43	1.95	2.52	2.82	17	1.20	1.41	1.86	2.35	2.61
34 weeks	48	1.45	1.71	2.22	2.79	3.08	65	1.47	1.68	2.13	2.64	2.90
35 weeks	128	1.70	1.95	2.47	3.03	3.32	114	1.71	1.92	2.38	2.89	3.16
36 weeks	323	1.93	2.18	2.63	3.25	3.54	293	1.92	2.14	2.60	3.12	3.39
37 weeks	857	2.13	2.38	2.89	3.45	2.74	803	2.11	2.33	2.80	3.32	3.60
38 weeks	2045	2.32	2.57	3.07	3.63	3.92	1802	2.28	2.50	2.97	3.51	3.78
39 weeks	3009	2.49	2.73	3.24	3.79	4.08	2869	2.42	2.65	3.13	3.66	3.94
40 weeks	2568	2.63	2.88	3.38	3.94	4.22	2523	2.55	2.78	3.26	3.80	4.08
41 weeks	1179	2.76	3.01	3.51	4.06	4.35	1195	2.65	2.86	3.37	3.92	4.20
42 weeks	206	2.88	3.12	3.62	4.17	4.46	224	2.74	2.98	3.46	4.01	4.30
Total	10,397						9905					

From Villar J, Victora CG, O'Huma E, et al: International standards for newborn weight, length, and head circumference by gestational age and sex: the Newborn Cross-Sectional Study of the INTERGROWTH-21st Project. *Lancet*. 384:857-868, 2014, Table 2.



**TABLE B-6 Race/Ethnic-Specific Percentiles for Fetal Anthropometric Measurements by Gestational Age, as Reported in the National Institutes of Child Health and Human Development (NICHD) Fetal Growth Studies**

Gestational Age (wk)	PERCENTILE						
	3rd	5th	10th	50th	90th	95th	97th
<b>Biparietal Diameter (mm), White</b>							
10	10.4	10.6	10.9	12.1	13.5	13.9	14.2
11	13.4	13.6	14.0	15.5	17.2	17.7	18.0
12	16.6	16.9	17.4	19.2	21.1	21.7	22.1
13	20.0	20.3	20.9	22.9	25.2	25.9	26.3
14	23.3	23.7	24.3	26.7	29.2	30.0	30.5
15	26.6	27.1	27.7	30.3	33.0	33.9	34.4
16	29.8	30.3	31.0	33.7	36.7	37.6	38.2
17	32.8	33.3	34.1	37.0	40.1	41.0	41.7
18	35.8	36.3	37.1	40.1	43.4	44.3	45.0
19	38.7	39.2	40.0	43.2	46.6	47.6	48.3
20	41.6	42.2	43.0	46.3	49.8	50.9	51.5
21	44.6	45.2	46.1	49.4	53.1	54.1	54.9
22	47.6	48.2	49.1	52.6	56.3	57.4	58.2
23	50.5	51.2	52.1	55.7	59.6	60.7	61.5
24	53.5	54.1	55.1	58.9	62.8	64.0	64.8
25	56.4	57.1	58.1	61.9	66.0	67.2	68.0
26	59.3	60.0	61.0	65.0	69.2	70.4	71.2
27	62.1	62.8	63.9	68.0	72.3	73.5	74.4
28	64.8	65.5	66.7	70.8	75.3	76.6	77.5
29	67.4	68.2	69.4	73.6	78.2	79.6	80.4
30	70.0	70.7	71.9	76.4	81.0	82.4	83.3
31	72.4	73.2	74.4	78.9	83.7	85.2	86.1
32	74.6	75.4	76.7	81.4	86.3	87.7	88.7
33	76.7	77.6	78.8	83.6	88.6	90.1	91.1
34	78.6	79.5	80.8	85.6	90.8	92.3	93.3
35	80.3	81.2	82.5	87.4	92.7	94.2	95.2
36	81.7	82.6	84.0	89.0	94.3	95.9	96.9
37	83.0	83.9	85.3	90.3	95.7	97.3	98.3
38	84.1	85.0	86.3	91.5	96.9	98.5	99.5
39	85.0	85.9	87.3	92.4	97.9	99.5	100.6
40	85.7	86.6	88.0	93.3	98.8	100.4	101.5
<b>Head Circumference (mm), White</b>							
10	41.4	42.1	43.1	47.1	51.3	52.6	53.5
11	52.2	53.0	54.3	59.0	64.2	65.7	66.8
12	63.9	64.9	66.3	71.9	77.9	79.6	80.8
13	76.1	77.2	78.9	85.1	91.9	93.9	95.3
14	88.4	89.6	91.5	98.5	106.0	108.2	109.7
15	100.7	102.0	104.0	111.6	119.7	122.1	123.7
16	112.7	114.1	116.3	124.3	132.9	135.4	137.1
17	124.4	125.8	128.1	136.6	145.6	148.2	150.0
18	135.8	137.3	139.7	148.5	157.8	160.6	162.4
19	147.1	148.7	151.2	160.3	169.9	172.7	174.6
20	158.6	160.3	162.8	172.2	182.1	185.0	186.9
21	170.2	171.9	174.5	184.1	194.2	197.2	199.2
22	181.7	183.5	186.2	196.0	206.4	209.4	211.4
23	193.2	195.0	197.7	207.8	218.4	221.5	223.5
24	204.4	206.3	209.1	219.4	230.2	233.4	235.5
25	215.4	217.3	220.2	230.8	241.8	245.1	247.2
26	226.1	228.0	231.0	241.8	253.1	256.4	258.6
27	236.3	238.3	241.3	252.5	264.1	267.5	269.7
28	246.1	248.1	251.3	262.7	274.7	278.2	280.5
29	255.3	257.4	260.7	272.5	284.8	288.4	290.8
30	264.0	266.2	269.5	281.8	294.5	298.2	300.7

**TABLE B-6 Race/Ethnic-Specific Percentiles for Fetal Anthropometric Measurements by Gestational Age, as Reported in the National Institutes of Child Health and Human Development (NICHD) Fetal Growth Studies—cont'd**

Gestational Age (wk)	PERCENTILE						
	3rd	5th	10th	50th	90th	95th	97th
31	272.1	274.3	277.8	290.4	303.7	307.5	310.0
32	279.5	281.8	285.4	298.5	312.2	316.2	318.8
33	286.2	288.6	292.3	305.9	320.1	324.2	326.9
34	292.1	294.6	298.5	312.5	327.2	331.5	334.3
35	297.3	299.8	303.8	318.4	333.6	338.0	341.0
36	301.7	304.3	308.5	323.5	339.2	343.8	346.9
37	305.4	308.2	312.4	327.9	344.2	348.9	352.1
38	308.6	311.4	315.8	331.8	348.5	353.4	356.7
39	311.2	314.1	318.6	335.1	352.4	357.4	360.8
40	313.4	316.4	321.0	338.0	355.8	361.1	364.5
<b>Abdominal Circumference (mm), White</b>							
10	30.5	31.1	32.1	35.8	40.0	41.3	42.1
11	38.8	39.6	40.8	45.4	50.5	52.0	53.0
12	48.1	49.0	50.4	55.9	61.9	63.8	65.0
13	58.1	59.2	60.9	67.2	74.2	76.3	77.7
14	68.7	69.9	71.8	79.0	86.9	89.3	90.9
15	79.7	81.0	83.2	91.2	99.9	102.6	104.3
16	90.8	92.3	94.7	103.4	112.9	115.8	117.7
17	102.0	103.6	106.2	115.6	125.8	128.9	131.0
18	113.2	114.9	117.6	127.7	138.6	141.8	144.0
19	124.4	126.2	129.1	139.7	151.2	154.6	156.9
20	135.6	137.6	140.6	151.7	163.7	167.3	169.7
21	146.8	148.9	152.0	163.6	176.2	179.9	182.4
22	157.9	160.0	163.3	175.4	188.4	192.3	194.8
23	168.9	171.0	174.4	187.0	200.5	204.5	207.1
24	179.6	181.8	185.4	198.4	212.3	216.4	219.2
25	190.1	192.4	196.1	209.6	224.0	228.2	231.0
26	200.4	202.8	206.6	220.6	235.5	239.9	242.8
27	210.5	213.0	217.0	231.4	246.9	251.5	254.5
28	220.5	223.1	227.2	242.3	258.4	263.1	266.3
29	230.5	233.2	237.5	253.2	270.0	274.9	278.2
30	240.5	243.4	247.8	264.3	281.8	287.0	290.4
31	250.5	253.5	258.2	275.4	293.8	299.3	302.9
32	260.3	263.4	268.4	286.5	305.9	311.6	315.4
33	269.9	273.2	278.4	297.5	318.0	324.0	328.0
34	279.2	282.7	288.1	308.3	329.9	336.3	340.5
35	288.0	291.7	297.5	318.8	341.6	348.3	352.8
36	296.4	300.2	306.3	328.8	352.9	360.1	364.8
37	304.0	308.1	314.5	338.2	363.7	371.2	376.2
38	310.9	315.2	321.9	346.9	373.8	381.8	387.0
39	316.8	321.4	328.4	354.7	383.0	391.4	397.0
40	321.7	326.4	333.8	361.4	391.2	400.1	406.0
<b>Femur Length (mm), White</b>							
10	1.7	1.8	1.9	2.4	3.0	3.2	3.3
11	2.9	3.1	3.2	4.0	5.0	5.3	5.5
12	4.7	4.9	5.1	6.3	7.7	8.2	8.5
13	6.9	7.1	7.5	9.1	11.0	11.6	12.0
14	9.5	9.8	10.3	12.3	14.8	15.5	16.0
15	12.4	12.8	13.4	15.8	18.7	19.6	20.2
16	15.3	15.8	16.5	19.3	22.5	23.5	24.2
17	18.3	18.8	19.6	22.6	26.1	27.2	28.0
18	21.1	21.7	22.5	25.7	29.5	30.6	31.4
19	23.9	24.5	25.4	28.7	32.6	33.7	34.5

Continued



**TABLE B-6 Race/Ethnic-Specific Percentiles for Fetal Anthropometric Measurements by Gestational Age, as Reported in the National Institutes of Child Health and Human Development (NICHD) Fetal Growth Studies—cont'd**

Gestational Age (wk)	PERCENTILE						
	3rd	5th	10th	50th	90th	95th	97th
20	26.7	27.3	28.2	31.7	35.6	36.8	37.5
21	29.5	30.1	31.0	34.6	38.5	39.7	40.5
22	32.3	32.9	33.8	37.4	41.3	42.5	43.3
23	35.0	35.6	36.5	40.1	44.0	45.2	46.0
24	37.5	38.2	39.1	42.7	46.6	47.8	48.5
25	40.0	40.6	41.6	45.2	49.1	50.2	51.0
26	42.3	43.0	43.9	47.5	51.4	52.6	53.4
27	44.6	45.2	46.2	49.8	53.7	54.9	55.7
28	46.7	47.3	48.3	52.0	56.0	57.2	57.9
29	48.7	49.3	50.4	54.1	58.2	59.4	60.2
30	50.6	51.3	52.4	56.3	60.4	61.7	62.5
31	52.5	53.2	54.3	58.4	62.7	64.0	64.8
32	54.4	55.1	56.2	60.4	64.9	66.2	67.1
33	56.1	56.9	58.1	62.4	67.0	68.4	69.3
34	57.8	58.6	59.8	64.3	69.1	70.5	71.4
35	59.4	60.2	61.5	66.1	71.0	72.5	73.4
36	60.9	61.7	63.0	67.7	72.8	74.3	75.3
37	62.3	63.1	64.4	69.3	74.5	76.0	77.0
38	63.5	64.4	65.7	70.6	75.9	77.5	78.5
39	64.6	65.4	66.8	71.8	77.2	78.8	79.9
40	65.4	66.3	67.7	72.8	78.3	79.9	81.0
<b>Humerus Length (mm), White</b>							
10	1.8	1.9	2.0	2.5	3.1	3.3	3.4
11	3.2	3.3	3.5	4.2	5.2	5.5	5.7
12	5.0	5.2	5.5	6.6	8.0	8.5	8.8
13	7.4	7.6	8.0	9.6	11.5	12.1	12.5
14	10.1	10.4	10.9	12.9	15.3	16.0	16.5
15	13.0	13.3	14.0	16.3	19.1	20.0	20.6
16	15.9	16.3	17.0	19.7	22.8	23.8	24.5
17	18.6	19.1	19.9	22.8	26.2	27.2	27.9
18	21.2	21.7	22.5	25.6	29.1	30.2	30.9
19	23.7	24.2	25.0	28.2	31.8	32.9	33.6
20	26.1	26.6	27.5	30.8	34.4	35.5	36.2
21	28.5	29.1	29.9	33.2	36.9	38.0	38.7
22	30.9	31.4	32.3	35.6	39.2	40.3	41.1
23	33.1	33.7	34.6	37.9	41.5	42.6	43.3
24	35.3	35.9	36.7	40.0	43.6	44.7	45.4
25	37.3	37.9	38.8	42.1	45.7	46.8	47.5
26	39.3	39.8	40.7	44.0	47.6	48.7	49.4
27	41.1	41.6	42.5	45.9	49.5	50.6	51.3
28	42.8	43.4	44.3	47.6	51.3	52.4	53.1
29	44.4	45.0	45.9	49.4	53.1	54.2	54.9
30	45.9	46.5	47.5	51.0	54.8	55.9	56.7
31	47.4	48.0	49.0	52.6	56.5	57.7	58.4
32	48.8	49.5	50.5	54.2	58.2	59.4	60.2
33	50.2	50.9	51.9	55.7	59.8	61.1	61.9
34	51.5	52.2	53.2	57.2	61.4	62.7	63.5
35	52.7	53.4	54.5	58.6	62.9	64.2	65.1
36	53.9	54.6	55.8	59.9	64.4	65.7	66.6
37	55.0	55.7	56.9	61.1	65.7	67.0	67.9
38	56.0	56.7	57.9	62.2	66.9	68.3	69.2
39	56.8	57.6	58.8	63.2	67.9	69.3	70.2
40	57.4	58.2	59.4	63.9	68.7	70.2	71.1

**TABLE B-6 Race/Ethnic-Specific Percentiles for Fetal Anthropometric Measurements by Gestational Age, as Reported in the National Institutes of Child Health and Human Development (NICHD) Fetal Growth Studies—cont'd**

Gestational Age (wk)	PERCENTILE						
	3rd	5th	10th	50th	90th	95th	97th
<b>Estimated Fetal Weight (g), White</b>							
10	23	23	25	29	35	37	38
11	31	32	33	39	46	48	49
12	42	43	45	52	60	63	65
13	55	57	59	68	78	82	84
14	72	73	76	88	101	105	108
15	92	94	98	113	129	135	138
16	116	119	124	143	164	170	175
17	146	150	156	179	205	213	219
18	181	186	193	222	255	265	272
19	222	228	237	273	313	325	334
20	271	278	289	332	381	396	407
21	327	335	349	401	460	479	491
22	391	401	417	479	551	573	588
23	464	476	495	569	654	681	698
24	546	560	583	671	771	803	824
25	638	655	682	785	903	940	964
26	741	760	791	911	1050	1092	1121
27	854	876	912	1052	1212	1262	1295
28	977	1003	1045	1205	1391	1449	1487
29	1111	1141	1188	1373	1587	1653	1697
30	1255	1289	1343	1555	1799	1875	1926
31	1409	1447	1509	1750	2029	2116	2174
32	1571	1615	1686	1958	2276	2374	2441
33	1741	1790	1869	2178	2537	2649	2724
34	1914	1969	2058	2404	2809	2936	3021
35	2086	2148	2247	2634	3088	3230	3326
36	2254	2323	2432	2862	3368	3527	3635
37	2413	2489	2609	3084	3645	3822	3942
38	2562	2645	2777	3299	3918	4114	4246
39	2701	2790	2934	3505	4186	4402	4548
40	2826	2924	3080	3702	4450	4688	4850
<b>Head Circumference/Abdominal Circumference (mm), White</b>							
10	1.219	1.231	1.250	1.317	1.388	1.409	1.422
11	1.209	1.220	1.238	1.304	1.373	1.393	1.406
12	1.194	1.206	1.223	1.287	1.354	1.374	1.387
13	1.177	1.188	1.205	1.267	1.333	1.352	1.365
14	1.158	1.168	1.185	1.246	1.310	1.329	1.341
15	1.138	1.148	1.165	1.224	1.286	1.305	1.317
16	1.118	1.128	1.144	1.202	1.263	1.281	1.293
17	1.099	1.109	1.125	1.182	1.241	1.259	1.270
18	1.083	1.092	1.108	1.163	1.222	1.239	1.250
19	1.068	1.078	1.093	1.148	1.205	1.222	1.233
20	1.057	1.066	1.081	1.135	1.192	1.209	1.220
21	1.047	1.057	1.072	1.126	1.182	1.199	1.210
22	1.040	1.049	1.064	1.118	1.174	1.191	1.202
23	1.034	1.043	1.058	1.112	1.168	1.185	1.196
24	1.028	1.037	1.052	1.106	1.163	1.180	1.190
25	1.023	1.032	1.047	1.101	1.158	1.175	1.186
26	1.017	1.027	1.042	1.096	1.154	1.171	1.182
27	1.011	1.021	1.036	1.091	1.149	1.166	1.177
28	1.004	1.013	1.029	1.084	1.143	1.160	1.171
29	0.995	1.004	1.020	1.076	1.135	1.152	1.164
30	0.984	0.994	1.009	1.066	1.126	1.143	1.155

Continued



**TABLE B-6 Race/Ethnic-Specific Percentiles for Fetal Anthropometric Measurements by Gestational Age, as Reported in the National Institutes of Child Health and Human Development (NICHD) Fetal Growth Studies—cont'd**

Gestational Age (wk)	PERCENTILE						
	3rd	5th	10th	50th	90th	95th	97th
31	0.972	0.982	0.997	1.055	1.115	1.133	1.144
32	0.958	0.968	0.984	1.042	1.103	1.121	1.133
33	0.944	0.954	0.970	1.028	1.090	1.109	1.121
34	0.928	0.938	0.955	1.014	1.077	1.095	1.108
35	0.912	0.922	0.939	0.999	1.063	1.082	1.094
36	0.896	0.906	0.923	0.984	1.049	1.068	1.081
37	0.880	0.890	0.907	0.969	1.036	1.055	1.068
38	0.865	0.876	0.893	0.956	1.024	1.044	1.057
39	0.851	0.862	0.880	0.945	1.014	1.035	1.048
40	0.839	0.851	0.869	0.935	1.007	1.029	1.043
<b>Biparietal Diameter (mm), Black</b>							
10	10.3	10.5	10.8	11.9	13.3	13.7	13.9
11	13.3	13.5	13.9	15.4	17.0	17.5	17.8
12	16.5	16.8	17.3	19.1	21.0	21.6	22.0
13	19.9	20.3	20.8	22.8	25.1	25.7	26.2
14	23.3	23.7	24.3	26.6	29.1	29.8	30.3
15	26.5	27.0	27.6	30.2	32.9	33.7	34.3
16	29.7	30.1	30.9	33.6	36.5	37.4	38.0
17	32.7	33.1	33.9	36.8	39.9	40.8	41.5
18	35.6	36.1	36.9	39.9	43.2	44.2	44.8
19	38.5	39.0	39.9	43.0	46.5	47.5	48.1
20	41.4	42.0	42.9	46.2	49.7	50.8	51.5
21	44.4	45.0	45.9	49.3	53.0	54.1	54.8
22	47.3	47.9	48.9	52.5	56.3	57.4	58.2
23	50.2	50.8	51.8	55.5	59.5	60.7	61.5
24	53.1	53.7	54.8	58.6	62.7	63.9	64.7
25	55.9	56.6	57.6	61.6	65.8	67.0	67.9
26	58.6	59.3	60.4	64.5	68.8	70.1	71.0
27	61.3	62.0	63.1	67.3	71.8	73.1	74.0
28	63.8	64.6	65.8	70.1	74.7	76.1	77.0
29	66.4	67.1	68.3	72.8	77.5	78.9	79.9
30	68.8	69.6	70.8	75.4	80.2	81.7	82.6
31	71.0	71.8	73.1	77.8	82.8	84.3	85.3
32	73.1	74.0	75.3	80.1	85.2	86.7	87.7
33	75.0	75.9	77.2	82.1	87.4	88.9	89.9
34	76.7	77.6	79.0	84.0	89.3	90.8	91.9
35	78.2	79.1	80.4	85.5	90.9	92.5	93.6
36	79.4	80.3	81.7	86.8	92.3	93.9	95.0
37	80.5	81.4	82.8	88.0	93.5	95.2	96.2
38	81.4	82.3	83.8	89.1	94.7	96.3	97.4
39	82.4	83.3	84.7	90.1	95.8	97.4	98.5
40	83.3	84.2	85.7	91.2	97.0	98.7	99.8
<b>Head Circumference (mm), Black</b>							
10	40.6	41.2	42.2	46.1	50.3	51.6	52.4
11	51.7	52.5	53.7	58.4	63.6	65.1	66.1
12	63.6	64.5	66.0	71.6	77.6	79.4	80.6
13	75.9	77.0	78.7	85.1	92.0	94.0	95.4
14	88.3	89.5	91.4	98.5	106.2	108.5	110.0
15	100.5	101.8	103.9	111.6	120.0	122.4	124.1
16	112.3	113.7	116.0	124.2	133.1	135.7	137.5
17	123.7	125.3	127.6	136.4	145.7	148.5	150.3
18	135.0	136.6	139.1	148.2	157.9	160.8	162.7
19	146.3	148.0	150.6	160.0	170.1	173.1	175.0

**TABLE B-6 Race/Ethnic-Specific Percentiles for Fetal Anthropometric Measurements by Gestational Age, as Reported in the National Institutes of Child Health and Human Development (NICHD) Fetal Growth Studies—cont'd**

Gestational Age (wk)	PERCENTILE						
	3rd	5th	10th	50th	90th	95th	97th
20	157.7	159.4	162.1	171.9	182.3	185.3	187.3
21	169.1	170.9	173.6	183.7	194.3	197.4	199.5
22	180.4	182.2	185.0	195.3	206.2	209.4	211.5
23	191.5	193.3	196.2	206.8	217.9	221.2	223.3
24	202.3	204.2	207.2	218.0	229.3	232.7	234.8
25	212.8	214.8	217.8	228.9	240.4	243.8	246.1
26	223.0	225.0	228.1	239.4	251.2	254.7	257.0
27	232.8	234.8	238.0	249.6	261.7	265.2	267.5
28	242.2	244.3	247.5	259.4	271.7	275.4	277.7
29	251.1	253.3	256.6	268.8	281.5	285.2	287.6
30	259.6	261.8	265.2	277.7	290.8	294.6	297.1
31	267.4	269.7	273.2	286.1	299.6	303.5	306.1
32	274.6	276.9	280.6	293.9	307.8	311.9	314.6
33	280.9	283.4	287.2	300.9	315.3	319.5	322.3
34	286.5	289.0	292.9	307.1	322.0	326.3	329.2
35	291.1	293.7	297.7	312.4	327.8	332.3	335.2
36	294.9	297.6	301.7	316.9	332.8	337.5	340.5
37	298.1	300.9	305.2	320.8	337.3	342.1	345.3
38	300.9	303.8	308.2	324.4	341.4	346.4	349.7
39	303.5	306.5	311.1	327.8	345.4	350.6	354.0
40	306.1	309.2	313.9	331.3	349.7	355.1	358.6
<b>Abdominal Circumference (mm), Black</b>							
10	30.8	31.4	32.4	35.9	39.7	40.9	41.7
11	39.2	39.9	41.1	45.3	50.0	51.4	52.4
12	48.5	49.3	50.6	55.7	61.2	62.9	64.0
13	58.4	59.4	60.9	66.8	73.1	75.1	76.3
14	68.8	69.9	71.6	78.2	85.5	87.6	89.0
15	79.4	80.7	82.6	89.9	97.9	100.3	101.9
16	90.1	91.5	93.7	101.7	110.4	113.0	114.7
17	100.9	102.3	104.7	113.3	122.7	125.5	127.3
18	111.5	113.1	115.6	124.9	134.8	137.8	139.8
19	122.2	123.9	126.6	136.4	146.9	150.1	152.2
20	132.8	134.6	137.4	147.8	158.9	162.2	164.4
21	143.2	145.1	148.1	159.0	170.7	174.2	176.5
22	153.5	155.4	158.5	170.0	182.3	185.9	188.3
23	163.4	165.5	168.8	180.8	193.6	197.4	199.9
24	173.1	175.3	178.7	191.3	204.7	208.7	211.4
25	182.6	184.9	188.5	201.6	215.7	219.9	222.6
26	191.9	194.3	198.1	211.8	226.6	230.9	233.8
27	201.2	203.7	207.6	222.0	237.5	242.0	245.1
28	210.4	213.0	217.2	232.3	248.5	253.3	256.5
29	219.8	222.6	226.9	242.8	259.9	264.9	268.3
30	229.4	232.3	236.8	253.6	271.6	276.9	280.4
31	239.0	242.1	246.8	264.5	283.5	289.1	292.8
32	248.5	251.7	256.8	275.4	295.4	301.3	305.3
33	257.8	261.2	266.5	286.1	307.2	313.4	317.6
34	266.6	270.2	275.8	296.4	318.6	325.2	329.5
35	274.9	278.6	284.5	306.1	329.4	336.4	340.9
36	282.7	286.6	292.7	315.4	339.8	347.1	351.9
37	290.1	294.2	300.6	324.3	349.9	357.5	362.5
38	297.3	301.6	308.3	333.1	359.9	367.9	373.1
39	304.6	309.1	316.0	342.0	370.1	378.5	384.0
40	312.0	316.7	324.0	351.3	380.9	389.7	395.6

Continued



**TABLE B-6 Race/Ethnic-Specific Percentiles for Fetal Anthropometric Measurements by Gestational Age, as Reported in the National Institutes of Child Health and Human Development (NICHD) Fetal Growth Studies—cont'd**

Gestational Age (wk)	PERCENTILE						
	3rd	5th	10th	50th	90th	95th	97th
<b>Femur Length (mm), Black</b>							
10	1.7	1.8	1.9	2.4	3.1	3.3	3.4
11	3.1	3.2	3.4	4.2	5.3	5.7	5.9
12	4.9	5.1	5.4	6.7	8.3	8.8	9.2
13	7.3	7.6	8.0	9.8	12.0	12.7	13.1
14	10.0	10.4	10.9	13.2	16.0	16.9	17.4
15	12.9	13.3	14.0	16.8	20.0	21.1	21.8
16	15.8	16.3	17.1	20.2	23.9	25.1	25.8
17	18.6	19.2	20.0	23.4	27.4	28.7	29.5
18	21.3	21.9	22.8	26.4	30.6	31.9	32.8
19	24.0	24.6	25.6	29.4	33.7	35.0	35.9
20	26.7	27.4	28.4	32.3	36.7	38.0	38.9
21	29.5	30.1	31.2	35.1	39.6	40.9	41.8
22	32.2	32.8	33.9	37.9	42.3	43.7	44.6
23	34.8	35.5	36.6	40.6	45.0	46.3	47.2
24	37.4	38.1	39.2	43.2	47.6	48.9	49.8
25	39.9	40.6	41.7	45.6	50.0	51.3	52.2
26	42.3	43.0	44.1	48.0	52.3	53.6	54.5
27	44.6	45.3	46.4	50.3	54.6	55.9	56.7
28	46.8	47.5	48.6	52.5	56.8	58.1	58.9
29	49.0	49.7	50.7	54.7	59.0	60.3	61.1
30	51.1	51.8	52.9	56.9	61.2	62.5	63.4
31	53.1	53.8	54.9	59.0	63.4	64.7	65.6
32	55.0	55.7	56.9	61.1	65.6	66.9	67.8
33	56.8	57.6	58.7	63.0	67.7	69.0	69.9
34	58.5	59.3	60.5	64.9	69.6	71.0	72.0
35	60.0	60.8	62.1	66.6	71.5	72.9	73.9
36	61.4	62.2	63.5	68.2	73.2	74.7	75.6
37	62.8	63.6	64.9	69.7	74.8	76.3	77.3
38	64.0	64.9	66.2	71.1	76.4	77.9	79.0
39	65.3	66.2	67.5	72.6	78.0	79.6	80.6
40	66.5	67.4	68.8	74.1	79.7	81.4	82.5
<b>Humerus Length (mm), Black</b>							
10	2.0	2.1	2.2	2.6	3.1	3.2	3.3
11	3.6	3.7	3.9	4.5	5.3	5.6	5.7
12	5.7	5.9	6.1	7.1	8.3	8.6	8.9
13	8.3	8.6	8.9	10.3	11.8	12.3	12.6
14	11.3	11.6	12.0	13.7	15.7	16.3	16.7
15	14.4	14.7	15.2	17.2	19.5	20.2	20.7
16	17.3	17.7	18.3	20.6	23.1	23.9	24.4
17	20.1	20.5	21.1	23.6	26.3	27.1	27.7
18	22.6	23.1	23.7	26.3	29.2	30.0	30.6
19	25.1	25.5	26.2	28.9	31.9	32.8	33.4
20	27.5	28.0	28.7	31.5	34.5	35.4	36.0
21	29.8	30.3	31.1	33.9	37.0	38.0	38.6
22	32.0	32.5	33.3	36.3	39.5	40.4	41.1
23	34.2	34.7	35.5	38.5	41.8	42.8	43.5
24	36.1	36.7	37.5	40.7	44.0	45.1	45.7
25	38.0	38.6	39.4	42.7	46.2	47.2	47.9
26	39.7	40.3	41.2	44.6	48.2	49.3	50.0
27	41.4	42.0	42.9	46.4	50.1	51.2	52.0
28	42.9	43.6	44.5	48.1	52.0	53.2	53.9
29	44.4	45.1	46.1	49.8	53.9	55.1	55.9
30	45.9	46.6	47.6	51.5	55.7	56.9	57.8

**TABLE B-6 Race/Ethnic-Specific Percentiles for Fetal Anthropometric Measurements by Gestational Age, as Reported in the National Institutes of Child Health and Human Development (NICHD) Fetal Growth Studies—cont'd**

Gestational Age (wk)	PERCENTILE						
	3rd	5th	10th	50th	90th	95th	97th
31	47.4	48.1	49.2	53.2	57.5	58.8	59.6
32	48.8	49.5	50.6	54.7	59.2	60.5	61.4
33	50.1	50.9	52.0	56.2	60.8	62.2	63.1
34	51.4	52.2	53.3	57.7	62.3	63.7	64.7
35	52.6	53.3	54.5	59.0	63.7	65.2	66.1
36	53.7	54.5	55.7	60.2	65.0	66.5	67.5
37	54.8	55.5	56.8	61.4	66.3	67.8	68.8
38	55.8	56.6	57.9	62.6	67.7	69.2	70.2
39	56.9	57.8	59.1	63.9	69.1	70.7	71.7
40	58.1	59.0	60.3	65.4	70.9	72.5	73.6
<b>Estimated Fetal Weight (g), Black</b>							
10	22	22	24	28	34	35	37
11	30	31	33	38	45	47	48
12	42	43	45	52	60	62	64
13	56	57	59	68	78	81	83
14	73	74	77	89	101	105	108
15	93	96	99	114	130	135	138
16	118	121	126	144	164	171	175
17	147	151	157	180	206	214	219
18	182	186	194	222	254	264	271
19	222	228	236	271	311	323	331
20	268	275	286	328	376	391	401
21	321	329	342	393	451	469	481
22	381	390	406	467	536	558	572
23	448	460	478	550	633	658	676
24	524	538	559	644	742	772	792
25	609	625	650	749	864	899	923
26	703	722	751	867	1000	1041	1069
27	807	828	863	996	1151	1199	1231
28	921	946	985	1139	1317	1372	1409
29	1044	1073	1118	1294	1498	1562	1604
30	1178	1210	1262	1463	1695	1768	1816
31	1321	1358	1416	1644	1908	1990	2045
32	1472	1513	1579	1836	2135	2228	2290
33	1629	1676	1749	2038	2373	2478	2548
34	1789	1841	1923	2244	2619	2737	2816
35	1948	2005	2096	2452	2868	2999	3087
36	2101	2164	2264	2655	3115	3259	3356
37	2249	2317	2427	2855	3359	3517	3624
38	2394	2468	2587	3054	3605	3779	3896
39	2541	2621	2751	3260	3863	4053	4182
40	2693	2781	2922	3479	4142	4352	4494
<b>Head Circumference/Abdominal Circumference (mm), Black</b>							
10	1.182	1.195	1.215	1.291	1.372	1.395	1.411
11	1.183	1.196	1.217	1.291	1.371	1.394	1.409
12	1.178	1.191	1.211	1.285	1.363	1.386	1.401
13	1.167	1.180	1.200	1.273	1.350	1.372	1.387
14	1.153	1.166	1.185	1.257	1.332	1.355	1.369
15	1.137	1.149	1.169	1.239	1.313	1.335	1.350
16	1.120	1.132	1.151	1.220	1.293	1.315	1.329
17	1.104	1.116	1.134	1.202	1.274	1.295	1.309
18	1.089	1.101	1.119	1.186	1.257	1.278	1.292
19	1.077	1.088	1.107	1.173	1.244	1.265	1.278

Continued



**TABLE B-6 Race/Ethnic-Specific Percentiles for Fetal Anthropometric Measurements by Gestational Age, as Reported in the National Institutes of Child Health and Human Development (NICHD) Fetal Growth Studies—cont'd**

Gestational Age (wk)	PERCENTILE						
	3rd	5th	10th	50th	90th	95th	97th
20	1.067	1.079	1.097	1.163	1.233	1.254	1.268
21	1.060	1.071	1.089	1.155	1.226	1.246	1.260
22	1.053	1.065	1.083	1.149	1.219	1.240	1.254
23	1.048	1.060	1.078	1.144	1.215	1.235	1.249
24	1.043	1.055	1.073	1.140	1.210	1.231	1.245
25	1.038	1.050	1.068	1.135	1.206	1.227	1.241
26	1.033	1.045	1.063	1.130	1.201	1.223	1.236
27	1.026	1.038	1.056	1.124	1.196	1.217	1.231
28	1.018	1.030	1.048	1.116	1.188	1.210	1.224
29	1.008	1.020	1.038	1.106	1.179	1.200	1.214
30	0.996	1.008	1.026	1.095	1.167	1.189	1.203
31	0.982	0.994	1.013	1.081	1.154	1.176	1.190
32	0.968	0.980	0.998	1.067	1.140	1.162	1.176
33	0.952	0.964	0.983	1.052	1.125	1.147	1.161
34	0.937	0.949	0.967	1.036	1.110	1.131	1.146
35	0.921	0.933	0.951	1.020	1.094	1.116	1.130
36	0.905	0.917	0.935	1.005	1.079	1.101	1.115
37	0.889	0.901	0.919	0.989	1.064	1.086	1.101
38	0.873	0.885	0.904	0.974	1.049	1.072	1.087
39	0.857	0.869	0.888	0.959	1.035	1.058	1.073
40	0.841	0.854	0.873	0.945	1.022	1.045	1.060
<b>Biparietal Diameter (mm), Hispanic</b>							
10	10.2	10.4	10.7	12.0	13.5	13.9	14.2
11	13.1	13.3	13.8	15.4	17.1	17.7	18.0
12	16.2	16.5	17.0	18.9	21.1	21.7	22.1
13	19.5	19.8	20.4	22.6	25.1	25.8	26.3
14	22.7	23.2	23.8	26.3	29.1	29.9	30.4
15	26.0	26.4	27.2	29.9	32.9	33.8	34.4
16	29.1	29.6	30.4	33.3	36.6	37.5	38.2
17	32.1	32.6	33.4	36.6	40.0	41.0	41.7
18	35.0	35.5	36.4	39.7	43.3	44.4	45.1
19	37.8	38.4	39.4	42.8	46.5	47.6	48.4
20	40.8	41.4	42.3	45.9	49.8	50.9	51.7
21	43.7	44.4	45.4	49.1	53.1	54.2	55.0
22	46.7	47.4	48.4	52.2	56.3	57.5	58.4
23	49.7	50.4	51.4	55.3	59.6	60.8	61.7
24	52.6	53.3	54.4	58.5	62.8	64.1	64.9
25	55.6	56.3	57.4	61.5	65.9	67.3	68.1
26	58.4	59.1	60.3	64.5	69.0	70.4	71.3
27	61.2	62.0	63.1	67.5	72.1	73.4	74.3
28	63.9	64.7	65.9	70.3	75.0	76.4	77.3
29	66.5	67.3	68.5	73.0	77.8	79.3	80.2
30	69.0	69.8	71.0	75.7	80.6	82.0	83.0
31	71.3	72.2	73.4	78.1	83.1	84.6	85.6
32	73.5	74.4	75.7	80.4	85.5	87.0	88.0
33	75.5	76.4	77.7	82.6	87.8	89.3	90.3
34	77.3	78.2	79.5	84.5	89.8	91.3	92.3
35	78.8	79.7	81.1	86.1	91.5	93.1	94.1
36	80.2	81.1	82.5	87.6	93.0	94.6	95.7
37	81.3	82.2	83.6	88.8	94.4	96.0	97.1
38	82.4	83.3	84.7	90.0	95.6	97.3	98.4
39	83.3	84.3	85.7	91.1	96.8	98.5	99.6
40	84.3	85.3	86.8	92.2	98.0	99.8	100.9

**TABLE B-6 Race/Ethnic-Specific Percentiles for Fetal Anthropometric Measurements by Gestational Age, as Reported in the National Institutes of Child Health and Human Development (NICHD) Fetal Growth Studies—cont'd**

Gestational Age (wk)	PERCENTILE						
	3rd	5th	10th	50th	90th	95th	97th
<b>Head Circumference (mm), Hispanic</b>							
10	38.7	39.5	40.7	45.5	50.8	52.4	53.5
11	49.2	50.2	51.7	57.5	64.0	65.9	67.2
12	60.7	61.8	63.6	70.5	78.0	80.3	81.8
13	72.7	74.0	76.1	83.9	92.5	95.1	96.8
14	84.9	86.4	88.7	97.4	106.9	109.8	111.7
15	97.0	98.6	101.2	110.6	121.0	124.1	126.2
16	108.9	110.6	113.3	123.5	134.5	137.8	140.0
17	120.4	122.2	125.1	135.8	147.4	150.9	153.2
18	131.7	133.6	136.6	147.7	159.8	163.3	165.7
19	142.9	144.9	148.0	159.5	171.9	175.6	178.0
20	154.2	156.2	159.4	171.3	184.0	187.8	190.2
21	165.6	167.7	170.9	183.1	196.1	199.9	202.4
22	176.9	179.0	182.4	194.8	208.0	211.9	214.5
23	188.1	190.3	193.8	206.4	219.8	223.8	226.4
24	199.2	201.4	204.9	217.7	231.3	235.4	238.0
25	209.9	212.2	215.8	228.8	242.6	246.7	249.4
26	220.4	222.7	226.3	239.6	253.6	257.7	260.4
27	230.5	232.8	236.5	250.0	264.2	268.4	271.1
28	240.1	242.5	246.3	260.0	274.4	278.7	281.4
29	249.3	251.8	255.6	269.5	284.3	288.6	291.4
30	258.0	260.5	264.4	278.7	293.7	298.1	301.0
31	266.1	268.6	272.6	287.2	302.6	307.1	310.1
32	273.5	276.1	280.2	295.2	310.9	315.6	318.6
33	280.2	282.9	287.1	302.5	318.6	323.4	326.5
34	286.1	288.9	293.2	309.0	325.6	330.4	333.6
35	291.2	294.1	298.5	314.6	331.7	336.7	339.9
36	295.5	298.4	302.9	319.5	337.0	342.1	345.5
37	299.0	302.0	306.6	323.6	341.6	346.8	350.3
38	301.9	305.0	309.7	327.1	345.5	350.9	354.4
39	304.3	307.4	312.3	330.1	348.9	354.5	358.1
40	306.2	309.4	314.4	332.7	352.0	357.7	361.4
<b>Abdominal Circumference (mm), Hispanic</b>							
10	30.5	31.2	32.2	35.9	40.1	41.3	42.2
11	38.7	39.4	40.6	45.2	50.3	51.8	52.8
12	47.7	48.6	50.1	55.5	61.5	63.4	64.6
13	57.5	58.5	60.2	66.6	73.6	75.7	77.1
14	67.8	69.0	70.9	78.2	86.2	88.6	90.2
15	78.5	79.8	82.0	90.1	99.1	101.8	103.5
16	89.3	90.8	93.2	102.2	112.0	115.0	116.9
17	100.2	101.9	104.5	114.2	124.9	128.1	130.2
18	111.1	112.9	115.7	126.2	137.6	141.0	143.3
19	121.9	123.8	126.8	138.0	150.2	153.8	156.2
20	132.8	134.8	138.0	149.8	162.6	166.4	169.0
21	143.5	145.6	149.0	161.4	174.9	178.9	181.6
22	154.0	156.3	159.8	172.8	186.9	191.1	193.9
23	164.4	166.7	170.4	184.0	198.7	203.1	206.0
24	174.5	177.0	180.8	195.0	210.2	214.8	217.8
25	184.5	187.0	191.0	205.7	221.6	226.3	229.4
26	194.2	196.9	201.0	216.3	232.8	237.7	240.9
27	203.9	206.6	211.0	226.9	244.0	249.1	252.4
28	213.5	216.4	220.9	237.5	255.3	260.5	264.0
29	223.3	226.3	231.0	248.2	266.8	272.3	275.9
30	233.2	236.3	241.2	259.3	278.7	284.4	288.2

Continued



**TABLE B-6 Race/Ethnic-Specific Percentiles for Fetal Anthropometric Measurements by Gestational Age, as Reported in the National Institutes of Child Health and Human Development (NICHD) Fetal Growth Studies—cont'd**

Gestational Age (wk)	PERCENTILE						
	3rd	5th	10th	50th	90th	95th	97th
31	243.1	246.4	251.5	270.4	290.8	296.8	300.8
32	253.0	256.4	261.8	281.6	303.0	309.3	313.5
33	262.5	266.1	271.8	292.6	315.0	321.7	326.1
34	271.7	275.5	281.4	303.2	326.8	333.8	338.5
35	280.2	284.2	290.4	313.3	338.1	345.4	350.3
36	288.0	292.2	298.7	322.7	348.8	356.5	361.6
37	295.2	299.6	306.4	331.6	358.9	367.1	372.5
38	301.9	306.4	313.6	340.0	368.7	377.2	382.9
39	308.1	312.9	320.3	348.0	378.1	387.1	393.1
40	313.9	318.9	326.7	355.8	387.5	397.0	403.3
<b>Femur Length (mm), Hispanic</b>							
10	1.7	1.7	1.9	2.4	3.0	3.2	3.4
11	2.9	3.0	3.2	4.0	5.1	5.4	5.6
12	4.6	4.8	5.1	6.3	7.9	8.3	8.7
13	6.8	7.1	7.5	9.2	11.2	11.9	12.3
14	9.4	9.7	10.2	12.4	15.0	15.8	16.4
15	12.2	12.6	13.2	15.8	18.9	19.9	20.6
16	15.0	15.5	16.3	19.2	22.8	23.9	24.6
17	17.9	18.4	19.2	22.5	26.3	27.6	28.4
18	20.6	21.2	22.1	25.6	29.6	30.9	31.7
19	23.3	23.9	24.9	28.5	32.7	34.0	34.9
20	26.1	26.7	27.7	31.4	35.7	37.0	37.9
21	28.9	29.5	30.5	34.3	38.6	39.9	40.8
22	31.6	32.2	33.2	37.1	41.4	42.7	43.5
23	34.3	34.9	35.9	39.8	44.0	45.3	46.1
24	36.9	37.5	38.5	42.3	46.5	47.8	48.6
25	39.4	40.0	41.0	44.8	48.9	50.1	51.0
26	41.7	42.4	43.4	47.1	51.2	52.4	53.2
27	44.0	44.7	45.7	49.4	53.4	54.6	55.4
28	46.2	46.9	47.9	51.6	55.5	56.7	57.5
29	48.3	49.0	50.0	53.7	57.7	58.9	59.7
30	50.4	51.1	52.1	55.8	59.9	61.1	61.9
31	52.4	53.1	54.1	58.0	62.1	63.3	64.1
32	54.3	55.0	56.1	60.0	64.2	65.4	66.3
33	56.1	56.8	57.9	62.0	66.3	67.6	68.4
34	57.8	58.5	59.6	63.8	68.2	69.6	70.4
35	59.3	60.0	61.2	65.5	70.1	71.4	72.3
36	60.7	61.4	62.6	67.0	71.7	73.1	74.0
37	61.9	62.7	63.9	68.5	73.3	74.7	75.7
38	63.1	63.9	65.2	69.8	74.8	76.2	77.2
39	64.3	65.1	66.4	71.2	76.2	77.7	78.7
40	65.5	66.3	67.6	72.5	77.8	79.3	80.4
<b>Humerus Length (mm), Hispanic</b>							
10	1.7	1.8	1.9	2.4	3.0	3.2	3.3
11	3.1	3.2	3.4	4.2	5.1	5.5	5.7
12	4.9	5.1	5.4	6.6	8.1	8.5	8.8
13	7.3	7.5	8.0	9.6	11.6	12.2	12.6
14	10.0	10.3	10.9	12.9	15.4	16.2	16.8
15	12.9	13.3	13.9	16.4	19.3	20.2	20.9
16	15.7	16.1	16.9	19.7	23.0	24.0	24.7
17	18.4	18.9	19.7	22.7	26.2	27.3	28.0
18	20.9	21.4	22.2	25.4	29.1	30.2	30.9
19	23.3	23.8	24.7	28.0	31.7	32.8	33.6

**TABLE B-6 Race/Ethnic-Specific Percentiles for Fetal Anthropometric Measurements by Gestational Age, as Reported in the National Institutes of Child Health and Human Development (NICHD) Fetal Growth Studies—cont'd**

Gestational Age (wk)	PERCENTILE						
	3rd	5th	10th	50th	90th	95th	97th
20	25.7	26.3	27.1	30.5	34.2	35.3	36.1
21	28.1	28.7	29.5	32.9	36.6	37.8	38.5
22	30.4	31.0	31.9	35.2	39.0	40.1	40.8
23	32.7	33.2	34.1	37.5	41.2	42.3	43.0
24	34.8	35.4	36.3	39.6	43.3	44.4	45.1
25	36.9	37.4	38.3	41.6	45.2	46.3	47.0
26	38.8	39.4	40.2	43.6	47.1	48.2	48.9
27	40.6	41.2	42.1	45.4	49.0	50.0	50.7
28	42.3	42.9	43.8	47.1	50.7	51.8	52.5
29	43.9	44.5	45.4	48.8	52.5	53.6	54.3
30	45.4	46.0	47.0	50.4	54.2	55.3	56.0
31	46.9	47.5	48.5	52.0	55.9	57.0	57.8
32	48.2	48.9	49.9	53.6	57.5	58.7	59.5
33	49.5	50.2	51.2	55.0	59.1	60.3	61.1
34	50.8	51.5	52.5	56.4	60.6	61.9	62.7
35	51.9	52.6	53.7	57.7	62.1	63.3	64.2
36	53.0	53.7	54.8	58.9	63.4	64.7	65.6
37	54.0	54.7	55.9	60.1	64.6	66.0	66.9
38	54.9	55.7	56.8	61.1	65.8	67.2	68.1
39	55.8	56.6	57.8	62.2	66.9	68.3	69.2
40	56.6	57.4	58.6	63.1	68.0	69.4	70.4
<b>Estimated Fetal Weight (g), Hispanic</b>							
10	19	20	21	26	31	33	34
11	28	28	30	36	42	44	46
12	38	39	41	48	57	59	61
13	51	53	55	64	75	79	81
14	68	70	73	85	98	103	106
15	88	90	94	109	127	133	136
16	112	115	120	140	162	169	174
17	141	145	151	176	204	213	219
18	175	180	188	218	254	265	272
19	215	221	230	268	312	325	334
20	260	268	279	325	379	395	407
21	313	322	336	391	456	476	489
22	372	383	400	466	544	568	584
23	440	453	473	551	643	672	691
24	516	531	555	647	755	789	812
25	601	619	646	755	882	921	948
26	696	716	749	875	1023	1069	1100
27	801	825	862	1009	1180	1234	1270
28	917	944	987	1156	1353	1415	1457
29	1043	1074	1123	1316	1543	1614	1662
30	1178	1214	1270	1490	1749	1830	1885
31	1324	1364	1428	1677	1971	2063	2126
32	1478	1523	1595	1877	2209	2313	2384
33	1638	1688	1769	2086	2460	2577	2657
34	1801	1857	1947	2301	2719	2851	2940
35	1963	2025	2125	2518	2983	3130	3229
36	2120	2189	2298	2731	3245	3408	3517
37	2269	2344	2463	2937	3502	3681	3802
38	2410	2491	2621	3138	3756	3953	4086
39	2545	2633	2774	3336	4011	4226	4372
40	2675	2770	2923	3534	4273	4510	4670

Continued



**TABLE B-6 Race/Ethnic-Specific Percentiles for Fetal Anthropometric Measurements by Gestational Age, as Reported in the National Institutes of Child Health and Human Development (NICHD) Fetal Growth Studies—cont'd**

Gestational Age (wk)	PERCENTILE						
	3rd	5th	10th	50th	90th	95th	97th
<b>Head Circumference/Abdominal Circumference (mm), Hispanic</b>							
10	1.142	1.158	1.184	1.278	1.379	1.409	1.429
11	1.148	1.163	1.188	1.278	1.375	1.404	1.424
12	1.146	1.161	1.184	1.272	1.365	1.393	1.412
13	1.138	1.153	1.176	1.260	1.350	1.377	1.394
14	1.127	1.141	1.163	1.244	1.331	1.356	1.373
15	1.113	1.127	1.148	1.226	1.309	1.333	1.350
16	1.098	1.111	1.132	1.206	1.286	1.310	1.325
17	1.083	1.096	1.115	1.187	1.264	1.287	1.301
18	1.069	1.081	1.100	1.170	1.244	1.265	1.280
19	1.057	1.069	1.088	1.155	1.227	1.248	1.262
20	1.048	1.060	1.078	1.143	1.213	1.234	1.247
21	1.041	1.052	1.070	1.134	1.203	1.223	1.236
22	1.035	1.046	1.064	1.127	1.195	1.215	1.228
23	1.031	1.042	1.059	1.122	1.188	1.208	1.221
24	1.026	1.037	1.054	1.117	1.183	1.203	1.216
25	1.022	1.033	1.050	1.112	1.179	1.198	1.211
26	1.017	1.028	1.045	1.108	1.174	1.194	1.206
27	1.011	1.022	1.039	1.102	1.169	1.188	1.201
28	1.003	1.014	1.031	1.095	1.162	1.182	1.195
29	0.993	1.004	1.022	1.086	1.154	1.174	1.187
30	0.981	0.992	1.010	1.074	1.143	1.163	1.177
31	0.968	0.979	0.997	1.062	1.131	1.152	1.165
32	0.953	0.964	0.982	1.048	1.118	1.139	1.153
33	0.937	0.949	0.967	1.034	1.105	1.126	1.140
34	0.921	0.933	0.951	1.019	1.091	1.113	1.127
35	0.905	0.917	0.936	1.004	1.078	1.100	1.114
36	0.890	0.902	0.920	0.990	1.065	1.087	1.102
37	0.874	0.886	0.905	0.976	1.052	1.075	1.090
38	0.859	0.871	0.891	0.963	1.041	1.064	1.079
39	0.844	0.857	0.877	0.950	1.030	1.053	1.069
40	0.830	0.842	0.863	0.938	1.019	1.044	1.060
<b>Biparietal Diameter (mm), Asian</b>							
10	10.0	10.2	10.5	11.8	13.3	13.8	14.1
11	12.9	13.2	13.6	15.2	17.0	17.6	17.9
12	16.1	16.4	16.9	18.9	21.0	21.7	22.1
13	19.4	19.8	20.4	22.6	25.1	25.9	26.4
14	22.8	23.2	23.9	26.4	29.2	30.1	30.6
15	26.1	26.6	27.3	30.1	33.1	34.1	34.7
16	29.3	29.8	30.6	33.6	36.9	37.8	38.5
17	32.4	32.9	33.7	36.9	40.3	41.4	42.1
18	35.3	35.8	36.7	40.0	43.6	44.7	45.4
19	38.1	38.7	39.6	43.1	46.8	47.9	48.6
20	41.0	41.6	42.6	46.1	49.9	51.1	51.8
21	44.0	44.6	45.6	49.2	53.1	54.3	55.1
22	47.0	47.6	48.6	52.3	56.4	57.6	58.4
23	49.9	50.6	51.6	55.5	59.6	60.8	61.6
24	52.9	53.6	54.7	58.6	62.8	64.1	64.9
25	55.9	56.6	57.7	61.7	66.0	67.3	68.1
26	58.8	59.5	60.6	64.7	69.1	70.4	71.3
27	61.6	62.4	63.5	67.7	72.2	73.5	74.3
28	64.4	65.1	66.3	70.6	75.1	76.5	77.3
29	67.0	67.8	69.0	73.3	78.0	79.3	80.2
30	69.5	70.3	71.5	76.0	80.7	82.1	83.0

**TABLE B-6 Race/Ethnic-Specific Percentiles for Fetal Anthropometric Measurements by Gestational Age, as Reported in the National Institutes of Child Health and Human Development (NICHD) Fetal Growth Studies—cont'd**

Gestational Age (wk)	PERCENTILE						
	3rd	5th	10th	50th	90th	95th	97th
31	71.9	72.7	73.9	78.5	83.3	84.7	85.6
32	74.1	74.9	76.2	80.8	85.7	87.2	88.1
33	76.2	77.0	78.3	83.0	88.0	89.5	90.4
34	78.0	78.9	80.2	85.0	90.1	91.6	92.6
35	79.7	80.6	81.9	86.8	92.0	93.5	94.5
36	81.2	82.1	83.5	88.5	93.7	95.3	96.3
37	82.6	83.5	84.8	89.9	95.3	96.8	97.9
38	83.7	84.6	86.0	91.1	96.6	98.2	99.2
39	84.6	85.5	87.0	92.1	97.7	99.3	100.3
40	85.3	86.2	87.7	93.0	98.6	100.2	101.3
<b>Head Circumference (mm), Asian</b>							
10	39.9	40.6	41.7	45.9	50.4	51.8	52.7
11	50.6	51.5	52.8	57.8	63.3	64.9	66.0
12	62.2	63.2	64.8	70.6	77.0	78.9	80.2
13	74.3	75.4	77.2	83.9	91.1	93.3	94.7
14	86.6	87.9	89.9	97.3	105.3	107.7	109.3
15	98.9	100.3	102.5	110.5	119.2	121.8	123.5
16	110.9	112.4	114.7	123.3	132.6	135.3	137.1
17	122.6	124.2	126.6	135.6	145.3	148.1	150.0
18	133.9	135.6	138.1	147.5	157.4	160.4	162.3
19	145.1	146.8	149.4	159.0	169.3	172.3	174.3
20	156.4	158.1	160.8	170.7	181.1	184.2	186.2
21	167.8	169.6	172.3	182.4	193.0	196.1	198.1
22	179.3	181.1	183.9	194.0	204.8	208.0	210.0
23	190.7	192.5	195.3	205.7	216.6	219.7	221.8
24	201.9	203.8	206.6	217.1	228.1	231.3	233.5
25	212.9	214.8	217.7	228.3	239.5	242.7	244.9
26	223.6	225.5	228.4	239.2	250.5	253.8	256.0
27	233.8	235.8	238.8	249.7	261.2	264.5	266.7
28	243.6	245.6	248.6	259.8	271.5	274.9	277.1
29	252.8	254.8	257.9	269.3	281.3	284.7	287.0
30	261.3	263.4	266.6	278.3	290.6	294.1	296.5
31	269.2	271.3	274.7	286.7	299.3	303.0	305.4
32	276.4	278.6	282.1	294.5	307.5	311.3	313.8
33	282.9	285.2	288.8	301.7	315.2	319.1	321.7
34	288.8	291.2	294.9	308.3	322.3	326.4	329.0
35	294.0	296.5	300.3	314.2	328.8	333.0	335.8
36	298.5	301.1	305.0	319.5	334.7	339.1	342.0
37	302.3	304.9	309.0	324.1	339.8	344.4	347.5
38	305.2	308.0	312.2	327.8	344.2	349.0	352.1
39	307.3	310.1	314.5	330.7	347.7	352.7	355.9
40	308.3	311.3	315.9	332.6	350.3	355.4	358.8
<b>Abdominal Circumference (mm), Asian</b>							
10	30.9	31.5	32.4	36.0	40.0	41.2	42.0
11	39.2	39.9	41.1	45.4	50.1	51.6	52.5
12	48.4	49.2	50.6	55.7	61.3	63.0	64.1
13	58.3	59.3	60.9	66.8	73.3	75.2	76.5
14	68.8	70.0	71.8	78.4	85.7	87.9	89.4
15	79.7	81.0	83.0	90.4	98.5	100.9	102.5
16	90.8	92.2	94.3	102.5	111.3	113.9	115.6
17	101.8	103.3	105.7	114.5	123.9	126.8	128.6
18	112.9	114.5	117.0	126.3	136.4	139.4	141.4
19	123.8	125.5	128.1	138.0	148.7	151.8	153.9

Continued



**TABLE B-6 Race/Ethnic-Specific Percentiles for Fetal Anthropometric Measurements by Gestational Age, as Reported in the National Institutes of Child Health and Human Development (NICHD) Fetal Growth Studies—cont'd**

Gestational Age (wk)	PERCENTILE						
	3rd	5th	10th	50th	90th	95th	97th
20	134.6	136.4	139.2	149.6	160.8	164.1	166.3
21	145.3	147.2	150.2	161.1	172.8	176.3	178.6
22	155.9	157.9	161.0	172.4	184.6	188.2	190.6
23	166.2	168.3	171.5	183.4	196.2	200.0	202.5
24	176.3	178.4	181.8	194.3	207.6	211.5	214.1
25	186.1	188.4	191.9	204.9	218.8	222.9	225.6
26	195.7	198.1	201.8	215.4	229.9	234.2	237.0
27	205.2	207.6	211.5	225.8	241.0	245.5	248.4
28	214.5	217.1	221.2	236.1	252.1	256.8	259.9
29	223.9	226.7	230.9	246.7	263.4	268.4	271.7
30	233.4	236.3	240.8	257.3	275.0	280.3	283.7
31	242.8	245.8	250.5	268.0	286.7	292.3	295.9
32	252.0	255.2	260.2	278.7	298.5	304.3	308.2
33	260.9	264.3	269.6	289.1	310.1	316.3	320.4
34	269.5	273.1	278.7	299.3	321.4	328.0	332.3
35	277.6	281.4	287.3	309.0	332.4	339.3	343.9
36	285.2	289.2	295.4	318.3	342.9	350.3	355.1
37	292.4	296.6	303.1	327.2	353.2	360.9	366.0
38	299.4	303.7	310.6	335.9	363.2	371.4	376.8
39	306.2	310.7	317.9	344.5	373.4	382.0	387.7
40	312.9	317.7	325.2	353.3	383.8	392.9	398.9
<b>Femur Length (mm), Asian</b>							
10	1.6	1.7	1.8	2.2	2.6	2.8	2.9
11	2.9	3.0	3.2	3.8	4.6	4.8	5.0
12	4.7	4.9	5.1	6.1	7.2	7.6	7.8
13	7.0	7.3	7.6	8.9	10.5	11.0	11.3
14	9.8	10.0	10.5	12.2	14.2	14.8	15.3
15	12.7	13.1	13.6	15.7	18.1	18.8	19.3
16	15.7	16.1	16.8	19.1	21.9	22.7	23.3
17	18.7	19.1	19.8	22.4	25.4	26.3	26.9
18	21.4	21.9	22.6	25.4	28.5	29.5	30.1
19	24.1	24.6	25.3	28.2	31.5	32.4	33.1
20	26.7	27.2	28.0	31.0	34.3	35.3	36.0
21	29.4	29.9	30.7	33.8	37.1	38.1	38.8
22	32.1	32.6	33.4	36.5	39.9	40.9	41.5
23	34.7	35.2	36.0	39.1	42.5	43.6	44.2
24	37.2	37.7	38.6	41.7	45.1	46.2	46.8
25	39.6	40.2	41.0	44.2	47.7	48.7	49.4
26	42.0	42.5	43.4	46.6	50.1	51.2	51.8
27	44.2	44.8	45.7	49.0	52.5	53.5	54.2
28	46.3	46.9	47.8	51.2	54.8	55.9	56.6
29	48.4	49.0	49.9	53.4	57.1	58.2	58.9
30	50.4	51.0	51.9	55.5	59.3	60.4	61.1
31	52.3	52.9	53.9	57.5	61.4	62.6	63.4
32	54.1	54.7	55.7	59.5	63.5	64.7	65.5
33	55.8	56.5	57.5	61.4	65.6	66.8	67.6
34	57.5	58.1	59.2	63.2	67.5	68.8	69.6
35	59.0	59.8	60.9	65.0	69.4	70.7	71.5
36	60.6	61.3	62.4	66.7	71.2	72.5	73.4
37	62.0	62.7	63.9	68.3	72.9	74.2	75.1
38	63.3	64.1	65.3	69.7	74.5	75.9	76.8
39	64.5	65.3	66.6	71.1	76.0	77.4	78.3
40	65.6	66.4	67.7	72.4	77.4	78.9	79.9

**TABLE B-6 Race/Ethnic-Specific Percentiles for Fetal Anthropometric Measurements by Gestational Age, as Reported in the National Institutes of Child Health and Human Development (NICHD) Fetal Growth Studies—cont'd**

Gestational Age (wk)	PERCENTILE						
	3rd	5th	10th	50th	90th	95th	97th
<b>Humerus Length (mm), Asian</b>							
10	1.8	1.8	1.9	2.3	2.8	3.0	3.1
11	3.2	3.3	3.4	4.1	4.8	5.1	5.2
12	5.1	5.2	5.5	6.4	7.6	7.9	8.2
13	7.5	7.7	8.1	9.4	10.9	11.4	11.7
14	10.3	10.6	11.0	12.7	14.6	15.2	15.6
15	13.3	13.6	14.1	16.1	18.4	19.1	19.6
16	16.2	16.6	17.2	19.4	22.0	22.8	23.3
17	19.0	19.4	20.0	22.5	25.3	26.1	26.7
18	21.5	22.0	22.6	25.2	28.1	29.0	29.5
19	23.9	24.3	25.0	27.7	30.6	31.5	32.1
20	26.2	26.6	27.4	30.0	33.0	33.9	34.5
21	28.5	28.9	29.7	32.4	35.4	36.3	36.9
22	30.7	31.2	31.9	34.7	37.7	38.6	39.2
23	32.9	33.4	34.1	36.9	39.9	40.8	41.4
24	35.0	35.5	36.3	39.1	42.1	43.0	43.6
25	37.0	37.5	38.3	41.2	44.2	45.2	45.8
26	38.9	39.4	40.2	43.1	46.3	47.2	47.8
27	40.6	41.2	42.0	45.0	48.3	49.2	49.9
28	42.3	42.8	43.7	46.8	50.1	51.1	51.8
29	43.8	44.4	45.3	48.5	52.0	53.0	53.7
30	45.3	45.8	46.8	50.1	53.7	54.8	55.5
31	46.6	47.2	48.2	51.6	55.4	56.5	57.2
32	47.9	48.5	49.5	53.1	57.0	58.2	58.9
33	49.1	49.8	50.8	54.5	58.6	59.7	60.5
34	50.3	51.0	52.0	55.9	60.1	61.3	62.1
35	51.5	52.2	53.3	57.3	61.5	62.8	63.6
36	52.7	53.4	54.5	58.6	63.0	64.3	65.1
37	53.8	54.5	55.6	59.8	64.3	65.6	66.5
38	54.8	55.5	56.7	60.9	65.5	66.9	67.8
39	55.7	56.4	57.6	61.9	66.6	68.0	68.9
40	56.4	57.1	58.3	62.7	67.5	68.9	69.8
<b>Estimated Fetal Weight (g), Asian</b>							
10	18	19	20	24	30	31	33
11	26	27	28	34	41	43	44
12	36	38	39	47	55	58	60
13	50	51	53	63	74	77	79
14	66	68	71	83	97	101	104
15	86	88	92	108	125	131	135
16	110	113	118	138	160	167	172
17	139	143	149	173	202	211	216
18	172	177	185	215	250	261	269
19	211	217	227	264	307	321	330
20	257	264	275	320	373	389	400
21	308	317	331	385	447	467	480
22	367	378	394	458	532	556	571
23	434	446	466	541	628	656	674
24	509	524	546	634	737	769	790
25	594	611	637	740	859	896	921
26	690	709	740	859	997	1040	1069
27	796	818	853	990	1149	1199	1232
28	913	938	978	1136	1318	1375	1413
29	1039	1068	1114	1293	1501	1566	1609
30	1175	1208	1260	1463	1698	1772	1821

Continued



**TABLE B-6 Race/Ethnic-Specific Percentiles for Fetal Anthropometric Measurements by Gestational Age, as Reported in the National Institutes of Child Health and Human Development (NICHD) Fetal Growth Studies—cont'd**

Gestational Age (wk)	PERCENTILE						
	3rd	5th	10th	50th	90th	95th	97th
31	1318	1355	1414	1642	1908	1991	2047
32	1467	1508	1574	1830	2129	2222	2284
33	1620	1667	1740	2026	2360	2464	2534
34	1778	1829	1911	2229	2600	2717	2795
35	1938	1995	2085	2438	2851	2980	3067
36	2100	2162	2262	2653	3111	3255	3352
37	2259	2327	2437	2869	3376	3536	3644
38	2408	2483	2604	3077	3637	3814	3933
39	2539	2621	2752	3269	3884	4078	4210
40	2643	2731	2873	3434	4105	4318	4462
<b>Head Circumference/Abdominal Circumference (mm), Asian</b>							
10	1.198	1.209	1.227	1.293	1.362	1.382	1.395
11	1.192	1.203	1.221	1.284	1.350	1.370	1.383
12	1.181	1.192	1.209	1.271	1.336	1.355	1.368
13	1.167	1.178	1.194	1.255	1.319	1.338	1.351
14	1.150	1.161	1.177	1.238	1.301	1.319	1.332
15	1.132	1.143	1.159	1.219	1.281	1.300	1.312
16	1.115	1.125	1.141	1.200	1.262	1.280	1.292
17	1.098	1.108	1.124	1.182	1.243	1.261	1.273
18	1.082	1.092	1.108	1.166	1.226	1.244	1.256
19	1.068	1.078	1.094	1.152	1.212	1.230	1.242
20	1.057	1.068	1.083	1.141	1.201	1.219	1.231
21	1.049	1.059	1.075	1.133	1.194	1.211	1.223
22	1.042	1.053	1.069	1.127	1.188	1.206	1.218
23	1.037	1.047	1.063	1.122	1.184	1.202	1.214
24	1.032	1.043	1.059	1.118	1.181	1.199	1.211
25	1.028	1.038	1.055	1.115	1.178	1.197	1.209
26	1.023	1.033	1.050	1.111	1.175	1.194	1.207
27	1.017	1.028	1.044	1.106	1.171	1.191	1.203
28	1.009	1.020	1.037	1.100	1.166	1.185	1.198
29	1.000	1.011	1.028	1.091	1.159	1.178	1.191
30	0.989	1.000	1.017	1.081	1.149	1.169	1.182
31	0.976	0.987	1.005	1.069	1.138	1.158	1.172
32	0.962	0.974	0.991	1.057	1.126	1.147	1.160
33	0.948	0.959	0.977	1.043	1.114	1.135	1.148
34	0.933	0.945	0.963	1.030	1.101	1.123	1.136
35	0.919	0.931	0.949	1.017	1.089	1.111	1.125
36	0.905	0.916	0.935	1.004	1.077	1.099	1.114
37	0.890	0.902	0.921	0.990	1.065	1.087	1.102
38	0.874	0.886	0.905	0.976	1.052	1.075	1.090
39	0.857	0.870	0.889	0.960	1.038	1.061	1.076
40	0.839	0.851	0.871	0.943	1.022	1.046	1.061

From Buck Louis GM, Jagtshwar G, Albert PS, et al: Racial/ethnic standards for fetal growth: the NICHD Fetal Growth Studies. Am J Obstet Gynecol 449:e1-e41, October 2015, Table 2.

**TABLE B-7 Nomogram of Estimated Fetal Weight in Twin Gestations**

Gestational Age (wk)	ESTIMATED FETAL WEIGHT (g) BY PERCENTILE				
	5th	25th	50th	75th	95th
16	132	141	154	189	207
17	173	194	215	239	249
18	214	248	276	289	291
19	223	253	300	333	412
20	232	259	324	378	534
21	275	355	432	482	705
22	319	452	540	586	876
23	347	497	598	684	880
24	376	543	656	783	885
25	549	677	793	916	1118
26	722	812	931	1049	1352
27	755	978	1087	1193	1563
28	789	1145	1244	1337	1774
29	900	1266	1395	1509	1883
30	1011	1387	1546	1682	1992
31	1198	1532	1693	1875	2392
32	1385	1677	1840	2068	2793
33	1491	1771	2032	2334	3000
34	1597	1866	2224	2601	3208
35	1703	2093	2427	2716	3336
36	1809	2321	2631	2832	3465
37	2239	2540	2824	3035	3679
38	2669	2760	3017	3239	3894

From Yarkoni S, Reece EA, Holford T, et al: Estimated fetal weight in the evaluation of growth in twin gestations: a prospective longitudinal study. *Obstet Gynecol* 69:636, 1987. Reprinted with permission from The American College of Obstetricians and Gynecologists.

**TABLE B-8 Growth Parameters in Triplets Generated From Regression Equations**

Gestational age (wk)	BPD (cm)	HC (cm)	Bicerebellar Diameter (cm)	Humerus Length (cm)	FL (cm)	Tibia Length (cm)	Fibula Length (cm)	AC (cm)
16	3.5	12.8	1.5	2.1	2.0	1.7	1.6	10.7
17	3.9	14.1	1.6	2.3	2.3	2.0	1.9	11.9
18	4.2	15.3	1.7	2.6	2.6	2.3	2.2	13.1
19	4.5	16.5	1.9	2.8	2.9	2.5	2.4	14.2
20	4.8	17.6	2.0	3.1	3.2	2.8	2.7	15.3
21	5.1	18.7	2.2	3.3	3.5	3.1	2.9	16.4
22	5.4	19.8	2.3	3.5	3.7	3.3	3.2	17.4
23	5.7	20.8	2.5	3.7	4.0	3.5	3.4	18.4
24	6.0	21.8	2.6	3.9	4.2	3.7	3.6	19.4
25	6.2	22.7	2.7	4.1	4.4	3.9	3.7	20.3
26	6.5	23.6	2.8	4.2	4.6	4.1	3.9	21.2
27	6.7	24.5	3.0	4.4	4.8	4.2	4.1	22.1
28	6.9	25.3	3.1	4.6	5.0	4.4	4.2	22.9
29	7.1	26.1	3.2	4.7	5.2	4.5	4.3	23.7
30	7.3	26.8	3.4	4.8	5.4	4.7	4.4	24.5
31	7.5	27.5	3.5	4.9	5.5	4.8	4.6	25.2
32	7.7	28.1	3.6	5.0	5.7	4.9	4.6	25.9
33	7.8	28.7	3.8	5.1	5.8	4.9	4.7	26.6
34	8.0	29.2	3.9	5.2	5.9	5.0	4.8	27.2
35	8.1	29.7	4.0	5.2	6.0	5.1	4.8	27.8

AC, abdominal circumference; BPD, biparietal diameter; FL, femur length; HC, head circumference.

From Rodis JF, Arky L, Egan JF, et al: Comprehensive fetal ultrasonographic growth measurements in triplet gestations. *Am J Obstet Gynecol* 181:1128, 1999.



TABLE B-9 Estimates of Fetal Weight (g) Based on Abdominal Circumference and Femur Length

Femur Length (cm)	ABDOMINAL CIRCUMFERENCE (cm)																				
	20.0	20.5	21.0	21.5	22.0	22.5	23.0	23.5	24.0	24.5	25.0	25.5	26.0	26.5	27.0	27.5	28.0	28.5	29.0	29.5	30.0
4.0	663	691	720	751	783	816	851	887	925	964	1006	1048	1093	1139	1188	1239	1291	1346	1403	1463	1525
4.1	680	709	738	769	802	836	871	907	946	986	1027	1070	1115	1162	1211	1262	1315	1371	1429	1489	1551
4.2	697	726	757	788	821	855	891	928	967	1007	1049	1093	1138	1186	1235	1287	1340	1396	1454	1515	1578
4.3	715	745	776	808	841	875	912	949	988	1029	1071	1116	1162	1209	1259	1311	1365	1422	1480	1541	1605
4.4	734	764	795	827	861	896	933	971	1010	1051	1094	1139	1185	1234	1284	1336	1391	1448	1507	1568	1632
4.5	753	783	815	847	882	917	954	993	1033	1074	1118	1163	1210	1259	1309	1362	1417	1474	1534	1596	1660
4.6	772	803	835	868	903	939	976	1015	1056	1098	1142	1187	1235	1284	1335	1388	1444	1501	1561	1623	1688
4.7	792	823	856	889	924	961	999	1038	1079	1122	1166	1212	1260	1310	1361	1415	1471	1529	1589	1652	1717
4.8	812	844	877	911	947	984	1022	1062	1103	1146	1191	1237	1286	1336	1388	1442	1498	1557	1618	1681	1746
4.9	833	865	899	933	969	1007	1046	1086	1128	1171	1216	1263	1312	1363	1415	1470	1527	1585	1647	1710	1776
5.0	855	887	921	956	993	1031	1070	1111	1153	1197	1243	1290	1339	1390	1443	1498	1555	1615	1676	1740	1806
5.1	877	910	944	980	1016	1055	1095	1136	1179	1223	1269	1317	1367	1418	1471	1527	1584	1644	1706	1770	1837
5.2	899	933	967	1004	1041	1080	1120	1162	1205	1250	1296	1344	1395	1447	1500	1556	1614	1674	1737	1801	1868
5.3	922	956	992	1028	1066	1105	1146	1188	1232	1277	1324	1373	1423	1476	1530	1586	1645	1705	1768	1833	1900
5.4	946	981	1016	1053	1091	1131	1172	1215	1259	1305	1352	1401	1452	1505	1560	1617	1675	1736	1799	1865	1933
5.5	971	1005	1041	1079	1118	1158	1199	1242	1287	1333	1381	1431	1482	1535	1591	1648	1707	1768	1832	1897	1966
5.6	995	1031	1067	1105	1144	1185	1227	1271	1316	1362	1411	1461	1513	1566	1622	1679	1739	1801	1864	1931	1999
5.7	1021	1057	1094	1132	1172	1213	1255	1299	1345	1392	1441	1491	1544	1598	1654	1712	1772	1834	1898	1964	2033
5.8	1047	1084	1121	1160	1200	1242	1285	1329	1375	1422	1472	1523	1575	1630	1686	1744	1805	1867	1932	1999	2068
5.9	1074	1111	1149	1188	1229	1271	1314	1359	1406	1454	1503	1555	1608	1663	1719	1778	1839	1902	1966	2034	2103
6.0	1102	1139	1178	1217	1258	1301	1345	1390	1437	1485	1535	1587	1641	1696	1753	1812	1873	1936	2002	2069	2139
6.1	1130	1168	1207	1247	1289	1331	1376	1421	1469	1518	1568	1620	1674	1730	1788	1847	1908	1972	2038	2105	2175
6.2	1160	1198	1237	1278	1319	1363	1408	1454	1501	1551	1602	1654	1709	1765	1823	1882	1944	2008	2074	2142	2212
6.3	1189	1228	1268	1309	1351	1395	1440	1487	1535	1585	1636	1689	1744	1800	1858	1919	1981	2045	2111	2180	2250
6.4	1220	1259	1299	1341	1384	1428	1473	1520	1569	1619	1671	1724	1779	1836	1895	1956	2018	2082	2149	2218	2289
6.5	1251	1291	1332	1373	1417	1461	1507	1555	1604	1655	1707	1760	1816	1873	1932	1993	2056	2121	2188	2256	2328
6.6	1284	1324	1365	1407	1451	1496	1542	1590	1640	1691	1743	1797	1853	1911	1970	2031	2094	2160	2227	2296	2367
6.7	1317	1357	1399	1441	1486	1531	1578	1626	1676	1728	1780	1835	1891	1949	2009	2070	2134	2199	2267	2336	2408
6.8	1351	1391	1433	1477	1521	1567	1615	1663	1713	1765	1819	1873	1930	1988	2048	2110	2174	2240	2307	2377	2449
6.9	1385	1427	1469	1513	1558	1604	1652	1701	1752	1804	1857	1913	1970	2028	2089	2151	2215	2281	2348	2418	2490
7.0	1421	1463	1506	1550	1595	1642	1690	1740	1791	1843	1897	1953	2010	2069	2130	2192	2256	2322	2391	2461	2533
7.1	1458	1500	1543	1588	1633	1681	1729	1779	1830	1883	1938	1994	2051	2110	2171	2234	2299	2365	2433	2504	2576
7.2	1495	1538	1581	1626	1673	1720	1769	1819	1871	1924	1979	2035	2093	2153	2214	2277	2342	2408	2477	2547	2620
7.3	1534	1577	1621	1666	1713	1761	1810	1861	1913	1966	2021	2078	2136	2196	2258	2321	2386	2453	2521	2592	2665
7.4	1573	1616	1661	1707	1754	1802	1852	1903	1955	2009	2065	2122	2180	2240	2302	2365	2431	2498	2566	2637	2710
7.5	1614	1657	1702	1749	1796	1845	1895	1946	1999	2053	2109	2166	2225	2285	2347	2411	2476	2543	2612	2683	2756
7.6	1655	1699	1745	1791	1839	1888	1939	1990	2043	2098	2154	2211	2270	2331	2393	2457	2523	2590	2659	2730	2803
7.7	1698	1742	1788	1835	1883	1933	1983	2035	2089	2144	2200	2258	2317	2378	2440	2504	2570	2638	2707	2778	2851
7.8	1741	1786	1833	1880	1928	1978	2029	2082	2135	2191	2247	2305	2365	2426	2488	2553	2618	2686	2755	2827	2899
7.9	1786	1832	1878	1926	1975	2025	2076	2129	2183	2238	2295	2353	2413	2474	2537	2602	2668	2735	2805	2876	2949
8.0	1832	1878	1925	1973	2022	2073	2124	2177	2232	2287	2344	2403	2463	2524	2587	2652	2718	2785	2855	2926	2999
8.1	1879	1926	1973	2021	2071	2121	2173	2227	2281	2337	2394	2453	2513	2575	2638	2702	2769	2837	2906	2977	3050
8.2	1928	1974	2022	2070	2120	2171	2224	2277	2332	2388	2446	2504	2565	2626	2690	2754	2821	2889	2958	3029	3102
8.3	1978	2024	2072	2121	2171	2223	2275	2329	2384	2440	2498	2557	2617	2679	2743	2807	2874	2942	3011	3082	3155



TABLE B-10 Estimates of Fetal Weight (g) Based on Abdominal Circumference and Femur Length—Continued

Femur Length (cm)	ABDOMINAL CIRCUMFERENCE (cm)																			
	30.5	31.0	31.5	32.0	32.5	33.0	33.5	34.0	34.5	35.0	35.5	36.0	36.5	37.0	37.5	38.0	38.5	39.0	39.5	40.0
4.0	1590	1658	1729	1802	1879	1959	2042	2129	2220	2314	2413	2515	2622	2734	2850	2972	3098	3230	3367	3511
4.1	1617	1685	1756	1830	1907	1987	2071	2158	2249	2344	2442	2545	2652	2764	2880	3002	3128	3260	3397	3540
4.2	1644	1712	1783	1858	1935	2016	2100	2187	2279	2373	2472	2575	2683	2794	2911	3032	3159	3290	3427	3570
4.3	1671	1740	1812	1886	1964	2045	2129	2217	2308	2404	2503	2606	2713	2825	2942	3063	3189	3321	3458	3600
4.4	1699	1768	1840	1915	1993	2075	2159	2247	2339	2434	2533	2637	2744	2856	2973	3094	3220	3352	3488	3630
4.5	1727	1797	1869	1944	2023	2105	2189	2278	2370	2465	2565	2668	2776	2888	3004	3125	3251	3383	3519	3661
4.6	1756	1826	1898	1974	2053	2135	2220	2309	2401	2497	2596	2700	2807	2919	3036	3157	3283	3414	3550	3692
4.7	1785	1855	1928	2004	2084	2166	2251	2340	2432	2528	2628	2732	2840	2952	3068	3189	3315	3446	3582	3723
4.8	1814	1885	1959	2035	2115	2197	2283	2372	2464	2560	2660	2764	2872	2984	3100	3221	3347	3478	3613	3754
4.9	1845	1916	1990	2066	2146	2229	2315	2404	2497	2593	2693	2797	2905	3017	3133	3254	3380	3510	3645	3786
5.0	1875	1947	2021	2098	2178	2261	2347	2437	2530	2626	2726	2830	2938	3050	3166	3287	3412	3542	3677	3818
5.1	1906	1978	2053	2130	2210	2294	2380	2470	2563	2659	2760	2864	2972	3084	3200	3320	3445	3575	3710	3850
5.2	1938	2010	2085	2163	2243	2327	2413	2503	2597	2693	2794	2898	3006	3117	3234	3354	3479	3608	3743	3882
5.3	1970	2043	2118	2196	2277	2360	2447	2537	2631	2728	2828	2932	3040	3152	3268	3388	3513	3642	3776	3915
5.4	2003	2076	2151	2229	2311	2395	2482	2572	2665	2762	2863	2967	3075	3186	3302	3422	3547	3676	3809	3948
5.5	2036	2109	2185	2264	2345	2429	2516	2607	2700	2797	2898	3002	3110	3221	3337	3457	3581	3710	3843	3981
5.6	2070	2143	2220	2298	2380	2464	2552	2642	2736	2833	2933	3038	3145	3257	3372	3492	3616	3744	3877	4015
5.7	2104	2178	2254	2333	2415	2500	2587	2678	2772	2869	2970	3074	3181	3293	3408	3527	3651	3779	3911	4048
5.8	2139	2213	2290	2369	2451	2536	2624	2714	2808	2905	3006	3110	3218	3329	3444	3563	3686	3814	3946	4082
5.9	2175	2249	2326	2405	2488	2573	2660	2751	2845	2942	3043	3147	3254	3366	3480	3599	3722	3849	3981	4117
6.0	2211	2286	2363	2442	2525	2610	2698	2789	2883	2980	3080	3184	3292	3403	3517	3636	3758	3885	4016	4151
6.1	2248	2323	2400	2480	2562	2647	2736	2827	2921	3018	3118	3222	3329	3440	3554	3673	3795	3921	4052	4186
6.2	2285	2360	2438	2518	2600	2686	2774	2865	2959	3056	3157	3260	3367	3478	3592	3710	3832	3957	4087	4222
6.3	2323	2398	2476	2556	2639	2725	2813	2904	2998	3095	3195	3299	3406	3516	3630	3747	3869	3994	4124	4257
6.4	2362	2437	2515	2595	2678	2764	2852	2943	3037	3134	3235	3338	3445	3555	3668	3785	3906	4031	4160	4293
6.5	2401	2477	2555	2635	2718	2804	2892	2983	3077	3174	3274	3378	3484	3594	3707	3824	3944	4069	4197	4329
6.6	2441	2517	2595	2675	2759	2844	2933	3024	3118	3215	3315	3418	3524	3633	3746	3863	3983	4106	4234	4366
6.7	2481	2557	2636	2716	2800	2885	2974	3065	3159	3256	3355	3458	3564	3673	3786	3902	4021	4144	4271	4402
6.8	2523	2599	2677	2758	2841	2927	3016	3107	3200	3297	3397	3499	3605	3714	3826	3941	4060	4183	4309	4439
6.9	2564	2641	2719	2800	2884	2969	3058	3149	3242	3339	3438	3541	3646	3754	3866	3981	4100	4222	4347	4477
7.0	2607	2683	2762	2843	2927	3012	3101	3192	3285	3381	3481	3583	3688	3796	3907	4022	4140	4261	4386	4514
7.1	2650	2727	2806	2887	2970	3056	3144	3235	3328	3424	3523	3625	3730	3838	3948	4062	4180	4300	4425	4552
7.2	2694	2771	2850	2931	3014	3100	3188	3279	3372	3468	3567	3668	3772	3880	3990	4104	4220	4340	4464	4591
7.3	2739	2816	2895	2976	3059	3145	3233	3323	3416	3512	3610	3712	3816	3922	4032	4145	4261	4381	4503	4629
7.4	2785	2861	2940	3021	3105	3190	3278	3369	3461	3557	3655	3756	3859	3966	4075	4187	4303	4421	4543	4668
7.5	2831	2908	2987	3068	3151	3236	3324	3414	3507	3602	3700	3800	3903	4009	4118	4230	4344	4462	4583	4708
7.6	2878	2955	3034	3115	3198	3283	3371	3461	3553	3648	3745	3845	3948	4053	4161	4272	4387	4504	4624	4747
7.7	2926	3003	3081	3162	3245	3331	3418	3508	3600	3694	3791	3891	3993	4098	4205	4316	4429	4545	4665	4787
7.8	2974	3051	3130	3211	3294	3379	3466	3555	3647	3741	3838	3937	4039	4143	4250	4360	4472	4588	4706	4827
7.9	3024	3100	3179	3260	3343	3427	3514	3604	3695	3789	3885	3984	4085	4188	4295	4404	4515	4630	4748	4868
8.0	3074	3151	3229	3310	3392	3477	3564	3653	3744	3837	3933	4031	4131	4234	4340	4448	4559	4673	4790	4909
8.1	3125	3202	3280	3360	3443	3527	3614	3702	3793	3886	3981	4079	4179	4281	4386	4493	4604	4716	4832	4950
8.2	3177	3253	3332	3412	3494	3578	3664	3752	3843	3935	4030	4127	4226	4328	4432	4539	4648	4760	4875	4992
8.3	3230	3306	3384	3464	3546	3630	3716	3803	3893	3985	4080	4176	4275	4376	4479	4585	4693	4804	4918	5034

From Hadlock FP, Harrist RB, Carpenter RJ, et al: Sonographic estimation of fetal weight. Radiology 150:535, 1984.



TABLE B-11 Normal Body Ratio Data (14 to 21 Weeks)

Menstrual Age (wk)	Cephalic Index (SD = 3.7)*	Femur/BPD × 100 (SD = 4.0) <sup>†</sup>	Femur/HC × 100 (SD = 1.0) <sup>†</sup>	Femur/AC × 100 (SD = 1.3) <sup>†</sup>
14	81.5	58.0	15.0	19.0
15	81.0	59.0	15.7	19.3
16	80.5	61.0	16.4	19.8
17	80.1	63.0	16.9	20.3
18	79.7	65.0	17.5	20.8
19	79.4	67.0	18.1	21.0
20	79.1	69.0	18.4	21.3
21	78.8	70.0	18.6	21.5

AC, abdominal circumference; BPD, biparietal diameter; HC, head circumference; SD, standard deviation.

\*Data from Gray DL, Songster GS, Parvin CA, et al: Cephalic index: a gestational age-dependent biometric parameter. *Obstet Gynecol* 74:600, 1989.

<sup>†</sup>Data from Hadlock FP, Harrist RB, Martinez-Poyer J: Fetal body ratios in second trimester: a useful tool for identifying chromosomal abnormalities? *J Ultrasound Med* 11:81, 1992.

TABLE B-12 Normal Fetal Body Ratios (22 to 40 Weeks)

Menstrual Age (wk)	Cephalic Index (SD = 4.4)*	Femur/BPD × 100 (SD = 5.0) <sup>†</sup>	Femur/HC × 100 (SD = 1.1) <sup>†</sup>	Femur/AC × 100 (SD = 1.3) <sup>§</sup>
22	78.3	77.4	18.6	21.6
23	78.3	77.6	18.8	21.7
24	78.3	77.8	19.0	21.7
25	78.3	78.0	19.2	21.8
26	78.3	78.2	19.4	21.8
27	78.3	78.4	19.6	21.9
28	78.3	78.6	19.8	21.9
29	78.3	78.8	20.0	21.9
30	78.3	79.0	20.3	22.0
31	78.3	79.2	20.5	22.0
32	78.3	79.4	20.7	22.1
33	78.3	79.6	20.9	22.1
34	78.3	79.8	21.1	22.2
35	78.3	80.0	21.4	22.2
36	78.3	80.2	21.6	22.2
37	78.3	80.4	21.8	22.3
38	78.3	80.6	22.0	22.3
39	78.3	80.8	22.2	22.3
40	78.3	81.0	22.4	22.4

AC, abdominal circumference; BPD, biparietal diameter; HC, head circumference; SD, standard deviation.

\*Data from Hadlock FP, Deter RL, Carpenter RJ, et al: The effect of head shape on the accuracy of BPD in estimating fetal gestational age. *AJR* 137:83, 1981.

<sup>†</sup>Data from Hohler CW, Quetel TA: The relationship between fetal femur length and biparietal diameter in the last half of pregnancy. *Am J Obstet Gynecol* 141:759, 1981.

<sup>‡</sup>Data from Hadlock FP, Harrist RB, Shah YP, et al: The use of femur length/head circumference relation in obstetrical sonography. *J Ultrasound Med* 3:439, 1984.

<sup>§</sup>Data from Hadlock FP, Deter RL, Harrist RB, et al: A date-independent predictor of intrauterine growth retardation: femur length/abdominal circumference ratio. *AJR* 141:979, 1983.

**TABLE B-13 Comparison of Fetal Parameters in LGA and AGA Fetuses**

Parameter	AGA Group (mean ± SD)	LGA Group (mean ± SD)	P Value
BPD (cm)	9.2 ± 0.4	9.6 ± 0.4	<.0001
HC (cm)	33.7 ± 1.1	35.2 ± 1.3	<.0001
AC (cm)	33.6 ± 1.6	37.4 ± 1.3	<.0001
FL (cm)	7.4 ± 0.4	7.6 ± 0.3	<.0001
HC/AC	1.0 ± 0.05	0.94 ± 0.04	<.0001
FL/AC*	22.0 ± 1.0	20.5 ± 1.0	<.0001

AC, abdominal circumference; AGA, appropriate for gestational age; BPD, biparietal diameter; FL, femur length; HC, head circumference; LGA, large for gestational age.

\*FL/AC expressed as FL/AC × 100.

From Hadlock FP, Harrist RB, Fearneyhough TC, et al: Use of femur length/abdominal circumference ratio in detecting the macrosomic fetus. *Radiology* 154:503, 1985.

**TABLE B-14 Conventional Sonographic Criteria for Fetal Growth Restriction: Performance Characteristics**

Criterion	Sensitivity (%)*	Specificity (%)*	PREDICTIVE VALUES (%)**†	
			Positive	Negative
Advanced placental grade	62	64	16	94
Elevated FL/AC	34-49	78-83	18-20	92-93
Low TIUV	57-80	72-76	21-24	92-97
Small BPD	24-88	62-94	21-44	92-98
Small BPD and advanced placental grade	59	86	32	95
Slow rate of BPD growth	75	84	35	97
Low EFW	89	88	45	99
Decreased AFV	24	98	55	92
Elevated HC/AC	82	94	62	98

AFV, amniotic fluid volume; BPD, biparietal diameter; EFW, estimated fetal weight; FL/AC, femur length/abdominal circumference ratio; HC/AC, head circumference/abdominal circumference ratio; TIUV, total intrauterine volume.

\*A range of values is given for a criterion when different studies apply that criterion in two or more ways.

†Computed using Bayes' theorem and assuming a fetal growth restriction prevalence rate of 10%.

From Benson CB, Doubilet PM, Saltzman DH: Intrauterine growth retardation: predictive value of US criteria for antenatal diagnosis. *Radiology* 160:415, 1986.



## Measurements for Amniotic Fluid Assessment

**TABLE C-1 Amniotic Fluid Index Values in Normal Pregnancy**

Gestational age (wk)	AMNIOTIC FLUID INDEX (mm) BY PERCENTILE				
	3rd	5th	50th	95th	97th
16	73	79	121	185	201
17	77	83	127	194	211
18	80	87	133	202	220
19	83	90	137	207	225
20	86	93	141	212	230
21	88	95	143	214	233
22	89	97	145	216	235
23	90	98	146	218	237
24	90	98	147	219	238
25	89	97	147	221	240
26	89	97	147	223	242
27	85	95	146	226	245
28	86	94	146	228	249
29	84	92	145	231	254
30	82	90	145	234	258
31	79	88	144	238	263
32	77	86	144	242	269
33	74	83	143	245	274
34	72	81	142	248	278
35	70	79	140	249	279
36	68	77	138	249	279
37	66	75	135	244	275
38	65	73	132	239	269
39	64	72	127	226	255
40	63	71	123	214	240
41	63	70	116	194	216
42	63	69	110	175	192

Adapted from Moore TR, Cayle JE: The amniotic fluid index in normal human pregnancy. *Am J Obstet Gynecol* 162:1168, 1990.

TABLE C-2 Amniotic Fluid Index Values in Normal Pregnancy

Menstrual Age (wk)	AMNIOTIC FLUID INDEX (cm) BY PERCENTILE					
	5th	10th	50th	Mean	90th	95th
14	2.8	3.1	5.0	5.4	8.0	8.6
15	3.2	3.6	5.4	5.7	8.2	9.1
16	3.6	4.1	5.8	6.1	8.5	9.6
17	4.1	4.0	6.3	6.6	9.0	10.3
18	4.6	5.1	6.8	7.1	9.7	11.1
19	5.1	5.6	7.4	7.7	10.4	12.0
20	5.5	6.1	8.0	8.3	11.3	12.9
21	5.9	6.6	8.7	8.9	12.2	13.9
22	6.3	7.1	9.3	9.6	13.2	14.9
23	6.7	7.5	10.0	10.3	14.2	15.9
24	7.0	7.9	10.7	11.0	15.2	16.9
25	7.3	8.2	11.4	11.7	16.1	17.8
26	7.5	8.4	12.0	12.3	17.0	18.7
27	7.6	8.6	12.6	12.8	17.8	19.4
28	7.6	8.6	13.0	13.3	18.4	19.9
29	7.6	8.6	13.4	13.6	18.8	20.4
30	7.5	8.5	13.6	13.8	18.9	20.6
31	7.3	8.4	13.6	13.8	18.9	20.6
32	7.1	8.1	13.6	13.7	18.7	20.4
33	6.8	7.8	13.3	13.4	18.2	20.0
34	6.4	7.4	13.9	13.0	17.7	19.4
35	6.0	7.0	12.4	12.5	16.9	18.7
36	5.6	6.5	11.8	11.8	16.2	17.9
37	5.1	6.0	11.1	11.1	15.3	16.9
38	4.7	5.5	10.3	10.3	14.4	15.9
39	4.2	5.0	9.4	9.4	13.7	14.9
40	3.7	4.5	8.6	8.6	12.9	13.9
41	3.3	4.0	7.8	7.7	12.3	12.9

From Magann EF, Sanderson M, Martin JN Jr, et al: The amniotic fluid index, single deepest pocket and two diameter pocket in normal pregnancy. *Am J Obstet Gynecol* 182:1581, 2000.



**TABLE C-3 Single Deepest Pocket Values of Amniotic Fluid During Normal Pregnancy**

Menstrual Age (wk)	SINGLE DEEPEST POCKET (cm) BY PERCENTILE					
	5th	10th	50th	Mean	90th	95th
14	1.7	1.9	2.9	3.1	4.7	5.0
15	2.0	2.2	3.4	3.5	5.1	5.5
16	2.3	2.5	3.6	3.8	5.4	5.9
17	2.5	2.7	3.9	4.0	5.7	6.2
18	2.7	2.9	4.1	4.2	5.9	6.4
19	2.8	3.1	4.3	4.4	6.1	6.6
20	2.9	3.2	4.4	4.5	6.2	6.7
21	2.9	3.3	4.5	4.6	6.3	6.8
22	3.0	3.3	4.6	4.7	6.3	6.8
23	3.0	3.4	4.6	4.7	6.3	6.8
24	3.1	3.4	4.7	4.8	6.3	6.8
25	3.0	3.3	4.7	4.8	6.3	6.8
26	3.0	3.3	4.8	4.8	6.4	6.8
27	3.0	3.3	4.8	4.8	6.4	6.9
28	3.0	3.3	4.8	4.8	6.4	6.9
29	2.9	3.3	4.8	4.8	6.4	6.9
30	2.9	3.3	4.8	4.8	6.4	6.9
31	2.9	3.2	4.8	4.9	6.5	7.0
32	2.9	3.2	4.8	4.9	6.6	7.1
33	2.9	3.2	4.82	4.9	6.6	7.2
34	2.8	3.2	4.8	4.8	6.6	7.2
35	2.8	3.1	4.7	4.8	6.6	7.2
36	2.7	3.1	4.7	4.7	6.6	7.1
37	2.6	2.9	4.5	4.6	6.5	7.0
38	2.4	2.8	4.4	4.5	6.3	6.8
39	2.3	2.7	4.2	4.3	6.1	6.6
40	2.1	2.5	3.9	4.0	5.8	6.2
41	1.9	2.2	3.7	3.7	5.4	5.7

From Magann EF, Sanderson M, Martin JN Jr, et al: The amniotic fluid index, single deepest pocket and two diameter pocket in normal pregnancy. *Am J Obstet Gynecol* 182:1581, 2000.

**TABLE C-4 Amniotic Fluid Volume Values in Relation to Gestational Age by Second Order Quantile Regression**

Week of Gestation	AMNIOTIC FLUID VOLUME (mL) BY PERCENTILE				
	5th	25th	50th	75th	95th
16	134.0	334.5	377.1	503.2	694.7
17	132.3	322.0	389.6	552.2	937.2
18	130.9	311.1	401.9	602.0	1233.7
19	129.9	301.7	414.0	652.1	1584.8
20	129.2	293.7	425.8	701.8	1986.6
21	128.9	286.9	437.2	750.4	2430.0
22	128.9	281.4	448.3	797.2	2900.5
23	129.2	277.0	459.0	841.5	3378.4
24	129.8	273.7	469.2	882.5	3839.9
25	130.8	271.4	478.9	919.5	4258.8
26	132.1	270.2	488.1	951.9	4609.3
27	133.8	270.0	496.7	979.1	4868.0
28	135.8	270.8	504.7	1000.5	5016.9
29	138.3	272.6	512.1	1015.9	5045.3
30	141.1	275.4	518.8	1024.8	4951.1
31	144.4	279.3	524.8	1027.1	4741.3
32	148.1	284.4	530.0	1022.8	4430.5
33	152.3	290.6	534.5	1012.0	4040.0
34	157.0	298.0	538.2	994.8	3594.8
35	162.3	306.8	541.1	971.6	3121.4
36	168.2	317.0	543.2	942.8	2644.7
37	174.7	328.8	544.5	909.0	2186.7
38	182.0	342.3	545.0	870.7	1764.2
39	190.0	357.7	544.7	828.7	1389.0
40	198.2	375.2	543.5	783.6	1067.1
41	207.9	395.0	541.5	736.2	800.0

From Sandlin AT, Ounpraseuth ST, Spencer HJ, et al: Amniotic fluid volume in normal singleton pregnancies: modeling with quantile regression. Arch Gynecol Obstet 289:967-972, 2014, used with permission.



## Fetal Doppler Assessment (Noncardiac)

**TABLE D-1 Resistance Index of the Uterine Artery**

Gestation (wk)	5th Percentile	50th Percentile	95th Percentile
18	0.222	0.447	0.659
19	0.204	0.429	0.641
20	0.194	0.419	0.630
21	0.186	0.411	0.622
22	0.180	0.405	0.615
23	0.175	0.400	0.610
24	0.171	0.395	0.605
25	0.167	0.391	0.601
26	0.163	0.387	0.597
27	0.160	0.384	0.593
28	0.157	0.380	0.590
29	0.154	0.378	0.587
30	0.152	0.375	0.584
31	0.150	0.372	0.581
32	0.147	0.370	0.578
33	0.145	0.368	0.576
34	0.144	0.366	0.574
35	0.142	0.364	0.571
36	0.140	0.362	0.569
37	0.139	0.360	0.567
38	0.137	0.358	0.566
39	0.136	0.357	0.564
40	0.135	0.355	0.562

From Merz E (ed): *Ultrasonography in Obstetrics and Gynecology*. Stuttgart, Thieme, 2005, pp 469-480, 613, 614.

**TABLE D-2 Pulsatility Index of the Uterine Artery**

Gestation (wk)	5th Percentile	50th Percentile	95th Percentile
18	0.509	0.888	1.407
19	0.460	0.838	1.356
20	0.436	0.812	1.328
21	0.420	0.795	1.309
22	0.407	0.781	1.293
23	0.397	0.769	1.280
24	0.388	0.759	1.268
25	0.381	0.751	1.258
26	0.374	0.743	1.248
27	0.369	0.736	1.239
28	0.363	0.729	1.230
29	0.358	0.722	1.222
30	0.354	0.716	1.214
31	0.349	0.711	1.207
32	0.345	0.705	1.199
33	0.341	0.700	1.192
34	0.337	0.695	1.185
35	0.333	0.690	1.178
36	0.330	0.684	1.171
37	0.326	0.679	1.164
38	0.322	0.674	1.157
39	0.318	0.669	1.150
40	0.313	0.663	1.143

From Merz E (ed): *Ultrasonography in Obstetrics and Gynecology*. Stuttgart, Thieme, 2005, pp 469-480, 613, 614.

**TABLE D-3 Reference Values for Serial Measurements of the Umbilical Artery Systolic/Diastolic Ratio**

Gestational age (wk)	UMBILICAL ARTERY SYSTOLIC/DIASTOLIC RATIO BY PERCENTILE								
	2.5th	5th	10th	25th	50th	75th	90th	95th	97.5th
19	2.73	2.93	3.19	3.67	4.28	5.00	5.75	6.26	6.73
20	2.63	2.83	3.07	3.53	4.11	4.80	5.51	5.99	6.43
21	2.51	2.70	2.93	3.36	3.91	4.55	5.22	5.67	6.09
22	2.43	2.60	2.83	3.24	3.77	4.38	5.03	5.45	5.85
23	2.34	2.51	2.72	3.11	3.62	4.21	4.82	5.22	5.61
24	2.25	2.41	2.62	2.99	3.48	4.04	4.63	5.02	5.38
25	2.17	2.33	2.52	2.88	3.35	3.89	4.45	4.83	5.18
26	2.09	2.24	2.43	2.78	3.23	3.75	4.30	4.66	5.00
27	2.02	2.17	2.35	2.69	3.12	3.63	4.15	4.50	4.83
28	1.95	2.09	2.27	2.60	3.02	3.51	4.02	4.36	4.67
29	1.89	2.03	2.20	2.52	2.92	3.40	3.89	4.22	4.53
30	1.83	1.96	2.13	2.44	2.83	3.30	3.78	4.10	4.40
31	1.77	1.90	2.06	2.36	2.75	3.20	3.67	3.98	4.27
32	1.71	1.84	2.00	2.29	2.67	3.11	3.57	3.87	4.16
33	1.66	1.79	1.94	2.23	2.60	3.03	3.48	3.77	4.06
34	1.61	1.73	1.88	2.16	2.53	2.95	3.39	3.68	3.96
35	1.57	1.68	1.83	2.11	2.46	2.87	3.30	3.59	3.86
36	1.52	1.64	1.78	2.05	2.40	2.80	3.23	3.51	3.78
37	1.48	1.59	1.73	2.00	2.34	2.74	3.15	3.43	3.69
38	1.44	1.55	1.69	1.95	2.28	2.67	3.08	3.36	3.62
39	1.40	1.51	1.64	1.90	2.23	2.61	3.02	3.29	3.54
40	1.36	1.47	1.60	1.85	2.18	2.56	2.96	3.22	3.48
41	1.33	1.43	1.56	1.81	2.13	2.50	2.90	3.16	3.41

From Acharya G, Wilsgaard T, Bernsten GKR, et al: Reference ranges for serial measurements of umbilical artery Doppler indices in the second half of pregnancy. *Am J Obstet Gynecol* 192:937, 2005.

**TABLE D-4 Resistance Index of the Umbilical Artery Between 20 and 40 Weeks of Gestation**

Gestation (wk)	5th Percentile	50th Percentile	95th Percentile
20	0.567	0.690	0.802
21	0.557	0.680	0.793
22	0.548	0.671	0.784
23	0.539	0.663	0.776
24	0.530	0.655	0.768
25	0.522	0.646	0.760
26	0.514	0.639	0.752
27	0.506	0.631	0.745
28	0.498	0.623	0.737
29	0.490	0.615	0.730
30	0.482	0.608	0.723
31	0.474	0.600	0.715
32	0.465	0.592	0.707
33	0.457	0.584	0.700
34	0.449	0.576	0.692
35	0.440	0.567	0.684
36	0.431	0.559	0.675
37	0.422	0.550	0.667
38	0.412	0.540	0.657
39	0.402	0.530	0.648
40	0.390	0.519	0.637

From Merz E (ed): *Ultrasonography in Obstetrics and Gynecology*. Stuttgart, Thieme, 2005, pp 469-480, 613, 614.

**TABLE D-5 Pulsatility Index of the Umbilical Artery Between 20 and 40 Weeks of Gestation**

Gestation (wk)	5th Percentile	50th Percentile	95th Percentile
20	0.940	1.216	1.505
21	0.913	1.189	1.476
22	0.890	1.165	1.450
23	0.869	1.142	1.427
24	0.849	1.122	1.405
25	0.831	1.102	1.385
26	0.813	1.084	1.365
27	0.798	1.065	1.346
28	0.780	1.048	1.327
29	0.764	1.031	1.308
30	0.748	1.014	1.290
31	0.732	0.997	1.272
32	0.716	0.980	1.254
33	0.700	0.963	1.236
34	0.684	0.946	1.218
35	0.668	0.928	1.199
36	0.651	0.910	1.180
37	0.634	0.891	1.160
38	0.615	0.872	1.139
39	0.595	0.851	1.117
40	0.573	0.828	1.093

From Merz E (ed): *Ultrasonography in Obstetrics and Gynecology*. Stuttgart, Thieme, 2005, pp 469-480, 613, 614.



TABLE D-6 Umbilical Vein Mean Velocity

Gestational age (wk)	MEAN VELOCITY (cm/sec)			Gestational age (wk)	MEAN VELOCITY (cm/sec)		
	BY PERCENTILE				BY PERCENTILE		
	5th	50th	95th		5th	50th	95th
20	5.70	7.90	10.70	31	7.04	9.67	13.02
21	5.82	8.06	10.91	32	7.17	9.83	13.23
22	5.94	8.22	11.12	33	7.29	9.99	13.44
23	6.07	8.38	11.33	34	7.41	10.16	13.66
24	6.19	8.54	11.54	35	7.53	10.32	13.87
25	6.31	8.71	11.76	36	7.65	10.48	14.08
26	6.43	8.87	11.97	37	7.78	10.64	14.29
27	6.56	9.03	12.18	38	7.90	10.80	14.50
28	6.68	9.19	12.39	39	8.02	10.96	14.71
29	6.80	9.35	12.60	40	8.14	11.12	14.92
30	6.92	9.51	12.81				

From Barbera A, Galan HL, Ferrazzi E, et al: Relationship of umbilical vein blood flow to growth parameters in the human fetus. Am J Obstet Gynecol 181:174, 1999.

TABLE D-7 Reference Values for the Resistance Index of Umbilical and Middle Cerebral Arteries, as Well as the UA/MCA Ratio

Gestation (wk)	UMBILICAL ARTERY RESISTANCE INDEX (UA RI)			MIDDLE CEREBRAL ARTERY RESISTANCE INDEX (MCA RI)			UA RI/MCA RI RATIO		
	5th	50th	95th	5th	50th	95th	5th	50th	95th
	Percentile	Percentile	Percentile	Percentile	Percentile	Percentile	Percentile	Percentile	Percentile
24	0.615	0.717	0.828	0.778	0.867	—	0.696	0.809	0.968
25	0.605	0.707	0.819	0.789	0.881	—	0.676	0.791	0.955
26	0.594	0.697	0.810	0.795	0.892	—	0.658	0.775	0.945
27	0.583	0.687	0.802	0.798	0.898	—	0.642	0.761	0.937
28	0.572	0.678	0.793	0.797	0.901	—	0.628	0.750	0.932
29	0.562	0.668	0.785	0.793	0.900	—	0.616	0.740	0.929
30	0.551	0.658	0.776	0.786	0.897	—	0.606	0.732	0.928
31	0.540	0.648	0.767	0.776	0.891	—	0.597	0.726	0.929
32	0.530	0.638	0.759	0.764	0.883	—	0.590	0.722	0.931
33	0.519	0.629	0.750	0.750	0.872	—	0.585	0.719	0.936
34	0.508	0.619	0.742	0.734	0.860	—	0.581	0.717	0.941
35	0.498	0.609	0.733	0.717	0.846	—	0.578	0.717	0.949
36	0.487	0.599	0.724	0.698	0.831	—	0.576	0.718	0.957
37	0.476	0.589	0.716	0.677	0.814	—	0.575	0.720	0.967
38	0.465	0.580	0.707	0.655	0.795	—	0.576	0.724	0.978
39	0.455	0.570	0.699	0.632	0.776	—	0.577	0.728	0.991
40	0.444	0.560	0.690	0.607	0.755	—	0.580	0.734	1.004
41	0.433	0.550	0.681	0.582	0.734	—	0.583	0.740	1.018
42	0.423	0.540	0.673	0.556	0.711	—	0.588	0.747	1.034

From Kurmanavicius J, Florio I, Wisser J, et al: Reference resistance indices of the umbilical, fetal middle cerebral and uterine arteries at 24–42 weeks of gestation. Ultrasound Obstet Gynecol 10:112, 1997.

**TABLE D-8 Ductus Venosus Preload Index (a/S)**

Gestational age (wk)	PRELOAD INDEX (a/S)		
	5th Percentile	50th Percentile	95th Percentile
20	0.342	0.508	0.674
21	0.341	0.507	0.673
22	0.341	0.507	0.673
23	0.340	0.506	0.672
24	0.339	0.505	0.671
25	0.339	0.505	0.671
26	0.338	0.504	0.670
27	0.338	0.504	0.670
28	0.337	0.503	0.669
29	0.336	0.502	0.668
30	0.336	0.502	0.668
31	0.335	0.501	0.667
32	0.335	0.501	0.667
33	0.334	0.500	0.666
34	0.333	0.499	0.665
35	0.333	0.499	0.665
36	0.332	0.498	0.664
37	0.332	0.498	0.664
38	0.331	0.497	0.663
39	0.330	0.496	0.662
40	0.330	0.496	0.662

a, atrial systolic peak blood flow velocity; S, systolic peak blood flow velocity.

From Baschat AA: Relationship between placental blood flow resistance and precordial venous Doppler indices. *Ultrasound Obstet Gynecol* 22:561, 2003.

**TABLE D-10 Ductus Venosus Peak Velocity Index**

Gestational age (wk)	PEAK VELOCITY INDEX (S – a)/D		
	5th Percentile	50th Percentile	95th Percentile
20	0.381	0.580	0.779
21	0.380	0.579	0.779
22	0.380	0.579	0.778
23	0.379	0.578	0.777
24	0.378	0.578	0.777
25	0.378	0.577	0.776
26	0.377	0.576	0.776
27	0.377	0.576	0.775
28	0.376	0.575	0.774
29	0.375	0.575	0.774
30	0.375	0.574	0.773
31	0.374	0.573	0.773
32	0.374	0.573	0.772
33	0.373	0.572	0.771
34	0.372	0.572	0.771
35	0.372	0.571	0.770
36	0.371	0.570	0.770
37	0.371	0.570	0.769
38	0.370	0.569	0.768
39	0.369	0.569	0.768
40	0.369	0.568	0.767

a, atrial systolic peak blood flow velocity; D, diastolic peak blood flow velocity; S, systolic peak blood flow velocity.

From Baschat AA: Relationship between placental blood flow resistance and precordial venous Doppler indices. *Ultrasound Obstet Gynecol* 22:561, 2003.

**TABLE D-9 Ductus Venosus Pulsatility Index**

Gestational age (wk)	PULSATILITY INDEX (S – a)/TAMX		
	5th Percentile	50th Percentile	95th Percentile
20	0.410	0.643	0.875
21	0.409	0.642	0.874
22	0.408	0.641	0.873
23	0.407	0.640	0.872
24	0.406	0.639	0.871
25	0.405	0.638	0.870
26	0.404	0.637	0.869
27	0.403	0.636	0.868
28	0.402	0.635	0.867
29	0.401	0.634	0.866
30	0.400	0.633	0.865
31	0.399	0.632	0.864
32	0.398	0.631	0.863
33	0.397	0.630	0.862
34	0.396	0.629	0.861
35	0.395	0.628	0.860
36	0.394	0.627	0.859
37	0.393	0.626	0.858
38	0.392	0.625	0.857
39	0.391	0.624	0.856
40	0.390	0.623	0.855

a, atrial systolic peak blood flow velocity; S, systolic peak blood flow velocity; TAMX, time-averaged maximum velocity.

From Baschat AA: Relationship between placental blood flow resistance and precordial venous Doppler indices. *Ultrasound Obstet Gynecol* 22:561, 2003.

**TABLE D-11 Ductus Venosus Systolic/a-Wave (S/a) Ratio**

Gestational age (wk)	S/a RATIO		
	5th Percentile	50th Percentile	95th Percentile
20	1.331	2.161	2.991
21	1.329	2.159	2.989
22	1.327	2.157	2.987
23	1.324	2.154	2.984
24	1.322	2.152	2.982
25	1.320	2.150	2.980
26	1.318	2.148	2.978
27	1.315	2.145	2.975
28	1.313	2.143	2.973
29	1.311	2.141	2.971
30	1.308	2.138	2.968
31	1.306	2.136	2.966
32	1.304	2.134	2.964
33	1.301	2.131	2.961
34	1.299	2.129	2.959
35	1.297	2.127	2.957
36	1.295	2.125	2.955
37	1.292	2.122	2.952
38	1.290	2.120	2.950
39	1.288	2.118	2.948
40	1.285	2.115	2.945

From Baschat AA: Relationship between placental blood flow resistance and precordial venous Doppler indices. *Ultrasound Obstet Gynecol* 22:561, 2003.



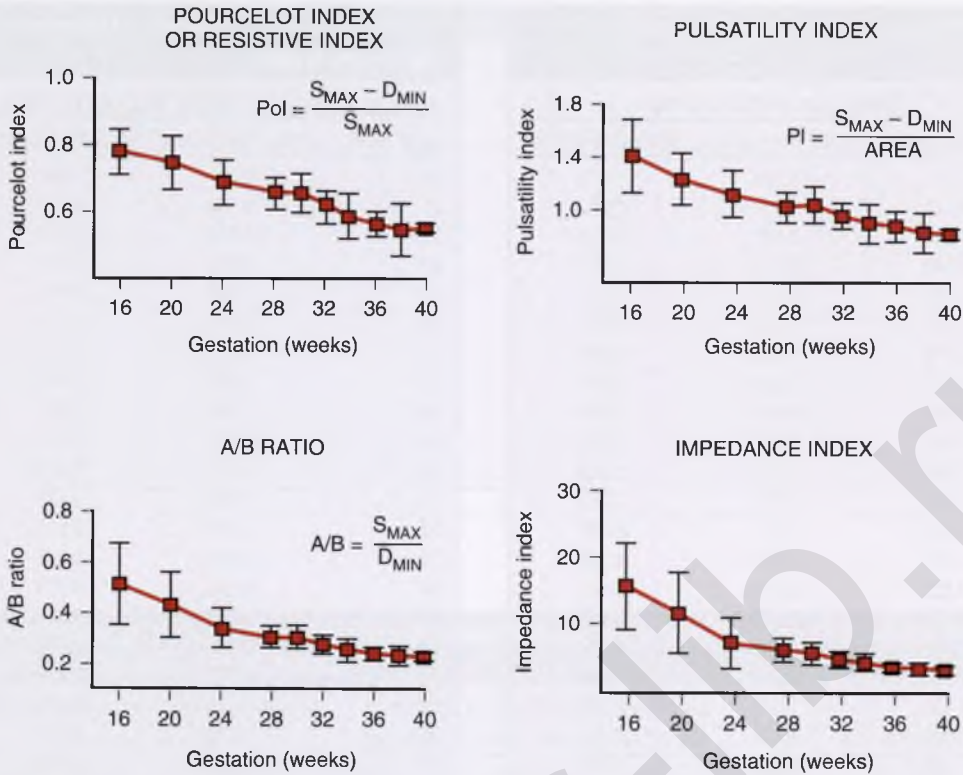


**FIG D-1** Doppler waveform analysis of the fetal umbilical artery. With advancing gestation and increasing compliance of the placenta, there is a progressive decrease in the systolic/diastolic ratio (A/B ratio), Pourcelot index (Pol), and pulsatility index (PI) of the umbilical artery that is a result of increased placental flow owing to decreased resistance. (Modified from Erskine RLA, Ritchie JWK: Umbilical artery blood flow characteristics in normal and growth retarded fetuses. *Br J Obstet Gynecol* 92:605, 1985.)

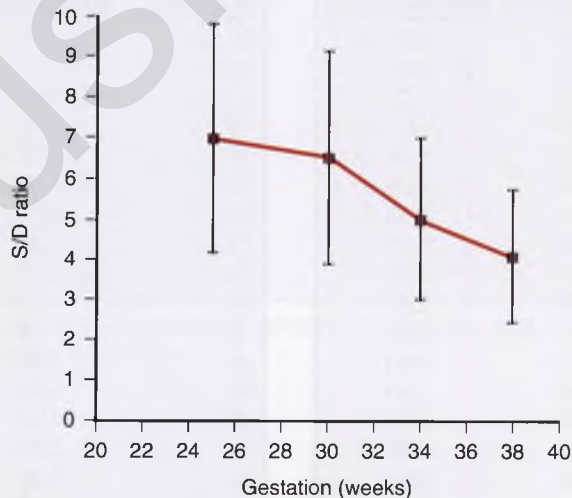


**FIG D-2** Middle cerebral artery Doppler systolic/diastolic (S/D) ratios. (Modified from Woo JSK, Liang ST, Lo RL, Chan FY: Middle cerebral artery Doppler flow velocity waveforms. *Obstet Gynecol* 70:613, 1987. Reprinted with permission from the American College of Obstetricians and Gynecologists.)

## Doppler of the Middle Cerebral Artery to Assess Fetal Anemia

**TABLE E-1 Threshold of Peak Velocity of Systolic Blood Flow in the Middle Cerebral Artery Above Which Mild, Moderate, and Severe Anemia Occurs**

THRESHOLD OF PEAK VELOCITY OF MIDDLE CEREBRAL ARTERY (cm/sec) ABOVE WHICH DEGREE OF ANEMIA IS CLASSIFIED				
Gestation (wk)	1.00 (Median)	Mild Anemia (1.29 MoM)	Moderate Anemia (1.50 MoM)	Severe Anemia (1.55 MoM)
18	23.2	29.9	34.8	36.0
20	25.5	32.8	38.2	39.5
22	27.9	36.0	41.9	43.3
24	30.7	39.5	46.0	47.5
26	33.6	43.3	50.4	52.1
28	36.9	47.6	55.4	57.2
30	40.5	52.2	60.7	62.8
32	44.4	57.3	66.6	68.9
34	48.7	62.9	73.1	75.6
36	53.5	69.0	80.2	82.9
38	58.7	75.7	88.0	91.0
40	64.4	83.0	96.6	99.8

MoM, multiple of median.

From Mari G, Deter RL, Carpenter RL, et al: Non-invasive diagnosis by Doppler ultrasonography of fetal anemia due to maternal red-cell alloimmunization. Collaborative Group for Doppler Assessment of the Blood Velocity in Anemic Fetuses. *N Engl J Med* 342:9, 2000.



## Fetal Cardiac Measurements and Doppler Assessment

**TABLE F-1 Mitral and Tricuspid Valve E/A Ratios**

Gestation (wk)	MITRAL VALVE E/A RATIO			TRICUSPID VALVE E/A RATIO		
	2.5th Percentile	50th Percentile	97.5th Percentile	2.5th Percentile	50th Percentile	97.5th Percentile
20	0.40	0.59	0.77	0.47	0.65	0.83
21	0.42	0.60	0.79	0.49	0.66	0.84
22	0.43	0.62	0.80	0.50	0.68	0.85
23	0.45	0.63	0.82	0.52	0.69	0.86
24	0.46	0.65	0.83	0.53	0.70	0.87
25	0.48	0.66	0.84	0.54	0.71	0.88
26	0.49	0.68	0.86	0.55	0.72	0.89
27	0.50	0.69	0.87	0.56	0.73	0.90
28	0.52	0.70	0.88	0.57	0.74	0.90
29	0.53	0.71	0.89	0.58	0.74	0.91
30	0.54	0.73	0.90	0.58	0.75	0.91
31	0.55	0.74	0.91	0.59	0.75	0.92
32	0.56	0.75	0.92	0.59	0.76	0.92
33	0.57	0.76	0.93	0.60	0.76	0.92
34	0.58	0.76	0.93	0.60	0.76	0.92
35	0.59	0.77	0.94	0.60	0.76	0.92
36	0.59	0.78	0.95	0.60	0.76	0.92
37	0.60	0.79	0.95	0.60	0.76	0.92
38	0.61	0.79	0.96	0.60	0.76	0.92

Note: A represents atrial contraction in late diastole; E represents passive ventricular filling in early diastole.

From DeVore GR: Pulsed Doppler examination of the fetal heart. In Goldberg BB, McGahan JP (eds): Atlas of Ultrasound Measurements, 2nd ed. Philadelphia, Mosby/Elsevier, 2006.

akus  
snrye



FIGURE 1-10  
Fetal Cardiac Measurements and Doppler Assessment

TABLE F-2 Peak or Maximum Velocity of the Aorta and Main Pulmonary Artery

Gestation (wk)	AORTA PEAK VELOCITY (cm/sec)			PULMONARY ARTERY PEAK VELOCITY (cm/sec)		
	2.5th Percentile	50th Percentile	97.5th Percentile	2.5th Percentile	50th Percentile	97.5th Percentile
20	29	62	95	23	53	80
21	30	63	96	24	54	81
22	32	65	98	25	56	82
23	33	66	99	27	57	84
24	34	67	100	28	58	85
25	36	68	101	29	59	86
26	37	70	103	30	61	87
27	38	71	104	31	62	89
28	40	72	105	32	63	90
29	41	74	107	34	64	91
30	42	75	108	35	65	92
31	44	76	109	36	67	93
32	45	77	110	37	68	95
33	46	79	112	38	69	96
34	48	80	113	39	70	97
35	49	81	114	41	72	98
36	50	82	115	42	73	100
37	52	84	117	43	74	101
38	53	85	118	44	78	102

From DeVore GR: Pulsed Doppler examination of the fetal heart. In Goldberg BB, McGahan JP (eds): Atlas of Ultrasound Measurements, 2nd ed. Philadelphia, Mosby/Elsevier, 2006.



**TABLE F-3 Longitudinal Reference Ranges for Peak Systolic Velocity in the Ductus Venosus Based on 547 Observations in 160 Low-Risk Pregnancies**

Gestational Age (wk)	PEAK SYSTOLIC VELOCITY IN DUCTUS VENOSUS (cm/sec) BY PERCENTILE								
	2.5th	5th	10th	25th	50th	75th	90th	95th	97.5th
21	46.2	48.0	50.2	54.3	59.3	65.1	70.9	74.8	78.5
22	48.3	50.1	52.4	56.6	61.8	67.6	73.7	77.7	81.4
23	50.1	52.0	54.3	58.6	63.9	69.9	76.1	80.1	83.9
24	51.6	53.5	55.9	60.3	65.7	71.9	78.2	82.3	86.2
25	52.8	54.8	57.2	61.7	67.2	73.5	79.9	84.2	88.1
26	53.8	55.8	58.3	62.8	68.5	74.9	81.4	85.7	89.7
27	54.5	56.6	59.1	63.8	69.5	76.0	82.7	87.1	91.1
28	55.1	57.2	59.7	64.4	70.3	76.9	83.7	88.1	92.3
29	55.4	57.6	60.2	64.9	70.8	77.6	84.5	89.0	93.2
30	55.6	57.7	60.4	65.2	71.2	78.0	85.0	89.7	94.0
31	55.6	57.8	60.5	65.3	71.4	78.3	85.4	90.1	94.5
32	55.5	57.7	60.4	65.3	71.4	78.5	85.7	90.4	94.9
33	55.3	57.5	60.2	65.2	71.4	78.5	85.8	90.6	95.1
34	55.0	57.2	59.9	64.9	71.2	78.3	85.7	90.6	95.2
35	54.6	56.8	59.5	64.5	70.8	78.1	85.5	90.5	95.1
36	54.1	56.3	59.1	64.1	70.4	77.7	85.2	90.3	94.9
37	53.6	55.8	58.6	63.6	70.0	77.3	84.9	89.9	94.7
38	53.0	55.2	58.0	63.0	69.4	76.8	84.4	89.5	94.3
39	52.4	54.6	57.4	62.4	68.8	76.2	83.9	89.0	93.8

From Kessler J, Rasmussen S, Hanson M, et al: Longitudinal reference ranges for ductus venosus flow velocities and waveform indices. *Ultrasound Obstet Gynecol* 28:890, 2006.

**TABLE F-4 Longitudinal Reference Ranges for End-Diastolic Velocity in the Ductus Venosus Based on 547 Observations in 160 Low-Risk Pregnancies**

Gestational Age (wk)	END-DIASTOLIC VELOCITY IN DUCTUS VENOSUS (cm/sec) BY PERCENTILE								
	2.5th	5th	10th	25th	50th	75th	90th	95th	97.5th
21	15.8	18.1	20.8	25.5	31.0	36.7	42.0	45.3	48.1
22	17.1	19.4	22.2	27.0	32.5	38.3	43.6	46.9	49.8
23	18.3	20.6	23.4	28.3	33.9	39.7	45.1	48.4	51.2
24	19.3	21.7	24.5	29.4	35.1	40.9	46.3	49.6	52.5
25	20.3	22.7	25.5	30.5	36.1	42.0	47.5	50.8	53.7
26	21.1	23.5	26.4	31.4	37.1	43.0	48.4	51.8	54.7
27	21.8	24.3	27.2	32.1	37.9	43.8	49.3	52.7	55.6
28	22.5	24.9	27.8	32.8	38.6	44.6	50.1	53.4	56.4
29	23.0	25.5	28.4	33.5	39.3	45.2	50.8	54.1	57.1
30	23.5	26.0	29.0	34.0	39.8	45.8	51.4	54.7	57.7
31	24.0	26.5	29.4	34.5	40.3	46.3	51.9	55.3	58.2
32	24.4	26.9	29.8	34.9	40.8	46.8	52.3	55.7	58.7
33	24.7	27.2	30.2	35.3	41.1	47.2	52.7	56.1	59.1
34	25.0	27.5	30.5	35.6	41.5	47.5	53.1	56.5	59.5
35	25.3	27.8	30.8	35.9	41.7	47.8	53.4	56.8	59.8
36	25.5	28.0	31.0	36.1	42.0	48.0	53.6	57.1	60.1
37	25.7	28.2	31.2	36.3	42.2	48.3	53.9	57.3	60.3
38	25.8	28.4	31.3	36.5	42.4	48.4	54.0	57.5	60.5
39	25.9	28.5	31.5	36.6	42.5	48.6	54.2	57.6	60.6

From Kessler J, Rasmussen S, Hanson M, et al: Longitudinal reference ranges for ductus venosus flow velocities and waveform indices. *Ultrasound Obstet Gynecol* 28:890, 2006.

**TABLE F-5 Normal Echocardiographic Values for Fetal Cardiovascular Structures**

Gestational Age (wk)	TRICUSPID ANNULUS RIGHT-LEFT DIAMETER (cm)		
	2.5%	50.0%	97.5%
16	0.242	0.312	0.381
17	0.274	0.355	0.436
18	0.306	0.398	0.491
19	0.338	0.442	0.546
20	0.369	0.485	0.601
21	0.401	0.528	0.655
22	0.433	0.572	0.710
23	0.465	0.615	0.765
24	0.496	0.658	0.820
25	0.528	0.702	0.875
26	0.560	0.745	0.930
27	0.592	0.788	0.985
28	0.623	0.832	1.040
29	0.655	0.875	1.095
30	0.687	0.918	1.150
31	0.719	0.962	1.205
32	0.751	1.005	1.260
33	0.782	1.048	1.315
34	0.814	1.092	1.369
35	0.846	1.135	1.424
36	0.878	1.178	1.479
37	0.909	1.222	1.534
38	0.941	1.265	1.589
39	0.973	1.308	1.644
40	1.005	1.352	1.699

Mean = 0.04334 \* GA - 0.38183  
SD = -0.05801 + 0.00579 \* GA

Gestational Age (wk)	MITRAL ANNULUS RIGHT-LEFT DIAMETER (cm)		
	2.5%	50.0%	97.5%
16	0.242	0.347	0.452
17	0.272	0.382	0.491
18	0.303	0.416	0.530
19	0.333	0.451	0.570
20	0.363	0.486	0.609
21	0.394	0.521	0.648
22	0.424	0.556	0.687
23	0.454	0.591	0.727
24	0.485	0.625	0.766
25	0.515	0.660	0.805
26	0.546	0.695	0.844
27	0.576	0.730	0.884
28	0.606	0.765	0.923
29	0.637	0.799	0.962
30	0.667	0.834	1.001
31	0.697	0.869	1.041
32	0.728	0.904	1.080
33	0.758	0.939	1.119
34	0.789	0.974	1.158
35	0.819	1.008	1.198
36	0.849	1.043	1.237
37	0.880	1.078	1.276
38	0.910	1.113	1.315
39	0.941	1.148	1.355
40	0.971	1.182	1.394

Mean = 0.03482 \* GA - 0.21035  
SD = 0.01698 + 0.00222 \* GA

Gestational Age (wk)	PULMONARY ANNULUS DIAMETER (cm)		
	2.5%	50.0%	97.5%
16	0.190	0.251	0.313
17	0.214	0.282	0.350
18	0.239	0.313	0.387
19	0.263	0.343	0.424
20	0.287	0.374	0.461
21	0.312	0.405	0.498
22	0.336	0.436	0.535
23	0.360	0.466	0.572
24	0.385	0.497	0.609
25	0.409	0.528	0.647
26	0.434	0.559	0.684
27	0.458	0.589	0.721
28	0.482	0.620	0.758
29	0.507	0.651	0.795
30	0.531	0.682	0.832
31	0.556	0.712	0.869
32	0.580	0.743	0.906
33	0.604	0.774	0.943
34	0.629	0.805	0.980
35	0.653	0.835	1.018
36	0.677	0.866	1.055
37	0.702	0.897	1.092
38	0.726	0.927	1.129
39	0.751	0.958	1.166
40	0.775	0.989	1.203

Mean = 0.03074 \* GA - 0.24064  
SD = -0.02018 + 0.00318 \* GA

Gestational Age (wk)	MAIN PULMONARY ARTERY DIAMETER (cm)		
	2.5%	50.0%	97.5%
16	0.188	0.255	0.321
17	0.214	0.290	0.365
18	0.241	0.325	0.409
19	0.267	0.360	0.453
20	0.293	0.395	0.497
21	0.320	0.430	0.541
22	0.346	0.466	0.585
23	0.372	0.501	0.629
24	0.399	0.536	0.673
25	0.425	0.571	0.717
26	0.451	0.606	0.761
27	0.478	0.641	0.805
28	0.504	0.676	0.849
29	0.530	0.712	0.893
30	0.557	0.747	0.937
31	0.583	0.782	0.981
32	0.609	0.817	1.025
33	0.636	0.852	1.069
34	0.662	0.887	1.112
35	0.689	0.922	1.156
36	0.715	0.958	1.200
37	0.741	0.993	1.244
38	0.768	1.028	1.288
39	0.794	1.063	1.332
40	0.820	1.098	1.376

Mean = 0.03515 \* GA - 0.30778  
SD = -0.03702 + 0.0044 \* GA



**TABLE F-5 Normal Echocardiographic Values for Fetal Cardiovascular Structures—cont'd**

Gestational Age (wk)	RIGHT PULMONARY ARTERY DIAMETER (cm)		
	2.5%	50.0%	97.5%
16	0.096	0.123	0.150
17	0.108	0.141	0.174
18	0.121	0.159	0.197
19	0.133	0.177	0.221
20	0.146	0.195	0.244
21	0.158	0.213	0.268
22	0.171	0.231	0.292
23	0.183	0.249	0.315
24	0.196	0.267	0.339
25	0.208	0.285	0.363
26	0.220	0.303	0.386
27	0.233	0.321	0.410
28	0.245	0.339	0.433
29	0.258	0.357	0.457
30	0.270	0.376	0.481
31	0.283	0.394	0.504
32	0.295	0.412	0.528
33	0.308	0.430	0.551
34	0.320	0.448	0.575
35	0.333	0.466	0.599
36	0.345	0.484	0.622
37	0.358	0.502	0.646
38	0.370	0.520	0.669
39	0.383	0.538	0.693
40	0.395	0.556	0.717

Mean = 0.01805 \* GA - 0.166  
SD = -0.03087 + 0.00278 \* GA

Gestational Age (wk)	LEFT PULMONARY ARTERY DIAMETER (cm)		
	2.5%	50.0%	97.5%
16	0.018	0.124	0.230
17	0.030	0.141	0.251
18	0.043	0.158	0.273
19	0.055	0.175	0.295
20	0.068	0.192	0.317
21	0.080	0.209	0.338
22	0.092	0.226	0.360
23	0.105	0.243	0.382
24	0.117	0.260	0.403
25	0.130	0.278	0.425
26	0.142	0.295	0.447
27	0.155	0.312	0.469
28	0.167	0.329	0.490
29	0.180	0.346	0.512
30	0.192	0.363	0.534
31	0.205	0.380	0.556
32	0.217	0.397	0.577
33	0.229	0.414	0.599
34	0.242	0.431	0.621
35	0.254	0.449	0.643
36	0.267	0.466	0.664
37	0.279	0.483	0.686
38	0.292	0.500	0.708
39	0.304	0.517	0.730
40	0.317	0.534	0.751

Mean = 0.0171 \* GA - 0.15  
SD = 0.01585 + 0.00232 \* GA

Gestational Age (wk)	AORTIC ANNULUS DIAMETER (cm)		
	2.5%	50.0%	97.5%
16	0.159	0.215	0.270
17	0.179	0.239	0.299
18	0.199	0.263	0.327
19	0.219	0.287	0.355
20	0.239	0.311	0.383
21	0.259	0.336	0.412
22	0.279	0.360	0.440
23	0.299	0.384	0.468
24	0.320	0.408	0.497
25	0.340	0.432	0.525
26	0.360	0.456	0.553
27	0.380	0.480	0.581
28	0.400	0.505	0.610
29	0.420	0.529	0.638
30	0.440	0.553	0.666
31	0.460	0.577	0.694
32	0.480	0.601	0.723
33	0.500	0.625	0.751
34	0.520	0.650	0.779
35	0.540	0.674	0.807
36	0.560	0.698	0.836
37	0.580	0.722	0.864
38	0.600	0.746	0.892
39	0.620	0.770	0.921
40	0.640	0.794	0.949

Mean = 0.02415 \* GA - 0.17158  
SD = -0.00519 + 0.00206 \* GA

Gestational Age (wk)	AORTIC ROOT DIAMETER (cm)		
	2.5%	50.0%	97.5%
16	0.211	0.307	0.404
17	0.233	0.329	0.425
18	0.255	0.351	0.447
19	0.276	0.372	0.468
20	0.298	0.394	0.489
21	0.320	0.416	0.511
22	0.342	0.437	0.532
23	0.363	0.459	0.554
24	0.385	0.480	0.576
25	0.407	0.502	0.597
26	0.428	0.524	0.619
27	0.450	0.545	0.641
28	0.472	0.567	0.662
29	0.493	0.589	0.684
30	0.515	0.610	0.706
31	0.536	0.632	0.728
32	0.557	0.653	0.749
33	0.579	0.675	0.771
34	0.600	0.697	0.793
35	0.622	0.718	0.815
36	0.643	0.740	0.837
37	0.664	0.762	0.859
38	0.685	0.783	0.881
39	0.707	0.805	0.903
40	0.728	0.826	0.925

Mean = 0.02163 \* GA - 0.03873  
SD = SQRT (0.00224 \* (1 + (1/83) + (((GA - 24.99)<sup>2</sup>)/2945)))

**TABLE F-5 Normal Echocardiographic Values for Fetal Cardiovascular Structures—cont'd**

Gestational Age (wk)	ASCENDING AORTA DIAMETER (cm)		
	2.5%	50.0%	97.5%
16	0.183	0.260	0.338
17	0.203	0.284	0.366
18	0.223	0.308	0.394
19	0.243	0.333	0.422
20	0.263	0.357	0.450
21	0.283	0.381	0.479
22	0.303	0.405	0.507
23	0.323	0.429	0.535
24	0.343	0.453	0.563
25	0.363	0.477	0.592
26	0.383	0.502	0.620
27	0.403	0.526	0.648
28	0.423	0.550	0.676
29	0.443	0.574	0.705
30	0.463	0.598	0.733
31	0.483	0.622	0.761
32	0.503	0.646	0.789
33	0.523	0.670	0.817
34	0.543	0.695	0.846
35	0.563	0.719	0.874
36	0.583	0.743	0.902
37	0.603	0.767	0.930
38	0.624	0.791	0.959
39	0.644	0.815	0.987
40	0.664	0.839	1.015

Mean = 0.02413 \* GA - 0.12588  
SD = 0.00587 + 0.00205 \* GA

Gestational Age (wk)	AORTIC ISTHMUS DIAMETER (cm)		
	2.5%	50.0%	97.5%
16	0.124	0.198	0.272
17	0.137	0.213	0.289
18	0.150	0.228	0.306
19	0.164	0.244	0.323
20	0.177	0.259	0.341
21	0.191	0.274	0.358
22	0.204	0.290	0.375
23	0.217	0.305	0.392
24	0.231	0.320	0.410
25	0.244	0.335	0.427
26	0.258	0.351	0.444
27	0.271	0.366	0.461
28	0.284	0.381	0.479
29	0.298	0.397	0.496
30	0.311	0.412	0.513
31	0.324	0.427	0.530
32	0.338	0.443	0.548
33	0.351	0.458	0.565
34	0.365	0.473	0.582
35	0.378	0.489	0.599
36	0.391	0.504	0.617
37	0.405	0.519	0.634
38	0.418	0.535	0.651
39	0.431	0.550	0.668
40	0.445	0.565	0.686

Mean = 0.01532 \* GA - 0.04751  
SD = 0.02143 + 0.00097 \* GA

Gestational Age (wk)	TRANSVERSE ARCH DIAMETER (cm)		
	2.5%	50.0%	97.5%
16	0.137	0.223	0.308
17	0.154	0.241	0.329
18	0.170	0.260	0.350
19	0.187	0.279	0.371
20	0.203	0.297	0.391
21	0.219	0.316	0.412
22	0.236	0.334	0.433
23	0.252	0.353	0.453
24	0.269	0.371	0.474
25	0.285	0.390	0.495
26	0.302	0.408	0.515
27	0.318	0.427	0.536
28	0.334	0.446	0.557
29	0.351	0.464	0.577
30	0.367	0.483	0.598
31	0.384	0.501	0.619
32	0.400	0.520	0.639
33	0.416	0.538	0.660
34	0.433	0.557	0.681
35	0.449	0.575	0.702
36	0.466	0.594	0.722
37	0.482	0.612	0.743
38	0.498	0.631	0.764
39	0.515	0.650	0.784
40	0.531	0.668	0.805

Mean = 0.01855 \* GA - 0.07386  
SD = 0.02563 + 0.00107 \* GA

Gestational Age (wk)	DESCENDING AORTA DIAMETER (cm)		
	2.5%	50.0%	97.5%
16	0.142	0.236	0.331
17	0.163	0.257	0.351
18	0.184	0.278	0.372
19	0.205	0.299	0.393
20	0.226	0.320	0.413
21	0.247	0.341	0.434
22	0.268	0.361	0.455
23	0.289	0.382	0.476
24	0.310	0.403	0.496
25	0.331	0.424	0.517
26	0.351	0.445	0.538
27	0.372	0.466	0.559
28	0.393	0.486	0.580
29	0.414	0.507	0.601
30	0.434	0.528	0.622
31	0.455	0.549	0.643
32	0.476	0.570	0.664
33	0.496	0.591	0.685
34	0.517	0.611	0.706
35	0.537	0.632	0.727
36	0.558	0.653	0.748
37	0.578	0.674	0.770
38	0.599	0.695	0.791
39	0.619	0.716	0.812
40	0.640	0.737	0.833

Mean = 0.02084 \* GA - 0.09708  
SD = SQRT (0.00215 \* (1 + (1/88)) + (((GA - 24.81)²)/2958))



**TABLE F-5 Normal Echocardiographic Values for Fetal Cardiovascular Structures—cont'd**

Gestational Age (wk)	AORTIC/PULMONARY VALVE ANNULUS DIAMETER RATIO		
	2.5%	50.0%	97.5%
16	0.638	0.844	1.049
17	0.635	0.842	1.048
18	0.632	0.839	1.047
19	0.629	0.837	1.046
20	0.626	0.835	1.044
21	0.623	0.833	1.043
22	0.620	0.831	1.042
23	0.617	0.829	1.041
24	0.614	0.827	1.039
25	0.611	0.824	1.038
26	0.608	0.822	1.037
27	0.605	0.820	1.036
28	0.601	0.818	1.034
29	0.598	0.816	1.033
30	0.595	0.814	1.032
31	0.592	0.812	1.031
32	0.589	0.809	1.029
33	0.586	0.807	1.028
34	0.583	0.805	1.027
35	0.580	0.803	1.026
36	0.577	0.801	1.024
37	0.574	0.799	1.023
38	0.571	0.796	1.022
39	0.568	0.794	1.021
40	0.565	0.792	1.019

Mean =  $-0.00215 * GA + 0.87816$   
 SD =  $0.09565 + 0.00045 * GA$

Gestational Age (wk)	LEFT VENTRICULAR RIGHT-LEFT SHORT-AXIS DIMENSION (cm)		
	2.5%	50.0%	97.5%
16	0.060	0.437	0.813
17	0.105	0.497	0.889
18	0.149	0.557	0.964
19	0.193	0.616	1.040
20	0.237	0.676	1.115
21	0.281	0.736	1.191
22	0.325	0.796	1.266
23	0.369	0.856	1.342
24	0.414	0.915	1.417
25	0.458	0.975	1.493
26	0.502	1.035	1.568
27	0.546	1.095	1.644
28	0.590	1.155	1.719
29	0.634	1.215	1.795
30	0.678	1.274	1.870
31	0.722	1.334	1.946
32	0.767	1.394	2.021
33	0.811	1.454	2.097
34	0.855	1.514	2.172
35	0.899	1.573	2.248
36	0.943	1.633	2.323
37	0.987	1.693	2.399
38	1.031	1.753	2.474
39	1.075	1.813	2.550
40	1.120	1.872	2.625

Mean =  $0.05981 * GA - 0.51997$   
 SD =  $0.06281 + 0.00784 * GA$

Gestational Age (wk)	LEFT VENTRICULAR LONG-AXIS DIMENSION (cm)		
	2.5%	50.0%	97.5%
16	0.743	0.974	1.204
17	0.816	1.069	1.322
18	0.888	1.164	1.440
19	0.961	1.260	1.559
20	1.033	1.355	1.677
21	1.106	1.451	1.796
22	1.178	1.546	1.914
23	1.250	1.641	2.032
24	1.323	1.737	2.151
25	1.395	1.832	2.269
26	1.468	1.928	2.388
27	1.540	2.023	2.506
28	1.613	2.118	2.624
29	1.685	2.214	2.743
30	1.757	2.309	2.861
31	1.830	2.405	2.980
32	1.902	2.500	3.098
33	1.975	2.595	3.216
34	2.047	2.691	3.335
35	2.120	2.786	3.453
36	2.192	2.882	3.571
37	2.264	2.977	3.690
38	2.337	3.073	3.808
39	2.409	3.168	3.927
40	2.482	3.263	4.045

Mean =  $0.09541 * GA - 0.55304$   
 SD =  $-0.06876 + 0.01149 * GA$

Gestational Age (wk)	RIGHT VENTRICULAR LONG-AXIS DIMENSION (cm)		
	2.5%	50.0%	97.5%
16	0.582	0.834	1.086
17	0.659	0.929	1.198
18	0.736	1.024	1.311
19	0.814	1.119	1.424
20	0.891	1.214	1.537
21	0.968	1.309	1.650
22	1.046	1.404	1.763
23	1.123	1.499	1.876
24	1.200	1.595	1.989
25	1.278	1.690	2.102
26	1.355	1.785	2.215
27	1.432	1.880	2.328
28	1.509	1.975	2.441
29	1.587	2.070	2.554
30	1.664	2.165	2.666
31	1.741	2.260	2.779
32	1.819	2.356	2.892
33	1.896	2.451	3.005
34	1.973	2.546	3.118
35	2.051	2.641	3.231
36	2.128	2.736	3.344
37	2.205	2.831	3.457
38	2.283	2.926	3.570
39	2.360	3.021	3.683
40	2.437	3.116	3.796

Mean =  $0.09512 * GA - 0.68831$   
 SD =  $-0.01642 + 0.0089 * GA$

**TABLE F-5 Normal Echocardiographic Values for Fetal Cardiovascular Structures—cont'd**

Gestational Age (wk)	RIGHT VENTRICULAR SHORT-AXIS RIGHT-LEFT DIAMETER (cm)		
	2.5%	50.0%	97.5%
16	0.311	0.442	0.574
17	0.356	0.499	0.643
18	0.401	0.556	0.711
19	0.446	0.613	0.780
20	0.492	0.670	0.848
21	0.537	0.727	0.917
22	0.582	0.784	0.985
23	0.627	0.841	1.054
24	0.673	0.898	1.123
25	0.718	0.954	1.191
26	0.763	1.011	1.260
27	0.808	1.068	1.328
28	0.853	1.125	1.397
29	0.899	1.182	1.466
30	0.944	1.239	1.534
31	0.989	1.296	1.603
32	1.034	1.353	1.671
33	1.080	1.410	1.740
34	1.125	1.467	1.809
35	1.170	1.524	1.877
36	1.215	1.581	1.946
37	1.261	1.637	2.014
38	1.306	1.694	2.083
39	1.351	1.751	2.151
40	1.396	1.808	2.220

Mean = 0.05691 \* GA - 0.46826

SD = -0.02763 + 0.00584 \* GA

Courtesy Steven D. Colan, MD, Cardiology, Boston Children's Hospital.

**TABLE F-6 Average ( $\pm$  Standard Deviation) Values for Each Measure of Myocardial Deformation and for Myocardial Performance Indices**

Gestational Age (wk)	CS-LV (%)	CSr-LV (s <sup>-1</sup> )	LS-LV (%)	LSr-LV (s <sup>-1</sup> )	LS-RV(%)	LSr-RV (s <sup>-1</sup> )	LV MPI	RV MPI	HR
20-21 (N = 59)	-20.42 $\pm$ 4.45	-2.46 $\pm$ 0.60	-19.61 $\pm$ 3.71	-2.15 $\pm$ 0.60	-18.82 $\pm$ 3.13	-2.04 $\pm$ 0.70	0.31 $\pm$ 0.10	0.31 $\pm$ 0.10	146 $\pm$ 9
24-25 (N = 56)	-19.34 $\pm$ 4.30	-2.16 $\pm$ 0.40	-20.08 $\pm$ 2.66	-2.03 $\pm$ 0.43	-18.16 $\pm$ 2.95	-1.78 $\pm$ 0.41	0.29 $\pm$ 0.10	0.29 $\pm$ 0.11	144 $\pm$ 9
28-29 (N = 53)	-19.97 $\pm$ 3.50	-2.21 $\pm$ 0.52	-20.95 $\pm$ 2.92	-2.00 $\pm$ 0.41	-19.47 $\pm$ 2.93	-1.78 $\pm$ 0.41	0.28 $\pm$ 0.10	0.30 $\pm$ 0.17	141 $\pm$ 11
32-33 (N = 52)	-19.56 $\pm$ 3.48	-2.14 $\pm$ 0.40	-20.40 $\pm$ 3.13	-1.88 $\pm$ 0.37	-19.30 $\pm$ 2.75	-1.68 $\pm$ 0.37	0.34 $\pm$ 0.12	0.33 $\pm$ 0.10	138 $\pm$ 10
36-37 (N = 52)	-18.99 $\pm$ 4.12	-2.11 $\pm$ 0.48	-21.13 $\pm$ 2.90	-1.98 $\pm$ 0.40	-19.54 $\pm$ 2.56	-1.68 $\pm$ 0.33	0.32 $\pm$ 0.12	0.33 $\pm$ 0.09	138 $\pm$ 13
Postnatal (N = 53)	-17.83 $\pm$ 3.18	-1.72 $\pm$ 0.34	-19.98 $\pm$ 2.87	-1.57 $\pm$ 0.30	-24.68 $\pm$ 3.90	-2.08 $\pm$ 0.28	0.33 $\pm$ 0.11	0.20 $\pm$ 0.09	147 $\pm$ 14

CS-LV, global circumferential strain, left ventricle; CSr-LV, global circumferential strain rate, left ventricle; HR, heart rate; LS-LV, global longitudinal strain, left ventricle; LSr-LV, global longitudinal strain rate, left ventricle; LSr-RV, global longitudinal strain rate, right ventricle; LV MPI, left ventricular myocardial performance index; RV MPI, right ventricular myocardial performance index.

From Longitudinal changes and interobserver variability of systolic myocardial deformation values in a prospective cohort of healthy fetuses across gestation and after delivery. J Am Soc Echocardiogr 29:341-349, 2016.



**TABLE F-7 Average ( $\pm$  Standard Deviation) Values for Each Measure of Diastolic Strain Rate and E/A Ratios**

Gestational Age (wk)	CSr-LVe (s <sup>-1</sup> )	CSr-LVa (s <sup>-1</sup> )	LSr-LVe (s <sup>-1</sup> )	LSr-LVa (s <sup>-1</sup> )	LSr-RVe (s <sup>-1</sup> )	LSr-RVa (s <sup>-1</sup> )	MV E/A	TV E/A
20-21 (N = 59)	2.93 $\pm$ 1.04	2.22 $\pm$ 0.92	2.56 $\pm$ 1.00	2.40 $\pm$ 1.01 <sup>†</sup>	2.37 $\pm$ 0.76 <sup>†</sup>	2.13 $\pm$ 1.04	0.62 $\pm$ 0.12 <sup>†</sup>	0.63 $\pm$ 0.06
24-25 (N = 56)	2.60 $\pm$ 0.84	1.84 $\pm$ 0.91*	2.34 $\pm$ 0.66	2.28 $\pm$ 0.70	2.33 $\pm$ 0.74 <sup>†</sup>	2.00 $\pm$ 0.80 <sup>†</sup>	0.66 $\pm$ 0.10 <sup>†</sup>	0.65 $\pm$ 0.15 <sup>†</sup>
28-29 (N = 53)	2.39 $\pm$ 0.73*	1.49 $\pm$ 0.50*	2.49 $\pm$ 0.67	2.20 $\pm$ 0.63	2.37 $\pm$ 0.64 <sup>†</sup>	2.15 $\pm$ 0.66	0.66 $\pm$ 0.13 <sup>†</sup>	0.69 $\pm$ 0.19 <sup>†</sup>
32-33 (N = 52)	2.31 $\pm$ 0.70*	1.52 $\pm$ 0.62*	2.41 $\pm$ 0.67*	1.94 $\pm$ 0.51*	2.20 $\pm$ 0.57 <sup>†</sup>	1.81 $\pm$ 0.47 <sup>†</sup>	0.75 $\pm$ 0.12 <sup>†</sup>	0.70 $\pm$ 0.18*
36-38 (N = 52)	2.21 $\pm$ 0.84* <sup>†</sup>	1.35 $\pm$ 0.63*	2.33 $\pm$ 0.66*	1.87 $\pm$ 0.51*	1.98 $\pm$ 0.53 <sup>†</sup>	1.90 $\pm$ 0.46 <sup>†</sup>	0.76 $\pm$ 0.12 <sup>†</sup>	0.68 $\pm$ 0.22*
Postnatal (N = 53)	2.76 $\pm$ 0.63	1.53 $\pm$ 0.58*	2.65 $\pm$ 0.51*	1.91 $\pm$ 0.62*	3.09 $\pm$ 0.96	2.41 $\pm$ 0.89	1.05 $\pm$ 0.21	0.78 $\pm$ 0.18*

\*Intercept variance.

<sup>†</sup>Error variance.

CSr-LVa, global circumferential late peak left ventricular strain rate; CSr-LVe, global circumferential early peak left ventricular strain rate; LSr-LVa, global longitudinal late peak left ventricular diastolic strain rate; LSr-LVe, global longitudinal early peak left ventricular diastolic strain rate; LSr-RVa, global longitudinal late peak right ventricular diastolic strain rate; LSr-RVe, global longitudinal early peak right ventricular diastolic strain rate; MV E/A, mitral Doppler inflow pattern E to A ratio; TV E/A, tricuspid Doppler inflow pattern E to A ratio.

From Fetal and neonatal diastolic myocardial strain rate: normal reference ranges and reproducibility in a prospective, longitudinal cohort of pregnancies. J Am Soc Echocardiogr 2016 Apr 1. pii: S0894-7317(16)00165-6.

**TABLE F-8 Mathematical Equations for the Expected Values and Variances of Myocardial Deformation and for Myocardial Performance Indices**

Parameter (P)	Expected Value of (P)	Variance of (P)
CSr-LV	$-4.6496 + (0.1561 \times GA) + (-0.0024 \times GA^2)$	$0.03878^a + 0.2381^b$
GLSLV	$-17.9329 + (-0.08745 \times GA)$	$0.07613^a + 9.4234^b$
LSr-LV	$-2.3898 + (0.01351 \times GA)$	$0.04^a + 0.1672^b$
LSr-RV	$-16.7401 + (-0.07918 \times GA)$	$0.1527^a + 10.2806^b$
LSr-RV	$-2.4008 + (0.02134 \times GA)$	$0.005139^a + 0.2176^b$
RV MPI*	$-1.4526 + (0.008281 \times GA)$	$0.01753^a + 0.1051^b$
LV MPI*	$-1.39 + (0.004916 \times GA)$	$0.03726^a + 0.1074^b$

<sup>a</sup>Intercept variance.<sup>b</sup>Error variance.\*The equation provides the expected value of log<sub>e</sub> (P).

GA, gestational age; GCS, global circumferential strain; GCSr, global circumferential strain rate; GLSLV, global longitudinal strain, left ventricle; GLSLV, global longitudinal strain rate, left ventricle; GLSLRV, global longitudinal strain rate, right ventricle; GLSRV, global longitudinal strain, right ventricle; LV MPI, left ventricular myocardial performance index; RV MPI, right ventricular myocardial performance index.

From Longitudinal changes and interobserver variability of systolic myocardial deformation values in a prospective cohort of healthy fetuses across gestation and after delivery. J Am Soc Echocardiogr 29:341-349, 2016.

**TABLE F-9 Mathematical Equations for the Expected Values and Variances of Diastolic Strain Rate and E/A Ratio Measurements by Gestational Age**

Parameter (P)	Expected Value of Log <sub>e</sub> (P)	Variance of Log <sub>e</sub> (P)
CSr-LVe	$1.3702 + (-0.01809 \times GA)$	$0.008835^a + 0.09989^b$
CSr-LVa	$1.2356 + (-0.02862 \times GA)$	$0.008908^a + 0.2102^b$
LSr-LVe	$0.9570 + (-0.00389 \times GA)$	$0.004639^a + 0.07606^b$
LSr-LVa	$1.1122 + (-0.01436 \times GA)$	$0.008844^a + 0.1164^b$
LSr-RVe	$1.0426 + (-0.00964 \times GA)$	$0.01355^a + 0.06866^b$
LSr-RVa	$0.7718 + (-0.00485 \times GA)$	$0.005965^a + 0.1248^b$
MV E/A	$-0.7702 + (0.01378 \times GA)$	$0.006462^a + 0.03864^b$
TV E/A	$-0.6518 + (0.009869 \times GA)$	$0.003489^a + 0.01483^b$

<sup>a</sup>Intercept variance.<sup>b</sup>Error variance.

CSr-LVa, global circumferential late peak left ventricular strain rate; CSr-LVe, global circumferential early peak left ventricular strain rate; GA, gestational age in weeks; LSr-LVa, global longitudinal late peak left ventricular diastolic strain rate; LSr-LVe, global longitudinal early peak left ventricular diastolic strain rate; LSr-RVa, global longitudinal late peak right ventricular diastolic strain rate; LSr-RVe, global longitudinal early peak right ventricular diastolic strain rate; MV E/A, mitral Doppler inflow pattern E to A ratio; TV E/A, tricuspid Doppler inflow pattern E to A ratio.

From Fetal and neonatal diastolic myocardial strain rate: normal reference ranges and reproducibility in a prospective, longitudinal cohort of pregnancies. J Am Soc Echocardiogr 2016 Apr 1. pii: S0894-7317(16)00165-6.

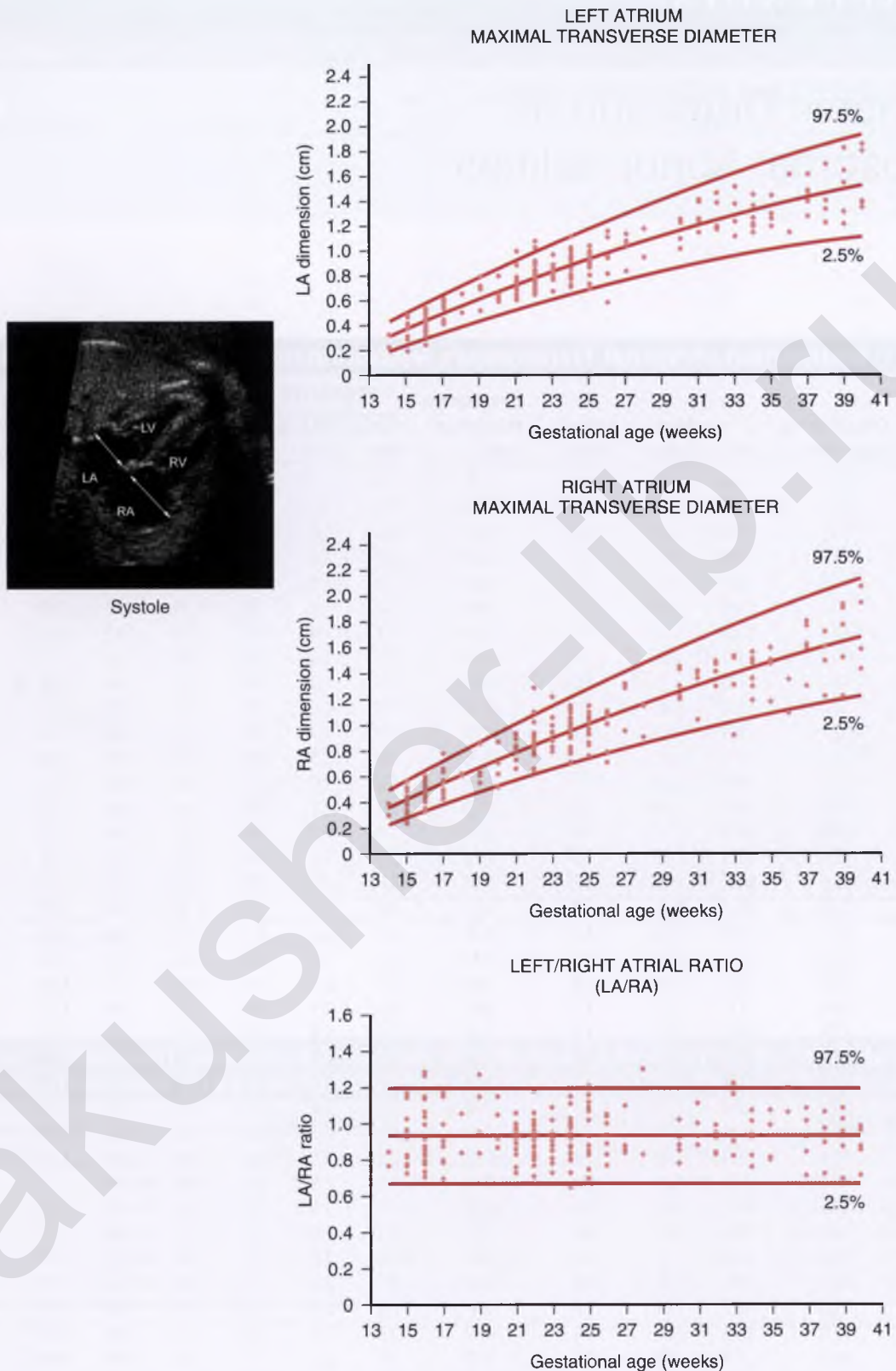


**FIG F-1** Left atrial (LA) and right atrial (RA) dimensions and LA/RA ratio. Measurements should be taken from a systolic four-chamber view. (Modified from Shapiro I, Degani S, Leibovitz Z, et al: Fetal cardiac measurements derived by transvaginal and transabdominal cross-sectional echocardiography from 14 weeks of gestation to term. *Ultrasound Obstet Gynecol* 12:404, 1998, used with permission. Figure by Shi-Joon Yoo, MD, The Hospital for Sick Children, Toronto, Canada.)



## Sonographic Detection of Chromosomal Abnormalities

**TABLE G-1 Distribution of Nuchal Translucency Measurements by Crown-Rump Length**

Crown-Rump Length (mm)	Gestational Age (wk)	N	Mean (mm)	Median (mm)	Standard Deviation (mm)	PERCENTILE CUTPOINT (mm)			PERCENTILE CUTPOINT (MoM)			Percentile Equivalent at 3.5 mm
						90th	95th	99th	90th	95th	99th	
45.0	11.3	404	1.17	1.1	0.31	1.5	1.7	2.0	1.31	1.42	1.82	99.8
46.0	11.4	620	1.22	1.2	0.38	1.6	1.8	2.9	1.37	1.58	2.45	99.6
47.0	11.5	667	1.21	1.2	0.33	1.6	1.8	2.2	1.30	1.44	2.02	99.8
48.0	11.6	796	1.26	1.2	0.39	1.7	1.9	2.9	1.35	1.55	2.32	99.6
49.0	11.7	853	1.25	1.2	0.33	1.6	1.8	2.5	1.28	1.45	1.90	99.8
50.0	11.7	1048	1.29	1.2	0.36	1.7	1.8	2.6	1.34	1.49	2.08	99.7
51.0	11.8	1256	1.31	1.2	0.38	1.7	1.9	2.8	1.34	1.53	2.17	99.8
52.0	11.9	1401	1.31	1.3	0.30	1.7	1.8	2.3	1.29	1.40	1.71	99.9
53.0	12.0	1783	1.35	1.3	0.39	1.7	1.9	2.6	1.32	1.44	1.98	99.7
54.0	12.0	1919	1.37	1.3	0.34	1.8	2.0	2.4	1.33	1.47	1.83	99.8
55.0	12.1	2089	1.41	1.4	0.42	1.8	2.0	2.6	1.32	1.46	2.02	99.6
56.0	12.2	2247	1.42	1.4	0.36	1.8	2.0	2.6	1.33	1.45	1.89	99.7
57.0	12.3	2439	1.44	1.4	0.35	1.8	2.0	2.5	1.33	1.46	1.85	99.9
58.0	12.3	2695	1.48	1.4	0.39	1.9	2.1	2.6	1.35	1.48	1.92	99.6
59.0	12.4	2831	1.51	1.5	0.42	1.9	2.1	2.8	1.35	1.49	1.93	99.6
60.0	12.5	3011	1.54	1.5	0.39	2.0	2.2	2.7	1.38	1.50	1.98	99.7
61.0	12.6	3050	1.55	1.5	0.37	2.0	2.2	2.6	1.35	1.50	1.79	99.8
62.0	12.6	3185	1.57	1.5	0.37	2.0	2.2	2.8	1.36	1.48	1.91	99.8
63.0	12.7	3156	1.60	1.5	0.38	2.1	2.3	2.7	1.35	1.48	1.85	99.8
64.0	12.8	3217	1.62	1.6	0.41	2.1	2.3	2.8	1.38	1.51	1.81	99.8
65.0	12.8	3125	1.64	1.6	0.39	2.1	2.3	2.8	1.35	1.47	1.83	99.7
66.0	12.9	3171	1.67	1.6	0.42	2.2	2.4	2.9	1.37	1.50	1.91	99.6
67.0	13.0	3083	1.69	1.6	0.42	2.2	2.4	2.8	1.37	1.51	1.81	99.7
68.0	13.1	2872	1.70	1.7	0.40	2.2	2.4	2.8	1.35	1.50	1.76	99.9
69.0	13.1	2779	1.72	1.7	0.41	2.2	2.4	2.9	1.35	1.46	1.80	99.8
70.0	13.2	2662	1.74	1.7	0.40	2.2	2.4	2.9	1.35	1.46	1.78	99.8
71.0	13.3	2483	1.79	1.7	0.41	2.3	2.5	3.0	1.37	1.48	1.77	99.7
72.0	13.4	2337	1.78	1.7	0.43	2.3	2.5	3.0	1.34	1.48	1.79	99.7
73.0	13.4	2150	1.79	1.8	0.43	2.3	2.5	2.9	1.34	1.45	1.74	99.7
74.0	13.5	2015	1.82	1.8	0.44	2.3	2.5	3.0	1.34	1.45	1.83	99.7
75.0	13.6	1920	1.80	1.8	0.43	2.3	2.5	3.1	1.31	1.49	1.75	99.7
76.0	13.7	1799	1.83	1.8	0.44	2.4	2.6	3.1	1.30	1.42	1.75	99.6
77.0	13.8	1542	1.85	1.8	0.45	2.4	2.6	3.3	1.30	1.43	1.75	99.4
78.0	13.8	1477	1.81	1.8	0.44	2.4	2.5	3.1	1.29	1.42	1.73	99.5
79.0	13.9	1215	1.85	1.8	0.47	2.4	2.5	3.0	1.27	1.38	1.65	99.7
80.0	14.0	778	1.84	1.8	0.43	2.4	2.7	3.1	1.27	1.39	1.69	99.8
81.0	14.1	625	1.86	1.8	0.45	2.4	2.7	3.2	1.24	1.39	1.67	99.6
82.0	14.2	592	1.86	1.8	0.45	2.4	2.6	3.3	1.23	1.33	1.66	99.4
83.0	14.2	611	1.85	1.8	0.44	2.4	2.6	2.8	1.18	1.27	1.47	99.8
84.0	14.2	383	1.86	1.8	0.45	2.5	2.6	3.1	1.23	1.35	1.84	99.7

MoM, multiples of the median.

From Jelliffe-Pawlowski LL, Norton ME, Shaw GM, et al: Risk of critical congenital heart defects by nuchal translucency norms. Am J Obstet Gynecol 212(4):518.e1-518.e10, 2015.

**TABLE G-2 Normal Percentile Ranges for Nasal Bone Lengths (*N* = 3537) for a Specific Menstrual Age**

Gestational Age (wk)	Subjects ( <i>n</i> )	NASAL BONE LENGTHS (mm) BY PERCENTILE				
		2.5th	5th	50th	95th	97.5th
11	16	1.3	1.4	2.3	3.3	3.4
12	54	1.7	1.8	2.8	4.2	4.3
13	59	2.2	2.3	3.1	4.6	4.8
14	82	2.2	2.5	3.8	5.3	5.7
15	103	2.8	3.0	4.3	5.7	6.0
16	134	3.2	3.4	4.7	6.2	6.2
17	203	3.7	4.0	5.3	6.6	6.9
18	252	4.0	4.3	5.7	7.0	7.3
19	388	4.6	5.0	6.3	7.9	8.2
20	440	5.0	5.2	6.7	8.3	8.6
21	322	5.1	5.6	7.1	9.0	9.3
22	208	5.6	5.8	7.5	9.3	10.2
23	157	6.0	6.4	7.9	9.6	9.9
24	121	6.6	6.8	9.3	10.0	10.3
25	123	6.3	6.5	8.5	10.7	10.8
26	96	6.8	7.4	8.9	10.9	11.3
27	80	7.0	7.5	9.2	11.3	11.6
28	103	7.2	7.6	9.8	12.1	13.4
29	95	7.2	7.7	9.8	11.8	12.3
30	104	7.3	7.9	10.0	12.6	13.2
31	92	7.9	8.2	10.4	12.6	13.2
32	66	8.1	8.6	10.5	13.6	13.7
33	54	8.6	8.7	10.8	12.8	13.0
34	41	9.0	9.1	10.9	12.8	13.5
35	37	7.5	8.5	11.0	14.1	15.0
36	40	7.3	7.8	10.8	12.8	13.6
37	36	8.4	8.7	11.4	14.5	15.0
38	13	9.2	9.3	11.7	15.7	16.6
39	12	9.1	9.2	10.9	14.0	14.8
40	6	10.3	10.4	12.1	14.5	14.7

From Sonok JD, McKenna D, Webb D, et al: Nasal bone length throughout gestation: normal ranges based on 3537 fetal ultrasound measurements. *Ultrasound Obstet Gynecol* 21:152, 2003.

**TABLE G-3 Observed Number of Trisomies 21, 18, and 13 in Relation to Fetal Nuchal Translucency Thickness and Expected Number of Trisomies on the Basis of Maternal Age**

Nuchal Translucency Thickness (mm)	<i>n</i>	OBSERVED			EXPECTED BY AGE			OBSERVED/EXPECTED		
		21	18/13	21/18/13	21	18/13	21/18/13	21	18/13	21/18/13
3	383	16	7	23	4.20	1.81	6.01	3.8	3.9	3.8
4	67	16	5	21	0.71	0.31	1.02	22.5	16.0	20.6
5	41	13	7	20	0.53	0.23	0.76	24.5	30.0	26.3
≥6	69	16	22	38	0.65	0.28	0.93	24.6	78.6	40.9
Total	560	61	41	102	6.09	2.63	8.72	10.0	15.6	11.7

From Pandya PP, Beizot ML, Kuhn P, et al: First-trimester fetal nuchal translucency thickness and risk of trisomies. *Obstet Gynecol* 84:420, 1994.



**TABLE G-4 Nuchal Thickness at 14 to 24 Weeks' Gestation by Maternal Age and Prenatal Detection of Down Syndrome**

Parameter	NUCHAL SKINFOLD THICKNESS					
	5 mm		6 mm		7 mm	
	<35 y	≥35 y	<35 y	≥35 y	<35 y	≥35 y
Sensitivity	75% (6/8)	46% (11/24)	62% (5/8)	38% (9/24)	38% (3/8)	21% (5/24)
95% confidence interval	35%-97%	26%-68%	24%-91%	19%-59%	8%-75%	7%-42%
Specificity	92.3%	95.5%	98.8%	99.2%	99.7%	99.7%
Positive predictive value	1/168	1/42	1/34	1/11	1/14	1/7
Positive screens	7.8%	4.8%	1.3%	1.0%	0.3%	0.4%

From Gray DL, Crane JP: Optimal nuchal skin-fold thresholds based on gestational age for prenatal detection of Down syndrome. Am J Obstet Gynecol 171:1282, 1994.

**TABLE G-5 Common Microdeletion Syndromes**

Syndrome	Location	Frequency
Prader-Willi	15q11-13	1/10,000-1/30,000
Angelman	15q11-13	1/12,000-1/20,000
22q11.2 deletion (velocardiofacial, Di George)	22q11.2	1/4000
Smith-Magenis	17p11.2	1/15,000-1/25,000
Williams	7q11.23	1/7500
Alagille	20p12	1/30,000-1/50,000
Rubenstein-Taybi	16p13.3	1/100,000
WAGR	11p13	1/40,000
Miller-Dieker	17p13.3	1/85,000
Wolf-Hirschhorn	4p16.3	1/50,000
Cri du chat	5p15.2	1/20,000-1/50,000
Retinoblastoma	13q14.2	1/15,000-1/20,000

## Medications and Reported Associated Malformations

**TABLE H-1 Selected Medications and Reported Associated Malformations\***

Drug	Malformation(s)
Acetazolamide	Sacroccygeal teratoma
Acyclovir	CDH, neural tube defect, cleft lip, clubfoot, transposition
Alprazolam	Umbilical hernia, clubfoot
Albuterol	Cleft palate, cranioschisis, cardiovascular defect, spina bifida, polydactyly, fetal tachycardia
Amantadine	Cardiac defects
Aminopterin	Neural tube defects, hydrocephalus, limb shortening, cleft lip/palate, clubfoot
p-Aminosalicylic acid	Ear deformity, limb deformity, hypospadias
Amiodarone	FGR, ventricular septal defect, micrognathia
Amitriptyline	Limb reduction, micrognathia, hypospadias, cleft palate, thanatophoric dysplasia
Ampicillin	Transposition of the great vessels
Amobarbital	Anencephaly, cardiac defects, limb deformity, cleft lip/palate, polydactyly, genitourinary defects, clubfoot
Amphetamine	Cerebral injury in neonates
Aspirin	Intracranial hemorrhage, FGR
Atenolol	Hypospadias, cardiovascular defects
Atropine	Polydactyly, limb reduction
Azatadine	Oral cleft, limb reduction
Baclofen	Spina bifida
Belladonna	Eye/ear malformations, hypospadias
Benztropine	Cardiovascular defects
Bromides	Polydactyly, gastrointestinal anomalies, clubfoot, FGR
Busulfan	FGR, cleft palate, neural tube defects
Captopril	Second-trimester hypocalvaria, oligohydramnios, renal dysfunction
Carbamazepine	Neural tube defects, cardiac defects
Carisoprodol	Oral clefts
Cephalexin	Cardiovascular defects, oral clefts
Cephradine	Cardiovascular defects
Chlorambucil	Renal agenesis, cardiac defects
Chlordiazepoxide	Microcephaly, duodenal atresia, cardiac defects
Chloroquine	Wilms tumor, hemihypertrophy, tetralogy of Fallot
Chlorothiazide	Fetal bradycardia
Chlorpheniramine	Polydactyly, gastrointestinal defects, hydrocephalus
Chlorpromazine	Microcephaly, syndactyly
Chlorpropamide	Microcephaly, hand anomalies
Ciprofloxacin	Hypospadias, cerebellar hypoplasia, cardiovascular defect, femoral aplasia
Clarithromycin	Craniofacial abnormalities, absent clavicles, spina bifida, cleft lip, pulmonary hypoplasia; coloboma, heart anomaly, choanal atresia, retardation (mental and somatic), genital and ear anomalies (CHARGE) association
Clomiphene	Microcephaly, neural tube defects, cleft lip/palate, cardiac defects, syndactyly, clubfoot, hypospadias
Clonazepam	Cardiovascular defects
Clorazepate	Bifid foot, absent scrotum, short femur, absent fibula, absent metacarpal bones, renal agenesis
Cloxacillin	Cardiovascular defects
Cocaine	Spontaneous abortion, placental abruption, cardiac defects, urinary tract and limb abnormalities, bowel atresias, FGR
Codeine	Pulmonary and genitourinary defects, hydrocephalus, cleft lip/palate
Colchicine	Cardiac malformation, syndactyly, cleft palate
Cortisone	Cataracts, cyclopia, VSD, coarctation of the aorta, clubfoot, cleft lip, gastroschisis
Coumarin derivatives	Spontaneous abortion, FGR, neural tube defects (open and closed) (dorsal midline dysplasia), cardiac defects, scoliosis, limb hypoplasia, cleft palate

Continued



TABLE H-1 Selected Medications and Reported Associated Malformations\*—cont'd

Drug	Malformation(s)
Cyclophosphamide	Cleft palate, hand abnormalities, cardiac defects, FGR
Cyclosporine	Limb hypoplasia, agenesis of the corpus callosum, anencephaly, FGR
Cyproheptadine	Cleft lip/palate, hypospadias
Cytarabine	Hand abnormalities (lobster claw deformity), lower limb defects, neural tube defects, cardiac defects
Dacarbazine	Limb reduction defects, cleft palate, encephalocele
Danazol	Ambiguous genitalia
Daunorubicin	FGR
Dexfenfluramine	Hand malformation, anencephaly, vertebral abnormality
Diazepam	Cleft lip/palate, cardiac defects
Dicyclomine	Polydactyly
Dilantin	Microcephaly, hypertelorism, cleft lip/palate, hypoplasia of distal phalanges, short neck, broad nasal ridge
Diltiazem	Cardiovascular defects
Dimenhydrinate	Cardiovascular defects
Diphenhydramine	Cleft lip/palate, genitourinary defects, clubfoot, cardiac defects
Disulfiram	Clubfoot, vertebral defects, anal atresia, cardiac anomalies, tracheoesophageal fistula with esophageal atresia, renal anomalies, limb anomalies (VACTERL) syndrome, phocomelia
Doxepin	Oral clefts, polydactyly
Droperidol	Hydrocephalus, cerebral hypoplasia
Enalapril	Hypocalvaria, renal defects
Ephedrine	Clubfoot
Ethanol (alcohol)	FGR, microphthalmia, micrognathia, microcephaly, hypoplastic maxilla, cardiac defects, genitourinary defects, radioulnar synostosis, Klippel-Feil anomaly, diaphragmatic hernia
Ethoheptazine	Umbilical hernia, hip dislocation
Ethotoin	Cleft lip/palate, patent ductus arteriosus
Ethosuximide	Cleft lip/palate, hydrocephalus, patent ductus arteriosus, spontaneous hemorrhage in the neonate
Etretinate	Neural tube defects, facial dysmorphia, multiple synostoses, syndactylies, limb reduction
Fluconazole	Craniosynostosis, cleft palate, limb shortening
Fluorouracil	Radial aplasia, pulmonary hypoplasia, esophageal and duodenal atresia, cloacal malformation
Fluphenazine	Ocular hypertelorism, cleft lip/palate, imperforate anus
Furosemide	Hypospadias
Griseofulvin	Conjoined twins
Haloperidol	Limb reduction, aortic valve defect
Heparin	Cardiovascular defects
Heroin	FGR, multiple and varied congenital malformations
Hydroxyprogesterone	Spina bifida, anencephaly, tetralogy of Fallot, truncus arteriosus, VSD
Hydroxyzine	Oral clefts
Hyoscyamine	Polydactyly, limb reduction
Ibuprofen	Oligohydramnios, premature closure of patent ductus arteriosus
Imipramine	Diaphragmatic hernia, cleft palate, exencephaly, renal cystic dysplasia, amelia
Indomethacin	Oligohydramnios, premature closure of patent ductus arteriosus, phocomelia, penile agenesis
Isoetharine	Clubfoot
Isotretinoin	Hydrocephalus, neural tube defects, microphthalmia, microcephaly, cardiac defects, limb abnormalities, cleft palate
Itraconazole	Limb defect
Ketoconazole	Limb defect
Ketorolac	Constriction of the ductus arteriosus, fetal renal impairment
Levothyroxine	Cardiac defects, polydactyly
Lindane	Hypospadias
Lisinopril	Hypocalvaria, polydactyly, oligohydramnios
Lithium	Cardiac defects (Ebstein anomaly, VSD, coarctation, mitral atresia), neural tube defects
Lovastatin	Aortic hypoplasia, VSD, anal atresia, renal dysplasia, radial aplasia
Lysergic acid diethylamide	FGR, limb reduction, neural tube defects, cardiac defects
Marijuana	FGR, facial anomalies
Mechlorethamine	FGR, oligodactyly, malformed kidneys
Medroxyprogesterone	Cardiovascular defect
Meclizine	Eye and ear defects, hypoplastic heart, respiratory defects
Mefenamic acid	Constriction of the ductus arteriosus
Melphalan	FGR
Meprobamate	Cardiac defects, omphalocele, joint abnormalities

TABLE H-1 Selected Medications and Reported Associated Malformations\*—cont'd

Drug	Malformation(s)
Mercaptopurine	Cleft palate, microphthalmia, FGR
Metaproterenol	Polydactyly
Methimazole	Patent urachus
Methotrexate	FGR, hypertelorism, dextroposition of the heart, absent digits, absence of frontal bone
Methotrimeprazine	Hydrocephalus, cardiac defects
Metronidazole	Spontaneous abortion, limb, cardiac, urinary, and facial abnormalities
Mifepristone	Sirenomelia, caudal regression syndrome
Minoxidil	Omphalocele, clinodactyly, cardiac defects (VSD and transposition)
Misoprostol	Limb defects, hypocalvaria, cleft lip, clubfoot, gastroschisis
Norethindrone	Neural tube defects, hydrocephalus
Norethynodrel	Cardiac defects, hypospadias
Nortriptyline	Limb reduction
Ofloxacin	Myelomeningocele, hydrocephalus, hypospadias
Omeprazole	Anencephaly, hydranencephaly, clubfoot
Oxazepam	Neural tube defects, FGR
Paramethadione	Spontaneous abortions, FGR, cardiac defects
Penicillamine	Hydrocephalus, flexion deformities, perforated bowel
Pentoxifylline	Cardiac defects
Phenacetin	Craniosynostosis and atresia, musculoskeletal and urinary tract defects
Phenobarbital	Cardiovascular defects
Phensuximide	Ambiguous genitalia
Phenylephrine	Eye and ear abnormalities, syndactyly, clubfoot, musculoskeletal defects
Phenylpropanolamine	Eye and ear abnormalities, polydactyly, hypospadias
Phenytoin	Microcephaly, hypertelorism, cleft lip/palate, hypoplasia of distal phalanges, short neck, broad nasal ridge
Podophyllum	Limb reduction
Procarbazine	FGR, cardiac defects, oligodactyly, malformed kidneys
Prochlorperazine	Cleft palate/micrognathia, cardiac defects, skeletal defects
Propoxyphene	Limb abnormalities, omphalocele, micrognathia, clubfoot, microcephaly
Quinacrine	Renal agenesis, neural tube defects
Quinine	Neural tube defects, hydrocephalus, limb defects, facial defects, cardiac defects, urogenital abnormalities, vertebral abnormality, gastrointestinal anomaly
Reserpine	Microcephaly, hydronephrosis
Retinoic acid	Hydrocephalus, neural tube defects, microphthalmia, microcephaly, cardiac defects, limb abnormalities, cleft palate
Rifampin	Anencephaly, hydrocephalus, limb malformation
Sodium iodide	Ablation of fetal thyroid gland
Sulfasalazine	Cleft lip/palate, hydrocephalus, cardiac defects, urinary tract abnormalities
Sulfonamides	Limb hypoplasia, urinary tract abnormalities
Sumatriptan	Phocomelia, tibial aplasia, clubfoot, cleft palate
Tamoxifen	Ambiguous genitalia
Tazarotene	Reduced skeletal ossification, hydrocephaly, spina bifida, cardiac defects
Temazepam	Oral clefts
Terfenadine	Polydactyly
Tetracycline	Hypospadias, limb hypoplasia
Thioguanine	Absent digits
Tolbutamide	Syndactyly, cardiac defects, clubfoot
Trifluoperazine	Phocomelia, transposition of the great vessels
Trimethadione	FGR, microcephaly, cleft lip/palate, cardiac defects, malformed hand, clubfoot, ambiguous genitalia, esophageal atresia, tracheoesophageal fistula
Trimethoprim	Cardiovascular defects
Valproic acid	Neural tube defects, cardiac defects, facial dysmorphism, hypertelorism, protruding eyes, micrognathia, hydrocephalus, cleft lip/palate, microcephaly, limb reduction, scoliosis, renal hypoplasia, duodenal atresia, hand deformity
Zidovudine	Renal agenesis, microphthalmus, polydactyly, cleft lip/palate, clubfoot, VSD

CDH, congenital diaphragmatic hernia; FGR, fetal growth restriction; VSD, ventricular septal defect.

\*This list represents selected medications and their possible associations with fetal structural abnormalities. Many of the listed associations are based on isolated case reports that have appeared in the medical literature for which the association is unproved or in animal studies in which the dosage of medication far exceeded the clinical amount normally used. It is likely that in many cases the reported association was coincidental to, rather than resultant from, the medication. This list is not intended for patient counseling regarding the likelihood of fetal malformations or abnormalities. The table should be used by the sonologist/sonographer as a guide for evaluating specific organ systems in addition to a thorough sonographic examination. In all cases of suspected teratogenic effects, a reproductive geneticist or teratologist and the drug manufacturer should be consulted.

Modified from Briggs GG, Freeman RK, Yaffe SJ: *Drugs in Pregnancy and Lactation*, 7th ed. Philadelphia, Lippincott Williams & Wilkins, 2005.



## Estimated Radiation Exposure to the Fetus During Radiographic Examinations

**TABLE I-1 Estimated Fetal Radiation Dose From Abdominopelvic Radiography\***

PROCEDURE TYPE (# OF CASES)	FETAL DOSE (mGy)		RANGE OF GESTATIONAL AGE
	Range of Dose	Mean	Weeks + Days
Abdominal radiography (n = 19)	0.45–7.20	2.44	1w + 0d–17w + 2d
Abdominopelvic radiography (n = 1)	3.60	3.60	11w + 0d
Pelvic radiography (n = 12)	1.70–9.45	4.77	3w + 1d–18w + 5d

\*Adapted and reprinted with permission from: Ozbayrak M, Cavdar I, Seven M, et al. Determining and managing fetal radiation dose from diagnostic radiology procedures in Turkey. *Korean J Radiol* 2015;16(6):1276-1282.

**TABLE I-2 Estimated Fetal Radiation Dose per 100 mAs<sub>eff</sub> From Adominopelvic CT for Several Different MDCT Scanners\***

Scanner Model	Tube Voltage (kVp)	Collimation (mm)	Fetal Dose (mGy) per 100 mAs <sub>eff</sub>	Scanner Model	Tube Voltage (kVp)	Collimation (mm)	Fetal Dose (mGy) per 100 mAs <sub>eff</sub>
LightSpeed VCT <sup>a</sup>	120	20	14.35	Sensation 16 <sup>b</sup>	120	24	9.9
	140	40	17.92		120	18	10.08
	140	20	19.31		140	24	14.78
LightSpeed 16 Pro <sup>a</sup>	120	20	11.54	Brilliance 64 <sup>c</sup>	140	18	15.04
	120	10	13.54		120	40	8.63
	140	20	17.92		120	25	10.12
LightSpeed 16 <sup>a</sup>	140	10	20.91	140	40	13.65	
	120	20	14.18	Brilliance 16 <sup>c</sup>	140	25	16.02
	120	10	16.56		120	24	10.26
140	20	19.94	120		12	11.43	
Sensation 64 <sup>b</sup>	140	10	23.29	140	24	14.8	
	120	28.8	9.64	Aquilion 16 <sup>d</sup>	140	12	16.5
		19.2	10.4		120	32	17.34
	140	28.8	15.56	120	16	19.08	
140	19.2	16.79	135	32	21.05		
				135	16	23.39	

<sup>a</sup>GE Healthcare

<sup>b</sup>Siemens Healthcare

<sup>c</sup>Philips Healthcare

<sup>d</sup>Toshiba Medical Systems

\*Adapted and reprinted with permission from: Goldberg-Stein SA, Liu B, Hahn PF, Lee SI. Radiation dose management: part 2, estimating fetal radiation risk from CT during pregnancy. *AJR* 2012; 198:W352–W356.

**TABLE I-3 How to Estimate Fetal Radiation Dose From an Abdominopelvic CT Examination\***

An estimate of fetal radiation dose from an abdominopelvic CT examination is calculated as follows:

1. Determine your scanner model type and detector collimation.
2. Calculate total beam collimation using the following equation:

$$\text{Total beam collimation} = \# \text{ of detector rows} \times \text{detector collimation}$$

3. Select the desired kVp for scanning.
4. Use Table I-2 (above) to identify the corresponding estimated fetal radiation dose, specified in units of mGy per 100 mAs<sub>eff</sub>.
5. Calculate the mAs<sub>eff</sub> using the following equation:

$$\text{mAs}_{\text{eff}} = \text{current (mA)} \times \text{time per rotation (s)} / \text{pitch}$$

If Automatic Tube Current Modulation (ATCM) is enabled, tube current (mA) is automatically adjusted. This adjustment occurs according to the size of the patient and to the attenuation values of the anatomy being imaged. If ATCM is used, a mean mA value should be used here. Because the mean mA will vary with each patient, the mean value can only be estimated. If the calculation is being performed after scanning, the mean mA can be obtained from the mA range in the examination dose report.

6. Estimated fetal radiation dose (mGy) = mGy/100 mAs<sub>eff</sub> (result of step 4) × mAs<sub>eff</sub> (result of step 5) / 100.

Example:

1. LightSpeed VCT (GE Healthcare) 64 MDCT scanner with a detector collimation of 0.625 mm
2. Total beam collimation = 64 × 0.625 = 40 mm
3. 140 kVp selected for scanning
4. With these parameters, Table 2 indicates an estimated fetal radiation dose of 17.92 mGy per 100 mAs<sub>eff</sub>.
5. Calculate mAs<sub>eff</sub>. For example, with a current setting of 300 mA, time per rotation of 0.6 sec, and a pitch of 1.375:

$$\text{mAs}_{\text{eff}} = 300 \times 0.6 / 1.375 = 130.9$$

6. Estimated fetal radiation dose (mGy) = 17.92 mGy per 100 mAs<sub>eff</sub> (result of step 4) × 130.9 mAs (result of step 5) / 100 = 23.45 mGy.

\*Adapted and reprinted with permission from: Goldberg-Stein SA, Liu B, Hahn PF, Lee SI. Radiation dose management: part 2, estimating fetal radiation risk from CT during pregnancy. *AJR* 2012; 198:W352–W356.



## Magnetic Resonance Imaging of the Female Pelvis: Representative Protocols\*

**TABLE J-1 Pelvic Mass Magnetic Resonance Imaging Protocol**

**Sequences**

- **Sag T2 Fast Spin Echo (FSE)**
  - Free breathing
  - May need to try phase S/I and A/P to see which gives best quality
  - Consider anterior or superior suppression pulses
- **Axial T2 FSE Fat Saturation (FS)**
  - Free breathing
  - Phase L/R
- **Axial T2 FSE**
  - Free breathing
  - Phase L/R
- **Coronal T2 FSE**
  - Free breathing
  - Phase L/R
- **Axial T1 In and Opposed Phase**
  - End expiration is preferred. Inspiration is acceptable.
- **Axial Isotropic T1 FS pre (3D Vibe)**
  - Free breathing
  - **PHASE L/R** (not A/P)
- **Inject Contrast**
- **Axial Isotropic T1 FS post (start 1 minute following initiation of the injection)**
  - Free breathing
- **Axial Vibe (only if necessary to cover the anatomy)**
  - End inspiration is acceptable
  - FS

If the pelvic pathology is too large to perform the isotropic T1 FS images in a reasonable amount of time, use Vibe pre- and post-contrast images similar to a Liver Mass Protocol and acquire breath hold axial, sagittal, and coronal pre- and post-contrast images.

**TABLE J-2 Uterine Anomaly Magnetic Resonance Imaging Protocol**

**Sequences**

- **LOCALIZER free breathing**
  - Run in ISO mode to see where the uterus is centered in the coil.
- **LOCALIZER free breathing**
  - Run in ISO mode.
  - Center the uterus in the center of the field view.
  - When this is finished, remove the previous series from the sequence list and remove its images from the thumbnails. If you prescribe off this localizer using the REF mode, the uterus will remain in the center of the magnet.
- **HASTE LOCALIZER (T2)**
  - Run in the following planes centered on the uterus. Make sure you are in reference mode and prescribe off the second localizer above.
    - *Straight Axial*
    - *Straight Sagittal*
    - *Straight Coronal*
- **"Coronal of Uterus" T2 Fast Spin Echo (FSE)**
  - Use the above HASTE localizers to create a plane that parallels the endometrium to make a true coronal of the uterus.
  - Free breathing
  - Phase L/R
- **"Sagittal of Uterus" T2 FSE**
  - Use of the above HASTE localizers to create a parasagittal plane that parallels the endometrium.
  - Free breathing
  - May need to try phase S/I and A/P to see which gives best quality.
  - Consider anterior or superior suppression pulses.
- **"Axial of Uterus" T2 FSE**
  - Use the above HASTE localizers to create a plane that is perpendicular to the plane of the endometrium.
  - Free breathing
  - Phase L/R
- **3D T2 SPACE SAG**
  - Free breathing
- **Axial T1 In and Opposed Phase**
  - End expiration is preferred. End inspiration is acceptable.
- **Axial Isotropic T1 Fat Saturation (FS) pre (3D Vibe)**
  - Free breathing
  - **PHASE L/R** not A/P
- **Axial Isotropic T1 FS post (only if giving contrast) (3D Vibe)**
  - Free Breathing
  - **PHASE L/R** not A/P
- **CORONAL HASTE (T2) to include kidneys**

\*Protocols will vary depending upon indication, institution, and manufacturer. These representative protocols were provided courtesy of Dr. Steffen Huber, Department of Radiology and Biomedical Imaging, Yale University School of Medicine, New Haven, CT.

### TABLE J-3 Magnetic Resonance Imaging Protocol for the Pregnant Patient With Right Lower Quadrant Pain

#### • Patient Position

- Head first
- Supine

#### • Coils

- Place sufficient matrix coils to cover the abdomen and pelvis (or chest, abdomen, and pelvis if necessary).
- Make supercoils if the patient is large and there are enough (4) matrix coils.
- **“Zero” the scanner at the center of the top coil.**
- **Assess the patient’s ability to breath hold.**

#### Sequences

- **Axial T2 HASTE (2 station Set-and-Go)**
  - Multiple short and expiration breath holds.
  - Send the composed images to PACS.
- **Coronal T2 HASTE**
  - Navigator triggered or short end expiration breath holds.
- **Sagittal T2 HASTE**
  - Navigator triggered or short end expiration breath holds.
- **Axial T2 HASTE Fat Saturation (FS) (2 Station Set-and-Go)**
  - Multiple short end expiration breath holds.
  - Send the composed images to PACS.
- **T1 In and Out of Phase (cover Uterus and Adnexa)**
  - End expiration is preferred. End inspiration is acceptable.

#### Notes:

##### **IMPORTANT! These HASTE Sequences Are Different!**

- 5 mm thick with 10% slice spacing
- Matrix of 256 x 256 is acceptable, but 320-256 is preferable if signal is OK.
- HASTE in these cases is run without parallel imaging. If you want to turn on parallel imaging, then phase oversample (with no time penalty) to avoid artifact.
- **Image the cecum in all planes.** (Since the appendix is attached to the cecum, if you image the cecum, you will also include the appendix.)
- **Do not let the images “bounce.”** The appendix measures 5mm. Each pixel is 2mm. Even 2 mm of bouncing can make the appendix “disappear.” Use *breath holds if possible* and only use navigator as the last resort. You can Navigator off the bottom of the liver, spleen, or even the top of a moderate sized uterus!

#### HASTE Coverage

- Axial: gallbladder to pubis in the axial plane
- Coronal: front to back to include from the gallbladder superiorly to the pubis inferiorly
- Sagittal: midline to right skin surface

#### **Axial Dual Echo VIBE Through the Uterus and Pelvis Is a Breath Hold Image.**

- The purpose of this image is to look for hemorrhage in the uterus (placenta, fibroids) or fat in the adnexa (dermoid cysts).
- Use iPAT 2
- Choose from the appropriate breath hold protocol
- If these images are blurry, use free breathing T1 protocol. Copy the slices from the Axial T2 HASTE.

#### Abbreviations:

HASTE: Single shot T2 weighted sequence

VIBE: Volume interpolated gradient echo T1 weighted sequence

iPAT: Parallel imaging

FS: Fat suppression



**TABLE J-4 Urethral Diverticulum Magnetic Resonance Imaging Protocol**

Feet first  
Supine  
Coil coverage over deep pelvis and perineum

**Sequences**

- **Sagittal Hi Res T2 Fast Spin Echo (FSE) Fat Saturation (FS)**
  - Free breathing
  - Since there is rarely motion this deep in the pelvis, set phase A/P.
- **Axial Hi Res T2 FSE**
  - Free breathing
  - Phase L/R
- **Axial T1 FSE**
  - Free breathing
  - Phase L/R
- **Axial Isotropic T1 FS pre (3D Vibe)**
  - Free breathing
  - **PHASE L/R** not A/P
- **Inject Contrast**
- **Axial Isotropic T1 FS post (start 30 seconds following initiation of the injection) (3D Vibe)**
  - Free breathing
  - **PHASE L/R** not A/P

**Note: These T2's Are Different.**

- Small FOV, 180-220 depending on patient size. Important to cone down on the urethra. Use enough phase oversampling on the axial images to avoid wrap into the image.
- Axial images should be *perpendicular* to the urethra. This is almost always a straight axial. Phase is placed L/R. Use enough oversampling to avoid wrap. Image from the top of the bladder to the perineum.
- On the sagittal images set phase A/P as there is almost never respiratory motion at the level of the pubis.
- The slices for the Axial T1 FSE can be copied from the Axial T2.

**TABLE J-5 Endometrial Cancer Magnetic Resonance Imaging Protocol (for Local Staging)**

Place patient feet first, supine.

Use enough coils to cover from perineum to aortic bifurcation.

10ccs of ultrasound gel should be inserted into the vagina (via syringe, preferably by patient).

1 mg Glucagon IM prior to scout sequence.

#### Sequences

- **LOCALIZER free breathing**
  - Run in ISO mode to see where the uterus is centered in the coil.
- **LOCALIZER free breathing**
  - Run in ISO mode.
  - Center the cervix in the center of the field of view.
  - When this is finished, remove the previous series from the sequence list and its images from the thumbnails. If you prescribe off this localizer using the REF mode, the uterus will remain in the center of the magnet.
- **HASTE LOCALIZER (T2)**
  - Run in the following planes centered on the cervix.
  - Make sure you are in Reference Mode.
  - Prescribe off the second localizer above.
  - *Straight Axial*
  - *Straight Sagittal*
  - *Straight Coronal*
- **Diffusion Weighted Imaging (DWI) in the "Sagittal Plane of Uterus"**
  - B values (50, 400, 800)
  - Apparent Diffusion Co-efficient (ADC) maps
- **"Transverse of Uterus" T2 FSE**
  - Use the above HASTE localizers to create a plane that runs perpendicular to the uterus.
  - Free breathing
  - Phase L/R
- **"Coronal of Uterus" T2 FSE**
  - Use the above HASTE localizers to create an oblique coronal that parallels the uterus.
  - Free breathing
  - May need to try phase S/I and A/P to see which gives best quality.
  - Consider anterior or superior suppression pulses.
- **"Sagittal of Uterus" T2 FSE**
  - Small FOV
  - Use the above HASTE localizers to create a parasagittal plane that is parallel to the plane of the uterus.
  - Free breathing
  - Phase L/R
  - Only cover the uterus
- **3D T2 SPACE**
  - Free breathing
  - Only cover the uterus
- **Axial Isotropic T1 Fat Saturation (FS) pre**
  - Free breathing
  - **PHASE L/R** not A/P
- **Optional Sagittal Dynamic Contrast Enhanced (DCE) (depending on protocol)**
  - Free breathing
- **Isotropic T1 FS post (30 seconds after injection)**
  - Free breathing
  - **PHASE L/R** not A/P
- **Vibe post from bifurcation down**



**TABLE J-6 Cervical Cancer Magnetic Resonance Imaging Protocol (for Local Staging)**

Place patient feet first, supine.

Use enough coils to cover from perineum to aortic bifurcation.

10cc of ultrasound gel should be inserted into the vagina (via syringe, preferably by patient).

1 mg Glucagon IM prior to scout sequence.

### Sequences

- **LOCALIZER free breathing**

- Run in ISO mode to see where the uterus is centered in the coil.

- **LOCALIZER free breathing**

- Run in ISO mode.
- Center the cervix in the center of the field of view.
- When this is finished, remove the previous series from the sequence list and its images from the thumbnails. If you prescribe off this localizer using the REF mode, the uterus will remain in the center of the magnet.

- **HASTE LOCALIZER (T2)**

- Run in the following planes centered on the cervix.
- Make sure you are in Reference Mode.
- Prescribe off the second localizer above.
- *Straight Axial*
- *Straight Sagittal*
- *Straight Coronal*

- **Diffusion Weighted Imaging (DWI) in the "transverse plane of cervix"**

- B values (50, 400, 800)
- Apparent Diffusion Co-efficient (ADC) maps

- **"Transverse of Cervix" T2 FSE**

- Use the above HASTE localizers to create a plane that runs perpendicular to the cervix.
- Free breathing
- Phase L/R

- **"Coronal of Cervix" T2 FSE**

- Use the above HASTE localizers to create an oblique coronal that parallels the cervix.
- Free breathing
- May need to try phase S/I and A/P to see which gives best quality.
- Consider anterior or superior suppression pulses.

- **"Sagittal of Cervix" T2 FSE**

- Small FOV
- Use the above HASTE localizers to create a parasagittal plane that is parallel to the plane of the cervix.
- Free breathing
- Phase L/R
- Only cover the uterus

- **3D T2 SPACE**

- Free breathing
- Only cover the uterus/cervix
- Sagittal

- **Axial Isotropic T1 Fat Saturation (FS) pre**

- Free breathing
- **PHASE L/R** not A/P

- **Optional Sagittal Dynamic Contrast Enhanced (DCE) (depending on protocol)**

- Free breathing

- **Axial Isotropic T1 FS post (30 seconds after injection)**

- Free breathing
- **PHASE L/R** not A/P

- **Axial Vibe post from bifurcation down**

Page numbers followed by “f” indicate figures, and “t” indicate tables.

## A

- Aase syndrome, 322
- Abdomen. *see also specific structures*
- fetal
    - abnormalities in, MRI evaluation for, 762-763, 765f-767f
    - ultrasound imaging of, artifacts, pitfalls, and normal variants, 1135-1143, 1135f-1142f
  - in first trimester
    - abnormal ultrasound findings of, 111-113
    - normal ultrasound findings of, 106-107, 106f
  - maternal
    - CT and MRI imaging of, 751
    - planes of, 162f
    - neonatal, 157, 159f
- Abdominal circumference (AC), second and third trimester dating by, 121, 123f
- Abdominal cyst, first trimester, 482-483, 483f
- Abdominal diameter (AD), second and third trimester dating by, 121, 123f
- Abdominal ectopic pregnancy, 991-993, 994f-995f
- Abdominal mass, 1140f
- Abdominal pain, hepatobiliary causes of, 751
- Abdominal wall
- anterior, focal laxity of, 1136f
  - defects of, 607-610, 763
    - Beckwith-Wiedemann syndrome, 607-609, 607f
    - earlobe groove in, 608f
    - organomegaly in, 608f
  - cloacal exstrophy sequence, 609
  - first trimester ultrasound of, 111-112
  - prune-belly syndrome as, 609-610, 610f
  - musculature of, 183, 183f
  - ultrasound evaluation of, 460-502
- Abdominal wall endometriotic implant, 898f
- Aberrant cephalad migration, 520, 520f
- Aberrant right subclavian artery (ARSA), in Down syndrome, 74
- Abnormal imprinting, in Prader-Willi critical region, 617
- Abnormal uterine bleeding. *see* Uterine bleeding, abnormal
- Abortion, inevitable, cervical ectopic pregnancy and, 990f
- Abruptio placentae, 689
- diagnosis of, 16
- ABS. *see* Amniotic band syndrome (ABS)
- Abscess
- in assisted reproduction, 963, 963f
  - diverticular, 939-940, 945f
  - tubo-ovarian, 892f, 939-940, 943f-944f
  - mimicking ectopic pregnancy, 984f
- Absent limbs, syndromes with, 318-319
- AC. *see* Abdominal circumference (AC)
- Acardiac fetus, 782
- radiofrequency ablation of, 784f
- Acardiac twin, 144-145, 146f-147f
- ACC. *see* Agenesis of corpus callosum (ACC)
- Accelerations, in fetal heart rate, 722
- Accurate detailed anatomic diagnosis, 775
- Achondrogenesis, 307-309, 308f, 308t, 577, 578f
- nosology of, 278t-282t
  - prevalence of, 275, 277t
  - three-dimensional ultrasound in, 290t
  - type I, 577
  - type II, 577
- Achondroplasia, 303-305, 304f, 581-582, 581f-582f
- heterozygous, 305
  - prevalence of, 275, 277t
  - severe, with developmental delay and acanthosis nigricans, 305
  - three-dimensional ultrasound in, 290t
- Acinar dysplasia, 351
- ACOG. *see* American College of Obstetricians and Gynecologists (ACOG)
- ACR. *see* American College of Radiology (ACR)
- Acrania, 222-223
- Acrocephalopolysyndactyly type II, 565
- Acrocephalosyndactyly
- type 1, 562
  - type 3, 566
  - type 5, 565
- Acrocephaly, in Apert syndrome, 562
- Acromelia, 277
- Actinomycosis, 947f
- Acyclovir, for varicella zoster, 548
- AD. *see* Abdominal diameter (AD)
- Adams-Oliver syndrome, 319, 585
- Additional imaging modalities, leiomyomas, uterine and, 900
- Adenoma malignum, 1059-1060
- Adenomyoma, 858
- focal, 904-906
- Adenomyosis, 857-858, 859f-861f, 900, 1056
- clinical aspects of, 1056
  - definition and epidemiology of, 1056
  - diagnosis of, 1056
  - features of, 858t
  - focal, 858
  - imaging characteristics of, 1056, 1057f
  - imaging features of, 857-858
  - leiomyoma and, 1053f, 1055f
  - pathophysiology of, 1056
  - sonographic imaging of, 955, 956f
  - ultrasound findings of, 907f
- Adnexa
- cyst in, 1113f
  - first trimester ultrasound examination of, 13
  - second and third trimester ultrasound examinations of, 17
  - torsion of, 884-887
    - clinical presentation of, 884
    - pelvic inflammatory disease, 891-892
    - peritoneal inclusion cyst, 897-899
    - ultrasound of, 1018, 1018f
- Adnexal mass(es), 1065-1070
- benign and malignant lesions in, differentiation of, 1067
  - complex or solid, 87
  - in ectopic pregnancy, 972, 973f-977f
  - endometrioma, 894-895, 894f
  - epidemiology and clinical significance of, 1065-1066
  - hemorrhagic corpus luteum cyst, 890, 890f
  - mature cystic teratoma, 887f, 891
  - MRI for
    - cystic malignant-appearing lesions, 1067, 1070f
    - with distinctive imaging features, 1067, 1068f-1069f
    - imaging diagnosis of, 1066-1067
    - predominantly solid lesions, 1067-1068, 1071f
    - preoperative staging, 1068-1070
    - specific diagnosis of, 1067-1070
  - ovarian, 927-928
    - in pelvic inflammatory disease, 891-892, 891f
    - peritoneal inclusion pseudocyst, 928, 928f
    - solid, 1103f
    - sonography in, 1066-1067
- ADPKD (autosomal dominant polycystic kidney disease), 522, 523f
- Adrenal cyst, 482, 482f
- Adrenal glands
- fetal, 200, 202f, 529-531
  - disorders of, 530-531
    - adrenogenital syndrome, 530, 530f
    - cysts of, 531f
    - hemorrhage, 530f
    - masses as, 530, 531t
    - neuroblastoma as, 530-531, 531f
    - normal, 529-531, 529f-530f
  - Adrenal neuroblastoma, cystic, 482f
  - Adrenogenital syndrome, 530, 530f
- AFI. *see* Amniotic fluid index (AFI)
- AFP. *see* Alpha-fetoprotein (AFP)
- Afterload, and fetal growth restriction, 747
- AFV. *see* Amniotic fluid volume (AFV)
- Agenesis of corpus callosum (ACC), 226, 756f
- with absence of septum pellucidum, 229, 232f
  - in aneuploidy, 61-62, 64f
  - complete, 227, 229f
  - MRI of, 754
  - partial, 227, 230f
  - schematic diagram of, 229f
  - syndrome associated with, 227, 231t
- Aglossia-adaactylia syndrome, 318
- Aicardi syndrome, 32, 227, 553-554, 554f
- AIUM. *see* American Institute of Ultrasound in Medicine (AIUM)
- Akinesia, fetal, 615, 615f
- genes associated with, 616t
- Alagille syndrome, 596, 596f
- Albumin, fetal, and hydrops fetalis, 638
- Alcohol
- exposure to, 36t
  - in utero, 548
  - as teratogen, 549
- Allantois, 504, 693-694
- Alloimmunization, maternal, 635-636, 637f
- prevention of, 638
- Alpha-fetoprotein (AFP)
- elevated maternal serum levels of, 41, 42f
  - causes of, 42t
  - other abnormalities and, 41
  - in second trimester, 42-43, 43t
  - in Meckel syndrome, 555-556
  - neural tube defects and, 223
  - open neural tube defects and, 40-41
- Alveolar phase, of lung development, 349
- Ambiguous genitalia, 1009-1011, 1011t, 1012f-1015f
- Amenorrhea, primary, 1015-1018, 1018f
- American College of Obstetricians and Gynecologists (ACOG), guidelines of, 7t-11t
- verbiage used in, 17-18
- American College of Radiology (ACR), guidelines of, 7t-11t
- verbiage used in, 17-18
- American Fertility Society Classification System, in mullerian anomalies, 1080, 1080f, 1080t
- American Institute of Ultrasound in Medicine (AIUM), guidelines of, 6, 7t-11t
- for imaging of uterus, 847
  - verbiage used in, 17-18
- American Society for Reproductive Medicine (ASRM) system, in reproductive tract, anomalies of, 1004, 1005f, 1005t
- Amiodarone, 650t
- Amniocentesis, 46, 46f
- complications of, 46
  - for fetal blood type assessment, 638-639
  - in multiple gestations, 48
  - for prediction of anemia, 639
  - therapeutic, in twin-to-twin transfusion syndrome, 778
- Amnioinfusion, 712
- Annion
- development of, 83, 84t, 85f-86f
  - in first trimester gestations, 1119f
  - pregnancy failure and
  - empty sign of, 90, 91f
  - expanded sign of, 90-91, 91f
  - rupture of, in early pregnancy, 628
- Amnionicity, 17
- in multiple gestations, 136-137, 137t, 138f-139f
- Amnioreduction, 649
- in twin-to-twin transfusion syndrome, 779
- Amniotic band sequence, 628-631, 629f-630f, 692-693, 694f
- Amniotic band syndrome (ABS), 497
- fetal surgery and, 791-792, 792f



- Amniotic fluid, 704-719, 705f  
 excess of, 705-706  
 intramembranous movement and, 705-706  
 maternal fluid status and, 706  
 membranes and, ultrasound imaging of, artifacts,  
 pitfalls, and normal variants, 1143-1146,  
 1143f-1145f  
 physiology and dynamics of, 704-706, 706f  
 Amniotic fluid index (AFI), 706-707, 706f  
 with biophysical profile, 727, 727f  
 fetal position and, 707-708, 709f  
 values, in normal pregnancy, 710t  
 Amniotic fluid volume (AFV), 15-16, 704. *see also*  
 Oligohydramnios; Polyhydramnios  
 abnormally low, 708  
 assessment of, in high-risk patient, 712-715  
 and fetal growth restriction, 714  
 polyhydramnios in, 712-714, 713f  
 in twin pregnancies, 714-715, 715f-716f  
 in biophysical profiling, 728  
 determination of, 706-707, 706f-707f  
 dye-determined calculation of, at cesarean delivery,  
 707  
 estimation of, using ultrasound, difficulties in,  
 707-708, 709f  
 and fetal growth restriction, 714  
 and gestational age, 708, 710t  
 increased, 708  
 in multiple gestations, 16  
 in obese patients, 15  
 population-specific curves for, 710  
 pregnancy outcomes and, 710-712  
 oligohydramnios, 711  
 pulmonary hypoplasia, 711-712  
 in singleton pregnancies, 708-710, 710f  
 subjective assessment of, 707, 707f  
 urinary tract assessment and, 504f  
 Amniotic sac. *see* Gestational sac  
 Amniotic sheet, 692, 693f  
 Ampulla, 934-935  
 Anal atresia, 471-472  
 Anal incontinence, 1025  
 endoanal sonography for, 1027-1029, 1028f-1029f  
 MRI in, 1036-1037, 1038f  
 Anal sphincter  
 tears in, 1028-1029, 1029f  
 transperineal sonography of, 1029-1030, 1030f  
 ultrasound in, 1028f  
 Anemia, fetal  
 hematologic disorders causing, and nonimmune  
 hydrops, 645t-647t  
 hydrops fetalis and, 637  
 fetal response to, 639-640  
 paternal testing for, 638  
 prediction of, 637f, 639-641, 639t, 640f  
 severe, 638  
 sinusoidal fetal heart rate in, 723, 724f  
 Anencephaly, 108, 222-223, 224f  
 in first trimester, 1119f  
 incidence of, 223t  
 Aneuploidy. *see also* Chromosomal abnormalities  
 definition of, 27  
 fetal  
 congenital anomalies in, 58t  
 cystic hygroma and, 67  
 genetic screening of, 41  
 sonography of, 57  
 ultrasound evaluation of, 57-81  
 cerebellar abnormalities in, 61-62, 62f-63f  
 first trimester markers for, 63-69  
 minor markers for, 69, 70t  
 second trimester genetic sonogram, 69-75  
 structural abnormalities in, 58-63  
 in first trimester, 42  
 monochorionic twins discordant for, 789  
 polyhydramnios and, 713  
 single umbilical artery and, 697  
 sonographic "soft markers" for, 43  
 umbilical vein varix and, 698  
 Aneurysm, of vein of Galen, 237, 238f  
 Angiogenesis, 676f  
 Angiotensin-converting enzyme (ACE) inhibitors,  
 36t  
 Angular pregnancies, 978  
 Aniridia, congenital, 525  
 Anomalous pulmonary venous connection, 430-434  
 anatomy of, 430-433  
 birth prevalence/epidemiology of, 430  
 definition of, 430, 432f  
 diagnostic imaging features of, 433-434  
 genetic considerations of, 433  
 interventions and prognosis of, 433  
 Anophthalmia, 63, 253-255, 260f  
 Anorectal malformations, 471-475, 471f-472f  
 associated anomalies of, 472  
 neonatal management of, 475  
 persistent cloaca, 473-475, 473f-475f  
 prevalence of, 472  
 sonographic diagnosis of, 472-473, 473f-474f  
 Anosteogenesis. *see* Achondrogenesis  
 Antepartum fetal surveillance, 720-732  
 assessment of fetal movement in, 720-721  
 biophysical profile for, 726-730, 727f, 728t  
 amniotic fluid volume component of, 728  
 gradual hypoxia concept, 726-727  
 modified, 729-730  
 tone in, 726  
 contraction stress test for, 724-726  
 contraindications to, 726  
 indications for, 721t  
 nonstress test for, 721-724, 722f  
 nonreactive, 723-724  
 and prevention of stillbirth, 724  
 reactive, 723-724  
 risk of stillborn in, 721t  
 serial, 720  
 umbilical artery Doppler velocimetry, 730, 731f  
 Anterior sacral meningocele, cysts and, 481  
 Anti-D gamma globulin, 634-635  
 Anti-D immune globulin, dosage of, 638  
 Antiarrhythmic medication, for nonimmune hydrops  
 fetalis, 647  
 Antiepileptic drugs (AEDs), 35  
 Antley-Bixler syndrome, 561-562  
 Anus, fetal, 195, 196f  
 Anxiolytics, in MRI techniques, 750  
 Aorta  
 fetal, 186-187, 188f  
 in first trimester, 105-106, 106f  
 Aorta bifurcates, common iliac arteries into, 816  
 Aortic arch, long-axis view of, 392, 393f  
 Aortic valves, 390  
 Aortic valvuloplasty, 790f  
 Apert-Crouzon disease, 562  
 Apert syndrome, 263, 265f, 290t, 562, 563f-564f  
 genetics of, 562  
 Apparent missing digits, 1150f  
 Apparent spinal defect, 1151f  
 Appearing twin, 94, 95f  
 Appendicitis  
 acute, 751, 907-908, 911f, 939-940, 945f  
 magnetic resonance image of, 910f  
 ultrasound of, 1019-1020, 1021f  
 ruptured, 752f  
 Appendicular skeleton, bones of, fetal, 164, 168f-170f  
 Appendix  
 inflamed, ultrasound examination, 908  
 mucocele of, 908, 911f  
 Arachnoid cysts, 230, 232, 236f  
 Arcuate artery, 816-820, 819f  
 calcifications, 825, 825f  
 Arcuate uterus, 856, 857f  
 Mullerian duct anomalies and, 1049, 1049f  
 Arcuate veins, 851-852  
 Arcuate venous plexus, 820, 820f  
 ARPKD (autosomal recessive polycystic kidney disease),  
 521-522, 522f  
 Arrhythmias, fetal, 440-444  
 diagnostic imaging features of, 443-444  
 general features of, 440  
 nonimmune hydrops and, 645t-647t, 647  
 medications for, 650t  
 Arterial outflow tracts, 390-391  
 Arteriovenous malformations (AVMs), of uterus,  
 871-872  
 Arthrogryposis, 323-325, 324f, 324t  
 syndrome, distal, 617  
 Artifacts  
 echoes, 1097f  
 in fetal duodenum, 1096f  
 Artifacts (*Continued*)  
 in fetal stomach, 1096f  
 mirror image, 1095-1098, 1095f-1096f  
 pitfalls, and normal variants, 1092-1151  
 side lobe, 1096f  
 Artifactual short cervix, 1106f  
 ARTs. *see* Assisted reproductive technologies (ARTs)  
 Ascites, 474, 478-479, 478f, 479t  
 fetal, 1139f  
 isolated, in cytomegalovirus infections, 542  
 Asherman syndrome, 954-955  
 endometrial interventions in, 1082-1083  
 Ashkenazi Jewish population, carrier screening in, 38, 39t  
 Asphyxiating thoracic dysplasia, 313-314  
 Asplenia, 601  
 ASRM system. *see* American Society for Reproductive  
 Medicine (ASRM) system  
 Assisted reproduction, complications of, 962-963  
 abscess as, 963, 963f  
 hemoperitoneum as, 963, 963f  
 ovarian hyperstimulation syndrome as, 962-963, 962f  
 Assisted reproductive technologies (ARTs), twinning and,  
 133  
 Association, 25-27, 540  
 Atelosteogenesis, 307  
 type 2, 580  
 Atresia  
 bronchial, 355-356, 357f-358f  
 urethral, 515, 515f  
 Atrial bradycardia, low, 441  
 Atrial chambers, 387-389  
 Atrial flutter, 443, 445f  
 Atrial septal aneurysm, 387  
 Atrioventricular canal defects (AVCDs), 405-409  
 anatomy of, 407, 410f  
 definition of, 405, 408f  
 diagnostic imaging features of, 408-409  
 epidemiology of, 407, 409f  
 genetic considerations of, 407  
 interventions and prognosis of, 407  
 Atrioventricular junction, 389-390  
 Atrioventricular valves, 389-390  
 Doppler waveforms in, 745, 745f, 745t  
 Autonomic nervous system, fetal heart rate and, 721-722  
 Autosomal-dominant inheritance, 30f-31f, 31-32  
 paternal age and risk of, 31, 31f  
 penetrance and expression in, 31-32  
 Autosomal dominant polycystic kidney disease  
 (ADPKD), 522, 523f  
 Autosomal-recessive disorders, 30f-31f, 32  
 Autosomal recessive polycystic kidney disease (ARPKD),  
 521-522, 522f  
 Autosomes, 27  
 AVMs. *see* Arteriovenous malformations (AVMs)
- B**
- Balanced steady-state free precession (bSSFP), 750-751  
 triplanar, 750  
 Banana sign, 223  
 Bannayan-Riley-Ruvalcaba syndrome, 618  
 Baraitser-Winter syndrome, and lissencephaly, 556  
 Bardet-Biedl syndrome, 523  
 Basal plate, 675  
 Battledore placenta, 681  
 Beckwith-Wiedemann syndrome (BWS), 32, 257, 261f,  
 525, 607-609, 607f  
 earlobe groove in, 608f  
 organomegaly in, 608f  
 Benzathine penicillin, for fetal syphilis infection, 546  
 B-flow rendering, 400, 400f-401f  
 Bicaval view, of heart, 392, 393f  
 Bicornuate uterus, 855, 856f, 1004-1006, 1005f-1006f  
 Mullerian duct anomalies and, 1049, 1049f-1050f  
 repair of, 1082  
 Bilateral open lip schizencephaly, MRI of, 758f  
 Bilateral renal agenesis, 518-519, 519f  
 Biometric parameters  
 in diagnosis of pulmonary hypoplasia, 293, 297t  
 in diagnosis of skeletal dysplasias, 277-288  
 Biophysical profile (BPP), 726-730, 727f, 728t  
 amniotic fluid volume component of, 728  
 and cerebral palsy, 730f  
 and cord artery base excess, 729f

- Biophysical profile (BPP)** (*Continued*)  
 and cord artery bicarbonate level, 729f  
 and cord artery pH, 728f  
 and fetal umbilical venous pH, 728f  
 gradual hypoxia concept, 726-727  
 modified, 729-730  
 and perinatal morbidity rate, 729f  
 and perinatal mortality rate, 730f  
 tone in, 726  
 ultrasound in, 726
- Biopsies**  
 endometrial, 838, 841f  
 in pelvic masses, 1088, 1089f
- Biparietal diameter (BPD)**  
 gestational age estimation by, 124t  
 second and third trimester dating by, 119, 122f-123f
- Biparietal diameter/nasal bone length (BPD/NBL)**, fetal, 72
- Birth defects.** *see also* Congenital anomalies  
 genetics and, 25  
 structural, screening for, 40-41
- Birth weights.** *see also* Fetal weight  
 percentiles in third trimester, 126t  
 prenatal ultrasound and, 4
- Bladder**  
 fetal, 158-159, 199-200, 504, 506f  
 absent or nonvisualized, 526  
 development of, 504, 505f, 507f  
 enlargement of, 512, 513f  
 causes of, 514t  
 filling and emptying of, 504  
 nonobstructive anomalies of, 526-528  
 and umbilical arteries, 504, 506f  
 first trimester ultrasound of, 107, 108f  
 full, in ultrasonography of cervix, 656  
 maternal, filling for transabdominal sonography, 805
- Bladder exstrophy**, 492f-493f, 496-497, 527-528, 528f  
 embryology of, 496  
 neonatal management of, 497  
 sonographic diagnosis of, 496-497
- Bladder outlet obstruction**, 515
- Bladder-serosal interface**, 684
- Blake pouch**, 216  
 cyst of, 229  
 MRI of, 757f
- Blastocyst**, 83f
- Bone(s).** *see also* Ossification; Skeletal dysplasias; *specific bones*  
 bowing of, 292f  
 cartilaginous portions of, fetal, 164, 168f-170f  
 visualization of, 176, 177f  
 demineralization of, 291, 292f  
 development of, 273, 273f  
 endochondral, 273-275, 274f  
 imaging of, 274-275  
 long  
 degree of curvature of, 291, 292f  
 degree of mineralization of, 291, 292f  
 fractures of, 292, 293f-294f  
 length of. *see also* Femur length (FL); Humerus, length of  
 head circumference and, 277, 287f  
 normal values for, 287t-288t  
 measurements of, 291  
 metaphyseal flaring of, 291-292  
 ossification of, 273-275, 274f-276f
- Borderline epithelial ovarian tumor**, 1070f
- Borderline mucinous neoplasm**, 925f
- Bourneville disease**, 558
- Bourneville sclerosis**, 558
- Bowel.** *see also* Colon; Small intestine  
 fetal, pseudo-hyperechoic, 1137f  
 first trimester ultrasound of, 107, 107f  
 inflammatory conditions of, 910-912  
 simulating ovarian cystic teratoma, 1100f
- BPD.** *see* Biparietal diameter (BPD)
- BPP.** *see* Biophysical profile (BPP)
- BPS.** *see* Bronchopulmonary sequestration (BPS)
- Brachmann-de Lange syndrome**, 585
- Brachycephaly**, in Apert syndrome, 562
- Brachydactyly**, 298-299, 299t
- Bradycardia**, fetal, 441
- Brain.** *see also specific disorders*  
 fetal, 200, 203f  
 disruption of, in varicella zoster, 548  
 sonoluculent, 1130f  
 transverse axial sonogram of, 1129f  
 in lissencephaly, 556  
 neonatal, 157, 158f
- Branchiooculofacial syndrome**, 566
- Breathing**, fetal, 726
- Breech presentation**, 13, 15f-16f
- Brenner tumors**, 926
- Bridging vascular sign**, 899-900
- Bridging vessels**, 684, 685f
- Brittle bone disease**, 575
- Broad ligaments**, 811, 817f
- Bronchial atresia**, 355-356, 357f-358f
- Bronchogenic cyst**, 354-355, 356f
- Bronchopulmonary sequestration (BPS)**, 351, 353f, 761-762
- bSSFP.** *see* Balanced steady-state free precession (bSSFP)
- Bubble sign**, pseudo-double, 1138f
- BWS.** *see* Beckwith-Wiedemann syndrome (BWS)
- C**
- CACI.** *see* California Civil Jury Instructions (CACI)
- Calcar avis**, 211-214
- Calcarine fissure**, 211-214
- Calcification**, placental, 688, 689f
- Calcified myoma**, 1111f
- Calcified uterine arcuate vessels**, 825
- California Civil Jury Instructions (CACI)**, 20-21
- Campomelic dysplasia**, 312-313, 312f, 579, 579f
- Canalicular phase**, of lung development, 349
- Carbamazepine**, 35, 36t
- Cardiac anomalies**, congenital, and single umbilical artery, 696-697
- Cardiac axis**, 386
- Cardiac chambers**, 386
- Cardiac disease**, first trimester ultrasound of, 111, 111f
- Cardiac dysfunction**, in hydrops fetalis, 638
- Cardiac evaluation**, fetal  
 3D and 4D sonography, 396-401  
 accuracy and reproducibility of, 400-401  
 acquisition of volume datasets with, 396-397  
 display modalities in, 397-400  
 first and early second trimester 4D fetal echocardiography, 401  
 rendering techniques in, 400  
 in first and early second trimester, 372-378  
 cardiac examination, 372-376, 375f-378f  
 effectiveness of early gestation in, 376-378  
 in second trimester, 378-396  
 rationale and effectiveness, 378, 378t  
 screening, 378-391  
 standard views in, 381-384  
 four-chamber view, 381, 384f-385f, 386t  
 left ventricular outflow tract view, 381, 386f  
 right ventricular outflow tract view, 381, 387f  
 three-vessel and trachea view, 384, 388f  
 three-vessel view, 381-382, 388f  
 transabdominal view, 381, 384f  
 standardized scan planes in, 379-381, 379f-382f
- Cardiac features**, imaging of, 102-106, 104f
- Cardiac hemangiomas**  
 anatomy of, 438  
 diagnostic imaging features of, 439
- Cardiac interventions**, fetal, 789-790
- Cardiac malformations**, identification of, 58
- Cardiac masses**, 437-440  
 anatomy of, 438  
 definition of, 437, 437f  
 epidemiology of, 437-438  
 genetic considerations of, 438  
 outcomes of, 438
- Cardiac output (CO)**, 394
- Cardiac rhythm**, fetal, echocardiographic assessment of, 440, 441f
- Cardiac tumors**, 437-440  
 anatomy of, 438  
 definition of, 437, 437f  
 epidemiology of, 437-438  
 genetic considerations of, 438
- Cardiac tumors** (*Continued*)  
 outcomes of, 438  
 in tuberous sclerosis, 559
- Cardiomegaly**, 384-386
- Cardiomyopathy**, 445, 447f
- Cardiovascular disease**, fetal, 401-447  
 cardiac masses and tumors, 437-440  
 ectopia cordis/pentology of Cantrell, 439-440  
 congenital heart lesions, 402-436  
 anomalous pulmonary venous connection, 430-434  
 atrioventricular canal defects, 405-409  
 congenitally corrected transposition of the great arteries, 419-421  
 double-outlet right ventricle, 414-417  
 hypoplastic left heart syndrome, 421-428  
 situs abnormalities, 434-436  
 tetralogy of Fallot and pulmonary atresia with ventricular septal defect, 409-412  
 transposition of the great arteries, 417-419  
 tricuspid valve atresia, 428-430  
 truncus arteriosus, 413-414  
 ventricular septal defect, 402-405  
 epidemiology of, 401  
 etiology of, 401-402, 402f  
 extracardiac masses, 445-447  
 fetal cardiac arrhythmias, 440-444  
 fetal heart failure/impaired cardiovascular performance, 444-445, 446f  
 neurodevelopmental outcomes of, 402  
 pericardial effusions, 444
- Cardiovascular function**, assessment of, 393-396, 395f-396f
- Cardiovascular physiology**, fetal, 372, 373f-375f
- Cardiovascular Profile Score (CPS)**, 393-394, 395f
- Cardiovascular system**, fetal anatomy of, 183-191, 184f-191f
- Carmi syndrome**, 606
- Carpenter syndrome**, 565
- Cartilage**, development of, 273
- Cataracts**  
 congenital, 255  
 unilateral, 255
- Caudal dysplasia sequence**, 551
- Caudal regression syndrome**, 551-553, 552f-553f  
 sirenomelia and, 590
- Cavernous hemangiomas**, 267
- Cavitation**, 3
- Cavum septi pellucidi**, 212f, 216
- Cavum septum pellucidum (CSP)**, 1129f  
 absence of, in septo-optic dysplasia, 558  
 MRI of, 760f
- Cavum vergae**, 216
- CCAM.** *see* Congenital cystic adenomatoid malformation (CCAM)
- CCTGA.** *see* Congenitally corrected transposition of the great arteries (CCTGA)
- CDH.** *see* Congenital diaphragmatic hernia (CDH)
- Cell-free DNA screening**, 43-45, 44f  
 fetal, 638-639
- Central endocervical canal**, 851
- Central nervous system (CNS)**  
 congenital anomalies of, 553-560  
 Aicardi syndrome as, 553-554, 554f  
 LI syndrome as, 560  
 lissencephaly as, 556-557, 557f  
 Baraitser-Winter syndrome, 556  
 with cerebellar hypoplasia, 556  
 classic types of, 556  
 cobblestone cortical malformation, 556  
 microlissencephaly, 556  
 Neu-Laxova syndrome, 557  
 X-linked, with ambiguous genitalia, 556
- Meckel syndrome** as, 554-556, 555f  
 cystic dysplastic kidneys in, 555-556, 555f  
 genetics of, 555  
 occipital encephalocele in, 555f  
 oligohydramnios in, 555-556  
 polydactyly in, 555, 555f  
 septo-optic dysplasia as, 557-558, 558f  
 tuberous sclerosis as, 558-560, 559f-560f  
 cardiac tumors in, 559  
 genetics of, 560  
 main aspects of, 559t  
 renal angiofibromas in, 559



- Central nervous system (CNS) (*Continued*)
- fetal
    - anatomy of, 200-217, 203f-217f
    - anomalies in, MRI of, 752-755, 753f, 759f
    - embryology of, 221-232, 221f-222f
    - in first trimester
      - abnormal ultrasound findings in, 108-109
      - division of, 101
      - normal ultrasound findings in, 101-102, 101f
    - intracranial cysts and tumors in, 232-240, 236f-237f
    - ultrasound evaluation of, 220-242
  - Central placenta previa, 770f
  - Central precocious puberty, 1014
  - Cephalic presentation, of fetus, 13, 15f
  - Cephalocele, 224-225
    - conditions associated with, 226t
    - outcome of, 224-225
  - Cerclage
    - for cervical insufficiency, 668, 668t
    - transvaginal sonography in, 664
  - Cerebellar abnormalities, in aneuploidy, 61-62, 62f-63f
  - Cerebellar vermis, 207, 216
    - in Dandy-Walker malformation, 229-230
  - Cerebellum
    - hyperplasia of, with lissencephaly, 556
    - normal ultrasound findings in, 102
  - Cerebral gigantism, 622
  - Cerebral ventricle, dilated, sonogram in, 1129f
  - Cerebrocostomandibular syndrome, and Pierre Robin sequence, 569-572
  - Cerebrohepato renal syndrome, 627
  - Cervical atresia, 1007
  - Cervical cancer, 1057-1063
    - clinical staging of, 1060, 1060t
    - diagnosis of, 1060
    - epidemiology and clinical presentation of, 1057-1059
    - histopathology of, 1059-1060
    - imaging of, 1060-1063
      - early stage, 1060-1062, 1061f
      - lymph node assessment, 1062-1063
      - parametrial extension, 1062, 1062f
      - stage III, 1062, 1062f
      - stage IV, 1062, 1063f
      - tumor size assessment, 1062
    - treatment of, 1060
  - Cervical carcinoma, 878, 881f
  - Cervical cysts, 878, 878f
  - Cervical ectopic pregnancy, 986-990, 990f
  - Cervical leiomyomas, 880f
  - Cervical length
    - measurement of, in prediction of preterm birth, 657-658, 659f-660f
    - normal vs. abnormal, 660-661
    - for preterm birth prevention, 667-670
      - for asymptomatic multiple gestations, 668-669
      - for asymptomatic singletons with prior spontaneous preterm birth, 668, 668t
      - for asymptomatic singletons without prior spontaneous preterm birth, 667-668, 667f
    - in predicting success of labor induction and mode of delivery, 670
    - in prediction of start of spontaneous labor, 669, 669f
    - in preterm labor, 669, 669f
    - in preterm premature rupture of the membranes, 669
    - short, and preterm birth, 666-667
  - Cervical stenosis, endometrial interventions in, 1082-1083
  - Cervicitis, 939
  - Cervicofacial teratomas, MRI of, 755-761
  - Cervix, 825-826, 854f
    - anatomy of, 854f, 1046-1047, 1046f
    - normal zonal, 878
    - artifactual short, 1106f
    - dynamic changes of, 1107f
    - gravid, ultrasound evaluation of, 653-673
    - clinical applications of, 657-660
    - dynamic changes, 660
    - transvaginal, 655, 655f-656f, 657t, 661-665, 664t
    - for prediction of preterm birth, 657-660
    - singleton with a prior spontaneous preterm birth, 664
  - Cervix (*Continued*)
    - singleton without prior spontaneous preterm birth, 663-664
    - in triplets, 665
    - in twins, 665
    - in women with cerclage, 664
    - in women with pessary, 664-665
    - gestational age and frequency of examinations, 661
    - limitations and pitfalls of, 656-657
    - contraction in, 656, 658f
    - excessive pressure in, 656, 658f
    - full bladder in, 656
    - underdeveloped lower uterine segment in, 656-657
    - three-dimensional transvaginal, 665-666, 665f-666f
    - transabdominal, 653-654, 654t, 656f
    - translabial, 654-655, 654f, 656f
    - longitudinal transvaginal sonogram in, 1102f
    - manual examination of, 657
    - physiology of, 1046-1047, 1046f
  - Cesarean delivery
    - after hysterotomy, 776
    - placenta accreta and, 684
    - scar pregnancy after, 686-687, 687f
    - ectopic, 990-991, 991f-993f
  - CF. *see* Cystic fibrosis (CF)
  - CGH. *see* Comparative genomic hybridization (CGH)
  - CHAOS. *see* Congenital high airway obstruction syndrome (CHAOS)
  - CHARGE syndrome, 464, 464t, 597
    - major characteristics of, 597t
  - CHD. *see* Congenital heart disease (CHD)
  - Chemotherapeutic agents, teratogenicity of, 36t
  - Chest. *see also* Thorax
    - fetal, ultrasound findings of, 189f
    - in first trimester
      - abnormal ultrasound findings in, 110-111
      - normal ultrasound findings in, 102-106, 104f
  - Chiari II malformation
    - frequency of brain and spine anomalies with, 225t
    - MRI of, 758f
    - spina bifida and, 223
  - CHILD syndrome. *see* Congenital hemidysplasia with ichthyosiform erythroderma and limb defects (CHILD) syndrome
  - Chlamydia trachomatis*, 939
  - Choledochal cysts, 475
  - Choledochal malformation, types of, 477f
  - Chondrodysplasia, punctata, 278t-282t
  - Chondroectodermal dysplasia, 315-316, 316f
  - Chorangiosis, 690-691
  - Chorioamniotic separation, 777f
  - Chorioangioma, 689-691, 691f, 792-793
    - placental, 792f
  - Chorionic bridge, 677
  - Chorionic plate, 675-676
  - Chorionic villus sampling, 46-47, 47f
  - Chorionicity, 17
    - in multiple gestations, 48, 135-137, 135f, 136t-137t, 137f-138f
  - Choroid plexus
    - cysts, 75, 75f-76f, 233, 237f, 1127f
    - fetal, 200-201
      - development of, 203f
    - heterogeneous, 1128f
    - normal ultrasound findings in, 101, 101f
  - Chromosomal aberrations, and nonimmune hydrops, 645t-647t
  - Chromosomal abnormalities
    - cystic hygroma and, 110, 110t
    - facial profile abnormalities and, 62-63, 65f
    - genitourinary abnormalities and, 63
    - ocular anomalies and, 63, 66f
    - risk of, 27t
  - Chromosomal defects, 27-29
  - Chromosomal disorders, population frequency of, 28t
  - Chromosomal microarray, 51-52, 540, 542f
    - for 22q11.2 deletion, 595
    - microdeletion in, 50, 50f
  - Chromosomal rearrangements, types of, 29
  - Chromosome 22q11.2 deletion syndrome, 412t
  - Chromosome identification, 50-51, 51f
  - Chromosome number, abnormalities of, 27-29
    - Klinefelter syndrome in, 28-29
    - triploidy in, 29
    - trisomy 13 in, 28
  - Chromosome number, abnormalities of (*Continued*)
    - trisomy 18 in, 28
    - trisomy 21 in, 27-28
    - Turner syndrome in, 28
  - Chromosomes structure, abnormalities of, 29
  - Chronic ectopic pregnancy, 995-996
  - Cine clip technology, 159-160
  - Cingulate sulcus, 211-214, 213f
  - Circle of Willis, 187, 191f
    - fetal arterial Doppler sonography for, 735, 736f
  - Circulation
    - fetal vs. adult, 744-745
    - pulmonary, 347, 347f
  - Circumvallate placenta, sonogram in, 1103f
  - Cisterna magna, 1126f-1127f
    - in Dandy-Walker malformation, 229-230
  - Clavicles
    - fetal, 165, 171f-172f
    - ossification of, 275
  - Clear cell carcinoma, 1059f
  - Cleft lip/palate, 63, 66f, 300
    - bilateral, 248, 251f, 253t-254t
    - in first trimester, 109
    - median, 250, 257f
    - recurrence risk of, 248-250, 257t
    - unilateral, 248, 251f, 253f, 253t-254t
  - Cleidocranial dysplasia, 316, 317f
  - Clinical pregnancy, defined, 955
  - Clinodactyly, 277
  - CLO. *see* Congenital lobar overinflation (CLO)
  - Cloaca, 504
    - division of, 471f
    - persistent, 471-475, 473f-475f
  - Cloacal extrophy, 492f-493f, 496-497, 528, 529f
    - embryology of, 496
    - neonatal management of, 497
    - sonographic diagnosis of, 496-497
  - Cloacal extrophy sequence, 609
  - Cloacal malformation, 515, 516f, 1011, 1014f-1015f
  - Cloverleaf skull, 300f
  - Clubfoot, 77, 77f, 325, 325f
    - three-dimensional imaging of, 167f
  - Clubhand deformities, 321-325, 321t-322t
  - CNS. *see* Central nervous system (CNS)
  - CO. *see* Cardiac output (CO)
  - Cobblestone cortical malformation, and lissencephaly, 556
  - Cocaine, teratogenicity of, 36t
  - Collet-Edwards classification, of truncus arteriosus, 413
  - Colon
    - fetal, 195, 195f
    - normal, 469f
    - in third trimester, 1138f
    - rectosigmoid, 829-832, 832f
  - Color flow Doppler sonography, for placental evaluation, 139-140
  - Colpocephaly, in aneuploidy, 61-62
  - Community-acquired *Clostridium difficile* colitis, MRI and, 752f
  - Comparative genomic hybridization (CGH), 51-52, 52f
  - Computed tomography (CT), 751
    - in adnexal masses, 1069
    - in gynecologic disease, 1045-1075
    - for ovarian malignancy, 919
    - three-dimensional helical, in skeletal dysplasias, 289, 291f
  - Conal septal defects, 403, 405, 407f
  - Conceptual age, 118
  - Confined placental mosaicism (CPM), 47
  - Congenital adrenal hyperplasia, 532, 1013f-1014f
  - Congenital amputations, 317-318, 317t, 318f
  - Congenital anomalies, 540, 541f-542f
    - abnormal fetal movement as, 613-618
    - association, 540
    - of central nervous system, 553-560
    - of cranium/face, 561-573
    - deformations, 540
    - disruption, 540
    - dysplasia, 540
    - fetal growth restriction as, 623-624
    - fetal overgrowth as, 618-622
    - of gastrointestinal system/abdominal wall, 605-610
    - of genitourinary tract, 611-613
    - of heart, 594-605
    - malformation, 540, 628-632

- Congenital anomalies (*Continued*)  
 metabolic syndromes, 626-628  
 microdeletion syndromes, 624-626  
 of musculoskeletal system, 573-590  
 syndrome, 540  
 of thorax, 590-594
- Congenital complete heart block, 442-443, 443f
- Congenital cystic adenomatoid malformation (CCAM), 351, 352f-356f, 590, 788
- Congenital diaphragmatic hernia (CDH), 59-60, 60f, 362-367, 362f-367f, 761, 763f, 785-788, 786f-788f  
 first trimester ultrasound of, 111  
 left, 1141f
- Congenital heart defects  
 prenatal ultrasound of, 50  
 in trisomy 21, 27-28
- Congenital heart disease (CHD), 371-372  
 and associated clinical characteristics, 378t  
 chondroectodermal dysplasia and, 315  
 4D sonography in, 400-401  
 first trimester ultrasound of, 111  
 in Noonan syndrome, 601-603
- Congenital heart lesions, 402-436
- Congenital hemidysplasia with ichthyosiform erythroderma and limb defects (CHILD) syndrome, 319
- Congenital high airway obstruction syndrome (CHAOS), 357-359, 358f-360f, 590-591, 591f, 761, 762f
- Congenital ichthyosis, 613
- Congenital lobar emphysema, 357
- Congenital lobar overinflation (CLO), 761-762, 764f
- Congenital lymphangiectasia, 265-266
- Congenital malformations  
 mortality due to, 17  
 prenatal testing for, 49-52
- Congenital megalourethra, 515, 516f
- Congenital myasthenic syndromes, 614
- Congenital neuroblastoma, metastases from, 476
- Congenital pulmonary airway malformation (CPAM), 351-354, 352f-356f, 761-762, 764f, 788-789, 789f
- Congenital rubella syndrome, 545
- Congenital short femur, 320, 320f
- Congenitally corrected transposition of the great arteries (CCTGA), 419-421  
 anatomy of, 419  
 definition of, 419, 420f  
 diagnostic imaging features of, 421  
 epidemiology of, 419  
 genetic considerations of, 419-420  
 interventions and prognosis of, 420-421  
 rhythm abnormalities of, 419
- Conjoined twins, 144, 144t, 145f-146f  
 MRI evaluation of, 765
- Conotruncal defects, in 22q11.2 deletion syndrome, 595
- Conoventricular ventricular septal defect, 404, 405f
- Constriction rings, in amniotic band sequence, 628
- Contraction stress test, 724-726  
 contraindications to, 726
- Contrast agents, 157-158
- Contrast-enhanced computed tomography, ruptured hemorrhagic ovarian cyst at, 890f
- Conus medullaris, 302, 302f
- Copper IUD, 1087-1088
- Cordocentesis, for prediction of anemia, 639
- Cornelia de Lange syndrome, 585
- Cornual pregnancy, 978
- Corpus callosum, 214, 215f  
 agenesis of, 226, 756f  
 with absence of septum pellucidum, 229, 232f  
 complete, 227, 229f  
 MRI of, 754  
 partial, 227, 230f  
 schematic diagram of, 229f  
 syndrome associated with, 227, 231t  
 dysgenesis of, 553  
 MRI of, 755f
- Corpus luteum, 826-827, 827f  
 appearances of, 889f  
 ectopic pregnancy and, 972, 977, 982f-983f  
 sonographic imaging of, 956-957, 958f
- Cortical formation  
 abnormal, MRI of, 758f  
 disorders of, 754
- Cortical malformations, 237-240, 239f-240f, 239t-240t
- Corticosteroids, for congenital pulmonary airway malformation, 353
- Coumadin exposure, 551
- Coumarin anticoagulants, teratogenicity of, 36t
- Counseling, about examination results, 19-20
- CPAM. *see* Congenital pulmonary airway malformation (CPAM)
- CPM. *see* Confined placental mosaicism (CPM)
- CPS. *see* Cardiovascular Profile Score (CPS)
- Cranial abnormalities, and nonimmune hydrops, 645t-647t
- Cranial meningocele, 224-225, 227f
- Craniofacial anomalies, 245-262  
 facial clefts  
 atypical, 250-252, 257f-259f  
 typical, 245-250, 249f-251f, 252t-254t, 253f-257f, 257t  
 facial tumors, 257-262, 261f-262f  
 holoprosencephaly, 250-252  
 macroglossia, 257, 261f  
 micrognathia and retrognathia, 255-257, 261f  
 orbital and ocular defects, 252-255, 260f  
 3D ultrasound of, 243-244
- Craniofacial skeleton, ossification of, 275
- Craniofacial surgery, multistage, for frontonasal dysplasia, 567
- Craniosynostosis, 262-265, 264f-265f, 561-566, 561t  
 in Antley-Bixler syndrome, 561-562  
 in Apert syndrome, 562, 563f-564f  
 genetics of, 562  
 in Carpenter syndrome, 565  
 in Crouzon syndrome, 565  
 in Pfeiffer syndrome, 565-566  
 type I, 565  
 type II, 565  
 type III, 565  
 in Saethre-Chotzen syndrome, 566
- Cranium, fluid-filled intracranial area in, of embryo, 1119f
- Cri du Chat syndrome, 625
- CRL. *see* Crown-rump length (CRL)
- Crossed fused renal ectopia, 521
- Crouzon syndrome, 263, 565
- Crown-rump length (CRL), 12  
 gestational dating by, 119, 121t, 122f  
 in multiple gestations, 133, 136f  
 in pregnancy failure  
 definitive, 88, 89f  
 suspicious, 90, 90f
- Cryptophthalmos-syndactyly syndrome, 611
- CSP. *see* Cavum septum pellucidum (CSP)
- CT. *see* Computed tomography (CT)
- Cul-de-sac, 971-977, 979f-980f
- Curved linear array transducers, 847
- Cyclopia, 63, 65f  
 holoprosencephaly and, 226
- Cystadenofibroma  
 adnexal masses and, 1067  
 serous, 926f
- Cystadenoma  
 mucinous, 885f, 895f, 925f  
 serous, 888f
- Cystic benign-appearing lesions, 1067
- Cystic dysplastic kidneys, in Meckel syndrome, 555-556, 555f
- Cystic fibrosis (CF), 605, 606f  
 as autosomal-recessive disorders, 32  
 carrier screening for, 39t  
 Down syndrome and, 466-467  
 genetic screening, 38-40, 38t  
 hypercholechoic bowel in, 40f
- Cystic hygroma, 67, 68f  
 chromosomal abnormalities and, 110, 110t  
 cranial meningocele and, 224-225  
 first trimester ultrasound of, 110, 110f  
 hydrops fetalis and, 58-59, 60f  
 nuchal, 265-266, 266f-267f  
 nuchal translucency and, in twin pregnancies, 138, 140f
- Cystic lymphangiomas, 755-761
- Cystic malignant-appearing lesions, 1067, 1070f
- Cystic masses, MRI of, 763
- Cystic renal disorders, 523
- Cystocele, magnetic resonance imaging of, 1038, 1040f
- Cysts, 479-483  
 arachnoid, 230, 232, 236f  
 Blake pouch, 229  
 MRI of, 757f  
 bronchogenic, 354-355, 356f  
 cervical, 878, 878f  
 choroid plexus, 233, 237f  
 decidual, 972f  
 dermoid  
 adnexal masses and, 1067  
 ovarian, 923-924, 923f  
 differential diagnosis of, 479-480, 479t  
 enteric duplication, 481, 481f  
 Gartner duct, 828, 829f  
 nabothian, 878, 878f  
 ovarian, 480-481, 480f  
 hemorrhagic. *see* Hemorrhagic ovarian cysts  
 with indeterminate features, 925  
 with multiple thin, 925  
 ruptured, 887-891  
 ruptured, hemoperitoneum from, 809f  
 simple, 921, 921f  
 theca lutein, 929, 929f  
 with typical benign features, 920-924  
 with typical malignant features, 924  
 paratubal, 828, 829f, 937f  
 peritoneal inclusion, 897-899, 900f  
 rare causes of, 481-483  
 in umbilical cord, 694-695, 695f
- Cytomegalovirus (CMV) infections  
 congenital, 542-543, 543f  
 Down syndrome and, 467  
 intrauterine, 35, 36t, 231, 235f
- Cytotrophoblasts, 674-675, 675f
- D**
- D antigen, 636
- Dacrocystoceles, 255, 260f
- Dandy-Walker malformation (DWM), 61-62, 62f-63f, 229-230  
 abnormalities associated with, 234t  
 MRI of, 757f
- Dandy-Walker variant, 230
- de Morsier syndrome, 229, 558
- Decelerations, in fetal heart rate, 722-723, 723f
- Decidua basalis, veins in, 1110f
- Decidual cysts, 972f
- Deep pelvic endometriosis, 894-895
- Deepest vertical pocket (DVP), 706-707, 707f
- Deformations, 25, 540  
 due to oligohydramnios, 711
- Degenerated exophytic leiomyoma, 903f
- Degenerated pedunculated myoma, ectopic pregnancy and, 984f
- Dehydration, and amniotic fluid, 706
- Deletion 4p, 624
- Deletions, 29
- Delivery  
 cesarean  
 after hysterotomy, 776  
 placenta accreta and, 684  
 scar pregnancy after, 686-687, 687f  
 ectopic, 990-991, 991f-993f  
 transvaginal sonography of cervix to predict mode of, 670
- Depakote exposure, 550
- Dermatomyotomes, 275
- Dermoid cysts  
 adnexal masses and, 1067  
 ovarian, 923-924, 923f
- Developmental disorders, 25-27
- Diabetes and renal cyst syndrome, 526f
- Diamond-Blackfan syndrome, 322
- Diaphragm, structure of, 347
- Diastrophic dysplasia, 310-311, 311f
- Dichorionic twins, 1152f
- Didelphys uterus, 855, 856f, 1004-1006, 1005f-1006f
- Diethylstilbestrol, 36t  
 exposure  
 Mullerian duct anomalies and, 1049-1051, 1049f  
 uterine anomalies, 855f, 856-857
- Diffusion-weighted imaging (DWI), 751, 903-904, 1046
- Digoxin, 650t



- Discordant twin, unequal placental sharing with, 148, 153f  
 Discriminatory zone, of human chorionic gonadotropin, 84, 1093-1094  
 Disinfection, of transvaginal probe, 808  
 Disorders of sex development (DSD), classification for, 1009, 1011t  
 Display modalities, in 4D sonography and STIC, 397-400  
 Disruption, 25, 540  
 Distal ureteral calculus, 831f  
 Distended urinary bladder, 1104f  
 Diverticular abscess, 939-940, 945f  
 Diverticulitis, acute, 908-910  
   sigmoid, 912f  
 Diverticulum, respiratory, 347  
 Dizygotic twins, 132-133  
 Doppler analysis, molecular techniques for, 51  
 Dolichocephaly, 1125f  
 Donnai-Barrow syndrome, 592  
 Doppler assessment, of tracheal fluid flow, 298  
 Doppler effect, 733-734, 734f  
 Doppler indices, 734, 734f  
   in echocardiography, 744, 745f  
 Doppler of the Middle Cerebral Artery to Assess Fetal Anemia (Appendix E), 1209  
 Doppler ultrasonography, 733-748  
   for amniotic fluid volume determination, 707, 708f  
   embryonic effects from, 3  
   for evaluation of amniotic fluid in setting of polyhydramnios, 713  
   fetal arterial, 734-738  
   of middle cerebral artery, 735-736, 736f, 737t-738t, 738f-739f  
   of umbilical artery, 734-735, 734f-735f, 735t-737t  
   of uterine artery, 736-738, 739f, 740t  
   fetal cardiac, 744-745, 745f-746f, 745t-746t  
   echocardiography settings in, 744  
   optimizing image in, 744-745  
   fetal growth restriction and, 745-747  
   in management of, 747  
   as predictor of perinatal death, 746  
   fetal venous, 738-739, 740f-742f, 743t-744t, 744f  
   in first trimester, temperature elevation due to, 3  
   of inferior vena cava, 738, 741f-742f  
   physical principles, 733-734, 734f  
   of placenta, 676-677, 677f  
   bridging vessels, 684, 685f  
   cesarean scar pregnancy, 686, 687f  
   chorioangioma, 689-690, 691f  
   cord insertion, 681, 681f  
   placental lacunae, 684, 685f  
   placental sonolucencies, 687, 688f  
   succenturiate lobe, 677, 678f  
   uterine synechia, 692, 693f  
   vasa previa, 683, 683f  
   velamentous cord insertion, 681, 682f  
   for predicting pulmonary hypoplasia, 712  
   of semilunar valves, 745, 746f, 746t  
   of umbilical arteries, 504, 506f, 694, 695f  
   of umbilical cord  
   coiling, 695, 696f  
   persistent right umbilical vein, 697, 697f  
   single umbilical cord artery, 695, 696f  
   umbilical cord entanglement, 698, 699f  
   umbilical cord knot, 698, 698f  
   umbilical vein varix, 697-698, 697f  
 Doppler velocimetry  
   of pulmonary arteries, 298  
   of umbilical artery, 730, 731f  
   of uterine arteries, 737  
 Dorsal sac, 225, 228f  
 DORV. *see* Double-outlet right ventricle (DORV)  
 Double decidual sac sign, 972  
 Double-inlet left ventricle, by two-dimensional imaging, 389f  
 Double-outlet right ventricle (DORV), 414-417  
   anatomy of, 415, 415f-416f  
   definition of, 414-415  
   diagnostic imaging features of, 416-417  
   epidemiology of, 415  
   genetic considerations of, 415  
   interventions and prognosis of, 415-416  
 Double sac sign, 86, 86f  
 Down syndrome, 25-27  
   cardiac defects in, 58, 58f-59f  
   duodenal atresia in, 58, 59f  
   Down syndrome (*Continued*)  
   echogenic bowel and, 465-466  
   genetic sonogram for, 69  
   minor markers for, 74-75  
   in multiple gestations, 47-48  
   pleural effusion and, 59  
   prenatal thickness in, 74  
   pyelectasis in, 73  
   thickened nuchal fold in, 70, 71f  
   in twin pregnancies, 137-138  
 Drainages, in pelvic masses, 1088, 1089f  
 Drash syndrome, 525  
 DSD. *see* Disorders of sex development (DSD)  
 Du Pan syndrome, 319  
 Ductal arch, long-axis view of, 393, 394f  
 Ductus arteriosus, 376f, 744-745  
   absence of, 414, 414f  
   ductus-dependent congenital heart disease, 378t  
 Ductus venosus  
   Doppler studies in, 68-69, 72f  
   Doppler waveform of, 739, 742f  
   in fetal circulation, 184  
   peak velocity index of, 743t  
   preload index of, 743t  
   pulsatility index of, 743t  
   reversed flow in, 739, 744f  
   S/a ratio of, 743t  
 Duodenal atresia, in Down syndrome, 58, 59f  
 Duodenal obstruction, 465, 466f  
   "double bubble sign" of, 465  
 Duodenum, fetal, artifacts in, 1096f  
 Duplex collecting system, 509-511, 512f-513f  
 Duplications, 29  
 Dura, 206-207, 206f  
 Dural sinuses, thrombosis of, 237, 238f  
 DVP. *see* Deepest vertical pocket (DVP)  
 DWI. *see* Diffusion-weighted imaging (DWI)  
 Dynamic multiphase contrast-enhanced MRI (DCE-MRI), 1046  
 Dysencephalia splanchnocystica, 554  
 Dysgerminoma, 1068  
   ovarian, 927f, 1020, 1022f  
 Dysplasia, 540  
 Dysplastic kidneys, 521-523, 521f  
 Dyssegmental dysplasia, 312
- E**
- E/A ratio, 745, 745t  
 Eagle-Barrett syndrome, 609  
 Ears  
   anomalies of, 262, 263f  
   fetal, superficial anatomy of, 161, 165f  
 EAS. *see* External anal sphincter (EAS)  
 Ebstein malformation, of tricuspid valve, 390f  
 Echocardiography  
   fetal, 391-396  
   common indications for referral for, 391t  
   components of, 392t  
   first and early second trimester 4D, 401  
   guidelines of, 391  
   timing of, 391  
   views of, 391-393  
   bicaval view, 392, 393f  
   high short-axis view-great arteries, 393, 394f  
   long-axis view of aortic arch, 392, 393f  
   long-axis view of ductal arch, 393, 394f  
   low short-axis view-ventricles, 393, 395f  
   fetal, Doppler indices in, 744, 745f  
 Echoes, artifactual, 1097f  
 Echogenic bowel, 465-469  
   association with adverse outcomes, 465-468, 465t  
   congenital infection, 467  
   cystic fibrosis, 466-467  
   Down syndrome, 465-466  
   fetal growth restriction and stillbirth, 467-468  
   definition of, 465, 467f-468f  
   etiology of, 465  
   management of, 468-469  
 Echogenic foci, 475, 920  
 Echogenic intracardiac focus, 1134f  
   in second trimester, 73-74, 74f  
 Echogenic myocardium, 1133f  
 Echogenicity, of fetal lung, 1132f  
 Ectoderm, in female reproductive tract, 1003  
 Ectodermal dysplasia, chondroectodermal dysplasia and, 315  
 Ectopia cordis/pentology of Cantrell, 439-440  
   anatomy of, 439  
   definition of, 439, 439f  
   diagnostic imaging features of, 440  
   epidemiology of, 439  
   genetic considerations of, 439-440  
   interventions and prognosis of, 440  
   outcomes of, 440  
 Ectopic pregnancy (EP), 966-1000, 1019  
   abdominal, 991-993, 994f-995f  
   cervical, 986-990, 990f  
   cesarean scar, 990-991, 991f-993f  
   chronic, 995-996  
   clinical presentation of, 969, 969f  
   diagnostic tests for, 969-971  
   transvaginal sonography, 970-971, 971f  
   human chorionic gonadotropin in, 969-970  
   molecular biomarkers, 970  
   epidemiology of, 967  
   gestational sacs in, 86, 87f-88f  
   heterotopic pregnancies and, 996, 997f  
   interstitial, 978-985, 985f-989f  
   locations of, 967f  
   management of, 996-998  
   MRI of, 751, 751f  
   ovarian, 991, 994f  
   pathophysiology of, 968-969, 968f  
   posthysterectomy, 996  
   pseudogestational sac in, 85  
   retroperitoneal, 993-995, 995f  
   risk factors for, 967-968, 967t  
   rudimentary horn, 985-986, 989f  
   sonographic diagnosis of, 971-978  
   adnexal findings, 972, 974f-978f  
   cul-de-sac findings, 972-977, 979f-980f  
   pitfalls, 977-978, 981f-984f  
   uterine findings, 971-972, 972f-973f  
   in unusual locations, 978-995  
 Ectopic ureters, bilateral single, 529-531  
 Ectrodactyly ectodermal dysplasia-cleft lip/palate syndrome, 320-321  
 Ectrodactyly-ectodermal dysplasia-clefting syndrome, 586, 586f  
 EDC. *see* Estimated date of confinement (EDC)  
 EDD. *see* Estimated due date (EDD)  
 Elbow, fetal, 172f  
 Ellis-van Creveld syndrome, 315-316, 316f  
 Embryo  
   cranium of, 1119f  
   detecting gestational sac without yolk sac or, 84  
   development in first trimester, 83, 84t, 85f-86f  
   sonogram of, 1118f  
   in uterus, transvaginal sonogram, 1112f  
 Embryoblast, 674-675, 675f  
 Embryonic/fetal number, 12  
 Embryonic heart rate, slow, 92-93, 92f  
 Embryonic heartbeat, pregnancy failure and, 91-93, 92t  
   slow embryonic heart rate, 92-93, 92f  
   small gestational sac size, 93, 93f  
   subchorionic hematoma, 93, 93f  
 Embryonic period, fetal development in, 99-101  
 Embryonic phase, of lung development, 349  
 Embryonic tumors, in Beckwith-Wiedemann syndrome, 608  
 Empty amnion sign, of pregnancy failure, 90, 91f  
 Empty renal fossa, 518-519  
 Encephalitis, maternal, in varicella zoster, 548  
 Encephaloceles, 109, 224-225, 227f  
 Endoanal sonography  
   for anal incontinence, 1027-1029, 1028f-1029f  
   for fistulas, 1029, 1029f  
   for perianal abscesses, 1029, 1029f  
 Endocervical polyps, 878, 879f  
 Endocrine system, in septo-optic dysplasia, 558  
 Endoderm, in female reproductive tract, 1003  
 Endometrial ablation, 1077-1078  
   contraindications to, 1077t  
 Endometrial atrophy, 839-840, 840f  
 Endometrial biopsy (EMB), 838, 841f  
 Endometrial cancer, 1063-1065  
   diagnosis of, 1063  
   epidemiology and clinical presentation of, 1063

- Endometrial cancer (*Continued*)  
 histopathology of, 1063  
 imaging of, 1064-1065, 1065f-1066f  
 staging of, 1064-1065, 1064t  
 treatment of, 1063-1064
- Endometrial carcinoma, 839, 842, 843f-844f  
 incidence of, 840
- Endometrial cavity, blood in, 837-838
- Endometrial curettage, 835-836
- Endometrial hyperplasia, 840, 840f-841f
- Endometrial interventions, guidance for, 1082-1083, 1085f
- Endometrial polyps, 840-841, 841f-843f, 857  
 sonographic imaging of, 954-955, 955f-956f
- Endometrioma, 894-895, 922-923, 923f  
 complex, mimicking ovarian neoplasm, 896f  
 decidualized, 929, 930f  
 infected, 899f  
 mimics of, 895f  
 MRI of, 1067  
 ruptured, 898f  
 sonographic imaging of, 959f  
 ultrasound examination findings of, 895
- Endometriosis, 892-897, 894f, 898f, 1056-1057  
 clinicopathologic aspects of, 1057  
 definition and epidemiology of, 1056  
 in ectopic pregnancy, 968  
 etiology of, 1056  
 imaging of, 1057, 1058f-1059f  
 involving fallopian tube with hematosalpinx, 897f
- Endometriotic implant  
 abdominal wall, 898f  
 at posterior serosal surface of uterus, 898f
- Endometritis, 891f
- Endometrium, 823-824  
 abnormalities, 858  
 anatomy and physiology of, 1047, 1047f  
 decidualized, gestational sac in, 1114f  
 early proliferative phase, 824f  
 fluid, 825f  
 during menstrual cycle, 848, 849f  
 normal postmenopausal, 825f  
 periovulatory, 824f  
 polyp, 824f  
 secretory, 824f  
 sonographic imaging of, 954-955, 955f  
 changes in, 960, 960f  
 thickness of, 824, 876-877
- Endorectal sonography, 1041
- Transvaginal sonography (TVS), 953, 1094f-1095f  
 for adenomyosis, 1056  
 advantages of, 805-807  
 of cervix, 655, 655f-656f  
 for prediction of preterm birth, 657-660  
 with cerclage, 659-660, 662f-663f  
 cervical length, 657-658, 659f-660f  
 funneling, 658-659, 661f-662f  
 screening test criteria, 657, 659t  
 sludge, 659  
 total time for, 655  
 recommendations for, 657t  
 three-dimensional, 665-666, 665f-666f  
 chaperone, 808  
 contraindications for, 805-807  
 diagrammatic representation for, 806f  
 for ectopic pregnancy, 970-971, 971f  
 in evolution of endometrial assessment, 836, 836f  
 of fallopian tube, 827-828  
 free fluid in posterior cul-de-sac in normal patients, 811  
 imaging technique of, 808-811, 812f  
 indications to, 805-807  
 of intrauterine device, 1115f  
 of intrauterine pregnancy, 1095f, 1115f  
 longitudinal, in nongravid uterus, 1102f  
 normal anatomy, 804-834, 814f  
 ovarian morphologic appearance with, 806f  
 of ovaries, 826-827, 1113f  
 patient and probe preparation for, 808  
 of pelvic anatomy, 811  
 probe during, 810f-811f  
 protocols for, 807-808  
 of rectosigmoid colon, 829-832, 832f  
 of urinary bladder, distal ureters, and urethra, 829, 830f-831f
- Transvaginal sonography (TVS) (*Continued*)  
 of uterus, 821-826, 1112f  
 for vascular anatomy, 816-821
- Transvaginal transducers, for fetal anatomy, 158, 159f
- Transvaginal ultrasound-guided biopsy, in pelvic lymphoma, 1088, 1089f
- Endovascular trophoblasts, 675-676
- Entanglement, of umbilical cord, 698, 698f-699f
- Enteric duplication cysts, 481, 481f
- Enterocoele, on magnetic resonance imaging, 1038, 1041f  
 EP. *see* Ectopic pregnancy (EP)
- Epidermolysis bullosa, with pyloric atresia, 606-607
- Epignathus, 257-262, 261f-262f
- Epiphyseal ossification centers, 1149f
- Epiphyses, 274
- Epiploic appendagitis, 910, 913f
- Epispadias, 527, 613
- Epithelial tumors, adnexal masses and, 1067
- Erythroblastosis, in medullary hematopoiesis, 637-638
- Erythrocyte  
 excessive loss of, and nonimmune hydrops, 645t-647t  
 underproduction of, and nonimmune hydrops, 645t-647t
- Erythropoiesis, fetal, 637
- Esophageal atresia, 461-465, 462f-463f, 463t  
 abnormalities associated with, 461  
 antepartum management of, 464, 464t  
 differential diagnosis of, 463t  
 etiology of, 463t  
 MRI of, 761, 762f  
 neonatal management of, 464-465  
 sonographic diagnosis of, 461-464  
 types of, 463f
- Esophagus, 461-465, 462f  
 fetal, 193, 193f-194f
- Essure device, 950f-951f
- Essure microinsert, for tubal sterilization, 1084-1086, 1085f-1086f
- Estimated date of confinement (EDC), 118
- Estimated due date (EDD), 118
- Estimated Radiation Exposure to the Fetus During Radiographic Examinations (Appendix I), 1226
- Ethnicity, carrier screening and, 38, 39t
- European Society for Gynaecological Endoscopy (ESGE)  
 classification, of female genital tract congenital anomalies, 1080, 1082f-1083f
- European Society of Human Reproduction and Embryology (ESHRE) classification, of female genital tract congenital anomalies, 1080, 1082f-1083f
- Ex utero intrapartum therapy (EXIT), 777-778, 777f
- Exencephaly, 108
- EXIT procedure, MRI for, 755
- Expanded amnion sign, of pregnancy failure, 90-91, 91f
- External anal sphincter (EAS), 1026-1027  
 defects in, 1028-1029
- External genitalia, development of, 1003-1004
- Extracardiac masses, 445-447  
 first trimester ultrasound of, 111
- Extrachorial placentation, 691, 692f-693f
- Extravillous cytotrophoblasts, 675-676
- Extremities  
 abnormal ultrasound findings in, 113, 113f  
 abnormalities of, 76-77  
 normal ultrasound findings in, 107-108, 108f
- Eyes, 243  
 ocular parameters, 245t
- F**
- Face, fetal  
 anomalies of, 245-262, 318-319, 566-573, 755-762. *see*  
*also* Craniofacial anomalies  
 atypical clefts, 250-252, 257f-259f  
 branchiooculofacial syndrome as, 566  
 frontonasal dysplasia, 566-567  
 Goldenhar syndrome as, 567  
 Gorlin syndrome, 567-568  
 Hallerman-Streif syndrome as, 568  
 lateral clefts, 252, 259f  
 macroglossia, 257, 261f  
 micrognathia and retrognathia, 255-257, 261f  
 Nager syndrome, 568  
 oral-facial-digital syndrome, type I, 568-569  
 orbital and ocular defects, 252-255, 260f
- Face, fetal (*Continued*)  
 Pierre Robin sequence, 569-572  
 Treacher Collins syndrome as, 572  
 tumors, 257-262, 261f-262f  
 typical clefts, 245-250, 249f-251f, 252t-254t, 253f-257f, 257t  
 Van der Woude syndrome as, 572-573, 572f  
 X-linked Opitz G/BBB syndrome, 573
- coronal plane of, 1123f
- in first trimester  
 abnormal ultrasound findings in, 109  
 normal ultrasound findings in, 102, 103f
- images of  
 growth of ocular parameters, 245t  
 planes for, 243, 244f, 244t  
 reverse view of, 244-245, 247f  
 3D ultrasound, 243, 246f-248f  
 normal sonographic anatomy of, 243-245  
 pseudocleft of, 1122f  
 superficial anatomy of, 161, 163f-165f  
 ultrasound evaluation of, 243-271
- facial profile  
 in alobar holoprosencephaly, 65f  
 in chromosomal abnormalities, 62-63, 65f
- Faciooculoacousticorenal (FOAR) syndrome, 592
- Fallopian tube, 817f, 827-828  
 abnormal, sonographic signs of, 935, 937f-939f  
 carcinoma, 949f  
 embryology and normal anatomy of, 934-935, 935f  
 hematosalpinx, 946, 947f  
 hydrosalpinx, 892  
 interstitial portion of, 828f  
 isolated torsion of, 948f  
 malignancy of, 946-949, 949f  
 normal, 935, 936f  
 pelvic inflammatory disease and, 939-940, 941f-945f  
 simulating ovarian cysts, 1099f  
 sonographic imaging of, in infertility, 958-959, 959f  
 torsion of, 767f, 884, 946, 948f  
 isolated, 887, 888f  
 tubal patency, evaluation of, 949-951, 950f-951f  
 ultrasound evaluation of, 934-952  
 uncommon tubal infections, 940-946, 946f-947f
- Fanconi anemia, 321-322, 586
- FAS (fetal alcohol syndrome), 548-550  
 ear characteristic features in, 549f  
 facial features in, 549f  
 hand characteristic features in, 549f
- Fast imaging with steady-state precession and fast imaging employing steady-state acquisition (FIESTA), 750-751
- FaSTER trial, for Down syndrome, 801
- Fecal incontinence (FI), 1027-1028
- Federation of Gynecology and Obstetrics (FIGO)  
 classification system  
 in carcinoma, of ovary/fallopian tube, 1068-1069, 1072t  
 in cervical cancer, 1060, 1060t  
 in endometrial cancer, 1064, 1064t
- Female genitalia, fetal, 161, 167f
- Femoral angle, 292
- Femoral hypoplasia-unusual facies syndrome (FHUFS), 323f, 589
- Femoral length, short, significance of, 1147f
- Femur, fetal, 168f, 170f, 1146f  
 distal epiphysis of, 164, 168f-169f, 275f  
 distal point of, 176-177  
 measurement of, 176-177, 177f  
 ossification of, 165-176, 176f-177f  
 shortened, in achondroplasia, 581
- Femur length (FL), 277-288  
 gestational age estimation by, 125t  
 measurement of, 121, 124f  
 relationship between, foot length, 298-299, 299f  
 in skeletal dysplasias, 277-288  
 lethality and, 293
- Fetal abnormalities, observation of, 21f
- Fetal age, 6
- Fetal alcohol effects, 548-550  
 ear characteristic features in, 549f  
 facial features of, 549f  
 hand characteristic features in, 549f
- Fetal alcohol syndrome (FAS), 548-550  
 ear characteristic features in, 549f  
 facial features of, 549f  
 hand characteristic features in, 549f



- "Fetal Anatomic Survey", 17
- Fetal anatomy, ultrasound evaluation of, 157-219
- cardiovascular system in, 183-191, 184f-191f
  - central nervous system in, 200-217, 203f-217f
  - gastrointestinal system in, 191-196, 191f-197f
  - genitourinary system in, 199-200, 201f-202f
  - musculoskeletal system in, 161-183, 167f-183f
  - respiratory system in, 197-199, 197f-200f
  - superficial anatomy in, 161, 163f-167f
  - technique for, 160, 160f
- Fetal anomalies
- associated with abnormal biometry, 127-128
  - factors of, 200
- Fetal arterial Doppler, 734-738
- of middle cerebral artery, 735-736, 736f, 738f
  - peak velocity of systolic blood flow in, 738f-739f, 738t
  - resistance index of, 737t
  - of umbilical artery, 734-735, 734f-735f
  - pulsatility index of, 736t
  - resistance index of, 736t-737t
  - serial measurements of, reference values for, 735t
  - of uterine artery, 736-738, 739f
  - pulsatility index of, 740t
  - resistance index of, 740t
- Fetal biometry, 118-131
- abnormal, fetal anomalies associated with, 127-128
  - gestational age in, assignment of, 119, 126t
  - based on last menstrual period, 119
  - in second and third trimester, 119-122, 124t-125t
  - weight, estimation and percentiles of, 123-126, 126t
- Fetal blood sampling, 48
- for fetal blood type assessment, 638-639
  - example setup for, 644t
- Fetal Cardiac Measurements and Doppler Assessment (Appendix F), 1210
- Fetal Doppler Assessment (Noncardiac) (Appendix D), 1204
- Fetal endoscopic tracheal occlusion (FETO), 787-788
- Fetal growth
- abnormal, 126-127
  - biometry and, 118-131
  - studies, in multiple gestations, 140-143, 142f-143f
- Fetal growth restriction, 126-127, 467-468, 623-624
- amniotic fluid volume and, 714
  - diagnosis of, 127
  - fetal Doppler for, 745-747
  - in management of, 747
  - myocardial contractility in, 747
  - as predictor of perinatal death, 746
  - Russell-Silver syndrome, 623
  - Seckel syndrome, 623-624
  - selective, 148, 153f
  - single umbilical artery and, 697
- Fetal heart rate, 384-386
- accelerations in, 722
  - baseline, 721-722
  - with contraction stress test, 724-726
  - decelerations in, 722-723, 723f
  - interpretation of, 723-724, 725f-726f, 727t
  - measurement of, by nonstress test, 721
  - sinusoidal, 723, 724f
  - variability in, 722, 723f
- Fetal life, 13
- Fetal lung maturity, testing of, for hydrops fetalis, 641
- Fetal malformations
- comprehensive scan for, 17
  - second and third trimester ultrasound examinations for, 17
- Fetal malpresentation, 13
- Fetal-maternal hemorrhage, and maternal alloimmunization, 636
- Fetal monitoring, for nonimmune hydrops fetalis, 647-648
- Fetal movement, 302
- abnormal, 613-618
  - congenital ichthyosis, 613
  - congenital myasthenic syndromes, 614
  - congenital myotonic dystrophy, type 1, 614-615
  - fetal akinesia, 615, 615f
  - genes associated with, 616t
  - Freeman-Sheldon syndrome, 617
  - Prader-Willi syndrome, 617-618
  - assessment of, 720-721
  - randomized controlled trial for, 721
- Fetal number, 13
- Fetal overgrowth, 618-622
- Bannayan-Riley-Ruvalcaba syndrome, 618
  - Klippel-Trenaunay syndrome, 619, 619f
  - megalencephaly-polymicrogyria-polydactyly-hydrocephalus syndrome, 619-620
  - Perlman syndrome, 620
  - Proteus syndrome, 620-621
  - Simpson-Golabi-Behmel syndrome, 621
  - Sotos syndrome, 622
  - Weaver syndrome, 622
- Fetal period, 101
- Fetal phase, teratogenic susceptibility in, 35
- Fetal pole, 6
- Fetal position
- in organ imaging, 161, 162f
  - in second and third trimester ultrasound examinations, 13, 14f-15f
  - sonographic technique and, 159
  - in sonography, 158
- Fetal presentation
- breech, 13, 15f-16f
  - cephalic, 13, 15f
  - malpresentation, 13
- Fetal rubella effects, 545
- Fetal sex, evaluation of, 17-18
- Fetal stroke, 231, 235f
- Fetal surgery
- for amniotic band syndrome, 791-792, 792f
  - for cardiac interventions, 789-790
  - for chorioangioma, 792-793
  - conditions amenable to fetal therapy, 778-793
  - congenital cystic adenomatoid malformation, 788
  - for congenital diaphragmatic hernia, 785-788, 786f-788f
  - for congenital pulmonary airway malformation, 788-789, 789f
  - ex utero intrapartum therapy, 777-778, 777f
  - indications of, 776-777
  - for lower urinary tract obstruction, 790-791, 791f
  - minimally invasive maternal, 776-777, 777t
  - for monozygotic twins complications, 778-783, 779f-780f
  - selective fetal growth restriction, 780-781
  - twin anemia-polycythemia sequence, 781-782, 782f
  - twin reversed arterial perfusion sequence, 782-783, 783f
  - twin-twin transfusion syndrome, 778-780
  - twins with discordant structural anomalies, 783
  - for myelomeningocele, 776, 783-785, 786f
  - fetal therapy of, 778-793
  - lumbar, 785f
  - open maternal, 776
  - for pleural effusion, 789
  - procedures for, 775-798
  - fetoscopy, 776-777, 777t
  - laparotomy/hysterotomy, 776
  - shunt placement, 776-777
  - for sacrococcygeal teratoma, 791
- Fetal swallowing, and amniotic fluid, 705
- Fetal syndromes, ultrasound features of, 539-632
- Fetal therapy, conditions amenable to, 778-793
- Fetal thoracic circumference measurements, 351t
- Fetal urine production, 504, 526
- as source of amniotic fluid, 705
- Fetal venous Doppler, 738-739, 740f-742f, 743t-744t, 744f
- Fetal viability, 6
- Fetal weight
- determination of, 18
  - estimation and percentiles of, 123-126, 126t
- FETO. *see* Fetal endoscopic tracheal occlusion (FETO)
- Fetoscopic laser surgery, 782
- Fetoscopy, operative, 776-777
- Fetus, 6
- second trimester
  - amnion in, 1144f
  - integument in, 1120f
- FGFR genes, and craniosynostosis, 561, 561t
- FHUFs. *see* Femoral hypoplasia-unusual facies syndrome (FHUFs)
- FI. *see* Fecal incontinence (FI)
- Fibroblast growth factors (FGFs), in skeletogenesis, 273
- Fibrochondrogenesis, 306-307, 580
- Fibroids. *see* Leiomyomas, uterine
- Fibromas (Continued)
- anatomy of, 438
  - diagnostic imaging features of, 439
  - ovarian, 926, 927f
- Fibrothecomas, ovarian, 926
- Fibrous cervical stroma, 851
- Fibula, fetal, 165, 175f
- Fibula aplasia complex brachydactyly, 319
- FIESTA. *see* Fast imaging with steady-state precession and fast imaging employing steady-state acquisition (FIESTA)
- Fifth disease, 543
- First trimester
- abnormal ultrasound findings in, 108-113
  - abdomen, 111-113
  - chest, 110-111
  - extremities, 113, 113f
  - head and neck, 108-110
  - anatomy, 98-117
  - dating, 119, 120f
  - fetal anatomic survey
  - cost effectiveness of, 114
  - detection rates in, 114, 114t
  - limitations of, 113-114
  - safety of, 114-115
  - fetal development in, 98-101, 99f
  - normal ultrasound findings in, 100t, 101-108
  - abdomen, 106-107, 106f
  - chest, 102-106, 104f
  - extremities, 107-108, 108f
  - head and neck, 101-102
  - risk assessment in, 41-42
- First trimester ultrasound examination, 6-13
- artifacts, pitfalls, and normal variants, 1114-1122, 1114f-1121f
  - to detect morphologic abnormalities, 12
  - early, 82-97
  - assignment of gestational age by, 87-88
  - intrauterine pregnancies in
  - confirmation or exclusion of, when no yolk sac or embryo is seen, 84-87
  - failed, 88-91
  - normal sonographic findings in, 83, 84t
  - pregnancy failure. *see also* Pregnancy failure
  - risk factors of, 91-93, 92t
  - pregnancy number in, 93-94
  - appearing twin, 94, 95f
  - vanishing twin, 94, 94f
  - to estimate gestational age, 12
  - to evaluate placenta, 12
  - to evaluate uterus and adnexa, 13
  - to identify embryonic/fetal number, 12
  - to identify intrauterine pregnancy, 6-12, 12t
  - markers of aneuploidy, 63-69
  - absent nasal bone as, 67-68, 68f
  - cystic hygroma as, 67, 68f
  - ductus venosus Doppler studies as, 68-69, 72f
  - frontomaxillary facial angle as, 69
  - nuchal translucency as, 63-67, 67f
  - tricuspid regurgitation as, 69, 73f
- Fistulas, endoanal sonography for, 1029, 1029f
- FL. *see* Femur length (FL)
- Flecainide, 650t
- Fluid-filled endometrial cavity, 891
- Fluid resuscitation, for duodenal obstruction, 465
- Fluorescence in situ hybridization, 51
- for 22q11.2 deletion, 595
  - microdeletion in, 50, 50f
- FMR1 gene, 32
- FOAR syndrome. *see* Faciooculoacousticorenal (FOAR) syndrome
- Focal adenomyoma, 904-906
- Focal adenomyosis, 858
- Focal laxity, of anterior abdominal wall, 1136f
- Folic acid antagonists, teratogenicity of, 36t
- Follicular ring sign, 884-886, 886f
- Folliculogenesis, ultrasound in, 960-961, 960f
- Fontanelles, 178-179, 179f-180f, 206f
- Foot
- abnormalities of
  - clubfoot, 77, 77f, 325, 325f
  - "rocker-bottom feet", 77
  - length of, 299t
  - relationship with femur length, 298-299, 299f
- Forebrain, normal ultrasound findings in, 101

- Foregut, 460-461, 461f  
 Forehead, 243, 244f  
 Fossa of Waldeyer, 826  
 Four-chamber view, of fetal heart, 381, 384f-385f, 386t  
 Four-dimensional (4D) ultrasonography  
 accuracy and reproducibility of, 400-401  
 acquisition of volume datasets with, 396-397  
 volume acquisition with matrix array technology, 396-397  
 volume acquisition with mechanical transducers, 396  
 display modalities in, 397-400  
 automated display of multiple slices, 397-400, 399f  
 dynamic multiplanar display, 397, 397f-399f  
 first and early second trimester 4D fetal echocardiography, 401  
 rendering techniques in, 400  
 B-flow rendering, 400, 400f-401f  
 inversion mode, 400, 400f  
 transparency modes, 400  
 Four-dimensional spatiotemporal image correlation (4D STIC), 111  
 limitations of, 113-114  
 Fractures, 292, 293f-294f  
 Fragile X syndrome, 32  
 carrier screening for, 39t  
 Fraser syndrome, 611-612, 611f-612f  
 Fraternal twins, 132-133  
 Free pelvic fluid, 816f  
 Free radical damage, in hydrops fetalis, 638  
 Freeman-Sheldon syndrome, 617  
 Frequency shift, 733-734, 734f  
 Frontal bossing, 300f  
 Frontomaxillary facial angle, 69  
 increased, 109  
 Frontonasal dysplasia, 252, 566-567  
 Fryns syndrome, 592-593, 592f  
 Fukuyama congenital muscular dystrophy, 556  
 Full mutation, 32  
 Funneling, in prediction of preterm birth, 658-659, 661f-662f  
 cervical length vs., 658-659
- G**
- G banding, 50-51, 51f  
 Gadolinium, 750  
 Gallbladder, 476-478, 477f  
 fetal, 193, 194f  
 Gallstones, fetal, 1139f  
 Gartner duct cyst, 828, 829f  
 Gastric decompression, for duodenal obstruction, 465  
 Gastrointestinal malformations, first trimester ultrasound of, 111-112  
 Gastrointestinal system, fetal  
 anatomy of, 191-196, 191f-197f  
 disorders, 605-607  
 cystic fibrosis as, 605, 606f  
 epidermolysis bullosa with pyloric atresia, 606-607  
 megacystis-microcolon-intestinal hypoperistalsis syndrome, 607  
 nonimmune hydrops and abnormalities of, 645t-647t  
 Gastrointestinal tract, fetal  
 ascites, 478-479, 478f, 479t  
 cysts of, 479-483  
 differential diagnosis of, 479-480, 479t  
 enteric duplication, 481, 481f  
 ovarian, 480-481, 480f  
 rare causes of, 481-483  
 embryology of, 460-461, 461f  
 esophagus and stomach, 461-465, 462f  
 first trimester ultrasound of, 107  
 gallbladder, 476-478, 477f  
 liver, 475-476, 476f-477f  
 rectum, 471-475  
 small intestine, 465-471  
 spleen, 478, 478f  
 ultrasound evaluation of, 460-502  
 ventral wall defects, 483-497, 484t  
 Gastroschisis, 488f-491f, 493-496  
 adverse obstetric outcomes of, 495-496  
 associated anomalies of, 495  
 definition of, 493  
 first trimester ultrasound for, 111-112, 112f  
 neonatal management of, 496  
 Gastroschisis (*Continued*)  
 pathophysiology of, 495  
 prevalence and risk factors of, 493-495  
 in second trimester pregnancy, 1136f  
 sonographic diagnosis and obstetric management of, 496  
 GEA. *see* Global endometrial ablation (GEA)  
 Genetic analysis, techniques of, 50  
 Genetic counseling, 37  
 genetic screening and, 38  
 before prenatal diagnostic procedures, 46  
 Genetic diagnosis, in pregnancy, 45-49  
 Genetic screening  
 alpha-fetoprotein in  
 elevated maternal serum levels of, 41, 42f  
 open neural tube defects and, 40-41  
 carrier (heterozygote) screening in, 38-40  
 cell-free DNA screening in, 43-45, 44f  
 for fetal chromosomal aneuploidy, 41  
 in pregnancy, 37-41  
 for structural birth defects, 40-41  
 third-trimester complications after abnormal serum screening, 45  
 Genetics, 24-56  
 birth defects and, 25  
 chromosomal defects in, 27-29  
 developmental disorders, 25-27  
 imprinting in, 32, 33f  
 prevalence of genetic diseases, 25, 25f  
 risk assessment in  
 combined first and second, 43-45  
 in first trimester, 41-42  
 in second trimester, 42-43  
 single gene disorders, 29-34  
 teratology in, 34-37, 34f  
 Genital anomalies, 613  
 Genital hernia, ultrasound of, 1020, 1021f  
 Genital tract, fetal  
 anomalies in, 531-532  
 male, epispadias, 527  
 sonography of, 531  
 normal, 532f  
 Genitalia, fetal  
 first trimester ultrasound of, 107  
 superficial anatomy of, 161, 167f  
 Genitourinary anomalies, MRI of, 763  
 Genitourinary system, fetal  
 abnormalities, first trimester ultrasound of, 112-113  
 anatomy of, 199-200, 201f-202f  
 Genitourinary tract, fetal, 503-538  
 embryology of, 504  
 first trimester ultrasound of, 107  
 Germ cell neoplasms, 926-927  
 German measles, 545  
 Germline mosaicism, 31  
 Gestation, in cardiovascular evaluation, 376-378  
 Gestational age, 6, 118  
 assignment of, 119, 126t  
 based on last menstrual period, 119  
 in second and third trimester, 119-122, 124t-125t  
 first trimester ultrasound examination for, 12  
 weight and, assigning, 13  
 Gestational sac  
 in decidualized endometrium, 1114f  
 intradecidual sign, 972  
 small size of, in relation to embryo, 93, 93f  
 ultrasound detection of, 83, 83f-84f, 84t  
 double sac sign in, 86, 86f  
 gestational age and, 83  
 intradecidual sign in, 86, 86f  
 without an embryo or yolk sac, 84  
 Gestational trophoblastic disease (GTD), 678, 866-868, 869f-870f  
 Gestational trophoblastic neoplasia, 866, 869f-870f  
 Giant omphalocele, 486  
 Giemsa staining, 50-51  
 Gingival ridge, 192-193  
 Global endometrial ablation (GEA), 1077  
 contraindications to, 1077t  
 Glomerulocystic kidneys, 523, 526f  
 causes of, 525t  
 Goiter, fetal, 268, 268f  
 Goldenhar syndrome, 253-255, 322, 567  
 Gonadal vein thrombosis, 907, 910f  
 Gonadotropin-independent (peripheral) precocious puberty, 1014  
 Gonads, development of, 1003  
 Gorlin syndrome, 567-568  
 Gradual hypoxia concept, 726-727  
 Granulosa cell tumor, 1020, 1022f  
 of ovary, 1071f  
 Great arteries, high short-axis view of, 393, 394f  
 Grebe-Quelez-Salgado chondrodystrophy, 320  
 Grebe syndrome, 320  
 Growth, delayed, from fetal alcohol syndrome, 549-550  
 Growth hormone (GH), for achondroplasia, 305  
 GTD. *see* Gestational trophoblastic disease (GTD)  
 Gut tube, primitive, 460-461, 461f  
 Gynecologic interventions, ultrasound in, 1076-1091  
 endometrial ablation, 1077-1078, 1077f, 1077t  
 endometrial interventions, 1082-1083, 1085f  
 malpositioned intrauterine device, 1086-1088, 1087f-1088f  
 pelvic biopsies and drainage, 1088  
 tubal sterilization, correct Essure microinsert placement for, 1084-1086, 1085f-1086f  
 uterine artery embolization, 1078-1079, 1079f, 1079t  
 uterus, congenital anomalies of, repair of, 1079-1082, 1080f, 1080-1081t, 1082f-1083f  
 agenesis, 1080-1081  
 lateral fusion defects, 1081-1082  
 vertical fusion defects, 1082  
 Gynecologic ultrasound, in pediatric and adolescent patient, 1001-1024  
 ambiguous genitalia, 1009-1011, 1011t, 1012f-1015f  
 external genitalia, 1003-1004  
 gonads, 1003  
 gynecologic pelvic masses, 1020-1022  
 ovarian masses, 1020  
 ovarian tumors, 1020-1022, 1021f-1023f  
 pregnancy, 1022  
 normal anatomy in, 1002, 1002f  
 pelvic pain, 1018-1020  
 acute appendicitis, 1019-1020, 1021f  
 adnexal torsion, 1018, 1018f  
 ectopic pregnancy, 1019  
 genital hernia, 1020, 1021f  
 ovarian cyst, 1018-1019, 1019f  
 pelvic inflammatory disease, 1019, 1020f  
 prepubertal bleeding, 1011-1015  
 precocious puberty, 1011-1014, 1016f  
 vaginal foreign body, 1014, 1016f  
 vaginal masses, 1014-1015, 1017f  
 primary amenorrhea, 1015-1018, 1018f  
 reproductive tract  
 development, 1002-1004, 1004f  
 structural anomalies of, 1004-1009, 1005f-1010f, 1005t  
 technique in, 1001, 1002f
- H**
- Hair, fetal, in third trimester, 1124f  
 Half-Fourier acquisition single shot turbo spin echo (HASTE), 750  
 Hallerman-Streiff syndrome, 568  
 Hands, abnormalities of  
 clenched hand, 75f-76f  
 clinodactyly, 277  
 clubhand, 321-325, 321t-322t  
 polydactyly, 77, 323, 323f, 1150f  
 split hand and foot deformities, 320  
 trident hand in achondroplasia, 581  
 in trisomy 18, 75f-76f  
 Hard palate, 192-193  
 Harlequin ichthyosis, 613  
 HASTE. *see* Half-Fourier acquisition single shot turbo spin echo (HASTE)  
 HC. *see* Head circumference (HC)  
 hCG. *see* Human chorionic gonadotropin (hCG)  
 Head, fetal, ultrasound imaging of, artifacts, pitfalls, and normal variants, 1122-1132, 1122f-1131f  
 Head circumference (HC)  
 gestational age estimation by, 125t  
 relationship with other biometric parameters, long bone length, 277, 287f  
 second and third trimester dating by, 119-121, 122f-123f



- Heart**
- congenital anomalies of, 594-605
    - Alagille syndrome, 596, 596f
    - CHARGE syndrome, 597
      - major characteristics of, 597t
    - heterotaxy syndromes, 598-601, 600f
      - defects seen in, 598t-599t
    - Noonan syndrome, 601-603, 602f
      - management guidelines in, 601t-602t
    - Pentalogy of Cantrell, 603-605, 603f-605f
    - 22q11.2 deletion syndrome, 595, 595f
  - fetal
    - description of, 381, 382f-383f
    - fetal cardiovascular physiology of, 372, 373f-375f
    - first and early second trimester evaluation of, 372-378
      - effectiveness of early gestation in, 376-378
      - examination of, 372-376, 375f-378f
    - first trimester ultrasound of, 104-105, 105f
    - second trimester evaluation of, 378-396
      - rationale and effectiveness of, 378, 378t
      - screening of, 378-391
    - size of, 384-386
    - sonographic evaluation of, 371-459
      - standard views of, 381-384
        - four-chamber view, 381, 384f-385f, 386t
        - left ventricular outflow tract view, 381, 386f
        - right ventricular outflow tract view, 381, 387f
        - three-vessel and trachea view, 384, 388f
        - three-vessel view, 381-382, 388f
      - transabdominal view, 381, 384f
      - standardized scan planes for, 379-381, 379f-382f
      - ultrasound equipment for, 372
  - Heart defects
    - in fetal valproic acid syndrome, 550
    - in Holt-Oram syndrome, 587
  - Heart failure, fetal, 444-445, 446f
    - assessment parameters of, 445
  - Heart-hand syndrome, 586
  - Heavy metal, teratogenicity of, 36t
  - Hemangioendotheliomas, 476
  - Hemangiomas, 267, 476
  - Hematomas
    - endometrial ablation in, 1077-1078, 1077f
    - placental, 688-689, 689f-690f
    - subchorionic, 688-689
      - in pregnancy failure, 93, 93f
  - Hematosalpinx, 895
    - endometriosis involving fallopian tube with, 897f
  - Hematosalpinx, fallopian tube and, 946, 947f
  - Hemihyperplasia, in Beckwith-Wiedemann syndrome, 608
  - Hemimegalencephaly, MRI of, 759f
  - Hemivertebra, 277, 286f
  - Hemoglobin, fetal, and gestational age, 637-638, 637f
    - reference ranges for, 639t
  - Hemoglobinopathies, carrier screening for, 39t
  - Hemoperitoneum, ectopic pregnancy in, 969f, 970, 972-977, 979f-980f
  - Hemoperitoneum, in assisted reproduction, 963, 963f
  - Hemophilia A, 32
  - Hemorrhagic ovarian cysts, 887-891, 921-922, 921f
    - ruptured, 890, 890f
    - at contrast-enhanced computed tomography, 890f
    - subacute, 922f
  - Hepatic calcifications, 475
  - Hepatic fibrosis, autosomal recessive polycystic kidney disease and, 522
  - Hepatic vein, fetal, 185-186, 185f
  - Hepatoblastomas, 476
  - Herald bleed, 679
  - Heterogeneous choroid plexus, 1128f
  - Heterotaxy, 434
  - Heterotaxy syndromes, 598-601, 600f
    - defects seen in, 598t-599t
  - Heterotopic pregnancies, 996, 997f
  - High short-axis view, of great arteries, 393, 394f
  - Hindgut, 460-461, 461f
  - Hip joint, fetal, 165, 173f-174f
  - Hirschsprung disease, and L1 syndrome, 560
  - Hitchhiker thumb, in diastrophic dysplasia, 310, 311f
  - HLHS. *see* Hypoplastic left heart syndrome (HLHS)
  - Holoprosencephalies, 62, 64f-65f, 109, 225
    - with absent septum pellucidum, 225
    - alobar, 225, 228f
  - Holoprosencephalies (*Continued*)
    - classification of, 225, 227f
    - facial anomalies and, 226, 228f
    - lobar, 225-226, 228f
    - middle hemispheric variant of, 225-226
    - MRI of, 754
    - prenatal diagnosis of, 226
    - semilobar, 225-226, 756f
    - spectrum, 756f
  - Holoprosencephaly, facial anomalies and, median cleft lip, 250-252, 257f-259f
  - Holt-Oram syndrome, 322, 586-588, 587f
  - Horseshoe kidney, 520-521, 520f
  - HPV. *see* Human papillomavirus (HPV)
  - Human chorionic gonadotropin (hCG)
    - discriminatory zone of, 84
    - in ectopic pregnancy, 969-970
    - management algorithms based on discriminatory level of, 84-85
  - Human genome project, 31
  - Human papillomavirus (HPV), in cervical cancer, 1059
  - Humerus
    - fetal, 165, 171f-172f
    - ossification, 175f
    - length of, relationship with ulna length, 285f
    - proximal epiphyseal ossification center of, 274f
  - Hyaloid artery, in second trimester, 1131f
  - HyCoSy. *see* Hysterosalpingo-contrast-sonography (HyCoSy)
  - Hydantoin, 36t
  - Hydatid cyst of Morgagni, 828
  - Hydatid of Morgagni, 935
  - Hydration, and amniotic fluid, 706
  - Hydrocephalus, 61, 62f, 1130f
    - cephalocele and, 224-225
      - Dandy-Walker malformation and, 229-230
      - spina bifida and, 223-224
    - Hydrocolpos, 473-474, 474f-475f, 534
      - cysts and, 481
      - isolated, 474f
  - Hydrometrocolpos, 533f, 534
    - MRI of, 763, 766f
  - Hydronephrosis, MRI of, 751
  - Hydropic degeneration, of placenta, 870f
  - Hydropic placenta, 1108f
  - Hydrops fetalis, 634f-635f
    - background for, 633-635
    - cystic hygroma and, 58-59, 60f
    - defined, 633
    - evaluation of, 633-652
    - fetal parvovirus B19 infections and, 543-544
    - immune, 633-643
      - intrauterine transfusion for, 641-643, 642f, 642t-644t
      - management of, 638-639
      - mechanism of, 635-638, 636t, 637f
      - prediction of anemia in, 637f, 639-641, 639t, 640f
      - prognosis of, 643
    - incidence of, 635
    - maternal risks from, 649
    - nonimmune, 633-634, 643-649
      - ascites and, 58-59, 60f
      - causes and associations of, 645t-647t
      - diagnosis and management of, 649f
      - evaluation and management of, 644-647, 648f
      - mechanism of, 643-644
      - mortality rates in, 648-649
      - prognosis of, 648-649
      - therapy for selected etiologic categories of, 650t
      - treatment of, 647-648
  - Hydrosalpinx, 892, 893f, 958-959, 959f
    - appearance of, 938f-939f
    - pelvic varix mimicking, 937f
  - Hydrothorax, 789
    - aneuploidy and, 59, 60f
    - congenital, 359-362, 361f
  - Hypercohenicity, within fetal abdomen, 1137f
  - Hypercholechoic bowel, in second trimester genetic sonogram, 72
  - Hypercholechoic kidneys, 522, 522f-523f, 525f-526f
    - bilateral, causes of, 524t
  - Hyperreactio luteinalis, 929
  - Hypertelorism, 63, 252-253, 300, 302t
  - Hypertrophy, pericardial effusion on, 386-387, 388f
  - Hypervascular stalk, 864f-865f
  - Hypochondrogenesis, 307, 308t
  - Hypochondroplasia, 306
  - Hypopharynx, fetal, 1132f
  - Hypophosphatasia, 278t-282t, 310
  - Hypophosphatasia congenita, 579-580
  - Hypoplastic heart, 58, 58f
  - Hypoplastic left heart syndrome (HLHS), 421-428, 789-790
    - anatomy of, 421-423, 423f-427f
    - birth prevalence/epidemiology of, 421
    - definition of, 421, 422f
    - diagnostic imaging features of, 426-428
    - genetic considerations of, 423
    - interventions and prognosis of, 423-426
  - Hypoplastic thorax, skeletal dysplasias and, 313-316, 313t, 314f
  - Hypospadias, 532, 533f, 613
  - Hypotelorism, 63, 252-253
  - Hypoxemia, adaptive mechanisms for, and fetal heart, 747
  - Hysterectomy, for leiomyoma, 1053
  - Hysterosalpingo-contrast-sonography (HyCoSy), 958-959
  - Hysterotomy, 776
- I**
- iAREDF. *see* Intermittent absent or reversed end-diastolic flow (iAREDF)
  - IAS. *see* Internal anal sphincter (IAS)
  - Iatrogenic processes, 871-877
  - ICH. *see* Intracranial hemorrhage (ICH)
  - Identical twins, 132-133
  - IgG antibodies
    - in fetal erythropoiesis, 637
    - in Rh system, 636
  - Ileal atresia, in second half of pregnancy, 469t
  - Immune prophylaxis, for immune hydrops fetalis, 638
  - Immunoglobulin M (IgM), 636
    - detection of, in parvovirus B19 infection, 544
  - Impaired cardiovascular performance, 444-445, 446f
    - assessment parameters of, 445
  - Imperforate anus, 471-472
  - Imperforate hymen, in female reproductive tract, 1008-1009, 1010f
  - Imprinting, genetic, 32, 33f
    - abnormal, in Prader-Willi critical region, 617
  - In vitro fertilization (IVF), in ectopic pregnancy, 968
  - Incarcerated uterus, 850, 853f, 1112f
  - Indomethacin, for tocolysis, during fetoscopy, 776
  - Inevitable abortion, cervical ectopic pregnancy and, 990f
  - Infarcted necrotic ovary, ovarian torsion with, 886f
  - Infections
    - in assisted reproduction, 963, 963f
    - intrauterine, 35, 36t
      - cytomegalovirus, 231, 235f
    - maternal, 542-548
      - fetal cytomegalovirus, 542-543, 543f
      - fetal parvovirus B19, 543-544, 544f
      - fetal rubella syndrome, 544-545
      - fetal syphilis, 545-546, 546f
      - fetal toxoplasmosis syndrome, 546-547, 547f
      - fetal varicella zoster, 547-548, 548f
    - nonimmune hydrops and, 645t-647t
    - pelvic inflammatory disease and, 891
    - short TVS-CL and, 667
    - tubo-ovarian abscess, 892f
    - uncommon tubal, 940-946, 946f-947f
  - Infectious disease, prevent spread of, 808
  - Inferior vena cava
    - Doppler waveforms of, 738, 741f-742f
    - interruption of, in heterotaxy syndromes, 598
  - Infertility, 892-894
    - assisted reproduction in, complications of, 962-963
    - abscess as, 963f
    - hemoperitoneum as, 963f
    - ovarian hyperstimulation syndrome as, 962f
    - definition of, 953
    - sonographic imaging in, 953-965
      - fallopian tube, 958-959, 959f
      - hydrosalpinx, 959f
    - initial evaluation of, 953
    - ovary, 956-958, 958f
      - corpus luteum, 956-957, 958f

- Infertility (Continued)**  
 endometrioma, 959f  
 polycystic ovary syndrome, 956-957, 959f  
 treatment monitoring, 959-962, 960f-961f  
 uterus, 954-956  
 adenomyosis, 955, 956f  
 calcified intrauterine material, 956f  
 endometrial polyp, 954-955, 955f-956f  
 endometrium, 954-955, 955f  
 leiomyoma, 955, 957f  
 septate, 954f
- Intracardiac total anomalous pulmonary venous connection**, 432
- Infundibulopelvic ligament**, 884
- Inheritance, modes of**, 30f-31f
- Inner myometrial-endometrial junction**, 823
- Institutional review board (IRB)**, 750
- Integument, in second trimester fetus**, 1120f
- Intellectual disability, from fetal alcohol syndrome**, 549-550
- Intermediate villi**, 675
- Intermittent absent or reversed end-diastolic flow (iAREDF)**, 781
- Internal anal sphincter (IAS)**, 1026-1027  
 defects in, 1028-1029
- International Nomenclature and Classification of Constitutional Disorders of Bone**, 275
- International Skeletal Dysplasia Society (ISDS)**, 275-277
- Interstitial ectopic pregnancy**, 978-985, 985f-989f
- Interstitial line sign**, 978-985
- Interstitial trophoblasts**, 675-676
- Intestine, fetal**, 1139f  
 in second trimester, 467f
- Intracavitary (transvaginal) transducer, for fetal anatomy**, 158, 159f
- Intracavitary leiomyoma, submucosal**, 867f
- Intracranial cystic lesions, differential diagnosis of**, 755
- Intracranial cysts**, 232-240
- Intracranial hemorrhage (ICH)**, 231, 234t, 235f  
 imaging of, 755f
- Intracranial teratoma, MRI of**, 768f
- Intracranial tumors**, 232-240  
 congenital, 237t  
 fetal, 233-234, 238f
- Intradecidual sign**, 86, 86f, 972
- Intramural leiomyoma**, 858, 1051, 1052f
- Intrapericardial teratoma**, 438  
 diagnostic imaging features of, 439
- Intraperitoneal transfusions, for immune hydrops fetalis**, 642-643
- Intrauterine arteriovenous malformations**, 874f
- Intrauterine cerebral injuries**, 231
- Intrauterine devices (IUDs)**, 811, 813f, 872, 875f, 909f, 1087f  
 in ectopic pregnancy, 968  
 intrauterine pregnancy and, 1089f  
 malpositioned, 906, 1086-1088, 1088f  
 transvaginal sonogram of, 1115f
- Intrauterine fluid collection, ultrasound demonstrating**, 85-87  
 absence of, 84-85
- Intrauterine pregnancies**  
 confirmation or exclusion of, 84-87  
 ectopic pregnancy vs., 86  
 failed, 88-91. *see also* Pregnancy failure  
 large yolk sac, 91, 92f  
 sonographic findings definitive for, 88-89, 88t  
 sonographic findings suspicious for, 90-91, 90t  
 transvaginal sonogram of, 1115f  
 identification of, 6-12, 12t
- Intrauterine transfusion**  
 for immune hydrops fetalis, 641-643, 642f, 642t-643t  
 example setup for, 644t  
 for severe fetal anemia, 775
- Intravenous immunoglobulin (IVIG)**  
 for immune hydrops fetalis, 643  
 for nonimmune hydrops fetalis, 647
- Inversion mode**, 400, 400f
- Ionizing radiation**, 35
- Ipsilateral renal agenesis syndrome**, 855
- Ipsilateral ureter, diagram of**, 818f
- IRB. *see* Institutional review board (IRB)**
- Iron overload, in hydrops fetalis**, 638
- Irregular fetal rhythm**, 440-441, 442f
- ISDS. *see* International Skeletal Dysplasia Society (ISDS)**
- Isochromosome, in Pallister-Killian syndrome**, 593
- Isotretinoin**, 36t
- Isthmus**, 821  
 in horseshoe kidney, 520-521, 520f
- IUDs. *see* Intrauterine devices (IUDs)**
- Ivemark II syndrome**, 525f
- IVF. *see* In vitro fertilization (IVF)**
- IVIG. *see* Intravenous immunoglobulin (IVIG)**
- J**
- Jacobsen syndrome**, 625-626
- Jarcho-Levin syndrome**, 313, 314f
- Jejunal atresia, in second half of pregnancy**, 469t
- Jejunioileal obstruction**, 469-470, 469f, 469t  
 antenatal management of, 470  
 etiology of, 470  
 evaluation of, 470  
 evolution of, 468f  
 neonatal management of, 470
- Jeune syndrome**, 313-314
- Joubert syndrome**, 230, 234f, 555
- Jugular lymphatic-obstruction sequence**, 265-266
- K**
- Kick counts**, 720-721
- Kidneys, fetal**, 195, 195f, 199, 201f  
 agenesis of  
 bilateral, 518-519, 519f  
 unilateral, 519, 520f  
 corticomedullary differentiation of, 504, 506f  
 cystic diseases of, 523-525  
 differential diagnosis for, 525t  
 cystic dysplastic, in Meckel syndrome, 555-556, 555f  
 development of, 505f  
 duplication of, 509, 512f-513f  
 dysplastic, 521-523, 521f  
 ectopia of, 520  
 crossed fused, 521  
 embryonic, 504  
 first trimester ultrasound of, 107, 107f  
 fusion abnormalities of, 520-521  
 glomerulocystic, 523, 526f  
 causes of, 525t  
 growth throughout gestation, 199  
 horseshoe, 520-521, 520f  
 hyperechoic, 522, 522f-523f, 525f-526f  
 bilateral, causes of, 524t  
 imaging of, 504, 506f  
 multicystic dysplastic, 509, 521, 523-525, 526f-527f  
 nonvisualization of, 518-519  
 oval paraspinous soft tissue structure in, 1140f  
 pelvic, 520, 520f  
 threshold measurement for, 506-509  
 tumors of, 525, 528f  
 in urinary tract dilation, 506-509, 507f, 511f  
 "Kissing contractions," of lower uterine segment, 1106f
- Klinefelter syndrome**, 28-29
- Klippel-Feil syndrome**, 322-323, 583, 583f
- Klippel-Trenaunay syndrome**, 619, 619f  
 MRI of, 765, 768f
- Knee, fetal**, 165, 168f, 174f-175f, 177f
- Kniest dysplasia**, 278t-282t
- Kniest-like disorders**, 311-312
- Kniest syndrome**, 311-312
- L**
- LI syndrome**, 560
- LICAM gene**, 37
- Labia, hypertrophy of**, 531-532
- Labor induction, success of, cervical length in**, 670
- Lambda sign**, 135-136, 137f
- Laparoscopy, for ectopic pregnancy**, 996
- Laparotomy, for ectopic pregnancy**, 996
- Large for gestational age fetuses**, 127
- Laryngeal pharynx, fetal**, 192-193, 193f
- Larynx, fetal**, 197
- Last menstrual period (LMP)**, 118
- Lateral fusion defects, repair of**, 1081-1082
- Lateral ventricles, normal ultrasound findings in**, 101-102, 101f
- Left congenital diaphragmatic hernia**, 1141f
- Left ovarian vein**, 907
- Left ventricle**, 389
- Left ventricular outflow tract view, of fetal heart**, 381, 386f
- Leiomyomas, uterine**, 858-861, 862f, 866f, 899, 1051-1056  
 acute complications of, 901-903  
 additional imaging modalities and, 900  
 adenomyosis and, 904-906  
 appearance of, 864f-865f  
 classification of, 1051, 1052f  
 clinical aspects of, 1051, 1052f  
 definition and epidemiology of, 1051  
 degenerated exophytic, 903f  
 diagnosis of, 1053  
 focal adenomyosis mimicking, 908f  
 growth of, 858-861  
 imaging characteristics of, 1053-1056, 1055f  
 imaging spectrum of, 901f  
 infected and infarcted, 904f  
 intramural, 866f  
 large  
 classification of, 863f  
 echogenic, 866f  
 large intramural, 902f  
 lipoleiomyoma and, 900-901, 902f  
 locations of, 862f  
 lower uterine segment, 863f  
 malpositioned intrauterine device, 906  
 pathophysiology of, 1052, 1053f-1055f  
 sonographic imaging of, 955, 957f  
 submucosal, 861, 901f  
 treatment of, 1053
- Leiomyosarcoma**, 873f, 905f  
 cellular leiomyoma with imaging features, 906f
- Lemon sign**, 223, 1125f
- Leptomeninges, fetal**, 206-207, 206f, 216-217
- LHR. *see* Lung-to-head ratio (LHR)**
- Ligaments, broad**, 811, 817f
- Likelihood ratio (LR), Down syndrome and**, 465-466
- Limb-body wall complex**, 495f, 497, 692
- Limb deficiency**, 317-318, 317t, 318f
- Limb reduction defects**, 319-320
- Linea terminalis**, 811
- Lipoleiomyoma**, 900-901, 902f  
 spectrum of, 868f
- Lipoma, closed spina bifida with**, 224, 226f
- Lipomatous uterine tumors**, 866, 868f
- Lips**, 243, 244f, 244t  
 imaging of, 102, 103f  
 pseudocleft of, 1123f
- Lissencephaly**, 556-557, 557f  
 Baraitser-Winter syndrome, 556  
 with cerebellar hypoplasia, 556  
 classic types of, 556  
 cobblestone cortical malformation, 556  
 microlissencephaly, 556  
 Neu-Laxova syndrome, 557  
 X-linked, with ambiguous genitalia, 556
- Lithium**, 36t
- Liver, fetal**, 184-185, 187f, 195-196, 197f, 475-476, 476f-477f  
 malformations of, 476f
- LMP. *see* Last menstrual period (LMP)**
- Long-axis view**  
 of aortic arch, 392, 393f  
 of ductal arch, 393, 394f
- Longitudinal vaginal septum, repair of**, 1082
- Low short-axis view, of ventricles**, 393, 395f
- Lower extremity anomalies**, 589-590  
 femoral hypoplasia-unusual facies syndrome, 589  
 Pallister-Killian syndrome, 593, 593f  
 Scimitar syndrome as, 594  
 sirenomelia, 589-590, 590f
- Lower urinary tract obstruction (LUTO)**, 790-791, 791f  
 megacystis and, 113
- LR. *see* Likelihood ratio (LR)**
- Lumbar myelomeningocele**, 785f
- Lung, fetal**  
 development of, 347, 347f-348f  
 dimensions, by two-dimensional ultrasound, 293, 294f-295f, 295t-297t  
 echogenicity of, 1132f  
 secretion of fluid, and amniotic fluid, 705



- Lung bud, 347  
 Lung fluid, secretion of, and amniotic fluid, 705  
 Lung-to-head ratio (LHR), congenital diaphragmatic hernia and, 365-366  
 Lung volumetry, by three-dimensional sonography, 293-298, 297f  
 LUTO. *see* Lower urinary tract obstruction (LUTO)  
 Lying-down adrenal sign, 519f, 529-530  
 Lymphangiectasia, aneuploidy and, 58-59, 60f  
 Lymphangiomas, 257-262, 267, 267f  
   cystic, 755-761  
   in MRI, 765  
 Lymphovenous malformations, 755-761  
 Lynch syndrome, 930
- M**
- Macrocephaly, holoprosencephaly and, 225  
 Macroglossia, 257, 261f  
 Macrosomia, 127  
 Macrostomia, 252  
 Magnetic resonance imaging (MRI), 749-774  
   abnormal placentation, 765-768  
   abnormalities in fetal abdomen, 762-763  
   acquisitions, 751  
   in adenomyosis, 1056, 1057f  
   in adnexal masses  
     cystic malignant-appearing lesions, 1067, 1070f  
     with distinctive imaging features, 1067, 1068f-1069f  
     imaging diagnosis of, 1066-1067  
     predominantly solid lesions, 1067-1068, 1071f  
     preoperative staging, 1068-1070  
     specific diagnosis of, 1067-1070  
   advantages of, 749  
   balanced steady-state free precession, 750-751  
   biologic risks of, 749  
   in central nervous system anomalies, 752-755, 753f, 759f  
   in cervical cancer, 1057-1063, 1061f-1062f  
   in congenital anomalies, 1048-1051  
     agenesis/hypoplasia, 1048  
     arcuate uterus, 1049  
     bicornuate uterus, 1049, 1050f  
     diethylstilbestrol exposure, 1049-1051  
     mullerian duct, 1048-1051, 1049f  
     ovarian, 1051  
     septate uterus, 1049, 1050f  
     unicornuate uterus, 1048-1049  
     uterus didelphys, 1049, 1050f  
     vaginal, 1051, 1051f  
   diffusion-weighted, 751  
   emerging concepts of, 768-769  
   in endometrial cancer, 1063-1065, 1065f-1066f  
   in endometriosis, 1056-1057, 1058f-1059f  
   estimation of pulmonary hypoplasia by, 298  
   in face, neck, thorax anomalies, 755-762  
   fetal, 752-769, 753t  
   of fetus, 157, 159f  
   in gynecologic disease, 1045-1075  
   in leiomyomas, 1051-1056, 1052f-1055f  
   maternal, 751-752, 753f  
   of maternal hydronephrosis, 751  
   monochorionic twins, 765, 768f  
   for pelvic floor, 1027, 1034-1040  
     abnormal findings on, 1036-1039, 1038f-1041f  
     limitations of, 1039-1040  
     reference lines, 1036, 1037f  
     technical considerations in, 1034-1036  
   for placenta accreta, 684-686, 686f  
   safety in, 749-750  
   T1-weighted, 750  
   T2-weighted, 750  
   rapid acquisition with relaxation enhancement, 750  
   techniques for, 750-751  
   in tumors, 763-765  
   in urogynecology, 1025-1044  
 Magnetic Resonance Imaging of the Female Pelvis: Representative Protocols (Appendix J), 1228  
 Malformations, 25, 540, 628-632  
   amniotic band sequence, 628-631, 629f-630f  
   VACTERL association, 631-632, 631f-632f  
 Malpositioned intrauterine device, 906  
 Malpractice, 20  
 Mandible, fetal, 178-179, 192f, 244f  
 Mandible width/maxilla width (MD/MX) ratio, 300, 301f  
 Mandibulofacial dysostosis, 572  
 Maternal diabetes, 551-553, 552f-553f  
 Maternal-fetal ABO incompatibility, 638  
 Maternal-fetal surgery  
   minimally invasive, 776-777, 777t  
   open, 776  
 Maternal floor infarction, 688  
 Maternal serum alpha-fetoprotein (MSAFP), 783  
 Maternal spiral arterioles, invasion of, 736-737  
 Matrix array technology, volume acquisition with, 396-397  
 Mature cystic teratoma, 887f, 891, 923-924  
   ruptured, 891f  
 Maxilla, fetal, 178-179  
 Maximal vertical pocket (MVP), 142-143, 143f, 706-707  
 Mayer-Rokitansky-Küster-Hauser (MRKH) syndrome, 612, 852, 1048, 1080-1081  
 MCA. *see* Middle cerebral artery (MCA)  
 MCD (medullary cystic dysplasia), 523, 525f  
 MCDK (multicystic dysplastic kidney), 509, 521, 523-525, 526f-527f  
 Mean sac diameter  
   gestational dating by, 119, 120f, 121t  
   in pregnancy failure  
     definitive, 88-89, 89f  
     suspicious, 90, 91f  
 Measurements for Amniotic Fluid Assessment (Appendix C), 1200  
 Measurements Frequently Used to Estimate Gestational Age and Fetal Biometry (Appendix A), 1155  
 Measurements Used in Assessing Fetal Weight, Growth, and Body Proportions (Appendix B), 1174  
 Mechanical transducer, volume acquisition with, 396  
 Meckel-Gruber syndrome, 109, 525f, 554  
 Meckel syndrome, 554-556, 555f  
   cystic dysplastic kidneys in, 555-556, 555f  
   genetics of, 555  
   occipital encephalocele in, 555f  
   oligohydramnios in, 555-556  
   polydactyly in, 555, 555f  
 Meconium ileus, MRI of, 765f  
 Meconium peritonitis, 470-471, 470f  
 Meconium pseudocyst, 471  
 Median cleft face syndrome, 252  
 Mediastinal abnormalities, and nonimmune hydrops, 645t-647t  
 Medications and Reported Associated Malformations (Appendix H), 1223  
 Medullary cystic dysplasia (MCD), 523, 525f  
 Medullary hematopoiesis, 637-638  
 Mega-cisterna magna, 229  
 Megacystis, 515f  
   first trimester ultrasound of, 113  
 Megacystis-microcolon-intestinal hypoperistalsis syndrome, 515-516, 607  
 Megalencephaly, 232  
 Megalencephaly-capillary malformation, 620  
 Megalin, in Donnai-Barrow syndrome, 592  
 Megalourethra, 515, 516f  
 Megaureter, nonobstructive, 517-518, 518f  
 Membranes, ultrasound evaluation of, 674-703  
 Membranous ventricular septal defect, 403-404, 404f  
 Meningocele, 224  
   cranial, 224-225, 227f  
 Menstrual age, 6, 118  
 Menstrual cycle, endometrium during, 848, 849f  
 Mental retardation aphasia, spastic paraplegia, adducted thumbs (MASA) syndrome, 560  
 Mercury, organic, 36t  
 Mermaid syndrome, 590  
 Mesenchymal hamartomas, 476  
 Mesenteric cyst, 481  
 Mesentery, inflammatory conditions of, 910-912  
 Meso-ovarium, endovaginal sonography of, 817f  
 Mesoblastic nephroma, 525  
 Mesoderm, in female reproductive tract, 1003  
 Mesomelia, 277, 285f, 285t  
 Mesonephric ducts, 828  
 Mesonephros, 504, 505f  
 Metabolic disorders, and nonimmune hydrops, 645t-647t  
 Metabolic syndromes, 626-628  
   Neu-Laxova syndrome, 626  
   Smith-Lemli-Opitz syndrome as, 626-627  
   anomalies associated with, 627t  
   Zellweger syndrome, 627-628  
 Metanephros, 504, 505f  
 Metaphyseal flaring, 291-292  
 Metastases, from congenital neuroblastoma, 476  
 Metatropic dysplasia, 278t-282t  
 Methotrexate (MTX), for ectopic pregnancy, 996, 998  
 Meyer-Weigert rule, 512f  
 Microcephaly, 231-232  
   etiologic classification of, 236t  
   holoprosencephaly and, 225  
 Microdeletion syndromes, 29, 29t, 540, 624-626  
   deletion 4p (Wolf-Hirschhorn syndrome), 624  
   deletion 5p (Cri du Chat syndrome), 625  
   deletion 11q (Jacobsen syndrome), 625-626  
   detection of, 50, 50f  
 Microduplication syndromes, 540  
 Micrognathia, 62-63, 65f, 109, 255-257, 261f, 300, 301f, 301t  
   MRI of, 761  
   in Pierre Robin syndrome, 569, 571f  
 Microlissencephaly, 556  
 Micromelia, 277, 285f, 285t  
 Microphthalmia, 63, 253-255  
 Midbrain  
   fetal, 207f  
   normal ultrasound findings in, 101  
 Middle cerebral artery (MCA)  
   color Doppler of, 640, 640f  
   fetal Doppler of, 735-736, 736f, 738f  
   peak velocity of systolic blood flow in, 738f-739f, 738t  
   resistance index of, 737t  
   peak systolic velocity in, measurement of, 639-641, 639t  
   elevated, 641  
 Midgut, 460-461, 461f  
   physiologic herniation of, 106, 106f, 111  
 Midline anomalies, 225-229  
 Midpubic line, in pelvic floor, 1036  
 Miller-Dieker syndrome, and lissencephaly, 557f  
 Minimally invasive maternal-fetal surgery, 776-777, 777t  
 Minimum projection mode (MPM), 400  
 Mirena IUD, 1087-1088  
 Mirror image artifact, 1095-1098, 1095f-1096f  
 Mirror syndrome, 649  
 Miscarriage, 88-91. *see also* Pregnancy failure  
 Misoprostol, 36t  
 Missing digits, apparent, 1150f  
 Mitochondria, 32-33  
 Mitochondrial disorders, 32-33  
 Mitral valves, 389, 389f  
 Mittelschmerz, defined, 887-888  
 Mixed total anomalous pulmonary venous connection, 433  
 MLPA. *see* Multiplex ligation-dependent probe amplification (MLPA)  
 MMC. *see* Myelomeningocele (MMC)  
 Moebius sequence, 318-319  
 Molecular biomarkers, in ectopic pregnancy, 970  
 Molecular-Pathogenetic Classification of Skeletal Dysplasias, 275-277, 278t-282t  
 Monoamniotic twins, 143-144, 143f-144f  
 Monochorionic diamniotic twin pregnancy, with twin-to-twin transfusion syndrome, 1153f  
 Monochorionic twins, 1152f  
   complicated, 778-783, 779f-780f  
   selective fetal growth restriction, 780-781  
   twin anemia-polycythemia sequence, 781-782, 782f  
   twin reversed arterial perfusion sequence, 782-783, 783f  
   twin-twin transfusion syndrome, 778-780  
   twins with discordant structural anomalies, 783  
   MRI of, 765, 768f  
 Monosomy, 27  
 Monozygotic twins, 132-133  
   types of, 136t  
 Morphogenesis, errors in, 25, 26f, 541f  
 Morphologic abnormalities, first trimester ultrasound examination for, 12  
 Mosaicism, 27  
   confined placental, 47  
   germline, 31  
 MPI. *see* Myocardial performance index (MPI)  
 MRI. *see* Magnetic resonance imaging (MRI)  
 MRKH syndrome. *see* Mayer-Rokitansky-Küster-Hauser (MRKH) syndrome  
 MSAFP. *see* Maternal serum alpha-fetoprotein (MSAFP)

- Mucinous cystadenoma, 885*f*, 895*f*, 1020-1022, 1023*f*  
 Mucosal star, 1029-1030  
 Mullerian duct  
 anomalies of, 852, 1048-1051  
 agenesis/hypoplasia, 1048, 1049*f*  
 in American Fertility Society Classification System, 1080, 1080*f*, 1080*r*  
 arcuate uterus, 1049, 1049*f*  
 bicornuate uterus, 1049, 1049*f*-1050*f*  
 classification of, 1004, 1005*f*, 1049*f*  
 diethylstilbestrol exposure, 1049-1051, 1049*f*  
 septate uterus, 1049, 1049*f*-1050*f*  
 unicornuate uterus, 1048-1049, 1049*f*  
 uterus didelphys, 1049, 1049*f*-1050*f*  
 development of, 1003-1004  
 unilateral, 852  
 Multicompartmental prolapse, magnetic resonance imaging of, 1038, 1040*f*  
 Multicystic dysplastic kidney (MCDK), 509, 521, 523-525, 526*f*-527*f*  
 Multifactorial inheritance, 33-34  
 Multifetal pregnancies, selective termination of, 48  
 Multiplanar display, dynamic, 397, 397*f*-399*f*  
 Multiple gestations  
 amniotic fluid volume in, 16  
 asymptomatic, cervical length in prevention of preterm birth in, 668-669  
 postprocedural loss rates in, 48  
 prenatal diagnosis in, 47-48  
 prenatal screening in, 45  
 rates of, 133*f*, 135*t*  
 timing of cleavage in, 133, 136*f*, 136*t*  
 ultrasound evaluation of, 132-156, 154*t*  
 amniocentesis in, 136-137, 137*t*, 138*f*-139*f*  
 anatomic survey in, 138-139, 140*f*  
 cervical length in, 140  
 chorionicity in, 135-137, 135*f*, 136*t*-137*t*, 137*f*-138*f*  
 fetal growth studies in, 140-143, 142*f*-143*f*  
 nuchal translucency in, 137-138, 139*f*-140*f*  
 placental evaluation in, 139-140, 141*f*-142*f*  
 pregnancy dating in, 133  
 serial surveillance in, 143-150  
 ultrasound examination of, artifacts, pitfalls, and normal variants, 1151, 1151*f*-1154*f*  
 Multiple slices, automated display of, 397-400, 399*f*  
 Multiplex ligation-dependent probe amplification (MLPA), for 22q11.2 deletion, 595  
 MURCS association, 612  
 Muscle-eye-brain disease, 556  
 Muscular ventricular septal defects, 404, 406*f*  
 Musculoskeletal system  
 congenital anomalies of, 573-590  
 lower extremity, 589-590  
 skeletal dysplasias as, 573-580  
 upper extremity, 585-589  
 vertebral, 583-585  
 fetal, 272-345  
 anatomy of, 161-183, 167*f*-183*f*  
 development of, 273-275, 273*f*  
 skeletal dysplasias, 275-303  
 Myelomeningocele (MMC), 108, 223, 225*f*, 776, 783-785, 786*f*, 1125*f*  
 Chiari II malformation and, 223, 225*t*  
 fetal therapy for, 778-793  
 lumbar, 785*f*  
 MRI of, 754  
 Myocardial cell damage, in fetal growth restriction, 747  
 Myocardial contractility, reduced, in fetal growth restriction, 747  
 Myocardial deformation imaging, 394-396  
 Myocardial performance index (MPI), 394, 396*f*  
 Myocarditis, 445, 447*f*  
 Myocardium, echogenic, 1133*f*  
 Myoma. *see also* Leiomyomas, uterine  
 calcified, 1111*f*  
 large uterine, 863*f*  
 myometrial contraction in, 1105*f*  
 pedunculated submucosal, 1079, 1079*f*  
 Myomectomy, for leiomyoma, 1053  
 Myometrial contractions  
 of lower uterine segment, 1105*f*-1106*f*  
 in myoma, 1105*f*  
 in trimester sonograms, 1104*f*  
 Myometrial layers, 823*f*  
 Myometrium, 848  
 inner, 823*f*  
 veins in, 1110*f*  
 Myotonic dystrophy, congenital, type 1, 614-615  
 Myxoma  
 anatomy of, 438  
 diagnostic imaging features of, 439  
**N**  
 Nabothian cysts, 878, 878*f*  
 Nager syndrome, 568  
 Nasal bone, fetal, 244*t*  
 absent, 67-68, 68*f*, 109  
 in second trimester, 70-72, 71*f*  
 in first trimester, 1121*f*  
 hypoplastic, in second trimester, 70-72, 71*f*  
 NBCCS. *see* Nevoid basal cell carcinoma syndrome (NBCCS)  
 Neck, fetal  
 anomalies of, 265-268, 266*f*  
 MRI of, 755-762  
 artifacts, pitfalls, and normal variants in imaging of, 1122-1132  
 normal ultrasound findings in, 102  
 ultrasound evaluation of, 243-271  
 webbed, 266  
 Neck masses, 266-268  
 Neisseria gonorrhoeae, 939  
 Neonates  
 managing urinary tract dilatation in, 517, 517*f*  
 ultrasonic imaging of, 157, 158*f*-159*f*  
 Neoplasm, in right ventricle, 1133*f*  
 Nephrogenesis, 522  
 Nephroma, mesoblastic, 525  
 Nephron, 504, 505*f*  
 Neu-Laxova syndrome, 626  
 and lissencephaly, 557  
 Neural tube defects (NTDs), 35, 108, 222-225, 550  
 anencephaly, 222-223, 224*f*  
 causes of, 224*t*  
 cephalocele, 224-225, 226*t*, 227*f*  
 incidence of, 222, 223*t*-224*t*  
 inheritance of, 34  
 open, alpha-fetoprotein and, 40-41, 40*f*  
 risk factors for, 224*t*  
 spina bifida, 223, 225*f*-226*f*  
 Neuroblastoma, 530-531, 531*f*  
 Neuronal migration, anomalies of, 237-240, 239*f*-240*f*, 239*t*-240*t*  
 Nevoid basal cell carcinoma syndrome (NBCCS), 567  
 Newborn  
 evaluation of, 302-303  
 skeleton of, 276*f*  
 Nondisjunction, 27  
 Nonobstructive megaureter, 517-518, 518*f*  
 Nonstress test, 721-724, 722*f*  
 nonreactive, 723-724  
 and prevention of stillbirth, 724  
 reactive, 723-724  
 Nonviable fetuses, 6  
 Noonan syndrome, 601-603, 602*f*  
 management guidelines in, 601*t*-602*t*  
 Nose, 243  
 NTDs. *see* Neural tube defects (NTDs)  
 Nuchal cords, of umbilical cord, 698  
 Nuchal fold, 1124*f*  
 thickened, in second trimester, 70, 71*f*  
 Nuchal translucency, 41-42, 63-67  
 erroneous measurement of, 1120*f*  
 first trimester ultrasound of, 102, 104*f*  
 measurement of, 66, 67*f*  
 in multiple gestations, 137-138, 139*f*-140*f*  
 cystic hygroma and, 138, 140*f*  
 in Noonan syndrome, 601-603, 602*f*  
 as risk factor for aneuploidy, 109-110, 110*f*  
 skeletal dysplasias and, 303, 303*t*  
 thickness, cardiac anomalies in, 109-110, 109*t*  
**O**  
 Obese gravidas, 799  
 Down syndrome in, 801  
 ultrasound image quality in, 801*t*  
 Obesity  
 and amniotic fluid volume, 708, 709*f*  
 maternal  
 fetal anomalies associated with, 800*t*  
 fetal head scan in, 802*f*  
 risk associated with, 800*t*  
 obstetric ultrasound and, 799-803, 800*f*-801*f*  
 BMI category, 800*t*  
 fetal head scan in, 802*f*  
 Obstructed defecation, MRI for, 1038  
 Obstructed hemivagina and ipsilateral renal anomaly (OHVIRA), 855  
 Obstructed hemivagina syndrome, 855  
 Obstructive uropathy, 912  
 Occipital encephalocele, in Meckel syndrome, 555*f*  
 Occipitofrontal diameter (OFD), second and third trimester dating by, 121, 122*f*  
 Occupational Safety and Health Administration (OSHA), 808  
 Ocular anomalies, in chromosomal abnormalities, 63, 66*f*  
 Ocular defects, 252-255, 260*f*  
 Ocular parameters, 245*t*  
 OEIS complex (omphalocele, cloacal exstrophy, imperforate anus, and spinal anomalies), 496-497, 528  
 embryology of, 496  
 neonatal management of, 497  
 sonographic diagnosis of, 496-497  
 OFD. *see* Occipitofrontal diameter (OFD)  
 Offset atrioventricular valves, 389-390, 390*f*  
 OHSS, Ovarian hyperstimulation syndrome (OHSS)  
 OHVIRA. *see* Obstructed hemivagina and ipsilateral renal anomaly (OHVIRA)  
 OI. *see* Osteogenesis imperfecta (OI)  
 Oligohydramnios, 708  
 autosomal recessive polycystic kidney disease, 522  
 cause of, 711  
 diagnosis of, 15-16  
 in fetal growth restriction, 714  
 in lower urinary tract obstruction, 512  
 in Meckel syndrome, 555-556  
 and pregnancy outcomes, 711  
 setting of, prediction of pulmonary hypoplasia in, 712  
 Omental cyst, 481  
 Omphalocele, 483-493, 484*t*  
 aneuploidy and, 60-61, 61*f*  
 associated aneuploidies in, 484  
 associated syndromes of, 484-485  
 counseling and obstetric management of, 490-493  
 diagnosis of, 486-490, 486*t*  
 first trimester ultrasound of, 111  
 giant, MRI of, 767*f*  
 neonatal management of, 493  
 nonchromosomal anomalies of, 485  
 nuchal translucency and, 110*f*  
 prevalence of, 483-484, 484*t*  
 prognosis of, 486  
 sonographic diagnosis of, 485-486, 485*f*-487*f*  
 Oocyte retrieval, transabdominal ultrasound for, 960-961, 961*f*  
 Open fetal myelomeningocele repair, 785*f*  
 Open maternal-fetal surgery, 776  
 Oral cavity, 244*t*  
 Orbit, fetal, 178-179, 179*f*  
 Orbital defects, 252-255, 260*f*  
 Orbital teratoma, 257-262, 262*f*  
 Orchiopexy, for prune-belly syndrome, 610  
 Organic mercury, teratogenicity of, 36*t*  
 Orofacial clefts, 245  
 anomalies associated with, 248, 252*t*  
 embryonic development and, 248, 249*f*-251*f*  
 prognosis for, 250  
 Oronasal cavity, and amniotic fluid, 706  
 Oropharyngeal teratoma, large, MRI of, 761*f*  
 Oropharynx, fetal, 192-193, 193*f*  
 OSHA. *see* Occupational Safety and Health Administration (OSHA)  
 Ossification, 273-275, 274*f*-276*f*  
 centers of, 273-274, 276*f*  
 epiphyseal, 1149*f*  
 femoral, 274-275, 275*f*  
 primary, 274  
 secondary, 274  
 tibial, 275*f*



Ossification (*Continued*)

- endochondral, 273-275, 274f
- intramembranous, 275
- Osteochondrodysplasias, 303-320
- Osteogenesis imperfecta (OI), 309-310, 575-577, 576f-577f
  - classification of, 309, 309t
  - nosology of, 278t-282t
  - prevalence of, 275, 277t
- Ovarian abnormality, absence of associated, 884
- Ovarian artery, transvaginal sonography of, 817f, 821f
- Ovarian carcinoma, coexistent, pregnancy with, 1101f
- Ovarian cysts, 480-481, 480f, 887-888, 889f, 1018-1019, 1019f, 1097f
  - dilated fallopian tubes simulating, 1099f
  - fetal, 532-534, 533f
  - hemorrhagic, 887-891, 921-922, 921f
    - ruptured, 890, 890f
    - at contrast-enhanced computed tomography, 890f
    - subacute, 922f
  - with indeterminate features, 925
  - with multiple thin, 925
  - ruptured, hemoperitoneum from, 809f
  - simple, 921, 921f
  - teratoma, bowel simulating, 1100f
  - theca lutein, 929, 929f
  - with typical benign features, 920-924
  - with typical malignant features, 924
- Ovarian dysgerminoma, 1020, 1022f
- Ovarian ectopic pregnancy, 991, 994f
- Ovarian follicle, 920
  - development of, 920f
  - dominant, 826-827, 827f
- Ovarian hyperstimulation syndrome (OHSS), 962-963, 962f
- Ovarian mass(es), 1020
  - Doppler imaging and, 928
  - endometriosis, 892-897, 898f
  - enlarging found on serial sonograms, 899f
  - in pregnancy, 929
  - solid, 926-928
- Ovarian torsion, 767f, 884-886, 885f
  - CT in, 887f
  - with infarcted necrotic ovary, 886f
  - MRI in, 888f
  - with mucinous cystadenoma, 885f
- Ovarian tumors, 1020-1022, 1021f-1023f
- Ovarian vein
  - left, 907
  - thrombophlebitis, 907
- Ovarian volume, 826
- Ovary(ies), 826-827
  - anatomy and physiology of, 1047-1048, 1048f
  - anomalies in, 1051-1056
  - benign mature cystic teratoma of, 1068f
  - calcification, 920f
  - clear cell cystadenocarcinoma of, 924f
  - diagram of, 816f, 818f
  - endometrioma in, 1058f-1059f
  - granulosa cell tumor of, 1071f
  - inferior aspect of, 826
  - lateral surface of, 826
  - metastases to, 927, 927f
  - neonatal, anatomy of, 1002, 1002f
  - normal, 826f
  - normal and inconsequential findings, 920
  - pelvic inflammatory disease and, 939
  - pitfalls in evaluating, 928, 929f
  - postmenopausal, 821f, 828f
  - serous cystadenocarcinoma of, 925f, 1070f
  - serous cystadenofibroma of, 926f
  - soft tissue mass in, 1113f
  - sonographic imaging of, in infertility, 956-958, 958f
    - corpus luteum, 956-957, 958f
    - endometrioma, 959f
    - on follicular monitoring studies, 960-961, 961f
    - following oocyte retrieval, 960-961, 961f
    - polycystic ovary syndrome, 956-957, 959f
  - tiny echogenic foci in, 920f
  - ultrasound evaluation of, 919-933
    - dermoids, 923-924, 923f
    - endometriomas, 922-923, 923f
    - mature cystic teratomas, 923-924
    - neoplasms, 924
    - syndromes and diseases associated with, 929-930

## P

- Pachymeninx, fetal, 206-207, 206f
- Palate, fetal, 244-245, 244t, 247f
  - development of, 248, 249f-251f
  - imaging of, 102, 103f
- Pallister-Killian syndrome, 593, 593f
- Pancreas, fetal, 191-192, 191f
- Papillon-Léage-Psaume syndrome, 568
- Paraovarian cyst, 928f
- Parasitic leiomyoma, 858
- Parasympathetic innervation, fetal heart rate and, 721-722
- Paratubal cysts, 829f, 937f
- Parfait sign, 1057
- Partial anomalous pulmonary venous connection or drainage (PAPVC), 433
- Partial molar pregnancy, 871f
- Parvovirus B19 infection, fetal, 543-544, 544f
  - and hydrops fetalis, 543-544
- Passive immunoglobulin administration, 638
- Patent urachus, 694
- Paternal testing, for fetal anemia, 638
- PATSS. *see* Postablation tubal sterilization syndrome (PATSS)
- PCL. *see* Pubococcygeal line (PCL)
- PCS. *see* Pelvic congestion syndrome (PCS)
- Peak systolic velocity, measurement of, for fetal anemia prediction, 639-641, 639t
  - elevated, 641
- Pedigrees, of modes of inheritance, 31f
- Pedunculated myoma, degenerated, ectopic pregnancy and, 84f
- Pedunculated submucosal myomas, 1079, 1079f
- Pelvic brim, 811
- Pelvic congestion syndrome (PCS), 906-907, 909f
- Pelvic floor
  - anatomy of, 1026-1027, 1026f, 1031f
  - disorders of, risk factors for, 1027
  - exercises, 1031
  - function of, 1026-1027
  - hiatus, 1031, 1032f
  - imaging of
    - indications for, 1027
    - MRI in, 1034-1040
    - ultrasound, 1027-1034
  - musculature, 1031, 1032f
  - sonography, 1027, 1030-1034, 1031f-1032f
    - endoanal, 1027-1029, 1028f-1029f
    - in pelvic organ prolapse, 1033-1034, 1035f
    - postintervention imaging in, 1031-1033, 1033f
    - transperineal, 1029-1030, 1030f
    - urethral diverticulum, 1033, 1034f-1035f
    - urinary incontinence, 1031
- Pelvic inflammatory disease (PID), 891-892, 891f-893f, 939-940, 941f-945f
  - fallopian tube and, 939-940, 941f-945f
  - ultrasound of, 1019, 1020f
- Pelvic masses, biopsies and drainages in, 1088, 1089f
- Pelvic musculature, 829
- Pelvic organ prolapse (POP), pelvic floor sonography in, 1033-1034, 1035f
- Pelvic Organ Prolapse Quantification (POP-Q) system, 1033-1034
- Pelvic pain
  - adnexal causes of, 884-899
  - evaluation of, reproductive age patient in, 883-918
  - nongynecologic causes of, 907-912
  - uterine causes of, 899-906
  - vascular causes of, 906-907
- Pelvic sonography, 805
  - advantages of, 805-807
  - chaperone for, 808
  - contraindications to, 805-807
  - fallopian tube, 827-828
  - free fluid in posterior cul-de-sac in normal patients, 811
  - imaging technique of, 808-811, 812f
  - indications for, 805-807
  - normal anatomy of, 804-834, 814f
  - ovarian morphologic appearance with, 806f
  - ovaries, 826-827
  - patient and probe preparation of, 808
  - pelvic anatomy, 811
  - probe during, 810f-811f
- Pelvic sonography (*Continued*)
  - protocols for, 807-808, 809f
  - rectosigmoid colon, 829-832, 832f
  - ultrasound examination, 806f
  - urinary bladder, distal ureters, and urethra, 829, 830f-831f
  - uterus and, 821-826, 822f
  - vascular anatomy and, 816-821, 818f
- Pelvis, 811
  - anatomy of, 811, 816f
  - visualization of, 809-811
  - artifacts, pitfalls, and normal variants in imaging of, 1098-1114, 1098f-1113f
  - bowel in, ovarian cysts and, 1097f
  - false, 811
  - female
    - diagram of, 814f-815f
    - normal anatomy of, 804-834, 814f
    - true, 829-832
- Penicillin, for nonimmune hydrops fetalis, 647
- Penis, fetal, superficial anatomy of, 167f
- Pentology of Cantrell, 494f, 497, 603-605, 603f-605f
- Percutaneous umbilical blood sampling (PUBS), 48
- Perianal abscesses, endoanal sonography for, 1029, 1029f
- Perianal fistulas, MRI for, 1037-1038, 1039f
- Pericallosal artery, 230f
- Pericardial effusions, 444
  - on hypertrophy, 386-387, 388f
- Perinatal lethal hypophosphatasia, 579
- Perinatal outcome, 780f
  - in monozygotic twins, 778, 779f
- Periovarian endometrium, 824f
- Peritoneal implants, 926f
- Peritoneal inclusion cyst, 897-899, 900f
- Peritoneal inclusion pseudocyst, 928, 928f
- Peritonitis, meconium, 470-471, 470f
- Perlman syndrome, 525, 620
- Persistent cloaca, 471-475, 473f-475f
  - prenatal diagnosis of, 474-475
- Persistent trophoblastic neoplasia, 868, 872f
- Pessary, transvaginal sonograph with, 664-665
- Pfeiffer syndrome, 263, 565-566
  - type I, 565
  - type II, 565
  - type III, 565
- PFTC. *see* Primary fallopian tube carcinoma (PFTC)
- Phalanges, fetal, 164-165, 170f-171f, 173f
- Pharynx, fetal, 192-193, 193f
- Phocomelia, 319
- Pia-arachnoid, fetal, 206-207, 206f
- Picture archiving and communication systems (PACS), 6
- PID. *see* Pelvic inflammatory disease (PID)
- Pierre Robin sequence, 255-256, 569-572
  - and cerebrocostomandibular syndrome, 569-572
  - micrognathia in, 569, 571f
  - and Stickler syndrome, 569
  - syndromes and chromosomal abnormalities associated with, 569f-571t
- Pierre Robin syndrome, 761f
- Placenta
  - abnormal shape, 677
  - abnormal thickness, 677-678
  - anomalies, and nonimmune hydrops, 645t-647t
  - battledore, 681
  - bilobed, 677
  - chorioangioma, 689-691, 691f
  - circummarginate, 691
  - circumvallate, 691, 692f-693f
  - sonogram in, 1103f
  - cord insertion abnormalities in, 681-683, 681f
  - vasa previa, 682-683, 683f
  - velamentous cord insertion, 681-682, 682f
  - development of, 674-677
  - evaluation, in multiple gestations, 139-140, 141f-142f
  - first trimester ultrasound examination of, 12
  - hydropic, 1108f
  - hydropic degeneration of, 870f
  - hypochoic region in, 1110f
  - location of, abnormalities in, 678-681, 679f
    - low-lying, 680-681, 681f
    - placenta previa, 679-680, 680f
    - low-lying, 680-681, 681f
    - management of, 681

- Placenta (Continued)**  
 membrane abnormalities, 691-693, 691f, 692t  
 amniotic band sequence, 692-693, 694f  
 extrachorial placentation as, 691, 692f-693f  
 uterine synechia, 692, 693f  
 morbidly adherent, 683-687  
 multilobate, 677  
 normal, 676-677  
 ring-shaped, 677  
 second trimester ultrasound examination of, 676-677, 677f  
 and third trimester, 16-17  
 succenturiate lobe, 677, 677f-678f  
 ultrasound evaluation of, 674-703  
 vascular abnormalities of, 687-689  
 placental abruption as, 689, 690f  
 placental calcification as, 688, 689f  
 placental hematomas as, 688-689, 689f-690f  
 placental sonolucencies as, 687-688, 688f
- Placenta accreta**, 683-687, 684f, 770f  
 epidemiology and risk factors of, 684  
 first trimester, and cesarean scar pregnancy, 686-687, 687f  
 magnetic resonance imaging for, 684-686, 686f  
 risk in subsequent pregnancies after hysterotomy, 776  
 sonographic findings in, 684, 685f
- Placenta fenestrata**, 677
- Placenta membranacea**, 677
- Placenta percreta**, 684, 771f
- Placenta previa**, 679-680, 680f  
 complete, 680  
 management of, 680  
 marginal, 680  
 partial, 680  
 placental "migration" in, 680  
 prevalence of, 679  
 risk factors for, 679  
 terminology, 679-680  
 transabdominal longitudinal sonogram in, 1109f
- Placental abruption**, 689, 690f  
 hypoechoic area in, 1111f
- Placental chorioangioma**, 792f
- Placental increta**, 683
- Placental lacunae**, 684, 685f, 688
- Placental lakes**, 688
- Placental sonolucencies**, 687-688, 688f
- Placentomegaly**, 677-678, 679f
- Platyspondyly**, 277, 286f, 301
- Pleural effusion**, 789  
 aneuploidy and, 59, 60f  
 isolated fetal, 789
- Pneumonia, maternal**, in varicella zoster, 548
- Polycystic kidney disease**, 521  
 autosomal dominant, 522, 523f  
 autosomal recessive, 521-522, 522f
- Polycystic ovary syndrome (PCOS)**, 1015, 1018f  
 sonographic imaging of, 956-957, 959f
- Polydactyly**, 77, 323, 323f, 1150f  
 in Bardet-Biedl syndrome, 523  
 definition of, 277  
 in Meckel syndrome, 555, 555f  
 postaxial, 315, 316f  
 short rib-polydactyly syndrome, 278t-282t  
 skeletal dysplasias with, 299t, 313t
- Polyhydramnios**, 708, 713f-714f, 1125f  
 AFV measurement and, 713  
 in Apert syndrome, 562  
 and congenital abnormalities, 713  
 diagnosis of, 16  
 in fetal growth restriction, 714  
 in high-risk patient, 712-714, 713f  
 idiopathic, 712  
 in twin pregnancies, 715
- Polymerase chain reaction (PCR)**, for cytomegalovirus infection, 542
- Polyps**  
 endocervical, 878, 879f  
 endometrial, 824f, 840-841, 841f-843f, 857
- Pontocerebellar hypoplasia**, fetal MRI of, 757f
- POP**. *see* Pelvic organ prolapse (POP)
- Portal vein**, fetal, 184, 186f
- Positive predictive value (PPV)**, 886
- Postablation tubal sterilization syndrome (PATSS)**, 1078
- Postabortive uterus**, 872-877, 876f-877f
- Postembolization syndrome**, 902-903
- Posterior compartment laxity**, 1038-1039
- Posterior cul-de-sac**, 811, 812f, 816f
- Posterior fossa**, cystic and cyst-like abnormalities of, 229-231, 232t, 233f
- Posterior fossa**, normal ultrasound findings in, 102
- Posterior urethral valve (PUV)**, 512, 513f-514f
- Posterior vaginal fornix**, 816f
- Posthysterectomy ectopic pregnancy**, 996
- Postmenopausal endometrium**, 825  
 normal, 825f
- Potter sequence**, 25-27
- PPV**. *see* Positive predictive value (PPV)
- Practice Guideline for the Performance of an Antepartum Obstetric Ultrasound Examination**, 6
- Prader-Willi syndrome**, 32, 617-618
- Preaxial acrofacial dysostosis**, 568
- Precocious puberty**, 1011-1014, 1016f
- Predominantly solid lesions**, 1067-1068, 1071f
- Pregnancies**, alloimmunized, 641, 641f
- Pregnancy**  
 with coexistent ovarian carcinoma, 1101f  
 endometrial ablation in, 1078  
 jejunal and ileal atresia in second half of, 469t  
 luteoma of, 929  
 obese women risk for, 799  
 ovarian masses of, 929  
 partial molar, 871f  
 second trimester, amniotic fluid in, 1143f  
 termination of  
 for fetal cytomegalovirus infection, 543  
 for fetal rubella infection, 545  
 for fetal varicella zoster, 548  
 for osteogenesis imperfecta, 577  
 uterine artery embolization in, 1079  
 vaginal bleeding during, 1116f
- Pregnancy-associated plasma protein A (PAPP-A)**, 41-42
- Pregnancy failure**  
 empty amnion sign of, 90, 91f  
 expanded amnion sign of, 90-91, 91f  
 risk factors for, with embryonic heartbeat, 91-93, 92t  
 slow embryonic heart rate, 92-93, 92f  
 small gestational sac size, 93, 93f  
 subchorionic hematoma, 93, 93f  
 sonographic findings definitive for crown rump length in, 88, 89f  
 mean sac diameter in, 88-89, 89f  
 time-based criteria for, 89  
 sonographic findings suspicious for crown rump length in, 90, 90f  
 mean sac diameter in, 90, 91f  
 time-based criteria for, 90
- Pregnancy number**, assessment of, 93-94  
 appearing twin, 94, 95f  
 vanishing twin, 94, 94f
- Pregnancy of unknown location (PUL)**, 970  
 management algorithms in, 85
- Preimplantation genetic diagnosis**, 49, 49f
- Preload**, and fetal growth restriction, 747
- Premature centromere separation**, in Roberts syndrome, 588
- Premenopausal women**, ovarian volume and, 826
- Premutation**, 32
- Prenatal diagnosis**  
 fetal blood sampling in, 48  
 fetal tissue biopsy in, 48  
 genetic counseling before, 46  
 in multiple gestations, 47-48  
 in preimplantation genetic diagnosis, 49, 49f  
 techniques for, 46-47  
 amniocentesis, 46, 46f  
 chorionic villus sampling, 46-47, 47f
- Preorganogenetic phase**, teratogenic susceptibility in, 34-35
- Prepubertal uterus**, 850, 854f
- Pressure**, excessive, in ultrasonography of cervix, 656, 658f
- Preterm birth**  
 prediction of, with transvaginal sonography, 657-660  
 measurements in, 657-660, 662f  
 with cerclage, 659-660, 663f  
 cervical length, 657-658, 659f-660f  
 funneling, 658-659, 661f-662f  
 sludge, 659  
 screening test criteria, 657, 659t  
 accuracy of, 657
- Preterm birth (Continued)**  
 important and prevalent conditions of, 657  
 recognizable early asymptomatic phase, 657  
 reliable/reproducible, 657  
 safe and acceptable, 657  
 and short cervical length, 666-667  
 prevention of, with cervical length, 667-670  
 for asymptomatic multiple gestations, 668-669  
 for asymptomatic singletons with prior spontaneous preterm birth, 668, 668t  
 for asymptomatic singletons without prior spontaneous preterm birth, 667-668, 667f  
 in predicting success of labor induction and mode of delivery, 670  
 in prediction of start of spontaneous labor, 669, 669f  
 in preterm labor, 669, 669f  
 in preterm premature rupture of the membranes, 669
- Preterm labor**, cervical length in, 669, 669f
- Preterm premature rupture of membranes (PPROM)**, after fetal surgical procedures, hysterotomy, 776, 776f
- Preterm premature rupture of the membranes**, cervical length in, 669
- Primary ciliary dyskinesia**, 598
- Primary fallopian tube carcinoma (PFTC)**, 946
- Primary villi**, 674-675, 676f
- Proctodeum**, 460-461
- Prolapse**, MRI in, 1038-1039, 1040f-1041f
- Prolapsing submucosal leiomyoma**, 903f
- Pronephros**, 504, 505f
- Proteus syndrome**, 620-621
- Proximal femoral focal deficiency**, 320, 320f
- Prune-belly syndrome**, 515, 609-610, 610f
- PSAs**. *see* Pseudoaneurysms (PSAs), uterus
- Pseudo-double bubble sign**, 1138f
- Pseudo-hyperechogenic fetal bowel**, 1137f
- Pseudo-omphalocele**, 1135f
- Pseudo-ulnar hypoplasia**, 1149f
- Pseudoaneurysms (PSAs)**, uterus and, 871
- Pseudoascites**, 1136f
- Pseudochorioamniotic separation**, 1144f
- Pseudocleft**  
 of face, 1122f  
 of lip, 1123f
- Pseudocyst**  
 meconium, 471  
 peritoneal inclusion, 928, 928f
- Pseudogastroschisis**, 1136f
- Pseudogestational sac**, 972, 973f  
 in ectopic pregnancy, 85
- Pseudoglandular phase**, of lung development, 349
- Pseudolimb reduction**, 1148f
- Pseudomyxoma peritonei**, 908
- Pseudosac**, 972
- Pseudothalidomide syndrome**, 588
- Pubococcygeal line (PCL)**, in pelvic floor, 1036
- PUL**. *see* Pregnancy of unknown location (PUL)
- Pulmonary abnormalities**, and nonimmune hydrops, 645t-647t
- Pulmonary arteries**, Doppler velocimetry of, 298
- Pulmonary atresia**, with ventricular septal defect, 409-412  
 anatomy of, 409-410, 411f  
 definition of, 409, 410f  
 diagnostic imaging features of, 411-412  
 epidemiology of, 409  
 genetic considerations of, 410-411, 412t  
 interventions and prognosis of, 411
- Pulmonary circulation**, 347, 347f
- Pulmonary edema**, 649
- Pulmonary hypoplasia**, 350-351, 350f, 351t, 352f  
 fetal, due to oligohydramnios, 711  
 lethal, 712  
 prediction of, 292-298  
 biometric parameters of, 293, 297t  
 Doppler assessment of tracheal fluid flow, 298  
 Doppler velocimetry of the pulmonary arteries, 298  
 evaluation of thoracic and lung dimensions by two-dimensional ultrasound, 293, 294f-295f, 295t-297t  
 lung volumetry by three-dimensional sonography, 293-298, 297f  
 by magnetic resonance imaging, 298



- Pulmonary hypoplasia (*Continued*)  
 short femur length and prediction of lethality in skeletal dysplasias, 293  
 prediction of, in setting of oligohydramnios, 712 and pregnancy outcomes, 711-712
- Pulmonary valves, 390
- Pulmonary vasculature, 347
- Pulmonary venolobar syndrome, 594
- Pyelectasis, 73
- Pyloric atresia, epidermolysis bullosa with, 606-607
- Pyomyoma, 904f
- Pyosalpinx, 892f, 939-940, 941f, 1019, 1020f
- Pyrimethamine, for fetal toxoplasmosis syndrome, 547
- Q**
- Quickening, 720
- Quintero staging, of twin-twin transfusion syndrome, 146, 150t
- R**
- Radial aplasia thrombocytopenia syndrome, 588
- Radial artery, uterine, 820f
- Radial clubhand, 321  
 hematologic disorders and, 321-322  
 other conditions associated with, 323  
 scoliosis and, 322-323
- Radial ray defects, 321t
- Radiation, teratogenicity of, 35
- Radiation therapy, for endometrial cancer, 1063-1064
- Radiofrequency ablation (RFA), 781
- Radiotherapy, for Gorlin syndrome, 568
- Radius, fetal, 165, 172f
- RADIUS (Routine Antenatal Diagnostic Imaging with Ultrasound) trial, 109
- Radius syndrome, thrombocytopenia-absent, 588-589
- Rapid acquisition with relaxation enhancement (RARE), MRI technique, 750
- RARE. *see* Rapid acquisition with relaxation enhancement (RARE)
- Real-time sonographic systems, 159-160
- Recessive osteogenesis imperfecta, 214f
- Rectocele, on magnetic resonance imaging, 1038, 1041f
- Rectosigmoid colon, 829-832, 832f
- Rectouterine pouch, vagina and, 811
- Rectum, fetal, 195, 196f, 471-475  
 in second and third trimester, 1138f
- Remnants, in umbilical cord, 694-695
- Renal abnormalities, and nonimmune hydrops, 645t-647t
- Renal agenesis  
 bilateral, 518-519, 519f  
 ipsilateral, 852  
 unilateral, 519, 520f
- Renal angiofibromas, in tuberous sclerosis, 559
- Renal anomalies  
 in Beckwith-Wiedemann syndrome, 608  
 congenital, and single umbilical artery, 696-697  
 Mayer-Rokitansky-Küster-Hauser (MRKH) syndrome and, 852
- Renal cystic diseases  
 genetic  
 autosomal dominant polycystic kidney disease, 522, 523f  
 autosomal recessive polycystic kidney disease, 521-522, 522f  
 differential diagnosis for, 525t  
 glomerulocystic kidneys, 523, 525t, 526f  
 medullary cystic dysplasia, 523, 525f  
 nongenetic  
 multicystic dysplastic kidney, 509, 521, 523-525, 526f-527f  
 renal tumors, 525, 528f  
 unclassified, 523-525
- Renal duplication, 509, 512f-513f
- Renal dysplasia, 521, 521f
- Renal ectopia, 520  
 crossed fused, 521
- Renal medullary pyramids, fetal, 1139f
- Renal tract, congenital anomalies of, 611-613  
 Fraser syndrome as, 611-612, 611f-612f  
 MURCS association, 612
- Residual anastomosis (RA), 779-780
- Respiratory diverticulum, 347
- Respiratory insufficiency, surgical management for, 314
- Respiratory system, fetal anatomy of, 197-199, 197f-200f
- Retained products of conception (RPOC), 876f
- Retrognathia, 62-63, 255-257, 261f
- Retronasal triangle, 109
- Retroperitoneal ectopic pregnancy, 993-995, 995f
- Retroplacental clear space, 684
- Retroplacental myometrium, thinning of, 684, 685f
- RFA (radiofrequency ablation), 781
- Rh system, genetics of, 636
- Rhabdomyoma  
 anatomy of, 438  
 diagnostic imaging features of, 438  
 in tuberous sclerosis, 559
- Rhabdomyosarcoma, vaginal, 1014-1015, 1017f
- RhD antigen, 635-636  
 repeat antibody screen for, 638
- RhD iso-immunization, 635-636
- RhD pseudogene, 636
- Rhizomelia, 277, 285f, 285t
- Rhizomelic chondrodysplasia punctata, type I, 581
- Right umbilical vein, persistent, 1142f
- Right ventricle, 389
- Right ventricular outflow tract view, of fetal heart, 381, 387f
- Risk assessment, genetic  
 combined first and second, 43-45  
 in first trimester, 41-42  
 in second trimester, 42-43
- Roberts syndrome, 319-320, 588
- Robertsonian translocation, 27, 29
- Robinow-Sorauf syndrome, 566
- "Rocker-bottom feet", 77
- Rokitansky nodule, 923
- RPOC. *see* Retained products of conception (RPOC)
- Rubella syndrome, fetal, 544-545
- Rubella virus infections, intrauterine, 35, 36f
- Rudimentary horn ectopic pregnancy, 985-986, 989f
- S**
- Saccular phase, of lung development, 349
- Sacral agenesis, 551
- Sacrococcygeal teratoma (SCT)  
 cysts and, 481  
 fetal surgery for repair of, 777t, 791  
 MRI of, 763, 767f
- SADDAN. *see* Severe achondroplasia with developmental delay and acanthosis nigricans (SADDAN)
- Saethre-Chotzen syndrome, 566
- Safety, of MRI, in obstetric patients, 749-750
- Sagittal sign, 531
- Saline infusion sonography  
 in evolution of endometrial assessment, 836-837  
 technique for, 837, 837f
- Saline infusion sonohysterography (SIS), 867f  
 technique for, 848, 850f
- Salpingectomy, for ectopic pregnancy, 996
- Salpingitis, 940f  
 acute, 941f  
 xanthogranulomatous, 947f
- Sarcomas, uterine, 868-871
- Scalp hair, fetal, superficial anatomy of, 161, 166f
- Scapula, fetal, 165, 171f
- Schizencephaly, MRI of, 760f
- Scimitar syndrome, 594
- Sclerosis, tuberous, 558-560, 559f-560f  
 cardiac tumors in, 559  
 genetics of, 560  
 main aspects of, 559t  
 renal angiofibromas in, 559
- Sclerotome, 275
- Scoliosis, 277, 286f, 302  
 radial clubhand and, 322-323  
 three-dimensional ultrasound image of, 286f
- SCT. *see* Sacrococcygeal teratoma (SCT)
- SDP. *see* Single deepest pocket (SDP)
- Seckel syndrome, 623-624
- Second and third trimester  
 assigning gestational age in, 119-122, 124f-125t  
 gestational dating of, 119-122  
 measurements in, 119-121
- Second and third trimester ultrasound examinations, 13-17  
 to assess amniotic fluid volume, 15-16  
 to assign gestational age and weight, 13  
 to detect fetal malformations, 17  
 to determine fetal life, 13  
 to determine fetal number, 13  
 to determine fetal position, 13, 14f-15f  
 to evaluate placenta, 16-17  
 to evaluate uterus and adnexa, 17  
 Level 1, 5  
 Level 2, 5  
 technical limitations in, 18
- Second-degree heart block, 441
- Second trimester genetic sonogram, 69-75  
 absent/hypoplastic nasal bone in, 70-72, 71f  
 echogenic intracardiac focus in, 73-74, 74f  
 femoral/humeral shortening in, 72-73  
 hyperechoic bowel in, 72  
 minor markers for Down syndrome in, 74-75  
 pyelectasis in, 73  
 thickened nuchal fold in, 70, 71f
- Secondary villi, 675, 676f
- Secretory endometrium, 824f
- Selective estrogen receptor modulator (SERM), 842-843
- Selective fetal growth restriction (sFGR), 148, 153f, 780-781  
 late-onset, 781  
 type I, 781
- Selective laser photocoagulation of communicating vessels (SLPCV), 778-779  
 surgical goal of, 779-780
- Semilobar holoprosencephaly, MRI of, 756f
- Semilunar valves, Doppler waveforms in, 745, 746f, 746t
- Septate uterus, 855-856, 857f, 954f, 1004-1006, 1005f-1006f  
 lateral fusion defects and, 1081  
 Mullerian duct anomalies and, 1049, 1049f-1050f  
 repair of, 1081
- Septo-optic dysplasia, 557-558, 558f
- Septum pellucidum, absence of  
 agenesis of the corpus callosum and, 229, 232f  
 lobar holoprosencephaly and, 225
- Sequence, 25-27, 540, 692-693
- Serial surveillance, in multiple gestations, 143-150
- Serine-deficiency, in Neu-Laxova syndrome, 626
- SERM. *see* Selective estrogen receptor modulator (SERM)
- Serous cystadenofibroma, 926f
- Severe achondroplasia with developmental delay and acanthosis nigricans (SADDAN), 305
- Sex cord-stromal neoplasms, 924
- Sex determination, 1003
- Sex differentiation, 1003
- Sexual development, disorders of, 532, 532f  
 due to congenital adrenal hyperplasia, 532  
 hypospadias, 532, 533f
- sFGR. *see* Selective fetal growth restriction (sFGR)
- SGA. *see* Small for gestational age (SGA)
- SGF syndrome. *see* Splenogonadal fusion (SGF) syndrome
- Shading, ultrasound examination findings of, 895
- Short femoral length, significance of, 1147f
- Short rib-polydactyly syndrome, 278t-282t, 314-315, 315f, 580
- Shunting, vesicoamniotic, 514
- Side lobe artifact, 1096f
- Sigmoid colon, 829-832
- Sigmoid vaginoplasty, for agenesis, 1081
- Simpson-Golabi-Behmel syndrome, 621
- Sims position, 802, 802f
- Single deepest pocket (SDP), 706-707, 707f
- Single gene disorders, 29-34  
 autosomal-dominant inheritance in, 30f-31f, 31-32  
 autosomal-recessive disorders in, 30f-31f, 32  
 carrier (heterozygote) screening for, 38-40  
 multifactorial inheritance in, 33-34  
 novel genetic mechanisms in, 32-33  
 X-linked inheritance in, 30f-31f, 32
- Single nucleotide polymorphism (SNP), 51-52
- Single shot fast spin echo (SSFSE), 750
- Single suture synostosis, 263
- Single twin demise, 148-150, 154f
- Single umbilical artery, 75-76, 76f, 695-697, 696f  
 isolated, 695-696
- Sinus bradycardia, 441

- Sinus tachycardia, 443, 444f  
 Sirenomelia, 553, 589-590, 590f  
 SIS. *see* Saline infusion sonohysterography (SIS)  
 Situs abnormalities, 434-436  
 anatomy of, 434, 436f  
 birth prevalence/epidemiology of, 434  
 definition of, 434, 435f  
 diagnostic imaging features of, 436  
 genetic considerations of, 434-435  
 interventions and prognosis of, 435-436  
 Skeletal dysplasias, 275-303, 573-580  
 achondrogenesis, 577, 578f  
 type I, 577  
 type II, 577  
 achondroplasia, 581-582, 581f-582f  
 atelosteogenesis, type 2, 580  
 at birth, 277, 282t-283t  
 birth prevalence of, 275, 277t  
 campomelic, 579, 579f  
 classification of, 275-277  
 clinical presentation of, 288  
 clinically oriented classification of, 277, 284t  
 diagnosis approach to, 291-303, 292t  
 evaluation of fetal cranium, 299, 300f, 301t  
 evaluation of fetal face, 299-300, 301f, 301t-302t  
 evaluation of fetal spine, 301-302  
 evaluation of hands and feet, 298-299, 298f-299f, 299t  
 evaluation of internal organs, 302  
 evaluation of long bones, 291-292  
 fetal movements, 302  
 newborn evaluation, 302-303  
 prediction of pulmonary hypoplasia, 292-298  
 diagnostic imaging and prenatal diagnosis of, 288-290  
 3D ultrasonography of, 289, 290f, 290t  
 fetal magnetic resonance imaging of, 290  
 sonography of, 289, 289t  
 three-dimensional helical computed tomography of, 289, 291f  
 fibrochondrogenesis, 580  
 hypophosphatasia congenita as, 579-580  
 lethal, 275  
 long bone biometry in, 277, 287f, 287t-288t  
 molecular-pathogenetic classification of, 275-277, 278t-282t  
 nuchal translucency and, 303, 303t  
 osteogenesis imperfecta, 575-577, 576f-577f  
 perinatal mortality and, 275  
 with predominant membranous bone involvement, 316-317  
 relative frequency of, 275, 277t  
 rhizomelic chondrodysplasia punctata, type I as, 581  
 short-rib polydactyly syndromes, 580  
 terminology for, 277-288  
 thanatophoric, 574-575, 574f-575f  
 type I, 574  
 type II, 574  
 Skeletal structures, in first trimester  
 abnormal ultrasound findings in, 109  
 normal ultrasound findings in, 102  
 Skeletogenesis, 273  
 Skeleton  
 fetal, imaging of, artifacts, pitfalls, and normal variants, 1146-1151, 1146f-1151f  
 of newborn, 276f  
 Skin, fetal, keratinizing, 704-705  
 Skull, fetal, 178-179, 179f  
 imaging of, three-dimensional, 246f  
 normal ultrasound findings in, 102, 103f  
 Sludge, in prediction of preterm birth, 659  
 Small biparietal diameter (BPD), myelomeningocele and, 108  
 Small bowel, fetal, 194-195, 194f  
 Small for gestational age (SGA), 126-127  
 Small intestine, 465-471  
 echogenic, management of, 468-469  
 Smith-Lemli-Opitz syndrome, 45, 626-627  
 anomalies associated with, 627t  
 Smooth muscle tumor of uncertain malignant potential (STUMP), 903  
 Sodium iodide, teratogenicity of, 36t  
 Soft markers, sonographic, for aneuploidy, 43  
 Sonographic Detection of Chromosomal Abnormalities (Appendix G), 1220  
 Sonohysterography, 949-951  
 technique for, 848  
 Sotalol, 650t  
 Sotos syndrome, 622  
 Spatiotemporal image correlation (STIC), 396-401  
 acquisition of volume datasets with, 396-397  
 volume acquisition with matrix array technology, 396-397  
 volume acquisition with mechanical transducers, 396  
 display modalities in, 397-400  
 automated display of multiple slices, 397-400, 399f  
 dynamic multiplanar display, 397, 397f-399f  
 rendering techniques in, 400  
 B-flow rendering, 400, 400f-401f  
 inversion mode, 400, 400f  
 transparency modes, 400  
 Spina bifida, 61, 62f, 216-217, 223. *see also* Neural tube defects  
 alpha-fetoprotein levels and, 223  
 Chiari II malformation and, 223, 226t  
 closed, 224, 226f  
 hydrocephalus and, 223-224  
 incidence of, 223t  
 open, 223, 225f  
 outcome of, 224  
 Spina bifida, fetal surgery for repair of, 783  
 Spinal curvature, 302  
 Spinal defect, apparent, 1151f  
 Spinal dysgenesis, 301, 302f  
 Spinal muscular atrophy, carrier screening for, 39t  
 Spine, fetal, 179-180, 180f-183f  
 cartilaginous structures in, 183  
 normal ultrasound findings in, 102, 102f  
 Spiral artery, 820f  
 Spiramycin, for fetal toxoplasmosis syndrome, 547  
 Spleen, 478, 478f  
 Splenic cyst, 1140f  
 Splenogonadal fusion (SGF) syndrome, 319  
 Split hand and foot deformities, 320  
 Spondylocostal dysostosis, 584-585, 584t  
 Spontaneous abortion, and fetal rubella infection, 545  
 Spontaneous labor, start of, cervical length in, 669, 669f  
 SSFSE. *see* Single shot fast spin echo (SSFSE)  
 Standard of Care for Health Care Professionals, 20-21  
 STIC. *see* Spatiotemporal image correlation (STIC)  
 Stickler syndrome, and Pierre Robin sequence, 569  
 Stillbirth, 467-468  
 prevention of, with nonstress testing, 724  
 Stomach, fetal, 192f, 193-194, 461-465, 462f  
 artifacts in, 1096f  
 debris within, 1137f  
 first trimester ultrasound of, 107, 107f  
 persistently small or absent, 463t  
 Stomodeum, 460-461  
 Stress urinary incontinence, 1025  
 Subchorionic hematoma, in pregnancy failure, 93, 93f  
 Submucosal intracavitary leiomyoma, 867f  
 Submucosal leiomyomas, 901f, 1051, 1052f  
 endometrial ablation in, 1077, 1077f  
 sonographic imaging of, 957f  
 Subserosal leiomyoma, 1051, 1052f  
 Succenturiate lobe, 677, 677f-678f  
 Sulfadiazine, for fetal toxoplasmosis syndrome, 547  
 Supracardiac total anomalous pulmonary venous connection, 431-432  
 Supratentorial ventricular system, fetal, 201-202  
 Supraventricular tachycardia, 443  
 Suspensory ligament, transvaginal sonography of, 817f  
 Sutures, 178-179, 179f, 206f  
 overlapping, in fetus, 1125f  
 Sylvian cistern, 201-202  
 Sympathetic nervous system, fetal heart rate and, 721-722  
 Syncytiotrophoblast, 674-675, 675f  
 Syndactyly  
 in Apert syndrome, 562, 563f  
 definition of, 277  
 Syndrome, 25-27, 540, 692-693  
 Synechia, uterine, 1102f  
 Syphilis, fetal, 545-546, 546f  
 early, 545  
 late, 545-546  
 T  
 T-sign, 135-136, 138f  
 T1-weighted images, 1046  
 T2-weighted images, 1046  
 Tachycardia, fetal, 443  
 Talipes equinovarus, 77, 77f. *see also* Clubfoot  
 Tamoxifen, 842-843, 844f  
 TAPVC. *see* Total anomalous pulmonary venous connection (TAPVC)  
 TAR syndrome. *see* Thrombocytopenia-absent radius (TAR) syndrome  
 TAS. *see* Transabdominal sonography (TAS)  
 Taussig-Bing anatomy, 417  
 Tay-Sachs disease, genetic screening for, 38  
 Tei index, 394, 396f  
 Telemedicine, 6  
 Teratogenic agents, recognized, 35, 36t  
 Teratogens, 548-553  
 fetal alcohol syndrome/fetal alcohol effects, 548-550  
 ear characteristic features in, 549f  
 facial features of, 549f  
 hand characteristic features in, 549f  
 fetal valproic acid syndrome, 550, 550f  
 fetal warfarin syndrome, 551, 551f  
 maternal diabetes/caudal regression syndrome, 551-553, 552f-553f  
 Teratology, 34-37, 34f  
 maternal factors in, 35-37  
 maternal infections and, 35  
 mechanical factors of, 37  
 medications in, 35  
 radiation in, 35  
 recognized teratogenic agents in, 35, 36t  
 Teratoma, 267-268, 267f-268f  
 cervicofacial, MRI of, 755-761  
 intracranial, MRI of, 768f  
 intrapericardial, 438  
 diagnostic imaging features of, 439  
 mature cystic, 923-924  
 orbital, 257-262, 262f  
 oropharyngeal, large, MRI of, 761f  
 ovarian cystic, bowel simulating, 1100f  
 sacrococcygeal  
 cysts and, 481  
 fetal surgery for repair of, 777t, 791  
 MRI of, 763, 767f  
 Terminal villi, 675  
 Tertiary villi, 675, 676f  
 Teschler-Nicola/Killian syndrome, 593  
 Tetralogy of Fallot  
 with ventricular septal defect, 409-412  
 anatomy of, 409-410, 411f  
 definition of, 409, 410f  
 diagnostic imaging features of, 411-412  
 epidemiology of, 409  
 genetic considerations of, 410-411, 412t  
 interventions and prognosis of, 411  
 Tetrasomy 12p, 593  
 Thalidomide, 34-35, 36t  
 Thanatophoric dysplasia, 305-306, 305f-306f, 574-575, 574f-575f  
 nosology of, 278t-282t  
 prevalence of, 275, 277t  
 type I, 574  
 type II, 574  
 Theca lutein cysts, 929, 929f  
 Thermal index (TI), of ultrasound wave, 3  
 Third-degree heart block, 442-443, 443f  
 Thoracic abnormalities, and nonimmune hydrops, 645t-647t  
 Thoracic dimensions, by two-dimensional ultrasound, 293, 294f-295f, 295t-297t  
 Thoraco-omphalopagus conjoined twins, MRI for, 769f  
 Thorax  
 anomalies of, 590-594, 755-762  
 congenital high airway obstruction syndrome, 590-591, 591f  
 Donnai-Barrow syndrome, 592  
 Fryns syndrome, 592-593, 592f  
 fetal  
 bronchial atresia and, 355-356, 357f-358f  
 bronchogenic cyst and, 354-355, 356f  
 congenital diaphragmatic hernia and, 362-367, 362f-367f  
 congenital high airway obstruction syndrome and, 357-359, 358f-360f  
 congenital hydrothorax and, 359-362, 361f  
 congenital lobar emphysema and, 357



- Thorax (*Continued*)  
 congenital pulmonary airway malformation and, 351-354, 352f-356f  
 embryology of, 346-349, 347f-348f  
 alveolar phase, 349  
 canalicular phase, 349  
 embryonic phase, 349  
 pseudoglandular phase, 349  
 sacular phase, 349  
 imaging of, artifacts, pitfalls, and normal variants, 1132-1135, 1132f-1135f  
 key features for assessment of, 349-350, 349f-350f  
 pulmonary hypoplasia and, 350-351, 350f, 351t, 352f  
 ultrasound evaluation of, 346-370  
 heart, fetal, "four-chamber view," ultrasound findings of, 187, 188f
- Three-dimensional (3D) ultrasonography  
 fetal cardiac evaluation, 396-401  
 of fetal face and neck, 243, 246f-248f  
 lung volumetry by, 293-298, 297f  
 in skeletal dysplasias, 289, 290f, 290t  
 of skull, 246f
- Three-dimensional imaging, 160, 160f  
 for fetal skeletal structures, 161, 167f
- Three-vessel view, of fetal heart, 381-382, 388f  
 trachea view and, 384, 388f
- Thrombocytopenia-absent radius (TAR) syndrome, 320, 322, 588-589
- Thrombophlebitis, ovarian vein, 907
- Thrombosis  
 of dural sinuses, 237, 238f  
 gonadal vein, 907, 910f
- Thrombus, in right ventricle, 1133f
- Thymus, 1135f
- Tl. *see* Thermal index (TI)
- Tibia, fetal, 165, 175f  
 length of, relationship with femur, 285f  
 proximal, 275f
- Time-based criteria, for pregnancy failure  
 definitive, 89  
 suspicious, 90
- TOA. *see* Tubo-ovarian abscess (TOA)
- TOC. *see* Tubo-ovarian complex (TOC)
- Tocolysis  
 during fetoscopy, 776  
 indomethacin for, 776
- Tone, in biophysical profile, 726
- Tongue, fetal, 165f, 192-193, 192f
- Toothbuds, 244f
- Total anomalous pulmonary venous connection (TAPVC)  
 to heart, 432  
 imaging features of, 434  
 to right atrium, 432-433
- Townes-Brocks syndrome, 589
- Toxoplasma*, intrauterine infection, 36t
- Toxoplasma gondii*, 546
- Toxoplasmosis syndrome, fetal, 546-547, 547f
- Trachea, fetal, 197
- Tracheal atresia, in congenital high airway obstruction syndrome, 590-591
- Tracheal fluid flow, Doppler assessment of, 298
- Tracheolaryngeal airway obstruction, MRI of, 761
- Transabdominal sonography (TAS), 805, 808f  
 bladder filling for, 805  
 of cervix, 653-654, 654t, 656f  
 in ectopic pregnancy, 970  
 of gravid uterus, 1119f  
 longitudinal, in placenta previa, 1109f  
 of placenta previa, 680  
 for placental location, 678-679, 679f
- Transabdominal transducers, of fetuses, 158
- Transabdominal view, of fetal heart, 381, 384f
- Transducer, excessive pressure on, and amniotic fluid volume, 708
- Transducers, for ultrasound examination, 6
- Transfundal pressure, dynamic changes of cervix after, 660
- Transient clitoromegaly, 531-532
- Transitional cell tumors, 926
- Translabial sonography, of cervix, 654-655, 654f, 656f
- Translocations, 27
- Translucency, nuchal, erroneous measurement of, 1120f
- Transparency modes, 400
- Transperineal sonography  
 of anal sphincter, 1029-1030, 1030f  
 of cervix, 654-655, 654f
- Transposition of the great arteries, 417-419  
 anatomy of, 417  
 congenitally corrected, 419-421  
 anatomy of, 419  
 definition of, 419, 420f  
 diagnostic imaging features of, 421  
 epidemiology of, 419  
 genetic considerations of, 419-420  
 interventions and prognosis of, 420-421  
 rhythm abnormalities of, 419  
 definition of, 417, 418f  
 diagnostic imaging features of, 417-419  
 epidemiology of, 417  
 genetic considerations of, 417  
 imaging tips of, 419  
 interventions and prognosis of, 417
- Transrectal scan, of anteverted uterus, 833f
- Transverse abdominal sonogram, 862f
- Transverse axial sonogram  
 of fetal brain, 1129f  
 of pelvis, 1101f
- Transverse vaginal septum, 1006-1007, 1008f, 1082
- Trapezioccephaly-multiple synostosis syndrome, 561
- Traumatized endometrial-myometrial interface, 904
- Treacher Collins-Franceschetti syndrome, 572
- Treacher Collins syndrome, 567, 572
- Treponema pallidum*, 545  
 intrauterine infection, 36t
- Triad syndrome, 609
- Tricuspid regurgitation, 69, 73f
- Tricuspid valve atresia (TVA), 428-430  
 anatomy of, 428-429  
 birth prevalence/epidemiology of, 428  
 definition of, 428, 428f  
 diagnostic imaging features of, 429-430, 430f-431f  
 genetic considerations of, 429  
 interventions and prognosis of, 429
- Tricuspid valves, 389, 389f
- Trigonocephaly, 263
- Trimethadione, teratogenicity of, 36t
- Triplets, transvaginal sonography in, 665
- Triploidy, 29
- Trisomy 9, facial profile of, 65f
- Trisomy 13, 28  
 congenital anomalies in, 58t  
 holoprosencephaly in, 62  
 postaxial polydactyly in, 77  
 urethrovaginal obstruction, 63
- Trisomy 18, 28  
 choroid plexus cysts in, 75, 75f  
 congenital anomalies in, 58t  
 facial profile of, 65f  
 fetal extremities of, abnormalities in, 76-77  
 "rocker-bottom feet" in, 77  
 urethrovaginal obstruction, 63
- Trisomy 21, 27-28, 28f. *see also* Down syndrome  
 congenital anomalies in, 58t  
 first trimester markers of, 64
- Trisomy rescue, 47, 47f
- Trophoblast, 674-675
- Trophotropism, 680
- Truncus arteriosus, 413-414  
 anatomy of, 413, 413f-414f  
 definition of, 413  
 diagnostic imaging features of, 414  
 epidemiology of, 413  
 genetic considerations of, 413  
 interventions and prognosis of, 413
- Tubal actinomycosis, 940
- Tubal infections, uncommon, 940-946, 946f-947f
- Tubal patency, evaluation of, 949-951, 950f-951f
- Tubal sterilization, Essure microinsert placement for, 1084-1086, 1085f-1086f
- Tubal torsion, 946, 948f
- Tuberculosis, 946f
- Tuberous sclerosis, 234, 558-560, 559f-560f  
 cardiac tumors in, 559  
 genetics of, 560  
 main aspects of, 559t  
 renal angiofibromas in, 559
- Tuberous sclerosis, renal macrocysts in, 523
- Tubers, 559
- Tubo-ovarian abscess (TOA), 892f, 939-940, 943f-944f  
 mimicking ectopic pregnancy, 984f  
 secondary to diverticulitis, 893f
- Tubo-ovarian complex (TOC), 939
- Tubular adnexal masses, in ectopic pregnancies, 977f
- Tumors  
 cardiac, 437-440  
 anatomy of, 438  
 definition of, 437, 437f  
 epidemiology of, 437-438  
 genetic considerations of, 438  
 outcomes of, 438  
 in tuberous sclerosis, 559  
 face, 257-262, 261f-262f  
 intracranial, 232-240  
 congenital, 237t  
 fetal, 233-234, 238f  
 MRI for, 763-765  
 nonimmune hydrops and, 645t-647t  
 ovarian, 1020-1022, 1021f-1023f  
 renal, 525, 528f  
 sacrococcygeal teratoma, 777t, 791  
 uterine, lipomatous, 866, 868f  
 uterine, malignant, 903-904
- Turner syndrome, 28, 644, 1009, 1012f  
 TVA. *see* Tricuspid valve atresia (TVA)
- TVS. *see* Transvaginal sonography (TVS)
- 22q11.2 deletion syndrome, 595, 595f
- Twin anemia-polycythemia sequence, 147-148, 153f, 781-782, 782f
- Twin ectopic pregnancies, 972, 978f
- Twin peak sign, 135-136, 138f
- Twin pregnancies, amniotic fluid volume in, 714-715, 715f-716f  
 normal, 714  
 pregnancy outcomes in, 715, 716f  
 subjective estimation of, 715  
 ultrasound estimation of, 714-715
- Twin reversed arterial perfusion sequence, 782-783, 783f
- Twin reversed arterial perfusion syndrome, 144-145, 146f-147f
- Twin-twin transfusion syndrome, 145-147, 148f-153f, 778-780, 1152f  
 amniotic fluid volume in, 715, 716f  
 diagnosis of, 778  
 fetal growth studies in, 142-143, 143f  
 laser for, 780f  
 monochorionic diamniotic twin pregnancy with, 1153f  
 Quintero staging of, 146, 150t  
 stage-based perinatal survival after laser surgery for, 780t  
 staging of, 779t
- Twins  
 appearing, 94, 95f  
 dichorionic, 1152f  
 with discordant structural anomalies, 783  
 embryology of, 132-133, 133f-134f  
 transvaginal sonography for, 665  
 monochorionic, 1152f  
 monochorionic, MRI for, 765, 768f  
 in second trimester, 1151f  
 twin anemia-polycythemia sequence, 781-782, 782f  
 twin reversed arterial perfusion sequence, 782-783, 783f  
 twin-twin transfusion syndrome, 778-780  
 vanishing, 94, 94f
- Twisted vascular pedicle, 886
- Two-diameter pocket, 706-707
- Two-dimensional ultrasound, thoracic and lung  
 dimensions by, 293, 294f-295f, 295t-297t

## U

- UAE. *see* Uterine artery embolization (UAE)
- Ulna, fetal, 165, 172f  
 length of, relationship between humerus and, 285f
- Ulnar clubhand, 323
- Ulnar ray defects, 322t
- Ultrasound beam, and obese patient, 799-800
- Ultrasound examination, 1-23  
 ALARA (as low as reasonably achievable) principle in, 4, 4f  
 categories of, 5  
 collaboration in, 5

- Ultrasound examination (*Continued*)  
 discussing with patients, 19-20  
 equipment and documentation of, 6  
 evaluating literature on, 20, 20t  
 of fetal anatomy, 157-219  
 fetal anomaly detection, 4  
 of fetal movements, 159-160  
 guidelines for, 4-5, 7t-12t, 8f  
 indications for, 4-6  
 interpretation of, 18-20  
 malpractice and, 20  
 nonmedical use of, 5  
 obstetric, 1-23  
 pathologic process in, identification of, 21, 21f  
 performance of, 5  
 pitfalls in, 18  
 reporting results in, 18-19  
 safety of, 3-4, 4f  
 self-referral, 5  
 spatial resolution and contrast in, 157-158  
 technique for, 158  
 terminology for, 5  
 thermal index in, 3  
 training for performance and interpretation of, 5  
 transducers in, 6
- Ultrasound lexicon, 6
- Umbilical arteries, 693-694, 695f  
 end-diastolic flow in, 745-746  
 and fetal bladder, 504, 506f  
 fetal Doppler of, 734-735, 734f-735f  
 pulsatility index of, 736t  
 resistance index of, 736t-737t  
 serial measurements of, reference values for, 735t  
 single, 695-697, 696f
- Umbilical artery Doppler velocimetry, 730, 731f
- Umbilical coiling index, 695
- Umbilical cord, 184, 184f-186f, 693-698, 695f  
 anomalies, and nonimmune hydrops, 645t-647t  
 cyst, 1117f  
 dimensions and coiling of, 695  
 hypercoiled, 696f  
 hypo-coiled, 696f  
 insertion of, 681, 681f  
 abnormalities in, 681-683, 681f  
 marginal, 681  
 vasa previa, 682-683, 683f  
 velamentous, 681-682, 682f  
 normal development of, 693-694  
 remnants and cysts, 694-695, 695f  
 short-axis view of, 1145f  
 thick, 1145f  
 ultrasound evaluation of, 674-703  
 vascular abnormalities of, 695-698  
 cord entanglement, 698, 698f-699f  
 knots, 698, 698f  
 nuchal cords, 698  
 persistent right umbilical vein, 697, 697f  
 single umbilical artery, 695-697, 696f  
 umbilical vein varix, 697-698, 697f
- Umbilical vein, 184  
 blood flow through, 739, 740f  
 mean velocity of, 744t  
 Doppler waveform of, 742f  
 persistent right, 475, 697, 697f
- Umbilical vein varix, 697-698, 697f, 1142f
- Unicornuate uterus, 852, 1004-1006, 1005f, 1007f  
 in lateral fusion defects, 1081  
 müllerian duct anomalies and, 1048-1049, 1049f  
 repair of, 1081
- Unilateral renal agenesis, 519, 520f
- Uniparental disomy (UPD), 47, 47f
- Universal CL screening, 667-668
- UPD. *see* Uniparental disomy (UPD)
- UPJ obstruction. *see* Ureteropelvic junction (UPJ) obstruction
- Upper extremity anomalies, 585-589  
 Adams-Oliver syndrome, 585  
 Cornelia de Lange syndrome, 585  
 ectrodactyly-ectodermal dysplasia-clefting syndrome, 586, 586f  
 Fanconi anemia as, 586  
 Holt-Oram syndrome, 586-588, 587f  
 Roberts syndrome, 588  
 thrombocytopenia-absent radius syndrome, 588-589  
 Townes-Brocks syndrome, 589
- Urachal cyst, 495f, 497
- Urachus, 504
- Ureter, distal, 829, 830f
- Ureteric bud, 504, 505f  
 divisions of, 504
- Ureterocele, 509-511, 512f  
 ectopic, 517
- Ureteropelvic junction (UPJ) obstruction, 506-509  
 differential diagnosis of, 509
- Ureterovesical junction (UVJ), 829, 935  
 obstruction, 509, 511f
- Ureters, fetal, 505f  
 bilateral single ectopic, 528-529
- Urethra, fetal, 200, 829, 830f-831f  
 atresia of, 515, 515f  
 megalourethra, 515, 516f  
 transperineal image of, 807f
- Urethral diverticulum, 832f, 1033, 1034f-1035f
- Urethrovesical obstruction, 63
- Urgency urinary incontinence, 1025
- Urinary ascites, 478-479
- Urinary bladder, 808, 829, 830f  
 distended, 1104f  
 transvaginal evaluation, 847  
 examination technique of, 837  
 normal, 830f
- Urinary incontinence, 1025, 1031
- Urinary tract, fetal, 503-538  
 and aberrant cephalad migration, 520, 520f  
 bladder, 158-159  
 dilation of, 504-506, 510f  
 causes of  
 duplex collecting system/ureterocele as, 509-511, 512f-513f  
 lower urinary tract obstruction as, 512-515, 513f, 515t  
 transient, 506  
 ureteropelvic junction obstruction as, 506-509  
 ureterovesical junction obstruction, 509, 511f  
 vesicoureteral reflux as, 511, 513f  
 classification system for, 504-506, 510f  
 normal values for, 509t  
 ultrasound parameters in, 507t  
 and cloacal malformation, 515, 516f  
 and congenital megalourethra, 515, 516f  
 etiology of, 510t  
 imaging of, 507f-508f, 510f-514f  
 kidney response to, 506-509, 507f, 511f  
 management of  
 after birth, 516-517, 517f  
 scheme for, 509f  
 and megacystis-microcolon-intestinal hypoperistalsis syndrome, 515-516  
 non-specific, 516-517  
 and prune-belly syndrome, 515  
 risk-based management of, 518f  
 threshold measurement for, 506-509  
 and urethral atresia, 515, 515f  
 embryology of, 504  
 empty renal fossa and, 518-519  
 nonobstructive anomalies of, 517-521  
 nonobstructive megaureter as, 517-518, 518f  
 normal, 504  
 obstructive abnormalities of, 504-517  
 and unilateral renal agenesis, 519, 520f
- Urine, fetal  
 electrolytes in, as prognostic factor in urinary tract dilatation, 513-514  
 production of, 504, 526
- Urine prognostic thresholds, fetal, 790t
- Urinoma, 514f
- Urogenital sinus, 504  
 persistent, 534, 534f
- Urogenital sinus malformations, 471-472
- Urography  
 CT and MRI, 751  
 MR, 751
- Uroynecology, ultrasound and magnetic resonance  
 imaging in, 1025-1044
- Urolithiasis, 913f
- Uropathy, obstructive, 912
- Uterine artery, 816-820  
 diagram of, 819f
- Uterine artery (*Continued*)  
 fetal Doppler of, 736-738, 739f  
 pulsatility index of, 740t  
 resistance index of, 740t  
 normal, 821f
- Uterine artery embolization (UAE), 857, 1078-1079, 1079f  
 contraindications to, 1079t  
 for leiomyoma, 1053
- Uterine bleeding, abnormal, 838-839  
 endometrial carcinoma, 842, 843f-844f  
 endometrial pathology of, 839-843  
 atrophy, 839-840, 840f  
 hyperplasia, 840, 840f-841f  
 evolution of endometrial assessment, 835-838  
 algorithm for, 838f  
 challenges, 837-838, 837f  
 curettage, 835-836  
 transvaginal sonography, 836, 836f  
 examination technique, 837, 837f  
 Pipelle biopsy, 835-836  
 preprocedure considerations, 837  
 saline infusion sonohysterography, 836-837  
 postmenopausal bleeding, 838-839  
 premenopausal bleeding, 839  
 tamoxifen, 842-843, 844f
- Uterine leiomyomas, 858-861, 862f, 866f, 899  
 acute complications of, 901-903  
 additional imaging modalities and, 900  
 adenomyosis and, 904-906  
 appearance of, 864f-865f  
 degenerated exophytic, 903f  
 focal adenomyosis mimicking, 908f  
 growth of, 858-861  
 imaging spectrum of, 901f  
 infected and infarcted, 904f  
 intramural, 866f  
 large  
 classification of, 863f  
 echogenic, 866f  
 large intramural, 902f  
 lipoleiomyoma and, 900-901, 902f  
 locations of, 862f  
 lower uterine segment, 863f  
 malpositioned intrauterine device, 906  
 submucosal, 861, 901f
- Uterine myoma, large, 863f
- Uterine position, 821-822
- Uterine radial artery, 820f
- Uterine segment  
 contractions, ultrasonography of, 656, 658f  
 lower, underdeveloped, 656-657
- Uterine synechia, 692, 693f, 1102f
- Uterine tumors, malignant, 903-904
- Uterus  
 anatomy and physiology of, 1046-1047, 1047f-1048f  
 anomalies, 1004, 1005f  
 antelexion of, 821-822, 822f, 851f  
 anterior surface of, 811  
 anteversion of, 810f-811f, 822-823, 851f  
 arcuate, 856, 857f, 1049, 1049f  
 benign conditions, 857-866  
 adenomyosis, 857-858  
 leiomyomas, 858-861, 862f, 864f-866f  
 lipomatous uterine tumors, 866, 868f  
 bicornuate, 855, 856f, 1049, 1049f-1050f  
 cervical cysts, 878  
 congenital anomalies of, repair of, 1079-1082, 1084f  
 agenesis, 1080-1081  
 American Fertility Society Classification System in, 1080, 1080f, 1080t  
 European Society for Gynaecological Endoscopy (ESGE) classification, 1080, 1082f-1083f  
 European Society of Human Reproduction and Embryology (ESHRE) classification, 1080, 1082f-1083f  
 lateral fusion defects, 1081-1082  
 Vagina Cervix Uterus Adnexa-associated Malformation (VCUAM) classification system, 1080, 1081t  
 vertical fusion defects, 1082  
 congenital malformations of, 852-857  
 diethylstilbestrol exposure, 855f  
 diagram of, 816f, 818f  
 didelphys, 852-855, 856f, 1049, 1049f-1050f



Uterus (*Continued*)

- embryologic development of, 1004f
- endometriotic implant at posterior serosal surface of, 898f
- transvaginal gray-scale of, 848f
- first trimester ultrasound examination of, 13 gravid, 14f-15f
  - ultrasound imaging of
    - artifacts, pitfalls, and normal variants, 1098-1114, 1102f-1103f, 1111f, 1115f, 1119f, 1121f
- iatrogenic processes, 871-877
  - arteriovenous malformations, 871-872
  - intrauterine contraceptive devices, 872
  - postpartum and postabortive uterus, 872-877, 876f-877f
- imaging, 847-852
  - anatomy of, 848-852, 854f
  - guidelines of, 847
  - techniques of, 847-848, 847f-848f
- imaging of, artifacts, pitfalls, and normal variants, 1098-1114, 1102f-1106f, 1108f, 1111f-1112f, 1115f-1116f, 1119f
- improved visualization of, 806f
  - incarcerated, 853f
  - leiomyosarcoma in, leiomyoma and, 1052 malformations, 852
  - malignant conditions of, 866-871
    - gestational trophoblastic disease, 866-868
    - uterine sarcomas, 868-871
  - myomatous, 1053f
  - myometrium of, 823, 851
  - neonatal, anatomy of, 1002, 1002f-1003f
  - nongravid, 823
    - ultrasound imaging of, artifacts, pitfalls, and normal variants, 1098-1114, 1102f
  - polyps and, 878
  - prepubertal, 850, 854f
  - retroflexion of, 813f, 821-822, 822f, 851f, 855f
  - retroversion of, 813f, 822-823, 852f, 855f
  - sarcoma in, 1055f
  - second and third trimester ultrasound examinations of, 17
  - segment leiomyoma, 863f
  - septate, 855-856, 857f, 1049, 1049f-1050f
  - shape and size of, 850
  - sonographic findings of, in ectopic pregnancy, 971-972, 972f-973f
  - sonographic imaging of, in infertility, 954-956
    - adenomyosis, 955, 956f
    - calcified intrauterine material, 956f
    - endometrial polyp, 954-955, 955f-956f
    - endometrium, 954-955, 955f
    - septate uterus, 954f, 955
    - submucosal leiomyomas, 957f
  - 3D sonography of, 813f
    - ultrasound evaluation of, 846-882
  - unicornuate, 852, 1048-1049, 1049f
- Uterus didelphys, repair of, 1082
- UVJ. *see* Ureterovesical junction (UVJ)

## V

- VACTERL association, 25-27, 464, 464f, 631-632, 631f-632f
- Vagina
  - agenesis, 1007-1008, 1008f-1009f
  - anomalies in, 1004, 1051, 1051f
  - atresia, 1010f

Vagina (*Continued*)

- azygos arteries of, 816-820
  - embryologic development of, 1004f
  - foreign body in, 1014, 1016f
  - masses in, 1014-1015, 1017f
  - rhabdomyosarcoma, 1014-1015, 1017f
  - septum in, transverse, 1006-1007, 1008f
- Vagina Cervix Uterus Adnexa-associated Malformation (VCUAM) classification, 1004, 1005t
  - for genital malformations, 1080, 1081t
- Vaginal arteries, diagram of, 818f
- Vaginal bleeding, during early pregnancy, 1116f
- Vaginal septum, 852-855
- Vaginal veins, diagram of, 818f
- Valproate, teratogenicity of, 35, 36t
- Valproic acid syndrome, fetal, 550, 550f
- Van der Woude syndrome, 572-573, 572f
- Van Praagh classification, of truncus arteriosus, 413
- Vanishing twin, 94, 94f
- Variability, in fetal heart rate, 722, 723f
- Varicella zoster, fetal, 547-548, 548f
- Varicella-zoster virus, intrauterine infection, 36t
- Vasa previa, 16-17, 682-683, 683f
  - in multiple gestations, 139
- Vascular abnormalities, 237
- Vascular disorders, and nonimmune hydrops, 645t-647t
- VATER/VACTER association, 322
- VCUAM. *see* Vagina Cervix Uterus Adnexa-associated Malformation (VCUAM) classification
- VCUG (voiding cystourethrogram), 516-517
- Vecchiotti procedure, for agenesia, 1081
- Vein of Galen, aneurysm of, 237, 238f
- Velum interpositum, cyst of, 1130f
- Venolymphatic malformation, MRI of, 760f
- Venous pressure, in hydrops fetalis, 638
- Ventral wall defects, 483-497, 484t
  - bladder and cloacal extrophy/OEIS complex, 496-497
  - gastroschisis, 493-496
  - limb-body wall complex/amniotic band syndrome, 495f, 497
  - omphalocele, 483-493, 484t
  - pentalogy of Cantrell, 494f, 497
  - urachal cyst, 495f, 497
- Ventricles
  - imaging of, 104-105
  - low short-axis view of, 393, 395f
- Ventricular chambers, 389
- Ventricular ejection force, in fetal growth restriction, 747
- Ventricular septal defect (VSD), 402-405
  - anatomy of, 403, 403f-407f
  - atrioventricular canal type, 404, 406f
  - definition of, 402
  - diagnostic imaging features of, 403
  - diagnostic imaging tips of, 403-405
  - epidemiology of, 402-403
  - genetic considerations of, 403
  - interventions and prognosis of, 403
  - nomenclature of, 402t
  - tetralogy of Fallot and pulmonary atresia with, 409-412
    - anatomy of, 409-410, 411f
    - definition of, 409, 410f
    - diagnostic imaging features of, 411-412
    - epidemiology of, 409
    - genetic considerations of, 410-411, 412t
    - interventions and prognosis of, 411
- Ventricular septum, 1133f
- Ventricular tachycardia, 443
- Ventriculoarterial junction, 390-391

## Ventriculoarterial valves, 390-391

- Ventriculomegaly, 222, 223f
  - aneuploidy and, 61, 61f
  - holoprosencephaly and, 109
  - mild, 222, 223f
  - MRI of, 754, 754f
  - severe, 222, 223f
- Vermian agenesis/hypoplasia, 230
- Vertebrae
  - flattening of, 277, 286f
  - hemivertebra, 277, 286f
- Vertebral anomalies, 583-585
  - Klippel-Feil syndrome, 583, 583f
  - spondylocostal dysostosis, 584-585, 584t
- Vertebral bodies, 301-302, 302f
- Vertical fusion defects, repair of, 1082
- Vesicoamniotic shunting, 514
- Vesicoureteral reflux (VUR), 511, 513f
- Viability. *see* Fetal viability
- Vibroacoustic stimulation, 724
  - in modified biophysical profile, 729
- Villous trophoblasts, 675-676
- Vitelline arterial steal, 590
- Voiding cystourethrogram (VCUG), 516-517
- Volume imaging, 160, 160f
  - for fetal skeletal structures, 161, 167f
- VSD. *see* Ventricular septal defect (VSD)
- VUR (vesicoureteral reflux), 511, 513f

## W

- Walker-Warburg syndrome, 556
- Warfarin embryopathy, 551
- Warfarin syndrome, fetal, 551, 551f
- Weaver syndrome, 622
- Webbed neck, 266
- Wharton jelly, 694
- "Whirlpool sign", 886
- Williams vaginoplasty, for agenesia, 1081
- Wolf-Hirschhorn syndrome, 624
- Wolffian duct, development of, 1003-1004
- World Federation for Ultrasound in Medicine and Biology, 3

## X

- X-linked hydrocephalus with stenosis of the aqueduct of Sylvius (HSAS), 560
- X-linked inheritance, 30f-31f, 32
- X-linked Opitz G, 573
- Xanthogranulomatous inflammation, 940-946
- Xanthogranulomatous salpingitis, 947f

## Y

- Yolk sac
  - detecting gestational sac without embryo or, 84
  - large, in pregnancy failure, 91, 92f
  - in uterus, transvaginal sonogram, 1112f
- Yunis-Varon syndrome, 316-317

## Z

- Zellweger syndrome, 627-628
- Zona functionalis, 823-824